Infrared Study of Aniline Adsorbed on Aluminum Halides and on Gallium Chloride

Hiroyasu SATO and Shin-ichi ARASE*

College of Liberal Arts, Kagoshima University, Kagoshima 890

(Received March 4, 1975)

Infrared study was made on aniline adsorbed on aluminum chloride, bromide and iodide. Aniline-d_0 ($C_6H_5NH_2$), aniline-*N,N*-d_2, aniline-d_5 ($C_6D_5NH_2$) and aniline-d_7 were used. Aniline-d_0–gallium chloride system was studied for comparison. Only the bands associated with amino group showed large frequency shifts on complex formation. The structures of adsorbed molecules were discussed in terms of the frequency shift of bands, especially of those assigned to C–N stretching and ND_2 bending modes. The interaction of adsorbed aniline with aluminum chloride is rather weak and predominantly ionic. A strong chemisorption with the formation of an essentially covalent N···Al bond can be deduced for aniline adsorbed on aluminum bromide, iodide and gallium chloride. Such an ionic adsorption on aluminum chloride can be understood by considering the ionic structure of solid aluminum chloride. Some of the observed bands for aniline-d_5 are (cm^{-1}); 3424, 3350, 3312 (NH str.), 1620 (NH_2 bend.) and 1300 (CN str.).

Considering the importance of aluminum halides as catalysts for a large number of organic reactions, the spectroscopic study of organic molecules adsorbed on solid aluminum halides is of much interest. One of the authors (H. S.) studied the UV spectrum (300—150 nm) of aniline adsorbed on aluminum chloride, showing that it has an intermediate feature between free aniline molecule and toluene.[1] This was interpreted by assuming the interaction of the lone pair on the nitrogen atom in aniline molecule with the vacant sp^3-type orbital on the aluminum atom in aluminum chloride.[2] Thus, it is clear that some kind of adsorption complex is formed. Measurement of the IR spectrum is essential for a more detailed discussion on the structures of the adsorption complexes. Such a study, however, has not so far been made.[3] We have measured IR spectra for aniline adsorbed on aluminum chloride, bromide and iodide. The study of aniline adsorbed on aluminum bromide in comparison with that on aluminum chloride is interesting if one considers the difference of these two halides as regards their crystal structures and the physical properties in the solid phase. It is known that the dimeric structure Al_2X_6 (X=Cl, Br) in the gas phase[4] remains on transition to the liquid phase,[5-7] but in the solid phase aluminum chloride has a crystal structure based on an ionic bonding scheme,[8] while solid aluminum bromide retains the dimeric structure.[9] The difference of structure in the solid phase is also reflected in their physical properties. Solid aluminum chloride has a significant electric conductivity; the conductivity increases as the melting point is approached but falls abruptly nearly to zero on melting; the volume increases sharply on melting.[10] Pershina and Raskin[11] showed that the Raman spectrum of solid aluminum chloride differs from that of liquid aluminum chloride, while the Raman spectra of these two phases coincide for aluminum bromide.[12] In the present study, three deuterium-labelled compounds, *i.e.*, aniline-*N,N*-d_2 ($C_6H_5ND_2$), aniline-d_5 ($C_6D_5NH_2$) and aniline-d_7 ($C_6D_5ND_2$) were used together with aniline-d_0 ($C_6H_5NH_2$) to make the assignments of IR bands unambiguously by separating the bands related to the modes in amino group from those related to the modes in phenyl group. Aniline-d_0–gallium chloride system was studied for comparison.

Experimental

Materials. Aluminum chloride was prepared from aluminum and silver chloride *in vacuo*.[1] Aluminum bromide or iodide was prepared in a similar way using the corresponding silver halide. Gallium chloride was prepared from gallium and silver chloride. All the compounds were stored in ampoules with break-off seals. Aniline-d_0 was distilled under reduced pressure, dried over potassium hydroxide and distilled again *in vacuo* before use. Aniline-*N,N*-d_2 was prepared by treating aniline with heavy water. Aniline-d_7 of minimum isotope purity of 99 atom% (J. T. Baker Chemical Co., Philipsburg, N. J., U. S. A.) was distilled under reduced pressure. Aniline-d_5 was prepared by treating aniline-d_7 with water. The three compounds were dried over anhydrous potassium carbonate and distilled *in vacuo* before use.

Procedure. The cell assembly used in IR measurement was similar to the one used previously,[1] but was provided with NaCl or KBr windows. This was degassed thoroughly (more than two hours at 10^{-3} Torr) before use. After aluminum halide or gallium chloride was sublimed onto the NaCl or KBr window plate, aniline vapor was introduced into the cell. After evacuation, IR spectra were recorded on JASCO IRA-1 (for 4000—650 cm^{-1}) or IRA-2 (for 4000—400 cm^{-1}) recording spectrophotometers.[13]

Results

The following symbols are used: aniline-d_0 (**1**) aniline-*N,N*-d_2 (**2**), aniline-d_5 (**3**), aniline-d_7 (**4**), aluminum chloride (A), aluminum bromide (B), aluminum iodide (C), gallium chloride (D). The complexes are also shown by these symbols (*e.g.* **1**A for aniline-d_0–aluminum chloride complex).

Complexes of Aniline-d_0 *and Aniline*-N,N-d_2. IR spectra of **1**, **1**A, **1**B, **1**C and **1**D are shown in Fig. 1, and those of **2**, **2**A and **2**B in Fig. 2. The assignment of IR bands for **1** and **2** was well established by Tsuboi[14] and Evans.[15] The bands of **1** or **2** can be classified into two groups, those associated with (a) the phenyl group, and (b) the amino group (C–N stretching in-

* Present Address: Faculty of Education, Kagoshima University.

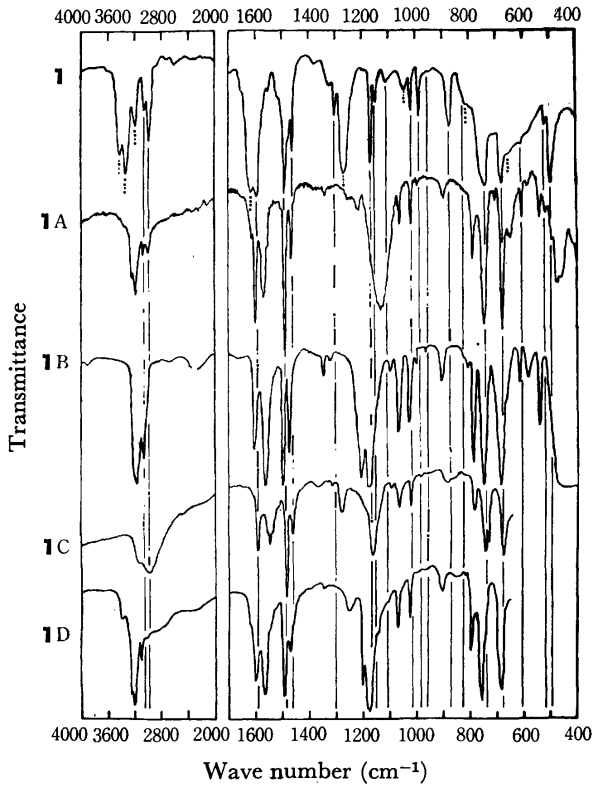

Fig. 1. IR spectra.
(1) aniline-d_0 (liq.).
(1A) aniline-d_0–aluminum chloride.
(1B) aniline-d_0–aluminum bromide.
(1C) aniline-d_0–aluminum iodide.
(1D) aniline-d_0–gallium chloride.

clusive). The full lines show the positions of bands belonging to group (a), dotted lines those of group (b). Some of the bands of complexes fell in the close vicinity of the bands belonging to group (a) of the free molecules, essentially retaining their relative intensities. These bands can be attributed to the modes within the phenyl group of the complex. The complex formation clearly

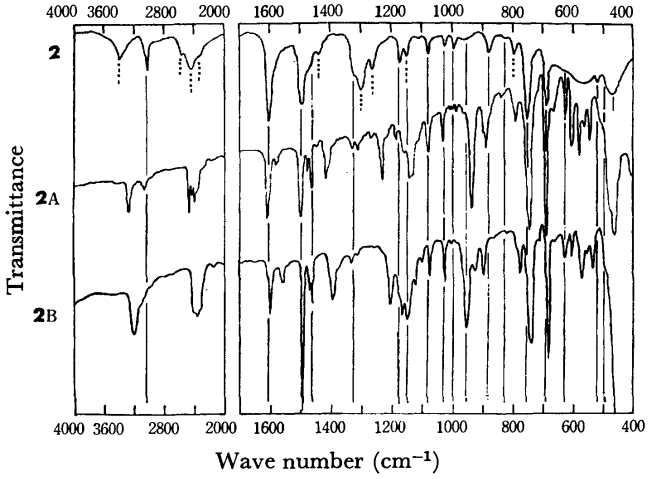

Fig. 2. IR spectra.
(2) aniline-*N*-*N*-d_2 (liq.).
(2A) aniline-*N*,*N*-d_2–aluminum chloride.
(2B) aniline-*N*,*N*-d_2–aluminum bromide.

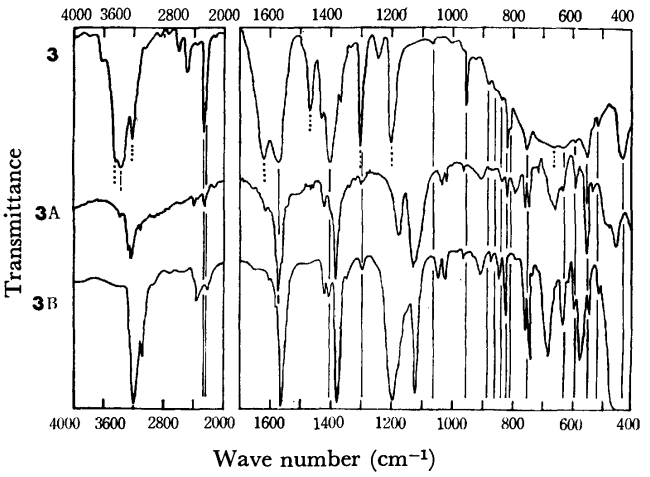

Fig. 3. IR spectra.
(3) aniline-d_5 (liq.).
(3A) aniline-d_5–aluminum chloride
(3B) aniline-d_5–aluminum bromide.

gave little effect on the vibrations within the phenyl moiety. On the other hand, the bands of group (b) showed a large shift on complex formation. This shows that it is the amino group and C–N bond that are affected by complex formation and that the coordination of the amino group occurs on adsorption. The positions of bands thus attributed to amino group (C–N stretching inclusive) are listed in Table 1.

Complexes of Aniline-d_5 *and Aniline*-d_7. IR spectra of **3**, **3A** and **3B** are shown in Fig. 3, and those of **4**, **4A** and **4B** in Fig. 4. No IR spectrum of **3** seems to have been published. As to **4**, Ostrowska and Tramer[16] published the wave numbers of IR bands in the region above 700 cm^{-1}. They gave assignments for some of the bands. Rai and Maheshwari[17] gave the wave numbers of seven bands without assignments. The positions of bands in our spectrum are in line with theirs.[18] Complete assignments of the bands for **3** and **4** were made. They are given in the Appendix. Since Ostrowska and Tramer[16] did not give assignments

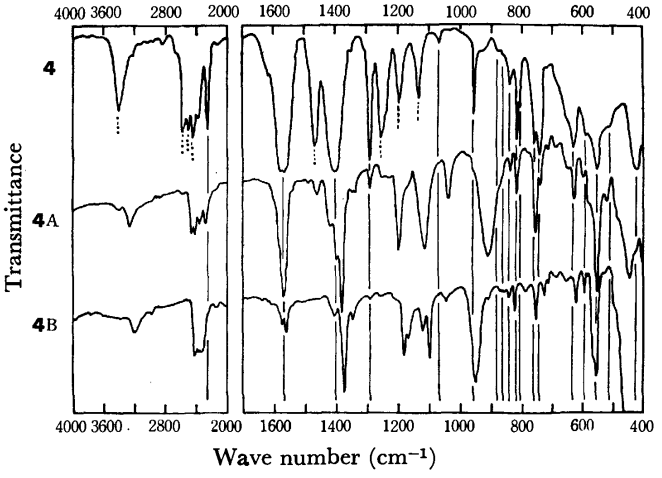

Fig. 4. IR spectra.
(4) aniline-d_7 (liq.).
(4A) aniline-d_7–aluminum chloride.
(4B) aniline-d_7–aluminum bromide.

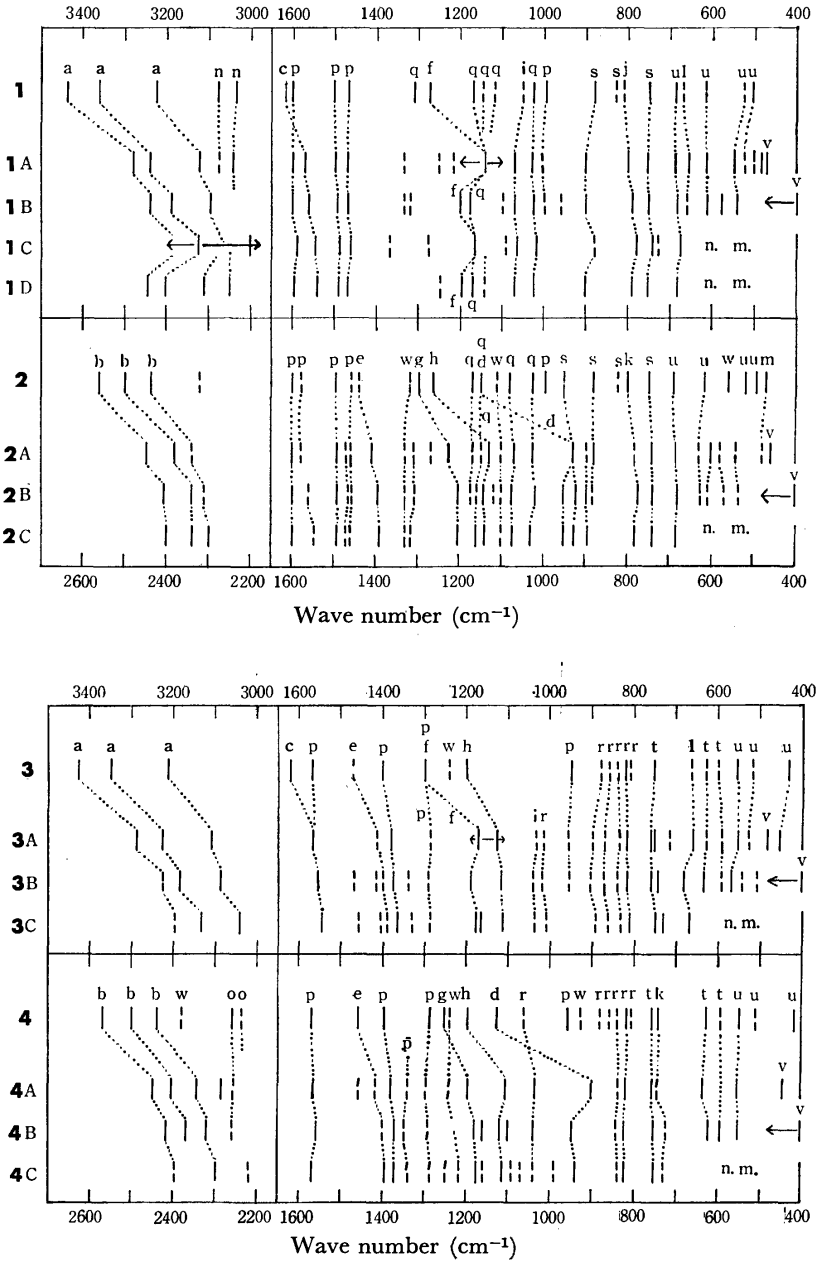

Fig. 5. IR spectra of aniline–aluminum halide and –gallium chloride complexes; positions of the bands. Solid lines show strong bands. Broken lines indicate weak bands (or a shoulder). Horizontal arrow shows the region covered by a very broad band. Corresponding bands are connected. **1.** aniline-d_0, **2.** aniline-N,N-d_2, **3.** aniline-d_5, **4.** aniline-d_7, A. aluminum chloride, B. aluminum bromide, C. aluminum iodide, D. gallium chloride, a. NH str., b. ND str., c. NH_2 bend., d. ND_2 bend., e. NHD bend., f. CN str. (NH_2), g. CN str. (ND_2), h. CN str. (NHD), i. NH_2 tw., j. NH_2 rock., k. ND_2 rock. (or tw.), l. NH_2 wag., m. ND_2 wag., n. CH str., o. CD str., p. ring str., q. CH in-plane bend., r. CD in-plane bend., s. CH out-of-plane bend., t. CD out-of-plane bend., u. ring def., v. AlX_3 skeletal vibration, w. combination band; n.m. region not measured.

for all the bands, those for **4** are given here for comparison with the assignments of bands in **3**. After these assignments were made, the IR bands of **3** and **4** were classified into groups (a) and (b) as for **1** and **2**. It was found that only the bands of group (b) showed a large shift on complex formation. The positions of bands thus attributed to the amino group (C–N stretching inclusive) are listed in Table 1.

The positions of observed bands for all the systems studied are shown in Fig. 5, with their assignments given by symbols.

Table 1. Bands ascribable to the amino-group, positions of bands in cm^{-1}

Aniline-d_0 ($C_6H_5NH_2$)					Assignment	Aniline-d_5 ($C_6D_5NH_2$)			
free[a]	$AlCl_3$	$AlBr_3$	AlI_3	$GaCl_3$		free[a]	$AlCl_3$	$AlBr_3$	AlI_3
3436	3282	3238		3246	NH str.	3424	3290	3230sh	3200sh
3360	3238	3190	3124	3204		3350	3226	3184	3134
3222	3122	3094	3000			3212	3110	3084	3044
1617	1572	1559	1545	1562	NH_2 bend.	1620	1565[b]	1555[b]	1547[b]
					NHD bend.	1470	1415	1401	1389
1272	1140	1201	1164	1169	CN str.	1300	1165[c]	1191	1172
					CN str. (NHD)	1197	1125[c]	1119	1114
1051	1070	1071	1064	1067	NH_2 tw.		1033	1041	1035
810	799	789	781	791	NH_2 rock.				
670	655	660sh			NH_2 wag.	660	655	677	667
—	483 468	≲400[d]			AlX_3	—	480	≲400[d]	

Aniline-*N*,*N*-d_2 ($C_6H_5ND_2$)				Assignment	Aniline-d_7 ($C_6D_5ND_2$)			
free[a]	$AlCl_3$	$AlBr_3$	AlI_3		free[a]	$AlCl_3$	$AlBr_3$	AlI_3
3400	3258	3200	3165	NH str. (NHD)	3400	3244	3200	3178
2560	2446	2406	2400	ND str.	2570	2450	2414	2398
2500	2382	2340	2340		2500	2404	2360	2300
2438	2340sh	2310sh	2300		2442	2344	2320	2218
1440sh	1409	1393	1390	NHD bend.	1461	1415	1401	1398
1300	1227[e]	1203[e]	1203[e]	CN str.	1253	1196[e]	1178[e]	1173[e]
1260	1129	1145	1140	CN str. (NHD)	1197	1110	1120	1117
1150	931[e]	953[e]	950[e]	ND_2 bend.	1130	902[e]	948[e]	941[e]
798	784	775	780	ND_2 rock. (or tw.)	741	740	726	725
470	480			ND_2 wag.				
—	460	≲400[d]		AlX_3	—	446	≲400[d]	

a) Liq. film. b) The positions of bands ascribable to ring vibration. Bands related to NH_2 bending vibration seem to be superimposed on these bands. c) See Ref. 22. d) A strong band was present around or below 400 cm^{-1}. e) These two bands are attributed to the modes given by the coupling of CN stretching and ND_2 bending modes. (See Text.)

Discussion

Some characteristic bands of complexes are discussed below. Detailed information on the structures of adsorption complexes was obtained by examination of direction and magnitude of the frequency shifts. C–N stretching modes for NH_2 and ND_2 are shown as C–NH_2 and C–ND_2 stretching, respectively.

1) Aluminum Halide Complexes. NH_2 (and ND_2) Stretching Vibration: Substantial reduction was observed in the NH_2 stretching frequencies. The magnitude of the frequency shift for the complexes of **1** and **3** increased in the order: A<B<C. It amounted to about 160 cm^{-1} and more than 200 cm^{-1} for the complex of B and that of C, respectively. The relative order of the frequency shift was the same for ND_2 stretching frequencies (in the complexes of **2** and **4**).

NH_2 Bending Vibration: The band assigned to this mode shifted to lower frequencies in the complexes of **1**. The result is in line with that of aniline adsorbed on alumina.[3] The magnitude of the frequency shift was in the order: **1**A<**1**B<**1**C. In the complexes of **3**, this mode seems to be superimposed on the benzene ring stretching mode and the relative order of magnitude in the frequency shift was the same as above.

C–NH_2 Stretching Vibration: The 1272 cm^{-1} band of **1** has been assigned to the C–NH_2 stretching mode, which is lowered in frequency by the coupling with the NH_2 bending mode.[15] This band is higher in frequency than the corresponding band in aliphatic amines (*e.g.* 1044 cm^{-1} in methylamine[19]) due to the double bond character in the C–N bond.[15,20] The double bond character is given by the partial conjugation of the lone pair on the nitrogen atom with π-electrons in the phenyl group. The band in **1**A, **1**B or **1**C which is to be correlated with this band is at 1140 cm^{-1}, 1201 cm^{-1} or 1164 cm^{-1}, respectively. The relative order of magnitude of the shift was **1**B<**1**C<**1**A. An abnormally large shift for **1**A is to be noted. The 1140 cm^{-1} band in **1**A is peculiar as regards its very high intensity and broadness. The shifts to lower frequencies in the complexes **1**B and **1**C can be explained in terms of the decrease in the double bond character of C–N bond caused by the partial consumption of the lone pair on the nitrogen atom by the formation of N–Al coordination bond. However, the abnormally large shift in

1A can not be explained along this line, because the interaction of the lone pair with aluminum atom in **1**A is weaker than in **1**B, as revealed by their UV spectra.[21] For complexes **3**A, **3**B and **3**C, the band appearing in a position similar to that in the case of **1**A, **1**B and **1**C, respectively, can be assigned as due to this mode (Table 1), and the relative order of magnitude in the frequency shift was the same as above.[22,23]

C–ND_2 Stretching and ND_2 Bending Vibrations: A strong band near 1200 cm^{-1} in each of the complexes of **2** and **4** can be correlated to C–ND_2 stretching vibration.[23,24] The relative order of the magnitude in the frequency shift for the complexes of **2** and **4** is as follows; complex of A< that of B≲ that of C.

A strong band was found in the 900—950 cm^{-1} region in each of the complexes of **2** and **4**. This does not correspond to the bands of phenyl group. When the band around 1200 cm^{-1} was correlated to C–ND_2 stretching vibration, it remains as the only one to be correlated to ND_2 bending vibration. The frequency shift on complex formation is very large, the relative order of magnitude being as follows; complex of B< that of C< that of A. This order is exactly the same as that of the bands attributed to C–NH_2 stretching vibration. An extensive coupling should be assumed between C–ND_2 stretching and ND_2 bending modes in the complexes.

AlX_3 Skeletal Vibration: A strong band was found in the 450—480 cm^{-1} region or near (or lower than) 400 cm^{-1} for the complexes of A or those of B, respectively. The band can be attributed to AlX_3 skeletal vibration, since a band with a similar position and band shape was found in the NH_3–AlX_3 complex (X=Cl or Br).[25]

N···Al Stretching Vibration: No band with considerable intensity was found.

2*)* *Aniline-d_0–Gallium Chloride Complex*: IR spectrum was similar to that of **1**B.

The abnormally low frequency of the band attributed to C–NH_2 stretching vibration in aluminum chloride complexes (**1**A and **3**A) can be explained by assuming a large ionic character and the elongation of C–N bond in these complexes. The presence of such an ionic character in C–N bond can be understood if we consider the "ionic structure" of solid aluminum chloride. The aluminum atom in aluminum chloride carries some positive charge. On the other hand, aniline molecule is rather weakly adsorbed on the surface of aluminum chloride as revealed by its UV spectrum.[21] The IR spectrum shows that the coordination of the amino group occurs on adsorption. The positive charge on the aluminum atom polarizes the C–N bond giving large ionic character in this bond with the bond elongation. The abnormally high intensity of 1140 cm^{-1} band in **1**A would support the assumption of such an ionic C–N bond, since a large change in dipole moment is expected to accompany the C–N stretching vibration.

The abnormally large frequency shift of the bands associated with ND_2 bending vibration in **2**A and **4**A can be explained by considering the coupling of the modes. It is known that C–ND_2 stretching vibration and ND_2 bending vibration have little coupling with each other in the free molecule, though the two belong to the same symmetry species.[14] This situation changes, however, in the complexes we studied. If C–ND_2 stretching frequency is lowered by some ionic character brought into C–N bond and/or by a decrease in the double bond character of C–N bond, the separation between this and ND_2 bending frequencies becomes smaller, and the two modes will be brought into coupling. In the complexes of A, the pronounced reduction of C–ND_2 stretching frequency due to the ionic character of C–N bond brings this mode into an extensive coupling with ND_2 bending mode, the coupling causing two bands widely separated. It is probable that C–ND_2 stretching frequency falls down to nearly equal to or even lower than the ND_2 bending frequency in the free molecule, and these two modes are extensively mixed. As a result the higher wave number member of the coupled modes in the complex has apparently only a small shift toward a lower wave number as compared with the C–ND_2 stretching mode in the free molecule. The lower wave number member in the complex shows an abnormally large shift toward the lower wave number as compared with the ND_2 bending mode in the free molecule. This coupling is shown schematically in

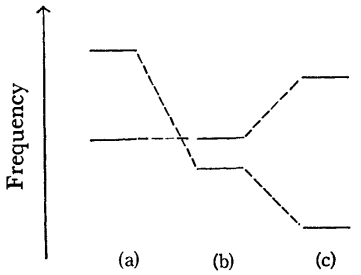

Fig. 6. Diagram showing the coupling of C–ND_2 stretching mode and ND_2 bending mode by complex formation.
(1) in free molecule (**2** or **4**).
(2) hypothetical case in which C–ND_2 stretching mode decreased in frequency and not coupled with ND_2 bending mode.
(3) (2)+coupling, the real case in the complex.

Fig. 6. It can be deduced that the adsorption of aniline on aluminum chloride is rather weak and predomiantly ionic, with a highly polarized C–N bond.

In the complexes of B and C, the interaction of the lone pair on the nitrogen atom in aniline molecule with aluminum halide is larger than in the case of complex of A, as revealed by their UV spectra.[21] The lone pair is partially consumed in the formation of the coordination bond to the aluminum atom, more or less covalent N···Al bond being formed. The hybridization of the nitrogen atom becomes closer to sp^3, and the double bond character of C–N bond decreases. In the complexes of B, the aluminum atom has no large positive charge and the polarization effect on C–N bond is small. If any polarization occurs, the effect will be compensated by the flow of electron from nitrogen atom to aluminum atom. The situation will be similar in the complex of C. In these complexes, the decrease in frequency of C–N stretching mode occurs by the reduction of double bond character of C–N bond.

TABLE 2. POSITIONS OF BANDS AND THEIR ASSIGNMENTS FOR ANILINE-d_5 AND ANILINE-d_7 (liq. film)

Aniline-d_5 ($C_6D_5NH_2$)	Aniline-d_7 ($C_6D_5ND_2$)	Assignment[a]	Corresponding band in	
			$C_6D_5CD_3$[b,d]	C_6D_6[c,d]
3424 s	—	NH str.		
—	3400 m	NH str. (NHD)		
3350 s	—	NH str.		
3212 m	—	NH str.		
2599 w	—	1300×2		
—	2570 m	ND str.		
—	2500 m	ND str.		
—	2442 m	ND str.		
	2382 sh	1197×2		
2260 m	2260 m	CD str.	2276 (ν_{20b})	2288 (ν_{20})
2240 sh	2240 sh	CD str.	2262 (ν_{20a})	
1620 s	—	NH_2 bend.		
1570 s	1570*s	ring str.	1583 (ν_{8a})	1558 (ν_8)
			1570 (ν_{8b})	
1470 w	1461 m	NHD bend.		
1400 s	1400*s	ring str.	1388 (ν_{19a})	1333 (ν_{19})
			1332 (ν_{19b})	
1300 s		CN str. (NH_2) + ring str.		
	1288 s	ring str.	1375 (ν_{14})	1282 (ν_{14})
	1253*m	CN str. (ND_2)		
1240 w	1240 sh	804+431?		
1197 m	1197 m	CN str. (NHD)		
	1130*m	ND_2 bend.		
	1066 w	CD bend. i.p.	972 (ν_3)	1059 (ν_3)
953 m	955 m	ring str.	961 (ν_{12})	970 (ν_{12})
	928 w	508+420		946 (ν_1)
880 vw	880*vw	CD bend. i.p.	880 (ν_{9a})	868 (ν_9)
860 vw	860*vw	CD bend. i.p.	869 (ν_{9b})	
				827 (ν_5)
				824 (ν_{15})
838 vw	838*w	CD bend. i.p.	840 (ν_{18a})	814 (ν_{18})
818 m	818*m	CD bend. i.p.	819 (ν_{18b})	
804 sh	804 sh	CD bend. i.p.	785 (ν_5)	
750 m	755 m	CD bend. o.p.	717 (ν_1, ν_{17b})	793 (ν_{17})
	741*m	ND_2 rock (or tw.)		
660 w		NH_2 wag.		
626 w	628 m	CD bend. o.p.	658 (ν_{10a})	664 (ν_{10})
594 w	593 vw	CD bend. o.p.	605 (ν_{11}, ν_{6b})	601 (ν_4)
552 s	553 s	ring def.	541 (ν_4)	579 (ν_6)
515 w	508 vw	ring def.	490 (ν_{6a})	496 (ν_{11})
431 s	420 s	ring def.		

a) i.p.=in plane, o.p.=out of plane. b) From Ref. 28. All the strong bands (with relative intensity greater than 8 in Table 2 in Ref. 28 except those assigned to CD_3 group vibrations) are listed. c) From Ref. 27. d) Numbering is after Refs. 27 and 28. * Ostrowska and Tramer (Ref. 16) gave assignments for these bands.

This will bring C–ND_2 mode into coupling with ND_2 bending mode to some extent, which will cause the low frequency shift of the bands associated with the ND_2 bending mode in these complexes. Since the reduction of C–ND_2 stretching frequency for these complexes is smaller than for the complex of A, the extent of this coupling should be smaller and hence the frequency shift in ND_2 bending mode also smaller. Thus, the adsorption of aniline on aluminum bromide and iodide can be shown to be a stronger chemisorption (with an essentially covalent N···Al bond) with C–N bond of less polarity than the adsorption on aluminum chloride. Judging from the magnitude of the frequency shifts of bands, the chemisorption on C is stronger than that on B.

In the complex **1D**, the IR spectrum was similar to that of **1B**, and the structure of the adsorbed complex would thus be similar to that of the complex **1B**.

A brief comment will be necessary as to the frequency shifts of NH stretching vibrations. The polarization of C–N bond in the complexes of A accompanies the polarization of N–H bond, reducing the frequencies of N–H stretching vibrations. The frequency shifts of N–H stretching vibrations in these complexes might be larger than in the complexes of B and C owing to this effect, as is the case for the C–N stretching vibrations. However, the observed magnitude of the shifts was in

the order: A<B<C. This can be explained in the following way. There is another factor for reducing the frequencies of N–H stretching vibrations in the complexes of B and C, namely the substantial change in hybridization of the nitrogen atom toward sp^3.

Thus, detailed information on the structures of adsorbed molecules and also on the nature of adsorption (ionic or covalent) was obtained by analyses of the IR spectra.[26]

Our thanks are due to Dr. Taruo Kurokawa, Kogaiboshi Kyokai, Kagoshima Pref., who allowed us the use of their JASCO IRA-2 infrared spectrophotometer.

Appendix

IR Bands of Aniline-d_5 and Aniline-d_7 and Their Assignments. Observed IR bands are listed in Table 2. For aniline-d_7, the positions of bands are in line with the data of Ostrowska and Tramer.[16,18] The assignments of these bands were made as follows. The liquid film of aniline-d_7 was exposed to the air with repeated IR measurement at certain intervals. The content of aniline-d_7 decreased with an increase in aniline-d_5. The bands common to all the spectra were attributed to C_6D_5-group. The assignments were confirmed by comparison with IR bands of benzene-d_6[27] and toluene-d_8.[28] The bands found only in aniline-d_7 or in aniline-d_5 were associated to ND_2- or NH_2-group, respectively. The bands remaining in the intermediate state were assigned to NHD-group. The assignments were compared with those of the corresponding bands in aniline-*N*,*N*-d_2 and aniline-d_0.[14,15] For aniline-d_7, Ostrowska and Tramer[16] gave the assignments of nine bands (shown by asterisks in Table 2). Our assignments for these nine bands agree with theirs except for the band at 741 cm^{-1} which was assigned to CD out-of-plane bending mode.[16] Although this assignment can not be ruled out completely, the band was assigned to ND_2 rocking (or twisting) mode in this paper, since no corresponding band was found in aniline-d_5.

References

1) H. Sato, K. Hirota, and S. Nagakura, This Bulletin, **38**, 962 (1965).
2) H. Sato, S. Nagakura, and K. Hirota, *ibid.*, **38**, 1730 (1965).
3) IR study of aniline adsorbed on alumina was reported: M. Tanaka and S. Ogasawara, *J. Catal.*, **25**, 111 (1972). Their study was limited to the regions of ring stretching and NH_2 bending modes (1400—1700 cm^{-1}) and NH stretching mode.
4) K.J. Palmer and N. Elliot, *J. Amer. Chem. Soc.*, **60**, 1852 (1938).
5) H. Gerding and E. Smit, *Z. Phys. Chem.* (Leibzig), **B50**, 171 (1941).
6) K.W.F. Kohlrausch and I. Wagner, *ibid.*, **B52**, 185 (1942).
7) R. L. Harris, R. E. Wood, and H. L. Ritter, *J. Amer. Chem. Soc.*, **73**, 3151 (1951).
8) J. A. A. Ketelaar, C. H. McGillavry, and P. A. Renes, *Rec. Trav. Chim. Pays-Bas*, **66**, 501 (1947).
9) P. A. Renes and C. H. McGillavry, *ibid.*, **64**, 275 (1945).
10) W. Biltz and A. Voigt, *Z. Anorg. Allg. Chem.*, **126**, 39 (1923).
11) E. V. Pershina and Sh. Sh. Raskin, *Opt. Spektrosk.*, **13**, 488 (1962).
12) Pershina and Raskin (Ref. 11) found that the Raman spectrum of evaporated film of aluminum chloride was identical to that of single crystal. The Raman spectrum of sublimed film of aluminum chloride we obtained was found to be essentially the same as that of evaporated film of these authors. Our sublimed film is of polycrystalline nature and therefore has an ionic structure. Our measurement was made on a JASCO R-300 laser-Raman spectrophotometer by courtesy of JASCO, Co., Hino, Tokyo.
13) The IRA-2 spectrophotometer is installed in the Kogaiboshi Kyokai, Kagoshima Pref.
14) M. Tsuboi, *Spectrochim. Acta*, **16**, 505 (1960).
15) J. C. Evans, *ibid.*, **16**, 428 (1960).
16) B. Ostrowska and A. Tramer, *Acta Phys. Pol.*, **33**, 111 (1967).
17) J. N. Rai and R. C. Maheshwari, *Indian J. Pure Appl. Phys.*, **9**, 27 (1971).
18) Five bands (711, 1025, 1350, 1580, 2276 cm^{-1}) of the 27 bands were not observed. Three bands (3400, 1066, 928 cm^{-1}) in our spectrum are not reported.[16]
19) A. P. Gray and R. C. Lord, *J. Chem. Phys.*, **26**, 690 (1957).
20) N. B. Colthup, L. H. Daly, and S. Wiberley, "Introduction to Infrared and Raman Spectroscopy," Academic Press, New York, N. Y. (1964), p. 280.
21) The UV spectrum of **1B** was measured on a Shimadzu MPS-50L recording spectrophotometer. The shift of the bands toward shorter wavelength was larger than that in the case of **1A** (Ref. 1). The positions of observed UV bands for **1B** (253, 259, 265 nm, the highest peak being that of 259 nm.) were very close to those of anilinium ion $C_6H_5NH_3^+$ (248, 254, 260 nm in H_2SO_4 aq.; "DMS UV Atlas," Vol. IV, Butterworths, London, D6/4 (1968)). The species giving this UV spectrum, however, was not the anilinium ion, but the aluminum bromide complex, since the IR measurement on the same sample gave the characteristics of the complex. The UV spectrum of **1C** gave a broad band in the 246—274 nm region, with an absorption maximum at 258 nm. The location of this band is similar to that of **1B**.
22) For **3A**, two broad bands (1165 and 1125 cm^{-1}) were found in this region. The latter was assigned to C–NHD stretching mode. However, these two bands might result from two types of adsorbed molecules (adsorbed on two types of sites). If this is the case, the band associated to C–NHD stretching mode may be involved in the 1125 cm^{-1} band. It might be possible that the broad 1140 cm^{-1} band of **1A** is actually composed of two bands, one around 1165 cm^{-1} and the other around 1125 cm^{-1}.
23) The bands appearing in 1100—1120 cm^{-1} region seem to be attributable to NHD species, since they were found at the same positions (within experimental error) in the complexes of **3** and **4**, and at the positions close to these in the complex of **2**. (For the 1125 cm^{-1} band of **3A**, see footnote 22).
24) In the complexes of **2** and **4** with B and C, some of the bands assigned to CN stretching vibration were accompanied by another weak band, the nature of which is not clear. This may result from some chemical reaction occuring on these aluminum halides.
25) H. Sato, unpublished result.
26) The relative order of strength in chemisorption was revealed also in the difference of chemical stability of the complexes **1A** and **1B** when the cell systems were exposed to the air. The complex **1A** decomposed immediately to give the IR spectrum of anilinium ion salt, while the IR spectrum of **1B** did not change appreciably for hours.
27) The Chemical Society of Japan, ed., "Kagaku Benran," Maruzen, Tokyo (1966), p. 1157.
28) N. Fuson, C. Garrigou-Lagrange, and M. L. Josien, *Spectrochim. Acta*, **16**, 106 (1960).

pH-Dependence of Spectral Sensitization at Semiconductor Electrodes

Tadashi WATANABE, Akira FUJISHIMA,* Osamu TATSUOKI, and Ken-ichi HONDA

Department of Industrial Chemistry, Faculty of Engineering, University of Tokyo, Hongo, Bunkyo-ku, Tokyo 113

**Department of Applied Chemistry, Faculty of Technology, Kanagawa University, Rokkakubashi, Kanagawa-ku, Yokohama 221*

(Received April 7, 1975)

For an interpretation of the pH-dependence of the sensitized photocurrent at semiconductor electrodes, measurements have been carried out on n-type TiO_2 and CdS single crystal electrodes. As sensitizing dyes, rhodamine B and 3,3'-diethylthiacarbocyanine iodide which remain stable in a sufficiently wide pH range were used. It has been found that the logarithm of the sensitized photocurrent at TiO_2 electrode depends linearly on the pH of the electrolyte solution, whereas the sensitized photocurrent shows practically no pH-dependence at CdS electrode. These observations have been accounted for on the basis of the different pH-dependence of flatband potentials of these semiconductor electrodes.

Investigations of spectral sensitization by means of electrochemical arrangements have so far been carried out by a number of authors on ZnO,[1-14] TiO_2,[15] CdS,[16,17] GaAs,[4] GaP,[4,18] AgCl,[12,19] AgBr,[12,19] SnO_2,[20] Cu_2O,[12,21] and organic semiconductors[1,22,23] such as perylene, chrysene and anthracene. By addition of a suitable dye to the electrolyte solution and by subsequent illumination of the semiconductor-electrolyte interface with light of the optical absorption band of the dye, an enhancement of the photocurrent (sensitized photocurrent) is observed. For most n-type and p-type semiconductor electrodes, the sensitized photocurrent is produced under anodic and cathodic polarizations, respectively.

The magnitude of the sensitized photocurrent can be influenced by several factors such as light intensity, dye concentration, additives (reducing or oxidizing agents in particular), and the pH value of the electrolyte solution.

As regards the effect of pH on the sensitized photocurrent, three examples have so far been reported uniquely on ZnO electrode. Gerischer *et al.*[1] measured the rose bengale-sensitized photocurrent as a function of the pH of the solution. The sensitized photocurrent exhibited only a slight pH-dependence in the alkaline region and completely disappeared below pH 3.8 (owing presumably to the protonation of the dye). However, their results show a remarkable increase in the sensitized photocurrent as the pH decreases from 5.5 to 4.5.

Hauffe *et al.*[8] measured the fluorescein-sensitized photocurrent with varying pH. The magnitude of the sensitized photocurrent showed a maximum when the solution pH was around 7.0, and decreased both in alkaline and acidic solutions. However, the decrease in the photocurrent in the acidic condition is due to some structural change of the sensitizing dye, as is indicated by a remarkable decrease in the fluorescent intensity when compared with that in neutral and alkaline solutions.

Gerischer and Tributsch,[2] using rhodamine B as a sensitizing dye, found that the logarithm of the sensitized photocurrent increased almost linearly with the pH of the solution as it decreased from 9.0 to 1.5, but they did not give any plausible interpretation.

The examples cited above suggest that in the pH range where the sensitizing dye undergoes no structural change, the sensitized photocurrent increases as the pH of the electrolyte solution decreases.

In order to obtain further information on the pH-dependence of the sensitized photocurrent, we have investigated the pH-dependence of the sensitized photocurrent at two different semiconductor electrodes, using two kinds of sensitizing dyes which remain quite stable in a sufficiently wide pH range.

Experimental

Materials and Measuring Setup. Single crystals of TiO_2 and CdS, supplied from Nakazumi Crystals Co., Ltd. and Teikoku Tsushin Co., Ltd., respectively, were used as the n-type semiconductor electrodes. Both were in the form of platelets with a surface area of 1.0 cm^2 and thickness of 1.0 mm. In the case of TiO_2, the crystal was treated at around 600 °C under high vacuum for three hours, prior to the preparation of the electrode, in order to increase the electrical conductivity. The crystals were then cemented with an epoxy resin so that usually the (001) face and the (0001) face of TiO_2 and CdS, respectively, were in contact with the electrolyte solution. The opposite face was used for a barrier-free electrical contact by means of vacuum evaporated indium. Before measurements, the electrodes were polished with alumina paste. The CdS electrode surface was chemically etched with concentrated HCl for a few seconds.

As the sensitizing dyes, rhodamine B and 3,3'-diethylthiacarbocyanine iodide were used. The electrolyte was 0.2 M Na_2SO_4 aqueous solution, and the pH of the electrolyte solution was varied by adding a small amount of H_2SO_4 or NaOH aqueous solution. All the chemicals used were of reagent grade.

A 500-W xenon lamp was used as the light source. The wavelength of the illuminating light was selected with the use of colored glass filters or a Shimadzu monochromator. Illumination of the electrode-electrolyte interface was carried out either through the electrode attached as the window of the electrochemical cell or through a quartz window and the dye-containing electrolyte solution. The photocurrent was detected by means of a Keithley picoammeter Model 417.

Adsorption Measurements. Since direct measurement of adsorption of dyes with single crystals is difficult, a powdered TiO_2 (Kishida Kagaku Co., Ltd.) was used as an adsorbent. 0.5 g of TiO_2 powder was added to 20 ml of a dye solution of various concentrations containing 0.2 M of Na_2SO_4. The

mixture was put into a glass tube assembled on a stirring machine. The TiO_2 powder was kept in contact with the solution for 30 min at 20 °C, and then separated by centrifuging. The absorbance change of the dye solution was determined by means of a Shimadzu spectrophotometer MPS-5000.

Results and Discussion

Since TiO_2 and CdS are n-type semiconductors with relatively large band gaps (3.0 eV and 2.4 eV, respectively), only a small current flows in darkness under anodic polarization, owing to the formation of a depletion layer for the majority carrier at the surface of the electrode. Figure 1 shows typical current-potential curves for the TiO_2 electrode at two different pH values. In the absence of a sensitizing dye and under illumination with light of longer wavelengths than the intrinsic absorption of TiO_2, a small photocurrent is produced, which is almost independent of the pH of the electrolyte solution. By addition of a sensitizing dye, 3,3′-diethylthiacarbocyanine in the present case, a further photocurrent (sensitized photocurrent) was observed, whose spectral dependence is close to that of the optical absorption of the dye adsorbed to TiO_2. The sensitized photocurrent reaches a saturation value under a slight anodic polarization. As can be seen in Fig. 1, with a decrease in pH from 6.15 to 2.2, the saturation value of the sensitized photocurrent shows a remarkable increase by a factor of more than ten.

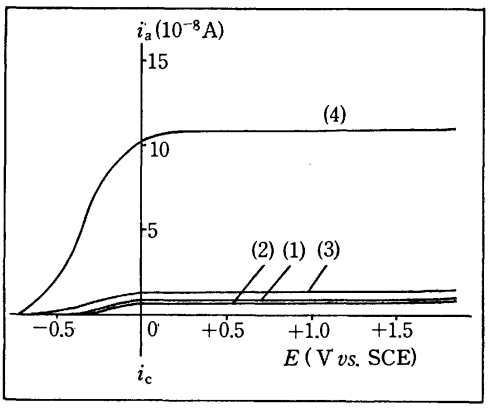

Fig. 1. Current-potential curves for TiO_2 electrode under illumination with $\lambda > 460$ nm.
(1): Blank photocurrent at pH 6.15, (2): same as (1) at pH 2.2, (3): photocurrent by addition of 2×10^{-5} M of 3,3′-diethylthiacarbocyanine at pH 6.15, (4): same as (3) at pH 2.2.

When the sensitized photocurrent is plotted against the dye concentration, in a log-log scale, an almost straight line with a slope of *ca.* 1.0 is obtained in the relatively low concentration region. Figure 2 shows such curves for two different pH values. Decrease in pH enhances the sensitized photocurrent by approximately the same factor, irrespective of the dye concentration.

In the case of the CdS electrode, in contrast to TiO_2 electrode, no pH-dependence of the sensitized photocurrent was observed. Fugure 3 shows the spectra

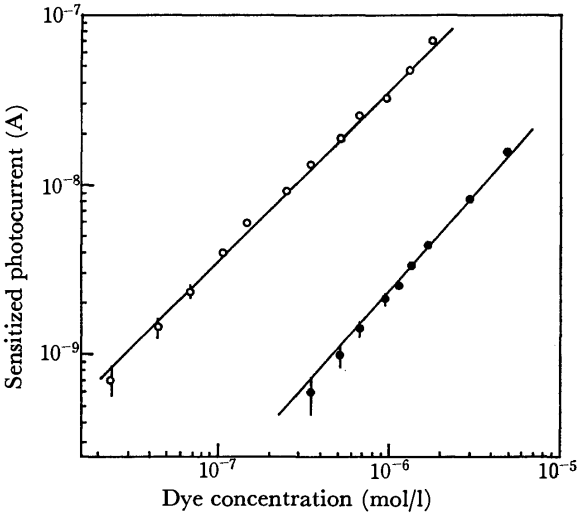

Fig. 2. Dependence of the sensitized photocurrent at TiO_2 electrode upon the concentration of the sentitizing dye (3,3′-diethylthiacarbocyanine iodide) at two different pH values; —○—: pH 2.2, —●—: pH 6.15.

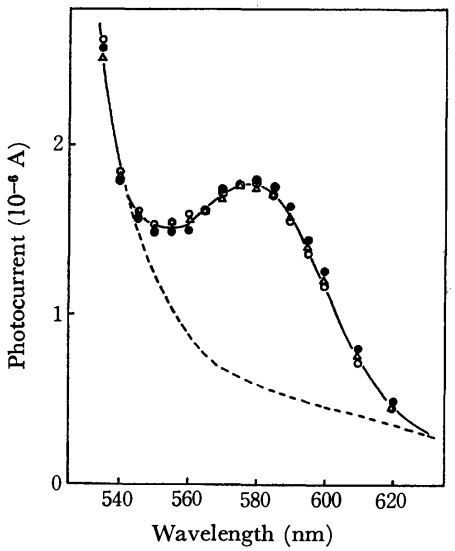

Fig. 3. Spectral dependence of the sensitized photocurrent at CdS electrode with varying pH: ——: pH 5.2, —○—: pH 4.0, —△—: pH 3.0, —●—: pH 2.4, ·····: blank photocurrent.

of the rhodamine B-sensitized photocurrent at CdS electrode for four different pH values.

The experimental results of spectral sensitization measurements at TiO_2 and CdS electrodes are summarized in Fig. 4 as a function of pH of the electrolyte solution, together with the data reported by Gerischer and Tributsch[2] on ZnO electrode. In the cases of TiO_2 and ZnO electrodes, the logarithm of the sensitized photocurrent depends almost linearly upon the pH of the solution containing rhodamine B or 3,3′-diethylthiacarbocyanine iodide as a sensitizing dye, while no detectable dependence being observed for the CdS electrode.

As regards the pH-dependence of the sensitized photocurrent at TiO_2 electrode, it is necessary in the first place to check the possible contributions from any

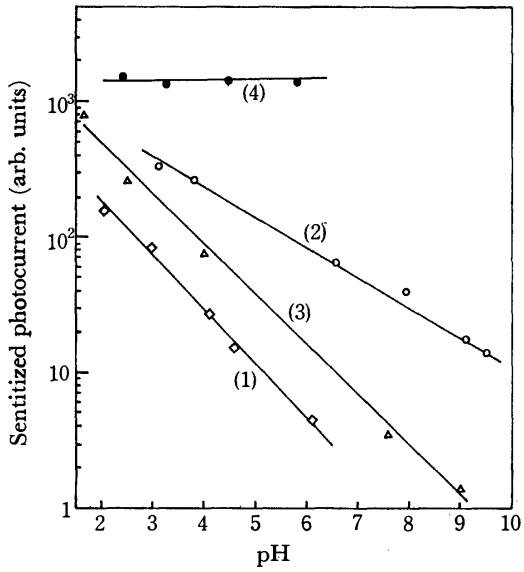

Fig. 4. pH-dependence of the sensitized photocurrents at several semiconductor electrodes;
(1): TiO_2 with 3,3′-diethylthiacarbocyanine, (2) TiO_2 with rhodamine B (3) ZnO with rhodamine B (Gerischer and Tributsch[2]), (4) CdS with rhodamine B.

pH-assisted structural change of the dye molecule and from the pH-dependence of the adsorption characteristics of dyes on TiO_2. The absorption spectra of rhodamine B and 3,3′-diethylthiacarbocyanine iodide were measured in the pH range 2—12, but no detectable change was observed. From this the possibility of the structural change of dye molecules through pH could be ruled out.

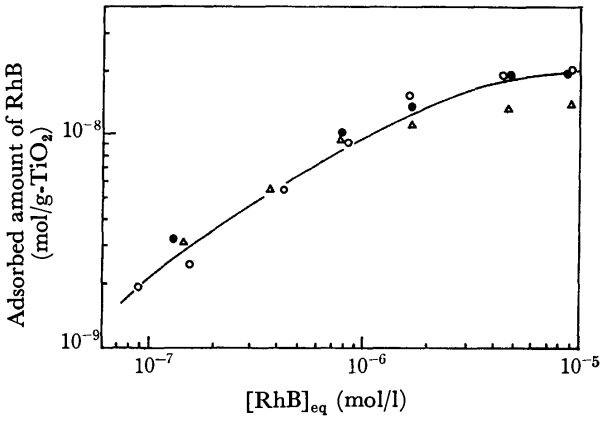

Fig. 5. Adsorption characteristics of rhodamine B on TiO_2 at 20 °C at different pH values; —○—: pH 2.0, —●—: pH 6.15, —△—: pH 10.0.

The adsorption characteristics of the two dyes employed here on TiO_2 have been measured with varying pH of the solution. The results for rhodamine B are shown in Fig. 5. We see that the adsorbability of rhodamine B in the pH range 2—12 falls on the same curve within experimental error. The adsorption of 3,3′-diethylthiacarbocyanine iodide on TiO_2 also is hardly affected by the pH of the solution.

The observations suggest that, in the case of the TiO_2 electrode, a decrease in pH of the electrolyte solution brings about a favorable condition for the occurrence of the spectral sensitization (possibly the electron transfer from the excited dye molecule to the conduction band of the semiconductor).

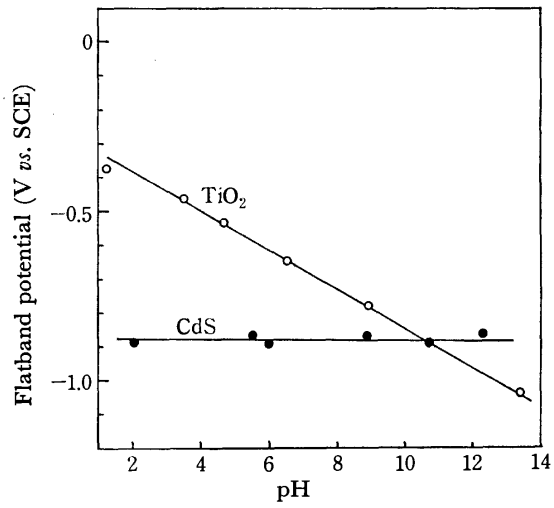

Fig. 6. pH-dependence of flatband potentials of TiO_2 and CdS single crystal electrodes.

In this connection we notice a quite good correlation between the results shown in Fig. 4 and the pH-dependence of the flatband potentials of TiO_2 and CdS electrodes (Fig. 6).[24] The pH-dependence of the flatband potential of the TiO_2 electrode could be elucidated by assuming a dissociation equilibrium[25] at the electrode surface facing the electrolyte solution, such as

$$\text{Ti-O}^{2-} + \text{H}^+ \rightleftarrows \text{Ti-OH}^- \qquad (1)$$

where Ti-O^{2-} denotes a lattice element of the TiO_2 surface, H^+ a proton in the bulk of the electrolyte solution, and Ti-OH^- the lattice element protonized. A thermodynamic consideration on the dissociation equilibrium (1) leads to the following formula:

$$\mu^\circ_{\text{Ti-O}^{2-}} + RT\ln a_{\text{Ti-O}^{2-}} - 2F\Phi_e + \mu^\circ_{H^+} + RT\ln a_{H^+} + F\Phi_s = \mu^\circ_{\text{Ti-OH}^-} + RT\ln a_{\text{Ti-OH}^-} - F\Phi_e \qquad (2)$$

where Φ_e and Φ_s are the potentials of the electrode surface and of the bulk of the solution, respectively. Other symbols have their usual meanings. It follows that the potential difference $\Delta\Phi$ ($=\Phi_e-\Phi_s$) at the phase boundary TiO_2—electrolyte is expressed as

$$\Delta\Phi = \text{const.} + \frac{RT}{F}\ln\frac{a_{\text{Ti-O}^{2-}}}{a_{\text{Ti-OH}^-}} - \frac{2.3RT}{F}\text{pH} \qquad (3)$$

Provided that the second term in Eq. (3) is not significantly affected by the pH change of the electrolyte solution, the electrode potential of TiO_2 shifts by *ca.* 60 mV (at room temperature) per unit decrease in the pH value. This is shown in Fig. 6.

In the ordinary polarization of a semiconductor electrode through the external circuit, most part of the applied voltage operates within the space charge region inside the semiconductor, and the potential difference across the electrical double layer (in the solution-side of the interface) can hardly be changed, owing to much lower carrier concentration in the electrode than

in the bulk of the electrolyte solution. Therefore, the rate of the electron transfer from the excited dye to the semiconductor (sensitized photocurrent) exhibits no detectable dependence on the anodic polarization (practically up to 10 V or more *vs.* S.C.E.) as shown in Fig. 1. The effect of polarization appears only under cathodic polarization where an accumulation layer, which obstructs the electron transfer towards the electrode, is formed at the surface of the semiconductor electrode.

Since the potential difference $\Delta\Phi$ due to pH change of the electrolyte solution is brought about at the electrode surface-electrolyte interface, as is ordinarily the case for the polarization of metal electrodes, the rate of the electron transfer from the excited dye to a semiconductor is expected to depend on the pH of the solution. Postulating an ordinary rate equation for the anodic process and tentatively assuming the one-electron transfer, the anodic sensitized photocurrent i_s can be expressed as

$$i_s \propto \exp\left(\frac{\alpha F}{RT}\eta\right) \tag{4}$$

where α is the transfer coefficient and η the overpotential. In view of the above discussion, the latter can be written as

$$\eta = \text{const.}' + \Delta\Phi \tag{5}$$

Combining Eqs. (3)—(5), one obtains the following formula for the sensitized photocurrent:

$$\log i_s = \text{const.}'' - \alpha\text{pH} \tag{6}$$

This equation seems to hold for the pH-dependence of the sensitized photocurrent at TiO_2 and ZnO electrodes shown in Fig. 4. The value of α falls within 0.26—0.40.

A similar treatment has been reported by Vetter and Gorn[26] concerning the corrosion process taking place at the iron oxide-electrolyte interface. They demonstrated a pH-dependence of the corrosion current, which they accounted for by assuming the potential variation caused by the dissolution equilibrium of oxygen ions at the phase boundary.

In contrast to the sensitized photocurrent, the rate-determining step for the blank photocurrent under long wavelength illumination would be the transport of positively-charged species such as ionized donors from interior to the surface of the electrode, since the latter current originates from light absorption inside the semiconductor. This assumption can be verified by the fact that the magnitude of the blank photocurrent shows practically no pH-dependence (Fig. 1) and that it increases gradually with the increase in the anodic polarization.

The fact that no pH-dependence of the sensitized photocurrent was observed at the CdS electrode would be ascribed to the pH-independence of the potential difference within the double layer, as is indicated by the pH-independence of the flatband potential (Fig. 6). This suggests that no dissociation equilibrium, similar to Eq. (1), could be established at the surface of the CdS electrode.

References

1) H. Gerischer, M. E. Michel-Beyerle, F. Rebentrost, and H. Tributsch, *Electrochim. Acta*, **13**, 1509 (1968).
2) H. Gerischer and H. Tributsch, *Ber. Bunsenges. Phys. Chem.*, **72**, 437 (1968).
3) H. Tributsch and H. Gerischer, *ibid.*, **73**, 251 (1969).
4) H. Tributsch and H. Gerischer, *ibid.*, **73**, 850 (1969).
5) H. Tributsch, *ibid.*, **73**, 582 (1969).
6) H. Tributsch and M. Calvin, *Photochem. Photobiol.*, **14**, 95 (1971).
7) K. Hauffe and J. Range, *Z. Naturforsch.*, **236**, 736 (1968).
8) K. Hauffe, H. Pusch, and J. Range, *Z. Phys. Chem. N. F.*, **64**, 122 (1969).
9) K. Hauffe, H. J. Danzmann, H. Pusch, J. Range, and H. Volz, *J. Electrochem. Soc.*, **117**, 993 (1970).
10) K. Hauffe and O. Haeggqwist, *Z. Phys. Chem. N. F.*, **85**, 191 (1973).
11) U. Bode, K. Hauffe, Y. Ishikawa, and H. Pusch, *ibid.*, **85**, 144 (1973).
12) H. Gerischer, *Photochem. Photobiol.*, **16**, 243 (1972).
13) H. Tributsch, *ibid.*, **16**, 261 (1972).
14) A. Fujishima, E. Hayashitani, and K. Honda, *Seisan Kenkyu*, **23**, 31 (1971).
15) A. Fujishima, E. Hayashitani, and K. Honda, *ibid.*, **23**, 363 (1971).
16) A. Fujishima, T. Watanabe, O. Tatsuoki, and K. Honda, *Chem. Lett.*, **1975**, 13.
17) A. Fujishima, T. Iwase, T. Watanabe, and K. Honda, *J. Amer. Chem. Soc.*, **97**, 4134 (1975).
18) R. Memming and H. Tributsch, *J. Phys. Chem.*, **75**, 562 (1971).
19) H. Gerischer and H. Selzle, *Electrochim. Acta*, **18**, 799 (1973).
20) H. Kim, Thesis at Univ. of Illinois (1973).
21) H. R. Schoeppel and H. Gerischer, *Ber. Bunsenges. Phys. Chem.*, **75**, 1237 (1971).
22) J. W. Steketee and J. De Jonge, *Proc. Koninkl. Ned. Akad. Wetenschap*, **B66**, 76 (1963).
23) B. J. Mulder and J. De Jonge, *ibid.*, **B66**, 303 (1963).
24) T. Watanabe, A. Fujishima, and K. Honda, *Chem. Lett.*, **1974**, 897.
25) H. Gerischer, in Physical Chemistry: An Advanced Treatise, pp. 487—488, ed. by H. Eyring *et al.*, Academic Press, New York (1970).
26) K. J. Vetter and F. Gorn, *Electrochim. Acta*, **18**, 321 (1973).

Studies of MoO_3–Al_2O_3 Catalyst in Ethylene Polymerization. III. The Nature of Mo(V) and Its Relation with Activity

Keizi HASHIMOTO, Shozi WATANABE, and Kimio TARAMA*

The Osaka Municipal Technical Research Institute, Ogimati, Kita-ku, Osaka 530

**Department of Hydrocarbon Chemistry, Faculty of Engineering, Kyoto University, Yoshida, Sakyo-ku, Kyoto 606*

(Received May 16, 1975)

In order to determine the active center of ethylene polymerization over MoO_3–Al_2O_3, the *g*-tensor and the amount of molybdenum(V) in each chemical state were determined by means of ESR measurement. The anisotropy of the *g*-tensor revealed the strength of the crystal field in the state; the decreasing order of the strengths was as follows: state(S)>state(M)>state(W)>MoO_3–SiO_2≒free MoO_3. In the state(S) molybdenum oxide is insoluble in aq.10M–NH_3, in the state(M) it is soluble in aq. NH_3 but insoluble in water, and in the state(W) it is soluble in water. The amount of molybdenum(V) in the state(W) was studied in connection with the activity, because only the state(W) was suitable for polymerization. The behavior of the activity was in fair agreement with that of the molybdenum(V) content in the state(W) and this content depedned on the amount of supported MoO_3 and on the extent of reduction. The amount of molybdenum(V) in the state (W) corresponded to the amount of chemisorbed hydrogen, which was a polymerization initiator. The chemisorption of oxygen on the catalyst caused a complete disappearance of both the activity and the molybdenum(V) content in the state(W). Therefore, it was concluded that the active center of the polymerization was molybdenum(V) in the state(W).

The polymerization over MoO_3–Al_2O_3 has been studied. In the first paper,[1] we reported about the activity of the catalyst and the kinetics of the polymerization. In the second paper,[2] we reported the relation between the activity and the chemical states of molybdenum oxide on Al_2O_3 and concluded that the oxide on Al_2O_3 might be classified into three chemical states: the state(W) in which molybdenum oxide is soluble in water, the state(M), insoluble in water but soluble in aq.NH_3, and the state(S), insoluble in aq.10M-NH_3.

In general it is known that the activity may be attributed to the low valence of molybdenum on the basis of the fact that an olefin is polymerized in a reducing atmosphere.[3] Emelyanov *et al.*[4] and Voevodskii[5] attempted to relate the polymerization activity to molybdenum(V). However, they did not obtain a clear relation between the activity and the molybdenum(V) content. The explanation for the unfavorable results is that they regarded the molybdenum oxide on Al_2O_3 as a single state without considering the properties of the three chemical states.

The present paper deals with a part of an investigation of the active center, in view of the states. The anisotropy of the *g*-tensor of molybdenum(V) in each chemical states is measured by ESR. The strength of crystal field and the field suitable for polymerization will be discussed on the basis of the ESR data and the activity. In order to show the valence of molybdenum ion as an active center, the molybdenum(V) content in the state(W) is determined by the ESR measurement. The activity is compared with this content, which is due to the amount of supported MoO_3 and the extent of reduction. The amount of polymerization initiator, chemisorbed hydrogen, is determined and compared with the molybdenum(V) content in the state(W). The poisoning effects of oxygen chemisorbed on the catalyst are studied. One interesting conclusion to be drawn from these results in the fact that the polymerization activity in MoO_3–Al_2O_3 is related to the strength of the crystal field and the amount of the molybdenum(V) in the state(W).

Experimental

Preparation of Catalyst. MoO_3–Al_2O_3 and MoO_3–SiO_2 were prepared according to the procedure described previously.[1]

Reactants. Hydrogen and oxygen (more than 99.9%) were used without further purification. Ethylene (99.5%, Seitetu Chemical Co.) was used without further purification. Most of the impurities were methane or ethane.

Treatment of Catalyst. The catalyst were reduced under a hydrogen pressure of 170 Torr at 400 °C before the ESR measurement and the ethylene polymerization. The extent of reduction was determined on the basis of the amount of oxygen completely reoxydating the catalyst. The extent shows the conversion ratio of MoO_3 to MoO_2.

ESR Measurement. The catalysts were placed into a reaction vessel equipped with a pyrex-tube for ESR measurement. The measurement was carried out at room temperature. ESR spectra were obtained with a JES-ME-IX spectrometer (Japan Electron Optics Laboratory Co.) using manganese (II) as an internal standard. The amount of molybdenum (V) in the catalyst was determined by Seshadri's method[6] using copper(II) as an internal standard.

Polymerization. The ethylene was polymerized at 0 °C using the procedure described previously.[1]

Results and Discussion

Crystal Field of Molybdenum Oxide. After reduction in each chemical state, the presence of molybdenum(V) was recognized from ESR studies. The molybdenum(V) in each chemical state showed an anisotropy of the *g*-tensor. The values of the anisotropy are shown in Table 1. The value in MoO_3–SiO_2 is also added in

TABLE 1. *g*-VALUE OF MOLYBDENUM (V)

Sample	$g_\perp$	$g_{//}$
MoO_3–SiO_2	1.952±0.001	1.867±0.001
(W)–Al_2O_3	1.953±0.001	1.896±0.001
(M)–Al_2O_3	1.955±0.001	1.909±0.001
(S)–Al_2O_3	1.955±0.001	1.914±0.001

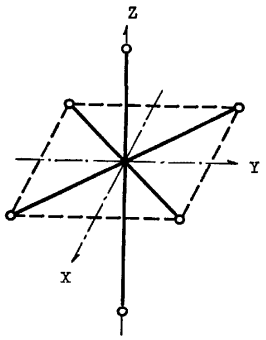

Fig. 1. Model of molybdenum oxide on Al_2O_3.
●: Mo^{6+} ion, ○: O^{2-} ion.

Table 1. As Table 1 shows, the $g_\perp$-value was almost constant in the different states. The $g_{//}$-value varied with the kinds of states and of carriers. The decreasing order of $g_{//}$-values was in agreement with the increase of the interaction between the state and the carrier.[2] The strength of the crystal field in the state was determined on the basis of the anisotropy. According to Andersson's report,[7] the crystal structure of free MoO_3 is a distorted octahedron. Therefore, the structure of molybdenum oxide on Al_2O_3 was supposed to be a distorted octahedron, as shown in Fig. 1. The five-fold degenerate levels of d^1-ion are split into 4-levels in the model and the energy levels decrease in the following order: $a_1(d_{z^2})$, $b_1(d_{x^2-y^2})$, $e(d_{zx}, d_{yz})$, and $b_2(d_{xy})$. Several authors have derived equations for the $g_{//}$ and $g_\perp$ expected in a d^1-model of a distorted octahedron, using a set of molecular orbitals as the basis functions for the calculation. Ballhausen *et al.*[8] placed the unpaired electron in a non-bonding b_2-orbital(d_{xy}), defined the antibonding orbital as $\Phi^*=C_1^*\Phi(\text{metal})+C_2^*\Phi(\text{ligand})$, and derived

$$g_{//}=2\left[1-\frac{4(C_1^*)^2\xi_M}{\Delta E(^2B_2-{}^2B_1)}\right] \quad (1)$$

$$g_\perp=2\left[1-\frac{(C_1^*)^2\xi_M}{\Delta E(^2B_2-{}^2E)}\right] \quad (2)$$

Where ξ_M is the single electron spin-orbit coupling constant for molybdenum. $\Delta E(^2B_2-{}^2B_1)$ is a function of the equatorial Mo–O distance and $\Delta E(^2B_2-{}^2E)$ is a function of both the equatorial and the Mo–O distance along the C_{4v} axis. Since the $g_\perp$-value in Table 1 is almost constant, the quantitative variation of $\Delta E(^2B_2-{}^2E)$ might be small in the different chemical states. The values of $\Delta E(^2B_2-{}^2B_1)$ and $\Delta E(^2B_2-{}^2E)$ were determined as follows. In the previous paper, we reported that state(W) and state(M) occupied most of the alumina surface in 16.7wt%MoO_3–Al_2O_3 and (0—6)wt%MoO_3–Al_2O_3, respectively. The catalysts were prepared in the way that Asmolov *et al.*[9] described. They reported that the adsorption bands in 16.7wt%-MoO_3–Al_2O_3 and (0.2—1.8)wt%MoO_3–Al_2O_3 appeared at 31250 and 33900 cm^{-1}, respectively. In the molybdenyl complexes having a similarly distorted octahedron, the values of $\Delta E(^2B_2-{}^2E)$ and $\Delta E(^2B_2-{}^2B_1)$ were (10000—20000) and (20000—30000) cm^{-1}, respectively.[10,11] Therefore, the values of $\Delta E(^2B_2-{}^2B_1)$ in the state(W) and the state(M) were 31250 and 33900 cm^{-1}. The values of $\Delta E(^2B_2-{}^2E)$ in the state(W) and the state(M) were calculated to be 17300 and 17100 cm^{-1} on the basis of a substitution of these values, the $g_\perp$ and $g_{//}$-values, in Eqs. (1) and (2). Thus, the variation of $\Delta E(^2B_2-{}^2E)$ was small, as expected from the $g_\perp$-values in Table 1. Consequently, the value of $\Delta E(^2B_2-{}^2E)$ was assumed to be 17200 cm^{-1} in both the state(S) and the MoO_3–SiO_2 and those of $\Delta E(^2B_2-{}^2B_1)$ in the state(S) and the MoO_3–SiO_2 were calculated to be 36000 and 24800 cm^{-1}, respectively (Table 2). As Table 2 shows, the value of $\Delta E(^2B_2-{}^2B_1)$ decreased in the following order of states: state(S), state(M), state(W), and MoO_3–SiO_2. Since the value of ΔE-$(^2B_2-{}^2B_1)$ in MoO_3–SiO_2, 24800 cm^{-1}, was nearly equal to that in the single crystal of MoO_3, 24250 cm^{-1},[12] the molybdenum oxide on the SiO_2 had little interaction between the oxide and the SiO_2. The value of ΔE-$(^2B_2-{}^2B_1)$ in the state(S), 36000 cm^{-1}, supported the idea that the state(S) had a strong crystal field. The quantity of $\Delta E(^2B_2-{}^2B_1)$ is a function of the equatorial Mo–O distance as described above and the shortening of the equatorial distance leads to an increase of ΔE-$(^2B_2-{}^2B_1)$. The equatorial Mo–O distance was shortened in the following order of states: MoO_3–SiO_2, state(W), state(M), and state(S). This shortening order was in agreement with the increasing order of the interaction between the molybdenum oxide and the carrier.[2] From the facts presented above, the strengths of the crystal field in each chemical state were not equal and that in the state(W) led the value of $\Delta E(^2B_2-{}^2B_1)$ of molybdenum(V) to *ca.* 31000 cm^{-1}. This strength was suitable for ethylene polymerization and only the state(W) was suitable for it, as described previously.[2]

Table 2. Spectral parameters of molybdenum(V) signals

Sample	$(^2B_2-{}^2B_1)$, (cm^{-1})	$(^2B_2-{}^2E)$, (cm^{-1})
MoO_3–SiO_2	24800	17200[a]
(W)-Al_2O_3	31250[b]	17300
(M)-Al_2O_3	33900[b]	17100
(S)-Al_2O_3	36000	17200[a]

a) Estimated value. b) Ref. 9.

Relation between Activity and Molybdenum(V) content. In order to reveal the valence states of the active molybdenum which was present in the state(W) suitable for polymerization, the catalytic activity was studied in connection with the molybdenum(V) content in the catalysts. The amount of molybdenum(V) in MoO_3–Al_2O_3 is expressed as a sum of the molybdenum(V) contents in three chemical states, that is:

$$(Mo^{5+})_{total}=(Mo^{5+})_W+(Mo^{5+})_M+(Mo^{5+})_S, \quad (3)$$

Where (Mo^{5+}) is the amount of molybdenum(V) and W, M, and S subscripts refer to state(W), state(M), and state(S), respectively. The apparent $g_{//}'$-value of molybdenum(V) in MoO_3–Al_2O_3 varied with the composition of molybdenum(V) in the three states. The apparent $g_{//}'$-values in various comopsitions were determined by the simulation on the basis of the ESR spectra of molybdenum(V) in each state. Figure 2 shows an ESR spectrum simulated in the following composition: $(Mo^{5+})_W$, $(Mo^{5+})_M$, and $(Mo^{5+})_S$ are

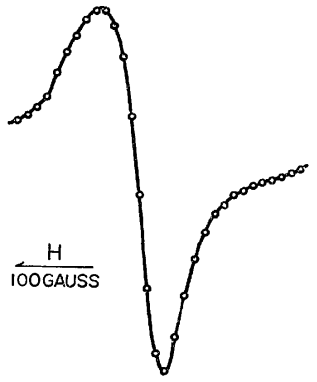

Fig. 2. ESR spectrum of Mo^{5+} in the composition, $(Mo^{5+})_W$, $(Mo^{5+})_M$ and $(Mo^{5+})_S$, respectively, 4.30×10^{18}, 2.14×10^{18} and 3.00×10^{18} spins/g-cat.
○: Points of simulated spectrum, —: measured spectrum.

respectively 4.30×10^{18}, 2.14×10^{18} and 3.00×10^{18} spins/g-cat.. These $g_{//}'$-values of simulated spectra are shown in Table 3. The apparent $g_{//}'$-value was assumed to be approximately expressed as a function of the content, $(Mo^{5+})_W$, $(Mo^{5+})_M$, and $(Mo^{5+})_S$, by the following equation:

$$g_{//}' = \frac{1.8960(Mo^{5+})_W + 1.9086(Mo^{5+})_M + 1.9140(Mo^{5+})_S}{(Mo^{5+})_{total}}, \quad (4)$$

Table 3. Apparent $g_{//}'$-value of molybdenum(V)

Composition (mol%)			$g_{//}'$-Value of simulated spectra	Approximated $g_{//}'$-value
$(Mo^{5+})_W$	$(Mo^{5+})_M$	$(Mo^{5+})_S$		
0	80	20	1.9097	1.9097
20	60	20	1.0973	1.9072
40	40	20	1.9047	1.9046
60	20	20	1.9020	1.9021
0	60	40	1.9107	1.9108
40	30	40	1.9070	1.9070
50	10	40	1.9047	1.9045
60	0	40	1.9030	1.9032
0	40	60	1.9116	1.9118
20	20	60	1.9093	1.9093
30	10	60	1.9080	1.9081

The apparent $g_{//}'$-values calculated from Eq. 4 are shown in Table 3. As Table 3 shows, the apparent $g_{//}'$-value calculated is in fair agreement with the apparent $g_{//}'$-value of the simulated spectrum. Therefore, the apparent $g_{//}'$-value might be approximately expressed by Eq. 4. The substitution of $(Mo^{5+})_{total}$, $(Mo^{5+})_S$, and the apparent $g_{//}'$-value in both Eqs. 3 and 4 determined $(Mo^{5+})_W$, which was present in the crystal field of suitable strength for polymerization.

In order to reveal the relation between $(Mo^{5+})_W$ and the supported molybdite-content, the relations of the molybdite-content to $(Mo^{5+})_{total}$, $(Mo^{5+})_S$, and the apparent $g_{//}'$-value were studied and is shown in Fig. 3. Before the ESR measurement, the catalysts were reduced under a hydrogen pressure of 170 Torr at 400 °C for 15 min. The molybdenum oxide in the state(S) was prepared by the removal of molybdenum oxides in

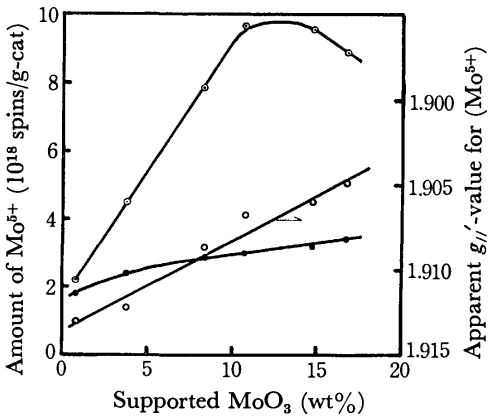

Fig. 3. Relation of the molybdite-content to $(Mo^{5+})_{total}$, $(Mo^{5+})_S$ or the apparent $g_{//}'$-value
○: $(Mo^{5+})_{total}$, ●: $(Mo^{5+})_S$, ○: apparent $g_{//}'$-value for $(Mo^{5+})_{total}$.

both state(W) and state(M) from MoO_3–Al_2O_3 with aq.10 M-NH_3 and reduced under the same conditions before the determination of $(Mo^{5+})_S$. As Fig. 3 shows, $(Mo^{5+})_{total}$ was maximum at a molybdite-content of 10 to 15wt%. The apparent $g_{//}'$-value decreased with an increase of the molybdite-content and $(Mo^{5+})_S$ increased gradually with an increase of the molybdite-content. The behavior of $(Mo^{5+})_{total}$ was in agreement with Voevodskii's result.[5] $(Mo^{5+})_W$ was calculated by substitution of $(Mo^{5+})_S$, $(Mo^{5+})_{total}$, and the apparent $g_{//}'$-value in Fig. 3 into Eqs. 3 and 4. The relation between $(Mo^{5+})_W$ and molybdite-content is shown in Fig. 4. $(Mo^{5+})_W$ was small in the molybdite-content, less than several percents. $(Mo^{5+})_W$ increased with the further molybdite-content. The behavior of $(Mo^{5+})_W$ differed from that of $(Mo^{5+})_{total}$ in Fig. 3.

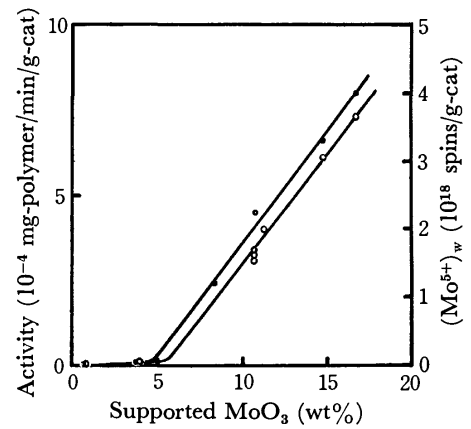

Fig. 4. Relation between the activity and $(Mo^{5+})_W$.
●: $(Mo^{5+})_W$, ○: activity.

Moreover, the relation between the catalytic activity and the molybdite-content is shown in Fig. 4. The catalysts were reduced under a hydrogen pressure of 170 Torr at 400 °C for 15 min before ethylene polymerization. In order to avoid solvent effects and a further reduction of the catalyst with ethylene, ethylene was polymerized under a pressure of 100 to 200 Torr at 0 °C in a gas-solid phase. The activity showed the polymerization rate. As Fig. 4 shows, the behavior

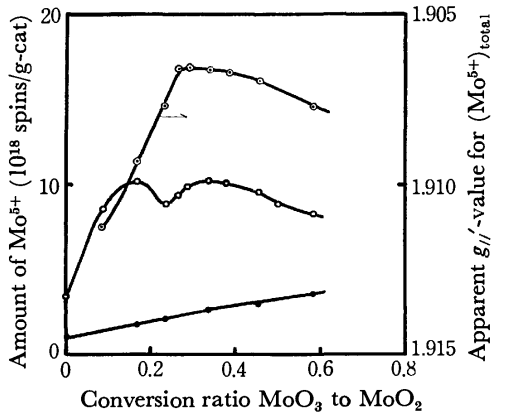

Fig. 5. Relation of the extent of reduction to $(Mo^{5+})_{total}$, $(Mo^{5+})_S$ or the apparent $g_{//}'$-value in 10.7 wt% MoO_3–Al_2O_3.
○: $(Mo^{5+})_{total}$, ●: $(Mo^{5+})_S$, ⊙: apparent $g_{//}'$-value for $(Mo^{5+})_{total}$.

of the activity was in fair agreement with that of $(Mo^{5+})_w$. Therefore, the activity might be attributed to molybdenum(V) in the state(W).

In order to confirm this conclusion, the relation between the conversion ratio of MoO_3 to MoO_2 and either $(Mo^{5+})_w$ or polymerization activity was studied, because $(Mo^{5+})_w$ must vary with the ratio. The relation of the ratio to $(Mo^{5+})_{total}$, the apparent $g_{//}'$-value, and $(Mo^{5+})_S$ were studied in 10.7wt%MoO_3–Al_2O_3 and are shown in Fig. 5. $(Mo^{5+})_S$ was determined by the ESR measurement of the state(S), which was prepared by the same procedure as described above. Before the measurement, the molybdenum oxide in the state(S) and 10.7wt%MoO_3–Al_2O_3 were reduced under a hydrogen pressure of 170 Torr at 400 °C. As Fig. 5 shows, $(Mo^{5+})_{total}$ had two variation points. The apparent $g_{//}'$-value was minimum in the ratio of 0.25 to 0.50. $(Mo^{5+})_S$ increased gradually with an increase of the ratio.

$(Mo^{5+})_S$ was calculated by substitution of $(Mo^{5+})_{total}$, $(Mo^{5+})_S$, and the apparent $g_{//}'$-value in Fig. 5 into Eqs. 3 and 4. The relation between the ratio and $(Mo^{5+})_w$ is shown in Fig. 6. $(Mo^{5+})_w$ was small in the ratio less than 0.20. However, $(Mo^{5+})_w$ increased remarkably in the ratio of 0.20 to 0.24 and showed

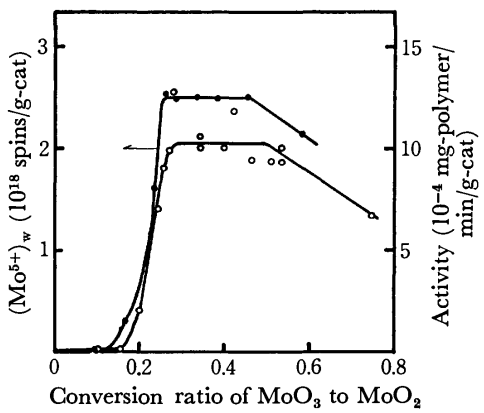

Fig. 6. Relation between the conversion ratio of MoO_3 to MoO_2 and either activity or $(Mo^{5+})_w$.
○: Activity, ●: $(Mo^{5+})_w$.

constant value of *ca.* 2.5×10^{18} spins/g-cat. in the ratio of 0.25 to 0.45. $(Mo^{5+})_w$ decreased gradually for higher ratios.

The relation between the ratio and the catalytic activity is shown in Fig. 6. For the determination of the activity, ethylene was polymerized under the same conditions as described above. As Fig. 6 shows, the behavior of the activity was in fair agreement with that of $(Mo^{5+})_w$.

The polyethylene, which was produced at 50 °C for 5 hr over 10.7wt%MoO_3–Al_2O_3, had an average value of 19000 in polymerization degree. The amount of chemisorbed hydrogen, the polymerization initiator, was calculated on the basis of this polymerization degree and from a consideration of the reaction mechanism.[1] The amount of chemisorbed hydrogen had a value of 1.0×10^{18} site/g-cat. This value corresponded closely to 2.5×10^{18} spin/g-cat. of $(Mo^{5+})_w$.

Exposure to oxygen poisoned completely the active 10.7wt%MoO_3–Al_2O_3 which had been reduced to the ratio of 0.35 and increased the apparent $g_{//}'$-value from 1.907 to 1.910. This increase could be explained by the assumption of the disappearance of $(Mo^{5+})_w$ from the active catalyst in which $(Mo^{5+})_{total}$, $(Mo^{5+})_S$, and $(Mo^{5+})_w$ were 10.2×10^{18}, 2.6×10^{18} and 2.5×10^{18} spin/g-cat, respectively, as Figs. 5 and 6 show. $(Mo^{5+})_w$ was determined to be 5.1×10^{18} spin/g-cat. by the substitution of these values in Eq. 3. The apparent $g_{//}'$-value was determined to be 1.910 by the substitution of $(Mo^{5+})_S$ and $(Mo^{5+})_w$ into Eq. 4. This $g_{//}'$-value was in fair agreement with the experimental one. Exposure to oxygen accompanied the complete disappearance of both catalytic acitivity and $(Mo^{5+})_w$ in 16.7wt%MoO_3–Al_2O_3 as well. Therefore, exposure to oxygen was proved to cause the complete disappearance of both catalytic activity and $(Mo^{5+})_w$.

From the facts described above, it was concluded that the activity should be attributed to molybdenum(V) in the state(W).

References

1) K. Hashimoto, S. Watanabe, and K. Tarama, *Nippon Kagaku Kaishi*, **1974**, 409.
2) K. Hashimoto, S. Watanabe, and K. Tarama, *ibid.*, **1975**, 591.
3) A. V. Topchiev, B. A. Krentsel, A. I. Perelman, and K. G. Miesserov, *J. Polym. Sci.*, XXXIV, 129 (1959).
4) V. M. Emelyanov and G. K. Boreskov, *Dokl. Akad. Nauk. SSSR*, **150**, 829 (1963).
5) V. V. Voevodskii, "Proc. 3rd Intern., Congr. Catalysis, Amsterdam," **2**, 88 (1964).
6) K. S. Seshadri and L. Petrakis, *J. Catal.*, **30**, 195 (1973).
7) G. Andersson and A. Magneli, *Acta Chem. Scand.*, **4**, 793 (1973).
8) C. J. Ballhausen and H. B. Gray, *Inorg. Chem.*, **1**, 111 (1962).
9) G. N. Asmolov and O. V. Krylov, *Kinet. Katal.*, **11**, 1028 (1970).
10) P. T. Manoharan and M. T. Rogers, *J. Chem. Phys.*, **49**, 5510 (1968).
11) R. D. Dowsing and J. F. Gibson, *J. Chem. Soc. A*, **1967**, 655.
12) S. K. Deb, *Proc. Roy. Soc. Ser. A*, **304**, 215 (1968).

Semiempirical Relations in Molecular Liquids. II. Estimation of Thermal Expansivity

Yoshitsugu Oono

Department of Applied Science, Faculty of Engineering, Kyushu University, Higashi-ku, Fukuoka 812

(Received June 2, 1975)

A simple method for the estimation of thermal expansivity of the molecular liquid is proposed. Thermal expansivity α can be calculated by

$$\alpha = T^{-1}\phi(y)/y\phi'(y),$$

where $\phi(y)=p_h/\rho kT$, $y=\pi\rho a^3/6$, p_h is the pressure of a hard sphere fluid, a the effective hard core diameter of the molecule, ρ the number density, and k, T have their usual meanings. For the molecular liquids consisting of compact molecules, the equation gives a fairly accurate estimation of α, which is practically applicable to the estimation of the density of the liquids at 1 atm at desired temperature.

If the effective hard core diameter of the molecule and the density of the liquid are known, then the scaled particle theory (SPT) allows one to calculate surface tension, compressibility, *etc.* of the molecular liquids.[1] From knowledge of the density at room temperature and the approximate value of melting temperature, which are both easily measurable, hard core diameter a at desired temperature can be estimated by the method given in the preceding paper.[2]

If the value of thermal expansivity α calculated by the SPT were accurate, then the density at desired temperature could be estimated from the melting point and the density at room temperature. However, α estimated by the SPT is not sufficiently accurate for practical use.

The purpose of the present paper is to propose a method for the fairly accurate estimation of α from the effective hard core diameter of molecule and density. This method enables one to calculate the density at desired temperature at 1 atm from the melting point and the density at room temperature.

Theory

It is an oversimplified assumption that the volume change at higher densities is mainly due to the repacking of molecular hard cores.[1] Hence the effect of intermolecular attractive forces on the equation of state must be taken into account. The simplest method is to adopt the so-called augmented van der Waals (AVdW) equation of state,[3]

$$p = p_h - \varepsilon\rho^2, \tag{1}$$

where ρ is the number density, p the pressure, p_h the pressure of a hard sphere fluid with hard core diameter a, and ε a constant. Since $p_h/\rho kT$ is the function of $y=\pi\rho a^3/6$ only, we put $p_h=\rho kT\phi(y)$. Thermal expansivity α is given by

$$(\alpha T)^{-1} = (\partial \ln T/\partial \ln V)_p. \tag{2}$$

From Eqs. (1) and (2), taking into account that $p \ll \varepsilon\rho^2$ at higher densities, we obtain

$$(\alpha T)^{-1} = -1 + y\phi'(y)/\phi(y). \tag{3}$$

If $\varepsilon=0$, *i.e.*, $dp=dp_h$, then[1]

$$(\alpha T)^{-1} = 1 + y\phi'(y)/\phi(y). \tag{4}$$

However, the value of αT predicted by Eq. (3) is too large and that by Eq. (4) is too small.

According to the computer experiment by Alder and Hecht,[4] ε strongly depends on y at higher densities. Hence it is suggested that the crudest modification of the AVdW equation of state is to assume ε to be proportional to y^{-1} at higher densities ($y \gtrsim 0.4$). After modification of Eq. (1), we obtain

$$(\alpha T)^{-1} = y\phi'(y)/\phi(y). \tag{5}$$

In deriving Eqs. (3)—(5), the contribution of da/dT is not taken into account, since all the quantities are calculated for the model liquid consisting of hard spheres exerting attractive forces. The diameter of the hard sphere is so chosen after all the calculations are completed to describe the molecular liquid at temperature T. Note that αT does not depend on the details of the intermolecular attractive forces. In the following, we adopt the Carnahan-Stahling equation of state[5] for $\phi(y)$.

Comparison with Observed Data

The observed values of αT at 298 K for organic liquids of nearly spherical molecules and the calculated values of αT given by Eqs. (3)—(5) are plotted *vs.* y which is obtained by means of

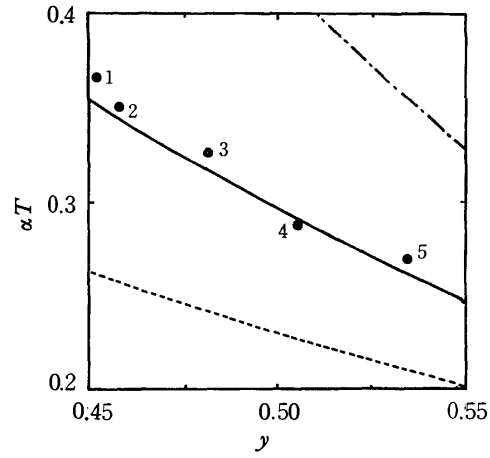

Fig. 1. Thermal expansivities of haloalkanes.
-·-·-: Eq. (3), ·····: Eq. (4), ——: Eq. (5).
1: Carbon tetrachloride, 2: 1,2-dichloroethane, 3: bromotrichloromethane, 4: 1,2-dibromoethane, 5: 1,3-dibromopropane.

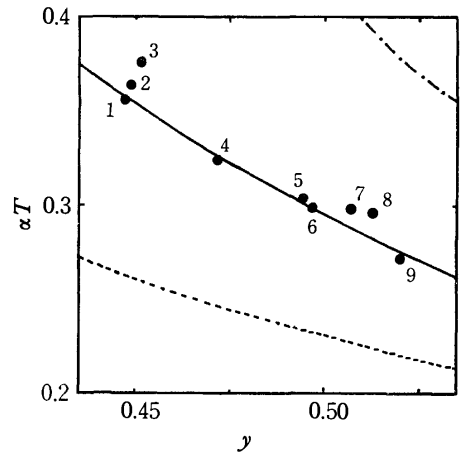

Fig. 2. Themal expansivities of benzene and mono-substituted benzenes.
-·-·-: Eq. (3), ·····: Eq. (4), ——: Eq. (5).
1: Fluorobenzene, 2: benzene, 3: (trifluoromethyl)-benzene, 4: toluene, 5: ethylbenzene, 6: chlorobenzene, 7: cumene, 8: propylbenzene, 9: bromobenzene.

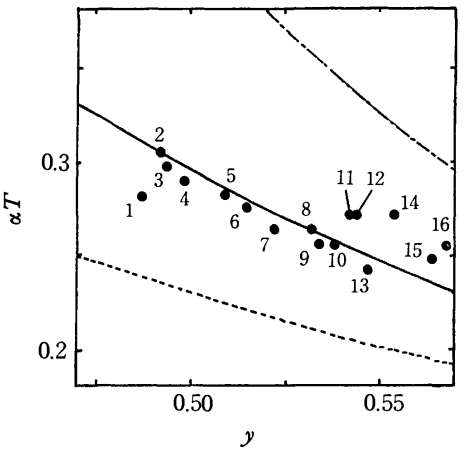

Fig. 3. Thermal expansivities of di- and tri-substituted benzenes.
-·-·-: Eq. (3), ·····: Eq. (4), ——: Eq. (5).
1: *p*-Dichlorobenzene, 2: *p*-xylene, 3: *m*-xylene, 4: *o*-xylene, 5: 1,3,5-trimethylbenzene, 6: 1,2,4-trimethylbenzene, 7: 1,2,3-trimethylbenzene, 8: *m*-dichlorobenzene, 9: *o*-dichlorobenzene, 10: *o*-cresol, 11: *p*-ethylpropylbenzene, 12: *p*-*t*-butyltoluene, 13: 3,4-dichlorotoluene, 14: *p*-diisopropylbenzene, 15: *o*-ethylnitrobenzene, 16: *o*-diisopropylbenzene.

$$\sigma T^{-1}\rho^{-2/3} = 4.28\times 10^{-17} y^{1/3}(2+y)/(1-y)^2, \qquad (6)$$

where σ is the surface tension in dyn/cm.[1,2] (Figs. 1—5). The observed data on thermal expansivity at 298 K are calculated by $(\rho_{293\,K}-\rho_{303\,K})/5(\rho_{293\,K}+\rho_{303\,K})$. The data on density and surface tension are obtained from Refs. 6—8. Surface tension scarcely depends on the details of the intermolecular attractive forces,[2] so that use of y estimated from Eq. (6) is suitable. Figures 1—5 show that αT of organic liquids of nearly spherical molecules without strong dipole moments and strongly hydrogen-bonding abilities satisfy Eq. (5), but not Eqs. (3) and (4).

Figure 6 shows that organic liquids of long chain-like molecules deviate considerably from Eq. (5). The deviation is not surprising since the SPT is so constructed as to treat liquids of spherical molecules.

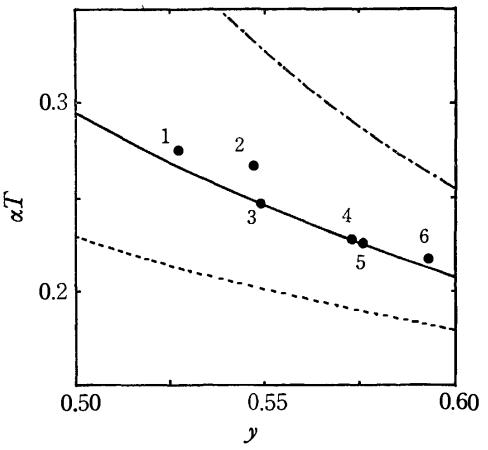

Fig. 4. Thermal expansivities of naphthalenes *etc.*
-·-·-: Eq. (3), ·····: Eq. (4), ——: Eq. (5).
1: *trans*-Decalin, 2: *cis*-decalin, 3: tetralin, 4: 5-methyl-1,2,3,4-tetrahydronaphthalene, 5: 1-methylnaphthalene, 6: 2-butylnaphthalene.

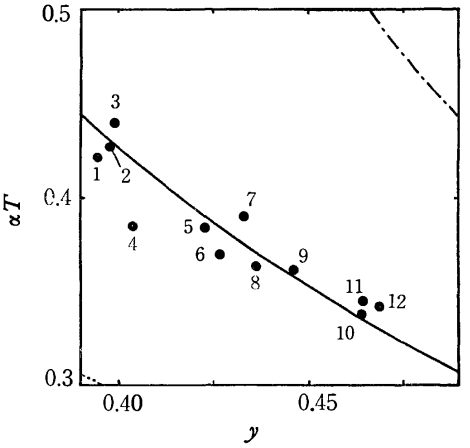

Fig. 5. Thermal expansivities of aliphatic compounds.
-·-·-: Eq. (3), ·····: Eq. (4), ——: Eq. (5).
1: 2,3-Dimethylbutane, 2: 2-methylpentane, 3: 2-pentyne, 4: propionitrile, 5: ethyl methyl sulfide, 6: 2,2,3-trimethylbutane, 7: 2,3-dimethyl-2-butene, 8: 3,3-dimethylpentane, 9: 2,2,4-trimethylpentane, 10: butyronitrile, 11: 2-methylhexane, 12: 3-ethyl-2-methylpentane.

Applications

Estimation of ρ–T *Relation at 1 atm.* As an application of the results of the preceding and the present papers, we show how to estimate ρ at T from the melting point and the density ρ_0 at temperature T_0. The effective hard core diameter a at melting point can be calculated from the melting point and the molecular structure. The effective hard core diameter a_0 at T_0 can be obtained by Eq. (6) from ρ_0 and parachor. Then we can calculate α at T_0 by means of Eq. (5). With the value of α obtained, we can estimate the density at $T_0+\Delta T$ by $\rho=(1-\alpha\Delta T)\rho_0$. The procedure is repeated until the desired temperature is reached. Some examples are given in Tables 1—4, where ΔT is

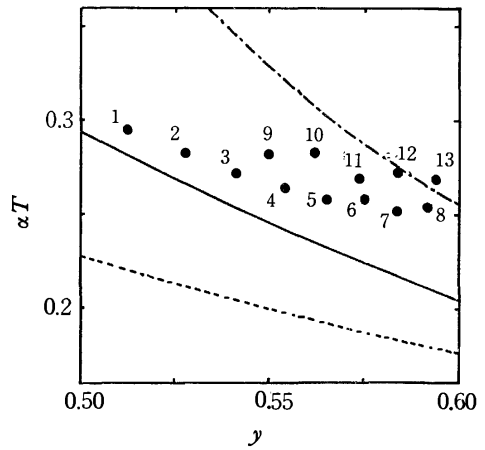

Fig. 6. Thermal expansivities of normal alkanes and their phenyl derivatives.
-----: Eq. (3), ·····: Eq. (4), ——: Eq. (5).
1: Propylbenzene, 2: butylbenzene, 3: pentylbenzene, 4: hexylbenzene, 5: heptylbenzene, 6: octylbenzene, 7: nonylbenzene, 8: decylbenzene, 9: dodecane, 10: tridecane, 11: tetradecane, 12: pentadecane, 13: hexadecane.

10 K. It can be concluded that the method mentioned above provides a fairly accurate and practical procedure for the estimation of ρ–T relation at 1 atm.

Table 1. Estimation of the specific volume of chloroform

The density at 293 K is 1.4894 g/cm^3,[13] which is assumed to be known. From this data and the melting point 210 K, da/dT becomes 4.14×10^{-3} Å/K. The specific volume at supercooled state is predicted accurately.

T(K)	Specific volume (cm^3/g)	
	Obsd[13]	Calcd
283	0.6634	0.6630
273	0.6554	0.6546
263	0.6473	0.6465
253	0.6393	0.6388
243	0.6321	0.6313
233	0.6243	0.6241
223	0.6172	0.6172
213	0.6106	0.6106
203	0.6039	0.6042

Table 2. Estimation of the specific volume of chlorobenzene

The density at 293 K is 1.055 g/cm^3,[13] which is assumed to be known. From this data and the melting point 228 K, da/dT becomes 2.45×10^{-3}Å/K.

T(K)	Specific volume (cm^3/g)	
	Obsd[13]	Calcd
283	0.8956	0.8957
273	0.8868	0.8870
263	0.8789	0.8784
253	0.8696	0.8700
243	0.8621	0.8616
233	0.8532	0.8534
228	0.8494	0.8494

Table 3. Estimation of the specific volume of bromobenzene

The density at 293 K is 1.4954 g/cm^3,[13] which is assumed to be known. From this data and the melting point 243 K, da/dT becomes 2.22×10^{-3}/K.

T(K)	Specific volume (cm^3/g)	
	Obsd[13]	Calcd
323	0.6877	0.6876
313	0.6813	0.6812
303	0.6746	0.6749
283	0.6632	0.6626
273	0.6566	0.6566
263	0.6507	0.6507
253	0.6452	0.6449
243	0.6397	0.6392
234.5	0.6353	0.6343

Table 4. Estimation of the specific volume of nitrobenzene

The density at 293 K is 1.2019 g/cm^3,[13] which is assumed to be kmnown. From this data and the melting point 278.8 K, da/dT becomes 4.07×10^{-3}Å/K.

T(K)	Specific volume (cm^3/g)	
	Obsd[13]	Calcd
283	0.8258	0.8251
303	0.8380	0.8389
313	0.8452	0.8457
323	0.8517	0.8525

Liquid Argon at Triple Point. We have proposed the modification of the AVdW equation of state. This equation of state gives good estimation of α and isothermal compressibility β of liquid argon at triple point.

Longuet-Higgins and Widom[3] and Guggenheim[9] estimated α and β of liquid argon at triple point using the AVdW equation of state. The values obtained by Longuet-Higgins and Widom are $\alpha T=0.50$ and $\rho kT\beta=0.058$. Guggenheim estimated y at triple point to be 0.427 from the data of internal pressure, and obtained $\alpha T=0.57$ and $\rho kT\beta=0.0663$. The observed values are $\alpha T=0.37$ and $\rho kT\beta=0.0495$.[3]

Using the modified AVdW equation of state,

$$\frac{p}{\rho kT}=\frac{1+y+y^2-y^3}{(1-y)^3}-\varepsilon' y, \tag{7}$$

where ε' is a constant, and the data of internal pressure used by Guggenheim, we obtain $y=0.422$ at triple point. From this value of y we obtain $\alpha T=0.39$ and $\rho kT\beta=0.050$. These values agree well with the observed data.

Discussion

The effective hard core diameter can be calculated also from the data of isothermal compressibility.[1] The expression of isothermal compressibility in terms of y has been derived from the following considerations.[1] At higher densities the isothermal compression can be regarded as a process of repacking hard spheres. Thus

$$dp = dp_h. \quad (8)$$

The isothermal compressibility can be approximately expressed by

$$\beta = \rho^{-1}(\partial\rho/\partial p_h)_T. \quad (9)$$

If we adopt the equation of state of hard sphere fluid obtained from the original SPT, then we have in cgs unit

$$\rho\beta T = 7.2\times 10^{15} f(y), \quad (10)$$

where

$$f(y) = (1-y)^4/(1+2y)^2. \quad (11)$$

If we adopt the Carnahan-Stahling equation of state, then Eq. (11) is replaced by

$$f_{SC}(y) = (1-y)^4/[(1+2y)^2+y^4-4y^3]. \quad (12)$$

Function $f_{SC}(y)$ is slightly larger than $f(y)$. Using the observed values for ρ, β, and T, we can calculate the effective hard core diameter a_β of the molecule from Eq. (10).

Calculating a_β from Eq. (10) and Eq. (11), and a from Eq. (6), Mayer[10] has shown that a_β and a coincide with each other at room temperature. However, da/dT is about twice as large as da_β/dT. This suggests that the temperature range in which a_β and a are nearly equal is not wide and that there is no universal relation between σ and β. If there is a certain general relation between σ and β (as suggested by the SPT), the observed value of $\rho\beta T$ should be a one-valued function of y obtained from Eq. (6). Some examples of $\rho\beta T$–y relations are shown in Fig. 7 together with those calculated by using Eqs. (11) and (12). Figure 7 shows that, as expected, no universal relation exists between β and σ. At higher densities Eq. (12) is more accurate than Eq. (11). This corresponds to the accuracy of the Carnahan-Stahling equation of state at higher densities.

Since σ scarcely depends on the details of intermolecular forces, it can be concluded that β depends on the details of intermolecular forces in comparison with σ. Thus the assumption (8) is concluded to be oversimplified.

In contrast to this $\rho\beta T$–y relation, the temperature range in which Eq. (5) holds is not very narrow as is shown in Fig. 8.

The internal pressure calculated from the modified

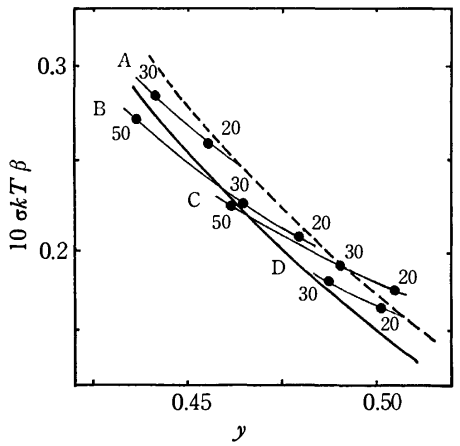

Fig. 7. Relation between compressibility and y. The numbers in the figure denote temperature in °C.
A: Benzene, B: toluene, C: chlorobenzene, D: *m*-xylene.
——: Eq. (11), ·····: Eq. (12).

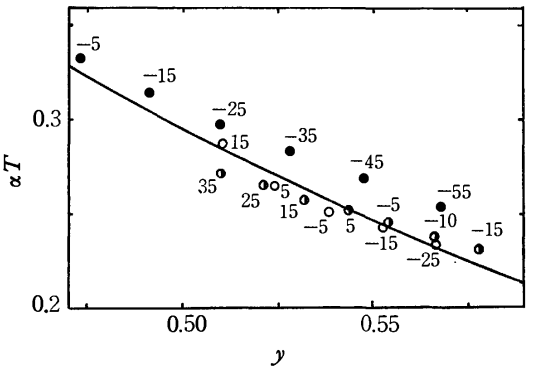

Fig. 8. Relation between thermal expansivity and y. The numbers in the figure denote temperature in °C.
●: Chloroform, ◑: bromobenzene, ○: chlorobenzene.
——: Eq. (5).

AVdW equation of state (7) is proportional not to ρ^2 but to ρ. This contradicts with the observation by Bianchi *et al.*[11] and also with an intuitive picture of the liquid state.[12] However, the modified AVdW equation of state predicts α fairly accurately and thus has a practical value. The original AVdW equation of state, which gives the internal pressure in proportion to ρ^2, gives poor results for α of molecular liquids and for the properties of liquid argon at triple point. As long as we use the van der Waals type equation of state, *i.e.*, $p=p_h-$(effect of intermolecular attractive forces), it is very difficult to work out the equation of state which predicts α accurately and at the same time gives the internal pressure in proportion to ρ^2. Thus there seems to be a limitation to the van der Waals type equation of state even at lower temperatures.

The author wishes to express his appreciation to Professor T. Oyama for a critical reading of the manuscript.

References

1) H. Reiss, "Advances in Chemical Physics," Vol. 9, ed. by I. Prigogine and S. A. Rice, Wiley, New York (1965), p. 1.
2) Y. Oono, This Bulletin, **48**, 2270 (1975).
3) H. C. Longuet-Higgins and B. Widom, *Mol. Phys.*, **8**, 549 (1964).
4) B. J. Alder and C. E. Hecht, *J. Chem. Phys.*, **50**, 2032 (1969). *cf.* Fig. 1.
5) N. F. Carnahan and K. E. Stahling, *ibid.*, **51**, 635 (1969).
6) R. R. Dreisbach, "Physical Properties of Chemical Compounds," American Chemical Society, Washington D. C. (1955).
7) R. R. Dreisbach, "Physical Properties of Chemical Compounds II," American Chemical Society, Washington D. C. (1959).
8) R. R. Dreisbach, "Physical Properties of Chemical Compounds III," American Chemical Society, Washington D. C. (1961).
9) E. A. Guggenheim, *Mol. Phys.*, **9**, 43 (1965).
10) S. W. Mayer, *J. Phys. Chem.*, **67**, 2160 (1963).
11) U. Bianchi, G. Agabio, and A. Turturro, *ibid.*, **69**, 4392 (1965).
12) B. Widom, *J. Chem. Phys.*, **39**, 2808 (1963).
13) S. Mallikarjun and N. E. Hill, *Trans. Faraday Soc.*, **61**, 1389 (1965).

Ionic Adsorption of Lithium Bromide at the Mercury-Dimethyl Sulfoxide Interface

Kohichi YAMAMOTO and Shigeo HAYANO
Institute of Industrial Science, University of Tokyo, Minato-ku, Tokyo 106
(Received June 23, 1975)

The specific adsorption of bromide ions on a mercury electrode from lithium bromide solutions of dimethyl sulfoxide (DMSO) has been studied through the measurement of the differential capacity and the interfacial tension. The capacity data showed the evidence that anions are more weakly, but cations are more strongly, solvated by DMSO molecules than by H_2O. The amounts of specifically adsorbed bromide ions are greater than those values in water at the same electrode charge. The specific adsorption of cations (Li^+) was not found in this study. The inner layer capacity due to the amounts of specific adsorbed anions was calculated, and the ratio of the distances from the metal to the inner Helmholtz plane and to the outer Helmholtz plane were deduced. These values are comparable to those for LiCl in DMSO, but are greater than for water.

Many works on the specific adsorption and the inner layer structure of the electrical double layer have been reported in aqueous system. However, these have been few on non-aqueous systems, especially aprotic solvent systems. It is well known that the role of solvent molecules is very important in the structure of the electrical double layer. An aprotic solvent like dimethyl sulfoxide (DMSO) is very favourable for investigating the electrical double layer, for we can exclude the contribution due to protons. On the other hand, DMSO has been the subject of many recent electrochemical studies[1-4] directed towards the design of new battery systems. The specific adsorption of the supporting electrolyte on the electrode surface has a great influence on these studies. Furthermore, it will be necessary, for a detailed description of electrode kinetics, to analyze the structure of the electrical double layer.

Kolthoff and Reddy[5] obtained an electrocapillary curve of the 0.1M NaCl solution in DMSO. Payne[6] measured the electrocapillary curves and differencial capacities of the double layer for various inorganic salts in DMSO and in mixtures of DMSO and water. However, these studies did not attempt to go into any quantitative discussion of adsorbed ions because of the lack of thermodynamic data. Kim *et al.*[7] discussed the structure of the electrical dorble layer in the presence of LiCl from the measurement of the electrocapillary curves. Hills and Reeves[8] measured the activity coefficients of $LiNO_3$ in DMSO and investigated the degree of ionic adsorption from the measurement of the differential capacities. These two recent detailed studies, however, are different from each other in several points (*e.g.* regarding the solvent effect) in spite of the similar method of data analysis. It is important to investigate systematically halide ions (*e.g.* LiCl, LiB, LiI) in DMSO for the purpose of describing the structure of the electrical double layer and the ionic adsorption in detail. Therefore, a comparison of the above data with the corresponding data for aqueous systems will be useful in discussing the role of solvent molecules.

In the present paper, we will attempt to examine the structure of the electrical double layer in mercury–DMSO containing LiBr. The thermodynamic parameters for the double layer were calculated through measurements of the differential capacity and the interfacial tension.

Experimental

Differential capacity-potential curves were obtained by measuring the in- and out of-phase components of the AC admittance of the mercury electrode–DMSO solution interface by the use of a PAR model 170 electrochemistry system. A 10 mV (peak to peak) amplitude AC voltage with a frequency of 80 Hz was superimposed on the DC voltage applied between the dropping mercuy electrode (DME) and the platinum counter electrode. The scan rate of the DC voltage was 1 mV/s. The drop time of mercury was mechanically controlled at 5 s, and the capillary constant, m, for DME was 0.739 mg/s. The amplitudes of the in- and out of-phase components were recorded as a function of the DME potential. The differential capacity, C, was calculated from:

$$C = \frac{I_1^2 + I_0^2}{2\pi f I_0 V A} \quad (1)$$

where I_1 is the AC current of the in-phase, I_0 is that of the out of-phas,e f is the frequency (Hz), V is its amplitude, and A is the area of the electrode at the end of the drop life, as calculated from the flow rate and the drop time. The precision of the data obtained in this manner was about 0.5%.

The interfacial tension between the mercury electrode and the DMSO solution was measured at the electrocapillary maximum (*i.e.*, point of zero charge) to determine the integral constant in the process of the integration of the capacity-potential curve. This has been done by using a modified Lippmann type capillary electrometer. The capillary electrometer used in this work was constructed by taking several ideas presented by previous workers.[9-11] The tapering capillary was made of a Pyrex capillary tubing with an internal diameter of 1 mm. The tubing was drawn out in a gas flame so as to have the internal diameter of 15—20 μ. Then the capillary was cut at this point. The gas pressure above the mercury reservoir was controlled by a nitrogen gas pressure control system which consists of a series combination of two precision-variable bellows mounted over a screwdriven press. The gas pressure was measured with a Texas Instruments, Inc. Fused-Quartz Precision Pressure Gauge instead of a mercury manometer. A stereomicroscope was employed to observe the capillary tip. The window of the cell was finished to an optically plane to eliminate distortion. The precision of the interfacial tension in this methods is within 0.02%. For the measurements of both the differential capacity and the interfacial tension, the temperature of the cell was controlled at 25.0±0.1 °C. Prior to each measurement the solution was flushed with a high-purity nitrogen which had been deoxygenated, dehydrated in an anhydrous

calcium chloride column, and then presaturated by bubbling it through DMSO. DMSO was refluxed for several hours on calcium hydride and then fractionated through an efficient distillation column at a reduced pressure of about 5 Torr. The water content of the solvent was checked by means of Karl Fisher titration. The analytical reagent grade mercury was used without further purification, while the analytical grade anhydrous LiBr was used after have been dried at 180 °C under a vacuum for 24 hr.

Results and Discussion

Differential capacity *vs.* potential curves for LiBr in DMSO at six concentration levels between 0.753 M and 0.0196 M were obtained in the potential range of −0.35∼−1.65 V (*vs.* aqueous SCE), where no significant DC current and no frequency dispersion of capacity was observed. At more positive potentials, the measurements were not reproducible, this is due to the faradaic admittance. The aqueous SCE was used as a reference electrode, the junction between the reference electrode and the DMSO solution was kept constant in each experiment by employing the 0.200 M LiBr solution in DMSO. The liquid junction between 0.200 M solution and the test solution was made through a fritted glass. The measured potentials, E_m, were converted to the potential scale of the reference electrode reversible to the anion (*i.e.*, to the E^- scale) according to this equation:

$$E^- = E_m + E_{ljp} + \frac{RT}{F} \ln a_\pm \quad (2)$$

Here, E_{ljp} is the liquid junction potential between 0.200 M and x M LiBr in DMSO (test solution); it was calculated using the following equation:

$$E_{ljp} = (2t^+ - 1)\frac{RT}{F} \ln \frac{a_\pm}{a_{\pm 0.200M}} \quad (3)$$

The mean ionic activities, $a_\pm$, were taken form the data of Salomon.[12] The transference number for Li^+ in DMSO, t^+, was estimated to be 0.324 from the mobility data of Dunnett and Gasser.[13] The observed differential capacity *vs.* potential (converted to E^- scale) curves are shown in Fig. 1. The curves are featureless like those of the LiCl[7] and $LiNO_3$[8] solutions in DMSO. The capacity increases rapidly in the anodic branch; this is due to the specific adsorption of the anion. The anodic hump in the capacity curves observed in the cases of $LiClO_4$[6] and KPF_6[6,14] in DMSO were not found anywhere in the concentration range studied. The diffuse layer capacity minimum, which was observed with KPF_6,[6] $LiNO_3$,[8] KNO_3[14] in DMSO, was not detected even in the 0.0196 M LiBr solution. The diffuse layer capacity minimum appears in the vicinity of pzc if there is no significant ionic specific adsorption; *i.e.*, the structure of the double layer can be assumed to be a simple Stern model. Therefore, the differential capacity curves shown in Fig. 1 lead us to the conclusion that Br^- is more specifically adsorbed on the mercury electrode than PF_6^-, ClO_4^- and NO_3^-. In the cathodic branch, the capacity decreases monotonously with the electrode potential to the value of about 7 $\mu F/cm^2$. This limiting value is comparable with that obtained in DMSO containing lithium salt.[6-8] In aqueous systems, in general, at higher cathodic potentials a rise in the capacity curves is observed. This is due to the onset of the faradaic reaction. In the present system, such behaviour was not detectable, so, in the potential region of the invariant capacity (*i.e.*, at extreme cathodic potentials), the structure of the electrical double layer may be determined mainly by the Li^+ cation, which is more firmly solvated in DMSO than in aqueous solutions. This point will be discussed later in detail. The difference in the limiting value in DMSO from those in aqueous solutions (about 16 $\mu F/cm^2$) can be expected from the lower dielectric constant of DMSO, since, in these potential regions, we can assume that there is no ionic specific adsorption.

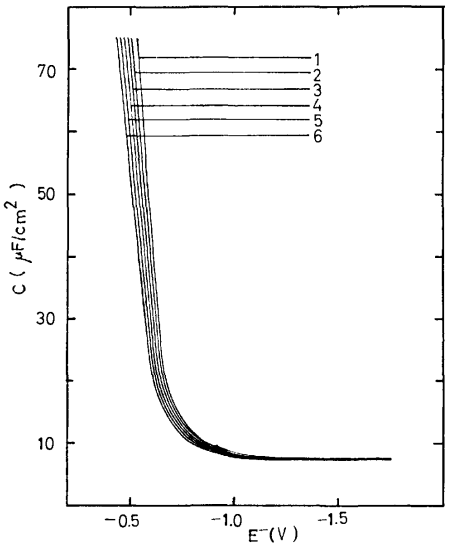

Fig. 1. Differential capacity of electrical double layer at mercury electrode in contact with LiBr solutions in DMSO at 25 °C: (1): 0.753 M, (2): 0.497 M, (3): 0.196 M, (4): 0.0979 M, (5): 0.0497 M, (6): 0.0196 M.

For a detailed discussion, it is a matter of prime importance to establish to what degree bromide ions are specifically adsorbed from DMSO. The capacity *vs.* potential data were integrated to obtain the charge density on the electrode, q_m, and the interfacial tension, γ, over the entire range of concentrations and potentials with the aid of a computer (FACOM 230-55) using a program written in FORTRAN. Then Parsons' auxiliary function, ξ,[15] was evaluated from this equation:

$$\xi_- = \gamma + q_m E^- \quad (4)$$

The surface excess of Li^+ cations, Γ_+, was then calculated from this relationship:

$$\left(\frac{\partial \xi_-}{2RT\partial \ln a_\pm}\right)_{q_m} = -\Gamma_+ = -\frac{q_+}{F} \quad (5)$$

This calculation was carried out first by computer differentiation and then checked manually. The results, expressed as q_+ (*i.e.*, the charge due to the excess of cations), are shown in Fig. 2. This shows that the bromide ion is adsorbed so strongly that the surface excess of lithium ions is positive at all concentrations and all values of q_m. Figure 2 also shows a minimum at all concentrations which is similar to those found with

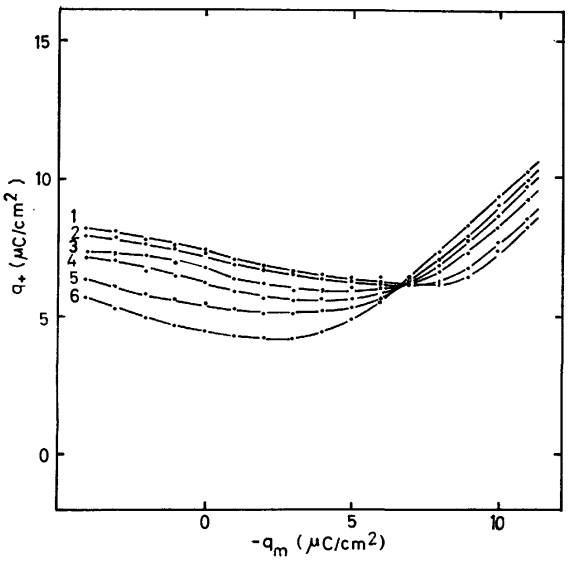

Fig. 2. Charge due to the cations as a function of the electrode charge (q_m) at the corresponding concentration as given in Fig. 1.

LiCl[7] and $LiNO_3$[8] in DMSO and with aqueous solutions of strongly adsorbed species, such as halide ions.[16] The appearence of the invariant point at $q_m = -7\ \mu C/cm^2$ is interesting; such a point is also found in the comparable study of LiCl in DMSO.[7] This invariant point, however, is more negative than those of chloride ions ($q_m = -4\ \mu C/cm^2$).

From the similarity of the surface excess curve with those for aqueous alkali halide solutions[16-17] and the results obtained in the present work, it seems reasonable to assume that lithium ions are present only in the diffuse layer. That is, $q_+ = q_+^{2-s}$, where q_+^{2-s} is the charge in the diffuse layer. On the basis of this assumption, we calculated the potential of the outer Helmholtz plane, ϕ_2, from q_+^{2-s} according to the diffuse layer theory;[18]

$$q_+^{2-s} = \left(\frac{RT\varepsilon C^s}{2\pi}\right)^{1/2}\left[\exp\left(-\frac{F}{2RT}\phi_2\right) - 1\right] \qquad (6)$$

Here, C^s is the electrolyte concentration and ε is the dielectric constant in the diffuse layer, assuming it to be equal to the bulk dielectric constant of DMSO (46.7).[19] Then the charge due to the bromide ions, q_-, and that distributed in the diffuse (q_-^{2-s}) and inner (q_-^1) fouble layer were evaluated according to:

$$-q_m = q_+^{2-s} + q_- \qquad (7)$$

$$q_- = q_-^{2-s} + q_-^1 \qquad (8)$$

$$q_-^{2-s} = -\left(\frac{RT\varepsilon C^s}{2\pi}\right)^{1/2}\left[\exp\left(\frac{F}{2RT}\phi_2\right) - 1\right] \qquad (9)$$

The plots of ϕ_2 *vs.* q_m as a function of the LiBr concentration are shown in Fig. 3. The curves have a striking resemblance to those of the LiCl solution.[7] In the absence of a specific adsorption such as in NaF aqueous solutions,[20-21] the sign of ϕ_2 changes at pzc. However, in the present system, the specific adsorption of bromide ions is so strong that ϕ_2 is negative over the entire range of q_m and the values of ϕ_2 are more negative than those obtained in chloride ions.

The specifically adsorbed charge due to bromide ions

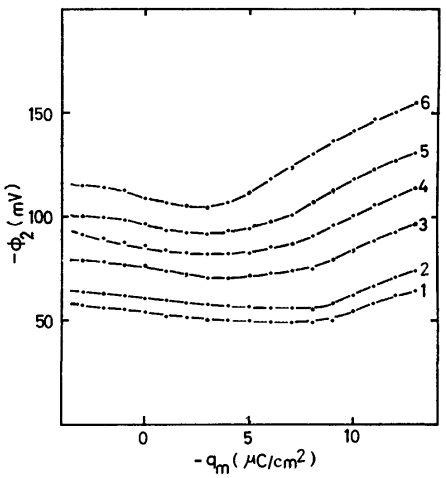

Fig. 3. Potential of outer Helmholtz plane (ϕ_2) as a function of the value of q_m at various LiBr concentrations.

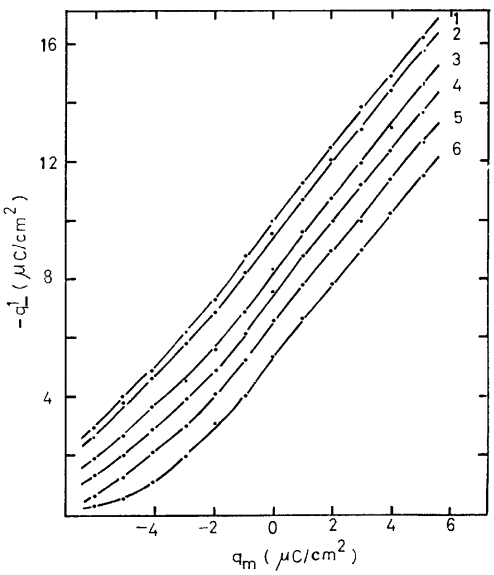

Fig. 4. Charge due to specifically adsorbed bromide ions (q_-^1) as a function of the electrode charge at the corresponding concentration as given in Fig. 1.

(q_-^1) is shown in Fig. 4 as a function of q_m and the LiBr concentration. The figure shows that q_-^1 is a monotonous function of q_m and that the degree of the concentration dependence of q_-^1 changes with q_m, that is, increases with the electrode charge. This behaviour is similar to that found in chloride ions[7] in DMSO and is different from that in nitrate ions[8] in DMSO (*i.e.*, the nitrate-ions system shows a reversed tendency.). At $q_m > 0$ the curves become virtually parallel lines. At the same concentration, say at 0.1 M, some comparisons can be made with the system of other electrolytes in DMSO and with the aqueous potassium bromide solution. The minimum q_m value ($0\ \mu C/cm^2$), the $q_-^1 - q_m$ curves of which in Fig. 4 deviate from a straight line, is more negative than those obtained in chloride ions[7] and nitrate ions[8] in DMSO (*ca.* 2 and 4 $\mu C/cm^2$ respectively), but it is more positive than that with potassium iodide in formamide[22] (*ca.* $-2\ \mu C/cm^2$). The values of the specifically adsorbed charge at pzc are as

follows; −7.5 (in the present system), −5.1 (in KBr aqueous solution),[17] −4.5 (in LiCl solution in DMSO),[7] −3.6 (in $LiNO_3$ solution in DMSO)[8] and −1.2 (in KPF_6 solution in DMSO)[14] (unit is $\mu C/cm^2$). From these results, it may be concluded that the degree of the specific adsorption of anions in DMSO changes in the following order:

$$PF_6^- < NO_3^- < Cl^- < Br^-$$

and the specific adsorption of bromide ions is stronger in DMSO than in H_2O.

The limiting values of the slope at positive q_m values were −1.26~−1.35. These values of the dq_-^1/dq_m will be discussed in the section on Esin and Markov effects below.

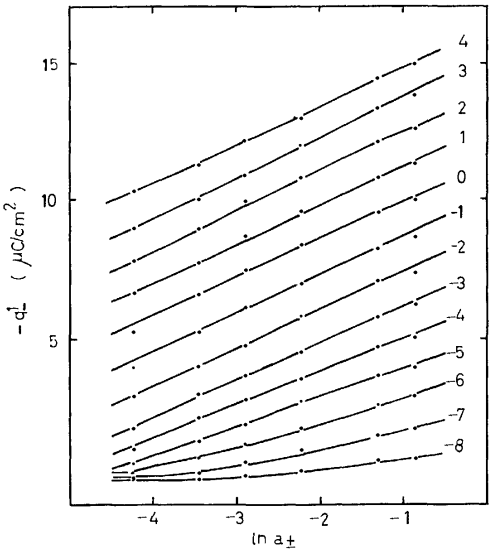

Fig. 5. Charge due to specifically adsorbed bromide ions (q_-^1) as a function of ln $a_\pm$ at the constant value of charge on electrode (q_m). The value of q_m is indicated by each line in $\mu C/cm^2$.

We also show the logarithmic isotherms at a constant q_m in Fig. 5. The figure is similar in character to that obtained for aqueous bromide and iodide solutions.

It is usual to invenstigate the degree of specific adsorption in terms of the Esin and Markov coefficients, defined as:[23-24]

$$\left(\frac{\partial E^+}{\partial \mu}\right)_{q_m} = -\left(\frac{\partial \Gamma_-}{\partial q_m}\right)_\mu \tag{10}$$

or

$$\left(\frac{\partial E^+}{\partial \ln a_\pm}\right)_{q_m} = \frac{2RT}{F}\left[\left(\frac{\partial q_-^1}{\partial q_m}\right)_\mu + \left(\frac{\partial q_-^{2-s}}{\partial q_m}\right)_\mu\right] \tag{11}$$

where E^+ is the potential with respect to the reference electrode reversible to the cation. The right-hand sides of Eq. (10) and (11) can be predicted as follows from the diffiuse double layer theory in the absence of any specific adsorption:

$$\left(\frac{\partial E^+}{\partial \ln a_\pm}\right)_{q_m} = -\frac{1}{2}\exp\left[\sinh^{-1}\left(\frac{q_m}{2A}\right)\right]\left[1+\left(\frac{q_m}{2A}\right)^2\right]^{-1/2}$$

$$A = \left(\frac{RT\varepsilon C^s}{2\pi}\right)^{1/2} \tag{12}$$

The observed results are shown in Fig. 6. According to Eq. (12), if any specific adsorption is absent, two

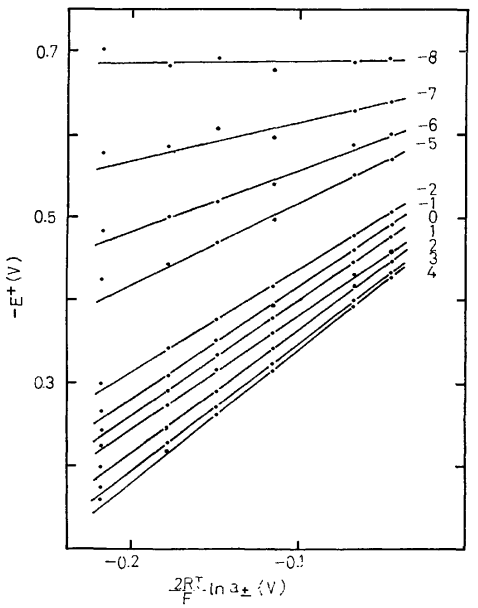

Fig. 6. Esin and Markov plots for LiBr in DMSO at 25 °C. The value of q_m in $\mu C/cm^2$ is incicated by each line.

limiting slopes can be found, *i.e.*, 0 for $q_m \to -\infty$ and −1 for $q_m \to +\infty$ respectively. Furthermore, the value of the slope is −0.5 at pzc (*i.e.*, at $q_m=0$). In this study, however, the values of the slope evidently deviate from those given by Eq. (12); that is because of the significant specific adsorption of bromide ions. The slope becomes steeper with an increase in the electrode charge. At pzc this value is −1.2, and it reaches the limiting value of −1.3 at $q_m=4\,\mu C/cm^2$. This limiting value is compared with those obtained for other electrolytes in DMSO in Table 1. In the second row, the values of $-(\partial q_-^1/\partial q_m)_\mu$ (*i.e.*, the derivatives of the adsorbed anion charge with respect to the electrode charge at a constant chemical potential) are shown. It is well known that the Esin and Markov coefficients are approximately equal to this value[7-8,25] (*cf.* Eq. (11)). In the present work, the two values agree well. This shows the consistency of the experimental data. The values for LiBr in the first row and in the second row in Table 1 are the highest among the electrolytes. The high specific adsorptivity of the bromide ions was confirmed again by these results.

In the discussion of the specific adsorption of ions, we must take into account two important factors. One is the solvation energy of ions, and the other is the interaction between the metal surface and solvent molecules. According to Parker,[26] such dipolar aprotic

Table 1. The limiting values of Esin and Markov coefficient for various anions in DMSO

	LiBr	LiCl	$LiNO_3$	KPF_6
$-\frac{F}{2RT}\left(\frac{\partial E^+}{\partial \ln a_\pm}\right)_{q_m}$	1.3	1.2	1.18	1.26
$-\left(\frac{\partial q_-^1}{\partial q_m}\right)_\mu$	1.26—1.35	1.1—1.3	1.17[a]	1.26[a]
Reference		7)	8)	25)

a) The value was taken for 0.1 M solution.

solvents as DMSO poorly solvate anion.[12,27] Salomon has reported that the free energy of transfer of LiBr from H_2O to DMSO at 25 °C is 2.515 kcal/mol, and concluded that the order of increasing solvation by DMSO molecules is:

$$Cl^- < Br^- < I^-$$

in spite of the solvation being poorer than the H_2O system. This behaviour is reflected in our study by the rapid rise on the capacity curves in the anodic potential in Fig. 1. Furthermore, as for the ionic solvation, we may infer that the small cations like Li^+ are solvated more steadily in DMSO than in H_2O. This is supported by the evidence that the significant capacity rise found in the case of an aqueous system was not observed in Fig. 1. From these results, the higher specific adsorptivity of bromide ions in the DMSO system seems to be attributable to the difference in the degree of ionic solvation. However, the second factor (*i.e.*, the interction of the mercury electrode surface and the DMSO molecules) is also important, as was pointed out by Hills *et al.*[8] The effect of this factor can be observed on the values of the Esin and Markov coefficients and $-(\partial q_-^1/\partial q_m)_\mu$. These values in Table 1 are higher than those of aqueous solutions for other electrolytes. This may be the influence of the property of the solvent molecules. Hills *et al.*[8] stressed this factor in their study of $LiNO_3$ in DMSO, since the value of $-(\partial q_-^1/\partial q_m)_\mu$ rises with the electrode charge. These values are higher in their system than in the corresponding aqueous system (up to 1.3 for DMSO and 1.22 for water). In our present work, however, we did not observed such a significant difference between these two systems. It is difficult and dangerous to conclude which factor predominantly governs the specific adsorption of ions from only these data. Independent measurements from this point of view are desirable.

For the detailed discussion of the structure of the inner layer, the potential drop across the layer between the electrode surface and the outer Helmholtz plane (oHp), ϕ_{m-2}, was calculated from this relationship:[7,22]

$$\phi_{m-2} = E_m + E_{ljp} - \phi_2 \qquad (13)$$

Here, it should be mentioned that the ϕ_{m-2} potential computed in this way is not equal to the rational potential in the sense of Grahame's definition. ϕ_{m-2} is shown in Fig. 7 as a function of q_-^1 at constant values of q_m. The relationship shown in Fig. 7 indicates a linear function of q_-^1 and the slopes of these straight lines are almost the same except at very negatives of q_m. This slope has the relationship with the standard free energy of adsorption, ΔG:[28-30]

$$\left(\frac{\partial\phi_{m-2}}{\partial q_-^1}\right)_{q_m} = \frac{RT}{F}\left(\frac{\partial(-\Delta G/RT)}{\partial q_m}\right)_{T,P} \qquad (14)$$

Therefore, if we base our discussion on Eq. (14), we may infer that the free energy of adsorption is a linear fuction of q_m and is independent of q_-^1. This behaviour has been shown in the aqueous solution of ions with high specific adsorptivity ions such as I^-[17] and Cl^-[7] in the DMSO solution.[7] However, Eq. (14) is only an approximation because it does not take into account the contribution of the diffuse double layer. This contribution may be very small in the potential range where the specific adsorption of ions is predominant. On the other hand, it becomes effective in other potential ranges. This is supported by the results that the deviation from the constant slope in Fig. 7 increases with the decrease in q_m (*i.e.*, becoming more negative).

The potential of ϕ_{m-2} can be divided into two components according to the following equation:[31]

$$d\phi_{m-2} = \left(\frac{\partial\phi_{m-2}}{\partial q_-^1}\right)_{q_m} dq_-^1 + \left(\frac{\partial\phi_{m-2}}{\partial q_m}\right)_{q_-^1} dq_m. \qquad (15)$$

In Eq. (15), we define the corresponding integral capacities, ${}_{q_-^1}C^i$ and ${}_{q_m}C^i$, according to Grahame and Parsons by:[32]

$$\begin{aligned} {}_{q_-^1}C^i &= 1/(\partial\phi_{m-2}/\partial q_-^1)_{q_m} \\ {}_{q_m}C^i &= 1/(\partial\phi_{m-2}/\partial q_m)_{q_-^1} \end{aligned} \qquad (16)$$

As a first approximation, we assumed that the inner layer can be represented by two condensers in series,

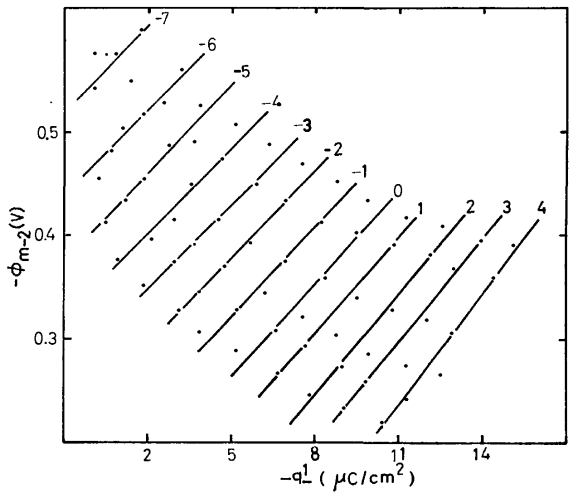

Fig. 7. Potential difference across the inner layer generated by specifically adsorbed anion (ϕ_{m-2}), as a function of the charge due to specifically adsorbed bromide ions (q_-^1) at the constant electrode charge. The value of electrode charge is indicated by each line in μC/cm^2.

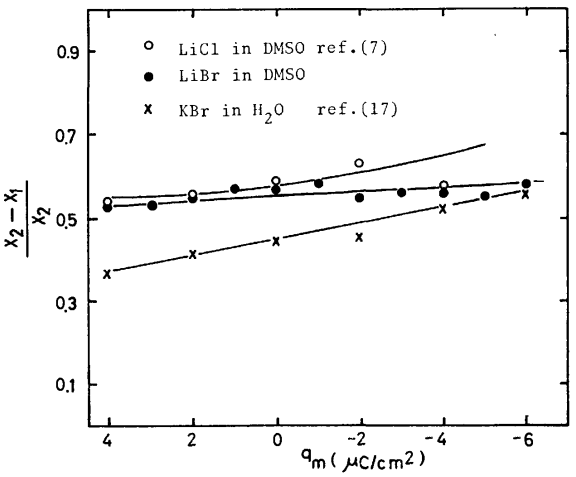

Fig. 8. Variation of distance ratio ($(x_2-x_1)/x_2$) as a function of the electrode charge and comparison it with other data.

the mercuy surface to the inner Helmholtz plane (iHp) and the iHp to the oHp; furthermore, we assumed that the dielectric constants are equal in these two layers. Then we computed the distance ratio $(x_2-x_1)/x_2$ from this relationship:

$$\frac{x_2-x_1}{x_2}=\frac{{}_{q_m}C^i}{{}_{q^-}C^i}, \qquad (17)$$

where x_1 and x_2 are the distances from the metal surface to the iHp and to the oHp respectively. From the results of Fig. 7 we found the integral capacities to be ${}_{q^-}C^i=30\sim36$ μF/cm² and ${}_{q_m}C^i=16\sim21$ μF/cm². These values are comparable to those for LiCl in DMSO. The distance ratios mentioned above found to be 0.52—0.58; the dependence of this ratio on q_m is shown in Fig. 8, where it is also compared with other electrolytes and aqueous system. The plot in the present study seems to be constant over the range of q_m studied and does not show a definite tendency to increase with a decrease in the q_m values. The values of the distance ratio are greater than the corresponding values of bromide ions in an aqueous system[17] (0.35—0.55) in the range of $q_m>0$. However, they are nearly the same at negative values of q_m. If we assume x_2 to be the sum of the thickness of DMSO monolayer (4.8 Å)[33] and the crystallographic radius of the lithium ion of 0.68 Å,[34] the resulting value of x_1 (*i.e.*, the thickness of the iHp) varies from 2.3 Å to 2.6 Å. These are greater than the crystallographic radius of the bromide ion (1.96 Å).[34] If x_1 is assumed to be 1.96 Å, the thickness of the oHp becomes from 4.1 to 4.7 Å. Considering the incompliteness of the solvent monolayer formation, we may say that some of the lithium ions sit inside the DMSO monolayer and that others are present on the outside of the monolayer of solvent molecules. However, this discussion has been based on a simple condenser model; it is only a qualitative discussion. For more detailed discussion, it will be necessary for us to take into consideration the dependence of the dielectric constant on the distance from electrode surface, the influence of the variation in solvent dipoles, and so on.

The authors with to thank Miss Masako Arai and Mr. Masami Iiyama who assisted them extensively in this study.

References

1) J. N. Butler, *J. Electroanal. Chem.*, **14**, 89 (1967).
2) R. Jasinski, "High Energy Batteries," Plenum Press, New York (1967).
3) J. N. Butler," Advances in Electrochemistry and Electrochemical Engineering," Vol. 7, Wiley-Interscience, New York (1970), p. 77.
4) B. Burrows, *J. Electrochem. Soc.*, **118**, 1130 (1971).
5) I. M. Kolthoff and T. B. Reddy, *ibid.*, **108**, 980 (1961).
6) R. Payne, *J. Amer. Chem. Soc.*, **89**, 489 (1967).
7) S. H. Kim, T. N. Andersen, and H. Eyring, *J. Phys. Chem.* **74**, 4555 (1970).
8) G. J. Hills and R. M. Reeves, *J. Electroanal. Chem.*, **41**, 213 (1973).
9) R. S. Hansen, D. J. Kelsh, and D. H. Grantham, *J. Phys. Chem.*, **67**, 2316 (1963).
10) D. E. Broadhead, R. S. Hansen, and G. W. Jr. Potter, *J. Colloid Interface Sci.*, **31**, 61 (1969).
11) Y. Inoue and K. Niki, *Rev. Polarography* (Kyoto), **18**, 49 (1972).
12) M. Salomon, *J. Electrochem. Soc.*, **116**, 1392 (1969).
13) J. S. Dunnett and R. P. H. Gasser, *Trans. Faraday Soc.*, **61**, 922 (1965).
14) K. Yamamoto, unpublished data.
15) R. Parsons, *Trans. Faraday Soc.*, **64**, 1638 (1968).
16) M. A. V. Devanathan and B. V. K. S. R. A. Tilak, *Chem. Rev.*, **65**, 635 (1965).
17) J. Lawrence and R. Parsons, *J. Electroanal. Chem.*, **16**, 193 (1968).
18) D. C. Grahame and B. Sorderberg, *J. Chem. Phys.*, **22**, 449 (1954).
19) R. A. Hovermale and P. G. Sears, *J. Phys. Chem.*, **60**, 1579 (1956).
20) P. Delahay, "Double Layer and Electrode Kinetics," Wiley, New York, 1965.
21) R. Payne, *J. Electroanal. Chem.*, **7**, 343 (1964).
22) R. Payne, *J. Chem. Phys.*, **42**, 3371 (1965).
23) R. Parsons, Proc. Intern. Congr. Surface Activity, 2nd, London, 3, 38 (1957).
24) D. M. Mohilner, "Electroanalytical Chemistry," Vol. 1, Mercel Dekker, New York (1966), p. 291.
25) G. J. Hills and R. M. Reeves, *J. Electroanal. Chem.*, **38**, 1 (1972).
26) A. J. Parker, *Quart. Rev.* (London), **16**, 163 (1962).
27) M. Salomon, *J. Electrochem. Soc.*, **117**, 325 (1970).
28) R. Parsons, *Trans. Faraday Soc.*, **55**, 999 (1959).
29) J. M. Parry and R. Parsons, *ibid.*, **59**, 241 (1961).
30) J. Lawrence and R. Parsons, *ibid.*, **64**, 751 (1968).
31) R. Parsons, "Advance in Electrochemistry and Electrochemical Engineering," Vol. 1, 1, Willey-Interscience, New York (1961).
32) D. C. Grahame and R. Parsons, *J. Amer. Chem. Soc.*, **83**, 1291 (1961).
33) R. Thomas, C. R. Shoemaker, and K. Eriks, *Acta Crystallogr.*, **21**, 12 (1966).
34) R. C. Weast, Ed., "Handbook of Chemistry and Physics," 50th ed. The Chemical Rubber Publishing Co., Cleveland, Ohio (1969).

Theory for Longitudinal Ion Cyclotron Resonance Power Absorption: Application to Line Shape for Nonreactive Ion

Katsuyuki AOYAGI

JEOL Ltd., 1418 Nakagami, Akishima-shi, Tokyo 196

(Received July 2, 1975)

The rf electric field in circular concave electrodes for longitudinal ion cyclotron resonance is investigated. The potential equation of this rf electric field is theoretically derived from Laplace's equation. The equation of the motion of an ion which moves under the simultaneous application of the magnetic field and this rf electric field was solved. The solution of this equation is used to obtain the instantaneous and total power absorptions of the ion from the rf electric field. The power absorption expression is used to derive the line-shape expresssions of the longitudinal ion cyclotron resonance.

Ion cyclotron single- and multiple-resonances have been used extensively in recent years to study a wide field of gas-phase chemistry. The reviews[1] describe the use of ion cyclotron resonance (ICR) in the determination of reaction mechanisms, reaction rates, ion structures, relative acidities and basicities, photodetachment processes, the detection of excited states, thermochemistry, and other properties of ions. Recently, the technique of Fourier transform ion cyclotron resonance (FT-ICR) was developed by Comisarow and Marshall,[2] it improves the ICR spectral resolution by orders of magnitude. By combining the high resolution with the inherent high sensitivity of ICR, FT-ICR makes possible new fields of diamagnetic resonance spectroscopy, such as mass spectrometry with regard to organic chemistry, biology, and medicine.

The principle of ICR is based phenomenologically on the classical motion of charged particles in the magnetic and electric fields. An ion moving in a homogeneous magnetic field describes a helical path which is a combination of a translation along the field line and a circular motion in a plane perpendicular to the direction of the magnetic field. The angular frequency or cyclotron frequency, ω, of the circular motion is given by $\omega=eH/me$, where e/m is the charge-to-mass ratio; H, the magnetic field strength, and c, the speed of light. If an rf electric field with the frequency of ω_1 is applied perpendicular to the magnetic field, and the magnetic field or the rf frequency is swept, the ion resonates at $\omega=\omega_1$ and absorbs energy from the rf electric field; then the ions of a particular e/m ratio are accelerated and the radius of its orbit increases with the time.

ICR is of two types, longitudinal ICR and transverse ICR. In the case of transverse ICR,[1] the guiding center of the circular motion of the ion is migrated at right angles to both the magnetic and electric fields with a uniform drift velocity of v_d. In the other case of longitudinal ICR,[3] the guiding center of the circular motion of the ion is migrated along the magnetic line of force with a uniform traveling velocity of v_z.

In an application of FT-ICR to a wide mass range, a more intence magnetic field than that of the electromagnet used widely is required. Super conducting magnet (SCM)[4] satisfies the requirement mentioned above, and longitudinal ICR is suitable for FT-ICR using SCM.

In this paper, we will propose a potential equation for the longitudinal ICR cell and an exact solution of the equation of the motion of the ion used for driving the power absorption of an ion.

Result and Discussion

RF Electric Field in the ICR Cell. In order to treat the problem, we consider the rf electric field in a vacuum produced by circular concave electrodes arranged cylindrically as is shown in Fig. 1. Let us assume that the frequency of the rf electric field is sufficiently low enough for the displacement current to be neglected, and let us also ignor the axial component of the electric field in the ICR cell. The problem can be reduced to that of solving Laplace's equation:

$$\Delta V = 0, \tag{1}$$

under given conditions, where V is a scalar electric potential. Electric field, $\mathbf{E}$, can be obtained from the potential, V, by using this relation:

$$\mathbf{E} = -grad\, V. \tag{2}$$

Equation (1) is expressed in cylindrical coordinates (r, θ) as:

$$\frac{1}{r}\cdot\frac{\partial}{\partial r}\left(r\frac{\partial V}{\partial r}\right)+\frac{1\partial^2 V}{r^2\partial\theta^2}=0. \tag{3}$$

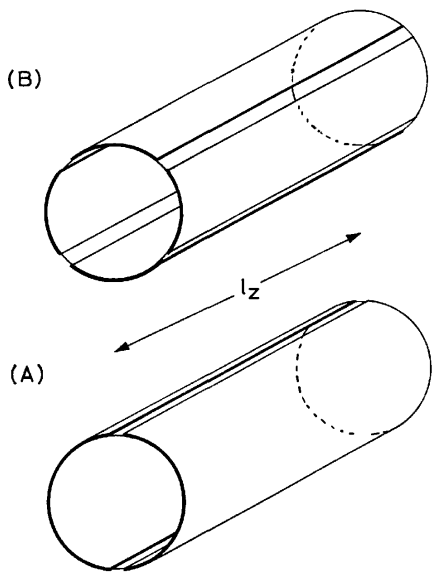

Fig. 1. Electrodes arrangement for theoretical analysis. (A) 2-Split electrodes, (B) 4-split electrodes.

After some analytical treatment, we solve Eq. (3), the result is given by Eq. (A4) (see Appendix). By substituting Eq. (A4) into Eq. (2), we then obtain the expressions of the rf electric field in the case of 2-split electrodes as follows:

$$\mathbf{E}(r)_2 = \left\{ -\frac{2(V_1-V_2)}{\pi} \sum_{k=1}^{k=\infty} \frac{(-1)^{k-1}}{r} \left(\frac{r}{R}\right)^{2k-1} \times \cos(2k-1)\theta \right\} \sin(\omega_1 t+\phi_1) \quad (4a)$$

$$\mathbf{E}(\theta)_2 = \left\{ \frac{2(V_1-V_2)}{\pi} \sum_{k=1}^{k=\infty} \frac{(-1)^{k-1}}{r} \left(\frac{r}{R}\right)^{2k-1} \times \sin(2k-1)\theta \right\} \sin(\omega_1 t+\phi_1), \quad (4b)$$

where V_1 and V_2 are the electric potentials applied to electrodes, and R, the radius of the cylinder indicated in Fig. 1.

Solution of the Equation of Motion. In absence of reactive collisions, the motion of an ion in the ICR cell can be described as follows:

$$\frac{d\mathbf{v}}{dt} = \frac{e}{m}\mathbf{E}(t) + \frac{e}{mc}\mathbf{v}\times\mathbf{H} - \xi\mathbf{v}, \quad (5)$$

where ξ is the reduced collision frequency that specifies the rate of the momentum relaxation of the ion.[5a]

The Cartesian coordinates system is chosen so that the static magnetic field, H, is parallel to the z axis and the rf electric field is perpendicular to the z axis. Therefore, the expressions of the rf electric field in the cylindrical coordinates are transformed to those of the Cartesian coordinates.[6] Equation (4) is transformed as follows:

$$\mathbf{E}(\mathbf{x})_2 = \left\{ -\frac{2(V_1-V_2)}{\pi R}\left[1 - \frac{x^2-y^2}{R^2} + \frac{x^4-6x^2y^2+y^4}{R^4} - \cdots\right]\right\} \sin(\omega_1 t+\phi_1), \quad (6a)$$

$$\mathbf{E}(\mathrm{y})_2 = \left\{ -\frac{2(V_1-V_2)}{\pi R}\left[\frac{2xy}{R^2} - \frac{4x^3y-4xy^3}{R^4} + \frac{6x^5y-20x^3y^3+6xy^5}{R^6} - \cdots\right]\right\} \sin(\omega_1 t+\phi_1). \quad (6b)$$

Equation (5) is now separated into an equation of $\mathbf{v}_z$ only and two coupled equations of $\mathbf{v}_x$ and $\mathbf{v}_y$. The relevant equations of motion are, then:

$$\frac{d\mathbf{v}_x}{dt} = \frac{e}{m}\mathbf{E}_x \sin(\omega_1 t+\phi_1) + \omega\mathbf{v}_y - \xi\mathbf{v}_x, \quad (7a)$$

$$\frac{d\mathbf{v}_y}{dt} = \frac{e}{m}\mathbf{E}_y \sin(\omega_1 t+\phi_1) - \omega\mathbf{v}_x - \xi\mathbf{v}_y, \quad (7b)$$

where $\mathbf{E}_x$ or $\mathbf{E}_y$ only denotes the expression in the brace of Eq. (6).

An ion whose initial velocity, $\mathbf{v}_0$, is due to the thermal velocity leads to a circular motion with the phase angle of ϕ_0; then, $\mathbf{v}_x(0) = -\mathbf{v}_0 \sin\phi_0$ and $\mathbf{v}_y(0) = \mathbf{v}_0 \cos\phi_0$ at $t=0$. The exact solution of Eq. (7) is given by:

$$\mathbf{v}_x = \mathbf{v}_0 \sin(\omega t-\phi_0)\exp(-\xi t) + \frac{e}{m}(\alpha\mathbf{E}_x - \beta\mathbf{E}_y), \quad (8a)$$

$$\mathbf{v}_y = \mathbf{v}_0 \cos(\omega t-\phi_0)\exp(-\xi t) + \frac{e}{m}(\beta\mathbf{E}_x + \alpha\mathbf{E}_y), \quad (8b)$$

where;

$$\alpha = A\sin(\omega_1 t+\phi_1) - B\cos(\omega_1 t+\phi_1) - [(A\cos\omega t + D\sin\omega t)\sin\phi_1 - (B\cos\omega t - C\sin\omega t)\cos\phi_1]\exp(-\xi t),$$

$$\beta = D\sin(\omega_1 t+\phi_1) + C\cos(\omega_1 t+\phi_1) + [(A\sin\omega t - D\cos\omega t)\sin\phi_1 - (B\sin\omega t + C\cos\omega t)\cos\phi_1]\exp(-\xi t),$$

A, B, C, and D are given in the Appendix.

Line-shape Expression for Nonreactive Ion. *a) Power Absorption of an Average Nonreactive Ion*: The power absorption, A, of an ion from the rf electric field is given by:

$$A = \langle e\mathbf{E}(t)\cdot(\mathbf{v}_x+\mathbf{v}_y)\rangle. \quad (9)$$

The initial velocity of an ion with the phase angle of ϕ_0 will not contribute to the actual power absorption. Substituting Eq. (8) into Eq. (9), the power absorption can be obtained by averaging over the ϕ_1 phase angle, since all the values of ϕ_1 are equally probable. With the approximation that:

$$\omega_1 + \omega \approx 2\omega, \qquad \xi \ll \omega_1, \quad (10)$$

the instantaneous power absorption of an average ion is found to be:

$$A(\omega_1 \mp \omega) = \frac{e^2(\mathbf{E}_x^2+\mathbf{E}_y^2)}{4m[(\omega_1-\omega)^2+\xi^2]}\{\xi + [(\omega_1-\omega)\sin(\omega_1-\omega)t - \xi\cos(\omega_1-\omega)t]\exp(-\xi t)\}. \quad (11)$$

b) Total Power Absorption for Nonreactive Ion: Ions are produced in a source region with electron impact at a rate of n_0 ions per second; then they move towards the ion collector through an analyzer region at a constant traveling velocity. It has been assumed that the length of the analyzer region is considerably longer than the diameter of the ICR cell and that the distribution of ions is uniform inside the ICR cell. There are a constant number, $n_0\tau$, of ions in the time τ for an ion move through the analyzer, each absorbing energy at the rate given in Eq. (11). Thus, the total power absorption $A(T)$, is obtained by averaging the integration from 0 to τ, the time required for the ions to absorb energy from the applied rf electric field. The averaged total power absorption is given by:

$$A(T, \omega_1 \mp \omega) = \frac{1}{\tau}\int_0^\tau n_0\tau A(\omega_1 \mp \omega)d\tau = \frac{n_0e^2(\mathbf{E}_x^2+\mathbf{E}_y^2)}{4m[(\omega_1-\omega)^2+\xi^2]}\left\langle \xi\tau + \frac{(\omega_1-\omega)^2-\xi^2}{(\omega_1+\omega)^2+\xi^2} - \left\{\frac{[(\omega_1-\omega)^2-\xi^2]\cos(\omega_1-\omega)\tau + 2\xi(\omega_1-\omega)\sin(\omega_1-\omega)\tau}{(\omega_1-\omega)^2+\xi^2}\right\} \times \exp(-\xi\tau)\right\rangle, \quad (12a)$$

and:

$$A(T, \omega_1=\omega) = \frac{n_0e^2(\mathbf{E}_x^2+\mathbf{E}_y^2)}{4m\xi^2}\left\{1 - \frac{1}{\xi\tau}[1-\exp(-\xi\tau)]\right\}. \quad (12b)$$

If the pressure is sufficiently high for each ion to undergo many nonreactive collisions, Eq. (12a) is reduced to:

$$A(T, \text{high-pressure}) = \frac{n_0 e^2(\mathbf{E}_x^2+\mathbf{E}_y^2)\tau}{4m}\frac{\xi}{(\omega_1-\omega)^2+\xi^2} \quad (13)$$

by the application of the $\xi t \gg 1$ approximation. This high-pressure power absorption represents the Lorentzian line shape. In the collisionless limit, $\xi \to 0$, Eq. (12a) is reduced to:

$$A(T, \text{low-pressure}) = \frac{n_0 e^2(\mathbf{E}_x^2+\mathbf{E}_y^2)}{4m(\omega_1-\omega)^2}[1-\cos(\omega_1-\omega)\tau]. \quad (14)$$

The line shapes of the total power absorption of longitudinal ICR for the ensemble of ions are represented by Eqs. (12)—(14).

Furthermore, the total power absorption and the line-shape expressions for such reactive ions as the primary, secondary, and tertiary ions are formularized theoretically; results similar to those reported previously[5b] have been obtained. A detailed discussion of the longitudinal ICR power absorption for the reactive ions will be published in the near future.

Appendix

a) Solution of Eq. (3).

To solve Eq. (3), we shall assume V in the following form:

$$V(r, \theta) = R(r)G(\theta)\sin(\omega_1 t+\phi_1). \quad (A1)$$

By substituting (A1) into Eq. (3) and by solving the resultant differential equations, we get the general solution of Eq. (3):[7]

$$V(r, \theta) = \sum_{n=0}^{n=\infty}[(r^n(A_n\cos n\theta + B_n \sin n\theta) + r^{-n}(C_n\cos n\theta + D_n \sin n\theta)]\sin(\omega_1 t+\phi_1), \quad (A2)$$

where A_n, B_n, C_n, and D_n are constants which should be determined from the boundary conditions. If we impose these boundary conditions:

$$\mathbf{E} \neq \infty \quad \text{for } r = 0$$
$$V(\theta) = V(-\theta) \quad \text{for } -\pi < \theta < \pi$$

on Eq. (A2), V becomes:

$$V(r, \theta) = \left[a_0+\sum_{n=1}^{n=\infty}\left(\frac{r}{R}\right)^n a_n \cos n\theta\right]\sin(\omega_1 t+\phi_1), \quad (A3)$$

where R is the radius of the cylinder. The potential distribution on the circle at $r=R$ can be expressed by periodic even function of θ as is shown in Fig. 2. Therefore, we can express V by means of a Fourier series. After some algebra, we obtain:

$$a_0 = (V_1+V_2)/2,$$

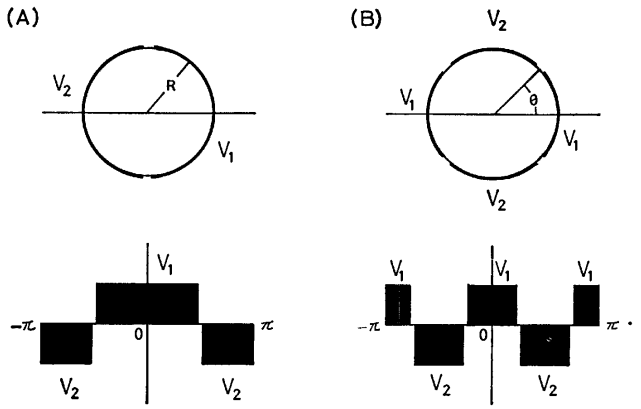

Fig. 2. Potential distribution on circle at $r=R$ of the electrodes (A) and (B), respectively.

$$a_n = [2(V_1-V_2)/n\pi]\sin(n\pi/2)$$

in the case of 2-split electrodes.

When $k=1, 2, 3, \cdots\cdots$, a_n becomes:

$$a_{2k} = 0 \quad \text{for } n=2k$$
$$a_{2k-1} = 2(V_1-V_2)(-1)^{k-1}/\pi(2k-1) \quad \text{for } n=2k-1.$$

Thus, we finally obtain:

$$V(r, \theta)_2 = \left\{\frac{V_1+V_2}{2}+\frac{2(V_1-V_2)}{\pi}\sum_{k=1}^{k=\infty}\frac{(-1)^{k-1}}{2k-1}\left(\frac{r}{R}\right)^{2k-1} \times\cos(2k-1)\theta\right\}\sin(\omega_1 t+\phi_1)$$
for 2 splits. (A4)

In a similar way, Eq. (A4) can be generalized to the potential equation for $2m$-split electrodes as follows:

$$V(r, \theta)_{2m} = \left\{\frac{V_1+V_2}{2}+\frac{2(V_1-V_2)}{\pi}\sum_{k=1}^{k=\infty}\frac{(-1)^{k-1}}{2k-1}\left(\frac{r}{R}\right)^{m(2k-1)} \times\cos[m(2k-1)\theta]\right\}\sin(\omega_1 t+\phi_1)$$
for $2m$ splits, (A5)

where $m=1, 2, 3, \cdots\cdots$.

By substituting Eq. (A5) into Eq. (2), we obtain this expression of the rf electric field for $2m$-split electrodes:

$$\mathbf{E}(r)_{2m} = \left\{-\frac{2(V_1-V_2)}{\pi}\sum_{k=1}^{k=\infty}\frac{m(-1)^{k-1}}{r}\left(\frac{r}{R}\right)^{m(2k-1)} \times\cos[m(2k-1)\theta]\right\}\sin(\omega_1 t+\phi_1), \quad (A6a)$$

$$\mathbf{E}(\theta)_{2m} = \left\{\frac{2(V_1-V_2)}{\pi}\sum_{k=1}^{k=\infty}\frac{m(-1)^{k-1}}{r}\left(\frac{r}{R}\right)^{m(2k-1)} \times\sin[m(2k-1)\theta]\right\}\sin(\omega_1 t+\phi_1)$$
for $2m$ splits. (A6b)

b) List of Notations Used in the Text.

$$A = [\xi(\xi^2+\omega_1^2-\omega^2)+2\xi\omega^2]/F,$$
$$B = \omega_1(\xi^2+\omega_1^2-\omega^2)/F,$$
$$C = 2\xi\omega\omega_1/F,$$
$$D = [\omega(\xi^2+\omega_1^2-\omega^2)-2\xi^2\omega]/F,$$
$$F = [(\omega_1-\omega)^2+\xi^2][(\omega_1+\omega)^2+\xi^2].$$

References

1) (a) J. L. Beauchamp, *Ann. Rev. Phys. Chem.*, **22**, 527 (1971); (b) J. H. Futrell, "Dynamic Mass Spectrometry," Vol. 2, ed. by D. Price, Heyden and Son, New York, (1971); (c) J. D. Baldeschwieler and S. S. Woodgate, *Accounts Chem. Res.*, **4**, 114 (1971); (d) K. Aoyagi, *Bunseki-kiki*, **10**, 703 (1972); (e) J. I. Brauman and I. K. Blair, "Determination of Organic Structures by Physical Methods," Vol. 5, ed. by F. C. Nachod and J. J. Zuckerman, Academic Press, New York, (1973).

2) M. B. Comisarow and A. G. Marshall, *J. Chem. Phys.*, **62**, 293 (1975).

3) D. Wobshall, J. R. Graham, Jr., and D. P. Malone, *Phys. Rev.*, **131**, 1565 (1963).

4) K. Nishikage, T. Iinuma, and S. Takahashi, Preprint of 12th Annual Conference on Cryogenic Engineering, (1973).

5) (a) M. B. Comisarow, *J. Chem. Phys.*, **55**, 205 (1971); (b) K. Aoyagi, This Bulletin, **47**, 519 (1974).

6) The exact solution of Eq. (5), at present, can not be obtained analytically in the cylindrical coordinates.

7) T. Nakamura, *Oyo Butsuri*, **31**, 253 (1962).

The Vibrational Spectra and Rotational Isomerism of Chloro(chloromethyl)silanes

Keiichi SERA, Keigo SUEHIRO, Michiro HAYASHI, and Hiromu MURATA
Department of Chemistry, Faculty of Science, Hiroshima University, Hiroshima 730
(Received July 11, 1975)

The infrared spectra of chloro(chloromethyl)methylsilanes $ClCH_2SiCl_{3-n}(CH_3)_n$ (n=0—2) in the liquid and crystalline states and a part of the Raman spectra in the liquid state have been measured. It has become apparent that, for $ClCH_2SiCl_2CH_3$ and $ClCH_2SiCl(CH_3)_2$, two rotational isomers coexist in the liquid state, while only one isomer persists in the crystalline state. The fundamental vibrations for these molecules have been assigned, and the normal vibrations have been calculated on the basis of a modified Urey-Bradley force field. The solvent effects and the calculation of the normal vibrations have indicated that the *gauche* form for $ClCH_2SiCl_2CH_3$ and the *trans* form for $ClCH_2SiCl(CH_3)_2$ persist in the crystalline state. For $ClCH_2SiCl_3$, the barrier height, $V_3(SiCl_3)$, has been estimated to be 4.6 kcal/mol from the torsional force constant.

In our previous papers,[1] we have reported the existence of rotational isomers in the XCH_2SiH_2Y-type (X,Y=Cl or CH_3) molecules. However, with regard to chloro(chloromethyl)dimethylsilane (CCDS) and chloro(ethyl)dimethylsilane, one of the present authors (M. H.) published a paper about fifteen years ago which mentioned that rotational isomers may not exist in these molecules, juaging from the Raman spectra in the liquid and solid states, while the dipole moments of CCDS at various temperatures do indicate the possibility of the existence of the rotational isomers.[2] The Raman spectra of the $ClCH_2SiCl_{3-n}(CH_3)_n$ molecules (n=0—2)[3] and the infrared spectrum of dichloro(chloromethyl)methylsilane (DCMS)[4] have been reported, but no detailed vibrational analyses have been made. The vibrational spectra and assignments of CCDS have been reported by one of the present authors (M. H.),[2] by Goubeau *et al.*,[5] and by Kriegmann *et al.*,[6] but the assignments of the C–Si and C–Cl stretching vibrations have not been consistent with each other.

In the present paper, we will deal anew with the molecular vibrations of the $ClCH_2SiCl_{3-n}(CH_3)_n$ series of molecules (n=0—2) in order to show the existence of the rotational isomers, information about the barrier height around a C–Si bond, and reasonable vibrational assignments for this series of molecules.

Experimental

Trichlorochloromethylsilane (TCS) was prepared by the reaction of tetrachlorosilane with diazomethane.[7] The samples of DCMS and CCDS were commercial products purified by redistillation.

The infrared spectra in the 200—4000 cm^{-1} region were recorded on a Perkin–Elmer instrument (Model 621). For the measurements in the crystalline state, the vapor of the sample was directly condensed on a CsI window cooled with liquid nitrogen in a vacuum and was annealed several times near the melting point. The solution spectra were measured using a sealed KRS-5 cell (0.5 mm thick), with carbon disulfide and acetonitrile as solvents. The Raman spectra in the liquid state were recorded on a JEOL Raman spectrometer (Model JRS-02AS), using an argon-ion laser (488.0 nm) for excitation.

Results and Discussion

Rotational Isomerism and Vibrational Assignments. Figure 1 shows the infrared spectra of TCS, DCMS, and CCDS in the liquid and crystalline states. It has been reported, on the basis of microwave study, that staggered configurations are more stable around a C–Si bond in such molecules as chloromethylsilane[8] and dimethylsilane.[9] For DCMS and CCDS, the two rotational isomers in Fig. 2 are expected. Actually, not for TCS, but for DCMS and CCDS, a few bands observed in the liquid state vanish in the crystalline

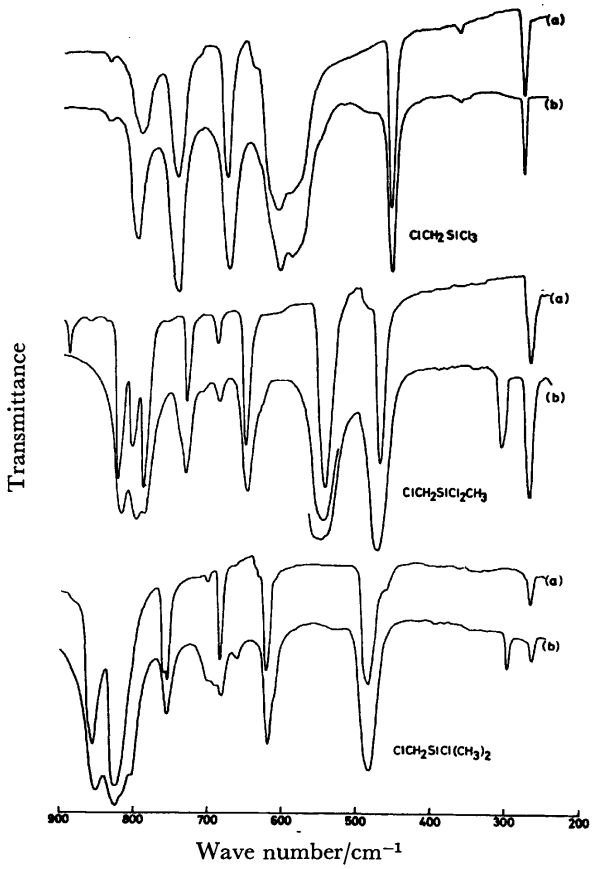

Fig. 1. Infrared spectra of the $ClCH_2SiCl_{3-n}(CH_3)_n$ molecules (n=0—2).
(a): In the crystalline state, (b): in the liquid state.

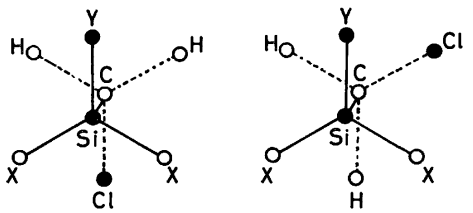

Fig. 2. Possible molecular forms for $ClCH_2SiCl_2CH_3$ and $ClCH_2SiCl(CH_3)_2$.

state. For CCDS, the Raman spectrum in the solid state has previously been reported by one of the present authors (M. H). Unfortunately, the Raman lines which correspond to the disappeared infrared bands in the crystalline state have not vanished completely, though the relative intensities of these lines have remarkably decreased in the solid state.[2] From the above results and the relative intensity changes in the infrared bands in the solution spectra, it may be concluded that, for DCMS and CCDS, two rotational isomers coexist in the liquid state, while only one isomer persists in the crystalline state.

On the other hand, the fundamental vibrations are assigned on the basis of the spectra in the $ClCH_2SiCl_{3-n}(CH_3)_n$ series of molecules (n=0—3) and on the basis of the relative intensities between the infrared bands and Raman lines. Figure 3 shows the correlation of the vibrational assignments of TCS, DCMS, and CCDS, together with that of chloromethyltrimethylsilane.[10] The assignment for CCDS is consistent with that by Goubeua *et al.*[5]

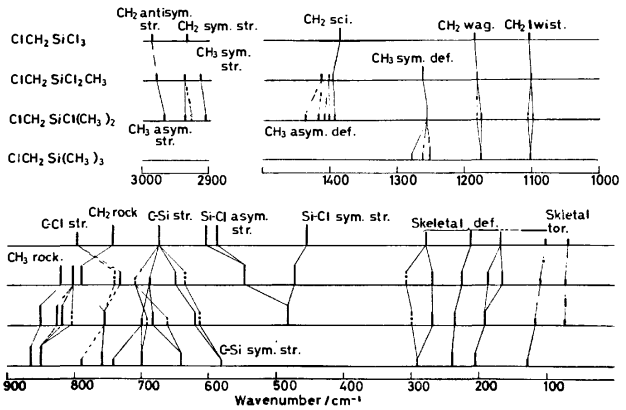

Fig. 3. Correlation of the vibrational assignments of the $ClCH_2SiCl_{3-n}(CH_3)_n$ series of molecules (n=0—3), where the lines in the region below 400 cm^{-1} and above 400 cm^{-1} are the observed Raman lines and the infrared bands respectively.

Solvent Effects. The solvent effects can be used for the determination of the molecular forms for DCMS and CCDS, because the dipole moments are expected to change considerably with an azimuthal angle of internal rotation. The dipole moment calculation based on the bond moments indicates that, for DCMS, the *trans* form is more polar than the *gauche* form, while for CCDS the *gauche* form is more polar than the *trans* form.

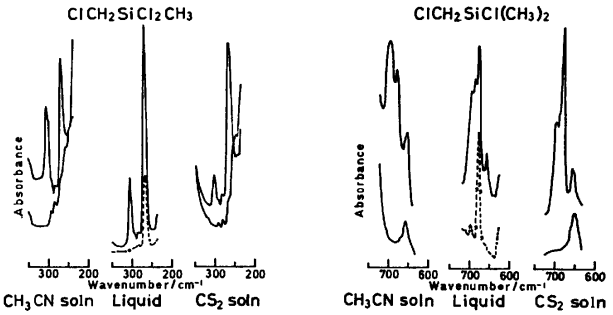

Fig. 4. The solvent effects of the infrared bands for $ClCH_2SiCl_2CH_3$ and $ClCH_2SiCl(CH_3)_2$.
·····: The spectra in the crystalline state.

For DCMS, the solvent effects of the infrared spectra are measured, using the bands at 308 and 269 cm^{-1} assigned to the skeletal deformation vibrations. The band at 308 cm^{-1} vanishes in the crystalline state. Figure 4 shows the solvent effects of the infrared bands. The A_{308}/A_{269} ratio increases when it is mixed with a polar solvent such as acetonitrile, while the reverse is true in a mixture with a non-polar solvent such as carbon disulfide. Therefore, the isomer disappearing in the crystalline state (the *trans* form) is more polar than the other (the *gauche* form).

For CCDS, the solvent effects of the bands at 692 and 683 cm^{-1} assigned to the C–Si stretching vibrations indicate that the isomer disappearing in the crystalline state (the *gauche* form) is more polar than the other

Table 1. Observed and calculated frequencies of trichloro(chloromethyl)silane[a] (cm^{-1})

Infrared Liquid Int.	Raman Liquid Int.	Calcd C_s	P. E. D.
2987 w	2987 w	2993 A″	$\nu_a(CH_2)$
2934 m	2936 ms	2948 A′	$\nu_s(CH_2)$
1386 ms	1387 w	1421 A′	$s(CH_2)$
1185 w	1186 vw	1167 A′	$w(CH)_2$
1103 w	1104 vw	1115 A″	$t(CH_2)$
838 vw			
798 ms	799 w	745 A′	ν(C–Cl), ν(C–Si)
743 vs		748 A″	$r(CH_2)$
674 s	676 m	676 A′	ν(C–Si), ν(C–Cl)
604 s	597 sh	606 A′	$\nu_a(SiCl_3)$
588 s	586 w	594 A″	$\nu_a(SiCl_3)$
454 s	456 vvs	456 A′	$\nu_s(SiCl_3)$
361 vw			
276 m	277 s	263 A′	δ(ClCSi), $\delta_s(SiCl_3)$
	212 s	230 A″	$r(SiCl_3)$, $\delta_a(SiCl_3)$
		208 A′	$\delta_s(SiCl_3)$, $\delta_a(SiCl_3)$
	167 s	167 A″	$\delta_a(SiCl_3)$, $r(SiCl_3)$
		156 A′	$\delta_a(SiCl_3)$
	101 m	101 A′	$r(SiCl_3)$, δ(ClCSi)
	68 m	67 A″	$\tau(SiCl_3)$

a) Int.=intensity; s, m, w=strong, medium, weak; v=very; sh=shoulder; A′, A″=A′ symmetry species, A″ symmetry species; P.E.D.=potential energy distributions; ν, s, w, t, r, δ, τ=stretching, scissoring, wagging, twisting, rocking, deformation, torsion; potential energy distributions greater than 20% are included.

(the *trans* form), as is shown in Fig. 4.

Normal Vibration Calculation. In order to confirm the results of the molecular forms and the vibrational assignments, the normal vibrations of the $ClCH_2SiCl_{3-n}(CH_3)_n$ molecules (n=0—2) were calculated, using Wilson's **GF**-matrix method. The bond lengths used were C–Cl=1.788 Å, CH_2–Si=1.889 Å, CH_3–Si=1.868 Å, Si–Cl=2.021 Å, and C–H=1.095 Å.[8,9,11] All the valence angles were assumed to be tetrahedral, and the internal rotation angles were 180° (*trans*) and 60° (*gauche*). The force constants in the modified Urey-Bradley force field were transferred from those of trichloromethylsilane,[11] chloromethylsilane,[12] and dichloroethylmethylsilane;[13] only the force constants of the skeletal torsions were adjusted to reproduce well the observed torsional frequencies.

The observed and calculated frequencies are summarized in Tables 1—3, together with the predominant potential energy distributions in the internal symmetry coordinates. The force constants are listed in Table 4. The vibrational assignments in Fig. 3 are consistent with the results of the calculations, though the potential energy distributions indicate large mixings between the C–Si and C–Cl stretching vibrations and between the

Table 2. Observed and calculated frequencies of dichloro(chloromethyl)methylsilane[a] (cm^{-1})

Infrared		Raman[b]	Calcd[c]		P. E. D.
Liq. Int.	Cryst. Int.	Liq. Int.	T form	G form	
2979 vw	2974 vw		2992 A″	2992	$\nu_a(CH_2)$
			2964 A′	2964	$\nu_a(CH_3)$
			2964 A″	2964	$\nu_a(CH_3)$
2938 w	2938 w		2944 A′	2944	$\nu_s(CH_2)$
2914 vw	2914 vw		2900 A′	2900	$\nu_s(CH_3)$
1402 m	1407 sh, 1403 m		1416 A″	1416	$\delta_a(CH_3)$
			1416 A′	1416	$\delta_a(CH_3)$
1396 m	1396 m		1421 A′	1421	$s(CH_2)$
1384 sh w	—				
1375 sh w	1373 w				
1262 s	1261 s		1283 A′	1283	$\delta_s(CH_3)$
1181 w	1182, 1179 w		1165 A′	1166	$w(CH_2)$
1101 w	1101, 1097 w		1115 A″	1115	$t(CH_2)$
	941 vw				
	897 w				
821 vs	825 vs	823 w	836 A′	837	$r(CH_3)$
802 vs	807 vs	804 w	832 A″	831	$r(CH_3)$
790 vs	792 vs	791 vw		763	$r(CH_2)$, ν_a(C–Si)
741sh m	—		746 A′		ν(C–Cl), ν_a(C–Si)
			741 A″		$r(CH_2)$
734 s	735 s	735 ms		736	ν(C–Cl), ν_a(C–Si)
710 vw	—		704 A′		ν_s(C–Si)
689 w	693 w	690 w		700	ν_s(C–Si), ν(C–Cl), $r(CH_2)$
650 s	654 s	651 vs		648	ν_s(C–Si), ν(C–Cl)
635 sh w	—	635 sh w	644 A′		ν_a(C–Si), ν(C–Cl)
547 vs	547 vs	552 w	531 A″	542	$\nu_a(SiCl_2)$
473 vs	473 vs	472 vvs	461 A′	471	$\nu_s(SiCl_2)$
308 m	—	307 w	281 A′		δ(ClCSi), $w(SiCl_2)$
269 m	271 m	268 s		265	δ(ClCSi), $w(SiCl_2)$, δ(CSiC)
			231 A″		$r(SiCl_2)$
		225 s		239	δ(CSiC), $w(SiCl_2)$, $r(SiCl_2)$
			220 A′		δ(CSiC), $s(SiCl_2)$
				218	$w(SiCl_2)$, $r(SiCl_2)$
		186 ms	183 A″		$t(SiCl_2)$
				179	$t(SiCl_2)$, $s(SiCl_2)$
			169 A′		$s(SiCl_2)$, δ(CSiC)
		165 ms		162	$s(SiCl_2)$
			165 A″	165	$\tau(SiCH_3)$
		109 mw	107 A′		$w(SiCl_2)$, δ(ClCSi), δ(CSiC)
				111	$t(SiCl_2)$, δ(ClCSi)
		73 w	70 A″	75	τ(skel)

a) See footnote a) of Table 1. b) The Raman spectrum is measured in the region below 900 cm^{-1}.
c) T, G=*trans*, *gauche*.

skeletal deformation vibrations. For the molecular forms of DCMS and CCDS, the conclusion regarding the solvent effects is consistent with that obtained from the comparison of the observed frequencies with the calculated frequencies of the highest-frequency skeletal deformation for each molecular form.

Barriers to Internal Rotation. The barrier height, V_3, assuming the harmonic oscillation ($V=(1/2)V_3(1-\cos 3\alpha)$, $V_3>2.5$ kcal/mol) can be calculated by the use of the torsional frequency or its force constants as

TABLE 3. OBSERVED AND CALCULATED FREQUENCIES OF CHLORO(CHLOROMETHYL)DIMETHYLSILANE[a] (cm^{-1})

Infrared		Raman[b]	Calcd[c]		P. E. D.
Liq. Int.	Cryst. Int.	Liq. Int.	T form	G form	
	2981 vw				
2967 m	2969 w	2976 7b	2992 A″	2993	$\nu_a(CH_2)$
			2964 A′	2964	$\nu_a(CH_3)$
			2964 A′	2964	$\nu_a(CH_3)$
			2963 A″	2963	$\nu_a(CH_3)$
			2963 A″	2963	$\nu_a(CH_3)$
2936 m	2943 w	2932 5	2948 A′		$\nu_s(CH_2)$
2927 m	—			2949	$\nu_s(CH_2)$
2905 vw	2902 vw	2908 7b	2900 A″	2900	$\nu_s(CH_3)$
			2900 A′	2900	$\nu_s(CH_3)$
1437 vw	1438 w		1416 A′	1417	$\delta_a(CH_3)$
1417 vw	1414 w		1416 A′	1416	$\delta_a(CH_3)$
1408sh m			1416 A″	1416	$\delta_a(CH_3)$
1401sh m	1399 m		1415 A″	1415	$\delta_a(CH_3)$
1393 m	1389 m	1397 5b	1421 A′	1421	$s(CH_2)$
		1361 1			
1256 vs	1260 vs	1258 3	1282 A′	1282	$\delta_s(CH_3)$
	1255 vs		1282 A″	1282	$\delta_s(CH_3)$
1181sh m	—			1166	$w(CH_2)$
1175 m	1178 s	1174 3	1166 A′		$w(CH_2)$
1104 w	—			1115	$t(CH_2)$
1096 m	1097 m	1101 1	1115 A″		$t(CH_2)$
851 vs	855 vs	853 1	851 A′	859	$r(CH_3)$
			843 A′	844	$r(CH_3)$
826 vs	827 vs	822 1	833 A″	832	$r(CH_3)$
818 sh			816 A″		$r(CH_3)$
804 sh	—	806 1		816	$r(CH_3)$
756 s	759 s	756 4	761 A″	751	$r(CH_2)$, ν_a(C–Si)
	755 s		733 A′	732	ν(C–Cl), ν_s(C–Si)
700	700 vw	709 2	695 A″		ν_a(C–Si), $r(CH_2)$
692 m	—			718	ν_a(C–Si), $r(CH_2)$
683 s	684 s	686 1	690 A′		ν_a(C–Si), ν(C–Cl)
661 w	—	663 1		667	ν_a(C–Si), ν(C–Cl)
620 s	619 s	620 10b	612 A′		ν_s(C–Si), ν_a(C–Si), ν(C–Cl)
613sh s	—			634	ν_s(C–Si) ν_a(C–Si)
483 vs	481 s	482 9b	493 A′	473	ν(Si–Cl)
298 m	—	299 4		278	δ(ClCSi), δ_a(CSiC)
266 m	265 w	268 4	262 A′		δ(ClCSi), δ_s(CSiC), δ_a(CSiC)
			242 A″		δ_a(CSiC)
		235 5b		235	δ_s(CSiC)
			228 A′		δ_a(CSiC), δ_s(CSiC)
				221	δ_s(CSiC), δ(CSiCl)
			190 A″	198	δ(CSiCl), δ_a(CSiC)
				182	δ(CSiCl), δ_a(CSiC)
		191 5b	172 A′		δ(CSiCl), δ(ClCSi)
			166 A″	165	$\tau(SiCH_3)$
			165 A′	164	$\tau(SiCH_3)$
		117 1	119 A′		δ_s(CSiC), δ(ClCSi), δ(CSiCl)
				116	δ_a(CSiC), δ(ClCSi)
		73 1	77 A″	70	τ(skel)

a) See footnote a) of Table 1. b) The Raman spectrum is remeasured in the region below 100 cm^{-1}.
c) See footnote c) of Table 2.

Table 4. Force constants for chloro-(chloromethyl) methylsilanes[a)]

Force const.		Force const.	
K(C–H), CH_3	4.403	$k(CH_3)$	0.014
K(C–H), CH_2	4.390	$k(CH_2)$	0.027
K(C–Cl)	1.697	$\kappa(CSiCl_3)$	0.170
K(C–Si)	1.991	$\kappa(C_2SiCl_2)$	0.149
K(Si–Cl), SiCl	2.166	$\kappa(C_3SiCl)$	0.090
K(Si–Cl), $SiCl_2$	2.226	$p(SiCl_2)$	0.174
K(Si–Cl), $SiCl_3$	2.590	p(C–H)	−0.084
H(Si–C–Cl)	0.100	F(Si·C·Cl)	0.210
H(Si–C–H), CH_2	0.104	F(Si·C·H), CH_2	0.271
H(Si–C–H), CH_3	0.123	F(Si·C·H), CH_3	0.271
H(Cl–C–H)	0.147	F(Cl·C·H)	0.588
H(H–C–H)	0.349	F(H·C·H)	0.200
H(C–Si–Cl)	0.085	F(C·Si·Cl)	0.162
H(C–Si–C)	0.133	F(C·Si·C)	0.040
H(Cl–Si–Cl)	0.059	F(Cl·Si·Cl)	0.290
Y(Si–CH_3)	0.051	Y(C–$SiCl_2CH_3$)	0.149
Y(C–$SiCl_3$)	0.143	Y(C–$SiCl(CH_3)_2$)	0.130

a) The units of the force constants are in md/Å for stretching, K; bending, H; repulsion, F; bond interaction, p; and in md.Å for intramolecular tension, κ; torsion, Y.

follows: V_3 (kcal/mol)$=2.858\times10^{-3}\,\nu^2/(9F)$ or $k=(\partial^2V/\partial\alpha^2)_{\alpha=0}=9/2V_3$, that is, k (md. Å)$=0.03126\ V_3$ (kcal/mol), where F is the reduced rotational constant for internal rotation ($F(SiCl_3)=0.3859$ cm^{-1}); ν, the observed torsional frequency in cm^{-1}, and k, the torsional force constant.[14] For TCS, the barrier heights, V_3, calculated from the torsional frequency (68 cm^{-1}) and its force constant (0.143 md. Å) are 3.8 and 4.6 kcal/mol respectively. For the former, the interactions between the torsional vibration and the other vibrations are neglected, while for the latter the kinetic effect of the other vibrations (the **G**-matrix elements between the torsional vibration and the other vibrations) is taken into account. Actually, the potential energy distributions of the skeletal torsion are skeletal tor (79), $SiCl_3$ rock(14), and CH_2 rock(6). The torsional force constants of DCMS and CCDS are 0.149 and 0.130 md.Å, and the barrier heights of $V_3(SiCl_2CH_3)$ and $V_3(SiCl(CH_3)_2)$, assuming a symmetrical-three fold barrier, are 4.8 and 4.2 kcal/mol respectively.

On the other hand, for 1,1,1,2-tetrachloroethane, $V_3(CCl_3)$, has been reported to be 10.2 kcal/mol.[15] Therefore, the barrier height of V_3 for $ClCH_2SiCl_3$ is considerably smaller than that for $ClCH_2CCl_3$, but is higher than that of the free rotation (*ca.* 0.6 kcal/mol).

The authors wish to express their thanks to Dr. Teizo Kitagawa of Osaka University for the use of the Raman spectrophotometer.

References

1) M. Hayashi, K. Ohno, and H. Murata, This Bulletin, **46**, 797, 2044 (1973).
2) M. Hayashi, *Nippon Kagaku Zasshi*, **79**, 508 (1956).
3) M. I. Batvev, V. A. Ponomarenko, A. D. Matveeva, and A. D. Snegova, *Izvest, Akad. Nauk S.S.S.R., Otdel. Khim. Nauk*, **1958**, 996.
4) M. T. Filippov, R. V. Dzhagatspanyan, G. V. Motsarev, and V. I. Zetkin, *Russian J. Phys. Chem.*, **36**, 942 (1962).
5) Von J. Goubeau, G. R. Hein, and I. Hein, *Z. Anorg. Allg. Chem.*, **312**, 110 (1961).
6) H. Kriegsmann and G. E. Engelhardt, *Z. Chem.*, **2**, 95 (1962).
7) D. Seyferth and E. G. Rochow, *J. Amer. Chem. Soc.*, **77**, 907 (1955).
8) R. H. Schwendeman and G. D. Jacobs, *J. Chem. Phys.*, **36**, 1251 (1962).
9) L. Pierce, *J. Chem. Phys.*, **34**, 498 (1961).
10) W. Mowat, A. Shortland, G. Yagupsky, N, J. Hill, M. Yagupsky, and G. Wilkinson, *J. Chem. Soc., A*, **1972**, 533.
11) K. Shimizu and H. Murata, *J. Mol. Spectrosc.*, **4**, 214 (1960).
12) K. Ohno and H. Murata, This Bulletin, **45**, 3333 (1972).
13) K. Ohno, Y. Shiro, and H. Murata, *ibid.*, **47**, 2962 (1974).
14) J. R. Durig, "Vibrational Spectra and Structure," Dekker Inc., New York (1972).
15) G. Allen, P. N. Brier, and G. Lane, *Trans Faraday Soc.*, **63**, 824 (1967).

The Effect of Organic Additives on the Thermodynamic Parameters of Micellization

Shigeyoshi MIYAGISHI

Department of Industrial Chemistry, Faculty of Technology, Kanazawa University, Kodatsuno, Kanazawa 920

(Received July 12, 1975)

The CMC values of dodecylammonium chloride and iodide and of hexadecylammonium chloride were measured in water upon the addition of acetone, 1-propanol, and urea at several temperatures. The effects of the additives were most remarkable on the CMC of hexadecylammonium chloride at 45.0 °C. Urea was less effective on the disruption of micelles than acetone, while the addition of 1-propanol was most effective. The enthalpy of micellization became more negative, while the entropy of micellization became less positive, as the additive concentration increased. We divided the standard free energy of micellization into the hydrophobic term, ΔG_n°, and the hydrophilic term, ΔG_p°. The value of ΔG_p° became more negative with the additive concentration and contributed to the stabilization of the micelle, while ΔG_n° became less negative. Therefore, it was concluded that the disruption of the micelle in the presence of these organic additives results from an increase in the free energy in the hydrophobic group of the surfactant molecule.

It is well known that the addition of a protein denaturant to a surfactant solution brings about the disruption of a micelle. The two phenomena, *i.e.*, protein denaturation and micelle disruption, are qualitatively similar, and so the effects of the organic additives on the micellar properties have received much attention.

On the other hand, the association of the surfactant molecule itself is a significant problem in physical chemistry, apart from biology. In the investigation of the effect of organic additives, nonionic surfactants have often been used;[1-6] there have been fewer systematic studies of ionic surfactant solutions[7-9] because of the complexity of the electrostatic interaction. However, we could previously obtain some significant results in the alkylammonium halide solutions.[10,11]

In the present investigation, our studies were extended to the effect of the additives on the thermodynamic parameters of micellization. Here we reached the significant conclusion that the increase in the CMC in the presence of the organic additives results from the increase in the free energy of the hydrophobic group in the surfactant molecule.

Experimental

The materials and the experimental procedure were almost the same as those described in previous papers.[10,11] That is, dodecylammonium chloride (DAC), iodide (DAI) and hexadecyammonium chloride (HAC) were used. Their CMC's were measured by the electric conductivity method. The CMC of HAC was not measured in the urea solutions because of the appearance of turbidity.

Results and Discussion

The Effect of the Additives on the CMC. The effect of three organic additives on the micellization of alkylammonium halides was examined. 1-Propanol is a protonic solvent, acetone is aprotic, and urea is well known to be a typical protein denaturant.

The additives affect the micellizations through the breakage of the water structure around the hydrocarbon chain of a surfactant molecule[12] and the modification of the electrostatic interaction.[13] The chloride ion may be a stronger water-structure breaker than the iodide ion, and therefore the water around the hydrocarbon chain may be less ordered and less susceptible to modification by the organic additives in the presence of the chloride ion than in that of the iodide ion. Therefore, the surfactant molecule with a longer hydrocarbon chain or a weaker structure-breaking ion is expected to be more subject to the effect of the additive. The experimental results that the CMC increasing effects of the additives were most remarkable in HAC and less in DAC than in DAI were in accord with these expectations.

TABLE 1. THE EFFECT OF PROPANOL ON CMC

Temp. (°C)	CMC × 10^4 (mole fraction) (CMC/CMC$_0$) 1-Propanol (mol/1000 g) 0	0.659	1.318	1.977	2.636	3.294
			DAC			
25.0	2.66	1.96	1.69		2.12	2.74
	(1.00)	(0.74)	(0.64)		(0.80)	(1.03)
35.0	2.79	2.14	1.92		2.44	3.45
	(1.00)	(0.77)	(0.69)		(0.87)	(1.24)
45.0	2.88	2.31	2.00		3.26	5.23
	(1.00)	(0.80)	(0.69)		(1.13)	(1.82)
			DAI			
25.0	1.69	1.50	1.31	2.65	3.26	4.04
	(1.00)	(0.89)	(0.78)	(1.57)	(1.93)	(2.39)
35.0	1.76	1.58			3.36	
	(1.00)	(0.90)			(1.91)	
45.0	1.96	1.64	1.60	2.77	3.71	4.60
	(1.00)	(0.84)	(0.82)	(1.41)	(1.89)	(2.34)
			HAC			
25.0			0.173		0.458	0.834
35.0	0.162	0.162	0.234		0.611	1.15
	(1.00)	(1.00)	(1.44)		(3.77)	(7.10)
45.0	0.175	0.252	0.404		1.02	1.63
	(1.00)	(1.44)	(2.31)		(5.83)	(9.31)

CMC$_0$: The CMC in the absence of propanol. The relative CMC is given in the parenthesis under each row.

Table 2. The effect of acetone on CMC

Temp. (°C)	CMC × 10^4 (mole fraction) (CMC/CMC$_0$) Acetone (mol/1000 g) 0	0.675	1.350	2.701	3.376
	DAC				
25.0	2.66	2.61	3.34	3.94	6.88
	(1.00)	(0.98)	(1.26)	(1.48)	(2.59)
35.0	2.79	2.95	3.59	4.88	9.17
	(1.00)	(1.06)	(1.29)	(1.75)	(3.29)
45.0	2.88	3.13	3.76	5.60	9.17
	(1.00)	(1.09)	(1.31)	(1.94)	(3.18)
	HAC				
35.0	0.162	0.228	0.392	0.830	
	(1.00)	(1.41)	(2.42)	(5.12)	
45.0	0.175	0.246	0.444	1.04	
	(1.00)	(1.41)	(2.54)	(5.93)	

	Acetone (mol/1000 g) 0	0.174	0.906	1.913	2.701
	DAI				
25.0	1.69	1.71	2.07	2.56	3.11
	(1.00)	(1.01)	(1.22)	(1.51)	(1.84)
35.0	1.76	1.86	2.20	2.73	3.61
	(1.00)	(1.06)	(1.25)	(1.55)	(2.05)
45.0	1.96	2.04	2.45	3.07	4.25
	(1.00)	(1.04)	(1.25)	(1.57)	(2.17)

CMC$_0$: The CMC in the absence of acetone.

Table 3. The effect of urea on CMC

Temp. (°C)	CMC × 10^4 (mole fraction) (CMC/CMC$_0$) Urea (M) 0	1	3	4.5	5	6
	DAC					
25.0	2.66	2.96	3.88		4.66	
	(1.00)	(1.11)	(1.46)		(1.75)	
35.0	2.79	3.06	3.88		4.72	
	(1.00)	(1.10)	(1.39)		(1.69)	
45.0	2.88	3.15	4.17		4.86	
	(1.00)	(1.09)	(1.45)		(1.69)	
	SDS[a)]					
25.0	1.30	1.37	1.78	2.12		2.63
	(1.00)	(1.05)	(1.37)	(1.63)		(2.02)
45.0	1.37		1.79			2.52
	(1.00)		(1.31)			(1.84)

CMC$_0$: The CMC in the absence of urea. a) From Ref. 12.

The CMC values in Tables 1—3 are seen to increase with the temperature, irrespective of the presence or absence of the additive, and the increment in HAC is remarkable in the presence of additives. The addition of 1-propanol and acetone affects the micellization to a considerable extent, while urea is least effective.

The CMC values of sodium dodecylsulfate (SDS) in the presence of urea reported by Schick[12] are denoted in Table 3 for comparison with our data. The difference between these two sets of data is relatively small. Therefore, in the absence of a strong structure-breaking ion or a strong structure-making ion, the increments in the CMC values on urea addition seem to be determined mainly by its effect on the hydrophobic group of a surfactant molecule.

Thermodynamic Parameters of Micellization. The standard free energy of micellization can be represented by Eq. (1), and the enthalpy may be calculated from the dependence of the CMC on the temperature by means of Eq. (2):

$$\Delta G^\circ = (1+K_g)RT \ln \text{CMC (mole fraction)} \quad (1)$$

$$\Delta H^\circ = -(1+K_g)RT^2 \frac{d \ln \text{CMC}}{dT} \quad (2)$$

The value of K_g does not change largely with the temperature[14] or with the concentration of the organic additive.[11] The thermodynamic parameters in the present work have been calculated by assuming that $K_g=0.7$.

From the usual relation among thermodynamic functions, the standard entropy of micellization is obtained. In the micellization, the entropy generally has a relatively large positive value, while the enthalpy is small or even negative in an aqueous solution. Shinoda[15] explained these phenomena by taking into account the iceberg formation of the water surrounding a surfactant molecule. Urea is known to denature a protein through the disruption of the iceberg. However, in the present work, acetone, a weaker denaturant, was found to be more effective in the breakage of micelles than urea. Similar phenomena were also suggested by Bruning and Holtzer.[16] A comparison of Fig. 3 with Figs. 1—2 reveals that the effect of urea on the thermodynamic parameters is weaker than those of acetone and 1-propanol and that the enthalpy scarcely changes upon the addition of urea.

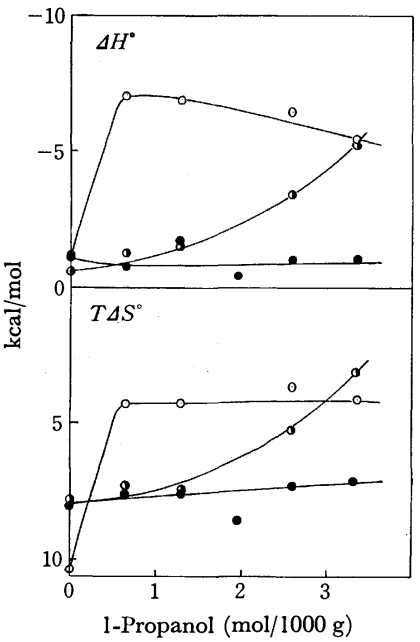

Fig. 1. The effect of 1-propanol on thermodynamic parameters of micellization at 35.0 °C.
—◑—: DAC, —●—: DAI, —○—: HAC.

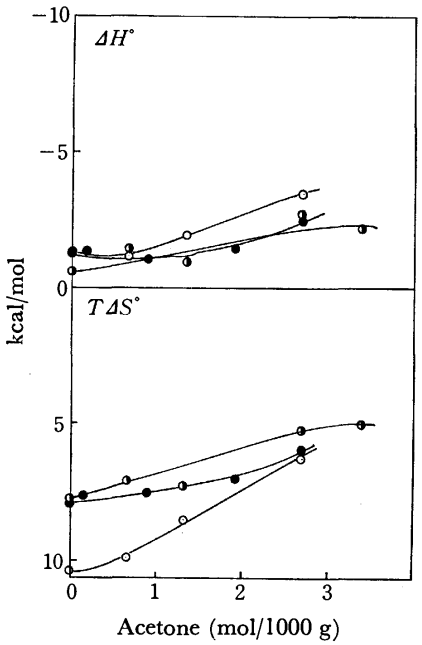

Fig. 2. The effect of acetone on thermodynamic parameters of micellization at 35.0 °C.
Symbols are identical with them in Fig. 1.

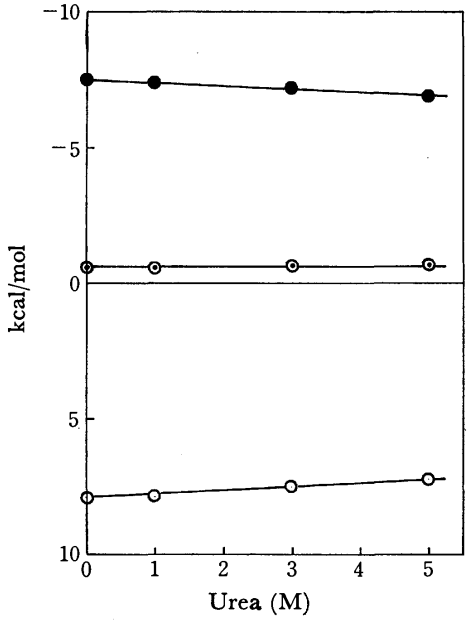

Fig. 3. The effect of urea on thermodynamic parameters of micellization at 35.0 °C.
—●—: $\Delta G°$, —⊙—: $\Delta H°$, —○—: $T\Delta S°$.

Therefore, acetone and 1-propanol seem to affect the micellization through other mechanisms, in addition to the disruption of iceberg; for example, the preferential solvation of the hydrocarbon chain by the additives or the more appropriate solubility parameter of the mixed solvent.

The effects of additives on the enthalpy and the entropy were remarkable in the HAC solution; the difference between their effects in the DAC and DAI solutions was small at low concentrations of the additives. These results suggest that their effects are operative primarily on the hydrophobic group of the surfactant, while only secondarily on the hydrophilic group.

Furthermore, the entalpy is more negative, and the entropy is less positive, in the presence of additives; therefore, the contribution of the enthalpy to the micellization becomes increasingly important with the additive concentrations, in contrast to the predominance of entropy in the aqueous solutions. Such more negative enthalpy in the presence of organic additives has also been observed in other systems.[2-5] We consider these phenomena to result from the decrease in the highly ordered structure through hydrogen bonding in an aqueous solution. Further investigations, however, will be required before a detailed discussion can be done.

The Hydrophobic and the Hydrophilic Terms in the Free Energy. It is possible to divide the standard free energy of micellization in the DAC solution, $\Delta G°_{DAC}$, into two components, one due to the hydrophobic group of the surfactant molecule, $\Delta G°_n$, and the other, due to the hydrophilic group, $\Delta G°_p$. We will represent the standard free energy of micellization in the HAC solutions as $\Delta G°_{HAC}$ and will assume the following equation, similar equations have been used by some other authors:[4,5,9]

$$\Delta G°_n = 3(\Delta G°_{HAC} - \Delta G°_{DAC}) \quad (3)$$

$$\Delta G°_p = \Delta G°_{DAC} - \Delta G°_n \quad (4)$$

Such a division may give further detailed knowledge about the effects of additives. The variations in $\Delta G°_n$ and $\Delta G°_p$ with additive concentrations are represented in Figs. 4—5. The value of $\Delta G°_n$ becomes less negative as the additive concentration increases, while $\Delta G°_p$, surprisingly, becomes more negative. Consequently, we reach the significant conclusion that the increase in $\Delta G°_{DAC}$ in the presence of organic additives should be ascribed to the increase in $\Delta G°_n$. The stabilization of the micelles at the lower concentrations of additives is explained by the more negative $\Delta G°_p$. A similar calculation made with the HAC solutions gave values of $\Delta G°_p$ identical with those in the DAC solution, but the values of $\Delta G°_n$ were more negative.

On the other hand, a comparison between Figs. 4

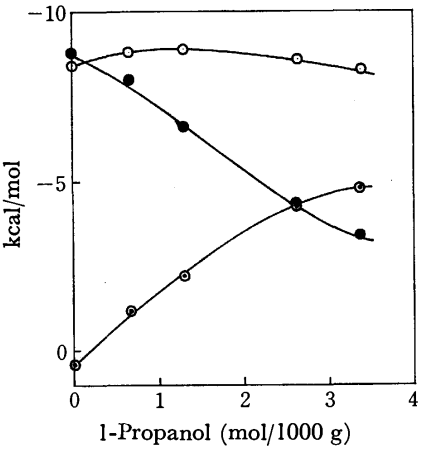

Fig. 4. The effect of 1-propanol on free energy of micellization of DAC at 35.0 °C.
—●—: $\Delta G°_n$, —⊙—: $\Delta G°_p$, —○—: $\Delta G°_{DAC}$.

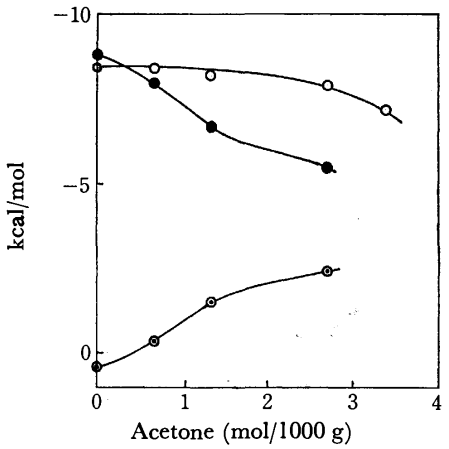

Fig. 5. The effect of acetone on free energy of micellization of DAC at 35.0 °C.
Symbols are identical with them in Fig. 4.

and 5 suggests that 1-propanol increases $-\Delta G_p^\circ$ more than acetone does. According to a previous paper,[10] propanol is more solubilized in the DAC micelle than is acetone. The increase in the solubilizate may produce the decrease in the surface-charge density of the micelle. Therefore, the fact reported above can be explained by the difference in their solubilized amounts.

The author wishes to express his hearty thanks to Professor Ryohei Matuura of Kyushu University and Professor Morie Nishida for their kind discussions throughout this study.

References

1) W. B. Gratzer and G. H. Beaven, *J. Phys. Chem.*, **73**, 2270 (1969).
2) J. M. Corkill, J. F. Goodman, S. P. Harrold, and J. R. Tate, *Trans. Faraday Soc.*, **63**, 240 (1967).
3) C. McDonald, *J. Pharm. Pharm.*, **22**, 148 (1970); **22**, 774 (1970).
4) A. Ray and G. Nemethy, *J. Phys. Chem.*, **75**, 809 (1971).
5) P. Becher and S. E. Trifiletti, *J. Colloid Interface Sci.*, **43**, 485 (1973).
6) N. Nishikido, Y. Moroi, H. Uehara, and R. Matuura, This Bulletin, **47**, 2634 (1974).
7) K. Shinoda, *J. Phys. Chem.*, **58**, 1136 (1954).
8) M. F. Emerson and A. Holtzer, *ibid.*, **71**, 3320 (1967).
9) K. Shirahama, M. Hayashi, and R. Matuura, This Bulletin, **42**, 1206 (1969); **42**, 2123 (1969).
10) S. Miyagishi, *ibid.*, **47**, 2972 (1974).
11) S. Miyagishi, *ibid.*, **48**, 2349 (1975).
12) M. J. Schick, *J. Phys. Chem.*, **68**, 3585 (1964).
13) K. Shirahama and R. Matuura, This Bulletin, **38**, **38**, 373 (1965).
14) Y. Moroi, N. Nishikido, H. Uehara, and R. Matuura, *J. Colloid Interface Sci.*, **50**, 254 (1975).
15) K. Shinoda, Proc. 6th Int. Congr. Surface Active Agent, 891 (1973).
16) W. Bruning and A. Holtzer, *J. Amer. Chem. Soc.*, **83**, 4865 (1961).

Photoreactions of the Uranyl Ion with Arylaldehydes in Solution

Ryoka MATSUSHIMA,* Kenichi MORI, and Morio SUZUKI

Department of Industrial Chemistry, Faculty of Engineering, Shizuoka University, Hamamatsu 432

(Received July 23, 1975)

Irradiation of benzaldehyde in a deoxygenated aqueous acetone solution in the presence of the uranyl ion with light of $\lambda \geqq 365$ nm gives the U(IV) species and benzil (**1**) as the main photoredox products, and small amounts of 4-hydroxy-4-phenylbutan-2-one (**2**), *trans*-4-phenyl-3-buten-2-one (**3**), and an unidentified product (**4**). None of them are formed in the absence of the uranyl ion. The products **2** and **3** are assumed to be formed by the uranyl ion-photocatalyzed condensation of benzaldehyde with acetone. Irradiation of acetophenone in the presence of the uranyl ion gives no photoproducts, though the uranyl emission is effectively quenched. *p*-Methoxybenzaldehyde and *p*-chlorobenzaldehyde give the corresponding 4,4′-disubstituted benzils respectively by irradiation under similar conditions. The quantum yield for the formation of the U(IV) species decreases whereas the quenching constant increases with the increase in the electron donating power of the substituent. The physical quenching process appears to compete significantly with the chemical (redox) process. The relative importance of the physical quenching to the chemical quenching process has been estimated. As to the photocatalyzed aldol condensation, the excess vibrational energy, which the quencher and/or the quenchee would possess during or immediately after the quenching interactions, may possibly be converted into the energy of the chemical reaction.

Primary interactions of the excited uranyl ion with organic compounds in solutions may be classified into three types: a) electronic energy transfer,[1,2] b) chemical (redox) interactions such as the abstraction of active hydrogen atoms,[3-5] and c) physical quenching *via* formation and decay of excited state π-complexes[6] (with aromatic molecules). In the previous paper the formation of biacetyl by the photooxidation of acetaldehyde with the uranyl ion has been reported,[5] where the only important interactions is the chemical one.

Arylaldehydes have both physical (π-electron cloud) and chemical (aldehyde hydrogen) quenching centers in one molecule. The present paper is concerned with the photochemistry of the uranyl ion with arylaldehydes, where it may be questioned whether physical and chemical interactions are simply competitive or whether they can be interconverted to some extent.

Experimental

Materials. Benzaldehyde (guaranteed grade) was freshly distilled under reduced nitrogen pressure before use. Other chemicals were of guaranteed reagent grade and were used without further purification. Water was distilled after passing through ion exchange resins.

Quenching Constants. The relative intensities of the uranyl emission near the 510 nm peak were measured with the 436 nm excitation in 60 vol% aqueous acetone solutions containing 0.02 M uranyl nitrate, 0.1 M perchloric acid, and various concentrations of the quenchers, at 25 ± 2 °C. Since the quenching constants were not significantly influenced by the dissolved oxygen, they were measured without deoxygenation. The measurements were carried out by means of a Hitachi 204-type fluorescence spectrophotometer.

Photolysis. 60 vol% aqueous acetone solutions of 0.2 M benzaldehydes in the presence of 0.02 M uranyl nitrate (hexahydrate) and 0.1 M perchloric acid were deoxygenated with oxygen-free nitrogen current, and were sealed in identical 7 ml ampoules. They were irradiated with light of $\lambda \geqq 365$ nm from a 100 or 400 W high pressure mercury lamp. For the quantitative experiments, a merry-go-round irradiation apparatus in a thermostat (10 ± 1 °C) or an optical train with a suitable arrangement for obtaining a parallel light beam perpendicular to the plane of the windows of the photoreaction cells was used. Actinometry was carried out with the ferric oxalate actinometer solution. No correction was made of the quantum yields for formation of the products, though under these conditions some errors might be involved due to the inner filter effects by benzaldehyde or products and the quenching of the excited state uranyl ion by the products.

Analysis of the Photoproducts. After the elimination of acetone from the photolyzed mixture solution, the residual aqueous solution was extracted with chloroform. The chloroform layer was washed with aqueous sodium bisulfate solution to eliminate benzoic acid. The chloroform layer was, after drying and condensation, separated on PLC (silica gel 60 PF-254, Merck) into four portions (**1**, **2**, **3**, and **4**). **2**: IR, 1700 (s), 3400 (broad) cm^{-1}; NMR, δ 2.0 (s, 3H), 2.6 (d, 2H), 4.0 (s, 1H), 5.0 (dd, 1H), 7.2 (m, 5H). **4**: mp, 120.5—122 °C; IR, 1690 cm^{-1}, no OH; NMR, δ 7.1 (s, 1H), 7.5—8.4 (m, 13H). Found: C, 80.32; H, 5.45%. Calcd for $C_{14}H_{10}O_2$: C, 80.00; H, 4.76%.

The amounts of the organic products were determined by densitometry on TLC after conversion into the corresponding 2,4-dinitrophenylhydrazone derivatives. The densitometer was an OZUMOR-82 (Meika KK). The measurements of NMR and IR spectra were carried out by means of a high resolution NMR spectrometer (Hitachi R-24) and an IR spectrometer (Japan Spectroscopic IR-S).

Results and Discussion

Formation of Organic Products. From the photolysis of benzaldehyde–uranyl solution, the products **1** and **3** have been identified respectively as benzil and *trans*-4-

TABLE 1. APPROXIMATE QUANTUM YIELDS OF THE PRODUCTS FROM THE PHOTOLYSIS OF BENZALDEHYDE WITH THE URANYL ION[a]

Product	Quantum yield
U (IV)	0.14
1	0.12
2	0.01
3	0.02
4	<0.01

a) Benzaldehyde: 0.2 M; uranyl ion: 0.02 M; perchloric acid: 0.1 M; in 60 vol % aqueous acetone at 10 °C, $\lambda \geqq 365$ nm.

phenyl-3-buten-2-one by comparing their IR and NMR spectra with those of authentic samples, while the product **2** has been assigned to 4-hydroxy-4-phenyl-butan-2-one on the basis of its IR and NMR spectra. The structure of the product **4** has not been clarified, though it may be tentatively assumed to be 2-phenyl-2,3-dihydrobenzofuran-3-one. The approximate quantum yields for the products from the photolysis of uranyl-benzaldehyde solution are listed in Table 1. Benzil (**1**), which was not formed by thermal reaction at 50 °C, is the main organic product, while the products **2**, **3**, and **4** are minor ones. In the absence of the uranyl ion, however, none of them was formed by the photolysis of benzaldehyde under similar conditions. Benzoic acid which is produced by thermal autooxidation of benzaldehyde on oxposure to the air, was unlikely to be an important product of the photoreactions under the present experimental conditions.

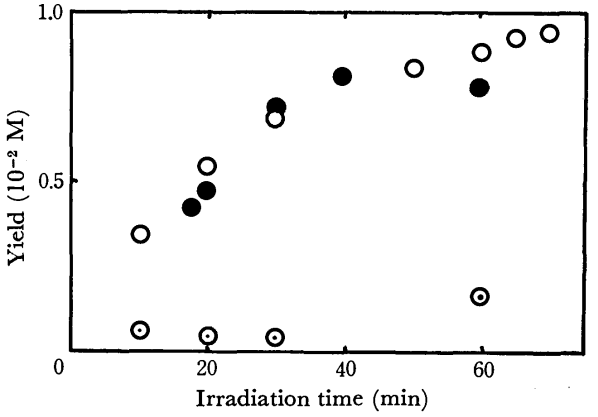

Fig. 1. Product yields at various extents of the photoreaction of benzaldehyde with the uranyl ion. Conditions are similar to those in Table 1. ○: U(IV) species, ●: product **1**, ⊙: product **2**.

Figure 1 shows that the molar ratio of the product **1** to the U(IV) species is close to unity, regardless of the extent of the photoreaction; thus **1** is the main oxidation product and it probably does not undergo any subsequent reactions. *p*-Methoxybenzaldehyde and *p*-chlorobenzaldehyde also gave the corresponding 4,4'-disubstituted benzils as the main organic products by irradiation in the presence of the uranyl ion under similar conditions. The reaction scheme for the formation of the product **1** (and also 4,4'-disubstituted benzils) may be assumed as follows, in analogy to that for the formation of biacetyl by the photooxidation of acetaldehyde with the uranyl ion:[5]

$$*UO_2^{2+} + ArCH{=}O \longrightarrow UO_2^{+} + H^{+} + Ar\dot{C}{=}O$$

$$2Ar\dot{C}{=}O \longrightarrow ArCOCOAr$$

$$2UO_2^{+} \xrightarrow{H^{+}} UO_2^{2+} + U(IV)\ species$$

Unlike the product **1** which is the photoredox product, the products **2** and **3** are formally not the redox products but are aldol condensation products of benzaldehyde with acetone, catalyzed by the excited state uranyl ion. As to the catalyzed aldol condensation by transition metal ions in the ground states, Iwata and Emoto have recently reported the cupric ion-catalyzed condensation of aromatic aldehydes with acetone.[7] Thermal reaction of the uranyl–benzaldehyde mixture for 30 hours at 50 °C also gave the products **2** and **3**, but their amounts were much less compared to those obtained by irradiation of an identical solution for 2 hours at 10 °C with a 100 W high pressure mercury lamp. Direct irradiation (*i.e.*, in the absence of the uranyl ion) with light of 254 nm (from a 160 W low pressure mercury lamp) for 9 hours at 10 °C gave no such condensation products. These facts suggest a photocatalytic action of the uranyl ion, *i.e.*, the condensation of benzaldehyde with acetone is much more accelerated by the excited uranyl ion than by the ground state uranyl ion. In the sense that the uranyl ion is not reduced, the process is a photocatalytic one.

$$ArCH{=}O + CH_3COCH_3 \xrightarrow{*UO_2^{2+}} ArCH(OH)CH_2COCH_3$$

The product **3** is assumed to be formed from the product **2** by dehydration during the analytical procedures, since **2** is easily converted into **3** by similar treatments. Hence the relative yield of the product **2** to **3** is changeable. In order to clarify the possible route for the formation of the product **4**, an investigation was made on the solution conditions of the photoreaction to give **4** (Table 2). The results show that the product **1** is unlikely to be the source of **4**, but that **4** is probably formed only by the photoreaction of benzaldehyde with the uranyl ion. The structure of **4** is, however, uncertain as yet.

Table 2. Conditions of the photoreaction to give the product **4**

Initially added concentrations[a]			Formation of **4**
Uranyl ion, M	Benzaldehyde, M	Benzil, M	
0.00	0.10	0.02	no
0.02	0.00	0.10	no
0.02	0.10	0.00	yes

a) Other conditions were similar to those in Table 1.

Stability of the U(IV) Species. The stabilities of the U(IV) species in solutions exposed to the air were preliminarily examined. Figure 2 shows that the stability of the U(IV) species is significantly solvent-dependent. The stability was higher at low temperature. The amount of the U(IV) species formed was determined either by rapid colorimetric analysis with arsenazo-III[8] immediately after breaking the ampoules or by the direct measurements of the absorbance at its 650 nm peak in the ampoules without exposure to the air.

Formation Quantum Yield of the U(IV) Species. Irradiation with $\lambda \geqq 365$ nm of a deoxygenated 60 vol% aqueous acetone solution of 0.2 M benzaldehyde in the presence of 0.02 M uranyl ion and 0.1 M perchloric acid leads to the reduction of the uranyl ion to give the U(IV) species which is easily identified by its characteristic absorption spectrum (430—700 nm). A series of the substituted benzaldehydes also lead to the formation of the U(IV) species upon irradiation under similar conditions. The formation quantum yields of the

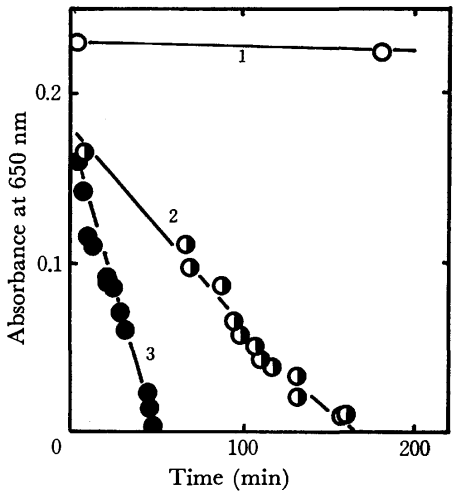

Fig. 2. Stabilities of the U(IV) species in solutions under the air. U(IV) species: 0.02 M, perchloric acid: 0.1 M; (1): in aqueous solution, (2): in 60 vol % aqueous acetone solution, (3): in 60 vol % aqueous acetone solutionin the presence of 0.2 M benzaldehyde.

Table 3. Quenching constants (K) and the quantum yields (ϕ) of the U(IV) formation for substituted benzaldehydes

Substituent	$K\times10^{-2}$. M^{-1}	ϕ	$\sigma^{+a)}$
p-$N(CH_3)_2$	93		−1.7
p-OCH_3	17	0.06	−0.778
p-CH_3	8.0	0.13	−0.311
H	5.0	0.16	0.000
p-Cl	4.0	0.23	0.114
m-Cl	3.3	0.25	0.391
p-NO_2	2.0	0.6[b)]	0.790

a) Polar substituent constants. b) Because of the low solubility, the initial concentration of *p*-nitrobenzaldehyde was 0.017 M.

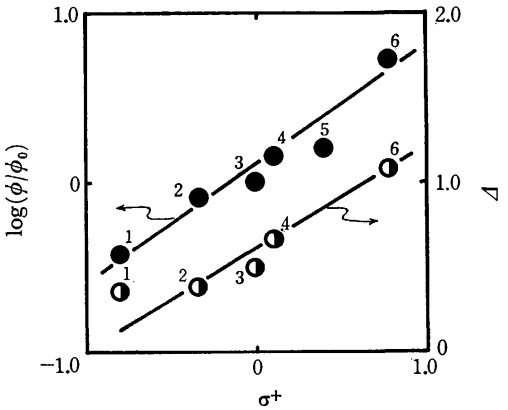

Fig. 3. Plots of $\log(\phi/\phi_0)$ and Δ *vs.* σ^+. Δ is the difference in the ordinates for benzaldehydes (b) and acetophenones (a) in Fig. 4. The numbering is the same as that in Fig. 4.

U(IV) are listed in Table 3. A plot of log (ϕ/ϕ_0) *vs* σ^+ is shown in Fig. 3, where ϕ and ϕ_0 are the formation quantum yields of the U(IV) species for the substituted and parent benzaldehydes respectively.

Unlike the systems of the uranyl–benzaldehydes, neither significant formation of the U(IV) species nor formation of organic photoproducts were detected upon irradiation of the uranyl–acetophenone system under conditions similar to those of the uranyl–benzaldehyde system.

Physical and Chemical Quenching. Quenching constants (K) of substituted benzaldehydes, obtained from the Stern-Volmer plots for the quenching of the uranyl emission in 60% aqueous acetone (containing 0.1 M perchloric acid), are listed in Table 3. The Stern-Volmer plots, $I^\circ/I=1+K[\mathrm{ArCH{=}O}]$, did not always give straight lines; sometimes the lines were concave downward at high concentrations of the quenchers. The quenching constants were obtained at low concentrations of the quenchers (usually, $[\mathrm{ArCH{=}O}]\leqq 2\times10^{-3}$ M).

It may be noted that the photoredox quantum yield inversely proportional to the quenching constant, which indicates that the physical and the chemical quenching processes are competing. The plot of log (K/K_0) *vs* σ^+ shows a straight line with a slope of $\rho=-0.7$ (where K_0 is the quenching constant of benzaldehyde), while similar plot for substituted acetophenones gives a straight line with a slope of $\rho=-1.0$ (Fig. 4). The difference in the slope of the two lines may be noted.

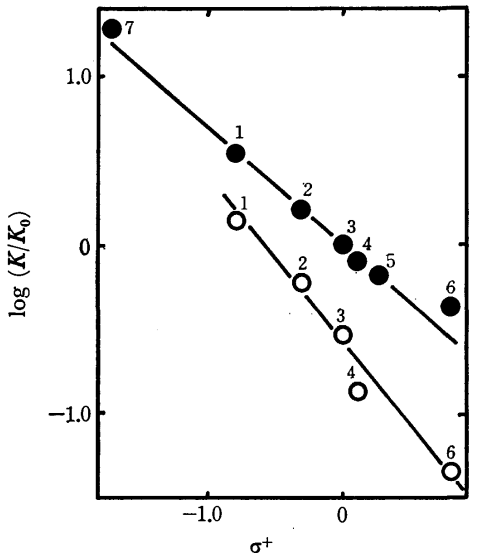

Fig. 4. Plots of $\log(K/K_0)$ *vs.* σ^+ for substituted benzaldehydes (●) and acetophenones (○). The substituents are, 1: *p*-methoxy, 2: *p*-methyl, 3: nonsubstituted, 4: *p*-chloro, 5: *m*-chloro, 6: *p*-nitro, and 7: *p*-dimethylamino, groups.

An electronic excitation energy transfer from the uranyl ion to these substrates will not occur, since it is a highly endothermic process. Quenching of the uranyl emission by acetophenone may be assumed to be essentially a physical quenching process, since it occurs without final chemical changes, while quenching by benzaldehydes involves both chemical and physical processes. From this point of view, the difference in the slope of the two lines in Fig. 4 may be assumed to reflect the chemical quenching of benzaldehydes. Thus the

difference in the ordinate of the two plots in Fig. 4, $\Delta=\log (K/K_0)_b-\log (K/K_0)_a$, which is assumed to be a measure of the chemical part of the quenching interactions, is plotted against σ^+ (open circles in Fig. 3). Here, a and b refer to the series of acetophenones and benzaldehydes, respectively. Figure 3 shows that Δ and $\log (\phi/\phi_0)$ are roughly parallel and suggests that the rate-determining steps are similar (abstration of the aldehyde hydrogen atoms). The apparent positive slope (ρ) in Fig. 3 may indicate that the chemical process is depressed by the competitive physical quenching process as the efficiency of the latter process is increased with the decrease in σ^+.

On the assumption of a simple scheme for the quenching of the uranyl emission by benzaldehydes, an approximate estimation of the relative importance of the physical and chemical (redox) quenching processes may be available. The main scheme may be drawn as follows for the photoredox reaction:

$$*UO_2^{2+} + ArCH{=}O \underset{k_d}{\overset{k_e}{\rightleftharpoons}} *UO_2^{2+} \cdots ArCH{=}O$$

$$\xrightarrow{k_p} UO_2^{2+} + ArCH{=}O + \text{heat} \quad (1)$$

$$\xrightarrow{k_r} UO_2^{+} + Ar\dot{C}{=}O + H^+ \quad (2)$$

$$2UO_2^{+} \xrightarrow[\text{rapid}]{H^+} UO_2^{2+} + \text{U(IV) species} \quad (3)$$

$$2Ar\dot{C}{=}O \xrightarrow[\text{rapid}]{} ArCOCOAr \quad (4)$$

Since the molar ratio of the redox products (benzils and the U(IV) species) is near unity, the following processes are assumed to be less important:

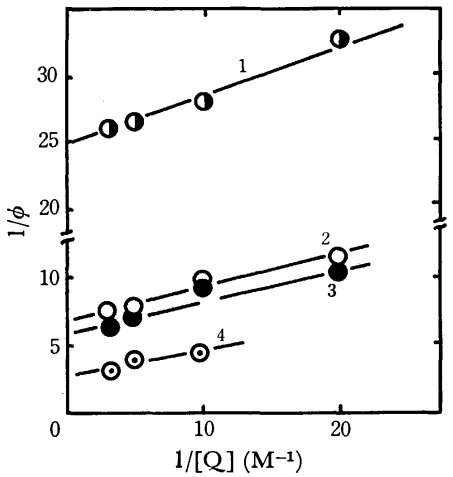

Fig. 5. Plots of $1/\phi$ *vs.* 1/[ArCH=O], for *p*-methoxy (1), *p*-methyl (2), nonsubstituted (3), and *p*-chloro (4), benzaldehydes. Conditions are similar to those in Table 1.

$$Ar\dot{C}{=}O + U(IV) \xrightarrow{H^+} UO_2^{+} + ArCH{=}O$$

$$UO_2^{+} + ArCH{=}O \longrightarrow U(IV) + Ar\dot{C}{=}O + H^+$$

The steady state approximation to $*UO_2^{2+}$, $*UO_2^{2+}\cdots$ ArCH=O, $Ar\dot{C}$=O and UO_2^{+} may eventually yield

$$\frac{1}{\phi} = \left(2+\frac{2k_p}{k_r}\right) + \frac{2(k_d+k_p+k_r)}{\tau_0 k_e k_r[ArCH{=}O]} \quad (5)$$

Here, τ_0 is the emission lifetime of the excited uranyl ion in the absence of benzaldehydes. Equation 5 indicates that the plots of ϕ^{-1} *vs* [benzaldehyde]$^{-1}$ should give a straight line with an intercept not smaller than 2. Figure 5 agrees with Eq. 5. From Eq. 5 the ratio of the physical and the chemical (redox) quenching rate constants, k_p/k_r, is given by $k_p/k_r=$(intercept$-2)/2$. The values obtained from Fig. 5 are listed in Table 4.

Table 4. Rate parameters for the photooxidation of substituted benzaldehydes with the uranyl ion

Substituent	I_s [a]	k_p/k_r [b]
p-OCH_3	25	11.5
p-CH_3	6.8	2.4
H	6.0	2.0
p-Cl	2.5	0.25

a) Intercept of the plot in Fig. 5. b) $k_p/k_r=(I_s-2)/2$.

These results shows that significant physical quenching is competing with the chemical (redox) quenching process, or that the excess vibrational energy (which the quencher and/or the quenchee would possess during or immediately after the physical quenching interactions) is unlikely to be effective for causing the redox reaction. On the other hand, the uranyl ion-photocatalyzed aldol condensation can be assumed to involve the conversion of the excess vibrational energy to that for the chemical process.

References

1) H. D. Burrows and T. J. Kemp, *Chem. Revs.* (London), **3**, 139 (1974).
2) R. Matsushima and S. Sakuraba, *Chem. Lett.*, **1973**, 1077.
3) R. J. Hill, T. J. Kemp, D. M. Allen, and A. Cox, *J. Chem. Soc., Faraday I*, **70**, 847 (1974).
4) S. Sakuraba and R. Matsushima, This Bulletin, **43**, 2359 (1970).
5) S. Sakuraba and R. Matsushima, *Chem. Lett.*, **1972**, 911.
6) R. Matsushima and S. Sakuraba, *J. Amer. Chem. Soc.*, **93**, 7143 (1971).
7) M. Iwata and S. Emoto, *Chem. Lett.*, **1974**, 959.
8) H. Onishi and Y. Toita, *Bunseki Kagaku*, **14**, 1141 (1965).

Inter- and Intramolecular Exciplexes and EDA Complexes in the 9,10-Dicyanoanthracene and Alkylbenzene Systems

Michiya Itoh,* Yoshiro Kumano, and Toshihiko Okamoto
Faculty of Pharmaceutical Sciences, The University of Tokyo, Bunkyo-ku, Tokyo 113
(Received July 29, 1975)

The exciplex (above ~150 K) and EDA complex (below ~120 K) fluorescence were observed in the 9,10-dicyanoanthracene and several alkylbenzene systems and also in the intramolecular system of (9,10-dicyanoanthracene)-$(CH_2)_3$-(pentamethylbenzene) in the nonpolar solvents. The exciplex fluorescence lifetimes and maxima both in the inter- and intramolecular systems exhibit the continuous change to those of the corresponding EDA complex, which implies the identical fluorescent state of the exciplex and EDA complex. The fluorescence lifetimes and the fluorescence polarization suggest that the fluorescent state of both exciplex and EDA complex may be mostly locally excited state of electron acceptor.

Steady-state and transient spectroscopies, and also theoretical consideration of the electron donor-acceptor (EDA) system in the excited state suggest that the exciplex and the EDA complex may be essentially identical each other. It has been believed, however, that the EDA complex stable in the ground state can not be formed in the EDA system which exhibits the fluorescence of the exciplex stable only in the excited state.[1,2] Itoh and Mimura reported the exciplex and also the EDA complex formation in the nonpolar solution of 9,10-dicyanoanthracene (DCA) and several alkylnaphthalenes, and demonstrated a direct evidence for an identical fluorescent state of the exciplex and EDA complex.[3,4] Recently, Gaweda and Prochorow[5] reported similar evidence for the identical fluorescent state in the tetracyanobenzene and *p*-xylene system from their measurements of the decay times of fluorescence and investigation of the influence of solvent polarity on the fluorescence spectra.

On the other hand, the experimental and theoretical studies in the previous papers revealed that there are two different fluorescent state of the exciplex and EDA complex in the intramolecular system of (9,10-dicyanoanthracene)-$(CH_2)_3$-(naphthalene) (DCAN).[6,7] These two different fluorescent states were attributed to the unsymmetric property of the naphthyl moiety around the trimethylene chain in DCAN. Therefore, an intramolecular system containing an electron donor which has C_2 symmetry around the trimethylene was predicted to show the exciplex and EDA complex fluorescences from the identical fluorescent state. This paper describes further investigation of the exciplex and the EDA complex in the DCA-alkylnaphthalene system and in the intramolecular system of (9,10-dicyanoanthracene)-$(CH_2)_3$-(pentamethylbenzene).

Experimental

Materials and Measurements. Purification of materials and solvents were described in the previous papers. Commercial zone-refined samples of hexamethylbenzene were used after recrystallization (three times) from ethanol. Pentamethylbenzene and durene were recrystallized six or seven times from ethanol.

Determination of the fluorescence and absorption spectra, and the fluorescence polarization were described previously.[4,6] The fluorescence lifetimes and time-resolved fluorescence spectra were determined by analyzing exponential decay curves measured by an oscilloscope (Tektronix 465), and by a coaxial N_2 gas laser excitation (3371 Å, ~20 kW, ~5 ns width).

Synthesis of 1-(9,10-Dicyano-2-anthryl)-3-(pentamethylphenyl)-propane. The sample of *1-(9,10-dicyano-2-anthryl)-3-(pentamethylphenyl)propane* was synthesized by bromination and cyanogenation of 1-(2-anthryl)-3-(pentamethylphenyl)propane, which was prepared by the similar route to that of 1,3-dinaphthylpropane.[8] The unsaturated ketone, *1-(2-anthryl)-3-(pentamethylphenyl)-2-propen-1-one*, was prepared from 2-acetylanthracene and pentamethylbenzaldehyde: mp 214—216 °C.

Found: C, 88.22; H, 6.19%. Calcd for $C_{28}H_{26}O$: C, 88.85; H, 6.92%.

A solution of the unsaturated ketone (400 mg) in tetrahydrofuran (100 ml) was hydrogenated over 5% Pd/C for about 8 hr. The ketone, *1-(2-anthryl)-3-(pentamethylphenyl)-1-propanone* was obtained: mp 190 °C.

Found: C, 87.99; H, 7.49%. Calcd for $C_{28}H_{28}O$: C, 88.38; H, 7.42%.

The ketone (300 mg) was reduced in refluxing (4 hr) diethylene glycol (5 ml) containing hydrazine (1 ml, ~95%) and sodium hydroxide (500 mg). The mixture was diluted with water and extracted with benzene. The yellow product was purified through silica gel with benzene–hexane, and recrystallized from benzene–hexane: mp 181 °C.

Found: C, 91.48; H, 7.49%. Calcd for $C_{28}H_{30}$: C, 91.75; H, 8.25%.

The hydrocarbon was brominated and cyanogenated in the way described in the previous paper.

1-(9,10-Dibromo-2-anthryl)-3-(pentamethylphenyl)propane. Recrystallized from benzene: mp 157 °C.

Found: C, 64.01; H, 5.42%. Calcd for $C_{28}H_{28}Br_2$: C, 64.13; H, 5.38%.

1-(9,10-Dicyano-2-anthryl)-3-(pentamethylphenyl)propane. Purifiedaby preparative thin layer chromatography and recrystallized from hexane: mp 264 °C.

Found: C, 86.43; H, 6.75; N, 6.54%. Calcd for $C_{30}H_{28}N_2$: C, 86.49; H, 6.78; N, 6.73%.

Results and Discussion

The exciplex formation between DCA and aromatic hydrocarbons was reported first by Chandross and Ferguson.[9] The exciplex fluorescence in the 3-methylpentane (MP) solutions of DCA and several alkylbenzenes were observed at room temperature. The exciplex fluorescence was almost quenched below ~150 K, while the fluorescence due to the EDA complex was observed in the nonpolar solution of these

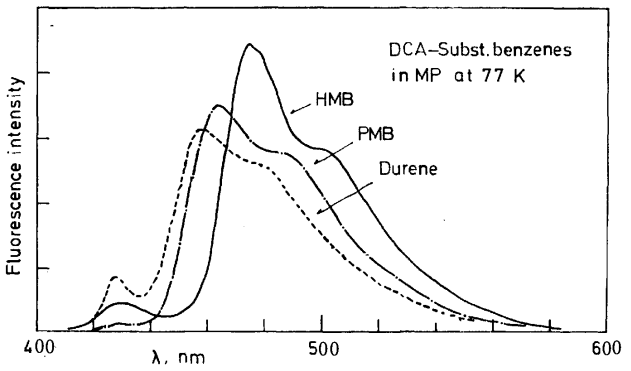

Fig. 1. Fluorescence spectra of MP solutions of DCA and several alkylbenzenes at 77 K (concentrations: DCA, 2×10^{-6} M; HMB, 6×10^{-3} M; pentamethylbenzene, 1×10^{-2} M; durene, 9×10^{-3} M).

EDA systems below ~120 K. The fluorescence spectra of the EDA complexes at 77 K are shown in Fig. 1. These exciplex and EDA complex were characterized by their fluorescence excitation and the absorption spectra at room temperature and at low temperature. The EDA complex fluorescence was observed only in the nonpolar solvents such as MP and methylcyclohexane (MC), but none in the polar solvents.[3,6] The fluorescence behavior in DCA-alkylbenzene is quite similar to the results in DCA-alkylnaphthalene reported previously.[3,4,6] Fluorescence lifetimes of these exciplex and EDA complex are considerably smaller in the DCA–alkylbenzene system (summarized in Table 1) than in the DCA–alkylnaphthalene system (~40—100 ns).

Table 1. Fluorescence maxima and life times of the exciplex (at room temperature) and the EDA complex (at 77 K) in MP solution of DCA and several alkylbenzenes, and of DCAB

DCA–alkylbenzenes and DCAB	Exciplex		EDA complex	
	λ, nm	τ, ns[a]	λ, nm	τ, ns[a]
Hexamethylbenzene	494	19	476	32
Pentamethylbenzene	482	21	465	34
Durene	467	21	~460	34
DCAB	501	72	~507[b]	106

a) Errors are approximately ±1 ns. b) Determined by time-resolved fluorescence spectra.

The fluorescence of the EDA complex in the MP solution of DCA and hexamethylbenzene (HMB) was determined at 77 K to exhibit very small positive polarization with the excitation at 360 nm, as shown in Fig. 2. In the DCA and alkylnaphthalene systems reported previously, the fluorescence polarization of the MP solution of the EDA complex at 77 K with the excitation at 370 nm (LE band in DCA) decreased from negative to more negative value, and the fluorescence lifetimes increased with decreasing ionization potential of alkylnaphthalenes.[4] The results of these fluorescence lifetimes and polarizations in DCA-alkylnaphthalenes were attributed to the considerable charge-transfer

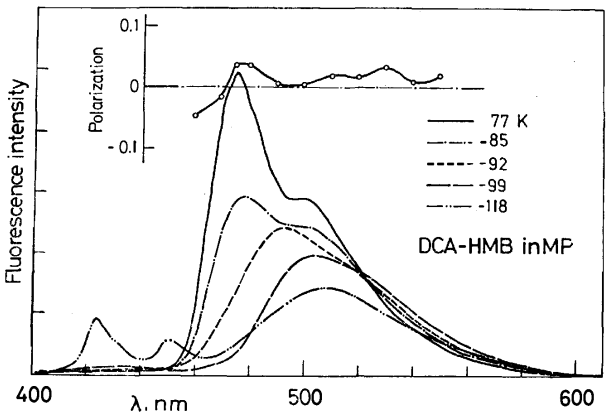

Fig. 2. Fluorescence spectra of an MP solution of DCA and HMB at several temperatures and fluorescence polarization at 77 K excitation at 360 nm). Concentration: DCA, 5×10^{-6} M; HMB, 1×10^{-3} M.

character in the fluorescent state of the EDA complex. From the small fluorescence lifetimes and small positive polarization obtained in DCA–alkylbenzenes, the fluorescent state of the EDA complex in this system seems to consist mostly of the locally excited state of DCA. The fluorescence lifetimes in the MP or MC solution of DCA–HMB exhibit continuous variation from room temperature (exciplex) to 77 K (EDA complex) as shown in Fig. 3, which implies the identical fluorescent state of the exciplex and the EDA complex.

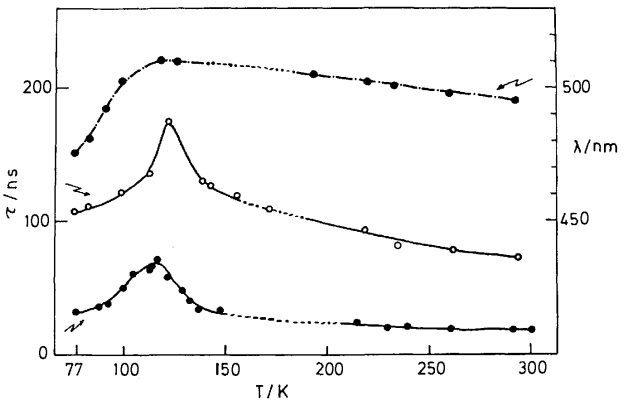

Fig. 3. Temperature dependence of fluorescence maxima and lifetimes of the exciplex and EDA complex in MP (lifetimes monitored at 540 nm); -·-·-●-·-·-and —●— are fluorescence maxima and lifetimes in DCA–HMB, respectively, and —○— is the fluorescence lifetimes in DCAB.

The fluorescences of an MP solution of (9,10-dicyanoanthracene)-$(CH_2)_3$-(pentamethylbenzene) (abbreviated to DCAB) at several temperatures are shown in Fig. 4. The exciplex fluorescence (λ_{max} ~500 nm) was completely quenched below ~150 K, and no fluorescence maximum in this wavelength region was detected at 77 K. However, the time-resolved fluorescence spectra of this solution at 77 K revealed that the fluorescence with a maximum at ~510 nm was hidden by a strong fluorescence of the DCA moiety in DCAB, as shown in Fig. 5. The fluorescence excitation spectrum of this

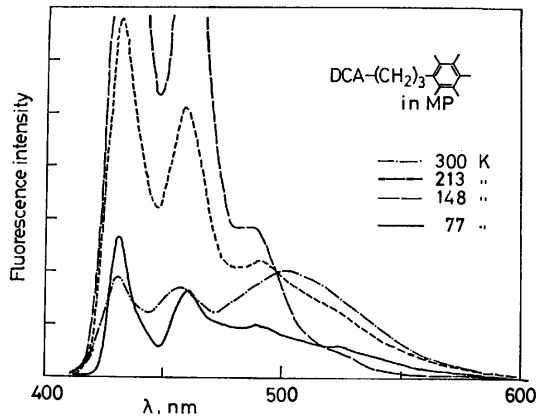

Fig. 4. Fluorescence spectra of an MP solution of DCAB at several temperatures (concentration: ~4×10^{-5} M).

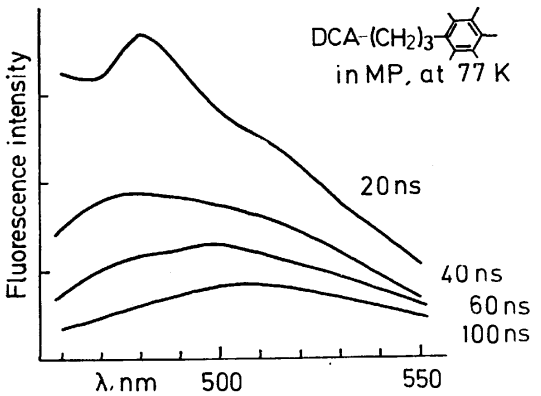

Fig. 5. Time-resolved fluorescence spectra of an MP solution of DCAB at 77 K.

solution (77 K) monitored at 530 nm showed significantly different from the spectrum monitored at 430 nm. Furthermore, the absorption spectrum of DCAB in dilute solution of MP (~10^{-5} M) demonstrated considerable EDA complex formation at 77—140 K. Therefore, the weak fluorescence of an MP solution of DCAB shown in Fig. 5 may be ascribed to the fluorescence of the intramolecular EDA complex.

The rise and decay curves of the exciplex fluorescence were observed in a dioxane solution of DCAB at room temperature by nanosecond laser excitation, while neither rise time of the exciplex fluorescence was detected in less viscous solution such as MP or 2-methyltetrahydrofuran at room temperature, nor rise time was detected in the viscous solution of DCAB in MP at ~100 K where the intramolecular EDA complex was formed. Similar time-development of the exciplex fluorescence was also observed in the intermolecular system of DCA–HMB. They are shown in Fig. 6. These results suggest that the fluorescence in the ~500 nm region at room temperature is ascribed to the exciplex different from the EDA complex at low temperature, though the characterization of the exciplex and the EDA complex was already suggested by the absorption and fluorescence excitation spectra, as mentioned above.

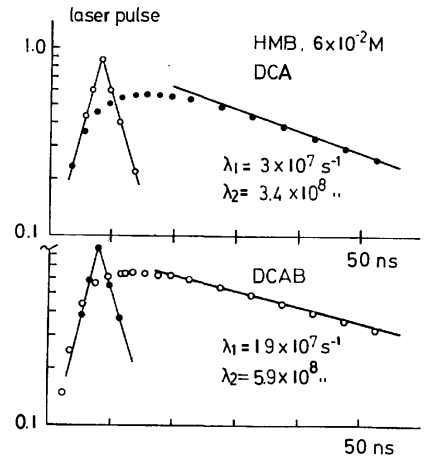

Fig. 6. Time-developments of the exciplex fluorescence (monitored at 560 nm) in the dioxane solutions of DCA–HMB and DCAB at room temperature. Time dependent exciplex concentration is expressed as a following equation; $[(DA)^*]=\frac{C}{\lambda_2-\lambda_1}\{\exp(-\lambda_1 t)-\exp(-\lambda_2 t)\}$. The time constant, λ_1 was obtained from the decay curve, and λ_2 was obtained from λ_1 and the time lag between the maxima of [(DA)*] and the exciting laser pulse; $t_1=\frac{\ln(\lambda_2/\lambda_1)}{\lambda_2-\lambda_1}$.

The fluorescence liferimes of the exciplex (room temperature) in the MP solution of DCAB were observed to vary continuously to that of the EDA complex (77 K). This temperature dependence of the fluorescence lifetimes in DCAB is almost same as that in the DCA–HMB system, as shown in Fig. 3. The continuous change of the fluorescence lifetimes means that there is no different fluorescent state in the exciplex and the EDA complex.[3,4] This fact seems to be attributable to the C_2 symmetry of the pentamethylphenyl moiety around the trimethylene chain in DCAB as metnioned in the introductory section.

As seen in Fig. 3, it is noteworthy that a remarkable temperature dependence of the fluorescence lifetimes of the EDA complex at ~120—77 K. The solvent viscosity increases markedly below ~120 K to make a rigid glass at 77 K.[10] Decrease of fluorescence lifetimes both in the inter- and intramolecular EDA complexes from ~120 K to 77 K are ascribed to the solvent viscosity, and this is consistent with the remarkable temperature dependence of the fluorescence spectra of DCA–HMB shown in Fig. 2. The solvent viscosity reduces the extent which molecular reorientation can occur during the excited state, and as the results the fluorescence lifetime of the EDA complex is reduced. Therefore, the fluorescence emmits from near Franck-Condon excited state of EDA complex at 77 K,[11] which seems to be almost locally excited state of DCA. It is because the fluorescence of the EDA complex of DCA–alkylbenzenes at 77 K has a vibrational progression ($\bar{\nu}$=~1260 cm^{-1}) and positive polarization with the local excitation in the EDA complex, as mentioned above.

The authors wish to acnowledge useful suggestions of Dr. Keitaro Yoshihara and Mr. Minoru Sumitani for making a coaxial nitrogen gas laser.

References

1) For comprehensive books: (a) R. S. Mulliken and W. B. Person "Molecular Complexes, A Lecture and Reprint Volume," Willy-Interscience, New York, N.Y., 1969; (b) N. Mataga and T. Kubota, "Molecular Interactions and Electronic Spectra," Marcel Dekker, New York, N. Y. 1970.

2) See references Ref. (1).

3) M. Itoh and T. Mimura, *Chem. Phys. Lett.*, **24**, 551 (1974).

4) M. Itoh, *J. Amer. Chem. Soc.*, **96**, 7390 (1974); *Chem. Phys. Lett.*, **26**, 505 (1974).

5) E. Gaweda and J. Prochorow, *Chem. Phys. Lett.*, **30**, 155 (1975).

6) M. Itoh, T. Mimura, H. Usui, and T. Okamoto, *J. Amer. Chem. Soc.*, **95**, 4388 (1973).

7) T. Mimura, M. Itoh, T. Ohta, and T. Okamoto, This Bulletin, **48**, 2245 (1975).

8) E. A. Chandross and C. J. Dempster, *J. Amer. Chem, Soc.*, **92**, 3586 (1970).

9) E. Chandross and J. Ferguson, *J. Chem. Phys.*, **47.** 2557 (1967).

10) T. Kobayashi, K. Yoshihara, and S. Nagakura, This Bulletin, **44**, 2603 (1971).

11) N. G. Bakshiev, *Opt. Spectrosk.*, **16**, 821 (1964); *Opt. spectrosk.*, **16**, 446 (1964); **20**, 542(1966).

Vibrational Spectra and Rotational Isomerism of Alkyl Vinyl Ethers

Masaaki SAKAKIBARA, Fuyuhiko INAGAKI, Issei HARADA, and Takehiko SHIMANOUCHI
Department of Chemistry, Faculty of Science, The University of Tokyo, Hongo, Bunkyo-ku, Tokyo 113
(Received August 1, 1975)

The rotational isomerism of methyl vinyl ether, ethyl vinyl ether, and *n*-butyl vinyl ether has been studied by means of the vibrational spectra and normal frequency calculations. The enthalpy difference between the *skew* and *cis* isomers in the liquid state of methyl vinyl ether has been determined to be 1440 ± 160 cal/mol. Series of C–O torsional transitions in the *cis* well have been observed for methyl vinyl ether and methyl-d_3 vinyl ether in the region near 230 cm^{-1} and analyzed. It has been concluded for ethyl vinyl ether that the *cis-trans* form (CT) is stable in the solid state and that three forms, CT, SG′, and ST, coexist in the liquid and gaseous states. The spectra in the solid state of *n*-butyl vinyl ether are consistent with the calculated frequencies of the CTTT form.

In a preceding paper the analysis of the mid-infrared spectra in the various states with the support by the normal coordinate treatment was successful for the determination of the rotational isomerism about the C–C axis neighboring a C=C double bond.[1] It was concluded that the *cis* and *skew* conformations are stable for the C–C bond neighboring the *trans* C=C bond, and only the *skew* conformation is stable for the C–C bond neighboring the *cis* C=C bond. As an extension of the work, the rotational isomerism about the C–O bond neighboring a C=C double bond has been studied for methyl vinyl ether, ethyl vinyl ether, and *n*-butyl vinyl ether with the additional information of the Raman spectra. The enthalpy differences among the rotational isomers in the liquid state have also been determined.

In the case of methyl vinyl ether and methyl-d_3 vinyl ether, series of the C–O torsional transitions in the *cis* well have been observed and analyzed by the method described in a preceding paper.[2]

The details and the results are reported in the present paper.

Experimental

Methyl vinyl ether, ethyl vinyl ether, and *n*-butyl vinyl ether were obtained commercially. Methyl vinyl ether was used without further purification. Ethyl vinyl ether and *n*-butyl vinyl ether were purified by fractional distillations. Methyl-d_3 vinyl ether was prepared by the interchange reaction,

$$CD_3OD + ROCH{=}CH_2 \rightleftharpoons ROD + CD_3OCH{=}CH_2,$$

with $Hg(OAc)_2$ as the catalyst and *n*-butyl vinyl ether as the starting alkyl vinyl ether. The purity of the sample was checked by means of infrared spectroscopy.

The infrared spectra were recorded on a Hitachi EPI-L double beam grating spectrometer in the region 700—250 cm^{-1} and on a Hitachi FIS-1 vacuum double beam grating spectrometer in the region 300—60 cm^{-1}. The spectra in the gaseous state were obtained by using the 10-cm and 4.9-m cells with white polyethylene windows and those in the liquid state were taken with 0.025—0.01 mm cells of KBr, KRS-5, or polyethylene windows. The spectra in the solid state were observed at the temperature of liquid nitrogen. Sample deposited on a cooled window of KRS-5, silicon, or KBr was repeatedly annealed until no further spectral change was observed. A low-temperature cell and a Hitachi 205 double beam grating spectrometer at the Institute for Protein Research of Osaka University[3] were used for the measurement of the infrared spectra of methyl vinyl ether in the liquid state.

The Raman spectra were obtained on a JEOL JRS-400D spectrophotometer with the 5145 Å line of a Coherent Radiation CR-3 argon ion laser as the exciting line and on a Spex 1401 spectrophotometer equipped with an NEC He-Cd laser and an NEC He–Ne laser. The He–Cd laser line at 4416 Å and the He–Ne laser line at 6328 Å were used as exciting lines. The latter instrument was calibrated with neon gas emission lines and the observed Raman frequencies are believed accurate to 2 cm^{-1}. The Raman spectra at low temperatures were obtained with a simple glass Dewar-type low temperature cell. The temperature of the sample was controlled by the amount of liquid nitrogen or of Dry Ice added to the cell. The temperature was measured with a thermocouple directly inserted into the sample.

The mid-infrared spectra of the three compounds in the gaseous, liquid, and solid states are shown in Figs. 1—3. The far-infrared spectra of methyl vinyl ether and methyl-d_3 vinyl ether are shown in Fig. 4. The Raman spectra of the three compounds are shown in Figs. 5—7. The observed frequencies are listed in Table 1.

Normal Vibration Calculations

For the purpose to correlate the observed vibration bands with the normal modes of the rotational isomers, the normal vibrations have been calculated by Program NCTB, which is a combination of GCCC, BGLZ, and LSMB,[4] and the HITAC 8800/8700 Computer of the

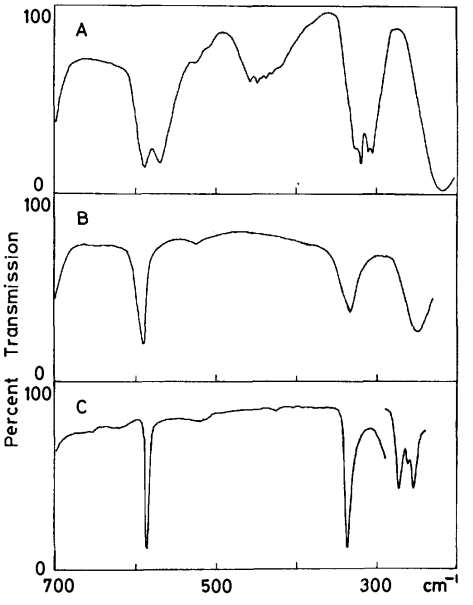

Fig. 1. Infrared spectra of methyl vinyl ether.
A: Gas, B: liquid, C: solid.

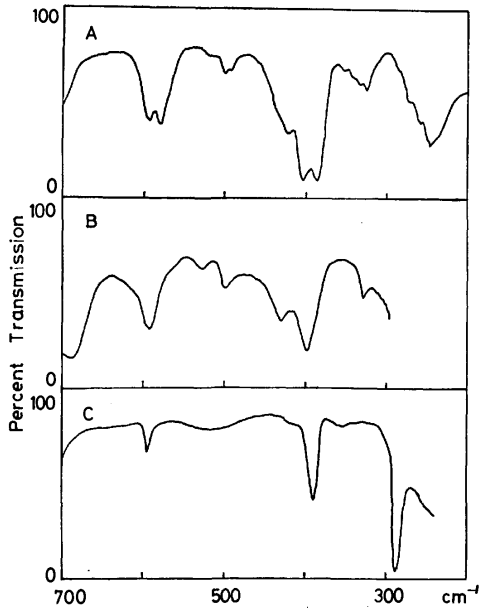

Fig. 2. Infrared spectra of ethyl vinyl ether.
A: Gas, B: liquid, C: solid.

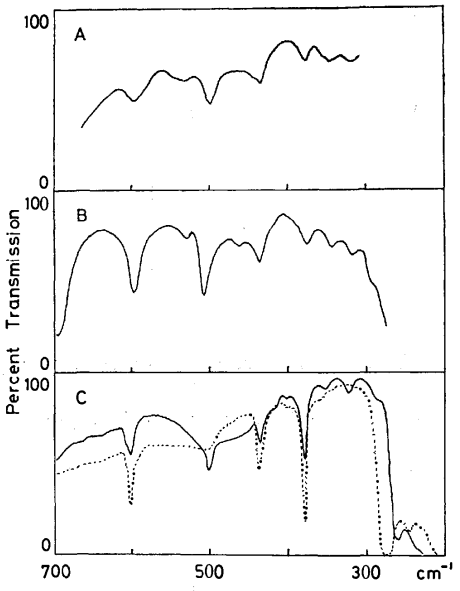

Fig. 3. Infrared spectra of *n*-butyl vinyl ether.
A: Gas, B: liquid, C: —— amorphous solid,
····· annealed solid.

Table 1. Observed frequencies of methyl vinyl ether, ethyl vinyl ether, and *n*-butyl vinyl ether in cm^{-1}

Gas		Liquid		Solid	
IR	R	IR	R	IR	R
Methyl vinyl ether					
702 *C*		707	707	720	722
				714	718
585 *B*	590	591	591	595	591
	525	525	527		
464 *C*					
456 *C*					
451 *C*					
444 *C*					
435 *C*					
	413[a)]				
328 *AB*	326	336	333	340	344
234 *C*	232	250	248	273	280
230 *C*				263	264
226 *C*				256	254
					119
					90
					84
					68
					39
					28
Ethyl vinyl ether					
700 *C*		704	708	710	719
				704	710
594 *B*	598	595	600	598	605
					599
523	525	530	533		
500 *B*	496	500	500		
425	435	437	436		
395 *B*	396	400	398	395	397
				280	280
247	238		245		248
			215		228
					217

Gas		Liquid		Solid	
IR	R	IR	R	IR	R
					136
					80
					68
					50
					40
					33
					27
					20
n-Butyl vinyl ether					
700		700	702	710	709
602		600	600	605	611
				598	
534		530	538		
498		505	497		
		455	459		
437		437	437	436	440
380		380	378	378	380
344		350	350		
			337		
		320	322		
			265		289
			246	278	276
				268	
					251
					162
					141
					133
					95
					72
					59
					42
					31
					26

a) Origin unknown.

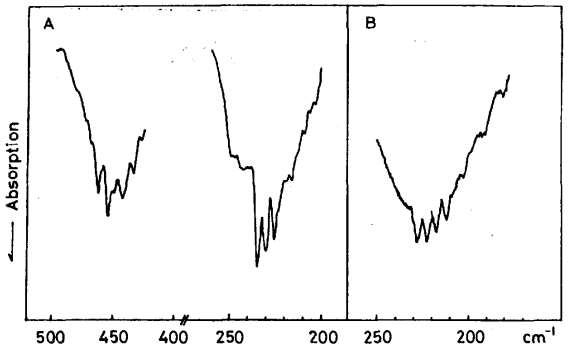

Fig. 4. Far-infrared spectra of gaseous methyl vinyl ether.
A: Methyl vinyl ether, B: methyl-d_3 vinyl ether.

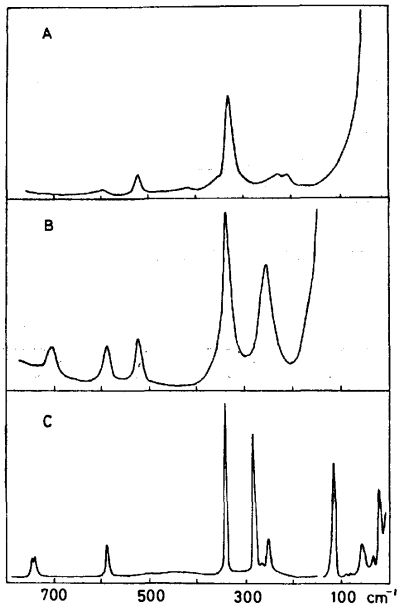

Fig. 5. Raman spectra of methyl vinyl ether.
A: Gas 500 mmHg, B: liquid, C: solid.

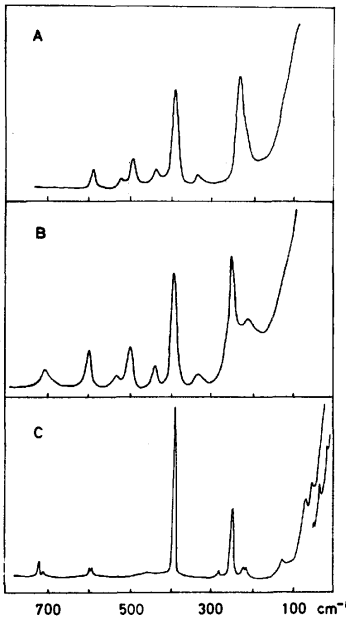

Fig. 6. Raman spectra of ethyl vinyl ether.
A: Gas 420 mmHg, B: liquid, C: solid.

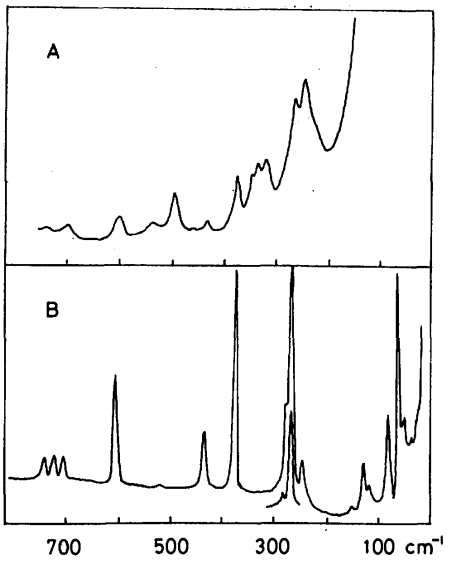

Fig. 7. Raman spectra of *n*-butyl vinyl ether.
A: Liquid, B: solid.

Computer Center of the University of Tokyo. The bond lengths and the bond angles of methyl vinyl ether determined by microwave spectroscopy[5] were used for the CH_2=CH–O–CH_2 part and 1.522 Å, 1.09 Å, and the tetrahedral angle were assumed for the other C–C bonds, C–H bonds, and the rest of the angles. The values of force constants were transferred from those of 1-alkenes,[1] except for those given in Table 2. The

Table 2. Force constants of methyl vinyl ether[a] (MUBFF)

K(C–O)	2.40 md/Å	W(=CH)	0.37md·Å
H(C=C–O)	0.487	W(=CH_2)	0.28
H(C–O–C)	0.26	Y(C=C)	0.518
F(C=C–O)	0.40	Y(=C–O)	0.147
F(C–O–C)	0.40	Y(O–CH_3)	0.11
R(*cis* C=C–O–C)	0.369	WY(=CH_2, C=C)	0.049
		WY(=CH, C=C)	0.145
		YY(=C–O, O–CH_3)	0.064

a) Only the values of modified force constants are listed in the table. Other force constants are transferred from those of olefins (see Table III of Ref. 1).

values given in this table were determined so as to give the best fit with the observed frequencies for the *cis* form of methyl vinyl ether. These values were transferred to ethyl vinyl ether with various conformations and the CTTT form of *n*-butyl vinyl ether. The torsion angles are taken to be 0°, 60°, 120°, and 180° for the *cis*, *gauche*, *skew*, and *trans* forms, respectively.

As in the case of 1-alkene molecules, the *cis* repulsion constant R were taken into account for the two carbon atoms of the =CH_2 and –O–C parts in the *cis* position. The inclusion of this constant explains the C–O–C bending and C=C–O bending vibrations simultaneously.

Results and Discussion

Methyl Vinyl Ether. Since the bands with frequencies less than 750 cm^{-1} are significantly related

Table 3. Calculated and observed frequencies of methyl vinyl ether in cm^{-1}

Calculated (Observed)					Assignment
0° (*cis*)		90°, 120° (*skew*)	180° (*trans*)		
ip	op		ip	op	
	700(707)	713, 712(707[a])		702	=CH wag.
586(591)		533, 515(526)	504		C=CO bend.
326(335)		347, 341(335[a])	280		COC bend.
	244(249[a])	248, 253(249[a])		281	CH_3 tor.
	227(249)	158, 154(—)		155	=C–O tor.

a) Overlapped.

to the molecular conformation, the frequencies observed in this region are summarized and compared with the calculated frequencies in Table 3. The infrared and electron diffraction studies by Owen and Sheppard[6] and Owen and Seip[7] show that this molecule has the two rotational isomers, the *cis* form and the *skew* form with the torsion angle 80—110°. This fact is in agreement with the result for the 1-butene molecule which has *cis* and *skew* for the stable conformations.[8] Accordingly, we assigned the observed bands to the vibrations of the *cis* and *skew* forms, by taking into account the possibility of a considerable deviation of the *skew* form torsion angle.

As shown in Table 3, the strong bands observed in the gaseous state at 702 cm^{-1} (*C* type), 585 cm^{-1} (*B* type), and 328 cm^{-1} (*A* and *B* hybrid) are assigned reasonably to the =CH– wagging, C=C–O in-plane, and C–O–C in-plane bending vibrations of the *cis* isomer, respectively. The two low frequency vibrations, methyl torsion and C–O torsion, are predicted to appear at 225±20 cm^{-1} and 219±20 cm^{-1} from the microwave study.[5] The fairly strong band at about 230 cm^{-1} is composed of three distinct equally separated sharp absorptions (Fig. 4). The corresponding band of the methyl deuterated compound is composed of a quartet and is observed lower than that of the undeuterated compound by 4 cm^{-1} (Fig. 4). We assign this band to =C–O– torsion, taking the small isotopic shift in frequency into account. The methyl torsion may be weak and overlapped with this band. The weak and broad band with some structure near 450 cm^{-1} is explained as the progression of =C–O– torsional transitions for $\Delta v=2$. The details about the potential of internal rotation will be discussed in the later part of this paper.

The band observed at about 525 cm^{-1} in the Raman spectra in the gaseous and liquid states is missing in the spectrum in the solid state. This band is the only band assigned to the *skew* form. This fact is justified by the large enthalpy difference to be described below.

The situation about the key band sensitive to the conformation of this molecule is different from that of 1-alkenes. For the latter case the *cis* conformation gives a band near 550 cm^{-1} which is assigned to one of the CH out-of-plane vibrations of the vinyl group and the *skew* conformation gives a band near 640 cm^{-1}, the frequency shift being caused by the coupling between this vibration and the skeletal deformation vibration. In the case of methyl vinyl ether, this vibration has a higher frequency near 700 cm^{-1} and the coupling with the skeletal deformation is small in the *skew* conformation. The C=C–O bending vibration, on the other hand, seems to be the key band to the conformation. The calculated frequency for the C=C–O bending mode varies from 586 cm^{-1} to 504 cm^{-1} as the torsion angle changes from 0° (*cis*) to 180° (*trans*).

The barrier to internal rotation of the C–O axis has been studied in one-dimensional approximation by the use of three $\Delta v=1$ and four $\Delta v=2$ torsional transitions of methyl vinyl ether and four $\Delta v=1$ transitions of methyl-d_3 vinyl ether. The method described in the preceding paper[2] was used for the analysis. $F(\alpha)$'s were calculated numerically by Pitzer's method[9] and expanded in Fourier cosine series. $F(\alpha)_{cis}$ was calculated with the structural parameters determined for the *cis* form by microwave spectroscopy.[5] $F(\alpha)_{skew}$ was calculated with the same structural parameters as those for $F(\alpha)_{cis}$ except the value of the angle C–O–C, 112°, determined by the electron diffraction analysis.[7] Then, $F(\alpha)_{\text{hybrid}}$ was determined so that it may be continuous as going from the *cis* form to the *skew* form. $F(\alpha)$ determined in this way corresponds to the situation that the angle C–O–C varies as the OCH_3 group rotates around the C–O axis. $F(\alpha)_{cis}$ and $F(\alpha)_{\text{hybrid}}$ were used in the calculation. The values of parameters of $F(\alpha)_{cis}$ and $F(\alpha)_{\text{hybrid}}$ are as follows:

$$F(\alpha)_{cis} = \underset{(2.4960)}{2.8807} + \underset{(0.4485)}{0.6620}\cos\alpha + \underset{(0.2191)}{0.2940}\cos 2\alpha + \underset{(0.0545)}{0.0826}\cos 3\alpha + \underset{(0.0167)}{0.0260}\cos 4\alpha + \underset{(0.0047)}{0.0079}\cos 5\alpha + \underset{(0.0014)}{0.0024}\cos 6\alpha$$

$$F(\alpha)_{\text{hybrid}} = \underset{(2.4246)}{2.7724} + \underset{(0.4008)}{0.5905}\cos\alpha + \underset{(0.2187)}{0.2840}\cos 2\alpha + \underset{(0.0533)}{0.0786}\cos 3\alpha + \underset{(0.0172)}{0.0255}\cos 4\alpha + \underset{(0.0048)}{0.0078}\cos 5\alpha + \underset{(0.0015)}{0.0024}\cos 6\alpha$$

where the values in parentheses are for the deuterated species.

At first, several set values of V_1, V_2, and V_3 were estimated from the 1←0 and 2←1 transitions, 234 cm^{-1} and 230 cm^{-1}, and the enthalpy differences, 1150±250 cal/mol (402±87 cm^{-1})[6] and the energy levels were calculated. After preliminary calculations the value of V_2 was fixed at 628.4 cm^{-1}. The least squares adjustment was performed for the following four cases:

Case A: $F(\alpha)_{cis}$ and the data of methyl vinyl ether are used.

Case B: $F(\alpha)_{cis}$ and the data of methyl-d_3 vinyl ether are used.

Case C: $F(\alpha)_{cis}$ and the data of methyl vinyl ether and methyl-d_3 vinyl ether are used.

Case D: $F(\alpha)_{\text{hybrid}}$ and the data of methyl vinyl ether and methyl-d_3 vinyl ether are used.

The results are given in Table 4. The agreement between the observed and the calculated is satisfactory for both Case A and Case B, but the obtained potential parameters are different for these two cases. In Case C, the calculated frequencies of the normal species are higher than the observed and those of the deuterated

Table 4. Observed and calculated C–O torsional transitions[a] in cm^{-1}

Transition (*cis*)	ν_{obsd}	ν_{calcd} Case A	Case B	Case C	Case D
Methyl vinyl ether					
1←0	234	233.3		240.8	238.6
2←1	230	229.8		235.4	233.1
3←2	226	225.1		229.1	226.8
2←0	464	463.2		476.2	471.7
3←1	456	454.9		464.5	459.8
4←2	444	444.4		451.1	446.5
5←3	435	431.6		435.9	431.7
Methyl-d_3 vinyl ether					
1←0	227		226.4	218.7	218.0
2←1	222		222.1	214.6	213.7
3←2	217		217.1	209.7	208.7
4←3	212		211.5	204.3	203.3

a) Potential parameters and dispersions are as follows in the order of Cases A, B, C, and D; V_1, −19.6 (8.1), −27.0(11.7), −3.4(14.8), and −3.8(13.5); V_2, 628.4 fixed; V_3, 1765.8(62.8), 1908.2(119.6), 1775.6(85.2), and 1810.1(83.1); V_6, −119.7(25.8), −91.0(48.6), −90.0(39.9), and −83.8(38.1).

species are lower than the observed. This inconvenience cannot be overcome even in Case D, where different structures are assumed for the different internal rotation angles. All these are explained by the difference of vibrational couplings in the normal and the deuterated species. In the normal species, the C–O torsion may couple with the methyl torsion, which is estimated at about 240 cm^{-1} by microwave study.[5] On the other hand, the methyl torsion shifts to lower frequency region on methyl deuteration and the coupling between C–O torsion and methyl-d_3 torsion becomes small; thus the one dimensional model approximation may work better for the deuterated species. This interpretation is verified by the normal coordinate analysis. The potential energy distribution shows that the methyl torsion and C–O torsion couple in the ratio of one to two in the normal species and in the ratio of one to six in the deuterated species. It is concluded that the set of potential parameters obtained with the data of methyl-d_3 vinyl ether is the most probable of the four cases. The values of the parameters for Case B are as follows: $V_1=-27.0$, $V_2=628.4$, $V_3=1908.0$, and $V_6=-91.0$ cm^{-1} (See also the footnote of Table 4). The *skew* transitions are calculated at about 160 cm^{-1}, but no distinct band has yet been observed.

The observed frequency, 234 cm^{-1}, of C–O torsion of methyl vinyl ether is much higher than that of methyl ethyl ether,[3] 113 cm^{-1}. This may be explained by the conjugation between the vinyl group and the lone pair electron of the oxygen atom.

Ethyl Vinyl Ether. The observed frequencies are compared with the calculated in Table 5. Owen and Sheppard analyzed the rotational fine structure of the band at 813 cm^{-1} and suggested that the stable conformer is the planar "sickle shaped" form (the *cis-trans* form).[10] From the comparison of the infrared spectra of gaseous, liquid, and solid states (Fig. 2), it is clear that

Table 5. Calculated and observed frequencies of ethyl vinyl ether in cm^{-1}

Calculated (Observed) CT	CG	SG′	SG	ST	Assignment
654(706)	654	712(—)	692	690(—)	=CH wag.
588(598)	614	510(500)	559	526(532)	C=CO bend.
389(399)	421	441(437)	417	394(399)[a]	OCC bend.
	315	308(330)	305		COC bend., CH_3 tor.
267(—)				267(—)	CH_3 tor.
235(245)				259(—)	COC bend.
	221	231(215)	232		CH_3 tor., COC bend.
138(—)	126	145(—)	111	136(—)	=C–O tor.
109(—)	97	65(—)	82	71(—)	–O–C tor.

a) Overlapped.

the dominant isomer in the gaseous state is also dominant in the liquid state and remains in the solid state. The weak bands at 523, 500, 425, and 330 cm^{-1} in the spectrum of the gaseous state are also observed in the spectrum of the liquid state and are assigned to the less stable forms. The intensity dependence on temperature was examined for the Raman bands at 600, 533, 500, 436, and 398 cm^{-1} as will be given below. The results indicate that the bands at 600 and 398 cm^{-1} belong to the most stable isomer (the CT form) and the two bands at 500 and 436 cm^{-1} and the band at 533 cm^{-1} are due to the other two less stable isomers. In other words, three rotational isomers coexist in the liquid and gaseous states of ethyl vinyl ether. The obtained enthalpy differences of the two less stable isomers to the CT form are of the same order as the enthalpy difference of the *skew* isomer to the *cis* isomer of methyl vinyl ether. This fact suggests that the two isomers take the *skew* conformation around the C–O axis.

The above discussion is supported by the results of the normal frequency calculations. The key bands to the conformation are the C=C–O bending vibration and the C–O–C bending vibration in the case of ethyl vinyl ether. It is noticed that the *cis* and *skew* forms around the =C–O– axis give frequencies of about 600 and 500 cm^{-1} and the *trans* and *gauche* forms around the –O–C– axis give frequencies of about 400 and 430 cm^{-1}, respectively. The observed frequencies in the solid state correspond well to the calculated frequencies of the CT form. Among the observed frequencies in the liquid state, 500 and 436 cm^{-1} correspond to the calculated frequencies, 510 and 441 cm^{-1}, of the SG′ form (the stretched form). The band at 533 cm^{-1} is assigned to the ST form, the calculated frequency being 526 cm^{-1}. The CG form may be eliminated from the discussion on conformation because of its steric instability.

n-*Butyl Vinyl Ether.* The observed frequencies and the calculated frequencies for the CTTT form are given in Table 6. The complex features of the spectra in the gaseous and liquid states indicate the coexistence of rotational isomers. The situation of the rotational isomerism around the C–C axis next to the O–C axis seems to be rather peculiar. The small repulsive interaction between the oxygen atom and the CH_2

TABLE 6. CALCULATED AND OBSERVED FREQUENCIES OF *n*-BUTYL VINYL ETHER IN cm^{-1}

Calculated (Observed) CTTT form		Assignment[a]
ip	op	
	654 (701)	=CH wag.
599 (600)		C=CO bend.
426 (437)		$C_2C_3C_4$ def., OC_1C_2 def.
334 (379)		$C_1C_2C_3$ def., OC_1C_2 def.
	261 (265)	CH_3 tor.
256 (246)		$C_2C_3C_4$ def., COC_1 bend.
	172 (—)	=C–O tor.
	148 (—)	–O–C tor.
124 (—)		$C_1C_2C_3$ def., OC_1C_2 def.
	96 (—)	=C–O tor., C_1–C_2 tor.
	70 (—)	–O–C tor., C_2–C_3 tor.

a) The alkyl carbon atoms are numbered as –O–C_1–C_2–C_3–C_4.

group in the O–CH_2–CH_2–CH_2 part of *n*-butyl vinyl ether makes the *gauche* form more stable than that in the case of the ordinary *n*-hydrocarbons. The complex features of the spectra may partly be due to this situation. The spectra in the solid state, however, are rather simple and have similar patterns to those of methyl vinyl ether and ethyl vinyl ether in the region 600—300 cm^{-1}, with an additional band at 440 cm^{-1}. The bands at 611 and 380 cm^{-1} correspond to those at 591 and 344 cm^{-1} of methyl vinyl ether and those at 603 and 395 cm^{-1} of ethyl vinyl ether, respectively. This fact suggests that the stable isomer in the solid state is the *cis* conformer around the =C–O– axis and the *trans* conformer around the –O–C– axis. An extra band at 440 cm^{-1} may be assigned to the CCC deformation of the extended form of the *n*-butyl group. The corresponding vibration of trans *n*-butane is observed at 425 cm^{-1} in the solid state.[11]

The observed frequencies of the solid state are well

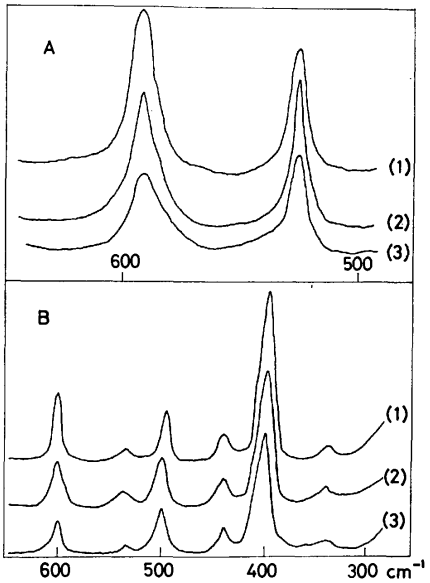

Fig. 8. Temperature dependence of Raman spectra.
A: Methyl vinyl ether, (1) 198 K (2) 215 K (3) 233 K.
B: Ethyl vinyl ether, (1) 206 K (2) 238 K (3) 297 K.

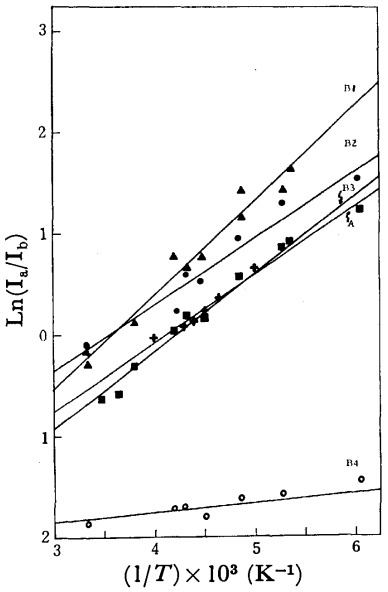

Fig. 9. Plots of Raman intensity *vs.* temperature.
A: +, methyl vinyl ether; a: 591 cm^{-1}, b: 527 cm^{-1}.
B: Ethyl vinyl ether; B1. ▲, a: 600 cm^{-1}, b: 533 cm^{-1}.
B2: ●, a: 600 cm^{-1}, b: 436 cm^{-1}. B3. ■, a: 600 cm^{-1}, b: 500 cm^{-1}. B4: ○, a: 600 cm^{-1}, b: 398 cm^{-1}.

explained by the calculated frequencies of the CTTT form. The calculated frequency at 426 cm^{-1} corresponds to the observed frequency at 440 cm^{-1} in the solid state.

Enthalpy Differences in the Liquid State. The Raman spectra of methyl vinyl ether and ethyl vinyl ether at different temperatures are shown in Fig. 8 and $\ln(I_a/I_b)$ plots *vs* $1/T$ are shown in Fig. 9, where I_a and I_b are the intensities of the Raman bands, a and b, belonging to the two rotational isomers.

For methyl vinyl ether, the enthalpy difference between the two isomers, the *skew* and *cis* forms, is obtained as 1440±160 cal/mol from the intensity dependence of the two bands at 527 and 591 cm^{-1} on temperature (Fig. 8A and plot A of Fig. 9). This value is consistent with the values 1150 and 1200 cal/mol obtained for the gaseous state by infrared[6] and electron diffraction[7] methods within the experimental errors.

In the case of ethyl vinyl ether, the intensity dependence on temperature has been examined for the Raman bands at 600, 533, 500, 436, and 398 cm^{-1} and the enthalpy differences obtained for the band pairs, 533 and 600 cm^{-1}, 436 and 600 cm^{-1}, 500 and 600 cm^{-1}, and 398 and 600 cm^{-1} are 1840±130, 1330±130, 1520±60, and 240±60 cal/mol, respectively (Fig. 8B and plots, B1, B2, B3, and B4 of Fig. 9). The enthalpy difference, 240±60 cal/mol, obtained for the bands at 398 and 600 cm^{-1} does not necessarily indicate that these bands are of different origins. It is possible that the band at 398 cm^{-1} is overlapped by the band due to the ST form (See Table 5).

The authors are indebted to Dr. Teizo Kitagawa of the Institute for Protein Research of Osaka University for the use of the low-temperature cell and the Hitachi 205 spectrometer.

References

1) T. Shimanouchi, Y. Abe, and Y. Alaki, *Polym. J.*, **2**, 199 (1971).
2) F. Inagaki, I. Harada, and T. Shimanouchi, *J. Mol. Spectrosc.*, **46**, 381 (1973).
3) T. Kitagawa, K. Ohno, H. Sugeta, and T. Miyazawa, This Bulletin, **45**, 969 (1972).
4) T. Shimanouchi, "Computer Program for Normal Coordinate Treatment of Molecules," Department of Chemistry, University of Tokyo, 1975.
5) P. Cahill, L. P. Gold, and N. L. Owen, *J. Chem. Phys.*, **48**, 1620 (1968).
6) N. L. Owen and N. Sheppard, *Trans. Faraday Soc.*, **60**, 634 (1963).
7) N. L. Owen and H. M. Seip, *Chem. Phys. Lett.*, **5**, 162 (1970).
8) S. Kondo, E. Hirota, and Y. Morino, *J. Mol. Spectrosc.*, **28**, 471 (1968).
9) K. S. Pitzer, *J. Chem. Phys.*, **14**, 239 (1946).
10) N. L. Owen and N. Sheppard, *Spectrochim. Acta*, **22A**, 1101 (1965).
11) S. Mizushima and T. Shimanouchi, *J. Amer. Chem. Soc.*, **71**, 1320 (1949).

Formation of Diacetylene Ion ($A^2\Pi_u$) by Controlled Electron Impact on Unsaturated Molecules

Masaharu TSUJI,* Teiichiro OGAWA, Totaro IMASAKA, Yukio NISHIMURA,* and Nobuhiko ISHIBASHI

Faculty of Engineering, Kyushu University, Hakozaki, Fukuoka 812

(Received August 2, 1975)

By the impact of an electron beam (100—450 eV) on aliphatic hydrocarbons (C_2H_2, C_2H_4, C_4H_6), cyclooctadienes, and aromatic molecules (C_6H_6, $C_{10}H_8$, $C_{12}H_{10}$, *etc.*) at about 10^{-3} Torr, the Schüler's T spectrum of diacetylene ion ($A^2\Pi_u$–$X^2\Pi_g$) was observed in the 505—570 nm region, in addition to the well-known systems of H(Balmer), CH(A–X), and C_2(Swan). Three different kinds of mechanisms for the formation of $C_4H_2^+$ (A) were derived from the dependence of the emission intensity on the electron-beam current and the gas pressure: (a) the primary excitation process (C_4H_6), (b) the secondary excitation process (aromatic molecules, cyclooctadienes), and (c) the dimerization excitation process (C_2H_2, C_2H_4). The intensity ratio ($C_4D_2^+/C_4H_2^+$) of the T spectrum from C_6H_6 and C_6D_6 was 0.83 ± 0.04 for the (0,0) sequence at 300 eV excitation.

Schüler and Reinebeck observed a new spectrum in low current discharges through a number of organic vapors (acetylene, benzene, naphthalene, *etc.*), usually in a carrier gas such as helium.[1] This spectrum was labelled "T". Calloman assigned the "T" spectrum to the diacetylene (1,3-butadiyne) ion, $C_4H_2^+(A^2\Pi_u-X^2\Pi_g)$, through isotopic studies and detailed analysis under a high resolution.[2]

Mass-spectrometric measurements have provided information on the mechanism of the formation of $C_4H_2^+$ under electron impact; this ion is produced through a primary collision of an electron with a molecule in the cases of aromatic molecules,[3] and through some ion-molecule reactions at high pressures in the cases of C_2H_2[4] and C_2H_4.[5] In addition, the dimeric ion, $C_4H_2^+$, has been found to be formed by ion-molecule reactions in the α-particle radiolysis of C_2H_2[6] and C_2H_4[7] and in the photoionization of C_2H_2,[8] and by the chemi-ionization reaction between excited- and ground-states of C_2H_2.[9] However, no studies have been carried out on the mechanism of the formation of $C_4H_2^+$ in the excited state.

The photometric measurement on the collision of an electron beam with a molecular jet is of great advantage for the investigation of the excitation, the ionization, and the dissociation processes and of the reactions of the species thus produced.[10–14] We have observed the Schüler's T spectrum by electron impact on aromatic molecules and aliphatic hydrocarbons.[11] It has been found that the excited $C_4H_2^+$ species were formed from naphthalene by a secondary collision of an electron with a primary product.[11] The purpose of this investigation is to elucidate the mechanism for the formation of $C_4H_2^+$ (A) under controlled electron-impact excitation (100—450 eV) on such organic vapors as aromatic molecules, cyclooctadienes, and aliphatic hydrocarbons.

Experimental

The electron-impact apparatus and the experimental procedure are essentially identical with those described previously.[11] An electron beam of a variable energy (100—450 eV) and a variable current (1—3000 μA) passes through the collision chamber so as to collide with the sample gas introduced from a nozzle. The pressure in the collision region was estimated by a penning gauge to be of the order of 10^{-3} Torr when the sample gas was introduced and of the order of 10^{-5} Torr when it was shut off. The pressure in the gas reservoir measured by a mercury manometer was estimated to be proportional to that in the actual collision region.

The photoemission of the excited species was measured in the visible region (400—660 nm) with a JASCO CT-50 monochromator equipped with a 1200 groove/mm grating blazed for 500 nm. The photons were detected by either an EMI 9558QB photomultiplier with a DC amplifier or an HTV R585 photomultiplier with an NF-PC545A photon counter. The isotope effect on the emission intensity of the T spectrum from C_6H_6 and C_6D_6 was measured by exchanging the reagent gases alternatively several times under identical conditions. The intensities were measured in the band area. The wavelength was calibrated by means of a low-pressure mercury lamp; its error was estimated to be within ±2 Å.

The gas samples used were of Research Grade from the Takachiho Trading Co. (C_2H_2 99.6%, C_2H_4 99.8%, 1,3-C_4H_6 99.5%); the other compounds, of the best grade, were obtained from Wako Pure Chemical Ind. or the Kishida Chemical Co., except for C_6D_6, which was obtained from Merck. The samples were subjected to several freeze-pump-thaw cycles before use.

Results

Aromatic Molecules. Most aromatic molecules show the photoemissions of the parent molecule (S_1-S_0) and a few fragment species in the 240—450 nm region under electron-impact excitation.[10–14] The spectra in the visible region (400—660 nm) are found to consist of various bands of fragment species. Typical spectra of C_6H_6 and C_6D_6 are shown in Figs. 1 and 2, in which most features of interest appear.

The sharp lines at 656 (not shown in Figs. 1 and 2), 486, 434, and 410 nm with high peak intensities are identified as the hydrogen Balmer serires ($H_{\alpha,\beta,\gamma,\delta}$ and $D_{\alpha,\beta,\gamma,\delta}$). The 4300 Å system ($A^2\Delta-X^2\Pi$) of the CH or CD radical and the Swan system ($d^3\Pi_g-a^3\Pi_u$) of C_2 are also identified. It should be noticed that, upon deuterium substitution, the intensities of the Balmer

* Research Institute of Industrial Science, Kyushu University, Hakozaki, Fukuoka 812

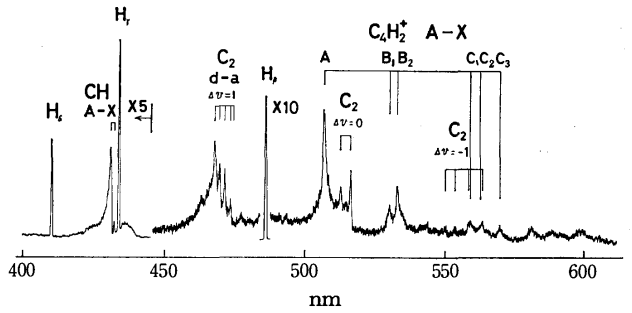

Fig. 1. Emission spectrum of C_6H_6 by controlled electron impact. Electron energy 300 eV, electron-beam current 1 mA, monochromator resolution 4 Å (FWHM).

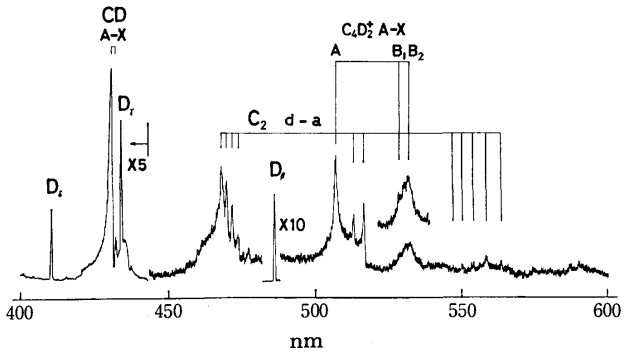

Fig. 2. Emission spectrum of C_6D_6 by controlled electron impact. Electron energy 300 eV, electron-beam current 1 mA, monochromator resolution 4 Å (FWHM). Upper spectrum of group B of $C_4D_2^+$ (A–X); electron energy 300 eV, electron-beam current 2 mA, monochromator resolution 3 Å (FWHM).

lines decrease, while those of the methylidyne radical increase.

The strong band at 5069 Å and the doublet band at 5303 and 5331 Å in the spectrum of C_6H_6 are assigned to the Schüler's T spectrum of $C_4H_2^+$ ($A^2\Pi_u - X^2\Pi_g$).[2] In the spectrum of C_6D_6, the corresponding bands appear at 5064, 5285, and 5318 Å. The doublet band can be resolved more clearly with a higher resolution, because a shoulder at about 530 nm makes the spectrum broad, as is shown in Fig. 2.

The band at around 507 nm, which shows the smallest isotope shift, is assigned to the (0,0) sequence, which is designated as A.[1,2] The bands at 530 and 533 nm, designated as B_1 and B_2, are assigned to the (0, ν_3'') and (0, $2\nu_7''$) sequences. The shoulder at 530 nm in C_6D_6 is ascribed to other strong sequence bands of the group B_2, as was reported by Calloman.[2] The groups C_1 (0, $\nu_3''+2\nu_7''$), C_2 (0, $4\nu_7''$) and C_3 (0, ν_2'') are observed in C_6H_6 at 559, 563, and 570 nm respectively, although the former two bands are partially overlapped on the (1, 2) and (0, 1) bands of the C_2 Swan system. The assignments of the vibrational modes are as follows: ν_2 is symmetric C≡C stretching, ν_3 C–C stretching and ν_7 symmetric bending.

The relative intensity of the T spectrum from C_6D_6 to that from C_6H_6 is measured for group A under 300 eV —1 mA excitation. The $C_4D_2^+/C_4H_2^+$ ratio is found to be 0.83 ± 0.04.

The Schüler's T spectrum is observed for various aromatic molecules, such as benzene, hydrocarbons (toluene, *o*, *m*, *p*-xylenes, cumene, *p*-cymene, phenylacetylene, naphthalene and biphenyl), halides (fluoro-, chloro-, iodo-benzenes, *p*-chlorotoluene and benzyl chloride), and nitrogen derivatives (benzonitrile, aniline and 2-naphthylamine). Schüler and Reinebeck reported that the intensity of the T spectrum was greatly reduced by the substitution of Cl or NH_2.[1] However, no such significant change in intensity can be found in chlorobenzene, aniline, and 2-naphthylamine in the present study. Meanwhile, oxygen derivatives (phenol, anisole, phenetol and benzophenone) and nitrobenzene do not show appreciable bands of $C_4H_2^+$, as in the case of phenol by discharge[1]; this is partly because the intense comet-tail system of CO^+ occupies the wavelength region of the strongest band of $C_4H_2^+$.

All the aromatic molecules described above give the bands of such fragment species as H(Balmer), CH(A-X), and C_2(d-a). Their intensities in C_6H_6 are found to be linear both to the electron-beam current and the gas pressure, as has partly been reported previously.[10] However, the band intensity of $C_4H_2^+$ in C_6H_6 is found to be proportional to the second power of the electron-beam current, although it is also proportional to the gas pressure, as is shown in Fig. 3. Similar results are obtained for H, CH, C_2, and $C_4H_2^+$ in most of the other aromatic molecules described above.

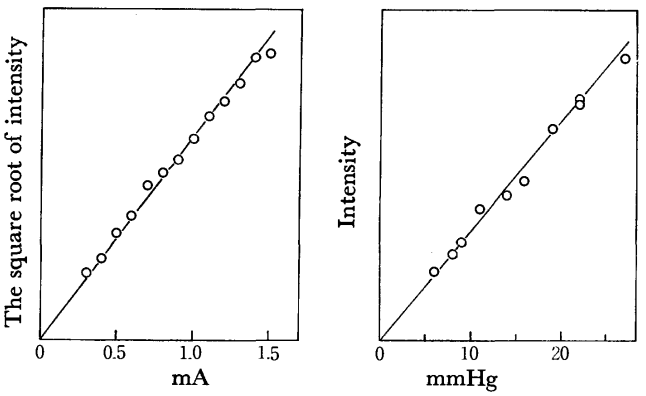

Fig. 3. Dependence of photoemission intensity (arbitrary units) of C_6H_6 on the electron-beam current (mA) and the pressure in the gas reservoir (mmHg).
Left; $C_4H_2^+$ (507 nm), electron energy 300 eV.
Right; $C_4H_2^+$ (507 nm), electron energy 300 eV, electron-beam current 300 μA.

Cyclooctadienes. The emission spectra of such cyclic dienes as 1,3- and 1,5-cyclooctadienes under electron-impact excitation were investigated to see whether these dienes showed the T spectrum, and if, they did, whether the difference in the conjugation of the two double bonds in these isomers affected the mechanism of the formation of $C_4H_2^+$ (A).

Both dienes are found to give the T spectrum with almost the same intensity, in addition to the band systems of H, CH, and C_2. The relationships between their intensities and the electron-beam current are identical with those of C_6H_6 for both isomers; the intensity of the $C_4H_2^+$ band is proportional to the

second power, and that of the other bands to the first power, in the region of 400—1500 μA. However, the pressure dependence of the intensities was difficult to determine because of the low vapor pressures of cyclooctadienes.

Aliphatic Hydrocarbons. Acetylene, ethylene, diacetylene, and butadiene are known to give the strong T spectrum in the positive column of the discharge tube.[1,2] In the present study, this spectrum is observed for acetylene, ethylene, and 1,3-butadiene; besides this spectrum, these molecules show relatively strong bands of H, CH, C_2, and CH^+ (A–X). It should be noticed that the dimeric ion, $C_4H_2^+$, is obtained from C_2H_2 and C_2H_4 at low pressures of about 10^{-3} Torr. However, the intensity is so weak that only the strongest band at 507 nm is appreciable, with a high electron-beam current. Thus, there are significant differences in the intensities of the T spectrum; the order is generally: aromatic molecules>1,3-butadiene≈cyclooctadienes≫acetylene≈ethylene, as compared at 100—450 eV, 1 mA excitation.

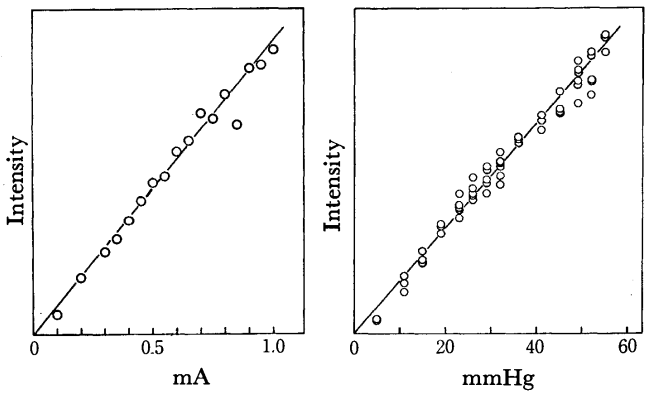

Fig. 4. Dependence of photoemission intensity (arbitrary units) of 1,3-C_4H_6 on the electron-beam current (mA) and the pressure in the gas reservoir (mmHg).
Left; $C_4H_2^+$ (507 nm), electron energy 300 eV.
Right; $C_4H_2^+$ (533 nm), electron energy 300 eV, electron-beam current 100 μA.

The current dependence of the intensity of the $C_4H_2^+$ band from 1,3-butadiene differs from that in the cases of the aromatic molecules; the band intensity of $C_4H_2^+$ as well as those of H, CH, C_2, and CH^+, is proportional to the first power of the electron-beam current and the gas pressure, as is shown in Fig. 4. In the cases of C_2H_2 and C_2H_4, similar quantitative measurements could not be carried out because of the weakness of the T spectrum and because of the band overlap of the group A with the tail band of the C_2 $\Delta v=0$ sequence.

Discussion

The Schüler's T spectrum consists of the (0, 0) and (0, v_i'') sequences and the (0, 0) sequence is the most intense; thus, the Franck-Condon principle indicates that the molecular dimensions of this ion are not very different in the excited- and the ground-states.

The mechanism of the formation of the excited species by electron impact can be discussed in terms of the dependence of the emission intensity on the electron-beam current and the gas pressure. Schüler and Reinebeck reported that they almost exclusively obtained the emissions of C_2, CH, and H_2 with high current densities in a discharge tube through various organic vapors (C_2H_2, C_6H_6, *etc.*).[1] Upon a decrease in the current, the diatomic bands became weak and the T spectrum came out. However, no quantitative measurements have been carried out on the changes in the intensity upon variations in the current density and the gas pressure.

In the present crossed electron-beam and molecular-jet method, most emitting excited species have been confirmed to be produced by a single collision of an electron with a molecule at low pressures;[10–14] such examples are excited fragments as H, CH, and C_2 in the present study, since their emission intensities are proportional both to the electron-beam current and to the gas pressure. Two kinds of exceptions have been pointed out:[13] (1) the excited CN, CO, and CO^+ species produced through the scission of two aromatic bonds (*e.g.*, CO^+ from dimethoxybenzenes[13]), and (2) the excited species produced through the formation of a new chemical bond (*e.g.*, HCl^+ from chlorobenzene[11]). The band intensities in these exceptional cases have often been found to be apparently proportional to the fractional power (1.0—2.0) of the electron-beam current. The deviation from the linearity can be interpreted by the competitive reactions between a one-electron process and a two-electron process, as was reported in the case of CO^+ from dimethoxybenzenes.[13] The formation of $C_4H_2^+$ (A), however, proceeds through either a one-electron process or a two-electron process; the mechanisms can be classified in the following three groups.

(a) The Primary Excitation Process. This process is applicable to 1,3-butadiene. The linear dependence of the emission intensity on the electron-beam current and the gas pressure shows that $C_4H_2^+$ (A) is produced through a unimolecular dissociative excitation induced by a collision with an electron and that the probability of collisional deactivation is negligible within its radiative lifetime:

$$1,3\text{-}C_4H_6 + e \longrightarrow C_4H_2^{+}*$$

where the asterisk denotes the emitting excited state of $A^2\Pi_u$. This result indicates that excited $C_4H_2^+$ (m/e= 50) should be produced in the ionization chamber of a conventional mass spectrometer.

(b) The Secondary Excitation Process. Since the band intensity is proportional to the second power of the electron-beam current and to the first power of the gas pressure, the formation of $C_4H_2^+$ (A) from C_6H_6 proceeds through the two-electron and unimolecular dissociative excitation:

$$M + e \longrightarrow X$$
$$X + e \longrightarrow C_4H_2^{+}*$$

where M represents an incident molecule and where X stands for some kinds of intermediates. The possible intermediates are the ground state of $C_4H_2^+$, C_4H_2, and other larger neutral or ionic species. This process is also applicable to other aromatic molecules.

A number of mass-spectrometric measurements show that $C_4H_2^+$ is produced by the unimolecular decomposition of aromatic molecules.[3] Most of the $C_4H_2^+$ species thus produced in the ionization chamber are expected to be in the ground state.

(c) The Dimerization Excitation Process. One of the most prominent features of C_2H_2 and C_2H_4 in their photolysis and radiolysis is that these olefins are apt to polymerize mainly through consecutive ion-molecule reactions.[4-9] Hence, C_2H_2 and C_2H_4 may dimerize under the present experimental conditions. Meanwhile, since the T spectrum can be observed only at a high electron-beam current, two electrons should participate in the formation of $C_4H_2^+$ (A). These results lead to the conclusion that $C_4H_2^+$ (A) is produced from C_2H_2 and C_2H_4 through collisions of intermediates (neutral or ionic dimerization products) with another electron. The weakness of the intensity of the T spectrum in the present method indicates that the probabilities of such secondary reactions are much smaller than those in the discharge tube.

A number of mass-spectrometric studies of the ion-molecule reactions of C_2H_2 by electron impact[4] and α-particle radiolysis[6] occurring in the ionization chamber at elevated pressures show that the major secondary reactions of the primary ions at about 10^{-3} Torr are the formation of $C_4H_3^+$ and $C_4H_2^+$ as follows:

$$C_2H_2^+ + C_2H_2 \longrightarrow C_4H_2^+ + H_2 \quad (1)$$

$$\searrow C_4H_3^+ + H \quad (2)$$

$$C_2H^+ + C_2H_2 \longrightarrow C_4H_2^+ + H \quad (3)$$

Meanwhile, Koyano *et al.*[9] have reported that $C_4H_3^+$ and $C_4H_2^+$ are formed by the chemi-ionization reaction between excited- and ground-states of C_2H_2 at $5—50 \times 10^{-3}$ Torr. Since the energy-loss spectra of C_2H_2 above 8.0 eV at incident electron energies of 40 and 50 eV have been reported to agree well with the UV spectrum,[15] dimeric ions may be produced *via* chemi-ionization under electron-impact excitation. However, no evidence for chemi-ionization induced by electron impact has been reported in the mass-spectrometric studies.[4] Consequently, the $C_4H_3^+$ and $C_4H_2^+$ formed through the ion-molecule reactions of (1)—(3) would be important intermediates. Besides them, some neutral dimerization products (*e.g.*, C_4H_2 and C_4H_4), as has been shown by VUV photolysis at high pressures,[16] are possible intermediates of $C_4H_2^+$ (A).

The mechanism for the formation of $C_4H_2^+$ (A) from C_2H_4 is probably similar to that from C_2H_2. Possible intermediates are the predominant secondary ions observed in the mass-spectrometric studies[5] (*e.g.*, $C_4H_5^+$ and $C_4H_7^+$) and such neutral species as C_4H_2 and C_4H_4.

The T spectrum can be observed from the non-conjugated cyclic diene as well as from the conjugated one. The formation of $C_4H_2^+$ (A) is confirmed to proceed through a two-electron process, (b) or (c), independent of the conjugation of the two double bonds. Since the intensity of the T spectrum from cyclooctadienes is much stronger than that from C_2H_2 and C_2H_4, and since the possibilities of the secondary reactions are expected to be smaller than those in the cases of C_2H_2 and C_2H_4, the corresponding mechanism for cyclooctadienes is concluded to be (b). The intermediates are probably alike, because no significant difference is found in the intensities of the T spectra of the two isomers.

The reason for the loss of the T spectrum in the oxygen derivatives (PhOH, $PhOCH_3$, $PhOC_2H_5$, and $(Ph)_2CO$) and nitrobenzene, all of which give strong CO^+ emissions, may be partly that another fast dissociative process, probably CO or CO^+ elimination, competes with the $C_4H_2^+$ (A) formation in the first or the second reaction of the (b) mechanism.

The isotope effect on the relative intensity of the T spectrum from C_6H_6 and C_6D_6 should originate from the contributions of the competitive processes of the excitation, the ionization, the dissociation, and the photoemission. The competition between dissociation and preionization in the superexcited states has been pointed out as being responsible for the isotope effect of the hydrogen Balmer emission by electron-impact excitation.[17-21] However, the increase in the intensity of the methylidyne radical upon deuterium substitution established in the present study seems to contradict such an interpretation. It, rather, seems to be caused by the slower rate of the competitive dissociation process, the cleavage of the C-D bond. Thus, the competition of various dissociation channels in the superexcited states plays an important role in determining the isotope effect in such a large molecule as benzene; this effect should also participate in the isotope effect of the diacetylene ion. In addition, differences in various non-radiative decay rates from the excited states of diacetylene ion induced by changes in the vibrational frequencies should be taken into account. Since unidentified secondary processes are involved in the reaction, a detailed interpretation of the isotope effect requires further investigation.

The authors wish to express their thanks to Professor Fumiyuki Nakashio and Dr. Minoru Toyoda for their discussions. Thanks are also due to Professor Tomoo Oyama for the use of his CT-50 monochromator.

References

1) H. Schüler and L. Reinebeck, *Z. Naturforsch.*, **6a**, 160, 270 (1951); **7a**, 285 (1952); **9a**, 350 (1954).

2) J. H. Calloman, *Can. J. Phys.*, **34**, 1046 (1956).

3) E. Stenhagen, S. Abrahamsson, and F. W. Mclafferty, "Registry of Mass Spectral Data," John Wiley & Sons (1974).

4) M. S. B. Munson, *J. Phys. Chem.*, **69**, 572 (1965); G. A. W. Derwish, A. Galli, A. Giardini-Guidoni, and G. G. Volpi, *J. Amer. Chem. Soc.*, **87**, 1159 (1965); J. H. Futrell and T. O. Tiernan, *J. Phys. Chem.*, **72**, 158 (1968); J. J. Myher and A. G. Harrison, *Can. J. Chem.*, **46**, 1755 (1968); P. G. Miasek and J. L. Beauchamp, *Int. J. Mass Spectrom. Ion Phys.*, **15**, 49 (1974).

5) T. O. Tiernan and J. H. Furtell, *J. Phys. Chem.*, **72**, 3080 (1968); M. T. Bowers, D. D. Elleman, and J. L. Beauchamp, *ibid.*, **72**, 3599 (1968); J. J. Myher and A. G. Harrison, *Can. J. Chem.*, **46**, 101 (1968).

6) P. S. Rudolph and C. E. Melton, *J. Phys. Chem.*, **63**, 916 (1959).

7) C. E. Melton and P. S. Rudolph, *J. Chem. Phys.*, **32**, 1128 (1960).

8) V. P. Warneck, *Ber. Bunsenges. Phys. Chem.*, **76**, 421 (1972).
9) I. Koyano, I. Tanaka, and I. Omura, *J. Chem. Phys.*, **40**, 2734 (1964).
10) T. Ogawa, M. Tsuji, M. Toyoda, and N. Ishibashi, This Bulletin, **46**, 1063 (1973).
11) T. Ogawa, M. Tsuji, M. Toyoda, and N. Ishibashi, *ibid.*, **46**, 2637 (1973); M. Tsuji, T. Ogawa, and N. Ishibashi, *Chem. Phys. Lett.*, **26**, 586 (1974); M. Tsuji, T. Ogawa, Y. Nishimura, and N. Ishibashi, *Chem. Lett.*, **1975**, 317.
12) M. Tsuji, T. Ogawa, and N. Ishibashi, This Bulletin, **46**, 3380 (1973).
13) T. Ogawa, T. Imasaka, M. Toyoda, M. Tsuji, and N. Ishibashi, *ibid.*, **48**, 645 (1975).
14) K. Hirota, M. Hatada, and T. Ogawa, *Int. J. Rad. Phys. Chem.*, in press.
15) E. N. Lassettre, A. Skerbele, M. A. Dillon, and K. J. Ross, *J. Chem. Phys.*, **48**, 5066 (1968).
16) S. Takita, Y. Mori, and I. Tanaka, *J. Phys. Chem.*, **73**, 2929 (1969).
17) R. L. Platzman, *Vortex*, **23**, 372 (1962); *Radiation Res.*, **17**, 419 (1962).
18) D. A. Vroom and F. J. de Heer, *J. Chem. Phys.*, **50**, 573 (1969).
19) I. Fujita, M. Hatada, T. Ogawa, and K. Hirota, This Bulletin, **44**, 1751 (1971).
20) K. Fukui, I. Fujita, and K. Kuwata, *ibid.*, **45**, 2278 (1972).
21) I. Tokue, I. Nishiyama, and K. Kuchitsu, *Chem. Phys. Lett.*, **35**, 69 (1975).

The Crystal and Molecular Structure of Zinc Complex of 2-Chlorobenzoic Acid. I. The Crystal and Molecular Structure of Bis(2-chlorobenzoato)zinc(II)

Yoshifumi NAKACHO, Takeshi MISAWA, Takaji FUJIWARA,* Akio WAKAHARA,* and Ken-ichi TOMITA*

Otsuka Chemical Co., Ltd., Satoura, Naruto, Tokushima 772
**Faculty of Pharmaceutical Sciences, Osaka University, Yamada-kami, Suita, Osaka 565*

(Received August 22, 1975)

The crystal of bis(2-chlorobenzoato)zinc(II) is monoclinic, space group $P2_1/c$, $a=7.284$, $b=10.480$, $c=19.091$ Å, $\beta=95.59°$, and $Z=4$. The structure was solved by usual heavy atom method and refined to the final R-value of 0.052. In the crystalline state, the complex forms a chain. Each zinc atom is bonded to four oxygen atoms from four different ligands.

Benzoic acid is able to react with metal ion to produce metal complexes in a similar way to aliphatic carboxylic acid, *e.g.*, those in copper(II) formate and copper(II) acetate. We have intended to investigate the influence of chlorine atom at ortho-position on the complex formation between zinc ion and 2-chlorobenzoate ion. Ferguson and Sim determined the crystal structure of 2-chlorobenzoic acid which consists of centrosymmetrically hydrogen-bonded dimers.[1] They found that the steric repulsion between carbonyl group and chlorine atom causes to allow the rotation of carboxyl group about the exocyclic C-C bond, and the chlorine atom and the exocyclic carbon atom are slightly displaced out of the plane of the benzene ring.

In the course of the synthesis of mefenamic acid used as an anti-inflammation drug, a derivative of anthranilic acid, we noticed that zinc complex of 2-chlorobenzoic acid crystallized in two different forms, prismatic and hexagonal pillar-shaped. One of these with a 1:2 ratio of zinc and 2-chlorobenzoic acid, was inactive for the following condensation reaction with 2,3-xylidine and only the other with a 2:3 ratio was reactive.[2] These two complexes could be separated by application of a solvent effect.

The present paper deals with the crystal structure of bis(2-chlorobenzoato)zinc(II), an inactive form of the two different complexes. We will present the structure analysis of the other form of the zinc complex in the following paper.

Experimental

Adding two-molar sodium 2-chlorobenzoate to one-molar zinc chloride in aqueous or methanol solution at room temperature, the white precipitate of zinc complex appeared after a few seconds, which was filtrated, washed several times with water and dissolved in anhydrous acetone. After a few days, transparent prismatic crystals were grown up to a proper size ($0.2\times0.1\times0.1$ mm) for X-ray investigation.

The cell dimensions were first determined from Weissenberg and precession photographs and were refined by remeasurement on a diffractometer. According to the systematic absences of reflection, $h0l$ with $l=2n+1$, and $0k0$ with $k=2n+1$, the crystal belongs to the space group of $P2_1/c$. The density was measured by flotation method in a carbon tetrachloride and ethylene dibromide mixture. The crystallographic data are listed in Table 1. The intensity data were

TABLE 1. CRYSTAL DATA OF BIS(2-CHLOROBENZOATO)ZINC
$C_{14}H_8O_4Cl_2Zn$: M.W=376.5

Crystal system:	monoclinic
Cell constants :	$a=7.284\ \pm0.005$ Å
	$b=10.480\pm0.004$ Å
	$c=19.091\pm0.008$ Å
	$\beta=95.59\ \pm0.05$ °
	$U=1448.05$ Å^3
Space group :	$P2_1/c$
Z :	4
Density (obsd):	$D_m=1.729\pm0.002$ g/cm^3
(calcd):	$D_x=1.726$ g/cm^3

TABLE 2. THE FINAL FRACTIONAL COORDINATES WITH THEIR STANDARD DEVIATIONS IN PARENTHESES

Atom	x	y	z	Atom	x	y	z
Zn	0.2484 (1)	0.0349 (1)	0.4869 (1)	CB2	0.7892 (11)	0.5261 (7)	0.5937 (4)
ClA	0.9250 (3)	0.0502 (2)	0.3322 (1)	CB3	0.9527 (13)	0.5796 (8)	0.6239 (5)
ClB	0.5849 (3)	0.3433 (2)	0.5281 (1)	CB4	1.1160 (11)	0.5133 (9)	0.6254 (4)
OA1	0.6340 (7)	0.0020 (5)	0.4197 (2)	CB5	1.1154 (10)	0.3922 (8)	0.5963 (4)
OA2	0.3773 (6)	0.1148 (5)	0.4142 (2)	CB6	0.9526 (9)	0.3356 (6)	0.5678 (3)
OB1	0.8399 (6)	0.1249 (4)	0.5525 (2)	CB7	0.9635 (9)	0.2030 (7)	0.5391 (3)
OB2	1.0996 (7)	0.1783 (4)	0.5068 (3)	HA1	0.898 (10)	0.196 (8)	0.217 (4)
CA1	0.7410 (9)	0.1434 (7)	0.2975 (3)	HA2	0.658 (11)	0.337 (8)	0.161 (4)
CA2	0.7730 (10)	0.2118 (8)	0.2374 (4)	HA3	0.346 (11)	0.360 (8)	0.215 (4)
CA3	0.6374 (12)	0.2852 (8)	0.2062 (4)	HA4	0.313 (9)	0.226 (7)	0.311 (3)
CA4	0.4666 (12)	0.2936 (8)	0.2316 (4)	HB1	0.655 (11)	0.579 (8)	0.600 (4)
CA5	0.4362 (10)	0.2266 (7)	0.2919 (3)	HB2	0.953 (13)	0.674 (9)	0.649 (5)
CA6	0.5719 (8)	0.1503 (6)	0.3259 (3)	HB3	1.259 (12)	0.545 (9)	0.644 (4)
CA7	0.5256 (9)	0.0830 (6)	0.3916 (3)	HB4	1.241 (11)	0.338 (8)	0.595 (4)
CB1	0.7937 (9)	0.4051 (6)	0.5667 (4)				

collected on a Rigaku-Denki four-circle diffractometer with Cu-$K\alpha$ radiation using the ω-2θ scan technique. A total of 1520 independent reflections in the range of $\sin\theta/\lambda \leq 0.53$ Å^{-1} were collected. The observed structure factors were converted into absolute values by Wilson's statistics. No absorption correction was applied.

Structure Determination and Refinement

The structure was solved by the usual heavy atom method. By successive Fourier synthesis, the positional parameters of all non-hydrogen atoms were determined (R-value, $R=\sum||F_o|-|F_c||/\sum|F_o|=0.183$). Further refinements were carried out by the block-diagonal least-squares method with isotropic temperature factors ($R=0.122$) and then anisotropic ones ($R=0.062$). A difference Fourier synthesis calculated at this stage revealed the positions of all eight hydrogen atoms with reasonable peak heights. The final refinement including the hydrogen atoms with isotropic temperature factor ($B=3.9$ Å^2) reduced the R-value to 0.052 (0.046 except $|F_o|=0$). The final atomic coordinats and temperature factors together with their estimated standard deviations are given in Table 2 and 3. The observed and calculated structure factors are listed in Table 4.[3] The atomic scattering factors employed were those listed in the International Tables for X-ray Crystallography.[4] All the numerical calculations were carried out on the NEAC 2200-700 in the Computation Center of Osaka University, using the UNICS programs.[5]

Table 3. The final temperature factors and their standard deviations ($\times 10^4$)

The anisotropic temperature factors are in the form of $\exp[-(\beta_{11}h^2+\beta_{22}k^2+\beta_{33}l^2+\beta_{12}hk+\beta_{13}hl+\beta_{23}kl)]$.

Atom	β_{11}	β_{22}	β_{33}	β_{12}	β_{13}	β_{23}
Zn	141(2)	65(1)	22(0)	27(2)	45(1)	6(1)
ClA	168(4)	163(3)	40(1)	55(6)	25(3)	19(2)
ClB	202(5)	109(2)	61(1)	67(5)	−53(3)	−21(3)
OA1	294(14)	109(6)	20(1)	89(15)	45(7)	22(5)
OA2	189(11)	124(6)	26(2)	−5(14)	74(7)	26(5)
OB1	220(12)	74(5)	33(2)	−5(13)	52(7)	−12(5)
OB2	228(13)	75(5)	35(2)	79(14)	88(8)	19(5)
CA1	167(16)	90(8)	20(2)	−10(18)	18(9)	−4(7)
CA2	225(19)	121(10)	29(3)	4(23)	73(11)	5(8)
CA3	341(24)	142(11)	24(3)	10(27)	78(12)	35(9)
CA4	325(24)	115(10)	31(3)	92(25)	30(13)	29(9)
CA5	237(18)	93(8)	21(2)	72(20)	48(10)	34(7)
CA6	153(14)	50(7)	14(2)	−20(15)	33(8)	0(5)
CA7	170(15)	74(7)	17(2)	−24(17)	3(9)	−9(6)
CB1	194(17)	56(7)	31(3)	35(18)	8(10)	−14(7)
CB2	254(20)	86(9)	39(3)	70(22)	21(12)	−21(8)
CB3	373(26)	92(10)	50(4)	−11(26)	49(16)	−52(10)
CB4	248(21)	141(11)	42(3)	−87(26)	41(13)	−45(10)
CB5	198(18)	112(10)	36(3)	6(22)	48(11)	−21(9)
CB6	183(16)	58(7)	19(2)	16(17)	29(9)	−11(6)
CB7	166(15)	92(8)	17(2)	28(18)	19(9)	13(7)

Table 5. The bond lengths (Å) and angles (°), with estimated standard deviations in parentheses

From To	Length	From To	Length	From To	Length
Zn–OA1	1.940(5) Å	Zn–OA2′[a]	1.939(5) Å	CA2–HA1	1.04(8) Å
Zn–OB1	1.922(5)	Zn–OB2″[a]	1.912(5)	CA3–HA2	1.04(8)
ClA–CA1	1.737(7)	ClB–CB1	1.748(7)	CA4–HA3	1.14(9)
OA1–CA7	1.245(8)	OB1–CB7	1.260(8)	CA5–HA4	1.01(7)
OA2–CA7	1.247(8)	OB2–CB7	1.245(9)	CB2–HB1	1.14(8)
CA1–CA2	1.391(11)	CB1–CB2	1.372(11)	CB3–HB2	1.10(10)
CA1–CA6	1.396(9)	CB1–CB6	1.366(10)	CB4–HB3	1.12(9)
CA2–CA3	1.345(12)	CB2–CB3	1.389(12)	CB5–HB4	1.08(9)
CA3–CA4	1.380(13)	CB3–CB4	1.376(13)		
CA4–CA5	1.384(11)	CB4–CB5	1.386(12)		
CA5–CA6	1.383(9)	CB5–CB6	1.388(10)		
CA6–CA7	1.505(9)	CB6–CB7	1.499(10)		

	Angle		Angle
OA1–An–OA2′	122.8(2)°	OA1–Zn–OB1	106.6(2)°
OA1–Zn–OB2″	100.5(2)	OA2′–Zn–OB1	105.2(2)
OA2′–Zn–OB2″	97.3(2)	OB2″–Zn–OB1	126.0(2)
ClA–CA1–CA2	114.8(6)	ClB–CB1–CB2	116.7(6)
ClA–CA1–CA6	123.9(5)	ClB–CB1–CB6	120.7(5)
CA2–CA1–CA6	121.3(6)	CB2–CB1–CB6	122.5(7)
CA1–CA2–CA3	119.0(7)	CB1–CB2–CB3	118.6(7)
CA2–CA3–CA4	122.0(8)	CB2–CB3–CB4	120.6(8)
CA3–CA4–CA5	118.8(8)	CB3–CB4–CB5	119.0(8)
CA4–CA5–CA6	121.3(7)	CB4–CB5–CB6	121.1(7)
CA1–CA6–CA5	117.6(6)	CB1–CB6–CB5	118.0(6)
CA1–CA6–CA7	125.3(6)	CB1–CB6–CB7	124.2(6)
CA5–CA6–CA7	117.1(6)	CB5–CB6–CB7	117.7(6)
OA1–CA7–OA2	124.5(6)	OB1–CB7–OB2	125.7(6)
OA1–CA7–CA6	119.6(6)	OB1–CB7–CB6	117.6(6)
OA2–CA7–CA6	115.8(6)	OB2–CB7–CB6	116.5(6)

The bond angles involving the hydrogen atoms were all nearly $120\pm9°$ (E.S.D$\cong$5°)

a) The coordinates of the single and double primed atoms are obtained by the translational operations of $(1-x, -y, 1-z)$ and $(2-x, -y, 1-z)$ from that of original atoms (x,y,z).

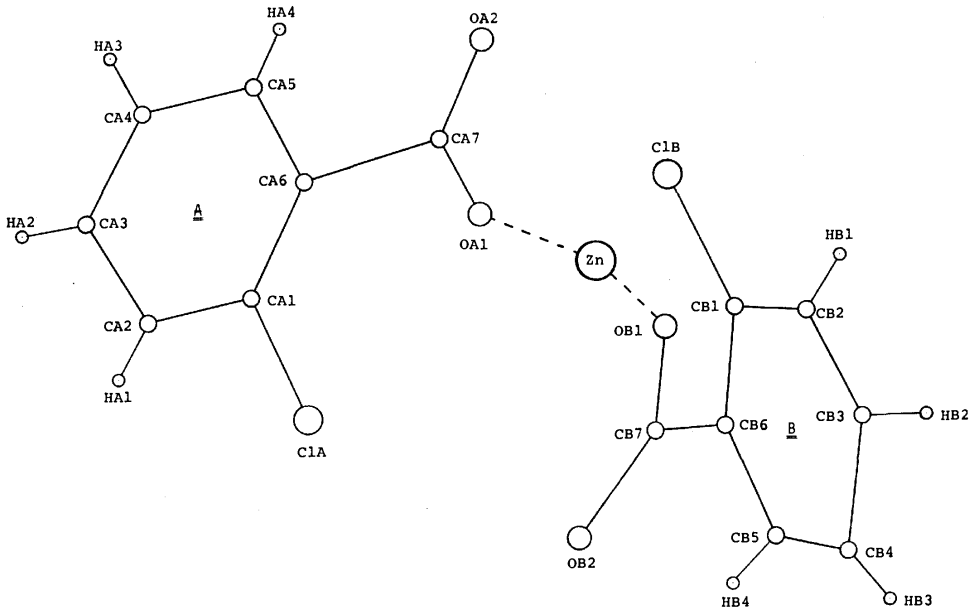

Fig. 1. The atomic numbering scheme of bis(2-chlorobenzoato)zinc(II).

Results and Discussion

The numbering of each atom is represented in Fig. 1. The bond lengths and angles are listed in Table 5, which indicate no significant differences between two independent benzoate ligands. Two C–O bond lengths in carboxyl group range from 1.24 to 1.26 Å which represent the double-bond character, while C_6–C_7 bonds (1.499 and 1.505 Å) are almost pure single-bond which allows the rotation of carboxyl group. The torsion angles between the plane of carboxyl group and that of benzene ring are 9° for ligand A and 41° for ligand B. Such twisting between carboxyl group and the benzene ring plane was also found in the crystal structure of 2-chlorobenzoic acid (14°)[1] and 2-chloro-5-nitrobenzoic acid (23°).[6]

The four carboxyl oxygen atoms coordinate tetrahedrally to each zinc atom as shown in Fig. 2. It is

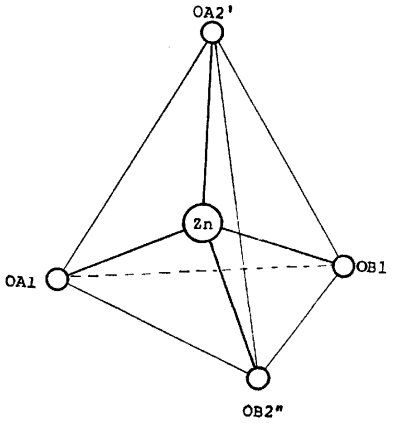

Fig. 2. The coordination of zinc atom.
About the single and double primed atoms, refer to the footnote in Table 5.

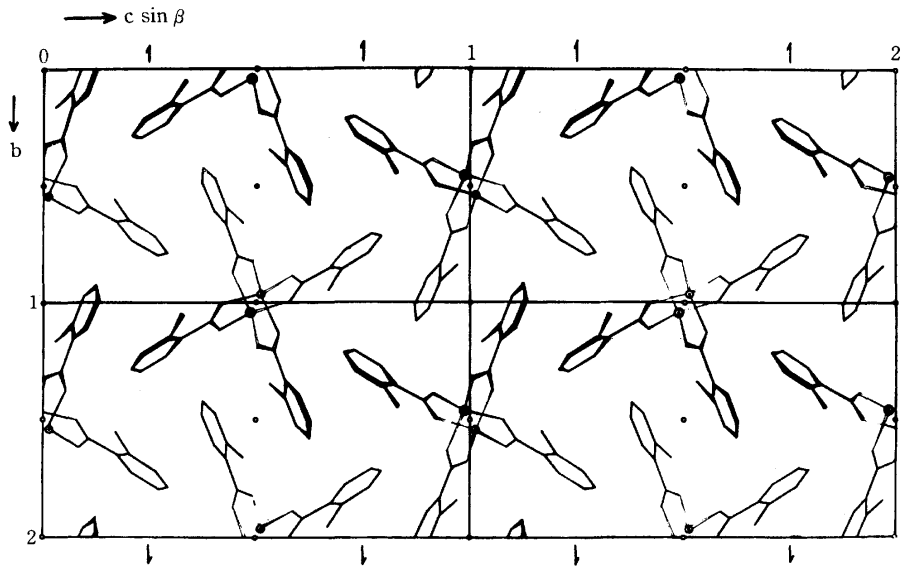

Fig. 3a. The view of the structure looking down the a-axis.

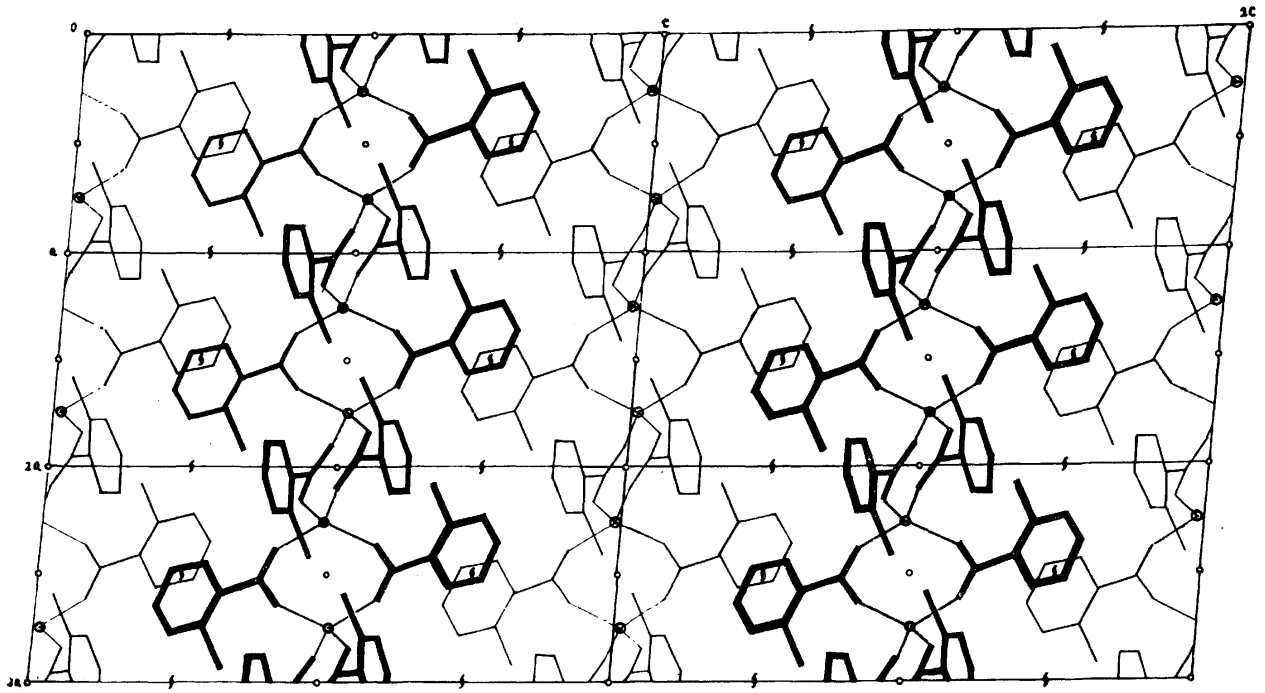

Fig. 3b. The view of the structure looking down the b-axis.

very interesting that four coordinated carboxyl oxygen atoms consist of O_1 of A and B, and O_2 of next neighboring A and B. That is to say, carboxyl oxygen atoms (O_1 and O_2) connect two adjacent zinc atoms to form the infinite chain extending in the direction of the a-axis. The stable coordination number of zinc atom is usually four or six; the former is found in zinc oxyacetate,[7] zinc salicylate dihydrate,[8] di(L-histidino)zinc dihydrate,[9] di(histidino)zinc pentahydrate[10] and the latter in zinc acetate dihydrate,[11] zinc 8-hydroxyquinolate dihydrate.[12] In this crystal, four oxygen atoms coordinate tetrahedrally to the central zinc atom and this sort of coordination may be more stable than that of the pentaligand zinc complex described in the following paper. The arrangements of molecules in the a- and b-axes projections are shown in Fig. 3(a) and 3(b), respectively. Looking down through the a-axis, the plane of each benzene ring sticks out with rotation angle of about 90°. The orientations of the ligands within two chains related by c-glide plane differ by 45° around the a-axis, and therefore, the arrangement of the infinite chains in the [011] direction looks like $+\times+\times+\times\cdots\cdots$ when viewed along the a-axis. Each chain contacts with normal van der Waals distances.

References

1) G. Ferguson and G. A. Sim, *Acta Crystallogr.*, **14**, 1262 (1961).

2) S. Koomura, R. Harima, T. Misawa, T. Goto, T. Masatomi, T. Nishi, Y. Shimizu, and Y. Nakacho, Japan, Kokai 50-70343 (1975).

3) Table 4 has been deposited at the office of Chemical Society of Japan (Document No. 7601).

4) "International Tables for X-ray Crystallography," Vol. 4, Kynoch Press, Birmingham (1974).

5) The Universal Crystallographic Computing System (Library Programs in the Computing Center of Osaka University, 1973). The Crystallographic Society of Japan.

6) G. Ferguson and G. A. Sim, *J. Chem. Soc.*, **1962**, 1767.

7) H. Koyama and Y. Saito, This Bulletin, **27**, 112 (1954).

8) H. P. Klug, L. E. Alexander, and G. G. Sumner, *Acta Crystallogr.*, **11**, 41 (1958).

9) R. H. Kretsinger, F. A. Cotton, and R. F. Bryan, *Acta Crystallogr.*, **16**, 651 (1963).

10) M. M. Harding and S. J. Cole, *ibid.*, **16**, 643 (1963).

11) J. N. van Niekerk, F. R. L. Schoening, and J. H. Talbot, *ibid.*, **6**, 720 (1953).

12) L. Merritt, R. T. Cady, and B. W. Mundy, *ibid.*, **7**, 473 (1954).

A Structure Analysis of a Bromoacetate of Hydroxypiperenone by the X-Ray Diffraction Method

Kuniaki MATSUI,* Keiichi FUKUYAMA, Kumiko TSUKIHARA, Tomitake TSUKIHARA, Yukiteru KATSUBE, and Katsura MUNAKATA**

Faculty of Engineering, Tottori University, Koyama, Tottori 680
**Department of Agricultural Chemistry, Tottori University, Koyama, Tottori 680*
***Department of Agricultural Chemistry, Nagoya University, Nagoya 464*

(Received September 5, 1975)

The structure of a bromoacetate of hydroxypiperenone, $C_{24}H_{31}O_7Br$, has been determined by the X-ray diffraction method. The compound crystallized in the space group $P2_1$, with $a=8.296$, $b=13.247$, $c=11.400$ Å, and $\beta=102.8°$. The structure was solved by the heavy-atom method and refined to $R=0.075$ for 1614 reflections. The present analysis has established that the five- and six-membered rings are fused in the *cis* fashion. The absolute configuration of the molecule has been determined by using the anomalous dispersion effect of the bromine atom for Cu $K\alpha$ radiation.

Piperenone isolated from the leaves of *Piper futokadzura* Sieb. et Zucc. shows a distinct antifeeding activity in response to the larvae of *Spodoptera litura* F. The structural formula of piperenone has been shown to be (I),[1] and the configurations at the C(7) and C(8) atoms (refer to Fig. 1) have been presumed to be *S*-form[2] on the basis of chemical and spectroscopic methods. However, the configurations at the C(9) and C(14) atoms could not be determined by these methods. In order to confirm the presumption, and, further, in order to determine the absolute configuration, a bromoacetate of hydroxypiperenone (II) has now been investigated by means of the X-ray diffraction method.

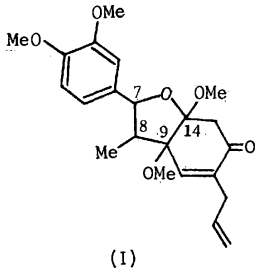

(I)

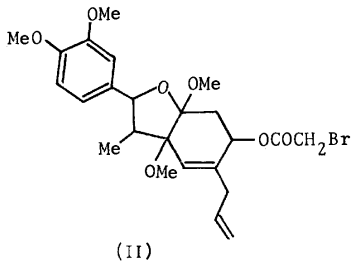

(II)

Experimental

The bromoacetate of hydroxypiperenone was prepared by the reaction of bromoacetyl bromide and hydroxypiperenone, one of the epimers obtained by the reduction of piperenone with lithium aluminum hydride. The compound crystallized from the hexane–ethyl acetate solution in the form of colorless plates.

A preliminary photographic investigation showed that the crystals were monoclinic with the b axis along the most developed axis, and that the intensities fell off fairly rapidly with an increase in θ. The systematic absence ($0k0$ when k is odd) and optical activity indicated the space group to be $P2_1$. The unit-cell constants were obtained from the Bragg angles measured by a Toshiba four-circle diffractometer using Ni-filtered Cu$K\alpha$ radiation. The crystal data were as follows: $C_{24}H_{31}O_7Br$, mp 153—155 °C, $M=511.4$, monoclinic, $P2_1$, $a=8.296(5)$, $b=13.247(7)$, $c=11.400(6)$ Å, $\beta=102.8(1)°$, $V=1222$ Å^3, $Z=2$, $D_0=1.38$ g/cm^3, $D_x=1.39$ g/cm^3, $\mu=28.6$ cm^{-1} (for Cu$K\alpha$).

A crystal with dimensions of *ca.* $0.12\times0.35\times0.22$ mm^3 was mounted with its b axis parallel to the ϕ axis of the diffractometer. The stationary-crystal stationary-counter technique was applied, with a counting time of 30 s. The intensities of 1616 independent reflections were measured up to $\sin\theta/\lambda=0.53$, with Ni-filtered Cu$K\alpha$ radiation. The background for each reflection was taken from the plots of the background as a function of 2θ. The intensities were corrected for the Lorentz and polarization factors, but not for absorption.

Determination of the Structure

The coordinates of the bromine atom were easily determined from the Patterson map. The locations of the remaining non-hydrogen atoms were determined by successive Fourier syntheses. The coordinates and isotropic temperature factors were initially refined by a block-diagonal least-squares method, using carbon and bromine scattering factors. The atomic species were determined on the bases of the temperature factors and chemical sense. The refinement with anisotropic temperature factors reduced the R value to 0.08. Two

TABLE 1. DETERMINATION OF THE ABSOLUTE CONFIGURATION

h	k	l	$F_c(hkl)$	$F_c(\bar{h}\bar{k}\bar{l})$	$I_0(hkl)$ $I_0(\bar{h}\bar{k}\bar{l})$
0	1	1	486	533	<
0	3	1	564	513	>
1	1	−3	581	553	>
1	3	−3	414	390	>
1	1	−2	255	287	<
1	2	1	254	272	<
2	1	−4	436	470	<
2	4	−3	510	484	>
2	4	−2	290	306	<
2	5	−2	370	395	<
2	6	−2	273	255	>
2	2	−1	203	160	>
2	6	−1	278	302	<
2	3	0	322	304	>
2	5	0	316	297	>
2	1	3	273	246	>
3	1	−4	429	400	>
3	2	−1	357	379	<
4	1	0	391	417	<

The right-handed coordinate system is adopted.
The values of F_c are multiplied by 10.

TABLE 2. FINAL ATOMIC PARAMETERS AND e.s.d.'s ($\times 10^4$) FOR NON-HYDROGEN ATOMS
The anisotropic temperature factors are of the form; $\exp[-(\beta_{11}h^2+\beta_{22}k^2+\beta_{33}l^2+\beta_{12}hk+\beta_{13}hl+\beta_{23}kl)]$.

	x	y	z	β_{11}	β_{22}	β_{33}	β_{12}	β_{13}	β_{23}
Br	698(2)	2500(2)	7354(1)	232(2)	100(1)	182(2)	61(3)	103(3)	25(3)
C(1)	6604(14)	1517(9)	3363(10)	192(21)	68(8)	101(11)	28(22)	64(23)	−19(16)
C(2)	5178(16)	1382(10)	2459(11)	249(24)	73(9)	105(11)	−5(26)	39(26)	0(17)
C(3)	4945(20)	1897(13)	1389(12)	343(35)	99(11)	107(12)	−36(33)	83(33)	1(20)
C(4)	6163(16)	2587(13)	1174(10)	300(26)	81(9)	115(11)	−16(35)	122(27)	−20(23)
C(5)	7541(18)	2766(10)	2084(13)	293(28)	65(11)	157(14)	−6(26)	185(34)	−23(19)
C(6)	7737(15)	2232(9)	3179(11)	216(22)	70(10)	116(12)	1(22)	98(25)	−17(16)
C(7)	6912(13)	928(9)	4504(11)	141(18)	61(8)	136(13)	3(19)	64(25)	17(16)
C(8)	7983(13)	−15(10)	4488(10)	126(17)	76(8)	122(12)	−2(20)	58(22)	4(17)
C(9)	7438(13)	−663(9)	5463(11)	152(18)	69(8)	123(12)	10(20)	74(23)	−14(16)
C(10)	8159(13)	−291(10)	6709(11)	131(17)	71(8)	129(12)	18(20)	43(23)	1(17)
C(11)	7320(14)	27(11)	7478(12)	154(19)	79(9)	147(14)	−20(23)	−5(26)	17(19)
C(12)	5458(13)	−51(10)	7260(10)	154(19)	74(8)	119(12)	−18(21)	50(24)	−5(17)
C(13)	4654(13)	−627(10)	6142(10)	161(19)	82(9)	96(10)	14(22)	75(22)	−12(16)
C(14)	5558(12)	−510(10)	5113(10)	127(17)	77(9)	110(11)	4(21)	15(22)	0(17)
C(15)	3377(15)	1131(9)	7471(10)	208(22)	71(9)	99(11)	74(23)	39(25)	−4(16)
C(16)	3010(14)	2272(10)	7488(11)	169(19)	94(13)	127(12)	60(24)	64(24)	2(18)
C(17)	3166(15)	−1198(15)	3655(13)	146(20)	155(16)	148(15)	−63(31)	70(28)	−90(27)
C(18)	2130(19)	1413(14)	661(14)	258(29)	125(14)	145(16)	−73(36)	4(34)	−11(26)
C(19)	7153(33)	3737(17)	−124(17)	754(76)	132(17)	152(19)	−280(64)	264(61)	−6(30)
C(20)	9865(16)	195(11)	4705(12)	163(20)	97(12)	142(16)	−14(25)	113(30)	13(21)
C(21)	7521(17)	−2448(16)	6021(14)	271(27)	95(11)	198(17)	39(40)	169(35)	63(32)
C(22)	8156(16)	422(12)	8724(10)	229(24)	122(12)	92(11)	−73(30)	−7(26)	−5(21)
C(23)	8136(20)	−307(15)	9716(14)	305(32)	130(15)	135(15)	35(37)	−13(35)	27(25)
C(24)	7672(37)	−48(20)	10722(18)	831(91)	157(20)	152(21)	−60(77)	246(68)	29(36)
O(1)	5349(8)	522(6)	4703(6)	146(12)	77(6)	109(7)	24(14)	61(14)	10(11)
O(2)	4966(9)	−1170(7)	4161(7)	141(12)	109(7)	129(8)	−14(16)	78(16)	−67(14)
O(3)	3556(14)	1845(10)	442(8)	355(25)	166(11)	101(8)	−111(28)	−58(23)	48(17)
O(4)	5884(17)	3047(9)	76(9)	562(37)	116(9)	123(10)	−89(30)	107(32)	60(16)
O(5)	7999(10)	−1668(7)	5318(8)	180(14)	67(5)	156(9)	23(14)	102(18)	8(12)
O(6)	4849(9)	995(6)	7224(7)	182(14)	67(6)	121(8)	5(14)	73(17)	−4(11)
O(7)	2504(10)	486(7)	7719(8)	180(14)	71(6)	170(10)	−1(15)	111(19)	14(13)

intense reflections, -121 and 013, were rejected from the subsequent calculations.

The absolute configuration of the molecule was determined using the anomalous dispersion effect of the bromine atom ($\Delta f'=-0.9$ and $\Delta f''=1.5$) for Cu$K\alpha$ radiation. The intensities of the Friedel-pair reflections were measured by the ω-2θ scan technique, using Ni-filtered Cu $K\alpha$ radiation with a specimen with dimensions of *ca.* $0.08\times0.20\times0.10$ mm^3. A comparison of the observed and calculated intensities between the Friedel-pair reflections is given in Table 1. Of the 31 hydrogen atoms in the molecule, twelve atoms were located from a difference Fourier map. The final refinement was made by including these hydrogen atoms with fixed parameters and the anomalous dispersion effect of the bromine atom, and by using the following weighting scheme; $w=0.34$ for $F_o=0.0$, $w=1.0$ for $0<F_o\leqq15$, and $w=1.0/(1.0+0.1(F_o-15))$ for $15<F_o$. The final R value was 0.075 for 1614 independent reflections. The final atomic parameters are given in Table 2.***

The atomic scattering factors were taken from the International Tables for X-ray Crystallography.[3] The computations were performed on a TOSBAC-3400 computer at the Tottori University Computing Center, and on a NEAC 2200-N700 computer at the Computation Center of Osaka University.

Results and Discussion

The structural formula and the absolute configuration of the molecule have been established by the present

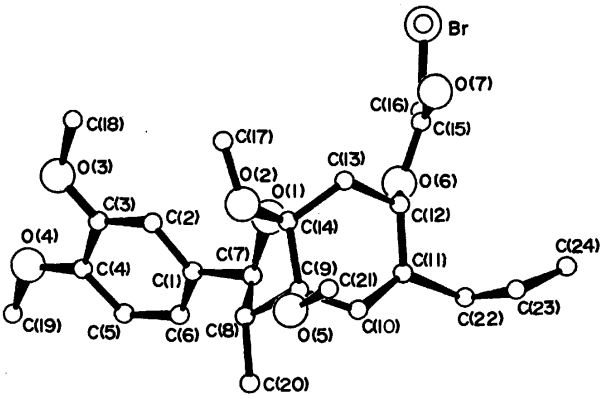

Fig. 1. Perspective view of the molecule and the scheme of atomic numbering.

*** A list of the observed and calculated structure factors is kept by the office of the Chemical Society of Japan (Document No. 7602).

X-ray analysis. The absolute configuration of the molecule is correctly represented by the parameters in Table 2 if the right-handed coordinate system is adopted. A perspective drawing of the molecule and the numbering of atoms are shown in Fig. 1, and a stereoscopic view of the molecule, in Fig. 2. Both figures are drawn with a correct absolute configuration. The least-squares planes and the deviations of atoms from each plane are listed in Table 3. The two methoxy groups bonded to the C(9) and C(14) atoms are in the *cis*-form to each other; the torsion angles† of O(2)–C(14)–C(9)–O(5) and C(8)–C(9)–C(14)–O(1) are −33° and −36° respectively. The torsion angle of H–C(7)–C(8)–

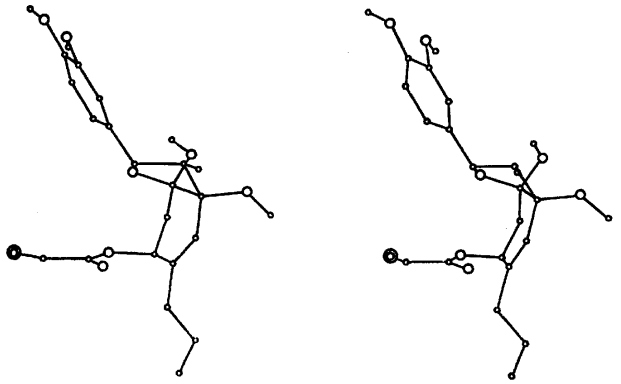

Fig. 2. Stereoscopic drawing of the molecule.

Table 3(a). Least-squares planes and deviations of atoms

In the equation of each plane, X, Y, and Z are defined to be $ax+cz\cos\beta$, by, and $cz\sin\beta$, respectively.

(1) Benzene ring

$0.568X-0.730Y-0.381Z=-0.288$ (I)

C (1)	0.03 Å	C (2)	0.00 Å
C (3)	0.00	C (4)	0.03
C (5)	−0.01	C (6)	−0.03
C (7)*	0.10	O (3)*	−0.07
O (4)*	0.07	C (18)*	−0.45
C (19)*	0.12		

(2) The plane through the C(7), C(8), C(9), C(14), and O(1) atoms

$0.143X+0.400Y+0.905Z=5.533$ (II)

C (7)	−0.15 Å	C (8)	0.24 Å
C (9)	−0.30	C (14)	0.18
O (1)	0.06	C (1)*	0.68
C (20)*	−0.31	O (5)*	0.31
O (2)*	1.53	C (10)*	−1.79
C (13)*	−0.65		

(3) The plane through the C(9), C(10), C(11), C (12), and C(22) atoms

$0.019X+0.928Y-0.371Z=-2.995$ (III)

C (9)	0.02 Å	C (10)	−0.03 Å
C (11)	0.02	C (12)	−0.01
C (22)	0.00	C (13)*	−0.26
C (14)*	0.32		

(4) The plane through the C(15), C(16), O(6), and O(7) atoms

$0.238X+0.056Y+0.970Z=8.377$ (IV)

C (15)	0.02 Å	C (16)	−0.01 Å
O (6)	−0.01	O (7)	−0.01
C (12)*	−0.09	Br*	0.57

*) Not included in least-squares calculation.

(b) Dihedral angles

	I	II	III
II	56°	—	—
III	122°	92°	—
IV	74°	21°	72°

Table 4(a). Bond lengths and their estimated standard deviations

Br–C(16)	1.92(1) Å	O(1)–C(7)	1.47(2) Å
O(1)–C(14)	1.44(2)	O(2)–C(14)	1.40(2)
O(2)–C(17)	1.48(2)	O(3)–C(3)	1.40(2)
O(3)–C(18)	1.39(2)	O(4)–C(4)	1.37(2)
O(4)–C(19)	1.45(3)	O(5)–C(9)	1.43(2)
O(5)–C(21)	1.42(2)	O(6)–C(12)	1.47(2)
O(6)–C(15)	1.33(2)	O(7)–C(15)	1.19(2)
C(1)–C(2)	1.40(2)	C(1)–C(6)	1.38(2)
C(1)–C(7)	1.49(2)	C(2)–C(3)	1.37(2)
C(3)–C(4)	1.42(2)	C(4)–C(5)	1.38(2)
C(5)–C(6)	1.41(2)	C(7)–C(8)	1.54(2)
C(8)–C(9)	1.55(2)	C(8)–C(20)	1.55(2)
C(9)–C(10)	1.50(2)	C(9)–C(14)	1.54(2)
C(10)–C(11)	1.30(2)	C(11)–C(12)	1.51(2)
C(11)–C(22)	1.53(2)	C(12)–C(13)	1.51(2)
C(13)–C(14)	1.53(2)	C(15)–C(16)	1.54(2)
C(22)–C(23)	1.49(3)	C(23)–C(24)	1.33(4)

Table 4(b). Bond angles and their estimated standard deviations

C(7)–O(1)–C(14)	111(1)°	C(14)–O(2)–C(17)	118(1)°
C(3)–O(3)–C(18)	118(1)	C(4)–O(4)–C(19)	116(2)
C(9)–O(5)–C(21)	118(1)	C(12)–O(6)–C(15)	117(1)
C(2)–C(1)–C(6)	118(1)	C(2)–C(1)–C(7)	122(1)
C(6)–C(1)–C(7)	120(1)	C(1)–C(2)–C(3)	121(1)
O(3)–C(3)–C(2)	126(1)	O(3)–C(3)–C(4)	113(1)
C(2)–C(3)–C(4)	120(2)	O(4)–C(4)–C(3)	117(2)
O(4)–C(4)–C(5)	124(2)	C(3)–C(4)–C(5)	119(2)
C(4)–C(5)–C(6)	119(1)	C(1)–C(6)–C(5)	122(1)
O(1)–C(7)–C(1)	110(1)	O(1)–C(7)–C(8)	104(1)
C(1)–C(7)–C(8)	114(1)	C(7)–C(8)–C(9)	100(1)
C(7)–C(8)–C(20)	115(1)	C(9)–C(8)–C(20)	115(1)
O(5)–C(9)–C(8)	106(1)	O(5)–C(9)–C(10)	110(1)
O(5)–C(9)–C(14)	115(1)	C(8)–C(9)–C(10)	112(1)
C(8)–C(9)–C(14)	100(1)	C(10)–C(9)–C(14)	112(1)
C(9)–C(10)–C(11)	126(1)	C(10)–C(11)–C(12)	123(1)
C(10)–C(11)–C(22)	122(1)	C(12)–C(11)–C(22)	114(1)
O(6)–C(12)–C(11)	106(1)	O(6)–C(12)–C(13)	112(1)
C(11)–C(12)–C(13)	115(1)	C(12)–C(13)–C(14)	113(1)
O(1)–C(14)–O(2)	110(1)	O(1)–C(14)–C(9)	105(1)
O(1)–C(14)–C(13)	107(1)	O(2)–C(14)–C(9)	106(1)
O(2)–C(14)–C(13)	113(1)	C(9)–C(14)–C(13)	115(1)
O(6)–C(15)–O(7)	126(1)	O(6)–C(15)–C(16)	109(1)
O(7)–C(15)–C(16)	125(1)	Br–C(16)–C(15)	111(1)
C(11)–C(22)–C(23)	114(1)	C(22)–C(23)–C(24)	123(2)

† In this paper, the torsion angle A–B–C–D is a projected angle between the A–B and C–D bonds. When viewed down the B–C bond, the clockwise rotation of the C–D bond with reference to the A–B bond is taken to be positive.

Table 5. Intermolecular contacts for non-hydrogen atoms (<3.8 Å)

O(7) ···C(10)^{i}	3.68 Å	O(7) ···C(20)^{i}	3.66 Å
C(17)···C(20)^{i}	3.71	Br·····O(5)^{ii}	3.62
O(1) ···C(21)^{ii}	3.57	C(2) ···C(21)^{ii}	3.49
C(5) ···O(7)^{ii}	3.61	C(5) ···C(13)^{ii}	3.68
C(6) ···C(13)^{ii}	3.64	C(16)···O(2)^{ii}	3.47
C(16)···O(5)^{ii}	3.42	C(19)···O(7)^{ii}	3.55
O(7) ···O(3)^{iii}	3.53	O(7) ···C(18)^{iii}	3.65
C(15)···O(3)^{iii}	3.49	C(16)···O(3)^{iii}	3.35
C(16)···O(4)^{iii}	3.51	C(24)···C(2)^{iii}	3.69
C(24)···C(3)^{iii}	3.62	C(24)···C(4)^{iii}	3.78
C(19)···C(18)^{iv}	3.67		

Symmetry code: (i) $-1+x, y, z$ (ii) $1-x, 1/2+y, 1-z$ (iii) $x, y, 1+z$ (iv) $1-x, 1/2+y, -z$.

H derived from the X-ray analysis is about −168°. This value can be correlated with the coupling constant (11 Hz) of these hydrogen atoms, derived by an analysis of the NMR spectrum.[4] The five-membered ring comprising the C(7), C(8), C(9), C(14), and O(1) atoms takes a half-chair conformation, and the C_2 axis lies on a line connecting the midpoint of the C(8)–C(9) bond and the O(1) atom. This is one of two conformations of the cyclopentane. As is usually found in the cyclohexene and the heterocyclic rings,[5,6] the six-membered ring comprising the C(9), C(10), C(11), C(12), C(13), and C(14) atoms is also in the form of a half-chair. The ethylenic carbon atoms (C(10) and C(11)) and the two adjacent allylic carbon atoms (C(9) and C(12)) lie approximately on a plane, while the C(13) and C(14) atoms on the other side deviate by 0.26 Å above and 0.32 Å below the plane respectively. The torsion angles in the ring, C(13)–C(14)–C(9)–C(10), C(12)–C(13)–C(14)–C(9), and C(11)–C(12)–C(13)–C(14), are calculated to be −34°, 48°, and −33° respectively. One of the two methoxy groups attached to the benzene ring is approximately coplanar with the benzene ring; the torsion angles of C(5)–C(4)–O(4)–C(19) and C(2)–C(3)–O(3)–C(18) are 2° and 15° respectively. The bond lengths and angles of the molecule are listed in Table 4. They seem to be normal for the respective bond types within the limits of experimental error. The intermolecular distances between the non-hydrogen atoms less than 3.8 Å are listed in Table 5; the table indicates the absence of any abnormally short contact.

The authors wish to thank Mr. Tetsuya Ikeda for his technical assistance in this work, and Professor Tamaichi Ashida of Nagoya University for his permission to use the block-diagonal least-squares program.

References

1) K. Matsui and K. Munakata, *Tetrahedron Lett.*, **1975**, 1905.
2) K. Matsui and K. Munakata, to be published.
3) "International Tables for X-Ray Crystallography," Vol. III, Kynoch Press, Birmingham (1962), p. 202.
4) R. U. Lemieux and J. W. Lown, *Can. J. Chem.*, **42**, 898 (1964).
5) J. Konnert, I. L. Karle and J. Karle, *Acta Crystallogr.*, **B26**, 770 (1970).
6) D. C. Rohrer and M. Sundaralingam, *ibid.*, **B26**, 546 (1970).

Studies of Fragment Ion Distribution and Reaction with a Charge Spectrometer. VIII. Fragmentation Processes of Various Alkyl Halides

Shigeru IKUTA, Kenji YOSHIHARA, and Takanobu SHIOKAWA

Department of Chemistry, Faculty of Science, Tohoku University, Aoba, Aramaki, Sendai 980

(Received December 13, 1974)

The breakdown curves for C_2H_5X, n-C_3H_7X, and n-C_4H_9X (X=Cl, Br, and I) were obtained by the use of a double mass spectrometer of the perpendicular type. The charge exchange mass spectra for alkyl bromide and alkyl iodide are found to be similar, although those for alkyl chloride are somewhat different from these for bromide and iodide. According to the molecular orbital calculation, the difference of the electronic configuration between chloride and bromide or iodide is found to correspond to the difference of the breakdown curves. The results obtained in this study using larger molecules support our previous analysis on the breakdown processes in smaller molecules: (1) direct scission of the bond which has lost one electron by the charge exchange reaction, (2) electron redistribution, and (3) secondary decomposition (and those of higher order) from the primary fragments. In the case of alkyl chloride, formation of the ion $C_nH_{2n}^+$ is ascribed to the elimination of HX from the molecular ion in its electronically ground but vibrationally excited state.

Fragmentation processes of molecules by electron or photon impact have usually been interpreted by the quasi-equilibrium theory (QET)[1] based on the unimolecular decomposition of the molecular ion in its vibrationally excited state. Contrary to this widely accepted interpretation, some evidence of fragmentation of the molecular ion in its electronically excited state has recently been highlighted.[2-5]

On the other hand Hirota[6] and Lorquet[7] found that the scission probability of the skeletal bond was proportional to the electron density of the corresponding bond in the highest occupied MO. Although this molecular orbital theory applied to fragmentation is interesting, the validity of the theory has been shown to be doubtful.[8] In a word, a theory which is universally applicable has not been available so far.

Therefore, in order to approach the solution of these difficulties, we have proposed some new fragmentation mechanisms on the basis of a MO treatment involving the inner occupied MO's.[9] The fragmentation processes of various CH_3X (X=NH_2, OH, SH, Cl, Br, and I),[5,9] C_2H_5OH, $C_2H_5NH_2$,[10] various alcohols,[11] and various mercaptans[12] have been successfully explained by our interpretation.

In this paper, the breakdown curves of various alkyl halides RX (R=ethyl, propyl, and butyl, and X=Cl, Br, and I) are studied by charge exchange reactions and the effects of the length of the alkyl group (R) and that of the substituent (X) on the fragmentation processes are investigated.

Experimental

Fragmentation processes of various molecular ions produced by charge exchange reactions were studied using a double mass spectrometer of the perpendicular type. Details of the apparatus have already been described.[13] In the work, H_2S^+, $C_2H_2^+$, Xe^+, Kr^+, N_2^+, Ar^+, Xe^{++}, Ne^+, and He^+ ions were used as primary incident ions and admitted into the reaction chamber. The pressure in the reaction chamber was below 6×10^{-6} Torr.

Calculation

Eigenvectors of molecular orbitals of various alkyl halides were calculated according to the Extended Hückel Molecular Orbital method.[14] Details of the calculation were already described in the previous paper.[9] The calculation was performed at the Computer Center of Tohoku University. The models employed for this calculation are shown in Fig. 1.

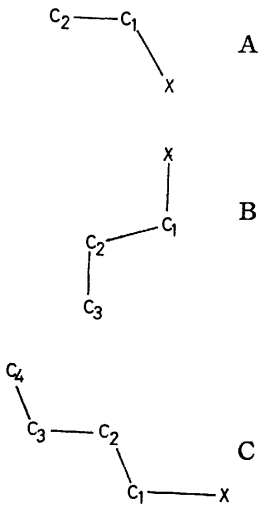

Fig. 1. Models employed for calculation (hydrogens are omitted).
A: Ethyl halide. B: Propyl halide. C: Butyl halide.

Results

(A) Ethyl Halides. The breakdown curves of ethyl chloride and ethyl iodide obtained by charge exchange reactions are shown in Fig. 2 (A) and (B). In the figure the abscissa indicates the recombination energy of the incident positive ions and the ordinate indicates the abundance of the fragment ions. The curves are normalized so that the sum of the abundances of the constituent ions at each energy is equal to 100. The production of the molecular ions must start at

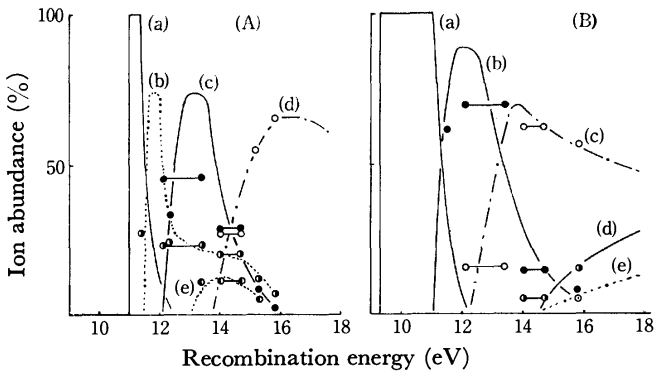

Fig. 2. Breakdown curves of ethyl chloride (A) and ethyl iodide (B).
(A) (a) $C_2H_5Cl^+$ (b) $C_2H_4^+$ (c) $C_2H_5^+$ (d) $C_2H_3^+$ (e) CH_2Cl^+
(B) (a) $C_2H_5I^+$ (b) $C_2H_5^+$ (c) $C_2H_3^+$ (d) I^+ (e) $C_2H_2^+$

the recombination energy equal to the spectroscopic ionization potential.

In ethyl chloride, the $C_2H_4^+$ ion produced by the loss of HCl from the molecular ion in the vibrationally excited state[15] follows the stable molecular ion. Formation of $C_2H_5^+$ ion starts at about 12 eV. The CH_2Cl^+ ion appears at about 13 eV as a result of scission of the C–C bond and its maximum abundance is about 15%. Formation of $C_2H_3^+$ ion produced by unimolecular decomposition of the $C_2H_5^+$ ion starts at 13.5—14.0 eV. The appearance potential of $C_2H_5^+$ ion is equal to that of the second band in the photoelectron spectrum.[16] Therefore, it is thought that the primary fragment ions from the molecular ions are $C_2H_4^+$, $C_2H_5^+$, and CH_2Cl^+, among which the $C_2H_5^+$ and CH_2Cl^+ ions are correlated to the direct fragmentation of the molecular ion in its electronically excited state.

On the other hand, in ethyl iodide the $C_2H_5^+$ ion follows the stable molecular ion. The appearance potential of this ion is equal to that of the second band in the photoelectron spectrum.[16] Formation of the $C_2H_3^+$ ion produced by unimolecular decomposition of the $C_2H_5^+$ ion starts at about 12.5 eV. Formation of the

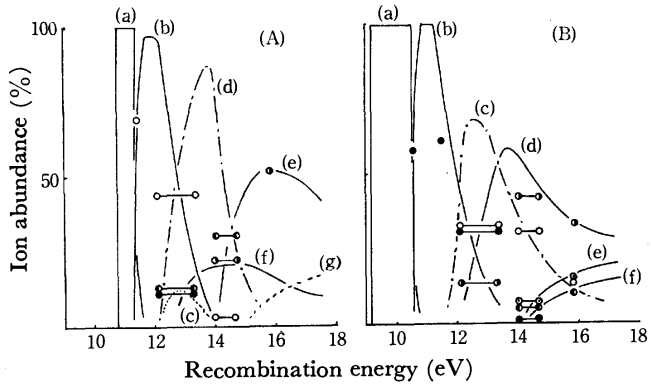

Fig. 3. Breakdown curves of propyl chloride (A) and propyl iodide (B).
(A) (a) $C_3H_7Cl^+$ (b) $C_3H_6^+$ (c) $C_3H_7^+$ (d) $C_2H_5^+$ (e) $C_2H_3^+$ (f) $C_3H_5^+$ (g) $C_3H_3^+$
(B) (a) $C_3H_7I^+$ (b) $C_3H_7^+$ (c) $C_3H_5^+$ (d) $C_2H_3^+$ (e) $C_3H_3^+$ (f) I^+

I^+ and $C_2H_2^+$ ions starts at about 14.5 eV, but the CH_2I^+ ion produced by scission of the C–C bond comprises only a few percent. Therefore, it is concluded that the product of the primary scission of the molecular ions is only the $C_2H_5^+$ ion in the low energy region (<15 eV).

(B) Propyl Halides. The breakdown curves of propyl chloride and propyl iodide obtained by charge exchange reactions are shown in Fig. 3.

In propyl chloride, formation of the $C_3H_6^+$ ion which is produced from the molecular ion in its vibrationally excited state[15] follows that of the stable molecular ion. Formation of the $C_2H_5^+$ ion starts at about 12.0 eV after that of the $C_3H_6^+$ ion and it is thought that this $C_2H_5^+$ ion is produced by the primary scission of the molecular ion. Formation of the $C_3H_7^+$ ion also starts at about 12.0 eV and the maximum abundance of this ion is about 15%. The $C_3H_5^+$ and $C_2H_3^+$ ions are formed as a result of the consecutive decomposition of the $C_3H_6^+$, $C_3H_7^+$, and $C_2H_5^+$ ions. Therefore, these results show that the primary fragment ions of the molecular ion are $C_3H_6^+$, $C_2H_5^+$, and $C_3H_7^+$ ions, among which the $C_2H_5^+$ and $C_3H_7^+$ ions are correlated to the direct fragmentation of the molecular ion in its electronically excited state.

On the other hand, in propyl iodide the formation of $C_3H_7^+$ ion follows that of the stable molecular ion, and this $C_3H_7^+$ ion decomposes further to smaller ions ($C_3H_5^+$, $C_2H_3^+$,……). It is thought that the primary fragment ion is the $C_3H_7^+$ ion alone in the low energy region (<15 eV).

(C) Butyl Halides. The breakdown curves of butyl chloride and butyl iodide obtained by charge exchange reactions are shown in Fig. 4.

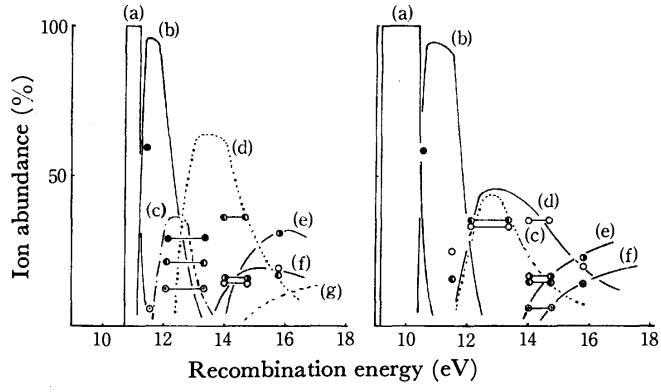

Fig. 4. Breakdown curves of butyl chloride (A) and butyl iodide (B).
(A) (a) $C_4H_9Cl^+$ (b) $C_4H_8^+$ (c) $C_3H_7^+$ (d) $C_3H_5^+$ (e) $C_2H_3^+$ (f) $C_3H_3^+$
(B) (a) $C_4H_9I^+$ (b) $C_4H_9^+$ (c) $C_3H_5^+$ (d) $C_2H_5^+$ (e) $C_2H_3^+$ (f) $C_3H_3^+$

In butyl chloride formation of the $C_4H_8^+$ ion produced by the elimination of hydrogen chloride from the molecular ion in its vibrationally excited state[15] follows that of the stable molecular ion. Formation of the $C_3H_7^+$ ion starts after the appearance of the $C_4H_8^+$ ion and this $C_3H_7^+$ ion is considered to be produced by the primary scission of the molecular ion. Formation of $C_2H_5^+$ starts at about 12.5 eV, after that of the $C_3H_7^+$ ion.

The $C_4H_8^+$, $C_3H_7^+$, and $C_2H_5^+$ ions decompose further to smaller ions. These results and Figure 4 show that the primary fragment ions of the molecular ions are the $C_4H_8^+$, $C_3H_7^+$, and $C_2H_5^+$ ions, among which the $C_3H_7^+$ and $C_2H_5^+$ ions are correlated to the decomposition of the molecular ion in its electronically excited state.

On the other hand, in butyl iodide formation of the $C_4H_9^+$ ion follows that of the stable molecular ion. This $C_4H_9^+$ ion decomposes further to smaller ions ($C_3H_5^+$, $C_2H_5^+$,……). The primary fragment ion of the molecular ion is the $C_4H_9^+$ ion alone in the low energy region (<15 eV).

From these results the dissociation schemes of various molecular ions are shown in Fig. 5.

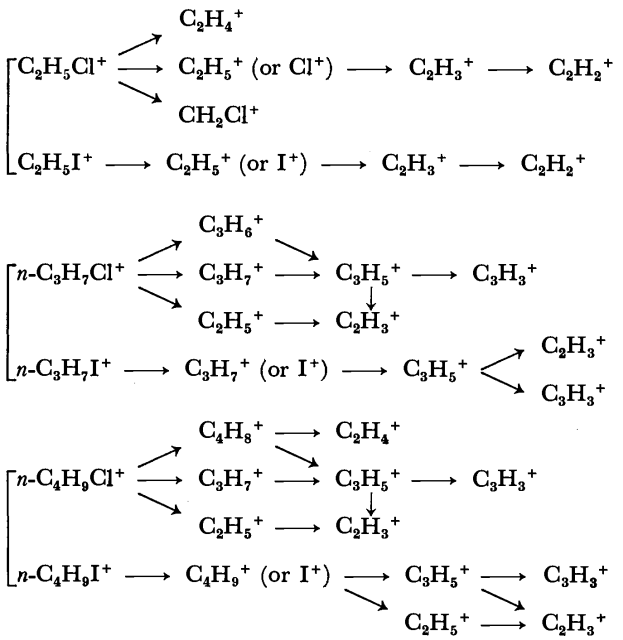

Fig. 5. Dissociation ionization schemes of various alkyl halide-moleular ions.

Discussion

Instead of an interpretation of the mass spectra using the QET[1] and Hirota's theory,[6] we have already set up a new interpretation of fragmentation processes based on the MO treatment.[5,9-12] The scission probabilities of the C–X and C–H bonds in various CH_3X^+ have been well explained by our proposal.[5,9] And the fragmentation processes of various alcohols[11] and mercaptans[12] have been also successfully accounted for. Our interpretation is composed of three basic suppositions, as follows:

(1) The scission first occurs where the electrons are exist densely in the particular occupied MO correlated to the particular ionization.

(2) Process (1) competes with the electron redistribution process after the event of ionization.

(3) In a higher energy region, secondary scission (and those of higher orders) also occurs.

Based on process(1), the primary fragment ions of the molecular ions can be predicted by the main character of the particular MO which correlates to the particular ionization, and the over-all features of the energy dependence of the fragmentation phenomena can be explained by processes (2) and (3) in addition to process (1).

Table 1. Calculated MO energy, observed ionization potential and calculated bonding character in alkyl iodides

		Calculated MO energy (−eV)	Observed I. P. (eV)[16]	Calculated Bonding character
C_2H_5I	HOMO	10.47	9.34	non-bonding
		10.48	9.93	
	SOMO	12.36	11.66	C–I bonding
	TOMO	13.68	12.90	C–H bonding
	FOMO	13.93	13.85	C–C bonding
C_3H_7I	HOMO	10.46	9.27	non-bonding
		10.48	9.82	
	SOMO	12.36	11.43	C_1–I bonding
	TOMO	13.29	12.22	C–H bonding
	FOMO	13.48	12.78	C_1–C_2 bonding
C_4H_9I	HOMO	10.46	9.24	non-bonding
		10.48	9.79	
	SOMO	12.28	11.22	C_1–I bonding
	TOMO	13.24	11.90	C–H bonding
	FOMO	13.26	12.3	C_1–C_2 bonding

The calculated MO energy, the observed ionization potential, and the general character of the occupied MO for alkyl iodide are shown in Table 1. The highest occupied MO which is degenerated is non-bonding and the second occupied MO is C–I bonding. Therefore, the ionization of the electron in the highest occupied MO results in formation of the stable molecular ion, and the ionization of the electron in the second occupied MO results in formation of the alkyl ion, as shown in the figures. The appearance potential of the alkyl ion is equal to that of the second band in the corresponding photoelectron spectrum.[16] The primary fragment ion of the molecular ion is the alkyl ion alone in the low energy region. No formation of any fragment ions originating from ionization of the electron above the second occupied MO was observed in the present experiments. Therefore, it is considered that the molecular ion in its electronically excited state easily falls into its electronically ground state (or at least into its low-lying electronically excited states) before it decomposes. Similar considerations can be applied to the fragmentation of the molecular ion in alkyl bromide.

The MO energy and the general character of the occupied MO calculated in this work for alkyl chloride are shown in Table 2. The fragment ion produced by the elimination of hydrogen chloride is ascribed to the presence of the molecular ion in its vibrationally excited state.[15] The breakdown curves in ethyl chloride are similar to those of ethyl bromide and ethyl iodide, except for the formation of the $C_2H_4^+$ ion. Therefore, it is assumed that the general character of the various occupied MO's in ethyl chloride is similar to those of ethyl bromide and ethyl iodide.

Table 2. MO energy and bonding character calculated in this work on alkyl chlorides

		MO energy (−eV)	Bonding character
C_2H_5Cl	HOMO	12.88	non-bonding
	SOMO	13.72	C–H bonding
	TOMO	13.90	C–C bonding
	FOMO	14.12	C–Cl bonding
C_3H_7Cl	HOMO	12.84 12.93	non-bonding
	SOMO	13.30	C–H bonding
	TOMO	13.42	C_1–C_2 bonding> C_1–Cl bonding
	FOMO	13.73	C_2–C_3 bonding
C_4H_9Cl	HOMO	12.76 12.91	non-bonding
	SOMO	13.20	C_1–C_2, C_2–C_3,··· bondings
	TOMO	13.25	C–H bonding
	FOMO	13.50	C_2–C_3 bonding

In propyl chloride the highest occupied MO is degenerated n(Cl). The third occupied MO is both C_1–C_2 bonding and C_1–Cl bonding. The calculated partial bond population of C_1–C_2 bonding comprises 75% and that of C_1–Cl bonding comprises 25%. Therefore, ionization of an electron in the third occupied MO results in formation of the $C_2H_5^+$ ion in abundance and a small amount of the $C_3H_7^+$ ion, as shown in Fig. 3. It is thought that the general character of the various occupied MO's in propyl chloride shown in Table 2 is correct.

In butyl chloride the calculated bonding character of the second occupied MO is C_1–C_2, C_2–C_3,·····bondings. From the experimentally obtained breakdown curve, the most dominant one is thought to be C_1–C_2 bonding.

In the molecular ions of alkyl bromide and alkyl iodide, the C–X bond dominantly dissociates and the fragment ions produced by the scission of the other bond can be scarcely observed, in contrast to the fragmentation of molecular ions of alkyl amine, alkyl alcohol, and alkyl mercaptan. This difference is explained by the difference of the general character of the various occupied MO's.

No formation of fragment ions originating from the ionization of an electron above the second occupied MO was observed. Therefore, it is considered that the molecular ion in its electronically excited state easily falls into its electronically ground state or into a less excited electronic one. Although the degree of transition between the electronic states is considered to be large in alkyl bromide and alkyl iodide, as shown in the figures, it seems this is not the case in alkyl chloride. It is likely that this degree decreases in the order of of butyl>propyl>ethyl chloride.

From these results it is shown that the electron redistribution process of our proposal also plays an important role in the higher energy region in the breakdown curve of alkyl halides. Thus, the general trends of fragmentation processes of molecular ions are concluded to be interpreted satisfactorily by our approach, although efforts to make the results more quantitative will be necessary in the future.

References

1) H. M. Rosenstock, M. B. Wallenstein, A. L. Wahrhaftig and H. Eyring, *Proc. Nat. Acad. Sci., U.S.*, **38**, 667 (1952).
2) E. Lindholm, "Ion-Molecule Reactions," Vol. 2, ed. by Franklin, Plenum Press, New York (1972), p. 457.
3) I. G. Simm, C. J. Danby, and J. H. D. Eland, *Chem. Commun.*, **1973**, 832.
4) H. M. Rosenstock, J. T. Larkins, and J. A. Walker, *Int. J. Mass Spectrom. Ion Phys.*, **11**, 309 (1973).
5) S. Ikuta, K. Yoshihara, and T. Shiokawa, *Mass Spectroscopy, Japan*, **22**, 233 (1974).
6) K. Hirota, *Nippon Kagaku Zasshi*, **81**, 585 (1970).
7) J. C. Lorquet, *Mol. Phys.*, **9**, 101 (1965).
8) S. Ikuta, K. Yoshihara, and T. Shiokawa, This Bulletin, **46**, 3648 (1973).
9) S. Ikuta, K. Yoshihara, and T. Shiokawa, *ibid.*, **48**, 2134 (1975).
10) S. Ikuta, K. Harada, K. Yoshihara, and T. Shiokawa, *Mass Spectroscopy, Japan*, **22**, 239 (1974).
11) S. Ikuta, K. Yoshihara, and T. Shiokawa, *ibid.*, **22**, 245 (1974).
12) K. Yoshihara, M. Kobayashi, S. Ikuta, and T. Shiokawa, This Bulletin, **48**, 2433 (1975).
13) T. Shiokawa, K. Yoshihara, M. Yagi, T. Omori, H, Kaji, M. Hiraga, T. Nagatani, and Y. Takita, *Mass Spectroscopy, Japan*, **18**, 1230 (1970).
14) R. Hoffmann, *J. Chem. Phys.*, **39**, 1397 (1963).
15) K. C. Kim, J. H. Beynon, and R. G. Cooks, *J. Chem. Phys.*, **61**, 1305 (1974).
16) K. Kimura, S. Katsumata, Y. Achiba, H. Matsumoto, and S. Nagakura, This Bulletin, **46**, 373 (1973).

The Chemical Behavior of Low Valence Sulfur Compounds. X.[1] Disproportionation of Thiosulfate, Trithionate, Tetrathionate and Sulfite under Acidic Conditions

Tadaaki MIZOGUCHI,* Yoshiaki TAKEI,** and Taijiro OKABE

Department of Applied Chemistry, Faculty of Engineering, Tohoku University, Sendai 980

(Received February 25, 1975)

The disproportionation of thiosulfate, trithionate, tetrathionate and sulfite in acidic solutions has been studied at relatively high temperatures. Thiosulfate hardly decomposes in the absence of sulfuric acid, even at 150 °C, but decomposes very easily in the presence of sulfuric acid at 70 °C, forming elemental sulfur, tetrathionate and sulfite. Trithionate decomposes to thiosulfate and sulfate at 70 °C, while tetrathionate decomposes only at temperatures above 130 °C after an induction period forming thiosulfate as an intermediate. Sulfite undergoes disproportionation, giving thiosulfate and sulfate at 150 °C, and then elemental sulfur and sulfate accompanied by intermediate formation of tetrathionate. A disproportionation pathway of low valence sulfur oxyacids including thiosulfate, trithionate, tetrathionate and sulfite has been proposed.

Investigations of disproportionation of low valence sulfur compounds such as thiosulfate,[2-4] polythionates[4-8] and sulfite[9-11] have been carried out by a number of workers. It has been shown that some kinds of polythionates play important roles as intermediates in these reactions, but no systematic study seems to have been made, partly because of the lack of a simple and accurate method of analysis. A photometric method for thiosulfate and polythionates[1] described in the previous paper, has been found to be useful.

The disproportionation of thiosulfate, trithionate, tetrathionate and sulfite has been investigated in acidic solutions at relatively high temperatures to obtain the basic data concerning the treatment of waste waters containing low valence sulfur compounds. Sulfuric acid was used as an acidic medium, as this acid is used most widely in industrial fields.

Experimental

Materials. All chemicals except polythionates were of analytical reagent grade. Potassium trithionate and potassium tetrathionate were prepared by Stamm's method[12] and Martin's method,[13] respectively. The concentrations of the stock solution of trithionate and tetrathionate were determined by Procedures C and B, respectively.[1]

Procedure. The reactions were carried out in 25 ml sealed glass tubes. Each tube was sealed soon after the transfer of 15 ml of sample solution together with 0.5 ml of sulfuric acid of different concentration, and placed in a glycerol bath regulated at the desired temperature. The sealed tubes were removed from the bath after a definite period of time, and quickly cooled to room temperature, when necessary, in an ice bath.

Analysis. The seals of the glass tubes were removed and a clear supernatant solution was withdrawn. The sample solution was diluted to a suitable concentration and analyzed for thiosulfate, trithionate, tetrathionate, sulfite and sulfate as follows:

Thiosulfate, Trithionate and Tetrathionate: Since the higher polythionates above tetrathionate were proved by paper chromatography to be absent in the reaction mixtures,[14] the photometric method[1] was used for the determination of the concentrations of thiosulfate, trithionate and tetrathionate. The calibration curves were prepared with a standard thiosulfate solution. The standard addition method was employed to eliminate interferences caused by various chemical compositions of the samples.

Sulfite: The total amount of thiosulfate and sulfite was determined by iodometry. The amount of sulfite was determined by substracting the amount of thiosulfate obtained by photometry from the total amount of thiosulfate and sulfite.

Sulfate: The total amount of sulfite and sulfate was determined gravimetrically as barium sulfate, after oxidizing thiosulfate and sulfite with iodine to tetrathionate and sulfate, respectively. The amount of sulfate formed in the disproportionation was determined by substracting the amount of sulfite and that of sulfuric acid added.

Elemental Sulfur: The elemental sulfur deposited in the glass tubes was dissolved in carbon disulfide. After being washed with water, the carbon disulfide layer was poured into a 200 ml beaker, and then warmed to about 35 °C to evaporate carbon disulfide. The residual elemental sulfur was determined gravimetrically as barium sulfate after oxidation to sulfate with a mixture of potassium chlorate and nitric acid.

Results and Discussion

Disproportionation of Thiosulfate Solution. The effect of reaction time on the decomposition degree of thio-

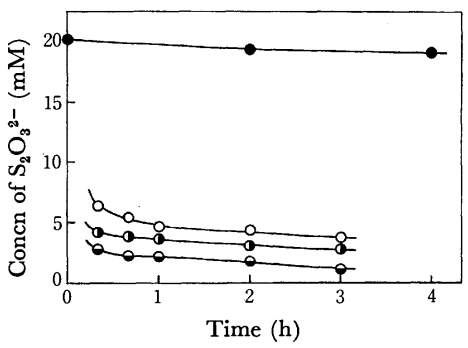

Fig. 1. Effect of reaction time on the decomposition degree of thiosulfate solution.
Initial concn of H_2SO_4: 20 mM, temp (°C): ○70, ◑110, ◒150. Without H_2SO_4, temp. (°C): ●150.

* Present address: Chemical Research Institute of Non-Aqueous Solutions, Tohoku University, Sendai 980

** Present address: Konishiroku Photo Ind. Co., Ltd., Hino, Tokyo 191

TABLE 1. EFFECT OF REACTION TEMPERATURE ON THE DISPROPORTIONATION OF ACIDIC THIOSULFATE SOLUTION

Temp (°C)	Composition of the reaction mixtures (mg atom-S/l)								pH
	$S_2O_3^{2-}$	S	$S_3O_6^{2-}$	$S_4O_6^{2-}$	HSO_3^-	SO_4^{2-}	Total-S	S_{calcd}[a]	
70	8.9	13.5	1.0	4.8	11.3	1.2[b]	40.7	13.6	2.25
90	7.3	12.2	0.5	11.0	8.5	1.1[b]	40.6	12.3	2.00
110	5.9	11.5	0.5	13.6	6.9	1.4[b]	39.8	11.7	1.95
130	4.7	10.6	0	17.0	5.2	2.0[b]	39.4	11.4	2.17
150	3.6	14.6	0	11.0	4.6	6.1[b]	39.6	13.5	1.98

Initial concn of $Na_2S_2O_3$: 39.7 mg atom-S/l, initial concn of H_2SO_4: 20 mM, time: 2 h. a) Calculated values obtained by assuming that the first stage of thiosulfate decomposition is represented by the reactions shown by Eqs. (1) and (2), and also that the formation of sulfate is attributed to air oxidation of sulfite formed according to the reaction shown by Eq. (2). b) The amount of sulfuric acid added was substracted.

sulfate is shown in Fig. 1. We see that thiosulfate hardly decomposes in the absence of sulfuric acid even at 150 °C, while it decomposes very easily in the presence of sulfuric acid at 70 °C.

The effect of reaction temperature was determined in the range 70—150 °C. The material balance of sulfur atoms can be explained well, taking into consideration elemental sulfur, trithionate, tetrathionate, sulfite and sulfate as reaction products (Table 1). Trithionate can be regarded to be of minor importance as a decomposition product. Thiosulfate decomposes in acidic solution, forming elemental sulfur as a lower oxidation state species, and tetrathionate, sulfite and sulfate as higher oxidation state species. The reactions can be represented by the following equations:

$$5S_2O_3^{2-} + 6H^+ = 2S + 2S_4O_6^{2-} + 3H_2O \quad (1)$$

$$S_2O_3^{2-} + H^+ = S + HSO_3^- \quad (2)$$

$$3S_2O_3^{2-} + 2H^+ = 4S + 2SO_4^{2-} + H_2O \quad (3)$$

When considered thermodynamically,[11,15] hydrogen sulfide besides elemental sulfur is considered to be formed as a lower oxidation state species. However, all the reaction mixtures in the present investigation gave no characteristic odor of hydrogen sulfide.

The amount of tetrathionate formed increases with an increase of reaction temperature in the range 70—130 °C, while that of sulfite decreases with an increase of reaction temperature (Table 1). On the other hand, the amount of sulfate formed is independent of reaction temperature and is as low as about 1 mg atom-S/l. The values of S_{calcd} (Table 1) were calculated by

$$S_{calcd}(\text{mg atom-S/l}) = 0.25(S_4O_6^{2-})\ (\text{mg atom-S/l}) + (HSO_3^-)\ (\text{mg atom-S/l}) + (SO_4^{2-})\ (\text{mg atom-S/l}).$$

The amount of elemental sulfur formed is in good agreement with the calculated values of S_{calcd} in the temperature range 70—130 °C. Therefore, it can be said that tetrathionate and sulfite are formed according to the reactions shown by Eqs. (1) and (2), respectively, and that the formation of sulfate is not attributed to disproportionation of tetrathionate or sulfite but rather to air oxidation of sulfite formed as shown by Eq. (2). On the other hand, it is noted that at the reaction temperature of 150 °C, yields of elemental sulfur and sulfate are higher than those at 130 °C, while the yield of tetrathionate is correspondingly lower. It seems

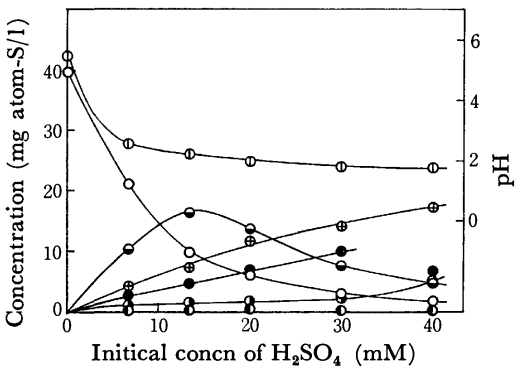

Fig. 2. Effect of sulfuric acid concentration on the disproportionation of thiosulfate solution.
Initial concn of $S_2O_3^{2-}$: 19.9 mM, temp: 110 °C, time: 2 hr.
⊕: S, ○: $S_2O_3^{2-}$, ◐: $S_3O_6^{2-}$, ◒: $S_4O_6^{2-}$, ●: HSO_3^-, ◑: SO_4^{2-},[a] ⓘ: pH.
a) The amount of sulfuric acid added was substracted.

that the reaction shown by Eq. (3) proceeds favorably at 150 °C. The successive occurrence of reactions shown by Eqs. (1) and (8) or Eqs. (2) and (11), however, lead to the overall reaction of Eq. (3), which therefore need not necessarily be considered as a separate reaction.

The decomposition of thiosulfate was carried out in sulfuric acid solutions of barious concentrations at 110 °C. From the results (Fig. 2), it is evident that the amount of tetrathionate increases gradually with an increase of sulfuric acid concentration, and after reaching a maximum, finally falls off. On the other hand, the amount of sulfite shows a steady increase with an increase of sulfuric acid concentration. The reason why the amount of sulfite is not so high as to compensate the decrease in the amount of tetrathionate at sulfuric acid concentrations of 30 and 40 mM is that the sulfite formed escapes to the gaseous phase.

Figure 3 shows the tetrathionate concentrations in the final reaction mixtures as functions of temperature and sulfuric acid concentration. At a definite acid concentration, the amount of tetrathionate formed increases with an increase of reaction temperature in the range 70—130 °C. Tetrathionate, however, decomposes above 130 °C, the final concentration decreasing with increasing temperature in the temperature range. The reason why the amount of tetrathionate shows a maximum at a certain concentration of sulfuric acid is not clear.

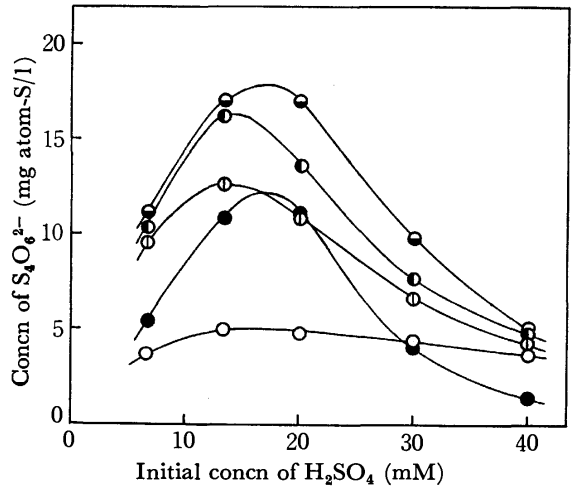

Fig. 3. Effect of reaction temperature and sulfuric acid concentration on the formation of tetrathionate from thiosulfate.
Initial concn of $S_2O_3^{2-}$: 19.9 mM, time: 2 h.
Temp (°C): ○70, ⓘ90, ◐110, ◒130, ●150.

In the experiments shown in Figs. 2 and 3, a fixed reaction time of 2 h was used. However, the decomposition velocity of thiosulfate is very high at even 70 °C, while tetrathionate decomposes hardly below 130 °C. Thus, the amount of tetrathionate formed might not change much even if the reaction time is extended.

It is well known that some kinds of polythionates as well as elemental sulfur and sulfite are formed in the acid decomposition of thiosulfate.[2-4] Many investigators reported that the reaction

$$S_nO_6^{2-} + S_2O_3^{2-} + H^+ \rightleftharpoons S_{n+1}O_6^{2-} + HSO_3^- \quad (n \geqq 3) \qquad (4)$$

played an important role not only in the formation of polythionates[6,7,16,17] but also in their decomposition.[2] The amount of trithionate in the final reaction mixtures was extremely small, compared with that of tetrathionate (Table 1 and Fig. 2). Blasius and Krämer[3] suggested that tetrathionate is formed exclusively in the reaction of thiosulfate with concentrated hydrochloric acid at room temperature. Thus, it may be said that tetrathionate does not always exist in equilibrium with trithionate as shown by Eq. (4), and that the formation reaction of trithionate is represented by

$$4HSO_3^- + S_2O_3^{2-} + 2H^+ = 2S_3O_6^{2-} + 3H_2O \qquad (5).^{18,19}$$

Polythionates except tetrathionate are unstable and decompose readily at high temperature, so the formation reaction of tetrathionate shown by Eq. (1) is the most important in the acid decomposition of thiosulfate solution at relatively high temperature. Janickis[2] reported abnormally higher polythionates, but they might be formed only in highly concentrated acid solutions at a low temperature.

Disproportionation of Trithionate Solution. Trithionate solution undergoes a noticeable decomposition at relatively low temperature.[5,20] The decomposition reaction which takes place in weakly acidic to weakly alkaline solution is represented by

$$S_3O_6^{2-} + H_2O = S_2O_3^{2-} + SO_4^{2-} + 2H^+ \qquad (6)^{5-7}$$

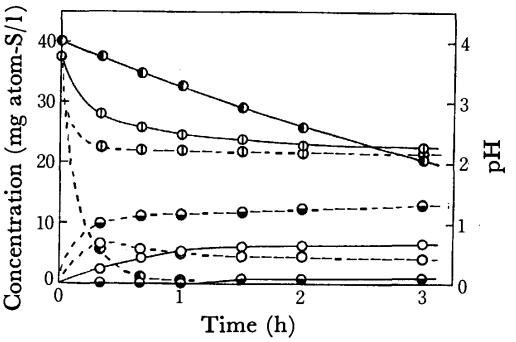

Fig. 4. Disproportionation of potassium trithionate solution.
—○—: $S_2O_3^{2-}$ (70 °C), —◐—: $S_3O_6^{2-}$ (70 °C), —◒—: $S_4O_6^{2-}$ (70 °C), —ⓘ—: pH (70 °C), ---○---: $S_2O_3^{2-}$ (110 °C), ---◐---: $S_3O_6^{2-}$ (110 °C), ---◒---: $S_4O_6^{2-}$ (110 °C), ---ⓘ---: pH (110 °C).
The numbers in parentheses represent reaction temperatures.
The amounts of elemental sulfur, sulfite and sulfate formed were not determined.

The results of the thermal decomposition of potassium trithionate solution at 70 and 110 °C are shown in Fig. 4. Trithionate solution is very unstable and tends to decompose readily without the addition of acid at as low as 70 °C, as compared with the case of thiosulfate and tetrathionate. The decomposition at 110 °C is characterized by the fact that the velocity is considerably high, and that the amount of tetrathionate formed is large. The phenomena that the amount of tetrathionate formed at 110 °C is larger than that formed at 70 °C is consistent with the results obtained in the present experiments on acid decomposition of thiosulfate solution.

The results of the disproportionation of trithionate solution in the presence of sulfuric acid are shown in Fig. 5. It is seen that elemental sulfur, thiosulfate, tetrathionate, sulfite and sulfate are formed in the decomposition of trithionate solution, and that the composition of reaction mixtures at sulfuric acid concentrations of 0, 10 and 20 mM are almost the same as that of decomposition products of thiosulfate at

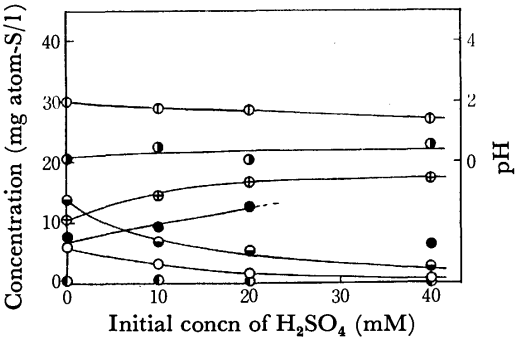

Fig. 5. Effect of sulfuric acid concentration on the disproportionation of trithionate solution.
Initial concn of $S_3O_6^{2-}$: 19.5 mM, temp: 110 °C, time: 2 h.
⊕: S, ○: $S_2O_3^{2-}$, ◐: $S_3O_6^{2-}$, ◒: $S_4O_6^{2-}$, ●: HSO_3^-, ◑: SO_4^{2-},[a] ⓘ: pH.
a) The amount of sulfuric acid added was substracted.

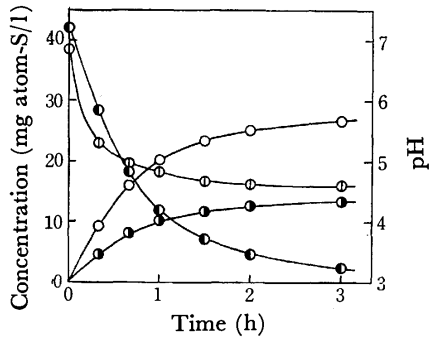

Fig. 6. Disproportionation of trithionate in the presence of acetate buffer solution.
Temp: 90 °C, concn of ammonium acetate: 50 mM.
○: $S_2O_3^{2-}$, ◐: $S_3O_6^{2-}$, ◑: SO_4^{2-}, ⓟ: pH.

sulfuric acid concentrations of 20, 30 and 40 mM, respectively (Fig. 2). The only difference is that the amount of sulfate formed is about 20 mM (Fig. 5), which indicates that trithionate decomposes to form equimolar amount of sulfuric acid. Equimolar amounts of thiosulfate and sulfate were exclusively formed from trithionate solution at pH 4.6 (Fig. 6). It seems that trithionate decomposes to thiosulfate, sulfate and hydrogen ions according to Eq. (6), and that the formation of elemental sulfur, tetrathionate and sulfite (Fig. 5) are related to the acid decomposition of thiosulfate thus formed.

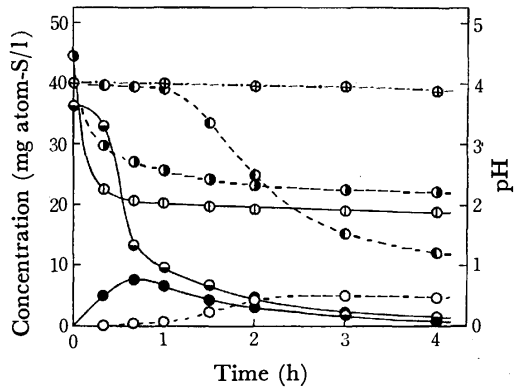

Fig. 7. Disproportionation of potassium tetrathionate solution.
⋯⊕⋯: $S_4O_6^{2-}$ (130 °C), —○—: $S_2O_3^{2-}$ (150 °C), —◐—: $S_4O_6^{2-}$ (150 °C), —◑—: pH (150 °C), —●— $S_2O_3^{2-}$(170 °C), —◒—: $S_4O_6^{2-}$ (170 °C), —ⓟ—: pH (170 °C).
The numbers in parentheses represent reaction temperatures. The amounts of elemental sulfur, sulfite and sulfate formed were not determined.

Disproportionation of Tetrathionate Solution. Figure 7 shows the results of the disproportionation of potassium tetrathionate solution at various temperatures. It is seen that tetrathionate scarcely undergoes thermal decomposition at 130 °C, while it decomposes at temperature above 150 °C after an induction period, forming thiosulfate as an intermediate. The reason why the pH of the solution decreases to 3.0 after 20 min of the initiation of experiment is that a small amount of sulfuric acid is formed due to disproportionation of

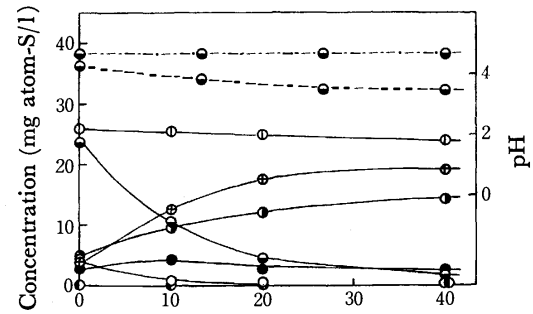

Figre. 8. Effect of reaction temperature and sulfuric acid concentration on the disproportionation of tetrathionate solution.
Initial concn of $S_4O_6^{2-}$: 9.7 mM, time: 2 h.
-·-◒-·-: $S_4O_6^{2-}$ (110 °C), —◒—: $S_4O_6^{2-}$ (130 °C), —⊕—: S (150 °C), —○—: $S_2O_3^{2-}$ (150 °C), —◐—: $S_3O_6^{2-}$ (150 °C), —◒—: $S_4O_6^{2-}$ (150 °C), —●—: HSO_3^- (150 °C), —◑—: SO_4^{2-} (150 °C),[a] —ⓟ—: pH (150 °C).
The numbers in parentheses represent reaction temperatures.
a) The amount of sulfuric acid added was substracted.

tetrathionate.

The results of the disproportionation of tetrathionate solution in the presence of sulfuric acid are shown in Fig. 8. The decomposition degree is fairly high at 150 °C and increases with increasing sulfuric acid concentration. The molar ratio of elemental sulfur to sulfate reaches 1.34 when the initial concentration of sulfuric acid is 40 mM. Accordingly, the decomposition reaction of tetrathionate under the acidic conditions can be represented virtually by

$$3S_4O_6^{2-} + 2H_2O = 7S + 5SO_4^{2-} + 4H^+ \quad (7).$$

However, it is evident from the results shown in Figs. 7 and 8 that thiosulfate is also formed as a decomposition product. Some 80% of sulfur atoms was converted into thiosulfate, the remainder of the sulfur atoms being sulfate under the conditions where thiosulfate was not subjected to acid decomposition (Fig. 9). Thus, the first stage of the disproportionation of tetrathionate could be represented by

$$4S_4O_6^{2-} + 5H_2O = 7S_2O_3^{2-} + 2SO_4^{2-} + 10H^+ \quad (8).$$

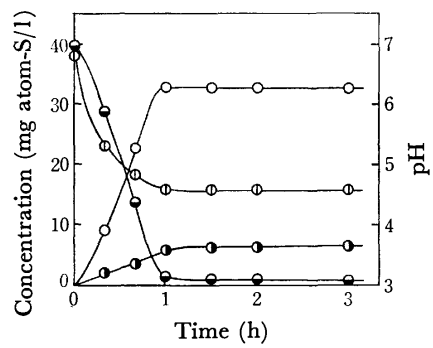

Fig. 9. Disproportionation of tetrathionate in the presence of acetate buffer solution.
Temp: 150 °C, concn of ammonium acetate: 50 mM.
○: $S_2O_3^{2-}$, ◒: $S_4O_6^{2-}$, ◑: SO_4^{2-}, ⓟ: pH.

The formation of elemental sulfur and sulfite (Fig. 8) would be attributed to the acid decomposition of thiosulfate thus formed. Sulfite, however, also decomposes easily under the conditions as seen in Fig. 8,[11] resulting in a small amount of sulfite in the final reaction mixtures. From the results, the relation between decomposition degree of tetrathionate at 150 °C and acidity of solution can be summarized as follows: the decomposition degree of tetrathionate at near pH 5—6 (Fig. 9) is higher than that at near pH 2—3 (Fig. 7), although the decomposition degree increases with increasing sulfuric acid concentration (Fig. 8). Tetrathionate solution at 150 °C seems to be the most stable at near pH 2—3. This tendency is similar to the results obtained by Kurtenacker *et al.*[7] that tetrathionate solution at 50 °C is the most stable at near pH 0—3. Thus, the reactions shown by Eqs. (7) and (8) are important in the decomposition of tetrathionate under the acidic conditions. However, the successive occurrence of reactions shown by Eqs. (8) and (1) or (8), (2) and (11) lead to the overall reaction of (7), and the reaction shown by Eq. (7) is not necessarily considered as a separate reaction.

The equation to represent the decomposition of tetrathionate in acidic solutions has been considered to be as follows:[7,8]

$$2S_4O_6^{2-} = S_3O_6^{2-} + S_5O_6^{2-} \quad (9).$$

The decomposition of potassium pentathionate accompanied by the precipitation of elemental sulfur took place under the same conditions (Fig. 9), whereas no elemental sulfur was formed from tetrathionate. The decomosition of tetrathionate is not represented by Eq. (9). By thermodynamical consideration[11,15] the reactions which reasonably proceed under acidic conditions are restrictedly expressed by Eqs. (7) and (8). Reactions such as those given by Eqs. (9) and (10) which are considered to express the occurrence of decomposition of tetrathionate[7] can be ruled out.

$$4S_4O_6^{2-} + 3H_2O = 5S_2O_3^{2-} + 2S_3O_6^{2-} + 6H^+ \quad (10)$$

Disproportionation of Sulfite Solution. It is well known that sulfurous acid is subjected to disproportionation at 150—200 °C to give elemental sulfur and sulfuric acid.[9,10] Acidic sulfite solution also decomposes to elemental sulfur and acidic sulfate accompanied by intermediate formation of thiosulfate. The reaction is largely accelerated by the presence of thiosulfate.[11] The formation of polythionate, however, has not been verified. Experiments were carried out in order to elucidate the role of polythionates participating in the disproportionation of mixed solutions consisting of sodium sulfite, sodium thiosulfate and sulfuric acid. From the results (Fig. 10) it is evident that thiosulfate does not undergo a remarkable change up to a sulfuric acid concentration of 20 mM. The decrease in sulfite concentration below the acid concentration of 20 mM is caused by air oxidation. The increase in thiosulfate concentration at a sulfuric acid concentration of about 25 mM could be related to the formation of another thiosulfate according to the reaction

$$4HSO_3^- = S_2O_3^{2-} + 2SO_4^{2-} + 2H^+ + H_2O \quad (11).$$

It is seen that the formation of tetrathionate becomes predominant under the conditions where sulfite undergoes disproportionation.

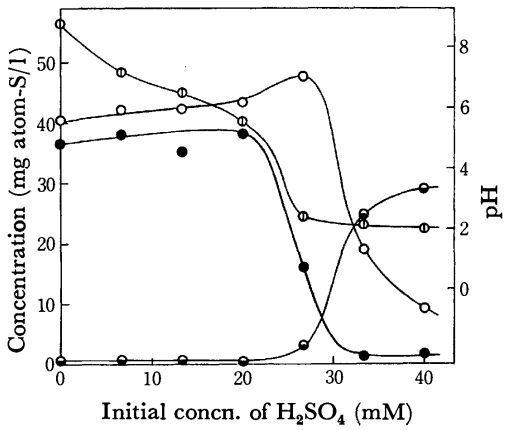

Fig. 10. Disproportionation of mixed solutions of sulfite, thiosulfate and sulfuric acid.
Initial concn of $Na_2S_2O_3$: 21 mM, initial concn of Na_2SO_3: 50 mM, temp: 150 °C, time: 2 h.
○: $S_2O_3^{2-}$, ◒: $S_4O_6^{2-}$, ●: HSO_3^-, ⦶: pH.
The amounts of elemental sulfur and sulfate formed were not determined. When the initial concentration of sulfuric acid is 0, 25, and 40 mM, the initial composition of the solution is given approximately as follows: $Na_2S_2O_3$ (21 mM)—Na_2SO_3 (50 mM), $Na_2S_2O_3$ (21 mM)—$NaHSO_3$ (50 mM), and $Na_2S_2O_3$ (21 mM)—$NaHSO_3$ (20 mM)—H_2SO_3 (30 mM), respectively.

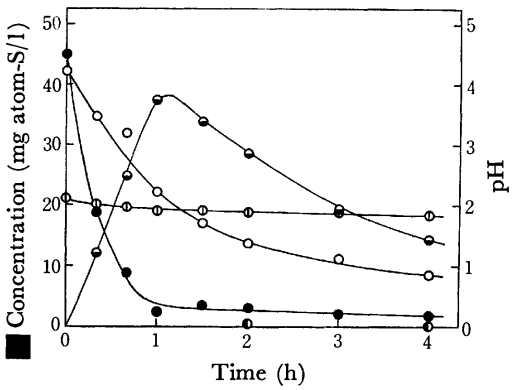

Fig. 11. Time course of the disproportionation of a mixed solution of sulfite, thiosulfate and sulfuric acid.
Initial concn of $Na_2S_2O_3$: 21 mM, initial concn of Na_2SO_3: 45 mM, initial concn of H_2SO_4: 40 mM, temp: 150 °C.
○: $S_2O_3^{2-}$, ◐: $S_3O_6^{2-}$, ◒: $S_4O_6^{2-}$, ●: HSO_3^-, ⦶: pH.
The amounts of elemental sulfur and sulfate formed were not determined.

Figure 11 shows the acid decomposition of a mixed solution of thiosulfate and sulfite with the lapse of time, showing that the decomposition velocity is extremely high, and that the concentration of tetrathionate increases linearly with the lapse of time. The increase in tetrathionate concentration after 1 h from the beginning of experiment is about twice as high as the decrease in thiosulfate concentration, indicating that tetrathionate is formed not only from thiosulfate but also from sulfite. On the other hand, most of the sulfite disappears upon disproportionation within 1 h,

and so tetrathionate is not supplied thereafter, which begins to decrease suddenly. The reason why thiosulfate decomposes at a slower speed than that as seen in Fig. 1 is that, under the conditions shown in Fig. 11, the decomposition of thiosulfate is caused by the proton released in the disproportionation of tetrathionate.

It cannot be made clear from the present experiments what kinds of intermediates are formed in the disproportionation of sulfite. It has been concluded that sulfite firstly decomposes according to Eq. (11) to give thiosulfate and sulfate.[11] Thus, the formation of tetrathionate from sulfite may be explained on the basis of reactions (11) and (1).

Pathway of Disproportionation of Low Valence Sulfur Oxyacids. Tetrathionate undergoes sulfite degradation in faintly acidic to alkaline solution, forming thiosulfate and trithionate as shown by

$$S_4O_6^{2-} + HSO_3^- = S_3O_6^{2-} + S_2O_3^{2-} + H^+ \quad (12).$$

Taking this reaction into consideration, the pathway of disproportionation of low valence sulfur oxyacids including thiosulfate, trithionate, tetrathionate and sulfite is shown to be as follows (Fig. 12). Tetrathionate

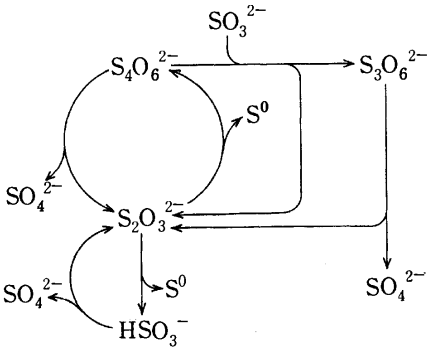

Fig. 12. Pathway of disproportionation of low valence sulfur oxyacids under the acidic conditions.

is decomposed with sulfite to give thiosulfate and trithionate. Trithionate is subjected to hydrolysis to give thiosulfate and sulfate, only if the temperature is high enough. On the other hand, tetrathionate decomposes to thiosulfate and sulfate at the temperature above 130 °C in the absence of sulfite. The thiosulfate thus formed undergoes disproportionation to elemental sulfur and tetrathionate, or elemental sulfur and sulfite. Sulfite undergoes disproportionation to give thiosulfate and sulfate, and then elemental sulfur and sulfate accompanied by intermediate formation of tetrathionate.

The reaction pathway shown in Fig. 12 has been proposed to explain the species detected in the course of the present experiments, such reactions as shown by Eq. (5) thus being excluded. Further study is necessary to clarify the details of the reactions. The reaction pathway (Fig. 12), however, may be useful in understanding the manner in which low valence sulfur oxyacids decompose and the kinds of intermediates formed in acidic solutions at relatively high temperatures.

References

1) Part IX of this series: T. Mizoguchi and T. Okabe, This Bulletin, **48**, 1799 (1975).
2) J. Janickis, *Z. Anorg. Allg. Chem.*, **234**, 193 (1937).
3) E. Blasium and R. Krämer, *ibid.*, **318**, 113 (1962).
4) F. H. Pollard, G. Nickless, and R. B. Glover, *J. Chromatog.*, **15**, 518 (1964).
5) F. Foerster, *Z. Anorg. Allg. Chem.*, **139**, 246 (1924); *ibid.*, **144**, 337 (1925).
6) A. Kurtenacker and M. Kaufmann, *ibid.*, **148**, 43, 369 (1925).
7) A. Kurtenacker, A. Mutschin, and F. Stastny, *ibid.*, **224**, 399 (1935).
8) E. Blasius and G. Wermbter, *ibid.*, **316**, 251 (1962).
9) T. Marusawa, *Kogyo Kagaku Zasshi*, **20**, 737 (1917).
10) F. Foerster, F. Lange, O. Droßbach, and W. Seidel, *Z. Anorg. Allg. Chem.*, **128**, 245 (1923).
11) T. Okabe, G. Otoshi, and S. Hori, *Kogyo Kagaku Zasshi*, **61**, 662 (1958); T. Okabe, M. Owaku, and S. Hori, *Nippon Kagaku Zasshi*, **81**, 1818 (1960).
12) H. Stamm, M. Goehring, and U. Feldmann, *Z. Anorg. Allg. Chem.*, **250**, 226 (1942).
13) F. Martin and L. Metz, *ibid.*, **127**, 83 (1923).
14) P. A. Trudinger, *J. Bacteriol.*, **93**, 550 (1967).
15) R. M. Garrels and C. L. Christ, "Solutions, Minerals, and Equilibria," Harper and Row, New York (1965).
16) A. Kurtenacker and M. Kaufmann, *Z. Anorg. Allg. Chem.*, **148**, 225 (1925).
17) E. Blasius and W. Burmeister, *Z. Anal. Chem.*, **168**, 1 (1959).
18) C. J. Battaglia and W. J. Miller, *Phot. Sci. Eng.*, **12**, 46 (1968).
19) T. Koh and K. Taniguchi, *Anal. Chem.*, **46**, 1679 (1974).
20) T. Koh, A. Wagai, and Y. Miura, *Anal. Chim. Acta*, **71**, 367 (1974).

Semi-empirical UHF-MO Studies of the Spin Distribution and the Bonding Character of Iron-group Fluorides and Some Other Similar Transition Metal Halides

Shigeyoshi SAKAKI,* Hisamichi KIKKAWA, Hiroshi KATO,** and Satohiro YOSHIDA

Department of Hydrocarbon Chemistry, Faculty of Engineering, Kyoto University, Sakyo-ku, Kyoto 606

***Department of General Education, Nagoya University, Chikusa-ku, Nagoya 464*

(Received April 21, 1975)

CNDO- and INDO-type UHF-MO calculations are carried out on MF_6^{n-} (M=V(II), Cr(III), Mn(II), Fe(III), Ni(II)), $NiCl_6^{4-}$, $MnCl_6^{4-}$, $MnCl_4^{2-}$, $MnBr_6^{4-}$, and $CuCl_4^{2-}$. The calculated spin fractions on the ligand orbitals agree well with the experimental values, with a few exceptions. Spin transfers to ligands are mainly attributed to the spin delocalization (SD) mechanism, except those to the 2s and $2p_\sigma$ orbitals of the F ligand in CrF_6^{3-} and VF_6^{4-}, in which spin transfer to those orbitals results from the spin polarization (SP) mechanism. Unpaired electrons are also transferred into the 4s and 4p orbitals of the central metal ion by the SP mechanism. The spin transfers to the ligand due to both the SD and SP mechanisms increase in the order of F<Cl<Br in MnX_6^{4-} and NiX_6^{4-}. The following characterisities of metal-halogen bonds are established; (1) the covalent interaction between the metal d-orbital and the fluorine atom increases in the order Ni(II)<Mn(II)~Fe(III)<Cr(III)~V(II) in MF_6^{n-}, and (2) in metal-halogen covalent interactions, the s-character of halogen decreases in the order F>Cl>Br, while the p-character increases in the same order.

^{19}F NMR studies of open-shell iron-group fluorides have revealed the existence of hyperfine interaction between the fluorine nuclei and the magnetic electrons.[1-7] Similar hyperfine interactions have also been observed in ESR studies of those complexes.[2,8-13] These hyperfine interactions have been explained in terms of the spin fractions on the F ligand.[2-15] It has been accepted that unpaired electrons have been brought into the s and p orbitals of the ligand by metal-fluorine covalency (the spin delocalization (SD) mechanism),[2-16] except in the cases of CrF_6^{3-} and VF_6^{4-}, in which the spin fractions on the 2s orbital of the F ligand are considered to result from the mixing of the excited states (the spin polarization (SP) mechanism).[4,10] However, the spin transfer due to the SP mechanism has not been ascertained theoretically.

Although some theoretical works have been carried out on the electronic structures of these complexes,[14-24] only a few UHF-MO calculations have been presented[19,20,23] which are suitable for studying the spin distribution. Only one INDO-type semi-empirical UHF-MO study of iron-group fluorides has been carried out, by Brown *et al.*[19] In that study, however, the fluorine's 2s orbital was neglected in the basis set, although this orbital is expected to contribute significantly to the metal-fluorine bond. There exists a possibility that this neglect leads to an incorrect conclusion as to the spin distribution.

In this work, semi-empirical UHF-MO calculations, which explicitly included all the valence orbitals, were carried out for iron-group fluorides and some other similar halides, such as $NiCl_6^{4-}$, $MnCl_6^{4-}$, $MnCl_4^{2-}$, $MnBr_6^{4-}$, and $CuCl_4^{2-}$. None of the latter compounds except $CuCl_4^{2-}$ and $MnCl_4^{2-}$ have ever been studied by means of the method, as for as we know. The MO method is a powerful means for studying the electronic structure of transition metal complexes. Especially we need much theoretical support when we attempt to interpret the results of NMR, ESR, *etc.* Thus, the purposes of this work are; (1) to investigate the electronic structures of these complexes, and (2) to ascertain how useful the semi-empirical SCF-MO method is in interpreting the NMR and ESR results of these complexes.

* Present address: Department of Industrial Chemistry, Faculty of Engineering, Kumamoto University, Kurokami, Kumamoto 860

Method, Parametrization, and Geometries

Method. A semi-empirical UHF-MO method is used, in which either a CNDO- or INDO-type approximation is included. The approximations used here are the same as our previous ones for the CNDO-type MO method[25] and the same as Konishi's for the INDO-type one[26] respectively. Only the one-electron part of the Fock-matrix elements, H_{rt}, in the INDO-type MO method will be reiterated here:

$$H_{rr} = -I_r - (N_r - 1)\gamma_{rr} - \sum_{t\neq r}^{A} N_r(\gamma_{rt} - 0.5\kappa_{rt}) - \sum_{B\neq A}\sum_{s}^{B} N_s\gamma_{rs} \quad (1)$$

$$H_{rt} = -0.5KS_{rt}(I_r + I_t) \quad (2)$$

where r-AO is on the A atom and where $\sum^A$ means the summation on the A atom. H_{rr} in the CNDO-type MO method is obtained by the use of Eq. (1) by neglecting κ_{rt}. For the Wolfsberg-Helmholz parameter, K,[27] the values of 1.0 and 0.8 are used in the AO pair including the d-orbital and in that including only the s and p orbitals[25b] respectively.

Parametrization. The elements of the first transition series have $d^{n-2}s^2$ configurations in their ground states, except for the Cr atom, which contains the d^5s configuration, where n represents the number of valence electrons. Thus, for metal atoms, the following ionization processes may be considered as valence-state ionizations:

(1) 3d orbital ionization potential (IP); $3d^{n-2}4s^2 \rightarrow 3d^{n-3}4s^2$,

(2) 4s orbital IP; $3d^{n-2}4s^2 \rightarrow 3d^{n-2}4s$,

(3) 4p orbital IP; $3d^{n-2}4s4p \rightarrow 3d^{n-2}4s$.

These values are calculated by using the data of Di Sipio *et al.*[28] The values of the one-center Coulomb repulsion integrals are also taken from the same work.[28] For ligand atoms, the values of the VSIP and one-center Coulomb repulsion integrals are taken from Hinze's work.[29] The values of one-center exchange repulsion intergrals are adopted from Di Sipio's work[30] for metal atoms and from Kato's report[31] for ligand atoms.

In INDO-type MO calculations, the values of the one-center Coulomb repulsion integrals, γ_{ds} and γ_{dp}, are evaluated from Slater-Condon parameters.[30]

The double-ζ type orbitals of Richardson *et al.*[32] are used only for the d-orbitals,[33] while single Slater-type orbitals[34] are used for the s and p orbitals.

Bond Index. The contribution of the AB bond to the total energy, E_{AB}, is used as the bond index.[35,36] This quantity is represented as follows under both approximations, CNDO- and INDO-type used here;

$$E_{AB} = \sum_r^A \sum_t^B [2P_{rt}H_{rt} - \{(P_{rt}^{\alpha})^2 + (P_{rt}^{\beta})^2\}\gamma_{rt}] + \sum_r^A \sum_t^B (P_{rr} - N_r)(P_{tt} - N_t)\gamma_{rt} \quad (3)$$

where $P_{rt} = P_{rt}^{\alpha} + P_{rt}^{\beta}$. The first term on the right-hand side represents approximately the contribution of the covalent bonding interaction, and the second one, approximately that of the electrostatic one. In order to investigate the metal-halogen bonding nature, the first term is divided into individual AO-pair terms, such as $E_{AB(s)}$, $E_{AB(p)}$, and $E_{AB(d)}$;

$$E_{AB(s)} = \sum_r^A [2P_{rs}H_{rs} - \{(P_{rs}^{\alpha})^2 + (P_{rs}^{\beta})^2\}\gamma_{rs}] \quad (4)$$

$$E_{AB(p)} = \sum_r^A \sum_t^{B(p)} [2P_{rt}H_{rt} - \{(P_{rt}^{\alpha})^2 + (P_{rt}^{\beta})^2\}\gamma_{rt}] \quad (5)$$

where $\sum^{B(p)}$ means the summation on the p-orbitals of the B atom. $E_{AB(d)}$ is similarly defined. The quantity, $E_{AB(s)}$, represents the contribution of the B atom's s-orbital to the A-B bond; $E_{AB(p)}$, that of the B atom's p-orbital, and $E_{AB(d)}$, that of the B atom's d-orbital. The second term in Eq. (3) is not divided into individual AO-pair terms, since it approximately represents the electrostatic interaction, and so the division described above is meaningless.

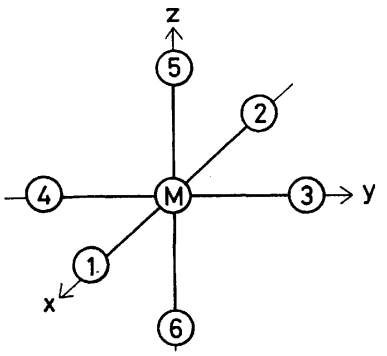

Fig. 1. The coordinate system of MX_6^{n-}.
In $CuCl_4^{2-}$ and $MnCl_4^{2-}$, x, y, and z axis are defined corresponding to their C_4 and C_2 axis respectively.
M–X bond lengths (Å unit): Ni–F=2.00, W. H. Bauer, *Acta Crystallogr.*, **11**, 588 (1958); Mn–F=2.095,[7] and 2.31,[11] see the footnote (f) of Table 3; Fe–F=1.994[11]; Cr–F=1.933;[4] V–F=1.994;[2] Ni–Cl=2.43;[40] Mn–Cl (Oh)=2.63;[13] Mn–Cl (Td)=2.32;[13]; Mn–Br=2.75 (the estimated value); Cu–Cl=2.26.[39]

Geometries. The structure of MX_6^{n-} is assumed for simplicitly to be a rigid octahedron, while its true structure is slightly distorted.[3,4,6] The coordinate system of MX_6^{n-} is shown in Fig. 1. The structures of $CuCl_4^{2-}$ and $MnCl_4^{2-}$ are considered to obey D_{4h}[37] and T_d[13] symmetries respectively.

Results and Discussion

Electron Densities. Table 1 gives the electron distributions calculated by the INDO-type MO method.

The INDO- and CNDO-type MO methods give similar electron densities on the 3d, 4s, and 4p orbitals of the central metal atom; for example, in the CNDO-

Table 1. Electron densities and atomic charges[a]

Compounds	Total density: Metal atom 3d	4s	4p	Halogen atom s	p_σ	p_π	Atomic charge: Metal	Halogen
NiF_6^{4-}	8.138	0.251	0.465	1.922	1.945	3.991	+1.146	−0.858
M–H–H–B[b]	8.023	0.071	0.060	1.985	5.986		+1.818	−0.970
$NiCl_6^{4-}$	8.151	0.449	0.764	1.923	1.864	3.985	+0.636	−0.773
FeF_6^{3-}	5.373	0.272	0.500	1.908	1.926	3.974	+1.855	−0.809
Obsd[c]							+1.33	
MnF_6^{4-} [d]	5.190	0.212	0.429	1.922	1.954	3.985	+1.169	−0.861
$MnCl_6^{4-}$	5.193	0.404	0.711	1.929	1.872	3.980	+0.692	−0.782
$MnBr_6^{4-}$	5.190	0.444	0.760	1.936	1.852	3.980	+0.607	−0.768
CrF_6^{3-}	3.701	0.226	0.479	1.878	1.919	3.968	+1.594	−0.766
Obsd[c]							+1.53	
VF_6^{4-}	3.449	0.192	0.447	1.885	1.956	3.977	+0.913	−0.819
$MnCl_4^{2-}$	5.247	0.394	0.780	1.864	1.933	3.848	+0.579	−0.645
$CuCl_4^{2-}$	9.197	0.471	0.599	1.904	1.807	3.973	+0.732	−0.683
D–V–W[e]	9.08	0.10[g]	0.15[g]	1.97[g]	1.92[g]	3.99[g]	+1.54	−0.88

a) The INDO-type MO method. The single annihilation scarcely affects on these results. b) Ref. 23. c) Ref. 38. d) Mn–F=2.095 Å. e) Ref. 39. g) These values are estimated by assuming that the core AO's are fully occupied.

type MO calculation of NiF_6^{4-}, the electron density on the 3d orbital is 8.201, that on the 4s one is 0.256, and that on the 4p one is 0.502. See also the results of the INDO-type MO calculation of NiF_6^{4-} in Table 1.

In NiF_6^{4-} and $CuCl_4^{2-}$, the electron densities on the 3d orbitals of the central metal atom agree well with those obtained by *ab initio* MO calculations,[23,38] while the electron densities on the 4s and 4p orbitals are remarkably larger than those obtained by the *ab initio* MO calculations. Generally speaking, the *ab initio* MO method gives reasonable electron densities. In transition metal complexes, however, the electron densities on 4s and 4p orbitals depend very much upon the orbital expandings.[39] Thus, the *ab initio* MO method, in which re-optimized AO exponents are not used, does not always give good results for the electron densities in transition metal complexes.

In FeF_6^{3-} and CrF_6^{3-}, the calculated net charges on the central metal ion agree fairly well with the experimental values, as is shown in Table 1. These agreements are better than those of the previous INDO-type method.[19]

In NiX_6^{4-} and MnX_6^{4-} (X=F, Cl, Br), the positive net charge on the central metal ion and the negative net charge on the ligand decrease in this order: F>Cl>Br. This result is reasonable considering the electronegativities of the halogens. While the electron densities on the p_π orbital of the halogen scarcely depend on the kind of halogen, those on the p_σ orbital decrease in this order: F>Cl>Br, and those on the s orbital increase slightly in this order: F<Cl<Br. Since the metal-halogen coordination bond is formed by the electron donation from the halogen anion to metal, and since the stronger interaction should bring about less electron density on the halogen, this result suggests that the contribution of the halogen's p_σ orbital to the metal-halogen bond increases in the order of F<Cl<Br, while that of the s orbital decreases. On this issue, a more detailed discussion will be presented in the following paragraph.

In $MnCl_4^{2-}$, the net charges on the Mn and Cl atoms are smaller than those of $MnCl_6^{4-}$. This suggests that more electrons are donated from ligands to the metal ion in $MnCl_4^{2-}$ than in $MnCl_6^{4-}$. A more precise inspection of the electron densities reveals that the strong electron donation in $MnCl_4^{2-}$ results from the formation of a strong π-bond between the Mn and Cl atoms; in $MnCl_4^{2-}$, the electron densities on the $3p_\pi$ orbitals of the Cl ligand are considerably smaller than those of $MnCl_6^{4-}$, while that on the $3p_\sigma$ orbital in $MnCl_4^{2-}$ is larger than that in $MnCl_6^{4-}$.

Metal-halogen Bonding Nature. In order to investigate the metal-halogen bonding nature, E_{MX} (M= metal atom, X=halogen atom) is divided into $E_{MX(s)}$, $E_{MX(p)}$, $E_{M(d)X}$, and $E_{M(s+p)X}$. The results are given in Table 2.

The absolute values of $E_{M(s+p)X}$ are remarkably large and do not depend very much on the kind of central metal, which suggests the 4s and 4p orbitals participate in the metal-halogen covalent bond to almost the same degree in all complexes. The absolute values of $E_{M(d)X}$ depend largely on the kinds of the metal atoms and increase in this order; Ni(II)<Mn(II)~Fe(III)< Cr(III)~V(II), which suggests that the contribution of the 3d orbitals to the metal-halogen bond increases in this order. This increasing order agrees with the decreasing tendency of the numbers of electrons held in the molecule; *i.e.*, as is shown in Fig. 2, the increasing numbers of electrons result in more electrons in the anti-bonding MO's, e_g^* and t_{2g}^*, and as a consequence

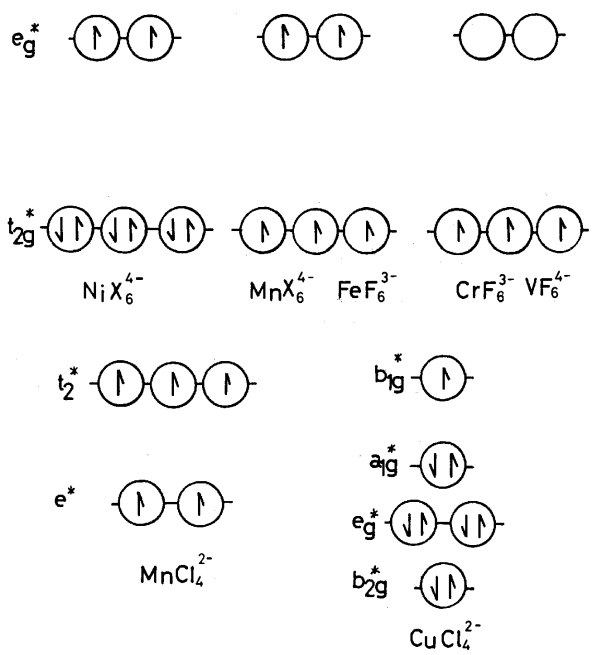

Fig. 2. Schematic MO's mainly contributed from d orbitals of the central metal ion.
These MO's have weak anti-bonding character.

TABLE 2. METAL-HALOGEN BONDING NATURES[a]

(A) Effect of metal atom on metal-halogen covalent bond

Metal atom	Ni(II)	Fe(III)	Mn(II)[b]	Cr(III)	V(II)
$E_{M(d)X}$ (eV)	−0.882	−1.903	−1.383	−4.909	−4.445
$E_{M(s+p)X}$ (eV)	−7.042	−7.451	−6.405	−7.622	−7.229

(B) Effect of halogen atom on metal-halogen covalent bond

Halogen atom	MnX_6^{4-}			NiX_6^{2-}	
	F[b]	Cl	Br	F	Cl
$E_{MX(s)}$ (eV)	−5.770	−3.349	−2.925	−5.844	−3.779
$E_{MX(p)}$ (eV)	−2.018	−3.793	−4.012	−2.079	−4.117

a) The INDO-type MO method. After a single annihilation. b) Mn–F=2.095 Å.

TABLE 3. SPIN FRACTIONS ON THE F⁻ LIGAND (%)

	Method	NiF_6^{4-}		MnF_6^{4-}		FeF_6^{3-}		CrF_6^{3-}		VF_6^{4-}	
		f_s	$f_{p_\sigma}-f_{p_\pi}$	f_s	$f_{p_\sigma}-f_{p_\pi}$	f_s	$f_{p_\sigma}-f_{p_\pi}$	f_s	$f_{p_\sigma}-f_{p_\pi}$	f_s	$f_{p_\sigma}-f_{p_\pi}$
Ours	CNDO	0.72	2.78	0.66	2.32	1.40	4.23	0.0	−1.79	0.0	−0.92
	INDO	0.49	1.80	0.38	1.05	0.94	3.76	−0.19	−1.79	−0.17	−0.88
				0.71	1.29[f]						
	INDO-aa	0.50	1.79	0.40	1.09	0.96	3.75	−0.11	−1.49	−0.10	−0.78
Clack[b]	CNDO-B	0.02	0.33	0.12	1.17	0.15	7.97	−0.003	−0.415	0.0	−0.2002
	CNDO-G	0.15	1.39	0.34	2.25	0.44	7.38	−0.01	−0.74	0.0	−0.30
Brown[c]	MCZDO	—	0.46	—	1.98	—	5.14	—	−4.74	—	—
Obsd	NMR	0.538	3.78[d]	0.52	0.18[g]	—	—	−0.021	−4.90[g]	—	—
	ESR	0.490	4.51[e]	0.47	0.80[e]	0.763	3.3[e]	−0.031	−4.76[e]	−0.072	−2.8[h]
				0.41	1.30[e]						

a) "aa" means the results after a single annihilation. b) Ref. 20). c) Ref. 19). d) Ref. 7). e) Ref. 11). f) Mn–F=2.095 Å. Since the ESR data (Mn–F=2.31 Å) is considerably different from NMR one (Mn–F=2.095 Å), two bond lengths of Mn–F are examined. g) Ref. 4). h) Ref. 2).

of this, the metal-halogen bond becomes weak.

The $E_{MX(s)}$ and $E_{MX(p)}$ of MnX_6^{4-} and NiX_6^{4-} are also given in Table 2. The absolute value of $E_{MX(s)}$ decreases in this order; F>Cl>Br, while that of $E_{MX(p)}$ increases in this order; F<Cl<Br. These results suggest that the contribution of the halogen's s orbital to the metal-halogen bond decreases in this order; F>Cl>Br and that the contribution of the halogen's p orbital increases in this order; F<Cl<Br. This bonding nature is consistent with that discussed in the previous paragraph on the basis of electron density.

Spin Fraction on the Ligands. Results are given in Tables 3 and 4, compared with the experimental values[2,4,7,11] and the previously calculated ones.[19,20] In Table 3, "aa" represents the results after a single annihilation.

TABLE 4. SPIN FRACTIONS ON THE Cl⁻ LIGAND[a]

Compounds	f_s (%)		$f_{p_\sigma}-f_{p_\pi}$ (%)	
	Calcd	Obsd	Calcd	Obsd
$NiCl_6^{4-}$	0.33	0.58[b]	2.10	7.3[b]
$MnCl_6^{4-}$	0.37	0.4[c]	1.50	3.9[c]
$MnCl_4^{2-}$	0.25	—	−2.71[d]	—
$CuCl_4^{2-}$	0.27[d]	0.61	5.09	11.9[d]

a) The INDO-type MO method. After a single annihilation. b) Ref. 40). c) Ref. 13). d) This value is the one before annihilation, since our coordinate system cannot give spin fractions on p_σ and p_π orbitals after annihilation.

INDO-type MO calculations give smaller values of f_s and $f_{p_\sigma}-f_{p_\pi}$ than the CNDO-type MO calculations in all complexes.

As is shown in Fig. 2, NiF_6^{4-} has a $t_{2g}^{*6}e_g^{*2}$ configuration, and MnF_6^{4-} and FeF_6^{3-} have $t_{2g}^{*3}e_g^{*2}$ one. Metal-fluorine covalency results in positive spin fractions on the 2s and $2p_\sigma$ orbitals of the F ligand in NiF_6^{4-} and positive ones on the 2s, $2p_\sigma$, and $2p_\pi$ orbitals in MnF_6^{4-} and FeF_6^{3-}. In these complexes, both CNDO- and INDO-type MO methods can give reasonable results on spin fractions, as is shown in Table 3. Our results are in better agreement with the experiments than the previously calculated ones.[19,20] Single annihilations affect the values of f_s and $f_{p_\sigma}-f_{p_\pi}$ hardly at all.

In CrF_6^{3-} and VF_6^{4-}, which contain t_{2g}^{*3} configurations, as is shown in Fig. 2, metal-fluorine covalency brings positive spin fractions into only two $2p_\pi$ orbitals of the F ligand. Negative spin fraction is also observed on the 2s orbital of the F ligand in these complexes; this is thought to be due to the spin polarization.[4,10] While the CNDO-type MO method fails to give this spin fraction, the INDO-type one can give it. The single annihilation, which gives almost complete eigenvalues of $\mathbf{S}^2$ (See Table 5), brings about remarkably large changes in the values of f_s and $f_{p_\sigma}-f_{p_\pi}$. Although, in these complexes, the values of f_s and $f_{p_\sigma}-f_{p_\pi}$ do not fit in with the experimental values except for the f_s value of VF_6^{4-}, these calculated values are better than the results obtained by the previous CNDO/II calculation[20] and seem reasonable considering the relatively large uncertainty in the experimental values.

The results for chloro complexes are given in Table 4; they were calculated by the INDO-type MO method. The calculated values of f_s agree fairly well with the experimental values except for the case of $CuCl_4^{2-}$. The $f_{p_\sigma}-f_{p_\pi}$ value in chloro complexes are larger than those in fluoro complexes, which is reproduced by our calculations. These calculated values, however, are considerably smaller than the experimental values, as is shown in Table 4.

Spin-transfer Mechanism. Spin fractions are divided into two components according to the method of Nakatsuji *et al.*;[42] the components due to the SD mechanism and the others due to the SP mechanism. The results are given in Table 5, together with the expected values of $\mathbf{S}^2$ before and after a single annihilation.

The expectation values of $\mathbf{S}^2$ before annihilation are almost the same to the eigenvalues of $\mathbf{S}^2$ in all complexes, although there is a little difference between the two values in CrF_6^{3-} and VF_6^{4-}. This shows that we can investigate the electronic structures of these complexes with a single Slater determinant. In all the complexes, unpaired electrons are localized in the d orbitals of the central metal ion; this shows that it is reasonable to use the crystal field theory in the qualitative discussion of the electronic structures of these complexes.

TABLE 5. SPIN APPEARING MECHANISM[a)]

Complex		Metal ion (%)				Ligand ion (%)			S^{2} [b)]	
		$3d_{t_{2g}}$	$3d_{e_g}$	4s	4p	s	p_σ	p_π	ba	aa
NiF_6^{4-}	SD	0.0	93.12	0.0	0.0	0.51	1.78	0.0	2.000	2.000
	SP	0.0	0.0	0.11	0.0	−0.01	0.01	0.0		
$NiCl_6^{4-}$	SD	0.0	92.45	0.0	0.0	0.35	2.16	0.0	2.000	2.000
	SP	0.0	0.0	0.28	0.09	−0.02	−0.05	−0.01		
FeF_6^{3-}	SD	96.98	85.86	0.0	0.0	1.00	3.71	0.75	8.750	8.750
	SP	0.0	0.0	0.14	0.02	−0.04	0.03	−0.01		
MnF_6^{4-} [c)]	SD	99.34	94.53	0.01	0.0	0.46	1.37	0.16	8.750	8.750
	SP	0.0	0.0	0.61	0.18	−0.06	−0.12	0.0		
$MnCl_6^{4-}$	SD	98.77	92.16	0.03	0.0	0.47	2.15	0.30	8.751	8.750
	SP	0.01	0.01	1.42	0.52	−0.10	−0.37	−0.03		
$MnBr_6^{4-}$	SD	98.81	92.24	0.04	0.01	0.39	2.20	0.29	8.752	8.750
	SP	0.02	0.02	1.77	0.66	−0.09	−0.50	−0.02		
CrF_6^{3-}	SD	95.76	−0.04	0.0	0.0	0.0	0.01	1.04	3.753	3.750
	SP	0.03	1.34	0.30	0.14	−0.11	−0.46	0.0		
VF_6^{4-}	SD	97.42	0.01	0.0	0.0	0.0	0.0	0.64	3.751	3.750
	SP	0.0	0.49	0.21	0.11	−0.10	−0.15	0.0		
$MnCl_4^{2-}$ [d)]	SD	91.43	96.59	0.02	2.54	0.52	1.90[e)]		8.752	8.750
	SP	0.12	0.02	1.26	0.74	−0.27	−0.23[e)]			
		$d_{x^2-y^2}$	d_{z^2}	4s	4p	3s	$3p_\sigma$	$3p_\pi$		
$CuCl_4^{2-}$ [f)]	SD	79.00%	0.0%	0.0%	0.0%	0.27%	4.98%	0.0%	0.750	0.750
	SP	0.0	0.04	−0.21	−0.11	0.0	0.10	−0.10		

a) The INDO-type MO method. These data are spin fraction per an orbital after annihilation. b) "aa" and "ba" mean after and before a single annihilation, respectively. c) Mn–F=2.31 Å. d) In $MnCl_4^{2-}$, t_{2g} and e_g should be replaced by t_2 and e, respectively. e) These values are spin fraction on a p-orbital. In our coordinate system, spin fractions on p-orbital after annihilation can not be divided into those on p_σ and p_π orbitals. f) In $CuCl_4^{2-}$, the other 3d-orbitals and $4p_\pi$-orbital do not have spin fractions.

Spin transfer to the ligands is mainly contributed to by the SD mechanism in NiX_6^{4-}, MnX_6^{4-}, and FeF_6^{3-}. It should be noted, however, that the SP mechanism brings a little negative spin fractions on the P_π orbitals of the ligand in MnX_6^{4-}. In these complexes, spin transfer to the halogen s orbital through the SD mechanism roughly decreases in this order; F≳Cl>Br, while that to the halogen p orbital through the same mechanism increases in the same order; F<Cl<Br. It is interesting that the former decreasing order agrees with decreasing order of the halogen's s orbital contribution to the metal-halogen bond, and that the latter increasing one agrees with the increasing order of the halogen's p-orbital contribution (See Table 2-B). The spin fraction due to the SP mechanism increases in this order; F<Cl<Br. It is also interesting that this order agrees with the reverse order of the spectrochemical series. These interesting features should be investigated in more detail.

In CrF_6^{3-} and VF_6^{4-}, the SD mechanism brings about positive spin fractions on the two $2p_\pi$ orbitals of the F ligand, while the SP mechanism induces negative spin fractions on the 2s and $2p_\sigma$ orbitals of the F ligand. These results support the previous proposal of spin transfer in these complexes.[3,10] In $MnCl_4^{2-}$ and $CuCl_4^{2-}$, the spin fractions on the ligand are mainly due to the SD mechanism, while in $MnCl_4^{2-}$ the SP mechanism contributes considerably to f_s and f_p. In $MnCl_4^{2-}$, spin transfer to the Cl ligand is larger than that in the $MnCl_6^{4-}$.

The SP mechanism also induces spin fractions on the 4s and 4p orbitals of the central metal ion in all the complexes. Furthermore, in CrF_6^{3-} and VF_6^{4-} its mechanism also induces positive spin fractions on the $3d_{e_g}$ orbitals.

Comparison between the CNDO- and INDO-type Methods. The CNDO-type MO method can not give the spin fraction due to the SP mechanism, while the INDO-type one can; in CrF_6^{3-} and VF_6^{4-}, the CNDO-type MO method can not give the spin fraction on the 2s and $2p_\sigma$ orbitals of the F ligand which is induced by the SP mechanism, as has been described in the previous paragraph and shown in Table 5. Thus, the CNDO-type method is inferior to the INDO-type method in treating the spin fraction induced by the SP mechanism. It is worthwhile to compare these two methods in the MO calculation of such complexes as NiF_6^{4-}, where the SD mechanism mainly brings about the spin fraction on the ligand (See Table 5) and where the CNDO-type MO method gives good results for the spin distribution. Table 6 gives the MO energies and MO coefficients of NiF_6^{4-}. The CNDO-type MO method gives quite the same MO energies and the same MO coefficients between α-spin and β-spin MO's, while the INDO-type method gives considerably different values. Thus, the CNDO-type method does not show the polarization effects on the MO energy and MO coefficients sufficiently well and is not satisfactory even in NiF_6^{4-}.

In conclusion, the INDO-type MO method used here can give good results on spin fractions. It is expected that this can be used in studies of the electronic structures of open-shell transition metal complexes and

Table 6. Comparison between the CNDO-type and INDO-type MO methods
$2t_{2g}$* MO of NiF_6^{4-}

Method		ε (eV)[a]	Eigenvector[b]
CNDO	α-spin	7.848	$0.783\,d_{xz} - 0.311[(1z)-(2z)+(5x)-(6x)]$
	β-spin	7.848	$0.783\,d_{xz} - 0.311[(1z)-(2z)+(5x)-(6x)]$
INDO	α-spin	7.621	$0.201\,d_{xz} - 0.201[(1z)-(2z)+(5x)-(6x)]$
	β-sinp	8.818	$0.952\,d_{xz} - 0.153[(1z)-(2z)+(5x)-(6x)]$

a) These positive MO energies would be due to the neglect of effects of cation and/or crystal lattice[19]. The extra potential, such as crystal lattice, do not give so great effect on spin fraction.[19] b) $(1z)$ *etc.* means the p_z orbital of the ligand 1 (See Fig. 1.).

can be of great help in interpreting the results of NMR, ESR, *etc.*

These calculations were carried out using the Facom 230-75 Computer of the Data Processing Center in Kyoto University.

The authors wish to thank Professor Kimio Tarama for his generous support of this work. They also wish to thank Dr. Hideyuki Konishi for his help in the calculation and Dr. Hiroshi Nakatsuji for his help in the single annihilation.

References

1) R. G. Shulman and V. Jaccarino, *Phys. Rev.*, **103**, 1126 (1956).
2) J. Owen and J. H. M. Thornley, *Rept. Progr. Phys.*, **29**, 675 (1966).
3) R. G. Shulman and V. Jaccarino, *Phys. Rev.*, **108**, 1219 (1957).
4) R. G. Shulman and K. Knox, *Phys. Rev. Lett.*, **4**, 603 (1960).
5) R. G. Shulman and K. Knox, *Phys. Rev.*, **119**, 94 (1960).
6) R. G. Shulman, *ibid.*, **121**, 125 (1961).
7) R. G. Shulman and S. Sugano, *ibid.*, **130**, 506 (1963).
8) M. Tinkham, *Proc. Roy. Soc., Ser. A*, **236**, 535, 549 (1956).
9) L. Helmholz, *J. Chem. Phys.*, **31**, 172 (1959).
10) L. Helmholz, A. V. Guzzo, and R. N. Sanders, *J. Chem. Phys.*, **35**, 1349 (1961).
11) T. P. P. Hall, W. Hayes, R. W. H. Stevenson, and J. Wilkens, *ibid.*, **38**, 1977 (1963).
12) T. P. P. Hall, W. Hayes, R. W. H. Stevenson, and J. Wilkens, *ibid.*, **39**, 35 (1963).
13) F.-D. Tsay and L. Helmholz, *ibid.*, **50**, 2642 (1969).
14) L. Shields, *J. Chem. Soc., A*, **1971**, 1048.
15) W. Marshall and R. Stuart, *Phys. Rev.*, **123**, 2048 (1961).
16) S. Sugano and R. G. Shulman, *ibid.*, **130**, 517 (1963).
17) R. E. Watson and A. J. Freeman, *ibid.*, **134**, A1526 (1964).
18) A. Dutta-Ahmed and E. A. Boudreaux, *Inorg. Chem.*, **12**, 159 (1973).
19) R. D. Brown and P. G. Burton, *Theoret. Chim. Acta*, **18**, 309 (1970).
20) D. W. Clack, N. S. Hush, and J. R. Yandle, *J. Chem. Phys.*, **57**, 3503 (1972).
21) H. M. Gladney and A. Veillard, *Phys. Rev.*, **180**, 385 (1969).
22) J. W. Richardson, D. M. Vaught, T. F. Soules, and R. R. Powell, *J. Chem. Phys.*, **50**, 3633 (1969).
23) J. W. Moskowitz, C. Hollister, C. J. Hornback, and H. Basch, *J. Chem. Phys.*, **53**, 2570 (1970).
24) G. De Brouchére, N. J. Trappeniers, and C. A. Ten Seldam, *Chem. Phys. Lett.*, **21**, 230 (1973).
25) (a) S. Sakaki and H. Kato, This Bulletin, **46**, 2227 (1973); (b) S. Sakaki, H. Kato, H. Kanai, and K. Tarama, This Bulletin, **47**, 377 (1974).
26) T. Yonezawa, H. Konishi, and H. Kato, This Bulletin, **42**, 933 (1969).
27) M. Wolfsberg and L. Helmholz, *J. Chem. Phys.*, **20**, 837 (1952).
28) L. Di Sipio, E. Tondello, G. De Michelis, and G. Oleari, *Chem. Phys. Lett.*, **11**, 287 (1971).
29) J. Hinze and H. H. Jaffé, *J. Amer. Chem. Soc.*, **84**, 540 (1962).
30) E. Tondello. G. De Michelis, L. Oleari, and L. Di Sipio, *Coord. Chem. Rev.*, **2**, 65 (1967).
31) H. Kato, K. Hirao, H. Konishi, and T. Yonezawa, This Bulletin, **44**, 2062 (1971).
32) J. W. Richardson, W. C. Nieuwpoort, R. R. Powell, and W. F. Edgell, *J. Chem. Phys.*, **36**, 1057 (1962).
33) When the d-function for the $d^{n-2}s^2$ configuration is used, too small spin fractions are obtained. The use of the d-function for d^n-one gives better results on spin distribution. Thus, although the valence state is taken as the $d^{n-2}s^2$ configuration, the d-function for the d^n configuration is used in this work; this does not seem unreasonable considering that the d-function is used only in calculating the overlap integrals induced in the empirical Wolfsberg-Helmholz approximation.
34) E. Clementi and D. L. Raimondi, *J. Chem. Phys.*, **38**, 2686 (1963).
35) M. S. Gordon, *J. Amer. Chem. Soc.*, **91**, 3122 (1969).
36) S. Ehrenson and S. Seltzer, *Theoret. Chim. Acta*, **20**, 17 (1971).
37) H. Rinneberg, H. Haas, and H. Hartman, *J. Chem. Phys.*, **50**, 3064 (1969).
38) J. Demuynck, A. Veillard, and U. Wahlgren, *J. Amer. Chem. Soc.*, **95**, 5563 (1973).
39) In *ab initio* MO calculations on MnO_4^-, the use of the self-consistent AO's for the Mn atom gave remarkably small electron densities on the 4s and 4p AO's of the Mn atom (0.08109e on the 4s and 0.44193e on the 4p AO) (A. P. Mortola, H. Basch, and J. W. Moskowitz, *Int. J. Quant. Chem.*, **7**, 725 (1973)), and the use of the re-optimized AO's gave relatively large ones on those orbitals (*ca.* 0.328e on the 4s AO and *ca.* 0.747e on the 4p AO) (H. Johansen, *Chem. Phys. Lett.*, **17**, 569 (1972)).
40) G. Leonhart and A. Meisel, *J. Chem. Phys.*, **52**, 6189 (1970).
41) T. Amos and L. C. Snyder, *ibid.*, **41**, 1773 (1964).
42) H. Nakatsuji, H. Kato, and T. Yonezawa, *ibid.*, **51**, 3175 (1969).
43) S. Larsson and J. W. D. Connolly, *ibid.*, **60**, 1514 (1974). In the course of our study, this report has been presented, in which spin-polarized multiple scattering X_α calculations are presented on some MF_6^{-n}. Those results fairly agree with experiments to the almost same degree as ours.

A Spectrophotometric Study of Copper(I) Chloro-Complexes in Aqueous 5 M Na(Cl, ClO_4) Solutions

Kazuhiko SUGASAKA and Ayako FUJII

Government Industrial Research Institute, Shikoku, Hananomiya Takamatsu, Kagawa 760

(Received May 6, 1975)

The complex formation of copper(I) ions in aqueous 5 M Na(Cl, ClO_4) solutions was studied by spectrophotometry covering a pH range from acidic to alkaline. Over the range of the chloride concentration of 0.05—5 M in acidic solutions, the complexes $CuCl_2^-$ and $CuCl_3^{2-}$ were found. The molar extinction coefficients of the complexes were determined at various wavelengths from 220 to 320 nm. The equilibrium constant for the reaction $CuCl_2^- + Cl^- = CuCl_3^{2-}$ was determined to be 1.95. Chloro-hydroxo mixed complexes of copper(I), such as $CuClOH^-$, $CuCl_2OH^{2-}$, and $CuCl(OH)_2^{2-}$ were formed in alkaline solutions and the molar extinction coefficients of these species were estimated. The formation constants $\beta_{pq}=[CuCl_{2+p}(OH)^q]/[CuCl_2][Cl]^p[OH]^q$ of the complexes were evaluated to be as follows: $\beta_{-11}=(1.1\pm0.1)\times10^4$, $\beta_{01}=(4.1\pm0.3)\times10^3$, and $\beta_{-12}=(3.8\pm0.7)\times10^6$. No polynuclear complex was formed in the solutions.

It is known that the color of copper(I) oxide changes from yellow to red depending upon the conditions of preparation. Red copper(I) oxide is usually prepared by the electrolysis of a concentrated sodium chloride solution using copper electrodes, while yellow copper(I) oxide is precipitated by the hydrolysis of copper(I) chloride in dilute sodium chloride solutions, the former being used for ship bottom paint for antifouling.

As reported in previous publications[1,2] a search was made for favorable conditions for the preparation of red copper(I) oxide. The present study was undertaken as a continuation of this series of studies.

Since the solubility of copper(I) chloride in water is low, reliable results for the formation of copper(I) chloro-complexes have hitherto scarcely been obtained. The oxidation of copper(I) ions causes another difficulty for the experimental procedures of the study. We first note an investigation by Bodländer and Storbeck[3] who interpreted their results of the solubility measurements of copper(I) chloride in sodium chloride solutions by postulating the formation of the complexes $CuCl_2^-$ and $CuCl_3^{2-}$. More than a quarter century after Bodländer's pioneering work, Fromherz and Menshik[4] showed that the absorption maximum of copper(I) chloro-complexes appeared at 272 nm in a concentrated solution of potassium chloride. Glasner and Avinur[5] found an absorption maximum at 273 nm together with a shoulder at 234 nm in an acidic copper(I) solution containing potassium chloride. The formation of the $CuCl_2^-$ complex in a concentrated hydrochloric acid solution was confirmed by an extraction method and Raman spectrophotometry.[6] The formation constants of copper(I) chloro-complexes have been reported to be $[CuCl_2^-]/[Cu^+][Cl^-]^2=(1.00\pm0.05)\times10^6$, $[CuCl_3^{2-}]/[Cu^+][Cl^-]^3=(0.97\pm0.05)\times10^6$, and hence $[CuCl_3^{2-}]/[CuCl_2^-][Cl^-]=0.97$ by the solubility method.[7]

In all previous studies of copper(I) complexes in chloride solutions, measurements were carried out in acidic solutions.[3-8] It is a well-known fact that an increase in the pH of a copper(I) chloride solution results in precipitates which dissolves with a further increase of pH.[9] Nevertheless, no quantitative investigation has yet been made of alkaline solutions of copper(I) chloride. The aim of the present work is to elucidate the reaction equilibria of copper(I) ions in aqueous chloride solutions over a wide pH range.

Experimental

Reagents. Reagent grade copper(I) chloride was recrystallized from hydrochloric acid and dried at 130 °C in a nitrogen atmosphere after washing the crystals with acetic acid.[10] Copper(I) chloride crystals were dissolved into a 0.5 M sodium chloride solution containing sufficient amounts of sodium perchlorate and perchloric acid in order to maintain the ionic strength and pH at 5 and 1, respectively. Sample solutions were prepared by diluting the stock solution by the addition of sodium chloride and sodium hydroxide solutions. Pure copper wire (99.99% purity) was added to the stock solution for reducing a trace amount of copper(II) ions. The amount of copper(II) ions in the stock solution was calculated not to exceed 4.4×10^{-8} M by using the equilibrium constant of the disproportionation reaction[11] and the formation constants[11] of copper(I) and (II) chloro-complexes reported in the literature. Sodium chloride and sodium perchlorate solutions were prepared from reagent grade chemicals by dissolving them in oxygen free water. All the experimental procedures were carried out in an atmosphere of nitrogen.

Spectrophotometric Measurements were carried out with a Hitachi EPS-3T spectrophotometer. Sample solutions were referred to blank solutions which were identical in composition to the sample solutions except for copper(I) chloride. The influence of copper(II) ions on the measurement of the absorption spectrum was neglected because the amount of copper(II) ions in the sample solution was calculated to not exceed 7.5×10^{-9} M and log ε of the copper(II) chloro-complexes over the wavelength range examined is about 2 to 3.[12] Cells with 1, 2, 10, and 20 mm optical pathlengths were used for the measurements at 25 °C.

Determination of Concentrations of Ions in Solution. The concentration of copper(I) ions in the stock solution was determined by atomic absorption spectrophotometry. The concentration of chloride ions was determined by Mohr's method. Since the concentration of chloride ions was greatly in excess of the copper(I) ions, the concentration of free chloride ions $[Cl^-]$ was equated to the total concentration of sodium chloride in the solution.

pH Measurements. Beckman No. 39013 combination electrodes were used for pH measurements with a Hitachi-Horiba F-5 type expanded-scale pH meter at 25 °C. The electrodes were calibrated against standard solutions of perchloric acid in 5 M Na(Cl, ClO_4) media. In an alkaline region, a series of sodium hydroxide solutions at a constant

ionic medium of 5 M Na(Cl, ClO_4) was used as a series of standard pH buffer solutions. The potentials of the cell obeyed Nernst's equation over the range of the concentration of hydroxide ions from 1×10^{-4} to 3×10^{-2} M to within an uncertainty of ±1 mV.

Results and Discussion

Spectra of Copper(I) Chloride Solutions. Absorption spectra of copper(I) chloride solutions containing various amounts of sodium chloride and sodium hydroxide are shown in Fig. 1. Absorption maxima appeared at 226, 233, and 273 nm depending on the concentrations of chloride and hydroxide ions. In Table 1 are summarized the results of absorption spectra of the solutions. Spectra observed in acidic solutions ($-\log[OH^-]\simeq12$) are similar to those reported by Froherz[4] and Glasner[5] and showed two maxima at wavelengths longer than 200 nm. The absorbance at 273 nm decreased as the concentration of chloride ions decreased.

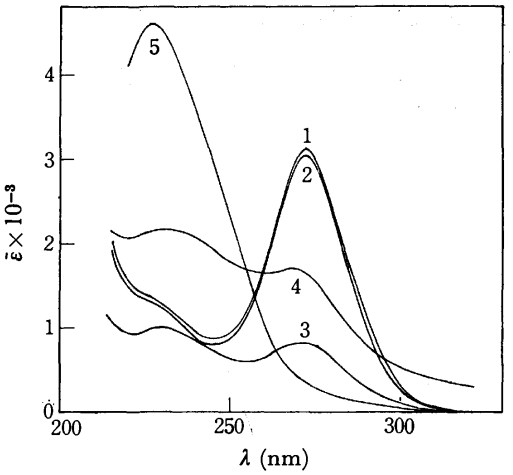

Fig. 1. Spectra of copper(I) chloride aqueous solutions. The compositions of the sample solutions numbered on the curves are shown in Table 1.

The absorption maximum at 226 nm in an alkaline solution has been previously observed.[13] The absorbance at this wavelength increased with the concentration of hydroxide ions, whereas the absorbance at 273 nm decreased.

Table 1. Wavelengths of maximum absorption of copper(I) chloride solutions

No	[Cl⁻] (M)	$-\log[OH^-]$	λ_{max} (nm)
1	5	~12	233(shoulder), 273(sharp)
2	4	~12	233(shoulder), 273(sharp)
3	0.1	~12	233(broad), 270
4	4	2.5[a]	230(broad), 270
5	4	0.25[a]	226(sharp)

a) These values were calculated from the analytical concentrations of hydroxide ions.

Species of Copper(I) Chloro-complexes in Acidic Solutions Containing Sodium Chloride. The apparent molar extinction coefficient $\bar{\varepsilon}=E/[Cu(I)]_{TOT}$ (E denotes the absorbance of a solution for a unit optical length) at 233 and 273 nm varied with the concentration of chloride ions as shown in Fig. 2. $\bar{\varepsilon}$ was independent of the concentration of copper(I) chloride. This result shows that no polynuclear complex of copper(I) was formed in the solution.

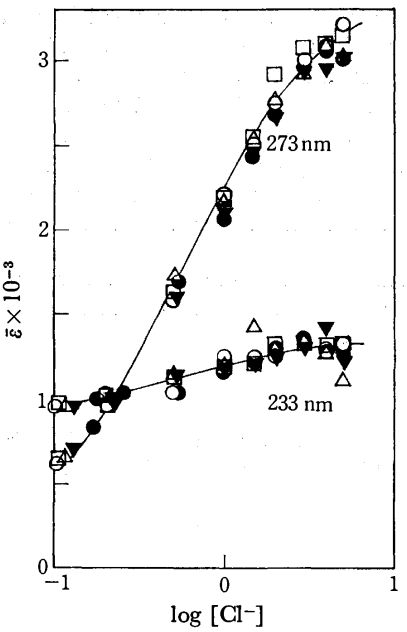

Fig. 2. Plots of $\bar{\varepsilon}$ against log[Cl⁻] ($\mu=5$, $-\log[OH^-]=12$, at 25 °C).
[Cu(I)]=○2.4×10^{-4}, □4.7×10^{-4}, △9.4×10^{-4}, ▼ 1.9×10^{-3}, ●4.7×10^{-3} M.

Copper(I) chloride, which is only slightly soluble in water, becomes soluble in an aqueous solution containing chloride ions to form $CuCl_m^{(m-1)-}$ complexes, where $m\geq2$. Therefore, it may be reasonable to assume that the complex $CuCl_2^-$ is formed at the first stage of complex formation in a chloride solution and formation reactions of higher complexes in solution may be described by the following equation:

$$CuCl_2^- + nCl^- = CuCl_{2+n}^{(n+1)-}. \quad (1)$$

From the material balance of copper(I), the following equation is derived:

$$[Cu(I)]_{TOT} = [CuCl_2^-] + \sum_n \beta_n[CuCl_2^-][Cl^-]^n \quad (2)$$

where $\beta_n=[CuCl_{2+n}^{(n+1)-}]/[CuCl_2^-][Cl^-]^n$. Since the ligand shows no absorption over the entire range studied, the absorbance E per unit path is given by

$$E = \varepsilon_0[CuCl_2^-] + \sum_n \varepsilon_n\beta_n[CuCl_2^-][Cl^-]^n. \quad (3)$$

Then, $\bar{\varepsilon}$ is given by

$$\bar{\varepsilon} = \frac{\varepsilon_0+\sum_n \varepsilon_n\beta_n[Cl^-]^n}{1+\sum_n \beta_n[Cl^-]^n}. \quad (4)$$

The plots of $\bar{\varepsilon}$ *vs.* log[Cl⁻] were fitted to a normalized curve, $y=\log\{a/(1+x)\}$, by choosing a suitable value of a. From this it was found that $n=1$, and thus Eq. (4) is rewritten as

$$\bar{\varepsilon} = \frac{\varepsilon_0+\varepsilon_1\beta_1[Cl^-]}{1+\beta_1[Cl^-]} = \varepsilon_1 + \frac{\varepsilon_0-\varepsilon_1}{1+\beta_1[Cl^-]}. \quad (5)$$

From the best fit to the $\bar{\varepsilon}$ curves at 233 and 273 nm, the following values were obtained: at 273 nm ε_0 (*i.e.*, the molar extinction coefficient of the $CuCl_2^-$ complex) $=0$, $\varepsilon_1=3.5\times10^3$, $\beta_1=1.95$ and at 233 nm $\varepsilon_0=0.9\times10^3$, $\varepsilon_1=1.4\times10^3$ and $\beta_1=1.80$. The formation constant β_1 and the values of ε_0 and ε_1 at 273 and 233 nm were refined with the aid of an electronic computer by means of least squares calculations as shown in Table 2.

Table 2. The molar extinction coefficients and the formation constant of the complexes

λ_{max} (nm)	ε_0	ε_1	β_1
233	$(0.80\pm0.02)\times10^3$	$(1.45\pm0.01)\times10^3$	1.95
273	$(0.00\pm0.08)\times10^3$	$(3.33\pm0.05)\times10^3$	

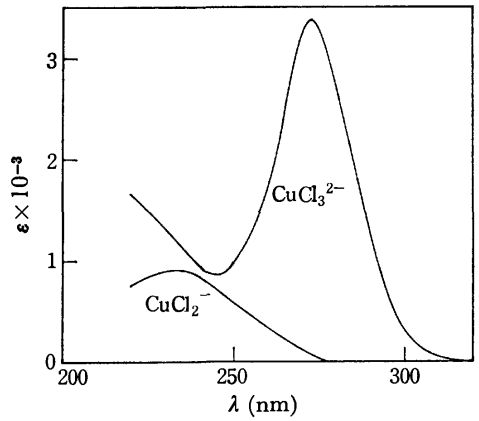

Fig. 3. Calculated spectra for the species of $CuCl_2^-$ and $CuCl_3^{2-}$ in acidic solution.

Figure 3 shows the spectra of the $CuCl_2^-$ and $CuCl_3^{2-}$ complexes calculated from spectrophotometric data at various wavelengths using the constants given in Table 2.

Copper(I) Chloro-complexes in Alkaline Solutions. As shown in Fig. 1, $\bar{\varepsilon}$ at 226 nm increases with the hydroxide ion concentration, whereas $\bar{\varepsilon}$ at 273 nm decreased. Typical examples of the change in $\bar{\varepsilon}$ at 273 and 226 nm with the hydroxide ion concentration are shown in Figs. 4 and 5. $\bar{\varepsilon}$ at 273 and 226 nm also changed with the chloride ion concentration. Therefore, both chloride and hydroxide ions must be taken into consideration in the reaction equilibria of copper(I) chloro-complexes in alkaline solutions. It is obvious that the formation of any polynuclear complex is ruled out because $\bar{\varepsilon}$ was independent of the concentration of copper(I) ions. From the fact that $\bar{\varepsilon}$ at 226 nm at the highest hydroxide ion concentration decreased as the concentration of chloride ions increased, it can be concluded that some $CuCl_{2+p}(OH)_q$ complexes with $p<0$ are formed in the alkaline solution, thus

$$CuCl_2^- + pCl^- + qOH^- = CuCl_{2+p}(OH)_q^{(p+q+1)-}. \quad (6)$$

The material balance for copper(I) ions can be represented by

$$[Cu(I)]_{TOT} = [CuCl_2^-] + \beta_1[CuCl_2][Cl^-] + \sum_p\sum_q \beta_{pq}[CuCl_2^-][Cl^-]^p[OH^-]^q, \quad (7)$$

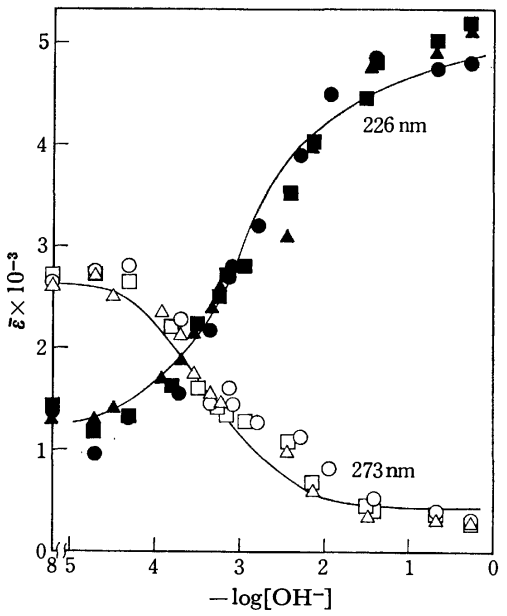

Fig. 4. Plots of $\bar{\varepsilon}$ against the concentration of hydroxide ion.
[Cu(I)]=○2.4×10⁻⁴, □4.6×10⁻⁴, △9.4×10⁻⁴ M, [Cl⁻]=2 M.

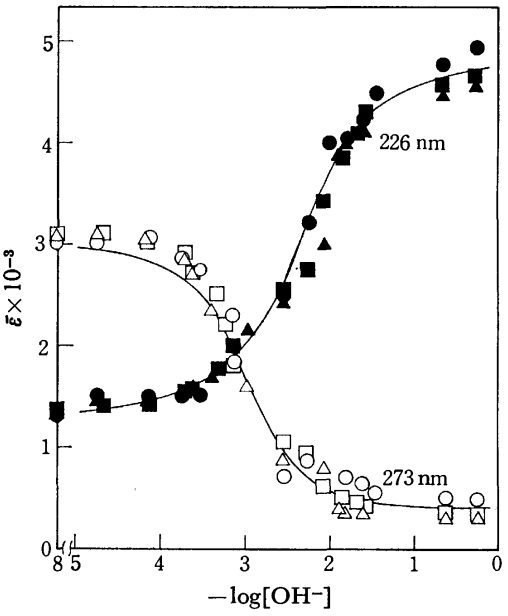

Fig. 5. Plots of $\bar{\varepsilon}$ against the concentration of hydroxide ion.
[Cu(I)]=○2.4×10⁻⁴, □4.6×10⁻⁴, △9.4×10⁻⁴ M [Cl⁻]=4 M.

where p is either positive, zero or negative, and q is zero or a positive integer. The apparent molar extinction coefficient $\bar{\varepsilon}$ may be written as follows:

$$\bar{\varepsilon} = \frac{\varepsilon_0+\varepsilon_1\beta_1[Cl^-]+\sum_p\sum_q\varepsilon_{pq}\beta_{pq}[Cl^-]^p[OH^-]^q}{1+\beta_1[Cl^-]+\sum_p\sum_q\beta_{pq}[Cl^-]^p[OH^-]^q}. \quad (8)$$

By comparing the family of normalized curves, $y=\log\{a/(1+x^b)\}=f(\log x)$, having various values of a and b with the $\bar{\varepsilon}$ *vs.* $\log[OH^-]$ curves at constant $[Cl^-]$, q in the $CuCl_{2+p}(OH)_q^{(p+q+1)-}$ complex can be

roughly estimated. The normalized curve with $b=1$ is less steep and that with $b=2$ is steeper than the experimental ones. These facts suggest that complexes with $q=1$ and 2 are formed in the solution.

In the first approach, the formation of $CuCl_{2+p}OH^{(p+2)-}$ complexes with varying p in the region of relatively low $[OH^-]$ concentration ($-\log[OH^-] \gtrsim 3$) was assumed. With this assumption, Eq. (8) may be rewritten as

$$\bar{\varepsilon} = \frac{\varepsilon_0+\varepsilon_1\beta_1[Cl^-]+\sum_p \varepsilon_{p1}\beta_{p1}[Cl^-]^p[OH^-]}{1+\beta_1[Cl^-]+\sum_p \beta_{p1}[Cl^-]^p[OH^-]}. \quad (9)$$

By rearranging this equation, the following is obtained:

$$F \equiv \{\bar{\varepsilon}(1+\beta_1[Cl^-])-(\varepsilon_0+\varepsilon_1\beta_1[Cl^-])\}[OH^-]^{-1} = \sum_p \varepsilon_{p1}\beta_{p1}[Cl^-]^p - \bar{\varepsilon}\sum_p \beta_{p1}[Cl^-]^p. \quad (10)$$

The plots of F *vs.* $\bar{\varepsilon}$ are shown in Fig. 6 in which three straight lines are seen. The values of $\sum_p \beta_{p1}[Cl^-]^p$ and $\sum_p \varepsilon_{p1}\beta_{p1}[Cl^-]^p$ were obtained from the slopes and intercepts, respectively, of the lines. If it is simply assumed that only one complex is formed, *i.e.*, $p=P$, the values of $\beta_{P1}[Cl^-]^P$ and $\varepsilon_{P1}\beta_{P1}[Cl^-]^P$ are obtained.

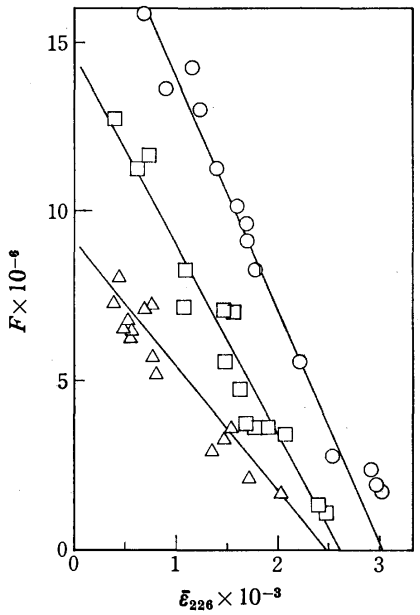

Fig. 6. Plots of F against $\bar{\varepsilon}_{226}$.
$[Cl^-]$=○2, □3, △4 M.

These values are almost inversely proportional to $[Cl^-]$. However, both β_{P1} and $\varepsilon_{P1}\beta_{P1}$ calculated assuming $P=-1$ were not constant but decreased slightly with $[Cl^-]$. Therefore, it is concluded that the $CuCl_2OH^{2-}$ complex must be taken into consideration, in addition to the main product of $CuClOH^-$. On the assumption of the formation of complexes with $P=0$ and -1, β_{-11}, β_{01}, ε_{-11} and ε_{01} were obtained by the simultaneous solution of Eq. (10) at various chloride and hydroxide ion concentrations. At high hydroxide ion concentrations $CuCl_{2+p'}(OH)_2^{(p'+3)-}$ may be formed. Taking into consideration the formation of dihydroxo-complexes, Eq. (8) can be rewritten as

$$\bar{\varepsilon} = \frac{\varepsilon_0+\varepsilon_1\beta_1[Cl^-]+\varepsilon_{-11}\beta_{-11}[Cl^-]^{-1}[OH^-]+\varepsilon_{01}\beta_{01}[OH^-]+\sum_{p'} \varepsilon_{p'2}\beta_{p'2}[Cl^-]^{p'}[OH^-]^2}{1+\beta_1[Cl^-]+\beta_{-11}[Cl^-]^{-1}[OH^-]+\beta_{01}[OH^-]+\sum_{p'} \beta_{p'2}[Cl^-]^{p'}[OH^-]^2}. \quad (11)$$

Rearrangement of Eq. (11) leads to

$$F' \equiv \{\bar{\varepsilon}(1+\beta_1[Cl^-]+(\beta_{-11}[Cl^-]^{-1}+\beta_{01})[OH^-]) -(\varepsilon_0+\varepsilon_1\beta_1[Cl^-]+(\varepsilon_{-11}\beta_{-11}[Cl^-]^{-1} +\varepsilon_{01}\beta_{01})[OH^-])\}[OH^-]^{-2} = \sum_{p'} \varepsilon_{p'2}\beta_{p'2}[Cl^-]^{p'} - \bar{\varepsilon}\sum_{p'} \beta_{p'2}[Cl^-]^{p'}. \quad (12)$$

The left-hand side of Eq. (12), F', can be calculated from the experimental data by the insertion of the values ε_{-11}, ε_{01}, β_{-11} and β_{01} determined in the previous section. The plots of $F'\times[Cl^-]$ *vs.* $\bar{\varepsilon}$ are shown in Fig. 7. The points fall on a single straight line, the

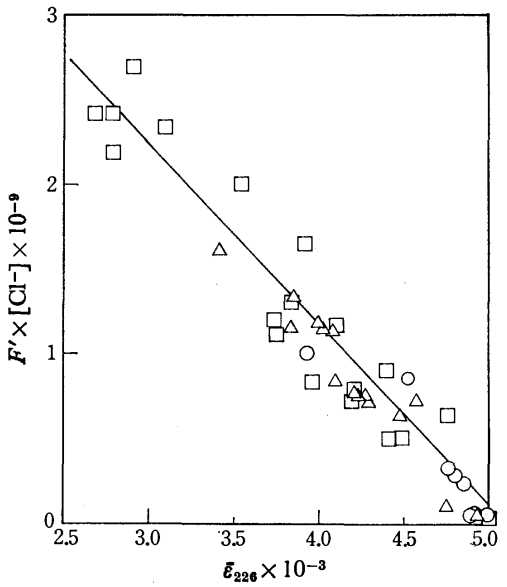

Fig. 7. Plots of $F'\times[Cl^-]$ against $\bar{\varepsilon}_{226}$.
$[Cl^-]$=○2, □3, △4 M.

spread of the points being probably due to experimental uncertainties. From the plot, it can be seen that the values of $F'\times[Cl^-]$ are independent of the chloride ion concentration, and thus $p'=-1$, *i.e.*, $CuCl(OH)_2^{2-}$. From the slope and intercept of the line, the values of β_{-12} and ε_{-12} were obtained.

Finally the formation constants and the molar extinction coefficients of the complexes proposed were refined with the aid of an electronic computer and the results are summarized in Table 3.

Table 3. The molar extinction coefficients and formation constants of copper(I) chloro-hydroxo-complexes

Species	$\varepsilon_{pq}(cm^{-1}\cdot M^{-1})$ 226 nm	273 nm	β_{pq}
$CuClOH^-$	5080	300	$(1.1\pm0.1)\times10^4$
$CuCl_2OH^{2-}$	0	0	$(4.1\pm0.3)\times10^3$
$CuCl(OH)_2^{2-}$	4760	500	$(3.8\pm0.7)\times10^6$

The solid lines in Figs. 4 and 5 show the curves calculated using the constants finally obtained. Although slightly systematic deviations were found in the plots of $\bar{\varepsilon}$ *vs.* $-\log[OH^-]$ at 273 nm, it is expected that better results cannot be obtained assuming additional complexes because of the relatively large uncertainties in the pH measurements and the reproducibility of the data for the alkaline solutions.

The distribution of the complexes in 2 and 4 M chloride solutions at an ionic strength of 5 over the $-\log[OH^-]$ range from 5 to 0 is shown in Fig. 8.

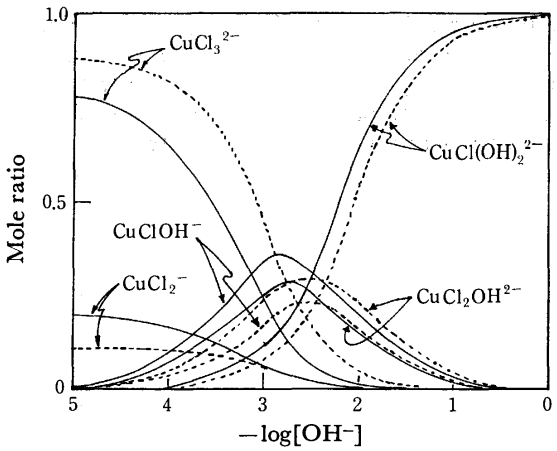

Fig. 8. Distribution of the species of copper(I). $[Cl^-]$=—2, —4 M.

The following equilibrium constants were also obtained from the results in Table 3.

$$CuCl_2^- + OH^- \rightleftharpoons CuClOH^- + Cl^-$$
$$K_{-11} = \beta_{-11} = (1.1\pm0.1)\times10^4 \quad (13)$$
$$CuCl_2^- + OH^- \rightleftharpoons CuCl_2OH^{2-}$$
$$K_{01} = \beta_{01} = (4.1\pm0.3)\times10^3 \quad (14)$$
$$CuCl_3^{2-} + OH^- \rightleftharpoons CuCl_2OH^{2-} + Cl^-$$
$$K_{01}' = \beta_{01}/\beta_1 = (2.1\pm0.2)\times10^3 \quad (15)$$
$$CuClOH^- + OH^- \rightleftharpoons CuCl(OH)_2^{2-}$$
$$K_{-12} = \beta_{-12}/\beta_{-11} = (3.5\pm1.0)\times10^2 \quad (16)$$
$$CuCl_2OH^{2-} + OH^- \rightleftharpoons CuCl(OH)_2^{2-} + Cl^-$$
$$K_{-12}' = \beta_{-12}/\beta_{01} = (0.9\pm0.2)\times10^3 \quad (17)$$

The authors wish to express their grateful thanks to Professor Hitoshi Ohtaki of the Tokyo Institute of Technology for guidance and helpful discussions. We also thank Dr. Shin-ichi Ishiguro for programming the computer calculations.

References

1) K. Sugasaka and T. Kobayashi, *Kogyo Kagaku Zasshi*, **71**, 335 (1968).
2) K. Sugasaka, A. Fujii, and J. Mizuguchi, *Kogyo Kagaku Zasshi*, **71**, 1107 (1968).
3) G. Bodländer and O. Storbeck, *Z. Anorg. Chem.*, **31**, 1 (1902).
4) H. Fromherz and W. Menshik, *Z. Phys. Chem.*, **3**, 1 (1929).
5) A. Glasner and P. Avinur, *Anal. Chem.*, **33**, 1122 (1961).
6) J. A. Creighton and E. R. Lippincott, *J. Chem. Soc.*, **1963**, 5134.
7) H. Hikita, H. Ishikawa, and N. Esaka, *Nippon Kagaku Kaishi*, **1973**, 13.
8) S. Ahrland and J. Rawsthorne, *Acta Chem. Scand.*, **24**, 157 (1970).
9) L. Wilson, *Australia, Commonwealth Dept. Supply, Aeron. Res. Lab., Note*, **19**, 7 (1964).
10) "Jikken Kagaku Koza" Vol. 9, Maruzen, Tokyo (1958), p. 379.
11) "Stability Constants," Chem. Soc., London, No. 17 (1974), pp. 17, 285, 286.
12) H. McConnel and N. Davidson, *J. Amer. Chem. Soc.*, **72**, 3164 (1950).
13) K. Sugasaka, A. Fujii, S. Katoh, and J. Mizuguchi, *Kogyo Kagaku Zasshi*, **72**, 1238 (1969).

Heteropolytungstates Containing Cobalt(II) or Cobalt(III)

Akitoshi KOMURA, Mutsuo HAYASHI, and Hiroto IMANAGA
Faculty of Technology, Kanazawa University, Kanazawa 920
(Received May 14, 1975)

The reactions of tungstophosphate with cobalt ion and the properties of heteropolytungstates containing cobalt have been investigated. Unsaturated heteropolyanion $PW_{11}O_{39}^{7-}$ produced by the partial degradation of the parent 12-tungstophosphoric acid reacts with cobalt ion to give 11-tungstocobaltophosphate $PCoW_{11}O_{40}H_2^{5-}$. Discussion is given on the presence of cobalt in the heteropolyanion and on the above reaction. Both 12-tungstocobaltate-(II) and -(III) are very resistant to acid, but 11-tungstocobaltophosphates lose cobalt ion in strongly acidic solutions to give the parent 12-acid. Some aspects of the spectra of the heteropolytungstates, in which cobalt(II) and cobalt(III), respectively, are present in the specific site, are discussed.

The characteristic of molybdenum and tungsten is the formation of numerous isopoly and heteropoly acids and their salts. The heteropolyanions containing two different heteroatoms have been reported.[1-3] Baker and Figgis[4] showed that in heteropolyanions an octahedrally coordinated transition metal atom replaces one of the 12 octahedral tungsten atoms of conventional Keggin structure,[5] being simultaneously coordinated to a water molecule (constitutional water). Malic and Weakley[1,2] prepared many ternary heteropolyanions from the solutions containing unsaturated heteropolyanions which were isolated as solid by Tourné and Tourné,[6] and formulated the ternary heteropolyanions. Weakley[7] reported the replacement of the constitutional water by other ligands mainly in the heteropolyanions containing cobalt. On the other hand, there are some ternary heteropolyanions which can not be interpreted on the basis of the Keggin structure.[8] The anions probably formed through addition reactions appear to have the composition X: Z: W or Mo=1: 1: 12, where both X and Z are heteroatoms. The heteropolyanions containing metal heteroatoms form an important class of coordination compounds, but their chemistry remains unclarified. In order to obtain information on heteropoly complexes, we have investigated the chemical and spectroscopic properties of heteropolytungstates containing cobalt, reported by Weakley.[7] The present paper deals with the formation process of the heteropolyanions and the formulation proposed by Baker and Figgis.[4]

Experimental

Dodeca-tungstophosphoric acid was obtained from Wako Pure Chemical Industries Ltd. (Found: P, 1.0; W, 64.4%). Potassium monohydrogen 12-tungstocobaltate(II) was prepared by Baker's method.[9] The cerimetric titration gave 3550 as its equivalent weight. Found: K, 5.3; Co, 1.7; W, 62.0%. Calcd for $K_5HCoW_{12}O_{40}\cdot 24H_2O$: K, 5.5; Co, 1.7; W, 62.4%, equiv. wt, 3534.

Potassium 11-Tungstophosphate. Preparation was carried out by a modification of Tourné's method.[6] To a solution of 12-tungstophosphoric acid (25 g) in water (300 ml) at 90—100 °C was added 0.5 M-potassium bicarbonate dropwise with stirring until a large portion of the precipitate of the resulting potassium 12-tungstophosphate disappeared (the pH of the solution being then about 5). A small quantity of the residual precipitate was filtered off and the pH of the filtrate was adjusted to 5.25 with potassium acetate buffer solution. The filtrate was concentrated to one third of its original volume and then kept at 5 °C for a few days while white crystals formed. These were filtered off, washed with water, and air-dried at room temperature. Found: K, 8.1; P, 1.0; W, 58.6%. Calcd for $K_7PW_{11}O_{39}\cdot 28H_2O$: K, 7.9; P, 0.9; W, 58.5%.

Potassium 11-Tungstocobalto(II)phosphate. The procedure was based on that for 11-tungstocobalto(II)silicate.[1] A solution of cobalt nitrate (2.2 g) in water (20 ml) was added with stirring to a heated solution (pH 5.3) of 12-tungstophosphoric acid partly degraded in a similar manner to that above. The mixture was concentrated to two thirds of its original volume after being filtered at 60 °C. The solution was kept at 5 °C for a few days while deep red crystals separated. Found: K, 6.8; P, 1.0; Co, 1.6; W, 61.0%. Calcd for $K_5PCoW_{11}O_{40}H_2\cdot 20H_2O$: K, 6.0; P, 0.9; Co, 1.8; W, 61.1%. Weakley[7] gave 15 molecules of water of hydration to the complex.

Pyridinium 11-Tungstocobalto(II)phosphate. This compound was isolated in an attempt to coordinate pyridine to the cobalt atom of potassium 11-tungstocobalto(II)phosphate. Thirty milliliters of 0.1 M-aqueous solution of pyridine was added to a solution of potassium 11-tungstocobalto(II)phosphate (3.34 g) in water (20 ml) with stirring. A pink precipitate which formed immediately was filtered off, washed with an aqueous solution of pyridine and methanol, and air-dried at room temperature. Found: Co, 1.7; W, 64.0%. Calcd for $C_{25}H_{30}N_5PCoW_{11}O_{40}H_2\cdot 5H_2O$: Co, 1.8; W, 62.3%.

Solutions containing cobalt(III) were obtained by constant current electrolysis on a platinum anode placed in a H cell with a fine sintered glass frit separating two compartments. Completion of oxidation was confirmed spectrophotometrically. Electronic and IR spectra were recorded on Hitachi 124 and Nihonbunko DS 301 spectrophotometers, respectively. X-ray powder diffraction data were obtained by use of a Rigaku Denki D-9C X-ray generator with a SG-7 diffractometer. Cu$K\alpha$ radiation and a nickel filter were used in all measurements. Differential thermal analytic (DTA) curves were obtained with a Rigaku Denki 8001 at a heating rate of 15 °C/min. The reference material was α-alumina. Potassium was precipitated and weighed as tetraphenylborate. The remaining elements were determined after alkaline decomposition of the hereropolyanions. Cobalt was precipitated as hydroxide, dissolved in hydrochloric acid, and estimated by EDTA titration. Tungsten was precipitated and weighed as trioxide. Phosphorous was separated as magnesium ammonium phosphate and was weighed as magnesium pyrophosphate after a second precipitation.

Results and Discussion

The DTA curves of heteropolytungstates are given in Fig. 1. All the heteropoly salts showed characteristic

two endothermic peaks which probably correspond to dehydration. The first large endothermic peak was observed at about 130 °C for all the salts. Ignition of the salts at 175 °C gave 60—80% loss of the water of hydration. All the heteropoly salts lost practically all the water above 400 °C with the change in color. The 12-tungstophosphoric acid showed a prominent exothermic peak at 637 °C. Both 11-tungstophosphate and 11-tungstocobalto(II)phosphate showed a complicated feature at high temperature. The X-ray diffraction pattern showed that 11-tungstophosphate and 11-tungstocobalto(II)phosphate belong to the tetragonal series, $a=12.2$, $c=9.08$ Å and $a=12.4$, $c=9.10$ Å, respectively; 12-tungstocobaltate(II) is simple cubic ($a=10.7$ Å). The 12-tungstophosphoric acid was shown to be cubic by Keggin.[5]

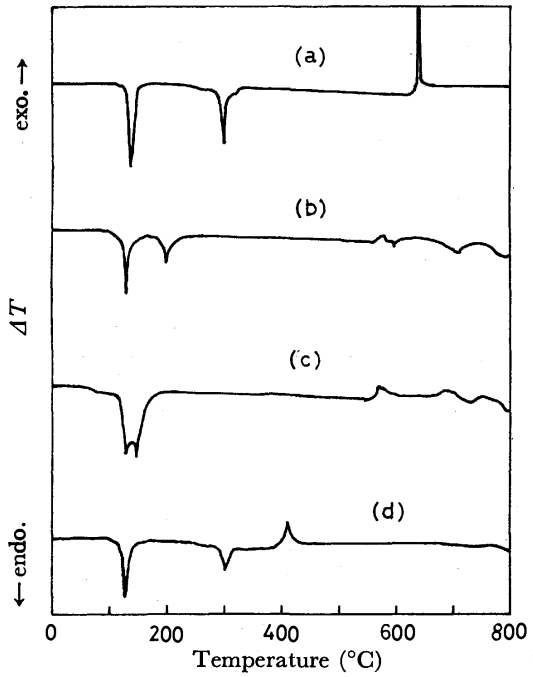

Fig. 1. DTA curves of heteropolytungstates.
(a): 12-tungstophosphoric acid, (b): 11-tungstophosphate, (c): 11-tungstocobalto(II)phosphate, (d): 12-tungstocobaltate(II).

Infrared Spectra. The positions and assignments of the main bands are given in Table 1. All the compounds have strong bands at 740—980 cm^{-1} characteristic of polytungstates. The bands at 880—980 cm^{-1} might be assigned to the independent W–O stretching vibration and the broad bands at 740—820 cm^{-1} to the W–O–W bridge vibrations. Such peaks are also observed in the infrared spectra of several heteropolymolybdovanadates.[10] The 12-tungstophosphoric acid having high symmetry Td gives the triply degenerated γ_3 of PO_4 at 1080 cm^{-1}. The band is split into 1085 and 1040 cm^{-1} in 11-tungstophosphate. There is probably a lowering of symmetry from Td in 11-tungstophosphate owing to the lack of one tungsten and the unshared oxygen. The reduction in symmetry of PO_4 should result in the splitting of the degenerate mode γ_3. The complication of the vibration of WO_6 in 11-tungstophosphate can also be attributed to the structural distortion. The splitting of the γ_3 band is also observed in 11-tungstocobaltophosphate where the PO_4 tetrahedron is also distorted because one tungsten atom of 12-tungstophosphate is replaced by cobalt atom. The spectrum of the heteropoly salt with pyridines is similar to that of the potassium 11-tungstocobaltophosphate, except for bands of pyridine at 3060s, 1635m, 1531m, 1482m, 1330w, 1245w, 1200w, and 1165w cm^{-1}. Gill *et al.* distinguished a pyridinium ion from the pyridine coordinated to metals according to infrared spectra.[11] Absorption bands of C=C and C=N bonds in the heteropoly salt with pyridine were shifted to higher wave number than those in pure pyridine in agreement with the observation of Murata and Ikeda.[12] The infrared spectrum shows that the compound is not a pyridine complex but pyridinium salt.

Reactions. The parent 12-heteropolyanions probably

TABLE 1. IR SPECTRA OF THE HETEROPOLYTUNGSTATES[a]

Compound	Assignments			
	$\nu(H_2O)$	$\delta(H_2O)$	ν(P–O)	ν(W–O)
$H_3PW_{12}O_{40}\cdot 29H_2O$	3440s, b	1620m, b	1080s	983s 890s 810s, b
$K_7PW_{11}O_{39}\cdot 28H_2O$	3450s, b	1625m, b	1085m 1040m	950s 900s, b 863s 814s 740s, b
$K_5PCoW_{11}O_{40}H_2\cdot 20H_2O$	3440s, b	1620m, b	1075m 1055m	960s 887s 820s, b 755s
$(pyH)_5PCoW_{11}O_{40}H_2\cdot 5H_2O$	3450s, b	1615m, b	1075m 1057s	955s 890s 820s, b 750s
$K_5HCoW_{12}O_{40}\cdot 24H_2O$	3440s, b	1620m, b		950s 882s, b 745s, b

a) All values in cm^{-1}. Abbreviations; s: strong, m: medium, w: weak, b: broad.

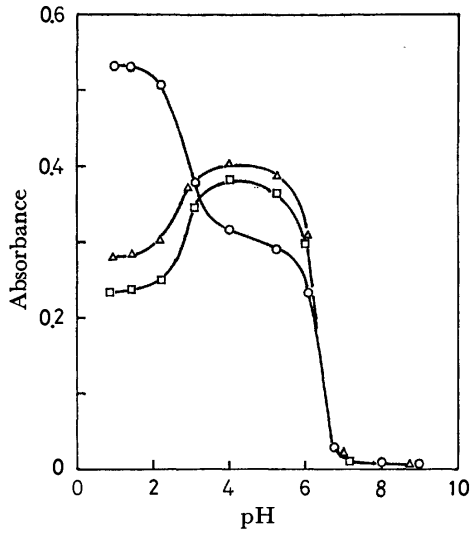

Fig. 2. Relation between the absorbance of 12-tungstophosphate solution and the pH.
The concentration of 12-tungstophosphate is 10^{-5} M.
○: 264 nm, △: 247 nm, □: 235 nm.

undergo gradual degradation on alkalization.[6] The 12-tungstophosphoric acid exihibits a characteristic intense absorption band ($\varepsilon=5.2\times10^4$ 1 $mol^{-1}cm^{-1}$) at 264 nm in acidic solutions. The position of the absorption maximum shifts to shorter wavelength with an increase in pH, no maximum being observed above pH 7. Figure 2 shows the relation between the absorbance of 12-tungstophosphate solution and the pH at different wavelengths. The absorbances show abrupt changes at pH 2.7 and 6.2, a distinct plateau occurring in the 3.5—6 pH region. This suggests that the parent 12-tungstophosphoric acid is transformed into a certain species in this region, and further decomposes into other species above pH 7 (ultimately to WO_4^{2-} and PO_4^{3-}). On the basis of the measurement of pH on rapid neutralization, Schwarzenbach *et al.* presumed the initial process of the degradation as follows.[13]

$$PW_{12}O_{40}^{3-} + 9/2\ OH^- \rightleftharpoons PW_{11}O_{39}^{7-} + 1/12H_2W_{12}O_{40}^{6-} + 13/6H_2O \quad (1)$$

In equilibrium (1) the metatungstate $H_2W_{12}O_{40}^{6-}$ may be some other species. The equilibrium can explain the fact that an aqueous solution of 12-tungstophosphoric acid contains 3–4 titratable H^+ per molecule. Tourné and Tourné isolated solid potassium 11-tungstates by the partial degradation of 12-heteropolyanions.[6] A hydrolysis product which we isolated from the weakly acidic solution of 12-tungstophosphate could also be formulated as potassium 11-tungstophosphate according to the analytical data. The latter compound seems to be further decomposed by base into species such as $P_2W_{19}O_{69}^{14-}$, $(PW_9O_{34}^{9-})_n$, *etc.*[14] On the other hand, 12-tungstocobaltate(II) seems to be considerably resistant to the degradation. Its spectrum showed no change at all on alkalization up to pH 7 though the anion decomposed completely above pH 10.5. The 11-tungstophosphate reacts with cobalt ion under weakly acidic conditions.[6] The stoichiometry of the reaction was examined spectrophotometrically by the molar ratio method (Fig. 3). An inflection in the

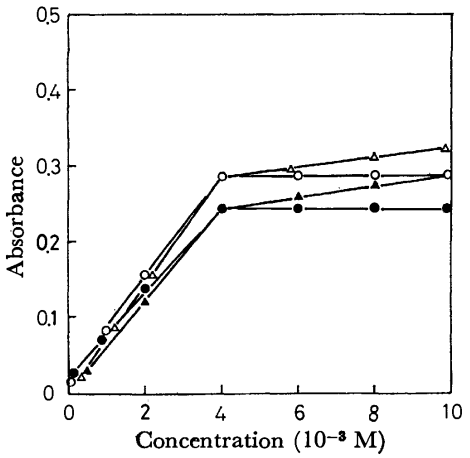

Fig. 3. Absorbances of the solutions containing 11-tungstophosphate and cobalt ion.
Circle; the concentration of cobalt ion is 4×10^{-3} M and that of 11-tungstophosphate is shown on the abscissa.
Triangle; the concentration of 11-tungstophosphate is 4×10^{-3} M and that of cobalt ion is shown on the abscissa. Open: 540 nm, close: 511 nm.

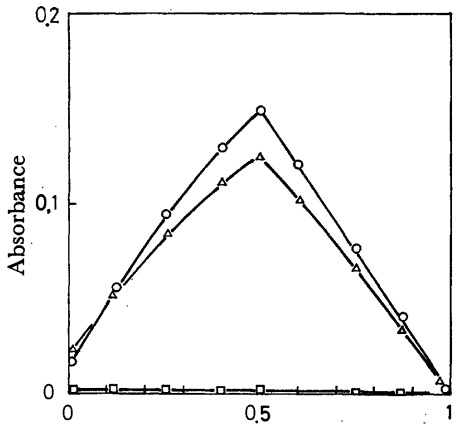

Fig. 4. Continuous variations plots of the reaction of 12-tungstophosphate with cobalt ion.
Total concentration were 4×10^{-3} M. ○: pH 5.2, 540 nm. △: pH 5.2, 511 nm. □: in 0.1 M-HCl, 540 nm.

absorbance occurred at a heteropolyanion: cobalt ratio of 1 : 1. This indicates the formation of a complex of stoichiometry 1 heteropolyanion: 1 cobalt. As shown in Fig. 4, a similar result was also obtained when the parent 12-acid was allowed to react with cobalt ion at pH 5.2 (whereas no reaction occurred in 0.1 M-hydrochloric acid). This implies that equilibrium (1) lies sufficiently to the right or that the reaction is fairly rapid. We isolated a ternary heteropoly salt from the solution which might contain 11-tungstophosphate and cobalt ion. The analytical data agreed with the values calculated for 11-tungstate rather than for 12-tungstate. The formation of the complex is probably a simple reaction as follows.

$$Co(H_2O)_6^{2+} + PW_{11}O_{39}^{7-} \longrightarrow PCoW_{11}O_{40}H_2^{5-} + 5H_2O \quad (2)$$

Absence of the complex in 0.1 M-HCl can be inter-

preted in terms of equilibria (1) and (2). If we suppose that 11-tungstophosphate remains unchanged when it is dissolved in water, we can estimate the stability constant of the complex, using the molar absorption coefficient (ε) of the species participating in the formation of the complex. The ε values at 540 nm were 75 for 11-tungstocabalto(II)phosphate, 0 for 11-tungstophosphate, and 3.0 l mol^{-1}cm^{-1} for cobalt ion. The stability constant of 11-tungstocobalto(II)phosphate was estimated to be log K=5 at 25 °C.

If 11-tungstocobalto(II)phosphate has the structure of the type proposed by Baker and Figgis,[4] an oxygen atom, probably of a water molecule (or hydroxide ion[15]), should occupy a coordination position of cobalt pointing to the exterior of the heteropoly part. It was difficult to determine from the analytical data whether a water or hydroxide ion occupied the sixth coordination position of the cobalt atom (the charge of anion is different in the two cases). If the above formulation is correct, the water or hydroxide ion coordinated to cobalt should be replaceable by other ligands in aqueous solution. Weakley reported spectrophotometrical indications of the replacement of the constitutional water by other ligands, with the isolation of pyridine complexes.[7] We attempted to replace the water or hydroxide ion with monodentate ligands such as thiocyanate, chloride, ammonia, and pyridine, but could not confirm the formation of any new complex. In the presence of pyridine, an increase in the intensity of the d-d band of 11-tungstocobalto(II)phosphate was observed, but the molar ratio plot at pH 5 was linear until about 5 molar ratio of pyridine to the heteropolytungstate. In larger excess of pyridine, the solid probably corresponding to the pyridinium salt of 11-tungstocobalto(II)phosphate was obtained in disagreement with the results of Weakley.[7] With the other ligands, there were no spectral changes, molar ratio plots at pH 5 being straight lines parallel to the abscissa (molar ratio). Since the replacement at only one of 6 coordination positions of cobalt causes no significant change in the spectrum, it might be difficult to examine spectrophotometrically the replacement of the constitutional water.

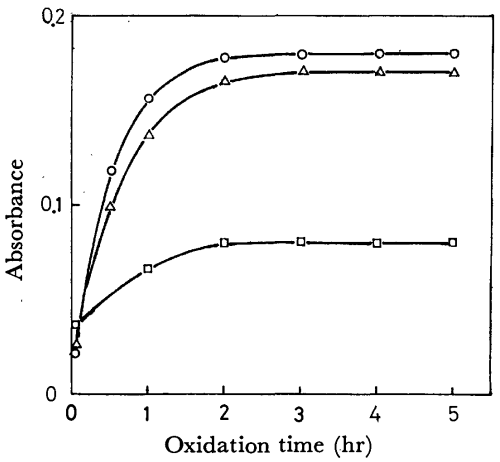

Fig. 5. Variations of the absorbance of the heteropolytungstates containing cobalt with oxidation time.
△: 5×10^{-4} M 11-tungstocobalto(II)phosphate in borate buffer (pH 5), 457 nm. □: the same as above, 540 nm. ○: 7.5×10^{-4} M 12-tungstocobaltate(II) in 0.1 M-sulfuric acid, 390 nm, absorbance (1/5).

It is known that the transition elements in heteropolyanions can be oxidized to higher oxidation states, with only the change in oxidation number of the elements apart from the charge of anions. We carried out the electrolytic oxidation of 11-tungstocobalto(II)-phosphate and 12-tungstocobaltate(II). The complete oxidation of the cobalt(II)-anions could be confirmed spectrophotometrically (Fig. 5). When the oxidized solutions were left to stand, 11-tungstocobalto(III)-phosphate was slowly reduced to 11-tungstocobalto-(II)phosphate, whereas 12-tungstocobaltate(III) was stable and isolated as pure crystals by Baker and McCutcheon.[9] The electrolysis of 11-tungstocobalto-(II)phosphate with phosphate as a buffer solution gave solutions with higher absorbance than those in the case of borate buffer solution, and gave variable molar absorption coefficients depending upon the concentration of the original 11-tungstocobalto(II)phosphate. Other heteropolyanions besides 11-tungstocobalto(III)-phosphate might be formed by the electrolysis of 11-tungstocobalto(II)phosphate in the presence of excess phosphate.

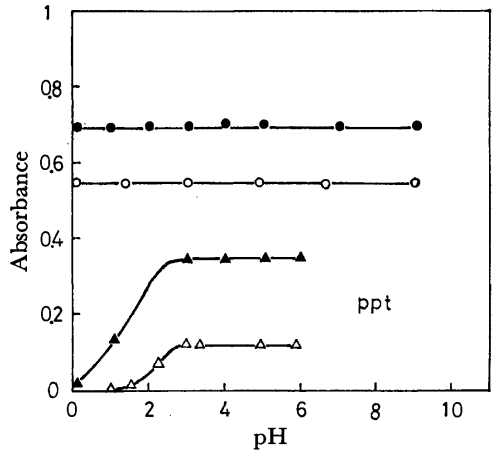

Fig. 6. Variations of the absorbance of the heteropolytungstates with pH.
▲: 10^{-3} M 11-tungstocobalto(III)phosphate, 457 nm. △: 2×10^{-3} M 11-tungstocobalto(II)phosphate, 540 nm. ●: 5×10^{-4} M 12-tungstocobaltate(III), 390 nm. ○: 3×10^{-3} M 12-tungstocobaltate(II), 624 nm.

Figure 6 shows the stability of the heteropolyanions towards acid and base. Both 12-tungstocobaltates are stable in wide pH range below 9 regardless of the oxidation state of cobalt. This does not mean that the anions remain actually unchanged. The anions probably undergo partial degradation at higher pH, but cobalt ions are still present in approximately tetrahedral environment. The 11-tungstocobalto(III)phosphate is slightly more stable towards acid than 11-tungstocobalto-(II)phosphate, but both lose cobalt ion in strongly acidic solutions to give the parent 12-acid. On the other hand, all heteropolyanions are decomposed by strong alkali.

Electronic Spectra. The positions, intensities, and assignments of the absorption maxima are given in

Table 2. Visible spectra of the heteropolyanions[a)]

Compound	ν_{max} (10^3 cm^{-1})	Assignments
11-tungstocobalto(II)-phosphate	14.1(2)	$^4T_{1g}(F) \rightarrow {}^4A_{2g}(F)$
	18.5(75)	$^4T_{1g}(F) \rightarrow {}^4T_{1g}(P)$
	19.0(75)	
	19.8sh	
11-tungstocobalt(III)-phosphate	13.9(140)	$^1A_{1g} \rightarrow {}^1T_{1g}$
	21.9(340)	$^1A_{1g} \rightarrow {}^1T_{2g}$
12-tungstocobaltate(II)	16.0(180)	$^4A_2(F) \rightarrow {}^4T_1(P)$
	16.8sh	
	17.7sh	
12-tungstocobaltate(III)	25.7(1060)	$^5E \rightarrow {}^5T_2$

a) Molar absorption coefficients (1 mol^{-1} cm^{-1}) are given in parentheses.

Table 2. The spectra assignments for 11-tungstocobaltophosphates are made on the basis of O_h symmetry, though the true site symmetry around cobalt is probably lower.[1,16)] The spectrum of 11-tungstocobalto-(II)phosphate differs distinctly from that of 12-tungstocobaltate(II) having Td symmetry, resembling that of the well-known cobalt(II) aqua-ion, except in intensity.[1)] This is also the case for the corresponding cobalt(III) complex. When metal heteroatoms are present in octahedral sites, the spectra should resemble those of the corresponding aqua-ions, the ligand-field parameters being of similar magnitude.[1)] Thus, a comparison of the spectra presents evidence supporting the view that cobalt atom in 11-tungstocobaltophosphates is present in essentially octahedral site. In the 12-heteropolyanions, tungsten or molybdenum atoms are effectively in tetragonal oxide environments.[17)] When cobalt replaces a single tungsten, it is to be expected that the CoO_6 group will also be distorted. The splitting of the second band in the 11-tungstocobalto(II)phosphate spectrum might be attributed to the lower site symmetry around cobalt atom. Thus the ε value for 11-tungstocobalto(II)phosphate is 15 times as great as that for the cobalt(II) aqua-ion. The remarkable band in the spectrum of 11-tungstocobalto(III)phosphate is also 5—15 times as intense as the corresponding bands for the cobalt(III) aqua-ion and centrosymmetric 6-molybdocobaltate(III).[1,18,19)] The spectrum of 11-tungstocobalto(III)phosphate indicates that the cobalt(III) is certainly of low-spin and the ligand-field stabilization energy is less even than in the cobalt(III) aqua-ion.[16)] The latter is also the case for the corresponding cobalt-(II) complex. The 12-tungstocobaltate(III) seems to be the first compound containing cobalt(III) in any tetrahedral site.[20)] The band of 25700 cm^{-1} was assigned tentatively to the transition $^5E \rightarrow {}^5T_2$. The ε value is *ca.* 50 times as great as that for 6-molybdocobaltate(III) with cobalt(III) in octahedral site. The heteropolyanions all show an intense absorption in the ultraviolet (Fig. 7). This is characteristic of polytungstates, and is to be ascribed to charge transfer from oxygen to tungsten.[16)] The ultraviolet absorption band for 12-tungstophosphate is shifted 2—3 kK to higher energies in 11-tungstophosphate and 11-tungstocobalto(II)-phosphate, with decreasing ε value. In heteropolyanions containing cobalt, a broad, relatively weak band ($\varepsilon \sim 220$) is superimposed on the ultraviolet absorption edge (spectra 5 and 6 in Fig. 7). This has been ascribed

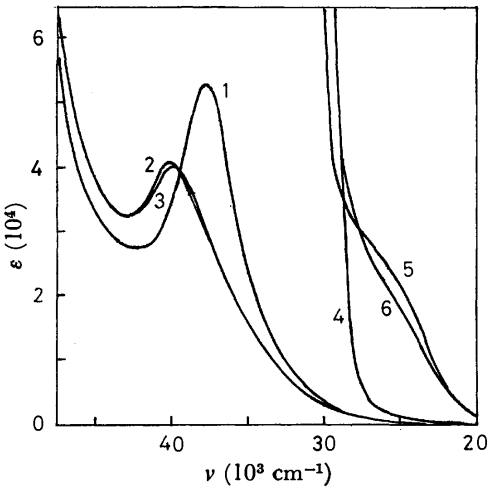

Fig. 7. Ultraviolet absorption spectra of the heteropolyanions. 1,4: 12-tungstophosphoric acid. 2: 11-tungstophosphate. 3,5: 11-tungstocobalto(II)phosphate. 6: 12-tungstocobaltate(II). Ordinate: 4,5,6 (100ε).

by Malik and Weakley[16)] to the charge transfer between cobalt and polytungstate, either from cobalt(II) to tungsten or from oxygen to cobalt(III). The charge transfer from oxygen to cobalt(III) should result in a stabilization of the (III) oxidation state of cobalt.

References

1) T. J. R. Weakley and S. A. Malik, *J. Inorg. Nucl. Chem.*, **29**, 2935 (1967).
2) C. M. Tourné, G. F. Tourné, S. A. Malik, and T. J. R. Weakley, *ibid.*, **32**, 3875 (1970).
3) R. D. Peacock and T. J. R. Weakley, *J. Chem. Soc., A*, **1971**, 1836.
4) L. C. W. Baker and J. S. Figgis, *J. Amer. Chem. Soc.*, **92**, 3794 (1970).
5) J. F. Keggin, *Proc. Roy. Soc. Ser. A*, **144**, 75 (1934).
6) C. M. Tourné and G. F. Tourné, *Bull. Soc. Chim. Fr.*, **1969**, 1124.
7) T. J. R. Weakley, *J. Chem. Soc., Dalton*, **1973**, 341.
8) R. A. Chalmers, *Proc. Soc. Analyt. Chem.*, **1966**, 157.
9) L. C. W. Baker and T. P. McCutcheon, *J. Amer. Chem. Soc.*, **78**, 4503 (1956).
10) G. A. Tsigdinos and C. J. Hallada, *Inorg. Chem.*, **7**, 437 (1968).
11) N. S. Gill, R. H. Nuttall, D. E. Scaife, and D. W. A. Sharp, *J. Inorg. Nucl. Chem.*, **18**, 79 (1961).
12) K. Murata and S. Ikeda, *Anal. Chim. Acta*, **51**, 489 (1970).
13) G. Schwarzenbach, G. Geier, and J. Littler, *Helv. Chim. Acta*, **45**, 2601 (1962).
14) C. M. Tourné, A. Revel, and G. F. Tourné, *Chem. Abstr.*, **80**, 55394p (1974).
15) R. Ripan and M. Puscasiu, *Z. Anorg. Allg. Chem.*, **380**, 102 (1971).
16) S. A. Malik and T. J. R. Weakley, *J. Chem. Soc., A*, **1968**, 2647.
17) G. M. Varga, E. Papaconstantinou, and M. T. Pope, *Inorg. Chem.*, **9**, 662 (1970); J. W. Linnett, *J. Chem. Soc.*, **1961**, 3796.
18) D. Sutton, "Electronic Spectra of Transition Metal Complexes," McGraw-Hill Publishers, New York, N. Y. (1968), p. 103.
19) Y. Shimura, H. Ito, and R. Thuchida, *Nippon Kagaku Zasshi* **75**, 560 (1954).
20) L. C. W. Baker and V. E. Simmons, *J. Amer. Chem. Soc.*, **81**, 4744 (1959).

Effect of Water on Crystallization Process of Coesite

Tetsuya KAMEYAMA and Shigeharu NAKA

Synthetic Crystal Research Laboratory, Faculty of Engineering, Nagoya University, Chikusa-ku, Nagoya 464

(Received May 19, 1975)

The effect of water on crystallization process of coesite was studied at 450 to 700 °C under 30 kbars by using different starting materials. The presence of water under compression and heating was found to have remarkable effects not only on the kinetics of crystallization of coesite also on the morphology of metastable quartz, consequently of coesite crystals. Under anhydrous condition, from amorphous silica and silica glass, the spherulitic aggregates of metastable quartz appeared. The coesite crystals were developed in the spherulites of quartz as elongated crystals with different sizes and appeared to be defective. When synthetic quartz was used as a starting material, however, no formation of spherulitic aggregates of quartz was observed and granular coesite crystals were obtained. Under hydrous condition, granular coesite crystals with homogeneous size were developed rapidly at 450 °C from both amorphous silica and silica glass through the discrete particles of metastable quartz.

Water plays a very important role in the crystallization and phase transformation of silica.[1-7] Previously,[8] the effect of water on the crystal growth of coesite under 30 kbars at 900 °C has been discussed from crystal morphology and size of coesite formed; in anhydrous condition the coesite grains are sintered and appeared to be defective, whereas in hydrous condition the coesite crystals are euhedral and less defective. It has also been pointed out that the transformation of amorphous silica to coesite is a consecutive process through the metastable phase of quartz and that water accelerates both steps in the consecutive process.[9,10] The formation of spherulitic aggregates of metastable quartz has been briefly reported under anhydrous condition.[11]

In the present paper, the effect of water on the crystallization process of coesite was studied in detail, particularly paying attention to morphology and aggregation state of metastable quartz, by using various starting materials between 450 and 700 °C under 30 kbars.

Experimental

Materials. The starting materials used were noncrystalline silicas, so-called amorphous silica and silica glass, and synthetic quartz. Amorphous silica with particle size of 0.1—10 μm was prepared by hydrolysis of silicon ethoxide and then heating at 1200 °C for 2 h. Silica glass with particle size of 0.5—1.0 μm was prepared by mechanical grinding of the commercial silica glass rods and by means of elutriation. The silica glass was heated at 800 °C for 2 h in order to remove the strain and the adsorbed water. The quartz powder with particle size of 0.5—1.0 μm was prepared by the method similar to the preparation of silica glass. Heating at 800 °C for 48 h was necessary for removing water adsorbed.

High Pressure Treatment. The crystallization of coesite was performed at the temperature range of 450 °C to 700 °C under 30 kbars for various durations up to 96 hr, with a girdle type high pressure apparatus,[10] either with or without water. Amount of water added into the sample was 4, 10, or 16 wt%. The samples were heated with the heating rate of 200 °C/min and after the programmed duration at a desired temperature quenched in the cell under compression.

Characterization of Specimen. The phases formed were identified with the X-ray powder technique and optical microscopy. The proportions of the phases were determined from the relative peak intensities of diffraction lines.[10] The crystallite size of metastable quartz was evaluated from the half widths of X-ray diffraction lines according to Hall's equation. The crystals of metastable quartz and coesite were examined by optical and scanning electron microscopes.

Results and Discussion

Crystallization from Amorphous Silica. In Fig. 1, the variations of proportion of the original amorphous silica, metastable phase of quartz and coesite with heating time are shown in both cases, without water and with 10 wt% water, at 450 °C. The kinetic process of the transformation changes by the addition of water.[9] The effect of water addition was seen not only from kinetics also from morphology of metastable quartz and coesite. Under anhydrous condition, metastable phase of quartz crystallized into spherulitic aggregates with the apparent size up to 50 μm after 4 h heating. These spherulites of quartz were formed in the matrix of unchanged amorphous matrix. The aggregate consisted of fine quartz crystals with the size of 0.5—1.0 μm, of which c-axes oriented radially. The size of the aggragates increased with the increase of heating time. It became up to 300 μm after 48 h. In the center of the spherulitic aggragates, where the radial orientation of crystals of quartz collapsed, needle-like crystals of coesite with the size of 20—50 μm were often found (Fig. 2-A). After 96 h quartz completely transformed to coesite, but the size of coesite crystals did not show any detectable increase. With 10 wt% water, on the other hand,

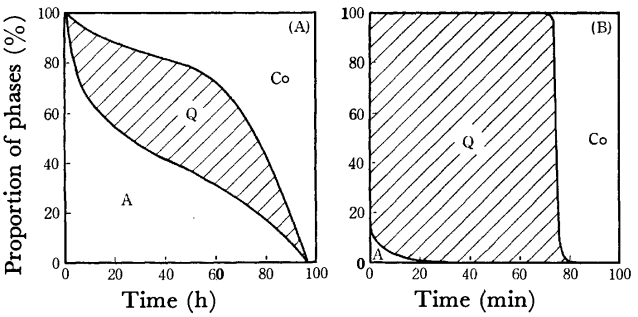

Fig. 1. Variations in proportions for phases obtained from amorphous silica at 450 °C under 30 kb.
A: Without water, B: with 10 wt % water.
Abbreviations; A: amorphous phase, Q: quartz, Co: coesite.

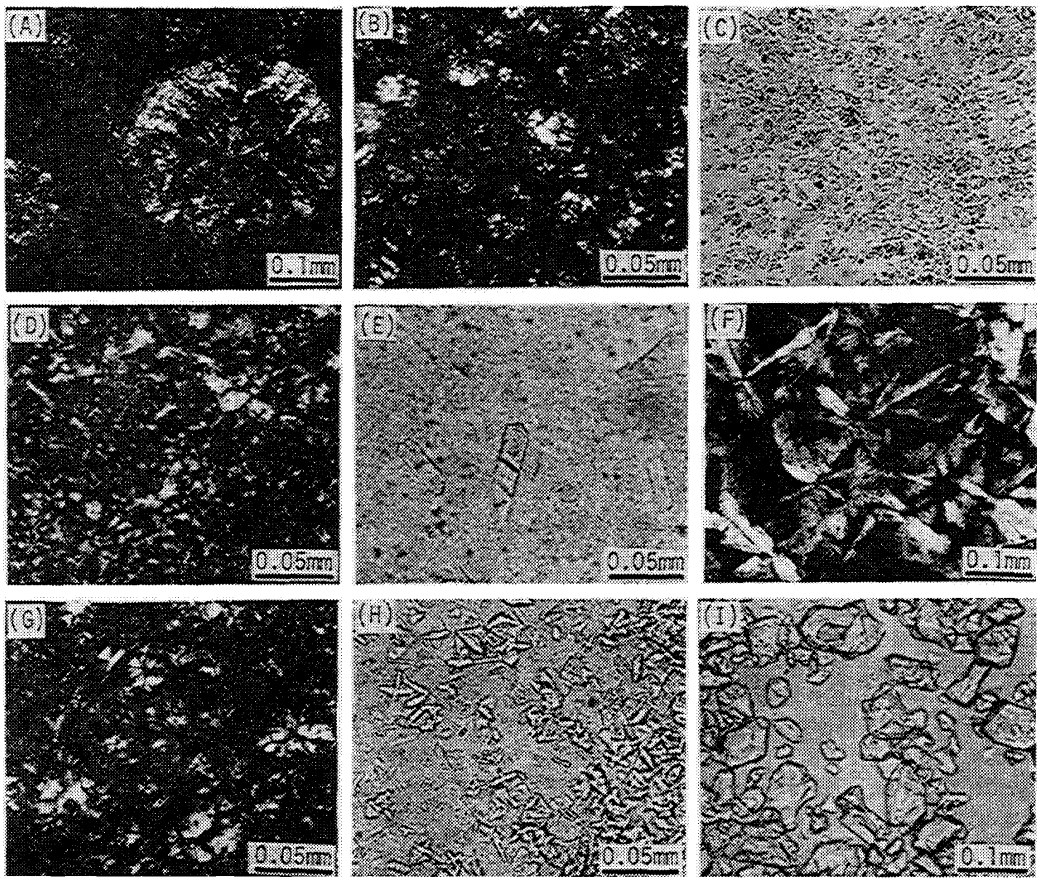

Fig. 2. Microphotographs of crystallization process of coesite from amorphous silica under 30 kb.

A: Spherulitic aggregates of metastable quartz in amorphous silica and radial growth of coesite at the center of the spherulite after heating at 450 °C for 48 h without water (under crossed nicols).

B: Small quartz aggregates in amorphous silica matrix heated at 450 °C for 1 h in the presence of 10 wt % water (under crossed nicols).

C: Granular coesite crystals formed after heating at 450 °C for 80 min in the presence of 10 wt % water (under open nicol).

D: Quartz aggregates in sintered state after heating for 10 min at 600 °C without water (under crossed nicols).

E: Lath-shaped and needle-like coesite crystals developed in quartz matrix of sintered state after heating for 60 min at 600 °C without water (under open nicol).

F: Penetration twins and lath-shaped coesite crystals grown after heating for 3 h at 600 °C without water (under crossed nicols).

G: Quartz spherulitic aggregates in amorphous silica matrix heated at 600 °C for 3 min in the presence of 4 wt % water (under crossed nicols).

H: Tiny penetration twins and granular crystals of coesite developed in quartz matrix after heating for 10 min at 600 °C in the presence of 4 wt % water (under open nicol).

I: Granular and euhedral coesite crystals grown after heating for 3 h at 600 °C in the presence of 16 wt % water (under open nicol).

most of the original amorphous silica was converted, within a few minutes, to quartz of discrete particles with the size of 0.02—0.03 μm. Many quartz aggregates were also observed in the fine particles of quartz. After 60 minutes, single phase of quartz was obtained and its crystal size increased up to 0.05—0.06 μm (Fig. 2-B). After 80 minutes metastable quartz transformed rapidly to coesite, of which crystal grew to 2—5 μm (Fig. 2-C).

The similar effect of water on crystal morphology was observed during the crystallization process at 600 °C. Some micrographs are shown in Figs. 2-D~I. Under the anhydrous condition (Fig. 2-D~F), amorphous silica completely transformed within 10 minutes to sintered quartz and the size of single crystal region was 1—3 μm (Fig. 2-D). In this case, the crystallization of metastable quartz is rather fast and the crystals sintered each other. This may be why we could not recognize the spherulitic aggregates of quartz crystals. After 60 minutes, the lath-shaped and needle-like crystals of coesite with the size of about 70 μm were developed in

quartz matrix, as shown in Fig. 2-F. The coesite crystals occurred mostly at grain boundaries of quartz crystals, and they grew along the c-axis. After 3 h, single phase of coesite was obtained. Most of the crystals were in lath-shape and 100—300 μm in size. They showed wavy extinction under microscope. The penetration twins of coesite crystals were often observed[12] (Fig. 2-F). With 4 wt% water, amorphous silica crystallized completely to quartz after 3 minutes. In this case, many spherulitic aggregates of quartz crystals were also observed in the matrix of the fine quartz crystals with the size of 0.5—1.0 μm (Fig. 2-G). After 10 minutes, however, the spherulitic aggregates disappeared. The granular crystals and penetration twins of coesite were formed in the matrix of fine quartz crystals (Fig. 2-H). After 60 minutes, the number of twins decreased and the granular coesite crystals with the size of 20—50 μm were formed. In the crystallization with 16 wt% of water, both steps of the consecutive process were so accelerated that only the morphology of coesite crystals could be discussed. The metastable quartz which was formed from amorphous silica in very short time transformed completely to coesite within 10 minutes. The spherulitic aggregates of quartz crystals and also penetration twins of coesite were hardly observed (Fig. 2-I). The granular coesite crystals grew with the increase in heating time. After 3 h, the coesite crystals as large as 100 μm were found, which were transparent and showed clear extinction.

The observation by electron scanning microscope agreed in the sizes and morphology of crystals with the results mentioned above.

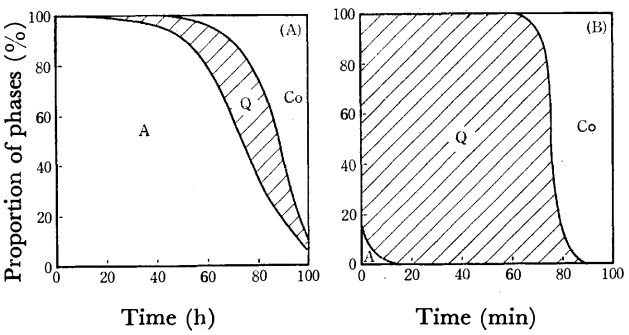

Fig. 3. Variations in proportions of phases obtained from silica glass under 30 kb;
A: without water at 600 °C.
B: with 10 wt % water at 450 °C.

Crystallization from Silica Glass. Under anhydrous condition, silica glass remained in amorphous state even after 96 h at 450 °C. At 600 °C, the crystallization of silica glass to coesite through metastable quartz was observed (Fig. 3-A). This kinetics is rather similar to that from amorphous silica to coesite at 450 °C (Fig. 1-A). The morphological changes during crystallization were found to be also similar to those which were observed at 450 °C on amorphous silica. After 48 h, the spherulitic aggregates of quartz crystals with the size of 20—200 μm were found to be scattered in amosphous matrix (Fig. 4-A). In the spherulite, the c-axes of quartz crystals oriented mostly to the radial direction. The coesite crystals were also developed radially from the center of the quartz spherulites (Fig. 4-B). It seemed likely that before the transformation to coesite the radial arrangement of quartz crystals were destroyed to be random. After 96 h, lath-shaped and needle-like coesite were developed, but the spherulitic texture remained even after the complete transformation to coesite (Fig. 4-C). With 10 wt% water at 450 °C, however, the kinetics and morphological changes to coesite from silica glass was found to be similar to the case from amorphous silica under the same condition, that is, at 450 °C with 10 wt% water (Fig. 3-B).

Crystallization from Quartz. Under anhydrous condition at 450 °C, the starting quartz remained

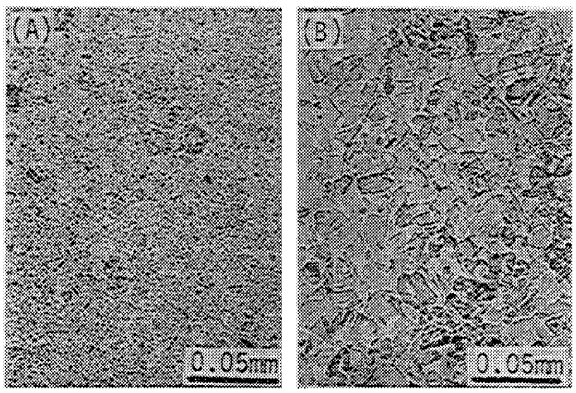

Fig. 5. Microphotographs of coesite prepared from quartz;
A: heated at 700 °C for 24 h without water (under open nicol).
B: heated at 450 °C for 4 h with 10 wt % water (under open nicol).

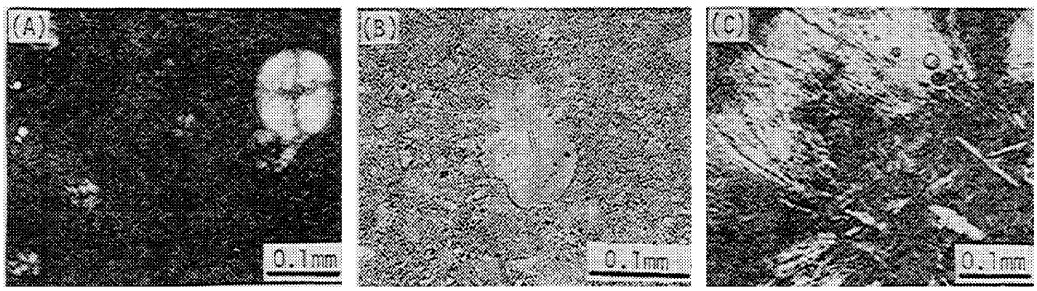

Fig. 4. Microphotographs of crystallization process of coesite from silica glass heated at 600 °C under 30 kb without water;
A, B: for 48 h (under crossed nicols).
C: for 96 h (under crossed nicols).

Table 1. Crystallization of coesite prepared from various starting materials at 450°C under 30 kb with 10 wt% water

Starting materials	Crystallite size of metastable quartz (Å)	Nucleation period (min)	Nucleation rate (s^{-1})	Growth rate (s^{-1})
Amorphous silica, silica glass	200~500	60	2.8×10^{-4}	7.5×10^{-2}
Quartz	5000	80	9.3×10^{-5}	2.8×10^{-2}

unaltered in a powdered state even after 96 h, although the broadening of X-ray diffraction profiles and the undulatory extinction under optical microscope were observed. The single phase of coesite was obtained from the quartz only after 2 h at 700 °C. The coesite crystals formed are in granular shape with the size of 2—5 μm (Fig. 5-A). With 10 wt% water at 450 °C, coesite crystallized after an induction period of about 3 h. After 4 h, 90% of the starting quartz was converted into the granular coesite crystals with the size of 20—40 μm (Fig. 5-B).

Effect of Water on Crystallization of Coesite. Under anhydrous condition, the crystallization rate of coesite is different from the starting materials; amorphous silica changes completely to coesite at 450 °C after 96 hr, but silica glass needs 600 °C and quartz 700 °C for complete transformation to coestite. During the crystallization from amorphous silica and silica glass, the formation of spherulitic aggregates of metastable quartz was observed. The spherulites formed in the silica glass appeared to have better orientation (Fig. 4-A) and are less in number than those in amorphous silica, probably due to the slow rate of transformation of glass to metastable quartz. The formation of spherulitic aggregates may be explained by the surface tension developed in amorphous state, similar to the devitrification of glass.[13] Mostly from the center of the spherulites, the growth of coesite crystals is found to start. Therefore, the formation of spherulites and also orientation of quartz crystals in spherulites restrict the morphology and size of coesite crystals.

Under hydrous condition, no difference in the crystallization rate of coesite is observed between amorphous silica and silica glass. They transform to coesite much faster than quartz. The process of transformation of metastable quartz to coesite seems to be the rate determining step. Since the formation curve of coesite could not be refered to a paraboric law, no long range diffusion process should be involved in the crystallization process of coesite. Thus, the crystallization rate of coesite was analyzed by adopting the linear law,[14] which had been commonly used for the rate determining process of interfacial reaction. The nucleation period of coesite from metastable quartz, the nucleation rate, and the growth rate evaluated from the slope of the formation curve are summarized in Table 1. The crystallite size of metastable quartz is also shown in Table 1. Both the nucleation rate and the growth rate of coesite crystals are found to be larger for amorphous silica and silica glass than for quartz. This difference in the rates may be due to the smaller particle size of metastable quartz formed from amorphous silica and silica glass than that from quartz. It has been well known that the dimension and the microstructure of the starting crystal affect both speed and temperature of its phase transformation.[15]

The coesite crystals prepared from the amorphous phases under anhydrous condition have an elongated form with heterogeneous size and appears to be defective, but well sintered. The crystals prepared under hydrous condition, however, are granular in shape, homogeneous in size and also less defective. With more than 10 wt% of water, the granular crystals of metastable quartz and also of coesite are obtained from any starting materials. Water may prevent the aggragation of metastable quartz. Even in the presence of water the elongated crystals and penetration twins of coesite were often observed at the beginning of crystallization, but they disappeared after prolonged heating. These experimental results may suggest the growth mechanism of coesite as the dissolution and precipitation through a solvent of water. This mechanism may be understood from the fact that water of even 4 wt% is largely enough to cover the surface of quartz and coesite grains by water layer of few tens molecular thickness.

When quartz was used as a starting material, the penetration twins and needle-like crystals of coesite were hardly observed even under anhydrous condition. Random orientation and rigid boundaries of the original quartz particles may prevent the aggregation of quartz and the preferential growth of coesite.

Conclusively, the crystallization process of coesite is found to depend strongly on the morphological characteristics of metastable quartz as well as on the significant roles of water. The granular coesite having homogeneous size could be obtained under hydrous condition through the discrete crystals of metastable quartz. The crystal size of coesite could also be controlled by the selection of heating temperature and time.

The authors wish to thank Dr. M. Inagaki and Dr. Y. Suwa who offered valuable discussion and encouragement on this work.

References

1) F. C. Kracek, "Phase Transformation in Solids," Wiley, New York, Ch. IX, (1953), pp. 257—277.
2) R. J. Zeto, F. Dachille, and R. Roy, *Amer. Ceram. Soc. Bull.*, **41**, 245 (1962), abstract.
3) F. E. Wagstaff, S. D. Brown, and I. B. Cutler, *Phys. Chem. Glasses*, **5**, 76 (1964).
4) F. E. Wagstaff and K. J. Richards, *J. Amer. Ceram. Soc.*, **49**, 118 (1966).
5) D. R. Uhlmann, J. F. Hays, and D. Turnbull, *Phys. Chem. Glasses*, **7**, 159 (1966).
6) F. R. Boyd and J. L. England. *J. Geophys. Res.*, **65**, 749 (1960).

7) C. B. Sclar, L. C. Carrison, and C. M. Schwartz, *Amer. Mineral.*, **47**, 1292 (1962).
8) S. Naka, M. Inagaki, T. Kameyama, and K. Suwa, *J. Cryst. Growth*, **24/25**, 614 (1974).
9) T. Kameyama and S. Naka, *J. Amer. Ceram. Soc.*, **57**, 499 (1974).
10) S. Naka, S. Ito, and M. Inagaki, *ibid.*, **57**, 217 (1974).
11) S. Naka, T. Kameyama, S. Ito, and M. Inagaki, *Chem. Lett.*, **1974**, 1313.
12) S. Naka, T. Kameyama, and K. Suwa, *Amer. Mineral.*, **60**, 726 (1975).
13) L. Hillert and M. Hillert, *J. Mat. Sci.*, **5**, 610 (1970).
14) A. G. Verduch, *J. Amer. Ceram. Soc.*, **41**[11], 427 (1958).
15) M. J. Buerger, "Phase Transformation in Solids," Wiley, New York, Ch. VI, (1953), pp. 183—211.

Studies on the Electrode Processes of Oxovanadium (IV). II. Electrolytic Reduction of Vanadyl Acetylacetonate in Acetonitrile Solution at Mercury Electrode

Mitsutaka KITAMURA, Kazuo YAMASHITA, and Hideo IMAI

Faculty of Integrated Arts and Sciences, Hiroshima University, Hiroshima 730

(Received June 9, 1975)

The electrolytic reduction of vanadyl acetylacetonate in acetonitrile solution was investigated by means of conventional and AC polarography, cyclic voltammetry and controlled-potential electrolysis. A well-defined polarographic cathodic wave was obtained in a solution containing excess acetylacetone. The wave-form was outwardly a single step with two-electron transfer. However, logarithmic analysis revealed that it consists of two steps. The first step is slightly irreversible, being accompanied by V–O bond breaking, and the second one is controlled by the rate of coupled chemical reactions. The reaction mechanism is discussed in detail. The reversible half-wave potentials of the species $[VO(acac)_2]$ and $[V(acac)_3]$ were determined to be -1.93 and -1.78 V *vs.* Ag/0.1 M $AgClO_4$, respectively, from the logarithmic analysis.

Invesigations on the electrolytic reduction of vanadyl ion and its complexes have been made by many authors. Lingane,[1] reporting on the polarographic behavior in aqueous media, found an irreversible cathodic process with two-electron transfer. Later, Lingane and Meites[2] reported that the reduction wave is accompanied by a pre-wave in an unbuffered solution, assumed to be caused by the rate-controlled reduction of $VOOH^+$ formed by the hydrolysis of VO^{2+}. They found that the pre-wave is no longer observed in an oxalate solution, the main-wave being excessively large. They attributed this to a catalytic reduction of hydrogen oxalate ion. Pecsok and Juvet[3] studied the polarographic reduction of vanadyl-versene complex. They attributed the pre-wave to the reduction of +4 to +3 vanadium, and the main-wave to the reduction of +3 to +2 vanadium. The pre-wave in both studies was observed in a limited pH range, and in a strongly acidic or alkaline solution it was completely eradicated. Meites and Moros[4] reported on the electrolytic reduction in an acidic solution, and found that the process consumes a much larger quantity of electricity than expected. This so-called induced current was extensively studied by Israel and Meites,[5] who found that the reduction proceeds in two consecutive steps. They analysed the rate-controlled process and induced current, and pointed out the oligomer formation and deprotonation of the reduced species.

In a previous paper[6] the polarographic cathodic process of vanadyl ion in M potassium oxalate was described. It was pointed out that the irreversible cathodic wave with two-electron transfer shows a trend to split into two waves when the vanadyl ion concentration exceeds 4 mM. The linearity of the wave-height *versus* concentration plot was recognized only up to 2 mM, the dependence of the wave-height on the head of mercury showing a characteristic of diffusion control. In order to clarify the above-mentioned anomalous behavior the present authors investigated the electrolytic reduction of vanadyl acetylacetonate in acetonitrile solution. The results obtained by means of conventional and AC polarography, cyclic voltammetry and controlled-potential electrolysis are presented in this paper.

Experimental

The polarographic current-potential curve was recorded on a Shimadzu Model RP-50 polarograph with an ohmic drop compensator. An AC attachment, Model BF-50 was used for AC polarography. Controlled-potential electrolysis was carried out with a Shimadzu Model PS-2 potentiostat and cyclic voltammetry with a Yanaco Electronic Scanner and Hokuto Denko Model HA-104 potentiostat.

The working electrodes used were a dropping mercury electrode(DME) for the polarography, a hanging mercury drop for the cyclic voltammetry and a mercury pool for the controlled-potential electrolysis. The characteristics of DME are as follows; mercury head=49 cm, rate of mercury flow= 0.71 mg/s, life time=7.2 s in open circuit. A platinum cylinder with a surface area of 1 cm^2 was used as an auxiliary electrode. The reference electrode was $Ag/AgClO_4$ (0.1 M in acetonitrile).

Vanadyl acetylacetonate (bis(2,4-pentanediono)oxovanadium (IV)), $[VO(acac)_2]$, was prepared by the method given by Rowe and Jones,[7] and was recrystallized from a chloroform solution. Acetonitrile (AN) used as a solvent was purified by distillation with phosphorus pentoxide in nitrogen atmosphere.

In order to prevent aerial oxidation, all the solutions of supporting electrolyte and vanadyl acetylacetonate were sufficiently bubbled with purified nitrogen prior to mixing. The prepared solution contained 1 mM vanadyl acetylacetonate, 20 mM acetylacetone (Hacac) and 0.1 M tetraethylammonium perchlorate (TEAP). Purified nitrogen was passed over the solution during the course of electrolysis. The temperature was kept at 20 °C with a water jacket attached to the cell.

Results and Discussion

Polarographic Current-Potential and Current-Time Curves. Vanadyl acetylacetonate usually gives an ill-defined polarographic cathodic wave in an AN solution containing 0.1 M TEAP. When excess Hacac was added to the solution, the wave-form was modified as shown in Fig. 1. A well-defined wave was obtained at least outwardly by adding 20 mM Hacac to 1 mM vanadyl acetylacetonate. Subsequent experiment were carried out under these conditions.

The apparent half-wave potential of the cathodic wave was -2.00 V, the overall electrons transferred per molecule being two. The logarithmic analysis of

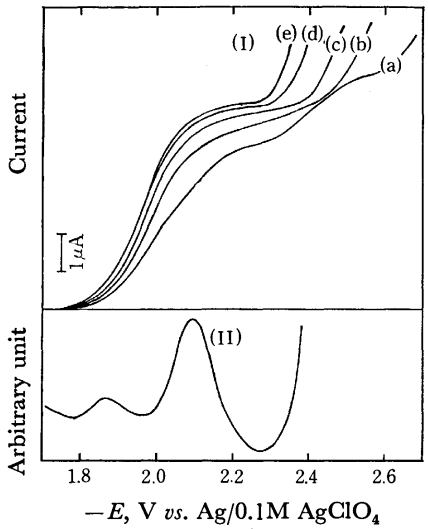

Fig. 1. (I) DC polarograms of 1 mM [VO(acac)$_2$] in AN solution containing 0.1 M TEAP at different concentrations of excess Hacac.
(a) 0, (b) 1 mM, (c) 5 mM, (d) 20 mM, (e) 40 mM Hacac
(II) AC polarogram of the same solution as (I) with 20 mM Hacac (applied sinusoidal voltage=10 mV).

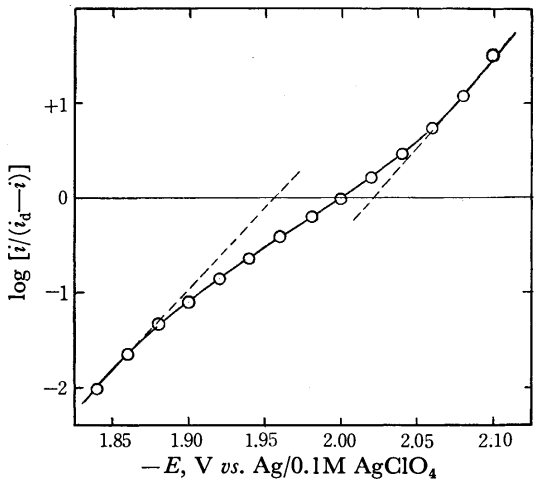

Fig. 2. Logarithmic plot of overall cathodic processes of [VO(acac)$_2$].

the current-potential curve gave a nonlinear plot as shown in Fig. 2. The distorted plot can be divided into three portions, *i.e.*, first and last linear portions and a middle curvilinear portion. The slopes of the first and last portions are 58 and 53 mV, respectively. Both values are approximately equal to the theoretical value of 58 mV for a reversible one-electron transfer process.

The current-time curves during one drop-growth of the DME were recorded at different potentials along the polarographic wave, and the exponent, γ, in $i=kt^{\gamma}$ (i: the current, k: the constant, t: the time) was estimated. In the estimation the rising portion of the i-t curve was omitted because of distortion by the dilution effect. The result is illustrated in Fig. 3.

Vlček[8] classified the varied values of γ as follows:
(a) $\gamma=0.17-0.2$; diffusion-controlled process

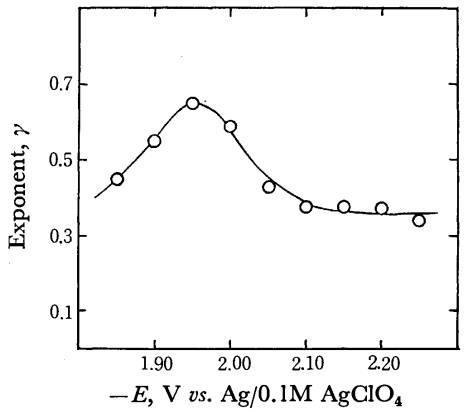

Fig. 3. Variation of exponent, γ, in $i=kt^{\gamma}$ with electrode potential.

(b) $\gamma=0.67$; reaction-rate control
(c) $\gamma=0.2-0.67$; diffusion and reaction-rate in competition
(d) γ changes with t during a drop-growth from 0.67 to 0.2; irreversible process
(e) γ changes with increasing i/i_1 (i_1: the limiting current) or E (E: the applied potential) from $\simeq$0.4 to 0.17 through a maximum; slightly irreversible process

In the present case the value of γ changes with increasing i/i_1 from 0.45 at −1.85 V to 0.34 at −2.25 V through a maximum of 0.65 at −1.95 V. In view of the above-mentioned classification the electrode reaction seems to proceed slightly irreversibly in the first step, proceeding thereafter with diffusion and reaction-rate control in competition.

In relation to the irreversible electrode process of VO^{2+} in M HCl solution, Suchomel and Vlček[8] pointed out that the reaction proceeds inherently in two stages as follows:

$$VO^{2+}\ aq \xrightarrow{+e^-} V(H_2O)_6^{3+} \xrightarrow{+e^-} V(H_2O)_6^{2+}$$

The first step proceeds highly irreversibly and the second one with only a very small overvoltage. No separate waves, corresponding to these two stages, could be observed in the conventional polarogram, but two separate waves appeared (Fig. 1) in the AC polarogram. The first AC peak at −1.85 V is more rounded, showing its irreversible characteristic. The second peak at −2.1 V is rather sharp, reflecting its reversibility. The effect of kinetic currents on an AC polarogram is small compared with the DC polarogram because the reaction time in an AC cycle is small. This supports the fact that the AC polarogram shows distinctly separated peaks.

Controlled-Potential Electrolysis and Cyclic Voltammetry. The controlled-potential electrolysis was carried out in a cell with the anode and cathode compartments separated by a sintered glass disc. By electrolysis at −2.1 V the solution color turned from light-blue (λ_{max} of the optical absorption band=710, 591 and 393 nm) to greenish-yellow. By continuation of electrolysis it turned to dark-green especially in the vicinity of the cathode surface. However, the dark-green color promptly

faded to yellow (λ_{max}=275 nm) on being left to stand in nitrogen atmosphere.

A similar trend was observed in the reduction of VO^{2+} with zinc amalgam. In an acidic aqueous solution vanadyl acetylacetonate was reduced easily by zinc amalgam. The color turned from light-blue to purple, showing the formation of V(II) entities. In AN solution, however, the reduction did not proceed markedly, but it proceeded slowly in the presence of excess Hacac. The reduction product was yellow, giving a polarographic cathodic wave at −1.78 V. On being left to stand in the air, no noticeable change was observed in the yellow coloration after a few hours, but the color faded very slowly in a few days.

The current-potential curve obtained *in situ* in the electrolysis cell is shown in Fig. 4. The greenish-yellow solution gave a cathodic wave at −1.78 V and an anodic wave at about −0.45 V. In addition to these waves the dark-green solution gave an unstable anodic wave at −1.70 V, but it could no longer be observed on being left to stand, the coloration of the solution turning to yellow. The yellow solution obtained finally gave a cathodic wave at −1.78 V and an anodic wave at −0.45 V (A similar anodic wave was observed in 20 mM Hacac solution containing 0.1 M TEAP after controlled-potential electrolysis at −2.3 V. For the cathodic process of Hacac in aqueous solution refer to 9).).

The slope of the logarithmic plot of the cathodic wave developed in the yellow solution was about 65 mV, the initial value being 55 mV (Fig. 6). The exponent, γ, of the current-time relationship varies with increase of i/i_1 from 0.32 at −1.80 V to 0.34 at −1.85 V, 0.35 at −1.90 V and 0.34 at −2.00 and −2.10 V. These results indicate that the cathodic process is a slightly irreversible one-electron transfer one, coupled with a reaction-rate controlled process.

The cyclic voltammogram of vanadyl acetylacetonate in AN solution is shown in Fig. 5. A sharp cathodic peak and a rounded anodic peak appear in the first

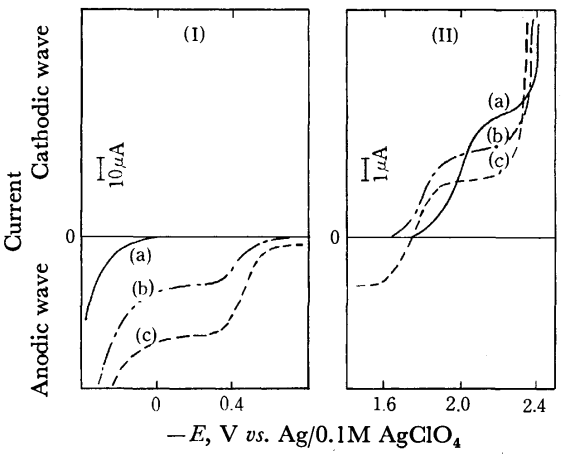

Fig. 4. Polarograms recorded *in situ* in course of controlled-potential electrolysis of [VO(acac)$_2$] in AN solution containing 0.1 M TEAP and 20 mM Hacac at −2.1 V.
(I) Anodic wave, (II) Cathodic wave; (a) 0 hr, (b) 1 hr, (c) 3 hr electrolysis.

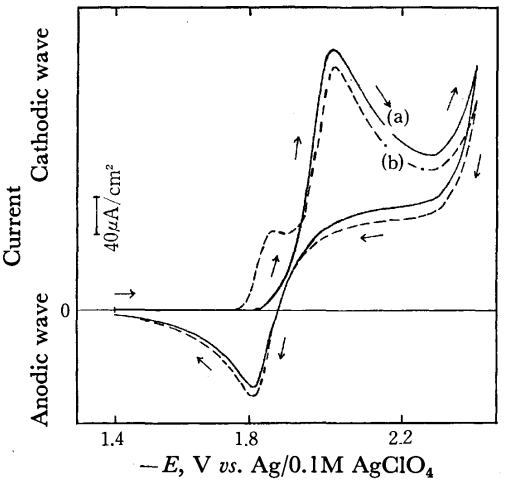

Fig. 5. Cyclic voltammograms of 1 mM [VO(acac)$_2$] in AN solution containing 0.1 M TEAP and 20 mM Hacac.
(a) First cycle of triangular sweep, (b) Second cycle of triangular sweep; scan-rate=50 mV/s.

cycle of the applied triangular voltage. The cathodic peak potential, E_p^c, was −2.02 V, and the anodic peak potential, E_p^a, was −1.80 V. The difference between E_p^a and E_p^c is noticeable as compared with the theoretical value of $E_p^a - E_p^c = 0.058/n$ V[10,11] for a reversible process at 20 °C. However, in the second and the following cycles a new cathodic peak appeared at −1.85 V, its peak-height gradually increasing in the consecutive cycles of the applied sweep. The new peak corresponds to the anodic peak at −1.80 V. When the scan-rate of the triangular voltage decreased from 50 mV/s to 20 and 10 mV/s, the ratio of the anodic and cathodic peak-heights decreased noticeably, the anodic peak disappearing completely under the scan-rate of 5 mV/s. It seems that the entity, which gives an anodic peak at −1.80 V, is unstable in solution, corresponding to the unstable anodic wave developed by the dark-green solution at −1.70 V. It is concluded that the cathodic peaks at −2.02 and −1.85 V and anodic peak at −1.80 V can be assigned to the cathodic waves at −2.00 and −1.78 V and the anodic wave at −1.70 V, respectively, in the conventional polarography.

Reaction Mechanism of Electrode Processes. Vanadyl acetylacetonate is stable and soluble in a large number of solvents without exchange of ligands. Dodge, Templeton and Zalkin[12] reported the composition and structure of anhydrous vanadyl acetylacetonates as five-coordinated complex with VO^{2+} perpendicular to the oxygen base of a square pyramid. The complex presumably retains its VO^{2+} identity in solution forming a distorted octahedral array. The vanadyl oxygen is expected to dominate the electrostatic interactions between the central ion and the ligand by virtue of its close approach to vanadium. The sixth ligand, *trans* to the vanadyl oxygen, is open and can be coordinated by solvent molecules as pointed out by Bernal and Rieger.[13] Ballhausen and Gray[14] investigated the complex by the MO theory, and pointed out the significance of the π-bonding in VO^{2+}. It seems that

at least two factors have to be considered in relation to the irreversible electrode process. The predominant factor is the extreme stability of the V–O bond. Since all the orbitals are occupied and the lowest vacant orbitals in a σ-antibonding orbital are of relatively high energy, the strong V–O bond has to be broken and the low-lying orbital must be vacated for the electron transfer. The second minor factor is a structural change of ligands, *i.e.*, a breaking of the V–O bond accompanies the rearrangement of bidentate ligands, ($acac^-$).

Since the kinetic current is reduced to minimum at the plateau potential of the cathodic wave, the diffusion-controlled current for the first electron transfer can be approximated by one half of the overall limiting current. By using this value a logarithmic plot for the first electron transfer process is obtained as shown in Fig. 6. The reversible half-wave potential of the first electron transfer is estimated to be −1.93 V. The reductant by the first electron transfer would necessitate a ligand rearrangement. Accordingly, the middle portion of the cathodic wave is affected by this rearrangement reaction. Once the reaction is over, the following electron transfer would proceed with a close resemblance to the atomic configuration in the environment. However, the internuclear distance should change due to the ionic valency change of the central atom. The cathodic process developed by the yellow solution seems to correspond to this case. The reversible half-wave potential is estimated to be −1.78 V by logarithmic analysis (Fig. 6). It is noteworthy that this process proceeds at a less negative potential by 0.15 V than the first electron transfer. The discrepancy seems to be attributed mainly to the V–O bond strength. Newton and Baker[15] studied the second-order rate law of the reduction of V(IV) species by V(II) species in an aqueous solution. This reaction seems to play the role of the kinetic current in the present case, causing deformation in the middle portion of the cathodic wave. At the plateau of the polarogram the formation of V(II) species dominates, and the V(IV) entity diffusing toward the electrode from the solution bulk will be depleted in the reaction layer by the reaction of V(II) with V(IV). Thus, the last portion of the polarogram is hardly affected at all by the rate-controlled process. Another possible coupled chemical reaction is the oligomer formation of the reduced species as pointed out by Israel and Meites.[5] No convincing evidence for this process, however, was found in the present investigation.

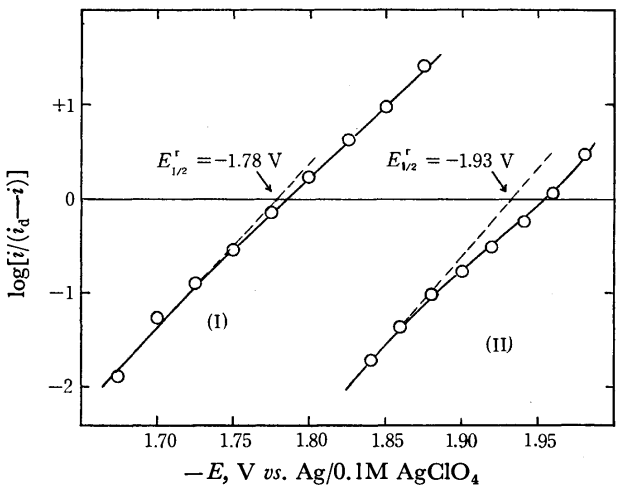

Fig. 6. Logarithmic plots of cathodic processes of (I) $[V(acac)_3]$ and (II) $[VO(acac)_2]$ as assumed to be one-electron transfer process.

The reaction mechanism can be summarized as follows:

(1) The first electron transfer to $[VO(acac)_2]$:

$$[VO(acac)_2] + Hacac + e^- \longrightarrow (V(acac)_2 \cdot O \cdot Hacac^-)^*$$

where * denotes the activated state.

(2) The successive electron transfer to the activated state:

$$(V(acac)_2 \cdot O \cdot Hacac^-)^* + e^- \longrightarrow [V(acac)_3]^- + OH^-$$

(3) The second electron transfer after the ligands rearrangement:

$$[V(acac)_3] + e^- \longrightarrow [V(acac)_3]^-$$

(4) The coupled chemical reactions:
(4-1) the ligands rearrangement:

$$(V(acac)_2 \cdot O \cdot Hacac^-)^* \longrightarrow [V(acac)_3] + OH^-$$

(4-2) A possible following reaction of (4-1):

$$OH^- + Hacac \longrightarrow acac^- + H_2O$$

(4-3) the reduction of V(IV) by V(II):

$$[VO(acac)_2] + [V(acac)_3]^- + Hacac \longrightarrow 2[V(acac)_3] + OH^-$$

References

1) J. J. Ligane, *J. Amer. Chem. Soc.*, **67**, 182 (1945).
2) J. J. Lingane and L. Meites, Jr., *ibid.*, **69**, 1021 (1947).
3) R. L. Pecsok and R. S. Juvet, Jr., *ibid.*, **75**, 1202 (1953).
4) L. Meites and S. A. Moros, *Anal. Chem.*, **31**, 23 (1959).
5) Y. Israel and L. Meites, *J. Electroanal. Chem.*, **8**, 99 (1964).
6) M. Kitamura and H. Imai, This Bulletin, **48**, 1459 (1975).
7) R. A. Rowe and M. M. Jones "Inorganic Syntheses," ed. by T. Moeller, Vol. 5, McGraw-Hill Book Co. Inc., New York (1957), p. 113.
8) A. A. Vlček in "Progress in Inorganic Chemistry," ed. by F. A. Cotton, Vol. 5, Interscience Publishers, New York-London (1963), p. 243.
9) S. Patai, "The Chemistry of the Carbonyl Group," Interscience Publishers, London-New York-Sydney-Toronto (1966), p. 527.
10) A. Sevčik, *Coll. Czech. Chem. Commun.*, **13**, 349 (1948).
11) H. Matsuda and Y. Ayabe, *Z. Electrochem.*, **59**, 494 (1955).
12) R. P. Dodge, D. H. Templeton, and A. Zalkin, *J. Chem. Phys.*, **35**, 55 (1961).
13) I. Bernal and P. H. Rieger, *Inorg. Chem.*, **2**, 256 (1963).
14) C. J. Ballhausen and H. B. Gray, *ibid.*, **1**, 111 (1962).
15) T. W. Newton and F. B. Baker, *J. Phys. Chem.*, **68**, 228 (1964).

Circular Dichroism of *trans*-Dichlorocobalt(III) Complexes with Chiral 1,2-Diamines

Shigenobu YANO, Masahiko SABURI, Sadao YOSHIKAWA, and Junnosuke FUJITA*

Department of Synthetic Chemistry, Faculty of Engineering, University of Tokyo, Tokyo 113
**Department of Chemistry, Faculty of Science, Nagoya University, Nagoya 464*

(Received June 12, 1975)

The circular dichroism (CD) spectra of *trans*-dichlorobis(diamine)cobalt(III) complexes were measured in methanol solution in the 700—200 nm region, where the diamines have the general formula of $NH_2CH(R)CH_2NH_2$ (R=isopropyl, isobutyl, *sec*-butyl, benzyl and phenyl) and belong to the *S* configuration except the phenyl-substituted one. The spectra are essentially the same as the spectrum of the (*S*)-propylenediamine ((*S*)-pn; R=methyl) complex, except for the (*R*)-*C*-phenylethylenediamine ((*R*)-phenen) complex. The variation of the *C*-substituted alkyl groups has hardly any influence on the CD of the *trans*-$[CoCl_2(diamine)_2]^+$ type complexes, demonstrating that the vicinal contribution from the *C*-substituents can be disregarded in these compounds. The *trans*-$[CoCl_2((R)\text{-phenen})_2]^+$ ion shows a CD pattern differing significantly from that of the *trans*-$[CoCl_2((R)\text{-pn})_2]^+$ ion in the first absorption band region, suggesting the significance of the vicinal effect due to the *C*-substituted phenyl group. The CD curve of *trans*-$[CoCl_2((-)_D\text{-stien})_2]^+$ ion (stien=stilbenediamine) was found to be antimeric to that of the (*R*)-phenen complex. Taking into account the anomalous vicinal effect of the phenyl groups, the absolute configuration of the $(-)_D$-stien was assigned to the (*S,S*) configuration.

Stereochemical features which can contribute to the circular dichroism (CD) of a dissymmetric metal complex have been classified as follows: (1) a distribution of chelate rings about the metal ion (configurational effect), (2) the puckered dissymmetric conformation of individual chelate rings (conformational effect) and (3) the presence of asymmetric groups on the ligands (vicinal effect).[1,2] Some papers indicate that ligand field CD spectra of Co(III) complexes can be differentiated between the configurational and the other two effects in such systems as tris(diamine)Co(III) ion,[3] (*S*)-aminoacidatobis(ethylenediamine)Co(III) ion[4] and tris(aminoacidato)Co(III) complexes.[5] However, it has been pointed out that differentiation between the conformational and vicinal effect is rather difficult, though the latter effect is considered to have minor contributions with respect to the 1,2-diamine chelate rings.[1-2] This may be due to the fact that restriction of the conformation is usually caused by the substitution at the C atom(s) of diamine chelates such as (*R*)-propylenediamine, 2(*R*),3(*R*)-butanediamine and 1(*R*),-2(*R*)-cyclohexanediamine.

Bosnich and Harrowfield reported that the CD spectra of *trans*-$[CoCl_2((R)\text{-pn})_2]^+$ ion ((*R*)-pn=(*R*)-propylenediamine) and *trans*-$[CoCl_2((R)\text{-bn})_2]^+$ ion ((*R*)-bn=2(*R*),3(*R*)-butanediamine) are nearly the same, and the contribution of vicinal effect to optical activity is small.[2] This implies that the introduction of an alkyl group larger than the methyl group into a diamine chelate ring would result in minor changes in the shape and magnitude of CD. In order to confirm the assumption, we have prepared chiral 1,2-diamines with the general formula, $NH_2CH(R)CH_2NH_2$ (*R*=isopyl, isobutyl, *sec*-butyl and benzyl),[6] from the corresponding (*S*)-amino acids, *i.e.*, (*S*)-valine, (*S*)-leucine, (*S*)-isoleucine and (*S*)-phenylalanine, respectively, and obtained *trans*-dichlorocobalt(III) complexes with these diamines. We have also prepared (*R*)-*C*-phenylethylenediamine ((*R*)-phenen)[6] from the corresponding amino acid, (*R*)-*C*-phenylglycine, the absolute configuration of which has been established.[7] The CD spectra of the (*R*)-phenen complex and of the closely related $(-)_D$-stien (stien=stilbenediamine) complex will also be discussed in this report.

Experimental

Preparation of 1,2-Diamines. (*S*)-Valine, (*S*)-leucine and (*S*)-phenylalanine were converted into the amides according to the procedure described by Yang and Rising.[8] (*S*)-Isoleucine amide hydrochloride was obtained by the method of Smith *et al.*[9] (*R*)-phenylglycine amide was also prepared by the known method.[10] All the amino acid amides and their hydrochloride were treated with $LiAlH_4$ in dry tetrahydrofuran according to the procedure of Schnell and Karrer[11] with slight modifications as follows.

To a suspension of $LiAlH_4$ (11.4 g, 0.3 mol) in dry tetrahydrofuran (250 ml) was added 0.1 mol of amino acid amide in small portions. The mixture was stirred and heated under reflux for 24 hr, and then cooled to room temperature. Water (22 ml) was added dropwise with vigorous stirring, and the resulting slurry was stirred for further 1 hr at room temperature. The slurry was filtered by suction; the residue was extracted with tetrahydrofuran (100 ml) under reflux for 1 hr, and filtered again. The extraction was repeated once more, and the filtrate and extracts of tetrahydrofuran were combined. Excess concentrated hydrochloric acid was added, and the mixture was evaporated under reduced pressure almost to dryness. The residue was dissolved in a small volume of water, and then a concentrated sodium hydroxide solution was added in order to make the solution strongly alkaline. The separated amine layer was extracted with ether (total 300 ml). The ether extracts were dried over potassium hydroxide pellets overnight, and ether was removed by distillation under atmospheric pressure. The remaining oily liquid was distilled over potassium hydroxide pellets under atmospheric or reduced pressure. The crude diamines thus obtained were used for preparing cobalt (III) complexes without further purification.

$(-)_D$-Stilbenediamine was prepared and resolved by the known method.[12]

Preparation of Complexes. The *trans*-$[CoCl_2(diamine)_2]$-ClO_4 type complexes of (*S*)-ipren, (*S*)-*i*-buen and (*S*)-*sec*-buen were obtained in aqueous solution by the usual air-oxidation

procedure. To an aqueous solution of $CoCl_2 \cdot 6H_2O$ were added twice the molar amounts of 1,2-diamine, and the resulting solution was aerated for 5 hr at room temperature. Concentrated hydrochloric acid (about 5 ml for 0.01 mol scale) was added, and mixture was evaporated on a water bath until a small amount of green crystals began to separate. To the mixture was added excess perchloric acid (60%), and the green crystals separated were collected and washed with ethanol and ether, and air-dried. The crude products were recrystallized from methanol by adding ether. Found: C, 27.77; H, 6.46; N, 12.71%. Calcd for *trans*-$[CoCl_2((S)\text{-ipren})_2]ClO_4$: C, 27.70; H, 6.51; N, 12.92%. Found:C, 30.93; H, 7.03; N, 11.71%. Calcd for *trans*-$[CoCl_2((S)\text{-}i\text{-buen})_2]ClO_4$: C, 31.22; H, 6.99; N, 12.14%. Found: C, 31.81; H, 7.06; N, 12.24%. Calcd for *trans*-$[CoCl_2((S)\text{-buen})_2]ClO_4$: C, 31.22; H, 6.99; N, 12.14%.

The air-oxidation process was carried out in aqueous methanol and methanol solution for obtaining the (*S*)-benen, (*R*)-phenen complex and $(-)_D$-stien. The subsequent procedures were the same as those mentioned above. Found: C, 39.14; H, 5.66; N, 10.03%. Calcd for *trans*-$[CoCl_2((S)\text{-benen})_2]ClO_4 \cdot H_2O$: C, 39.47; H, 5.52; N, 10.23%. Found: C, 38.54; H, 5.02; N, 11.19%. Calcd for *trans*-$[CoCl_2((R)\text{-phenen})_2]ClO_4$: C, 38.31; H, 4.82; N, 11.17%. Found: C, 53.64; H, 5.46; N, 9.02%. Calcd for *trans*-$[CoCl_2((-)_D\text{-stien})_2]Cl \cdot 2H_2O$: C, 53.73; H, 5.80; N, 8.95%.

Measurements. Visible and ultraviolet absorption spectra were obtained with a Shimadzu MPS 50L recording spectrophotometer. CD spectra were obtained with a JASCO J-20 automatic spectropolarimeter. All the spectra were measured in methanol solution.

Results and Discussion

It has been acknowledged that substituting groups on carbon atoms of puckered 1,2-diamine chelate rings always tend to take the equatorial orientation both in the solid state[13-14] and in solution.[15] Thus, the (*R*)- and (*S*)-pn chelates adopt the *δ*- and *λ-gauche* conformation, respectively, (Fig. 1), according to the nomenclature of the conformation of a diamine chelate ring based on the proposal in the reference.[16]

The alkyl-substituted 1,2-diamine prepared from (*S*)-amino acid should have the *S* configuration with respect to the asymmetric C atoms of the diamine moiety.. Sor far as the alkyl substituents adopts preferably the equatorial orientation upon coordination, the chelate ring of substituted diamine should have the *δ* conformation as well as the (*S*)-pn chelate. Since most investigations on the CD of *trans*-dichloro complexes have dealt with the (*R*)-pn or (*S*)-pn complex, we will discuss the CD spectra of our complexes by comparing them with those of the *trans*-$[CoCl_2((R)\text{-pn})_2]^+$ ion or *trans*-$[CoCl_2((S)\text{-pn})_2]^+$ ion.

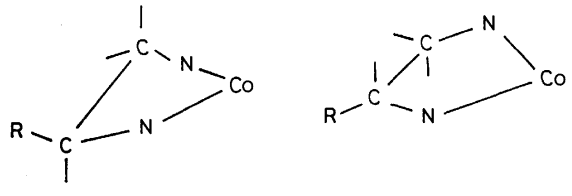

Fig. 1. Conformations of a 1,2-diamine chelate ring: (a) *δ-gauche*; (b) *λ-gauche*.

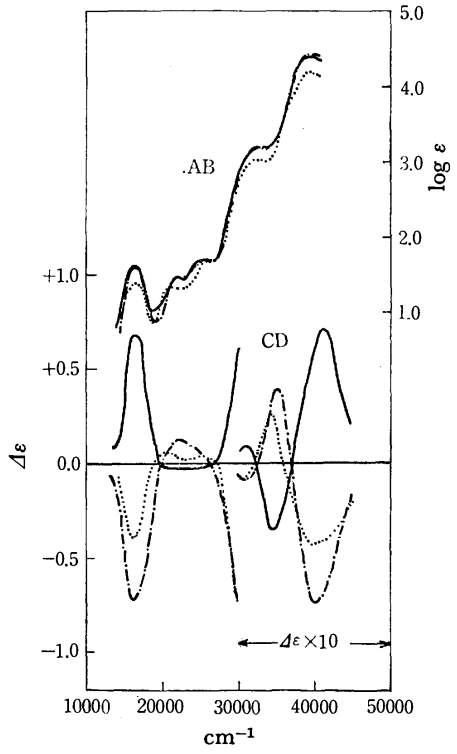

Fig. 2. Absorption (AB) and circular dichroism (CD) spectra of
(—) *trans*-$[CoCl_2((R)\text{-pn})_2]^+$, (···) *trans*-$[CoCl_2((S)\text{-benen})_2]^+$, and (-·-) *trans*-$[CoCl_2((S)\text{-ipren})_2]^+$.

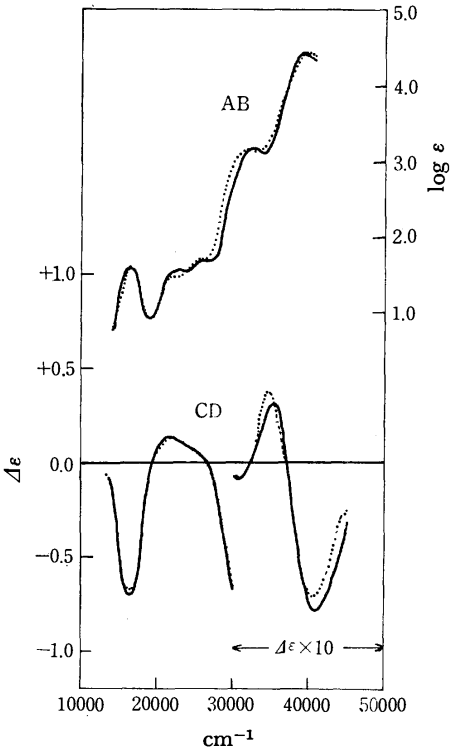

Fig. 3. Absorption (AB) and circular dichroism (CD) spectra of
(—) *trans*-$[CoCl_2((S)\text{-}sec\text{-buen})_2]^+$ and (···) *trans*-$[CoCl_2((S)\text{-}i\text{-buen})_2]^+$.

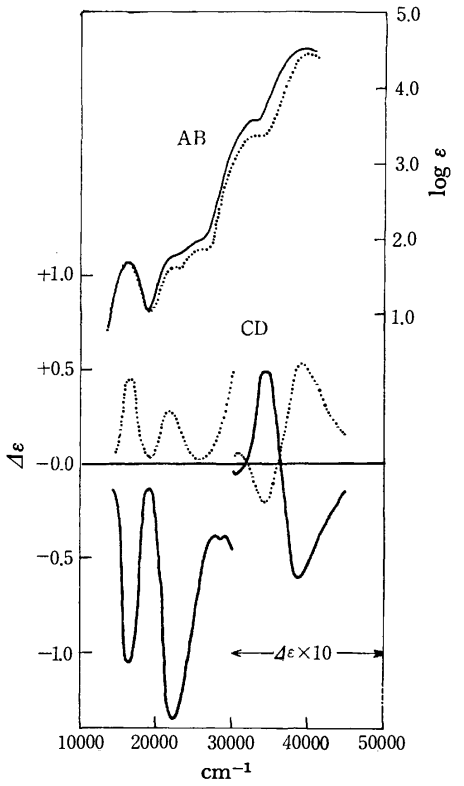

Fig. 4. Absorption (AB) and circular dichroism (CD) spectra of
(—) *trans*-$[CoCl_2((-)_D\text{-stien})_2]^+$ and (···) *trans*-$[CoCl_2$-$((R)\text{-phenen})_2]^+$.

CD of C-Alkylsubstituted 1,2-Diamine Complexes. The absorption spectra and circular dichroism spectra are given in Figs. 2—4 and Table 1. The first ligand field transition in the absorption spectrum of cobalt(III) in an octahedral field is $^1A_{1g}\rightarrow{}^1T_{1g}(O_h)$ which splits in a tetragonal field (*e.g.* *trans*-$[CoCl_2(NH_3)_4]^+$) into $^1A_{1g}\rightarrow{}^1E_g(D_{4h})$ and $^1A_{2g}(D_{4h})$ component, respectively.[17] The band of *trans*-$[CoCl_2(en)_2]^+$ ion at 16000 cm^{-1} was assigned to the $^1A_{1g}\rightarrow{}^1E_g(D_{4h})$ transition (I_a), and that at 22000 cm^{-1} to the $^1A_{1g}\rightarrow{}^1A_{2g}(D_{4h})$ transition (I_b).[17,18] The 1,2-diamine chelate with the λ conformation, such as (*R*)-pn or (*R*)-chxn ((*R*)-chxn= 1(*R*),2(*R*)-diaminocyclohexane), gives a positive and a negative CD band for the I_a band and the I_b band respectively.[19]

In the near-ultraviolet and ultraviolet regions, the *trans*-$[CoCl_2(NH_3)_4]^+$ ion gives two strong absorption bands which have been assigned to the charge transfer bands from the halides to the central metal ion, The longer wave length band involving the $p_\pi\rightarrow d_{z^2}$ and the shorter wave length band involving the $p_\sigma\rightarrow d_{z^2}$ transition.[20] It was observed that the *trans*-$[CoCl_2((R)$-chxn$)_2]^+$ ion shows a positive and a negative CD bands for the $p_\pi\rightarrow d_{z^2}$ transition and a positive CD band for the $p_\sigma\rightarrow d_{z^2}$ transition band.[21] The (*R*)-pn complex gives a similar CD pattern to that of the (*R*)-chxn complex in the charge transfer region (Fig. 2).[32]

As shown in Figs. 2 and 3, the CD spectra of the *trans*-$[CoCl_2((S)\text{-ipren})_2]^+$, *trans*-$[CoCl_2((S)$-*i*-buen$)_2]^+$, *trans*-$[CoCl_2((S)$-*sec*-buen$)_2]^+$ and *trans*-$[CoCl_2((S)$-benen$)_2]^+$ ion are very similar to each other and to the spectrum of the (*S*)-pn complex (the enantiomorph of (*R*)-pn complex) both in the ligand field and in the charge transfer region. It is apparent from these results that, so far as the methyl, isopropyl, isobutyl, *sec*-butyl and benzyl groups are concerned, the change of the substituting groups on the asymmetric C atom of the diamine chelate makes little contribution to the CD pattern. This means that the optical activity of *trans*-$[CoCl_2(diamine)_2]^+$ system is affected strongly by the conformational contribution and weakly by the vicinal effect.

The (*S*)-*sec*-buen has two asymmetric C atoms, one on the chelate ring and the other in the substituting *sec*-butyl group ((*S*) configuration). A marked resemblance of the CD curves between the (*S*)-*sec*-buen complex

Table 1. Electronic absorption (AB) and circular dichroism (CD) data of *trans*-$[CoCl_2(diamine)_2]^+$ ions ν in 10^3 cm^{-1}, (log ε) and ($\varepsilon_1-\varepsilon_r$)

Diamine	AB	max(log ε)	CD	max ($\varepsilon_1-\varepsilon_r$)
(*R*)-pn	16.50	1.62	16.50	+0.68
	21.97	1.48	21.50	−0.01
	25.97	1.74		
	32.60	3.13	31.15	+0.94
			34.72	−3.60
	39.70	4.40	41.51	+7.01
(*S*)-*i*-buen	16.50	1.60	16.50	−0.67
	21.97	1.48	21.61	+0.14
	25.97	1.71		
	32.78	3.16	30.91	−0.92
			34.72	+3.76
	39.70	4.41	40.65	−7.16
(*S*)-*sec*-buen	16.50	1.61	16.34	−0.71
	22.70	1.53	21.50	+0.13
	26.24	1.74		
	32.78	3.16	30.91	−0.91
			35.08	+3.18
	39.70	4.41	40.65	−7.86
(*S*)-benen	16.50	1.41	16.38	−0.39
	21.97	1.35	20.49	+0.06
	25.97	1.73		
	32.70	3.02	30.76	−0.86
			34.48	+2.47
	39.70	4.17	40.00	−4.26
(*S*)-ipren	16.50	1.61	16.26	−0.73
	22.47	1.48	21.80	+0.12
	25.78	1.71		
	32.70	3.01	30.91	−0.93
			35.08	+3.96
	39.70	4.16	40.32	−7.56
(*R*)-phenen	16.50	1.66	16.26	+0.45
	21.97	1.61	21.50	+0.28
	25.97	1.85		
	32.78	3.37	30.48	+0.58
			34.24	−2.01
	39.70	4.44	38.91	+5.34
(−)-stien	16.50	1.70	16.13	−1.06
	22.98	1.78	21.73	−1.36
	25.97	1.97		
	32.78	3.56	30.03	−0.46
			34.35	+4.98
	39.37	4.52	38.46	−6.10

and the (*S*)-*i*-buen complex (and others) suggests that the additional asymmetric center in the (*S*)-*sec*-buen contributes very little to the CD. This also suggests that the vicinal effect does not contribute much to optical activity.

CD of C-*Phenylsubstituted 1,2-Diamine Complexes.* It has been indicated that the (*R*)-phenen chelate ring has the *λ-gauche* conformation with an equatorially situated phenyl group.[23] The CD pattern of the *trans*-$[CoCl_2((R)\text{-phenen})_2]^+$ ion shown in Fig. 4 obviously differes from that of the (*R*)-pn complex. The (*R*)-phenen complex shows positive maxima both in the I_a and in the I_b region. Both CD peaks have comparable intensities with each other. In the case of the *trans*-$[CoCl_2((R)\text{-pn})_2]^+$ ion, its CD is negative in the I_b and positive in the I_a region. The former CD band is considerably weaker than that of the latter.

Bonich and Harrowfield[2] revealed that the CD sign of the $^1A_{1g}\rightarrow{}^1A_{2g}(D_{4h})$ transition region varies with the change of solvents or the states of the samples (crystal or solution state) in a series of *trans*-$[CoCl_2(1,2\text{-diamine})_2]^+$ complexes, where 1,2-diamines are mono- or disubstituted with alkyl groups. However, a minority of the CD in the A_{2g} transition was still recognized in all cases.[2] The anomalous CD behavior of *trans*-$[CoCl_2((R)\text{-phenen})_2]^+$ ion observed in the first absorption band region would be ascribed to the influence of the phenyl group on the chelate ring.

On the other hand, the CD behavior of the (*R*)-phenen complex resembles closely that of the (*R*)-pn complex in the charge transfer region. This indicates that the phenyl group on the chelate ring has little effect on the CD spectrum in this region. We consider that the CD signs of the charge transfer band region can be regarded as a good indication for determining the conformation of 1,2-diamine chelate rings.

It was found that the CD spectrum of the *trans*-$[CoCl_2((-)_D\text{-stien})_2]^+$ ion, shown in Fig. 4, closely resembles that of the (*R*)-phenen complex, though each corresponding peak has the opposite sign. It is significant that in the charge transfer region, where the phenyl group shows little contribution to determining the CD as described above, both the $(-)_D$-stien and the (*R*)-phenen complexes show the same CD pattern with the opposite signs. This indicates that the $(-)_D$-stein and (*R*)-phenen chelate rings take an antimeric conformation to each other.

The (*R*)-phenen complex should have the λ conformation, in which the phenyl group can adopt the equatorial orientation. Hence, the $(-)_D$-stien chelate should have the δ conformation. It has been shown that the two phenyl groups of $(-)_D$-stien take the equatorial orientation simultaneously.[23] The absolute configuration of stien satisfies the requirements that the diamine has the δ conformation and the equatorial phenyl groups must be of the (*S,S*) configuration.

It has recently been reported that the CD spectra of the Zn(II) complexes of $(-)_D$-stien suggest the (*S,S*) configuration for the ligand in these complexes.[25]

The absolute configuration of $(-)_D$-stien has been assigned to the (*R,R*) configuration,[2,24] based on the examination of the equilibrium between the Δ and Λ isomers of $[Co((-)_D\text{-stien})_3]^{3+}$ ion, or the exciton analysis of the CD of $(-)_D$-isomarine, the precursor of $(-)_D$-stien. Bosnich and Harrowfield, however, raised some questions on their assignments. Our assignment mentioned above is entirely reverse to these assignments.

If the $(-)_D$-stien has the (*R,R*) configuration, it would be difficult to explain the remarkable difference in CD between the *trans*-dichloro complexes of $(-)_D$-stien and of (*R*)-phenen. On the other hand, if the $(-)_D$-stien has the (*S,S*) configuration, a very significant problem would arise with regard to the assignment of the Δ and Λ isomers of tris(diamine) complex. Although the true configuration of $(-)_D$-stien should be clarified by X-ray analysis study, we assign the $(-)_D$-stien to the (*S,S*) configuration, since the visible CD curve of the *trans*-$[CoCl_2((-)_D\text{-stien})_2]^+$ ion can be explained by taking into account the vicinal effect of the phenyl group.

By comparing the CD of (*R*)-phenen complex with that of (*R*)-pn complex, it is apparent that the phenyl group affects especially the CD in the I_b ($^1A_{1g}\rightarrow{}^1A_{2g}(D_{4h})$) transition. A strong CD band with negative sign is observed for the *trans*-$[CoCl_2((-)_D\text{-stien})_2]^+$ ion in the I_b region, demonstrating the vicinal effect of the phenyl groups. The visible CD band of the $(-)_D$-stien complex is considerably stronger than that of the (*R*)-phenen complex. This may be due to the difference in the number of phenyl groups between the ligands. The remarkable vicinal effect observed for the phenen, having only one phenyl group, should appear twice as much in the case of stien with two phenyl groups.

It is interesting to note that the (*S*)-benen complex which also has a phenyl group in the ligand shows no obvious influence of the phenyl group in its CD curve. In this case, the phenyl group is separated by a methylene group from the diamine chelate ring. It is suggested, that only the phenyl group attached directly to the 1,2-diamine moiety gives rise to the anomalous vicinal effect in the first absorption band region.

This research was aided in part by a Scientific Research Grant of the Ministry of Education.

References

1) C. J. Hawkins, "Absolute Configuration of Metal Complexes," Wiley-Interscience, New York, N. Y. (1971), Chapter 5.

2) B. Bosnich and J. MacB. Harrowfield, *J. Amer. Chem. Soc.*, **94**, 3425 (1972).

3) B. E. Douglas, *Inorg. Chem.*, **4**, 1813 (1965).

4) C. T. Liu and B. E. Douglas, *ibid.*, **3**, 1356 (1964); S. K. Hall and B. E. Douglas, *ibid.*, **8**, 372 (1969).

5) M. Shibata, N. Nishikawa, and Y. Nishida, *Inorg. Chem.*, **7**, 9 (1968).

6) Nomenclature and abbreviations of diamines (abbreviations are given in the parentheses). R=isopropyl; 1,2(*S*)-diamino-3-methylbutane, or (*S*)-*C*-isopropylethylenediamine ((*S*)-ipren). R=isobutyl; 1,2(*S*)-diamino-4-methylpentane, or (*S*)-*C*-(isobutyl)ethylenediamine ((*S*)-*i*-buen). R=*sec*-butyl; 1,2(*S*)-diamino-3(*S*)-methylpentane, or (*S*)-*C*-(*sec*-butyl)ethylenediamine ((*S*)-*sec*-buen). R=benzyl; 1,2(*S*)-diamino-3-phenylpropane, or (*S*)-*C*-benzylethylenediamine ((*S*)-benen). R=phenyl; 1(*R*), 2-diamino-1-phenylethane,

or (*R*)-*C*-phenylethylenediamine ((*R*)-phenen).
7) J. P. Greenstein and M. Winitz, "Chemistry of Amino Acids," John-Wiley & Sons, New York, N. Y. (1961), p. 69.
8) P. S. Yang and M. M. Rising, *J. Amer. Chem. Soc.*, **53**, 3183 (1931).
9) E. L. Smith, D. H. Speckman, and W. J. Polglase, *J. Biol. Chem.*, **199**, 801 (1952).
10) L. Arpesella, A. La Manna, and M. Grassi, *Gazz. Chim. Ital.*, **85**, 1354 (1955).
11) S. Schnell and P. Karrer, *Helv. Chim. Acta*, **38**, 2036 (1955).
12) I. Lifschitz and J. G. Bos, *Rec. Trav. Chim.*, **59**, 173 (1940).
13) Y. Saito and H. Iwasaki, This Bulletin, **35**, 1131 (1962).
14) H. Iwasaki and Y. Saito, *ibid.*, **39**, 92 (1966).
15) S. Yano, H. Ito, Y. Koike, J. Fujita, and K. Saito, *ibid.*, **42**, 3184 (1969).
16) *Inorg. Chem.*, **9**, 1 (1970).
17) H. Yamatera, This Bulletin, **31**, 95 (1958).
18) R. Dingle, *J. Chem. Phys.*, **46**, 1 (1967).
19) C. J. Hawkins, E. Larsen, and I. Olsen, *Acta Chem. Scand.*, **19**, 1915 (1965).
20) H. Yamatera, *J. Inorg. Nucl. Chem.*, **15**, 50 (1960).
21) R. S. Treptow, *Inorg. Chem.*, **5**, 1593 (1966).
22) H. Ito, J. Fujita, and K. Saito, This Bulletin, **42**, 1286 (1969).
23) S. Yano, the doctoral thesis.
24) P. L. Fereday and S. F. Mason, *Chem. Commun.*, **1971**, 1314.
25) S. F. Mason and R. H. Seal, *ibid.*, **1973**, 422.

The Crystal Structure of Ammonium Pentamolybdodisulfate(IV) (4-) Trihydrate $(NH_4)_4[S^{IV}_2Mo_5O_{21}]\cdot 3H_2O$

Kazuko Y. MATSUMOTO, Masao KATO, and Yukiyoshi SASAKI

Department of Chemistry, Faculty of Science, The University of Tokyo, Hongo, Bunkyo-ku, Tokyo 113

(Received July 16, 1975)

The crystal of $(NH_4)_4S_2Mo_5O_{21}\cdot 3H_2O$ contains a discrete polyanion, $S_2Mo_5O_{21}^{4-}$, formed by reactions in an aqueous solution:

$$5Mo_7O_{24}^{6-} + 14SO_2 + 2H^+ \rightleftarrows 7S_2Mo_5O_{21}^{4-} + H_2O$$

or

$$5MoO_4^{2-} + 2SO_2 + 6H^+ \rightleftarrows S_2Mo_5O_{21}^{4-} + 3H_2O$$

It is orthorhombic, with the space group Pbcn and with $a=15.096(9)$, $b=13.375(8)$, $c=23.734(7)$ Å, $D_m=2.79$, and $D_x=2.79$ g cm^{-3} for $Z=8$. The crystal consists of $S_2Mo_5O_{21}^{4-}$ anions connected with each other by hydrogen bonds, with intervening water molecules and ammonium cations. In the polyanion, five MoO_6 octahedra are connected by edge sharing, and the two octahedra at the two ends are connected by corner sharing to complete the Mo_5O_{21} ring; the two SO_3 trigonal pyramids are attached to the ring from above and below the ring.

Three polymolybdosulfate(IV)(4—) ions, $S_2Mo_8O_{31}^{6-}$,[1] $S_2Mo_5O_{21}^{4-}$,[2] and $S_3Mo_{10}O_{40}^{8-}$,[3] are found in the literature, but the existence of the last species was once regarded as doubtful.[2] Our preparative work, together with powder X-ray diffraction and IR measurements, confirmed the first two polyanions as ammonium salts, $(NH_4)_6S_2Mo_8O_{31}\cdot 5H_2O$ and $(NH_4)_4S_2Mo_5O_{21}\cdot 3H_2O$.

Both samples were examined by means of the single crystal X-ray diffraction technique; the former was found only as twinned crystals. The present structure work deals with the structure of ammonium pentamolybdodisulfate(IV)(4—); the results show that the material is neither an inclusion nor a clathrate compound of SO_2 gas, but contains a discrete polyanion consisting of two SO_3 trigonal pyramids and five MoO_6 octahedra.

Experimental

Preparation. Crystals of $(NH_4)_4S_2Mo_5O_{21}\cdot 3H_2O$ were prepared according to the method described by Rosenheim:[2] a 9 g portion of ammonium paramolybdate was dissolved in 30 ml of water, and SO_2 gas was dissolved in this solution; during this procedure the color of the solution gradually changed to yellow. After the solution had become saturated with SO_2, it was rapidly cooled in an ice-water bath; pale yellow needles of $(NH_4)_4S_2Mo_5O_{21}\cdot 3H_2O$ were thus obtained. If the solution was kept in a desiccator at room temperature, $(NH_4)_6S_2Mo_8O_{31}\cdot 5H_2O$ was crystallized. The results of the elemental analyses of $(NH_4)_4S_2Mo_5O_{21}\cdot 3H_2O$ were as follows: Found: Mo, 47.3; S, 6.4; N, 5.55; H, 1.91%. Calcd: Mo, 47.6; S, 6.4; N, 5.51; H, 2.18%.

The solid sample is stable in air and on X-ray irradiation at room temperature.

IR Measurement. The IR spectra were measured from 400 to 4000 cm^{-1} using Nujol mull and a KBr disk on a Hitachi EPI-G2 spectrometer.

Crystal Data. Preliminary photographs revealed that the crystal is orthorhombic, with the space group Pbcn. The unit-cell dimensions were refined with 12 θ values measured on a diffractometer with Mo$K\alpha$ radiation ($\lambda=0.7107$ Å). The crystal data are as follows:

$(NH_4)_4S_2Mo_5O_{21}\cdot 3H_2O$
F.W. = 1005.9
orthorhombic Pbcn
a = 15.096(9) Å
b = 13.375(8) Å
c = 23.734(7) Å
V = 4792.1 Å^3
D_m = 2.79 g cm^{-3}
D_x = 2.79 g cm^{-3}
Z = 8
μ = 30.4 cm^{-1} (for Mo$K\alpha$)

Data Collection. The intensity data were collected on a Rigaku four-circle automatic diffractometer with graphite-monochromated Mo$K\alpha$ radiation. The ω-2θ scan tachnique, with a scan rate of 2θ 2° min^{-1}, was employed. The scan range was determined for each reflection according to this formula: $\Delta\omega=1.4+0.6\tan\theta$, while the background was counted at each scan end for ten seconds. As a check on the crystal stability during the data collection, three standard reflections were monitored every 50 measurements, but no significant deterioration of the crystal was observed. After applying Lorentz and polarization corrections, 6698 $|F_o|$'s were obtained; of those, 3295 reflections with $|F_o|\geq 3\sigma(F)$ were used for further computation. The crystal used for the intensity measurement was pillar-shaped, approximately 0.3 mm long and 0.1 mm in diameter. No absorption correction was made because of the relatively low absorption coefficient.

Structure Determination

The structure was solved by the heavy atom method. Refinement with anisotropic temperature factors for the molybdenum in the anion and with isotropics for the sulfur and oxygen reduced R_1 to 0.112. This was followed by a difference Fourier synthesis, which revealed the positions of all the other non-hydrogen atoms. Eight peaks on the Fourier projection map were attributed to oxygen atoms of water and nitrogen atoms of ammonium cations.

In order to discern the nitrogen atoms in ammonium cations from the oxygens in water molecules, reference was made to the empirical effective radius for NH_4^+, which was determined from the NH_4^+–O distances in a number of ammonium salts.[4] In crystals containing ammonium cations with high coordination numbers, such as 7, 8 or 9, as in the present crystal, the ammonium cations may be considered to be approximate spheres with an effective radius of 1.65 Å. Accordingly, interatomic distances shorter than 3.5 Å were assigned to nitrogen-oxygen contacts. The most probable assign-

TABLE 1. FINAL POSITIONAL AND THERMAL PARAMETERS ($\times 10^4$) WITH THEIR ESTIMATED STANDARD DEVIATIONS IN PARENTHESES

The B_{ij}'s are defined by: $\exp[-(h^2B_{11}+k^2B_{22}+l^2B_{33}+2hkB_{12}+2hlB_{13}+2klB_{23})]$.

	x	y	z	B_{11}	B_{22}	B_{33}	B_{12}	B_{13}	B_{23}
Mo(1)	278(1)	1521(1)	1285(1)	11(1)	18(1)	6(0)	−1(1)	1(0)	0(0)
Mo(2)	1622(1)	538(1)	2270(1)	18(1)	24(1)	5(0)	0(1)	2(0)	3(0)
Mo(3)	3733(1)	1043(1)	1919(1)	13(1)	21(1)	6(0)	1(1)	−1(0)	0(0)
Mo(4)	3782(1)	2104(1)	612(1)	12(1)	15(1)	6(0)	−2(1)	2(0)	1(0)
Mo(5)	1715(1)	2040(1)	77(1)	14(1)	18(1)	5(0)	−1(1)	0(0)	2(0)
S(1)	2274(3)	37(3)	905(1)	15(1)	9(1)	5(0)	−1(1)	0(0)	−1(0)
S(2)	2203(3)	2828(3)	1526(2)	14(2)	10(2)	6(1)	0(2)	1(1)	−1(1)
O(1)	713(99)	1821(9)	558(5)	23(6)	12(7)	4(2)	2(5)	3(3)	−1(3)
O(2)	−326(8)	449(10)	1114(6)	9(5)	25(8)	10(3)	1(5)	−1(3)	−1(4)
O(3)	−517(9)	2400(11)	1357(7)	10(6)	26(8)	13(3)	0(5)	6(3)	0(4)
O(4)	586(8)	1306(10)	2030(6)	8(5)	27(8)	7(2)	6(5)	0(3)	−4(4)
O(5)	1219(9)	2879(10)	1497(6)	18(6)	15(6)	7(2)	6(6)	4(3)	2(4)
O(6)	1559(9)	480(10)	1318(5)	22(6)	18(7)	2(2)	−3(5)	0(3)	0(4)
O(7)	1744(12)	1008(15)	2935(6)	41(9)	67(13)	5(2)	2(10)	−3(4)	3(5)
O(8)	1139(11)	−619(12)	2380(8)	25(7)	34(9)	19(4)	−10(7)	2(5)	5(5)
O(9)	2807(10)	130(10)	2143(6)	26(7)	18(8)	7(2)	6(6)	2(3)	5(4)
O(10)	2421(9)	1945(10)	1913(6)	15(5)	14(7)	8(2)	4(5)	0(3)	2(4)
O(11)	4037(11)	1616(13)	2545(7)	35(9)	43(10)	11(3)	−6(8)	−5(4)	−3(5)
O(12)	4599(9)	225(10)	1809(7)	15(6)	26(9)	12(3)	6(6)	−2(3)	0(4)
O(13)	4046(9)	2098(10)	1397(6)	22(6)	13(7)	8(2)	−10(6)	−4(3)	1(4)
O(14)	3144(8)	608(10)	1028(5)	10(5)	19(7)	4(2)	3(5)	2(3)	2(3)
O(15)	4624(9)	1321(11)	375(6)	18(6)	23(8)	10(3)	−2(6)	3(3)	−2(4)
O(16)	4213(12)	3277(11)	462(8)	39(9)	14(8)	18(4)	−12(7)	2(5)	6(5)
O(17)	2986(9)	1947(9)	−26(6)	22(6)	13(7)	5(2)	0(5)	6(3)	3(4)
O(18)	2441(9)	2449(10)	925(6)	13(5)	8(6)	8(2)	7(5)	6(3)	3(4)
O(19)	1349(9)	1515(12)	−540(6)	20(6)	41(9)	5(2)	−3(7)	−3(3)	2(4)
O(20)	1612(11)	3284(11)	−58(7)	31(7)	20(8)	13(3)	−1(6)	−2(4)	14(4)
O(21)	1974(9)	401(10)	345(6)	24(6)	13(7)	6(2)	0(5)	−5(3)	−1(4)
N(1)	1970(19)	3388(19)	2974(11)	86(19)	48(16)	19(6)	−28(15)	14(8)	−12(8)
N(2)	241(12)	4202(13)	714(8)	19(8)	31(10)	9(3)	−5(7)	0(4)	0(5)
N(3)	4585(13)	3486(15)	3339(8)	37(10)	28(11)	13(4)	3(9)	0(5)	−3(6)
N(4)	2146(16)	830(20)	4190(10)	38(12)	78(19)	17(5)	−8(12)	−9(6)	3(9)
$H_2O(1)$	0(0)	0(0)	0(0)	30(10)	26(12)	11(4)	3(10)	0(6)	−2(7)
$H_2O(2)$	1638(12)	4225(13)	4037(8)	25(8)	48(12)	19(4)	3(8)	−1(5)	6(6)
$H_2O(3)$	0(0)	3367(22)	2500(0)	49(16)	59(20)	20(6)	0(0)	8(8)	0(0)
$H_2O(4)$	3755(14)	1571(16)	3711(8)	57(11)	61(13)	15(4)	−11(11)	9(6)	−4(6)

ment and the proposed model of the ammonium and water arrangement in the crystal are given in Table 1 and in Fig. 3.

After six cycles of refinement with anisotropic temperature factors, all the shifts in the parameters were less than their standard deviations and refinement was terminated. The final value of $R_1(=\sum[|F_o|-|F_c|]/\sum|F_o|)$ was 0.060, and that of $R_2(=[\sum w(|F_o|-|F_c|)^2/\sum w|F_o|^2]^{1/2})$ was 0.084.

In the block-diagonal least-squares refinement, the quantity minimized was $\sum w(|F_o|-k|F_c|)^2$; the weighting scheme adopted was $w=0.2$ for $|F_o|<75$ and $w=1.0$ for all the others.

The atomic scattering factors used were taken from Ref. 5, while corrections of the effect of anomalous dispersion for molybdenum and sulfur were based on Ref. 6.

A difference Fourier synthesis was calculated with the reflections in the range of $0\leq\sin\theta\leq0.45$, but no definitive conclusion was drawn about the positions of hydrogens.

The final coordinates and temperature factors are listed in Table. 1. The observed and calculated structure factors are available at the office of this Bulletin as Document No. 7603.

The calculations were performed on a HITAC 8700/8800 computer at the Computer Centre of the University of Tokyo, using a local version of the UNICS programs.[7]

Description and Discussion of the Structure

Molecular Structure. The $S_2Mo_5O_{21}^{4-}$ anion can be described as an assemblage of five distorted MoO_6 octahedra, which are joined through four sharings of edges and one corner sharing nearly on a plane to form a Mo_5O_{21} pentagon. The two SO_3 trigonal pyramids

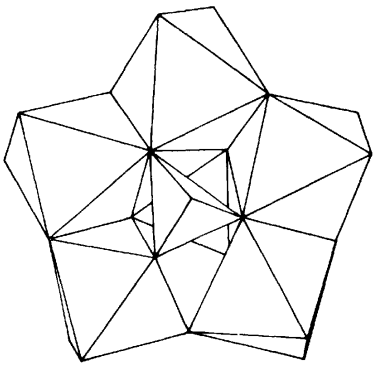

Fig. 1. The structure of $S_2Mo_5O_{21}^{4-}$ anion. Sulfur atoms occupy the apexes of the central trigonal pyramids. Five molybdenum atoms lie nearly on a plane to form a pentagon.

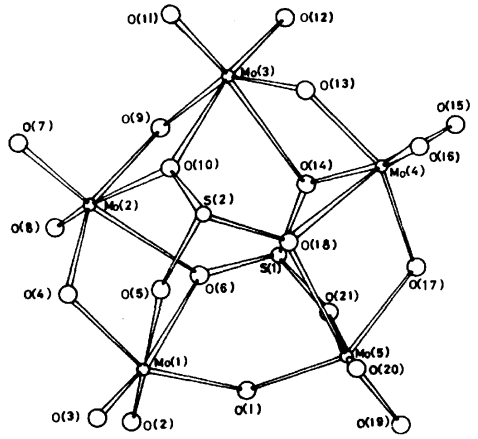

Fig. 2. The structure of $S_2Mo_5O_{21}^{4-}$ anion and its numbering scheme.

are situated so that the Mo_5O_{21} pentagon is capped on both sides by SO_3 pyramids through sharing the oxygens. Figures 1 and 2 show the structure of the anion and numbering scheme adopted for it. The five Mo atoms in the anion are almost co-planar. The equation of the plane through the molybdenum atoms obtained by the least-squares method is:

$$0.03055x - 0.92493y - 0.37892z + 2.82437 = 0.0$$

(x, y, and z are in Å unit)

while the deviations (Å) of each molybdenum from the plane are:

Mo(1) −0.2172, Mo(2) 0.1809, Mo(3) −0.0291
Mo(4) −0.1661, Mo(5) 0.2938

The vector from S(1) to S(2) is almost perpendicular to this plane; the angle between them is 89.25°. The anion has a pseudo twofold axis passing from Mo(3) to O(1).

The structure of the $S_2Mo_5O_{21}^{4-}$ anion is very similar to those of $P_2Mo_5O_{23}^{6-}$,[8] $HP_2Mo_5O_{23}^{5-}$,[9] and $H_2P_2Mo_5O_{23}^{4-}$[10] (Fig. 3). However, the latter anions have hetero atom P's tetrahedrally coordinated by four oxygen atoms; that is, each phosphorus has one unshared atom, while the trigonal pyramidal SO_3 has no such

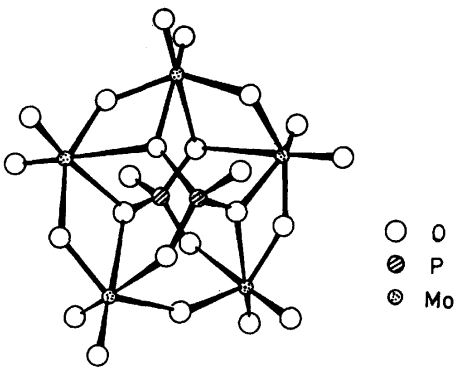

Fig. 3. The structure of $P_2Mo_5O_{23}^{6-}$anion.

terminal oxygen. The bond lengths and angles within the anion are listed in Tables 2 and 3. All the MoO_6 octahedra are disorted, and the Mo–O distances can be grouped into three groups, *i.e.*, Mo–O (unshared, terminal) 1.69—1.74 Å, Mo–O (shared between molybdenums) 1.89—1.95 Å, and Mo–O (shared between molybdenum and sulfur atom) 2.32—2.43 Å. These values are almost equal to the corresponding lengths in the $P_2Mo_5O_{23}^{6-}$ anions.[8-10]

Of the three S–O bondings of the SO_3 trigonal pyramid, two are relatively long; for example, the S(1)–O(6), S(1)–O(4) and S(2)–O(10), S(2)–O(18) distances are comparable to those in the SO_3^{2-} anions, while the other ones, S(1)–O(21) and S(2)–O(5), are as short as the S–O bonds in the SO_4^{2-} ions (1.47—1.49 Å).[11,12] These two types of bonds are different in their bonding schemes as well. O(6), O(14), O(10) and

Table 2. Bond distances (Å) within the anion with their estimated standard deviations in parentheses

Mo(1)···Mo(2)	3.364(2)	Mo(4)—O(13)	1.905(14)
Mo(2)···Mo(3)	3.361(2)	Mo(4)—O(14)	2.431(13)
Mo(3)···Mo(4)	3.413(2)	Mo(4)—O(15)	1.740(14)
Mo(4)···Mo(5)	3.368(2)	Mo(4)—O(16)	1.737(15)
Mo(5)···Mo(1)	3.662(2)	Mo(4)—O(17)	1.945(13)
		Mo(4)—O(18)	2.204(13)
Mo(1)—O(1)	1.890(13)		
Mo(1)—O(2)	1.748(14)	Mo(5)—O(17)	1.936(13)
Mo(1)—O(3)	1.688(14)	Mo(5)—O(18)	2.354(13)
Mo(1)—O(4)	1.851(13)	Mo(5)—O(19)	1.718(14)
Mo(1)—O(5)	2.359(13)	Mo(5)—O(20)	1.703(14)
Mo(1)—O(6)	2.384(13)	Mo(5)—O(21)	2.318(13)
		Mo(5)—O(1)	1.917(13)
Mo(2)—O(4)	1.957(13)		
Mo(2)—O(6)	2.264(12)	S(1)—O(6)	1.574(13)
Mo(2)—O(7)	1.708(16)	S(1)—O(14)	1.547(13)
Mo(2)—O(8)	1.713(17)	S(1)—O(21)	1.486(14)
Mo(2)—O(9)	1.894(15)		
Mo(2)—O(10)	2.391(13)	S(2)—O(5)	1.488(14)
		S(2)—O(10)	1.533(14)
Mo(3)—O(9)	1.931(14)	S(2)—O(18)	1.558(14)
Mo(3)—O(10)	2.318(13)		
Mo(3)—O(11)	1.733(17)		
Mo(3)—O(12)	1.725(14)		
Mo(3)—O(13)	1.937(14)		
Mo(3)—O(14)	2.367(12)		

Table 3. Bond angles (°) within the anion with their estimated standard deviations in parentheses

Mo(1)···Mo(2)···Mo(3)	108.67(6)	O(11)—Mo(3)—O(12)	102.15(74)
Mo(2)···Mo(3)···Mo(4)	109.25(6)	O(11)—Mo(3)—O(13)	99.30(71)
Mo(3)···Mo(4)···Mo(5)	108.19(6)	O(12)—Mo(3)—O(13)	100.41(62)
Mo(4)···Mo(5)···Mo(1)	104.95(6)	O(12)—Mo(3)—O(14)	89.54(55)
Mo(5)···Mo(1)···Mo(2)	105.16(6)	O(13)—Mo(3)—O(14)	72.49(50)
		O(13)—Mo(4)—O(14)	71.47(51)
O(2)—Mo(1)—O(3)	103.00(65)	O(13)—Mo(4)—O(18)	82.19(54)
O(2)—Mo(1)—O(6)	87.16(55)	O(13)—Mo(4)—O(16)	97.23(66)
O(2)—Mo(1)—O(4)	103.01(60)	O(13)—Mo(4)—O(15)	99.25(62)
O(2)—Mo(1)—O(1)	98.23(60)	O(14)—Mo(4)—O(18)	70.86(46)
O(3)—Mo(1)—O(4)	100.98(62)	O(14)—Mo(4)—O(17)	89.04(49)
O(3)—Mo(1)—O(5)	82.49(57)	O(14)—Mo(4)—O(15)	85.69(55)
O(3)—Mo(1)—O(1)	101.02(61)	O(18)—Mo(4)—O(17)	73.58(51)
O(4)—Mo(1)—O(5)	76.41(52)	O(18)—Mo(4)—O(16)	102.92(62)
O(4)—Mo(1)—O(6)	70.98(52)	O(17)—Mo(4)—O(16)	99.73(64)
O(5)—Mo(1)—O(6)	87.45(46)	O(17)—Mo(4)—O(15)	97.74(60)
O(5)—Mo(1)—O(1)	79.78(51)	O(16)—Mo(4)—O(15)	101.80(69)
O(6)—Mo(1)—O(1)	82.66(51)	O(17)—Mo(5)—O(21)	78.89(50)
O(4)—Mo(2)—O(10)	83.40(49)	O(18)—Mo(5)—O(17)	70.30(50)
O(4)—Mo(2)—O(6)	72.11(48)	O(18)—Mo(5)—O(21)	84.68(46)
O(8)—Mo(2)—O(7)	103.64(76)	O(18)—Mo(5)—O(1)	83.91(51)
O(8)—Mo(2)—O(9)	99.44(70)	O(19)—Mo(5)—O(17)	100.63(60)
O(8)—Mo(2)—O(4)	100.25(67)	O(19)—Mo(5)—O(21)	84.28(56)
O(8)—Mo(2)—O(6)	95.87(62)	O(19)—Mo(5)—O(1)	101.01(61)
O(7)—Mo(2)—O(9)	98.74(68)	O(20)—Mo(5)—O(19)	102.09(66)
O(7)—Mo(2)—O(4)	99.31(65)	O(20)—Mo(5)—O(18)	88.70(58)
O(7)—Mo(2)—O(10)	89.03(61)	O(20)—Mo(5)—O(17)	97.43(61)
O(9)—Mo(2)—O(10)	72.20(54)	O(20)—Mo(5)—O(1)	100.97(63)
O(9)—Mo(2)—O(6)	82.56(53)	O(21)—Mo(5)—O(1)	79.90(52)
O(10)—Mo(2)—O(6)	72.18(43)		
O(9)—Mo(3)—O(10)	73.35(53)	O(6)—S(1)—O(14)	106.10(70)
O(9)—Mo(3)—O(12)	100.80(63)	O(6)—S(1)—O(21)	103.05(74)
O(9)—Mo(3)—O(14)	79.51(51)	O(14)—S(1)—O(21)	105.43(73)
O(10)—Mo(3)—O(13)	79.93(52)	O(5)—S(2)—O(10)	106.13(76)
O(10)—Mo(3)—O(14)	78.56(44)	O(5)—S(2)—O(18)	101.68(76)
O(11)—Mo(3)—O(9)	103.66(72)	O(10)—S(2)—O(18)	104.41(73)
O(11)—Mo(3)—O(10)	90.11(66)		

Table 4. Intermolecular contact distances less than 3.1 Å with their estimated standard deviations in parentheses

N(1)···$H_2O(2)$	2.804(33)	$H_2O(1)$···O(1)	2.975(13)
N(1)···$H_2O(3^{i})$	3.013(32)	$H_2O(1)$···$O(16^{viii})$	2.818(16)
N(1)···$H_2O(9^{ii})$	3.081(30)	$H_2O(2)$···N(1)	2.804(33)
N(2)···$H_2O(5)$	2.961(23)	$H_2O(2)$···$O(17^{iv})$	2.778(23)
N(2)···$H_2O(3)$	3.074(24)	$H_2O(2)$···$N(2^{i})$	2.897(25)
N(2)···$H_2O(20)$	3.025(25)	$H_2O(2)$···$N(4^{ii})$	2.849(32)
N(2)···$H_2O(2^{i})$	2.897(25)	$H_2O(3)$···O(5)	3.078(15)
N(2)···$H_2O(12^{ii})$	2.948(24)	$H_2O(3)$···$O(12^{ii})$	3.036(29)
N(2)···$H_2O(15^{ii})$	2.959(23)	$H_2O(4)$···O(11)	2.803(26)
N(2)···$H_2O(15^{iii})$	2.837(24)	$H_2O(4)$···N(3)	2.986(30)
N(3)···$H_2O(19^{iv})$	3.011(25)	$H_2O(4)$···N(4)	2.858(33)
N(3)···$H_2O(2^{v})$	2.935(25)	$H_2O(4)$···$O(20^{iv})$	2.979(27)
N(3)···$H_2HO(8^{ii})$	2.791(27)	i $-x$, y,	$0.5-z$
N(3)···$H_2O(13^{vi})$	2.848(25)	ii $0.5-x$, $0.5+y$,	z
N(3)···$H_2H_2O(4)$	2.986(30)	iii $-0.5+x$, $0.5-y$,	$-z$
N(4)···$H_2O(7)$	3.051(29)	iv $0.5-x$, $0.5-y$,	$0.5+z$
N(4)···$H_2O(20^{iv})$	2.849(30)	v $0.5+x$, $0.5+y$,	$0.5-z$
N(4)···$H_2O(2^{i})$	2.885(28)	vi $1.0-x$, y,	$0.5-z$
N(4)···$H_2O(2^{viii})$	2.840(32)	vii x, $-y$,	$0.5+z$
N(4)···$H_2O(4)$	2.858(33)	viii $0.5-x$, $-0.5+y$,	z
$H_2O(1)$···O(2)	2.757(14)	xi $-x$, $-y$,	$-z$

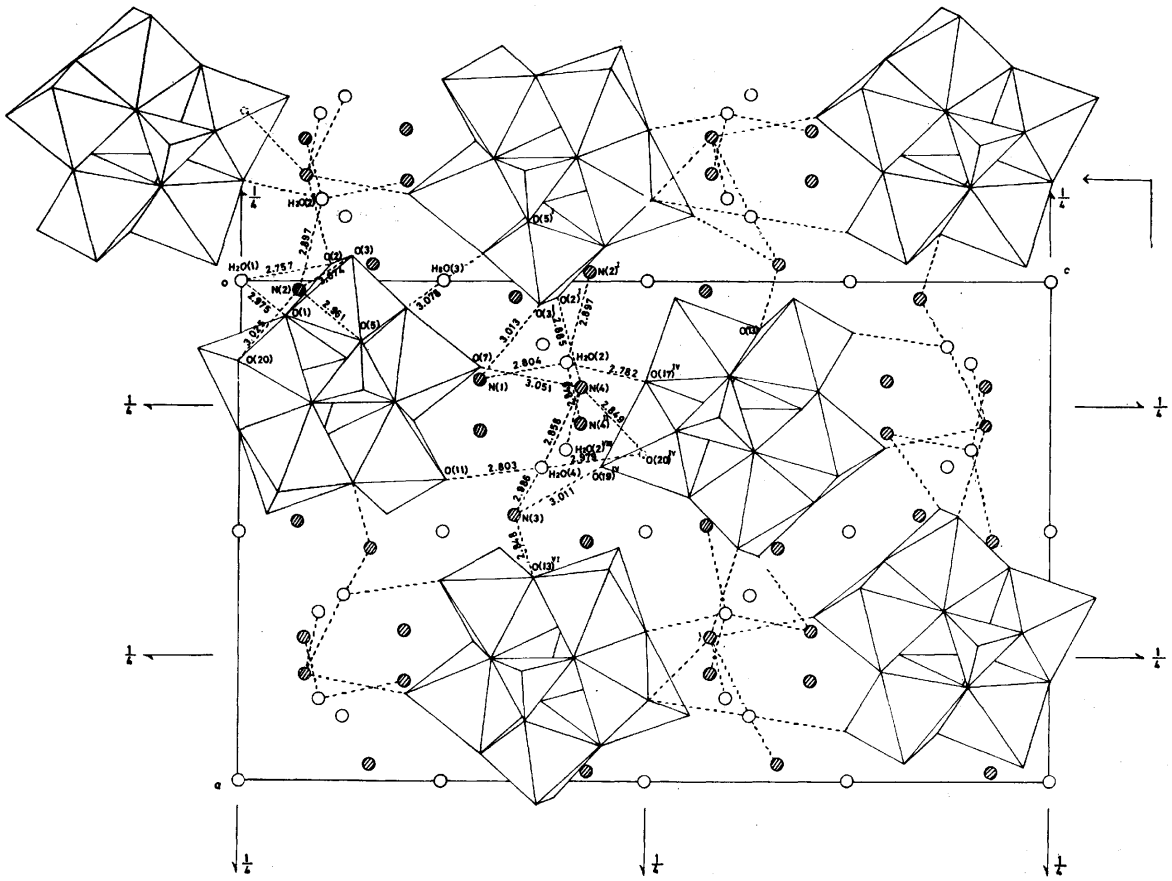

Fig. 4. The crystal structure of $(NH_4)_4S_2Mo_5O_{21}\cdot 3H_2O$. Open circles represent oxygen atoms in the water molecules and shaded circles nitrogen atoms. Only seven anions which lie in the range $y=0.0$—0.5 are depicted for easy viewing.

O(18), all of which make long S–O bonds, are all shared by two Mo atoms, whereas O(21) and O(5) are each bonded to only one Mo atom and make shorter bonds with the sulfur atom. This relation between the S–O lengths and the bonding schemes of the SO_3^{2-} ions corresponds to the general tendency of the elongating effect of a metal atom attached to the oxygen in SO_3^{2-}.[12] The IR spectra of the sample compound show a strong band at *ca.* 1020 cm^{-1} which is assigned to the S–O stretching of the short S–O bonding according to the relationship between the S–O lengths and the stretching frequencies.[11] It does not seem that either of the two lone pairs of S atoms coordinates to any particular atom. The crystal is held by hydrogen bondings between the anions, the cations, and the water of crystallization. Probable hydrogen bondings and van der Waals contacts less than 3.1 Å are given in Fig. 4 and Table 4.

References

1) A. Rosenheim, *Z. Anorg. Chem.* **7**, 177 (1894).
2) A. Rosenheim, *ibid.*, **15**, 183 (1897).
3) E. Péchard, *Ann. Chim. Phys.*, [6], **30**, 401 (1893).
4) A. A. Khan and W. H. Baur, *Acta Crystallogr.*, **B28**, 683 (1972).
5) "International Tables for X-Ray Crystallography," Kynoch Press, Birmingham (1962) Vol. III.
6) D. T. Cromer, *Acta Crystallogr.*, **18**, 17 (1965).
7) "The Universal Crystallographic Computation Program System," Crystallographic Society of Japan (1967).
8) R. Strandberg, *Acta Chem. Scand.*, **27**, 1004 (1973).
9) J. Fischer, L. Ricard, and P. Toledano, *J. Chem. Soc., Dalton Trans.*, **1974**, 941.
10) B. Hedman, *Acta Chem. Scand.*, **27**, 3335 (1973).
11) B. Nyberg and R. Larsson, *ibid.*, **27**, 63 (1973).
12) P. Kierkegaard, L. O. Larsson, and B. Nyberg, *ibid.*, **26**, 218 (1973).

Studies of the Hydrous Titanium Oxide Ion Exchanger. II. The Equivalence of the Exchange Adsorption of Cations and the Dissociation Constant

Yasushi INOUE and Masamichi TSUJI

Department of Nuclear Engineering, Faculty of Engineering, Tohoku University, Aramaki, Sendai 980

(Received July 18, 1975)

In order to elucidate the fundamental properties of hydrous titanium oxide as a cation exchanger, the authors examined the stoichiometry of cation exchange and the acid-base property of the exchanger by means of titration curves. The results may be summarized as follows: 1. The equivalent exchange between the hydrogen ion and either the sodium or strontium ion holds over a wide range of conditions, such as the pH, the ionic strength, and the particle size of the exchanger. 2. The method of conditioning for obtaining the exchanger in the pure hydrogen form has been established. 3. The water content in the exchanger depends on the ionic composition. 4. This hydrous titanium oxide is a four-functional, weakly acidic cation exchanger and has the following apparent pK values: pK_1 6.7±0.1, pK_2 10.3±0.2, pK_3 12.3±0.2, and pK_4 13.2±0.2. The corresponding apparent ion exchange capacities are 2.2±0.1, 1.2±0.2, 0.7±0.3, and 0.2±0.3 meq. Na^+/g respectively.

Hydrous titanium oxide ion exchangers were synthesized by various methods, and their composition, ion exchange capacity, stability against various chemicals, and thermal stability were investigated, in the previous paper.[1] The exchangers in the hydrogen form have the composition of $TiO_2 \cdot (2.0—2.2)H_2O$ and a larger exchange capacity (about 3 meq.Cu(II)/g) than the value (1.6 meq.Cu(II)/g) obtained by Heitner-Wirguin *et al.*[2,3] The exchanger is semitransparent, consisting of nearly amorphous particles which are hard enough to be ground into fine particles suitable for column operations. It is stable in both alkaline and dilute acid solutions(<0.1 M).

The release of hydrogen ions by the adsorption of cations on this material strongly suggests that the mechanism of adsorption is ion exchange, but to substantiate the mechanism unambiguously it is necessary to confirm quantitatively the stoichiometric exchange of the ions concerned. This has been undertaken by using the relation that, for the stoichiometric uptake of ions, the plot of the logarithm of the distribution coefficient *vs.* the pH should be a straight line with a slope corresponding to the valency of cations exchanged.[4] However, this relation is valid only if the concentration of exchanging metal ions is very small in comparison with both the hydrogen-ion concentration and the adsorption capacity of the adsorbent; hence, it is limited to a rather narrow range of experimental conditions. Therefore, from papers hitherto published we cannot exclude the possible participation of mechanisms, such as some specific chemical reaction, surface adsorption, or coprecipitation, other than an ion-exchange reaction.

The purpose of the present investigation is to understand the fundamental properties of hydrous titanium oxide as a cation exchanger through examinations of the validity of the equivalent exchange of cations and of the titration curves, which are useful for understanding the acid-base property of the exchanger.

Experimental

Reagents and Apparatus. The strontium and cesium hydroxide solutions were prepared by passing strontium and cesium chloride solutions through a column packed with Dowex-I anion exchange resin in the OH^- form. All the other reagents were the same as have previously been described.[1]

β-Ray counting was undertaken by the use of a Kobe Kogyo Corp. G. M. counter, Model EA-11, coupled with a Kobe Kogyo scaler, Model SA-250. Except for it, all the apparatuses were the same as have previously been described.

Analytical Method. Alkali metal ions were converted to the corresponding pure chloride and indirectly determined by titrating Cl^- ions by means of Fajans' method. Sr^{2+} was determined chelatometrically.[5] OH^- and CO_3^{2-} were determined by a differential titration, using phenolphthalein and methyl orange as indicators. Cl^- was determined by means of Fajans' method, except for cases where the Cl^- ion was not intentionally added, but came from the ^{22}Na tracer solution. In the latter case, it was estimated by means of the electroneutrality relationship.

Synthesis. The synthetic method No. 7′ described in the preceding paper was used throughout this work. The outline was as follows. Into 200 ml of a 2.2 M $TiCl_4$ solution prepared by diluting liquid $TiCl_4$ with water, 800 ml of a 2.8 M NaOH solution was added at an average rate of 25—30 ml/min. Immediately after the addition, the precipitate was filtered through Toyo No. 1 filter paper under suction, removed from the funnel, dispersed into fresh water, and aged. This procedure was repeated until the pH of the filtrate approached a constant value (about 10). Finally, the precipitate was filtered and air-dried. Since the ion exchange capacity of the material thus prepared fluctuated from batch to batch (3.4—3.7 meq./g), samples of the same batch were employed throughout each series of experiments.

Ion-exchange Stoichiometry. The test samples employed were subjected to three kinds of chemical pretreatments by means of the column method to be described below. The columns used for treating 10 g and 5 g portions of the exchanger were 1.0 cmϕ × 15 cm and 0.7 cmϕ × 15 cm respectively. About a 500 ml portion of the conditioning solution per 10 g of the exchanger was passed through at a flow rate of 0.7—1 ml/min.

Sample A: No pretreatment.

Sample B: Sample A was treated with a 0.1 M HCl solution.

Sample C: About 5 g of Sample A was immersed in 100 ml of a 1 M NaOH solution for 2 days and then treated with the 0.1 M HCl solution.

Sample D: Sample B was treated with a 0.1 M NaOH solution and next with the 0.1 M HCl solution.

Following each single treatment, the exchanger was washed until the effluent was neutral. The particle sizes of the material employed were 65—100, 100—200, and 200—350 meshes.

A half-gram portion of each sample was immersed in 50 ml of a suitable solution (NaOH spiked with ^{22}Na, NaOH–NaCl with ^{22}Na, or $Sr(OH)_2$ with ^{89}Sr) in a tightly stoppered vessel for longer than two days at room temperature, with intermittent shaking. This was followed by chemical analysis and by the measurement of the radioactivity of the solution in a suitable aliquot.

Titration Curve. In 50 ml of a MOH or MOH–MCl solution (M=Na, K, Cs) of a suitable concentration (ionic strength: 0.10 or 1.0 M), 0.5 g of the sample was immersed for 2—3 days at room temperature, followed by the pH measurement and by the chemical analysis of the solution. When the ionic strength was 0.10 M, the amount of ion taken up by the exchanger was evaluated from the difference between the initial and the final concentrations of the ions present in the solution. In the case of the ionic strength of 1.0 M, the amount of uptake was estimated either from the decreased amount of the OH^- ion in the solution or from the weight increase in the exchanger. For the latter, the solid phase was weighed after it had been separated from the solution; it was then washed with acetone, air-dried, and humidiated over a desiccator containing a saturated NH_4Cl solution. This method is warranted by the results, to be described later.

Results and Discussion

Weight Change in the Exchanger with the Change in the Ionic Composition. The change in weight of the exchanger with that of the ionic composition was measured by directly weighing the exchanger before and after a suitable treatment which produced a desired ionic composition. The ionic composition was obtained from the difference in the alkali-metal-ion concentrations of the solution before and after treating the exchanger. The weight increment obtained by direct weighing is plotted in Fig. 1 against that calculated from the change in the ionic composition by assuming that only the difference in the weight of the ions exchanged affects the weight of the exchanger. If this assumption is valid, a straight line with a unit slope passing through the point of origin should be obtained (broken line in Fig. 1). For the sodium ion this relation hold except for the large amount of uptake and can be used for the determination of sodium ion in the exchanger, as has been decribed earlier. In the cases of potassium and cesium ions, the curves deviate appreciably from the broken line. This deviation can naturally be considered to be mainly due to the change in the water content in a hydrous oxide such as this. On the basis of this consideration, we can estimate the change in the water content of the exchanger from the data in Fig. 1.

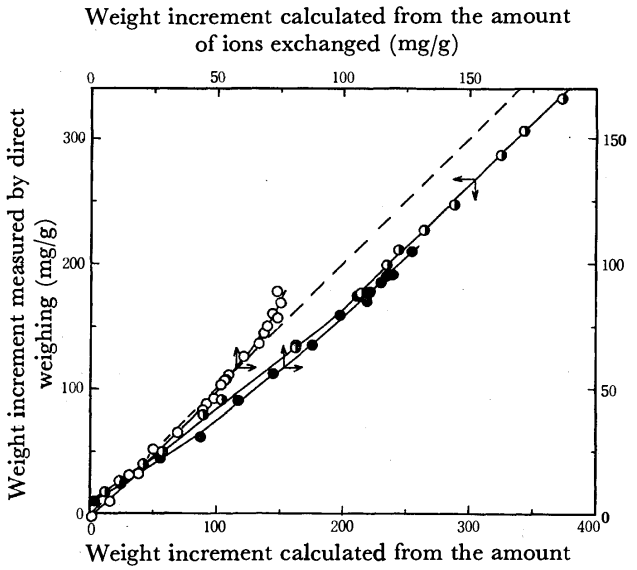

Fig. 1. Weight increase of the exchanger by ion exchange.
○: Na^+ 0.10M; ●: K^+ 0.10M; ◑: Cs^+ 0.10M.

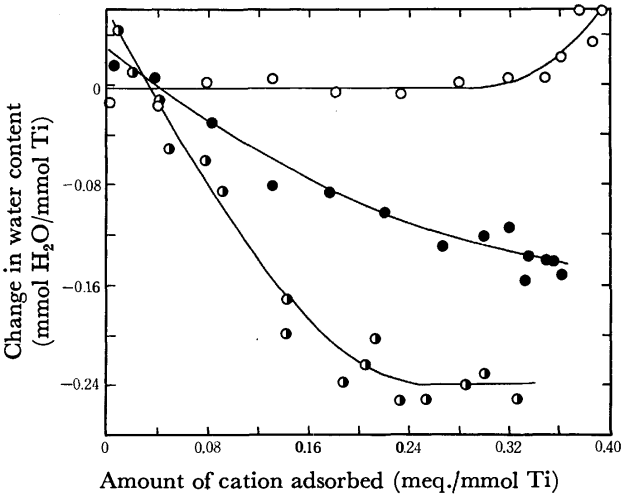

Fig. 2. Change in water content of the exchanger by cation exchange. Marks are the same as used in Fig. 1.

Figure 2 shows the change in the water content of the exchanger in mmol H_2O/mmol Ti against the amount of alkali metal ions taken up in meq./mmol Ti. The horizontal line observed in the case of the sodium ion leads to the conclusion that the exchange between sodium and hydrogen ions causes no change in the water content. The slight deviation from the line in the range of large amounts of sodium-ion uptake is probably due to the reaction with carbon dioxide in the atmosphere during the course of air-drying and humidiating. This explanation is supported by the observations to be described in the next section. Since the same phenomena should also be observed in potassium and cesium exchanges, the curves in Fig. 2 do not show the change in water content quantitatively, especially in the range of higher alkali contents, but the effect is not very large. Therefore, it is evident from Fig. 2 that the ion with the larger ionic radius—that is, with the weaker hydration power, can expel a larger amount of water in the exchanger.

Stoichiometry of the Exchange Reactions. Table 1 represents the experimental results concerning the stoichiometry of the exchange reaction on Samples A

TABLE 1. THE VERIFICATION OF EQUIVALENT EXCHANGE ON THE HYDROUS TITANIUM OXIDE

Sample and mesh size	Run	Added (meq./g)			
		Na^+	OH^-	CO_3^{2-}	Cl^-
A 65–100	c) 1	10.20±0.00	9.97±0.00	0.15±0.02	0.08±0.02
	c) 2	10.28±0.00	10.05±0.00	0.15±0.02	0.08±0.02
	c) 3	0	0	0	0
	d) 1	10.20±0.00	9.97±0.00	0.15±0.02	0.08±0.02
	d) 2	10.28±0.00	10.05±0.00	0.15±0.02	0.08±0.02
	d) 3	0	0	0	0
B 65–100	1	9.60±0.02	9.43±0.02	0.16±0.01	0.01±0.05
	2	9.54±0.02	9.37±0.02	0.16±0.01	0.01±0.05
	3	0	0	0	0

Sample and mesh size	Run	Remaining (meq./g)				
		Na^+		OH^-	CO_3^{2-}	Cl^-
		1[a]	2[b]			
A 65–100	c) 1	7.21±0.15	9.28±0.03	8.79±0.03	0.42±0.01	0.07±0.07
	c) 2	7.42±0.15	9.36±0.03	8.90±0.01	0.39±0.01	0.07±0.05
	c) 3	—	0.23±0.01	−0.02±0.01	0.22±0.01	—
	d) 1	—	9.01±0.06	8.79±0.03	0.15±0.02	0.07±0.11
	d) 2	—	9.12±0.06	8.90±0.01	0.15±0.02	0.07±0.09
	d) 3	—	0	0	0	0
B 65–100	1	7.18±0.18	7.30±0.04	7.10±0.01	0.14±0.02	0.06±0.07
	2	7.07±0.18	7.25±0.01	7.01±0.01	0.14±0.00	0.10±0.02
	3	—	0.00±0.00	0.00±0.00	0.00±0.00	—

Sample and mesh size	Run	(i) meq./Na^+ adsorbed/g		(ii) meq./H^+ released/g	(ii)/(i)	
		1[a]	2[b]		1[a]	2[b]
A 65–100	c) 1	2.99±0.15	0.92±0.03	1.18±0.03	0.40±0.03	1.28±0.07
	c) 2	2.86±0.15	0.92±0.03	1.15±0.01	0.40±0.03	1.25±0.05
	c) 3	—	—	—	—	—
	d) 1	—	1.19±0.06	1.18±0.03	—	0.99±0.08
	d) 2	—	1.16±0.06	1.15±0.01	—	0.99±0.06
	d) 3	—	—	—	—	—
B 65–100	1	2.42±0.20	2.30±0.06	2.33±0.03	0.97±0.10	1.01±0.04
	2	2.47±0.20	2.29±0.03	2.36±0.03	0.96±0.09	1.03±0.03
	3	—	—	—	—	—

a) γ-Counting. b) Titration. c) Experimental values. d) Corrected values.

and B For Sample A, the ratio of hydrogen ions released to the sodium ions adsorbed was 1.26 (an average of the data on the last column of the table) if we determine the sodium-ion concentration by Fajans' method. This value is somewhat greater than unity, which would be obtained if the ion-exchange stoichiometry holds. The blank Run No. 3 shows that, even in distilled water, some sodium carbonate is released. Assuming that the sodium carbonate comes entirely from the sample, and that the sodium carbonate in the sample completely dissolves in the solution, we may conclude that Sample A contains 0.23 meq. sodium ion/g as a carbonate. This value is also in good agreement with the increase in the carbonate-ion concentration in the sodium hydroxide solution during equilibration with the exchanger. Therefore, the sodium ions originating from the sodium carbonate in the sample can be estimated from the increment in the carbonate ions in solution. When such an amount of sodium ions is subtracted from that in the equilibrium solution, it is revealed that the equivalent exchange holds in each run, as is indicated by the corrected values in the same table.

On the other hand, an average of the ratios of the hydrogen ions released to the sodium ions adsorbed was 0.40, if we calculated the amount of sodium ions adsorbed simply from the difference between the initial and the final activities of the sodium-22 present in solution, assuming a constant specific activity throughout the experiment. This value contradicts the one mentioned above. This discrepancy can be understood by considering that Sample A is not in the pure hydrogen form, but partly in the sodium form.

Assuming that the sodium ion in the exchanger is present as sodium carbonate and fixed ions which are distributed uniformly, and that the specific activity of sodium-22 becomes constant throughout the system after the equilibrium is reached, we obtain the following

equations from the conservations of the sodium ion and radioactivity:

$$\bar{w}_i(m_i - Me/2000) + e + w_i V_i = \bar{w}_f m_f + w_f V_f \quad (1)$$

$$a_i V_i = a_f V_f + S\bar{w}_f m_f \quad (2)$$

$$S = a_i V_i / [\bar{w}_i(m_i - Me/2000) + e + w_i V_i] \quad (3)$$

where w represents the concentration of sodium ions in the liquid phase in meq.Na^+/ml; $\bar{w}$, the concentration of sodium ions fixed in the exchange site in meq.Na^+/g; V, the volume of the liquid phase in ml; m, the weight of the exchanger in g; a, the activity concentration in the solution in cpm/ml; e, the amount of sodium carbonate in the sample in meq.; M, the molecular weight of the sodium carbonate, and S, the specific activity of sodium-22 in cpm/meq.Na^+ after the equilibrium was reached. Furthermore, the i and f suffixes refer to the initial and the final states respectively.

TABLE 2. THE COMPARISON BETWEEN CALCULATED AND EXPERIMENTAL VALUES OF $\bar{w}_i$

Sample	Run	m_i (g)	$\bar{w}_i^{calcd}$ meq./g	$\bar{w}_i^{calcd}$ based on H^+ form	$\bar{w}_i^{exp}$ meq./g
A	1	0.5017	2.71±0.32	2.90±0.35	2.32
	2	0.4979	2.48±0.32	2.64±0.34	
B	1	0.4983	0.15±0.32	0.15±0.32	0.08
	2	0.5016	0.11±0.42	0.11±0.42	

Since the water content of the exchanger does not change in the exchange between sodium and hydrogen ions, as is shown in Fig. 1, $V_i = V_f = V$. Combining Eqs. (1)—(3), we obtain:

$$\bar{w}_i = 2000[(a_i w_f/a_f - w_i)V - e]/(2000 m_i - Me) \quad (4)$$

We can calculate $\bar{w}_i$ by substituting the data in Table 1 into Eq. (4). Table 2 shows the results, together with the values determined directly by chemical analysis. The average of these results, 2.60±0.32 meq.Na^+/g of Sample A, agrees with the analytical value, 2.32 meq.Na^+/g of Sample A, within the limits of experimental error. Accordingly, the isotopic-exchange equilibrium is reached in the exchanger. Furthermore, the average of $\bar{w}_i^{calcd}$ in terms of meq./g of the hydrogen form is 2.77±0.35, as is indicated in the next to the last column of the same table. It is nearly equal to the apparent capacity, 2.6 meq./g (Fig. 4), at pH 10.4, which corresponds to that of the filtrate in the final stage of synthesis. The amount of sodium ions adsorbed by Sample A is 1.18±0.06 meq./g, which corresponds to 1.23±0.06 meq./g of the hydrogen form. This value plus $\bar{w}_i^{calcd}$ is 4.00±0.41 meq./g, which agrees, within the limits of experimental error, with the ion-exchange capacity obtained with the 0.10 M sodium hydroxide solution. From these results, one can conclude that about 75% of the exchange sites are occupied by sodium ion in the stage of synthesis and that some sodium carbonate is also present. The sodium carbonate may be admixed in the stage of aging and/or during storage, when the sodium ions in the exchanger are expelled to form carbonate by means of the action of atmospheric carbon dioxide.

In Sample B, the ratio of hydrogen ions released to sodium ions adsorbed is 1.02±0.04, as is shown in the last column of Table 1. Therefore, the equivalent exchange is also valid for this sample. The one obtained by the radiometric method is also nearly unity, but it seems a little lower. The results of the blank Run No. 3 show that this sample does not contain carbonate. The sodium content, calculated from the data in Table 1 by means of Eq. (4), is 0.13±0.37 meq./g (Table 2), which agrees with the analytical value, 0.08 meq./g, within the limits of experimental error. The conclusion can be derived directly from these results that the treatment with the 0.1 M hydrochloric acid solution can remove carbonate and most of the sodium ions.

The amount of sodium ions adsorbed plus the $\bar{w}_i^{calcd}$ value obtained by the radiometric method, 2.43±0.42 meq./g of the hydrogen form, is smaller than the value on Samples C and D, about 3.5 meq./g. The reason for this discrepancy is not clear, but the treatment with 0.1 M hydrochloric acid solution alone is not sufficient to activate all the exchange sites and so is incomplete.

The results on Samples C and D were obtained by means of the radiometric method. Table 3 shows the equivalent exchange between sodium and hydrogen ions

TABLE 3. THE VERIFICATION OF EQUIVALENT EXCHANGE ON THE HYDROUS TITANIUM OXIDE

Sample and mesh size	Ionic strength (M)	Run	(i) meq. Na^+ adsorbed/g	(ii) meq./H^+ released/g	(ii)/(i)
C 65—100	0.10	1	3.42±0.17	3.43±0.01	1.00±0.05
		2	3.35±0.17	3.36±0.02	1.00±0.06
		3	3.42±0.17	3.38±0.03	0.99±0.06
D 65—100	0.10	1	3.69±0.19	3.62±0.04	0.97±0.05
		2	3.51±0.20	3.69±0.04	1.05±0.07
D 100—200	0.10 (OH^-/Cl^-=0.20)[a]	1	1.71±0.18	1.70±0.01	1.01±0.12
		2	1.67±0.18	1.71±0.01	1.04±0.11
		3	1.70±0.18	1.70±0.01	1.01±0.12
D 200—350	0.10	1	3.73±0.15	3.85±0.02	1.03±0.05
		2	3.82±0.15	3.86±0.02	1.01±0.05
D 200—350	0.028 (OH^-/Cl^-=1.6)[a]	1	1.70±0.04	1.68±0.01	1.00±0.03
		2	1.70±0.05	1.69±0.01	1.00±0.04
		3	1.72±0.03	1.69±0.01	0.98±0.03

a) Molar ratio.

TABLE 4. THE VERIFICATION OF EQUIVALENT EXCHANGE ON THE HYDROUS TITANIUM OXIDE

Sample and mesh size	Ionic strength (M)	Run	(i) meq. Sr^{2+} adsorbed/g		(ii) meq. H^+ released/g	(ii)/(i)	
			1[a]	2[b]		1[a]	2[b]
D 65—100	0.068	1	3.77±0.01	3.79±0.01	3.74±0.04	0.99±0.02	0.99±0.02
		2	3.77±0.01	3.79±0.00	3.73±0.07	0.99±0.02	0.98±0.02
		3	3.79±0.01	3.80±0.00	3.76±0.06	0.99±0.02	0.99±0.02

a) γ-Counting. b) Titration.

which takes place in these samples. This relationship holds exactly, irrespective of the particle size, the ionic strength, and the kind of anion.

Table 4 shows that the same is also true when the strontium ion is used as the exchanging cation. Since the carbonate-ion concentration decreased in this run, the amount of hydrogen ions released was estimated from the difference in the sum of carbonate and hydroxide ions before and after the equilibration.

As the results presented above show, the pure-hydrogen-form exchanger can be obtained by treating the air-dried gel first with the 0.1 M hydrochloric acid solution and next with the 0.1 M sodium hydroxide solution, followed by the 0.1 M hydrochloric acid solution. It acts as an ideal cation exchanger, and an equivalent exchange of cations occurs on the exchange sites uniformly distributed in it.

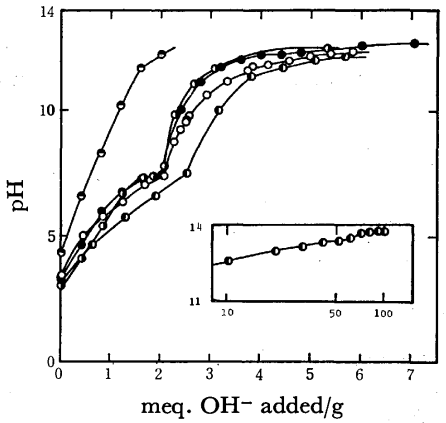

Fig. 3. Titration curves of the exchanger for various alkali metal ions. ◐: Na^+ 1.0M; ◓: K^+ (Ref. 6) 0.1M; ○: Na^+ 0.10M; ●: K^+ 0.10M; ◑: Cs^+ 0.10M.

Acid-base Properties. In order to study the acid-base property of the exchanger, titration curves were constructed by various alkali metal hydroxides, as is shown in Fig. 3. The features are not different from each other except in minor details. The curves obtained with a solution with an ionic strength of 0.10 M present a steep pH jump at pH 7.4. The curve for the potassium ion possesses a small flat portion at pH 12.2, whereas those for the other ions do not.

The titration curve with the sodium hydroxide-sodium chloride mixed solution with an ionic strength of 1.0M also shows a steep pH jump at pH 7.4 and another, less pronounced one at pH 13.5. From these observations, this exchanger can be inferred to possess four kinds of exchange sites.

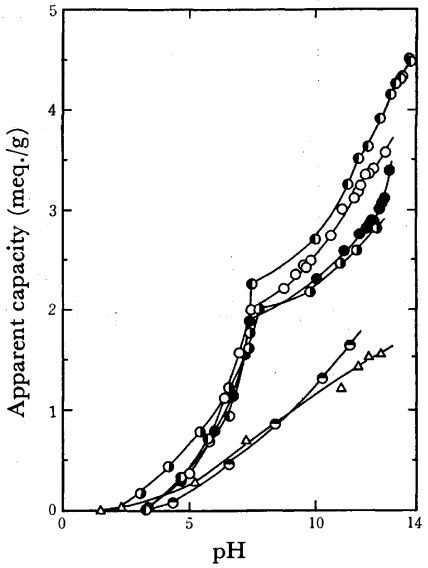

Fig. 4. Apparent capacity of the exchanger as a function of pH. △: Na^+ (Ref. 7); other marks are the same as those in Fig. 3.

The apparent exchange capacity is plotted as a function of the pH in Fig. 4. The curves are consistent with the titration curves, but show some features more clearly. Irrespective of the ionic strength and the kind of ion employed, the first inflecting point appears at pH 7.4, where the first pH jump is observed in the titration curves. While the point indicating the beginning of the participation of the third exchange site is not distinctly observed in the titration curves, it appears more clearly in the cases of the potassium and sodium ions for μ=0.10 at pH 12.2 and 12.0 and in the case of the sodium ion for μ=1.0 at pH 11.7 in Fig. 4. In the latter case, an additional jump in pH is observed at pH 13.5, where a corresponding discontinuity is also observed in Fig. 4.

Another interesting fact may well be noted here. The exchange rate shown in Fig. 5 indicates that the exchange of sodium ions occurs step by step. The amount of sodium ions taken up at the end of each step is nearly the same as the value observed at the inflection point of Fig. 4. This fact not only shows that the rate of exchange is faster in the more acidic site, but also strengthens the observation about the position of the inflection point mentioned above. It can be concluded from these facts that this exchanger possesses four kinds of exchange sites. This conclusion is quite different from the findings by other workers.[6,7] The hydrous titanium oxide prepared by them shows an apparent exchange capacity of about 1.6 meq./g at

Table 5. pK values and apparent capacities of the exchanger for alkali metal ions

Ion	Ionic strength (M)		Steps 1	2	3	4	Total ion exchange capacity
Na^+	0.10	pK	5.20±0.04	9.00±0.15	—	—	3.4±0.1
		$C^{a)}$	2.01±0.07	1.33±0.19	—	—	
	1.0	pK	6.7 ±0.1	10.3±0.2	12.3±0.2	13.2±0.2	4.5±0.2
		$C^{a)}$	2.2 ±0.1	1.2 ±0.2	0.7±0.3	0.2 ±0.3	
K^+	0.10	pK	5.42±0.03	9.27±0.03	—	—	3.4±0.1
		$C^{a)}$	1.90±0.02	0.99±0.04	—	—	
	1.0		—	—	—	—	4.5±0.1
Cs^+	0.10	pK	5.05±0.03	—	—	—	2.8±0.1
		$C^{a)}$	2.00±0.03	—	—	—	
	0.50		—	—	—	—	3.4±0.2
Cs^+ (Ref. 4)	2.5×10^{-3}	pK	5.7	6.7	8.5	—	(0.299)
		$C^{b)}$	0.100	0.090	(0.109)	—	
	5.0×10^{-3}	pK	5.7	6.8	8.4	—	(0.292)
		$C^{b)}$	0.100	0.096	0.096	—	
	1.2×10^{-2}	pK	5.7	7.0	8.7	—	(0.298)
		$C^{b)}$	0.100	0.098	0.100	—	

a) Ion exchange capacity in meq./g. b) Ion exchange capacity in g-eq./molTiO_2.

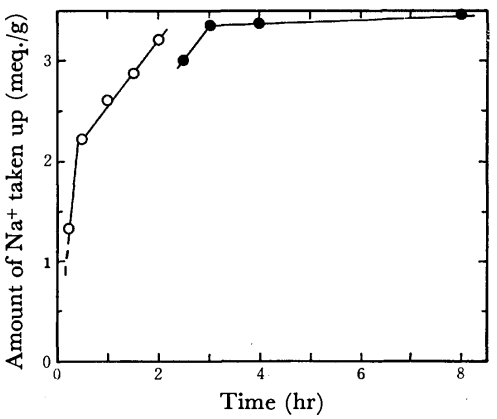

Fig. 5. Ion exchange rate of Na^+ ion. Conditions: 50 ml of 0.106 M NaOH/0.50 g of H^+ form exchanger 65—100 mesh. Temperature, ○: 22 °C, ●: 19—22 °C.

pH 12, and up to this pH the inflection point is not observed. This difference is probably attributable to the difference in their synthetic method from the present authors'.

The apparent pK values can be calculated by applying the following equation[8] to the titration curve (Fig. 3) and to the dependency of the apparent capacity on the pH (Fig. 4):

$$pK_i = pH_i + \log (M^+)_i - \log (\bar{X})_i/2$$

where $(M^+)_i$ and pH_i are the alkali-metal-ion concentration and the pH at the half-conversion point of the i-th exchange site respectively. The results are presented in Table 5, together with the results reported by Schiewer.[4] It can be concluded from the table that all the functional groups in the exchanger are weakly acidic. Since the experimental conditions used by Schiewer are appreciably different from ours, we cannot compare the results strictly, but, interestingly enough, the pK_1 value of this exchanger is almost the same as that of Schiewer, 5.7. However, the pK_2 and pK_3 values are completely different from those of Schiewer. This discrepancy may arise from the difference in structure; that is, Schiewer employed a hydrous titanium oxide suspension as an exchanger, whereas the present authors used an exchanger possessing a hard, three-dimensional network.

References

1) Y. Inoue and M. Tsuji, *J. Nucl. Sci. Technol.*, in press, "Studies on Hydrous Titanium Oxide Ion Exchanger. I. Method of Synthesis and Some Properties."
2) C. Heitner-Wirguin and A. Albu-Yaron, *J. Appl. Chem.*, **15**, 445 (1965).
3) V. Veselý and V. Pekárek, *Talanta*, **19**, 219 (1972).
4) E. Schiewer, Dissertation, Technische Universität Berlin (1967).
5) T. J. Manns, M. U. Reschowsky, and A. J. Certa, *Anal. Chem.*, **24**, 908 (1952).
6) M. Abe and T. Ito, *Nippon Kagaku Zasshi*, **86**, 1259 (1965).
7) N. J. Keen, *J. Brit. Nucl. Soc.*, **7**, 178 (1968).
8) F. Helfferrich, "Ion Exchange," McGraw-Hill, New York (1962), p. 85.

The Crystal Structure of the Trinuclear Complex, $[Cu_3\{(C_2H_5)_2N(CH_2)_2NH(CH_2)_3O\}_2(OH)_2](ClO_4)_2$

Naohide MATSUMOTO, Yuzo NISHIDA, Sigeo KIDA, and Ikuhiko UEDA*

Department of Chemistry, Faculty of Science, Kyushu University, Hakozaki, Fukuoka 812

**Department of Physics, Faculty of General Education, Kyushu University, Ropponmatsu, Fukuoka 810*

(Received July 18, 1975)

The structure of the trinuclear complex, formed from *N,N*-diethyl-*N'*-(3-hydroxypropyl)ethylenediamine and copper(II) perchlorate, has been determined from three dimensional X-ray diffraction data. The crystals are monoclinic with the space group $P2_1/c$. The cell dimensions are $a=7.759(6)$, $b=13.21(1)$, $c=15.00(1)$ Å and $\beta=103.95(6)°$. The unit cell contains two molecules and the molecule has a centre of symmetry. The structure has been determined by the heavy atom method and refined by the block diagonal least squares method to give $R=6.83\%$ for 1368 observed reflections. Three copper atoms are arrayed on a straight line, the separations being 2.902 Å. The geometry around the two end copper atoms is best described as a slightly distorted tetragonal pyramid. The central copper atom has a square planar environment.

In the previous paper Nishida and Kida[1] reported the preparation of the binuclear (green) and the trinuclear (blue) copper(II) complexes from *N,N*-dialkyl-*N'*-(3-hydroxypropyl)ethylenediamine, $R_2N(CH_2)_2NH(CH_2)_3OH$ ($R=CH_3$, C_2H_5), copper(II) perchlorate and sodium hydroxide.

When the ligand, copper(II) perchlorate and sodium hydroxide were mixed with the mole ratio 1:1.2:1, green crystals were obtained. This complex was assumed to be binuclear on the bases of the elemental analysis and the magnetic susceptibility measurements over the temperature range 80—300 K. This was verified from the single crystal X-ray diffraction method by Villa *et al.*[2]

On the other hand, when the ligand, copper(II) perchlorate and sodium hydroxide were mixed with the mole ratio 1:2:1, blue crystals were obtained, which were assumed to be of a linear trinuclear structure on the bases of the elemental analysis and the magnetic susceptibility measurements (80—300 K). In the present work a single crystal X-ray diffraction study has been carried out for this compound in order to confirm the above assumption. The detailed structural data are desirable for the elucidation of magnetisms and electronic spectra of the alkoxo-bridged copper(II) complexes.

Experimental

The complex was prepared according to Ref. 1. Single crystals of the complex for the X-ray work were obtained as violet blue needles by slow evaporation of 99% methanol solution at room temperature. For cell parameter determination and intensity measurement an approximately cubic crystal of dimension 0.2 mm was prepared by cutting a larger specimen. The cell parameters were determined from fifteen reflections measured on Syntex $P\bar{1}$ diffractometer by the autoindexing and least squares programs.

The Crystal Data: $Cu_3Cl_2O_{12}N_4C_{18}H_{44}$, formula weight 770.1, monoclinic, space group $P2_1/c$, $a=7.759(6)$, $b=13.21(1)$, $c=15.00(1)$ Å, $\beta=103.95(6)°$, $V=1493.03$ Å^3, $Z=2$, $D_m=1.704$ g·cm^{-3} (by floatation), $D_x=1.712$ g·cm^{-3}, μ(Mo $K\alpha$)$=23.90$ cm^{-1}. Three dimensional intensity data were collected by the θ—2θ scan technique with a variable scan rate from 4.0 to 24.0°/min on a Syntex $P\bar{1}$ four-circle diffractometer using Mo$K\alpha$ radiation monochromated by a graphite plate. Three reflections were monitored after every measurement of 47 reflections, and the monitored data showed good stability. Of the 2650 reflections recorded, 1368 had intensities greater than 2.33 times their estimated standard deviations, and only these unique reflections were used for the structure determination. The data were corrected for Lorentz and polarization effects. Correction for absorption was not applied.

Determination and Refinement of Structure

In the space group $P2_1/c$, the general positions are fourfold. In this crystal, there are only two molecules in a unit cell and each molecule includes three copper atoms. Therefore, each molecule has a center of symmetry, which corresponds to the special position 0, 0, 0 or 0, 1/2, 1/2, and the central copper atom of each molecule is required to be in this special position.

TABLE 1. FRACTIONAL ATOMIC COORDINATES AND THEIR STANDARD DEVIATIONS IN PARENTHESES

	x	y	z
Cu(1)	0.0	1/2	1/2
Cu(2)	0.1320(1)	0.3363(0)	0.4056(0)
Cl	0.3066(4)	0.5661(2)	0.2998(2)
O(1)	0.1750(9)	0.3942(5)	0.5252(4)
O(2)	−0.0764(8)	0.4169(4)	0.3940(3)
N(1)	0.0580(10)	0.2770(6)	0.2813(4)
N(2)	0.3361(10)	0.2329(6)	0.4263(5)
C(1)	0.2173(14)	0.2360(8)	0.2603(6)
C(2)	0.3099(13)	0.1731(8)	0.3397(6)
C(3)	−0.0478(15)	0.3423(8)	0.2093(6)
C(4)	−0.2123(14)	0.3792(8)	0.2345(7)
C(5)	−0.1839(14)	0.4567(7)	0.3082(6)
C(6)	0.5088(14)	0.2923(8)	0.4433(7)
C(7)	0.6789(16)	0.2279(11)	0.4628(9)
C(8)	0.3386(14)	0.1654(8)	0.5072(6)
C(9)	0.1597(17)	0.1252(11)	0.5082(9)
O(3)[a]	0.3077(17)	0.4771(9)	0.3395(8)
O(4)[b]	0.1874(19)	0.6124(13)	0.3644(11)
O(5)	0.4547(11)	0.6289(7)	0.3222(6)
O(6)	0.1851(14)	0.5943(8)	0.2228(7)
O(7)[c]	0.3756(25)	0.4882(14)	0.2316(13)

a) Occupancy 0.82. b) Occupancy 0.65. c) Occupancy 0.53.

TABLE 2. FINAL ANISOTROPIC TEMPERATURE FACTORS ($\times 10^4$) AND THEIR STANDARD DEVIATIONS IN PARENTHESES
The temperature factor is of the form $\exp[-(B_{11}h^2+B_{22}k^2+B_{33}l^2+B_{12}hk+B_{13}hl+B_{23}kl)]$.

	B_{11}	B_{22}	B_{33}	B_{12}	B_{13}	B_{23}
Cu(1)	137(3)	44(1)	28(0)	38(3)	18(2)	−21(1)
Cu(2)	131(2)	41(0)	25(0)	32(2)	17(1)	−11(1)
Cl	166(7)	71(2)	84(2)	−42(6)	−57(5)	61(3)
O(1)	216(18)	51(4)	29(3)	25(14)	42(12)	−28(6)
O(2)	173(16)	43(4)	29(3)	23(13)	11(10)	−16(5)
N(1)	166(20)	63(6)	20(3)	59(18)	−11(12)	−5(7)
N(2)	155(19)	39(5)	41(4)	35(16)	45(14)	−6(7)
C(1)	190(26)	64(7)	26(4)	106(23)	27(16)	−32(9)
C(2)	186(27)	56(7)	37(5)	68(23)	29(17)	−26(10)
C(3)	287(30)	50(7)	32(5)	−2(26)	17(19)	−16(10)
C(4)	146(26)	62(8)	54(6)	60(23)	−46(19)	−59(11)
C(5)	164(24)	48(6)	32(5)	73(21)	−45(16)	6(9)
C(6)	157(25)	52(7)	50(6)	5(22)	33(19)	1(10)
C(7)	159(29)	108(12)	79(8)	−15(31)	41(24)	30(17)
C(8)	225(27)	52(6)	34(4)	17(24)	9(17)	34(10)
C(9)	238(34)	110(12)	72(8)	−27(32)	87(27)	12(16)
O(3)	412(37)	95(10)	121(10)	−64(31)	−11(30)	168(16)
O(4)	264(39)	139(15)	120(15)	34(40)	185(36)	−10(22)
O(5)	218(21)	104(8)	86(6)	−91(20)	75(17)	−30(11)
O(6)	404(31)	121(9)	92(7)	40(29)	−40(23)	54(13)
O(7)	336(51)	91(15)	118(15)	−72(47)	−52(44)	−69(25)

TABLE 3. FRACTIONAL ATOMIC COORDINATES AND ISOTROPIC TEMPERATURE FACTORS OF HYDROGEN ATOMS
The average estimated standard deviations of the isotropic temperature factors is 2.0Å².

	x	y	z	B(Å²)
H(1)	0.234(19)	0.382(11)	0.557(9)	8.0
H(2)	0.190(13)	0.204(7)	0.202(6)	2.5
H(3)	0.304(14)	0.294(8)	0.246(7)	4.3
H(4)	0.430(13)	0.131(7)	0.329(6)	3.1
H(5)	0.240(13)	0.110(8)	0.350(7)	3.2
H(6)	−0.079(17)	0.301(10)	0.150(8)	6.6
H(7)	0.022(17)	0.399(10)	0.197(8)	6.6
H(8)	−0.285(13)	0.318(7)	0.244(6)	2.8
H(9)	−0.297(13)	0.407(8)	0.177(6)	3.0
H(10)	−0.299(14)	0.495(9)	0.313(7)	4.2
H(11)	−0.122(14)	0.522(8)	0.288(7)	3.8
H(12)	0.515(13)	0.348(7)	0.495(6)	2.4
H(13)	0.496(14)	0.342(8)	0.389(7)	4.1
H(14)	0.383(16)	0.199(9)	0.564(7)	6.2
H(15)	0.421(15)	0.100(9)	0.508(8)	5.4
H(16)	−0.026(17)	0.218(9)	0.275(8)	6.1
H(17)	0.598(17)	0.179(10)	0.435(8)	6.4
H(18)	0.657(16)	0.197(9)	0.501(8)	5.8
H(19)	0.786(13)	0.275(8)	0.465(8)	3.5
H(20)	0.080(15)	0.198(8)	0.484(7)	4.9
H(21)	0.068(17)	0.094(10)	0.464(7)	6.3
H(22)	0.140(17)	0.357(10)	0.052(8)	6.7

The structure was solved by the heavy atom method. The coordinates of the copper atoms could be easily determined from the three-dimensional Patterson synthesis. The position of the chlorine atom was deduced from the minimum function based on the copper atoms. A three dimensional electron density map was then calculated with all observed reflections phased by the copper and chlorine atoms. The resulting map showed the peaks corresponding to all the remaining non-hydrogen atoms except two oxygen atoms in perchlorate anion. The atomic positions and isotropic temperature factors were refined by the block diagonal least squares method. Further refinement was carried out, introducing anisotropic temperature factors, and the disagreement factor decreased to 11.67%. At this step a difference Fourier synthesis was calculated. The difference Fourier map showed three diffuse peaks, though only two peaks of the two oxygen atoms in perchlorate ion were expected. Accordingly, the occupancy factors of the oxygen atoms were assigned in proportion to the peak values, as shown in Table 1. Six cycles of the block diagonal least squares refinement were applied to the positional and anisotropic thermal parameters of all the non-hydrogen atoms. The disagreement factor was decreased from 8.96 to 7.69% for the observed 1368 reflections. At this stage a difference Fourier synthesis was calculated and the positions of about half of the hydrogen atoms could be determined. The positions of the remaining hydrogen atoms were assigned from the calculation. Introducing these hydrogen atoms, the final set of the least squares calculation was carried out.

The final disagreement factor was 6.83% for the observed 1368 reflections.** Maximum shifts of the positional and thermal parameters in the final cycle did not exceed half their standard deviations. In the least squares procedure, the quantity minimized was $\sum w(k|F_o|-|F_c|)^2$, where k is a scale factor and $w=1$ for $|F_o|\geqq 5.0$ and $w=0$ for $|F_o|<5.0$. The scattering factors for all the atoms were taken from the literature.[3] The final positional and thermal parameters are shown in Tables 1, 2 and 3.

* The observed and calculated structure factors are available at the office of this Bulletin as Document No. 7604.

Description and Discussion of the Structure

A perspective drawing of the complex and the numbering system used in this text are illustrated in Fig. 1. The bond distances and the bond angles within a molecule are listed in Tables 4 and 5.

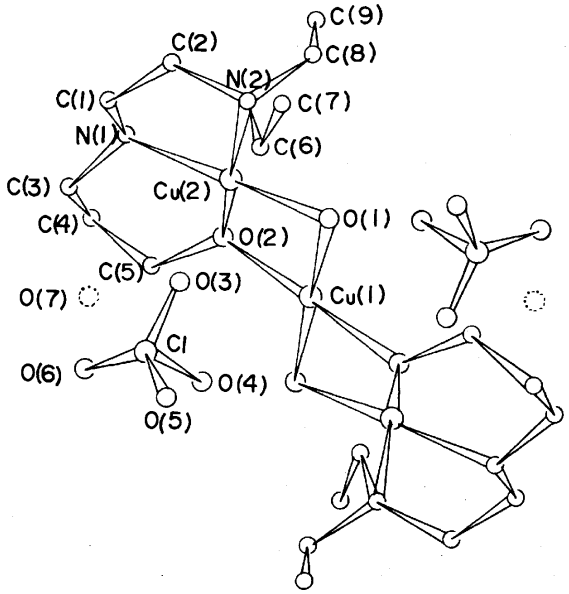

Fig. 1. A perspective drawing of the molecule.

Table 4. Interatomic distances

Coordination sphere		
Cu(1)	Cu(2)	2.902(1)Å
Cu(1)	O(1)	1.922(7)
Cu(1)	O(2)	1.904(7)
Cu(1)	O(4)	3.13(1)
Cu(2)	O(1)	1.904(7)
Cu(2)	O(2)	1.910(7)
Cu(2)	N(1)	1.977(9)
Cu(2)	N(2)	2.059(9)
Cu(2)	O(3)	2.63(1)
Six-membered ring		
N(1)	C(3)	1.46(1)Å
C(3)	C(4)	1.50(1)
C(4)	C(5)	1.48(1)
C(5)	O(2)	1.45(1)
Five-membered ring		
N(1)	C(1)	1.45(1)Å
C(1)	C(2)	1.49(1)
C(2)	N(2)	1.49(1)
Ethyl group		
N(2)	C(6)	1.52(1)Å
C(6)	C(7)	1.53(1)
N(2)	C(8)	1.50(1)
C(8)	C(9)	1.49(1)
Perchlorate ion		
Cl	O(3)	1.31(1)Å
Cl	O(4)	1.62(1)
Cl	O(5)	1.39(1)
Cl	O(6)	1.35(1)
Cl	O(7)	1.62(2)

Table 5. Bond angles

Coordination sphere			
Cu(1)	O(1)	Cu(2)	98.6(3)°
Cu(1)	O(2)	Cu(2)	99.1(3)
O(1)	Cu(1)	O(2)	79.0(3)
O(1)	Cu(2)	O(2)	79.3(3)
O(1)	Cu(2)	N(2)	99.8(3)
O(2)	Cu(2)	N(1)	95.0(3)
N(1)	Cu(2)	N(2)	85.2(3)
Six-membered ring			
Cu(2)	N(1)	C(3)	116.4(6)°
N(1)	C(3)	C(4)	111.2(9)
C(3)	C(4)	C(5)	115.2(9)
C(4)	C(5)	O(2)	111.0(8)
C(5)	O(2)	Cu(2)	125.1(6)
Five-membered ring			
Cu(2)	N(2)	C(2)	106.3(8)°
N(2)	C(2)	C(1)	109.8(8)
C(2)	C(1)	N(1)	107.6(8)
C(1)	N(1)	Cu(2)	106.4(6)
Ethyl group			
Cu(2)	N(2)	C(6)	107.2(9)°
C(2)	N(2)	C(6)	110.4(8)
N(2)	C(6)	C(7)	114.9(9)
Cu(2)	N(2)	C(8)	112.0(9)
C(2)	N(2)	C(8)	111.2(8)
N(2)	C(8)	C(9)	112.7(9)
Perchlorate ion			
O(5)	Cl	O(6)	113.9(6)°
O(5)	Cl	O(3)	120.6(7)
O(5)	Cl	O(7)	98.8(8)
O(5)	Cl	O(4)	100.6(7)
O(6)	Cl	O(3)	123.8(8)
O(6)	Cl	O(7)	84.4(9)
O(6)	Cl	O(4)	91.6(8)
O(3)	Cl	O(7)	75.6(9)
O(3)	Cl	O(4)	90.5(8)
O(7)	Cl	O(4)	160.0(9)

Three copper atoms are arrayed on a straight line, the separations being 2.902(1) Å. This arrangement has been expected from the magnetic susceptibility measurements over the temperature range 80—300 K.[1] The geometry around the two end copper atoms is best described as a slightly distorted tetragonal pyramid. One of the axial coordination site is occupied by an oxygen atom of perchlorate ion. The bond distance, Cu(2)–O(3), is 2.63(1) Å. The central copper atom has a square planar environment. The Cu–Cu distance (2.902(1) Å), the Cu–O distances (1.904(7)—1.922(7) Å) and the bridging Cu–O–Cu angles(98.6(3), 99.1(3)°) are very close to the corresponding values (2.953(3) Å, 1.915(6)—1.953(6) Å, 99.3(2)° and 99.5(2)°) in the green binuclear complex with the same ligand,[2] and are within the range of ones found in other di-μ-alkoxo copper(II) and di-μ-hydroxo copper(II) complexes.[4-9] The Cu(2)–N(2) distance(2.059(9) Å) is longer than the Cu(2)–N(1) distance(1.977(9) Å), such a tendency was also observed in the green binuclear complex.[2] The C–N, C–O and C–C bond distances of the chelate ring are also similar to those of the green binuclear

TABLE 6. BEST LEAST-SQUARE PLANES DEFINED BY ATOMIC POSITIONS

1) Plane defined by Cu(2), O(1), O(2), N(1), N(2)
$0.6176x+0.7193y-0.4572z=0.9609$
Distances of atoms from this plane (Å)

Cu(2)	0.08Å	N(1)	0.02Å
O(1)	0.02	N(2)	−0.06
O(2)	−0.06	O(3)	2.71

2) Plane defined by Cu(1), Cu(2), O(1), O(2)
$0.6453x+0.6563y-0.5373z=0.1818$
Distances of atoms from this plane (Å)

Cu(1)	0.12Å	O(1)	−0.12Å
Cu(2)	0.12	O(2)	−0.12

3) Plane defined by Cu(1), Cu(2), C(5)
$0.6989x+0.6419y-0.4744z=0.6817$
Distances of atoms from this plane (Å)

O(2)	−0.36Å		

4) Plane defined by Cu(2), N(1), N(2)
$0.6686x+0.6645y-0.4849z=0.6868$
Distances of atoms from this plane (Å)

C(1)	0.61Å	C(2)	−0.02Å

5) Plane defined by N(1), O(2), C(3), C(9)
$0.7713x+0.6461y-0.1665z=2.017$
Distances of atoms from this plane (Å)

Cu(2)	0.58Å	C(4)	−0.68Å
N(1)	0.04	C(3)	0.05
O(1)	−0.04	C(5)	−0.05

x, y, and z denote atomic fractional coordinates.

complex.[2] The ethyl C(8)–C(9) bond length is a little shorter than the normal C–C bond length, and may be explained in terms of heavy thermal motion of C(9) atom. It is noteworthy that a second oxygen atom O(4) of perchlorate ion appears to be in proximity of the axial coordination site of the central copper atom, although the Cu(1)–O(4) separation of 3.13(1) Å is too large for any bonding to be assumed. The positions of oxygens of perchlorate ion were not determined unequivocally and the geometry of the perchlorate ion is different from that of tetrahedron. This may be due to the disorder and the hindered rotation. We attempted to interpret the disorder and the hindered rotation of the perchlorate ion, but no satisfactory interpretation was obtained.

Some least squares planes are given in Table 6, together with the distances of the individual atoms from these planes. The basal plane of pyramidal unit, consisting of Cu(1), O(1), O(2), N(1), N(2), is essentially planar, the deviation of Cu(2) being 0.08 Å in the direction of the axial site. The dihedral angle between the planes passing through Cu(1), O(1), O(2) and Cu(2), O(1), O(2) is 3.5°. The five membered chelate ring has an unsymmetrical skew conformation and C(1) and C(2) are at 0.61 Å and −0.02 Å respectively from the plane through Cu(2), N(1) and N(2). The six membered chelate ring has a chair conformation and Cu(2) and C(4) are at 0.58 Å and −0.68 Å respectively from the plane through N(1), O(2), C(3) and C(5).

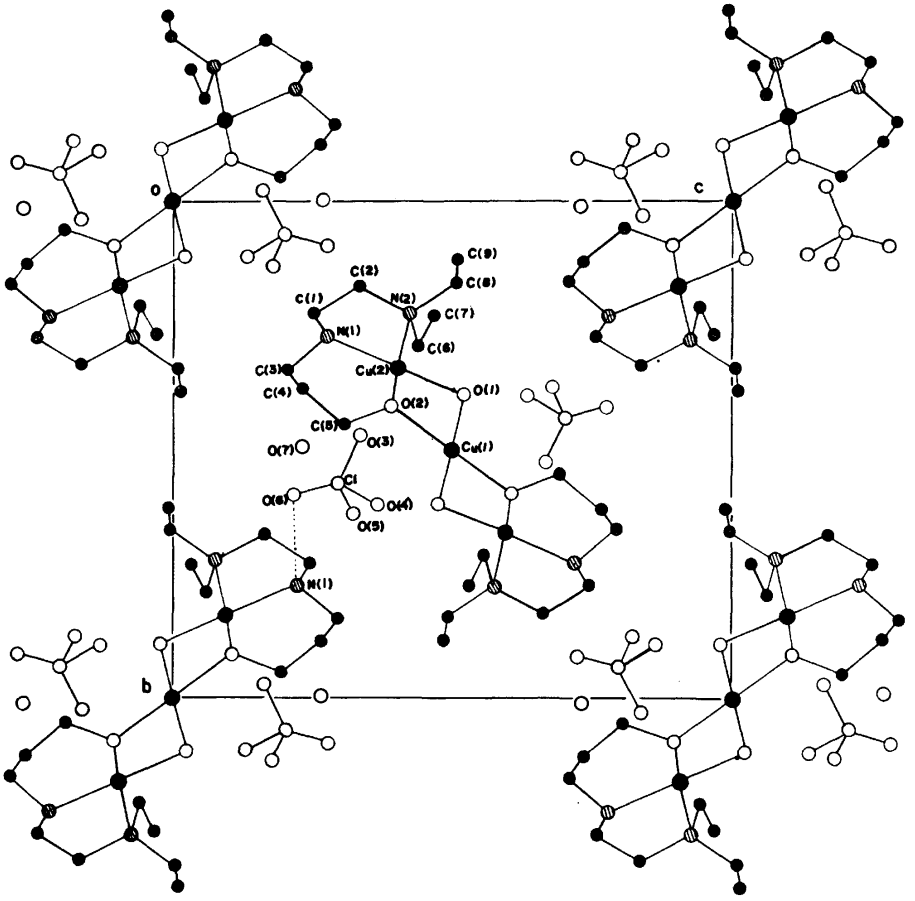

Fig. 2. Molecular configuration along a-axis.

Table 7. Intermolecular distances below 3.5Å

O(2)..... C(1)	III	3.39Å
O(2)..... C(2)	III	3.42
O(6)..... N(1)	III	3.05
N(1)..... O(4)	III	3.34
C(3)..... N(1)	IV	3.32

Key to symmetry operations

I	x	y	z
II	$-x$	$-y$	$-z$
III	x	$1/2+y$	$1/2-z$
IV	x	$1/2-y$	$1/2+z$

The crystal structure projected along the a-axis is presented in Fig. 2. Intermolecular distances less than 3.5 Å are listed in Table 7. The molecules in the crystal are in contact at the normal van der Waals distances. There may be weak hydrogen bond between N(1) and O(6), whose distance is 3.05 Å.

We are grateful to Professor T. Komori of Kyushu University for his kind advice and allowing us to use the Syntex P$\bar{1}$ automatic diffractometer. Thanks are also due to Mr. T. Uechi of this unversity for valuable advice and discussions.

References

1) Y. Nishida and S. Kida, *Chem. Lett.*, **1974**, 339.
2) C. Villa, L. Coghi, G. Manfredotti, and C. Guastini, *Cryst. Str. Commun.*, **3**, **1974**, 543.
3) "International Tables for X-Ray Crystallography," Vol. 3, Kynoch Press, Birmingham, England (1962).
4) D. L. Lewis, W. E. Hatfield, and D. J. Hodgson, *Inorg. Chemun.*, **11**, 2216 (1972).
5) E. D. Estes, W. E. Hatfield, and D. J. Hodgson, *ibid.*, **13**, 1654 (1974).
6) E. D. Estes and D. J. Hodgson, *ibid.*, **14**, 334 (1975).
7) Y. Iitaka, K. Shimazu, and T. Kwan, *Acta Crystallogr.*, **20**, 803 (1966).
8) T. P. Mitchel and W. H. Bernard, *ibid.*, **26**, 2096 (1970).
9) R. J. Majeste and E. A. Meyers, *J. Phys. Chem.*, **74**, 3497 (1970).

Analytical Application of Catalytic Polarographic Current of Nickel(II) in Acidified Thiocyanate Solutions Containing Cobalt(II)

Eiki ITABASHI and Ikuko YUSA
Miyagi University of Education, Aoba, Aramaki, Sendai 980
(Received June 6, 1975)

Simple and sensitive methods have been developed for the determination of nickel(II), based on the catalytic polarographic current in acidic thiocyanate solution in the presence and absence of cobalt(II). The basis of the methods and the effect of variables have been investigated and elucidated. In the absence of cobalt(II), thiocyanate solution containing large amounts of hydrogen ions serves a supporting electrolyte, while an acidic thiocyanate solution containing tetra-*n*-butylammonium salts is suitable for the determination of nickel(II) in the presence of cobalt(II). These methods are applicable to the determination 2×10^{-6} M nickel(II) in the presence and absence of 1×10^{-3} M cobalt(II).

Polarographic as well as anodic stripping methods have been applied for the analysis of nickel(II). It has been found that pyridine is a good supporting electrolyte for the polarographic simultaneous determination of nickel(II) and cobalt(II). Thiocyanate electrolyte serves a good supporting electrolyte when only nickel(II) is to be determined in neutral solution.[1,2] The anodic stripping method has been applied by employing sodium thiocyanate as a supporting electrolyte;[3] however, thiocyanate electrolyte is not suitable for the anodic stripping analysis of nickel, because during the reduction of nickel(II) at both mercury and platinum electrodes the reduction of thiocyanate ions takes place with the formation of sulfides and cyanides.[4-7]

The polarographic reduction of nickel(II) in acidified thiocyanate solution in the presence and absence of tetraalkylammonium salts has previously been reported to exhibit a catalytic wave having the shape of a "maximum".[8] The mechanism of this catalytic wave was thought to involve the cyclic regeneration of the electroactive nickel(II) according to the following reaction sequence:[5,8]

$$NiNCS^{+}_{ads} + 2e \xrightarrow{\text{fast}} Ni(0)NCS^{-}$$

$$Ni(0)NCS^{-} + 3H^{+} \xrightarrow{\text{slow}} Ni^{2+} + HCN + H_2S$$

The cyclic regeneration of nickel(II) accounts for the enhancement of the limiting current. Hydrogen ions act as a neutralizing agent of the reduction products of thiocyanate ion, cyanide and sulfide ions. This catalytic wave is usually sensitive and selective. This immediately suggests the use of the present catalytic wave to determine the concentration of nickel(II). Previously polarographic catalytic current based on the oxidation-reduction,[9,10] dispropotionation,[11] hydrogen reduction wave,[12,13] and pre-wave[14,15] have been employed successfully for the determination of metal ions and nitrogen- or sulfur-containing organic compounds. The present paper reports on some analytical applications utilizing the catalytic current of nickel(II) in the presence and absence of cobalt(II).

Experimental

Chemicals. Nickel(II) perchlorate[16] and cobalt(II) perchlorate[17] were prepared and recrystallized using the procedures given in literatures. Tetra-*n*-butylammonium perchlorate(*n*-Bu_4NClO_4) was prepared by neutralizing a 40% tetra-*n*-butylammonium hydroxide solution with perchloric acid and recrystallized several times from ethyl alcohol, and then dried in a vacuum oven at 80 °C for 20 h. Extra pure grade sodium thiocyanate and perchloric acid were used. All the other chemicals were of chemical grade without further purification. Redistilled water was used and all solutions were deaerated with high-purity nitrogen.

Instrumentation and Electrode Assembly. Direct current (DC) polarographic experiments were carried out with a potentiostat constructed locally with operational amplifiers.[18] Polarograms were recorded with a X-Y recorder.

Two capillaries were used throughout this work. The rate of flow of mercury (m) and the drop time (t) of capillary I were 1.49_6 mg/s and 5.42 s, respectively, measured in deaerated 0.5 M NaCl solution under an applied pressure of 55 cm at −0.65 V *vs.* SCE. Capillary II had the characteristics $m=1.33_1$ mg/s and $t=4.95$ s, in deaerated 0.5 M $NaNO_3$ solution under an applied pressure of 40 cm at −0.56 V *vs.* SCE. Capillaries I and II were employed for the experiments of methods I and II, respectively.

The counter electrode was a platinum spiral electrode which was connected to the electrolytic solution through a glass sinter. The potential of the DME was measured against a saturated calomel electrode (SCE) which was connected to the test solution through a Luggin capillary with a pair of sintered glass discs.

Procedure for the Determination of Nickel(II) in the Presence of Cobalt(II). Because *n*-Bu_4NClO_4 is slightly soluble in water, the electrolytic solutions are usually prepared as follows Into a 25 ml volumetric flask, add 68 mg (8 mM) or 85 mg (10 mM) of *n*-Bu_4NClO_4, and then pour in 10 ml of 2.5 M NaSCN solution. Dissolve *n*-Bu_4NClO_4 in thiocyanate solution by shaking gently. After dissolution of *n*-Bu_4NClO_4 in thiocyanate solution, add perchloric acid and nickel (II) or cobalt(II) solution containing nickel(II), and dilute to 25 ml with distilled water and mix well. Prior separation of the precipitate of $(n\text{-}Bu_4N)_2[Co(NCS)_4]$ is used when the solution contains more than 2×10^{-4} M cobalt(II). Pour the solution into a 100 ml centrifuge tube and then centrifuge for 30 min at 3500 rpm. Transfer the solution into the cell and then analyze the solution by the conventional DC polarographic method.

Treatment of Data. The catalytic wave of nickel(II) in acidic thiocyanate solution appears as a maximum wave. The value of peak current denoted as i_p is measured at the peak potential of the maximum wave. All values are corrected for the residual current or for the limiting current caused to the reduction of metal ions such as iron(III) and copper(II), which are reduced at potentials less negative than nickel(II). The latter way can be done by extrapolation of the linear flat

portion of the limiting current before the maximum wave rises. The concentration of nickel(II) is evaluated with reference to a suitably prepared calibration curve.

Results and Discussion

In the Absence of Cobalt(II) [*Method I*]. Figure 1 shows the DC polarogram obtained in 0.5 M thiocyanate solution containing 2×10^{-5} M nickel(II) and 0.14 M $HClO_4$. Nickel(II) in acidic thiocyanate solution gives a peak current rather a limiting plateau. This peak occurs at about −0.82 V *vs.* SCE. The rise in current at potentials more negative than −1.0 V is attributed to the direct reduction of hydrogen ions. In the absence of nickel(II), hydrogen ions in 0.5 M thiocyanate solution containing 0.14 M $HClO_4$ are reduced at potentials more negative than about −0.87 V.

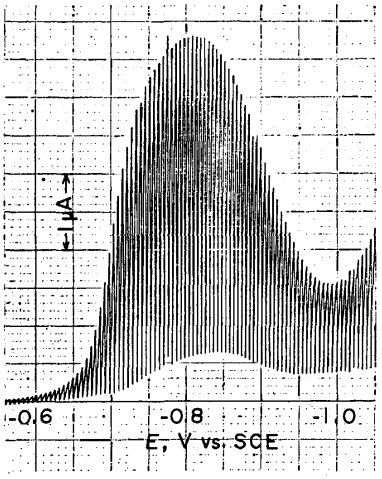

Fig. 1. Reduction wave of 2×10^{-5} M nickel(II) in 0.14 M $HClO_4$ and 0.5 M NaSCN.

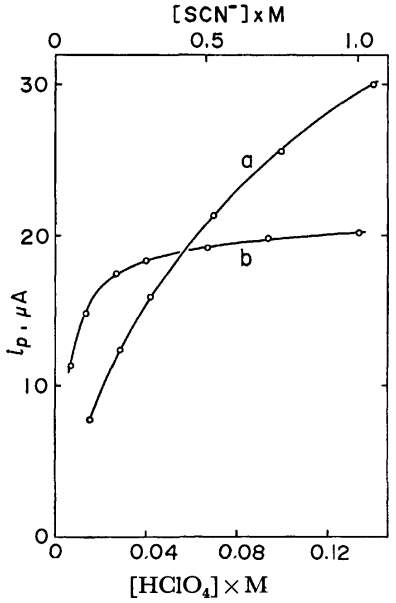

Fig. 2. Effect of concentrations of $HClO_4$ (a) in 0.5 M NaSCN, and NaSCN (b) in 0.056 M $HClO_4$ on the peak current of 1×10^{-4} M nickel(II).

The effect of the concentrations of thiocyanate and hydrogen ions on the peak current was studied to determine its applicability as a method for determing small amounts of nickel(II) polarographically. Figure 2 presents the relationships between the peak current and the concentrations of thiocyanate and hydrogen ions. The peak current increases in height with increase in hydrogen ion concentration. With further addition of $HClO_4$ above 0.2 M, the maximum wave appears as a shoulder on the hydrogen reduction wave. The concentrations 0.14 M in $HClO_4$ and 0.5 M in NaSCN have been selected for further experiments.

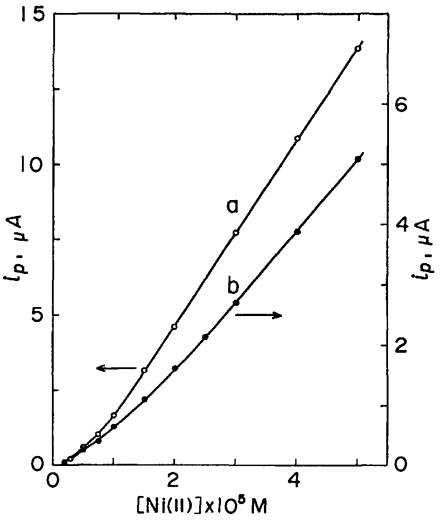

Fig. 3. Plots of i_p *vs.* nickel(II) concentration in 0.5 M NaSCN solution containing 0.14 M $HClO_4$ (a), and in 1.0 M NaSCN solution containing 7×10^{-3} M $HClO_4$ and 8×10^{-3} M *n*-Bu_4NClO_4 (b).

The height of the peak current as a function of the nickel(II) concentration is shown by curve a of Fig. 3. Two distinct portions are present on the curve. The first part at which the rise in the peak current with nickel(II) concentration is greater than linear extends from 2×10^{-6} to 1.5×10^{-5} M. The second portion at which the peak current is proportional to the nickel(II) concentration is observed in the concentration range from 2×10^{-5} to 1×10^{-4} M. This inflection on the calibration curve could indicate that the mechanism of the catalytic wave involves the sequence of reactions and a rate-determing step of the overall process changes over a wide range of nickel(II) concentration. The present method is suited for the determination of 2×10^{-6} to 1×10^{-4} M nickel(II) in the absence of cobalt(II).

In the Presence of Cobalt(II) [*Method II*]. With analysis of mixures, interference is always a possibility with any technique. The effect of cobalt(II) on the catalytic maximum wave of nickel(II) in acidic thiocyanate solution is presented in Fig. 4. These polarograms are drawn as the line through the maximum current observed just before the fall of a mercury drop. The peak height decreases with increase in cobalt(II) concentration. This may be due to the adsorption of

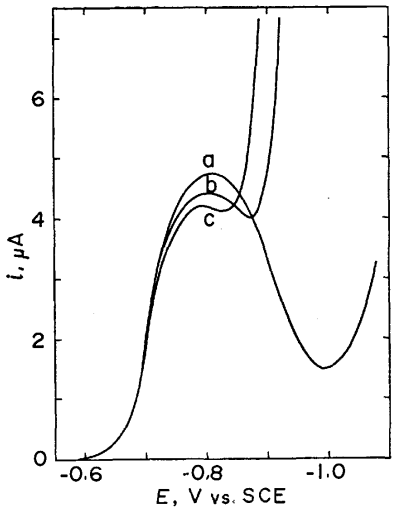

Fig. 4. Effect of cobalt(II) on the reduction waves of 2×10^{-5} M nickel(II) in 0.14 M $HClO_4$ and 0.5 M NaSCN.
[Co(II)]: a) 0, b) 2×10^{-4}, c) 5×10^{-4} M.

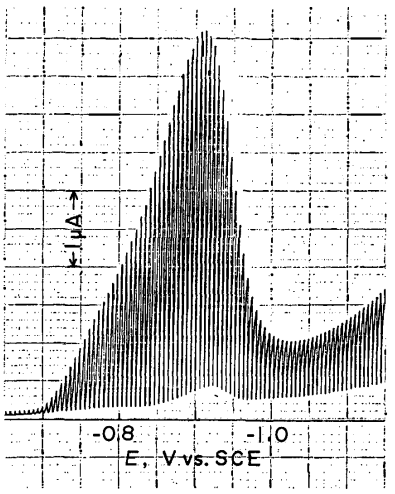

Fig. 5. Reduction wave of 5×10^{-5} M nickel(II) in 7×10^{-3} M $HClO_4$, 8×10^{-3} M n-Bu_4NClO_4 and 1.0 M NaSCN.

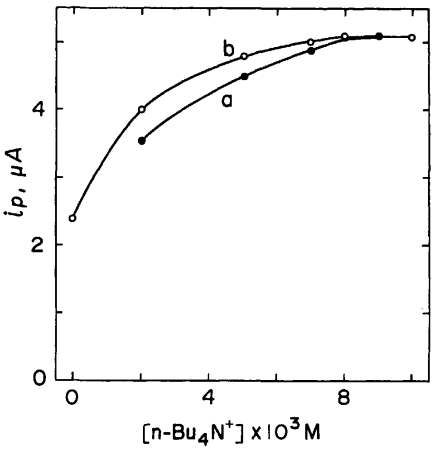

Fig. 6. Effect of concentration of n-Bu_4NClO_4 on the peak current of 5×10^{-5} M nickel(II) in 7×10^{-3} M $HClO_4$ and 1.0 M NaSCN solutions in the presence (a) and absence (b) of 5×10^{-4} M cobalt(II).

cobalt(II)-thiocyanate complexes. Cobalt(II) in thiocyanate solution containing perchloric acid or acetate buffer also exhibits a catalytic maximum wave.[19] This catalytic wave appears in the potential region where cobalt(II) exhibits a pre-wave which arises at less negative potentials than those for the usual hydrated cobalt(II) reduction wave. The catalytic current of cobalt(II) in acidic thiocyanate solution has a mixed adsorption-surface character.[19] If nickel(II)- and cobalt(II)-thiocyanate complexes are coadsorbed at the same potential region, the catalytic current of nickel(II) decreases because of decreasing adsorption of nickel(II)-thiocyanate complexes and hence of decreasing concentration of the active metallic nickel at the electrode surface.

It is therefore necessary to separate cobalt(II) from the solution containing nickel(II). Cobalt(II) in thiocyanate solution containing large cations such as tetraalkylammonium or tetraphenylarsonium ions yields the precipitate having the composition of $(Cat)_2[Co(NCS)_4]$, where Cat^+ is tetra-alkylammonium or -phenylarsonium ion.[20-22]

Of the many tetraalkylammonium salts investigated, n-Bu_4NClO_4 was the most suitable for the separation of cobalt(II) from the thiocyanate solution containing nickel(II).

The catalytic reaction of nickel(II) in acidic thiocyanate solution is also enhanced by the presence of various kinds of tetraalkylammonium ions.[5,8] Figure 5 shows the reduction wave of nickel(II) in acidic thiocyanate solution containing n-Bu_4NClO_4. The values of peak current of 5×10^{-5} M nickel(II) in 7×10^{-3} M $HClO_4$ and 1.0 M NaSCN solutions in the presence and absence of 8×10^{-3} M n-Bu_4NClO_4 are 5.02 and 2.45 μA, respectively.

Acceleration of the catalytic reaction of nickel(II) by the presence of n-Bu_4N^+ ions could be the result of the inhibition of the amalgamation of electrodeposited metallic nickel. The amalgamation of the deposited iron-group metals is known to be inhibited by the presence of some surface-active substances.[23-25]

The effect of concentration of n-Bu_4NClO_4 on the peak height of the catalytic wave of nickel(II) in the presence and absence of cobalt(II) is shown in Fig. 6. The peak current reaches a limiting value as the concentration of n-Bu_4NClO_4 increases. The difference between the peak currents in the presence and absence of cobalt(II) at lower concentrations of n-Bu_4NClO_4 is associated with a decrease in concentration of n-Bu_4N^+ ions in the bulk of solution.

Tetra-n-butylammonium ions in thiocyanate solution containing cobalt(II) are partially consumed for the precipitation of cobalt(II)-thiocyanate complex in the form of $(n\text{-}Bu_4N)_2[Co(NCS)_4]$. The peak current of nickel(II) in thiocyanate solution containing 8×10^{-3} M n-Bu_4NClO_4 remains unchanged with further addition of $HClO_4$ above 5×10^{-3} M, as shown in Fig. 7. Figure 8 presents the dependence of the peak current on the thiocyanate concentration. With further addition of NaSCN above 1.0 M, the peak current reaches a limiting value.

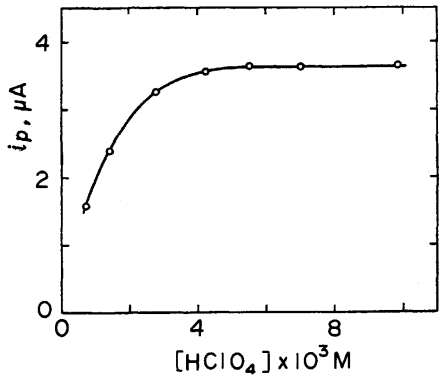

Fig. 7. Effect of concentration of $HClO_4$ on the peak current of 5×10^{-5} M nickel(II) in 8×10^{-3} M n-Bu_4NClO_4 and 0.5 M NaSCN.

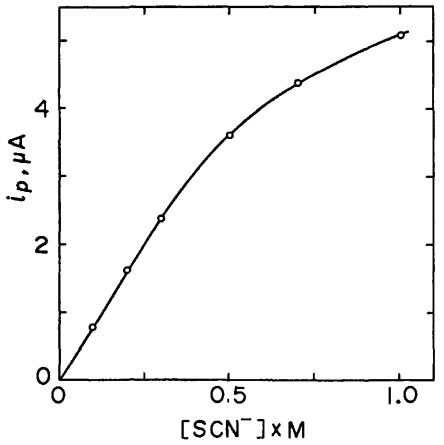

Fig. 8. Effect of thiocyanate concentration on the peak current of 5×10^{-5} M nickel(II) in 7×10^{-3} M $HClO_4$ and 8×10^{-3} M n-Bu_4NClO_4.

As a result of the experiments described above, it is possible to select the conditions and established a procedure for the determination of nickel(II) in the presence of cobalt(II). The experiments were performed with the solutions containing 7×10^{-3} M $HClO_4$, 8×10^{-3} M n-Bu_4NClO_4 and 1.0 M NaSCN. Over the entire range of nickel(II) between 2×10^{-6} and 2×10^{-4} M, the maximum waves were similar to that shown in Fig. 5. The present method has also two distinct portions on the calibration curve, as shown by curve b of Fig. 3. The first part at which the curve is a non-linear extends from 2×10^{-6} to 2×10^{-5} M nickel(II), and the second part at which the curve is a linear is observed in the nickel(II) concentration between 2.5×10^{-5} and 2×10^{-4} M. The quantity of nickel(II) in the presence of cobalt(II) was estimated from the calibration curve. Data compiled in Table 1 verify that in the presence of large excess of cobalt(II) nickel-(II) can be accurately determined within expected polarographic precision. When the solution contains 1×10^{-3} M cobalt(II) and nickel(II) of 2×10^{-5} M or greater, it is desirable to employ 10×10^{-3} M n-Bu_4NClO_4 instead of 8×10^{-3} M. With 1×10^{-3} M cobalt-(II) present, approximately 2×10^{-3} M n-Bu_4N^+ ions are consumed for the precipitation reaction of cobalt(II)-thiocyanate compound in the bulk of solution.

Table 1. Analysis of nickel(II)[a]

[n-Bu_4NClO_4] M×10^3	[Co(II)] M×10^3	[Ni(II)], Taken	M×10^6 Found[b]	Derivation M×10^6
8	1.0	2.0	1.9	−0.2—+0.1
8	0.5	5.0	5.1	−0.3—+0.1
8	1.0	20.0	19.8	−0.5—+0.4
10	1.0	20.0	19.8	−0.3—+0.2
8	0.5	50.0	49.3	−1.2—−0.7
10	0.5	50.0	50.2	−0.4—+0.5

a) Solution contains 7×10^{-3} M $HClO_4$ and 1.0 M NaSCN. b) Average of four replicate determinations on the different solutions.

Effect of Foreign Ions. Methods I and II described in this paper offer higher sensitivity than those being available in the literature.[2] Both methods were applied in a variety of situations to evaluate their effectiveness by employing the solutions containing 2×10^{-5} M nickel(II) and foreign ions.

In method I, the presence of 2×10^{-4} M aluminum-(III), iron(III), zinc(II), and lead(II) is tolerated. An error of 3% or greater occurs with these foreign ions of 5×10^{-4} M present. Chromium(III), copper(II) and cadmium(II) interfere in method I. Chromium(III) reduces the height of the peak current of nickel(II). An acidic thiocyanate solution containing nickel(II) and cadmium(II) gives a single round maximum wave in the potential region between −0.6 and −1.0 V. Copper(II) in acidic thiocyanate solution exhibits an ill-defined reduction wave. Halide, nitrate, sulfate, and oxalate ions are tolerated up to approximately 0.01 M.

In method II, chromium(III) and aluminum(III) are tolerated. Iron(III), copper(II), zinc(II), cadmium-(II), and lead(II) are precipitated in thiocyanate solution containing n-Bu_4N^+ ions. Copper(II), cadmium(II), and zinc(II) are tolerated at low concentration than 2×10^{-4} M. Iron(III) and lead(II) are tolerated up to 5×10^{-5} M. Anions such as bromide, iodide, sulfate, nitrate, and oxalate ions which are in part associated with n-Bu_4N^+ ions are tolerated up to 5×10^{-3} M.

In conclusion, method II is more sensitive than method I. Method II is applicable for the routine analysis of nickel(II) in various cobalt compounds by employing the calibration curve prepared carefully, although the calibration curve is a non-linear.

The authors thank the Ministry of Education for the financial support.

References

1) J. J. Lingane and H. Kerlinger, *Ind. Eng. Chem., Anal. Ed.*, **13**, 77 (1941).
2) J. M. Dale and C. V. Banks, "Treatise on Analytical Chemistry," Vol. 2, Part II-A, ed. by I. M. Kolthoff and P. J. Elving, Wiley-Interscience, New York (1962), p. 377.
3) M. M. Nicholson, *Anal. Chem.*, **32**, 1058 (1960).
4) H. Shirai, *Nippon Kagaku Zasshi*, **85**, 322 (1964).
5) E. Itabashi and S. Ikeda, *J. Electroanal. Chem.*, **27**, 243 (1970).
6) T. Hurlen and E. Eriksrud, *ibid.*, **54**, 331 (1974).

7) T. Krogules, A. Barański, and Z. Galus, *J. Electroanal. Chem.*, **57**, 63 (1974).
8) E. Itabashi, *ibid.*, **60**, 285 (1975).
9) I. M. Kolthoff and E. P. Parry, *J. Amer. Chem. Soc.*, **73**, 5315 (1951).
10) T. A. O'Shen and G. A. Parker, *Anal. Chem.*, **44**, 184 (1972).
11) W. E. Harris and I. M. Kolthoff, *J. Amer. Chem. Soc.*, **68**, 1175 (1946).
12) R. Brdička, *Collect. Czech. Chem. Commun.*, **5**, 238 (1933).
13) J. Heyrovský and J. Kůta, "Principle of Polarography," Academic Press, New York (1966), p. 407.
14) H. B. Mark, Jr. and C. N. Reilley, *Anal. Chem.*, **35**, 195 (1963).
15) L. R. McCoy and H. B. Mark, Jr., *ibid.*, **37**, 591 (1965).
16) A. E. Wickenden and R. A. Krause, *Inorg. Chem.*, **4**, 404 (1965).
17) N. A. Matwiyoff and S. V. Hooker, *ibid.*, **6**, 1127 (1967).
18) E. Itabashi and K. Oikawa, *Ann. Rept. Res. Inst. Sci. Educ., Miyagi Univ. Educ.*, **8**, 17 (1973).
19) E. Itabashi and M. Tan, *J. Electroanal. Chem.*, **60**, 299 (1975).
20) D. Forster and D. M. L. Goodgame, *Inorg. Chem.*, **4**, 715, 823 (1965).
21) A. Sabatini and I. Bertini, *ibid.*, **4**, 959 (1965).
22) H. Schmidtke, *Ber. Bunsenges. Phys. Chem.*, **71**, 1138 (1967).
23) V. F. Ivanov and Z. A. Iofa, *Russ. J. Phys. Chem., Engl. Trans.*, **36**, 571 (1962); **38**, 1026 (1964).
24) I. M. Kolthoff and P. Mader, *Anal. Chem.*, **41**, 924 (1969).
25) E. Itabashi and S. Ikeda, *J. Electroanal. Chem.*, **36**, 189 (1972).

The Crystal Structure of 1-(2-Thiazolylazo)-2-naphtholato-diaquacopper(II) Perchlorate

Masayasu KURAHASHI and Akira KAWASE*

National Research Institute for Metals, 2-3-12, Nakameguro, Meguro-ku, Tokyo 153

(Received July 22, 1975)

The crystal structure of 1-(2-thiazolylazo)-2-naphtholatodiaquacopper(II) perchlorate, $[Cu^{II}(TAN)(H_2O)_2]ClO_4$, has been determined from three-dimensional X-ray data collected by counter methods. The crystals are monoclinic, with the space group $P2_1/c$; $a=13.481(4)$, $b=8.060(4)$, $c=15.307(7)$ Å, $\beta=95.58(4)°$, and $Z=4$. The structure was refined to an R value of 0.086 for 952 non-zero reflections. The copper atom is five-coordinated and has a distorted square-pyramidal environment. The 1-(2-thiazolylazo)-2-naphtholato group (TAN) acts as a terdentate ligand, the phenolic oxygen, the azo nitrogen and the thiazole nitrogen atoms being coordinated to the copper atom to give two five-membered chelate rings. The remaining two positions are occupied by water molecules.

This work is part of a series of studies of the structures of metal chelates of 1-(2-thiazolylazo)-2-naphthol (abbr. as H-TAN). Recently, one of the present authors (M.K.) reported the structures of the Pd(II)-[1] and Ni(II)-chelates[2] and showed that the coordination configurations around the metals are square-planar and octahedral respectively (Fig. 1a and 1b). In both complexes, the 1-(2-thiazolylazo)-2-naphtholato group (abbr. as TAN) is exactly or nearly planar and acts as a terdentate ligand to form two five-membered chelate rings with the metal atom. It can easily be understood that a planar terdentate ligand like TAN can further form a five-coordinated square-pyramidal or trigonal-bipyramidal structure with a metal and two additional unidentate ligands (Fig. 1c and 1d). However, it is impossible for the TAN to give a tetrahedral coordination around the metal (Fig. 1e). In this paper, we will describe the structure of the five-coordinated Cu(II)–TAN complex, in which the copper atom has a square-pyramidal environment. A preliminary account of this work has already been given.[3]

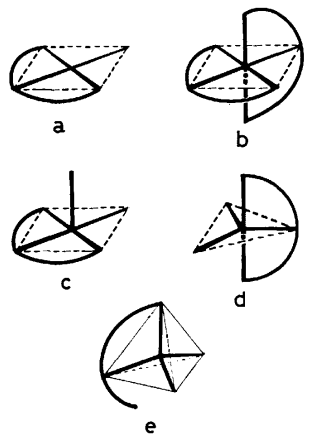

Fig. 1. Coordination of a planar terdentate ligand to the metal. The planar terdentate ligand can coordinate to the metal with (a) square-planar, (b) octahedral, (c) square-pyramidal, and (d) trigonal-bipyramidal environment; however, it is impossible to form a metal-complex with (e) tetrahedral environment.

* Present address: National Chemical Laboratory for Industry, 5-5, 1-Chome, Honmachi, Shibuya-ku, Tokyo, 151

The reaction of Cu(II) with H-TAN gives 1:1 as well as 1:2 Cu(II)–TAN chelates.[4] Furthermore, in view of the structures reported for the Cu(II)–complexes with analogous ligands,[5-7] it was thought that there probably exist various types of 1:1 Cu(II)–TAN complexes with the chemical formulae $[Cu^{II}(TAN)X]$, $[Cu^{II}(TAN)X_2]$, and $[Cu^{II}(TAN)XY]$, where X and Y are unidentate ligands. Accordingly, several attempts were made to produce the complexes using different reactants, different solvents, and different ratios of the reactants. Three crystalline forms (orthorhombic, monoclinic, and triclinic) of 1:1 Cu(II)–TAN complexes were obtained from the different solvents. The present study will deal with the structure of the monoclinic form, the crystallinity of which was comparatively better than the other two. An attempt to crystallize the complex with the composition of $[Cu^{II}Cl(TAN)]$, insoluble either in water or in most organic solvents, has been unsuccessful.

Experimental

An aqueous solution of $Cu^{II}(ClO_4)_2\cdot 6H_2O$ and a dioxane solution of H-TAN were mixed in an approximate molar ratio of 1:1. Blue needle crystals of $[Cu^{II}(TAN)(H_2O)_2]ClO_4$, elongated along the b-axis, were obtained by slow evaporation. The crystal used for the X-ray diffraction study had the dimensions of $0.1\times0.1\times0.25$ mm. The crystal data are listed in Table 1. The unit-cell dimensions were initially determined by Weissenberg photographs taken with Cu$K\alpha$ radiation; they were refined by the least-squares method, using 9 reflections

Table 1. Crystal data

$[Cu(C_{13}H_8N_3OS)(H_2O)_2]ClO_4$
F.W.=453.3
Monoclinic
$a=13.481\pm0.004$ Å
$b=8.060\pm0.004$ Å
$c=15.307\pm0.007$ Å
$\beta=95.58\pm0.04°$
$V=1655.1\pm1.2$ Å^3
$D_m=1.81$ g·cm^{-3}
$D_x=1.819$ g·cm^{-3}
$Z=4$
$\mu=17.0$ cm^{-1} (for Mo$K\alpha$)
Space group $P2_1/c$

measured by a diffractometer with Mo$K\alpha$ radiation. The density was measured by flotation in an aqueous solution of sodium iodide.

The intensity data were collected on a Rigaku automated four-circle diffractometer, using Mo$K\alpha$ radiation monochromatized with a graphite crystal. The ω-2θ scan technique was employed at a scan rate of 4°/min. The background countings were taken on both sides of each peak for 10 s. If the value of $\sigma(F)/F$ was larger than 0.03, the measurement was repeated and the average value was adopted. All unique reciprocal lattice points with $2\theta \leq 45°$ were examined; 953 reflections with $F > 3\sigma(F)$ were regarded as observed. The measured intensities were corrected for the Lorentz and polarization factors, but no corrections were made for absorption and extinction.

TABLE 2. ATOMIC PARAMETERS AND THEIR ESTIMATED STANDARD DEVIATIONS[a)]

Atom	x/a	y/b	z/c	B (Å^2)
Cu	0.7455(2)	0.4788(4)	0.4102(2)	*
S	0.7544(5)	0.4705(10)	0.6934(4)	*
Cl	0.4542(5)	0.8925(8)	0.3650(4)	*
O	0.8213(10)	0.4198(10)	0.3111(10)	3.1(3)
W(1)	0.6545(11)	0.6236(20)	0.3342(10)	4.5(4)
W(2)	0.6359(14)	0.2659(25)	0.3887(11)	6.1(5)
N(1)	0.8613(12)	0.3780(22)	0.4785(9)	2.6(4)
N(2)	0.8644(11)	0.3802(22)	0.5625(10)	2.6(4)
N(3)	0.7131(11)	0.5185(24)	0.5297(12)	3.6(4)
C(1)	0.9327(14)	0.3181(26)	0.4312(13)	2.4(5)
C(2)	0.9031(15)	0.3396(28)	0.3384(13)	2.9(5)
C(3)	0.9633(16)	0.2839(32)	0.2748(14)	3.6(5)
C(4)	1.0505(16)	0.2011(27)	0.3057(14)	3.8(5)
C(5)	1.0821(15)	0.1725(28)	0.3957(16)	4.2(6)
C(6)	1.1712(17)	0.0898(28)	0.4199(17)	4.0(6)
C(7)	1.1997(15)	0.0675(31)	0.5096(13)	4.4(6)
C(8)	1.1438(17)	0.1286(28)	0.5706(13)	3.8(5)
C(9)	1.0549(15)	0.2112(27)	0.5948(12)	3.2(5)
C(10)	1.0221(13)	0.2378(22)	0.4616(12)	2.3(4)
C(11)	0.7788(13)	0.4588(26)	0.5873(14)	2.7(4)
C(12)	0.6480(20)	0.5756(34)	0.6609(14)	5.4(7)
C(13)	0.6362(15)	0.5880(26)	0.5720(14)	3.1(5)
O(1)	0.4516(14)	0.7869(26)	0.2901(10)	6.0(5)
O(2)	0.5549(15)	0.8894(31)	0.4081(17)	9.9(7)
O(3)	0.3879(18)	0.8348(29)	0.4214(14)	9.1(7)
O(4)	0.4305(18)	1.0552(25)	0.3415(18)	9.8(7)
H(3)	0.9472	0.3100	0.2084	4.0
H(4)	1.0895	0.1587	0.2490	4.0
H(6)	1.2055	0.0357	0.3723	4.0
H(7)	1.2644	0.0016	0.5137	4.0
H(8)	1.1593	0.1224	0.6364	4.0
H(9)	1.0158	0.2460	0.5945	4.0
H(12)	0.5749	0.6104	0.7033	4.0
H(13)	0.5572	0.6532	0.5218	4.0

Anisotropic temperature factors ($\times 10^4$)[b)]

Atom	B_{11}	B_{22}	B_{33}	B_{12}	B_{13}	B_{23}
Cu	38(1)	112(6)	25(6)	26(6)	4(2)	9(5)
S	79(5)	227(16)	37(3)	3(16)	28(6)	−34(13)
Cl	59(4)	157(13)	53(3)	19(13)	25(6)	1(11)

a) E.s.d.'s in parentheses are in units of least significant digit. b) The anisotropic temperature factors are of the form:
$\exp\{-(B_{11}h^2+B_{22}k^2+B_{33}l^2+B_{12}hk+B_{13}hl+B_{23}kl)\}$

Structure Determination and Refinement

The structure was solved by the heavy-atom method. The positions of the copper and sulfur atoms were deduced from a three-dimensional Patterson map. From the Fourier synthesis phased on the heavy atoms only, the positions of all the non-hydrogen atoms could be found. Block-diagonal least-squares refinement using isotropic temperature factors for all the non-hydrogen atoms reduced R $(=\sum||F_o|-|F_c||/\sum|F_o|)$ to 0.105. A further three cycles of refinement with anisotropic thermal parameters for the copper, sulfur, and chlorine atoms improved R to 0.095. At this stage a difference synthesis was carried out and several hydrogen positions were revealed; however, a few ghost peaks as large as the hydrogen peaks appeared. Accordingly, the hydrogen positions of the ring systems were evaluated by assuming sp^2 hybrid bonds around the relevant carbon atoms and a C–H distance of 1.08 Å; these positions were included but not refined in the final least-squares cycles. The isotropic thermal parameter of 4.0 Å^2 was assigned to the hydrogen atoms. Convergence was reached at $R=0.086$ for all the 952 observed reflections. A unit weight was given to each reflection. The atomic scattering factors were taken from International Tables for X-ray Crystallography, Vol III.[8)] The final atomic parameters and their estimated standard deviations are listed in Table 2. The observed and calculated structure factors are given in Table 3.**

Description of the Structure and Discussion

Perspective drawings of the complex cation and perchlorate anion are shown in Fig. 2, along with the numbering of the atoms. The complex cation is composed of Cu, TAN, and $2H_2O$. The TAN, 1-(2-thiazolylazo)-2-naphtholato group, acts as a terdentate ligand; the phenolic oxygen atom, the azo nitrogen atom adjacent to the naphthol ring, and the thiazole nitrogen atom being coordinated jointly to the copper

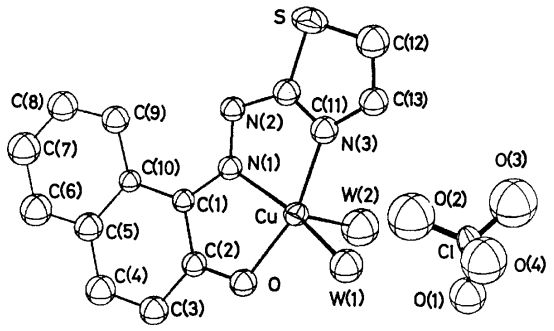

Fig. 2. Perspective drawings of $[Cu(TAN)(H_2O)_2]^+$ and ClO_4^- with numbering of atoms. The Thermal ellipsoids are drawn at 50% probability level (DEAM-4 diagram[11)]). W denotes the water oxygen atom.

** Table 3 is kept as Document No. 7605 at the Chemical Society of Japan, 1-5 Surugadai, Kanda, Chiyoda-ku, Tokyo, 101.

atom, thus giving two five-membered chelate rings. This mode of attachment of the TAN to the metal atom coincides with that observed in the crystals of Fe(II)-,[9] Co(III)-,[10] Ni(II)-,[2] and Pd(II)-chelate.[1] The thiazole sulfur atom does not coordinate to the metal in the present Cu(II)–TAN complex, either.

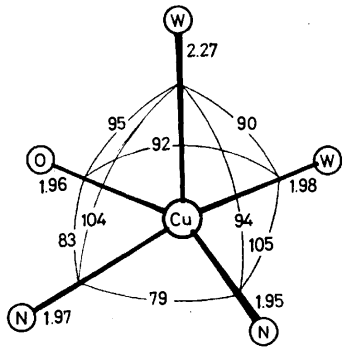

Fig. 3. Coordination geometry about the copper atom.

The coordination geometry about the copper atom is, as is shown in Fig. 3, a distorted square-pyramid whose basal plane consists of three coordinating atoms of TAN and a water-oxygen atom. The copper atom is displaced 0.18 Å from the basal plane toward an apical water oxygen atom.

It has been reported that a copper(II) complex of 1-(2-pyridylazo)-2-naphthol (abbr. as H-PAN), $[Cu^{II}(PAN)H_2O]ClO_4$, has a square-planar environment and that PAN is bonded to the copper atom through the phenolic oxygen atom, the azo nitrogen atom, and the pyridine nitrogen atom, thus giving two five-membered chelate rings.[5] Therefore, the coordination of TAN to the copper atom is similar to that of PAN. However, the coordination number and geometry around the metal are different between the $[Cu^{II}(TAN)(H_2O)_2]^+$ and $[Cu^{II}(PAN)H_2O]^+$ complexes.

The bond lengths and angles in the complex cation are shown in Figs. 4a and 4b respectively. The equatorial bond lengths, Cu–N(1), Cu–N(3), Cu–O, and Cu–W(1) (W refers to an oxygen of the water molecule), are 1.97, 1.95, 1.96, and 1.98 Å respectively, while the axial bond length, Cu–W(2), is 2.27 Å, longer by *ca.* 0.3 Å than any of the equatorial bond lengths. A similar feature has been observed in many copper complexes with a square-pyramidal coordination.[6,7,11] The bond angles around the metal, O–Cu–N(1) and N(1)–Cu–N(3), are compressed to 83 and 79° respectively. In relation to this deformation, Cu–N(3)–C(13), S–C(11)–N(2), N(2)–N(1)–C(1), and N(1)–C(1)–C(10) are enlarged to 134, 123, 127, and 127° respectively. Such deviations from the normal valence angles have been observed in all the metal-TAN complexes reported previously. The W(1)–Cu–W(2) angle is 90°. There is a close intra-ligand contact (2.3 Å) between N(2) and H(9) (hydrogen atom attached to C(9)), as is shown in Fig. 4.

The bond lengths and angles in the perchlorate anion are as follows: Cl–O(1)=1.42(2), Cl–O(2)=1.41(3), Cl–O(3)=1.39(3) and Cl–O(4)=1.41(3) Å, O(1)–Cl–O(2)=105(1), O(1)–Cl–O(3)=109(1), O(1)–Cl–O(4)=111(1), O(2)–Cl–O(3)=114(2), O(2)–Cl–O(4)=108(2),

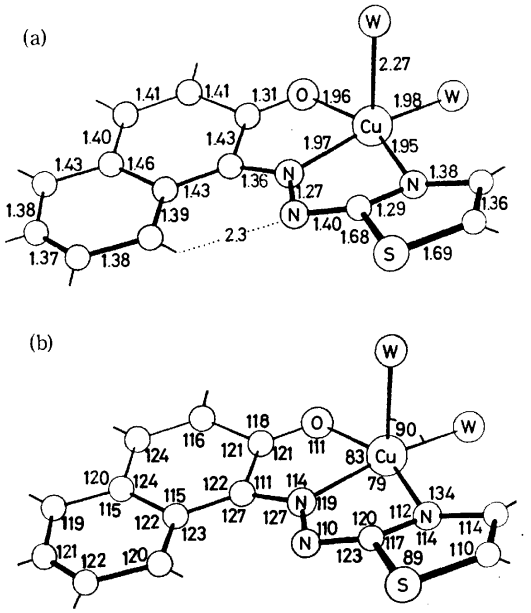

Fig. 4. Bond lengths (a) and bond angles (b) in $[Cu(TAN)(H_2O)_2]^+$. E. s. d.'s are as follows: 0.02Å for Cu–O, Cu–W, and Cu–N. 0.02—0.03 Å for S–C. 0.03 Å for C–O, N–N, and N–C. 0.03—0.04 Å for C–C. 1° for O–Cu–W, O–Cu–N, N–Cu–N, C–S–C, Cu–O–C, and Cu–N–N. 1—2° for N–N–C, C–N–C, and C–C–C.

TABLE 4. EQUATIONS OF THE LEAST-SQUARES PLANES[a] AND DEVIATIONS OF ATOMS FROM THE PLANES

Plane 1 The plane through Cu and TAN anion
$0.4790X+0.8769Y+0.0415Z=8.204$
Plane 2 The naphthalene ring plane
$0.4963X+0.8679Y+0.0207Z=8.293$
Plane 3 The basal plane of square-pyramid
$0.5559X+0.8249Y+0.1024Z=9.240$

Atoms	Plane 1	Plane 2	Plane 3
Cu	0.04*	0.13	0.18
S	0.07*	0.25	−0.04
O	−0.04*	−0.00	0.07*
W(1)	−0.42	−0.33	−0.06*
W(2)	2.25	2.33	2.42
N(1)	0.01*	0.08	−0.08*
N(2)	−0.02*	0.09	−0.18
N(3)	−0.02*	0.12	0.07*
C(1)	−0.03*	0.01*	−0.19
C(2)	0.00*	0.02*	−0.03
C(3)	−0.00*	−0.02*	−0.08
C(4)	0.03*	−0.01*	−0.21
C(5)	0.03*	0.01*	−0.33
C(6)	0.04*	0.01*	−0.47
C(7)	0.03*	0.01*	−0.60
C(8)	−0.04*	−0.01*	−0.62
C(9)	−0.06*	−0.01*	−0.49
C(10)	−0.03*	−0.01*	−0.35
C(11)	−0.02*	0.12	−0.07
C(12)	0.01*	0.21	0.09
C(13)	−0.01*	0.16	0.16

a) *X*, *Y*, *Z*, are orthogonal coordinate in Å and axes parallel a, b, c*.
b) Only the atoms marked with an asterisk are included in the calculation of each plane.

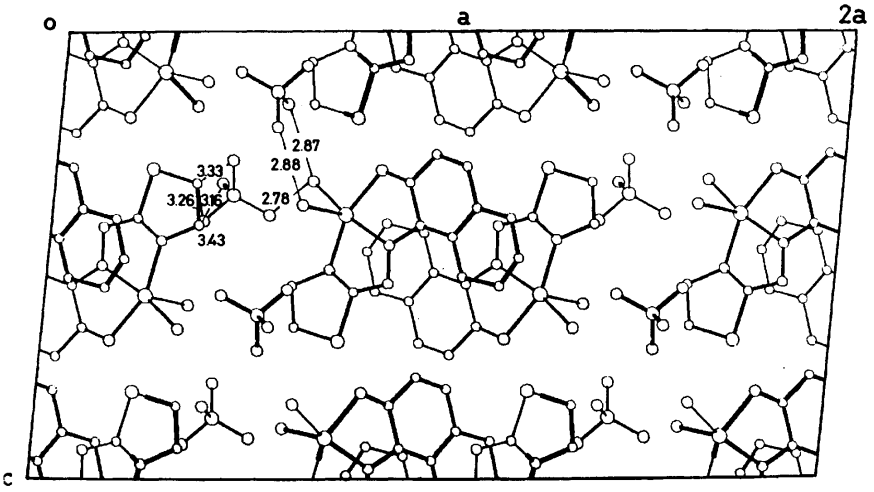

Fig. 5. Crystal structure projected along the b-axis (DEAM-4 diagram[12]).

and O(3)–Cl–O(4)=109(2)°. The perchlorate ion is slightly distorted from a regular tertrahedron. No close contact between Cu and oxygen of the perchlorate anion is observed. The isotropic temperature factors for the oxygen atoms of the perchlorate ion range from 6.0 to 9.9 Å^2, somewhat larger than those for the non-hydrogen atoms of the complex cation.

The deviations of atoms from the various planes are given in Table 4. The mean plane through the Cu and non-hydrogen atoms of the TAN ligand (plane 1) is significantly non-planar, and the S and C(9) atoms are displaced by +0.07 and −0.06 Å respectively. The distances of W(1) and W(2) from this plane are −0.42 and 2.25 Å respectively. On the other hand, the naphthalene ring (plane 2) is planar within a deviation of ±0.02 Å, and all the remaining atoms except oxygens are displaced from the naphthalene plane in the same direction; that is, the TAN ligand is slightly folded along the Cu–N(1) bond at an angle of 2.5°. The non-planarity of the TAN is probably the result of:

(1) the N(2)···H(9) intra-ligand repulsion mentioned above,
(2) the distorted square-pyramidal environment of the Cu atom, or
(3) interionic interactions; relatively short interatomic distances are found between thiazole-ring atoms and perchlorate-oxygen atoms.

The crystal structure projected along the b-axis is shown in Fig. 5. Interatomic distances less than 3.4 Å are listed in Table 5. $[Cu^{II}(TAN)(H_2O)_2]^+$ cations related by the center of symmetry at (0, 0, 0) are stacked alternately along the b-axis to form columns. The columns are held together by van der Waals forces, forming layers parallel to the (001) plane. Perchlorate anions are located around $x=1/2$ between the layers of the complex cations. There are some close approaches between the water-oxygen atoms and the perchlorate-oxygen atoms (Table 5). As can be seen in Fig. 5, the van der Waals forces are predominant around $x=0$, whereas the ionic interactions are predominant around $x=1/2$.

Calculations were carried out on a HITAC 5020F computer at the Computer Center of the National Aerospace Laboratory, using such programs of the UNICS system as PAMI, HBLS-4, and SFR-5. Figures 2 and 5 were produced by the plotter program of DEAM-4.[12]

TABLE 5. INTERATOMIC DISTANCES LESS THAN 3.4 Å

Atoms		Symmetry operation	Distance (Å)
N(3)	O(3)	3	3.27
C(11)	O(3)	3	3.26
C(12)	O(1)	3	3.33
C(12)	O(4)	4	3.16
W(1)	O(2)	1	2.78
W(1)	O(4)	5	2.87
W(2)	O(1)	6	2.88
W(2)	O(2)	2	3.24
W(2)	O(3)	3	3.07
W(2)	O(4)	2	3.27
O(1)	O(4)	5	3.27

Symmetry operations

1 (x y z)
2 (x $y+1$ z)
3 ($1-x$ $1-y$ $1-z$)
4 ($1-x$ $2-y$ $1-z$)
5 ($1-x$ $y-\frac{1}{2}$ $\frac{1}{2}-z$)
6 ($1-x$ $\frac{1}{2}+y$ $\frac{1}{2}-z$)

References

1) M. Kurahashi, This Bulletin, **47**, 2045 (1974).
2) M. Kurahashi, *ibid.*, **47**, 2067 (1974).
3) M. Kurahashi, *Chem. Lett.*, **1974**, 63.
4) A. Kawase, *Bunseki Kagaku*, **11**, 628 (1962).
5) S. Ooi, D. Carter, and Q. Fernando, *Chem. Commun.*, **1967**, 1301.
6) T. Ueki, T. Ashida, Y. Sasada, and M. Kakudo, *Acta Crystallogr.*, B**24**, 1361 (1968).
7) J. Coetzer, *ibid.*, B**26**, 1414 (1970).
8) "International Tables for X-ray Crystallography," Vol. III, Kynoch Press, Birmingham (1962).
9) M. Kurahashi, A. Kawase, K. Hirotsu, M. Fukuyo, and A. Shimada, This Bulletin, **45**, 1940 (1972).
10) M. Kurahashi, *Chem. Lett.*, **1974**, 1271.
11) T. J. Kistenmacher and D. J. Szalda, *Acta Crystallogr.*, B**31**, 1659 (1975).
12) A. Takenaka, "Schematic Drawing of Crystal and Molecular Structures Containing Atomic Thermal Motions," APPLY 270/30-503-001, Tokyo, Fujitsu Ltd.

Reactions of the Di-μ-oxo-bis[aquaoxalatooxomolybdate(V)] Ion

Akitoshi KOMURA, Yasuzi IKEDA, and Hiroto IMANAGA

Faculty of Technology, Kanazawa University, Kanazawa 920

(Received July 23, 1975)

Reactions of the complex ion $[Mo_2O_4(C_2O_4)_2(H_2O)_2]^{2-}$ (I) have been investigated. On acidification with perchloric acid and hydrochloric acid, complex (I) gave molybdenum(V) aqua-dimer ion $[Mo_2O_4(H_2O)_6]^{2+}$, which was converted into the monomeric species $[MoOCl_5]^{2-}$ in concentrated hydrochloric acid. The initial reaction of complex (I) with mercaptoacetic acid, giving a complex of stoichiometry 1 ligand: 1 Mo, was followed by a slower reaction which probably gave higher complexes. In the reactions with *o*-aminophenol and 2,2′-bipyridyl, complexes of stoichiometry 1 ligand: 1 Mo and 1 ligand: 2 Mo, respectively, were formed in solutions. The following complexes have been isolated: $Mo_2O_4(dtc)_2$, $Mo_2O_3(dtc)_4$ (dtc=diethyldithiocarbamate), $MoOCl_3\cdot$phen (phen=1,10-phenanthroline), and $Mo_2O_3Cl_4(bpy)_2$ (bpy=2,2′-bipyridyl). The infrared and electronic spectra of the complexes and their probable structures are given. The relative ease of replacement of ligands from complex (I) has been discussed.

Complexes of molybdenum-(V) and -(VI) with L-cysteine,[1,2] other amino acids[3] and organic sulfur compounds[4] are of interest as models for molybdenum-containing enzymes. It has been established that most of such enzymes contain two molybdenum atoms at the active sites. Molybdenum(V) tends to produce the binuclear oxo complexes bridged with oxide ion. The property of molybdenum(V) complexes and also the variety in both the oxidation number and coordination number of molybdenum might account for the complicated conditions required in the enzymes. The presence of bridging oxygen and terminal oxygen (*i.e.* bonded to only one molybdenum) in binuclear molybdenum(V) complexes might determine the structures and reactivities of the complexes. The oxo-bridged binuclear molybdenum(V) complexes with cysteine,[1,2] dithiocarbamate,[5,6] histidine,[7] oxalate,[8] EDTA,[9] and 8-quinolinol (oxine)[10] have been studied in view of the interest in molybdenum–enzyme systems. Mitchell[11] investigated the substitution reactions of di-μ-oxo-bis-[aquaoxalatooxomolybdate(V)] ion (I), the structure of which was determined by a single-crystal X-ray diffraction study.[12] Further study on the reactions of molybdenum(V) oxalato-complex was undertaken in order to obtain a general picture of the relative ease of replacement of ligands from the binuclear complex.

Experimental

Preparations and reactions were carried out in anaerobic water under an atmosphere of nitrogen, unless otherwise stated. The solution of complex (I) was prepared from the corresponding barium salt and potassium sulfate. The barium salt $Ba[Mo_2O_4(C_2O_4)_2(H_2O)_2]\cdot 3H_2O$ was prepared according to procedures described in the literature.[8,13] Found: Mo, 29.0; C_2O_4, 26.7; Ba, 21.4%. Calcd for $BaMo_2O_{17}C_4H_{10}$: Mo, 29.1; C_2O_4, 26.7; Ba, 20.8%. The oxidation number of the molybdenum is 5.0.

Di-μ-oxo-bis[diethyldithiocarbamatooxomolybdenum(V)], $Mo_2O_4(dtc)_2$. A solution of complex (I) (1.5 mmol) in water (50 ml) was slowly added to a solution of sodium diethyldithiocarbamate (3 mmol) in water (100 ml). A yellow precipitate which formed immediately was collected by filtration, washed with water and ethanol, and dried *in vacuo* over silica gel. The complex was soluble in chloroform and 1,2-dichloroethane. Found: Mo, 35.0; C, 21.8; 5.3; H, 3.5%. Calcd for $Mo_2O_4C_{10}H_{20}N_2S_4$: Mo, 34.8; C, 21.7; N, 5.1; H, 3.6%.

μ-Oxo-bis[bis(diethyldithiocarbamato)oxomolybdenum(V)], $Mo_2O_3(dtc)_4$. A solution of complex (I) (1.25 mmol) in 0.1M-acetate buffer (50 ml, pH 3.0) was added to an ice-cold solution of diethyldithiocarbamate (10 mmol) in water (100 ml). A dark purple precipitate formed immediately and the suspension was stirred for ten minutes. The precipitate was filtered off, washed with water and ethyl ether, and dried *in vacuo* over silica gel. The complex was soluble in chloroform. Found: Mo, 23.3; C, 28.3; N, 7.0; H, 4.8%. Calcd for $Mo_2O_3C_{20}H_{40}N_4S_8$: Mo, 23.1; C, 28.8; N, 6.7; H, 4.8%.

Trichlorooxo(1,10-phenanthroline)molybdenum(V), $MoOCl_3\cdot phen$. We obtained the complex $[Mo_2O_3(C_2O_4)_2(phen)_2]\cdot 2H_2O$ according to the method of Mitchell[11] by the reaction of complex (I) with 1,10-phenanthroline in phthalate buffer solution (pH 4). The former complex (46 mmol) was refluxed in 5M-HCl (50 ml) for twenty minutes. A dark red precipitate which formed was filtered off, washed with 5M-HCl and ethanol, and dried *in vacuo* over silica gel. The complex was insoluble in water. Found: Mo, 24.5; Cl, 26.3; N, 7.4%. Calcd for $MoOCl_3C_{12}H_8N_2$: Mo, 24.1; Cl, 26.7; N, 7.0%.

μ-Oxo-bis[(2,2′-bipyridyl)dichlorooxomolybdenum (V)], $Mo_2O_3Cl_4(bpy)_2$. A phthalate buffer solution (50 ml) containing 2,2′-bipyridyl (7 mmol) and 1M-sulfuric acid (10 ml) was added to a solution of complex (I) (3.5 mmol) in phthalate buffer (50 ml, pH 4). The solution was stirred for fifteen minutes while a buff precipitate formed. The precipitate was filtered off, washed with water and ethanol, and dried *in vacuo* over silica gel. The solid was little soluble in water. The solid contained both oxalate and 2,2′-bipyridyl, whereas it contained neither potassium nor sulfate. Typical analytical values: Mo, 32.6; N, 5.1; C_2O_4, 15.6%. When the solid was refluxed in 5M-HCl, a purple black precipitate was formed. The complex was insoluble in water and common organic solvents. Found: Mo, 27.8; Cl, 19.8; N, 8.0%. Calcd for $Mo_2O_3Cl_4C_{20}H_{16}N_4$: Mo, 27.6; Cl, 20.4; N, 8.1%.

Solutions of the aqua-ion $[Mo_2O_4(H_2O)_6]^{2+}$ were obtained by the following cation-exchange separation. A solution of 2×10^{-2} M-complex (I) in 5M-perchloric acid was aquated for two days under nitrogen. The solution was adsorbed on a cation-exchange column (Dowex 50W-X2) and a yellow band was eluted from the column with 1M-perchloric acid. The analysis of the eluted solution showed that the oxidation state of molybdenum was still 5+, and the solution was free from oxalate ion. UV and visible spectra of solutions were recorded on a Hitachi 124 spectrophotometer with the use of matched silica cells and appropriate reference solutions. IR

spectra of solids in potassium bromide discs were recorded on a Nihonbunko DS 301 spectrophotometer. Molybdenum was determined gravimetrically as molybdenum (VI) oxinate, $MoO_2(C_9H_6ON)_2$, after decomposition of the complexes by heating with a 1: 1 mixture of concentrated nitric and sulfuric acids. The oxidation number of molybdenum was determined by permanganate titration of the complexes, a correction being made for oxalate. Barium was determined gravimetrically as barium sulfate and chlorine as silver chloride. Carbon, hydrogen, and nitrogen were determined by standard microanalytical procedures.

Results and Discussion

Reactions in Solution. The electronic spectrum of complex (I) varied on acidification with perchloric acid. With increasing concentration of perchloric acid, a band at 304 nm in the complex (I) spectrum shifted to shorter wavelength (about 10 nm in 5 M-perchloric acid), whereas a band at 255 nm remained unchanged.

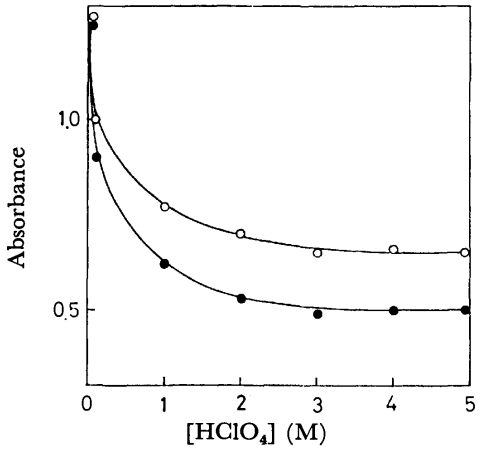

Fig. 1. The variation in absorbances of the complex (I) solution with concentration of perchloric acid. 1.5×10^{-4} M-complex (I). ○: 254 nm. ●: 304 nm.

Figure 1 shows the variation of the absorbances with the concentration of perchloric acid. We attempted to characterize the molybdenum(V) species in aqueous perchloric acid with ion-exchange method. The analytical evidence and the ion-exchange behavior indicate that the molybdenum(V) species is a +2 charged cation to which no oxalate is coordinated. It is well-known[14] that molybdenum(V) salts produce at least three species in aqueous solutions with oxo-molybdenum frameworks MoO^{3+}, $Mo_2O_3^{4+}$, and $Mo_2O_4^{2+}$, which are in an equilibrium dependent on hydrogen ion concentration. Ardon and Pernick[15] have proposed binuclear aqua-ion $[Mo_2O_4(H_2O)_6]^{2+}$ as a molybdenum(V) species in aqueous perchloric acid solutions. Sasaki and Sykes[16] conclude that the molybdenum(V) aqua-ion is stable in the concentration range of 0.5—5 M perchloric acid. Our observations are consistent with this assignment. The conclusion that we also have the molybdenum(V) aqua-dimer is supported by the measurement of the absorption characteristics. The absorption spectrum of the eluted solution has maxima at 294 nm (ε=3400 l mol^{-1} cm^{-1}) and 254 nm (ε=3900). The absorption spectrum is in good agreement with the spectra of Ardon and Pernick; 293 (3454) and 254 nm (3998),[15] and of Sasaki and Sykes; 295 (3546) and 255 nm (4320).[16] On neutralization of the molybdenum(V) aqua-dimer solution in the presence of oxalate, the peak at 294 nm shifted to longer wavelength with a significant increase in absorbance. This is probably consistent with equilibrium (1) in aqueous perchloric acid.

$$[Mo_2O_4(C_2O_4)_2(H_2O)_2]^{2-} + 4H_3O^+ \rightleftarrows [Mo_2O_4(H_2O)_6]^{2+} + 2H_2C_2O_4 \quad (1)$$

On the other hand, a number of studies have been made of the behavior of molybdenum(V) in hydrochloric acid solutions, and monomer-dimer equilibria have been proposed.[14] The electronic spectrum of complex (I) also varied on acidification with hydrochloric acid. With an increase in concentration of hydrochloric acid, the peak at 304 nm in complex (I) initially shifted to shorter wavelength, but the direction of the shift was reversed at [HCl]=1—2 M. Figure 2

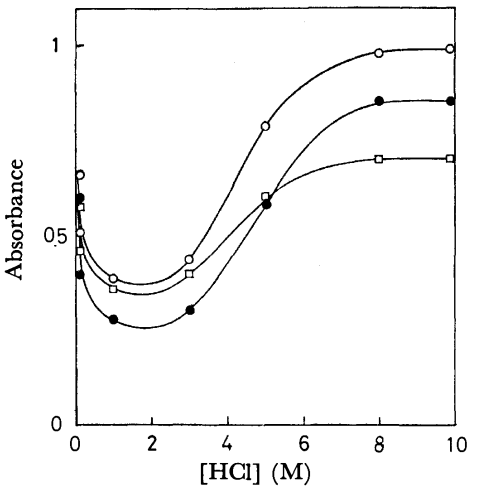

Fig. 2. The variation in absorbances of the complex (I) solution with concentration of hydrochloric acid. 10^{-4} M-complex (I). ○: 240 nm. □: 300 nm. ●: 310 nm.

shows the variation of absorbances with the concentration of hydrochloric acid. The absorbance at each wavelength shows a minimum at [HCl]=1—2 M and approaches a definite value in very high concentration of hydrochloric acid. With concentrated hydrochloric acid, the solution gave the characteristic green color of the pentachlorooxomolybdate(V) ion. Details of the absorption maxima (absorption coefficient per molybdenum), 720 (20), 443 (18), 355 (560), 310 (4700), and 241 nm (5400), are in good agreement with those of $MoOCl_5^{2-}$.[17] The change in the spectrum at [HCl]< 1M might be due to the aquation of complex (I), because the spectral change is identical with that in the aquation with perchloric acid. Ardon and Pernick[15] have shown that the main molybdenum(V) species in dilute hydrochloric acid (<1M) is the aqua-dimer $[Mo_2O_4(H_2O)_6]^{2+}$ as well as in perchloric acid. The change in spectrum of complex (I) at higher concentration of hydrochloric acid might be attributed to the conversion of the molybdenum(V)-dimer into the

monomeric species $[MoOCl_5]^{2-}$ according to the characteristic of the spectral change. When complex (I) was allowed to stand in basic solutions (pH 7—10), the band of 304 nm shifted to longer wavelength with a decrease in absorbance, whereas the band at 255 nm shifted to shorter wavelength with an increase in absorbance. The absorbance of the band at 304 nm remarkably decreased with time in higher pH, probably owing to the oxidation of molybdenum(V). Molybdenum(V) is too easily oxidizable in basic solutions to allow quantitative examination of the reaction.

Reactions of complex (I) with different ligands were carried out in aqueous solutions buffered at pH 4, in which complex (I) persists.[11] Continuous variations plots for 2,2'-bipyridyl are shown in Fig. 3. Maxima in ΔA, deviations of the absorbances of the mixed solutions from the sums of the absorbances of the components, occurred at a 2,2'-bipyridyl: complex (I) ratio of 1: 1 showing the formation of a complex of stoichiometry 1 bpy: 2 Mo. The spectrum of the mixed solution differed from that of complex (I) only in the enhanced absorbance above 350 nm and no new peaks were observed. The plot with *o*-aminophenol is shown

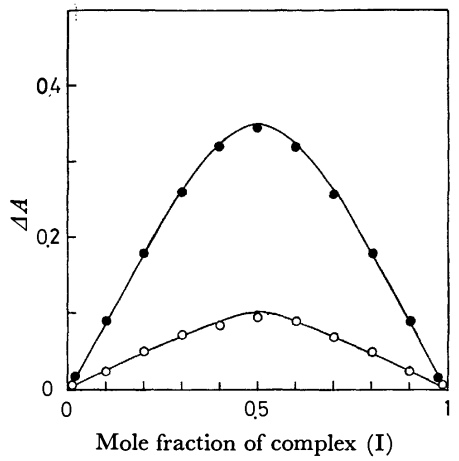

Fig. 3. Continuous variation plots for the reaction of complex (I) with 2,2'-bipyridyl.
The total concentration was 2.5×10^{-4} M. pH 4.0.
●: 400 nm. ○: 450 nm.

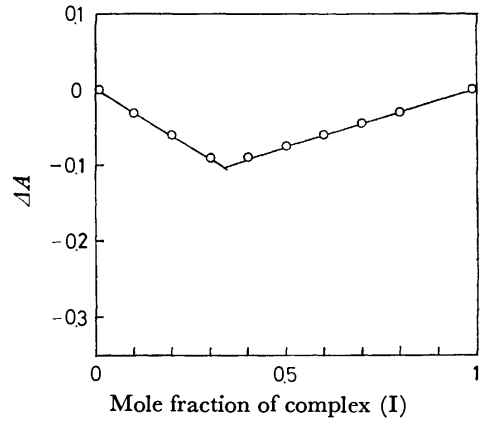

Fig. 4. The continuous variation plot for the reaction of complex (I) with *o*-aminophenol.
The total concentration was 2.5×10^{-4} M. pH 4.0, 435 nm.

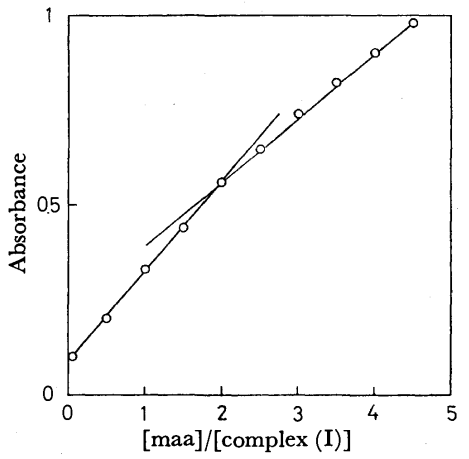

Fig. 5. The molar ratio plot at 30 min after mixing for the reaction of complex (I) with mercaptoacetic acid.
The concentration of complex (I) was 1.25×10^{-4} M. pH 4.0, 430 nm.

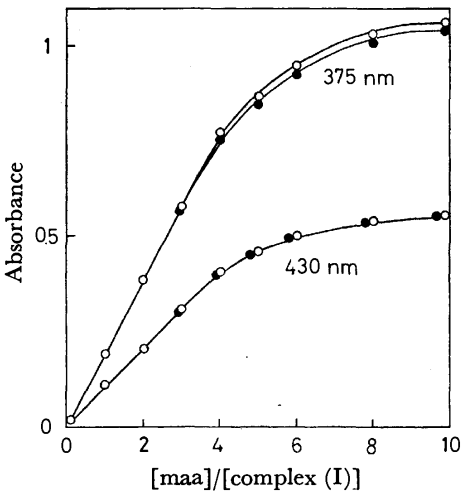

Fig. 6. Molar ratio plots at 15 and 40 hr after mixing for the reaction of complex (I) with mercaptoacetic acid. The concentration of complex (I) was 1.25×10^{-4} M. pH 4.0. ○: 40 hr. ●: 15 hr.

in Fig. 4. Minimum in ΔA occurred at a ligand: complex (I) ratio of 2: 1. This corresponds to the formation of a complex of stoichiometry 1 aminophenol: 1 Mo. Molar ratio plots for mercaptoacetic acid (maa) are shown in Figs. 5 and 6. The plot at 30 minutes after mixing shows the formation of a complex of stoichiometry 1 maa: 1 Mo. The plots after 15 and 40 hours are linear up to 4 molar ratio of mercaptoacetic acid to complex (I), above which ratio both absorbances gradually approach definite values. Thus the initial reaction, giving a 1: 1 complex, is followed by a slower reaction which might give higher complexes. With the following ions and molecules there were no spectral changes, continuous variations plots being straight lines; *O*-ethyl dithiocarbonate, glycine, tartrate, malonate, thiourea, biuret, thiosemicarbazide, and phosphate.

Complexes Isolated. The isolated complexes are listed in Tables 1 and 2. The formulas of the complexes

are based on analyses and physical measurements. For complexes with dithiocarbamate, the oxidation state of molybdenum could not be determined directly because of interference by oxidizable sulfur ligands. The complexes gave the characteristic green color of the $[MoOCl_5]^{2-}$ ion in concentrated hydrochloric acid. Immediate precipitation occurs on mixing complex (I) and dithiocarbamate solutions. Initial preparation gave the products with varying molybdenum percentage and color depending upon the conditions of reaction. A higher mixing-ratio of dithiocarbamate to complex (I) at pH 4 gave smaller molybdenum percentages (dark purple color). Higher pH at a given mixing-ratio gave higher molybdenum percentages (pink color). Visible and infrared spectra suggest that the product (pink) in higher pH and lower mixing-ratio corresponds mainly to complexes of the Mo_2O_4 type, and that (dark purple) in lower pH and higher mixing-ratio to the Mo_2O_3 type. We isolated analytically pure $Mo_2O_4(dtc)_2$ and $Mo_2O_3(dtc)_4$. Our observation is consistent with Kay and Mitchell's comment[2] that molybdenum(V) complexes of the type $Mo_2O_4L_2$ are obtained from aqueous solutions under more alkaline conditions than in the preparation of the complexes $Mo_2O_3L_4$. The complex $Mo_2O_4(dtc)_2$ has recently been prepared by refluxing an aqueous solution of pentachlorooxomolybdate(V) and dithiocarbamate.[6] The complex seems to have structures closely related to the molybdenum(V) complexes with L-cysteine esters, in which unique five-coordinate structures are formed.[18] The complex $Mo_2O_3(dtc)_4$ is considered to be structurally similar to the corresponding dithiocarbonate and phosphorothiolothionate complexes, the structures of which have been determined by single-crystal X-ray crystallography.[19,20] $Mo_2O_4(dtc)_2$ could be easily converted into $Mo_2O_3(dtc)_4$ by stirring with dithiocarbamate in chloroform–methanol (4: 1) solution. Confirming Mitchell's description,[11] we obtained μ-oxo-bis[oxobis(8-quinolinolato)molybdenum(V)]hydrate from a hot solution containing complex (I) and 8-quinolinol. In the reactions of complex (I) with 8-quinolinol one bridging oxo-group of the Mo_2O_4 group was replaced giving complexes of the Mo_2O_3 group. $MoOCl_3$·phen was obtained by refluxing the complex

TABLE 1. INFRARED SPECTRA[a]

$Ba[Mo_2O_4(C_2O_4)_2(H_2O)_2]\cdot 3H_2O$							
3450s	1708vs	1675vs	1645vs	1425s	1282m	976vs	
water			oxalate			Mo=O	
955m	910m	794m	728m				
Mo=O	oxalate		MoO_2Mo				
$Mo_2O_4(dtc)_2$							
1545s, sh	1530vs	1455s	1437s	1382m	1356m	1290w	
			dtc				
1278s	1200s	1152m	1100w	1080m	1065w	972vs	956m
		dtc				Mo=O	
910m	845m	780w	734m				
	dtc		MoO_2Mo				
$Mo_2O_3(dtc)_4$							
1512vs	1490s,sh	1455s	1434s	1382m	1358m	1297w	
			dtc				
1276s	1205s	1149m	1095w	1075w	1065w	1005m	937m
			dtc				Mo=O
913s	847m	781w	750w				
	dtc		MoOMo				
$[Mo_2O_3(C_2O_4)_2(phen)_2]\cdot 2H_2O$							
3420s	3050m	1705vs	1680vs	1630s	1540m	1518m	
water	phen		oxalate		phen		
1490w	1426s	1405s	1341m	1310w	1146m	1111m	1035w
phen		oxalate			phen		
958vs	910w	876m	852s	802m	745s	725s	
Mo=O	oxalate	phen		oxalate	MoOMo	phen	
$MoOCl_3\cdot$phen							
3030m	1625m	1601w	1575m	1516m	1489m	1426vs	
		phen					
1342m	1301w	1225m	1197w	1147m	1111m	1035w	
		phen					
963vs	874m	853vs	800m	785m	742m	725s	
Mo=O		phen			MoOMo	phen	
$Mo_2O_3Cl_4(bpy)_2$							
3040m	1660w	1598s	1560w	1490m	1468m	1440vs	
			bpy				
1315m	1280w	1242w	1171m	1157m	1075w	1044w	
			bpy				
1029m	1019m	963vs	903w	794m	777vs	753w	734m
bpy		Mo=O		bpy			MoOMo

a) All values in cm^{-1}. Abbreviations; vs: very strong, s: strong, m: medium, w: weak, sh: shoulder.

$[Mo_2O_3(C_2O_4)_2(phen)_2]\cdot 2H_2O$ in 5M-hydrochloric acid. In very prolonged refluxing, a green solution owing to $[MoOCl_5]^{2-}$ formed. The complex $MoOCl_3\cdot$phen was prepared by the reaction of the pentachlorooxomolybdate(V) with 1,10-phenanthroline in dehydrated ethanol.[21] For this complex three different isomeric forms (colored reddish-pink, pale brown, and green) are known to be interconvertible.[21] Judging from the color, our complex seems to be *cis*-isomer. A buff solid obtained by the reaction of complex (I) with 2,2'-bipyridyl at pH 4 seemed to be the Mo_2O_4 type according to the infrared spectrum. The analytical data corresponded to a Mo: oxalate: bpy ratio of 2: 1: 1. The same stoichiometry (2 Mo: 1 bpy) was also observed in the solution studies. However, no reasonable formula could be given. By refluxing the compound in 5M-hydrochloric acid we obtained the monooxo-bridged binuclear complex $Mo_2O_3Cl_4(bpy)_2$.

Infrared Spectra. The positions and assignments of the main bands are given in Table 1. All the complexes have a strong band at 930—980 cm^{-1} assigned to the stretching vibration of the Mo=O group. Bridge vibrations of the molybdenum-oxygen group occur at 700—800 cm^{-1}.[3,5,11] For molybdenum(V) the commonest binuclear oxo-species are the Mo_2O_3 and Mo_2O_4 groups each of which has one terminal oxygen per molybdenum and one or two bridging oxygens respectively. Wing and Callahan[22] showed that the molybdenum-oxygen stretching vibrations are a powerful tool for the characterization of the molybdenum-oxygen bridged complexes, but at present this does not seem to be always the case. Newton *et al.*[6] gave definite assignments for the infrared spectra of two series of molybdenum(V)–dithiocarbamate complexes. In the complexes with dithiocarbamate, the infrared spectra of the Mo_2O_4 groups contain two bands assigned to the terminal Mo=O vibrations and a medium band at *ca.* 740 cm^{-1} assigned to the MoO_2Mo bridge vibration. The higher (*ca.* 980 cm^{-1}) of the absorptions attributed to the terminal Mo=O vibrations is much stronger than the second band (*ca.* 960 cm^{-1}). The infrared spectra of the Mo_2O_3 groups have one band assigned to the terminal Mo=O vibration and a weak band at *ca.* 750 cm^{-1} assigned to the MoOMo bridge vibration. The split band at *ca.* 980 cm^{-1} and the medium absorption at *ca.* 740 cm^{-1} can be used as good indicators of the presence of the Mo_2O_4 moeity in complexes. These correlations are in line with those made in other complexes suggested to have the MoO_2Mo bridge.[23] Each band at about 730 cm^{-1} in complexes (I) and $Mo_2O_4(dtc)_2$ is therefore assigned to vibrations of the MoO_2Mo groups. For complexes with 1,10-phenanthroline and 2,2'-bipyridyl, assignments of bands to the MoOMo bridge vibrations are made uncertain because of ligand vibrations at 700—800 cm^{-1}. The infrared spectra of complexes (I) and $[Mo_2O_3(C_2O_4)_2(phen)_2]\cdot 2H_2O$ have characteristic bands at *ca.* 1630—1710 cm^{-1} assigned to the C=O stretching vibration of coordinated oxalate. As noted by Jowitt and Mitchell,[5] the vibration frequency (1488 cm^{-1}) of $N{=}CS_2$ group for dithiocarbamate increases on coordination because of an increased contribution of the canonical form $Et_2N^+{=}CS_2^{2-}$. In the complex $Mo_2O_3(dtc)_4$ this vibration splits into two bands (as a shoulder) indicating that the two dithiocarbamate groups are not equivalent.[19] The presence of 1,10-phenanthroline in the complexes $[Mo_2O_3(C_2O_4)_2(phen)_2]\cdot 2H_2O$ and $MoOCl_3\cdot$phen is shown by characteristic bands at *ca.* 1625 m, 1516 m, 1426s, 1341m, 1315w, 1147m, 853s, and 725s cm^{-1}. The spectrum of the complex obtained by the reaction of complex (I) with 2,2'-bipyridyl at pH 4 has bands at 955 and 937 cm^{-1} assigned to vibrations of the terminal Mo=O group, showing that the complex probably contains the Mo_2O_4 groups.

Electronic Spectra. The positions, intensities and assignments of the absorption maxima are shown in Table 2. Complex (I) has two peaks assigned to d-d transitions in the visible region, and two intense peaks assigned to charge-transfer transitions ($O^{2-}\rightarrow Mo$) in the UV region.[8] The spectrum of $Mo_2O_3(dtc)_4$ indicated a poorly resolved shoulder at 15600 cm^{-1} assigned to a d-d transition, which is at higher energy

Table 2. Electronic spectra[a]

Compound	ν_{max} ($10^3 cm^{-1}$)	Assignments
$[Mo_2O_4(C_2O_4)_2(H_2O)_2]^{2-}$	20.4sh(70)	d-d
in water	26.0(300)	d-d
	32.9(6700)	charge-transfer
	39.2(6600)	charge-transfer
$Mo_2O_4(dtc)_2$	31.5sh(7800)	charge-transfer
in chloroform		
$Mo_2O_3(dtc)_4$	15.6sh(600)	d-d
in chloroform	19.5(2000)	charge-transfer
	26.3(5200)	charge-transfer
	32.8sh(17700)	$\pi\rightarrow\pi^*$ of dtc
$[Mo_2O_3(C_2O_4)_2(phen)_2]\cdot 2H_2O$	28.2sh(2600)	charge-transfer
in water	36.0(38000)	$\pi\rightarrow\pi^*$ of phen
$MoOCl_3\cdot$phen	18.7(~400)	d-d
in acetone	23.8sh(~800)	charge-transfer
	27.7(2000)	charge-transfer
	32.9(11000)	$\pi\rightarrow\pi^*$ of phen

a) Molar absorption coefficients (l mol^{-1} cm^{-1}) are given in parentheses.

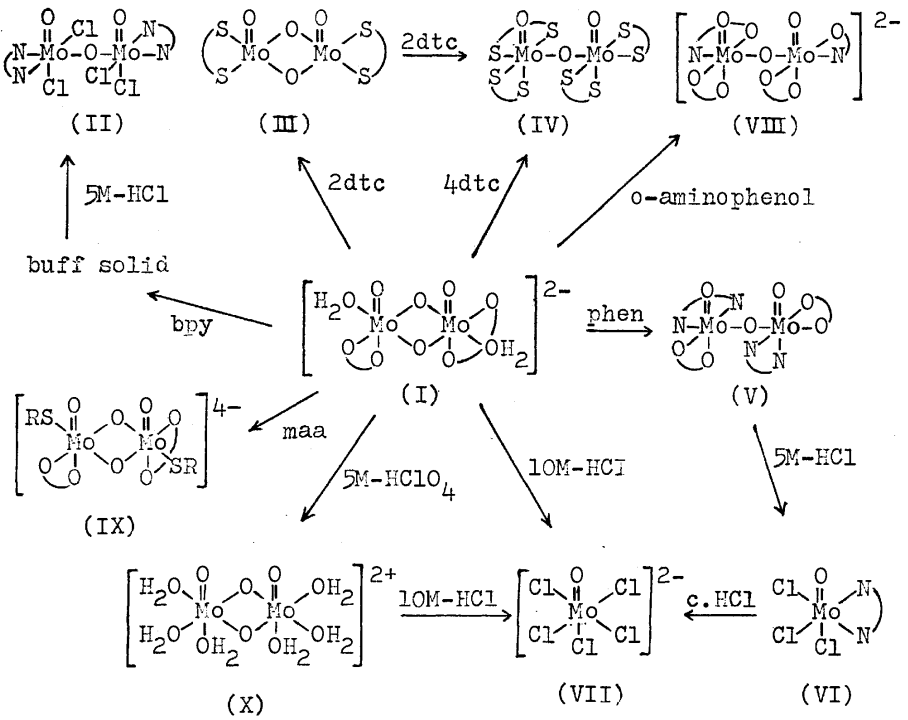

Scheme. Reaction scheme and proposed structures.

Complexes (I)—(VII) have been isolated, others being species postulated in aqueous solutions.

than the first d-d transition for the ion $[MoOCl_5]^{2-}$ (14100 cm^{-1}).[17] A peak or shoulder at less than 18000 cm^{-1} is observed for molybdenum(V) complexes, $Mo_2O_3L_4$ (L=dithiocarbamate, dithiocarbonate, or phosphorothiolothionate), and is assigned to a d-d transition.[5] Strong peaks at 18000—29000 cm^{-1} are characteristic of oxo molybdenum(V) complexes with polarizable ligands,[5] and cover peaks due to d-d transitions expected in this region. In agreement with Jowitt and Mitchell,[5,11] we assigned the peaks in this region in complexes $Mo_2O_3(dtc)_4$ and $[Mo_2O_3(C_2O_4)_2(phen)_2]\cdot 2H_2O$ to ligand-to-molybdenum charge-transfer transitions. The spectrum of $Mo_2O_4(dtc)_2$ was essentially featureless except for a poorly resolved shoulder at 31500 cm^{-1}. We assigned the peak to a charge-transfer transition because of its high absorption coefficient. $MoOCl_3\cdot$phen has only one peak below 20000 cm^{-1}. For the complex $MoOCl_3\cdot$phen (reddish-pink), Saha and Halder[21] observed two peaks at 13700 (ε=179) and 18900 cm^{-1} (ε=282) assigned to d-d transitions. The complex anion $[MoOCl_5]^{2-}$ has also two peaks at 14100 (20) and 22500 cm^{-1} (18) assigned to d-d transitions.[17] The complex $MoOCl_3\cdot$phen we prepared was too insoluble into common organic solvents to observe weak peaks of ε less than 200. Both peaks at 23800 and 27700 cm^{-1} in the complex are assigned to charge-transfer transitions according to the values of the absorption coefficient. A strong peak at 32900 cm^{-1} is assigned to the internal transition ($\pi\rightarrow\pi^*$) of coordinated 1,10-phenanthroline, which is at lower frequency than that of free 1,10-phenanthroline. Peaks at wave numbers greater than 32000 cm^{-1} are assigned to $\pi\rightarrow\pi^*$ transitions of the ligands except for complex (I).

Conclusion

Reactions involved in this paper are summarized in the Scheme. In the initial reaction with mercaptoacetic acid, a complex of stoichiometry 1 ligand: 1 Mo was formed in solution. Similarity of the spectrum of the mixed solution to that of complex (I) except for the enhancement of absorption above 360 nm suggests that no significant structural change occurs in the reaction. We assume that two coordinated waters are replaced by mercaptoacetic acid. With *o*-aminophenol a complex of stoichiometry 1 ligand: 1 Mo was formed in solution. Because of a strong absorption maximum of *o*-aminophenol at 435 nm, we cannot observe the remarkable characteristics in spectrum of the complex. The electrical migration studies showed that the complex was an anion. It is reasonable to assume that coordinated waters and one bridging oxygen were replaced by *o*-aminophenol, because the replacement of oxalate should produce a nonelectrolyte. As the substitution reactions of complex (I), there are four possible stages involving replacement of coordinated water, bridging oxygen, oxalate, and terminal oxygen, respectively. Mitchell[11] discussed the relative ease of replacement of ligands from complex (I) and showed that, qualitatively, the order of the ease was H_2O>one bridging oxygen>oxalate$\gg$terminal oxygen. We agree with Mitchell in concluding that the replacement of coordinated water is easiest. In reactions of complex (I) with 1,10-phenanthroline and *o*-aminophenol, the cleavage of one oxygen bridge of the Mo_2O_4 group occurred keeping oxalate. On the other hand, in the formation of $Mo_2O_4(dtc)_2$ and of $[Mo_2O_4(H_2O)_6]^{2+}$ the

replacement of oxalate occurred without any cleavage of oxygen bridge. The relative ease of replacement of one bridging oxygen and oxalate probably varies with nucleophiles in disagreement with Mitchell's conclusion.[11] Molybdenum(V) has a particular affinity for dithiocarbamate as well as 8-quinolinol. Nevertheless neither ligand can cleave all oxygen bridges of the Mo_2O_4 group and both ultimately give the single-bridged $Mo_2O_3L_4$ species. Strongly acidic conditions are required for the formation of a mononuclear species. Replacement of terminal oxygen whose bond order to molybdenum is approximately two[24] is very unlikely to occur in aqueous solutions (even in concentrated hydrochloric acid). Special stability of monooxo molybdenum(V) moiety MoO^{3+} in aqueous solutions has led to certain interesting investigations of the chemistry of the oxo molybdenum-(V) ions.[21,25]

References

1) L. R. Melby, *Inorg. Chem.*, **8**, 349 (1969); A. Kay and P. C. H. Mitchell, *J. Chem. Soc., Dalton*, **1973**, 1388.

2) A. Kay and P. C. H. Mitchell, *J. Chem. Soc., A*, **1970** 2421.

3) H. Eguchi, T. Takeuchi, A. Ouchi, and A. Furuhashi, This Bulletin, **42**, 3585 (1969).

4) L. S. Meriwether, W.F. Marzluff, and W. G. Hodgson, *Nature*, **212**, 465 (1966).

5) R. N. Jowitt and P. C. H. Mitchell, *J. Chem., Soc., A.* **1970**, 1702.

6) W. E. Newton, J. L. Corbin, D. C. Bravard, J. E. Searles, and J. W. Mcdonald, *Inorg. Chem.*, **13**, 1100 (1974).

7) L. R. Melby, *ibid.*, **8**, 1539 (1969); L. T. J. Delbaere and C. K. Prout, *Chem. Commun.*, **1971**, 162.

8) P. C. H. Mitchell, *J. Inorg. Nucl. Chem.*, **26**, 1967 (1964).

9) R. L. Pecsok and D. T. Sawyer, *J. Amer. Chem. Soc.*, **78**, 5496 (1956).

10) P. C. H. Mitchell and R. J. P. Williams, *J. Chem. Soc.*, **1962**, 4570; H. M. Stevens, *Anal. Chim. Acta*, **14**, 126 (1956).

11) P. C. H. Mitchell, *J. Chem. Soc., A*, **1969**, 146.

12) F. A. Cotton and S. M. Morehouse, *Inorg. Chem.*, **4**, 1377 (1965).

13) H. M. Spittle and W. Wardlaw, *J. Chem. Soc.*, **1928**, 2742.

14) F. A. Cotton and G. Wilkinson, "Advanced Inorganic Chemistry: A Comprehensive Text," Interscience Pub., New York (1972), p. 965.

15) M. Ardon and A. Pernick, *Inorg. Chem.*, **12**, 2484 (1973).

16) Y. Sasaki and A. G. Sykes, *J. Chem. Soc., Dalton*, **1974**, 1468.

17) H. B. Gray and C. R. Hare, *Inorg. Chem.*, **1**, 363 (1962).

18) M. G. B. Drew and A. Kay, *J. Chem. Soc., A*, **1971**, 1846, 1851.

19) A. B. Blake, F. A. Cotton, and J. S. Wood, *J. Amer. Chem. Soc.*, **86**, 3024 (1964).

20) J. R. Knox and C. K. Prout, *Acta Crystallogr.*, **25B**, 2281 (1969).

21) H. K. Saha and M. C. Halder, *J. Inorg. Nucl. Chem.*, **34**, 3097 (1972).

22) R. M. Wing and K. P. Callahan, *Inorg. Chem.*, **8**, 871 (1969).

23) B. J. Trzebiatowska, M. Rudolf, L. Natkaniec, and H. Sabat, *ibid.*, **13**, 617 (1974).

24) D. H. Brown, P. G. Perkins, and J. J. Stewart, *J. Chem. Soc., Dalton*, **1972**, 1105.

25) H. K. Saha, S. S. Mandal, and T. R. Chaudhuri, *J. Inorg. Nucl. Chem.*, **37**, 840 (1975).

N-Allylpyrazole as a Ligand. II. The Preparation and Reaction of Some Palladium(II) and Platinum(II) Complexes

Takeshi MIYAMOTO,* Kazuo FUKUSHIMA, Taro SAITO, and Yukiyoshi SASAKI

Department of Chemistry, Faculty of Science, The University of Tokyo, Hongo, Tokyo 113

(Received July 31, 1975)

New complexes of *N*-allylpyrazole(L) with Pd(II) and Pt(II) have been prepared and characterized; they have the general formulae of MX_2L_2 and MX_2L (X=Cl or Br). IR and ^1H NMR studies indicate that the latter complexes are *cis*-planar-chelate and involve both the pyrazolyl nitrogen and the olefinic group in bonding to the metal, while the former are *syn*- and *anti-trans*-planar and contain only uni-dentate pyrazole donor ligands. The treatment of the chelate complex $PtCl_2L$(L= 1-(2-methylallyl)-3,4,5-trimethylpyrazole) with donor ligands (L′) such as phosphines, $AsPh_3$, and py displaces the coordinated olefin,forming *cis*-$PtCl_2LL'$ with a retention of the *cis*-configuration.

Allylpyrazole (Fig. 1), which has both σ-donating nitrogen and π-accepting olefin, can be bound with metal ions in more than one way. We have already reported that the ligand forms bidentate complexes with copper(I) halide and silver nitrate; it also coordinates to metal halides of the first transition series by using only pyrazolyl nitrogen.[1] By analogy with other chelate olefin complexes,[2-9] the coordination chemistry of platinum(II) and palladium(II) has proved to be of interest because they form not only monodentate pyrazolyl-nitrogen complexes, but also stable olefin complexes, with the chelation of allylpyrazole through the nitrogen donor and the olefinic group.

We wish now to report the details of the preparation of palladium(II) and platinum(II) compounds and their properties, especially their spectroscopic characteristics and their substitution reactions.

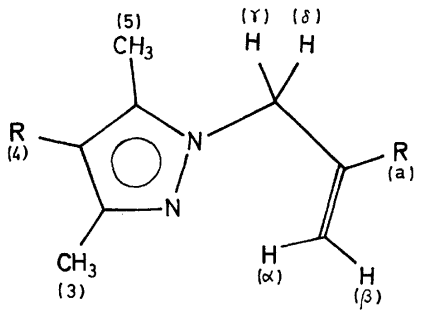

Fig. 1. *N*-Allylpyrazole, R_a, R_4=H or CH_3. Numbers and Greek letters represent the position of the hydrogen atoms.

Experimental

The molecular weight was determined by the Rast method. X-Ray powder diagrams were obtained by means of a Rigaku D-2F apparatus. The other physical measurements were made as has previously been described.[1] The IR and NMR data are collected in Tables 3 and 4 respectively.

Synthesis of Ligands. The four ligands were prepared by the method of Finar and Utting[10] in a *ca.* 40% yield. The names of the ligands are abbreviated thus, based on Fig. 1: admp(R_a=R_4=H); atmp (R_a=H, R_4=Me); amdmp(R_a=Me, R_4=H); amtmp(R_a=R_4=Me).

Preparation of trans-MX_2L_2 (*M=Pd or Pt; X=Cl or Br; L=substituted* N-*allylpyrazoles*). Dipotassium tetrachlorometallate (II) (0.01 M) was dissolved in water, and then an excess of allylpyrazole (0.10 M) was stirred in. Yellow crystals were obtained after stirring at 25 °C for a day and were recrystallized from cold chloroform. The complexes were also prepared by adding allylpyrazole to MCl_2L in cold chloroform. In general, throughout the reaction, the temperature must be maintained below 25 °C. If the temperature is allowed to rise above *ca.* 50 °C, a mixture of MCl_2L and MCl_2L_2 is obtained. The bromo-complex, MBr_2L_2 was prepared by the metathesis of the corresponding chloro-complex with lithium bromide. All the complexes are easily soluble in chloroform or dichloromethane. The analytical data and some properties of the complexes are shown in Table 1. The *trans* structure of $PtCl_2L_2$ was checked by Kurnakov's test.[11]

Preparation of PtX_2L. Dipotassium tetrachloroplatinate (II) (0.01 M) was dissolved in water (20 ml). Into this solution a mixture of allylpyrazole (0.01 M) and concd hydrochloric acid solution (*ca.* 5 ml) was vigorously stirred. Then, the reaction mixture was gently heated on a water bath for about half an hour. After they had been cooled to room temperature, the precipitated crystals were filtered, washed with water, and dried *in vacuo*. Crude products were recrystallized from chloroform(10)–ethanol(90) (yield: 95%). In boiling ethanol, these complexes partly decompose to yield platinum-(0) metal. The purified crystals are stable to light and air. The analytical data and physical properties are summarized in Table 2. The complexes were also obtained by a displacement reaction from bis(benzonitrile)dichloroplatinum(II) (0.01 M) or bis(dimethyl sulfide)dichloroplatinum(II) (0.01 M) with allylpyrazole (0.01 M) in chloroform (yield: *ca.* 80%).

Preparation of $PdCl_2L$. The palladium complexes are prepared by procedures similar to those used for the diolefin complexes.[12] A solution of $PdCl_2$ (0.01 M) in concd hydrochloric acid (5 ml) is diluted with 50 ml ethanol. To this solution, the ligand (0.01 M) is added. Immediately, brown crystals are precipitated. After stirring for 20 min, they are filtered, and washed successively with water, ethanol, and diethyl ether (yield: *ca.* 80%). The analytical data and some properties are given in Table 2. The complexes, except for the case of L=amtmp, are not soluble enough in any solvent to give meaningful structural information in a solution.

Substitution Reaction of 1-(2-Methylallyl)-3,4,5-trimethylpyrazole-dichloroplatinum(II) with Neutral Donor Ligands. The general scheme of the reaction is summarized in Fig. 2. The analytical data and some properties of new complexes are tabulated in Table 5. When tertiary alkylphosphines such as PBu^n_3, PPr^i_3 and PCy_3 were used, all the manipulations were carried out under a nitrogen atmosphere. Some typical reactions will be described:

With PPh_3: In 50 ml of benzene, the yellow complex, $PtCl_2L$ (2.1 g, 0.0051 M), was dispersed. When an equimolar

Table 1. Analytical data and properties of *trans*-MX_2L_2 type complexes

M	X	L[a]	Color	Mp (°C)[b]	% Found (Calcd)			
					C	H	N	X
Pt	Cl	admp	yellow	Nm	35.6 (35.7)	4.3 (4.5)	10.6 (10.4)	13.8 (13.2)
Pt	Cl	atmp	yellow	Nm	39.0 (38.2)	4·8 (5.0)	9.5 (9.9)	12.8 (12.5)
Pt	Cl	amtmp	yellow	207	40.5 (40.4)	5.5 (5.4)	9.4 (9.4)	11.8 (11.9)
Pt	Br	amtmp	yellow	214	35.6 (35.2)	4.8 (4.7)	7.9 (8.2)	22.6 (23.4)
Pd	Cl	amtmp	orange	198	47.9 (47.5)	6.8 (6.4)	11.2 (11.1)	13.8 (14.0)

a) Name of ligands, abbreviated in Experimental. b) All melting points were uncorrected.

Table 2. Analytical data and properties of MX_2L type complexes

M	X	L	Mp (°C)[a]	Color	% Found (Calcd)			
					C	H	N	X
Pt	Cl	admp	Nm	white	24.2 (23.9)	3.0 (3.0)	6.8 (7.0)	Nm
Pt	Cl	atmp	Nm	white	26.2 (26.0)	3.5 (3.4)	6.7 (6.7)	17.2 (17.0)
Pt	Cl	amdmp	248	light-yellow	26.2 (26.0)	3.1 (3.4)	6.7 (6.7)	16.7 (17.0)
Pt	Cl	amtmp[b]	238	light-yellow	28.2 (28.0)	3.5 (3.8)	6.5 (6.5)	16.2 (16.5)
Pt	Br	amtmp	215	yellow	23.3 (23.1)	3.1 (3.1)	5.1 (5.4)	Nm
Pd	Cl	amdmp	204	brown	33.3 (33.0)	4.2 (4.3)	8.5 (8.6)	21.4 (21.7)
Pd	Cl	amtmp	183	brown	35.2 (35.2)	4.5 (4.7)	7.9 (8.2)	21.0 (20.8)

a) All melting points were uncorrected. b) Molecular Weight: Found, 530; Calcd, 430.

quantity of triphenylphosphine (1.4 g, 0.0053 M) was added to the above mixture, the dispersed complex spontaneously dissolved in the solution. This light-yellow solution was then evacuated to dryness. The residue on crystallization from ethanol (20 ml)–hexane (60 ml) gave *cis*-$PtCl_2LPPh_3$ (yield: 3.2 g, 94% based on $PtCl_2L$). If two equivalents of PPh_3 (2.8 g) were used, snow-white crystals of *cis*-$PtCl_2(PPh_3)_2$ were precipitated from the benzene solution quantitatively.

With PCy_3: A benzene solution (100 ml) containing PCy_3 (7.0 g, 0.025 M) and $PtCl_2L$ (4.3 g, 0.010 M) was concentrated under reduced pressure at room temperature to about half its volume. White, puffy crystals of *cis*-$PtCl_2LPCy_3$ precipitated on the addition of hexane (100 ml). They could be recrystallized from ethanol (10)–hexane (90), even in the presence of excess PCy_3 (2.8 g, 0.01 M) (yield: 5.6 g, 79%).

With $P(OPh)_3$: The addition of $P(OPh)_3$ (3.1 g, 0.010 M) to $PtCl_2L$ (2.1 g, 0.0049 M) in benzene gave a homogeneous solution, from which white crystals of the empirical formula of $Pt_2Cl_4L(P(OPh)_3)_3$ were isolated (yield: 3.0 g, 85%). (Found: C, 39.1; H, 4.4; N, 2.6%, $C_{64}H_{61}N_2O_9P_3Cl_4Pt_2$ requires: C, 38.3; H, 4.5; N, 2.5% which corresponds to a 1: 1 mixture of *cis*-$PtCl_2LP(OPh)_3$ and *cis*-$PtCl_2(P(OPh)_3)_2$).

With Pyridine: A chloroform solution of pyridine (1.8 g, 0.023 M) and $PtCl_2L$ (4.3 g, 0.010 M) was evacuated to give an oily residue. On the addition of ethanol to it, crystals of *cis*-$PtCl_2Lpy$ were formed (yield: 2.5 g, 49%). The *cis* configuration of the product was confirmed by Kurnakov's reaction.[11]

With CO: A benzene solution in which the $PtCl_2L$ complex had been dispersed was bubbled with CO gas. After about 10 min, a homogeneous yellow solution was obtained. The IR spectrum of this solution showed an absorption of a C–O stretching vibration at 2060 cm^{-1}. However, on crystallization, the original comples, $PtCl_2L$, was recovered.

Results and Discussion

The complexing ability of allylpyrazole has been investigated with Ni(II), Pd(II), and Pt(II) ions. As for Pd(II) and Pt(II), two types of complexes, MX_2L and MX_2L_2, have been obtained. The blue nickel complex has been prepared in the presence of a large excess of the ligand, but, unfortunately, its extreme sensitivity to moisture has prevented any accurate analysis or characterization.

Bis-allylpyrazole Complexes, MX_2L_2. The KBr disk or Nujol mull IR spectra of the complexes closely resemble those of the free ligands. Particularly, the C=C vibration of the allyl group found at 1660 or 1640 cm^{-1} does not differ from that of the free ligands (Table 3). This indicates that the olefinic part is free and that only the pyrazolyl nitrogen coordinates to the metal.

The *trans* configuration of PtX_2L_2 has been confirmed by Kurnakov's test. Attempts to isolate *cis*-PtX_2L_2 have been unsuccessful; probably the bulky nature of the ligands hinders the formation of the *cis*-isomer. In the case of palladium complexes, although it has not been

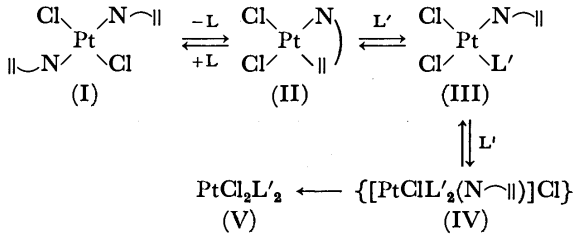

Fig. 2. Scheme.
N⌒|| =amtmp; III, L'=py, $AsPh_3$, PR_3 (R=Ph, Bu^n, Pr^i, Cy, OMe, OPh); IV ionic intermediate (not isolated); V, L'=$AsPh_3$; *trans*, PR_3; *cis* when R=Ph, OMe, OPh; *trans* when R=Bu^n, Pr^i.

definitely determined, the *trans* structure (Fig. 2-I) seems most likely in view of the following NMR results, similar to those for platinum complexes.

The NMR spectra of MX_2L_2 as a whole shift towards a lower magnetic field from the position of the free ligands, also indicating the apparent absence of the coordinated olefin; the coordinated olefin in metal complexes usually shows a remarkable shielding of olefinic protons.[9] Both 3-Me and allyl protons, except for H_β, have two sets of signals as is shown in Table 4. These signals can be assigned to two possible stereoisomers, *syn* and *anti*, which have been assumed in the NMR analysis of tetrazole complexes.[13] It is likely that the low symmetry of the ligand, together with its restricted rotation about M–N bonds, generates these rotational isomers.

Mono-allylpyrazole Complexes, MX_2L. The IR spectra of palladium complexes (Table 3) exhibit a sharp band at 1525 cm^{-1} for L=amdmp and at 1520 cm^{-1} for L=amtmp. No band was observed in the vicinity of 1660 cm^{-1}, the position of the C=C vibration for the free ligand. The above sharp band probably indicates the presence of a palladium-olefin bond (a lowering from the free ligand of $\Delta\nu$=135 or 140 cm^{-1}

Table 3. Vibration frequencies (in cm^{-1}) of the olefin part in MCl_2L_n

	Free ligand	$PdCl_2L_2$	$PdCl_2L$	*trans*-$PdCl_2L_2$	$PtCl_2L$
		L=admp			
$\nu_{CH_2=}$	3080 w	—	—	3075 m	3080 m
$\nu_{C=C}$ + δ_{C-H}	1640 m			1640 m	1500ms
δ_{C-H}	995 s	—	—	980 s	1000 s
ν_{M-C_2}	920 s			930 s	—
					515ms
		L=atmp			
$\nu_{CH_2=}$	3080 m	3080mw	—	3080mw	3075 w
$\nu_{C=C}$ + δ_{C-H}	1640 s	1640 m		1640 m	1500ms
$\nu_{C=C}$	1320 m	1320 s		1320vs	1290vs
		1005 s	—	1005 s	1005 s
δ_{C-H}	985vs				
ν_{M-C_2}		940 s		940vs	
					525ms
		L=amdmp			
$\nu_{CH_2=}$	3090mw	—	3075 w	—	3075 w
$\nu_{C=C}$ + δ_{C-H}	1660 s		1525 s		1500ms
$\nu_{C=C}$	1320 m		1295 s		1290 s
			1075 s		1080ms
			1040 s		1045 s
			1005 s		
		—		—	995 s
δ_{C-H}	980 w		980 s		
			965ms		970ms
			955sh		
			930ms		925ms
	900vs				
ν_{M-C_2}		—	480ms	—	505 s
		L=amtmp			
$\nu_{CH_2=}$	3070 m	3090 w	3075 m	3080 m	3080 m
$\nu_{C=C}$ + δ_{C-H}	1660ms	1660 m	1520 s	1660ms	1500ms
$\nu_{C=C}$	1320 s	1335 s	1320 s	1335 s	1300 s
			1255 s		1250 s
	1240 s	1240 m	1240 s	1245 s	1230 s
			1040ms		1040 s
			975 s		990br s
δ_{C-H}	900vs	900vs	875ms	900vs	870ms
ν_{M-C_2}			840ms		840ms
			490ms		510 s

TABLE 4. NMR DATA[a] IN $CDCl_3$ (relative to TMS τ 10 ppm)

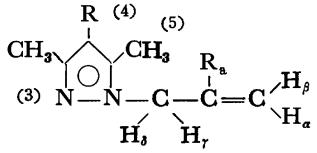

	3-Me	R_4 4-Me	4-H	5-Me	R_a a-Me	a-H	H_α	H_β	H_γ	H_δ
L=admp										
Free ligand	7.94		4.35	7.91		4.20	5.12	4.98	5.54	
$PtCl_2L_2$	7.31		4.11	7.73		3.61	4.83	4.71	4.45	
	7.24					3.70	4.77		4.53	
L=atmp										
Free ligand	8.00	8.28		8.08		4.19	5.15	4.97	5.53	
$PtCl_2L_2$	7.44	8.26		7.98		3.72	4.95	4.85	4.57	
	7.36					3.83	4.90		4.64	
$PdCl_2L_2$	7.27	8.13		7.86		3.60	4.78	4.69	4.45	
	7.20					3.68	4.74		4.54	
L=amdmp										
Free ligand	7.80		4.25	7.86	8.34		5.52	5.20	5.53	
$PtCl_2L$	7.46		4.01	7.66	7.99		6·54	5.46	6.38	5.58
	(4)		(14)	(—)	(40)		(65)	(60)	(50)	(14)
L=amtmp										
Free ligand	7.90	8.21		8.01	8.37		5.51	5.27	5.56	
$PtCl_2L_2$	7.32	8.10		7.80	8.13		5.42	5.00	4.52	
	7.26				8.18		5.36		4.58	
$PtBr_2L_2$	7.36	8.10		7.80	8.13		5.42	5.02	4.50	
	7.28				8.18		5.36		4.56	
$PdCl_2L_2$	7.26	8.12		7.88	8.06		6.32	4.95	4.52	
	7.16				8.16		5.25		4.60	
$PtCl_2L_2$	7.55	8.08		7.82	8.00		6.53	5.50	6.30	5.78
	(5)	(—)		(—)	(40)		(66)	(62)	(51)	(14)
$PtBr_2L$	7.55	8.08		7.70	8.09		6.49	5.50	6.35	5.57
	(5)	(—)		(—)	(44)		(64)	(63)	(54)	(15)
$PdCl_2L$	7.56	8.11		7.73	7.70		5.64	4.98	5.70	5.24

a) Coupling constants ($|J_{Pt-H}|$, Hz) in parentheses.

respectively). The sharp bands of medium intensity at 480 cm^{-1} (amdmp) and 490 cm^{-1} (amtmp) may be assigned to ν(Pd–C_2). These bands are present in the region thought to indicate Pd-olefin stretching, as has been found for $PdCl_2$[tri(2-butenyl)arsine][3] (425 cm^{-1}) and $Pd_2Cl_4(C_2H_4)_2$ (427 cm^{-1}). The ^1H NMR spectrum of $PdCl_2L$ (L=amtmp) in $CDCl_3$ shows that the H_γ- and H_δ-protons differ in their chemical shifts ($|J_{H_\gamma-H_\delta}|=16$ Hz), while in the free ligand in $PdCl_2L_2$, the two protons are equivalent (Table 4). This inequality in the chemical shifts suggests that the olefinic group coordinates to palladium.

The platinum(II) complexes, PtX_2L, are generally more soluble than $PdCl_2L$ and can be well characterized by ^1H NMR (Table 4). All the protons of the allyl group in PtX_2L, except for a-Me, are shifted towards higher fields. Changes in the chemical shifts similar to that of the above spectra have been reported for pnicogen-olefin chelate complexes by several workers.[9,14,15] Since a rapid, bonded⇌non-bonded equilibrium of the Pt-olefin bond shows a rather small spin coupling ($|J_{Pt-H_\alpha}|=23$ Hz),[16] the large coupling constants ($|J_{Pt-H}|=60$ Hz) on the present complexes indicate that the allyl group is not liberated from platinum. The IR spectra of platinum complexes also show a characteristic band (*ca.* 1500 cm^{-1}) of the coordinated olefin ($\Delta\nu=140$—160 cm^{-1}). The band in the range of 500—530 cm^{-1} in the PtX_2L series may be assigned to ν(Pt–C_2).

The above IR and NMR results of MX_2L support Fig. 2-II as a possible structure. The molecular weight of $PtCl_2$(amtmp) confirms that the structure of the complex is not that of a chlorine-bridged dimer with monodentate amtmp. The measurement of powder X-ray diagrams has revealed isomorphism in both the palladium and platinum complexes; this also indirectly supports the idea that both Pd(II) and Pt(II) complexes have the same structure (Fig. 2-II).

The observation that the chemical shifts of the allyl protons of MCl_2L, where M=Pd or Pt and L=amtmp, move downfield when platinum is replaced by palladium is consistent with the lower olefin-metal interaction present in the palladium complex, such as in MX_2-(diolefin)[17] and olefinic tertiary phosphine complexes.[9]

Substitution Reaction of $PtCl_2L$ with Donor Molecules. The reaction scheme is outlined in Fig. 2. Only the 1-(2-methylallyl)-3,4,5-trimethylpyrazole complex, $PtCl_2L$, was investigated in detail.

In the reaction of an equivalent donor ligand with $PtCl_2L$ in benzene at room temperature, stable com-

Table 5. Analytical data and properties of the isolated new complexes (L=amtmp)

	Color	Mp (°C)[a]	% Found (Calcd) C	H	N
cis-$PtCl_2LPPh_3$[b]	white	208 (dec.)	49.2 (48.6)	4.0 (4.5)	4.1 (4.1)
cis-$PtCl_2LPBu^n_3$[b]	white	128	40.8 (41.8)	6.1 (6.9)	4.1 (4.4)
cis-$PtCl_2LPr^i_3$[b]	white	177	39.0 (38.7)	6.2 (6.3)	5.0 (4.7)
cis-$PtCl_2LPCy_3$[b]	white	217 (dec.)	47.3 (47.3)	6.7 (7.0)	3.8 (3.9)
cis-$PtCl_2LPy$	light-yellow	135	35.4 (35.4)	3.9 (4.2)	8.1 (8.3)
cis-$PtCl_2LAsPh_3$	light-yellow	174	46.0 (45.7)	4.1 (4.2)	3.6 (3.8)

a) All melting points were uncorrected. b) *cis*-Configuration of the complexes is judged from their color.

plexes with the empirical formula of $PtCl_2LL'$ (L'=PR_3, $AsPh_3$ or py) have been isolated and characterized (Table 5). All the new complexes, which are easily soluble in benzene, have a sharp IR absorption at *ca.* 1660 cm^{-1}, indicating the existence of free olefin.

In our system, "mixed" complexes of the *cis*-configuration have been specifically obtained, maintaining the *cis*-configuration of the original chelate complex, whereas the bridge-splitting reaction of Chatt and Venanzi[18] has usually been used in the laboratory to prepare mixed complexes with a *trans*-configuration. This selectivity of the *cis*-configuration can be explained by the relatively higher lability of olefin and the *cis*-directing power of the pyrazolyl nitrogen to the incoming ligand.

With one more equivalent donor (L'=PPh_3, PBu^n_3, PPr^i_3 or $AsPh_3$), the mixed complex, $PtCl_2LL'$, reacted to give a complex of the $PtCl_2L'_2$ type, displacing an equivalent allylpyrazole. The configurations of the isolated complexes depended upon the entering ligand; that is, a configuration favorable to each ligand was observed: *cis* to PPh_3, *trans* to PBu^n_3, PPr^i_3 and $AsPh_3$. These results can be interpreted by means of the consecutive displacement mechanism[19-21] *via* an ionic intermediate, as is shown in Fig. 2.

The equilibrium for the formation of $PtCl_2LL'$ lies too far to the left to permit the isolation of the complexes when L'=CO or $PhNH_2$, and, for steric reasons,[22,23] excess PCy_3 does not displace L from *cis*-$PtCl_2L(PCy_3)$.

When phosphite is used as a donor ligand, a mixture of *cis*-$PtCl_2LP(OR)_3$ and *cis*-$PtCl_2(P(OR)_3)_2$ is obtained. This is attributable to the analogous solubilities of the two compounds.

References

1) Part I: K. Fukushima, T. Miyamoto, and Y. Sasaki, *Inorg. Chim. Acta*, **15**, 105 (1975).
2) R. S. Nyholm, *Rev. Pure Appl. Chem.*, **27**, 127 (1970).
3) C. A. McAuliffe and D. G. Watson, *J. Chem. Soc., Dalton*, **1974**, 1531.
4) R. E. Yingst and B. E. Douglas, *Inorg. Chem.*, **3**, 1177 (1964).
5) R. G. Dening and L. M. Venanzi, *J. Chem. Soc.*, **1963**, 3241.
6) M. A. Bennett, W. R. Kneen, and R. S. Nyholm, *Inorg. Chem.*, **7**, 556 (1968).
7) J. C. Chottard, E. Mulliez, J. P. Girault, and D. Mansuy, *Chem. Commun.*, **1974**, 780.
8) M. K. Cooper and D. W. Yaniuk, *J. Organometal. Chem.*, **74**, C 11 (1974).
9) P. E. Garrou and G. E. Hartwell, *ibid.*, **71**, 443 (1974).
10) L. L. Finar and K. Utting, *J. Chem. Soc.*, **1960**, 5272.
11) N. S. Kurnakov, *J. Russ. Phys. Chem. Soc.*, **25**, 565 (1893).
12) D. Drew and J. R. Doyle, *Inorg. Syn.*, XIII, 52 (1972).
13) D. A. Redfield, J. H. Nelson, R. A. Henry, D. W. Moor, and H. B. Jonassen, *J. Amer. Chem. Soc.*, **96**, 6298 (1974).
14) J. L. S. Curtis and G. E. Hartwell, *J. Chem. Soc. Dalton*, **1974**, 1808.
15) M. A. Bennett, R. N. Johnson, and I. B. Tomkins, *Inorg. Chem.*, **13**, 346 (1974).
16) D. I. Hall and R. S. Nyholm, *Chem. Commun.*, **1970**, 488. *Idem*, *J. Chem. Soc., A*, **1971**, 1491.
17) F. R. Hartley, "The Chemistry of Platinum and Palladium," Applied Science Publishers, (1973), pp. 367—372.
18) J. Chatt and L. M. Venanzi, *J. Chem. Soc.*, **1955**, 3858.
19) D. G. Cooper and J. Powell, *J. Amer. Chem. Soc.*, **95**, 1102 (1973).
20) D. G. Cooper and J. Powell, *Can. J. Chem.*, **51**, 1634 (1973).
21) J. Powell and D. G. Cooper, *Chem. Commun.*, **1974**, 749
22) C. A. Rolman, *J. Amer. Chem. Soc.*, **92**, 2956 (1970).
23) C. A. Tolman, W. C. Seidel, and L. W. Gosser, *ibid.*, **96**, 53 (1974).

N-Allylprazole as a Ligand. III.* The Crystal and Molecular Structure of (1-Allyl-3,5-dimethylpyrazole)-copper(I) Chloride

Kazuo FUKUSHIMA, Akiko KOBAYASHI, Takeshi MIYAMOTO, and Yukiyoshi SASAKI
Department of Chemistry, Faculty of Science, The University of Tokyo, Hongo, Tokyo 113
(Received July 31, 1975)

The crystal structure of (1-allyl-3,5-dimethylpyrazole)copper(I) chloride, $CuCl(C_8H_{12}N_2)$, has been determined by the three-dimensional X-ray analysis. The crystal is triclinic, space group $P\bar{1}$; $a=8.442(4)$, $b=8.873(6)$, $c=8.112(3)$ Å, $\alpha=103.44(3)$, $\beta=116.42(3)$, $\gamma=63.37(3)°$ and $Z=2$. The structure was refined to an R value of 0.056 for 1196 collected reflections. The complex has a dimeric structure in which the copper(I) ion is surrounded quasi-tetrahedrally by two bridging chlorines, a pyrazole-nitrogen and the olefinic part of the allyl group. The C=C bond distance (1.34 Å) scarcely shows any increase upon coordination to the metal. The olefin plane is almost perpendicular to the Cu-olefin bond axis and shows no significant bendings of the olefinic atoms out of the plane.

We have reported that *N*-allylpyrazole forms complexes with transition metals and in certain metal complexes (M=Cu(I), Ag(I)[1], Pd(II) and Pt(II)[2]) the coordination of the olefin site of the allyl group was indicated. In the Cu(I) and Ag(I) complexes, the coordination of the allyl site was evidenced by the decrease of the C=C vibration frequencies in the solid state. It is well known that Cu(I) ion easily forms complexes with olefins and together with Ag(I) presents the extreme of the transition metal-olefin compounds, in which the σ-donation of the olefinic electrons to the metal might be predominant. Up to present, however, the crystal structures of only a few Cu(I)-olefin complexes have been determined by the X-ray analysis and sufficient structural data are uavailable for the discussion. We now report the crystal structure of CuCl(admp (admp=1-allyl-3,5-dimethylpyrazole), one of the chelate olefin complex of Cu(I).

Experimental

The crystals of CuCl(admp) were grown from an ethanol solution as described in Ref. 1. They were stable in air. Oscillation and Weissenberg photographs were taken to determine the cell dimensions and the space group of the crystals, using the Cu$K\alpha$ radiation ($\lambda=1.5418$ Å).

Crystal data: $CuClC_8H_{12}N_2$, MW=235.1; triclinic, $a=8.442(4)$, $b=8.873(6)$, $c=8.112$ (3) Å, $\alpha=103.44(3)°$, $\beta=116.42(3)°$, $\gamma=63.37(3)°$, $V=486.1$ Å^3; $Z=2$, $D_m=1.67$ g cm^{-3}, $D_x=1.61$ g cm^{-3}; $\mu=0.47$ cm^{-1}; space group $P\bar{1}$.

The intensities of the reflections were measured on a Rigaku automated four-circle diffractometer. The dimensions of the specimen used for the data collection were about $0.1\times0.3\times0.5$ mm. The ω-2θ scan technique was employed. The scan speed was 2°/min in 2θ. The background counts of ten seconds duration were taken at both limits of the scan. The Mo$K\alpha$ radiation ($\lambda=0.71068$ Å) monochromated by a graphite crystal was used. Three standard reflections were measured during the data collection to check any deterioration of the crystal. Independent 1196 reflections ($|F_o|\geq3\sigma(|F_o|)$) were collected up to $2\theta=50°$.

The structure was solved by the conventional heavy atom method. Copper and chlorine atoms were found on a three dimensional Patterson map. All the carbon and nitrogen atoms were located from the successive Fourier and difference syntheses. The parameters of these atoms were refined by a block-diagonal least-squares method to $R=0.091$ with the isotropic temperature factors and to a $R=0.064$ with anisotropic ones. The calculated hydrogen positions were affirmed by the difference syntheses including six methyl hydrogens. Their parameters were refined using isotropic temperature factors. The final R value was 0.056. Atomic scattering factors were taken from International Tables for X-ray Crystallography.[3] Calculations were performed by a HITAC 8800/8700 computer at the Computer Centre of this University, using a local version of the Universal Crystallographic Computation Program System, UNICS.[4]

Description of the Structure

The final atomic parameters are listed in Table 1. The molecular and crystal structures of CuCl(admp) are shown in Figs. 1 and 2. The interatomic distances and bond angles within a molecule are listed in Tables 2 and 3. No unusual intermolecular proximity in the adjacent units is observed.

The complex has a centrosymmetric dimeric structure in which each copper atom is surrounded quasi-tetrahedrally by two bridging chlorines, a nitrogen and an olefinic part of the allyl group (Fig. 1). The olefinic carbons C7 and C8 are 2.13(1) Å and 2.15(1) Å apart

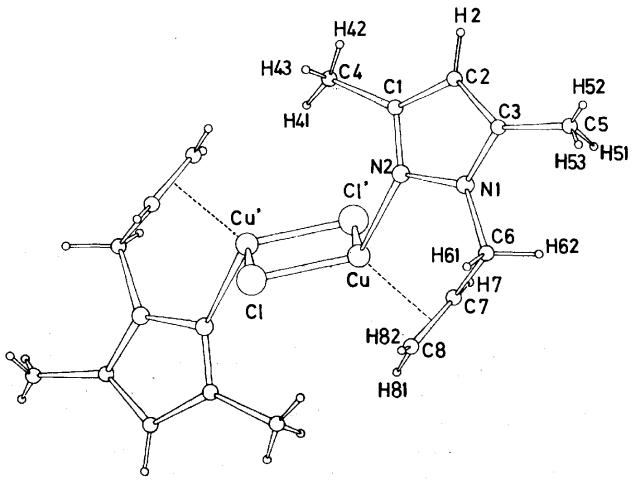

Fig. 1. The molecular structure of CuCl (admp).

* Part II, see Ref. 2.

Table 1(a). Final and temperature parameters for nonhydrogen atoms with their standard deviations in parentheses ($\times 10^4$)

Atom	x	y	z	B_{11}[a)]	B_{22}	B_{33}	B_{12}	B_{13}	B_{23}
Cu	−829(2)	260(2)	1504(2)	217(3)	162(3)	179(3)	−100(2)	77(2)	10(2)
Cl	1673(4)	781(4)	1828(4)	187(6)	191(5)	145(5)	−106(5)	51(5)	−11(4)
N1	−2013(11)	−1432(10)	3011(10)	149(19)	132(15)	125(17)	−60(14)	49(15)	5(12)
N2	−514(12)	−1779(10)	2570(11)	168(20)	145(16)	139(18)	−71(15)	66(15)	−2(13)
C1	364(14)	−3458(12)	2500(13)	154(23)	123(18)	114(20)	−28(16)	32(17)	14(14)
C2	−566(14)	−4188(13)	2915(13)	176(25)	148(20)	119(20)	−58(18)	30(18)	13(15)
C3	−2103(14)	−2863(12)	3216(12)	173(23)	138(18)	102(19)	−78(17)	24(17)	19(14)
C4	2140(17)	−4301(15)	2053(18)	222(30)	191(25)	283(33)	−49(22)	144(27)	4(22)
C5	−3634(16)	−2848(15)	3712(16)	206(27)	198(23)	219(27)	−107(21)	92(22)	16(19)
C6	−3209(15)	358(13)	3276(14)	190(25)	118(18)	185(24)	−49(17)	91(20)	1(16)
C7	−3514(16)	1362(13)	1786(16)	199(27)	120(19)	227(27)	−48(19)	101(23)	−2(17)
C8	−2869(16)	2583(13)	2167(16)	235(28)	116(18)	253(28)	−55(19)	140(24)	−13(18)

a) The form of the anisotropic temperature parameters is $\exp[-(B_{11}h^2+B_{22}k^2+B_{33}l^2+2B_{12}hk+2B_{13}hl+2B_{23}kl)]$.

Table 1(b). Final positional and temperature parameters for hydrogen atoms

Atom	$x\times 10^3$	$y\times 10^3$	$z\times 10^3$	B(A^2)	Atom	$x\times 10^3$	$y\times 10^3$	$z\times 10^3$	B(A^2)
H41	213(18)	−367(16)	146(17)	7.0(35)	H53	−365(15)	−234(13)	466(14)	4.5(27)
H42	208(19)	−525(16)	149(18)	8.0(38)	H61	−244(19)	72(17)	431(18)	8.0(38)
H43	333(18)	−451(15)	323(17)	6.9(35)	H62	−452(13)	40(11)	318(12)	2.8(22)
H2	−20(13)	−537(11)	288(12)	2.5(20)	H7	−425(14)	125(12)	82(13)	3.4(23)
H51	−476(14)	−233(12)	292(13)	3.6(24)	H81	−317(16)	322(14)	124(15)	5.2(29)
H52	−332(14)	−403(12)	386(14)	4.0(25)	H82	−216(14)	275(12)	343(13)	3.3(23)

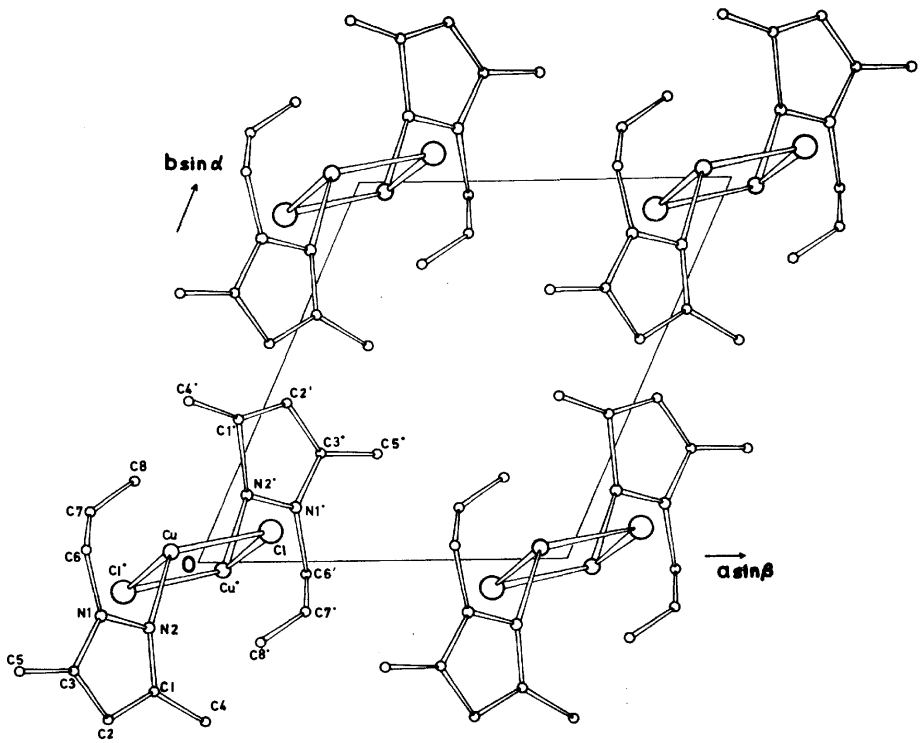

Fig. 2. The crystal structure of CuCl(admp) projected along the c-axis.

from Cu respectively. The distance between Cu and M, the middle point of C7–C8, is 2.03 Å, which indicates an evident bonding of Cu and olefin (Fig. 3). The dihedral angle between the two planes Cl–Cu–Cl′ and N2–Cu–M is 105.2°, and deviates to some extent from the theoretical 90° of a regular tetrahedron. Chlorine is bonded unequivalently to two copper atoms, 2.525(3) Å apart from one copper and 2.252(4) Å apart from the other. The pyrazole ring and two methyl carbons C4 and C5 make a perfect plane, from which the vectors Cu–N2 and C6–N1 are bent 15.8° and 2.9° respectively to the opposite directions of the plane.

The bond length of the coordinated C=C double bond is 1.34(2) Å. The vector Cu–M is perpendicular

Table 2. Interatomic distances (Å) with their standard deviations in the parentheses

Cu–Cu′	3.172(3)	C2–H2	0.95(10)
Cu–Cl	2.252(4)	C4–H41	0.82(18)
Cu–Cl′	2.525(3)	C4–H42	0.89(14)
Cu–N2	2.045(11)	C4–H43	1.00(14)
Cu–C7	2.126(13)	C5–H51	0.85(8)
Cu–C8	2.151(11)	C5–H52	0.98(12)
N1–N2	1.351(15)	C5–H53	0.81(11)
N2–C1	1.334(12)	C6–H61	0.92(13)
C1–C4	1.513(18)	C6–H62	1.05(13)
C1–C2	1.393(24)	C7–H7	0.77(8)
C2–C3	1.380(16)	C8–H81	0.92(14)
C3–C5	1.509(23)	C8–H82	0.95(9)
C3–N1	1.357(19)		
N1–C6	1.478(11)		
C6–C7	1.529(20)		
C7–C8	1.338(20)		

Table 3. Bond angle (degree)

Cl–Cu–Cl′	97.01(14)	C1–C4–H41	109(11)
Cu–Cl–Cu′	82.99(11)	C1–C4–H42	104(10)
N2–Cu–Cl	123.35(32)	C1–C4–H43	109(8)
N2–Cu–Cl′	98.29(31)	H41–C4–H42	116(15)
N2–N1–C6	118.0(10)	H41–C4–H43	108(14)
N2–N1–C3	111.6(9)	H42–C4–H43	111(13)
C3–N1–C6	130.4(11)	C1–C2–H2	123(6)
Cu–N2–N1	111.5(6)	C3–C2–H2	131(6)
Cu–N2–C1	139.0(9)	C3–C5–H51	111(8)
N1–N2–C1	105.9(10)	C3–C5–H52	107(7)
N2–C1–C4	120.3(12)	C3–C5–H53	113(9)
N2–C1–C2	110.4(12)	H51–C5–H52	115(11)
C2–C1–C4	129.2(11)	H51–C5–H53	104(12)
C1–C2–C3	105.9(12)	H52–C5–H53	108(11)
C2–C3–C5	130.9(14)	N1–C6–H61	105(10)
C2–C3–N1	106.2(13)	N1–C6–H62	107(6)
C5–C3–N1	122.9(11)	C7–C6–H61	103(10)
N1–C6–C7	108.4(10)	C7–C6–H62	112(6)
C6–C7–C8	122.9(11)	H61–C6–H62	121(12)
		C6–C7–H7	115(9)
		C8–C7–H7	121(9)
		C7–C8–H81	120(8)
		C7–C8–H82	115(7)
		H81–C8–H82	125(11)

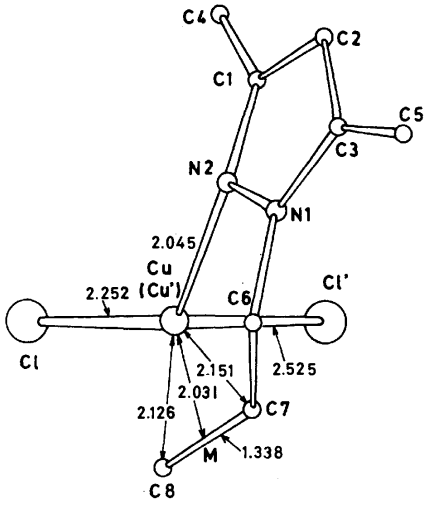

Fig. 3. The structure of the coordination sphere projected along the Cu–Cu′ axis.

to the C7–C8 bond (88.9(15)°). The deviations of the olefinic atoms from their least-squares plane are less than 0.1 Å and any distinctive features such as a bending out of the plane are not observed. The angle between this plane and Cu–M axis is 87.8°.

Discussion

Preceding studies by Bennett and co-workers have revealed that phosphine-olefin and arsine-olefin type of ligands successfully form stable olefin complexes with a number of transition metals,[5] making much use of the coordination ability of the donor atom. Among them, the structures of Mo(0),[6] Fe(0),[7] Ag(I)[8] and Rh(I)[9,10] complexes have been determined by the single crystal X-ray analysis, whereby a bridging bidentate in the Ag(I) complex and chelating bi- or quadridentate coordination in other complexes were known. Our nitrogen-olefin type ligand, admp, shows an analogous ability of the complex-formation with several transition metals to these chelate olefin type ligands.

As for Cu(I), several N-olefin,[11] P-olefin and As-olefin[12] complexes are known. They were assumed to contain a chelating bidentate coordination but none of them has been devoted to the X-ray analysis. With respect to the simple olefin complexes, up to now, the crystal structures of only three Cu(II)-olefin complexes have been determined by the X-ray analysis. The tetrahedral coordination form is found in CuCl(1,5-cyclooctadiene) dimer,[13] in which Cu is surrounded quasi-tetrahedrally by two bridging chlorines and two C=C moieties. Another coordination form is found in CuCl(1,3,5,7-cyclooctatetraene)[14] and CuCl (2,5-norbornadiene),[15] where two chlorines and one C=C make a trigonal plane around the central copper. The molecular structure of our admp complex, a dimeric tetrahedral coordination, is very analogous to that of the cyclooctadiene complex.

The most remarkable characteristic of the metal-olefin bond present in Cu(I)-admp is that the bond length of the coordinated C=C (1.34(2) Å) is scarcely increased compared with those of the free olefins (1.33—1.35 Å) and the C=C sp^2 plane scarcely shows a distortion upon coordination to Cu. In many metal-olefin complexes, a significant increase of the C=C distance upon complex formation is observed and hence regarded as the most important structural evidence to be explained in the metal-olefin bond nature. For instance, in above cited Fe(0) complex,[7] the bond length of the coordinated C=C is 1.45(2) Å, while that of the uncoordinated C=C is 1.33(2) Å. In Ag(I)[8] and Mo[6] complexes, the coordinated C=C shows a length of 1.41(6) Å and 1.39(2) Å respectively. This indicates that in Cu(I)-admp the metal-olefin interaction may be very weak.

It is known that Cu(I) and Ag(I) are able to form complexes with olefins which mainly consist of the σ-donation of the olefinic electrons to the metal. The IR spectra of Cu(I)- and Ag(I)-admp show the lowering shifts of the ν(C=C) band in the solid states but in solutions, free ν(C=C) and little change of

^{1}H-NMR of the olefinic protons are observed, which may be due to the liberation of the metal-olefin bond. Similar trends of the ^{1}H-NMR were noticed in the P-olefin and As-olefin type complexes of these metals. Such a lability in the Cu(I)-olefin and Ag(I)-olefin bonds is frequently observed.[16,17] It also indicates a weak metal-olefin interaction in these olefin complexes.

The weak metal-olefin interaction of CuCl(admp) is very likely but there remains some curiosity behind. The former X-ray studies on the crystal structures of Cu(I)- and Ag(I)-olefin compounds have reported the small but significant increases of the coordinated C=C bond distances.[18] Hence the metal-olefin interaction in CuCl(admp) should be considered to be particularly weak, although the stretching frequency, ν(C=C), is lowered by 103 cm^{-1}, which is much larger than those of Ag(I)-olefin (50—75 cm^{-1}) and is one of the largest value among the Cu(I)-olefin complexes (80—100 cm^{-1}).[11,12,19] Since the data are too limited and some are old, more investigations of many Cu(I)-olefin complexes will be required, in order to find the reason of this contradiction.

References

1) K. Fukushima, T. Miyamoto, and Y. Sasaki, *Inorg. Chim. Acta*, **15**, 105 (1975).
2) T. Miyamoto, K. Fukushima, T. Saito, and Y. Sasaki, This Bulletin, **49**, 138 (1976).
3) "International Tables for X-Ray Crystallography," Vol. III, Kynoch Press, Birmingham (1962).
4) "The Universal Crystallographic Computation Program System," The Crystallographic Society of Japan (1967).
5) R. S. Nyholm, *Rev. Pure Appl. Chem.*, **27**, 127 (1971).
6) H. Luth, M. R. Truter, and A. Robson, *J. Chem. Soc. A*, **1969**, 28.
7) M. A. Bennett, G. B. Robertson, I. B. Tomkins, and P. O. Whimp, *Chem. Commun.*, **1971**, 341.
8) M. K. Cooper and R. S. Nyholm, *ibid.*, **1974**, 343.
9) M. O. Visscher, J. C. Huffman, and W. E. Streib, *Inorg. Chem.*, **13**, 792 (1974).
10) C. Nave and M. R. Truter, *Chem. Commun.*, **1971**, 1253.
11) R. E. Yingst and B. E. Douglas, *Inorg. Chem.*, **3**, 1177 (1964).
12) M. A. Bennett, W. R. Kneen, and R. S. Nyholm, *ibid.*, **7**, 552 (1968).
13) J. H. van den Hende and W. C. Baird, *J. Amer. Chem. Soc.*, **85**, 1009 (1963).
14) N. C. Baenziger, G. F. Richards, and J. R. Doyle, *Inorg. Chem.*, **3**, 1529 (1964).
15) N. C. Baenziger, H. L. Haight, and J. R. Doyle, *ibid.*, **3**, 1535 (1964).
16) R. G. Salomon and J. K. Kochi, *J. Organometal. Chem.*, **43**, C7 (1972).
17) J. Solodar and J. P. Petrovich, *Inorg. Chem.*, **10**, 395 (1971).
18) H. W. Quinn and J. H. Tsai, *Advan. Inorg. Radiochem.*, **12**, 217 (1969), and references cited therein.
19) G. N. Schrauzer and S. Eichler, *Chem. Ber.*, **95**, 260 (1962).

The Preparation, Infrared Spectra, and Thermal Stability in the Solid State of Nickel(II) Complexes with edda-type Polyamino Carboxylic Acids

Ichiro HIRAKO, Tasuku MURAKAMI, and Masahiro HATANO

Chemical Research Institute of Non-Aqueous Solutions, Tohoku University, 2-1-1 Katahira, Sendai 980

(Received September 9, 1975)

Some nickel(II) complexes with optically active ethylenediamine-*N,N'*-diacetic acid(edda)-type polyamino carboxylic acids were prepared. Their electronic and infrared spectra and thermogravimetric curves were measured in the solid state. The stretching frequencies of the coordinated carboxylate group and the thermal stability of these complexes in the solid state were quite different from those of bis(amino acidato) complexes.

On the structures and thermal stabilities in the solid state of diaquabis(amino acidato)nickel(II) complexes, extensive works have been reported. The crystal structure of diaquabis(glycinato)nickel(II) is a slightly distorted octahedral, with two glycinate anions of a *trans(N,N)*-configuration in a plane, and with two water molecules occupying its apical positions.[1,2] The diaquabis(amino acidato) complexes are easily dehydrated on heating to form their anhydrous complexes, which are polymeric with bridging through the non-donating oxygen atom in the carboxylate group.[3,4]

On the other hand, not so much has been reported concerning the nickel(II) complexes with edda-type polyamino carboxylic acids, which are expected to form complexes with a *cis(N,N)*-configuration in a plane. In order to obtain information on the differences in structures and thermal stabilities between the edda-type complexes and the bis(amino acidato) complexes, we have now prepared new edda-type complexes and measured their electronic and infrared(IR) spectra and thermogravimetric(TG) curves.

Experimental

Preparation of Ligands. Ethylenediamine-*N,N'*-di-L-α-propionic acid (abbreviated to H_2eddp), ethylenediamine-*N,N'*-di-L-α-isovaleric acid (H_2eddv), ethylenediamine-*N,N'*-di-L-α-hydrocinnamic acid (H_2eddc), ethylenediamine-*N,N'*-di-L-α-(β-hydroxy)propionic acid (H_2eddh), and (*S,S*)-1,1'-ethylenedipyrrolidine-2,2'-dicarboxylic acid (H_2epro) were prepared from L-alanine (L-alaH), L-valine (L-valH), L-phenylalanine (L-phalaH), L-serine (L-serH), and L-proline (L-proH) respectively by a method similar to that described in the literature.[5] These acids were identified by their elementary analyses. The ethylenediamine-*N,N'*-diacetic acid (H_2edda) was obtained commercially. The structural formulas of these polyamino carboxylic acids are shown in Fig. 1.

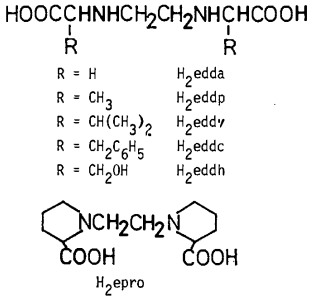

Fig. 1. edda-Type polyamino carboxylic acids. Except for H_2edda these acids are optically active.

Preparation of Nickel(II) Complexes. Hydrated Complexes: The hydrated nickel(II) complexes of these edda-type polyamino carboxylic acids were prepared by the following procedures. Basic nickel(II) carbonate was mixed with an equimolar amount of each polyamino carboxylic acid in an aqueous solution. The solution was concentrated at 70—80 °C on a water bath, and then allowed to stand. Within a few days, blue crystals separated out; they were recrystallized from water. The analytical data of these complexes are summarized in Table 1.

TABLE 1. ANALYTICAL DATA

Complex	C% Obsd (Calcd)	H% Obsd (Calcd)	N% Obsd (Calcd)
$[Ni(edda)(H_2O)_2]\cdot H_2O$	25.26 (25.06)	5.59 (5.57)	9.86 (9.76)
$[Ni(eddp)(H_2O)_2]$	32.41 (32.21)	6.61 (6.06)	9.41 (9.40)
[Ni(eddp)]	36.58 (36.52)	5.59 (5.33)	10.66 (10.63)
$[Ni(eddv)(H_2O)_2]$	42.19 (40.80)	7.55 (7.43)	7.87 (7.94)
[Ni(eddv)]	45.17 (45.40)	6.95 (6.64)	8.61 (8.84)
$[Ni(eddc)(H_2O)_2]\cdot H_2O$	50.80 (51.20)	5.69 (5.55)	6.08 (6.10)
[Ni(eddc)]	56.95 (57.82)	5.66 (5.35)	6.68 (6.67)
$[Ni(eddh)(H_2O)_2]$	29.14 (29.21)	5.47 (5.48)	9.01 (8.54)
$[Ni(epro)(H_2O)_2]$	41.00 (41.30)	5.92 (6.35)	8.10 (8.03)

Anhydrous Complexes: The anhydrous complexes of eddc and eddv were separated out from concentrated hot (70—80 °C) aqueous solutions. The anhydrous eddp complex was obtained on heating its hydrate *in vacuo* at 250 °C. See Table 1 for the results of analyses.

Bis(amino acidato) Complexes: Some bis(L-amino acidato)-nickel(II) complexes were prepared from basic nickel(II) carbonate and L-amino acids according to the method in the literature.[6] These bis(amino acidato) complexes were identified by means of their elementary analyses.

Measurements. The electronic and IR spectra were recorded with Hitachi EPS-3T and EPI-S_2 or EPI-G_2 spectrophotometers respectively, using KBr pellets. The TG curves were obtained with a Perkin-Elmer TGS-1 thermobalance at a heating rate of 8 °C/min in a nitrogen stream. All of the samples used for the TG measurements were ground

and sieved to obtain finely powdered fractions below 100 mesh.

Results and Discussion

The electronic spectra in the solid state of the hydrated nickel(II) complexes of edda, eddp, and eddc exhibited three absorption peaks, at about 10200, 13300 and 16200 cm^{-1}, which are characteristic of the octahedrally coordinated nickel(II) ion. Their anhydrous complexes also showed similar spectra, the peaks of which shifted to slightly lower wave numbers. This spectral profile of the edda-type complexes is identical with that of bis(amino acidato) nickel(II) complexes, suggesting that the anhydrous edda-type complexes are also polymeric, with bridging through the carboxylate groups, like the anhydrous bis(amino acidato) complexes.[4]

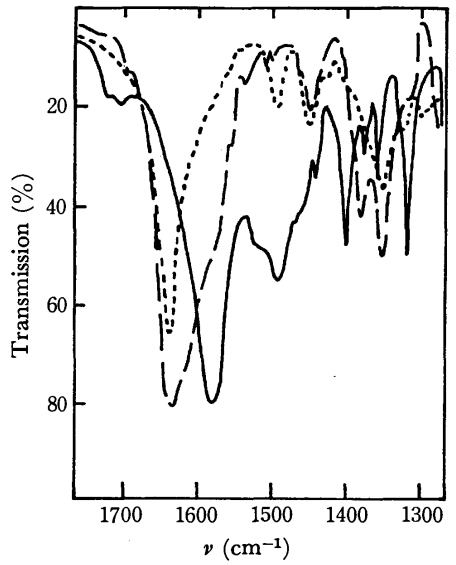

Fig. 2. IR spectra (1700—1300 cm^{-1}) of [Ni(eddp)-$(H_2O)_2$] (—), [Ni(eddp)](—), and [Ni(eddc)] (···).

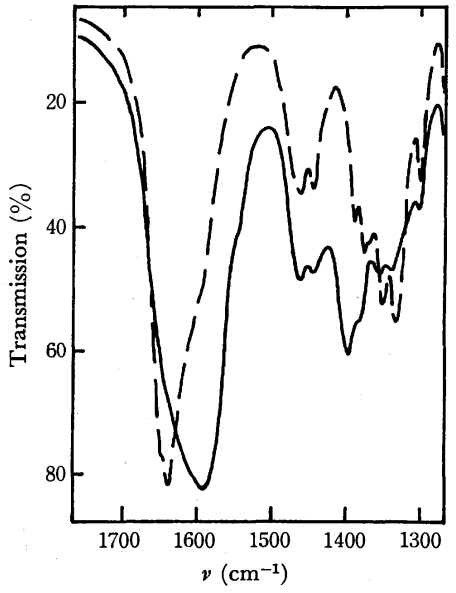

Fig. 3. IR spectra (1700—1300 cm^{-1}) of [Ni(eddv)-$(H_2O)_2$] (—) and [Ni(eddv)] (– –).

Figures 2 and 3 show the IR spectra of the complexes of eddp, eddv, and eddc in the region of 1300—1700 cm^{-1}. The strong band at 1590 cm^{-1} and the medium band at 1400 cm^{-1}, both of which appeared for the hydrated complex of eddp, can be assigned to the antisymmetric and symmetric stretching vibrations of the coordinated COO^- group respectively, as in the case of the bis(amino acidato) complexes.[4,6] When the hydrate was dehydrated on heating, the strong band shifted to 1640 cm^{-1}, with a shoulder at 1580 cm^{-1}. Similarly, the strong band at 1590 cm^{-1} which appeared for the hydrated complex of eddv shifted to 1640 cm^{-1} in its anhydrous complex. Further, the anhydrous eddc complex exhibited the strong band at 1640 cm^{-1}, Therefore, it can be concluded that the antisymmetric COO^- vibration appears at 1640 cm^{-1} for the anhydrous nickel(II) complexes of the edda-type polyamino carboxylic acids. Such a high frequency of the antisymmetric COO^- stretching vibration has also appeared for palladium(II) and platinum(II) complexes of amino acids.[7]

On the other hand, the medium band at 1400 cm^{-1} disappeared in the anhydrous complexes, as may be seen in the figures. Instead of this band, two medium bands appeared at 1380 and 1350 cm^{-1} for the anhydrous eddp complex. Either of these two bands can be expected to correspond to the symmetric COO^- vibration. The anhydrous eddv complexes also exhibited two bands at 1350 and 1330 cm^{-1}. For the anhydrous eddc complex, only one band appeared at 1350 cm^{-1} with a medium strength. From these findings, it seems plausible to assign the band at 1350 cm^{-1} to the symmetric COO^- stretching vibration of the anhydrous complexes.

TABLE 2. THE COO^- STRETCHING FREQUENCIES (cm^{-1})

Complex	ν_{asym}	ν_{sym}	$\Delta\nu$
$[Ni(edda)(H_2O)_2]\cdot H_2O$	1585	1393	192
[Ni(edda)]	1580	1395	185
	1640sh	1350sh	290
$[Ni(eddp)(H_2O)_2]$	1580	1400	180
[Ni(eddp)]	1640	1350	290
		(1380)	(260)
$[Ni(eddv)(H_2O)_2]$	1590	1400	190
[Ni(eddv)]	1640	1350	290
		(1330)	(310)
[Ni(eddc)]	1640	1350	290
$[Ni(eddh)(H_2O)_2]$	1600	1400	200
$[Ni(epro)(H_2O)_2]$	1595	1395	200
$[Ni(L\text{-}ser)_2(H_2O)_2]$	1600	1420	180
$[Ni(L\text{-}ser)_2]$	1580	1410	170
$[Ni(gly)_2(H_2O)_2]$[a]	1599	1410	189
$[Ni(gly)_2]$[a]	1583	1400	183

a) From Ref. 4.

Table 2 lists the symmetric (ν_{sym}) and antisymmetric (ν_{asym}) stretching frequencies of the coordinated COO^- group observed for the hydrated or anhydrous complexes of the edda-type polyamino carboxylic acids, together with those of the bis(L-serinato) and bis(glycinato) complexes. It is very interesting that the frequency separation ($\Delta\nu$) between

Table 3. Temperature range and mass loss

Complex	Dehydration		Decomposition	
	Temperature range, °C	Mass loss, % Obsd (Calcd)	Temperature range, °C	Mass loss, % Obsd(Calcd)[a]
$[Ni(edda)(H_2O)_2]\cdot H_2O$	70—140(H_2O) 140—180($2H_2O$)	16.6 (18.8)	310—460	55.6 (55.5)
$[Ni(eddp)(H_2O)_2]$	150—230	13.2 (12.2)	310—470	56.3 (62.6)
[Ni(eddv)]			310—440	77.0 (76.3)
$[Ni(eddc)(H_2O)_2]\cdot H_2O$	50—320	8.2 (11.5)	330—490	72.1 (72.7)
$[Ni(gly)_2(H_2O)_2]$	140—210	15.8 (14.8)	330—385	53.9 (54.5)
$[Ni(L\text{-}ala)_2(H_2O)_2]\cdot 2H_2O$	50—110($2H_2O$) 110—130($2H_2O$)	23.5 (23.2)	280—325	56.6 (52.5)
$[Ni(L\text{-}val)_2(H_2O)_2]$	50—150	11.7 (11.0)	275—340	70.2 (66.1)
$[Ni(L\text{-}phala)_2(H_2O)_2]$	80—140	8.4 (8.5)	280—410	71.8 (74.0)
$[Ni(L\text{-}ser)_2(H_2O)_2]$	90—180	14.1 (12.0)	230—375	57.4 (63.0)

a) For a residue of nickel oxide.

the antisymmetric and symmetric COO^- vibrations is much greater for the anhydrous edda-type complexes than for their hydrates, while in the bis(amino acidato) complexes the $\Delta\nu$ values of the hydrates are slightly greater than those of their anhydrous complexes.[4] It has been accepted by several authors[6,7] that, as the covalent character of the bond between the metal ion and the coordinated oxygen atom increases, the coordinated carboxylate group becomes more asymmetric, and that, as a result, the increase in the covalent character results in an increase in the frequency separation ($\Delta\nu$) between the two COO^- stretching bands. For example, large $\Delta\nu$ values(about 270 cm^{-1}) have been obtained for the bis(glycinato)palladium(II) and -platinum(II) complexes, in which the covalent character of the metal-oxygen bond is said to be very strong.[7] Therefore, the abnormal large values of $\Delta\nu$ observed for the anhydrous edda-type complexes suggest that the coordinated carboxylate group becomes more asymmetric on dehydration, in spite of the polymerization through the non-donating oxygen atom in the carboxylate group; we might conclude that the covalent character of the metal-oxygen bond in one complex molecule increases also.

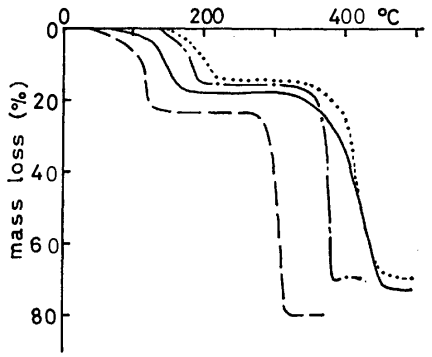

Fig. 4. TG curves of $[Ni(edda)(H_2O)_2]\cdot H_2O$ (—), $[Ni(eddp)(H_2O)_2]$ (···), $[Ni(gly)_2(H_2O)_2]$ (-·-), and $[Ni(L\text{-}ala)_2(H_2O)_2]\cdot 2H_2O$ (—).

Figure 4 shows the TG curves of the hydrated complexes of edda, eddp, glycine and L-alanine. The temperature range and the percentage of mass loss obtained from the TG curves are summarized in Table 3. As may be seen in Fig. 4, the hydrated complexes of edda and L-alanine released three or four moles of water in two steps in the temperature range from 50 to 180 °C. The step in the lower temperature range corresponds to the dehydration of lattice water(s), and the other step, to that of coordinated waters. However, the lattice water was dehydrated over a wider temperature range than the coordinated water. Though the hydrated eddc complex has three moles of water, the two steps corresponding to the dehydrations of lattice and coordinated waters were not distinguished.

The anhydrous edda-type complexes decomposed at a higher temperature than the anhydrous bis(amino acidato) complexes; further, the decomposition of the edda-type complexes was very slow, as may be seen in Fig. 4. These findings show that the edda-type anhydrous complexes are thermally more stable than the bis(amino acidato) complexes in the solid state. This high thermal stability of the edda-type complexes probably results from the increase in the covalent character in the intra-molecular metal-oxygen bond, as is to be expected from the behavior of the COO^- vibrations.

As may be seen in Table 3, bis(L-serinato)nickel(II), which has been established by X-ray analysis to have a *cis*(*N*,*N*)-configuration,[8] decomposed in a lower temperature range than did the edda-type complexes. Similarly, the bis(glycinato) complex, with a *trans*(*N*,*N*)-configuration, also decomposed in the lower temperature range. Further, the bis(L-serinato) complex shows a difference($\Delta\nu$) between the two COO^- vibrations similar to that of the bis(glycinato) complex (Table 2). These findings indicate that the *cis-trans* isomerism is not very significant for the thermal stability and the COO^- vibrations. Therefore, the high stability and the abnormal behavior in the COO^- vibrations observed for the edda-type complexes are expected to result from some structural factors, such as the tetradentate character of the ligands, other than the *cis-trans* isomerism.

The authors wish to thank Professor Takuji Kanno and Dr. Katsuo Itoh of this university for their permission to use the Perkin Elmer thermobalance.

References

1) A. J. Stosick, *J. Amer. Chem. Soc.*, **67**, 365 (1945).
2) H. C. Freeman, J. M. Guss, and R. L. Sinclair, *Chem. Commun.*, **1968**, 485.
3) S. E. Livingstone and J. D. Nolan, *Inorg. Chem.*, **7**, 1447 (1968).
4) C. A. McAuliffe and W. D. Perry, *J. Chem. Soc., A*, **1969**, 634.
5) L. N. Schoenberg, D. W. Cooke, and C. F. Liu, *Inorg. Chem.*, **7**, 2386 (1968).
6) K. Nakamoto, Y. Morimoto, and A. E. Martell, *J. Amer. Chem. Soc.*, **83**, 4523 (1961), and references therein.
7) K. Nakamoto "Spectroscopy and Structure of Metal Chelate Compounds," ed. K. Nakamoto and P. J. McCarthy, John Wiley and Sons, New York (1968), p. 268.
8) D. V. Helm and M. B. Hossain, *Acta Crystallogr.*, **B25**, 457 (1968).

The X-Ray Structure of the $(+)_{589}$-*cis*(O)*trans*(N_α)*cis*(N_δ)-Bis(L-ornithinato)cobalt(III) Complex

Yasuji NAKAYAMA, Shun'ichiro OOI, and Hisao KUROYA

Department of Chemistry, Faculty of Science, Osaka City University, Sumiyoshi-ku, Osaka 558

(Received September 16, 1975)

$(+)_{589}$-Bis(L-ornithinato)cobalt(III) nitrate monohydrate was isolated by ion-exchange chromatography from a reaction mixture of trinitratotriamminecobalt(III) with L-ornithine at pH 9, and was assigned to the *cis*-(O)*trans*(N_α)*cis*(N_δ) isomer on the basis of the absorption and circular dichroism spectra. Then, the geometry of the complex was confirmed by X-ray structure analysis. The red crystal is orthorhombic, with these cell dimensions: $a=14.380$, $b=16.493$, and $c=6.787$ Å. The space group is $P2_12_12_1$, and $Z=4$. The crystal structure was solved by the Patterson and Fourier techniques and was refined by the least-squares method to R 0.099. The Co atom is surrounded by 2 O and 4 N atoms, the former being in *cis* positions. Each of the L-ornithinato ligands assumes the facial coordination, and the complex cation has an approximate two-fold axis by which the ligand are correlated.

The ornithinate ion, H_2N_δ–$(H_2C)_3$–$HC(H_2N_\alpha)$–COO^-, has three donor atoms ($O_{(carboxyl)}$, N_α, N_δ) and is capable of coordinating facially to a metal ion with octahedral stereochemistry,[1] while it acts as a bidentate ligand for the metal ion amenable to a square-planar or an elongated octahedral coordination.[2,3] We have prepared the bis(L-ornithinato)-cobalt(III) complex, $[Co(L\text{-}C_5H_{11}N_2O_2)_2]NO_3\cdot H_2O$, by the reaction of trinitratotriamminecobalt(III) with L-ornithine at pH 9. The complex cation may exist in three geometrical isomers, as is shown in Fig. 1. Actually,

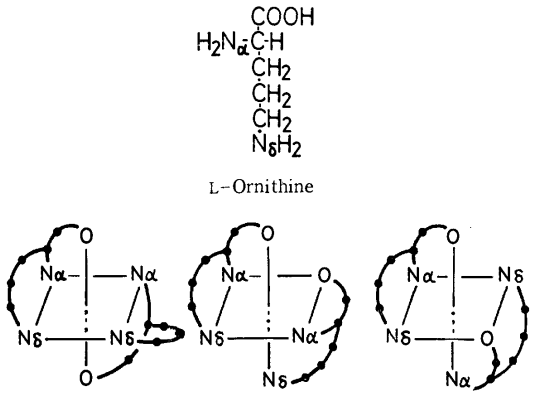

Fig. 1. Possible geometrical isomers of bis(L-ornithinato)-cobalt(III) ion.

the three bands could be separated from the reaction mixture by means of a cation-exchange column. The compound obtained from the most predominant band was inferred to be the *cis*(O)*trans*(N_α)*cis*(N_δ) isomer from its absorption and circular dichroism spectra. In order to confirm the geometry of the complex and in order to examine the conformational details of the chelate rings, the single crystal X-ray structure analysis was performed.

Experimental

Preparation of the Complex. From 1.5 g (0.009 mol) of L-ornithine hydrochloride and 1.5 g (0.009 mol) of silver nitrate, L-ornithine hydrogen nitrate was prepared as an aqueous solution of 40 ml, in which 1.3 g (0.0045 mol) of trinitratotriamminecobalt(III) was suspended. Then, 0.7 g (0.018 mol) of sodium hydroxide in 15 ml of water was added, and the solution was stirred at 50 °C for 5 h in the presence of activated charcoal. After the filtration of the charcoal and dilution to 100 ml, the reaction mixture was sorbed on the cation-exchange column (100—200 mesh Dowex 50W-X8 in the ammonium form). Three main bands developed upon elution with a 0.1 M NH_4NO_3 solution; the fastest band is red-violet in color, while the other two are red, the second band being overwhelmingly most abundant. Red, needle-like crystals were obtained by the slow evaporation of the solution from the second band; they were subsequently recrystallized from water.

Found: C, 29.69; H, 6.16; N, 17.34%; Calcd for $C_{10}H_{24}O_8N_5Co$: C, 29.93; H, 6.04; N, 17.45%.

Spectroscopic Measurements. The AB and CD spectra were recorded at room temperature using a Hitachi EPS-3T Recording Spectrophotometer and a JASCO J-20 Automatic Recording Spectropolarimeter respectively.

X-Ray Data Measurement. Crystal Data: *cis*(O)*trans*-(N_α)*cis*(N_δ)-$[Co(L\text{-}C_5H_{11}O_2N_2)_2]NO_3\cdot H_2O$, $FW=401.32$, orthorhombic, $a=14.380(4)$, $b=16.493(3)$, $c=6.787(2)$ Å, $V=1609.7$ Å^3, $Z=4$, $D_m=1.66$ (flotation), $D_x=1.66$ g cm^{-3}, space group $P2_12_12_1$, $\mu(NiK_\alpha)=25.3$ cm^{-1}. The unit-cell dimensions were determined by the least-squares analysis of the θ values from 45 high-angle reflections on zero-level Weissenberg photographs calibrated with silicon powder.

Multiple-film equi-inclination Weissenberg photographs were taken about a (0—7kl) and c (hk0—6) axes with NiK_α radiation. Crystals with the dimensions of $0.20\times0.15\times0.15$ and $0.15\times0.17\times0.18$ mm were used for the intensity-data collections about the a and c axes respectively. The intensities were measured visually by the use of a calibrated intensity strip and were corrected for Lp factors, spot shape, and absorption. The structure amplitudes were placed on a common arbitrary scale by the least-squares method. A total of 1636 independent reflections was obtained; of those, the intensities of 172 reflections were too weak to be observed.

Determination and Refinement of Crystal Structure

The coordinate of the Co atom was derived from the three-dimensional Patterson synthesis. Approximate coordinates of the other non-hydrogen atoms were obtained from successive Fourier syntheses. The positional and thermal parameters were refined by the block-diagonal-matrix least-squares method, the function minimized being $w(F_o-|F_c|)^2$. Five cycles of refine-

TABLE 1. THE ATOMIC COORDINATES, TEMPERATURE FACTORS, AND THEIR e.s.d.'s.
Temperature factors are of the form
$\exp[-(h^2B_{11}+k^2B_{22}+l^2B_{33}+hkB_{12}+hlB_{13}+klB_{23})]$

Atom	x	y	z	B_{11}	B_{22}	B_{33}	B_{12}	B_{13}	B_{23}
Co	0.4359(1)	0.4361(1)	−0.0661(3)	0.0011(1)	0.0012(1)	0.0055(4)	−0.0001(1)	0.0000(3)	−0.0006(3)
N(1)	0.4054(6)	0.3229(6)	−0.1283(15)	0.0011(4)	0.0012(3)	0.0089(22)	−0.0004(6)	0.0000(16)	0.0024(14)
N(2)	0.3958(8)	0.4312(7)	0.2100(15)	0.0026(5)	0.0025(4)	0.0066(20)	0.0000(9)	−0.0002(17)	−0.0013(17)
N′(1)	0.4584(7)	0.5522(6)	−0.0346(15)	0.0024(5)	0.0017(4)	0.0088(22)	0.0007(7)	−0.0048(17)	−0.0015(16)
N′(2)	0.5648(7)	0.4031(7)	−0.0024(15)	0.0008(4)	0.0028(4)	0.0072(20)	0.0007(8)	0.0016(17)	−0.0010(15)
O(1)	0.3117(6)	0.4605(4)	−0.1467(13)	0.0016(4)	0.0008(2)	0.0121(19)	−0.0003(5)	0.0042(15)	0.0014(12)
O(2)	0.1818(6)	0.4045(6)	−0.2689(16)	0.0019(4)	0.0023(3)	0.0229(27)	0.0006(7)	0.0081(19)	−0.0023(17)
O′(1)	0.4723(6)	0.4518(4)	−0.3372(12)	0.0025(4)	0.0008(3)	0.0082(17)	−0.0003(5)	−0.0017(15)	−0.0013(12)
O′(2)	0.5214(7)	0.5431(5)	−0.5525(13)	0.0044(5)	0.0020(3)	0.0086(19)	0.0017(7)	−0.0007(19)	0.0017(14)
C(1)	0.2606(8)	0.3986(7)	−0.1971(18)	0.0014(5)	0.0016(4)	0.0113(28)	−0.0018(8)	0.0017(20)	0.0018(19)
C(2)	0.3012(7)	0.3153(6)	−0.1517(18)	0.0011(5)	0.0009(4)	0.0117(25)	0.0004(7)	0.0006(19)	−0.0021(17)
C(3)	0.2565(9)	0.2811(7)	0.0332(20)	0.0023(6)	0.0017(4)	0.0117(30)	0.0011(8)	−0.0022(23)	0.0004(19)
C(4)	0.2558(9)	0.3398(9)	0.2148(20)	0.0027(6)	0.0027(5)	0.0103(28)	−0.0016(10)	−0.0018(23)	−0.0029(21)
C(5)	0.3505(10)	0.3609(8)	0.3030(17)	0.0031(7)	0.0026(5)	0.0039(24)	0.0009(10)	0.0007(22)	0.0001(18)
C′(1)	0.5000(8)	0.5241(8)	−0.3802(18)	0.0019(5)	0.0023(5)	0.0090(28)	0.0015(8)	−0.0010(20)	−0.0032(18)
C′(2)	0.5094(9)	0.5840(7)	−0.2138(18)	0.0033(7)	0.0018(4)	0.0089(27)	0.0018(9)	−0.0059(23)	−0.0036(18)
C′(3)	0.6105(10)	0.5965(9)	−0.1563(22)	0.0028(7)	0.0028(5)	0.0140(31)	0.0030(10)	−0.0042(26)	−0.0053(23)
C′(4)	0.6698(10)	0.5171(10)	−0.1206(24)	0.0017(6)	0.0037(6)	0.0204(40)	0.0013(10)	0.0001(25)	−0.0027(26)
C′(5)	0.6406(8)	0.4647(9)	0.0508(21)	0.0014(5)	0.0039(6)	0.0116(29)	0.0011(9)	0.0013(23)	−0.0009(24)
N(3)	0.6086(7)	0.3079(6)	0.5119(15)	0.0027(5)	0.0012(3)	0.0088(22)	−0.0031(7)	−0.0018(18)	0.0006(14)
O(3)	0.6277(12)	0.3111(10)	0.3371(18)	0.0105(11)	0.0064(7)	0.0126(27)	0.0004(17)	−0.0038(32)	0.0021(26)
O(4)	0.5455(10)	0.2669(7)	0.5802(28)	0.0074(9)	0.0031(5)	0.0559(62)	−0.0023(11)	−0.0258(44)	−0.0024(29)
O(5)	0.6628(10)	0.3430(9)	0.6343(22)	0.0056(8)	0.0060(7)	0.0309(41)	−0.0037(12)	0.0100(31)	−0.0144(30)
H_2O	0.4906(10)	0.2066(7)	0.1406(19)	0.0094(10)	0.0026(4)	0.0223(31)	−0.0053(11)	0.0142(32)	−0.0052(20)

ment ($w=1$ for all reflections) with isotropic temperature factors reduced R and R' ($=[\Sigma w(F_o-|F_c|)^2/\Sigma wF_o^2]^{1/2}$) to 0.116 and 0.152 respectively. In the subsequent refinements, the following weighting scheme was employed:

$$w = 0.3 \quad \text{for } F_o < F_{min}$$
$$w = 1.0 \quad \text{for } F_{min} \leq F_o \leq F_{max}$$
$$w = F_{max}/F_o \quad \text{for } F_{max} < F_o$$

F_{max} and F_{min} were varied as is indicated by F_o and $(\sin\theta/\lambda)$ analysis of $w(F_o-|F_c|)^2$. Moreover, four reflections (020, 080, 120, 200) thought to be suffering from extinction errors were omitted in the least-squares calculation. Anisotropic thermal parameters were introduced in the following step-by-step order: i) first, to the Co atom only; then, ii) to the O atoms of the water molecule and the nitrate ion, and finally, iii) to all the atoms. R' was thus improved in an order of 0.151, 0.143, and 0.133 ($R=0.099$). R'-ratio tests at each stage showed the introduction of thermal anisotropy to be significant at the 0.01 level of significance.[4] In the final cycle of the least-squares refinement, the shifts of the parameters were $<0.3\sigma$, F_{max} and F_{min} being 20.2 and 4.7 respectively. The absolute configuration of the complex cation was derived from the well-established configuration of the L-ornithine.

The atomic scattering factors for C, N, O, and neutral Co atoms were employed from Ref. 5. The real part of the anomalous dispersion was taken into account for the Co atom. The final atomic coordinates and thermal parameters are listed in Table 1. The atomic coordinates correspond exactly to the absolute crystal structure. A complete list of the F_o and $|F_c|$ values is preserved by the Chemical Society of Japan (Document No. 7608). All the computations were carried out by means of the FACOM 270-30 computer at Osaka City University. The computer programs used were RSSFR-4 (Fourier synthesis) and HBLS-IV (least-squares calculation).

Results and Discussion

The AB and CD spectra are shown in Fig. 2, and they are summarized in Table 2. The pattern of the first absorption band (Band I) indicates that the present complex has two O atoms in the *cis* positions. In the figure, the CD curves for the bis(L-2,3-diaminopropionato)cobalt(III) and bis(L-2,4-diaminobutyrato)-cobalt(III) ions are also shown as references.[6,7] In these ions, the amino acidato ligand has the facial coordination *via* 2 N and O atoms and forms a 5-membered ring composed of the carboxyl and α-amino groups as well as a 5- or 6-membered chelate ring involving α- and β- or γ-amino groups. These two complexes have been assigned to the *cis*(O)*trans*(N_α)*cis*(N_β or N_γ) isomers by Liu *et al.*[6,7] The three complexes in Fig. 2 show similar Cotton effects in the Band I region. This

TABLE 2. DATA OF THE ABSORPTION AND CIRCULAR DICHROISM SPECTRA

	$\tilde{\nu}_{max}$ [a]	ε_{max}	$\tilde{\nu}_{ext}$ [a]	$\Delta\varepsilon_{ext}$
Band I	20.3	121	18.3	+1.27
			20.3	−0.32
Band II	28.0	172	27.7	−0.44

a) $\tilde{\nu}$ in $cm^{-1}\times10^{-3}$.

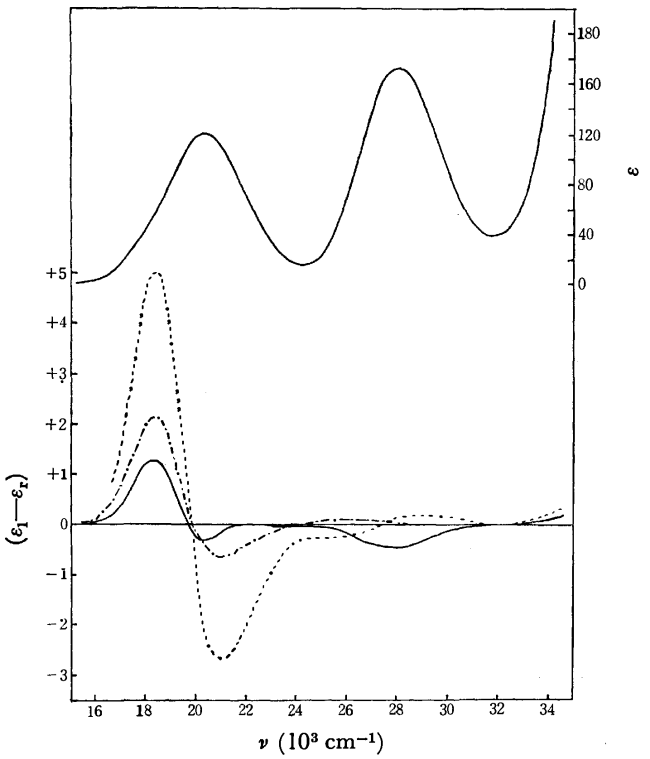

Fig. 2. AB and CD spectra (—) of the present bis(L-ornithinato)cobalt(III) ion, and CD spectra of: (···) *cis*(O)*trans*(N_α)*cis*(N_β) isomer of bis(L-2,3-diaminopropionato)cobalt(III) ion; (-·-) *cis*(O)*trans*(N_α)*cis*(N_γ) isomer of bis(L-2,4-diaminobutyrato)cobalt(III) ion.

implies that the present complex can be assigned to the *cis*(O)*trans*(N_α)*cis*(N_δ) isomer, though the sign of the CD band in the second absorption-band region (Band II) is opposite to the signs of the complexes cited for comparison. However, since the correlation between the CD spectrum and the absolute configuration of the Co(III) chelate of the tridentate α-amino acidato ligand has not yet been established, X-ray structure analysis was undertaken in order to establish the stereochemistry of the present complex.

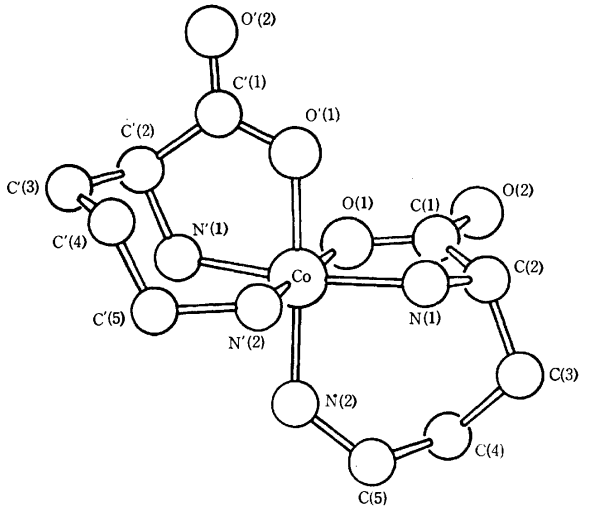

Fig. 3. Absolute configuration of *cis*(O)*trans*(N_α)*cis*(N_δ) isomer of bis(L-ornithinato)cobalt(III) cation.

Table 3. Bond lengths and angles

Co–N(1)	1.96(1)Å	N(1)–Co–N'(2)	89.7(4)°
Co–N(2)	1.96(1)	N'(1)–Co–N(2)	89.1(5)
Co–N'(1)	1.95(1)	N(1)–Co–O'(1)	89.1(4)
Co–N'(2)	1.98(1)	N'(1)–Co–O(1)	88.8(4)
Co–O(1)	1.91(1)	N(2)–Co–N'(2)	93.2(5)
Co–O'(1)	1.93(1)	O(1)–Co–O'(1)	87.2(4)
N(1)–C(2)	1.51(2)	Co–N(1)–C(2)	109(1)
C(2)–C(3)	1.52(2)	N(1)–C(2)–C(3)	111(1)
C(3)–C(4)	1.57(2)	C(2)–C(3)–C(4)	115(1)
C(4)–C(5)	1.53(2)	C(3)–C(4)–C(5)	116(1)
C(5)–N(2)	1.47(2)	C(4)–C(5)–N(2)	114(1)
C(1)–C(2)	1.53(2)	C(5)–N(2)–Co	125(1)
C(1)–O(1)	1.30(2)	C(1)–C(2)–C(3)	110(1)
C(1)–O(2)	1.24(2)	C(1)–C(2)–N(1)	109(1)
		O(1)–C(1)–C(2)	116(1)
N'(1)–C'(2)	1.51(2)	O(2)–C(1)–C(2)	120(1)
C'(2)–C'(3)	1.52(2)	O(1)–C(1)–O(2)	124(2)
C'(3)–C'(4)	1.58(2)		
C'(4)–C'(5)	1.51(2)	Co–N'(1)–C'(2)	109(1)
C'(5)–N'(2)	1.53(2)	N'(1)–C'(2)–C'(3)	108(1)
C'(1)–C'(2)	1.51(2)	C'(2)–C'(3)–C'(4)	116(1)
C'(1)–O'(1)	1.29(2)	C'(3)–C'(4)–C'(5)	116(1)
C'(1)–O'(2)	1.25(2)	C'(4)–C'(5)'–N'(2)	113(1)
		C'(5)–N'(2)–Co	122(1)
N(3)–O(3)	1.22(2)	C'(1)–C'(2)–C'(3)	112(1)
N(3)–O(4)	1.22(2)	C'(1)–C'(2)–N'(1)	109(1)
N(3)–O(5)	1.28(2)	O'(1)–C'(1)–C'(2)	118(1)
		O'(2)–C'(1)–C'(2)	121(1)
N(1)–Co–N(2)	95.8(5)°	O'(1)–C'(1)–O'(2)	121(1)
N(1)–Co–O(1)	86.0(4)		
N(2)–Co–O(1)	90.4(4)	O(3)–N(3)–O(4)	124(2)
N'(1)–Co–N'(2)	95.2(4)	O(4)–N(3)–O(5)	117(1)
N'(1)–Co–O'(1)	85.9(4)	O(5)–N(3)–O(3)	118(1)
N'(2)–Co–O'(1)	89.5(4)		

Figure 3 shows the absolute configuration of the complex cation. This has a pseudo two-fold axis which passes through the Co atom and bisects N(2)–Co–N'(2) bond angle. This axis correlates the primed and unprimed atoms in Fig. 3. In the bond lengths and angles (Table 3), those related by the two-fold axis are in good agreement within the limits of experimental error.

In the 7-membered chelate ring composed of $N_\alpha(1)$, $C_\alpha(2)$, $C_\beta(3)$, $C_\gamma(4)$, $C_\delta(5)$, $N_\delta(2)$, and Co atoms, the N_α–Co–N_δ bond angle is larger than 90°, the average value being 95.5°; this can be ascribed to the repulsion between two confronting H atoms—H($N_\alpha H_2$) and H($C_\delta H_2$). This value is comparable to that (92°—95°) in the 6-membered ring formed by the trimethylenediamine molecule (tn) and the Co atom.[8,9] The bond angle of Co–N_α–C_α is close to the tetrahedral angle, while that of Co–N_δ–C_δ is much greater than 109.5°, but compares with the corresponding one in the tn ring. The C–C–C and N–C–C angles range from 108° to 116°. They are also similar to those in the tn ring of $[Co(tn)_3]^{3+}$ and the 7-membered ring found in bis(L-ornithinato)palladium(II), but are larger by 2°—5° than those in the L-ornithine hydrochloride[10] and hydrobromide.[11]

The $-CH-CH_2-CH_2-CH_2-$, $-CH_2-CH_2-CH_2-NH_2-$ and $-CH_2-CH_2-NH_2-Co-$ fragments in the 7-membered ring assume a *gauche* conformation. However, the $-H_2C(3)-H_2C(4)-H_2C(5)-H_2N(2)-$ fragment and the corresponding one composed of the primed atoms are somewhat close to the eclipsed conformation; the torsional angles between the two terminal bonds about the central C–C bond are 88° for the unprimed fragment and 87° for the primed one. These values agree well within the limits of experimental error (88° on the average).

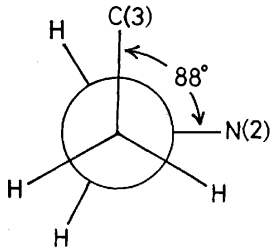

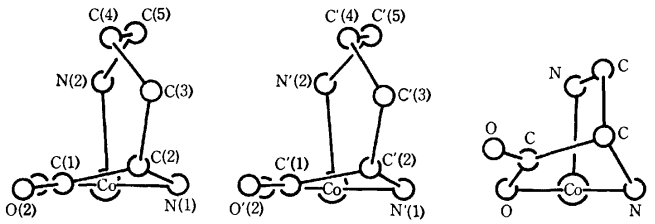

Fig. 4. Elevation of the chelate ring in: (a) and (b), bis(L-ornithinato)cobalt(III) nitrate monohydrate; (c), *cis* (O) *trans* (N_a) *cis* (N_β)-bis (L-2,3-diaminopropionato)-cobalt(III) bromide. Numbers in parentheses indicate the deviation (Å) of the C_α atoms in 5-membered glycinato ring from the (Co, N_α, O) planes.

The elevation of the 5-membered rings (or glycinato rings) formed by the N_α, C_α, $C_{(carboxyl)}$, O, and Co atoms are shown in Fig. 4, where the glycinato ring in bis(L-2,3-diaminopropionato)cobalt(III) bromide is also drawn for comparison.[12] Although the bond lengths and angles in the glycinato ring of the present complex are in good harmony with those in the planar chelate ring made by a glycinate ion and a Co atom,[13] the C(2) and C'(2) atoms are pulled upward from the $Co\langle^{N(1)}_{O(1)}$ and $Co\langle^{N'(1)}_{O'(1)}$ planes by the wing composed of C_α, C_β, C_γ, C_δ, N_δ, and Co atoms. In the glycinato ring of tridentate α-amino acid, the deviation of the C_α atom from the (Co, N_α, O) plane appears to be reduced as the members of the wings are increased.

TABLE 4. PLANES DEFINED BY THE O, Co, AND N_α ATOMS
Deviations(Å) of atoms from the plane are given in square brackets.

(O(1), Co, $N_\alpha(1)$) plane
$-0.318X-0.317Y+0.938Z=-3.40$
[C(1) 0.05, $C_\alpha(2)$ 0.35]
(O'(1), Co, $N'_\alpha(1)$) plane
$-0.951X+0.188Y-0.244Z=-4.50$
[C'(1) 0.08, $C'_\alpha(2)$ 0.30]

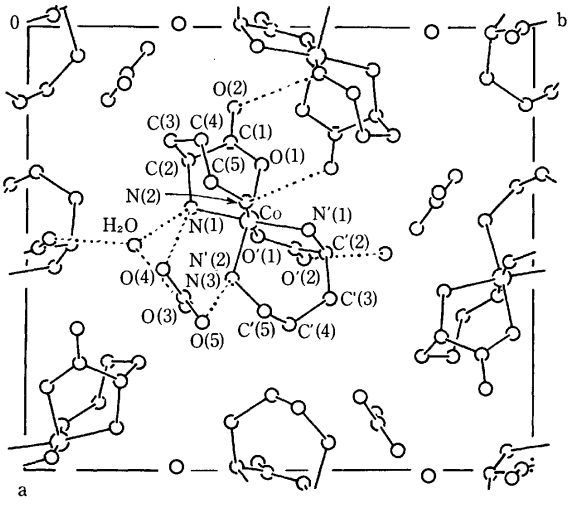

Fig. 5. Crystal structure viewed down the c axis. Broken lines indicate the hydrogen bonds.

TABLE 5. DATA OF THE HYDROGEN BONDS

A–H···B		A···B	H···B	A–H···B	Positions[a] of A	B
N(1)	H_2O	2.92(2)Å	1.91Å	165°	1	1
N(1)	O(4)	2.97(2)	2.01	155	1	3
N(2)	O(2)	2.94(2)	1.98	153	1	4
N(2)	O'(2)	3.05(2)	2.19	139	1	2
N'(1)	O(2)	2.80(2)	2.05	128	1	4
N'(2)	O(3)	2.90(2)	1.99	146	1	1
N'(2)	O(5)	3.01(2)	2.02	161	1	3
H_2O	O(3)	2.94(2)			1	1
H_2O	O'(2)	2.77(2)			1	5

a) Numerals refer to the following equivalent positions:
1 x, y, z 2 $x, y, 1+z$ 3 $x, y, -1+z$
4 $1/2-x, 1-y, 1/2+z$ 5 $1-x, -1/2+y, -1/2-z$

The crystal structure viewed down the c axis is depicted in Fig. 5. There are N–H···O and O–H···O hydrogen bonds in the crystal (Table 5), though they are rather weak in view of the distance between the proton donor and the acceptor. The positions of the H atoms of the amino groups are calculated on the assumption that the N–H distance is 1.03 Å. Both of the H atoms in the $N(1)H_2$ group and in the water molecule, and one of those in the $N(2)H_2$ and $N'(2)H_2$ groups participate in the hydrogen bonding, while none of those in $N'(1)H_2$ groups do.

The authors wish to express their thanks to the Ministry of Education for financial support of this work. They are also grateful to Dr. Ken Hirotsu who adapted the computer programs to FACOM 270-30 computer at Osaka City University.

References

1) M. Watabe and S. Yoshikawa, Proceeding of the 28th Meeting of the Chemical Society of Japan, I (1973), p. 554.
2) Y. Nakayama, K. Matsumoto, S. Ooi, and H. Kuroya, *Chem. Commun.*, **1973**, 170.

3) S. Guha and N. Saha, *Acta Crystallogr.*, **B26**, 2073 (1970).
4) W. C. Hamilton, *ibid.*, **18**, 502 (1965).
5) "International Tables for X-Ray Crystallography," Vol. III, Kynoch Press, Birmingham (1962).
6) W. A. Freeman and C. F. Liu, *Inorg. Chem.*, **7**, 764 (1968).
7) W. A. Freeman and C. F. Liu, *ibid.*, **9**, 1191 (1970).
8) R. Nagao, F. Marumo, and Y. Saito, *Acta Crystallogr.*, **B29**, 2438 (1973).
9) K. Matsumoto, H. Kawaguchi, H. Kuroya, and S. Kawaguchi, This Bulletin, **46**, 2424 (1973).
10) S. Guha, S. K. Mazumdar, and N. N. Saha, *Z. Kristallogr.*, **129**, 84 (1969).
11) R. Schaffrin and J. Trotter, *J. Chem. Soc., A*, **1970**, 25.
12) C. F. Liu and J. A. Ibers, *Inorg. Chem.* **8**, 1911 (1969).
13) S. Yamaguchi, S. Ooi, and H. Kuroya, unpublished work.

The Crystal Structure of α-$K_8SiW_{11}O_{39}\cdot 13H_2O$

Kazuko Y. MATSUMOTO and Yukiyoshi SASAKI

Department of Chemistry, Faculty of Science, The University of Tokyo, Hongo, Bunkyo-ku, Tokyo 113

(Received September 17, 1975)

α-$K_8SiW_{11}O_{39}\cdot 13H_2O$ is cubic with the space group $P\bar{4}3m$ and $a=10.654(1)$ Å; $D_m=4.40$ g cm^{-3}, $D_x=4.42$ g cm^{-3} for $Z=1$. The crystal contains a discrete $SiW_{11}O_{39}^{8-}$ ion, which is almost identical to α-$SiW_{12}O_{40}^{4-}$ anion in shape and in size but one tungsten atom and the exterior terminal oxygen atom are absent. The position of the vacant hole could not be located because of the seemingly high symmetry of T_d of the polyanion caused by the orientational randomness of the anions. The silicon atom at the center of the polyanion lies on the origin of the cubic lattice and the potassium cations linking α-$SiW_{11}O_{39}^{8-}$ ions are at the middle points of adjacent polyanions.

The 11-tungstosilicate salts were first prepared by Marignac,[1] however he described the compounds as 10-tungstosilicates, $M_8^I SiW_{10}O_{36}$. Most of the 10-tungstosilicates given in the Gmelin's Handbook[2] are now believed to be 11-tungstosilicates.

This heteropoly anion can be regarded as an hydrolytic degradation product of α-$SiW_{12}O_{40}^{4-}$ anion and the reaction is as follows;

$$\alpha\text{-}SiW_{12}O_{40}^{4-} + 6OH^- \rightleftharpoons \alpha\text{-}SiW_{11}O_{39}^{8-} + WO_4^{2-} + 3H_2O$$

This reaction is reversible and addition of acid to a solution of α-$SiW_{11}O_{39}^{8-}$ in the presence of WO_4^{2-} yields α-$SiW_{12}O_{40}^{4-}$ immediately. Even in the absence of WO_4^{2-}, α-$SiW_{12}O_{40}^{4-}$ is formed on acidification from α-$SiW_{11}O_{39}^{8-}$.

Recent investigation by Souchay *et al.*[3] has shown that the α-$SiW_{11}O_{39}^{8-}$ anion is an important intermediate product in the formation of α-$SiW_{12}O_{40}^{4-}$ and the reaction proceeds as follows;

$$SiO(OH)_3^- + 11WO_4^{2-} + 15H^+ \longrightarrow \alpha\text{-}SiW_{11}O_{39}^{8-} + 9H_2O$$

$$\alpha\text{-}SiW_{11}O_{39}^{8-} + WO_4^{2-} + 6H^+ \longrightarrow \alpha\text{-}SiW_{12}O_{40}^{4-} + 3H_2O$$

On the other hand, addition of acidified sodium silicate to a solution of acidified sodium tungstate gives β-$SiW_{11}O_{39}^{8-}$ and β-$SiW_{12}O_{40}^{4-}$ as is shown in Fig. 1. As for the structure of α- and β-$SiW_{12}O_{40}^{4-}$, we have already published the results.[5-7] Recently the formation of three isomers of β-$SiW_{11}O_{39}^{8-}$, β_1, β_2, and β_3, through $SiW_9O_{34}^{10-}$ and $HSiW_9O_{34}^{9-}$ have been reported by Contant *et al.*[4] However these isomers are outscope of the present study. The reaction

$$SiW_{11}O_{39}^{8-} + M^{n+} \longrightarrow SiW_{11}MO_{40}^{(8-n)-}$$

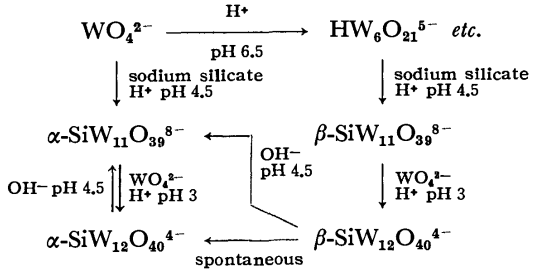

Fig. 1. Formation condition of $SiW_{11}O_{39}^{8-}$ and $SiW_{12}O_{40}^{4-}$ anions at room temperature.

where M is Mn(II), Fe(II), Co(II), Ni(II), Cu(II), Fe(III), Cr(III), V(IV), V(V), and Mo(VI) were reported[8] and the resultant $SiW_{11}MO_{40}^{(8-n)-}$ anions have Keggin structure,[9] in which one of the twelve tungsten atoms is substituted by M. But lanthanide cations (Ln) may be too large to be included in the Keggin structure and form salts of the type $K_{10}Ln(SiW_{11}O_{39})_2\cdot nH_2O$.[10]

Present crystal-structure determination of α-$K_8SiW_{11}O_{39}\cdot 13H_2O$ have revealed that the structure of the α-$SiW_{11}O_{39}^{8-}$ is very similar to that of α-$SiW_{12}O_{40}^{4-}$, which has the Keggin structure, but one tungsten atom and its terminal oxygen atom are missing.

Experimental

Potassium hydroxide was added to a hot concentrated solution of α-$K_4SiW_{12}O_{40}$ with mole-ratio of 6:1; the pH of the solution was increased to 4.5. The crystals of α-$K_8SiW_{11}O_{39}\cdot 13H_2O$ were precipitated on cooling and was recrystallized from water. They are colorless, stable in air and more resistant to reduction that the α-$SiW_{12}O_{40}^{4-}$.

Preliminary oscillation and Weissenberg photographs showed that the crystal is cubic. No systematic absence of the reflections was observed, therefore three space groups, $P\bar{4}3m$, P432, and Pm3m were possible, however further structure analysis determined the space group to be $P\bar{4}3m$. The intensities of the reflections up to $2\theta=60°$ were measured on the Rigaku four-circle diffractometer with graphite-monochromated Mo$K\alpha$ radiation ($\lambda=0.71069$ Å). The ω-2θ scan technique was employed and a total of 312 independent reflections, whose intensities were larger than 3σ, were used for the structure analysis. The data were corrected for Lorentz and polarization factors. No corrections were made for absorption and extinction effects. The crystal used for intensity measurement was of the dimensions $0.1\times0.1\times0.1$ mm and the crystal data are as follows;

α-$K_8SiW_{11}O_{39}\cdot 13H_2O$
F.W. = 3220.7
cubic $P\bar{4}3m$
$a = 10.654(1)$ Å
$V = 1209.3$ Å^3
$Z = 1$
$D_m = 4.40$ g cm^{-1}, $D_x = 4.42$ g cm^{-1}
$\mu = 302.0$ cm^{-1} (for Mo$K\alpha$ radiation)

Structure Determination

The structure was solved by the heavy atom method. The three dimensional Patterson map could not be at

TABLE 1. ATOMIC PARAMETERS

Positional and thermal parameters ($\times 10^4$) with their estimated standard deviations in parentheses. The β_{ij}'s are defined by: $\exp[-(\beta_{11}h^2+\beta_{22}k^2+\beta_{33}l^2+2\beta_{12}hk+2\beta_{13}hl+2\beta_{23}kl)]$.

	x	y	z	β_{11}	β_{22}	β_{33}	β_{12}	β_{13}	β_{23}
W	2349(2)	2349(2)	38(10)	25(1)	25(1)	54(3)	−5(2)	−0(4)	−0(4)
Si	0(0)	0(0)	0(0)	72(34)	72(34)	72(34)	0(0)	0(0)	0(0)
O(1)	877(50)	877(50)	−877(50)	50(39)	50(39)	50(39)	−19(41)	19(41)	19(41)
O(2)	3328(65)	1412(41)	−1412(41)	77(70)	90(46)	90(46)	22(40)	−22(40)	33(67)
O(3)	2908(46)	1120(32)	1120(32)	45(49)	28(24)	28(24)	−4(28)	−4(28)	1(34)
O(4)	3438(39)	3438(39)	285(69)	36(29)	36(29)	89(119)	19(40)	−16(37)	−16(37)
K	5000(0)	0(0)	0(0)	11(21)	108(26)	108(26)	0(0)	0(0)	0(0)

first solved with the three possible space groups assuming eleven tungsten atoms per molecule, but satisfactory solution was obtained assuming that eleven tungsten atoms occupy the twelve tungsten positions of the Keggin structure[9] with equal statistical weight and that the space group is $P\bar{4}3m$. All the other atoms, except five potassium cations and thirteen water molecules, were located from the Fourier synthesis based on the coordinates of tungsten atoms. The structure was refined by the block diagonal least-squares technique with a local version of UNICS[11] program. A weighting scheme, $w=0.2$ for $|F_o|<41$ and $w=1$ otherwise, was employed. At the last stage of the refinement, the temperature factors were assumed to be anisotropic and the last R value, $R=\sum||F_o|-|F_c||/\sum|F_o|$, was 0.069.

The atomic scattering factors used were taken from the International Tables for X-Ray Crystallography.[12] The calculations were performed on a HITAC 8700/8800 computer at the Computer Centre of the University of Tokyo. The atomic coordinates and the temperature factors are listed in Table 1. The final F_o-F_c table is kept at the office of Chemical Society of Japan as Document No. 7607.

Results and Discussion

The structure of the α-$SiW_{11}O_{39}^{8-}$ anion results from removing one WO_6 octahedron from the α-$SiW_{12}O_{40}^{4-}$, which has the Keggin structure, and is illustrated in Fig. 2 as a coordination polyhedra model. The result of the structure determination has shown that α-$SiW_{11}O_{39}^{8-}$ is required to have T_d symmetry and Keggin structure. This apparent high symmetry is effected by orientational randomness of the polyanions in the crystal. The α-$SiW_{11}O_{39}^{8-}$ anion can be regarded as a "deficient Keggin ion," in which one of the twelve equivalent positions of metals and its terminal oxygen, is vacant. This deficient Keggin ion lies in the crystal with its vacant site oriented randomly to one of the twelve positions and with the statistical weight of 11/12. The deformation of the Keggin structure caused by the removal of one tungsten atom could not be studied in detail because of this randomness. The standard deviations of the coordinates of the heavy atoms and the thermal parameters are not so large and accordingly it is inferred that the α-$SiW_{11}O_{39}^{8-}$ is not much deformed from the α-$SiW_{12}O_{40}^{4-}$. The tungsten-oxygen and silicon-oxygen interatomic distances given in Table 2 should be understood as average values for this hypothetical Keggin ion and agree well with those of the α-$SiW_{12}O_{40}^{4-}$ anion.[5]

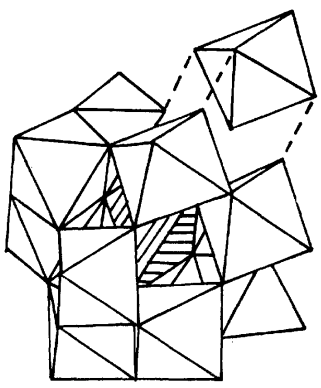

Fig. 2. The structure of the α-$SiW_{11}O_{39}^{8-}$ anion and its structural relation to the α-$SiW_{12}O_{40}^{4-}$ anion.

TABLE 2. INTERATOMIC DISTANCES WITH THEIR ESTIMATED STANDARD DEVIATIONS

W—O(1)	2.422(54)Å	O(2)—O(3)	2.752(85)
O(2)	2.114(70)	O(4)	2.817(101)
O(3)	1.843(50)	O(3)—O(4)	2.684(89)
O(4)	1.662(74)	Si—O(1)	1.617(53)
O(1)—O(2)	2.733(87)	K—O(2)	2.774(70)
O(3)	3.045(72)	K—O(3)	2.795(49)

Three equivalent potassium cations per formula unit were located and are shown in Fig. 3. The potassium ion is octacoordinated by four O(2) and four O(3) in the form of skewed antiprism. The molecular center is at the origin of the cubic cell and the potassium atoms lie at the middle points of the cell edges. There are large straight channels through the center of the unit cell parallel to the three axes and on the Fourier map low electron-density peaks were found in this space, however they could not be interpreted even by assuming random distribution of the unlocated five potassium cations and/or water molecules. Similar situation was encountered when Baker *et al.* solved the crystal structure of ammonium salt of $Co^{III}Co^{II}W_{11}O_{40}^{9-}$, in which he could not locate the ammonium cations and water of crystallization probably because of the disorder in the channels and large pockets formed by the exterior oxygens of the anions.[13] Although this anion is not exactly the same as that of the present compound because the former has the Keggin structure with one

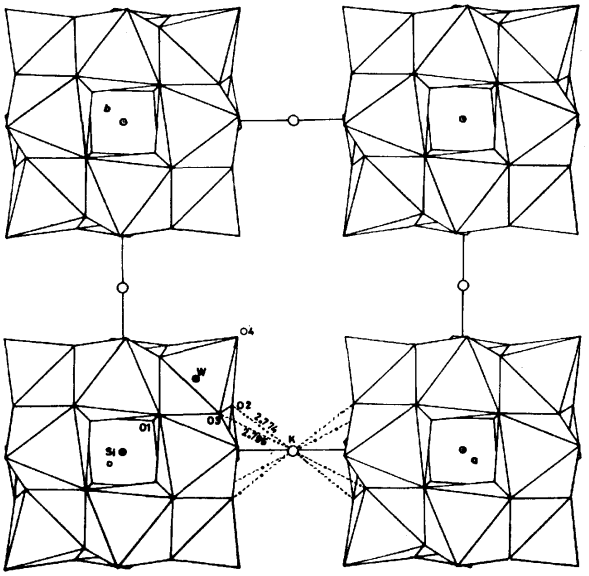

Fig. 3. The crystal structure of α-$K_8SiW_{11}O_{39}\cdot 13H_2O$ showing the coordination around potassium atoms.

of the twelve tungstens replaced by Co^{II}, their crystal structures resemble each other; the ammonium salt of $Co^{III}Co^{II}W_{11}O_{40}^{9-}$ is cubic with the space group Fm3m, the cell constant is just the double of that of the present compound and $Z=8$. The arrangement of anions is an enlarged NaCl type, with the Na^+ ions replaced by a set of Keggin units having one unique orientation and the Cl^- ions replaced by Keggin units with an orientation at right angles to the first set. Therefore if there have not been for the two sets of orientations, the unit-cell dimensions would be the half and the arrangement of the anions would be the same as in the present compound. Single crystal X-ray work of $(NH_4)_7Na_2[GaH_2W_{11}O_{40}]\cdot 15H_2O$, $(NH_4)_{7.3}H_{2.7}[Co^{II}Co^{II}W_{11}O_{40}]\cdot 17H_2O$, $Rb_{6.5}Co_{0.4}H_{2.7}[Co^{II}Co^{II}W_{11}O_{40}]\cdot 15H_2O$, $K_{6.5}H_{2.5}[Co^{II}Co^{II}W_{11}O_{40}]\cdot 13H_2O$, $K_7H[Co^{III}Co^{III}W_{11}O_{40}]\cdot 14H_2O$[13,14] have shown that these compounds are isomorphous with the ammonium salt of $Co^{III}Co^{II}W_{11}O_{40}^{9-}$ in spite of their various number of cations and water of crystallization. The unit-cell edge of $(NH_4)_7Na_2[GaH_2W_{11}O_{40}]\cdot 15H_2O$ shrinks reversibly and continuously with increasing temperature. From these facts, fairly high degree of freedom in the arrangement of cations and water molecules in the channels can be inferred. In the crystal-structure analysis of $K_4SiW_{12}O_{40}\cdot 17H_2O$,[15] some of the potassium atoms could not be located and some works[7,14,16] have reported that crystals of heteropoly acids often contain zeolitic water. These facts suggest that the unlocated potassium atoms and water molecules in the present crystal are a characteristic result of disorder in the cavities between the polyanions.

References

1) C. Marignac, *Ann. Chim. Phys.*, [4], **3**, 5 (1864).
2) Gmelin, "Handbuch der Anorganischen Chemie," 8th Ed., Verlag Chemie Berlin, (1935).
3) P. Souchay, A. Tézé, and G. Hervé, *C. R. Acad. Sci. Paris, Ser. C*, **275**, 1013 (1972).
4) R. Contant, J.-M. Fruchart, G. Hervé, and A. Tézé, *ibid.*, **278**, 199 (1974).
5) A. Kobayashi and Y. Sasaki, This Bulletin, **48**, 885 (1975).
6) K. Yamamura and Y. Sasaki, *Chem. Comm.*, **1973**, 648.
7) K. Y. Matsumoto, A. Kobayashi, and Y. Sasaki, This Bulletin, **48**, 3146 (1975).
8) C. Tourné and G. Tourné, *Bull. Soc. Chim. Fr.* **1969**, 1124.
9) J. F. Keggin, *Proc. Roy. Soc., Ser. A*, **144**, 75 (1934).
10) R. D. Peacock and T. J. R. Weakley, *J. Chem. Soc., A.*, **1971**, 1836.
11) "The Universal Crystallographic Computation Program System," Crystallographic Society of Japan (1967).
12) "International Tables for X-ray Crystallography," Vol. III, Kynoch Press, Birmingham (1962).
13) L. C. W. Baker, V. S. Baker, K. Eriks, M. T. Pope, M. Shibata, O. W. Rollins, J. H. Fang, and L. L. Koh, *J. Amer. Chem. Soc.*, **88**, 2329 (1966).
14) H. T. Evans "Perspectives in Structural Chemistry," Vol. IV, John Wiley, N. Y. (1971).
15) P. M. Smith, Ph. D. Thesis, Georgetown University, 1972, *Dissert. Abstr.*, **32**, 5136-B (1972).
16) S. F. West and L. F. Audrieth, *J. Phys. Chem.*, **59**, 1069 (1955).

Isomerism of the Metal Complexes Containing Multidentate Ligands. VII.[1] The Conformational Analysis of the Isomers of [Co(linpen)]$^{3+}$ *

Yuzo Yoshikawa

Department of Chemistry, Faculty of Science, Nagoya University, Chikusa-ku, Nagoya 464

(Received September 22, 1975)

The conformational analysis of the $[Co(dien)_2]^{3+}$ and $[Co(linpen)]^{3+}$ (dien=$H_2N(CH_2CH_2NH)_2H$, linpen=$H_2N(CH_2CH_2NH)_5H$) complexes has been carried out. The former, which can exist in three geometric isomers, was selected as a standard for the determination of several parameters in the strain-energy calculation; they were determined so that the calculated geometries of these isomers were almost the same as those obtained from the crystal structure analysis studies. These results were applied to the strain-energy calculation for the latter, $[Co(linpen)]^{3+}$, which can exist in four geometric isomers. Further, in three of these isomers, some conformational isomers are possible. From the results of the energy-minimized conformational-analysis calculations of these isomers, it has turned out that the assignment of the structures of the configurational and conformational isomers is possible.

A conformational analysis technique has been effectively used to obtain information about the conformational structures of molecules. The strain-energy-minimization technique developed by Boyd[2] has been very frequently applied not only to organic molecules, but also to metal complexes.

Recently Toriumi and Saito[3] modified Boyd's method and reported the results of:

$(+)_{589}$*cis*-β-$[Co(CO_3)(S,S\text{-}3,8\text{-dimetrien})]^+$ [4] calculated by it.

In the present study we have adopted the method of Toriumi and Saito, the main part of which is the same as Boyd's, and calculated the strain energies of the isomers of $[Co(dien)_2]^{3+}$ and $[Co(linpen)]^{3+}$. The force field in this calculation includes contributions from bond stretching, nonbonded interactions, angle bending, and torsional potentials. In the calculations of the nonbonded interactions, only those between nonbonded atoms (except between atoms bonded to the same atom) up to distances of 1.2 times the sum of each van der Waas radius (1.50 Å for N, 1.55 Å for C and 1.20 Å for H atoms) have been treated; the interactions containing a cobalt atom have been omitted. The purpose of this study is to investigate the details of the molecular structures of $[Co(linpen)]^{3+}$ isomers, the isolation and characterization of which have already been reported in this Bulletin.[5] We will first carry out a conformational analysis of the isomers of $[Co(dien)_2]^{3+}$ in order to determine the adequate parameters in the calculation of strain energies by comparing the energy-minimized structures with those determined by X-ray studies.

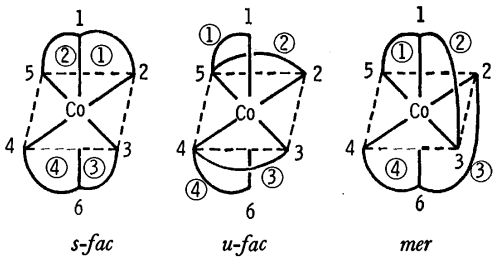

Fig. 1. Three possible geometric isomers of $[Co(dien)_2]^{3+}$. Figures in the circles show the numberings for the chelate rings.

The complex ion, $[Co(dien)_2]^{3+}$, can exist in three geometric isomers, as Fig. 1 shows, and they have all been isolated.[6] Saito *et al.* determined the molecular structures of *s-facial* and *u-facial* isomers of $[Co(dien)_2]^{3+}$ by the X-ray crystal analysis of *s-fac*-$[Co(dien)_2]Br_3$[7] and $\{-\}_{502}$*u-fac*-$[Co(dien)_2][Co(CN)_6]\cdot 2H_2O$**,[8] respectively. According to these results, *s-fac*-$[Co(dien)_2]^{3+}$ has approximately the C_{2h} symmetry and $\{-\}_{502}$*u-fac*-$[Co(dien)_2]^{3+}$ (there are two conformational isomers in the crystals of this complex hexacyanocobaltate(III)), the C_2 symmetry. The conformations of the four

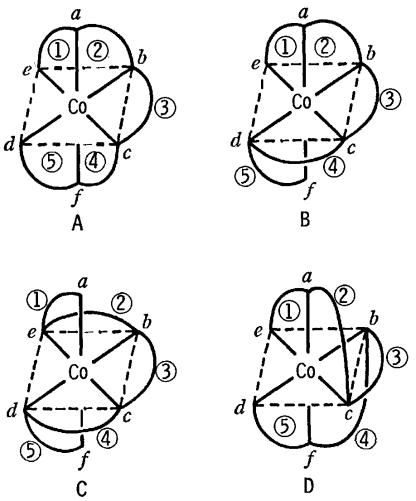

Fig. 2. Four possible geometric isomers of $[Co(linpen)]^{3+}$. Letters, *a*—*f*, are the locant designators according to the nomenclature proposed by IUPAC.[9]

* Presented at the 24th Symposium on Coordination Chemistry, Kanazawa, October, 1974.

** The $\{+\}_\lambda$ or $\{-\}_\lambda$ symbol represents the sign of the CD spectrum at a certain wavelength, λ nm, and $\{-\}_{502}$ corresponds to $(-)_{589}$ in the *u-fac*-$[Co(dien)_2]^{3+}$ complex. This symbol is convenient for characterizing an optically active compound, because there is no need to measure an optical rotation. For the λ, wavelength, it is advisable to adopt that of a maximum CD intensity in a suitable band.

chelate rings in the former are $\lambda\delta\lambda\delta$ (or $\delta\lambda\delta\lambda$), in the order of the numbers of the chelate rings in Fig. 1, while those of the latter are $\lambda\delta\delta\lambda$ and $\lambda\lambda\lambda\lambda$ (denoted as *u-fac*-1 and *u-fac*-2 respectively) for the determined absolute configuration, that is to say, they are skew chelate pairs $\Delta\Lambda\Delta$ (Fig. 1). On the other hand, the structure of *mer*-$[Co(dien)_2]^{3+}$ has not yet been determined. However, it is expected to have a two-fold axis.

The linpen ligand consists of two dien linearly linked by an ethylene group ($-CH_2CH_2-$) between the individual primary amine-N atoms. Therefore, the structures of $[Co(linpen)]^{3+}$, which can exist in four different configurational isomers (Fig. 2), are closely related to those of $[Co(dien)_2]^{3+}$. For example, the A and C isomers are formed by linking N2 to N3 by an ethylene group in the *s-facial* and *u-facial* isomers respectively.

Results and Discussion

The Conformational Analysis of the Isomers of $[Co(dien)_2]^{3+}$. Dwyer *et al.* have attempted the conformational analysis of $[Co(dien)_2]^{3+}$ isomers by using the strain-energy-minimization technique.[10] We analyzed these isomers independently.

The initial molecular structure of each isomer was constructed from the internuclear bond distances; Co–N (primary amine): 1.97 Å, Co–N (secondary amine): 1.95 Å, N–C: 1.49 Å, C–C: 1.51 Å, N–H: 1.03 Å, and C–H: 1.09 Å; the valency angles, ∠NCoN (chelate ring): 86.0°, ∠CoNC: 105—114°, ∠NCC: 105—114°, ∠CNC: 106—118° (*facial*) and 121° (*meridional*), and the angles related to H atoms: 109.5°. Their strain-energy-minimizations were carried out for several sets of equilibrium internuclear bond distances, Co–N, N–C, and C–C, the other parameters[11] being kept constant. Consequently, it was found to be adequate to use the values of 1.935, 1.485, and 1.51 Å for the Co–N, N–C, and C–C equilibrium bond distances respectively, for better fitting the resulting molecular structures to those obtained by X-ray methods. The energy terms obtained from these minimizations, where the root-mean-square coordinate deviations are smaller than 0.005 Å, are shown in Table 1. There are not large differences among these total energies.

Table 1. Final energy terms for the isomers of $[Co(dien)_2]^{3+}$

Isomer	Bond	Nonbond	Angle	Torsion	Total	
s-fac	0.19	1.45	0.55	1.88	4.08	kJ/mol
u-fac-1	0.20	1.46	0.57	1.89	4.12	
u-fac-2	0.26	1.49	0.67	1.70	4.12	
mer	0.26	1.22	1.30	1.29	4.06	

On the other hand, the formation ratios found experimentally in the equilibrium mixture of bromides (25 °C) were *s-fac*: *u-fac*: *mer*=7: 30: 63.

Therefore, the correlation between the minimized strain-energy and the formation percentage of each isomer is not necessarily good. In this case, there may be an inadequate choice for any parameters in the minimization and/or zero level imbalances.[10] The presently calculated molecular geometries (Table 2) are, nevertheless, presumed to be sufficiently accurate by comparison with the experimental structures. Some of these values will be used to construct the molecular structures of $[Co(linpen)]^{3+}$ isomers in the next section.

The Conformational Analysis of the Isomers of $[Co(linpen)]^{3+}$. Figure 2 shows the four geometric isomers of $[Co(linpen)]^{3+}$. The A structure has only secondary amine; the >NH groups of its facial structure are formed in *facial* isomers of $[Co(dien)_2]^{3+}$, but none of the meridional structure. Therefore, this is represented by f_4.*** The B structure contains one >NH group of the meridional structure and is represented by f_2mf (or fmf_2).*** Both the C and D structures have two >NH groups of each structure; they are represented by fm_2f and mf_2m*** respectively.

When the absolute configurations around the secondary amine-N atoms are taken into account for each structure in Fig. 2, the number of isomers is 1 (f_4-*RSSR*= I) for the A, 2 each (f_2mf-*RSRS*, -*RSSS*=II-1, II-2 and fm_2f-*SRRS*, -*SSSS*=III, IV) for B and C respectively, and 3 (mf_2m-*RRRR*, -*RRRS*, -*SRRS*=V, VI, VII) for the D structure, making a total of 8, where *R* and *S*

Table 2. Molecular geometries of the isomers of $[Co(dien)_2]^{3+}$

	Co–NH_2[a] / Co–NH	C–NH_2[a] / C–NH	C–C[a]	∠NCoN Chelate ring	∠CNC[a]
s-fac	1.966Å (1.97Å)[b]	1.491Å (1.48Å)	1.515Å (1.51Å)	88.3—88.9° (86.6—87.2°)	113.8° (116.0°)
	1.944 (1.95)	1.494 (1.505)			
u-fac-1	{1.958, 1.968} ({1.957, 1.969})	1.490 (1.491)	1.513 (1.516)	87.0—88.3 (85.4—86.4)	113.0 (113.9)
	1.960 (1.970)	1.495 (1.496)			
u-fac-2	{1.952, 1.973} ({1.951, 1.968})	1.488 (1.488)	1.514 (1.509)	86.8—87.0 (84.9—85.7)	110.3 (110.4)
	1.971 (1.970)	1.497 (1.499)			
mer	1.976	1.495	1.514	86.0—86.1	114.5
	1.942	1.486			

a) Averages of corresponding values are given. b) Figures in parentheses are the values determined from X-ray crystal structure analysis.[7,8]

*** These designations, f_4, f_2mf, fm_2f, and mf_2m, can be represented by *acbfed*, *acbfde*, *aebcdf*, and *acfbed* respectively by the use of the locant designators according to the nomenclature proposed by IUPAC.[9] The former can also be used as such for optical isomers the absolute configurations of which are not known.

represent the absolute configurations around the secondary amine-N atoms; they are written in the same order as that of *f* and *m*. These eight isomers (I, II-1, II-2, III—VII) have actually been found by means of column chromatography on SP-Sephadex and thus characterized.[5] The II-1 and II-2 isomers, however, were labile and isomerized into a mixture with the formation ratio of about 1 : 1 during the isolation, so they could not be obtained in pure states. All the isomers have the corresponding catoptric forms. In the calculation, the catoptromers shown in Fig. 2 were used. The averages of the individual geometrical values based upon the minimum strain energies of the $[Co(dien)_2]^{3+}$ isomers were mainly used to construct the initial molecular structures of $[Co(linpen)]^{3+}$ isomers with the corresponding ones. In this case, the valency angles, ∠CNC, were 110—114° for the facial and 115—122° for the meridional structures. The force constants and the other parameters in the minimization were the same as for the isomers of $[Co(dien)_2]^{3+}$.

The highest symmetries for *f_4-RSSR*, *fm_2f-SRRS*, *-SSSS*, *mf_2m-RRRR*, and *-SRRS* are C_2, so the calculations for these isomers were initiated from the structures with C_2 symmetry, whereas the *f_2mf-RSRS*, *-RSSS*, and *mf_2m-RRRS* isomers possess only the C_1 symmetry. In the course of the minimization, the symmetry of each isomer was not considered, but all the isomers possessing C_2 symmetry except for *f_4-RSSR* were energy-minimized retaining this symmetry, within the limits of error. The symmetry of the energy-minimized structure of the *f_4-RSSR* isomer was C_1, and its energy was smaller than that of the structure the C_2 symmetry of which was retained in the course of the minimization. The final energy terms are presented in Table 3. All the terms coordinate deviations were smaller than 0.005 Å. The formation percentages in Table 3 are those in the equilibrium mixture of chlorides (25 °C). The III and IV isomers were assigned to *fm_2f-SRRS* and *-SSSS* for the first time on the basis of these results. As a whole, there is a rough tendency for the isomer of a large percentage to have a low minimized energy. When the data in Table 3 are plotted, with the minimized energy as the ordinate and the logarithm of the formation percentage as the abscissa, a very rough linear relationship is obtained (Fig. 3).

If the conformational structure (δ, λ) of each chelate ring is not taken into consideration, only the *f_2mf* II-1 and II-2 isomers have the C_1 symmetry, while all the others have the C_2 symmetry. Therefore, the former are favored by a statistical factor of two over the latter; those formation percentages were divided by two when their data were plotted in Fig. 3. The relatively high abundances of the VI and VII isomers, when considered with their energies, may account for the conformational equilibria being almost independent of those among the configurational isomers; that is to say, the very high stability of the V isomer may make the VI and VII isomers form more abundantly. These results show that conformational analysis may be a technique for the assignment of the structures of the configurational isomers.

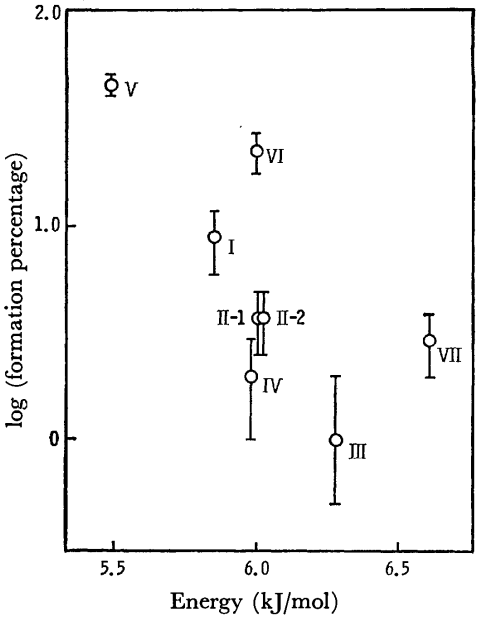

Fig. 3. Plot of log(formation percentage) *vs.* minimized energy for the isomers of $[Co(linpen)]^{3+}$. The formation percentages of both the II-1 and II-2 isomers were divided by two because of the statistical preference for these structures.

In all the calculations described here, the complexes are dealt with as free molecules. In practice, however, they have some mutual interactions with their surroundings. Therefore, it is an important problem awaiting solution to take into account these effects in order to obtain more accurate energies.

All the molecular geometries obtained by the method of the conformational analysis are presented in Table 4.

Table 3. Final energy terms for the isomers of $[Co(linpen)]^{3+}$ (Fig. 2)

Isomer	Sign of CD	Absolute configuration	Proposed[a] prefix	Bond	Nonbond	Angle	Torsion	Total		Formation percentage
I	$\{+\}_{502}$	*ΛΛΛΔ*	*f_4-RSSR*	0.33	2.22	0.86	2.45	5.85	kJ/mol	9%
II-1	$\{+\}_{492}$	*ΛΛΛΛΔ*	*f_2mf-RSRS*	0.32	2.04	1.33	2.34	6.02		15
II-2	$\{+\}_{492}$	*ΛΛΛΛΔ*	*f_2mf-RSSS*	0.35	2.08	1.30	2.27	6.00		
III	$\{+\}_{485}$	*ΛΛΛΔΔ*	*fm_2f-SRRS*	0.32	1.71	2.28	1.97	6.28		1
IV	$\{+\}_{453}$	*ΛΛΛΔΔ*	*fm_2f-SSSS*	0.32	1.82	1.97	1.87	5.98		2
V	$\{+\}_{475}$	*ΛΛΛΛΔΔ*	*mf_2m-RRRR*	0.33	1.79	1.30	2.06	5.48		47
VI	$\{+\}_{469}$	*ΛΛΛΛΔΔ*	*mf_2m-RRRS*	0.38	1.84	1.89	1.89	5.99		23
VII	$\{+\}_{469}$	*ΛΛΛΛΔΔ*	*mf_2m-SRRS*	0.42	2.06	2.23	1.90	6.60		3

a) For example, the full designation for the isomer, $\{+\}_{502}$ I is *ΛΛΛΔ-f_4(RSSR)*-$[Co(linpen)\delta\lambda\delta\lambda\delta]^{3+}$, where the last small Greek letters show the conformations of chelate rings from one end to the other.

Table 4. Molecular geometries of the isomers of [Co(linpen)]$^{3+}$ (Fig. 2)

Isomer	Bond length Co–N					
	N(*a*)	N(*b*)	N(*c*)	N(*d*)	N(*e*)	N(*f*)
I, f_4-*RSSR*	1.958	1.967	1.973	1.971	1.974	1.969 Å
I, f_4-*RSSR**	1.963	1.968	1.972	1.973	1.975	1.970
II-1, f_2mf-*RSRS*	1.965	1.961	1.952	1.970	1.977	1.975
II-2, f_2mf-*RSSS*	1.983	1.964	1.948	1.974	1.976	1.966
III, fm_2f-*SRRS*	1.982	1.943	1.943	1.963	1.963	1.982
IV, fm_2f-*SSSS*	1.980	1.936	1.937	1.958	1.958	1.981
V, mf_2m-*RRRR*	1.947	1.969	1.969	1.982	1.982	1.947
VI, mf_2m-*RRRS*	1.953	1.986	1.974	1.974	1.985	1.947
VII, mf_2m-*SRRS*	1.953	1.990	1.991	1.978	1.978	1.952

Isomer	Valence angle ∠NCoN chelate ring				
	1	2	3	4	5
I, f_4-*RSSR*	87.2	88.6	86.9	87.1	86.1°
I, f_4-*RSSR**	86.9	88.2	87.1	87.3	86.1
II-1, f_2mf-*RSRS*	85.3	89.3	84.9	87.0	86.8
II-2, f_2mf-*RSSS*	85.2	87.4	86.7	84.5	88.2
III, fm_2f-*SRRS*	85.0	87.5	86.3	87.5	85.0
IV, fm_2f-*SSSS*	88.1	86.8	87.3	86.8	88.0
V, mf_2m-*RRRR*	85.7	85.0	89.0	85.0	85.7
VI, mf_2m-*RRRS*	84.6	84.9	87.3	85.8	85.5
VII, mf_2m-*SRRS*	84.0	85.8	86.1	85.8	84.0

Isomer	Dihedral angle ∠NCCN[a] chelate ring				
	1	2	3	4	5
I, f_4-*RSSR*	+43.4	−39.4	+41.7	−41.5	+39.0°
I, f_4-*RSSR**	+42.5	−40.1	+41.5	−41.7	+39.2
II-1, f_2mf-*RSRS*	+38.9	−46.1	−37.1	+46.6	−40.6
II-2, f_2mf-*RSSS*	+41.0	−40.6	+45.8	−35.1	−49.2
III, fm_2f-*SRRS*	−41.7	+44.0	−52.4	+44.1	−41.7
IV, fm_2f-*SSSS*	−50.2	−39.0	+53.0	−39.0	−49.7
V, mf_2m-*RRRR*	+48.6	−36.4	−52.2	−36.5	+48.7
VI, mf_2m-*RRRS*	−47.6	−37.0	−47.2	+44.5	+49.6
VII, mf_2m-*SRRS*	−44.5	+47.4	−40.7	+47.4	−44.4

a) Positive and negative signs represent δ and λ conformations of chelate rings, respectively.

* As the initial molecular coordinates, those from the X-ray analysis[12] were used.

Generally, the Co–N bond lengths are 1.97—1.98 Å for primary amines, and 1.96—1.97 and 1.94—1.95 Å for secondary amines, with facial and meridional structures respectively, except for a part of the II-2, VI, and VII isomers. The valency angles, ∠NCoN (chelate ring), in the meridional structure are smaller than those in the facial structure.

As the I isomer contains only the facial structure, it can be predicted that the strain for the valency angles in this isomer is smaller than those in all the others which contain the meridional structures; this is in accord with the result shown in Table 3. On the other hand, the III—VII isomers, which contain two meridional structures, have appreciably large strains for all the valency angles except for the V isomer. The strain of the V isomer may be moderately released at the sacrifice of that for the torsion.

During the course of the present study, Sato and Saito have determined the molecular structure of the {+}$_{502}$I isomer from an X-ray analysis of {+}$_{502}$[Co(linpen)][Co(CN)$_6$]·3H$_2$O.[12] The structure which we predicted and energy-minimized agreed completely in its conformations and configurations with that determined by them.

We also carried out the minimization for the I isomer by using the molecular coordinates obtained from the X-ray analysis[12] as the initial ones. These results are also included in Table 4. The agreement between this structure and that obtained previously is excellent.

Thus, we can obtain accurate information on the molecular structures of cobalt(III) complexes from the energy-minimized conformational analysis calculation.

We wish to thank Mr. Koshiro Toriumi and Professor Yoshihiko Saito of the Institute for Solid State Physics, the University of Tokyo, for the permission to use their computer programs and for their valuable discussions. Mr. Koshiro Toriumi also provided helpful advice. We are also indebted to Professors Shoichi Sato and Yoshihiko Saito for obtaining the X-ray crystal analysis data on the {+}$_{502}$I isomer of [Co(linpen)]$^{3+}$. Thanks are also due to the Nagoya University Computer Center for the use of the FACOM 230-60 computer. This research was supported in part by the Matsunaga Science Foundation.

References

1) Parts V and VI were published in this Bulletin, **48**, 879 and 2801 (1975).

2) R. H. Boyd, *J. Chem. Phys.*, **49**, 2574 (1968).

3) K. Toriumi and Y. Saito, The 29th Annual Meeting of the Chemical Society of Japan, Hiroshima, October, 1973, Proceedings Vol. II, p. 1108.

4) K. Toriumi and Y. Saito, *Acta Crystallogr.*, **B31**, 1247 (1975).

5) Y. Yoshikawa and K. Yamasaki, This Bulletin, **46**, 3448 (1973).

6) Y. Yoshikawa and K. Yamasaki, *ibid.*, **45**, 179 (1972); F. R. Keene and G. H. Searle, *Inorg. Chem.*, **11**, 148 (1972).

7) M. Kobayashi, F. Marumo, and Y. Saito, *Acta Crystallogr.*, **B28**, 470 (1972).

8) M. Konno, F. Marumo, and Y. Saito, *ibid.*, **B29**, 739 (1973).

9) IUPAC Nomenclature of Inorganic Chemistry, Definitive Rules 1970, Butterworths, London (1971).

10) M. Dwyer and G. H. Searle, *Chem. Commun.*, **1972**, 726; M. Dwyer, R. J. Geue, and M. R. Snow, *Inorg. Chem.*, **12**, 2057 (1973).

11) D. A. Buckingham, I. E. Maxwell, A. W. Sargeson, and M. R. Snow, *J. Amer. Chem. Soc.*, **92**, 3619 (1970).

12) S. Sato and Y. Saito, Private communication; *Acta Crystallogr.*, **B31** (1975), in press, The Crystal Structure of (+)$_{589}$-*AAAA*-Linear Pentaethylenehexaminecobalt(III) Hexacyanocobaltate(III) Trihydrate.

The Effect of Steric Condition in Cobalt(II), Nickel(II) and Copper(II) Complexes with Schiff Bases Obtained from Salicylaldehyde Derivatives and Diphenylmethylamine

Kuniko YAMANOUCHI and Shoichiro YAMADA

Institute of Chemistry, College of General Education, Osaka University, Toyonaka, Osaka 560

(Received September 26, 1975)

Cobalt(II), nickel(II) and copper(II) complexes with *N*-diphenylmethyl-ring-substituted salicylideneiminates (abbreviated as X-Sal-Dpm) have been synthesized, in order to examine the steric and electronic effect of a substituent diphenylmethyl group on the structure of the metal complexes. Compounds of the type $M(X\text{-}Sal\text{-}Dpm)_2$ and their adducts of the type $M(X\text{-}Sal\text{-}Dpm)_2 \cdot nL$ have been isolated in crystals, n being 2 or 4 and L being benzene, acetone or pyridine. Both in the solid state and in non-donor solvents, the complexes $Co(X\text{-}Sal\text{-}Dpm)_2$ have a tetrahedral configuration, and $Ni(X\text{-}Sal\text{-}Dpm)_2$ and $Cu(X\text{-}Sal\text{-}Dpm)_2$ have a square-planar configuration, irrespectively of substituents X. The results so far available seem to indicate that the steric hindrance caused by the substituent diphenylmethyl group against the square-planar configuration of the metal complexes may be smaller than that by isopropyl group.

Numerous studies have so far been carried out on 3d transition metal complexes with *N*-substituted salicylideneiminates, which are abbreviated as X-Sal-R (I) in the present paper. These studies have shown that metal complexes of the type $M(X\text{-}Sal\text{-}R)_2$ vary widely in the structure, depending upon the steric condition arising from R and also upon the electronic effect caused by R on the nitrogen atom.[1-3] For instance, the structure of $M(X\text{-}Sal\text{-}n\text{-}alkyl)_2$ often differs from that of the complexes with α-branched alkyl for R, mainly because the steric hindrance arising from the α-branched alkyl is remarkably larger than that from *n*-alkyl. The 3d transition metal complexes with *N*-isopropylsalicylideneiminate and its derivatives have been studied, in comparison with the corresponding *n*-alkyl complexes.[4-6] Since diphenylmethyl, abbreviated as Dpm, is related to isopropyl, bearing two phenyl groups instead of two methyl groups in isopropyl, it is thought to be interesting to investigate metal complexes with Schiff bases having diphenylmethyl for R and compare the steric and electronic effects of the substituent Dpm upon the structure of their metal complexes with those of α-branched alkyls.

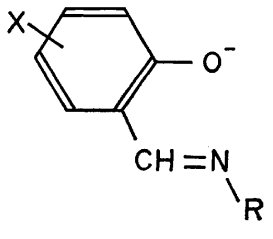

I

In the present work, cobalt(II), nickel(II) and copper(II) complexes with *N*-diphenylmethyl-ring-substituted salicylideneiminates have been synthesized and their structures examined mainly on the basis of their electronic absorption spectra and magnetic data.

Experimental

Materials. Analytical data of new complexes prepared in the present work are shown in Tables 1 and 2.

Bis(N-diphenylmethylsalicylideneiminato)copper(II), Cu(H-Sal-Dpm)₂. Diphenylmethylamine (0.01 mol) was added to a suspension of bis(salicylaldehydato)copper(II) (0.01 mol) in ethanol (50 ml) at about 60 °C and heated with stirring at this temperature for about 30 min. A brown precipitate was recrystallized from chloroform to yield olive-green crystals.

Bis(N-diphenylmethyl-5-chlorosalicylideneiminato)copper(II), Bis(N-diphenylmethyl-5-bromosalicylideneiminato)copper(II) and *Bis(N-diphenylmethyl-3-methoxysalicylideneiminato)copper(II)* were prepared as crystals by a method similar to that described above. These copper(II) complexes are olive-green (X=5-Cl, 5-Br) or brown ($X=3\text{-}CH_3O$). They are highly soluble in chloroform and benzene, moderately soluble in acetone and pyridine, and sparingly soluble in methanol and ethanol.

Bis(N-diphenylmethyl-5-chlorosalicylideneiminato)copper(II) Bis(pyridine)-adduct, Cu(5-Cl-Sal-Dpm)₂·2py. The parent complex was dissolved in pyridine at 50—60 °C, filtered while the solution was hot, and allowed to stand overnight in a refrigerator. Green crystals of the bis(pyridine)-adduct were collected by filtration.

Bis(N-diphenylmethyl-5-bromosalicylideneiminato)copper(II) Tetrakis(pyridine)-adduct, Cu(5-Br-Sal-Dpm)₂·4py. A similar procedure to that described above yielded green crystals of the tetrakis(pyridine)-adduct.

Bis(pyridine)-adduct of the same parent complex was isolated, when recrystallization was carried out from pyridine–ethanol (2:1) or pyridine–chloroform (2:1) mixture instead of pyridine itself.

Both these adducts readily lose pyridine molecules, when left in the atmosphere.

Bis(N-diphenylmethyl-ring-substituted salicylideneiminato)nickel(II), Ni(X-Sal-Dpm)₂ (X=H, 5-Cl, 5-Br, 3-CH₃O). Complexes of this type were prepared by a method similar to that for the copper(II) complexes. They are olive-green (X=H, 5-Cl, 5-Br) or greenish brown ($X=3\text{-}CH_3O$). They are highly soluble in chloroform and benzene, moderately soluble in acetone and hot pyridine, and sparingly soluble in methanol, ethanol and cold pyridine.

Bis(N-diphenylmethyl-3-methoxysalicylideneiminato)nickel(II) Tetrakis(pyridine)-adduct, Ni(3-CH₃O-Sal-Dpm)₂·4py. was obtained in green crystals, when the parent complex was recrystallized from pyridine. Bis(pyridine)-adduct could not be isolated by procedures similar to those described above.

All these pyridine adducts of the nickel(II) complexes are much more stable in the atmosphere than the corresponding adducts of the copper(II) and cobalt(II) complexes. They are soluble in benzene, chloroform and acetone, but only

TABLE 1. ANALYTICAL DATA OF COMPLEXES OF THE TYPE M(X-Sal-Dpm)$_2$ AND RELATED COMPOUNDS

Compound	Calcd, %			Found, %			μ
	C	H	N	C	H	N	
Cu(H-Sal-Dpm)$_2$	75.51	5.07	4.40	74.75	5.06	4.45	1.9
Cu(5-Br-Sal-Dpm)$_2$	60.50	3.81	3.53	60.94	4.01	3.50	1.9
Cu(5-Cl-Sal-DPM)$_2$	69.55	4.29	3.97	69.33	4.28	4.01	1.9
Cu(3-CH_3O-Sal-Dpm)$_2$	72.46	5.21	4.02	72.51	5.23	4.03	2.0
Ni(H-Sal-Dpm)$_2$	76.09	5.11	4.44	75.92	5.20	4.56	dia
Ni(5-Br-Sal-Dpm)$_2$	60.87	3.83	3.55	60.23	3.78	3.44	dia
Ni(5-Cl-Sal-Dpm)$_2$	68.63	4.32	4.00	68.73	4.32	3.89	dia
Ni(3-CH_3O-Sal-Dpm)$_2$	72.95	5.25	4.05	72.77	5.18	3.98	dia
Co(H-Sal-Dpm)$_2$	76.06	5.11	4.44	76.24	5.08	4.48	4.5
Co(5-Br-Sal-Dpm)$_2$	60.85	3.83	3.55	60.82	3.85	3.56	4.2
Co(5-Cl-Sal-Dpm)$_2$	68.58	4.32	4.00	68.52	4.49	4.04	4.4
Co(5-Br-Sal-Dpm)$_2$·2bz	68.53	5.37	3.56	68.08	5.12	3.47	4.5
Co(5-Br-Sal-Dpm)$_2$·2ac	60.85	3.83	3.55	60.82	3.85	3.56	4.6
Co(5-Cl-Sal-Dpm)$_2$·2bz	72.90	4.94	3.27	71.49	5.05	3.17	4.2
Co(5-Cl-Sal-Dpm)$_2$·2ac	61.01	4.68	3.09	61.10	4.64	3.08	4.2

μ: BM, at room temperature dia: diamagnetic bz: benzene ac: acetone

TABLE 2. ANALYTICAL DATA OF ADDUCTS WITH PYRIDINE

Compound	Calcd, %			Found, %			μ
	C	H	N	C	H	N	
Cu(5-Br-Sal-Dpm)$_2$·2py	63.06	4.23	5.88	63.13	4.17	5.94	
Cu(5-Br-Sal-Dpm)$_2$·4py	64.89	4.54	7.57	64.29	4.54	7.42	
Cu(5-Cl-Sal-Dpm)$_2$·2py	69.56	4.67	6.49	69.68	4.64	6.42	2.0
Ni(H-Sal-Dpm)$_2$·2py	76.06	5.36	7.10	75.89	5.46	7.22	3.0
Ni(5-Br-Sal-Dpm)$_2$·2py	63.39	4.26	5.91	63.15	4.25	5.89	3.2
Ni(5-Br-Sal-Dpm)$_2$·4py	65.18	4.56	7.60	65.57	4.58	7.83	2.9
Ni(5-Cl-Sal-Dpm)$_2$·2py	69.93	4.70	6.52	70.56	4.78	6.87	3.1
Ni(3-CH_3O-Sal-Dpm)$_2$·4py	73.88	5.60	8.34	74.35	5.65	8.34	3.0
Co(H-Sal-Dpm)$_2$·2py	76.03	5.36	7.09	75.88	5.51	7.29	4.8
Co(5-Br-Sal-Dpm)$_2$·2py	63.37	4.25	5.91	63.12	4.42	5.88	4.9
Co(5-Br-Sal-Dpm)$_2$·4py	65.16	4.56	7.60	65.85	4.62	7.65	4.8
Co(5-Cl-Sal-Dpm)$_2$·2py	69.56	4.67	6.49	69.68	4.64	6.42	5.0
Co(3-CH_3O-Sal-Dpm)$_2$·4py	73.87	5.60	8.34	73.72	5.67	8.01	5.0
Co(5-Br-Sal-*i*-pr)$_2$·2py	51.52	4.61	8.01	51.38	4.68	8.11	4.9
Co(5-NO_2-Sal-*i*-pr)$_2$·2py	57.05	5.11	13.30	57.33	5.16	13.37	4.8
Co(5-NO_2-Sal-Ch)$_2$·2py	60.75	5.67	11.81	61.14	5.60	12.01	4.9
Co(3-CH_3O-Sal-Ch)$_2$·2py	66.95	6.80	8.22	66.87	6.75	8.16	4.9

μ: BM, at room temperature py: pyridine pr: propyl Ch: cyclohexyl

slightly soluble in methanol, ethanol and cold pyridine.

Bis(N-*diphenylmethylsalicylideneiminato*)*cobalt*(*II*), *Co*(*H-Sal-Dpm*)$_2$. This complex was synthesized in the same way as the corresponding copper(II) complex. Recrystallization of the crude product from benzene or chloroform yielded red-orange crystals of the pure complex.

Bis(N-*diphenylmethyl-5-halogenosalicylideneiminato*)*cobalt* (*II*), *Co*(*X-Sal-Dpm*)$_2$ (*X=5-Cl, 5-Br*). The crude products of these complexes were prepared in the same way as described above for Co(H-Sal-Dpm)$_2$. It was not possible to find a suitable solvent for recrystallization. Attempts to recrystallize them yielded either products of insignificant composition or adducts with solvents used in the recrystallization, instead of the pure parent complex.

The pure complexes of the type Co(X-Sal-Dpm)$_2$ were obtained by heating bis(benzene)- or bis(acetone)-adduct (*vide infra*) for about 4 hr at about 80 °C under reduced pressure.

These cobalt(II) complexes are soluble in chloroform, benzene and acetone, but sparingly soluble in methanol, ethanol and cold pyridine.

Bis(N-*diphenylmethyl-5-halogenosalicylideneiminato*)*cobalt*(*II*) *Bis*-(*benzene*)- *and Bis*(*acetone*)-*adducts*, *Co*(*X-Sal-Dpm*)$_2$·2*L* (*X=5-Cl, 5-Br*; *L=benzene, acetone*). Crude products of the parent complexes, which were prepared as described above, were recrystallized from benzene or acetone to yield red-orange crystals of the bis(benzene)- or bis(acetone)-adducts.

Bis(N-*diphenylmethyl-ring-substituted salicylideneiminato*)*cobalt*-(*II*) *Bis*(*pyridine*)-*adducts*, *Co*(*X-Sal-Dpm*)$_2$·2*py* (*X=H, 5-Cl*). Compounds of this type were isolated in yellow-orange crystals by a method similar to that for the corresponding nickel(II) compounds.

Bis(N-*diphenylmethyl-5-bromosalicylideneiminato*)*cobalt*(*II*) *Tetra-kis*(*pyridine*)- *and Bis*(*pyridine*)-*adducts*, *Co*(*5-Br-Sal-Dpm*)$_2$·n*py* (*n*=2,4) were isolated in yellow-orange crystals by a method similar to that for the corresponding nickel(II) compounds.

Bis(N-*diphenylmethyl-3-methoxysalicylideneiminato*)*cobalt*(*II*)

Tetrakis(pyridine)-adduct, Co(3-CH_3O-Sal-Dpm)$_2$·4py, was obtained in yellow-orange crystals in the same way as described above for the corresponding nickel(II) complex. It has not been possible so far to isolate crystals of the parent complex, Co(3-CH_3O-Sal-Dpm)$_2$.

All these pyridine adducts of the cobalt(II) complexes lose pyridine molecules comparatively slowly, when left in the atmosphere. They are considerably soluble in benzene, chloroform and acetone, but only slightly soluble in methanol, ethanol and cold pyridine.

With the cobalt(II), nickel(II) and copper(II) complexes, only bis- and/or tetrakis(pyridine)-adducts were obtained, and adducts of another type, such as mono- and tris-(pyridine)-adducts, have not been isolated.

Bis(N-isopropyl-ring-substituted salicylideneiminato)cobalt(II) Bis-(pyridine)-adducts, Co(X-Sal-i-C_3H_7)$_2$·2py (X=5-Br, 5-NO_2), were obtained in yellow-orange crystals by recrystallizing the parent complex from pyridine or by adding *n*-hexane into a hot solution of the parent complex in pyridine.

Bis(N-cyclohexyl-ring-substituted salicylideneiminato)cobalt(II), Co(X-Sal-Ch)$_2$ (X=5-Cl, 5-Br, 5-NO_2, 3-CH_3O), were prepared, as previously reported, Ch being cyclohexyl.[6]

Bis(N-cyclohexyl-ring-substituted salicylideneiminato)cobalt(II)bis-(pyridine)-adducts, Co(X-Sal-Ch)$_2$·2py (X=5-NO_2, 3-CH_3O) were obtained in yellow-orange crystals by recrystallizing the parent complexes from pyridine or by adding hexane into a hot solution of the parent complexes in pyridine.

Measurements. Electronic absorption spectra of the complexes were measured on a Shimadzu MPS-50L spectrophotometer. Infrared spectra were obtained from Nujol mulls using a Hitachi EPI-S2 infrared spectrophotometer.

Magnetic measurements were carried out by the Gouy method at room temperature using $CoHg(SCN)_4$ as a calibrant.

Since many of the adducts underwent decomposition during the measurements, only those data which may be regarded as accurate and reliable enough for discussion are shown in the tables. Solubility of complexes Co(X-Sal-Dpm)$_2$ and Ni-(X-Sal-Dpm)$_2$ in appropriate solvents including pyridine is not high enough for spectral measurements.

Results and Discussion

Cobalt(II) Complexes. When cobalt(II) acetate, salicylaldehyde and diphenylmethylamine are refluxed in the atmosphere in the presence of alkali, such as sodium carbonate, bis(*N*-diphenylmethylsalicylideneiminato)cobalt(II) is readily obtained, oxidation to the cobalt(III) complex hardly being observed. Any attempt to isolate the tris(Schiff base)cobalt(III) complex has not so far been successful even with hydrogen peroxide.

Previous studies have shown that a similar procedure in the atmosphere readily yields the cobalt(III) complexes of the corresponding Schiff bases, when *n*-alkylamines are employed instead of diphenylmethylamine.[2a] A similar procedure using isopropylamine, *t*-butylamine or arylamines yields only bis(Schiff base)-cobalt(II) complex.[6] Tris(*N*-isopropyl-ring-substituted salicylideneiminato)cobalt(III) complexes,[7] as well as tris(*N*-arylsalicylideneiminato)cobalt(III),[8] are obtained by more effective oxidation using hydrogen peroxide.

Comparison seems to indicate that greater difficulty is encountered in obtaining Co(X-Sal-Dpm)$_3$ than Co(X-Sal-*i*-C_3H_7)$_3$, although it may not be plausible to say definitely that Co(X-Sal-Dpm)$_3$ cannot be isolated at all. The difference in this respect between Dpm and isopropyl may be discussed in terms of the two factors: (a) ligand field strength and (b) steric condition.

It is known that the higher stability of the sexa-coordinated cobalt(III) complex is attained with ligands producing a stronger ligand field. It is expected and has also been confirmed by some experimental results[1,2] that the ligand field of X-Sal-R depends upon the nature of substituents R and decreases in the following order: aryl<CH(ph)$_2$<CH_2ph<*n*-alkyl<*i*-C_3H_7, where ph denotes phenyl group. Thus X-Sal-Dpm would produce a slightly weaker ligand field than X-Sal-*i*-C_3H_7. Therefore, so far as the factor of the ligand field strength is concerned, X-Sal-Dpm would form the tris(Schiff base)-cobalt(III) less readily than X-Sal-*i*-C_3H_7, in agreement with the experimental results.

Alternatively, in order to explain the observed results, one might argue that larger steric hindrance against formation of the tris(Schiff base)cobalt(III) complex would be created by X-Sal-Dpm than by X-Sal-*i*-C_3H_7. This explanation, however, may not be adequate, since in fact, the reverse seems to be the case. The truth is that larger steric hindrance may be exercised by X-Sal-*i*-C_3H_7 than by X-Sal-Dpm in formation of both th square-planar bis(Schiff base)-nickel(II) complexes and the sexa-coordinated bis(pyridine)-adducts of the cobalt(II) complexes, as will be discussed later in this paper. Nevertheless, the steric factor, besides the electronic factor, is also considered to play at least a minor role in preventing the tris-complex formation.

It should be noted that benzene or acetone adducts are obtained, when recrystallization of Co(X-Sal-Dpm)$_2$ is carried out from benzene or acetone, X being Cl and Br. As shown in Table 3, spectra of the benzene adducts are typical of the tetrahedral cobalt(II) complexes. It is presumed that the benzene adducts consist of tetrahedral cobalt(II) complexes and non-coordinated benzene molecules, which presumably occupy interstice in the crystal lattices. The benzene adducts, when dissolved in benzene, show nearly the same electronic spectra as those of the parent complexes, which are typical of the tetrahearal cobalt(II) complexes, as shown in Table 3.

The acetone adducts also show electronic spectra, which are essentially the same as those of the parent complexes. Moreover, the adducts show a strong infrared band at 1700 cm^{-1}, which is assigned to a C=O stretching frequency of a free acetone molecule. It is, therefore, reasonable to consider that they consist of the tetrahedral cobalt(II) complexes and non-coordinated acetone molecules. This conclusion is also supported by the finding that the spectrum of Co(5-Cl-Sal-Dpm)$_2$ in acetone is almost identical with that of the same complex in benzene, showing that the acetone molecule is not bound with the cobalt(II) ion.

It is interesting to note that both bis(pyridine)- and tetrakis(pyridine)-adducts of the cobalt(II) complexes are isolated for X=H, 5-Cl, 5-Br and 3-CH_3O. Although they lose pyridine molecules slowly, they are

TABLE 3. MAIN d-d ABSORPTION MAXIMA OF M(X-Sal-Dpm)$_2$ AND THEIR BENZENE AND ACETONE ADDUCTS

Compound	Solvent	ν (log ε)
Ni(H-Sal-Dpm)$_2$	CH_2Cl_2	16.5 (1.94), 19.5 (2.05) sh
Ni(5-Cl-Sal-Dpm)$_2$	CH_2Cl_2	16.4 (2.01), 19.3 (2.10) sh
Ni(5-Br-Sal-Dpm)$_2$	CH_2Cl_2	16.4 (2.00), 19.4 (2.10) sh
Ni(3-CH_3O-Sal-Dpm)$_2$	CH_2Cl_2	16.3 (2.06), 19.3 (2.10) sh
Co(H-Sal-Dpm)$_2$	CH_2Cl_2	8.3 (1.79), 10.8 (1.50) sh, 18.6 (1.80)
Co(5-Br-Sal-Dpm)$_2$	$CHCl_3$	8.1 (1.84), 10.5 (1.55) sh, 18.1 (1.80) sh
Co(5-Cl-Sal-Dpm)$_2$	$CHCl_3$	8.1 (1.82), 10.6 (1.45) sh, 18.2 (1.80) sh
	benzene	8.2 (1.81), 10.6 (1.60) sh, 18.2 (1.90) sh
	acetone	8.2 (1.81), 10.5 (1.60) sh, 18.3 (1.98) sh
Co(5-Cl-Sal-Dpm)$_2$·2bz	Nujol	8.2, 10.5, 18.2
Co(5-Br-Sal-Dpm)$_2$·2ac	Nujol	8.2, 10.5, 18.3

ν: kK

crystalline and their analytical data agree only with either the bis- or tetrakis(pyridine)-adduct. The reason why another type of adduct, for example, mono- or tris-(pyridine)-adduct does not occur is not clear. Both the bis- and tetrakis-(pyridine)-adducts show electronic spectra typical of sexa-coordinated bis-(pyridine)bis(*N*-substituted salicylideneiminato)cobalt-(II) complexes, as shown in Table 4. The d-d band at about 10 kK may be assigned to a transition $^4T_{2g} \leftarrow {}^4T_{1g}$ in the scheme of the O_h ligand field symmetry. It is, therefore, presumed that they contain sexa-coordinated bis(pyridine)-cobalt(II) complexes, which probably have a *cis*-structure, judging from the steric condition.

Now we may compare the data in the present work with those for complexes of the type Co(X-Sal-*i*-C_3H_7)$_2$. In previous papers,[2] Co(H-Sal-*i*-C_3H_7)$_2$ was reported to have very low capacity to form a sexa-coordinated bis(pyridine)-adduct, which has not been isolated in crystals so far. Even in pyridine, at least 90% of it exists as the original tetrahedral cobalt(II) complex.[6,9] This is in contrast to the behavior of Co(H-Sal-Dpm)$_2$, which readily forms a bis(pyridine)-adduct. The difference in this respect between these two series of cobalt(II) complexes may be ascribed mainly to the steric factor. The steric factor, however, seems to be rather delicate and not the only dominant factor in this case. The effect of the substituent X on the electronic state of the nitrogen atom in the Schiff base may also play a significant part. As shown in Table 4, when dissolved in pyridine, the complexes Co(X-Sal-*i*-C_3H_7)$_2$, X being 5-Cl, 5-Br and 5-NO_2, consist almost entirely of sexa-coordinated bis(pyridine)-adducts, some of which can be isolated in crystals from their pyridine solutions. The bis(pyridine)-adducts have magnetic moments of 4.8 to 5.1 BM and show electronic spectra typical of the sexacoordinated cobalt(II) complex with a d-d band maximum at about 10 kK. The remarkable difference between Co(H-Sal-*i*-C_3H_7)$_2$ and Co(X-Sal-*i*-C_3H_7)$_2$, X being 5-Cl, 5-Br and 5-NO_2, seems to be noteworthy. The effect of the substituent X is found to be significant.

TABLE 4. MAIN d-d ABSORPTION MAXIMA OF M(X-Sal-Dpm)$_2$·*n*py AND RELATED COMPOUNDS

Compound	Solvent	ν (log ε)
Ni(H-Sal-Dpm)$_2$·2py	Nujol	11.0, 17.9
Ni(5-Br-Sal-Dpm)$_2$·2py	Nujol	11.0, 17.9
Ni(5-Br-Sal-Dpm)$_2$·4py	Nujol	11.0, 17.8
Ni(5-Cl-Sal-Dpm)$_2$·2py	Nujol	10.7, 17.8
Ni(3-CH_3O-Sal-Dpm)$_2$·4py	Nujol	10.9, 17.9
Co(H-Sal-Dpm)$_2$·2py	Nujol	10.7, 17.8 sh
Co(5-Br-Sal-Dpm)$_2$·2py	Nujol	10.6, 17.5 sh
Co(5-Br-Sal-Dpm)$_2$·4py	Nujol	10.6, 17.7 sh
Co(5-Cl-Sal-Dpm)$_2$·2py	Nujol	10.6, 17.7 sh
Co(3-CH_3O-Sal-Dpm)$_2$·4py	Nujol	10.7, 17.5 sh
Co(5-Br-Sal-*i*-pr)$_2$	pyridine	10.3 (1.02), 17.8 (1.32) sh
Co(5-Br-Sal-*i*-pr)$_2$·2py	Nujol	10.2, 17.8
Co(5-Cl-Sal-*i*-pr)$_2$	pyridine	10.3 (1.08), 17.9 (1.35) sh
Co(5-NO_2-Sal-*i*-pr)$_2$	pyridine	10.0 (1.12), 17.6 (1.35) sh
Co(5-NO_2-Sal-*i*-pr)$_2$·2py	Nujol	10.1, 17.8 sh
Co(5-Br-Sal-Ch)$_2$	pyridine	10.3 (0.95), 17.7 (1.32) sh
Co(5-Cl-Sal-Ch)$_2$	pyridine	10.1 (1.01), 17.7 (1.33) sh
Co(5-NO_2-Sal-Ch)$_2$	pyridine	10.0 (1.16), 17.8 (1.40) sh
Co(5-NO_2-Sal-Ch)$_2$·2py	Nujol	10.2, 17.6
Co(3-CH_3O-Sal-Ch)$_2$	pyridine	10.2 (1.10), 17.7 (1.35) sh
Co(3-CH_3O-Sal-Ch)$_2$·2py	Nujol	10.2, 17.6

ν: kK pr: propyl Ch: cyclohexyl

Comparison of Co(X-Sal-Dpm)$_2$ with Co(X-Sal-Ch)$_2$, Ch being cyclohexyl group, may also be interesting. Previous studies have shown that in pyridine, nearly 50% of Co(H-Sal-Ch)$_2$ exists as the original tetrahedral cobalt(II) complex.[6,9] However, it has not so far been possible to isolate bis(pyridine)-adduct. Instead, mono-pyridine-adduct was isolated as red crystals.[10] The effect of the substituent X is again found to be remarkable in the cyclohexyl complexes. As shown in Table 4, electronic spectra indicate that the complexes Co(X-Sal-Ch)$_2$ in pyridine, X being 5-Cl, 5-Br, 5-NO_2 and 5-CH_3O, exist totally as sexa-coordinated bis(pyridine)-adducts. Some of them can also be isolated in crystals from their pyridine solutions, as shown in Table 2. Electronic spectra of these bis(pyridine)-adducts have a d-d band with a maximum at about 10 kK, which is typical of the sexa-coordinated cobalt(II) complex.

Inspection of the data so far available indicates that the relative tendency of Co(X-Sal-R)$_2$ to form sexa-coordinated bis(pyridine)-adducts increases according to the substituent R in the following order: $CH(ph)_2 < Ch < CH(CH_3)_2 < C(CH_3)_3$. This order seems to be in agreement with the order for the steric hindrance arising from the substituent.

Nickel(II) and Copper(II) Complexes. As shown in Tables 1 and 3, complexes of the type Ni(X-Sal-Dpm)$_2$ are diamagnetic in the solid state and show electronic absorption spectra typical of the square-planar nickel(II) complex in non-donor solvents. No absorption band is observed at about 10—11 kK or lower frequencies, where the octahedral or tetrahedral nickel(II) complex is expected to absorb. So far, any tetrahedral species has been neither isolated in crystals, nor detected in the solutions at room temperature for nickel(II) complexes of the type Ni(X-Sal-Dpm)$_2$. This result is in contrast to the result previously reported for complexes of the type Ni(X-Sal-*i*-C_3H_7)$_2$, which exist in non-donor solvents at room temperature in a conformational equilibrium of the planar diamagnetic and pseudo-tetrahedral paramagnetic forms.[4] The equilibrium depends upon the nature of the substituents R; Ni(H-Sal-*i*-C_3H_7)$_2$ in non-donor solvents at room temperature exists almost totally as the tetrahedral species. Moreover, both tetrahedral and squre-planar species of Ni(X-Sal-*i*-C_3H_7)$_2$ were previously isolated.[2b,4,5,11] Comparison indicates that the steric hindrance against the square-planar configuration in the complexes Ni(X-Sal-Dpm)$_2$ is smaller than in Ni(X-Sal-*i*-C_3H_7)$_2$.

Just like the corresponding cobalt(II) complexes, both bis- and tetrakis-(pyridine)-adducts of the nickel(II) complexes are readily isolated. They are of a high spin type and show electronic absorption spectra typical of sexa-coordinated nickel(II) complexes, having a d-d band at about 11 kK, as shown in Table 4. The band at about 11 kK may be assigned to a $^3T_{2g} \leftarrow {}^3A_{2g}$ transition in the scheme of O_h field symmetry. It is presumed, therefore, that they all contain sexa-coordinated bis(pyridine)nickel(II) complexes. A similar trend was previously reported for complexes of the type Ni(X-Sal-*i*-C_3H_7)$_2$, which form sexa-coordinated bis-(pyridine)-adducts, when dissolved in pyridine.[12]

Electronic absorption spectra of copper(II) complexes of the type Cu(X-Sal-Dpm)$_2$ in non-donor solvents are similar to each other and nearly identical with the spectra of complexes Cu(X-Sal-*n*-alkyl)$_2$, having the first d-d band with a maximum at about 17 kK (log ε 2—2.2) and a shoulder at about 22 kK (log ε 2.8—3.0). It may, therefore, be reasonable to presume that these complexes in non-donor solvents have an essentially square-planar configuration.

It should be noted that the spectra of Cu(H-Sal-Dpm)$_2$ in non-donor solvents are remarkably different from those of Cu(H-Sal-*i*-C_3H_7)$_2$,[4,5] which was concluded to contain pseudo-tetrahedral species. The latter complex shows the first d-d band with a maximum at about 15.7 kK, which is found to be shifted toward a considerably lower frequency than that of the former (17 kK). The difference between these two complexes also seems to be in agreement with the assumption that the steric hindrance against the square-planar configuration is smaller in the complexes Cu(X-Sal-Dpm)$_2$ than in Cu(X-Sal-*i*-C_3H_7)$_2$.

Spectra of Cu(X-Sal-Dpm)$_2$ in pyridine differ significantly from their spectra in non-donor solvents; the latter have more broad d-d bands at about 15.5 kK, which is found to be shifted toward lower frequencies, as compared with the corresponding band of the solutions in non-donor solvents. The spectral change in the d-d band region of these copper(II) complexes on going from a non-donor solvent to pyridine is similar to the change observed previously when the quadri-coordinated complex of copper(II) takes up one or two additional pyridine molecules to form a penta- or sexa-coordinated complex.[13]

The pyridine adducts, Cu(X-Sal-Dpm)$_2 \cdot n$py, n being 2 and 4, are isolated in crystals. However, they lose pyridine molecules so readily that it has not been possible to obtain reliable data of electronic absorption spectra and magnetic susceptibilities in most cases. Judging from their behavior in the pyridine solutions, it is most likely that some number of pyridine molecules may be bound with the copper(II) ion. From the experimental data so far available, however, it is difficult to know the exact number of pyridine molecules bound with the copper(II) ion.

References

1) R. H. Holm and M. J. O'Connor, *Progr. Inorg. Chem.*, **14**, 241 (1972).

2) (a) S. Yamada, *Coord. Chem. Rev.*, **1**, 415 (1966); (b) S. Yamada, "Novel in Coordination Chemistry. Section Lectures of the XIII. I. C. C. C.," ed. by B. J. -Trzebiatowska and M. Rudolph, Polish Academy of Sciences (1974), p. 189.

3) L. Sacconi, *Coord. Chem. Rev.*, **1**, 192 (1966).

4) L. Sacconi, *ibid.*, **1**, 126 (1966); *Exper. Suppl.*, **9**, 148 (1964); R. H. Holm and K. Swaminathan, *Inorg. Chem.*, **2**, 181 (1963).

5) S. Yamada and H. Nishikawa, This Bulletin, **36**, 755 (1963).

6) H. Nishikawa and S. Yamada, *ibid.*, **37**, 1154 (1964); L. Sacconi and M. Ciampolini, *J. Chem. Soc.*, **1964**, 274.

7) S. Yamada, E. Ohno, and K. Yamanouchi, This Bulletin, **41**, 535 (1968).

8) B. O. West, *J. Chem. Soc.*, **1960**, 4944.

9) L. Sacconi, M. Ciampolini, F. Maggio, and F. P. Cavasino, *J. Amer. Chem., Soc.*, **84**, 3246 (1962).
10) S. Yamada and H. Nishikawa, This Bulletin, **38**, 683 (1965).
11) A. Takeuchi and S. Yamada, *ibid.*, **42**, 3046 (1969); *Inorg. Chim. Acta*, **8**, 225 (1974).
12) S. Yamada, Y. Kuge, and K. Yamanouchi, This Bulletin, **40**, 1864 (1967); S. Yamada, E. Ohno, Y. Yamanouchi, *ibid.*, **40**, 1864 (1967); S. Yamada, E. Ohno, Y. Kuge, A. Takeuchi, K. Yamanouchi, and K. Iwasaki, *Coord. Chem. Rev.*, **3**, 247 (1968).
13) S. Yamada, H. Nishikawa, and E. Yoshida, This Bulletin, **39**, 994 (1966); S. Yamada, A. Takeuchi, K. Yamanouchi, and K. Iwasaki, *ibid.*, **42**, 131 (1969).

Mixed Ligand Copper(II) Complexes of α-Amino Acids with Ligand-Ligand Interactions

Takeshi SAKURAI, Osamu YAMAUCHI, and Akitsugu NAKAHARA

Institute of Chemistry, College of General Education, Osaka University, Toyonaka, Osaka 560

(Received October 6, 1975)

Synthetic and spectroscopic studies have been made on the ternary copper(II) complexes containing two optically active α-amino acids with charged groups in their side chains. Thus, for all combinations of ligands A and B, where A refers to aspartic or glutamic acid and B to arginine, lysine, or ornithine, the mixed ligand complexes, [Cu(L-A)(L-B)] and [Cu(D-A)(L-B)] except [Cu(L-aspartate)(L-ornithine)], were isolated as crystals. Infrared spectra of the isolated complexes suggested the presence of the geometrical isomers. By comparing the observed circular dichroism spectra of the ternary systems with the spectra estimated from those of the corresponding binary systems, the magnitude enhancements were detected for all the Cu(L-A)(L-B) systems, whereas no such enhancement was observed when one of the ligands was L-alanine or L-valine. The spectral behaviors as well as the solid complexes isolated have been interpreted as indicative of the existence of the intramolecular electrostatic bonding between the oppositely charged groups in the side chains of the ligands and their significance as an effective driving force leading to the ternary complex formation.

A mixed ligand metal complex is regarded as a simplified chemical model for the enzyme-metal-substrate complex formed in the course of the enzymatic reaction with a metal ion at the active center. As has been shown for the carboxypeptidase A–peptide complex by the X-ray studies,[1] the electrostatic bonding between the coordinated ligands is certainly one of the important driving forces leading to the formation of mixed ligand complexes. We reported in a previous paper[2] the synthetic and spectroscopic evidence, which suggests that such electrostatic or hydrogen bondings exist between the oppositely charged groups in the side chains of the two ligands in several copper(II)-containing ternary systems and that they affect the formation of mixed ligand complexes. Brookes and Pettit[3] recently showed by potentiometric studies that the ternary systems composed of copper(II), L- or D-histidine, and an amino acid with a positively charged side chain, such as L-arginine, L-lysine, and L-ornithine, exhibit appreciable stereoselectivity, which they ascribed to the electrostatic interaction between the positive group and the carboxylate oxygen of histidine in the systems with two L-ligands.

With a view to obtaining further information about the factors governing the mixed ligand complex formation and finding clues to the mechanism of the enzymatic reactions, we now extended the previous study to the copper(II) complexes of optically active α-amino acids and carried out synthetic and spectroscopic investigations on the possibilities of the electrostatic ligand-ligand interactions within the complex molecules. For the present purpose, we employed L- and D-glutamic acid (L- and D-Glu) and L- and D-aspartic acid (L- and D-Asp) as ligands with negatively charged side chains (referred to as A ligands hereinafter), and L-arginine (L-Arg), L-lysine (L-Lys), and L-ornithine (L-Orn) as ligands with positively charged side chains (referred to as B ligands). Based on the expected chelate structures **1** and **2**, which impose the steric and the mentioned electrostatic requirements on the formation of the ternary complex, Cu(A)(B), we attempted the isolation of the complexes with all combinations of A and B. The present paper deals with the synthesis of the chelates and the discussions of their structures and the intramolecular bondings.

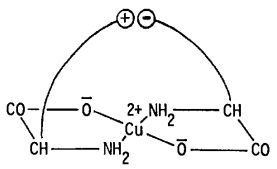

Cu(L-A)(L-B)

1

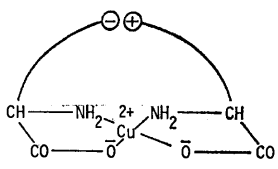

Cu(D-A)(L-B)

2

Experimental

Materials. L-Arginine, L-lysine dihydrochloride, L-ornithine monohydrochloride, L- and D-glutamic acid, L- and D-aspartic acid, L-valine, and L-alanine were purchased from Nakarai Chemicals, Ltd. The optical purities of the enantiomers of glutamic and aspartic acids were checked by their specific rotations, $[\alpha]_{20}^{589}$, which were +11.2 and −10.9 (in H_2O) for L- and D-glutamic acid, respectively, and +25.1 and −22.1 (in 3M HCl) for L- and D-aspartic acid, respectively, indicating that the optical purity of D-aspartic acid was slightly lower.

All the chemicals used were of reagent grade or of highest grade available.

Preparation of Mixed Ligand Copper(II) Complexes. The complexes were prepared by essentially the same procedure as typically described below for [Cu(L-Glu)(L-Arg)]. Copper(II) perchlorate hexahydrate (1.85 g, 5 mmol), L-arginine (0.85 g, 5 mmol), and L-glutamic acid (0.74 g, 5 mmol) were dissolved in 30 ml of water, and the pH of the resulting solution was adjusted to *ca.* 9 with aqueous sodium hydroxide. The reaction mixture was stirred for 1 h at room temperature and concentrated *in vacuo* to a small volume at temperatures below 50 °C. Addition of methanol to the residue gave blue crystals, which were recrystallized from aqueous methanol–ethanol.

The pH values of the reaction mixtures containing L-ornithine or L-lysine as B ligands were adjusted to *ca.* 7.

The analytical data for the isolated complexes are shown in Table 1.

Measurements of Absorption and Circular Dichroism (CD) Spectra. The spectroscopic measurements were performed in water at room temperature for the systems with the Cu(II):

TABLE 1. ELEMENTAL ANALYSIS OF MIXED LIGAND COPPER(II) COMPLEXES OF α-AMINO ACIDS

Complex	Formula	Found (%)			Calcd (%)		
		C	H	N	C	H	N
[Cu(L-Glu)(L-Arg)]·2H_2O	$C_{11}H_{21}N_5O_6Cu\cdot 2H_2O$	31.45	5.64	16.77	31.54	6.02	16.72
[Cu(D-Glu)(L-Arg)]·H_2O	$C_{11}H_{21}N_5O_6Cu\cdot H_2O$	32.71	5.66	17.44	32.96	5.78	17.47
[Cu(L-Asp)(L-Arg)]·H_2O	$C_{10}H_{19}N_5O_6Cu\cdot H_2O$	30.77	5.59	18.17	31.05	5.47	18.11
[Cu(D-Asp)(L-Arg)]·1.5H_2O	$C_{10}H_{19}N_5O_6Cu\cdot 1.5H_2O$	30.10	5.47	17.49	30.34	5.60	17.69
[Cu(L-Glu)(L-Lys)]·1.5H_2O	$C_{11}H_{21}N_3O_6Cu\cdot 1.5H_2O$	34.52	5.97	11.19	34.59	6.34	11.01
[Cu(D-Glu)(L-Lys)]·H_2O	$C_{11}H_{21}N_3O_6Cu\cdot H_2O$	35.49	5.81	11.29	35.43	6.22	11.27
[Cu(L-Asp)(L-Lys)]·1.5H_2O	$C_{10}H_{19}N_3O_6Cu\cdot 1.5H_2O$	32.89	5·84	11.41	32.65	6.02	11.42
[Cu(D-Asp)(L-Lys)]·H_2O	$C_{10}H_{19}N_3O_6Cu\cdot H_2O$	33.51	5.79	11.90	33.66	5.90	11.71
[Cu(L-Glu)(L-Orn)]·2H_2O	$C_{10}H_{19}N_3O_6Cu\cdot 2H_2O$	32.05	5.63	11.28	31.87	6.14	11.15
[Cu(D-Glu)(L-Orn)]·2H_2O	$C_{10}H_{19}N_3O_6Cu\cdot 2H_2O$	31.85	5.71	11.45	31.87	6.14	11.15
[Cu(D-Asp)(L-Orn)]·2.5H_2O	$C_9H_{17}N_3O_6Cu\cdot 2.5H_2O$	28.92	5.39	11.34	29.07	5.97	11.30

A: B ratios of 1: 1: 1 (ternary systems) and 1: 2: 0 and 1: 0: 2 (binary systems) at pH 5—11 at a constant Cu(II) concentration of 5×10^{-3} M. The spectral samples were prepared from 0.1 M stock solutions of copper (II) perchlorate and the amino acids. The pH values, which were roughly adjusted with aqueous sodium hydroxide and dilute perchloric acid, were finally determined after the spectroscopic measurements. The ionic strength (μ) of the solutions was not adjusted at a constant value (μ=variable). Absorption spectra were recorded in the range 400—800 nm on a Union Giken SM-401 high sensitivity recording spectrophotometer. CD spectra were measured in a 1-cm path length quartz cell in the range 350—800 nm with a JASCO MOE-1 spectropolarimeter. Infrared spectra were obtained in the range 4000—650 cm^{-1} with a Hitachi EPI-S2 infrared spectrophotometer with the KBr disk method and in the range 700—200 cm^{-1} with a Hitachi EPI-L grating infrared spectrophotometer in the dry air with the Nujol mull method.

Results and Discussion

Preparation of Mixed Ligand Complexes. As shown in Table 1, all the expected ternary complexes except [Cu(L-Asp)(L-Orn)] were isolated as crystals in good yields. Although it was difficult to obtain pure crystals of [Cu(L-Asp)(L-Orn)], we may assume its formation from the analytical data.[4]

The structures of these complexes are expected from the space-filling models to be such as are expressed by **1** and **2**, which suggest that the (L-A)(L-B) pairs of ligands favor the *trans* structure around the central copper(II) ion (**1**), whereas the (D-A)(L-B) pairs prefer the *cis* structure (**2**). Both structures are more puckered and may be sterically less stable as compared with those without ligand-ligand interactions, but the synthetic results seem to indicate the existence of the electrostatic bondings, which supplement the steric disadvantage incurred. Although the complexes with pairs of A and B containing longer side chains, *e.g.* Glu–Arg and Glu–Lys, were isolated easily, the total length of the two side chains may not be the sole factor affecting the isolation, because [Cu(L-Glu)(L-Orn)] was more easily isolated than [Cu(L-Asp)(L-Lys)] which has the same side chain length as the former. The difficulty encountered in isolation of [Cu(L-Asp)(L-Orn)] with the shortest chain length nevertheless suggests that the chain lengths as well as the solubility and the *cis-trans* geometry around the copper(II) ion exert influence over the formation and crystallization of the complexes.

IR Spectra and cis-trans *Isomerism.* Figure 1 shows the IR spectra of the mixed ligand complexes in the range 4000—650 cm^{-1}. The spectral patterns in the fingerprint region are different from those of the corresponding binary complexes. Subtle spectral differences in this region are also detected between the Cu(L-A)-(L-B) and Cu(D-A)(L-B) series with all combinations

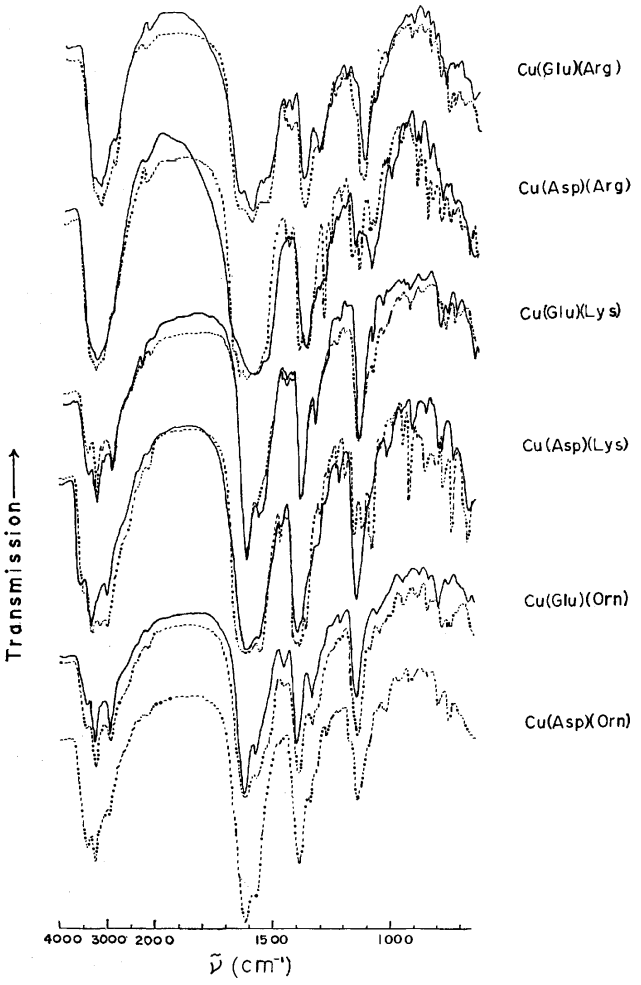

Fig. 1. Infrared spectra of copper(II) complexes in the range 4000—650 cm^{-1}.
Cu(L-A)(L-B)—; Cu(D-A)(L-B)---.

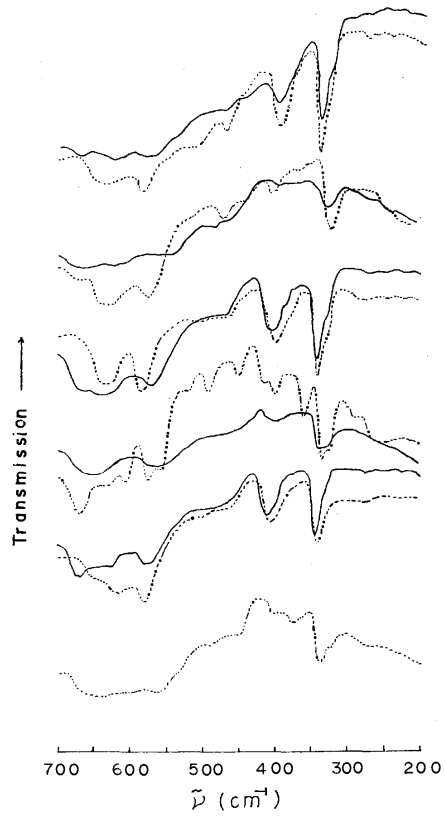

Fig. 2. Infrared spectra of copper(II) complexes in the range 700—200 cm^{-1}.
Cu(L-A)(L-B)—; Cu(D-A)(L-B)—.

of A and B except the Asp-Orn pair, which may reflect the structural differences as illustrated by **1** and **2**.

Geometrical isomerism has been known to give rise to characteristic bands due to metal-ligand bonds in the range below 700 cm^{-1}.[5] Thus, the spectral patterns of *cis*- and *trans*-[Cu(glycine)$_2$] in this region[6] are considerably different from each other. We see from Fig. 2 that at 700—500 cm^{-1} and 400—330 cm^{-1} the complexes with (L-A)(L-B) pairs give the spectra, which are typical of the A ligands and differ from those exhibited by the complexes [Cu(D-A)(L-B)]. This suggests the presence of the *cis-trans* isomers expressed by **1** and **2**, and since the side chains in these systems are comparable, the isomerism in turn points to the intramolecular ligand-ligand bonding. The stereoselectivity as observed for the histidine-containing ternary copper(II) complexes[3] would implicate the preference of one geometrical isomer over the other in the present ternary systems.

Absorption and CD Spectra and Interpretation of the CD Magnitudes. The CD spectra obtained for each of the systems at various pH values between 5 and 11 were satisfactorily reproducible. The spectral data are summarized in Table 2 and some examples of the curves are depicted in Figs. 3 and 4 (solid lines). The CD magnitudes of the ternary systems increase with pH, indicating that the mixed ligand complexes are the major species present at pH 9—10. The systems with L-Orn show marked spectral changes at pH>8 owing to the apical coordination by the δ-amino group,[2,7,8] while the other systems including those with Asp show

Table 2. Relative CD magnitude in water (μ=variable)[a]

Complex	pH	$\Delta\varepsilon_{max}$ (Found)	Relative magnitude	λ_{max} (nm) Found	λ_{max} (nm) Calcd[b]
[Cu(L-Val)(L-Arg)]	7.2	0.19	1.0	590	590
	8.6	0.19	1.0	580—590	590
[Cu(L-Val)(L-Glu)]	7.4	0.19	1.0	600	600
	8.8	0.19	1.0	600	600
[Cu(L-Ala)(L-Arg)]	9.4	0.10	1.0	610	600
[Cu(L-Ala)(L-Glu)]	7.8	0.10	1.0	610	610
[Cu(L-Ala)(L-Asp)]	9.3	0.06	1.0	630	630
[Cu(L-Glu)(L-Arg)]	7.3	0.14	1.4	600	610
	8.5	0.15	1.3	600	600
[Cu(L-Glu)(L-Lys)]	7.3	0.13	1.2	600	610
	9.0	0.13	1.1	600	600
[Cu(L-Glu)(L-Orn)]	7.5	0.13	1.4	600	600
[Cu(L-Asp)(L-Arg)]	7.2	0.09	1.4	630	630
	9.5	0.09	1.3	630	630
[Cu(L-Asp)(L-Lys)]	7.2	0.08	1.2	640	630—640
	9.6	0.08	1.1	640—650	630—640
[Cu(L-Asp)(L-Orn)]	7.1	0.07	1.5	640	640

a) Relative CD magnitude refers to $\Delta\varepsilon_{max}$ (found)/$\Delta\varepsilon_{max}$ (calcd). b) The approximate maximum wavelength estimated from the CD spectral curves.

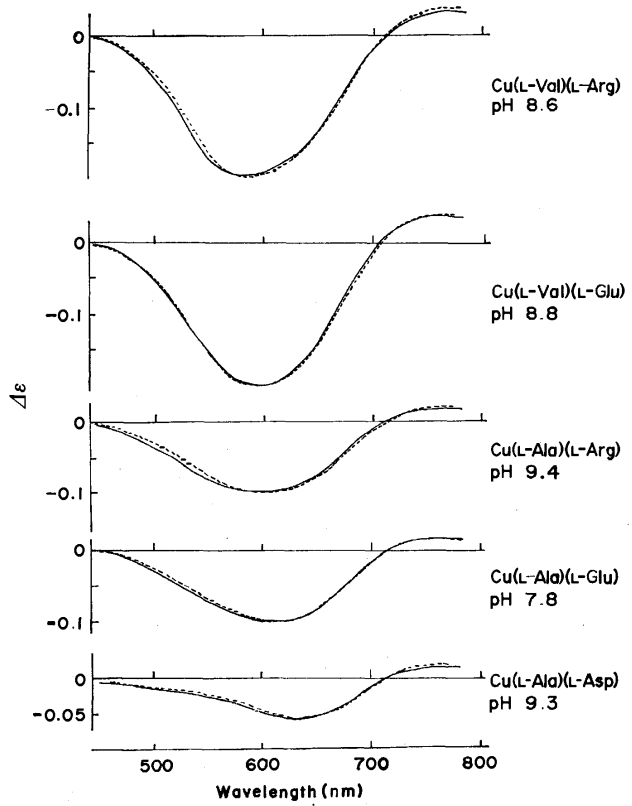

Fig. 3. Circular dichroism curves of ternary copper(II) systems without electrostatic ligand-ligand interactions.
Experimental curves:—, estimated curves:—.

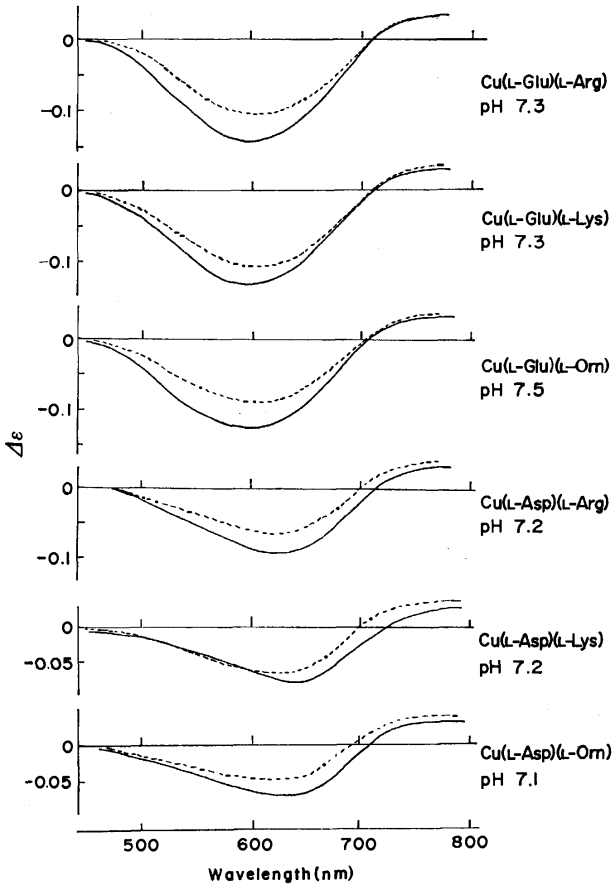

Fig. 4. Circular dichroism curves of ternary copper(II) systems containing ligands with oppositely charged side chains.
Experimental curves:—
Estimated curves:---.

moderate changes.

On the assumption that the CD magnitude is an additive function under the present conditions, we estimated the theoretical CD curves for the ternary systems (broken lines in Figs. 3 and 4) by summing up half the magnitude ($1/2\Delta\varepsilon$) of CuA_2 and of CuB_2 at every wavelength. As is apparent from Fig. 3, the L-Val- or L-Ala-containing ternary systems, where no intramolecular ligand-ligand interaction is expected, exhibit excellent fits of the calculated curves to the experimental ones. On the other hand, serious deviations of the curves are observed most remarkably for the systems with two L-ligands each of which have an oppositely charged side chain that can form intramolecular electrostatic bonds (Fig. 4). Since the spectra were obtained for 5×10^{-3} M solutions, these observations may imply that such discrepancies arise from the intramolecular bonds, which cause fixation of the complex structures and reduce the freedom of motion of the side chains. Regarding the Cu(D-A)(L-B) systems, the experimental curves do not deviate greatly from the expected ones. Because the absolute values of $\Delta\varepsilon$ for these systems are much smaller than those for the Cu(L-A)(L-B) systems and the deviations are roughly in the range of experimental errors, it is difficult to find any significant difference between them.

Inspection of the curve fit of the L-Orn-containing systems was made at pH 7—8, because, as mentioned earlier, they exhibit spectral changes at pH>8 due to apical coordination. These systems give anomalous CD curves which are difficult to interpret, and further investigations will be necessary.

The observed CD magnitudes may be explained by the hexadecant (D_{4h}) rule,[9,10] according to which the side chains of the L-ligands in [Cu(L-A)(L-B)] with the *trans* geometry (**1**) are located in the sectors with negative sign, and this configuration may contribute to the observed magnitude enhancement. Although the complex formation in the binary systems are supposed to be nearly complete at pH 9—10[11] from the pH dependence of the CD magnitude, the above argument is contingent on the species distributions in the ternary systems at equilibrium and a more quantitative comparison of the CD magnitudes should be made from the study of the solution equilibria.

The absorption spectral data in the visible region are

Table 3. Absorption spectral data

Complex	pH	λ_{max} (nm)	ε	Remarks
[Cu(L-Glu)(L-Arg)]	5.2	670	36	
	7.3	625	57	
	8.5	622	56	
[Cu(D-Glu)(L-Arg)]	5.4	651	55	
	7.3	626	58	
	9.4	(620)[a]	(60)[a]	turbid
[Cu(L-Glu)(L-Lys)]	5.8	677	35	
	7.3	626	53	
	9.0	(622)	(56)	turbid
[Cu(D-Glu)(L-Lys)]	5.5	659	39	
	7.4	625	52	
	9.3	(623)	(56)	turbid
[Cu(L-Glu)(L-Orn)]	5.2	660	39	
	7.5	625	56	
	9.2	626	59	
[Cu(D-Glu)(L-Orn)]	5.5	643	44	
	7.8	620	57	
	9.3	626	59	
[Cu(L-Asp)(L-Arg)]	5.3	(622)	(40)	cryst[b]
	7.2	633	53	
	9.5	(630)	(55)	ppt[c]
[Cu(D-Asp)(L-Arg)]	5.5	(654)	(38)	cryst
	7.3	634	53	
	9.8	(641)	(54)	ppt
[Cu(L-Asp)(L-Lys)]	5.3	659	37	
	7.2	632	50	
	9.6	630	52	
[Cu(D-Asp)(L-Lys)]	5.7	651	40	
	7.4	633	49	
	9.7	(629)	(55)	turbid
[Cu(L-Asp)(L-Orn)]	7.1	630	51	
	9.4	630	54	
	10.8	634	56	
[Cu(D-Asp)(L-Orn)]	7.3	634	51	
	9.4	630	54	
	10.8	636	57	

a) Numbers in parentheses are approximate values.
b) Crystals separated. c) A precipitate was formed.

listed in Table 3, which indicates that the peaks of the ternary systems are between those of the corresponding binary systems. The maximum wavelengths and the ε values do not explicitly reflect the effects of the ligand-ligand interactions and the differences due to L- and D-enantiomers, although there are observed slight disagreements in the shapes of the curves. This may not be unexpected, because all the chelate rings of the systems in consideration have the same structures around the copper(II) ion and the ε values of the absorption spectra are more than a hundred times greater than the $\Delta\varepsilon$ values of the CD spectra.

As regards α-amino acids as ligands, only a small number of mixed ligand copper(II) complexes have so far been reported,[12] and we may take this as an indication that isolation of such labile complexes is not always feasible under normal conditions but requires additional factors favoring or stabilizing ternary systems. The present results of the synthesis and the relevant CD spectral information strongly suggest the existence of the ligand-ligand bonding and lead us to the conclusion that such intramolecular bondings serve as an effective driving force for the mixed ligand complex formation.

We thank Miss Tazuko Ikebata for technical assistance and to Miss Teruko Kuroe for elemental analysis. This work was supported by a grant from the Ministry of Education.

References

1) W. N. Lipscomb, *Accounts Chem. Res.*, **3**, 81 (1970).
2) O. Yamauchi, Y. Nakao, and A. Nakahara, This Bulletin, **48**, 2572 (1975).
3) G. Brookes and L. D. Pettit, *Chem. Commun.*, **1975**, 385.
4) On addition of methanol to the reaction mixture, this complex usually separated as an oil, which could occasionally be crystallized by washing with ethanol. Analytical data for the crystals obtained in this way are as follows: Found: C, 29.63; H, 5.29; N, 10.56%. Calcd for $C_9H_{17}N_3O_6Cu \cdot 2.5H_2O$: C, 29.07; H, 5.97; N, 11.30%.
5) K. Nakamoto, "Infrared Spectra of Inorganic and Coordination Compounds," Wiley-Interscience, New York (1970), p. 212.
6) R. A. Condrate and K. Nakamoto, *J. Chem. Phys.*, **42**, 2590 (1965).
7) K. M. Wellman, T. G. Mecca, W. Mungall, and C. R. Hare, *J. Amer. Chem. Soc.*, **90**, 805 (1968).
8) E. W. Wilson, Jr., M. H. Kasperian, and R. B. Martin, *ibid.*, **92**, 5365 (1970).
9) J. M. Tsangaris and R. B. Martin, *ibid.*, **92**, 4255 (1970).
10) R. B. Martin, "Metal Ions in Biological Systems," Vol. 1, ed. by H. Sigel, Marcel Dekker, New York (1974), p. 140.
11) Although the actual CD magnitude of a complex can be greater than the observed value owing to the dissociation of the complex (V. A. Davankov and P. R. Mitchell, *J. Chem. Soc., Dalton*, **1972**, 1012), the magnitude of the system with the Cu(II): L-Val ratio of 1:2 was found to be the same as that with the ratio of 1:4.
12) R. P. Martin, M. M. Petit-Ramel, and J. P. Scharff, "Metal Ions in Biological Systems," Vol. 2, ed. by H. Sigel, Marcel Dekker, New York (1973), p. 1.

The Estimation of the *G*-Values for Ionization and Excitation of Ten-Electron Molecules: Methane, Ammonia, and Water Irradiated by 100 keV Electrons

Kiyoshi OKAZAKI, Shin SATO, and Shin-ichi OHNO*

Department of Applied Physics, Tokyo Institute of Technology, Ookayama, Meguro-ku, Tokyo 152
**Japan Atomic Energy Research Institute, Tokai-mura, Ibaraki 319-11*

(Received May 31, 1975)

The binary-encounter collision theory is applied to calculate the *G*-values for the ionization and excitation of methane, ammonia, and water irradiated by 100 keV electrons. Double collision of the incident electron in a molecule is also taken into account. On the assumption of the occurrence of certain reactions in the systems, the *G*-values for electrons, various radicals, and several final products were estimated. Some of the results are as follows: the *G*-values for electrons were 3.60 for methane, 3.56 for ammonia, and 3.00 for water. These values are in fair agreement with the experimental values: 3.6 for methane, 3.8 for ammonia, and 3.3 for water. The calculated *G*-value for hot hydrogen atoms was about 1.0 for all three compounds. The ratios of the *G*-value for excitation to that for electrons are 1.1 for methane, 1.5 for ammonia, and 1.7 for water. An estimation was also made of the *G*-value for the emission of highly-excited hydrogen atoms using reported cross sections. The *G*-values are 0.1 for methane and ammonia, and 0.2 for water.

Methane, ammonia, and water are iso-electronic with neon. The radiolyses of these compounds have been extensively investigated by many radiation chemists.[1-9] They measured the *G*-values of the final products both in the pure state and in systems containing electrons or radical scavengers. On the basis of these results, they constructed reaction sequences consisting of ion-molecule reactions and radical reactions, and estimated the *G*-values for the primary products such as electrons, radicals, and singlet- and triplet-excited states of the parent molecules. On the other hand, radiation physicists are concerned with the *W*-values of these gases (the *W*-value is equal to $100/G$(electrons)) and have measured them accurately.[10-13] They also reported various physical processes occuring during irradiation, such as the emissions of intermediate species and the lifetimes of the highly-excited atoms produced.[14] At present, therefore, we are in a good position to view generally the entire sequence of the radiolyses of methane, ammonia, and water.

Previously, the authors calculated the degradation spectra of electrons in noble gases from He to Xe, and estimated the *G*-values of electrons and singlet- and triplet-excited states.[15,16] Although the method was a classical one, the calculations are in fair agreement with the experimental results. After the calculation on noble gases, they extended the calculation to water irradiated by 10 keV electrons.[17] Since the method of calculation was established, the estimation of the *G*-values for electrons and excited states was straightforward. The main concern in Ref. 17, therefore, was the estimation of the *G*-values of the various products which are of interest to radiation chemists. In order to estimate these values, all of the available spectroscopic, photochemical, and radiation chemical data were considered.

The present paper is an extension of Ref. 17, and treats the radiolyses of methane, ammonia, and water. The water molecule was again chosen as one of the objects of research, since the above three compounds are iso-electronic and it is thought worthwhile to compare them on the same basis.

Method of Calculation

The differential cross section, $\sigma_E(T)$, and the total cross sections for ionization and excitation, $Q_s(T)$, at an electron energy T were estimated using the classical binary-encounter theory, the details of which have been described in previous papers.[15-17] Only the parameters, the binding energy (I_i), the average kinetic energy (E_i), the energy of the first excited singlet state (E_s) and that of the lowest triplet state (E_t) have to be replaced by the values corresponding to those for the molecular orbitals.

The formulation of the stopping power, $S(T)$, is the same as that given in Ref. 17. Once $\sigma_E(T)$ and $S(T)$ are obtained, we can calculate the degradation spectra for electrons, $y(T)$, in the three compounds on the assumption of continuous slowing down. The procedure for the calculation of $y(T)$ is the same as that given in Ref. 15. Since we know that the contribution from double collisions to the *G*-values for electrons cannot be ignored, they were calculated for the three compounds. The cross sections for different types of double collisions have been formulated in Ref. 16. Then, as stated in Ref. 15, we can estimate the *G*-value of any process by integrating $Ty(T)\,Q_s(T)$ over $\ln T$.

Constants Used for Calculation

Tables 1 and 2 summarize all the constants used for the calculations for methane, ammonia, and water. Each value was determined as follows.

$CH_4(1a_1)^2(2a_1)^2(1t_2)^6$: The binding energies ($I_i$) were taken from ESCA data.[18,19] The average kinetic energies (E_i) were calculated from the SCF functions proposed by Palke and Lipscomb.[20] Since the absorption spectrum of methane begins at 1455 Å,[21] the energy of the first excited singlet state, $E_{s,1t_2}$, was assumed to be 8.5 eV. No experimental data on the energies of the inner-shell excited states (E_s and E_t) are available. Therefore, these values were tentatively estimated as shown in Table 1. The equations used

Table 1. Binding energies (I_i), average kinetic energies (E_i), and energies to the first excited singlet state (E_s) and to the lowest triplet state (E_t)

Orbital		No. of electrons	I_i (eV)[a]	E_i (eV)	E_s (eV)	E_t (eV)
CH_4	$1t_2$	6	13.0	20.31	8.52[b]	6.5[c]
	$2a_1$	2	23.1	30.34	19[d]	17[c]
	$1a_1$	2	290.7	437.1	286[d]	284[c]
NH_3	$1a_2''$	2	10.85	52.53	6.5[e]	4.5[c]
	$1e'$	4	15.8	28.48	11.5[f]	9.5[c]
	$2a_1'$	2	21.22	42.60	17[f]	15[c]
	$1a_1'$	2	405.6	605.3	401[f]	339[c]
H_2O	$1b_1$	2	12.6	70.40	7.42[g]	5.0[h]
	$3a_1$	2	14.7	66.46	9.5[i]	7[j]
	$1b_2$	2	18.4	28.41	13[k]	11[j]
	$2a_1$	2	32.2	74.94	27[k]	25[j]
	$1a_1$	2	539.7	799.6	535[k]	533[j]

a) Refs. 18, 19. b) Ref. 21. c) $E_t=E_s-(E_s-E_t)_{H_2O,1b_1}=E_s-2$. d) $E_s=I_i-(I_i-E_s)_{1t_2}=I_i-4.5$. e) Ref. 24. f) $E_s=I_i-(I_i-E_s)_{1a_2''}=I_i-4.4$. g) Ref. 24. h) Ref. 25. i) Ref. 22. j) $E_t=I_i-(I_i-E_t)_{1b_1}=I_i-7.6$. k) $E_s=I_i-(I_i-E_s)_{1b_1}=I_i-5.2$.

Table 2. The constants used for double collisions

	CH_4	NH_3	H_2O	Ne
No. of electrons	6	6	6	6
Orbitals involved	$1t_2$	$1a_2''$, $1e'$	$1b_1$, $3a_1$, $1b_2$	2p
$\bar{I}_i$ (eV)	13.0	14.2	15.2	21.56
$\bar{E}_s$	8.52	10.0	10.0	16.8
$\bar{E}_t$	6.5	8.0	9.0	16.7
$\bar{E}_i$	20.31	36.5	55.0	112.8
I_{ii}	25.0	27.0	29.0	41.07
E^{**}	25.0	28.0	30.0	45.0
E^{+*}	31.5	35.0	37.0	57.6
$\bar{r}$ (Å)	0.86	0.79	0.75	0.45

for the estimations are summarized in the footnotes of Table 1.

$NH_3(1a_1')^2(2a_1')^2(1e')^4(1a_2'')^2$: The values of I_i were taken from ESCA data, and the E_i values were calculated from the SCF functions proposed by Duncan.[23] The energy of the first excited singlet state, $E_{s,1a_2''}$, was estimated from the electron-impact spectrum data reported by Lassettre *et al.*[24] Other values of E_s and E_t were estimated in a manner similar to those of methane.

$H_2O(1a_1)^2(2a_1)^2(1b_2)^2(3a_1)^2(1b_1)^2$: The values of I_i, $E_{s,1b_1}$ and $E_{t,1b_1}$ are the same as those used in Ref. 17, except for the E_t of the inner shells, which were estimated in a manner similar to that for the values of E_t for methane. The E_i values were calculated from the SCF functions proposed by Ellison and Shull.[26]

Table 2 shows the constants used for the calculations for double collisions. The values for $\bar{I}_i$, $\bar{E}_s$, $\bar{E}_t$, and $\bar{E}_i$ are the averages of the I_i, E_s, E_t, and E_i for the corresponding molecular orbitals.[16,17] The second ionization potential, I_{ii}, of neon is 1.9 times the first ionization potential, I_i.[16] It is assumed that the values of I_{ii} for methane, ammonia, and water are 1.9 times the average first ionization potentials ($\bar{I}_i$). The I_{ii} value calculated for methane is in good agreement with those obtained experimentally[27] and theoretically.[28] The energy of the doubly-excited state (E^{**}) and that of the excited ion (E^{+*}) were determined in a manner similar to those for the rare gases.[16] The mean distance between valence electrons ($\bar{r}$) was calculated by placing them uniformly on a sphere whose radius is the bond length. The bond lengths of C–H, N–H, and O–H are reported to be 1.1, 1.0, and 0.96 Å, respectively.[29]

Results

Figure 1 shows the degradation spectra, $y(T)$, for methane, ammonia, water, and neon. The results for neon were reproduced from a previous paper.[15] At low electron energies (<100 eV), the $y(T)$ for neon is different from those for the iso-electronic molecules. Figure 2 shows the $Ty(T)$ $Q_s(T)$ for the ionization and

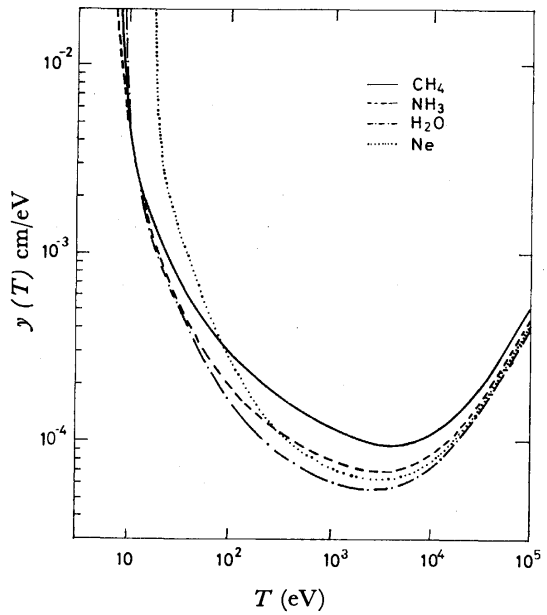

Fig. 1. Degradation spectra in methane, ammonia, water, and neon.

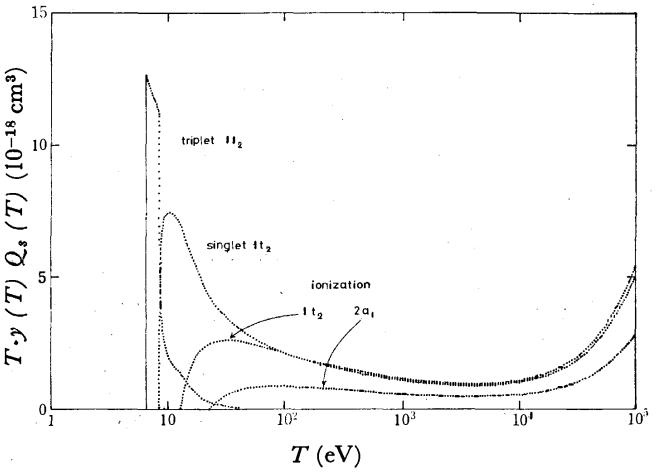

Fig. 2. Contribution of different portions of the electron degradation spectrum to the ionization and excitation in methane.

Table 3. The G-values for ionizations and singlet and triplet excitation. The values in parentheses are those obtained in Ref. 17.

	Orbital	G_i	$G_{ex,s}$	$G_{ex,t}$
CH_4	$1t_2$	2.59	3.45	0.78
	$2a_1$	0.36	0.15	0.0070
	$1a_1$	0.018	0.0005	0.000009
NH_3	$1a_2''$	1.55	3.48	1.12
	$1e'$	1.06	0.89	0.052
	$2a_1'$	0.38	0.19	0.0079
	$1a_1'$	0.0098	0.0002	0.000003
H_2O	$1b_1$	1.17 (1.26)	2.67 (2.80)	0.93 (1.00)
	$3a_1$	0.83 (0.68)	1.22 (0.96)	0.081 (0.029)
	$1b_2$	0.34 (0.44)	0.31 (0.39)	0.015 (0.011)
	$2a_1$	0.21 (0.21)	0.076 (0.076)	0.002 (0.0016)
	$1a_1$	0.0062 (0.005)	0.0001 (0.000079)	1×10^{-6} (1.5×10^{-6})

excitation of methane as a function of ln T. Similar figures can be obtained for ammonia and water. Table 3 summarizes the G-values for the ionization and excitation from each molecular orbital. The values for water in parentheses are those reported previously.[17] Although the values (E_t and E_i) used in the present calculation are slightly different from those in Ref. 17, the G-values obtained are in fair agreement with each other. The difference in the energies of the incident electrons, 10 and 100 keV, produces no noticeable change in the calculated G-values. Table 4 shows the G-values for the double collisions. The yields for double collision for the three compounds are approximately the same.

Table 4. The G-values for doubly-charged ions, doubly-excited molecules, and excited ions

	CH_4	NH_3	H_2O	Ne
M^{++}	0.11	0.10	0.10	0.15
M^{**}	0.16	0.11	0.13	0.11
M^{+*}	0.54	0.43	0.49	0.26

Reaction Sequences and the Product Yields

The calculated G-values which are shown in Tables 3 and 4 cannot be compared directly with the observed values, because most of the ions and excited states initially produced are too short-lived to be measured experimentally. We, therefore, have to consider the reaction sequences for each compound. Since fragmental reports on these reaction mechanisms are abundant,[1-9,17,21,30-57] they were collected and the reaction sequences were reconstructed. The most perplexing problem arises when the branching ratios have to be taken into consideration. Such a case is often encountered in reconstructing the reaction sequence of methane. Therefore, the relative abundances based on the branching ratios are somewhat tentative.

CH_4: The fragmentation modes assumed for the ions and excited states produced are summarized as follows:

	orbital		relative abundance[3,30-34]
Ionization from $(1t_2)$	$\longrightarrow$	$CH_4^+ + e^-$	0.6
	$\searrow$	$CH_3^+ + H + e^-$	0.4
$(2a_1)$	$\longrightarrow$	$CH_4^+ + e^-$	0.6
	$\searrow$	$CH_3^+ + H' + e^-$	0.4
$(1a_1)$	$\longrightarrow$	$CH_4^{6+} + 6e^-$	

where H′ denotes a hot hydrogen atom. When an electron in the $(1a_1)$ orbital is ejected, the Auger effect is expected to occur and fragmentation of the ion will take place, however, since there is no available information for the mode of this fragmentation and the G-value of this process is very small, it was assumed that only ionization occurs and the ions produced react as follows:

$$CH_4^{6+} + 11CH_4 \longrightarrow 6CH_5^+ + 6CH_3$$

The number of electrons ejected in the Auger effect was estimated by the method described in Ref. 15.

Excitation from $(1t_2)$ triplet	$\longrightarrow$	$CH_3 + H$		
singlet	$\longrightarrow$	$CH_3 + H$	0.4	[1,21,35-44]
	$\longrightarrow$	$CH_2 + H_2$	0.4	
	$\longrightarrow$	$CH + H_2 + H$	0.15	
	$\longrightarrow$	$C + 2H_2$	0.05	
$(2a_1)$	$\longrightarrow$	$CH_4^+ + e^-$	0.6	[3,32-34]
	$\searrow$	$CH_3^+ + H' + e^-$	0.4	
$(1a_1)$	$\longrightarrow$	$CH_4^{6+} + 6e^-$	(Auger effect)	

Double collisions:

CH_4^{2+}	$\longrightarrow$	$CH_3^+ + H^+$	0.5	[16,32-34]
	$\searrow$	$CH_2^+ + H^+ + H'$	0.5	
CH_4^{**}	$\longrightarrow$	$CH_4^+ + e^-$	0.6	
	$\searrow$	$CH_3^+ + H' + e^-$	0.4	
CH_4^{+*}	$\longrightarrow$	$CH_3^+ + H'$	0.5	
	$\searrow$	$CH_2^+ + H_2$	0.5	

The successive reactions of these fragment ions have been investigated by many researchers.

Ion-molecule reactions: [3,45]

$CH_4^+ + CH_4$	$\longrightarrow$	$CH_5^+ + CH_3$	
$CH_3^+ + CH_4$	$\longrightarrow$	$C_2H_5^+ + H_2$	
$CH_2^+ + CH_4$	$\nearrow$	$C_2H_5^+ + H$	1/3
	$\longrightarrow$	$C_2H_4^+ + H_2$	1/3
	$\searrow$	$C_2H_3^+ + H_2 + H$	1/3
$C_2H_3^+ + CH_4$	$\longrightarrow$	$C_3H_5^+ + H_2$	
$C_3H_5^+ + CH_4$	$\xrightarrow{+M}$	$C_4H_9^+$	
$H^+ + CH_4$	$\xrightarrow{+M}$	CH_5^+	

Neutralization reaction: [1-3]

$$CH_5^+ + e^- \longrightarrow CH_4 + H$$
$$C_2H_5^+ + e^- \longrightarrow C_2H_4^* + H$$

$$C_2H_4^+ + e^- \xrightarrow{+M} C_2H_4^*$$
$$C_4H_9^+ + e^- \longrightarrow C_3H_6 + CH_3$$

A part of the excited ethylene produced will decompose into acetylene and a hydrogen molecule.[1)]

$$C_2H_4^* \longrightarrow C_2H_4 \quad 2/3$$
$$C_2H_4^* \longrightarrow C_2H_2 + H_2 \quad 1/3$$

Radical reactions: The hot hydrogen atoms produced will react with the substrate, methane.[46)]

$$H' + CH_4 \longrightarrow H_2 + CH_3$$

The radicals, CH_2, CH, and C will undergo the following reactions.[1,2)] Here, it is assumed that the ratio of the amount of singlet methylene ($^1CH_2$) to that of the triplet methylene ($^3CH_2$) is unity and C is in ^1S or ^1D state.

$$^1CH_2 + CH_4 \longrightarrow C_2H_6^*$$
$$C_2H_6^* \longrightarrow C_2H_6$$
$$^3CH_2 + CH_3 \longrightarrow C_2H_5^*$$
$$C_2H_5^* \longrightarrow C_2H_4 + H$$
$$CH + CH_4 \longrightarrow C_2H_4 + H$$
$$C + CH_4 \longrightarrow C_2H_2 + H_2$$

Since hydrogen atoms are not reactive with methane at room temperature, they will remain as one of the most abundant radicals in the system together with methyl radicals.

$$2CH_3 \longrightarrow C_2H_6 \quad k_1$$[9)]
$$CH_3 + H \longrightarrow CH_4 \quad k_2$$
$$2H \longrightarrow H_2 \quad k_3$$

The relative rate constants were assumed to be in the ratio 5: 57: 1 for k_1: k_2: k_3. This ratio is for the reactions of OH radicals and H atoms.[9)] Thus, we can calculate the *G*-values of the intermediate species and final products using the *G*-values of the initial processes shown in Tables 3 and 4. The results are summarized in Table 5 together with the reactions that produced them.

NH_3: A reaction sequence similar to that for methane was constructed as is shown below. This mechanism is much simpler than that for methane because branching is much less common in the case of ammonia.

Ionization from $(1a_2'') \longrightarrow NH_3^+ + e^-$ [47-50)]
$(1e') \longrightarrow NH_2^+ + H + e^-$
$(2a_1') \longrightarrow NH_2^+ + H' + e^-$
$(1a_1') \longrightarrow NH_3^{8+} + 8e^-$ (Auger effect)

Excitation from $(1a_2'') \longrightarrow NH_2 + H$ [51-54)]
$(1e') \longrightarrow NH + 2H \quad 0.85$
$(1e') \longrightarrow NH + H' + H \quad 0.15$
$(2a_1') \longrightarrow NH_3^+ + e^-$ (Autoionization)
$(1a_1') \longrightarrow NH_3^{8+} + 8e^-$ (Auger effect)

Double collisions:

$$NH_3^{2+} \longrightarrow NH_2^+ + H^+$$ [16,49)]
$$NH_3^{**} \longrightarrow NH_3^+ + e^- \text{ (Autoionization)}$$
$$NH_3^{+*} \longrightarrow NH_2^+ + H'$$

Ion-molecule reactions:[47,55)]

$$NH_3^+ + NH_3 \longrightarrow NH_4^+ + NH_2$$
$$NH_2^+ + NH_3 \longrightarrow NH_3^+ + NH_2$$
$$H^+ + NH_3 \longrightarrow NH_4^+$$

TABLE 5. THE *G*-VALUES FOR INTERMEDIATE AND FINAL PRODUCTS FROM METHANE

	Ionization	Excitation	Ion-molecule reaction	Neutralization	Hot-atom reaction	Total intermediate	Radical reaction		Final products
e^-	3.60			0					
CH_4^+	1.63		0						
CH_3^+	1.42		0						
CH_2^+	0.32		0						
H^+	0.11		0						
CH_4^{6+}	0.02		0						
CH_5^+			1.86	0					
$C_2H_5^+$			1.52	0					
$C_2H_4^+$			0.12	0					
$C_4H_9^+$			0.10	0					
H	0.82	2.05	0.20	3.38		6.45	1.11	0	
H'	0.59	0.48			0				
CH_3		2.05	1.75	0.10	1.07	4.97		0	
CH_2		1.27				1.27	0		
CH		0.48				0.48	0		
C		0.16				0.16	0		
H_2	0.27	2.07	1.74	0.55	1.07	5.70	0.16	1.32	7.18
C_2H_2				0.55		0.55	0.16		0.71
C_2H_4				1.09		1.09	1.11		2.20
C_2H_6							0.64	0.03	0.67
C_3H_6				0.10		0.10			0.10
$-CH_4$	3.39	3.96	3.90	—1.86	1.07	10.46	1.91	—4.91	7.46

Table 6. The *G*-values for intermediate and final products from ammonia

	Ionization	Excitation	Ion-molecule reaction	Neutralization	Hot-atom reaction	Total intermediate	Radical reaction	Final products
e^-	3.56			0				
NH_3^+	1.59		0					
NH_2^+	1.79		0					
H^+	0.10		0					
NH_3^{8+}	0.01		0					
NH_4^+			3.56	0				
H	0.88	6.12		3.56		10.56	0	
H′	0.81	0.14			0			
NH_2		4.44	5.25		0.95	10.64	0	
NH		0.91				0.91	0	
H_2					0.95	0.95	2.84	3.79
N_2							1.18	1.18
N_2H_4							0.24	0.24
$-NH_3$	3.39	5.35	5.42	−3.56	0.95	11.55	−8.70	2.85

$$NH_3^{8+} + 15NH_3 \longrightarrow 8NH_4^+ + 8NH_2$$

Neutralization reactions:[5,6,56]

$$e^- + NH_4^+ \longrightarrow NH_3 + H$$

Hot-atom reaction:[46]

$$H' + NH_3 \longrightarrow H_2 + NH_2$$

Radical reactions:[6]

$$2NH_2 \longrightarrow N_2H_4$$
$$\searrow\ NH + NH_3$$
$$NH_2 + H \longrightarrow NH_3$$
$$\searrow\ NH + H_2$$
$$2H \longrightarrow H_2$$
$$2NH \longrightarrow N_2 + H_2$$

The rate constants of these radical reactions have been summarized by Willis *et al.*[6] The *G*-values thus estimated are listed in Table 6.

H_2O: The reaction mechanism for water has already been discussed in detail in a previous paper.[17] Here, it is summarized.

Ionization from $(1b_1) \longrightarrow H_2O^+ + e^-$

$(3a_1) \longrightarrow H_2O^+ + e^-$

$(1b_2) \longrightarrow H^+ + OH + e^-$ 0.5

$(2a_1) \longrightarrow H' + OH^+ + e^-$ 0.5

$(1a_1) \longrightarrow H_2O^{8+} + 8e^-$ (Auger effect)

Excitation from $(1b_1) \longrightarrow H + OH$

$(3a_1) \longrightarrow H + OH$ 0.75

$\searrow\ H_2 + O$ 0.25

$(1b_2) \longrightarrow H' + OH$ 0.75

$\searrow\ H_2 + O$ 0.25

$(2a_1) \longrightarrow H^+ + OH + e^-$ 0.5

$\searrow\ H' + OH^+ + e^-$ 0.5

$(1a_1) \longrightarrow H_2O^{8+} + 8e^-$ (Auger effect)

It has been assumed in Ref. 17 that the Auger effect accompanied with the ejection of an electron from the $(1a_1)$ orbital results in the formation of only one H_2O^+ ion. Energetically the reaction assumed above is more probable.

Double collisions:

$$H_2O^{2+} \longrightarrow H^+ + OH^+$$
$$H_2O^{**} \longrightarrow H_2O^+ + e^-$$
$$H_2O^{+*} \longrightarrow H^+ + OH \quad 0.5$$
$$\searrow\ H' + OH^+ \quad 0.5$$

Ion-molecule reactions:

$$H_2O^+ + H_2O \longrightarrow H_3O^+ + OH$$
$$OH^+ + H_2O \longrightarrow H_3O^+ + O$$
$$H^+ + H_2O \longrightarrow H_3O^+$$
$$H_2O^{8+} + 15H_2O \longrightarrow 8H_3O^+ + 8OH$$

Neutralization reaction:

$$H_3O^+ + e^- \longrightarrow H_2O + H$$

Hot-atom reaction:

$$H' + H_2O \longrightarrow H_2 + OH$$

The radicals accumulated in the present system through the foregoing reactions are H, OH, and O atoms. The rate constants of the reactions involving these radicals are not all available, so that we cannot write explicitly the reactions of these radicals.

Table 7 summarizes the *G*-values of several intermediate species calculated on the basis of the reactions assumed above.

Discussion

Comparison of Calculation with Experiment. Table 8 summarizes the *G*-values of the final products from methane. Since methane is one of the most stable hydrocarbons, the results obtained at low dose rates cannot be used for comparison, because the secondary reactions of the products play an important role. The experimental results quoted in Table 8 were obtained using a Febetron at a high dose rate[2,4] and a mass spectrometer.[3] The *G*-values estimated in the present calculation agree fairly well with the experimental values. The calculated *G*-values for hydrogen, ethylene,

Table 7. The G-values for intermediate roducts from water

	Ionization	Excitation	Ion-molecule reaction	Neutralization	Hot-atom reaction	Total Intermediate
e^-	3.00			0		
H_2O^+	1.71		0			
OH^+	0.62		0			
H^+	0.62		0			
H_2O^{s+}	0.006		0			
H_3O^+			3.00	0		
H		4.37		3.00		7.37
H′	0.52	0.24			0	
OH	0.52	4.61	1.76		0.76	7.65
O		0.39	0.62			1.01
H_2		0.39			0.76	1.15
$-H_2O$	2.96	4.86	3.04	−3.00	0.76	8.62

Table 8. The G-values for final products from methane

	Present estimation	Experimental		
		(a)	(b)	(c)
H_2	7.18	5.44	6.9	
C_2H_2	0.71	0.76—0.81	0.7	0.85
C_2H_4	2.20	0.71—1.60	1.6	1.05
C_2H_6	0.67	0.75—1.05	0.6	1.93
C_3H_6	0.10	0.06—0.11	0.2	
C_3H_8		0.03—0.09	0.2	
$-CH_4$	7.46	6.92	7.8	

(a) Ref. 2. (b) Ref. 3. (c) Ref. 4.

and propylene, however, are a little larger than those obtained experimentally. This may be due to the secondary reactions of olefins with hydrogen atoms. Even at the high dose rates obtained using the Febetron, the occurrence of some of the fast secondary reactions cannot be avoided.

Tables 9 and 10 compare the G-values of various products obtained in the radiolysis of ammonia.[5,7,8,56,57] The agreement between calculation and experiment is again good. The calculated G-values of the intermediate products from water are listed in Table 7. These values may be compared with those reported in Ref. 17. Most of the G-values are in good agreement with each other. The G-value for hydrogen atoms listed here should be compared with the $G(H)+G(H_3O^+)-G(H')$ in Table 5 of Ref. 17.

Table 9. Comparison of the G-values obtained experimentally with the G-values calculated for the radiolysis of ammonia

	Present estimation	Experimental			
		(a)	(b)	(c)	(d)
H_2	0.95	0.75	0.70	0.80	0.74
H	7.0		7.0	7.2	
e^-+H	10.56	12.5	10.4		
NH_2+2NH	12.46		11.9		
e^-	3.56	3.77	3.4	3.9	
$-NH_3$	11.55	14.0			

(a) Ref. 7. (b) Ref. 8. (c) Ref. 56. (d) Ref. 5.

G-values for Ionization and Excitation. Table 11 compares the W-values obtained theoretically and experimentally.[10-13] The agreement is again satisfactory, although the values calculated here are a little higher than those obtained experimentally. Consider-

Table 10. The G-values for final products from ammonia

	Present estimation	Experimental				
		High dose rate		Low dose rate		
		(a)	(b)	(c)	(d)	(e)
H_2	3.79	3.58	2.9	5.4	4.4	5.5
N_2	1.18	1.0	0.9	1.8	1.45	1.0
N_2H_4	0.24	0.58	0.1			0.4

(a) Ref. 5. (b) Ref. 57. (c) Ref. 7. (d) Ref. 8. (e) Ref. 56.

Table 11. W-values obtained theorecially and experimentally

	Present estimation	Experimental		
CH_4	27.8	26.7[a]	27.5[b]	27.6[c]
NH_3	28.1	26.5[a]	26.5[c]	
H_2O	33.3	30.2[d]	29.9[b]	
Ne	38.9[f]	36.3[e]		

a) Ref. 10. b) Ref. 11. c) Ref. 13. d) Ref. 12. e) Ref. 58. f) This value is slightly smaller than that reported in Ref. 16 ($W=39.5$). In the present calculation, inner-shell excitation has been included in the estimation of the stopping power.

Table 12. The ratio between the G-value for excitation and that for electrons, and the G-value for total loss of the substrate

	Present estimation		Santar and Bednar[59]	
	G_{ex}/G_e	$G(-M)$	G_{ex}/G_e	$G(-M)$
CH_4	1.10	7.36	0.8—0.9	6.4— 6.9
NH_3	1.50	8.74	1.2—1.6	7.4—10.0
H_2O	1.67	7.86	0.7—1.3	5.5— 7.6
Ne	0.57	3.77	0.4	3.7

ing the number of rough approximations involved in the present calculation, the agreement is surprisingly good.

Table 12 shows the ratios of the *G*-values for excitation to those for electrons and the *G*-values for the total loss of the substrate. The same values were calculated by Santar and Bednar[59] using the "optical approximation" proposed by Platzman.[58] Both methods seem to be consistent.

Table 13. The calculated *G*-values for emission from excited hydrogen atoms and other species

		CH_4	NH_3	H_2O
H Lyman	α	0.06[a]	0.05[b]	0.04[b]
		0.006[b]		0.16[d]
	β	0.001[a]		0.005[d]
Balmer	α	0.01[a]		0.03[d]
	β	0.003[a]		0.005[d]
	γ	0.001[a]		0.002[d]
	δ	0.0008[a]		0.0008[d]
2s→1s		0.006[a]		
CH		0.008[c]		
C		0.0007[b]		
N			0.008[b]	

The cross section used for the calculation was quoted from Ref. 14 for a), Ref. 39 for b), Ref. 38 for c), and Ref. 60 for d).

The G-value for Emission. Recently, the emission from the excited species produced by electron impact have been measured by several investigators.[14,38,39,60–62] They reported the cross sections for these processes as a function of the energy of incident electrons. Using these cross sections and the degradation spectra obtained here, it is possible to calculate the *G*-values of various emissions for the substrate excited by 100 keV electrons. Table 13 summarizes the calculated results. The total *G*-values for emission from excited hydrogen atoms produced by 100- keV-electron radiolysis are about 0.1 for methane and ammonia, and 0.2 for water.

References

1) R. E. Rebbert, S. G. Lias, and P. Ausloos, *J. Res. Nat. Bur. Stand.*, **77A**, 249 (1973).
2) R. E. Rebbert and P. Ausloos, *ibid.*, **77A**, 109 (1973).
3) P. S. Rudolph, *Advan. Chem. Ser.*, **82**, 101 (1968).
4) R. W. Hummel and J. A. Hearne, *J. Phys. Chem.*, **75**, 1164 (1971).
5) C. Willis, A. W. Boyd, and O. A. Miller, *Can. J. Chem.*, **47**, 3007 (1969).
6) A. W. Boyd, C. Willis, and O. A. Miller, *ibid.*, **49**, 2283 (1971).
7) F. T. Jones and T. J. Sworski, *Trans. Faraday Soc.*, **63**, 2411, 2426 (1967).
8) J. A. Eyre and D. Smithies, *ibid.*, **66**, 2199 (1970).
9) A. W. Boyd, C. Willis, and O. A. Miller, *Can. J. Chem.*, **51**, 4048 (1973).
10) G. G. Meisels, *J. Chem. Phys.*, **41**, 51 (1964).
11) P. Adler and H. K. Bothe, *Z. Naturforsch.*, **20a**, 1700 (1965).
12) R. Cooper and R. M. Mooring, *Aust. J. Chem.*, **21**, 2417 (1968).
13) R. M. Leblanc and J. A. Herman, *J. Chim. Phys.*, **63**, 1055 (1966).
14) D. A. Vroom and F. J. de Heer, *J. Chem. Phys.*, **50**, 573 (1969).
15) S. Sato, K. Okazaki, and S. Ohno, This Bulletin, **47**, 2174 (1974).
16) K. Okazaki, S. Sato, and S. Ohno, *ibid.*, **48**, 1411 (1975).
17) S. Ohno, H. Nagayama, K. Okazaki, and S. Sato, *ibid.*, **48**, 2153 (1975).
18) K. Siegbahn *et al.*, "ESCA Applied to Free Molecules," North-Holland, Amsterdam (1969).
19) K. Hamrin, G. Johansson, H. Gelius, A. Fahlman, C. Nordling, and K. Siegbahn. *Chem. Phys. Lett.*, **1**, 613 (1968).
20) W. E. Palke and W. N. Lipscomb, *J. Amer. Chem. Soc.*, **88**, 2384 (1966).
21) G. Herzberg, "Molecular Spectra and Molecular Structure," Van Nostrand, Princeton, N. J., Vol. III (1966).
22) S. J. Trajmar, W. Williams, and A. Kuppermann, *J. Chem. Phys.*, **58**, 2512 (1973).
23) A. B. Duncan, *J. Chem. Phys.*, **27**, 423 (1957).
24) E. N. Lassettre, A. Skerbele, M. A. Dillon, and K. J. Ross, *ibid.*, **48**, 5066 (1968).
25) C. R. Claydon, G. A. Segal, and H. S. Taylor, *ibid.*, **54**, 3799 (1971).
26) E. O. Ellison and H. Shull, *ibid.*, **23**, 2348 (1955).
27) J. Appell, J. Durup, F. C. Fehsenfeld, and P. Fourier, *J. Phys., B*, **7**, 406 (1974).
28) E. Clementi and H. Popkie, *J. Amer. Chem. Soc.*, **94**, 4057 (1972).
29) "Handbook of Chemistry and Physics," ed. by R. C. West, The Chemical Rubber Co., Ohio, 51, F-156 (1970—71).
30) V. H. Dibeler, M. Kraus, R. M. Resse, and F. N. Harlee, *J. Chem. Phys.*, **42**, 3791 (1965).
31) C. R. Brundle, M. B. Robin, and H. Basch, *ibid.*, **53**, 2196 (1970).
32) B. Adamczyk, A. J. H. Boerboom, B. L. Schram, and J. Kistemaker, *ibid.*, **44**, 4640 (1966).
33) C. E. Melton and P. S. Rudolph, *ibid.*, **47**, 1771 (1967).
34) D. C. Walker and R. A. Back, *ibid.*, **38**, 1526 (1963).
35) P. H. Metzger and G. R. Cook, *ibid.*, **41**, 642 (1964).
36) J. R. McNesby and H. Okabe, "Advances in Photochemistry," Vol. 3, ed. by W. A. Noyes *et al.*, John Willey & Sons, New York (1964), p. 157.
37) W. Sroka, *Z. Naturforsch*, **24a**, 1724 (1969).
38) J. F. M. Aarts, C. I. M. Beenakker, and F. J. de Heer, *Physica*, **53**, 32 (1971).
39) H. D. Morgan and J. E. Mentall, *J. Chem. Phys.*, **60**, 4734 (1974).
40) B. H. Mahan and R. Mandal, *ibid.*, **37**, 207 (1962).
41) P. Ausloos, R. Gorden, Jr., and S. G. Lias, *ibid.*, **40**, 1854 (1964).
42) R. Gorden, Jr., and P. Ausloos, *ibid.*, **46**, 4823 (1967).
43) A. R. Welch and D. L. Judge, *ibid.*, **57**, 286 (1972).
44) W. Braun, K. H. Welge, and J. R. McNesby, *ibid.*, **45**, 2650 (1966).
45) F. P. Abramson and J. H. Futrell, *ibid.*, **45**, 1925 (1966).
46) R. L. Platzman, *Radiat. Res.*, **17**, 419 (1962).
47) V. H. Dibeler, J. A. Walker, and H. M. Rosenstock, *J. Res. Nat. Bur. Stand.*, **70A**, 459 (1966).
48) D. W. Turner *et al.*, "Molecular Photoelectron Spectroscopy," John Willey & Sons, New York (1969).
49) L. M. Dorfman and P. C. Noble, *J. Phys. Chem.*, **63**, 980 (1959).
50) C. E. Melton, *J. Chem. Phys.*, **45**, 4414 (1966).
51) K. D. Bayes, K. H. Becker, and K. H. Welge, *Z. Naturforsch.*, **17a**, 676 (1962).
52) F. Stuhl and K. H. Welge, *ibid.*, **18a**, 900 (1963).

53) J. R. McNesby, I. Tanaka, and H. Okabe, *J. Chem. Phys.*, **36**, 605 (1962).
54) O. Dressler and K. Schnepp, *ibid.*, **32**, 1682 (1960).
55) A. G. Harrison and J. C. J. Thynne, *Trans. Faraday Soc.*, **62**, 2804 (1968).
56) G. R. A. Johnson and M. Simic, *Advan. Chem. Ser.*, **82**, 197 (1968).
57) G. M. Meaburn and S. Gordon, *J. Phys. Chem.*, **72**, 1592 (1968).
58) R. L. Platzman, *Int. J. Appl. Radiat. Isotopes*, **10**, 116 (1961).
59) I. Santar and J. Bednar, *Coll. Czech. Chem. Commun.*, **32**, 953 (1967); **33**, 1 (1968); **34**, 1 (1969).
60) D. A. Vroom and F. J. de Heer, *J. Chem. Phys.*, **50**, 1883 (1969).
61) N. Bose and W. Sroka, *Z. Naturforsch.*, **26a**, 1491 (1971).
62) J. W. McGowan, J. F. Williams, and D. A. Vroom, *Chem. Phys. Lett.*, **3**, 614 (1969).

Solvent Inclusion Effects on the Structure and Electrical Conductivity of Benzidine-TCNQ Complex

Noriaki TAKAHASHI, Kyuya YAKUSHI, Kikujiro ISHII,* and Haruo KURODA
Department of Chemistry, Faculty of Science, University of Tokyo, Hongo, Tokyo 113
(Received August 9, 1975)

The solvent-containing modification of benzidine (BD)-tetracyanoquinodimethane (TCNQ) complex is a new type of inclusion compound where solvent molecules are included in the channels of the host lattice formed by hydrogen bonding and charge-transfer interaction between BD and TCNQ. The electrical conductivity at 18 °C is 7×10^{-10} ohm^{-1}·cm^{-1} and the activation energy of semiconduction is 0.54 eV in the solvent-free state, but they change to 10^{-4}—10^{-6} ohm^{-1}·cm^{-1} and 0.1—0.2 eV, respectively, when an aliphatic solvent is included, and to 10^{-6}—10^{-9} ohm^{-1}·cm^{-1} and 0.3—0.5 eV, when benzene or its derivatives is included. By examining the changes of the electrical conductivity and the spin density of BD·TCNQ·[CH_2Cl_2] system with the pressure change of the ambient dichloromethane vapor, it is concluded that the conductivity of BD·TCNQ·[CH_2Cl_2] is strongly controlled by the amount of solvent vacancies in the crystal lattice. The correlations between the electrical properties and crystal structures of solvent-containing modifications are discussed.

In the earlier investigations by Ohmasa *et al.*[1] it was first found that the electronic properties of the solid molecular complex between benzidine (BD) and tetracyano-*p*-quinodimethane (TCNQ) were significantly dependent on the solvent used in the preparation of the crystals, and these phenomena were concluded to be due to the solvent inclusion in the crystal lattice of BD·TCNQ complex. They reported that dichloromethane, 1,2-dichloroethane, dibromomethane, bromoethane, acetonitrile, nitromethane and acetone were able to be included in BD·TCNQ complex, while chloroform and 1,1-dichloroethane were not.

Later, we found that a variety of aromatic solvents such as benzene, chlorobenzene, bromobenzene, toluene, benzonitrile and nitrobenzene can be included in BD·TCNQ complex. By carrying out crystal structure analysis on the solvent-free modification as well as on several solvent-containing modifications, we have concluded that the solvent-containing modifications of BD·TCNQ complex are to be regarded as a new type of inclusion compound where the hydrogen bonding and charge-transfer interaction between donor and acceptor molecules are playing an important role in the formation of the channeled structure of the host lattice.[2-4]

In the present paper, we report the effects of the solvent inclusion on the electrical conductivity of the BD·TCNQ system, and their relations with the crystal structures.

Experimental

The solvent-containing modifications of BD·TCNQ complex were obtained by the following procedures; an appropriate amount of benzidine was dissolved in a hot solution which had been almost saturated with TCNQ, and this solution was gradually cooled and kept at room temperature for about one day yielding the crystals of BD·TCNQ complex from the solution. The solvent-free modification was prepared by the same method using chloroform as the solvent.

Since the included solvent is gradually lost when a crystal of a solvent-containing modification is kept in the ordinary atmosphere at room temperature, we took out the crystals from their mother solutions immediately before each experiment.

The X-ray diffraction patterns of the powder samples were observed with a diffractometer, Geigerflex. The presence of the included solvent was examined by thermogravimetric analysis (TG) combined with differential scanning calorimetry (DSC), which were carried out with a Rigaku TG-DSC apparatus. The infrared absorption spectra were examined by use of Nujol mull method.

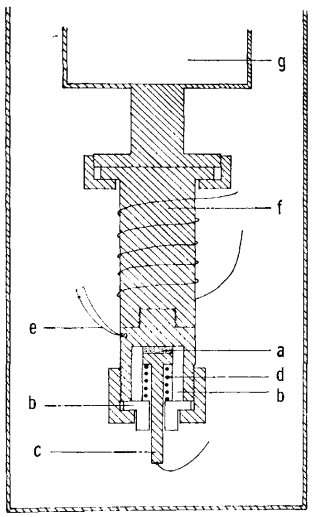

Fig. 1. Apparatus for conductivity measurement: (a) sample, (b) Teflon cylinder, (c) electrode, (d) spring, (e) thermo-couple (Cu-constantan), (f) heat-conductor with a heater, (g) liquid N_2.

The DC conductivity of each modification was measured on a polycrystalline sample by using the apparatus illustrated in Fig. 1. The crystalline powder[5] was packed in the sample cell, and compressed to a polycrystalline disc between the electrodes using a pressure of about 16 kg·cm^{-2}. In this way, the sample was tightly sealed in the cell so as to prevent the evolution of the included solvent during the measurement. To minimize the solvent evolution, we carried out the measurement only at lower temperatures. The size of the polycrystalline disc of the sample was measured after the conductivity experiment. Typically, it was about 8 mm in diameter and about 0.5 mm thick. Applying a DC voltage of 1—20 volt between the electrodes, we measured the current through the sample with an electrometer, Takeda Riken TR-8651.

* Present address: Institute for Solid State Physics, University of Tokyo, Roppongi, Tokyo.

Results and Discussion

Structural Aspects of Solvent Inclusion. From the examination of the powder X-ray diffraction patterns of various modifications of BD·TCNQ complex, with and without solvent inclusion, we concluded that there are, at least, three different types of crystal lattice for the BD·TCNQ system: The first one (Type I) is the crystal lattice of the solvent-free modification, BD·TCNQ·[n], the second one (Type II) is that of a modification containing an aliphatic solvent, and the third one (Type III) is that of a modification containing an aromatic solvent.

We have carried out the crystal structure analysis on a representative example of each of the above three types; the solvent-free modification, BD·TCNQ·[n], as Type I, the one containing dichloromethane, BD·TCNQ·[CH_2Cl_2], for Type II, and the one containing benzene, BD·TCNQ·[C_6H_6], for Type III. The details of the crystal structure analysis of each modification have been separately reported elsewhere.[2-4] In the crystal of BD·TCNQ·[n],[3] benzidine and TCNQ molecules are alternately stacked on each other to form molecular columns along the c-axis, and those molecular columns are closely packed together without leaving any free space to accommodate solvent molecules.

The crystal structure of BD·TCNQ·[CH_2Cl_2] is reproduced in Fig. 2.[2] Benzidine and TCNQ molecules are alternately stacked on each other to form molecular columns which are almost the same as in BD·TCNQ·[n], but these columns are arranged so as to leave channels running through the crystal along the c-axis, in which solvent molecules are accommodated. There seems to be no specific interaction between the included dichloromethane molecules and the BD·TCNQ host lattice.

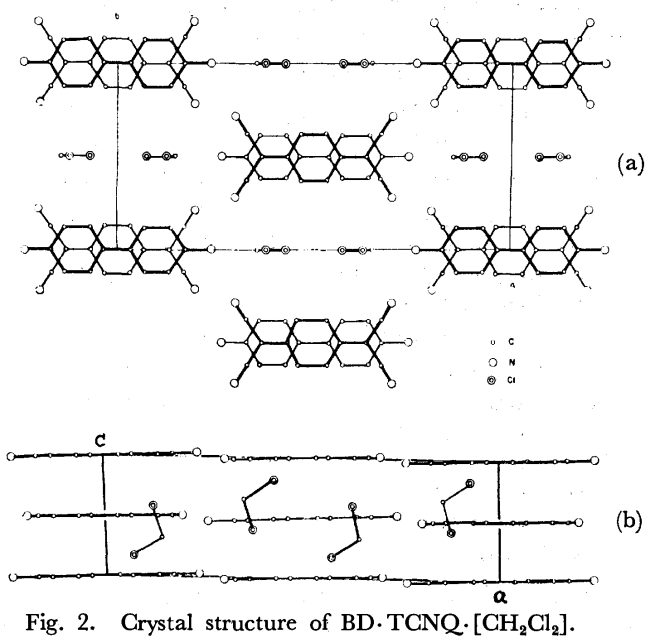

Fig. 2. Crystal structure of BD·TCNQ·[CH_2Cl_2]. (a) projection to the (001) plane, (b) projection to the (010) plane.

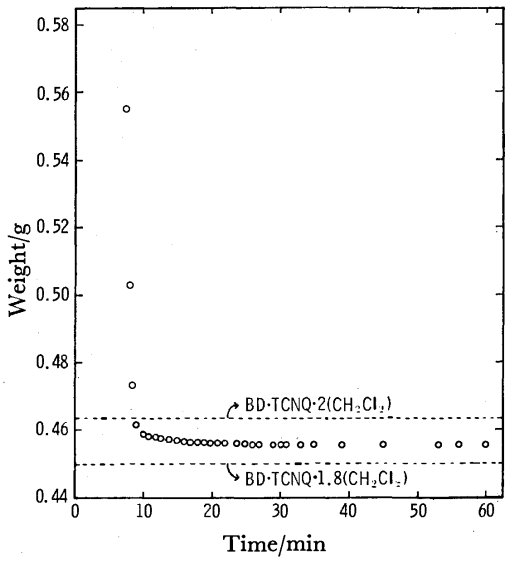

Fig. 3. Weight change of BD·TCNQ·[CH_2Cl_2] powder in the ordinary atmosphere, starting from the state wet with dichloromethane liquid. Note that the weight settles at the value corresponding to BD·TCNQ·1.8 (CH_2Cl_2), and remains the same after that. The mole ratio was calculated from the weight loss of the sample heated in vacuum.

According to the crystal structure, the ideal composition of the BD·TCNQ·[CH_2Cl_2] system is to be BD·TCNQ·2(CH_2Cl_2), but the actual composition was BD·TCNQ·1.8(CH_2Cl_2) under normal conditions. This means that about 10 percent of dichloromethane molecules are missing from the crystal lattice of BD·TCNQ·[CH_2Cl_2] creating the corresponding amount of vacancies at the solvents sites without producing any significant distortion of the host lattice. When the crystalline powder of BD·TCNQ·[CH_2Cl_2], which was wet with an excess dichloromethane, was kept in the ordinary atmosphere, the amount of the included solvent changed with time as shown in Fig. 3. The amount of the included solvent decreased to the value corresponding to BD·TCNQ·1.8(CH_2Cl_2), and thereafter it stayed at the same value for a long period. Further loss of the included solvent took place when the powder was heated to about 60 °C in vacuum, but, in this case, the solvent evolution was accompanied by conversion

Table 1. Crystal data of BD·TCNQ

	Space group	*a*	*b*	*c*	*β*	*Z*
BD·TCNQ·[n]	C2/m	12.231	12.679	6.477	104.84	2
BD·TCNQ·[CH_2Cl_2]	I2/m	20.892	9.950	6.445	91.92	2
BD·TCNQ·[CH_2ClCH_2Cl]	Immm	10.199	20.765	6.529		2
BD·TCNQ·[CH_2BrCH_2Br]	Immm	10.205	20.785	6.525		2
BD·TCNQ·[C_6H_6]	$P2_1/m$	17.184	9.852	7.680	100.3	2

of the crystals to BD·TCNQ·[n]. Seemingly, BD·TCNQ·1.8(CH_2Cl_2) is the limiting composition for keeping the channeled structure of the host lattice.

The crystal data of other two modifications of Type II are compared in Table 1 with those of BD·TCNQ·[CH_2Cl_2]. Above three modifications are almost isomorphous to each other. In effect, preliminary analyses of the crystal structures of BD·TCNQ·[CH_2ClCH_2Cl] and BD·TCNQ·[CH_2BrCH_2Br] have shown that, in these cases, the host lattice is almost the same as in BD·TCNQ·[CH_2Cl_2]. The amount of included solvent was found to be 1.6 mole per one mole of BD·TCNQ in BD·TCNQ·[CH_2ClCH_2Cl] as well as in BD·TCNQ·[CH_2BrCH_2Br], which is approximately equal to the value that is expected to fill up the channels with dichloroethane or dibromoethane. The analyses of the diffraction patterns have led us to conclude the presence of a considerable disorder as regards the arrangement of solvent molecules in the channels. Seemingly, such a disorder has been inevitably introduced to fill up the channels with the solvent molecules. Although a detailed investigation has not yet been carried out on the crystal structure of other modifications of Type II, we believe that all of them commonly possess the same type of host lattice.

The crystal structure of BD·TCNQ·[C_6H_6][4] is different from the structures of the modifications of Type II; The BD·TCNQ column is composed of BD·TCNQ pairs[6] and one benzene molecule is surrounded by four BD·TCNQ pairs. The amount of the included benzene was found to be one mole per one mole of BD·TCNQ as it is expected from the crystal structure. When a crystal of BD·TCNQ·[C_6H_6] is kept in the ordinary atmosphere at room temperature, the included benzene is gradually lost converting the crystal to the solvent-free modification. There seems to be no stable phase which has some fixed amount of solvent vacancies in this case.

As we have already mentioned, the modifications which contain aromatic solvents, exhibit diffraction patterns similar to that of BD·TCNQ·[C_6H_6], and the mole ratio of included solvent is always one mole per one mole of BD·TCNQ as in BD·TCNQ·[C_6H_6]. Thus, the structure of the host lattice is likely to be essentially the same in all of these cases.

Electrical Conductivities of Solvent-containing Modifications. Although some of the solvent-containing modifications were obtainable as a single crystal sufficiently large for performing the measurement of electrical conductivity, we carried out the measurement exclusively on the compressed polycrystalline samples by the method described in the earlier part of this paper because it is more difficult to prevent a loss of the included solvent during the conductivity measurement when we use a small single crystal.

In Fig. 4, we show the experimental results obtained for three representative modifications. For all modifications, the temperature dependence of electrical conductivity was reproducible between the cooling and heating processes, and the relation between the conductivity σ and the temperature was describable with a single exponential function (Eq. (1)).

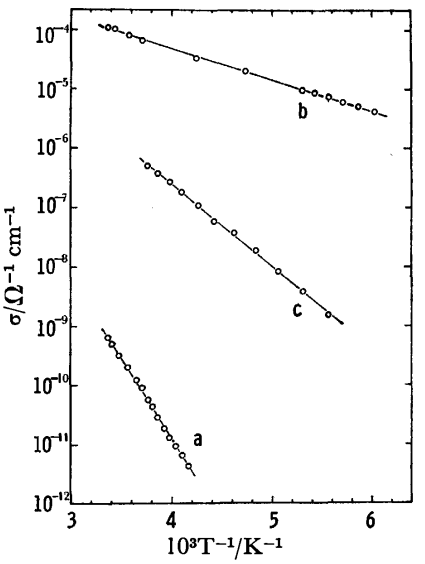

Fig. 4. Temperature dependence of conductivity.
(a) BD·TCNQ·[n], (b) BD·TCNQ·[CH_2Cl_2], and (c) BD·TCNQ·[C_6H_6].

$$\sigma = \sigma_0 \exp(-\Delta E/kT) \quad (1)$$

These facts imply that we were practically able to avoid the solvent loss during the conductivity measurements.

The electrical conductivities at 18 °C and the activation energies of semiconduction are summarized in Table 2, where the results reported by Ohmasa *et al.*[1] are also included for comparison.

TABLE 2. CONDUCTIVITY DATA OF BD·TCNQ

	Included solvent (mole ratio)	Crystal lattice	σ (18°C) [$ohm^{-1}\cdot cm^{-1}$]	ΔE [eV]
(1)	solvent-free	I	7×10^{-10}	0.54
(2)	CH_2Cl_2 (1.8)	II	1×10^{-4}	0.11
(3)	C_2H_5Br (1.8)	II	2×10^{-4}	0.12[a]
(4)	CH_2ClCH_2Cl (1.6)	II	1×10^{-5}	0.14
(5)	CH_3CN (0.8)	II	1×10^{-5}	0.16[a]
(6)	CH_3COCH_3 (0.8)	II	3×10^{-6}	0.21[a]
(7)	C_6H_6 (1.0)	III	1×10^{-6}	0.28
(8)	C_6H_5Cl (1.0)	III	3×10^{-7}	0.38
(9)	C_6H_5Br (1.0)	III	1×10^{-7}	0.40
(10)	$C_6H_5CH_3$ (1.0)	III	3×10^{-8}	0.43
(11)	C_6H_5CN (1.0)	III	2×10^{-9}	0.44
(12)	$C_6H_5NO_2$ (1.1)	III	3×10^{-9}	0.50

a) Ref. 1.

First of all, we note that a large increase of conductivity and a marked lowering of activation energy are caused by the solvent inclusion. These changes are most significant in the modifications which have been classified as Type II. In these cases the conductivities at 18 °C are of the order of 10^{-4}—10^{-6} $ohm^{-1}\cdot cm^{-1}$ and the activation energies are only 0.1—0.2 eV while the former is 10^{-9} $ohm^{-1}\cdot cm^{-1}$ and the latter is 0.54 eV in the case of BD·TCNQ·[n].

According to Eq. (1), the relation between the conductivity at 18 °C, σ (18 °C), and the activation energy of semiconduction, ΔE (in eV units), can be expressed as follows;

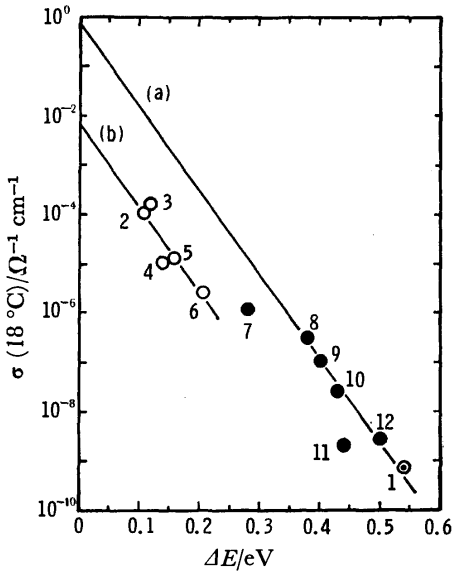

Fig. 5. Plots of the conductivity at 18 °C *versus* the activation energy of semiconduction. (See text for the meanings of lines (a) and (b). Their inclinations corresponds to $-1/kT$ (T=291 K).) Refer Table 2 for the numbering of the systems.

$$\log \sigma\,(18°C) = \log \sigma_0 - 17.32\Delta E \qquad (2)$$

Therefore, if σ_0 is the same for different modifications, we should have a straight line when we plot log σ (18 °C) versus ΔE. We show the log σ (18 °C) *vs.* ΔE plots in Fig. 5. Interestingly, the plots in the ΔE region of 0.4—0.6 eV are on the line (a) which correspond to σ_0=1 ohm^{-1}·cm^{-1}. These plots are concerned with the modifications of Type III and the solvent-free modification. On the other hand, the plots concerned with the modifications of Type II fall on another line (b) which corresponds to σ_0 of about 10^{-2} ohm^{-1}·cm^{-1}. If we assume that the density of states are of the same order of magnitude as the number of BD·TCNQ units per unit volume, and the mobilities of charge carriers are 10^{-2}—10^{-1} cm^2·V^{-1}·s^{-1} as reported for several charge-transfer complexes,[7-9] σ_0 is expected to be 10^{0}—10^{1} ohm^{-1}·cm^{-1} for the intrinsic semiconduction. Naturally, it is difficult to make a quantitative discussion on σ_0 by using the conductivity data obtained of polycrystalline samples, but we could say that the σ_0 value corresponding to the line (a) is not unreasonable for the intrinsic semiconduction while that corresponding to the line (b) is too small.

The value of activation energy provides another criterion. In the case of a charge-transfer complex, the energy gap (*i.e.*, the energy required for the intrinsic carrier formation) can be estimated by the following relation;

$$\varepsilon = I(\mathrm{D}) - A(\mathrm{A}) - \{P(\mathrm{D}^+) + P(\mathrm{A}^-)\} \qquad (3)$$

where I(D) and A(A) are the ionization potential of the donor (D) and the electron affinity of the acceptor (A), respectively, and P(D$^+$) and P(A$^-$) are the polarization energies associated with the formations of D$^+$ and A$^-$ ions in the crystal, respectively. Ionization potential of benzidine is estimated as 7.15 eV from the charge-transfer band of the benzidine-chloranil complex in solution,[10] and the electron affinity of TCNQ has been reported to be 2.8 eV.[11,12] According to Batley and Lyons,[13] the photoionization threshold of BD·TCNQ complex is at 5.03 eV. Since the ionization potential of TCNQ, 9.6 eV,[14] is more than 2 eV higher than that of benzidine, the photoionization threshold corresponds to the energy for the ionization of a benzidine molecule in the crystal of the complex. This energy can be related to I(D) and P(D$^+$) as follows;

$$I(\mathrm{D};\ \text{solid DA}) = I(\mathrm{D}) - P(\mathrm{D}^+) \qquad (4)$$

By substituting I(D; solid DA)=5.03 eV and I(D)=7.15 eV into Eq. (4), we obtain P(D$^+$)=2.12 eV. At present, P(A$^-$) can not be experimentally estimated, but one could reasonably assume it as 1.5—2 eV. If we put these figures into Eq. (3), the energy gap is estimated to be less than 1 eV, which is rather smaller than the twice of the activation energy actually observed of the solvent-free modification. Thus it is not unreasonable to consider that the observed conductivity is due to the intrinsic carrier formation in this case.

We may expect two kinds of effects of solvent inclusion on the activation energy of semiconduction in the BD·TCNQ system. The first is the one associated with the formation of hydrogen bonds between benzidine and TCNQ. We have found that the crystal of the molecular complex which has an infinite hydrogen-bonded chain of donor and acceptor as in quinhydrone, generally exhibits a charge-transfer band at an energy lower by 0.4—0.6 eV than the value that is expected simply from the ionization potential of donor and the electron affinity of acceptor.[16] Seemingly, the value of I(D)$-A$(A) is reduced when a hydrogen-bonded chain or network is formed between donor and acceptor. From this point of view, we can expect that the solvent inclusion of BD·TCNQ complex will cause a decrease of the activation energy of semiconduction, since benzidine and TCNQ molecules are forming hydrogen-bonded networks when solvent molecules are included, while not in the solvent-free state.[17]

The second effect of solvent inclusion is the one associated with a change in the polarization energy term. The values of P(D$^+$) and P(A$^-$) will naturally be affected by the solvent inclusion. Although it is not easy to quantify this effect we can qualitatively predict that the polarization energy term will be a little smaller in the solvent-containing modifications than in the solvent-free modification. Therefore, this effect of solvent inclusion is likely to cause an increase of activation energy.

Since the above two effects are giving mutually opposite contributions, the solvent inclusion will cause a relatively small change in the intrinsic energy gap. In this sense, the activation energies observed of the modification of Type III are quite understandable, but those observed of the modifications of Type II seem to be too small for the intrinsic carrier formation.

Solvent Vacancies and Electrical Conductivity. As we have already mentioned, the amount of the included solvent can vary within a certain range without changing the structure of the host lattice in the case of the modifications of Type II. This is typically the case in BD·TCNQ·[CH_2Cl_2]. Thus we examined the correlation

between the electrical conductivity and the amount of solvent vacancies by varying the pressure of the ambient dichloromethane vapor. For this purpose the crystalline powder of BD·TCNQ·[CH_2Cl_2], still wet with dichloromethane, was packed between two gold-mesh electrodes so as to keep a good contact with the ambient vapor, and put in a glass cell for the conductivity measurement. This cell was connected to the system for controlling the pressure of the dichloromethane vapor. When the vapor pressure was stepwisely varied after the removal of excess dichloromethane, the current changed rather rapidly settling to a new stationary state within 5—10 minutes at each vapor

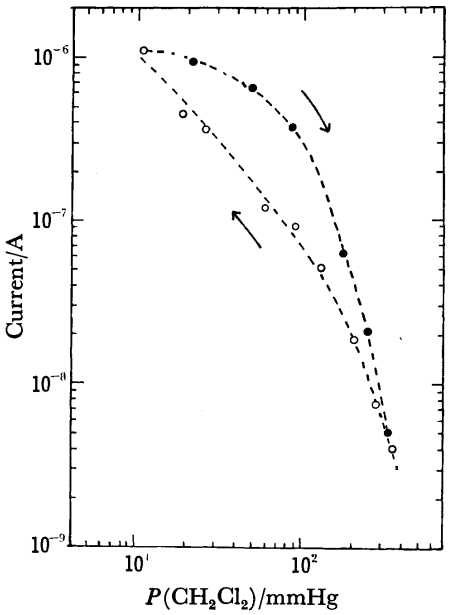

Fig. 6. Dependence of the conductivity of BD·TCNQ·[CH_2Cl_2] on the vapor pressure of dichloromethane in the ambient atmosphere. The current observed at a constant applied field is directly plotted instead of the conductivity.

pressure. In Fig. 6, we plotted the observed steady-state current against the vapor pressure of dichloromethane. In the pressure region above 6 mmHg, the steady-state current significantly increased on decreasing the vapor pressure, and conversely, decreased on increasing the vapor pressure, but there appeared an appreciable hysteresis in the current *vs* pressure curve. The current reached a maximum value at about 6 mmHg, and remained at almost the same value at lower vapor pressures. Examining the amounts of included solvent in the powders which have been subjected to the conditions similar to those in the above experiments, we concluded that the results shown in Fig. 6, are giving the conductivity change due to the variation of the composition, BD·TCNQ·$x(CH_2Cl_2)$ in the range of $1.8 \leq x \leq 2$. The experimental results described above, most clearly demonstrate that the electrical conductivity of the BD·TCNQ·[CH_2Cl_2] system is strongly controlled by the amount of solvent vacancies, and the conductivity data obtained under the ordinary condition, where the composition of the sample is BD·TCNQ·$1.8(CH_2Cl_2)$, should be regarded as primarily associated with an extrinsic semiconduction caused by the presence of solvent vacancies.

In this connection, it is interesting to see that the BD·TCNQ·[CH_2Cl_2] system exhibits a strong ESR absorption in the presence of solvent vacancies. It was reported by Ohmasa *et al.*[1] that BD·TCNQ·[CH_2Cl_2] did not exhibit ESR signal when measured with its well-grown crystals immediately after preparation, but gave strong ESR signals when ground to a fine powder. They observed also that a strong ESR signal appeared when a pulverized sample of BD·TCNQ·[n] was exposed to the vapor of dichloromethane.

In order to elucidate the relation between spin centers and solvent vacancies, we examined the ESR signal of BD·TCNQ·[CH_2Cl_2] powder in the dichloromethane vapor. The powder sample, still wet with an excess dichloromethane, was put into the ESR sample tube which had a stopcock and a joint so that it could be connected to the vacuum system for controlling the vapor pressure of dichloromethane. The ESR signal was first observed in the presence an excess dichloromethane, then its change was observed by stepwisely reducing the vapor pressure of the dichloromethane in the sample tube. At each vapor pressure, we waited for about 45 min before the ESR measurement so that the sample had settled in an equilibrium state with the ambient dichloromethane vapor. The results are shown in Fig. 7, in which we have plotted the spin density against the vapor pressure, both in logarithmic scale.

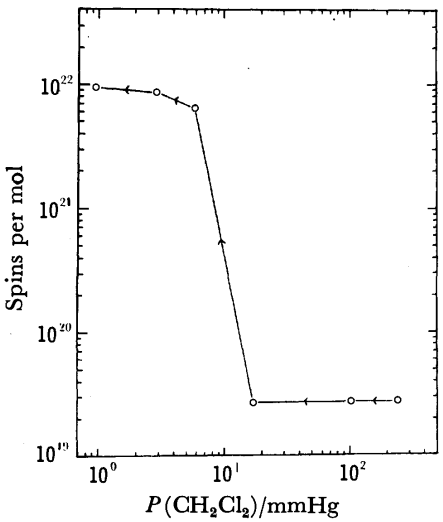

Fig. 7. Dependence of the spin concentration of BD·TCNQ·[CH_2Cl_2] on the vapor pressure of dichloromethane.

Since we had pulverized the crystals, the sample exhibited a weak ESR signal even in the presence of an excess dichloromethane. On driving off the excess dichloromethane, the spin density increased slightly, but after a small initial change it remained almost at a constant magnitude down to 20 mmHg. A steep rise of spin density was observed on decreasing the vapor pressure from 20 mmHg to about 6 mmHg,[15] then the change was leveled off in the lower pressure region. The above data clearly demonstrate that the spin density is closely related to the amount of solvent

vacancies. Although benzidine and TCNQ molecules are essentially in non-ionic states when they are at their regular sites, radical ions could be easily formed through electron transfer from benzidine to TCNQ at the crystal sites which possess features favouring ion-formation, since benzidine has a low ionization potential and TCNQ has a very high electron affinity. Seemingly the solvent vacancies are contributing somehow to the creation of such sites in the crystal. If a radical ion of benzidine and/or that of TCNQ are formed in the crystal, they could also contribute as the origins of extrinsic charge carriers. However, it is not possible to find out a direct correlation between the vapor pressure dependence of spin density (Fig. 7) and that of electrical conductivity (Fig. 6). Possibly, this is because the latter is, to some extent, reflecting the properties of the surface regions of crystals, while the former is more related to the bulk properties.

We examined the temperature dependence of magnetic susceptibility on the powder of BD·TCNQ·1.8(CH_2Cl_2) by means of Faraday method. The observed results are shown in Fig. 8. We found that the

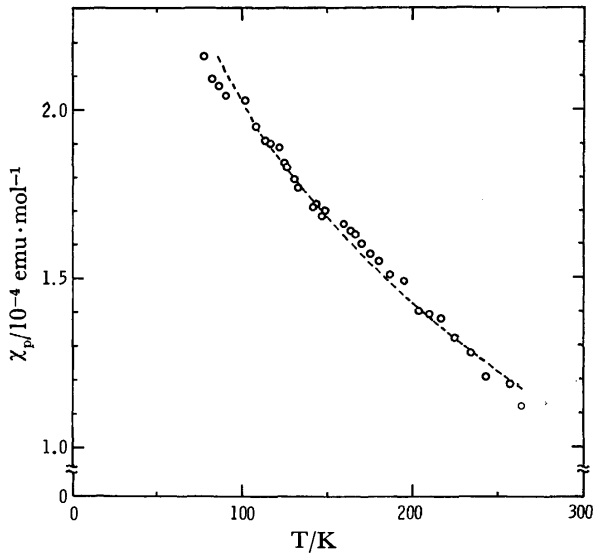

Fig. 8. Temperature dependence of the paramagnetic susceptibility of BD·TCNQ·1.8(CH_2Cl_2).

paramagnetic susceptibility, which was obtained by subtracting the diamagnetic term, $\chi_d=-336\times10^{-6}$ emu·mol^{-1}, from the observed molar susceptibility, followed the Curie-Weiss law with the Weiss temperature of about −130K and the Curie constant $C=0.047$ emu·K. This seems to suggest that the spin centers are not entirely isolated from each other, but are distributed in the state that allows a weak interaction between them.

References

1) M. Ohmasa, M. Kinoshita, and H. Akamatu, This Bulletin, **44**, 391, 395 (1971).
2) I. Ikemoto, K. Chikaishi, K. Yakushi, and H. Kuroda, *Acta Crystallogr.*, **B28**, 3502 (1972).
3) K. Yakushi, I. Ikemoto, and H. Kuroda, *ibid.*, **B30**, 835 (1974).
4) K. Yakushi, I. Ikemoto, and H. Kuroda, *ibid.*, **B30**, 1738 (1974).
5) A freshly prepared crystalline powder was used without grinding to a fine powder, to avoid the loss of the included solvent.
6) The mean separation between the molecular planes of benzidine and TCNQ is 3.09 Å in the pair shorter one, but 3.29 Å, between pairs.
7) H. Kuroda, K. Yoshihara, and H. Akamatu, This Bulletin, **36**, 1365 (1963).
8) H. Möhwald, D. Haarer, and G. Castro, *Chem. Phys. Lett.*, **32**, 433 (1975).
9) N. Karl and J. Ziegler, *ibid.*, **32**, 438 (1975).
10) T. Amano, H. Kuroda, and H. Akamatu, This Bulletin, **42**, 671 (1969).
11) A. L. Ferragher and F. M. Page, *Trans. Faraday Soc.*, **63**, 2369 (1967).
12) C. E. Klots, R. N. Compton, and V. Raasen, Private communication.
13) M. Batley and L. E. Lyons, *Mol. Cryst.*, **3**, 357 (1968).
14) I. Ikemoto, K. Samizo, T. Fujikawa, K. Ishii, T. Ohta, and H. Kuroda, *Chem. Lett.*, **1974**, 785.
15) The ESR signal was of a Lorentzian shape with $g=2.002$ and with a half width of about 1 G.
16) T. Amano; Thesis, University of Tokyo (1968).
17) The maximum of the first charge-transfer band is located at 0.81 eV in the case of BD·TCNQ·[CH_2Cl_2] while it is at 0.94 eV in the case of BD·TCNQ·[n].

Mass Spectrometric Study of the Primary Processes in Photochemical Reactions. III. Primary Steps in Simple Ketone Photolysis and Mass Spectrum of Acetyl Radical

Shigeru YAMASHITA

Department of Chemistry, Faculty of Liberal Arts and Sciences, University of Osaka Prefecture, Mozu-Umemachi, Sakai, Osaka 591

(Received August 20, 1975)

The primary processes of the photolyses of acetone, methyl ethyl ketone, and methyl vinyl ketone have been studied using a high intensity UV light beam and collision-free photochemical reactor incorporated in the ion-source of a mass spectrometer. Photofragment radicals are directly detected from the mass spectrum of the photolyte flow and the primary processes are determined. Mass spectrum of acetyl radical has been obtained in addition to the mass spectra of hydrocarbon free radicals reported in previous papers. As for the ketones investigated, C–C bond rupture between acetyl and the remainder of the molecule is found predominant in the primary process of the photolysis in the region 290—320 nm.

The photolyses of simple ketones have been reported by many workers and the primary processes of these photochemical reactions have been studied on many compounds.[1] Most of the mechanisms, however, were proposed by the analyses of reaction products after the light-off of the experiments. Direct identification of the photofragments produced in the primary processes has been attempted and successful detections of free radicals from photolyses have been reported since the pioneering works in mass spectrometry[2] and in flash photolysis.[3] In most of the mass spectrometric studies for identification of free radicals in photochemical reactions, only the parent-ion peaks of free radicals have been detected.[4-6]

In the previous paper[7] photolysis of methyl and ethyl iodide was carried out using a light source incorporated in the ion-source of a mass spectrometer and the photofragments recorded in the mass spectrum were assigned to CH_3, C_2H_5, and I. The mass spectra of methyl and ethyl radicals thus obtained were in good agreement with the results of previous workers[8] and with theoretical estimation recently reported.[9]

In the present paper, the primary processes of the photolyses of acetone, methyl ethyl ketone and methyl vinyl ketone have been studied by direct identification of the primary photofragments from the mass spectra of photolyte mixtures.

In the case of these simple ketones, possible primary steps are as following since "Norrish Type II" process can be excluded because of the absence of γ-hydrogen atom:

$$CH_3COR + h\nu \longrightarrow CH_3CO + R \quad (1)$$
$$\longrightarrow CH_3 + COR \quad (2)$$
$$\longrightarrow CH_3 + R + CO \quad (3)$$

here, R denotes CH_3, C_2H_5, or C_2H_3 appropriately.

The purpose of the present paper is to detect directly the photofragments expected from processes (1)—(3) and thereby estimate the contribution from each process although the estimation has been reported by the previous workers[1] from the results of conventional analysis of final products.

Experimental

Acetone and methyl ethyl ketone obtained from Wako Pure Chemical Industry Ltd. and methyl vinyl ketone from Aldrich Chemical Co. were purified by vacuum distillation.

The apparatus and procedure were reported elsewhere.[7,10] The molecular flow of the reactant gas was supplied from a 5 l reservoir kept in the dark into the reactor installed in the ion-source of a Hitachi RMU-5 mass spectrometer through an orifice and a Pyrex glass gas-lead.

The light source was a USH-500D 500W high-pressure mercury lamp (Ushio Electric Co.) and the light flux was focused on the molecular flow of the reactant in the reactor through a quartz window of the ion-source.

Considering the absorption spectra of the reactant ketones[1,11] and the transmission of the Pyrex glass of the reactor, the effective wavelength for photolyses was estimated to be in the range 290—320 nm of the mercury lamp output.

The mass spectrum obtained at 50 eV for each run was a superposition of the cracking patterns of the photofragments and that of the unchanged reactant. The mass spectrum of the photofragment mixture was obtained by subtracting the contribution from unreacted reactant ketones.

Results and Discussion

Photolysis of Acetone. Table 1 shows an example of the mass spectrum of photolyte flow of acetone photolysis. By subtracting the contribution from unreacted acetone from the recorded peak height in the second column at each mass number, the residue Δ is obtained

Table 1. Recorded mass spectrum of the photolyte flow of acetone at 50 eV (in arbitrary units)

m/e	Peak height	Acetone contribution	Δ
13	0.2	0.1	0.1
14	1.3	0.9	0.4
15	7.1	5.8	1.3
26	1.1	1.0	0.1
27	1.9	1.7	0.2
28	1.9	1.5	0.4
29	1.3	1.2	0.1
39	1.0	0.9	0.1
41	1.3	1.1	0.2
42	1.7	1.6	0.1
43	27.4	25.0	2.4
58	7.1	7.1	—

as the superposition of the mass spectrum of each photofragment.

The averaged value of Δ obtained from fifteen runs is shown in Table 2 where abundance is normalized at *m/e* 43. The peak height ratio at mass number 15, 14, and 13 is 55: 12: 6, which is equal to 100: 22: 11. This ratio is almost the same as the cracking pattern of methyl radical previously reported.[7] This means that the primary process of acetone photolysis at $\lambda > 290$ nm is almost exclusively the following one:

$$CH_3COCH_3 + h\nu \longrightarrow CH_3CO + CH_3 \quad (4)$$

The above-mentioned observation is consistent with the results of previous works where the formation of acetyl radical was deduced by the static studies.[12]

Table 2. Mass spectrum of photofragment mixture of acetone photolysis

m/e	Abundance	Assignment
13	6±2	CH_3
14	12±4	
15	55±10	
26	7±3	CH_3CO
27	9±3	
28	12±3	
29	8±4	
39	7±3	
41	12±4	
42	9±3	
43	100	

In Table 2, the peaks at *m/e* 26, 27, 28, 29, 39, 41, 42, and 43 are assigned to acetyl radical. That is, peak *m/e* 43 is the base peak in the mass spectrum of acetyl radical and the cracking pattern coefficients of other peaks are shown.

Photolysis of Methyl Ethyl Ketone. Mass spectrum of the photofragment mixture of methyl ethyl ketone photolysis, which was obtained by subtracting the contribution of unreacted ketone from recorded mass spectrum in similar way to the case of acetone photolysis in Table 1, is shown in the second column of Table 3 in the form of relative abundance normalized at *m/e* 43. This abundance ratio is an average obtained from fifteen runs. The peaks *m/e* 43, 42, 41, and 39 are completely due to CH_3CO since the peak height ratio of these peaks is nearly the same as the cracking pattern of acetyl radical mentioned before. In the peaks *m/e* 29, 28, 27, and 26, there are partial contribution from acetyl radical. Since the cracking pattern of CH_3CO is known in Table 2, the residue Δ_1 is obtained by subtracting the contribution of CH_3CO.

In the residue Δ_1, the peaks *m/e* 26—29 may entirely be attributed to ethyl radical C_2H_5 since the peak height ratio in these mass numbers is close to the cracking pattern of C_2H_5 previously reported.[7] By subtracting the contribution of C_2H_5 from Δ_1, small residue Δ_2 is obtained. The peaks *m/e* 15 and 14 are due to CH_3, and *m/e* 57 peak may be assigned to photofragment C_2H_5CO.

Then, besides the major process (5)

$$CH_3COC_2H_5 + h\nu \longrightarrow CH_3CO + C_2H_5 \quad (5)$$

Table 3. Mass spectrum of photofragment mixture of methyl ethyl ketone photolysis

m/e	Abundance	CH_3CO contribution	Δ_1	C_2H_5 contribution	Δ_2
14	4±2		4		4 (CH_3)
15	11±3		11		11
26	8±3	7	1	1	—
27	20±6	9	11	11	—
28	16±6	12	4	4	—
29	21±4	8	13	13	—
39	6±2	6	—		—
41	12±2	12	—		—
42	10±3	10	—		—
43	100	100	—		—
57	8±4		8		8 (C_2H_5CO)

the following process (6) is taken into account as a minor process in the primary step of methyl ethyl ketone photolysis in the wavelength range of this work:

$$CH_3COC_2H_5 + h\nu \longrightarrow CH_3 + C_2H_5CO \quad (6)$$

The quantum yield ratio Φ_5/Φ_6 may be estimated to be 8.4 considering the total ion current ratio $[\sum I(CH_3CO) + \sum I(C_2H_5)]/[\sum I(C_2H_5CO) + \sum I(CH_3)]$ from Table 3 under the assumption of equal ionization cross section of each photofragment radical. Here, $\sum I(R)$ denotes the sum of all of the ion intensities originated from photofragment R.

Pitts and Blacet reported[13] that $\Phi_5/\Phi_6 = 40$ at 313 nm and $\Phi_5/\Phi_6 = 5.5$ at 265 nm by analyzing the final products in the photolysis of methyl ethyl ketone. Considering the effective wavelength range of 290—320 nm in the present work, the estimated Φ_5/Φ_6 value in this work is consistent with their results.

Photolysis of Methyl Vinyl Ketone. Primary process of the photochemical reaction of methyl vinyl ketone in gas phase seems to have not been explored although a number of works have been reported on the polymerization reaction.

An example of the mass spectrum of the photolyte flow of methyl vinyl ketone photolysis is shown in the second column of Table 4. By subtracting the contribution from unreacted methyl vinyl ketone, the residue Δ_1 is obtained as a superposition of the ion current from each photofragment. The residue Δ_2 is obtained by subtracting the CH_3CO contribution from Δ_1. Since the most intense peak in Δ_2 is found at *m/e* 27, the mass number of the base peak in the mass spectrum of vinyl radical recently reported,[14] the contribution from C_2H_3 is subtracted from Δ_2 resulting in the small residue Δ_3.

Because of the small peaks in Δ_3, the minor process (8) is considered although major process is evidently process (7) in the primary step of methyl vinyl ketone photolysis:

$$CH_3COC_2H_3 + h\nu \longrightarrow CH_3CO + C_2H_3 \quad (7)$$

$$CH_3COC_2H_3 + h\nu \longrightarrow C_2H_3CO + CH_3 \quad (8)$$

In the residue Δ_3, the peak *m/e* 15 suggests the formation of CH_3 and the peak *m/e* 55 may be due to C_2H_3CO. Small peaks at *m/e* 39 and 42 are presumably the frag-

TABLE 4. MASS SPECTRUM OF PHOTOFRAGMENT MIXTURE OF METHYL VINYL KETONE PHOTOLYSIS

m/e	Peak height	$CH_3COC_2H_3$ contribution	Δ_1	CH_3CO contribution	Δ_2	C_2H_3 contribution	Δ_3
14	2.1	2.1	—		—		—
15	5.3	5.1	0.2		0.2	0.1	0.1
26	3.4	3.2	0.2	0.1	0.1	0.1	—
27	11.4	10.2	1.2	0.1	1.1	1.1	—
28	1.7	1.6	0.1	0.1	—		—
39	1.7	1.5	0.2	0.1	0.1		0.1
41	1.3	1.2	0.1	0.1	—		—
42	2.3	2.1	0.2	0.1	0.1		0.1
43	13.4	12.6	0.8	0.8	—		—
55	16.1	15.8	0.3		0.3		0.3
70	6.2	6.2	—		—		—

ment ions from C_2H_3CO. As for the mass spectra of free radicals previously studied,[7,8,14] the parent-ion peak is always the most intense base peak.

The reproducibility in the mass spectrum of the photolyte flow is poor in the photolysis of methyl vinyl ketone compared with the case of acetone and methyl ethyl ketone under the present experimental conditions probably because of some deposit on the reactor wall, although the predominance of process (7) over process (8) is always found in every run of methyl vinyl ketone photolysis. The contribution ratio (7)/(8) may roughly be estimated about 10.

Summary. As for the simple ketones studied in this work, the following process (I) producing acetyl radical is always found predominant in the primary step of the photolysis of these ketones by mass spectrometric detection of photofragment radicals:

$$CH_3COR + h\nu \longrightarrow CH_3CO + R \qquad (I)$$

($R = CH_3$, C_2H_5 and C_2H_3)

In the case of methyl ethyl ketone and methyl vinyl ketone, the minor process (II) is found by the detection of CH_3 and RCO:

$$CH_3COR + h\nu \longrightarrow CH_3 + RCO \qquad (II)$$

The predominance of process (I) over (II) might be due to the high stability of acetyl radical whose heat of formation is known to be -11 kcal/mol.[15]

The author is grateful to Professor Teruo Hayakawa for encouragement and discussion. This work was supported by research grant from the Ministry of Education.

References

1) J. G. Calvert and J. N. Pitts, Jr., "Photochemistry," John Wiley and Sons, New York, N. Y. (1966), p. 377.
2) a) F. P. Lossing, D. G. Marsden, and J. B. Farmer, *Can. J. Chem.*, **34**, 701 (1956). b) H. D. Beckey and W. Groth, *Z. Phys. Chem.* (Frankfurt), **20**, 307 (1959).
3) a) R. G. W. Norrish and G. Porter, *Nature*, **164**, 658 (1949). b) G. Herzberg and D. A. Ramsay, *J. Chem. Phys.*, **20**, 347 (1952).
4) R. F. Pottie, A. G. Harrison, and F. P. Lossing, *Can. J. Chem.*, **39**, 102 (1961).
5) A. Jones, S. Yamashita, and F. P. Lossing, *ibid.*, **46**, 833 (1968).
6) K. O. McFadden and C. L. Currie, *J. Chem. Phys.*, **58**, 1213 (1973).
7) S. Yamashita, This Bulletin, **47**, 1373 (1974).
8) O. Osberghaus and R. Taubert, *Z. Phys. Chem.*, **4**, 264 (1955).
9) S. Ikuta, K. Yoshihara, and T. Shiokawa, *Chem. Lett.*, **1975**, 289.
10) S. Yamashita and T. Hayakawa, This Bulletin, **46**, 2290 (1973).
11) A. F. Moskvin, O. P. Yablonski, and L. F. Border, *Teor. Eksp. Khim.*, **2**, 635 (1966).
12) a) R. Doepker and G. J. Mains, *J. Amer. Chem. Soc.*, **83**, 294 (1961). b) J. Heicklen and W. A. Noyes, Jr., *ibid.*, **81**, 3858 (1959). c) P. Ausloos and E. Murad, *J. Phys. Chem.*, **65**, 1519 (1961).
13) J. N. Pitts, Jr. and F. E. Blacet, *J. Amer. Chem. Soc.*, **72**, 2810 (1950).
14) S. Yamashita, *Chem. Lett.*, **1975**, 967.
15) a) A. Langer, J. A. Hipple, and D. P. Stevenson, *J. Chem. Phys.*, **22**, 1836 (1954). b) K. Watanabe and T. Namioka, *ibid.*, **24**, 915 (1956).

Study of Organo(2,2'-bipyridine)nickel Complexes. III. NMR Studies on the Interaction of Dialkyl(2,2'-bipyridine)nickel with Solvents and Olefins[1]

Takakazu YAMAMOTO, Yoshiyuki NAKAMURA, and Akio YAMAMOTO
Research Laboratory of Resources Utilization, Tokyo Institute of Technology, Meguro, Tokyo 152
(Received August 23, 1975)

The ^{1}H-NMR spectra of $NiR_2(bpy)$ (bpy=2,2'-bipyridine; R=CH_3, C_2H_5, and C_3H_7) and $Ni(C_2H_5)_2(bpy)$–olefin systems (olefin=acrylonitrile and acrylaldehyde) have been studied in a temperature range from −70 °C to 80 °C. The temperature dependence of the chemical shifts of ethyl and 2,2'-bipyridine protons of $Ni(C_2H_5)_2$-(bpy) in non-aromatic solvents (acetonitrile, *N,N*-dimethylformamide, acetone and tetrahydrofuran) is analyzed on the basis of the formation of 1 : 1 solvent-solute complex. The formation constant of the 1 : 1 comples, K_1, and the thermodynamic parameters $\Delta F_1°$, $\Delta H_1°$, and $\Delta S_1°$ are given. The NMR spectra of $NiR_2(bpy)$ in aromatic solvents show the aromatic induced solvent shifts, and the chemical shifts of CH_2 and CH_3 of $Ni(C_2H_5)_2(bpy)$ coincide at 76 °C in benzene to give a sharp singlet peak. The ^{13}C-NMR spectrum of $Ni(C_2H_5)_2(bpy)$ in benzene shows a triplet at 10.63 ppm (CH_2, $J(^{13}C–H)=132$ Hz) and a quartet at 15.97 ppm (CH_3, $J(^{13}C–H)=128$ Hz). The formation constant of $Ni(C_2H_5)_2(bpy)$(olefin), K_2, and the thermodynamic parameters, $\Delta F_2°$, $\Delta H_2°$, and $\Delta S_2°$ have been obtained from the temperature dependence of the NMR spectra of the $Ni(C_2H_5)(bpy)$–olefin systems. The values of the chemical shift differences between CH_2 and CH_3 ($\Delta=\delta_{CH_2}-\delta_{CH_3}$) for $Ni(C_2H_5)_2(bpy)$, $Ni(C_2H_5)_2$-(bpy)(acrylaldehyde), and $Ni(C_2H_5)_2(bpy)$(acrylonitrile) are −0.30, 0.94 and 0.83, respectively. The increase of the values of Δ by the coordination of the electronegative olefins with nickel is regarded as indicating the increase of the electronegativity of nickel due to the back-donation from nickel to the olefin.

Variable temperature NMR study provides a powerful means for clarifying the behavior of various important compounds in solution and extensive NMR studies have been made on the behavior of non-transition metal alkyls.[2] Alkyltransition metal compounds, on the other hand, have received much less attention, and very few systematic NMR studies have been made[3] despite their significance as models for active species in various catalytic reactions such as olefin hydrogenation, isomerization, hydroformylation and polymerization.[4,5] This is mainly due to the lack of suitable diamagnetic alkyltransition metal compounds which are stable enough to allow the NMR study. Dialkyl(2,2'-bipyridine)nickel(II)[6] is suitable for detailed NMR study because of the following advantages. (1) It is thermally stable in the range from −80 to 80 °C, having sufficient solubilities in various organic solvents. (2) A series of alkyl homologs can be readily prepared which allow the study of the effect of chemical environment on each nickel alkyl. (3) It interacts with olefins to form olefin-coordinated complexes, and the effect of olefin coordination on the nature of the alkylnickel complex can be investigated. The study of the interaction of an alkyltransition metal complex with olefins is particularly important in understanding the mechanism of activation of transition metal-to-carbon bond by coordination of olefin since it constitutes a key elementary step in catalytic reactions involving olefins.[5]

Experimental

$NiR_2(bpy)$ was prepared as reported in previous papers.[6] Deuterated solvents were used as purchased from Merck and Co., Inc. Acrylonitrile and acrylaldehyde were dehydrated and purified by distillation. The solvent, olefin, and tetramethylsilane were added to an NMR tube containing NiR_2-(bpy) by a trap-to-trap distillation in a vacuum, and the NMR tube was sealed. The ^{1}H-NMR spectra were obtained with a Japan Electron Optics Laboratory PS-100 spectrometer or a Varian HR-220 spectrometer. The ^{13}C-NMR spectra were obtained with the Japan Electron Optics Laboratory PS-100 spectrometer in the pulsed Fourier transform mode at 25.15 MHz. Chemical shifts are referred to internal TMS both in ^{1}H-NMR and ^{13}C-NMR.

Results and Discussion

NMR Spectra of $NiR_2(bpy)$ in Various Solvents. NMR Spectra of $Ni(C_2H_5)_2(bpy)$ 1 at Various Temperatures: The NMR spectrum of $Ni(C_2H_5)_2(bpy)$ **1** shows a triplet (at lower field) and a quartet (at higher field) of an

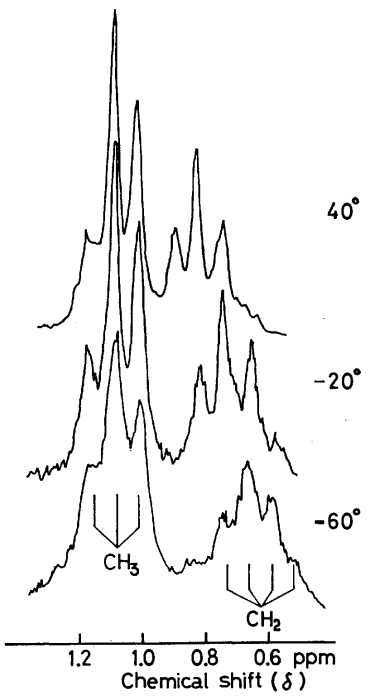

Fig. 1. 100 MHz ^{1}H-NMR spectra of C_2H_5 of $Ni(C_2H_5)_2(bpy)$ in acetone-d_6 at various temperatures.

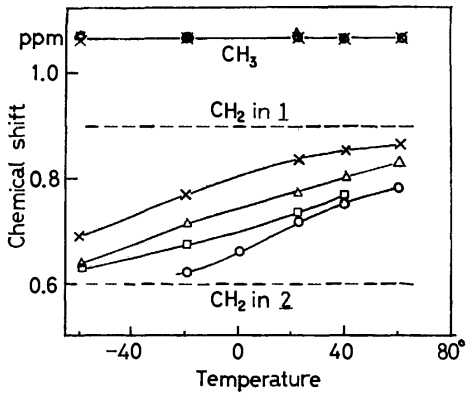

Fig. 2. Temperature dependence of the chemical shifts of CH_2 and CH_3 signals in tetrahydrofuran-d_8 (×), in acetone-d_6(△), in dimethylformamide-d_7(□), and in acetonitrile-d_3(○). Broken lines show the chemical shifts of CH_2 in **1** and **2** (see the text).

area ratio of 3: 2, which were assigned to methyl and methylene protons.[6b]

When a non-aromatic solvent is employed, only the chemical shifts of the methylene protons of the ethyl group varies with temperature in the ethyl region, the chemical shift of methyl protons being essentially temperature independent (Fig. 1). The change of the chemical shifts of CH_3 and CH_2 signals with temperature is shown in Fig. 2.

It is seen that the chemical shift of CH_2 approaches limiting values on cooling and heating. The temperature dependence of the chemical shift of the methylene protons may be accounted for on the basis of the formation of a 1: 1 solvent-solute complex (Eq. 1).[6c,7]

$$\underset{\mathbf{1}}{Ni(C_2H_5)_2(bpy)} + \text{solvent} \overset{K_1}{\rightleftarrows} \underset{\mathbf{2}}{Ni(C_2H_5)_2(bpy)(solvent)} \quad (1)$$

$$K_1 = \frac{[\mathbf{2}]}{[\mathbf{1}][\text{solvent}]} \quad (2)$$

The coordination of solvent with the four coordinate nickel to form a five coordinate nickel compound **2** will cause a change of magnetic character of nickel, which affects the chemical shift of the CH_2 protons. Since the chemical shift of the CH_2 protons in three different solvents (acetonitrile, *N,N*-dimethylformamide, and acetone) approaches the same value (0.60 ppm from TMS) on cooling, we assume that the chemical shift of the CH_2 protons in the solvated species is virtually independent of the solvent coordinated. On heating, **1** becomes predominant and the chemical shift of CH_2 protons approaches 0.90 ppm.

When one assumes a rapid exchange between **1** and **2** in solutions, the ratio [**2**]/[**1**] can be calculated from the chemical shift of $CH_2(\delta)$, which is a weighted mean of the chemical shifts of CH_2 of **1** and **2**, as $(0.90-\delta)/(\delta-0.60)$.

Table 1. Values of $[Ni(C_2H_5)_2(bpy)(solvent)]/[Ni(C_2H_5)_2(bpy)]$

(°C)	Acetonitrile	*N,N*-Dimethylformamide	Acetone	Tetrahydrofuran
−60				3.0
−20		3.0	1.60	0.82
0	4.0			
22	1.5	1.2	0.77	0.28
40	1.0	0.82	0.50	0.20
60	0.67			0.14

Table 1 gives the values of [**2**]/[**1**] at various temperatures.

The value of [**2**]/[**1**] at certain temperatures decreases in the order acetonitrile>*N,N*-dimethylformamide>acetone>tetrahydrofuran. The order agrees with the decreasing order of coordination ability of solvent to **1** estimated with visible spectra.[6c]

The plot of the value of [**2**]/[**1**] against $1/T$ gives a straight line. The equilibrium constant K_1 for the solvation of **1** and thermodynamic data are summarized in Table 2. The reproducibility of the curves in Fig. 2 is good.

Table 2 indicates that the enthalpy changes favor the formation of the solvent coordinated species but are compensated by the large negative entropy changes.

The signals of 2,2'-bipyridine protons of diethyl(2,2'-bipyridine)nickel appear in the range 7.5—9.0 ppm in the non-aromatic solvents. On cooling and heating diethyl(2,2'-bipyridine)nickel in the solutions, the chemical shift of each 2,2'-bipyridine proton also approaches a limiting value as in the case of the chemical shift of the methylene protons.

The chemical shifts of the 2,2'-bipyridine protons of **1** and **2**, as numbered below, were estimated from the limiting values and are listed in Table 3.

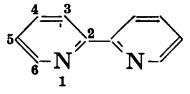

The ethyl signals of the ethyl nickel complex in aromatic solvents (benzene and toluene) show a large downfield shift presumably due to the aromatic induced solvent shift (AISS).[7,9] In contrast to the temperature

Table 2. Equilibrium constant K_1 at 22°C and thermodynamic data for the coordination of solvent with $Ni(C_2H_5)_2(bpy)$

Solvent[a]	K_1[b] (l/mol)	$\Delta F_1°$ (kcal/mol)	$\Delta H_1°$ (kcal/mol)	$\Delta S_1°$ (e.u.)
Acetonitrile	8.0×10^{-2}	1.5	−4.3	−20
N,N-Dimethylformamide	9.1×10^{-2}	1.4	−3.7	−17
Acetone	5.9×10^{-2}	1.7	−3.1	−16
Tetrahydrofuran	2.3×10^{-2}	2.2	−3.7	−20

a) Protons of solvents are deuterated. b) The value of [**2**]/[**1**] is divided by the molarity of the neat solvent.

Table 3. Chemical shifts of 2,2′-bipyridine protons of **1** and **2** in non-aromatic solvents (acetonitrile, *N,N*-dimethylformamide, acetone, and tetrahydrofuran)[a)]

Compound	3-H and 4-H[b)]	5-H	6-H
1	8.0±0.1m	7.5t	9.0d
2	8.4±0.1m	7.8t	8.9d

a) In ppm from TMS (downfield positive). The assignment of the 2,2′-bipyridine protons in 1,2-dimethoxyethane has been given elsewhere;[8)] d: double, t: triplet, m: multiplet.
b) Signals of 3-H and 4-H were not separated from each other at 100 MHz.

independence of the chemical shift of CH_3 protons in non-aromatic solvents, both chemical shifts of CH_2 and CH_3 protons are temperature dependent in aromatic solvents. The chemical shifts of CH_2 and CH_3 in toluene at various temperatures are given in Table 4.

Table 4. Chemical shift of CH_2 and CH_3 signals in toluene[a)]

Temp. (°C)	CH_2	CH_3
−60	1.66	1.94
−20	1.60	1.87
20	1.57	1.65
40	1.60[b)]	
60	1.52[b)]	

a) In ppm from TMS (downfield positive).
b) CH_2 and CH_3 signals overlap with each other.

In benzene-d_6 the CH_2 and CH_3 signals are resolved at 20 °C or below (Fig. 3), although at 40 °C or above they overlap each other even at 220 MHz. At 40 °C and 59 °C the ^{1}H-NMR spectra of the ethyl region show an A_2B_3 pattern where the chemical shift difference between A and B is comparable to the coupling constant between A and B (Figs. 3b, 3c).[10,11)] At 76 °C in benzene the chemical shifts of CH_2 and CH_3 coincide to give a sharp singlet peak (Fig. 3d). Further increase

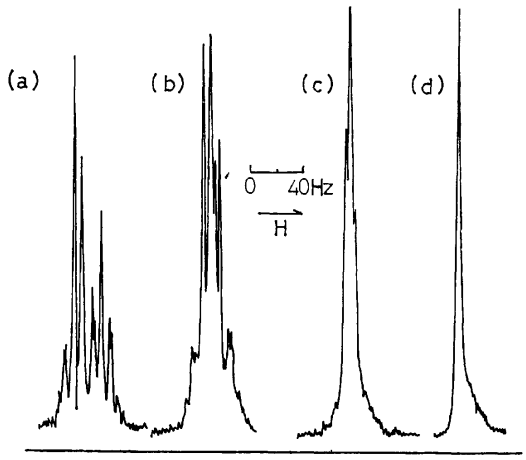

Fig. 3. NMR spectra of the ethyl protons of Ni-$(C_2H_5)_2$(bpy) in benzene-d_6 at 220 MHz. (a) 20 °C, (b) 40 °C, (c) 59 °C, and (d) 76 °C.

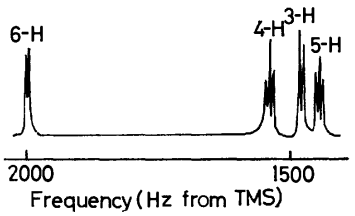

Fig. 4. NMR spectrum of bipyridine protons of Ni-$(C_2H_5)_2$(bpy) in benzene-d_6 at 220 MHz (at 20 °C).

in the temperature led to the decomposition of the ethyl nickel complex.

Signals of 3-H and 4-H of 2,2′-bipyridine, which overlap each other in the non-aromatic solvent, separate in the aromatic solvents (Fig. 4). The enhancements of higher field portions of the 6-H doublet and 4-H triplet and lower field portion of the 3-H doublet and 5-H triplet are consistent with the coupling between 5-H and 6-H, 3-H and 4-H, and 4-H and 5-H.

The ^{1}H-NMR spectrum of $Ni(C_2H_5)_2$(bpy) in pyridine or styrene is essentially the same as that in benzene or toluene, suggesting a coordination of pyridine and styrene with nickel through the aromatic π-ring. However, in contrast to the considerable stability of **1** even in boiling benzene,[6a)] standing of the pyridine or styrene solution at room temperature for some time (30 min or more) caused a scission of Ni–C_2H_5 bonds to form butane.[6c)]

Table 5. ^{13}C-NMR spectrum of $Ni(C_2H_5)_2$(bpy) in benzene at 68 °C (25.15 MHz)

Chemical shift (ppm from TMS)	$J(^{13}C-H)$ (Hz)	Assignment
10.63	132	CH_2
15.97	128	CH_3
120.3∼147.6		2,2′-bipyridine carbons

Although CH_2 and CH_3 signals of **1** in aromatic solvents overlap each other in ^{1}H-NMR at 40 °C or above, the ^{13}C-NMR at 68 °C in benzene gave well separated CH_2 and CH_3 signals at 10.63 and 15.97 ppm from TMS, respectively. The good separation of CH_2 and CH_3 signals in ^{13}C-NMR is considered to be due to a difference of anisotropic character between CH_2 and CH_3 positions to which the ^{13}C-NMR is more sensitive than ^{1}H-NMR.[12)] The ^{13}C-NMR spectroscopic data are listed in Table 5. The magnitude of $J(^{13}C-H)$ indicates that the electronic configuration of carbon is essentially sp^3 both in CH_2 and CH_3 groups of the ethyl nickel complex suggesting a covalent bond between Ni and C_2H_5 rather than an ionic bond.

$Ni(CH_3)_2$(bpy) and $Ni(C_3H_7)_2$(bpy). The ^{1}H-NMR spectrum of $Ni(CH_3)_2$(bpy) in non-aromatic solvent at 100 MHz showed a singlet at δ 0.10 ppm for CH_3, a multiplet at 8.18 ppm for 3-H and 4-H protons of 2,2′-bipyridine, a triplet at 7.62 ppm for 5-H, and a doublet at 8.96 ppm for 6-H. The ^{1}H-NMR spectrum of $Ni(CH_3)_2$(bpy) in aromatic solvents showed the aromatic induced solvent shifts. The NMR spectroscopic data for $Ni(CH_3)_2$(bpy) both in non-aromatic and aromatic solvents are listed in Table 6 together with those for $Ni(C_3H_7)_2$(bpy).

TABLE 6. ^{1}H-NMR SPECTRA OF $Ni(CH_3)_2(bpy)$ AND $Ni(C_3H_7)_2(bpy)$ AT 24 °C (100 MHz, ppm from TMS)[a]

$Ni(CH_3)_2(bpy)$	CH_3	2,2'-bipyridine			
		3-H	4-H	5-H	6-H
In acetone-d_6	−0.10 s	8.18m[b]		7.62t	8.96 d
In toluene-d_8	0.74 s	6.81 d	8.52t	6.60t	9.00 d

$Ni(C_3H_7)_2(bpy)$	α-CH_2	CH_3	β-CH_2	2,2'-bipyridine			
				3-H	4-H	5-H	6-H
In *N,N*-dimethylformamide-d_7	0.8t	1.05t	1.52m	8.27m[b]		7.71t	8.99 d
In benzene-d_6	1.7∼1.8m[b]		2.23m	6.78 d	7.07t	6.65t	9.16 d

a) s=singlet, d=doublet, t=triplet, m=multiplet. b) Unresolved.

^{1}H-NMR spectrum of $Ni(C_3H_7)_2(bpy)$ showed signals of β-methylene at the lowest field amongst the signals of the propyl group similar to the NMR spectrum of $Al(C_3H_7)_3$. No signals assignable to $Ni(i\text{-}C_3H_7)_2(bpy)$, which might be formed through a thermal isomerization of $Ni(C_3H_7)_2(bpy)$, were observed in the NMR spectrum. Chemical shift of each signal of $Ni(CH_3)_2$-(bpy) and $Ni(C_3H_7)_2(bpy)$ showed temperature dependence which may be accounted for on the basis of the solvation of the methyl and propyl nickel complexes as in the case of the ethyl nickel complex.

$Ni(C_2H_5)_2(bpy)$–Olefin System. On addition of olefins (acrylonitrile and acrylaldehyde) to the deep green tetrahydrofuran solution of $Ni(C_2H_5)_2(bpy)$ at

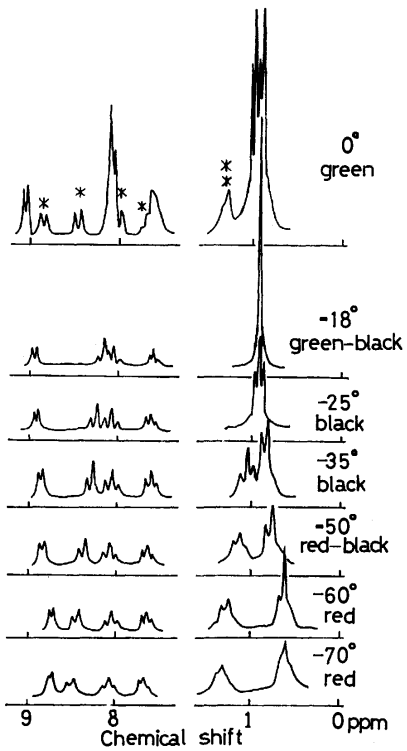

Fig. 5. Temperature dependence of the NMR spectrum of the **1**–acrylonitrile system in tetrahydrofuran-d_8. [acrylonitrile]=1.4 mol/l. [**1**]+[**3**]=0.2 mol/l. At 0 °C the partial scission of the Ni–C_2H_5 bonds takes place to give Ni(bpy)(acrylonitrile) and C_4H_{10}. The signals with * and ‡ show bpy signals of Ni(bpy)(acrylonitrile) and CH_2 signals of butane evolved, respectively.

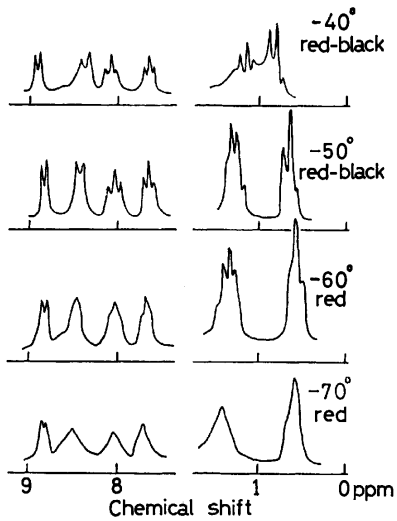

Fig. 6. Temperature dependence of the NMR spectrum of the **1**–acrylaldehyde system in tetrahydrofuran-d_8. [acrylaldehyde]=2.3 mol/l. [**1**]+[**3**]=0.2 mol/l.

−70 °C the color of the solution turned deep red, the NMR spectrum of the **1**–olefin system showing the CH_3 signals of C_2H_5 at higher field than CH_2 signals in contrast to the NMR spectrum of **1** in tetrahydrofuran without olefin. On warming the solution, the coloration turned from deep red to deep green *via* black, the chemical shift of CH_2 and CH_3 signals changing with the coloration (Figs. 5 and 6).

Dialkyl(2,2'-bipyridine)nickel (deep green) forms complexes of the type $NiR_2(bpy)(olefin)$ (deep red) with acrylonitrile and acrylaldehyde at low temperatures.[1,6c] By a visual method based on the change of the color from deep red to deep green on warming the NiR_2-(bpy)–olefin system, the equilibrium constant expressed by Eq. (4) was estimated.[1]

$$\underset{\mathbf{1}}{NiR_2(bpy)} + \text{olefin} \rightleftarrows \underset{\mathbf{3}}{NiR_2(bpy)(olefin)} \qquad (3)$$

$$K_2 = \frac{[NiR_2(bpy)(olefin)]}{[NiR_2(bpy)][olefin]} \qquad (4)$$

From the change of the NMR spectrum of the **1**–olefin system at various temperatures we can estimate the equilibrium constants more accurately than with the visual method. Corresponding to the color change, the NMR spectrum of the **1**–olefin system varies with temperature and the variation of the chemical shifts can

Table 7. Values of [3]/[1] and K_2 calculated from the data in Fig. 7[a)]

[Acryonitrile]=6.5 mol/l				[Acrylonitrile]=1.4 mol/l			
Temp. (°C)	(ppm)	[3]/[1]	K_2 (l/mol)	Temp. (°C)	(ppm)	[3]/[1]	K_2 (l/mol)
−50	0.51	14	2.2	−70	0.52	11	7.9
−40	0.53	9.0	1.4	−60	0.54	7.6	5.4
−30	0.57	5.0	0.77	−50	0.60	3.6	2.6
−20	0.63	2.8	0.43	−42	0.72	1.4	1.0
−10	0.69	1.7	0.26	−35	0.77	1.0	0.72
				−18	0.50	0.4	0.29

a) Solvent=tetrahydrofuran-d_8

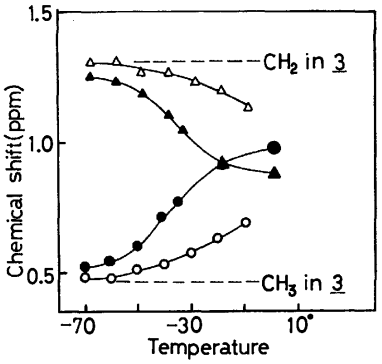

Fig. 7. Chemical shifts of CH_2 and CH_3 protons of the **1**–acrylonitrile systems in tetrahydrofuran-d_8 at various temperatures. ○CH_3 and △CH_2 for [acrylonitrile]=6.5 mol/l, ●CH_3 and ▲CH_2 for [acrylonitrile]=1.4 mol/l.

be explained in terms of a 1 : 1 adduct (**3**) formation and its rapid exchange with the uncoordinated ethylnickel complex **1**. At lower temperatures the olefin-coordinated complex **3** is predominant and the chemical shifts of the CH_3 and CH_2 protons approach the limiting values 0.47 and 1.3 ppm, respectively, corresponding to $Ni(C_2H_5)_2(bpy)$(acrylonitrile) as shown in Fig. 7. On warming the solution, the CH_3 signals shift to lower field and the CH_2 signals to higher field. The extent of the shifts depends on the concentration of acrylonitrile in the solution. In a system containing a lower concentration of acrylonitrile (1.4 mol/l in Fig. 7), the crossing of two signals was observed and the CH_3 and CH_2 protons appeared as a sharp singlet at −18 °C with identical chemical shift values for the CH_3 and CH_2 protons. The CH_3 and CH_2 signals separate again with the CH_3 signals at a lower field than the CH_2 signals by raising the temperature to 0 °C. Further increase of the temperature caused the decomposition of the ethylnickel complex. The decomposition set in at a lower temperature when a higher concentration of acrylonitrile was employed.

From the temperature dependence of the chemical shifts of CH_2 and CH_3 one can calculate the ratio of the concentration of **3** to that of **1**. The ratio [3]/[1] is calculated from the chemical shift of $CH_3(\delta_{CH_3})$ of the **1**–olefin system at the temperature as

$$\frac{[3]}{[1]} = \frac{\delta_{CH_3}(\text{in } 1) - \delta_{CH_3}}{\delta_{CH_3} - \delta_{CH_3}(\text{in } 3)} = \frac{1.07 - \delta_{CH_3}}{\delta_{CH_3} - 0.47} \quad (5)$$

In the equation 1.07 and 0.47 are the limiting chemical shifts of the CH_3 protons in the uncoordinated and fully coordinated ethylnickel complexes **1** and **3**.

The values of [3]/[1] for **1**–acrylonitrile system at various temperatures as well as the equilibrium constant expressed by Eq. (4) are given in Table 7.

The plot of log K_2 against $1/T$ gives a straight line (Fig. 8).

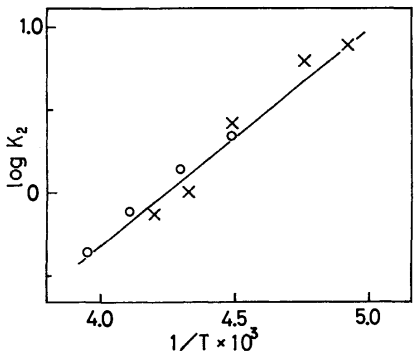

Fig. 8. log K_2 *vs.* $1/T$ for the coordination of acrylonitrile with **1**. ○ for [acrylonitrile]=6.5 mol/l, ● for [acrylonitrile]=1.4 mol/l.

The temperature dependence of the 2,2'-bipyridine signals of the **1**–acrylonitrile system is also accounted for by assuming the equilibrium expressed by Eq. (3).

The 2,2'-bipyridine signals observed at −70 °C can be assigned to those of **3**. On warming, the chemical shift of each 2,2'-bipyridine signal approaches that of **1** (Table 3).

A similar temperature variation of ^{1}H-NMR spectrum to that for the **1**–acrylonitrile system was observed for **1**–acrylaldehyde system. The stability constants of the complexes of the type $Ni(C_2H_5)_2(bpy)$(olefin) and the thermodynamic data for the coordination of olefin with **1** are given in Table 8.

Table 8. Stability constant of $Ni(C_2H_5)_2$-(bpy)(olefin) K_2 at −50 °C and thermodynamic data

Olefin	log K_2	$\Delta F_2°$ kcal/mol	$\Delta H_2°$ kcal/mol	$\Delta S_2°$ e.u.
Acrylonitrile	0.38	−0.4	−6.4	−27
Acrylaldehyde	0.080	−0.1	−7.4	−31

The enthalpy changes for the coordination of olefin are fairly large as compared with those of solvents (*cf.* Table 2).

In the case of **1**–acrylaldehyde system both ethyl and

2,2'-bipyridine signals showed a broadening at low temperatures (−50——70 °C).

Since the signals of solvent impurities (tetrahydrofuran-d_7's) and TMS did not show any broadening at low temperatures, the broadening of the ethyl and 2,2'-bipyridine signals is not considered to be due to the increase of viscosity of the solution but to the decrease of the exchange rate between **1** and **3** at the low temperatures. At −40 °C or above, both the ethyl and 2,2'-bipyridine signals are sharp and the half widths of the signals are constant.

Approximate rates of the coordination and dissociation of olefin and, consequently, the rate constants k_1 and k_{-1} in the following equation have been calculated from the half widths of C_2H_5 and 2,2'-bipyridine signals.[13]

$$\underset{\mathbf{1}}{Ni(C_2H_5)_2(bpy)} + \text{acrylaldehyde} \underset{k_{-1}}{\overset{k_1}{\rightleftharpoons}} \underset{\mathbf{3}}{Ni(C_2H_5)_2(bpy)(\text{acrylaldehyde})} \quad (6)$$

The values of k_1 and k_{-1} are *ca.* 1×10^3 l/mol·s and 1×10^3 s^{-1} at −60 °C respectively.

Electronegativities of Nickel in 1 and 3. As for the NMR spectrum of an ethyl group bonded with various atoms Narasimhan and Rogers[14] proposed the straight-line correlation

$$\chi = 0.62\Delta + 2.07 \quad (7)$$

where χ is the electronegativity of M for M–C_2H_5 compounds and Δ is the chemical shift difference between the CH_2 and CH_3 singals ($\Delta = \delta_{CH_2} - \delta_{CH_3}$).

When Eq. (7) is applied to the present nickel complexes, the electronegativities of the nickel in **1**, $Ni(C_2H_5)_2$(bpy)(acrylonitrile), $Ni(C_2H_5)_2$(bpy)(acrylaldehyde) are 1.89, 2.58, and 2.65, respectively (Table 9).

Table 9. Electronegativity of nickel in complexes calculated according to Eq. (7)

Complex	Δ	χ
$Ni(C_2H_5)_2$(bpy)	−0.30	1.89
$Ni(C_2H_5)_2$(bpy)(acrylonitrile)	0.83	2.58
$Ni(C_2H_5)_2$(bpy)(acrylaldehyde)	0.94	2.65

The electronegativity of nickel in **1** is close to Pauling's electronegativity of nickel ($\chi = 1.7$).[6b] When an olefin is coordinated with **1**, the electronegativity of nickel markedly increases almost to the value of carbon ($\chi =$ 2.5—2.6); the chemical shifts of CH_3 and CH_2 of **3** are close to those of butane. The increase of the electronegativity of nickel by the coordination of olefin can be interpreted as due to the back-donation of electron from nickel to the olefin. The result is consistent with the lowering of the highest occupied energy level of nickel by coordination of olefin with **1** as observed in the strong blue shift of a charge-transfer band (Ni→bpy).[1,6c]

The coordination of olefin with **1** makes a homolytic scission of Ni–C_2H_5 bond much easier by a factor of 10^{11} at room temperature than without the coordination of olefin.[15] Since the nickel-carbon bond of **1** is considered to be polarized as $Ni^{\delta+}$—$C^{\delta-}$, the homolytic scission of the nickel-carbon bond in **1**, leading to liberation of an electrically neutral molecule butane, seems to require the migration of electron from carbon to nickel.[16] The scission of the Ni–C bond in **3**, however, may require only a minor migration of electron because of minor polarization of the Ni–C bond as judged from the small difference in electronegativity between Ni and C in **3**. This may account for the easier scission of Ni–C bond by the coordination of olefin.

The authors are grateful to Prof. I. Morishima, Kyoto University, and Mr. K. Kosaka, Japan Electron Optics Laboratory Co. Ltd. for measurements of the 220 MHz ^{1}H- and ^{13}C-NMR spectra, respectively. The authors express appreciation to Professor R. Chujo of our Institute for his helpful discussion on the ^{1}H-NMR spectra of **1** in solutions.

References

1) For the preceding report of this series on a study of organo(dipyridyl)nickel complexes II, see T. Yamamoto, A. Yamamoto, and S. Ikeda, *J. Amer. Chem. Soc.*, **93**, 3360 (1971).

2) For example (a) J. R. Holmes and H. D. Kaesz; *ibid.*, **83**, 3903 (1961); (b) J. V. Hatton, W. G. Schneider, W. Sieband, *J. Chem. Phys.*, **39**, 1330 (1963); (c) T. L. Brown and L. L. Murrell, *J. Amer. Chem. Soc.*, **94**, 378 (1972); (d) R. G. Kidd, "Characterization of Organometallic Compounds," M. Tsutsui, Ed. Part II, Wiley-Interscience (1971).

3) (a) T. L. Brown, L. M. Ludwick, and R. S. Stewart, *J. Amer. Chem. Soc.*, **94**, 384 (1972); (b) W. Herlinger and T. L. Brown, *ibid.*, **94**, 388 (1972); (c) F. A. Cotton, B. A. Frenz, and D. L. Hunter, *ibid.*, **96**, 4820 (1974).

4) (a) C. W. Bird, *Chem. Rev.*, **62**, 283 (1962); (b) G. E. Coates, M. L. H. Green, and K. Wade, "Organometallic Compounds," Vol. 2, Methuen and Co. Ltd., London (1968); (c) M. M. Taqui Khan and A. E. Martell, "Homogeneous Catalysis by Metal Complexes," Vol. II, Academic Press (1974).

5) (a) P. Cossee, *Tetrahedron Lett.*, **17**, 12, 17 (1960); (b) *J. Catal.*, **3**, 80 (1964); (c) E. J. Arlman and P. Cossee, *ibid.*, **3**, 99 (1964); (d) F. Basolo and R. G. Pearson, "Mechanisms of Inorganic Reactions," p. 601, John Wiley and Sons, New York, London, Sydney (1967).

6) (a) A. Yamamoto, K. Morifuji, S. Ikeda, T. Saito, Y. Uchida, and A. Misono, *J. Amer. Chem. Soc.*, **87**, 4652 (1965); (b) T. Saito, Y. Uchida, A. Misono, K. Morifuji, A. Yamamoto, and S. Ikeda, *ibid.*, **88**, 5198 (1966); (c) T. Yamamoto, A. Yamamoto, and S. Ikeda, *ibid.*, **93**, 3350 (1971).

7) (a) J. H. Bowie, J. Ronayne, and D. H. Williams, *J. Chem. Soc., B*, **1966**, 785; (b) *ibid.*, **1967**, 535; (c) J. Ronayne and D. H. Williams, *ibid.*, **1967**, 540; (d) J. Ronayne, M. V. Sargent, and D. H. Williams, *J. Amer. Chem. Soc.*, **88**, 5288 (1966).,

8) T. Saito, M. Araki, Y. Uhcida, and A. Misono, *J. Phys. Chem.*, **71**, 2370 (1967).

9) (a) J. Ronayne and D. H. Williams, "Annual Review of NMR Spectroscopy," Vol. 2, Academic Press, London and New York (1969), p. 106; (b) P. Laszlo "Progress in NMR spectroscopy," Vol. 3, Pergamon Press, Oxford (1967), p. 348.

10) H. Schmidbauer and F. Schindler, *J. Organometal. Chem.*, **2**, 466 (1964).

11) (a) B. R. McGarvey and G. Slomp, Jr., *J. Chem. Phys.*, **30**, 1586 (1959); (b) J. S. Waugh and E. L. Wei, *ibid.*, **43**, 2308 (1965).

12) (a) E. F. Mooney and P. H. Winson, "Annual Review of NMR Spectroscopy" Vol. 2, Academic Press, London and New York (1969), p. 153; (b) J. B. Stothers "Carbon-13 NMR spectroscopy," Academic Press, London and New York (1972).

13) A. Carrington and A. D. McLachlan, "Magnetic Resonance," A Harper International Edition, Tokyo (1967).

14) P. T. Narasimhan and M. T. Rogers, *J. Amer. Chem. Soc.*, **82**, 5983 (1960).

15) The first-order rate constant k for the thermolysis of **1** obtained at high temperature (97—113 °C), $\mathbf{1} \xrightarrow{k} Ni(bpy) + C_4H_{10}$, is extrapolated to 20 °C to give a value of *ca.* 1×10^{-11} s^{-1}.[6c] The stability constant K_2 at 20 °C for $Ni(C_2H_5)_2(bpy)$-(acrylaldehyde) is estimated from the thermodynamic data (Table 8) to be *ca.* 1×10^{-2} l/mol, while the rate constant k_2K_2 for the reaction, $\mathbf{1}$ + acrolein $\overset{K_2}{\rightleftharpoons} \mathbf{3} \overset{k_2}{\rightarrow}$ Ni(bpy)(acrylaldehyde) + butane, is *ca.* 1×10^{-2} l/mol·s at 20 °C,[6c] which gives the value of k_2, the rate constant for the splitting of $Ni-C_2H_5$ bond in $Ni(C_2H_5)_2(bpy)$(acrylaldehyde), 1×10^0 s^{-1}. Therefore we obtain the value of 1×10^{11} for the ratio of k_2 to k.

16) The migration of electron was represented as a promotion of electron from σ_{Ni-C} orbital to the lowest vacant orbital of nickel.[6c]

The Electronic Spectra of α,ω-Di-1-anthrylpolyenes in Solution and in Solid State

Krishnagopal MANDAL and T. N. MISRA

Department of Physics, North Bengal University, Darjeeling, Pin-734430, India

(Received January 6, 1975)

The electronic absorption spectra of a number of α,ω-Di-1-anthrylpolyenes have been studied in solution and in crystals. Three intense and two weak band systems have been observed. The plots of λ^2-n and $\varepsilon-n$ result in a good straight line in lower members. These results suggest that long anthrylpolyenes are not in *all-trans* form. Highest energy emission and lowest energy absorption bands show good overlap and identical solvent behavior. It has been concluded that in anthrylpolyenes the lowest excited state is an allowed ^1B_u type. The terminal anthryl-group interaction effect is such that ^1A_g is not lowered relative to ^1B_u in these polyenes. The absorption bands of anthrylpolyenes in the crystalline state could be explained in terms of factor group split components.

A systematic investigation of spectroscopic properties of conjugated polyenes in different states has been undertaken in this laboratory. It has already been established[1-4] in many linear polyenes with the general structure $R_1-(CH=CH)_n-R_2$ that there exists a low energy excited state below the strongly allowed electronic transition previously observed and that fluorescence of polyenes originates from this state. Here R_1 and R_2 are the end groups. The ground electronic state of these polyenes is ^1A_g and the excited states in increasing energy order are ^1B_u, ^1A_g, ^1A_g, ^1B_u according to the Pariser-Parr-Pople (PPP) method.[5] The ordering of the excited electronic states is altered when double-excited configuration interaction is included.[2] One of the two excited states (^1A_g) is significantly lowered in energy and the ordering of the excited electronic states changes to ^1A_g, ^1B_u, ^1A_g, ^1B_u in butadiene.[2] The high energy ^1B_u and ^1A_g state energies are altered less by inclusion of double-excited configuration, although in hexatriene and octatetraene the higher ^1B_u appears below the highest ^1A_g state.[2] The effect of the end groups on the electronic states of these molecules is well known.[6-9] The first intense transition $^1A_g \rightarrow {}^1B_u$ is at longer wavelength for the end group C_6H_5 than for the end group H or CH_3 when the polyene has the same number (n) of double bonds. In order to study the effect of the terminal groups on the electronic excitation of polyacetylene chromophore, it was thought worthwhile to extend the investigation to other polyenes terminated with aromatic groups. The present paper deals with the results of our investigation on the electronic absorption spectra of a number of anthrylpolyenes in solution and also in the solid state.

Experimental

Highly pure, synthetic α,ω-di-1-anthrylpolyene was obtained from Prof. Nakagawa, Osaka University, Japan as a gift. It was used without further purification. Solvent tetrahydrofuran (THF) used was of spectrograde quality. The electronic absorption spectra were measured at room temperature using a well-matched pair of 1-cm cells with a Spektromom-202 spectrophotometer of Hungarian Optical Works. The electronic spectra in the solid state were obtained in the same spectrophotometer by making a thin crystal film on the quartz plate by gently rubbing the polyene powder. The thickness of the film has been estimated from the absorption spectrum of the solid film. An absorption band unsplit in the crystalline state and its molar extinction coefficient in the solution spectrum have been taken to estimate the thickness. Six α,ω-di-1-anthrylpolyenes of type $R-(CH=CH)_n-R$, which is abbreviated as I_n, have been studied. Here R stands for the anthryl group and $n=1$—6.

Results and Discussion

I. Solution Spectra. The electronic absorption

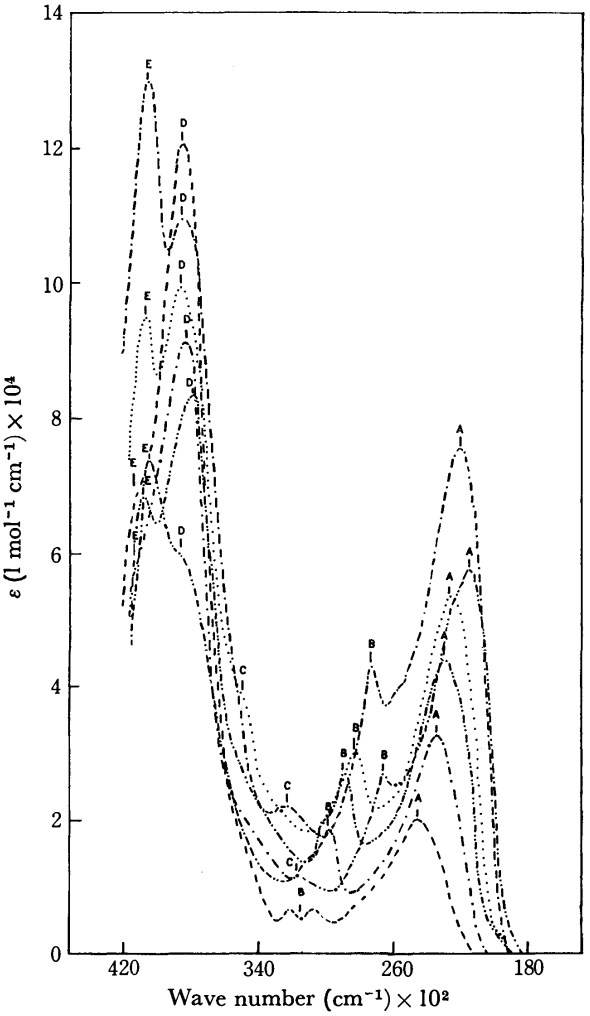

Fig. 1. Absorption spectra of anthrylpolyenes in THF solution.
--------: I_1, -·-·-: I_2, -·-·-: I_3, ·····: I_4, -·-·-: I_5, -··-··-: I_6.

TABLE 1. ABSORPTION BANDS OF ANTHRYLPOLYENES

No. of double bonds (n)	Bands in solution (Solvent: THF) Wave number (cm^{-1})	Assignment	Bands in crystalline state Wave number (cm^{-1})	Assignment
1	24630(s)	$A(O_1)$	22400	A
	30864(w)	$B(O_2)$		
	32258(w)	$B(O_2+1400)$		
	38610(vs)	$D(O_4)$	41322	D_1
			36496	D_2
	41493(vw)	$E(O_5)$		
2	23529(s)	$A(O_1)$	24630	A_1
			22624	A_2
	29940(s)	$B(O_2)$		
	31250(w)	$B(O_2+1310)$		
	38314(vs)	$D(O_4)$	43478	D_1
			37037	D_2
	41493(w)	$E(O_5)$	45455	E_1
			40322	E_2
3	23094(s)	$A(O_1)$	23200	A
	29069	$B(O_2)$		
	30120(w)	$B(O_2+1061)$		
	37878(vs)	$D(O_4)$	44052	D_1
			38167	D_2
	40983(s)	$E(O_5)$	44052	E_1
			38167	E_2
4	22727(vs)	$A(O_1)$	22800	A_1
			21100	A_2
	28328(s)	$B(O_2)$	26800	B
	34965(w)	$C(O_3)$	32400	C
	38610(s)	$D(O_4)$	44444	D_1
			36900	D_2
	40650(s)	$E(O_5)$	44444	E_1
			36900	E_2
5	22123(vs)	$A(O_1)$	21978	A_1
			20618	A_2
	27472(w)	$B(O_2)$	27000	B
	32258	$C(O_3)$	30800	C
	38610(s)	$D(O_4)$	41016	D_1
			34722	D_2
	40650(vs)	$E(O_5)$	44642	E_1
			35971	E_2
6	21739(vs)	$A(O_1)$	21459	A_1
			20000	A_2
	26737(w)	$B(O_2)$	26737	B
	31847(w)	$C(O_3)$	28900	C
	38610(vw)	$D(O_4)$	40983	D_1?
			34722	D_2?
	40650(vs)	$E(O_2)$	40983	E_1
			34722	E_2

s: strong, w: weak, v: very.

spectra of di-1-anthrylpolyene in THF are shown in Fig. 1. Results are summarized in Table 1. The electronic absorption spectrum seems to be composed of three distinct intense electronic band systems. Two more bands are also observed for higher members. The first band system observed in the region 4000—5000 Å is very intense and structureless: its intensity increases with the increase of the number of double bonds. This band is designated as A in the diagram. The band system in the region 3200—3800 Å designated as B is of moderate intensity and shows some structures in the spectra of lower polyenes. The vibronic band represents the upper state fundamental frequency of about 1400 cm^{-1} in I_1, 1310 cm^{-1} in I_2 and 1061 cm^{-1} in I_3. The band system in the high energy region (2500 Å) is also very intense in all the polyenes. This system consists of two bands with a separation of about 200 cm^{-1} between them. These two bands (D and E) seem to belong to two different systems. Finally a weak broad band (C) in the region 2900 Å is observed in the higher members of the group. These results are in complete agreement with that reported by Takeuchi *et al.*[10]

As can be seem from Fig. 1 and Table 1, the longest wavelength maxima and second-longest wavelength maxima both undergo redshift with the increase in length of polyene chain. For linear polyenes, it has generally been accepted[11] that for the longest wavelength band

$$\lambda^2_{max} = A + Bn$$

where n is the number of conjugated double bonds, A and B are constants. This relation has been seen to hold well also for phenylpolyenes, diphenylpolyenes and triphenylpolyenes.[9] We have attempted such a plot for these anthrylpolyenes. For the longest wavelength band a reasonably good straight line is obtained for the lower polyenes only. Owing to broadness of the band, exact estimation of λ_{max} is, however, difficult. For the second band the plot of λ^2_{max} against n-values results in a straight line. These plots are shown in Fig. 2. Shift of other bands with the increase of n is negligible.

For long polyenes the transition moment for the first $^1A_g \rightarrow {}^1B_u$ transition is along the long axis of the molecule and is proportional to the length of the molecule.[12] Molecular orbital theory predicts the same.[12] The

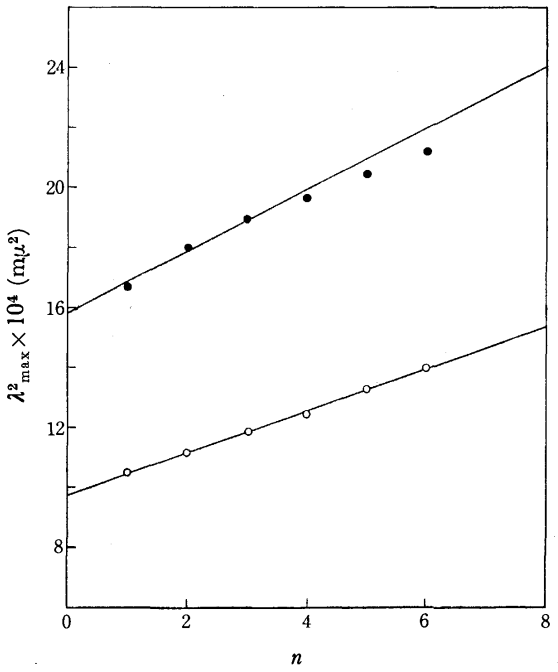

Fig. 2. Plot of λ^2_{max} against n.
—●—: Longest wavelength maxima,
—○—: Second-longest-wavelength maxima.

TABLE 2. OBSERVED OSCILLATOR STRENGTH OF ABSORPTION BANDS OF ANTHRYLPOLYENES IN SOLUTION

No. of double bonds n	Oscillator strength for bands			
	A	B	D	E
1	0.377	0.036	2.50	0.01
2	0.634	0.101	1.96	0.01
3	0.883	0.151	1.84	0.30
4	1.220	0.172	1.60	1.30
5	1.690	0.211	1.34	2.48
6	1.225	0.103	0.304	1.47

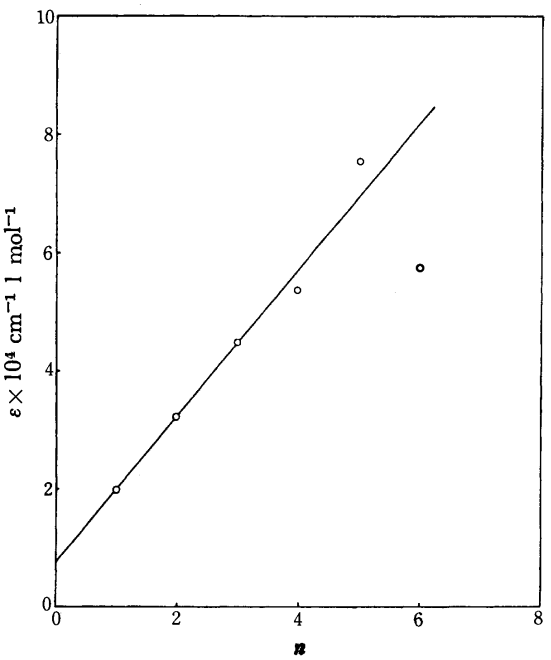

Fig. 3. Plot of ε against n for the longest wavelength maxima.

experimentally obtained oscillator strength values, as presented in Table 2, agree satisfactorily with the prediction. A plot of ε, molar extinction coefficient, *vs.* n, the number of double bonds, gives a good straight line for the first three polyenes. This linear plot (shown in Fig. 3) is also taken as a proof[9] of *all-trans* configuration of the polyene. That I_4—I_6 do not fall in the straight line proves that the higher anthrylpolyenes are not purely *trans*. Both in λ^2–n and ε–n plots, I_6 deviates significantly from the straight line and the molecule is definitely not in *trans* form. Small deviation is also observed in I_4 and I_5 and these two polyenes also do not seem to be in purely *all-trans* form. The high energy symmetry allowed band $^1A_g \rightarrow {}^1B_u$ (^{1}D in Platt's notation) is intense in *all-trans* polyenes. It has, however, generally been observed that the low energy $^1A_g \rightarrow {}^1B_u$ (^{1}B in Platt's notation) is more intense than the high energy $^1A_g \rightarrow {}^1B_u$ transition. In *all-trans* lycopene[13] the molar extinction coefficient have values 186×10^3 and 52×10^3 respectively for the two transitions. As can be seen from Table 2, in anthrylpolyenes the low energy allowed transition is less intense than the high energy allowed transition. This possibly is due to intensity "stealing" from the adjacent intense band E on the high energy side. Of the two bands D and E the lower energy one at about 2620 Å is intense in lower polyenes. As the number of double bonds increases, this band becomes weaker whereas the other at higher energy at about 2430 Å gains in intensity. This high energy band possibly arises from the interaction between ^1B_u state of *all-trans* polyene and the $^1B_{3u}$ state of the anthryl group.

The plots of λ^2 against n, ε against n and the enhancement in intensity of 2430 Å band in I_5 and I_6 perhaps indicates that the long polyenes are not in *all-trans* form. The long polyene chromophore with the large anthryl terminal group may bend the $(CH{=}CH)_n$ chain. In such *cis* form, the transition moment of the $^1A_{1g} \rightarrow {}^1B_{3u}$ transition along the long axis of the anthracene molecule makes a smaller angle with the direction of the transition moment of $^1A_g \rightarrow {}^1B_u$ of the polyene chromophore and the intensity of 2430 Å band may be enhanced in higher members. This *cis* configuration of long anthrylpolyenes is further supported by increased intensity of the *cis* peak at 3640 Å and 3740 Å at I_5 and I_6 respectively and also by the appearance of another symmetry forbidden band (as evidenced from its low intensity) at about 3100 Å and 3140 Å in I_5 and I_6 respectively.

II. Solvent Behavior. In some linear conjugated polyenes there exists a low-lying π-electronic state, transition to which is normally forbidden in *all-trans* form. Emission is observed from this low-lying state and as a result no overlap is usually observed between the intense lowest energy absorption band and the emission band of this *trans* polyene.[14] In the anthrylpolyenes we have observed two weak bands around 3500 Å (B) and 3000 Å (C). These are of forbidden nature and possibly belong to the ^1A_g states of polyene. In addition, three allowed type strong bands A, D, and E have been observed. A and D most likely are transitions to the ^1B_u state of polyene. The E band seems to be related to the $^1B_{3u}$ band of anthracene nucleus. It, therefore, appears that in these polyenes the first excited ^1A_g state is not below the ^1B_u state of polyene. Significant overlap has been observed between the absorption and emission bands in I_1. Solvent effect is a good clue as to the identity of the absorbing and emitting states. The major contribution to the solvent shift of the strong transition can be written in the form[3,15]

$$\bar{\nu} - \bar{\nu}_{gas} = Kf_{eg}\frac{n^2-1}{n^2+2}$$

where $\bar{\nu}$ is the transition energy in cm^{-1}, K is a parameter which is constant for a given molecule, f_{eg} is the oscillator strength for a particular transition of the molecule, n is the solvent refractive index and $(n^2-1)/(n^2+2)$ is the solvent polarizability. A plot of $\bar{\nu}$ for the first absorption and the emission bands of I_1 *versus* $(n^2-1)/(n^2+2)$ is shown in Fig. 4. The slopes of the lines are the same indicating similar value for the absorption and emission oscillator strengths. This result is different from that usually observed[1,16] in linear conjugated polyenes where ^1A_g state has been established to be the lowest excited electronic state. State ordering may as well be different for polyenes with different substituents. We conclude that in α,ω-di-1-anthrylpolyenes the lowest excited state is an allowed ^1B_u type. The terminal anthryl group

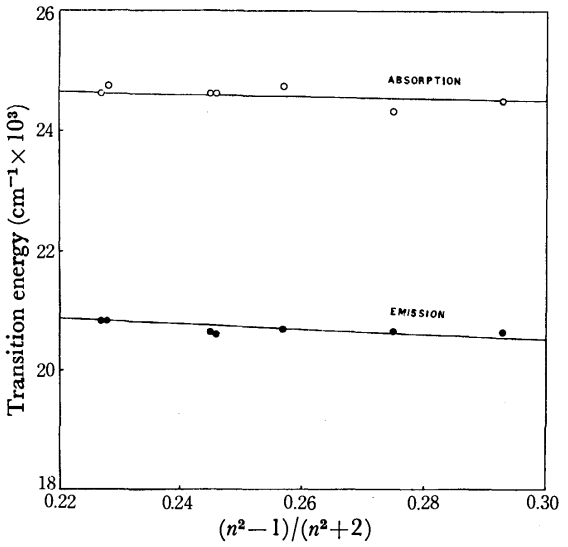

Fig. 4. The positions of the highest energy emission band and lowest energy strong absorption band of I_1 as a function of $(n^2-1)/(n^2+2)$.

interaction effect is such that the electronic state of the acetylene chromophore is lowered in energy with ^1A_g as the ground state and with ^1B_u, ^1A_g, ^1A_g, ^1B_u as the excited states in increasing energy order, the same as when only single-excitation configuration interaction is considered in PPP calculation.

III. Solid Film Spectra. The electronic absorption spectra of anthrylpolyenes in crystalline state are shown in Fig. 5. The bands are broad and there is overlapping between bands. The ordinate shows the intensity of a band relative to others in the same spectrum.

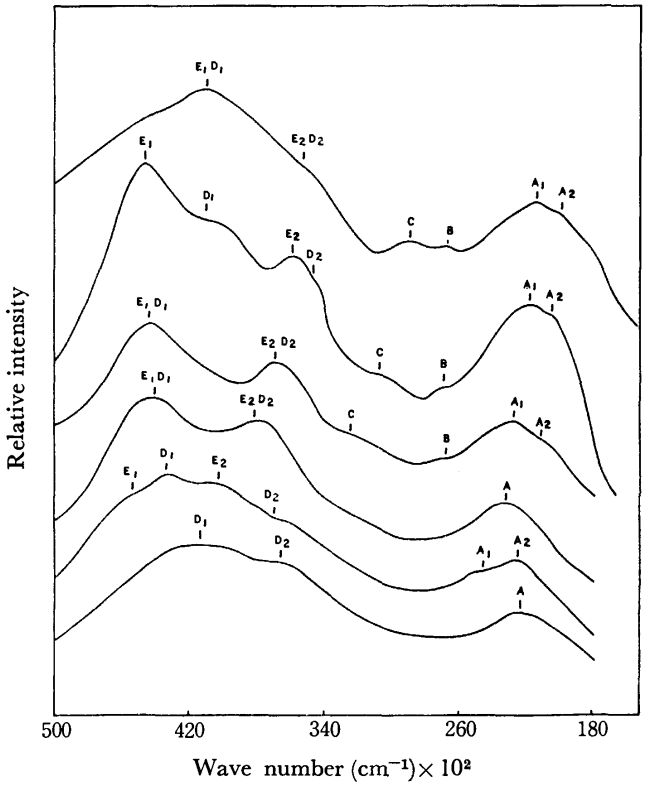

Fig. 5. Absorption spectra of di-1-anthrylpolyenes (I_n) in the solid state. The curves ($n=1-6$) have been displaced upward successively on the ordinate axis from the curve immediately below for clarity.

The band B in the region 3200—3800 Å, which is of moderate intensity in solution, seems to be absent in the lower member in the crystalline state. In the higher members, this band appears with moderate intensity. Further, the other weak band at about 3140 Å appears with moderate intensity in higher polyene crystal spectra but is absent in lower polyenes. These observations indicate that in the crystalline state also lower anthrylpolyenes remain in *all-trans* form but the higher members are in *cis* form: this is likely in view of the longer chain between the two anthryl terminal groups.

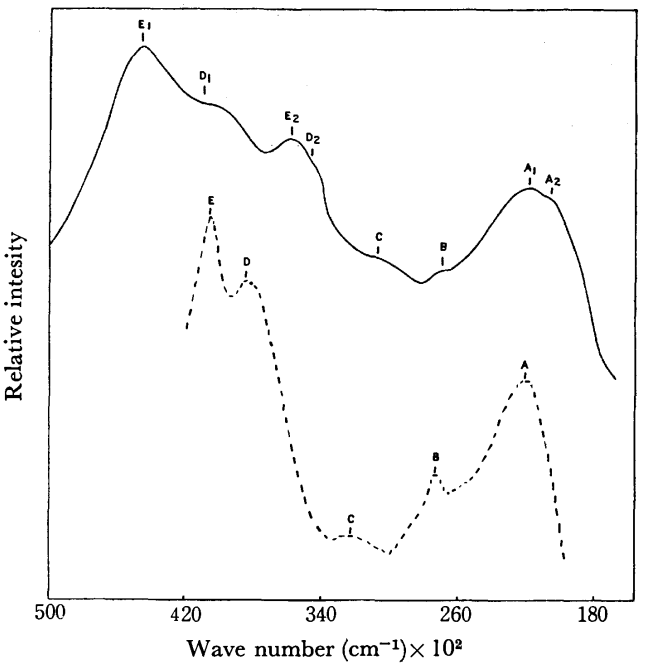

Fig. 6. Absorption spectrum of I_5.
---: Spectrum in THF solution, —: Solid film spectrum.

The crystal spectra differ from the spectra of free molecules in that in the solid state there are more number of bands than in solution and these bands are on both high and low energy sides of the intense solution bands. Some of these bands seem to be the factor group split components of the intense free molecular bands. This is better observed in the solid film spectrum of I_5 which shows structures and better resolution (Fig. 6). Solid state bands A_1 and A_2 on high and low energy sides of solution band A respectively seem to be the split components of A. Identification of weak B and C solution bands in solid film is obvious and no additional structure is observed in this region. In the region of solution bands D and E there are four distinct resolved bands in the crystal spectra. From the structures of the bands it seems that the band D is split into D_1 and D_2 and E is split into E_1 and E_2 in the solid state. Assignments of the bands in the crystal spectra of other anthrylpolyenes are less straightforward. We have, however, attempted a tentative identification of these bands in terms of solu-

tion band in other anthrylpolyenes (Fig. 5). The assignment of the factor group split components in Table 1 is only tentative and numerical values of splitting are of no significance. Study of single crystal polarized spectra at liquid N_2 or liquid He temperature is required for any inequivocal identification of factor group split components.

The authors are thankful to Prof. Nakagawa for his generous gift of anthrylpolyenes. One of the authors (K.G.M.) expressess his thanks to the University Grants Commission, India for a fellowship.

References

1) B. S. Hudson and B. E. Kohler, *Chem. Phys. Lett.*, **14**, 299 (1972).
2) K. Schulten and M. Karplus, *ibid.*, **14**, 305 (1972).
3) B. S. Hudson and B. E. Kohler, *J. Chem. Phys.*, **59**, 4988 (1973).
4) K. G. Mandal and T. N. Misra, *Chem. Phys. Lett.*, **27**, 57 (1974).
5) H. Suzuki, "Electronic Absorption Spectra and Geometry of Organic Molecules," Academic Press, New York (1967).
6) J. H. Pinckard, B. Wille, and L. Zechmeister, *J. Amer. Chem. Soc.*, **70**, 1938 (1948).
7) L. Zechmeister and J. H. Pinckard, *ibid.*, **76**, 4144 (1954).
8) K. Lunde and L. Zechmeister, *ibid.*, **76**, 2308 (1954).
9) H. M. Walborsky and J. F. Pendleton, *ibid.*, **82**, 1405 (1960).
10) Y. Takeuchi, S. Akiyama, and M. Nakagawa, This Bulletin, **45**, 3183 (1972).
11) L. N. Ferguson, *Chem. Rev.*, **43**, 408 (1948).
12) J. N. Murrell, "The Theory of the Electronic Spectra of Organic Molecules," Chapman and Hall, London (1971), p. 74.
13) L. Zechmeister, A. L. LeRosen, W. A. Schroeder, A. Polgar, and L. Pauling, *J. Amer. Chem. Soc.*, **65**, 1940 (1943).
14) A. J. Thomson, *J. Chem. Phys.*, **51**, 4106 (1969).
15) S. Basu, *Adv. Quantum Chem.*, **1**, 145 (1964).
16) K. G. Mandal, B. Mallik, and T. N. Misra, *Indian J. Pure Appl. Phys.*, **13**, 699 (1975).

Effect of Water on the Conductance of Hydrogen Halides in Diethylene Glycol

V. SRINIVAS RAO and C. KALIDAS*

Department of Chemistry, Indian Institute of Technology, Madras, 600036, India

(Received May 2, 1975)

The effect of addition of small amounts of water on the conductance of hydrogen chloride and hydrogen bromide in diethylene glycol at 25 °C was investigated. The Λ_0 of both acids sharply decreases with the addition of water, passes through a minimum at about 1.23 wt% of water and then increases. This was explained on the basis of the changes in the proton jump mechanism due to shift of the proton transfer equilibrium, $ROH_2^+ + H_2O \rightleftarrows ROH + H_3O^+$. The role of water in this equilibrium was shown to be similar to the protonation of a Hammett indicator base in acid solutions.

Conductance studies on hydrogen halides in amphiprotic solvents, especially the monohydric alcohols and their aqueous mixtures have received[1–4] some attention in recent years. Such studies are useful[5] in elucidating the effect of solvent structure on the proton migration mechanism in these solvents. Despite this, practically no conductance measurements have been reported[6] in glycols or their aqueous mixtures. The present work, which is in continuation of our earlier work on the subject,[7,8] therefore, deals with the effect of addition of small amounts of water on the conductance of hydrogen chloride and bromide in diethylene glycol in order to elucidate the nature of solute-solvent interactions in these systems.

Experimental

BDH (LR) grade sample of diethylene glycol, purified according to the method described earlier[9] was used. The distilled sample had a bp 120 °C at 10 mmHg, $d^{25\,°C} = 1.115$ g ml^{-1}, and the specific conductivity 9.5×10^{-9} ohm^{-1} cm^{-1} at 25 °C. Conductivity water, obtained by repeatedly distilling double distilled water to which a pinch of permanganate and a trace of sodium hydroxide were added, was used. *p*-Nitroaniline, recrystallised twice from alcohol (mp = 147 °C) was employed as the indicator in H_0 measurements, details of which are given elsewhere.[10] The preparation, purification and standardization of stock HCl and HBr solutions in diethylene glycol are similar to that described[8,9] earlier. The conductance measurements were carried out with a precision conductivity bridge (Model WBR/TAV, WTW, West Germany). A logarithmic indicator amplifier with built-in 1000 Hz generator served as the balance indicator. Further details of the conductance measurements are given[6] elsewhere. All measurements were made at 25.00±0.01 °C employing high boiling liquid paraffin as bath liquid. All solutions were prepared by weight and converted to volume concentrations by appropriate density data. The physical constants of the various solvent mixtures used were identified with the pure solvent in all calculations.

Results and Discussion

The conductance data of the acids are given in Tables 1 and 2. Computer analysis of these data with the Fuoss-Onsager 1965 three parameter equation[11] revealed no significant association of the halides either in the pure solvents[8] or the mixtures. The data were hence analyzed by the Fuoss-Onsager 1965 two parameter equation[11] given by

$$\Lambda = \Lambda_0 - SC^{1/2} + 2EC\log(\tau) + LC \qquad (1)$$

where the various terms have their usual significance. The Λ_0 obtained for the acids in the various solvent mixtures are presented in Table 3. It is seen from this Table that the Λ_0 of the acids decreases continuously as the amount of water added to a solution of HCl or HBr in diethylene glycol increases gradually, passes through a minimum at about 1.23 wt% of water and then increases again with further additions of water. This variation can be qualitatively accounted for in terms of the changes in the proton jump mechanism arising due to the shift of the equilibrium

Table 1. Conductance data of hydrogen chloride in diethylene glycol containing added water at 25 °C

C=concn of acid in eq/l, Λ in ohm^{-1}·cm^2·mol^{-1}

Wt% water	0.2494		0.3737		0.4975	
	$C\times10^4$	Λ	$C\times10^4$	Λ	$C\times10^4$	Λ
	10.10	7.21	9.90	7.05	9.90	6.85
	15.4	7.20	15.4	6.98	15.30	6.80
	21.6	7.10	21.5	6.96	21.50	6.75
	25.7	7.08	25.7	6.94	25.70	6.73
	37.3	7.07	37.3	6.91	37.20	6.71
	42.4	7.04	42.4	6.84	42.30	6.60
	46.1	6.95	46.0	6.80	46.00	6.52
Wt% water	0.6212		0.7444		0.8676	
	$C\times10^4$	Λ	$C\times10^4$	Λ	$C\times10^4$	Λ
	9.90	6.70	9.90	6.65	9.90	6.54
	15.30	6.63	15.30	6.58	15.30	6.50
	21.50	6.60	25.60	6.55	21.40	6.49
	25.60	6.57	37.10	6.49	25.60	6.43
	37.20	6.54	42.20	6.43	37.10	6.42
	42.30	6.52	45.80	6.38	42.20	6.40
	45.90	6.48			45.80	6.31
Wt% water	0.9902		1.234		1.356	
	$C\times10^4$	Λ	$C\times10^4$	Λ	$C\times10^4$	Λ
	9.90	6.49	10.00	6.52	9.80	6.59
	15.30	6.47	15.20	6.46	15.20	6.53
	25.60	6.45	21.30	6.45	21.30	6.47
	37.00	6.39	25.50	6.44	25.50	6.43
	42.10	6.35	36.90	6.38	36.90	6.41
	45.70	6.30	42.00	6.34	42.00	6.37
			45.60	6.30	45.60	6.30

* To whom correspondence should be addressed.

Table 2. Conductance data of hydrogen bromide in diethylene glycol containing added water at 25 °C

C=concn of acid in eq/l, Λ in ohm^{-1}·cm^2·mol^{-1}

Wt% water	0.2494		0.3737		0.4975	
	$C\times10^4$	Λ	$C\times10^4$	Λ	$C\times10^4$	Λ
	11.10	7.52	11.10	7.15	11.10	6.92
	18.30	7.51	18.20	7.13	18.20	6.91
	32.80	7.45	23.90	7.11	23.90	6.90
	40.80	7.44	32.80	7.10	32.70	6.87
	58.60	7.38	40.70	7.09	40.70	6.85
			58.50	7.00	58.40	6.77
Wt% water	0.6212		0.7444		0.9902	
	$C\times10^4$	Λ	$C\times10^4$	Λ	$C\times10^4$	Λ
	11.10	6.80	11.10	6.63	11.10	6.52
	18.20	6.79	18.20	6.62	18.10	6.51
	23.90	6.78	23.80	6.61	23.80	6.50
	32.70	6.72	32.70	6.58	32.50	6.48
	40.60	6.70	40.60	6.56	40.50	6.42
	58.40	6.68	58.30	6.50	58.20	6.34
Wt% water	1.234		1.356			
	$C\times10^4$	Λ	$C\times10^4$	Λ		
	11.00	6.51	11.00	6.55		
	18.10	6.49	18.00	6.53		
	23.70	6.48	23.70	6.52		
	32.50	6.41	32.50	6.43		
	40.40	6.40	40.30	6.42		
	58.00	6.31	57.90	6.32		

Table 3. Limiting equivalent conductances, Λ_0, of HCl and HBr in diethylene glycol–water mixture at 25 °C

Wt% water	Λ_0 (HCl) $\Omega^{-1}\cdot cm^2\cdot mol^{-1}$	Λ_0 (HBr) $\Omega^{-1}\cdot cm^2\cdot mol^{-1}$
0.2494	7.62±0.04	7.96±0.06
0.3737	7.44±0.03	7.55±0.05
0.4975	7.29±0.05	7.32±0.05
0.6212	7.06±0.02	7.17±0.03
0.7444	7.04±0.04	7.01±0.04
0.8676	6.92±0.04	—
0.9902	6.90±0.04	6.92±0.04
1.234	6.89±0.03	6.89±0.04
1.356	6.97±0.03	6.95±0.04

$$ROH_2^+ + H_2O \rightleftharpoons ROH + H_3O^+ \qquad (2)$$

in which the initial decrease of Λ_0 is caused by the replacement of protons of abnormal conductance (ROH_2^+) by protons of normal conductance (H_3O^+) at low concentrations of water. At higher concentrations of water, the H_3O^+ ions are increasingly surrounded by water molecules and their proton jump mechanism is restored resulting in abnormal conductance of these ions. Similar observations have been made by Goffredi *et al.* in propanol-water mixtures and Selvarajan and Kalidas[7] in ethylene glycol-water and propylene glycol-water mixtures. The equilibrium constant K, of Reaction (2) was evaluated[12] according to

$$\frac{1}{\Lambda_0^\circ-\Lambda_0} = \frac{1}{\Lambda_0^\circ-\Lambda_0^w} + \frac{1-x}{xK(\Lambda_0^\circ-\Lambda_0^w)} \qquad (3)$$

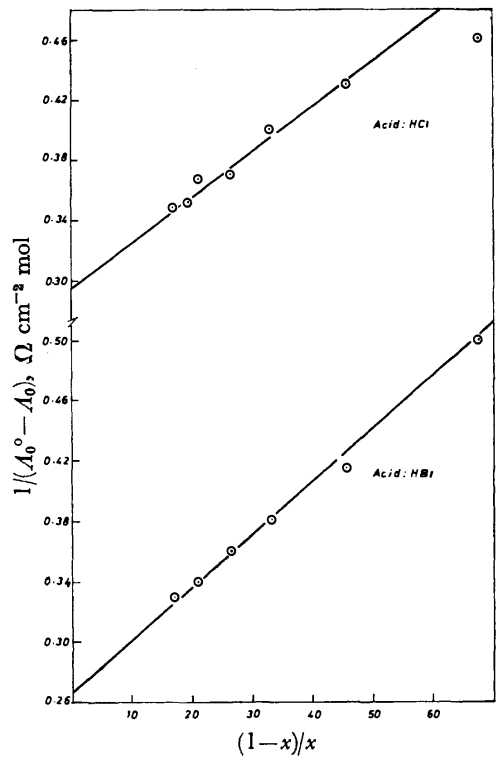

Fig. 1. Plot of $1/(\Lambda_0^\circ-\Lambda_0)$ *vs.* $(1-x)/x$ at 25 °C in diethylene glycol for HCl and HBr.

where Λ_0° represents the conductance of the hydrogen halide in diethylene glycol with the protons in the form of ROH_2^+, Λ_0^w is the (hypothetical) conductance of the same acid in the solvent with the protons in the form of H_3O^+ and Λ_0 is the conductance at a mole fraction x of water. A plot of $1/(\Lambda_0^\circ-\Lambda_0)$ *vs.* $(1-x)/x$ for the two acids is shown in Fig. 1. The average value of K obtained (from the slopes of these plots) corresponding to the least squares fitting of the best straight lines (for the two acids) is 88±12. Although it might be expected that the equilibrium constant of Reaction (2) in different alcohols is related to the basic strengths of these molecules, a comparison of the values in different alcohols shows that this is not true. This is most probably due to the structural influence of the solvent on the proton migration mechanism in amphiprotic solvents, *viz.*, through the free solvent molecules and through hydrogen bonded net works in the solvents as proposed by Goffredi *et al.*[5] It is, however, significant that the role of water in Reaction (2) can be likened to that of a Hammett indicator base in protonation equilibria according to

$$SH^+ + B \rightleftharpoons S + BH^+ \qquad (4)$$

and hence the H_0 difference between two solvents S_1 and S_2 can be related to

$$H_{0(S_2)} - H_{0(S_1)} = \log \frac{K_{(S_2)}}{K_{(S_1)}} \qquad (5)$$

where $K_{(S_2)}$ and $K_{(S_1)}$ are the equilibrium constants of Reaction (2) in the two solvents. Considering S_1 and S_2 to be diethylene glycol and propylene glycol respectively, the H_0 difference was found to be 0.22 (at 0.1 mol/kg concn) while the log ratio of equilibrium constants is 0.31 ($K_{P,G}$=43)[7] which shows the approximate

validity of Equation(5) and hence of the assumption made above.

Our thanks are due to C.S.I.R. for the award of a senior research fellowship to one of us (V.S.R.). We also express our sincere thanks to Prof. M. Goffredi, of the University of Palermo, Italy for providing us with the computer program for the analysis of the conductance data presented in this paper.

References

1) G. J. Janz and S. S. Danyluk, *Chem. Rev.*, **60**, 209 (1960).
2) M. Goffredi and T. Shedlovsky, *J. Phys. Chem.*, **71**, 2182 (1967).
3) H. O. Spivey and T. Shedlovsky, *ibid.*, **71**, 2187 (1967).
4) R. DeLisi and M. Goffredi, *Electrochim. Acta*, **17**, 2001 (1972).
5) R. DeLisi and M. Goffredi, *J. Chem. Soc., Faraday Trans.*, **70**, 787 (1974).
6) T. Erdey Gruz, E. Kugler, and L. Majthenyi, *Acta Chim. Acad. Sci. Hung.*, **19**, 363 (1959).
7) V. M. Selvarajan and C. Kalidas, *Trans SAEST.*, **9**, 111 (1974).
8) C. Kalidas and V. Srinivas Rao, *Ind. J. Chem.*, in press.
9) C. Kalidas and V. Srinivas Rao, *J. Chem. Eng. Data*, **19**, 201 (1974).
10) C. Kalidas and S. R. Palit, *J. Chem. Soc.*, **1961**, 3998.
11) R. M. Fuoss, L. Onsager, and J. F. Skinner, *J. Phys. Chem.*, **69**, 2581 (1965).
12) H. Strehlow, *Z. Phys. Chem., N. F.*, **24**, 240 (1960).

Electric Dipole Moment of 4-Chloro-2,3-tetra-, penta-, and hexamethylene Quinoline

Miss DIPTI and Pushti Prakash RASTOGI*
Department of Chemistry, University of Lucknow, Lucknow, India
(Received June 6, 1975)

Electric dipole moments of 4-chloro-2,3-tetra-, penta-, and hexamethylene quinolines[1-3] have been determined in benzene solution at a frequency of 1 MHz by Guggenheim method.[4] The reported results indicate that these compounds are non-planar and the dipole moment increases with the increase in the size of substituted methylene ring.

Recently a series of useful antidepressant and biologically active compounds like, 4-chloro-2,3-tetra-, penta- and hexamethylene quinolines have been prepared and their physical properties have been reported.[1-3] It has been found[6-8] that the dipole moment measurements of substituted quinolines and naphthalenes provide valuable information regarding the mode of interaction and the distribution of π-electrons to assign the structural configuration of these compounds. From this point of view the present series of organic compounds has been selected for the measurement of electric dipole moment and thereby to examine the influence of the size of the substituted methylene ring on the π-electron distribution of 4-chloroquinoline.

Experimental

The dielectric constant measurements were carried out at 25 °C at a radio frequency of 1 MHz with the help of a "Toshniwal" Dipole Meter type RLO9 supplied by Scientific and Industrial Instrument Co., India. The instrument works on a well known principle of heterodyne beat method. The resulting beat frequency is projected on the screen of a cathode ray tube with a 50 cycles per second. A Lissajous figure is obtained on the screen. The readings were recorded at the resonance point indicated on the CRT screen by the formation of a single loop pattern, *i.e.*, an ellipse or a circle.

Refractive indices of the solvent and solutions were determined at 25 °C with the help of "ASCO" Abbe-Refractometer (made in India). The range of this instrument is 1.3000 to 1.7000, the maximum precision attainable being 0.0002. Sodium D-line was used as a source of light and the refractometer was standardized with the help of a glass slab of known refractive index. The instrument directly gives the value of refractive index which is measured with the reading telescope.

The compounds 4-chloro-2,3-tetra-, penta-, and hexamethylene quinolines obtained from Central Drug Research Institute, Lucknow, India were recrystallized from benzene, dried and kept in a vacuum desiccator.

The dipole moment has been calculated by Guggenheim method,[4] *i.e.* by plotting** a quantity Δ against the concentration C, in moles of polar solute per cm^3 given by the relation:

$$\Delta = (\varepsilon_{12}-n_{12}^2) - (\varepsilon_1-n_1^2) \qquad (1)$$

where ε_1, n_1 and ε_{12}, n_{12} represent the dielectric constant and refractive index of pure solvent and solution respectively.

The slope $(\Delta/C)_0$ of the curve at $C=0$ is then used to calculate the dipole moment by means of the equation[9] given below:

$$\mu^2 = \frac{9kT}{4\pi N}\frac{3}{(\varepsilon_1+2)(n_1^2+2)}\left(\frac{\Delta}{C}\right)_0 \qquad (2)$$

The dipole moment, μ, has also been calculated from Eq. (2) by determining the slope (Δ/C), using the mathematical relation based on least squares method,[5] namely

$$\left(\frac{\Delta}{C}\right) = \frac{\sum\Delta\sum C - n\sum(\Delta C)}{(\sum C)^2 - n\sum(C^2)} \qquad (3)$$

where Δ and C represent their usual meaning and that n is the number of observations recorded.

In order to make an estimate of the precision of equipments (Dipole Meter & Refractometer), the dipole moments of some of the liquids like, methanol, pyridine, acetone, and nitrobenzene are determined in benzene solution and are given in Table 1 along with their reported values for the sake of comparison. The experimental and literature values are found to be within the maximum deviation of $\pm 3\%$.

TABLE 1. DIPOLE MOMENT (μ) OF METHANOL, PYRIDINE, ACETONE, AND NITROBENZENE IN BENZENE SOLUTION AT 25 °C

Substance	$\mu \times 10^{18}$ e.s.u.	
	Experimental	Literature[a]
Methanol	1.73	1.68
Pyridine	2.22	2.20
Acetone	2.84	2.76[b]
Nitrobenzene	3.86	3.98

a) G.C. Pimentel and A.L. McClellan, "The Hydrogen Bond," Reinhold Publishing Co., New York, N.Y. (1960), p. 15. b) C.P. Smyth, "Dielectric Behaviour and Structure," McGraw Hill Book Co., New York (1955), p. 48.

Results

The refractive index, n_{12}, and dielectric constant, ε_{12}, of 4-chloro-2,3-tetra-, penta-, and hexamethylene quinolines are determined in benzene solution at different concentrations at 25 °C and are recorded in Table 2. The Δ values calculated from Eq. (1) are also given in Table 2. These Δ values are plotted against C as shown in Fig. 1. The slopes (Δ/C), evaluated from these linear plots as well as from least-squares relation[5] have been used to determine dipole moment μ, by Guggenheim method.[4] The obtained (Δ/C) and μ values are summarized in Table 3.

* Visiting Scientist, Chemistry Department, University of Leicester, Leicester, England, U. K.

** The slope is directly obtained from the plot of $(\varepsilon_{12}-n_{12}^2)$ against C as the second term on the right hand side in Eq. (1) is constant.

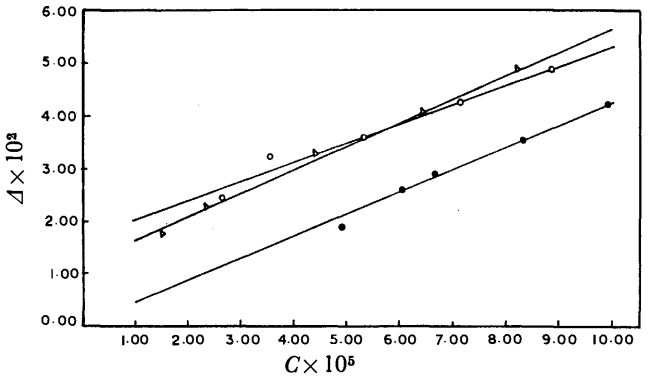

Fig. 1. Plot of Δ *vs.* C for tetra, penta, and hexa salts in benzene solutions at 25 °C.
△: 4-Chloro-2,3-hexamethylene quinoline, ○: 4-chloro-2,3-tetramethylene quinoline, ●: 4-chloro-2,3-pentamethylene quinoline.

Table 2. Refractive index (n_{12}), dielectric constant (ε_{12}), and Δ values of 4-chloro-2,3-tetra-, penta-, and hexamethylene quinolines in benzene at different concentrations (25 °C)

Concn $C\times 10^5$	Refractive index n_{12}	Dielectric constant ε_{12}	$\Delta\times 10^2$ $[\Delta=(\varepsilon_{12}-n_{12}^2)]$
4-Chloro-2,3-tetramethylene quinoline			
0.00	1.5026	2.274	—
2.65	1.5032	2.284	2.44
3.56	1.5036	2.293	3.22
5.34	1.5040	2.298	3.60
7.16	1.5049	2.307	4.23
8.87	1.5054	2.315	4.88
4-Chloro-2,3-pentamethylene quinoline			
4.94	1.5037	2.280	1.89
6.06	1.5040	2.288	2.60
6.67	1.5047	2.293	2.89
8.38	1.5052	2.301	3.54
9.94	1.5056	2.309	4.22
4-Chloro-2,3-hexamethylene quinoline			
1.56	1.5032	2.277	1.74
2.39	1.5034	2.283	2.28
4.47	1.5038	2.294	3.26
6.49	1.5041	2.303	4.07
8.26	1.5044	2.312	4.88

Table 3. (Δ/C) and dipole moment (μ) of tetra-, penta-, and hexa salts in benzene solution at 25 °C

Salt	Graphical method / Least squares method $(\Delta/C)\times 10^{-3}$	$\mu\times 10^{18}$ e.s.u.	
Tetra	0.365 0.365[a)]	1.70 1.70[a)]	1.70
Penta	0.425 0.415[a)]	1.84 1.82[a)]	1.83
Hexa	0.445 0.460[a)]	1.88 1.92[a)]	1.90

a) Slope (Δ/C), evaluated from least-squares method (Ref. 5).

Discussion

It may be observed from Table 3 that the dipole moments of 4-chloro-2,3-tetra-, penta-, and hexamethylene quinolines in benzene solution determined by using (Δ/C) values obtained from graphical and least squares[5] methods are found to be in an excellent agreement and are within the maximum deviation of 2%. It may also be noted that the dipole moment of these compounds increases in the increasing order of the size of substituted methylene ring, *i.e.*, μ tetra$<\mu$ penta$<\mu$ hexa as 4-chloroquinoline being the common constituent to all the above investigated polar compounds.

The geometrical structures and dipole moments[6-8] of 1-chloronaphthalene, quinoline, 4-chloroquinoline, and 4-chloro-2,3-tetra-, penta-, and hexamethylene quinolines are represented in Fig. 2 (see I, II, III, IV, V, and VI respectively).

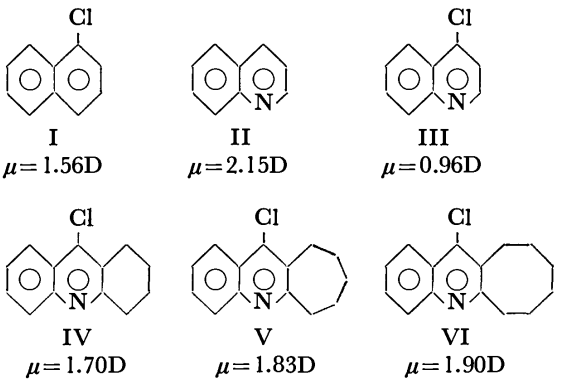

Fig. 2.

It is clear from Fig. 2 (see III) that the 4-chloroquinoline has two dipoles of similar magnitudes that of quinoline itself (2.15D) and the other associated with the C–Cl bond (1.56D). The Cl-substituent increases the electronegativity of the carbon atom to which it is attached and this consequently modifies the π-electron distribution of the quinoline ring. The p-electrons of chlorine atom interacts with the π-electrons of quinoline ring which reduced the net dipole moment of the 4-chloroquinoline (0.96D).

The dipole moments of 4-chloro-2,3-tetra-, penta-, and hexamethylene quinoline are not only in the regular increasing order but are almost twice that of 4-chloroquinoline, which establishes that the substitution of methylene ring is definitely on the different plane to that of the quinoline ring. The dipole moment of these compounds can be considered as the sum of the moments of 4-chloroquinoline and substituent methylene ring, which interact with one another thereby resulting in an increase of the net magnitude of dipole moment.

The authors are grateful to the State C. S. I. R. Lucknow for their valuable financial assistance and to Direcfor, Central Drug Research Institute, Lucknow for providing organic compounds. The thanks are also due to the Indian National Science Academy, New Delhi for their constant encouragement and appreciation.

References

1) L. J. Sargent and L. Small, *J. Org. Chem.*, **11**, 359 (1946).
2) M. V. Saigal, Jr., B. J. Brent, and P. Marchini, U. S. 3232945 (1966).
3) W. E. Parham, R. W. Davenport, and J. B. Biasotti, *J. Org. Chem.*, **35**, 3775 (1970).
4) E. A. Guggenheim, *Trans. Faraday Soc.*, **45**, 714 (1949).
5) J. W. Mellor. "Higher Mathematics for Students of Chemistry and Physics," Dover, New York (1954), p. 326.
6) G. C. Hampson and A. Weissberger, *J. Chem. Soc.* **1936**, 393.
7) C. W. N. Cumper and A. I. Vogel, *ibid.*, **1960**, 4723.
8) C. W. N. Cumper D. G. Redford, and A. I. Vogel, *ibid.*, **1962**, 1176, 1183.
9) C. P. Smyth, "Dielectric Behaviour and Structure," McGraw Hill Book Co., New York (1955), p. 225.

Lactone Carboxylic Acids. VIII.[1] A Synthesis of γ-Substituted α-Amino-butyrolactones from Ethyl γ-Substituted α-Hydroxyaminoaconates

Sigeru TORII,* Masasi UKIDA, Hiromichi KANO, Takuya FURUTA, and Hideo TANAKA
Department of Industrial Chemistry, School of Engineering, Okayama University, Okayama 700
(Received November 2, 1974)

The conversion of α-hydroxyaminoaconates **1a** and **1b** to α-aminoaconates **2a** and **2c** was described, involving a novel reduction of the α-hydroxyamines on treatment with *p*-toluenesulfonyl chloridep–yridine in 62.1—89.5% yields. In the case of the reduction of **1b** *N*-tosyloxy derivative **11b** was isolated. α-Amino-γ-butyrolactones **3** and **4** could be obtained by hydrogenation of *N*-acetates of **2a** and **2c**. Ammonolysis of 2-hydroxy-2-butenolides **5a** and **7a** prepared from acid-hydrolysis of **1b** also gave α-aminobutyrolactones **6**, **8a**, **8b**, **9**, and **10**.

α-Amino-γ-butyrolactones have been used extensively for a variety of synthetic purposes,[2-8] above all in the field of antibiotics synthesis.[9] In this connection, neccessity of the α-aminobutyrolactones as a synthetic intermediate is increasing in recent years. Thus, many attempts have been made to obtain appropriate aminolactones starting from α-halogenobutyrolactone,[2] 2-hydroxy-2-butenolide,[3] α-azidobutyrolactone,[4] 2-carboxy-2-butenolide,[5] α-cyanobutyrolactone,[6] β,γ-dihydroxy-α-amino acid,[7] and others.[8] We wish to report here a convenient synthetic method of γ-substituted α-amino-γ-butyrolactones and its derivatives. The procedure involves initial reduction of ethyl γ-substituted α-hydroxyaminoaconates **1a** and **1b** on treatment with *p*-toluenesulfonyl chloride–pyridine to form the corresponding α-aminoaconates **2a** and **2c** and the subsequent hydrogenation to form α-acetylamino-γ-butyrolactones **3** and **4**.

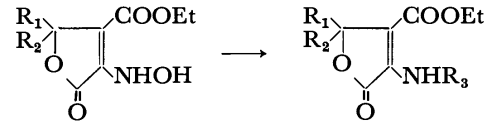

1a $R_1=R_2=Me$
1b R_1, $R_2=-(CH_2)_5-$

2a $R_1=R_2=Me$, $R_3=H$
2b $R_1=R_2=Me$, $R_3=Ac$
2c R_1, $R_2=-(CH_2)_5-$, $R_3=H$
2d R_1, $R_2=-(CH_2)_5-$, $R_3=Ac$

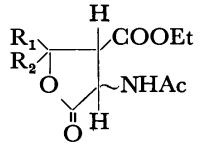

3a $R_1=R_2=Me$ (*trans*)
3b $R_1=R_2=Me$ (*cis*)
4a R_1, $R_2=-(CH_2)_5-$ (*trans*)
4b R_1, $R_2=-(CH_2)_5-$ (*cis*)

Nitrosation of β-ethoxycarbonyl-α-carboxy-γ-butyrolactones with an equimolar amount of sodium nitrite in acetic acid at −5—0 °C gave ethyl α-hydroxyaminoaconates **1a** and **1b** in excellent yields.[10] The infrared spectrum of **1b** showed characteristic bands at 3520 and 3460 cm^{-1} corresponding to NH and OH functions and a broad band at 1744 due to lactone and ester carbonyls. Reduction of **1a** and **1b** to the corresponding primary amines **2a** and **2c** were carried out on treatment with *p*-toluenesulfonyl chloride–pyridine at room temperature for 2 days to afford ethyl γ-substituted α-aminoaconates **2a** and **2c** in 62.1—89.5% yields. The infrared spectrum of **2c** exhibited two sharp bands at 3410 and 3320 cm^{-1} due to primary amine and bands at 1762 and 1692 corresponding to lactone and conjugated ester carbonyls.

Acetylation of **2c** giving α-acetylaminoaconate **2d** and the subsequent hydrogenation in ethanol containing a small amount of acetic acid over platinum oxide at room temperature gave a mixture of the corresponding α-acetylamino-γ-butyrolactones **4a** and **4b** in quantitative yield. Separation of *cis* and *trans* isomers was accomplished by column chromatography over silica gel to afford 22.2% of **4a** and 77.5% of **4b**, respectively. In the similar manner, conversion of **2a** into the corresponding **3a** and **3b** *via* **2b** was achieved in quantitative yield.

The α-hydroxyaminoaconate **1b** underwent hydrolysis on treatment with concentrated hydrochloric acid at room temperature for 7 days to give ethyl α-hydroxyaconate **5a** as a major product together with **5c** (3.6%). Spectral evidences and the formation of **5b** from **5a** support assignment of the structure of **5a**.

The α-hydroxybutenolides **5a** and **7a** are considered to be a good precursor for α-aminolactone synthesis.[3] Thus, treatment of **5a** with ammonium acetate at 110—120 °C for 6 h afforded **6** in 81.1% yield.

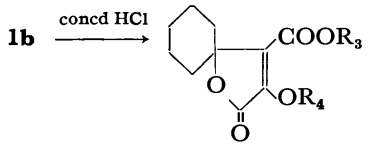

5a $R_3=Et$, $R_4=H$
5b $R_3=Et$, $R_4=Me$
5c $R_3=H$, $R_4=H$
5d $R_3=Me$, $R_4=Me$

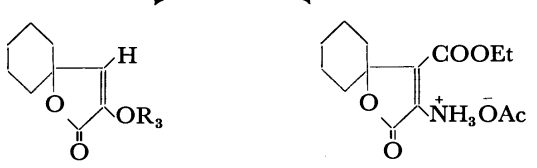

7a $R_3=H$
7b $R_3=Me$

6

Acid-hydrolysis of **5a** under refluxing for 20 h afforded 2-hydroxy-2-butenolide **7a** in 79.6% yield. Ammonolysis of **7a** with 11.3 equivalents of ammonium

acetate at 104 °C for 30 min gave the α-aminobutenolide **8a** in 92.1% yield. However, in the ammonolysis reaction decrease of the amount of ammonium acetate to 7.6 equivalents provided the dimeric compound **10** as a minor product, whose structure was confirmed by spectral data and elemental analysis.

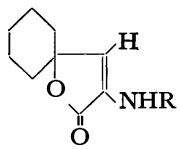

8a R=H
8b R=Ac

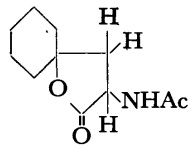

9

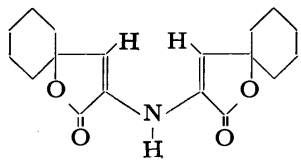

10

The conversion of **8a** into the α-aminobutyrolactone **9** *via* **8b** was carried out successfully. Treatment of **8a** with acetic anhydride in the presence of a catalytic amount of *p*-toluenesulfonic acid resulted in the acetate **8b** in 95.9% yield. The subsequent hydrogenation of **8b** in ethanol containing a trace of acetic acid over platinum oxide gave **9** in 95% yield.

From the reaction products of **1b** with *p*-tolenesulfonyl chloride–pyridine 7.1% of (tosyloxyamino)aconate **11b** was isolated. Similarly, when **1b** was treated with equimolar amount of butyllithium followed by treatment with *p*-toluenesulfonyl chloride, the reaction produced 26.4% of **11b** in addition to the formation of **2c** (68.7%). The conversion of the tosylate **11b** into **2c** could be carried out by stirring in pyridine at room temperature.

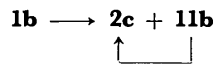

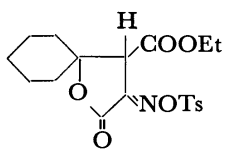

11b

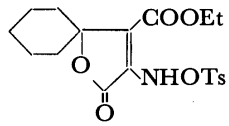

11a

One possible pathway for the formation of **2c** and **11b** from **1b** may involve an unstable intermediate **11a**, a tautomer of **11b**. In the conversion of **11b** into **2c** the

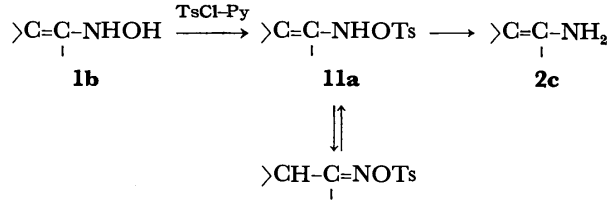

1b **11a** **2c**

11b

reaction may also proceed *via* the intermediate **11a**, which would provide **2c** promptly in contrast to the slow change of **11b** into **11a**.

Discrimination of *cis* and *trans* isomers of α-amino-β-ethoxycarbonylbutyrolactones **3** and **4** was accomplished by comparison with related compounds **12**,[11] **13**,[12] and **14**.[13] Aminobutyrolactones **3a** and **4a**, which were separated from hydrogenation products of **2b** and **2d** by column chromatography, have PMR coupling constants ($J_{\alpha,\beta}$) of 10.5 and 11.1 Hz respectively, indicating that structure of **3a** and **4a** should be assigned to the *trans* isomers. The butyrolactones **12** and **13**, which are considered to be thermodynamically favorable *trans* isomers, have coupling constants in the range of 10.0—13.0 Hz (Table 1).

Table 1. Coupling constants between H_α and H_β of α,β-substituted butyrolactones

Compound	H_α (δ)		H_β (δ)	$J_{\alpha,\beta}$ (Hz)	
	cis	*trans*		*cis*	*trans*
3a	—	4.73	3.65	—	11.1
3b	5.29	—	3.43	7.5	—
4a	—	4.76	3.50	—	10.5
4b	5.25	—	3.46	7.5	—
12a	—	4.17	3.54	—	11.0
12b	—	3.96	3.39	—	11.5
12c	—	4.15	3.55	—	11.0
13a	—	3.47	3.04	—	12.8
13b	—	3.30	2.82	—	11.5
14	2.80	2.60[a]	3.07	7.0	11.0

a) The coupling constant of geminal hydrogen atoms at the α position was 18.0 Hz.

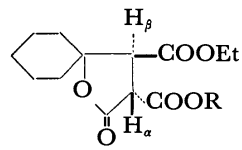

12a R=H; **12b** R=Me
12c R=Et

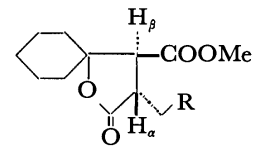

13a R=CHO
13b R=HC=CH$_2$

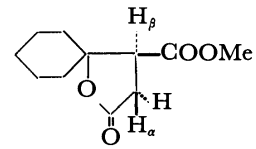

14

On the other hand, the isomers **3b** and **4b** have identical coupling constant ($J_{\alpha,\beta}$: 7.5 Hz), being assigned to the *cis* isomer based on the result observed in the resemble *cis* substituted cyclopentane system[14] and on the calculation from the Karplus equation.[15]

Experimental

Melting points and boiling points are uncorrected. NMR spectra were recorded on Hitachi R-24 and/or R-20 instruments. IR spectra were determined with a Hitachi EPI-S2, with only major absorptions being cited. Wako gel C-200 silica gel was used for elution chromatography. Elemental analysis was performed by Mr. Tsutomu Okamoto of our Laboratory.

γ,γ-Pentamethylene-β-ethoxycarbonyl-α-carboxy-γ-butyrolactone (12a). Hydrolysis of γ,γ-pentamethylene-α,β-diethoxycarbonyl-γ-butyrolactone (**12c**)[11] (8.9 g, 0.03 mol) with NaOH (3.42 g, 0.09 mol) in aqueous 20% EtOH (18 ml) afforded 7.1 g (87.5%) of **12a** as a white solid: mp 130.0—131.0 °C (from water); IR (neat) 3600—2200 (COOH),

1785, 1740 cm^{-1}; NMR (CCl_4) δ 1.32 (t, J=6.8 Hz, 3H, CH_3), 1.00—2.10 (m, 10H), 3.54 (d, J=11.0 Hz, 1H, H_β), 4.17 (d, J=11.0 Hz, 1H, H_α), 4.27 (q, J=7.0 Hz, 2H, CH_2O). Treatment of the acid with diazomethane gave the corresponding methyl ester **12b**: bp 82.0—86.0 °C/1 mmHg; IR (neat) 1790, 1742 cm^{-1}; NMR ($CDCl_3$) δ 1.29 (t, J=7.0 Hz, 3H, CH_3), 1.00—2.20 (m, 10H), 3.39 (d, J=11.5 Hz, 1H, H_β), 3.76 (s, 3H, CH_3O), 3.96 (d, J=11.5 Hz, 1H, H_α), 4.16 (q, J=7.0 Hz, CH_2O). Found: C, 59.26; H, 7.18%. Calcd for $C_{14}H_{20}O_6$: C, 59.14; H, 7.09%.

*Ethyl γ,γ-Pentamethylene-α-hydroxyaminoaconate (**1b**).* To a stirred solution of **12a** (5.0 g, 18.5 mmol) in AcOH (15 ml) a solution of $NaNO_2$ (1.28 g, 18.5 mmol) in water (3.0 ml) was added dropwise for 10 min at −5—0 °C. The mixture was stirred for 40 min at 5 °C and then diluted with water. After stirring for additional 40 min at 10 °C the organic phase was extracted with ether. The extracts were washed with water, with aqueous $NaHCO_3$, and with water and dried (Na_2SO_4). Evaporation of the solvent under reduced pressure afforded a light yellow oil which was triturated with a small amount of hexane–$CHCl_3$ (3: 1) to give 4.5 g (92%) of **1b** as white crystals: mp 61.5—62.0 °C (from hexane–$CHCl_3$); IR (Nujol) 3520, 3460, 1744, 1660, 1529 cm^{-1}; NMR ($CDCl_3$) δ 1.27 (t, J=7.0 Hz, 3H, CH_3), 1.69 (s, 10H), 2.50—3.10 (broad, 2H, HO–N, 1/2H_2O), 3.81 (s, 1H, NH), 4.19 (q, J=7.0 Hz, 2H, CH_2O).

Found: C, 54.62; H, 6.89%. Calcd for $C_{12}H_{17}NO_5 \cdot 1/2H_2O$: C, 54.54; H, 6.86%.

*Ethyl γ,γ-Pentamethylene-α-aminoaconate (**2c**).* To a stirred solution of **1b** (96.0 mg, 0.36 mmol) in anhydrous pyridine (0.5 ml) *p*-toluenesulfonyl chloride (140 mg, 0.73 mmol) was added portionwise for 30 min. The mixture was stirred for additional 1 h at 0—5 °C under nitrogen and for 2 days at room temperature. After cooling in an ice bath the mixture was poured into 10% HCl and adjusted to pH 7 and extracted with ether. The extracts were washed with aqueous $NaHCO_3$ and with water, dried (Na_2SO_4), and concentrated. The residual oil was chromatographed over silica gel. The first comming elution from the column with CH_2Cl_2(*ca.* 5 ml) gave 10.5 mg (7.1%) of an oil. Upon standing for several days, the oily material bigan to crystallize to give white crystals **11b**, mp 115.0—116.0 °C (from hexane–benzene); IR (Nujol) 1792 (lactone C=O), 1759, 1635, 1596 cm^{-1}; NMR ($CDCl_3$) δ 1.36 (t, J=7.0 Hz, 3H, CH_3), 0.70—2.20 (m, 11H), 2.46 (s, 3H, CH_3C=C), 4.35 (q, J=7.0 Hz, 2H, CH_2O), 7.34 (d, J=8.0 Hz, 2H, HC=C), 7.89 (d, J=8.0 Hz, 2H, HC=C). Found: C, 55.58; H, 5.49%. Calcd for $C_{19}H_{23}NO_7S$: C, 55.74; H, 5.66%.

The second elution with CH_2Cl_2 (*ca.* 20 ml) gave 54.0 mg (62.1%) of **2c**: mp 139.0—139.5 °C (from hexane–CH_2Cl_2); IR (Nujol) 3410, 3320, 1762, 1692, 1661 cm^{-1}; NMR ($CDCl_3$) δ 1.35 (t, J=7.0 Hz, 3H, CH_3), 1.52—2.52 (m, 10H), 4.28 (q, J=7.0 Hz, 2H, CH_2O), 5.59 (broad s, 2H, NH_2). Found: C, 60.45; H, 6.99%. Calcd for $C_{12}H_{17}NO_4$: C, 60.24; H, 7.16%.

The following elution with CH_2Cl_2–AcOEt (10: 1, *ca.* 10 ml) gave 3.0 mg (1.6%) of an amorphous, glassy solid: IR (neat) 3450—2700, 1775, 1731, 1650, 1590, 1563, 1497 cm^{-1}; NMR ($CDCl_3$) δ 1.26 (t, J=7.0 Hz, 3H, CH_3), 1.00—2.50 (m, 10H), 2.40 (s, 3H, CH_3C=C), 4.30 (q, J=7.0 Hz, 2H, CH_2O), 5.50 (broad, 1H, NH), 7.00—7.46 (m, 5H, HC=C), 7.95 (d, J=8.0 Hz, 2H), 8.46 (d, J=6.0 Hz, 2H). Difficulty was encountered in obtaining a pure sample for elemental analysis by recrystallization.

In the similar manner, ethyl γ,γ-dimethyl-α-aminoaconate (**2a**) was obtained in 89.5% yield, mp 120.0 °C (lit,[10] mp 120.0 °C).

*Ethyl γ,γ-Pentamethylene-α-acetylaminoaconate (**2d**).* A mixture of **2c** (126 mg, 0.527 mmol), Ac_2O(1.0 ml) and anhydrous *p*-toluenesulfonic acid (9.0 mg, 0.05 mmol) was stirred for 18 h under nitrogen at room temperature. Upon cooling with an ice-bath the mixture was poured into water and the aqueous solution was adjusted to weak alkaline solution by addition of solid $NaHCO_3$ (1.0 g) and then extracted with ether. The extracts were washed with water, dried (Na_2SO_4) and concentrated. The residue was chromatographed over silica gel using CH_2Cl_2, giving 147.0 mg (99.2%) of **2d**: mp 118.0—119.0 °C (from hexane–CH_2Cl_2), IR (Nujol) 3310 (NH), 1746, 1725, 1668 cm^{-1}; NMR ($CDCl_3$) δ 1.33 (t, J=7.0 Hz, 3H, CH_3), 1.49—2.01 (m, 10H), 2.19 (s, 3H, CH_3CO), 4.33 (q, J=7.0 Hz, 2H, CH_2O), 8.04 (broad, 1H, NH). Found: C, 59.85; H, 6.88%. Calcd for $C_{14}H_{19}NO_5$: C, 59.78; H, 6.81%.

In the similar manner, ethyl γ,γ-dimethyl-α-acetylaminoaconate (**2b**) was obtained in 93.5% yield: mp 115.5—116.5 °C (from hexane–benzene); IR (Nujol) 3320 (NH), 1755, 1724, 1678 cm^{-1}; NMR ($CDCl_3$) δ 1.34 (t, J=7.2 Hz, 3H, CH_3), 1.65 (s, 6H, *gem* CH_3), 2.22 (s, 3H, CH_3CO), 4.37 (q, J=7.2 Hz, CH_2O), 8.18 (broad, 1H, NH). Found: C, 54.90; H, 6.30%. Calcd for $C_{11}H_{15}NO_5$: C, 54.77; H, 6.27%.

*γ,γ-Pentamethylene-β-ethoxycarbonyl-α-acetylamino-γ-butyrolactones (**4a** and **4b**).* Hydrogenation of **2d** (102 mg, 0.36 mmol) was carried out in ethanol (1 ml) containing one drop of AcOH in the presence of platinum oxide (25 mg) for 43 h until 8 ml of hydrogen gas was absorbed. The catalyst was filtered off and washed with ethanol. The filtrate was concentrated under reduced pressure to give 106 mg of a light yellow oil, which was chromatographed over silica gel. Elution of the column with 10—30 ml of benzene–AcOEt (3: 2) gave 79.6 mg (77.5%) of **4b** (*cis*); mp 116.5—117.0 °C (from hexane–CH_2Cl_2): IR (Nujol) 3250 (NH), 3050, 1780, 1736, 1643 cm^{-1}; NMR ($CDCl_3$) δ 1.28 (t, J=7.5 Hz, 3H, CH_3), 1.40—1.95 (m, 10H), 2.03 (s, 3H, CH_3CO), 3.46 (d, J=7.5 Hz, 1H, H_β), 4.23 (q, J=7.0 Hz, 2H, CH_2O), 5.25 (q, J=7.5 Hz, J=7.0 Hz, 1H, H_α), 6.65 (d, J=7.0 Hz, 1H, NH). Found: C, 59.31; H, 7.38%. Calcd for $C_{14}H_{21}NO_5$: C, 59.35; H, 7.47%.

Following elution of the column with 30—40 ml of benzene–AcOEt (3: 2) gave 22.8 mg (22.2%) of **4a** (*trans*): mp 147.5—148.0 °C (from hexane–CH_2Cl_2); IR (Nujol) 3280 (NH), 3080, 1783, 1732, 1658 cm^{-1}; NMR ($CDCl_3$) δ 1.31 (t, J=7.0 Hz, 3H, CH_3), 1.40—1.95 (m, 10H), 2.01 (s, 3H, CH_3CO), 3.50 (d, J=10.5 Hz, 1H, H_β), 4.22 (q, J=7.0 Hz, 2H, CH_2-O); 4.76 (q, J=10.5 Hz, J=7.0 Hz, 1H, H_α), 6.86 (d, J=7.0 Hz, 1H, NH). Found: C, 59.07; H, 7.50%. Calcd for $C_{14}H_{21}NO_5$: C, 59.35; H, 7.47%.

In the similar manner, γ,γ-dimethyl-β-ethoxycarbonyl-α-acetylamino-γ-butyrolactones (**3a** and **3b**) were obtained in quantitative yield. Analytical samples of **3a** and **3b** were obtained by preparative glpc (3a/3b: 1/1.1; Column SE-30, 3 m×4 mm, carrier gas H_2 27 ml/min at 160 °C). **3a** (*trans*, glpc retention time 3.2 min): IR (neat) 3290 (NH), 1790, 1738, 1661 cm^{-1}; NMR ($CDCl_3$) δ 1.32 (t, J=7.1 Hz, 3H, CH_3), 1.33 (s, 6H, *gem* CH_3), 2.05 (s, CH_3CO), 3.65 (d, J=11.1 Hz, 1H, H_β), 4.25 (q, J=7.1 Hz, 2H, CH_2O), 4.73 (q, J=11.1 Hz, 1H, H_α), 6.74 (d, J=6.8 Hz, 1H, NH). Found: C, 54.33; H, 6.98%. Calcd for $C_{11}H_{17}NO_5$: C, 54.31; H, 7.04%.

The compound **3b** (*cis*, glpc retention time 9.0 min): IR (neat) 3310 (NH), 1797, 1736, 1668 cm^{-1}; NMR ($CDCl_3$) δ 1.32 (t, J=7.1 Hz, 3H, CH_3), 1.49, 1.59 (each s, 6H, *gem* CH_3), 3.43 (d, J=7.5 Hz, 1H, H_β), 4.22 (q, J=7.1 Hz, 2H, CH_2O), 5.29 (t, J=7.5 Hz, 1H, H_α), 6.33 (d, J=7.5 Hz, 1H, NH). Found: C, 54.34; H, 7.14%. Calcd for $C_{11}H_{17}NO_5$: C, 54.31; H, 7.04%.

Ethyl γ,γ-Pentamethylene-α-hydroxyaconate (5a). A mixture of **1b** (1.0 g, 3.78 mmol) in concd HCl (25 ml) was allowed to stand for 7 days at room temperature. The precipitate was collected by filtration. The precipitate was taken up in CH_2Cl_2 and the solution was washed with water, dried (Na_2SO_4), and concentrated to give 607 mg (66.8%) of **5a**: mp 118.0—119.0 °C (from hexane–CH_2Cl_2) (lit.[16] mp 119.0—119.5 °C); IR (Nujol) 3235 (OH), 1753, 1713, 1660 cm^{-1}; NMR ($CDCl_3$) δ 1.39 (t, J=7.0 Hz, 3H, CH_3), 1.52—2.36 (m, 10H), 4.35 (q, J=7.0 Hz, 2H, CH_2O), 8.84 (broad s, 1H, OH).

The filtrate was concentrated and extracted with ether. The extracts were washed with water, dried (Na_2SO_4), and concentrated to give 188 mg of an oily material, which was triturated with hexane–CH_2Cl_2 (3: 1) to give 29 mg (3.6%) of **5c**: mp 119.0—119.5 °C (decomp.); IR (Nujol) 3450—2100 (COOH), 1762, 1705, 1680, 1630 cm^{-1}. During recrystallization partial decarboxylation of **5c** was encountered. Thus, the crude acid **5c** (10.0 mg, 0.047 mmol) was treated with excess amount of diazomethane in ether for 30 min at 0—5 °C and then the solvent was evaporated. The residue was chromatographed over silica gel using CH_2Cl_2, which eluted 10.8 mg (95.4%) of **5d**: mp 64.5—65.0 °C (from hexane–CH_2Cl_2); IR (Nujol) 1755, 1698, 1642 cm^{-1}; NMR (CCl_4) δ 1.00—2.70 (m, 10H), 3.79 (s, 3H, CH_3O), 4.19 (s, 3H, CH_3O). Found: C, 60.08; H, 6.66%. Calcd for $C_{12}H_{16}O_5$: C, 59.99; H, 6.71%.

From the residual filtrate 60 mg (6.6%) of **5a** was recovered along with 74 mg (7.4%) of **1b**.

Ethyl γ,γ-Pentamethylene-α-methoxyaconate (5b). The α-hydroxyaconate **5a** (100 mg, 0.42 mmol) was treated with an excess amount of diazomethane in ether for 30 min at 0—5 °C and then the solvent was evaporated. The residue was chromatographed over silica gel using hexane–CH_2Cl_2 (1: 1), which eluted 100 mg (94.5%) of **5b**: mp 84.5—85.0 °C (from hexane–CH_2Cl_2); IR (Nujol) 1763, 1700, 1646 cm^{-1}; NMR (CCl_4) δ 1.32 (t, J=7.0 Hz, 3H, CH_3), 1.48—2.40 (m, 10H), 4.12 (s, 3H, CH_3O), 4.18 (q, J=7.0 Hz, 2H, CH_2O). Found: C, 61.38; H, 7.08%. Calcd for $C_{13}H_{18}O_5$: C, 61.41; H, 7.14%.

4,4-Pentemethylene-3-ethoxycarbonyl-2-ammonio-2-butenolide Acetate (6). A mixture of **5a** (100 mg, 0.416 mmol) and $AcONH_4$ (32.0 mg, 0.416 mmol) was allowed to stand at 110—120 °C under nitrogen for 6 h, and then the resulting white solid was sublimed at 110—120 °C to afford 101 mg (81.1%) of **6**: IR (Nujol) 3220 (NH), 1756, 1682, 1568 (COO^-) cm^{-1}; NMR ($CDCl_3$) δ 1.40 (t, J=7.0 Hz, 3H, CH_3), 1.56—2.10 (m, 10H). 2.15 (s, 3H, CH_3CO), 4.40 (q, J=7.0 Hz, 2H, CH_2O), 6.30—8.00 (broad, 3H, NH_3^+). Found: C, 56.21; H, 7.13%. Calcd for $C_{14}H_{21}NO_6$: C, 56.18; H, 7.07%.

Hydrolysis of 5a. A solution of **5a** (510 mg, 2.12 mmol) in EtOH (4 ml) and concd HCl (12 ml) was stirred for 20 h at 90 °C. The mixture was cooled and filtered with suction. The filtrate was concentrated and extracted with ether. The extracts were washed with aqueous $NaHCO_3$ and water and dried (Na_2SO_4). Removal of the solvent gave 284 mg (79.6%) of **7a**: mp 132.5—133.5 °C (from hexane–CH_2Cl_2)(lit.[16] 136—137 °C); IR (Nujol) 3185 (OH), 1748, 1644 cm^{-1}; NMR ($CDCl_3$) δ 1.64 (broad s, 10H), 5.51—6.81 (broad s, 1H, OH), 6.24 (s, 1H, H_β).

The alkaline solution was acidified to pH 3 with 10% HCl and extracted with ether. After usual work-up, there was obtained 38.0 mg (8.4%) of **5c**: mp 119.0—119.5 °C.

γ,γ-Pentamethylene-α-methoxybutenolide (7b). The α-hydroxybutenolide **7a** (20.0 mg, 0.119 mmol) was treated with an excess amount of diazomethane in ether at 0—5 °C for 30 min. After work-up as an usual manner, there was obtained 21.0 mg (96.8%) of **7b**: mp 73.0—73.5 °C (from hexane–CH_2Cl_2); IR (Nujol) 1770, 1690, 1655 cm^{-1}; NMR (CCl_4) δ 1.64 (s, 10H), 3.29 (s, 3H, CH_3O), 6.15 (s, 1H, H_β). Found: C, 65.73; H, 7.83%. Calcd for $C_{10}H_{14}O_3$: C, 65.92; H, 7.74%.

4,4-Pentamethylene-2-amino-2-butenolide (8a) and its dimer (10). *Procedure A*: A mixture of **7a** (84.1 mg, 0.50 mmol) and $AcONH_4$ (436 mg, 5.65 mmol) was heated for 30 min at 104 °C under nitrogen. The mixture was taken up in $CHCl_3$ and the $CHCl_3$ solution was washed with aqueous $NaHCO_3$, and with water, and dried (Na_2SO_4). Removal of the solvent gave 80 mg of **8a** as a solid. Purification was achieved by chromatography over silica gel using hexane–CH_2Cl_2 to give 77.0 mg (92.1%) of **8a**: mp 139.0—139.5 °C (from hexane–CH_2Cl_2); IR (Nujol) 3420, 3320 (NH), 1740, 1670, 1608 cm^{-1}; NMR ($CDCl_3$) δ 1.62 (s, 10H), 3.75 (broad, 2H, NH), 6.01 (s, 1H, H_β). Found: C, 64.54; H, 7.95%. Calcd for $C_9H_{13}NO_2$: C, 64.65; H, 7.84%.

Procedure B: A mixture of **7a** (172 mg, 1.02 mmol) and $AcONH_4$ (598 mg, 7.76 mmol) was heated to 100 °C for 30 min under nitrogen. After work-up as described above, there was obtained 126 mg (73.7%) of **8a**; mp 139.0—139.5 °C, 12 mg (7.4%) of **10**; mp 187.5—188.5 °C (from hexane–CH_2Cl_2), and 12 mg (7.0%) of the starting material **7a**.

The spectral data together with the result of elemental analysis of **10** are as follows: IR (Nujol) 3380 (NH), 3100, 1770, 1745, 1665 cm^{-1}; NMR ($CDCl_3$) δ 1.70 (s, 20H), 6.19 (s, 2H, H_β), 6.63 (broad s, 1H, NH). Found: C, 68.21; H, 7.30%. Calcd for $C_{18}H_{23}NO_4$: C, 68.12; H, 7.30%.

4,4-Pentamethylene-2-acetylamino-2-butenolide (8b). A mixture of **8a** (25.0 mg, 0.15 mmol), Ac_2O (0.5 ml), and *p*-toluenesulfonic acid (2.5 mg, 0.015 mmol) was stirred under nitrogen for 13 h at room temperature. After work-up as an usual manner, there was obtained 30 mg (95.9%) of **8b**: mp 136.0—137.0 °C (from hexane–CH_2Cl_2); IR (Nujol) 3310 (NH), 1770, 1740, 1693, 1655 cm^{-1}; NMR ($CDCl_3$) δ 1.69 (s, 10H), 2.21 (s, 3H, CH_3CO), 7.53 (s, 1H, H_β), 8.09 (broad s, 1H, NH). Found: C, 63.32; H, 7.19%. Calcd for $C_{11}H_{15}NO_3$: C, 63.14; H, 7.23%.

γ,γ-Pentamethylene-α-acetylamino-γ-butyrolactone (9). Hydrogenation of **8b** (25.0 mg, 0.12 mmol) was carried out in EtOH (0.5 ml) containing AcOH (0.01 ml) in the presence of platinum oxide (5.0 mg) for 38 h at room temperature until 3 ml of hydrogen gas was absorbed. The catalyst was filtered off and washed with EtOH. The combined filtrates were concentrated. The residual oil (31 mg) was cooled at 0—5 °C and triturated with ether to give 24.0 mg (95.0%) of **9** as a white crystal: mp 134.5—135.0 °C (from hexane–CH_2Cl_2); IR (Nujol) 3280 (NH), 3090, 1775, 1655 cm^{-1}; NMR ($CDCl_3$) δ 1.30—1.90 (broad s, 10H), 2.03 (s, 3H, CH_3CO), 2.24 (m, 2H, H_β), 4.80 (m, 1H, H_α), 6.89 (d, J=7.0 Hz, 1H, NH). Found: C, 62.60; H, 8.11%. Calcd. for $C_{11}H_{17}NO_3$: C, 62.54; H, 8.11%.

Reaction of 1b with p-Toluenesulfonyl Chloride–Butyllithium. To a THF solution (1.0 ml) of **1b** (66.2 mg, 0.25 mmol) 1.1 M butyllithium in ether (0.25 ml, 0.275 mmol) was added at −78 °C under nitrogen. After stirring for 30 min at −78 °C *p*-toluenesulfonyl chloride (50.0 mg, 0.26 mmol) was added. The mixture was allowed to warm slowly to room temperature during 2 h and stirring was continued for additional 3 h. The mixture was poured into 1.0 ml of ice-cooled diluted HCl and extracted with $CHCl_3$. The extracts were washed with water, dried (Na_2SO_4), and concentrated. The residue was chromatographed over silica gel. Elution of the column with benzene (2—3 ml) gave 27.1 mg (26.4%) of **11b**. Following elution with benzene–AcOEt (30: 1, 10 ml) gave 41.2 mg (68.7%) of **2c**. The structure of both **11b** and **2c** were identified spectroscopically in comparison with authentic samples.

Reaction of 11b with Pyridine. A solution of **11b** (10.0 mg, 0.024 mmol) in pyridine (0.5 ml) was heated to 110 °C in

a sealed tube for 15 h. The mixture was concentrated *in vacuo* and the residue was chromatographed over silica gel using benzene to give 4.7 mg (80%) of **2c**. IR and NMR spectra were identical with those of authentic sample.

Alternative Procedure: A solution of **11b** (13.5 mg, 0.033 mmol) in pyridine (0.5 ml) was stirred at room temperature under nitrogen for 2 days. The mixture was worked up in the same manner as described above to give 3.3 mg (41.9%) of **2c** and 6.3 mg (46.7%) of **11b** (recovered).

References

1) For preceding article in the series, see S. Torii and T. Furuta, This Bulletin, **43**, 2544 (1970).

2) (a) H. Plieninger, *Chem. Ber.*, **83**, 268 (1950); (b) Badische Anilin- & Soda-Fabrik, Ger. 812.077, Aug. 27, 1951 (Cl, 12q, 6ol); *Chem. Abstr.*, **47**, P606^{c} (1953); (c) R. Sudo, Y. Akiyama, T. Kato, and M. Ohta, *Nippon Kagaku Zasshi*, **74**, 1009 (1953); Japan 2075, 2076 (1954), Apr. 19; *Chem. Abstr.*, **49**, P14800^{e} (1955); (d) A. C. J. Opfermann, Ger. 922168, Jan. 10, 1955 (Cl. 12q, 6ol); *Chem. Abstr.*, **51**, P17984^{h} (1957); Brit. 734.928, Aug. 10, 1955; *Chem. Abstr.*, **50**, P8717^{c} (1956); (e) T. Sheradsky, Y. Knobler, and M. Frankel, *J. Org. Chem.*, **26**, 1482 (1961) and references cited therein; (f) L. Pichat, G. Madegard, and M. Herbert, *Bull. Soc. Chim. France*, **1961**, 2420.

3) E. Galantay, H. Engel, A. Szabo, and J. Fried, *J. Org. Chem.*, **29**, 3560 (1964) and references cited therein.

4) (a) M. Frankel, Y. Knobler, and T. Sheradsky, *J. Chem. Soc.*, **1959**, 3642; (b) U. Kraatz, W. Hasenbrink, H. Wamhoff, and F. Korte, *Chem. Ber.*, **104**, 2458 (1971).

5) W. Haefliger and T. Petrzilka, *Helv. Chim. Acta*, **49**, 1937 (1966).

6) P. L. Pacini and R. G. Ghirardelli, *J. Org. Chem.*, **31**, 4133 (1966).

7) K. Isono and S. Suzuki, *Tetrahedron Lett.*, **1968**, 1133.

8) (a) H. R. Snyder, J. H. Andreen, G. W. Cannon, and C. F. Peters, *J. Amer. Chem. Soc.*, **64**, 2082 (1942) and references cited therein; (b) E. Galantay, A. Szabo, and J. Fried, *J. Org. Chem.*, **28**, 98 (1963); (c) M. Fedorchuk and F. T. Seminiuk, *J. Pharm. Sci.*, **52**, 733 (1963); *Chem. Abstr.*, **63**, 11350^{a} (1965); (d) Ref. 2c.

9) J. E. Dolfini, J. Schwartz, and F. Weisenborn, *J. Org. Chem.*, **34**, 1582 (1968).

10) S. Torii, S. Endo, H. Oka, and Y. Kariya, This Bulletin, **41**, 2707 (1968).

11) M. Mousseron, R. Richaud, R. Granger, F. Winternitz, G. Combes, E. Canals, L. Souches, M. Cabanes, and P. Froger, *Bull. Soc. Chim. France*, **1946**, 629.

12) S. Torii, T. Okamoto, and S. Kadono, unpublished work.

13) F. Bourelle-Wargnier and B. Gastambide, *Bull. Soc. Chim. France*, **1965**, 1405.

14) J. D. Park, R. L. Settine, B. A. Parkin, Jr., and G. W. Hedrick, *J. Org. Chem.*, **27**, 898 (1962).

15) L. M. Jackman and S. Sternhell, "Applications of Nuclear Magnetic Resonance Spectroscopy in Organic Chemistry," 2nd Ed., Pergamon Press, Oxford (1969), p. 280.

16) (a) G. W. Stacy, J. Wm. Cleary, and M. J. Gortatowski, *J. Org. Chem.*, **22**, 765 (1957); (b) G. W. Stacy, J. Wm. Cleary, and M. J. Gortatowski, *J. Amer. Chem. Soc.*, **79**, 1451 (1957).

Equilibria and Substrate Specificity Studies with Alcohol Dehydrogenases

Charles C. PRICE and Mitsuhiro IWASA*

Department of Chemistry, University of Pennsylvania, Philadelphia, Pennsylvania 19174, U.S.A.

(Received February 10, 1975)

While secondary alcohols and NAD^+, and ketones and NADH react much slowly than the ethanol–acetaldehyde system in the presence of yeast and liver alcohol dehydrogenases, by starting near equilibrium concentrations, it has been shown that expected thermodynamic equilibria are obtained. With liver ADH, cycloalkanols are remarkably reactive, while with yeast ADH those with six or more carbon atoms in the ring are unreactive. Horse liver ADH shows stereospecificity for 2-octanol, but no stereospecificity for 2-butanol. On the other hand, yeast ADH shows the same stereoselectivity for both alcohols. In the presence of yeast ADH, R(−)-isomers of 2-butanol, 2-octanol and 1-methoxy-2-propanol are not reactive, comparing to the big reactivity of $S(+)$-isomers of these alcohols, but $R(-)$-isomer of propylene glycol is also slightly reactive as $S(+)$-isomer. Further, the reactivity of secondary alcohols with NAD^+ in the presence of liver ADH is following, 2-octanol>2-butanol>2-propanol. These results suggest that horse liver ADH is much less sterically hindered at its active site than yeast ADH and that not only the steric factor but also hydrophobic bonding between the end alkyl group of alcohol and the hydrophobic region of enzyme might be another important factor to determine stereospecificity and reactivity of enzyme.

The stereoselective reduction of acetol to $R(-)$-propylene glycol by fermenting yeast was reported many years ago by Levene and Walti.[1] To improve the convenience of workup, we studied the fermenting yeast reduction of acetol benzoate; to our surprise, the product was the benzoate of $S(+)$-propylene glycol.[2]

The pure enzyme, yeast alcohol dehydrogenase (yeast ADH), has been shown to be stereoselective in the interconversion of ethanol and acetaldehyde.[3] It was the purpose of this investigation to determine whether the enzyme was also stereoselective for ketone reduction and, especially, whether this could explain the reversal of the steric sense of reduction for acetol and acetol benzoate. Kaplan and Van Eys[4] have shown that yeast ADH is indeed stereoselective in oxidizing only the $S(+)$-isomers of 2-butanol and 2-octanol. In this case, the isolated enzyme result accords with the observation that fermenting yeast reduced 2-octanone to the $S(+)$-enantiomer.[5] The absolute optical specificity of the yeast enzyme towards 2-alkanols and its unreactivity towards 3-pentanol, 3-hexanol and 3-heptanol were explained by its inability to accept alkyl groups larger than methyl in the unbound positions in a viable ternary complex.[6] Liver ADH, however, has been reported to lack such stereoselectivity.[7]

While Burton and Wilson[8] have established the equilibrium for 2-propanol–acetone ($K_{eq}=7.19\times10^{-9}$) by starting with mixtures containing three of the four

$$NAD^+ + R_2CHOH \overset{YADH}{\rightleftharpoons} NADH + R_2C{=}O + H^+$$

$$K_{eq} = \frac{[NADH][R_2C{=}O][H^+]}{[NAD^+][R_2CHOH]}$$

organic components, there are reports that cyclic ketones and higher homologs of 2-butanone are not reduced by either yeast or liver alcohol dehydrogenases.[9-11]

Preliminary investigations of the propylene glycol–acetol system were therefore initiated from the alcohol oxidation side.[12] In this early work, 2-hydroxypropyl benzoate was found inactive to enzymic oxidation. 1-Methoxy-2-propanol was, however, reactive. Furthermore, it was shown that methoxyacetone was stereoselectively reduced by fermenting yeast to $S(+)$-1-methoxy-2-propanol. The methoxy group thus provides the same reversal sense as does the benzoate group.

While these preliminary studies[12] showed that oxidation of 1,2-propanediol with yeast ADH did proceed, the reactions were much slower than for ethanol oxidation. Furthermore, the reactions stopped in several hours far short of true equilibrium. It has now been shown that this was due to inactivation of the enzyme during the time required for the slow oxidation of glycol derivatives.

By starting with reaction mixture near equilibrium, it has been possible to show that thermodynamic equilibrium is reached. Based on equilibrium constants and optical density changes at 340 nm, the factors determining stereospecificity of enzymes are discussed.

Experimental

Twice-crystallized yeast ADH and β-NAD⁺ were purchased from Sigma Chemical Co. and further purified. Once-crystallized horse liver ADH was purchased from Worthington Biochemicals and purified in the same way as yeast ADH.

Commercial NAD⁺ (grade III) was further purified by DEAE cellulose column chromatography.[13]

S(+)-1,2-Propanediol was prepared either through yeast reduction of acetol benzoate[α]$_D^{30}$=+26.2 °C (C=1, $CHCl_3$), or from $S(+)$-lactic acid by lithium alminum hydride reduction,[14], [α]$_D^{25}$=+29.10 (C=1, $CHCl_3$).

Acetol[15] was converted to $R(-)$-1,2-propanediol, [α]$_D^{25}$=−27.7 (C=1, $CHCl_3$) by yeast fermentation.

S(+)-and R(−)-Octanol, [α]$_D^{25}$=+8.37 and −8.66, respectively (C=5, 95% ethanol), were prepared by Ingersoll's procedure.[16] $S(+)$-2-Butanol was similarly prepared.[16]

Measurement of Equilibrium Constant. Solutions of different composition were prepared by mixing 1.0 ml of variable mol ratio of alcohol to ketone solutions and 1.90 ml of mixed coenzyme solution (NAD^+ and NaDH in tris buffer) in test tubes. A blank was also made up from 1.0 ml of water and

* Present Address: Mitsui Toatsu Chemicals, Inc. 2—5, Kasumigaseki 3-Chome, Chiyoda-Ku, Tokyo 100, Japan.

1.9 ml of the same coenzyme solution.

These solutions were kept standing for an hour in the 25.0 °C constant temperature bath. Preserved horse liver ADH in the frozen state was diluted with phosphate buffer (near 0 °C). This diluted ADH solution (0.1 ml each) was added to each solution at 25 °C.

Just after adding ADH, the optical density of the blank solution was measured at 340 nm. All the solutions were kept standing at 25.0 °C, usually for 4 h, and then the optical density of each solution was measured at 340 nm. At the same time, the pH of the solution was measured. The amount and direction of shift from the initial concentrations was calculated from the difference of optical density of each solutions from that of the blank.

Results and discussion

Equilibrium Constants. A typical example of the experimental data used to calculate equilibrium constant K_{eq} is summarized in Table 1. Values thus obtained are listed in Table 2.

From the equilibrium constants in Table 2, the standard free energy change for the reaction is readily estimated ($\Delta G = -RT \ln K_{eq}$). With the known $\Delta G^0 = 5.22$ kcal/mol for the NAD$^+$–NADH couple,[8] this leads to values for the ketone–alcohol couples listed in Table 2.

In these experiments we measured the amount of alcohol oxidized by NAD$^+$ through increase in absorbance at 340 nm, a λ_{max} for NADH. It has, however, been shown that ketones, especially acetol and methoxyacetone, undergo a base catalyzed reaction with NAD$^+$ producing compounds with a λ_{max} near 340 nm.[17] In Fig. 1, data on the reaction of several ketones with

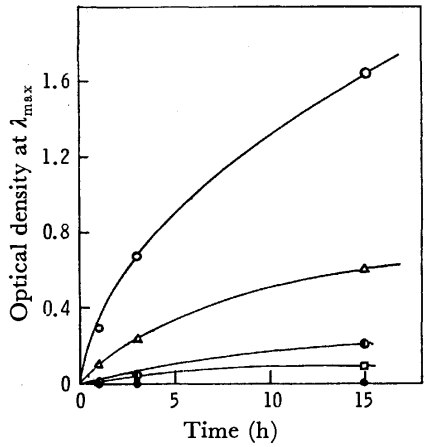

Fig. 1. Rate of reaction of NAD$^+$ and ketones at pH 9; initial concentration of NAD$^+$, 6.2×10^{-4}M; ○ acetol, 1.03×10^{-2} M; △ methoxyacetone, 6.90×10^{-3} M; ◐ cyclohexanone, 6.90×10^{-3} M; □ cyclopentanone, 3.30×10^{-3} M; ● acetone, 6.90×10^{-3} M; Tris buffer, 0.02 M; 25.0°C; no ADH. (No reaction at pH 7.0 under the same conditions.) λ_{max}: 340—345 nm.

Table 1. Experimental data used to estimate K_{ep} for the $S(+)$-2-butanol–2-butanone system with horse liver ADH[a]

[ROH][b]	[ketone]/[ROH]	OD[c]$_{340nm}$	ΔOD	K'[d]
5.56	0.075	1.31	+0.12	
5.22	0.15	1.275	+0.085	5.7×10^{-9} (K'_A)
4.14	0.45	1.16	−0.03	1.4×10^{-8} (K'_B)
3.15	0.90	1.03	−0.16	

a) 25°C, $[NAD^+]_0 = 5.87\times10^{-4}$ M; $[NADH]_0 = 2.09\times10^{-4}$ M; [ADH] $= 1.5\times10^{-7}$ N; Tris chloride buffer, 0.02 M. b) $\times10^{-3}$ M. c) Optical density at 340 nm after 15 h; pH=7.01. d) $K' = [NADH][2\text{-Butanone}][H^+]/[NAD^+][2\text{-Butanol}]$ at 15 h; $K_{eq} = \{K_A + \Delta OD_A\ (K_B - K_A)\}/(\Delta OD_A + \Delta OD_B \cdot p)$ where $p = [Ketone]_B[ROH]_A/[ROH]_B[Ketone]_A$.

Table 2. Summary of equilibrium constants of various alcohol–ketone systems with yeast and horse liver ADH

Alcohol–Ketone System	Catalyst: Yeast ADH	Catalyst: Liver ADH	Average
2-Propanol–acetone	8.6×10^{-9}	8.5×10^{-9}	8.6×10^{-9}
(+)-2-Butanol–butanone	1.2×10^{-8}	9.7×10^{-9}	1.1×10^{-8}
dl-2-Butanol–butanone[a]	(5.1×10^{-9})	(7.1×10^{-9})	—
(+)-2-Octanol–octanone	2.7×10^{-8}	3.1×10^{-8}	2.9×10^{-8}
dl-2-Octanol–octanone[a]	(1.5×10^{-8})	(1.2×10^{-8})	—
(−)-2-Octanol–octanone	N. R.	N. R.	
Cyclopentanol–cyclopentanone	3.5×10^{-8}	3.7×10^{-8}	3.6×10^{-8}
Cyclohexanol–cyclohexanone	N. R.	3.6×10^{-10}	3.6×10^{-10}
dl-1-Methoxy-2-propanol–methoxyacetone	4.7×10^{-11}	1.0×10^{-10}	7.4×10^{-11}
(+)-1,2-Propanediol–acetol[b]	8.9×10^{-11}	9.3×10^{-11}	9.1×10^{-11}
dl-1,2-Propanediol–acetol[a]	7.5×10^{-11}	1.1×10^{-10}	9.3×10^{-11}
(−)-1,2-Propanediol–acetol[b]	7.9×10^{-11}	7.7×10^{-11}	7.8×10^{-11}

a) K_{ap} using total ROH; since only one enantiomer reacts, the values in parentheses are not proper K_{eq}.
b) To obtain the equilibrium data, acetol was used, although the real system may involve lactaldehyde as well.

NAD^+ at pH 9.1 are summarized.

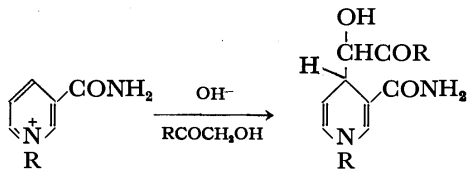

The ΔOD for acetol and methoxyacetone are so great that the values for K_{eq} would be seriously in error at this pH. At pH 7, there was no increase in OD, even for acetol.

NADH is also known to react with acids[18] to lose optical density at 340 nm.

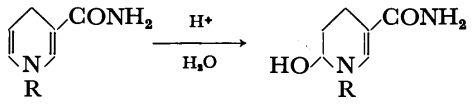

We found that NADH was rapidly destroyed at pH 6 (*ca.* 20—25% in 19 h, 25°C) and even at pH 7, about 6% reacts in 19 h. The presence of either yeast or liver ADH markedly enhances NADH stability, less than 1% disappearing in 19 h at 25°C. We therefore chose pH 7 as the most suitable pH, both for NADH stability to acid and NAD^+ stability to ketone.

Table 3. The standard free energy changes for various alcohol–ketone systems

Alcohol–ketone system	$\Delta G°$ (kcal mol^{-1})	$\Delta G°$ (lit)
2-Propanol–acetone	5.8	5.89(8), 6.0(19)(20)
2-Butanol–2-butanone[a]	5.7	5.7(19), (20)
2-Octanol–2-octanone[a]	5.1	not available
Cyclopentanol–cyclopentanone	5.0	5.7(19)
Cyclohexanol–cyclohexanone	7.7	7.5(19)
1-Methoxy-2-propanol–methoxyacetone	8.7	8.8(19)
1,2-Propanediol–acetol	8.6	not available

a) K_{eq} for $S(+)$-isomers were used to calculate ΔG, since these are reactive isomers.

The equilibrium data in Table 2 and 3 are in reasonably satisfactory agreement with earlier data obtained by chemical equilibration[19,20] and with the YADH equilibration for 2-propanol–acetone.[8] The fact that yeast and liver ADH give values essentially the same is support for the conclusion that the procedure used has given true equilibrium. The catalyst should, of course, contribute only to the rate and, at the low relative concentrations used, should not influence the equilibrium position.

Stereospecificity of Liver and Yeast ADH for 2-Butanol and 2-Octanol. The data in Table 2 support the earlier proposal[4] that yeast ADH is stereoselective for the $S(+)$-isomers of 2-butanol and 2-octanol, since the "apparent" K_{eq} for the racemates is nearly half of K_{eq} for the $S(+)$-isomers. We found, however, that liver ADH shows optical specificity for 2-octanol and even for 2-butanol it seems to show small optical specificity. Stereospecificity of horse liver ADH for 2-octanol was confirmed by the initial rate of oxidation of secondary alcohols, but that for 2-butanol was not clear as shown in Table 4.

Table 4. Initial rate of oxidation reaction of various alcohols with NAD^+ in the presence of horse liver ADH.

Alcohol	ΔOD at 340/min
2-Propanol	0.012
(+)-2-Butanol	0.016
dl-2-Butanol	0.016
(+)-2-Octanol	0.048
dl-2-Octanol	0.024
(−)-2-Octanol	0.004
(+)-1,2-Propanediol	0.024
dl-1,2-Propanediol	0.018
(−)-1,2-Propanediol	0.016
1-Methoxy-2-propanol	0.024

Initial conc.: NAD^+, 6×10^{-3} M; horse liver ADH, 1.5×10^{-7} N; Tris chloride buffer, 0.02 M; 25.0 °C; pH, 7.1—7.3.

Stereospecificity of ADHs for 1-Methoxy-2-propanol and 1,2-Propanediol. Yeast ADH is probably stereoselective for 1-methoxy-2-propanol, because the "apparent" K_{eq} of yeast ADH is just half of that of horse liver ADH.

As for the motivating reason for this investigation, there appears to be no stereoselection between the $S(+)$- and $R(-)$-1,2-propanediol enantiomers in the presence of ADHs and NAD^+.

There is one complication with propylene glycol oxidation in that it can oxidize at either the primary alcohol group to give lactaldehyde or the secondary to give acetol. Huff[21] reports that liver ADH oxidizes 1,2-propanediol preferentially to lactaldehyde while Tjioe[12] detected acetol (as the 2,4-dinitrophenylhydrazone) using yeast ADH. If the two equilibria for the glycol are established independently, then the overall observed K_{eq} should be $K_{10}+K_{20}$. If we assume that the K_{10} is approximately the same as for ethanol (1.2×10^{-11}) and for K_{20} approximately the same as for 1-methoxy-2-propanol (1.0×10^{-10}), the sum (1.1×10^{-10}) is close to the experimental values for propylene glycol.

Propylene glycol shows different character comparing to other examined secondary alcohols on the points that $R(-)$-isomer shows the same low reactivity as the $S(+)$-isomer even in the presence of yeast ADH. This result is surprising in view of the fact that whole yeast cell catalyze the reduction of acetol to only $R(-)$-1,2-propanediol and the reduction of methoxy acetone and acetol benzoate to $S(+)$-isomer of 1-methoxy-2-propanol and 2-hydroxypropyl benzoate, respectively.[2,12,15]

Effect of Ring Size on Substrate Specificity of ADHs for Cyclic Secondary Alcohols. The reactivity of various cyclic alcohols was examined from optical density changes with horse liver ADH and yeast ADH. Table 5 shows the optical density change of cycloalkanols after 3 hours of oxidation reaction. With horse liver ADH, all the cyclic alkanols show big reactivities which is almost independent of ring size. In the presence of yeast ADH, reactivity of cycloalkanol decreases with

Table 5. Effect of ring size of cyclic alcohols on substrate specificity of alcohol dehydrogenase[a)]

Cycloalkanol	Yeast ADH		Horse liver ADH	
	pH 9.0	pH 7.2	pH 9.0	pH 7.2
C_4	2.0	1.5	1.9	1.5
C_5	0.55	0.4	1.9	1.2
C_6	0	0	1.8	0.8
C_8	0	0	1.9	1.8
C_{12}	0	0	0.2	0.1

a) Initial concentration: NAD^+, 2.0×10^{-4} M; Cyclic alcohols 6.0×10^{-3} except cyclododecanol, about 10^{-3} M; Yeast ADH, 8.4×10^{-7} N; Horse liver ADH, 5.2×10^{-7} N; Tris chloride buffer, 0.02 M, 25.0°C; Unit, ΔOD (340 nm) at 3 h.

increasing ring size and when the number of ring carbon becomes more than 6, it becomes completely non-reactive.

These results indicate that the active site of yeast ADH is much more sterically hindered than horse liver ADH.[6)]

Factors to Determine an Optical Specificity of ADHs for Secondary Alcohols. Dalziel and Dickinson[6,7)] explained the lack of stereospecificity of liver ADH for secondary alcohols with the absence of steric hindrance of the binding site of enzyme.

However, we noted that liver ADH also exhibits optical specificity for higher secondary alcohols even though steric hindrance at the active site of liver ADH is estimated to be small. Therefore, another factor should be considered to explain stereospecificity of enzymes in addition to steric hindrance.

Sigman[22)] determined the dissociation constants $K_{e,s}$(=[E][S]/[ES]) for complexes of liver ADH with various primary alcohols by measuring the diminution that complexes cause in the intensity of enzyme-bipyridine spectrum and showed that bigger alkyl groups interact more strongly with lipophilic site of enzyme.

A plot of initial rate (ΔOD/min) of oxidation reaction of various secondary alcohols shown in Table 4 *vs.* $1/K_{e,s}$ of primary alcohols obtained by Sigman shows that initial rate of oxidation reaction increases with the increases of $1/K_{e,s}$ as shown in Fig. 2. Thus, the reactivity of the alcohols is much influenced by the hydrophobic interaction of end-alkyl group of alcohols with enzyme.

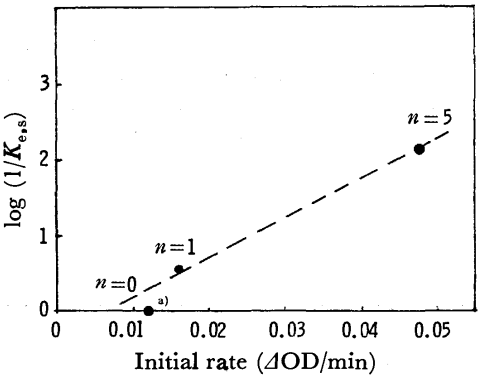

Fig. 2. Plots of the reciprocal of the dissociation constants log ($1/K_{e,s}$) of primary alcohol, $CH_3(CH_2)_n$-OH *vs.* initial rate of oxidation (ΔOD/min) of secondary alcohol, $CH_3(CH_2)_n\rangle CHOH$ (CH_3)

a) $K_{e,s}$ of CH_3OH was estimated to be 1.0 from Sigman's data.[22)]

Stereospecificities of alcohol dehydrogenases for secondary alcohols are summarized in Table 6, which shows a common tendency to three enzymes; $S(+)$-isomers are more reactive in secondary alcohols whose end groups are both normal alkyl or aromatic and $R(-)$-isomers are more reactive or reactive as $S(+)$-isomer in secondary alcohols where one of the end groups is hydroxyl.

If we apply the idea of hydrophobic bonding between substrate and lipophilic site of the enzyme in addition to steric hindrance, we can explain well the optical specificity of the enzymes; thus for 2-butanol, 2-octanol, 1-methoxy-2-propanol and 2-hydroxypropyl benzoate, the C_2H_5–, C_6H_{13}–, CH_3– of $-CH_2OCH_3$ and C_6H_5– of $-CH_2OCOC_6H_5$ group, respectively, binds more strongly with the lipophilic site of the enzyme than does the CH_3-group attached to α-carbon. Hexyl group binds more strongly with lipophilic site of enzyme than ethyl group and this might be a reason why liver ADH shows clear stereospecificity to 2-octanol, in spite it shows small stereospecificity to 2-butanol.

For 1,2-propanediol, the CH_2OH group binds more weakly with the enzyme than CH_3– group attached to α-carbon. As Tsai[23)] observed that the introduction of polar groups such as amino, carbonyl or halogen to primary alcohols renders substrates inactive or inhibitory, generally the introduction of polar groups such as –OH, $-NH_2$, –COOH, $-NO_2$ or halogen to the

Table 6. Reactive optical isomer of various secondary alcohols in the presence of ADHs and that produced from ketone in the presence of yeast cell

Sec. alcohol	Enzyme and Coenzyme		
	Yeast ADH and NAD^+	Horse liver ADH and NAD^+	Yeast cell
2-Butanol	(+)	(+) and (−)	mostly (+)[a)]
2-Octanol	(+)	(+)	no data
1-Methoxy-2-propanol	(+) ?	(+) and (−)	(+)[12)]
1,2-Propanediol	(+) and (−)	(+) and (−)	(−)[15)]
2-Hydroxypropyl benzoate	no data	no data	(+)[2)]

a) According to our experiments, from 20 g of 2-butanone 0.48 g of 2-butanol, which consists of about 80% of (+)-isomer and $[\alpha]_D^{25}=+8.8°$ in 95% ethanol, was obtained in the presence of sugar and yeast cell.

end of one of the alkyl group of secondary alcohol seems $R(-)$-isomer make more reactive or as reactive as $S(+)$-isomer. Although $S(+)$-1,2-propanediol is as reactive as $R(-)$-isomer in the presence of liver ADH, in the presence of yeast cell $S(+)$-isomer losses its reactivity. Further study is necessary to elucidate above difference.

The authors wish to acknowledge Dr. B. Cooperman and Dr. I. Noguchi, Department of Chemistry, University of Pennsylvania, for their advice and contribution to this work.

This work is partly supported by the National Institutes of Health Research Grant in U.S.A.

References

1) P. A. Levene and A. Walti, *J. Biol. Chem.*, **68**, 415 (1926).
2) N. Shieh and C. C. Price, *J. Org. Chem.*, **24**, 1169 (1959).
3) F. A. Loewus, F. H. Westheimer, and B. Vennesland, *J. Amer. Chem. Soc.*, **77**, 3391 (1955).
4) J. Van Eys and N. O. Kaplan, *ibid.*, **79**, 2782 (1957).
5) C. Newberg and F. F. Nord, *Ber.*, **52**, 2237 (1919).
6) F. M. Dickinson and K. Dalziel, *Biochem. J.*, **104**, 165 (1967).
7) F. M. Dickinson and K. Dalziel, *Nature*, **214**, 31 (1967).
8) K. Burton and T. H. Wilson, *Biochem. J.*, **54**, 86 (1953).
9) W. A. Buhler, *Arch. Biochem. Biophys.*, **62**, 173 (1956).
10) A. D. Winer, *Acta Chem. Scand.*, **12**, 1695 (1958).
11) A. D. Merritt and C. M. Tompkins, *J. Biol. Chem.*, **234**, 2778 (1959).
12) G. B. Tjioe, "Rate and Equilibria Studies of Enzymatic Oxidation of Propylene Glycol and 1-Methoxy-2-propanol," Ph. D. Thesis, University of Pennsylvania (1968).
13) A. D. Winer, *J. Biol. Chem.*, **239**, 3598 (1964).
14) C. C. Price, M. K. Akkapeddi, B. T. Debona, and B. C. Furie, *J. Amer. Chem. Soc.*, **94**, 3964 (1972).
15) P. A. Levene and A. J. Walti, *Org. Syn.*, **10**, 1 (1930).
16) A. W. Inersoll, "Organic Reactions," Vol. II, John Wiley & Sons (1944), p. 376.
17) R. M. Burton and N. O. Kaplan, *J. Biol. Chem.*, **206**, 283 (1954) and **211**, 447 (1954).
18) E. Haas, *Biochem. Z.*, **288**, 123 (1936); P. Karrer and F. J. Stare, *Helv. Chim. Acta*, **20**, 418 (1937); P. Karrer and F. W. Kahnt, *ibid.*, **21**, 223 (1938).
19) H. Adkins, R. M. Elofson, A. G. Rossow, and C. C. Robinson, *J. Amer. Chem. Soc.*, **71**, 3672 (1949).
20) R. A. Day, Jr., A. E. Robinson, Jr., J. M. Bellis, and S. B. Till, *ibid.*, **72**, 1379 (1950).
21) E. Huff, *Biochim. Biophys. Acta*, **48**, 506 (1961).
22) D. S. Sigman, *J. Biol. Chem.*, **242**, 3815 (1967).
23) C. S. Tsai, *Can. J. Biol. Chem.*, **46**, 381 (1968).

Studies of the Isomerization of Unsaturated Carboxylic Acids. II.[1] The Thermal Rearrangement of Citraconic Acid to Itaconic Acid in Aqueous Solutions

Mutsuji SAKAI

Department of Textile Chemistry, Faculty of Textile Science, Kyoto University of Industrial Arts and Textile Fibers, Matsugasaki, Sakyo-ku, Kyoto 606

(Received March 22, 1975)

The thermal reaction of citraconic acid (**2**) in water gives a mixture of products similar to that obtained from itaconic acid (**1**) in water. After 22 h at 170 °C, the equilibrium composition about 74%, 18%, and 8% **1**, **2**, and mesaconic acid respectively. At the optimum conditions (170 °C for 3 h), the yield of **1** is 65%. The mechanism of the reaction is discussed.

Itaconic acid (**1**) is a relatively innocuous vinyl monomer and has been used extensively in industry.[2] This important acid has been conveniently prepared from citraconic anhydride.[3] It is interesting that, in this preparative method, terminal olefin **1** is obtained from citraconic acid (**2**) by thermal rearrangement in water;[4] this is in contrast to the general concept that internal olefins are thermodynamically more stable than the corresponding terminal ones. In spite of extensive studies of base-catalyzed rearrangements[5] and isomerizations[5] of unsaturated acids[6-8] and other compounds,[9,10] similar reactions[5] under neutral to acidic conditions have not received much attention.

The present report will describe the results of studies of the factors that govern equilibration between **1** and **2** under neutral to acidic conditions, and a plausible mechanism of the reaction will be proposed. Under the present conditions, **1** is the most abundant component of the three acids, whereas, under basic conditions, mesaconic acid (**3**) predominates over the others. Thus, the equilibrium between **1** and **2** is practically more important than that between **2** and **3**.

Experimental

All the melting and boiling points are uncorrected.

Materials. Commercial-grade itaconic acid (methylenesuccinic acid) (**1**) was purified by recrystallization from water. The following compounds were prepared by the methods described in the literature: citraconic acid (methylmaleic acid)[11] (**2**), mp 90 °C; mesaconic acid (methylfumalic acid)[11] (**3**), mp 204 °C; citramalic acid (2-hydroxy-2-methylbutanedioic acid)[12] (**4**), mp 116 °C, and paraconic acid (3-carboxy-4-butanolide)[13] (**5**), mp 54 °C.

The methyl ester of **5** was isolated by distillation from the reaction mixture obtained under the conditions that give **5** in the highest yield (170 °C, 22 h) and was identified by the aid of NMR and elemental analyses.

The water was distilled prior to use, and the deuterium oxide was 99.8% pure. The organic solvents were purified by ordinary methods. The other reagents were of a reagent grade.

Procedure. *Reactions in Aqueous Solutions*: A mixture of 1.0 g (7.7 mmol) of **2** and 2.0 g (0.11 mol) of water was sealed into a glass tube, which was then heated to an appropriate temperature in an autoclave filled with water. For the analysis, all the acids were converted into the corresponding methyl esters by the following treatment. From the reaction mixture, the water was removed as benzene azeotrope, and the acids in the residue, together with the glutaric acid added as an internal standard of gas chromatography, were esterified with methanol by refluxing for 5 h in the presence of sulfuric acid. After the removal of the methanol, the mixture was neutralized with an aqueous sodium carbonate and the esters were extracted with benzene. For runs under basic conditions, the reaction mixture was neutralized with sulfuric acid before the water was removed from the mixture. The organic acids were extracted from the residue with hot methanol and worked up similarly. The reactions of the other acids in water were carried out similarly.

Reactions in Deuterium Oxide: A mixture of 1.0 g of **1** and 2.2 g of deuterium oxide was heated at 170 °C for 3 h. The compositions of the products were determined from glc, as will be described below. The deuterium content in α-methylene of **1** was calculated from the relative intensities at δ 6.3 ($=CH_2$), 5.8 ($=CH_2$), and 3.3 ($-CH_2-$) in the NMR spectrum (in D_2O).

Analysis. The benzene extracts were analyzed by gas chromatography using a BDS 90m capillary column with Hitachi Perkin-Elmer F6-D at 150 °C. It was confirmed that no rearrangement took place in the course of the esterification and the gas-chromatographic analysis. The NMR spectra were recorded on a Varian T-60A spectrometer.

Results and Discussion

Thermal Reaction of 2 in an Aqueous Solution. Reactions were carried out in the temperature range from 140 °C to 200 °C. No reaction occurred at 100 °C. The gas chromatogram of the reaction mixture revealed that the mixture consisted of five components (**1**—**5**). The main product of the reaction

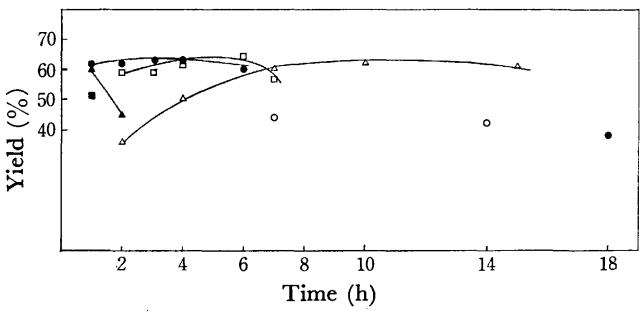

Fig 1. The yield of **1** from the rearrangement of **2** in an aqueous solution.
2, 1.0 g; H_2O, 2.0 g.
○; 140 °C, △; 150 °C, □; 160 °C, ●; 170 °C, ▲; 180 °C, ■; 200 °C.

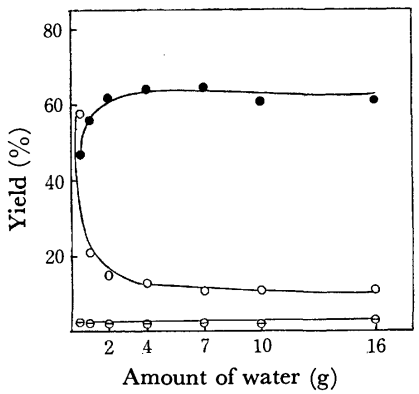

Fig. 2. Effect of the amount of water on the products.
2, 1.0 g; Temp, 170 °C; Time, 3 h.
●; **1**, ○; **2**, ⊖; **3**.

was **1**, and the yield was 65%, as is shown in Figs. 1 and 2. Figure 2 also reveals that the maximum yield of **1** can be achieved when the reaction mixture contains at least twice as much water as **2** in weight. Small amounts of other products (**3**, **4**, and **5**) besides **1** and **2** were formed at higher temperatures or by prolonged heating.

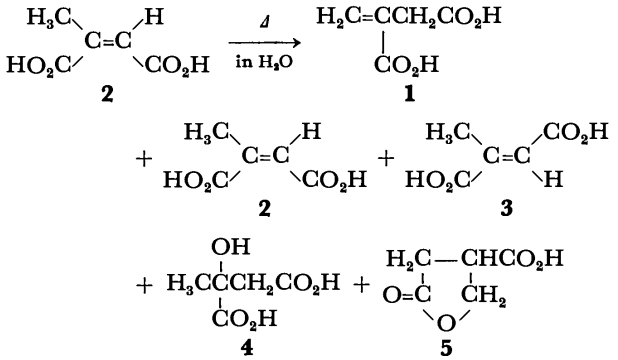

An Equilibrium between the Reaction Products. Reactions starting from **1** and **2** gave mixtures with the same equilibrium composition, whereas those from **3**, **4**, and **5** took place with difficulty and large portions of the starting acids were recovered (Table 1). Table 1 and Fig. 3 show the presence of an equilibrium between **1** and **2**, from which the equilibrium composition at

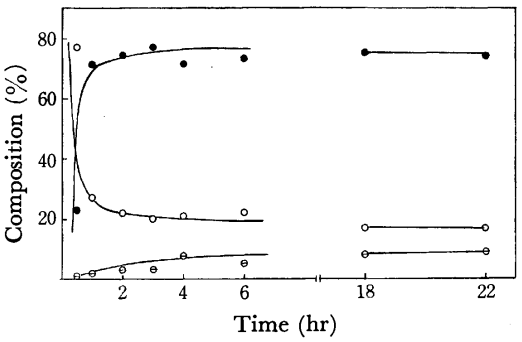

Fig. 3. An equilibrium between **1** and **2**.
2, 1.0 g; H_2O, 2.0 g; Temp, 170 °C.
●; **1**, ○; **2**, ⊖; **3**.

170 °C was calculated to be 74% **1**, 18% **2**, and 8% **3**. Neither aprotic (acetonitrile, acetone, and diglyme) nor protic (isovaleric acid and methanol) organic solvents were effective for the reaction at 170 °C, which implies that water is acting not only as a solvent but also as a reagent.

Since both the formation of **3** from **2** and reactions starting from **3**, **4**, or **5** are too slow to account for the rapid rearrangement between **1** and **2**, the possibility of these acids being intermediates of the reaction can be discarded.

It is quite plausible that the reaction proceeds *via* a protonation-deprotonation process, because the reaction mixture is slightly acidic under the present conditions.

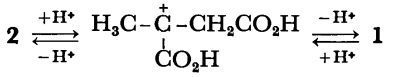

However, this mechanism cannot explain the rapid hydrogen-deuterium exchange that accompanies the rearrangement. The NMR analyses of the recovered **1** showed that 65% of the α-methylene protons were exchanged by deuterium when **1** was heated in deuterium oxide for 3 h at 170 °C, whereas practically no exchange was observed at the terminal methylene group. The exchange did not take place when the mixture was heated at 110 °C for 3 h. When **2** was heated in deuterium oxide at 170 °C for 3 h, no exchange was observed at the methyl protons of the

TABLE 1. THERMAL REACTION OF FIVE ACIDS IN AQUEOUS SOLUTION[a)]

Starting acid	Reaction time, h	Yield, %						Composition, %		
		1	**2**	**3**	**4**	**5**	Total	**1**	**2**	**3**
1	3	62.5	13.8	2.2	3.4	1.1	83.0	79.6	17.6	2.8
2	3	63.4	13.4	2.2	9.1	1.0	89.1	80.2	17.0	2.8
3	3	3.9	0.9	94.0	—	—	98.8	3.9	0.9	95.1
4	3	2.2	1.7	0.4	89.8	—	94.1			
5	3	1.7	0.2	—	0.4	84.7	86.9			
1	22	34.0	8.2	3.7	5.8	21.0	72.6	74.2	17.8	8.0
2	22	33.2	7.6	4.1	11.2	18.6	74.6	74.0	17.0	9.0
3	22	7.8	2.1	62.8	2.0	2.5	83.4	10.7	2.9	86.4
4	22	6.6	1.9	1.5	84.3	1.0	94.3	65.7	19.4	14.7
5	22	11.7	2.3	0.6	1.3	53.8	69.8	80.0	16.0	4.0
1[b)]	3							91.5	5.8	2.6
2[b)]	3							66.1	33.0	0.9

a) Acid, 1.0 g; H_2O, 2.0 g; Temp, 170 °C. b) Reaction in D_2O; composition from glc analysis.

Table 2. Effect of additives on the reaction[a)]

Starting acid	Additive (mg)	Reaction time, h	Yield, %						Composition, %		
			1	2	3	4	5	Total	1	2	3
1	None	4	65.3	14.2	1.2	1.0	1.1	82.7	81.8	17.6	1.4
2	None	4	62.5	14.7	2.6	7.6	1.3	88.7	78.4	18.4	3.3
1	H_2SO_4(0.1)	4	57.8	13.4	0.9	1.6	7.2	80.9	80.2	18.5	1.3
1	H_2SO_4(10)	4	61.4	11.2	0.7	0.9	6.1	80.3	83.8	15.3	0.9
2	H_2SO_4(100)	4	44.2	32.6	2.5	15.3	2.0	96.6	55.7	41.1	3.2
1	H_2SO_4(2000)[b)]	5	51.2	1.3	1.4	—	31.7	85.5	95.0	2.4	2.6
2	H_2SO_4(2000)[b)]	5	1.7	57.0	3.2	26.8	—	88.7	2.7	92.1	5.2
3	H_2SO_4(2000)[b)]	5	0.5	1.2	79.0	1.4	—	82.0	0.6	1.5	97.9
2	NaOH(16)	4	14.9	49.4	3.7	—	—	68.0	21.9	72.7	5.4
1	NaOH(50)	4	49.6	21.4	19.8	—	3.9	94.7	54.7	23.6	21.8
1	NaOH(240)	4	14.5	17.9	53.8	0.8	2.2	89.2	16.8	20.8	62.4
1	NaOH(1500)[c)]	10	20.1	23.2	39.6	3.9	2.6	89.4	24.2	28.0	47.8
2	NaOH(1500)[c)]	10	16.0	17.4	43.2	4.7	4.7	86.0	20.9	22.7	56.0
3	NaOH(1500)[c)]	10	16.6	19.2	48.4	5.5	7.4	97.2	19.7	22.8	57.4

a) Acid, 1.0 g; H_2O, 2.0 g; Temp, 170 °C. b) Refluxed. c) Refluxed with 5.0 g of 30% NaOH solution.

recovered **2**, whereas 85% of the α-methylene protons in **1** produced were exchanged by deuterium. If the intermediate carbonium ion is responsible for the reaction, the terminal methylene-protons must be exchanged by deuterium faster than those in the α-methylene group.

The above observation as well as the effect of additives (*vide infra*) establishes that the reaction involves a carbanion as an intermediate, or that water acts as a general base, in spite of acidic reaction conditions.

The Effect of Additives on the Reaction. The addition of sulfuric acid not only dramatically retards the rearrangement between **1** and **2**, but also changes the product distribution completely (namely, the distribution of **4** and **5**). This fact again disproves the protonation-deprotonation mechanism for the equilibration. On the other hand, the increase in the yields of **4** and **5** (from **2** and **1** respectively) indicates that these products might be produced *via* carbonium ion intermediates. It should be noted that even *cis-trans* interconversion (**2**⇌**3**) does not proceed in the presence of sulfuric acid.

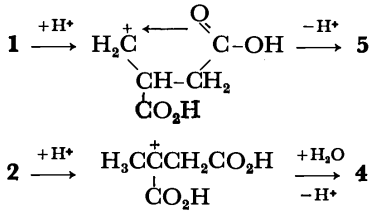

Sodium hydroxide also retards the rearrangement, but increases the yield of the isomerized product, **3**. The dependency of the product composition (at 170 °C, after 4 h) on the amount of sodium hydroxide added is exemplified by the reaction of **2**, shown in Fig. 4. That these are not equilibrium compositions (except for the values at the zero sodium hydroxide concentration) was confirmed by the fact that the yield of **3** predominated over those of other acids at longer reaction times.

The effect of sodium hydroxide can be interpreted as follows. The added base facilitates the dissociation of carboxylic acids to the corresponding carboxylate anions. Since proton abstraction from a carboxylate anion is a more difficult process than that from an undissociated acid, the rearrangement which proceeds *via* a carbanion intermediate takes place with difficulty from a carboxylate anion. Thus, the species[14)] that undergo the rearrangement are undissociated acids in the range of $0 \leqq [NaOH]/[2] < 1$, whereas a slower rearrangement takes place only from monocarboxylate anions of dicarboxylic acids in the range of $1 \leqq [NaOH]/[2] \leqq 2$. As may be seen from Fig. 4, dicarboxylate anions do not undergo the rearrangement without a specific hydroxide ion catalyst, whereas excess sodium hydroxide ($[NaOH]/[2] > 2$) catalyzes the reaction of dicarboxylate anions.

Undissociated *cis*-acid (**2**) might be stabilized by intramolecular hydrogen bonding,[15)] which is expected to be overcome by ion-pair formation when sodium hydroxide is added to this acid.

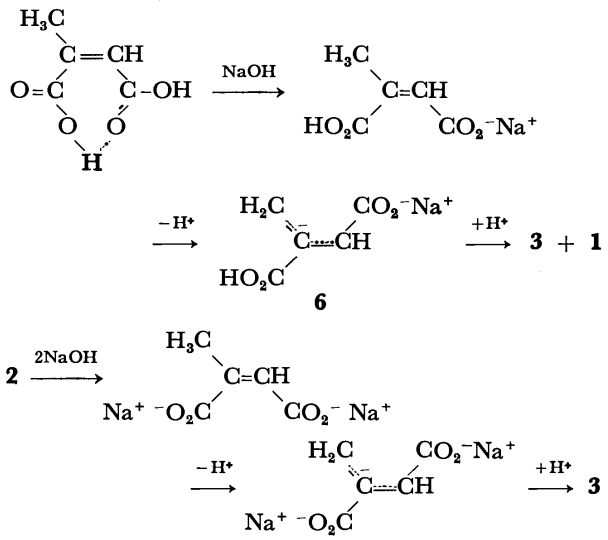

Since **6** no more retains the force to hold the *cis*-configuration, it affords a more stable *trans*-acids rather than **2** when reprotonation takes place. The same is true for **1**.

Although the intramolecular hydrogen bonding in **1** and **2** has not been proved directly, its importance in

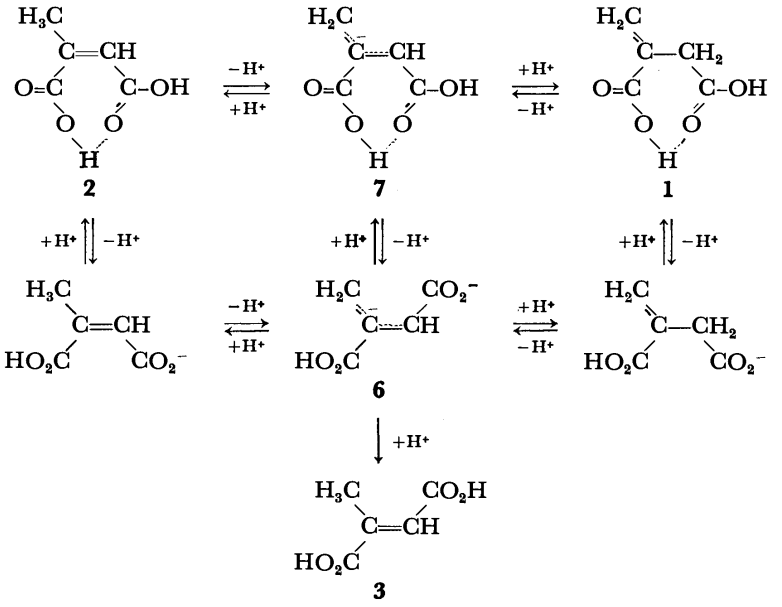

Scheme 1.

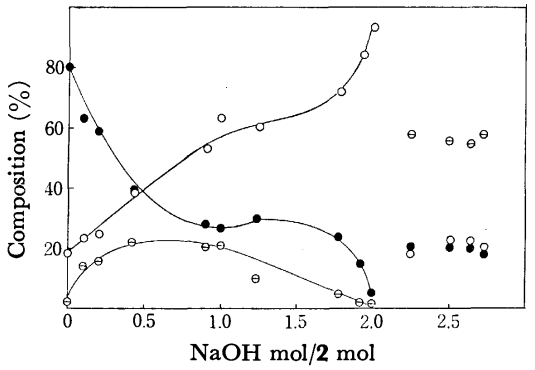

Fig. 4. The effect of sodium hydroxide on the composition.
2, 1.0 g; H_2O, 2.0 g; Temp, 170 °C; Time, 4 h.
●; **1**, ○; **2**, ⊖; **3**.

keeping **3** a minor component under acidic conditions and a major one under basic conditions is supported by the following evidence: the dimethyl ester of **2** isomerized to the *trans*-isomer under neutral conditions,[16] and crotonic acid is the main product in the thermal rearrangement of butenoic acids in an aqueous solution.[17] Thus, the *cis*-configuration is more stable than the *trans*-configuration only for dicarboxylic acids.

All of the present results support the idea that the most plausible mechanism for interconversion between **1**, **2**, and **3** in an aqueous solution is that shown in Scheme 1.

Isotope Effect. When the reaction is carried out in deuterium oxide, the rearrangement from **2** to **1** proceeds as quickly as that in water (protium oxide), whereas that from **1** to **2** is dramatically retarded (Table 1). This result is not accounted for by the solvent-isotope effect, because proton abstractions from **1** and **2** should result in inverse isotope effects and protonation to the intermediate carbanion (**7**) is a process which the two reactions have in common. It should be remembered that **1** undergoes hydrogen-deuterium exchange at the α-methylene group faster than it does the rearrangement under the present conditions, and that the reaction of **1** in deuterium oxide is that of the α-deuterated compound. On the other hand, rather small portions of **2** are deuterated under the same conditions; the intermediate carbanion (**7**) formed from **2** prefers to give the rearranged product, **1**, and only small portions of it return to **2** by deuteration. Thus, the present author believes that the isotope effect observed presently indicates that the rate-determining step of the rearrangement is the process of proton abstraction to form **7**; this is in accord with the discussion in the previous section. The energy diagram may be visualized as is illustrated in Fig. 5.

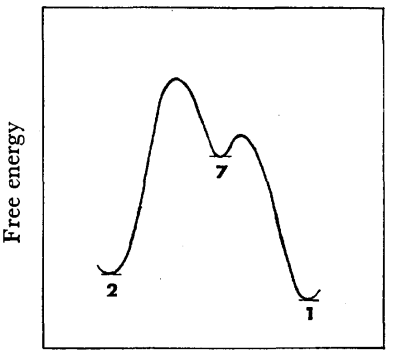

Fig. 5. Schematic energy profile for the rearrangement between **1** and **2**.

Since the reaction is run in a sealed tube at an elevated temperature, the author unfortunately has no device to obtain precise kinetic data to support the mechanism proposed here.

The author wishes to thank Professor Emeritus Sango Kunichika of Kyoto University for his encouragement throughtout this work. He is also grateful to Professors Shinzaburo Oka, Yasumasa Sakakibara, and Atsuyoshi

Ohno for their continuous guidance and helpful discussions.

References

1) Part I of this series: M. Sakai, N. Kawarabayashi, Y. Sakakibara, N. Uchino, and S. Oka, *Nippon Kagaku Kaishi*, **1973**, 1715.

2) B. E. Tate, "High Polymers, Vol. XXIV, Vinyl and Diene Monomers," Part 1, ed. by E. C. Leonard, Wiley-Interscience, New York, N. Y. (1970), p. 205.

3) S. Kunichika, S. Oka, and K. Tanaka, *Bull. Inst. Chem. Research Kyoto Univ.*, **44**, 221 (1966).

4) R. Fittig and A. Landolt, *Ann. Chem.*, **188**, 71 (1877).

5) Rearrangement is defined as the migration of a double bond, whereas isomerization stands for the *cis-trans* interconversion. Reaction means a transformation that includes both rearrangement and isomerization.

6) A. Delisle, *Ann. Chem.*, **269**, 74 (1893).

7) R. Fittig and C. F. Langworthy, *ibid.*, **304**, 145 (1898).

8) R. P. Linstead and J. T. W. Mann, *J. Chem. Soc.*, **1931**, 726.

9) H. Henecka, "Methoden der Organischen Chemie, Allgemeine Chemische Methoden," Teil 2, 4th. ed. by E. Müllar, Georg Thieme Verlag, Stuttgart (1957), p. 48.

10) D. J. Cram, "Foundamentals of Carbanion Chemistry," Academic Press, New York, N. Y. (1965), p. 175.

11) R. L. Shriner, S. G. Ford, and L. J. Roll, "Organic Synthesis," Coll. Vol., II (1943), pp. 140, 368, and 382.

12) H. A. Barker and A. H. Blair, *Biochem. Preps.*, **9**, 25 (1962).

13) R. Fittig and A. Beer, *Ann. Chem.*, **216**, 77 (1882).

14) There are several examples in which the species that exist in smaller amount contribute to the rearrangement. See, for example, J. March, "Advanced Organic Chemistry," McGraw-Hill Book, Co., New York, N. Y. (1968), p. 517.

15) This is true even in aqueous solution because intramolecular hydrogen bonding is stronger than intermolecular one; (a) E. S. Gould, "Mechanism and Structure in Organic Chemistry," Holt, Reinhart and Winston, Inc., New York, N. Y. (1959), p. 211. The acidity of **2** is larger than that of water; (b) $pK_a=2.3$, 6.1 for **2**, H. W. Ashton and J. R. Partington, *Trans. Faraday Soc.*, **30**, 598 (1934); (c) $pK_a=16$ for water, R. P. Bell, "The Proton in Chemistry," Cornell University Press, Ithaca, N. Y. (1959).

16) M. Sakai, unpublished result, which will be submitted elsewhere.

17) M. B. Hocking, *Can. J. Chem.*, **49**, 3807 (1971); *ibid.*, **50**, 1224 (1972).

An External Heavy Atom Effect upon the Photoreaction of *N*-Acetyldiphenylmethyleneamine in Toluene

Shuichiro Asao, Naoki Toshima, and Hidefumi Hirai

Department of Industrial Chemistry, Faculty of Engineering, The University of Tokyo, Bunkyo-ku, Tokyo 113

(Received March 28, 1975)

The photochemical conversion of *N*-acetyldiphenylmethyleneamine (I) in toluene to produce an addition product *N*-(1,1,2-triphenylethyl)acetamide and a hydrogenation product *N*-(diphenylmethyl)acetamide has been found to increase remarkably by displacement of *para*-hydrogen of toluene with a halogen (chlorine or bromine). A number of halogenated solvents, especially brominated solvents such as dibromomethane and bromobenzene, also promoted the photoreaction of the imine I with toluene. The extent of the promotion depends on the kind of a halogen atom of the solvent molecule. The reaction rate was accelerated with the number of halogen atoms of the solvent molecule. The conversion rate increased very remarkably when the concentration of bromobenzene increased from 0 to 1 mol/l. The reaction *via* chemical sensitization by benzophenone, a contaminant in imine I, was shown to be insensitive to the heavy atom solvent. The heavy atom effect can be attributed to an increase in the rate of intersystem crossing from the excited singlet state to the triplet state of the imine I. Imine I in the excited state was confirmed to have a hydrogen abstracting character.

The heavy atom effect in the field of molecular photochemistry is known to be a unique phenomenon for spectroscopists.[1-8] It is thought to arise from the increased spin-orbit coupling due to the interaction of the electronic spin with the nucleus of the heavy atom.[9] This effect cannot be observed in the photochemistry of the carbonyl compound. The asymmetry inherent in a carbonyl group was pointed out to produce a sufficient spin-orbit coupling greatly enhancing the rates of T–S transitions involving the n,π^* excited state. Such transitions were predicted to be hardly susceptible to heavy atom effects.[7,9]

Although there are many spectroscopic investigations on the heavy atom effect, little is known of the actual increase of the photoreaction yield due to it.[10-14]

Irradiation of a toluene solution of *N*-acetyldiphenylmethyleneamine (*N*-acetyldiphenylketimine, I), an *N*-analogue of α,β-unsaturated ketone, gave *N*-(1,1,2-triphenylethyl)acetamide (II) and *N*-(diphenylmethyl)-acetamide (III) in 11 and 4.4% yields, respectively.[15]

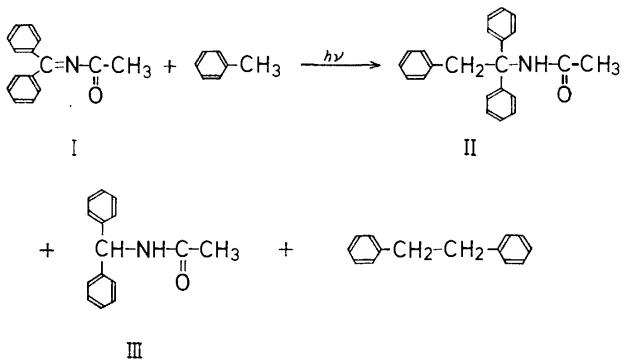

I II

III

This photoreaction was proposed to proceed not only by the "chemical sensitization" mechanism, but also by the mechanism through the excited state of imine I. In the "chemical sensitization" mechanism, the reaction proceeds *via* an α-acetylamino radical formed by hydrogen atom transfer to imine I from a ketyl radical.[16] The benzophenone ketyl radical is photochemically derived from benzophenone present in the starting imine I as an impurity. Almost all the photoreduction of the imino compounds were proposed to be brought about *via* "chemical sensitization",[17] since the imino compound was easily hydrolyzed to the carbonyl compound which has a hydrogen abstracting character in the excited state.[16] However, we showed that[15] imine I in the excited state has a hydrogen abstracting character, from the fact that the relative reactivity of the substituted toluenes to imine I differs from that to benzophenone,[18] and that the products can be given in the absence of benzophenone based on the investigation of the dependence of the reaction yields on the concentration of benzophenone.

We wish to report the noticeable promotion of the photoreaction rate of imine I with toluene by the heavy atom solvent and the results of research on the heavy atom solvent effects.[19]

Results

Photoreaction of N-*Acetylketimine I with* p-*Halotoluene.* On irradiation of the *p*-halotoluene solution of *N*-acetylketimine I in a Pyrex vessel with a high pressure mercury lamp, the adduct, *N*-[1,1-diphenyl-2-(*p*-halophenyl)ethyl]acetamide (IV) and the hydrogenation product, *N*-(diphenylmethyl)acetamide (III) were obtained. *p*-Fluorotoluene, *p*-chlorotoluene, and *p*-bromotoluene were used as *p*-halotoluenes. The results are shown in Table 1 together with those of toluene as a standard.

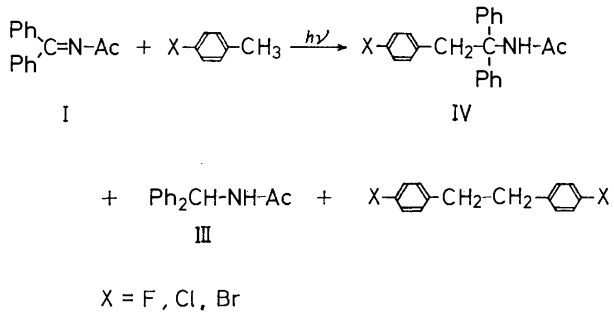

I IV

III

X = F, Cl, Br

The structures of the products were determined from spectroscopic data and elemental analyses (see Experimental).

Table 1. Photoreaction of *N*-acetylketimine I with *p*-halotoluene[a)]

Solvent	Yield (%)[b)]			Relative reactivity	
	Adduct (IV)	Hydrogenation product (III)	Total	I	$^3Ph_2CO$[c)]
Toluene	4.6	1.2	5.8	1.00[d)]	1.00[d)]
p-Fluorotoluene	4.2	1.2	5.4	0.93	1.2
p-Chlorotoluene	11.0	4.0	15.0	2.6	0.97
p-Bromotoluene	20.3	24.5	44.8	7.7	—

a) Irradiation was carried out in benzene (5 ml) solution, of 0.23 mol/l of I with *p*-halotoluene (5 ml) in a Pyrex tube for 50 hr with a high pressure Hg lamp. b) Total yield indicates the conversion of the imine I, in this paper, since the remainder is the starting imine only. See Ref. 20. c) Relative reactivity of alkylbenzenes to the triplet state of benzophenone. See Ref. 18. d) Standard.

The results show that the excited state of I has a quite different photoreactivity from that of benzophenone, *viz.*, in the photoreaction of imine I the total yield increased in the order, *p*-fluoro-<*p*-chloro-<*p*-bromotoluene, *p*-bromotoluene vigorously reacting with I. The extremely high reactivity of *p*-bromotoluene to I suggests the contribution of the so-called heavy atom effect on the photoreaction of I.

Heavy Atom Solvent Effects on the Photoreaction of N-*Acetylketimine I with Toluene.* The effect of the heavy atom solvent was investigated as regards the results of the photoreaction of I with *p*-halotoluene. The results are given in Table 2, with the use of 1 or 5 ml of propyl chloride, chlorobenzene, chloroform, propyl bromide, bromobenzene, or dibromomethane as a halogen-containing solvent in 10 ml of the solution of I (0.23 mol/l). The yields[20)] increased in the presence of halogenated solvents, especially in brominated ones. Propyl chloride and chlorobenzene showed no significant heavy atom effect in a low (1 ml) concentration, but chloroform showed clearly since it contains a larger number of chlorine in the molecule. Increasing the amount of the chlorinated solvent from 1 ml to 5 ml enhanced the effect. The brominated solvents, on the other hand, were remarkably effective. The reaction yields[20)] increased with the bromine content of the solvent molecules in a low (1 ml) concentration, although increasing the amount of the solvent to 5 ml altered the tendency. On irradiation of I in toluene in the presence of ethyl iodide, a deep coloration appeared indicating the depression of the reaction. The yields in the presence of 5 ml of the heavy atom solvent sometimes happened to be lower than those in the presence of 1 ml of the same solvent depending on concentration of toluene (Table 2).

Dependence of the Yield of Photoreaction of N-*Acetylketimine I with Toluene on the Concentration of the Heavy Atom Solvent.* The external heavy atom effect was clarified by the investigation of the relationship between the yield and the concentration of the heavy atom solvent. The photoreaction of I with toluene was carried out using the various concentrations of bromobenzene. The results are shown in Fig. 1. The product yield increased noticeably as the concentration of bromobenzene was increased from 0 to 1.5 mol/l. Further increase in the concentration of the heavy atom solvent, however, resulted in saturation of the increasing yield.

Dependence of the Yield of Photoreaction of N-*Acetylketimine I with Toluene on the Concentration of Benzophenone in the Presence of the Heavy Atom Solvent.* The dependence of the reaction yield upon the concentration of benzophenone was investigated in the presence of bromobenzene. The results are given in Fig. 2 together with those in the absence of bromobenzene.

The amount of benzophenone is the sum of that in the

Table 2. Solvent effect on the yields of the photoreaction of *N*-acetylketimine I with toluene[a)]

Solvent	Volume of solvent added					
	1 ml[b)]			5 ml[c)]		
	Adduct, II (%)	Hydrogenation product, III(%)	Total (%)	Adduct, II (%)	Hydrogenation product, III(%)	Total (%)
Benzene	3.4	0.8	4.2	1.3	0.4	1.7
Acetonitrile	—	—	—	1.4	0.2	1.6
Propyl chloride	3.1	0.7	3.8	2.0	1.4	3.4
Chlorobenzene	3.1	0.7	3.8	3.7	1.9	5.6
Chloroform	5.0	2.0	7.0	6.0	2.2	8.2
Propyl bromide	6.8	3.6	10.4	17.6	5.8	23.4
Bromobenzene	8.3	5.2	13.5	15.5	6.1	21.6
Dibromomethane	13.5	4.3	17.8	14.3	5.5	19.8

a) Irradiation was carried out with 0.23 mol/l of I in a Pyrex tube with the merry-go-round type apparatus for 30 hr. b) One milliliter of the solvent listed and 9 ml of toluene were used. c) Five milliliter of the solvent listed and 5 ml of toluene were used.

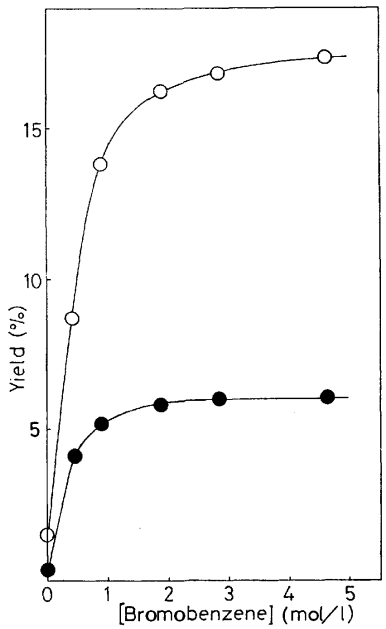

Fig. 1. Dependence of the yields of the photoreaction of *N*-acetylketimine I upon the concentration of bromobenzene in toluene: Adduct (○), hydrogenation product (●); [*N*-Acetylketimine] 0.23 mol/l, [Toluene] 5 ml: Irradiation was carried out above 300 nm for 30 hr at 25 °C.

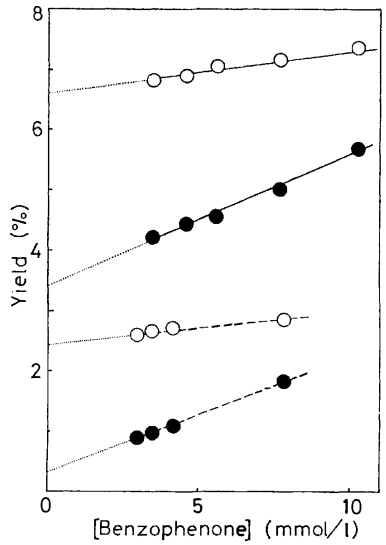

Fig. 2. Dependence of the yields of the photoreaction of *N*-acetylketimine I (0.23 mol/l) with toluene upon the concentration of benzophenone in the presence (—) (Toluene, 9 ml; Bromobenzene, 1 ml), and the absence (---) (Toluene, 10 ml) of bromobenzene: Adduct (○), hydrogenation product (●); irradiation was carried out above 300 nm for 30 hr at 25 °C.

starting imine I as an impurity determined by glpc and that added separately. The yields of both products increased linearly with the concentration of benzophenone, each slope in the presence of bromobenzene being nearly the same as that in its absence, respectively. The full and dashed lines indicate the experimental data and the dotted lines show the extrapolation of the results.

Discussion

The heteroaromatic compound containing a nitrogen atom has been thoroughly investigated both in spectroscopy and in photochemical reactions.[21] The simple acyclic compound containing a C=N bond shows very low photoreactivity,[17,22] and no photoemission.[17] Since the excited state of *N*-acetylketimine I cannot be clarified in spectroscopy, it is difficult to determine its photoreaction mechanism. The sensitization experiment, a procedure for determining the excited triplet state energy indirectly, are not useful for estimating the energy level of the triplet state, since the sensitizers with the hydrogen abstracting character in their excited states can act as the so-called "chemical sensitizer."[17] Sensitization technique is inadequate for determining the triplet state of I, since the sensitizer of a low triplet energy with a hydrogen abstracting character can promote the reaction of I.

Reaction Processes and Heavy Atom Effects. From the results of previous investigation, we proposed a reaction scheme as follows:[15]

Scheme 1.

$$D \xrightarrow{h\nu} {}^3D \quad (1)$$

$${}^3D + RH \xrightarrow{k_a} \cdot DH + \cdot R \quad (2)$$

$$\cdot DH + \cdot R \xrightarrow{k_{cc}} DHR \quad (3)$$

$$2\dot{D}H \xrightarrow{k_D} DH_2 + D \quad (4)$$

$$2\dot{R} \xrightarrow{k_c} R_2 \quad (5)$$

$$B \xrightarrow{h\nu} {}^3B \quad (6)$$

$${}^3B + RH \xrightarrow{k_a'} \cdot BH + \cdot R \quad (7)$$

$$\cdot BH + D \xrightarrow{k_h} \cdot DH + B \quad (8)$$

where D is *N*-acetylketimine I, RH is toluene, B is benzophenone, ·DH is the α-amino radical derived from D by the hydrogen atom abstraction, ·BH is a benzophenone ketyl radical, and DHR and DH_2 are the adduct and the hydrogenation product, respectively.

For a detailed discussion of the external heavy atom effect, the primary processes (Eqs. 1 and 6) should be separated more precisely as shown in Scheme 2.

Scheme 2.

$$D \xrightarrow{h\nu} {}^1D \quad (1a)$$

$${}^1D \xrightarrow{k_{1e}} D \quad (1b)$$

$${}^1D \xrightarrow{k_{1s}} {}^3D \quad (1c)$$

$${}^3D \xrightarrow{k_d} D \quad (1d)$$

$$D \xrightarrow{h\nu'} {}^3D \quad (1e)$$

$$B \xrightarrow{h\nu''} {}^1B \quad (6a)$$

$$ {}^1B \xrightarrow{k_{ic}'} B \quad (6b) $$

$$ {}^1B \xrightarrow{k_{is}'} {}^3B \quad (6c) $$

$$ {}^3B \xrightarrow{k_d'} B \quad (6d) $$

$$ B \xrightarrow{h\nu'''} {}^3B \quad (6e) $$

All possible processes influenced by the heavy atom effect should be considered. They are: (a) an intersystem crossing from the lowest singlet state to the triplet state of the imine I or benzophenone (Eqs. 1c and 6c), (b) a radiative or radiationless decay from the lowest triplet state to the ground state (Eqs. 1d and 6d), (c) light absorption to the triplet state directly from the ground state (Eqs. 1e and 6e), and (d) coupling of two radicals (Eqs. 3 and 5).

A heavy atom promotes the S–T_{π,π^*} transition, but not S–T_{n,π^*} transition.[7,23] In fact, no external heavy atom effect on the yield of the photoreaction of I with toluene was observed on irradiation with light over 390 nm in the presence of benzil. Since light in this region can be absorbed by benzil[24] but not by I or benzophenone, the lowest n,π^* triplet state of benzil not being influenced by the heavy atom effect, the reaction yields were insensitive to the heavy atom solvent. Consequently the processes of Eqs. 6c and 6d (the rate constants of which are k'_{is} and k'_d, respectively) and the transition from the ground singlet state to the excited triplet state of benzophenone (Eq. 6e) should not be susceptible to the heavy atom effect.

The heavy atom effect was negligible for the direct excitation from a ground state to a triplet state of imine I (Eq. 1e), since the toluene solution of imine I under the usual reaction conditions exhibited no S_0–T absorption in the presence of the heavy atom solvent.

A possible process influenced by a heavy atom solvent other than those described above is the hydrogen abstraction step of imine I (Eq. 2). In this process the halo-solvent would act as a polar solvent rather than as a heavy atom solvent. But this is not true since acetonitrile, a polar solvent, exerts no solvent effect (see Table 2). Another possibility is that the halo-solvent decomposes on irradiation to produce radicals which accelerate the photoreaction of I with toluene. In order to exclude this possibility, the heavy atom effect of 1-bromopropane and 2-bromopropane were compared. If the breaking of the C–Br bond occurred on irradiation of bromopropane under the present conditions, the effect of 2-bromopropane would be much larger than that of 1-bromopropane. The experiments indicated a tendency rather contrary to the hypothesis. (Total yield in 1-bromopropane is 5.2% and in 2-bromopropane 3.9% under the same conditions with the use of a merry-go-round type apparatus.)

Consequently, the processes of Eqs. 1c and 1d (k_{is} and k_d, respectively) are noticeably susceptible to the heavy atom solvent.

Comparison of the Two Main Processes Effected by the Heavy Atom Solvent. A heavy atom solvent influences the rate of the processes of Eqs. 1c and 1d. The next problem is whether the rate of the process of Eq. 1c or that of Eq. 1d is much more influenced by a heavy atom solvent. The heavy atom effect on the rate constant k_{is} causes an increase in the product yield, and the effect on the rate constant k_d a decrease in it.

The increasing reactivity of imine I in the heavy atom solvent demonstrates the influence of the heavy atom effect on the increase in the rate of process of Eq. 1c (k_{is}) in the present case. The results of the photoreaction of imine I with toluene in the presence of various amounts of bromobenzene are shown in Fig. 1, which shows a typical saturation curve.[10]

There are two possible mechanisms to explain the saturation in yields when a large amount of bromobenzene is added: One is the balance between the two successive processes, *i.e.*, the intersystem crossing process from the excited singlet state to the triplet state and the deactivation process from the excited triplet state to the ground state. The quantum yield of the intersystem crossing is known to increase greatly in the presence of a small amount of the heavy atom solvent, being effected to a greater extent by the heavy atom solvent than that of the radiative and radiationless decay.[4] However, when a greater amount of a heavy atom solvent is added, the increment of the intersystem crossing quantum yield becomes small, and the rate of the radiative and radiationless deactivation processes begins to increase gradually, the total yield of the photoreaction of imine I with toluene reaching saturation. If an extremely heavy atom solvent is used, the balance would break resulting in a decrease in the product yield.[25] However, this has not yet been reported to occur in the brominated solvent.

As regards the other explanation for the saturation, the total yield of the photoreaction depends only on the quantum yields of the intersystem crossing, which reach the upper limit at a high concentration of a heavy atom solvent, since only a limited number of heavy atoms can exist in the definite surroundings of an imine molecule under these conditions according to the special interaction between imine I and a heavy atom solvent molecule. In this case, it is assumed that the rate of deactivation of the excited triplet to the ground state is not so susceptible to the heavy atom solvent, or the rate of the intersystem crossing is great enough to neglect that of the deactivation process. The assumption is valid since the deactivation process of an imino compound from its excited triplet to the ground state has been proposed to be very rapid.[17] It is impossible in the present stage to determine which of the two views is adequate because of the absence of the means to see the excited state of *N*-acetylketimine I precisely.

Dependence of the Heavy Atom Effect upon the Kind of Halogenated Solvents. A strong evidence for the external heavy atom effect on the present photoreaction is that the photoreaction yield is dependent on the kind of solvent (Table 2). On irradiation of imine I in toluene with 1 ml of a chlorinated solvent, the reaction rate was promoted only by chloroform which contains three chlorine atoms in a molecule, while no promotion of the reaction rate was observed with 1 ml of propyl chloride or chlorobenzene having one chlorine atom in a molecule. However, the presence of 5 ml of each kind of chlorinated solvent in the solution slightly

increased the reaction yield. On the other hand, 1 ml of each kind of brominated solvent in the reaction system drastically promoted the reaction of imine I to the same extent as did 5 ml of the bromo-solvent. The dependence of the yield on the kind of 1 ml of brominated solvent is contrary in the order to that of 5 ml of the solvent. The curious result suggests that the concentration of the bromo-solvent where the saturation of the heavy atom effect occurs is depending on the kind of brominated solvent. Namely, the reaction yield in the presence of 1 ml of dibromomethane could already start to saturated by the same way as shown in Fig. 2 or to decrease from the upper limit by the same way as proposed by Cowan and Koziar.[25]

The effect of a heavy atom solvent on the probability of the transitions in the present photoreaction can be attributed to the indirect mixing mechanism.[8,9,26,27] The singlet state of the solute is mixed electrostatically with the singlet state of the solvent, while the triplet state of the solute is mixed with the triplet state of the solvent. Since the solvent contains a heavy atom, the singlet and triplet states of the solvent are strongly mixed by a spin-orbit interaction. The allowedness of the solvent S–T transition relaxes the spin forbiddenness of the solute S–T transition under consideration.

The probability (P) of the transition has been proposed to be proportional to the square of the spin-orbit coupling parameter (ζ) of the solvent:

$$P \propto \zeta^2$$

Some experimental results were discussed in terms of ζ.[1,4,10] A certain correlation between the photoreaction of N-acetylketimine I and the ζ values of the heavy atom solvent is expected. The total product yields in the presence of 1 ml of the halo-solvent of Table 2 are plotted in Fig. 3 against the square of the ζ value of the various kinds of solvents. The yield and the square of the ζ value roughly show a linear relationship. This clarifies the fact that the solvent in this reaction shows an external heavy atom effect and that the

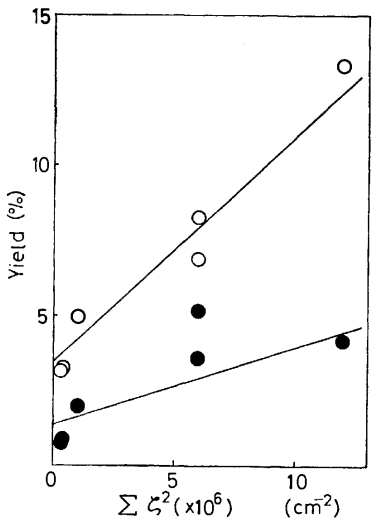

Fig. 3. Dependence of the yields of the photoreaction of N-acetylketimine I with toluene on $\sum$ (ζ^2) values of the heavy atom solvents: Adduct (○), hydrogenation product (●).

mechanism we proposed is in good agreement with the experimental results.

The other explanation proposed for the external heavy atom effect is the charge transfer complexation between the solute and the solvent.[4] The contribution of the charge transfer interaction might be small in our case, since the toluene solution of imine I in dibromomethane showed no absorption in an electronic spectrum. However, the yield in the presence of 1 ml of bromobenzene was larger than in propyl bromide, which result might be due to the acceptor character of the solvents, since no difference is expected in their ζ values. The charge transfer mechanism would be concluded to contribute a little to the photoreaction of imine I.

Relationship between Heavy Atom Effects and Chemical Sensitization. The spectroscopic data from the excited benzophenone was insensitive to the heavy atom solvent.[7] This is in line with the present finding that the effect of benzophenone exhibits no difference in the presence and the absence of a heavy atom solvent in the photoreaction of imine I with toluene. The product yields increase linearly with increasing amount of benzophenone both in benzene and bromobenzene, and the slopes of the line for the adduct and the hydrogenation product yields in the presence of the heavy atom solvent are nearly the same as those without any heavy atom solvent, as shown in Fig. 2. The photoreaction influenced by benzophenone is indifferent to the heavy atom effect. This result is in line with the conclusion that benzophenone can act only as a chemical sensitizer.[15]

The polar effect by the halogenated solvents was not observed in the reaction (Fig. 2), just as the photoreaction of I with toluene in acetonitrile showed no difference from that in benzene (Table 2). This result shows that the reaction *via* chemical sensitization by benzophenone is not influenced by the polar effect. It can be concluded that most parts of the products were produced *via* the excited state of imine I not *via* chemical sensitization in the presence of the heavy atom solvent.

Reaction State of N-*Acetylketimine I.* A point of further interest in connection with the photoreaction of imine I was its reactive state. In the present photoreaction, a high pressure mercury lamp with a Pyrex filter was used for irradiation. Imine I has a π-π^* absorption maximum at 250 nm and tailing with shoulders above 300 nm.[15] It is difficult to say whether the lowest excited singlet state is a π,π^* state or a n,π^*. On the basis of our previous work and the present results of the heavy atom effect,[15] it was confirmed that the reactive state was the excited triplet state of imine I. The observed heavy atom effects on its photochemical behavior support the view that the lowest excited triplet state has a π,π^* character. However, a hydrogen abstracting character may usually belong to the $T_{n,\pi}$ state.[28] Consequently, it could be concluded that $T_{\pi,\pi}$ and $T_{n,\pi}$ states lie closely and are mixed with each other in the case of imine I.

The photoreaction of N-acetylketimine I with toluene was noticeably susceptible to the heavy atom solvent and the yields of the adduct and the hydrogenation product remarkably increases in the presence of the

heavy atom solvent. Though the imino compound has been explained to be not the active hydrogen-abstracting species on irradiation and the photoreduction of the imino compound has been interpreted by a chemical sensitization mechanism, the hydrogen abstracting character of the excited state of imine I is strongly supported by the external heavy atom effect.

Experimental

Materials. Toluene and benzene (Yoneyama Chemical Industry) were dried over sodium by refluxing and distilled. *p*-Fluorotoluene, *p*-chlorotoluene, *p*-bromotoluene, propyl chloride, propyl bromide, and dibromomethane (Tokyo Chemical Industry), and chlorobenzene and bromobenzene (Yoneyama Chemical Inductry) were dried over anhydrous magnesium sulfate and distilled. Benzophenone (Yoneyama Chemical Industry) and benzil (Tokyo Chemical Imdustry) were recrystallized from ethanol. *N*-Acetyldiphenylmethyleneamine (I), bp 168—170 °C/1 mmHg (lit,[29] bp 168—170 °C/1 mmHg), was prepared by the reaction of diphenylmethyleneamine[29] with acetic anhydride and distilled repeatedly.[30]

Instrumentation. Most comparative runs were carried out on a "merry-go-round" type reactor (Riko Kagaku Ltd.) with a turntable device holding ten rotating Pyrex tubes. This turntable also rotates around the irradiation lamp in a water cooled quartz immersion well. The turntable and tubes are held in a constant temperature water bath maintained at 25 °C. Irradiation was carried out with a 500 W high pressure mercury lamp (Eikōsha Ltd.). Glpc analysis was accomplished on an Ohkura Rikagaku gas chromatograph employing a 2 m×3 mmϕ stainless steel column packed with 10% Apiezon Grease L on 60—80 mesh Chromosorb W (HP). High speed liquid chromatography was taken on a Waters ALC-202 high speed liquid chromatograph with a 600 type high pressure pump, a U6K universal injector, and a 660 type solvent programmer. A stainless steel column with Microporasil and chloroform as an eluting solvent were used. Infrared spectra were obtained on a JASCO IR-E spectrometer. NMR spectra were recorded on a JEOL PS-100 or a Hitachi Perkin-Elmer R-20B spectrometer. Mass Spectra were taken on a Hitachi RMS-4 spectrometer. Melting point was determined on a Yanagimoto micro melting point apparatus, and was not corrected.

Photoreaction of N-*Acetylketimine I with* p-*Fluorotoluene.* A *p*-fluorotoluene (30 ml) solution of *N*-acetylketimine I (0.14 mol/l) in a Pyrex tube was degassed in three successive freeze-thaw cycles, and was irradiated under nitrogen with a 500 W high pressure mercury lamp for 100 hr. After irradiation, *p*-fluorotoluene was distilled off at a reduced pressure and the residue were separated by a column chromatography on 100 mesh Marincrodt silica gel. The fraction eluted with benzene contained I. The adduct and the hydrogenation product were eluted separately with chloroform in 4.2 and 1.2% yields, respectively. Yields mean per cent conversion of the starting imine I.[20] The remainder of the imine was recovered in each case. These products were purified by repeated recrystallization from the mixed solvent of cyclohexane and ethanol. The hydrogenation product was identified by comparing the spectral data and by the fact that no melting point depression took place with an authentic sample.[22] The structure of the adduct (mp 197.0—197.7 °C) was inferred from its composition (Found: C, 79.52; H, 6.18; N, 4.49; F, 5.60%; mol wt, 333 by mass spectra. Calcd for $C_{22}H_{20}NOF$: C, 79.23; H, 6.06; N, 4.20; F, 5.70%; mol wt, 333.2.) and the spectral data: The infrared spectra had an amide absorption (ν_{NH}, 3400; ν_{CO}, 1600; δ_{NH} 1530 cm^{-1}) and NMR spectra in $CDCl_3$ showed ten phenyl protons at δ 7.32—6.84, an NH proton at δ 6.15, two methylene protons at δ3.92, and three acetyl protons at δ1.95. The A_2B_2 pattern of four phenyl protons of *p*-fluorobenzyl group splitts into two quartets (δ 6.82, 6.74, 6.60, 6.52; J=8 Hz: δ 6.74, 6.66, 6.54, 6.46; J=8 Hz).

Photoreaction of N-*Acetylketimine I with* p-*Chlorotoluene.* A *p*-chlorotoluene (30 ml) solution of *N*-acetylketimine I (0.14 mol/l) was irradiated under the same conditions as in the photoreaction of imine I with *p*-fluorotoluene, the adduct and the hydrogenation product being obtained in 11.0 and 4.0% yields, respectively. The structure of the adduct was identified as *N*-[1,1-diphenyl-2-(*p*-chlorophenyl)ethyl]acetamide mp 224.0—224.8 °C. Found: C, 75.80; H, 5.57; N, 4.30; Cl, 10.37%; mol wt, 349 by mass spectra. Calcd for $C_{22}H_{20}NOCl$; C, 75.51; H, 5.78; N, 4.00; Cl, 10.14%; mol wt, 349.6. Infrared spectra had an amide absorption (ν_{NH}, 3325; ν_{CO}, 1657; δ_{NH}, 1525 cm^{-1}). NMR spectra showed ten phenyl protons at δ 7.60—6.85, four phenyl protons of A_2B_2 pattern specific for *p*-disubstituted benzene at δ 7.02, 6.96, 6.53, and 6.47 with J=6 Hz, an NH proton at δ 6.10, two methylene protons at δ 3.93, and three methyl protons at δ 1.94.

Photoreaction of N-*Acetylketimine I with* p-*Bromotoluene.* A solution of *N*-acetylketimine I (0.14 mol/l) with *p*-bromotoluene (30 ml) was irradiated under similar conditions to those described before, the adduct and the hydrogenation product being obtained in 20.3 and 24.5% yields, respectively. The adduct was determined as *N*-[1,1-diphenyl-2-(*p*-bromophenyl)ethyl]acetamide: mp 223.0—223.6 °C. Found: C, 67.04; H, 5.12; N, 3.60; Br, 20.24%; mol wt, 394 by mass spectra. Calcd for $C_{22}H_{20}NOBr$: C, 66.99; H, 5.13; N, 3.55; Br, 20.25%; mol wt, 394.1. NMR analysis (in $CDCl_3$) showed ten phenyl protons (δ 7.46—6.78), four phenyl protons of A_2B_2 pattern specific for *p*-disubstituted benzene (δ 7.17, 7.09, 6.52, 6.44; J=8 Hz), an NH proton (δ 6.15), two methylene protons (δ 3.92), and three acetyl protons (δ 1.96), and IR spectra had an amide absorption (ν_{NH}, 3325; ν_{CO}, 1657; δ_{NH}, 1530 cm^{-1}).

Effect of the Solvents and Benzophenone Added. The benzene solution of *N*-acetylketimine I (2.3 mmol) and toluene (5 ml) with or without benzophenone in the presence of a certain amount of heavy atom solvents in a Pyrex tube was degassed in three successive freeze-thaw cycles and irradiated under nitrogen with a 500 W high pressure mercury lamp at 25±1 °C for 30 hr using a merry-go-round type reactor. After irradiation, toluene was distilled off at reduced pressure and the residue was analyzed by a gas chromatography equipped with a 2 m×3 mmϕ column on 10% Apiezon Grease L 60—80 mesh Chromosorb W(HP) or a high speed liquid chromatography on Microporasil using chloroform as an elution solvent. Yields were shown in terms of per cent conversion of the starting imine I. The remainder of the imine was recovered in each case.[20]

Dependence of the Yields of the Photoreaction of N-*Acetylketimine I upon the Concentration of Bromobenzene.* Ten milliliters of benzene solutions containing 0.23 mol/l of *N*-acetylketimine *I*, 5 ml of toluene, and various amounts of bromobenzene (0—4.3 mol/l) were placed in Pyrex tubes, which were then degassed in three freeze-pump-thaw cycles, substituted by nitrogen, and irradiated with 500 W high pressure mercury lamp at 25±1 °C for 30 hr using a merry-go-round type reactor. The reaction mixtures were analyzed by a high speed liquid chromatography employing a stainless steel column with Microporasil using chloroform as an eluting solvent. Results are shown in Fig. 1. Yields are given in terms of per cent conversion of the starting imine I.[20]

References

1) D. S. McClure, *J. Chem. Phys.*, **17**, 905 (1949).

2) M. Kasha, *ibid.*, **20**, 71 (1952). M. R. Padhye, S. P. McGlynn, and M. Kasha, *ibid.*, **24**, 588 (1956).

3) M. Z. Hoffman and G. Porter, *Proc. Roy. Soc., Ser. A*, **268**, 46 (1962).

4) S. P. McGlynn, R. Sunseri, and N. D. Christodouleas, *J. Chem. Phys.*, **37**, 1818 (1962). S. P. McGlynn, M. J. Reynolds, G. W. Daigre, and N. D. Christodouleas, *J. Phys. Chem.*, **66**, 2499 (1962). S. P. McGlynn, T. Azumi, and K. Kasha, *J. Chem. Phys.*, **40**, 507 (1964). S. P. McGlynn, J. Daigre, and F. J. Smith, *ibid.*, **39**, 675 (1963).

5) S. Siegel and H. J. Judeikis, *ibid.*, **42**, 3060 (1965).

6) K. B. Eisenthal and M. A. El-Sayed, *ibid.*, **42**, 794 (1965).

7) R. F. Borkman and D. R. Kearns, *Chem. Commun.*, **1966**, 446. M. S. El-Sayed, *J. Chem. Phys.*, **41**, 2462 (1964). D. R. Kearns and W. A. Case, *J. Amer. Chem. Soc.*, **88**, 5087 (1966).

8) G. G. Gianchino and D. R. Kearns, *J. Chem. Phys.*, **52**, 2964 (1969).

9) M. A. El-Sayed, *Accounts Chem. Res.*, **1**, 8 (1968). S. K. Lower and M. A. El-Sayed, *Chem. Rev.*, **66**, 199 (1966).

10) D. O. Cowan and R. L. Drisco, *Tetrahedron Lett.*, **1967**, 1255; *J. Amer. Chem. Soc.*, **89**, 3068 (1967); **92**, 6281 (1970).

11) G. Fischer, K. A. Muszkat, and E. Fischer, *Isr. J. Chem.*, **6**, 965, (1968). B. F. Plummer and R. A. Hall, *Chem. Commun.*, **1970**, 44.

12) J. Meinwald, G. E. Samuelson, and M. Ikeda, *J. Amer. Chem. Soc.*, **92**, 7604 (1970). J. E. Shields, D. Gavrilovic, and J. Kopecký, *Tetrahedron Lett.*, **1971**, 271. W. Hartmann and H. -G. Heine, *Angew. Chem. Int. Ed. Engl.*, **10**, 272 (1971).

13) B. F. Plummer and D. M. Chiral, *J. Amer. Chem. Soc.*, **93**, 2071 (1971). W. I. Ferree, Jr. and B. F. Plummer, *ibid.*, **95**, 6709 (1973).

14) J. Saltiel, D. W. -L. Chang, and E. D. Megarity, *ibid.*, **96**, 6521 (1974). J. Saltiel, *et al.*, *Org. Photochem.*, **3**, 1 (1973).

15) S. Asao, N. Toshima, and H. Hirai, This Bulletin, **48**, 2068 (1975).

16) B. M. Monroe and S. A. Weiner, *J. Amer. Chem. Soc.*, **91**, 450 (1969). J. G. Pacifici and G. Irick, Jr., *Tetrahedron Lett.*, **1969**, 2207. H. E. Zimmerman and V. J. Hull, *J. Amer. Chem. Soc.*, **92**, 6515 (1970). M. B. Rubin and J. M. Ben-Bassat, *Mol. Photochem.*, **3**, 155 (1971). P. S. Engel and B.M. Monroe, "Advances in Photochemistry," W. A. Noyes, Jr., G. S. Hammond, and J. N. Pitts, Jr., Ed., Wiley-Interscience, New York, 1971, Vol. 8, p. 245.

17) M. Fischer, *Tetrahedron Lett.*, **1966**, 5273; *Chem. Ber.*, **100**, 3599 (1967). A Padwa, W. Bergmark, and D. Pashayan, *J. Amer. Chem. Soc.*, **90**, 4458 (1968); **91**, 2653 (1969). P. Beak and C. R. Payet, *J. Org. Chem.*, **35**, 3281 (1970). A. Padwa and M. Dharan, *Tetrahedron Lett.*, **1972**, 1053.

18) C. Walling and M. J. Gibian, *J. Amer. Chem. Soc.*, **87**, 3361 (1965).

19) Preliminary communication; N. Toshima, S. Asao, and H. Hirai, *Chem. Lett.*, **1975**, 451.

20) The yield indicates the product percentage based on the amount of the reactant imine under the given conditions. The remainder of the reactant can be recovered without change. Thus, the total yield indicates the conversion of the reactant imine I. As the adduct II and the hydrogenation product III are produced selectively from imine I, the product yields increase with irradiation time.

21) For example, F. R. Stermitz, C. C. Wei, and W. H. Huang, *Chem. Commun.*, **1968**, 482. R. M. Kellog, T. J. van Bergen, and H. Wynberg, *Tetrahedron Lett.*, **1969**, 5211. Y. Ogata and K. Takagi, *Tetrahedron*, **27**, 2785 (1971).

22) N. Toshima and H. Hirai, *Tetrahedron Lett.*, **1970**, 433. N. Toshima, H. Hirai, and S. Makishima, *Kogyo Kagaku Zasshi*, **72**, 184 (1969). N. Toshima, S. Asao, K. Takada, and H. Hirai, *Tetrahedron Lett.*, **1970**, 5123. H. Ohta and K. Tokymaru, *ibid.*, **1974**, 2965; *Chem. Lett.*, **1974**, 1403. T. H. Koch and R. M. Rodehorst, *Tetrahedron Lett.*, **1972**, 4039, T. H. Koch, J. A. Olesen, and J. Deniro, *J. Org. Chem.*, **40**, 14 (1975).

23) P. J. Wagner, *J. Chem. Phys.*, **45**, 2335 (1966).

24) Benzil exhibits maximum at 370 nm (ε_{max} 78) with tailing over 390 nm indicating n-π^* absorption. N. J. Leonard and E. R. Blout, *J. Amer. Chem. Soc.*, **72**, 484 (1950).

25) D. O. Cowan and J. C. Koziar, *J. Amer. Chem. Soc.*, **96**, 1229 (1974); **97**, 249 (1975).

26) S. P. McGlynn, T. Azumi, and N. Kinoshita, "The Triplet State," Prentice-Hall, Englewood Cliffs, N. J., 1969.

27) G. W. Robinson and R. Frosch, *J. Chem. Phys.*, **37**, 1962 (1962); **38**, 1187 (1963).

28) Some compounds such as 1-methylcyclopentane and 1,1-diphenylethylene were reported to undergo a hydrogen abstraction reaction *via* π,π^* triplet states, usually their hydrogen abstracting ability being very small. P. J. Kropp, *J. Amer. Chem. Soc.*, **89**, 3650 (1967). H. Rosenberg and P. Servé, *ibid.*, **92** 4746 (1970). A. C. Pratt, *Chem. Commun.*, **1974**, 183. J. M. Hornbanck, *J. Amer.* [*Chem. Soc.*, **96**, 6773 (1974).

29) J. E. Banfield, G. M. Brown, F. D. Davey, D. Davies, and T. H. Ramsay, *Aust. J. Sci. Res.*, **A1**, 330 (1948). W. E. Bachman, *J. Amer. Chem. Soc.*, **55**, 391 (1933).

30) The UV spectrum of *N*-acetyldiphenylmethyleneamine (I) is shown in Ref. 15.

Cation, Solvent, and Substituent Effects on the Optical Spectra of Alkali Metal Salts of Arylthiolate Anions

Tokuji MIYASHITA, Takao AOKI, and Minoru MATSUDA

Chemical Research Institute of Non-aqueous Solutions, Tohoku University, Katahira, Sendai 980

(Received May 19, 1975)

The optical spectra of the alkali metal salts of arylthiolate anions have been studied in the two aprotic solvents, tetrahydrofuran (THF) and dimethylformamide (DMF). In the former solvent the position of the absorption maxima depends on the size of the counter cations, even at low temperatures (−72 to −76 °C); nearly linear relationships were observed between the inverse of the alkali metal radius (r_c) and the wave number of the transition ($\bar{\nu}_{max}$) for both room and low temperatures. The intercepts for the extrapolation of both lines for $1/r_c \to 0$ agree with the $\bar{\nu}_{max}$ of the ion pairs observed in DMF at room temperature, and the absorption maxima for this solvent are independent of the size of the counter cations. Thus, the existence of contact ion pairs in THF over the temperature range investigated and that of the solvent-separated ion pairs in DMF at room temperature were revealed. In the latter solvent, however, a hypsochromic shift was observed on lowering the temperature. The substituent effect of arylthiolate anions and the solvent effect of dimethoxyethane and dioxane on the absorption maxima are also discussed. From an inspection of optical spectral data it has been suggested that negative charge of arylthiolate anions is localized mainly on the sulfur atom.

Since the first suggestion by Weinstein that the equilibrium between contact (or intimate) and solvent-separated ion pairs may be established in solutions of low dielectric constant[1] and the further development of this idea by Grunwald,[2] there have been extensive investigations of ion pairs in solutions.[3] Direct evidence for the existence of two distinct types of ion pairs was first demonstrated by optical spectra on cooling a THF solution of alkali metal salts of fluorenyl anions (carbanions)[4] and, though not simultaneously, by ESR studies of alkali metal naphthalenides (radical anions).[5]

In this paper the cation, solvent, and substituent effects on the optical spectra of alkali metal salts of arylthiolate anions is reported. The optical spectra of ion pairs other than carbanions have been studied with the alkali metal salts of phenols and enols[6] and with tetraalkylammonium iodides,[7] but there is no information about the thiolate anions which have a negative charge on the sulfur atom. The phenylthiolate anion is said to be a stronger nucleophile than the corresponding isoelectronic phenoxide ion,[8] and interesting results have been reported in other reactions of thiolate anions to double and triple bonds and also to carbonyl groups.[9,10] Nucleophilic substitutions with these anions are also interesting; the rate increases in dipolar aprotic solvents (*e.g.*, DMF)[11] and electron transfer from the *n*-butylthiolate anion to oxygen in solutions is accelerated in the order methanol<THF< dimethoxyethane (DME)<DMF and is also affected by counter cations ($Na^+ < K^+ < Rb^+ < Cs^+$).[12] These results can be explained by an increase in reactivity caused by changes in the strength of the thiolate anion-counter cation binding.

Thus, it is interesting to investigate the optical spectra of the solutions of alkali metal salts of arylthiolate anions; the effects of the size of the counter cation, solvent, and of the introduction of substituents at the *para*-position on the absorption spectra give some information about the nature of thiolate anions, *i.e.*, the stronger nucleophilic character of thiolate anions can be revealed by an inspection of spectral data.

Experimental

Diphenyl disulfide, acquired commercially, was recrystallized three times from ethanol. Di-*p*-chlorophenyl-, di-*p*-methylphenyl-, di-*p*-methoxyphenyl-, and di-*p*-*t*-butylphenyl disulfide were synthesized from the oxidation of the corresponding thiols and recrystallized three times from ethanol.

Alkali metal salts of arylthiolate anions were prepared from the reduction of the corresponding symmetric aryl disulfides with an appropriate alkali metal in THF,

$$\text{RS–SR} + \text{alkali metal} \xrightarrow{\text{in THF}} \text{RS}^-, \text{M}^+ + \text{RS}\cdot$$

$$\text{RS}\cdot + \text{alkali metal} \longrightarrow \text{RS}^-, \text{M}^+$$

$$\text{RS}\cdot + \text{RS}\cdot \longrightarrow \text{RS–SR}$$

The purification of solvents and the reduction of the disulfides with alkali metals in the solvents were carried out on a high vacuum line using a technique described in Ref. 3b.

Solutions of thiolate anions in solvents other than THF were usually prepared from the corresponding THF solution by removing the THF under vacuum and distilling the appropriate solvent onto the dry salt.

Electronic spectra were recorded with a Cary 14-UV spectrophotometer, using 0.2 cm quartz optical vacuum cells with some measurements made with a 0.18 cm spacer. Concentrations of thiolate anions could be varied by transferring a part of the sample to an adjacent glass ampoule and by distilling the solvent back by cooling the cell. Using this technique, concentrations were adjusted to give optical densities of 0 to 2. A quartz dewar with optical windows was used for the low temperature measurements and precooled methanol with liquid nitrogen was chosen as the cooling liquid. Dry nitrogen gas was blown onto the optical windows to prevent the formation of a frost covering. The temperature of methanol was recorded with a copper-constantan thermocouple located in the vicinity of the cell.

The concentrations of the sodium salt of phenylthiolate anion in THF were determined by the titration of thiolate anions with silver nitrate using a dithizone as an indicator or by electron transfer from thiolate anions to chloranil in THF forming chloranil radical anions having a known molar extinction coefficient,[13] and then, by estimating the molar extinction coefficient of the sodium salt of phenylthiolate anion.

Results

The alkali metal salts of thiolate anions were found to be stable in both THF and DMF over the temperature range investigated (25 to −76 °C) and the optical spectra exhibited sharp absorption bands at 280 nm in THF and at 308 nm in DMF at room temperature. The decimal extinction coefficient of the sodium salt of phenylthiolate anion in THF was found to be about 10^4 l/mol·cm. However, the spectrum of the cesium salt of phenylthiolate anion in THF showed a rather broad band.

Optical Spectra in THF. The position of the absorption maxima (λ_{max}) in THF depended upon the size of the counter cation, temperature, and structure of the thiolate anions. However, it was found that a 100-fold dilution of a *ca.* 10^{-3} mol/l solution did not alter the position; the independence of the position of the absorption maximum on the concentration excludes the possibility of an association of ion pairs under the conditions of the experiment (the concentrations were usually about 10^{-4} mol/l). The position of the absorption maxima of the phenylthiolate anion in THF was shifted toward longer wavelengths when the radius of the counter cations increased and the same phenomenon was observed even at low temperature (−72 to −76 °C); nearly linear relationships were observed between the inverse of the counter cation radius ($1/r_c$) and the wave number of the transition ($\bar{\nu}_{max}$) for both room and low temperatures, as depicted in Fig. 1 (see also Table 1). It is interesting to note that the alkali metal salts of phenylthiolate anions in THF exhibit a single sharp absorption band regardless of the temperature, and at intermediate temperatures the two isolated bands were not observed and no shoulder appeared.

The effect of *para*-substituents of the alkali metal salts of arylthiolate anions on the λ_{max} in THF is shown in

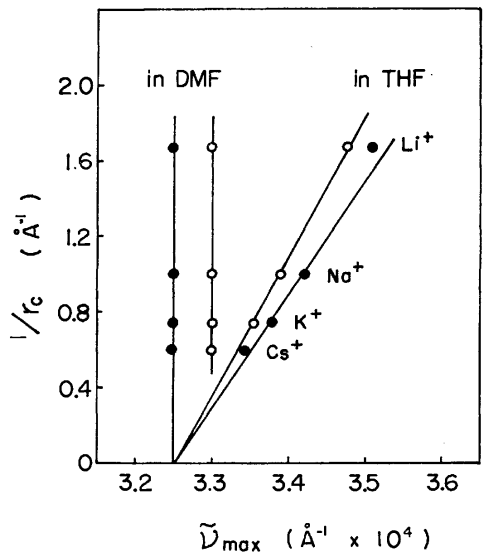

Fig. 1. Relationships between the inverse of the counter cation radius ($1/r_c$) of alkali metal salts of phenylthiolate anions and the wave number of the transition ($\bar{\nu}_{max}$) in THF and DMF. Black and open circles represent the values obtained in room and low temperatures, respectively.

Table 1. Dependence of λ_{max} on the radius of the counter cation (r_c) for alkali thiolate salts in THF and DMF at room and low temperatures

Counter cation	r_c Å	λ_{max}, nm in THF		in DMF	
		20 °C	low temp.(°C)	20 °C	low temp.(°C)
Li^+	0.60	285	287(−72)	308	303(−63)
Na^+	0.96	292	295(−75)	307	303(−43)
K^+	1.33	296	298(−76)	308	303(−62)
Cs^+	1.66	299		308	303(−60)

Table 2, and Fig. 2 shows a plot of the wave number against the Brown-Okamoto substituent constants.

Optical Spectra in DMF. The λ_{max} observed at both room and low temperatures are assembled in Table 1 and depicted in Fig. 1 together with the data in THF. The position of the absorption maximum was not affected by the counter cation (308 nm) and agreed with the extrapolated wave number of both lines obtained in THF for $1/r_c \to 0$. On lowering the temperature to *ca.* −70 °C a hypsochromic shift was observed (303 nm).

Table 2. Substituent effects of sodium arylthiolate anions on λ_{max} in THF at 20 °C

Substituent	CH_3O–	CH_3–	t-C_4H_9–	H–	Cl–
λ_{max}(nm)	279	290	292	292	297

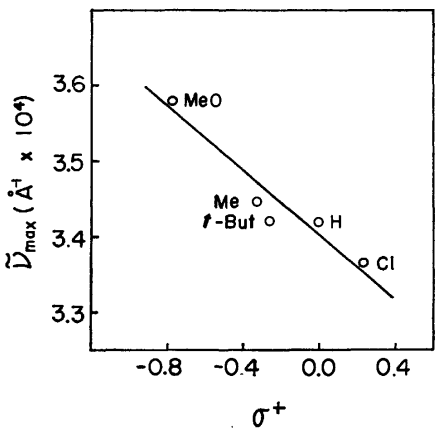

Fig. 2. Relationship between $\bar{\nu}_{max}$ of sodium arylthiolate anions in THF at room temperature and Brown-Okamoto's substituent constant in the Hammett equation (σ^+).

Optical spectra in other solvents, dimethoxyethane (DME) and dioxane, were also measured. These salts were also found to be stable in the solvents. The λ_{max} are given in Table 3.

Table 3. Solvent effects of phenylthiolate salts on λ_{max}(nm) at 20 °C

	Dioxane	THF	DME	DMF
$C_6H_5S^-$, Li^+		285	286	308
$C_6H_5S^-$, Na^+	279	292	292	307

Discussion

The sharp absorption bands observed in THF depended upon both the counter cation and the temperature; even at low temperatures (−72 to −76 °C) the position of the absorption maximum was shifted toward longer wavelengths with increasing size of the counter cation and a nearly linear relationship is observed between the inverse of the counter cation radius r_c and $\bar{\nu}_{max}$ (Fig. 1). A similar bathochromic shift for increasing size of the counter cation has been found for alkali metal salts of fluorenyl anions,[14] phenoxide ions,[6] and ketyl radical anions.[15] The independence of λ_{max} on the concentration has been observed for the sodium salt of phenylthiolate anion in THF. Thus, the shift in THF can be explained as a result of the formation of contact ion pairs, and the cause of the shift has been explained[4] as a perturbation of the molecular energy levels by the positive field of the cation, and a perturbation depends on the electrostatic interaction energy. The excited state is less stable due to the counter cation than the ground state, since in the ground state of an ion pair, the cation is located so as to form the smallest dipole, and a redistribution of charge occurs upon excitation, but as expected from the Franck-Condon principle, the cation has no time to readjust its position. Thus, the smaller the cation the larger the transition energy.[14]

As has been described above the relations for THF depicted in Fig. 1 strongly suggest that the alkali metal salts of phenylthiolate anions in THF exist as contact ion pairs and on lowering the temperature these may interact strongly with the surrounding THF molecules to form on its periphery a slight rigid coordination shell. Such an interaction is expected to be exothermic; the counter cations in contact ion pairs may interact more strongly with THF molecules on lowering the temperature. Although the alkali metal salts of phenylthiolate anions in THF at low temperature may still be classified as tight ion pairs, the strong interaction of THF with counter cations apparently results in a dispersion of positive charge (external solvation) and thus in a slight increase in the average interionic distance between the metal cation and thiolate anion, causing the bathochromic shift.

The process which is responsible for the shift of the position of the absorption maxima is reversible with temperature, but no new isolated band or shoulder appeared at intermediate temperatures, indicating that no discrete types of ion pairs such as contact and solvent-separated ion pairs were present in THF over the temperature range investigated. However, sodium fluorenyl salt in the same solvent exists as discrete types of ion pairs at intermediate temperatures (−30 °C).[14] This is probably attributable to a difference in the nucleophilic characters of carbanions and thiolate anions. The interionic interaction between anions and counter cations may be strengthened by the localization of the negative charge. This appears to be the case for our thiolate anions, since bathochromic shifts with counter cations are observed in THF even on lowering the temperature. Furthermore, this may be supported by the fact that the sodium phenoxide ion and the sodium benzyl carbanion, isoelectronic anions of the thiolate anion, have absorption bands at 303[6] and 355[16] nm, respectively. On the other hand, the λ_{max} of the thiolate anions appears at 285 to 290 nm depending on the counter cation, solvent, and substituent, indicating that the localization of the negative charge on the sulfur atom of thiolate anion could be greater than that on the carbon atom of carbanions.

The intercept $\bar{\nu}^{\circ}_{max}$ obtained on extrapolation of both lines plotted for THF as $1/r_c \rightarrow 0$ agrees with the wave number of the ion pairs observed in DMF at room temperature and no bathochromic shift with counter cation is observed at all in DMF. Thus, it may be safely stated that the entity observed in DMF is solvent-separated ion pairs or solvated free ions, even at room temperature (no difference has been reported in the positions of the absorption maxima of the solvent-separated ion pair and free ion[14]), since the position of the absorption maxima of the ion pairs in DMF at low temperature was not subject to the influence of counter cation (308 nm) (the fraction of free thiolate anions in the investigated solutions should be less than a few percent on the basis of the data reported for solutions containing alkali metal salts of carbanions and radical anions (*e.g.*, Ref. 14). The interionic interaction between a thiolate anion and a counter cation may be weakened by the DMF molecules separating both ions; the anion in the solvent-separated ion pairs is not subject to the influence of the counter cation. A similar observation was made on some alkali metal salts of phenols and enols in DMF.[6] The hypsochromic shift observed on lowering the temperature in DMF (308 to 303 nm) is quite interesting. Two causes could account for such a hypsochromic shift. (1) The negative charge of the thiolate anions may localize on the sulfur atom and hence such anions may exist as a dipolar molecules and be stabilized by an interaction with DMF molecules in the ground state. However, in an excited state, such solvating DMF molecules cannot be rearranged as expected from the Franck-Condon principle giving rise to orientational strain,[17] and thus stablilizing ion pairs. Therefore, thiolate anions in DMF are stabilized on lowering the temperature in the ground state and, on the contrary, the excited state is destabilized, and a hypsochromic shift is expected. (2) It is apparent that thiolate anions in DMF are solvent-separated ion pairs, even at room temperature. On lowering the temperature, however, the strength of the interaction of the DMF separating an ion pair with both the counter cation and the thiolate anion (for more detail, see the discussion of the solvent effect) may increase; *i.e.*, the average interionic distance between the metal cation and the thiolate anion may decrease on lowering the temperature, causing the hypsochromic shift.

As shown in Table 3, the positions of the absorption maxima of the lithium and sodium salts of phenylthiolate anions in the four aprotic solvents shifted toward longer wavelengths; the ease of solvation to the counter cation can be evaluated from the extent of the shift of the position of the absorption maxima, thus, dioxane<

THF<DME<DMF. This order is essentially the same as in the case of the formation of the solvent-separated ion pairs of the alkali metal salts of fluorenyl anions[14] except for DMF (in that study no DMF was used), and is also consistent with the order reported for electron transfer from sodium *n*-butylthiolate anions in solutions to oxygen which was described in the introduction,[12] indicating that the case of electron transfer depends upon the solvation state of the ion pair. Dioxane appears to be a poor solvating agent for alkali cations in view of the reported data on the shift of the absorption spectra of some ion pairs with changing solvents[14] and the position occupied by THF in this order is reasonable. A comparison of the solvating ability of DMF with that of DME can be made for the proton hyperfine coupling constants of alkali metal salts of fluorenone radical anion;[20] DMF yields free ions while DME produces contact ion pairs. Thus, the order obtained here seems, on the whole, plausible. At first sight, the behavior of DME for the lithium salt of phenylthiolate anion may appear strange, since fluorenyl lithium undoubtedly forms a solvent-separated ion pair, even at room temperature. Since the negative charge on thiolate anions is localized mainly on the sulfur atom, arylthiolate anions exist as tight ion pairs even in DME.

It is well known that DMF is a polarizable powerful base like dimethyl sulfoxide and hexamethylphosphoric triamide and the negative charge on the DMF is localized on a bare oxygen atom (the nucleophilicity is centered on this oxygen atom[18]) and DMF possesses a positively-charged nitrogen atom (this is conceivable from NMR data). DMF has a higher dielectric constant (36.7 at 25 °C) than THF (7.4 at 25 °C), but it is obvious that the solvating properties of the solvent rather than its dielectric constant are of prime importance;[19] thus the DMF yields solvent-separated ion pairs by utilizing both sites, one negatively- and the other positively-charged.

As can be seen from Table 2 and Fig. 2, the effects of substituents are reflected on the position of the absorption maxima. As has been described above, the negative charge of the thiolate anions is localized mainly on the sulfur atom, and thus, conjugation between the negative charge located on the sulfur atom and the phenyl ring is not so large. This is also obvious realized from the fact that pK_a of hydrogen sulfide (7.5) roughly equals that of phenylthiol (6.5). In oxide homologues, pK_a of water is 15.8 and that of phenol is 10, thus the oxide anions are stabilized by conjugation with the phenyl ring.[9] Therefore, no substituent effect on the position of the absorption maxima can be expected in the ground state. In general, in $\pi \rightarrow \pi^*$ transitions of odd alternant benzyl-type aromatic hydrocarbons, the excited state is stabilized by conjugation with the substituent, causing a bathochromic shift, *i.e.*, the contribution of the structure 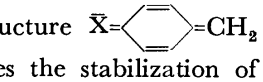 (I) to the excited state produces the stabilization of the excited state (an inductive substituent effect results in only a slight bathochromic shift).[21] This appears to be the case for the substituent effects observed in the optical spectra of sodium metal salts of arylthiolate anions. The greater the localization of the negative charge on the sulfur atom in the ground state, the larger the contribution of structure (I) in the excited state should be, thus a larger bathochromic shift is expected than those caused by the effects of the counter cation and the solvent.

References

1) S. Weinstein, E. Clippinger, A. H. Fainberg, and R. C. Robinson, *J. Amer. Chem. Soc.*, **76**, 2597 (1954).

2) E. Grunwald, *Anal. Chem.*, **26**, 1696 (1954).

3) For reviews on this subject, see (a) "Ions and Ion Pairs in Organic Reactions," Vol. 1 (1972) and Vol. 2 (1974), ed. by M. Szwarc, Wiley-Interscience, New York, N. Y. ; (b) M. Szwarc, "Carbanions, Living Polymers and Electron Transfers," Wiley-Interscience, New York, N. Y., (1968).

4) T. E. Hogen-Esch and J. Smid, *J. Amer. Chem. Soc.*, **87**, 669 (1965).

5) (a) N. Hirota, *J. Phys. Chem.*, **71**, 127 (1967); (b) M. C. R. Symons, *ibid.*, **71**, 172 (1967).

6) H. E. Zaugg and A. D. Shaefer, *J. Amer. Chem. Soc.*, **87**, 1857 (1965).

7) T. R. Griffiths and M. C. R. Symons, *Mol. Phys.*, **3**. 90 (1960).

8) R. G. Pearson, H. Sobel, and J. Songstad, *J. Amer. Chem. Soc.*, **90**, 319 (1968).

9) W. E. Truce, "Organic Sulfur Compounds," Vol. 1, ed. by N. Kharasch, Pergamon Press Inc., (1961), Chap. 12.

10) M. J. Janssen, "Sulfur in Organic and Inorganic Chemistry," Vol. 3, ed. by A. Senning, Marcel Dekker, Inc., New York, (1972), Chap. 29.

11) (a) B. O. Coniglio, D. E. Giles, W. A. McDonald, and A. J. Parker, *J. Chem. Soc., B*, **1966**, 152; (b) B. W. Clare, D. Cook. E. C. F. Ko, Y. C. Mac, and A. J. Parker, *J. Amer. Chem. Soc.*, **88**, 1911 (1966).

12) T. J. Wallace and A. Schriesheim, *J. Org. Chem.*, **27**, 1514 (1962).

13) C. N. Rao, V. Kalyanaraman, and V. George, "Applied Spectroscopy Reviews," ed. by E. G. Brame, Marcel Dekker, Inc., (1970) p. 153.

14) T. E. Hogen-Esch and J. Smid, *J. Amer. Chem. Soc.*, **88**, 307 (1966).

15) H. V. Carter, B. J. McClelland, and E. Wahurst, *Trans. Faraday Soc.*, **56**, 455 (1960).

16) B. Bockrath and L. M. Dorfman, *J. Amer. Chem. Soc.*, **96**, 5708 (1974).

17) N. S. Bagliss and E. G. McRae, *J. Phys. Chem.*, **58**, 1002 (1954).

18) A. J. Parker, *Chem. Revs.*, **69**, 1 (1969).

19) V. Gutmann, "Coordination Chemistry in Non-Aqueous Solutions," Springer-Verlag Berlin (1968).

20) N. Hirota, "Radical Ions," ed. by E. T. Kaiser and L. Kevan, Interscience Publishers, New York, N. Y., (1968) p. 35.

21) A. Streitwieser, "Molecular Orbital Theory for Organic Chemists," John Wiley & Sons Inc., New York, N. Y. (1961), Chap. 8.

Substituent Effects for the Benzene Ring on Solvolysis of 3,4-Benzotricyclo[4.3.1.0^{1,6}]dec-3-en-2-yl *p*-Nitrobenzoate

Katsuo OHKATA

Chemistry Department, Faculty of Science, Hiroshima University, Higashi-senda-cho, Hiroshima 730

(Received May 23, 1975)

Preparations of *anti*-4′-substituted 3,4-benzotricyclo[4. 3. 1. 0^{1,6}]dec-3-en-2-yl *p*-nitrobenzoates (**1a—d**) are described. The solvolysis of these esters was examined in 80% aqueous acetone. The rates were relatively high but the sensitivity to substituents on the benzene ring was low in comparison with other secondary systems. It is considered that σ-participation rather than π-conjugation might contribute to the rate accelerative effect. In the presence of a base, **1a—d** gave *anti*-alcohol (**12a—d**) (13 to 17%), *syn*-alcohol (**13a—d**) (31 to 78%), and *tert*-alcohol (**14a—d**) (5 to 54%). The product distributions are explained in terms of a nonclassical homonaphthalenium cation (**24**).

There is abundant experimental evidence for selective product formation,[1] rate acceleration,[1a,1b,2] and transmittance of the substituent effect[3] in the solvolysis of various types of substrates in which bent, electron-releasing systems like cyclopropyl groups are situated at the reaction center.[4] The remarkable effect of the cyclopropyl group in stabilizing an adjacent carbocation is well documented for a large number of solvolyses.[1,2,4] Also, a π-electron system such as a phenyl or a vinyl group is similarly capable of conjugation with an adjacent cationic center.[5]

Deno *et al.*[6] and Brown *et al.*[7] reported that a cyclopropyl group contributes to stabilization of the cationic center to a greater extent than does a phenyl group. In contrast, Olah *et al.* reported that the relative effectiveness in delocalizing the positive charge decreases in the following order, Ph>cyclo-C_3H_5>CH_3, on the basis of the ^{13}C chemical shift for the carbocation in various stable species.[8] Then, they suggested that the cyclopropyl group is a more actively participating group in solvolysis than the phenyl group, which delocalizes the charge away from the cationic center better than the cyclopropyl group in the intermediate carbocation.[8] In other words, the effectiveness of charge delocalization (π-conjugation and σ-participation[9,10,17]) by two groups (such π-electron systems as phenyl groups and bent-σ-electron systems as cyclopropyl groups) in the transition state, might be different from that in the intermediate.

These comparisons have been made by studies on the intermolecular competition of different molecules, so that there may be some lack of clarity due to other factors like the steric effect and the solvent effect of the reactivity of the different substrates. The author wishes here to report on the study of the solvolysis of a series of cyclopropylphenylmethyl esters in which the steric environments in the vicinity of the reactive site are essentially identical and a comparison between two substituents can be made intramolecularly.

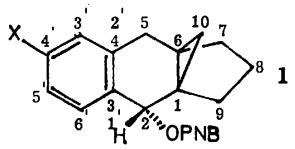

1a X=MeO
1b X=Me
1c X=H
1d X=Cl

Fig. 1. *p*-Nitrobenzoate (**1**).

From a synthesis and solvolytic study of **1c**, it is regarded as a suitable cyclopropylphenylmethyl derivative for examining the above competitive effects.[10] It is now interesting to investigate the substituent effects at the *para*-position of the reactive center of **1** on both the solvolysis rate and the distribution of the solvolysis products. Much information on σ-participation and π-conjugation may be expected from such studies.

Results

Synthesis. Each *p*-nitrobenzoate (**1a—d**) was prepared by the sequence outlined in Scheme 1, which is the same route as in the case of **1c**.[10] 2-(*m*-Substituted benzyl)-2-methoxycarbonylcyclopentanones (**2a—d**)

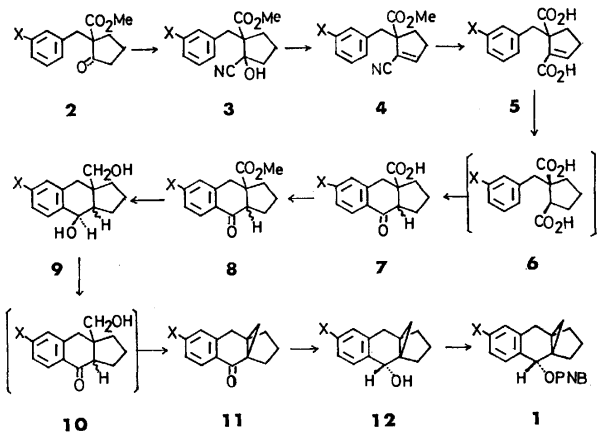

Scheme 1.

were prepared by the condensation of 2-methoxycarbonylcyclopentanone with *m*-substituted benzyl chloride. The addition of hydrogen cyanide to **2a—d** gave the cyanohydrins (**3a—d**), which were dehydrated by phosphoryl chloride in dry pyridine to afford the unsaturated cyano esters (**4a—d**), and then the unsaturated dicarboxylic acids (**5a—d**) were obtained by the hydrolysis of these cyano esters. Hydrogenation of **5a—d** with Adams' catalyst in ethyl acetate produced the saturated acids (**6a—d**) in high yields. Intramolecular cyclization of **6a—d** with concentrated sulfuric acid gave rise to the keto acids (**7a—d**). Esterification with diazomethane converted **7a—d** almost completely

into the esters (**8a—d**) which were reduced by lithium aluminum hydride to give a mixture of at least two diols in good yields, the ratio being about 3: 1 in each case. Contrary to the fact that the above minor products were not oxidized with active manganese dioxide, the oxidation of the major diols (**9a—d**) easily afforded the keto alcohols (**10a—d**). These keto alcohols (**10a—d**) were transformed to their tosylates, followed by heating under reflux in dry pyridine to give the ketones (**11a—d**). Spectroscopic and elemental analyses support the structure of the assigned cyclopropyl phenyl ketones. The NMR spectra of **11a—d** show that the aliphatic proton signals are similar to each other and that each substituent on the benzene ring is at a *para*-position to the carbonyl carbon (Table 5).

Reduction of **11a—d** with lithium aluminum hydride in ether gave the alcohols (**12a—d**), in 85—90% yields, concomitant with a traces of other epimers (**13a—d**) (2—5%). The stereochemical assignment of C_2 (reactive center) is based upon a comparison of the NMR spectra of both epimeric alcohols and upon the inference for the direction of the hydride reduction of **11a—d**. Since it has been confirmed by NMR spectroscopy that a proton which is located above the plane of a cyclopropane ring should be shielded in contrast with a proton in the same plane as that of the cyclopropane, a comparison of the chemical shifts of α-carbinyl protons in two epimers was made.[11] The results are shown in Table 1. As is seen, the *anti* geometry of a hydroxyl group relative to a cyclopropane is assigned to **12a—d**, the main reduction product, in which the α-proton was more shielded, and *vice versa*. The expectation for hydride reduction also leads to the same assignment. It may be expected that the reduction of **11a—d** with lithium aluminum hydride predominantly give the *anti* alcohols (**12a—d**), since the hydride attacks from the less hindered side of the carbonyl group.[12]

Kinetic Studies. The rates of solvolysis of *p*-nitrobenzoates (**1a—d**) were determined by titration of *para*-nitrobenzoic acid in 80% aqueous acetone. The results are summarized in Table 2.

Product Studies. Studies of solvolysis products of **1a—d** were carried out in the presence of 2,6-lutidine. After about ten half-lives, the products were extracted

Table 1. Observed α-hydrogen shifts and their differences due to neighboring cyclopropane

X	Compound	a)	δ[b]	$\Delta\delta$[c]	lit.
MeO	**12a**	*anti*	4.84	0.16	d)
	13a	*syn*	5.00		
Me	**12b**	*anti*	4.83	0.16	d)
	13b	*syn*	4.99		
H	**12c**	*anti*	4.83	0.21	e)
	13c	*syn*	5.04		
Cl	**12d**	*anti*	4.82	0.19	d)
	13d	*syn*	5.01		
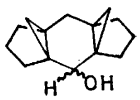		*anti*	3.48	0.69	f)
		syn	4.17		

a) The relation between the OH group and cyclopropane methylene. b) Chemical shifts are given in δ (ppm) relative to the internal reference, tetramethylsilane. c) $\Delta\delta=\delta$ *syn*$-\delta$ *anti*. d) Present study. e) Ref. 10. f) Ref. 11.

Table 3. Product distributions of solvolysis of **1a—d** in the presence of 2,6-lutidine

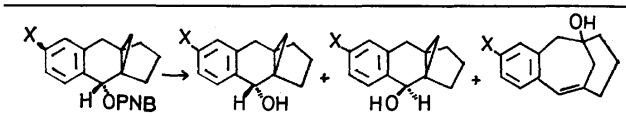

(1)	(**12**) %, (δ)[a]	(**13**) %, (δ)[a]	(**14**) %, (δ)[a]
1a (X=MeO)	17, (4.84)	78, (5.00)	5, (6.10)
1b (X=Me)	15, (4.83)	46, (4.99)	39, (6.11)
1c[b] (X=H)	13, (4.83)	42, (5.04)	45, (6.17)
1d (X=Cl)	15, (4.82)	31, (5.01)	54, (6.08)
	15±2%[c]	85±2%[c]	

a) (δ): ^{1}H-NMR chemical shifts for characteristic signals in $CDCl_3$ (α-proton of OH-group for **12** and **13**, vinyl proton for **14**) in the solvolysis products.
b) Ref. 10.
c) **13**+**14**/**12**=85±2/15±2=const. The ratio is independent of substituents.

Table 2. Rates of solvolysis of *p*-nitrobenzoate (**1a**, **1b**, **1c**, and **1d**) in 80% aqueous acetone

Compound	T, °C	10^4k, s^{-1}	ΔH^*, kcal/mol	ΔS^*, e.u.	k_{rel}, 25 °C[a]
1a	0.0	1.10 ±0.1			
(X=MeO)	25.0	37.9 ±0.4[b]	22.3	+5.3	44.1[b]
1b	0.0	0.108±0.005			
(X=Me)	25.0	3.22 ±0.1	21.4	−4.7	3.74
1c	25.0	0.860±0.05[c]	20.6	−8.0	1.00
(X=H)	30.0	1.51 ±0.04[c]			
	40.0	4.86 ±0.03[c]			
1d	25.0	0.287±0.021	22.8	−2.9	0.334
(X=Cl)	45.0	3.58 ±0.08			

a) $k_{rel}=k_X/k_H$. The Hammett plots against σ^+ gave an acceptable linear relation ($\rho=-2.11$).
b) Owing to the high reactivity of **1a** (X=MeO), this rate constant at 25 °C may be an upper limit, so that k_{MeO}/k_H is also an upper limit.
c) Ref. 10.

and analyzed using NMR spectroscopy. The product in each series was a mixture of alcohols consisting of **12**, **13**, and **14**, from a comparison of the NMR spectra with those of authentic samples of the **c**-series (X=H).[10] The product distributions were determined from the integral ratio for the characteristic signals in the NMR spectra. The results are summarized in Table 3. The primary alcohols (**15a—d**) could not be detected by way of the extraneous singlet signal due to the hydroxymethyl protons in each case.[10]

The following points may be important in the consideration of the reaction intermediate in the solvolysis of **1a—d**:

1) The ratio, **13a—d**/**12a—d**, was varied with the substituent on the benzene ring.

2) Secondary alcohols (**13a—d** and **12a—d**) increased in the case of the MeO-group, but tertiary alcohols (**14a—d**) increased in the case of the Cl-group.

3) The proportions between (**13a—d**)+(**14a—d**) and (**12a—d**) remained almost unchanged with substituent on the benzene ring.

Discussion

Solvolysis Rate. The rate measurements of S_N1 reactions, *i.e.*, the solvolyses of halides, sulfonates and *p*-nitrobenzoates, have been utilized for the purpose of obtaining information as to the factors influencing the stability or the electronic delocalization in an intermediate carbocation for these reactions.[13] A substituent at the *para*-position of a benzene ring in the benzylic substrate does not affect the steric environment near the reactive center, but does affect the ability of electronic conjugation with the site bearing a positive charge in the reaction intermediate.[14] The reaction constant, ρ, in the Hammett equation, or the effect of a single substituent (for instance, k_{MeO}/k_H) may serve for an approximate measure of the variation between the ground state and the transition state on the benzenoid system. Accordingly, the greater the positive charge on the benzene ring at the trasition state in the rate determining step, the greater the rate enhancement provided by *p*-methoxy substitution.

The rate ratios and the rho values obtained in the present study and in certain related systems are listed in Table 4. The rate ratios, k_{MeO}/k_H, for most of these substrates (**16**, **17**, **18**, **20**, and **21**) are fairly large, 0.7—1.5$\times 10^4$, demonstrating that π-conjugation of the intermediate carbocation with the anisyl group contributes considerably to increasing the solvolysis rate, as is generally observed. On the other hand, the rate ratio, 1.4$\times 10^2$, for **19** is rather smaller than the above examples. Since the substituent effect for a highly reactive system like the *tert*-arylmethyl ester is ordinarily smaller, this may be reasonable taking account of the faster rate of **19** by a factor of 10^2—10^4 compared with the other substrates cited above. This is consistent with the postulation that the more stable the carbocation, the less demand for additional stabilization through neighboring group participation.[18] Compared with these values, the ratio, 44, for **1** is the smallest among that for a number of arylmethyl *p*-nitrobenzoates. The relative reactivity of **1** to **19** under the same conditions is about 0.4, namely the reactivity of **1** is similar to or even less than that of **19**, the tertiary ester, but the ratio k_{MeO}/k_H, for **1** is unexpectedly smaller than one half of the ratio for **19**. This is in contrast with the above discussion. This also shows that the conjugative effect of the *p*-MeO-group in **1** might be quite small at the transition state for solvolysis.

On account of the lower rate ratio, k_{MeO}/k_H, and the lower reactivity of this series of compounds, **1**, compared with *tert*-cyclopropylphenylmethyl systems, it is reasonable to assume that the cyclopropane ring is oriented favorably in the 1-bicyclo[3.1.0]hexyl group of **1** against the reactive center and that its bent σ-bond could participate very well to the ionization process in the transition state (σ-participation). As compared with the π-conjugation which stabilizes the intermediate carbocation and reduces the energy of activation in solvolysis indirectly,[19] σ-participation can immediately contribute to the transition state for ionization in solvolysis and might be more effective for the rate than π-conjugation if the stereochemistry is satisfied. This is a result of the present experiments for the rate determination of **1a—d** at 25 °C, but for more detail it will be necessary to obtain further thermodynamic parameters such as the enthalpy and entropy of activation.

Recently Eaton and Traylor[20] suggested that the

Table 4. Relative rates (k_X/k_H and k_H/k_{1H}) and reaction constants (ρ) in Hammett's equation of the solvolysis of various *p*-nitrobenzoates in 80% aqueous acetone at 25 °C

	a)	b)	b)	d)	d)	c)	c)
	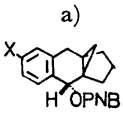	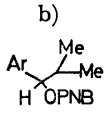	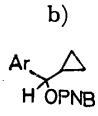	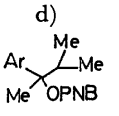	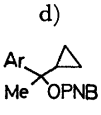	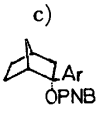	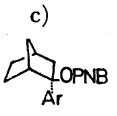
	(1)	(16)	(17)	(18)	(19)	(20)	(21)
k_{MeO}/k_H	44.1	804	780	686	~137	785.5	1521
k_{Me}/k_H	3.74	2.47	10.9	—	—	—	—
k_{Cl}/k_H	0.334	0.77	0.3	—	—	—	—
ρ[e]	−2.11	—	−3.61	−4.65	−2.78	−3.77	−3.96
$k_{rel.}$	1.0	~10^{-6} [f]	~10^{-2} [f]	1.1$\times 10^{-4}$	2.4	6.2$\times 10^{-4}$	8.8$\times 10^{-2}$

a) Present study. b) Ref. 15. c) Ref. 16. d) Ref. 17.

e) Reaction constant, ρ, in ρ-σ^+ plot.

f) Calculated from data in other solvents (60% aqueous acetone or 65% aqueous dioxane) using the Grunwald-Winstein equation (*Y*-value).

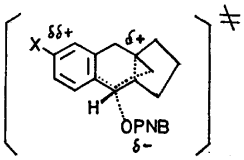

Fig. 2. Transition state in solvolysis of **1**.

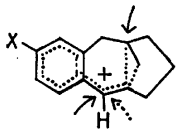

(**24**)

Fig. 4. Reaction intermediate in solvolysis of **1**.

rigid cyclopropyl carbinyl system (**23**) affords at least as much stabilization as in the freely rotating system (**22**). However, the model for comparison cited by them is not necessarily a favorable system for solvolysis. A favorable configuration should also be an important factor for vertical stabilization[22] in an electron transition (vertical process) such as Kosower *et al.* have reported.[23]

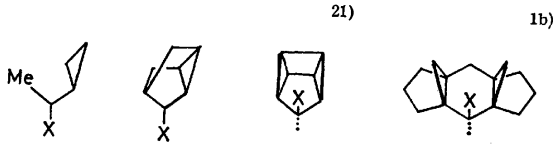

22 **23**

krel. 1 10^4 10^6

Fig. 3. Relative rates of solvolysis of rigid cyclopropyl systems.

Products. It has been established by Olah *et al.* that the charge density of each carbon atom in a stable carbocation is closely related to their ^{13}C chemical shifts.[24] It is also expected that the above charge distribution resembles, to a certain extent, that of the unstable intermediate ions in solvolysis. They suggested that the π-electron system of the phenyl group, when not hindered by steric effects, can conjugatively delocalize charge more effectively than hyperconjugation with bent C–C bonds.[8] Generally, the distribution of substitution products in solvolysis may depend upon a number of effects, for instance, the charge density and steric factors of the carbon atoms which the solvent attacks.

It may be noted from the present result that the distribution of the hydroxylic products varies considerably with the substituent at the *para*-position of the benzene ring in spite of an almost identical steric environment around the reactive site. The proportions between **13** and **12** changed from 2.1 to 4.6 with various substituents on the benzene ring. Therefore, they are dependent upon the properties of intermediate carbocation rather than the steric factor. These discussions result in the proposition that the intermediate carbocation is essentially not the classical carbocation of the benzyl type. The most remarkable feature is the fact that the proportions between **12** and (**13**+**14**) remain almost constant with the substituents on the benzene ring while the yield for **14** increases from the MeO- to the Cl-group.

The result might be explained on the basis of the formation of an intermediate carbocation in which the positive charge would be highly delocalized not only on the aromatic part but also on the cyclopropane ring as in **24**. Since it is usually recognized that the formation of a bridge-head carbocation in relatively small polycyclic systems is an extraordinarily slow process,[25] the localized or classical C-6 carbocation could be excluded in such reactive species as the present substrates. As the primary homo-allylic alcohols (**15a**—**d**) could not be detected in the product analysis, the positive charge might be delocalized even slightly into the primary carbon (C_{10}) in the intermediate ion (**24**).

In the case of a *p*-MeO-derivative, the positive charge may be principally stabilized by the powerful conjugative effect of the *p*-MeO-group, so that the positive charge density at the C_6 carbon is decreased. This results in the formation of **14** in a low yield in comparison with the other cases. Nevertheless, electron delocalization might expand through C_2–C_1–C_6 to a certain extent and cover the side below this planar ionic species. Consequently, a nucleophilic solvent attack would mostly take place from the upper side of the ion to afford **13** rather than **12** which would be produced by a solvent attack from below. A steric effect around the C_2 position, which does not vary with the substituents on the benzene ring, would have to be incorporated in such a nucleophilic substitution at the C_2 position, but a clear distinction between the effects could not be made in the present study.

As the conjugative effect of a substituent decreases, the positive charge density at the C-6 position might increase proportionately and the ratio of the formation of **14** increase also. If it is assumed that the solvent attack at C_6 and C_2 from the upper side depends substantially on the electron delocalization over the aromatic ring and the C_2–C_1–C_6, plane below which the filled orbital rejects the approach of a nucleophilic solvent molecule, the sum of the two products, **13** and **14**, reflects such electronic circumstances of the intermediate ion (**24**). On the other hand, the solvent attack at C_2 from below would occur responding to the degree that the C_1–C_{10} bonding electrons contribute to this intermediate ion when the steric factors offset each other. It has been reported that nucleophilic solvents enter from the *cis* side to a methylene of the cyclopropane in a large number of solvolyses in which a homo-allylic or homo-aromatic carbocation intervenes.[1b,1c,4,26]

In summary, the rates of solvolysis of **1a**—**d** in 80% aqueous acetone were greatly increased and their sensitivity to a substituent on the benzene ring is small in comparison with other cyclopropylphenylmethyl systems. These results indicate that σ-participation rather than π-conjugation might contribute to the rate accelerative effect due to the earlier transition state in which the hybridization of C_2 (reactive carbon) might not be a complete sp^2-hybridization. On the other hand, in the intermediate, the conjugation between the vacant *p*-orbital at C_2 and the aromatic nucleus

would contribute to the stabilization of the intermediate (**24**). The degree of such stabilization by π-conjugation might be varied with the substituent on the benzene ring.

Experimental

All the melting points are uncorrected. The IR spectra were obtained with a Hitachi 215 grating IR spectrophotometer. NMR measurements were carried out on a Varian T-60 spectrometer, using tetramethylsilane as an internal reference.

The details of synthesis of **1c** will be provided in a future publication.[10]

m-*Substituted Benzyl Chloride.* The chlorides were prepared by the reported methods: *m*-methoxy bp 88—89 °C/4 mmHg (lit,[27] bp 124 °C/13 mmHg), *m*-methyl bp 91—92 °C/22 mmHg (lit,[28] 101—102 °C/30 mmHg), and *m*-chloro derivatives bp 103—105 °C/20 mmHg (lit,[29] 104 °C/17 mmHg).

*2-(*m-*Substituted benzyl)-2-methoxycarbonylcyclopentanone (**2a**, **2b**, and **2d**).* *(a) 2-*m-*Methoxybenzyl-2-methoxycarbonylcyclopentanone (**2a**):* To a suspension of 11 g (0.48 mol) of finely dispersed sodium in 150 ml of dry toluene was added a solution of 69 g (0.48 mol) of 2-methoxycarbonylcyclopentanone[30] in 350 ml of dry benzene with stirring in a nitrogen atmosphere for 2 h. After the mixture was heated under reflux for 2.5 h, a solution of 50 g (0.32 mol) of *m*-methoxybenzyl chloride in 100 ml of dry benzene was added in one portion. Then, the reaction mixture was heated under reflux for 25 h. The usual work-up gave 68 g of colorless **2a** in an 80% yield (bp 189—191 °C/5 mmHg).

*(b) 2-*m-*Methylbenzyl-2-methoxycarbonylcyclopentanone (**2b**):* By a similar method to that used in the preparation of **2a**, **2b** (bp 145—150 °C/2 mmHg, 62 g, 83%) was obtained from *m*-methylbenzyl chloride (78 g, 0.56 mol) and 2-methoxycarbonylcyclopentanone (53 g, 0.38 mol).

*(d) 2-*m-*Chlorobenzyl-2-methoxycarbonylcyclopentanone (**2d**):* By a method similar to that used in the preparation of **2a**, **2d** (bp 173—177 °C/5 mmHg, 88 g, 82%) was obtained from *m*-chlorobenzyl chloride (64 g, 0.4 mol) and 2-methoxycarbonylcyclopentanone (71 g, 0.5 mol).

*2-(*m-*Substituted benzyl)-1-hydroxy-2-methoxycarbonylcyclopentanecarbonitrile (**3a**, **3b**, and **3d**).* *(a) 2-*m-*Methoxybenzyl-1-hydroxy-2-methoxycarbonylcyclopentanecarbonitrile (**3a**):* Into an aqueous solution (150 ml) of sodium cyanide (73 g, 1.5 mol) was added an ethereal solution (90 ml of ether) of **2a** (68 g, 0.26 mol) with vigorous stirring and cooling with ice water. Concentrated hydrochloric acid (82 ml) was added to the above mixture at 5—10 °C; vigorous stirring was continued for 30 h. Crude cyanohydrin (**3a**) (64 g) was obtained in an 85% yield by the ordinary extraction procedure, and used for the following dehydration without further purification. Pure sample, mp 90—98 °C (dec), was obtained by recrystallization from carbon tetrachloride. Found: C, 66.17; H, 6.53; N, 4.87%. Calcd for $C_{16}H_{19}NO_4$: C, 66.42; H, 6.62; N, 4.84%.

*(b) 2-*m-*Methylbenzyl-1-hydroxy-2-methoxycarbonylcyclopentanecarbonitrile (**3b**):* By a method similar to that used in the preparation of **3a**, **3b** (mp 105—107 °C (dec), 109 g, 80%) was obtained from **2b** (120 g, 0.49 mol) and sodium cyanide (115 g, 2.4 mol). Found: C, 70.19; H, 6.92; N, 5.15%. Calcd for $C_{16}H_{17}NO_2$: C, 70.31; H, 7.01; N, 5.12%.

*(d) 2-*m-*Chlorobenzyl-1-hydroxy-2-methoxycarbonylcyclopentanecarbonitrile (**3d**):* By a method similar to that used in the preparation of **3a**, **3d** (mp 102—106 °C (dec), 72 g, 73%) was obtained from **2d** (95 g, 0.36 mol) and sodium cyanide (88 g, 1.8 mol). Found: C, 61.52; H, 5.35; N, 4.59; Cl, 12.22%. Calcd for $C_{15}H_{14}NO_2Cl$: C, 61.33; H, 5.49; N, 4.77; Cl, 12.07%.

*5-(*m-*Substituted benzyl)-5-methoxycarbonyl-1-cyclopentenecarbonitrile (**4a**, **4b**, and **4d**).* *(a) 5-*m-*Methoxybenzyl-5-methoxycarbonyl-1-cyclopentenecarbonitrile (**4a**):* To a solution of **3a** (64 g, 0.22 mol) in 220 ml of anhydrous pyridine was added phosphorus oxychloride (100 g, 0.67 mol) with vigorous stirring and cooling below 10 °C. Stirring was continued for 3 h in an ice-water bath, for 12 h at room temperature, and then for 2 h under reflux. After the reaction mixture was poured onto a mixture of crushed ice (100 g) and concd hydrochloric acid (100 ml), 47 g, of **4a** (78% yield) was obtained by the usual work-up; bp 185—190 °C/2 mmHg.

*(b) 5-*m-*Methylbenzyl-5-methoxycarbonyl-1-cyclopentenecarbonitrile (**4b**):* By a method similar to that used in the preparation of **4a**, **4b** (bp 175—184 °C/4 mmHg, 80 g, 89%) was obtained from **3b** (95 g, 0.35 mol) and phosphorus oxychloride (150 g, 1.05 mol).

*(d) 5-*m-*Chlorobenzyl-5-methoxycarbonyl-1-cyclopentenecarbonitrile (**4d**):* The reaction of **3d** (69 g, 0.24 mol) with phosphorus oxychloride (105 g, 0.705 mol) afforded **4d** (bp 192—198 °C/4 mmHg, 55 g, 85%).

*5-(*m-*Substituted benzyl)-1-cyclopentene-1,5-dicarboxylic Acid (**5a**, **5b**, and **5d**).* *(a) 5-*m-*Methoxybenzyl-1-cyclopentene-1,5-dicarboxylic Acid (**5a**).* Hydrolysis of **4a** (38 g, 0.14 mol) was accomplished using 100 ml of concd hydrochloric acid and 50 ml of glacial acetic acid under reflux with stirring for 10 h. The crude **5a** (21 g) was obtained in a 54% yield, and recrystallized from ethyl acetate, mp 196—200 °C. Found: C, 65.09; H, 5.91%. Calcd for $C_{15}H_{16}O_5$: C, 65.21; H, 5.84%.

*(b) 5-*m-*Methylbenzyl-1-cyclopentene-1,5-dicarboxylic Acid (**5b**):* Crude dicarboxylic acid (**5b**) (34 g) obtained from **4b** (40 g, 0.16 mol) in an 82% yield was recrystallized from ethyl acetate to afford pure **5b**, mp 195—198 °C. Found: C, 69.39; H, 6.18%. Calcd for $C_{15}H_{16}O_4$: C, 69.22; H, 6.20%.

*(d) 5-*m-*Chlorobenzyl-1-cyclopentene-1,5-dicarboxylic Acid (**5d**):* Hydrolysis of **4d** (44 g, 0.16 mol) yielded **5d** (33 g, 73%) which was recrystallized from ethyl acetate–petroleum ether to give a pure compound, mp 183—184 °C. Found: C, 59.69; H, 4.54; Cl, 12.71%. Calcd for $C_{14}H_{13}ClO_4$: C, 59.90; H, 4.66; Cl, 12.63%.

*1-(*m-*Substituted benzyl) cyclopentane-1,2-dicarboxylic Acid (**6a**, **6b**, and **6d**).* *(a) 1-*m-*Methoxybenzylcyclopentane-1,2-dicarboxylic Acid (**6a**):* A mixture of 9.0 g (0.033 mol) of **5a** suspended in 500 ml of ethyl acetate and 100 mg of Adams-Pt catalyst was stirred in a hydrogen atmosphere at room temperature; 750 ml (theoretically 728 ml) of hydrogen was absorbed. After the catalyst was filtered out, the solvent was removed under reduced pressure. Saturated dicarboxylic acid (**6a**) was obtained quantitatively and used without further purification for the subsequent dehydration.

*(b) 1-*m-*Methylbenzylcyclopentane-1,2-dicarboxylic Acid (**6b**):* Hydrogenation of **5b** (20 g, 0.077 mol) yielded **6b**.

*(d) 1-*m-*Chlorobenzylcyclopentane-1,2-dicarboxylic Acid (**6d**):* Hydrogenation of **5d** (20 g, 0.071 mol) yielded **6d**.

*3,4-(4'-Substituted benzo)-5-oxo-bicyclo[4.3.0]non-3-ene-1-carboxylic Acid (**7a**, **7b**, and **7d**).* *(a) 3,4-(4'-Methoxybenzo)-5-oxo-bicyclo[4.3.0]non-3-ene-1-carboxylic Acid (**7a**):* A solution of **6a** (9.0 g, 0.033 mol) in a mixture of 80 ml of concd sulfuric acid and 20 ml of water was stirred for 24 h at room temperature. From the reaction mixture, **7a** (5.8 g, mp 146—147 °C) was obtained by the usual work-up in a 67% yield. Found: C, 69.14; H, 6.16%. Calcd for $C_{15}H_{16}O_4$: C, 69.22; H, 6.20%.

*(b) 3,4-(4'-Methylbenzo)-5-oxo-bicyclo[4.3.0]non-3-ene-1-carboxylic Acid (**7b**):* To a solution of **6b** (20 g, 0.076 mol) in 100

ml of benzene was added 100 ml of concentrated sulfuric acid. The mixture was stirred at room temperature for 24 h. By the usual procedure, **7b** (9.0 g, mp 123—124 °C) was obtained in a 48% yield. Found: C, 73.65; H, 6.61%. Calcd for $C_{15}H_{16}O_3$: C, 73.75; H, 6.60%.

(d) 3,4-(4'-Chlorobenzo)-5-oxo-bicyclo[4.3.0]non-3-ene-1-carboxylic Acid (7d): By a method similar to that used in the preparation of **7b**, **7d** (mp 182—184 °C, 12.4 g) was obtained from **5d** (20 g, 0.071 mol) in a 66% yield Found: C, 63.52; H, 4.80; Cl, 13.59%. Calcd for $C_{14}H_{13}O_3Cl$: C, 63.52; H, 4.95; Cl, 13.39%.

3,4-(4'-Substituted benzo)-1-hydroxymethyl-5-hydroxybicyclo-[4.3.0]non-3-ene (9a, 9b, and 9d). (a) 3,4-(4'-Methoxybenzo)-1-hydroxymethyl-5-hydrobicyclo [4.3.0] non-3-ene (9a): A solution of 9.8 g (0.038 mol) of **7a** in 50 ml of ether was treated with a distilled solution of diazomethane in 350 ml of ether, prepared from 40 g (*ca.* 0.19 mol) of *p*-toluenesulfonylmethylnitrosoamide. The reaction mixture was kept in an ice bath for 5 h, ether was removed under reduced pressure, and the keto ester (**8a**) (mp 88—89 °C, 8.5 g, 81%) was obtained. Found: C, 69.86; H, 6.64%. Calcd for $C_{16}H_{18}O_4$: C, 70.06; H, 6.61%.

A solution of **8a** (6.27 g, 0.023 mol) in 350 ml of ether was gradually added into a mixture of 5.3 g of $LiAlH_4$ and 100 ml of ether with stirring in an ice bath. After the mixture was stirred at room temperature for 24 h, a minimum amount (12 ml) of water was added to the mixture. Repeated extraction with $CHCl_3$ yielded the crude product, which was recrystallized from $CHCl_3$ to give 3.06 g (54%) (mp 156—157 °C) of **9a** and 2.47 g (43%) (mp 130—135 °C) of a mixture consisting of **9a** and its epimer. The minor diol was not oxidized with active MnO_2 in benzene, while under the same conditions **9a** was smoothly oxidized into keto alcohol (**10a**). Elemental Analysis for **9a**, Found: C, 72.65; H, 8.00%. Calcd for $C_{15}H_{20}O_3$: C, 72.55; H, 8.12%.

(b) 3,4-(4'-Methylbenzo)-1-hydroxymethyl-5-hydroxybicyclo [4.3.0] non-3-ene (9b). Esterification of **7b** (12.2 g) with diazomethane yielded keto ester (**8b**) (mp 66—67 °C, 12.0 g). Found: C, 74.20; H, 7.06%. Calcd for $C_{16}H_{18}O_3$: C, 74.40; H, 7.02%.

Reduction of **8b** (5.3 g, 0.02 mol) with $LiAlH_4$ (3.8 g) yielded **9b** (2.3 g, 47%), a mixture of **9b** and its epimer (1.4 g, mp 114—118 °C, 29%), and an oily product (0.9 g). **9b** was purified by recrystallization from $CHCl_3$, mp 164—165 °C. The epimer of **9b** was not oxidized with active MnO_2 in benzene as above.

(d) 3,4-(4'-Chlorobenzo)-1-hydroxymethyl-5-hydroxybicyclo [4.3.0] non-3-ene (9d): By a method similar to that used in the preparation of **9a**, **9d** (3.0 g, mp 162—163 °C, 56%) and the mixture of **9d** and its epimer (1.5 g, mp 115—125 °C, 28%) were obtained from **8d** (mp 88—89 °C) prepared by esterification of **7d** (5.6 g, 0.021 mol). Elemental analysis for **8d**, Found: C, 64.44; H, 5.22; Cl, 12.81%. Calcd for $C_{15}H_{15}O_3Cl$: C, 64.64; H, 5.43; Cl, 12.71%. **9d**, Found: C, 66.38; H, 6.66; Cl, 13.96%. Calcd for $C_{15}H_{17}O_2Cl$: C, 66.53; H, 6.78; Cl, 14.02%.

3,4-(4'-Substituted benzo)-tricyclo [4.3.1.0^{1,6}] dec-3-en-2-one (11a, 11b, and 11d). (a) 3,4-(4'-Methoxybenzo)-tricyclo [4.3.1.0^{1,6}] dec-3-en-2-one (11a): A mixture of 890 mg (3.58 mmol) of diol (**9a**) (mp 156—157 °C) and 2 g of active MnO_2, crushed immediately before reaction, was suspended in 100 ml of dry benzene. Stirring was continued for 24 hr at room temperature, followed by filtration and then the solvent was removed under reduced pressure. Without further purification 20 ml of dry pyridine and 1.4 g of *p*-toluenesulfonyl chloride were added with cooling in an ice-water bath. Stirring was continued for 15 h at room temperature, then for 3 h under reflux. The reaction mixture was poured onto a mixture of 50 ml of concentrated hydrochloric acid and ice, followed by extraction with ether. The organic layer was washed with 6M-hydrochloric acid and water, and dried over anhydrous sodium sulfate. Removing the solvent, the residue was treated with petroleum ether followed by filtration through neutral alumina. Evaporation of the solvent under reduced pressure gave an oily product. Crystallization and purification gave rise to 602 mg of **11a** (mp 87—88 °C) in a 74% yield based on **9a**. Found: C, 78.75; H, 6.98%. Calcd for $C_{15}H_{16}O_2$: C, 78.92; H, 7.06%.

(b) 3,4-(4'-Methylbenzo)-tricyclo [4.3.1.0^{1,6}] dec-3-en-2-one (11b): By a method similar to that used in the preparation of **11a**, **11b** (mp 89—90 °C, 270 mg, 27%) was obtained from **9b** (mp 164—165 °C, 1.1 g, 4.7 mmol). Found: C, 84.81; H, 7.55%. Calcd for $C_{15}H_{16}O$: C, 84.87; H, 7.60%.

(d) 3,4-(4'-Chlorobenzo)-tricyclo [4.3.1.0^{1,6}] dec-3-en-2-one (11d): Similar oxidation and elimination of **9d** (mp 162—163 °C, 1.73 g, 6.8 mmol) gave rise to **11d** (mp 105—106 °C, 780 mg, 49%). Found: C, 72.10; H, 5.62; Cl, 15.05%. Calcd for $C_{14}H_{13}OCl$: C, 72.26; H, 5.63; Cl, 15.23%.

3,4-(4'-Substituted benzo)-tricyclo [4.3.1.0^{1,6}] dec-3-en-2-ol (12a, 12b, and 12d). (a) 3,4-(4'-Methoxybenzo)-tricyclo [4.3.1.0^{1,6}] dec-3-en-2-ol (12a): To a stirred suspension of 130 mg of $LiAlH_4$ in 120 ml of dry ether was added a solution of 560 mg (2.5 mmol) of **11a** in 100 ml of ether. The mixture was stirred for 1 h at 0 °C and for 20 h at room temperature before the excess hydride was carefully decomposed with 0.5 ml of water. The ether layer was decanted and the precipitate was washed several times with ether. The combined organic layer was dried with anhydrous K_2CO_3. The solvent was removed under reduced pressure to yield 550 mg of a colorless solid. Recrystallization from petroleum ether gave a pure product (**12a**) (460 mg, 80%), mp 135—136 °C, and an oily residue (70 mg). It was found from its NMR spectrum that the oily residue consisted of two components **12a** and **13a**. Found: C, 78.44; H, 7.92%. Calcd for $C_{15}H_{18}O_2$: C, 78.23; H, 7.88%.

(b) 3,4-(4'-Methylbenzo)-tricyclo [4.3.1.0^{1,6}] dec-3-en-2-ol (12b): Reduction of **11b** (1.06 g, 4.9 mmol) with $LiAlH_4$ (185 mg) yielded **12b** (940 mg, 89%) which was recrystallized from petroleum ether to give a pure product, mp 68—69 °C and an oily residue (50 mg) which consisted of two components, **12b** and **13b**. Found: C, 83.88; H, 8.68%. Calcd for $C_{15}H_{18}O_2$: C, 84.07; H, 8.47%.

(d) 3,4-(4'-Chlorobenzo)-tricyclo [4.3.1.0^{1,6}] dec-3-en-2-ol (12d): Reduction of **11d** (240 mg, 1.0 mmol) with $LiAlH_4$ (200 mg) yielded **12d** (mp 108—109 °C, 200 mg, 85%) and an oily residue (20 mg) which consisted of two components, **12d** and **13d**. Mass: m^+/e 236 (M^+) and 234 ($C_{14}H_{15}OCl$).

p-*Nitrobenzoate (1a, 1b, and 1d)*. The *p*-nitrobenzoate was prepared by allowing 150 mg (0.065 mmol) of **12a** to react with 240 mg (1.3 mmol) of *p*-nitrobenzoyl chloride in 5 ml of dry pyridine at 5 °C for 24 h. The product was extracted with ether and the organic layer was washed with water, 1M-hydrochloric acid, 5% aqueous sodium hydrogen carbonate, and water. The ether layer was dried over anhydrous sodium sulfate and concentrated under reduced pressure. A light yellow solid was recrystallized from cyclohexane to give **1a** (84 mg, 34%), mp 120—121 °C. Found: C, 69.69; H, 5.43; N, 3.65%. Calcd for $C_{22}H_{21}NO_5$: C, 69.64; H, 5.58; N, 3.69%. By a similar method **1b** (mp 121—122 °C, 58%) and **1d** (mp 144—145 °C, 60%) were obtained. Elemental analysis for **1b**; Found: C, 72.43; H, 5.73; N, 3.80%. Calcd for $C_{22}H_{21}NO_3$: C, 72.71; H, 5.82; N, 3.85%. For **1d**; Found: C, 66.25; H, 4.63; N, 3.50; Calcd for $C_{21}H_{18}NO_4Cl$: C, 65.71; H, 4.73; N, 3.65.

General Kinetic Procedures. For each run approximately 50 mg (*ca.* 0.15 mmol) of *p*-nitrobenzoate (**1a—d**) was weighed into a 50 ml volumetric flask and dissolved in 80% aqueous acetone (*ca.* 3×10^{-3}M). The rate at each temperature (to an accuracy of ±0.03 °C at 25 and 45 °C, and ±0.1 °C at 0 °C) was measured by seven quenching 5.00 ml aliquotes in 20 ml of dry acetone and immediately titrated with a standard aqueous sodium hydroxide solution (*ca.* 0.01M) to a blue end point, using 2 drops of a 1% methanol sodium of Bromothymol Blue as an indicator. The reported values are the average of two runs (Table 2). In all cases infinite titers were measured after *ca.* 10 half-lives and 97 to 102% of the *p*-nitrobenzoic acid was removed. In the case of **1a** (X=MeO), the rate was so fast even at 25 °C that the rate constant was determined by three quenching titers at this temperature.

Preparative Solvolysis of p-*Nitrobenzoate (**1a**, **1b**, **1c**, and **1d**).* *General Method.* A solution of 0.26 mmol of **1c** and 0.5 ml (*ca.* 2.5 mmol) of 2,6-lutidine in 100 ml of 80% acetone–water was heated at 40 °C for *ca.* 40 half-lives. The solution was concentrated under reduced pressure, 50 ml of water was added and the resulting suspension was extracted with ether. The combined ether extracts were washed with water and dried over anhydrous K_2CO_3. Removing the solvent under reduced pressure gave 50 mg of a light yellow oil. Starting from **1c**, the NMR spectrum of the product thus obtained in $CDCl_3$ was essentially identical with the spectrum of a mixture of **12c**, **13c**, and **14c** in the ratio cited previously from five independent experiments.[10] On the basis of this result, the solvolysis product was determined to consist of **12**, **13**, and **14** in each substituent series by comparison of the NMR spectrum with that of the **c**-series (X=H). Then, product distributions were determined by the average ratio of NMR integral values of the vinyl proton signal for **14**, to those of the α-proton signals for **12** and **13** in five runs. The chemical shifts (δ) of the α-proton and vinyl proton signals of the products and the product distributions are

Table 5. IR and ^{1}H-NMR spectral data of **1a—d** to **12a—d**

Compound	IR[a] (cm^{-1})	^{1}H-NMR δ (ppm) in $CDCl_3$			
		Aromatic	Benzylic	Cyclopentyl	Others
1a	1710 (CO_2R), 1600 1520 (NO_2), 1340 (NO_2)	8.33 (s, 4H), 7.10 (d, J=9.0 Hz, 1H), 6.77 (dd, J=9.0, 2.0 Hz, 1H), 6.67 (d, 2.0 Hz, 1H)	3.26, 2.90 (ABq, J=15.0 Hz, 2H)	2.1—1.2 (m, 6H)	6.60 (s, 1H, α-hydrogen), 3.80 (s, 3H, methyl), 0.70, 0.53 (ABq, J=6.0 Hz, 2H, cyclopropyl)
1b	1715 (CO_2R), 1600 1515 (NO_2), 1345 (NO_2)	8.28 (s, 4H), 6.98 (s, 3H)	3.22, 2.90 (ABq, J=15.0 Hz, 2H)	2.1—1.2 (m, 6H)	6.54 (s, 1H, α-hydrogen), 2.31 (s, 3H, methyl), 0.66, 0.52 (ABq, J=6.0 Hz, 2H, cyclopropyl)
1c	1715 (CO_2R), 1605 1530 (NO_2), 1345 (NO_2)	8.37 (s, 4H), 7.23 (s, 4H)	3.22, 2.90 (ABq, J=15.0 Hz, 2H)	2.1—1.2 (m, 6H)	6.69 (s, 1H, α-hydrogen), 0.66, 0.52 (ABq, J=6.0 Hz, 2H, cyclopropyl)
1d	1715 (CO_2R), 1605 1510 (NO_2), 1345 (NO_2)	8.36 (s, 4H), 7.16(s, 3H)	3.29, 2.93 (ABq, J=16.0 Hz, 2H)	2.1—1.4 (m, 6H)	6.60 (s, 1H, α-hydrogen), 0.64, 0.50 (ABq, J=6.0 Hz, 2H, cyclopropyl)
2a	1750, 1730 (CO) 1600	7.20—6.90 (m, 1H) 6.65—6.55 (m, 3H)	3.00 (s, 2H)	2.5—1.4 (m, 6H)	3.68 (s, 3H, methyl), 3.70 (s, 3H, methyl)
2b	1750, 1730 (CO), 1610	7.18—6.90 (m, 4H)	3.10 (s, 2H)	2.5—1.4 (m, 6H)	3.70 (s, 3H, methyl), 2.28 (s, 3H, methyl)
2c	1730 (CO), 1600	7.20 (s, 5H)	3.10 (s, 2H)	2.5—1.4 (m, 6H)	3.70 (s, 3H, methyl)
2d	1750, 1730 (CO), 1600	7.3—7.0 (m, 4H)	3.25, 2.90 (ABq, J=13.5 Hz, 2H)	2.5—1.4 (m, 6H)	3.70 (s, 3H, methyl)
3a	3380 (OH), 2250 (CN), 1740 (CO_2Me), 1600	7.32—7.06 (m, 1H), 6.90—6.60 (m, 3H)	3.38, 2.63 (ABq, J=13.5 Hz, 2H)	2.5—1.5 (m, 7H, contained OH)	3.75 (s, 3H, methyl), 3.66 (s, 3H, methyl)
3b	3340 (OH), 2250 (CN), 1730 (CO_2Me)	7.30—6.80 (m, 4H)	3.37, 2.62 (ABq, J=13.5 Hz, 2H)	2.5—1.5 (m, 7H, contained OH)	3.66 (s, 3H, methyl), 2.31 (s, 3H, methyl)
3c	3380 (OH), 2250 (CN), 1735 (CO_2Me),	7.42—7.02 (m, 5H)	3.30, 2.70 (ABq, J=13.5 Hz, 2H)	2.4—1.7 (m, 7H, contained OH)	3.70 (s, 3H, methyl)
3d	3340 (OH), 2250 (CN), 1740, 1600	7.26—6.95 (m, 4H)	3.38, 2.64 (ABq, J=13.5 Hz, 2H)	2.5—1.7 (m, 7H, contained OH)	3.68 (s, 3H, methyl)
4a	2210 (CN), 1720 (CO_2Me), 1600	7.25—6.97 (m, 1H) 6.75—6.55 (m, 3H)	3.20, 2.95 (ABq, J=13.0 Hz, 2H)	2.70—2.0(m, 4H)	6.63(t, J=1.5 Hz, 1H, vinyl), 3.76 (s, 3H, methyl), 3.70 (s, 3H, methyl)
4b	2210 (CN), 1730 (CO_2Me), 1610	7.24—6.99 (m, 4H)	3.25, 2.95 (ABq, J=13.0 Hz, 2H)	2.8—1.9 (m, 4H)	6.64 (t, J=1.5 Hz, 1H, vinyl), 3.76(s, 3H, methyl), 2.31 (s, 3H, methyl)

Table 5. (continued)

Compound	IR[a] (cm^{-1})	^{1}H-NMR δ (ppm) in $CDCl_3$			
		Aromatic	Benzylic	Cyclopentyl	Others
4c	2230 (CN), 1730 (CO_2Me)	7.28 (s, 5H)	3.25, 2.95 (ABq, J=13.5 Hz, 2H)	2.6—1.85(m, 4H)	6.69 (t, J=2.5 Hz, 1H, vinyl), 3.78 (s, 3H, methyl)
4d	2220 (CN), 1735 (CO_2Me), 1600	7.26—7.05 (m, 4H)	3.29, 2.99 (ABq, J=13.0 Hz, 2H)	2.7—1.95(m, 4H)	6.69 (t, J=1.5 Hz, 1H, vinyl), 3.77 (s, 3H, methyl)
5a	2600, 1690(CO_2H), 1630				
5b	2600, 1690(CO_2H), 1630				
5c	2600, 1690(CO_2H), 1620				
5d	2600, 1700(CO_2H), 1650, 1600				
6a	1700(CO_2H), 1600	7.25—7.00 (m, 1H), 6.77—6.65 (m, 3H)	3.31, 2.74 (ABq, J=13.5 Hz, 2H)	2.4—1.6 (m, 6H)	10.90 (s, 2H, carboxyl), 3.70 (s, 3H, methyl), 3.31 (m, 1H, methine)
6b	1700(CO_2H), 1600	7.00 (s, 4H)	3.30, 2.73 (ABq, J=13.5 Hz, 2H)	2.0—1.7(m, 6H)	11.60 (s, 2H, carboxyl), 3.30 (m, 1H, methine), 2.25 (s, 3H, methyl)
6c	1685 (CO_2H)	7.20 (s, 5H)	3.34, 2.78 (ABq, J=13.5 Hz, 2H)	2.2—1.7(m, 6H)	11.35 (s, 2H, carboxyl), 3.32 (m, 1H, methine)
6d	1700(CO_2H), 1600	7.16 (s, 4H)	3.36, 2.73 (ABq, J=13.5 Hz, 2H)	2.2—1.6(m, 6H)	11.96 (s, 2H, carboxyl), 3.33 (m, 1H, methine)
7a	1700 (CO_2H), 1675 (CO)	7.95 (d, J=9.0 Hz, 1H), 6.95 (dd, J=9.0, 1.5 Hz, 1H), 6.69 (d, 1.5 Hz, 1H)	3.28, 2.90 (ABq, J=18.0 Hz, 2H)	2.5—1.5(m, 6H)	9.21 (s, 1H, carboxyl), 3.80 (s, 3H, methyl), 3.30 (m, 1H, methine)
7b	1690 (CO_2H, CO)	7.86 (d, J=9.0 Hz, 1H), 7.08 (dd, J=9.0, 1.5 Hz), 7.00 (d, J=1.5 Hz)	3.28, 2.90 (ABq, J=18.0 Hz, 2H)	2.5—1.5(m, 6H)	9.95 (s, 1H, carboxyl), 3.30 (m, 1H,methine), 2.35 (s, 3H, methyl)
7c	1680 (CO_2H), 1670 (CO)	8.20—7.7 (m, 1H), 7.65—7.00 (m, 3H)	3.31, 2.96 (ABq, J=18.0 Hz, 2H)	2.5—1.5(m, 6H)	11.08 (s, 1H, carboxyl), 3.35 (m, 1H, methine)
7d	1700 (CO_2H, CO), 1600	7.93 (d, J=9.0 Hz, 1H), 7.30 (dd, J=9.0, 1.5 Hz, 1H), 7.22 (d, J=1.5 Hz, 1H)	3.30, 2.93 (ABq, J=18.0 Hz, 2H)	2.5—1.5(m, 6H)	10.20 (s, 1H, carboxyl), 3.33 (m, 1H, methine)
8a	1725 (CO_2Me), 1665 (CO), 1595	7.97 (d, J=9.0 Hz, 1H), 6.81 (dd, J=9.0, 1.5 Hz, 1H), 6.72 (d, J=1.5 Hz, 1H)	3.28, 2.91 (ABq, J=17.0 Hz, 2H)	2.4—1.6(m, 6H)	3.81 (s, 3H, methyl), 3.59 (s, 3H, methyl), 3.30 (m, 1H, methine)
8b	1730 (CO_2Me), 1675 (CO), 1610	7.92 (d, J=9.0 Hz, 1H), 7.14 (dd, J=9.0, 1.5 Hz, 1H), 7.06 (d, J=1.5 Hz, 1H)	3.33, 2.96 (ABq, J=17.0 Hz, 2H)	2.4—1.6(m, 6H)	3.61 (s, 3H, methyl), 3.40 (m, 1H, methine)
8c	1730 (CO_2Me) 1670 (CO)	8.00 (dd, J=8.0, 1.5 Hz, 1H), 7.65—7.05 (m, 3H)	3.37, 2.97 (ABq, J=16.0 Hz, 2H)	2.3—1.7(m, 6H)	3.60 (s, 3H, methyl), 3.40 (m, 1H, methine)
8d	1725 (CO_2Me), 1680(CO), 1595	7.93 (d, J=9.0 Hz, 1H), 7.30 (dd, J=9.0, 1.5 Hz, 1H), 7.23 (d, J=1.5 Hz, 1H)	3.33, 2.93 (ABq, J=17.0 Hz, 2H)	2.4—1.6(m, 6H)	3.60 (s, 3H, methyl) 3.36 (m, 1H, methine)
9a	3300 (OH), 1620, 1595				
9b	3250 (OH), 1620				
9c	3300 (OH)				

Table 5. (continued)

Compound	IR[a] (cm^{-1})	^{1}H-NMR δ (ppm) in $CDCl_3$			
		Aromatic	Benzylic	Cyclopentyl	Others
9d	3300 (OH), 1625				
10a	3400 (OH), 1660 (CO), 1595	7.94(d, J=9.0Hz, 1H), 6.79(dd, J=9.0, 2.0 Hz, 1H), 6.70 (d, J=2.0 Hz, 1H)	3.59, 3.40 (ABq, J=12.0 Hz, 2H)	2.3—1.5(m, 6H)	3.82 (s, 3H, methyl), 2.89 (s, 2H, oxmethyl), 2.75 (m, 1H, methine), 2.78 (s, 1H, hydroxyl)
10b	3400 (OH), 1660 (CO), 1605	7.86 (d, J=8.0 Hz, 1H), 7.10(dd, J=8.0, 1.5 Hz, 1H), 7.04(d, J=1.5 Hz, 1H)	3.16, 3.41 (ABq, J=11.0 Hz, 2H)	2.2—1.6(m, 6H)	2.90 (s, 2H, oxymethyl), 2.47 (s, 3H, methyl), 2.65 (m, 1H, methine), 1.90 (s, 1H, hydroxyl)
10c	3430 (OH), 1670 (CO)	8.06 7.80 (m, 1H) 7.70 7.05 (m, 3H)	3.52 (s, 2H)	2.5—1.6(m, 7H contained OH)	2.95 (s, 2H, oxmethyl), 2.70 (m, 1H, methine)
10d	3450 (OH), 1660 (CO), 1595	7.89 (d, J=9.0 Hz, 1H), 7.26(dd, J=9.0, 1.0 Hz, 1H), 7.20 (d, J=1.0 Hz, 1H)	3.59, 3.40 (ABq, J=12.0 Hz, 2H)	2.3—1.6(m, 7H contained OH)	2.93 (s, 2H, oxymethyl) 2.75—2.60(m, 1H, methine)
11a	1645 (CO)	7.88 (d, J=8.2 Hz, 1H), 6.81 (dd, J=8.2, 2.2 Hz, 1H), 6.68 (d, J=2.2 Hz, 1H)	3.37, 3.00 (ABq, J=18.0 Hz, 2H)	2.4—1.5(m, 6H)	3.80 (s, 3H, methyl), 1.23, 1.00 (ABq, J=6.0 Hz, 2H cyclopropyl)
11b	1650 (CO), 1605	7.80 (d, J=8.0 Hz, 1H), 7.10(dd, J=8.0, 2.0 Hz, 1H), 7.00 (d, J=2.0Hz, 1H)	3.36, 3.00 (ABq, J=17.0 Hz, 2H)	2.3—1.5(m, 6H)	2.33 (s, 3H, methyl), 1.22, 1.00 (ABq, J=6.0 Hz, 2H, cyclopropyl)
11c	1665 (CO), 1600	8.00—7.60 (m, 1H) 7.55—6.96 (m, 3H)	3.39, 3.02 (ABq, J=18.9 Hz, 2H)	2.4—1.4(m, 6H)	1.24, 1.05 (ABq, J=6.0 Hz, 2H, cyclopropyl)
11d	1655 (CO), 1595	7.80 (d, J=8.0 Hz, 1H), 7.23 (dd, J=8.0, 1.5 Hz, 1H), 7.15 (d, J=1.5 Hz, 1H)	3.35, 2.98 (ABq, J=16.5 Hz, 2H)	2.3—1.5(m, 6H)	1.25, 1.03 (ABq, J=6.0 Hz, 2H, cyclopropyl)
12a	3350 (OH), 1610	7.56 (d, J=9.0 Hz, 1H), 6.76 (dd, J=9.0, 2.0 Hz, 1H), 6.61 (d, J=2.0 Hz, 1H)	3.16, 2.82 (ABq, J=16.0 Hz, 2H)	2.4—1.4(m, 7H contained OH)	4.84 (s, 1H, α-hydrogen), 3.80 (s, 3H, methyl), 0.36 (s, 2H, cyclopropyl)
12b	3350 (OH), 1610	7.56 (d, J=9.0 Hz, 1H), 7.03 (dd, J=9.0, 2.0 Hz, 1H), 6.90 (d, J=2.0 Hz, 1H)	3.16, 2.82 (ABq, J=16.0 Hz, 2H)	2.4—1.2(m, 7H contained OH)	4.83 (s, 1H, α-hydrogen), 2.30 (s, 3H, methyl). 0.36 (s, 2H, cyclopropyl)
12c	3350 (OH)	7.70—7.40 (m, 1H) 7.30—6.90 (m, 3H)	3.15, 2.79 (ABq, J=16.0 Hz, 2H)	2.5—1.3(m, 7H contained OH)	4.83 (s, 1H, α-hydrogen), 0.36 (s, 2H, cyclopropyl)
12d	3250 (OH), 1600	7.60 (d, J=9.0, 1H), 7.2—7.0 (m, 2H)	3.14, 2.77 (ABq, J=16.0 Hz, 2H)	2.4—1.4(m, 7H contained OH)	4.82 (s, 1H, α-hydrogen), 0.35 (s, 2H, cyclopropyl)

a) Infrared spectra of **2a—d** and **4a—d** were recorded in neat and those of the other compounds in Nujol mulls.

summarized in Table 3.

This work was supported in part by a grant from the Ministry of Education of Japan, 774136, in 1972 and 874145, in 1973. The athor wishes to thank Professor Terukiyo Hanafusa for his helpful advice and encouragement.

References

1) a) S. Winstein and E. M. Kosower, *J. Amer. Chem. Soc.*, **81**, 4399 (1959). b) L. Birladeanu, T. Hanafusa, B. Johnson, and S. Winstein, *ibid.*, **88**, 2316 (1966). c) C. D. Poulter, E. C. Friedrich, and S. Winstein, *ibid.*, **92**, 4274 (1970). d) A. S. Kende, J. K. Jenkins, and L. E. Friedrich, *Chem. Commun.*, **1971**, 1215.

2) a) T. Tsuji, I. Moritani, and S. Nishida, This Bulletin, **40**, 2338 (1967). b) H. Hart and J. M. Sandri, *J. Amer. Chem. Soc.*, **81**, 320 (1959).

3) a) P. v. R. Schleyer and G. W. Van Dine, *ibid.*, **88**, 2321 (1961). b) P. v. R. Schleyer, P. J. Stang, and D. J. Robert, *ibid.*, **92**, 4725 (1970). c) C. F. Wilcox, L. M. Loew, and R. Hoffmann, *ibid.*, **95**, 8192 (1973). d) R. S. Brown and T. G. Traylor, *ibid.*, **59**, 8025 (1973) and references cited therein.

4) Review: "Carbonium Ions," Vol. III, ed. by G. A. Olah and P. v. R. Scheyer, Wiley-Interscience, New York, N. Y. (1969).

5) A. Streitwieser, Jr., "Solvolytic Displacement Reaction," McGraw-Hill, New York (1962), p. 13.
6) N. C. Deno, H. G. Richey, Jr., J. S. Liu, D. N. Lincoln, and J. O. Turner, *J. Amer. Chem. Soc.*, **87**, 4533 (1965).
7) H. C. Brown and E. N. Peters, *ibid.*, **95**, 2400 (1973).
8) G. A. Olah and P. W. Westerman, *ibid.*, **95**, 7530 (1973). G. A. Olah, P. W. Westerman, and J. Nishimura, *ibid.*, **96**, 3548 (1974).
9) A. S. Kende, J. K. Jenkins, and L. E. Friedrich, *Chem. Commun.*, **1971**, 1215.
10) The details of synthesis and solvolysis of **1c** will be provied in a furture publication.
11) C. D. Poulter, R. S. Boikess, J. I. Brauman, and S. Winstein, *J. Amer. Chem. Soc.*, **94**, 2291 (1972) and references cited therein.
12) H. C. Brown and J. Muzzio, *ibid.*, **88**, 2811 (1966); H. C. Brown and H. R. Deck, *ibid.*, **87**, 5620 (1965).
13) C. K. Ingold, "Structure and Mechanism in Organic Chemistry," 2nd ed, Cornell University Press, Ithaka, N. Y. (1970).
14) A. Streitwieser, Jr., "Solvolytic Displacement Reactions," McGraw-Hill, New York (1962), p. 75.
15) R. A. Sneen and A. L. Baron, *J. Amer. Chem. Soc.*, **83**, 614 (1961). T. Shono, A. Oku, and R. Oda, *Tetrahedron*, **24**, 421 (1967).
16) K. Takeuchi and H. C. Brown, *J. Amer. Chem. Soc.*, **90**, 2693 (1968).
17) E. N. Peters and H. C. Brown, *ibid.*, **95**, 2397 (1973).
18) S. Winstein, R. K. Morse, E. Grunwark, K. C. Shreiber, and J. Corse, *ibid.*, **74**, 1113 (1952).
19) G. S. Hammond, *ibid.*, **77**, 334 (1955).
20) D. F. Eaton and T. G. Traylor, *ibid.*, **96**, 1226 (1974).
21) H. G. Richey, Jr. and N. C. Buckley, *ibid.*, **85**, 3057 (1963).
22) T. G. Traylor, W. Hanstein, H. J. Berwin, N. A. Clinton, and R. S. Brown, *ibid.*, **93**, 5715 (1971).
23) E. M. Kosower and M. Ito, *Proc. Chem. Soc.*, **1962**, 25.
24) G. A. Olah and A. M. White, *J. Amer. Chem. Soc.*, **91**, 5801 (1969); *ibid.*, **90**, 1884 (1968).
25) W. von E. Doering, M. Levitz, A. Sayigh, M. Sprecher, and W. P. Whelan, *J. Amer. Chem. Soc.*, **75**, 1008 (1953); R.C. Fort, Jr. and P. v. R. Schleyer, *Adv. Alicyclic Chem.*, **1**, 284 (1966).
26) S. Winstein and J. Sonnenberg, *J. Amer. Chem. Soc.*, **83**, 3235, 3244 (1961); R. F. Childs and S. Winstein, *ibid.*, **89**, 6348 (1967); S. Winstein, *Quart. Rev.*, **23**, 141 (1969); R. Huisgen and G. Boche, *Tetrahedron Lett.* **1965**, 1769.
27) M. Simonetta and G. Favini, *J. Chem. Soc.*, **1954**, 1840.
28) M. S. Kharasch and H. C. Brown, *J. Amer. Chem. Soc.*, **61**, 2141 (1939).
29) G. M. Bennett and B. Jones, *J. Chem. Soc.*, **1935**, 1815.
30) P. S. Pinkney, "Organic Syntheses," Coll. Vol. II, p. 116 (1943).

Solvolysis of 2,3-Cyclopenteno-4*H*-homochromen-4-ol Acetate: Comparison with the Corresponding Carbocyclic System

Hiroshi YAMAOKA, Katsuo OHKATA, and Terukiyo HANAFUSA

Chemistry Department, Faculty of Science, Hiroshima University, Higashi-senda-cho, Hiroshima 730

(Received February 26, 1975)

A novel secondary cyclopropylphenylmethyl acetate was prepared from a chromone skeleton *via* homochromone derivatives in order to study solvolytic behavior. Reduction of the cyclopropyl ketone (homochromone) with lithium aluminum hydride in ether to the corresponding secondary alcohol, was found to be highly stereospecific giving only one of the geometrical isomers. The alcohol was converted into its acetate and subjected to solvolysis in 80% acetone–water. The acetate was hydrolyzed at the rate of 3×10^{-5} s^{-1} (25 °C) undergoing alkyl-oxygen fission. This rate constant was as high as the most reactive secondary esters in solvolyses ever reported, and about 20 times as high as the corresponding carbocyclic ester by estimation of the same leaving group. Product studies were undertaken in the presence of sodium hydrogencarbonate, and seven-membered hemiacetal was obtained in good yield. The structural characteristics of the homochromenol ester in the solvolysis are discussed and benzohomopyrylium ion, an extremely delocalized homoaromatic species, is proposed as an intermediate carbocation.

A large number of studies have been made on solvolytic behavior in various cyclopropane derivatives since newer convenient synthetic routes for producing a cyclopropyl group have been reported. Thus, one of the attractive concepts from these studies may be homoconjugation or homoaromaticity in carbocations as the solvolytic intermediate.[1]

Here, a novel secondary cyclopropylphenyl methanol derivative (**1-OAc**) is presented, which is closely related to the corresponding carbocyclic system (**2-OPNB**).[2] The structural characteristics of these systems are: (i) the benzene ring and cyclopropane are connected to each other with both a carbon of the reaction center and an etherial oxygen (or methylene) group, and then a heterocyclic or a carbocyclic six-membered ring is formed, (ii) such a carbon skeleton enables two geometric isomers (*syn*, *anti*) between hydroxyl group and cyclopropane, and (iii) the cyclopropane ring is also fused with a trimethylene group (scissors effect).

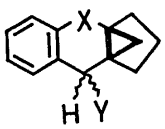

	X	Y
1-OH	O	OH
1-OAc	O	OAc
2-OH	CH_2	OH
2-OPNB	CH_2	OPNB
2-H	CH_2	H

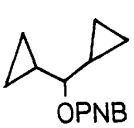

3-OPNB

	X
4-OH	OH
4-OPNB	OPNB

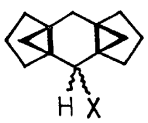

	X
5-OH	OH
5-OPNB	OPNB
5-OAc	OAc

* *a* (*anti*) and *s* (*syn*) are referred between hydroxyl and cyclopropane

** -OPNB; paranitrobenzoate

In both systems, the phenyl and cyclopropyl groups are situated in the α-position to the carbon of the reactive center, where both groups can be effective for high reactivity in solvolysis.[3] It is one of the special interests in these substrates that the accelerative effects of each of these two groups seem to compete with each other in the solvolysis. Another interesting point is the difference between **1** and **2** due to the bridged oxygen or the bridged methylene.

Various carbocations may be predicted as solvolytic intermediates of **1-OAc**, and are shown in Fig. 1. From the available data in the literature, we may speculate upon the relative importance of these cations. In the case of a heterocyclic system (**1**), it is interesting that the cation (**e**) is taken for a fully-conjugated homopyrylium ion.[4]

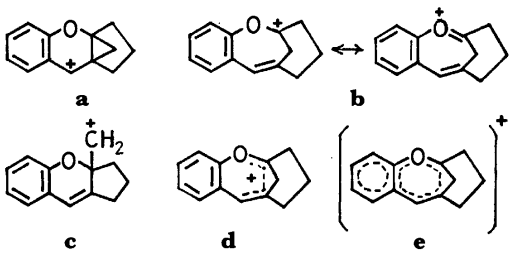

Fig. 1. Cabocations predicted as a solvolytic intermediate of **1-OAc**.

Both **1** and **2** have the cyclopropane fused with a trimethylene bridge which was suggested to be effective in contributing to the anchimeric assistance of the cyclopropane ring in solvolysis.[5] A similar effect of bridged methylene (forming a six-membered ring) in the biscyclopropylmethyl system was reported.[5,6] Regarding the first-order rate constants, the relative rate ratio of **3-OPNB** to **4s-OPNB** to **5s-OPNB** was $1:10^2:3\times10^3$, respectively. The reactivity of **1** is also interesting from another point of view, in which **1** is regarded as a 2-aryloxycyclopropyl methanol derivative. Julia *et al.* reported the isomerization of 2-alkoxy- and 2-aryloxycyclopropyl methanol into an β,γ-unsaturated carbonyl compound and an alcohol or a phenol with sulfuric acid.[7] The solvolytic study of **1-OAc** will be

referred to in the order: (1) synthetic procedure, (2) product study, and (3) kinetic results.

Results and Discussion

Syntheses. Preparation of the Homochromone: It was pointed out by Corey *et al.* that dimethyloxosulfonium methylide is convenient in preparing a cyclopropane ring from corresponding α,β-unsaturated ketones.[8] Chromones, regarded as unsaturated carbonyl compounds, were treated with the above reagent in dimethyl sulfoxide by Ollis *et al.* and three types of additional products were reported:[9] (**i**) 2,3-methanochroman-4-one (homochromone) derivatives, (**ii**) ketophenols obtained from further reaction (hydrolysis) of (**i**), and (**iii**) five-membered ketones including a non-conjugated double bond.

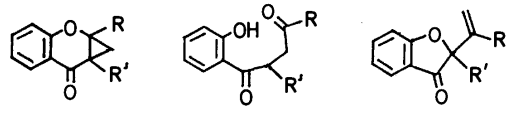

i **ii** **iii**

2,3-Cyclopentenochromone (**6**), an important precursor for producing homochromenol derivatives (**1**), was prepared according to the procedure reported by Boyd *et al.*[10] The reaction of **6** with dimethyloxosulfonium methylide gave homochromone (**7**) (type **i**) in good yield, which was purified using column chromatography on neutral alumina, but the other products (**ii** and **iii**) were not found in this experiment. Though chemical shifts of the protons belonging to the cyclopropane ring in **7** were not obvious owing to the duplication with the signals of a trimethylene group in its NMR spectrum, the wave number of maximum absorption ($\nu_{C=O}$) in the IR spectrum of **7** shifted to higher frequency (20 cm^{-1}) because of the change of the properties of the carbonyl function compared with the corresponding chromone (**6**).

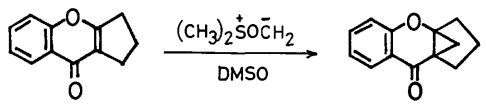

6 **7**

Reduction of the Homochromone (7): Reduction of homochromone (**7**) with lithium aluminum hydride (LAH) in ether gave a secondary alcohol (**1-OH**) in *ca.* 70% yield, which was fairly unstable. Contrary to **7**, **1-OH** showed a typical AB quartet (J=6.5 Hz) due to cyclopropyl methylene protons (δ=1.15, 0.55 ppm) separated from other methylene protons (δ=2.5−1.5 ppm) in its NMR spectrum. Also **1-OH** showed a singlet at δ=4.65 ppm for α-hydrogen, while another singlet was observed at δ=4.92 ppm in the crude minor epimeric alcohol, which was obtained from the mother liquor after repeated recrystallization of the former. An attempt to obtain pure minor alcohol was not successful because of the high stereospecificity of the reduction. Moreover, facile decomposition often occurred (cleavage of the cyclopropane ring) during purification of the mixture of these epimers. Reduction of **7** with sodium borohydride (NBH) in 2-propanol was also stereospecific and gave only one isomer; the spectroscopic data agree well with those of the major product obtained by LAH reduction. The reduction of the closely related ketone (**8**) with both LAH and NBH was also stereospecific, giving only one stereoisomer.[2] It is interesting that the reaction of both **7** and **8** with LAH yielded single alcohols in contrast to **9**, which gave both epimeric alcohols in nearly equal amounts upon reduction with LAH.[5]

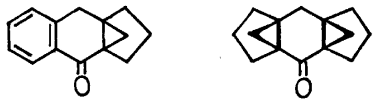

8 **9**

Stereochemistry of Homochromenol: It is generally accepted that α-proton *syn* to such a cyclopropane ring as in bicyclo[*m.* 1. 0]- or tricyclo[*m. n.* 1. 0]alkane-2-ol should be more shielded by the cyclopropane than the *anti* proton.[11] Also in the reduction of **7** and **8**, hydride addition with the carbonyl function should predominantly occur from less hindered *syn* to a cyclopropane ring in analogy with the reduction of the related ketone.

On the basis of these prospects, the structure of the main reduction product from **7** is assigned for the *anti* alcohol (between hydroxyl and cyclopropane) at this stage, though this assignment is tentative because of the following equivocal factors: (i) the difference between the carbocyclic and oxacyclic systems, and (ii) the existence of the benzene ring, which may play various roles affecting the magnetic properties of α-hydrogen of **7**.

Recently the stereochemistry of the reduction products from 1,3,5,7-tetramethyltricyclo[5.1.0.$0^{3,5}$]octan-2-one and its derivatives was discussed in another approach to interpreting the NMR spectrum.[12] According to Ref. 12, the reduction took place quite stereospecifically and gave only one isomer assigned to be *syn* alcohol. It is necessary to study from various viewpoints for the stereochemical problem of **1-OH**. This will be discussed by means of the NMR spectra of some substrates including a homochromenol skeleton in a forthcoming paper.

Preparation of the Ester: Attempts to prepare *p*-nitrobenzoate (**1-OPNB**) with *p*-nitrobenzoyl chloride in pyridine were unsuccessful owing to the production of a complex mixture. Then, **1-OH** was transformed into its acetate (**1-OAc**), a colorless liquid, with acetic anhydride in pyridine. The acetate was so unstable that a decomposition occurred in the course of the purification process in column chromatography over neutral alumina. The structure of the acetate was determined by spectroscopic analysis (*cf.* Experimental). This acetate was then subjected to a solvolytic study without further purification.

Product Study in Solvolysis. In the presence of sodium hydrogencarbonate as a suspension in 80% acetone–water at 25 °C for 4 days (*ca.* 10 half-lives), the major solvolysis product of **1-OAc** was a hemiacetal (**10**). Another alcohol (**11**) was contaminated with **10** though the **10**/**11** ratios were somewhat variable from the information of the NMR spectra. The structural determination of these products will now be discussed.

Structural Problem of **10**: On the basis of combustion

analysis, both **10** and **11** are structural isomers of the parent alcohol (**1-OH**). The major product showed a strong absorption at 1640 cm^{-1} in the IR spectrum, and a singlet at $\delta=5.87$ ppm (vinyl) and $\delta=3.55$ ppm (methylene) in the NMR spectrum. Two possible structures are expected from this data: (i) primary alcohol (**12**) produced by b-c bond cleavage of the cyclopropane ring, (ii) tertiary alcohol (hemiacetal) (**10**) produced by a-b bond cleavage of the cyclopropane ring. The signal at $\delta=3.55$ ppm may be assigned to the methylene proton of neopentyl group (i), and not to the allylic (bridged) methylene (ii), according to an estimation from the available data listed in Table 1.

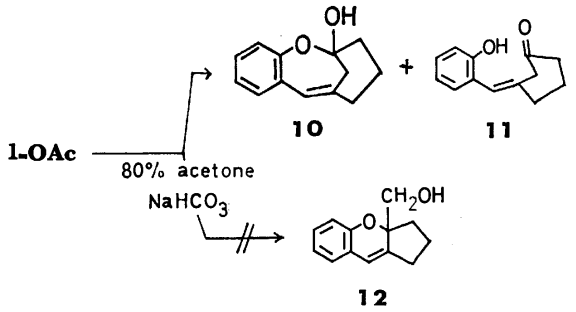

Table 1. Chemical shifts for dual type methylene signals (corresponding to **10** and **12**, respectively)

Substrate	Methylene (ppm)	Reference
>C-CH_2-O-	3.36—4.48	13[a,c]
H_3C-CH_2-OH	3.26	14[a,e]
F_3C-CH_2-OH	3.93	14[a,e]
16	3.28	2[a]
>C-CH_2-C=C<	1.86—2.12	13[b,d]
H_3C-CH_2-C=C<	2.02	14[b,e]
F_3C-CH_2-C=C<	2.69	14[b,e]
17	2.6	15[b]
18	2.43	22[b]
10	3.55	f

a) Examples for primary alcohol **12**. b) Examples for hemiacetal **10**. c) Summed for 42 substrates. d) Summed for 11 substrates. e) Calculated value by means of Shoolery's effective shielding constants. f) Observed chemical shift of the major solvolysis product obtained from **1-OAc**.

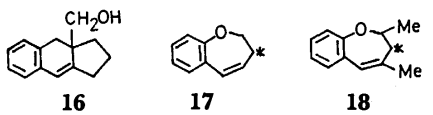

16 **17** **18**

Acetylation of the alcohol was performed with acetic anhydride in pyridine for the purpose of distinguishing between primary and tertiary alcohols. In contrast to the expectation based on the chemical shift, downfield shift of the signal at $\delta=3.55$ ppm was not observed at all, but a slight upfield shift (0.1 ppm) occurred. Thus, the alcohol was assigned preferably to be tertiary alcohol (ii) from these observations of the NMR spectra.

Europium dipivaloyl methanate, $Eu(dpm)_3$, was utilized in order to obtain further information about the structure. In general, a characteristic downfield shift is expected for methylene adjacent to a hydroxyl group if the substrate is a primary alcohol. On the other hand, such a phenomenon is not expected for tertiary alcohol (hemiacetal). The experimental results for the alcohol obtained in solvolysis are shown in Fig. 2. The extent of the induced downfield shift of both the methylene signal at $\delta=3.55$ ppm and the signals assigned as part of the trimethylene group at $\delta=1.7$—2.6 ppm may be worth noticing in comparison to those of other signals. According to the situation, the structure of this alcohol may be characterized as tertiary alcohol (**10**) rather than primary alcohol (**12**), on the basis of the result from acetylation. The major solvolysis product from **1-OAc** is concluded to be a hemiacetal (**10**). Though the chemical shift of the bridged methylene group of **10** appears at a fairly lower field value ($\delta=3.55$ ppm) than expected, this might be due to steric compression as has been mentioned for cage molecules.[16]

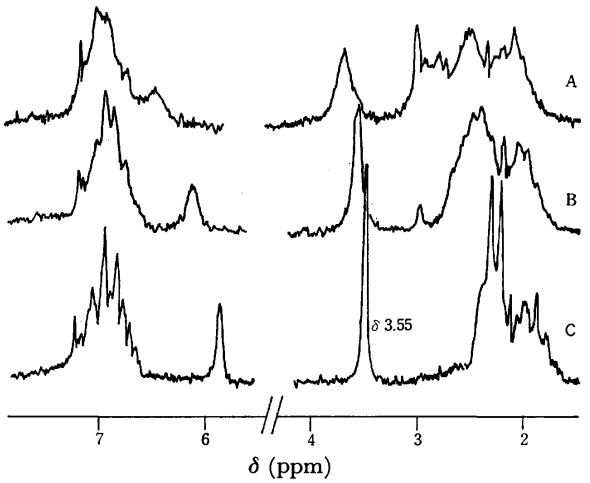

Fig. 2. The NMR spectra of **10** (spectrum C) in $CDCl_3$. After the addition of $Eu(dpm)_3$ into the solution, the spectrum B (10.0 mg) and the spectrum A (18.0 mg) were recorded. Signals for hydroxyl proton were not shown in both spectra A and B owing to enormous downfield shift.

Structural Problem of 11: Characteristics of the minor solvolysis product of **1-OAc** are: (i) positive for $FeCl_3$ in chloroform–phenolic material, (ii) typical IR and UV absorption bands for the aliphatic carbonyl group at 1720 cm^{-1}, and 315 nm ($\varepsilon=350$), respectively, and (iii) the presence of an allylic methylene group adjacent to a carbonyl function ($\delta=3.05$ ppm) based on the NMR spectra. From speculation based on these data, ketophenol (**11**) might be proposed as the structure of this material. Hemiacetal (**10**) was transformed into **11** in the presence of **11** in the medium, *e.g.*, in $CDCl_3$ prepared for the measurement of a NMR spectrum. It is probably due to the phenolic function of **11**. On the basis of this phenomenon, the uncertainty of the ratio **10**/**11** in the solvolysis may be explained satisfactorily.

When the NMR spectrum of **10** in trifluoroacetic acid (TFA) was observed at room temperature, a mixture of **10** and **11** was produced and the former was predominant under the condition. Similarly when the

spectrum of **11** was recorded in TFA, the same mixture as above was evidently produced. In both cases, the mixture could be isolated in good yield by quenching the solution. It is interesting that **10** and **11** are converted into each other in TFA. Such a mutual exchange suggests the validity of each structure, since **10** is an intramolecular hemiacetal of a ketophenol (**11**). It was, moreover, found that homochromenol (**1-OH**) was clearly converted into a mixture analogous to the above in TFA at room temperature. Isolation of the mixture was similarly achieved, thus

$$\underset{(\mathbf{1\text{-}OH})}{\text{Parent alcohol}} \xrightarrow[\text{in TFA}]{} \underset{(\mathbf{10})}{\text{Hemiacetal}} \underset{\text{in TFA}}{\overset{\text{in TFA or 11}}{\rightleftharpoons}} \underset{(\mathbf{11})}{\text{Ketophenol}}$$

Solvolysis in Another Condition: The hemiacetal (**10**) was also obtained in solvolysis of **1-OAc** in the presence of either pyridine or 2,6-lutidine instead of in the presence of sodium hydrogencarbonate as described above. However, a complex mixture was obtained if any acid was used in order to remove the alkali during a work-up process. It is suggested that the hemiacetal (**10**) may be highly sensitive to acidic substances.

In the absence of any alkali, solvolysis of **1-OAc** gives a yellowish oil whose NMR spectrum suggested the production of complex mixtures, and **10** was not observed at all. Thus, the presence of an alkali is obviously essential to the production of **10** in such reaction conditions.

A Comparison of the Solvolysis Products of 1-OAc with Those from the Corresponding Carbocyclic Ester: According to the product study of a closely related ester (**2-OPNB**), the mixture of **2a-OH**, **2s-OH** and a tertiary alcohol (**13**) was obtained in the ratio of 1.0: 3.3: 3.5 in 80% acetone–water at 25 °C in the presence of the alkali.[2] This is somewhat different from the result for **1-OAc**. A parent alcohol (**2a-OH**) was isomerized into the thermodynamically more stable isomer **13** in the presence of *p*-nitrobenzoic acid, but both parent alcohols (**2a-OH**) and (**2s-OH**) were stable in the presence of the alkali under solvolytic conditions. The alcohol (**13**) is produced in a mode similar to the cleavage of the cyclopropane ring (a-b cleavage), as in the case of hemiacetal (**10**). It is noteworthy that considerably strained bridgehead alcohols, **10** and **13**, were thermodynamically the most stable products in both cases, although a partial ketonization sometimes occurred for **10**. Together with the kinetic results discussed later, these facts might support possible intervention of the homoallylically conjugated or homoaromatically conjugated carbocation in these solvolyses.

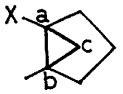

Modes of the cleavage of cyclopropane

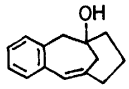

13

Alkyl-oxygen Fission of Homochromenol Acetate (1-OAc) during Solvolysis: The parent alcohol (**1-OH**) was found to be stable in the presence of sodium hydrogencarbonate under the solvolytic condition. So alkyl-oxygen fission may occur during the solvolysis of **1-OAc** based on the fact that rearranged alcohols **10** and **11** were isolated as solvolysis products of **1-OAc**.

The mode of fission may be confirmed by means of solvolysis in anhydrous methanol (methanolysis). If the solvolysis of **1-OAc** proceeds with an acyl-oxygen fission, the products should be alcohol(s) and methyl acetate. But methyl ether and acetic acid should be obtained in the case of an alkyl-oxygen fission. The reaction scheme is as follows:

$$\mathrm{RO\text{-}\overset{\overset{\mathrm{O}}{\|}}{C}CH_3} \xrightarrow{\text{SO-H}} \mathrm{RO\text{-}H} + \mathrm{SO\text{-}\overset{\overset{\mathrm{O}}{\|}}{C}CH_3}$$

acyl-oxygen fission

$$\mathrm{R\text{-}O\overset{\overset{\mathrm{O}}{\|}}{C}CH_3} \xrightarrow{\text{SO-H}} \mathrm{R\text{-}OS} + \mathrm{H\text{-}O\overset{\overset{\mathrm{O}}{\|}}{C}CH_3}$$

alkyl-oxygen fission

SO- = MeO-, HO-

Methanolysis of **1-OAc** was carried out in the presence of pyridine at 25 °C for 4 days, the methyl ether (**14**) of **10** was obtained as the sole product, and the ether was determined from its spectra. Thus, alkyl-oxygen fission of **1-OAc** during solvolysis may be more plausible.

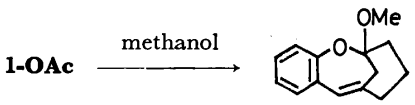

14

Trapping a Reactive Carbocation with a Hydride Reagent: A high solvolytic reactivity of appropriate esters provides an effective route to the parent (or isomerized) hydrocarbon, which is called *trapping* an intermediate carbocation.[17] The acetate (**1-OAc**), could be converted to a seven-membered unsaturated ether (**15**), as the sole product in 50% aqueous diglyme containing excess NBH. From these product studies in various reactions for **1-OAc** it has been shown that a nucleophile attacks specifically at the bridgehead carbon adjacent to etherial oxygen in the intermediate cation. This is contrary to the fact that the *p*-nitrobenzoate (**2-OPNB**) was converted to a mixture of isomeric alcohols (**2a-OH**, **2s-OH** and **13**) upon solvolysis or to the *parent* hydrocarbon (**2-H**) by the hydride reagent. The difference between the products from the two systems (**1-OAc** and **2-OPNB**) may correspond to the properties of the intermediate carbocation in the reactions, although the leaving groups are different.

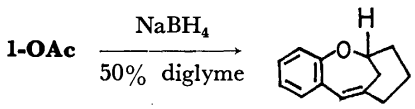

15

Kinetic Study of the Solvolysis. The rates of the solvolysis of **1-OAc** were determined in 80% acetone–water solution at 25—40 °C by tracing the increment of the acetic acid produced with 18 aliquots at regular intervals. Each aliquot was quenched by acetone, followed by means of the usual alkaline titration using bromothymol blue as an indicator. All runs showed

Table 2. Solvolysis rates of **1-OAc** and **2-OPNB** in 80% acetone–water[a)]

Substrate	Temperature[b)] °C	k s^{-1}	$\Delta H^{\neq}$ kcal/mol	$\Delta S^{\neq}$ e.u.	Relative rate[c)]	Reference
1-OAc	25	$3.2_4\times10^{-5}$	21.2	−5.8	1.0	This work
	35	$9.5_1\times10^{-5}$				
	40	$1.9_0\times10^{-4}$				
2a-OPNB	25	$8.6_0\times10^{-5}$	20.6	−8.0	0.052	2
2s-OPNB	25	$1.7_3\times10^{-4}$			0.10	2

a) The rate constants (k) are first-order, and the mean values obtained from several runs are shown. b) Accuracy was ±0.03 °C. c) Estimation was based on available data in Ref. 5 as the same leaving group.

Table 3. Relative rates of solvolysis for related secondary esters on the basis of **1-OAc**

Substrate	**4-sOPNB**	**5-OAc**	**19-OAc**	**20-OPNB**	**21-OPNB**	**22-OPNB**
Relative rate[a)]	0.15	a : 2.4 s : 4.6	0.39	6.1	$\times10^{-4}$	$\times10^{-8}$
Solvolysis product	b	b	c	d	b	b
References	5, 6	5	19	20	18	18

a) Calculated as the same leaving group, solvent (80% acetone–water), and temperature (25 °C, or 30 °C if necessary). b) Parent alcohol (in aqueous acetone). c) Anthracene. d) Tetralin.

strictly first-order kinetics up to almost two half-lives (Fig. 3.), despite the fact that the purification of **1-OAc** was difficult. The observed kinetic data are shown in Table 2, and the relative rates of solvolysis for related systems in Table 3.

Thus, **1-OAc** was solvolyzed accompanying alkyl-oxygen fission in 80% acetone–water at the rate of $3.2_4\times10^{-5}$ s^{-1} (25 °C), which is as high as those of the most reactive secondary esters (**5a-OAc**, **5s-OAc**, **19-OAc**, and **20-OPNB**) that have ever been measured in solvolysis.[5,19,20)] The acetate (**1-OAc**) was about 20 times as reactive as the corresponding carbocyclic system (**2a-OPNB**), by estimation of the same leaving group as shown in Table 2, and was solvolyzed *ca.* 10^4 times faster than the secondary cyclopropylphenylmethyl

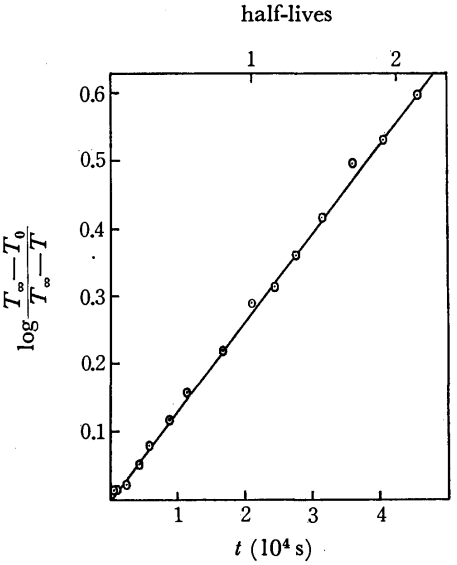

Fig. 3. Plots of the first-order function *vs.* reaction time (or half-lives) for **1-OAc** at 25 °C in 80% acetone–water.

p-nitrobenzoate (**21-OPNB**).[18)] In the following discussion, **21-OPNB** may be chosen as the standard substrate.

Since the benzene ring and the cyclopropane are connected to each other by the bridged oxygen in **1-OAc**, dual types of contributions may be expected for such a high reactivity due to the etherial oxygen: (i) the effect of an *ortho*-alkoxy group on the benzene ring, and (ii) a contribution as β-phenoxy substitution of the cyclopropane. Now the role of the bridged oxygen in the solvolysis will be discussed from such viewpoints.

Substituent Effect of the Benzene Ring: According to the study of Shono *et al.* for the *para* substituent effect of the benzene ring (–OMe, –Me, –H, and –Cl) on **21-OPNB**, the *para*-methoxy ester was 780 times more reactive than the corresponding parent ester (**21-OPNB**): $\rho=-3.61$ *vs.* σ^+.[18)] From these results, an *ortho*-alkoxy substitution in the benzene ring seems to be one of the important factors for the high reactivity of **1-OAc**, though the accelerative effect of the *ortho*-alkoxy group may be usually smaller than that of the *para*-alkoxy group according to available data.[21)]

Effects of Substitution on the Cyclopropane: Rate enhancement due to the substitution was reported for *primary* cyclopropylmethyl 3,5-dinitrobenzoate (**23-ODNB**) such that every methyl substitution at the β-position increased the rate about 10 times that of the corresponding ester, and the substitution of a *trans* β-ethoxy group caused a great acceleration (nearly 10^3 times).[23)] But the substituent effect of the cyclopropane ring for **21-OPNB** has not been reported to date. Therefore, *trans* 2-phenoxycyclopropylphenylmethyl acetate (**24-OAc**) was adopted as an acyclic model system corresponding to its cyclic acetate (**1-OAc**). If a clear rate enhancement in comparison with **21-OPNB** should be observed, the β-aryloxy substitution may be an important cause of the high reactivity of **1-OAc**.

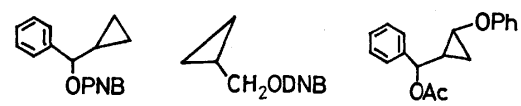

21-OPNB **23-ODNB** **24-OAc**

* -ODNB; 3,5-dinitrobenzoate

In our preliminary experiments, **24-OAc** was not hydrolyzed appreciably under similar solvolytic conditions for **1-OAc.**[22] The effect of the β-aryloxy substitution, therefore, should be explained by means of another contribution, probably due to a *cis* substitution which constitutes a six-membered heterocycle, **1-OAc**. Since it has been pointed out that both the phenyl group and the cyclopropyl group are effective in increasing the reactivity in **21-OPNB,**[18] these are perturbations of such relatively highly reactive systems. The ester (**1-OAc**) involves many complex factors which cause difficulty in determining the origins of the increase in reactivity compared with the standard substrate (**21-OPNB**). Consequently, it appears risky to interpret the observed kinetic data on the basis of the simple additional summation of the effects of *ortho*-alkoxy group of the benzene ring and of the substitution of the cyclopropane in such a sophisticated system as **1-OAc**. The structural characteristics of **1-OAc** may play an important role in solvolysis, since a homochromenol ester is, in general, suitable for creating high reactivity.

Intermediate Carbocation in the Solvolysis. As shown in the product studies of **1-OAc**, each nucleophile attacks at the carbon adjacent to the etherial oxygen quite specifically in spite of different reaction conditions. According to these product studies, the cation (**b**) appears at first sight to be suitable as a solvolytic intermediate of **1-OAc**.

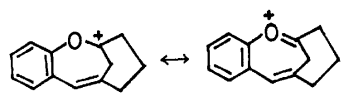

b

The difficulty in the production of the bridgehead cation is well known, in general. Owing to the assistance of the oxygen adjacent to the carbon of the cationic center, the bridgehead cation (**b**) might be an exception to the above general rule though such a phenomenon has not yet been reported.

Otherwise, the presence of the double bond on the opposite bridge ead carbon diminishes the possibility of **b**. Recently, the relative stability between the norcaradiene form (**f**) and the cycloheptatriene form (**g**) using the NMR spectra was discussed by Vogel *et al.*[24] According to their report, the former (**f**) is much more stable than the latter (**g**) in case of the presence of a trimethylene group. The cation (**b**) is *isoelectronic* to the cycloheptatriene form (**g**), so that **b** may be invalid as a solvolytic intermediate for **1-OAc**.

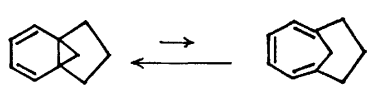

f **g**

Norcaradiene form Cycloheptatriene form

Aromatization sometimes occurs in the solvolysis of highly reactive systems, as shown in Table 3, where the intermediate carbocation may be somewhat stabilized by means of its aromaticity, *e.g.*,

19-OAc ⟶ anthracene[19]

and

20-OPNB ⟶ tetralin[20]

From these prospects, the benzohomopyrylium ion (**e**) might be proposed as the cationic intermediate in the solvolysis of **1-OAc**, and the formation of such extremely delocalized homoaromatic species might greatly contribute to decreasing the activation energy for solvolysis.[1]

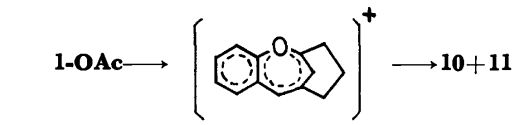

e

Benzohomopyrylium ion

Experimental

General. All melting points are uncorrected. The IR spectra were measured using a Hitachi 215 spectrometer, the UV spectra on a Yanaco spectrometer, the mass spectra on a Hitachi RMS-4 spectrometer, and the NMR spectra on a Hitachi R-20 spectrometer. The chemical shifts of the NMR spectra are given in δ, with tetramethylsilane as an internal standard.

Materials. The preparation of 2,3-cyclopentenochromone (**6**) was carried out according to the procedure reported by Boyd *et al.*[10] Mp 127—128 °C (lit,[10] 122—123 °C) (60% yield, colorless prisms, from cyclohexane).

2,3-Cyclopentenohomochromone (2,3-trimethylene-2,3-methanochroman-4-one) (7): To mineral oil-free sodium hydride (NaH), prepared from commercial NaH (3.4 g, 0.071 mol; mineral oil dispersion) by means of triple decantation with light petroleum, was added trimethyloxosulfonium iodide[8] (12.1 g, 0.055 mol) in one portion followed by the addition of anhydrous dimethyl sulfoxide (DMSO) (50 ml) with stirring over a period of 20 min, at first carefully at 20 °C. After the cessation of the violent evolution of hydrogen, the milky-white solution was kept in a nitrogen atmosphere. To the dimethyloxosulfonium methylide produced in DMSO, was added a saturated solution of **6** (9.3 g, 0.05 mol) in DMSO (100 ml) with stirring over a period of 40 min at a temperature of 17—20 °C. The solution turned to grayish green, and then to reddish violet. The mixture was then allowed to stand at room temperature for 2.5 h under nitrogen, warmed to 40° C, maintained for 5 min then cooled in an ice-bath, and anhydrous ether (100 ml) was then added to the solution. The mixture was poured into ice-water, separated, and the aqueous layer was extracted thoroughly with ether. The combined extract was satisfactorily washed with water, and dried on anhydrous sodium sulfate. During the work-up process, separation was sometimes difficult probably due to the poor solubility of unreacted **6**, when the reaction was not complete. The ether was evaporated *in vacuo*, and a yellowish viscous syrup (7.6 g) was obtained, chromatographed on neutral alumina (30 g, activity III, short column) using petroleum ether (boiling range below 40 °C) as an eluent, and the solvent was removed *in vacuo* to give a colorless syrup (7.4 g), which crystallized slowly in a refrigerator. Mp 60—61 °C (6.9 g, 70% yield, colorless prisms, from petroleum ether). IR

(Nujol): 1660, 1610, 1235, 1065 cm^{-1}. NMR (CCl_4): 7.9—6.7 (4H, m, aromatic), 2.6—1.3 (8H, m, trimethylene and cyclopropane). Found: C, 78.15; H, 6.04%. Calcd for $C_{13}H_{12}O_2$: C, 77.98; H, 6.04%.

*2,3-Cyclopenteno-4H-homochromen-4-ol (Homochromenol) (**1-OH**)*: *(a) Reduction of **7** with $LiAlH_4$ in ether.* A solution of **7** (2.00 g) in ether (30 ml) was added portionwise to the well-stirred suspension of lithium aluminum hydride (0.40 g, excess) in ether (10 ml) with ice-cooling. Then the mixture was allowed to sit at room temperature, stirred overnight, and quenched by adding 5 ml of water carefully over 30 min with ice-cooling. The resulting clear solution was decanted and the residue was washed twice with ether. The combined organic solutions were dried over anhydrous potassium carbonate, evaporated *in vacuo* without externel heating to give a colorless oil (2.00 g, quantitative yield), which crystallized in a refrigerator. This material was recrystallized from petroleum ether to yield pure **1-OH** (1.15 g, 57% yield), mp 101—102 °C. IR (nujol): 3350, 1605, 1230, 1070 cm^{-1}. NMR (CCl_4): 7.6—6.5 (4H, m, aromatic), 4.65 (1H, s, α-proton, 2.5—1.5 (7H, m. trimethylene and hydroxyl), 1.15, 0.55 (2H, AB quartet, J=6.5 Hz, cyclopropane). Found: C, 76.95; H, 7.10%. Calcd for $C_{13}H_{14}O_2$: C, 77.20; H, 6.98%.

*(b) Reduction of **7** with $NaBH_4$ in aqueous 2-propanol.* A solution of sodium borohydride (90 mg) in 2-propanol–water (60 ml; 2: 1, by volume) was added to a stirred solution of **7** (1.00 g, 5 mmol) in 2-propanol (40 ml). After being stirred for 2 days at room temperature, 2-propanol was evaporated slowly *in vacuo* without heating and the residue was extracted twice with ether (20 ml). The extracts were combined, washed with water, and dried over anhydrous potassium carbonate. The extract was condensed *in vacuo* to give a colorless oil, whose spectroscopic data agreed well with those of **1-OH** prepared by the above procedure. Pure material (mp 98—100 °C) (0.40 g, 40% yield) was obtained by recrystallization from cyclohexane.

*2,3-Cyclopenteno-4H-homochromen-4-ol Acetate (Homochromenol Acetate) (**1-OAc**)*: To a magnetically-stirred solution of **1-OH** (0.30 g) in pyridine (8 ml), was added a solution of acetic anhydride (0.3 ml) in pyridine (2 ml) over a period of 5 min in an ice–salt bath. After being stirred overnight at room temperature, dry ether (20 ml) was added to the solution, and the mixture was worked up by pouring into ice–water (300 ml). The organic layer was separated, and the aqueous layer was extracted twice with ether (50 ml). The extract was combined, washed with cold water, with ice-cold dilute hydrochloric acid, with water, with 5% sodium hydrogencarbonate and finally with water, and then dried over anhydrous sodium sulfate. The extract was concentrated *in vacuo* without heating to give a colorless oil (0.33 g, 85%). IR (neat): 1730, 1580, 1235, 745 cm^{-1}. MS: (*m/e*) 244 (M^+). NMR (CCl_4): 7.3—6.7 (4H, m, aromatic), 6.05 (1H, s, α-proton), 2.10(3H, s, acetoxy), 2.4—1.2(6H, m, trimethylene), 1.15, 0.75 (2H, AB quartet, J=6.5 Hz, cyclopropane).

For the purpose of purification, the oil was chromatographed on a neutral alumina column. Elution with benzene–petroleum ether (1: 1) produced decomposed substances. When heated for 30 min at 130 °C in a neat condition in a capillary, the oil decomposed.

*Product Studies. Homochromenol Acetate (**1-OAc**) in 80% Acetone–Water*: A solution of the acetate (750 mg) in 80% acetone–water (250 ml) containing sodium hydrogencarbonate (250 mg) was allowed to sit at 25 °C (in a thermostatic bath) for 4 days (*ca.* 12 half-lives). Most of the acetone was evaporated *in vacuo* without heating, and the remaining suspension was extracted with three 50-ml portions of ether. The ether extract was washed with water. After drying over anhydrous sodium sulfate, the ether was removed and the residual partially-crystallized material (602.4 mg, 97% yield) was recrystallyzed from cyclohexane to give pure **10** (310.0 mg, 50% yield). Mp 126—128 °C. IR (Nujol): 3140, 1640, 1270, 1250, 755 cm^{-1}. MS (*m/e*): 202 (M^+). UV λ_{max} (ε) (ethanol): 235 (14000), 277 (2900) nm. NMR ($CDCl_3$): 7.4—6.7 (4H, m, aromatic), 5.87 (1H, s, vinyl), 3.55 (2H, s, allylic bridged methylene), 2.7—1.7 (7H, m, trimethylene and hydroxyl) *cf.* Fig. 2. Found: C, 77.39; H, 6.88%. Calcd for $C_{13}H_{14}O_2$: C, 77.20; H, 6.98%. Acetylation of **10** in a similar manner as described above (from **1-OH** to **1-OAc**) was accomplished to give a colorless oil. IR ($CHCl_3$): 2960, 1770, 1750, 1660 cm^{-1}. NMR ($CDCl_3$): 7.4—6.9 (4H, m, aromatic), 5.87 (1H, s, vinyl), 3.45 (2H, s, allylic bridged methylene), 2.23 (s, acetoxy), 2.6—1.7 (m, others). The above crude product from **1-OAc** in such a solvolytic condition was dissolved in $CDCl_3$, and the NMR measurement was carried out immediately, at which time **10** was found to be almost the sole product, though small amounts of **11** and traces of unidentified materials were present.

When the solvolysis of **1-OAc** was carried out in 80% acetone–water in the presence of pyridine or 2,6-lutidine (a slightly excess amount of the ester), **10** was obtained as a major product. But using any acidic material for removing the alkali during the work-up process, a complex mixture was obtained as a solvolysis product and **10** was not found at all. Similarly, solvolysis of **1-OAc** in 80% acetone–water in the absence of alkali gave a complex mixture. Particular attention should be paid to the treatment of hemiacetal (**10**), since it is highly sensitive to acidic materials.

In addition, parent alcohol (**1-OH**) was stable under the solvolytic condition (in 80% acetone–water at 25 °C for 4 days in the presence of sodium hydrogencarbonate).

*Methanolysis of **1-OAc***: The ester (**1-OAc**) (100 mg) was dissolved in absolute methanol (100 ml) containing pyridine (0.5 ml), and the mixture was allowed to sit at 25 °C for 4 days. After removing the methanol *in vacuo* without heating, CCl_4 (40 ml) was added to the residue and the solvent was removed azeotropically. The residue was dissolved in CCl_4, filtered, and the filtrate was analyzed by NMR spectroscopy. The solvent was removed, ether (50 ml) was added to the residue, the mixture was poured into ice-cold 1M-HCl (70 ml), extracted twice with ether (50 ml), washed with water (50 ml), with 5% sodium hydrogencarbonate (50 ml), and finally with water (50 ml), and then dried over anhydrous sodium sulfate. The colorless oil (96.3 mg) obtained by evaporation of the extract was difficult to crystallize, and produced the same NMR spectrum as the pre-measured NMR spectra made during the work-up process. IR (CCl_4); 3380, 2940, 1480, 1240, 1110, 1050 cm^{-1}. MS (*m/e*): 216 (M^+). NMR (CCl_4); 7.3—6.65 (4H, m, aromatic), 6.08 (1H, s, vinyl), 3.12 (3H, s, methoxy; *cf.* 3.37 for MeO–H), 2.5—1.15 (*ca.* 8H, m, others).

Trapping a Reactive Carbocation with Hydride Reagent: A solution of sodium borohydride (2.0 g) in 50% aqueous diglyme (30 ml) including sodium hydroxide (80 mg) was added to the homochromenol ester (**1-OAc**) (183.2 mg). After being stirred overnight at room temperature, *n*-pentane (50 ml) and water (50 ml) were added to the reaction mixture, separated, and the aqueous layer was extracted twice with *n*-pentane (30 ml). The combined organic layers were washed with water (30 ml), and dried over anhydrous sodium sulfate. The colorless oil (250.4 mg) obtained by evaporation of the extract *in vacuo*, included the remaining diglyme. After distillation, **15** was obtained; bp *ca.* 130 °C/2 mmHg (bath temp) (40 mg). No isomerization (or decomposition) occurred during the distillation as verified by IR, NMR, and GC data. IR (neat): 2900, 1470, 1440, 1180, 1110 cm^{-1}. MS (*m/e*): 186 (M^+). UV (ethanol) λ_{max} 254.5 nm. NMR (CCl_4): 7.4—6.5 (4H,

m, aromatic), 6.10 (1H, s, vinyl), 5.03 (1H, m, bridgehead methine), 3.0—1.7 (8H, m, others).

Kinetic Studies. The rates of solvolysis of homochromenol acetate (**1-OAc**) in 80% acetone–water were determined using solutions in about 0.004 mol concentration and titrating the liberated acetic acid with 0.01 M NaOH in methanol to a bromothymol blue end-point. The base was frequently restandardized against oxalic acid during the course of the work.

Solutions of the acetate in 80% acetone–water (by volume) were prepared in the following manner. The weighed **1-OAc** was dissolved in anhydrous acetone (40 ml). Then, a 75% acetone–water (by volume, 160 ml) solution was prepared, and both solutions were set in a thermostatic bath and maintained at 25 °C (±0.03 °C). About 10 min later, the latter solution poured into the former, and the mixture (**1-OAc** in 80% acetone–water) was well shaken, then dipped in the thermostatic bath. The first aliquot (10 ml) was pipetted after 5—10 min and taken as the zero point. Periodically, each aliquot was taken, quenched by anhydrous acetone (20 ml) and then subjected to titration. Infinity titrations were determined after 10 or more half-lives, and in those cases the liberated acetic acid reached 95—98% of the theoretical amount. Rate constants were calculated to the first-order, and mean values from several runs are shown in Table 2. Typical first-order plots are shown in Fig. 3.

Isomerization of the Parent Alcohol and Interconversion between Hemiacetal and Ketophenol in Trifluoroacetic Acid. A wine red solution of the parent alcohol (**1-OH**) (0.20 g) in trifluoroacetic acid (TFA) (1 ml) was analyzed by NMR spectroscopy. NMR (TFA) 7.5—6.7 (>4H, m, aromatic), 6.0 (<1H, s, vinyl), 3.72, 3.10 (2H, s, s, allylic methylene), 3.1—1.8 (7H, m, others). The ratio **10/11** in TFA was *ca.* 3: 1 in comparison with the characteristic signals of the NMR spectra. The ratio was variable though **10** always predominates in TFA at room temperature even after 3 days. The solution was poured into an ice-cold aqueous sodium hydrogencarbonate solution, extracted three times with ether, next the combined organic layer was washed with cold aqueous sodium hydrogencarbonate and with water, and then dried over anhydrous potassium carbonate. A pale yellow syrup (181.3 mg, 90%) obtained by evaporation of the ether, was pumping *in vacuo* to give **11** (mp 76—78 °C) as the sole product of the NMR spectrum in $CDCl_3$, which was dissolved in benzene and passed through a short column of alumina (activity III). Concentration of the filtrate produced pure **11**, mp 78—80 °C, IR (Nujol): 2950, 1720, 1580, 1240, 750 cm^{-1}. MS (*m/e*): 202 (M^+). UV λ_{max} (ε) (ethanol): 279 (2900), 315 (350) nm. NMR ($CDCl_3$): 7.5—6.6 (5H, m, aromatic and vinyl), 3.05 (2H, s, allylic methylene), 3.0—1.7 (7H, m, trimethylene and hydroxyl). Positive for the $FeCl_3$ test in $CDCl_3$. Found: C, 76.78; H, 6.86%. Calcd for $C_{13}H_{14}O_2$: C, 77.20; H, 6.98%.

When dry ether was added to the above TFA solution before the work-up process, a mixture of **10** and **11** was isolated after similar treatment, and the former was found to be predominant (*ca.* 2: 1) in the NMR spectra in $CDCl_3$. Heating the contents of the $CDCl_3$ solution at 50 °C for 30 min, **11** was obtained as the sole product.

When **11** (40 mg) was dissolved in TFA (0.3 ml) the ratio of **10/11** was *ca.* 9: 4 from the NMR spectrum. NMR (TFA): 7.5, 6.7 (>4H, m, aromatic), 6.02 (<1H, s, vinyl), 3.76, 3.14 (2H, s, s, methylene), 3.0—1.8 (*ca.* 7H, m, others). Ether was added to the solution, then the mixture was treated in the same manner as described above. The yellowish oil (35.8 mg, 90%) obtained was dissolved in $CDCl_3$ for measuring both the IR and NMR spectra. The IR spectrum of this oil was found to be consist of duplicates of **10** and **11**, and the former was at first predominant depending on the relative intensity of each characteristic absorption band (especially 1640 cm^{-1} for **10**, and 1720 cm^{-1} for **11**). However, after several hours the relative intensities were clearly reversed, and the information from NMR spectroscopy agreed well with these results. Similarly, a mixture of **10** and **11** was obtained from **10** in TFA. According to the NMR study, the ratios of **10/11** derivated from **1-OH**, **10**, or **11** in TFA appear to depend on the temperature.

We are indebted to Mr. T. Sugiura for assistance during the experiments, and we also wish to thank to Mrs. S. Kurokawa and Miss S. Eguchi for obtaining the NMR and the mass spectra, respectively. This work was partially supported by a grant in aid from the Ministry of Education, No. 747019 in 1972 and 1973.

References

1) S. Winstein, *Quart. Rev.*, **23**, 141 (1969).
2) K. Ohkata, to be published.
3) A. C. Nixon and G. E. K. Branch, *J. Amer. Chem. Soc.*, **58**, 492 (1936); H. Hart and P. A. Law, *ibid.*, **86**, 1957 (1964).
4) Recently homopyrylium ion was proposed as intermediate of acid-catalyzed isomerization; H. Klein and W. Grimme, *Angew. Chem. Internat. Ed., Engl.*, **13**, 672 (1974).
5) L. Birladeanu, T. Hanafusa, and S. Winstein, *J. Amer. Chem. Soc.*, **88**, 2315 (1966); L. Birladeanu, T. Hanafusa, B. Johnson, and S. Winstein, *ibid.*, **88**, 2316 (1966).
6) J. B. Lambert, F. R. Koeng, and J. W. Hamersma, *J. Org. Chem.*, **36**, 2941 (1971).
7) M. Julia and G. L. Thuillier, *Bull. Soc. Chim. Fr.*, **1966**, 717; M. Julia and M. Baillarge, *ibid.*, **1966**, 734, 743.
8) E. J. Corey and M. Chaykovsky, *J. Amer. Chem. Soc.*, **87**, 1353 (1965).
9) G. A. Chaplin, W. D. Ollis, and I. O. Sutherland, *Chem. Commun.*, **1967**, 575; *J. Chem. Soc. C*, **1968**, 2302.
10) G. V. Boyd, D. Hewson, and R. A. Neuberry, *ibid., C*, **1969**, 935.
11) C. D. Poulter, R. S. Boikess, J. I. Brauman, and S. Winstein, *J. Amer. Chem. Soc.*, **94**, 2291 (1972).
12) M. Gordon, W. C. Howell, C. H. Jackson, and J. B. Stothers, *Can. J. Chem.*, **49**, 143 (1971); L. Birladeanu, D. L. Harris, and S. Winstein, *J. Amer. Chem. Soc.*, **92**, 6387 (1970).
13) K. Nukada, O. Yamamoto, T. Suzuki, M. Ohnishi, and T. Takeuchi, *Anal. Chem.*, **35**, 1892 (1963).
14) B. P. Dailey and J. N. Shoolery, *J. Amer. Chem. Soc.*, **77**, 3977 (1955).
15) E. E. Schweizer and R. Schepers, *Tetrahedron Lett.*, **1963**, 979.
16) S. Winstein, P. Carter, F. A. L. Anet, and A. J. R. Bourne, *J. Amer. Chem. Soc.*, **87**, 5247 (1965).
17) H. C. Brown and H. M. Bell, *ibid.*, **85**, 2324 (1963); *J. Org. Chem.*, **27**, 1928 (1962).
18) R. A. Sneen and A. C. Baron, *J. Amer. Chem. Soc.*, **83**, 614 (1961); T. Shono, A. Oku, and R. Oda, *Tetrahedron*, **24**, 421 (1968).
19) R. Leute and S. Winstein, *Tetrahedron Lett.*, **1967**, 2475.
20) E. C. Friedrich and S. Winstein, *ibid.*, **1962**, 475.
21) J. F. Norris and C. Banta, *J. Amer. Chem. Soc.*, **50**, 1804 (1928); M. Simonetta and G. Favini, *J. Chem. Soc.*, **1954**, 1840.
22) Unpublished work.
23) P. von R. Schleyer and G. W. van Dine, *J. Amer. Chem. Soc.*, **88**, 2321 (1966); P. von R. Schleyer, P. J. Stang, and D. J. Raber, *ibid.*, **92**, 4725 (1970).
24) E. Vogel, W. Wiedemann, H. D. Roth, J. Eimer, and H. Günther, *Ann. Chem.*, **759**, 1 (1972).

Reaction of a Stable Free Nitrogen-centered Radical, 3,4-Dihydro-2,4,6-triphenyl-2*H*-1,2,4,5-tetrazin-1-yl, with Grignard Reagents[1)]

Yozo Miura, Yuzo Morimoto, and Masayoshi Kinoshita

Department of Applied Chemistry, Faculty of Engineering, Osaka City University, Sumiyoshi-ku, Osaka 558

(Received June 12, 1975)

The reactions of 3,4-dihydro-2,4,6-triphenyl-2*H*-1,2,4,5-tetrazin-1-yl (**1**) with Grignard reagents such as ethyl-, isopropyl-, butyl-, isobutyl-, *s*-butyl-, *t*-butyl-, cyclohexyl-, phenethyl-, phenyl-, and 2-naphthylmagnesium bromides and benzylmagnesium chloride were examined. In the reactions with the alkylmagnesium halides, coupling compounds (**2**) of **1** with alkyl radicals derived from the alkylmagnesium halides were isolated in 41—50% yields. On the other hand, in the reactions with arylmagnesium bromides the corresponding coupling compounds were not isolated, but biphenyl and 2,2′-binaphthyl were isolated in 87 and 86% yields, respectively. From these results, the reactions of **1** with Grignard reagents are concluded to proceed through a homolytic process.

Recently, many reactions of oxygen-centered radicals with organometallic compounds have been investigated,[2)] and these reactions have been demonstrated to proceed through a homolytic process at metal centers, by stereochemical, kinetic, and ESR studies. However, only a few examples of homolytic reactions with nitrogen-centered radicals have been so far reported.[3)]

In the course of preparation of polymers containing stable free radicals,[4)] the reactions of 3,4-dihydro-2,4,6-triphenyl-2*H*-1,2,4,5-tetrazin-1-yl (**1**, 1,3,5-triphenylverdazyl),[5)] which is a typical stable free nitrogen-centered radical, with alkylmagnesium halides or alkyllithiums used as an initiator, were examined. It was found that coupling compounds of **1**, 1-alkyl-2,4,6-triphenyl-1,2,3,4-tetrahydro-1,2,4,5-tetrazines (**2**), with radicals derived from these organometallic compounds were formed.[6)] The formation of **2** suggests that the reactions proceed through a homolytic process.

In this paper, the results of the reactions of **1** with various Grignard reagents are described, and the reaction mechanisms will be discussed.

Results and Discussion

Reaction of 1 with Alkylmagnesium Halides. As a Grignard reagent was added gradually to a tetrahydrofuran (THF) solution of **1**, the characteristic dark green color of **1** slowly faded, and turned finally to light yellow within *ca.* 10 min after the Grignard reagent had been added. This yellow solution maintained its color in the absence of moisture. However, when the solution was poured into water, its color retured immediately to green, the coloration indicating that **1** was regenerated. The solution was extracted with benzene, and thin layer chromatography (tlc) revealed the presence of three components in the benzene solution. One of them was easily identified to be **1** on the basis of the green color and the R_f value. One of the other spots disappeared when the benzene solution was allowed to stand for two days under ambient conditions, and the amount of **1** recovered was found to increase gradually from the measurement of absorbance at 720 nm. The spot also disappeared immediatelly upon the addition of catalytic amounts of lead dioxide. A leuco compound (**4**) of **1** is known to be easily oxidized to **1** even by atmospheric oxygen,[5)] and thus, the component was identified to be **4**. This was also ascertained by the R_f value. From these results it is clear that **1** is formed by the oxidation of **4**. The amount of **1** recovered was determined by measuring the absorbance at 720 nm after **4** was oxidized thoroughly to **1**. The results are summarised in Table 1.

Next, the benzene solution was concentrated and subjected to column chromatography. The results indicate the formation of a coupling compound (**2**) of **1** with an alkyl radical derived from the Grignard reagent in 41—50% yields (based on the amount of **1** used).

Reaction of 1 with Arylmagnesium Bromides. The reactions of **1** with arylmagnesium bromides such as phenyl- and 2-naphthylmagnesium bromides were examined. In these cases, the green solution turned to light yellow within *ca.* 2 hr after the addition of the Grignard reagent, and the reaction proceeded much more slowly than that with alkylmagnesium halides. In the extracted benzene solution three components were found. Two of them were identified to be **1** and **4**, respectively. However, the corresponding coupling compound (**2**) was not detected. The amounts of **1** recovered were determined by the same procedure as described above to be 79 and 81% yields (Table 1).

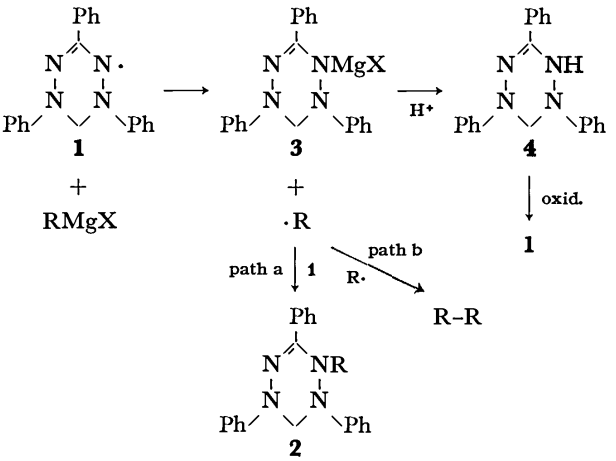

2a : R = C_2H_5 **2f** : R = t-C_4H_9
2b : R = i-C_3H_7 **2g** : R =
2c : R = n-C_4H_9 **2h** : R = CH_2Ph
2d : R = i-C_4H_9 **2i** : R = CH_2CH_2Ph
2e : R = s-C_4H_9

Scheme 1.

These values are much larger than those for alkylmagnesium halides. The benzene solution was then concentrated and subjected to column chromatography to give biphenyl and 2,2'-binaphthyl in almost quantitative yields (Table 1).

Reaction Mechanism. From these results a reasonable reaction mechanism may be illustrated as shown in Scheme. In the reactions of **1** with alkylmagnesium halides, **1** and a Grignard reagent are converted into the corresponding magnesium salt (**3**) and an alkyl radical. The alkyl radical formed is captured exclusively by another **1** to give a coupling compound (**2**, path a). This is also supported by the fact that **1** has been found to be an efficient inhibitor in radical polymerization,[7] and that the amount of octane detected in the reaction of **1** with butylmagnesium bromide was almost the same as found in the course of the preparation of the Grignard reagent. Although **3** is stable under anhydrous conditions, it decomposes immediately in contact with water to give a lueco compound (**4**), which is oxidized gradually by atmospheric oxygen to **1**.

In the reactions with arylmagnesium bromides, aryl radicals formed are not captured by **1**, but are coupled with each other to give the biarlys (path b), and therefore, the amounts of **1** recovered were much larger than those for the alkylmagnesium halides.

In order to confirm whether **1** reacts with a phenyl radical, an attempted reaction of **1** with phenylazotriphenylmethane[8] was examined. A benzene solution containing **1** and two equivalents of the azo-compound was refluxed for a few hours. The resulting reaction mixture was examined by tlc, but the corresponding coupling compoung was not detected.

Experimental

All melting points were uncorrected. Thin layer chromatography was performed on Kieselgel GF_{254} according to Stahl Type 60 (E. Merck, Darmstadt, West Germany), using benzene, and detection was effected by UV irradiation. The NMR spectra were recorded using a Hitachi-Perkin Elmer R-20 Spectrometer in $CDCl_3$, using TMS as an internal standard. The visible spectra were measured with a Hitachi Recording Spectrometer Model EPS-3T.

THF was distilled from KOH, sodium wire, and from $LiAlH_4$ before use. All Grignard reagents were prepared by treating alkyl and aryl halides [2.0 ml except for 2-bromonaphthalene (2.0 g)] with a slight excess of magnesium in THF (50 ml), and the conversions were determined by the method of Gilman *et al.*[9]

3,4-Dihydro-2,4,6-triphenyl-2*H*-1,2,4,5-tetrazin-1-yl (**1**) was prepared by treating 1,3,5-triphenylformazan with 37% formalin in the presence of potassium hydrogensulfate according to the procedure of Kuhn and Trischmann,[5] and was recrystallized from methanol, mp 141—142 °C (lit,[5] 139—140 °C).

General Procedure for the Reactions of 1 with Grignard Reagents. **1** (0.50 g, 1.6 mmol) and THF (15 ml) were put in a vessel with a rubber-capped neck. After the dark green THF solution was degassed by freeze-and-thaw cycles, the vessel was sealed. A Grignard reagent was then added gradually to the THF solution at 0 °C through the rubber-cap with a syringe. The green reaction mixture was allowed to stand for *ca.* 10 min (in the reactions with alkylmagnesium halides) and *ca.* 2 hr (for arylmagnesium bromides) at the same temperature, after which, turned to light yellow. After 2 hr, the solution was poured into water, and extracted with benzene. The benzene solution was washed with dilute hydrochloric acid (*ca.* 1 M), and with water, and dried over sodium sulfate. The amount of **1** recovered was determined by the measurement of absorbance at 720 nm (ε 4330 in benzene) in the benzene solution (total volume 3000 ml). Next benzene was evaporated under reduced pressure and the residue obtained was subjected to chromatography on a silica-gel column (Mallinckrodt 100 mesh, 25×400 cm) with benzene, giving a coupling compound (**2**) in the case of reactions with alkylmagnesium halides, and biaryls with arylmagnesium bromides. All results of the reactions are summarized in Tables 1 and 2.

The biphenyl isolated by this method was in the form of pure crystals, 0.12 g (0.78 mmol), mp 70—71 °C (lit,[10] 71 °C). The isolated 2,2'-binaphthyl contained small amounts of naphthalene, which was removed by recrystallization from ethanol, 0.19 g (0.75 mmol), mp 184—185 °C (lit,[11] 185—186 °C). The amounts of biaryls which arise from the preparation procedure of arylmagnesium bromides were determined as follows; the same amounts of arylmagnesium bromides used in the reactions were hydrolyzed, and extracted with benzene. The benzene solution was concentrated, and the residue was analyzed by column chromatography. The amounts of biphenyl and 2,2'-binaphthyl isolated were 0.013 g (0.084 mmol) and 0.015 g (0.059 mmol), respectively.[12] The yields of the

Table 1. The results of the reactions of 3,4-dihydro-2,4,6-triphenyl-2*H*-1,2,4,5-tetrazin-1-yl (**1**) with Grignard reagents[a]

Grignard reagent	mmol[b]	Recovered **1** (%)	Isolated coupling compound	(%)[c]
Ethylmagnesium bromide	1.6	36	**2a**	47
Isopropylmagnesium bromide	1.5	39	**2b**	41
Butylmagnesium bromide	1.0	40	**2c**	43
Isobutylmagnesium bromide	1.5	39	**2d**	50
s-Butylmagnesium bromide	1.3	38	**2e**	46
t-Butylmagnesium bromide	1.5	37	**2f**	46
Cyclohexylmagnesium bromide	1.6	34	**2g**	43
Benzylmagnesium chloride	1.4	42	**2h**	50
Phenethylmagnesium bromide	1.5	33	**2i**	48
Phenylmagnesium bromide	1.9	81	Biphenyl	87
2-Naphthylmagnesium bromide	2.2	78	2,2'-Binaphthyl	86

a) Reaction condition: **1**, 0.50 g (1.6 mmol); tetrahydrofuran, 15 ml, at 0 °C. b) Molar amount required for the completion of the reaction. c) Based on the amount of **1** used.

TABLE 2. PHYSICAL AND ANALYTICAL DATA OF 1-ALKYL-2,4,6-TRIPHENYL-1,2,3,4-TETRAHYDRO-1,2,4,5-TETRAZINE (**2**)

2	Mp (°C) (lit)	Formula	Anal (%) Found / Calcd C	H	N	NMR ($CDCl_3$) δ (ppm)
2a	133—134	$C_{22}H_{22}N_4$	77.12	6.54	16.43	1.28(t, J=8 Hz, 3H), 2.50—3.60(b, 2H), 4.20—4.70
			77.16	6.48	16.36	(b, 1H), 5.35—5.90(b, 1H), 6.70—8.00(m, 15H)
2b	124—125	$C_{23}H_{24}N_4$	77.25	6.73	15.57	1.10(d, J=7 Hz, 3H), 1.17(d, J=7 Hz, 3H), 3.95
			77.49	6.97	15.72	(q, J=7 Hz, 1H), 4.86(q, J=12 Hz, 2H), 6.63—7.93 (m, 15H)
2c	109—111	$C_{24}H_{26}N_4$	77.67	6.88	15.08	0.65—2.10(m, 7H), 2.50—3.65(b, 2H), 4.13—4.70
			77.80	7.07	15.12	(b,1H), 4.35—5.90(b, 1H), 6.70—8.00(m, 15H)
2d	158—160	$C_{24}H_{26}N_4$	78.16	7.18	15.25	0.65—1.30 (b, 6H), 1.80—2.63(m, 1H), 2.65—3.20
			77.80	7.07	15.12	(b, 2H), 4.98(q, J=12 Hz, 2H), 6.70—8.13(m, 15H)
2e[a]	104—105	$C_{24}H_{26}N_4$	78.02	7.04	14.93	0.75 and 0.80(t, J=7 Hz, 3H), 1.06 and 1.14(d, J=
			77.80	7.07	15.12	7 Hz, 3H), 1.20—1.92(m, 2H), 3.68(q, J=7 Hz, 1H), 4.90 and 4.98(q, J=12 Hz, 2H), 6.60—7.90(m, 15H)
2f	189—190	$C_{24}H_{26}N_4$	77.82	6.97	15.10	1.26(s, 9H), 5.25(q, J=13 Hz, 2H), 6.70—7.79(m,
			77.80	7.07	15.12	15 H)
2g	142—144	$C_{26}H_{28}N_4$	78.93	7.10	13.97	0.65—2.15(b, 10H), 3.25—3.80(b, 1H), 4.98(q, J=
			78.75	7.12	14.13	12 Hz, 2H), 6.55—7.96(m, 15H)
2h	168—169 (172)[13]					
2i	116—118	$C_{28}H_{26}N_4$	80.30	6.19	13.59	2.80—3.70(b, 4H), 4.20—4.80(b, 1H), 5.40—6.00
			80.36	6.26	13.39	(b, 1H), 6.55—7.85(m, 20H)

a) A mixture of diastereoisomers.

biaryls in Table 1 were determined on the basis of these reductions.

References

1) A preliminary report: Y. Miura, Y. Morimoto, and M. Kinoshita, *Chem. Lett.*, **1975**, 19.

2) a) K. U. Ingold and B. P. Roberts, "Free Radical Substitution Reaction," Interscience, New York, N. Y. (1970), p. 10. b) A. G. Davies and B. P. Roberts, *Accounts Chem.. Res.*, **5**, 387 (1972). c) A. G. Davies and B. P. Roberts, "Free Radicals," Vol. 1, ed. by J. K. Kochi, Interscience, New York, N. Y. (1973), p. 547.

3) a) A. G. Davies, S. C. W. Hook, and B. P. Roberts, *J. Organometal. Chem.*, **22**, C 11 (1970). b) A. G. Davies, S. C. W. Hook, B. P. Roberts, and J. M. Smith, *J. Chem. Soc., Perkin II*, **1972**, 993.

4) For a recent report, see, Y. Miura and M. Kinoshita, *Makromol. Chem.*, **175**, 33 (1974).

5) R. Kuhn and H. Trischmann, *Monatsh. Chem.*, **95**, 457 (1964).

6) Y. Miura, Y. Morimoto, and M. Kinoshita, *Makromol. Chem.*, **175**, 3487 (1974).

7) M. Kinoshita and Y. Miura, *ibid.*, **124**, 211 (1969).

8) R. F. Bridger and G. A. Russell, *J. Amer. Chem. Soc.*, **85**, 3754 (1963).

9) H. Gilman, E. A. Zoellner, and J. B. Dickey, *ibid.*, **51**, 1576 (1929).

10) R. Fittig, *Ann.*, **121**, 361 (1862).

11) S. Chooker and L. K. Fieser, *J. Amer. Chem. Soc.*, **63**, 2316 (1936).

12) M. S. Kharasch and E. K. Fields, *ibid.*, **63**, 2316 (1941).

13) M. Kinoshita, N. Yoshizumi, and M. Imoto, *Makromol. Chem.*, **127**, 185 (1969).

β-Disulfoxides. II. The Preparation of Some Optically Active β-Disulfoxides

Norio KUNIEDA, Junzo NOKAMI, and Masayoshi KINOSHITA

Department of Applied Chemistry, Faculty of Engineering, Osaka City University, Sumiyoshi-ku, Osaka 558

(Received June 16, 1975)

α-Sulfinylcarbanions (**1**) derived from methyl-substituted sulfoxides readily react with arenesulfinic esters (**2**) to give the corresponding β-disulfoxides (**3**) in good yields. The reaction was conducted using (−)-menthyl (−)-(*S*)-benzenesulfinate ((−)-(*S*)-**2b**), (−)-menthyl (−)-(*S*)-*p*-toluenesulfinate ((−)-(*S*)-**2c**), and α-*p*-tolylsulfinylcarbanion derived from (+)-(*R*)- or (−)-(*S*)-methyl *p*-tolyl sulfoxide to produce (*R,S*)- and/or (*S,S*)-diastereoisomers of five β-disulfoxides (**3a—e**). The configurational assignment for the diastereoisomers obtained was accomplished by a combination of NMR and polarimetric analyses.

Recently, we have reported a facile one-step synthesis of β-disulfoxides, starting from arenesulfinic esters and α-sulfinylcarbanions derived from the corresponding methyl-substituted sulfoxides.[1] This reaction is of great advantage in synthesizing optically active β-disulfoxides, because one can readily prepare either optically active methyl-substituted sulfoxides or optically active arenesulfinic esters in a state of high enantiomeric purity.[2] In order to study the stereochemistry of β-disulfoxides,[6] we have now investigated the application of this reaction to the synthesis of some diastereomerically pure β-disulfoxides[(+)-(*S*)-[(*S*)-α-methylsulfinyl]-methyl phenyl sulfoxide((*S,S*)-**3a**), (+)-(*S*)-[(*S*)-α-methylsulfinyl]methyl *p*-tolyl sulfoxide((*S,S*)-**3b**), (+)-(*S*)-[(*R*)-α-methylsulfinyl]methyl *p*-tolyl sulfoxide((*R,S*)-**3b**), (+)-(*S,S*)- and (*R,S*)-bis(phenylsulfinyl)methanes-((*S,S*)- and (*R,S*)-**3c**), (+)-(*S*)-[(*S*)-α-*p*-tolylsulfinyl]-methyl phenyl sulfoxide((*S,S*)-**3d**), and (+)-(*S,S*)- and (*R,S*)-bis(*p*-tolylsulfinyl)methanes((*S,S*)- and (*R,S*)-**3e**)], using (+)-(*R*)- and (−)-(*S*)-methyl *p*-tolyl sulfoxides, (−)-menthyl (−)-(*S*)-benzenesulfinate((−)-(*S*)-**2b**), and (−)-menthyl (−)-(*S*)-*p*-toluenesulfinate((−)-(*S*)-**2c**) as chiral precursors.

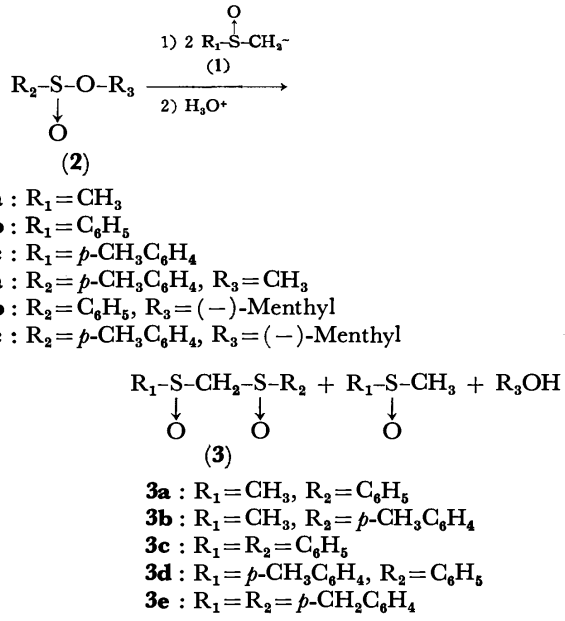

Scheme 1.

Results and Discussion

When 2 equivalents of arenesulfinic esters(**2**) were allowed to react with α-sulfinylcarbanions(**1**) in tetrahydrofuran at 0 °C,[8] a diastereomeric mixture of β-disulfoxides(**3**) was produced in a good yield, in a fashion analogous to the case of the reaction of α-methylsulfinylcarbanion with carboxylic esters.[9]

In typical reactions, when (−)-(*S*)-**2c** was treated with 2 equivalents of α-methylsulfinylcarbanion(**1a**) (derived from dimethyl sulfoxide and sodium hydride)[9d] in tetrahydrofuran at 0 °C, dextrorotatory α-methylsulfinylmethyl *p*-tolyl sulfoxides(**3b**) [(*R,S*)-**3b**: (*S,S*)-**3b**=59: 41%][10] was produced in a 85% yield. From the resulting **3b**, diastereomerically pure (*S,S*)-**3b**, $[\alpha]_D^{19}$ +346° (acetone), was isolated by fractional crystallization from benzene. The structural assignment of (*S,S*)-**3b** was supported by the NMR spectrum, which exhibited resonances at 2.76 ppm(s) and 4.00 ppm(s) due to the methyl protons of the methylsulfinyl group and the methylene protons respectively. Though we have not isolated pure (*R,S*)-**3b**, the concentration of the mother liquid, followed by the recrystallization of the residue from hexane–benzene, led to an enrichment in (*R,S*)-**3b**. The NMR spectrum of (*R,S*)-**3b** shows an AB quartet at 4.00 ppm (J_{AB}=7.8 Hz) due to the non-equivalent methylene protons[11] and a singlet at 2.94 ppm due to the methyl protons of the methylsulfinyl group.

When 2 equivalents of α-*p*-tolylsulfinylcarbanion, (*R*)-**1c**, derived from (+)-(*R*)-methyl *p*-tolyl sulfoxide and lithium diethylamide, were allowed to react with racemic methyl *p*-toluenesulfinate(**2a**) in tetrahydrofuran at 0 °C, a diastereomeric mixture of bis(*p*-tolylsulfinyl)methanes(**3e**) [(*R,S*)-**3e**: (*S,S*)-**3e**=62: 38%] was produced. Column chromatography, followed by the fractional crystallization of the resulting **3e**, afforded (*S,S*)-**3e**(*dl*-form) (mp 137.5 °C, $[\alpha]_D^{20}$ +318°(acetone) and optically inactive (*R,S*)-**3e** (*meso*-form) (mp 124.5—125 °C). The NMR spectra (in $CDCl_3$) of each diastereoisomer showed singlets due to methylene protons at 4.05 ppm for (*S,S*)-**3e** and at 4.18 ppm for (*R,S*)-**3e**.[12] In addition, the treatment of (−)-(*S*)-**2c** with 2 equivalents of (*R*)-**1c** afforded a single diastereoisomer (*S,S*)-**3e**; its physical properties as well as specific rotation were found to be identical with those of the (*S,S*)-**3e** mentioned above. Only one diastereoisomer, optically inactive (*R,S*)-**3e**, was also obtained on the treatment of (−)-(*S*)-**2c** with 2 equivalents of (*S*)-**1c**

Table 1. Reaction of α-sulfinylcarbanions (**1**) with arenesulfinic esters (**2**) in tetrahydrofuran at 0 °C

1	2	3 (Yields, %)[a]	Diastereomeric ratio of **3**, (*R*, *S*)/(*S*, *S*)	Isolated diastereoisomers[f]
1a	(−)-(*S*)-**2b**	**3a** (75)[b]	63/37	(*S*, *S*)-**3a**, $[\alpha]_D^{19}$ +403°[e]
1a	(−)-(*S*)-**2c**	**3b** (85)[b]	59/41	(*S*, *S*)-**3b**, $[\alpha]_D^{19}$ +346° (*R*,*S*)-**3b**, $[\alpha]_D^{19}$ +170°[d]
1b	(−)-(*S*)-**2b**	**3c** (78)[b]	57/43	(*S*, *S*)-**3c**, $[\alpha]_D^{15}$ +358° (*R*,*S*)-**3c**, inactive
1b	(−)-(*S*)-**2c**	**3d** (71)[b]	58/42	(*S*, *S*)-**3d**, $[\alpha]_D^{20}$ +334°[e]
1c	(−)-(*S*)-**2c**	**3e** (80)[b]	64/36	(*S*, *S*)-**3e**, $[\alpha]_D^{20}$ +318°[e]
(*R*)-**1c**	**2a**	**3e** (56)[b]	62/38	(*S*, *S*)-**3e**, $[\alpha]_D^{20}$ +318° (*R*,*S*)-**3e**, inactive
(*R*)-**1c**	(−)-(*S*)-**2c**	**3e** (35)[c]	0/100	(*S*, *S*)-**3e**, $[\alpha]_D^{20}$ +318°
(*S*)-**1c**	(−)-(*S*)-**2c**	**3e** (45)[c]	100/0	(*R*,*S*)-**3e**, inactive

a) Yields are based on the starting arenesulfinic esters (**2**). b) Yields of a mixture of diastereoisomers. c) Yields after recrystallization. d) It includes 9.8% (*S*,*S*)-**3b**. e) In this case, no attempt was made to separate (*R*,*S*)-diastereoisomer. f) Specific rotations were determined in acetone.

Table 2. NMR data of β-disulfoxides (**3a**—**e**) in $CDCl_3$

β-Disulfoxides	NMR chemical shift, δ (multiplicity, *J*, Hz), ppm		
	$-CH_2-$	CH_3SO-	$\underline{CH_3}C_6H_4-$
3a (*R*,*S*)	4.03(q, 8.0)	2.96(s)	
(*S*, *S*)	4.02(s)	2.80(s)	
3b (*R*,*S*)	4.00(q, 7.8)	2.94(s)	2.45(s)
(*S*, *S*)	4.00(s)	2.76(s)	2.45(s)
3c (*R*,*S*)	4.12(s)		
(*S*, *S*)	3.92(s)		
3d (*R*,*S*)	4.11(s)		2.39(s)
(*S*, *S*)	3.99(s)		2.39(s)
3e (*R*,*S*)	4.18(s)		2.43(s)
(*S*, *S*)	4.05(s)		2.43(s)

derived from (−)-(*S*)-methyl *p*-tolyl sulfoxide and lithium diethylamide.

By a similar procedure, (+)-(*S*,*S*)-**3a**, (+)-(*S*,*S*)-**3c**, optically inactive (*R*,*S*)-**3c**, and (+)-(*S*,*S*)-**3d** were also prepared, using (−)-(*S*)-**2b** and (−)-(*S*)-**2c** as chiral precursors.

The results of these reactions are summarized in Table 1, while the NMR data of isolated diastereomeric β-disulfoxides are compiled in Table 2.

Incidentally, an attempt was made to confirm that the reaction takes place without any loss of stereochemical integrity in the precursors (see Scheme 2). The treatment of (+)-(*S*)-α-bromomethyl *p*-tolyl sulfoxide(**4**), $[\alpha]_D^{14}$ +208° (acetone), with sodium *p*-tolyl sulfide afforded (+)-(*S*)-*p*-tolyl *p*-tolylthiomethyl sulfoxide(**5**), $[\alpha]_D^{15}$ +76.8° (acetone). The oxidation of **5** with hydrogen peroxide in acetic acid yielded a mixture of diastereoisomers of **3e**[(*R*,*S*)-**3e**: (*S*,*S*)-**3e**= 53: 47%]. The fractional crystallization of the mixture furnished dextrorotatory (*S*,*S*)-**3e** and optically inactive (*R*,*S*)-**3e**; their physical properties were found to be identical with those of the compounds obtained from (*R*)-**1c** and **2a**.

An inspection of these results reveals that the nucleophilic substitution at the sulfur atom of sulfinic esters, the entering α-sulfinylcarbanion and the outgoing alkoxy group, proceeds through an S_N2 process with a complete inversion of configuration, in a fashion

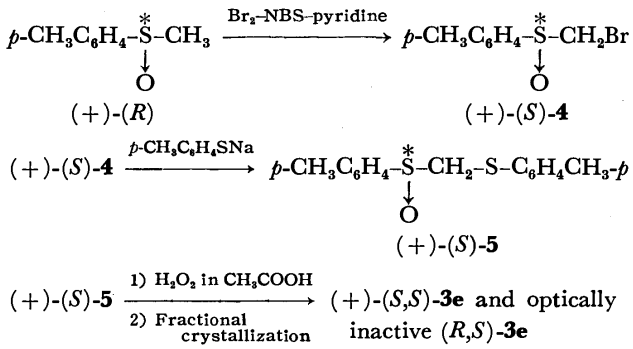

Scheme 2.

similar to the case of normal S_N2-type reactions between sulfinic esters and nucleophiles.[13] Therefore, this reaction is very convenient for obtaining β-disulfoxides in optically and diastereomerically pure states. Moreover, as is revealed in Table 1, in the products of the reaction of **1** with **2** (*R*,*S*)-**3** predominates over (*S*,*S*)-**3**. Though the stereoselectivity may be attributed to the chiralities of both α-sulfinylcarbanions and sulfinic esters, the stereochemical implications of this problem are not yet clear; they will be the subject of our forthcoming paper in this series.

Experimental

General. The optical rotations were measured with a Jasco DPI-4-type polarimeter. The NMR spectra were determined with a Hitachi-Perkin-Elmer R-20 Spectrometer or a Jeol-PS-100 Spectrometer; the chemical shifts are reported in δ units, using tetramethylsilane as the internal reference. The NMR characteristics of β-disulfoxides described here are summarized in Table 2. The IR spectra were obtained with a Jasco IR-G-type spectrometer. All the melting points were taken in a Yanaco MP-type apparatus.

Starting Materials. *(−)-Menthyl (−)-(S)-p-Toluenesulfinate* [(−)-*(S)*-**2c**] was prepared by the reaction of (−)-menthol (Nakarai Chemical Ltd., Kyoto, mp 42—42.5 °C, $[\alpha]_D$ −50 °C (EtOH)) with *p*-toluenesulfinyl chloride according to the method developed by Phillips;[13a] mp 107—107.5 °C, $[\alpha]_D^{25}$ −201° (acetone) [lit,[14] mp 106—107 °C, $[\alpha]_D^{25}$ −199.2° (acetone)]. *(−)-Menthyl (−)-(S)-Benzenesulfinate* [(−)-*(S)*-**2b**] was prepared by the reaction of (−)-menthol

with benzenesulfinyl chloride; mp 50 °C, $[\alpha]_D^{20}$ −200° (acetone) [lit,[15] mp 49—51 °C, $[\alpha]_D$ −205.5° (acetone)]. *(+)-(R)-Methyl p-Tolyl Sulfoxide* was prepared from (−)-(*S*)-**2c** and methylmagnesium iodide according to the method developed by Andersen;[13c] mp 74 °C, $[\alpha]_D^{20}$ +146 °(acetone) [lit,[13f] mp 73—74.5 °C, $[\alpha]_D$ +145.5° (acetone)]. *(−)-(S)-Methyl p-Tolyl Sulfoxide* was prepared by the hydrolysis of the ethoxysulfonium salt of (+)-(*R*)-methyl *p*-tolyl sulfoxide according to the method of Johnson and McCants;[16] mp 74.5 °C, $[\alpha]_D^{20}$ −146 ° (acetone). *Dimethyl Sulfoxide* was freshly distilled from calcium hydride; bp 53 °C/1 mmHg. *Racemic Methyl Phenyl Sulfoxide* was prepared by the periodate oxidation of methyl phenyl sulfide;[17] bp 98—99 °C/1 mmHg(lit,[18] bp 84 °C/0.25 mmHg).

Reaction of **1a** *with (−)-(S)-***2c**. A solution of 2.94 g (0.01 mol) of (−)-(*S*)-**2c** in 10 ml of dry tetrahydrofuran was added, drop by drop to a solution of **1a** (prepared from 12 ml of dimethyl sulfoxide and 0.021 mol of sodium hydride)[9d] in 15 ml of dry tetrahydrofuran at 0 °C under nitrogen. The reaction mixture was then stirred for 1 h at 0 °C under nitrogen. After the addition of water (50 ml), the solution was acidified with 10% hydrochloric acid to a pH of about 3 and extracted with chloroform. The chloroform layer was washed with water and dried over anhydrous sodium sulfate. The column chromatography using a column packed with 100-mesh silica gel and using benzene as the eluent, afforded crude **3b** in an 80% yield; $[\alpha]_D^{19}$ +223° (*c* 0.207, acetone) [(*R,S*)-**3b**: (*S,S*)-**3b**=59: 41%]. (When the residue obtained from the chloroform layer was poured into a large amount of hexane, the hexane-insoluble **3b** was also obtained as a precipitate.) From the resulting **3b**, diastereomerically pure (*S,S*)-**3b** (250 mg) was isolated as colorless needles by fractional crystallization from benzene; mp 147 °C, $[\alpha]_D^{19}$ +346 ° (*c* 0.113, acetone), IR (KBr): 2980, 2900, 1602, 1500, 1430, 1415, 1355, 1300, 1120, 1085, 1055, 1040, 1020, 980, 850, and 715 cm^{-1}. Found: C, 49.85; H, 5.50%. Calcd for $C_9H_{12}O_2S_2$: C, 49.97; H, 5.59%. The concentration of the mother liquid and the crystallization of the residue from hexane–benzene yielded the (*R,S*)-rich diastereoisomer (78 mg) [(*S,S*)-**3b**: (*R,S*)-**3b**=9.8: 90.2%]; $[\alpha]_D^{19}$ +170° (*c* 0.299, acetone). Found: C, 49.88; H, 5.55%. Calcd for $C_9H_{12}O_2S_2$: C, 49.97; H, 5.59%.

Reaction of **1a** *with (−)-(S)-***2b**. A solution of 2.80 g (0.01 mol) of (−)-(*S*)-**2b** in 10 ml of dry tetrahydrofuran was added, drop by drop to a solution of **1a** (0.021 mol) in 15 ml of dry tetrahydrofuran at 0 °C under nitrogen. According to a work-up similar to that described above for **3b**, $[\alpha]_D^{19}$ +280° (*c* 0.180, acetone) [(*R,S*)-**3a**: (*S,S*)-**3a**=63: 37%] was obtained in a 75% yield. From the resulting **3a**, diastereomerically pure (*S,S*)-**3a** (130 mg) was isolated as colorless crystals by fractional crystallization from benzene; mp 138 °C, $[\alpha]_D^{19}$ +403 ° (*c* 0.054, acetone), IR (KBr): 2950, 2900, 1450, 1375, 1080, 1073, 1048, 1023, 993, 955, and 743 cm^{-1}. Found: C, 47.11; H, 4.72%. Calcd for $C_8H_{10}S_2O_2$: C, 47.50; H, 4.98%. No attempt was made to separate (*R,S*)-**3a**.

Reaction of **1b** *with (−)-(S)-***2b**. Methyl phenyl sulfoxide (1.12 g, 0.008 mol) was treated with a solution of lithium diethylamide (prepared from 5.2 ml of a 0.1 g/ml solution of butyllithium in hexane and 585 mg of diethylamine) in 15 ml of dry tetrahydrofuran at 0 °C under nitrogen. After 30 min, a solution of 1.12 g (0.004 mol) of (−)-(*S*)-**2b** in 10 ml of dry tetrahydrofuran was added, and the mixture was stirred for 1 h. The solution was then acidified (*ca.* pH 3) with 10% hydrochloric acid and extracted with chloroform. The chloroform layer was washed with water and dried over anhydrous sodium sulfate. The solvent was evaporated *in vacuo* and washed well with hexane in order to remove the *l*-menthol. Subsequent crystallization from carbon tetrachloride gave (*S,S*)-**3c** (300 mg); mp 136 °C, $[\alpha]_D^{15}$ +358°(*c* 0.190, acetone); IR (KBr): 1480, 1445, 1155, 1075, 1040, 1023, 785, and 738 cm^{-1}. Found: C, 58.55; H, 4.48%. Calcd for $C_{13}H_{12}O_2S_2$: C, 59.06; H, 4.58%. The concentration of the mother liquid and column chromatography on silica gel, using chloroform or benzene as the eluent, followed by recrystallization from hexane–benzene, yielded (*R,S*)-**3c** (250 mg); mp 123 °C. Found: C, 58.71; H, 4.41%. Calcd for $C_{13}H_{12}O_2S_2$: C, 59.06; H, 4.58%.

*Reaction of (R)-***1c** *with* **2a**. A solution of 851 mg (0.005 mol) of **2a** in 10 ml of dry tetrahydrofuran was added, drop by drop to a solution of (*R*)-**1c** (derived from 1.54 g (0.01 mol) of (+)-(*R*)-methyl *p*-tolyl sulfoxide, 6.4 ml of a 0.1 g/ml solution of butyllithium in hexane, and 732 mg of diethylamine in 5 ml of tetrahydrofuran) at 0 °C under nitrogen. A work-up similar to that described for **3c**, a mixture of diastereoisomers of **3e** [(*R,S*)-**3e**: (*S,S*)-**3e**=62: 38%] was produced in an 80% yield. From the mixture, (*S,S*)-**3e** (210 mg) and (*R,S*)-**3e** (135 mg) were obtained by fractional crystallization. (*S,S*)-**3e**: mp 137.5 °C, $[\alpha]_D^{20}$ +318° (*c* 0.110, acetone), IR (KBr): 1500, 1180, 1110, 1080, 1015, and 815 cm^{-1}. Found: C, 61.10; H, 5.38%. Calcd for $C_{15}H_{16}O_2S_2$: C, 61.61; H, 5.51%. Optically inactive (*R,S*)-**3e**: mp 124.5—125 °C.

*Reaction of (R)-***1c** *with (−)-(S)-***2c**. In a manner similar to that used for **3c**, the treatment of 442 mg (0.0015 mol) of (−)-(*S*)-**2c** in 5 ml of dry tetrahydrofuran with (*R*)-**1c** (derived from 463 mg (0.003 mol) of (+)-(*R*)-methyl *p*-tolyl sulfoxide, 0.0031 mol of butyllithium, and 0.0031 mol of diethylamine) afforded crude (*S,S*)-**3e** in an 87% yield. The recrystallization of the crude product from benzene yielded 152 mg of (*S,S*)-**3e** in a diastereomerically pure state; mp 137.5 °C, $[\alpha]_D^{20}$ +318° (*c* 0.190, acetone). Found: C, 61.14; H, 5.28%. Calcd for $C_{15}H_{16}O_2S_2$: C, 61.61; H, 5.51%.

*Reaction of (S)-***1c** *with (−)-(S)-***2c**. Using a procedure similar to that described for **3c**, 99 mg (45% yield) of optically inactive (*R,S*)-**3e** (mp 124.5—125 °C) was obtained from 221 mg (0.00075 mol) of (−)-(*S*)-**2c** and 0.0015 mol of (*S*)-**1c** (derived from 231 mg of (−)-(*S*)-methyl *p*-tolyl sulfoxide and 0.0016 mol of lithium diethylamide).

Reaction of **1b** *with (−)-(S)-***2c**. When a 2.94 g (0.01 mol) of (−)-(*S*)-**2c** was treated with **1b** (derived from 2.81 g of racemic methyl phenyl sulfoxide, 2.8 ml of a 0.1 g/ml solution of butyllithium, and 1.46 g of diethylamine) in dry tetrahydrofuran at 0 °C by a procedure similar to that described for **3c**, a mixture of diastereomeric **3d**[(*R,S*)-**3d**: (*S,S*)-**3d**= 58: 42%] was produced in a 71% yield. From the resulting mixture, (*S,S*)-**3d** was separated as white crystals by fractional crystallization from carbon tetrachloride; mp 100 °C, $[\alpha]_D^{20}$ +334° (*c* 0.205, acetone), IR (KBr): 2950, 2900, 1600, 1450, 1147, 1099, 1080, 1035, 1015, 995, 842, 810, and 740 cm^{-1}. Found: C, 59.10; H, 4.69%. Calcd for $C_{14}H_{14}O_2S_2$: C, 60.40; H, 5.07%. No attempt was made to separate (*R,S*)-**3d**.

*Preparation of (+)-(S)-***4**. (+)-(*R*)-Methyl *p*-tolyl sulfoxide (1.203 g, 0.0078 mol) was brominated with a mixed reagent of bromine (620 mg), *N*-bromosuccinimide (1.388 g), and pyridine (0.7 ml) in methylene chloride (50 ml) according to the published method.[19a] The crude product was recrystallized from hexane–benzene to give (+)-(*S*)-**4** (970 mg, 53% yield); mp 92 °C, $[\alpha]_D^{14}$ +208° (*c* 0.167, acetone). [lit,[19b] $[\alpha]_D^{25}$ +153°(acetone) (optical purity 73%)].

*Preparation of (+)-(S)-***5**. This compound was prepared by the reaction of (+)-(*S*)-**4**(473 mg, 0.00203 mol) with 1 equiv of sodium *p*-tolyl sulfide in acetonitrile–water using a procedure similar to that described by Numata and Oae.[19c] Recrystallization from hexane–benzene gave pure (+)-(*S*)-**5** (360 mg, 64% yield); mp 81.5—82 °C, $[\alpha]_D^{14}$ +76.8° (*c*

0.186, acetone), NMR ($CDCl_3$) δ 2.38 (s, 3H), 2.45 (s, 3H), 4.15 (s, 2H), and 7.45 (m, 8H).

Oxidation of (+)-(S)-5. The oxidation of (+)-(*S*)-**5** (200 mg, 0.000724 mol) was carried out in 5 ml of glacial acetic acid, using 123 mg (0.00108 mol) of 30% hydrogen peroxide, to yield 194 mg of a mixture of diastereoisomers of **3e** [(*R,S*)-**3e**: (*S,S*)-**3e**=53: 47%]. The fractionsl crystallization of the mixture from hexane–benzene afforded 55 mg of (*S,S*)-**3e** (mp 137.5 °C, $[\alpha]_D^{19}$ +318° (*c* 0.132, acetone)) and 45 mg of optically inactive (*R,S*)-**3e** (mp 124.5—125 °C).

References

1) N. Kunieda, J. Nokami, and M. Kinoshita, *Chem. Lett.*, **1973**, 871.

2) Recently, it has been reported that α-sulfinylcarbanions derived from optically active sulfoxides can serve as good chiral reagents in the asymmetric synthesis of optically active alcohols,[3] styrene oxide,[4] and amines.[5]

3) G. Tsuchihashi, S. Iriuchijima, and M. Ishibashi, *Tetrahedron Lett.*, **1972**, 4608.

4) C. R. Johnson and C. W. Schroeck, *J. Amer. Chem. Soc.*, **93**, 5303 (1971); **95**, 7424 (1973).

5) G. Tsuchihashi, S. Iriuchijima, and K. Maniwa, *Tetrahedron Lett.*, **1973**, 3389.

6) Only a few stereochemical studies for β-disulfoxides have hitherto been reported.[7]

7) a) R. Louw and H. Nieuwenhuyse, *Chem. Commun.*, **1968**, 1561; b) J. L. Greene, Jr. and P. B. Shevlin, *ibid.*, **1971**, 1092.

8) The treatment of **2** with 1 equiv of **1** resulted in at most 10% yield of **3**. This fact perhaps due to an acidic nature of β-disulfoxides of permitting the ready formation of an α,α-disulfinylcarbanion by base. For instance, the H–D exchange of methylene hydrogens of β-disulfoxides in the presence of base is very rapid. When (*S,S*)-**3d** was treated with 1 equiv of **1b** in dry tetrahydrofuran at 0 °C, followed by quenching with D_2O–D_2SO_4, the methylene hydrogens of recovered (*S,S*)-**3d** were found to be deuterated quantitatively.

9) H. -D. Becker, G. J. Mikol, and G. A. Russell, *J. Amer. Chem. Soc.*, **85**, 3410 (1963); b) H. -D. Becker and G. A. Russell, *J. Org. Chem.*, **28**, 1896 (1963); c) E. J. Corey and M. Chaykovsky, *J. Amer. Chem. Soc.*, **86**, 1639 (1964); d) E. J. Corey and M. Chaykovsky, *ibid.*, **87**, 1345 (1965).

10) The diastereomeric ratio can readily be evaluated from the NMR spectra of methylene protons or methyl protons of methylsulfinyl group by integration of the respective signals.

11) Low *et al.*[7a] have reported that the NMR spectrum of *meso*-2,4-dithiapentane 2,4-dioxide shows an AB quartet.

12) The spectra of the methylene protons of (*R,S*)-**3c** and (*R,S*)-**3e** were split into an AB quartet by tris(dipivaloylmethanato)europium in accord with the result of Greene and Shevlin.[7b]

13) a) H. Phillips, *J. Chem. Soc.*, **127**, 2552 (1925); b) J. Day and D. J. Cram, *J. Amer. Chem. Soc.*, **87**, 4398 (1965); c) K. K. Andersen, *Tetrahedron Lett.*, **1962**, 93; d) M. Kobayashi and M. Terao, This Bulletin, **39**, 1343 (1966); e) K. Mislow, M. M. Green, P. Laur, J. T. Melillo. T. Simmons, and A. L. Ternay, Jr., *J. Amer. Chem. Soc.*, **87**, 1958 (1965); f) M. Axelrod, P. Bickart, J. Jacobus, M. M. Green, and K. Mislow, *ibid.*, **90**, 4835 (1968).

14) H. F. Herbrandson, R. T. Dickerson, Jr., and J. Weinstein, *ibid.*, **78**, 2576 (1956).

15) H. F. Herbrandson and R. T. Dickerson, Jr., *ibid.*, **81**, 4102 (1959).

16) C. R. Johnson and D. McCants, Jr., *ibid.*, **87**, 5404 (1965).

17) N. J. Leonard and C. R. Johnson, *J. Org. Chem.*, **27**, 282 (1962).

18) K. K. Andersen, W. H. Edmonds, J. B. Biasotti, and R. A. Strecker, *ibid.*, **31**, 2859 (1966).

19) a) S. Iriuchijima and G. Tsuchihashi, *Synthesis*, **1970**, 588; b) M. Cinquini, S. Colonna, F. Fornasier, and F. Montanari, *J. Chem. Soc., Perkin I*, **1972**, 1886; c) T. Numata and S. Oae, This Bulletin, **45**, 2794 (1972).

Carbonization of Aromatic Hydrocarbons. II. Carbonization of Modified Pyrene in the Presence of Aluminum Chloride

Isao MOCHIDA, Noriyoshi FUKUDA, Keiko MAEDA, and Kenjiro TAKESHITA
Research Institute of Industrial Science, Kyushu University, Fukuoka 812
(Received June 19, 1975)

The carbonization of four hydrogenated and two methylated pyrene derivatives in the presence of aluminum chloride was investigated to elucidate the effects of the slight structural perturbation on the carbonization properties of pyrene. Hexahydropyrene was found to give coke having a needle-like structure *via* similar carbonization steps as naphthalene followed. In contrast, dihydropyrene formed coke of a mosaic structure for the most part. Although 1-methylpyrene produced coke with a needle-like structure, in part, reductively methylated pyrene was converted to a mosaic structure as was pyrene. In the case of needle-coke formation, the carbonization process of hydrogenated and methylated pyrene followed the steps of appearance, growth and coalescence of anisotropic spheres where the reaction started at a lower temperature and proceeded more moderately compared with the case of pyrene. It is thus indicated that a partially lowered aromaticity of pyrene may favor its carbonization into needle coke.

Two kinds of anisotropic graphitizable coke were reported in the carbonization of aromatic hydrocarbons in a previous paper.[1] The first type had a needle-like appearance, which was observed on the coke formed from naphthalene, anthracene, chrysene, *etc.* The second one obtained from pyrene and perylene showed a mosaic structure without any regularity in the arrangement of the anisotropic compounds. The size of orientated domains was found to depend on the rate of carbonization which could be modified by the carbonization conditions such as the holding temperature, time and quantity of the catalyst in the process. The carbonization reactivities should also be controlled by a modification of the aromaticity of the aromatic hydrocarbons. In fact, the carbonization properties of quinoline insoluble of pitches were improved by reductive alkylation and hydrogenation.[2,3]

In the present study, the carbonization of four hydrogenated and two methylated pyrene derivatives was investigated to learn the effect of slight structural changes on the condensation reactivity of the starting material, as well as, on the structures of the resulting coke. By following the carbonization process through microscopic observation, analysis of the evolved gases, and the solubility index, which may indicate the degree of carbonization, the mechanism of needle-like coke formation is discussed.

Experimental

Materials. The materials used in the present study are listed in Table 1. Commercially available materials (from the Wako Co. and the Tokyo Kasei Co.) were carbonized without further purification except for the perhydropyrene and the reductively methylated pyrene (RA-pyrene). Perhydropyrene was synthesized from pyrene by Birch reduction with lithium ethylenediamine.[4] Reductive methylation of pyrene was carried out according to the method reported by Sternberg *et al.*[5] NMR spectra indicated that RA-pyrene had 1.9 methyl groups on the average.

Procedure. Carbonization was carried out in the presence of aluminum chloride ($AlCl_3$/aromatics=0.1 mole ratio). The carbonization was carried out in flowing nitrogen. The rate of the temperature increase and the holding time at a fixed temperature were 150 °C/hr and 2 hr, respectively.

TABLE 1. AROMATIC SAMPLES

	Structure
Naphthalene	
Pyrene	
Dihydropyrene	
Tetrahydropyrene	
Hexahydropyrene	
Perhydropyrene	
1-Methylpyrene	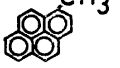
RA-pyrene	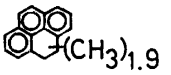

Experimental details in this study have been described in a previous paper.[1]

Analysis of Gases Evolved during Carbonization. Hydrogen and methane evolved during carbonization under a programmed temperature increase (150 °C/hr up to 560 °C) were analyzed by means of a gas chromatograph with a molecular sieve column, the evolved gas being sampled every 15 min.

Results

Carbonization of Hydrogenated Pyrene Derivatives.
Dihydropyrene: Microscopic photographs of coke obtained from dihydropyrene at several holding temperatures are shown in Fig. 1. Slightly warped spheres several microns in diameter were observed in the coke maintained at 380 °C (Fig. 1a). Within a narrow range beyond this temperature, the coke was completely converted into an anisotropic carbon with a disordered mosaic structure such as that observed in the coke from pyrene (Fig. 1b). Before small anisotropic spheres could grow into large oriented domains, the whole coke sample became anisotropic. It should be noted,

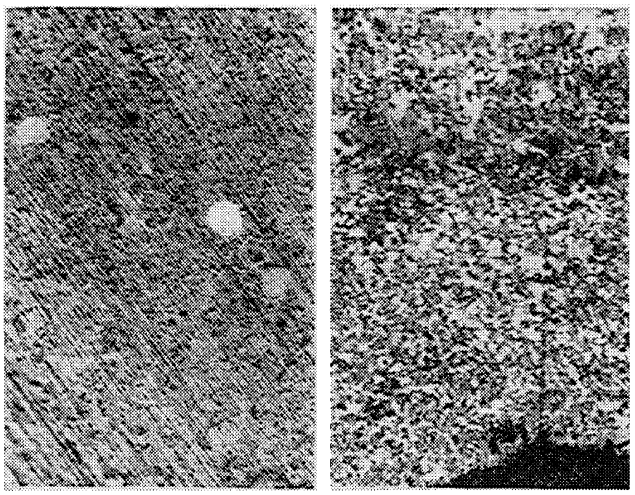

Fig. 1. Microphotographs of carbon obtained from dihydropyrene (under crossed nicols, ×200).
a; carbonization at 380 °C, b; carbonization at 500 °C.

however, that the temperature at which the anisotropy occurred was lower by 20—30 °C than that in the pyrene carbonization.[1)]

Tetrahydropyrene: The coke from tetrahydropyrene remained isotropic up to 380 °C, and then the coke became completely anisotropic at 400 °C, at which temperature the mixed appearance of the oriented and mosaic domains was observed (Fig. 2a). This result may indicate that the hydrogenation of pyrene into tetrahydropyrene produced the structure of a partial-flow pattern, and lowered the temperature for the appearance of anisotropy.

Hexahydropyrene: Hexahydropyrene gave such a sticky carbon below 360 °C that it was impossible to grind it for microscopic observation. As shown in Fig. 2b, the structure of the anisotropic flow pattern was observed for coke maintained at 520°, as well as 380 °C. This flow pattern was quite similar to that of the coke from naphthalene.

Perhydropyrene: In marked contrast, the coke from perhydropyrene remained entirely isotropic up to 500 °C. A photomicrograph of it is shown in Fig. 2c. The yield of carbon was only 5—10%. Because the carbon yield of hexahydropyrene, for example, was 58% at 500 °C, it should be noted that the yield of perhydropyrene was extraordinarily low in comparison with the three other hydropyrenes. Aluminum chloride may not work as a catalyst for the carbonization of non-aromatic hydrocarbons.

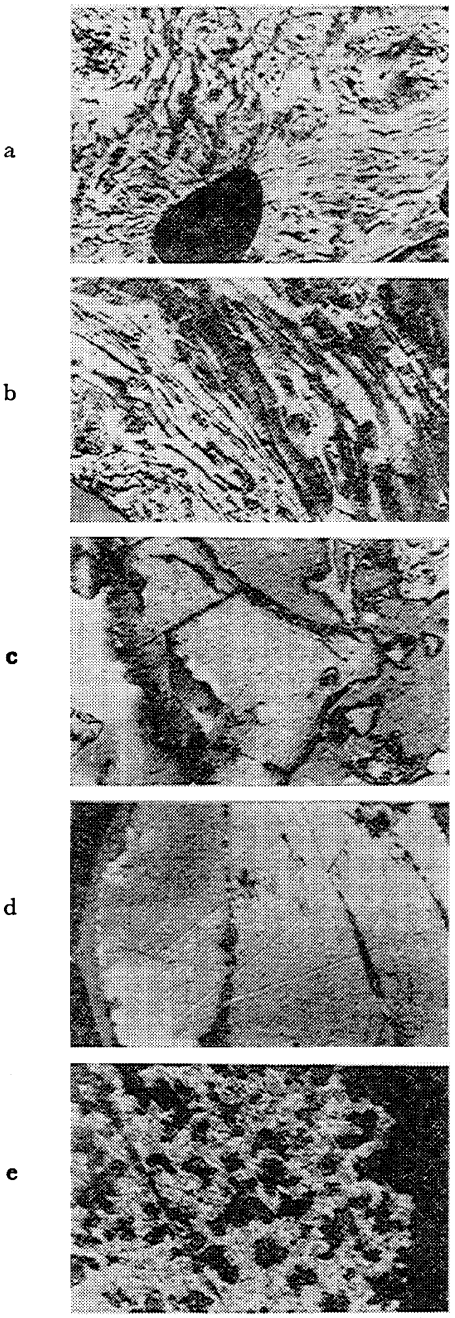

Fig. 2. Microphotographs of carbon obtained from modified pyrenes (under crossed nicols, ×200).
a; tetrahydropyrene at 560 °C, b; hexahydropyrene at 520 °C, c; perhydropyrene at 500 °C, d; 1-methylpyrene at 560 °C, e; RA-pyrene at 560 °C.

Table 2. Crystallographic parameters of types of coke soaking temp. and time; 2500 °C—0.5 hr pretreatment; 2 hr at 380 °C and 0.5 hr at 1250 °C

Samples	C_0(002) (Å)	L_c(002) (Å)	Feature of coke
Naphthalene	6.737	690	needle
Pyrene	6.744	450	mosaic
Dihydropyrene	6.734	540	mosaic
Tetrahydropyrene	6.747	370	needle and mosaic
Hexahydropyrene	6.734	510	needle

C_0(002); lattice constant (CuK_α). L_c(002); crystal size.

X-Ray Analysis of Coke from Hydrogenated Pyrenes. Table 2 shows the crystallographic parameters of coke obtained from pyrene derivatives at 2500 °C. All carbons showed considerable crystal growth indicating the formation of graphite except for the coke from perhydropyrene. No significant difference in the parameters obtained by X-ray analysis was observable among these types of coke in spite of the different structural features revealed with an optical microscope, as indicated in Table 2.

Carbonization of Methylated Pyrene Derivatives.
1-Methylpyrene: Photomicrographs of the coke obtained

from 1-methylpyrene are shown in Fig. 2d. Anisotropic spheres were observed in the coke maintained at 300 °C, and the coke was converted completely anisotropic having large oriented domains by further heat-treatment. Methylation of pyrene provided the flow pattern structure, and lowered the temperature necessary for the appearance of anisotropic structures.

RA-pyrene: As shown in Fig. 2e, a fine mosaic structure was observed for the coke maintained at 560 °C. It should be noted that reductive methylation of pyrene did not produce the same flow pattern structure as that of 1-methylpyrene, although both derivatives had methyl groups.

The Reactivity of Aromatic Hydrocarbons to Carbonization. The yields of benzene insoluble (BI %) in the cokes obtained from four kinds of aromatic hydrocarbons are plotted against the carbonization temperature in Fig. 3,

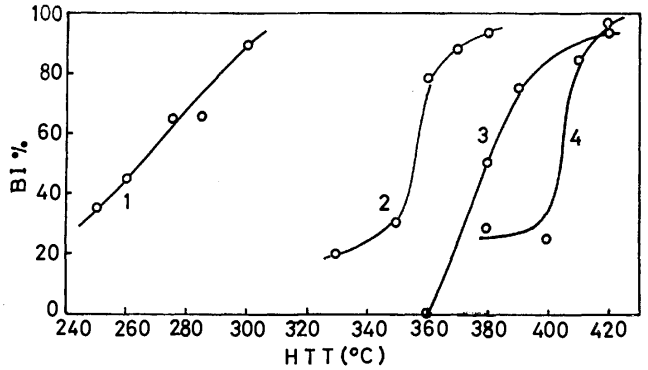

Fig. 3. BI content of carbon from modified pyrenes 1; naphthalene, 2; hexahydropyrene, 3; tetrahydropyrene, 4; pyrene.

because the value of BI% is considered to be one of the criteria for the degree of carbonization. The BI% of the coke from naphthalene increased from 37% at 250 °C to 90% at 300 °C. In contrast, that of the coke from pyrene increased rather rapidly from 25% at 400 °C to 85% at 410 °C. The profiles of the BI% increase in the carbonization of hexahydropyrene and tetrahydropyrene were located in the intermediate between pyrene and naphthalene, as shown in Fig. 3. Furthermore, it is interesting to note that the order of increasing size of the needle-like domains determined by microscopic observation (naphthalene>hexahydropyrene>tetrahydropyrene>pyrene) coincides with the decreasing carbonization temperature necessary for the coke to be insoluble in quinoline.

Hydrogen and methane evolved during the carbonization of dihydropyrene, hexahydropyrene, 1-methylpyrene, and RA-pyrene are shown in Figs. 4 and 5, where the temperature was programmed to rise at the rate of 150 °C/hr up to 560 °C. Analysis of the evolved gases indicated that the modified pyrenes of two pairs (dihydropyrene and hexahydropyrene, and 1-methylpyrene and RA-pyrene) followed different carbonization processes, giving the coke of a needle-like or a mosaic structure, respectively (see Figs. 1 and 2). There are some precautions necessary in the analysis of the present observation of the gases evolved during carbonization. First, the evolution of gases during the heat

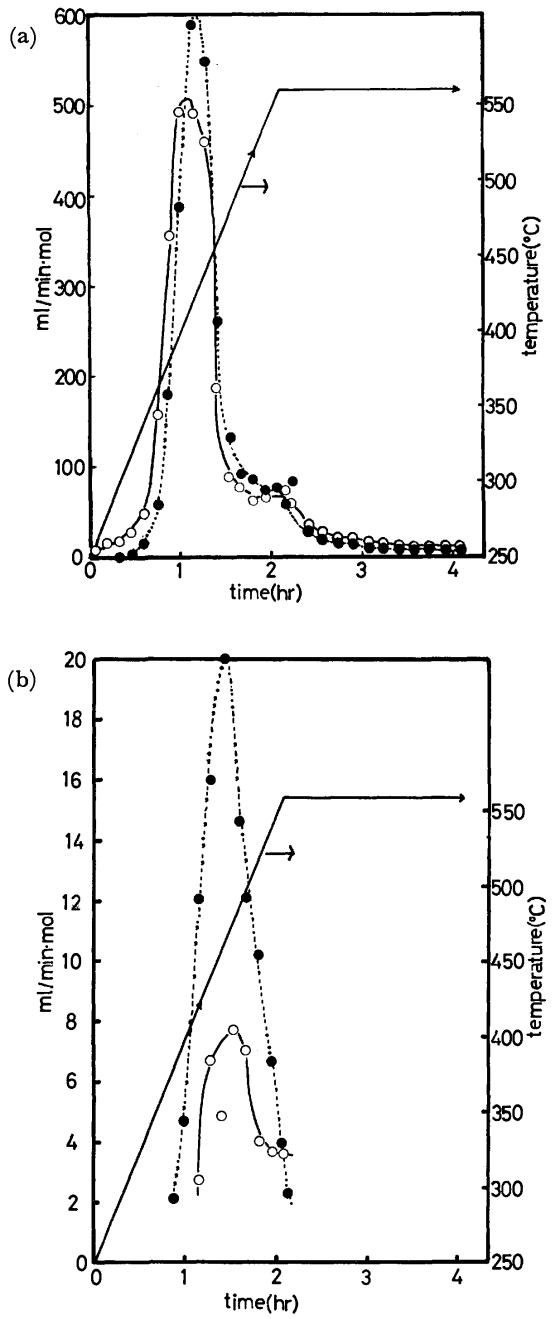

Fig. 4. Evolved gases during the carbonization of dihydropyrene and hexahydropyrene
(a); H_2, (b); CH_4,
—○—; dihydropyrene, —●—, hexahydropyrene.

treatment was ascribed to the elimination reaction, as well as the carbonization reaction, however these two reactions are rather difficult to distinguish clearly. Second, heating conditions for the analysis of the gases and the microscopic observation or BI% analysis were not the same as those described in the experimental section. Thus, a direct comparison of these results is not possible. In general, longer holding times may cause advanced carbonization. Thus, carbonization reactivities of these compounds should be discussed taking into account these conditions.

Three significant differences were noticed in the carbonizations of dihydropyrene and hexahydropyrene.

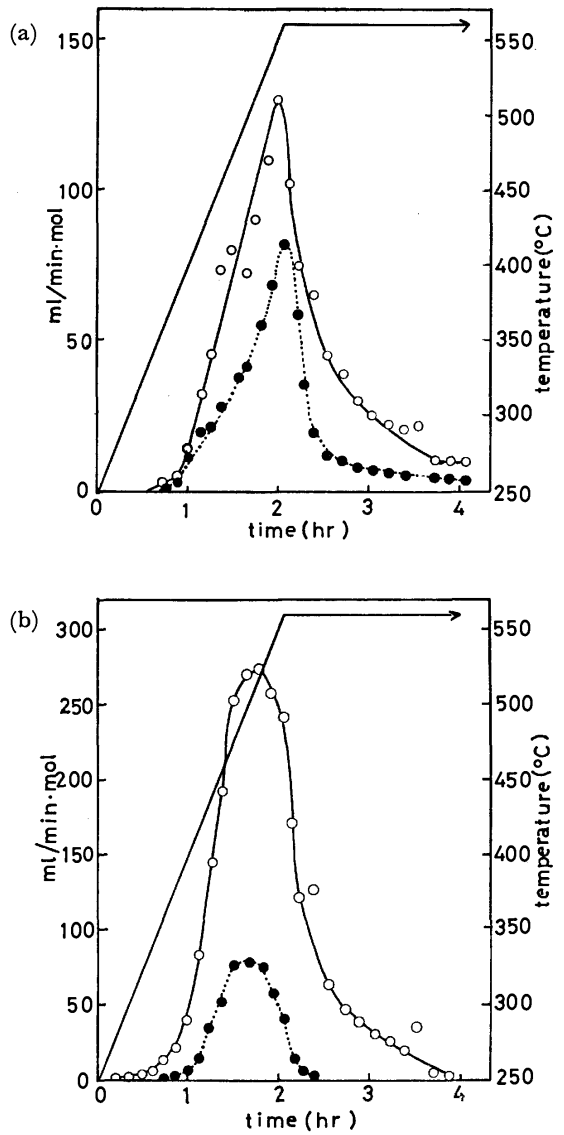

Fig. 5. Evolved gases during the carbonization of 1-methylpyrene and RA-pyrene.
(a); H_2, (b); CH_4,
—○—; RA-pyrene, ---●---; 1-methylpyrene.

First, dehydrogenation of dihydropyrene started at a temperature lower by 50 °C than that for hexahydropyrene perhaps indicating a faster reproduction of pyrene from dihydropyrene, although the total features were quite similar. Second, the amount of evolved methane was much less in the carbonization of dihydropyrene than in that of hexahydropyrene. Such a difference was also observed in the carbonization of pyrene and naphthalene, which resulted in mosaic and needle-like coke structures, respectively. Third, dehydrogenation and demethylation occurred almost simultaneously at 300 °C in the case of hexahydropyrene, indicating that "dehydrogenation" which may convert hexahydropyrene back to pyrene did not take place before carbonization. On the other hand, "dedehydrogenation" of dihyd ropyrene occurred 150 °C below that of demethylation, bringing about a reproduction of pyrene before carbonization.

Methyl groups of RA-pyrene started to evolve at *ca.* 250 °C which was lower by 100 °C and much more methane was evolved compared with 1-methylpyrene, as shown in Fig. 5, although the peaks of the evolution were located at closer temperatures. Methane started to evolve earlier than hydrogen in the case of RA-pyrene. In contrast, both gases started at the same temperature in 1-methylpyrene. Such results may indicate that "demethylation" of RA-pyrene started before the carbonization reaction occurred, converting RA-pyrene to pyrene.

Discussion

The results of X-ray analysis shown in Table 2 show that all carbonization processes of the five kinds of aromatic hydrocarbons may proceed *via* molten phases at the early stage of carbonization and that all of the cokes calcined at 2500 °C show considerable crystal growth, indicating the formation of graphite. However, it is revealed that the types of coke have two different anisotropic structures when examined with an optical microscope, namely, a mosaic structure with small domains and a flow pattern structure with large oriented domains. This fact again indicates that carbonization through the molten phase is not sufficient for the formation of a flow pattern structure, as discussed in a previous study.[1]

An improvement in the carbonization properties of pyrene into the needle-like coke is clearly achieved by partial hydrogenation and alkylation, as is shown in Figs. 1 and 2. Such an improvement may come from the modified reactivity of the pyrene by a slight structural change. Lowered aromaticity seems to favor the carbonization of pyrene into needle coke. It has been pointed in a previous paper[1] that the steps of appearance, coalescence, and growth of anisotropic spheres may be essential for the formation of the needle cokes as Taylor and Brooks have indicated,[6] and that the starting material should have the appropriate condensation reactivity for the carbonization process to follow these steps because the increase of the molecular weight and of the viscosity of the carbonizing material occurs at the same time during carbonization where molecular arrangement should be completed before solidification.

A change in the reactivity of pyrene by this modification is shown in Figs. 3, 4, and 5. In every case, hydrogenation lowers the temperature at which carbonization begins as indicated by the BI% increase in Fig. 3. If the temperature and the rate of carbonization are decreased enough by hydrogenation or alkylation, the carbon obtained shows a needle-like structure similar to that produced by hexahydropyrene. In such cases, modifying groups introduced should stay on the pyrene nuclei long enough until carbonization has progressed to some extent.

The structures of hexahydropyrene and tetrahydropyrene can be compared to naphthalene and diphenyl, respectively. In a previous paper,[1] the latter two compounds have been found to have quite different reactivities. The different reactivities of the former two compounds due to their structures may bring about the different features of the coke structures.

In contrast, if the introduced groups are eliminated at an early stage of the heat treatment, modification cannot longer be expected to produce a needle-like coke structure which does not occur in the case of pyrene. Dihydropyrene and RA-pyrene are such cases, although warped anisotropic spheres were observed on the coke from dihydropyrene. Dehydrogenation may take place before the anisotropic spheres grow into the flow-pattern structure.

A marked elimination of methyl groups from RA-pyrene should be noted. In reductive alkylation, the introduction of a methyl group should accompany the reduction of the aromatic double bond. Dealkylation of the alkyl-naphthene to form a double bond occurs more easily at elevated temperatures than for the alkyl-aromatic compound, so that the different features of carbonization may be observed as in the cases of 1-methylpyrene and RA-pyrene.

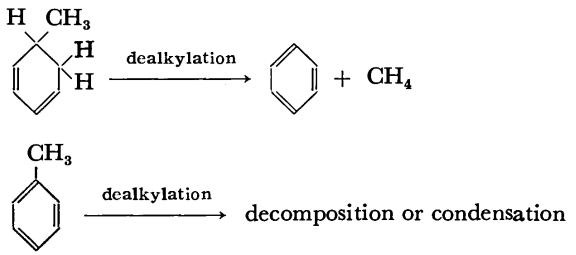

A modification of the carbonization properties of quinoline-insolubles in coal-tar and petroleum pitches has been reported for reductive alkylation and hydrogenation in previous papers,[2,3,7] where both methods could convert some parts of the QI soluble in the solvent (benzene or chloroform). However, hydrogenation produced fusibility at the same time resulting in anisotropic needle coke, whereas reductive alkylation did not. The same situation was observed for the model compounds of pitches in the present study. These results can be explained in terms of elimination reactivity of the groups introduced during the carbonization. The present study indicates that the alkylation may be expected to be effective for a modification of the carbonization properties, and its application to pitches is now in progress.

Reference

1) I. Mochida, K. Kudo, N. Fukuda, K. Takeshita, and R. Takahashi, *Carbon*, **13**, 135 (1975).
2) I. Mochida, K. Kudo, K. Takeshita, R. Takahashi, Y. Suetsugu, and J. Furumi, *Fuel*, **53**, 253 (1974).
3) I. Mochida, Y. Tomari, K. Maeda, and K. Takeshita, *ibid.*, **54**, 265 (1975).
4) L. Reggel, R. Raymond, S. Friedman, R. A. Freidel, and I. Wender, *ibid.*, **37**, 126 (1958).
5) H. W. Sternberg, C. L. Delle, Donne, P. Patages, E. C. Moroni, and R. E. Markby, *ibid.*, **50**, 452 (1971).
6) J. D. Brooks and G. H. Taylor, "Chemistry and Physics of Carbon," Vol. 4, ed. by P. L. Walker, Jr., Edward Arnold, New York (1968), p. 243.
7) I. Mochida, K. Maeda, and K. Takeshita, *Fuel.*, **55**, 70 (1976)

The Formation of Ethers from *dl*-Citronellol in the Presence of Boron Trifluoride Etherate

Kimiko NAGAI

Department of Chemistry, Faculty of Science, Hiroshima University, Higashisenda-machi, Hiroshima, 730

(Received June 23, 1975)

dl-Citronellol reacted with boron trifluoride etherate to give a mixture of a novel cyclic dicitronellyl ether (IX) and an acyclic dicitronellyl ether (X), along with eight minor products. Both major ethers were produced in equilibrium in the presence of the above reagent.

In previous papers it has been reported that a variety of ethers were obtained in reactions of boron trifluoride etherate with monoterpene alcohols, of allylic acyclic geraniol,[1] nerol,[2] and *l*-linalool,[2] of homoallylic cyclic *l*-isopulegol,[3] and of saturated bicyclic *d*-borneol[4] and *dl*-isoborneol.[4] The reactions may be regarded as the acid-catalyzed intermolecular dehydration of these alcohols and/or their isomers. In one case,[2] there was observed further cyclization of the ether, the primary product. In the present work, a study of an analogous acid-catalyzed reaction of *dl*-citronellol (I), in which one double bond is at the ζ-position for the hydroxyl group is reported. Some of the results have previously been reported.[5]

Results and Discussion

The reaction conditions and the product distributions in the present study are summarized in Table 1. In each run, the reaction mixture was roughly divided into two fractions by setting up the boundary at the boiling point of 130 °C in distillation under reduced pressure (3.5 mmHg).

Characterization of Monoterpene Products. Each low-boiling fraction was submitted to column chromatography with silica gel. The hydrocarbon portion thus obtained was small in all runs, and the analysis employing glc comparisons with authentic samples and a combined glc-mass spectrometric technique revealed this part to be a mixture of four compounds, namely, α-terpinene (II), dipentene (III), 2,4(8)-*p*-methadiene (IV), and terpinolene (V). The alcoholic portion was also found to be a mixture of the reactant and three other alcohols, the latter being identified as isopulegol (VI), menthol (VII),[6] and tetrahydrogeraniol (VIII) mainly from spectral data. VIII was the major product. The yields of these alcohols slightly increased with an increase in the amount of boron trifluoride etherate.

Characterization of Dimerized Products. Thin layer and gas chromatography of the high-boiling fractions indicated the production of two dimerized compounds in Experiments 1 and 2, and of three compounds in Experiment 3. Isolation and characterization of these compounds are as follows:

2,2,6,10,10,14-Hexamethyl-1,9-dioxacyclohexadecane (IX): The least polar compound in the column chromatography of the high-boiling fraction was isolated as colorless needles, mp 61—62 °C. Its molecular formula was determined to be $C_{20}H_{40}O_2$ corresponding to a dimerized molecule of the reactant from mass spectra analysis and using the method of Rast. Despite the hydrogen deficient formula, this compound was not hydrogenated over an Adams catalyst in acetic acid. It may be of particular significance that a singlet at δ 1.10 for twelve hydrogens and a doublet at δ 0.85 for six hydrogens with J=6 Hz were observed in the NMR spectrum. The former was assigned to two *gem*-dimethyl groups located on a tertiary carbon and the latter to two secondary methyls. In addition, a triplet at δ 3.28 for four hydrogens with J=6 Hz was assigned to two methylene groups adjacent to the oxygen atoms. In the IR spectrum there was no indication of the presence of a hydroxyl group, but a characteristic absorption band was observed at 1085 cm^{-1} for the ether linkage. These spectroscopic results strongly suggest a highly symmetric structure for this dimeric ether. Thus, the compound was determined to be 2,2,6,10,10,14-hexamethyl-1,9-dioxacyclohexadecane (IX). Additional evidence was obtained from the fact that the reaction of this ether with hydroiodic acid afforded tetra- and di-hydrogeranyl iodides which were prepared independently.

3,7,7,11,15-Pentamethyl-8-oxa-14-hexadecen-1-ol (X): The moderately polar compound eluted by column

Table 1. Reaction of citronellol with boron trifluoride etherate

Experiment No.	Reaction condition: Citronellol (I) (g)	$BF_3 \cdot Et_2O$ (ml)	React. temp. (°C)	React. period (hr)	Reaction product[a] (%): Low-boiling fraction (monoterpene): Hydrocarbons (I)	(II)	(III)	(IV)	(V)	Alcohols (VI)	(VII)	(VIII)	High-boiling fraction (dimer) (IX)	(X)	(XI)	Residue (polymer)
1	10	1	20	72	66.0	trace				0.1	0.1	0.8	32.0	1.0	—	—
2	10	2	20	24	62.0	0.4				0.7	0.6	3.3	16.0	8.0	—	9.0
3	10	3	20	48	53.7	0.3				1.0	1.0	4.0	10.0	19.0	2.0	9.0

a) Percentages of reaction products were determined by glc on a column of Silicon SE-30 10% on Uniport B (60—80 mesh) at 200 °C.

chromatography of the high-boiling fraction was isolated as a colorless oil in all three runs. Although its molecular weight obtained by mass spectrometry was the same as that of IX, this oil absorbed one equivalent of hydrogen under catalytic reduction. Distinctive bands at 3350 cm^{-1} and 1070 cm^{-1} were present in the IR spectrum due to a primary hydroxyl group and the oil afforded monoacetate upon treatment with acetic anhydride in dry pyridine. Together with the NMR spectrum, this evidence indicates the oil to be 3,7,7,11,-15-pentamethyl-8-oxa-14-hexadecen-1-ol (X). Reaction of the compound with phosphoryl chloride in dry pyridine converted it into an unsaturated ether ($C_{20}H_{38}O$), which was then hydrogenated. Further, the saturated ether was treated with hydroiodic acid giving the tetrahydrogeranyl iodide described above and 2,6-dimethyl-1-octene.[7]

3,7,9,9,13-Pentamethyl-7-pentadecene-1,15-diol (XI): The most polar compound was isolated in a small amount as a colorless oil only from the high-boiling fraction of Experiment 3. This compound was also an isomer of the other two fractions. Taking account of both the spectral data obtained for this product and experiments analogous to those described above, this may be characterized as an unsaturated diol. For determining the position of the double bond, the compound was submitted to osmium tetroxide oxidation followed by silylation with a mixed reagent of hexamethyldisilazane and trimethylchlorosilane to be converted into trimethylsilyl ether. From precise analysis of the mass spectrum of the silyl ether, the unsaturated diol was characterized as 3,7,9,9,13-pentamethyl-7-pentadecene-1,15-diol, as is shown in detail in the Experimental Section.

Reaction Sequence. As given in Table 1, three monoterpene alcohols and four hydrocarbons were found in the low-boiling fraction of the product. Of the monoterpene alcohols, tetrahydrogeraniol (VIII) was the major product in all three runs. Isopulegol (VI) was assumed to be produced by way of citronellal as a possible intermediate, since this cyclization took place with ease under similar conditions. Although citronellal could not be detected in the present study, VIII and citronellal should be produced by disproportionation of citronellol (I). Another alcohol, menthol (VII), was formed probably by cyclization of the reactant (I), in a manner similar to that described in an earlier report.[6] Since the four hydrocarbons were all cyclic diolefins, their precursor should be a cyclic unsaturated alcohol if acid-catalyzed dehydration follows. Isopulegol (VI), mentioned above, may be the most probable precursor in this reaction. These processes are summarized in Scheme 1.

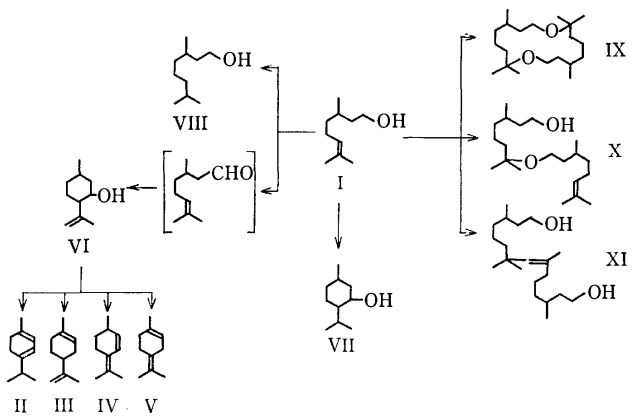

Scheme 1.

TABLE 2. CONVERSION OF CYCLIC (IX) AND ACYCLIC (X) ETHERS IN THE PRESENCE OF BORON TRIFLUORIDE ETHERATE

Composition after the treatment	Starting compound	
	Cyclic diether (IX)	Acyclic ether (X)
IX	86%	42%
X	11	33
XI	1	20
Others	2	5

In the present study, IX and X were the main products. The former, cyclic diether, was predominant when one ml of boron trifluoride etherate was used for ten grams of I, whereas the latter, its isomeric acyclic ether, was preferentially produced when three ml of the reagent was applied. Under the same conditions, IX, could be converted into X in an 11% yield and X was transformed into IX and XI in 42% and 20% yields respectively, as shown in Table 2. Thus, these compounds were in equilibrium under the reaction conditions. The distribution of these dimerized products was estimated by glc analysis where ten grams of citronellol (I) was treated with various amounts of boron trifluoride etherate. The results are given in Fig. 1. It is clearly shown that the distribution is markedly influenced by the molar ratio of the acidic reagent to I.

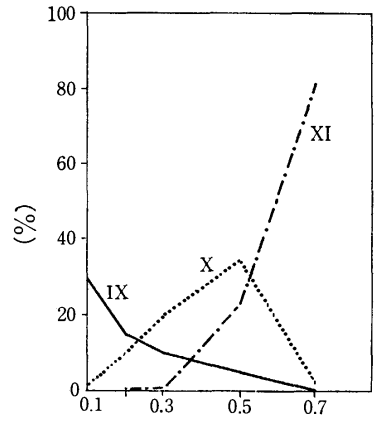

Fig. 1. Dependence of three dimerized species on the concentration of $BF_3 \cdot Et_2O$.
Citronellol each 10 g, no solvent, room temperature, 48 hr.

The formation of the cyclic diether (IX) in the presence of boron trifluoride etherate may be interesting in view of the natural occurrence of large membered cyclic compounds.

Experimental

Apparatus. The glc was carried out using a Hitachi-063, equipped with an FID detector, a stainless-steel separating column (3 mm×3 m) packed with Carbowax 6000 (10%) on Diasolid (60—80 mesh), DEGS (10%) on Shimalite W (60—80 mesh), and Silicon SE-30 (10%) on Uniport B (60—80 mesh); the flow rate of nitrogen, the carrier gas, 20 ml/min. The mass spectra were obtained using a combined apparatus, Shimadzu-LKB 9000 glc and mass spectrometer: a glass separating tube (3 mm×3 m) packed with Carbowax 20 M (10%) on Diasolid (60—80 mesh); temperature program, 5 °C/min from 50 °C to 120 °C; ionization energy, 70 eV; ion accelerating voltage, 3500 V; ionization chamber temperature, 200 °C. The NMR spectra were measured in a $CDCl_3$ solution using a 60 MHz spectrometer, Hitachi R-20, with TMS as an internal reference.

Materials. Commercial citronellol was used, after being purified through repeated fractionations. Bp 109 °C/4 mmHg, d_4^{25} 0.8530, n_D^{25} 1.4539, $[\alpha]_D^{25}$ ±0° ($CHCl_3$). A single peak was observed in glc in each case for separating columns of Carbowax 6000, Silicon SE-30, and DEGS, and the IR and NMR spectra coincided with those of authentic samples.

$BF_3 \cdot Et_2O$ of chemical grade (BF_3 47%) was used without purification.

Reaction of Citronellol with $BF_3 \cdot Et_2O$. To 10 g of citronellol 1, 2, or 3 ml of $BF_3 \cdot Et_2O$ was added drop by drop, the mixture being allowed to stand for 72, 24, and 48 hr at room temperature (*ca.* 20 °C). The mixture, after having been shaken with a saturated aqueous solution of sodium carbonate to decompose the excess of $BF_3 \cdot Et_2O$, was washed with water, dried over anhydrous sodium sulfate, and fractionated into low-boiling (bp 55—130 °C/3.5 mmHg) and high-boiling (bp 130 °C/3.5 mmHg) fractions under reduced pressure.

Characterization of Monoterpene Compounds. Each low-boiling fraction from Experiments 1—3 was eluted over a silica gel column with hexane and then with a mixture of ethyl acetate and hexane (v/v 15:85) for separation into hydrocarbons and alcohols.

Hydrocarbons: Gas chromatographic analysis of each hydrocarbon portion was carried out on a separating column packed with Carbowax 6000 by comparison with authentic samples. The mass spectra of these compounds were obtained using the combined glc-mass spectrometer. Thus, II, III, IV, and V were identified.

Alcohols: The alcohol portions showed three peaks in the glc on a DEGS-packed column in addition to the reactant peak. The gas chromatographic analysis of the portion was carried out using authentic samples, and also each compound was isolated by preparative glc for determining the IR and NMR spectra. The compounds were thus identified as VI, VII, and VIII.

Characterization of Dimerized Compounds. The high-boiling fractions from Experiments 1 and 2 were shown to consist of two compounds (R_f 0.7 and 0.6; t_R 5.3 and 6.3) from tlc with a mixed solvent of ethyl acetate and hexane (v/v 15:85) and from glc on a Silicon SE-30-packed separating column at 200 °C. The high-boiling fraction from Experiment 3 contained three compounds (R_f 0.7, 0.6, and 0.2; t_R 5.3, 6.3, and 10.5). Each fraction was chromatographed over a silica gel column with hexane and then with mixtures of hexane and ethyl acetate increasing in the concentration of ethyl acetate stepwise from 2% to 14%, each compound being isolated.

2,2,6,10,14-Hexamethyl-1,9-dioxacyclohexadecane (IX). The compound with R_f 0.7 and t_R 5.3 was isolated by elution chromatography as white needles, mp 61—62 °C. Mass: *m/e* 41 (36%), 43 (29), 55 (57), 69 (65), 81 (29), 83 (base, C_6H_{11}), 95 (21), 109 (18), 123 (21), 138 (25, $M^+-C_{10}H_{22}O_2$), 140 (50, $M^+-C_{10}H_{20}O_2$), 157 (25, $C_{10}H_{21}O$), 199 (11, $M^+-C_7H_{13}O$), 297 (11, M^+-CH_3), 312 (2, M^+, $C_{20}H_{40}O_2$). IR (CCl_4, cm^{-1}): 1380 and 1362 (CH_3-$\underset{|}{C}$-CH_3), 1085 (C-O-C). NMR ($CDCl_3$, ppm): 0.85 (6H, d, J=6 Hz, $C\underline{H}_3$-CH-), 1.10 (12H, s, $(C\underline{H}_3)_2$-C-O-), 3.28 (4H, t, J=6 Hz, -O-$C\underline{H}_2$-CH_2-).

Found: C, 76.72; H, 13.01%; mol wt (Rast), 317. Calcd for $C_{20}H_{40}O_2$: C, 76.86; H, 12.90%; mol wt, 312.5.

Ether Bond Cleavage of IX: Compound IX (100 mg) was heated with hydroiodic acid (d=1.7, 0.2 ml) under reflux for 10 min. The mixture, after having been poured into water (30 ml), was extracted with ether. After the organic layer was washed with a 10% aqueous solution of sodium bicarbonate and with water and dried over sodium sulfate, evaporation of the solvent gave a colorless oil in a 90% yield, showing two peaks at t_R 9.8 and 10.8 in glc on a Silicon SE-30-packed column. The oil was separated by elution chromatography over a silica gel column with hexane as an eluent.

Identification of Tetrahydrogeranyl Iodide: The compound with t_R 9.8 was a colorless oil, the yield of which was 75% of the ether-cleaved products. n_D^{20} 1.4748. The mass, IR, and NMR spectra were respectively superimposable on those of tetrahydrogeranyl iodide prepared as described below.

Identification of Dihydrogeranyl Iodide: The compound with t_R 10.8 of the ether-cleaved products was also a colorless oil, the yield of which was 25% of the ether-cleaved products. n_D^{20} 1.4978. The mass, IR, and NMR spectra were respectively coincident with those of dihydrogeranyl iodide which was prepared as described below.

Synthesis of Tetrahydrogeranyl Iodide. Tetrahydrogeraniol (2.5 g) was heated with a mixture of red phosphorus (0.15 g) and resublimed iodide (1.3 g) with stirring at 150 °C for 7 hr. The reaction product was taken up into ether. The solution was filtered, and the filtrate was washed successively with water, a 5% aqueous sodium hydroxide solution and water and then dried over anhydrous sodium sulfate. Evaporation of the solvent gave tetrahydrogeranyl iodide as a colorless oil in a 77% yield, which was further purified by elution chromatography over a silica gel column with hexane. n_D^{20} 1.4749. Mass: *m/e* 39 (45%), 41 (70), 43 (base), 55 (14), 57 (85), 71 (53), 85 (14), 99 (13), 127 (5, I^+), 141 (12, $C_{10}H_{21}$), 268 (2, M^+, $C_{10}H_{21}I$). IR (CCl_4, cm^{-1}): 1386, 1381, 1368, 1208, 1178. NMR ($CDCl_3$, ppm): 0.87 (9H, d, J=6 Hz, $C\underline{H}_3$-$\underset{|}{C}$H-$C\underline{H}_3$, $C\underline{H}_3$-$\underset{|}{C}$H-), 1.26 (8H, br.s, -$C\underline{H}_2$-), 3.21 (2H, t, J=6 Hz, -CH_2-$C\underline{H}_2$-I).

Synthesis of Dihydrogeranyl Iodide. A mixture of dihydrogeraniol (2.0 g), red phosphorus (0.1 g) and resublimed iodide (1.0 g) was heated at 150 °C for 3 hr. The mixture was treated similarly as in the case of the preparation of tetrahydrogeranyl iodide to give dihydrogeranyl iodide as a colorless oil in a 58% yield. n_D^{18} 1.4973. Mass: *m/e* 41 (67%), 55 (80), 69 (base), 83 (60), 95 (5), 97 (10), 109 (4), 127 (4, I^+), 139 (5, $C_{10}H_{19}$), 266 (3, M^+, $C_{10}H_{19}I$). IR (CCl_4, cm^{-1}): 1660, 1181, 830. NMR ($CDCl_3$, ppm): 0.87 (3H, d, J=6 Hz, $C\underline{H}_3$-$\underset{|}{C}$H-), 1.60 and 1.67 (each 3H, br.s, $C\underline{H}_3$-$\underset{|}{C}$=CH-), 3.22 (2H, t, J=6 Hz, -CH_2-$C\underline{H}_2$-I), 5.06 (1H, m, -$\underset{|}{C}$=C$\underline{H}$-).

3,7,7,11,15-Pentamethyl-8-oxa-14-hexadecen-1-ol (X). The compound with R_f 0.6 and t_R 6.3 of the high-boiling fraction was isolated as a colorless viscous oil by the above-mentioned elution chromatography. n_D^{27} 1.4601. Mass: *m/e* 41 (28%), 43 (20), 55 (42), 67 (10), 69 (90), 81 (33), 83 (base), 95 (15), 109 (6), 123 (16, C_9H_{15}), 138 (12), 139 (15, $C_{10}H_{19}$), 156 (13, $C_{10}H_{20}O$), 197 (23, $M^+-C_7H_{15}O$), 297 (2, M^+-CH_3), 312

(3, M^+, $C_{20}H_{40}O_2$). IR (CCl_4, cm^{-1}): 3350, 1070 (-OH), 1080 (C-O-C), 1650, 830 (-C=CH-), 1380, 1363 (CH_3-C-CH_3). NMR ($CDCl_3$, ppm): 0.85 (6H, d, J=6 Hz, C$\underline{H}_3$-CH-), 1.10 (6H, s, (C$\underline{H}_3$)$_2$-C-O-), 1.60, 1.68 (each 3H, br.s, C$\underline{H}_3$-C=CH-), 3.30 (2H, t, J=6 Hz, -C-O-C$\underline{H}_2$-CH_2-), 3.64 (2H, t, J=6 Hz, -CH_2-C$\underline{H}_2$-OH), 1.90 (1H, br.s, -O$\underline{H}$), 5.05 (1H, m, -C$\underline{H}$=C-).

Catalytic Hydrogenation of X: Compound X (300 mg) was hydrogenated over platinum oxide (30 mg) in acetic acid (7 ml) to take up one molar equivalent of hydrogen. The mixture was treated according to the usual procedure, dihydro X being obtained as a colorless oil in a good yield. Mass: *m/e* 41 (77%), 43 (base), 55 (77), 57(65), 69 (52), 83 (21), 85 (26), 87 (11), 141 (10), 199 (13), 314 (trace, M^+,$C_{20}H_{42}O$). IR (CCl_4, cm^{-1}): 3370, 1075 (-OH), 1070(C-O-C), 1380, 1368 (CH_3-CH-CH_3 and CH_3-C-CH_3). NMR ($CDCl_3$, ppm): 0.85 (12H, d, J=6 Hz, C$\underline{H}_3$-CH- and C$\underline{H}_3$-C-C$\underline{H}_3$), 1.10 (6H, s, (C$\underline{H}_3$)$_2$C-O-), 2.00 (1H, br.s, -O$\underline{H}$), 3.30 (2H, t, J=6 Hz, -O-C$\underline{H}_2$-CH_2-), 3.65 (2H, t, J=6 Hz, -CH_2-C$\underline{H}_2$-OH).

Acetylation of X: Acetic anhydride (1 ml) was added to a solution of X (500 mg) in dry pyridine (1 ml) and the mixture was allowed to stand overnight at room temperature. The mixture, after having been poured into water, was extracted with ether, and evaporation of the solvent gave monoacetate as an oily substance in a good yield. IR (CCl_4, cm^{-1}): 1745, 1245 (CH_3COO-), 1080 (C-O-C), 1382, 1370 (CH_3-C-CH_3). NMR ($CDCl_3$, ppm): 0.88 (6H, d, J=6 Hz, C$\underline{H}_3$-CH-), 1.10 (6H, s, C$\underline{H}_3$-C-C$\underline{H}_3$), 1.60, 1.68 (each 3H, br.s, C$\underline{H}_3$-C=CH-), 2.02 (3H, s, C$\underline{H}_3$COO-), 4.05 (2H, t, J=6 Hz, CH_3-COO-C$\underline{H}_2$-CH_2-), 5.05 (1H, m, -C$\underline{H}$=C-).

Dehydration of X: A solution of phosphoryl chloride (0.2 ml) in dry pyridine (1 ml) was added to a solution of X (500 mg) in the same solvent under cooling at −5 °C, and the mixture was allowed to stand at the same temperature for 24 hr. The mixture, after having been poured into a 10% ice-cooled aqueous solution of sodium bicarbonate, was taken up into ether. Evaporation of the solvent gave a dehydrated compound (X-A) as an oily substance in a good yield. IR (CCl_4, cm^{-1}): 1650, 890 (CH_2=C-), 1670, 830 (-CH=C-), 1080 (C-O-C), 1385, 1369 (CH_3-C-CH_3). NMR ($CDCl_3$, ppm): 0.88 (6H, d, J=6 Hz, C$\underline{H}_3$-CH-), 1.12 (6H, s, (C$\underline{H}_3$)$_2$=C-O-), 1.60, 1.68 (3H and 6H, each br.s, -C(C$\underline{H}_3$)=C(H)- and -C($\underline{H}_3$C)=C($\underline{H}$)-), 3.30 (2H, t, J=6 Hz, -O-C$\underline{H}_2$-CH_2-), 4.70 (2H, br.s, CH_2=C-), 5.10 (1H, m, -C$\underline{H}$=C-).

Catalytic Hydrogenation of Dehydrated Product X-A: Catalytic hydrogenation of the dehydrated product (X-A, 400 mg) over platinum oxide (40 mg) in acetic acid (6 ml) took up two molar equivalents of hydrogen to give a tetrahydroproduct (X-B) as an oily substance in a good yield. Mass: *m/e* 39 (20%), 41 (85), 43 (95), 55 (91), 57 (base), 69 (98), 81 (72), 83 (44), 85(54), 97 (22), 140 (6), 141 (21), 173 (27), 199 (50, M^+-C_7H_{15}), 265 (3, M^+-CH_3-H_2O), 280 (2, M^+-H_2O), 298 (trace, M^+, $C_{20}H_{42}O$). IR (CCl_4, cm^{-1}): 1382, 1365, 1082. NMR ($CDCl_3$, ppm): 0.85 (12H, d, J=6 Hz, C$\underline{H}_3$-CH-C$\underline{H}_3$ and C$\underline{H}_3$-CH-), 1.08 (6H, s, (C$\underline{H}_3$)$_2$C-O-), 3.25 (2H, t, J=6 Hz, -O-C$\underline{H}_2$-CH_2-).

Ether Bond Cleavage of the Tetrahydro-Compound X-B: X-B (300 mg) was heated with hydroiodic acid (d=1.7, 0.4 ml) under reflux for 10 min, and the reaction product was chromatographed over silica gel with hexane to give two compounds with t_R 7.6 and 9.8 in good yields.

Identification of 2,6-Dimethyl-1-octene: The compound with t_R 7.6 of the ether-cleaved products was obtained as a colorless oil in a relative yield of 30%. Mass: *m/e* 41 (36%), 43 (50), 55 (59), 57 (75), 69 (base), 83 (80), 95 (29), 97 (43), 111 (42), 126 (25), 140 (41, M^+, $C_{10}H_{20}$). The mass spectrum of this compound was in good agreement with that of 2,6-dimethyl-1-octene.[7]

Identification of Tetrahydrogeranyl Iodide: The compound with t_R 9.8 of the ether-cleaved products was obtained as a colorless oil in a relative yield of 70%. The mass, IR, and NMR spectra were respectively superimposable on those of the synthetic samples of tetrahydrogeranyl iodide mentioned above.

3,7,9,9,13-Pentamethyl-7-pentadecene-1,15-diol (XI). The most polar compound (R_f 0.20 and t_R 10.5) of the high-boiling fraction separated in Experiment 3 was isolated in elution chromatography as a colorless oil. n_D^{28} 1.4770. Mass: *m/e* 41 (base), 43 (86%), 55 (68), 57 (56), 59 (10), 67 (25), 69 (71), 70 (40), 71 (41), 81 (22), 83 (20), 95 (18), 112 (11), 123 (8), 138 (4), 156 (3), 269 (2, M^+−C_3H_7), 297 (2, M^+−CH_3), 312 (1, M^+, $C_{20}H_{40}O_2$). IR (CCl_4, cm^{-1}): 3350, 1065, 1020 (-OH), 1388, 1371 (CH_3-C-CH_3), 1650, 860 (-CH=C-). NMR ($CDCl_3$, ppm): 1.63 (3H, br.s, C$\underline{H}_3$-C=CH-), 0.85 (6H, s, C$\underline{H}_3$-C-C$\underline{H}_3$), 0.90 (6H, d, J=6 Hz, C$\underline{H}_3$-CH-), 3.59 (4H, t, J=6 Hz, -CH_2-C$\underline{H}_2$-OH), 3.80 (2H, br.s, -O$\underline{H}$), 5.09 (1H, m, -C$\underline{H}$=C-).

Found: C, 76.67; H, 13.04%; mol wt (Rast), 310. Calcd for $C_{20}H_{40}O_2$: C, 76.86; H, 12.90%; mol wt, 312.5.

Acetylation of XI: XI (100 mg) was treated with acetic anhydride (0.7 ml) in dry pyridine (1.0 ml) at room temperature according to the manner indicated above to give a diacetate as an oily substance in a good yield. IR (CCl_4, cm^{-1}): 1389, 1371 (CH_3-C-CH_3), 1740, 1250 (CH_3COO-), 1650, 855 (-CH=C-). NMR ($CDCl_3$, ppm): 0.82 (6H, s, C$\underline{H}_3$-C-C$\underline{H}_3$), 0.90 (6H, d, J=6 Hz, C$\underline{H}_3$-CH-), 2.02 (6H, s, C$\underline{H}_3$-COO-), 4.09 (4H, t, J=6 Hz, -CH_2-C$\underline{H}_2$-COOCH_3), 5.05 (1H, m, -C=C$\underline{H}$-).

Catalytic Hydrogenation of XI: XI (500 mg) was hydrogenated over platinum oxide (50 mg) in acetic acid (7 ml), and took up one molar equivalent of hydrogen to give a dihydroderivative as a colorless oil in a good yield. Mass: *m/e* 41 (68%), 43 (base), 55 (64), 56 (44), 57 (52), 59 (8), 67 (36), 69 (56), 70 (32), 71 (36), 77 (8), 81 (40), 83 (20), 95 (28), 112 (12), 121 (6), 123 (12), 141 (21), 199 (18), 296 (2, M^+-H_2O), 314 (trace, M^+, $C_{20}H_{42}O_2$). IR (CCl_4, cm^{-1}): 3350, 1065, 1020 (-OH), 1388, 1371 (CH_3-C-CH_3). NMR ($CDCl_3$, ppm): 0.85 (6H, s, C$\underline{H}_3$-C-C$\underline{H}_3$), 0.90 (6H, d, J=6 Hz, C$\underline{H}_3$-CH-), 3.14 (2H, br.s, -O$\underline{H}$), 3.65 (4H, t, J=6 Hz, -CH_2-C$\underline{H}_2$-OH).

Oxidation of XI: A solution of osmium tetroxide (500 mg) in 4 ml of dry benzene was added to a solution of XI (500 mg) in a mixture of dry benzene (5 ml) and dry pyridine (0.5 ml) and the mixture was allowed to stand at room temperature for 6 days. After benzene had been distilled out from the mixture, the residual portion was diluted with ethanol (10 ml), then the solution was refluxed with a 10% aqueous sodium sulfite solution (10 ml) for 2 hr. Brown precipitates thus formed were filtered off, and the filtrate was extracted with chloroform to give a glycol as a colorless oil in a 90% yield. IR (CCl_4, cm^{-1}): 3400, 1160, 1070 (-OH). NMR ($CDCl_3$, ppm): 0.90 (6H, d, J=6 Hz, C$\underline{H}_3$-CH-), 0.99 (6H, s, C$\underline{H}_3$-C-C$\underline{H}_3$), 1.25 (3H, s, C$\underline{H}_3$-C-OH), 2.84 (4H, br.s, -O$\underline{H}$), 3.40 (1H, m, -C-C$\underline{H}$-OH), 3.65 (4H, t, J=6 Hz, -CH_2-C$\underline{H}_2$-OH).

Trimethylsilylation of the Glycol: Hexamethyldisilazane (0.1 ml) and trimethylchlorosilane (0.05 ml) were successively added to a solution of the above glycol (3 mg) in dry pyridine (0.5 ml), and the mixture was heated at 65 °C for 7 min. The mixture was treated according to a usual procedure to give trimethylsilyl ether as an oily substance. Mass: *m/e* 69 (45%), 71 (25), 73 (40), 75 (45), 81 (50), 83 (95), 89 (10), 95 (67), 103 (48), 117 (27), 123 (30), 129 (62), 131 (60), 139 (40), 147 (45), 171 (55), 187 (45), 218 (50), 229 (26), 242 (10), 288 (base), 303 (18), 316 (15), 331 (12), 405 (2), 456 (16), 545 (5). This spectrum was reasonably explained by following fragmentation.

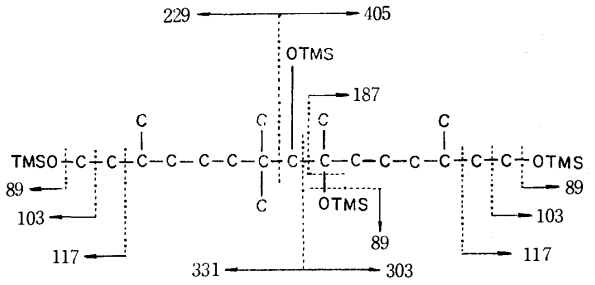

Conversion of Cyclic Diether (IX) and Acyclic Ether (X) by $BF_3 \cdot Et_2O$. A solution of IX (100 mg) in dry ether (1 ml) was mixed with 0.02 ml of $BF_3 \cdot Et_2O$ and the mixture was allowed to stand at room temperature for 48 hr. After the excess catalyst had been decomposed by the addition of a small amount of water, the separated oily layer was analyzed by glc with the Silicon SE-30 separation column. The conversion of acyclic ether was similarly examined. The results are given in Table 2.

The author wishes to express sincere gratitude to Professor Shûichi Hayashi of Hiroshima University for kind and continuous guidance in the course of this work, and also to Assistant Professor Mitsuru Nakayama of Hiroshima University for valuablesuggestions.

References

1) K. Nagai, *Chem. Pharm. Bull.*, **18**, 2123 (1970).
2) K. Nagai, This Bulletin, **48**, 2317 (1975).
3) K. Nagai, *J. Sci. Hiroshima Univ., Ser.* **A, 38**, 141 (1974).
4) K. Nagai, M. Nakayama, A. Matsuo, S. Eguchi, and S. Hayashi, This Bulletin **47**, 1193 (1974).
5) K. Nagai, M. Nakayama, and S. Hayashi, *Chem. Lett.*, **1973**, 665.
6) E. van Bruggen, *Rec. Trav. Chim. Pays-Bas*, **87**, 1134 (1968).
7) G. Ohloff, J. Seibl, and E. sz. Kováts, *Ann. Chem.*, **675**, 83 (1964).

Important Role of Fluorescence Reabsorption Mechanism in Sensitized Reaction of Unsaturated Lactones. Evidence against "the Orbital Symmetry Correlations in Sensitization"

Hirochika SAKURAGI, Isao ONO,* Norisuke HATA,* and Katsumi TOKUMARU[1]

Department of Chemistry, Faculty of Science, The University of Tokyo, Hongo, Bunkyo-ku, Tokyo 113
**Department of Chemistry, College of Science and Engineering, Aoyama Gakuin University, Chitosedai, Setagaya-ku, Tokyo 154*

(Received June 26, 1975)

Evidence are presented against Ullman's "the orbital symmetry correlations" between excited aromatic hydrocarbon sensitizers and 4-benzylidene-2-phenyl-5-oxazolone. It is now shown that the oxazolone efficiently quenches the triplet sensitizers regardless of Ullman's classification, and the fluorescence emitted from the sensitizers is reabsorbed by the oxazolone and its wavelength seems to govern the reported reaction course.

Previously Ullman and Baumann reported that under irradiation unsaturated lactones, 4-benzylidene-2-phenyl-5-oxazolone (I) and 2-benzylidene-4-phenyl-3-buten-4-olide (II), depending upon the wavelength of light irradiated or the sensitizers employed, either "selectively" undergo only geometrical isomerization or "unselectively" undergo hydrogen atom abstraction from solvent together with the isomerization.[2] Thus, on direct irradiation of the lactones, 313 nm light caused both reactions, whereas 366 nm light caused only the

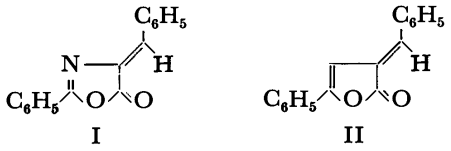

I II

isomerization. In sensitized reactions, sensitization with biphenyl, fluorene, and naphthalene led to both reactions, whereas sensitization with phenanthrene, triphenylene, and chrysene resulted in only the isomerization. In order to explain the relation between the selectivity of the reaction course and the structure of the sensitizers, they proposed the "orbital symmetry correlations between the excited sensitizers and the lactones" which implied that the close matching of the orbital symmetry between the lowest unfilled molecular orbital of the lactone and a certain part of the highest occupied orbital of the sensitizer led only to the "selective reaction," the isomerization. They stated that matching of the orbital symmetry between the sensitizer and the lactone molecules would lead to effective excitation of the lactone to its $T_1(\pi,\pi^*)$ state to cause the "selective reaction," whereas no matching of the symmetry would lead to inefficient unselective energy transfer to cause the "unselective reactions."[2]

In a previous communication[3] we presented an aspect against Ullman's postulate by showing that not the triplet but the singlet excited aromatic hydrocarbons played an important role in the sensitized reaction of the lactone II; fluorescence emitted from the hydrocarbon sensitizers was reabsorbed by the lactone and the fluorescence wavelength seemed to govern the course of the reaction.

In this paper we report firm evidence against Ullman and Baumann's postulate on "the orbital symmetry correlations between the excited sensitizer and the substrate." Contrary to their previous proposition, the oxazolone I is now shown to effectively quench the triplet states of the hydrocarbon sensitizers irrespective of "selective" or "unselective" sensitizers on the ground of direct determination of rate constants for the quenching of the triplet hydrocarbons by the oxazolone. Therefore the reported dependence of the reaction course on sensitizers employed does not result from the difference between the sensitizers in rate constants for the quenching of their triplet states by the oxazolone but is shown to be mostly governed by wavelengths of fluorescence emitted from the singlet excited sensitizers which is reabsorbed by the oxazolone.

Results and Discussion

Absorption and Emission Spectra. Figure 1 shows the absorption spectra of the oxazolone in EPA at 77 K and at ambient temperature together with its emission spectrum in EPA at 77 K. The emission was observed only at 77 K and it is attributable to fluorescence, since the emission starts from the end of absorption and shows mirror image relationship with the absorption. Lack of phosphorescence might be due to rapid radiationless deactivation of the triplet state probably resulting in the facile isomerization of the benzylidene group. The singlet excitation energy of the oxazolone is estimated to be 72 kcal/mol from the above result and its triplet excitation energy was reported to be 43 kcal/mol from its singlet-triplet absorption.[2]

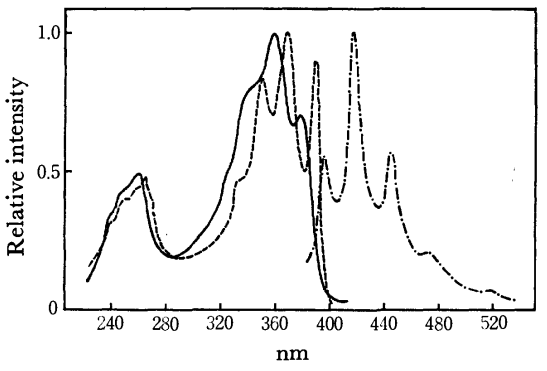

Fig. 1. Absorption and emission spectra of 4-benzylidene-2-phenyl-5-oxazolone in EPA. Absorption at ambient temperature: —, at 77 K: —, emission at 77 K: -·-·-.

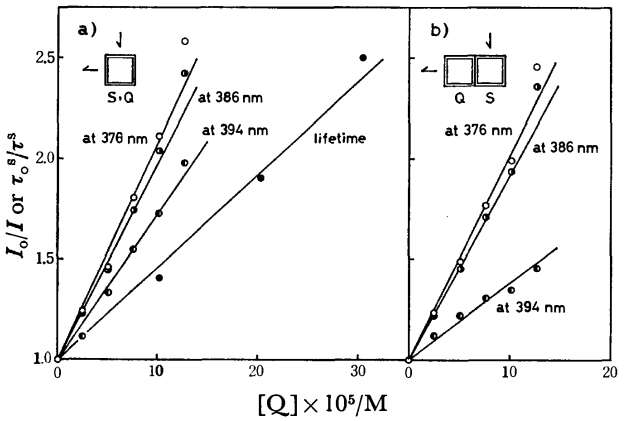

Fig. 2. Stern-Volmer plots. a) Quenching of fluorescence of pyrene (S) by 4-benzylidene-2-phenyl-5-oxazolone (Q) in benzene, b) reabsorption of fluorescence of pyrene (S) by the oxazolone (Q) in benzene.

Quenching of Hydrocarbon Fluorescence by the Oxazolone. Fluorescence of the aromatic hydrocarbons (10^{-5}—10^{-2} mol/l) such as biphenyl, fluorene, naphthalene, triphenylene, chrysene, *p*-terphenyl, phenanthrene, and pyrene was quenched for the intensity and the lifetime by the added oxazolone in benzene solution. Plots of the fluorescence intensity ratio, I_0/I, against the concentration of the oxazolone, [Q], (0—2×10^{-5} mol/l) were, for the most cases, linear only in the lower concentration range of the oxazolone and curved upwards in the higher concentration range as indicated in Fig. 2, where I_0 and I denote the fluorescence intensity of the hydrocarbon in the absence of the oxazolone and that in the presence of the oxazolone in concentration of [Q], respectively. If, in the lower concentration range of the oxazolone, the plots are assumed to obey the Stern-Volmer relationship

$$I_0/I = 1 + k_q^{app}\tau_0^S[Q] \quad (1)$$

(Eq. 1), the apparent quenching rate constants, k_q^{app}, can be obtained from their slopes divided by the lifetimes of the singlet states of the hydrocarbons in the absence of the oxazolone, τ_0^S. The shapes of fluorescence spectra of some hydrocarbons were varied with increase in the concentration of the oxazolone and the fluorescence intensity ratio, I_0/I, was also varied with wavelength at which the emission is observed. These results suggest, as will be discussed later, that the quenching of hydrocarbon fluorescence is mostly due to the reabsorption of fluorescence by the quencher. In Table 1 are listed the apparent quenching rate constants, k_q^{app}, measured at the emission maximum of each hydrocarbon.

For the quenching of the singlet lifetimes of the aromatic hydrocarbons by the oxazolone, plots of τ_0^S/τ^S against the concentration of the oxazolone fitted the

$$\tau_0^S/\tau^S = 1 + k_q^S\tau_0^S[Q] \quad (2)$$

Stern-Volmer relationship (Eq. 2) over the concentration range of the oxazolone employed (0—5×10^{-4} mol/l) (Fig. 2), where τ^S denotes the lifetime of a singlet hydrocarbon in the presence of the oxazolone in concentration [Q]. The bimolecular rate constants, k_q^S, for the quenching process of the excited singlet hydrocarbons by the oxazolone are summarized in Table 1, which shows that k_q^{app} values are several to eighty times larger than k_q^S values. Table 1 also contains I_0/I and τ_0^S/τ^S values obtained at $[Q]=2.0\times10^{-5}$ mol/l, showing that I_0/I values are significantly higher than the corresponding τ_0^S/τ^S values.

Table 1. Quenching of hydrocarbon fluorescence by 4-benzylidene-2-phenyl-5-oxazolone in benzene[a)]

Hydrocarbon	fl[b)]	k_q^{app} c) $\times10^{-12}$	k_q^S c) $\times10^{-11}$	I_0/I[d)]	$(I_0/I)_{reabs}$[d)]	τ_0^S/τ^S d)
Biphenyl	316	2.4	0.87	1.45	1.26	1.02
Fluorene	318	3.5	1.5	1.48	1.30	1.02
Naphthalene	336	2.8	4.9	1.98	1.63	1.17
p-Terphenyl	343	55	—	2.31	2.12	—
Triphenylene	364	8.3	1.1	3.27	2.10	1.03
Phenanthrene	366	9.4	4.2	2.95	2.51	1.06
Pyrene	376	7.4	27	3.64	3.34	1.95
Chrysene	383	6.5	3.9	2.72	1.97	1.11

a) Conducted under the aerated condition; the concentration of the hydrocarbon: 10^{-5}—10^{-2} M, the concentration of the oxazolone: 0—5×10^{-5} M for the intensity measurement and 0—10^{-4} M for the lifetime measurement. b) Maximum wavelength of fluorescence in nm. c) In $M^{-1}s^{-1}$. d) Values at the oxazolone concentration of 2×10^{-5} M.

The above difference between I_0/I and τ_0^S/τ^S values at the same concentration of the oxazolone is reasonably attributable to reabsorption of the fluorescence from the excited singlet hydrocarbons by the oxazolone by the following reasons. If the added oxazolone acts only to quench the excited singlet hydrocarbon with a rate constant of k_q^S, the fluorescence intensity of the hydrocarbon would be decreased to the same extent as the singlet lifetime, so I_0/I would be equal to τ_0^S/τ^S, but it is not the case. When the fluorescence from the hydrocarbon is reabsorbed by the oxazolone in the surrounding medium, the actually observed fluorescence is to be further reduced in intensity, so, as was actually observed, I_0/I value is to be higher than τ_0^S/τ^S value by an extent corresponding to the reabsorption. A possibility that apparent reduction of the sensitizer fluorescence by the oxazolone would be due to formation of complex between ground states of the sensitizer and the oxazolone is excluded since no new absorption appeared on the mixing of the both compounds in solution.

A fact that the absorption spectrum of the oxazolone effectively overlaps with the emission spectra of the hydrocarbon sensitizers suggests that the singlet hydrocarbons could undergo efficient radiative transfer to the oxazolone, which could cause distortion of the shape of the emission spectra. Actually, as mentioned previously, the emission spectra of some hydrocarbons were changed in the shape with the increase in the concentration of the oxazolone, and slopes of Stern-Volmer plots of I_0/I gave higher values in the region of 340—390 nm where the oxazolone shows higher molecular extinction coefficient. Thus, triphenylene, phenanthrene, and pyrene, which have emission maxima in the region of 360—380 nm, gave higher apparent quenching rate constants $k_q^{app}\tau_0^S$ than biphenyl and fluorene which have emission maxima near 320 nm.

Reabsorption of the fluorescence emitted from the hydrocarbons by the oxazolone was further confirmed

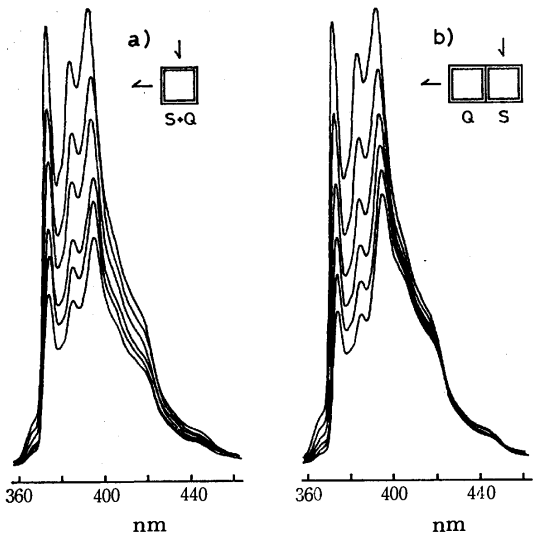

Fig. 3. Changes of fluorescence spectra with the concenration of 4-benzylidene-2-phenyl-5-oxazolone (Q). a) Quenching of fluorescence of pyrene (S) by the oxazolone in benzene, b) reabsorption of fluorescence of pyrene (S) by the oxazolone in benzene.

by the following experiment. A cell containing benzene solution of an emissive hydrocarbon without the oxazolone was placed adjacently to a cell containing benzene solution of the oxazolone in various concentrations, and the fluorescence emitted from the former solution was observed after passing the latter solution. A typical example is shown in Figs. 2 and 3 for pyrene, which has the highest k_q^S value among the sensitizers employed, showing that the spectral change of the fluorescence of the hydrocarbon with added oxazolone in the solution closely resembles that of the fluorescence of the hydrocarbon solution without the oxazolone observed through its reabsorption by the oxazolone solution.

These facts undoubtedly indicate that the fluorescence emitted from the hydrocarbons is effectively reabsorbed by the oxazolone in the surrounding medium, and the reported "selectivity" of the sensitized reaction course seems to depend on the fluorescence wavelength of the sensitizers. In Table 1 are listed $(I_0/I)_{reabs}$ values at $[Q]=2\times10^{-5}$ mol/l which denote estimated values for I_0/I when the decrease of the fluorescence intensity with the oxazolone is assumed to be due only to its reabsorption by the oxazolone, and these values are evaluated from k_q^{app}, k_q^S, and τ_0^S, according to Eq. 3.

$$(I_0/I)_{reabs} = 1 + (k_q^{app} - k_q^S)\tau_0^S[Q] \qquad (3)$$

Quenching of Hydrocarbon Triplet by the Oxazolone. Since the triplet energies of the aromatic hydrocarbons employed are in the range between 56.6 kcal/mol for chrysene and 68.0 kcal/mol for fluorene in a nonpolar solvent,[4] and the first excited triplet energy of the oxazolone has been estimated to be 43.0 kcal/mol[2] in chloroform, triplet energy transfer from the hydrocarbons to the oxazolone is expected to be sufficiently exothermic and to proceed with nearly diffusion-controlled rate constants.

In order to examine whether the quenching of the triplet states of the hydrocarbons by the oxazolone would proceed in different manner between "selective" and "unselective" hydrocarbon sensitizers as was proposed by Ullman, rate constants for the quenching of the triplet hydrocarbons by the oxazolone were measured by flash spectrophotometry. The oxazolone did not show any detectable transient absorption in the region of 380—600 nm on flash excitation. So, the decay of the triplet-triplet absorption of the hydrocarbon was followed in the absence and in the presence of various concentrations of the oxazolone in cyclohexane solution at room temperature.

Figures 4 and 5 show typical oscilloscopic traces of triplet-triplet absorption of naphthalene and triphenylene in the absence (a) and in the presence (b) of the oxazolone obtained by monitoring the absorption at 420 and 430 nm, respectively, and Figs. 6 and 7 contain

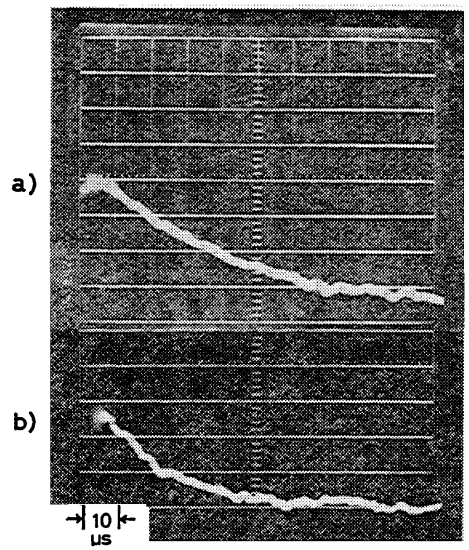

Fig. 4. Oscilloscopic traces of triplet-triplet absorption of naphthalene (7.5×10^{-5} M) in cyclohexane in the absence of 4-benzylidene-2-phenyl-5-oxazolone (a) and in the presence of the oxazolone in 5.5×10^{-6} M (b).

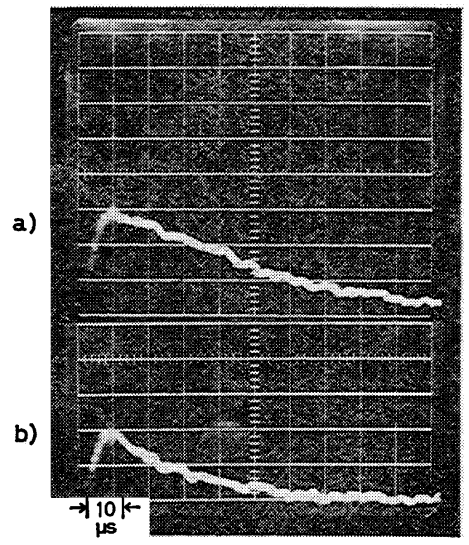

Fig. 5. Oscilloscopic traces of triplet-triplet absorption of triphenylene (3.5×10^{-5} M) in cyclohexane in the absence of 4-benzylidene-2-phenyl-5-oxazolone (a) and in the presence of the oxazolone in 5.5×10^{-6} M (b).

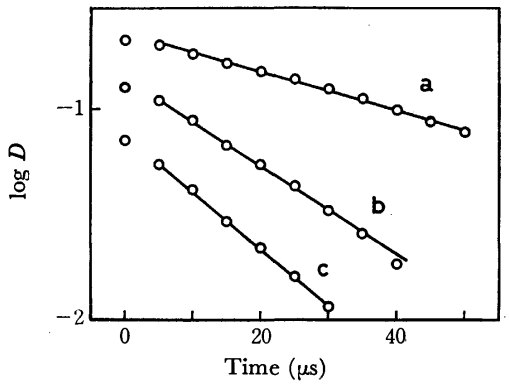

Fig. 6. First-order rate plots for the decay of triplet-triplet absorption (intensity: D) of naphthalene in cyclohexane in the absence of 4-benzylidene-2-phenyl-5-oxazolone (a), in the presence of the oxazolone in 5.5×10^{-6} M (b), and in 1.1×10^{-5} M (c).

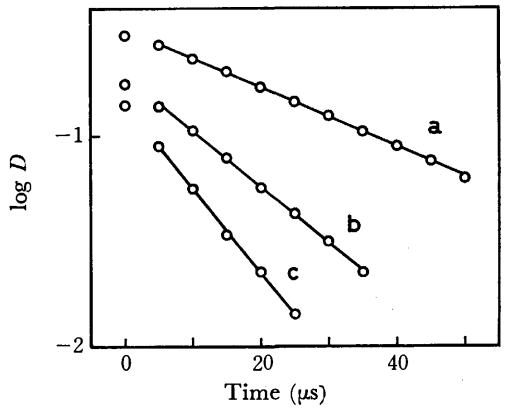

Fig. 7. First-order rate plots for the decay of triplet-triplet absorption (intensity: D) of triphenylene in cyclohexane in the absence of 4-benzylidene-2-phenyl-5-oxazolone (a), in the presence of the oxazolone in 5.5×10^{-6} M (b), and in 1.1×10^{-5} M (c).

first-order plots for the decays of the transients in the presence of different concentrations of the oxazolone. These figures indicate that intensities of triplet-triplet absorptions of the hydrocarbons were reduced and their decay rates were accelerated by the added oxazolone. The slope of the above plots yields the pseudo first-order overall decay coefficient, k', for a particular concentration of the added oxazolone. The coefficient, k', is expressed in the following form:

$$k' = k_d^T + k_q^T[Q] \quad (4)$$

where k_q^T is the second-order rate constant for the triplet quenching and k_d^T represents the first-order coefficient for the unimolecular decay. The observed k' values actually obeyed Eq. 4 to give k_q^T values. The obtained values for k_q^T are summarized in Table 2, together with k_q^{app}, k_q^S, singlet lifetimes, τ_0^S, quantum yields for fluorescence and intersystem crossing, Φ_f and Φ_{IS}, respectively.

Table 2 shows that the triplet states of all sensitizers employed are quenched by the oxazolone with rate constants close to the diffusion-controlled limit regardless of "selective" or "unselective" sensitizers, or of the triplet excitation energy and the structure of the sensitizer. The k_q^T values of fluorene, phenanthrene, and chrysene are larger than those of naphthalene and triphenylene. This result is in contrast with the previous postulate[2] that fluorene and naphthalene classified as "unselective" sensitizers would be more facilely quenched by the oxazolone than the other sensitizers classified as "selective" ones.

New Account for the Effect of the Sensitizers on the Reaction Course. The simplest mechanistic scheme to account for the sensitized reaction is shown in Eqs. 5—15, where S denotes the hydrocarbon sensitizer and Q denotes the oxazolone.

	rate constant	
$S \xrightarrow{h\nu} {}^1S^*$		(5)
${}^1S^* \longrightarrow S_0 + h\nu_f$	k_f	(6)
${}^1S^* \longrightarrow S_0$	k_d^S	(7)
${}^1S^* \longrightarrow {}^3S^*$	k_{IS}	(8)
${}^1S^* + Q \longrightarrow S_0 + {}^1Q^*$	k_q^S	(9)
$Q \xrightarrow{h\nu_f} {}^1Q^*$	k_{reabs}	(10)
${}^3S^* \longrightarrow S_0$	k_d^T	(11)
${}^3S^* + Q \longrightarrow S_0 + {}^3Q^*(\pi,\pi)$	k_q^T	(12)
${}^3Q^*(\pi,\pi) \longrightarrow$ isomerization		(13)
${}^1Q^* \longrightarrow {}^3Q^*(n,\pi)$		(14)
${}^3Q^*(n,\pi) \longrightarrow$ H-abstraction		(15)

Thus, a sensitizer molecule, on absorption of photon, is excited to its singlet state (Eq. 5). The singlet state either undergoes fluorescence emission (Eq. 6), radiationless deactivation to the ground state (Eq. 7), intersystem crossing to the triplet state (Eq. 8), or is quenched by the oxazolone (Eq. 9). The emitted fluorescence

Table 2. Quenching rate constants and spectral characteristics of aromatic hydrocarbons

Hydrocarbon	τ_0^S a) ns	k_q^{app} b) $\times10^{-12}$	k_q^S b) $\times10^{-12}$	τ_0^T c) μs	k_q^T c,d) $\times10^{-9}$	Φ_f e)	Φ_{IS} e)
Fluorene	10	3.5	0.15	10.4	14.8	0.68	0.31
Naphthalene	96	2.8	0.49	32.7	5.4	0.23	0.40
Triphenylene	37.4	8.3	0.11	39.5	4.1	0.10	0.90
Phenanthrene	57.5	9.4	0.42	15.3	13.0	0.13	0.82
Chrysene	43.7	6.5	0.39	19.5	10.0	0.14	0.69

a) I. B. Berlman, "Handbook of Fluorescence Spectra of Aromatic Molecules," 2nd Ed., Academic Press, New York, N. Y. (1971). b) In M^{-1} s^{-1}, in benzene. c) Conducted under nitrogen in cyclohexane; the concentration of the hydrocarbon: $(4—8)\times10^{-5}$ M, the concentration of the oxazolone: $0—1\times10^{-5}$ M. d) In M^{-1} s^{-1}. e) R. S. Becker, "Theory and Interpretation of Fluorescence and Phosphorescence," John Wiley and Sons, New York, N. Y. (1969) p. 118.

TABLE 3. ESTIMATED QUANTUM YIELDS FOR SENSITIZED REACTIONS OF THE OXAZOLONE IN 2×10^{-5} M THROUGH APPARENT FLUORESCENCE (Φ_f^{app}), INTERSYSTEM CROSSING (Φ_{IS}), QUENCHING OF THE SINGLET SENSITIZERS (Φ_q^S), REABSORPTION OF THE FLUORESCENCE FROM THE SINGLET SENSITIZERS (Φ_{reabs}), AND QUENCHING OF THE TRIPLET SENSITIZERS (Φ_q^T)

	Φ_f^{app}	Φ_{IS}	Φ_q^S	Φ_{reabs}	Φ_q^T
Fluorene	0.46	0.30	0.02	0.21	0.23
Naphthalene	0.19	0.33	0.18	0.05	0.26
Triphenylene	0.05	0.89	0.01	0.05	0.68
Phenanthrene	0.05	0.77	0.06	0.07	0.62
Chrysene	0.07	0.66	0.05	0.06	0.52

can be reabsorbed by the oxazolone and the latter is excited to its singlet state (Eq. 10). The triplet state of the sensitizer either undergoes radiationless deactivation (Eq. 11) or is quenched by the oxazolone to give the lowest triplet state of the latter (Eq. 12). The quantum yields for the singlet quenching (Φ_q^S), for the reabsorption of fluorescence (Φ_{reabs}), for the apparent fluorescence (Φ_f^{app}), and for the triplet quenching (Φ_q^T) by the oxazolone are estimated in the presence of 2×10^{-5} mol/l of the oxazolone according to the following equations 16—20 and summarized in Table 3.

$$\Phi_f^{app} = \frac{k_f\tau_0^S}{1+k_q^{app}\tau_0^S[Q]} \tag{16}$$

$$\Phi_{IS} = \frac{k_{IS}\tau_0^S}{1+k_q^S\tau_0^S[Q]} \tag{17}$$

$$\Phi_q^S = \frac{k_q^S\tau_0^S[Q]}{1+k_q^S\tau_0^S[Q]} \tag{18}$$

$$\Phi_{reabs} = \frac{k_f\tau_0^S}{1+k_q^S\tau_0^S[Q]} - \frac{k_f\tau_0^S}{1+k_q^{app}\tau_0^S[Q]} = \Phi_f - \Phi_f^{app} \tag{19}$$

$$\Phi_q^T = \Phi_{IS}\frac{k_q^T\tau_0^T[Q]}{1+k_q^T\tau_0^T[Q]} \tag{20}$$

Table 3 shows that fluorene and naphthalene, which fluoresce at shorter wavelengths, transfer singlet energy to the oxazolone more efficiently by both bimolecular interaction and reabsorption mechanism, but transfer triplet energy less efficiently than triphenylene, phenanthrene, and chrysene, which fluoresce at longer wavelengths; that is, the "unselective" sensitizers interact with the oxazolone in the singlet state as well as in the triplet state, while the "selective" sensitizers interact more effectively in the triplet state than in the singlet state. These results clearly account for Ullman's observation concerning the dependence of the sensitized reaction course on the structure of the sensitizers employed.

Thus, on taking account of an assumption by Ullman and Baumann that the lowest triplet state of the oxazolone undergoes isomerization and the higher triplet state abstracts hydrogen atom from a solvent, the oxazolone can be easily excited to its $T_1(\pi,\pi^*)$ state by all the sensitizers employed resulting in the isomerization (Eq. 13), but to its higher excited state, for example, T_2 (n, π^*) state, it would be efficiently excited through its singlet state only by sensitization with fluorene and naphthalene (Eqs. 10 and 14) resulting in hydrogen abstraction (Eq. 15).

Finally it should be stressed that reabsorption mechanism can play an important role in some photochemical systems.[5]

Experimental

Materials. 4-Benzylidene-2-phenyl-5-oxazolone was prepared by treating benzaldehyde with *N*-benzoylglycine and recrystallized from benzene.[6] Most sensitizers were purified by column chromatography and recrystallization, and their purities were checked by absorption and fluorescence spectra, and fluorescence lifetimes. Anthracene was prepared by reduction of anthraquinone and recrystallized.[7] Benzene (Wako special grade) was distilled over calcium hydride before use. Cyclohexane (Dotite Spectrosol) was used as received.

Spectra. Absorption spectra were measured with a Hitachi EPS-3 Recording Spectrophotometer. Emission spectra and fluorescence intensities were determined with a Hitachi MPF-2A Fluorescence Spectrophotometer. Reabsorbed emission spectra were measured by observing the emission from hydrocarbon solution in benzene placed in a quartz cell (1 cm in length and 1 cm in width) after passing through an adjacent quartz cell (1 cm in length and 1 cm in width) containing benzene solution of the varying concentration of the oxazolone.

Fluorescence lifetime was measured with a JASCO FL-10 Phase Fluorimeter.

Flash Spectrophotometry. A sample solution contained in a quartz cell (8 cm in length and 2 cm in diameter) was deaerated by bubbling nitrogen. A quartz flash photolysis lamp (10 cm in length and 2 cm in diameter) filled with xenon was operated at 11 kV and 2 μF, dissipating an energy of 120 J; the duration of the flash was 10 μs. The decays of triplet-triplet absorption of hydrocarbons were determined with a xenon lamp (Toshiba 500 W), a plane grating spectrograph (Shimadzu GE-100), a photomultiplier tube (RCA 1P28), and a synchroscope (Toshiba 3054).

The authors' thanks are due to Professor O. Simamura for his discussion, Dr. M. Takakusa, Electrotechnical Laboratory, for the use of a phase fluorimeter in his laboratory, and Professor S. Matsumoto, Aoyama Gakuin University, for the use of a flash spectrophotomeric apparatus.

References

1) Present address: Institute of Chemistry, The University of Tsukuba, Sakura-mura, Nihari-gun, Ibaraki-ken, 300-31.
2) E. F. Ullman and N. Baumann, *J. Amer. Chem. Soc.*, **92**, 5892 (1970).
3) K. Tokumaru, H. Sakuragi, and Y. Takahashi, *Chem. Lett.*, **1972**, 957.
4) S. L. Murov, "Handbook of Photochemistry," Marcel Dekker, New York, N. Y. (1973).
5) G. S. Hammond, C. A. Stout, and A. A. Lamola, *J. Amer. Chem. Soc.*, **86**, 3103 (1964); H. Ishikawa and M. Takiue, *Nuclear Instruments and Methods*, **112**, 431 (1973); M. Takiue and H. Ishikawa, *ibid.*, **118**, 51 (1974).
6) H. B. Gillespie and H. R. Snyder, "Organic Syntheses," Coll. Vol. II, p. 489 (1943).
7) L. F. Fieser, "Experiments in Organic Chemistry," translated by Y. Hirata and K. Nakanishi, Maruzen, Tokyo (1967), Chapter 29.

Studies on 8,9,10,11-Tetrahydro-7*H*-cycloocta[*de*]naphthalenes. I. Conformations of 8,8,10,10-Tetrasubstituted Derivatives of 8,9,10,11-Tetrahydro-7*H*-cycloocta[*de*]naphthalene

Toshihiro KAMADA, Nobuhide WASADA, and Osamu YAMAMOTO

National Chemical Laboratory for Industry, 1-1-5 Honmachi, Shibuya-ku, Tokyo 151

(Received June 28, 1975)

Several 8,8,10,10-tetrasubstituted 8,9,10,11-tetrahydro-7*H*-cycloocta[*de*]naphthalenes (**3**—**9**), novel pericyclic compounds of naphthalene, have been prepared through the alkylation reaction of 1,8-bis(bromomethyl)naphthalene and tetraethyl propane-1,1,3,3-tetracarboxylate, and the conformations of the cyclooctene ring in these compounds have been investigated on the basis of the PMR spectra. It is concluded that, at room temperature, the cyclooctene rings of (**3**—**9**) are frozen on the NMR time scale and exist exclusively in the boat form **15**, which is shown to be the most energetically stable conformation for the peri-eight-ring systems from models. Some discussion is also given on the configurations of the substituent groups in (**3**—**9**).

Although alicyclic ring systems, particularly six-membered rings, have been studied extensively by numerous investigators in the last two decades,[1] and although considerable attention has recently been focussed on the peri-interaction in naphthalene derivatives,[2] only a few reports have so far been presented on the pericyclic ring systems, in which methylene chains are fused to a naphthalene ring at the 1,8-positions, **1**. It seems that, in pericyclic naphthalene derivatives, the motions of the methylene chains of the peri-bridged ring are restricted by the naphthalene moiety, and that the rigid peri-bondings cause a large steric crowding in the molecules. This means that the peri-ring in these molecules exists under steric circumstances very different from those in the corresponding saturated cycloalkanes or structurally analogous benzo-derivatives. Among the pericyclic naphthalene derivatives **1**, little information has so far been available on the compounds with ring sizes larger than those of the commonly known acenaphthene (**1**, n=2), 2,3-dihydrophenalene (**1**, n=3) and 7,8,9,10-tetrahydrocyclohepta[*de*]naphthalene (**1**, n=4).[2]

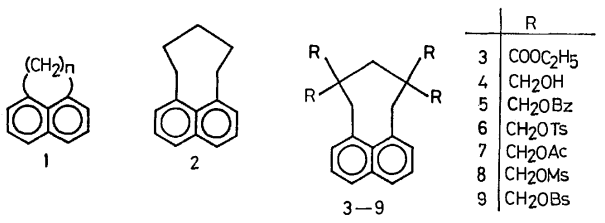

Our interest has been in the stereochemistry of these unknown pericyclic ring systems, particularly the 8,9,10,11-tetrahydro-7*H*-cycloocta[*de*]naphthalene ring **2**, which is the next higher homolog of the cyclohepta[*de*]naphthalene compound. Recently, the unsubstituted hydrocarbon **2** was first synthesized by Nelsen and Gillespie, and some suggestion was given as to its conformation.[3] However, no information has yet been obtained on the substituted derivatives of this compound.

In this paper, some new derivatives of 8,9,10,11-tetrahydro-7*H*-cycloocta[*de*]naphthalene (**3**—**9**) have been prepared, and their stable conformations have been determined on the basis of the PMR spectra.

TABLE 1. PHYSICAL PROPERTIES OF 8,8,10,10-TETRASUBSTITUTED 8,9,10,11-TETRAHYDRO-7*H*-CYCLOOCTA[*de*]NAPHTHALENES (**3**—**9**)

Compd	Mp (°C)	Molecular formula	Mol wt M+ (Calcd)	Found (Calcd) C%	H%	S%	IR data[b] (Nujol, cm^{-1})
3	112—112.5	$C_{27}H_{32}O_8$	484.212 (484.209)	66.75 (66.92)	6.77 (6.66)		1739, 1240, 1100
4	234—234.5	$C_{19}H_{24}O_4$	316.164 (316.167)	71.51 (72.12)	7.69 (7.65)		3350, 1030
5	196.5—197	$C_{47}H_{40}O_8$	732.267 (732.272)	76.97 (77.03)	5.37 (5.50)		1715, 1286, 1115
6[a]	178.5—179	$C_{47}H_{44}O_{12}S_4$	..... (932.203)	60.82 (60.50)	5.23 (5.19)	13.46 (13.74)	1367, 1174
7	205—205.5	$C_{27}H_{32}O_8$	484.211 (484.209)	67.02 (66.92)	6.59 (6.66)		1728, 1250
8	230—231	$C_{23}H_{32}O_{12}S_4$	628.079 (628.078)	43.95 (43.95)	5.01 (5.13)	20.43 (20.37)	1340, 1170
9[a]	190—191	$C_{43}H_{36}O_{12}S_4Br_4$	..... (1187.782)	43.00 (43.31)	2.90 (3.04)		1377, 1189

a) Attemps were also made to obtain molecular ions for compounds (**6**) and (**9**), but unsuccessful. b) Absorptions due to substituent groups.

Results

Syntheses. The compounds (**3**—**9**) used in this study were synthesized in the following reaction sequence, outlined in Scheme 1. The starting material was commercially available 1,8-naphthalenedicarboxylic anhydride, **10**, which was reduced with lithium aluminum hydride to 1,8-bis(hydroxymethyl)naphthalene, **11**.[4] Treatment of **11** with phosphorus tribromide and pyridine in ether led to the dibromide, **12**.[5] The next step was the formation of the eight-membered peri-ring. For this purpose, **12** was allowed to react with tetraethyl propane-1,1,3,3-tetracarboxylate, **13**, which had been prepared from diethyl malonate and paraformaldehyde by the condensation reaction in the presence of potassium hydroxide.[6,7] By the reaction between equimolar amounts of **12** and **13** in ethanol-dimethyl sulfoxide at 0 °C, using sodium ethoxide as a condensing agent, tetraethyl 8,9,10,11-tetrahydro-7*H*-cycloocta[*de*]naphthalene-8,8,10,10-tetracarboxylate, **3**, with the desired peri-8 ring, was obtained in 55% yield. Treatment of

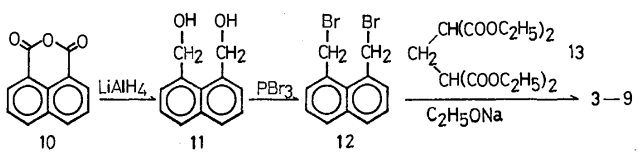

Scheme 1.

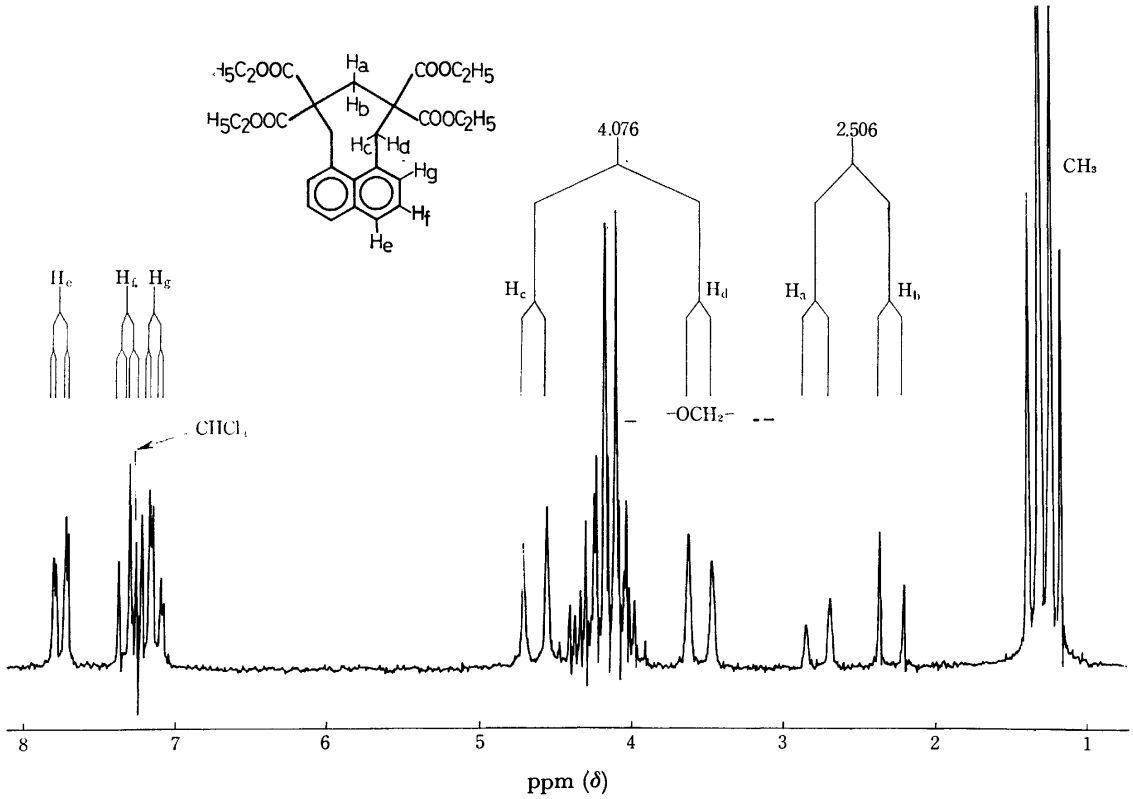

Fig. 1. PMR spectrum of tetraethyl 8,9,10,11-tetrahydro-7*H*-cycloocta[*de*]naphthalene-8,8,10,10-tetracarboxylate (**3**) at 100 MHz in $CDCl_3$ solution.

3 with excess lithium aluminum hydride in ether gave the tetrol **4**, which was then converted to the esters in the usual fashion. Thus, by treating **4** in pyridine with such acylating agents as benzoyl chloride, *p*-toluenesulfonyl chloride, acetic anhydride, methanesulfonyl chloride, and *p*-bromobenzenesulfonyl chloride, the corresponding tetraesters of **4** were obtained- namely, benzoate **5**, tosylate **6**, acetate **7**, mesylate **8**, and brosylate **9** respectively.

After purification, each compound (**3**—**9**) was proved to have the desired structure by elemental analysis as well as by a study of the IR, PMR, and high-resolution mass spectra. The data are summarized in Table 1 except for PMR, which will be given fully later.

PMR Spectra. The room-temperature 100-MHz PMR spectrum of tetraethyl 8,9,10,11-tetrahydro-7*H*-cycloocta[*de*]naphthalene-8,8,10,10-tetracarboxylate, **3**, in *ca.* 10% solution in deuteriochloroform consists of five distinct absorption groups, as is shown in Fig. 1. They are low-field naphthalene absorption bands (6H, e, f, g), a multiplet (8H) in the center of the spectrum due to the methylene protons of ester groups, a high-field methyl signal (12H), and two AB quartets centered at δ 4.076 (4H, c, d) and 2.506 (2H, a, b) respectively. From the positions and relative intensities of each peak, the low-field AB pattern can readily be assigned to the benzylic protons, and the high-field one, to the methylene protons on 9-carbon in the peri-ring. The lower-field portion, H_c, of the benzylic AB pattern can be assigned to hydrogens which point inward to the center of the molecule, since these hydrogens are expected to have a large steric interaction owing to their proximity with each other in the peri-eight ring systems.[8,9]

An important feature observed in the spectrum is that in the C_9-AB pattern, the higher-field methylene proton, H_b, appears as a sharp doublet, while the lower-field H_a affords a considerably broadened peak. The line broadening is also noted in the high-field H_d proton in the benzylic AB pattern, although it is not so remarkable as that for the C_9-methylene proton, H_a. An attempt to resolve these broadened lines by employing a degassed sample was unsuccessful. However, the line broadening in both AB patterns suggests that an appreciable long-range spin-spin interaction exists between one of the C_9-methylene protons, H_a, and an outward-pointing benzylic methylene proton, H_d. Actually, spin-decoupling experiments on **3** demonstrate the presence of this interaction, in which a sharpened doublet results for the C_9-methylene proton, H_a, upon irradiation at the higher-field portion, H_d, of the benzylic AB pattern.

The methyl and naphthalene absorptions are rather simple, as can be seen from the spectrum; thus, by a first-order analysis of the expanded spectra, two methyl groups at δ 1.287 and 1.208 (triplet, J=7.1 Hz, respectively), and three quartets for the aromatic protons at δ 7.730 (e, 2H, J=8.0 and 1.7 Hz), 7.279 (f, 2H, J=8.0 and 7.1 Hz), and 7.116 (g, 2H, J=7.1 and 1.7 Hz) are obtained. This means that two different types of methyl groups and three different types of aromatic protons are present in **3**. From the peak area and the values of the chemical shifts and the coupling constants, the aromatic protons can be assigned most reasonably as is shown in Fig. 1.

The methylene signals of the ester groups, appearing in the center of the spectrum as a complex multiplet rather than the usually observed simple pattern, can

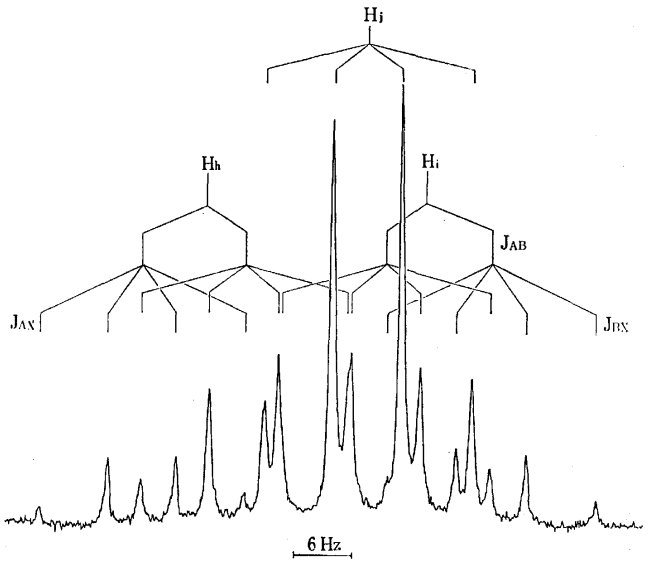

Fig. 2. *O*-Methylene proton signals of $-COOC_2H_5$ groups in compound (**3**). j; δ 4.131 (4H, quartet, J=7.1 Hz), h, i; δ 4.301 and 4.070, respectively (AB Part of ABX_3 system, 4H, J_{AB}=10.8, $J_{AX}=J_{BX}$ =7.1 Hz).

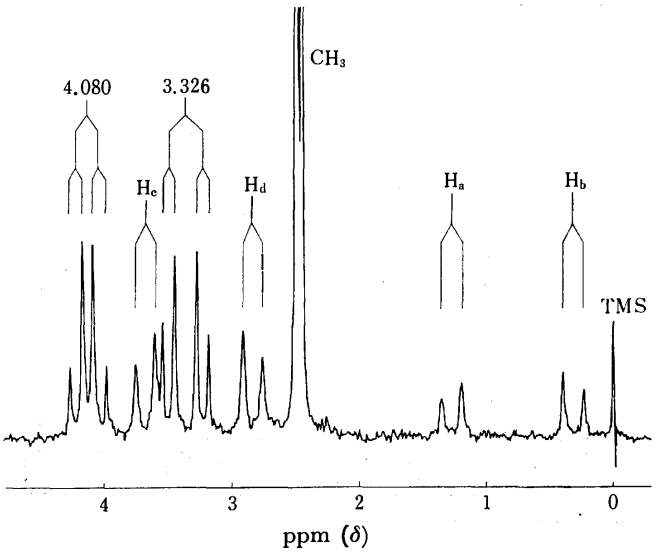

Fig. 3. PMR spectrum of aliphatic portion of tosylate (**6**).

also be completely analyzed, as is shown in Fig. 2. They consist of two distinct methylene groups, one of which resonates at δ 4.131, showing a simple, first-order quartet (j, 4H, J=7.1 Hz), while the other, with two components, resonates at δ 4.301 and 4.070, showing a multiplet of sixteen symmetric lines resulting from AB part of ABX_3 system (h, i, J_{AB}=10.8, $J_{AX}=J_{BX}$=7.1 Hz); *i.e.*, an AB quartet is formed, due to the nonequivalence of the methylene protons, and then each component further splits into a quartet by coupling with the neighboring methyl group. This is a fact of interest in connection with another previously reported compound, **14**, in which *O*-methylene protons of the ethoxycarbonyl group are known to be magnetically nonequivalent to each other.[10]

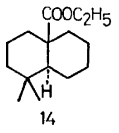

14

The 100-MHz PMR spectrum of the aliphatic portions of the tosylate **6** at ambient temperature is given in Fig. 3. All the spectra of the oxymethyl derivatives (**4**—**9**) in this region resemble each other well; they all contain four AB quartets, as may be seen in the figure. The high-field AB pattern (a, b, 2H) is readily assigned to the C_9-methylene protons in a manner similar to that described above, while the AB pattern (c, d, 4H) in the low-field region, with a larger coupling constant and a larger chemical-shift difference, can be assigned to the benzylic methylene protons. The remaining two AB patterns (4H), centered at δ 4.080 and 3.326 respectively, are responsible for the protons of oxymethyl groups ($-CH_2O-$) attached to the carbons-8 and -10 of the peri-ring; this means that two different types of methylene groups, belonging to a $\begin{matrix}X\\Y\end{matrix}\!\!\times\!\!CH_2^-$ moiety, are present in (**4**—**9**). The assignments of these methylene signals will be discussed later.

An additional doublet is also observed in the spctra of the tosylate **6** (δ 2.467 and 2.429), the acetate **7** (δ

Table 2. PMR spectra data of C_9 (a, b) and benzylic (c, d) methylene protons in compounds (**3**—**9**)[a]

Compd.	J_{gem}	$\delta_{a(c)}$	$\delta_{b(d)}$	$\triangle$	$\Delta\delta_{obsd}$	Solvent
3	16.0	2.735	2.277	2.506	0.458	$CDCl_3$
	(15.6	4.617	3.536	4.076	1.081)	
4	14.7	1.167	−0.032	0.568	1.199	DMSO-d_6
	(14.2	3.507	2.855	3.181	0.651)	
5	15.1	2.144	1.071	1.608	1.073	$CDCl_3$
	(14.9	4.163	3.466	3.815	0.697)	
6	15.0	1.261	0.330	0.796	0.931	$CDCl_3$
	(14.9	3.630	2.815	3.223	0.816)	
7	15.2	1.614	0.716	1.165	0.898	$CDCl_3$
	(14.9	3.881	2.965	3.423	0.916)	
8[b]	15.3	1.593	0.742	1.167	0.851	DMSO-d_6
	(15.1	4.111	2.940	3.526	1.171)	
9	15.2	1.390	0.540	0.965	0.850	$CDCl_3$
	(15.0	3.724	2.849	3.287	0.876)	
Cyclo-hexane	...	1.67[f]	1.21[f]	1.44[c]	0.46[d]	
Cyclo-hexane-d_8[e]	13.05	1.616	1.137	1.377	0.479	

J_{gem}; geminal coupling constant (Hz).
δ; chemical shift (ppm).
$\triangle$; absorption-center of AB protons (ppm).
$\Delta\delta_{obsd}$; differences in chemical shifts between AB protons (ppm).

a) In every compound, the data in parentheses correspond to those for the benzylic protons. b) Because of poor solubility in deuteriochloroform, the spectra of tetrol (**4**) and mesylate (**8**) were measured using dimethyl sulfoxide-d_6 as a solvent. The signals, however, seem little affected by this, since little change was observed in the spectra of brosylate (**9**) measured in both solutions. c) Ref. 11. d) Ref. 12. e) Ref. 13. f) Estimated from the values of $\triangle$ (1.44) amd $\Delta\delta_{obsd}$ (0.462) which were obtained from the high- and low-temperature spectra of cyclohexane, respectively.

TABLE 3. PMR SPECTRA DATA OF METHYLENE PROTONS OF $-CH_2O-$ GROUPS IN COMPOUNDS (**4**—**9**)[a]

Compound	J_{gem}	δ_A	δ_B	$\triangle$	$\Delta\delta$
4	11.0	3.813	3.654	3.733	0.158
	10.3	3.041	2.586	2.814	0.455
5	12.0	5.044	4.968	5.006	0.076
	11.2	4.402	4.185	4.294	0.217
6	10.0	4.156	4.003	4.080	0.152
	9.4	3.450	3.203	3.326	0.247
7	11.5	4.355	4.184	4.270	0.171
	10.9	3.735	3.464	3.599	0.271
8[b]	...	...	...	4.494	...
	9.8	3.749	3.654	3.702	0.094
9	9.9	4.223	4.104	4.164	0.119
	9.5	3.502	3.353	3.427	0.149

a) Symbols and units in this table are similar to those in Table 2. b) In the mesylate **8**, a methylene signal in the lower-field region appears as an unresolved broad singlet rather than an AB pattern.

TABLE 4. LINE-WIDTHS OF C_9- AND BENZILIC METHYLENE SIGNALS IN COMPOUNDS (**3**—**9**). (in Hz)

Compound	C_9-CH_2		Benzylic CH_2	
	H_a	H_b	H_c	H_d
3	3.0	1.1	2.1	2.7
4	3.8	3.1	3.9	3.0
5	3.5	2.6	a)	3.5
6	4.3	2.5	3.1	3.1
7	3.3	2.4	2.8	2.9
8	4.2	3.9	4.4	4.2
9	4.0	3.0	3.2	4.0

a) Because of overlapping of the peaks, line-width of this signal cannot be obtained.

2.096 and 2.072), and the mesylate **8** (δ 3.304 and 3.166); all similarly arise from two different types of methyl protons in the tosyl, acetyl, and mesyl groups respectively.

Again, line broadening is also observed in all the low-field doublets, H_a, of the C_9-methylene AB pattern as in **3**, although to a lesser extent, due to long-range spin-spin interactions with benzylic methylene protons, H_d. This fact suggests that all the molecules of this series (**3**—**9**) have a geometry very similar to one another in solution; this can also be supported by the other analogous spectral features described above. The PMR data for Compounds (**3**—**9**) are summarized in Tables 2,3, and 4.

Discussion

The PMR spectra of Compounds (**3**—**9**) at ambient temperature always give an AB pattern for each of the benzylic and the C_9-methylene protons. This suggests that, in all the compounds, the inversion of the peri-ring has been slow enough at this temperature on the NMR time scale; it also suggests that the molecules always assume only a single energetically stable conformation in solution.

The fact that only a single AB pattern is observed for the benzylic methylene groups in all the spectra indicates the equivalence of the two diastereomeric methylene protons on the benzylic positions in all the compounds, *i.e.*, the equivalence of the positions at carbon-7 and carbon-11. A similar situation can be expected for the positions of C-8 and C-10 in all of this series, since always only two absorption groups are shown for the four substituents at these positions (see spectra). This indicates that the most stable conformation of 8,9,10,11-tetrahydro-7*H*-cycloocta[*de*]naphthalene derivatives (**3**—**9**) has either a mirror plane (C_S) or a two-fold symmetry axis (C_2) passing through the C-9 and angular carbon atoms of the naphthalene nucleus. The simplicity of the naphthalene signals observed in **3** can also be accounted for by the above symmetric conformations. Furthermore, the fact that all the compounds clearly show an AB pattern for the C_9-methylene protons rules out the two-fold axis of symmetry in Compounds (**3**—**9**). If it were not the case, one would expect to find an A_2 singlet for these protons. On the other hand, the models of the 8,8,10,10-tetrasubstituted derivatives of 8,9,10,11-tetrahydro-7*H*-cycloocta[*de*]naphthalene show that the molecules are capable of existing in three conformations: *i.e.*, the boat, **15**, and the chair, **16**, with a C_S symmetry, and the twist-boat, **17**, with a

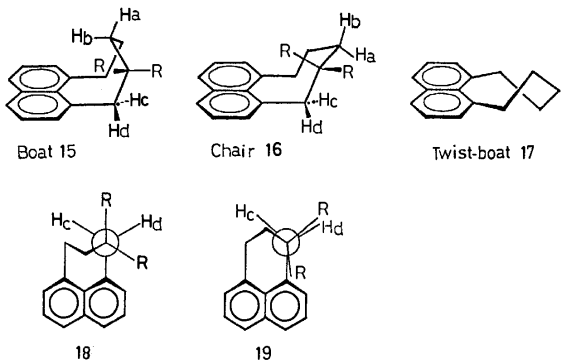

C_2 symmetry, as was recently suggested by Nelsen and Gillespie for the unsubstituted hydrocarbon **2**.[3] It is understandable, however, that the twist-boat can hardly exist at the ground state in Compounds (**3**—**9**), since the twist-boat is much more strained than the boat or the chair conformation.

Symmetry considerations cannot distinguish between the boat and the chair conformations, but fortunately this distinction can be made by using the values of the chemical shifts and line-widths of the C_9-methylene protons, together with an evaluation of the ring-current effects induced by the naphthalene nucleus. From the data for the 8,8,10,10-tetrasubstituted derivatives of 8,9,10,11-tetrahydro-7*H*-cycloocta[*de*]naphthalene (**3**—**9**) in Table 2, it is apparent that, generally in all the compounds except **3**, the C_9-methylene proton signals, particularly that of the high-field portion, H_b, shift remarkably to the high-field region as compared to the axial protons of cyclohexanes (δ 1.21[11,12] and 1.137[13] ppm); this makes the chemical-shift difference between the protons, H_a and H_b, of the C_9-methylene group in (**4**—**9**) much larger ($\Delta\delta_{obsd}$ 0.85—1.20 ppm) than that between the equatorial and the axial protons in cyclohexane (0.46[12] and 0.479[13] ppm). This comparison is not always accurate, since it is made between compounds with different ring systems and different sub-

stituents. Nevertheless, the above data do indicate the trends of the C_9-methylene protons in the peri-8 ring systems.

The anomalously large chemical-shift difference, $\Delta\delta_{obsd}$, observed for the C_9-geminal protons in the alicyclic ring systems of (**4**—**9**) suggests that these compounds (**4**—**9**) assume a conformation in which either of the methylene protons on C-9 experiences rather large ring-current effects of naphthalene. An examination of the models reveals that the proton, H_a, on C-9 is quite remote from the naphthalene moiety in both the boat and chair conformations; it can be expected to be little affected by the ring-current of naphthalene, while the H_b proton, which is spatially closer to the naphthalene ring in the boat conformation, can be expected to undergo larger ring-current effects; little effect is expected for the H_b proton, in the chair conformation (see diagram). This suggests that there exists a large chemical-shift difference in the C_9-geminal protons in the boat conformation of 8,9,10,11-tetrahydro-7*H*-cycloocta[*de*]-naphthalene ring.

Then, the effects of the ring-currents of naphthalene on the chemical shifts of the C_9-protons were evaluated for the boat and chair conformations of the 8,9,10,11-tetrahydro-7*H*-cycloocta[*de*]naphthalene ring. The calculation was done according to the method of Goldstein *et al.*[14] using Eq. (1), where the distances of hydrogens from the naphthalene nucleus necessary for the calculation were obtained from the models:

$$\sigma = \frac{-3434}{R^3}\left[(1-3\cos^2\alpha) + \frac{0.735}{R^2}(35\cos^4\alpha - 30\cos^2\alpha + 3)\right] \quad (1)$$

From the results of the calculation, shown in Table 5, it is clear that, in the boat conformation, the *endo*-orienting C_9-methylene proton, H_b, is shielded to a greater extent (1.50 ppm) than the *exo*-orienting proton, H_a (0.28 ppm), by the effect of the ring-current of naphthalene, while in the chair conformation, the ring-current deshields both the axial (H_a) and the equatorial (H_b) protons of the C_9-methylene group and the effect is very small (0.44 and 0.08 ppm, respectively). Consequently, the chemical-shift difference in the C_9-geminal protons responsible for the ring-current of naphthalene is much larger in the boat conformation (δ_r 1.22 ppm) than in the chair (δ_r 0.36 ppm).

In addition, in order to evaluate the chemical-shift difference in the C_9-geminal protons more accurately, one must also consider the chemical-shift difference in the C_9-geminal protons when the ring-current effects of naphthalene are absent. Since both the boat and chair conformations of the 8,9,10,11-tetrahydro-7*H*-cycloocta-[*de*]naphthalene ring can be considered to have a geometry similar to that of the cyclohexane with respect to the arrangement of the C-8, C-9, and C-10 portions of the peri-ring, the effect of the different configuration on the chemical shifts of the protons in the saturated ring system can be estimated from the experimental values observed in cyclohexane derivatives, in which the signal of the axial protons appears in a field higher than the equatorial protons by 0.1—0.7 ppm (δ_{ae}).[15]

Thus, considering both the effects of the ring-current, δ_r, and the configurational difference, δ_{ae}, the chemical-shift difference in the C_9-geminal protons $\Delta\delta_{calcd}$ for the boat and chair conformations of the 8,9,10,11-tetrahydro-7*H*-cycloocta[*de*]naphthalene ring are calculated as follows. Since, in the boat conformation, the hydrogens, H_a, and H_b, of the C_9-geminal group correspond to the equatorial and the axial protons of the cyclohexane respectively, the chemical-shift difference, $\Delta\delta_{calcd}$, is calculated to be 1.32—1.92 ppm. In the chair conformation, the H_a hydrogen corresponds to the axial, and the H_b hydrogen, to the equatorial; thus, the chemical-shift difference, $\Delta\delta_{calcd}$, is calculated to be −0.34—0.26 ppm (see diagram and Table 5). This result also indicates that the boat conformation has a large chemical-shift difference in the C_9-geminal protons, while the chair has a small one. A comparison of these calculated values $\Delta\delta_{calcd}$, with those observed, $\Delta\delta_{obsd}$, in (**4**—**9**) shows that the experimental values are much closer to that calculated for the boat conformation than that calculated for the chair. This makes it very possible that all the compounds (**4**—**9**) assume a boat form as the most stable conformation in solution at ambient temperature. Therefore, the high-field doublet (b) of the C_9-methylene signals observed in (**4**—**9**) can be assigned to the *endo*-orienting proton, H_b, and the low-field one (a), to the *exo*-orienting proton, H_a, of the boat conformation (see spectra).

The observed values in (**4**—**9**) ($\Delta\delta_{obsd}$ 0.85—1.20 ppm) are somewhat smaller than that calculated for the boat conformation ($\Delta\delta_{calcd}$ 1.32—1.92 ppm). In Compounds (**4**—**9**), however, the value of δ_{ae} is expected to be decreased to some extent by the effect of the axial $-CH_2O-$ groupings attached to the C-8 and C-10 positions.[15] Taking this fact into consideration, the chemical-shift difference calculated for the boat conformation can be expected to be a little smaller than that in Table 5; this results in a better agreement with the experimental values of (**4**—**9**).

It should be noted that there are some differences in the values of $\Delta\delta_{obsd}$ for (**4**—**9**), where **4** with hydroxyl groups exhibits a larger value than the others with more electronegative acyl or sulfonyl groups (**5**—**9**). From

Table 5. Calculation of chemical-shift difference in C_9-methylene protons in 8,9,10,11-tetrahydro-7*H*-cycloocta[*de*]-naphthalene ring (ppm unit)

	σH_a [a]	σH_b [a]	δ_r [b]	δ_{ae} [c]	$\Delta\delta_{calcd}$ [d]
Boat	0.28	1.50	1.22	0.1—0.7	1.32—1.92
Chair	−0.44	−0.08	0.36	0.1—0.7	−0.34—0.26
Observed in (**4**—**9**)					0.85—1.20 ($\Delta\delta_{obsd}$)

a) Ring-current effect of naphthalene on the chemical shift of the C_9-methylene protons, calculated from Eq. (1). A minus sign indicates a low-field shift. b) Chemical-shift difference in C_9-methylene protons responsible for the ring-current effect of naphthalene. c) Chemical-shift difference in C_9-methylene protons caused by configurational difference between these two protons, estimated from Ref. 15. d) Chemical-shift difference in C_9-methylene protons calculated from the values of δ_r and δ_{ae} (see text).

Tables 2 and 3 it may be seen that the low-field shifts of all the AB absorption-centers (△) including oxymethyl, benzylic, and C_9-protons increase in this order of the compounds: **4**,**6**,**9**,**7**,**8**,**5**. This clearly means that, in all the (**4**—**9**) compounds, not only the oxymethyl groups but also the benzylic and the C_9-methylene groups are substantially affected by the substituents, although they are remote from the benzylic and the C_9-methylene groups in these molecules (**4**—**9**). Table 2 also shows that, in all the (**5**—**9**) compounds, the low-field shift of the absorption-centers (△) is always larger in the C_9-methylene signals than that in the benzylic signals; that is, the C_9-methylene groups are more affected than the benzylic methylene groups by the four substituent groups attached to C-8 and C-10. In the cyclohexane chair conformation, it is known that the equatorial electronegative groups shield both the axial and equatorial protons attached to the adjacent carbon atom, whereas the axial substituents shield the equatorial protons, but cause an appreciable low-field shift of the corresponding axial protons on the contiguous carbon atom.[16] This means that the C_9-methylene proton, H_a, in the tetrasubstituted derivatives of the 8,9,10,11-tetrahydro-7*H*-cycloocta[*de*]naphthalene, with electronegative groupings at the C-8 and C-10 positions, is appreciably deshielded by the effect of the axial electronegative groups attached to the above positions, but the H_b proton is shielded, because the H_a proton in the boat conformation of the 8,9,10,11-tetrahydro-7*H*-cycloocta-[*de*]naphthalene ring corresponds to the equatorial proton of cyclohexane, and the H_b proton, to the axial. It is understandable, therefore, that the differences in chemical shifts between the C_9-methylene proton, H_a, and H_b, in **4** ($\Delta\delta_{obsd}$) are larger by 0.13—0.35 ppm than those in (**5**—**9**), since the signals of the H_b proton in Compounds (**5**—**9**) are expected to shift to a lower-field to a greater extent than in **4** as a result of the effect of acyl- or sulfonyloxymethyl groups on the carbon-8 and 10.

In the case of the benzylic methylene groups, the inward-pointing proton, H_c, is situated at the position *trans* to the equatorial substituents, and the spatial relationship between these two groups is similar to that between the H_b proton and the axial substituents described above. Thus, in contrast to the C_9-methylene protons, a large chemical-shift difference can be expected for the benzylic methylene protons in (**5**—**9**), since the inward-pointing proton, H_c, resonates at an appreciably lower field than the outward-pointing proton, H_d, because of the steric compression, and the H_c proton can be expected to be further deshielded by the acyl- or sulfonyloxymethyl groups in (**5**—**9**). The observed values of $\Delta\delta_{obsd}$ distinctly reveal this trend, where the value for **4** is smaller than those for (**5**—**9**) by 0.05—0.52 ppm (see Table 2). These results further support the predominance of the boat conformation over the chair in all the (**4**—**9**) compounds.

The only exception observed in Table 2 is the ethoxycarbonyl derivative, **3**, which shows a $\Delta\delta_{obsd}$ value of only 0.458 ppm, almost comparable to that of cyclohexane. However, as may be seen in the table, the absorption-centers of both the C_9- and benzylic methylene protons in **3** shift to a considerably lower field than those in other compounds (**4**—**9**); *i.e.*, in **3** both methylene groups are affected by the ethoxycarbonyl groups to a greater extent than in the other compounds, presumably because the electronegative ethoxycarbonyl groups directly attach to the ring carbons, C-8 and C-10, while in the other (**4**—**9**) compounds the acyloxy and sulfonyloxy groups attach to the substituent carbons. The chemical-shift difference in the C_9-methylene group in **3**, therefore, will be appreciably decreased by the effect of the ethoxycarbonyl groups, even if **3** exists in the boat conformation and even if the proton, H_b, in **3** is substantially shielded by the ring-current of naphthalene, as is observed in the other (**4**—**9**) compounds. This suggests a large possibility that the molecule of **3** also assumes the boat form as the most stable conformation at ambient temperature.

In the boat conformation, the four bonds between the C_9-methylene proton, H_a, and the outward-pointing benzylic methylene proton, H_d, lie in one plane in the W-arrangement, while in the chair such an arrangement is absent. Therefore, if the boat is the correct conformation for (**3**—**9**), an appreciably large long-range spin-spin interaction can be expected between these protons in all the (**3**—**9**) compounds.[17,18] Thus, as may be seen in the spectra and in Table 4, the fact that the signal of the C_9-methylene proton, H_a, is always broader than that of the proton, H_b, in (**3**—**9**) undoubtedly indicates the presence of this long-range coupling; hence, this is further evidence in favor of the boat conformation for (**3**—**9**). It may also be noted in Table 4 that the line-widths of both protons, H_a and H_b, are always larger in (**4**—**9**) than in **3**. This means that, in (**4**—**9**), both protons, H_a and H_b, are further coupled with oxymethyl groups attached to the contiguous carbon atoms, C-8 and C-10. It is also apparent from the table that this broadening of the signals is always more remarkable in the signals of H_b than those of H_a. This is presumably because the proton, H_b, in the boat conformation is coupled relatively strongly with the protons of the axial $-CH_2O-$ groups because of their *trans* arrangement.[19-22]

The effect of the substituents is also reflected in the geminal spin couplings of both the C_9- and the benzylic methylene groups in all the (**3**—**9**) compounds. Thus, as can be seen in Table 2, the geminal couplings, J_{gem}, of the C_9-methylene groups in (**3**—**9**) are appreciably larger (14.7—16.0 Hz) than those in the cyclohexanes (12—14 Hz). Moreover, the value of J_{gem} is much larger in the ethoxycarbonyl derivative, **3** (16.0 Hz), than those in the oxymethyl derivatives (**4**—**9**) (15.3—14.7 Hz), in which the value is the smallest in the hydroxy derivative **4**. Similar trends are also found in the geminal couplings of the benzylic methylene protons, in which, again, the value is the largest in **3** (15.6 Hz) and the smallest in **4** (14. 2Hz).

One point not yet discussed is the assignment of the two methylene signals arising from the 8- and 10-substituted groups ($-CH_2O-$ and $-COOC_2H_5$) to the axial and equatorial groups. In the oxymethyl derivatives (**4**—**9**), the axial methylene protons, involving the steric-compression effects, can be responsible for the low-field

AB quartet, and the equatorial ones, for the high-field signals.[16] This assignment is consistent with the results of the evaluation of the ring-current effect of the naphthalene nucleus on the methylene protons belonging to the axial and equatorial $-CH_2O-$ groups in (**4**—**9**), from which it is clear that the equatorial groups resonate at a field higher than the corresponding axials by *ca.* 0.46 ppm in the presence of the free rotations as a result of the ring-current effect.[10]

It is interesting that the nonequivalence of methylene protons is observed in the methylene signals of one of the $-COOC_2H_5$ groups in **3**. A detailed discussion of this point, however, as well as the assignment of methylene signals, must await further studies of the stereochemical properties inherent in these peri-8 ring systems.

All the results presented above provide conclusive evidence that all the (**3**—**9**) compounds exclusively exist in the boat conformation at room temperature in solution. Both the boat and chair conformations of (**3**—**9**) are expected to involve large van der Waals interactions caused by the two inward-pointing benzylic methylene protons, H_c,[8,9] and those caused by the two substituent groups in the 1,3-diaxial relationship to each other.[16] However, the chair conformation is expected to involve additional eclipsing interactions along the bonding between C-7 and C-8, and the bonding between C-10 and C-11 as well. Moreover, in the chair conformation, one can expect steric repulsions to be present between the axial substituents and the naphthalene ring because of their proximity to each other. On the other hand, the boat conformation lacks these additional interactions (see **15**, **16**, and the Newmann projections about the C_7–C_8 bonding, **18** for the boat and **19** for the chair conformation). The boat form, therefore, is the more energetically stable conformation for the 8,8,10,10-tetrasubstituted 8,9,10,11-tetrahydro-7*H*-cycloocta[*de*]-naphthalene ring, which well accounts for the predominance of the boat conformation over the chair observed in all the (**3**—**9**) compounds. A model of the boat conformation shows that the distance between the inward-pointing 7,11-hydrogens is *ca.* 0.7 Å, much smaller than the sum of the van der Waals radii of the two hydrogens (2.4 Å). Therefore, the molecules of (**3**—**9**) can be expected to assume a boat conformation which is strained to some extent in such a direction as to avoid the steric repulsions arising from the proximity of the two H_c hydrogens.

Experimental

All melting points were determined on a microscopic hot-stage melting-point apparatus and are reported uncorrected. All the solvents used in the reactions were dried and freshly distilled. Thin-layer chromatography was employed on silica gel to monitor the reactions and to check the purity of the products. After the solvents had been removed from the developed tlc sheets, the spots were detected by iodine vapor. The IR spectra were obtained on a JASCO Model IR-G Grating Infrared Spectrometer, using Uujol mulls. The positions of the absorption maxima are quoted in wave numbers (cm^{-1}), calibrated with polystyrene. The PMR spectra were obtained on a Varian HA-100 D spectrometer (100 MHz) at room temperature, using *ca.* 10% solution of compounds in deuteriochloroform or dimethyl sulfoxide-d_6; the chemical shifts are expressed in ppm (δ) downfield from the internal standard, tetramethylsilane, and the coupling constants (J), in Hz. High-resolution molecular-weight determinations were carried out on a CEC high-resolution mass spectrometer, Model 21-110 B, with a direct-inlet system and an ionization potential of 70 eV.

*1,8-Bis(hydroxymethyl)naphthalene (**11**).* Although Boekelheide and Vick[4] have previously reported the preparation of 1,8-bis(hydroxymethyl)naphthalene by the lithium aluminum hydride reduction of 1,8-naphthalenedicarboxylic anhydride, **11** was obtained in a more excellent yield by the method described below.

To a stirred suspension of 50 g of lithium aluminum hydride in a mixture of 1.2 l of absolute ether and 1 l of dry benzene, there was added 125 g of 1,8-naphthalenedicalbyxylic anhydride at a rate sufficient to maintain gentle boiling. After the addition was complete, the mixture was heated under reflux with stirring for an additional 6 days. After the reaction mixture had then been cooled, the excess metal hydride was destroyed by the addition of ethyl acetate and water. The further addition of 2M-aqueous hydrochloric acid to the slurry gave a white solid. This solid was collected, dried, and then heated with benzene containing ether. The benzene solution was separated and evaporated to give a white solid. After washing with dilute acid, the solid was recrystallized from benzene–methanol, giving the diol **11** (99 g; yield, 84%) as colorless needles; mp 156—156.5 °C (lit., mp 157—158 °C[4]) (Found: C, 76.39; H, 6.38%).

*1,8-Bis(bromomethyl)naphthalene (**12**).* 1,8-Bis(bromomethyl)naphthalene, **12**, was prepared in 84% yield by the bromination of 1,8-bis(hydroxymethyl)naphthalene, **11**, with phosphorus tribromide, essentially as has been described by Mitchell and Sondheimer.[5] Mp 131—132 °C (lit., mp 131—132 °C[5]) (Found: C, 46.00; H, 3.20; Br, 51.09%).

*Tetraethyl propane-1,1,3,3-tetracarboxylate (**13**).* Tetraethyl propane-1,1,3,3-tetracarboxylate, **13**, was prepared from diethyl malonate and paraformaldehyde according to the method of Welch.[6] Fractional distillation of the reaction product *in vacuo* using a Vigreux column afforded the tetraester **13**; bp 132—145 °C/0.3 mmHg; mostly distilled at 138 °C (lit., bp 194—198 °C/20 mmHg,[6] bp 190—200 °C/12 mmHg, 210—215 °C/20 mmHg[7]).

*Tetraethyl 8,9,10,11-tetrahydro-7H-cycloocta[de]naphthalene-8,8,10,10-tetracarboxylate (**3**).* A solution of 54 g of tetraethyl propane-1,1,3,3-tetracarboxylate, **13**, in 60 ml of absolute ethanol and 100 ml of dry dimethyl sulfoxide (distilled on calcium hydride) was added quickly to a stirred and cooled (0 °C) solution of sodium ethoxide in ethanol, obtained by dissolving 7.2 g of sodium in 660 ml of absolute ethanol. After 5 min, to this mixture, was added a solution of 54 g of 1,8-bis(bromomethyl)naphthalene, **12**, in 720 ml of dry dimethyl sulfoxide over a period of 12 min. After the addition was complete, stirring and cooling were continued for an additional 1.5 hr. The reaction mixture was then poured into cracked ice and water, and the resulting cloudy solution was extracted with ethyl acetate (500 ml × 5). The ethyl acetate solutions were combined, dried over anhydrous sodium sulfate, and evaporated to leave a yellow oil, which solidified on standing at room temperature. The solid was crushed in cool ethanol, filtered off, and then further purified by recrystallization from ethanol, giving the desired peri-eight-membered ring compound, **3** (43 g; yield, 55%) as colorless prisms.

*8,8,10,10-Tetrakis(hydroxymethyl)-8,9,10,11-tetrahydro-7H-cycloocta[de]naphthalene (**4**).* To a stirred slurry of 10 g of lithium aluminum hydride in 1 l of absolute ether, there was added a suspension of 30 g of the ester **3** in 200 ml of absolute

ether at a rate sufficient to maintain gentle boiling. After the addition was complete, the mixture was boiled under reflux, with vigorous stirring for an additional 120 hr. The excess lithium aluminum hydride was then decomposed by the addition of ethyl acetate, followed by that of 2M-aqueous hydrochloric acid. The resulting white precipitate was collected and extracted with 2 l of boiling ethyl acetate for 3 hr. The extracts and filtrate were then combined, and the solvent was evaporated. The residual solid was washed with 100 ml of diluted hydrochloric acid and recrystallized from methanol, giving the tetrol **4** (16 g; yield, 80%), as fine, colorless needles.

8,8,10,10-Tetrakis(benzoyloxymethyl)-8, 9, 10, 11-tetrahydro-7H-cycloocta[de]*naphthalene (5).* The tetrol **4** (0.1 g), was treated with benzoyl chloride (2 ml) in pyridine (3 ml) at 60 °C for 1 hr, after which the mixture was left at room temperature for 2 days. After the reaction had been completed, the reaction mixture was poured into ice and water and extracted with ethyl acetate. The usual work-up of the ethyl acetate solution gave a brown oil, which crystallized on the addition of cool methanol. After separation, the crystals were further purified by two recrystallizations from benzene–methanol to give the benzoate **5** as colorless needles (0.16 g; yield, 70%).

*8,8,10,10-Tetrakis(*p*-toluenesulfonyloxymethyl)-8, 9, 10, 11-tetrahydro-7H-cycloocta*[de]*naphthalene (6).* To a stirred suspension of 3 g of the tetrol **4** in 19 ml of pyridine, there was added a solution containing 12 g of *p*-toluenesulfonyl chloride and 12 ml of pyridine. The mixture was shaken vigorously for 1 min and then left at room temperature for 7 days. The reaction mixture was poured into 70 ml of ice and water, and the mixture was stirred well for 1 hr at 0 °C. The resulting precipitates were collected and recrystallized from methanol–benzene, yielding 8.6 g (yield, 97%) of the tosylate **6** as colorless needles.

8, 8, 10, 10-Tetrakis(acetoxymethyl)-8, 9, 10, 11-tetrahydro-7H-cycloocta[de]*naphthalene (7).* A mixture of the tetrol **4** (0.1 g), acetic anhydride (5 ml), and pyridine (5 ml) was heated at 60 °C on a water bath, with occasional shaking, for 30 min. The resulting clear solution was then allowed to stand at room temperature for 3 days to complete the reaction. The reaction mixture was poured into 50 ml of ice water; the mixture was stirred at 0 °C for 30 min and then left at room temperature for an additional 3 hr. The solid thus precipitated was collected and recrystallized from ethanol to give the acetate **7** (0.14 g; yield, 92%), as colorless needles.

8, 8, 10, 10-Tetrakis(methanesulfonyloxymethyl)-8, 9, 10, 11-tetrahydro-7H-cycloocta[de]*naphthalene (8).* To a suspension of 0.2 g of the tetrol **4** in 2 ml of pyridine, there was added 1 ml of methanesulfonyl chloride, after which the mixture was shaken vigorously for 10 min. After being left at 0 °C for 1 hr, the reaction mixture was poured into 100 ml of ice water and the mixture was stirred well at 0 °C for 30 min. The solid thus precipitated was filtered off, washed with methanol, and dried *in vacuo*. Recrystallization of this solid from dimethyl sulfoxide–methanol–water yielded the mesylate **8** as a colorless microcrystalline solid (0.3 g; 76%).

*8, 8, 10, 10-Tetrakis(*p*-bromobenzenesulfonyloxymethyl)-8, 9, 10,-11-tetrahydro-7H-cycloocta*[de]*naphthalene (9).* To a stirred suspension of 0.2 g of the tetrol **4** in 2 ml of pyridine, was added a solution of *p*-bromobenzenesulfonyl chloride (1.2 g) in pyridine (2 ml). The mixture was stirred at room temperature for 30 min and then left at room temperature for an additional 2 days. The reaction mixture was poured into 50 ml of ice water, and the mixture was stirred well for 30 min. The white solid thus precipitated was filtered off, washed with methanol, and dried *in vacuo*. Then it was purified by recrystallization from chloroform–methanol–water to give the brosylate **9** (0.56 g; 75%), as microcrystals.

References

1) (a) E. L. Eliel, N. L. Allinger, S. J. Angyal, and G. A. Morrison, "Conformational Analysis," Interscience Publishers, New York, N. Y. (1965). (b) H. Hanack, "Conformation Theory," Academic Press, New York, N. Y. (1965). (c) G. Binsch, "Topics in Stereochemistry," Vol. 3, ed. by E. L. Eliel and N. L. Allinger, Interscience Publishers, New York, N. Y. (1968), p. 97. (d) H. Booth, "Progress in NMR Spectroscopy," Vol. 5, ed. by J. W. Emsley, J. Feeney, and C. H. Sutcliffe, Pergamon Press, Oxford (1969), p. 149.

2) V. Balasubramanian, *Chem. Rev.*, **66**, 567 (1966).

3) S. F. Nelsen and J. P. Gillespie, *J. Amer. Chem. Soc.*, **95**, 2940 (1973).

4) V. Boekelheide and G. K. Vick, *ibid.*, **78**, 653 (1956).

5) R. H. Mitchell and F. Sondheimer, *Tetrahedron*, **34**, 1397 (1968).

6) K. N. Welch, *J. Chem. Soc.*, **1931**, 673.

7) T. J. Otterbacher, "Organic syntheses," Coll. Vol. I, p. 290 (1941).

8) J. G. Colson, P. T. Lansbury, and F. D. Saeva, *J. Amer. Chem. Soc.*, **89**, 4987 (1967), and references cited therein.

9) A. W. Brinkmann, M. Gordon, R. G. Harvey, P. W. Rabideau, J. B. Stothers, and A. L. Ternay, Jr, *ibid.*, **92**, 5912 (1970).

10) W. L. Meyer, D. L. Davis, L. Foster, A. S. Levinson, V. L. Sawin, D. C. Shew, and R. F. Weddleton, *ibid.*, **87**, 1573 (1965).

11) G. V. Tiers, *J. Phys. Chem.*, **62**, 1151 (1958).

12) F. R. Jensen, D. S. Noyce, C. H. Sederholm, and A. J. Berlin, *J. Amer. Chem. Soc.*, **82**, 1256 (1960).

13) E. W. Garbisch and M. G. Griffith, *ibid.*, **90**, 6543 (1968).

14) R. E. Mayo and J. H. Goldstein, *Mol. Phys.*, **10**, 301 (1966).

15) L. M. Jackman, "Applications of Nuclear Magnetic Resonance Spectroscopy in Organic Chemistry," Pergamon Press, London (1959), Chapter 7.

16) N. S. Bhacca and D. H. Williams, "Applications of NMR Spectroscopy in Organic Chemistry," Holden-Day, San Francisco (1964), p. 183.

17) K. B. Wiberg, B. R. Lowry, and B. J. Nist, *J. Amer. Chem. Soc.*, **84**, 1594 (1962).

18) A. Rassat, C. W. Jefford, J. M. Lehn, and B. Waegell, *Tetrahedron Lett.*, **1964**, 233.

19) M. J. T. Robinson, *ibid.*, **1965**, 1685.

20) D. R. Davis and J. D. Roberts, *J. Amer. Chem. Soc.*, **84**, 2252 (1962).

21) D. H. Williams and N. S. Bhacca, *ibid.*, **85**, 2861 (1963).

22) N. S. Bhacca, J. E. Gurst, and D. H. Williams, *ibid.*, **87**, 302 (1965).

Esters of Phosphorus Oxy Acids as Alkylating Agents. IV. *N*-Alkylation of Imidazole and Its Analogs with Alkyl Esters of Phosphonic and Phosphinic Acids

Masahiro HAYASHI, Kiyoshi YAMAUCHI, and Masayoshi KINOSHITA

Department of Applied Chemistry, Osaka City University, Sumiyoshi-ku, Osaka 558

(Received August 1, 1975)

Methyl, ethyl esters of phosphonic and phosphinic acids were found to be efficient alkylating agents for imidazole, benzimidazole, 1,2,4-triazole, 1,2,3-benzotriazole and pyrazole, giving the corresponding *N*-methyl or *N*-ethyl derivatives.

In a previous paper a report was given on the *N*-alkylation reactions of imidazoles with trialkyl phosphates.[1] Since phosphonic and phosphinic acid esters are also considered to be potentially useful as alkylating agents, we investigated the *N*-alkylation of imidazoles with these phosphorus oxy-acid esters, and found simple methods of alkylation for this class of heterocycles.

Reactions were carried out by heating a base in an ester, and the products were isolated by distillation or extraction.

Table 1 gives a summary of the alkylation reactions of imidazole (**I**, R=H), benzimidazole (**II**, R=H), 1,2,4-triazole (**III**, R=H), 1,2,3-benzotriazole (**IV**, R=H), and pyrazole (**VI**, R=H).

All the bases underwent *N*-alkylation to give the corresponding products in fairly good yields. Especially, in triazole, reactions brought into substitution at the N-1 position only to afford 1-alkyltriazole (**III**, R=Me, Et). In benzotriazole, the N-1 position was alkylated preferentially to the N-2 position to give 1-alkyl derivatives (**IV**, R=Me, Et) as a main product. High selective alkylation in the present method would be very useful, since other alkylating agents such as alkyl halide, diazomethane and dimethyl sulfate showed much lower selectivity,[2-8] giving a mixture of 1- and 2-alkyl isomers in approximately 5 to 3, 3 to 10, and 2 to 1 mole ratios, respectively.

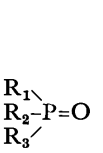

a: $R_1=R_2=OMe$, $R_3=Me$
Dimethyl methylphosphonate
b: $R_1=R_2=OEt$, $R_3=Et$
Diethyl ethylphosphonate
c: $R_1=OMe$, $R_2=R_3=Me$
Methyl dimethylphosphinate
d: $R_1=OEt$, $R_2=Et$, $R_3=Ph$
Ethyl ethylphenylphosphinate

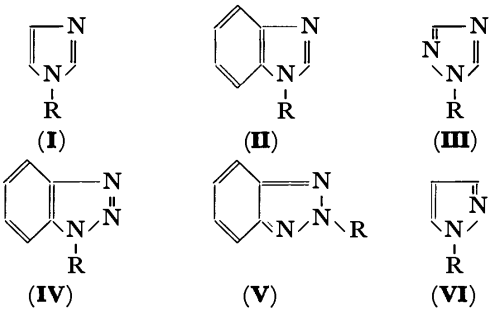

(**I**) (**II**) (**III**)

(**IV**) (**V**) (**VI**)

Alkyl-imidazoles, benzimidazoles, triazoles and pyrazoles were isolated by direct distillation of the reaction mixtures. Separation of 1-methyl and 2-methylbenzotriazole was carried out easily through fractionating the reaction mixture between a dilute hydrochloric acid and chloroform, since the former is soluble in a dilute acid while the latter goes into the organic layer.

The results suggest that alkyl esters of phosphonic and phosphinic acids could be utilized as convenient alkylating agents for the preparation of *N*-alkyl derivatives of imidazole and its analogs.

TABLE 1. REACTIONS OF IMIDAZOLE AND ITS ANALOGS WITH ESTERS OF PHOSPHONIC AND PHOSPHINIC ACIDS

Base (B)	Ester (E)	Mole ratio (E/B)	React. temp (°C)	React. time (hr)	Product	Yield (%)
Imidazole (**I**)	**a**	0.5	200	1	1-methylimidazole	54
	c	1	200	10.5	1-methylimidazole	50
	b	0.5	200	1	1-ethylimidazole	39
	d	0.5	193	6	1-ethylimidazole	37
Benzimidazole (**II**)	**a**	1	200	5	1-methylbenzimidazole	37
	b	1	200	5	1-ethylbenzimidazole	59
	d	0.5	198	6	1-ethylbenzimidazole	34
1,2,4-Triazole (**III**)	**a**	0.5	200	2	1-methyltriazole	36
	b	0.5	200	1.3	1-ethyltriazole	32
Benzotriazole (**IV**)	**a**	0.5	200	1.5	1-methylbenzotriazole 2-methylbenzotriazole	80 7
	a	0.5	200	3	1-methylbenzotriazole 2-methylbenzotriazole	87 8
	b	0.5	200	2	1-ethylbenzotriazole	71
Pyrazole (**VI**)	**a**	0.5	150	1	1-methylpyrazole	67
	b	0.5	170	1	1-ethyltriazole	62

Experimental

IR were measured with a JASCO IR-G spectrometer. NMR spectra were recorded on a Hitachi-Perkin Elmer R-20 spectrometer with a dilute solution in deuteriochloroform using tetramethylsilane as an internal standard.

Materials. Commercial imidazole, benzimidazole, triazole, benzotriazole and pyrazole were used without further purification. Dimethyl methyl- and diethyl ethylphosphonate were synthesized *via* Arbuzov reaction of the corresponding trialkyl phosphites with alkyl iodides. Methyl dimethyl- and ethyl ethylphenylphosphinates were prepared by the procedure of Reinhardt *et al.*[9]

The following reactions are typical. Reaction conditions are listed in Table 1.

1-Methylimidazole. A mixture of **I** (6.35 g, 0.092 mol) and **a** (5.80 g, 0.047 mol) was heated at 200 °C with stirring for 1 hr. The reaction mixture was treated with aqueous sodium bicarbonate and extracted with chloroform. The organic solution was concentrated and the residue was distilled under diminished pressure to give 1-methylimidazole as a liquid; (4.14 g, 54%), bp 75—76 °C/11 mmHg (lit,[5] 94—95 °C/14 mmHg). The IR spectrum of the product was identical with that of an authentic sample.

1-Ethylbenzimidazole. A mixture of **II** (3.00 g, 0.025 mol) and **d** (2.52 g, 0.014 mol) was heated at 198 °C for 6 hr. The reaction mixture was treated in a manner similar to the alkylation of **I** to give 1.27 g (34%) of 1-ethylbenzimidazole; bp 90—98 °C/1 mmHg (lit,[10] 160—162 °C/12 mmHg); picrate mp 216—217 °C (from ethanol) (lit,[10] 219 °C); IR (neat): 3300 (broad s), 3050 (m), 2970 (s), 2920 (s), 1610 (m), 1500 (s), 1460 (s), 1330 (s), 740 (s), and 700 cm^{-1} (m); NMR: τ 2.43 (complex m, 2H, ring), 2.70 (complex m, 3H, ring), 6.27 (q, J=7 Hz, 2H, $-CH_2-$), and 9.00 (t, J=8 Hz, 3H, $-CH_3$).

1-Methyl-1,2,4-Triazole. *1,2,4*-Triazole (III) (0.95 g, 0.0138 mol) was allowed to react with **a** (0.85 g, 0.0069 mol) to give 0.41 g (46%) of 1-methyl-1,2,4-triazole; bp 60 °C/10 mmHg (lit,[11] 175—176 °C); IR (neat): 3350 (broad s), 3100 (m), 2950 (w), 1520 (s), 1280 (s), 1220 (m), 1140 (s), 1010(m), 990 (m), and 680 cm^{-1} (s); NMR: τ 1.90 (s, 1H, ring) 2.12 (s, 1H, ring), and 6.10 (s, 3H, $-CH_3$).

Methylation of 1,2,3-Benzotriazole. A mixture of **IV** (5.75 g, 0.0482 mol) and **a** (2.99 g, 0.024 mol) was refluxed for 1.5 hr. The reaction mixture was subsequently made alkaline with aqueous sodium bicarbonate and extracted with chloroform (40 ml). The organic layer showed the presence of only two products in thin-layer chromatography (R_f=0.82 and 0.45, $CHCl_3$: CH_3OH=9: 1, Silica-Gel Merck Art-7730). The residue (5.5 g) obtained after evaporation of the solvent was dissolved in deuteriochloroform for study of the NMR spectrum. Only peaks, which are attributed to those of 1-methyl- and 2-methyl-benzotriazoles, were observed. From the area ratio (35: 3) of singlet peaks of CH_3 groups of both isomers (τ 5.74 for 1-methyl- and τ 5.50 for 2-methyl derivative, respectively), the yields of 1-methyl- and 2-methylbenzotriazole were calculated to be 80% and 7%, respectively. The residue (5.5 g) was then dissolved in benzene and fractionated with dilute hydrochloric acid. Neutralization of the acid layer, extraction with chloroform and subsequent recrystallization with hexane gave pure 1-methylbenzotriazole, 3.85 g (60%); mp 64 °C (from hexane) (lit,[12] 65 °C); IR (KBr): 3050 (m), 2950 (m), 1620 (m), 1590 (m), 1500 (s), 1450 (s), 1300 (s), 1270 (s), 1200 (s), 1030 (s), 740 (s), and 660 cm^{-1} (s); NMR: τ 1.95—2.00 (complex m, 1H, ring), 2.50—2.90 (complex m, 3H, ring), and 5.74 (s, 3H, $-CH_3$). Evaporation of benzene gave 2-methylbenzotriazole; 0.32 g (5%): bp 90—95 °C/10 mmHg (lit,[12] 104 °C/15 mmHg); NMR: τ 1.85—2.10 (complex m, 2H, ring), 2.43—2.60 (complex m, 2H, ring), and 5.50 (s, 3H, $-CH_3$).

Ethylation of 1,2,3-Benzotriazole. Benzotriazole (2.97 g, 0.0234 mol) was heated with **b** (2.07 g, 0.0125 mol) at 200 °C for 2 hr. The reaction mixture was neutralized with aqueous sodium bicarbonate and the solution was extracted with chloroform (10 ml×3). The organic layer was concentrated and the residue was distilled to give the product. The NMR spectrum of the distillate showed a set of signals consistent with the expected structure; bp 117 °C/2 mmHg (lit,[11] 150—151 °C/13 mmHg); IR (neat) 3300 (broad s), 3050 (s), 2970 (s), 2920 (s), 1610 (m), 1495 (s), 1469 (s), 1230 (s), 740 (s), and 700 cm^{-1} (m); NMR: τ 1.95—2.30 (complex m, 1H, ring), 2.50—2.90 (complex m, 3H, ring), 5.45 (q, J=8 Hz, 2H, $-CH_2-$), and 8.53 (t, J=8 Hz, 3H, $-CH_3$).

1-Methylpyrazole. 1-Methylpyrazole was distilled at 127 °C during heating of the reaction mixture through a distillating column as a clear liquid; 0.81 g (67%), bp (lit,[13] 127 °C); IR (neat): 3350 (broad s), 3100 (s), 2920 (s), 1515 (s), 1440 (m), 1390 (s), 1275 (s), 1205 (s), 1085 (s), 1065 (m), 1025 (s), 960 (s), 875 (m), 750 (broad s), 675 (s), and 605 cm^{-1} (s); NMR: τ 2.40 —2.80 (complex m, 2H, ring), 3.75—3.85 (complex m, 1H, ring), and 6.22 (s, 3H, $-CH_3$).

References

1) K. Yamauchi and M. Kinoshita, *J. Chem. Soc., Perkin I*, **1973**, 2506.
2) F. R. Benson and W. L. Savell, *Chem. Rev.*, **46**, 1 (1950).
3) M. A. Phillips, *J. Chem. Soc.*, **1921**, 2920 and **1931**, 1143.
4) M. R. Atkinson and J. B. Polya, *ibid.*, **1954**, 141.
5) L. P. Kyrides, F. B. Zienty, G. W. Steahly, and H. L. Morrill, *J. Org. Chem.*, **12**, 577 (1947).
6) F. L. Pyman and L. Light, *J. Chem. Soc.*, **121**, 2616 (1922).
7) J. G. Buchman, A. W. Johnson, J. A. Mills, and A. R. Todd, *ibid.*, **1950**, 2845.
8) F. Krollpfeiffer, *Ber.*, **71B**, 596 (1938).
9) H. Reinhardt, D. Bianch, and D. Möle, *ibid.*, **90**, 1656 (1957).
10) K. v. Auwers and W. Mauss, *ibid.*, **61B**, 2411 (1928).
11) P. A. Olifson and R. V. Kendel, *J. Org. Chem.*, **35**, 2246 (1970).
12) F. Krollpfeiffer, A. Rosenberg, and C. Muhlhausen, *Ann.*, **515**, 113 (1935).
13) K. v. Auwers, *ibid.*, **437**, 52 (1924).

Studies on O→N Acyl Migration in *O*-Acyl-2-deoxystreptamines

Takao KURISU,* Michio YAMASHITA,* Yoshio NISHIMURA, Toshiaki MIYAKE,*
Tsutomu TSUCHIYA, and Sumio UMEZAWA

Institute of Bioorganic Chemistry, 1614 Ida, Nakahara-ku, Kawasaki-shi 211
**Department of Applied Chemistry, Faculty of Engineering Keio University, Hiyoshi, Kohoku-ku, Yokohama 223*

(Received August 4, 1975)

Preparations of mono-*N*-protected 2-deoxystreptamines (racemates of **5**, **8**, **9**, **10**, **11**, **12**) from 4(and 6)-*O*-acyl-1,3-di-*N*-benzyloxycarbonyl-2-deoxystreptamines by O→N acyl migration were described. O→N Acyl migration of 2-deoxy-tri-*O*-ethoxycarbonylstreptamine (**15**) led to several protected derivatives (racemates of **16**, **17**, **18**) which also should serve for the preparation of glycosides and other derivatives of 2-deoxystreptamine.

In the course of our synthetic studies of aminoglycoside antibiotics, it was often necessary to protect selectively some of the amino and hydroxyl groups of 2-deoxystreptamine to effect a chemical reaction solely at other sites of the molecule remained intact. In this paper we describe the synthesis of a number of 2-deoxystreptamine derivatives that should serve for the preparation of their glycosides and other derivatives. The syntheses were achieved by way of O→N acyl migration.

The mono-*N*-di-*O*-protected derivatives (**5**,**8**,**9**) were prepared as follows: 1,3-Di-*N*-benzyloxycarbonyl-2-deoxystreptamine[1] was converted to a racemic mixture of 4,5-*O*- and 5,6-*O*-cyclohexylidene derivatives (**1**) by the acetal exchange reaction[2] with 1,1-dimethoxycyclohexane and *p*-toluenesulfonic acid in dimethylformamide. Acetylation or benzoylation or ethoxycarbonylation of **1** gave the corresponding racemic mixture of 6- and 4-*O*-acyl derivatives (**2**,**3**,**4**), respectively.

Deblocking of the *N*-protecting groups of the acetyl derivative (**2**) by catalytic hydrogenation with palladium resulted in the formation of 1 (and 3)-*N*-acetyl-4,5(and 5,6)-*O*-cyclohexylidene derivative (**5**, a racemate), which formed a monohydrochloride. This result showed that deblocking was followed by O→N migration.

In the case of similar hydrogenolysis of the benzoyl derivative (**3**), no O→N migration occurred, giving the racemic mixture of 6 (and 4)-*O*-benzoyl-4,5(and 5,6)-*O*-cyclohexylidene-2-deoxystreptamine (**6**), which formed a dihydrochloride. However, when the diacetate of **6** was treated with pyridine[3] at 50 °C for 2 days, migration occurred to give the *N*-benzoyl derivative (**8**), which formed a monohydrochloride.

Similar hydrogenolysis of the ethoxycarbonyl derivative (**4**) also was not followed by O→N migration and gave the racemic mixture of 4,5(and 5,6)-*O*-cyclohexylidene-2-deoxy-6(and 4)-*O*-ethoxycarbonylstreptamine (**7**), whereas similar treatment of **7** with pyridine gave, by way of O→N migration, the *N*-ethoxycarbonyl derivative (**9**), which formed a monohydrochloride.

Removal of the cycloxylidene group from **5**, **8**, and **9** with acid gave mono-*N*-protected 2-deoxystreptamines (**10**, **11**, **12**), respectively.

Next, we investigated the O→N migration of tri-*O*-ethoxycarbonyl derivative (**15**) of 2-deoxystreptamine. Di-*N*-(*p*-methylbenzylidene)-2-deoxystreptamine (**13**) was prepared and made to react with ethyl chloroformate in pyridine to give the tri-*O*-ethoxycarbonyl derivative (**14**), which was treated with 50% acetic acid to give **15**.

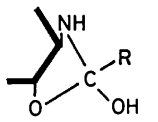

I: R=OC_2H_5
II: R=CH_3

Preliminary analysis for the reaction products of **15** with pyridine at various reaction temperatures and periods was made by tlc analysis of the fractions of reaction mixtures, and it was found that the first O→N migration giving mono-*N*-ethoxycarbonyl-di-*O*-ethoxycarbonyl derivative (**16**) was accompanied by the second O→N migration that is much slower to give di-*N*-ethoxycarbonyl-5-*O*-ethoxycarbonyl derivative (**17**). (See Preliminary Experiment on Treatment of **15** with Pyridine in the Experimental Section). However, when **16** was treated with pyridine similarly, it was readily converted to **17**. These results suggested that the migration of ethoxycarbonyl group probably proceeded through an unstable orthoester-amide structure (I) which may retard the second migration for some stereochemical reason. Although the orthoester-amide intermediate could not be isolated in the present work,

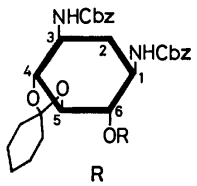

R	
2	Ac
3	Bz
4	Cbe

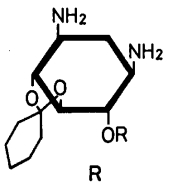

R	
6	Bz
7	Cbe

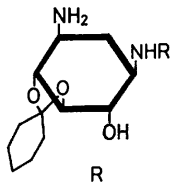

R	
5	Ac
8	Bz
9	Cbe

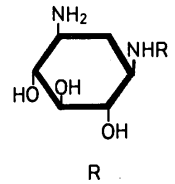

R	
10	Ac
11	Bz
12	Cbe

Cbe: $CO_2CH_2CH_3$
Cbz: $CO_2CH_2C_6H_5$

Only one isomer was shown in each compound.

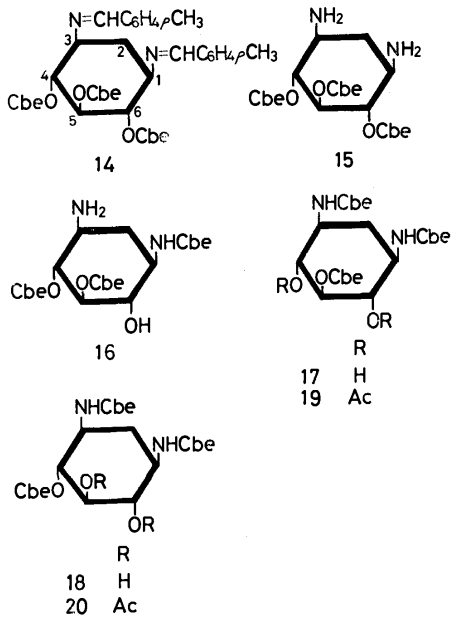

Only one isomer was shown in each compound.

formation of a related structure (II) has been reported by G. Fodor *et al.*,[4] who showed it by IR and PMR spectroscopy.

Furthermore, O→O migration was found to occur at higher temperature (100 °C) and prolonged reaction to give the racemic mixture of 2-deoxy-1,3-di-*N*-ethoxycarbonyl-4(and 6)-*O*-ethoxycarbonylstreptamine (**18**).

Confirmation of the structures of **17** and **18** was carried out by PMR spectral studies of their di-*O*-acetyl derivatives (**19**, **20**). The compound **19** showed a 6-proton singlet of acetyls in each of the $CDCl_3$ and pyridine-d_5, whereas another compound **20** showed two 3-proton singlets of acetyls in each of the above media, indicating that **20** (and also **18**) has an unsymmetrical structure. Periodate oxidation studies of **17** and **18** also afforded the same conclusion.

Experimental

*Racemic Mixture of 1,3-Di-*N*-benzyloxycarbonyl-4,5-*O*-cyclohexylidene-2-deoxystreptamine (1).* To a solution of 1,3-di-*N*-benzyloxycarbonyl-2-deoxystreptamine[1] (14.0 g) in dry DMF (280 ml), *p*-toluenesulfonic acid (0.54 g) and 1,1-dimethoxycyclohexane (9.4 ml) were added and the solution was heated at 50 °C under reduced pressure (~40 Torr). After 5 hr, the same amounts of both reagents were added and the solution was treated similarly. On tlc with benzene–methanol (6: 1), the starting material (R_f 0.33) disappeared and **1** (R_f 0.8) appeared as a single spot. The solution was neutralized with Amberlite IRA 400 (OH form, 25 ml), filtered, and concentrated under reduced pressure to approximately 100 ml, and the concentrate was poured into 0.1% sodium hydrogen carbonate solution (2 l) to deposit an amorphous powder, which was purified by reprecipitation with acetone–water, 15.8 g (95%), mp 149—151 °C.

Found: C, 66.02; H, 6.46; N, 5.39%. Calcd for $C_{28}H_{34}N_2O_7$: C, 65.86; H, 6.71; N, 5.49%.

*Racemic Mixture of 4-O-Acetyl-1,3-di-*N*-benzyloxycarbonyl-5,6-O-cyclohexylidene-2-deoxystreptamine (2).* A sample of **1** was treated in a usual manner with acetic anhydride in pyridine. Reprecipitation from cyclohexane gave **2** in 97% yield, mp 162—163 °C; PMR (in $CDCl_3$) δ: 1.97 (3H, s, OAc).

Found: C, 65.19; H, 6.58; N, 5.07%. Calcd for $C_{30}H_{36}N_2O_8$: C, 65.20; H, 6.57; N, 5.07%.

*Racemic Mixture of 4-O-Benzoyl-1,3-di-*N*-benzyloxycarbonyl-5,6-O-cyclohexylidene-2-deoxystreptamine (3).* A sample of **1** was treated with benzoyl chloride in pyridine in a usual manner to give **3** in 95% yield; Recrystallization from hot ether, mp 182—183 °C; IR (KBr): 1700, 1735 cm^{-1}.

Found: C, 68.49; H, 6.23; N, 4.58%. Calcd for $C_{35}H_{38}N_2O_8$: C, 68.39; H, 6.23; N, 4.56%.

*Racemic Mixture of 1,3-Di-*N*-benzyloxycarbonyl-4,5-O-cyclohexylidene-2-deoxy-6-O-ethoxycarbonylstreptamine (4).* To a solution of **1** (4.99 g) in pyridine (30 ml), ethyl chloroformate (3.1 ml) was added and the solution was allowed to stand at 5 °C overnight. On tlc with benzene–ethanol (20: 1), **1** (R_f 0.43) disappeared and **4** (R_f 0.66) appeared as a single spot. The solution was poured into ice-water and the precipitate was reprecipitated from ether, 5.36 g (94%), mp 150 °C; IR (KBr): 1765 (ν_{CO} of OCbe), 1690 (ν_{CO} of NCbe), 1535 cm^{-1}; PMR (in $CDCl_3$) δ: 1.26 (3H, t, $OCO_2CH_2C\underline{H}_3$).

Found: C, 64.04; H, 6.66; N, 4.83%. Calcd for $C_{31}H_{38}N_2O_9$: C, 63.90; H, 6.57; N, 4.81%.

*Racemic Mixture of 1-*N*-Acetyl-4,5-O-cyclohexylidene-2-deoxystreptamine (5).* A solution of **2** (5.22 g) in aqueous dioxane (1: 5, 25 ml), acetic acid (0.2 ml) was added and the solution was hydrogenated over palladium black at 40 °C overnight. On tlc with benzene–methanol (1: 1), **2** (R_f 1.0) disappeared and **5** (R_f 0.6) appeared as a single spot. The reaction mixture was filtered and the filtrate was evaporated. To the resulting syrup, 0.01 M hydrochloric acid was added until the mixture became weak acidic (pH~4.5) and the solution was evaporated to give a syrup. Addition of acetone gave precipitates, 2.62 g (82%), mp 112—113 °C; IR (KBr): 1635, 1550 cm^{-1}; PMR (in pyridine-d_5+D_2O) δ: 2.13 (3H, s, NAc).

Found: C, 49.67; H, 8.04; N, 7.95; Cl, 10.65%. Calcd for $C_{14}H_{24}N_2O_4 \cdot HCl \cdot H_2O$: C, 49.62; H, 8.03; N, 8.27; Cl, 10.4%.

Racemic Mixture of 4-O-Benzoyl-5,6-O-cyclohexylidene-2-deoxystreptamine (6). A sample of **3** (5.70 g) was hydrogenated in a similar manner as above. On tlc with benzene–methanol (1: 1), **3** (R_f 1.0) disappeared and **6** (R_f 0.3) appeared as a single spot. The reaction mixture was similarly treated as described above, 3.66 g (100%); IR (KBr): 1725 cm^{-1}; no peaks between 1650—1700 cm^{-1}.

Found: C, 54.67; H, 6.98; N, 6.44; Cl, 16.49%. Calcd for $C_{19}H_{26}N_2O_4 \cdot 2HCl$: C, 54.41; H, 6.73; N, 6.68; Cl, 16.91%.

Diacetate of **6** was obtained by using acetic acid instead of hydrochloric acid in the preparation described above, mp 92—93 °C.

Found: C, 59.49; H, 7.39; N, 6.19%. Calcd for $C_{19}H_{26}N_2O_4 \cdot 2CH_3CO_2H$: C, 59.21; H, 7.35; N, 6.01%.

Racemic Mixture of 4,5-O-Cyclohexylidene-2-deoxy-6-O-ethoxycarbonylstreptamine (7). A sample of **4** (5.36 g) was hydrogenated in a similar manner as described in the preparation of **5**. The crude product was recrystallized from acetone containing acetic acid to give **7**, 3.06 g (77%), mp 116—117 °C; tlc: R_f 0.2 (benzene–methanol 2: 1); IR (KBr): 1760 cm^{-1}; PMR (in D_2O) δ: 1.28 (3H, t, $OCO_2CH_2C\underline{H}_3$), 1.90 (6H s, AcOH).

Found: C, 52.72; H, 7.76; N, 6.29%. Calcd for $C_{15}H_{26}N_2O_5 \cdot 2CH_3CO_2H$: C, 52.52; H, 7.89; N, 6.45%.

*Racemic Mixture of 1-*N*-Benzoyl-4,5-O-cyclohexylidene-2-deoxystreptamine (8).* A solution of diacetate (3.66 g) of **6** in pyridine (73 ml) was maintained at 50 °C for 2 days. On tlc with benzene–methanol (3: 1), **6** (R_f 0.16) disappeared and **8** (R_f 0.56) appeared as a single spot. The solution was evaporated and then coevaporated with toluene to leave a residue, which was dissolved in aqueous methanol (1: 1). Addition of

0.01 M hydrochloric acid (pH~4.5) followed by evaporation gave a syrup. The procedure was repeated twice more. The methanol solution of the syrup was treated with charcoal to give the hydrochloride of **8**, 2.49 g (91%), mp 139—140 °C; IR (KBr): 1640, 1535 cm^{-1}.

Found: C, 57.16; H, 6.90; N, 6.47; Cl, 8.95%. Calcd for $C_{19}H_{26}N_2O_4 \cdot HCl \cdot H_2O$: C, 56.92; H, 7.29; N, 6.99; Cl, 8.84%.

Racemic Mixture of 4,5-O-Cyclohexylidene-2-deoxy-1-N-ethoxycarbonylstreptamine (9). The diacetate (3.06 g) of **7** was similarly treated in pyridine as described above. On tlc with benzene–methanol (1: 1), **7** (R_f 0.32) disappeared and **9** (R_f 0.74) appeared as a single spot. The solution was evaporated and then coevaporated with toluene. The residue was dissolved in aqueous methanol (1: 1) containing acetic acid (0.5 ml), treated with charcoal, and the solution was evaporated to give a solid, 2.99 g (82%); IR (KBr): 1690, 1620, 1540 cm^{-1}; PMR (in pyridine-d_5) δ: 1.13 (3H, t, $NCO_2CH_2C\underline{H}_3$), 2.12 (3H, s, AcOH).

Found: C, 54.20; H, 8.41; N, 7.79%. Calcd for $C_{15}H_{26}N_2O_5 \cdot CH_3CO_2H$: C, 54.53; H, 8.08; N, 7.48%.

Removal of Cyclohexylidene Group from 5, 8, and 9. The solution of 0.3 mmol of the starting material in 1M hydrochloric acid (2 ml) was allowed to stand at room temperature overnight. The product was purified by precipitation with acetone.

Racemic Mixture of 1-N-Acetyl-2-deoxystreptamine Hydrochloride (10): yield 82%, mp 171—172 °C. Found: C, 37.63; H, 7.11; N, 10.48, Cl, 13.56%. Calcd for $C_8H_{16}N_2O_4 \cdot HCl \cdot H_2O$: C, 37.14; N, 7.40; N, 10.83; Cl, 13.71%.

Racemic Mixture of 1-N-Benzoyl-2-deoxystreptamine Hydrochloride (11): yield 82%, mp 214—215 °C. Found: C, 50.28; H, 6.18; N, 8.55; Cl, 11.60%. Calcd for $C_{13}H_{18}N_2O_4 \cdot HCl \cdot 1/2H_2O$: C, 50.08; H, 6.47; N, 8.99; Cl, 11.37%.

Racemic Mixture of 2-Deoxy-1-N-ethoxycarbonylstreptamine Hydrochloride (12): yield 89%, mp 207—208 °C. Found: C, 40.06; H, 7.21; N, 10.52; Cl, 13.25%. Calcd for $C_9H_{18}N_2O_5 \cdot HCl$: C, 39.93; H, 7.07; N, 10.35; Cl, 13.10%.

1,3-Di-N-(p-methylbenzylidene)-2-deoxystreptamine (13). To a mixture of 2-deoxystreptamine dihydrochloride (1.02 g) and anhydrous potassium carbonate (6.9 g) in methanol (12 ml), *p*-methylbenzaldehyde (1.3 ml) was added under the atmosphere of nitrogen and the mixture was stirred at room temperature overnight. Evaporation gave a residue, which was extracted with chloroform. The solution was washed with water, dried over sodium sulfate and concentrated to give a syrup. Addition of hexane gave a solid, 1.09 g (63%); IR (KBr): 1630, 1605, 1100, 1030, 815, 500 cm^{-1}; PMR (in $CDCl_3$) δ: 2.31 (6H, s, $C\underline{H}_3C_6H_4$), 8.31 (2H, s, =CH–N).

Found: C, 68.35; H, 7.14; N, 6.96%. Calcd for $C_{22}H_{26}N_2O_3 \cdot H_2O$: C, 68.72; H, 7.34; N, 7.29%.

2-Deoxy-4,5,6-tri-O-ethoxycarbonyl-1,3-di-N-(p-methylbenzylidene)streptamine (14). To a solution of **13** (1.86 g, dried at 80 °C under reduced pressure) in pyridine (19 ml), a small amount of calcium hydride (to remove a trace of moisture) and ethyl chloroformate (2.9 ml) were added and the mixture was stirred at 50 °C overnight. Another ethyl chloroformate (0.8 ml) was added and the mixture was stirred for 1 hr. On tlc with benzene–ethyl acetate–triethylamine (6: 1: 0.01), **13** (R_f 0.2) disappeared and **14** (R_f 0.38) appeared. The mixture was poured into saturated sodium hydrogen carbonate solution (150 ml) and the mixture was stirred for 1 hr. The lower layer separated was extracted with chloroform and the solution was washed with water, dried over sodium sulfate and evaporated to give a syrup. Addition of hexane gave a solid, 2.45 g (85%); IR (KBr): 1750, 1710, 1640, 1610, 1370, 1290—1240 (s), 1010, 880, 820, 790, 510 cm^{-1}; PMR (in $CDCl_3$) δ: 1.08 (6H, t, $OCO_2CH_2C\underline{H}_3$), 1.29 (3H, t, $OCO_2CH_2C\underline{H}_3$), 2.40 (6H, s, $C\underline{H}_3C_6H_4$), 4.08 (4H, q, $OCO_2C\underline{H}_2CH_3$), 4.26 (2H, q, $OCO_2C\underline{H}_2CH_3$), 8.40 (2H, s, =CH–N).

Found: C, 63.50; H, 6.47; N, 4.68%. Calcd for $C_{31}H_{33}N_2O_9$: C, 63.90; H, 6.57; N, 4.81%.

2-Deoxy-4,5,6-tri-O-ethoxycarbonylstreptamine (15) Diacetate. A sample of **14** (3.70 g) was dissolved in 50% acetic acid (60 ml). Monitoring by tlc showed that **14** disappeared immediately, and **15** (R_f 0.5 with the lower layer of chloroform–ethanol–8% aqueous ammonia (2: 1: 1)) appeared. The solution was evaporated to give a syrup. Addition of ether gave a solid, 2.51 g (84%), mp 85—86 °C; IR (KBr): 1760, 1620 (w), 1400, 1280, 1250, 1020, 1000, 880, 780 cm^{-1}.

Found: C, 45.49; H, 6.52; N, 5.25%. Calcd for $C_{15}H_{26}N_2O_9 \cdot 2CH_3CO_2H$: C, 45.78; H, 6.87; N, 5.62%.

Preliminary Experimemt on Treatment of 15 with Pyridine. A solution of **15** (10 mg) in dry pyridine (0.2 ml) was allowed to stand at various temperatures and the change in the reaction was monitored by tlc (Wakogel B5, Wako Pure Chemicals Ind.) with ethyl acetate–ethanol–water (45: 5: 3) (Solvent A) and with chloroform–ethanol–8% aqueous ammonia (6: 1: 1) (lower layer) (Solvent B). Four spots A, B, C, and D appeared: A (R_f 0.1 by Solvent A and 0.1 by Solvent B, **15**), B (R_f 0.35 and 0.38, **16**), C (R_f 0.6 and 0.38, **17**) and D (R_f 0.6 and 0.3, **18**). At 20 °C: after 7 hr: *A* (卅), B(±); 24 hr: A (+), B(卅), C(±); 48 hr; A(±), B(卅), C(+). At 50 °C: 4 hr: A(卄), B(+), C(±); 5.5 hr: A(卄), B(卄), C(±); 7.5 hr: A(±), B(卅), C(+); 10 hr: A(±), B(卄), C(卄); 22 hr: B(卄), C(卄); 46 hr: B(+), C(卅); 50 hr: C(卅), D(+). At 100 °C: 0.5 hr: A(卄), B(+), C(±); 1 hr: A(+), B(卅), C(+); 2 hr: A(±), B(卄), C(卄), D(±); 3 hr: B(+), C(卄), D(卄); 5 hr: C(卄), D(卄).

Racemic Mixture of 2-Deoxy-1-N-ethoxycarbonyl-4,5-di-O-ethoxycarbonylstreptamine (16) and 1,3-Di-N-ethoxycarbonyl-5-O-ethoxycarbonyl-2-deoxystreptamine (17). A solution of **15** (1.18 g) in dry pyridine (21 ml) was allowed to stand at 50 °C for 46 hr. Evaporation of the solution gave a solid, which was charged on a column of silica gel (Wakogel C-200, Wako Pure Chemicals Ind.) and eluted with ethyl acetate–ethanol–water (45: 5: 3). From the earlier fraction, **17** was obtained, 425 mg (47%); Recrystallization from ethyl acetate gave needles, mp 112—113 °C; IR (KBr): 1740 (carbonate), 1700 (carbamate), 1540, 1270 (s), 1040, 880, 780 cm^{-1}; PMR (in $CDCl_3$) δ: 1.25 (6H, t, $NCO_2CH_2C\underline{H}_3$), 1.34 (3H, d, $OCO_2CH_2C\underline{H}_3$), 4.21 (4H, q, $CO_2C\underline{H}_2CH_3$).

Found: C, 47.30; H, 6.70; N, 7.13%. Calcd for $C_{15}H_{26}N_2O_9$: C, 47.61; H, 6.93; N, 7.40%.

From the later fraction, a solid of **16**, 172 mg (free base) (19%) was obtained, IR (KBr): 1750, 1700, 1540, 1270, 1030, 1000, 870, 780 cm^{-1}; PMR (in $CDCl_3$) δ: 1.23 (3H, t, $OCO_2CH_2C\underline{H}_3$), 1.30 (6H, t, $NCO_2CH_2C\underline{H}_3$); no peaks at ~$\delta$ 2 (acetate) was observed.

The hydrochloride of **16**. PMR (in CD_3OD) δ: 1.20 (3H, t, $OCO_2CH_2C\underline{H}_3$), 1.26 and 1.28 (each 3H, t, $NCO_2CH_2C\underline{H}_3$).

Found: C, 43.62; H, 6.44; N, 6.37; Cl, 8.46%. Calcd for $C_{15}H_{26}N_2O_9 \cdot HCl$: C, 43.43; H, 6.56; N, 6.75; Cl, 8.55%.

***17* from *16*.** A solution of **16** (free base, 115 mg) in pyridine (2 ml) was allowed to stand at 35 °C for 12 hr. On tlc, the solution gave a single spot. The solution was evaporated and the residue was similarly purified by chromatography as described above to give **17**, 52 mg (52%).

4,6-Di-O-acetyl-2-deoxy-1,3-di-N-ethoxycarbonyl-5-O-ethoxycarbonylstreptamine (19). A solution of **17** in pyridine was acetylated with acetic anhydride in a usual manner to give **19** almost quantitatively, mp 154—155 °C; IR (KBr): 1760, 1730, 1700, 1530, 1380, 1270, 1230, 1040 cm^{-1}; PMR (in

$CDCl_3$) δ: 1.23 (6H, t, $NCO_2CH_2C\underline{H}_3$), 1.30 (3H, t, $OCO_2CH_2C\underline{H}_3$), 2.07 (6H, s, Ac), 4.15 (6H, q, $CO_2C\underline{H}_2CH_3$).

Found: C, 49.31; H, 6.42; N, 6.01%. Calcd for $C_{19}H_{30}N_2O_{11}$: C, 49.35; H, 6.54; N, 6.05%.

Racemic Mixture of 2-Deoxy-1,3-di-N-ethoxycarbonyl-4-O-ethoxycarbonylstreptamine (18). A solution of the diacetate (1.0 g) of **15** in dry pyridine (20 ml) was heated at 100 °C for 5 hr. Evaporation of the solution gave a solid. The solid was chromatographed on a column of silica gel with ethyl acetate. From the earlier fraction **17** was obtained, 280 mg (37%) and from the later fraction **18**, 258 mg (34%) was obtained; Recrystallization from ethyl acetate gave needles, mp 120—121 °C; IR (KBr): 1740, 1700, 1540, 1270, 1030, 1010, 880, 780 cm^{-1}; PMR (in $CDCl_3$) δ: 1.22 and 1.23 (each 3H, t, $NHCO_2CH_2C\underline{H}_3$), 1.30 (3H, t, $OCO_2CH_2C\underline{H}_3$).

Found: C, 47.66; H, 6.89; N, 7.15%. Calcd for $C_{15}H_{26}N_2O_9$: C, 47.61; H, 6.93; N, 7.40%.

Racemic Mixture of 4,5-Di-O-acetyl-2-deoxy-1,3-di-N-ethoxycarbonyl-6-O-ethoxycarbonylstreptamine (20). A sample of **18** was similarly treated as described in the preparation of **19**, mp 169—170 °C. The IR spectrum was substantially similar to that of **19**. PMR (in $CDCl_3$) δ: 1.21 (6H, t, $NHCO_2CH_2C\underline{H}_3$), 1.27 (3H, t, $OCO_2CH_2C\underline{H}_3$), 2.10 and 2.12 (each 3H, s, Ac), 4.05 (6H, q, $CO_2C\underline{H}_2CH_3$).

Found: C, 49.84; H, 6.51; N, 5.98%. Calcd for $C_{19}H_{30}N_2O_{11}$: C, 49.35; H, 6.54; N, 6.05%.

Periodate Oxidation of the Mixture of 17 and 18. The reaction mixture of **17** and **18** described in the preparation of **18** was evaporated. The residue showed two spots at R_f 0.7 (**17**) and 0.55 (**18**) in almost equal strength on tlc with chloroform–ethanol–8% aqueous ammonia (6: 1: 1). To the solution of the residue (20.1 mg) in aqueous dioxane (1: 1, 0.5 ml), periodic acid (6.1 mg) was added and the solution was allowed to stand at room temperature for 1 hr. The reaction mixture showed a clear spot at R_f 0.7, but the spot at R_f 0.55 disappeared completely.

References

1) S. Umezawa and Y. Ito, This Bulletin, **34**, 1540 (1961).
2) F. H. Bissett, M. E. Evans, and F. W. Parrish, *Carbohyd. Res.*, **5**, 184 (1967).
3) For the use of pyridine, see, for exanple, F. P. van de Kamp, and F. Micheel, *Chem. Ber.*, **90**, 2054 (1957). For O→N migration in amino sugars, see A. B. Foster and D. Horton, *Advan. Carbohyd. Chem.*, **14**, 213 (1959).
4) G. Fodor, F. Letourneau, and N. Mandava, *Can. J. Chem.*, **48**, 1465 (1970).

Racemization Catalyst for Amino Acids. III.* Racemization of Alanine Induced by 4-Nitrosophenol

Kazuhiro HIROTA, Hisanori KOIZUMI,** Yoshio HIRONAKA, and Yoshiharu IZUMI

Division of Organic Chemistry, Institute for Protein Research, Osaka University, Suita, Osaka 565

(Received March 7, 1975)

The racemization of D-alanine was carried out with several derivatives of 4-nitrosophenol in the presence of cupric ion. Their racemization activities have been found to decrease with an increase in the bulk of alkyl group in 4-nitrosophenol. The racemization is accompanied with the decomposition of 4-nitrosophenol, and has been found to be catalyzed by an unidentified product generated in the reaction mixture. The proposed mechanism involves an autoaccelerating reaction.

In the course of studies on the racemization of amino acids, derivatives of 2- or 4-nitrosophenol[1,2] were found to be good catalyst for the racemization of alanine. The catalytic function of these compounds in the reaction was first expected to be the same as that of pyridoxal, since they require similar reaction conditions to those of the pyridoxal-catalyzed racemization.[3] Further they are able to form a Schiff's base with alanine, as pyridoxal does in a step of the racemization reaction. However rate studies of the racemization with 4-nitrosophenol revealed that these compounds are not the actual catalyst but they induce the formation of catalysts for the racemization whose mechanism differs from that of pyridoxal.

In this paper the functions of 4-nitrosophenols in the racemization reaction of D-alanine are explained.

Results and Discussion

Effect of the Substituent on 2,6 or 3,5 Positions in 4-Nitrosophenol on the Racemization. The racemization of D-alanine was performed with several derivatives of 4-nitrosophenol in the presence of cupric ion. The racemization yields and the recoveries of 4-nitrosophenols are shown in Figs. 1 and 2 (Fig. 2 includes some data used in Fig. 1). The time course is sigmoid, consisting of an induced stage and a subsequent steep rise, suggesting an autoaccelerating reaction. The induced period of the racemizations with 2-alkyl substituted 4-nitrosophenols, as seen in Fig. 1, are in the oder: 4-nitrosophenol $<$ 2-methyl-4-nitrosophenol $\simeq$ 2-ethyl-4-nitrosophenol $<$ 2-isopropyl-4-nitrosophenol $<$ 2-*tert*-butyl-4-nitrosophenol. Thus the apparent catalytic activity increases with decreasing steric bulk of the groups in the position *ortho* to the hydroxyl group of the 4-nitrosophenol derivatives. This suggests the contribution of the hydroxyl group of 4-nitrosophenol (**1**) to the initial stage of reaction. With this regard, the Schiff's base formed with alanine and the carbony

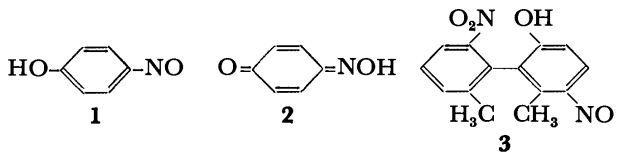

1 **2** **3**

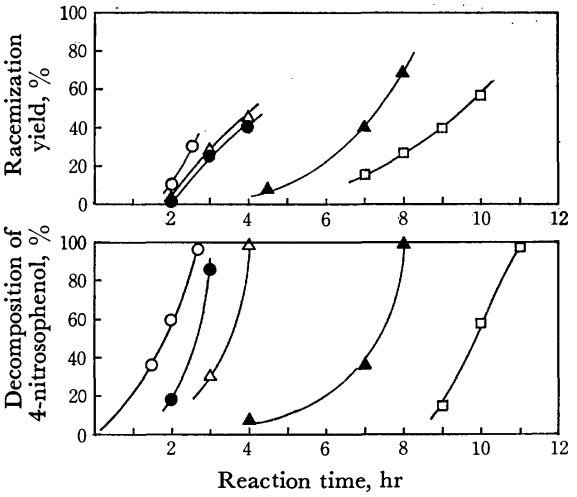

Fig. 1. Effect of 2-alkyl substituted 4-nitrosophenol on the racemization. Reaction mixture (0.5 ml, pH 10.4) containing 0.5 mmol D-alanine, 0.05 mmol $CuSO_4 \cdot 5H_2O$ and 0.0125 mmol one of the 4-nitrosophenol derivatives was shaken at 50 °C.
○: 4-Nitrosophenol, ●: 2-methyl-4-nitrosophenol, △: 2-ethyl-4-nitrosophenol, ▲: 2-isopropyl-4-nitrosophenol, □: 2-*tert*-butyl-4-nitrosophenol.

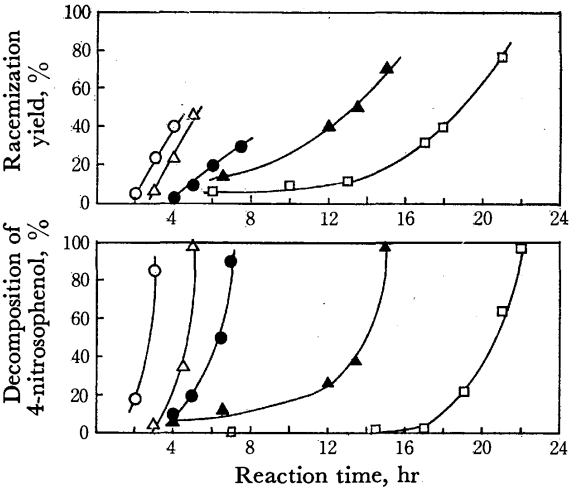

Fig. 2. Effect of 3-alkyl substituted 4-nitrosophenol on the racemization. The reaction condition of each experiment is same as that shown in Fig. 1.
○: 2-Methyl-4-nitrosophenol, ●: 3-methyl-4-nitrosophenol, △: 2,6-dimethyl-4-nitrosophenol, ▲: 3,5-dimethyl-4-nitrosophenol, □: 2-isopropyl-5-methyl-4-nitrosophenol.

* Presented at the 30th Annual Meeting of the Chemical Society of Japan, Osaka, April, 1974.

** Present adress: Nippon Senka Chemical Ind. Ltd. 1-83 Naka Hanatencho, Jyotoku, Osaka.

group of the quinone form (**2**) of 4-nitrosophenol would play an important role in the initial stage of the reaction.

On the other hand, a function of the nitroso group in the phenol form, **1** in the racemization was suggested by the experiment shown in Fig. 2. The apparent catalytic activity of 3,5-dimethyl-4-nitrosophenol, in which the nitroso group is protected by steric hindrance of the two methyl groups, is lower than that of 3-methyl-4-nitrosophenol. These results indicate that the catalytic activity of the 4-nitrosophenols depends not only on the carbonyl group in **2**, but also on the nitroso group in **1**. Consistent with this is the fact that the lowest activity of racemization among the derivatives of 4-nitrosophenol employed is observed with 2-isopropyl-5-methyl-4-nitrosophenol, in which both of the functional groups are sterically hindered by alkyl groups.

The relative reactivities of the two functional groups, were determined by comparing racemization activities of two structural isomers. The apparent catalytic activities, as seen in Fig. 2, are in the order: 2-methyl-4-nitrosophenol>3-methyl-4-nitrosophenol and 2,6-dimethyl-4-nitrosophenol > 3,5-dimethyl-4-nitrosophenol, respectively. These orders show that the participation of the nitroso group in **1** in the racemization is greater than that of the carbonyl group in **2**.

Relationship between the Racemization of D-*Alanine and the Decomposition of 4-Nitrosophenol.* The racemizations with 4-nitrosophenol, as seen in Figs. 1 and 2, are accompanied by the decomposition of 4-nitrosophenol.

A more detailed rate experiment was performed with 2'-nitro-2-hydroxy-5-nitroso-6,6'-dimethylbiphenyl (**3**). The result, comparing the rates of racemization and the decomposition of **3**, is shown in Fig. 3. The induction period of the racemization corresponds to that of the decomposition of **3** and increases when the concentration of **3** is decreased as seen in comparing A and B of Fig. 3. This indicates that the racemization of D-alanine is actually catalyzed by an unidentified product (X) generated in the reaction mixture, and suggests that the initiation of racemization activity might be a response to the appearance of this product, which is the actual catalyst.

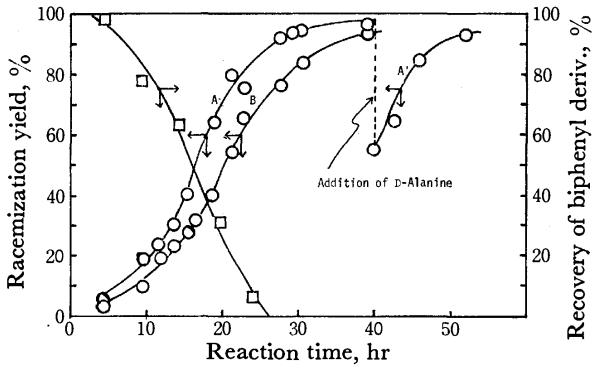

Fig. 3. Time courses of racemization yield and recovery of 2'-nitro-2-hydroxy-5-nitroso-6,6'-dimethylbiphenyl (**3**).
○: Racemization yield of alanine,
A: The reaction mixture of which initial composition consists of D-alanine 445 mg, $CuSO_4 \cdot 5H_2O$ 125 mg, **3** 3.4 mg, and borate buffer (0.05 M, pH 10.4 at 50 °C) was incubated at 50 °C.
A': To the reaction mixture of A at the final stage of racemization, D-alanine 445 mg and $CuSO_4 \cdot 5H_2O$ 125 mg were added. In this manner, the initial racemization yield of the reaction mixture becomes 50%. The mixture was reincuvated another 10 hr at 50 °C.
B: The reaction condition and the initial composition of reaction mixture are same as A, except the amount of **3** (14 mg).
□: Recovery of **3** in the system of A.

The above conclusion is also supported by the experiment shown in A' of Fig. 3; D-alanine and cupric sulfate pentahydrate were added again to the reaction mixture at the final stage of the reaction A in which **3** had already disappeared, and the racemization time course was followed. Additional D-alanine is racemized immediately without the induced period seen in curves A and its initial racemization rate corresponds to the previous maximum observed in curve A. This indicates that the relatively stable compound, X, has accumulated in the reaction mixture and that additional D-alanine can undergo racemization catalyzed by X already present.

Proposed Mechanism of the Racemization. Because the decomposition of 4-nitrosophenol in the reaction condition requires the presence of both D-alanine and cupric ions, the decomposition should proceed *via* a cupric complex DN–Cu containing D-alanine and 4-nitrosophenol. The resulting decomposition product, X, catalyzes both the racemization of D-alanine and the decomposition of DN–Cu in an autoaccelerating reaction. The proposed mechanism of racemization for D-alanine is shown in Eq. 1.

$$\mathrm{D} + \mathrm{N} \overset{Cu^{2+}}{\rightleftharpoons} \mathrm{DN\text{-}Cu} \longrightarrow \mathrm{X} \qquad (1)$$

$$\mathrm{D} \overset{\mathrm{X}}{\rightleftharpoons} \mathrm{L}$$

$$\mathrm{D} + \mathrm{N} \overset{Cu^{2+}}{\rightleftharpoons} \mathrm{DN\text{-}Cu} \rightleftharpoons \mathrm{LN\text{-}Cu} \overset{Cu^{2+}}{\rightleftharpoons} \mathrm{L} + \mathrm{N} \qquad (2)$$

D: D-alanine, L: L-alanine, N: 4-nitrosophenol, X: an unidentified compound.

Since the initial rate of racemization is negligible, the chief role of DN–Cu may be as a promoter to produce X rather than an intermediate in the racemization of D-alanine *via* reaction shown in Eq.(2). The racemization mechanism with 4-nitrosophenol, in this respect, is quite different from that with pyridoxal[3] which forms the metal-amino acid complex to catalyze the racemization.

We have no information about the composition or the structure of X, but we are currently working to confirm them.

Experimental

All melting points are uncorrected. The IR spectra were taken with a Shimadzu 27-G spectrometer. The NMR spectra were recorded by a Hitachi R-24 spectrometer using TMS as the internal standard. Thin layer chromatography was performed on precoated plates of silica gel (E. Merck). The glc analyses were carried on a Shimadzu 4APF apparatus, using neopentylglycolsuccinate (1.5%)-Chromosorb W (300 cm × 0.5 cm).

Materials. 4-Nitrosophenol,[4] 2-methyl-4-nitrosophe-

nol,[5] 3-methyl-4-nitrosophenol,[5] 2,6-dimethyl-4-nitrosophenol,[6] 3,5-dimethyl-4-nitrosophenol,[7] and 2-isopropyl-5-methyl-4-nitrosophenol[8] were prepared from substituted phenols and sodium nitrite according to the methods described previously.

2-Ethyl-4-nitrosophenol. To a solution of sodium nitrite (2.5 g) in water (2000 ml), 2-ethylphenol (6.0 g) was dissolved and 1.5% sulfuric acid (200 ml) was added dropwise while stirring at 0—5 °C for 2 hr. A brown yellow precipitate was collected and recrystallized from benzene with a small amount of charcoal. Yield, 3.0 g (40%); mp 101—102 °C. Found: C, 63.85; H, 6.06; N, 9.13%. Calcd for $C_8H_9N_1O_2$: C, 63.57; H, 6.00; N, 9.27%.

2-Isopropyl-4-nitrosophenol. Concentrated hydrochloric acid (30 ml) was added to a solution of 2-isopropylphenol (13.6 g) dissolved in ethanol (40 ml). The second solution of sodium nitrite (7.0 g) dissolved in water (10 ml) was poured with continuous stirring into the 2-isopropylphenol solution at 0—5 °C. The reaction mixture was allowed to stand for 2 hr at this temperature. After the addition of a solution of urea (0.5 g) in water (2.0 ml), it was evaporated to dryness. The residue was extracted with ether (50 ml). The extract was washed with water and dried over anhydrous sodium sulfate. The ether solution was chromatographed on a column of alumina and eluted with ether to separate an orange yellow fraction from the pitch-like material. Further purification was carried out with this layer chromatography on silica gel in a solvent system of ether–hexane (1 : 1 v/v). A yellow band which gave a positive Liebermann test was scraped off the plate, and extracted with ethyl acetate. After removing the solvent, the residue was recrystallized from 30% ethanol. Yield, 1.0 g (6%); mp 106—107 °C. Found: C, 65.25; H, 6.77; N, 8.61%. Calcd for $C_9H_{11}N_1O_2$: C, 65.44; H, 6.71; N, 8.48%.

2-tert-Butyl-4-nitrosophenol. 2-*tert*-Butylphenol (4.0 g) and sodium nitrite (4.0 g) were dissolved in 0.3% sodium hydroxide (1000 ml). To this solution 6% sulfuric acid (100 ml) was added dropwise with stirring over one hour at 0—3 °C. After standing for 2 hr., a red brown material precipitated. On cooling more of the precipitate formed. The precipitate was recrystallized twice from 25% ethanol to give yellow crystals. Yield, 1.0 g (21%); mp 136—137 °C. Found: C, 67.34; H, 7.35; N, 7.70%. Calcd for $C_{10}H_{13}N_1O_2$: C, 67.02; H, 7.31; N, 7.82%.

2′-Nitro-2-hydroxy-5-nitroso-6,6′-dimethylbiphenyl. 2-Hydroxy-2′-nitro-6,6′-dimethylbiphenyl (243 mg)[9] was dissolved in glacial acetic acid (1.0 ml) and then water (0.2 ml) was added. A solution of sodium nitrite (83 mg) in water (0.2 ml) was added dropwise with stirring at 0—3 °C. The mixture was allowed to stand overnight at the same temperature. The reddish yellow precipitate was collected on a filter and washed twice with 10% ethanol (1.5 ml). The crystals were recrystallized from 30% ethanol with a small amount of charcoal. Yield, 90 mg (33%); mp 200—202 °C. Found: C, 61.10: H, 4.26; N, 10.00%. Calcd for $C_{14}H_{12}N_2O_4$: C, 61.76; H, 4.44; N, 10.29%. IR ($CHCl_3$): 2550 cm^{-1} (OH). NMR (CD_3COCD_3): δ 12.5 (OH), 1.96 and 2.22 (CH_3).

Racemization Reaction. An aqueous solution of D-alanine (0.5 mmol), cupric sulfate pentahydrate (0.05 mmol), and one of the 4-nitrosophenol derivatives (0.0125 mmol) was made. The pH was adjusted to 10.4 (at 50 °C) with 1 M sodium hydroxide and diluted to a total volume of 0.25 ml. After diluting with 0.05 M borate buffer (0.25 ml, pH 10.4 at 50 °C), the mixture was shaken at 50 °C in a sealed tube. At specific time intervals the reaction was stopped by the addition of 0.25 ml of 6 M hydrochloric acid.

Determination of the Racemization Yield. The reaction mixture (0.2 ml) was dried *in vacuo*. The residue was heated with *l*-menthol (1.0 g) 110—120 °C and bubbled with dry hydrogen chloride for 1.5 hr to prepare the *l*-menthyl ester of alanine. Excess *l*-menthol was removed by sublimation at 110—120 °C under reduced pressure. Trifluoroacetic anhydride (0.05 ml) was added and allowed to stand overnight at room temperature to obtain *l*-menthyl L- and D-trifluoroacetylalaninate. After diluting with tetrahydrofuran (0.5 ml), the diastereomers were gas chromatographed at 170 °C. From the ratio of the diastereomers, the racemization yield of D-alanine was calculated.

Determination of the Recovery of 4-Nitrosophenol. The reaction mixture (0.2 ml) was extracted with ethyl acetate (2.0 ml) and the extract (120 μl) was chromatographed on a silica gel with ether–hexane (1 : 1 v/v) as the developing solvent. A yellow band containing 4-nitrosophenols was scraped off the plate and extracted with 0.5 M sodium hydroxide (5.0 ml). The absorption of the extract was measured at 403 nm and the concentration was calculated.

The authors wish to thank Mrs. Kiku Hara and Miss Aiko Yamanouchi for the elemental analyses.

References

1) K. Hirota and Y. Izumi, This Bulletin, **40**, 178 (1967).
2) K. Hirota, K. Miyamoto, and Y. Izumi, This Bulletin, **40**, 182 (1967).
3) J. Olivard, D. E. Metzler, and E. E. Snell, *J. Biol. Chem.*, **199**, 669 (1952).
4) J. L. Bridge, *Ann. Chem.*, **277**, 85 (1893).
5) J. L. Bridge and W. C. Morgan, *J. Amer. Chem. Soc.*, **20**, 766 (1898).
6) V. Ershov, G. A. Zlobina, and G. A. Nikiforov, *Akad. Nauk SSSR Izv.*, **1963**, 1877.
7) K. V. Auwers and E. Borshe, *Ber.*, **48**, 1715 (1915).
8) E. Kremers, N. Wakemann, and R. M. Hixon, "Organic Syntheses," Coll. Vol. 2, p. 511.
9) A. Angeletti, *Gazz. Chim. Ital.*, **61**, 832 (1931).

Dehydroannulenes. I. Synthesis and Properties of 1,5,10,14-Tetramethyl-6,8,15,17-tetrakisdehydro[18]annulene[1]

Jūro OJIMA,* Tsutomu KATAKAMI, Gen NAKAMINAMI, and Masazumi NAKAGAWA**

Department of Chemistry, Faculty of Science, Osaka University, Toyonaka, Osaka 560

(Received August 18, 1975)

1,6,10,15-Tetramethyl-7,9,15,17-cyclooctadecatetraene-2,4,11,13-tetrayne-1,6-diol (VII), a 18-membered cyclic glycol, was synthesized by a stepwise reaction sequence starting from 3-methyl-2-penten-4-ynal (III). Treatment of the cyclic glycol (VII) with stannous chloride dihydrate in concentrated hydrochloric acid yielded tetramethyltetrakisdehydro[18]annulene (VIII). Examination of the NMR spectra clearly indicates that the tetrakisdehydro[18]annulene (VIII) containing formal diacetylene and hexapentaene units sustains a strong diamagnetic ring current and has a high conformational stability.

1,8-Bisdehydro[14]annulene (I) obtained by Sondheimer and Gaoni[2] holds an unique position in a wide variety of dehydroannulenes, *i.e.*, the annulene (I) contains formal acetylenic and cumulenic linkages in the

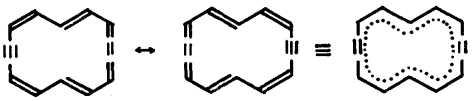

I I'

cyclic system, and equivalent Kekulé structures can be written in contrast to ordinary dehydroannulenes containing one or more acetylenic bonds in which no such type of equivalent resonance structures can be drawn. Bisdehydro[14]annulene (I) can be represented most properly by a symmetrical formula (I'). We have been interested in the synthesis and properties of such symmetrical dehydroannulenes containing linkages of sp-hybridized carbon atoms in the cyclic conjugated system. In this paper, we wish to report the synthesis and properties of tetramethyltetrakisdehydro[18]annulene (VIII) containing formal diacetylene and hexapentaene units in the conjugated ring.[3] The NMR spectrum of VIII provides a clear evidence for the existence of strong diamagnetic ring current in the 18π-electron system.

Ethynyl alcohol (II) prepared by the reaction of ethynylmagnesium bromide with β-chlorovinyl methyl ketone[4] in a high yield was treated with diluted sulfuric acid according to the reported method.[5] Examination of NMR spectrum of the resulting 2-penten-4-ynal reveals that the aldehyde largely consists of the *cis*-isomer (III) (*ca.* 95%) with respect to the ethynyl and the formyl groups consistent with the reported equilibration study of III in acidic conditions[6] being most suitable for the construction of desired 18-membered ring. The aldehyde without separating into pure *cis*-isomer (III) was condensed with acetone by the reported method[5b] with modification to give dieneyne ketone (IV). *trans*-Configuration of the newly formed double bond in IV was confirmed by IR and NMR spectroscopy. Oxidative coupling of IV by cupric acetate in pyridine[7] yielded diketone (V) in an almost quantitative

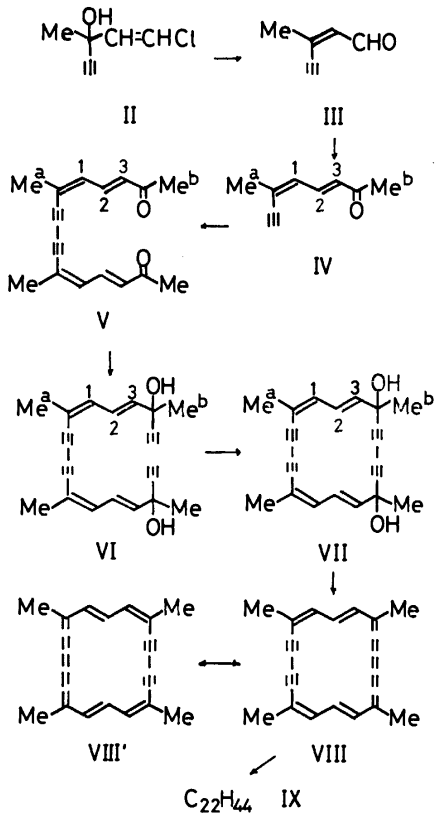

II III IV V VI VII VIII' VIII $C_{22}H_{44}$ IX

yield. Attempts of bis-ethynylation of the diketone using sodium, lithium or calcium acetylide[8] in liquid ammonia, ethynylmagnesium bromide in tetrahydrofuran and sodium acetylide in *N,N*-dimethylformamide[9] gave fruitless results. Finally, it was found that the diketone (V) can be ethynylated with lithium acetylide-ethylenediamine complex[10] in tetrahydrofuran. The product was chromatographed on alumina. The first substance to be eluted from the column was presumably monoethynylated derivative of V. Desired bis-ethynyl glycol (VI) was obtained from fractions eluted with benzene–ether (4: 6) and ether–ethyl acetate (6: 4) as a yellow viscous liquid in 63% yield. Oxidative coupling of the acyclic glycol (VI) by cupric acetate monohydrate in pyridine–methanol under high dilution conditions using ether as an entraining solvent resulted in a mixture of 18-membered cyclic glycol (VII) in a yield of 69.3%, which, upon chromatography on alumina, yielded a high melting isomer (VIIa) and a low melting isomer (VIIb) in a ratio of *ca.* 1.5: 1. The

* Present address, Faculty of Literature and Science, Toyama University, Gofuku, Toyama 930.

** Correspondence should be addressed to this author.

analytical and spectroscopic data, and the molecular weights determined by vapor osmometry were found to be identical. However, mixed melting point determination showed an appreciable depression. The isomerism can be reasonably attributed to *meso*- and *rac*-isomers. Recrystallization of the cyclic glycol (VIIa or VIIb) from acetone, methanol or ethyl acetate gave crystals containing solvent of crystallization in ratio of 1 : 1, 1 : 1 and 1 : 0.5, respectively. Formation of similar adducts has been reported for some 2,4-hexadiyne-1,6-diols and 2-butyne-1,4-diols.[11]

A solution of stannous chloride dihydrate in concentrated hydrochloric acid[12] was added to a vigorously stirred suspension of the cyclic glycol (VIIa or VIIb, or a mixture of them) at room temperature under nitrogen atmosphere. Instantaneous development of deep reddish color was observed. Chromatography of the product in benzene on alumina followed by elution with petroleum ether–benzene yielded a black purple crystalline powder, which gave black purple cubic crystals with metallic lustre upon recrystallization from benzene–petroleum ether (1 : 1) at a low temperature. The crystals gave a reddish purple solution similar to a permanganate solution. Full hydrogenation of the crystals in acetic acid over pre-reduced platinum oxide catalyst gave colorless crystals with low melting point. Absorption of 12.75 moles of hydrogen was observed (theoretical amount for the tetramethyltetrakisdehydro[18]-annulene is 13 moles). The elemental analysis, NMR spectrum and the appearance of molecular ion peak (M^+) at 308 in the mass spectrum provide the support that the low melting hydrocarbon should be tetramethylcycloctadecane (IX, Mol. wt., 308), thus suggesting the black purple crystals is the desired 1,5,10,14-tetramethyl-6,8,15,17-tetradehydro[18]annulene (VIII). The tetrakisdehydro[18]annulene (VIII) was found to be rather unstable compound. Exposure of crystals of VIII to air and diffused daylight at room temperature caused a complete decomposition in a few hours. But a solution of VIII in benzene–petroleum ether could be kept for two weeks without decomposition in a refrigerator.

The measurement of NMR spectrum of the tetrakisdehydro[18]annulene (VIII) was encoutered by some difficulties owing to the poor solubility. As illustrated in Fig. 1, the NMR spectrum in deuteriotetrahydrofuran exhibited signals at τ 0.34 (d, J=16.0 Hz) and τ 7.42 (s), which could be assigned to the outer and the methyl protons, respectively. Although, the presence of high field signal due to the inner protons was expected in view of the appearance of the outer proton signal at a fairly low field, only a weak signal could be scarcely observed at an extremely high field. Therefore, high field portion of spectrum was scanned 10 times and treated with C.A.T. technique clearly revealing the presence of signal of the inner protons at a extremely high field (τ 15.24, t, J=16.0 Hz). The NMR spectrum clearly indicates that the tetrakisdehydro[18]-annulene (VIII) containing formal diacetylene and hexapentaene units sustains a strong diamagnetic ring current. Also, the NMR spectral pattern of VIII suggests the equivalence of the outer protons. The electronic spectrum of VIII in tetrahydrofuran, consisting of three main absorption bands, shows features characteristic of [4n+2]annulenes (Fig. 2). Consequently, the tetrakisdehydro[18]annulene (VIII) can be regarded as an aromatic system with delocalized 18π-electrons being resonance hybrid of two equivalent Kekulé structures (VIII and VIII'). In the other words, the tetrakisdehydro[18]annulene (VIII) can be represented most properly by a symmetrical formula (VIII").

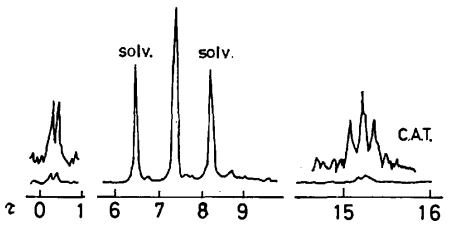

Fig. 1. 100 MHz NMR spectrum of VIII in THF-d_8.

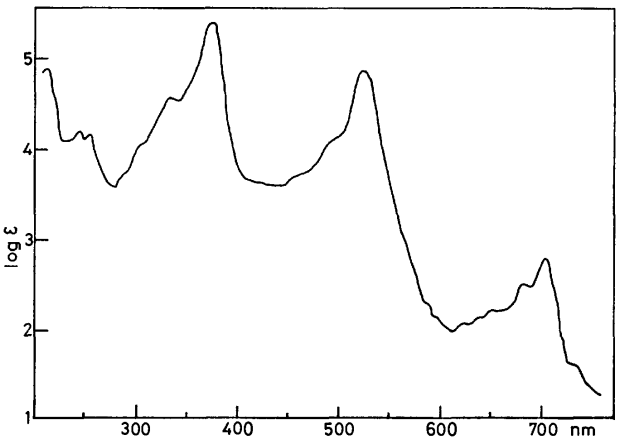

Fig. 2. Electronic spectrum of VIII in THF.

Table 1. NMR spectral parameters of VIII in THF-d_8 (100 MHz, τ-values)

Temperature °C	Outer protons d	Methyl protons s	Inner protons t
−60	0.10	6.65	15.66
−40	0.15	6.81	15.56
−20	0.19	6.98	15.49
0	0.27	7.20	15.38
22.5	0.34	7.42	15.23
40	0.41	7.60	15.09
64	0.44	7.78	14.99

As summarized in Table 1, the NMR spectra of VIII were found to be essentially temperature independent over a range of −60 to +64 °C, reflecting a high conformational stability of the tetrakisdehydro[18]annulene skelton provided by the presence of straight linkages of diacetylene and hexapentaene units. Attempts to

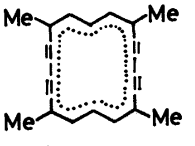

VIII"

measure the spectrum at higher temperatures than 64 °C were failed owing to a rapid decomposition of VIII. Increase of diatropicity along with decrease of temperature can be reasonably attributed to an increase of planarity of the 18-membered ring due to diminishing vibration of ring carbon atoms about their equilibrium positions.

The tetrakisdehydro[18]annulene (VIII) forms 1:1 CT complex with 2,4,7-trinitrofluorenone. Attempt to nitrate VIII with cupric nitrate in acetic anhydride[13,14] or with tetranitromethane in pyridine–methanol[15] or with silver nitrate and benzoyl chloride[16] gave fruitless results. Also, no substituted product could be obtained on treatment of VIII with acetic anhydride in the presence of boron trifluoride etherate under various reaction conditions. Because it has been found that substituent is introduced to the carbon atom adjacent to sp-hydridized carbon atoms in electropholic substitution reactions of dehydroannulenes,[14,17] at least one of the causes of the failure of electrophilic substitution seems to be attributable to the fact that the reactive sites in VIII are blocked by the methyl groups. VIII gave no adduct with maleic anhydride.

In view of the strong diatropicity and high conformational stability found in the tetrakisdehydro[18]annulene (VIII), dehydro-annulenes of this type seems to have the most adequate structure for the study of aromaticity of macrocyclic system.

Experimental

All experiments were performed under nitrogen atmosphere under shielding from light. A high dilution appratus was used for the oxidative cyclization reactions of acyclic glycols. The intermediates were stored usually as diluted solutions in a refigerator to minimize decomposition. All melting and boiling points are uncorrected. Brockmann alumina (Act. II—III) was for chromatography, unless otherwise stated. The IR, UV and mass spectra were obtained on a Hitachi EPI-2, a Hitachi EPS-3 and a Hitachi RMU-7HR spectrometers, respectively. Shoulders in UV spectra are indicated by sh, and strong, medium and weak bands in IR spectra are denoted by S, M, and W, respectively. NMR spectra were measured with a Varian A-60 and JNM-RA-I Spectral Accumlator. The chemical shifts are recorded in τ-values with respect to TMS as an internal standard, and the coupling constants are given in Hz. A Hitachi-Perkin Elmer 115 vapor osmometer was used for the measurements of molecular weights.

1-Chloro-3-methyl-1-penten-4-yn-3-ol (II). To an ice-cooled solution of ethynylmagnesium bromide in tetrahydrofuran (305 ml), prepared from magnesium 12.12 g (0.50 mol) and ethyl bromide 60 g (0.56 mol),[18] was added a solution of β-chlorovinyl methyl ketone (35.2 g, 0.34 mol)[4] in the same solvent (120 ml) over 1.5 hr-period. After the mixture had been stirred overnight at room temperature, saturated ammonium chloride solution was added to the mixture under cooling. The organic layer and ethereal extracts of the aqueous layer were combined, and worked up in the usual way. Dark red liquid thus obtained was distilled under reduced pressure in the presence of a small amount of hydroquinone. Ethynyl alcohol (II) was obtained as a colorless liquid, bp 63—68 °C/1596 Pa, 25—30 g (55—66%). In a run performed under similar conditions, II was obtained in 81% yield.

The reaction of β-chlorovinyl methyl ketone with sodium acetylide in liquid ammonia[5b] gave less satisfactory result.

3-Methyl-2-penten-4-ynal (III). Anionotropic rearrangement of II was carried out with diluted sulfuric acid by the reported method.[5b] The aldehyde (III) was obtained as a pale yellow liquid, bp 45.5—51 °C/1463 Pa, 38.8 g, 86%, NMR (60 MHz, CCl_4): 7.87 (d, J=2, 3H, CH_3), 6.37 (s, 1H, -C≡CH), 3.78 (dd, J=8 and 2, 1H, olefinic H), −0.3 (d, J=8, 1H, -CHO). Weak signals of the *trans*-isomer could be observed at 7.68 (d, J=2, CH_3) and 6.5 (s, -C≡CH). The ratio of *cis*- and *trans*-isomers was estimated to be 95:5 on the basis of the relative intensities of the methyl proton signals.

6-Methyl-3,5-octadien-7-yn-2-one (IV). Diene ketone (IV) was prepared by the reported method[5b] with considerable modification. An ice-cooled mixture of 2.6% aqueous sodium hydroxide (27 ml) and ethanol (27 ml) was added in a portion to a stirred and ice-cooled solution of the aldehyde (III, 11.25 g, 0.119 mol) in acetone (54 ml) under nitrogen atmosphere. After being stirred for 1 hr at the same temperature, the reaction was quenched with 1 M sulfuric acid (11 ml). A dark red liquid obtained from ether extracts was distilled in the presence of hydroquinone under reduced pressure to give dieneyne ketone (IV, bp 42—48 °C/4 Pa, light yellow liquid, 7.39 g, 47%, NMR (60 MHz, CCl_4): 7.79 (d, J=2, 3H, Me^a), 7.78 (s, 3H, Me^b), 6.52 (s, 1H, -C≡CH), 3.97 (d, J=15, 1H, olefinic H^3), 3.62 (dd, J=11 and 2, 1H, olefinic H^1), 2.58 (dd, J=15 and 11, 1H, olefinic H^2).

6,11-Dimethyl-3,5,11,13-hexadecatetraene-7,9-diyne-2,15-dione (V). A solution of the dieneyne ketone (IV, 4.8 g, 0.036 mol) in methanol (51 ml) was added over 40 min-period at room temperature to a homogeneous mixture of cupric acetate monohydrate (14.7 g, 0.074 mol), methanol (149 ml) and pyridine (149 ml). The reaction mixture, after being stirred for 3 hr at the same temperature, was poured into 1 M sulfuric acid (1600 ml) under ice-cooling. The mixture containing fine yellow crystals was extracted with ether, and the extracts were washed with water and dried over sodium sulfate. The most part of the solvent was removed under reduced pressure. Further concentration under ordinary pressure yielded fairly pure diketone (V) as pale yellow crystals (4.734 g, 98.7%). The crystals were recrystallized 4 times from methanol to give an analytical specimen, mp 94—95 °C, IR (KBr-disk): 1650—1690 (triplet, C=O), 1590 (*trans* C=C), 980 (*cis* C=C) cm^{-1}, UV: λ_{max}^{EtOH} 248 sh (12700), 260 (17900), 298 (27500), 346 sh (30600), 364 (30900), 388 (24500), NMR (60 MHz, CCl_4): 7.92 (d, J=2, 6H, Me^a), 7.75 (s, 6H, Me^b), 3.97 (d, J=15, 2H, olefinic H^3), 3.45 (dd, J=11 and 2, 2H, olefinic H^1), 2.64 (dd, J=15 and 11, 2H, olefinic H^2).

Found: C, 81.27; H, 6.83%. Calcd for $C_{18}H_{18}O_2$: C, 81.17; H, 6.81%.

3,7,12,16-Tetramethyl-4,6,12,14-octadecatetraene-1,8,10,17-tetrayne-3,16-diol (VI). To a mixture of lithium acetylide-ethylenediamine complex[10] (6.5 g, 0.07 mol) and tetrahydrofuran (100 ml) saturated with acetylene was added at 35 °C a solution of the diketone (V, 3.1 g, 0.012 mol) in the same solvent (35 ml) over a period of 40 min under stirring and bubbling with acetylene. After the mixture had been stirred vigorously for further 3 hr at 30 °C under slow introduction of acetylene, cold water (30 ml) and saturated sodium chloride solution were added successively to the reaction mixture at 10 °C. The organic layer obtained by salting-out the mixture with sodium chloride was combined with ethereal extracts of the aqueous layer, and washed successively with 2 M hydrochloric acid (2 times), water (3 times) and saturated sodium chloride solution (3 times). The solvent was removed, after being dried over sodium sulfate, under reduced pressure to give a dark red liquid. The liquid dissolved in benzene was absorbed on alumina (Woelm, Grade I, 90 g) and eluted with

solvents with increasing polarity. The fractions eluted with benzene–ether–methanol gave bis-ethynyl diol, yellow viscous liquid, 2.32 g (63%). The bis-ethynylation was repeated in nearly the same scale as described above, and total 17 g of the diketone was converted into crude product. The crude product was chromatographed on alumina (Brockmann Act. I, 600 g). A mixture of starting material (V) and mono-ethynylated product was obtained from benzene–ether (19: 1—3: 2) eluates (1.296 g). Following fractions eluted with benzene–ether (3: 2—2: 3) yielded monoethynylated product (1.303 g). Elution with benzene–ether (2: 3) and ether–ethyl acetate (3: 2) gave desired VI (9.503 g). Although all attempts to crystallize VI were failed, the IR (neat): 3370 (broad, OH), 3330 (-C≡CH), 2190, 2050 (-C≡C-), 960 (*trans* C=C) cm^{-1}, NMR (60 MHz, CCl_4): 8.46 (s, 6H, Me^b), 8.05 (d, J=2, 6H, Me^a), 7.46 (s, 2H, -C≡CH), 6.90 (broad, 2H, OH, disappeared on addition of D_2O), 4.20 (d, J=15, 2H, H^3), 3.70 (dd, J=11 and 2, 2H, H^1), 3.07 (dd, J=15 and 11, 2H, H^2) and UV: λ_{max}^{MeOH} 232 sh, 239 sh, 253, 262, 276, 291, 308, 312, 336, 359 were found to be consistent with the assigned structure.

1,6,10,15-Tetramethyl-7,9,15,17-cyclooctadecatetraene-2, 4, 11,13-tetrayne-1,6-diol (VII). A solution of the acyclic glycol (VI, 2.003 g, 0.0063 mol) in ether (70 ml), methanol (70 ml) and pyridine (280 ml) was added over 9.5 hr-period to a stirred and refluxing mixture of cupric acetate monohydrate (5.04 g, 0.025 mol), pyridine (2000 ml) and ether (400 ml). After being refluxed for further 1 hr, the mixture was allowed to stand overnight at room temperature. The reaction mixture was concentrated to 200 ml under pressure on a water-bath kept below 50 °C. The concentrate was chilled and poured into 1M hydrochloric acid (2500 ml) under ice-cooling over 30 min-period. The mixture was extracted 5 times with ether, and the extracts were washed with saturated sodium chloride solution and dried over sodium sulfate. Dark brown oily residue obtained by evaporation of the extracts under reduced pressure below 25 °C was dissolved in benzene and chromatographed on alumina (500 g). Elution with ether–ethyl acetate (9: 1—1: 1) yielded a diastereomeric mixture of the cyclic glycol (VII, 1.376 g, 69.3%). The mixture of VII was chromatographed on alumina and careful elution with solvents with increasing polarity resulted in separation of diastereomers. Fractions eluted with ether–ethyl acetate (9: 1—3: 2) yielded a high melting isomer (VIIa, colorless cubes (from dichloromethane), mp 228—230 °C (dec.), IR (KBr-disk): 3360 (singlet, OH), 2190, 2150 (-C≡C-), 968 (*trans* C=C) cm^{-1}, UV: λ_{max}^{EtOH} 245 sh (28600), 254 (49400), 263.5 (61400), 292 (5120), 308 sh (6570), 327 (11600), 344 (18800), 368 (20100).

Found: C, 83.17; H, 6.22%, Mol. wt., 325 (vapor osmometry). Calcd for $C_{22}H_{20}O_2$: C, 83.51; H, 6.37%, Mol. wt., 316.

When VIIa was recrystallized from methanol, crystals containing 1 mol of methanol were obtained. Removal of the solvent of crystallization was found to be difficult even upon heating to 70 °C *in vacuo* for 39 hr.

Further elution with ether–ethyl acetate (1: 1) and ethyl acetate gave a low melting isomer (VIIb, colorless cubes (from dichloromethane), mp 220—223 °C (dec.), IR (KBr-disk): 3330, 3270 (doublet, OH), 2190, 2150 (-C≡C-), 972 (*trans* (C=C) cm^{-1}, UV: λ_{max}^{EtOH} 246 sh (27700), 254 (49500), 263 (63500), 292 (3330), 307 sh (5110), 326 (10500), 344 (17600), 369 (19300), NMR (60 MHz, DMSO-d_6): 8.53 (s, 6H, Me^b), 8.07 (d, J=2, 6H, Me^a), 6.67 (broad, 2H, disappeared on addition of D_2O), 4.07 (d, J=15, 2H, H^3), 3.34 (dd, J=11 and 2, 2H, H^1), 2.98 (dd, J=15 and 11, 2H, H^2).

Found: C, 83.61; H, 6.38%, Mol. wt., 312 (vapor osmometry). Calcd for $C_{22}H_{20}O_2$: C, 83.51; H, 6.37%, Mol. wt., 316.

VIIb forms crystals containing 1 mol of acetone and 1/2 mol of ethyl acetate. The acetone could be removed upon heating the crystals to 70 °C *in vacuo* for 23 hr.

Melting point of *ca.* 1: 1 mixture of VIIa and VIIb (203—210 °C) showed an appreciable depression.

1,5,10,14-Tetramethyl-6,8,15,17-tetrakisdehydro[18]annulene (VIII). To a vigorously stirred suspension of a diastereomeric mixture of VII (154 mg, 4.87×10^{-4} mol) in pentane (6 ml) and benzene (3 ml) was added at room temperature under nitrogen atmosphere a solution of stannous chloride dihydrate (270 mg, 1.19×10^{-3} mol) in concentrated hydrochloric acid (3 ml). After 10 min, benzene (15 ml) was added in 3 ml portions over 25 min-period. The reddish purple reaction mixture was poured into water (50 ml), and the organic layer was separated. The aqueous layer was extracted 4 times with ether. The combined organic layer and extracts, after being washed successively with water, aqueous sodium hydrogencarbonate and dried over magnesium sulfate for 3 hr, was concentrated to 50 ml under reduced pressure below 18 °C. Benzene was added to the concentrate and again concentrated under reduced pressure to give a benzene solution of the product (30 ml). The benzene solution thus obtained was passed through a column of alumina (50 g). Elution with benzene–petroleum ether gave VIII as a black purple crystalline powder (77 mg, 56%). Cyclic glycol (VII, 20 mg) was recovered from ether–ethyl acetate eluates. A solution of crude VIII in benzene–petroleum ether (1: 1) was kept in a refrigerator (−14 °C) to give pure VIII as black purple cubes with metallic lustre, which showed no melting point, but underwent color change to yellowish brown at *ca.* 180 °C, IR (KBr-disk): 2940 (M), 2910 (S), 2840 (M), 1535 (W), 1495 (W), 1485 (M, broad), 1365 (M), 1350 (M), 1277(M), 1265(W), 1150 (W), 1020(W), 953 (S), 880 (W, broad) cm^{-1}, UV: λ_{max}^{THF} 217.5 (78000), 237 (15200), 248.5 (14700), 259 sh (5150), 266 sh (4120), 272 sh (3670), 290 sh (4810), 306 sh (10400), 334.5 (35100), 371 (228000), 440 sh (2160), 452 (3230), 490 (11400), 520.5 (74200), 582 sh (185), 596 (124), 622 (121), 639 sh (129), 652 (164), 682 (318), 705 (614), 740 sh (37), NMR (60 MHz, CH_3, s): 6.37 (CCl_4), 6.73 (C_6D_6), 6.79 (DMSO-d_6).

Found: C, 93.56; H, 6.40%. Calcd for $C_{22}H_{18}$: C, 93.57; H, 6.43%.

The high and low melting isomers (VIIa and VIIb) gave VIII in almost the same yields as the case of diastereomeric mixture.

A solution of pure VIII could be kept for 2 weeks without any change under shielding from light at −14 °C, but as shown in Table 2, at room temperature, decrease of relative absorption intensity (ε_r) of the maximum at 520.5 nm of a solution of VIII in THF (15 mg/l) along with the elapse of time was observed.

Table 2. Decrease of relative absorption intensity

Time (day)	0	1	16	39	79
ε_r	1.00	0.89	0.83	0.61	0.06

Tetramethylcyclooctadecane (IX). VIII (16.618 mg, 5.885×10^{-3} mol) in acetic acid (10 ml) was reduced over pre-reduced platinum oxide catalyst ($PtO_2\cdot2H_2O$, 69.5 mg). Absorption of hydrogen ceased after 3.5 hr (12.75 mol, theoretical value, 13 mol). A solution of the reduction product in pentane was chromatographed on alumina, and eluted with pentane. The eluates were concentrated under reduced pressure to give colorless liquid, which was dissolved in ethyl

acetate–methanol (15:8). Crystals deposited on strong cooling of the solution were recrystallized from the same solvent to yield tetramethylcyclooctadecane (IX), colorless low melting crystals, IR (neat): 2950 (S), 2925 (S), 1460 (M), 1380 (M), 725 (W) cm^{-1}, NMR (60 MHz, CCl_4): 9.15 (CH_3), 8.73 (CH_2), 8.20 (CH).

Found: C, 85.60; H, 14.02%, M^+ 308. Calcd for $C_{22}H_{44}$: C, 85.63; H, 14.37%, Mol. wt., 308.

CT Complex of VIII with Trinitrofluorenone. A mixture of VIII (53 mg, 0.187 mmol), 2,4,7-trinitrofluorenone (80 mg, 0.253 mmol), benzene (4 ml) and methanol (3 ml) was refluxed for 5 min to give a homogeneous solution. The solution was kept at 0 °C overnight. Black purple needles deposited were collected and washed successively with petroleum ether and benzene to give pure 1: 1 CT complex, which decomposed at 210 °C forming a grey material.

Found: C, 69.46; H, 3.86; N, 7.14%. Calcd for $C_{35}H_{23}N_3O_7$: C, 70.34; H, 3.88; N, 7.03%.

The author wish to thank Dr. K. Hatada and Mr. Y. Terawaki of the Faculty of Scientific Engineering, Osaka University for the measurements of 100 MHz NMR spectra.

References

1) The trivial nomenclature of dehydroannulenes recently proposed by T. M. Cresp and F. Sondheimer (*J. Amer. Chem. Soc.*, **97**, 4412 (1975), *cf.*, P. J. Garatt and K. Grohmann, "Houben-Weyl, Methoden der Organischen Chemie," Vol. V, Part 1d, Georg Thieme Verlag, Stuttgart, (1972), p. 527) will be used in this series of papers.

2) F. Sondheimer and Y. Gaoni, *J. Amer. Chem. Soc.*, **82**, 5765 (1960); F. Sondheimer, Y. Gaoni, L. M. Jackman, N. A. Bailey, and R. Mason, *ibid.*, **84**, 4595 (1962).

3) For a preliminary report, see, J. Ojima, T. Katakami, G. Nakaminami, and M. Nakagawa, *Tetrahedron Lett.*, **1968**, 1115.

4) *cf.*, C. C. Price and J. A. Pappalardo, "Organic Syntheses," **32**, 27 (1954).

5) a) E. R. H. Jones and B. C. L. Weedon, *J. Chem. Soc.*, **1946**, 937. b) I. Heilbrom, E. R. H. Jones, and M. Julia, *ibid.*, **1949**, 1430.

6) E. E. Boehm, V. Thaller, and M. C. Whiting, *J. Chem. Soc.*, **1963**, 2535.

7) G. Eglinton and A. R. Galbraith, *Chem. Ind.*, **1956**, 737; *idem.*, *J. Chem. Soc.*, **1959**, 889.

8) W. Oroshnick and A. D. Mebane, *J. Amer. Chem. Soc.*, **71**, 2062 (1944).

9) B. Görlich and G. Hildebrandt, *Chem. Ber.*, **91**, 2388 (1958).

10) D. F. Beumel, Jr. and R. F. Harris, *J. Org. Chem.*, **28**, 2775 (1963); *ibid.*, **29**, 1872 (1964).

11) F. Toda and K. Akagi, *Tetrahedron Lett.*, **1968**, 3695.

12) R. Kuhn and H. Krauch, *Chem. Ber.*, **88**, 309 (1955); M. Morimoto, S. Akiyama, S. Misumi, and M. Nakagawa, This Bulletin, **35**, 857 (1962); S. Misumi, *ibid.*, **34**, 1827 (1961).

13) A. G. Anderson, Jr., J. A. Nelson, and J. J. Tazuma, *J. Amer. Chem. Soc.*, **75**, 4980 (1953).

14) I. C. Calder, P. J. Garratt, H. C. Longuet-Higgins, R. Wolovsky, and F. Sondheimer, *J. Chem. Soc., C*, **1967**, 1041.

15) I. M. Aitkin and D. H. Reid. *J. Chem. Soc.*, **1956**, 3487.

16) D. J. Cram and R. D. Parts, *J. Amer. Chem. Soc.*, **85**, 1273 (1963).

17) Y. Gaoni and F. Sondheimer, *J. Amer. Chem. Soc.*, **86**, 521 (1964).

18) E. R. H. Jones, L. Skatteböl, and M. C. Whiting, *J. Chem. Soc.*, **1956**, 4765; L. Skatteböl, E. R. H. Jones, and M. C. Whiting, "Organic Syntheses," Coll. Vol. IV, p. 792 (1963).

Dehydroannulenes. II. Syntheses of Diatropic Dimethyldiphenyl- and Tetraphenyl-tetrakisdehydro[18]annulenes

Tsutomu KATAKAMI, Kunisuke FUKUI, Tetsuhiko OKAMOTO, and Masazumi NAKAGAWA*

Department of Chemistry, Faculty of Science, Osaka University, Toyonaka, Osaka 560

(Received August 18, 1975)

Syntheses of dimethyldiphenyl-(VI and XII) and tetraphenyltetrakisdehydro[18]annulenes (XVII) have been performed. It was found that the reaction sequence used for the synthesis of tetramethyltetrakisdehydro[18]-annulene can be used generally for the preparation of tetrakisdehydro[18]annulenes having various substituents. The annulenes (VI, XII, and XVII) were found to be strongly diatropic having high conformational stability. Remarkable stability is provided by introduction of phenyl groups accompanied with decrease in solubility of the annulene. Dimethyldiphenyl derivative was prepared by two different routes which will lead to isomers (VI and XII) with respect to the relative positions of the diacetylene and hexapentaene linkages to the substituent groups. The isomers (VI and XII) can be regarded as presumably identical, but precise agreement of NMR and UV spectra could not be attained. Bathochromic shift of UV spectra of phenyl substituted annulenes compared with tetramethyl analogue indicated that phenyl groups exert prominent perturbation on the annulene system.

As reported in the previous papers,[1] tetramethyltetrakisdehydro[18]annulene showed a strong diastropicity and a high conformational stability, but was found to be rather unstable. Therefore, the syntheses of tetradehydro[18]annulenes having various substituent groups are considerable interest from various points of view. Firstly, the preparation should offer information on the scope of validity of the reaction sequence used for the synthesis of tetramethyl derivative.[1] Secondly, it can be expected to find out substituent which stabilizes the tetradehydro[18]annulene system making possible further investigation on this type of dehydroannulenes. Finally, information on conjugative effects between the annulene ring and substituent group will be obtained from these studies.

The present paper deals with the synthesis and properties of dimethyldiphenyl- (VI, XII) and tetraphenyltetrakisdehydro[18]annulenes (XVIII).[2]

Synthesis. Synthesis of dimethyldiphenyltetrakisdehydro[18]annulene was performed according to two different route outlined in Scheme.

Dieneyne ketone (II) was obtained by the aldol condensation of 3-methyl-2-penten-4-ynal (I)[1,3] with acetophenone by the reported method[3b] with modification. Oxidative coupling of the ketone (II) by cupric acetate in pyridine–methanol[4] gave sparlingly soluble diketone (III) as yellow crystals. A solution of the diketone (III) in hot benzene was added to a suspension of lithium acetylide–ethylenediamine complex[5] in the same solvent saturated with acetylene to give acyclic glycol (IV). 18-Membered cyclic glycol (V) was obtained as a viscous yellow liquid by the oxidative coupling of IV under high dilution conditions. Treatment of the cyclic glycol (V) with stannous chloride in concentrated hydrochloric acid yielded 5,10-dimethyl-1,14-diphenyl-6,8,-15,17-tetrakisdehydro[18]annulene (VI) as black purple needles in an almost quantitative yield. Full hydrogenation of VI in ethyl acetate over platinum oxide catalyst yielded a liquid hydrocarbon corresponding to dimethyldiphenylcyclooctadecane.

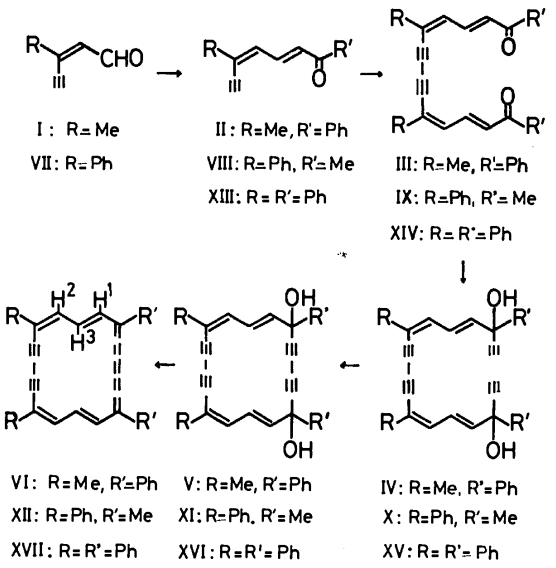

β-Chlorovinyl ketone was prepared by the reported method[6] with modification, which was converted into 1-chloro-3-phenyl-1-penten-4-yn-3-ol in a high yield on treatment with sodium acetylide in liquid ammonia. Anionotropic rearrangement of the alcohol by acid treatment yielded 3-phenyl-2-penten-4-ynal (VII). NMR spectrometry reveals that the aldehyde (VII) is pure *cis*-isomer with respect to the formyl and ethynyl groups. Diene ketone (VIII) obtained by the aldol condensation of VII with acetone was oxidatively coupled by cupric acetate in pyridine[4] to give diketone (IX). Bis-ethynyl alcohol (X) prepared by the reaction of lithium acetylide–ethylenediamine complex[5] with IX yielded cyclic glycol (XI) on treatment with cupric acetate in pyridine–methanol–ether under high dilution conditions. Reduction of the crude cyclic glycol (XI) with stannous chloride dihydrate in concentrated hydrochloric acid gave 9,10-dimethyl-1,14-diphenyl-6,8,15,-17-tetrakisdehydro[18]annulene (XII) as black purple crystals.

The aldol condensation of acetophenone with VII gave diphenyldiene ketone (XIII) in a high yield. The ketone (XIII) was converted into 1,5,10,14-tetraphenyl-6,8,15,17-tetrakisdehydro[18]annulene (XVII, black purple needles) by similar reaction sequence *via* diketone (IXV), acyclic glycol (XV) and cyclic glycol (XVI).

* The author to whom correspondence should be addressed.

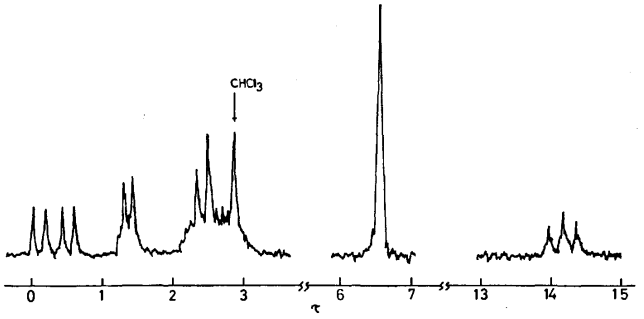

Fig. 1. 60 MHz NMR spectrum of VI in $CDCl_3$.

Properties. The NMR spectrum indicates that 1,14-dimethyl-5,10-diphenyl-6,8,15,17-tetrakisdehydro-[18]annulene (VI) is strongly diatropic exhibiting the inner proton (H^3) signal at extremely high-field (t, τ 14.20) and the outer proton (H^1 and H^2) signals at low-field (H^1, d, τ 0.12; H^2, d, τ 0.54) (Fig. 1). A low-field multiplet (τ 1.36) in the aromatic region could be assigned to *o*-protons of the phenyl groups, which suffer the deshielding effect of diamagnetic ring current of the annulene ring, and the higher-field multiplet at *ca.* τ 2.5 to the *m,p*-protons of the phenyl groups. The signal of methyl protons observed at τ 6.56 as a sharp singlet. As recorded in Table 1, VI showed essentially temperature independent NMR spectra similar to the tetramethyl analogue[1] indicating a high conformational stability of the tetrakisdehydro[18]annulene skelton. The electronic spectrum of VI illustrated in Fig. 2 showed characteristic feature of [4*n*+2]annulenes consisting of three main absorption band.

The dimethyldiphenyltetrakisdehydro[18]annulene (XII) gave an identical IR spectrum with that of VI. However, perfect coincidence of NMR and electronic spectra between VI and XII could not be attained, presumably owing to their instability, and to slight difference in their purity. In spite of the minor difference in physical property, the tetrakisdehydro[18]-annulenes (VI and XII) seemed to be an identical compound.[7]

TABLE 1. NMR PARAMETERS OF VI IN $CDCl_3$
(τ-Values, 100 MHz)

Temperature (°C)	H^1	H^2	*o*-H of phenyl	Methyl-H	H^3
−60	−0.08	0.40	1.18	6.45	14.61
−40	−0.13	0.34	1.17	6.45	14.45
−20	−0.09	0.34	1.20	6.47	14.41
− 6	−0.06	0.40	1.23	6.51	14.35
+25	0.00	0.46	1.26	6.53	14.27
+37	−0.02	0.44	1.29	6.51	14.14
+61	0.01	0.46	1.30	6.53	14.00

Tetraphenyltetrakisdehydro[18]annulene (XVIII) also showed an aromatic NMR spectrum exhibiting the inner proton (H^3) signal at τ 13.19 (t) and the outer proton (H^1 and H^2) signal at τ-0.31 (d). It is to be noted that the replacement of methyl with phenyl groups causes an appreciable down-field shift of all signals (Fig. 3).[8]

The stability of tetrasubstituted tetrakisdehydro[18]-annulenes was found to increase with the increase of phenyl substitution in the sequence of tetramethyl-<dimethyldiphenyl- (VI or XII)<tetraphenyl-derivatives (XVIII). However, as can be seen from Fig. 2, phenyl substitution caused remarkable bathochromic shift of absorption bands and intensification of the longest wavelength band indicating the perturbation of phenyl group on the annulene system. Furthermore, poor solubility of the tetraphenyl derivative (XVIII) in NMR solvents brought about experimental difficulty. In spite of the fairly effectual stabilization effect, phenyl group, aside from its interesting conjugative effect, can not be regarded as the most adequate substituent for the study of aromaticity of annulene system.

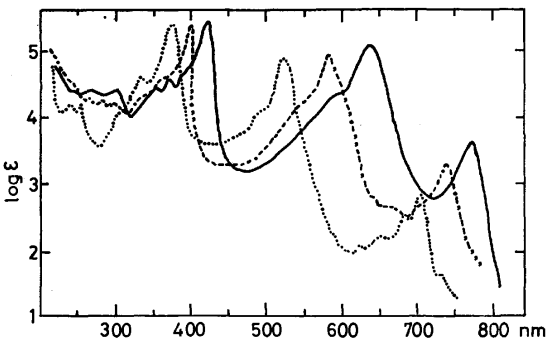

Fig. 2. Electronic spectra of tetrasubstituted tetrakisdehydro[18]annulenes. VI (---), XVII (—) and the tetramethyl analogue (···) in THF.

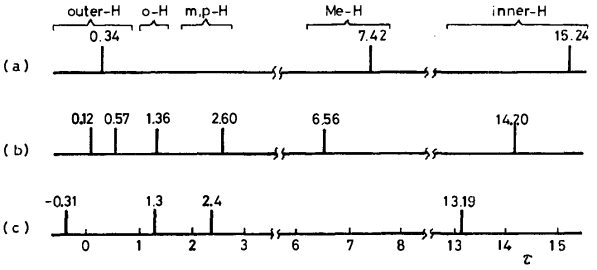

Fig. 3. Chemical shifts of tetrasubstituted tetrakisdehydro [18]annulenes. (a) tetramethyl-, (b) dimethyldiphenyl- (VI), and (c) tetraphenyl- (XVII) derivatives.

Experimental

All melting and boiling points are uncorrected. Brockmann alumina (Act. II—III) was used for chromatography. Evaporation of solvent was performed under reduced pressure in nitrogen atmosphere under shielding from light. A high dilution apparatus was used for the oxidative cyclization reaction of acyclic glycols. The IR, UV and mass spectra were obtained on a Hitachi EPI-2, a Hitachi EPS-3 and a Hitachi RMU-7HR spectrometers, respectively. Shoulder in UV spectrum is denoted by sh, and wavelength of absorption maximum is recorded in nm and ε-value is given in parentheses. NMR spectra were obtained on a Varian A-60 and JNM-4H-100 spectrometers. Chemical shift and coupling constant are given in τ-value with respect to TMS as an internal standard and in Hz, respectively.

1-Benzoyl-4-methyl-1,3-hexadien-5-yne (II). To a water-cooled and stirred mixture of I (2.04 g, 0.0217 mol)[1,3] and acetophenone (2.50 g, 0.0208 mol) was added dropwise a

mixture of 20% aqueous sodium hydroxide (8 ml) and ethanol (4 ml). After being stirred for 15 min, 1M sulfuric acid (30 ml) was added to the reaction mixture, and extracted with ether. The ethereal extracts were worked up in the usual way. The product dissolved in benzene was chromatographed on alumina, and eluted with the same solvent to give II, pale yellow rods, mp 83—87 °C (lit, 86—88 °C),[3b] 1.751 g (40%), IR (Nujol): 3230, 2090, 1655, 1590, 1575, 1360, 1280, 890, 770 cm^{-1}.

1,12-Dibenzoyl-4,9-dimethyl-1,3,9,11-dodecatetraene-5,7-diyne (III). A solution of II (2.23 g, 0.0114 mol) in benzene (50 ml) and methanol (30 ml) was added to a stirred solution of cupric acetate monohydrate (4.5 g) in pyridine (150 ml) and methanol (150 ml). The mixture containing yellow crystals was stirred overnight at room temperature. After the reaction mixture had been concentrated, the insoluble material was collected by filtration and washed throughly with water. The material thus obtained was dried and dissolved in boiling benzene. The hot benzene solution was passed through a short column of alumina. Upon cooling the filtrate, III was obtained as sparingly soluble yellow needles, mp *ca.* 150 °C (dec.), 1.33 g (60%), IR (KBr-disk): 3042, 3002, 1655, 1597, 1585, 1573, 1445, 1432, 1355, 1272, 1220, 1185, 1033, 1020, 980, 903, 853, 840, 774, 688, 658 cm.$^{-1}$

Found: C, 86.29; H, 5.88%. Calcd for $C_{28}H_{22}O_2$: C, 86.12; H, 5.68%.

7,12-Dimethyl-3,16-diphenyl-4,6,12,14-octadecatetraene-1,8,10,17-tetrayne-3,16-diol (IV). A solution of III (1.20 g, 0.00307 mol) in hot benzene (2000 ml) was added over 1.5 hr-period to a stirred suspension of lithium acetylide–ethylenediamine complex (10 g) in the same solvent (200 ml) saturated with acetylene at 35 °C. After acetylene had been introduced for further 3.5 hr at 35—38 °C, the reaction mixture was cooled to 5—7 °C, and water (50 ml) was added. The mixture was worked up in the usual manner. The product dissolved in benzene was chromatographed on alumina (40 g). Fractions obtained by elution with benzene and ethyl acetate, which showed satisfactory IR spectra, were combined and rechromatographed on alumina (10 g). IV was obtained as an amorphous yellow solid, 0.90 g (67%), IR (KBr-disk): 3500, 3350, 3260, 3050, 3020, 2920, 2850, 2190, 2110, 1600, 1580, 1470, 1445, 1370, 1345, 1280, 1170, 1070, 1030, 1015, 1000, 970, 930, 760, 690, 670 cm^{-1}.

Attempts to crystallized this material were failed.

10,15-Dimethyl-1,6-diphenyl-7,9,15,17-cyclooctadecatetraene-2,4,11,13-tetrayne-1,6-diol (V). To a stirred and refluxing solution of cupric acetate monohydrate (1.63 g) in pyridine (2000 ml), methanol (500 ml) and ether (500 ml) was added at 70±3 °C a solution of acyclic glycol (IV, 0.90 g, 2.05mmol) in pyridine (300 ml), methanol (100 ml) and ether (100 ml) over a period of 18 hr. After being stirred for further 1.5 hr at the same temperature, the reaction mixture was concentrated to *ca.* 100 ml at 40±2 °C. The concentrate was poured into 1M hydrochloric acid (3600 ml) under ice-cooling, and extracted with benzene and ethyl acetate. Combined extracts were worked up in the usual way. The product dissolved in benzene was chromatographed on alumina (150 g). Elution with ethyl acetate–benzene gave V as partly crystallized liquid, 242 mg (26.8%), IR (neat): 3300, 2180, 1600, 1580, 1480, 1450, 1035, 970, 760, 695, 670 cm^{-1}.

This material was used directly for the following reaction.

5,10-Dimethyl-1,14-diphenyl-6,8,15,17-tetrakisdehydro[18]annulene (VI). A solution of stannous chloride dihydrate (143.4 mg, 0.0637 mmol) in concentrated hydrochloric acid (3 ml) was added to a stirred suspension of the cyclic glycol (V, 113.7 mg, 0.0258 mmol) in pentane (10 ml) and benzene (5 ml). After being stirred for 10 min, benzene (10 ml) was added to the reaction mixture. After 20 min, ether (30 ml) and water were added to the mixture, and organic layer was treated in the usual fashion. The product dissolved in benzene was chromatographed on alumina (20 g). Elution with the same solvent yielded VI, black purple needles, 102.0 mg (97%), which was recrystallized from petroleum ether–benzene to give analytical specimen of VI, decomposed at 94 °C without fusion, UV: λ_{max}^{THF} 244 (16700), 249.5 (15800), 255.5 (18400), 261 sh (15600), 270 sh (15400), 278 (17600), 298 (13800), 299 (14200), 325 sh (14800), 348 sh (29300), 354 sh (30200), 370 sh (38200), 384 sh (61400), 400 (21800), 544 sh (17900), 584 (88900), 650 sh (738), 670 (443), 715 sh (560), 742 (1930), NMR (60 MHz, $CDCl_3$): 0.12 (d, J=14, H^1), 0.54 (d, J=14, H^2), 1.36 (m, *o*-H of phenyl), 2.3—2.9 (m. *m,p*-H of phenyl), 6.56 (s, CH_3), 14.20 (t, H^3).

Found: C, 94.23; H, 5.61%. Calcd for $C_{32}H_{22}$: C, 94.54; H, 5.46%.

1,6-Dimethyl-10,15-diphenylcyclooctadecane. The annulene (VI, 16.9 mg) in ethyl acetate (15 ml) was reduced over pre-reduced platinum oxide catalyst ($PtO_2 \cdot 2H_2O$, 12.6 mg). The reduction product was chromatographed on alumina and eluted with pentane. Dimethyldiphenylcyclooctadecane was obtained as a colorless liquid, M^+ 432 (Calcd for $C_{32}H_{48}$: 432), IR (neat): 3040, 3010, 2950—2850, 1455, 1375, 1600, 1493, 757, 695 cm^{-1}.

β-Chlorovinyl Phenyl Ketone. To an ice-cooled solution of benzoyl chloride (37 g, 0.264 mol) in chloroform (80 ml) was added crashed anhydrous aluminum chloride (37 g, 0.278 mol) in a rate to keep the temperature below 10 °C. Vinyl chloride was introduced to the mixture below 20 °C until no more absorption could be observed (*ca.* 3 hr). The reaction mixture was poured onto ice (300 g).[6] The organic layer was separated and the aqueous layer was extracted with chloroform. The combined organic layer and extracts were worked up in the usual way. Distillation of the product under reduced pressure yielded β-chlorovinyl phenyl ketone in a high yield under elimination of hydrogen chloride, bp 134—136 °C/2395 Pa, 36.2 g (83%).

1-Chloro-3-phenyl-1-penten-4-yn-3-ol. 1) To a solution of ethynylmagnesium bromide in tetrahydrofuran (120 ml) prepared from ethyl bromide (12 g, 0.11 mol) and magnesium (2.4 g, 0.10 mol)[9] was added over 20 min-period a solution of β-chlorovinyl phenyl ketone (11.0 g, 0.066 mol) in the same solvent (15 ml). After being stirred overnight at room temperature, saturated aqueous ammonium chloride solution was added to the reaction mixture under cooling in an ice-salt bath. The aqueous layer was extracted with ether and combined with the organic layer. The organic solution was worked up in the usual manner, and the crude product was distilled under reduced pressure to give pure ethynyl alcohol, bp 118—119 °C/465.5 Pa, 8.3 g (63%). Explosive decomposition sometimes occurred at the final stage of distillation. 2) A solution of β-chlorovinyl phenyl ketone (87.1 g, 0.523 mol) in tetrahydrofuran (270 ml) was added over 40 min-period at −60 °C to a stirred solution of lithium acetylide (from lithium, 4.1 g, 0.587 mol) in liquid ammonia (600 ml). After the mixture had been stirred overnight at −60∼−30 °C, the ammonia was allowed to evaporate. Saturated ammonium chloride solution was added to the residue under strong cooling with ice-salt bath. The aqueous layer was extracted with ether, and combined with the organic layer. The product, obtained by working up the organic solution in the usual way, was distilled under reduced pressure to give pure alcohol, bp 92—97 °C/66.5 Pa, 77.5 g (77%).

3-Phenyl-2-penten-4-ynal (VII). A mixture of 1-chloro-3-phenyl-1-penten-4-yn-3-ol (77.5 g, 0.403 mol), tetrahydrofuran (300 ml) and 1M sulfuric acid (1800 ml) was stirred

under nitrogen atmosphere for 3 days at room temperature. Sodium chloride was added to the reaction mixture, and the aqueous layer was extracted with ether. The extracts combined with the organic layer was worked up in the usual way. The crude crystals deposited on concentration of the organic solution were recrystallized from carbon tetrachloride–cyclohexane (2: 1) to give pure VII, unstable crystals, mp *ca.* 65 °C, 38.2 g (61%), NMR (60 MHz, CCl_4): 6.25 (s, 1H, ethynyl H), 3.20 (d, J=7, 1H, olefinic H), 2.50 (m, 3H, *m, p*–H of phenyl), 2.15 (m, 2H, *o*–H of phenyl), −0.25 (d, J=7, formyl H). NMR spectrum indicates that VII thus prepared is pure *cis*–isomer with respect to the formyl and ethynyl groups.

Found: C, 84.39; H, 5.23%. Calcd for $C_{11}H_8O$: C, 84.54; H, 5.16%.

2,4-Dinitrophenylhydrazone: orange needles, mp 177—178 °C.

Found: C, 60.71; H, 3.59; N, 16.70%. Calcd for $C_{17}H_{12}N_4O_4$: C, 60.71; H, 3.60; N, 16.66%.

6-Phenyl-3,5-octadien-7-yn-2-one (VIII). A solution of sodium hydroxide (0.70 g, 17.5 mmol) in ethanol (4 ml) and water (4 ml) was added to an ice-cooled solution of VII (2.70 g, 17.3 mmol) in acetone (28 ml). After being stirred for 2 hr at the same temperature, the reaction mixture was neutralized with 1M hydrochloric acid and mixed with water (300 ml). The mixture was extracted with benzene. After working up in the usual way, the product dissolved in carbon tetrachloride was passed through a column of alumina. The crystals obtained from the filtrate (1.16 g, 47%) were dissolved in the same solvent and again passed through a column of alumina. Pure VIII was obtained by recrystallization from ethanol, yellow crystals, mp 70.0—72.0 °C, IR (KBr–disk): 3250, 2080, 1662, 985, 953 $cm.^{-1}$

Found: C, 85.32; H, 6.06%. Calcd for $C_{14}H_{12}O$: C, 85.68 H, 6.10%.

2,4-Dinitrophenylhydrazone: mp 180—190 °C (dec.).

Found: C, 64.13; H, 4.92; N, 14.84%. Calcd for $C_{20}H_{16}N_4O_4$: C, 63.82; H, 4.29; N, 14.89%.

6,11-Diphenyl-3,5,11,13-hexadecatetraen-7,9-diyn-2,15-dione (IX). A mixture of VIII (1.00 g, 5.10 mmol), cupric acetate monohydrate (5.0 g), pyridine (25 ml) and methanol (25 ml) was stirred for 3 hr at room temperature. The reaction mixture was poured into ice-cooled 3M hydrochloric acid (150 ml) and extracted with benzene. After washing and drying, the extracts were concentrated and chromatographed on alumina. Recrystallization of crude crystals from benzene gave pure IX, yellow crystals, mp 130—150 °C (dec.), 0.62 g (63%), IR (KBr–disk): 1663, 1643, 998, 963 cm^{-1}.

Found: C, 86.07; H, 5.70%. Calcd for $C_{28}H_{22}O_2$: C, 86.12; H, 5.68%.

3,16-Dimethyl-7,12-diphenyl-4,6,12,14-octadecatetraene-1,8,10,17-tetrayne-3,16-diol (X). To an ice-cooled and stirred suspension of lithium acetylide–ethylenediamine complex[5] (0.5 g 5.4 mmol) in tetrahydrofuran (50 ml) was added over 10 min-period a solution of IX (300 mg, 0.77 mmol) in the same solvent (30 ml). After being stirred for 3 hr, saturated aqueous solution of ammonium chloride was added to the reaction mixture, and the aqueous layer was extracted with ether. The extracts were combined with the organic layer, and worked up in the usual way. Crude product was chromatographed on alumina, and eluted with benzene–ether. Crude X (208 mg) obtained as light brown liquid on concentrating the eluates was used without further purification for the following reaction.

1,4-Dimethyl-5,10-diphenyl-2,4,10,12-cyclooctadecatetraene-6,8,15,17-tetrayne-1,14-diol (XI). To a stirred and refluxing mixture of cupric acetate monohydrate (3.0 g, 1.5 mmol), pyridine (40 ml), methanol (20 ml) and ether (40 ml) was added over 2 hr-period a solution of crude X (208 mg) in pyridine (25 ml) and ether (25 ml). After being stirred and refluxed for further 2 hr, the reaction mixture was concentrated to *ca.* 80 ml. The concentrate was poured into 3M hydrochloric acid (200 ml) and extracted with benzene. The extracts, after being washed and dried, were concentrated to give crude cyclic glycol (XI), which was chromatographed on alumina, and eluted with benzene–ether. XI (133 mg) obtained from the eluates as light brown liquid was subjected to the further reaction.

1,14-Dimethyl-5,10-diphenyl-6,8,15,17-tetrakisdehydro[18]annulene (XII). The crude cyclic glycol (XI, 133 mg) dissolved in benzene (40 ml) was mixed under nitrogen atmosphere with a solution of stannous chloride dihydrate (0.4 g, 1.8 mmol) in concentrated hydrochloric acid (30 ml). After being stirred for 1 hr at room temperature, the reaction mixture was poured into cold water. The organic layer, after washing and drying, was concentrated, and the residue redissolved in benzene was chromatographed on alumina. Black purple crystals (63 mg, 17% based on IX) obtained from benzene eluates were recrystallized from benzene–cyclohexane, and dried *in vacuo* (0.4 Pa) for 5 hr at room temperature to give pure XII, decomposed at 94 °C without fusion, UV: λ_{max}^{THF} 244 (16600), 256 (19700), 270 sh (15300), 277.5 (17800), 292 sh (13900), 299 (14300), 324 sh (14600), 346 sh (30000), 354 sh (30800), 368 sh (38300), 385 sh (62300), 401 (212000), 542 sh (17400), 582 (85700), 666 sh (371), 715 sh (495), 742 (1790) [A maximum at 249 nm in XII which was also observed in VI disappeared on drying the crystals *in vacuo* for 5 hr.], NMR (60 MHz, $CDCl_3$): 0.05 (d, J=14, H^2), 0.49 (d, J=14, H^1), 1.35 (m, *o*–H of phenyl), 2.4 (m, *m,p*–H of phenyl), 6.54 (s, CH_3), 14.20 (t, H^3). The IR spectrum of XII (KBr–disk) was found to be perfectly identical with that of VI. Found: C, 94.46; H, 5.49%. Calcd for $C_{32}H_{22}$: C, 94.54; H, 5.46%.

CT Complex of XII with Trinitrofluorenone. A solution of XII (28 mg, 0.070 mmol) and 2,4,7-trinitrofluorenone (30 mg, 0.095 mmol) in benzene (15 ml) and methanol (15 ml) was allowed to stand in a refrigerator. Black purple crystals deposited decomposed at *ca.* 180 °C forming colorless solid. Elemental analysis indicates that the 1: 1 CT complex contains 1 mol of benzene as a solvent of crystallization.

Found: C, 76.42; H, 4.20; N, 5.16%. Calcd for $C_{32}H_{22}\cdot C_6H_6\cdot C_{13}H_5N_3O_7$: C, 76.58; H, 4.16; N, 5.25%.

1,5-Diphenyl-2,4-heptadien-6-yn-1-one (XIII). To an ice-cooled and stirred solution of phenylpentynal (VII, 2.70 g, 17.3 mmol) and acetophenone (2.08 g, 17.3 mmol) in ethanol (30 ml) was added a solution of sodium hydroxide (0.8 g, 22 mmol) in ethanol (3 ml) and water (3 ml). After 20 min, crystals deposited were collected by filtration and washed with water and ethanol. The crystals (3.70 g, 83%) were recrystallized from ethanol to give pure XIII, yellow crystals, mp 82.8—83.4 °C, IR (KBr–disk): 3240, 2070, 1653, 1016, 976 cm^{-1}.

Found: C, 88.01; H, 5.44%. Calcd for $C_{19}H_{14}O$: C, 88.34; H, 5.46%.

1,5,10,14-Tetraphenyl-2,4,10,12-tetradecatetraene-6,8-diyne-1,14-dione (XIV). A solution of XIII (3.70 g, 14.3 mmol) in pyridine (25 ml) was added at room temperature to a mixture of cupric acetate monohydrate (7.6 g, 38 mmol), pyridine (25 ml) and methanol (25 ml). After being stirred for 2 hr at the same temperature, the reaction mixture containing crystals was cooled in an ice-bath, and the crystals were collected and washed with methanol and water (3.2 g, 87%). The filtrate and washings were concentrated and poured into 2M hydrochloric acid, and extracted with benzene. The benzene extracts were worked up in the usual way. The residue dissolved

in benzene was passed through a column of alumina. Second crop of XIV (0.1 g) was obtained from the filtrate. Recrystallization of the crystals from benzene gave pure diketone (XIV), orange crystals, mp 159.7—160.2 °C, IR (KBr-disk): 1648, 1015, 971 cm^{-1}.

Found: C, 88.55; H, 5.00%. Calcd for $C_{38}H_{26}O_2$: C, 88.69; H, 5.09%.

3,7,12,16-Tetraphenyl-4,6,12,14-octadecatetraene-1,8,10,17-tetrayne-3,16-diol (XV). A solution of XIV (500 mg, 0.89 mmol) in tetrahydrofuran (44 ml) was added over 20 min-period to a stirred suspension of lithium acetylide-ethylenediamine complex[5] (5.6 g) in benzene (98 ml) saturated with acetylene at 15 °C, and the mixture was stirred for further 3 hr at 30—45 °C. The reaction mixture was poured onto ice-water (20 ml) and mixed with saturated sodium chloride solution (100 ml). The aqueous layer was extracted with benzene, and the extracts were combined with the organic layer. The combined organic layer was concentrated and chromatographed on alumina (8.7 g). Crude XV (352 mg) was obtained as a light brown liquid from the benzene–ether eluates.

1,5,10,14-Tetraphenyl-2,4,9,12-cyclooctadecatetraene-6,8,15,17-tetrayne-1,14-diol (XVI). Oxidative coupling of the crude XV (352 mg) by cupric acetate–pyridine–methanol–ether under similar high dilution conditions used for the preparation of XI gave crude XV (312 mg) as a viscous light brown liquid. The crude material was used for the subsequent reaction.

1,5,10,14-Tetraphenyl-6,8,15,17-tetrakisdehydro[18]annulene (XVII). The crude cyclic glycol (VI, 312 mg) was converted into XVII by the reaction with stannous chloride in concentrated hydrochloric acid under analogous conditions employed for the conversion of XI to XII. Slightly crude XVII, obtained as black purple crystals (159 mg, 31% based on XIV), was recrystallized from benzene to give pure XVII, black purple needles. XVII showed no melting point, but underwent color change at 180—190 °C, UV: λ_{max}^{THF} 245 (23300), 261 (24800), 302 (27000), 351 (26300), 373 (38000), 472 (273000), 635 (108000), 772 (4110), NMR (60 MHz, THF-d_8), −0.31 (d, J=13, H^1, H^2), 1.3 (m, *o*-H of phenyl), 2.4 (m, *m,p*-H of phenyl), 13.19 (t, J=13, H^3). XVII gave, green solutions in organic solvents.

Found: C, 94.83; H, 4.98%. Calcd for $C_{42}H_{26}$: C, 95.06; 95.06; H, 4.94%.

CT Complex of XVII with Trinitrofluorenone. A mixture of XVII (27 mg, 0.051 mmol), 2,4,7-trinitrofluorenone (22 mg, 0.070 mmol), benzene (50 ml) and methanol (25 ml) was refluxed for 3 min. CT complex deposited as black purple needles on standing the homogeneous solution in a refrigerator, which showed color change at *ca.* 240 °C without fusion.

Found: C, 77.26; H, 3.69; N, 4.83%. Calcd for $C_{42}H_{26}\cdot C_{13}H_5N_3O_7$: C, 78.09; H, 3.69; N, 4.99%.

References

1) J. Ojima, T. Katakami, G. Nakaminami, and M. Nakagawa, *Tetrahedtron Lett.*, **1968**, 1115; This Bulletin, **49**, 292 (1976).

2) For preliminary reports of a part of this paper, see, K. Fukui, T. Okamoto, and M. Nakagawa, *Tetrahedron Lett.*, **1971**, 3121 and T. Katakami, S. Tomita, K. Fukui, and M. Nakagawa, *Chem. Lett.*, **1972**, 225.

3) a) E. R. H. Jones and B. C. L. Weedon, *J. Chem. Soc.*, **1946**, 937. b) I. Heilbron, E. R. H. Jones, and M. Julia, *ibid.*, **1949**, 1430.

4) G. Eglinton and A. R. Galbraith, *Chem. Ind.*, **1956**, 737; *J. Chem. Soc.*, **1959**, 889.

5) O. F. Beumel, Jr. and R. F. Harris, *J. Org. Chem.*, **28**, 2775 (1963); *ibid.*, **29**, 1872 (1964).

6) V. T. Klimko, V. A. Mikhalev, and A. P. Skaldinov, *J. Gen. Chem.*, **27**, 415 (1957).

7) Further study along this line has been reported preliminary, see, T. Nomoto, K. Fukui, and M. Nakagawa, *Tetrahedron Lett.*, **1972**, 3253. The detail will be reported in a following paper of this series.

8) Effect of substituents on the NMR spectra of dehydroannulenes will be discussed in a following paper of this series.

9) L. Skatteböl, E. R. H. Jones, and M. C. Whiting, "Organic Syntheses," Coll. Vol. IV, p. 792 (1963).

Dehydroannulenes. III. Synthesis and Properties of 1,5,10,14-Tetra-*tert*-butyl-6,8,15,17-tetrakisdehydro[18]annulene

Sachiyo TOMITA and Masazumi NAKAGAWA*

Department of Chemistry, Faculty of Science, Osaka University, Toyonaka, Osaka 560

(Received August 18, 1975)

In order to find out substituent groups which provide stability and solubility to tetrakisdehydro[18]annulene system without appreciable electronic interaction with the annulene ring, the synthesis of 1,5,10,14-tetra-*tert*-butyl-6,8,15,17-tetrakisdehydro[18]annulene (VIII) has been catrried out starting from 3-*tert*-butyl-2-penten-4-ynal (III). It was found that the tetra-*tert*-butyl derivative (VIII) is strongly diatropic, and more stable and much more soluble than tetramethyl-, dimethyl-, diphenyl-, and tetraphenyl-analogues. The electronic spectrum of tetra-*tert*-butyl derivative (VIII) was found to be closely related with that of tetramethyltetrakisdehydro[18]annulene indicating a minor electronic perturbation of *tert*-butyl groups on the annulene ring.

As reported in previous papers,[1,2] replacement of methyl groups in 1,5,10,14-tetramethyl-6,8,15,17-tetrakisdehydro[18]annulene with two or four phenyl groups enhances the stability of phenyl substituted annulenes accompanying with marked decrease of their solubility in NMR solvents. Bathochromic shift of electronic spectra of the phenyl substituted annulenes as compared with that of tetramethyl analogue indicates that phenyl group exerts prominent electronic perturbation on the dehydroannulene nucleus. Consequently, it was desired to find out substituent group which provides stability and solubility without appreciable electronic interaction with annulene system. The present paper is concerned with the synthesis and properties of tetra-*tert*-butyltetrakisdehydro[18]annulene (VIII).

tert-Butyl β-chlorovinyl ketone (I), prepared from pinacolone *via* *tert*-butyl β-hydroxyvinyl ketone by the reported method,[3] was ethynylated with lithium acetylide in liquid ammonia. Ethynyl alcohol (II), thus obtained, was converted into 3-*tert*-butyl-2-penten-4-ynal by acid treatment. The aldehyde was found to be pure *cis*-isomer (III) with respect to the formyl and the ethynyl groups on the basis of NMR spectroscopy. The aldol condensation of pinacolone with III yielded dieneyne ketone (IV) as pale yellow crystals. Oxidative coupling of IV by cupric acetate in pyridine[4] gave diketone (V) in a high yield. The reaction of lithium acetylide–ethylenediamine complex[5] in tetrahydrofuran with the diketone (V) gave bis-ethynyl alcohol (VI) in 91.5% yield. Oxidative coupling of VI performed under high dilution conditions by cupric acetate in pyridine–methanol–ether yielded 18-membered cyclic glycol (VII) in an almost quantitative yield. Treatment of a suspension of the cyclic glycol (VII) in benzene with a solution of stannous chloride dihydrate in concentrated hydrochloric acid followed by chromatography on alumina yielded tetra-*tert*-butyltetrakisdehydro[18]annulene (VIII) as deep brown crystals. VIII gave reddish purple solution in organic solvents. Catalytic reduction of VIII in ethyl acetate over platinum catalyst yielded crystalline hydrocarbon (IX) corresponding to tetra-*tert*-butylcyclooctadecane. VIII forms 1 : 1 CT complex with 2,4,7-trinitrofluorenone, which seems to dissociate into components in a tetrahydrofuran solution, because the electronic spectrum was found to be a superposition of the components, and no CT band could be observed.

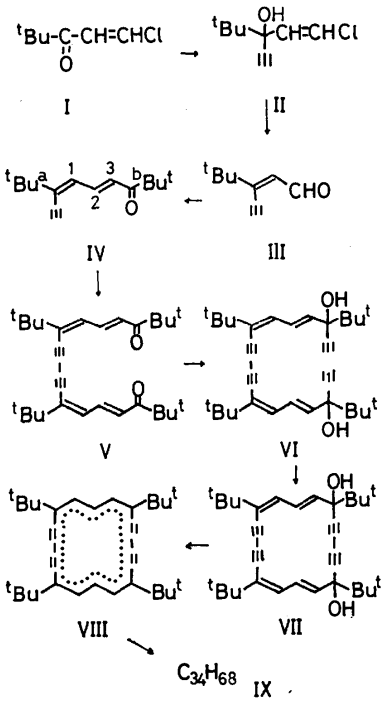

As illustrated in Fig. 1, 60 MHz NMR spectrum

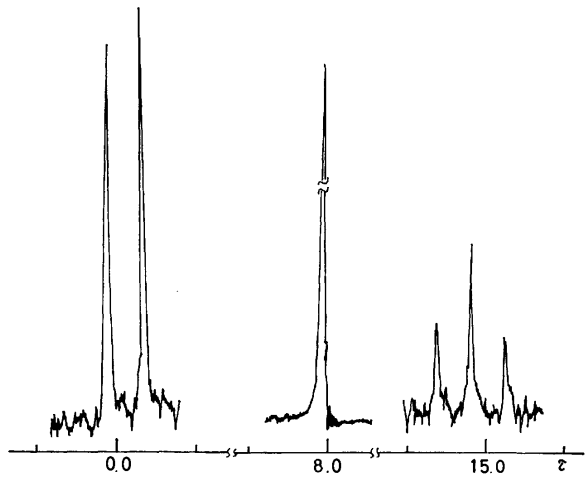

Fig. 1. 60 MHz NMR spectrum of VIII in $CDCl_3$. The signals of inner and outer protons are amplified.

* Author to whom correspondence should be addressed.

clearly indicates that the annulene (VIII) is strongly diatropic exhibiting the inner proton signal at a extremely high field (t, J=13 Hz, τ 14.89 ($CDCl_3$)) and the outer proton signal at a fairly low field (d, J=13 Hz, τ 0.04, ($CDCl_3$)).[6] An appreciable down-field shift of the signal of *tert*-butyl protons (s, τ 7.98 ($CDCl_3$)) can be reasonably ascribed to the deshielding effect of diamagnetic ring current in the 18π-electron system.

Tetra-*tert*-butyltetrakisdehydro[18]annulene (VIII) was found to be more stable and much more soluble than the tetramethyl-,[1] dimethyldiphenyl-[2b,c] and tetraphenyl analogues.[2a,c] The electronic spectrum of VIII shown in Fig. 2 was found to be closely related with that of tetramethyltetrakisdehydro[18]annulene[1] except for a minor bathochromic shift in tetra-*tert*-butyl derivative, thus indicating that the electronic interaction of *tert*-butyl group upon the tetrakisdehydro[18]annulene nucleus is nearly the same as that of methyl group.

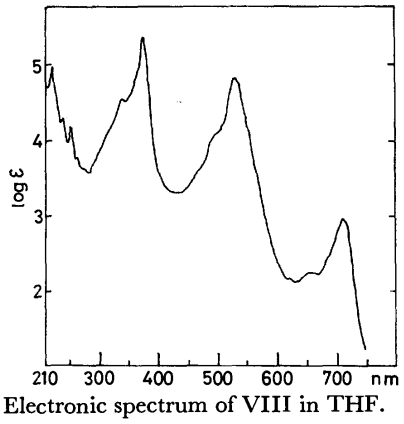

Fig. 2. Electronic spectrum of VIII in THF.

The properties found in tetra-*tert*-butyltetradehydro-[18]annulene (VIII) indicate that the requisite of the substituent, *i.e.*, increase of stability and solubility without enhancement of electronic perturbation, is essentially fulfilled by *tert*-butyl group.

Experimental

All melting and boiling points are not corrected. The IR spectra were measured on a Hitachi EPI-2 or EPI-G3 spectrometer, and the strong, medium and weak bands were indicated by S, M, and W, respectively. The UV spectra, obtained on a Hitachi EPS-3T spectrophotometer, were recorded in nm and the ε-values were given in parentheses. Shoulder was denoted by sh. The mass spectra were measured on a Hitachi RM-50 spectrometer. The NMR spectra were obtained on a Varian A-60 spectrometer. The chemical shifts are given in τ-values with respect to TMS as an internal standard, and the coupling constants are recorded in Hz.

tert-*Butyl β-Chlorovinyl Ketone (I).* The β-chlorovinyl ketone (I) was obtained from *tert*-butyl β-hydroxyvinyl ketone by the reported method[3] in 86% yield as pale yellow liquid, bp 61.5—73 °C/2793 Pa, n_D^{20} 1.4578 (lit, value, bp 65—70 °C/3990 Pa, n_D^{20} 1.4598),[3] NMR (neat): 8.86 (s, 9H, *tert*-butyl-H), 2.62—3.32 (dd, J=13, 2H, olefinic H).

*1-Chloro-3-*tert*-butyl-1-penten-4-yn-3-ol (II).* To a solution of lithium acetylide (from lithium 2.45 g, 0.35 mol) in liquid ammonia (450 ml) was added slowly a solution of the β-chlorovinyl ketone (I, 25.30 g, 0.172 mol) in ether (100 ml). The ammonia was allowed to evaporate under continuous stirring. The residue was mixed with ether (300 ml) and chilled to −30 °C, and then saturated aqueous ammonium chloride solution (150 ml) was slowly added to the mixture. The organic layer was separated and the aqueous layer was extracted with ether. The combined ethereal solution was dried (magnesium sulfate), and the solvent was removed under reduced pressure. The residue on distillation under reduced pressure gave forerun, colorless liquid, bp 50—55 °C/266 Pa, 5.24 g, 17%, and then gave II, colorless liquid, bp 55—59 °C/266 Pa, 20.17 g, 67%, IR (neat): 3600—3360 (OH), 3320 (-C≡CH), 1055 (C-O), 1620 (C=C) cm^{-1}, NMR (CCl_4): 8.98 (s, 9H, *tert*-butyl-H), 7.36 (s, 1H, ethynyl-H), 6.87 (s, 1H, -OH), 3.38—4.08 (dd, J=13, 2H, olefinic-H).

Found: C, 62.29; H, 7.59; Cl, 20.37%. Calcd for $C_9H_{13}OCl$: C, 62.61; H, 7.59; Cl, 20.53%.

The forerun was found to be fairly pure and could be used without purification for the subsequent reaction.

*3-*tert*-Butyl-2-penten-4-ynal (III).* A mixture of the β-chlorovinyl alcohol (III, 10.7 g, 0.062 mol), 2M sulfuric acid (300 ml) and tetrahydrofuran (10 ml) was stirred at 40 °C under nitrogen atmosphere for 46 hr under shielding from light. The reaction mixture was saturated with ammonium sulfate, and the aqueous layer was extracted with ether. The extracts were combined with the organic layer and worked up in the usual way. The residue obtained on evaporating the solvent under reduced pressure was dissolved in carbon tetrachloride and chromatographed on alumina (Brockmann, Act. II—III, 50 g). The carbon tetrachloride eluates were concentrated under reduced pressure, and the residue was distilled *in vacuo*. The pentynal (III) was obtained as an unstable pale yellow liquid, bp 60—62 °C/665 Pa, 5.32 g, 63%, IR (neat): 3270 (-C≡CH), 2750 (-CHO), 1680 (C=O) cm^{-1}, NMR (CCl_4): 8.77 (s, 9H, *tert*-butyl-H), 6.05 (s, ethynyl-H), 3.73 (d, J=8, 1H, olefinic-H), −0.20 (d, J=8, 1H, -CHO).

The aldehyde (III) containing a small amount of II was used in the following reaction, because it was difficult to remove a minor quantity of II in III by distillation and chromatography. Found: C, 78.02; H, 8.82%. Calcd for $C_9H_{12}O$: C, 79.37; H, 8.88%.

*1,5-Di-*tert*-butyl-2,4-pentadien-5-yn-1-one (IV).* An ice-cooled solution of sodium hydroxide (0.622 g, 15.2 mmol) in 99% ethanol (4 ml) and water (4 ml) was added in a portion to a stirred solution of the pentynal (III, 0.833 g, 6.12 mmol) and pinacolone (0.632 g, 6.32 mmol) in 99% ethanol (33 ml) under cooling on an ice-bath. After 24 hr, the reaction was quenched on addition of 1M sulfuric acid (10 ml). The mixture was extracted with ether. The extracts, after being washed and dried, were concentrated under reduced pressure to yield reddish brown liquid. The liquid dissolved in petroleum ether was passed through a column of silica gel (Merck, 10 g). The crystals obtained on concentrating the filtrate were collected and washed with a small amount of cold petroleum ether to give pure IV, pale yellow cubes, mp 52.9—54.9 °C, 0.377 g, IR (neat): 3330 (-C≡CH), 1660 (C=O), 1595 (C=C), 975 (*trans* C=C) cm,$^{-1}$ NMR (CCl_4): 8.87 (s, 9H, *tert*-butyl^a-H), 8.82 (s, 9H, *tert*-butyl^b-H), 6.45 (s, 1H, ethynyl-H), 3.56 (d, J=11, olefinic-H^1), 3.43 (d, J=14, olefinic-H^2). Found: C, 82.52; H, 10.02%. Calcd for $C_{15}H_{22}O$: C, 82.51; H, 10.16%.

The silica gel column was further eluted with ether or benzene. Concentration of the eluates under reduced pressure yielded reddish orange liquid (0.796 g), which showed identical IR and NMR spectra with those of crystalline IV, and could be used without further purification for the subsequent reaction.

*1,5,10,14-Tetra-*tert*-butyl-2,4,10,12-tetradecatetraene-6,8-diyne-1,14-dione (V).* To a stirred solution of cupric acetate monohydrate (6.314 g, 31.8 mmol) in pyridine (19.5 ml) and

methanol (19.5 ml) was added a solution of IV (1.388 g, 6.36 mmol) in methanol (15.7 ml). After being stirred overnight at room temperature, the reaction mixture was poured into ice-cooled 1M sulfuric acid (150 ml). The mixture containing yellow crystals was extracted with ether. The extracts, after washing and drying, were concentrated under reduced pressure. Yellow crystals thus obtained were dissolved in benzene, and the solution was passed through a column of alumina (Brockmann, Act. II—III, 10 g). Crystals obtained from the yellow cubes, mp 202.8—205.0 °C (dec.), 1.198 g, IR (KBr-disk): 1675 (C=O), 1592 (C=C), 1000—990 (doublet, filtrate were recrystallized from benzene to give diketone (V), *trans* C=C) cm^{-1}. Found: C, 82.66; H, 9.63%. Calcd for $C_{30}H_{42}O_2$: C, 82.90; H, 9.74%.

3,7,12,16-Tetra-tert-*butyl-4,6,12,14-octadecatetraene-1, 8, 10, 17-tetrayne-3,16-diol (VI).* To an ice-cooled and stirred suspension of lithium acetylide–ethylenediamine complex[5] (1.288 g) in tetrahydrofuran (90 ml) was added a solution of the diketone (III, 0.410 g, 0.95 mmol) in the same solvent (55 ml). After the cooling bath was removed, the mixture was stirred for further 2 hr at room temperature. Saturated aqueous ammonium chloride solution (100 ml) was added to the reaction mixture under ice-cooling. The aqueous layer was extracted with ether, and the extracts were combined with the organic layer. The combined organic layer was washed 3 times with saturated sodium chloride solution and dried, and evaporated under reduced pressure to give light brown solid. The solid dissolved in ethyl acetate was passed through a short column of alumina (Brockmann, Act. II—III, 3 g). Evaporation of the filtrate under reduced pressure gave faintly orange fine crystals, 0.420 g, 91.5%, which were recrystallized from cyclohexane to give pure VI, colorless crystals, mp 185.8—187.9 °C (dec.), IR (KBr-disk): 3560—3400 (doublet, OH), 3300—3260 (doublet, -C≡CH), 980—965 (doublet, *trans* C=C) cm^{-1}. Found: C, 83.90; H, 9.53%. Calcd for $C_{34}H_{46}O_2$: C, 83.65; H, 9.79%.

3,7,12,16-Tetra-tert-*butyl-4,6,12,14-cyclooctadecatetraene-1,8,10,-17-tetrayne-3,16-diol (VII).* A solution of VI (0.359 g) in pyridine (25 ml) and ether (25 ml) was added over 5 hr-period to a vigorously stirred and refluxing solution of cupric acetate monohydrate (1.16 g) in pyridine (45 ml) and ether (45 ml) using a high dilution apparatus. After the mixture had been stirred for further 2 hr at the same temperature, stirring was continued for 1 hr at room temperature. The ice-cooled reaction mixture, after *ca.* 1/3 volume of the solvents had been removed under reduced pressure, was poured into ice-cooled 2M hydrochloric acid (450 ml). The organic layer was separated, and the aqueous layer was extracted with ether. The extracts combined with the organic layer were worked up in the usual way. Brown solid obtained on evaporating the solvent was dissolved in ethyl acetate, and the solution was passed through a short column of alumina (Brockmann, Act. II—III, 3 g). Slightly crude VI, faintly brown fine crystals, 0.347 g, 96.0%, obtained on evaporating the filtrate, were recrystallized twice from ethanol to give analytical specimen, colorless crystals, mp 239.8—240.3 °C (dec.). The crystals contained 1 mol of ethanol as a solvent of crystallization, which could be removed upon heating to 70 °C *in vacuo* for 48 hr.

Combusion of the cyclic glycol (VI) was found to be difficult, and satisfactory elemental analysis could be obtained on a sample admixed with sucrose. Found: C, 84.74; H, 9.39%. Calcd for $C_{34}H_{44}O_2$: C, 84.25; H, 9.15%.

1,5,10,14-Tetra-tert-*butyl-6, 8,15,17-tetrakisdehydro[18]annulene (VIII).* A solution of stannous chloride dihydrate (0.6 g) in concentrated hydrochloric acid (4 ml) was added in a portion to a vigorously stirred suspension of the cyclic glycol (VII, 0.149 g, 0.308 mmol) in benzene (15 ml) under nitrogen atmosphere. After 30 min, cold water was added to the deep reddish purple reaction mixture. The organic layer was washed with water (3 times), saturated sodium hydrogencarbonate–sodium chloride solution and water, and dried over sodium sulfate in a refrigerator for 3 hr. Residue obtained on concentrating the organic layer under reduced pressure was dissolved in cyclohexane, and passed through a column of alumina (Merck, Act. I, 5 g) and eluted with the same solvent. The filtrate and eluates were combined, and concentrated under reduced pressure. Deep brown fine crystals deposited were collected and washed twice with a small amount of cold petroleum ether to give pure tetra-*tert*-butyltetrakisdehydro-[18]annulene (VIII), mp *ca.* 180 °C (dec.), 0.127 g, 90%, UV: λ_{max}^{THF} 219.5 (97600), 237.8 (19400), 250 (16300), 261 (5740), 275 (4240), 337 (35500), 374 (231000), 407.5 sh (12800), 524.5 (68700), 621 (151), 656 (186), 707 (932), IR (KBr-disk): 2950 (S), 2900 (M), 2870 (S), 1525 (W), 1480 (M), 1460 (S), 1395 (W), 1365 (M), 1285 (M), 1235 (S), 1195 (S), 1065 (M), 1025 (S), 1010 (S), 965 (M), 885(S), 858(S) cm^{-1}, NMR (THF-d_8): 7.98 (s, *tert*-butyl-H), 14.92 (t, J=13, inner-H), 0.02 (d, J=13, outer-H). Found: C, 90.56; H, 9.44%. Calcd for $C_{34}H_{42}$: C, 90.61; H, 9.39%.

VIII was found to be fairly stable even in crystalline state. Crystals of VIII which were placed in a refrigerator (−20 °C) for 3 days still held 70% purity indicating higher stability of VIII than the tetramethyl analogue.[1]

1,5,10,14-Tetra-tert-*butylcyclooctadecane (IX).* VIII (207.3 mg, 0.4277 mmol) in ethyl acetate (90 ml) was hydrogenated over pre-reduced platinum oxide catalyst ($PtO_2 \cdot 2H_2O$, 536.2 mg). After 1.5 hr, 139 ml (27 °C) of hydrogen was absorbed (theoretical volume, 136.9 ml). Yellowish solid obtained was dissolved in petroleum ether, and the solution was passed through a short column of alumina (Merck, Act. I, 2 g). Residue obtained on evaporating the filtrate was recrystallized from ethyl acetate to give tetra-*tert*-butylcyclooctadecane (IX), colorless crystals, mp 189—190 °C. Found: C, 86.08; H, 13.74%, M^+ 476. Calcd for $C_{34}H_{68}$: C, 85.63; H, 14.37%, Mol. wt., 476.9.

CT Complex of VIII with Trinitrofluorenone. A mixture of VIII (30.46 mg, 0.0676 mmol), 2,4,7-trinitrofluorenone (41.05 mg, 0.130 mmol), benzene (3 ml) and methanol (3 ml) was refluxed for a short period, and allowed to stand overnight in a refrigerator. Reddish purple crystals deposited were collected and washed successively with petroleum ether and benzene to give pure complex, reddish purple crystals, which showed no melting point, but underwent color change at *ca.* 215 °C. Found: C, 73.60; H, 6.09; N, 5.46%. Calcd for $C_{34}H_{42} \cdot C_{13}H_5O_7N_3$: C, 73.70; H, 6.19; N, 5.49%.

References

1) J. Ojima, T. Katakami, G. Nakaminami, and M. Nakagawa, *Tetrahedron Lett.*, **1968**, 1115; This Bulletin, **49**, 292 (1976).

2) a) K. Fukui, T. Okamoto, and M. Nakagawa, *Tetrahedron Lett.*, **1971**, 3121; b) T. Katakami, S. Tomita, K. Fukui, and M. Nakagawa, *Chem. Lett.*, **1972**, 225; c) T. Katakami, K. Fukui, T. Okamoto, and M. Nakagawa, This Bulletin, **49**, 297 (1976).

3) N. K. Kochetkov, I. Ambrush, T. I. Ambrush, and E. S. Severin, *J. Gen. Chem. USSR*, **28**, 3053 (1958).

4) G. Eglinton and A. R. Galbraith, *J. Chem. Soc.*, **1959**, 889.

5) D. F. Beumel, Jr. and R. F. Harris, *J. Org. Chem.*, **28**, 2775 (1963); **29**, 1872 (1964).

6) The chemical shifts of the outer protons given in the preliminary report (Ref. 2b) (−0.02 in THF-d_8 and −0.04 in $CDCl_3$) were erroneous.

Dehydroannulenes. IV. Synthesis and Properties of 1,14-Di-*tert*-butyl-5,10-diphenyl-6,8,15,17-tetrakisdehydro[18]annulene. Evidence for the Identity of Diacetylene and Hexapentaene Units in the 18π-Electron System

Tateo NOMOTO, Kunisuke FUKUI, and Masazumi NAKAGAWA*

Department of Chemistry, Faculty of Science, Osaka University, Toyonaka, Osaka 560

(Received August 18, 1975)

The synthesis designed to lead to isomeric di-*tert*-butyldiphenyl-tetrakisdehydro[18]annulenes (VII and XIII) have been performed. It was found that the isomeric tetrakisdehydro[18]annulenes (VII and XIII) are identical in all respects, thus providing chemical evidence for the identity of diacetylene and hexapentaene units incorporated in the aromatic 18π-electron system. Argon laster Raman spectra of VII and XIII exhibited single absorption due to stretching vibration of sp-hybridized carbon-carbon bond at 2080 cm^{-1} indicating equalized nature of acetylenic and cumulenic linkages in the aromatic dehydroannulene system.

It has been proved that tetrasubstituted tetrakisdehydro[18]annulene such as I_a, I_b, and I_c[1,2,3] sustain strong diamagnetic ring current suggesting that the acetylenic and cumulenic carbon atoms equally offer their p-electrons in the orbitals perpendicular to the molecular plane for the formation of π-molecular

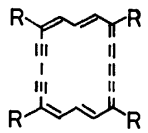

I_a: R=Me

I_b: R=Ph

I_c: R=t-Bu

orbital. Furthermore, the NMR spectral pattern of the symmetrical tetrakisdehydro[18]annulenes (Ia, Ib, and Ic) indicates the equivalence of outer protons. These facts suggest the identity of diacetylene and hexapentaene units in the aromatic system just as formal signle and double bonds in benzene. It is of considerable interest to get further evidence for the identity of diacetylene and cumulene in tetrakisdehydro[18]annulene system. The syntheses of formally isomeric dimethyldiphenyltetrakisdehydro[18]annulenes have been reported in a previous paper.[2b] However, perfect agreement in their physical properties could not be obtained presumably owing to minor difference in purity and to their instability. The present paper is concerned with the syntheses of isomeric di-*tert*-butyldiphenyltetrakisdehydro[18]annulenes (VII and XIII), which can be expected to have higher stability than the dimethyldiphenyl analogue.[3]

Syntheses. The aldol condensation of acetophenone with 3-*tert*-butyl-2-penten-4-ynal (II)[3] yielded dieneyne ketone (III). Oxidative coupling of III by cupric acetate in pyridine[4] gave diketone (IV) in an almost quantitative yield. The diketone (IV) was treated with lithium acetylide-ethylenediamine complex[5] in tetrahydrofuran to give acyclic glycol (V). Oxidation of V by cupric acetate in pyridine-methanol-ether under high dilution conditions resulted in 18-membered cyclic glycol (VI) in 85% yield. A solution

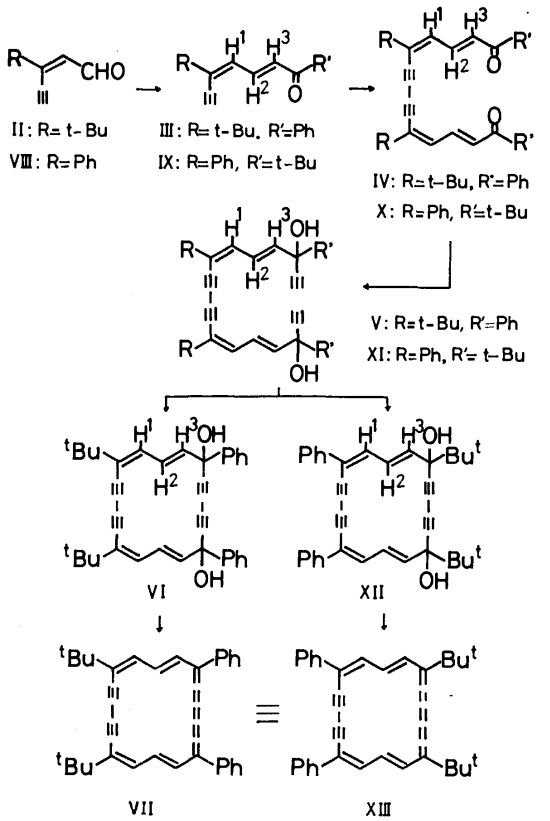

of the cyclic glycol (VI) in ether was mixed with a solution of stannous chloride dihydrate in concentrated hydrochloric acid at a low temperature. Di-*tert*-butyldiphenyltetrakisdehydro[18]annulene (VII) was obtained in 85% yield.

Alternatively, dieneyne ketone (IX) obtained by the aldol condensation of 3-phenyl-2-penten-4-ynal (VIII)[2a] with pinacolone was oxidatively coupled to give diketone (X) in a high yield. Bis-ethynylation of the diketone (X) by lithium acetylide-ethylenediamine comples[5] yielded XI in 97% yield. Oxidative coupling of XI under high dilution conditions gave cyclic glycol (XII), an isomer of VI, in 71% yield. XII could be converted into di-*tert*-butyldiphenyltetrakisdehydro[18]-annulene (XIII) on treatment with stannous chloride in ether saturated with hydrogen chloride.

* Author to whom correspondence should be addressed.

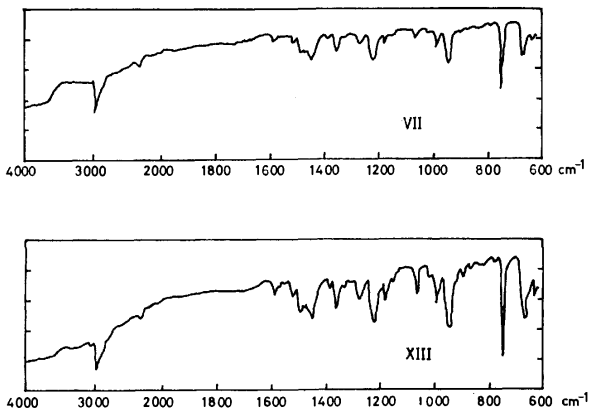

Fig. 1. IR spectra of VII and XIII (KBr-disk).

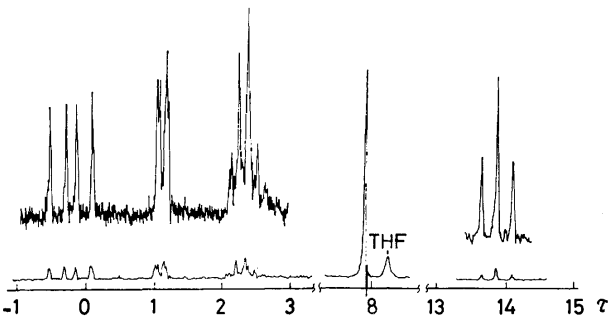

Fig. 2. 60 MHz NMR spectrum of VII in THF-d_8.

Properties. The IR spectra of di-*tert*-butyldiphenyltetrakisdehydro[18]annulenes (VII and XIII) were found to be superimposable as illustrated in Fig. 1. The NMR spectrum of VII shown in Fig. 2 indicates induction of a strong diamagnetic ring current in the tetrakisdehydro[18]annulene ring showing inner proton signal at a fairly high-field and outer proton signals at a low-field. Among two multiplets appeared at medium field, the lower field one could be assigned to *o*-protons of phenyl groups, which suffer deshielding effect of diatropicity of the annulene ring. The higher field multiplet could be reasonably ascribed to *m,p*-protons of phenyl groups, which are disposed in a less deshielding region. Down-field shift of *tert*-butyl proton signal also reflects the diatropicity of the annulene ring. The NMR parameters of VII and XIII are summarized in Table 1. As can be seen from the table, the chemical shifts and coupling constants of all signals of both tetrakisdehydro[18]annulenes (VII and XIII) were found to be identical within the experimental error, the difference of chemical shifts between the corresponding signals being $\tau \pm 0.02$.

Table 1. 60 MHz NMR parameters of VII and XIII in THF-d_8

	VII		XIII	
Outer protons adjacent to phenyl	−0.40 d (14 Hz)	1H	−0.40 d (14 Hz)	1H
Outer protons adjacent to *tert*-butyl	−0.01 d (14 Hz)	1H	0.01 d (14 Hz)	1H
o-Protons of phenyl	1.13m	2H	1.15m	2H
m,p-Protons of phenyl	2.37m	3H	2.39m	3H
Protons of *tert*-butyl	7.93 s	9H	7.93 s	9H
Inner protons	13.90 t (14 Hz)	1H	13.90 t (14 Hz)	1H

The chemical shifts are given in τ-values.

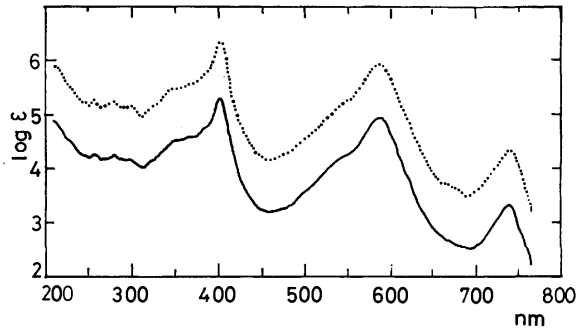

Fig. 3. Electronic spectra of VI (—) and XIII (···) in THF. The curve of XIII has been displaced upward by 1.0 log ε unit increment.

Table 2. Electronic spectra of VII and XIII in THF

λ_{max} in nm ($\varepsilon \times 10^{-2}$)

VII	231 sh (288),	245 sh (160),	256.5 (179),
	270 sh (153),	277.5 (176),	299 (142),
	325 sh (152),	347 sh (303),	368 sh (373),
	386 sh (616),	402 (2200),	544 sh (164),
	587 (875),	670 sh (4.80),	740 (21.7)
XIII	231 sh (285),	245 sh (162),	256.5 (177),
	270 sh (152),	277.7 (175),	299 (142),
	325 sh (151),	347 sh (303),	368 sh (374),
	386 sh (614),	402 (2190),	544 sh (164),
	587 (873),	670 sh (4.72),	740 (21.6)

Shoulder is denoted by sh.

The electronic spectra of VII and XIII are illustrated in Fig. 3, and the numerical data are recorded in Table 2. The wavelength of all absorption maxima were found to be identical in both tetrakisdehydro[18]annulenes (VII and XIII), and the absorption intensities also agreed within the experimental error being the difference between the corresponding maxima *ca.* ±1% at short wavelength region.

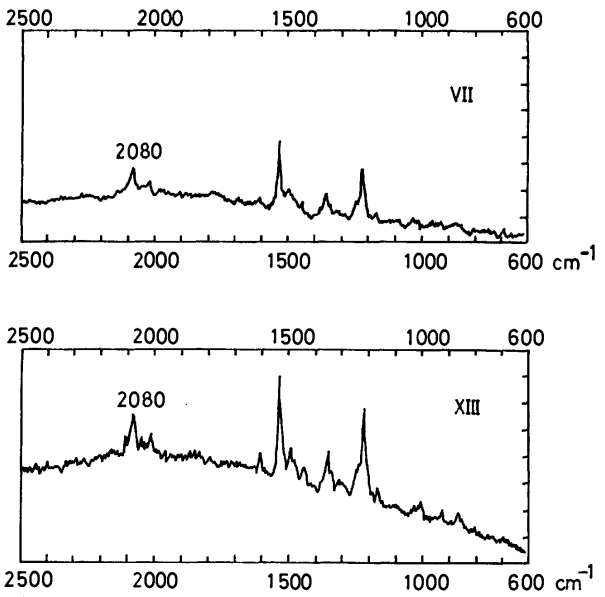

Fig. 4. Argon laser Raman spectra of VII and XIII (KBr-disk).

Argon laser Raman spectra of VII and XIII measured with KBr-disk method at a temperature of liquid nitrogen showed single absorption due to stretching vibration of sp-hybridized carbon-carbon linkage at 2080 cm^{-1} (Fig. 4), thus indicating equalized nature of the diacetylene and hexapentaene linkages incorporated in the aromatic system.

VII and XIII gave identical 1 : 1 CT complexes with 2,4,7-trinitrofluorenone.

The above-stated results provide confirmative evidences for the identity of diacetylenic and cumulenic linkages in the 18π-electron system. Consequently, it can be concluded reasonably that the tetrakisdehydro-[18]annulene ring has a highly delocalized π-electron system consisting of equalized sp-hybridized carbon-carbon linkages and polyene system with minor bond-alternation.

Experimental

All melting points are uncorrected. The IR spectra were obtained on a Hitachi EPI-2 spectrometer, and strong, medium and weak bands are denoted by S, M, and W, respectively. The electronic spectra were measured with a Hitachi EPS-3T spectrophotometer using well-matched pair of quartz cells, and the wavelengths were calibrated with the spectrum of benzene vapor and a didymium glass filter. A Varian A-60 spectrometer was used for the measurements of NMR spectra, and the chemical shifts with respect to TMS as an internal standard and coupling constants are given in τ-values and Hz, respectively. The mass spectra were obtained on a Hitachi RM-50 spectrometer. Laser Raman spectra were measured on a JASCO R750 spectrometer using argon laser (514.5 nm). KBr-disk was prepared under nitrogen atmosphere and measurements were performed in a high vacuum at liquid nitrogen temperature. Merck alumina (Act. II—III) and Merck silica gel (70—325 mesh) were used in chromatography, unless otherwise stated.

Measurements of physical properties of the tetradehydro-[18]annulenes (VII and XIII) were carried out successively using freshly prepared samples.

*1-Phenyl-5-*tert*-butyl-2,4-heptadien-6-yn-1-one (III).* To a stirred solution of II[3] (12.0 g, 0.0881 mol) and acetophenone (10.57 g, 0.0881 mol) in ethanol (55 ml) was added over 15 min-period a solution of sodium hydroxide (4.5 g) in ethanol (12 ml) and water (12 ml) at $-10\sim-5$ °C. The mixture was stirred for further 3—4 hr under ice-cooling (2 °C). Crystals deposited were collected and washed successively with ethanol–water (1: 1) and water to give III, pale yellow crystals, 13.0 g, 62.1%, which were recrystallized from hexane to yield pure III, pale yellow rods, mp 82.1—83.4 °C, IR (KBr-disk): 3280 (M, -C≡CH), 1655 (S, C=O), 1600, 1580 (s, vS, aromatic C=C) cm^{-1}, NMR (CCl_4): 8.75 (s, 9H, *tert*-butyl-H), 6.40 (s, 1H, ethynyl-H), 3.43 (d, $J_{12}=11$, 1H, H^1), 3.03 (d, $J_{23}=15$, 1H, H^3), 2.50 (m, 3.5H, *m*, *p*-H of phenyl and H^2), 2.13 (m, 2.5H, *o*-H of phenyl and H^2).

Found: C, 85.93; H, 7.61%. Calcd for $C_{17}H_{18}O$: C, 85.67; H, 7.61%.

The ketone (III) decomposed gradually on stading at room temperature, but could be kept without change in a refrigerator.

*1,14-Diphenyl-5,10-di-*tert*-butyl-2,4, 10, 12-tetradecatetraene-6, 8-diyne-1,14-dione (IV).* A solution of III (1.5 g, 0.0063 mol) in pyridine (6 ml) and methanol (6 ml) was added over 30 min-period to a stirred solution of cupric acetate monohydrate (3.8 g, 0.019 mol) in pyridine (24 ml) and methanol (24 ml) at room temperature. After being stirred for further 9 hr at the same temperature, the reaction mixture was poured into cold 1M sulfuric acid (300 ml), and extracted with benzene. The extracts were worked up in the usual way, and the solvent was removed under reduced pressure. Yellow amorphous solid, thus obtained, could be crystallized from hexane, 1.30 g, 97.7%. Recrystallization of the crystals from hexane containing trace of benzene gave pure IV, yellow leaflets, mp 144—146 °C, IR (KBr-disk): 1655 (S, C=O), 1580 (vS, aromatic C=C) cm^{-1}, NMR (CCl_4): 8.73 (s, 9H, *tert*-butyl-H), 3.34 (d, $J_{12}=11$, 1H, H^1), 3.04 (d, $J_{23}=15$, 1H, H^3), 2.52 (m, 3.5H, *m*,*p*-H of phenyl and H^2), 2.13 (m, 2.5H, *o*-H of phenyl and H^2).

Found: C, 85.97; H, 7.24%. Calcd for $C_{34}H_{34}O_2$: C, 86.04; H, 7.22%.

*3,16-Diphenyl-7,12-di-*tert*-butyl-4,6, 12, 14-octadecatetraene-1,8,-10,17-tetrayne-3,16-diol (V).* To a stirred suspension of lithium acetylide–ethylenediamine complex[5] (4.8 g) in tetrahydrofuran (260 ml) saturated with acetylene was added at room temperature over 1 hr-period a solution of IV (2.0 g, 0.00421 mol) in the same solvent (100 ml) under slow introduction of acetylene. Introduction of acetylene was stopped after 10 min, and the mixture was stirred for further 2.5 hr at the same temperature. Saturated aqueous ammonium chloride solution (30 ml) was added to the reaction mixture under cooling on an ice-bath. The mixture was extracted with ether. Dark colored oily residue obtained on concentrating the extracts *in vacuo* was chromatographed on silica gel (40 g), and eluted with benzene and benzene–ether (95: 5). V (2.2 g, *ca.* 90%) was obtained as a viscous yellow liquid on concentrating the eluates, IR (neat): 3400 (OH), 3280 (-C≡CH) cm^{-1}, NMR (CCl_4): 8.8 (s, 9H, *tert*-butyl-H), 7.5 (broad s, 1H, OH, disappeared on addition of D_2O), 7.25 (s, 1H, ethynyl-H), 4.13 (d, $J_{23}=15$, 1H, H^3), 3.62 (d, $J_{12}=11$, 1H, H^1), 2.83 (m, 4H, *m*, *p*-H of phenyl and H^2), 2.47 (m, 2H, *o*-H of phenyl).

Attempts to crystallize V were failed.

*1,6-Diphenyl-10,15-di-*tert*-butyl-7, 9, 15, 17-cyclooctadecatetraene-2,4,11,13-tetrayne-1,6-diol (VI).* To a stirred and refluxing solution of cupric acetate monohydrate (3.6 g) in pyridine (100 ml), ether (100 ml) and methanol (50 ml) was added over 8.5 hr-period a solution of V (0.7785 g, 0.00148 mol) in pyridine (50 ml), ether (50 ml) and methanol (50 ml) using a high dilution apparatus, and stirring was continued for further 9 hr at the same temperature. The reaction mixture was then stirred at room temperature for 6 hr, and concentrated to 1/3 volume under reduced pressure on a water-bath kept at 40 °C. The concentrate was extracted with ether, and the extracts were washed thoroughly with water, diluted hydrochloric acid, aqueous sodium hydrogencarbonate solution and saturated aqueous sodium chloride solution, successively, and dried over magnesium sulfate. Brown crystalline powder obtained on concentrating the extracts was chromatographed on alumina (25 g). Elution with benzene and benzene–ether (95: 5) yielded pale yellow crystalline powder, which was crystallized from hexane to give pale yellow crystals, 0.661 g, 85.2%. Recrystallization of the crystals from hexane yielded pure cyclic glycol (VI), colorless leaflets, mp *ca.* 160 °C (dec.), IR (KBr-disk): 3390 (broad, OH) cm^{-1}, NMR ($CDCl_3$): 8.82 (s, 9H, *tert*-butyl-H), 7.47 (broad s, 1H, OH, disappeared on addition of D_2O), 4.05 (d, $J_{23}=15$, 1H, H^3), 3.52 (d, $J_{12}=11$, H^1), 2.49 (m, 6H, H^2 and phenyl-H).

Found: C, 86.99; H, 7.18%. Calcd for $C_{38}H_{36}O_2$: C, 86.98; H, 6.91%.

*1,14-Diphenyl-5,10-di-*tert*-butyl-6,8,15,17-tetrakisdehydro[18]-annulene (VII).* A solution of stannous chloride dihydrate (320 mg) in concentrated hydrochloric acid (4 ml) was added

to a stirred solution of VI (150 mg, 0.286 mmol) in ether (35 ml) under nitrogen atmosphere at −12 °C (on an ice–salt-bath). After being stirred for 30 min at the same temperature, ether (30 ml) and ice–water (30 ml) were added to the deep blue violet reaction mixture. The organic layer was washed successively with water, aqueous sodium hydrogencarbonate solution and saturated sodium chloride solution, and passed through a short column of anhydrous potassium carbonate. Reddish purple powder obtained on evaporating the filtrate under reduced pressure was dissolved in hexane–ether (9: 1) and chromatographed on alumina (50 g). Elution with the same solvent yielded reddish purple crystals, 0.112 g, 80.0%. Recrystallization of the crystals from hexane–ether (3: 1) gave pure VII, reddish purple leaflets, mp 189.0—191.0 °C (dec.).

Found: C, 92.77; H, 7.05%, M^+ 490. Calcd for $C_{38}H_{34}$: C, 93.02; H, 6.98%, Mol. wt., 490.7.

CT Complex of VII with Trinitrofluorenone. A solution of 2,4,7-trinitrofluorenone (20 mg) in ether (15 ml) and methanol (15 ml) was added to a solution of VII (30 mg) in ether–methanol (1: 1, 30 ml). After being warmed to 50 °C for 5 min, the mixture was allowed to stand in a refrigerator for 30 min. Fine bluish purple crystals were collected and washed with ether and dried *in vacuo* for 1.5 hr, 34 mg, 69.4%. On attempted melting point determination, the color of the crystals faded at 240—241 °C.

Found: C, 75.87; H, 4.96; N, 5.25%. Calcd for $C_{38}H_{34}\cdot C_{13}H_5N_3O_7$: C, 76.01; H, 4.88; N, 5.21%.

2,2-Dimethyl-7-phenyl-4,6-nonadien-8-yn-3-one (IX). To a stirred solution of 3-phenyl-2-penten-4-ynal[2a] (VIII, 6.0 g, 0.0384 mol) and pinacolone (4.6 g, 0.0461 mol) in ethanol (90 ml) was added under nitrogen atmosphere over 30 min-period at −2 °C a solution of potassium hydroxide (2.16 g, 0.0384 mol) in ethanol (4 ml) and water (4 ml). The mixture was stirred for further 3.5 hr at 2 °C, and then for 15 hr at 14°C. The reaction mixture was mixed with cold diluted hydrochloric acid, and extracted with ether. The extracts, after being worked up in the usual way, were concentrated under reduced pressure. Dark colored oily residue dissolved in carbon tetrachloride–benzene (1: 9) was passed through a column of silica gel (Wakogel, 120 g). Orange yellow liquid obtained on concentrating the filtrate was dissolved in cyclohexane and passed through a column of alumina (60 g). Pale yellow liquid obtained from the filtrate was mixed with a small amount of cyclohexane–hexane (1: 1) to give pale yellow crystals, 3.8 g, 41.6%, which were recrystallized 3 times from the same solvent to give pure IX, pale yellow leaflets, mp 75.5—76.2 °C, IR (KBr-disk): 3250 (S, −C≡CH), 1675 (vS, C=O), 1600, 1575 (sh, vS, aromatic C=C) cm^{-1}, NMR (CCl_4): 8.83 (s, 9H, *tert*-butyl–H), 6.35 (s, 1H, ethynyl–H), 3.33 (d, $J_{23}=15$, 1H, H^3), 3.0 (d, $J_{12}=11$, 1H, H^1), 2.73 (m, 3H, *m,p*-H of phenyl), 2.37 m, 2.71 dd, $J_{23}=15$, $J_{12}=11$ (3H, *o*-H of phenyl and H^2).

Found: C, 85.91; H, 7.64%. Calcd for $C_{17}H_{18}O$: C, 85.67; H, 7.61%.

1,14-Di-tert-*butyl-5,10-diphenyl-2,4,10,12-tetradecatetraene-6,8-diyne-1,14-dione (X).* A solution of IX (3.5 g, 0.0147 mol) in pyridine–methanol (1: 1, 30 ml) was added at room temperature over 20 min-period to a stirred solution of cupric acetate monohydrate (8.8 g) in pyridine–methanol (1: 1, 108 ml). After being stirred for further 3 hr at the same temperature, the reaction mixture was poured into cold 1M sulfuric acid (700 ml), and extracted with ether. The extracts, after being worked up in the usual manner, were evaporated under reduced pressure to give yellowish brown powder. The material dissolved in carbon tetrachloride was passed through a column of alumina (30 g). Yellow powder obtained on concentrating the filtrate under reduced pressure was crystallized from hexane, thus yielding X, yellow crystals, 3.4 g, 98.3%, which were recrystallized from hexane–benzene (2: 1) to give analytical specimen, yellow needles, mp 154—156 °C, IR (KBr-disk): 1680 (M, C=O), 1585 (vS, aromatic C=C) cm^{-1}, NMR ($CDCl_3$): 8.8 (s, 9H, *tert*-butyl-H), 3.23 (d, $J_{23}=15$, 1H, H^3), 2.92 (d, $J_{12}=11$, 1H, H^1), 2.7 (m, 3H, *m,p*-H of phenyl), 2.4, m, 2.31, dd, $J_{12}=11$, $J_{23}=15$ (3H, *o*-H of phenyl and H^2).

Found: C, 86.00; H, 7.17%. Calcd for $C_{34}H_{34}O_2$: C, 86.04; H, 7.22%.

3,16-Di-tert-*butyl-7,12-diphenyl-4,6,12,14-octadecatetraene-1,8,-10,17-tetrayne-3,16-diol (XI).* Bis-ethynylation of X (2.0 g, 0.00421 mol) with lithium acetylide–ethylenediamine complex[5] (4.8 g) was carried out under the same reaction conditions as the case of preparation of V. Dark colored oily product was chromatographed on silica gel (40 g). Viscous yellow liquid obtained from benzene and benzene–ether (95: 5) eluates was mixed with hexane, and the solution was allowed to stand overnight in a refrigerator to yield pale yellow crystals, 2.15 g, 97.3%. Recrystallization of the crystals from hexane containing trace of benzene gave pure XI, pale yellow fine crystals, mp 145.5—148.5 °C, IR (KBr-disk): 3560 (M, OH), 3920 (M, −C≡CH), 1600 (W, aromatic (C=C) cm^{-1}, NMR ($CDCl_3$): 8.93 (s, 9H, *tert*-butyl–H), 7.92 (s, 1H, OH, disappeared on addition of D_2O), 7.33 (s, 1H, ethynyl–H), 3.80 (d, $J_{23}=15$, 1H, H^3), 2.77 (m, 5H, *m,p*–H of phenyl and H^2, H^1), 2.38 (m, 2H, *o*–H of phenyl).

Found: C, 86.42; H, 7.31%. Calcd for $C_{38}H_{38}O_2$: C, 86.65; H, 7.27%.

1,6-Di-tert-*butyl-10,15-diphenyl-7,9,15,17-cyclooctadecatetraene-2,4,11,13-tetrayne-1,6-diol (XII).* A solution of XI (1.29 g, 0.00245 mol) in pyridine–ether–methanol (1: 1: 1, 150 ml) was added over 10.5 hr-period to a stirred and refluxing solution of cupric acetate monohydrate (8.8 g) in pyridine (140 ml), ether (100 ml) and methanol (100 ml). After being refluxed under stirring for further 10 hr, a part of solvents was distilled out (bp 40—60 °C, 110 ml), and stirring under reflux was continued for further 4 hr. The reaction mixture was concentrated to 1/3 of its volume under reduced pressure at 40 °C. The concentrate was extracted with ether. The ethereal extracts were worked up in the usual way. Deep brown solid obtained on evaporating the extracts was dissolved in benzene and chromatographed on alumina (25 g). Yellow crystalline powder obtained from benzene and benzene–ether eluates was triturated with a small amount of carbon tetrachloride to give pale yellow crystals, 0.911 g, 70.8%. The crystals were recrystallized from carbon tetrachloride and carbon tetrachloride–hexane (1: 1) to give pure XII, pale yellow needles, mp 156.0—158.0 °C (dec.), IR (KBr-disk): 3400 (OH) cm^{-1}, NMR ($CDCl_3$): 8.89 (s, 9H, *tert*-butyl-H), 8.0 (broad s, 1H, OH, disappeared on addition of D_2O), 3.83 (d, $J_{23}=15$, 1H, H^3), 2.73 (m, 5H, *m,p*-H of phenyl and H^1, H^2), 2.33 (m, 2H, *o*–H of phenyl).

XII recrystallized from carbon tetrachloride or carbon tetrachloride–hexane contained tenaciously a small amount of the chloride and gave unsatisfacotry elemental analysis.

1,14-Diphenyl-5,10-di-tert-*butyl-6,8,15,17-tetrakisdehydro[18]-annulene (XIII).* To a stirred solution of XII (200 mg, 0.381 mmol) in ether (35 ml) cooled to −12 °C was added a mixture of stannous chloride dihydrate (400 mg) in ether (6 ml) saturated with hydrogen chloride. Deep bluish purple solution was stirred for 30 min at the same temperature, and then ether (30 ml) and ice–water (30 ml) were added successively to the reaction mixture. The organic layer was washed thoroughly with cold water, aqueous sodium hydrogencarbonate and sodium chloride solutions, successively. The organic layer, after being passed through a short column of

anhydrous potassium carbonate, was concentrated to give reddish purple powder. The powder dissolved in hexane–ether (9: 1) was chromatographed on alumina (30 g), and eluted with the same solvent. Evaporation of the eluates *in vacuo* yielded reddish purple crystals, 0.126 g, 67.4%, which were recrystallized 3 times from hexane–ether (3: 1) to give analytical specimen of XIII, reddish purple leaflets, mp 189.0—191.0 °C (dec.).

Found: C, 92.60; H, 7.04%, M^+ 490. Calcd for $C_{38}H_{34}$: C, 93.02; H, 6.98%, Mol. wt., 490.7.

CT Complex of XIII with Trinitrofluorenone. A solution of XIII (30 mg) in ether–methanol (1: 1, 30 ml) was mixed with a solution of 2,4,7-trinitrofluorenone (20 mg) in the same solvent (30 ml), and the mixture was kept at 50 °C for 5 min. According to similar procedure as that for the preparation of CT complex of VII, CT complex of XIII was obtained as purple fine crystals, 39 mg, 79.6%. The color of the crystals faded at 240—240.5 °C.

Found: C, 75.82; H, 4.84; N, 5.18%. Calcd for $C_{38}H_{34}\cdot C_{13}H_5N_3O_7$: C, 76.01; H, 4.88; N, 5.21%.

References

1) J. Ojima, T. Katakami, G. Nakaminami, and M. Nakagawa, *Tetrahedron Lett.*, **1968**, 1115; This Bulletin, **48**, 292 (1975).

2) a) K. Fukui, T. Okamoto, and M. Nakagawa, *Tetrahedron Lett.*, **1971**, 3121; b) T. Katakami, K. Fukui, T. Okamoto, and M. Nakagawa, This Bulletin, **48**, 297 (1975).

3) T. Katakami, S. Tomita, K. Fukui, and M. Nakagawa, *Chem. Lett.*, **1972**, 225; S. Tomita and M. Nakagawa, This Bulletin, **48**, 302 (1975).

4) G. Eglinton and R. A. Galbraith, *J. Chem. Soc.*, **1959**, 889.

5) D. F. Beumel, Jr. and R. F. Harris, *J. Org. Chem.*, **28**, 2775 (1963); *idem.*, *ibid.*, **29**, 1872 (1964).

Racemization of Alanine Induced by Copper(I) Oxide

Akira TAI, Kotaro OKADA, Tsutomu MASUDA, and Yoshiharu IZUMI
Division of Organic Chemistry, Institute for Protein Research, Osaka University, Suita, Osaka 565
(Received August 22, 1975)

Copper(I) oxide was found to be an excellent initiator for the racemization of alanine in alkaline aqueous solutions. The rate studies indicate that copper(I) oxide itself is not a catalyst for the racemization but is a pre-catalyst producing real racemization catalysts in the reaction system. The real catalytic system for racemization was found to consist of acetaldehyde and copper(II) ions. Acetaldehyde and copper(II) ions were produced by the oxidation of alanine and copper(I) oxide with oxygen in air, respectively. The function of copper(I) oxide is considered to produce oxidants by reaction with oxygen, which effects the oxidation of alanine.

In the course of studies on the catalytic racemization of alanine with nitrosophenol and copper(II) ions,[1] it was found that the addition of copper(I) oxide to the reaction system accelerates the rate of racemization. Further investigations revealed that even in the absence of nitrosophenol, racemization proceeded at a high rate so long as a catalytic amount of copper(I) oxide was present in the system.

The present paper describes the results of this finding and the function of the copper(I) oxide in this reaction.

Results and Discussion

The experimental systems are listed in Table 1 and the results of experiments 1, 2, and 3 are shown in Fig. 1.

Racemization proceeded at a high rate in the system of experiment 1. Since no detectable racemization was observed in experiment 2 carried out in a nitrogen atmosphere, copper(I) oxide itself was found to be inactive for racemization. From the results of experiment 3, it is also clear that copper(II) ions alone produce no racemization activity. Thus, the presence of copper(I) oxide and air appears to be an essential factor for racemization.

TABLE 1. COMPOSITION OF REACTION SYSTEM[a]

Experiment	Copper compound	Additives	Atmosphere
1	Cu_2O	···	air
2	Cu_2O	···	nitrogen
3	$CuSO_4$	···	air
4	Cu_2O	pyruvic acid[b]	air
5	$CuSO_4$	pyruvic acid	air
6	Cu_2O	pyruvic acid	nitrogen
7	Cu_2O	acetaldehyde[b]	air
8	Cu_2O	acetaldehyde	nitrogen
9	$CuSO_4$	acetaldehyde	air

a) The amounts of alanine, the copper compounds and the buffer solution are given in the experimental section.
b) The amount is adjusted to the maximum amount found in the system of experiment 1; pyruvic acid: 59 mg, acetaldehyde: 20 mg.

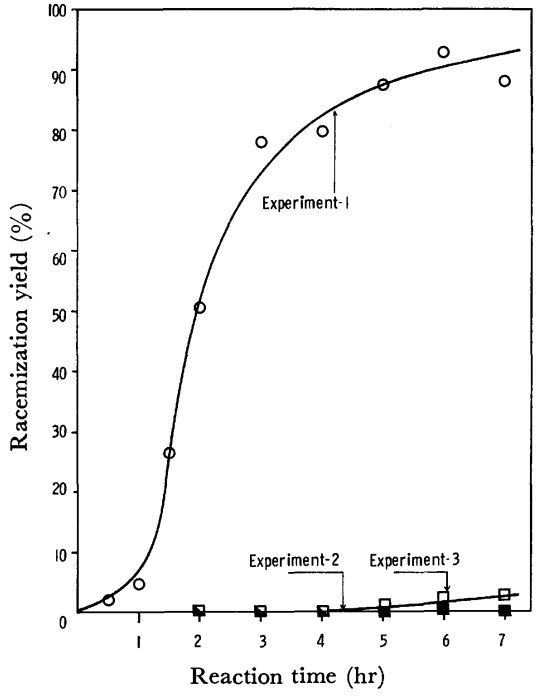

Fig. 1. Time course of racemization of D-alanine. The reaction condition of each experiment is shown in Table 1.

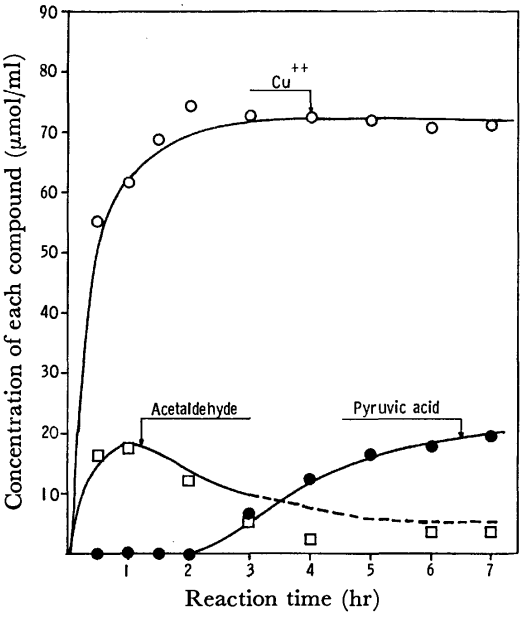

Fig. 2. Concentrations of cupric ion, acetaldehyde and pyruvic acid in the reaction mixture of experiment 1. The concentrations of acetaldehyde shown in a part of broken line are estimated by the average of scatterd analytical resalts caused by the interference of pyruvic acid.

When the presence of the induction period in the course of experiment 1 is taken into account, real racemization catalysts appear to be produced from the reaction mixture in the course of the reaction.

Analysis of the products of experiment 1 during the reaction revealed the presence of small amounts of pyruvic acid and acetaldehyde. The formation of copper(II) ions was suggested by a deep blue coloration of the reaction mixture. Fig. 2 shows the amounts of copper(II) ions, pyruvic acid and acetaldehyde produced during the reaction of experiment 1.

The role of the pyruvic acid in racemization was investigated with systems containing pyruvic acid (experiments 4, 5, and 6 in Table 1). The time courses of racemization in experiments 4, 5, and 6 are shown in Fig. 3.

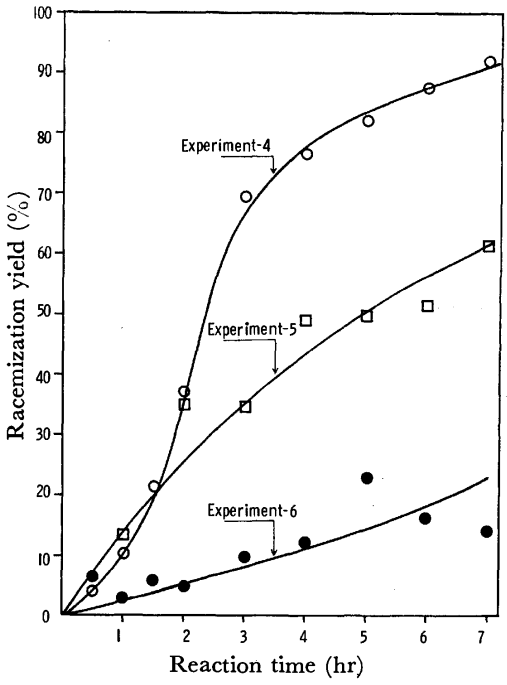

Fig. 3. Time course of racemization of D-alanine. The reaction condition of each experiment is shown in Table 1.

If the racemization of experiment 1 is catalyzed by pyruvic acid or by substances produced from pyruvic acid in the presence of copper(I) oxide or copper(II) ions, these experiments must result in an increase in the racemization rate and a reduction in the induction period. However, experiment 4 almost had the same rate and time course of racemization as did experiment 1 and experiments 5 and 6 resulted in racemization at very low or almost negligible rates.

Although the catalytic action of pyruvic acid is not completely neglected, it is not reasonable to consider pyruvic acid a primary factor governing the racemization in experiment 1.

A major part of the racemization in experiment 5 could be achieved by the transamination between alanine and pyruvic acid.[2]

The action of acetaldehyde in the racemization was also examined with systems containing acetaldehyde

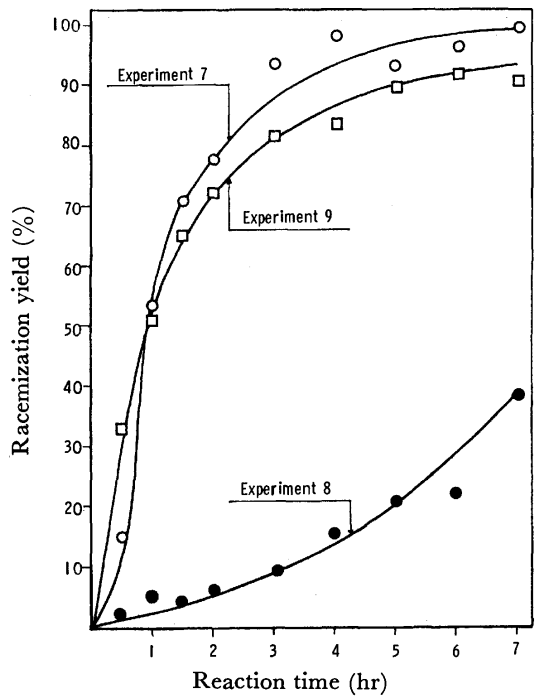

Fig. 4. Time course of racemization of D-alanine. The reaction condition of each experiment is shown in Table 1.

(experiments 7, 8, and 9 in Table 1). The time course of racemization of each experiment is shown in Fig. 4.

The results of experiment 7 reveal that acetaldehyde plays an important role in racemization. However, results of experiment 8 indicate that if there is no oxygen in the system, the rate of racemization becomes negligible even if sufficient amounts of acetaldehyde and copper(I) oxide are present. The fact that experiment 9 resulted in the absence of an induction period and high initial rate of racemization suggests that acetaldehyde is one of the essential components for the catalytic system and requires cupric ions to promote the racemization.

Since negligible effects of substances expected to be produced by the decomposition of alanine such as carbon dioxide, ammonia and ethylamine were confirmed experimentally, the real catalytic system participating in the racemization of experiment 1 was ascertained to consist of acetaldehyde and copper(II) ions.

The mechanism of racemization of alanine in experiment 1 is summarized in two steps: 1) oxidation of copper(I) oxide with oxygen produces copper(II) ions and oxidants, and the reaction of the oxidants with alanine results in the formation of acetaldehyde, and 2) catalytic racemization of alanine with acetaldehyde and copper(II) ions.

The detailed mechanism of catalytic racemization with acetaldehyde and copper(II) ions is not clear at the present time. Work is currently in progress to confirm this. Racemizations catalyzed by nitrosophenol, pyridoxal and their analogues are also being reinvestigated on the basis of this work.

Although the mechanism of the reaction between

copper(I) oxide and oxygen in the present experimental conditions has not been clarified, the formation of oxidants such as superoxide or hydroxy radicals can be expected from the reduction of oxygen with copper-(I) oxide.

The formation of acetaldehyde is considered to proceed by means of the oxidative decarboxylation of alanine because the results of experiments 4 and 5 exclude the possibility of its formation by means of the decarboxylation of pyruvic acid, as does the fact that the formation of acetaldehyde precedes that of pyruvic acid, as is shown in Fig. 2.

The direct formation of acetaldehyde and pyruvic acid from alanine and oxygen in the presence of copper-(I) oxide is interesting as a model reaction of amino acid oxidase. Studies along this line are also under way.

Experimental

All chemicals except those listed below were obtained from commercial sources and used without further purification. Copper(I) oxide was prepared by the reduction of copper(II) sulfate in an aqueous solution with glucose in the presence of potassium sodium tartrate and sodium hydroxide. Acetaldehyde was generated by the decomposition of paraldehyde in the presence of sulfuric acid. Diethyl ether was purified by the method described in Ref. 3).

The infrared spectra were recorded using a Shimadzu IR-27G spectrometer. Colorimetric determination was performed using a Hitachi 124 spectrometer. Gas chromatographic analysis was carried out with a Shimadzu 4APF gas chromatograph using a 300×0.5 cm glass column packed with neopentylglycol succinate (1.5%) on Chromosorb W. Thin-layer chromatography was performed on a precoated plate of Silica-gel HF (E. Merk) with Solvent 1 (hexane/ethyl formate=6/4) or Solvent 2 (butanol/ethanol/12% aqueous ammonia=7/1/2).

Racemization. In a shaker flask, D-alanine (25 m mol), a copper compound (2.5 m mol) and other additives as necessary were dissolved in 23 ml of an alkaline stock solution consisting of a 0.05 M solution of sodium borate and a 1M solution of sodium hydroxide in such a ratio that the pH of the resulting reaction mixture became 10.4 at 50 °C. The mixture was shaken at 50 °C in air or nitrogen. At specific time intervals, a small portion of the reaction mixture was taken out as a sample for analysis. The composition of each experiment is listed in Table 1.

Determination of Racemization Yield. The reaction mixture (0.2 ml) was acidified and dried *in vacuo*. The residue was heated with *l*-menthol (1.0 g). When the temperature of the mixture reached 120 °C, dry hydrogen chloride was passed into the mixture until the esterification of alanine was completed (requiring 1.5 hr). Excess *l*-menthol was removed from the mixture by sublimation at 110 °C at reduced pressure and the residue was allowed to react with trifluoroacetic anhydride (0.4 ml) at room temperature. The resulting *l*-menthyl L- and D-trifluoroacetylalaninate were subjected to gas chromatography at 170 °C. From the ratio of diastereomers, the racemization yield of D-alanine was calculated.

Determination of Copper(II) Ions. Copper(II) ions in the reaction mixture were determined by EDTA titration. The reaction mixture (2 ml) was acidified with 1 M sulfuric acid to pH 4—5, and was then diluted with 20 ml of an acetate buffer (pH 4.5). The solution was titrated with a 1/100 M EDTA solution in the presence of PAN as an indicator.

Characterization of Acetaldehyde and Pyruvic Acid. The reaction mixture of experiment 1 (20 ml) was acidified with hydrochloric acid and mixed with 20 ml of a 0.4% solution of 2,4-dinitrophenylhydrazine in 2 M hydrochloric acid. The reaction products were extracted three times with a 20 ml portion of ether. The combined extracts were extracted twice with a 30 ml portion of a 10% aqueous sodium carbonate solution.

The organic layer was concentrated to 0.5 ml and the reddish-orange crystals that precipitated were collected. The crystals (mp 162.0 °C) were identical with 2,4-dinitrophenylhydrazone of acetaldehyde (**1**) from a mixed melting-point determination, IR spectra and the R_f values (0.65) of tlc (developed with Solvent 1).

The aqueous layer was acidified with 2 M hydrochloric acid and the acid insoluble substance was extracted with a 30 ml portion of ethyl acetate. A yellow precipitate which appeared when the extract was concentrated to 0.3 ml was collected and recrystallized from ethyl acetate to give 2,4-dinitrophenylhydrazone of pyruvic acid (**2**) as yellow crystals (mp 162.5 °C), which was confirmed by a mixed melting-point determination with an authentic sample and by comparison of its IR spectrum and tlc R_f values of tlc (0.57) (developed with Solvent 2) with those of an authentic sample.

Determination of Acetaldehyde and Pyruvic Acid. The amounts of acetaldehyde and pyruvic acid in the reaction mixture were evaluated from those of their 2,4-dinitrophenylhydrazones, which were found in the reaction mixture treated with 2,4-dinitrophenylhydrazine.

The reaction mixture (0.3 ml) was treated with 1 ml of a 0.4% solution of 2,4-dinitrophenylhydrazine in 2 M hydrochloric acid. The products were extracted five times with a 4 ml portion of ether. The combined extracts were made up to 25 ml with ether in a volumetric flask.

a) Isolation and Determination of **1**. A 2 ml portion of the extract was concentrated to 0.1 ml and applied on a tlc plate. The plate was developed with Solvent 1. **1** separated as a yellow band on the plate was recovered by scraping the corresponding part of the silica gel and eluting with 5 ml of methanol. The amount of **1** in the eluate was determined by colorimetry with the absorbance at 355 mμ.

b) Isolation and Determination of **2**. A 0.6 ml portion of the extract was subjected to chromatography on a tlc plate with Solvent 2. **2** separated on the plate was recovered in the same way as in a) except for the use of a 0.1 M sodium bicarbonate solution instead of methanol. The amount of **2** in the eluate was determined by colorimetry with the absorbance at 355 mμ.

References

1) K. Hirota and Y. Izumi, This bulletin, **40**, 178 (1967). K. Hirota and Y. Izumi, *ibid.*, **44**, 2287 (1971).
2) H. Mix, *Z. Physiol. Chem.*, **315**, 1 (1959).
3) J. A. Riddick and E. E. Toops, Jr., "Organic Solvent", Interscience Publishers, Inc., 1955, p. 366.

Synthesis of 2-Amino-2,3-dideoxy-L-ribohexose

Hiroshi SANO, Tsutomu TSUCHIYA, Yoshihiro BAN,* and Sumio UMEZAWA

Institute of Bioorganic Chemistry, 1614 Ida, Nakahara-ku, Kawasaki 211

Department of Applied Chemistry, Faculty of Engineering, Keio University, Hiyoshi, Yokohama* **223

(Received September 16, 1975)

2-Amino-2,3-dideoxy-L-glucose (**1**) was synthesized from 2-amino-2-deoxy-L-glucose (**2**). The synthesis was achieved without protection of the anomeric hydroxyl group throughout the reaction sequence. The masked derivative (**9**) of **1** was prepared from **2** by sequential *N*-methoxycarbonylation, benzylidene acetal formation, mesylation, displacement with iodide, and hydrogenolysis. Alkaline hydrolysis of the debenzylidenated product (**10**) led to ring contraction and yielded the 1,2-oxazolidinone derivative (**11**) of a furanose. Acidic hydrolysis of **11** underwent ring expansion and successfully gave **1**.

2-Amino-2,3-dideoxy-L-ribohexose (**1**), an amino L-sugar, is the 3-deoxy derivative of a component of streptomycin. Since the mechanism of resistance of resistant bacteria to streptomycin has been revealed,[1,2,3] and it has been found that the C-3 hydroxyl group of the 2-deoxy-2-methylamino-L-glucose moiety of streptomycin was adenylylated or phosphorylated by ATP and streptomycin adenylyl transferase or streptomycin phosphate transferase, we intended to prepare the unnatural 2-amino-3-deoxy L-sugar (**1**) as an approach to the synthesis of a deoxy variant of streptomycin which does not contain the hydroxyl group masked by the resistant bacteria.

As for the corresponding D-sugar, namely, 2-amino-2,3-dideoxy-D-glucose, Meyer zu Reckendorf and Bonner[4] have reported its synthesis from methyl 2-benzamide-4,6-*O*-benzylidene-2-deoxy-3-*O*-mesyl-β-D-glucopyranoside through 3-thioacetylation followed by catalytic desulfuration, and, subsequently, the amino D-sugar was found in nature as a component of lividomycin.[5] Matsushima and coworkers[6] also prepared 2-acetamido-2,3-dideoxy-D-glucose from benzyl 2-acetamido-4,6-*O*-benzylidene-2-deoxy-β-D-glucopyranoside through 3-chlorination with sulfuryl chloride followed by reduction with tri-*n*-butyltin hydride and α,α′-azobisisobutyronitrile.

In the present paper, we wish to report a novel method for the preparation of the aminodeoxy L-sugar (**1**) from 2-amino-2-deoxy-L-glucose (**2**) that was achieved without protection of the anomeric hydroxyl group throughout the reaction sequence.

The starting L-sugar (**2**) was prepared from L-arabinose by the method of Kuhn and Kirschenlohr.[7] The 4,6-*O*-benzylidene-*N*-methoxycarbonyl derivative (**4**) was prepared through (**3**) similarly to the preparation of *N*-benzyloxycarbonyl-4,6-*O*-benzylidene derivative of 2-amino-2-deoxy-D-glucose by Wesemann and Zilliken.[8] The position of the acetal group (at 4,6-*O*, not at 5,6-*O* of furanose structure) was confirmed by the PMR spectral studies of the mesyl derivatives (**5**,**5**′), the next compounds. Treatment of **4** with mesyl chloride in pyridine containing triethylamine followed by column chromatography gave two crystalline 3-*O*-mesyl derivatives of α-L- (**5**, 47%) and β-L-glucopyranose form (**5**′, 17%). PMR studies of **5** and **5**′ showed the coupling constants, $J_{2,3}$ and $J_{3,4}$=9.5—10 Hz in each of the anomers and $J_{1,2}$=3.5 Hz (in **5**) and 8 Hz (in **5**′). The anomeric proton of **5** or **5**′ also coupled with the anomeric hydroxyl proton, respectively, and, on deuteration, the anomeric proton collapsed to a clear doublet, respectively. These results indicated that the anomeric hydroxyl groups of the both compounds were free and that the both compounds have the glucopyranose structure. It can therefore be assumed that, in the mesylation reaction, an unstable 1-chloride or 1-*O*-mesyl derivative would be formed and hydrolyzed during the subsequent isolation procedure.

The structures of **5** and **5**′ were further confirmed by the PMR spectral studies of their acetyl derivatives. Treatment of the α-anomer (**5**) with acetic anhydride and pyridine followed by chromatographic separation gave 1-*O*-acetyl-α (**6**) and β-derivative (**6**′) in a yield of 72 and 12%, respectively. Acetylation of the β-anomer (**5**′) gave **6** and **6**′ in a yield of 25 and 56%, respectively.

Hydrolysis of **5** or **5**′ with 70% acetic acid readily gave the debenzylidenated compound (**7**).

Next, displacement of the 3-*O*-mesyl group of **5** or **5**′ with iodine was achieved by treatment with sodium iodide in DMF. In general, displacement reaction of 3-sulfonyloxy group by a nucleophile readily proceeds in the case of β-D-glucopyranosides, whereas α-D-glucopyranosides resistant to the displacement owing to 1,3-diaxial type interaction[9,10] in the transition state. We[11] experienced, however, that iodination of 3-sulfonyloxy group in a 2-benzyloxycarbonylamino-α-D-glucoside structure smoothly proceeded in the synthseis of tobramycin from kanamycin B, although the displacement was carried out in high concentration of sodium iodide in DMF. Possibly, the iodination was facilitated by the neighboring group participation of the 2-acylamino group.[12] Also, in the present case, the displacement was carried out with a high concentration of sodium iodide to give almost equal amounts of two iodination products, **8** (35%) and **8**′ (35%), from both of **5** and **5**′. When the concentration of sodium iodide was reduced, the yields of iodinated products became lower. Further details of the structures of **8** and **8**′ were not studied, however, since both of **8** and **8**′ showed $J_{1,2}$=3—3.5 Hz in their PMR spectra, one of them was assumed to have α-L-glucopyranose structure and the other α-L-allopyranose structure.

Catalytic hydrogenation of **8** or **8**′ with Raney nickel gave the 3-deoxy-α-L-pyranose derivative (**9**) in high yield, giving no β-anomer.

Hydrolysis of **9** with 70% acetic acid removed its

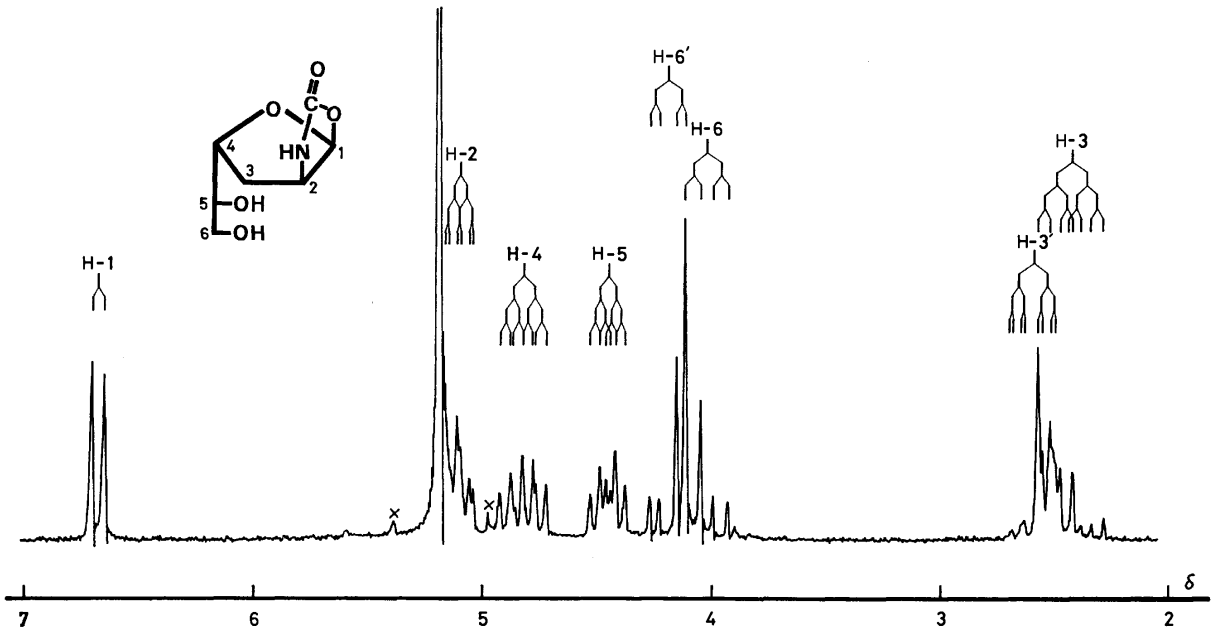

Fig. 1. PMR spectrum of **11**.

benzylidene group to give 2,3-dideoxy-2-methoxycarbonylamino-L-ribohexose (**10**). The compounds **9** and **10** are useful intermediates for the synthesis of related glycosyl halides and glycosides.

Alkaline hydrolysis of **10** with barium hydroxide to remove its methoxycarbonyl group led exclusively to ring contraction, giving an oxazolidinone derivative of α-L-ribohexofuranose (**11**) in 94% yield. Reactions of **11** with ninhydrin and triphenyltetrazolium chloride (TTC) were negative and, in the IR spectrum, **11** showed an absorption at 1730 cm^{-1}. These facts suggested that **11** was a 1,2-oxazolidinone derivative. The PMR spectrum of **11** (Fig. 1) showed the coupling constants, $J_{1,2}=5.5$, $J_{2,3}=5.5$, $J_{2,3'}=-1.5$, $J_{3,4}=10$, $J_{3',4}=5.5$ Hz and these values indicated that **11** has a furanoside structure and that the oxazolidinone is formed in a *cis* configuration at C-1 and C-2.

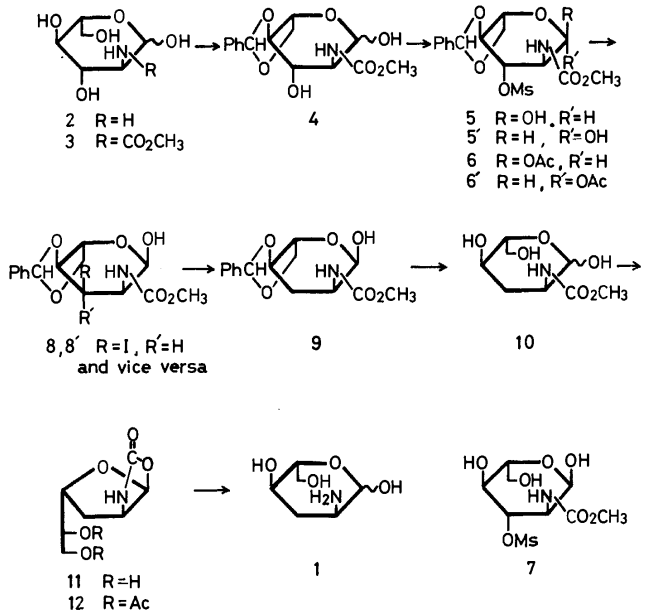

For further confirmation of the structure of **11**, it was acetylated to give the di-*O*-acetyl derivative (**12**). The PMR spectrum of **12** showed that only the shift values of H-5, 6, and 6' moved to downfield in comparison with those of the corresponding protons of **11**. This indicated that the hydroxyl groups at C-5 and C-6 of **11** were acetylated.

Naturally, it became of interest to investigate the alkaline hydrolysis of **3**. However, similar treatment of **3** with barium hydroxide failed to give a definite product. It seems therefore that the absence of 3-hydroxyl group in **10** facilitates the formation of oxazolidinone.

Acidic hydrolysis of **11** was found to undergo ring expansion of the furanose to a pyranose. Treatment of **11** with 1 M hydrochloric acid under warming successfully gave, in 78% yield, 2-amino-2,3-dideoxy-L-ribohexose (**1**) which showed a specific rotation numerically compatible with that of D-isomer[5] but opposite in direction.

Experimental

Tlc was carried out on 7.5×2.5 cm slides coated with silica gel (Wakogel B-5, Wako Pure Chemicals Co., Ltd., Osaka) and silica gel column chromatography was performed with Wakogel C-200.

2-Deoxy-2-methoxycarbonylamino-L-glucose (**3**). To an ice-cold suspension of 2-amino-2-deoxy-L-glucose hydrochloride[7] (26.3 g) and anhydrous sodium carbonate (16.9 g) in aqueous acetone (1 : 1, 440 ml), methyl chloroformate (19.7 ml) was added and the mixture was stirred for 1.5 hr in the cold and then for 1.5 hr at room temperature. Evaporation of the reaction mixture gave a residue, which was washed with methanol. The colorless residue was extracted with DMF (200 ml×5) to remove inorganic matter. Evaporation of the extract gave a solid, which was washed with methanol, 21.7 g (75%). Recrystallization from methanol gave crystals of **3**, mp 195—197 °C (decomp.) (*cf.* 2-deoxy-2-methoxycarbonylamino-D-glucose: mp 196—197 °C[13]); $[\alpha]_D^{26}$ −14.4°→−33.4°

(*c* 1, H_2O) (D-isomer: +34°,[13] +27°[14]).

Found: C, 40.49; H, 6.63; N, 5.72%. Calcd for $C_8H_{15}NO_7$: C, 40.50; H, 6.37; N, 5.91%.

4,6-O-Benzylidene-2-deoxy-2-methoxycarbonylamino-L-glucopyranose (4). A mixture of **3** (33.2 g), fuse-dried zinc chloride (33.5 g) and benzaldehyde (96 ml) was stirred at room temperature for 20 hr. The resulting viscous solution was poured into water. The oily precipitate was separated and washed with petroleum ether. The solidified mass was washed further with water and petroleum ether. Recrystallization from methanol gave needles of **4**, 32.5 g (71%), mp 238 °C (decomp.); $[\alpha]_D^{26}$ +55 °→+16.2 ° (*c* 0.5, dioxane); PMR (in $(CD_3)_2SO$) δ: 3.28 (3H s, CO_2CH_3), 5.57 (1H s, PhC<u>H</u>), 7.37 (5H s, Ph).

Found: C, 55.05; H, 5.70; N, 4.09%. Calcd for $C_{15}H_{19}NO_7$: C, 55.38; H, 5.89; N, 4.31%.

4,6-O-Benzylidene-2-deoxy-3-O-mesyl-2-methoxycarbonylamino-α- and β-L-glucopyranose (5 and 5′). To an ice-cold solution of **4** (10.0 g, 30.7 mmols) in pyridine (250 ml), triethylamine (8.6 ml) and mesyl chloride (8.6 ml, 111 mmol) were added and the solution was allowed to stand for 2 hr in the cold. The solution was poured, with stirring, into a mixture of chloroform-1% aqueous sodium carbonate solution. The chloroform layer was washed with water, dried over sodium sulfate and evaporated to give a red-colored solid. The solid was shaken with a mixture of benzene–ethyl acetate (2: 1) and the suspension was filtered to remove the insoluble matter. The filtrate was chromatographed on a column of silica gel with the same solvent system described above. From the eluate, **5** was obtained as a colorless solid, 5.76 g (47%). It was recrystallized from ethanol to give needles, mp 161—161.5 °C (decomp.); $[\alpha]_D^{15}$ −3.3 °→0 ° (*c* 1.5, acetone); R_f 0.25 (benzene–ethyl acetate 2: 1); positive to TTC; PMR (in $(CD_3)_2CO$) δ: 3.04 (3H s, SO_2CH_3), 3.64 (3H s, CO_2CH_3), 4.05—4.3 (2H m), 4.85 (1H q, H-3; $J_{2,3}$=9.5 or 10 Hz, $J_{3,4}$=9.5 or 10 Hz), 5.28 (1H incomplete t, which collapsed to a doublet ($J_{1,2}$=3.5 Hz) on deuteration, H-1), 5.73 (1H, s, PhCH), 6.13 (1H d with small couplings (<0.5 Hz), OH; J=~4 Hz; disappeared on deuteration). Irradiation of the deuterated sample at δ 3.99 collapsed the doublet of H-1 into a singlet and the quartet of H-3 into a broad singlet. Irradiation at δ 3.89 collapsed the quartet of H-3 into a doublet (J=~8 Hz).

Found: C, 47.59; H, 5.21; N, 3.25; S, 7.96%. Calcd for $C_{16}H_{21}NO_9S$: C, 47.64; H, 5.25; N, 3.47; S, 7.95%.

The insoluble matter described above was recrystallized from ethanol to give colorless needles of **5′**, 2.09 g (17%), mp 153.5—154.5 °C (decomp.); $[\alpha]_D^{15}$ +29 °→−3 ° (*c* 1.5, acetone); R_f 0.25 (benzene–ethyl acetate 2: 1); active for TTC; PMR (in $(CD_3)_2CO$) δ: 3.00 (3H s, SO_2CH_3), 3.62 (3H s, CO_2CH_3), 4.32 (1H q, H-6?$_{eq}$; J=4.5 and 10.5 Hz), 4.92 (1H t, H-3; J=9.5 Hz), 5.06 (1H t, H-1; J=~7.5 Hz; collapsed to a doublet ($J_{1,2}$=8 Hz) on deuteration), 5.74 (1H s, PhC<u>H</u>), 6.17 (1H d, OH; J=7.5 Hz;disappeared on deuteration), 7.3—7.6 (5H m, Ph).

Irradiation at δ 6.17 (OH) collapsed the triplet of H-1 to a doublet (J=8 Hz). Irradiation of the deuterated sample at δ 3.70 (H-2 resonated here) collapsed the doublet of H-1 to a singlet and the triplet of H-3 to a doublet (J=~8 Hz).

Found: C, 47.51; H, 5.18; N, 3.22; S, 7.66%.

2-Deoxy-3-O-mesyl-2-methoxycarbonylamino-α-L-glucopyranose (7). A suspension of **5** or **5′** in 70% aqueous acetic acid was heated at 95 °C for 5 min. The resulting clear solution was evaporated to give a solid, which was thoroughly washed with ether and recrystallized from ethanol to give needles of **7**, mp 151.5—153 °C (decomp.); $[\alpha]_D^{22}$ −86 °→−36 ° (*c* 1, methanol); R_f 0.33 (chloroform–methanol 7: 1); PMR (in $CDCl_3$) δ: 3.13 (3H s, SO_2CH_3), 3.67 (3H s, CO_2CH_3), 5.13 (1H d, H-1; $J_{1,2}$=3.5 Hz).

Found: C, 34.45; H, 5.32; N, 4.24; S, 10.10%. Calcd for $C_9H_{17}NO_9S$: C, 34.28; H, 5.44; N, 4.44; S, 10.17%.

1-O-Acetyl-4,6-O-benzylidene-2-deoxy-3-O-mesyl-2-methoxycarbonylamino-α- and β-L-glucopyranose (6 and 6′). *From 5*: A solution of **5** (200 mg) in pyridine (4.6 ml), acetic anhydride (0.05 ml) was added and the solution was allowed to stand at room temperature overnight. After addition of a drop of water, the solution was poured into ice-water. The precipitate was dissolved in chloroform and the solution was washed with water, dried over sodium sulfate and evaporated to give a solid. The solid was shaken with benzene–ethyl acetate (5: 1, 3 ml) and the insoluble product was filtered, washed with the same solvent mixture to give **6**, 60 mg (27%). The filtrate was evaporated and the residue was chromatographed on a column of silica gel with the above solvent mixture. From the earlier fraction, **6′** was obtained, 27 mg (12%), mp 158—159.5 °C (decomp.); $[\alpha]_D^{23}$ −65 ° (*c* 1, $CHCl_3$); R_f 0.48 (benzene–ethyl acetate 2: 1); PMR (in $CDCl_3$) δ: 2.20 (3H s, Ac), 2.98 (3H s, CO_2CH_3), 3.72 (3H s, SO_2CH_3), 3.75—4.0 (3H m, H-4,6$_{ax}$,6$_{eq}$ (or 5)), 4.1—4.45 (2H m, H-2 and 5 (or 6$_{eq}$)), 4.83 (1H t, H-3; J=~10 Hz), 5.19 (1H d, NH; $J_{2,NH}$=9 Hz; disappeared on addition of D_2O and NaOD), 5.59 (1H s, PhC<u>H</u>), 6.24 (1H d, H-1; $J_{1,2}$=3.5 Hz).

Irradiation of H-1 slightly changed the signal bush near 4.3 but not other signals. Irradiation at δ 4.33 (at which H-2 resonated) collapsed the triplet of H-3 (δ 4.83) into a doublet ($J_{2,3}$=~10 Hz), the doublet of N<u>H</u> (δ 5.19) into a singlet and the doublet of H-1 (δ 6.24) into a singlet. Irradiation at δ 3.87 (H-4) collapsed the triplet of H-3 into a doublet (11 Hz=$J_{3,4}$). Irradiation at 5.19 caused the signals at δ 4.1—4.45 to change.

Found: C, 48.64; H, 5.22; N, 2.85; S, 7.39%. Calcd for $C_{18}H_{23}NO_{10}S$: C, 48.54; H, 5.20; N, 3.14; S, 7.20%.

From the later fraction, **6** was obtained, 100 mg (45%). Thus the total yield of **6** is 72%, mp 156.5—158 °C (decomp.); $[\alpha]_D^{23}$ +9 ° (*c* 1, $CHCl_3$); R_f 0.50 (benzene–ethyl acetate 2: 1); PMR (in $CDCl_3$) δ: 2.15 (3H s, Ac), 2.93 (3H s, CO_2CH_3), 3.72 (3H s, SO_2CH_3), 3.6—4.0 (4H m, H-2,4,6$_{ax}$,5(or 6$_{eq}$)), 4.3—4.5 (1H m, H-6$_{eq}$ or 5), 4.98 (1H t, H-3; J=10 Hz), 5.32 (1H d, NH; $J_{2,NH}$=9 Hz; disappeared on addition of D_2O and DCl), 5.55 (1H s, PhC<u>H</u>), 5.95 (1H d, H-1; $J_{1,2}$=8.5 Hz).

Irradiation of H-1 changed the signals at δ 3.75—4.0. Irradiation at δ 3.84 (H-2,4,6$_{ax}$(or 6$_{eq}$)) caused the signals at δ 4.4 (H-6$_{eq}$ or 5), 4.98 (H-3), 5.32 (NH) and 5.95 (H-1) to a singlet, respectively.

Found: C, 48.77; H, 5.22; N, 3.08; S, 7.07%.

From 5′. Prepared in the same way as described above from **5′** (100 mg) giving **6**, 28 mg (25%) and **6′**, 62 mg (56%).

4,6-O-Benzylidene-2-deoxy-3-iodo-2-methoxycarbonylamino-α-L-gluco and α-L-allo(?)-hexopyranose (8 and 8′). A solution of **5** or **5′** (2.5 g) and sodium iodide (25 g) in DMF (30 ml) was heated at 100 °C for 1.5 hr. After addition of chloroform (350 ml), the organic layer was washed with 10% sodium thiosulfate solution (400 ml) and water (400 ml). The solution was dried over sodium sulfate and evaporated to leave a residue, which was shaken with benzene–ethyl acetate (3: 1, 20 ml). The insoluble product was recrystallized from methanol to give needles of **8**, 878 mg (35%), mp 219—221 °C (decomp.); $[\alpha]_D^{22}$ +93.5 °→+29.5 ° (*c* 1, pyridine); R_f 0.36 (benzene–ethyl acetate 2: 1); PMR (in $CDCl_3$+D_2O) δ: 3.69 (1H s, CO_2CH_3), 5.28 (1H d, H-1; $J_{1,2}$=3 Hz), 5.72 (1H s, PhC<u>H</u>).

Found: C, 40.81; H, 4. 08; N, 2.90; I, 28.70%. Calcd for $C_{15}H_{18}NO_6I$: C, 41.40; H, 4.17; N, 3.22; I, 29.16%.

The benzene–ethyl acetate soluble product was purified by

column chromatography with benzene–ethyl acetate (3: 1) to give **8′**, 945 mg (35%), mp 190—192 °C (decomp.); $[\alpha]_D^{23}$ +59.4 ° (*c* 1, $CHCl_3$) (the value kept constant for 20 hr), $[\alpha]_D^{23}$ +59.1 °→+20.1 ° (*c* 0.7, pyridine); R_f 0.36 (benzene–ethyl acetate 2: 1); PMR (in $CDCl_3+D_2O$) δ: 3.73 (3H s, CO_2CH_3), 5.15 (1H d, H-1; $J_{1,2}$=3.5 Hz), 5.70 (1H s, PhCH). Due to its unstable nature, the compound could not be successfully analyzed.

4,6-O-Benzylidene-2, 3-dideoxy-2-methoxycarbonylamino-α-L-ribo-hexopyranose (9). To a solution of **8** (641 mg) in dioxane (25 ml), triethylamine (0.08 ml) and Raney nickel were added and the mixture was shaken under hydrogen (50 lb. in^{-2}) at room temperature. After 5 hr, Raney nickel was replaced with the fresh one and the reaction was continued for further 6 hr. The solution was evaporated and the residue was extracted with ethyl acetate. The solution was washed successively with saturated sodium hydrogen sulfate solution, sodium hydrogen carbonate solution, and water, dried over sodium sulfate and evaporated to give a solid of **9**, 443 mg (97%).

A similar preparation from **8′** (616 mg) gave **9**, 413 mg (94%), mp 201—203 °C; $[\alpha]_D^{22}$ −11.7 ° (*c* 1, dioxane; the value kept constant for 20 hr); R_f 0.32 (benzene–ethyl acetate 2: 1); positive to TTC; PMR (in $CDCl_3$ $+D_2O$) δ: 1.75—2.35 (2H m, H-3,3′), 3.74 (3H s, CO_2CH_3), 5.19 (1H d, H-1; $J_{1,2}$=3.5 Hz), 5.66 (1H s, PhCH).

Found: C, 58.04; H, 6.13; N, 4.50%. Calcd for $C_{15}H_{19}NO_6$: C, 58.24; H, 6.19; N, 4.53%.

2, 3-Dideoxy-2-methoxycarbonylamino-L-ribo-hexose (10). A suspension of **9** (594 mg) in 70% aqueous acetic acid (21 ml) was heated at 95 °C for 5 min. Evaporation *in vacuo* and coevaporation with water gave a syrup. An aqueous solution (40 ml) of the syrup was washed with ether (40 ml ×2) and evaporated to give a solid, 405 mg (95%); $[\alpha]_D^{23}$ −56 °→−38 ° (*c* 1, methanol).

Found: C, 43.21; H, 6.74; N, 6.10%. Calcd for $C_8H_{15}NO_6$: C, 43.43; H, 6.84; N, 6.33%.

3-Deoxy-α-L-ribo-hexofurano[2, 1-d]-2-oxazolidinone (11). An aqueous solution (4.7 ml) of **10** (238 mg) and barium hydroxide octahydrate (470 mg) was heated at 70 °C for 5 min. After cooling, carbon dioxide was introduced and the reaction mixture was centrifuged. The aqueous layer separated was evaporated to give a residue, which was chromatographed on a column of silica gel with chloroform–ethanol–17% aqueous ammonia (10: 4: 0.6). Evaporation of the fraction containing the main product gave a glassy solid. Recrystallization from methanol–ether gave needles of **11**, 184 mg (94%), mp 127—128 °C; $[\alpha]_D^{23}$ +43 ° (*c* 1, methanol); IR (KBr): 1730, 1750 (sh) cm^{-1}; PMR (in D_2O) δ: 1.96 (1H octet, H-3; J=5.5, 10, 13 Hz), 2.07 (1H octet, H-3′; J=1.5, 5.5, 13 Hz), 3.56 (1H q, H-6; J=6.5, 11.5 Hz), 3.67 (1H q, H-6′; J=4, 11.5 Hz), 3.95 (1H d, H-5; J=~4.5, ~4.5, 6.5 Hz), 4.33 (1H m, H-4), 4.60 (1H d, H-2; J=~1.5, ~5.5, ~5.5 Hz), 6.18 (1H d, H-1; J=5.5 Hz); $J_{1,2}$=5.5 Hz, $J_{2,3}$=5.5 Hz, $J_{2,3'}$=−1.5 Hz, $J_{3,3'}$=13 Hz, $J_{3,4}$=10 Hz, $J_{3',4}$=5.5 Hz, $J_{4,5}$=4.5 Hz, $J_{5,6}$=6.5 Hz, $J_{5,6'}$=4 Hz, $J_{6,6'}$=11.5 Hz; mass spectrum: *m/e* 190 (M^+ +1).

Found: C, 44.69; H, 5.75; N, 7.22%. Calcd for $C_7H_{11}NO_5$: C, 44.44; H, 5.86; N, 7.41%.

5,6-Di-O-acetyl-3-deoxy-α-L-ribo-hexofurano[2,1-d]-2-oxazolidinone (12). To a solution of **11** (35 mg) in pyridine (1 ml), acetic anhydride (0.09 ml) was added and the solution was allowed to stand at room temperature overnight. After a drop of water was added, the solution was evaporated and the residue was extracted with chloroform. The solution was washed with water, dried over sodium sulfate and evaporated to give a syrup, 37 mg (74%), which was crystallized from ether to give needles of **12**, mp 89—91 °C; $[\alpha]_D^{23}$ −6 ° (*c* 0.7, methanol); IR (KBr): 1740 cm^{-1}; PMR (in $CDCl_3$–D_2O) δ: 1.75—2.3 (2H m, H-3,3′), 2.07 and 2.09 (each 3H s, Ac), 4.11 (1H q, H-6; J=6, 12 Hz), 4.41 (1H q, H-6′; J=3.5, 12 Hz), 4.3—4.55 (3H m, H-2,4,6), 5.23 (1H d, H-5; J=3.5, 5.5, 5.5 Hz), 6.08 (1H d, H-1; J=5.5 Hz); mass spectrum: *m/e* 274 (M^+ +1).

Found: C, 48.15; H, 5.41; N, 4.83%. Calcd for $C_{11}H_{15}NO_7$: C, 48.35; H, 5.53; N, 5.13%.

2-Amino-2, 3-dideoxy-L-ribo-hexopyranose Hydrochloride (1). A solution of **11** (28 mg) in 1M hydrochloric acid (0.9 ml) was kept at 40 °C for 17 hr. Evaporation *in vacuo* gave a syrup, which was precipitated from methanol–acetone to give a solid of **1**, 23 mg (78%); $[\alpha]_D^{23}$ −48.6 ° (*c* 1.4, water; final value) (D-isomer[5]), $[\alpha]_D^{25}$ +43.9 ° (water)); $R_{f\,2\text{-amino-2-deoxy-L-glucose}}$ 1.26 (ppc with 1-butanol–pyridine–water–acetic acid 6: 4:3: 1 and Toyo-Roshi No. 51 of Toyo-Roshi Co.).

Found: C, 36.45; H, 6.78; N, 6.82; Cl, 17.99%. Calcd for $C_6H_{13}NO_4 \cdot HCl$: C, 36.10; H, 7.07; N, 7.02; Cl, 17.76%.

The authors are grateful to Dr. Hamao Umezawa, Director of Institute of Microbial Chemistry, for his support and encouragement.

References

1) S. Takasawa, R. Utahara, M. Okanishi, K. Maeda, and H. Umezawa, *J. Antibiot.* (Tokyo), **21**, 477 (1968).
2) T. Yamada, D. Tipper, and J. Davies, *Nature*, **219**, 288 (1968).
3) H. Naganawa, S. Kondo, K. Maeda, and H. Umezawa, *J. Antibiot.* (Tokyo), **24**, 823 (1971).
4) W. Meyer zu Reckendorf and W. A. Bonner, *Tetrahedron*, **19**, 1711 (1963).
5) T. Oda, T. Mori, and Y. Kyotani, *J. Antibiot.* (Tokyo), **24**, 503 (1971).
6) H. Arita, K. Fukukawa, and Y. Matsushima, This Bulletin, **45**, 3614 (1972).
7) R. Kuhn and W. Kirschenlohr, *Justus Liebigs Ann. Chem.*, **600**, 115 (1956).
8) W. Wesemann and F. Zilliken, *ibid.*, **695**, 209 (1966).
9) N. A. Hughes and P. R. H. Speakman, *J. Chem. Soc.*, **1965**, 2236.
10) A. C. Richardson, *Carbohyd. Res.*, **10**, 395 (1969).
11) Y. Takagi, T. Miyake, T. Tsuchiya, S. Umezawa, and H. Umezawa, *J. Antibiot.* (Tokyo), **26**, 403 (1973).
12) A. C. Richardson, *J. Chem. Soc.*, **1964**, 5364.
13) W. H. Bromund and R. M. Herbst, *J. Org. Chem.*, **10**, 267 (1945).
14) M. Viscontini and J. Meier, *Helv. Chim. Acta*, **35**, 807 (1952).

Influence of Anhydrous Hydrogen Fluoride on Hen Egg-White Lysozyme. II. Effects on Reduced Hen Egg-White Lysozyme

Saburo AIMOTO and Yasutsugu SHIMONISHI

Institute for Protein Research, Osaka University, Yamada-kami, Suita, Osaka 565

(Received October 8, 1975)

The influences of anhydrous hydrogen fluoride on reduced hen egg-white lysozyme were investigated under standard conditions for peptide synthesis. 1) Enzymatically fully active protein was recovered in poor yield (5%) from reduced hen egg-white lysozyme after treatment with hydrogen fluoride. 2) The yield (29—33%) was improved by addition of 1,4-butanedithiol or L-cysteine during treatment of reduced hen egg-white lysozyme with hydrogen fluoride. 3) Tetragonal crystals which were indistinguishable from those of native hen egg-white lysozyme were recovered after treatment of reduced hen egg-white lysozyme with hydrogen fluoride in the presence of 1,4-butanedithiol, anisole and amino acid derivatives. Thus, the original intact lysozyme could be recovered from an HF-solution of the reduced form.

In studies on the chemical synthesis of the well-characterized protein molecule, native hen egg-white lysozyme (HEL), we examined its recovery after exposure of this enzyme and its derivatives to anhydrous liquid hydrogen fluoride (HF) under usual conditions for peptide synthesis. In the previous paper[1] we reported the effect of HF on the native form of HEL under usual conditions of peptide synthesis and a method for recovering fully active HEL from an HF-solution of native HEL.

This paper reports studies on the influence of HF on the reduced form of HEL. It was found that when reduced HEL was treated with HF under usual conditions for peptide synthesis, its enzymatic activity decreased. In contrast when native HEL was treated with HF, fully active HEL was recovered in good yield (about 50%). Thus there was a difference in the effects of HF on the native and reduced forms of HEL. Next, the effect of thiol compounds during treatment of reduced HEL with HF was examined, because thiol compounds prevent modifications, such as oxidation of proteins. Studies were also made on the effect of treating reduced HEL with HF in the presence of amino acid derivatives, which liberate cations on treatment with HF. Anisole has generally been used as a scavenger of cations liberated from protected amino acids and peptides in acidic medium[2] or on treatment with HF[3]. Therefore, we also examined the effect of the presence of anisole in preliminary experiments on deblocking reactions of protected derivatives[4] of HEL. The results showed that intact, regenerated HEL could be recovered after treating reduced HEL with HF under conditions for peptide synthesis.

Experimental

Materials. Hen egg-white lysozyme (6×crystallized Lot. No. 7103) and spray-dried cells of *Micrococcus lysodeikticus* (Lot. No. 21—88—778) were purchased from Seikagaku Biochemicals (Tokyo). Sephadex was purchased from Pharmacia Co. (Uppsala). Hydrogen fluoride was a product of Daikin Ind. Co. (Osaka). Urea of reagent grade was recrystallized from ethanol before use. All other chemicals used were of analytical grade.

Treatment of Reduced HEL with HF. Reduced HEL was prepared from native HEL by the method of Saxena and Wetlaufer,[5] and after desalting, it was frozen and lyophilized. The freeze-dried powder of reduced HEL (*ca.* 15 mg) was treated with HF (9 ml) under similar conditions to those used with native HEL.[1] The residue of the HF-treated reduced HEL was dissolved in 0.2 M sodium phosphate buffer solution (15 ml) at pH 8.5 containing 1 M mercaptoethanol, 8 M urea and 0.2 mM EDTA·2Na and the solution was stirred overnight at room temperature. Then it was adjusted to below pH 4 by addition of glacial acetic acid and passed through a column of Sephadex G-10 (3.2×60 cm) in 1 M acetic acid. The fractions containing protein were collected and treated under the conditions described below for refolding reduced HEL. Then, the solution containing regenerated HEL was adjusted to pH 4.5—5 with glacial acetic acid. The regenerated HEL was adsorpted on a CM-cellulose column (carboxylic acid cycle), and eluted with 0.3 M sodium phosphate buffer solution at pH 8.0.

Refolding of Reduced HEL to Native HEL. Refolding of reduced HEL (*ca.* 10^{-6} M) to form native HEL was achieved in 0.08 M tris-buffer solution at pH 8.0 containing 5.4×10^{-3}M L-cysteine and 4.8×10^{-4} M L-cystine at 37 °C following the procedure of Saxena and Wetlaufer.[5]

Gel-filtration and Ion-exchange Chromatography of HF-treated Reduced HEL. HF-treated HEL refolded as described above was chromatographed on Sephadex G-50 (2×95 cm) using buffer containing 1M acetic acid and 5 M urea, using the method described in the previous paper.[1] The fractions separated by gel-filtration on Sephadex G-50 were chromatographed on Bio-rex 70 (1×78 cm) using 0.2 M sodium phosphate buffer solution at pH 7.18.

Enzyme Assays. The specific activity of HF-treated HEL was determined by measuring the initial rate of lysis of *Micrococcus lysodeikticus* cells spectrophotometrically at 540 nm following the method described previously,[1] with native HEL, purified on Sephadex G-50, as a standard.

Ultraviolet Spectra. UV-absorption spectra were measured using a Hitachi-spectrophotometer, type-124, equipped with a recording attachment. Spectra were measured at 25 °C.

Crystallization of HF-treated HEL. Crystallization was carried out by the method of Berthou and Jolles[6] with the modifications described in the previous paper.[1]

Results and Discussion

First reduced HEL was treated with HF at 0 °C for 60 min, since it has been found that intact HEL is recovered in good yield (about 50%), when native HEL is treated with HF under these conditions. The HF was completely evaporated off from the HF-solution

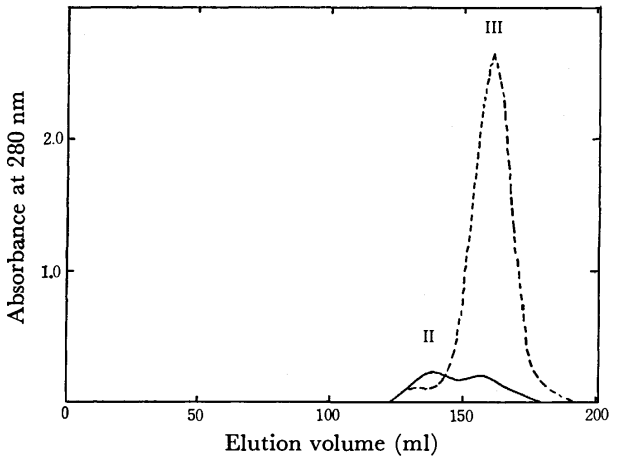

Fig. 1. Sephadex G-50 gel-filtration of reduced HEL after treatment with HF at 0 °C for 60 min and refolding at pH 8.0. The column (2.2×95 cm) was eluted with buffer containing 1M acetic acid and 5M urea. The flow rate was 10 ml per hr.
—: reduced HEL refolded after HF-treatment, — : reduced HEL refolded without HF-treatment.

of reduced HEL *in vacuo*, and the residue was mixed with 0.2 M sodium phosphate buffer solution at pH 8.5 containing 1 M mercaptoethanol, 8 M urea and 0.2 mM EDTA·2Na. This buffer was used because it was thought that reduced HEL might aggregate by forming random disulfide linkages in HF and that this buffer solution might dissociate the aggregates, because it has been used for reducing native enzyme.[5] In fact the residue did aggregate. However, the aggregates did not easily dissolve in this buffer solution. The supernatant was separated from aggregated material and desalted and then treated under the conditions used for refolding reduced HEL. The refolded protein was desalted, lyophilized and chromatographed on Sephadex G–50 in 1 M acetic acid and 5 M urea buffer solution, as shown in Fig. 1. The recovery of a fraction (named fraction III), eluted in the same position as native HEL, corresponded to only 5% of the original native HEL. The recovery of this fraction was low probably because reduced HEL aggregated to sparingly soluble material on treatment with HF.

Next, reduced HEL was treated with HF under the same conditions but in the presence of the thiol compounds listed in Table 1. The residue of HF-treated reduced HEL dissolved in 0.2 M sodium phosphate buffer solution containing 1 M mercaptoethanol, 8 M urea and 0.2 mM EDTA·2Na. This protein fraction was desalted by gel-filtration on Sephadex G-10, treated under the conditions leading to refolding of reduced HEL and then chromatographed on Sephadex G-50. It was found that the recovery of original HEL, eluted in the same position as native HEL, was improved considerably using L-cysteine or 1,4-butanedithiol as the thiol compound and was improved slightly using dithiothreitol. However, scarcely any fraction III was obtained using 2-mercaptoethanol. The chromatogram of regenerated protein on Sephadex G–50 obtained using 1,4-butanedithiol as a thiol compound is shown in Fig. 2. The amount of fraction III in Fig. 2 corresponds to the recovery shown in Table 1.

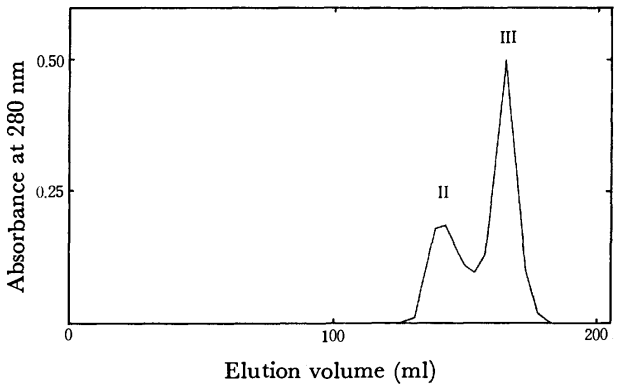

Fig. 2. Sephadex G-50 gel-filtration of reduced HEL after treatment with HF at 0 °C for 60 min in the presence of 1,4-butanedithiol and refolding at pH 8.0. The column (2.0×95 cm) was eluted with buffer containing 1M acetic acid and 5M urea. The flow rate was 10 ml per hr.

TABLE 1. EFFECTS OF THIOL COMPOUNDS ON THE RECOVERY OF FRACTION III FROM HF-TREATED REDUCED HEL

Exp. No.	Thiol compound	HF-treatment	Recovery of fraction III (%)	Specific activity[a] of fraction III (%)
1	—	—[b]	65	98
2	—	0 °C, 60 min	5	95
3	$HSCH_2CH_2OH$[c]	0 °C, 60 min	0—1	43
4	L-Cysteine·HCl ·H_2O[c]	0 °C, 60 min	24	97
5	L-Cysteine[c]	0 °C, 60 min	29	98
6	1,4-Butane-dithiol	0 °C, 60 min	33	99
7	Dithiothreitol[d]	0 °C, 60 min	19	100

a) 6x recrystallized HEL purified on Sephadex G-50 was used as a standard, b) reduced HEL was refolded without HF-treatment, c) 0.8 mmole of thiol compound was added per μmol of protein, d) 0.4 mmole of thiol compound was added per μmol of protein.

Next, we made preliminary experiments on the effect of removal of protecting groups from protected derivatives[4] of HEL. Reduced HEL was first treated with HF in the presence of anisole. 1,4-Butanedithiol was also added to the reaction mixture, because among the thiol compounds tested it caused the greatest improvement in recovery of the original enzyme, as shown in Table 1. When reduced HEL was treated with HF at 0 °C for 60 min with 1,4-butanedithiol, the recovery of the original enzyme was 14% in the presence of anisole and 33% in its absence. The reason for this lower recovery in the presence of anisole seemed to be that the excess anisole could not easily be removed from the HF-reaction mixture, so that the HF could not be removed rapidly. On increase in the time of reaction (120—240 min) of reduced HEL with HF at 0 °C, the amount of fraction III decreased. Furthermore, the yield of fraction III was very low when reduced HEL was treated with HF at a higher temperature (25 °C), even after reaction for only 30 min. These results are summarized in Table 2.

Table 2. Recoveries (%) of fraction III, from reduced HEL (15 mg) treated with HF (9 ml) under various conditions in the presence of 1,4-butanedithiol (0.3 ml) and anisole (1 ml), refolded at pH 8.0 and chromatographed on Sephadex G-50

	30 min	60 min	120 min	240 min
0 °C	17	14	4.1	2.4
25 °C	1.1	0.5	0.6	0.3

Reduced HEL was treated with HF in the presence of anisole, 1,4-butanedithiol and amino acid derivatives, which bind protecting groups and liberate them as cations on treatment with HF. The amino acid derivatives used were N^{ε}-benzyloxycarbonyl-L-lysine, N^{α}-benzyloxycarbonyl-*S*-benzyl-L-cysteine and *S*-*p*-methoxybenzyl-L-cysteine which liberate the benzyl group on treatment with HF, N^{α}-benzyloxycarbonyl-N^{ω}-tosyl-L-arginine which liberates a tosyl group, *t*-butyloxycarbonyl-glycine which liberate a *t*-butyl group and N^{ω}-nitro-L-arginine which liberates a nitro group. The results in Table 3 show that most of these amino acid derivatives did not affect the yield of fraction III but N^{ω}-nitro-L-arginine decreased the yield greatly. The reason for this is unknown.

Table 3. Effects of various amino acid derivatives on the recovery of fraction III from HF-treated reduced HEL

Exp. No.	Amino acid derivative	(mmole)[a]	Recovery of fraction III (%)
1	H-Lys(Z)-OH	1.0	13
2	Z-Cys(Bzl)-OH	0.5	15
3	H-Cys(Bzl(OMe))-OH	1.0	13
4	Z-Arg(Tos)-OH	1.0	16
5	Boc-Gly-OH	1.0	14
6	H-Arg(NO_2)-OH	1.0	3

a) Reduced HEL (15 mg), 1,4-butanedithiol (0.3 ml), anisole (1 ml) and the indicated amino acid derivatives (0.5 mmol or 1.0 mmol) were mixed and treated with HF (9 ml) at 0 °C for 60 min.

Reduced HEL was treated with HF 0 °C for 60 min in the presence of the mixture of amino acid derivatives given in Fig. 3. The regenerated protein fraction was chromatographed on Sephadex G-50 using buffer solution containing 1 M acetic acid and 5 M urea, as shown in Fig. 3. The amount of fraction III obtained was 33% of the initial amount of enzyme. This yield was better than those obtained on treatment of reduced HEL with HF in the presence of any of the amino acid derivatives alone. When fraction III of Fig. 3 was subjected to chromatography on Bio-rex 70 at pH 7.18, the main fraction eluted in the position of native HEL (Fig. 4) was fully active on *Micrococcus lysodeikticus* cells, and it had the same UV-spectrum as native HEL, as shown in Fig. 5. During this chromatography, a fairly large fraction with biological activity was eluted in front of the main fraction, but its properties were not examined. The main fraction in Fig. 4 was desalted on Sephadex G-10 and lyophilized. The lyophilized

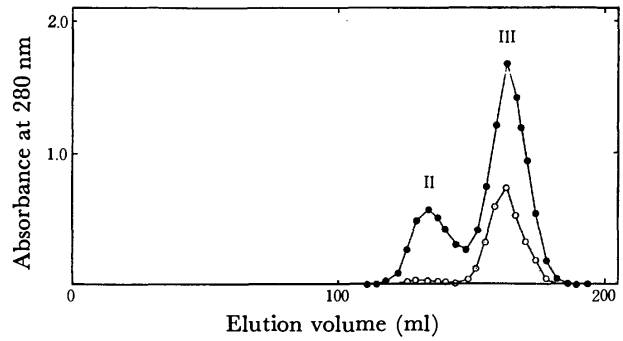

Fig. 3. Sephadex G-50 gel-filtration of reduced HEL treated with HF. The column (2.0×95 cm) was eluted with buffer containing 1M acid acetic and 5M urea. Reduced HEL (38 mg) was mixed with anisole (1.5 ml, 14 mmol), 1,4-butanedithiol (1.0 ml, 8.8 mmol), Z-Arg(Tos)-OH (231 mg, 0.5 mmol), H-Cys (Bzl)-OH (106 mg, 0.5 mmol), H-Cys(Bzl(OMe))-OH·HCl (130 mg, 0.5 mmol) and Boc-Gly-OH (88 mg, 0.5 mmol), treated with HF (15 ml) and refolded at pH 8.0. -●-: HF-treated reduced HEL, -○-: Native HEL.

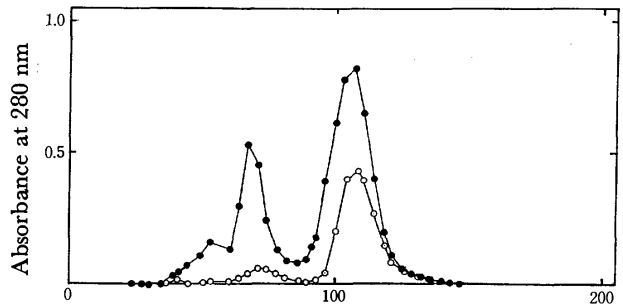

Fig. 4. Ion-exchange chromatogram of HEL on Bio-rex 70. The column (1×78 cm) was eluted with 0.2 M sodium phosphate buffer solution (pH 7.18). The flow rate was 16 ml per hr.
-●-: Fraction III of Fig. 3, -○-: Native HEL.

Table 4. Effects of various compounds on the recovery of fraction III from HF-treated native HEL

Compound	Average recovery of fraction III (%)	Ratio
1) —[a]	65	100
2) None	25	38
3) 1,4-Butanedithiol[b]	36	55
4) L-Cysteine[b]	32	49
5) L-Cysteine·HCl·H_2O[b]	32	49
6) $HSCH_2CH_2OH$[b]	0	0
7) L-Methionine[b]	34	52
8) L-Alanine[c]	26	40
9) L-Tryptophan[d]	18	28
10) L-Tryptophan[e]	3	5
11) L-Tryptophan[f]	0	0

a) Native HEL was reduced and refolded without HF-treatment. The amounts of compounds added per μmole of native HEL were: b) 2.5 mmol, c) 4.0 mmole, d) 0.5 mmol, e) 1.8 mmol and f) 2.4 mmol.

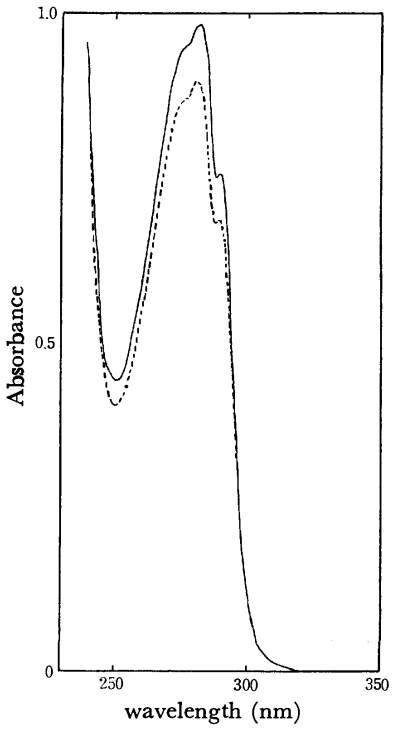

Fig. 5. Ultra-violet absorption spectra of the main fraction of Fig. 4 (—) and native HEL (—). Solvent: 0.2 M sodium phosphate buffer (pH 7.18).

powder was treated under conditions inducing crystallization. The crystals obtained were like those of native HEL, as shown in Fig. 6.

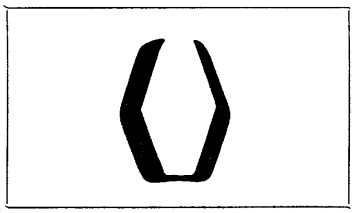

Fig. 6. Microphotograph of crystals of the material from the main fraction of Fig. 4. Crystals were obtained by the method of Berthou and Jolles.[6]

Native HEL was treated with HF under the same conditions as reduced HEL in the presence of various thiol compounds. After treatments similar to those used with reduced HEL the regenerated protein was subjected to chromatography on Sephadex G-50 using buffer solution containing 1 M acetic acid and 5 M urea. The yields of fraction III, eluted at the same position as native HEL, are summarized in Table 4. The recovery of the original enzyme from native HEL treated with in the presence of 1,4-butanedithiol and L-cysteine were 32 and 36%, respectively, while the recovery of original enzyme from native HEL treated with HF in the absence of thiol compounds was 25%. Thus thiol compounds also improved the yield on treatment of native HEL with HF. Since native HEL aggregates slightly in HF,[1] the thiol compounds seemed to prevent both this aggregation and also structural modification of HEL. It was also found that the presence of L-tryptophan during treatment of native HEL with HF greatly decreased the recovery of the original enzyme under the present conditions (Table 4).

The present results show that material with similar properties to original HEL could be recovered in fairly good yield and also in a crystalline state after treatment of reduced HEL with HF in the presence of a thiol compound such as 1,4-butanedithiol under usual conditions for peptide synthesis. In further studies on the chemical synthesis of HEL attempts are in progress to recover HEL with the same properties as native HEL from the *N*-benzyloxycarbonyl derivative of native HEL and the *S*-*p*-methoxybenzyl-derivative of reduced HEL.[4]

References

1) S. Aimoto and Y. Shimonishi, This Bulletin, **48**, 3293 (1975).

2) F. Weygand and W. Steglich, *Z. Naturforsch.*, **14b**, 472 (1959).

3) S. Sakakibara, Y. Shimonishi, M. Okada, and Y. Kishida, "Peptides," Proc, 8th European Peptide Symp., ed. by H. C. Beyermann, *et al.*, North Holland Publishing Co., Amsterdam (1967), p. 44; S. Sakakibara, Y. Shimonishi, Y. Kishida, M. Okada, and H. Sugihara, This Bulletin, **40**, 2164 (1967).

4) S. Aimoto and Y. Shimonishi, unpublished data; the derivatives synthesized include the *N*-bezyloxycarbonyl-derivative of native HEL and the *S*-benzyl, *S*-*p*-methoxybenzyl-, and *N*-benzyloxycarbonyl-*S*-*p*-methoxybenzyl-derivatives of reduced HEL.

5) V. P. Saxena and D. B. Wetlaufer, *Biochemistry*, **9**, 5015 (1970).

6) J. Berthou and P. Jolles, *FEBS Lett.*, **31**, 189 (1973).

Reaction of Dimethylphenacylsulfonium Bromide with *N*-Nitrosoacetarylamides and Reactions of the Products with Nucleophiles†

A. Sami SHAWALI* and A. Osman ABDELHAMID**

Department of Chemistry, Faculty of Science, University of Kuwait, State of Kuwait

***Department of Chemistry, Faculty of Science, University of Cairo, Giza, Egypt*

(Received December 7, 1974)

The azo coupling of dimethylphenacylsulfonium bromides (I) with *N*-nitrosoacetanilides in nonaqueous solvents, and with diazotized aniline in aqueous media gave 2-bromophenylglyoxal 2-arylhydrazones (V) and the tetrazine (VI), respectively. V reacted with nucleophiles displacing the bromide. Treatment of V with bases gave VI *via* benzoylphenylnitrilimine (X). 1,3-Dipolar cycloadditions of X onto ethyl acrylate and acrylonitrile afforded the expected cycloadducts. The mechanisms of the reactions are outlined.

Recently it has been reported that the nitrosation of dimethylphenacylsulfonium bromide (Ia) affords II[1] or III[2] depending on the reaction conditions. In view of the similarity between the azo coupling and nitrosation reaction, it was of interest to investigate the azo coupling of I in aqueous and nonaquous media to see whether or not similar effects would be observed. An earlier report[3] claimed that coupling of benzenediazonium sulfate to Ia gives IV. The structure of the latter cannot be sustained, however. The azo coupling of I in nonaqueous media has not yet been explored. We now report the results of this reaction and some properties of the product formed.

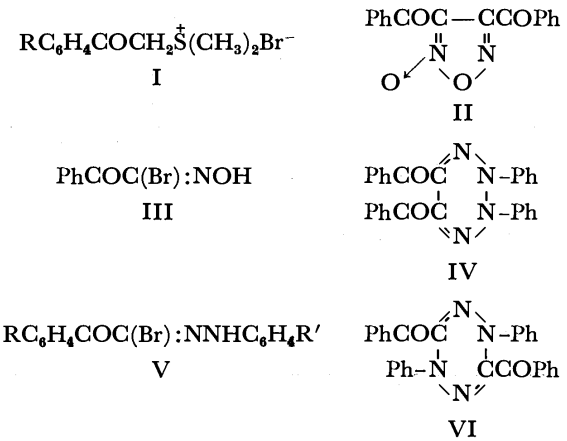

a, R=H; b, R=4-Me; c, R=4-Br; d, R=4-NO_2

Results and Discussion

Treatment of Ia with *N*-nitrosoacetanilide in ether gave 2-bromophenylglyoxal 2-phenylhydrazone (Va, R=R′=H). The latter was also obtained when other organic solvents were used in place of ether. The structure of Va was established by elemental analysis, by molecular weight determination, and by analysis of its spectra (see Experimental). The reactions summarized in Scheme 2 also support structure Va for the reaction product. Similar treatments of Ib—d with *N*-nitrosoacetanilides in EtOH gave the products Vb—g (Table1).

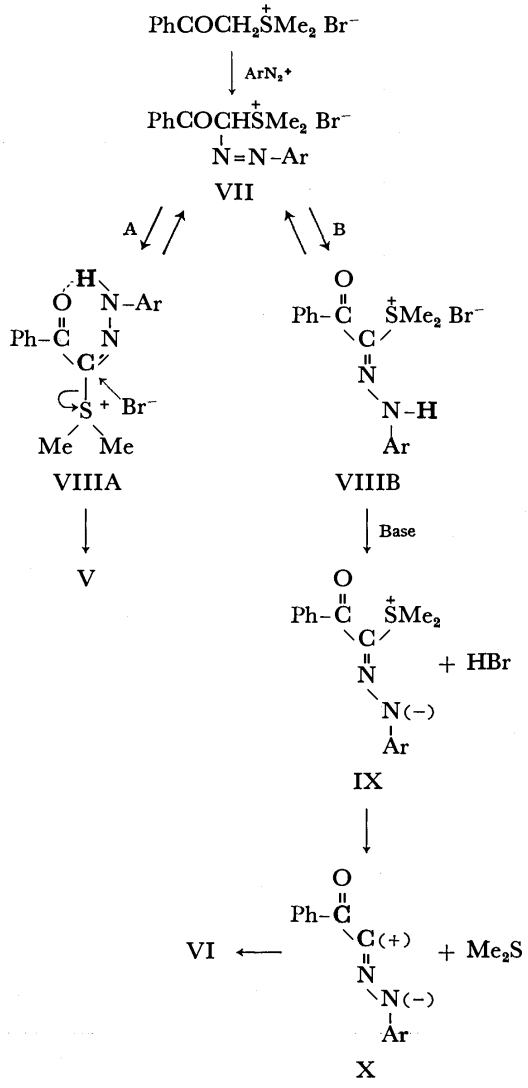

A, in nonaqueous media; B, in aqueous media

Scheme 1.

Reaction of Ia with benzenediazonium chloride in NaOAc buffered solutions gave 1,4-diphenyl-3,6-dibenzoyl-1,4-dihydro-1,2,4,5-tetrazine (VI). The latter was identified by mixed melting point with an authentic sample[4] and by spectral analysis. In addition, the formation of VI from Va upon treatment with bases

* To whom all inquiries should be addressed.

† Taken in part from the Ph. D. Thesis of one of the authors (A. O. A).

Table 1. 2-Bromophenylglyoxal 2-arylhydrazones (V)
$RC_6H_4COC(Br):NNHC_6H_4R'$

Compound No.	R	R′	Mp[a] °C	Formula	Bromine, % Calcd	Bromine, % Found	λ_{max}^{EtOH} (log ε)
Va	H	H	114[c]	$C_{14}H_{11}BrN_2O$	26.36	26.11	372(4.169); 253(4.257)
Vb	H	4-Me	152	$C_{15}H_{13}BrN_2O$[b]	25.19	24.89	378(4.198); 253(4.258)
Vc	H	4-MeO	141	$C_{15}H_{13}BrN_2O_2$	23.98	24.10	386(4.223); 310(3.727); 253(4.329)
Vd	H	4-Cl	188	$C_{14}H_{10}ClBrN_2O$	23.67	23.48	372(4.205); 257(4.332); 229(4.333)
Ve	4-Me	H	125	$C_{15}H_{13}BrN_2O$	25.19	25.00	368(4.195); 257(4.214); 229(4.268)
Vf	4-Br	H	185	$C_{14}H_{10}Br_2N_2O$	41.83	41.78	374(4.178); 261(4.266); 227(4.296)
Vg	4-NO_2	H	188	$C_{14}H_{10}BrN_3O_3$	22.95	22.90	384(4.014); 320(3.908); 270(4.197) 229(4.364)

a) All compounds were crystallized from AcOH, except Va and Ve from EtOH. b) Anal. Calcd (Found): C, 56.80 (56.62); H, 4.13 (4.00); N, 8.83 (8.57)%. c) Lit., mp 113—114 °C.

Table 2. Substituted 2-(phenylthio)phenylglyoxal 2-phenylhydrazones (XI)

Compound No.	R	R′	Mp[a] °C	Formula	Sulfur, % Calcd	Sulfur, % Found	λ_{max}^{EtOH} (log ε)
	$RC_6H_4COC(SC_6H_5):NNHC_6H_4R'$						
XIa	H	H	122	$C_{20}H_{16}N_2OS$[b]	9.64	9.41	370(4.278); 275(4.057); 243(4.306)
XIb	H	4-Me	137	$C_{21}H_{18}N_2OS$	9.26	9.31	376(4.258); 278(3.986); 245(4.275)
XIc	H	4-Cl	170	$C_{20}H_{15}ClN_2OS$	8.74	8.58	370(3.429); 290(3.304); 250(4.543)
XId	H	4-MeO	130	$C_{21}H_{18}N_2O_2S$	8.85	8.54	386(4.476); 310(3.945); 242(4.506)
XIe	4-Br	H	129	$C_{20}H_{15}BrN_2OS$	7.79	7.60	372(4.185); 270(4.171); 242(4.221)
	$RC_6H_4COC(SC_6H_4Me\text{-}p):NNHC_6H_4R'$						
XIf	H	H	171	$C_{21}H_{18}N_2OS$[c]	9.26	9.30	368(4.443); 280(4.262); 242(4.522)
XIg	H	4-Me	126	$C_{22}H_{20}N_2OS$	8.89	8.79	378(4.335); 280(4.089); 244(4.390)
XIh	H	4-MeO	120	$C_{22}H_{20}N_2O_2S$	8.51	8.38	386(4.091); 285(3.811); 244(4.158)
XIi	H	4-Cl	145	$C_{21}H_{17}ClN_2OS$	8.42	8.51	374(4.306); 275(4.155); 245(4.348)
XIj	4-Br	H	132	$C_{21}H_{17}BrN_2OS$	7.54	7.32	374(4.189); 270(4.189); 245(4.246)

a) All compounds were recrystallized from EtOH. b) Anal. Calcd (Found): C, 72.25 (72.00); H, 4.85 (4.51); N, 8.42 (8.33)%. c) Anal. Calcd (Found): C, 72.80 (72.54); H, 5.23 (5.10); N, 8.08 (7.89)%.

Table 3. 2-(*p*-Tolylsulfonyl)phenylglyoxal 2-arylhydrazones (XII)
$RC_6H_4COC(SO_2C_6H_4Me\text{-}p):NNHC_6H_4R'$

Compound No.	R	R′	Mp[a] °C	Formula	Sulfur, % Calcd	Sulfur, % Found	λ_{max}^{EtOH} (log ε)
XIIa	H	H	174	$C_{21}H_{18}N_2O_3S$[b]	8.47	8.24	352(4.262); 270(4.123); 249(4.229)
XIIb	H	4-Me	184	$C_{22}H_{20}N_2O_3S$	8.17	8.08	374(4.357); 273(4.163); 253(4.326)
XIIc	H	4-Cl	180	$C_{21}H_{17}N_2O_3SCl$	7.76	7.81	365(4.360); 272(4.218); 247(4.355)
XIId	H	4-MeO	154	$C_{22}H_{20}N_2O_4S$	7.85	7.70	390(4.399); 255(4.366); 229(4.399)
XIIe	4-Me	H	178	$C_{22}H_{20}N_2O_3S$	8.17	8.00	364(4.308); 275(4.201); 230(4.364)
XIIf	4-Br	H	158	$C_{21}H_{17}BrN_2O_3S$	7.01	6.96	369(4.301); 275(4.267); 255(4.274) 231(4.356)
XIIg	4-NO_2	H	200	$C_{21}H_{17}N_3O_5S$	7.57	7.39	370(4.156); 270(4.190); 255(4.210) 235(4.197)

a) All compounds were crystallized from AcOH. b) Anal. Calcd (Found): C, 66.64 (66.38); H, 4.79 (4.59); N, 7.41 (7.52)%.

supports its structure. These results indicate that the diazonium coupling product of Ia in aqueous media is VI, and not IV as proposed[3] previously.

The probable mechanism that accounts for the foregoing results is presented in Scheme 1. It is assumed that the configurations of the hydrazone intermediate VIII in the solvents determined the products obtained.[1]

A brief chemical study of the product V is summarized in Scheme 2. The results show that V is highly reactive and reacts with nucleophiles with displacement of its halogen atom, and with bases to form the 1,3-dipolar intermediate X, that readily undergoes dimerization and 1,3-dipolar cycloaddition reactions. The structures of the products XI—XV follow from their method of preparation, the physical data, and their independent syntheses. The orientation of the cycloadditions of X

Table 4. Substituted 2-cyanophenylglyoxal 2-phenylhydrazones (XIII)
$RC_6H_4COC(CN):NNHC_6H_4R'$

Compound No.	R	R′	Mp[a] °C	Formula	Nitrogen, % Calcd	Nitrogen, % Found	λ_{max}^{EtOH} (log ε)
XIIIa	H	H	135	$C_{15}H_{11}N_3O$	16.86	16.71	373(3.732); 280(3.605); 248(3.893)
XIIIb	H	4-Me	154	$C_{16}H_{13}N_3O$	15.96	16.01	384(4.301); 280(3.801)sh; 250(4.037)
XIIIc	H	4-Cl	174	$C_{15}H_{10}ClN_3O$	14.81	14.64	378(4.390); 280(3.869); 298(4.153)
XIIId	H	4-MeO	146	$C_{16}H_{13}N_3O_2$	15.04	14.88	400(4.185); 290(3.693)[b]; 250(3.914)
XIIIe	4-Me	H	149	$C_{16}H_{13}N_3O$	15.96	16.00	374(4.356); 285(3.909); 247(4.131)
XIIIf	4-Br	H	181	$C_{15}H_{10}BrN_3O$	12.80	12.63	370(4.375); 280(4.165); 245(4.376)
XIIIg	4-NO_2	H	233	$C_{15}H_{10}N_4O_3$	19.04	18.89	376(4.467); 265(4.200)

a) All compounds were recrystallized from EtOH. b) Broad band.

Table 5.

Compound No.	R	R′	Mp[a] °C	Formula	Nitrogen, % Calcd	Nitrogen, % Found	λ_{max}^{EtOH} (log ε)
1-Aryl-3-aroyl-5-ethoxycarbonyl-2-pyrazolines (XIV)							
XIVa	H	H	105	$C_{19}H_{18}N_2O_3$[b]	8.69	8.60	390(4.374); 254(4.244)
XIVb	H	4-Me	125	$C_{20}H_{20}N_2O_3$	8.33	8.07	400(4.299); 256(4.187)
XIVc	H	4-Cl	126	$C_{19}H_{17}ClN_2O_3$	7.85	7.69	390(4.330); 310sh(3.518); 260(4.179)
XIVd	4-Me	H	92	$C_{20}H_{20}N_2O_3$	8.33	8.11	392(4.375); 290sh(4.003); 253(4.189)
XIVe	4-Br	H	107	$C_{19}H_{17}BrN_2O_3$	6.98	6.69	398(4.283); 275sh(4.084); 260(4.126)
1-Aryl-3-aroyl-5-cyano-2-pyrazolines (XV)							
XVa	H	H	139	$C_{17}H_{13}N_3O$[c]	15.26	15.09	376(4.214); 240(4.142)
XVb	H	4-Me	118	$C_{18}H_{15}N_3O$	14.52	14.31	386(4.196); 248(4.134)
XVc	H	4-Cl	135	$C_{17}H_{12}ClN_3O$	13.56	13.48	374(4.442); 254(4.448)
XVd	H	4-MeO	135	$C_{18}H_{15}N_3O_2$	13.76	13.59	396(4.214); 244(4.181)
XVe	4-Br	H	165	$C_{17}H_{12}BrN_3O$	11.86	11.70	380(4.200); 270(4.200)

a) All compounds were recrystallized from EtOH. b) Anal. Calcd (Found): C, 70.79 (70.54); H, 5.63 (5.48)%.
c) Anal. Calcd (Found): C, 74.17 (73.88); H, 4.76 (4.54)%.

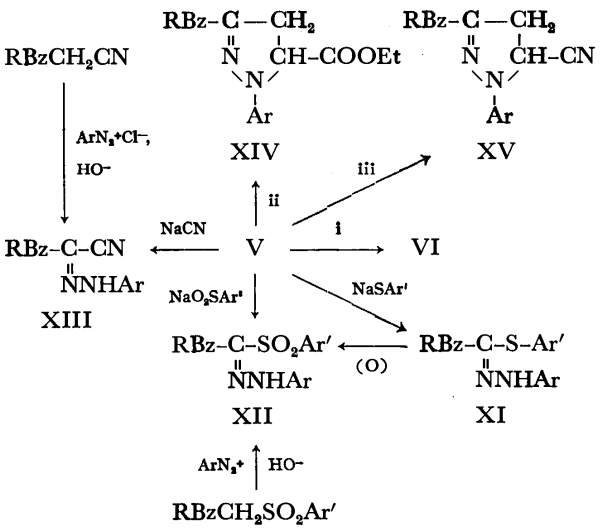

Reagents: i, Et_3N, NaOH, NaOPh, or NaOAc; ii, CH_2=CHCOOEt; iii, CH_2=CHCN
RBz=RC_6H_4CO; Ar=$R'C_6H_4$; Ar′=C_6H_5 or *p*-MeC_6H_4

Scheme 2.

can be interpreted in a manner similar to that proposed for benzoyl cyanide *N*-oxide;[11] *i.e.*, the resonance structures of X would be XVI, XVII, and XVIII, and its principal polarized structure would be XVIII:

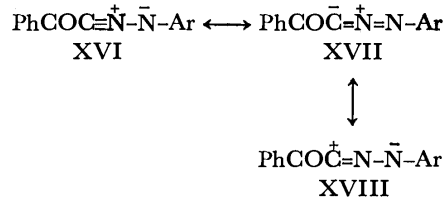

Experimental

Mp's are uncorrected. IR and UV spectra were recorded on Unicam SP1000 and Unicam SP8000 spectrophotometers respectively. NMR spectra were recorded on Varian T60-A spectrometer with TMS as an internal standard. Microanalyses were carried out by Alfred Bernhardt, Mikroanalytisches Laboratorium, West Germany.

Reaction of I with N-Nitrosoacetanilides. A mixture of Ia[9] (0.1 mol) and *N*-nitrosoacetanilide[10] (0.12 mol) was stirred in ether for 8 hr at room temperature. Removal of the solvent gave Va (62%), mp 114 °C (EtOH); spectral characteristics: ν_{max} (KBr) 1650 (PhCO), β3240 (NH) cm^{-1}; λ_{max}^{EtOH} (log ε) 372 (4.169), 253 (4.257) nm; δ ($CDCl_3$) 7.5—6.5 (m, 10, ArH), 8.05 (s, 1, NH) ppm. The product Va was also obtained (55—80%) when the reaction was repeated using dioxane, chloroform, acetone, or EtOH in place of ether. The products Vb—g (Table 1) were similarly prepared using EtOH as a solvent.

Reaction of Ia with Benzenediazonium Chloride. To Ia (0.02 mol) in 50 ml EtOH was added NaOAc (8 g, in 30 ml water). The mixture was chilled (0—5 °C), vigorously stirred, treated dropwise (25 min) with PhN_2Cl (0.021 mol), and kept in an ice chest (3 hr). The solid was collected, washed with water, and recrystallized from EtOH to give VI (67%), mp and mixed mp[4] 198 °C; λ_{max}^{EtOH} (log ε): 390 (2.749), 290sh (4.412), 265 (4.542); IR ν_{max} (KBr) 1670 (PhCO) cm^{-1}, NH band was absent; its NMR spectrum ($CDCl_3$) showed only an aromatic proton multiplet.

Reaction of Va with Bases. A mixture of Va (0.01 mol) in EtOH (30 ml) and NaOAc (1 g) in water (5 ml) was refluxed for 30 min and cooled. Working up the reaction mixture gave VI (70%); mp and mixed mp with the sample above 198 °C. VI was similarly obtained by using one equivalent of NaOH or two equivalents of Et_3N in place of NaOAc.

Reactions of V with Nucleophiles, General. Equimolecular quantities of V and the appropriate nucleophile (NaSAr, NaO_2SAr, or NaCN) in EtOH were stirred for 0.5—2 hr and left overnight at room temperature. The product was collected, washed with water and recrystallized from EtOH or AcOH. The compounds XI—XIII prepared are listed in Tables 2—4. The products XIIh and XIIIa proved to be identical with authentic samples.[6,7] Reaction of Va with NaOPh, when carried out in a similar manner, gave VI (68%). IR (KBr) of XII showed bands at 1314 and 1140 cm^{-1} due to $-SO_2-$ asymmetric and symmetric stretchings, and that of XIII exhibited a nitrile band at 2225 cm^{-1}. Both XII and XIII showed common bands at 1650 (PhCO) and 3260—3220 (hydrazone NH) cm^{-1}. UV spectral characteristics of XI—XIII are given in Tables 2—4.

Oxidation of XI. To a solution of XI (2 mmol) in AcOH was added 2 ml of hydrogen peroxide solution (33%); the mixture was left for two days at room temperature, then poured on water. Recrystallization of the product from AcOH gave the corresponding XII (73—78%). Mixed mp with samples prepared above showed no depression.

Formation of XIV and XV, General. A stirred cold solution of equimolecular quantities (5 mmol each) of V and ethyl acrylate (or acrylonitrile) in dry benzene (50 ml) was treated dropwise (30 min) with triethylamine (0.4 ml) in 10 ml of benzene. The mixture was then refluxed for 30 min and left overnight at room temperature, and filtered. The oil residue left after removal of the solvent solidified on trituration with petroleum ether (60/80 °C). Recrystallization from EtOH gave XIV (and XV) (Table 5) in 50—60% yields. The spectral characteristics of XIVa and XVb, taken as typical examples of the series prepared, are as follows: XIVa: ν_{max} (KBr) 1650 (3-PhCO), 1755 (5-EtOCO) cm^{-1}; δ ($CDCl_3$) 7.0—8.5 (m, 10, ArH), 4.95 (t, 1, J=10 Hz, 5-CH), 3.65 (d, 2, J=10 Hz, 4-CH_2), 4.25 (q, 2, J=7 Hz, $-COO\underline{CH_2}-CH_3$), 1.25 (t, 3, J=7 Hz, $-COOCH_2-\underline{CH_3}$) ppm. XVa: ν_{max} (KBr) 1650 (PhCO) cm^{-1}; δ ($CDCl_3$) 7.1—8.5 (m, 10, ArH), 3.77 (d, 2, J=10.5 Hz, 4-CH_2), 5.12 (t, 1, J=10.5 Hz, 5-CH) ppm. The UV maxima of XIV and XV are given in Table 5. The absence of nitrile absorption in the IR spectrum of XVa supports its 5-cyano structure.[8]

References

1) Y. Otsuji, Y. Tsuji, A. Yoshida, and E. Imoto, This Bulletin, **41**, 223 (1971).
2) T. Mukayama, K. Saigo, and H. Takei, *ibid.*, **44**, 190 (1971).
3) F. Krollpfeiffer and H. Hartmann, *Chem. Ber.*, **83**, 90 (1950).
4) R. Huisgen, E. Aufderhaar, and G. Wallbillich, *ibid.*, **98**, 1476 (1965).
5) J. S. Clovis, A. Eckell, R. Huisgen, and R. Sustmann, *ibid.*, **100**, 60 (1967); R. Huisgen, *Bull. Soc. Chim. Fr.*, **1965**, 3431; *J. Org. Chem.*, **33**, 2291 (1968); A. F. Hegarty, M. P. Cashman, and F. L. Scott, *Chem. Commun.*, **13**, 684 (1971).
6) A. S. Shawali, M. I. Ali, M. M. Naoum, and A. L. Elansari, *Tetrahedron*, **28**, 3808 (1972).
7) Haller, *C. R. Acad. Sci. Paris*, **108**, 1116 (1889).
8) L. J. Bellamy, "The IR Spectra of Complex Molecules," Methuen & Co., New York, N. Y. (1969), p. 266.
9) K. W. Ratts and A. Yao, *J. Org. Chem.*, **31**, 1185 (1966).
10) O. Eischer, *Chem. Ber.*, **9**, 463 (1876); H. S. Wechester, *Ann.*, **325**, 237 (1902).
11) T. Sasaki, T. Yoshioka, and Y. Suzuki, This Bulletin, **44**, 185 (1971).

NOTES

BULLETIN OF THE CHEMICAL SOCIETY OF JAPAN, VOL. 49(1), 325—326 (1976)

Threshold Switching of Violanthrone in a Sandwich-type Cell

Yoshihiko SADAOKA and Yoshiro SAKAI

Department of Industrial Chemistry, Faculty of Engineering, Ehime University, Matsuyama 790

(Received July 9, 1975)

Synopsis. Threshold switching between two impedance states has been observed at room temperature in a sandwich-type cell of violanthrone thin film with the use of silver electrodes. The conductivity of the "on state" is larger than that of the "off state" by a factor of 10^4.

Memory- and threshold-switching phenomena have recently received considerable attention. They were observed in many inorganic compounds,[1,2] memory-switching being observed in evaporated aromatic hydrocarbon thin films[3,4] and in electron-beam-deposited polymer films.[5] In a previous paper[6] we reported the memory switching in a surface-type cell of pyranthrone film.

In the present work threshold switching has been observed in evaporated thin violanthrone film sandwiched between silver electrodes.

Experimental

Violanthrone was purified by sublimation *in vacuo* (10^{-6} Torr). The geometry of the sample was of sandwich type, where violanthrone was deposited over a silver electrode prepared by vacuum evaporation onto the glass substrate through an etched stainless steel mask, the counter silver electrode being plated on top of the film. A schematic illustration of the sample is given in Fig. 1. The lead wires were placed on the electrodes by means of silver paste. The area of the electrode was *ca.* 0.01 cm^2 and the thickness of the violanthrone layer *ca.* 100 nm. Switching behaviour was observed with an AC generator and a synchroscope. Electrical measurements were carried out in the atmosphere.

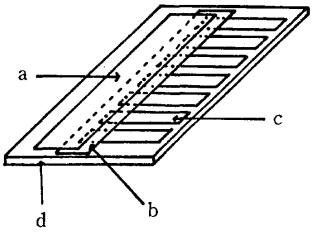

Fig. 1. Sandwich-type cell.
(a) silver electrode, (b) violanthrone film, (c) counter silver electrode, (d) microscope slide.

The microscopic distribution of the temperature on the surface of the sample during the course of switching was recorded with a Nikon 725 thermal plotter having an InSb infrared detector. The detectable spot size with this apparatus is 22 μm and the position of the view can be shifted with the aid of a mobile stage. The state of the film during switching was also observed with an optical microscope. Inspection under the polarizing microscope and the scanning electron microscope showed that the freshly prepared violanthrone films are essentially amorphous.

Results and Discussion

A typical current variation with the applied voltage of 60 Hz for the reversible threshold switching device of violanthrone of the sandwich type is shown in Fig. 2. The film has very low conductance ("off state") as long as the applied voltage is lower than a certain value, so that the current-voltage curve can not be observed in this region. When the voltage exceeded the threshold value, the conductance abruptly increased to the order of 10^{-5} ohm^{-1} and the curve (a) in Fig. 2 appeared. This state is called "on state". The threshold voltage for this device was estimated to be *ca.* 10 V.

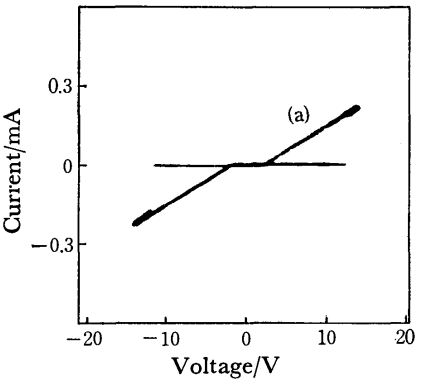

Fig. 2. Response of switching device to 60 Hz voltage.

In general, switching has been interpreted in terms of either a purely electronic effect or a thermal effect. The thermal effect interpretation is based on the premise that the highly localized Joule-heating is occasionally accompanied by structural changes such as crystallization. However, in the present case no difference in temperature was observed on the sample between the switching state and the non-switching state with the aid of a thermal plotter. Inspection of the film under the optical microscope showed no changes after the stable switching had occurred. In some cases unstable switching curves were obtained. In such cases the structural changes were observed during the switching. Observation with the thermal plotter revealed that an electrothermal breakdown had occurred. Thus the electronic effect is distinguishable from the electrothermal effect.

In order to elucidate the switching mechanism, it is desirable to investigate the effect of the film thickness on the switching. However, since it was difficult to prepare a thick and uniform film, surface type cells with various electrode distances were prepared. The minimum distance was 4×10^{-3} cm. In the surface type cell having an electrode distance of 4×10^{-3} cm or more, the

high field conduction in the high resistance state was found to agree with the Richardson-Schottky equation,[7] $\sigma=\sigma_0\exp(\beta_s V^{1/2}/d^{1/2}kT)$. This indicates the existence of the potential barrier at the violanthrone-electrode contact. The thickness of the space-charge-layer was estimated to be 10^{-3} cm.

No reversible threshold switching* occurred in the surface type cell of violanthrone having an electrode distance larger than the thickness of the space-charge-layer and an inspection of the film under the optical microscope showed no change after the threshold switching had occurred in the sandwich type cell of violanthrone. Therefore the threshold switching in the sandwich type cell having an electrode distance smaller than the thickness of the space-charge-layer may be interpreted in terms of the electronic effect such as space-charge-overlap.

* Although the transformation from the "off state" to the "on state" accompanied by structural changes at both interfaces of violanthrone-metal contacts was observed in the surface type cell, the "on state" could not be quenched by lowering the applied voltage in contrast to the case of pyranthrone.[6]

References

1) P. W. Pryor and H. K. Henisch, *J. Non-Cryst. Solids*, **7**, 181 (1972).
2) W. D. Buckley and S. H. Holmberg, *Solid-State Electronics*, **18**, 127 (1975).
3) S. G. E. Garrett, R. Pethig, and V. Soni, *J. Chem. Soc., Faraday II*, **70**, 1732 (1974).
4) J. Kevorkian, M. M. Labes, D. C. Larson, and D. C. Wu, *Discuss. Faraday Soc.*, **51**, 139 (1971).
5) W. P. Ballard and R. W. Christy, *J. Non-Cryst. Solids*, **17**, 81 (1975).
6) Y. Sakai and Y. Sadaoka, *Chem. Lett.*, **1975**, 315.
7) J. G. Simmons, *Phys. Rev.*, **155**, 657 (1967).

BULLETIN OF THE CHEMICAL SOCIETY OF JAPAN, VOL. 49(1), 327—328 (1976)

Absorption Spectrum of the Aggregated Radical Anion of Sulfur Dioxide Produced by γ-Irradiation

Osamu Ito, Shigeru Kuwashima, and Minoru Matsuda

Chemical Research Institute of Non-aqueous Solutions, Tohoku University, Katahira, Sendai 980

(Received September 18, 1975)

Synopsis. By γ-irradiation of sulfur dioxide in 2-methyltetrahydrofuran at -196 °C, blue glassy solution was obtained, although the monomer radical anion of sulfur dioxide was colorless. The absorption spectrum of the blue species was identical with that of the stable radical anion produced by the amalgam reduction of sulfur dioxide, which was attributed to the dimer or trimer radical anion.

The dimer radical cations formed by the γ-irradiation of aromatic hydrocarbons have been identified by the absorption bands appearing in the longer wavelength region than those of the monomer radical cations.[1] Recently, the dimer radical anions were studied by means of the absorption and ESR spectra.[2] From these studies, it is revealed that if the dimer or trimer radical anion in which an unpaired electron is delocalized was formed, it would be distinguishable from the monomer one by the characteristic absorption band. In this note, we will report that the γ-irradiation of SO_2 gives a colored radical anion at -196 °C, although a monomer one has been known to be colorless.[3]

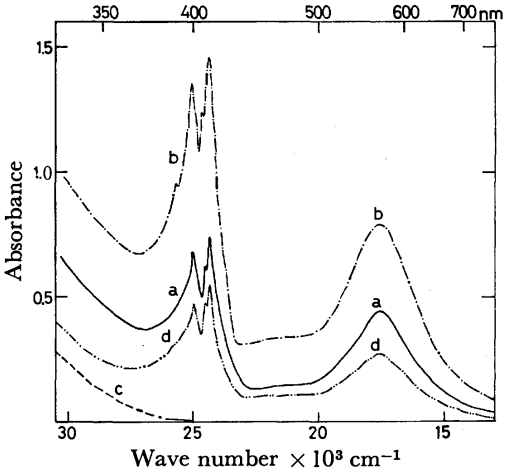

Fig. 1. Absorption spectra of the radical anion formed by γ-irradiation of SO_2 in MTHF at -196 °C (2 mm cell length).
a: $[SO_2]=0.15$ mol/l, b: after thermal annealing of a,
c: $[SO_2]=0.05$ mol/l, d: after thermal annealing of c.

γ-Irradiation of the concentrated SO_2 solution (>0.1 mol/l) in 2-methyltetrahydrofuran (MTHF) at -196 °C gave a blue glassy solution and the absorption bands appeared at 566 nm (band I) and 410 nm (band II) as shown in Fig. 1-a. When the blue glassy solution was warmed slightly, the solution changed to deep blue. By thermal annealing the intensities of the bands I and II, which were observed after recooling to -196 °C, increased with the same proportion without the shift of the positions of the absorption maxima (Fig. 1-b). By the γ-irradiation of the dilute SO_2 solution (<0.05 mol/l), the colorless solution was obtained and only the tail of absorption band appeared at shorter wavelength than 360 nm (Fig. 1-c). By slight melting, this colorless glassy solution turned to a blue solution, whose absorption maxima (Fig. 1-d) were the same as those obtained by the γ-irradiation of the concentrated solution (Fig. 1-a and -b). This suggests that the anionic species, probably monomer radical anion (SO_2^-), exists in the γ-irradiated colorless glass and the blue species, probably aggregated radical anion, may be formed by the collision of SO_2^- and SO_2 by thermal annealing. Although the absorption band due to SO_2^- was observed at 360 nm in aqueous solution by means of flash photolysis[3] and pulse radiolysis,[4] any clear peak was not observed at this region in MTHF glass. However, since SO_2^- may interact strongly with H_2O, this difference can be caused by the solvent effect on the electronic transition and the tail of the absorption band shown in Fig. 1-c may be attributed to SO_2^- in MTHF. Since the blue species was also formed by the γ-irradiation of the crystalline SO_2 at -196 °C, the blue species could not attributed to the reaction products formed by MTHF and SO_2. Furthermore, if SO and SO_3 were formed by γ-irradiation at -196 °C, SO^- and SO_3^- and their aggregates with SO_2 such as $SO^-(SO_2)_n$ and $SO_3^-(SO_2)_n$ must be taken into consideration as blue species. However, SO^-, SO_3^-, and $S_2O_3^-$ were known to be colorless in aqueous solution[3] or in crystalline phase.[5]

The results above indicate the following facts clearly; a) the absorption bands I and II shown in Fig. 1 were attributed to an identical species, since the relative intensities of both bands did not change by the thermal annealing, and b) the blue species increased by thermal annealing was identical with the blue species directly formed by the γ-irradiation of the concentrated solution, since the appreciable shift of the positions of the absorption maxima was not observed by thermal annealing. These results suggest that the blue radical anion can be attributed to the aggregated radical anion of sulfur dioxide, $(SO_2)_n^-$, which may be produced by the following scheme of reactions;

$$n\ SO_2 \rightleftharpoons (SO_2)_n \quad (1)$$

$$MTHF \xrightarrow{\gamma} MTHF^+ + e^- \quad (2)$$

$$(SO_2)_n + e^- \longrightarrow (SO_2)_n^- \quad (3)$$

$$SO_2 + e^- \longrightarrow SO_2^- \quad (4)$$

$$SO_2^- + n-1\ SO_2 \longrightarrow (SO_2)_n^- \quad (5)$$

The formation of the blue species by γ-irradiation of the concentrated solution indicates that the self-association of SO_2 occurred in MTHF at -196 °C before irradiation (reactions (1) and (3)),[6] or SO_2 migrated in MTHF

glass during γ-irradiation (reaction (5)). Increasing of the blue species by the thermal annealing may suggest that the collision of SO_2 and $SO_2^{\cdot-}$ (reaction (5)) occurs before $SO_2^{\cdot-}$ encounters with cationic species in MTHF glass. By the experiments of γ-irradiation, however, any information about a value n in $(SO_2)_n^{\cdot-}$ could not be obtained.

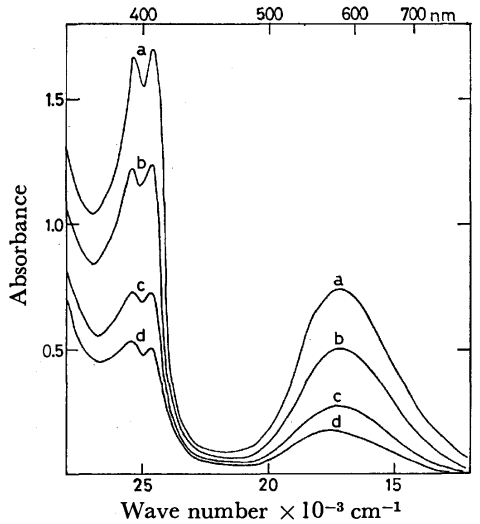

Fig. 2. Absorption spectra of the radical anion formed by sodium amalgam reduction of SO_2 in DMF at various temperatures ($[SO_2]=0.15$ mol/l in 2mm cell). a: 19 °C, b: 0 °C, c: −10 °C, d: −20 °C.

On the other hand, it is reported by Rinker and Lynn that the sodium amalgam reduction of SO_2 gave a stable radical anion having blue color in aprotic solvents.[7] The absorption spectrum of the stable species in dimethylformamide (DMF) was shown in Fig. 2. This absorption spectrum was essentially the same as that of the blue species obtained by γ-irradiation of SO_2. There is no doubt about that both blue species are the identical species. For the stable blue species formed by amalgam reduction or by electrolysis, two different structures have been speculated; bonded dimer radical anion ($O_2\bar{S}$–$\dot{S}O_2 \leftrightarrow O_2\dot{S}$–$\bar{S}O_2$) by Rinker and Lynn[7] and associated trimer ($(SO_2)^{\cdot-}(SO_2)_2$) by Dinse and Möbius.[8]

Before elucidating the structure of the stable blue species, we found that a diamagnetic colorless species coexist with the radical anion in the solution reduced by amalgam. As shown in Fig. 2, with varying temperature the intensities of the two bands at 580 nm (band I) and 400 nm (band II) changed in the same proportion reversibly. Increasing in the intensities of the bands was observed up to 70 °C, and upper limit may exist at higher temperature. With lowering temperature, the intensity of a singlet ESR signal ($g=2.006$) decreased with the same proportion of the intensities of the absorption bands I and II. Thus, it is apparent that the reversible change was caused by the equilibrium between the radical anion and a diamagnetic colorless species, probably a higher aggregate. From this fact it is impossible to elucidate whether the blue species can be attributed to the dimer or trimer radical anion.

It is noteworthy that the absorption spectra of $(SO_2)_n^{\cdot-}$ resemble that of the disulfone radical anion ($(R\text{–}SO_2\text{–}SO_2\text{–}R)^{\cdot-}$).[9] The dialkyl disulfone radical anion showed the absorption bands at 690 nm and 350 nm, although the dialkyl monosulfone radical anion showed a band at 400 nm. In the disulfone radical anion, the absorption band appearing at 690 nm was assigned to the transition having charge-resonance character, which indicates that an unpaired electron is delocalized between two sulfone moieties. Recently Kerr and Williams studied the radical anion of sulfuryl chloride (SO_2Cl_2) by means of the ESR measurements and proposed that $(SO_2Cl_2)^{\cdot-}$ can be thought as a resonance hybrid of ($SO_2^{\cdot-}$, Cl_2) and (SO_2, $Cl_2^{\cdot-}$) or equivalently, as radical anion complex in which the two molecules share an unpaired electron.[10] Supposing that the absorption bands of $(SO_2)_n^{\cdot-}$ appearing at 560—580 nm were assigned to the transition having charge-resonance character, $(SO_2)_n^{\cdot-}$ can be thought as that two or three SO_2 molecules share an unpaired electron in the dimer or trimer radical anion.[11]

References

1) B. Badger, B. Brocklehurst, and R. D. Russel, *Chem. Phys. Lett.*, **1**, 122 (1967); B. Badger and Brocklehurst, *Trans. Faraday Soc.*, **65**, 2582 (1969); M. A. J. Rogers, *Chem. Phys. Lett.*, **9**, 107 (1971).

2) E. D. Sprague, K. Takeda, and F. Williams, *Chem. Phys. Lett.*, **10**, 299 (1971); T. Shida and S. Iwata, *J. Chem. Phys.*, **56**, 2858 (1972); T. Shida, Y. Takahashi, H. Hatano, and M. Imamura, *Chem. Phys. Lett.*, **33**, 491 (1975).

3) E. Hayon, A. Treinin, and J. Wilf, *J. Amer. Chem. Soc.*, **94**, 47 (1972).

4) T. E. Eriksen, *J. Chem. Soc. Faraday I*, **70**, 208 (1974).

5) M. I. Samoilovich, *Geokhimiya*, **1971**, 477.

6) The self-association of sulfur dioxide, probably dimer, in nonpolar solvent at room temperature was reported; C. Deveze and P. Rumpf, *C. R. Acad. Sci., Paris, Ser. C*, **266**, 1001 (1968).

7) R. G. Rinker and S. Lynn, *J. Phys. Chem.*, **72**, 4706 (1968); *Ind. Eng. Chem.*, **8**, 338 (1969).

8) K. P. Dinse and K. Möbius, *Z. Naturforsch.*, **23a**, 695 (1968).

9) O. Ito and M. Matsuda, This Bulletin, **48**, 3389 (1975).

10) C. M. L. Kerr and Williams, *J. Amer. Chem. Soc.*, **94**, 5212 (1972).

11) There are some suggestions that the dimer radical anion is more probable than trimer one, although they are not sufficient. One of them is as follows; estimated value $n=2$ in $(SO_2)^{\cdot-}(SO_2)_n$ by Dinse and Möbius may be slightly larger, since the total intensities of the two ESR signals assigned to the monomer and trimer radical anions decreased with lowering temperature, indicating the formation of the diamagnetic species even by the electrolysis.[8]

BULLETIN OF THE CHEMICAL SOCIETY OF JAPAN, VOL. 49(1), 329—330 (1976)

Dielectric Behavior of *N*-Methylacetamide

Koichi ITOH, Hiroshi SATO, Hiroaki TAKAHASHI, and Keniti HIGASI
Department of Chemistry, Waseda University, Shinjuku, Tokyo 160

(Received September 27, 1975)

Synopsis. The dielectric constants and losses of liquid *N*-methylacetamide were measured in the frequency range 0.356—2.10 GHz at 31.4 °C. The result provides a definitive evidence for the validity of the simple Debye equation for the dielectric relaxation process of liquid *N*-methylacetamide.

The molecular structure of *N*-methylacetamide has been intensively studied by various physical methods. Infrared and Raman spectra,[1,2] dipole moment,[3] and electron diffraction[4] have been measured and discussed. Bass *et al.*[5] studied dielectric relaxation, but not in a sufficiently wide frequency range. They employed only the VHF range of 1—250 MHz. The present note provides complementary dielectric data for liquid *N*-methylacetamide in view of its great importance as a model compound of biological materials.

Experimental

Commercial *N*-methylacetamide was purified by vacuum distillation prior to use. The purity was examined by measurements of the infrared spectra.

Dielectric constants, ε', and losses, ε'', were measured at 31.4°C at the UHF frequencies of 0.356, 0.516, 0.698, 1.00, 1.50, and 2.10 GHz with an equipment reported in previous papers.[6,10] The errors of the measurement are of the order of a few per cent.

Relaxation time, τ, and the limiting low- and high-frequency dielectric constants, ε_0 and ε_∞, respectively, were calculated by the Debye equation:

$$\varepsilon' - j\varepsilon'' = \varepsilon_\infty + \frac{\varepsilon_0 - \varepsilon_\infty}{1 + j\omega\tau} \qquad (1)$$

where ω is the angular frequency. An iterative method by an electric computer was used for the calculation.

Results and Discussion

The ε' and ε'' values observed at 31.4 °C are summarized in Table 1. Figure 1 shows the Cole-Cole diagram (dashed line) constructed from the UHF data obtained by the present writers and the VHF data provided by Bass *et al.*[5] We see that all the measured points lie in a semi-circle with its center in the ε' axis.

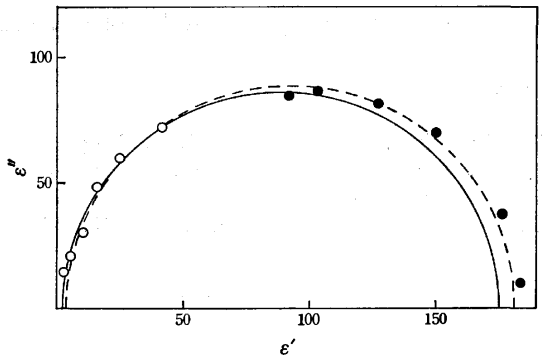

Fig. 1. Cole-Cole plots for liquid *N*-methylacetamide at 31.4 °C: open circles, results of the present investigation; closed circles, literature values from S. J. Bass *et al.*[5] The solid line corresponds to the values of ε_0, ε_∞, and τ of 175.5, 2.37, and 808 ps, respectively, and the dashed line to the values of 181.5, 3.44, and 769 ps, respectively.

Table 1. The observed and calculated ε' and ε'' values of liquid *N*-methylacetamide at 31.4 °C

Frequency (GHz)	ε'		ε''	
	Obsd	Calcd	Obsd	Calcd
2.10	2.43	3.87	14.4	16.0
1.50	5.28	5.31	21.0	22.4
1.00	10.4	8.80	30.3	32.8
0.698	15.7	15.1	48.3	45.3
0.516	25.0	24.4	59.9	57.7
0.356	41.8	42.9	71.9	73.3

The values of the parameters, ε_0, ε_∞ and τ, calculated by Eq. (1) and ε'_{obsd} and ε''_{obsd} in Table 1 are 175.5, 2.37, and 808 ps, respectively. The semi-circle (solid line, Fig. 1) is drawn with the use of this set of parameters. The values of ε'_{calcd} and ε''_{calcd} (Table 1) are those calculated by using the same values of the parameters. If the VHF values of ε' and ε'' reported by Bass *et al.*[5] are included in the calculation, the values of ε_0, ε_∞, and τ become 181.5, 3.44, and 769 ps, respectively—this set of parameters gives the semi-circle (dashed line, Fig. 1).

The experimental values were examined also by the use of the Cole-Cole equation:

$$\varepsilon' - j\varepsilon'' = \varepsilon_\infty + \frac{\varepsilon_0 - \varepsilon_\infty}{1 + (j\omega\tau)^{1-\alpha}} \qquad (2)$$

The distribution parameter, $\alpha=0$, was also obtained, confirming that the dielectric dispersion of liquid *N*-methylacetamide is of the Debye type.

The static dielectric constant of *N*-methylacetamide was reported to be 177.0 at 31.4 °C[5] which lies between 175.5 and 181.5 obtained in this work. The refractive index, n_D, of *N*-methylacetamide is reported to be 1.4185.[5] The fact that ε_∞ is larger than n_D^2 only by 15% suggests that the second and third dielectric relaxations in a higher frequency region, if they exist at all, would have very small values of dielectric absorption.

The results seem to show that all the data for *N*-methylacetamide can be represented by the simple Debye equation. As in the case of the principal dispersion of alcohols, the dielectric relaxation of this substance is governed by the simple exponential decay process. All the existing theories explaining the simple Debye dis-

persion[7,8] assume no interaction between orientating dipoles, which is not suitable for the system of strongly hydrogen-bonded liquids such as alcohols and *N*-substituted amides. The switch-over[9] and cluster[10] mechanisms have been tentatively proposed for the explanation of the dielectric relaxation of alcohols. For liquid *N*-methylacetamide, which is considered to be composed of the linear chains of the hydrogen-bonded molecules, the mechanism might be simpler than that of alcohols.

References

1) S. Mizushima, T. Shimanouchi, S. Nagakura, K. Kuratani, M. Tsuboi, H. Baba, and O. Fujioka, *J. Amer. Chem. Soc.*, **72**, 3490 (1950).
2) T. Miyazawa, T. Shimanouchi, and S. Mizushima, *J. Chem. Phys.*, **29**, 611 (1958).
3) R. M. Meighan and R. H. Cole, *J. Phys. Chem.*, **68**, 503 (1964).
4) M. Kitano, T. Fukuyama, and K. Kuchitsu, This Bulletin, **46**, 384 (1973).
5) S. J. Bass, W. I. Nathan, R. M. Meighan, and R. H. Cole, *J. Phys. Chem.*, **68**, 509 (1964).
6) T. Koshii, E. Arie, M. Nakamura, H. Takahashi, and K. Higasi, This Bulletin, **47**, 618 (1974).
7) P. Debye, "Polar Molecule," Chemical Catalog Company, New York (1929) and Dover Publications, New York (1945), p. 95.
8) H. Frölich, "Theory of Dielectrics," Clarendon Press, Oxford, England (1958), p. 78.
9) M. W. Sagal, *J. Chem. Phys.*, **36**, 2437 (1962).
10) H. Sato, T. Koshii, H. Takahashi, and K. Higasi, *Chem. Lett.*, **1975**, 491.

BULLETIN OF THE CHEMICAL SOCIETY OF JAPAN, VOL. 49 (1), 331—332 (1976)

Note on the Use of Linear Free Energy Relationships in Heterogeneously Catalyzed Reactions

A. P. G. KIEBOOM

Laboratory of Organic Chemistry, Delft University of Technology, Julianalaan 136, Delft 2208, The Netherlands

(Received June 3, 1975)

Synopsis. A critical examination of the use of linear free energy relationships in the study of the mechanism of heterogeneously catalyzed reactions is presented in the case of the ruthenium catalyzed hydrogenation of monoalkylbenzenes reported in the literature.[5] It is concluded that the use of both electronic and steric substituent parameters leads to a quite different mechanistic interpretation as compared to the statements made before in the literature on the basis of just the electronic substituent parameter.

One of the major purposes in the field of heterogeneous catalysis is a better understanding of the reaction mechanism in order to develop somewhat less empiric approximations towards the choice of the catalyst as well as the reaction conditions.[1-3] The study of a particular reaction with the aid of a series of structurally related compounds on a single catalyst has proved a further suitable tool for mechanistic studies. Thus, a systematic variation of the substrate by the introduction of suitable substituents gives a set of experimental data to be correlated by means of a linear free energy relationship (*e.g.* Hammett and Taft relations), from which conclusions about the reaction mechanism involved can be drawn.[4]

On the other hand, one has to be very cautious in correlating experimental data with structural parameters since the substituent itself will give electronic and/or steric (attractive or repulsive) interactions with the catalyst, *i.e.*, substituent effects are often more complicated than in the case of homogeneously catalyzed reactions. In this respect, the recent investigation of Yoshida[5] concerning the mechanism of the hydrogenation of monoalkylbenzenes over ruthenium metal is an illustrative example of ignoring the above-mentioned interactions between the substituents and the catalyst. As will be outlined below, these "secondary" substituent effects may bring about false conclusions concerning the mechanism and the transition state of the reaction studied.

Results and Discussion

Yoshida[5] has studied the hydrogenation of monoalkylbenzenes over ruthenium black at 30 °C and 1 atm with ethanol as the solvent and obtained the following data for the reaction rate constants (k) and adsorption equilibrium constants (K) (Table 1). In addition, both the electronic (σ^*) and steric (E_s) substituent parameters according to Taft[6] have been included in Table 1.

Table 1. Hydrogenation of R-substituted benzenes over ruthenium[a]

Substituent R	log k	log K	σ^*	E_s
H	−1.85	0.30	0.49	1.24
Me	−2.66	0.78	0.00	0.00
Et	−2.88	1.00	−0.10	−0.07
Pr	−3.12	1.18	−0.115	−0.36
i-Pr	−3.34	0.98	−0.19	−0.47

a) log k and log K derived from Fig. 2 of Ref. 5.

Although the size of the substituents at the aromatic nucleus varies considerably, the data of Table 1 were just correlated[5] with the electronic substituent parameter σ^* (Table 2, relations *1* and *4*). On this basis, it was concluded that (i) the initial state of hydrogenation is the adsorption step (in terms of the Horiuti-Polanyi mechanism) and (ii) the rate-determining step involves a nucleophilic attack of a hydride species from the catalyst surface.[5]

However, Table 2 shows that the experimental data may also (and even better) be correlated with the steric substituent parameter E_s (*2* and *5*). Correlation of the experimental data by both σ^* and E_s shows further that *the reaction rate constant is almost completely determined by steric interactions (3)*, whereas *the adsorption equilibrium constant is influenced by electronic as well as steric effects (6)*.

Table 2. Taft relations[a] for the hydrogenation of R-substituted benzenes over ruthenium[5]

No.	Reaction rate (k)	ρ_r^*	δ_r	log k°	R
1	$\log k/k^\circ=\rho_r^*\sigma^*$	2.05	—	−2.80	0.974
2	$\log k/k^\circ=\delta_r E_s$	—	0.82	−2.83	0.983
3	$\log k/k^\circ=\rho_r^*\sigma^*+\delta_r E_s$	0.06	0.81	−2.82	0.983

No.	Adsorption equilibrium (K)	ρ_a^*	δ_a	log K°	R
4	$\log K/K^\circ=\rho_a^*\sigma^*$	−1.16	—	0.87	0.942
5	$\log K/K^\circ=\delta_a E_s$	—	−0.47	0.88	0.944
6	$\log K/K^\circ=\rho_a^*\sigma^*+\delta_a E_s$	−0.40	−0.31	0.88	0.945

a) ρ^* and δ are the polar and steric reaction parameters,[6] respectively, with r=reaction and a=adsorption; k° and K° are the calculated data for toluene (R=Me); R is the correlation coefficient.

This result leads to the following conclusions: (i) *The reaction rate constant is independent of electronic effects, i.e.*, atomic hydrogen has to be considered as the reducing agent. Increase of the size of the substituent decreases the reaction rate, which implies relatively less disturbance in the initial state of hydrogenation as compared to the transition state, and (ii) *The adsorbed state is stabilized by electron-donating substituents, i.e.*, the higher electron density on the aromatic nucleus will result in a stronger

aryl-ruthenium donor bond by π-spd overlap. In addition, increase of the size of the substituent enhances the strength of adsorption, which may point to alkyl-ruthenium bond formation in the initially adsorbed state. This result is in agreement with the steric substituent effect on the rate of hydrogenation and may have some resemblance with the homogeneously ruthenium-catalyzed α-H/D-exchange of aliphatic alcohols.[7] The picture for the adsorbed state, however, remains somewhat uncertain because of the rather low correlation coefficient of the relations *4*—*6*.

Summarizing, it is evident that one has to be very cautious in correlating experimental data with structural parameters in the case of heterogeneously catalyzed reactions.

References

1) M. Kraus, *Advan. Catal. Relat. Subj.*, **17**, 75 (1967).
2) I. Mochida and Y. Yoneda, *J. Catal.*, **11**, 183 (1968).
3) A. P. G. Kieboom, "Substituent Effects in the Hydrogenation on Palladium," Thesis, Delft, 1971; *Diss. Abstr. Int.*, *B* **35**, 1203 (1974).
4) *Cf.* H. van Bekkum, A. P. G. Kieboom, and K. J. G. van de Putte, *Rec. Trav. Chim. Pays-Bas*, **88**, 52 (1969); V. Ruzicka, L. Cerveny, and J. Pachta, *Coll. Czech. Chem. Commun.*, **34**, 2074 (1969); J. Endrysova and M. Kraus, *ibid.*, **35**, 62 (1970); A. P. G. Kieboom, J. F. de Kreuk, and H. van Bekkum, *J. Catal.*, **20**, 58 (1971); M. Kraus and V. Bazant, *Proc. Intern. Congr. Catal. 5th*, **1972**, 1073; A. P. G. Kieboom and H. van Bekkum, *J. Catal.*, **25**, 342 (1972); J. Simonikova, A. Ralkova, and K. Kochloefl, *ibid.*, **29**, 412 (1973); A. W. van Muijlwijk, A. P. G. Kieboom, and H. van Bekkum, *Rec. Trav. Chim. Pays-Bas*, **93**, 204 (1974).
5) T. Yoshida, This Bulletin, **47**, 2061 (1974).
6) R. W. Taft, Jr., "Steric Effects in Organic Chemistry," ed. by M. S. Newman, J. Wiley & Sons, London (1956), pp. 598, 619.
7) S. L. Regen, *J. Org. Chem.*, **39**, 260 (1974).

BULLETIN OF THE CHEMICAL SOCIETY OF JAPAN, VOL. 49(1), 333—334 (1976)

Some Aspects of the Solid-solid Reaction Products between MgO and V_2O_3

Hirotoshi OSHIMA, Hiroshi YAMAMURA, and Shin-ichi SHIRASAKI

National Institute for Researches in Inorganic Materials, Kurakake, Sakuramura, Niihari-gun, Ibaraki 300-31

(Received April 28, 1975)

Synopsis. This report is concerned with the characterization of the metastably occurring reaction products with the spinel structure of a solid-solid reaction between MgO and V_2O_3 in an H_2 atmosphere. The measurements of the lattice constants and the magnetic properties suggest that the oxygen framework of the product is formed in an early stage of the reaction, followed by the ordering of the magnetic ions in the tetrahedral sites.

The present paper will deal the lattice constants and the magnetic properties of several reaction products obtained by solid-solid reactions between MgO and V_2O_3 in an H_2 atmosphere at different temperatures, the results give an insight into the characteristics of the metastably developed reaction products.

Two series of magnesio-vanadates, $MgO \cdot xV_2O_3$, with the spinel structure were prepared by firing oxide mixtures of MgO and V_2O_3 in different ratios; one of the species was fired at 1100 °C (A specimen series), and the other, at 1200 °C (B specimen series). The V^{3+} ion is stable in the $PO_2 \simeq 10^{-13}$—10^{-23} atm. region at 1100 °C—1200 °C, while the PO_2 in the H_2 atmosphere was measured to be $\sim 10^{-15}$ atm. therefore, only V^{3+} ions are supposed to be present in these materials throughout this investigation. X-Ray diffraction work was carried out in order to make precise lattice-constant measurements of the materials by the conventional method,[1] while the magnetic susceptibility was traced from 180 K to 100 K.

X-Ray diffraction patterns indicated that specimens of $1.0 < x < 1.13$ were monophasic, while specimens of $x > 1.13$ more or less involved vanadium sesquioxide together with the host magnesio-vanadate.

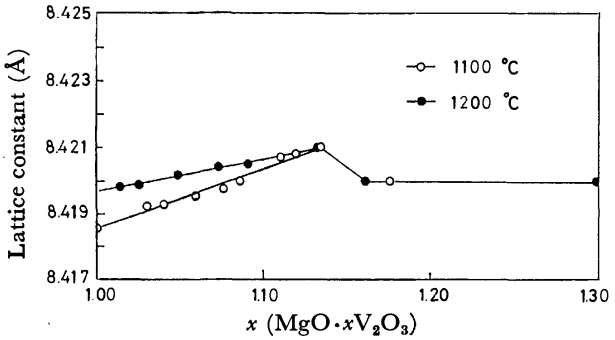

Fig. 1. Lattice constants of magnesio-vanadates with spinel structure.

Figure 1 gives the lattice constants as a function of the x value for the two series of materials. There is the general trend for the lattice constants for the two series to increase linearly with an increase in the x value up to $x = 1.13$. For the materials in this range, excess vanadium ions can occupy the tetrahedral sites of the spinel lattice, and as the result, cation vacancies in these sites may form to maintain the charge neutrality. Therefore, the general trend of present interest may be connected with such configuration change in the tetrahedral sites.

Figure 1 further shows that the respective lattice constants for the two series of materials approach each other with an increase in the x value, finally coinciding at $x = 1.13$. This fact suggests that materials with a larger x value have a larger number of cation vacancies and arrive at an "equilibrium structure" easily by means of the diffusion of oxygen. It is noticeable that at least two different lattice constants are possible for a fixed x value in the range of $1.0 < x < 1.13$. This fact strongly suggests that the A specimen series, with smaller x value, is metastable, in contrast to the B specimen series. The most probable model of the metastable structure is the Schottky-defect pairs of V_{mg}—V_o and V_v—V_o formed on the V_2O_3 side and the MgO side of the reaction product respectively, with their concentration ratio, $V_{mg}/V_v/V_o$, being always kept equal to the ratio of the constituent ions of MgV_2O_4, the number of vacancies decrease with an increase in the temperature. If this idea is correct, the lattice constant of the metastable

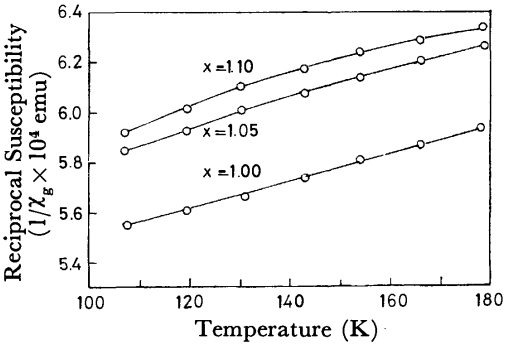

Fig. 2. The reciprocal values of the gram susceptibility ($1/\chi_g$) as a function of temperature for magnesio-vanadates fired at 1100 °C (A specimens).

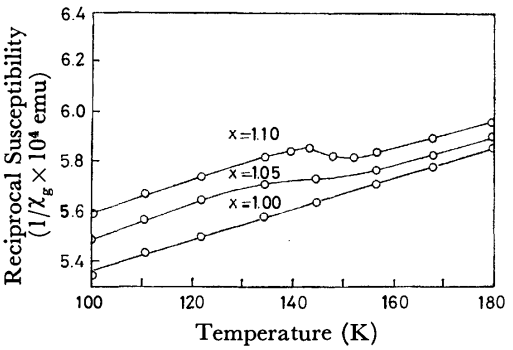

Fig. 3. The reciprocal values of the gram susceptibility ($1/\chi_g$) as a function of temperature for magnesio-vanadates fired at 1200 °C (B specimens).

structure can change by losing the respective vacancies without any change in its overall composition.

Figures 2 and 3 show the reciprocal susceptibility of A and B specimen series as a function of the temperature. The Curie-Weiss law held exactly over the entire range tested for the A specimen series, whereas deviation from the law began from the vicinity of 145 K for the $x=1.05$ and 1.10 materials in the B specimen series. It is unlikely that such anomalous magnetic behavior is associated with V^{3+} ions in the octahedral sites, which are occupied by V^{3+} in all the specimens. The deviation from the Curic-Weiss law may apear as a result of a contribution of an antiferromagnetic-like spin ordering partially occurring over the tetrahedral sites to the major paramagnetic disordering in the sites of the materials. This idea may be supported by the previous magnetic study of V_2O_3.[2] The occurrence of this anomaly, therefore, can be regarded as indirect evidence of cation ordering in the tetrahedral sites. Of the A specimen series and $MgO \cdot V_2O_3$ in the B specimen series, on the other hand, the lack of any cation order-disorder transition suggests cation disordering as well as spin disordering in the tetrahedral sites.

Figure 1 shows that the lattice constants of the two materials of $x=1.13$ fired at 1100 °C and 1200 °C respectively coincide, suggesting that the oxygen framework in the spinel lattice reached the equilibrium state in terms of structure. Nevertheless, the susceptibility versus temperature curves of the two materials are different from each other, thus, the $x=1.13$ material fired at 1200 °C can be regarded as being cation-ordered.

In summary, in the solid-solid reaction products between MgO and V_2O_3, the building of the oxygen framework takes place in an early stage of the reaction, followed by an ordering of the magnetic cations in the tetrahedral sites. A detailed study of this is in progress.

References

1) A. Taylor and H. Sinclair, *Proc. Phys. Soc.*, **57**, 126 (1945). J. B. Nelson and D. P. Riley, *ibid.*, **57**, 160 (1945).
2) H. Oshima, *Yogyo Kyokai Shi*, **81**, 162 (1973).

BULLETIN OF THE CHEMICAL SOCIETY OF JAPAN, VOL. 49(1), 335—336 (1976)

The Stability Constants of Nickel(II) Complexes with Chloride, Thiocyanate, Sulfate, Thiosulfate, and Oxalate Ions, as Determined by a Solvent Extraction Method

Ryokichi MURAI, Kiyoshi KURAKANE, and Tatsuya SEKINE

Department of Chemistry, Science University of Tokyo, Kagurazaka, Shinjuku-ku, Tokyo 162

(Received July 23, 1975)

Synopsis. The stability constants of nickel(II) complexes in 1 mol dm^{-3} sodium perchlorate media were determined at 25 °C by means of a solvent extraction method. The values thus obtained for log β_1 and log β_2 are: 0.0 and no second complex (Cl^-), 1.1 and 1.6 (SCN^-), 1.0 and 1.4 (SO_4^{2-}), 0.9 and 1.3 ($S_2O_3^{2-}$), and 3.7 and 6.6 ($C_2O_4^{2-}$), respectively.

Although there have been several reports on the stability constants of nickel(II) complexes with various common anions, most of them have been studied in dilute electrolyte solutions.[1,2] In order to obtain these constants at higher electrolyte concentrations, which are often necessary for various analytical purposes, experiments were made in 1 mol dm^{-3} sodium perchlorate media at 25 °C by means of a solvent extraction method.

Experimental

All the procedures, based on the synergic metal chelate extraction method,[3] were carried out at 25±0.3 °C in a way similar to that described in previous reports.[4,5] The aqueous phase was a 1 mol dm^{-3} $Na(ClO_4)$ medium containing about 10^{-4} mol dm^{-3} of nickel(II), 1×10^{-2} mol dm^{-3} of a sulfanilate buffer, and a certain amount of the ligand anion. This amount of buffer kept the hydrogen-ion concentration about 10^{-3} mol dm^{-3} and has a negligible effect on the extraction. The organic phase was carbon tetrachloride containing 5×10^{-2} mol dm^{-3} of thenoyltrifluoroacetone (TTA) and 3×10^{-2} mol dm^{-3} of trioctylphosphine oxide (TOPO). A 5 ml portion of each solution was placed in a stoppered glass tube and agitated mechanically until the distribution equilibrium was reached; then the whole was centrifuged. The optical absorbance of this organic phase was measured at 410 nm by means of a spectrophotometer. The hydrogen-ion concentration was measured by means of a potentiometer. A correction was made for the dissociation of the hydrogen oxalate ion by using a value of 3.54 for pKa_2 in 1 mol dm^{-3} perchlorate media at 25 °C.[6]

Statistical

The stability constants of complexes with a L_l^- ligand are:

$$\beta_n = [NiL^{2-nl}][Ni^{2+}]^{-1}[L^{l-}]^{-n} \quad (1)$$

The equilibrium constant for the extraction of the Ni^{2+} ion with a chelating extractant, HA, can be written as:

$$Kex = [NiA_2]_{org}[H^+]^2[Ni^{2+}]^{-1}[HA]_{org}^{-2} \quad (2)$$

where "org" denotes a species in the organic phase and where the lack of any subscript denotes a species in the aqueous phase. Even when a synergist which forms adduct chelates with the NiA_2 complex is present, its term can be omitted as long as its concentration is kept constant.[3] When nickel(II) is present in the organic phase as the NiA_2 species and in the aqueous phase as the Ni^{2+}, NiL^{2-l}, and NiL_2^{2-2l} species, the distribution ratio can be written as:

$$D = [NiA_2]_{org}/([Ni^{2+}]+[NiL^{2-l}]+[NiL_2^{2-2l}]) \quad (3)$$

When the distribution ratio in the absence of L^{l-} is denoted by D_0, the following equation can be obtained from Eqs. (1) to (3):

$$D[H^+]^2[HA]_{org}^{-2}Kex^{-1} = (1+\beta_1[L^{l-}]+\beta_2[L^{l-}]^2)^{-1} \quad (4)$$

When the results are plotted in the form of log $D[H^+]^2[HA]_{org}^{-2}Kex^{-1}$ vs. log $[L^{l-}]$, the stability constants can be determined by a curve-fitting method.[6]

Results and Discussion

In the absence of TOPO, the extraction of nickel(II) with TTA in carbon tetrachloride was poor and the

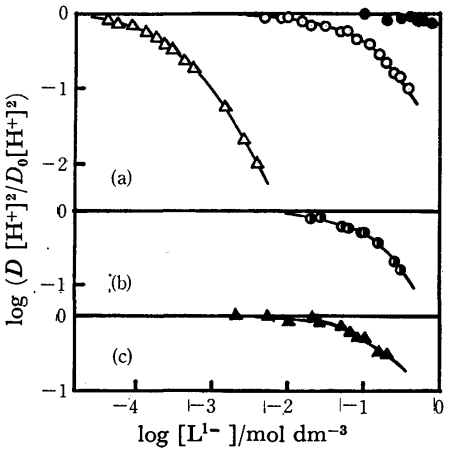

Fig. 1. Decrease in the extraction by complex formation. The ligands are as follows. (a) $C_2O_4^{2-}$ (△), SCN^- (○), and Cl^- (●), (b) SO_4^{2-} (◑), and (c) $S_2O_3^{2-}$ (▲). The curves were obtained by introducing the constants in Table 1 into Eq. (4).

TABLE 1. STABILITY CONSTANTS OF NICKEL(II) AND COBALT(II) COMPLEXES IN 1 mol dm^{-3} SODIUM PERCHLORATE SOLUTION AT 25 °C

Ligand	Ni(II)[a]		Co(II)[b]	
	log β_1	log β_2	log β_1	log β_2
Cl^-	0.0	—	−0.5	—
SCN^-	1.1	1.6	1.00	1.32
SO_4^{2-}	1.0	1.4	0.74	1.48
$S_2O_3^{2-}$	0.9	1.3	0.84	0.88
$C_2O_4^{2-}$	3.7	6.6	3.33	6.20

a) Present work. b) From Refs. 4 and 5.

results were not reproducible. In its presence, however, reasonable results, which can be represented by Eq. (4), were obtained in the range of $10^{-2}<D<10$. Figure 1 gives the experimental data. The stability constants obtained are listed in Table 1, together with those of the cobalt(II) complexes previously reported.[4,5] It may be seen from the table that the stability constants of the nickel(II) complexes are, in general, a little higher than those of the corresponding cobalt(II) complexes, as is to be expected from the natural order of stability, although the difference is not large.

The values of the stability constants for these complexes in the literature[1,2] are rather scattered, and, since many of them were obtained at low electrolyte concentrations, a direct comparison with the present results is not possible. However, the previous values for the β_1 of the chloride complex in 1.5 to 2 mol dm^{-3} perchlorate media are somewhat lower than the present values, while those for the β_1 of thiocyanate complexes in 1 to 2 mol dm^{-3} perchlorate media, about $10^{1.2}$, agree well with the present value.

We are grateful to Professor Masaakira Iguchi, who encouraged us to do this work.

References

1) A. E. Martell and L. G. Sillén, "Stability Constants," spec. pub. **17**, The Chemical Society, London (1964).
2) A Ringbom, "Complexation in Analytical Chemistry," John Wiley & Sons, New York (1963).
3) T. Sekine, M. Sakairi, F. Shimada, and Y. Hasegawa, This Bulletin, **38**, 847 (1965).
4) T. Sekine, R. Murai, and M. Iguchi, *Nippon Kagaku Zasshi*, **92**, 412 (1971).
5) R. Murai, T. Sekine, and M. Iguchi, *ibid.*, **92**, 1019 (1971).
6) T. Sekine, M. Sakairi, and Y. Hasegawa, This Bulletin, **39**, 2141 (1966).

BULLETIN OF THE CHEMICAL SOCIETY OF JAPAN, VOL. 49(1), 337—338 (1976)

Studies on Organic Semiconductors. XVIII. Photoconductivity of Heteroaromatic Compounds and Their Substituted Derivatives

Akira SUGIMOTO, Shinji KATO, Hiroo INOUE, and Eiji IMOTO

Department of Applied Chemistry, College of Engineering, University of Osaka Prefecture, Sakai-shi, Osaka 591

(Received February 6, 1975)

Synopsis. The effects of hetero atoms and substituents on the photocurrents of the parent compounds were investigated by comparison of the photocurrents of 52 specimens of the aza-benzenoid and oxa-benzenoid compounds.

Recently, we have reported the photoconductivity of condensed aromatic or heteroaromatic compounds and their substituted derivatives.[1-4] The photoconductivity of the compounds was found to depend strongly on their chemical structures.

The purpose of this paper is to summarize the effects of the substituents and the hetero atoms on the photoconductivity of the parent compounds.

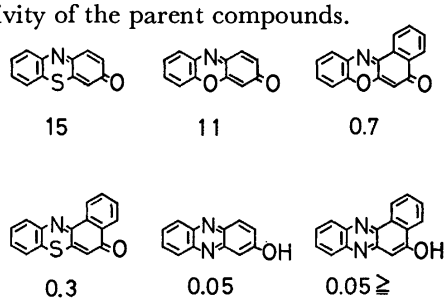

Fig. 1.
The values indicated below the chemical structures are the photocurrents (pico A).

TABLE 1. PHOTOCURRENTS OF OXA- AND AZA-BENZENOIDS, PARENT COMPOUNDS AND THEIR SUBSTITUTED COMPOUNDS

Compound	Hetero atom or substituent	Photocurrent (pico A)[a]
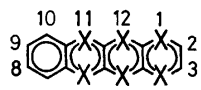	X=CH	10^3
	X (5,12)=N	0.4
	X (1,4,6,11)=N	0.2
	X (5,6,11,12)=N	0.2
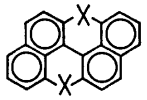	X=(-O-)	10^3
	X=(=CH-)	10^2—10^3
	X=(=N-)	0.1
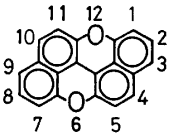	H	10^3
	1,10-$(NO_2)_2$	10^2
	4,10-$(NO_2)_2$	2
	1,4-$(NO_2)_2$	0.2
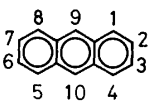	1,5-Cl_2	40 (410)
	H	35 (395)
	1,5-$(OCH_3)_2$	5 (410)
	1,5-$(COCH_3)_2$	5 (475)
	1,5-$(C_2H_5)_2$	1 (395)
	9-CN	0.07 (430)
	1-$COCH_3$	0.05 (430)
	9-$COCH_3$	<0.05

a) The values in parentheses are wavelength (nm).

TABLE 2. PHOTOCURRENTS OF SUBSTITUTED PHENAZINES

Substituent	Photocurrent (pico A)
2-NO_2	10^3
1-OCH_3-7-NO_2	10
2-OCH_3-8-NO_2	10
2-OCH_3-7-NO_2	1
1-OCH_3-8-NO_2	1
1-NO_2	0.1
1-OCH_3-6-NO_2	0.1
1-OCH_3-9-NO_2	<0.05
2-OCH_3-6-NO_2	<0.05
2-OCH_3-9-NO_2	<0.05
1,6-Cl_2	9
1,6-$(OCH_3)_2$	2
1,6-$(C(CH_3)_3)_2$	1
1,6-$(NO_2)_2$	0.6
1-Cl	0.3
2-OH	0.05
2-OCH_3	0.05
others[a]	<0.05

a) 1-OH, 1-OCH_3, 1-NH_2, 2-Cl, 2,7-$(OCH_3)_2$, 2,7-$(C(CH_3)_3)_2$, 2,7-Cl_2, 1,6-$(CH_3)_2$, 1,6-$(OH)_2$, 1,6-$(NH_2)_2$, 1,4,6-$(OCH_3)_3$, 1,4,6,9-$(OCH_3)_4$

The compounds are of two types; condensed aza-benzenoids containing pyridine-type nitrogen hetero atoms and condensed oxa-benzenoids containing pyran-type oxygen hetero atoms. The former is expressed by Albert[5] as a π-electron deficient system. The compounds belonging to the system are generally oxidized with difficulty by oxygen and apt to behave as an electron acceptor in the formation of a charge-transfer complex. In contrast, oxa-benzenoids are easily oxidized by oxygen and tend to behave as an electron donor in the formation of a charge-transfer complex. Thus, oxa-benzenoids are classified as a π-electron excessive system. The photocurrents of these compounds are summarized in Fig. 1 and Tables 1 and 2.

Effects of Hetero Atoms: Aza-benzenoid compounds show much smaller photocurrents than those of the parent aromatic hydrocarbons.[6] On the other hand, the photocurrent of the oxa-benzenoid compound becomes slightly larger (Table 1). No significant difference of photocurrent between the oxa- and thia-quinonoid compounds was observed. This indicates that the quinonoid structure is a dominant factor governing the photoconductive process (Fig. 1).

Effects of Substituents: (1) The electron-withdrawing substituent, such as a nitro group, gave rise to a decrease in the photocurrent of an oxa-benzenoid compound such as *peri*-xantheno[2,1,9,8-k,l,m,n,a]xanthene, and

an increase in the photocurrent of an aza-benzenoid compound such as phenazine.[2]

(2) The electron-releasing substituent, such as a methoxyl group, has no detectable effect on the photoconductivity of the aza-benzenoid compound. In the case of the oxa-benzenoid compound, the effect of the electron-releasing substituent was uncertain, since the photocurrent could not be measured due to instability in the air.

(3) The substituents at the *peri*-position of the nitrogen atom of phenazine, except for OH or NH_2 group, caused a rise in the photocurrent.[1]

(4) Introduction of the methoxyl, acetyl, ethyl, and cyano groups at 1-, 9-, or 1,5-positions of the anthracene ring resulted in a decrease in the photocurrent of the unsubstituted anthracene (Table 1).[3]

Experimental

Materials. All the samples, except 1,6-dimethyl-, 1,4,6-trimethoxy- and 1,4,6,9-tetramethoxyphenazine, were prepared by the methods described in literature[7] and purified by repeated recrystallization, vacuum sublimation and chromatography.

1,4,6,9-Tetramethoxyphenazine. A mixture of 2,5-dimethoxyaniline (1.5 g, 0.01 mol), 2,5-dimethoxynitrobenzene (5.5 g, 0.03 mol), a powdered KOH (50 g), and benzene (50 ml) was refluxed under stirring for 5 hr, then subjected to steam distillation. After being allowed to stand overnight, a gummy product was filtered off and washed successively with ethanol (100 ml) and benzene (50 ml) until it changed into powder. The powder was subjected to chromatography on alumina with chloroform eluent. From the first reddish fraction, 1,4,6,9-tetramethoxyphenazine was obtained. Recrystallization from benzene gave 300 mg (10%) of reddish vermilion needles: mp >360 °C; NMR (CF_3COOH) δ 7.70 (s, aromatic H, 4H) and 4.34 (s, CH_3, 12H).

Found: C, 63.71; H, 5.30; N, 9.39%. Calcd for $C_{16}H_{16}O_4N_2$: C, 63.99; H, 5.37; N, 9.33%.

1,4,6-Trimethoxyphenazine. This compound was prepared with 6.85 g of *o*-anisidine, 29 g of 2,5-dimethoxynitrobenzene, 80 g of KOH, and 150 ml of benzene according to the method used in the preparation of 1,4,6,9-tetramethoxyphenazine. Recrystallization from benzene gave 1,4,6-trimethoxyphenazine as red crystals (600 mg): mp 254—254.5 °C; NMR (CF_3COOH) δ 8.55—8.12 (m, aromatic H, 2H), 7.81—7.40 (m, aromatic H, 3H), 4.30 (s, CH_3, 6H), and 4.35 (s, CH_3, 3H).

Found: C, 66.42; H, 5.07; N, 10.09%. Calcd for $C_{15}H_{14}O_3N_2$: C, 66.65; H, 5.22; N, 10.37%.

1,6-Dimethylphenazine. A mixture of 3-methyl-2-methoxyaniline (3.5 g), 2-methoxy-3-nitrotoluene (8 g), and KOH (20 g) was added to 150 ml of toluene and refluxed for 5 hr. 1,6-Dimethylphenazine was obtained according to the reported method[8]: mp 218.5—219 °C (lit,[9] 221—222 °C).

Measurements. The surface-type cells of the samples were prepared according to methods given in previous papers and their photocurrents measured under conditions similar to those reported[1-4] (nitrogen atmosphere, 1900 lux, 200 V/cm). The photocurrents of the substituted anthracenes (Table 1) were measured by irradiating the surface-type cell with a monochromatic light, the wavelength of which is shown in parentheses in Table 1. In the case of the other compounds, the cells were irradiated with a white light (320—800 nm).

References

1) A. Sugimoto, S. Furuyama, H. Inoue, and E. Imoto, *Nippon Kagaku Kaichi*, **1974**, 1289.

2) A. Sugimoto, K. Inoue, H. Inoue, and E. Imoto, *ibid.*, **1974**, 1294.

3) A. Sugimoto, S. Kato, H. Inoue, and E. Imoto, *ibid.*, **1974**, 1299.

4) A. Sugimoto, S. Furuyama, H. Inoue, and E. Imoto, *ibid.*, **1974**, 1814.

5) A. Albert, "Current Trends in Heterocyclic Chemistry," ed. by A. Albert, G. M. Badger, and C. W. Shoppee, Butterworths Scientific Publications, London (1958), p. 20.

6) M. Y. Kleinermann and S. P. McGlynn, "Organic Semiconductors, Proceedings of an Inter-Industry Conference," ed. by J. J. Brophy and J. W. Buttrey, Maruzen, Tokyo (1962), p. 108.

7) L. F. Fieser, *J. Amer. Chem. Soc.*, **53**, 2329 (1931); O. Hinsberg, *Ann. Chem.*, **319**, 257 (1901); A. Sugimoto, K. Inoue, and H. Inoue, *Nippon Kagaku Kaishi*, **1973**, 2429; R. Kuhn, P. Skrabal, and P. H. H. Fischer, *Tetrahedron*, **24**, 1843 (1968); R. Pummerer, E. Prell, and A. Rieche, *Chem. Ber.*, **59**, 2159 (1926); E. Clar, *ibid.*, **72**, 1645 (1939); A. Rieche, W. Rudolph, and R. Seifert, *ibid.*, **73**, 343 (1940); R. Pummerer, E. Buchta, W. Gundel, W. Kiessling, K. Pfeiffer, H. Rath, K. Schuler, and H. Stinzendorfer, *Ann. Chem.*, **553**, 103 (1942); The other references are cited in Refs. 1), 2), 3), and 4).

8) I. J. Pachter and M. C. Kloetzel, *J. Amer. Chem. Soc.*, **73**, 4958 (1951).

9) Y. Kindani and H. Otomasu, *Chem. Pharm. Bull.* (Tokyo), **4**, 391 (1956).

BULLETIN OF THE CHEMICAL SOCIETY OF JAPAN, VOL. 49(1), 339—340 (1976)

Spectroscopic Study of Alkyl Vinyl Ketones

Ikuo NAITO, Akihiro KINOSHITA, and Tadashi YONEMITSU

Department of Photography, Kyushu Sangyo University, Matsugadai, Higashi-ku, Fukuoka 813

(Received February 10, 1975)

Synopsis. Alkyl vinyl ketones have two conformations, *s-cis* and *s-trans*. The ratios of the two conformers are given by comparing their IR with NMR data. The conformer of *s-cis* is given by the equation, Percentage of *s-cis*=180·($\Delta\delta$ −0.15) (%), where $\Delta\delta$ is the chemical shift difference between *cis* and *trans* protons for carbonyl group. The value of ΔF obtained by means of the equation is related to steric factors Es^c of bearing alkyl groups. The ratio *s-cis*/*s-trans* is determined by the bulkiness of the alkyl group.

Alkyl vinyl ketones (AVK) are in equilibrium between two comparatively stable conformations, *s-cis* and *s-trans*. NMR spectra of AVK were studied and discussed as regards mono substituted ethylene.[1] Kossanyi[2] determined seven kinds of AVK in arbitrary units (δ *cis*+δ*trans*+δ*gem*=0) and reported the effect of the alkyl group. The chemical shift of each vinylic proton can not be compared with other AVK, nor considered to be caused by conformation. The relation between conformations of β,β disubstituted enone and its chemical shift difference, reported by Cottee and Timmons,[3] and Faulk and Fry,[4] seems to be applicable to AVK.

NMR measurement of AVK (CH_2=CH–CO–R, R= Me, *n*-Pr, *i*-Pr, cyclo-Hex, *tert*-Bu and Ph) was carried out in carbon tetrachloride. The chemical shifts of vinylic protons are listed in Table 1. The chemical shift of *cis* proton is shifted to lower magnetic field with the decrease of Taft's σ^* value,[5] contrary to the tendency of *trans* proton. No different effects of alkyl substituent seem to be found for the protons. For 2 methylene cycloalkanones, Klose[6] and Kaiser and Hooper[7] showed a correlation between the chemical shift difference of two geminal olefinic protons and dihedral angle about central C–C bond from the diamagnetic anisotropy of carbonyl group. Similary, the chemical shifts of AVK are greatly affected by its carbonyl group. Since the ketones seem to consist of two comparatively stable conformers, the observed values are the mean values of *s-cis* and *s-trans*, and seem to be proportional to Taft's σ^* values. For the sake of clarification chemical shift differences ($\Delta\delta$=δ*cis*—δ*trans*) are compared with the proportion of $\varepsilon^{a}_{C=O\ s\text{-}cis}$, $(\varepsilon^{a}_{C=O\ s\text{-}cis}/(\varepsilon^{a}_{C=O\ s\text{-}cis}+\varepsilon^{a}_{C=O\ s\text{-}trans}))$ *s-trans* which does not indicate the exact proportion but suggests the part of *s-cis*, as shown Fig. 1. Linearity is found to hold. The conformer of *s-cis* in conjugated enone is given by means of the following equation,

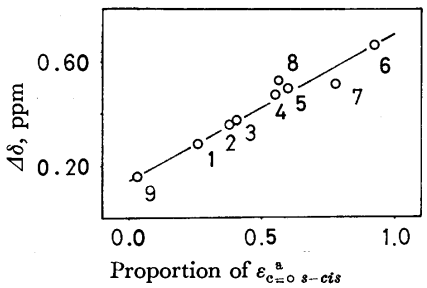

Fig. 1. Relation between the proportion of $\varepsilon_{C=O\ s\text{-}cis}$ and $\Delta\delta$.
(1=Me, 2=Et, 3=*n*-Pr, 4=cyclo-Hex, 5=*i*-Pr, 6=*t*-Bu, 7=Ph, 8=Methyl propenoate, 9=Propenal and 3-Methylbut-3-ene-2-one)

TABLE 1. NMR CHEMICAL SHIFTS OF VINYLIC PROTONS, RATIOS OF THE C=O *s-cis* TO C=O *s-trans* STRETCHING BAND ABSORBANCE AND Taft's σ^* VALUES OF BEARING ALKYL GROUP

Compound (R)	Chemical Shift (ppm)			Ratio of Absorbances	σ^*
	cis	*trans*	geminal		
1 Me	6.11	5.82	6.31	0.37	0.0
2 Et	6.12	5.76	6.35	0.61	−0.10
3 n-Pr	6.12	5.74	6.35	0.69	−0.115
4 iso-Pr	6.16	5.66	6.40	1.47	−0.19
5 cyclo-Hex	6.16	5.68	6.42	1.13	−0.15
6 tert-Bu	6.26	5.60	6.88	9.27	−0.30
7 Ph	6.35	5.83	7.09	4.17	0.60
8 H (Propenal)[a]	6.07	6.23	6.25	—	0.49
9 3-Methylbut-3-ene-2-one[b]	5.87	5.71	1.80 (CH_3)	0.03	
10 Methyl propenoate	0.533[c]			1.29[d]	

NMR spectra were measured in carbon tetrachloride (*ca.* 0.5 mol/l) with TMS at 35 °C, using Hitachi R-22 and Japan Electron Optics 4H-100. The chemical shifts were obtained from the spectra which were approximated to ABX type systems.

IR spectra were measured in carbon tetrachloride ($4.0—8.0\times10^{-2}$ mol/l) by the use of Shimadzu IR-27G type and NaCl and 0.2 mm spacer. Each AVK has C=O streching bands near 1700 cm^{-1}.

Higher frequency peak is assigned to *s-cis* the lower frequency peak to *s-trans* conformations.

a) Ref. 8, b) This value was given under the same condition as for the measurements of AVK. c) Ref. 10, d) This value gives the ratio of the C=C *s-cis* to C=C *s-trans* stretching band absorbance.[9]

Percentage of *s-cis*=180 ($\Delta\delta$−0.15) (%). Since propeophenone contains high diamagnetic aromatic group, $\Delta\delta$ of propeophenone deviates from linearity. The value of *s-trans* (0.15 ppm) agrees completely with that of 2-methylene cycloalkanones reported by Kaiser and Hooper,[7] and that proposed for but-3-ene-2-one (R=Me) from carbonyl anisotropy by Barlet *et al.*[11] However, $\Delta\delta$ of *s-cis* (0.72 ppm) appears higher than both the former value[7] (0.64 ppm) and the latter value[11] (0.63 ppm). Since calculated values of AVK by means of Pople's data[12] are 0.79 ppm for *s-cis* and 0.19 ppm for *s-trans* (0.80 ppm and 0.12 ppm for but-3-ene-2-one, respectively),* $\Delta\delta$ of *s-cis* is acceptable. The results support the view that the relation is suitable for CH_2=C–C=O compounds, propenal,[8]** methyl propenoate[9,10] and 3 methyl but-3-ene-2-one, which have stable *s-cis* and *s-trans* but not effective shielding groups.

The *s-cis*/*s-trans* ratio and free energy difference ($\Delta F = F_{s\text{-}cis} - F_{s\text{-}trans}$) are calculated by means of the ratio of *s-cis* (Table 2). Since ΔF seems to be affected by its alkyl groups, it is compared with Hancock's steric factor (Es^c) which does not involve hyperconjugation term (Fig. 2). We see that a linear relation holds and that the *s-cis*/*s-trans* ratio of AVK is determined by the bulkiness of the bearing alkyl group.

TABLE 2. K AND ΔF OF AVK BY EMPLOYING THE EQUATION

Compound R	$\Delta\delta$ (ppm)	*s-cis* (%)	K *s-cis*/*s-trans*	$\Delta F \times 10^{a)}$ (kcal/mol)	E_s^c
Me	0.29	25	0.34	6.63	0.0
Et	0.36	38	0.61	3.03	−0.38
n-Pr	0.38	41	0.71	2.12	−0.67
i-Pr	0.50	63	1.70	−3.23	−1.09
cyclo-Hex	0.48	59	1.46	−2.30	−1.40
tert-Bu	0.66	92	11.2	−14.73	−2.46
H (Propenal)	0.16	2	0.02	*ca.* 25	
3-Methylbut-3-ene-2-one	0.16	2	0.02	*ca.* 25	

a) $\Delta F = F_{s\text{-}cis} - F_{s\text{-}trans}$.

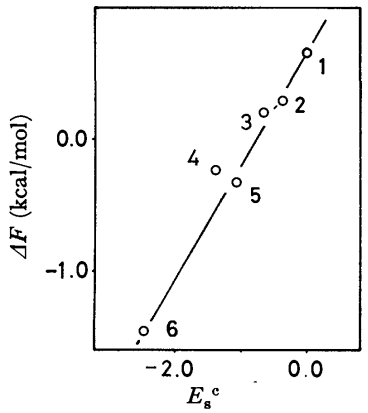

Fig. 2. Relation between ΔF and E_s^c (1=Me, 2=Et, 3=*N*-Pr, 4=cyclo-Hex, 5=*i*-Pr, 6=*t*-Bu)

* The calculation was carried out using ideal molecular coordinates. ($r_{C=C}$=1.34 Å, $r_{=C-H}$=1.08 Å, $r_{=C-C=}$=1.48 Å, $r_{C=O}$=1.21 Å, r_{C-CH_3}=1.54 Å, r_{C-H}=1.10 Å (1.09 Å at position of carbonyl group), $\angle^{C}_{(SP^3)}$=108° 28′ $\angle^{C}_{(SP^2)}$=120°) χ_x^c=10.8, χ_y^c=17.9, χ_z^c=10.8, χ_x^o=18.0, χ_y^o=16.7, χ_z^o=7.2 on carbonyl group, x^{C-C}=5.3 paramagnetic term on C–C single bond. The value of x^{C-H} and x^{C-C} on C–C single bonds which are out of the conjugated plane are neglected.

** Courtieu *et al.*[15] reported that propenal is *s-trans* form above 90% from NMR measurement. As $\nu_{c-o\ s\text{-}cis}$ could not be found, it is possible to consider that propenal is almost of s-*trans* conformation.

Conclusion

The *s-cis*/*s-trans* ratio of AVK is determined by the bulkiness of the alkyl group. Its chemical shift difference of two geminal olefinic protons is determined by the ratio of conformers. ΔH and potential barrier of rotation can be roughly estimated by means of the relation between $\Delta\delta$ and *s-cis* percentage. The ΔH value of but-3-ene-2-one (R=Me) is determined by means of the change of temperature in NMR (0.34 kcal/mol). The result agrees with the value reported by Bowles *et al.*[14] The change of the chemical shifts of vinylic protons are calculated for each conformations by the relation we obtained. Each chemical shift obtained is proportional to Taft's σ^* values of the bearing alkyl group.

References

1) For example, W. Brugel, Th. Ankel, and F. Kruckeberg, *Z. Electrochem.*, **64**, 1121 (1960). S. Castllano and J. S. Waugh, *J. Chem. Phys.*, **37**, 1951 (1962). K. Takahashi, This Bulletin, **37**, 963 (1962).
2) J. Kossanyi, *Bull. Soc. Chim. Fr.*, **1965**, 704.
3) F. H. Cottee and C. J. Timmons, *J. Chem. Soc., B*, **1968**, 326.
4) D. D. Faulk and A. Fry, *J. Org. Chem.*, **35**, 364 (1970).
5) R. W. Taft, M. S. Newman edited "Steric Effects in Organic Chemistry," John Wiley & Sons, (1956) p. 591.
6) G. Klose, *Mol. Phys.*, **6**, 585 (1965).
7) R. Kaiser and D. J. Hooper, *Mol. Phys.*, **8**, 403 (1964).
8) A. W. Douglas and J. H. Goldstein, *Spectrochem. Acta*, **16**, 1 (1965).
9) W. H. T. Davison and G. R. Bates, *J. Chem. Soc.*, **1953**, 2607.
10) H. S. Gutowsky, *J. Chem. Phys.*, **34**, 295 (1966).
11) R. Barlet, J. L. Pierre, and P. Arnand, *C. R. Acad. Sci. C*, **262**, 855 (1966).
12) L. M. Jackman and S. Sternhell, "Applications of Nuclear Magnetic Resonance in Organic Chemistry," 2nd edition, Pergamon Press, (1969) p. 88.
13) C. K. Hancock, E. A. Meyers, and S. J. Yager, *J. Amer. Chem. Soc.*, **83**, 4211 (1961).
14) A. K. Bowles, W. O. Gerorge, and W. F. Maddams, *J. Chem. Soc., B*, **1969**, 810.
15) J. Courtieu, Y. Gounelle, D. Gonord, and S. K. Kar, *Org. Magnetic Resonance*, **6**, 151 (1974).

BULLETIN OF THE CHEMICAL SOCIETY OF JAPAN, VOL. 49(1), 341—342 (1976)

Photochemical Reaction of Ethyl 3-Methyl-3-phenylglycidate in Methanol and Ether Solvents

Vo Van CHUNG, Masao TOKUDA,* Akira SUZUKI, and Mitsuomi ITOH
Department of Chemical Process Engineering, Hokkaido University, Sapporo 060

(Received May 26, 1975)

Synopsis. Irradiation of ethyl 3-methyl-3-phenylglycidate (**1**) in methanol gave an ionic addition product of the solvent, whereas in ether solvent different reaction paths leading to β-keto esters and carbene were observed.

It was previously reported that irradiation of aliphatic α,β-epoxy esters in an aprotic solvent gave corresponding β-keto esters,[1] while in a protic solvent completely different types of products were obtained.[2] In this note, we wish to report that the photochemical reaction of α,β-epoxy ester with a β-phenyl substituent in methanol gave an ionic addition product, but in ether solvent the reaction occurred with two competing pathway: a fragmentation to carbene and ketone and a rearrangement to β-keto ester. The photochemical fragmentation of aryl-substituted oxiranes to arylcarbenes has been studied extensively by Griffin and his co-workers.[3] The present work provides an additional example to the few reported ones where fragmentation occurs in the absence of vicinal diaryl substitution on the oxirane ring.[4]

Results and Discussion

Irradiation of ethyl 3-methyl-3-phenylglycidate (**1**) in methanol with 253.7 nm light for 45 hr gave a diastereoisomeric mixture of ethyl 2-hydroxy-3-methoxy-3-phenylbutyrate (**2**). The structure of **2** was determined by spectral data and by the following chemical transformations. Oxidation of **2** with chromium trioxide-pyridine complex gave α-keto ester (**3**), while treatment with warm sulfuric acid–acetic acid solution gave ethyl 2-acetoxy-3-phenyl-3-butenoate (**4**). Furthermore, a thermal reaction of **1** in methanol with a small amount of hydrochloric acid also gave **2** and its methyl ester in 45% and 19% yields, respectively.

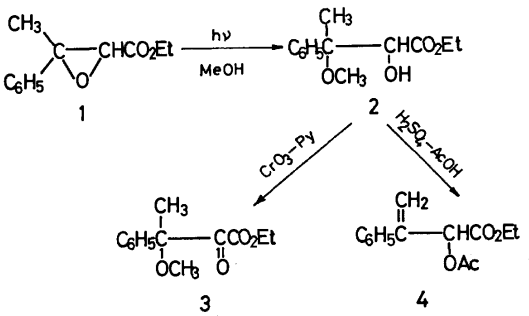

Scheme 1.

The results obtained under various conditions are summarized in Table 1. When the irradiation was carried out in the presence of hydrochloric acid or under oxygen atmosphere, an increased amount of **2** was obtained. The dark reaction of **1** in methanol did not give a detectable amount of **2**. In addition, it was also established that irradiation of **1** in methanol involving a small amount of alkali did not give **2**. These results demonstrate that this photochemical ionic reaction probably proceeds *via* a protonation of α,β-epoxy ester under irradiation. Photolysis of methanol in the presence of oxygen was reported to produce an acidic substance, which initiated the ionic reaction.[5] However, irradiation of degassed solution of **1** gave a 10% yield of **2**. Moreover, in a similar photochemical reaction of ethyl 1-oxaspiro[2,4]heptane-2-carboxylate, it was reported that the presence or absence of oxygen did not affect the yield of the ionic addition product of methanol.[2] Accordingly, although it is unknown what the nature of the acidic substance is, these results indicate that some acidic substances produced photochemically from the starting epoxy ester or solvent probably play an important role in these reactions.[5c]

Table 1. IRRADIATION OF **1** IN METHANOL UNDER VARIOUS CONDITIONS

Irradiation condition[a]	Yield of **2** (%)	Conversion of **1** (%)
N_2	20	97
N_2[b]	37	100
O_2	36	88
Degassed (1×10^{-4} mmHg)	10	65
Degassed, dark	0	58
Dark, in air	0	67
Dark, in air[b]	7	100

a) Irradiations were carried out with a 15 W low pressure mercury vapor lamp for 45 hr and dark reactions for 45 hr. b) A small amount of HCl was added.

The photochemical reaction of **1** in an aprotic solvent gave the following products mainly *via* two types of reaction paths, namely, a photolytic path leading to acetophenone and carbethoxycarbene (*a*)[3a] and a rearrangement to β-keto ester (*b*).[1] Irradiation of **1** in ether with a high pressure mercury vapor lamp for 90 hr gave acetophenone (**5**, 13%), ethyl acetate (**6**, 3%), 3-ethoxy-2-phenyl-2-butanol (**7**, 7%), 2,3-diethoxybutane (**8**, 40%), ethyl 3-hydroxy-2-methyl-3-phenylpropionate (**10**, 11%), and ethyl 4-ethoxy-3-hydroxy-2-methyl-3-phenylpentanoate (**11**, 32%) in a 95% conversion. Products **7**, **8**, **10**, and **11** involved an almost

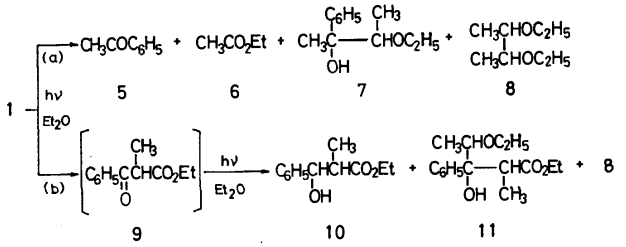

Scheme 2

equal amount of diastereoisomers.

The formation of **5**, **7**, and **6** indicates that a photochemical cleavage of **1** occurred mainly at the C_α–O and C_α–C_β bonds. Products **7** and **8** have been shown to be produced by the photochemical reaction of acetophenone in ether,[6] while **6** may result from carbethoxycarbene. Ethyl acetate was shown to be produced by photolysis of ethyl diazoacetate in ether. The photolytic path to **10**, **11**, and **8** through β-keto ester (**9**) was confirmed by the fact that irradiation of **9** under the same conditions gave a mixture of **10**, **11**, and **8**. It was shown that β-methyl substituent migrates to α-carbon in preference to the phenyl group.[1,7]

Experimental

Ethyl 3-methyl-3-phenylglycidate (**1**) was prepared by the procedure of the Darzens synthesis.[8] Ethyl 2-methyl-3-oxo-3-phenylpropionate (**9**) was prepared according to the procedure of Marvel.[9] Quantitative glpc analyses were carried out with the internal standard.

Photochemistry of **1** *in Methanol.* A mixture of **1** and methanol (0.08 M) in a quartz tube was cooled in water and externally irradiated with a 15W low pressure mercury vapor lamp for 45 hr. Nitrogen gas was allowed to pass through the mixture during the irradiation. Distillation and a preparative glpc of the irradiation mixture gave diastereoisomeric ethyl 2-hydroxy-3-methoxy-3-phenylbutyrate (**2**): bp 250 °C; n_D^{23} 1.5050; IR (CCl_4) 3540, 1735 cm^{-1}; NMR (CCl_4) τ 9.02 and 8.92 (t, 3H), 8.42 and 8.40 (s, 3H), 6.85 and 6.90 (s, 3H), 7.42 (s, 1H, OH), 5.98 (s, 1H), 6.10 (q, 2H); *m/e* 238 (M^+), 135, 103. Found: C, 65.32; H, 7.89%. Calcd for $C_{13}H_{18}O_4$: C, 65.53; H, 7.61%.

Oxidation of **2** with chromium trioxide and pyridine[10] produced ethyl 3-methoxy-2-oxo-3-phenylbutyrate (**3**): n_D^{20} 1.4980; IR (CCl_4) 1740, 1725 cm^{-1}; NMR (CCl_4) τ 8.82 (t, 3H), 8.37 (s, 3H), 6.80 (s, 3H), 5.87 (q, 2H), 2.7 (s, 5H); *m/e* 135 (M^+–$COCO_2Et$), 104, 73. Found: C, 65.68; H, 7.02%. Calcd for $C_{13}H_{16}O_4$: C, 66.08; H, 6.83%.

Treatment of **2** with freshly prepared warm sulfuric acid–acetic acid solution[11] gave ethyl 2-acetoxy-3-phenyl-3-butenoate (**4**): n_D^{20} 1.5115; IR (CCl_4) 1750, 865 cm^{-1}; NMR (CCl_4) τ 8.90 (t, 3H), 7.90 (s, 3H), 5.92 (q, 2H), 4.56 (s, 1H), 4.46 (s, 1H), 4.25 (s, 1H), 2.72 (m, 5H); *m/e* 248 (M^+), 189, 175, 145. Found: C, 67.87; H, 6.59%. Calcd for $C_{14}H_{16}O_4$: C, 67.73, H, 6.50%.

Thermal reaction of **1** in methanol in the presence of a small amount of HCl for 2 hr gave **2** and diastereoisomeric methyl 2-hydroxy-3-methoxy-3-phenylbutyrate: bp 230 °C, n_D^{23} 1.5160.

Photochemistry of **1** *in Ether.* An etheral solution of **1** (0.08 M) was irradiated with a 500 W high pressure mercury vapor lamp for 90 hr. Distillation and a preparative glpc gave **5**, **6**, **7**, **8**, **10**, and **11**. The identities of **7**, **8**, and **10** were established by comparison of IR, NMR, and mass spectr awith those of authentic samples.[6] β-Hydroxy ester **10** was prepared by a reduction of ethyl 2-methyl-3-oxo-3-phenylpropionate (**9**) with sodium borohydride in ethanol: bp 148—150 °C/11 mmHg (lit,[12] 109—110 °C/0.5 mmHg), n_D^{20} 1.5085 (lit,[12] n_D^{23} 1.5007). The spectral data of **11** were completely identical to those of the product obtained by the irradiation of **9** in ether: IR (CCl_4) 3475, 1735 cm^{-1}; *m/e* 207 (M^+–CH-(OC_2H_5)CH_3), 105, 77. Found: C, 68.53; H, 8.47%. Calcd for $C_{16}H_{24}O_4$: C, 68.54; H, 8.63%.

Photochemistry of **9** *in Ether.* An etheral solution of **9** (0.08 M) was irradiated with a 500 W high pressure mercury vapor lamp for 25 hr. Distillation and a preparative glpc gave **10**, **11**, and **8**. The spectral data of the former two were completely identical to those of **10** and **11** obtained by the irradiation of **1** in ether.

Photochemistry of Ethyl Diazoacetate in Ether. An etheral solution of ethyl diazoacetate (0.3 M) was irradiated with a 500 W high pressure mercury vapor lamp for 15 hr. Distillation and a preparative glpc gave ethyl acetate (**6**), diethyl maleate, diethyl fumarate, ethyl 2-ethoxyacetate, and ethyl 3-ethoxybutanoate. The structure of ethyl 3-ethoxybutanoate was identified by comparison with an authentic sample[13]: n_D^{20} 1.4125 (lit,[13] n_D^{19} 1.4092); IR (CCl_4) 1735, 1200, 1100 cm^{-1}; NMR (CCl_4) τ 8.87 (t, 3H), 8.74 (t, 3H), 8.84 (d, 2H), 7.57 and 7.73 (d, 2H), 6.56 (q, 2H), 5.92 (q, 2H), 6.23 (sex, 1H); *m/e* 160 (M^+), 145, 131, 85, 73.

References

1) M. Tokuda, M. Hataya, J. Imai, M. Itoh, and A. Suzuki, *Tetrahedron Lett.*, 3133 (1971).

2) M. Tokuda, V. V. Chung, A. Suzuki, and M. Itoh, *J. Org. Chem.*, **40**, 1858 (1975).

3) a) N. R. Bertoniere and G. W. Griffin, "Organic Photochemistry," Vol. 3, ed. by O. L. Chapman, Marcel Dekker, Inc., New York (1973), p. 115. b) T. I. Temnikova and I. P. Stepanov, *Zh. Org. Khim.*, **3**, 2253 (1967).

4) P. C. Petrellis, H. Dietrich, E. Meyer, and G. W. Griffin, *J. Amer. Chem. Soc.*, **89**, 1967 (1967).

5) a) S. J. Cristol, G. A. Lee, and A. L. Noreen, *Tetrahedron Lett.*, **1971**, 4175. b) G. Roussi and R. Beugelmans, *ibid.*, 1333 (1972). c) M. Hisaoka and K. Tokumaru, *Chem. Lett.*, **1973**, 351.

6) M. Tokuda, M. Hasegawa, A. Suzuki, and M. Itoh, This Bulletin, **47**, 2619 (1974).

7) C. S. Marcos and W. Reusch, *J. Amer. Chem. Soc.*, **89**, 3363 (1967).

8) R. H. Hunt, L. J. Chinn, and W. S. Johnson, "Organic Syntheses," Coll. Vol. IV, p. 459 (1963).

9) C. S. Marvel and F. D. Hager, "Organic Syntheses," Coll. Vol. I, p. 248 (1941).

10) P. J. Pasto and C. R. Johnson, "Organic Structure Determination," Pretice-Hall Inc., Engelwood Cliffs, N. J. (1969), p. 361.

11) E. W. Garbisch, Jr., *J. Org. Chem.*, **26**, 4165 (1961).

12) M. B. Floyd and G. R. Allen, Jr., *ibid.*, **35**, 2647 (1970).

13) H. Schinz and M. Hinder, *Helv. Chim. Acta*, **30**, 1369 (1947).

BULLETIN OF THE CHEMICAL SOCIETY OF JAPAN, VOL. 49(1), 343—344 (1976)

The Mass Spectra of 3-Aryl-1,2,3-oxathiazolidine 2-Oxides

Fukiko YAMADA, Tomihiro NISHIYAMA, Hiroshi SAMUKAWA, and Yasunari TAKEUCHI

Department of Applied Chemistry, Faculty of Engineering, Kansai University, Senriyama, Suita, Osaka 564

(Received July 7, 1975)

Synopsis. The mass spectra of a series of 3-aryl-1,2,-3-oxathiazolidine 2-oxides were obtained. The fragment ions were chiefly formed by the elimination of SO_2 from the M^+ ion. In this step, both the effects of the ring substituent and the torsion angle of the oxathiazolidine ring on the rate of the elimination were observed.

Recently, the authors reported the mass spectra of a number of 3-aryl-1,2,3-oxathiazolidine 2-oxides and a series of 3-aryl-5-methyl-, or 3-aryl-5-chloromethyl-1,2,3-oxathiazolidine 2-oxides.[1-3] In order to obtain further information about structural influence on the fragmentation pathways, the authors now deal with the correlations of the elimination rates with the substituents of the following 3-aryl-1,2,3-oxathiazolidine 2-oxides (**1**) and with the torsion angles of the oxathiazolidine ring determined from the vicinal coupling constants between the four methylene protons by means of NMR spectroscopy.[4]

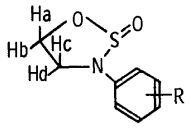

1

(2)

I, R=H
IIa, R=*o*-CH_3
IIb, R=*m*-CH_3
IIc, R=*p*-CH_3
IIIa, R=*o*-OCH_3
IIIb, R=*m*-OCH_3
IIIc, R=*p*-OCH_3
IV, R=*p*-Br
Va, R=*o*-Cl
Vb, R=*m*-Cl
Vc, R=*p*-Cl
VI, R=2,4,6-tri-Cl

Experimental

Compounds. A series of **1** was prepared and purified by a previously reported method.[5] The reaction conditions and the physical properties of **1** were reported in a previous paper by the authors.[4]

Measurements. The mass spectra were obtained with a Japan Electron Optics Co., Ltd., JMS-01SG Mattauch-Herzog double-focusing mass spectrometer at an ionizing energy of 75 eV, an emission current of 200 μA, an accelerating voltage of 6.4 kV, and a vapor pressure of 1.0×10^{-6} mmHg. The ion-source temperature varied between 100 and 150 °C. The accurate masses and elemental compositions were determined by a previously-reported method.[1]

Results and Discussion

The mass spectral data of I—VI are shown in Table 1, while the main fragmentation pathway is shown in Scheme 1. There are three steps of cleavage in the oxathiazolidine ring, the elimination of SO_2 (step 1), of the methyl radical (step 2), and of HCN (step 3).[1] Examination of the data in Table 1 indicates there is a relation between the rate of elimination and the Hammett σ constant of an *m*- or *p*-substituent.[6] Then, the log Z/Z_0 (relative intensities) in step 1 were plotted against σ, except for the data with *o*- and 2,4,6-tri-substituents, as is shown in Fig. 1. In the case of the I,IIb, IIIb, Vb, and Vc, a reasonably good linear correlation is obtained, and the slope is $\rho=+0.81$. On the contrary, the values for IIc, IIIc, and IV deviated from the line. In the cases of steps 2 and 3, no noticeable substituent effect was found.

In a previous paper by the present authors,[4] it was reported that oxathiazolidines tend to form twist-envelope conformations, that their torsion angles vary with both the position and the nature of the ring substituent,

Table 1. Mass spectral data and torsion angles of the compounds

Compd. No.	Rel. Int. (%) M	A	B	C	Torsion[a] angle (θ°)
I	55	16	100	78	15
IIa	92	13	100	33	−11
IIb	87	23	100	90	12
IIc	84	22	100	80	11
IIIa	100	14	97	22	−5
IIIb	100	37	99	63	14
IIIc	78	26	100	13	4
IV	48	27	100	67	14
Va	69	13	100	36	−11
Vb	50	28	100	65	15
Vc	56	27	100	55	12
VI	14	21	100	21	30

a) These values are taken from Ref. 4.

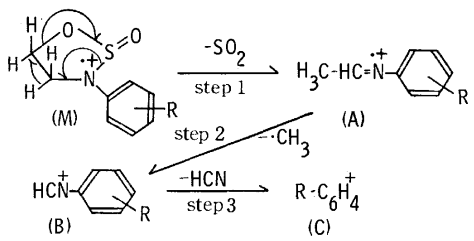

Scheme 1. The main fragmentation pathway of the **1** compounds.

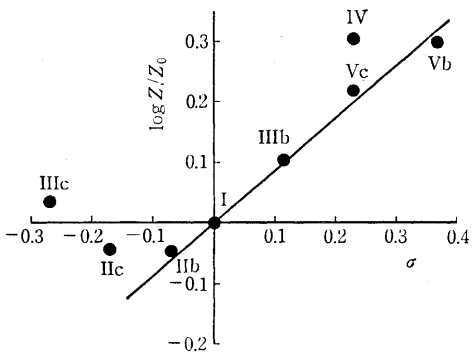

Fig. 1. Correlation of the intensities of the A ion in the 75 eV mass spectra of the **1** compounds. Slope=0.81.

and that the distortions of the oxathiazolidine ring of the compounds with *m*- and *p*-substituents are in the direction of the projection **2**, while those with an *o*-substituent cause a distortion toward the projection **3**, as can be seen in the diagram. The values of the torsion angles are listed in Table 1.

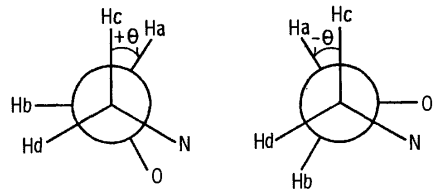

2 **3**

θ; Torsion angle

Regarding the greater deviation from the Hammett correlation in the case of IIIc (Fig. 1), it was considered that there is another energy factor for the elimination of SO_2 because of the small torsion angle for IIIc given in Table 1. The torsion angles of the compounds showed in Fig. 1 are in the range of 11—15 °C except for IIIc.

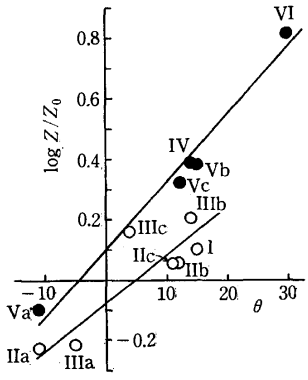

Fig. 2. The plot of the *Z*-values of the initial fragmentation of the **1** compounds against torsion angles (θ).
Z_o-value is obtained from the curve plotted of θ *vs.* *A*/*M* and is 23% at θ=0°.
$Z=[R\text{-}C_6H_4\text{-}\overset{+}{N}\text{-}CHCH_3]/[M^+]$
●: Electron-withdrawing group, ○: electron-donating group.

Therefore, an attempt was made to plot the *z*-values of all the compounds against their torsion angles (Fig. 2). As can be seen in Fig. 2, two kinds of linear correlation are obtained. The upper line due to the data of the compounds with an electron-withdrawing group and the lower line due to those with an electron-donating group.

As is indicated in Scheme 1, the transfer of a hydrogen atom from the C-4 to the C-5 position and the ring cleavage of the molecular ion afford the elimination of the SO_2 group. In the molecular ion, the positive charge is distributed over the nitrogen atom and the aromatic ring. Figure 1 indicates that an electron-withdrawing substituent strongly enhances the formation of the elimination product and the value of approximately +0.81 is relatively large compared with any previously reported values for the rate of an electron-impact collision.[7] Thus, it appears that the reaction is enhanced by an increased positive charge at the reaction site. Figure 2 indicates that, in general, an electron-withdrawing group enhances the rate of elimination, and an electron-donating group supresses it. Moreover, the magnitude of the distortion of the oxathiazolidine ring may markedly affect the rate of elimination. The above two factors, the magnitude of the positive charge at the reaction site and the torsion angle of the oxathiazolidine ring, should make an important contribution to the driving force for an electron-impact collision.

References

1) F. Yamada, T. Nishiyama, Y. Fujimoto, and M. Kinugasa, This Bulletin, 44, 1152 (1971).
2) T. Nishiyama and F. Yamada, *ibid.*, **45**, 928 (1972).
3) T. Nishiyama and F. Yamada, *ibid.*, **46**, 2166 (1973).
4) F. Yamada, T. Nishiyama, and H. Samukawa, *ibid.*, **48**, 1878 (1975).
5) F. Yamada, T. Nishiyama, M. Kinugasa, and M. Nakatani, *ibid.*, **43**, 3611 (1970).
6) (a) M. M. Bursey and F. W. McLafferty, *J. Amer. Chem. Soc.*, **88**, 529 (1966). (b) M. M. Bursey and F. W. McLafferty, *ibid.*, **88**, 4484 (1966). (c) M. M. Bursey and F. W. McLafferty, *ibid.*, **89**, 1 (1967).
7) P. Brown and C. Djerassi, *ibid.*, **89**, 2711 (1967).

BULLETIN OF THE CHEMICAL SOCIETY OF JAPAN, VOL. 49(1), 345—346 (1976)

The Chlorination of Norbornadiene by Various Chlorinating Agents

Akira ONOE, Sakae UEMURA,* and Masaya OKANO
Institute for Chemical Research, Kyoto University, Uji, Kyoto 611

(Received July 15, 1975)

Synopsis. The chlorination of norbornadiene by $CuCl_2$, $TlCl_3 \cdot 4H_2O$, $SbCl_5$, $SeCl_4$, and VCl_4 in CCl_4 or CH_3CN afforded mainly *trans*-3,5-(**1**) and *exo-cis*-3,5-dichloronortricyclene (**2**). In the reaction with $PbCl_4$, Cl_2, SO_2Cl_2, and PCl_5, appreciable amounts of *exo*-5-*syn*-7-(**3**) and/or *exo-cis*-5,6-dichloronorbornene (**4**) were obtained besides **1** and **2**.

Concerning the chlorination of norbornadiene, the reactions with $CuCl_2$ (gas-phase),[1] Cl_2,[2] $PhICl_2$,[2] $AuCl_3$,[3] and $MoCl_5$[4] have so far been reported. We now give the results of chlorination by various other chlorinating agents. Among the chlorinating agents examined the following were found to be effective: $CuCl_2$, $TlCl_3 \cdot 4H_2O$, $SbCl_5$, $SeCl_4$, VCl_4, $PbCl_4$, SO_2Cl_2, and PCl_5. The products were two isomeric dichloronortricyclenes [*trans*-3,5-(**1**) and *exo-cis*-3,5-(**2**)] and two isomeric dichloronorbornenes [*exo*-5-*syn*-7-(**3**) *exo-cis*-5,6-(**4**)], the distribution of the products depending a great deal on the kind of chlorinating agent and the reaction conditions. The results are shown in the Table together with our previous data on $MoCl_5$.[4]

1 **2** **3** **4**

The product distribution suggests that the chlorinating agents can be classified for convenience into three categories. The first class consists of $CuCl_2$, $TlCl_3 \cdot 4H_2O$, $SbCl_5$, $SeCl_4$, and VCl_4, which gave almost entirely **1** and **2**. Although a radical mechanism has been proposed for the formation of **1** and **2** by $PhICl_2$,[2] it was found that the reactions by these metal chlorides were ionic since no effect was observed by the addition of radical scavengers such as *m*-dinitrobenzene (*m*-DNB) and oxygen, or even when the reactions were carried out under N_2. Furthermore we have observed that the reaction of other olefins such as cyclohexene[5] and norbornene[6] with these metal chlorides proceeds by an ionic mechanism under nearly the same reaction contions. The ability of $SeCl_4$ and VCl_4 to chlorinate olefin, which was firstly found in the reaction with norbornene,[6] was also confirmed in this case (Runs 4 and 5), but no favorable *exo-cis*-addition by VCl_4 as observed in the case of norbornene[6] was found (Run 5).

The second class consists of $PbCl_4$, Cl_2, SO_2Cl_2, and PCl_5, which generally afforded a mixture of **1**, **2**, and **3**. The reactions with SO_2Cl_2 and PCl_5 at higher temperature gave **4** as an additional product (Runs 9 and 11). It is evident that at least **4** is formed by a radical pathway,[7] since the addition of *m*-DNB profoundly decreased the total yield of the products, affording none of **4**. In contrast, in the reactions with chlorine (in the dark) the formation of **4** was only slight (Run 7) and *m*-DNB and bubbling oxygen gave no effect on product distribution, suggesting an ionic process. The ionic nature of $PbCl_4$ was previously reported in the chlorination of norbornene.[6]

The mechanism for the formation of **1**—**3** might be essentially the same as that proposed by Winstein[8] in the bromination of norbornadiene. The attack of anion on C_3 and C_1 of a nonclassical chloronorbornyl cation

TABLE CHLORINATION OF NORBORNADIENE

Run	Norbornadiene (mmol)	Chlorinating agent (mmol)	Solvent (50 ml)	React temp (°C)	React time (hr)	Products Isomer distribution (%) 1	2	3	4	Yield (%)[a]
1	25	$CuCl_2$[b]	25 CH_3CN	80	2	49	50	1	0	82
2	25	$TlCl_3 \cdot 4H_2O$	12.5 CCl_4	76	2	51	49	0	0	86
3	25	$SbCl_5$	12.5 CCl_4	27	0.2	56	41	3	0	80
4	25	$SeCl_4$	2.8 CCl_4	76	12	40	55	5	0	28
5	20	VCl_4	3 CCl_4	76	2	64	33	1	2	38[c]
6	25	$PbCl_4$	5 CH_2Cl_2	−40	2	49	22	29	0	78[d]
7	25	Cl_2	70 CCl_4	−20	2	40	14	43	3	91
8	50	SO_2Cl_2	25 CCl_4	20	20	63	25	12	0	36
9	50	SO_2Cl_2	25 CCl_4	76	2	39	18	29	14	95
10	50	PCl_5	25 CH_2Cl_2	40	5	46	24	29	1	89
11	25	PCl_5	12.5 CCl_4	76	2	41	41	13	5	58
12[e]	5	$MoCl_5$	2 CCl_4	25	2	22	10	<0.5	68	20

a) Based on the chlorinating agent. Determined by glc. b) LiCl (25 mmol) was added. c) Other products; nortricyclyl chloride (0.2 mmol). d) Other products; nortricyclyl chloride (1.26 mmol) and *exo*-5-chloro-2-norbornene (3.6 mmol). e) Ref. 4.

* To whom all correspondence should be addressed.

(**A**) gives a mixture of **1** and **2**, and **3**, respectively. However, the reason why only the chlorinating agents in this class give **3** is not yet clear. The attack on C_6, which affords **4**, might be sterically unfavorable.

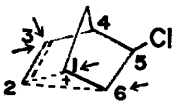

(**A**)

The last class contains only $MoCl_5$ which gave mainly **4** probably by molecular *cis*-addition mechanism.[4]

From a synthetic viewpoint chlorination by $SbCl_5$ is recommended for preparation of **1** and **2** because of its simplicity and high yields of the products. For **3** and **4**, the reactions with PCl_5 (in CH_2Cl_2) and $MoCl_5$, respectively, should be employed, though it is necessary to use preparative glc for isolating each isomer in a pure state.

Experimental

All materials except $PbCl_4$ were commercial products and used without further purification. The reactions were usually carried out by mixing all the reagents at room temperature and then keeping the mixture at reaction temperature under the presence of atmospheric oxygen. In the case of VCl_4, a CCl_4 solution of VCl_4 was added to a CCl_4 solution of norbornadiene in order to avoid the polymerization of diene. In the case of Cl_2, chlorine gas was introduced to a CCl_4 solution of norbornadiene at -20 °C. The identification of each product, **1**—**4**, was described previously.[4] The product mixtures were analyzed by glc by the use of Shimadzu apparatus 5APTF and 4BMPF on both EGSS-X(15%)-Chromosorb-W (3 m) and PEG 6000 (25%)-Chromosorb-W (3 m) columns (carrier gas, N_2; bromobenzene or *trans*-dichlorocyclohexane as internal standard).

Reaction with $PbCl_4$. A solution of CH_2Cl_2 (50 ml) containing $Pb(OAc)_4$ (2.22 g, 5.0 mmol) was kept at -60 °C and was introduced by HCl gas for 10 min.[9] To this solution was slowly added norbornadiene (2.3 g, 25 mmol) at -40 °C and the solution was stirred for 2 hr. After the usual work-up, the organic layer was evaporated to *ca.* 7 ml and analyzed by glc; *exo*-5-chloro-2-norbornene (3.6 mmol), nortricyclyl chloride (1.26 mmol), **1** (1.93 mmol), **2** (0.86 mmol), and **3** (1.13 mmol). The formation of the former two compounds by the reaction of norbornadiene with HCl has been reported.[10]

*Synthesis of **1** and **2**.* A CCl_4 (50 ml) solution of $SbCl_5$ (15 g, 50 mmol) was added to a CCl_4 (150 ml) solution of norbornadiene (9.2 g, 100 mmol) at 25 °C in *ca.* 1 min and the resulting clear solution was stirred for 10 min. To this solution was added water and the precipitated SbOCl was filtered and then CCl_4 layer was distilled to give 6.5 g (80% yield) of a mixture of **1** and **2** (**1**:**2**=58:42); bp 95—96 °C/22 mmHg. The NMR spectrum of both **1** and **2** (separated by preparative glc) was identical with the spectra reported.[2,3]

References

1) R. P. Arganbright and W. F. Yates, *J. Org. Chem.*, **27**, 1205 (1962).
2) S. Masson and A. Thuillier, *Bull. Soc., Chim. Fr.*, **1969**, 4368.
3) R. Hüttel, H. Reinheimer, and K. Nowak, *Chem. Ber.*, **101**, 3761 (1968).
4) S. Uemura, A. Onoe, and M. Okano, This Bulletin, **47**, 3121 (1974).
5) S. Uemura, A. Onoe, and M. Okano, *ibid.*, **47**, 692 (1974).
6) S. Uemura, A. Onoe, and M. Okano, *ibid.*, **48**, 3702 (1975).
7) The radical nature of SO_2Cl_2 and PCl_5 at high temperature is well-known; *e. g.*, a) M. S. Kharasch and H. C. Brown, *J. Amer. Chem. Soc.*, **61**, 3432 (1939). b) E. S. Huyser, *Synthesis*, **1970**, 7.
8) S. Winstein, *J. Amer. Chem. Soc.*, **83**, 1516 (1961).
9) P. W. Henniger, L. J. Dukker, and E. Havinga, *Rec. Trav. Chim. Pays-Bas*, **85**, 1177 (1966).
10) L. Schmerling, J. P. Luvisi, and R. W. Welch, *J. Amer. Chem. Soc.*, **78**, 2819 (1956).

BULLETIN OF THE CHEMICAL SOCIETY OF JAPAN, VOL. 49 (1), 347—348 (1976)

Extractive Spectrophotometric Determination of Chromium(III) with 1-(2-Pyridylazo)-2-naphthol

B. SUBRAHMANYAM and M. C. ESHWAR
Department of Chemistry, Indian Institute of Technology, Bombay-400076, India
(Received July 9, 1975)

Synopsis. 1-(2-Pyridylazo)-2-naphthol reacts with chromium(III), on heating at 80—90 °C for 35 min, at a pH of 3.2—3.7 in presence of acetate buffer. The reddish-brown chelate, extracted into 1-butanol, has two absorption maxima at 555 and 600 nm of equal intensity. The complex obeys Beer's law in the range 0.3—2.0 μg/ml, has molar absorptivity 1.28×10^4 at 555 nm.

1-(2-Pyridylazo)-2-naphthol, PAN, finds considerable application[1,2] as colorimetric reagent for determination of a number of metal ions. PAN has been found to be selective at lower pH values; hence a detailed investigation of chromium(III) has been carried out. This simple, sensitive and selective method is applied for the determination of chromium content in an alloy steel sample.

Experimental

Apparatus and Reagents. A CΦ4 quartz spectrophotometer with 10 mm quartz cells was used for the absorption measurements. The absorption spectra was recorded on a Perkin-Elmer recording spectrophotometer, Type 402. A cambridge pH meter was used for all pH measurements.

Stock solution of Cr(III) containing 2 mg/ml of chromium was prepared from chromium(III) nitrate (J. T. Baker) and standardized[3] volumetrically. Experimental solutions were obtained by appropriate dilution of stock solution.

1-(2-Pyridylazo)-2-naphthol. 0.1% solution of 1-(2-pyridylazo)-2-naphthol (PAN) was prepared in methyl alcohol.

Buffer solution of pH 3.5 was prepared from 0.2 M sodium acetate and 0.2 M acetic acid.

General Procedure. An aliquot of chromium(III) solution containing <20 μg of chromium was taken, to which were added 5 ml of sodium acetate-acetic acid buffer, pH 3.5, and 1 ml of 0.1% PAN. The contents were shaken thoroughly, made to 15 ml and heated in a boiling water bath for 35 min, allowed to cool, made to 25 ml, and extracted in a separating funnel with 10 ml of butanol for 20 s. After separation of layers, organic phase was collected in a 10 ml volumetric flask containing 1 g of anhydrous sodium sulfate and absorbance of reddish-brown chelate was measured at 555 nm against the reagent blank prepared under similar conditions.

Results and Discussion

Effect of pH. pH was varied from 0.5 to 7, and absorbance was found to be maximum (Fig. 1) in the pH range 3.2—3.7. Hence all studies were carried out at pH 3.5. Sodium acetate-acetic acid buffer was found to be the most suitable one.

Effect of Reagent Concentration. Reagent (0.1% PAN) concentration was varied from 0.1 to 5 ml with 13 μg of Cr(III) per 10 ml. Absorbance was found to be constant with amounts greater than 0.5 ml, hence 1 ml of reagent was used in all studies.

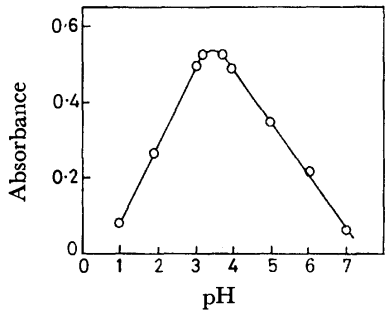

Fig. 1. Effect of pH.
[Chromium]$=3.95\times 10^{-4}$ M.

Effect of Heating and Stability. Reaction of chromium(III) with PAN was too slow at room temperature to be observed, probably due to inertness of $[Cr(H_2O)_6]^{3+}$. However, complexation resulted on heating the reactants to a temperature of 80—90 °C. The time of heating was varied from 5 min to 120 min and stable colour was formed from 30 min onwards. Hence reactants were heated for 35 min in all studies. The complex was found to be stable for more than 48 hr.

Choice of Solvent and Period of Equilibration. Various solvents, such as benzene, xylene, carbon tetrachloride, butanol, chloroform, butyl acetate were tried for extraction of the complex, but the complex was extracted only into chloroform and 1-butanol. As absorbance was found to be greater in 1-butanol than in chloroform, 1-butanol has been selected as suitable solvent.

Period of shaking for extraction of the complex into 1-butanol was varied from 5 s to 180 s, and the absorbance was found to be constant over this period. Hence, a period of 20 s was chosen for extraction.

Absorption Spectra. Absorption spectra of Cr-(III)-PAN chelate, extracted into butanol after heating for 35 min at pH 3.5 was recorded against a reagent blank prepared under similar conditions. The complex showed (Fig. 2) two absorption maxima at 555 and 600 nm, both of equal intensity. Hence, absorbance measurements can be carried out at 555 or 600 nm. The present studies were carried out at 555 nm.

Composition of the Complex. Composition of the complex was determined by Job's continuous variation method which gave a ratio of 1 : 2, metal-to-ligand, and the ratio was verified by mole ratio method.

Beer's Law. Beer's law was obeyed in the concentration range of 0.3 to 2.0 μg/ml of Cr(III). Molar absorptivity was 1.28×10^4 and Sandell's sensitivity was 0.004 μg of Cr(III) per cm^2.

Effect of Diverse Ions. Interference of about 46 ions in determination of 13 μg of Cr(III) per 10 ml was

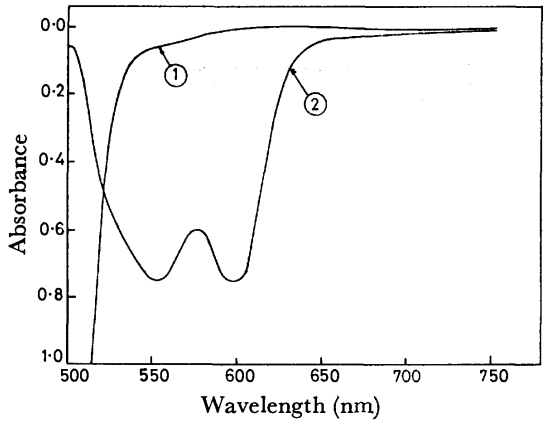

Fig. 2. Absorption spectrum of chromium(III)-PAN complex.
(1): Absorption spectrum of PAN *vs.* solvent,
(2): absorption spectrum of Cr(III)-PAN complex *vs.* reagent blank.
[Cr (III)]$=1.25\times10^{-4}$ M, [PAN]$=2.50\times10^{-4}$ M.

studied, setting the tolerance limit for interfering ions to cause an error of $\pm2\%$ in chromium recovery. Of the interfering ions, Fe(III), Cu(II), Co(II), Ga(III), In(III), and Tl(III) caused positive error, while CN^- and EDTA gave negative error. Interference due to Fe(III), was eliminated by prior extraction with mesityloxide[4] and those of Cu(II), Co(II), Ca(III), In(III), and Tl(III) was overcome by extracting their PAN complexes into chloroform before heating. The tolerance of some of the metal ions was due to decomposition of their chelates with PAN on heating. Most of the cations, associated with chromium, such as manganese, iron, cobalt, nickel, copper, titanium, zirconium, vanadium, niobium, tantalum, molybdenum and tungsten were tolerated, some of them in manyfold concentrations. The effect of foreign ions is shown in Table 1.

Table 1. Effect of diverse ions
Amount of Cr(III) taken: 13 μg/10 ml, pH=3.5

Foreign ion added	Tolerance limit μg
Ag(I), Mn(II), Pb(II), Fe(III)[a], F^-, Cl^-, Br^-, I^-, oxalate	5000
Sr(II), Ba(II), Ca(II), Mg(II), Zr(IV), Nb(V), AsO_4^{3-}, ReO_4^-, TeO_3^{2-}, SeO_3^{2-}, SO_4^{2-}	2000
Ge(IV), Ta(V), PO_4^{3-}, malonate	1000
Be(II), Bi(III)	500
Cd(II), Sb(III), Ti(IV), Zn(II)	200
Ni(II)[b], Cu(II)[c], Ga(III)[c], In(III)[c], Tl(III)[c], VO_3^-, $MO_7O_{24}^{6-}$, WO_4^-	50

a) Extracted with mesityl oxide. b) Masked with DMG.
c) Extracted as PAN complex before heating.

Precision and Accuracy. Relative standard deviation and relative error, calculated from ten repeat determinations with 1.3 μg of Cr(III) per ml, were found to be $\pm1.25\%$ and $\pm0.80\%$ respectively.

Application to the Analysis of Stainless Steel. 0.5 g of austenitic stainless steel (Bureau of Analysed Samples, Newham Hall, U. K., No. 332) was dissolved in 10 ml of 1:4 H_2SO_4 and diluted to 250 ml. Four ml of this solution was acidified with HCl to 3.5 M, transferred to a 100 ml separating funnel and iron was removed by extraction with 10 ml of mesityl oxide.[4] The aqueous layer was evaporated to dryness and made up to 100 ml. An aliquot of this solution was taken, adjusted to pH 3.5, and to it were added 1 ml of PAN, 1 ml of 0.5% DMG and 5 ml of acetate buffer (pH 3.5). The contents were heated for 35 min, transferred after cooling to a separating funnel, and chromium complex extracted with 10 ml of 1-butanol. Absorbance of the organic phase was measured at 555 nm. From duplicate analysis, recovery of chromium was found to be 12.50% and 12.60%, compared to the theoretical value of 12.8%. Other constituents of the alloy are Si–0.44%, S–0.02%, P–0.015%, Mn–0.800%, Ni–12.40% and rest iron.

Authors express their sincere thanks to Council of Scientific and Industrial Research (India) for the award of Junior Research Fellowship to one of them (BS).

References

1) R. G. Anderson and G. Nickless, *Analyst*, **92**, 207 (1967).
2) H. A. Flaschka and A. J. Barnard, Jr., "Chelates in Analytical Chemistry," Vol. 4, Marcel Dekker, New York (1972).
3) A. I. Vogel, "A Textbook of Quantitative Inorganic Analysis," Longman, Green Co. London (1961), p. 311.
4) V. M. Shinde and S. M. Khopkar, *Separation Science*, **4**, 161 (1969).

BULLETIN OF THE CHEMICAL SOCIETY OF JAPAN, VOL. 49(1), 349—350 (1976)

Template-Directed Synthesis of Oligonucleotide. Condensation of Nucleotide in the Presence of Polystyrene-Supported Neutral Oligonucleotide Derivative

Takeo SHIMIDZU and Akio IMAI

Department of Hydrocarbon Chemistry, Faculty of Engineering Kyoto University, Kyoto 606

(Received August 7, 1975)

Synopsis. A template-directed synthesis of oligonucleotide in the presence of polystyrene-supported neutral oligonucleotide derivative was studied. The oligonucleotide which has the sequence of the complementary base with the template, the neutral oligonucleotide derivative, yielded with a considerable amount, when the template with degree of oligomerization of 4 was used.

Chemically, we have two ways to synthesize the definite-sequence oligonucleotide: One is the stepwise synthesis of the oligonucleotide and the other is the template-directed synthesis. Several studies relating to the latter, the oligonucleotide syntheses using polynucleotides have been done,[1-8] but they were not necessarily successful.

Observations of those polynucleotide template-directed syntheses indicate a few problem. The complex formation between polynucleotide and condensing nucleotide in aqueous solution is not strong. Generally, that the equilibrium constant of the complex formation between nucleotide bases is remarkable in the aprotic solvent can be seen in IR[9] and NMR[10] studies. In addition, negatively charged phosphate groups both in the polynucleotide and the condensing nucleotide are undesirable for the complex formation. Disadvantage in the chemical reaction of the charged molecules on the polyelectrolyte having the same signed charge has been suggested by Ise.[11]

On the basis of those informations, a novel template-directed synthesis of the oligonucleotide has been tried. The material was synthesized by the method of so-called solid support.[12] In the present study, the cross-linked polystyrene anchored oligonucleotide of which phosphoric acid moiety was esterified by cyanoethyl alcohol was used. This material was synthesized by the method of the preceding paper.[13] The oligonucleotide derivative in the present template was neutral at its phosphate moiety and anchored in the polystyrene matrix. Figure 1 shows an example of the template. The anchored oligonucleotide derivative has a failure in its sequence, in part.

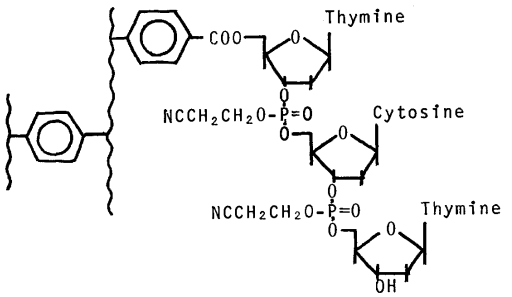

Fig. 1. [PSt]-TCT

Table 1 lists the result of the template-directed condensation of the nucleotide. In this condensation system, it is remarkable that the complementary oligonucleotide whose degree of condensation was more than two was obtained. However, the fully complementary oligonucleotide was scarecely obtained.

TABLE 1. CONDENSATION OF NUCLEOTIDE IN THE PRESENCE OF POLYSTYRENE-SUPPORTED NEUTRAL OLIGONUCLEOTIDE DERIVATIVE

Template	Nucleotide (mol%)	Relative yield of main product (optical density)
[PSt]-CH_3	pT(50) pdA(50)	pTpT(32) pdApdA(53) pTpdA(33) pdApT(38)
[PSt]-TTT[a]	pdA(100)	pdApdA(132) TpTpTpdA(66)
[PSt]-TTT[a]	pT(25) pdA(25) pdC(25) pdG(25)	pTpT(3) pdApdA(41) pdCpdC(34) pdGpdG(43) pTpdA(36) The others(62)
[PSt]-TTT[a]	pT(100)	pTpT(82)
[PSt]-TCT[b]	pT(25) pdA(25) pdC(25) pdG(25)	pTpT(11) pdApdA(41) pdCpdC(32) pdGpdG(65) pTpdA(32) The others(71) pdApdGpdA(0)
[PSt]-TCTC[c]	pT(25) pdA(25) pdC(25) pdG(25)	pTpT(14) pdApdA(49) pdCpdC(42) pdGpdG(84) pTpdA (29) pdApdGpdA (22) The others (88) Tetramer?(0)
[PSt]-TCTC[c]	pdA(50) pdG(50)	pdApdA (78) pdGpdG(132) pdApdG (175) pdGpdA(180) pdApdGpdA(39) pdGpdApdG(15) Tetramer ? (7)

a) TTT=96 mg/0.5 g-polymer support, % of the full sequence=79. b) TCT=85 mg/0.5 g-polymer support, % of the full sequence=78. c) TCTC=78 mg/0.5 g-polymer support, % of the full sequence=61. Total nucleotide (pyridinium form)=100 mg (calcd. as free acid). Pyridine=15 ml. Total DCCD=200 mg. Reaction time=24 hr. Room temperature.

In cases of [PSt]-CH_3 and [PSt]-TTT used, the rate of condensation of pdA was relatively high. In the product, the oligonucleotide which was additional product of the template oligonucleotide molecule, TpTpTpdA for example, was found. When four kinds of condensing nucleotides, pT, pdA, pdC, and pdG, were condensed in the presence of [PSt]-TTT or [PSt]-TCT, the maximum yield in the product was pdGpdG. And, in the case of [PSt]-TCT used, the fully complementary product, pdApdGpdA, was not found. On the other hand, when the tetramer template such as [PSt]-TCTC was used, though the fully complementary oligonucleotide, pdApdGpdApdG, was not found in the product, the partly complementary oligonucleotide yielded with a considerable amount. The yield of the partly complementary oligonucleotide appeared to be more prominent in the case that two kinds of condensing nucleotides, pdA and pdG, were used. In addition, the result showed that the yield of the oligonucleotide which was partly complementary with the template sequence close to the polystyrene solid support, *i.e.*, pdApdGpdA, was higher than that which not close to, *i.e.* pdGpdA-pdG. This shows the importance of a matrix constructed by the polymer that gives a hydrophobic enviroment.

Those results could lead the template-directed synthesis of oligonucleotide.

Support in part for this work by the Grant from the Ministry of Education (Grant in aid for Special Project Research 820828 and 911013). Thanks are due to Profeesor Kenichi Fukui for his encouragement. The authors are grateful to Dr. H. Hirai, Nagase Ind. Co., for kindly renting the Peptide Synthetizer Instrument (Schwartz Bioresearch).

References

1) R. Naylor and P. T. Gilham, *Biochemistry*, **5**, 2722 (1966).

2) J. Sulston, R. Lohrmann, L. E. Orgel, and H. T. Miles, *Proc. Nat. Acad. Sci., U. S.*, **60**, 409 (1968).

3) T. Shimidzu, and K. Fukui, *Annual Report Res. Inst. Chem. Fiber, Japan*, **25**, 87 (1968).

4) J. Sulston, R. Lohrmann, L. E. Orgel, H. Schneider-Bernloehr, B. J. Weimann, and H. T. Miles, *J. Mol. Biol.*, **40**, 227 (1969).

5) H. Schneider-Bernloehr, R. Lohrmann, J. Sulston, L. E. Orgel, and H. T. Miles, *J. Mol. Biol.*, **47**, 257 (1970).

6) Z. A. Shabarova, and M. A. Prokofiev, *FEBS Lett.*, **11**, 237 (1970).

7) S. Uesugi and P. O. P. Ts'O, *Biochemistry*, **13**, 3142 (1974).

8) L. E. Orgel, and Lohrmann, *Accounts Chem. Res.*, **7**, 368 (1974).

9) Y. Kyogoku, R. C. Lord, and A. Rich, *Science*, **154**, 518 (1966); *J. Amer. Chem. Soc.*, **89**, 496 (1967); *Proc. Nat. Acad. Sci. U. S.*, **57**, 250 (1969).

10) U. Krüger, H. Breyer, F. M. A. Klein, H. H. Perkampus, and K. H. Scheit, *Z. Naturforsch.*, **23B**, 1360 (1968).

11) N. Ise, *Nature*, **225**, 66 (1970).

12) R. L. Letsinger, and V. Mahadevan, *J. Amer. Chem. Soc.*, **87**, 3526 (1966); F. Cramer, R. Helbig, H. Hettler, K. H. Scheit, and H. Seliger, *Angew. Chem., Int. Ed.*, **5**, 601 (1966); G. M. Blackburn, M. J. Brown, and M. R. Harris, *J. Chem., Soc. C*, **1967**, 2438; L. R. Melby, and D. R. Strobach, *J. Amer. Chem. Soc.*, **89**, 450 (1969).

13) T. Shimidzu, and R. L. Letsinger, *J. Org. Chem.*, **33**, 708 (1968); This Bulletin, **44**, 1673 (1971).

BULLETIN OF THE CHEMICAL SOCIETY OF JAPAN, VOL. 49(1), 351—352 (1976)

The Dye-sensitized Photolysis of Aryl Aryldiazo Sulfone

Toshihiro YAMASE, Hiroshi HISADA, Sadao SUZUKI, and Tsuneo IKAWA

Research Laboratory of Resources Utilization, Tokyo Institute of Technology, Ookayama, Meguro-ku, Tokyo 152

(Received March 22, 1975)

Synopsis. The amethyst violet (AV)-sensitized photolysis of *p*-tolyl *p*-anilinobenzenediazo sulfone (TABS) has been investigated in a ethanol–water (9.3: 0.7, v/v) solution. The experimental data on the quantum yield of the sensitized photolysis and the AV fluorescence or phosphorescence intensity were explained in terms of AV-excited singlet sensitization. Studies of both the photoproducts and the heterogeneous photopolymerization of acrylamide supported the mechanism involving the homolytic dissociation of diazosulfone.

Brief reviews of the diazosulfones-imaging system have been published by Dinaburg.[1] When irradiated with actinic light, diazosulfones decompose in the areas illuminated, whereas the non-illuminated parts preserve the ability to undergo coupling reactions with the formation of azo dyes, like usual diazonium compounds. Our purpose was to find a dye-sensitized photolysis for this system, since the dye sensitization will ensure an increase in the overrall photosensitivity. The present note will describe the results of the amethyst violet (AV)-sensitized photolysis of *p*-tolyl *p*-anilinobenzenediazo sulfone (TABS) in an ethanol–water solution. The absorption spectra were recorded on a Hitachi 624 spectrophotometer. The fluorescence and phosphorescence measurements were carried out on a Hitachi MPF-2A spectrofluorimeter. The ESR spectra were recorded on a Varian E-12 X-band spectrometer with 100 kHz magnetic field modulation. Unless specified otherwise, all the experiments were performed at room temperature. Degassing from the solution was carried out by the usual freeze-pump-thaw cycle at 10^{-4} mmHg. The 546 nm irradiation was performed by the use of a 500-W super-high-pressure mercury lamp, equipped with two filters (Toshiba VO-52+KL-54). The light intensities were measured by Reineckate actinometry. The dark reaction of *p*-anilinobenzenediazonium sulfate ($2—4\times10^{-5}$ M) with sodium *p*-toluenesulfinate (STS) ($5\times10^{-4}—3\times10^{-3}$ M) to give TABS in ethanol–water solution was spectrophotometrically studied in order to measure the equilibrium constant (K) for the TABS formation.[2] Its value was determined from the straight line in Benesi-Hildebrand's plot;[3] the resulting value became greater with an increase in the ratio of ethanol in the ethanol–water solvent (Table 1). In the variation in the ethanol–water ratio, the extinction coefficient of TABS at the wavelength (450 nm) of its absorption maximum was unchanged at 2.9×10^{4} M^{-1} cm^{-1}. Some quantitative measurements were made with ethanol–water of 9.3: 0.7, v/v. TABS was stable in the dark during the experimental procedure. The dye-sensitized photolysis of TABS was followed by a change in the absorbance of the solutions at 450 nm. The absorbance of the solution at 546 nm was unchanged during continuous illumination, irrespective of the presence of oxygen.

TABLE 1. EQUILIBRIUM CONSTANTS FOR TABS FORMATION

Ethanol/water, (v/v)	9.6/0.4	9.4/0.6	9.3/0.7	9.2/0.8	9.1/1.0
K, 10^{3} M^{-1}	9.5	7.8	5.2	3.7	1.2

TABLE 2. EFFECTS OF OXYGEN, [AV], [TABS], AND 546 nm LIGHT INTENSITY (I_{abs}) ON QUANTYM YIELD (η)

I_{abs} 10^{-5} E/l min	[AV] 10^{-5} M	[TABS] 10^{-5} M	η	
8	3.3—3.5	5	0.038[a]	0.035[b]
			0.036[c]	0.038[d]
5.6	4	4	0.048[a]	
4	4	4	0.057[a]	
2	4	4	0.081[a]	
0.8	4	4	0.130[a]	
8	2.0	2.9	0.026[a]	
8	3	2.9	0.023[a]	
8	4	2.9	0.017[a]	
8	4	3.5	0.025[a]	

a) aerobic b) N_2 bubbled c) O_2 bubbled d) deaerated

With $\leq5\times10^{-5}$ M TABS and $\leq4\times10^{-5}$ M AV in an ethanol–water (9.3: 0.7, v/v) solution, the quantum yield (η) for TABS elimination was determined, based on the total absorbed intensity of the 546 nm irradiating light (Table 2). An oxygen effect seemed to be absent in this system at least, since the η value of about 0.04 was unchanged after a thorough degassing of the solution. The η value decreased with a decrease in the TABS concentration and with an increase in the AV concentration or the 546 nm light itensity ($\leq8\times10^{-5}$ E. absorbed/l min).

AV showed a strong fluorescence maximum at 565 nm in ethanol–water (9.3: 0.7, v/v). The steady-state fluorescence intensity decreased with an increase in the AV concentration ($\geq2\times10^{-5}$ M). To check whether or not AV singlets were involved in the sensitization, we examined the effect of added TABS upon the fluorescence intensity of AV (2×10^{-5} M) in degassed solutions. Figure 1 shows the Stern-Volmer plot for the quenching of the fluorescence of AV by TABS. No new emission was detected in the presence of TABS. The fluorescence quenching was scarcely affected by oxygen. STS and water also caused a decrease in the fluorescence intensity, but their quenching constants of 13 and 6.8×10^{-2} M^{-1} were very small in comparison with the value of TABS (3.9×10^{3} M^{-1}). The facts that the oxygen effect seemed to be absent in both the AV fluorescence intensity and the quantum yield of the sensitized TABS photolysis, that the AV fluorescence intensity decreased with an increase in the AV and TABS concentrations, and

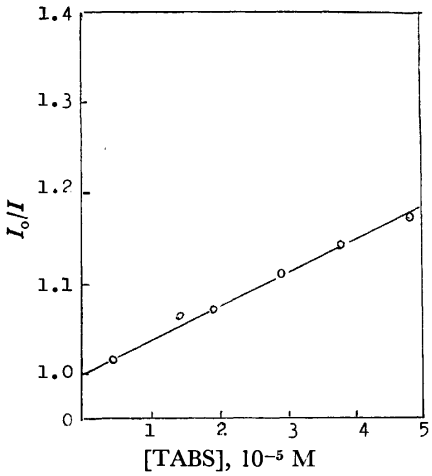

Fig. 1. Quenching of AV fluorescence by TABS, [AV]= 2×10^{-5} μ

that the quantum yield increased with a decrease in the AV concentration and an increase in the TABS concentration support the AV excited singlet sensitization.[4] In addition, AV (10^{-6}—10^{-5} M) emitted a phosphorescence exhibiting its maximum intensity at 730 nm in a deaerated EPA matrix (77 K), and its intensity was significantly reduced by oxygen. Those results may exclude the involvement of excited triplet AV in the sensitization, since the quantum yield of AV-sensitized photolysis should be significantly reduced by oxygen, if the above hypothesis occurs.[5]

The AV-sensitized photolysis of TABS induced the heterogeneous polymerization of acrylamide in a deaerated system without any permanent photobleaching of AV. The molecular weights of the polymers were of the order of thousands. The absence of TABS or the presence of oxygen caused no significant photopolymerization of acrylamide. The ESR spectrum of the polymer obtained showed a broadened single line at $g=2.009$, but the identity of the occluded radicals in the polyacrylamide particles seemed to be uncertain because of the lack of any observable hyperfine structure. The photopolymerization results suggest that the AV-sensitized photolysis of TABS leads to the production of free radical intermediates, which then initiate the polymerization of acrylamide.

Longer periods of the AV-sensitized photolysis of the TABS (~0.4 mmol) formed by a reaction between—0.4 mmol 4DS and ~15 mmol STS in 9.3: 0.7 ethanol-water (100 ml) containing ~0.06 mmol AV under nitrogen gave up to a 90% decomposition of TABS. Sodium *p*-toluenesulfonate readily precipitated out of the solution. The reaction mixture was then poured into 100 ml of a 5% sodium carbonate aqueous solution and filtered off. The filtrate was evaporated under reduced pressure, and the diphenylamine in the residue was separated by thin-layer chromatography on Kieselgel 60 F. Direct photolysis was carried out with the TABS (~0.2 mmol) formed by a reaction between 0.2 mmol 4DS and 5 mmol STS in 50 ml of 9.3: 0.7 ethanol–water. The final products isolated were essentially the same as in the case of AV-sensitized photolysis, sodium *p*-toluenesulfonate and diphenylamine. Photoproduct studies may indicate a similarity in the behabior of TABS decomposition in direct and sensitized photolyses. The direct photolysis of aryl aryldiazosulfone has been considered to undergo homolytic decomposition in neutral media.[6] This situation and the observation of the free radical photopolymerization of acrylamide make it likely that the homolytic dissociation has occurred in the AV-sensitized photolysis of TABS, thus yielding $CH_3C_6H_4SO_2\cdot$ and $C_6H_5NHC_6H_4N_2\cdot$ radicals. The loss of nitrogen from the latter may result in the formation of diphenylamine *via* a hydrogen abstraction from ethanol. The formation of sodium *p*-toluene-sulfonate may be ascribed to the disproportionation of the tosyl radical, as has been noted by da Silva Correa and Waters.[7]

References

1) M. S. Dianaburg, "Photosensitive Diazo Compounds and Their Uses," The Focal Press (1964), p. 82.

2) C. D. Ritchie, J. D. Saltiel, and E. S. Lewis, *J. Amer. Chem. Soc.*, **20**, 4601 (1961).

3) H. A. Benesi and J. H. Hildebrand, *ibid.*, **71**, 2703 (1949).

4) The tendency for the quantum yield to decrease with the increase in the incident light intensity may result from the quenching of the excited singlet AV by photoproducts or their precursors (free-radical intermediates) formed *via* the sensitized homolytic dissociation of TABS, although this is not clear from these observations alone.

5) Attempts to detect the TABS phosphorescence and to confirm the absence of any quenching of the AV phosphorescence by TABS failed, probably because of the lower solubility of TABS for EPA.

6) M. Kobayashi, S. Fujii, and H. Minato, This Bulletin, **45**, 2039, (1972).

7) C. M. M. da Silva Correa and W. A. Waters, *J. Chem. Soc. C*, **1968**, 1874.

BULLETIN OF THE CHEMICAL SOCIETY OF JAPAN, VOL. 49(1), 353—354 (1976)

A Single-step Synthesis of 2-Substituted Benzo-azoles

Nobutaka SUZUKI, Toshiyuki YAMABAYASHI, and Yasuji IZAWA*

Department of Industrial Chemistry, Faculty of Engineering, Mie University, Tsu 514

(Received July 28, 1975)

Synopsis. 2-Substituted benzimidazoles (**3a** and **5a**), benzothiazoles (**3b** and **5b**), and benzoxazole (**3c**) are readily synthesized in good yields by treating (thiobenzoylthio)-acetic acid (**1**) or ethyl dithioacetate (**4**) with the corresponding *o*-substituted anilines (**2a**, **2b**, and **2c**) in slightly alkaline media at room temperature.

Numerous methods have been reported for the preparation of 2-substituted benzo-azoles.[1] However, most of them require a procedure with several steps and/or severe reaction conditions.

In our attempt to prepare a series of 2-substituted thiazolines, (thiobenzoylthio)acetic acid[2] (**1**) or ethyl dithioacetate[3] (**4**) was treated with *o*-substituted anilines having a protic group, such as $-NH_2$, $-SH$, or $-OH$ (**2a**, **2b**, and **2c**), in a similar manner to that reported in a previous paper[4] to give the corresponding 2-substituted benzo-azoles (**3a**, **3b**, **3c**, **5a**, and **5b**) in good yields. However, **4** with **2c** gave only an acetanilide (**6c**) instead of 2-methylbenzoxazole (**5c**), in a moderate yield.

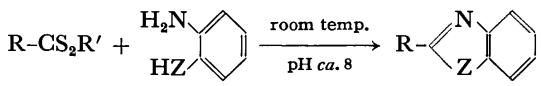

1: R=Ph; R'=CH_2CO_2H **2a—c** **3a—c**

4: R=Me; R'=Et **5a—b**

a: Z=NH, **b**: Z=S, **c**: Z=O

In a typical experiment, (thiobenzoylthio)acetic acid[2] (**1**: 2.0 mmol) and *o*-aminothiophenol (**2b**: 2.2 mmol) were dissolved in aqueous MeOH (3: 1) (40 ml), its pH being adjusted to *ca.* 8 with 1M NaOH. The solution was stirred at room temperature[5] under a slightly reduced pressure (aspirator) to remove H_2S generated until the red coloration of **1** disappeared. The progress of reaction was also monitored by tlc [silica gel, PF_{254}-gipshaltig (Merck), hexane–acetone (3: 1)]. The pH of the solution was checked occasionally and adjusted to *ca.* 8 with alkali. After being acidified with 1M HCl (to pH *ca.* 3), the resulting 2-phenylbenzothiazole (**3b**) was isolated from the reaction mixture by extraction with CH_2Cl_2 and $CHCl_3$. Evaporation of solvents followed by crystallization of the residue from aqueous EtOH afforded crystals of **3b**.

Similarly, except for the use of an aqueous EtOH (2: 1) as a solvent, **3a**, **3c**, **5a**, and **5b** were obtained in good yields from the corresponding starting materials (**1** and **4**, with **2a**, **2b**, and **2c**). In the case of **3c**, additional steam distillation of the extracts was necessary to obtain crystals. The reaction conditions and results are summarized in Table 1. The products (**3a**, **3b**, and **3c**) were identified by mp, IR, NMR and mass spectra. Structures of **5a** and **5b** were confirmed by comparison of their mp or bp, IR,[6] and mass spectra with those of the corresponding authentic samples.

An attempted synthesis of 2-methylbenzoxazole (**5c**) (treatment of **4** with **2c**) gave a colorless crystal, mp 204.5—206 °C (lit, bp of **5c**: 200—201 °C) in a moderate yield, which was identified as *N*-acetyl-*o*-aminophenol (**6c**) by its mp, IR,[6] and mass spectra. This seems to be a hydrolysis product of *N*-thioacetyl-*o*-aminophenol (**7**).

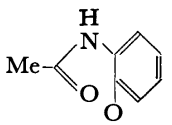

6c

Table 1. Synthesis and properties of 2-substituted benzo-azoles (**3a**, **3b**, **3c**, **5a**, and **5b**) and acetyl-*o*-aminophenol (**6c**)

Product	Reactn. time (hr)	Solv.[a]	Isolatn.[b]	Yield[c] (%)	mp (bp) [lit.]	*m/e* (M^+)
3a	74	E	A	89	288.5—291 °C [282 °C[1c], 294.5—295.5 °C[1d]]	194
3b	22	M	B	98	112—113 °C [112.7—113.9 °C[1d]]	211
3c	25	E	C	85	101.5—103 °C [102.5—103.9 °C[1d]]	195
5a	49	E	A	88	178.5—179.5 °C [178.5—179 °C[7]]	132
5b	66	E	A	85	(121.—123.5 °C/20 mmHg) [(235—239 °C[8])]	149
6c	49	E	A	57	204.5—206 °C [201—203 °C, 209 °C[9]]	151

a) M: aqueous MeOH (1: 1); E: aqueous EtOH (1: 1). b) A: Extd. with EtOAc and $CHCl_3$; B: Extd. with CH_2Cl_2 and $CHCl_3$; C: Extd. with $CHCl_3$, followed by steam distillation. c) Based on **1** or **4** used.

Experimental

The mp and bp are uncorrected. The following instruments were used for the spectral measurements: IR: JASCO IR-G; NMR: JEOL JNM-MH-100 (100 MHz) and MS: JEOL D-100.

The authentic 2-methyl-benzimidazole[7] (**5a**) and -benzothiazole[8] (**5b**) were prepared by the methods described in the lit. **5a**: Colorless fine-needles, mp 179—180 °C (64%). **5b**: Colorless liq. bp 121—122.5 °C/20 mmHg (44%). (Thiobenzoylthio)acetic acid[2] (**1**) and ethyl dithioacetate[3] (**4**) were prepared according to the methods described in the lit. **1**: Red fine needles, mp 125 °C (lit,[2] 121—124 °C). **4**: Orange-yellow liq., bp 47—50 °C/12 mmHg (lit,[3] 52 °C/12 mmHg). ν_{max} (neat) 1450, 1190, 1100 cm^{-1}, δ (ppm) (CCl_4) 1.31 (3H, t, J=7.6 Hz), 2.79 (3H, s), and 3.17 (2H, q, 7.6).

General Procedure of the synthesis of the azoles (**3a**, **3b**, **3c**, **5a**, and **5b**) is given in the text and their reaction conditions and results are shown in Table 1.

Attempted Synthesis of **5c** *(formation of* **6c**). Synthetic procedures were similar to the general procedure shown above. The conditions and results are also given in Table 1. **6c**: Colorless leaflets: ν_{max} (KBr) 3400, 1655, 1545 cm^{-1}.

References

1) For the reviews: (a) E. Haruki, *Yuki Gosei Kagaku Kyokai Shi*, **26**, 770 (1968); (b) P. N. Preston, *Chem. Revs.*, **74**, 279 (1974). For examples: (c) B. L. Bastic, R. P. Saper, and V. B. Glubovic, *Glasnik Khem. Drushtva Beograd*, **21**, 151 (1956); *Chem. Abstr.*, **54**, 4545a (1960); (d) D. W. Hein, R. J. Alheim, and J. J. Leavitt, *J. Amer. Chem. Soc.*, **79**, 427 (1957); (e) G. L. Jenkins, A. M. Knevel, and C. S. Davis, *J. Org. Chem.*, **26**, 274 (1961); (f) S. Seto, K. Ogura, and Y. Nishiyama, This Bulletin, **36**, 331 (1963); (g) B. L. Bastic and M. V. Piletic, *Glasnik Khem. Drushtva Beograd*, **29**, 139 (1965); *Chem. Abstr.*, **64**, 15863 (1965); (h) H. Fujita, T. Endo, J. Murayama, and T. Ichii, This Bulletin, **45**, 1581 (1972); (i) H. Igeta, T. Nakai, and T. Tsuchiya, *Chem. Commun.*, **1973**, 622; (j) C. Temple, Jr., B. H. Smith, Jr., and J. A. Montgomery, *J. Org. Chem.*, **38**, 613 (1973); (k) F. Hervans and H.-G. Viehe, *Angew. Chem.*, **85**, 446 (1973); (l) G. P. Ellis and R. T. Jones, *J. Chem. Soc. Perkin I*, **1974**, 903; (m) J. Takahashi, T. Suzuki, Y. Suzuki, H. Takeda, T. Zaima, and K. Mitsuhashi, *Nippon Kagaku Kaishi*, **1974**, 1595; (n) J. Chodowska-Palicka and M. Milsson, *Synthesis*, **1974**, 128; (o) B. Stanovnik and M. Tisler, *ibid.*, **1974**, 120, and references cited therein.

2) F. Kurzer and A. Lawson, "Org. Syntheses, Coll. Vol. V," p. 1046 (1973); F. Kurzer, *Chem. Ind.* (London), **1961**, 1333.

3) J. Meijer, P. Vermeer, and L. Vrandsma, *Rec. Trav. Chem. Pays-Bas*, **92**, 601 (1973).

4) N. Suzuki and Y. Izawa, *Tetrahedron Lett.*, **1974**, 1863, and references cited therein.

5) When the reaction mixtures were refluxed in aqueous EtOH or aqueous MeOH until the red coloration of **1** (red) or **4** (reddish orange) disappeared (*ca.* 3 hr), no corresponding benzo-azoles could be obtained.

6) C. J. Pouchert, "The Aldrich Library of Infrared Spectra," Aldrich Co., Inc., Milwaukee, Wisconsin (1970).

7) M. A. Phillips, *J. Chem. Soc.*, **1928**, 2395.

8) A. Hofmann, *Ber.*, **13**, 21, 1236, 1238 (1880).

9) E. Bamberger, *ibid.*, **36**, 2050 (1903).

Photoelectrochemical Reactions at $SrTiO_3$ Single Crystal Electrode

Tadashi WATANABE, Akira FUJISHIMA, and Ken-ichi HONDA

Department of Industrial Chemistry, Faculty of Engineering, University of Tokyo, Hongo, Bunkyo-ku, Tokyo 113

(Received July 14, 1975)

Electrode characteristics of strontium titanate ($SrTiO_3$) single crystal have been investigated under illumination with light of its intrinsic absorption region. It has been found that the photosensitized electrolytic oxidation of water, known heretofore uniquely on the TiO_2 electrode, can proceed also at the $SrTiO_3$ electrode whose anodic dissolution being negligible. Although the photosensitivity of the $SrTiO_3$ electrode is confined to a little shorter wavelength region than that of the TiO_2 electrode, the formal quantum efficiency of the photosensitized electrolytic oxidation of water is comparable for these two semiconductor electrodes under intrinsic absorption. In contrast to the case of the TiO_2 electrode, the electrochemical photocell consisted of the $SrTiO_3$ anode and platinum cathode can work efficiently even when the pH values of the anodic and cathodic compartments are close to each other. This point is discussed in terms of the flatband potential of these semiconductor electrodes.

We previously reported on the photosensitized electrolytic oxidation of water at the TiO_2 (n-type semiconductor) single crystal electrode,[1,2] and its utilization in an electrochemical photocell[3,4] where water is decomposed to hydrogen and oxygen gases through the light absorption by the electrode. However, no other semiconductor electrodes of this type have ever been reported so far.

Boddy and co-workers[5,6] studied the electrode characteristics of oxide semiconductors such as TiO_2, $KTaO_3$, Ta_2O_5 and $SrTiO_3$ without intended irradiation of the electrode surface. They noted oxygen evolution at the surface of these electrodes under strong anodic polarization, and elucidated this phenomenon on the basis of a tunneling of electrons from the surface oxide ions to the conduction band of the electrode. Since no evidence for the dissolution of the electrode surface was observed, they concluded that the surface oxide ions were supplied by water molecules. Provided that the electrode surface remains stable also at the excited state, the photosensitized electrolytic oxidation is expected to occur on these oxide semiconductor electrodes. However, the photoeffects on these electrodes, excluding TiO_2, have not been investigated in detail.

In the present study we carried out quantitative measurements of electrode characteristics of the $SrTiO_3$ single crystal under illumination with light of its intrinsic absorption range ($\lambda<390$ nm), and verified that the photosensitized electrolytic oxidation of water by surface holes does proceed effectively at the $SrTiO_3$ electrode.

Experimental

Electrode Preparation. Single crystals of $SrTiO_3$ were supplied by Fuji Titanium Industry, Ltd. The crystal was in the form of a platelet of 2.5 cm^2 in surface area and 1.0 mm in thickness. Prior to the preparation of the electrode, the crystal was treated at 600 °C under high vacuum (*ca.* 10^{-3} Torr) for several hours in order to increase the electric conductivity. After this treatment the crystal is colored in blue owing presumably to the formation of oxygen vacancies in the bulk of the crystal and the specific resistivity is found to be around 10^3 ohm·cm. The crystal was cemented with an epoxy resin in such a way that the (001) face of the crystal (perovskite-type) was exposed to the electrolyte solution. The opposite face was used for a barrier-free electrical contact with a conducting wire by means of electroplated indium. Before the measurements, the surface of the electrode thus prepared was polished with an alumina powder, washed with nitric acid and then with de-ionized water. A platinized platinum plate, having the apparent surface area of 10 cm^2, was employed as the counter electrode.

Experimental Setup. Figure 1 schematically shows the apparatus for photocurrent measurements. A 500 watt xenon lamp served as a light source. The wavelength of the illuminating light was selected by means of appropriate colored glass filters (Toshiba Kasei, Ltd.) or a monochromator (Shimadzu, Ltd.). The electrode-electrolyte interface was illuminated through a quartz window attached to the electrolytic cell. Photocurrents were detected by means of a potentiogalvanostat Type HA-101 of Hokuto Denko, Ltd.

The number of photons of the monochromatic light incident to the $SrTiO_3$ electrode surface was determined by the following procedure. (i) First, an exact number of photons at $\lambda=365$ nm was measured by means of chemical actinometry with 0.006 M potassium ferrioxalate aqueous solution, where the light leaving the monochromator was totally absorbed by the actinometer solution. (ii) Second, light energy was measured (in erg/s) at the same geometrical position as (i) in the wavelength range 350—600 nm by means of a JASCO thermopile, where 1 mm^2 of Au black absorbed the incident monochromatic light. Finally, the number of photons calculated from the results of (ii) was corrected on the basis of the results of (i). At the time of photocurrent measurements, the light flux reaching the surface of the $SrTiO_3$ electrode was the same as that incident to the actinometer cell.

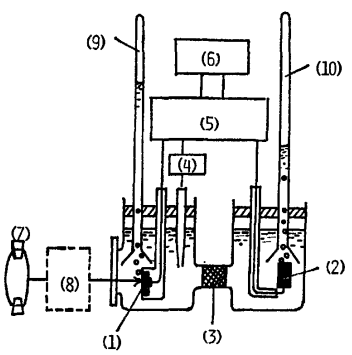

Fig. 1. Experimental setup.
(1) $SrTiO_3$ electrode (2) Platinum electrode (3) Agar salt bridge (4) SCE (5) Potentiostat (6) Recorder (7) Light source (8) Monochromator (9) Oxygen (10) Hydrogen.

Results and Discussion

Static Electrode Characteristics. The flatband potential of the $SrTiO_3$ single crystal electrode has been measured as a function of pH of the electrolyte solution. The determination of the flatband potential of an n-type semiconductor electrode is based on the application of the Mott-Schottky relationship[7]

$$\frac{1}{C_s^2} = \frac{2}{q\kappa\varepsilon_0 N}\left(E - E_{fb} - \frac{kT}{q}\right) \quad (1)$$

where C_s represents the space charge capacitance per unit area (measured by means of an AC bridge described elsewhere[8]), q the electronic charge, κ the dielectric constant of the semiconductor (332 for $SrTiO_3$ at 25 °C[9]), ε_0 the permittivity of vacuum, N the donor concentration, E the electrode potential against an appropriate reference electrode, and E_{fb} the flatband potential.

Figure 2 shows $1/C^2$ *vs.* E plots for the $SrTiO_3$ electrode at various pH values, from the slope of which the magnitude of N is calculated to obtain *ca.* 1.0×10^{19} cm^{-3}. From the intercepts of these curves on the E axis, the flatband potential of the $SrTiO_3$ electrode was determined and the results are shown in Fig. 3, together with those for the TiO_2 electrode reported elsewhere.[10] As is clearly seen, the flatband potential of the $SrTiO_3$ electrode depends almost linearly on pH of the electrolyte solution with the slope of *ca.* −60 mV/ΔpH. Such a dependence supposedly results from a dissociation equilibrium of proton at the oxide electrode surface.[7,8] The value of the flatband potential of the $SrTiO_3$ electrode at a given pH is about 0.30 volts more cathodic than that of the TiO_2 electrode. This point will be discussed later in connection with the electrochemical photocell characteristics of these two semiconductor electrodes.

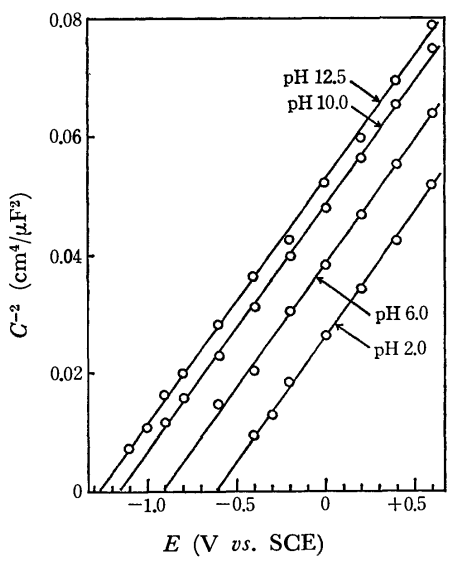

Fig. 2. Mott-Schottky plots for $SrTiO_3$ electrode.

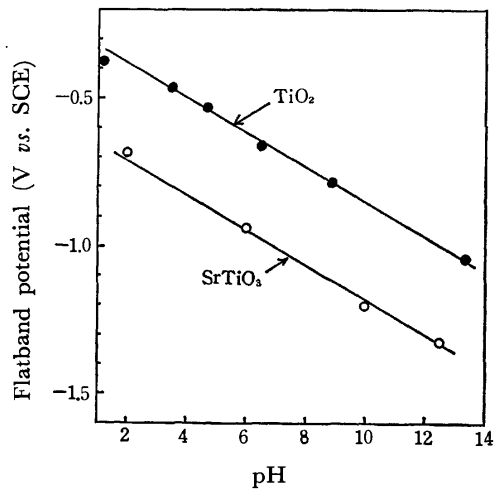

Fig. 3. Dependence of the flatband potentials of $SrTiO_3$ and TiO_2 single crystal electrodes on pH of the electrolyte solution.

Photosensitized Electrolytic Oxidation of Water. The reduced $SrTiO_3$ single crystal electrode behaves like a typical n-type semiconductor electrode. Figure 4 depicts the current-potential characteristics of the $SrTiO_3$ electrode at three different pH values. In darkness, owing to the formation of a depletion layer for the majority carrier (electrons) at the surface of the $SrTiO_3$ electrode, only a small current can be observed under anodic polarization. When the electrode surface is illuminated with light in the wavelength range

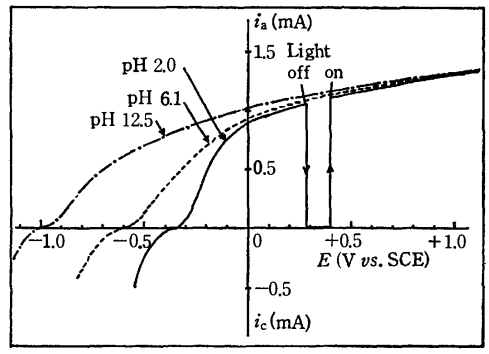

Fig. 4. Current-potential characteristics of $SrTiO_3$ electrode.

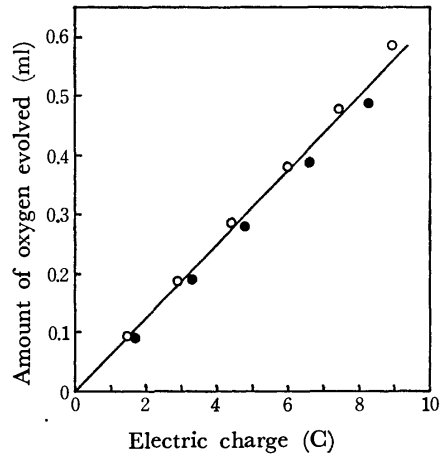

Fig. 5. Dependence of the amount of oxygen (as the standard state) evolved at the $SrTiO_3$ electrode surface on the amount of the electric charge passed through the external circuit. Solid line represents theoretical relationship.

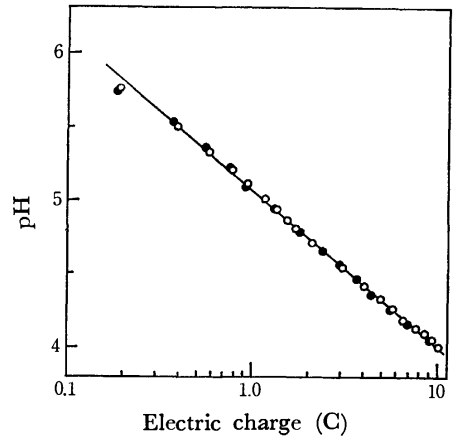

Fig. 6. Variation of pH value of the anodic compartment as a function of the amount of the electric charge passed through the external circuit.
—○—: $SrTiO_3$ (anode)-Pt (cathode) system; —●—: Pt (anode)-Pt (cathode) system under electrolysis.

$\lambda < 390$ nm, a large photocurrent is generated in the anodic polarization, while the cathodic branch remains practically unaffected. The electrode potential at which the anodic photocurrent starts to rise depends on pH of the solution with the slope of *ca.* —60 mV/ΔpH, which conforms to the pH-dependence of the flatband potential.

When the anodic photocurrent is flowing through the $SrTiO_3$ electrode, one can observe gases evolving from the surfaces of the $SrTiO_3$ electrode and of the platinum counter electrode with the apparent volume ratio of *ca.* 1 : 2. Through the examination on a gas chromatograph, these gases were found to be oxygen and hydrogen. The amounts of oxygen and hydrogen evolved have been measured as a function of the electric charge passed through the external circuit. Figure 5 shows the volume (as the standard state) of the oxygen gas evolved at the surface of the $SrTiO_3$ electrode as a function of the electric charge. The open and full circles represent independent measurements. From this figure it is evident that the current efficiency is approximately 100%. We could not notice any evidence for dissolution of the $SrTiO_3$ electrode surface during the electrolysis. The current efficiency for the hydrogen evolution from the platinum counter electrode was found in the range of 97±7%. These observations undoubtedly suggest that the photosensitized oxidation of water proceeds at the illuminated $SrTiO_3$ electrode surface as follows.

$$SrTiO_3 + h\nu \longrightarrow p^+ + e^- \quad (2)$$

$$4p^+ + 2H_2O \longrightarrow 4H^+ + O_2 \quad (3)$$

The residual electrons are transferred to the Pt electrode, where they react with protons to produce hydrogen.

$$2e^- + 2H^+ \longrightarrow H_2 \quad (4)$$

The occurrence of the reaction (3) can be verified by the fact that the value of pH of the anode ($SrTiO_3$) compartment is shifted by unity per decade increase in the amount of the electric charge passed through the electrode-electrolyte interface, as shown in Fig. 6. In this figure is also shown for comparison the variation of pH of the anode compartment for the Pt–Pt system

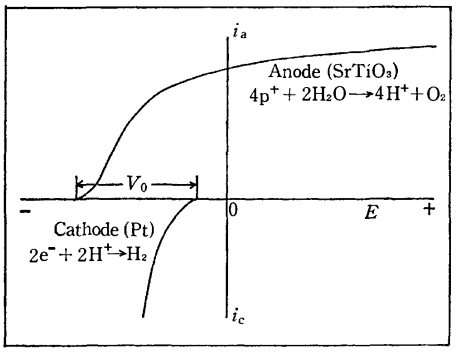

Fig. 7. Electrode reactions at $SrTiO_3$ (anode)-Pt (cathode) system under electrochemical photocell arrangement. V_0 represents the open-circuit cell voltage.

Table 1. Open-circuit cell voltages of $SrTiO_3$-Pt and TiO_2-Pt electrochemical photo-cells

	Common electrolyte solutions	Alkaline (anode)-acid (cathode) solutions
$SrTiO_3$-Pt	0.60 V (0.2 M Na_2SO_4)	1.25 V (1 M NaOH-0.5 M H_2SO_4)
TiO_2-Pt[4]	0.30 V (1 M NaOH)	0.64 V (1 M NaOH-0.5 M H_2SO_4)

during electrolysis.

The electrochemical reactions occurring on the anode ($SrTiO_3$) and cathode (Pt) under the electrochemical photocell arrangement[3,4] are summarized in Fig. 7. The electromotive force (and hence the value of the open-curcuit voltage, V_0) of the $SrTiO_3$ (anode)–Pt (cathode) electrochemical photocell is greater than that of the TiO_2–Pt system, owing to the fact that the flatband potential of the $SrTiO_3$ electrode is situated in the more cathodic region than that of the TiO_2 electrode. The data of V_0's for these semiconductor electrodes under the same illuminating light intensity are summarized in Table 1.

By illuminating the $SrTiO_3$ electrode surface with monochromatic light, the spectral response of the photocurrent has been measured. Since the forbidden gap width of $SrTiO_3$ is *ca.* 3.2 eV, the photosensitivity is confined to the wavelength range below 390 nm. For the estimation of the effectiveness of photocurrent production (and hence of the decomposition of water to hydrogen and oxygen gases), the formal quantum efficiency (*FQE*), defined by

$$FQE = \frac{\text{number of electrons flowing } (s^{-1})}{\text{number of incident photons } (s^{-1})} \quad (5)$$

was employed. The *FQE vs.* wavelength plot for the $SrTiO_3$ anode (0.0 V *vs.* SCE, in 1 M NaOH)–Pt (in 0.5 M H_2SO_4) system is shown in Fig. 8. The value of *FQE* reached 0.2 at 350 nm illumination. By the use of a common electrolyte solution (*e.g.*, 0.2 M Na_2SO_4) for both compartments, the values of *FQE* are lowered by a factor of about 1/2. This factor is much greater than that of the TiO_2–Pt system (*ca.* 1/30[4]), owing presumably to the greater emf of the $SrTiO_3$ anode–

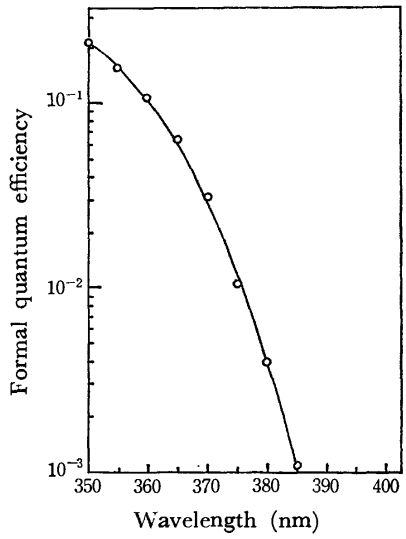

Fig. 8. Formal quantum efficiency of photocurrent production at $SrTiO_3$ anode (0.0 V *vs.* SCE) as a function of the wavelength of the incident light.

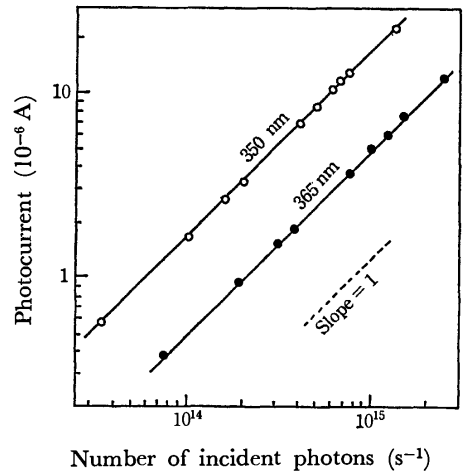

Fig. 9. Dependence of the photocurrent at $SrTiO_3$ electrode (0.0 V *vs.* SCE) on the intensity of the incident light.

Pt cathode electrochemical photocell than that of the TiO_2–Pt cell.

The true quantum efficiency would be much greater than *FQE* because of the high reflectivity of the $SrTiO_3$ crystal surface, whose precise measurement has not been carried out in the present study. For further enhancement of the quantum efficiency, it would be necessary to reduce the processes of electron trapping in the bulk of the semiconductor electrode and of the surface recombination of the charge carriers. These problems, possibly bearing on the thickness of the electrode[11] and/or the condition of the reduction treatment prior to the electrode preparation, are to be examined in the future investigation.

The magnitude of the photocurrent depends linearly on the incident light intensity, as depicted in Fig. 9. Even under the illumination by light with considerably high intensity (*e.g.*, 500 watt xenon lamp with no filters), the photocurrent did not show any saturation tendency.

Based upon the observations described above, it can be concluded that the $SrTiO_3$ single crystal is an excellent semiconductor electrode material for the decomposition of water by means of light energy.

The authors are grateful to Mr. Osamu Tatsuoki for his taking part in the experiments.

References

1) A. Fujishima, K. Honda, and S. Kikuchi, *Kogyo Kagaku Zasshi*, **72**, 108 (1969).
2) A. Fujishima and K. Honda, *ibid.*, **74**, 355 (1971).
3) A. Fujishima and K. Honda, *Nature*, **238**, 37 (1972).
4) A. Fujishima, K. Kohayakawa, and K. Honda, This Bulletin, **48**, 1041 (1975).
5) P. J. Boddy, D. Kahng, and Y. S. Chen, *Electrochim. Acta*, **13**, 1311 (1968).
6) P. J. Boddy, *J. Electrochem. Soc.*, **115**, 199 (1968).
7) H. Gerischer, "Physical Chemistry: An Advanced Treatise," ed. by H. Eyring *et al.*, Academic Press, New York (1970), pp. 487—489.
8) T. Watanabe, A. Fujishima, and K. Honda, *Chem. Lett.*, **1974**, 897.
9) "American Institute of Physics Handbook," 2nd ed., McGraw-Hill, New York (1963), pp. 9—95.
10) A Fujishima, A. Sakamoto, and K. Honda, *Seisan Kenkyu*, **21**, 450 (1969).
11) F. Moellers, H. J. Tolle, and R. Memming, *J. Electrochem. Soc.*, **121**, 1160 (1974).

The Gas-phase Emission Spectrum of Carbon Disulfide Excited by an N_2 Laser—Magnetic Quenching Effect

Akiyoshi MATSUZAKI and Saburo NAGAKURA

The Institute for Solid State Physics, The University of Tokyo, Roppongi, Minato, Tokyo 106

(Received July 8, 1975)

The time-resolved emission spectrum and its temperature dependence were observed with gaseous CS_2 excited by an N_2 laser. The spectrum was found to consist of three band systems, one of them being demonstrated to be emission from the $^1A_2$ state. The collision-free lifetimes and the collisional quenching constants were determined for the three band systems. The emission from the $^1A_2$ state was found to be quenched by a magnetic field because of the enhancement of an intramolecular energy-transfer process. This is the first observation of the magnetic quenching of emission from an excited singlet state.

The absorption spectrum of CS_2 in the region 290—370 nm has been studied by many researchers.[1-10] The longest wavelength absorption (the R system) in the region has been studied by Kleman,[4] by Douglas and Milton,[5] by Hougen,[6] and also by Hochstrasser and Wiersma[7] and has been assigned as the transition to the $^3A_2$ state which correlates with the $\pi\pi^*{}^3\Delta_u$ state of the linear CS_2 molecule. Jungen *et al.*[9,10] studied in detail much stronger absorption (the V system) and assigned it, in accord with Mulliken's prediction,[11] to the transition to the $^1B_2$ state, the upper Renner-Teller component of the $\pi\pi^*{}^1\Delta_u$ state of the linear molecule. Furthermore, they observed absorption due to the transition to the $^1A_2$ state, the corresponding lower component.

According to Jungen *et al.*,[9] there exist two absorption systems in the region of the N_2 laser wavelengths: one of them is due to a transition to a triplet state (the U band system) and the other to the transition to the $^1A_2$ state (the T band system). Brus[12] found that CS_2 emission excited by an N_2 laser shows two separate exponential decays. Mochiji *et al.* studied the emission spectrum of gaseous CS_2 and made a vibrational analysis with the aid of vibrational frequencies in the ground state.[13]

Under these circumstances, we have studied emission spectra of CS_2 excited by an N_2 laser, special attention being paid to the fluorescence from the $^1A_2$ state. We have found that the fluorescence is quenched by the magnetic field because of the enhancement of the intramolecular energy-transfer process. This is the first observation of magnetic quenching of emission from an excited singlet state.[14]

Experimental

An Avco Everett Model C950 N_2 laser was used for the excitation of CS_2. Emission from gaseous CS_2 was monochromatized by a Spex Model 1700 spectrometer and was detected by a combination of an EMI 6256S photomultiplier shielded by μ-metal and a PAR Model 160 boxcar integrator gated by a laser trigger. The signal is smoothed with an *RC* filter with a time constant of 0.2 μs. The N_2 laser intensity detected by this system was not affected by magnetic field. This shows that the shielding of the detecting system is good enough for our purpose. An electromagnet with a 6.5 cm gap was used for the magnetic quenching experiment, its field strength being calibrated by a Rowson-Lush gaussmeter indicator Type 789. A Pyrex glass cell of standard "cross" shaped design was used for the emission measurement which was made in the direction perpendicular to the excitation light. Temperature was controlled by flowing cooled nitrogen gas. Absorption spectra were measured by a Cary recording spectrophotometer model 14.

Wako reagent grade CS_2 was purified by distillation from calcium chloride. The sample pressure was measured by a calibrated Pirani gauge and an oil manometer. The vacuum system is free from Hg and background pressure is 10^{-6} Torr.

Results and Discussion

The Assignment of CS_2 Emission Excited by an N_2 Laser. Time-resolved emission spectra of CS_2 excited by the N_2 laser are shown in Fig. 1. The spectrum measured immediately after excitation ($t=0$) consists of sharp bands and a broad band. The latter decays more slowly than the former, as is clearly seen by a comparison of spectra a and b in Fig. 1.

Let us examine the sharp bands shown in Fig. 2. The most prominent band system labeled A forms a progression originating at the frequency of the N_2 laser, 29656 cm^{-1} and developing to the longer wavelength side with a interval of $2\nu''_2=850$ cm^{-1} [15]. The weaker bands labeled B, C, and D form similar progressions: their displacements from progression A are 210, 435, and 610 cm^{-1}, respectively. Progressions labeled a, b, c, and d appear at frequencies higher by 60 cm^{-1} than progressions A, B, C, and D, respectively. Pro-

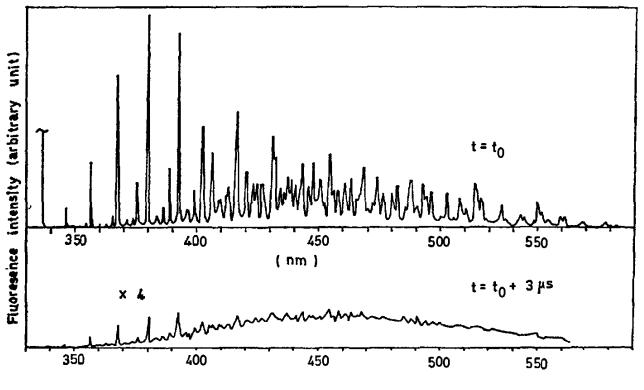

Fig. 1. The time-resolved emission spectra of CS_2 at 25 °C observed 0 μs (spectrum a) and 3 μs (spectrum b) after the fluorescence from the $^1A_2$ state of CS_2 reached the maximum intensity. The CS_2 pressure is 5×10^{-2} Torr.

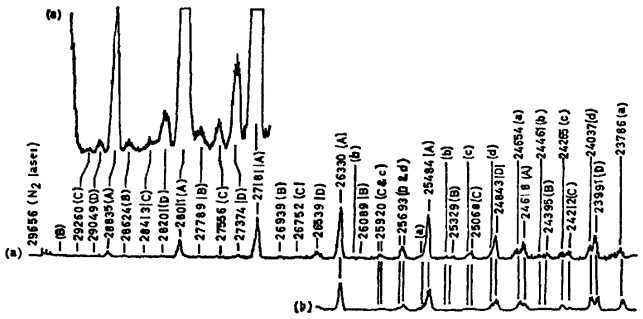

Fig. 2. The emission spectra of CS_2 at (a) 25 °C and (b) −90 °C. The pressure of CS_2 is 5×10^{-2} Torr.

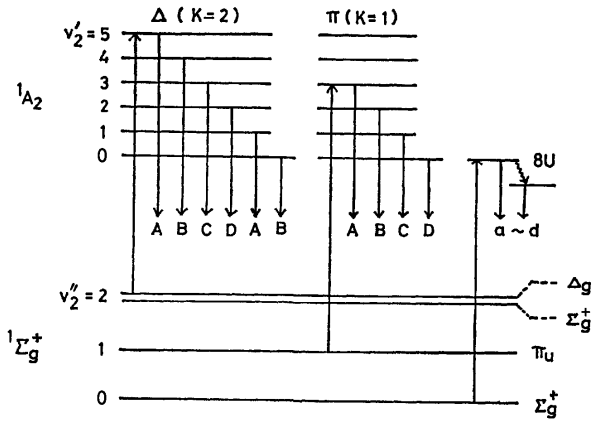

Fig. 3. The energy level diagram of CS_2: The $^1A_2$ and 8U excited states.

gressions a—d are too weak for their assignments to be made clear.

The temperature dependence of the emission spectra was studied at 25, −30, −45, and −90 °C. The spectra measured at 25 and −90 °C are shown in Fig. 2. The emission intensity at 25 °C is much stronger for progressions A—D than for progressions a—d. But progressions A—D rapidly decrease the intensity with lowering temperature and at −90 °C are weaker than progressions a—d. This means that progressions A—D and a—d belong to different electronic states.

According to Jungen *et al.*[9,10] who studied the absorption spectrum of CS_2, the N_2 laser excites the molecule to rovibronic levels of the $^1A_2$ state, say the 050(K=2) and 030(K=1) levels of $^1A_2$, and also to the upper level of the 8U band which corresponds to a transition to a triplet state and is known to display a Zeeman effect.[4] This is shown schematically in Fig. 3.

The transition from the ground state to the $^1A_2$ state is forbidden, but the mixing between the $^1A_2$ and $^1B_2$ components of the $^1\Delta_u$ state by the Renner-Teller effect can cause the hot bands to appear. In this case, the absorption intensity corresponding to the transition to the $^1A_2$ state is approximately proportional to K^2 [10] and also to the Boltzmann distribution in the lower state. This means that the fluorescence intensity from the $^1A_2$ state increases greatly with increasing temperature. Therefore, the A—D progressions sensitive to temperature are assigned to the transitions from the $^1A_2$ state. On the other hand, progressions a—d are regarded as emission from the excited levels of the 8U band system insensitive to temperature. The assignment of progressions A—D is supported by the fact that they shift each other by ~210 cm^{-1}, ν'_2 of the $^1A_2$ state reported by Jungen *et al.*[10] Furthermore, this assignment is consistent with the fact that the bands belonging to progressions A—D show no splitting or broadening under magnetic field of 13.3 kG.[16] Thus progressions A—D are assigned to the fluorescence from the 050(K=2) and 030(K=1) levels, the 040 (K=2) and 020(K=1) levels, the 030(K=2) and 010(K=1) levels, and the 020(K=2) and 000(K=1) levels, respectively. This is shown schematically in Fig. 3. Since their transition intensities are proportional to K^2, progression A is mainly from the 050(K=2) level of the $^1A_2$ state.

Let us turn to the broad band in Fig. 1 (b). This band is similar to emission of gaseous CS_2 excited optically at 290—330 nm,[17] excited by microwave discharge[18] or to that excited by electron impact of 200 eV[19] and also to emission of solid CS_2 or CS_2 in Ar and N_2 matrices excited at 260 nm.[19] The gas-phase emission was tentatively assigned by Douglas[17] and by others[18,19] to the transition from the excited state of the V system, say, the $^1B_2$ state. On the other hand, the solid-phase emission was assigned to the transition from the $^3A_2$ state. The decay times of the gas-phase emission and of the solid-phase emission are 15 μs and 1.8—2.1 ms, respectively. The former is very close to that of the broad band, 17 μs. This indicates that the broad band is tentatively assigned as the transition from the $^1B_2$ state.

Decay Times and Quenching Rates of the Emission. Figure 4 shows the plots of the decay rates, τ^{-1}, observed

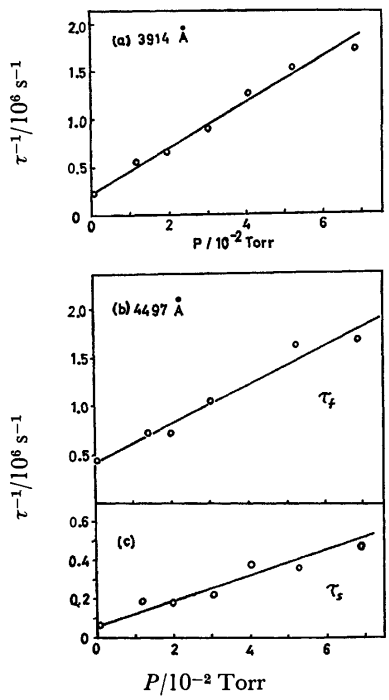

Fig. 4. The plots of decay rates *versus* the CS_2 pressure at 25 °C: (a) for the A band (391.4 nm); (b) for the a band (449.7 nm); (c) for the broad band (449.7 nm).

Table 1. Collision-free lifetimes (τ_0) and collisional quenching rate constants (k)

λ (Å)	Band	τ_0 (μs)	$k(10^{-10}$ cm^3/molecule s)
3923	A	4.5±0.2	5.6±0.2
4087	B	5.0±0.4	6.0±0.3
3988	C	5.0±0.5	8.1±0.2
4022	D	4.5±0.2	6.1±0.1
4475	a	2.9±0.3	6.0±0.3
4202	b	3.3±0.4	9.0±0.1
4475	broad	17.0±0.1	1.7±0.3

Table 2. The effect of the CS_2 pressure (P) on the fluorescence intensities

P (Torr)	$I_{A'}/I_A$[a)]	I_B/I_A[a)]	I_C/I_A[a)]	I_D/I_A[a)]
2×10^{-3}	1.1	0.07	0.12	0.29
2×10^{-2}	1.1	0.08	0.14	0.32
1×10^{-2}	1.1	0.09	0.15	0.35
10	1.1	0.10	0.17	0.36
49	1.1	0.11	0.19	0.38

a) $I_{A'}$, I_A, I_B, I_C, and I_D are the fluorescence intensities of the bands at 3797(band A), 3923(band A), 3832(band B), 3857(band C), 3891 Å(band D), respectively.

with the bands belonging to progressions A and a and with the broad band *versus* CS_2 pressure. We can see that the linear relationship is satisfied for each band. This indicates that a Stern-Volmer mechanism holds for collisional quenching by the ground-state CS_2 molecule. The slope and intercept give a collisional quenching rate constant and a collision-free lifetime, respectively. The result is shown in Table 1.

As pointed out by Kleman,[4] the $^1A_2$ state is perturbed by triplet states, as revealed by the observed perturbation to the vibrational and rotational structures of the corresponding absorption spectrum. However, since we can observe no effect of the magnetic field upon the positions and shapes of fluorescence bands belonging to progressions A, B, C, and D, it is clear that the mixing of triplet states is rather small and the singlet character is predominant for the $^1A_2$ state.

The appearance of the emission bands belonging to progression A suggests the "resonance limit". The effect of increasing collision frequency on the peak intensities of bands A—D is given in Table 2. Even at the CS_2 pressure of 10^{-3} Torr, under almost collision-free circumstances for instance, bands B—D have appreciable intensities.

Brus[12] observed the non-exponential decay of the unresolved emission of CS_2 excited by an N_2 laser and evaluated the collision-free lifetimes (τ_0) and collisional quenching rates (k): $\tau_0=2.9$ μs, $k=(7.9\pm1.2)\times10^{-10}$ cm^3/molecule s for the short-lived component; $\tau_0=17$ μs, $k=(1.2\pm1.0)\times10^{-10}$ cm^3/molecule s for the long-lived component. His results agree quite well with our results. He assigned the short and long-lived emissions to the transitions from the B_2 and degenerate A_1 and B_1 components of the $^3A_2$ state,[5,6] respectively, which has the zero-field splitting of 30—40 cm^{-1}.[7] However, this assignment is very improbable for the following reasons: (1) The N_2 laser wavelengths coincide with no absorption lines of the R system corresponding to the transition to the $^3A_2$ state. (2) The absorption band of the R system is insensitive to temperature, whereas progressions A—D under consideration are very sensitive to temperature. (3) The vibrational frequency, ν'_2 in the upper state of progressions A—D, ~210 cm^{-1}, is not equal to that in the R system, 311 cm^{-1} [4].

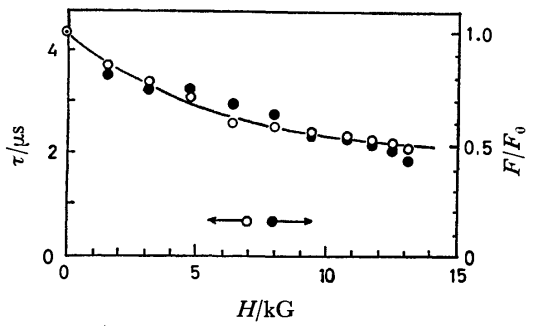

Fig. 5. Plots of F/F_0 and τ *versus* magnetic field(H): the pressure of CS_2 is 10^{-3} Torr.

Magnetic Quenching of Fluorescence. The effect of the magnetic field upon the emission intensity and lifetime of CS_2 was studied with a band at 379.7 nm which was assigned to the transition from the $^1A_2$ (0, 5, 0) state to the ground state. The lifetime, τ, and the integrated emission intensities in the absence and in the presence of the magnetic field, F_0 and F, respectively, were measured at 379.7 nm. The τ and F/F_0 values are plotted against the magnetic field in Fig. 5. As is clearly seen in this figure, the magnetic field effect is parallel for both quantities; they are reduced to about a half in the presence of the magnetic field of ~13 kG. This means that nonradiative energy-transfer (intramolecular or intermolecular) processes are enhanced in the magnetic field.

In order to study further the mechanism of the magnetic quenching observed with CS_2, we measured the pressure dependence of the fluorescence decay rate at 379.7 nm in the presence of the magnetic fields of 0, 4.7, and 12.6 kG. The Stern-Volmer plots of the observed decay rates *versus* the CS_2 pressure are shown in Fig. 6. From the straight lines obtained, the collision-free lifetimes, τ_0, and collisional quenching constants, k, were evaluated as given in Table 3. This table shows that the collision-free lifetime becomes shorter with an increase in the magnetic field, while the collisional quenching constant remains unchanged within the limits of experimental error.

The above-mentioned facts lead to the conclusion that the observed magnetic quenching of the fluorescence is due to an enhancement of an intramolecular nonradiative process. In view of the fact that the $^1A_2$ state is perturbed to some extent by the triplet states densely distributed in the appropriate energy region,[4] it is reasonable to consider that the intersystem crossing to these triplet states occurs as one of the nonradiative processes and is enhanced by the magnetic field.

According to our experimental result shown in

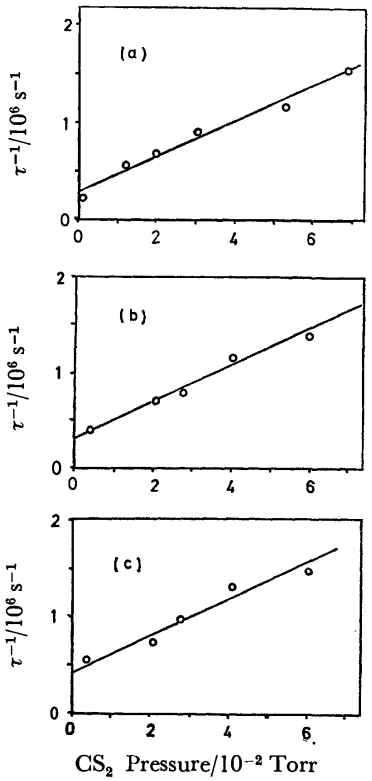

Fig. 6. Plots of τ^{-1} *versus* the CS_2 pressure.
(a) in the absence of magnetic field
(b) in the magnetic field of 4.7 kG
(c) in the magnetic field of 12.6 kG

TABLE 3. COLLISION FREE LIFETIMES (τ_0) AND COLLISIONAL QUENCHING CONSTANTS (k) IN THE PRESENCE OF MAGNETIC FIELD (H)

H (kG)	τ_0 (μs)	$k(10^{-10}$ cm^3/molecule s)
0	4.1±0.2	5.6±0.2
4.7	3.2±0.2	5.6±0.2
12.6	2.2±0.3	5.5±0.2

Fig. 7, the $(F_0/F)-1$ value is proportional to the square of the magnetic field in the range higher than 5 kG and decreases rapidly with decreasing magnetic field below 4 kG. The extrapolation of the straight line representing the relation between $(F_0/F)-1$ and H^2 does not pass the origin. We measured very carefully the magnetic-field effect upon the $(F_0/F)-1$ value in the low-field region. The result is also shown in Fig. 7. It is emphasized that, below 700 G, the $(F_0/F)-1$ value decreases once and thereafter increases steeply with increasing magnetic field. Atkins has made theoretical studies to explain this phenomenon.[20]

Emission from the $B^3\Pi\ 0_u^+$ state of iodine is known to be quenched by a magnetic field.[21,22] This phenomenon was explained by an induced predissociation caused by the magnetic mixing of an unbound 0_u^- state. Solarz *et al.* found that the fluorescence of nitrogen dioxide is quenched by magnetically induced collisional quenching.[23] The quenched states of iodine and nitrogen dioxide are triplet and doublet, respectively, and are paramagnetic. In the present study, we found

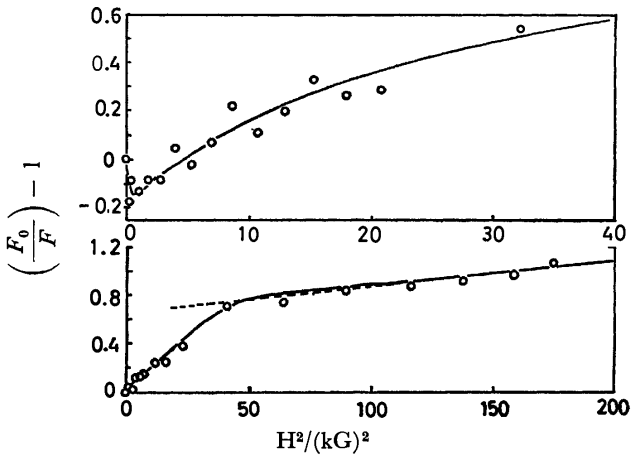

Fig. 7. Plots of $(F_0/F-1)$ *versus* the square of magnetic field: the pressure of CS_2 is 10^{-3} Torr.

that the fluorescence from the $^1A_2$ state of CS_2 was quenched by a magnetic field. This is the first example of the magnetic quenching of emission from a singlet state.

References

1) P. Kusch and F. W. Loomis, *Phys. Rev.*, **55**, 850 (1939).
2) L. N. Liebermann, *Phys. Rev.*, **58**, 183 (1940); **60**, 496 (1941).
3) C. Ramasastry, *Proc. Nat. Sci. Mdia*, **18**, 177, 622 (1952).
4) B. Kleman, *Can. J. Phys.*, **41**, 2034 (1963).
5) A. E. Douglas and E. R. V. Milton, *J. Chem. Phys.*, **41**, 357 (1964).
6) J. T. Hougen, *ibid.*, **41**, 363 (1964).
7) R. M. Hochstrasser and D. A. Wiersma, *ibid.*, **54**, 4165 (1971).
8) L. Bajema, M. Gouterman, and B. Meyer, *J. Phys. Chem.*, **75**, 2204 (1971).
9) Ch. Jungen, D. N. Malm, and A. J. Merer, *Chem. Phys. Lett.*, **16**, 302 (1972).
10) Ch. Jungen, D. N. Malm, and A. J. Merer, *Can. J. Phys.*, **51**, 1471 (1973).
11) R. S. Mulliken, *Can. J. Chem.*, **36**, 10 (1958).
12) L. E. Brus, *Chem. Phys. Lett.*, **12**, 116 (1971).
13) K. Mochiji, Y. Udagawa, and M. Ito, "Proceedings of the Symposium on Molecular Structure," October (1973), p. 255.
14) A preliminary report, A. Matsuzaki and S. Nagakura, *Chem. Lett.*, **1974**, 675.
15) D. F. Smith, Jr. and J. Overend, *J. Chem. Phys.*, **54**, 3632 (1971).
16) It is difficult to clarify whether or not the bands belonging to progressions a—d change their shapes by the magnetic field. This is because they are too weak to measure the magnetic field effect.
17) A. E. Douglas, *J. Chem. Phys.*, **45**, 1007 (1966).
18) S. J. Arnold and G. H. Kimbell, *Can. J. Chem.*, **49**, 4110 (1971).
19) M. Toyoda, T. Ogawa, and N. Ishibashi, This Bulletin, **47**, 95 (1974).
20) P. W. Atkins, private communication.
21) L. A. Turner, *Z. Phys.*, **65**, 464 (1930).
22) E. O. Degenkolb, J. I. Steinfeld, E. Wasserman, and W. Klemperer, *J. Chem. Phys.*, **51**, 615 (1969).
23) R. Solarz, S. Butler, and D. H. Levy, *J. Chem. Phys.*, **58**, 5172 (1973).

Thermal Separation Column with Vertical Barriers. I. Analytical Studies on the Thermal Separation Column Having Vertical Barriers

Kazuo SASAKI, Tsutomu YOSHITOMI, and Norio MIURA

Department of Applied Chemistry, Hiroshima University, Hiroshima 730

(Received January 30, 1975)

The effect of installing a couple of vertical flow barriers inside a double cylinder-type thermal separation column has been studied analytically. The method of analysis is entirely similar to that developed by Jones and Furry. The only change is that an additional parameter, which specifies the location of the barriers, has been introduced. The results indicated that the installation of barriers retards the convectional velocity and leads to a remarkable increase in the equilibrium separation. With the optimum design, which is achieved by locating barriers at 5/8 parts of the half-width of the wall spacing, the logarithmic equilibrium separation will become 4 times greater than that in the open column.

The use of thermal diffusion phenomena is practical enrichment of one component from a gaseous mixture was established by Clusius and Dickel[1] in 1938. The method is often useful in certain restricted purposes; however, it is still necessary to improve the operational characteristics of the Clusius-Dickel column for a wider application of the method.

Accordingly, various ideas have been introduced for improving the column efficiency. For instance, tilting the column, [9-11] use of column packing[12,13] or spiral wire[14,2] inside the annular space, and columns with moving wall[10,13] have been examined with more or less satisfactory results. It is interesting that almost all of these attempts for improving the thermal separation unit were made with liquid mixtures.

In contrast, most experiments with gaseous mixtures so far reported have been conducted by using the Clusius-Dickel column in its original form. In many papers of gaseous separation, attention was focused on the effectiveness of spacers, which are usually installed in a Clusius-Dickel type column in order to fix the central heating wire at a proper position. The first use of such spacers is seen in the work of Clusius and Dickel themselves in 1939.[3] In the experiment of separating an isotopic mixture of hydrogen chloride, they found that the introduction of spacers resulted in an increase of the separation efficiency. Later, Donaldson and Watson[4] found that simple wire crosses which were welded perpendicularly on the heating wire at given regular distances significantly increased the separation efficiency. According to Corbett and Watson,[5] however, the effect of spacers was insignificant and even disadvantageous when too many spacers were installed. Although discussion on the effectiveness of spacers have continued up to the present,[6,7] no unified theory seems to have been accepted.

In such a situation, the work of Treacy and Rich[15] seems exceptional. They examined the effect of installing several types of flow barriers inside the working space of the separation column. According to them, introduction of barriers usually resulted in the increase of both the magnitude and the rate of separation. Their work seems, however, unsystematic and lacks theoretical support.

In the following part of this paper, we shall examine the possibility of improving a thermal separation column by installing a couple of vertical flow barriers inside the column space.

Basic Idea and Analytical Approach

Basic Idea. As is well known, in a typical Clusius-Dickel apparatus, the velocity profile of vertical current has a maximum at a point having a finite distance from the wall surface. On the other hand, the maximum temperature difference, which is the driving force of the thermal diffusion, is attained undoubtedly at the wall surface. It is apparent that the convectional flow arises in an inefficient way. If we are able to move the position of maximum convectional velocity towards the wall surface, the efficiency will increase. This was our basic idea for the present study. We further thought that a vertical barrier will serve to separate functionally the column space to allow convection and thermal diffusion separately and this will lead to improvement of the column efficiency.

Analytical Approach-Modification of the Theory of Jones and Furry.[8] *Transport Equation by Jones and Furry*: Jones and Furry[8] developed a theory for the thermal separation in a Clusius-Dickel type column. Assuming the separation column to be a plane parallel type, they derived the following fundamental equations for the total transport of the lighter component, τ_1, in the upward direction:

$$\tau_1 = wB\rho\bar{v}(\alpha\Delta T/2\overline{T})c_1c_2 - \{wB\rho\bar{v}(\bar{v}w^2/D) + 2wB\rho D\}\frac{\partial c_1}{\partial z} \quad (1), \text{ (Eq. (52), Ref. 8)}$$

Alternatively,

$$\tau_1 = Hc_1(1-c_1) - (K_c+K_d)\frac{dc_1}{dz} \quad (2), \text{ (Eq. (53), Ref. 8)}$$

with the following abbreviations,

$$H = \frac{\alpha\rho^2 g w^3 B}{96\eta}\left(\frac{\Delta T}{\overline{T}}\right)^2 \quad (3), \text{ (Eq. (54), Ref. 8)}$$

$$K_c = \frac{\rho^3 g^3 w^7 B}{2304\eta^2 D}\left(\frac{\Delta T}{\overline{T}}\right)^2 \quad (4), \text{ (Eq. (55), Ref. 8)}$$

and

$$K_d = 2wB\rho D \quad (5), \text{ (Eq. (56), Ref. 8)}$$

Modification of the Theory: An entirely similar treatment can be applied to the present case, where a couple of plane parallel screens are installed vertically inside the column. We shall describe the procedure shortly. Prior to developing this analysis, we suppose the conditions of column operation to be as follows.

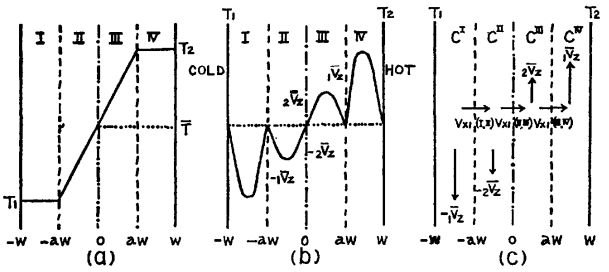

Fig. 1. Assumptions and notations for a column which equipped a couple of screens.
(a): Temperature gradient. (b) Convectional flow velocity as a function of x. (c) Notations.

1. The apparatus is of the plane parallel type having an interwall distance of $2w$.
2. Two screens are placed at positions $\pm aw$ parallel to the column wall.
3. A temperature gradient is set up between the pair of screens and the two gaps produced outside the screens, $|aw|<x<|w|$, are kept isothermal.[17]
4. The velocity of vertical gas flow is zero at $x=\pm aw$ where the two screens are located.

Accordingly, the space in the column are divided vertically into four sub-columns: column I ($-w\leq x\leq -aw$), II ($-aw\leq x\leq 0$), III ($0\leq x\leq aw$), and IV ($aw\leq x\leq w$). The symbols and coordinates necessary for the analytical treatment are given in Fig. 1 and are also listed at the end of this article. Unless otherwise stated, the symbols used by Jones and Furry will be used.

On account of the above assumptions, the basic equation to be solved for the region of $-aw<x<aw$ becomes

$$\eta\frac{\mathrm{d}^2{}_2v_z(x)}{\mathrm{d}x^2}=-\rho g\frac{x\Delta T}{2aw\overline{T}} \tag{6}$$

Under the boundary condition

$$\text{at } x=\pm aw;\ {}_2v_z(x)=0$$

Eq. (6) is solved to give

$${}_2v_z=\frac{\rho g\Delta T}{12\eta aw\overline{T}}\times(a^2w^2-x^2) \tag{7}$$

Denoting the average velocity of convectional flow in columns II and III as ${}_2\bar{v}_z$, we obtain

$${}_2\bar{v}_z=\frac{1}{aw}\int_0^{aw}{}_2v_z(x)\mathrm{d}x=\frac{\rho gw^2}{48\eta}\frac{\Delta T}{\overline{T}}a^2 \tag{8}$$

On the other hand, in column IV, where the region is specified by $aw\leq x\leq w$, the temperature must be the same everywhere, by assumption, and is given by

$$T=T_2=\overline{T}+\Delta T/2 \tag{9}$$

The convectional flow in column IV may be expressed as

$$\eta\frac{\mathrm{d}^2{}_1v_z(x)}{\mathrm{d}x^2}=-\rho g\frac{\Delta T}{2\overline{T}} \tag{10}$$

This equation is solved under the boundary condition

$${}_1v_z=0 \text{ at } x=aw \text{ and } x=w$$

to give the average vertical velocity in column IV (and also in column I)

$${}_1\bar{v}_z=\frac{\rho gw^2}{48\eta}\frac{\Delta T}{\overline{T}}\cdot 2(1-a)^2 \tag{11}$$

Since there will be a transport down the tube because of ordinary diffusion, the total transport of the lighter component up the tube will be

$$\tau_1'=\{(c_1^{IV}-c_1^{I})(1-\alpha){}_1\bar{v}_z+(c_1^{III}-c_1^{II})a\,{}_2\bar{v}_z\}\omega B\rho -2DwB\rho\frac{\partial c_1}{\partial z} \tag{12}$$

where $c_1{}^J$ stands for the average concentration of the lighter component in column J.

For the transverse flow, we have the following set of approximate equations:

$$\rho c_1v_{x1}(\mathrm{I,\ II})=-\rho D\ \mathrm{grad}\ c_1=-\frac{2(c_1^{II}-c_1^{I})\rho D}{w} \tag{13}$$

$$\rho c_1v_{x1}(\mathrm{II,\ III})=\rho D(\alpha c_1c_2\ \mathrm{grad}\ \ln T-\mathrm{grad}\ c_1)=\rho D\left(\alpha c_1c_2\frac{\Delta T}{2aw\overline{T}}-\frac{c_1^{III}-c_1^{II}}{aw}\right) \tag{14}$$

$$\rho c_1v_{x1}(\mathrm{III,\ IV})=-\rho D\ \mathrm{grad}\ c_1=-\frac{2(c_1^{IV}-c_1^{III})\rho D}{w} \tag{15}$$

where $v_{x1}(H,\ J)$ represents the rate of the horizontal transport of the lighter component from column H to J.

If we assume the concentration change from column to column is so small that c_1^{I}, c_1^{II}, c_1^{III}, and c_1^{IV} can be safely replaced by c_1, the terms $(c_1^{IV}-c_1^{I})$ and $(c_1^{III}-c_1^{II})$ appearing in Eq. (12) can be evaluated by the aid of Eqs. (13) through (15) to give

$$c_1^{III}-c_1^{II}=\alpha c_1c_2\frac{\Delta T}{2\overline{T}}+\frac{w^2}{D}\{(a^2-a){}_1\bar{v}_z-a^2{}_2\bar{v}_z\}\frac{\partial c_1}{\partial z} \tag{16}$$

$$c_1^{IV}-c_1^{I}=\alpha c_1c_2\frac{\Delta T}{2\overline{T}}+\frac{w^2}{D}\{(a^2-1){}_1\bar{v}_z-a^2{}_2\bar{v}_z\}\frac{\delta c_1}{\partial z} \tag{17}$$

Accordingly, Eq. (12) is now rewritten in the form of Eq. (2)

$$\tau_1'=H'c_1c_2-(K_c'+K_d')\frac{\mathrm{d}c_1}{\mathrm{d}z}\ . \tag{18}$$

Where the constants are defined as follows:

$$H'=\frac{\alpha\rho gw^3B}{96\eta}\left(\frac{\Delta T}{\overline{T}}\right)^2\{2(1-a)^3+a^3\}=\{2(1-a)^3+a^3\}H \tag{19}$$

$$K_c'=\frac{\rho^3g^2w^7B}{2304\eta^2D}\left(\frac{\Delta T}{\overline{T}}\right)^2\{4(1-a)^6(1+a)+4a^4(1-a)^3+a^7\}=\{4(1-a)^6(1+a)+4a^4(1-a)^3+a^7\}K_c \tag{20}$$

$$K_d'=K_d\ . \tag{21}$$

Operational Characteristics and Remarks

Several parameters which are important for describing the operational characteristics of the separation column have already been given by Jones and Furry.[8] We shall reproduce some of the results necessary in the following discussion.

The equilibrium separation factor, q_e, is given by

$$q_e=e^{2AL} \tag{22}$$

where the parameter A is defined as

$$A=H/2(K_c+K_d) \tag{23}$$

and L is the length of the separation column.

We now examine the separation characteristics of

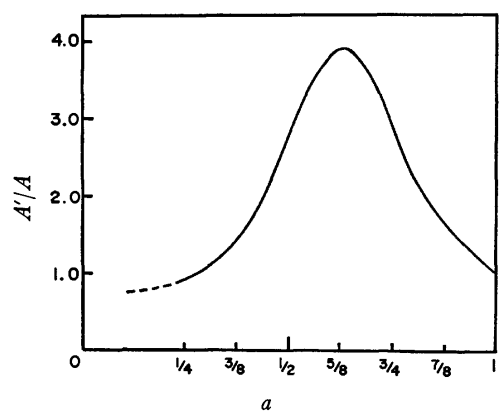

Fig. 2. The relative performance, A'/A, against design parameter a.

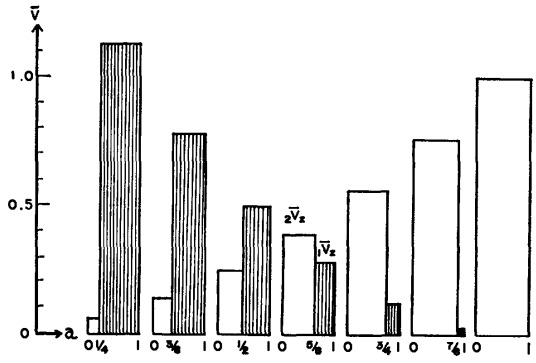

Fig. 3. Change in average convectional velocity in sub-columns I and IV ($_1\bar{v}_2$) and II and III ($_2\bar{v}_2$) with various value of design parameter a. Hatched bar represents $_1\bar{v}_z$ and empty bar $_2v_z$, respectively.

columns with and without screens. For simplicity, we suppose that the value of K_c is sufficiently greater than K_d, so that the contribution of the latter can be ignored in the expression of A in Eq. (23). As has been done already in Eqs. (18) through (21), the symbols corresponding to the column with screens will be primed to distinguish them from the ordinary column symbols. When K_d is ignorable, the change in A' with varying a can be expressed by a simple analytical function

$$\frac{A'}{A}=\frac{H'/2K_c'}{H/2K_c}=\frac{2(1-a)^3+a^3}{4(1-a)^6(1+a)+4a^4(1-a)^3+a^7} \qquad (24)$$

this function is graphicaly represented in Fig. 2. It is seen that the use of screens significantly increases the equilibrium separation factor. In order to see what was the cause of this improvement, we prepared Fig. 3, where the average velocity of convectional flow is indicated as a function of the design parameter a. It is indisputable that the vertical movement of gas is suppressed by the installation of screens and the supression becomes maximum at about $a=5/8$, where the separation becomes also maximum. This is predictable analytically also in the following manner. Eqs. (3) and (4) can be rewritten in terms of $\bar{v}$

$$H=\frac{1}{2}\alpha\bar{\rho}wB\bar{v}\left(\frac{\Delta T}{\bar{T}}\right)$$

$$K_c=\frac{\bar{\rho}w^2B\bar{v}^2}{D}$$

Accordingly, if K_d is ignored,

$$\ln q_e=\frac{HL}{K_c}=\frac{\alpha DL(\Delta T/\bar{T})}{2w^2\bar{v}}$$

The last equation indicates that q_e will increase when $\bar{v}$ decreases. Accordingly, our original idea, which anticipated an improvement by shifting the position of maximum vertical velocity towards the column wall, must be said to have been not wholly correct.

Treacy and Rich[15] studied the effect of barriers introduced in a double-cylinder type separation column. They found that the use of compound barriers made by cutting the vertical into sections of length suitable for insertion between horizontals exhibits a pronounced increase of column efficiency. Although they state that use of single vertical barriers is still effective for increasing efficiency, the data shown in the paper are not convincing. This is quite natural because they ignored the importance of the location of the barriers. In order to prove the result of the foregoing analysis to be acceptable, we need some experimental vertification. This will be reported in a following paper.[16]

Conclusion

It was confirmed analytically that the introduction of a couple of vertical barriers in a thermal separation column should increase the separation significantly. The improvement is rather sensitive to the design parameter a and the maximum improvement is expected at about $a=5/8$, where a four times greater value can be expected in $\ln q_e$ as compared with the ordinary column.

At the end of this article, it should be noted that in the foregoing treatment we have used somewhat particular boundary conditions according to which the temperature gradient exists only over the region specified by $-aw\leq x\leq aw$. This was necessary because of mathematical simplification. In an actual column, however, a finite temperature gradient may be unavoidable over the regions outside the screens. Errors due to this assumption will be larger for smaller values of design parameter a. This point will be examined in a future paper.

Table of Notation

$A=H/2(K_c+K_d)$, [cm^{-1}].
a=design parameter, $0<a<1$.
B=mean circumference, [cm].
c=either c_1 or c_2.
$\bar{c}=1-c$.
c_1=fractional molar concentration of the lighter component.
c_2=fractional molar concentration of the heavier component. $c_1+c_2=1$.
c_1^J=average concentration of the lighter component in column J.
D=coefficient of self-diffusion, [cm^2/s].
g=acceleration of gravity, [cm/s^2].
H, [g/s], K_c, K_d, [g cm/s]=transport coefficient.
L=length of column, $0\leq z\leq L$, [cm].

q=separation factor.
$q_e = e^{2AL}$=equilibrium separation factor.
T=absolute temperature, [K].
T_1=temperature of cold wall [K].
T_2=temperature of hot wall, $T_2 > T_1$, [K].
$\overline{T} = (T_1 + T_2)/2$, [K].
$\Delta T = T_2 - T_1$, [K].
v=velocity of convectional flow, [cm/s].
$\bar{v}$=average velocity of convectional flow, [cm/s].
${}_1\bar{v}_z$=average velocity of convectional flow in columns I and IV, [cm/s].
${}_2\bar{v}_z$=average velocity of convectional flow in columns II and III, [cm/s].
$v_{x1}(H,J)$=rate of the horizontal transport of the lighter component from column H to J, [cm/s].
w=one-half of the distance between the hot and cold walls. [cm].
x=coordinate perpendicular to the walls, $-w \leq x \leq w$, [cm].
z=coordinate along the column, $0 \leq x \leq L$, [cm].
α=thermal diffusion constant.
η=viscosity, [P].
ρ=density, [g/cm^3].
τ_1=transport of species 1 along the column, mass per unit time, [g/s].

References

1) K. Clusius and G. Dickel, *Naturwissenschaften*, **26**, 546 (1938).
2) H. M. Yeh and H. C. Ward, *Chem. Eng. Sci.*, **26**, 937 (1971).
3) K. Clusius and G. Dickel, *Z. Phys. Chem.*, **44**, 451 (1939).
4) J. Donaldson and W. W. Watson, *Phys. Rev.*, **82**, 909 (1951).
5) J. W. Corbett and W. W. Watson, *ibid.*, **101**, 519 (1956).
6) S. Raman, R. Paul, and W. W. Watson, *J. Chem. Phys.*, **46**, 3916 (1967).
7) S. Kimura and A. Kanagawa, *Nippon Gensiryoku Gakkaishi*, **14**, 52 (1972).
8) R. C. Jones and W. H. Furry, *Rev. Mod. Phys.*, **18**, 151 (1946).
9) P. L. Chueh and H. M. Yeh, *AIChE J.*, **13**, 37 (1967).
10) H. M. Yeh and C. S. Tsai, *Chem. Eng. Sci.*, **27**, 2065 (1972).
11) J. E. Powers and C. R. Wilke, *AIChE J.*, **3**, 213 (1957).
12) A. E. Emery, Jr. and M. Lorenz, *ibid.*, **9**, 660 (1963).
13) L. J. Sullivan, T. C. Russel, and C. B. Willingham, *Ind. Eng. Chem.*, **47**, 208 (1955).
14) T. A. Washall and F. W. Melpolder, *I & EC Process Design and Dev.*, **1**, 26 (1962).
15) J. C. Treacy and R. E. Rich, *Ind. Eng. Chem.*, **47**, 1544 (1955).
16) K. Sasaki, N. Miura, and T. Yoshitomi, This Bulletin, **49**, 367 (1976).
17) This assumption is necessary only for mathematical simplicity. In an actual column, however, there may be a finite temperature gradient in the gaps concerned. Because of this assumption, the question may arise whether "The comparison should be made with an open column having width of $2aw$ but not of $2w$". In fact, there may be two different views with regard to the installation of barriers: 1) screens are merely inserted in the column space of width of $2w$ and 2) additional spaces are produced outside the pair of screens. If, for an actual column, a finite temperature gradient is unavoidable over spaces outside the screens, the former view must be accepted. In the following part of this paper and also in the successive paper, the discussion has been developed on this standpoint.

Thermal Separation Column with Vertical Barriers. II. Performance of a Thermal Separation Column with Vertical Barriers

Kazuo SASAKI, Norio MIURA, and Tsutomu YOSHITOMI
Department of Applied Chemistry, Hiroshima University, Hiroshima 730

(Received January 30, 1975)

The performance of a newly designed thermal separation column has been examined. The apparatus was constructed along the line of mathematical analysis developed in the preceding paper. The column was basically composed of two coaxial cylinders inside of which two additional cylinders of fine stainless steel screen were installed to control the gas flows in the column. An equimolar mixture of argon and nitrogen was used as the test gas. A definite improvement in the magnitude of equilibrium separation was demonstrated in accordance with the theory. In addition, the rate of attainment of steady state was found not so much different from that with open column when temperature exceeded 140 °C or more.

As has been described in the preceding paper,[1] mathematical analysis predicted that the additional installation of a couple of wire gauzes or something like that, which effectively control the relative magnitude of convectional and horizontal flow of gas, will increase the performance of thermal separation markedly. Treacy and Rich[5] studied the effect of several sorts of flow barriers in a Clusius column and reported that the simultaneous use of horizontal and vertical barriers resulted in a remarkable increase in the separation. Their data seems to indicate that the single use of vertical barriers is not so much effective.

The design of column used by them, however, seems not suitable to test our theory and the data presented were so restricted. We thus attempted to construct a column which closely satisfies the assumptions made in the mathematical analysis.

The following is the first full report on the performance of thermal separation column having several types of barriers.

Experimental

Description of the Column. An outline of the column used are shown in Fig. 1. The inner tube (1) of the column was made of iron pipe of 21.7 mm o.d., and 970 mm in its effective length. On the outer surface of this tube, eight long iron bars (2) having square form cross section (2 mm in width, 4 mm in height) were welded parallelly along the direction of the length. Thus the horizontal cross section of the inner tube assembly has a form of a gear. Around this cylinder (30 mmϕ) a 100 mesh stainless steel screen (3) was tightly wound with thin wire.

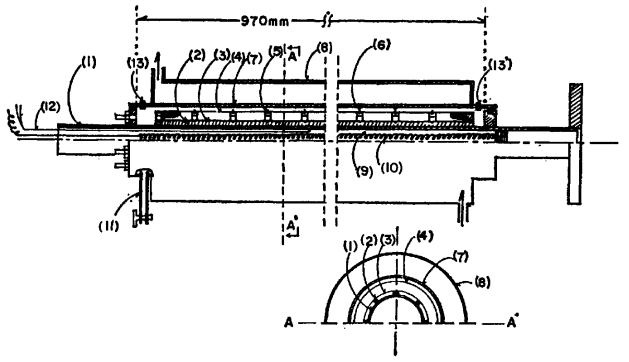

Fig. 1. Apparatus.
1: Inner tube, 2: square bar of iron, 3: inner screen, 4: outer screen, 5: aluminium O-ring, 6: binding wire, 7: outer tube, 8: water jacket, 9: heat mediator, 10: nichrome heater, 11: gas inlet, 12: thermocouple, and 13(13'): sampling port.

Outside the inner tube assembly, another cylindrical stainless steel screen was coaxially suspended (4). In order to keep the shape of cylinder, twenty aluminium O-rings of 38 mm i.d. and 44.8 mm o.d. (5) were placed with a regular distance (4 cm) and the screen was tightly bound onto the aluminium O-rings with steel wire. Each edge of the binding wire (6) was made to contact with the inner surface of the cold wall (52.7 mmϕ) (7) in order to keep, as far as possible, the temperature of the outer screen same as that of the cold wall. This benefited also to hold the suspended outer screen at a proper position. The size of the column and dimensions of each part were determined by purely technical reason except that the value of design parameter a was adjusted to be 1/2. The central hollow cylinder (9) of the inner tube was filled with a mineral oil as the heat mediator in which a 300 W nichrome wire (10) was immersed. The outer cylinder was surrounded by a water jacket (8) of vinyl chloride pipe through which tap water was flown.

The test gas inlet (11) was placed just below the top of the column. No particular gas reservoir was attached.

Operation of the Column. In an actual operation, the whole assembly was evacuated through the inlet tube (11) and the temperature difference was applied. After setting up the steady temperature difference, the test gas, 50% Ar–50% N_2, was introduced until a desired pressure was attained. The temperature of the hot wall was measured at the backside of it by means of a copper-constantan thermocouple (12), while that of cold plate was measured by a thermometer at exit of cooling water. The temperature variation along the direction of column was unable to detect by this method. Since oil was used as the heat mediator the highest temperature available was limited at 200 °C or so. Sample gas was withdrawn by a hypodermic syringe from two sampling ports (13) which were consisted of small silicone rubber stoppers. The progress of the thermal separation was monitored by periodical sampling and analysis with an ordinary gas chromatograph in which a 1 m column of molecular sieve 5 A was installed. By the aid of digital integrater maximum deviation of the readings was able to control within 0.1%.

As the control experiments, several series of data were collected with an open column which was an exact duplicate of the column described above except that no barrier was equipped.

Results

Equilibrium Separation and the Temperature Effect. In Fig. 2, are shown the results of two representative runnings observed with novel and ordinary columns under the same operational condition. In this figure, the scale of the ordinate is expressed by the ratio of direct reading of the gas-chromatographic peak areas of argon and nitrogen. A couple of curves drawn with solid line stand for the measurement with the novel column while another couple with dotted line for the ordinary column. Ascending curves stand for the measurement at the top of the column and descending curves at bottom. The couple of solid curves (novel column) in ascending and descending directions are not exactly symmetrical. The volume of free space at the column top was made slightly bigger than that of the bottom. Accordingly, if this structural assymmetry of the column was the cause, the depression of the curve would be more pronounced in the ascending curves. Local assymmetry of barrier location may be accounted for. On the other hand, the couple of curves observed with the ordinary column (dotted line) are exactly symmetrical. In any case, since the equilibrium was found to attain within five minutes in both columns, q_e data presented in the following were those observed after 20 minutes operation.

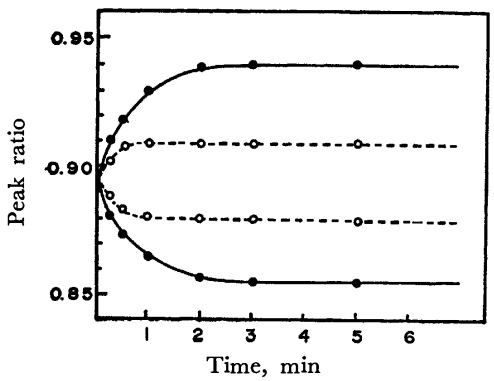

Fig. 2. Progress of separation with time.
Solid line: Column with barriers. Dotted line: Open coulmn. ΔT: 78 °C, pressure: 790 mmHg.

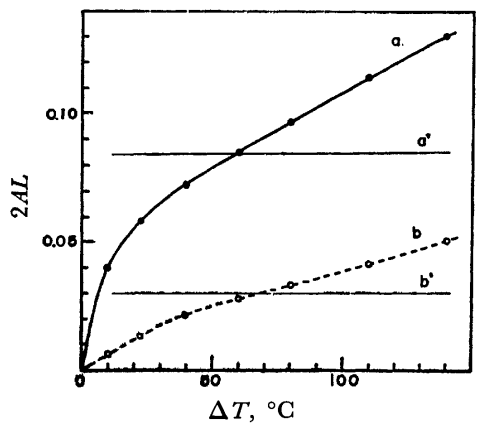

Fig. 3. Logarithm of equilibrium separation against temperature difference. Pressure: 790 mmHg.
Solid line: novel column. Dotted line: open column.

Results of a series of runnings in which the working pressure was kept constant and the temperature difference applied was varied are summarized in Fig. 3. The scale of the ordinate is logarithm of the equilibrium separation factor, ln q_e ($=2AL$).

The curves clearly indicate that, as the theoretical analysis predicted, the magnitude of the equilibrium separation is always greater with novel column (solid line) than with the ordinary one (dotted line). In this figure, the two horizontal lines indicates the theoretical values of the logarithmic equilibrium separation for the novel column (curve a') and ordinary column (b').[6] One thing to be stressed with this figure is not the dissimilarity[7] between the experimental and theoretical curve forms but is that the experimental separations are greater than the theoretical values when the temperature difference exceeds 70 °C or so regardless of the column type. As far as the authors are aware, it is usual that the experimental separation, particularly with hot-wire column, doesn't exceed theoretical value. The present result might be correlated with the shape and sizes of column used.

Pressure Effect. Similarly, the effect of pressure was studied under the condition of constant temperature difference. The results obtained are shown in Fig. 4 in which theoretical curves (a' and b') are drawn using the following relationship.

$$2AL = \frac{1.231 \times 24 \times \eta DL\alpha}{\rho g w^4 P^2} \qquad (1)$$

The numerical factor 1.231 is the correction factor for the cylindricity of the column used (see Eqs. (100) through (111) in Ref. 2). In accordance with the theory (curves a' and b'), the separation factor observed appears to decline with increasing pressure (curves a and b). Curve a, which stands for the observation with the novel column, appears to lie down at the lower pressure region. As has been frequently shown,[2,3] the separation factor makes a maximum at a low pressure. This effect is not seen in curve b which stands for the measurements with ordinary column. In any case, it is apparent that the performance of the novel

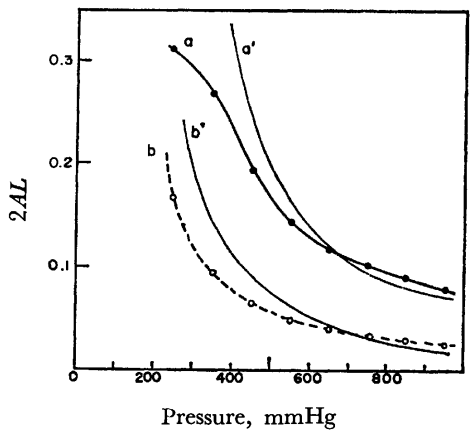

Fig. 4. Pressure effect on the logarithmic equilibrium separation.
a: observed with novel column, b: with ordinary column a' and b' are calculated on the base of Eq. (1). Temperature difference: 78 °C.

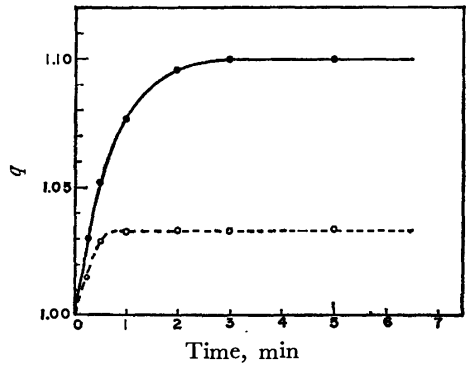

Fig. 5. Progress of thermal separation with time. Temperature difference: 78 °C, Pressure: 790 mmHg. Solid line: novel column, Dotted line: ordinary column.

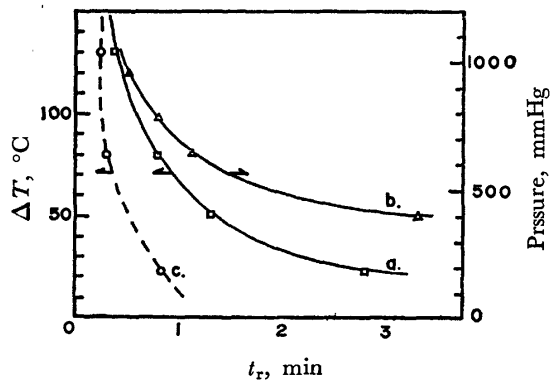

Fig. 6. Change in relaxation time, t_r, against ΔT (curve a) and pressure (curve b). Curve c represents the effect of ΔT observed with open column.

column is always better than that of the ordinary one.

Rate of Attainmnet of Equilibrium Separation. Although it is now undoubted that the magnitude of equilibrium separation is definitely improved, there is another important factor in the practice, *i.e.*, the rate of attainment of the equilibrium separation. This point is answered graphically in Fig. 5, where the scale of the ordinate is expressed by the separation factor q (not to be confused with q_e). It is clearly seen that the separation progresses with higher rate in the novel column than in the ordinary one. Although only two representative curves are shown in this figure, the situation was the same through all measurements in the present study.

The characteristics of the relaxation time was fully studied with the novel column. The effect of temperature difference was studied under a constant pressure of 790 mmHg, while the pressure effect was studied by keeping temperature difference 78 °C. These are shown in Fig. 6 with curves a and b respectively. The behavior of the curves are quite ordinary and the relaxation time decreases with the increase of both temperature difference and pressure.

Discussion

According to the original theory of Jones and Furry, the equilibrium separation does depend neither mean temperature nor the temperature difference, if the coefficient K_d is sufficiently less than K_c (see Eqs. (3), (4) and (23) in the foregoing paper). This was the case for the apparatus presently used (calculated K_c is 3×10^3 times greater than K_d). Accordingly, the experimental variation of the equilibrium separation with the change in applied temperature difference, as is exemplified by Fig. 3, is beyond the theory at present.

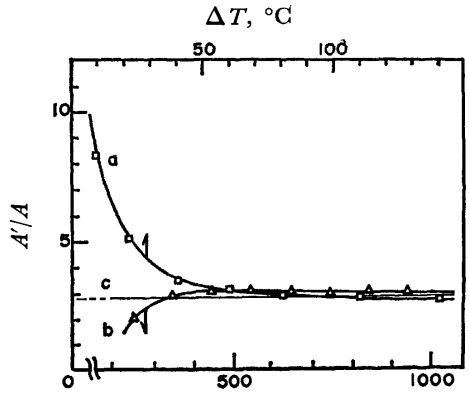

Fig. 7. Quality factor, A'/A, against ΔT (curve a) and pressure (curve b). Curve c represents theoretical value.

On the other hand, results shown in Fig. 4 indicate, regardless of the type of column, that the agreement between theory and experiment is quite good when the pressure effect is concerned.

The equilibrium separation factor is correlated with the theoretical transport coefficients by the equation

$$q_e = \exp(2AL), \text{ where } 2AL = HL/(K_c+K_d).$$

Accordingly, in order to see the relative performance of the two types of column, it will be worth to define the "quality factor" f as follows

$$f = \ln q_e'/\ln q_e = A'/A \qquad (2)$$

in which primed symbols stand for the novel column. On the base of experimental results shown in Figs. 3 and 4 the quality factor was calculated as a function of both the temperature difference and pressure respectively. This is shown in Fig. 7. It is interesting to see that the quality factor at a difference of 10 °C of temperature is 8.3 and reduces rapidly first and gradually later with increasing temperature difference. At the maximum temperature difference applied (140 °C), the quality factor takes a value of 2.6. This indicates that the performance of the novel column is equivalent to that of an ordinary column having 2.6 times longer length. A graphical estimation indicated that the quality factor will be still more than 2.3 at the temperature difference of 500 °C, which is thought as a practical condition in the gas phase operation.

Curve b in Fig. 7 is drawn for a series of experiments show in Fig. 4. In this case also, the quality factor becomes almost constant at higher pressure region but reduces strongly at lower pressure. The straight line c is the theoretical value[8] which is an only function of the design parameter a. It is obvious that at pressure more than 400 mmHg and the temperature difference exceeding 60 °C, the agreement between theory and

experiment is excellent.

According to Jones and Furry,[2] in cases where the equilibrium separation is sufficiently small so that $c(1-c)$ does not change appreciably along the column, the progress of the thermal separation is characterized by

$$\Delta = \Delta_e(1-e^{-t/t_r}) \quad (3)$$

where Δ is the concentration difference at top and bottom of column and suffix e means the value at equilibrium. The relaxation time, tr, is[9]

$$tr = 2mAL/H = mL/(K_c+K_d).$$

In the latter equation, m represents mass of gas in the positive reservoir. Since K_c is sufficiently greater than K_d the ratio of the relaxation times for the two types of column having the same dimension should be the ratio of K_c's.

$$t_r'/t_r = K_c/K_c'$$

According to this equation, the relaxation time of the novel column should be much longer than the ordinary column of the same dimension. Numerical evaluation indicated that the ratio of relaxation time becomes to 11.4 at maximum corresponding to $a=5/8$.

If this prediction was acceptable the benefit of using screens would be worthless because of a long time consumption. This was not the case, however. That the initial rise of curves in Fig. 5 is undoubtedly steeper in the novel column is an indisputable proof. Furthermore, as is seen in curve a in Fig. 6, the relaxation time of the novel column is certainly greater at smaller temperature difference but becomes almost indistinguishable at higher temperature difference. A similar behavior of t_r' is seen in curve b which represents the dependence on pressure. It is readily seen that the temperature difference was even smaller (ΔT was 78 °C in the measurement of curve b), the increase in pressure decreases the relaxation time. Treacy and Rich[5] also stated that the installation of barriers resulted in the increased rate of separation.

The authors are indeed grateful to Professors T. Chiba and M. Ohmori of Mechanical Engineering Department for their collaboration in constructing the separation columns. The authors are also indebted to Dr. Yoshimura of Chemical Engineering Department for his courtesy in giving every facility throughout this work.

Table of Notation

$A=H/2(K_c+K_d)$, [cm^{-1}].
D=self-diffusion coefficient, [cm^2/s].
H=transport coefficient, [g/s].
L=length of column, [cm].
K_c and K_d=transport coefficient, [g·cm/s].
P=dimensionless relative pressure.
g=acceleration of gravity, [cm/s^2].
m=mass of gas in positive reservoir, [g].
q=separation factor at transient state.
q_e=separation factor at steady state.
t_r=relaxation time, [s].
w=half-width of the annular space, [cm].
α=thermal diffusion constant.
ρ=density, [g/cm^3].
η=viscosity, [P].

References

1) K. Sasaki, T. Yoshitomi, and N. Miura, This Bulletin, **49**, 363 (1976).
2) R. C. Jones and W. H. Furry, *Rev. Mod. Phys.*, **18**, 151 (1946).
3) J. W. Corbett and W. W. Watson, *Phys. Rev.*, **101**, 519 (1956).
4) K. Hirota, "Molecular Structure and Related Problems", Monog. Ser. Res. Inst. Appl. Electricity, Hokkaido Univ., No. 4 (1954).
5) J. C. Treacy and R. E. Rich, *Ind. Eng. Chem.*, **47**, 1544 (1955).
6) Theoretical values were calculated by means of the following relationships

$$A = \frac{H}{2(K_c+K_d)} \fallingdotseq \frac{12\alpha\eta D}{\rho g w^4}$$

and

$$A' = \frac{H'}{2(K_c'+K_d')} \fallingdotseq 2.82\,A$$

for the ordinary and novel columns, respectively. In the evaluation of these equations, we adapted 0.102[4] as the α value which seems largest among we found.
7) When K_d is extremely less than K_c, theoretical value of equilibrium separation becomes independent of temperature difference as far as temperature dependence of characteristic constants, η, D, and ρ, are ignored. (see Eqs. (3), (4) and (23) in the preceeding paper).
8) See Eq. (24) in the foregoing paper.
9) This expression is applicable when the column has finite size of reservoirs at both ends (see Eq. (194) in Ref. 2) and thus inappropriate for the present case. It seems, however, the tentative use of this equation dosen't result in a serious error. For instance, if Eq. (163) in Ref. 2 was used in place of this equation, the result was unchanged.

Effects of Quinones on the Protonation Reaction of TCNQ Anion Radical; The Role of a Protonated Quinone as a Strong Electron Acceptor

Akihiko YAMAGISHI and Mutsuo YAMADA

Department of Chemistry, Faculty of Science, Hokkaido University, Sapporo 060

(Received March, 13, 1975)

Various kinds of substituted *p*-benzoquinones (Q) have been found to accelerate the rate of the reaction between 7,7,8,8-tetracyanoquinodimethane(TCNQ) anion radical and hydrogen chloride in acetonitrile. The stoichiometry of the reaction is altered by the presence of Q from $2TCNQ^- + 2H^+ = TCNQ + H_2TCNQ$ to $2TCNQ^- + 2H^+ + Q = 2TCNQ + QH_2$. In case of *p*-benzoquinone, the rate of the disappearance of $TCNQ^-$ is expressed by $v = k[TCNQ^-][Q][H^+]$, where $k = 3.0 \times 10^8$ M^{-2} s^{-1} at 8 °C. From these results, it is concluded that a protonated quinone QH^+ is an active species which accepts an electron from $TCNQ^-$.

In the previous paper, the protonation reaction of 7,7,8,8-tetracyanoquinodimethane (TCNQ) anion radical by hydrogen chloride was investigated in various organic solvents.[1] Comparing the protonation rate of $TCNQ^-$ with that of semiquinone ion (Q^-), it was revealed that $TCNQ^-$ reacts with a proton with the rate more than one order slower than Q^- does.

From these results it is expected that the reaction of $TCNQ^-$ with HCl is accelerated by Q, when Q rapidly accepts an electron from $TCNQ^-$ and is protonated to hydroquinone.

$$TCNQ^- + Q \rightleftharpoons TCNQ + Q^- \quad (1)$$

$$2Q^- + 2H^+ \rightarrow QH_2 + Q \quad (2)$$

Reaction paths (1) and (2) may proceed faster than the direct protonation of $TCNQ^-$, as far as a sufficient amount of Q^- is produced rapidly by reaction (1).[2]

Based on the above expectation, the effects of quinone on the protonation reaction of $TCNQ^-$ have been investigated using acetonitrile as a solvent. The present result may provide a new aspect as to the function of quinones in oxidation-reduction reactions especially in the acidic aprotic medium.

Experimental

p-Chloranil, *p*-benzoquinone, 1,4-naphthoquinone and di-*t*-butyl-*p*-benzoquinone were sublimed once. Chloro-*p*-benzoquinone was synthesized according to Levy and Schultz.[3] The product was identified with IR spectra.[4] Other reagents were prepared as described previously.[1]

The visible spectra were measured with a Hitachi EPS-3T spectrophotometer. The rate was measured in acetonitrile with a Union Giken RA-1300 rapid scan stopped-flow spectrophotometer. The rate was obtained by mixing the solution containing Na^+TCNQ^- and quinone with HCl. All measurements were performed at 8 °C. A Union Giken temperature-jump apparatus was used to try to detect a protonated quinone.

Results

As a preliminary experiment, the rate of the disappearance of $TCNQ^-$ is measured by mixing the solution of HCl with the solution containing both Na^+TCNQ^- and a quinone. The kinetic results are summarized in Table 1. All quinones except di-*t*-butyl-*p*-benzoquinone are found to accelerate the rate of the reaction. The accelerating capacity of quinone is expressed by the quantity, $\ln 2/\{t_{1/2}[Q][HCl]\}$, where [Q] is the concentration of quinone, [HCl] the initial concentration of HCl and $t_{1/2}$ the half-life of the reaction, although the decay of $TCNQ^-$ with time is either exponential or non-exponential, depending on the kind of quinone.

The detailed study of the kinetics of the reaction has

TABLE 1. THE EFFECT OF SUBSTITUTED *p*-BENZOQUINONES ON THE REACTION RATE OF Na^+TCNQ^- WITH HCl

[Q]/M	[HCl]/M	k_{obsd}/s^{-1}	$k_{obsd}/[HCl][Q]/M^{-2}\,s^{-1}$	$k_1/M^{-1}\,s^{-1}$ a)
No quinone b)	1.0×10^{-4}	7.5		
p-Chloranil	1.0×10^{-4}	1.0×10^{2}	6.9×10^{9}	6.0×10^{7}
(1.45×10^{-4}) c)	1.9×10^{-4}	1.6×10^{2}	5.8×10^{9}	
	2.9×10^{-4}	2.9×10^{2}	6.9×10^{9}	
	4.8×10^{-4}	3.8×10^{2}	5.4×10^{9}	
Chloro-*p*-benzoquinone	2.0×10^{-4}	5.8×10^{2}	1.5×10^{8}	35
(3.5×10^{-3}) c)				
p-Benzoquinone	1.0×10^{-4}	3.0×10^{2}	3.2×10^{8}	3.2×10^{-2}
(9.12×10^{-3}) c)				
1,4-Naphthoquinone	3.0×10^{-5}	3.4	2.0×10^{6}	8.5×10^{-6}
(5.6×10^{-2}) b)	1.2×10^{-4}	12	1.8×10^{6}	
	4.0×10^{-4}	69	3.0×10^{6}	
Di-*t*-butyl-*p*-benzoquinone	3.0×10^{-4}	1.2		3.7×10^{-6}
(1.6×10^{-2}) b)	1.2×10^{-4}	4.4		
	4.0×10^{-4}	5.8		

a) The forward rate constant of the reaction (1) according to the Eq. (7). ΔF^0 is calculated from the half-wave reduction potential reported by Peover.[7] b) The decay of $TCNQ^-$ is non-exponential with time. c) The decay of $TCNQ^-$ is almost exponential with time.

TABLE 2. THE STOICHIOMETRY OF THE REACTION OF Na^+TCNQ^- WITH HCl IN PRESENCE OF *p*-BENZOQUINONE

$[Na^+TCNQ^-]_0$/M	[HCl]/M	[Q]/M	[TCNQ]/M
6.58×10^{-6}	1.0×10^{-5}	0	3.43×10^{-6}
6.58×10^{-6}	1.0×10^{-5}	3.36×10^{-2}	6.48×10^{-6}
6.58×10^{-6}	5.0×10^{-5}	3.36×10^{-2}	6.48×10^{-6}

been performed in the case of *p*-benzoquinone. In Table 2, the stoichiometry of the reaction is presented. In the absence of quinone, the overall stoichiometry is expressed by

$$2TCNQ^- + 2H^+ = TCNQ + H_2TCNQ, \quad (3)$$

where H_2TCNQ denotes *p*-phenylenedimalononitrile.[1] On the other hand, when *p*-benzoquinone is present, almost 100% of Na^+TCNQ^- is converted to TCNQ. The same result is obtained for *p*-chloranil where the decrease of *p*-chloranil is found to be equal to 44% of the initial amount of Na^+TCNQ^-. Therefore, the stoichiometry of the reaction in the presence of quinone is expressed as below.

$$2TCNQ^- + Q + 2H^+ = 2TCNQ + H_2Q \quad (4)$$

This stoichiometry suggests that $TCNQ^-$ is oxidized to TCNQ by Q instead of being protonated and that it is Q^- that is protonated.

The decay of $TCNQ^-$ with time is shown in Fig. 1. In the absence of Q, $TCNQ^-$ decreases according to the following equation as established previously.[1]

$$-d[TCNQ^-]/dt = k[TCNQ^-]^2[H^+], \quad (5)$$

in which the initial concentration of $TCNQ^-$ is less than 10^{-5} M. On the other hand, $TCNQ^-$ decreases exponentially in the presence of a large excess of Q. The pseudo first-order rate constant k_{obsd} is linearly dependent on both the concentrations of *p*-benzoquinone and of HCl (Figs. 2 and 3). k_{obsd} is independent of both the concentrations of Na^+TCNQ^- and TCNQ (Figs. 4 and 5). Thus the decay rate is expressed as

$$-d[TCNQ^-]/dt = k_{ap}[TCNQ^-][Q][H^+], \quad (6)$$

and

$$k_{ap} = 3.0\times10^8\ M^{-2}\ s^{-1} \text{ at } 8\ ^\circ C,$$

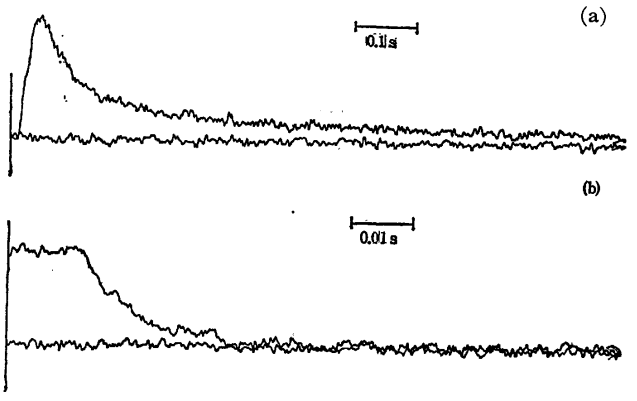

Fig. 1. (a) The decay of $TCNQ^-$ for the reaction of Na^+TCNQ^- with HCl; $[Na^+TCNQ^-]_0$ 3.0×10^{-6} M and $[HCl]_0$ 4.9×10^{-5} M. At 840 nm. (b) The decay of $TCNQ^-$ in the presence of 9.1×10^{-3} M *p*-benzoquinone; other experimental conditions are the same as in Fig. 1. (a).

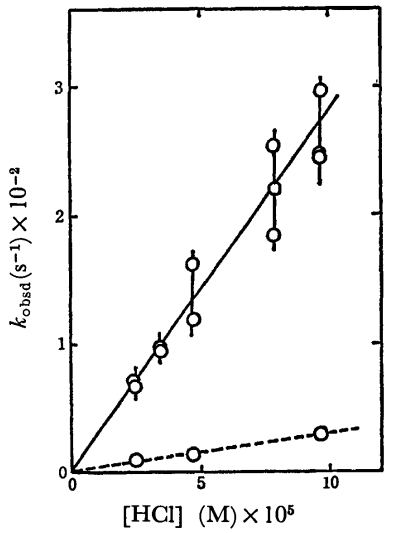

Fig. 2. The dependence of the pseudo first-order rate constant k_{obsd} on [HCl] in the absence (--○--) and in the presence of *p*-benzoquinone (—○—). $[Na^+TCNQ^-]_0$ 3.0×10^{-6} M and [*p*-benzoquinone] 9.1×10^{-3} M for the solid line.

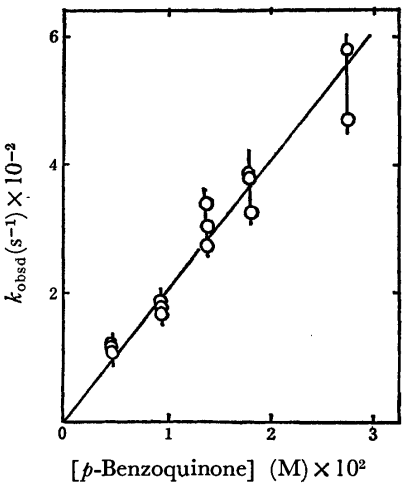

Fig. 3. The dependence of k_{obsd} on [*p*-benzoquinone]. $[Na^+TCNQ^-]_0$ 3.0×10^{-6} M and $[HCl]_0$ 6.2×10^{-5} M.

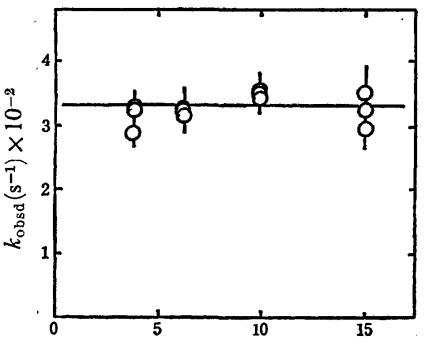

Fig. 4. The dependence of k_{obsd} on $[Na^+TCNQ^-]_0$. $[HCl]_0$ 1.1×10^{-4} M and [*p*-benzoquinone] 9.1×10^{-3} M.

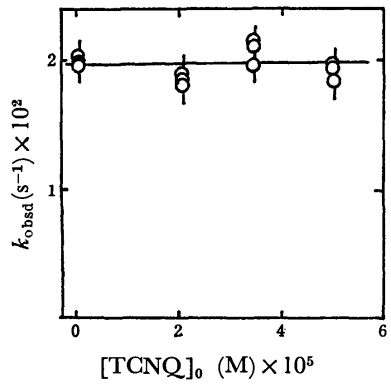

Fig. 5. The dependence of k_{obsd} on [TCNQ]$_0$. [Na^+TCNQ^-] 3.0×10^{-6} M, [HCl]$_0$ 6.2×10^{-3} M and [*p*-benzoquinone] 9.1×10^{-3} M.

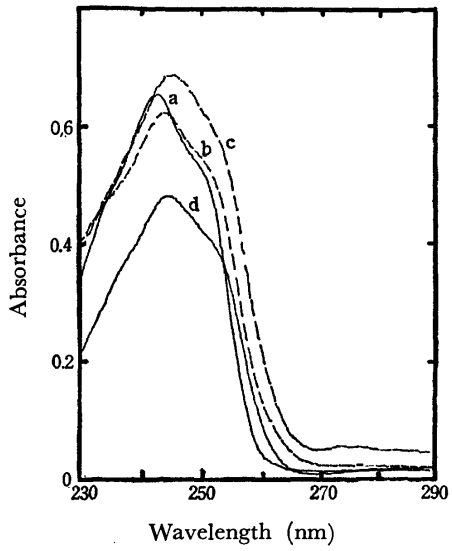

Fig. 6. The electronic spectra of *p*-benzoquinone in the following media; (a) acetonitrile, (b) acetonitrile contaning 20 vol% of concentrated $HClO_4$, (c) acetonitrile containing 40 vol% of concentrated $HClO_4$, and (d) acetonitrile containing 40 vol% of H_2O. [*p*-Benzoquinone] 3.3×10^{-5} M.

where HCl is considered to dissociate completely in acetonitrile.

In order to detect a protonated species of quinone, the ultraviolet spectra of *p*-benzoquinone are measured in the acetonitrile containing concentrated $HClO_4$ (Fig. 6). As $HClO_4$ is added, the peak at 243 nm is displaced by several nanometers to the longer wavelength. No new peak at 358 nm is detected contrary to the observation by Eggins and Chambers.[5] Comparing the present result with the red shift of the absorption peak at 245 nm of acetophenone in concentrated sulfuric acid due to the protonation of a carbonyl group,[6] this observation is considered to support the protonation of *p*-benzoquinone. It should be noted, however, that the observed change of electronic spectra may also include the change of medium properties, since the peak at 243 nm in acetonitrile displaces to 245 nm when acetonitrile contains 40 volume % of water. Although the temperature-jump measurements are performed for the solution containing *p*-benzoquinone and concentrated $HClO_4$, no change of the transmittance is detected at the temperature-jump in the wavelength region of 255—280 nm.

Discussion

The most striking feature of the present result is that quinones of low electron affinity like *p*-benzoquinone have an effect to accelerate the protonation rate of $TCNQ^-$.

At first, the accelerating effect by quinones seems to be ascribed to reaction paths (1) and (2). This may be true at least partially with *p*-chloranil and chloro-*p*-benzoquinone. In case of *p*-benzoquinone and other quinones, however, the participation of reaction (1) is negligible, since the forward rate of this reaction is too slow to give any effect on the reaction mechanism. The forward reaction rate constant k_1 is evaluated according to the following equation.[2]

$$k_1 = Z\exp(-\Delta F^\circ/RT) \text{ for } \Delta F^\circ > 0 \quad (7)$$

where Z is 10^{11} M^{-1} s^{-1} and ΔF° the change of the free energy of reaction (1). Assuming ΔF° to be the difference of the half-wave reduction potential between TCNQ and Q, k_1 thus estimated is given in the last column in Table 1.[7] Evidently k_1 except for *p*-chloranil is too small to explain the observed acceleration effect by quinones. To overcome this difficulty, two possible mechanisms are postulated by noticing the [H^+] dependence of the overall rate (Eq. (6)).

As a first possibility, it is assumed that there exists a pre-equilibrium of the protonation of $TCNQ^-$ (8), which is followed by the oxidation reaction by Q either through electron-transfer or through hydrogen atom transfer, (9) or (9)'.

$$TCNQ^- + H^+ \rightleftharpoons HTCNQ\cdot \quad (8)$$

$$HTCNQ\cdot + Q \rightarrow HTCNQ^+ + Q^- \quad (9)$$

or

$$HTCNQ\cdot + Q \rightarrow TCNQ + QH\cdot \quad (9)'$$

The [H^+] dependence of the rate may arise from reaction (8) which constitutes a pre-equilibrium in the overall reaction mechanisms. As K_8 was determined to be about 1.7 ± 0.6 M^{-1},[1] k_9 or $k_{9'}$ becomes about 2×10^8 M^{-1} s^{-1}. It is very unlikely, however, that reaction (9) or (9)' proceeds with such a large rate constant, considering that the oxidation of HTCNQ· is less favoured than that of $TCNQ^-$ itself from an energetic point of view.[1]

As a second possibility, it is assumed that there exists a pre-equilibrium where Q is protonated to QH^+, followed by the oxidation of $TCNQ^-$ by QH^+.

$$Q + H^+ \rightleftharpoons QH^+;\ K_{10} \quad (10)$$

$$TCNQ^- + QH^+ \rightarrow TCNQ + QH\cdot \quad (11)$$

The [H^+] dependence arises from reaction (10) under the condition that reaction (11) is rate-determining. If this is the case, k_{ap} in Eq. (6) is equated to

$$k_{ap} = K_{10}k_{11}, \quad (12)$$

where K_{10} and k_{11} are the equilibrium constant of reaction (10) and the forward rate constant of reaction

(11), respectively. The fact that the rate is independent of the TCNQ concentration is also consistent with this mechanism. Thus at the present stage of the investigation, it is concluded that protonated quinones QH^+ accelerate the protonation rate of $TCNQ^-$ by accepting an electron from $TCNQ^-$.

The validity of this conclusion is supported by the fact that QH^+ is a stronger electron-acceptor than Q itself. This fact is confirmed by evaluating the electron affinity of QH^+ as follows.

$$QH^+ + e \rightleftharpoons QH\cdot \quad (13)$$

$$Q + e \rightleftharpoons Q^- \quad (14)$$

The free energy change of reaction (13), ΔF_{13}, is related to the free energy change of reaction (14), ΔF_{14}, as below.

$$\Delta F_{13} - \Delta F_{14} = RT \ln K_{10} - RT \ln K_{16} \quad (15)$$

in which K_{10} and K_{16} are the equilibrium constants of the protonations of Q and Q^-, respectively.

$$Q + H^+ \rightleftharpoons QH^+ \quad (10)$$

$$Q^- + H^+ \rightleftharpoons QH\cdot \quad (16)$$

Using the values reported in Refs. 8 and 9, $K_{10} = 10^{-1.0}\,M^{-1}$ in water and $K_{16} = 10^{4.1}\,M^{-1}$ in water containing excess acetone and 2-propanol, $\Delta F_{13} - \Delta F_{14}$ is approximately estimated to be -6.6 kcal at 8 °C. If protonated *p*-benzoquinone QH^+ increases its electron affinity by this amount, QH^+ is as strong an electron acceptor as 2,5- or 2,6-dichloro-*p*-benzoquinone.

In the field of electrochemistry, it has been noted that the electrochemical reduction of quinone in the presence of proton donors displays the additional irreversible reduction wave at the less negative potential.[5,10] This additional wave indicates the existence of the more easily reducible species than neutral quinone. This species was suspected to be a protonated quinone.[5] The present conclusion that protonated quinone becomes a stronger electron-acceptor in homogeneous reaction is completely consistent with these electrochemical results, and confirms the above proposal.

Baxendale *et al.* studied the oxidation of Fe(II) by *p*-benzoquinone in aqueous solution.[11] In their study it is observed that the oxidation rate is independent of proton concentration from 0.35 to 0.15 M. This seems to contradict with the present results. However, since a proton in water is more stably solvated than in acetonitrile, K_{10} in aqueous solution is considered to be too small to produce the sufficient concentration of QH^+. Therefore, the present finding as to the high reactivity of QH^+ is important only in aprotic solvents where unstable proton leads to the large value of K_{10}.

The authors wish thanks to Prof. Masatoshi Fujimoto for his encouragement and also to Prof. Yoshio Matsunaga for his kind advices in synthesizing and identifiying chloro-*p*-benzoquinone.

References

1) A. Yamagishi and M. Sakamoto, This Bulletin, **47**, 2152 (1974).
2) A. Yamagishi, *Chem. Lett.*, **1975**, 899.
3) S. Levy and G. Schultz, *Ann.*, **210**, 133 (1881).
4) The authors owe the identification of chloro-*p*-benzoquinone to Prof. Y. Matsunaga.
5) B. R. Eggins and J. Q. Chambers, *J. Electrochem. Soc.*, **117**, 186 (1970).
6) L. A. Flexser, L. P. Hammett, and A. Dingwall, *J. Amer. Chem Soc.*, **57**, 2103 (1935).
7) M. E. Peover, *J. Chem. Soc.*, **1962**, 4540.
8) G. Biedermann, *Acta Chem. Scand.*, **10**, 1340 (1971).
9) R. L. Willson, *Trans. Faraday Soc.*, **67**, 3020 (1971).
10) L. Teftü and G. Manning, *J. Electroanal. Chem.*, **26**, 195 (1970).
11) J. H. Baxendale, H. R. Hardy, and L. H. Sutchlifee, *Trans. Faraday Soc.*, **47**, 963 (1951).

Gel Filtration of Aqueous Sodium Dodecyl Sulfate

Hitoshi SUZUKI

Department of Chemistry, Faculty of Science, Tokyo Metropolitan University, Setagaya, Tokyo 158

(Received March 31, 1975)

The tail analysis of gel filtration was applied to a sodium dodecyl sulfate (SDS) solution using Sephadex G-50. This method is more simple and useful than the frontal analysis method formerly reported. The relative elution rate of SDS micelle, R_m, increased with an increase in the SDS concentration above CMC, reached a maximum near 16 mmol/l and then decreased up to 100 mmol/l. The application of the Laurent-Killander equation gave a micellar radius of 17.6 Å at CMC and 11.7 Å at the maximum R_m, corresponding to aggregation numbers of 35 and 80, respectively. The apparent decrease of R_m observed above 20 mmol/l was due to an structural change of the Sephadex gel caused by the addition of SDS. The micellar weight was estimated referring to a substance of known molecular weight; it was found to be constant in the region from 15 to 100 mmol/l SDS. The results of gel filtration of the SDS solution using CPG-10 as a gel column were similar to the case of Sephadex G-50; a micellar weight and an aggregation number of 25000 and 88, respectively, in the constant R_m range were obtained.

As for the study of the dissolved state of the solute by gel filtration, zone and band analyses are possible. The former method is used to measure the position of a sharp peak of the elution curve obtained by charging a small amount of the sample, while the latter method is used to determine the positions of the front F and the tails M and S of the elution curve as shown in Fig. 1, obtained by charging a relatively large amount of material in band form. Band analysis enables the detection of species of solutes in rapid equilibrium with each other as has been mentioned previously.[1)]

Using the latter method, the present authors have measured the elution rate (R_m) of micelles, a measure of the micellar size, and the CMC from the elution rate of the front (R_f) for sodium dodecyl sulfate assuming the size of the micelles and the intermicellar concentration to be independent of the total concentration.[1)] Also the R_m have been measured directly using frontal analysis applying the extrapolation method[2)] and the same results as those employing the former method[1,2)] were obtained.

However, the frontal method with extrapolation, requires fairly large amounts of the substance and a troublesome procedure. Compared with this, tail analysis, namely, the analysis of the tail part of elution curve obtained by charging a large amount of the sample, proved to be quite simple and useful. Reliable information concerning the dissolved state of the surfactants, especially the state of the micelles, are directly obtained under some assumptions. The present paper reports the results obtained by applying the tail analysis of gel filtration to aqueous solutions of SDS using Sephadex G-50 and CPG-10 glass gel column.

Experimental

Materials. Sodium dodecyl sulfate was prepared by the same method as reported in a preceding paper.[2)] Sodium chloride of the first reagent grade was used after recrystallization. Distilled water was boiled and degassed before use. Blue Dextran 2000, a product of Pharmacia, Uppsala, was used for the measurement of the void volume of the gel bed used. Poly(vinyl alcohol)s (PVA) and the molecular weight marker kits of non-enzymatic proteins of known molecular weight were used as molecular weight standards. The PVA were kindly supplied by Nippon Gosei Kogyo Co., Ltd. and the proteins were obtained from Mann Research Laboratories Inc., New York.

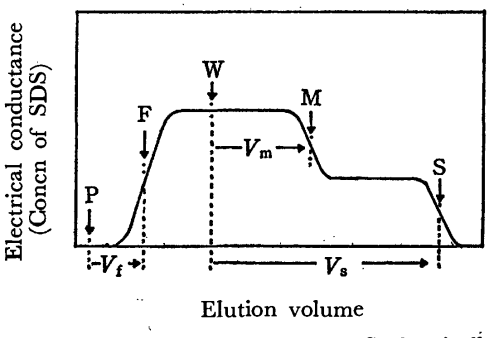

Fig. 1. The elution curve for an SDS micelle (frontal and tail analysis).
P and W: the points of sample and water charge, respectively, F: the front of the solution, M and S: the tails of micelles and single ion, V_f, V_m, and V_s: the elution volumes of front, micelles, and single ions, respectively.

The elution curve obtained is shown in Fig. 1. Elution volumes V_f, V_m, and V_s of the front F, the tails of the micelles M, and single ions S were measured as the volumes between the charge point of the sample P and the point F, between the charge point of water W, and between the points M and S on the elution curve, respectively. Relative elution rates of the front and micelles were respectively calculated from

$$R_f = V_s/V_f,\ R_m = V_s/V_m,\ \text{together with}\ R_s = 1, \quad (1)$$

R_s being the elution rate of the single ions.

Results and Discussion

Gel Filtration Using Sephadex Gel. (A) *SDS Solution*: The elution rate of micelles, R_m, calculated from V_m obtained by tail analysis is plotted against the total concentration of SDS as shown by open circles in Fig. 2. As is seen, R_m increases slightly at first, reaches a maximum near 16 mmol/l, and then decreases with increasing concentration of SDS, in agreement with previous results obtained by frontal analysis.[1,2)] A similar change with a change in the concentration was also observed with the Sephadex G-75 gel column. A linear relation between $(R_m - R_s)R_f/(R_m - R_f)$ and C predicted in a preceding paper[2)] was confirmed to be valid, and the CMC of 8.6 mmol/l

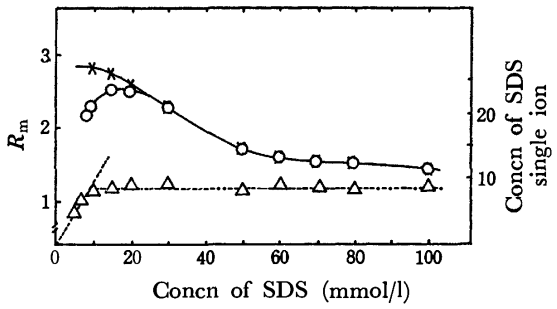

Fig. 2. R_m and the concn of SDS single ion *vs.* SDS concn using tail analysis.
×: Commercial SDS, ○: pure SDS, △: the concn of SDS single ion (CMC).

was obtained from the crossing point of this line with the horizontal straight line passing through unity on the ordinate; this CMC value is in agreement with the previous results.[2] However, the above plot deviates from linearity above 20 mmol/l, probably due to a change in gel matrix as discussed below. The lower plateau of the elution curve of Fig. 1 was also plotted against the concentration shown by the triangles in Fig. 2. As is seen, the value remains constant up to 100 mmol/l. This may indicate that the micelle-monomer equilibrium is relatively simple for SDS up to about 100 mmol/l, excluding the existence of the so-called second CMC.[3] But this does not necessarily mean that the intermicellar SDS concentration is constant. A detailed study will be reported in the near future on this subject.

(B) *Concentration Dependence of* R_m: The increase of R_m with C obtained from the tail analysis for pure SDS (open circles in Fig. 2) reflects the increase of micellar size up to about 16 mmol/l. The following experiment confirms this increase in micellar size.

An SDS solution of concentration C was charged on top of the gel which had been previously equilibrated with the SDS solution of the concentration C' between C and CMC, and was eluted with water. If the elution rate of micelles in the solution of higher concentration C is larger than that in the solution of lower concentration C', the front of the former solution goes ahead of the tail of the latter and a peak of high concentration $C+C'$ is expected to appear at the front. However, the peak was not actually observed and the front of the elution curve exhibited two simple plateaus corresponding to the concentrations C and C'. In addition, the R_f of the apparent front of the solution of concentration C is slightly but distinctly smaller than the R_m of the same solution. Since the elution volumes of NaCl and Blue Dextran confirm the absence of the effect of SDS below 20 mmol/l on the gel structure of Sephadex G-50, the above phenomena may be explained if we assume that the intermicellar concentration of single SDS ions is not equal in the solutions of differing concentrations C and C'. Figure 3 illustrates the phenomena which occurs according to such reasoning, where (a) is the initial and (b) the intermediate states of gel filtration. In this figure, the abscissa denotes the position and direction of the eluting solute, point 0 being the upper end of the gel column, and

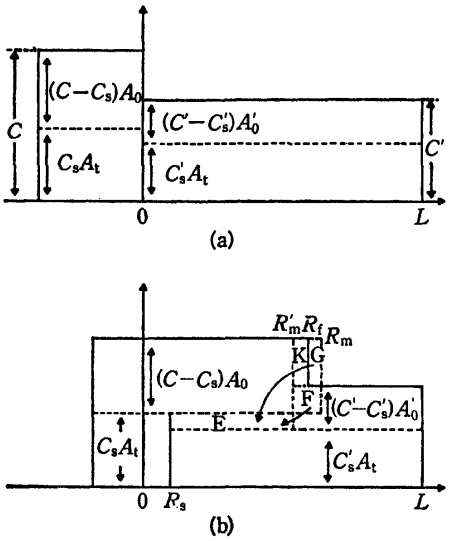

Fig. 3. The schematic representation of gel filtration of an SDS micellar solution near to the CMC.
(a) Initial and (b) intermediate state of gel filtration.

the ordinate shows the quantities of SDS single ions, (C_sA_t), and micelles, $(C-C_s)A_0$, per unit column length for both the solution of concentration C and that of concentration C'. Furthermore, $A_0(A_0')$ and A_t denoted the cross-sectional areas of the gel column through which the micelles and single ions, respectively, can pass. R_s, R_m, R_m', and R_f represent the elution rates of SDS single ions, of micelles in solution of concentrations C and C' and of the front of the solution of concentration C, respectively. In the course of gel filtration, the front of fast flowing micelles of concentration C advances ahead of the tail of the slowly flowing micelles in the solution of concentration C' by an amount $K+G+F$, as is shown in Fig. 3. Material balance gives the amount of SDS of

$$F = [(C'-C_s')A_0' + C_s'A_t - C_sA_t]\ (R_m - R_m') \quad (2)$$

and the amount of SDS of

$$G = [(C-C_s)A_0 + C_sA_t - (C'-C_s)A_0' - C_s'A_t](R_m - R_f) \quad (3)$$

that should fill the concentration gap of the portion

$$E = (C_sA_t - C_s'A_t)(R_m' - 1) \quad (4)$$

as indicated by the curved arrows in Fig. 3. Here, C_s and C_s' denote the intermicellar concentration of the solutions of concentrations C and C', respectively. Then, from Eqs. (1)—(4), the following equation results for CMC$<C'<C$

$$(C-C_s)(1-R_f/R_m) - (C'-C_s')(1-R_f'/R_m') = (C_s-C_s')(R_f-1) \quad (5)$$

From a similar consideration, the following equation is obtained instead of Eq. (5), in the case of

$C' <$ CMC $< C$

$$(1-R_f/R_m)(C-C_s) = (C_s-C')(R_f-1) \quad (6)$$

Gel filtration conducted for the system of $C=10$ mmol/l and $C'=8.5$ mmol/l solutions gave $R_f=2.24$. This value together with $R_m=2.37$ for $C=10$ mmol/l (Fig. 2) when substituted into Eq. (6) gives $C_s=8.55$ mmol/l

for $C=10$ mmol/l. Successive experiments for the system of $C'=10$ mmol/l and $C=14$ mmol/l solutions gave $R_f=2.44$. From this value together with $R_m=2.52$, $R_m'=2.37$, and $C_s'=8.55$ mmol/l, $C_s=8.73$ mmol/l for $C=14$ mmol/l was obtained using Eq. (5).

The data suggest a small but not negligible increase of the intermicellar concentration above CMC in accord with the results obtained by the electromotive force measurement.[4] A detailed gel filtration study of this problem will appear in the near future. A short extrapolation of the C_s *vs.* C relation at a point at which $C_s=C$ gives CMC=8.50 mmol/l, a value close to the value of 8.6 mmol/l obtained in a preceding paper[1,2] under the assumption of a constant intermicellar concentration.

As regards the decrease of R_m for SDS solutions of concentrations greater than 30 mmol/l, the change in gel structure as mentioned in below can be taken into account. However, a similar experiment as that shown in Fig. 3 also offers some information concerning the behavior of micelles flowing through a gel of high SDS concentration, where aqueous SDS solutions of $C=60$, 70, and 80 mmol/l were eluted through a gel column filled with a $C'=50$ mmol/l SDS solution. Figure 4(a) represents the initial and Fig. 4(b) the intermediate states during gel filtration. The notations used are the same as in Fig. 3. In this case, contrary to the dilute system described above, the apparent R_m for the solution of concentration C is considered to be smaller than that for the solution of concentration C'. Therefore, as the filtration proceeds, a gap or a space containing no micelles may form between the tail of foregoing micelles and the front of the micelles which follow, and an elution curve resembling the dotted line in Fig. 4 is expected. However, in this case as in the former case, two simple plateaus corresponding to the concentrations C and C' appeared without any gap. As in Fig. 3, the elution rate R_f

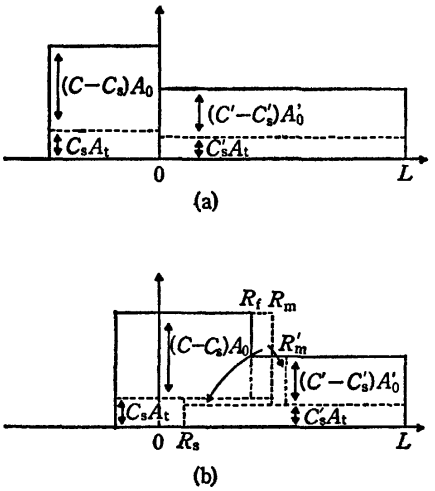

Fig. 4. The schematic representation of the front and the tail during gel filtration in higher concn of SDS. R_m': the tail of micelle in 50 mmol/l solution, R_m and R_f: the imaginary and actual fronts of micelles in C mmol/l solution, R_s: the tail of single ion in 50 mmol/l solutoin. The arrows indicates the eventual shift of solute.

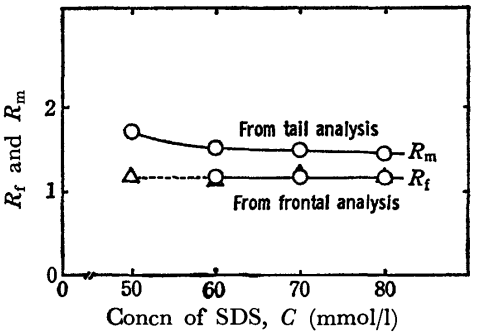

Fig. 5. The relationship between the elution rate for frontal analysis and that from tail analysis.
○: Observed, △: calculated.

observed in Fig. 4 is smaller than R_m, but the difference is fairly large compared with the case of Fig. 3, shown by circles in Fig. 5, and the value of R_f extrapolated to $C=50$ mmol/l does not agree with R_m at the same concentration, as was the case in the lower concentration region.[2]

These phenomena are explained by the higher concentration of micelles filling the above mentioned gap as is shown by the curved arrows in Fig. 4. Eq. (5) applies also in this case although the situation is somewhat different from the case shown in Fig. 3. The rate of the elution front, R_f, is calculated by putting the R_m obtained from the tail analysis into Eq. (5). The results are shown in Fig. 5 as triangles, which are seen to be in good agreement with observed values. By the trial-and-error-method best-fit values are obtained by setting $S_s=C_s'=8.7$ mmol/l. The results indicate the probable mechanism of filling at the elution front mentioned above and may suggest that the intermicellar concentration C_s is approximately constant over the region of SDS concentration from CMC to 80 mmol/l, further study being under way on this point.

(*C*) *Micellar Size*: The size of micelles can be estimated either from the theoretical formula taking account of the gel structure or from the elution volume using the appropriate substances as molecular weight standards. The former method utilizes the Laurent-Killander equation[5]

$$(V_e-V_o)/(V_t-V_o) = \exp[-\pi L(r_r-r_s)^2] \quad (7)$$

where V_t is the total volume of the gel bed, V_0 the void volume, V_e the elution volume of the substance, L and r_r are the concentration and radius of rods considered as an approximation of the structure of gel matrix (the values being 8.2×10^{12} cm/cm^3 and 7×10^{-8} cm, respectively, for Sephadex G-50) and r_s is the

Table 1. Micellar size of SDS

Concn of SDS	V_m	Radius(Å)	n
8.5 mmol/l	14.35 ml	17.6	35
10.0 mmol/l	13.20 ml	19.9	54
15.0 mmol/l	12.20 ml	22.7	80
20.0 mmol/l	12.47 ml	21.0	63

$n=89$ (K. J. Mysels)[9,10]
$n=40-70$ (H. V. Tartar)[8]

radius of the eluted particles. The hydrodynamic radii of the micelles calculated by setting $V_e = V_m$ in Eq. (7) are shown for SDS in Table 1.

The aggregation number of the micelles is calculated by dividing the micelle volume (calculated as a sphere of radius r_s) by 368.6 ml/mol, the molar volume of hydrated SDS molecules considered to be the constituent of hydrated micelles. Here, the amount of hydration was estimated from the conductivity measurement proposed by Nakagaki,[6] the value being in good agreement with that obtained from the intrinsic viscosity measurement.[7]

Calculation were not made for solutions with concentrations higher than 20 mmol/l because of the uncertainty of the V_m value due to the change in Sephadex gel structure. The aggregation numbers given by Tartar[8] and Mysels[9,10] are also listed in Table 1 for comparison. Table 1 suggests the possibility that the wide range of aggregation numbers reported is not due exclusively to experimental error but in part due to an actual increase in size with concentration. It may also be inferred that such a change in micellar size with concentration taking place in the solution near CMC may not be detectable by methods other than gel filtration.

It is noted that the micellar weight shown in Table 1 is in agreement with the value obtained by CPG gel filtration at 15 mmol/l SDS concentration, which is described below.

To confirm the probable change in the gel matrix of Sephadex beyond 20 mmol/l, and to determine the micellar weight of SDS more accurately, molecular weight standards were used. For each concentration of SDS with which the gel column is equilibrated, gel filtration was carried out with such standards of known molecular weight as sodium chloride, Blue Dextran, myoglobin, cytochrome C, and chymotrypsinogen. An calibration curve of the elution volume *vs.* molecular weight was obtained as shown in Fig. 6.

The actual molecular weight of the protein–SDS complex used for this plot was estimated by tail analysis of the elution curve, obtained by gel filtration of the protein–SDS solution in a manner similar to the measure-

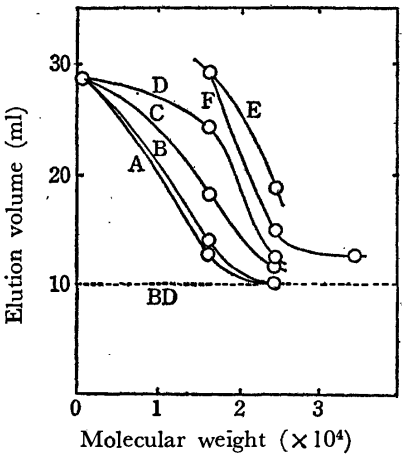

Fig. 6. The calibration curve for SDS solution.
(A): 8.5 mmol/l, (B): 15 mmol/l, (C): 30 mmol/l, (D): 50 mmol/l, (E): 70 mmol/l, (F): 100 mmol/l, BD: Blue Dextran.

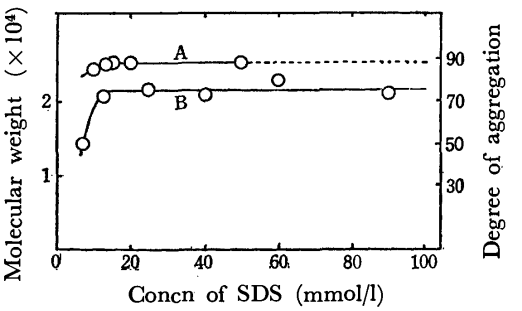

Fig. 7. The dependence of the micellar weight on the concentration of SDS measured using CPG-10 gel.
(A): CPG-10 gel, (B): Sephadex gel.

ment of the poly(vinyl acetate)–SDS system.[11] Further details of the measurement will be reported elsewhere. The results show that the protein–SDS complex contains 0.45 g of SDS per g of protein in the concentration range of SDS studied which is compared with the saturated amount of about 1 g per g of protein obtained after prolonged contact of SDS with the protein[12,13] as compared with about 1 hr contact in the present experiment.

As is seen in Fig. 6, a marked change in the gel structure was found to occur beyond 30 mmol/l. The micellar weights were calculated using these calibration curves and were plotted against the concentration, as is shown in Fig. 7. It is evident that the micellar size increases from CMC to about 15 mmol/l of SDS beyond which it remains constant over a wide range of concentrations contrary to the apparent R_m and the micellar weight decreases with increasing concentration in the case of Sephadex gel. The aggregation number of SDS micelles corresponding to this plateau is about 75. In the above calculation, hydration of the protein is assumed to be nearly equal to that of the SDS which may be permissible when both amounts of hydration[14] are compared.

Gel Filtration of an Aqueous SDS Solution by CPG-10. *(A) Elution Curve for Aqueous SDS Solution*: As mentioned above, the pore distribution of Sephadex gel is affected by a concentrated SDS solution. To avoid such a disturbance, CPG-10, a porous rigid glass gel was used instead of the Sephadex gel and the elution curve was measured for varying concentrations of SDS. A curve similar to that in Fig. 1 was obtained and the conductivity corresponding to the height of each plateau of the curve was plotted against the total concentration of SDS, as is shown in Fig. 8. Three straight lines met at one point giving CMC=8.6 mmol/l as in the case of Sephadex G-50[2]. From the observed values of V_f and V_m, R_f and R_m were calculated using Eq. (1). R_m, plotted against the SDS concentration, shows a slight increase in micellar size with concentration from CMC up to about 15 mmol/l beyond which it remains constant at least up to 50 mmol/l, as is shown in Fig. 9. This confirms the previous results obtained using Sephadex G-50 shown in Fig. 7.

Furthermore, the $(R_m - R_s)R_f/(R_m - T_f)R_s$ *vs.* C plot was made below and above CMC, and two straight lines, one passing through the origin and the other parallel to the c-axis, were obtained as shown in Fig.

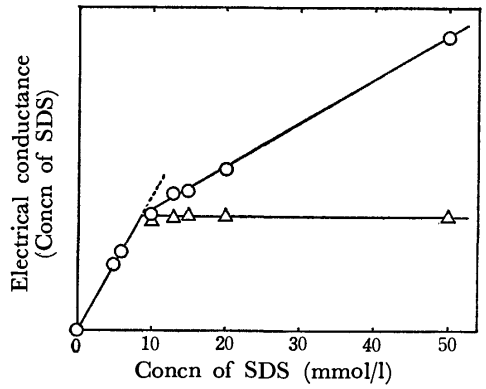

Fig. 8. The conductance of an SDS solution obtained by gel filtration using CPG-10.
○: conductance of the solution, △: conductance of the tail part of the solution (CMC).

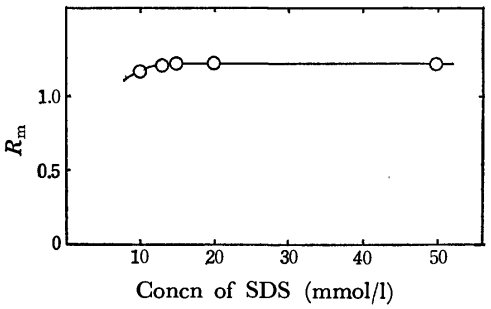

Fig. 9. The dependence of R_m on the concentration of SDS measured using CPG-10 gel.

10. The crossing point of these straight lines gives CMC=8.6 mmol/l in agreement with the value obtained previously. The fact that a straight line passes through the origin indicates the decomposition of micelle being instantaneous as was pointed out in a previous paper[2] using Sephadex G-50. It is emphasized in addition that the linearity shown in Fig. 10 extending up to and the probably beyond 50 mmol/l of SDS, as compared with the deviation from linearity over 20 mmol/l in the case of the Sephadex gel, clearly confirms the inert nature of CPG towards SDS.

(*B*) *Measurement of Micellar Weight*: To obtain the micellar weight of SDS, a calibration curve of the elution volume *vs.* molecular weight of the unhydrated SDS micelles, shown as SDS in Fig. 11, was constructed from the relation of the elution volume *vs.* molecular weight of the hydrated poly(vinyl alcohol) obtained by the conductance method,[6] shown as PVA in Fig. 11. To obtain the calibration curve, the amount of hydration of SDS (0.6 g of H_2O/g of SDS) was taken into account. To avoid disturbances due to the adsorption of poly(vinyl alcohol), the gel was treated with a dilute solution of albumin, then with a sufficient amount of concentrated SDS solution and washed with water. From this curve and the observed V_m, the micellar weight was calculated and plotted against the concentration as shown in Fig. 7. Again, a slight increase in the micellar weight is seen up to about 20 mmol/l, above which a constant micellar weight of approximately 25000 was obtained up to about 50 mmol/l. An aggregation number of about 88 was obtained for the maximum

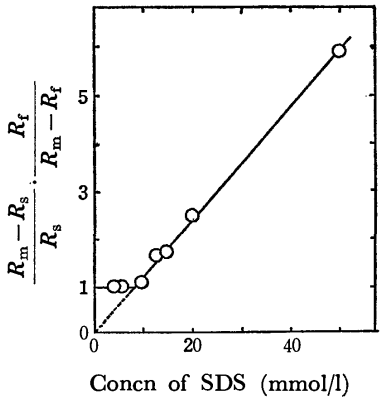

Fig. 10. The relationship between R_f and the concentration of SDS using CPG-10 gel.

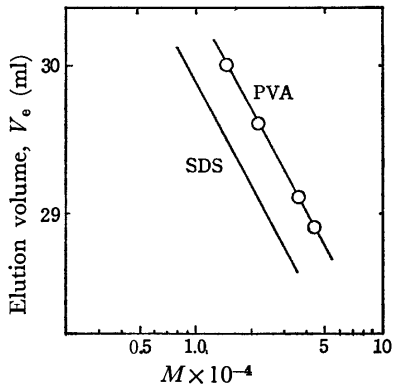

Fig. 11. The CPG-10 system calibration curve, showing the molecular weights of poly(v nyl alcohol)s relative to V_e plotted as a linear log function.

micellar weight. The value is larger than the value obtained using Sephadex G-50 with standards of known molecular weight but is near the maximum aggregation number shown in Table 1 calculated using the Laurent-Killander equation. The results obtained by the CPG gel method are considered to be more reliable considering the stability of the gel matrix.

In conclusion, it is emphasized that the frontal and tail analysis of gel filtration is useful for the study of the state and behavior of micelles in surfactant solutions. It is particularly suited for the study of micellar solutions near CMC, where other methods such as X-ray analysis, osmometry, and the light scattering method are not so effective.

The author wishes to express his deep gratitude to Professor Tsunetaka Sasaki for his kind direction and valuable criticism throughout the work.

References

1) T. Sasaki and Y. Ogihara, Proceedings of 5th International Congress on Surface Activity, Barcelona (1968).
2) H. Suzuki and T. Sasaki, This Bulletin, **44**, 2630 (1971).
3) M. Kodama and M. Miura, *ibid.*, **45**, 2259 (1972).
4) T. Sasaki, M. Hattori, J. Sasaki, and K. Nukina, *ibid.*, **48**, 1397 (1950).
5) T. C. Laurent and J. Killander, *J. Chromatog.*, **14**,

317 (1964).
6) M. Nakagaki and S. Shimabayashi, *Nippon Kagaku Kaishi*, **1973**, 207.
7) P. Mukerjee, *J. Colloid Sci.*, **19**, 722 (1964).
8) H. V. Tartar, *ibid.*, **14**, 115 (1959).
9) D. Stigter, R. J. Williams, and K. J. Mysels, *J. Phys. Chem.*, **59**, 330 (1955).
10) K. Shinoda, T. Nakagawa, B. Tamamushi, and T. Isemura, "Colloidal Surfactants," Academic Press, New York (1963).
11) T. Sasaki, K. Tanaka, and H. Suzuki, Proceedings of 6th International Congress on Surface Activity, Zürich (1972).
12) R. Pitt-Rivers and F. S. A. Impiombato, *Biochem. J.*, **109**, 829 (1968).
13) W. W. Fish, J. A. Reynolds, and C. Tanford, *J. Biol. Chem.*, **245**, 5166 (1970).
14) J. A. Reynolds and C. Tanford, *ibid.*, **245**, 5161 (1970).

Studies of the Effect of 1-Dodecanol on the Micellization of Sodium Dodecyl Sulfate by Gel Filtration

Hitoshi SUZUKI

Department of Chemistry, Faculty of Science, Tokyo Metropolitan University, Setagaya, Tokyo 158

(Received April 5, 1975)

The tail analysis of gel filtration was applied to an aqueous sodium dodecyl sulfate (SDS) solution containing solubilized 1-dodecanol. Commercial SDS containing 1-dodecanol as an impurity showed a maximum micellar size at CMC. The addition of 1-dodecanol caused an increase in the micellar size due to solubilization. The amount of 1-dodecanol impurity was estimated from the elution rate of the micelle, R_m, the result being in agreement with that obtained by surface tension measurements.

Concerning the property of aqueous solutions of surfactants employed for solubilizing long-chain alcohols which are sparingly soluble in water, studies have been mainly directed towards the effect of solubilization on the critical micelle concentration (CMC) and the determination of the amount solubilized. Studies on the estimation of the effect of the solubilizate on micellar size are rather few.[1]

The addition of solubilizates is known to lower the CMC and to increase the micellar size as measured by the visual dye method,[2] viscosity,[3] light scattering,[1] and others. However, the application of the gel filtration method affords a more simple and direct means of studying the solubilization by micelles especially near CMC. In the present report, the elution behavior of SDS micelles solubilizing 1-dodecanol was studied and the change of the CMC and the micellar size due to solubilization are discussed.

Experimental

Materials. Sodium dodecyl sulfate was prepared by the same method as described in a preceding paper,[4] and a commercial SDS without purification was also used. A solubilized system was prepared by dissolving known amounts of SDS and 1-dodecanol (DOH) or tritium labelled 1-dodecanol (TDOH) in ethanol, evaporating the ethanol and dissolving the residue in water. The labelled 1-dodecanol was kindly supplied by Dr. K. Tajima of our laboratory.

Procedures. The apparatus used for gel filtration was essentially the same as that reported in Ref. 4. The gel filtration experiments were made using two columns of 1.1×30.5 cm and 1.2×10 cm gel beds packed with Sephadex G-50 fine (Pharmacia, Uppsala, Sweden). To the gel column previously equilibrated with water, a known amount of the sample solution was added and was eluted with water. The elution curve was obtained by automatically recording the electrical conductance or the refractive index of solution eluted. All of the gel filtration experiments were carried out in an air thermostat at 30 °C. For the purpose of radioactivity measurement, eluates were taken in 1 ml fractions, and 30 μl of the eluate from each fraction was completely evaporated in a planchet at room temperature. The radioactivity of each eluate was determined by a 2π windowless gas flow counter.

As mentioned in a previous paper,[4] from the measurement of the elution volumes, V_f, V_m, V_s, the relative elution rates of the front and micelles were calculated from

$$R_f = V_s/V_f,\ R_m = V_s/V_m,\ R_s = 1$$

respectively, where, the elution rate of single ions was conventionally taken to be unity.

Surface tension measurements of aqueous solutions of SDS were carried out using a du Noüy tensiometer at room temperature (25 °C).

Results and Discussion

In order to study the solubilization by micelles by the tail analysis[5] of gel filtration, SDS solutions with solubilized TDOH were used. Figure 1 shows the elution curves obtained for SDS solutions with and without DOH, where A and B indicate the tails of the DOH and SDS micelles of the solubilized system measured by radioactivity and the electrical conductance, respectively, and C is the tail of SDS micelles measured by the electrical conductance for the system without any solubilizate. The elution curve A indicates the practical insolubility of 1-dodecanol in the intermicellar solution, and the agreement of elution volumes between A and B indicates the perfect incorporation of 1-dodecanol into micelles. Furthermore, a larger elution volume of C compared with A and B indicates the increase in size of the micelles due to solubilization.

Figure 2 shows the fronts of the elution curve of the solubilized system shown in Fig. 1. The shapes of the fronts for A and B are rather different compared with the similarity in the shapes of A and B tails shown in Fig. 1. Front A shows a sharp peak and is situated in advance of the front B which has a usual slope. This is explained as follows. A part of micelles containing the solubilizate decomposes at the front during gel filtration, resulting in the precipitation of solubilized 1-dodecanol, whereby a part of the precipitate is resolubilized and concentrated in the undecomposed

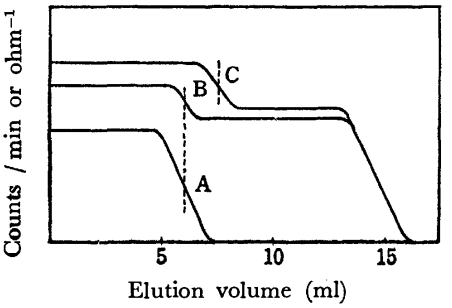

Fig. 1. Elution tail of micellar solution containing solubilized TDOH.
Curve A is from radioactivity measurement, curves B and C are from conductance, respectively (C, 1-dodecanol free).

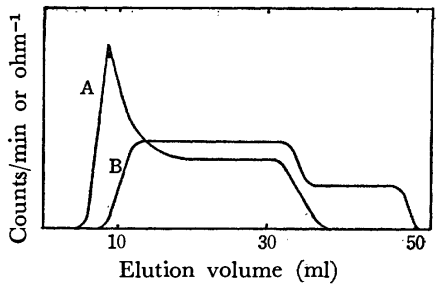

Fig. 2. Front of elution curve for micellar solution of SDS containing solubilized TDOH.
A, radioactivity measurement; B, conductance measurement.

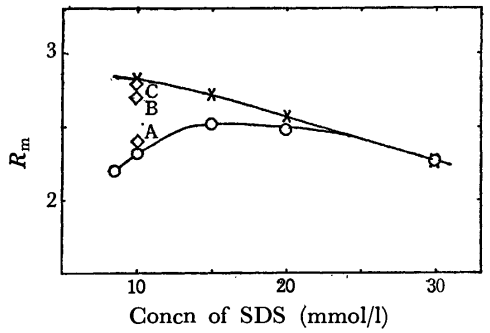

Fig. 3. Dependence of the R_m obtained by tail analysis on concentration of SDS.
○, pure SDS; ×, commercial SDS; ◇, SDS containing (A) 1.1×10^{-2}, (B) 1.5×10^{-2}, (C) 2.2×10^{-2} mol DOH/mol SDS.

micelles, while the rest of the precipitates being larger in size than the micelles advance faster than the micelles. Thus, 1-dodecanol is gradually concentrated in the micelles and forms a sharp peak in front of the micelles. The peak was also confirmed by detecting the front using a differential refractometer which has been described in detail.[6]

For the study of the change of the micellar size due to the solubilization, the R_m obtained with commercial SDS containing 1-dodecanol as impurities was plotted against the concentration shown by crosses in Fig. 3. As is seen, the commercial SDS shows remarkably larger R_m values than does a pure sample (open circles); R_m is largest at CMC and decreases with an increase in SDS concentration. At sufficiently high concentrations, both the pure and commercial products gave the same value of R_m. The marked increase of R_m for commercial SDS can be explained as follows. Although the total amount of 1-dodecanol contained as impurities in aqueous SDS solutions near CMC is not very large, the amount of 1-dodecanol solubilized per micelle may become fairly large since the number of micelles formed just above CMC is very few. This causes the formation of large micelles for impure SDS just above CMC. At higher concentrations, the number of micelles increases more rapidly than the amount of 1-dodecanol increases, and the effect of 1-dodecanol solubilization on micellar size becomes practically insignificant at sufficiently large concentrations of SDS. Thus, the micelle radius of commercial SDS, which contains 1-dodecanol as an impurity, is considerably larger than that of pure SDS near CMC. At higher concentrations of SDS, this difference tends to disappear. The hydrodynamic radii of the micelle calculated by the Laurent-Killander equation are shown for pure and impure (containing 1-dodecanol) SDS in Table 1. The increase in micellar size with the increase in the solubilized amount of DOH at a constant SDS concentration of 10 mmol/l was measured by the increase of R_m shown by squares in Fig. 3.

From a comparison of these R_m values with those

Table 1. Micellar size of SDS

Concn of SDS (mmol/l)	Pure SDS (Å)	Commercial SDS (Å)
8.5	17.6	—
10.0	19.9	27.3
15.0	22.7	25.3
20.0	21.0	23.0
8.12	21.5	(from D. Stigter and K. J. Mysels)[9]

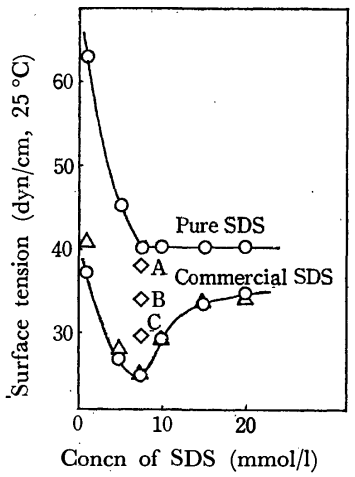

Fig. 4. Dependence of the surface tension on concentration of SDS containing solubilized DOH.
◇ A, ◇ B, ◇ C, △, SDS containing 0.07×10^{-2}, 0.26×10^{-2}, 1.03×10^{-2}, and 2.75×10^{-2} mol DOH per mol SDS, respectively.

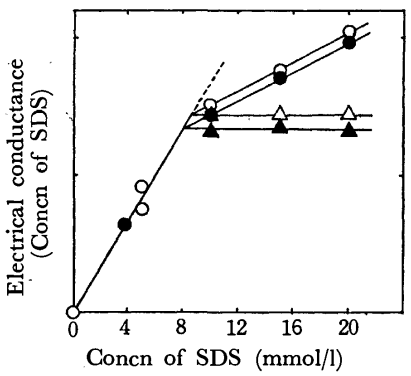

Fig. 5. Conductance of SDS solution obtained by gel filtration.
○, ●, conductance of the solution; △, ▲, conductance at the CMC; ○, △, pure SDS; ●, ▲, commercial SDS.

for commercial SDS used in the present experiment, the impurity (tentatively assumed to be 1-dodecanol) in the commercial SDS is estimated to be about 2.2×10^{-2} mol of DOH per mol of SDS. A similar amount was obtained from the surface tension measurement. Thus, the surface tensions of solutions containing the same amounts of SDS (near CMC) but varying amounts of 1-dodecanol were plotted against the concentrations of 1-dodecanol. Figure 4 shows the results together with the surface tension for commercial SDS. From this figure, about 2.75×10^{-2} mol of DOH/mol of SDS was obtained for the commercial SDS.

It was further confirmed from the plots of the plateau of the elution *vs.* concentration curve shown in Fig. 5[4] that the CMC of impure SDS, 7.8 mmol/l, was lower than that of pure SDS, 8.5 mmol/l, obtained from a similar plot which is in accordance with the general view on the effect of such a solubilizate.[7,8]

The author wishes to express his deep gratitude to Professor Tsunetaka Sasaki for his kind direction and valuable criticism throughout the work.

References

1) T. Nakagawa, K. Kuriyama, and H. Inoue, *J. Colloid Sci.*, **15**, 268 (1960).
2) S. H. Herzfeld, M. L. Corrin, and W. D. Harkins, *J. Phys. Chem.*, **54**, 271 (1950).
3) D. E. Clarke and D. G. Hall, *Colloid and Polymer Sci.*, **252**, 153 (1973).
4) H. Suzuki and T. Sasaki, This Bulletin, **44**, 2630 (1971).
5) H. Suzuki, manuscript in preparation.
6) M. Yasuoka, H. Suzuki, and T. Sasaki, manuscript in preparation.
7) K. Shinoda, T. Nakagawa, B. Tamamushi, and T. Isemura, "Colloidal Surfactants," Academic Press, New York (1963).
8) M. Miura and S. Arichi, *J. Sci. Hiroshima Univ., Ser. A*, **22**, No. 1 (1958).
9) D. Stigter and K. J. Mysels, *J. Phys. Chem.*, **59**, 45 (1955).

Formation of Excited Molecules and Atoms by Controlled Electron Impact on Hydrogen Chloride and Chlorinated Methanes

Minoru TOYODA, Teiichiro OGAWA, and Nobuhiko ISHIBASHI
Faculty of Engineering, Kyushu University, Hakozaki, Fukuoka 812

(Received April 14, 1975)

The dissociation, ionization, and excitation of hydrogen chloride and chlorinated methanes under controlled electron-impact excitation were studied at low pressures. The photoemissions (200—600 nm) were observed and assigned to HCl^+, CH, CH^+, CCl, H, and Cl^+. Such species as H and HCl^+ from HCl, and H and CH from CH_2Cl_2 were concluded to be produced by some one-electron processes. The photoemission of the HCl^+ produced from CH_2Cl_2 increases quadratically with the electron-beam current; in this case HCl^+ is mainly produced by the molecular elimination of HCl and the successive ionization excitation by the second electron. The threshold energies of the photoemissions were found to be 16.8 eV for HCl^{+*} from HCl, 19.8 eV for H* from HCl, and 17.6 eV for CH*(A) from $CHCl_3$. The processes of the excitation of these species near the threshold were discussed.

Information on the primary ionization, dissociation, and excitation of atoms and molecules can be obtained by the measurement of the emission spectrum excited by controlled electron impact at low pressures, since the excited molecule will normally emit radiation before undergoing a collision. This information is pertinent to various aspects of physics and chemistry, such as gaseous electrical discharges, collision phenomena, mass spectroscopy, and radiation chemistry. The emission spectra of aromatic molecules and of H_2S, CS_2, and thiols obtained by this method have been reported, and the processes of excitation have been discussed.[1-3]

The electronic spectrum of HCl^+ ($A^2\Sigma^+ - X^2\Pi$) has been measured by Brice and Jenkins,[4] Norling,[5] and Sheasley and Mathews.[6] The photoelectron spectrum of HCl was obtained by Lempka *et al*[7] and Turner *et al*.[8] Haugh[9,10] studied the collision of HCl with He^+, Ar^+, and Kr^+, and found an unusual vibrational distribution and the quadratic intensity dependence of the vibrational bands on the target-gas pressures.

Spectroscopic studies of the dissociative excitation of chlorinated methanes have been carried out by means of an electron-impact method[11] and by means of an electric discharge method.[12] The photoemission of HCl^+ was observed even though chlorinated methanes have no H-Cl bond. However, the mechanisms of their fragmentation and excitation processes have been left unsolved.

In the present report, the emission spectra of hydrogen chloride, dichloromethane, and chloroform under controlled electron-impact excitation will be presented, and compared with the results of the previous investigations. The mechanism of the excitation and dissociation by electron-impact will be discussed in terms of the intensity of the emission and threshold behavior.

Experimental

The experimental arrangement used in this work has been described elsewhere;[1,13] however, the apparatus has been partly modified in order to improve it. Thermal electrons emitted by a heated tungsten filament are accelerated and are then introduced into a collision chamber through a hole (4 mm in diameter). The energy of the electrons is externally controlled from 10 to 450 eV. The sample gas is jetted through a nozzle (0.1 mm in diameter) and collides with the electron beam. The pressure during the operation, as measured with a Penning gauge, is of the order of 10^{-4} mmHg, though the density of the gas in the middle of the molecular jet may be higher.

The collision cell used in the measurement with the electron energy near the threshold contains a brass cylinder inside the glass cell to remove the effect of space charges and secondary electrons. In order to avoid a space-charge effect, electron-beam currents of less than 5 μA have been used when the electron energy is below 30 eV. The electron energy scale is calibrated by thresholds of the molecular lines of N_2 (3371 Å, 11.1 eV[14]) and N_2^+ (3914 Å, 18.4 eV[14]).

The photoemission is observed perpendicularly to both the electron beam and the molecular beam. A JASCO CT-50 monochromator equipped with an EMI 9558Q B or an HTV R585 photomultiplier is used for the photoelectric detection. The monochromator has a 1200 line/mm grating blazed for 500 nm and has a reciprocal dispersion of 1.65 nm/mm. A Teledyne Philbric 1026-01 OP amplifier is used for the measurement of strong emissions, and an NF PC-545A photon counter, for the measurement of a weak signal near the threshold. The spectral sensitivity of the light detection system is determined by using a rohdamine B cell and by using an Ushio JC 24-150 halogen lamp.[15] The deviation of the two calibration curves is below 10% between 280 and 450 nm. The band intensities were determined by means of the peak height for the measurement of the intensity dependences on the electron-beam current and the gas pressure. However, the peak area was measured for the determination of the relative intensity of vibrational structures; the experimental uncertainty of the intensity measurements is, in this case, estimated to be about 20%.

The hydrogen chloride and deuterium chloride (99%) were obtained from the Takachiho Chemical Ind. and from Stohler. The dichloromethane and chloroform were obtained from Kishida, and the deuterated chloroform (99%) from Merk. Each sample was frozen and pumped repeatedly to remove any dissolved gases.

Results

Hydrogen Chloride and Deuterium Chloride. Typical emission spectra of HCl and DCl by controlled electron impact are shown in Fig. 1. A slit width of 50 μm was used for these measurements. The electron energy was 300 eV, and the electron-beam current was 1 mA. The dominant bands extending from 270 to 460 nm in these spectra are assigned to the $A^2\Sigma^+ - X^2\Pi$ transition of HCl^+. More than 6 vibrational levels of the upper

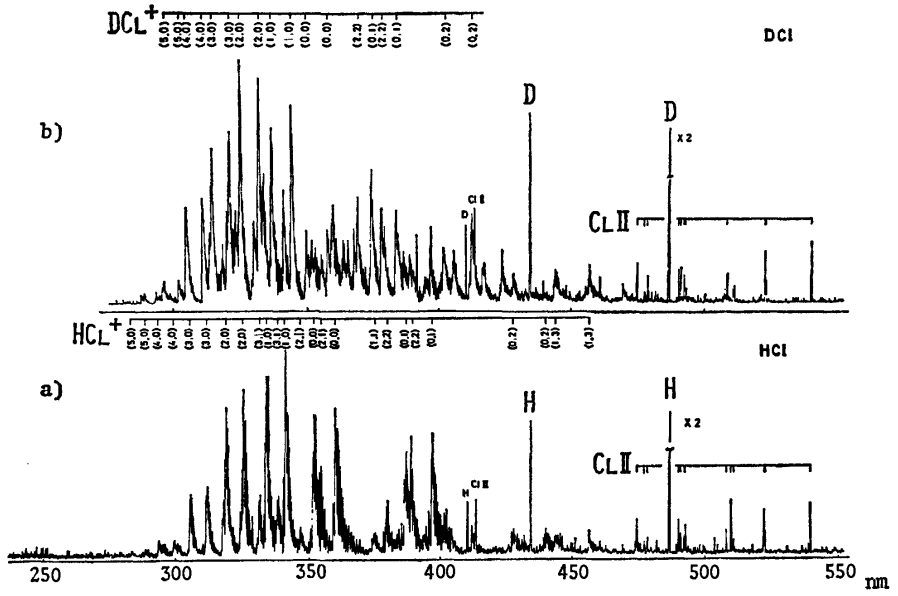

Fig. 1. Emission spectra of HCl (a) and DCl (b) by controlled electron impact. Electron energy 300 eV; electron-beam current 1 mA.

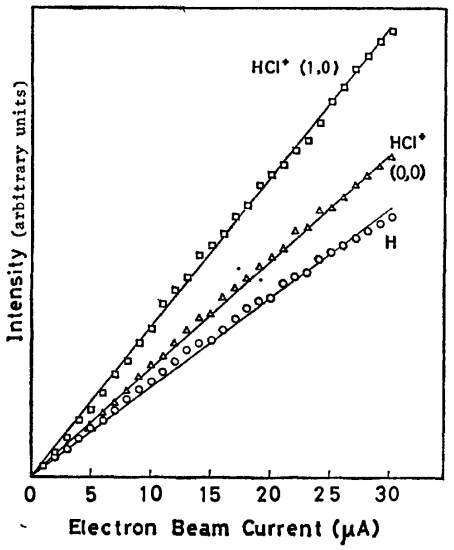

Fig. 2. Dependence of photoemission intensities of H (○) and HCl^+ (△ and □) on the electron-beam current. Electron energy was 300 eV.

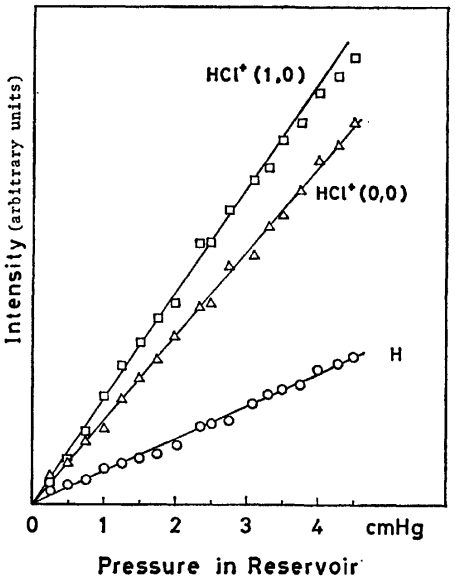

Fig. 3. Dependence of photoemission intensities of H (○) and HCl^+ (△ and □) on the gas pressure in the gas reservoir. Electron energy was 300 eV and the electron-beam current was 50 μA.

electronic state ($A^2\Sigma^+$) of HCl^+ are excited by electron impact. The strong bands of the $A-X$ system of HCl^+ are, in the order of calibrated intensities, (2, 0), (1, 0), (0, 0), and (0, 1). The intensity of the (v′, 0) band in a v″ progression is found to be the strongest; the intensity decreases at higher vibrational levels of v″. The DCl^+ spectrum shows an isotope shift in the vibrational structure. Such fragment species as H or D and Cl^+ are also observed, as is indicated in the figure.

The dependencies of the photoemission intensity of the H_β line and the HCl^+ bands from HCl on the incident electron-beam current and the target-gas pressure are shown in Figs. 2 and 3 respectively. The gas pressure was measured in the gas reservoir, where the pressure was estimated to be proportional to that in the collision chamber. Linear relations hold in all cases, and the intensity of the photoemissions of H and HCl^+ from HCl is given as follows:

$$I = k_1[e][HCl] \quad (1)$$

where I and k_1 stand for the emission intensity and a proportionality constant.

The threshold energies (minimum appearance potential) of the photoemissions of HCl^+ and H were measured; they are shown in Table 1, together with the calculated values. For the ionization excitation of HCl, the threshold energy was calculated by adding up the ionization energy of HCl and the excitation

Table 1. Threshold energy for ionization and dissociation excitation for HCl and $CHCl_3$

Process	Threshold energy (eV) Calcd	Obsd	
$HCl \xrightarrow{e} HCl^+*(0,0)$	16.3	16.8±1.0	(a)
$H^*(n=4)+Cl(3p^{52}P)$	17.2	19.8±1.0	(b)
$H^*(n=4)+Cl(4s^{14}P)$	26.1		(c)
$H^*(n=4)+Cl(4s^{12}P)$	26.4		(d)
$CHCl_3 \xrightarrow{e} CH^*(A)+Cl_2(X)+Cl(3p^{52}P)$	12.0		(e)
$CH^*(A)+Cl_2(A)+Cl(3p^{52}P)$	14.2		(f)
$CH^*(A)+3Cl(3p^{52}P)$	14.4	17.6±1.0	(g)
$CH^*(A)+Cl_2(C)+Cl(3p^{52}P)$	19.1		(h)

$I(HCl) = 12.82$ eV[16], $D(H\text{-}Cl) = 4.48$ eV[14]

$E_{calcd(e)}(CH^*) = D(CCl_3\text{-}H)+D(CCl_2\text{-}Cl)+D(CCl\text{-}Cl)+D(C\text{-}Cl)-D(C\text{-}H)-D(Cl\text{-}Cl)+h\nu$
$= 3.90^{17}+2.36^{18}+3.45^{18}+5.33^{18}-3.47^{14}-2.48^{14}+2.87$
$= 12.0$ eV

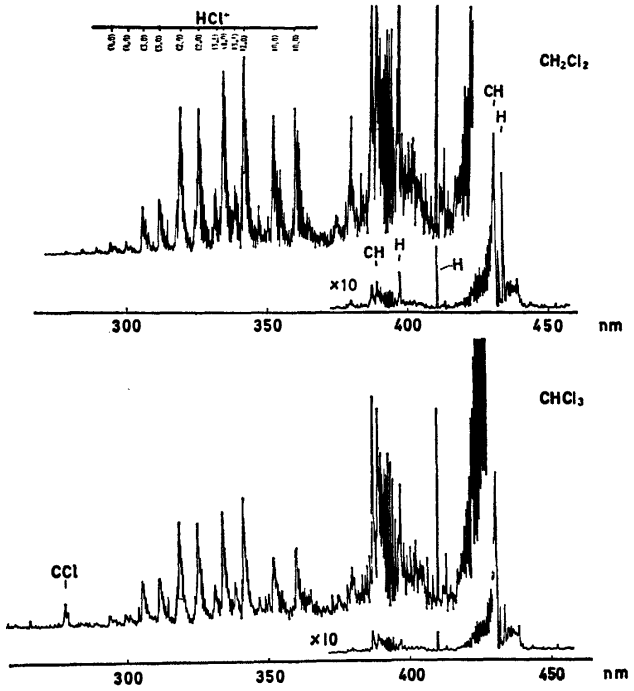

Fig. 4. Emission spectra of dichloromethane and chloroform by controlled electron impact. Electron energy 300 eV.

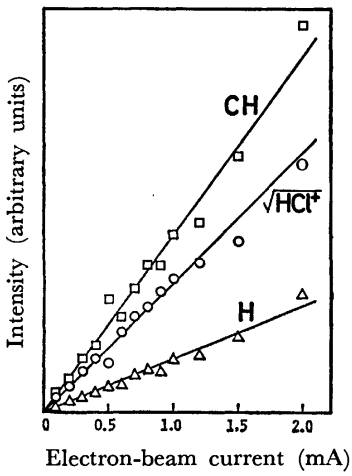

Fig. 5. Dependence of photoemission intensities of H (△), CH (□), and HCl^+ (○) on the electon-beam current. The square root of the intensity of HCl^+ is shown so that the quadratic dependence is clearly indicated. The electron energy was 300 eV.

energy of HCl^+. For the dissociation processes of HCl, the threshold energy was calculated by adding up the dissociation energy into fragments in their ground states and the relevant excitation energies of one or both of fragments, as given in Table 1. The calculated values can be expected to be smaller than the observed values by the amount of the kinetic, vibrational, and rotational energies of the species produced.

Dichloromethane and Chloroform. Typical emission spectra of dichloromethane and chloroform are shown in Fig. 4. The hydrogen Balmer series and HCl^+ doublet bands are obtained as in the case of HCl. The bands at 431 and 432 nm are assigned to the (0, 0) and (2, 2) bands of the $A^2\Delta-X^2\Pi$ transition of the CH radical, and the band at 387 nm, to its $B^2\Sigma^-$—$X^2\Pi$ transition. CCl shows a weak band at 278 nm, which is superimposed on the (6, 0) band of HCl^+. The emission at about 350 nm is assigned to CH^+ (see also Fig. 7). The 2800 Å and 2368 Å systems of CCl and the sharp line of the neutral carbon atom at 248 nm are also observed.

The spectrum of chloroform is identical to that of dichloromethane except for the relative amount of the fragments produced; for example, the ratio of the emission intensity of CH to that of H in $CHCl_3$ is much larger than that in CH_2Cl_2. Deuterated chloroform gives the bands of DCl^+.

The intensity of the photoemissions of H and CH produced from CH_2Cl_2 is proportional to both the electron-beam current and the gas pressure, as in the case of HCl, as is shown in Figs. 5 and 6. On the other hand, the square root of the emission intensity of HCl^+ is proportional to the electron-beam current (Fig. 5), while the pressure dependence of the intensity of HCl^+ is linear, as are H and CH (Fig. 6). The

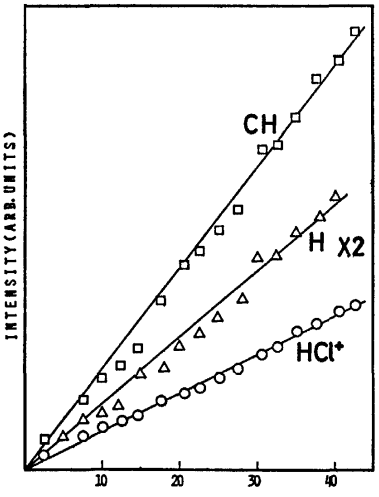

Fig. 6. Dependence of photoemission intensities of H (△), CH (□), and HCl^+ (○) on the gas pressure in the gas reservoir. The electron energy was 300 eV and the electron-beam current was 200 μA.

above findings give the following equations for the emission intensity of HCl^+ from CH_2Cl_2:

$$I = k_2[e]^2[CH_2Cl_2] \quad (2)$$

and for that of H and CH:

$$I = k_2[e][CH_2Cl_2] \quad (3)$$

The threshold energy of the photoemission of CH ($A^2\Delta - X^2\Pi$) was also measured; it is shown in Table 1, together with the calculated values.

Discussion

Hydrogen Chloride and Deuterium Chloride. The first vibrational quanta in the $A^2\Sigma^+$ and $X^2\Pi$ ionic states of HCl^+ and the ground state of the neutral molecule (HCl) are 1527, 2568, and 2886 cm^{-1} [14] respectively. The reduction of the vibrational quantum upon ionization in the $^2\Sigma^+$ state is much greater than that in the $^2\Pi$ state, as a result of the difference in the bonding nature of the orbital from which the electron is ejected for ionization. This is consistent with the difference in the bond length of the three species involved: 1.514 Å for HCl^+ ($^2\Sigma^+$), 1.315 Å for HCl^+ ($^2\Pi$) and 1.275 Å for the ground state of HCl.[14] This difference in the bond length is responsible for the greater population in the higher vibrational levels in the $^2\Sigma^+$ state, as is to be expected from the Franck-Condon factors for the transition between HCl (ground state) and HCl^+ ($A^2\Sigma^+$).

The emission intensity of a diatomic molecule in a transition from the v′ vibrational level of the upper state to the v″ vibrational level of the lower state is given by this expression:[14]

$$I_{v'v''} = KN_{v'}\nu^4 Re^2 q_{v'v''} \quad (4)$$

where K is a constant, $N_{v'}$ is the number of molecules in the upper state, Re is an electronic transition moment, and $q_{v'v''}$ is a Franck-Condon factor. If Re is constant for a series of transitions, the emission intensity of a band depends on the product of ν^4 and the Franck-Condon factor. Haugh[19] pointed out that Re decreases strongly at a large interatomic distance for the $A^2\Sigma^+ - X^2\Pi$ transition of HCl^+. In the present study, the intensities of the bands seem to give a displacement from the calculated Franck-Condon factors; the observed v′ progression with v″=0(v′, 0) is relatively more intense than the expected value. This displacement may be elucidated by Haugh's suggestion that the electronic transition moment decreases with an increase of v″.

The intensities of both H and HCl^+ are proportional to the electron-beam current and the gas pressure, as is shown in Equation (1). Thus, the ionization excitation and the dissociative excitation of HCl are concluded to proceed by one-electron unimolecular processes as follows:

$$HCl + e \rightarrow \begin{cases} HCl^{+*} \rightarrow HCl^+ + h\nu \\ H^*,\ Cl^{+*} \rightarrow H,\ Cl^+ + h\nu \end{cases}$$

where the asterisk stands for an excited state.

In the collision of HCl with He^+,[10] the ratio of the vibrational intensity of the (0, 0) band to the (1, 0) band at various target-gas pressures was not constant. The quadratic intensity dependence of the vibrational bands with the target-gas pressures has been obtained, and a reactive intermediate has been suggested. These are, however, not observed in the present case, and so no intermediate species need be considered in the present study. A difference in the method of the excitation sometimes results in a different distribution of the vibrational populations of the products, as may be seen also in the case of CN.[20]

The calculated and observed threshold values for the ionization excitation of hydrogen chloride agree well, as is shown in Table 1. This result shows that HCl^{+*} is also produced by a direct ionization-excitation of HCl near the threshold. For Balmer β of the hydrogen atom (4861 Å) from HCl, the observed onset potential is 19.8±1.0 eV. This onset is unambiguously due to the dissociation process (b), which is followed by the simultaneous formation of Cl in the ground state. In Reaction (b) the dissociation products carry off an excess energy of about 2.6 eV; the hydrogen atom shares 97% of the total excess energy. Ogawa *et al.*[21] measured the Doppler width of the light emission of H* formed by the 300 eV electron-impact on HCl and determined the kinetic energy to be 7.3 eV. Thus, the H atom produced by electron-impact seems to be hot.[21]

Dichloromethane and Chloroform. Though dichloromethane and chloroform have no direct H–Cl bond, the bands of the hydrogen chloride ion are clearly observed at high electron-beam currents. There are three plausible mechanisms for the formation of HCl^{+*}. The first one is a recombination of two atomic species:

$$H + Cl \rightarrow HCl^{+*}$$

where H and Cl, which may be ionic or excited, are produced in the primary processes. The second is an abstraction mechanism:

$$H(\text{or } Cl) + CH_2Cl_2 \rightarrow HCl^{+*}.$$

The third is a molecular elimination mechanism:

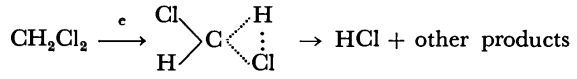

$$HCl \xrightarrow{e} HCl^{+*}.$$

The first and third mechanisms are compatible with the quadratic dependence of the emission intensity on the electron-beam current, while the second one is not. The third mechanism is supported by the linear relation between the photoemission intensity and the target-gas pressure, while the first and the second ones are not. The spectrum of a mixture of D_2O and CCl_4 was investigated; if either a recombination or an abstraction mechanism were correct, the emission from DCl^+ would be observed. No DCl^+ bands could be observed, however, even when the emissions of D and Cl^+ were very strong.

The spectrum of HCl^+ has well-resolved vibrational and rotational structures. The rotation-vibration bands of HCl^+ obtained from HCl were compared with those from CH_2Cl_2, as is shown in part in Fig. 7. The structures not only of the parts shown in Fig. 7, but also of the other parts of rotation-vibration bands were found to coincide completely. The relaxation processes of the electronically excited species can be ignored in the present study. Thus, this result reveals that the HCl^{+*} species obtained from CH_2Cl_2 may be formed *via* HCl in the ground state, since the intensity distribution of a band is related with the wave function of the initial and final states, as is given in Eq. (4). If these species were formed through other processes, the rotation-vibration bands would change clearly.

Dibeler and Bernstein[22] observed the CCl_2^+ ion from $CHCl_3$ and $CDCl_3$ by using a mass spectrometer. The impact voltages used in their study were 50 and 70 eV, smaller than the one used in the present study; however, no significant differences in emission spectra have been observed in this energy region, and their results can be carried over on the present study. They suggested that the CCl_2^+ ion was formed primarily by dissociation of neutral HCl or DCl molecules from $CHCl_3$ or $CDCl_3$, rather than by dissociation into the separated atoms, and that the amount of HCl thus produced was larger than that of HCl^+. These results support the molecular elimination mechanism suggested above.

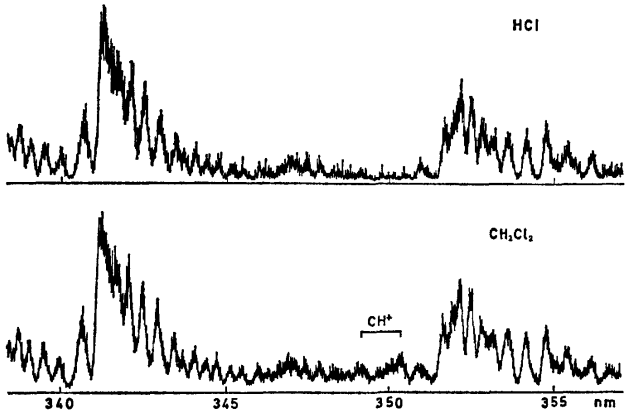

Fig. 7. Comparison of rotation-vibration bands of HCl^+ obtained from HCl with that from CH_2Cl_2. Slit width 50 μm.

Thus, the excited HCl^+ from chlorinated methanes is concluded to be produced mainly by the molecular elimination mechanism.

Since the intensity of the photoemissions of H and CH are expressed in Equation (3), it can be concluded that H and CH are produced in some one-electron unimolecular processes.

The relative intensity of the band of CH to the line of H from chloroform is larger than that in the case of dichloromethane. Since the formation of the CH radical requires the C–H bond rupture in CH_2Cl_2, and since the bond energy of a CH bond is larger than that of a C–Cl bond, the CH radical would be produced more easily from $CHCl_3$. The observation of the 2368 Å system of CCl and the C(I) atomic line in $CHCl_3$ can be explained in the same way.

For the dissociative excitation leading to CH* (4314 Å) from $CHCl_3$, the calculated and the observed threshold are also shown in Table 1. The energy consideration requires that the dissociation process involves Reactions (e)—(g) near the observed threshold. In Reaction (e), however, the excess energy is about 5.6 eV; this energy should be carried away mainly as the translational energy, since CH is not rotationally and vibrationally excited and since the rotational energy of Cl_2 would be small. This value seems to be too large for the total kinetic energy of CH*, Cl, and Cl_2. Even if Cl_2 were vibrationally excited up to the dissociation limit, CH*, Cl, and Cl_2 would still have about 3.2 eV as the kinetic energy. Reaction (e), therefore, makes only a small contribution to the formation of CH* near the threshold region.

The authors wish to thank Professor Tomoo Oyama for the use of his CT-50 monochromator and Mr. Masaharu Tsuji for his discussion. The authors are also indebted to Dr. Mamoru Susuki of the Electrotechnical Laboratory for the determination of spectral irradiance of a standard lamp.

References

1) T. Ogawa, M. Tsuji, M. Toyoda, and N. Ishibashi, This Bulletin, **46**, 1063 (1973).
2) T. Ogawa, M. Tsuji, M. Toyoda, and N. Ishibashi, *ibid.*, **46**, 2637, (1973).
3) M. Toyoda, T. Ogawa, and N. Ishibashi, *ibid.*, **47**, 95 (1974).
4) A. Brice and F. A. Jenkins, *Nature*, **123**, 944 (1929).
5) F. Norling, *Z. Phys.*, **104**, 638 (1937).
6) W. D. Sheasley and C. W. Mathews, *J. Mol. Spectrosc.*, **47**, 420, (1973).
7) J. H. Lempka, T. R. Passmore, and W. C. Price, *Proc. Roy. Soc. Ser. A*, **304**, 53, (1968).
8) D. W. Turner, C. Baker, A. D. Baker, and C. W. Brundle, "Molecular Photoelectron Spectroscopy," John Wiley & Sons, London (1970).
9) M. J. Haugh and K. D. Bayes, *Phys. Rev. A*, **2**, 1778 (1970).
10) M. J. Haugh, *J. Chem. Phys.*, **56**, 4001, (1972); **59**, 37 (1973).
11) T. Ogawa, I, Fujita, M. Hatada, and K. Hirota,

This Bulletin., **44**, 659 (1971).
12) G. Pannetier, L. Marsigny, P. Deschamps, J. Guillanme, and N. Luguet, *J. Chim. Phys.*, **61**, 1162 (1964).
13) T. Ogawa, M. Toyoda, M. Tsuji, and N. Ishibashi, *Technology Repts. Kyushu Univ.*, **45**, 427 (1972).
14) G. Herzberg. "Molecular Spectra and Molecular Structure," Vol. 1, Van Nostrand, New York (1950).
15) The spectral irradiance of the lamp was determined at the Electrotechnical Laboratory.
16) F. H. Field and J. L. Franklin, "Electron Impact Phenomena and the Properties of Gaseous Ions," Academic Press, New York (1970).
17) K. Tarama, "Constants of Organic Compounds," The Asakura Publishing Com., Tokyo (1963), p. 537.
18) R. I. Reed and W. Snedden, *Trans. Faraday Soc.*, **54**, 301 (1958).
19) M. J. Haugh, *J. Mol. Spectrosc.*, **51**, 123 (1974).
20) I. Tokue, T. Urisu, and K. Kuchitsu, *J. Photochem.*, **3**, 273 (1974).
21) T. Ogawa, F. Masumoto, and N. Ishibashi, *Chem. Lett.*, submitted.
22) V. H. Dibeler and R. B. Bernstein, *J. Chem. Phys.*, **19**, 404 (1951).

Epoxide Rearrangement III.[1] Isomerization of 1-Methylcyclohexene Oxide over TiO_2–ZrO_2, $NiSO_4$ and $FeSO_4$

Kazushi ARATA, Susumu AKUTAGAWA,* and Kozo TANABE**

Department of Chemistry, Hokkaido University of Education, Hachiman-cho, Hakodate-shi 400

**Central Research Laboratory, Takasago Perfumery Co., Kamata 5, Ohta-ku, Tokyo 144*

***Department of Chemistry, Faculty of Science, Hokkaido University, Sapporo-shi 060*

(Received April 24, 1975)

The reaction of 1-methylcyclohexene oxide at 108 °C was found to give predominantly 2-methylcyclohexanone (III) over $FeSO_4$, but predominantly allyl alcohols (VI) over TiO_2–ZrO_2 of various compositions. $NiSO_4$ gave the same amount of both products, III and VI. The selectivities over $FeSO_4$ and $NiSO_4$ were not much varied with calcination temperatures from 150 °C to 700 °C, while the catalytic activities were higher with $NiSO_4$ calcined at low temperature and with $FeSO_4$ calcined at high temperature. $FeSO_4$ and $NiSO_4$ gave the preferential formation of an allyl alcohol with *exo*-double bond, 2-methylene cyclohexanol (VIa), while TiO_2–ZrO_2 formed predominantly an allyl alcohol with *endo*-double bond, 2-methyl-2-cyclohexene-1-ol (VIb). Both the acidity and basicity of TiO_2–ZrO_2 were observed to increase by mixing each oxide and to correlate with the catalytic activity. The allyl alcohol formation was explained by an acid-base bifunctional mechanism.

We have recently reported some works on the isomerization of 1-methylcyclohexene oxide catalyzed by solid acids and bases,[1,2] where ketone (III) or allyl alcohols (VI) of five main products, with a small amount of 1-methylcyclohexene (I) and unidentified compound (II) (supposedly the dehydrated diene-compound of (VI)), was predominantly formed depending on the type of catalysts: $SiO_2 \cdot Al_2O_3$, H_2SO_4/SiO_2, low-temperature calcined solid H_3PO_4 and $LiClO_4$ produced almost 100% ketone, while Al_2O_3 and TiO_2 gave more than 80% of allyl alcohols (VI).[1]

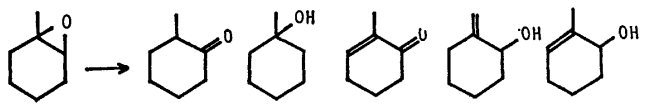

III IV V VIa VIb

In connection with our interests in the strikingly different selectivities, we have examined further the catalytic properties of TiO_2–ZrO_2, $NiSO_4$, and $FeSO_4$ for this isomerization reaction from the following several points of view: 1) TiO_2–ZrO_2 showed much higher catalytic activity with the predominant formation of allyl alcohol than TiO_2,[2] and the existence of basic sites on the surface was suggested from the catalytic action for the partial conversion of ethanol into butadiene;[3] 2) $NiSO_4$ gave the same amount of both ketone and allyl alcohol[2]; and 3) $FeSO_4$ was found to show the significant catalytic activity for a preferential formation of ketone and also exhibited a surprisingly high catalytic activity for the Friedel-Crafts benzylation of toluene with benzyl chloride when calcined at high temperature.[4]

In the present paper, we discuss more in detail the catalytic activity and selectivity of TiO_2–ZrO_2, $NiSO_4$, and $FeSO_4$ for the isomerization of 1-methylcyclohexene oxide, particularly the relationship between the surface property and the selectivity.

Experimental

1-Methylcyclohexene oxide, supplied from Takasago Perfumery Co., was fractionally distilled to purify to more than 98% and toluene, a guaranteed reagent, used as a solvent was redistilled over sodium metal.

$NiSO_4$ and $FeSO_4$ were prepared by calcining their heptahydrates, guaranteed reagents of Wako Pure Chemical Co and Kanto Chemical Co., respectively. TiO_2, ZrO_2 and TiO_2–ZrO_2 of various compositions were prepared by thermal decomposition of H_4TiO_4, $Zr(OH)_4$ and H_4TiO_4–$Zr(OH)_4$, respectively. The procedure for the preparation of these materials was described previously.[3] All the catalysts were calcined in air and stored in sealed ampoules until use.

The procedures of reaction and analysis of the products were followed by those of the previous experiment.[1]

The amounts of base of TiO_2–ZrO_2 catalysts were measured by titrating the 100 mesh powder suspended in benzene with 0.1 M benzoic acid benzene solution, using 2,4,6-trinitroaniline ($pK_{BH}=12.2$) as an indicator.

Results and Discussion

The reaction of 1-methylcyclohexene oxide over TiO_2–ZrO_2, $NiSO_4$ and $FeSO_4$ catalysts gave five main products, 2-methylcyclohexanone (III), 1-methylcyclohexanol (IV), 2-methyl-2-cyclohexene-1-one (V), 2-methylenecyclohexanol (VIa) and 2-methyl-2-cyclohexene-1-ol (VIb), as observed in our previous paper.[1]

Table 1 shows the catalytic activities and selectivities of these catalysts in 2 hr at 108 °C. The over-all reaction followed first order reaction kinetics with respect to the oxide concentration except those with $NiSO_4$ calcined at 250 °C and $FeSO_4$ heat-treated above 400 °C, in which the reaction rate was found to diminish greatly after 30 min, probably owing to the contamination of the catalyst surface with some polymers produced by those high catalytic activities.

The products are mainly divided into two groups, ketone (III) and allyl alcohols (VI). The former was formed predominantly over $FeSO_4$, while the latter was given by TiO_2, TiO_2–ZrO_2 and ZrO_2 with a marked amount of IV and V, obviously formed by hydrogen transfers from V to IV (approximately the same yield found). $NiSO_4$ gave the same amount of both products. It is of interest that the selectivities are almost the same over $NiSO_4$ and $FeSO_4$ heat-treated at any temperatures from 150 to 700 °C, though solid H_3PO_4 formed almost 100% ketone when calcined at 200 to 300 °C, but gave the same amount of both

Table 1. Catalytic activity and selectivity of TiO_2–ZrO_2, $NiSO_4$ and $FeSO_4$ for isomerization of 1-methylcyclohexene oxide at 108 °C in 2 hr

Catalyst and calcination temperature, °C	Catalyst amount (*A*), g	Conversion (*B*) %	Activity $B\times\frac{0.3}{A}$	Yields (%) I[a]	II[b]	III	IV	V	VI	(VIa,	VIb)
TiO_2, 500	0.455	31.3	20.6		0.6	2.1			27.7	(15.1,	12.6)
TiO_2–ZrO_2[c]											
3 : 1 500	0.393	83.0	63.3		0.9	6.5	1.5	1.6	72.5	(35.1,	37.4)
1 : 1 500	0.380	87.9	69.4		1.4	3.9	6.4	6.2	70.0	(28.1,	41.9)
1 : 1[d] 500	0.298	92.1	92.7		2.6	4.2	9.1	10.2	65.2	(26.4,	38.8)
1 : 3 500	0.350	49.0	42.0		0.9	2.9	3.2	3.1	38.9	(15.1,	23.8)
1 : 3[d] 500	0.290	52.8	54.6	0.6	0.8	3.5	3.7	4.7	38.9	(8.4,	30.5)
ZrO_2 500	0.329	3.3	3.0			0.7			2.6		
ZrO_2[e] 350	0.321	24.5				4.0	4.1	3.0	13.4	(6.5,	6.9)
$NiSO_4$ 150	0.257	55.4	64.7	0.3	1.2	22.9		0.9	26.8	(19.1,	7.7)
250	0.390	75.8	58.3	0.5	11.0	47.6			10.3	(10.3,	trace)
350	0.360	74.8	62.3			31.8			43.0	(35.7,	7.3)
400	0.324	34.4	31.9		0.3	12.9			18.4	(14.0,	4.4)
450	0.227	31.0	41.0	1.8	0.4	12.8			14.7		
500	0.210	17.8	25.4	trace	0.7	6.9			8.5		
600	0.250	13.3	16.0		0.5	5.8			6.7	(3.7,	3.0)
$FeSO_4$ 200	0.530	22.2	12.6			11.7			10.5	(7.6,	2.9)
300	0.315	65.9	62.7	4.0	3.8	40.9		0.8	11.4		
400	0.436	62.8	43.2	1.2	4.2	45.1		0.7	6.3		
500	0.339	72.2	63.9	3.9	2.4	56.3			4.3		
600	0.249	65.7	79.2		3.0	54.0			3.8		
700	0.166	37.8	68.3			24.4			12.3	(8.0,	4.3)

a) 1-Methylcyclohexene. b) Unidentified (supposedly dehydrated diene-compound of VI). c) Molar ratio. d) For those precipitated by ammonia following the method in Ref. 4. 4) Reaction carried out for 6 hr.

ketone and allyl alcohols when calcined at higher temperature, 400—900 °C, the formation of allyl alcohols being concluded to be due to the creation of basic sites on the surface at high temperature.[1] This indicates that the active sites of $NiSO_4$ and $FeSO_4$ catalysts for this isomerization are not altered even if these catalysts were prepared at the high temperature such as 500, 600 or 700 °C, though the structural and catalytic changes caused by calcination temperature are known in both cases of $NiSO_4$[5] and $FeSO_4$[6]

The isomerization between ketone and allyl alcohols was not found in every reaction under the present reaction conditions. Heats of formation of allyl alcohols and ketone in gas phase at 25° were calculated by use of Benson *et al.*'s second-order approximation which is the law of additivity of group properties.[7] They were −47.89 kcal/mol for 2-methylenecyclohexanol (VIa), −49.29 for 2-methyl-2-cyclohexene-1-ol (VIb) and −63.26 for 2-methylcyclohexanone (III). The differences in entropies of these materials were also calculated to be −1.94 e.u. for the entropy of ketonization of VIa to III, and +19.38 e.u. for that of VIb to III in gas phase at 25 °C. From these values, equilibrium constants of allyl alcohols to ketone were obtained to be 7.2×10^{10} for VIa to III and 3.6×10^{14} for VIb to III in gas phase at 25 °, indicating that the catalytic action of the present catalysts is quite selective.

An example of the time variation of the conversion to each product is shown in Fig. 1, where the catalyst is TiO_2–ZrO_2 (molar ratio = 1 : 1). The reaction entirely

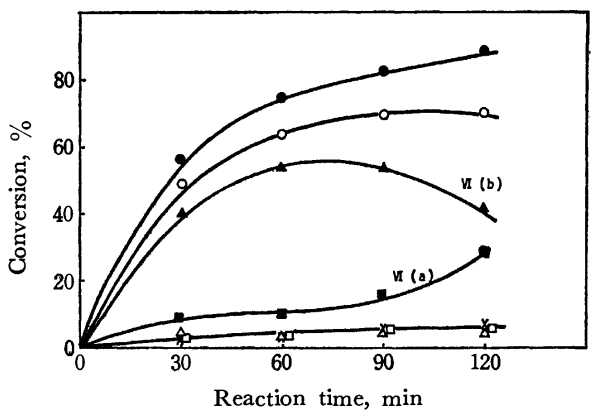

Fig. 1. Isomerization of 1-methylcyclohexene oxide over TiO_2–ZrO (1 : 1). (-●-) Total conversion, Conversion to III (-△-), IV (-×-), V (-□-), VI (-○-).

followed first-order reaction kinetics with respect to the oxide concentration, and the conversions to III, IV, V, and VI increased almost parallel to each other with time. It is also seen that, in the formation of allyl alcohol, VIb exceeded VIa and isomerized gradually to VIa after 60 min. On the contrary, $NiSO_4$ (350 °C) gave much more VIa than VIb (Table 1), and the isomerization between them with reaction time was not observed: 12.0% (VIa) and 1.6% (VIb) at 30 min; 25.0 and 2.0 at 1.0 hr; 35.2 and 3.7 at 1.5 hr; and 35.7 and 7.3 at 2.0 hr. VIa generally exceeds VIb because

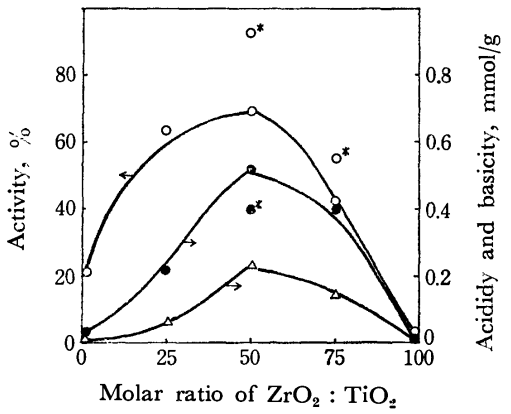

Fig. 2. Catalytic activity, acidity and basicity of TiO_2–ZrO_2 at various compositions. (-○-) Activity, (-●-) Acidity[4] ($pK_a = -3.0$), (-△-) Basicity ($pK_a = 12.2$) : Basicity per surface area was 3.4×10^{-4} mmol /m², 9.0×10^{-4} and 7.3×10^{-4} for TiO_2–ZrO_2 (3 : 1), (1 : 1), and (1 : 3), respectively.[13]
* The sample precipitated by NH_3 following the procedure of Ref. 4.

of the preference of primary proton abstraction over secondary one caused by the more enhanced acidity of primary hydrogen by the electronic effect. Our previous observations followed this rule: 51.1% (VIa) and 23.5% (VIb) over Al_2O_3; 6.7 and 1.9 over zeolite H-F9; and 9.2 and 8.3 over solid H_3PO_4 heat-treated at 400°C.[1] The similar observations, the preferential formations of allyl alcohol with *exo*-double bond in the rearrangement of cycloalkene oxides, are found in literatures: for 1-methylcyclohexene,[8] 1-methylcycloheptene[8] and α-pinene oxides[9] with lithium diethylamide; for menthene and limonene oxides with aluminum isopropoxide[10]; and for limonene [11],α-pinene,[11,12] 1-methylcyclopentene[12] and 3-carene oxides with alumina.[12] The example opposite to the above rule, the favorable formation of allyl alcohol with *endo*-double bond, has not been found except for the case of 1-methylcyclopentene oxide with lithium diethylamide[8] and alumina,[12] probably caused by the stereochemically preferred geometry. As seen in Table 1, the TiO_2–ZrO_2 catalysts gave the preferential formation of VIb, while $NiSO_4$ and $FeSO_4$ formed predominantly VIa. Figure 2 shows the relation between catalytic activity and acidity as well as basicity of TiO_2–ZrO_2 at various compositions, where the total conversion % of the oxide per 0.3 g of the catalyst was taken as activity. TiO_2–ZrO_2 (1 : 1) changed 2,4,6-trinitroaniline ($pK_{BH} = 12.2$) to the basic color, but TiO_2 and ZrO_2 did not change the acidic color of BTB ($pK_a = 7.2$) to its basic color. It should be noted that both acidity and basicity increase by mixing TiO_2 and ZrO_2 up to the equal composition, as seen in the figure.

The catalytic activity correlates well with both the acidity and basicity. It is known that acid sites alone are active for the selective formation of ketone and basic sites alone are almost inactive for the isomerization of 1-methylcyclohexene oxide.[1] Therefore, these facts indicate that allyl alcohol, main product produced by the TiO_2–ZrO_2 catalysts, is formed on both acidic and basic sites on the catalyst. In other words, the allyl alcohol formation is explained by acid-base bifunctional mechanism. Since the acidic sites on the surface of TiO_2 prepared by calcining H_4TiO_4 in air are determined to be the Brönsted type,[15] the reaction is considered to proceed by the following mechanism.

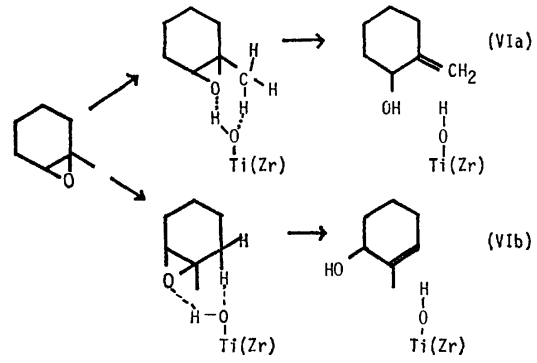

An oxygen atom of the oxide adsorbs on a proton of the catalyst, while a hydrogen atom of the methyl or methylene group on oxygen (basic site) of the catalyst surface, and both the opening of the epoxide ring and the hydrogen abstraction from the methyl or methylene group take place simultaneously to form the allyl alcohol. The breaking of α-bond of oxygen is much more favorable due to the electronic effect of the methyl group, since no compound formed by the breaking of β-bond is found in the products. The choice of the VIa or VIb formation seems to depend on the distance between acidic and basic sites on the catalyst. The distance of TiO_2–ZrO_2 is supposed to be different from those of $NiSO_4$ and $FeSO_4$, judging from the preferential formation of VIb or VIa.

The acidic and basic strength of catalysts must be an important factor which controls the ketone formation. If the acid strength is too strong, the α-bond cleavage prior to the hydrogen abstraction would occur to form the ketone, while, if it is too weak, the hydrogen abstraction would hardly occur.

ZrO_2 calcined at 350 °C showed higher activity than that treated at 500 °C. The similar phenomena were also observed for the dehydration reaction of ethanol over ZrO_2, where the catalytic activity of the catalyst heat-treated at 400 °C was more than two times as high as that calcined at 500 or 600 °C.[4]

It is of interest that TiO_2–ZrO_2 (1 : 1 and 1 : 3) prepared by the coprecipitation method with NH_3 showed higher activity than those with urea, though the acidity was opposite to the activity. This seems to suggest the unusual surface property of TiO_2–ZrO_2.

Figure 3 shows the relation between catalytic activity and acidity of $NiSO_4$ and $FeSO_4$ calcined at various temperatures. The activity of $NiSO_4$ calcined at higher temperature correlates with its acidity measured by the indicator method. However, no correlation was found for $NiSO_4$ calcined at lower temperature. The high activity at low calcination temperature is considered to be due to the relatively weak Brönsted acid, which can not be measured by the indicator method, proposed by Ben-Dor and Margalith.[17]

In the case of $NiSO_4$ calcined at 250 °C, the conversion to VI was low compared to that for other

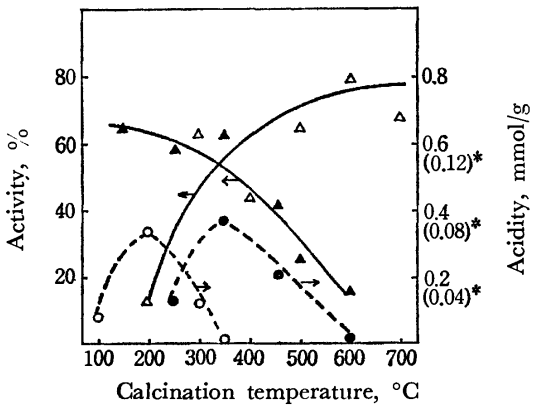

Fig. 3. Catalytic activity and acidity ($pK_a = 1.5$)[6,16] of $NiSO_4$ and $FeSO_4$ calcined at various temperatures.
(▲) $NiSO_4$, (△) and (○) $FeSO_4$.
*Scale in parenthesis correspounds to $NiSO_4$.

$NiSO_4$ catalysts (Table 1). Since both the decrease of VI and the increase of II were observed during the course of reaction, it seems that VI was dehydrated to give II by strong Brönsted acid, because the maximum of Brönsted acidity of $NiSO_4$ appears when calcined at 250 °C.[18] It is inferred from the explanation about the reaction mechanism of the allyl alcohol formation as mentioned already that $NiSO_4$ has also basic sites because of the considerable formation of allyl alcohols.

The activity of $FeSO_4$ is not related to the acidity. Figure 3 shows that the higher the calcination temperature, the higher the catalytic activity. Since the preferential formation of ketone was concluded to be given by strong acid, it is supposed that additional acid sites, which were not observed by the butylamine titration method, were created when calcined at high temperature. However, the possibility that the active sites are different from acid sites can not be excluded in the case of $FeSO_4$.

We thank Mr. Noboru Nishiyama and Mr. Hirotake Mori for their assistance with reaction experiments.

References

1) Part II: K. Arata, S. Akutagawa, and K. Tanabe, This Bulletin, **48**, 1097 (1975).
2) K. Arata and K. Tanabe, *Chem. Lett.* **1974**, 923.
3) K. Arata and H. Sawamura, in press.
4) K. Arata and I. Toyoshima, *Chem. Lett.*, **1974**, 929.
5) T. Takeshita, R. Ohnishi, T. Matsui, and K. Tanabe, *J. Phys. Chem.*, **69**, 4077 (1965).
6) I. Toyoshima, K. Tanabe, T. Yoshioka, J. Koizuka, and H. Ikoma, Ann. Meeting Chem. Soc. Japan, 22nd, Tokyo, Preprints of Paper, No. 06405 (1969).
7) S. W. Benson, F. R. Cruickshank, D. M. Golden, G. R. Haugen, E. H. O'Neal, A. S. Rodgers, R. Shaw, and R. Walsh, *Chem. Rev.*, **69**, 279 (1969). C-$(H)_3$ (C_d) and C-(O) (C) (C_d) (H) were assigned values identical to C-$(H)_3$ (C) and C-(O) $(C)_2$ (H), respectively.
8) J. K. Crandall and L. C. Lin, *J. Org. Chem.* **33**, 2375 (1968).
9) J. K. Crandall and L. C. Lin, *ibid.*, **32**, 435 (1967).
10) E. H. Eschinasi, *Israel J. Chem.* **6**, 713 (1968).
11) I. C. Nigam and L. Levi, *Can. J. Chem.* **46**, 1944 (1968).
12) V. S. Joshi, N. P. Damodaran, and S. Dev, *Tetrahedron*, **24**, 5817 (1968).
13) Specific surface area was cited from Shibata and Kiyoura's values.[14] The value of 177 m^2/g for TiO_2–ZrO_2 (3 : 1) was estimated from values of 145 and 210 for TiO_2–ZrO_2 (15 : 85) and 40 : 60, respectively.
14) K. Shibata and T. Kiyoura, *J. Res. Inst. Catalysis, Hokkaido Univ.*, **19**, 35 (1971).
15) K. Tanabe, C. Ishiya, I. Matsuzaki, I. Ichikawa, and H. Hattori, This Bulletin, **45**, 47 (1972).
16) K. Tanabe and R. Ohnishi, *J. Res. Inst. Catalysis, Hokkaido Univ.*, **10**, 229 (1962).
17) L. Ben-Dor and R. Margalith, *Inorg. Chim. Acta*, **1.**, 49 (1967).
18) K. Tanabe and T. Takeshita, "Advances in Catalysis", Academic Press, **17**, 315 (1967); H. Hattori, S. Miyashita, and K. Tanabe, This Bulletin, **44**, 893 (1971).

The Formation and Dissociation of the Solvated Ion-pair in the Excited Pyrene–Dicyanobenzene System

Tetsuro HINO, Hiroshi MASUHARA*, and Noboru MATAGA

Department of Chemistry, Faculty of Engineering Science, Osaka University, Toyonaka, Osaka 560

(Received June 18, 1975)

Nanosecond laser photolysis has been applied to investigate the photochemical primary processes of the pyrene-*p*-dicyanobenzene system in some solvents. The solvated ion-pair is formed by the excitation and its yield increases as the dielectric constant of the solvent does; this was explained with the empirical equation proposed previously. The dissociation of the solvated ion-pair to free ions was directly observed in moderately polar solvents and the rate constant of the dissociation was determined, which is in agreement with the values calculated by Eigen's equation. The role of the ion-pair formation in the fluorescence quenching was discussed on the basis of the present results, and it was concluded that some unknown quenching processes other than the triplet formation compete with the solvation to ion-pairs.

We have been studying the ionic photodissociation processes of the excited electron donor-acceptor (EDA) systems by using the nanosecond laser photolysis method. The excited singlet and triplet states of EDA complexes, which are stable in the ground state, and exciplexes are all called excited EDA systems in the present paper. These systems are suitable for clarifying the relation between photophysical as well as photochemical primary processes and molecular interactions. Ionic photodissociation to the donor cation and the acceptor anion in polar solvents is one of the important primary processes and has been referred to in many fields of chemistry. The results obtained by laser photolysis are summarized as follows: (1) Several different dissociation patterns have been demonstrated. Dissociations from the excited singlet or triplet states are known in the case of EDA complexes, while the problem in the case of exciplexes is not about the spin state but about the excited state relaxed or nonrelaxed with respect to the solvation.[1] (2) The important role of the nonrelaxed state in the dissociation process was confirmed.[1a,2] The dissociation of pyrene–*N*,*N*-dimethylaniline (DMA) and *s*-tetracyanobenzene–toluene systems occurs from the excited singlet state nonrelaxed with respect to the solvent orientation. (3) A new empirical equation for the relationship between the yield and the solvent dielectric constant was proposed. The solvent effect on the ionic photodissociation seems to be well explained in terms of the dielectric constant.[1a] (4) Ionic dissociation yields of several EDA systems in acetonitrile depend upon the chemical property of the quencher and not on the strength of the EDA interaction.[3]

In the present work we will show another kind of ionic dissociation process: namely, the results for the formation and dissociation processes of the solvated ion-pair will be shown in the case of the pyrene–*p*-dicyanobenzene(DCNB) system.

Experimental

The transient absorption spectral and photocurrent measurements were performed by using the same apparatus as reported previously.[4] The exciting pulse of 347 nm was produced through the ADP frequency doubler with a conversion efficiency of *ca.* 8%. The ADP crystal was set in an air bath to control the temperature. The fluctuation was ±0.6 °C. The temperature matched and phase matched ADP gives a constant output of the exciting pulse.

Pyrene was chromatographically purified. DCNB was recrystallized several times and sublimated. All the solvents were spectrograde (Dotite, Nakarai, or Merck) and used without further purification. Pyridine was dried over potassium hydroxide and distilled. The concentration of pyrene was adjusted to give an appropriate absorbance (0.1—0.4) at 347 nm, which is a suitable condition for the present laser photolysis measurements. The concentration of DCNB was determined so as to quench the pyrene fluorescence more than 90%. The solutions were completely degassed by usual freeze-pump-thaw method.

Results and Discussion

The Formation and Dissociation Processes of the Solvated Ion-Pair in the Pyrene–DCNB System. The transient absorption spectra of the pyrene–DCNB–dichloromethane system shown in Fig. 1 were obtained at 50 ns after the laser excitation. These spectra can be reproduced with the superposition of the bands of the pyrene cation, the DCNB anion, and the triplet pyrene. The ionic species and the triplet pyrene are produced immediately after the excitation with the pulse. The kinetic relation between the transmittance at 445 nm (the pyrene cation) and the photocurrent is given in Fig. 2. The transmittance is almost constant in the course of a few μs, while the peak photocurrent is attained in several hundred nanoseconds. The difference of the time dependence between the transmittance and the current may be ascribed to an ionic transient, which gives no current but shows an absorption similar to that of the pyrene cation. This transient may be an ion-pair of the pyrene cation and the DCNB anion or the pyrene–DCNB exciplex, since the absorption spectra of both species are expected to be reproduced with the superposition of the bands of the pyrene cation and the DCNB anion.[5] Because the lifetime of the exciplex in the dichloromethane solution is ~30 ns, a curve of photocurrent rising more quickly than the observed one should be found if the free ions were formed from the exciplex. Therefore, the present transient seems to be an ion-pair of the pyrene cation and the DCNB anion, which is of course completely solvated. The latter ion-pair is produced rapidly by

* To whom all correspondence should be addressed.

TABLE 1. THE DISSOCIATION RATE CONSTANTS OF THE SOLVATED ION-PAIR TO FREE IONS

Solvent	k_{exp}	τ_f	$1/\tau_f$	k_{diss}	τ_{max}[a]
Dichloromethane	1.3×10^7 s^{-1}	28 ns	3.5×10^7 s^{-1}	1.5×10^7	400 ns
1,2-Dichloroethane	0.9×10^7	short	large	2.4×10^7	
Pyridine	9×10^7	short	large	6.3×10^7	20 ns
Acetone	rapid[b]	—		1.4×10^9	immediately
Acetonitrile	rapid[b]	—		4.3×10^9	immediately

a) τ_{max} is the time when the peak photocurrent is attained after the excitation. b) The rising curve is identical with a time-integrated function of an exciting pulse.

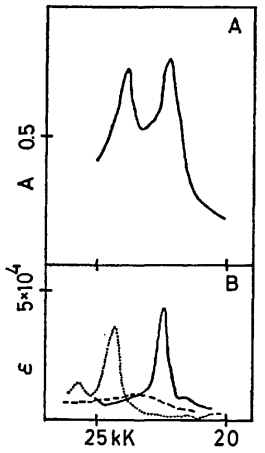

Fig. 1. The transient absorption spectra of the pyrene-DCNB-dichloromethane system obtained at 50 ns after the laser oscillation (A). The reference spectra (B) of the pyrene cation (——), the triplet pyrene (·····) and the DCNB anion (----).

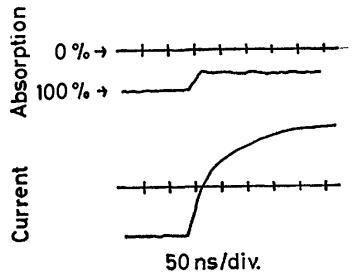

Fig. 2. The kinetic relation between the absorption (the pyrene cation at 445 nm) and the photocurrent of the pyrene-DCNB-dichloromethane system.

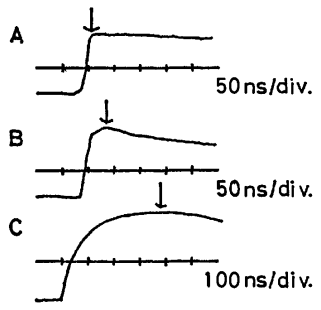

Fig. 3. The oscillogram of the rise of the transient photocurrent, (A) in acetonitrile, (B) in pyridine and (C) in dichloromethane. The vertical arrow (↓) shows the time when the maximum value was obtained.

laser excitation and dissociates gradually into free ions.

The solvent effect on the dissociation process is shown in Fig. 3. Faster rising curves are obtained in solvents with higher polarity, and the maximum value of the photocurrent in acetonitrile is reached immediately after excitation. These solvent effects are consistent with the following theoretical estimation of reaction rates. The rate constant of the diffusion-controlled dissociation was calculated by Eq. (1).[6,7]

$$k_{diss} = 4\pi N'(D_{A^-} + D_{D^+})a\delta/\Delta V(1-\exp(-\delta)) \quad (1)$$

where $\delta = e^2/\varepsilon kTa$ and $\Delta V = 4\pi N'a^3/3$. The notations are the same as in Ref. 7. The encounter distance a was assumed to be 7 Å. The experimental rate constant (k_{exp}) was determined from the exponential growth curve of the photocurrent. The results obtained are listed in Table 1. The k_{exp} in these solvents is almost identical with k_{diss}, but not with $1/\tau_f$. Thus the present solvent effect is well explained by assuming the diffusion-controlled dissociation mechanism.

As mentioned in the previous paper[1a], the ionic dissociation of the pyrene–DMA system occurs in the excited state nonrelaxed with respect to the solvation. Although the energy levels of the initial encounter complex, the solvated ion-pair, and the free ions of the pyrene–DMA system are almost equal to those of the pyrene–DCNB system, their dissociation processes are not similar. This difference may be characteristic of the "chemical property" of the quencher, although the precise nature of the "chemical property" is still unknown. Recently we have studied the ionic photodissociation of various pyrene-quencher systems in polar solvents and found no general relation between the yield of free ions and the strength of the EDA interaction.[3] It was emphasized that the "chemical property" of the quencher is a key for understanding the ionic photodissociation mechanism.

The Solvent Effect on the Yield of the Ion-pair Formation. The relative yield of ionic species (ion-pair or free ions) in acetonitrile and in dichloromethane was obtained by absorption spectral measurements. The ratio of the yields obtained immediately after the excitation in the former and the latter solvents was 1 : 0.25. On the other hand, the ratio obtained by comparing the maximum value of the transient photocurrent was 1 : 0.22. Since free ions are favored in acetonitrile,[8] the above agreement of the ratios for the spectral and the photocurrent data means that most of the ion-pair dissociate into ions even in dichloromethane. Therefore, the yield of ion-pair formation in some solvents may be estimated by examining the photo-

TABLE 2. QUANTUM YIELDS OF THE ION-PAIR FORMATION

Solvents	ε	ϕ_{pc}[a)]	ϕ_{ab}[b)]
Dichloromethane	8.93	0.08	0.25
1,2-Dichloroethane	10.4	0.11	
Pyridine	12.4	0.14	
Acetone	20.7	0.32	
Acetonitrile	37.5	0.38	1.00

a) ϕ_{pc} are the absolute yields obtained from the photocurrent data. b) ϕ_{ab} are the relative yields obtained from the absorption spectral measurements.

current data. As shown in Table 1, the rate constant of dissociation is larger than 10^7 s^{-1}, while the rate of the recombination of free ions is calculated to be 10^5—10^6 s^{-1}, since the rate constant of the diffusion-controlled process is 10^{10} M^{-1} s^{-1} and the concentration of ions is 10^{-4}—10^{-5} M. Since the decay of free ions due to the recombination is almost negligible at an early stage after the excitation, the dissociation may be approximately completed. Then the values of the current are proportional to the yield of the ion-pairs. The obtained yields are listed in Table 2.

The yield increases as the solvent polarity (dielectric constant) increases. The present results can be well explained with the following empirical equation for the relationship between the yield (ϕ) and the solvent dielectric constant (ε), proposed in the previous work[1a)].

$$\log\left(\frac{1}{\phi}-1\right)=\frac{p}{\varepsilon}+q \qquad (2)$$

where p and q represent constants. It has been pointed out[1a)] that the following two conclusions are given when Eq. (2) is satisfied: (1) The ionic photodissociation depending upon ε competes with the other radiationless processes independent of ε. (2) The identical dissociation mechanism is expected in various solvents. Therefore it may be concluded that the free ions in acetonitrile are also formed through the ion-pair and that some radiationless process independent of the solvent dielectric constant competes with the ion-pair formation.

Discussion on the Fluorescence Quenching Mechanism. The fluorescence quenching process has been studied in detail in various solvents by Mataga *et al.*[2,4b,9)] and by Weller *et al.*[7)] One of the main quenching processes has been pointed out to be the formation of the solvated ion-pair competing with the exciplex formation.[7)] However, there have been no observations concerning the dynamic behavior of the solvated ion-pair up to now, and the formation and dissociation processes of the solvated ion-pair have been made clear in the present work for the first time.

A quantitative analysis of the produced intermediates seems important for understanding the quenching processes. The yield of ions and the triplet molecule are estimated in the usual way.[4)] The yields of ions in acetonitrile and in dichloromethane were 0.38 and 0.08, respectively. On the other hand, the yields of the pyrene triplet in acetonitrile and in dichloromethane were 0.11 and 0.07, respectively. The sum of these yields is smaller than unity in both solvents and the residual radiationless transitions may compete with the above processes. This conclusion is in good agreement with the above result of the solvent effect on the ion-pair yield. Such a degradation process has not always been postulated in the previous papers. However, the former process seems to be important for elucidating the fluorescence quenching process due to the electron transfer in the excited EDA systems. This conclusion is consistent with the results of ionic photodissociation of pyrene–DMA, pyrene–electron acceptors, and tetracycnobenzene–aromatic hydrocarbon systems.[1,3,4a)]

Finally, the intersystem crossing process of the present system should be mentioned. In dichloromethane solution an appreciable amount of triplet molecules is formed at 50 ns (shown in Fig. 1) after the laser oscillation, when the decay of the ion-pair can be neglected. Therefore, a triplet formation through the solvated ion-pair of the present type may be excluded. Recently, similar results have been reported,[10)] although the nature of this particular behavior is not clear.

References

1) (a) H. Masuhara, T. Hino, and N. Mataga, *J. Phys. Chem.*, **79**, 994 (1975). (b) References cited therein.

2) Y. Taniguchi and N. Mataga, *Chem. Phys. Lett.*, **13**, 596 (1972); M. Shimada, H. Masuhara, and N. Mataga, *ibid.*, **15**, 364 (1972).

3) T. Hino, H. Akazawa, H. Masuhara, and N. Mataga, *J. Phys. Chem.*, **80**, 33 (1976).

4) (a) H. Masuhara, M. Shimada, N. Tujino, and N. Mataga, This Bulletin, **44**, 3310 (1971). (b) Y. Taniguchi, Y. Nishina, and N. Mataga, *ibid.*, **45**, 764 (1973).

5) H. Masuhara, N. Tsujino, and N. Mataga, *ibid.*, **46**, 1088 (1973); H. Masuhara and N. Mataga, *Z. Phys. Chem. N. F.* (Frankfurt am Main), **80**, 113 (1972); T. Kobayashi, S. Matsumoto, and S. Nagakura, *Chem. Lett.*, **1974**, 235.

6) M. Eigen, *Z. Phys. Chem. N. F.* (Frankfurt am Main), **1**, 176 (1954).

7) H. Knibbe, D. Rehm, and A. Weller, *Ber. Bunsenges. Phys. Chem.*, **72**, 257 (1968); H. Knibbe, Thesis, Free Univ., Amsterdam, 1969.

8) The concentration of free ions produced by exciting the pyrene–DMA–acetonitrile system was estimated by examining the absorption spectral and the photocurrent data. Within experimental errors both the estimations are in agreement which means that most of the produced ions are solvated separately.

9) T. Okada, H. Oohari, and N. Mataga, This Bulletin, **43**, 2750 (1970) and papers cited therein.

10) N. Orbach, J. Novros, and M. Ottolenghi, *J. Phys. Chem.*, **77**, 2831 (1973) and papers cited therein.

Proton Magnetic Resonance Spectra of Metal Ammine Complexes. VI.* The *trans*-Effect in Cobalt(III) Amine Compounds as Studied by the Rate of Hydrogen-Deuterium Exchange

Ushio SAKAGUCHI, Koichi MAEDA, and Hayami YONEDA
Department of Chemistry, Faculty of Science, Hiroshima University, Hiroshima 730

(Received June 30, 1975)

The rate of the isotopic deuterium exchange has been measured for several cobalt(III) amine complexes in D_2O. The substituents CN^-, NO_2^-, and possibly SO_3^{2-} decelerate the exchange of the amine protons *trans* to these ligands, leading in some cases to a smaller rate for these protons than for the *cis* ones. On the other hand, the *trans*-proton labilizing ligands include F^-, Cl^-, Br^-, H_2O, CO_3^{2-}, $OCONH_2^-$, N_3^-, CH_3NH_2, CH_3COO^-, and the malonate, fumarate, and oxalate ions. The above observation clearly indicates that the HD exchange rate can be a measure of the *trans*-effect of these ligand molecules.

In previous papers,[1-4] we have reported that the chemical shifts of amine protons of some cobalt(III) complexes are primarily determined by the magnetic anisotropy of the central metal ion. In pentaamine cobalt(III) compounds $[CoX(NH_3)_5]^{n+}$, the ammine proton chemical shifts could be quantitatively explained by using the theory based on the anisotropic magnetic field of the cobaltic ion along with the cobalt-59 chemical shifts. Small but significant discrepancies between the theory and the observations were noted for the *trans* hydrogens of the cyano- and nitro-pentaammine complexes. These hydrogens resonated at a field higher than that expected from the theory. The succeeding paper will deal with the assignment of the amine protons in the NMR spectra of bis(en) type complexes, where en is ethylenediamine. It will be shown that the chemical shifts of these protons can be explained in a manner similar to the pentaammines. The *trans* amine hydrogens of *cis*-$[Co(CN)_2en_2]^+$ appeared at a more shielded position than that the magnetic anisotropy of the metal ion would predict.

All the above phenomena seemed to point to an increase in the electron densities on these *trans* amine hydrogens. In other words, we attribute the discrepancies between the theory of chemical shift and the observed shift values to the inductive effects of the substituents. Thus, we expect that an increase or decrease in the electron density on a particular proton will be reflected in the rate of HD exchange of this proton. Here we report the results of measurements on the rate of hydrogen-deuterium exchange of ammine and amine protons of some cobalt(III) complexes. A part of the present paper has already been reported.[1]

Experimental

Materials. All the complexes investigated in this work are known compounds and were prepared by well-established methods. The identity of the complex was confirmed spectrophotometrically. Deuterium oxide (99.8 atom % D minimum) and dimethyl sulfoxide-d_6 (99.5 atom % D minimum) were purchased from Stohler Isotope Chemicals (Cal., U.S.A.).

Measurements. All the measurements were made on a Varian T-60 NMR spectrometer operating at 60 MHz and at a temperature of 30 °C. All the complexes except $[Co(NO_2)(NH_3)_5](NO_3)_2$ were dissolved in deuterium oxide to almost saturation and the signal intensities corresponding to amine hydrogens were measured at suitable time intervals. *t*-Buthyl alcohol was added as an internal reference for intensity if necessary. Since the solubility of the nitro-pentaammine compound in D_2O was too small, it was decided to use the dimethyl sulfoxide-d_6/D_2O mixed solution (90 : 10 wt%) as the solvent. Amine hydrogen signals of ethylenediamine overlapped, in some instances heavily, with the HDO signal, which tended to hamper an accurate measurement of intensities.

Results and Discussion

The rate of hydrogen exchange in cobalt(III) amine complexes was first reported by Anderson *et al.*[5] and the subsequent works of Block and Gold[6] and Basolo and his coworkers[7-9] established the following points: (i) the rate of HD exchange is specific hydroxide ion catalysed and is proportional to the concentration of OH^- ions, (ii) the observed pseudo-first-order rate constant is independent of the concentration of the metal ion, and (iii) the rate is unaffected by the added salt if the proper correction for the solution pH has been made according to (i). The results of Yamatera and Fujita[10] appeared to put forward an important objection to (iii). All these workers and others[11-16] reported that in a particular compound the amine protons *trans* to a substituent exchange faster than those *cis* to the substituent. However, this statement was necessarily non-definitive since these authors

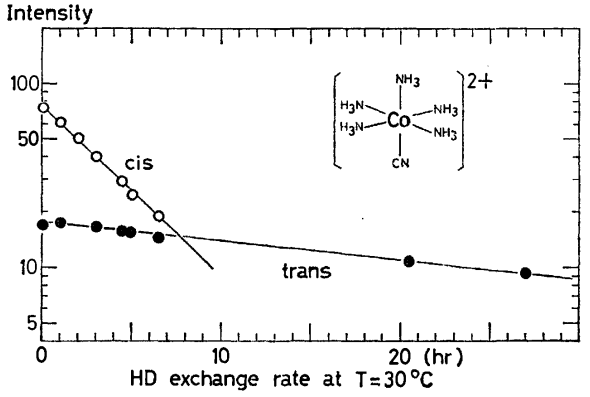

Fig. 1. The changes in ammine proton signal intensities of $[CoCN(NH_3)_5]^{2+}$ in D_2O.

* Part V: H. Yoneda, K. Maeda, and U. Sakaguchi, *Chem. Lett.*, **1975**, 107.

measured the overall rates. Separate rates for *cis* and *trans* hydrogens were first obtained by Clifton and Pratt[11] for fumaratopentaammine cobalt(III) ion, followed by the measurements of Buckingham *et al.*[14] on $[CoCl(NH_3)_5]^{2+}$ and $[CoCl(CH_3NH_2)_5]^{2+}$. Basolo *et al.*[7-9] obtained two rate constants for *cis*-$[Co(NO_2)_2(NH_3)_4]^+$ and *cis*-$[Co(NO_2)_2en_2]^+$ and Basolo and Pearson[17] stated, in their recent review, that it is not known whether the hydrogens exchanging faster are those *trans* to NO_2^- or to NH_3 and en. We solved this problem by obtaining a method for assigning NMR signals of coordinated NH_3 or en.[1-3] Thus, all the data described in the literature can now be considered to have reported that *trans* ammine protons are more labile against deuterium substitution than *cis* ones. Our present data offer another type of example, where the *trans* hydrogens are *less* labile. This is especially noted for compounds containing the cyanide, nitrite, and possibly sulfite ions.

Pentaamines. We have measured the exchange rate for cyano-, nitro-, and fluoro-pentaamine complexes. In this type of compounds, the assignment of the NMR signals follows immediately from their intensities. The result for the cyano compound is illustrated in Fig. 1. The data are summarized in Table 1 in terms of the pseudo-first-order rate constants. As is evident from Fig. 1, the *trans* hydrogens exchange an order of magnitude more slowly than the remaining four *cis* protons: $k_t=6.2\times10^{-6}$ s^{-1} and $k_c=6.0\times10^{-5}$ s^{-1}. k_t and k_c stand for the pseudo-first-order rate constants for *trans* and *cis* hydrogens. The nitropentaammine compound gives only a single absorption when it is dissolved in dimethyl sulfoxide or trifluoroacetic acid. This was shown[4] to be a mere coincidence of the *trans* and *cis* absorptions. For reasons mentioned previously, the rate for this compound was obtained in the dimethyl sulfoxide-d_6/D_2O mixed solvent. Separate rates for the *cis* and *trans* ammonia hydrogens can, however, be obtained by fitting the intensity-time data to an expression $[4\exp(-k_ct)+\exp(-k_tt)]$; see Fig. 2. It can readily be seen that the *trans* hydrogens are less labile than the *cis* ones. Since the rates of this compound were measured in mixed solvent, it may not pertinent to compare this data with those of the other complexes

TABLE 1.

Complex	k_c[a]	k_t[a]	Other rates[a]
$[CoCN(NH_3)_5](ClO_4)_2$	60	6.2	
$[CoNO_2(NH_3)_5](NO_3)_2$	180	17	
$[CoF(NH_3)_5](NO_3)_2$	58	(fast)	
cis-$[Co(CN)_2(NH_3)_4]Cl$	390	62	
$[Co\text{-}(CO_3)(NH_3)_4]_2SO_4$	1300	2200	
cis-$[Co(CH_3COO)_2\text{-}(NH_3)_4]ClO_4$	140	680	
cis-$NH_4[Co(SO_3)_2(NH_3)_4]$	(fast)	490[b]	
$[Co(NH_3)_4en](NO_3)_3$	1500	6500	3200[c]
cis-$[Co(CN)_2en_2]Cl$	680	310	

a) In units of 10^{-6} s^{-1}. b) For the assignment, see text. c) NH_2 protons.

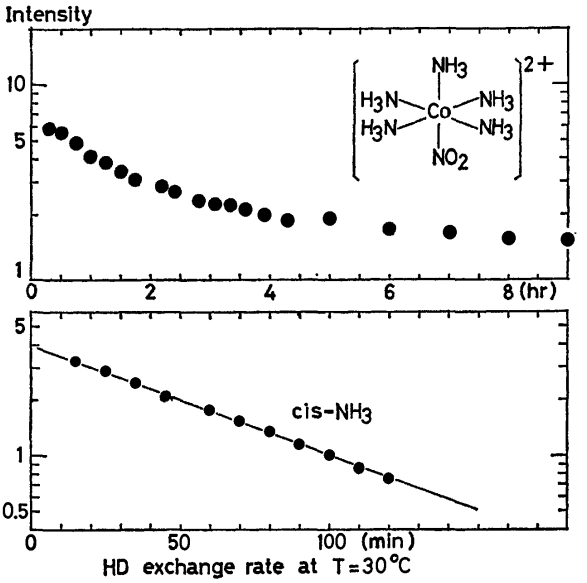

Fig. 2. HD exchange in $[Co(NO_2)(NH_3)_5]^{2+}$; (upper) experimental data, (lower) data analysed for *cis* ammine hydrogens.

for which deuterium oxide was used as the solvent.

Previously, Palmer and Basolo[8] obtained only a single rate constant for HD exchange in fluoro-, chloro-, bromo-, and nitro-pentaammine compounds. Basolo *et al.*[9] reported that all of the hydrogens of $[CoCl(NH_3)_5]^{2+}$ exchange at the same rate. Clifton and Pratt[11] showed that the rate of exchange of the *trans* ammonia protons is two orders of magnitude greater than that of the *cis* protons. Buckingham *et al.*[14] found that the *trans* hydrogens of $[CoCl(NH_3)_5]^{2+}$ and $[CoCl(CH_3NH_2)_5]^{2+}$ exchange with deuterium sixty times faster than the *cis* ones, thus invalidating the statement of Basolo *et al.* on the chloropentaammine complex. Further, for $[CoX(NH_3)_5]$ (X=H_2O, N_3^-, $OCONH_2^-$, Cl^-, and Br^-) they obtained spectra where the *trans* NH_3 was completely deuterated, leaving the four *cis* NH_3 groups substantially unaffected. Therefore, the *trans* ammine protons have been believed to be the more labile in pentaammine complexes containing H_2O, F^-, Cl^-, Br^-, N_3^-, $OCONH_2^-$, NO_2^-, and the fumarate ion.

In summary, the substituents X=CN^- and NO_2^- decelerate the *trans* hydrogens, while F^-, Cl^-, Br^-, H_2O, N_3^-, $OCONH_2^-$, CH_3NH_2, and the fumarate ion labilize the *trans* protons.

cis-*Tetraammine and* cis-*Bis(ethylenediamine) Complexes.* Block and Gold[6] and Basolo *et al.*[9] reported only one rate constant for $[Co(ox)(NH_3)_4]^+$ and *cis*-$[Co(NH_3)_2en_2]^{3+}$, where ox is the oxalate ion. Clifton and Pratt[11] observed that in *cis*-$[CoCl_2en_2]^+$ the *trans* protons are the faster, but their measurements of the rates were complicated by aquation and a subsequent isomerization of the complex. The only examples where separate rates for *trans* and *cis* hydrogens were obtained were *cis*-$[Co(NO_2)_2(NH_3)_4]^+$ and *cis*-$[Co(NO_2)_2en_2]^+$.[8]

The complexes of the types *cis*-$[CoX_2(NH_3)_4]$ and *cis*-$[CoX_2en_2]$ exhibit two singlets with an intensity

ratio 1 : 1 if these compounds are dissolved in D_2O. Thus, the signal assignment to the *trans* and *cis* hydrogens is not so straightforward as in pentaammine complexes. In the previous papers, we outlined the method for the assignment. Qualitatively, the *trans* hydrogens are more deshielded than the *cis* ones if the ligand X is a strong-field ligand, *e.g.*, CN^- or NO_2^-. For a weak ligand X, the *trans* hydrogens resonate at higher magnetic field. In this way we could assign almost all resonances examined in this work.

Figure 3 gives the result for *cis*-$[Co(CN)_2en_2]^+$. As in the case of the cyanopentaammine complex, the cyanide ion can be seen to decelerate the *trans* protons. The result for *cis*-$[Co(CN)_2(NH_3)_4]^+$ is illustrated in Fig. 4, which also shows that the *trans* hydrogens appearing at lower field than the *cis* ones are the less labile against deuterium substitution. The rate of the *trans* protons is about one-sixth of that of the *cis* protons. For *cis*-$[CoX_2(NH_3)_4]$ containing CH_3COO^-, en, and CO_3^{2-}, it was found that the *trans* protons are the more labile: see Fig. 5 and Table 1.

The complex *cis*-$[Co(SO_3)_2(NH_3)_4]^-$ shows two absorptions in water, while in D_2O only one signal can be observed, at a position coincident with that of the high field signal observed in water. This indicates that the low field signal disappears rapidly on dissolving in D_2O. Since no cobalt-59 chemical shift value is available for sulfito-containing compounds, we can make no assignment for these signals. However, it is highly probable that the high field signal which exchanges slowly is due to the *trans* ammonia. Numerous examples suggestive of a large *trans*-ligand labilizing effect of the sulfite ion are well documented.[17-20] Thus, it will be reasonable to assume that the *trans* hydrogens are upfield shifted owing to this *trans*-labilizing effect (see below). This deduction is not inconsistent with the slower rate for these *trans* hydrogens.

Separate rates for the *cis* and *trans* hydrogens of *cis*-$[Co(NO_2)_2en_2]^+$ and *cis*-$[Co(NO_2)_2(NH_3)_4]^+$ have been reported by Palmer and Basolo.[8] They noticed that the slower rates are about the same as the rates for the corresponding *trans* isomers and therefore they assigned the greater lability to the *trans* hydrogens. Their assignments, however, didn't seem to be sound enough and we re-examined both complexes. The complex *cis*-$[Co(NO_2)_2en_2]^+$ shows two NH_2 resonances. The signal situated at lower field exchanges with deuterium and disappears rapidly. The high field line exchanges much more slowly.

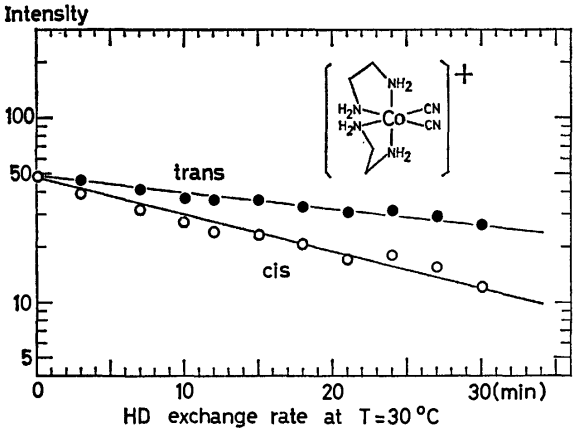

Fig. 3. The rate of hydrogen exchange in *cis*-$[Co(CN)_2en_2]^+$.

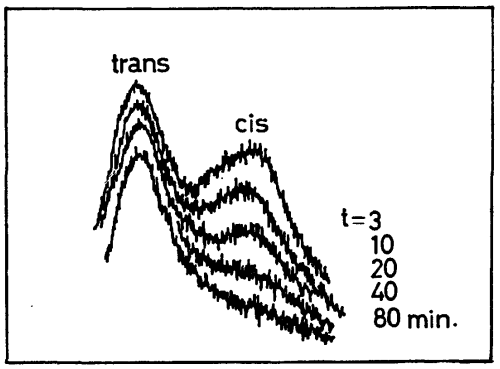

Fig. 4. The spectra of *cis*-$[Co(CN)_2(NH_3)_4]^+$ in D_2O observed at suitable time intervals after dissolution.

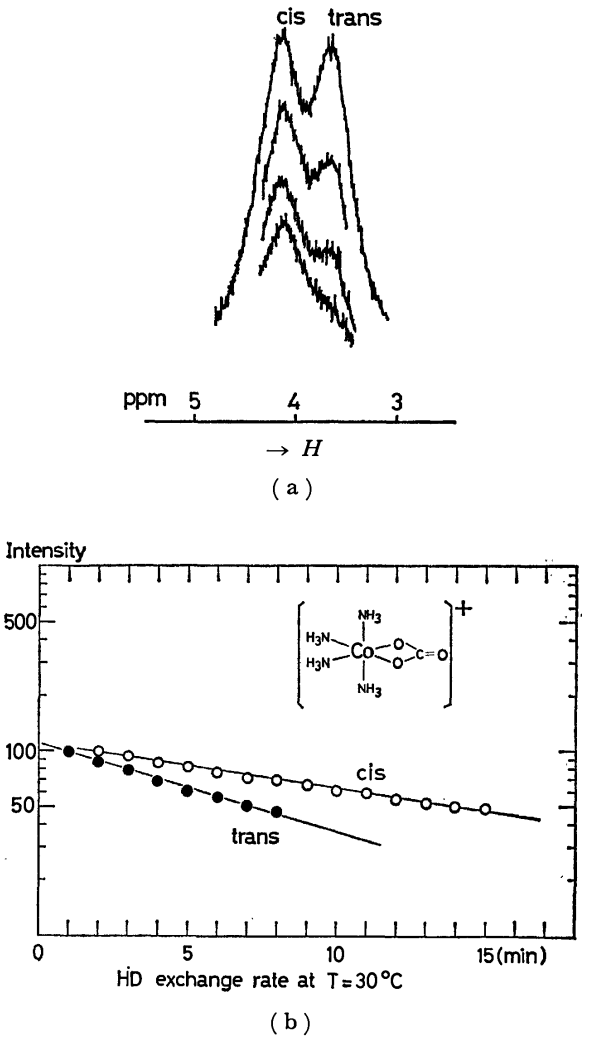

Fig. 5. (a) The spectra of $[CoCO_3(NH_3)_4]^+$ taken at every four minutes. (b) The plot of the signal intensities of ammine hydrogens in $[CoCO_3(NH_3)_4]^+$ against time.

In the preceding papers, we assigned the low field signal to the *trans* amines based on the magnetic anisotropy of the cobalt ion. If our assignment is correct, then it follows that the *trans* hydrogens are the more labile. This is in line with the deduction of Basolo and Palmer. *cis*-$[Co(NO_2)_2(NH_3)_4]^+$ exhibits only a single absorption in D_2O and in acidified D_2O. Therefore, we cannot tell which hydrogens are exchanging faster. It is to be noted that in $[Co(NO_2)(NH_3)_5]^{2+}$ the *trans* hydrogens are the slower, while in *cis*-$[Co(NO_2)_2en_2]^+$ and probably in *cis*-$[Co(NO_2)_2(NH_3)_4]^+$ they are the faster. We cannot at present give any explanation for this observation.

The trans-*Effect.* As is evident from the previous discussions, the exchange rate of amine hydrogens is greatly affected by the substituent *trans* to the protons under consideration. In conjunction with all the literature data, it can be concluded that the effect of the ligand X is primarily the most prominent on the *trans* (to X) hydrogens.

In general, coordinated ligand molecules are under the electron-withdrawing effect of the positively charged metal ions. Therefore, if the Co–NH_3 bond become strengthened for some reason, the electron density on this nitrogen atom will be decreased, with a concomitant labilization of the hydrogen atoms attached to this nitrogen. Conversely, if the Co–N bond is weakened, the electron density on this nitrogen atom will be restored, with the result that the hydrogen atoms bound to this nitrogen atom become less labile. This reasoning explains almost all the foregoing observations. Fujiwara *et al.*[21] have shown from the analysis of their cobalt-59 chemical shift data that the cobalt-cyanide, cobalt-nitro, and cobalt-sulfur bondings are much more covalent than the other Co-oxygen, Co-halogen(pseudohalogen), and Co-nitrogen bondings. Thus, if we presume that the cobalt-nitrogen bonds *trans* to the cyanide, nitrite, and sulfite ions assume the more ionic character, the deceleration of the exchange rates of the hydrogens attached to these nitrogen atoms may be expected.

If we assume that the rate of HD exchange results at least partially from the ground-state weakening of the *trans* Co–N bonds, we can expect the structural *trans*-effect especially for complexes with *trans*-decelerating ligands. It is rather difficult, as pointed out by Pratt and Thorp,[18] to decide whether any bond-length variation is significant and therefore whether this can be ascribed to effects of the lattice and the counter ion(s). With this in mind, we first note that Snow[22] added the carbonato ion to a growing list of anions including NO_2^-, Cl^-, thiosulfate, and thiocyanate (both sulfur ligands are sulfur-bonded) which do not show the structural *trans*-effect in ammine cobalt(III) compounds. The crystal and molecular structures of $[CoCN(NH_3)_5]Cl_2$ and $[CoCN(NH_3)_5](ClO_4)_2 \cdot 0.5H_2O$ have been determined by Ozbirn and Jacobson.[23] Although they did not state so explicitly in their paper, the *trans* Co–N bonds in both complexes are definitely longer than the *cis* ones. The differences of the bond lengths are 0.031 and 0.027 Å for the former and the latter compounds, respectively, which are well beyond the experimental uncertainties of thier work. Elder and Trkula[24] reported that the large *trans*-effect of sulfite ion is evident in the molecular structure of $[Co(SO_3)(NH_3)_5]^+$, where the *trans* Co–N bond length is 2.055(2)Å and the corresponding *cis* ones are 1.962—1.972(average= 1.966(4))Å. In *trans*-$[Co(SO_3)(NCS)en_2] \cdot 2H_2O$, the sulfite ion is reported,[25] however, to cause no significant bond lengthening. As is apparent from the examples of the sulfito- and nitro-containing compounds, the results of the molecular structure determination do not completely parallel the hydrogen exchange rates. In some cases, however, the *trans*-bond lengthening effect has really been observed.

Conclusion

Thr rate of HD exchange can be considered to be a manifestation of the *trans*-effect; the cyanide, nitrite, and possibly sulfite ions decelerate the exchange of *trans* hydrogens while F^-, Cl^-, Br^-, H_2O, N_3^-, CH_3COO^-, CO_3^{2-}, $OCONH_2^-$, ox, CH_3NH_2, and malonate ion tend to labilize the *trans* NH hydrogens. It will be noted that these *trans*-accelerating ligands are all weak-field ligands and are situated at lower positions than NH_3 or en in the spectrochemical series. This correlation of the HD exchange rate with the spectrochemical series has been rationalized qualitatively in terms of the electron donating or withdrawing power of the substituents. Furthermore, the crystal structure data seem to indicate that the effect of substituents, especially that of the *trans*-decelerating ligands, results at least partially from the ground-state weakening of the *trans* Co–N bonds.

References

1) H. Yoneda, U. Sakaguchi, and K. Maeda, *Chem. Lett.*, **1975**, 107.
2) Y. Nakashima, U. Sakaguchi, and H. Yoneda, This Bulletin, **48**, 762 (1975).
3) Y. Nakashima, *ibid.*, **48**, 766(1975).
4) Y. Nakashima, U. Sakaguchi, and H. Yoneda, *Chem. Lett.*, **1974**, 503.
5) J. S. Anderson, H. V. A. Briscoe, N. L. Spoor, *J. Chem. Soc.*, **1943**, 361.
6) H. Block and V. Gold, *ibid.*, **1959**, 966.
7) J. W. Palmer and F. Basolo, *J. Inorg. Nucl. Chem.*, **15**, 279 (1960).
8) J. W. Palmer and F. Basolo, *J. Phys. Chem.*, **64**, 778 (1960).
9) F. Basolo, J. W. Palmer, and R. G. Pearson, *J. Amer. Chem. Soc.*, **82**, 1073 (1960).
10) H. Yamatera and M. Fujita, This Bulletin, **42**, 3043 (1969).
11) P. Clifton and L. Pratt, *Proc. Chem. Soc.*, **1963**, 339.
12) D. A. Buckingham, I. I. Olsen, and A. M. Sargeson, *Aust. J. Chem.*, **20**, 597 (1967).
13) M. Parris, *J. Chem. Soc., A*, **1967**, 583.
14) D. A. Buckingham, B. M. Foxman, and A. M. Sargeson, *Inorg. Chem.*, **9**, 1970 (1970).
15) S. Hayashi, *Nippon Kagaku Zasshi*, **86**, 364 (1965).
16) C. K. Poon and H. W. Tong, *J. Chem. Soc., Dalton*, **1974**, 930.
17) F. Basolo and R. G. Pearson, *Prog. Inorg. Chem.*, **4**, 381 (1962).

18) J. M. Pratt and R. G. Thorp, *Advan. Inorg. Chem. Radiochem.*, **12**, 375 (1969).
19) T. G. Appleton, H. C. Clark, and L. E. Manzer, *Coord. Chem. Rev.*, **10**, 335 (1973).
20) F. R. Hartley, *Chem. Soc. Rev.*, **2**, 163 (1973).
21) S. Fujiwara, F. Yajima, and A. Yamasaki, *J. Magn. Resonance*, **1**, 203 (1969).
22) M. R. Snow, *Aust. J. Chem.*, **25**, 1307 (1972).
23) W. Ozbirn and R. A. Jacobson, *Inorg. Chim. Acta*, **4**, 377 (1970).
24) R. C. Elder and M. Trkula, *J. Amer. Chem. Soc.*, **96**, 2635 (1974).
25) S. Baggio and L. N. Becka, *Acta Crystallogr.*, **B25**, 946 (1969).

Proton Magnetic Resonance Spectra of Metal Ammine Complexes. VII.* Amine Proton Chemical Shifts in Bis(ethylenediamine)cobalt(III) Compounds

Ushio SAKAGUCHI, Shigeo YAMAZAKI, and Hayami YONEDA

Department of Chemistry, Faculty of Science, Hiroshima University, Hiroshima 730

(Received June 30, 1975)

Amine proton chemical shifts have been measured for some *cis*-bis(ethylenediamine)cobalt(III) complexes in trifluoroacetic acid. The shifts can be explained quantitatively by the magnetic anisotropy of the central metal ion and by assuming fast conformational inversion of chelate rings. Discrepancy between the observed and the computed shift values is apparent, however, for the *trans* hydrogens of the *cis*-dicyano compound, which may be due to the ground-state *trans*-effect of the cyanide ion. The chemical shifts of amine protons of *cis*-tetraammine and *cis*-bis(trimethylenediamine)compounds have been briefly discussed.

We have been interested in the proton chemical shifts of cobalt(III) ammine and amine compounds and have succeeded in explaining the ammine chemical shifts in pentaammine complexes $[CoX(NH_3)_5]^{n+}$.[1-5] In previous papers it was shown that the anisotropy of the paramagnetic term of the magnetic susceptibility of the central metal ion is responsible for the shift variation of coordinated ammonia molecules.

We here report the results of the chemical shift measurements on *cis*-bis(ethylenediamine)cobalt(III) compounds, *cis*-$[CoX_2en_2]$, in trifluoroacetic acid and the results are discussed in terms of the magnetic anisotropy of the cobalt ion. This paper makes the first step of our investigations on bis(en) complexes and an interpretation of the ethylenic part of the PMR spectra in relation to the conformation of en rings will be reported in subsequent publications. Although the PMR spectra of cobalt(III) ethylenediamine complexes have been studied by several workers,[6-21] no clear-cut explanation has been given, however, to chemical shifts and/or band shapes. Clifton and Pratt[12] enumerated several effects as probable causes of the different NH absorptions. These include the intramolecular hydrogen bonding between the *cis* amine groups and the ligand, the effects of magnetic anisotropy of the ligand, and a reduced polarity of the *trans* amine group due to polarization of the metal ion by the negative ligand. While it is clear that the substituent X must affect NH chemical shifts the reasons were not immediately apparent. Lantzke and Watts[11] considered similarly. Since they also had no quantitative measure of the extent of shielding or deshielding by each ligand, it was not possible to decide which hydrogens give rise to which resonance. Hendrickson and Jolly[15] may be the first to note the importance of the magnetic anisotropy of the central metal ion. Thus, they could predict that the *trans* protons resonate at higher field than the *cis* ones for weak-field ligand X and the opposite trend is possible for strong-field ligands.

Experimental

All the complexes used in this work are known compounds and were prepared by well-established methods. The complex prepared were identified spectrophotometrically. Trifluoroacetic acid of extra pure grade, purchased from Katayama Chemical Industries Co., Ltd., was used as the solvent. The measurement was made on a Varian A-60 or T-60 spectrometer at ambient probe temperature. Sodium 2,2-dimethyl-2-silapentane-5-sulfonate (DSS) was used as an internal standard for the chemical shift.

Method of Calculation

Theoretical. In this paper the chemical shift difference between the *cis* and *trans* ammine protons will be considered. If we attribute this difference to the anisotropy of the temperature-independent paramagnetism or the second-order paramagnetism of the cobalt(III) ion, and if the point-dipole approximation is appropriate to the problem, we can derive an equation for the chemical shift of ligand protons under the influence of the magnetic anisotropy of the cobalt(III) ion. Under these conditions Ramsey's expression for chemical shielding is reduced to[1-4]

$$\sigma = \left(\frac{1}{R^3} - \frac{3RR}{R^5}\right)\chi^{\mathrm{p}} \tag{1}$$

All the notations have their usual significances.[1-3] The paramagnetic term of the magnetic susceptibility of a cobalt(III) ion, χ^{p}, can generally be related[2,3] to the shielding constant of the cobalt-59 nucleus, $\sigma^{\mathrm{p}}(^{59}\mathrm{Co})$, as

$$\chi^{\mathrm{p}} = -\sigma^{\mathrm{p}}(^{59}\mathrm{Co})/2\langle r^{-3}\rangle \tag{2}$$

Here $\langle r^{-3}\rangle$ is an average of r^{-3} over a metal 3d orbital. Fujiwara *et al.*[22] discovered that the cobalt-59 chemical shift of the [Co(ABCDEF)] complex is given, to a good approximation, by the sum of contributions from each ligand A to F, see Fig. 1 and Ref. 3.

$$\sigma^{\mathrm{p}}_{\mathrm{iso}}(^{59}\mathrm{Co}) = \sum_{\mathrm{X}} (2/3)\sigma(\mathrm{X}) \tag{3}$$

In this equation $\sigma^{\mathrm{p}}_{\mathrm{iso}}(^{59}\mathrm{Co})$ is the observed shift of the cobalt-59 resonance and $\sigma(\mathrm{X})$ is the contribution from the ligand X. $\sigma(\mathrm{X})$ values for typical ligands are given in Ref. 3. This additivity originates from the relations[3]

$$\sigma^{\mathrm{p}}_{xx}(^{59}\mathrm{Co}) = \sigma(\mathrm{C}) + \sigma(\mathrm{D}) + \sigma(\mathrm{E}) + \sigma(\mathrm{F}) \tag{4}$$

$$\sigma^{\mathrm{p}}_{yy}(^{59}\mathrm{Co}) = \sigma(\mathrm{A}) + \sigma(\mathrm{B}) + \sigma(\mathrm{E}) + \sigma(\mathrm{F}) \tag{5}$$

$$\sigma^{\mathrm{p}}_{zz}(^{59}\mathrm{Co}) = \sigma(\mathrm{A}) + \sigma(\mathrm{B}) + \sigma(\mathrm{C}) + \sigma(\mathrm{D}) \tag{6}$$

Although these equations can predict cobalt-59 chemical shifts with few exceptions and with a good accuracy,[22] it is somewhat open to question, whether they can

* Part VI; U. Sakaguchi, K. Maeda, and H. Yoneda, This Bulletin, **49**, 397 (1976).

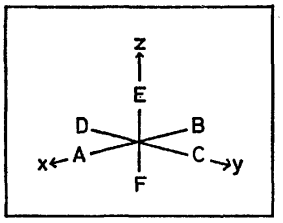

Fig. 1. The definition of the coordinate system for the complex [Co(ABCDEF)].

predict with any accuracy the anisotropy of cobalt-59 chemical shifts, which is relevant to the present investigation. In pentaammine cobalt(III) compounds, evidence has been given to their accuracy with which they predict the anisotropy.[4] If we assume the validity of the above additivity for *cis*-bis(en) complexes also, the proton chemical shift is given by an average of the following principal values of the shielding tensor.

$$\sigma_{xx} = -(1-3\sin^2\theta\cos^2\phi)(\sigma(C)+\sigma(D)+\sigma(E)+\sigma(F))/2R^3\langle r^{-3}\rangle \quad (7)$$

$$\sigma_{yy} = -(1-3\sin^2\theta\sin^2\phi)(\sigma(A)+\sigma(B)+\sigma(E)+\sigma(F))/2R^3\langle r^{-3}\rangle \quad (8)$$

$$\sigma_{zz} = -(1-3\cos^2\theta)(\sigma(A)+\sigma(B)+\sigma(C)+\sigma(D))/2R^3\langle r^{-3}\rangle \quad (9)$$

We will show that these expressions, along with the data of cobalt-59 chemical shifts, can give a good description of the chemical shift variation of amine hydrogens of *cis*-$[CoX_2en_2]$ ions.

Geometry of Complexes and Conformational Inversion of Chelate Rings. We approximate the arrangement of six nitrogen ligands around the cobalt ion to a regular octahedron and assume that all amine protons lie on the coordinate axes defined on this octahedron. The reason for this choice is as follows. First, we started with a more accurate model by using the crystallographically determined positions of amine protons in $(+)_{495}$-$[Coen_2(L\text{-glu})](ClO_4)$,[23] where L-glu represents the L-glutamate ion. In this molecule en rings assume the *gauche* conformation and the distance R between the amine proton(s) and the metal ion was calculated at around $R=2.53$ Å (4.77 a.u.). These geometrical factors coupled with Eqs. (7) to (9) render the chemical shift of eight amine protons of bis(en) compounds. For *cis*-$[CoCl(NO_2)en_2]^+$, the shift values ranging from -0.48 ppm to $+0.75$ ppm (relative to the shift of $[Coen_3]^{3+}$) were obtained. Thus, we should expect eight absorption lines, which is not in accord with the observation.[11] The discrepancies between the observed shift values and the computed ones are readily apparent for other *cis*-bis(en) complexes also. Therefore, we adopted a more realistic model, in which the fast conformational interconversion of the chelate rings are allowed. The shift values were calculated for amine protons situated at their averaged positions. In this model, four amine hydrogens *cis* to X are to appear as a single absorption, which should be the case with the *trans* protons. After taking the effect of fast conformational inversion into account, we obtain the chemical shift of *cis* NH_2 as

$$\sigma_{iso} \simeq -1.625(\sigma(en)/2 - \sigma(X))/6R^3\langle r^{-3}\rangle \quad (10)$$

For *trans* NH_2 we have

$$\sigma_{iso} \simeq 0.8125(\sigma(en)/2 - \sigma(X))/6R^3\langle r^{-3}\rangle \quad (11)$$

Likewise a singlet is expected for *trans*-$[CoXYen_2]$ at a position specified by

$$\sigma_{iso} \simeq 0.8125(\sigma(X) + \sigma(Y) - \sigma(en))/6R^3\langle r^{-3}\rangle \quad (12)$$

This model leads to four absorption lines for *cis*-$[CoXYen_2]$ corresponding to *trans* (to X) NH_2, *trans* (to Y) NH_2, and the two types of NH_2 groups both *cis* to X and Y. This expectation is not in line with the observation.[11] Further, these equations give shift values which are in poorer agreement with the measurement than does the next model. Thus, we are led to the simplest model where all amine hydrogens are on the coordinate axes of a regular octahedron. In this model the *cis* hydrogens of *cis*-bis(en) compounds appear at

$$\sigma_{iso} \simeq -2(\sigma(en)/2 - \sigma(X))/6R^3\langle r^{-3}\rangle \quad (13)$$

and the *trans* protons appear at

$$\sigma_{iso} \simeq (\sigma(en)/2 - \sigma(X))/6R^3\langle r^{-3}\rangle \quad (14)$$

The expected shift pattern may roughly be summarized as follows; (i) the *cis* hydrogens resonate at lower magnetic field than the *trans* ones if the ligand X is lower than en in the spectrochemical series, and (ii) if X is a strong-field ligand, then the opposite behavior is expected, see Fig. 2. In Fig. 2, the angle between the cone and the z-axis is 54°44′ corresponding to $(3\cos^2\theta-1)=0$. It should be noted that Eqs. (7) to (14) give shift values as measured from the chemical shift of $[Coen_3]^{3+}$. The value of $\langle r^{-3}\rangle$ was chosen to be 5.77 a.u.[2] of $[Co(NH_3)_6]^{3+}$ for all the complexes investigated here.

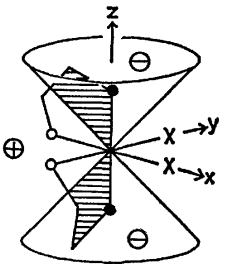

Fig. 2. A schematic presentation of the shift behavior expected for *cis*-$[CoX_2en_2]$, where X is assumed to be a weak-field ligand. Plus and minus refer to up- and down-field shifts, respectively.

Results

Typical examples of PMR spectra of *cis*-$[CoX_2en_2]$ complexes in trifluoroacetic acid are given in Fig. 3. In Fig. 3, the absorptions around $\tau=3$ ppm are due to methylene protons and those ranging from $\tau=4$ to 6 ppm due to amine hydrogens. The results of our measurements on *cis*-bis(en) compounds with substituents X=CN^-, NO_2^-, NCS^-, N_3^-, Cl^-, Br^-, CH_2ClCOO^-, and X_2=oxalate ion are illustrated in Fig. 4,

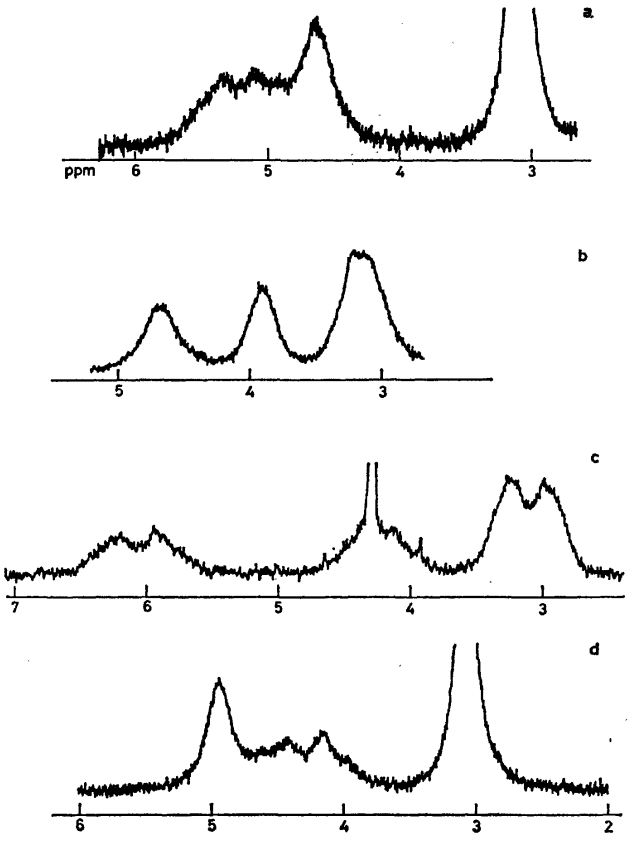

Fig. 3. Typical examples of the PMR spectra of *cis*-bis(en) complexes measured in trifluoroacetic acid. (a) *cis*-$[Co(ox)en_2]^+$, (b) *cis*-$[Co(CN)_2en_2]^+$, (c) *cis*-$[Co(CH_2ClCOO)_2en_2]^+$, and d) *cis*-$[Co(NO_2)_2en_2]^+$.

together with the computed shift values.

Discussion

cis-$[CoX_2en_2]$. We can see at once from Fig. 4 that the theory based on the magnetic anisotropy of the central cobalt(III) ion can explain not only the orders of magnitude of the chemical shifts of amine protons but also their exact values. From this we draw some important conclusions. First, it can be concluded that the chemical shift of these amine hydrogens are primarily determined by the anisotropy of the magnetic susceptibility of the metal ion. We employed several drastic approximations in computing the shielding constants. We approximated the symmetry around the cobalt ion to a regular octahedron and placed all amine protons on the coordinate axes. The same Co–H distances were assumed for all the complexes examined. Further, our model is based on the point-dipole approximation and the additivity of cobalt-59 chemical shifts. Fast conformational inversion was postulated to obtain a better agreement with the observation. The fact that we could obtain an excellent agreement with the observation notwithstanding all these approximations suggests that the magnetic anisotropy of the metal ion has the prime importance in determining the shift values of these compounds.

In our model the effect of covalency between the cobalt and nitrogen or X atoms are taken into consideration implicitly *via* the shielding constants of cobalt-59 nuclei. The abscissa in Fig. 4 is the wavelengths of the first absorption maxima of the corresponding compounds. No simple linear relation exists between the shift values and the wavelengths of the first absorption maxima. This may be a clear indication that we should take the covalency into account. Hendrickson and Jolly[15] argued that the trend of the chemical shifts of $[CoX(NH_3)_5]$ does not exactly match the spectrochemical series since in the shielding expression the exponential factor of the metal radial functions might be expected to vary.[24] With this reservation in mind we can expect the qualitative shift pattern as shown in Fig. 2.

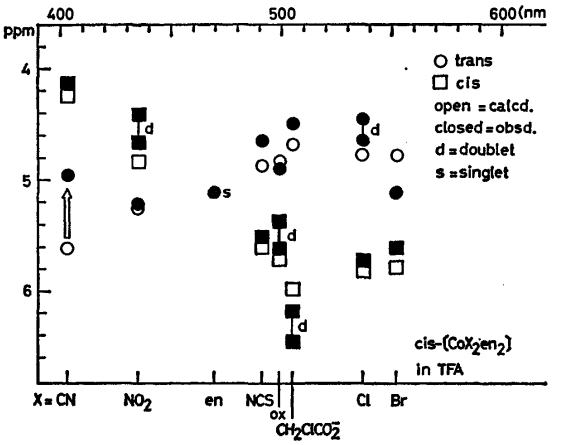

Fig. 4. A plot of the computed shift values of amine hydrogens against the observed shifts. TFA stands for trifluoroacetic acid.

While the agreement between the computed and the measured shifts is surprisingly good for complexes with NO_2^-, NCS^-, Cl^-, Br^-, CH_2ClCOO^-, and oxalate ion, the *trans* hydrogens of the dicyano compound appear at a position much higher than that expected from the theory. The shift of the *cis* hydrogens is fully explained. The discrepancy for the *trans* protons seems to be ascribed to the large inductive effect of the cyanide ion.[25] Fujiwara *et al.*[26] showed from the analysis of cobalt-59 chemical shifts that the Co–CN bond is the most covalent among the Co–O, Co–halogen, or Co–N bonds. Let us consider the CN–Co–NH_2 fragment with NH_2 *trans* to CN^-. The electron density on the NH_2 nitrogen atom will, thus, be restored to a great extent, with a concomitant weakening of the *trans* Co–NH_2 bonding. This will result in an enhanced shielding of the amine hydrogens under consideration, which is just in accord with the observation, see Fig. 4. These inductive effects were not properly taken into account in our model. An increase or decrease in electron density on an amine hydrogen atom will be detected as the rate of hydrogen deuterium exchange or as the pK_a value of the complex. Evidence supporting this deduction has really been obtained for pentaammine and *cis*-bis(en) complexes.[25,27] This result and its implication were discussed in Part VI of this series.

Tetraammines. We here discuss the empirical rule of Jolly *et al.*[14] for tetraammine cobalt(III) com-

plexes. They found that if we assume that the chemical shift of a coordinated ammonia molecule is the sum of five terms characteristic of the other five ligands and their positions, then it is possible, using the data of a series of compounds $[CoX(NH_3)_5]$, to estimate the chemical shift values of ammonia molecules in tetraammine complexes. It seems worthwhile to show that this empirical rule can be accomodated properly in our theory which is based on the magnetic anisotorpy of the cobalt(III) ion. For the pentaammine compound, we take the z-axis as the symmetry axis of the molecule. The chemical shift of the *trans* ammonia protons of this molecule is given by[3]

$$\sigma_{1so} \simeq (3\cos^2\theta-1)(\sigma(NH_3) - \sigma(X))/6R^3\langle r^{-3}\rangle \quad (15)$$

Similarly the shielding constant of the *cis* protons is given, after allowing for the rapid rotation of ammonia molecules around their C_3 axes, by the expression

$$\sigma_{1so} \simeq -(3\cos^2\theta-1)(\sigma(NH_3) - \sigma(X))/12R^3\langle r^{-3}\rangle \quad (16)$$

Here θ is the angle between the Co–N and Co–H axes and is unaffected by the NH_3 rotation. The above equations may be reinterpreted in the following way. If we define the quantity Δ_X, which is characteristic of the ligand X, by

$$\Delta_X \equiv (3\cos^2\theta-1)(\sigma(NH_3) - \sigma(X))/12R^3\langle r^{-3}\rangle \quad (17)$$

Eqs. (15) and (16) indicate that the contribution of the ligand X to the chemical shift of the *trans* protons is $2\Delta_X$ and that to the *cis* protons is $-\Delta_X$. On the other hand, in *cis*-$[CoXY(NH_3)_4]$ the chemical shift of the ammonia protons *cis* to both X and Y is shown, after taking the NH_3 rotation into account, to be given by

$$\sigma_{iso} \simeq (3\cos^2\theta-1)(\sigma(X) + \sigma(Y) - 2\sigma(NH_3))/12R^3\langle r^{-3}\rangle \quad (18)$$

$$\equiv (-\Delta_X) + (-\Delta_Y) \quad (19)$$

Likewise, for the ammonia molecule *trans* to X and *cis* to Y the following expression holds.

$$\sigma_{iso} \simeq (2\Delta_X) + (-\Delta_Y) \quad (20)$$

In view of the fact that Jolly *et al.* chose the chemical shift of $[Co(NH_3)_6]^{3+}$ as the reference and set it equal to zero, the above equations are just the analytical expressions of their empirical rule. More importantly the above results imply that the chemical shifts of coordinated ammonia molecules are dominated by the magnetic anisotropy of the central metal ion.

cis-Bis(trimethylenediamine) Complexes; Here we will briefly examine the chemical shift of amine protons of *cis*-$[CoX_2tn_2]$, where tn is trimethylenediamine. Kawaguchi and Kawaguchi[28] obtained the PMR spectra of *cis*-bis(tn) compounds containing the cyanide, azide, and thiocyanate ions as the ligand X. While the *trans* isomers exhibit a single absorption in the amine proton region, the *cis* compounds show a well-resolved doublet. Since it is highly probable that the chemical shifts of these amine protons are governed by the magnetic anisotropy of the metal ion, we would like to assign the amine signals according to Eqs. (13) and (14). The *trans* NH_2 may be more deshielded than the *cis* one when the substituent X is the cyanide ion. Thus, it follows that in *cis*-$[Co(CN)_2tn_2]^+$ the absorption centered at about 5.7 ppm from DSS is due to the *trans* hydrogens and that at 6.87 ppm is due to the *cis* ones. Similarly in the azido-containing complex the peak resonating at 6.1 ppm can be attributed to the *trans* amine protons.

References

1) H. Yoneda and Y. Nakashima, This Bulletin, **47**, 669 (1974).
2) Y. Nakashima, U. Sakaguchi, and H. Yoneda, *Chem. Lett.*, **1974**, 503.
3) Y. Nakashima, U. Sakaguchi, and H. Yoneda, This Bulletin, **48**, 762 (1975).
4) Y. Nakashima, *ibid.*, **48**, 766 (1975).
5) H. Yoneda, U. Sakaguchi, and Y. Nakashima, *ibid.*, **48**, 209 (1975).
6) J. K. Beattie, *Accounts Chem. Res.*, **4**, 253 (1971), and references cited therein.
7) J. K. Beattie and L. H. Novak, *J. Amer. Chem. Soc.*, **93**, 620 (1971).
8) J. K. Beattie, *Inorg. Chem.*, **10**, 426 (1971).
9) B. M. Fung, S. C. Wei, T. H. Martin, and I-yuan Wei, *ibid.*, **12**, 1203 (1973).
10) J. L. Sudmeier, G. L. Blackmer, C. H. Bradley, and F. A. L. Anet, *J. Amer. Chem. Soc.*, **94**, 757 (1974).
11) I. R. Lantzke and D. W. Watts, *Aust. J. Chem.*, **20**, 35 (1967).
12) P. Clifton and L. Pratt, *Proc. Chem. Soc.*, **1963**, 339.
13) D. A. Buckingham, L. Durham, and A. M. Sargeson, *Aust. J. Chem.*, **29**, 257 (1967).
14) W. L. Jolly, A. D. Harris, and T. S. Briggs, *Inorg. Chem.*, **4**, 1064 (1965).
15) D. N. Hendrickson and W. L. Jolly, *ibid.*, **9**, 1197 (1970).
16) T. E. MacDermott, *Inorg. Nucl. Chem. Lett.*, **5**, 463 (1969).
17) R. C. Henney, H. F. Holtzclaw, Jr., and R. C. Larson, *Inorg. Chem.*, **5**, 940, (1966).
18) J. G. Brushmiller and L. G. Stadtherr, *Inorg. Nucl. Chem. Lett.*, **3**, 525 (1967).
19) S. T. Spees, Jr., L. J. Durham, and A. M. Sargeson, *Inorg. Chem.*, **5**, 2103 (1966).
20) B. M. Fung, *J. Phys. Chem.*, **72**, 4708 (1968).
21) B. M. Fung, *J. Amer. Chem. Soc.*, **89**, 5788 (1967).
22) F. Yajima, Y. Koike, A. Yamasaki, and S. Fujiwara, This Bulletin, **47**, 1442 (1974).
23) R. D. Gillard, N. C. Payne, and G. B. Robertson, *J. Chem. Soc., A*, **1970**, 2579.
24) A. D. Buckingham and P. J. Stephens, *ibid.*, **1964**, 2747.
25) H. Yoneda, K. Maeda, and U. Sakaguchi, *Chem. Lett.*, **1975**, 107.
26) S. Fujiwara, F. Yajima, and A. Yamasaki, *J. Magn. Resonance*, **1**, 203 (1969).
27) U. Sakaguchi, K. Maeda, and H. Yoneda, This Bulletin, **49**, 397, (1976).
28) H. Kawaguchi and S. Kawaguchi, *ibid.*, **46**, 3453 (1973).

The Infrared and Raman Spectra of *p*-Azoxyanisole in the Crystalline, Nematic and Isotropic Liquid Phases

Kazuo SHIBATA, Masaki KUTSUKAKE, Hiroaki TAKAHASHI, and Keniti HIGASI
Department of Chemistry, School of Science and Engineering, Waseda University, Tokyo 160
(Received August 1, 1975)

The infrared and Raman spectra of *p*-azoxyanisole were measured in the crystalline, nematic, and isotropic liquid phases. In the internal vibrational region, abrupt changes in intensity were observed at the crystalline-nematic phase transition; however, no appreciable change was detected at the nematic-isotropic liquid phase transition. In the external vibrational region, some of the Raman lattice bands, which eventually vanish in the isotropic liquid phase, persist in the nematic phase, while some of the infrared lattice bands disappear and a new band appears as the crystalline-nematic phase transition point is reached and traversed. The assignments of the infrared and Raman bands which appear or disappear in the nematic phase are discussed.

The study of the infrared and Raman spectra of liquid crystal compounds provides an attractive approach for the elucidation of the forces that determine the order and molecular structure in the various phases exhibited by liquid crystal compounds. In spite of this, the number of investigations of infrared and Raman spectra with relation to this particular subject has been quite small.

The infrared spectra of a nematic liquid crystal compound, *p*-azoxyanisole (PAA), have been measured by Bulkin *et al.*[1,2] and by Gruger and Calvé.[3] Bulkin *et al.* reported the infrared spectra of the crystalline, nematic, and isotropic liquid phases in the 600—450 cm^{-1} and 200—50 cm^{-1} regions. They showed that the band at 509 cm^{-1} disappeared at the crystalline-nematic (c-n) phase transition,[1] and that the lattice bands below 150 cm^{-1} disappeared and a broad band emerged at about 100 cm^{-1} above the c-n phase transition temperature.[2] They also showed that the intensity of the disappearing bands began to decrease well below the transition temperature and suggested that there were pretransition effects.

The Raman spectra of PAA in the three phases have been measured by several investigators.[3-8] Amer *et al.*[4] measured the temperature dependence of the Raman bands in the 1300—1225 cm^{-1} and 100—30 cm^{-1} regions. They reported that the variation in the integrated intensity as well as in the bandwidth with the temperature has a characteristic quasi-discontinuity at the c-n phase transition. They also showed that the band at 75 cm^{-1} vanished completely, while the bands at 52 and 40 cm^{-1} persisted in the nematic phase. This result, however, does not agree with that obtained by Bulkin and Prochaska[5], who showed that the band at 52 cm^{-1} vanished while the bands at 70 and 45 cm^{-1} persisted in the nematic phase.

The purpose of this paper is to clarify the behavior of the Raman-active lattice modes of PAA in relation to the temperature variation and to explain the infrared and Raman bands, which change remarkably in intensity at the c-n phase transition.

Experimental

PAA purchased from Tokyo Kasei Kogyo Co., Ltd., was purified by recrystallization from methanol. The sample exhibited a nematic mesophase in the temperature range from 118 to 136 °C.

The infrared spectra were recorded with a Hitachi EPI-G3 spectrophotometer (4000—400 cm^{-1}) and a Hitachi FIS-3 spectrophotometer (400—30 cm^{-1}). The frequency accuracy is probably within ± 2 cm^{-1}. The spectra of the crystalline, nematic, and isotropic liquid phases were recorded as thin films sandwiched between KBr or silicon plates, depending on the frequency range. An electrically heated cell from Hitachi Co., Ltd., provided with an alumel-chromel thermocouple was used to measure the temperature variation.

The Raman spectra were obtained with a Shimadzu R-2D double monochromator equipped with a cooled photomultiplier (ITT FW 130) and a photon-counting system. The excitation source was an Ar^+ laser (Spectra Physics Model 165) operated at 514.5 nm. The output power at the laser-head was 80 mW for the crystalline phase, while it was 350 mW for the nematic and isotropic liquid phases. The frequencies were calibrated using emission lines from the laser and are believed accurate to ± 5 cm^{-1}. The spectral slitwidth was 1.2 cm^{-1} for the 1700—1000 cm^{-1} region, while it was 4.8 cm^{-1} for the 1000—100 cm^{-1} region. The sample cell was inserted in an electrically heated brass block and placed in a box packed with asbestos. The sample temperature was monitored constantly; the temperature fluctuations were less than 1 °C.

Results

The molecular structure of PAA, $CH_3O\text{-}C_6H_4\text{-}N(O)=N\text{-}C_6H_4\text{-}OCH_3$, has been determined by X-ray diffraction.[9] The –N=N– bond is twisted away from the planar *trans* form by 4.2°, and the angle between the normals of the two benzene rings is 22.6°. Hence, the molecule has no symmetry at all. The PAA crystal belongs to the monoclinic system, and the space group is C_{2h}^5–$P2_1/a$, with four molecules in a Bravais unit cell.

Intramolecular Mode The infrared spectra between 1800 and 400 cm^{-1} of PAA in the crystalline, nematic, and isotropic liquid phases are given in Fig. 1. The Raman spectra for the three phases are shown between 1700 and 100 cm^{-1} in Fig. 2. The Raman bands in the 1700—1000 cm^{-1} region are extremely intense compared with those in the lower-frequency range. The spectra in the 1700—1000 cm^{-1} region were recorded with the slit-width one fourth of that in the 1000—100 cm^{-1} region.

Neither the infrared nor the Raman spectra exhibit any significant change at the nematic-isotropic liquid (n-i) phase transition: the infrared and Raman spectra of the nematic phase are virtually the same as

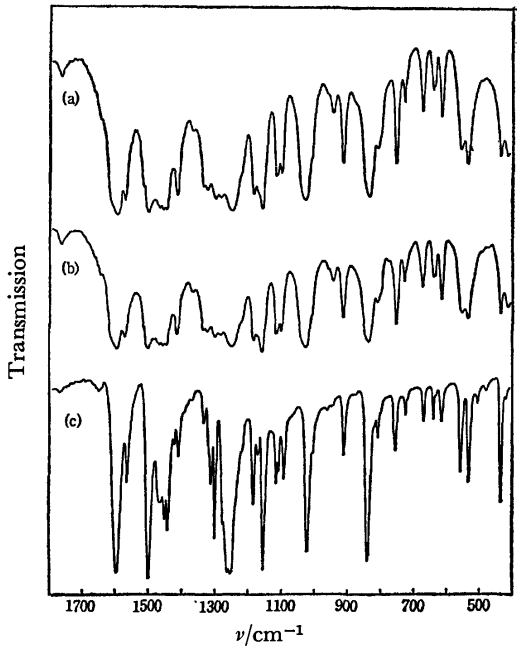

Fig. 1. Infrared spectra between 1800 and 400 cm^{-1} of PAA.
(a): isotropic liquid phase (at 140 °C). (b): nematic phase (at 125 °C). (c): crystalline phase (at 25 °C).

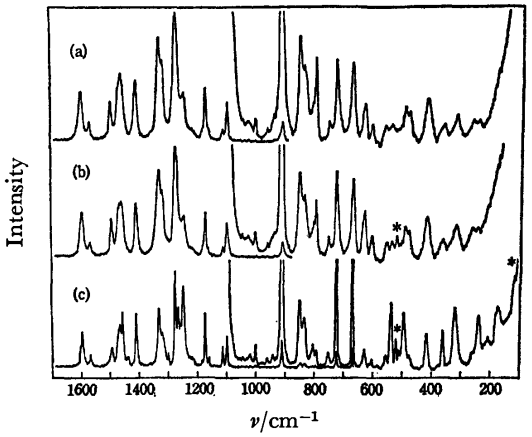

Fig. 2. Raman spectra between 1700 and 100 cm^{-1} of PAA. Spectral slit-width is 1.2 cm^{-1} for the 1700—1000 cm^{-1} region, while it is 4.8 cm^{-1} for the 1000—100 cm^{-1} region.
(a): isotropic liquid phase (at 140 °C). (b): nematic phase (at 125 °C). (c): crystalline phase (at 25 °C).
* denotes the emission lines from the Ar$^+$ laser.

those of the isotropic liquid phase, except for slightly different band-widths due to the different temperatures. In sharp contrast to this, several of the spectral features change almost abruptly at the c-n phase transition: many infrared and Raman bands change in their relative intensities, some increasing while others decrease. Most of the bands become broadened in the nematic phase. Further, some of the infrared and Raman bands exhibit small frequency shifts.

Of particular interest is the fact that the infrared bands at 1311, 509, and 482 cm^{-1} in the crystalline phase disappear above the c-n phase transition temperature (Fig. 3). Bulkin *et al.*[1] noticed that the

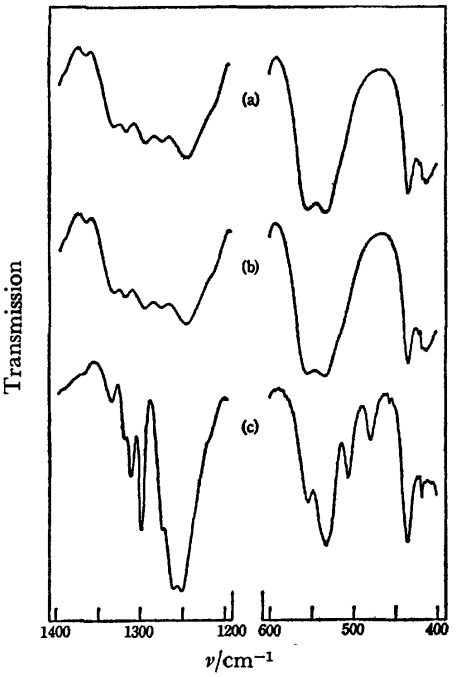

Fig. 3. Temperature dependence of the infrared bands at 1311, 509 and 482 cm^{-1}.
(a): isotropic liquid phase (at 140 °C). (b): nematic phase (at 125 °C). (c): crystalline phase (at 25 °C).

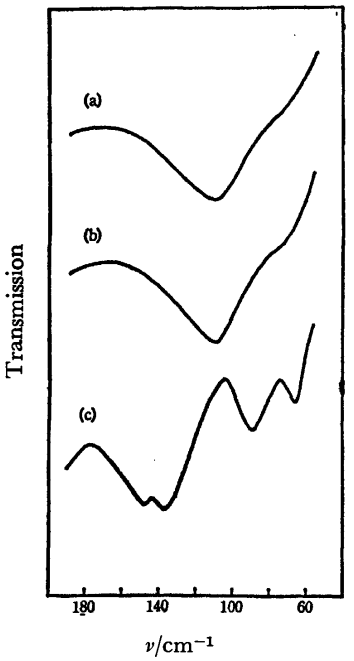

Fig. 4. Infrared spectra of PAA in the external vibrational region.
(a): isotropic liquid phase (at 140 °C). (b): nematic phase (at 125 °C). (c): crystalline phase (at 25 °C).

infrared band at 509 cm^{-1} vanishes at the c-n phase transition; however, they failed to observe the disappearance of the bands at 1311 and 482 cm^{-1}.

Intermolecular Modes The infrared spectra between 180 and 60 cm^{-1} of PAA in the crystalline, nematic, and isotropic liquid phases are reproduced in Fig. 4. In the crystalline phase, four bands are

observed at 150, 137, 89 and 67 cm^{-1}. In the nematic and isotropic liquid phases, some of the bands disappear, and, instead, an intense and broad band appears at about 108 cm^{-1}. This observation is in accord with that reported by Bulkin *et al.*[2]

The Raman spectra below 140 cm^{-1} for the three phases are shown in Fig. 5. Five bands are clearly seen at 94, 75, 56, 42 and 21 cm^{-1} in the crystalline phase. In the nematic phase, the 75 cm^{-1} band disappears and the bands at 56 and 42 cm^{-1} decrease in intensity. In the isotropic liquid phase, only the band at 94 cm^{-1} exists. The behavior of the band at 21 cm^{-1} is not clear because of the overlapping by the Rayleigh wing. This result agrees with that obtained by Amer *et al.*;[4,6] however, it does not agree with those obtained by Bulkin *et al.*[5] and Gruger and Calvé.[3] Bulkin *et al.* claimed that it was the 56 cm^{-1} band that disappeared in the nematic phase. On the other hand, Gruger and Calvé reported that the three bands at 75, 56, and 42 cm^{-1} all existed in the nematic phase at 119 °C, but at 125 °C (still in the nematic phase) only the 42 cm^{-1} band remained. The conclusions differ from one to another because of the extreme difficulty of obtaining high-quality Raman spectra below 100 cm^{-1} of the nematic and isotropic liquid phases as a result of the sudden broadening of the Rayleigh wing at the c-n phase transition. We examined the temperature dependence of these three lattice bands with great care and obtained good reproducible spectra, thus confirming that the band at 75 cm^{-1} vanishes unambiguously, whereas the bands at 56 and 42 cm^{-1}, although they become very much weakened, still exist in the nematic phase.

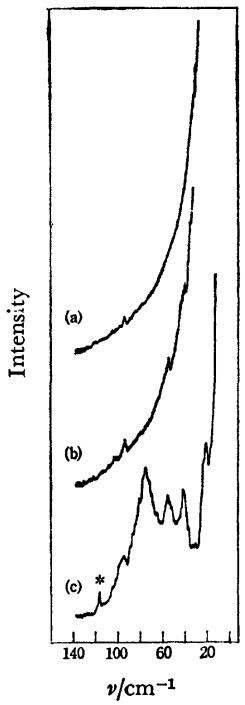

Fig. 5. Raman spectra of PAA in the external vibrational region.
(a): isotropic liquid phase (at 140 °C). (b): nematic phase (at 125 °C). (c): crystalline phase (at 25 °C).
* denotes the emission line from the Ar^+ laser.

Discussion

A nematic mesophase may be characterized by the tendency of all molecules to align themselves parallel to a preferred axis in space, although they are not fixed in position. Such a tendency, however, may still be present in the isotropic liquid phase, though among much smaller groups of molecules.[17]

McLoughlin *et al.*[10] concluded, from the volume changes at the c-n and n-i phase transitions, that there is, usually, no room for PAA molecules to rotate freely about their own long axes, in either the nematic or isotropic liquid phase. This suggests that the rotational motion about the long axis of a PAA molecule is hindered by neighboring molecules and becomes a librational oscillation even in the nematic and isotropic liquid phases; the frequency of the oscillation, however, is possibly different from that of the corresponding librational mode in the crystalline phase as a result of the different intermolecular force field.

The appearance of an intense and broad infrared band at 108 cm^{-1} at the c-n phase transition might be well explained if one could assume that this band originates from the librational oscillation about the molecular long axis, and further, that the short-range order is responsible for the librational oscillation appearing in the infrared spectra. It has been known that the polar molecules in the liquid state exhibit a broad and intense absorption in the far-infrared region (mostly below 100 cm^{-1});[11-13] this absorption band can be explained as due to the librational oscillation of each polar molecule within the cage formed by its neighbors.[14,15] Thus, it seems reasonable to assume that the infrared band at 108 cm^{-1} of PAA has the same origin as the absorption of polar molecules. Evans *et al.*[16] explained a strong band centered near 130 cm^{-1} of a liquid crystal compound, *N*-(*p*-methoxybenzylidene)-*p*-*n*-butylaniline (MBBA), in its nematic and isotropic liquid phases as being due to this type of absorption.

On the other hand, the disappearance of the Raman band at 75 cm^{-1} at the c-n phase transition may be interpreted on the assumption that this band is due to the Raman-active librational mode about the long axis, but the long-range order is essential to the appearance of the librational oscillation in the Raman spectra.

We have seen that the Raman bands at 56 cm^{-1} and 42 cm^{-1} persist in the nematic phase, although they vanish in the isotropic liquid phase. Thus, these bands can be assigned either to the librational modes about the molecular short axes or to the translational modes along the axes; along these axes, the long-range order still exists in the nematic phase. The Raman band at 94 cm^{-1} must be an internal mode because this band is seen in the isotropic liquid phase; besides, it does not exhibit any appreciable frequency shift through the phase transitions.

In the internal vibrational region, the infrared bands at 1311, 509, and 482 cm^{-1} vanish above the c-n phase transition point. These bands may be

assigned to combination modes between the librational mode about the molecular long axis and intramolecular modes; in the nematic phase, the librational mode disappears and, hence, its combination modes. It is difficult to explain these bands, except for the band at 1311 cm^{-1}, in terms of the crystal-field splitting, because they are far from any adjacent bands. The following combinations are, though, considered probable; 1247 (R)+67 (IR)=1314, 437 (IR)+75 (R)=512, and 418 (R)+67 (IR)=485.

In a nematic liquid crystal compound, *N*-anisyliden-*p*-aminophenyl acetate (APAPA), the infrared and Raman bands arising from rotational isomers which exist in the nematic and isotropic liquid phases were identified, and the energy difference between the isomers was estimated.[18] Therefore, it seems highly probable that more than one molecular conformation around the C–OCH_3 bonds are present for PAA in the nematic and isotropic liquid phases. The remarkable intensity changes at the c-n phase transition might be caused by the changes not only in the molecular orientation but also in the conformation.

Bulkin *et al.*[1,5] reported that there are pretransition effects at the c-n phase transition. It is true that the peak heights and band-widths of the infrared and Raman bands start to change well below the transition temperature, but this is what one would expect from the temperature variation in the spectra of any compounds, regardless of the phase transition. we found that the appearance or disappearance of the infrared and Raman bands took place almost abruptly at the transition temperature.

References

1) B. J. Bulkin, D. Grunbaum, and A. V. Santro, *J. Chem. Phys.*, **51**, 1602 (1969).
2) B. J. Bulkin and W. B. Lok, *J. Phys. Chem.*, **77**, 326 (1973).
3) A. Gruger and N. Calvé, *J. Mol. Structure*, **21**, 97 (1974).
4) N. M. Amer, Y. R. Shen, and H. Rosen, *Phys. Rev. Lett.*, **24**, 718 (1970).
5) B. J. Bulkin and F. T. Prochaska, *J. Chem. Phys.*, **54**, 635 (1971).
6) N. M. Amer and Y. R. Shen, *ibid.*, **56**, 2654 (1972).
7) J. M. Schnur, M. Hass, and W. B. Adair, *Phys. Lett.*, **41A**, 326 (1972).
8) J. M. Schnur, *Mol. Cryst. Liq. Cryst.*, **23**, 155 (1973).
9) W. B. Krigbaum, Y. Chatani, and P. G. Barker, *Acta Crystallogr.*, **B26**, 97 (1970).
10) E. McLaughlin, M. A. Shakespeare, and A. R. Ubbelohde, *Trans. Faraday Soc.*, **60**, 25 (1964).
11) H. A. Gebbie, *Nature*, **208**, 378 (1965).
12) M. Davies, G. W. F. Pardoe, J. E. Chamberlain, and H. A. Gebbie, *Trans. Faraday Soc.*, **64**, 847 (1968).
13) E. Constant, L. Galatry, Y. Leroy, and D. Robert, *J. Chim. Phys.*, **65**, 1022 (1965).
14). N. E. Hill, *Proc. Phys. Soc.*, **82**, 723 (1963).
15) K. Higasi, R. Minami, H. Takahashi, and A. Ohno, *J. Chem. Soc., Faraday II*, **69**, 1579 (1973).
16) M. Evans, M. Davies, and I. Larkin, *J. Chem. Soc., Faraday II*, **69**, 1011 (1973).
17) G. W. Stewart and R. M. Morrow, *Phys. Rev.*, **30**, 232 (1927).
18) M. Kutsukake, K. Shibata, and H. Takahashi, reported at the Symposium on Molecular Structure, Tokyo (1974).

Theoretical Calculations of the Infrared Absorption Intensities of Simultaneous Transitions

Hiroyuki SHINODA and Munehisa MITSUYA

Department of Applied Chemistry, Faculty of Science and Engineering, Waseda University, Nishi-Ohkubo, Shinjuku-ku, Tokyo 160

(Received August 13, 1975)

The formula of the infrared absorption intensity of a simultaneous transition has been derived on the basis of the vibronic expansion technique, with two simple assumptions. By the use of the foumula, the theoretical calculations of the intensities for the CO_2–N_2 and CO_2–H_2 systems have been done, the electronic wave functions being calculated by the CNDO/2 method. In both cases, it was found that the main contribution to the absorption intensity arises from the coupling between the electronic state of CO_2 and the nuclear vibration of the homonuclear diatomic molecule. Furthermore, the intensities of the fundamental, first-overtone, and combination bands of CO_2 have been calculated according to the formula corresponding to an intramolecular process, and the intensities of the overtone and combination bands caused by the intermolecular process have been calculated. These calculated results have been discussed in comparison with one another.

In their investigations of the infrared absorption spectra of the compressed gaseous mixture of carbon dioxide and nitrogen, Fahrenfort and Ketelaar[1] found new bands which were not observed in compressed gas of pure carbon dioxide. They attributed the bands to simultaneous transitions in each of the two compounds. The same phenomenon was found in the mixture of CO_2 and H_2 and also in CO_2 and O_2. Fahrenfort and Ketelaar suggested that the phenomena depend on the polarization of the symmetrical diatomic molecule under the influence of the electric field of the rather large quadrupole moment arising from the partial dipoles presented in CO_2. Ketelaar and his co-workers went on to investigate the simultaneous transitions in several liquified mixtures[2] and proposed a theoretical development of the simultaneous transition.[3] Their development is based on the idea that the dipole moment of the system is expanded in a power series of the vibrational normal coordinates. This idea has been used to explain the infrared absorption intensities of the vibrational transitions in a separate molecule;[4] in the expansion, the first derivatives with respect to the normal coordinates are related to the intensities of the fundamental tones, the second derivatives are related to the first overtones, and so on. For the intensity of a Raman scattering, a similar approach has been adopted in the form of the expansion of a molecular polarizability.[5] On the other hand, the formula of the Raman intensity has been derived by the use of the vibronic expansion technique,[6] which is different from that described above.

In this work the formulas of the infrared absorption intensities have been derived by the use of the vibronic expansion technique; the formula of the intensity for the simultaneous transition has also been derived. Moreover, by the use of these formulas, the intensities of the simultaneous transition for the CO_2–N_2 and CO_2–H_2 systems and of the fundamental, overtone, and combination bands of CO_2 have been calculated. The electronic wave functions have been evaluated by the CNDO/2 method.

Theoretical

Intramolecular Transition. The expression of the infrared absorption intensity for the vibrational transition from the ground state, o, to the excited state, m, of a molecule is given as:[7]

$$A_{m\leftarrow o} = \frac{8\pi^3}{3ch}\nu_{mo}(N_o - N_m)|\mu_{m,o}|^2; \quad (1)$$

$$\mu_{m,o} = \langle m|\hat{\mu}|o\rangle, \quad (2)$$

where c is the velocity of light; h, Planck's constant; ν_{mo}, the frequency of the absorbed light; N_o and N_m, the number of molecules per unit volume in the o and m states respectively, and $\hat{\mu}$, the electric dipole moment operator. The wave functions, $|o>$ and $|m>$, are described by the product of an electronic wave function and a vibrational wave function:

$$|o> = |\phi_g>|\varphi_o^g> \quad (3)$$

and:

$$|m> = |\psi_g>|\varphi_m^g>, \quad (4)$$

where $|\phi_g>$ is the wave function of the electronic ground state involving the nuclear coordinates as parameters and where $|\varphi_o^g>$ and $|\varphi_m^g>$ are the wave functions of the vibrational ground and the vibrational m-th states respectively, both of which belong to the electronic ground state. The Hamiltonian for the electronic system could be expanded in a Taylor series with respect to the normal coordinates, Q_a's, around the equilibrium nuclear position:

$$H = H_0 + \sum_a H_a'Q_a + \frac{1}{2}\sum_a\sum_b H_{ab}''Q_aQ_b + \textit{higher-order terms}, \quad (5)$$

where

$$H_a' = (\partial H/\partial Q_a)_0$$

and

$$H_{ab}'' = (\partial^2 H/\partial Q_a \partial Q_b)_0.$$

When H_0 is regarded as the unperturbed Hamiltonian which has the eigenvalues, ε_i^0's, and the corresponding eigenfunctions, $|\psi_i^0>$'s, and when the other terms on the right-hand side in Eq. (5) are regarded as the perturbation on H_0, we can make use of the perturbation method for obtaining the $|\psi_g>$. The expression of $|\psi_g>$ with the zeroth-, the first-, and the second-order terms of normal coordinates can be written as:[8]

$$|\psi_g> = |\psi_g^0> + \sum_a \sum_{i\neq g} \frac{\langle\psi_i^0|H_a'|\psi_g^0\rangle Q_a}{\varepsilon_g^0-\varepsilon_i^0}|\psi_i^0> + \sum_{a,b}\sum_{i\neq g}\left\{\frac{1}{2}\frac{\langle\psi_i^0|H_{ab}''|\psi_g^0\rangle}{\varepsilon_g^0-\varepsilon_i^0} + \sum_{j\neq g}\frac{\langle\psi_g^0|H_a'|\psi_j^0\rangle\langle\psi_j^0|H_b'|\psi_i^0\rangle}{(\varepsilon_g^0-\varepsilon_j^0)(\varepsilon_g^0-\varepsilon_i^0)} - \frac{\langle\psi_g^0|H_a'|\psi_g^0\rangle\langle\psi_g^0|H_b'|\psi_i^0\rangle}{(\varepsilon_g^0-\varepsilon_i^0)^2}\right\}Q_aQ_b|\psi_i^0\rangle. \quad (6)$$

It is convenient for the following development to show that $\hat{\boldsymbol{\mu}}$ can be expressed as follows:[9]

$$\hat{\boldsymbol{\mu}} = \hat{\boldsymbol{\mu}}_e + \hat{\boldsymbol{\mu}}_n = \hat{\boldsymbol{\mu}}_e + \hat{\boldsymbol{\mu}}_n^0 + \sum_a \mathbf{k}_a Q_a = \hat{\boldsymbol{\mu}}_0 + \sum \mathbf{k}_a Q_a, \quad (7)$$

where $\hat{\boldsymbol{\mu}}_e$ and $\hat{\boldsymbol{\mu}}_n$ are the electronic and nuclear parts of $\hat{\boldsymbol{\mu}}$ respectively, where $\hat{\boldsymbol{\mu}}_n^0$ is $\hat{\boldsymbol{\mu}}_n$ with the equilibrium nuclear position, and where $\hat{\boldsymbol{\mu}}_0$ is the sum of $\hat{\boldsymbol{\mu}}_e$ and $\hat{\boldsymbol{\mu}}_n^0$. By applying Eq. (6) to Eqs. (3) and (4), and considering the orthonormality between $|\psi_i^0>$'s, $\boldsymbol{\mu}_{m,o}$ is rewritten as:

$$\boldsymbol{\mu}_{m,o} = \langle\psi_g^0|\hat{\boldsymbol{\mu}}_0|\psi_g^0\rangle\langle\varphi_m^g|\varphi_o^g\rangle + \sum_a\left\{\mathbf{k}_a - 2\sum_{i\neq g}\frac{\langle\psi_g^0|H_a'|\psi_i^0\rangle\langle\psi_i^0|\hat{\boldsymbol{\mu}}_0|\psi_g^0\rangle}{\varepsilon_i^0-\varepsilon_g^0}\right\}\langle\varphi_m^g|Q_a|\varphi_o^g\rangle + \sum_{a,b}\left[\sum_{i\neq g}\sum_{j\neq g}\left\{\frac{\langle\psi_g^0|H_a'|\psi_i^0\rangle\langle\psi_i^0|\hat{\boldsymbol{\mu}}_0|\psi_j^0\rangle\langle\psi_j^0|H_b'|\psi_g^0\rangle}{(\varepsilon_i^0-\varepsilon_g^0)(\varepsilon_j^0-\varepsilon_g^0)} + 2\frac{\langle\psi_g^0|H_a'|\psi_i^0\rangle\langle\psi_i^0|H_b'|\psi_j^0\rangle\langle\psi_j^0|\hat{\boldsymbol{\mu}}_0|\psi_g^0\rangle}{(\varepsilon_i^0-\varepsilon_g^0)(\varepsilon_j^0-\varepsilon_g^0)}\right\} - \sum_{i\neq g}\left\{\frac{\langle\psi_g^0|H_{ab}''|\psi_i^0\rangle\langle\psi_i^0|\hat{\boldsymbol{\mu}}_0|\psi_g^0\rangle}{\varepsilon_i^0-\varepsilon_g^0} + 2\frac{\langle\psi_g^0|H_a'|\psi_g^0\rangle\langle\psi_g^0|H_b'|\psi_i^0\rangle\langle\psi_i^0|\hat{\boldsymbol{\mu}}_0|\psi_g^0\rangle}{(\varepsilon_i^0-\varepsilon_g^0)^2}\right\}\right]\langle\varphi_m^g|Q_aQ_b|\varphi_o^g\rangle. \quad (8)$$

with the harmonic oscillator approximation, the transition moments for the fundamental tone and the first overtone of the a normal vibration and for the combination tone of the a and b normal vibrations are given as:

Fundamental tone:

$$\boldsymbol{\mu}_{1,0}^a = \left\{\mathbf{k}_a - 2\sum_{i\neq g}\frac{\langle\psi_g^0|H_a'|\psi_i^0\rangle\langle\psi_i^0|\hat{\boldsymbol{\mu}}_0|\psi_g^0\rangle}{\varepsilon_i^0-\varepsilon_g^0}\right\}\langle\varphi_1^g|Q_a|\varphi_0^g\rangle: \quad (9)$$

First overtone:

$$\boldsymbol{\mu}_{2,0}^a = \left[\sum_{i\neq g}\sum_{j\neq g}\left\{\frac{\langle\psi_g^0|H_a'|\psi_i^0\rangle\langle\psi_i^0|\hat{\boldsymbol{\mu}}_0|\psi_j^0\rangle\langle\psi_j^0|H_a'|\psi_g^0\rangle}{(\varepsilon_i^0-\varepsilon_g^0)(\varepsilon_j^0-\varepsilon_g^0)} + 2\frac{\langle\psi_g^0|H_a'|\psi_i^0\rangle\langle\psi_i^0|H_a'|\psi_j^0\rangle\langle\psi_j^0|\hat{\boldsymbol{\mu}}_0|\psi_g^0\rangle}{(\varepsilon_i^0-\varepsilon_g^0)(\varepsilon_j^0-\varepsilon_g^0)}\right\} - \sum_{i\neq g}\left\{\frac{\langle\psi_g^0|H_{aa}''|\psi_i^0\rangle\langle\psi_i^0|\hat{\boldsymbol{\mu}}_0|\psi_g^0\rangle}{\varepsilon_i^0-\varepsilon_g^0} + 2\frac{\langle\psi_g^0|H_a'|\psi_g^0\rangle\langle\psi_g^0|H_a'|\psi_i^0\rangle\langle\psi_i^0|\hat{\boldsymbol{\mu}}_0|\psi_g^0\rangle}{(\varepsilon_i^0-\varepsilon_g^0)^2}\right\}\right]\langle\varphi_2^g|Q_a^2|\varphi_0^g\rangle: \quad (10)$$

Combination tone:

$$\boldsymbol{\mu}_{(1,1),0}^{a,b} = \left[2\sum_{i\neq g}\sum_{j\neq g}\left\{\frac{\langle\psi_g^0|H_a'|\psi_i^0\rangle\langle\psi_i^0|\hat{\boldsymbol{\mu}}_0|\psi_j^0|H_b'\rangle\langle\psi_i^0|\psi_g^0\rangle}{(\varepsilon_i^0-\varepsilon_g^0)(\varepsilon_j^0-\varepsilon_g^0)} + \frac{\langle\psi_g^0|H_a'|\psi_i^0\rangle\langle\psi_i^0|H_b'|\psi_j^0\rangle\langle\psi_j^0|\hat{\boldsymbol{\mu}}_0|\psi_g^0\rangle}{(\varepsilon_i^0-\varepsilon_g^0)(\varepsilon_j^0-\varepsilon_g^0)} + \frac{\langle\psi_g^0|H_b'|\psi_i^0\rangle\langle\psi_i^0|H_a'|\psi_j^0\rangle\langle\psi_j^0|\hat{\boldsymbol{\mu}}_0|\psi_g^0\rangle}{(\varepsilon_i^0-\varepsilon_g^0)(\varepsilon_j^0-\varepsilon_g^0)}\right\} - 2\sum_{i\neq g}\left\{\frac{\langle\psi_g^0|H_{ab}''|\psi_i^0\rangle\langle\psi_i^0|\hat{\boldsymbol{\mu}}_0|\psi_g^0\rangle}{\varepsilon_i^0-\varepsilon_g^0} + \frac{\langle\psi_g^0|H_a'|\psi_g^0\rangle\langle\psi_g^0|H_b'|\psi_i^0\rangle\langle\psi_i^0|\hat{\boldsymbol{\mu}}_0|\psi_g^0\rangle}{(\varepsilon_i^0-\varepsilon_g^0)^2} + \frac{\langle\psi_g^0|H_b'|\psi_g^0\rangle\langle\psi_g^0|H_a'|\psi_i^0\rangle\langle\psi_i^0|\hat{\boldsymbol{\mu}}_0|\psi_g^0\rangle}{(\varepsilon_i^0-\varepsilon_g^0)^2}\right\}\right]\langle\varphi_{(1,1)}^g|Q_aQ_b|\varphi_0^g\rangle. \quad (11)$$

Simultaneous Transition. In order to derive the expression of the transition moment for a simultaneous transition, we introduce two assumptions:

(i) The normal modes in a separate molecule remain in a two-molecule system.

(ii) The electron-transfer and -exchange between molecules do not appear.

The first assumption is supported by the experimental fact that the wave number of a simultaneous transition is equal to the sum of the wave numbers of the constituent fundamental tones. There is no experimental evidence to support the second assumption. On the basis of their theoretical investigation of intermolecular forces, however, Murrell *et al.*[10] suggested that the effect of the electron-exchange appears in the region of intermolecular distances shorter than 3 Å, as is shown in the figures in their report, and that the electron-transfer is not important when the charge-transfer states are not detected spectroscopically. Therefore, the use of the second assumption will not bring a fatal error into the results of the calculations for a gas phase; also, it has the merit that the expression of the transition moment becomes very simple, as will be shown later.

With the first assumption, the electronic Hamiltonian of two-molecule system is given as:

$$H = H^A + H^B + U^0 + \sum_a U_a'Q_a + \sum_b U_b'Q_b, \quad (12)$$

$$H^A = H_0^A + \sum_a H_a'Q_a \quad [\text{where } H_a' = (\partial H^A/\partial Q_a)_0], \quad (13)$$

$$H^B = H_0^B + \sum_b H_b'Q_b \quad [\text{where } H_b' = (\partial H^B/\partial Q_b)_0], \quad (14)$$

$$U_a' = (\partial U/\partial Q_a)_0, \quad (15)$$

and

$$U_b' = (\partial U/\partial Q_b)_0, \quad (16)$$

where H^A and H^B are the electronic Hamiltonians of the separate molecules, A and B respectively; U, the intermolecular interaction operator including the nuclear coordinates as parameter, and U^0, U with a specified molecular configuration, each molecule keeping the equilibrium geometry. Since the wave number of the simultaneous transition considered in this work is the sum of those of the constituent fundamental tones, it is sufficient to consider the first-order term in each normal coordinate. Hereafter, Q_a in the A

molecule and Q_b in the B molecule will be considered typical. The electronic wave function of the two-molecule system with an infinite separation is consistently given by the product of the wave functions of the separate molecules:

$$|\Psi^0_{ik}> = |\phi^A_i>|\phi^B_k>, \tag{17}$$

$$|\phi^A_i> = |\phi^{A0}_i> + \sum_{j\neq i} \frac{\langle\phi^{A0}_j|H_a'|\phi^{A0}_i\rangle Q_a}{\varepsilon^{A0}_i - \varepsilon^{A0}_j}|\phi^{A0}_j>, \tag{18}$$

and

$$|\phi^B_k> = |\phi^{B0}_k> + \sum_{l\neq k} \frac{\langle\phi^{B0}_l|H_b'|\phi^{B0}_k\rangle Q_b}{\varepsilon^{B0}_k - \varepsilon^{B0}_l}|\phi^{B0}_l>, \tag{19}$$

where the A and B superscripts indicate the separate molecules, A and B respectively, and where the 0 superscript in $|\Psi^0_{ik}>$ indicates the infinite separation. For the simultaneous transition, the initial state, o, and the final state, m, in Eq. (1) are given by the following expressions respectively:

$$|o> = |\Psi_g>|\Phi^g_{00}\rangle \tag{20}$$

and

$$|m> = |\Psi_g>|\Phi^g_{11}\rangle, \tag{21}$$

where $|\Psi_g>$ is the wave function of the electronic ground state of two-molecule system and where $|\Phi^g_{00}>$ and $|\Phi^g_{11}>$ are the wave functions of the vibrational initial and final states respectively. Regarding the last three terms in Eq. (12) as a perturbation caused by an interaction between neighbouring molecules, we can expand the wave function $|\Psi_g>$ by the use of the first-order perturbation method:

$$|\Psi_g> = |\Psi^0_{gg}> + \sum'_{(ik)} \frac{\langle\Psi^0_{ik}|U^0 + U_a'Q_a + U_b'Q_b|\Psi^0_{gg}\rangle}{E^0_{gg} - E^0_{ik}}|\Psi^0_{ik}>, \tag{22}$$

where E^0_{ik} is the energy of the $|\Psi^0_{ik}>$ state and where the prime in $\sum'$ indicates that the sum over (ik) does not include (gg). From the second assumption, the wave functions corresponding to the electron-transfers between molecules are also omitted. By substituting Eq. (22) into Eqs. (20) and (21), the following expression of $\mu_{m,o}$ in Eq. (2) can be obtained:

$$\mu_{m,o} = \langle\Phi^g_{11}|\mu_{m,o}(0) + \mu_{m,o}(1) + \mu_{m,o}(2)|\Phi^g_{00}\rangle, \tag{23}$$

where:

$$\mu_{m,o}(0) = \langle\Psi^0_{gg}|\hat{\mu}|\Psi^0_{gg}\rangle + 2\sum'_{(ik)} \frac{\langle\Psi^0_{gg}|\hat{\mu}|\Psi^0_{ik}\rangle\langle\Psi^0_{ik}|U_a'Q_a + U_b'Q_b|\Psi^0_{gg}\rangle}{E^0_{gg} - E^0_{ik}} + \sum'_{(ik)}\sum'_{(jl)} \frac{\langle\Psi^0_{gg}|U_a'Q_a + U_b'Q_b|\Psi^0_{ik}\rangle\langle\Psi^0_{ik}|\hat{\mu}|\Psi^0_{jl}\rangle\langle\Psi^0_{jl}|U_a'Q_a + U_b'Q_b|\Psi^0_{gg}\rangle}{(E^0_{gg} - E^0_{ik})(E^0_{gg} - E^0_{jl})}, \tag{24}$$

$$\mu_{m,o}(1) = 2\sum'_{(ik)} \frac{\langle\Psi^0_{gg}|\hat{\mu}|\Psi^0_{ik}\rangle\langle\Psi^0_{ik}|U^0|\Psi^0_{gg}\rangle}{E^0_{gg} - E^0_{ik}} + 2\sum'_{(ik)}\sum'_{(jl)} \frac{\langle\Psi^0_{gg}|U^0|\Psi^0_{ik}\rangle\langle\Psi^0_{ik}|\hat{\mu}|\Psi^0_{jl}\rangle\langle\Psi^0_{jl}|U_a'Q_a + U_b'Q_b|\Psi^0_{gg}\rangle}{(E^0_{gg} - E^0_{ik})(E^0_{gg} - E^0_{jl})} \tag{25}$$

and

$$\mu_{m,o}(2) = \sum'_{(ik)}\sum'_{(jl)} \frac{\langle\Psi^0_{gg}|U^0|\Psi^0_{ik}\rangle\langle\Psi^0_{ik}|\hat{\mu}|\Psi^0_{jl}\rangle\langle\Psi^0_{jl}|U^0|\Psi^0_{gg}\rangle}{(E^0_{gg} - E^0_{ik})(E^0_{gg} - E^0_{jl})} \tag{26}$$

In the above expressions, $\mu_{m,o}(0)$, $\mu_{m,o}(1)$, and $\mu_{m,o}(2)$ are the zeroth-, the first-, and the second-order terms of U^0 respectively. If the higher-order perturbations were considered in the expansion of $|\Psi_g>$, some other terms would be added to Eqs. (24)—(26). The terms contributing to the simultaneous transitions must include three kinds of matrix elements, two of them being those of the vibronic coupling operators referring to Q_a and Q_b respectively, and one of them being that of $\hat{\mu}$. Therefore, the lowest-order term contributing to the simultaneous transitions is the third-order one. The terms in $\mu_{m,o}(1)$ and $\mu_{m,o}(2)$ always include the matrix elements of U^0; therefore, their contributions to the simultaneous transitions arise from higher-order terms than the third-order one. In this work, the intensities of the simultaneous transitions have been calculated by considering only $\mu_{m,o}(0)$, which gives the lowest-order contribution. The influences of $\mu_{m,o}(1)$ and $\mu_{m,o}(2)$ will be investigated in the future. When $|\Psi^0_{ik}>$'s in Eq. (24) were rewritten by the use of the expressions in Eqs. (17)—(19), and only the terms including Q_aQ_b were retained, $\mu_{m,o}(0)$ was given as:

$$\begin{aligned}\mu_{m,o}(0) = {} & 2\sum_{i\neq g}\sum_{k\neq g} C^A_{ig}C^B_{kg}\{\langle gg|\hat{\mu}_0|ik\rangle + \langle ig|\hat{\mu}_0|gk\rangle\}Q_aQ_b + 2\sum'_{(ik)} \frac{1}{E^0_{gg} - E^0_{ik}}\Big[\sum_{n\neq i} C^A_{ni}\{\langle gg|U_b'|nk\rangle\langle ik|\hat{\mu}_0|gg\rangle \\ & + \langle gg|U_b'|ik\rangle\langle nk|\hat{\mu}_0|gg\rangle\} + \sum_{m\neq g} C^A_{mg}\{\langle mg|U_b'|ik\rangle\langle ik|\hat{\mu}_0|gg\rangle \\ & + \langle gg|U_b'|ik\rangle\langle ik|\hat{\mu}_0|mg\rangle\} + \sum_{s\neq k} C^B_{sk}\{\langle gg|U_a'|is\rangle\langle ik|\hat{\mu}_0|gg\rangle \\ & + \langle gg|U_a'|ik\rangle\langle is|\hat{\mu}_0|gg\rangle\} + \sum_{r\neq g} C^B_{rg}\{\langle gr|U_a'|ik\rangle\langle ik|\hat{\mu}_0|gg\rangle + \langle gg|U_a'|ik\rangle\langle ik|\hat{\mu}_0|gr\rangle\}\Big]Q_aQ_b \\ & + \sum'_{(ik)}\sum'_{(jl)} \frac{1}{(E^0_{gg} - E^0_{ik})(E^0_{gg} - E^0_{jl})}\{\langle gg|U_a'|ik\rangle\langle ik|\hat{\mu}_0|jl\rangle\langle jl|U_b'|gg\rangle + \langle gg|U_b'|ik\rangle\langle ik|\hat{\mu}_0|jl\rangle\langle jl|U_a'|gg\rangle\}Q_aQ_b,\end{aligned} \tag{27}$$

where $C^A_{ij} = \langle\phi^{A0}_i|H_a'|\phi^{A0}_j\rangle/(\varepsilon^{A0}_j - \varepsilon^{A0}_i)$; $C^B_{kl} = \langle\phi^{B0}_k|H_b'|\phi^{B0}_l\rangle/(\varepsilon^{B0}_l - \varepsilon^{B0}_k)$; and $|ij> = |\phi^{A0}_i>|\phi^{B0}_j>$. From the second assumption and the facts that the operators, U_a', U_b' and $\hat{\mu}_0$, are sums of the one-electron operators and that the electronic wave functions in the separated molecules are orthonormalized, the integrals on the right-hand side of Eq. (27) are reduced to one-molecule integrals as follows:

$$\left.\begin{aligned}\langle ij|U_a'|kl\rangle &= \langle\phi^{B0}_j|U_a'|\phi^{B0}_l\rangle\delta_{ik}, \\ \langle ij|U_b'|kl\rangle &= \langle\phi^{A0}_i|U_b'|\phi^{A0}_k\rangle\delta_{jl}, \\ \langle ij|\hat{\mu}_0|kl\rangle &= \langle\phi^{A0}_i|\hat{\mu}_0|\phi^{A0}_k\rangle\delta_{jl} + \langle\phi^{B0}_j|\hat{\mu}_0|\phi^{B0}_l\rangle\delta_{ik}.\end{aligned}\right\} \tag{28}$$

Considering Eq. (28) and adopting the approximation that $E^0_{ik}=\varepsilon^{A0}_i+\varepsilon^{B0}_k$, we can divide $\mu_{m,o}(0)$ into two parts:

$$\mu_{m,o}(0) = \{\mu^A_{m,o}(0)+\mu^B_{m,o}(0)\}Q_aQ_b, \tag{29}$$

where

$$\mu^A_{m,o}(0) = 2\Bigg[\sum_{i\neq g}\sum_{j\neq g}\left\{\frac{\langle\psi^{A0}_g|\hat{\mu}_0|\psi^{A0}_i\rangle\langle\psi^{A0}_i|U_b'|\psi^{A0}_j\rangle\langle\psi^{A0}_j|H_a'|\psi^{A0}_g\rangle}{(\varepsilon^{A0}_g-\varepsilon^{A0}_i)(\varepsilon^{A0}_g-\varepsilon^{A0}_j)}+\frac{\langle\psi^{A0}_g|U_b'|\psi^{A0}_i\rangle\langle\psi^{A0}_i|\hat{\mu}_0|\psi^{A0}_j\rangle\langle\psi^{A0}_j|H_a'|\psi^{A0}_g\rangle}{(\varepsilon^{A0}_g-\varepsilon^{A0}_i)(\varepsilon^{A0}_g-\varepsilon^{A0}_j)}\right\}$$
$$+\sum_{\substack{i\neq g\\(i\neq j)}}\sum_{j\neq g}\frac{\langle\psi^{A0}_g|U_b'|\psi^{A0}_i\rangle\langle\psi^{A0}_i|H_a'|\psi^{A0}_j\rangle\langle\psi^{A0}_j|\hat{\mu}_0|\psi^{A0}_g\rangle}{(\varepsilon^{A0}_g-\varepsilon^{A0}_i)(\varepsilon^{A0}_g-\varepsilon^{A0}_j)}-\sum_{i\neq g}\left\{\frac{\langle\psi^{A0}_g|U_b'|\psi^{A0}_g\rangle\langle\psi^{A0}_g|H_a'|\psi^{A0}_i\rangle\langle\psi^{A0}_i|\hat{\mu}_0|\psi^{A0}_g\rangle}{(\varepsilon^{A0}_g-\varepsilon^{A0}_i)^2}\right.$$
$$\left.+\frac{\langle\psi^{A0}_g|U_b'|\psi^{A0}_i\rangle\langle\psi^{A0}_i|H_a'|\psi^{A0}_g\rangle\langle\psi^{A0}_g|\hat{\mu}_0|\psi^{A0}_g\rangle}{(\varepsilon^{A0}_g-\varepsilon^{A0}_i)^2}\right\}\Bigg] \tag{30}$$

$$\mu^B_{m,o}(0) = 2\Bigg[\sum_{k\neq g}\sum_{l\neq g}\left\{\frac{\langle\psi^{B0}_g|\hat{\mu}_0|\psi^{B0}_k\rangle\langle\psi^{B0}_k|U_a'|\psi^{B0}_l\rangle\langle\psi^{B0}_l|H_b'|\psi^{B0}_g\rangle}{(\varepsilon^{B0}_g-\varepsilon^{B0}_k)(\varepsilon^{B0}_g-\varepsilon^{B0}_l)}+\frac{\langle\psi^{B0}_g|U_a'|\psi^{B0}_k\rangle\langle\psi^{B0}_k|\hat{\mu}_0|\psi^{B0}_l\rangle\langle\psi^{B0}_l|H_b'|\psi^{B0}_g\rangle}{(\varepsilon^{B0}_g-\varepsilon^{B0}_k)(\varepsilon^{B0}_g-\varepsilon^{B0}_l)}\right\}$$
$$+\sum_{\substack{k\neq g\\(k\neq l)}}\sum_{l\neq g}\frac{\langle\psi^{B0}_g|U_a'|\psi^{B0}_k\rangle\langle\psi^{B0}_k|H_b'|\psi^{B0}_l\rangle\langle\psi^{B0}_l|\hat{\mu}_0|\psi^{B0}_g\rangle}{(\varepsilon^{B0}_g-\varepsilon^{B0}_k)(\varepsilon^{B0}_g-\varepsilon^{B0}_l)}-\sum_{k\neq g}\left\{\frac{\langle\psi^{B0}_g|U_a'|\psi^{B0}_g\rangle\langle\psi^{B0}_g|H_b'|\psi^{B0}_k\rangle\langle\psi^{B0}_k|\hat{\mu}_0|\psi^{B0}_g\rangle}{(\varepsilon^{B0}_g-\varepsilon^{B0}_k)^2}\right.$$
$$\left.+\frac{\langle\psi^{B0}_g|U_a'|\psi^{B0}_k\rangle\langle\psi^{B0}_k|H_b'|\psi^{B0}_g\rangle\langle\psi^{B0}_g|\hat{\mu}_0|\psi^{B0}_g\rangle}{(\varepsilon^{B0}_g-\varepsilon^{B0}_k)^2}\right\}\Bigg]. \tag{31}$$

$\mu^A_{m,o}(0)$ indicates the contribution of the coupling between the electronic state of the A molecule and the nuclear vibration of the B molecule to the intensity of the simultaneous transition, and $\mu^B_{m,o}(0)$, the coupling between the electronic state of the B molecule and the nuclear vibration of the A molecule.

Methods of Calculations

In order to calculate the transition moment according to the expressions derived in the previous section, the electronic wave function, $|\psi^0_g>$, and the energy, ε^0_g, of the separate molecule in the ground state were obtained by the CNDO/2 method, an approximate elf-consistent molecular orbital theory, proposed by Pople *et al.*[11] The excited states, $|\psi^0_i>$'s, were approximated by the singly-excited configurations, χ^m_i's,[12] and their energies, ε^m_i's, were evaluated from the well-known expression:[13]

$$\varepsilon^m_i = \varepsilon^0_g - e_l + e_m - J_{lm} + 2K_{lm}, \tag{32}$$

where e_l and e_m are the orbital energies of the l-th and the m-th molecular orbitals respectively, and where J_{lm} and K_{lm} are the Coulomb- and exchange-integrals respectively. In this work, the terms including the operator, H''_{ab}, were neglected. The integrals in Eqs. (9)—(11), (30), and (31), *i.e.*, $\langle\psi^0_i|\hat{\mu}_0|\psi^0_j\rangle$, *etc.*, were expanded to the integral terms with the one-electron molecular orbitals and were calculated by the methods in Refs. 14 and 15. The calculations of the absorption intensities with reference to the intermolecular interaction were performed for 20 different arrangements, including variations in the intermolecular distance and in the orientation of the two molecules; the distances were fixed at 4.0, 6.0, 8.0, 15.0, and 30.0 Å, and the four kinds of the orientation shown in Fig. 1 were employed.

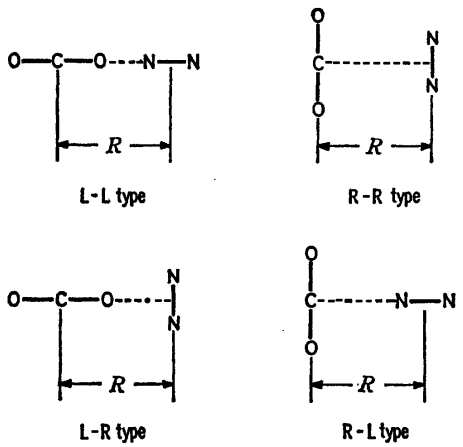

Fig. 1. The orientation of two molecures; R is the intermolecular distance.

Results and Discussion

The results will be discussed for the cases of the simultaneous transitions in the CO_2–N_2 and CO_2–H_2 systems and for the case of the vibrational transition of the CO_2 system, with reference to the intramolecular and intermolecular processes. In the following discussions, the same notations, ν_1, ν_2, and ν_3, for the fundamental bands of CO_2 as those in Ref. 16 are employed, while ν_{N_2} and ν_{H_2} denote the fundamental bands of N_2 and H_2 respectively. The L_x matrices, which are required in calculating the matrix elements of the vibronic coupling operator, were evaluated by the usual **GF** method, the **F** matrix elements in Ref. 16 being employed.

Simultaneous Transition. In the first place, in order to make a brief discussion of the results, the averaged values of the intensities of the simultaneous transition, as calculated for four kinds of orientations at a specified intermolecular distance, were compared with the experimental results. If a certain orientation between molecules should be considered in the compressed system, there will be a problem in the adoption of the averaged values as described above. However, in the level of the approximation used in this work, there was little reason to choose between the four orientations. The variations in the averaged value of the intensities with the intermolecular distance are shown in Figs. 2 and 3 for the CO_2–N_2 and CO_2–H_2 systems respectively. In the experiment with the CO_2–N_2 system,[1] the simultaneous transitions, $\nu_2+\nu_{N_2}$ and $\nu_3+\nu_{N_2}$, are observed, but $\nu_1+\nu_{N_2}$ is not ob-

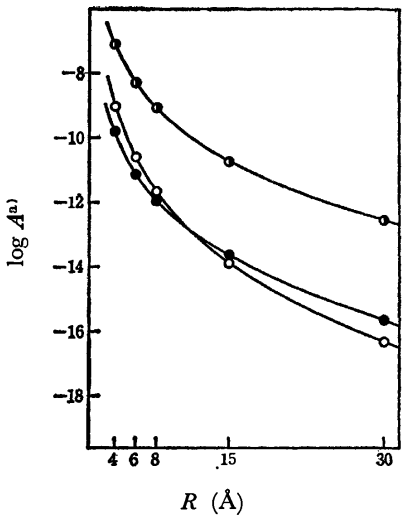

Fig. 2. The infrared absorption intensity of the simultaneous transition in the CO_2–N_2 system; a) A is the absolute intensity, unit of which is in cm^2 s^{-1} molecule-pair^{-1}.
○: $\nu_1+\nu_{N_2}$, ●: $\nu_2+\nu_{N_2}$, ◑: $\nu_3+\nu_{N_2}$.

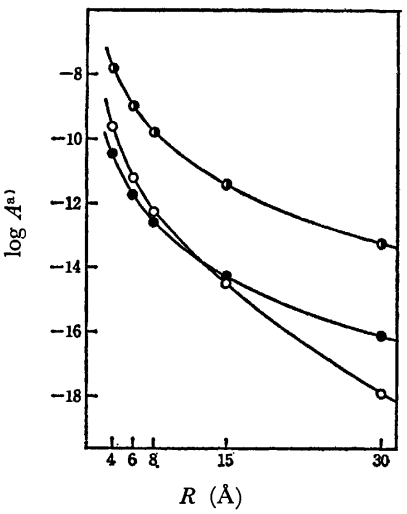

Fig. 3. The infrared absorption intensity of the simultaneous transition in the CO_2–H_2 system; a) A is the absolute intensity, unit of which is in cm^2 s^{-1} molecule-pair^{-1}.
○: $\nu_1+\nu_{H_2}$, ●: $\nu_2+\nu_{H_2}$, ◑: $\nu_3+\nu_{H_2}$.

served. There is difference between the observed and theoretical results with reference to the $\nu_1+\nu_{N_2}$ transition; the calculated intensity of $\nu_1+\nu_{N_2}$ was comparable to that of $\nu_2+\nu_{N_2}$. The difference may be derived from the overestimation in the approximate calculation of the integral which is required in the estimation of the matrix elements of the vibronic coupling operators, and which is connected with the intensities of the $\nu_1+\nu_{N_2}$ and $\nu_3+\nu_{N_2}$ transitions. There is a reason for this. That is, from the comparison between the values of the approximate and rigorous calculations of the integral which contributes to the absorption intensity related to the C–O stretching mode in CO_2, it is found that the difference between those values is remarkably large (see Fig. 4). The

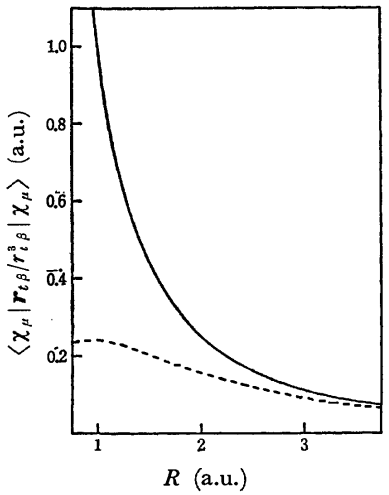

Fig. 4. Comparison between the approximate and rigorous values of the $\langle\chi_\mu|\boldsymbol{r}_{t\beta}/r^3_{t\beta}|\chi_\mu\rangle$ integral in Eq. (18) of Ref. 15. χ_μ is the $2p_x$ atomic orbital of carbon and R is the distance between the β atom and the carbon which are located on the z-axis.
——: Approximate, ----: Rigorous.

defect in the approximate calculation, however, has no influence on the value of the absorption intensity with reference to the bending mode of a linear molecule, because the scalar product in Eq. (17) in Ref. 15 is always equal to zero.

The theoretical intensities of the simultaneous transitions were calculated from the transition moments, which were divided into two parts, $\mu^A_{m,o}(0)$ and $\mu^B_{m,o}(0)$, as indicated in Eq. (29). In the CO_2–N_2 system, the A part is the transition moment derived from the coupling between the electronic state of CO_2 and the nuclear vibration of N_2, while the B part is that derived from the coupling between the electronic state of N_2 and the nuclear vibration of CO_2. The calculated intensities are listed in Tables 1—3, in which the first line indicates the value from the A part of the transition moment, and the second line, the value from the B part. In the cases of the L-R, R-R, and R-L types of orientation between the molecules, the intensities from the B part were affected by the degenerate bending vibrations, one of which is set on the plane involving the two molecules and the other one of which is set out of the plane; the intensities in the case of the out-of-plane bending vibration were zero. On the other hand, in cases of the other orientations, the intensities from the A and B parts were not affected by the different bending modes. Therefore, the values in Table 2 indicate only the case of the in-plane bending vibration. From the tables, it is found that the contributions of the A and B parts of the transition moment to the absorption intensity caused by the simultaneous transition differ from each other. The A part is effective on the intensities of $\nu_2+\nu_{N_2}$ and $\nu_3+\nu_{N_2}$ at all the orientations. The B part is, however, effective on the intensity of $\nu_2+\nu_{N_2}$ at the L-R and R-L types of orientation and on that of $\nu_3+\nu_{N_2}$ at the L-L and R-R types. The intensity of $\nu_1+\nu_{N_2}$ arises from the restricted parts, the A part at the L-L and L-R types of the orientation, and the

Table 1. The absorption intensity of the simultaneous transition, $\nu_1+\nu_{N_2}$ [$cm^2\,s^{-1}\,pair^{-1}$][a,b]

Orientation[c]	R[d] [Å]				
	4.0	6.0	8.0	15.0	30.0
L-L	0.389×10^{-8}	0.980×10^{-10}	0.851×10^{-11}	0.491×10^{-13}	0.185×10^{-15}
	0.515×10^{-10}	0.130×10^{-11}	0.113×10^{-12}	0.650×10^{-15}	0.245×10^{-17}
L-R	0.722×10^{-9}	0.219×10^{-10}	0.201×10^{-11}	0.121×10^{-13}	0.460×10^{-16}
	0.0	0.0	0.0	0.0	0.0
R-R	0.0	0.0	0.0	0.0	0.0
	0.0	0.0	0.0	0.0	0.0
R-L	0.0	0.0	0.0	0.0	0.0
	0.447×10^{-11}	0.207×10^{-12}	0.219×10^{-13}	0.151×10^{-15}	0.600×10^{-18}

a) The unit of the intensity is the cross section per unit time per molecule-pair. b) The upper values are calculated with the term of the coupling between the electronic state of CO_2 and the nuclear vibration of N_2 and the lower ones with the term of the coupling between the electronic state of N_2 and the nuclear vibration of CO_2. c) The orientation of the molecules is shown in Fig. 1. d) R is the intermolecular distance as shown in Fig. 1.

Table 2. The absorption intensity of the simulaneous transition, $\nu_2+\nu_{N_2}$ [$cm^2\,s^{-1}\,pair^{-1}$][a,b]

Orientation[c]	R[d] [Å]				
	4.0	6.0	8.0	15.0	30.0
L-L	0.469×10^{-9}	0.181×10^{-10}	0.239×10^{-11}	0.413×10^{-13}	0.591×10^{-15}
	0.0	0.0	0.0	0.0	0.0
L-R	0.900×10^{-10}	0.415×10^{-11}	0.572×10^{-12}	0.102×10^{-13}	0.147×10^{-15}
	0.332×10^{-11}	0.384×10^{-13}	0.328×10^{-14}	0.282×10^{-16}	0.294×10^{-18}
R-R	0.649×10^{-11}	0.127×10^{-11}	0.291×10^{-12}	0.841×10^{-14}	0.140×10^{-15}
	0.0	0.0	0.0	0.0	0.0
R-L	0.459×10^{-10}	0.643×10^{-11}	0.133×10^{-11}	0.349×10^{-13}	0.567×10^{-15}
	0.206×10^{-12}	0.305×10^{-17}	0.582×10^{-15}	0.460×10^{-16}	0.932×10^{-18}

a, b, c, d) See the footnotes in Table 1.

Table 3. The absorption intensity of the simultaneous transition, $\nu_3+\nu_{N_2}$ [$cm^2\,s^{-1}\,pair^{-1}$][a,b]

Orientation[c]	R[d] [Å]				
	4.0	6.0	8.0	15.0	30.0
L-L	0.196×10^{-6}	0.105×10^{-7}	0.159×10^{-8}	0.318×10^{-10}	0.476×10^{-12}
	0.428×10^{-11}	0.768×10^{-13}	0.614×10^{-14}	0.504×10^{-16}	0.520×10^{-18}
L-R	0.396×10^{-7}	0.244×10^{-8}	0.384×10^{-9}	0.786×10^{-11}	0.119×10^{-12}
	0.0	0.0	0.0	0.0	0.0
R-R	0.121×10^{-7}	0.143×10^{-8}	0.283×10^{-9}	0.720×10^{-11}	0.116×10^{-11}
	0.574×10^{-13}	0.226×10^{-15}	0.122×10^{-16}	0.413×10^{-17}	0.982×10^{-19}
R-L	0.637×10^{-7}	0.649×10^{-8}	0.122×10^{-8}	0.294×10^{-10}	0.467×10^{-12}
	0.0	0.0	0.0	0.0	0.0

a, b, c, d) See the footnotes in Table 1.

B part at the L-L and R-L types. For the intensities of all the simultaneous transitions, the A part at the L-L type of orientation makes the dominant contribution.

The following general considerations can be derived from these results. On the simultaneous transition of the A–B system, when the vibrational mode of the A molecule is infrared-active, the intermolecular vibronic coupling between the electronic state of the A molecule and the nuclear vibration of the B molecule is always effective. When both the vibrational modes of the molecules, A and B, are infrared-inactive, it does not necessarily follow that a simultaneous transition is not found. Rather, the finding of the phenomenon depends on the orientation of the molecules. Special attention should be paid to the latter conclusion.

These conclusions disagree with those suggested by Hooge and Ketelaar,[3] who discussed the problem on the basis of the expansion of the dipole moment with the normal coordinates. They suggested that the necessary condition for the appearance of a simul-

TABLE 4. THE INFRARED ABSORPTION INTENSITY OF CO_2

	Obsd	Intra.[a]	Inter.[a] [$cm^2\ s^{-1}$ pair^{-1}][b] R[c] [Å]				
	[$cm^2\ s^{-1}$ molecule^{-1}]		4.0	6.0	8.0	15.0	30.0
ν_1		0.0					
ν_2	0.18×10^{-6} [d]	0.196×10^{-7}					
	0.27×10^{-6} [e,f]						
ν_3	0.30×10^{-5} [d]	0.196×10^{-4}					
	0.33×10^{-5} [f]						
$2\nu_1$		0.0	0.173×10^{-8}	0.671×10^{-10}	0.662×10^{-11}	0.424×10^{-13}	0.165×10^{-15}
$2\nu_2$		0.0	0.582×10^{-11}	0.150×10^{-12}	0.154×10^{-12}	0.205×10^{-12}	0.140×10^{-14}
$2\nu_3$		0.0	0.192×10^{-7}	0.170×10^{-8}	0.346×10^{-9}	0.161×10^{-10}	0.817×10^{-12}
$\nu_1+\nu_2$	0.16×10^{-9} [d]	0.114×10^{-6}	0.169×10^{-8}	0.497×10^{-10}	0.743×10^{-11}	0.115×10^{-12}	0.169×10^{-14}
$\nu_1+\nu_3$	0.31×10^{-7} [d,g]	0.192×10^{-5}	0.793×10^{-6}	0.436×10^{-7}	0.699×10^{-8}	0.149×10^{-9}	0.228×10^{-11}
	0.44×10^{-7} [d,g]						
$\nu_2+\nu_3$		0.0	0.114×10^{-8}	0.273×10^{-9}	0.173×10^{-9}	0.228×10^{-11}	0.161×10^{-11}

a) The abbreviations, Intra. and Inter., mean the intramolecular and intermolecular processes, respectively. b) See the footnote a in Table 1. c) See the footnote d in Table 1. d) From Ref. 17. e) From Ref. 18. f) From Ref. 19. g) The assignment of these values was not exactly given because of the Fermi resonance between $\nu_1+\nu_3$ and $2\nu_2+\nu_3$.

taneous band is that one of the vibrational modes is infrared-active, while the other mode is Raman-active. The results of the CO_2–H_2 system are analogous to those of the CO_2–N_2 system. Therefore, their discussions are omitted.

Carbon Dioxide: The infrared absorption intensities of CO_2 have been measured by several investigators for the gas[17–19] and solid phases.[20] The calculated values of the intensities, with reference to the intramolecular and intermolecular processes, are shown in Table 4; the experimental results in the gas phase are also included. For the intensities from the intermolecular process, the averaged values are adopted for the same reason as has been presented before. The table shows that the intermolecular interaction contributes slightly to the absorption intensities at the atmospheric pressure and at the intermolecular distance of about 30 Å. Therefore, it is considered that the experimental results at the ordinary pressure correspond to the results caused by the intramolecular process. In the experiment, two fundamental bands, ν_2 and ν_3, with very strong intensities and two combination bands, $\nu_1+\nu_2$ and $\nu_1+\nu_3$, with medium and strong intensities respectively are observed. In the calculated results, the intensity of ν_3 is the strongest, while that of ν_2 is weaker than those of $\nu_1+\nu_2$ and $\nu_1+\nu_3$. From the comparison between the experimental and the calculated results, it is found that the calculated intensity of ν_2 is underestimated and that the theoretical values for the other absorption bands are overestimated. It is considered that these overestimations arise from the defect in the approximate calculation described before. It is noteworthy that the intensity from the intermolecular process increases with a decrease in the intermolecular distance (see Table 4). In any case, it is found that the intermolecular interaction contributes, more or less, to the intensities of the overtone and combination bands, some of which have no intensity from the intramolecular process. These results establish that the intermolecular vibronic coupling is an important factor for the infrared absorption intensity of the compressed gas of a one-component system. Also, the following statement might be made; in discussing the intensity of the vibrational spectra of the liquid phase, it is necessary to include an argument based on the intermolecular vibronic coupling.

Summary

The formulas of the infrared-absorption intensity for the intramolecular and intermolecular processes have been derived by the use of the vibronic expansion technique. The intensities for the simultaneous transitions of the CO_2–N_2 and CO_2–H_2 systems and for CO_2 have been calculated. Since the matrix elements of the vibronic coupling operator were only approximately calculated, quantitative conclusions could not be obtained. The qualitative conclusion is that, for any pair of vibrational modes between molecules, the intensities of the simultaneous transitions are not zero, although their magnitudes depend on the orientation of the molecules and are not always large enough to be observed. One remarkable suggestion is that the intermolecular interaction, like the intramolecular anharmonicities, is an important factor in discussing infrared absorption intensities in liquids and solutions. In that case, the method used in averaging the orientation of molecules will become an essential problem in the treatment of intermolecular interactions.

The authors would like to thank Professor Tomoo Miyazaki for his helpful advice and for his critical reading of the manuscript. In their calculations, they were also helped by "The University Contribution" of UNIVAC Japan, Ltd.

References

1) J. Fahrenfort and J. A. A. Ketelaar, *J. Chem. Phys.*, **22**, 1631 (1954).

2) J. A. A. Ketelaar and F. N. Hooge, *ibid.*, **23**, 749, 1549 (1955); *Rec. Trav. Chim. Pays-Bas.*, **76**, 529 (1957).

3) F. N. Hooge and J. A. A. Ketelaar, *Physica*, **23**, 423 (1957).

4) A. M. Thorndike, A. J. Wells, and E. B. Wilson, Jr., *J. Chem. Phys.*, **15**, 157 (1947); T. Miyazaki and H. Yamamoto, This Bulletin, **45**, 1669 (1972); T. Miyazaki, T. Shigetani, and H. Yamamoto, *ibid.*, **45**, 678 (1972); T. Miyazaki, M. Ikeda, and M. Shibata, *ibid.*, **48**, 1138 (1975); See Ref. 7, p. 39.

5) G. Placzek, "Handbuch der Radiologie," Vol. 6, ed. by E. Marx, Akademische Verlagsgesellschaft, Leipzig (1934), Pt. 2; H. Shinoda and T. Miyazaki, *Chem. Lett.*, **1973**, 563.

6) J. Tang and A. C. Albrecht, "Raman Spectroscopy," Vol. 2, ed. by. S. Szymanski, Plenum Press, New York-London (1970), p. 33; see also Ref. 15.

7) E. B. Wilson, Jr., J. C. Decius, and P. C. Cross, "Molecular Vibrations," McGraw-Hill Book Company, New York-Toronto-London (1955), p. 163.

8) L. I. Schiff, "Quantum Mechanics," 3rd Ed., McGraw-Hill Book Company, New York-Toronto-London (1968), p. 247.

9) When the translation and the rotation are neglected, $\hat{\boldsymbol{\mu}}_n$ can be expressed as $\hat{\boldsymbol{\mu}}_n=\sum_i Z_i(\mathbf{r}_i^0+\Delta\mathbf{r}_i)$, where Z_i is the nuclear charge of the i atom, $\mathbf{r}_i^0$ the vector of the equilibrium position of the i atom from the origin of the molecular fixed coordinate system, and $\Delta\mathbf{r}_i$ is the vector of the displacement of the i atom from the equilibrium position. $\hat{\boldsymbol{\mu}}_n^0$ in Eq. (7) means $\sum_i Z_i\mathbf{r}_i^0$ and $\sum_a \mathbf{k}_a Q_a$ in Eq. (7) is casily derived from $\sum_i Z_i\Delta\mathbf{r}_i$ by transforming $\Delta\mathbf{r}_i$ to Q_a by the use of the L_x matrix elements.

10) J. N. Murrell, M. Randic, and D. R. Williams, *Proc. Roy. Soc.* (London), *A*, **284**, 566 (1965).

11) J. A. Pople, D. P. Santry, and G. A. Segal, *J. Chem. Phys.*, **43**, S129 (1965); J. A. Pople and G. A. Segal, *ibid.*, **43**, S136 (1965); **44**, 3289 (1966).

12) The notation of the singly-excited configuration, χ_i^m, follows the Murrell and McEwen's in *J. Chem. Phys.*, **25**, 1143 (1956).

13) C. C. J. Roothaan, *Rev. Mod. Phys.*, **23**, 69 (1951).

14) T. Miyazaki and H. Shinoda, This Bulletin, **46**, 1216 (1973).

15) H. Shinoda, *ibid.*, **48**, 1777 (1975).

16) G. Herzberg, "Molecular Spectra and Molecular Structure," Vol. 1, 2nd Ed. (1950) and Vol. 2 (1945), Van Nostrand, New York.

17) D. F. Eggers, Jr., and B. L. Crawford, Jr., *J. Chem. Phys.*, **19**, 1554 (1951).

18) J. Overend, M. J. Youngquist, E. C. Curtis, and B. L. Crawford, Jr., *ibid.*, **30**, 532 (1959).

19) B. Schurin, *ibid.*, **33**, 1878 (1960).

20) H. Yamada and W. B. Person, *ibid.*, **41**, 2478 (1964)

Electronic Spectra of Perylene and Coronene Evaporated Films as a Function of Their Crystallinity

Yusuke KAMURA,* Ichimin SHIROTANI, Koichi OHNO,# Kazuhiko SEKI, and Hiroo INOKUCHI**

The Institute for Solid State Physics, The University of Tokyo, Roppongi, Minato-ku, Tokyo 106

#College of General Education, The University of Tokyo, Komaba, Meguro-ku, Tokyo 153

(Received August 20, 1975)

The absorption spectra of evaporated thin films of perylene and coronene have been studied as a function of their crystallinity. The amorphous films deposited on a low-temperature substrate *in vacuo* gave rise to "molecular" spectra which are very different from those of the polycrystalline films. The absorption spectra of amorphous films gradually changed with an increase in the substrate temperature to become similar to those of the polycrystalline films.

It has been found that the spectral responses of the evaporated thin films of polycyclic aromatic compounds depend on the temperature of their substrate during vacuum evaporation.[1-6] This behavior has been interpreted as being due to the difference in molecular aggregation in the films; that is, the evaporation of aromatics onto a high-temperature substrate yields oriented polycrystalline films, while evaporation onto a substrate kept at a low temperature gives rise to amorphous ones.

In a previous paper, we have reported[4,5] the absorption spectra and their pressure dependences of naphthacene and pentacene evaporated films. The Davydov splitting of the 0–0 band in their oriented polycrystalline films was found at atmospheric pressure, and the magnitude of this splitting increased with increasing pressure; on the other hand, no Davydov splitting could be observed in amorphous films, and the pressure-induced spectral red shifts were found to be slightly larger than those in the polycrystalline state.

Further, it was found that naphthacene and pentacene in the amorphous state are much more unstable and reactive than in the polycrystalline state under illumination and also under heat treatment in air.[4]

By means of a polarizing microscope, just after the evaporation a very dark image was observed for the naphthacene and pentacene amorphous films with a crossed nicol condition.[3] In a few days, however, several bright microcrystallites appeared in the dark background, their number increasing day by day. The change in the absorption spectrum due to crystallization was not measured because of the interference of a chemical reaction in the film.

In this paper, we will present the results of some studies of the electronic spectra of the perylene and coronene evaporated films as a function of the crystallinity and will also discuss the relation between the electronic states and the structures of the films.

Experimental

Synthesized perylene and synthesized coronene were purified by recrystallization and sublimation. Their thin films were prepared by evaporation onto a quartz substrate kept at room temperature (RT-film) or a low temperature (~170 K) (LT-film) in a vacuum of 10^{-4} Torr. The thickness of the films was monitored by means of a quartz-crystal oscillator and was estimated to be about 6×10^2 Å. The absorption spectra of the films were measured with a Cary 14 spectrophotometer.

The absorption spectra of the RT-film were measured at room temperature. The temperature dependence of the spectra of the LT-film was studied from 170 to 300 K *in vacuo*. The change in the X-ray diffraction patterns and also that in the absorption spectra of LT-films were investigated at room temperature. Further, the structures of these films were studied with a polarizing microscope.

In order to confirm the orientation of molecules in the film, and also in order to assign the absorption spectra, some additional experiments were carried out: the quartz substrate was inclined with respect to the incident light beam so that the transition with their polarization vector perpendicular to the plane of the substrate could be observed in the absorption spectra.

Results and Discussion

Absorption Spectra of Perylene and Coronene LT-films. We have already reported some findings on the absorption spectra of the naphthacene and pentacene evaporated films.[4] The characteristic absorption bands in the RT-film (oriented microcrystalline film) disappear in the LT-film (amorphous film); The absorption spectra in the LT-films resemble those of the corresponding free molecules in solution. Figures 1 and 2 show the absorption spectra of the LT- and RT-films and an ethanol solution for perylene and coronene respectively. The spectra of the LT-films at 170 K were similar to the molecular spectra in solution, but they were very different from those of the RT-films. These findings are similar to those for naphthacene and pentacene.[4]

Figure 3 shows the temperature dependence of the absorption spectra of the coronene LT-film. Its absorption bands gradually changed with an increase in the temperature. The absorption spectrum in the LT-film at room temperature agrees approximately with that of the RT-film. As is shown in Fig. 4, the absorption band of the perylene LT-film at room temperature was not similar to that of the RT-film.

By means of a polarizing microscope, a very dark image was observed for naphthacene and pentacene LT-films at room temperature using crossed nicols. However, in the case of perylene and coronene LT-

* Present address: Hatano Research Institute, F.D.S.C., Ochiai, Hatano-shi 257.

** Present address: Institute for Molecular Science, Okazaki 444.

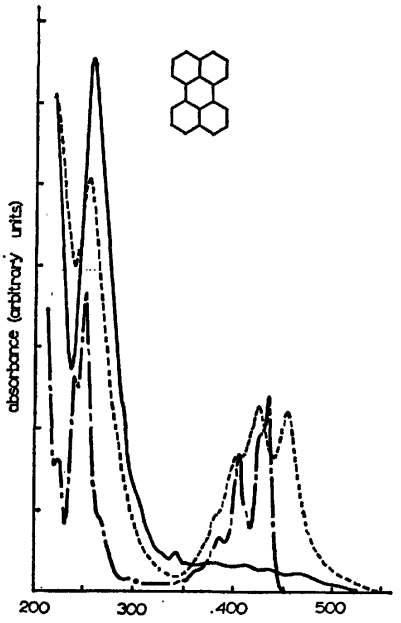

Fig. 1. Absorption spectra of perylene.
——: RT-film, – – –: LT-film at 170 K, ———: ethanol solution.

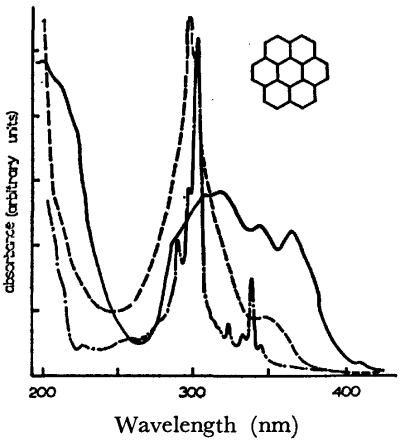

Fig. 2. Absorption spectra of coronene.
——: RT-film, – – –: LT-film at 170 K, ———: ethanol solution.

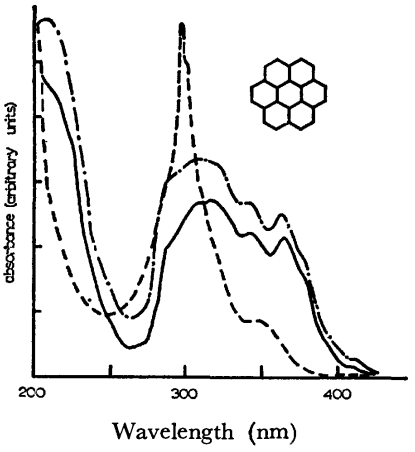

Fig. 3. Absorption spectra of coronene.
– – –: LT-film at 170 K, ———: annealed LT-film at 300 K, ——: RT-film.

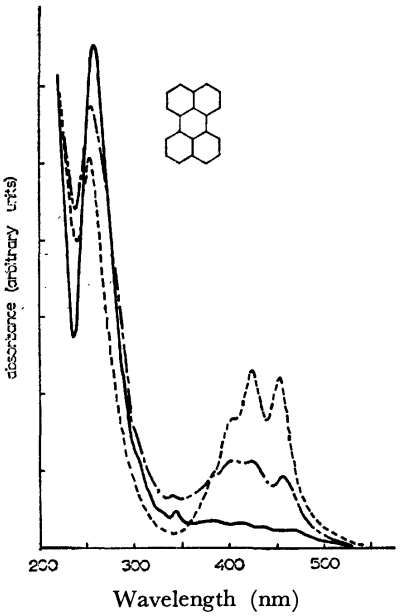

Fig. 4. Absorption spectra of perylene.
– – –: LT-film at 170 K, ———: annealed LT-film at 300 K, ——: RT-film.

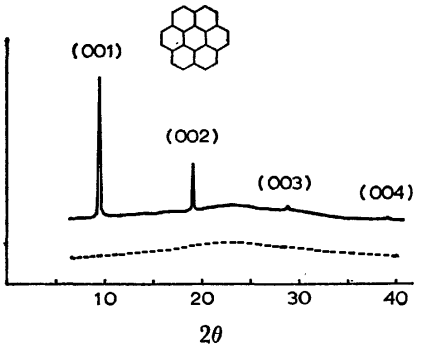

Fig. 5. X-Ray diffraction patterns of coronene evaporated films at room temperature.
——: RT-film, – – –: LT-film.

films at room temperature, a large number of bright crystallites were found against a dark background, and the number increased with the time.

From these facts we may conclude that the amorphous state in their LT-films undergoes a crystallization process with a change in the temperature and also with time.

Figure 5 shows the X-ray diffraction patterns of the LT- and RT-films of coronene at room temperature. The sharp peaks corresponding to the (00l) plane[7] were found for the RT-film, but no peaks could be observed for the LT-film. Similar results, in Fig. 6, were also found in perylene films.[8] As has been mentioned above, though LT-films at room temperature are partially crystallized, it should be noted that the sharp X-ray diffraction lines could not be found. This may be interpreted as follows: in the annealed films the crystallites are not oriented, and the thickness of the films is not sufficient for diffraction patterns to be observed.

The absorption bands of the naphthacene and pentacene LT-films are gradually changed with the

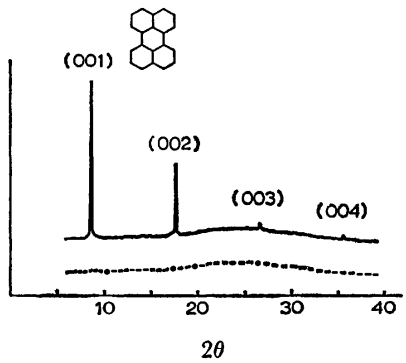

Fig. 6. X-Ray diffraction patterns of perylene evaporated films at room temperature.
——: RT-film, ----: LT-film.

passage of time at room temperature. Although the formation of microcrystals is observed in the LT-films, this spectral change arises mainly from the chemical reaction.[4]

Amorphous films of coronene and perylene, however, were easily annealed. In particular, the rate of the crystallization of amorphous coronene was very rapid. On the other hand, amorphous naphthacene and pentacene crystallized very slowly. These results suggest that the various effects of annealing on the amorphous organic films may be related to the difference in molecular shape.

Molecular Orientation in the Evaporated Films. The absorption spectra of the perylene single crystal has been studied in terms of the Davydov splitting of the exciton states by Tanaka.[9,10] The spectra were observed through the ab plane of the crystal, and the a-axis and b-axis polarization components were resolved. The absorption spectrum was found to be in good agreement with our spectrum of the RT-film when the plane of the substrate was set perpendicular to the incident light beam (Fig. 1). In our oriented microcrystalline film, however, only the bands of the b-axis polarization component could be found at 460 and 440 nm for the first electronic transition band between 400—500 nm. This is reasonable, since the b-axis polarization component in this spectral region is much larger than the a-axis one in the single crystal ab-plane spectra obtained by Tanaka. It has been shown that the first electronic transition band has its polarization vector along the long axis (L-axis) of the molecule.[9,10] As may be seen from Fig. 7,[8] the L-axis is almost perpendicular to the ab plane, whereas the short molecular axis (M-axis) is nearly parallel to the ab plane. Therefore, the L-axis polarized transitions in the crystals can be expected to be of a much reduced intensity in the ab-plane spectra in comparison with those observed for the LT-film and the solution. In fact, this can be seen from Fig. 1, where the 250—260 nm bands have been assigned as an M-axis transition;[9,10] therefore, they are considered to be slightly emphasized in the spectrum of the RT-film. The weakened L-axis transition bands, however, may be expected to appear when the ab planes of the single crystal on the oriented microcrystals are inclined nearly parallel to the direction of the

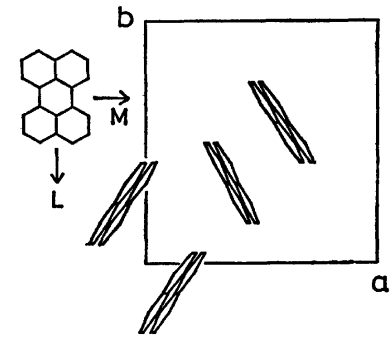

Fig. 7. Projection of perylene molecule onto the ab plane.

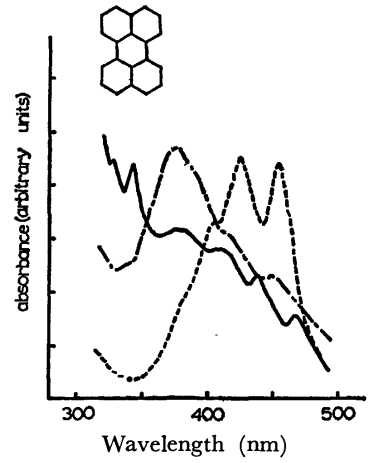

Fig. 8. Absorption spectra of perylene evaporated films.
——: Incident light with respect to the normal of the substrate is perpendicular, ——: incident light with respect to the normal of the substrate is set about 75°, ----: LT-film.

incident-light beam. An additional experiment for the RT-film of perylene, where the angle of the incident light with respect to the normal of the substrate was set at about 75° (Fig. 8), clearly revealed the ac polarization component of the exciton states, which should be much more polarized along the crystal c'-axis normal to the ab plane. The peaks at 405 and 445 nm observed in this spectrum were found to be in good agreement with those observed in the c-axis polarization component of the ab-plane crystal spectra. From the arguments given above, one can conclude that the perylene RT-film should be regarded as oriented microcrystalline films in which the crystallites are oriented with their ab planes parallel to the substrate planes. This is consistent with the orientation of the crystallites determined by X-ray diffraction in the previous subsection.

The spectral behavior of the evaporated films of coronene is very similar to that found for perylene. The absorption spectrum of the LT-film is shown in Fig. 2; it is found to agree well with the solution spectra. The most prominent band at about 300 nm in this spectrum of the LT-film may be assigned to a $^1A_{1g} \rightarrow {}^1E_{1u}$ transition, as in the case of the analogue in the solution spectra.[11] The absorption spectrum of the coronene RT-film, when the incident light beam was

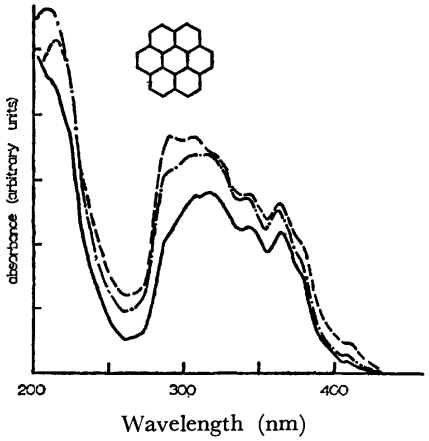

Fig. 9. Absorption spectra of coronene RT-film.
——: Incident light with respect to the normal of the substrate is perpendicular, ——: incident light with respect to the normal of the substrate is set about 45°, ——: incident light with respect to the normal of the substrate is set about 60°.

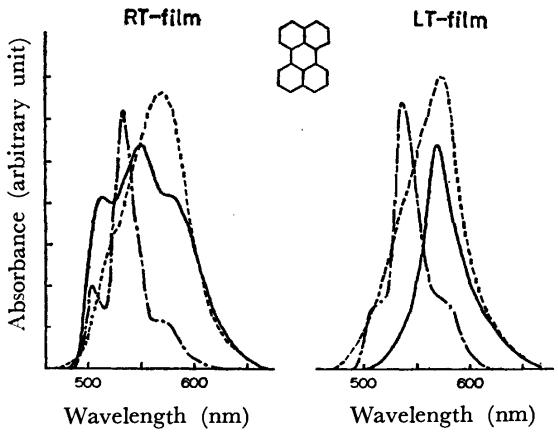

Fig. 10. Fluorescence spectra of perylene RT- (left side) and LT- (right side) films.
——: At liquid helium temperature, ——: at liquid nitrogen temperature, ——: at room temperature.

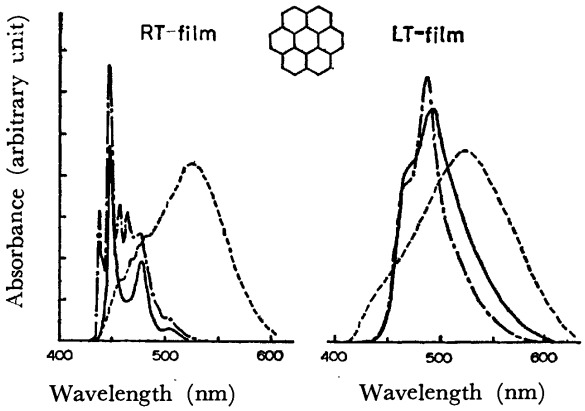

Fig. 11. Fluorescence spectra of coronene RT- (left side) and LT- (right side) films.
——: At liquid helium temperature, ——: at liquid nitrogen temperature, ——: at room temperature.

set perpendicular to the substrate, was found to be in good agreement with the ab-plane absorption spectra of the single crystals obtained by Tanaka.[11] His analysis showed that the bands between 280 and 320 nm could be assigned in terms of the Davydov splitting of the exciton states arising from a $^1E_{1u}$ state of the molecule. From our additional experiment, the band at 290 nm in the RT-film spectra increases in intensity on a decrease in the incident light angle with respect to the normal of the substrate: 0°, 45°, and 60° (Fig. 9), in this order. One can therefore assign the band at 290 nm to one of the ac polarization components of the exciton states arising from the $^1E_{1u}$ state, which should be much more polarized along the crystal c'-axis normal to the ab plane. This assignment of the 290 nm band is consistent with that made by Tanaka.[11] From the assignments given above, we can also conclude, for the coronene evaporated films, that the LT-film should be regarded as an amorphous film in which the orientation of the molecules is disordered, and that the RT-film is composed of a large number of crystals oriented with their ab planes parallel to the substrate.

Fluorescence Spectra of Perylene and Coronene Evaporated Films. Figure 10 shows the temperature dependence of the fluorescence spectra of the perylene RT- and LT-films. The fluorescence spectra of RT-film were similar to those of the α-type of perylene single crystal.[9] A broad emission band was observed in both films at room temperature. Judging from the results of the fluorescence of the perylene crystal,[9] the broad emission may arise from the excimer emission. This emission in the RT-film disappeared at the temperature of liquid nitrogen, where a monomer-like emission was observed. On the other hand, the excimer emission appeared in the LT-film at 77 K. This shows that the short-range molecular interaction in the amorphous state is rather stronger than that in the crystalline state. In a previous paper,[5] we have reported the pressure shift of the vibronic band in organic films; the pressure-induced spectral shifts in the amorphous state are slightly larger than those in the crystalline state. On the basis of the results of the emission spectra and the pressure shift, we may conclude that the intermolecular interactions in organic amorphous films are never weak in comparison with those in crystalline films. Figure 11 shows the temperature dependence of the fluorescence spectra of the coronene RT- and LT-films. Both the RT- and the LT-films of coronene showed an excimer-type emission at room temperature. However, at very low temperatures the excimer-type emission band could not be found in the fluorescence spectrum of the RT-film. In contrast, the LT-film showed an excimer-type emission at any temperature between room temperature and 4.2 K. It may, therefore, be suggested that, in the LT-film, the excited dimer state is rather more favorable than in the RT-film, where the emission spectrum may be affected by energy transfer through the exciton states.

Crystallization Processes in the Disordered Aggregates by Annealing. As has been mentioned in the previous subsections, the LT-films of coronene and

perylene undergo some annealing processes at room temperature, while for naphthacene and pentacene the LT-films are considered to be in amorphous states when they are left at room temperature for a few days. The absorption spectrum of the annealed LT-film coronene became very similar to that of the RT-film (Fig. 3). In connection with the results in the previous subsection, this may lead us to conclude that the annealed LT-film of coronene is in a microcrystalline state. Whether the annealed LT-film is oriented or not may be ascertained as follows. Since the absorption peaks in the spectrum of the annealed LT-film agree well with those of the RT-film and also with those of single crystals, the crystallites in the annealed LT-film may be considered as single crystals in which the arrangement and orientation of coronene molecules are almost perfect. Therefore, the diffuse X-ray diffraction pattern observed for the annealed LT-film may not be accounted for a disorder of the molecular orientation and arrangement in the microcrystals. As can be seen from Fig. 3, the 290 nm band for the annealed LT-film is slightly more intense than that for the RT-film. Furthermore, the spectra of the annealed LT-film were found to be independent of the incident-light angle. These facts indicate that the orientation of the crystallites is almost at random in the annealed LT-film. This may be the reason why the X-ray diffraction pattern was found to be still diffuse for the annealed LT-film.

The absorption spectrum of the annealed LT-film of perylene is shown in Fig. 4, together with those of the LT-film and the RT-film. For perylene, the absorption spectrum of the annealed LT-film did not become similar to that of the RT-film, but remained rather similar to that of the LT-film. The spectral peaks found in the L-axis transition bands for the annealed LT-film correspond well to those of the LT-film. The spectral intensities for these bands, however, were weakened in the annealed LT-film. These facts mean that the molecular orientation in the crystallites found through the microscope for the annealed LT-film is disordered to some extent and that the L-axis of the perylene molecules in the annealed LT-film is slightly oriented on average perpendicular to the plane of the substrate. Furthermore, the M-axis transition band at 250 nm for the annealed LT-film is found to be more intense than that observed for the LT-film; the M-axes of the perylene molecules in the annealed LT-film may also be slightly oriented on average parallel to the plane of the substrate. Since, for the annealed LT-film, crystallites were actually observed with a microscope, the molecules in the crystallites may be arranged in a way similar to that of the perfect crystals, especially for such a large disc-like-shaped planar molecule as perylene. One may, therefore, suggest that the annealed LT-film of perylene is composed of imperfect crystallites in which the orientation of the molecules within the molecular plane is disordered to some extent.

The various effects of annealing at room temperature on the LT-films may be related to the difference in their molecular shape. As was seen in the previous subsection, the fluorescence spectra of the LT-films and also of the annealed LT-films of perylene and coronene were found to be of the excimer type. This means that the molecules in the films are stacked in a similar way, with their planes parallel to one another. In the perfect crystals the molecules are regularly stacked. If such a stacking structure is well distributed in the LT-films of coronene and perylene, the rate-determining step lies in the molecular re-orientation within the crystal lattice. On the basis of this assumption the behavior of the annealed LT-films of coronene and perylene can be explained as follows. Since a coronene molecule has an almost disc-like shape, rotational motion along the normal-axis of the molecular plane may proceed in the aggregates without any serious change in the arrangements of the neighboring molecules; it follows that the LT-film of coronene may be almost perfectly annealed into a microcrystalline film. Since the perylene molecule is not so perfect in disc shape as coronene, rotational motion occurs less readily and may result in the imperfect crystal growth found in the annealed LT-film. On the other hand, for long-plate-like molecules, for example, naphthacene and pentacene, such a rotational motion may be inhibited because the re-orientation of the molecular axes should be quite difficult without the exclusion of neighboring molecules. One can, therefore, understand that the properties of the LT-films of naphthacene and pentacene are retained even if the films are left at room temperature for a few days.

The authors wish to thank Professor Satoshi Iwashima for his gift of the chemicals and Mr. Mikio Yagi for the measurements of the fluorescence spectra. Their thanks are also due to Dr. Yusei Maruyama for his helpful discussion.

References

1) H. Inokuchi, H. Kuroda, and H. Akamatu, This Bulletin, **34**, 749 (1961).
2) Y. Maruyama, T. Iwaki, T. Kajiwara, I. Shirotani, and H. Inokuchi, *ibid.*, **43**, 1259 (1970).
3) Y. Maruyama and N. Iwasaki, *Chem. Phys. Lett.*, **24**, 26 (1974).
4) Y. Kamura, I. Shirotani, H. Inokuchi, and Y. Maruyama, *Chem. Lett.*, **1974**, 627.
5) I. Shirotani, Y. Kamura, and H. Inokuchi, *Mol. Cryst. Liq. Cryst.*, **28**, 345 (1974).
6) Y. Kamura, K. Seki, and H. Inokuchi, *Chem. Phys. Lett.*, **30**, 35 (1975).
7) J. M. Robertson and J. G. White, *J. Chem. Soc.*, **1945**, 607.
8) D. M. Donaldson, J. M. Robertson, and J. G. White, *Proc. Roy. Soc.*, **A220**, 311 (1953).
9) J. Tanaka, This Bulletin, **36**, 1237 (1963).
10) J. Tanaka, T. Kishi, and M. Tanaka, *ibid.*, **47**, 2376 (1974).
11) J. Tanaka, *ibid.*, **38**, 86 (1964).

Kinetic Studies of the Crystallization of Vitreous Beryllium Fluoride

Seiichi TAMURA and Toshio YOKOKAWA

Department of Chemistry, Faculty of Science, Hokkaido University, Sapporo 060

(Received September 1, 1975)

The kinetics of the crystallization of vitreous beryllium fluoride were studied using the quantitative X-ray diffraction and calorimetric methods. Analysis of the data using the Johnson-Mehl-Avrami equation shows that the crystallization proceeds through spherulitic growth. The activation energy of 222 kJ mol^{-1} was obtained from the temperature dependence of the crystallization rate using a modified Johnson-Mehl-Avrami equation.

Investigations of the crystallization of beryllium fluoride from various fluoroberyllate glasses have been reported by many workers. However, no quantitative analysis of the crystallization of the pure vitreous beryllium fluoride has been performed. Several years ago, Batsanova *et al.* made a rough estimate of the rate of crystallization of pure vitreous beryllium fluoride at three temperatures.[1] The crystallization data, however, could not be analyzed because the data were very scarce; their main objective was to study the structure of the glasses.

Recently, enthalpy increments of the crystalline, liquid, and vitreous beryllium fluoride were measured between 456 and 1083 K by the normal drop method and by the transposed-temperature drop method in our laboratory.[2,3] In the transposed-temperature drop calorimetry, it was observed that the vitreous phase turned into the crystalline phase between 623 and 800 K. Qualitatively, the rate of crystallization at about 730 K was faster than those below and above that temperature. We measured the rate of crystallization by a calorimetric method using the enthalpy data as well as an X-ray diffraction method, and studied the kinetics of crystallization in detail using the Johnson-Mehl-Avrami equation.

Experimental

Materials. The beryllium fluoride used for this study was prepared from a commercial beryllium fluoride (Mitsuwa Kagaku Co., Ltd.) which was approximately 99.5 moles per cent pure. The sample was further purified by vacuum distillation at about 1070 K. Beryllium fluoride vapor was condensed onto the inner wall of a platinum crucible of about 800 K. Further analysis was not carried out for the purified beryllium fluoride. The vitreous sample was prepared by heating the sample in a sealed platinum container at 903 K and by then dropping it into the silver crucible at room temperature for rapid cooling. These vitreous samples were then submitted to the X-ray diffraction method and the calorimetric measurements.

Calorimetric Method. The calorimeter used for this study was a high-temperature calorimeter of the Calvet type which has been described previously.[4] The assembly of the apparatus is identical to that used previously in the normal drop method. However, the calorimeter was maintained at 730 or 760 K, and coarse silver powder was used instead of liquid mercury to aid heat conduction in the calorimeter cells. Although the electric furnace above the calorimeter had two different constant-temperature zones, only one of them was used for the present study. The vitreous sample (1.5 to 2.5 g) was loaded into a platinum container 8 mm in diameter, 45 mm in height, and 0.2 mm thick (2 to 2.5 g) and the top of the container was sealed by arc-welding in a glove box filled with nitrogen. The method of the quantitative determination of crystallization by the calorimeter is as follows. First, a vitreous sample of n moles is inserted into the furnace and maintained at a certain temperature, T_1, for the time t and then partially crystallized by the mole fraction, X. Then the sample is dropped into the calorimeter at another temperature, T_0, and crystallized completely in it. In this case, the measured heat, Q, contains both enthalpy increments, $\{H(T_1)-H(T_0)\}$, and the heat of crystallization,

$$\{H(\mathrm{gl},\ T_0)-H(\mathrm{c},\ T_0)\};$$

$$Q = nX\{H(\mathrm{c},\ T_1)-H(\mathrm{c},\ T_0)\}+n(1-X)\{H(\mathrm{gl},\ T_1)-H(\mathrm{gl},\ T_0)\}+n(1-X)\{H(\mathrm{gl},\ T_0)-H(\mathrm{c},\ T_0)\} \quad (1)$$

This equation can be rewritten in this form;

$$X = \frac{\{H(\mathrm{gl},\ T_1)-H(\mathrm{gl},\ T_0)\}+\{H(\mathrm{gl},\ T_0)-H(\mathrm{c},\ T_0)\}-Q/n}{\{H(\mathrm{gl},\ T_1)-H(\mathrm{gl},\ T_0)\}+\{H(\mathrm{gl},\ T_0)-H(\mathrm{c},\ T_0)\}-\{H(\mathrm{c},\ T_1)-H(\mathrm{c},\ T_0)\}} \quad (2)$$

Thus, the mole fraction of the crystalline phase, X, can be determined by means of the measured heat, Q, and the enthalpy data obtained previously. The temperatures used for measuring the crystallization rate ranged from 626 to 821 K.

X-Ray Diffraction Method. The further quantitative determination of the crystallization was done by means of X-ray diffraction analysis, using the powder method. Use was made of a Tokyo Shibaura Electric ADG-102 or ADG-301 diffractometer furnished with a fine focus copper tube, a nickel filter, and a SU-021E or SU-321 high-temperature sample holder attached to a goniometer, GD-2 or GD-3. The vitreous sample was grounded to 200 mesh in an agate mortar. Then the powder sample (0.1 g) was pressed on a platinum plate under a pressure of 8 MPa. The platinum plate with the sample was put on the heater in a high-temperature sample holder. Before heating, the sample was evacuated at 373 K for a day to evaporate the adsorbed water. Then the sample was heated at various constant temperatures. It took 5 min for the sample to attain thermal equilibrium in each heating. The integrated intensity of the strongest diffraction peak (101) at 27.5 degrees in 2θ was counted every two minutes. After these measurements, the sample was rapidly cooled to room temperature and then again heated at 730 K (optimum temperature of crystallization) for one hour in order to crystallize it completely. Then the sample was brought to the original temperature, and the intensity of the diffraction peak of this 100-per-cent-crystallized sample was counted in order to confirm the normalization. During these processes, the sample on the platinum plate was left as it had been in the high-temperature sample holder *in vacuo*. Mechanical mix-

tures of vitreous and crystalline powder of various compositions were prepared for the calibration experiment. The intensity of diffraction was proportional to the composition of the crystalline part within ±5 per cent. The temperatures for measurement ranged from 630 to 750 K.

Results and Discussion

The volume fraction of the crystallized part obtained by both the X-ray diffraction and calorimetric methods is shown at various temperatures as functions of the time in Fig. 1. The crystallization starts almost without induction time at each temperature and proceeds rapidly up to the 0.9-volume fraction, after which it proceeds very slowly. Although the temperature range covered is different in each method, the crystallization rate shows a maximum around 720 K and decays both below and above that temperature. The temperature ranges which the two experiments covered were different because (1) the calorimetry mainly covered higher-temperature ranges, since the scatter of the data is large at low temperatures, and so the time consumption for every experimental point became formidable and (2) the X-ray diffraction method covered low-temperature ranges since, because of the temperature inertia of the sample furnace, the crystallization during the heating period (especially around 720 K with a maximum crystallization rate) was too much to be neglected compared with that in time

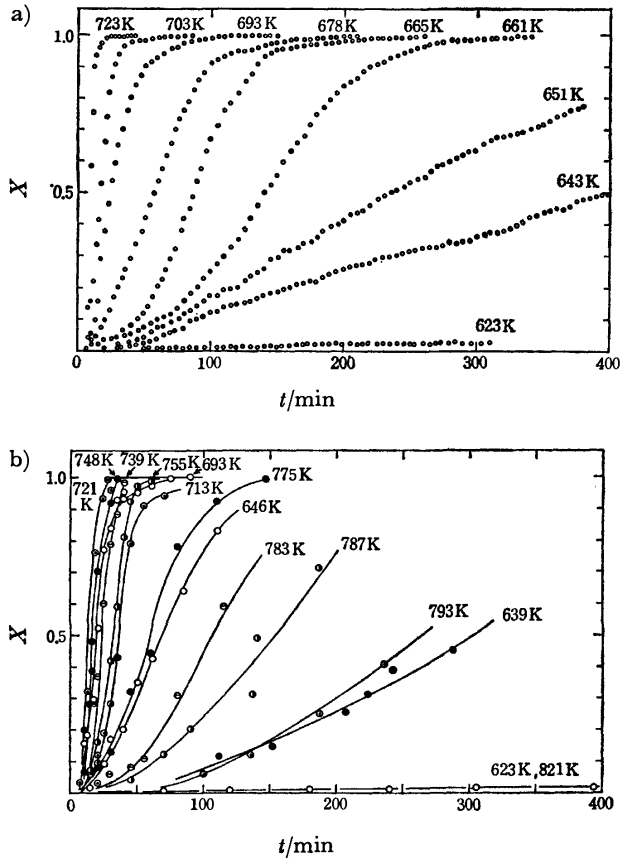

Fig. 1. a) Variation of crystallinity with time by the X-ray diffraction.
b) Variation of crystallinity with time by the calorimetric method.

intervals at the aimed-for temperature higher than 720 K.

The Johnson-Mehl-Avrami (J-M-A) equation has been developed to describe the kinetics of processes where nucleation and growth occur together.[5,6] Application of the J-M-A expression enables one to predict the volume fraction of a new phase that will form as a function of time, if suitable information about the nucleation and growth rates is available or if they can be assumed:

$$X = 1 - \exp\left\{-\int_{t'=0}^{t'=t} gIG^n(t-t')^n \mathrm{d}t'\right\} \quad (3)$$

Eq. (3) is the general form of the J-M-A equation: g is a shape factor; I, the nucleation rate; G, the growth rate; t', the time at which a given particle is nucleated; n, an integer which depends on the dimensionality of the growth mechanism, and X, the volume fraction of the new phase. In deriving this equation, the growth rate was assumed to be independent of the time. Eq. (3) may be integrated only by making specific assumptions about the variation in I with the time. If I is assumed to be independent of the time, Eq. (4) is obtained by integrating Eq. (3):

$$X = 1 - \exp\{-gIG^n t^{n+1}/(n+1)\} \quad (4)$$

If the nucleation rate, I, is assumed to be a rapidly decreasing function of the time—if, that is, the nucleation is completed at an early stage in the reaction, I may be replaced by the number of nuclei, N_0;

$$X = 1 - \exp(-gN_0G^n t^n/n) \quad (5)$$

For the present system, the latter assumption seems to be suitable since it has been found in our laboratory that, even at the same temperature, the crystallization rate of the "quenched glass," which has been quenched to room temperature before it is brought to the growth temperature, is very much greater than that of the "non-quenched glass" prepared by cooling a molten sample directly to the temperature of the growth experiment. This implies that the numbers of nuclei in the unit volumes of both the glasses are quite different at the beginning of the reaction. Thus, the nucleation in the quenched glass seems to have finished in an early stage of the reaction. Leadbetter and Whycherley also observed that the quenched glass of beryllium fluoride contained a number of small bubbles lined with a white powder which was identified with the quartz form of beryllium fluoride by means of X-ray diffraction.[7] When gN_0G^n/n in Eq. (5) is set equal to k_c, defined as a crystallization rate constant, one obtains Eq. (6), which is the same form as the so-called Kolmogorow-Avrami equation:[8]

$$X = 1 - \exp(-k_c t^n) \quad (6)$$

By taking the double logarithm of both sides of Eq. (6), one gets the following equation:

$$\ln\ln\left(\frac{1}{1-X}\right) = n\ln t + \ln k_c \quad (7)$$

If the left-hand side of Eq. (7) is plotted against $\ln t$, one may know the growth morphology of the transforming phase from the slope of the line, n. The curves

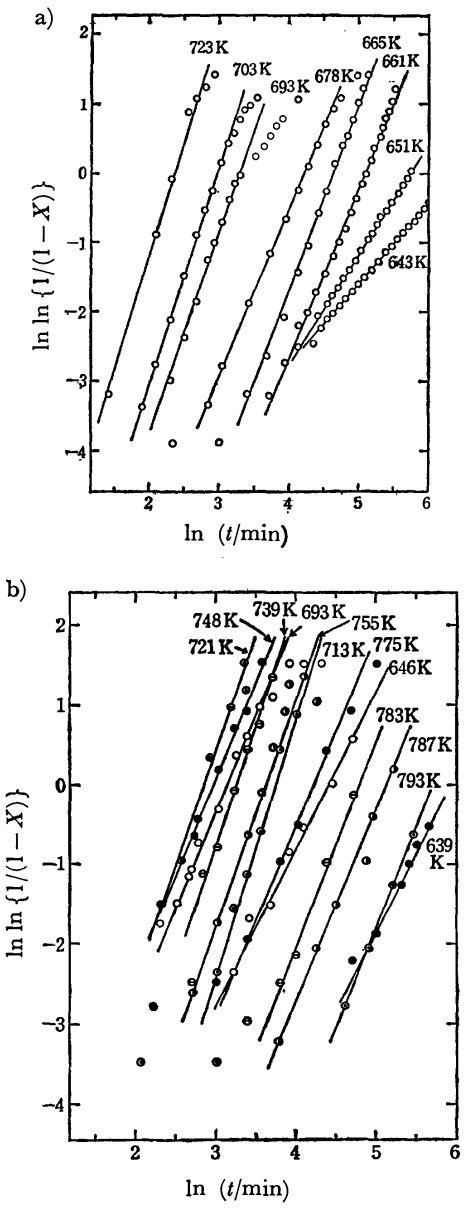

Fig. 2. a) Variation of ln ln $(1/(1-X))$ with ln t by the X-ray diffraction.
b) Variation of ln ln $(1/(1-X))$ with ln t by the calorimetric method.

are shown in Fig. 2. The values of the initial slopes of the curves before impingement occurs are presented in Table 1. Within the limits of experimental error, the values for the sample above 660 K are approximately 3, as is to be expected if the crystal growth during these periods is spherulitic in nature and if all the nuclei have been constituted at the beginning of the transformation. Below 660 K, the values of the slopes of the lines decrease to 2 or 1. Therefore, the growth mechanisms seem to be different from each other above and below this temperature, although much more information will be necessary before any conclusion can be drawn. A phenomenon similar to this was observed in the crystallization study of vitreous selenium.[9] Crystallization study by means of an electron micrograph or a photomicrograph is desirable to determine the more exact growth morphology of vitreous beryllium fluoride.

Table 1. Experimental slopes, n, in Eq. (6) and the time required for samples to reach 0.5-volume fraction, $t_{X=0.5}$.

T/K	n	$t_{X=0.5}$/min
	X-ray diffraction	
723	3.2	10
703	3.1	16
693	3.0	23
678	2.5	56
665	2.7	88
661	2.5	142
651	1.7	236
643	1.1	390
	calorimetric method	
793	2.5	265
787	2.4	155
783	2.6	105
775	2.4	60
755	2.8	32
748	2.6	15
739	3.1	22
721	2.9	13
713	3.1	37
693	2.5	20
646	1.9	69
639	2.1	304

The crystallization rate constant was determined from the plots of Eq. (7) using the values of n and $t_{X=0.5}$, which is referred to the time of $X=0.5$. As has been mentioned above, k_c was defined as gN_0G^n/n. Therefore,

$$\ln k_c(T) = \ln (gN_0(T)/n) + n \ln G(T) \tag{8}$$

As Strnad and Douglas noticed, it is implicitly assumed that the nuclei formed during the low-temperature treatment are not redissolved on heating to the growth temperature and, further, that the growth temperature must be chosen so that the nucleation rate at the growth temperature is negligible.[10] Thus,

$$N_0(T) = \text{constant.}$$

Then, as the first term on the right-hand side of Eq. (8) is independent of the temperature, one gets Eq. (9) when the temperature of 693 K is taken as the standard temperature:

$$\ln G'_{exp}(T) \equiv \ln \{G(T)/G(693\text{ K})\} = 1/n \ln\{k_c(T)/k_c(693\text{ K})\} \tag{9}$$

where $G'_{exp}(T)$ is defined as the relative growth rate. The logarithm of $G'_{exp}(T)$ is plotted against $1/T$ in Fig. 3.

On the other hand, Hillig and Turnbull proposed a semi-empirical equation for the growth rate.[11] Further, Ainslie *et al.* reduced this equation to Eq. (10) for vitreous silica using the Stokes-Einstein relation and other simple approximations:[12]

$$G(T) = f\Delta h(T_m - T)/(3\pi a_0^2 \eta T_m) \tag{10}$$

where f is the fraction of crystal surface sites to which

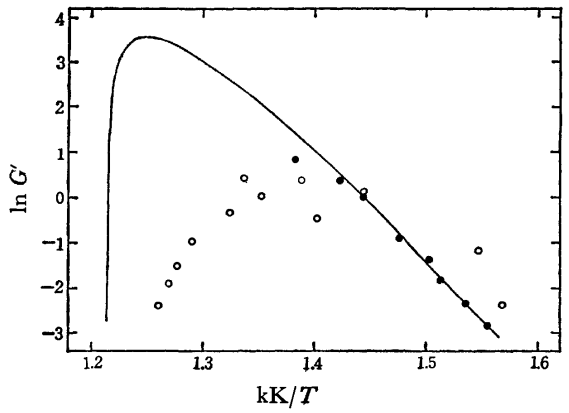

Fig. 3. Temperature dependence of relative growth rate.
——: Calculated from Eq. (11), ○: by calorimetric method, ●: by X-ray diffraction.

molecules can be attached in the growth process, Δh is the heat of fusion per molecule, T_m is the melting temperature, a_0 is the jump distance, and η is the viscosity. As a matter of fact, Wagstaff found from his experimental data for vitreous silica that the crystal-growth rate could be represented by an equation of the same type as Eq. (10).[13] This temperature dependence of the growth rate can be applied to vitreous beryllium fluoride since it is very similar to vitreous silica in structure and in thermodynamic properties, especially the entropy of fusion. The viscosity of beryllium fluoride was measured over 10 orders of magnitude; it was found that it could be represented by an Arrhenius-type equation.[14,15] Using this temperature equation for η in Eq. (10), one obtains the relative growth rate, $G'_{theor}(T)$:

$$\ln G'_{theor}(T) \equiv \ln\{G(T)/G(693\ \mathrm{K})\} = -Q_\eta'/RT + \ln(T_m - T) + 35.074 \qquad (11)$$

where R is the gas constant and where Q_η is the activation energy for the viscous flow, 230±12 kJ mol^{-1}.[15] The logarithm of $G'_{theor}(T)$ is also shown in Fig. 3. The two curves are consistent in the points that both have a maximum and behave similarly at both ends (especially at the lower temperatures). However, the temperature of the maximum is different by about 80 K and the behavior of decreasing after the maximum is dissimilar on the high-temperature side. Considering the consistency of the low-temperature side, it seems reasonable that the discrepancy cited above is attributable to the assumption of a constant N_0. It is interesting to note that the discrepancy can be eliminated if the nuclei partly redissolve on heating above 720 K and that the ratio of the number of the nuclei diminished to 10^{-1}, 10^{-3} and 10^{-6} at 730 K, 760 K, and 795 K respectively compared with that of 693 K.

Further, if the temperature dependence of the growth rate reported by Ainslie *et al.*, Eq. (10), is substituted into Eq. (5), one gets:

$$X = 1 - \exp\{(-gN_0t^n/n)[A(T_m - T)\exp(-Q_\eta/RT)]^n\} \qquad (12)$$

where A is equal to $f\Delta h/(3\pi a_0^2 T_m C)$; here C is a pre-

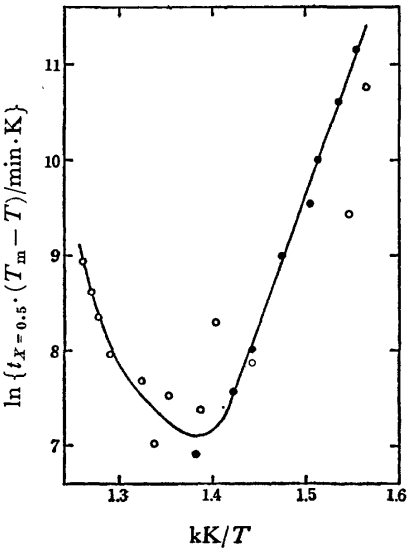

Fig. 4. Temperature dependence of $\ln\{(T_m - T)\cdot t_{X=0.5}\}$.
○: By calorimetric method, ●: by X-ray diffraction.

exponential factor in the viscosity expression. At a constant degree of crystallization, α, one obtains Eq. (13) by rearranging the terms of Eq. (12) and by taking the logarithms of both sides:

$$\ln\{t_{X=\alpha}\cdot(T_m - T)\} = Q_\eta/RT - \frac{\ln(A^n N_0 g/n)/\ln\left(\frac{1}{1-\alpha}\right)}{n} \qquad (13)$$

If the logarithm of the temperature difference, $(T_m - T)$, multiplied by the time needed to form a given volume fraction of the crystalline phase is plotted against $1/T$, when $N_0(T)$ is independent of the temperature, a straight line should be obtained with a slope of Q_η/R. The logarithm, $\ln\{t_{X=0.5}(T_m - T)\}$, is plotted as a function of $1/T$ in Fig. 4. We thus obtained, instead of a straight line, a curve which has a minimum value at about 720 K. However, a linearity holds true below 720 K. The activation energy for the viscous flow is evaluated from the slope of the straight line. The activation energies were obtained also when the temperature dependence of the times of X=0.4 and the 0.6-volume fraction were analyzed. The activation energy was estimated to be 222±4 kJ mol^{-1} as the mean value from the slopes of the lines of X=0.4, 0.5 and 0.6. This value is in excellent agreement with that obtained by the viscosity measurement, 230±12 kJ mol^{-1}. Above 720 K, depending on the crystallization temperature, some of the nuclei seem to redissolve on heating and seem not to contribute to the growth. This will correspond to the "deactivation of the crystallization centers" described in Dzhalilov's paper.[9]

References

1) L. R. Batsanova, G. S. Yurev, and V. P. Doronina, *Zh. Strukt. Khim.*, **9**, 79 (1968).
2) S. Tamura and T. Yokokawa, This Bulletin, **48**,

2542 (1975).
3) S. Tamura, T. Yokokawa, and K. Niwa, *J. Chem. Thermodynamics*, **7**, 633 (1975).
4) T. Maekawa, T. Yokokawa, and K. Niwa, *ibid.*, **3**, 143 (1971).
5) W. A. Johnson and R. F. Mehl, *Trans. AIME*, **135**, 416 (1939).
6) M. Avrami, *J. Chem. Phys.*, **7**, 1103 (1939).
7) A. J. Leadbetter and K. E. Wycherley, *Phys. Chem. Glasses*, **12**, 41 (1971).
8) A. N. Kolomogorov, *Izv. Akad. Nauk SSSR, Ser. Mat.*, **3**, 355 (1937).
9) S. U. Dzhalilov, *Russ. J. Phys. Chem.*, **39**, 1376 (1965).
10) Z. Strnad and R. W. Douglas, *Phys. Chem. Glasses*, **14**, 33 (1973).
11) W. B. Hilling and D. Turnbull, *J. Chem. Phys.*, **24**, 914 (1956).
12) N. G. Ainslie, C. R. Morelock, and D. Turnbull, "Symposium on Nucleation and Crystallization in Glasses and Melts," ed. by M. K. Reser, G. Smith, and H. Insley, The American Ceramic Society (1962), p. 97.
13) E. E. Wagstaff, *J. Amer. Ceramic Soc.*, **52**, 650 (1969).
14) C. T. Moynihan and S. Cantor, *J. Chem. Phys.*, **48**, 115 (1968).
15) S. V. Nemilov, *Fiz. Tverd. Tela*, **6**, 1375 (1964).

Photoelectron Ejection and Fluorescence from Molecular "Rydberg" States in Polar Solvents

Yoshihiro NAKATO, Akihiro NAKANE,* and Hiroshi TSUBOMURA

Department of Chemistry, Faculty of Engineering Science, Osaka University, Toyonaka, Osaka 560

(Received October 6, 1975)

Absorption and fluorescence spectra and photo-current yield curves of tetraaminoethylenes are studied. The UV absorption of these compounds is mostly attributable to the transitions from the ground state to the "vertical" Rydberg-like and ionized states. Their spectral shapes in ether and in pentane are nearly coincident with each other, showing that these states just after excitation are little affected by the solvent polarity. Based on this result and the results of photo-current measurements, the spontaneous formation of free, solvated electrons from the "vertical" Rydberg-like states in polar solvents has been verified. It is also found that the maximum wave numbers, the lifetimes and the yields of the fluorescence from the lowest "relaxed" Rydberg-like state depend strongly on solvent polarity, temperature and rigidity. These results are explained by taking account of the competition between electron ejection and relaxation processes and of the presence of a non-fluorescent, solvated cation-electron pair. The photo-electron ejection from other organic molecules in polar solvents reported before is shown to be explained by the same scheme as presented here.

So far, several different mechanisms on the electron ejection from organic molecules into polar solvents under illumination in the near ultraviolet region have been proposed, as reviewed previously.[1,2] This rather conflicting situation seems to arise mainly from the change of the ionization threshold with solvent polarity, causing varied degree of solvation for the ejected electron and parent cation.

The solvated cation-electron pair was proposed by some authors as a long-lived intermediate state caused by excitation in order to explain the appearance of the absorption spectra assigned to the cation not contributing to the photo-current.[1,3-5] Such a state is of great interest, but more experimental knowledge seems necessary for defining it clearly.

Recently, we reported the absorption spectra of some molecules assigned to transitions to Rydberg-like and ionized states in organic solvents.[2,6,7] From the measurements of photo-currents and absorption spectra, it was suggested that a spontaneous formation of the solvated electron from the Rydberg-like states occurred in polar solvents, competing with the relaxation to the lower excited states.[2] It was also found that the energy and yield of the fluorescence, conceivably originating from the lowest Rydberg-like state, decreased with increasing solvent polarity.[2,8]

In the present paper, we will report the results of our detailed studies on the photo-electron ejection and the Rydberg-like states of tetraaminoethylenes in polar solvents.

Experimental

The preparation and handling of tetrakis(dimethylamino)-ethylene (TMAE), and 1,1',3,3'-tetramethyl-2,2'-bi-imidazolidinylidene (TMBI), were described previously.[6]

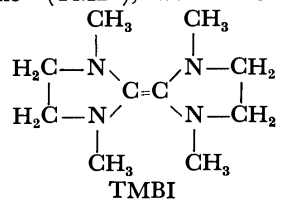

TMBI

* Present Address: Toray Industries Inc., Plastic Application Technology Dept., 9-1 Ooe-cho, Minato-ku, Nagoya 455-91, Japan.

Purification of solvents was made in a similar way as described elsewhere.[2,6] These solvents, especially the polar ones, were carefully dried with Na-K alloy in evacuated ampoules.

Absorption spectra were measured with a Cary Model 15 spectrophotometer. Fluorescence and its excitation spectra were measured with an Aminco-Bowman spectrophotofluorimeter, which was calibrated at Prof. Mataga's laboratory to obtain the correct fluorescence quantum spectrum by use of a standard lamp. The spectral distribution of the excitation light intensity of this apparatus was also obtained by the actinometry using the fluorescence of a concentrated Rhodamin B solution. Steady-state photo-currents were measured by using a quartz cell equipped with two parallel electrodes.[2] The temperatures of the sample solutions were controlled by putting the cell in a quartz Dewar containing isopentane cooled with nitrogen gas.

The fluorescence lifetime was measured with a nitrogen gas laser (λ 337.1 nm) as an exciting light source, having the duration of about 5 ns and a repetition frequency of *ca.* 50 Hz. The fluorescence decay was recorded by a photomultiplier, a sampling oscilloscope and an X-Y recorder.

Results

The absorption spectra of TMBI observed in pentane and diethyl ether are shown in Fig. 1. The absorption spectra, the photo-current yield curves and the fluorescence excitation spectra of TMAE in ether and hydrocarbons are shown in Fig. 2. The photo-

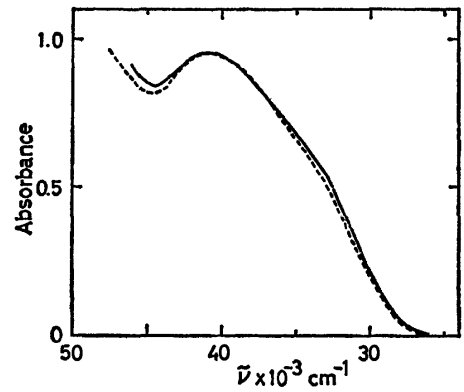

Fig. 1. The absorption spectra of TMBI in ether (----) and in pentane (——).

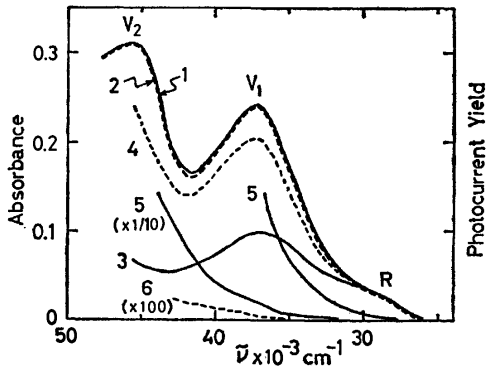

Fig. 2. The absorption spectra, the photo-current yield curves and the fluorescence excitation spectra of TMAE. Curve 1: The absorption spectrum in ether. Curve 2: That in pentane. Curve 3: The fluorescence excitation spectrum in ether. Curve 4: That in 3-methylpentane. Curve 5: The photo-current yield curve in ether. Curve 6: That in pentane. The fluorescence excitation spectra both in ether and in 3-methylpentane are adjusted so as to make their strengths agree with those of the corresponding absorption spectra in the lower energy region.

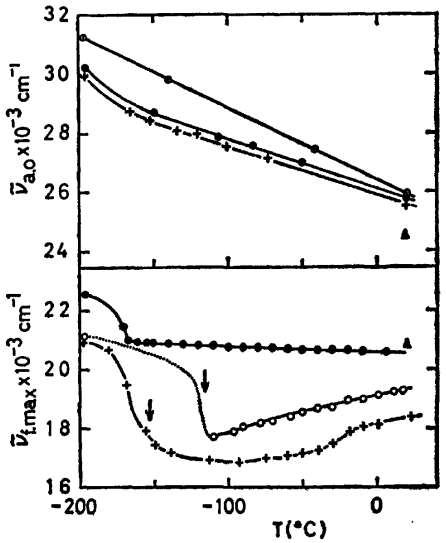

Fig. 3. The temperature dependence of the onset of the absorption band ($\tilde{\nu}_{ao}$) and the fluorescence maximum ($\tilde{\nu}_{f,max}$) of TMAE: (●) in 3-methylpentane, (○) ether, (+) 2-methyltetrahydrofuran (2-MTHF), (▲) the gas phase. The temperature dependence of the wave number of the absorption onset of TMBI in 3-methylpentane (⊙) is also included.[7] Arrows show the solidifying point of the solvent (the melting point in the case of ether and the temperature at which the dielectric constant abruptly changes in the case of 2-MTHF[13b]). Dotted lines are drawn by conjecture so that the temperature dependences of $\tilde{\nu}_{f,max}$, τ_f and ϕ_f^{rel} in Figs. 3 and 4 will be in harmony with each other in each solvent.

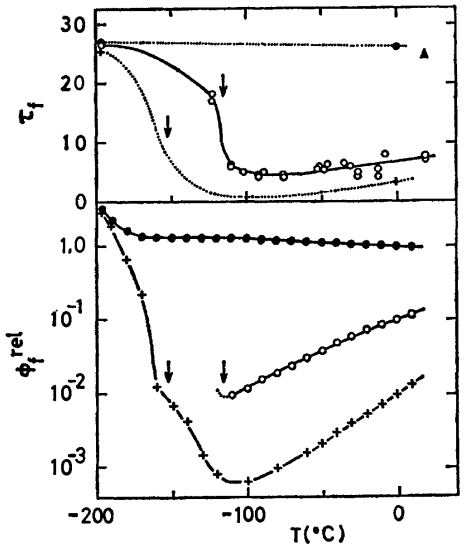

Fig. 4. The temperature dependence of the fluorescence lifetime (τ_f, in ns) and the relative fluorescence yield (ϕ_f^{rel}) of TMAE: (●) in 3-methylpentane, (○) ether, (+) 2-methyltetrahydrofuran, (▲) the gas phase. The wave number of excitation light is 30.3 kK for measurements of ϕ_f^{rel}, and 29.7 kK for τ_f. ϕ_f^{rel} is corrected for the change of the absorption intensity at 30.3 kK with temperature. The meanings of arrows and dotted lines are the same as those in Fig. 3.

current yield in the present work means $(\varepsilon \cdot i)/(I_0-I)$ in a relative scale,[9] where ε, i and (I_0-I) are the molar extinction coefficient, the steady-state photo-current and the light intensity absorbed by the sample solution, respectively.[10] The absolute photo-ionization yield in ether is about 0.9×10^{-5} electrons per absorbed photon at 29.4 kK ($\times10^3$ cm^{-1}) and that in pentane is about 1.6×10^{-7} at 40 kK.

Figure 3 shows the solvent and temperature dependences of the onset of the absorption spectrum and the fluorescence maximum of TMAE, and Fig. 4 shows those of the fluorescence lifetime and the relative yield. The absorption bands in polar solvents do not change much from those in nonpolar solvents. Both are gradually blue-shifted with decreasing temperature, while the fluorescence wave numbers, lifetimes and yields in polar solvents are quite different from those in nonpolar solvents. They show monotone decrease down to about −100 °C and abrupt increase below that due to solidification of these solvents.

The fluorescence of TMAE was quenched by atmospheric oxygen. When air was introduced into evacuated sample cells, the fluorescence intensity decreased instantaneously but the absorption intensity remained nearly the same at least for about ten minutes. The rate constant of the quenching reaction, calculated from the fluorescence lifetime, 7 ns, and an oxygen concentration, 4×10^{-3} M, is 1.9×10^{10} M^{-1} s^{-1}, the same order of magnitude as that for a diffusion-limited reaction.

Discussion

As reported previously,[6,7] the absorption spectrum of TMBI in the wave number region lower than 45 kK is assigned to the transitions to the Rydberg-like and ionized states. The transition to the lowest (π-π^*)-

type excited state of TMBI appears as the steeply rising absorption beginning at 45 kK. The close agreement of the spectra in pentane and ether (Fig. 1) shows that the Rydberg-like and ionized states just after the vertical excitations are little affected by the solvent polarity. This fact can also be regarded as a proof of the existence of "dry" electrons in polar solvents, first proposed by Hamill.[11]

In the absorption spectra of TMAE (Fig. 2), only the transitions to the lower Rydberg-like states appear as a shoulder (denoted by R in Fig. 2) and those to the higher Rydberg-like states and to the ionized state are hidden by the strong (π-π^*)-type absorption bands (denoted by V_1 and V_2).[2,6] However, the overall absorption spectrum in ether is identical with that in pentane.

Quite contrary, the photo-current yield curve and the fluorescence excitation spectrum in ether are much different from those in hydrocarbons (Fig. 2). Based on the above argument, this can be attributed to the relaxation processes from the vertical or Franck-Condon states, leading to different solvation states with solvent polarity.

Various relaxation processes expected for the ether solution are given in Fig. 5, including the ones already proposed and discussed in some detail in a previous paper.[2] Since the "vertical" ionization threshold in ether should be equal to that in pentane (~34 kK) as seen from the close agreement of the absorption spectra, the steeply rising photo-current in the region higher than 34 kK observed in ether (Fig. 2) is assigned to

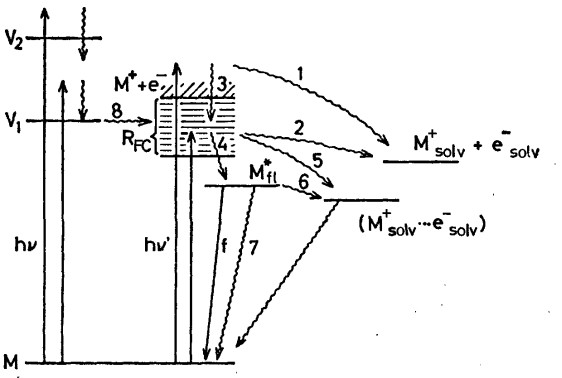

Fig. 5. The levels and processes showing photo-excitation and relaxation of TMAE in polar solvents such as ether. M: The ground state TMAE. V_1 and V_2: The (π-π^*)-type excited states of TMAE, each corresponding to the absorption bands denoted by V_1 and V_2 in Fig. 2. R_{FC}: The vertical (or Franck-Condon), Rydberg-like states. $M^+ + e^-$: The Franck-Condon, ionized state. M^*_{fl}: The fluorescent state (the solvated Rydberg state). $M^+_{solv} + e^-_{solv}$: The solvated cation and electron, free from each other. $(M^+_{solv} \cdots e^-_{solv})$: The non-fluorescent, solvated cation-electron pair. In nonpolar solvents, the state of free cation and electron contributing to photo-currents lies at almost the same energy as the Franck-Condon, ionized state. The solvated states such as $M^+_{solv} + e^-_{solv}$ and $(M^+_{solv} \cdots e^-_{solv})$ as well as the solvation processes (1), (2), (5), and (6) are of course absent in non-polar solvents and the fluorescent state is the Rydberg state situated in the solvent cavity.

the direct photoionization, and the photo-current in the lower energy region is assigned to process (2), the spontaneous formation of the solvated electrons from the "vertical" Rydberg states. The amount of charge carriers observed in ether at −65 °C is found to be twice as large as that at room temperature. This can be explained in view of the increase of the dielectric constant of ether (6.7 at −65 °C and 4.5 at room temperature). It is therefore expected that the ionization process (2) becomes more efficient in more polar solvents.

The shape of the fluorescence excitation spectrum in ether in the lower energy region nearly coincides with that of the Rydberg absorption band (R), while the shape of the photo-current yield curve in ether does not (Fig. 2). These results show that the ionization process *via* the fluorescent state ($R_{FC} \rightsquigarrow M^*_{fl} \rightsquigarrow M^+_{solv} + e^-_{solv}$) is not a main process, or in other words, process (2) competes, as shown in Fig. 5, with other relaxation processes (4) and (5), which will be discussed later.

The fluorescence excitation spectrum in ether extends into the region of the photo-current action spectrum, indicating the presence of processes (3) and (4), the relaxation from the vertical, ionized and Rydberg states to the fluorescent state in ether as well as in nonpolar solvents. Its shape in the higher energy region is rather different from the absorption spectrum, though the fluorescence excitation spectrum in 3-methylpentane is much more similar to the absorption spectrum. These results indicate that processes (2) and (5) exist and process (1) is more probable in ether.

These fluorescence excitation spectra show peaks corresponding to those of the absorption spectra (V_1),[12] suggesting the existence of non-radiative transition from the V_1-state to the Rydberg-like state (process (8)). One might thus expect that an auto-ionization from the V_1-state would occur in ether. The photo-current yield curve, however, shows very slight swelling at about 37 kK (Fig. 2). This fact can be explained by assuming that the molecules excited to the vibrationally excited V_1-state first relax to its lowest vibrational level lying near 30 kK, as shown in Fig. 5, and next pass into the Rydberg-like state, for which the photo-current yield is much smaller than for the case where the molecules are excited directly to the Rydberg-like or ionized states of the same energy as the vibrationally excited V_1-state.

The present results obtained in an extended temperature range (Fig. 3) are in good harmony with the structures of Rydberg states in solution discussed before,[2,8] and confirm them. Namely, the gradual blue-shifts of the lowest Rydberg absorption bands with lowering the temperature are attributed to the elevation of the solvent density surrounding the solute molecules increasing the repulsive interaction between the Rydberg electron and the solvents in the vertical Rydberg state. The relative constancy of the position of the fluorescence maximum with temperature in the case of fluid, 3-methylpentane solutions is ascribed to the presence of the relaxation from the vertical to the fluorescent state, leading to the expansion

of the solvent cavity so as to lower the Rydberg electron-solvent repulsive interaction. The red-shifts of the fluorescence maxima in fluid, polar solvents with decreasing temperature are also ascribed to the relaxation process leading to the solvated Rydberg state, going further by the increasing dielectric polarization at low temperature.[13] The blue-shifts of the fluorescence maxima on solidification of the solvents, both polar and nonpolar, are attributed to the restriction of such relaxations in rigid solutions.

The fluorescence lifetimes (τ_f) decrease greatly with increasing polarity and with decreasing temperature in polar solvents, but are restored to nearly the same level in the rigid solvents at 77 K as that in 3-methylpentane at room temperature, irrespective of whether they are polar or non-polar (Fig. 4). The Rydberg orbital in the fluorescent state in rigid solutions at 77 K must be largely distorted due to the repulsive interaction between the Rydberg electron and the surrounding solvent molecules as seen from the blue-shifts of the fluorescence maxima, while that in hydrocarbons at room temperature must be almost the same as that in the vapor phase, since the molecules in the Rydberg state are situated within the solvent cavity. These considerations lead to the conclusion that the fluorescence lifetime is hardly affected by distortion of the Rydberg orbital due to the surrounding solvent molecules.

We therefore tentatively assume that a non-fluorescent, solvated cation-electron pair, $(M^+_{solv}\cdots e^-_{solv})$, exists as an intermediate state attained by processes (5) and (6) in the case of polar solvents, as shown schematically in Fig. 5. The lifetime in polar solvents is then expressed by $\tau_f=1/(k_f+k_7+k_6)$, where k_f and k_7 are the rate constants of radiative and non-radiative processes from the fluorescent to the ground state, and k_6 is that of process (6). Since k_f and probably k_7 are nearly independent of the distortion of the Rydberg orbital and, therefore, of the solvent polarity, as discussed above, the decrease of τ_f with solvent polarity is mainly attributed to the increase of k_6.

The fluorescnce yield, ϕ_f, decreases with the solvent polarity much more than the fluorescence lifetime, τ_f, as seen from Fig. 4. The fluorescence yield in polar solvents is expressed by $\phi_f=k_4\cdot(k_4+k_5+k_2)^{-1}\cdot\tau_f\cdot k_f$. Based on the same reason as above, the decrease of (ϕ_f^{rel}/τ_f) with the solvent polarity must also be attributed to the increase of (k_2+k_5). Since the absolute value of k_2 is very small, as seen from the small absolute photo-current yield ($\sim10^{-5}$ at 30.3 kK in ether), the decrease of (ϕ_f^{rel}/τ_f) is mostly attributed to the increase of k_5. Thus, we can conclude that a large part of molecules excited to the Rydberg-like states near 30 kK in ether pass directly or *via* the fluorescent state into the solvated cation-electron pairs and only a small fraction turns to the free charge carriers or fluoresces. With increasing solvent polarity, process (2) will become more important.

The Photo-ionization of Other Organic Molecules in Polar Solvents. The ionization thresholds of organic molecules in nonpolar solvents are found to be 1.1—1.8 eV lower than the gas-phase ionization potentials, depending on the molecular size of solute and the molecular sphericity of solvent.[7,14-16] According to the scheme of the photo-electron ejection proposed in the present work, the ionization threshold in a polar solvent is expected to be further lowered, down to the lowest vertical Rydberg-like state.

The ionization threshold of *N,N,N',N'*-tetramethyl-*p*-phenylenediamine (TMPD) in hexane is measured to be about 5.0 eV,[15,16] 1.2 eV lower than the gas-phase ionization potential, 6.20 eV.[17] Richard and Thomas showed that TMPD was photo-ionized in water by illumination even at a photon energy of 3.57 eV.[4] The similar conclusion was also derived from an analysis of the fluorescence lifetimes and yields for TMPD in water–ethanol mixed solvents.[18] The lowest Rydberg states of aniline and its alkyl derivatives were reported to lie in the range 4.7—4.2 eV, being parallel to the sequence of decreasing ionization potentials.[19] Thus, the additional lowering of the ionization threshold of TMPD observed in polar solvents can be explained by the electron ejection from the lowest Rydberg-like state.

The ionization thresholds of aromatic hydrocarbons such as anthracene, pyrene and perylene in boric acid glass at room temperature were reported to be about 2.2—2.5 eV lower than the gas-phase ionization potentials.[20] These results can also be regarded as showing the electron ejection *via* the Rydberg-like state in polar solvents.[21]

The authors wish to thank Professor N. Mataga and Dr. T. Okada for letting us use a nitrogen gas laser for measurements of the fluorescence lifetime.

References

1) M. Ottolenghi, *Chem. Phys. Lett.*, **12**, 339 (1971).
2) Y. Nakato, M. Ozaki, and H. Tsubomura, *J. Phys. Chem.*, **76**, 2105 (1972).
3) T. Imura, N. Yamamoto, and H. Tsubomura, This Bulletin, **43**, 1670 (1970).
4) J. R. Richards and J. K. Thomas, *Trans. Faraday Soc.*, **66**, 621 (1970).
5) R. Potashnik, M. Ottolenghi, and R. Bensasson, *J. Phys. Chem.*, **73**, 1912 (1969).
6) Y. Nakato, M. Ozaki, and H. Tsubomura, This Bulletin, **45**, 1299 (1972).
7) Y. Nakato and H. Tsubomura, *J. Phys. Chem.*, **79**, 2135 (1975).
8) Y. Muto, Y. Nakato, and H. Tsubomura, *Chem. Phys. Lett.*, **9**, 597 (1971).
9) A plot of $i/(I_0-I)$ *vs.* photon energy shows a shoulder in the lower energy region, as reported in Fig. 4 of Ref. 2.
10) The steady-state photo-current may involve the effect of recombination of free charge carriers. This effect is not corrected in this work.
11) W. H. Hamill, *J. Phys. Chem.*, **73**, 1341 (1969).
12) The argument described as a preliminary result in Footnote 39 of Ref. 2 was found to be mistaken by recent detailed experiments.
13) The dielectric constant of ether is 4.6, 6.2 and 8.1 at 0, −50 and −100 °C, respectively,[a] and that of 2-methyltetrahydrofuran is 7.3, 9.2 and 12 at the same temperatures.[b] a) Landolt-Börnstein, 6 Auflage, II Band, 6 Teil, Springer Verlag, Berlin (1959), p. 635, 680; b) T. Furutsuka, T. Imura, T. Kojima, and K. Kawabe, *Tech. Rep. Osaka Univ.*,

24, 367 (1974).
14) Y. Nakato, T. Chiyoda, and H. Tsubomura, This Bulletin, **47**, 3001 (1974).
15) S. S. Takeda, N. E. Houser, and R. C. Jarnagin, *J. Chem. Phys.*, **54**, 3195 (1971).
16) R. A. Holroyd, *J. Chem. Phys.*, **57**, 3007 (1972); R. A. Holroyd and R. L. Russell, *J. Phys. Chem.*, **78**, 2128 (1974).
17) Y. Nakato, M. Ozaki, A. Egawa, and H. Tsubomura, *Chem. Phys. Lett.*, **9**, 615 (1971).
18) A. Alchalal and M. Ottolenghi, *ibid.*, **17**, 117 (1972).
19) H. Tsubomura and T. Sakata, *ibid.*, **21**, 511 (1973).
20) J. Joussot-Dubien and R. Lesclaux, "The Triplet State," ed. by A. B. Zahlan, Cambridge Univ. Press, London (1967), p. 197.
21) The ionization thresholds of anthracene and tetracene in boric acid glass agree fairly well with the energy of excitation to the optically allowed, lowest Rydberg state of each molecule. M. B. Robin, "Higher Excited States of Polyatomic Molecules," Vol. 2, Academic Press, New York (1975).

Solid-State Circular Dichroism Spectra of Tris(diamine)cobalt(III) Complexes: Decomposition into E and A_2 Components

Reiko KURODA* and Yoshihiko SAITO

The Institute for Solid State Physics, The University of Tokyo, Roppongi, Minato-ku, Tokyo 106

(Received October 15, 1975)

Solid-state circular dichroism spectra of some tris(diamine)cobalt(III) complexes were measured. Each CD band region was decomposed into E and A_2 components by combining the CD spectra in uniaxial single-crystals and in microcrystalline states. The observed values of $R(E)$ and $R(A_2)$ were compared with the theoretical calculation of Mason and Seal based on dynamic coupling method. The agreements are generally good for those complexes with five-membered chelate rings, however, there are some discrepancies for six- and seven-membered chelate ring cases.

Tris(diamine) cobalt(III) complexes usually exhibit two circular dichroism bands with opposite signs in the first absorption region ($A_{1g}\rightarrow T_{1g}$). The two bands correspond to the E and A_2 components of O_h parentage in D_3 environment. However, they are considered to be residual wing absorption resulting from extensive cancellation of the rotatory strengths of the two transitions, since the trigonal splitting is small. Single-crystal CD spectra are generally attended by difficulty of double refraction. Uniaxial crystals are usually employed for the measurement of single-crystal CD spectra. With the aid of the known crystal structures, an attempt has been made to decompose the CD spectra into two components by combining the single-crystal and the microcrystalline CD spectra of uniaxial crystals.

Principle of the Method

Figure 1 illustrates the interaction of circularly polarized light with the complex ion in a uniaxial crystal. The light propagates along the optic axis OZ. The direction of a threefold axis of the complex ion is indicated by a small closed triangle. The threefold axis is inclined at an angle of α with respect to the optic axis. Let OY be a projection of the threefold axis on a plane perpendicular to OZ. OX is chosen in such a way that OX, OY and OZ form a right-handed Cartesian coordinate system. When the circularly polarized light propagates along OZ, its electric vector $\boldsymbol{E}$ rotates on the XY plane. E component can be excited with the light whose electric vector is perpendicular to the threefold axis of the complex ion, whereas A_2 component can be excited when the electric vector is parallel to the threefold axis. At a given moment, let the electric vector $\boldsymbol{E}$ make an angle of φ with OX. The intensities of E and A_2 components excited at this moment will be proportional to

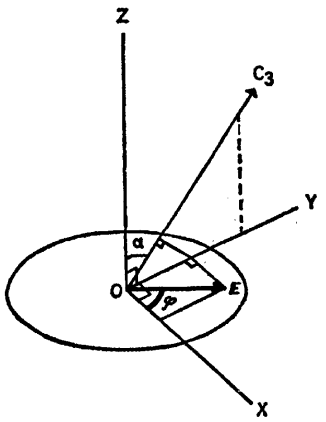

Fig. 1. Illustrating the interaction of circularly polarized light with the complex ion in a uniaxial crystal.

$$E^2\cos^2\alpha\sin^2\varphi + E^2\cos^2\varphi \quad \text{for E} \tag{1}$$

and

$$E^2\sin^2\alpha\sin^2\varphi \quad \text{for } A_2 \tag{2}$$

respectively. The averaged intensity over a period of rotation of the $\boldsymbol{E}$ vector will be obtained as follows:

$$1/2\pi\int_0^{2\pi}(E^2\cos^2\alpha\sin^2\varphi + E^2\cos^2\varphi)\mathrm{d}\varphi = E^2(1+\cos^2\alpha)/2 \quad \text{for E} \tag{3}$$

and

$$1/2\pi\int_0^{2\pi}(E^2\sin^2\alpha\sin^2\varphi)\mathrm{d}\varphi = E^2(\sin^2\alpha)/2 \quad \text{for } A_2 \tag{4}$$

Since E level is doubly degenerate, the difference between ε_l and ε_r of the single crystal, $\Delta\varepsilon_s$, can be written as a sum of the $\Delta\varepsilon(E_X)$, $\Delta\varepsilon(E_Y)$ and $\Delta\varepsilon(A_2)$ as follows:

$$\Delta\varepsilon_s = (1+\cos^2\alpha)/4\Delta\varepsilon(E_X) + (1+\cos^2\alpha)/4\Delta\varepsilon(E_Y) + (\sin^2\alpha)/2\Delta\varepsilon(A_2) \tag{5}$$

On the other hand, in microcrystalline state the threefold axes of the complex ions are randomly oriented, hence $\Delta\varepsilon$ in microcrystalline state, $\Delta\varepsilon_m$, can be written as

$$\Delta\varepsilon_m = 1/3\Delta\varepsilon(E_X) + 1/3\Delta\varepsilon(E_Y) + 1/3\Delta\varepsilon(A_2) \tag{6}$$

where 1/3 is a random orientation factor. Since $\Delta\varepsilon(E_X)=\Delta\varepsilon(E_Y)$, Eqs. (5) and (6) become

$$\Delta\varepsilon_s = (1+\cos^2\alpha)/2\Delta\varepsilon(E_X) + (\sin^2\alpha)/2\Delta\varepsilon(A_2) \tag{7}$$

and

$$\Delta\varepsilon_m = 2/3\Delta\varepsilon(E_X) + 1/3\Delta\varepsilon(A_2) \tag{8}$$

Now we obtain the two simultaneous Eqs. (7) and (8) involving $\Delta\varepsilon(E_X)$ and $\Delta\varepsilon(A_2)$ as two unknowns. Using $\Delta\varepsilon_s$ and $\Delta\varepsilon_m$ measured at an arbitrary wavelength, $\Delta\varepsilon(E_X)$ and $\Delta\varepsilon(A_2)$ can be easily calculated by Eqs. (7) and (8). In this way the observed CD spectra can be decomposed into E and A_2 components.

* Present address: Department of Chemistry, University of London, King's College, Strand, London WC2R 2LS, England.

Experimental

By the procedure described above, CD spectra of the following seven tris(diamine)cobalt(III) complexes of known crystal structures were decomposed.

	α	Ref.
Five-membered chelate rings		
Λ-2[Co(en)$_3$]Cl$_3$·NaCl·6H$_2$O	0°	1
Λ-[Co(en)$_3$]Br$_3$·H$_2$O	0	2
Δ-[Co(*R*-pn)$_3$]Br$_3$	0	3
Λ-[Co(*S*,*S*-chxn)$_3$]Cl$_3$·5H$_2$O	8	4
Δ-[Co(*R*,*R*-cptn)$_3$]Cl$_3$·4H$_2$O	22	5
Six-membered chelate rings		
Δ-[Co(*R*,*R*-ptn)$_3$]Cl$_3$·2H$_2$O	69.5	6
Seven-membered chelate rings		
Δ-[Co(tmd)$_3$]Br$_3$	0	7

Abbreviations: en ethylenediamine; pn propylenediamine; chxn *trans*-1,2-diaminocyclohexane; cptn *trans*-1,2-diaminocyclopentane; ptn 2,4-diaminopentane; tmd 1,4-diaminobutane.

These are all uniaxial crystals and the values of α are also shown.

The CD spectra of these D_3 complexes were measured for single-crystal and microcrystalline states except those of Δ-[Co(*R*,*R*-cptn)$_3$]Cl$_3$·4H$_2$O. For this complex Toftlund and Pedersen[8] measured the single-crystal CD spectra by diluting the complex ion in Δ-[Rh(*R*,*R*-chxn)$_3$]Cl$_3$·4H$_2$O. Though the crystal structure of this Rh(III) complex is not yet known, it is highly probable that the compound is isostructural with Δ-[Co(*R*,*R*-cptn)$_3$]Cl$_3$·4H$_2$O, in view of the fact that they belong to the same space group P6$_1$22 and form mixed crystals. Accordingly α was assumed to be 22° based on the known crystal structure of the cobalt complex[5].

The crystals of Λ-2[Co(en)$_3$]Cl$_3$·NaCl·6H$_2$O, Λ-[Co(en)$_3$]Br$_3$·H$_2$O, Δ-[Co(*R*-pn)$_3$]Br$_3$ and Λ-[Co(*S*,*S*-chxn)$_3$]Cl$_3$·5H$_2$O were prepared according to the method described by Nakatsu, Shiro, Saito and Kuroya[9], Werner[10], Iwasaki and Saito[3] and Jaeger and Bijkerk[11], respectively. The crystals of Δ-[Co(*R*,*R*-ptn)$_3$]Cl$_3$·2H$_2$O and Δ-[Co(tmd)$_3$]Br$_3$ were kindly supplied by Professor J. Fujita of Nagoya University.

CD Spectra. *a) Single-crystal CD Spectra*: Crystals were cut with a thin razor blade perpendicular to the optic axis and then they were polished on a filter paper moistened with water to the required thickness (0.01—0.08 mm). The thickness was measured by using a microscope fitted with a microscale. Direction of the optic axis for each specimen was checked by observing conoscopic figure under a polarizing microscope. The single-crystal CD spectra were measured over the range 300—650 nm by means of JASCO J-20 and partly by J-40, with the light beam parallel to the optic axis of the crystal. The measurements were repeated at least twice by employing different specimen in order to check the reproducibility except for Δ-[Co(tmd)$_3$]Br$_3$. For the latter case, the crystal was brittle and hard to manipulate. A specimen with suitable thickness for the measurement could not be obtained.

b) Preparation of KBr Disk and Measurement of CD Spectra in Microcrystalline State: About 180 mg of dry KBr and the required amount of complexes(*ca.* 1 mg) were weighed and powdered in a dental amalgam mill (Amalgamator) together with a stainless steel ball for about 150 s. In order to prevent from diffused reflections at grain boundaries, samples must be powdered elaborately. Dependence of CD spectra on duration of grinding was examined. $\Delta\varepsilon$ increases with the duration of grinding and tends to a constant value. The optimum duration of grinding was determined. The powdered samples were pressed in a standard KBr press at 9 t/cm^2 for five to ten minutes. The pellet was, after weighing, mounted on a KBr disk holder and placed normal to the light beam. CD spectra were measured over the range 300—650 nm by JASCO J-20. It was established that there exists a linear relationship between the circular dichroism deflection and the sample concentration, if the latter is less than 1% by weight.[12] Accordingly $\Delta\varepsilon$ values were calculated in the usual way.

The CD spectra under the second absorption band were recorded for those complexes containing chloride ions. The intensities were very weak, since the involved transitions are magnetically forbidden. The results are less reliable as compared to those under the first absorption band.

Results and Discussion

Figure 2 represents two typical CD spectra in single crystal and in microcrystalline state: Λ-[Co(*S*,*S*-chxn$_3$]Cl$_3$·5H$_2$O and Δ-[Co(*R*,*R*-ptn)$_3$]Cl$_3$·2H$_2$O. Table 1 gives the observed $\Delta\varepsilon_{max}$ and the peak positions for Λ-2[Co(en)$_3$]Cl$_3$·NaCl·6H$_2$O, Λ-[Co(*S*,*S*-chxn)$_3$]Cl$_3$·5H$_2$O and Δ-[Co(*R*,*R*-ptn)$_3$]Cl$_3$·2H$_2$O. In Fig. 3 are shown the results of decomposition into E and A_2 components of the CD spectra shown in Fig. 2. Table 2 summarizes the peak positions and $\Delta\varepsilon_{max}$ of the decomposed E and A_2 components in the first absorption region for all the seven D_3 complexes. Trigonal splitting param-

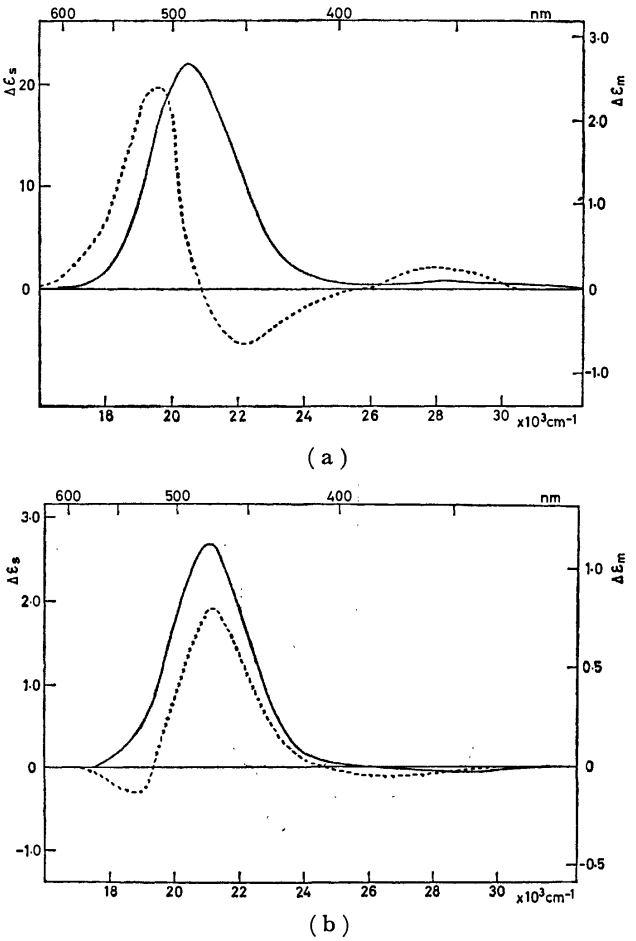

Fig. 2. The circular dichroism spectrum of a single-crystal (——) and that in KBr matrix (----).
(a) Λ-[Co(*S*,*S*-chxn)$_3$]Cl$_3$·5H$_2$O
(b) Δ-[Co(*R*,*R*-ptn)$_3$]Cl$_3$·2H$_2$O

eters $K(\equiv 2/3(\tilde{\nu}_E - \tilde{\nu}_{A_2}))$ are also included. Single-crystal CD spectra of some D_3 complexes with $\alpha=0°$ were reported by McCaffery and Mason[13] and Judkins and Royer[14]. General features of the spectra and peak positions obtained by these authors agree well with those of the present study. However, the $\Delta\varepsilon$ values are somewhat different, reflecting the experimental difficulties of this kind of measurement. The CD spectra of Λ-$[Co(S,S\text{-chxn})_3]Cl_3\cdot 5H_2O$ are broadly similar to those of Λ-$2[Co(en)_3]Cl_3\cdot NaCl\cdot 6H_2O$. The CD spectra in KBr matrix of Λ-$[Co(en)_3]^{3+}$ and Λ-$[Co(S,S\text{-chxn})]_3^{3+}$ are not so much different from their solution CD spectra. However, it is not true for Δ-$[Co(R,R\text{-ptn})_3]Cl_3\cdot 2H_2O$: in its microcrystalline state, it gives a weak negative peak at a longer wavelength side and a large positive peak at shorter wavelength side of the first absorption band and a very weak negative peak in the second absorption region, whereas in solution the peak heights in the first absorption region are inverted, suggesting a conformational change in solution.[15] From Table 2, it can be easily seen that $R(E)$ is positive and $R(A_2)$ is negative for the absolute configuration Λ, while $R(E)$ is negative and $R(A_2)$ is positive for Δ configuration, in agreement with the well-known empirical rule for the solution CD spectra. The sign of K is always negative throughout the series of the complexes. For the complexes with five-membered chelate rings, K ranges from -250 to $-130\ cm^{-1}$, while $\tilde{\nu}_{max}$ of the two bands nearly coincide and the sign of K is

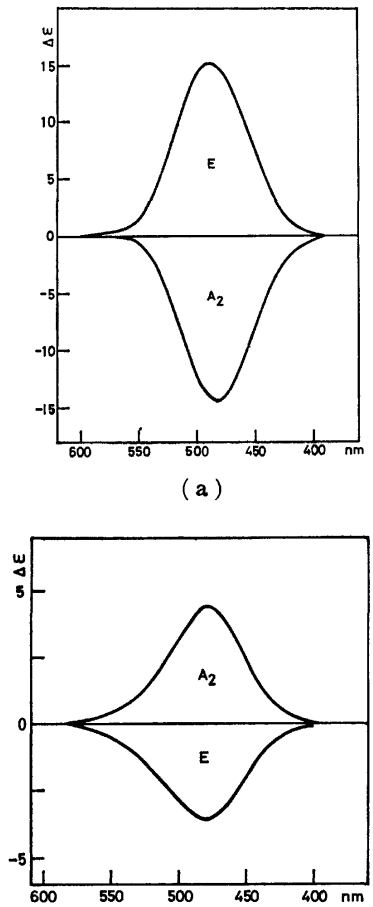

Fig. 3. The E and A_2 components obtained from the spectra shown in Fig. 2.
(a) Λ-$[Co(S,S\text{-chxn})_3]Cl_3\cdot 5H_2O$
(b) Δ-$[Co(R,R\text{-ptn})_3]Cl_3\cdot 2H_2O$

Table 1. CD spectra of single-crystal and in KBr matrix

		$\Delta\varepsilon_{max}$	λ_{max}
Λ-$2[Co(en)_3]Cl_3\cdot NaCl\cdot 6H_2O$	single-crystal	+24.4	489 nm
		+0.74	349
	KBr matrix	+2.0	505.5
		−0.59	445.5
		+0.19	352
Λ-$[Co(S,S\text{-chxn})_3]\cdot 5H_2O$	single-crystal	+22.17	488
		+0.58	350
	KBr matrix	+2.38	512.2
		−0.61	449.5
		+0.24	360
Δ-$[Co(R,R\text{-ptn})_3]Cl_3\cdot 2H_2O$	single-crystal	+2.7	478
		−0.064	345
	KBr matrix	−0.13	533.2
		+0.79	476.8
		−0.046	375

Table 2. E and A_2 components of solid-state CD spectra
The values of $\Delta\varepsilon(E)$ and $\Delta\varepsilon(A_2)$ are corrected by the fixed-orientation factors of 2/3 and 1/3 respectively.

Complex	E		A_2		K
	$\tilde{\nu}_{max}$	$\Delta\varepsilon_{max}$	$\tilde{\nu}_{max}$	$\Delta\varepsilon_{max}$	
Five-membered chelate rings	$\times 10^3\ cm^{-1}$		$\times 10^3\ cm^{-1}$		cm^{-1}
Λ-$2[Co(en)_3]Cl_3\cdot NaCl\cdot 6H_2O$	20.75	+15.9	20.97	−15.3	−150
Λ-$[Co(en)_3]Br_3\cdot H_2O$	20.76	+15.7	20.99	−15.1	−150
Δ-$[Co(R\text{-pn})_3]Br_3$	20.45	−10.9	20.83	+9.8	−253
Λ-$[Co(S,S\text{-chxn})_3]Cl_3\cdot 5H_2O$	20.45	+14.6	20.75	−13.7	−197
Δ-$[Co(R,R\text{-cptn})_3]Cl_3\cdot 4H_2O$[a]	19.6	−15.6	19.8	+14.3	−127
Six-membered chelate rings					
Δ-$[Co(R,R\text{-ptn})_3]Cl_3\cdot 2H_2O$	20.92	−3.6	20.94	+4.4	−13
Seven-membered chelate rings					
Δ-$[Co(tmd)_3]Br_3$	18.8[b]	−8.6[b]	19.3[b]	+10.2[b]	−333[b]

a) The decomposition was based on the CD spectra reported by Toftlund and Pedersen.[8] b) These values are not reliable. See text.

TABLE 3. ROTATORY STRENGTHS OF TRIS(DIAMINE)COBALT(III) COMPLEXES (10^{-40} c.g.s.)
Crystal values of $R(E)$ and $R(A_2)$ are corrected by the fixed-orientation factors of 2/3 and 1/3 respectively.

	Observed			Calculated by Mason and Seal[16,17]			$R(T_1)_{expt}$
	$R(E)$	$R(A_2)$	$R(T_1)$	$R(E)$	$R(A_2)$	$R(T_1)$	
Λ-2[Co(en)$_3$]Cl$_3$·NaCl·6H$_2$O	+62.9	−58.6	+4.3	+63.8	−59.8	+4.0	+4.4
Λ-[Co(en)$_3$]Br$_3$·H$_2$O	+59.9	−55.7	+4.2	+63.8	−59.8	+4.0	+4.4
Λ-[Co(*S*-pn)$_3$]Br$_3$[a]	+38.1	−36.6	+1.5	+65.1	−61.3	+3.8	+4.2
Λ-[Co(*S*,*S*-chxn)$_3$]Cl$_3$·5H$_2$O	+56.5	−51.1	+5.4	+78.1	−74.0	+4.1	+3.9
Λ-[Co(*S*,*S*-cptn)$_3$]Cl$_3$·4H$_2$O[b]	+57.3	−54.5	+2.8	+69.3	−65.4	+3.9	−4.3
Λ-[Co(*S*,*S*-ptn)$_3$]Cl$_3$·2H$_2$O[a]	+12.5	−14.5	−2.0	+57.7	−55.3	+2.4	+1.9
Λ-[Co(tmd)$_3$]Br$_3$[a]	+31.1	−38.7	−7.6	+93.0	−89.3	+3.7	−4.9

a) Experiments were carried out for the enantiomers. b) These values are based on the CD spectra measured by Toftlund and Petersen[8]. $R(T_1)=R(E)+R(A_2)$. $R(T_1)_{expt}$ are values observed for solution CD spectra.[16].

ambiguous in the six-membered chelate ring case. The K value for Δ-[Co(tmd)$_3$]$^{3+}$ was not so reliable and it may not be practicable to discuss further. Rotatory strengths of each component under the first absorption band were obtained from the band areas of the CD spectrum. Table 3 lists the values of $R(E)$ and $R(A_2)$. The net rotatory strengths, $R(T_1)=R(E)+R(A_2)$ are also included. The net rotatory strengths obtained from solution CD spectra are also included in Table 3 under the heading $R(T_1)_{expt}$.[16] For $R(E)$ of Λ-2[Co(en)$_3$]Cl$_3$·NaCl·6H$_2$O values of +52.6[13] and +50.9[14] are reported. +45.3 is given for $R(E)$ of Λ-[Co(en)$_3$]Br$_3$·H$_2$O.[13] All these values are somewhat smaller than those of the present study. $R(E)$ of −41.5 for Δ-[Co(*R*-pn)$_3$]Br$_3$ by Judkins and Royer[14] agrees well with −38.1 of the present study. As can be seen from Table 3, the absolute values of the observed rotatory strengths of the E and A_2 bands possess nearly the same magnitudes and opposite signs in conformity with the theoretical prediction. $R(E)$ and $R(A_2)$ are unequal: $|R(E)|>|R(A_2)|$ for the complexes with five-membered chelate rings, whereas $|R(E)|<|R(A_2)|$ for the complexes with six- and seven-membered chelate rings. $R(T_1)$'s obtained from solid state CD spectra generally agree well in magnitude and sign with those obtained from solution CD spectra except for Λ-[Co(*S*,*S*-cptn)$_3$]$^{3+}$, Λ-[Co(*S*,*S*-ptn)$_3$]$^{3+}$ and Λ-[Co(tmd)$_3$]$^{3+}$. For the latter three cases, some change in the conformation of the complex ion or in the mode of ion association may be expected in solution.[8,15]

Recently Mason and Seal calculated the d-electron optical activity of tris(diamine) cobalt(III) complex ions based on dipole-coupling ligand-polarization model.[16,17] All the computations are based on the crystal structures determined by us.[1-7] The results are listed in Table 3. The theoretical calculations correctly predict all the signs of $R(E)$ and $R(A_2)$. Moreover, theoretical values of $R(T_1)$ agree well in sign and magnitudes with those observed in solid-states for the complexes with five-membered chelate rings. Theoretical values of $R(E)$ and $R(A_2)$ for Λ-[Co(en)$_3$]$^{3+}$ agree satisfactorily with the observed values. For five-membered ring cases $R(E)$ and $R(A_2)$ agree pretty well with the observation. For the six- and seven-membered chelate ring cases, the agreement is less satisfactory. No explanation can be offered at present.

Unlike solution CD spectra, crystal CD spectra are free from the effect of conformational change which sometimes occurs in solution, on the other hand the effect of neighboring anion in the crystal cannot be ignored. This latter effect might not be of a primary importance, as can be seen from Table 3.

The authors wish to thank Professor C. E. Schäffer of University of Copenhagen for suggesting the method for decomposing solid-state CD spectra into E and A_2 components and for helpful discussion. They also thank Professor S. F. Mason of University of London for the theoretical results in advance of publication. Part of the cost of this reseach was met by a Scientific Research Grant from the Ministry of Education, to which the authors' thanks are due.

References

1) Y. Saito, K. Nakatsu, M. Shiro, and H. Kuroya, This Bulletin, **30**, 795 (1957).
2) K. Nakatsu, *ibid.*, **35**, 832 (1962).
3) H. Iwasaki and Y. Saito, *ibid.*, **39**, 92 (1966).
4) F. Marumo, Y. Utsumi, and Y. Saito, *Acta Crystallogr.*, **B26**, 1492 (1970).
5) M. Ito, F. Marumo, and Y. Saito, *ibid.*, **B27**, 2187 (1971).
6) A. Kobayashi, F. Marumo, and Y. Saito, *ibid.*, **B29**, 2443 (1973).
7) S. Sato and Y. Saito, *ibid.*, **B31**, 1378 (1975).
8) H. Toftlund and E. Pedersen, *Acta Chem. Scand.*, **26**, 4019 (1971).
9) K. Nakatsu, M. Shiro, Y. Saito, and H. Kuroya, This Bulletin, **30**, 158 (1957).
10) A. Werner, *Ber.*, **45**, 128 (1912).
11) F. M. Jaeger and L. Bijkerk, *Z. Anorg. Allg. Chem.*, **233**, 97 (1937).
12) B. Bosnich and J. M. Harrowfield, *J. Amer. Chem. Soc.*, **94**, 3245 (1972).
13) A. J. McCaffery and S. F. Mason, *Mol. Phys.*, **6**, 359 (1963).
14) R. R. Judkins and D. J. Royer, *Inorg. Chem.*, **13**, 945 (1974).
15) R. Kuroda, J. Fujita, and Y. Saito, *Chem. Lett.* **1975**, 225.
16) S. F. Mason and R. H. Seal, *Mol. Phys.*, to be published. R. H. Seal, Ph. D. Thesis, London University, 1974.
17) S. F. Mason and R. H. Seal, *Chem. Commun.*, **1975**, 331.

Triplet Excimer of Phenanthrene in Fluid Solution. Dynamic Analysis of Time-Resolved Phosphorescence

Masayuki AIKAWA, Takeshi TAKEMURA, and Hiroaki BABA

Division of Chemistry, Research Institute of Applied Electricity, Hokkaido University, Sapporo 060

(Received October 27, 1975)

The excimer phosphorescence of phenanthrene in isooctane at temperatures over a range of 300—77 K has been studied by means of a photon-counting technique. At temperatures above the melting point of isooctane a broad emission spectrum with its intensity maximum at 525 nm was obtained, which is essentially different from the structured phosphorescence spectrum obtained in rigid media at 77 K. The time dependence of the spectral shape and intensity of the phosphorescence emission affords strong evidence that the broad emission spectrum originates from the triplet excimer. A scheme of the triplet excimer formation involving a self-quenching pathway of the triplet monomer is proposed to interpret the time and concentration dependence of the monomer and excimer phosphorescence.

Although there have been many studies on the triplet excimer of aromatic hydrocarbons, the occurrence of excimer phosphorescence in solution has not yet been established.[1-4] In previous papers we have confirmed the existence of the triplet excimer for naphthalene and 1-chloronaphthalene in 2,2,4-trimethylpentane (isooctane) at 293 K through the photostationary and transient phosphorescence measurements.[5,6]

Langelaar *et al.* first reported the excimer phosphorescence of phenanthrene in viscous solution, but they have subsequently shown that the emission was due to an impurity.[7,8] They have also shown, however, kinetic evidence in favor of triplet excimer formation in some aromatic hydrocarbons including phenanthrene in fluid solutions.[9,10] On the other hand, in a study on the photo-dissociation of the *cis* dimer of 9-(hydroxymethyl)phenanthrene and other phenanthrene derivatives in a rigid matrix at 77 K, Chandross and Thomas have concluded that phenanthrene does not form a triplet excimer as well as a singlet excimer even under favorable conditions.[11] Thus, it is necessary to further study the phenanthrene triplet in fluid solution in order to settle the question whether the triplet excimer does exist.

In the present work, we have observed a broad phosphorescence spectrum with a maximum near 525 nm for phenanthrene in isooctane solution at 187 or 293 K. This spectrum is essentially different from the structured phosphorescence spectrum of phenanthrene obtained in EPA at 77 K. The broad spectrum may be attributed to emission either from an impurity triplet produced by T–T energy transfer or from the triplet excimer of phenanthrene. In order to elucidate this problem we measured time-resolved spectra of phenanthrene phosphorescence in fluid solution. An analysis of the time-dependent behavior of the phosphorescence after flash excitation leads to strong evidence that the phenanthrene triplet excimer exists even in fluid solution.

Experimental

A sample of commercial phenanthrene was purified carefully by the following successive processes. To remove a small quantity of anthracene from phenanthrene, the sample was refluxed with maleic anhydride in spectro-grade benzene for 20 hours. The mixture was filtered, the filtrate was shaken with a sodium hydroxide solution, and phenanthrene contained in the organic layer was freed from the solvent by distilling the latter under reduced pressure.[12,13] The sample was then recrystallized several times from spectro-quality ethanol, passed through a silica-gel column with petroleum benzine as the solvent, and finally sublimed *in vacuo*. Spectro-grade isooctane was also treated with a silica-gel column. The solution of phenanthrene in 1 cm square quartz cell was fully degassed by repeated freeze-thaw cycles (7 or 8 times).

Emission and excitation spectra were measured with a high-resolution, high-sensitivity photon-counting emission spectrophotometer constructed in our laboratory. The time-resolved phosphorescence spectra, as well as the intensity of phosphorescence or delayed fluorescence emission as a function of time, were measured with the aid of a spectro-phosphorimeter which was designed, on the basis of the photon-counting method, for obtaining emission decay curves in a time range of 10^2 to 10^{-5} s. In this phosphorimeter, either a continuous Xe arc lamp combined with a light-chopping system or a Xe flash lamp was used as a pulsed light source. The design and performance of these two apparatuses have been described in a previous paper.[6]

The phosphorescence spectra were corrected for the spectral sensitivity of the monochromator-photomultiplier system after the method reported in a previous paper[14] using a standard tungsten filament lamp. The phosphorescence quantum yields were determined by comparing the corrected phosphorescence spectra with a corrected fluorescence spectrum of quinine sulfate in 0.5 M sulfuric acid, which has a fluorescence quantum yield of 0.51.

Results

Figure 1 shows the phosphorescence spectra of phenanthrene in isooctane at 77 K and 187 K. In the spectrum at 187 K a broad emission band is seen near 525 nm which is absent at 77 K. A phosphorescence spectrum similar to that at 187 K was also obtained at 293 K. The structured phosphorescence band at 187 K or at 293 K in a region near 470 nm, which is practically identical with the spectrum at 77 K in location and band shape, can be attributed to the monomer phosphorescence emission of phenanthrene. The excitation spectrum in fluid solution monitored at the 520 nm emission peak (Fig. 1), as well as that monitored at 465 nm, is in good agreement with the absorption spectrum. This suggests that the broad emission band originates from phenanthrene itself.

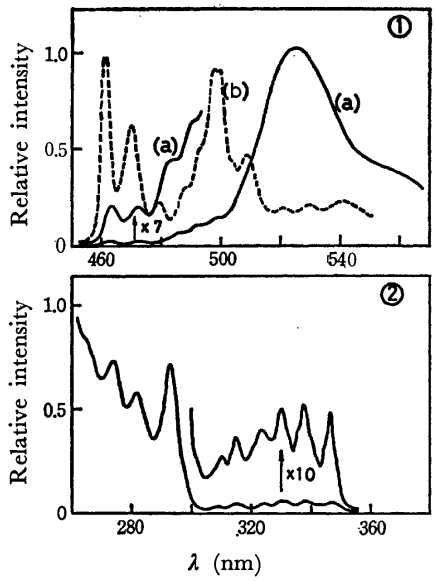

Fig. 1. Corrected phosphorescence and excitation spectra of phenanthrene in isooctane (2.5×10^{-5} M). (1) Phosphorescence spectrum: **a**, at 187 K; **b**, at 77 K. (2) Excitation spectrum at 187 K, monitored with respect to the 520 nm phosphorescence peak.

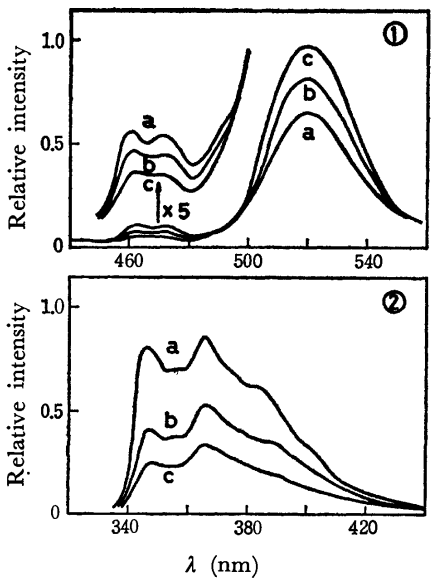

Fig. 2. Time-resolved phosphorescence (1) and delayed fluorescence (2) spectra in isooctane (1×10^{-4} M) at 293 K (uncorrected for instrumental response). The spectra denoted by **a**, **b**, and **c** were observed at 140, 305, and 635 μs, respectively, after flash excitation.

The time-resolved phosphorescence and delayed fluorescence spectra in isooctane at 293 K are shown in Fig. 2. The intensities of both the phosphorescence at about 465 nm and the delayed fluorescence decrease monotonously with time after flash excitation, whereas the broad structureless band with its maximum at about 525 nm grows with time.

The emission intensity as a function of time after flash excitation, monitored at a given wavelength, will be denoted by $I(t)$. Figure 3 illustrates the $I(t)$

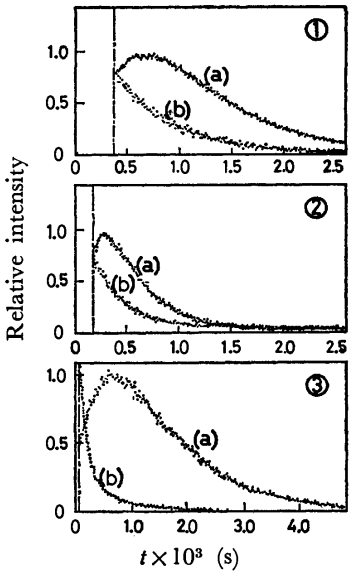

Fig. 3. Some representative $I(t)$ curves for phenanthrene in isooctane. Temperatures and solute concentrations: (1) 293 K, 1.8×10^{-4} M; (2) 293 K, 1.24×10^{-3} M; (3) 187 K, 2.1×10^{-3} M. Monitoring wavelengths: **a**, 465; **b**, 520 nm. Dashed lines show the time width of pulsed light source.

curves for phosphorescence in isooctane at 293 and 187 K. The $I(t)$ curve observed at 465 nm and at 187 K is composed of two exponential decays but that at 293 K represents a first order decay within our experimental errors. On the other hand, the $I(t)$ curve detected at 520 nm shows a rise for small values of t and decay for large t. It is also seen that the value of t at which $I(t)$ reaches a maximum becomes much smaller on increasing the phenanthrene concentration. We can thus assign the broad emission band with the intensity maximum at about 525 nm to the triplet excimer of phenanthrene on the basis of the following considerations.

Under our experimental conditions where the excitation intensity is low and the solution is of very low viscosity, the kinetic scheme for the deactivation of the triplet states involving the triplet excimer formation may be expressed in general as follows:[9,15]

$$^3M^* + {}^1M \underset{\overleftarrow{k}}{\overset{\overrightarrow{k}}{\rightleftharpoons}} {}^3D^* \qquad (1)$$

$^3M^*$ → k_{1r}, k_{1q}; $^3D^*$ → k_{2r}, k_{2q}

Here, ^1M, $^3M^*$, and $^3D^*$ stand for the ground singlet monomer, excited triplet monomer, and excited triplet dimer (triplet excimer), respectively; k_{1r}, k_{1q}, k_{2r}, and k_{2q} are the radiative (r) and non-radiative (q) decay constants for the triplet monomer and excimer; and $\overrightarrow{k}$ and $\overleftarrow{k}$ denote the rate constants for the formation and dissociation of the triplet excimer, respectively.

Delayed fluorescence could be observed because of its high intensity. The triplet–triplet annihilation, however, need not be considered in the scheme, since

the triplet concentration in our experiments was so low that the annihilation should not contribute appreciably to the triplet decay. The decay rate constant for the delayed fluorescence observed is twice the rate constant obtained from the tail portion of the phosphorescence $I(t)$ curve at 465 nm (see Fig. 2).

Solution of the rate equations for the kinetic scheme (1), under the appropriate initial conditions, yields the following expressions for the quantum intensity of the monomer and excimer phosphorescence at time t.

$$I_m(t) = \frac{k_{1r}(\theta_2 - X)}{(\theta_2 - \theta_1)}\{e^{-\theta_1 t} + Ae^{-\theta_2 t}\} \quad (2)$$

$$I_d(t) = \frac{k_{2r}\vec{k}[^1M]}{(\theta_2 - \theta_1)}\{e^{-\theta_1 t} - e^{-\theta_2 t}\} \quad (3)$$

where

$$\theta_{1,2} = \frac{1}{2}[X + Y \mp \{(Y-X)^2 + 4\vec{k}\overleftarrow{k}[^1M]\}^{1/2}] \quad (4)$$

and

$$A = (X-\theta_1)/(\theta_2 - X)$$
$$X \equiv k_1 + \vec{k}[^1M] \qquad k_1 = k_{1r} + k_{1q} \quad (5)$$
$$Y \equiv k_2 + \overleftarrow{k} \qquad k_2 = k_{2r} + k_{2q}$$

Equations (2) and (3) predict that the monomer should display a curve consisting of two exponential decays and that the excimer phosphorescence should yield a rise-and-decay curve. The $I(t)$ curves monitored at 465 and 520 nm correspond well to $I_m(t)$ given by Eq. (2) and $I_d(t)$ given by Eq. (3), respectively. This provides the conclusive evidence that the emission at 520 nm is due to the triplet excimer of phenanthrene.

For both $I(t)$ curves monitored at 465 and 520 nm, the plot of log $I(t)$ *vs.* t at long times after flash excitation gives the first-order decay constant, θ_1. The value of θ_2 can be obtained from the difference between the $I(t)$ curve observed for the excimer emission and the first order decay curve extrapolated towards shorter times by the use of θ_1. The θ_2 value can also be obtained by using the initial part of the $I(t)$ curve for the monomer.

The initial decay related to θ_2 was observed in the monomer $I(t)$ curve at 187 K, but not at 293 K. This is because the excitation pulse used was not sufficiently short to monitor the fast decay at 293 K.

There may be a possibility that the broad phosphorescence is ascribed to an impurity emission. Energetically, however, reversible energy transfer is not likely to occur[16,17] owing to a large energy difference between the phosphorescence 0–0 band at 463 nm and the phosphorescence maximum at 520 nm. Therefore, if the emission assigned to the excimer phosphorescence were to be due to an impurity triplet, $^3Q^*$, the broad phosphorescence should arise from irreversible triplet–triplet energy transfer from phenanthrene to the impurity. In this case, the kinetic scheme (1) is modified by substituting ^1Q for ^1M and $^3Q^*$ for $^3D^*$, and the following expression is obtained for the time dependence of the intensity of monomer emission:

$$I_m(t) = C\exp\{-(k_1 + \vec{k}[^1Q])t\} \quad (6)$$

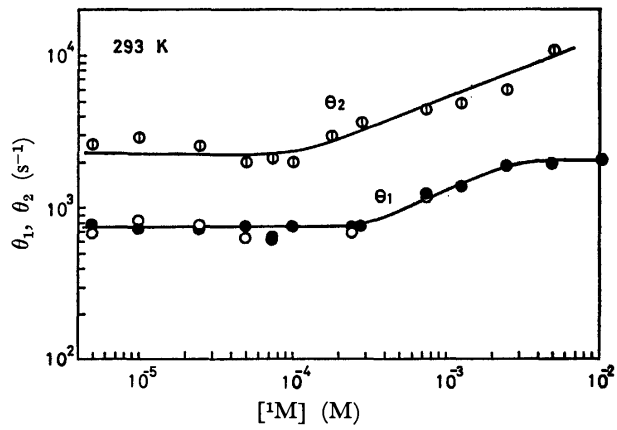

Fig. 4. Plots of θ_1 and θ_2 against the concentration of phenanthrene in isooctane at 293 K. The values of θ_1 are obtained from the $I(t)$ curves monitored at 465 (○) and 520 nm (●), and the values of θ_2 are obtained at 520 nm (ⓓ).

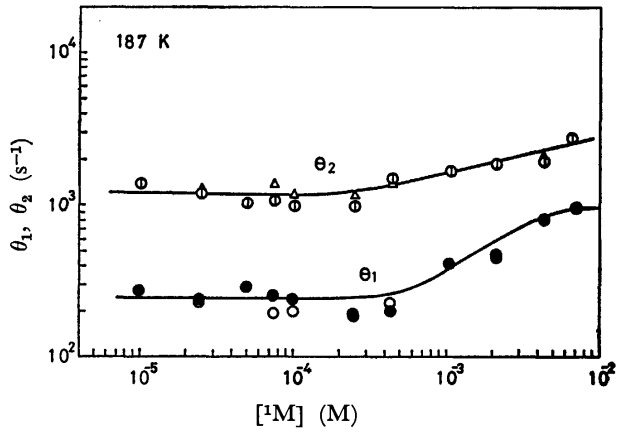

Fig. 5. Plots of θ_1 and θ_2 against the concentration of phenanthrene in isooctane at 187 K. The symbol (△) refers to the values of θ_2 which are obtained from the $I(t)$ curves monitored at 465 nm, and the other symbols are the same as in Fig. 4.

The $I(t)$ curve for the monomer phosphorescence observed at 465 nm is then expected to show a single exponential decay with a rate constant $k_1 + \vec{k}[^1Q]$. This expectation contradicts the experimental fact that the initial fast decay was observed in the monomer $I(t)$ curve at 187 K, and therefore the possibility of impurity emission is ruled out. Thus additional evidence is obtained that the emission at 525 nm is due to the triplet excimer of phenanthrene.

The plots of θ_1 and θ_2 obtained at 293 K and 187 K against [^{1}M] are shown in Figs. 4 and 5, respectively. As [^{1}M] increases, θ_1 first increases and then reaches a constant value at relatively high values of [^{1}M], while θ_2 increases monotonously. It is also seen from Fig. 5 that the monomer and the excimer $I(t)$ curves at 187 K lead to consistent values both for θ_1 and for θ_2.

The rate constants $\vec{k}$, $\overleftarrow{k}$, k_1, and k_2 at a given temperature can be evaluated from the data on θ_1 and θ_2 as a function of [^{1}M] by using the following limiting properties,[15] (i) As [^{1}M] becomes small, θ_1 and θ_2

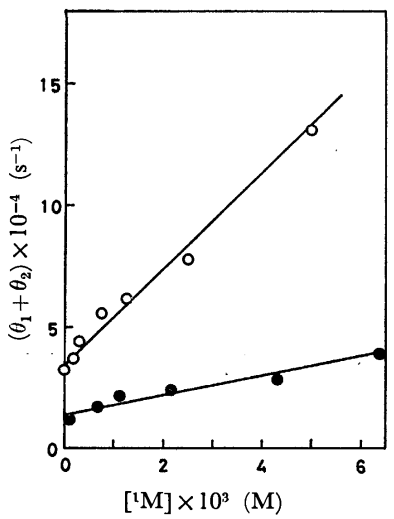

Fig. 6. Plots of $\theta_1+\theta_2$ against the concentration of phenanthrene at 293 (○) and 187 K (●).

TABLE 1. RATE CONSTANTS FOR PHENANTHRENE IN ISOOCTANE SOLUTION

Temperature K	$k_1\times10^{-2}$ s^{-1}	$k_2\times10^{-3}$ s^{-1}	$\vec{k}\times10^{-6}$ $M^{-1}s^{-1}$	$\overleftarrow{k}\times10^{-3}$ s^{-1}
187	2.5	1.0	0.4	0.2
293	7.5	1.9	2.0	0.6

approach constant values which represent k_1 and $k_2+\overleftarrow{k}$. As shown in Figs. 4 and 5, θ_1 and θ_2 become constant in the concentration range of 10^{-6}—10^{-4} M. (ii) At higher concentrations ($>10^{-2}$ M in the case of phenanthrene), θ_1 becomes k_2. (iii) At any value of $[^1M]$, Eq. (4) yields the following relation:

$$\theta_1+\theta_2=k_1+k_2+\overleftarrow{k}+\vec{k}[^1M] \quad (7)$$

As expected from Eq. (7), the plots of $\theta_1+\theta_2$ against $[^1M]$ (Fig. 6) give good straight lines with slopes, $\vec{k}$ equal to 2.0×10^6 and 0.4×10^6 $M^{-1}s^{-1}$, respectively, at 293 and 187 K. The behavior of θ_1 and θ_2 as predicted from the limiting conditions (i) through (iii) is consistent with our experimental results. The rate constants, $\vec{k}$, $\overleftarrow{k}$, k_1, and k_2 at 293 and 187 K thus determined are summarized in Table 1.

Discussion

The equilibrium constant of the excimer formation reaction (1) in the triplet state is defined as $K_e=\vec{k}/\overleftarrow{k}$, which is calculated to be 3.3×10^3 M^{-1} at 293 K and 2.0×10^3 M^{-1} at 187 K. The energy difference (ΔE) between the 0–0 phosphorescence band of the monomer at 463 nm and the phosphorescence maximum of the triplet excimer at 525 nm is about 2600 cm^{-1} (7.3 kcal). The value of K_e is much the same as those observed in singlet excimers, but the ΔE value is very small compared with the corresponding values for singlet excimers of aromatic hydrocarbons, in which ΔE is nearly constant and equal to ~6000 cm^{-1}.[16] The entropy change, ΔS, accompanying the triplet excimer formation is obtained from K_e and ΔE after the manner in which ΔS was estimated for the singlet excimer.[15] The absolute value of ΔS thus determined seems to be too small (less than 1 cal mol^{-1} deg^{-1} at 293 K).

In view of those circumstances, we introduce a self-quenching pathway of $^3M^*$ into the scheme (1):

$$^3M^* + {}^1M \underset{\overleftarrow{k}}{\overset{k_d}{\rightleftharpoons}} {}^3D^* \quad (9)$$

$^3M^*$ → k_1, $k_1'[^1M]$; $^3D^*$ → k_2

Evidently the rate constants k_1 and $\vec{k}$ defined in the scheme (1) correspond, respectively, to $k_1+k_1'[^1M]$ and k_d in the scheme (9). The values of $\vec{k}$ as determined from the dependence of $\theta_1+\theta_2$ on $[^1M]$ (Eq. (7) and Fig. 6) must then be identified as the values for $k_1'+k_d$. It is conceivable that most of the encounters of the triplet-state monomer with the ground-state lead to the quenching of the former, and thus it is possible that k_1' may be ten times as large as k_d. The rate constant k_d will then be smaller than $\vec{k}$ by a factor of 10; in other words, the photoassociation equilibrium constant, $K_a=k_d/\overleftarrow{k}$ in the scheme (9) may become far smaller than K_e. Thus, if we tentatively assume that $K_a=10^2$ M^{-1} at 300 K, we can obtain reasonable values for ΔS, the enthalpy of the triplet excimer formation ΔH, and the repulsion energy between two unexcited monomer molecules I_G, using $\Delta E=7.3$ kcal mol^{-1}. The results are: $\Delta S=-10$ cal mol^{-1} deg^{-1}, $\Delta H=-5.5$ kcal mol^{-1}, and $I_G=2$ kcal mol^{-1}.

We believe that the triplet excimer formation of aromatic hydrocarbons is a general phenomenon as in the case of the singlet excimer formation. It is probable that the stabilization responsible for the triplet excimer is due to the charge resonance interaction,[4,17,18] which depends critically on the distance, R, and the orbital overlap between the triplet and ground state molecules contrary to the dipole-dipole interaction.[19] Thus, the triplet excimer formation requires a specific arrangement between the two molecules within the solvent cage. This seems to correspond to the fact that the formation rate constant is much smaller than the diffusion-controlled rate constant, as is shown by our experimental results (Table 1). It may be concluded that the difference between those two rate constants results from the frequency factor.

It is well known that the T–T energy transfer rate in fluid solution is very nearly the diffusion-controlled rate when the triplet level of donor lies higher than that of the acceptor by 3—4 kcal/mol or more.[20-22] T–T energy transfer distance, 6—10 Å between donor and acceptor in fluid solution[23] is much larger than the interaction distance of triplet excimer which may be 3—3.5 Å on the analogy of singlet excimer. The difference between the T–T energy transfer and triplet excimer formation, though both processes require overlaps of the orbitals of the two molecules, is that the former can occur even within one or two encounter

with very weak interaction, in comparison with the latter which depends on the suitable overlap. There have been many negative results about the problem whether or not the orientation is detectable for the T–T energy transfer in solution.[24,25] Our result suggests, however, that the triplet excimer formation needs specific and critical requirement for the orientation between two molecules.

In the concentration range used in our experiments, the precursor of the triplet excimer is very likely the triplet monomer rather than the singlet excimer. In higher concentration region, the possibility of the latter cannot be ruled out.

References

1) G. Castro and R. M. Hochstrasser, *J. Chem. Phys.*, **45**, 4352 (1966).
2) E. C. Lim and S. K. Chakrabarti, *Mol. Phys.*, **13**, 293 (1967).
3) C. T. Lin and M. A. El-Sayed, *Chem. Phys.*, **5**, 315 (1974).
4) T. Azumi and S. P. McGlynn, *J. Chem. Phys.*, **41**, 3131 (1964).
5) T. Takemura, H. Baba, and Y. Shindo, *Chem. Lett.*, 1091 (1974).
6) T. Takemura, M. Aikawa, and H. Baba, *J. Amer. Chem. Soc.*, in press.
7) J. Langelaar, R. P. H. Rettschnick, A. M. F. Lambooy, and G. J. Hoytink, *Chem. Phys. Lett.*, **1**, 609 (1968).
8) J. Langelaar, Thesis, University of Amsterdam (1969).
9) J. Langelaar, R. P. H. Rettschnick, and G. J. Hoytink, *J. Chem. Phys.*, **54**, 1 (1971).
10) J. Langelaar, G. Jansen, R. P. H. Rettschnick, and G. J. Hoytink, *Chem. Phys. Lett.*, **12**, 86 (1971).
11) E. A. Chandross and H. T. Thomas, *J. Amer. Chem. Soc.*, **94**, 2421 (1972).
12) D. D. Phillips, "Organic Syntheses," Vol. 34, p. 31 (1954).
13) L. Feldman, P. Pantages, and M. Orchin, *J. Amer. Chem. Soc.*, **73**, 4341 (1951).
14) H. Baba and S. Suzuki, This Bulletin, **35**, 683 (1962).
15) J. B. Birks, "Photophysics of Aromatic Molecules," Wiley-Interscience, London (1970), p. 301.
16) J. B. Birks, M. D. Lumb, and I. H. Munro, *Proc. Roy. Soc.*, **A280**, 289 (1964).
17) J. N. Murrell and J. Tanaka, *Mol. Phys.*, **7**, 363 (1964).
18) S. I. Choi, J. Jortner, S. A. Rice, and R. Silbey, *J. Chem. Phys.*, **41**, 3294 (1964).
19) M. Inokuti and F. Hirayama, *ibid.*, **43**, 1978 (1965).
20) H. L. J. Bäckström and K. Sandros, *Acta Chem. Scand.*, **14**, 48 (1960); K. Sandros, *ibid.*, **18**, 2355 (1964).
21) W. G. Herkstroeter and G. S. Hammond, *J. Amer. Chem. Soc.*, **88**, 4769 (1966).
22) P. J. Wagner and I. Kochevar, *ibid.*, **90**, 2232 (1968).
23) T. Takemura, M. Aikawa, and H. Baba, This Bulletin, **47**, 2476 (1974).
24) K. B. Eisenthal, *J. Chem. Phys.*, **50**, 3120 (1969).
25) A. Adamczyk and D. Phillips, *J. Chem. Soc., Faraday II*, **70**, 537 (1974).

Sum Rule Consideration of Molecular Photoelectron Spectra: s-Type Bands of Butenes

Shunji KATSUMATA and Katsumi KIMURA

Physical Chemistry Laboratory, Institute of Applied Electricity, Hokkaido University, Sapporo 060

(Received November 17, 1975)

The s-type photoelectron bands of *cis*-, *trans*-2-butene, and 2-methylpropene in the gaseous phase have been measured in the region 17—27 eV by a He(II) resonance lamp which was constructed for the present purpose. The vertical ionization energies obtained here from the s-type bands have been interpreted with the Hückel method involving the Coulomb integrals of carbon 2s atomic orbitals which were estimated on the basis of the idea of sum rule from the available He(II) data of many other hydrocarbons reported by Potts *et al.*

In previous He(I) photoelectron studies of many aliphatic compounds,[1-5] total and partial sums of vertical ionization energies in the p-type region have been interpreted by Kimura *et al.* in terms of the empirical energies selected on the basis of the photoelectron data of simple molecules. The sum rule has also been applied to all the ionization energies obtained in the p- and s-type regions in mono-, di-, and trimethylamines,[6] using Hall's equivalent orbitals.[7] From the sum rule considerations of various chloro-substituted compounds[4] and ethylene derivatives,[5] the following substitution effects have been pointed out on the total sums of the p-type vertical ionization energies: 1) The total sum increases approximately linearly with number of substituents. 2) The total sums of the isomers are nearly the same. 3) The total sum may be approximately reproduced with the sums of the p-type empirical ionization energies. In connection with our previous studies, we have attempted to extend our study to the s-type region of butenes in the present He(II) photoelectron study.

Potts *et al.*[8-10] have published He(II) photoelectron spectra of many saturated and unsaturated hydrocarbons, together with the resulting complete sets of vertical ionization energies in the s-type region. They have interpreted the s-type ionization energies in terms of the Coulomb integrals of carbon 2s atomic orbitals on the basis of a simple Hückel theory. In the present work, we tried to employ their experimental data for a test of our sum rule in the present work. We wish to point out here that: 1) the total sums of the available s-type vertical ionization energies in the individual hydrocarbons may be reproduced by the sums of Coulomb integrals associated with the carbon skeletons of the hydrocarbons and 2) the He(II) bands of butenes which have not been published so far may be interpreted by the Hückel method with the Coulomb energies estimated from other hydrocarbons.

Experimental

Measurements of He(II) photoelectron spectra were carried out in the region up to about 27 eV with a high-resolution photoelectron spectrometer previously used,[1,2] a DC discharge He lamp of hollow-cathode type being used as a He(II) resonance source (304 Å) which was constructed for the present purpose. The cathode of the He(II) lamp was made of aluminum. During the photoelectron measurements, the He lamp was discharged at a pressure of about 0.06 Torr at a voltage of 700 V (0.4 A). Calibrations of ionization energies were carried out with Xe and He as internal standards. In the region below about I_1+17 in eV units, where I_1 represents the first ionization energy, He(II) spectra may be observed without overlapping with He(I) spectra. In the higher region the ionization bands produced by He(I) lines (584, 537, 522 Å, *etc.*) are mixed with those produced by He(II) line. No filter films were used here for separating He(II) line from He(I) line. Commercial gaseous samples of propene and *cis*- and *trans*-2-butene, and 2-metyhlpropene were used without further purification.

Results and Discussion

The photoelectron spectra of propene and *cis*- and *trans*-2-butene, and 2-methylpropene obtained here in the region 17—27 eV are shown in Fig. 1, suggesting three ionization bands indicated by vertical lines with the numbering. The propene spectrum in Fig. 1(a) is essentially the same as that reported by Potts *et al.*[10] It may be pointed out from the photoelectron spectra of butenes that the separations of the second and third

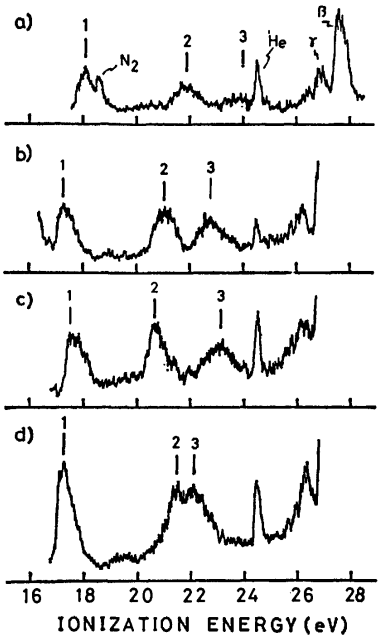

Fig. 1. The He(II) photoelectron spectra of (a) propene, (b) *cis*-2-butene, (c) *trans*-2-butene, and (d) 2-methylpropene in the region 17—27 eV. The peaks indicated by He are due to the ionization of helium gas by a He(II) line and those indicated by β and γ are due to the ionization of the samples by the 537- and 522-Å lines of He(I), respectively.

Table 1. Vertical ionization energies of propene and *cis*- and *trans*-2-butenes, and 2-methylpropene in the s-type region, together with the theoretical Koopmans' theorem ionization energies with orbital assignments

Propene		*cis*-2-Butene		*trans*-2-Butene		2-Methylpropene	
Expt[a]	Calcd	Expt	Calcd	Expt	Calcd	Expt	Calcd
18.30	18.30(a′)	17.5	17.42(a_1)	17.8	17.77(b_2)	17.5	17.77(b_u)
21.88	21.84(a′)	21.1	21.72(a_1)	20.8	20.60(a_1)	21.6	20.60(a_g)
24.16	24.18(a′)	22.9	22.17(b_2)	23.1	22.97(b_2)	22.2	22.97(b_u)
		[24.3]	24.46(a_1)	[24.1]	24.42(a_1)	[24.5]	24.42(a_g)

a) Ref. 10.

s-type bands remarkably differ from one another among the three isomers. The first s-type bands of the isomers are located approximately at the same position. The vertical ionization energies obtained from these photoelectron bands are summarized in Table 1. For *cis*- and *trans*-2-butene, and 2-methylpropene there are no available He(II) spectra for comparison.

In the previous He(I) photoelectron studies,[3,5] it has been indicated that all the p-type bands of methyl-substituted ethylenes appear below about 17 eV and may be interpreted in terms of p-type localized MO's. In the present work, we discuss only s-type bands in the photoelectron spectra. The number of such s-type MO's in a hydrocarbon is equal to that of carbon atoms. Propene has three carbon s-type MO's which probably correspond to the three bands in Fig. 1(a). Butene isomers show three bands, the remaining bands being not clear in Fig. 1(b—d). The theoretical treatments mentioned later suggest that the fourth bands may be located at about 24.5 eV.

Potts *et al.*[8-10] have indicated in their He(II) photoelectron studies that the s-type bands of hydrocarbons may be interpreted in terms of carbon 2s atomic orbitals. They estimated the Coulomb integrals of the C-2s orbitals on the basis of the He(II) data, and suggested that the Coulomb integrals depend on the number of hydrogen atoms attached to the carbon atoms. However, no formulas have been given for correlating the Coulomb integrals to the number of hydrogen atoms.

Using the ionization energy data of Potts *et al.*,[9,10] we found that there may be an approximately linear relationship between the Coulomb integrals ($\alpha_{CH_{4-m}}$) and the number (m) of hydrogen atoms lost from CH_4,

$$\alpha_{CH_{4-m}} = a + bm \qquad (1)$$
$$m = 0—4$$

where a means the Coulomb integral of CH_4 and bm a correcting term due to the change of CH_4 to CH_{4-m}. The Coulomb integrals α_{CH_i} (i=0—4) are hereafter represented by α_i for simplicity.

In the present work, we first estimated Coulomb integrals α_i's from the available s-type ionization energies of several hydrocarbons; $CH_{4-m}(CH_3)_m$ (m= 0—4), ethylene, and butadiene. From least squares calculations, we found that a=−22.90 eV and b= 0.73 eV. The Coulomb energies thus determined are summarized in Table 2, which are used in the present study of propene and butenes. Before going into the analysis of the He(II) spectra of the compounds studied, we examined how the α_i's in Table 2 can reproduce the experimental total sums of s-type vertical ionization energies for various other hydrocarbons.

Table 2. Coulomb integrals (in eV) of the carbon s-type orbitals in CH_i (i=0—4), estimated from the sum rule

α_0	α_1	α_2	α_3	α_4
−19.98	−20.71	−21.44	−22.17	−22.90

The traces of the Hückel determinants and their numerical values for fourteen hydrocarbons are given in Table 3, compared with the corresponding experimental sums (T_{expt}) based on the s-type ionization energies reported by Potts *et al.*[9,10] As seen from Table 3, excellent agreements are obtained between calculation and experiment, except for cyclopropane and benzene.

Applying the above sum rule to butenes, we may

Table 3. The traces of the Hückel determinants and the calculated and experimental total sums for various hydrocarbons (in eV units)

Compound	Trace	$-T_{calcd}$	$-T^{9,10)}_{expt}$
CH_4	$\alpha_4=a$	22.9	22.9
CH_3-CH_3	$2\alpha_3=2a+2b$	44.3	44.3
$CH_3CH_2CH_3$	$2\alpha_3+\alpha_2=3a+4b$	65.8	65.8
CH_3-$(CH_2)_2$-CH_3	$2\alpha_3+2\alpha_2=4a+6b$	87.2	87.2
$(CH_3)_3CH$	$3\alpha_3+\alpha_1=4a+6b$	87.2	87.0
CH_3-$(CH_2)_3$-CH_3	$2\alpha_3+3\alpha_2=5a+8b$	108.7	108.8
$(CH_3)_2CHCH_2CH_3$	$3\alpha_3+\alpha_2+\alpha_1=5a+8b$	108.7	108.9
$(CH_3)_4C$	$4\alpha_3+\alpha_0=5a+8b$	108.7	108.6
$[CH_2]_3$	$3\alpha_2=3a+6b$	64.3	65.6
$[CH_2]_6$	$6\alpha_2=6a+12b$	128.6	128.9
CH_2=CH_2	$2\alpha_2=2a+4b$	42.9	42.8
CH_3-CH=CH_2	$\alpha_3+\alpha_2+\alpha_1=3a+6b$	64.3	64.3
CH_2=CH-CH=CH_2	$2\alpha_2+2\alpha_1=4a+10b$	84.3	84.7
C_6H_6	$6\alpha_2=6a+12b$	124.4	125.3

Table 4. The traces of the Hückel determinants and the calculated total sums (eV) for *cis*- and *trans*-2-butene, and 2-methylpropene

Compound	Trace		$-T_{calcd}$
cis-CH_3-CH=CH-CH_3	$2\alpha_3+2\alpha_1$		
trans-CH_3-CH=CH-CH_3	$2\alpha_3+2\alpha_1$	$=4a+8b$	85.7
$(CH_3)_2C$=CH_2	$2\alpha_3+\alpha_2+\alpha_0$		

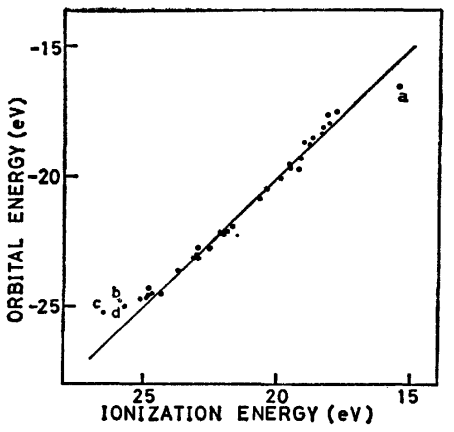

Fig. 2. A plot of the calculated (Hückel) orbital energies against the experimental vertical ionization energies in the s-type region for fourteen hydrocarbons given in Table 3. The solid line is drawn to show Koopmans' theorem. Points a and b are for the benzene b_{1u} and a_{1g} MO's, respectively; point c for the cyclopropane a_1 MO; and point d for the cyclohexane a_{1g} MO.

predict that the remaining s-type bands may appear at about 24.1—24.5 eV as shown in brackets in Table 1. The traces of the Hückel determinants of *cis*- and *trans*-2-butene, and 2-methylpropene are summarized in Table 4 which may be given simply by $4a+8b$.

In addition to the sum rule considerations mentioned above, we also calculated orbital energies by solving secular equations containing off-diagonal elements given by resonance integrals

$$\beta_{\mu\nu} = kS_{\mu\nu}(\alpha_\mu + \alpha_\nu) \qquad (2)$$

where $S_{\mu\nu}$ is the overlap integral between the nearest neighboring C-2s atomic orbitals and $k=0.12$ is used which was selected so as to reproduce the separation (3.48 eV) between two s-type vertical ionization energies of ethane. In order to test the validity of the parameter value (k) in Eq. (2), we calculated the orbital energies of s-type MO's for all the hydrocarbons given in Table 3. The resulting orbital energies are plotted against the available experimental ionization energies in Fig. 2, from which it may be seen that agreements between the orbital energies and the negative ionization energies are excellent except a few cases.

Similarly, solving secular equations, we also calculated the orbital energies of s-type MO's for *cis*- and *trans*-2-butene and 2-methylpropene. The calculated Koopmans' theorem ionization energies are also shown in Table 1, compared with the experimental ionization energies. Good agreements may be seen between experiment and theory.

The most interesting conclusions obtained in the present work are the following. 1) The sum rule of ionization energies approximately holds in the s-type region for the various hydrocarbons studied. 2) The s-type ionization energies in each of the hydrocarbons may well be interpreted in terms of the constant parameters a, b, and k. 3) The separation between the second and third s-type bands of 2-methylpropene is much smaller compared with that of *cis*-2-butene (or *trans*-2-butene) and such difference may be explained mainly with the difference in the Coulomb integrals of the C-2s atomic orbitals between the two isomers.

Further applications of the sum rule to many other organic compounds not only in the p-type region but also in the s-type region will be interesting subjects to be studied.

We would like to express our gratitude to Professor S. Kiyono, Dr. N. Ueno, and Dr. Y. Hayashi of Tohoku University for their valuable suggestions for the design of the He(II) lamp.

References

1) K. Kimura, S. Katsumata, Y. Achiba, H. Matsumoto, and S. Nagakura, This Bulletin, **46**, 373 (1973).
2) S. Katsumata and K. Kimura, *ibid.*, **46**, 1342 (1973); S, Katsumata, T. Iwai, and K. Kimura, *ibid.*, **46**, 3391 (1973).
3) K. Kimura, S. Katsumata, T. Yamazaki, and H. Wakabayashi, *J. Electron Spectrosc.*, **6**, 41 (1975).
4) S. Katsumata and K. Kimura, *ibid.*, **6**, 309 (1975).
5) T. Yamazaki and K. Kimura, This Bulletin, **48**, 1602 (1975).
6) K. Kimura and K. Osafune, *Mol. Phys.*, **29**, 1073 (1975).
7) G. G. Hall, *Proc. Roy. Soc., Ser. A*, **205**, 541 (1951).
8) A. W. Potts, T. A. Williams, and W. C. Price, *Faraday Diss. Chem. Soc.*, **54**, 104 (1972).
9) A. W. Potts and D. G. Streets, *J. Chem. Soc., Faraday Trans. II*, **70**, 875 (1974).
10) D. G. Streets and A. W. Potts, *ibid.*, **70**, 1505 (1974).

Substitution Reactions of Several Lead(II)–Polyamine-*N*-polyacetate Complexes with Indium(III) in Aqueous Solutions

Toru NOZAKI and Nagao SUEMITSU

Department of Industrial Chemistry, Faculty of Engineering, Ehime University, Matsuyama-shi 790

(Received January 13, 1975)

The kinetics of the substitution reactions of the lead(II) complexes of EDTA, EDTA·OH, CyDTA, and DTPA with the indium(III) ion have been studied in the pH range from 1.8 to 4.8 at 20 °C and at an ionic strength of 0.1 in the presence of an excess of lead(II) ions. The reaction for the CyDTA system seems to proceed through only the dissociative process, while those for the EDTA, EDTA·OH, and DTPA systems proceed through both the steps forming a binuclear intermediate and the dissociative steps, in which the reactions forming indium complexes proceed mainly through the paths involving $InOH^{2+}$.

Many of the substitution reactions of divalent metal complexes of ethylenediamine-*N,N,N',N'*-tetraacetate (EDTA) and 1,2-cyclohexanediaminetetraacetate (CyDTA) with other divalent metal ions have been reported. However, only a few substitution reactions of divalent metal complexes with trivalent metal ions have been studied. Recently, the reaction paths of this type of substitution reaction have been shown by Takahashi and his co-workers.[1]

In the same way as in the previous work,[2] the kinetics of the substitution reactions of the lead(II) complexes of EDTA, *N*-(hydroxyethyl)ethylenediamine-*N,N',N'*-triacetate (EDTA·OH), CyDTA, and diethylenetriamine-*N,N,N',N'',N''*-pentaacetate (DTPA) with the indium(III) ion, which has the same electronic configuration as the gallium(III) ion, have been studied in the pH range from 1.8 to 4.2 at 20 °C and at an ionic strength of 0.1 in order to investigate the effects of the ligand and of the species of the indium(III) ion on the rate and the reaction process, and in order to compare the rates with those for gallium(III). In the present paper the rate equations will be presented on the basis of the kinetic results, and the mechanisms of the reactions will be discussed by relating the terms in the observed rate constants of the reactions to the rate constants of the reaction paths of a known type.[1]

Experimental

Stock solutions of indium(III) and lead(II) were prepared by dissolving a weighed amount of metallic indium (99.99%) in perchloric acid, and by converting lead(II) nitrate into the perchlorate with perchloric acid, respectively. The solutions were diluted to a constant volume with redistilled water and were standardized by chelatometric titration with EDTA. Standard solutions of polyamine-*N*-polyacetate were prepared by dissolving a weighed amount of EDTA, EDTA·OH, CyDTA, or DTPA (Dotite reagent), which had been dried at 80 °C for 3 hr without further purification, in redistilled water containing equimolar quantities of sodium hydroxide.

The pH values of the solutions of the lead(II) complexes and indium(III) were adjusted to given values with sodium hydroxide and perchloric acid, using a pH meter equipped with a calomel electrode in which sodium chloride was substituted for potassium chloride to avoid potassium-perchlorate interference. After mixing, the pH of the resulting solutions was constant during the reactions. The ionic strength of each of the solutions was adjusted to 0.1 with sodium perchlorate. The initial concentrations of PbX_t, where X_t denotes all the species of the polyamine-*N*-polyacetate anions, In(III), and Pb^{2+} were 5.0×10^{-6}, 5.0×10^{-6}, and $(1.0-8.0)\times10^{-3}$ M respectively. The substitution reactions were run in the pH range from 1.8 to 4.2 at 20 °C and at an ionic strength of 0.1 in the presence of an excess of lead(II) ions and in the absence of a buffer solution.

The reactions were followed by measuring the changes in the percent transmittances of the mixed solutions of the lead(II)-EDTA, -EDTA·OH, -CyDTA, and -DTPA complexes at maximum absorption wavelengths[3] of 240, 240, 225, and 250 nm respectively. The reacted amount of PbX_t with In(III), x, in the molar concentration for the initial reaction time, t (min), can be expressed as follows:

$$x = \frac{a\cdot\varepsilon_{PbX_t} + b\cdot\varepsilon_{In} + c\cdot\varepsilon_{Pb} - D}{(\varepsilon_{PbX_t} - \varepsilon_{Pb}) - (\varepsilon_{InX_t} - \varepsilon_{In})}$$

where a, b, c are the initial concentrations of the lead complexes PbX_t, the In(III) ions, and Pb^{2+} respectively, and where ε_{PbX_t}, ε_{Pb}, ε_{InX_t}, and ε_{In} are the molar extinction coefficients for PbX_t, Pb^{2+}, all the species of the indium(III) complexes, InX_t, and the In(III) ions, again respectively, at the maximum absorption wavelengths of the lead complexes, and where D refers to the measured absorbance of the mixed solution.

Results and Discussion

Reaction Orders. The reaction orders with respect to the lead complexes and the indium(III) ions were examined by changing the concentration of the complexes from 2.0×10^{-6} to 9.0×10^{-6} M and that of the indium ions from 2.0×10^{-6} to 1.1×10^{-5} M in the presence of excessive lead ions at a constant pH. The reactions were found to be first-order in both $[PbX_t]$ and [In(III)].

Effects of an Excess of Lead(II) Ions. Using the Bydalek and Margerum method,[4] the effects of excessive lead ions on the rates were investigated. The rates for all the systems decreased with an increase in the concentration of added lead ions, as is shown in Fig. 1.

pH Dependences. The effects of the pH on the initial rates are shown in Fig. 2. The rates were too fast and too slow to be measured below and above the pH ranges from 2.6 to 4.1, from 3.2 to 4.3, from 2.6 to 3.6, and from 1.8 to 2.3 for the EDTA, EDTA·OH, CyDTA, and DTPA systems respectively. The slopes suggest that the rate equations involve the terms of $1/[H^+]$ and $[H^+]$ for the EDTA and EDTA·OH systems, $[H^+]$ for the CyDTA system, and $1/[H^+]$ for the DTPA system.

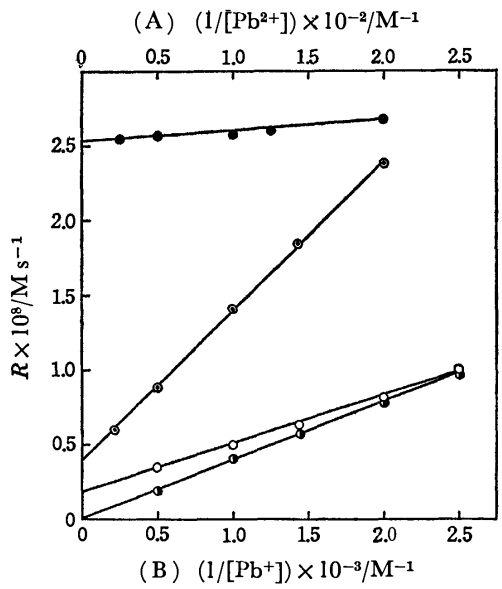

Fig. 1. Effect of the concentration of Pb^{2+} on the rate.
●: DTPA, pH 2.08, scale A; ⊙: EDTA·OH, pH 2.92, scale B; ○: EDTA, pH 2.64, scale B; ◑: CyDTA, pH 2.62, scale B; $[PbX_t]=[In(III)]=5.0\times10^{-6}$ M.

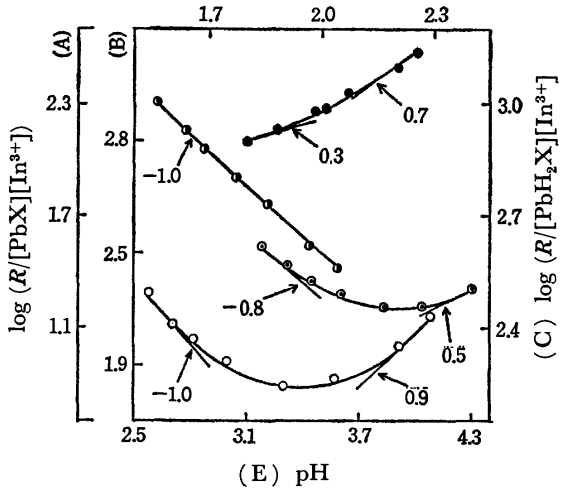

Fig. 2. pH Dependence on the rate R.

		$[Pb^{2+}]$(M)	
●:	DTPA	8.0×10^{-3}	C, D
◑:	CyDTA	1.0×10^{-3}	A, E
⊙:	EDTA·OH	1.0×10^{-3}	B, E
○:	EDTA	2.0×10^{-3}	B, E

$[PbX_t]=[In(III)]=5.0\times10^{-6}$ M.

Initial Rate Equations. In order to obtain the rate equations, the initial rates were measured by changing the pH in the presence of a large excess of lead(II) ions of 1.0×10^{-3} M and 2.0×10^{-3} M for the EDTA and EDTA·OH systems, 1.0×10^{-3} M for the CyDTA system, and 8.0×10^{-3} M and 4.0×10^{-2} M for the DTPA system. The concentrations of In^{3+}, PbX, and PbH_2X were calculated from the total concentrations of In(III) and PbX_t by use of the following equations: $[In^{3+}]=[In(III)]/(1+K_h/[H^+])$, $[PbX]=[PbX_t]/(1+K_H[Pb^{2+}])$, and $[PbH_2X]=[PbX_t]/(1+1/K_{2H}[H^+])$ respectively, and the values of $K_h=10^{-3.70}$M,[5] $K_H=66.1$,* 0, and 77.1 M^{-1} for EDTA, EDTA·OH, and CyDTA,[3] again respectively, and $K_{2H}=3.87\times10^4$ M^{-1} for DTPA.[3] The results are shown in Figs. 3, 4, and 5, and in Table 1. From the results and a consideration of the reaction orders and the effects of an excess of lead(II) ions and the pH dependence mentioned above, the initial rate equations can be

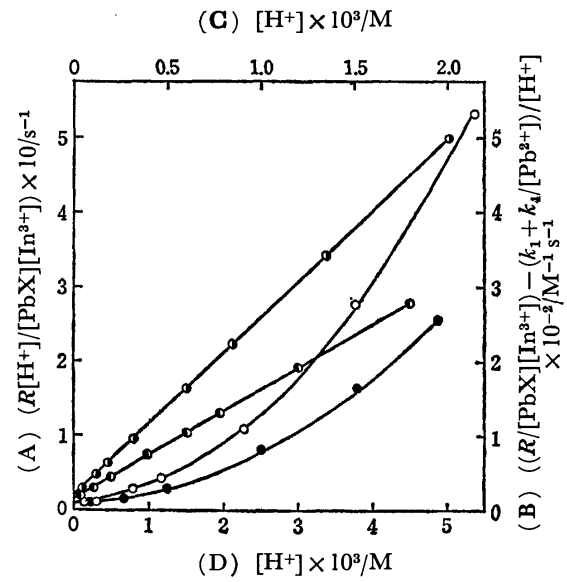

Fig. 3. The rate const for the reaction of the EDTA system.

	$[Pb^{2+}]$ (M)	
○:	1.0×10^{-3}	A, C
●:	2.0×10^{-3}	A, C
◑:	1.0×10^{-3}	B, D
◐:	2.0×10^{-3}	B, D

$[PbX_t]=[In(III)]=5.0\times10^{-6}$ M.

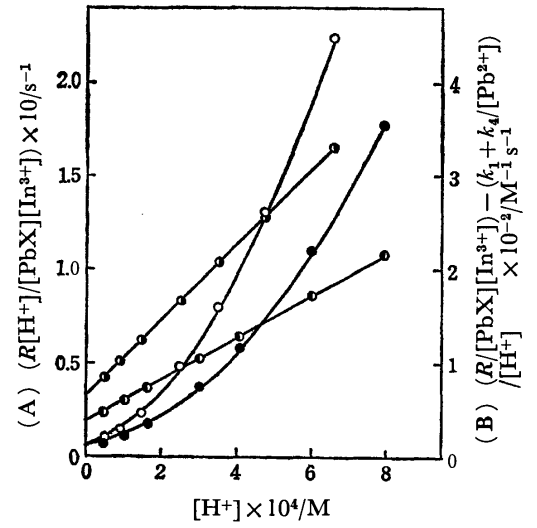

Fig. 4. The rate constants for the reaction of the EDTA·OH.

	$[Pb^{2+}]$ (M)	
○:	1.0×10^{-3}	A
●:	2.0×10^{-3}	A
◑:	1.0×10^{-3}	B
◐:	2.0×10^{-3}	B

$[PbXt]=[In(III)]=5.0\times10^{-6}$ M.

* Unpublised data.

Table 1. Rate constants

	EDTA	EDTA·OH	CyDTA	DTPA
k_1 (s^{-1})	1.0×10^{-2}	6.0×10^{-3}		
k_2 ($M^{-1}s^{-1}$)	1.2×10	1.0×10		
k_3 ($M^{-2}s^{-1}$)	1.0×10^{4}	4.3×10^{4}		k_3' 4.9 (s^{-1})
k_4 ($M\,s^{-1}$)	$\leq10^{-7}$	$\leq10^{-7}$	$\leq10^{-7}$	
k_5 (s^{-1})	8.0×10^{-3}	5.6×10^{-2}	5.0×10^{-3}	
k_6 ($M^{-1}s^{-1}$)	9.6×10	3.6×10^{2}	8.2×10	k_6' 1.5×10^{-3} ($M\,s^{-1}$)
k_7 ($M^{-1}s^{-1}$)				4.3×10^{2}
k_8 (s^{-1})				3.5×10^{-1}

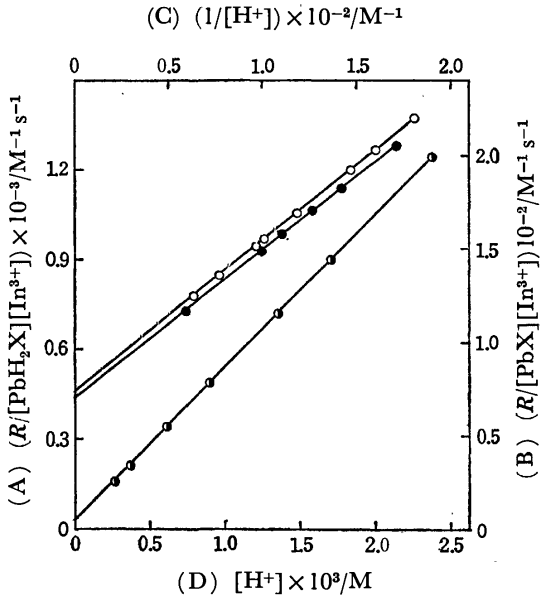

Fig. 5. The rate constants for the reactions of the DTPA and CyDTA systems.

		$[Pb^{2+}]$ (M)	
○:	DTPA	8.0×10^{-3}	A, C
●:	DTPA	4.0×10^{-2}	A, C
◑:	CyDTA	1.0×10^{-3}	B, D

$[PbX_t]=[In(III)]=5.0\times10^{-6}$ M.

expressed as follows:

For the EDTA and EDTA·OH systems:

$$R=\{(k_1+k_4/[Pb^{2+}])/[H^+]+(k_2+k_5/[Pb^{2+}])+(k_3+k_6/[Pb^{2+}])[H^+]\}[PbX][In^{3+}] \quad (1)$$

for the CyDTA system:

$$R=\{k_5+k_6[H^+]\}[PbX][In^{3+}]/[Pb^{2+}] \quad (2)$$

for the DTPA system:

$$R=\{(k'_3+k'_6/[Pb^{2+}])/[H^+]+(k_7+k_8/[Pb^{2+}])\}[PbH_2X][In^{3+}] \quad (3).$$

As has been concluded by previous workers,[1] such reactions proceed through simultaneous reaction paths of the electrophilic substitution reaction and the dissociation reaction of the metal complexes. From a consideration of the species of the indium(III) ions[5] and the lead and indium complexes in an equilibrium state, the following reaction paths from Eqs. (1a) to (6c) for the EDTA, EDTA·OH, and CyDTA systems, and from (2a) to (3b), (5a) to (6c), and (7a) to (8c) for the DTPA system may be considered:

$$PbX^{(n-2)-}+In^{3+}\xrightarrow{k_{1a}^+}InX^{(n-3)-}+Pb^{2+} \quad (1a)$$

$$PbX^{(n-2)-}+InOH^{2+}\xrightarrow{k_{1b}^+}In(OH)X^{(n-2)-}+Pb^{2+} \quad (1b)$$

$$PbHX^{(n-3)-}+In^{3+}\xrightarrow{k_{2a}^+}InHX^{(n-4)-}+Pb^{2+} \quad (2a)$$

$$PbHX^{(n-3)-}+InOH^{2+}\xrightarrow{k_{2b}^+}InX^{(n-3)-}+Pb^{2+}+H_2O \quad (2b)$$

$$PbH_2X^{(n-4)-}+In^{3+}\xrightarrow{k_{3a}^+}InH_2X^{(n-5)-}+Pb^{2+} \quad (3a)$$

$$PbH_2X^{(n-4)-}+InOH^{2+}\xrightarrow{k_{3b}^+}InHX^{(n-4)-}+Pb^{2+}+H_2O \quad (3b)$$

$$PbX^{(n-2)-}\underset{k_{4a}^-}{\overset{k_{4a}^+}{\rightleftharpoons}}Pb^{2+}+X^{n-} \quad (4a)$$

$$X^{n-}+In^{3+}\xrightarrow{k_{4b}^+}InX^{(n-3)-} \quad (4b)$$

$$X^{n-}+InOH^{2+}\xrightarrow{k_{4c}^+}In(OH)X^{(n-2)-} \quad (4c)$$

$$PbHX^{(n-3)-}\underset{k_{5a}^-}{\overset{k_{5a}^+}{\rightleftharpoons}}Pb^{2+}+HX^{(n-1)-} \quad (5a)$$

$$HX^{(n-1)-}+In^{3+}\xrightarrow{k_{5b}^+}InHX^{(n-4)-} \quad (5b)$$

$$HX^{(n-1)-}+InOH^{2+}\xrightarrow{k_{5c}^+}InX^{(n-3)-}+H_2O \quad (5c)$$

$$PbH_2X^{(n-4)-}\underset{k_{6a}^-}{\overset{k_{6a}^+}{\rightleftharpoons}}Pb^{2+}+H_2X^{(n-2)-} \quad (6a)$$

$$H_2X^{(n-2)-}+In^{3+}\xrightarrow{k_{6b}^+}InH_2X^{(n-5)-} \quad (6b)$$

$$H_2X^{(n-2)-}+InOH^{2+}\xrightarrow{k_{6c}^+}InHX^{(n-4)-}+H_2O \quad (6c)$$

$$PbH_2X+In^{3+}\xrightarrow{k_{7a}^+}InH_3X^{+}+Pb^{2+} \quad (7a)$$

$$PbH_3X+InOH^{2+}\xrightarrow{k_{7b}^+}InH_2X+Pb^{2+}+H_2O \quad (7b)$$

$$PbH_3X\underset{k_{8a}^-}{\overset{k_{8a}^+}{\rightleftharpoons}}Pb^{2+}+H_2X^{2-} \quad (8a)$$

$$H_3X^{2-}+In^{3+}\xrightarrow{k_{8b}^+}InH_3X^{+} \quad (8b)$$

$$H_3X^{2-}+InOH^{2+}\xrightarrow{k_{8c}^+}InH_2X+H_2O \quad (8c)$$

where X^{n-} denotes the polyamine-*N*-polyacetate anion.

According to Margerum's method,[6] the application of a steady-state approximation to $[X^{n-}]$ gives:

$$[X^{n-}]=\frac{k_{4a}^+[PbX]}{k_{4a}^-[Pb^{2+}]+k_{4b}^+[In^{3+}]+k_{4c}^+[InOH^{2+}]}.$$

From a consideration of the rate constants[6-10] for the exchange of water molecules from the first coordination spheres of metal ions and the experimental conditions,

the relation of $k_{4a}\cdot[Pb^{2+}] \gg k_{4b}\cdot[In^{3+}]+k_{4c}\cdot[InOH^{2+}]$ holds. Therefore, the above equation can be transformed to:

$$[X^{n-}] = (k_{4a}\cdot/k_{4a}\text{-})[PbX]/[Pb^{2+}].$$

Since the overall rate, R, is considered to be the sum of the rates of the individual reactions, the initial rate equations are derived as follows:

$$\begin{aligned}R &= k_{1a}\cdot[PbX][In^{3+}] + k_{1b}\cdot[PbX][InOH^{2+}] \\ &\quad + k_{2a}\cdot[PbHX][In^{3+}] + k_{2b}\cdot[PbHX][InOH^{2}] \\ &\quad + k_{3a}\cdot[PbH_2X][In^{3+}] + k_{3b}\cdot[PbH_2X][InOH^{2+}] \\ &\quad + k_{4b}\cdot\cdot k_{4a}\cdot[PbX][In^{3+}]/k_{4a}\text{-}[Pb^{2+}] \\ &\quad + k_{4c}\cdot\cdot k_{4a}\cdot[PbX][InOH^{2+}]/k_{4a}\text{-}[Pb^{2+}] \\ &\quad + k_{5b}\cdot\cdot k_{5a}\cdot[PbHX][In^{3+}]/k_{5a}\text{-}[Pb^{2+}] \\ &\quad + k_{5c}\cdot\cdot k_{5a}\cdot[PbHX][InOH^{2+}]/k_{5a}\text{-}[Pb^{2+}] \\ &\quad + k_{6c}\cdot\cdot k_{6a}\cdot[PbH_2X][In^{3+}]/k_{6a}\text{-}[Pb^{2+}] \\ &\quad + k_{6c}\cdot\cdot k_{6a}\cdot[PbH_2X][InOH^{2+}]/k_{6a}\text{-}[Pb^{2+}] \\ &= \{(k_1+k_4/[Pb^{2+}]/[H^+]+(k_2+k_5/[Pb^{2+}]) \\ &\quad +(k_3+k_6/[Pb^{2+}])[H^+] \\ &\quad +(k_3{*}+k_6{*}/[Pb^{2+}])[H^+]^2\}[PbX][In^{3+}]\end{aligned}$$

where

$$k_1 = k_{1b}\cdot\cdot K_h,\ k_2 = k_{1a}\cdot + k_{2b}\cdot\cdot K_H\cdot K_h$$

$$k_3 = k_{2a}\cdot\cdot K_H + k_{3b}\cdot\cdot K_{2H}\cdot K_h,\ k_4 = k_{4c}\cdot\cdot k_{4a}\cdot\cdot K_h/k_{4a}\text{-}$$

$$k_5 = k_{4b}\cdot\cdot k_{4a}\cdot/k_{4a}\text{-} + k_{5c}\cdot\cdot k_{5a}\cdot\cdot K_H\cdot K_h/k_{5a}\text{-}$$

$$k_6 = k_{5b}\cdot\cdot k_{5a}\cdot\cdot K_H/k_{5a}\text{-} + k_{6c}\cdot\cdot k_{6a}\cdot\cdot K_H\cdot K_{2H}\cdot K_h/k_{6a}\text{-}$$

$$k_3{*} = k_{3a}\cdot\cdot K_{2H}\cdot K_H,\ k_6{*} = k_{6b}\cdot\cdot k_{6a}\cdot\cdot K_H\cdot K_{2H}/k_{6a}\text{-}$$

$$K_h = [InOH^{2+}][H^+]/[In^{3+}],\ K_H = [PbHX]/[PbX][H^+]$$

$$K_{2H} = [PbH_2X]/[PbHX][H^+].$$

Neglecting the term of $[H^+]^2$, since it is not included in the above equations, Rate Equation (1) can be derived for the EDTA and EDTA·OH systems. For the CyDTA system, furthermore, considering that the plot of the rate, R, *vs.* $1/[Pb^{2+}]$ gives a straight line which passes through the point of origin of the coordinates, as may be seen in Fig. 1, and considering that the term of $1/[H^+]$ is not included, as has been mentioned above, Rate Equation (2) is obtained. In the same way, the rate equation for the DTPA system can be deduced as Equation (3), where $K_{3H}=[PbH_3X]/[PbH_2X][H^+]$

$$k_3' = k_{2a}\cdot/K_{2H} + k_{3b}\cdot\cdot K_h,$$

$$k_6' = k_{5b}\cdot\cdot k_{5a}\cdot/k_{5a}\text{-}\cdot\cdot K_{2H} + k_{6c}\cdot\cdot K_{6a}\cdot\cdot K_h/k_{6a}\text{-}$$

$$k_7 = k_{3a}\cdot + k_{7b}\cdot\cdot K_{3H}\cdot K_h,$$

$$k_8 = k_{6b}\cdot\cdot k_{6a}\cdot/k_{6a}\text{-} + k_{8c}\cdot\cdot k_{8a}\cdot\cdot K_{3H}\cdot K_h/k_{8a}\text{-}.$$

Reaction Mechanisms. The contribution of each reaction path to the overall rate of the reaction was estimated, the results are shown in Fig. 6, where the numbers of the curves, I, II, III, V, VI, VII, and VIII, denote Reaction Paths (1b), (1a)+(2b), (2a)+(3b), (4b)+(5c), (5b)+(6c), (3a)+(7b), and (6b)+(8c) respectively. For the EDTA, EDTA·OH, and DTPA systems the reactions proceed through the paths forming binuclear intermediate complexes, PbX_tIn, and the dissociative paths. For all the systems, the contribution of the dissociative path of PbX without acid is not found, while those of the other paths change with

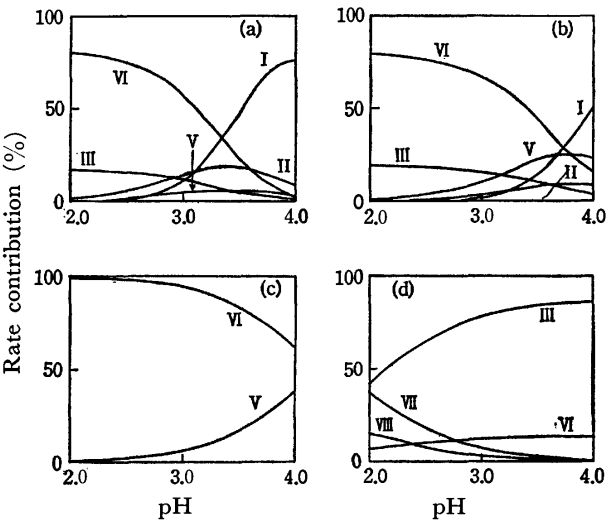

Fig. 6. The rate contribution of each path to the reaction rate.
(a): EDTA, (b): EDTA·OH, (c): CyDTA, (d): DTPA, $[Pb^{2+}]=2.0\times10^{-3}$ M
Number of curves, I, II, III, VI, VII, and VIII denotes reaction path (1b), (1a)+(2b), (2a)+(3b), (4b)+(5c), (5b)+(6c), (3a)+(7b), and (6b)+(8c), respectively.

the pH variation. Since the dissociation of the protonated lead complexes is rapid, the contributions of Paths (5b) and (6c) are predominant in the lower pH range for the EDTA and EDTA·OH systems, but the contribution decreases, and that of Path (1b) increases, with an increase in the pH, as the fractions of PbHX and PbH_2X decrease and those of PbX and $InOH^{2+}$ increase. For the CyDTA system only the contribution of the dissociative path is found, because the formation of a binuclear intermediate becomes difficult as a result of the steric hindrance of the cyclohexane ring, as Margerum and his co-workers have suggested in their study.[6] For the DTPA system the contributions of Paths (2a) and (3b) become predominant with an increase in the pH, since it is easier for the DTPA complex containing free coordinating groups to form a binuclear intermediate than for the complexes of the other ligands. From a consideration of the effect of the concentration of the lead ions, it is found that, in the dissociative paths, the rapid dissociative equilibria precede the formation of the indium complexes, as may be seen in the substitution reaction[11] of the lead(II)–EDTA complex with copper(II), for the systems other than the CyDTA system the contribution of the path forming a binuclear intermediate increases with an increase in the concentration of the lead(II) ions.

In order to determine the contribution of each path involving $InOH^{2+}$ to the rate of the formation of the indium complex through the dissociative step, the rate constants for the formation of InX, InHX, and InH_2X, k_5 and k_6 in Eqs. (1) and (2) for the EDTA, EDTA·OH, and CyDTA complexes, k'_6 and k_8 in Eq. (3) for the DTPA complexes, are rewritten as follows:

$$k_5 = k_{4b}\cdot/K_{PbX} + k_{5c}\cdot\cdot K_h/K_{PbX}\cdot K_{an} \qquad (4')$$

$$k_6 = k_{5b}\cdot/K_{PbX}\cdot K_{an} + k_{6c}\cdot\cdot K_h/K_{PbX}\cdot K_{an}\cdot K_{a(n-1)} \qquad (5')$$

for the EDTA, EDTA·OH and CyDTA systems and:

$$k_6' = k_{5b'}/K_{PbHX}\cdot K_{2H} + k_{6c'}\cdot K_h/K_{PbH_2X} \quad (6')$$

$$k_8 = k_{6b'}/K_{PbH_2X} + k_{8c'}\cdot K_h/K_{PbH_2X}\cdot K_{a3} \quad (7')$$

for the DTPA system, where K_{an}, K_{PbX}, K_{PbHX}, and K_{PbH_2X} represent the acid dissociation constants of the ligands and the stability constants of the lead complexes respectively. By a comparison of the values of the first terms and those of the second terms in Eqs. (4'), (5'), (6'), and (7'), using the values of K_h[5], K_{an},[12-15] K_{PbX},[12)16)] K_{PbHX},[17)] and K_{PbH_2X}[17)] obtained by the authors, and the products of the rate constants for the substitution of water molecules from the first coordination spheres of the In^{3+} and $InOH^{2+}$ ions and of the association constants[18)] of the ion-pairs according to Eigen,[19)] the first terms were found to be negligibly small. Therefore, the above equations are expressed as:

$$k_5 = k_{5c'}\cdot K_h/K_{PbX}\cdot K_{an} \quad (4)$$

$$k_6 = k_{6c'}\cdot K_h/K_{PbX}\cdot K_{an}\cdot K_{a(n-1)} \quad (5)$$

for the EDTA, EDTA·OH, and CyDTA systems, and as:

$$k_6 = k_{6c'}\cdot K_h/K_{PbH_2X} \quad (6)$$

$$k_8 = k_{8c'}\cdot K_h/K_{PbH_2X}\cdot K_{a3} \quad (7)$$

for the DTPA system.

As an example, the rate constants for the formation of the InHX of EDTA and CyDTA, and the InH_2X of DTPA and the InHX of EDTA·OH from $InOH^{2+}$ were calculated by means of Eqs. (5) and (7) to be 2.0×10^7, 2.9×10^7, 3.0×10^7, and 4.9×10^6 M^{-1} s^{-1} respectively. The rate constants for EDTA, CyDTA, DTPA, and EDTA·OH were in good agreement with the values of 2.5×10^7 and 5.0×10^6 M^{-1} s^{-1} of the complexes of $InOH^{2+}$ with SO_4^{2-} and of $InOH^{2+}$ with the semixylenol orange anion H_3SXO^-, which have the same charges as H_2X^{2-}, H_3X^{2-}, and H_2X^- respectively. This shows that the rate equations from (1) to (3) and the rate constants and the reaction mechanisms are suitable.

In addition, the reaction rate of indium(III) is 160 times faster than that of gallium(III) for the CyDTA system at pH 2.0. This may be attributed to the difference in the rate constants with regard to the substitution of the water molecules of the $InOH^{2+}$ and $GaOH^{2+}$ ions resulting from the difference in the effective nuclear charge.

The authors wish to thank Professor D.W. Margerum of Purdue University, U.S.A., for his useful discussions.

References

1) T. Takahashi, T. Koiso, and N. Tanaka, *Nippon Kagaku Zasshi*, **1973**, 64.
2) T. Nozaki and K. Kasuga, *ibid.*, **1973**, 2117.
3) T. Nozaki, K. Koshiba, and Y. Ono, *ibid.*, **90**, 1147 (1969).
4) T. J. Bydalek and D. W. Margerum, *J. Amer. Chem. Soc.*, **83**, 4326 (1961).
5) E. M. Hattox and T. DeVries, *ibid.*, **58**, 2128 (1936).
6) D. W. Margerum, P. J. Menardi, and D. L. Janes, *Inorg. Chem.*, **6**, 283 (1967).
7) M. Eigen and E. M. Eyring, *ibid.*, **2**, 636 (1963).
8) M. Eigen, *Pure Appl. Chem.*, **6**, 97 (1963).
9) J. Miceli and J. Stuehr, *J. Amer. Chem. Soc.*, **90**, 6967 (1968).
10) Y. Kawai, T. Takahashi, K. Hayashi, T. Imamura, H. Nakayama, and M. Fujimoto, This Bulletin, **45**, 1417 (1972).
11) N. Tanaka, K. Kato, and R. Tamamushi, *ibid.*, **31**, 238 (1958).
12) G. Schwarzenbach, R. Gut, and G. Anderegg, *Helv. Chim. Acta*, **37**, 937 (1954).
13) S. Chaderek and A. E. Martell, *J. Amer. Chem. Soc.*, **77**, 1477 (1955).
14) G. Schwarzenbach and H. Ackermann, *Helv. Chim. Acta*, **32**, 1682 (1949).
15) E. J. Durham and D. P. Ryskiewick, *J. Amer. Chem. Soc.*, **80**, 4813 (1958).
16) J. H. Holloway and C. N. Reilly, *Anal. Chem.*, **32**, 249 (1960).
17) log $K_{PbHX}=12.5$, log $K_{PbH_2X}=8.5$.
18) F. Basolo and R. G. Pearson, "Mechanism of Inorganic Reactions", J. Willey & Sons, Inc., N. Y. (1958), p. 34.
19) M. Eigen and K. Tamm, *Z. Elektrochem.*, **66**, 107 (1962).

Composition of Single Crystals of Chromium Chalcogenide Spinels Grown by Chemical Vapor Transport

Kohei AMETANI

RCA Research Laboratories, Inc., Zushi-machi, Machida-shi, Tokyo 194-02

(Received May 15, 1975)

Compositional analyses using atomic absorption spectrophotometry were carried out on the vapor-phase grown single crystals of copper-based spinels with the nominal formulas such as $CuCr_2S_3Cl$, $Cu_{1-x}Fe_xCr_2S_4$ ($x \leq 1$), $Cu_{0.5}In_{0.5}Cr_2S_4$, $CuCr_2Se_3Cl$, and $CuCr_2Se_3Br$, and the cadmium-based spinels of $CdCr_2S_4$ and $CdCr_2Se_4$, including crystals doped with indium, silver, and copper. The grown crystal usually had a composition different from the nominal formula and a tetrahedral-site deficiency of the copper-based spinels is reported for the first time. All crystals of $Cu_{1-x}Fe_xCr_2S_4$ and $Cu_{0.5}In_{0.5}Cr_2S_4$ were contaminated with a considerable amount of chlorine and some of the crystals had a substantial cation deficiency on the tetrahedral sites; the cation deficiency increases with increasing copper or chlorine content. For the $CuCr_2S_3Cl$ and $CuCr_2Se_3Br$ crystals, a large copper deficiency was also found while the halogen content was close to that expected for the nominal compositions, or somewhat higher. Of all the copper-based spinels, the least tetrahedral-site deficiency was observed in the $CuCr_2Se_3Cl$ crystals, but the chlorine content was much less than the stoichiometric content. The cadmium-based spinels usually satisfied the stoichiometric formula $CdCr_2S_4$ or $CdCr_2Se_4$.

The magnetic, electrical, and optical properties of chromium chalcogenide spinels have been extensively investigated. In spinels with the general formula ACr_2X_4, the A sites are usually filled with bivalent metal ions (M^{2+}) or a mixture of uni- and trivalent cations ($M^{+}_{0.5}M^{3+}_{0.5}$–). The X sites are occupied by a single chalcogen anion (–X^{2-}_4) or a combination of chalcogen with halogen anions (–$X^{2-}_3Y^{-}$; Y=halogen); in the latter case, the effective cation valence of the A sites is reduced to univalent. Single crystals are usually grown by the chemical vapor-transport method, using a halogen as a transport agent.[1-3] The crystals obtained are, at most, 3—4 mm on edge and weigh only several mg. A number of workers have spent a lot of time and effort to grow large single crystal using the chemical vapor-transport method and other methods, but the crystals obtained are size limited. Therefore, some of published papers reported the physical properties of the crystals without chemical analysis, or only a partial chemical analysis of impurities[4-11] and some of the main components[10-16] of the crystals has been made. Very little has been published about the compositional analysis of all the major constituents.[9,17] Most of the published papers described only the results of the analysis without details of the procedures for the analysis. In the present paper, we describe a method of chemical analysis to determine the composition of some single crystals of chromium chalcogenide spinels using AAS (Atomic Absorption Spectrophotometry) technique and present a serious problem regarding the composition of various samples; the grown crystals usually had compositions different from their nominal formula. The AAS technique provides a high sensitivity and selectivity so that the sample weight can be reduced to a minimum amount, and the major as well as minor constituents or impurities can be determined continuously or simultaneously from the same small sample. The use of the same sample would be recommended to obtain consistent analytical data. The present analytical method was developed from our previously reported procedures for chlorine[10] and sulfur.[15] Using 10 mg samples, the metallic elements were determined directly from their atomic absorptions. Chlorine and sulfur were determined indirectly from the silver and barium atomic absorptions after being captured in the form of silver chloride[10] and barium sulfate,[15] respectively.

The materials to be analyzed were the copper-based spinels with nominal formulas such as $CuCr_2S_3Cl$, $Cu_{1-x}Fe_xCr_2S_4(x \leq 1)$, $Cu_{0.5}In_{0.5}Cr_2S_4$, $CuCr_2Se_3Cl$, and $CuCr_2Se_3Br$, and the cadmium-based spinels of $CdCr_2S_4$ and $CdCr_2Se_4$, including crystals doped with indium, silver, and copper. Of these materials, the chlorine content for some of the copper-based and cadmium-based spinels,[10,11] the sulfur content of $CuCr_2S_3Cl$ and $CdCr_2S_4$ crystals,[15] and the content and site preference of dopants in $CdCr_2X_4$ crystals,[11] were reported previously. The single crystals, except for the halochalcogenides, were grown by the closed-tube vapor transport, where the starting materials with the above-described compositions were mixed with a solid transport agent $CrCl_3$, usually in ratio of 10 : 1. The halochalcogenide crystals were grown by transport either with an intrinsic copper halide present in the starting materials or an extra copper halide added as the halogen source. The details of the growth conditions can be found elsewhere.[1,11,18-20] All the crystals were prepared in these laboratories and the physical properties of some of the crystals have been reported.[18-23]

Experimental

Apparatus. Atomic absorption measurements were made in an air–acetylene flame using a Hitachi model 208 Atomic Absorption Spectrophotometer and Hitachi hollow-cathode lamps HLA-3, except the lamp used for the selenium measurement, which was obtained from Westinghouse. The analytical lines used were Cr 357.9 nm, Fe 372.0 nm, Cu 324.7 nm, Se 204.0 nm, Ag 328.1 nm, Cd 228.8 nm, In 303.9 nm, and Ba 553.5 nm.

Standard Solutions. (1) Solutions of metal chlorides: The chromium and iron solutions were prepared by dissolving metals (99.9%) in hydrochloric acid and diluting with deionized water. The copper, cadmium, and indium solutions were prepared by dissolving metals (99.9—99.99%) in nitric acid, removing the excess nitric acid by evaporation with hydrochloric acid, and then dissolving the residue in de-

Table 1. Confirmation of procedures using mixtures of standard solutions

Solution[a]	Analyte, mg									
	Cu		Cd		Cr		S		Cl	
	added	obsd	added	obsd	added	obsd	added	obsd	added	obsd
1	2.00	2.00	—		3.50	3.48	3.00	3.01	—	
2	2.00	2.00	—		3.50	3.48	3.50	3.52	—	
3	2.00	2.00	—		3.50	3.49	4.00	3.95	—	
4	—		3.00	3.01	3.00	2.98	4.00	3.95	—	
5	2.00	1.98	—		3.50	3.53	—		1.50	1.50
6	2.00	1.98	—		3.50	3.53	—		1.00	0.99
7	2.00	1.98	—		3.50	3.53	—		0.500	0.492
8	0.150	0.150	3.00	2.96	3.00	2.99	—		0.100	0.102
9	0.100	0.100	3.00	2.96	3.00	2.99	—		0.050	0.052
10	0.050	0.051	3.00	2.99	3.00	3.03	—		0.025	0.026
11	—		3.00	2.99	3.00	3.02	—		0.010	0.010

a) Solutions (5—7) and (8—11) also contained 3.50 and 4.00 mg of S, respectively, as Na_2SO_4.

ionized water. All the solutions were stocked as 0.1 M hydrochloric acid solutions with a concentration of 1 mg analyte/ml. (2) Solutions of metal nitrates: The chromium and iron solutions were prepared by dissolving the respective nitrates in deionized water and then standardizing by chelatometry using EDTA. The copper, cadmium, and indium solutions were prepared by dissolving metals (99.9—99.99%) in nitric acid and diluting with deionized water. All the solutions were stocked as 0.1 M nitric acid solutions with a concentration of 1 mg analyte/ml. (3) Other solutions: The selenium solution was prepared by dissolving elemental selenium (99.9%) in nitric acid and diluting with deionized water. The stock solution had a concentration of 1 mg Se/ml with 0.1 M nitric acid. The silver solutions (1, 0.5, or 0.25 mg Ag/ml) were prepared by dissolving silver nitrate (dried at 110 °C) in a minimum amount of deionized water, and then diluting with concentrated nitric acid. The silver solutions were used to dissolve samples as described below. The solutions containing 1 mg Ag/ml were also prepared from silver nitrate and stocked as 0.1 M nitric acid solutions. The barium solution (5 mg Ba/ml) was prepared by dissolving barium chloride dihydrate in deionized water and standardizing by chelatometry using EDTA. The sulfur and chlorine solutions (1 mg analyte/ml) were prepared by dissolving sodium sulfate and sodium chloride (dried at 110 °C), respectively, in deionized water. Reagents used were of analytical reagent grade.

Procedure (A). Pulverized crystals weighing 10 mg (usually 5—6 crystals) were dissolved in nitric acid containing excess silver ions of a known quantity and chlorine was simultaneously precipitated as silver chloride. For a sample containing several hundred μg to about 1 mg of chlorine, 5 ml of nitric acid containing 1 mg Ag/ml was used, and the solution was then diluted to about 50 ml. However, if the expected chlorine content in the sample was less than 100 μg, 2 ml of nitric acid containing 0.5 or 0.25 mg Ag/ml was used and the solution diluted to about 20 ml. The solution was aged for 30 min over a hot water bath. After the solution was cooled in ice water, the precipitated silver chloride was filtered and washed with six 5-ml portions of cold nitric acid (1 : 50), and dissolved in an aqueous ammonia solution. Both the ammoniacal solution and the filtrate were diluted to an appropriate concentration of analytes and the atomic absorptions measured. For the measurements, the concentrations of nitric acid and ammonia were adjusted to 0.05—0.3 M and 3%, respectively, because the interference effects of coexisting foreign elements at these concentrations were found to be negligible.[10,11] The chlorine content, except for the silver-doped $CdCr_2S_4$ and $CdCr_2Se_4$ crystals, was determined indirectly from the silver content, usually, in both the ammoniacal solution and the filtrate. For the silver-doped crystals, chlorine was determined from the silver content in the ammoniacal solution. Metallic elements, such as chromium, iron, copper, cadmium, and indium, and also selenium, were determined from the filtrate. The silver content in the silver-doped crystals was determined by comparing the total amount of silver in both the filtrate and the ammoniacal solution with the amount of silver contained in the nitric acid solution used to dissolve the crystals. The results obtained were corrected by the blank test in all cases.

Procedure (B). This procedure is applicable for the sulfides only, and not for the selenides. Pulverized crystals weighing 10 mg were dissolved in 2 ml of concentrated nitric acid containing bromine in order to oxidize the sulfurs into sulfate ions. The sample solution was evaporated nearly to dryness. After removal of the nitric acid by evaporation with hydrochloric acid, the residue was dissolved in deionized water. The sample solution was diluted to about 20 ml and warmed to about 80 °C. If iron was present in the solution, the iron(III) ions were reduced to iron(II) ions by adding a minimum amount of ascorbic acid. The acidity of the solution was adjusted to 0.05 M hydrochloric acid, and 5 ml of the standard barium solution (5 mg Ba/ml) was slowly added to the solution. The precipitated barium sulfate was allowed to settle for 1 hr over a hot water bath. After aging more than 20 hr, the precipitate was filtered and washed with six 5-ml portions of boiling water. The filtrate was diluted to an appropriate concentration of analytes and the atomic absorptions measured. For the measurements, the concentration of hydrochloric acid was adjusted to 0.05—0.2 M because the interference effects of coexisting foreign elements are negligible at these concentrations.[11,15] Metallic elements, except for silver, were determined directly by their atomic absorptions, and sulfur, indirectly by the atomic absorption of an excess of barium in the filtrate. Silver was not determined by this procedure.

The procedures (A) and (B) were confirmed by using mixtures of the standard solutions. Table 1 shows typical results for procedures (A) and (B). The tabulated values

Table 2. Results of single-crystal analysis for copper-based chromium spinels

Sample, nominal composition	Analyte, mole ratio								Lattice constant, a_0(Å)[d]
	Cu	Fe	In	Cr	X[a]	Y[a]	Cr/A[b]	M/(X+Y)[c]	
$CuCr_2S_3Cl$ (1)	0.87_3	—	—	2.04_3	2.97_5	1.10_6	2.33_8	0.71_4	9.902
$CuCr_2S_3Cl$ (2)	0.86_4	—	—	2.04_8	2.94_2	1.14_4	2.37_1	0.71_2	9.906
$CuCr_2S_3Cl$ (3)	0.85_2	—	—	1.99_6	2.78_5	1.18_6	2.34_1	0.71_7	9.907
$Cu_{0.8}Fe_{0.2}Cr_2S_4$	0.70_3	0.05_6		1.93_8	3.28_8	1.01_2	2.54_9	0.62_8	9.901
$Cu_{0.6}Fe_{0.4}Cr_2S_4$	0.81_3	0.07_3	—	2.01_1	3.34_1	0.76_0	2.26_9	0.70_6	9.880
$Cu_{0.4}Fe_{0.6}Cr_2S_4$	0.65_5	0.29_8	—	2.03_4	3.55_7	0.45_3	2.13_2	0.74_4	9.892
$Cu_{0.2}Fe_{0.8}Cr_2S_4$	0.32_0	0.69_5	—	2.04_5	3.70_2	0.23_5	2.01_2	0.77_7	9.936
$FeCr_2S_4$	—	0.96_8	—	2.01_1	3.95_2	0.06_6	2.07_6	0.74_1	10.083
$Cu_{0.5}In_{0.5}Cr_2S_4$ (1)	0.52_2	—	0.45_8	1.91_4	4.01_9	0.08_4	1.95_0	0.70_3	10.057
$Cu_{0.5}In_{0.5}Cr_2S_4$ (2)	0.57_3	—	0.35_9	1.94_3	3.85_5	0.26_6	2.08_1	0.69_5	10.089
$Cu_{0.5}In_{0.5}Cr_2S_4$ (3)	0.59_3	—	0.31_4	1.99_4	3.87_1	0.22_5	2.19_7	0.70_3	10.016
$CuCr_2Se_3Cl$	0.97_6	—	—	2.01_6	3.68_7	0.31_9	2.06_5	0.74_7	—
$CuCr_2Se_3Br$[e]	0.77_8	—	—	1.99_9	3.19_4	1.02_7	2.56_9	0.65_8	—
$CuCr_2Se_3Br$[e]	0.82_3	—	—	1.99_7	3.14_0	1.03_6	2.42_5	0.67_5	—

a) "X" designates S or Se and "Y" designates Cl or Br. b) The ratio expected for the formula is 2 for each sample, where "A" is Cu, Fe, and/or In. c) "M" designates cationic elements (Cu, Fe, In, and Cr) and the expected value of the ratio is 0.75 for each sample. d) Average of at least five determinations with the standard deviation 0.003—0.005 Å. e) Both sets of crystals were grown in the same batch. The first set was analyzed by procedure (A) of the present work and the second set was analyzed by the alternative method.[29]

for chlorine are the average of values obtained from the filtrate and the ammoniacal solution. Most of the observed values are in agreement with the added amounts, within 1—2%.

Results and Discussion

The results of analyses are presented as mole ratios of the analytes, as calculated from the observed wt% values, in order to easily understand the chemical composition of the present materials. Most of the results for metallic elements are the average of values obtained by the procedures of both (A) and (B). Table 2 shows the results for the copper-based chromium chalcogenide spinels. Table 3 compares the compositions determined by chemical analysis with those estimated from lattice parameters for crystals of the system $Cu_{1-x}Fe_xCr_2S_4$ ($x \leq 1$). Table 4 gives the results for the cadmium-based spinels including crystals doped with indium, silver, and copper.

$CuCr_2S_3Cl$. Samples grown in three different batches were analyzed. As can be seen in Table 2, all the results indicate that the crystal did not have the stoichiometric formula $CuCr_2S_3Cl$; the chlorine content is much higher than the stoichiometric amount.[10] The cation-to-anion ratio, (Cu+Cr)/(S+Cl), also shows that the total amount of the anionic elements was higher and that of the cations was lower than the expected amount. This is due to an insufficient amount of copper as shown in Table 2. Therefore, it can be concluded that the crystal has a copper deficiency on the tetrahedral sites in the spinel structure and the formula is written as $Cu_{1-x}\square_xCr_2S_{4-y}Cl_y$, where $\square$ designates the copper deficiency. When the mole ratios in Table 2 are normalized by the value of 2 for chromium, the empirical formulas for these crystals can be expressed as follows;

sample (1) $Cu_{0.86}\square_{0.14}Cr_2S_{2.91}Cl_{1.08}$,

sample (2) $Cu_{0.84}\square_{0.16}Cr_2S_{2.87}Cl_{1.12}$,

sample (3) $Cu_{0.85}\square_{0.15}Cr_2S_{2.80}Cl_{1.19}$.

Actually, Wada[24] of these laboratories successfully prepared polycrystalline powders of the copper-deficient chlorosulfospinels, $Cu_{1-x}\square_xCr_2S_3Cl$ ($x \leq 0.3$), by firing mixtures of copper(I) chloride, copper(II) chloride, chromium metal, elemental sulfur at high temperatures. He found that compounds with $x=0.2$—0.3 were the most pure of all the compositions, whereas the stoichiometric compound ($x=0$) always had a minor second phase of hexagonal $CuCrS_2$ as determined by X-ray diffraction; the degree of contamination by the second phase increased with the decreasing x. Another example of such metal-deficiencies are the trivalent metal-based sulfospinels $M_{16/9}\square_{3/9}Cr_{8/9}S_4$ with M= Al or In.[25]

The lattice constants of these crystals range from 9.902 to 9.907 Å, as given in Table 2. These values are nearly the same as those for single crystals with the composition close to $CuCr_2S_3Cl$ reported by Sleight and Jarrett.[12] They used a chemical analysis to determine the composition of crystals, but did not give the data for elements other than chlorine nor did they present the details of their chemical analysis. Presumably the crystal composition is dependent on the growth conditions.

$Cu_{1-x}Fe_xCr_2S_4$. For the system, samples with the nominal composition $x=0.2$, 0.4, 0.6, 0.8, or 1.0 were analyzed. For all of the crystals analyzed, the copper content was higher and the iron content much lower than the nominal amount, especially for the lower values of x. Colorimetric methods[26] also showed similar results. It seems that copper is transported more preferentially than iron during the vapor transport reaction, while, in the case of the $Cd_{1-x}Fe_xCr_2S_4$

system ($0 \leq x \leq 1$),[16] iron is incorporated more readily than the nominal content in the vapor-phase grown crystals. As can be seen in Table 2, a deficiency in the tetrahedral-site was also found for the crystals. For crystals containing the higher amount of iron, however, the degree of this deficiency was small; both ratios of chromium-to-copper and iron, Cr/(Cu+Fe), and cation-to-anion, (Cu+Fe+Cr)/(S+Cl), are closer to the expected values than those of crystals with the lower amount of iron. On the other hand, when the copper content increases or the iron content decreases, the tetrahedral-site cation deficiency increases when chlorine is easily incorporated in the crystals (see results for the $Cu_{0.8}Fe_{0.2}Cr_2S_4$ and $Cu_{0.6}Fe_{0.4}Cr_2S_4$ crystals). The $FeCr_2S_4$ crystal even seems to have a small deficiency on the tetrahedral sites as shown in Table 2. A similar result was reported by Goldstein *et al.*,[9] where the $FeCr_2S_4$ crystal was grown by use of $HCl+Cl_2$ gas as the transport agent. They found about 1% deviation in the chromium-to-iron ratio, Cr/Fe, but our result was about 3.5%. The discrepancy between the two results may be related to a variation of the chlorine content in the crystal; the mole ratio of chlorine presented in Table 2 corresponds to 0.8 wt%, whereas Goldstein *et al.*[9] reported only 0.01 wt%.

Haacke and Beegle[27] prepared polycrystalline samples in the entire composition range of the system $Cu_{1-x}Fe_xCr_2S_4$ ($0 \leq x \leq 1$), and found that the curve of lattice parameters *vs.* composition obeys Vegard's law. They used Vegard's law to determine the copper and iron content in single crystals grown by chemical vapor transport using HCl gas as the transport agent; the reported compositions ranged from $Cu_{0.59}Fe_{0.41}Cr_2S_4$ to $FeCr_2S_4$. However, the present results suggest that Vegard's law seems to be unsuitable for the determination of the copper and iron content in vapor-phase grown crystals of this system because of the tetrahedral-site deficiency and the observed higher incorporation of chlorine, (as described previously), which, in turn, cause the compositional variation of components other than copper and iron.

Table 3 compares the compositions determined by Vegard's law and our chemical analysis using this AAS technique for crystals of the system $Cu_{1-x}Fe_xCr_2S_4$. The compositions determined by chemical analysis are normalized by the value of 2 for chromium while those by Vegard's law are determined by the lattice constants, 9.819 and 9.989 Å for polycrystalline $CuCr_2S_4$ and $FeCr_2S_4$,[13] respectively. As can be seen in Table 3, the iron content determined by Vegard's law is usually much higher, particularly for crystals with a lower iron content than that obtained by chemical analysis. Banus[13] also obtained similar results for single crystals of this system by determining the copper, iron, and chromium content, using chemical analysis of crystals grown by transport with $CrCl_3$ as the transport agent. He found that the lattice constants of single crystals are 0.005 to 0.025 Å higher than those of polycrystals, assuming that both polycrystalline and single-crystal samples have the same value of x. This tendency indicates that the iron content determined by Vegard's law is apparently higher than the actual content because the lattice constant of $FeCr_2S_4$ is larger than that of $CuCr_2S_4$. In addition, Vegard's law does not suggest anything about components other than copper and iron. Our results for the $Cu_{0.2}Fe_{0.8}Cr_2S_4$ crystal showed that the composition of crystals of this system comes closer to the general formula $Cu_{1-x}Fe_xCr_2S_4$ when the iron content increases and the chlorine content decreases.

Table 3. Comparison of compositions determined by Vegard's law and chemical analysis for single crystals of the system $Cu_{1-x}Fe_xCr_2S_4$

Sample, nominal composition	Determined composition	
	by Vegard's law	by chemical analysis
$Cu_{0.8}Fe_{0.2}Cr_2S_4$	$Cu_{0.52}Fe_{0.48}Cr_2S_4$	$Cu_{0.73}Fe_{0.06}Cr_2S_{3.39}Cl_{1.04}$
$Cu_{0.6}Fe_{0.4}Cr_2S_4$	$Cu_{0.64}Fe_{0.36}Cr_2S_4$	$Cu_{0.81}Fe_{0.07}Cr_2S_{3.32}Cl_{0.76}$
$Cu_{0.4}Fe_{0.6}Cr_2S_4$	$Cu_{0.57}Fe_{0.43}Cr_2S_4$	$Cu_{0.64}Fe_{0.29}Cr_2S_{3.50}Cl_{0.45}$
$Cu_{0.2}Fe_{0.8}Cr_2S_4$	$Cu_{0.31}Fe_{0.69}Cr_2S_4$	$Cu_{0.31}Fe_{0.70}Cr_2S_{3.62}Cl_{0.23}$
$FeCr_2S_4$	——	$Fe_{0.96}Cr_2S_{3.93}Cl_{0.07}$

The reason Vegard's law gives apparent higher values for iron is due to the incorporation of chlorine in the crystals. Incorporating chlorine in the system $Cu_{1-x}Fe_xCr_2S_4$ will result in a chemical reduction of cationic species and give an increase in effective cation size so that there is an increase in unit cell volume. This tendency occurs because the lattice constant of crystals for the system $Cu_{1-x}Fe_xCr_2S_4$ decreases upon annealing in a sulfur atmosphere,[13] where the relative sulfur and chlorine content increases and decreases, respectively. Therefore, the present $FeCr_2S_4$ crystal has a lattice constant (10.083 Å) higher than that of the polycrystalline sample (9.989 Å),[13] where the former contains a substantial amount of chlorine, while the latter is believed to be a chlorine-free sample.

$Cu_{0.5}In_{0.5}Cr_2S_4$. The results for samples grown in three different batches showed that the anionic element content is higher than the expected content, as shown by the ratio of (Cu+In+Cr)/(S+Cl) in Table 2. The chlorine content is small when the indium content is large and/or the copper content is small. The copper-to-indium ratio, Cu/In, always exceeds unity, indicating a higher preferential incorporation of copper, as compared to indium, in crystals. This is consistent with the previous result obtained by X-ray fluorescence spectroscopy.[14] The ratio of chromium-to-copper and indium, Cr/(Cu+In), is lower than the expected value of 2 for the crystal with the relatively higher content of indium (sample (1)) but the ratio is higher than 2 for other crystals with a lower indium content (samples (2) and (3)). This indicates that indium in sample (1) may substitute partially for chromium on the octahedral sites in addition to occupancy of tetrahedral sites, just as was found for $CdCr_2S_4$ crystals heavily doped with indium.[11] For samples (2) and (3) a tetrahedral-site deficiency, as described earlier for $CuCr_2S_3Cl$ and $Cu_{1-x}Fe_xCr_2S_4$ crystals, was found. Among these crystals, sample (1) has the copper-to-indium ratio (Cu/In) nearest to unity and the lowest chlorine content. Samples (2) and (3) have a composition relatively similar to each other but the lattice constants of the samples differ as

shown in Table 2; the values of 10.089 Å (sample (2)) and 10.016 Å (sample (3)) bracket the 10.057 Å of sample (1), while the lattice constant of the polycrystalline sample is reported to be 10.065 Å.[28]

$CuCr_2Se_3Cl$ and $CuCr_2Se_3Br$. The $CuCr_2Se_3Cl$ crystal shows a tendency to have a different composition than the $CuCr_2S_3Cl$ crystal. The chlorine content is much less than the stoichiometric content, as shown in Table 2. This may be due to the difference between the chalcogenide elements sulfur and selenium. A comparison of the ionic radii of these elements indicates that the sulfur ionic size (S^{2-}; 1.84 Å) is nearly the same as chlorine (Cl^-; 1.81 Å) while selenium (Se^{2-}; 1.91 Å) is somewhat larger. This large difference in ionic radii is responsible for the reduced incorporation of chlorine in the $CuCr_2S_3Cl$ crystal, while chlorine is more easily incorporated in the $CuCr_2S_3Cl$ crystal as described previously, because the sulfur- and chlorine-ion sizes are comparable. However, the ratios of chromium-to-copper, Cr/Cu, and cation-to-anion, (Cu+Cr)/(Se+Cl), are close to the expected values as shown in Table 2. The formula, normalized by the value of 2 for chromium, is $Cu_{0.97}Cr_2Se_{3.66}Cl_{0.32}$. Similar results for crystals grown in different batches were found, while Miyatani *et al.*[19] reported without chemical analysis that the composition of crystals always ranged from $CuCr_2Se_{3.6}Cl_{0.4}$ to $CuCr_2Se_{3.5}Cl_{0.5}$. They determined the composition by comparing the lattice constant (Vegard's law) and the magnetic property of single crystals with those of polycrystalline samples having a known composition.

In the case of the $CuCr_2Se_3Br$ crystal, the compositional problem is expected to be similar to that of the $CuCr_2S_3Cl$ crystal because for both crystals the ionic size of the chalcogen is nearly equal to that of the corresponding halogen (Br^-; 1.96 Å). Although the present method of chemical analysis was established for materials containing chlorine, the use of procedure (A) to analyze the $CuCr_2Se_3Br$ crystal seems reasonable because the solubility of silver bromide in aqueous media is much smaller than that of silver chloride. For the analysis, 10 mg of the sample was dissolved in 5 ml of nitric acid containing 1 mg Ag/ml. The results showed that the total amount of the anionic elements is higher, and that of the cations lower, than the expected amount. As in the case of the $CuCr_2S_3Cl$ crystal, this is due to the tetrahedral-site deficiency of copper. An alternative method[29] showed a similar result for a crystal grown in the same batch as shown in Table 2. For another crystal grown in a different batch, the composition was found to be $Cu_{0.80}Cr_{2.01}Se_{3.06}Br_{1.13}$ by the alternative method.

The present crystal is one of samples for the system $CuCr_2Se_{4-x}Br_x$ reported by Miyatani *et al.*[19] The alternative method was used to analyze their both polycrystalline and single-crystal samples at that time. They reported that the actual compositions of their polycrystalline samples are found to be the same as those intended within 1% by chemical analysis but did not give the data of chemical analysis for single crystals; the composition of single crystals was determined by comparing the lattice constant (Vegard's law) and the magnetic property (the Curie temperature) of single crystals with those of polycrystalline samples. They concluded as follows: (1) No excess-bromine compounds ($x>1$) can be synthesized. (2) The ionic configuration assumed is $Cu^{1+}_{1-x}Cu^{+}_{x}Cr^{3+}_{2}Se^{2-}_{4-x}Br^{-}_{x}$. (3) The physical properties of crystals can be explained in terms of the x-value dependence; for example, both the Curie temperature and electrical resistivity vary drastically over the small range $0.98 \leq x \leq 1.0$.

From the present results, however, it is revealed that the physical properties of crystals cannot be explained in terms of the compositional (x-value) dependence. Near $x=1$, they considered that the Cu^{2+} ions concentration is negligibly small but the present results indicated that the Cu^{2+} ions concentration is larger than that of Cu^+ ions. When the values in Table 2 (the first set) are normarized by the value of 2 for chromium, taking into account the electroneutrality of crystal, the present crystal can be expressed by the ionic configuration $Cu^{2+}_{0.63}Cu^{+}_{0.15}Cr^{3+}_{2}Se^{2-}_{3.19}Br^{-}_{1.03}$, while they regarded the crystal as one of samples with the composition close to $CuCr_2Se_3Br$ and the effective copper valence as monovalent. Moreover, their experiments to determine the composition are clearly found to be very careless because the composition of the crystal with the lattice constant 10.414 Å was reported to be $CuCr_2Se_{3.5}Br_{0.5}$; the lattice constant for the system $CuCr_2Se_{4-x}Br_x$ increased linearly from 10.325 to 10.405 Å as x increased from 0 to 1. Therefore, we can now understand that their conclusions are very suspicious and a complete analysis for the composition is necessary to interpret the physical properties of crystals.

$CdCr_2S_4$ and $CdCr_2Se_4$. We have already described the chlorine contamination,[10,11] and the actual content and site preference of dopants such as indium, silver, and copper for the $CdCr_2S_4$ and $CdCr_2Se_4$ crystals.[11] To provide a review of all the constituents, data for the minor elements are summarized with the major constituents in Table 4. All the crystals are contaminated with chlorine, but the chlorine content is much less than that of the copper-based spinels. The chlorine content increases in the following order; indium-doped, undoped, silver-doped, and copper-doped crystals. The content of dopants is usually less than the nominal content, especially, in $Cd_{0.95}Ag_{0.05}Cr_2S_4$ and $Cd_{0.9}Ag_{0.1}Cr_2S_4$ crystals. There seems to be a solubility limit for dopants in the single crystals.[30] The tetrahedral-site deficiency was not usually observed, although the undoped $CdCr_2Se_4$ and $Cd_{0.99}Ag_{0.01}Cr_2Se_4$ crystals had a somewhat lower value for cadmium in comparison with the chromium content. The stoichiometric formula $CdCr_2X_4$ is more closely satisfied for $CdCr_2S_4$ than for $CdCr_2Se_4$.

In summary, for the copper-based spinels, single crystals with the nominal formula $Cu_{1-x}Fe_xCr_2S_4 (x \leq 1)$, $Cu_{0.5}In_{0.5}Cr_2S_4$, or $CuCr_2X_3Y$ (X=S or Se, and Y=Cl or Br) were not found. In crystals of the halo-chalocogenides, combinations such as S–Cl and Se–Br on the anionic sites caused a substantial cation deficiency on the copper sites, while the halogen content was close to stoichiometric, or somewhat higher, because in both cases chalcogens and halogens are of nearly the same ionic size. The combination of Se–Cl on the

TABLE 4. RESULTS OF ANALYSIS FOR $CdCr_2S_4$ AND $CdCr_2Se_4$ SINGLE CRYSTALS

Sample, nominal composition	Analyte, mole ratio				
	Cd	M[a]	Cr	X[a]	Cl
$CdCr_2S_4$	0.99_4	—	1.99_3	4.00_6	0.00_5
$CdCr_2S_4$[b]	1.00_9	—	1.99_7	3.98_4	0.00_8
$Cd_{0.99}In_{0.01}Cr_2S_4$	0.99_1	0.00_3	2.00_0	3.99_9	0.00_3
$Cd_{0.99}In_{0.01}Cr_2S_4$[b]	0.98_6	0.00_4	2.01_8	3.98_7	0.00_1
$Cd_{0.95}In_{0.05}Cr_2S_4$	0.98_9	0.04_6	1.99_2	3.96_2	0.00_7
$Cd_{0.99}Ag_{0.01}Cr_2S_4$[c]	0.98_6	0.01_6	1.99_7	—	—
$Cd_{0.95}Ag_{0.05}Cr_2S_4$	0.99_9	0.01_3	2.01_4	3.96_4	0.00_8
$Cd_{0.9}Ag_{0.1}Cr_2S_4$	0.98_6	0.01_5	2.00_9	3.97_4	0.01_3
$Cd_{0.95}Cu_{0.05}Cr_2S_4$	0.99_1	0.03_0	2.00_1	3.95_5	0.02_1
$Cd_{0.9}Cu_{0.1}Cr_2S_4$	0.95_1	0.06_4	2.01_5	3.93_4	0.03_3
$CdCr_2Se_4$	0.97_6	—	2.11_2	3.90_5	0.00_5
$Cd_{0.99}In_{0.01}Cr_2Se_4$	0.96_0	0.01_2	2.04_7	3.97_8	$<0.00_1$
$Cd_{0.95}In_{0.05}Cr_2Se_4$	0.96_0	0.05_1	2.01_7	3.96_4	0.00_4
$Cd_{0.9}In_{0.1}Cr_2Se_4$	0.93_8	0.05_8	2.01_9	3.97_5	0.00_7
$Cd_{0.99}Ag_{0.01}Cr_2Se_4$	0.97_4	0.00_9	2.08_7	3.91_8	0.00_8
$Cd_{0.9}Ag_{0.1}Cr_2Se_4$	0.96_3	0.04_4	1.99_1	3.97_5	0.02_3
$Cd_{0.95}Cu_{0.05}Cr_2Se_4$	0.95_7	0.03_3	2.00_8	3.97_9	0.02_0
$Cd_{0.9}Cu_{0.1}Cr_2Se_4$	0.94_7	0.05_3	1.99_7	3.98_0	0.02_1

a) "M" designates dopants (In, Ag, and Cu) and "X" designates S or Se. b) Annealed in vacuum at 600 °C for 48 hr. c) The crystal was dissolved in concd HNO_3 without Ag^+ ions. The intrinsic Ag and Cl present in the material were reacted with each other to form AgCl precipitates during the dissolution Only metals such as Cd, Ag, and Cr were determined subsequently using procedure (A) so that the observed Ag value was the sum of the Ag content in both the filtrate and precipitates.

anionic sites did not give the copper deficiency, but the chlorine content was much less than the stoichiometric content. The halochalocogenides, contrary to the general understanding, seem to contain a considerable amount of bivalent copper ions. For other crystals of the copper-based spinels, it was often observed that the total amount of metals was lower than that expected for the nominal composition and the amount of chlorine was high. The lower amounts of metals are mainly due to an insufficient amount of tetrahedral-site elements. The composition of single crystals of cadmium-based spinels, compared to that of the copper-based spinels, more closely approximated the nominal formula ($CdCr_2X_4$) but all the crystals were contaminated with a small amount of chlorine. The chlorine content was much less than that of the copper-based spinels and increased in the order of indium-doped, undoped, silver-doped, and copper-doped crystals. The content of dopants was usually less than the nominal content. From the present results, it can be concluded that Vegard's law is not useful to determine the intermediate composition of the vapor-phase-grown single-crystals of multicomponent systems such as $Cu_{1-x}Fe_xCr_2S_4$ and $CuCr_2X_{4-x}Y_x$, and that a complete analysis, including the determination of both major and minor constituents or impurities, is necessary to interpret the physical properties of crystals; a partial analysis fails to notice a compositional variation of components other than elements of interest. The present work also indicates that individual crystals in a growth batch can be characterized by AAS techniques if somewhat large crystals are grown.

The author would like to express his sincere appreciation to Drs. Bernard Hershenov and Fumio Okamoto for critical reading of the manuscript, and to Mr. Katsuhiro Kato for measurements of the lattice constants and discussions during the course of this work. He is also indebted to Drs. Fumio Okamoto and Yasuo Wada, and Messrs. Katsuhiro Kato and Takao Oka for providing samples. All the above-mentioned personnel are with RCA Research Laboratories, Inc., Tokyo.

References

1) F. Okamoto, T. Takahashi, and Y. Wada, *Oyo Butsuri*, **39**, 471 (1970).
2) K. Masumoto, T. Tsushima, H. Sekizawa, and A. Kiyosawa, *Nippon Kinzoku Gakkai Kaiho*, **10**, 113 (1971).
3) H. von Philipsborn, *J. Crystal Growth*, **9**, 296 (1971).
4) G. Harbeke and H. Pinch, *Phys. Rev. Lett.*, **17**, 1090 (1966).
5) H. von Philipsborn, *Helv. Phys. Acta*, **40**, 810 (1967).
6) S. B. Berger and H. L. Pinch, *J. Appl. Phys.*, **38**, 949 (1967).
7) H. L. Pinch and S. B. Berger, *J. Phys. Chem. Solids*, **29**, 2091 (1968).
8) K. G. Barraclough and A. Meyer, *J. Crystal Growth*, **16**, 265 (1972).
9) L. Goldstein, J. -L. Dormann, R. Druilhe, M. Guittard, and P. Gibart, *ibid.*, **20**, 24 (1973).
10) K. Ametani, This Bulletin, **47**, 242 (1974).
11) F. Okamoto, K. Ametani, and T. Oka, *Japan. J. Appl. Phys.*, **13**, 187 (1974).
12) A. W. Sleight and H. S. Jarrett, *J. Phys. Chem. Solids*, **29**, 868 (1968).
13) M. D. Banus, "Solid State Res," (**1971**: **2**) Lincoln Lab., M.I.T. (1971), p. 23.
14) K. Ametani and F. Okamoto, *Bunseki Kagaku*, **21**, 1229 (1972).
15) K. Ametani, *ibid.*, **23**, 745 (1974).
16) K. G. Barraclough, W. Lugscheider, A. Meyer, H. Schäfer, and L. Treitinger, *Phys. Stat. Sol. (a)*, **22**, 401 (1974).
17) M. D. Banus and M. C. Lavine, *J. Solid State Chem.*, **1**, 109 (1969).
18) K. Miyatani, Y. Wada, and F. Okamoto, *J. Phys. Soc. Japan*, **25**, 369 (1968).
19) K. Miyatani, K. Minematsu, Y. Wada, F. Okamoto, K. Kato, and P. K. Baltzer, *J. Appl. Phys.*, **41**, 1085 (1970); *J. Phys. Chem. Solids*, **32**, 1429 (1971).
20) K. I. Arai, O. Kubo, N. Tsuya, F. Okamoto, and P. K. Baltzer, *IEEE Trans. Mag.*, **Mag-8**, 479 (1972).
21) H. Fujita, Y. Okada, and F. Okamoto, *J. Phys. Soc. Japan*, **31**, 610 (1971).
22) M. Toda and S. Tosima, *J. Appl. Phys.*, **43**, 1751 (1972).
23) S. Osaka, T. Oka, and H. Fujita, *J. Phys. Soc. Japan*, **34**, 836 (1973).
24) Private communication: K. Minematsu, K. Miyatani, Y. Wada, and K. Kojima, Presented at the Spring Meeting of the Physical Society of Japan, Proceedings 6a-T-6, 1972, Tokyo.
25) F. K. Lotgering and G. H. A. M. van der Steen, *Solid State Commun.*, **7**, 1827 (1969).

26) Analyses were performed for one crystal in the individual growth batches. Pulverized crystals weighing 1 mg were dissolved in concentrated nitric acid. The sample solution was evaporated nearly to dryness. After removal of the nitric acid by evaporation with hydrochloric acid, the residue was dissolved in deionized water. Copper was determined by colorimetry using cupferazone as a color-producing reagent, where the absorbance was measured at 600 nm. Iron was determined by the absorbance at 470 nm using the colorimetric thiocyanate method.

27) G. Haacke and L. C. Beegle, *J. Phys. Chem. Solids*, **28**, 1699 (1967); *J. Appl. Phys.*, **39**, 656 (1968).

28) H. L. Pinch, M. J. Woods, and E. Lopatin, *Mat. Res. Bull.*, **5**, 425 (1970).

29) Two hundred mg of the sample was dissolved in concentrated nitric acid in a distillation flask and steam-distillation simultaneously performed until the sample completely dissolved, whereupon the distillate containing bromine was absorbed by a solution mixed with sodium hydroxide and hydrogen peroxide. Bromine in the distillate was determined by iodometry after removal of the excess hydrogen peroxide. The nitric acid solution remaining in the distillation flask was converted to hydrochloric acid solution and elemental selenium was precipitated by adding sulfurous acid. The precipitated selenium was filtered and determined by gravimetry. From the filtrate, copper and chromium were determined by chelatometry with EDTA using PAN and Zincon, respectively, as indicators. The procedure was confirmed using polycrystalline samples with the composition of $CuCr_2Se_{3.2}Br_{0.8}$ or $CuCr_2Se_3Br$, and satisfactory results were obtained.

30) A. R. Von Neida and L. K. Shick, *J. Appl. Phys.*, **40**, 1013 (1969).

Magnetic Circular Dichroism of the Iron(III) Porphins

Hiroshi KOBAYASHI, Tadatoshi HIGUCHI, and Ken EGUCHI

Department of Chemistry, Tokyo Institute of Technology, Ookayama, Meguro-ku, Tokyo 152

(Received July 5, 1975)

Magnetic circular dichroism(MCD) spectra were measured of some low-spin and high-spin Fe(III) porphins in a rigid matrix of polymethyl methacrylate(PMMA) for a variety of temperature. Some of the most prominent MCD extrema of the low-spin Fe(III) porphins showed a remarkable enhancement of the intensity at reduced temperatures, while no appreciable increase was observed in the absorption intensity. The temperature dependence of the MCD dispersion of the low-spin Fe(III) porphins arises, in principle, from a change in the Boltzmann distribution between the ground Kramers doublet splitting in a magnetic field, however, the MCD enhancement observed in the Soret region can correctly be interpreted only when the excited states described by a product wave function of the porphin B state and the spin-orbit coupling substates of low-spin iron(III) d^5 system are split by a configuration interaction with the "porphin to iron(III)" charge-transfer excited states.

The visible and near-ultraviolet absorption spectra of metalloporphyrins arise from the lowest spin-allowed (π, π^*) excitations.[1-3] The role of the central metal ion in the absorption spectra is of relatively minor in most metalloporphyrins, whereas the lifetime of the excited metalloporphyrins depends upon the structure of interactions between the π-electron system of porphyrin and the central transition metal ion.[4-9] In some metalloporphyrins with dπ-open shell such as high-spin iron(III) porphyrins and high-spin manganese(III) porphyrins, a participation of "porphyrin to metal" charge-transfer (CT) excited states in the lowest electronic excited states gives rise to an observable anomaly in the absorption spectra.[10]

The temperature-dependent *C*-term extrema in the (π, π^*) transitions of the ligand coordinated to a metal ion in a degenerate ground state should be observed only when an appreciable interaction between the π-electron system of the ligand and the open-shell orbital of the central metal ion is present. In this paper, a study of temperature changes of the MCD spectra in the lowest excitations of the iron-(III) porphyrins is presented.

Experimental

Synthesis of the Metal-free Base of Tetraphenylporphin (H_2TPP). H_2TPP was synthesized by the method of Adler *et al.*[11] Chromatographic purification was repeated on activated alumina columns using chloroform as solvent and also as eluent. The elute was concentrated, and then excess methanol was added. Purple needle crystals thus obtained were identified by elemental analysis.

Found: C, 86.18; H, 4.61; N, 8.96%. Calcd for $C_{44}H_{30}N_4$: C, 85.97; H, 4.92; N, 9.11%.

Synthesis of Tetraphenylporphinatoiron(III) Chloride (TPPFe(III)Cl). TPPFe(III)Cl was prepared in dimethylformamide (DMF). H_2TPP (0.3 g) and $FeCl_2 \cdot 4H_2O$ (1.5 g) were dissolved in DMF (200 ml) and refluxed for 3 hr. When the solution was cooled, portions of dilute hydrochloric acid were added by a small amount. The dark purple crystals thus precipitated were collected by filteration. The complex was recrystallized twice from a mixture of 1,2-dichloroethane and hexane.

Found: C, 74.94; H, 3.85; N, 7.92; Fe, 7.97; Cl, 5.10%. Calcd for $C_{44}H_{28}N_4FeCl$: C, 75.07; H, 4.01; N, 7.96; Fe, 7.93; Cl, 5.04%.

Synthesis of Bisimidazoletetraphenylporphinatoiron(III) Perchlorate ([TPPFe(III)(Im)$_2$]ClO$_4$). TPPFe(III)Cl (35 mg) was dissolved in benzene (5 ml). $AgClO_4$ (10 mg) was added to the solution. After reflux for 4 hr, AgCl was filtered off and then imidazole (6 mg) was added. Just after the addition of imidazole, reddish purple crystals precipitated. When the precipitation was completed, unreacted $AgClO_4$ and imidazole were dissolved by adding ethyl ether (5 ml). The residue was dissolved in 1,2-dichloroethane and then filtered for separation of the contaminating $AgClO_4$. The filtrate was condensed under reduced pressure and then benzene was added to it for precipitation. Pure crystals were obtained by recrystallization from a mixture of 1,2-dichloroethane and benzene.

Found: C, 66.18; H, 3.67; N, 12.50; Fe, 6.08%. Calcd for $C_{50}H_{36}N_8FeClO_4$: C, 66.42; H, 4.01; N, 12.39; Fe, 6.18%.

Synthesis of the Metal-free Bases of Octaethylporphin (H_2OEP). H_2OEP was prepared by refluxing 3,4-diethyl-5-hydroxymethylpyrrole-2-carboxylic acid and potassium ferricyanide in glacial acetic acid according to the method of Inhoffen *et al.*[12] Octaethylporphin thus obtained was recrystallized from a mixture of chloroform and methanol and purified by column chromatography.

Found: C, 80.55; H, 8.51; N, 10.44%. Calcd for $C_{36}H_{46}N_4$: C, 80.85; H, 8.67; N, 10.48%.

Synthesis of Octaethylporphinatoiron(III) Chloride (OEPFe(III)Cl). OEPFe(III)Cl was prepared by a method similar to the preparation of TPPFe(III)Cl. H_2OEP (250 mg) was dissolved in refluxing dimethylformamide (100 ml). $FeCl_2 \cdot 4H_2O$ (1.5 g) was added to the refluxing solution of the free base. After reflux for 3 hr, portions of dilute hydrochloric acid were added by a small amount when the refluxed solution was cooled. The product was recrystallized twice from a mixture of 1,2-dichloroethane and hexane.

Found: C, 68.60; H, 6.88; N, 9.16; Fe, 8.55; Cl, 6.00%. Calcd for $C_{36}H_{44}N_4FeCl$: C, 69.29; H, 7.11; N, 8.98; Fe, 8.95; Cl, 5.68%.

Synthesis of Bisimidazoleoctaethylporphinatoiron(III) Perchlorate ([OEPFe(III)(Im)$_2$]ClO$_4$). [OEPFe(III)(Im)$_2$]ClO_4 was prepared by the method of Ogoshi *et al.*[13] OEPFe(III)Cl (150 mg) was dissolved in benzene (50 ml), and $AgClO_4$ (200 mg) was added. The reaction mixture was refluxed for 3 hr. After imidazole (80 mg) dissolved in benzene (15 ml) was added, the reaction mixture was refluxed continuously until the solution became transparent. The precipitates were separated by filteration, and extracted with 1,2-dichloroethane. Crude crystals were obtained by removing the solvent under reduced pressure. Dark brown pure crystals were obtained by recrystallization from a mixture of 1,2-dichloroethane and benzene.

Other metal porphins TPPMn(III)Cl, TPPCo(II), and TPPZn(II) used in the present measurements were prepared

in our previous works[10,14,15] and used without further purification.

Measurements of Absorption and Magnetic Circular Dichroism Spectra. The electronic absorption spectra were recorded on a Shimadzu recording spectrophotometer Model MPS-50. Solvents were benzene and 1,2-dichloroethane purified by fractional distillation using a 1.5 m Dixson-ring packed column and dried by the usual procedure.[16]

The circular dichroism under an external magnetic field (MCD) was measured by a JASCO automatic recording spectropolarimeter Model ORD/UV-5 with its CD attachment and electromagnet. The magnetic field was set at 10000 gauss.

A cryostat was adopted for measurements of the spectra at liquid-nitrogen temperature and dry ice–methanol temperature. For the low-temperature measurements, the porphins were dispersed in an appropriate polymer film. In the case of TPPFe(III)Cl, OEPFe(III)Cl, [TPPFe(III)-$(Im)_2]ClO_4$, [OEPFe(III)$(Im)_2]ClO_4$, TPPMn(III)Cl, and TPPZn(II), polymethyl methacrylate was used for matrices. By spontaneous evaporation of a viscous solution, which was obtained by dissolving polymethyl methacrylate and porphin in 1,2-dichloroethane, a transparent film dispersing porphin was prepared on a clean glass plate. In the case of TPPFe-(III)Cl and TPPZn, polystyrene was also used. A polystyrene film was made on a glass plate by spontaneous evaporation of a viscous solution, which was obtained by dissolving polystyrene and porphin in 1,2-dichloroethane. After evacuation, the film was melted in a glass tube at about 200 °C under nitrogen atmosphere which was used for polystyrene not to be oxidized. The bubbles in polystyrene were eliminated by recycling evacuation of the atmosphere in the glass tube and introduction of nitrogen gas. The polystyrene gave a rigid glass without cracks and distortion when slowly cooled. The sample was cut in a disk and its faces were polished so as to make optical measurements possible. Since TPPCo(II) might be oxidized during preparation of the rigid glass sample, TPPCo(II) was directly fused in polystyrene under nitrogen atmosphere.

ESR Spectra. The ESR spectra were obtained by a Japan Electron Optics Laboratory spectrometer Model JES ME3X. The static magnetic field was calibrated by means of a proton-resonance gaussmeter.

Results and Discussion

The MCD spectra of TPPFe(III)Cl and OEPFe-(III)Cl, which are typical iron(III) porphins in the high spin state $S=5/2$, were observed in benzene. The results are presented in Figs. 1 and 2. The similar spectra were obtained in polystyrene. Quantitative spectrum, however, could not be obtained, since the back-ground absorption of polystyrene increased so fast in the higher wave number region that a reproducible calibration was impossible. In the case of PMMA matrices, reproducible spectra of the porphins were obtained. In fact, the spectra of the rigid polymer glass at room temperature were coincident with the solution spectra. The absorption and MCD spectra of TPPFe(III)Cl and OEPFe(III)Cl in PMMA were measured for a variety of temperature as shown in Figs. 3 and 4.

The MCD spectra of [TPPFe(III)$(Im)_2]ClO_4$ and [OEPFe(III)$(Im)_2]ClO_4$, which are typical iron(III) porphins in the low spin state $S=1/2$, were

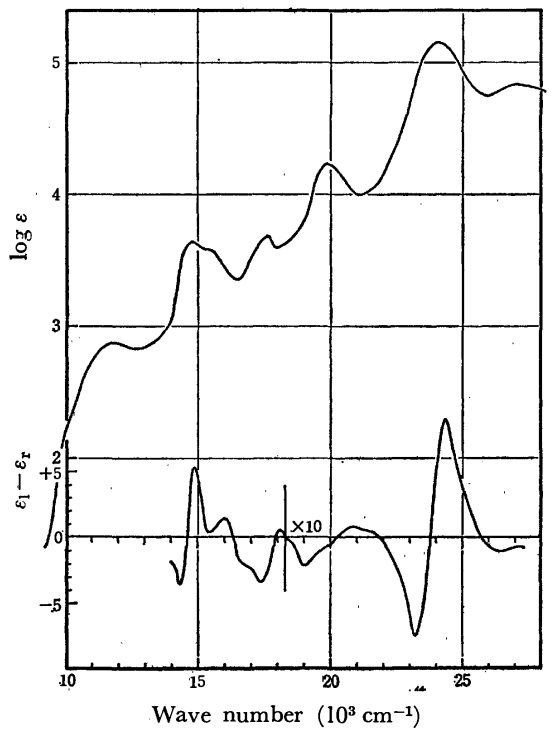

Fig. 1. The absorption and MCD spectra of TPPFe-(III)Cl in C_6H_6.

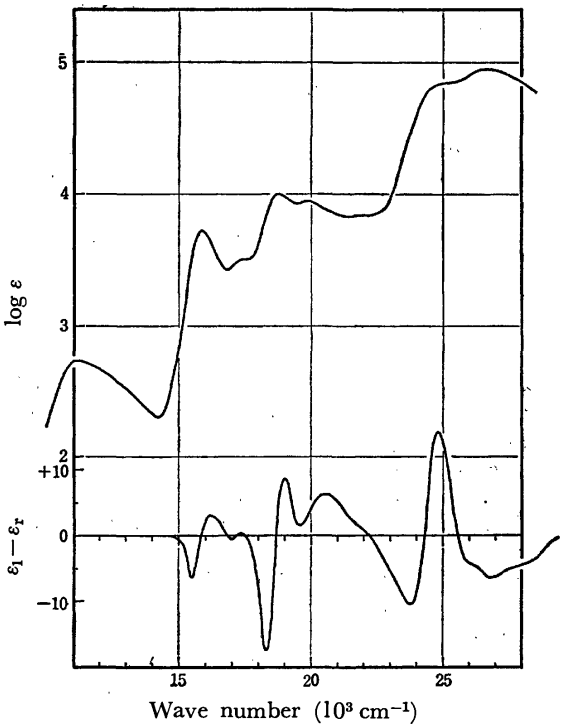

Fig. 2. The absorption and MCD spectra of OEPFe-(III)Cl in C_6H_6.

observed in $C_2H_4Cl_2$, and in PMMA for a variety of temperature. The results are presented in Figs. 5, 6, 7, and 8. The similar spectra were also obtained for [TPPFe(III)$(Im)_2]Cl$ and [TPPFe(III)$(Im)_2]ClO_4$ in chloroform which consists of ten times or more excess imidazole. La Mar and Walker also ob-

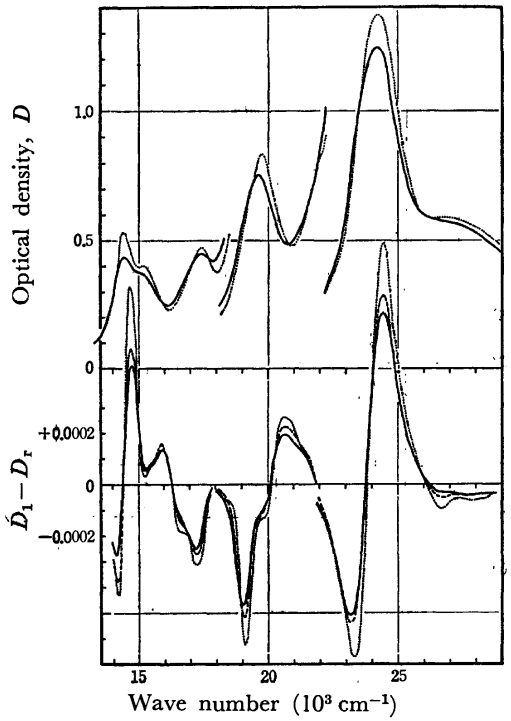

Fig. 3. The absorption and MCD spectra of TPPFe-(III)Cl in PMMA.
——: 310 K; – – –: 196 K; ·····: 79 K.

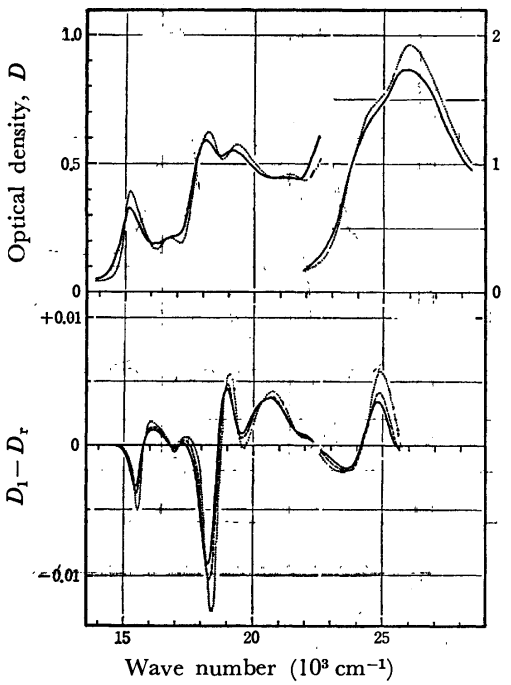

Fig. 4. The absorption and MCD spectra of OEPFe-(III)Cl in PMMA. ——: 310 K; – – –: 196 K; ·····: 79 K.

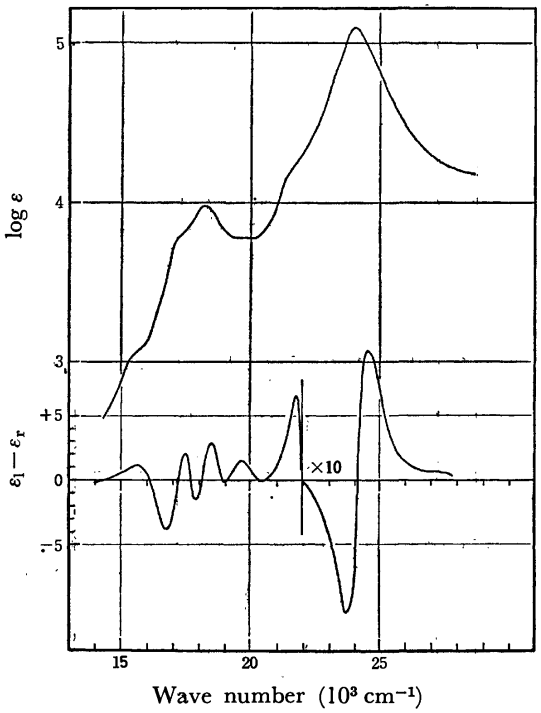

Fig. 5. The absorption and MCD spectra of [TPPFe-(III)$(Im)_2$]ClO_4 in $C_2H_4Cl_2$.

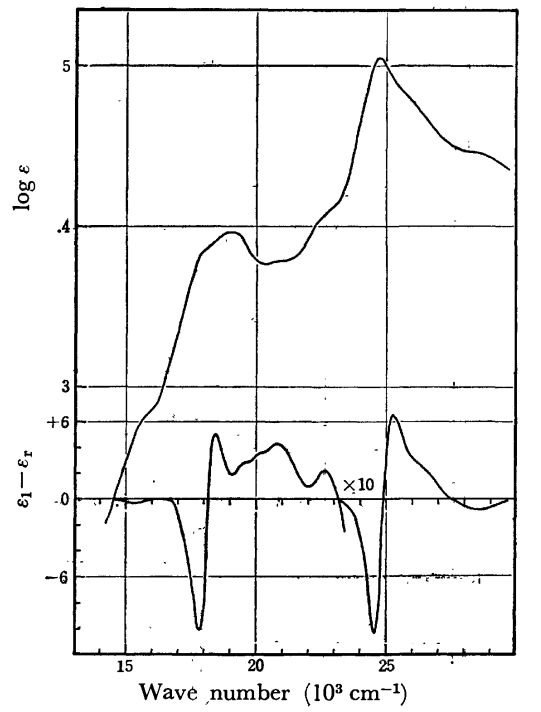

Fig. 6. The absorption and MCD spectra of [OEPFe-(III)$(Im)_2$]ClO_4 in $C_2H_4Cl_2$.

served in their NMR studies that the proton signals of the low-spin species were detected only in the presence of eight times excess imidazole in deutero-chloroform.[17] In chloroform, however, the dissociation of coordinated imidazole gives rise to a drift of the spectrum even in the presence of excess imidazole. In 1,2-dichloroethane, on the other hand, a spectrum characteristic of the low-spin iron(III) porphins did not change for a few days after the solid sample was dissolved in the absence of excess imidazole. The spectra obtained for TPPMn(III)Cl in PMMA, TPPCo(II) in polystyrene, and TPPZn(II) in PMMA are also shown in Figs. 9, 10, and 11.

A most remarkable enhancement of MCD extrema was observed in the low-spin iron(III) porphins when

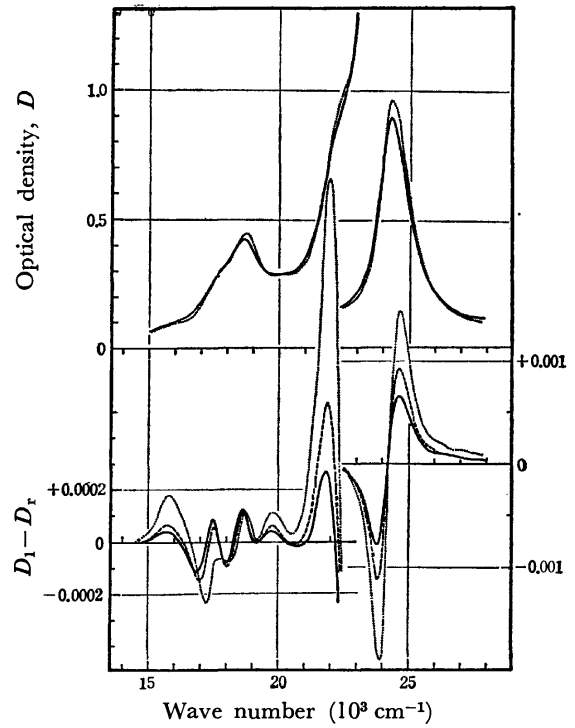

Fig. 7. The absorption and MCD spectra of [TPPFe(III)$(Im)_2$]ClO_4 in PMMA. ——: 310 K; ----: 196 K; ·····: 79 K.

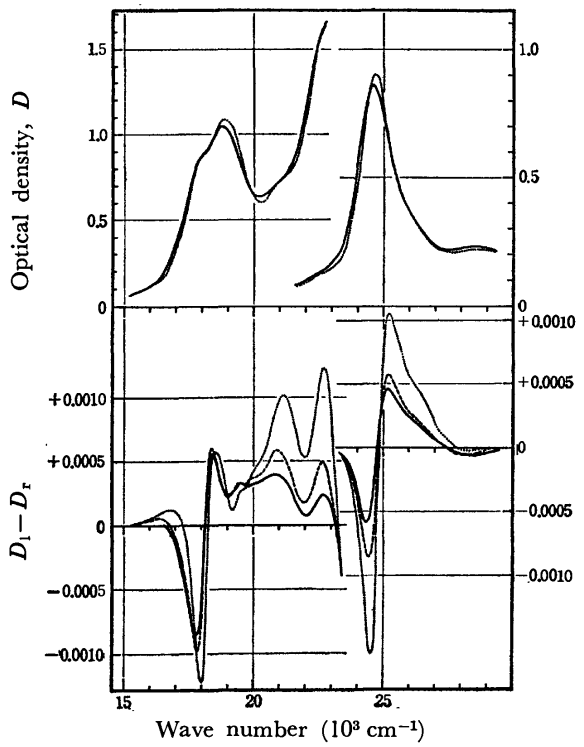

Fig. 8. The absorption and MCD spectra of [OEPFe(III)$(Im)_2$]ClO_4 in PMMA. ——: 310 K; ----: 196 K; ·····: 79 K.

the temperature is reduced. At the liquid-nitrogen temperature, two MCD peaks in the lower energy region of the B band increase their intensity up to several times greater than those at room temperature.

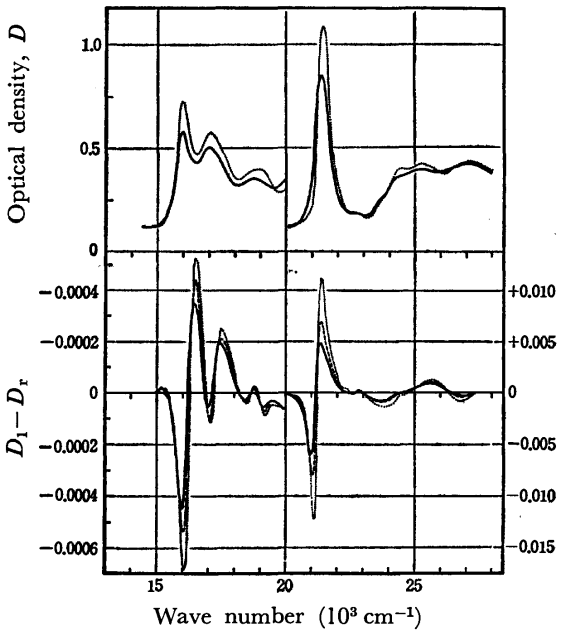

Fig. 9. The absorption and MCD spectra of TPPMn(III)Cl in PMMA. ——: 310 K; ----: 196 K; ·····: 79 K.

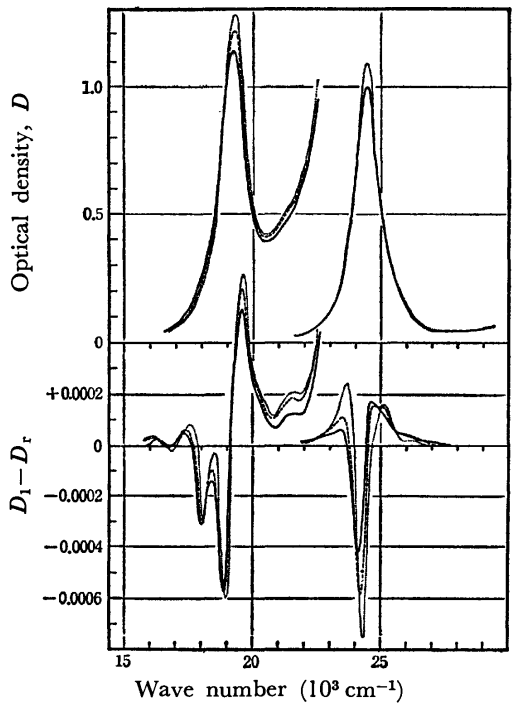

Fig. 10. The absorptioon and MCD spectra of TPPCo(II) in PMMA. ——: 310 K; ---- 196 K; ·····: 79 K.

The MCD extrema in the B band also increase their intensity at reduced temperatures. TPPCo(II) and TPPMn(III)Cl also exhibit the similar enhancement.

The absorption band is simulated by a damped oscillator or Gaussian spectral shape function.[18] Supposed that other factors are unchanged, the intensity of *A*-term dispersion extrema is inversely proportional to a square of the line width, while the intensities of *B*-term extrema and of absorption maxima are in-

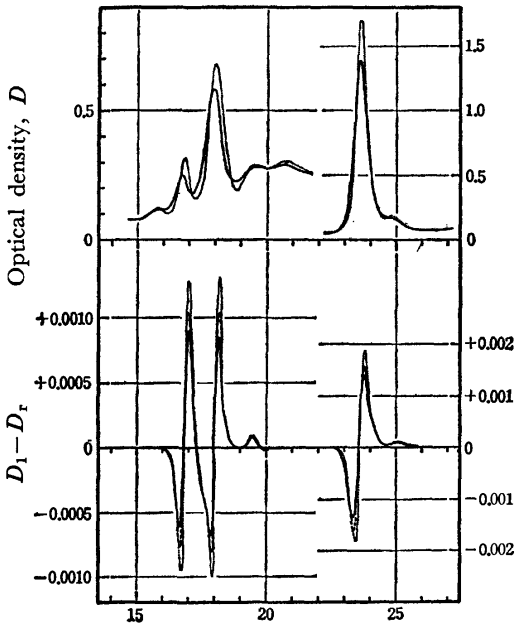

Fig. 11. The absorption and MCD spectra of TPPZn-(II) in PMMA. ——: 310 K; ----: 196 K; ……: 79 K.

versely proportional to the line width,

$$\theta^A_{max} \propto (1/\Gamma(T))^2,\ \theta^B_{max} \propto 1/\Gamma(T) \text{ and } \varepsilon^B_{max} \propto 1/\Gamma(T),$$

where Γ is the line width and a function of temperature T. Thus a ratio of the intensities of MCD extrema observed at two different temperatures is correlated with a ratio of the absorption intensities at the corresponding temperatures as follows:

$$\theta^A_{max}(T_2)/\theta^A_{max}(T_1) = \{\varepsilon_{max}(T_2)/\varepsilon_{max}(T_1)\}^2$$

and

$$\theta^B_{max}(T_2)/\theta^B_{max}(T_1) = \varepsilon_{max}(T_2)/\varepsilon_{max}(T_1).$$

Here it is noted that the ratio R_θ of the intensities of MCD extrema at liquid-nitrogen temperature and at ambient temperature is equal to or less than the square of the corresponding ratio R^2_ε of the absorption maxima. When R_θ is much greater than R^2_ε, a mechanism other than temperature-broadening of the line width should be working. The R_θ's and R^2_ε's observed for the samples studied in the present work are summarized in Fig. 12. The R_θ of TPPZn(II), in which only a small interaction between metal and porphin is present, is in good agreement with its corresponding R^2_ε. This implies that the MCD dispersions observed in the absorption bands of TPPZn(II) are assigned to A-term dispersions. A greater deviation was found in the case of two low-spin iron(III) porphins, TPPCo(II), and TPPMn(III)Cl. Here it is noted that a change of R_θ over the observed wave numbers was analogous in two different low-spin iron(III) porphins.

The ground state of the low-spin iron(III) porphin is described as a composite system of the ground state of porphin π system and the lowest Kramers doublet of low-spin iron d^5 system as follows:

$$A^+(+1) = |+4+\bar{4}-4-\bar{4}\,\zeta\,\bar{\zeta}+1+\bar{1}-1|,$$

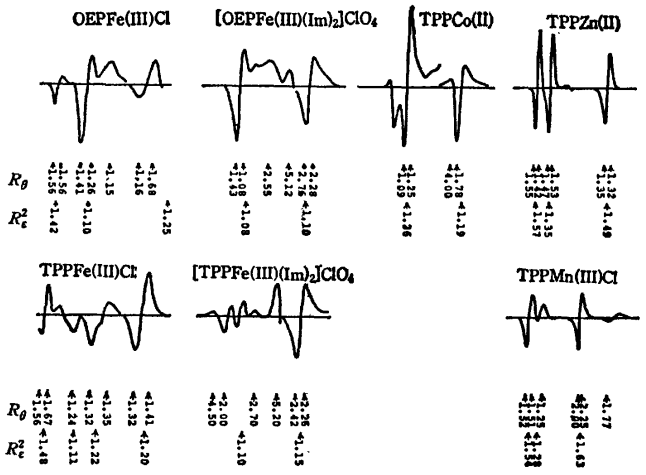

Fig. 12. $R_\theta = \left\{\dfrac{\theta_{max}(79\text{ K})}{\theta_{max}(310\text{ K})}\right\}$ and $R^2_\varepsilon = \left\{\dfrac{\varepsilon_{max}(79\text{ K})}{\varepsilon_{max}(310\text{ K})}\right\}^2$.

and

$$A^-(-1) = |+4+\bar{4}-4-\bar{4}\,\zeta\,\bar{\zeta}-1-\bar{1}+\bar{1}|,$$

where the numbers ±1 given in the parentheses are the orbital angular momenta, the superscripts $\pm$ indicate the α- and β-components of the Kramers doublet, ±4 are the highest occupied porphin π orbitals, ζ is iron xy orbital, ±1 are iron $d_{\pm1}$ orbitals, no bar implies spin α and a bar implies spin β. Thus the spin-allowed excited states of the low-spin iron(III) porphin should be spin-doublets. The composite doublets arise from products of the Kramers doublets of low-spin iron d^5 system and the porphin-localized lowest (π, π^*) excited states, not only of spin-singlet but also of triplet. The doublets given by the product wave funtions of the lowest Kramers' doublet of low-spin iron d^5 system and the porphin-localized Soret excited state B are denoted by $B^+(+2)$, $B^-(-2)$, $B^+(0)$, and $B^-(0)$:

$$B^+(+2) = \frac{1}{\sqrt{2}}\{|-4-\bar{4}+4+\bar{5}\,\zeta\,\bar{\zeta}+1+\bar{1}-1| - |-4-\bar{4}+\bar{4}+5\,\zeta\,\bar{\zeta}+1+\bar{1}-1|\}$$

$$B^-(-2) = \frac{1}{\sqrt{2}}\{|+4+\bar{4}-4-\bar{5}\,\zeta\,\bar{\zeta}-1-\bar{1}+\bar{1}| - |+4+\bar{4}-\bar{4}-5\,\zeta\,\bar{\zeta}-1-\bar{1}+\bar{1}|\}$$

$$B^+(0) = \frac{1}{\sqrt{2}}\{|+4+\bar{4}-4-\bar{5}\,\zeta\,\bar{\zeta}+1+\bar{1}-1| - |+4+\bar{4}-\bar{4}-5\,\zeta\,\bar{\zeta}+1+\bar{1}-1|\}$$

$$B^-(0) = \frac{1}{\sqrt{2}}\{|-4-\bar{4}+4+\bar{5}\,\zeta\,\bar{\zeta}-1-\bar{1}+\bar{1}| - |-4-\bar{4}+\bar{4}+5\,\zeta\,\bar{\zeta}-1-\bar{1}+\bar{1}|\}$$

Here the numbers given in the parentheses are the orbital angular momenta, the superscripts $\pm$ indicate the α- and β-components of the Kramers doublet, and ±5 are the lowest vacant porphin π orbitals. The excitations $A^+(+1)\rightarrow B^+(+2)$ and $A^-(-1)\rightarrow B^-(0)$ are left-handed circularly polarized, while the excitations $A^-(-1)\rightarrow B^-(-2)$ and $A^+(+1)\rightarrow B^+(0)$ are right-handed circularly polarized. An MCD dispersion occurs in the excitations $A^+(+1)\rightarrow B^+(+2)$ and $B^+(0)$

and also in the excitations $A^-(-1)\rightarrow B^-(-2)$ and $B^-(0)$. When the temperature is reduced, $A^-(-1)$ is more populated than $A^+(+1)$. However no practical change in MCD happens even at reduced temperatures if the B_1 states ($B^+(+2)$ and $B^-(-2)$), in which an orbital angular momentum induced upon excitation is in the direction of the resultant momentum of spin-orbit coupling at the central iron(III) ion, and the B_2 states ($B^+(0)$ and $B^-(0)$), in which an orbital angular momentum induced upon excitation is against the iron momentum, are degenerate.

Since the vacant $d\pi$ orbital and the lowest vacant porphin π^* orbital are equivalent in symmetry and thus, an electron-delocalization is possible between the $d\pi$ and π^* orbitals, the low-energy "porphin to iron(III)" CT excited states exhibit a configuration interaction against the lowest porphin-localized (π, π^*) excited states.[10] A difference in the configuration interactions of the "porphin to iron(III)" CT excited states against the porphin (π, π^*) excited states arises between the B_1 and B_2 states from a difference in symmetry of the doublet eigenfunctions of spin-orbit coupling in the low-spin iron(III) ion embedded in the excited porphin. The $B^+(0)$ and $B^-(0)$ states interact with the CT excited states $CT^+(+4)=|+4+\bar{4}-4\ \zeta\ \bar{\zeta}+1+\bar{1}-1-\bar{1}|$ and $CT^-(-4)=|-4-\bar{4}+\bar{4}\ \zeta\ \bar{\zeta}+1+\bar{1}-1-\bar{1}|$, respectively, while there is no such CT excited states interacting with the $B^+(+2)$ and $B^-(-2)$ states in a first-order approximation.

		$B^+(0)$ ($B^-(0)$)	$-CT^+(+4)$ ($CT^-(-4)$)
$B^+(0)$	($B^-(0)$)	$E+2K_1-\frac{1}{2}a$	$\frac{\sqrt{2}}{2}X$
$-CT^-(+4)$	($CT^-(-4)$)	$\frac{\sqrt{2}}{2}X$	E_{CT}

Here $E+2K_1$ and E_{CT} are the diagonal energies of the B state and the CT state, a is the spin-orbit coupling constant and X is the resonance integral between porphin ±5 orbital and iron $d_{\pm1}$ orbital. Since the "porphin to iron(III)" CT excited states in low-spin iron(III) porphins are lower than the B states,[10] the CT states raise the $B^\pm(0)$ states. The empirical values $E=13070\ cm^{-1}$, $K_1=4600\ cm^{-1}$, $X=-3000\ cm^{-1}$ [10] and $a=435\ cm^{-1}$ [19] predict an energy gap ΔE between $B^\pm(0)$ and $B^\pm(\pm2)$ as a function of E_{CT} as follows:

$E_{CT}=10000\ cm^{-1}$	$\Delta E=360\ cm^{-1}$
$E_{CT}=12500\ cm^{-1}$	$\Delta E=450\ cm^{-1}$
$E_{CT}=15000\ cm^{-1}$	$\Delta E=590\ cm^{-1}$

The mixing of the "porphin to iron(III)" CT excited states to B_1 states occurs to a less extent than the interaction to B_2 states even if in a higher approximation. In fact, the B band of low-spin iron(III) porphins is evidently broad as compared with the B band observed for a typical (π, π^*) transition in TPPZn(II). An MCD dispersion experimentally observed in the Soret region, however, indicates that a gap between the B_1 and B_2 states should be less than the band width ($1000\ cm^{-1}$) of each component absorption band. Since $A^-(-1)$ is more populated than $A^+(+1)$ at reduced temperatures, the low-energy component transition $A^-(-1)\rightarrow B^+(-2)$ which is right-handed circularly polarized and the high-energy component transition $A^-(-1)\rightarrow B^-(0)$ which is left-handed circularly polarized enhance their absorption intensities. An apparent dispersion is thus obtained by superposing two temperature-dependent *C*-term extrema with opposite sign for a small energy gap of the excitations to B_1 and B_2 states.

The ESR spectrum of powder $[TPPFe(III)(Im)_2]ClO_4$ at 77 K exhibits three different *g*-values at $g_{zz}=2.87$, $g_{yy}=2.26$, and $g_{xx}=1.65$. The *g*-values of powder $[TPPFe(III)(Im)_2]Cl$ prepared in the present work were $g_{zz}=2.91$, $g_{yy}=2.31$, and $g_{xx}=1.54$ and in good agreement with the values $g_1=2.9$, $g_2=2.3$, and $g_3=1.5$ reported for $[TPPFe(III)(Im)_2]Cl$ in a frozen chloroform solution containing excess imidazole.[20] These anisotropic *g*-values insist that the iron $d_{\pm1}$ orbitals are split by the π-interaction due to the axial ligands and the lowest Kramers doublet is predominantly made of a degenerate configuration ((xy) ($\overline{xy}$) (zx) ($\overline{zx}$) (yz); (xy) ($\overline{xy}$) (zx) ($\overline{zx}$) ($\overline{yz}$)). The lowest component of the spin-orbit coupling sublevels of low-spin d^5 system is about 99.3% occupied even at 300 K.[19] For such a ground state, the arguments similar to those given for the ground state $A^\pm(\pm1)$ can be applicable and predict a temperature-dependent MCD dispersion. As revealed by X-ray studies, two coordinated imidazole molecules are in almost coplanar in the crystal.[21,22] However an internal rotation of the coordinated imidazoles is not so hindered in solution and then the anisotropy becomes smaller than expected from three *g*-values observed for the solid sample.

In the course of the present work, an independent observation on the temperature-dependent MCD spectra of the low-spin iron(III) porphyrins in hemoproteins was informed the authors before its publication by Dr. T. Nozawa, Tohoku University. The authors' thanks are due to Dr. H. Ogoshi, Kyoto University, for his advice concerning the preparation of porphyrinatoiron(III) perchlorates. The authors are also indebted to Professor J. Higuchi and Dr. T. Ito for the measurements of ESR spectra.

References

1) M. Gouterman, *J. Chem. Phys.*, **30**, 1139 (1959).
2) H. Kobayashi, *ibid.*, **30**, 1362 (1959).
3) C. Weiss, H. Kobayashi, and M. Gouterman, *J. Mol. Spectrosc.*, **16**, 415 (1965).
4) B. E. Smith and M. Gouterman, *Chem. Phys. Lett.*, **2**, 517 (1968).
5) D. Eastwood and M. Gouterman, *J. Mol. Spectrosc.*, **30**, 437 (1969).
6) R. L. Ake and M. Gouterman, *Theoret. Chim. Acta* (Berl.), **15**, 20 (1969).
7) R. L. Ake and M. Gouterman, *ibid.*, **17**, 408 (1970).
8) M. Gouterman, R. A. Mathies, B. E. Smith, and W. S. Caughey, *J. Chem. Phys.*, **52**, 3795 (1970).
9) J. Bohandy, B. F. Kim, and C. K. Jen, *J. Mol. Spectrosc.*, **49**, 365 (1974).
10) H. Kobayashi, Y. Yanagawa, H. Osada, S. Minami,

and M. Shimizu, This Bulletin, **46**, 1471 (1973).
11) A. D. Adler, F. R. Longo, J. D. Finarelli, J. Goldmacher, J. Assour, and L. Korsakoff, *J. Org. Chem.*, **32**, 476 (1967).
12) H. H. Inhoffen, J. H. Fuhrhop, H. Voigt, and H. Brockmann, Jr., *Ann. Chem.*, **695**, 133 (1966).
13) H. Ogoshi, E. Watanabe, Z. Yoshida, J. Kincaid, and K. Nakamoto, *J. Amer. Chem. Soc.*, **95**, 2845 (1973).
14) H. Kobayashi, M. Shimizu, and I. Fujita, This Bulletin, **43**, 2335 (1970).
15) H. Kobayashi, T. Hara, and Y. Kaizu, *ibid.*, **45**, 2148 (1972).
16) D. D. Perrin, W. L. F. Armarego, and D. R. Perrin, "Purification of Laboratory Chemicals," Pergamon Press, Oxford (1966).
17) G. N. La Mar and F. A. Walker, *J. Amer. Chem. Soc.*, **94**, 8607 (1972).
18) P. J. Stephens, W. Suëtaka, and P. N. Schatz, *J. Chem. Phys.*, **44**, 4592 (1966).
19) M. Kotani, *Progr. Theoret. Phys. Suppl.*, **17**, 4 (1961).
20) G. N. La Mar and F. A. Walker, *J. Amer. Chem. Soc.*, **95**, 1782 (1973).
21) D. M. Collins, R. Countryman, and J. L. Hoard, *ibid.*, **87**, 2312 (1965).
22) A. Takenaka, Y. Sadasa, E. Watanabe, H. Ogoshi, and Z. Yoshida, *Chem. Lett.*, **1972**, 1235.

Cyanoalkyl Complexes of Transition Metals. IV. Geometry and Spectroscopic Properties of Cyanomethyl Complexes of Palladium(II) and Platinum(II)

Keinosuke SUZUKI, Junichi OOYAMA, and Masami SAKURAI

Inorganic Chemistry Laboratory, Faculty of Science, Nagoya University, Chikusa, Nagoya 464

(Received August 11, 1975)

A number of cyanomethyl complexes of palladium(II) and platinum(II) were prepared and characterized by proton nuclear magnetic resonance and infrared spectroscopy. It was shown that the methylene resonance, phenyl resonance, and a strong band at 550 ± 5 cm^{-1} are acceptable criteria for deducing the geometry of the complexes $MX(CH_2CN)(PPh_3)_2$ (M=Pd, Pt). The criteria allow us to assign the *cis* geometry to the bromo and iodo complexes of platinum(II) both of which showed an unusual methylene resonance. An approximately linear relationship holds between ^2J(Pt-H) of *trans*-$PtX(CH_2CN)(PPh_3)_2$ and that of *trans*-$PtX(CH_3)(PPh_3)_2$ (X=Cl, Br, I, N_3, NO_2, NO_3).

It has been well established that the stereochemistry of square-planar bis(phosphine)-transition metal complexes can be determined by ^{1}H NMR if the phosphines contain methyl or methylene groups attached to the phosphorus atom.[1-8] However, this method is inadequate when the phosphine is triphenylphosphine. Recently we reported the synthesis and spectroscopic properties of $PdCl(CH_2CN)(PPh_3)_2$[9] (**1a**), *trans*- and *cis*-$PtCl(CH_2CN)(PPh_3)_2$[10] (**1b**, **2**) and demonstrated that the gross geometry of these complexes could be determined by the ^{1}H NMR spectrum of the cyanomethyl protons. The methylene resonance of **1a** and **1b** appeared as a triplet due to spin-spin coupling with two equivalent phosphorus atoms. On the other hand the same resonance of **2** occurred as a 1 : 1 : 1 : 1 doublet of doublets because of the two non-equivalent phosphorus atoms. The cyanomethyl protons of PtCl(diphos) (**3**, diphos=$Ph_2PCH_2CH_2PPh_2$) also

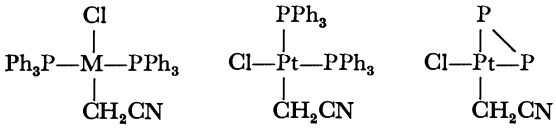

1a, M=Pd **2** **3**, P-P=diphos
1b, M=Pt

gave a doublet of doublets in accordance with *cis* geometry. The methylene resonance seems to be useful as a criterion for determining the stereochemistry of the complexes $MX(CH_2CN)(PPh_3)_2$. However, we found in the course of studies on cyanomethyl complexes that care should be taken in making deductions about the geometry of $MX(CH_2CN)(PPh_3)_2$ solely from the methylene resonance. In this paper we describe the preparation of several cyanomethyl complexes of palladium(II) and platinum(II) and discuss the method of establishing their geometry on the basis of IR and ^{1}H NMR spectral data.

Experimental

High frequency infrared spectra (4000—700 cm^{-1}) were recorded on a JASCO-DS-402G spectrometer with samples prepared as Nujol or hexachlorobutadiene mulls. Low frequency spectra (700—200 cm^{-1}) were recorded on a HITACHI EPI-L2 spectrometer with samples as Nujol mulls. The ^{1}H NMR spectra were recorded on a JEOL-C60H spectrometer with TMS as an internal standard.

Starting Materials. Chlorocyanomethylbis(triphenylphosphine)-palladium (II) **1a**, *trans*- and *cis*-chlorocyanomethylbis(triphenylphosphine)platinum(II) **1b** and **2**, were prepared as reported previously.[9,10] Commercial reagents and solvents were used without purification. Microanalyses were performed by Wako Pure Chemical Industries, Ltd.

Preparation of $PdX(CH_2CN)(PPh_3)_2$ (X=NCO, N_3, I, NO_2, $N(CO)_2C_6H_4$, CN). Potassium cyanate (0.07 g, 0.86 mmol) was added to a solution of **1a** (0.50 g, 0.71 mmol) dissolved in 150 ml of acetone and stirred for 3 hr at room temperature. The yellow color of the solution disappeared and a small amount of white solid was obtained. It was filtered off and the filtrate was concentrated to give a white precipitate of $Pd(NCO)(CH_2CN)(PPh_3)_2$. The precipitate was filtered, washed with acetone and dried *in vacuo*. The azido, iodo, nitro, and phthalimido complexes were prepared similarly in acetone (sodium azide, potassium iodide) or methanol (sodium nitrite, potassium phthalimide).

A suspension of potassium cyanide (0.046 g, 0.73 mmol) and **1a** (0.50 g, 0.71 mmol) in 150 ml of methanol was heated at 55—60 °C for 2 hr. The resulting yellow solution was allowed to stand at room temperature to afford pale yellow crystals of $Pd(CN)(CH_2CN)(PPh_3)_2$ containing two molecules of methanol.

Preparation of trans-*$PtX(CH_2CN)(PPh_3)_2$ (X=NCO, N_3, NO_2, $N(CO)_2C_6H_4$, NO_3, CH_3COO),* Potassium cyanate (0.045 g, 0.55 mmol) and **1b** (0.35 g, 0.44 mmol) were suspended in a mixed solvent of benzene (100 ml) and ethanol (50 ml) and refluxed for 5 hr. The resulting yellow solid was filtered and recrystallized from chloroform–diethyl ether to give *trans*-$Pt(NCO)(CH_2CN)(PPh_3)_2$. Similarly *trans*-$Pt[N(CO)_2C_6H_4](CH_2CN)(PPh_3)_2$ was prepared by the reaction of **1b** with potassium phthalimide in a mixed solvent of acetone and ethanol (1 : 1). *trans*-$Pt(N_3)(CH_2CN)(PPh_3)_2$ was synthesized by the reaction of **1b** with sodium azide in ethanol at room temperature.

A suspension of **1b** (0.50 g, 0.63 mmol) and silver nitrate (0.107 g, 0.63 mmol) in 150 ml of acetone was stirred for 12 hr at room temperature in the dark. The silver chloride formed was removed by filtration and the filtrate was concentrated to dryness *in vacuo*. The white residue was recrystallized from dichloromethane–diethyl ether to give white crystals of *trans*-$Pt(NO_3)(CH_2CN)(PPh_3)_2$. It contained one molecule of dichloromethane. *trans*-$Pt(CH_3COO)(CH_2CN)(PPh_3)_2$ was prepared in the same way with the use of silver acetate. *trans*-$Pt(NO_2)(CH_2CN)(PPh_3)_2$ was prepared by the reaction of *trans*-$Pt(NO_3)(CH_2CN)(PPh_3)_2$ with potassium nitrite in acetone.

Preparation of cis-*$PtX(CH_2CN)(PPh_3)_2$(X=NCO, N_3, NO_2, Br, I).* Lithium bromide (0.04 g, 0.46 mmol) and **2**

Table 1. Physical properties and analytical data of $MX(CH_2CN)(PPh_3)_2$

Complex M	Complex X	Color	Mp,[a] °C	Yield %	Analyses, % found (calcd) C	H	N
Pt (*trans*)	N_3	pale yellow	211—215	70	56.40(56.90)	4.05(4.03)	6.77(6.99)
	NCO	pale yellow	230—235	80	58.11(58.40)	4.16(4.03)	3.53(3.49)
	NO_2	white	223—226	50	56.13(56.62)	3.89(4.01)	3.23(3.48)
	$N(CO)_2C_6H_4$	white	260—272	70	60.52(60.83)	3.98(4.23)	2.80(3.09)
	$NO_3 \cdot CH_2Cl_2$[b]	white	185—200	50	51.55(51.64)	3.64(3.79)	3.05(3.09)
	CH_3CO_2	white	205—217	50	57.92(58.65)	4.41(4.32)	1.37(1.71)
Pt (*cis*)	N_3	white	190—220	60	56.60(56.90)	3.91(4.03)	7.13(6.99)
	NCO	white	240—260	80	57.86(58.40)	4.01(4.03)	3.22(3.49)
	NO_2	white	220—234	75	55.95(56.62)	3.96(4.01)	3.14(3.48)
	$Br \cdot CH_2Cl_2$[b]	pale yellow	240—250	60	49.99(50.67)	3.61(3.71)	1.47(1.51)
	I	yellow	235—241	75	51.10(51.45)	3.71(3.65)	1.65(1.58)
Pd	$N_3 \cdot CH_2Cl_2$[b]	yellow	155—161	65	58.73(58.69)	4.26(4.26)	7.03(7.02)
	$NCO \cdot (CH_3)_2CO$[b]	pale yellow	183—188	80	65.00(65.42)	4.72(4.93)	3.55(3.64)
	NO_2	white	178—185	50	63.26(63.65)	3.62(3.91)	4.25(4.50)
	$N(CO)_2C_6H_4$	white	192—198	60	66.86(67.63)	4.34(4.43)	3.28(3.43)
	$I \cdot (CH_3)_2CO$[b]	yellow	172—178	55	54.83(54.55)	3.95(4.35)	1.31(1.56)
	$CN \cdot 2CH_3OH$[b]	pale yellow	140—150	50	64.71(64.97)	5.29(4.98)	3.68(3.52)

a) All complexes melted with decomposition. b) The existence of one mole of dichloromethane and acetone and two moles of methanol was confirmed by ^1H NMR.

(0.20 g, 0.25 mmol) were dissolved in a mixed solvent of methanol (30 ml) and bromoform (15 ml). The solution was refluxed for 0.5 hr and then concentrated *in vacuo*. Addition of diethyl ether to the solution caused the precipitation of a pale yellow solid, which was recrystallized from dichloromethane–petroleum ether to afford pale yellow crystals of *cis*-$PtBr(CH_2CN)(PPh_3)_2$. It contained one molecule of dichloromethane.

A suspension of **2** (0.50 g, 0.63 mmol) and lithium iodide trihydrate (0.15 g, 0.80 mmol) in methanol (20 ml) was stirred for 5 hr at room temperature. The white suspension turned into a yellow solid. It was filtered and recrystallized from dichloromethane–diethyl ether to give yellow crystals of *cis*-$PtI(CH_2CN)(PPh_3)_2$. *cis*-$Pt(NCO)(CH_2CN)(PPh_3)_2$ and *cis*-$Pt(NO_2)(CH_2CN)(PPh_3)_2$ were synthesized by the reaction of **2** with potassium cyanate or potassium nitrite in a similar manner, after being stirred for 24 hr at room temperature. *cis*-$Pt(N_3)(CH_2CN)(PPh_3)_2$ was similarly prepared by the reaction of **2** with sodium azide. Heating under reflux for 5 hr was necessary.

Physical properties and analytical data of new cyanomethyl complexes are given in Table 1.

Results and Discussion

Most of the cyanomethyl complexes were prepared by simple metathesis according to

$$MCl(CH_2CN)(PPh_3)_2 + X^- \rightarrow MX(CH_2CN)(PPh_3)_2 + Cl^-$$

For the nitrato and acetato complexes of platinum(II), it was necessary to utilize silver nitrate or silver acetate in order to abstract the chloride ion. However, application of this method to **1a** and **2** was unsuccessful.

An interesting property of the palladium complexes is photochromism. In the solid state, all palladium complexes except the cyano derivative change color (B) when exposed to light, but revert to the original color (A) in the dark. This color change is reversible but not observed in solution. The observed color changes are summarized in Table 2. In contrast to the palladium complexes, neither *cis*- nor *trans*-$PtX(CH_2CN)(PPh_3)_2$ showed similar color changes. Thus the phenomenon seems to be characteristic of the cyanomethyl complexes of palladium(II), but the cause has not been clarified.

Table 2. Photochromism of $PdX(CH_2CN)(PPh_3)_2$

X	N_3	NCO	NO_2	$N(CO)_2C_6H_4$	I
A	yellow	pale yellow	white	white	yellow
B	orange	pale orange	pale orange	red	brown

All the complexes are stable in the air both in the solid state and in solution. They are soluble in chloroform and dichloromethane but sparingly soluble in diethyl ether.

Spectroscopic Features of $MX(CH_2CN)(PPh_3)_2$. ^1H NMR spectral data are given in Table 3. They show that the methylene resonance of complexes prepared from **1a** and **1b** consists of a 1 : 2 : 1 triplet without exception while the same resonance of azido, cyanato, and nitro complexes derived from **2** occurs as a 1 : 1 : 1 : 1 doublet of doublets. For the platinum complexes of the same composition, the triplet always appeared at much higher field relative to the doublet of doublets (*ca.* 0.6 ppm). The coupling constants, ^2J(Pt–H) of the triplets (90.0—109.5 Hz) are much larger than those for the doublet of doublets (76.5—79.5 Hz). The methylene resonance of two azide complexes of platinum (II) illustrates these spectroscopic features (Fig. 1). The results confirm the previous observation based on the spectral data of the chloro complexes and suggest that the methylene resonance, if it satisfies the conditions mentioned above, will provide a method to distinguish *cis*-$MX(CH_2CN)(PPh_3)_2$ from the corresponding *trans* isomer. The difference of the chemical shift of the methylene protons (0.6 ppm) is larger than

Table 3. ^{1}H NMR Data for the cyanomethyl complexes $MX(CH_2CN)(PPh_3)_2$[a]

M	X	$\tau(CH_2CN)$ ppm	^2J(Pt-H) Hz	^3J(P-H) Hz	τ(Ph)[b] ppm
Pt (*trans*)	N_3	9.09 t	102.0	7.5	2.5m, 2.3m
	NCO	9.12 t	103.5	8.0	2.5m, 2.3m
	NO_2	9.03 t	90.0	8.0	2.5m, 2.3m
	$N(CO)_2C_6H_4$	8.89 t	97.0	7.5	2.7m,[e] 2.3m
	NO_3	8.68 t	109.5	7.5	2.5m, 2.3m
	CH_3CO_2[c]	8.95 t	105.5	7.5	2.6m, 2.3m
Pt (*cis*)	N_3	8.50 dd	76.5	9.0, 5.0	2.6m
	NCO	8.52 dd	78.0	9.5, 6.0	2.7m
	NO_2	8.38 dd	78.0	8.5, 5.5	2.7m
	Br	8.19	78.0	[d]	2.6m
	I	7.91	79.5	[d]	2.7m
Pd	N_3	9.21 t		7.5	2.5m, 2.3m
	NCO	9.27 t		7.5	2.5m, 2.3m
	NO_2	9.27 t		7.5	2.5m, 2.3m
	$N(CO)_2C_6H_4$	9.10 t		7.5	2.7m,[e] 2.3m
	I	8.86 t		7.5	2.6m, 2.3m
	CN	9.48 t		7.5	2.5m, 2.3m

a) Spectra were recorded in $CDCl_3$ at 21 °C. Key: m, multiplet; dd, doublet of doublets; t, triplet. b) The approximate center of each multiplet is listed. c) $\tau(CH_3)=9.21$, ^4J(Pt−H)=~3 Hz. d) See text. e) An apparent doublet also appeared at τ 2.90.

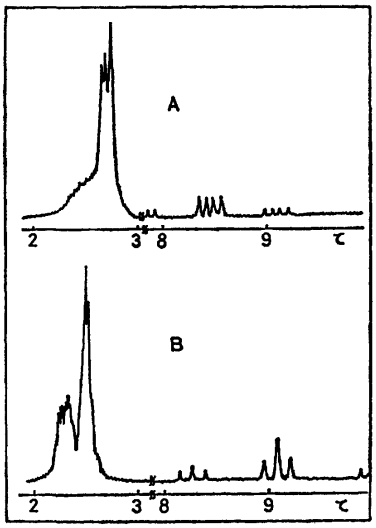

Fig. 1. ^{1}H NMR spectra of (A) *cis*- and (B) *trans*-$Pt(N_3)(CH_2CN)(PPh_3)_2$.

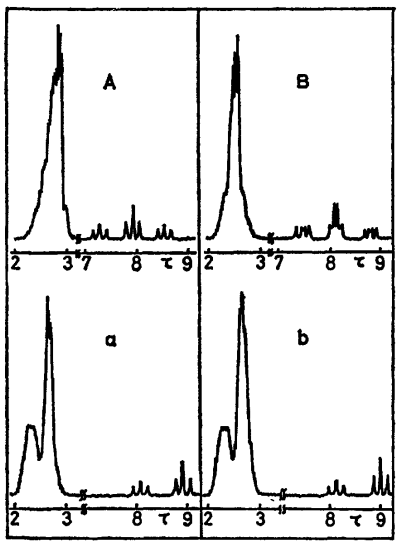

Fig. 2. ^{1}H NMR spectra of the bromo and iodo complexes of platinum(II). (A) *cis*-$PtI(CH_2CN)(PPh_3)_2$, (a) *trans*-$PtI(CH_2CN)(PPh_3)_2$, (B) *cis*-$PtBr(CH_2CN)(PPh_3)_2$, (b) *trans*-$PtBr(CH_2CN)(PPh_3)_2$.

that of the methyl protons for *cis*- and *trans*-$PtX(CH_3)(PEt_3)_2$[11] (*ca.* 0.2 ppm). The larger difference found in the cyanomethyl complexes might be due to the ring current of the coordinated triphenylphosphine.

Nelson *et al.*[12] showed that when two phenylphosphines, in square-planar complexes, are *trans* to one another the phenyl resonance occurs as two broad multiplets, whereas if they are *cis*, only one broad multiplet is usually observed. Figure 1 indicates this is true for the complexes we studied. The phenyl resonance of the cymplexes which exhibited a triplet occurred as two broad multiplets centered at τ 2.3 and 2.5—2.7 while only one multiplet was found for the complexes accompanied by a doublet of doublets. Thus the phenyl resonance of $MX(CH_2CN)(PPh_3)_2$ also provides identification of the stereochemistry of the cyanomethyl complexes.

Recently, Mastin[13] gave a convenient method for directly determining the stereochemistry of the complexes $PtXY(PPh_3)_2$ and proposed the use of the intensity of a band at 550±5 cm^{-1} as a simple criterion for assignment of their stereochemistry. The complexes which showed a doublet of doublets and one multiplet gave a strong absorption at 550±5 cm^{-1} without exception (Table 4). On the other hand, none of the complexes to which the *trans* geometry was assigned on the basis of the methylene and phenyl resonance showed any strong absorption in this region. Thus Mastin's proposal is a useful tool for determining

the geometry of $MX(CH_2CN)(PPh_3)_2$.

For the cyanomethyl complexes discussed so far, one of the three criteria was consistent with the other two, suggesting each of them is normally a reliable criterion in determining the stereochemistry of the complexes $MX(CH_2CN)(PPh_3)_2$.

Geometry of $PtX(CH_2CN)(PPh_3)_2$ (X=Br, I). ^1H NMR spectra of the bromo and iodo complexes of platinum(II) prepared from **2** are shown in Fig. 2, which includes the spectra of the corresponding *trans* isomers for the sake of comparison. The splitting pattern of the methylene resonance differs from that expected for the *cis* geometry. In particular the NMR spectrum of the iodo complex is of interest in that the methylene resonance appeared as a 1 : 2 : 1 triplet which is typical of *trans*-$PtX(CH_2CN)(PPh_3)_2$ (Figs. 1 and 2). However, this triplet is not due to the formation of *trans*-$PtI(CH_2CN)(PPh_3)_2$ since its chemical shift (τ 7.91) and the coupling constant ^2J(Pt-H) (79.5 Hz) are quite different from those of the *trans* isomer[10] (τ 8.88, ^2J(Pt–H)=102.0 Hz). Thus, in order to deduce their geometry, the other criteria were considered. First, the methylene resonance of the bromo (τ 8.19) and iodo (τ 7.91) complexes in question appear at much lower fields than those of the *trans* isomers (τ 8.98 (Br), τ 8.81(I)) and rather close to those of the diphosphine complexes (τ 8.27 (Br), τ 8.03(I)).[10] Furthermore, the coupling constant ^2J(Pt–H) of both complexes (Br= 78.0, I=79.5 Hz) is also comparable with the values found for the other *cis* isomers (Table 3) but smaller than those obtained for the *trans* isomers. Second, the phenyl resonance exhibits only one broad multiplet centered at τ 2.6 (Br) and 2.7 (I), while *trans* isomers gave two broad multiplets (Fig. 2). A strong absorption was observed at 545 cm^{-1} for both bromo and iodo complexes but not for the corresponding *trans* isomers. These spectroscopic data led us to assign the *cis* geometry to the bromo and iodo complexes, although their methylene resonance showed no expected nultiplets. This demonstrates that the spectral pattern of the methylene protons alone is insufficient for deducing the geometry of $MX(CH_2CN)(PPh_3)_2$.

The methylene resonance of *cis*-$PtBr(CH_2CN)(PPh_3)_2$ shows different multiplet structures in the side bands and in the center band (Fig. 2). Similar unusual spectra have been reported for some hydride complexes of platinum(II)[14] and interpreted on the basis of the relative magnitude of the chemical shift difference of two phosphorus atoms and the coupling constant J(Pt–P). Although we could not analyze the spectrum, the observed anomaly might be explained in a similar manner.

Recently, Ros *et al.*[15] have measured the proton decoupled ^{31}P NMR spectrum of *cis*-$PtCl(CH_2CN)(PPh_3)_2$ and observed two sets of doublet with equal intensity. Therefore we assumed an AMX_2 spin system (A=M=P, X=H) for the *cis* complexes which showed a doublet of doublets. The coupling constants ^3J(P–H) for these complexes are listed in Table 3. The unusual methylene resonance of the bromo and iodo complexes cannot be explained in terms of the same spin system. Instead of the ^3J(P–H) we tentatively report a separation between the two inside strong peaks (*ca.* 2.5 Hz) and one between the two outside peaks (*ca.* 14.5 Hz) for the bromo complex, and a separation between the central peak and one of the two outside peaks (*ca.* 7.5 Hz) for the iodo complex.

The methylene resonance of *cis*-$PtX(CH_2CN)(PPh_3)_2$ changes from a doublet of doublets (X=Cl)[10] to a triplet (X=I) through an intermediate pattern (X=Br), but no similar variations have been observed for $PtX(CH_2CN)(P\text{–}P)$ (X=Cl, Br, I). X-Ray structural analysis of $[Rh(P\text{–}P)_2]^+$ [16] and $[Ir(PMePh_2)_4]^+$ [17] indicates that the steric crowding around the central metal atom is larger for the latter. Since triphenylphosphine is more bulky than methyldiphenylphosphine, it is likely that greater distortion from the planar configuration is found in $PtX(CH_2CN)(PPh_3)_2$ than $PtX(CH_2CN)(P\text{–}P)$ and enhanced with increase in the size of a halogen atom. Thus, the observed variation in the methylene resonance might be partially due to this distortion.

^2J(Pt–H). The coupling constant, ^2J(Pt–H) of *trans*-$PtX(CH_2CN)(PPh_3)_2$ is larger than that of *trans*-$PtX(CH_3)(PPh_3)_2$.[18] These two coupling constants are related to one another by a reasonably linear relationship (Fig. 3). The dependence of ^2J(Pt–H) on the substituent R in the Pt–CH_2R moiety is not clear at present, but it is evident that the nitrile group increases the absolute value of ^2J(Pt–H) as is found for the coupling constant ^2J(H–H).[19]

The coupling constant ^2J(Pt–H) of *trans*-$PtX(CH_2CN)(PPh_3)_2$ increases in the order

$$NO_2 < N(CO)_2C_6H_4 < N_3,\ I < NCO,\ Br < Cl < CH_3CO_2 < NO_3^-$$

This is in line with the NMR *trans*-influence order given by Appleton, Clark, and Manzer.[20]

Infrared Spectra. All the complexes studied showed a sharp strong band due to ν(CN) at *ca.* 2200 cm^{-1}. The band is useful in identifying the presence of the CH_2CN group but gives little information on the geometry of the cyanomethyl complexes.

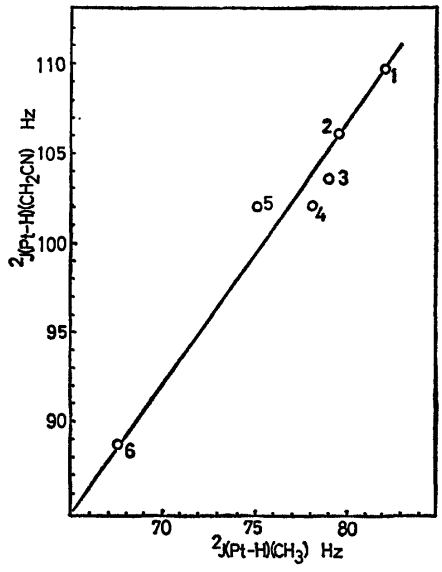

Fig. 3. A plot of ^2J(Pt–H) of *trans*-$PtX(CH_2CN)(PPh_3)_2$ *vs.* ^2J(Pt–H) of *trans*-$PtX(CH_3)(PPh_3)_2$. X=NO_3 (1), Cl (2), Br (3), I (4), N_3 (5), NO_2 (6).

Table 4. Characteristic infrared frequencies (cm^{-1}) in $MX(CH_2CN)(PPh_3)_2$

M	X	ν(CN)	ν(MX)	Band at *ca.* 550 cm^{-1} a)
Pt	N_3	2215 s	375 m	
(*trans*)	NCO	2210 s	335 w	
	NO_2	2220 s	286 m	543 w
	$N(CO)_2C_6H_4$	2215 s	353 m	
	NO_3	2210 s	292 m	546 w
	CH_3CO_2	2210 s		544 w
Pt	N_3	2210 s	378 m	548 s
(*cis*)	NCO	2200 s	360 m	550 s
	NO_2	2210 s	289 m	545 s
	Br	2200 s		545 s
	I	2200 s		545 s
Pd	N_3	2210 s	355 w	
	NCO	2220 s	330 w	
	NO_2	2220 s	280 m	
	$N(CO)_2C_6H_4$	2220 s	350 m	
	I	2200 s		
	CN	2210 s		

a) See text.

A comparison between ν(Pt–X) of *cis*- and *trans*-$PtX(CH_2CN)(PPh_3)_2$ (X=N_3, NCO, NO_2) indicates that the *trans*-influence of the CH_2CN group is slightly higher than that of triphenylphosphine.

We could not prepare *cis*-$PdX(CH_2CN)(PPh_3)_2$ and examine the presence or absence of a strong band at 550±5 cm^{-1}. Thus, for the palladium complexes, the validity of Mastin's criterion is uncertain, although none of the *trans*-$PdX(CH_2CN)(PPh_3)_2$ complexes showed a strong absorption in this region.

References

1) J. M. Jenkins and B. L. Shaw, *J. Chem. Soc., A*, **1966**, 770.
2) D. G. Cooper and J. Powell, *J. Amer. Chem. Soc.*, **95**, 1102 (1973).
3) D. A. Redfield and J. H. Nelson, *Inorg. Chem.*, **12**, 15 (1973).
4) B. E. Mann, B. L. Shaw, and, R. C. Stainbank, *Chem. Commun.*, **1972**, 151.
5) D. G. Cooper and J. Powell, *Can. J. Chem.*, **51**, 1634 (1973).
6) M. H. Chisholm and H. C. Clark, *Inorg. Chem.*, **12**, 991 (1973).
7) D. A. Redfield, J. H. Nelson, R. A. Henry, D. W. Moore, and H. B. Jonassen, *J. Amer. Chem. Soc.*, **96**, 6298 (1974).
8) D. A. Redfield, L. W. Carry, and J. H. Nelson, *Inorg. Chem.*, **14**, 50 (1975).
9) K. Suzuki and H. Yamamoto, *J. Organometal. Chem.*, **54**, 385 (1973).
10) K. Suzuki, H. Yamamoto, and S. Kanie, *J. Organometal. Chem.*, **73**, 131 (1974).
11) F. H. Allen and A. Pidcock, *J. Chem. Soc., A*, **1968**, 2700.
12) J. H. Nelson, A. W. Verstuyft, J. D. Kelly, and H. B. Jonassen, *Inorg. Chem.*, **13**, 27 (1974).
13) S. H. Mastin, *ibid.*, **13**, 1003 (1974).
14) T. W. Dingle and K. R. Dixon, *ibid.*, **13**, 846 (1974).
15) R. Ros, J. Renaud, and R. Roulet, *Helv. Chim. Acta*, **58**, 133 (1975).
16) M. C. Hall(nee Barrett), B. T. Kilbourn, and K. A. Taylor, *J. Chem. Soc., A*, **1970**, 2539.
17) G. R. Clark, B. W. Skelton, and T. N. Waters, *J. Organometal. Chem.*, **85**, 375 (1975).
18) C. D. Cook and K. Y. Wan, *ibid.*, **92**, 2595 (1970).
19) M. Barfield and D. M. Grant, *ibid.*, **85**, 1899 (1963).
20) T. G. Appleton, H. C. Clark, and L. E. Manzer, *Coord. Chem. Rev.*, **10**, 335 (1973).

Metal Complexes of EDTA and Its Related Compounds. II.[1] Geometric Isomers of [Co(X)(trimethylenediamine-*N,N,N'*-triacetate)] Complexes with X=H_2O, NH_3, Cl^-, and CN^-

Myung-Ki Doh,* Hiroshi Ogino, Junnosuke Fujita,** and Kazuo Saito

Department of Chemistry, Faculty of Science, Tohoku University, Aoba, Aramaki, Sendai 980

(Received August 25, 1975)

Three geometric isomers, equatorial-skew, polar-chair and polar-skew, of [Co(X)(trdtra)] ($trdtra^{3-}$=trimethylenediamine-*N,N,N'*-triacetate) have been prepared for each X=H_2O, NH_3 and Cl^-, and the structures assigned mainly by comparing their electronic spectra with those of the equatorial-skew and the polar-chair isomers of *N*-methyl-trdtra complexes reported previously. The cyano complex gives only the polar-chair isomer.

Cobalt(III) complexes containing a quinquedentate trimethylenediamine-*N,N,N'*-triacetate($trdtra^{3-}$) or its *N*-substituted derivatives can have three probable geometric isomers as shown in Fig. 1.[1] Of these, the equatorial-skew and the polar-chair isomers were found for aqua, ammine and chloro complexes of *N*-methyl-trimethylenediamine-*N,N',N'*-triacetate(*N*-Me-$trdtra^{3-}$).[1] In the present study, all the three isomers have been obtained for the aqua, ammine and chloro complexes with trdtra in place of *N*-Me-trdtra.

Experimental

Preparation of Sodium Trimethylenediamine-N,N,N'*-triacetate (Na₃trdtra).* This ligand was prepared by a method similar to that for Na_3*N*-Me-trdtra.[1] An aqueous solution containing 0.3 mol of chloroacetic acid, 0.1 mol of trimethylenediamine and 0.7 mol of sodium hydroxide was heated at 80 °C for 40 min, concentrated under a reduced pressure at 70 °C and filtered to remove sodium chloride. The filtrate was used for the preparation of cobalt(III) complexes without isolating the free ligand.

Preparation of Complexes. [$Co(H_2O)$(trdtra)]: The aqua complex was prepared from cobalt(II) nitrate and the aqueous Na_3trdtra solution and separated into geometric isomers by a method similar to that for [$Co(H_2O)$(*N*-Me-trdtra)]·H_2O.[1] On the separation of three isomers by column chromatography, the order of elution was bluish violet(polar-chair), reddish violet(polar-skew) and violet(equatorial-skew) isomer. Each eluate was evaporated to dryness under a reduced pressure below 40 °C. Pure isomers were obtained by dissolving the residues in a small amount of water and by adding ethanol. The solubility in water increases in the order of the bluish violet, the reddish violet and the violet isomer. Total yield of the three isomers based on trimethylenediamine was about 20% and the ratio of the bluish violet, the reddish violet and the violet isomer was 1 : 1 : 8.

[($Co(NH_3)$(trdra)]: Violet(equatorial-skew), reddish violet(polar-skew) and red(polar-chair) isomers of the complex were obtained by a similar method to that for [$Co(NH_3)$(*N*-Me-trdra]·$2H_2O$.[1] The isomers were eluted from the column in the order given above. The solubility in water increases in the order of the red, the reddish violet and the violet isomer.

H[(Co(Cl)(trdra)]: The violet(equatorial-skew), reddish violet(polar-skew) and bluish violet(polar-chair) isomers of [$Co(H_2O)$(trdtra)] were converted to bluish green(A)(equatorial-skew), bluish green(B)(polar-skew) and greenish blue (polar-chair) isomers, respectively, by a method similar to that for H[Co(Cl)(*N*-Me-trdtra)].[1] The greenish blue isomer includes one mole of crystalline ethanol which can hardly be removed by usual methods.

H[Co(CN)(trdra)]·$2H_2O$: The complex was prepared from the violet aqua complex by a method similar to that for H[Co(CN)(*N*-Me-trdtra)]·$2H_2O$.[1] The reactions with the other isomers of aqua complex gave also the same red cyano complex(polar-chair).

The analytical data for the complexes prepared in this work are summarized in Table 1.

Measurements. Visible and ultraviolet absorption spectra were recorded on a Hitachi 323 recording spectrophotometer. PMR spectra were obtained on a Varian HA-100 spectrometer in a D_2O solution containing sodium 3-trimethylsilyl-1-propanesulfonate(TMS*) as the internal standard. All the measurements were made at room temperature.

Results and Discussion

Figure 1 shows three geometric isomers of the complex [Co(X)(trdtra)]. This complex could have further possible geometric isomers than the three. They have two acetate groups on the tertiary nitrogen coordinated *trans* to each other. Such a form was found in [$Co(NO_2)$((*R*)-pdtra)]$^-$ [2] ((*R*)-pdtra=(*R*)-1,2-propanediaminetriacetate) and [Co(en)((*R*)-H_2pdta)]$^+$ [3] (en = ethylenediamine, (*R*)-pdta = *R*-1,2-propanediaminetetraacetate). However, this form is expected to be stable only for complexes of diamine-tri- or -tetraacetate with bulky groups on carbon atoms of the diamine moiety.[2] In fact, no indication for the presence of more than three isomers was found in the present syntheses of trdtra complexes. Thus, the three isomers for each aqua, ammine and chloro trdtra complex obtained here may have all the *cis* form in which two acetate groups on the tertiary nitrogen are coordinated *cis* to each other as shown in Fig. 1.

Both violet and bluish violet isomers of the aqua complex isomerize to each other in an acid aqueous

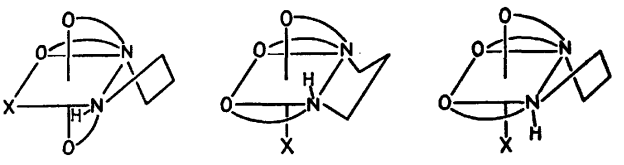

equatorial-skew polar-chair polar-skew

Fig. 1. Three geometric isomers of [Co(X)(trdtra)].

* Present address: Department of Chemistry, Yeung Nam University, Korea.

** Present address: Department of Chemistry, Faculty of Science, Nagoya University, Nagoya.

Table 1. Summary of analytical data for the complexes prepared in this work

Complex	C/%		H/%		N/%	
	Calcd	Found	Calcd	Found	Calcd	Found
Equatorial-skew isomer						
$[Co(H_2O)(trdtra)]\cdot 2H_2O$ (violet)	30.18	30.50	5.35	5.32	7.82	7.87
$[Co(NH_3)(trdtra)]$ (violet)	33.65	33.91	5.02	5.06	13.09	12.98
$H[Co(Cl)(trdtra)]\cdot 3H_2O$ (bluish green(A))	27.39	27.06	5.11	4.61	7.10	7.10
Polar-chair isomer						
$[Co(H_2O)(trdtra)]\cdot H_2O$ (bluish violet)	31.77	31.82	5.04	5.36	8.24	7.89
$[Co(NH_3)(trdtra)]$ (red)	33.65	33.35	5.02	5.00	13.09	12.94
$H[Co(Cl)(trdtra)]\cdot C_2H_5OH\cdot H_2O$ (greenish blue)	32.64	32.47	5.48	5.28	6.92	7.13
$H[Co(CN)(trdtra)]\cdot 2H_2O$ (red)	32.71	33.09	4.94	4.95	11.45	11.64
Polar-skew isomer						
$[Co(H_2O)(trdtra)]\cdot 2H_2O$ (reddish violet)	30.18	29.97	5.35	5.37	7.82	8.02
$[Co(NH_3)(trdtra)]\cdot 2H_2O$ (reddish violet)	30.26	30.82	5.64	5.49	11.77	11.30
$H[Co(Cl)(trdtra)]\cdot 3H_2O$ (bluish green(B))	27.39	27.53	5.11	4.78	7.10	7.55

Table 2. Visible and ultraviolet absorption data of $[Co(X)(trdtra)]$ complexes, $\tilde{\nu}/10^3\ cm^{-1}(\log \varepsilon)$

Equatorial-skew isomer			
$[Co(H_2O)(trdtra)]\cdot 2H_2O$ (violet)	19.53(1.82)	26.32(1.88)	43.86(4.30)
	17.70 sh(1.80)		
$[Co(NH_3)(trdtra)]$ (violet)	18.18(2.03)	26.82(2.19)	44.64(4.37)
$H[Co(Cl)(trdtra)]\cdot 3H_2O$ (bluish green)	19.31(1.75)	25.26(1.94)	40.81(4.30)
	16.18 sh(1.92)		
Polar-chair isomer			
$[Co(H_2O)(trdtra)]\cdot H_2O$ (bluish violet)	18.02(2.02)	26.18(2.02)	43.86(4.26)
$[Co(NH_3)(trdtra)]$ (red)	19.23(2.08)	27.40(1.93)	44.25(4.34)
$H[Co(Cl)(trdtra)]\cdot C_2H_5OH\cdot H_2O$ (greenish blue)	17.18(2.03)	25.12(2.06)	41.67(4.29)
$H[Co(CN)(trdtra)]\cdot 2H_2O$ (red)	20.41(2.15)	28.41(1.97)	43.64(4.33)
Polar-skew isomer			
$[Co(H_2O)(trdtra)]\cdot 2H_2O$ (reddish violet)	18.52(1.91)	26.46(2.01)	44.25(4.27)
$[Co(NH_3)(trdtra)]\cdot 2H_2O$ (reddish violet)	18.58(2.01)	26.98(2.16)	44.25(4.38)
$H[Co(Cl)(trdtra)]\cdot 3H_2O$ (bluish green)	17.12(1.93)	25.44(2.03)	41.32(4.30)

sh: shoulder band.

solution on warming. The equilibrium constant between the two isomers was 0.12 at 63 °C and pH 3, the violet isomer being predominant. On the other hand, the reddish violet isomer shows no spectral change under a similar condition. We reported that the isomerization between the equatorial-skew and the polar-chair isomer takes place more easily than do those between the polar-skew and the other two isomers.[1] Therefore, the violet and the bluish violet isomer can be assigned to either the equatorial-skew or the polar-chair, and the reddish violet isomer to the polar-skew. The assignment for the first two isomers was made by comparing the absorption spectra with those of the corresponding *N*-Me-trdtra complexes. As Fig. 2 and the Table 2 show, the bluish violet isomer exhibits a sharp first absorption band at longer wave length and an intense second absorption band as compared with those of the violet isomer. Such spectral differences resemble those between the two isomers of the aqua *N*-Me-trdtra complex, and the bluish violet isomer can be assigned to the polar-chair, and the violet isomer to the equatorial-skew.

Tanaka *et al.*[4] obtained the violet isomer by thermal decomposition of $K[Co(trdta)]\cdot 2H_2O$ ($trdta^{4-}$=trimethylenediaminetetraacetate) at 250 °C, but they did not describe its structure.

The absorption spectra of three isomers of the ammine complex are shown in Fig. 2. The equatorial and the polar structure correspond to *mer*- and *fac*-$[CoN_3O_3]$ type, respectively.

The red isomer shows a sharp first absorption band and can be assigned to *fac* type.[5] On the other hand, the violet and the reddish violet isomers give broad first absorption bands, indicating *mer* type, although only one *mer* type is expected. To assign the structure of these two isomers, PMR spectrum of the violet isomer was measured in deuterium oxide. The spectrum shows three AB patterns with coupling constants, 16.0, 18.3 and 18.5 Hz (Fig. 3). The AB pattern with 16.0 Hz is attributed to the in-plane acetate protons and those with 18.3 and 18.5 Hz to the out-of-plane acetate protons.[6] Thus, the violet isomer can be assigned to the equatorial-skew (*mer*) and hence, the reddish violet isomer to the *fac*. Of the two *fac* isomers, the red isomer can be assigned to the polar-chair structure, since its absorption spec-

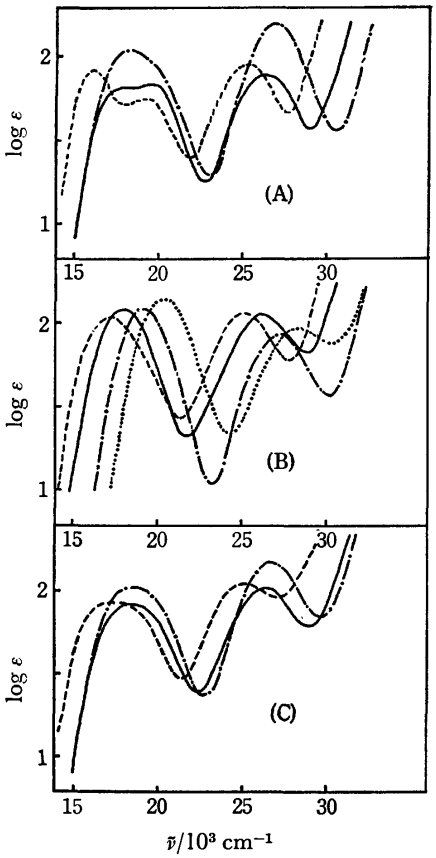

Fig. 2. Absorption spectra of (A): equatorial-skew, (B): polar-chair and (C): polar-skew isomers of [Co(X)(trdtra)] in water except chloro complexes (in 1 M HCl). ——: aqua, – – –: ammine, – – –: chloro, and ·····: cyano complexes.

trum resembles very closely that of the corresponding *N*-Me-trdtra complex. The remaining reddish violet isomer, therefore should have the polar-skew structure, although it gives a broad first absorption band. The broadening of the first absorption band seems to be characteristic of trdtra and its related complexes with a skew conformation in the trimethylenediamine moiety. The [Cotrdta]$^-$ in which the trimethylenediamine moiety takes a skew conformation[7] shows also a broad first absorption band.[8]

The chloro complexes were prepared from the aqua complexes by treating with hydrochloric acid. Since the substitution reactions would be configuration retention[1] under the present experimental condition, the bluish green(A), the bluish green(B) and the greenish blue isomer would have the structure of the equatorial-skew, the polar-skew and the polar-chair, respectively. The absorption spectra of these isomers are shown in Fig. 2. The first absorption bands of the two skew isomers are broader than that of the chair isomer, as seen in the aqua and ammine complexes. The equatorial-skew isomer shows the first absorption band split apparently into two components.

The cyano complex gives always only one red isomer

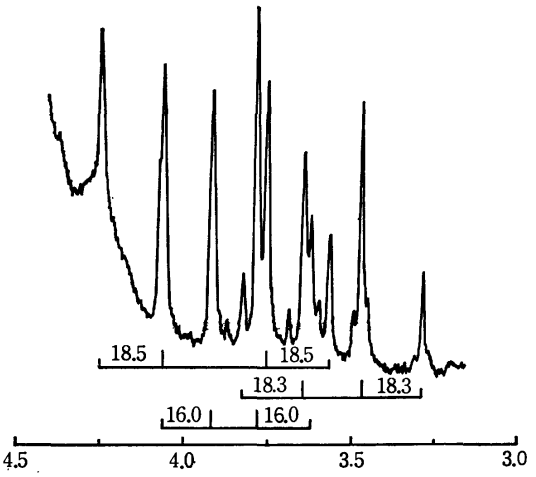

Fig. 3. PMR spectrum of violet (equatorial-skew) [Co(NH_3)(trdtra)] in D_2O (100 MHz). Numerical values in the figure indicate coupling constants in Hz for acetate protons.

on the reactions of any isomer of aqua complex with potassium cyanide. It exhibits a sharp and symmetrical first absorption band which is almost identical with that of the corresponding *N*-Me-trdtra complex (Fig. 2). Thus, the complex would have the same structure as that of the *N*-Me-trdtra complex, the polar-chair.

The absorption spectra of all the complexes obtained in the present study are compared in Fig. 2. As stated previously, the first absorption bands of the skew isomers are broader than those of the chair isomers. The equatorial-skew isomers of the aqua and the chloro complex give the first absorption band split into two components. When the kind of unidentate ligand is changed, the lower frequency components shift to a greater extent than do the higher frequency components, although all the bands shift in accordance with the spectrochemical series.

One of the authors (M. -K. D) is grateful to the Ministry of Education for the Japanese Government Scholarship.

References

1) Part I of this series: M. -K. Doh, J. Fujita, H. Ogino, and K. Saito, This Bulletin, **48**, 874 (1975).

2) C. W. Maricondi and C. Maricondi, *Inorg. Chem.*, **13**, 1110 (1974).

3) M. -K. Doh, H. Ogino, J. Fujita, K. Saito, and N. Tanaka, *Chem. Lett.*, **1974**, 1233.

4) N. Tanaka, K. Sato, and H. Ogino, *Inorg. Nucl. Chem. Lett.*, **8**, 93 (1972).

5) H. Yamatera, This Bulletin, **31**, 95 (1958).

6) G. L. Blackmer and J. L. Sudmeier, *Inorg. Chem.*, **10**, 2019 (1971).

7) H. Ogino, M. Takahashi, and N. Tanaka, This Bulletin, **43**, 424 (1970); R. Nagao, F. Marumo, and Y. Saito, *Acta Crystallogr.*, **B28**, 1852 (1972).

8) N. Tanaka and H. Ogino, This Bulletin, **37**, 877 (1964).

Metal Complexes of Amino Acids. IX.[1] Carbon-13 Nuclear Magnetic Resonances of Cobalt(III) Complexes

Tomoharu AMA and Takaji YASUI

Faculty of Arts and Sciences, Kochi University, Asakura, Kochi 780

(Received September 8, 1975)

The ^{13}C NMR spectra of cobalt(III) complexes containing various amino acids as unidentate or bidentate ligands were measured. The relation between the coordination types and the changes of the chemical shifts was clarified. The changes of chemical shift on coordination of α-amino acid to cobalt(III) (NH_3^+-R-COOH→ NH_3^+-R-COOCo) were about 7 and 1 ppm for the carboxy-carbon and α-carbon, respectively. On the other hand, those on chelation (NH_3^+-R-COOH→chelated amino acid) were about 15 and 5 ppm for each carbon, respectively. However, the changes of chemical shift on chelation of β-alanine were different from those of α-amino acids.

There have been numerous reports containing the application of ^{13}C NMR to organic compounds, and the technique has proven to be a very powerful tool for the structural investigation of organic compounds.[2,3] However, there have been few reports of application of the technique to transition metal complexes, except for organometallic compounds. As octahedrally coordinated Co(III) complexes (Werner type) are diamagnetic and there are no direct bonds between cobalt and carbon atoms in the complexes, many results in organic researches are applicable to these complexes with little modification.[4-10]

Previously we reported the ^{13}C NMR of the *trans(O)*-[Co en_2(aaH)$_2$]X_3 complexes containing various amino acids,[1,11] which were bound to cobalt(III) ion as unidentate ligands through their carboxylate groups, the $-NH_3^+$ groups being free. In the present paper, we wish to describe not only more detailed ^{13}C NMR study of the *trans(O)*-[Co en_2(aaH)$_2$]X_3 complexes, but also new ^{13}C NMR study of the [Co(NH_3)$_4$(aa)]X_2 complexes containing amino acids bound to cobalt(III) ions as bidentate ligands. The relation between the coordination types and the changes in the ^{13}C chemical shifts of amino acid-cobalt(III) complexes will be clarified from the results of ^{13}C NMR spectra.

Experimental

Preparation of Complexes. The *trans(O)*-[Co en_2(aaH)$_2$]-(ClO_4)$_3$ (aaH=glyH, L-alaH, L-valH, L-leuH, L-serH, L-thrH, L-proH, L-hyproH, β-alaH, and γ-ambH (γ-aminobutyric acid)) complexes were prepared by the procedure similar to those described in previous papers.[12,13]

trans(O)-[*Co en_2(ac)$_2$*]*Cl·0.5 NaCl·3.5 H_2O*: This complex was obtained by the modification of Linhard's method.[14] To an aqueous solution containing 5 g of [Co en_2(OH_2)$_2$]-(ClO_4)$_3$ in 10 ml of water, 5 ml of 1 M aqueous solution of NaOH and 10 ml of acetic acid (acH) were added. The mixture was evaporated almost to dryness on steam-bath. After cooling, the resultant was dissolved in 50 ml of water. The solution was poured into a SP-sephadex column (C-25, Na^+ form) and eluted with 5% aqueous solution of NaCl. The first eluted solution (reddish violet) was concentrated in vacuum evaporator till a large excess of NaCl was deposited out. The deposited NaCl was removed off by filtration. A dark red complex, *trans(O)*-[Co en_2(ac)$_2$]Cl, contaminated with some sodium chloride, was obtained by adding ethanol and ether to the filtrate. The crude product was recrystallized from water by adding ethanol and ether.

Found: C, 22.92; H, 6.83; N, 12.95%. Calcd for $C_8H_{29}N_4O_{7.5}Cl_{1.5}Na_{0.5}Co$: C, 22.61; H, 6.88; N, 13.19%.

trans(O)-[*Co en_2(pr)$_2$*]*Cl·0.5 H_2O*: This complex was prepared by a similar method to that for the acetato complex except for using propionic acid (prH).

Found: C, 32.64; H, 7.37; N, 15.26%. Calcd for $C_{10}H_{27}N_4O_{4.5}ClCo$: C, 32.48; H, 7.36; N, 15.15%.

trans(O)-[*Co en_2(bu)$_2$*]*ClO_4·0.5 H_2O*: The complex of butyric acid (buH) was prepared by a procedure similar to those described above. However, this complex was obtained directly from the reacted solution as crystals of perchlorate salt without using SP-sephadex column. The crude product was recrystallized from warm water.

Found: C, 31.34; H, 6.78; N, 11.75%. Calcd for $C_{12}H_{31}N_4O_{8.5}ClCo$: C, 31.20; H, 6.75; N, 12.13%.

[*Co(NH_3)$_4$gly*]*Cl_2·0.5 H_2O*: To an aqueous solution containing 6 g of [Co(NH_3)$_6$]Cl_3 and 1.5 g of glycine in 100 ml of water, about 2 g of activated carbon was added. The mixture was warmed at 60 °C for 30 min with stirring. After filtering off a large amount of insoluble materials, the filtrate was poured into a column containing SP-sephadex (C-25, Ca^{2+} form) and eluted with 3% aqueous solution of calcium chloride. The eluted solution from the orange band was evaporated to about 5 ml in vaccum evaporator. To the concentrated solution 200 ml of ethanol was added, and the desired complex deposited was filtered. The complex was recrystallized from water by adding ethanol.

Found: C, 8.38; H, 6.08; N, 24.54%. Calcd for $C_2H_{17}N_5O_{2.5}Cl_2Co$: C, 8.55; H, 6.10; N, 24.93%.

[*Co(NH_3)$_4$(aa)*]*SO_4 (aa=*L-*ala*, L-*val*, L-*leu*, L-*ser*, L-*thr*, L-*pro*, and L-hypro)*: These complexes were prepared by modification of the methods described in previous papers.[12,15]

[*Co(NH_3)$_4$(β-ala)*]*Cl_2·H_2O*: To an aqueous solution containing 5 g of [Co(NH_3)$_5$(β-alaH)](ClO_4)$_3$[13] in 50 ml of water, 2 g of activated carbon was added. The mixture was warmed at 60 °C for 5 min with stirring. After the solution was filtered, the filtrate was poured into SP-sephadex column. The adsorbed band was eluted with 3% calcium chloride solution, and the solution eluted from the orange band was concentrated by using a vacuum evaporator. The crude complex was deposited by adding ethanol to the concentrated solution. The complex was recrystallized from water by adding ethanol.

Found: C, 11.82; H, 6.59; N, 23.13%. Calcd for $C_3H_{20}N_5O_3Cl_2Co$: C, 11.85; H, 6.64; N, 23.03%.

Measurements. ^{13}C NMR spectra at 25.15 MHz were recorded on a JEOL MFT-100 spectrometer with JEC-6 spectrum computer, in pulsed Fourier transform/proton noise decoupled mode. The field frequency ratio was stabilized by locking to internal D_2O. Peak positions were measured relative to external benzene (capillary). Chemical shifts in

TABLE 1. ^{13}C CHEMICAL SHIFTS AND CHEMICAL SHIFTS-CHANGES OF C_0-CARBONS IN AMINO ACIDS AND FATTY ACIDS

	NH_3^+-R-COOH or R-COOH	NH_3^+-R-COO$^-$ or R-COO$^-$		NH_2-R-COO$^-$		NH_3^+-R-COOCo or R-COOCo		Chelated amino-acids	
	δ (C_0)	δ_{-H} (C_0)	Δ_{-H} (C_0)[a]	δ_{-H_2} (C_0)	Δ_{-H_2} (C_0)[b]	δ_{Co} (C_0)	Δ_{Co} (C_0)	δ_{ch} (C_0)	Δ_{ch} (C_0)
gly	171.1ppm	174.0ppm	+2.9ppm	183.5ppm	+12.4ppm	177.9ppm	+6.8ppm	187.1ppm	+16.0ppm
L-ala	174.0	177.3	+3.3	186.4	+12.4	181.3	+7.3	188.0	+14.0
L-val	172.9	175.8	+2.9	184.7	+11.8	180.2	+7.3	187.0	+14.1
L-leu	172.9			185.7	+12.8	180.0	+7.1	188.0	+15.1
L-ser	171.5	174.1	+2.6	182.6	+11.1	178.4	+6.9	186.6	+15.1
L-thr	171.8	174.2	+2.4	182.7	+10.9	178.7	+6.9	186.7	+14.9
L-pro	173.0	176.1	+3.1	184.4	+11.4	180.1	+7.1	188.0	+15.0
L-hypro	172.8	175.8	+3.0	183.7	+10.9	179.7	+6.9	187.5	+14.7
β-ala	175.9	180.1	+4.2	183.3	+7.4	184.1	+8.2	181.8	+5.9
γ-amb	178.4	183.1	+4.7	185.0	+6.6	187.5	+9.1		
ac	177.5	183.1	+5.6			187.2	+9.7		
pr	180.4	186.3	+5.9			190.7	+10.3		
bu	180.3	185.5	+5.2			189.9	+9.6		
asp[c]	176.6	179.1	+2.5			184.4[e]	+7.8[e]		
glu[d]	178.7	183.5	+4.8			187.4[e]	+8.7[e]		

a) $\Delta_{-H}(C_0)=\delta_{-H}(C_0)-\delta(C_0)$. b) $\Delta_{-H_2}(C_0)=\delta_{-H_2}(C_0)-\delta(C_0)$. c) "asp" indicates the chelated L-aspartate with uncoordinated γ-carboxyl group in $[Co\,en_2(L\text{-asp})]^+$. d) "glu" indicates the chelated L-glutamate with uncoordinated δ-carboxyl group in $[Co\,en_2(L\text{-glu})]^+$. e) These values are for the trinuclear complexes, *trans(O)*-$[en_2Co\{(L\text{-asp})Co\,en_2\}_2]^{5+}$ and -$[en_2Co\{(L\text{-glu})Co\,en_2\}_2]^{5+}$. (Ref. 1)

TABLE 2. ^{13}C CHEMICAL SHIFTS AND CHEMICAL SHIFT-CHANGES OF C_α-CARBONS IN AMINO ACIDS AND FATTY ACIDS

	NH_3^+-R-COOH or R-COOH	NH_3^+-R-COO$^-$ or R-COO$^-$		NH_2-R-COO$^-$		NH_3^+-R-COOCo or R-COOCo		Chelated amino acids	
	δ (C_α)	δ_{-H} (C_α)	Δ_{-H} (C_α)[a]	δ_{-H_2} (C_α)	Δ_{-H_2} (C_α)[b]	δ_{Co} (C_α)	Δ_{Co} (C_α)	δ_{ch} (C_α)	Δ_{ch} (C_α)
gly	40.0ppm	41.5ppm	+1.1ppm	45.4ppm	+5.0ppm	41.3ppm	+0.9ppm	46.1ppm	+5.7ppm
L-ala	49.2	50.7	+1.5	51.8	+2.6	50.1	+0.9	53.4	+4.2
L-val	58.9	60.8	+1.9	62.4	+3.5	60.1	+1.2	62.9	+4.0
L-leu	52.1			54.9	+2.8	52.8	+0.8	55.9	+3.8
L-ser	55.1	56.7	+1.6	58.3	+3.2	56.1	+1.0	58.9	+3.8
L-thr	58.9	60.7	+1.8	62.4	+3.5	59.6	+0.7	62.7	+3.8
L-pro	60.0	61.7	+1.7	62.3	+2.3	61.0	+1.0	65.4	+5.4
L-hypro	58.6	60.3	+1.7	60.9	+2.3	59.6	+1.0	63.8	+5.2
β-ala	31.2	33.6	+2.4	38.1	+6.9	34.1	+2.9	33.4	+2.2
γ-amb	30.8	34.5	+3.7	35.2	+4.4	34.5	+3.7		
ac	19.8	23.7	+3.9			24.3	+4.5		
pr	26.7	30.7	+4.0			31.1	+4.4		
bu	35.7	39.8	+4.1			39.9	+4.2		
asp[c]	36.6	38.7	+2.1			38.5[e]	+1.9[e]		
glu[d]	30.1	33.6	+3.5			33.7[e]	+3.6[e]		

a) $\Delta_{-H}(C_\alpha)=\delta_{-H}(C_\alpha)-\delta(C_\alpha)$. b) $\Delta_{-H_2}(C_\alpha)=\delta_{-H_2}(C_\alpha)-\delta(C_\alpha)$. c), d) and e); see Table 1.

Figures and Tables are reported relative to TMS using the relation $\delta_{TMS}=\delta_{benzene}-128.5$ ppm.

Amino acids, of which concentrations in D_2O, 10% NaOD-D_2O and 10% DCl-D_2O were 2 mmol/ml, were used for NMR measurements. However, L-alaH, L-thrH and L-valH were sparingly soluble in D_2O, so that these amino acids were measured with saturated solutions in D_2O. Acetic and propionic acids which were dissolved in equivolumes of D_2O containing small amount of DCl, and butyric acid which was saturated in D_2O containing small amount of DCl were used. For the measurements of fatty acidate anions, the saturated solutions of their sodium salts in D_2O containing small amount of 10% NaOD were used.

The perchlorate or sulfate salts of the complexes were converted to the more soluble chlorides by treating with anion-exchange resin (Cl^- form). The saturated solutions of the *trans(O)*-$[Co\,en_2(aaH)_2]Cl_3$ complexes which have free $-NH_3^+$ groups were acidified with a small amount of 20% DCl to obtain the complete protonation of free amino groups. The other complexes were examined in saturated solutions. Experimental errors were within ± 0.1 ppm.

Results and Discussion

The ^{13}C chemical shifts of carboxy-carbons (C_0) and α-carbons (C_α) of amino acids and fatty acids are summerized in Tables 1 and 2. The symbols of

$\delta(C_0)$ and $\delta(C_\alpha)$ represent the chemical shifts of the carbons of C_0 and C_α of NH_3^+–R–COOH or R–COOH (in acidic solution), $\delta_{-H}(C_0)$ and $\delta_{-H}(C_\alpha)$ those of NH_3^+–R–COO^- or R–COO^-, and δ_{-H_2} (C_0) and δ_{-H_2} (C_α) those of NH_2–R–COO^-. The chemical shifts of C_0 and C_α of unidentate ligands in *trans(O)*-[Co en_2-$(acid)_2]^+$ and -[Co $en_2(aaH)_2]^{3+}$ complex ions are given by the symbols of $\delta_{Co}(C_0)$ and $\delta_{Co}(C_\alpha)$, respectively. The chemical shifts of C_0 and C_α of the chelated amino acidates in $[Co(NH_3)_4$(amino acidato)$]^{2+}$ complex ions are denoted in the symbols of $\delta_{ch}(C_0)$ and $\delta_{ch}(C_\alpha)$, respectively.

The $\delta(C_0)$ values for α-amino acids were found in the range of 171—174 ppm. However, those for β- and γ-amino acids and fatty acids were observed at a furthermore lower magnetic field region (175.9—180.4 ppm).

The resonances for C_α were observed over a fairly wide region, 18.9—60.0 ppm, for the fatty acids and amino acids having various α-substituted groups.[16,17]

trans*(O)*-[*Co* en_2*(OCO-R)*$_2$] *Type Complexes.* It is known that a large number of amino acids and fatty acids form inert complexes in which they coordinate to cobalt(III) with only carboxyl-groups. When the proton attaching to the carboxyl group was substituted with Co(III), down-field shift was observed in the resonance of carboxy-carbon ($\Delta_{Co}(C_0)$: $\delta_{Co}(C_0)$ minus $\delta(C_0)$). Similar down-field shifts were also observed when the corresponding carboxylate anions were formed. It is interesting that the chemical shifts of coordinated carboxy-carbon ($\delta_{Co}(C_0)$) are closer to those of the deprotonated carboxy-carbon ($\delta_{-H}(C_0)$) than to those of the protonated carboxy-carbon($\delta(C_0)$), (though the $\delta_{Co}(C_0)$ located at lower field region than the $\delta_{-H}(C_0)$) (Table 1).

The $\Delta_{Co}(C_0)$ values of α-amino acids were 7.0± 0.3 ppm. Those of the β- and γ-amino acids and fatty acids were rather diverse, showing 7.8—10.3 ppm. These $\Delta_{Co}(C_0)$ values increase with increasing $\delta_{-H}(C_0)$ values, and it appears that there are linear correlation between them (Fig. 1). For the practical purpose in predicting the $\Delta_{Co}(C_0)$ value, we propose the following relation (Eq. (1)).

$$\Delta_{Co}(C_0) = 0.268\,\delta_{-H}(C_0) - 40.00 \quad (1)$$

We could also obtain linear correlation between Δ_{Co}-(C_0) and $\delta(C_0)$ values in a similar manner as above, though the deviation of the data from the calculated straight line was larger than those in Fig. 1.

The resonances of the C_α in α-amino acids appear over the wide region, compared with those of the carboxy-carbons. This is caused by the different character of the groups attaching to the α-carbon in α-amino acid. In spite of the fairly large difference of the chemical shifts ($\delta(C_\alpha)$), the $\Delta_{Co}(C_\alpha)$ values ($\delta_{Co}(C_\alpha)$ minus $\delta(C_\alpha)$) were approximately constant in α-amino acids, showing 1.0±0.2 ppm.

Similarly to the C_0, the chemical shifts of the C_α in the unidentate coordination form ($\delta_{Co}(C_\alpha)$) are closer to those in the deprotonated form ($\delta_{-H}(C_\alpha)$) than to those in the protonated form ($\delta(C_\alpha)$) (Table 2). In the α-amino acids, the chemical shifts, $\delta_{Co}(C_\alpha)$, appear in a field higher than $\delta_{-H}(C_\alpha)$. This behavior

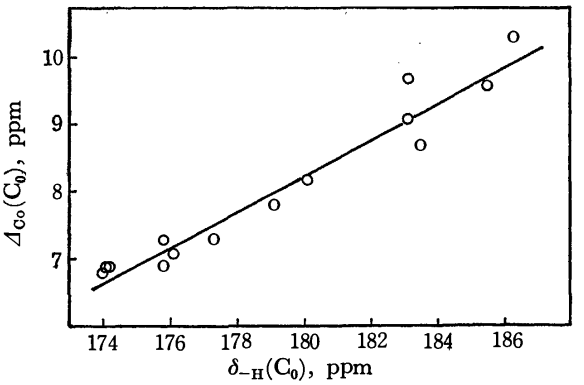

Fig. 1. Variation of $\Delta_{Co}(C_0)$ for the unidenate complexes with $\delta_{-H}(C_0)$ for the fatty acids and amino acids. The line is determined by Eq. (1).

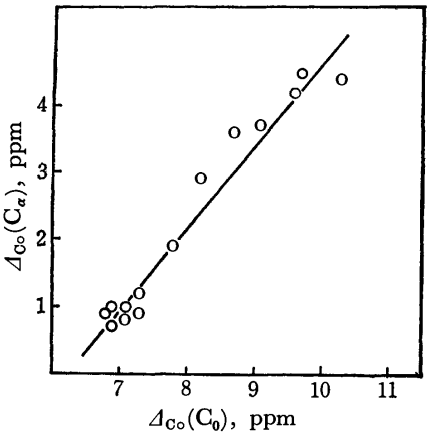

Fig. 2. Variation of $\Delta_{Co}(C_\alpha)$ with $\Delta_{Co}(C_0)$ for the unidentae complexes. The line is determined by Eq. (2).

is different from that of carboxy-carbon, that is, $\delta_{Co}(C_0)$ appears in a field lower than $\delta_{-H}(C_0)$. On the other hand, in β- and γ-amino acids and fatty acids, the $\delta_{Co}(C_\alpha)$ values were observed in a field lower than $\delta_{-H}(C_\alpha)$.

Figure 2 shows the relationship between the $\Delta_{Co}(C_0)$ and $\Delta_{Co}(C_\alpha)$ values. It is evident from the figure that the acid showing a large $\Delta_{Co}(C_0)$ value possesses a large $\Delta_{Co}(C_\alpha)$ value. It is probable that the change in chemical shift of α-carbon, which is neighboring to the carboxy-carbon, becomes larger as the change in chemical shift of carboxy carbon becomes larger. It appears that there are a simple linear correlation between the $\Delta_{Co}(C_0)$ and $\Delta_{Co}(C_\alpha)$ values (Eq. (2)).

$$\Delta_{Co}(C_\alpha) = 1.228\,\Delta_{Co}(C_0) - 7.67 \quad (2)$$

If the extrapolation of linear plot to the smaller value is correct, the following results will be obtained. In the case where the $\Delta_{Co}(C_0)$ value is equal to 0 ppm, that is, in the case where the chemical shift of the coordinated carboxy-carbon is equal to that of the protonated carboxy-carbon, the $\Delta_{Co}(C_\alpha)$ value will be about −8 ppm. Some portion of the −8 ppm may be caused by the direct interaction between the α-carbon and Co(III).

$[Co(NH_3)_4$*(amino acidato)*$]^{2+}$ *Type Complexes.* It is well known that the α-amino acid also forms an

inert complex chelated to Co(III) with both carboxyl and amino groups. The chemical shifts of the carboxy-carbon in the chelated α-amino acids were observed in a field lower than those of the carboxy-carbons in the protonated α-amino acids, that is, the $\Delta_{ch}(C_0)$ values ($\delta_{ch}(C_0)$ minus $\delta(C_0)$) are 15.0±1.0 ppm. The chemical shifts of the chelated carboxy-carbons of α-amino acids are closer to those of their carboxy-carbons in basic solution rather than in acidic and neutral solutions (Table 1).

Figure 3 shows the plots of $\Delta_{ch}(C_0)$ against $\delta(C_0)$ for some α-amino acids. It appears that the $\Delta_{ch}(C_0)$ values decrease with increasing $\delta(C_0)$ values. On the contrary, $\Delta_{Co}(C_0)$ values increase with increasing $\delta(C_0)$ values, as previously described.

Chemical shifts of C_α in chelated α-amino acids, $\delta_{ch}(C_\alpha)$, are closer to $\delta_{-H_2}(C_\alpha)$ than $\delta(C_\alpha)$, $\delta_{-H}(C_\alpha)$ and $\delta_{Co}(C_\alpha)$. The $\Delta_{ch}(C_\alpha)$ ($\delta_{ch}(C_\alpha)$ minus $\delta(C_\alpha)$) values are 4.8±1.0 ppm and independent from $\delta_{ch}(C_0)$, $\delta(C_\alpha)$ and $\delta_{ch}(C_\alpha)$ values. Difference of the interaction between substituting group on the C_α of α-amino acids and the other ligands in the complex, and difference among the natures of amino-nitrogen will be responsible for the variance of the $\Delta_{ch}(C_\alpha)$ values. The α-amino acids with pyrrolidine ring, *i.e.*, L-proline and hydroxy-L-proline, show larger $\Delta_{ch}(C_\alpha)$ values than the other α-amino acids (except for glycine). This may be caused by the large steric interactions between the pyrrolidine ring and the other ligands in the complex, and/or by the coordination of the secondary amino-nitrogen to cobalt(III). However, the $\Delta_{Co}(C_\alpha)$ values of L-proline and hydroxy-L-proline in the complexes in which the amino acids are coordinated to Co(III)

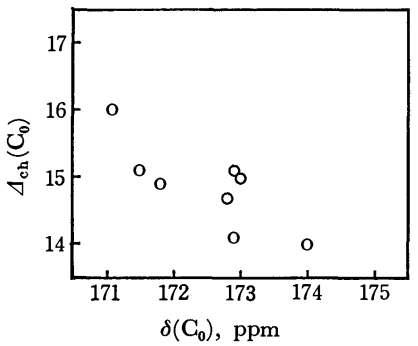

Fig. 3. Plots of $\Delta_{ch}(C_0)$ for the chelated α-amino acids *vs.* $\delta(C_0)$ for the α-amino acids.

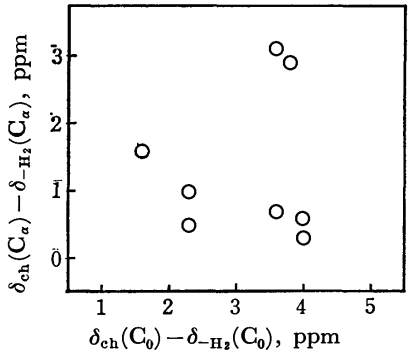

Fig. 4. Plots of $\delta_{ch}(C_0)-\delta_{-H_2}(C_0)$ *vs.* $\delta_{ch}(C_\alpha)-\delta_{-H_2}(C_\alpha)$ for the α-amino acids.

Table 3. Chemical shifts of C_0-carbons in cobalt(III) complexes containing chelated glycine

Complex	δ_{ch} (C_0)	
$[Co(NH_3)_4(gly)]Cl_2$	187.1 ppm	
[Co en$_2$ (gly)]Cl_2[a]	186.7	
C_1-*cis*(*O*)-[Co en (gly)$_2$]Cl[a]	186.0	187.4
trans(*O*)-[Co en (gly)$_2$]Cl[a]	187.5	
C_1-*cis*(*N*)-Li[Co ox (gly)$_2$][a]	186.8	187.2
C_2-*cis*(*N*)-Li[Co ox (gly)$_2$][a]	187.0	
trans(*N*)-Li[Co ox (gly)$_2$][a]	188.6	

a) Preparation; Ref. 18.

with their carboxyl groups as unidentate ligands are nearly equal to those of the other amino acids in the corresponding complexes. This means that there are no steric interactions in these unidentate complexes.

Figure 4 illustrates plots of $\delta_{ch}(C_0)$ minus $\delta_{-H_2}(C_0)$ *versus* $\delta_{ch}(C_\alpha)$ minus $\delta_{-H_2}(C_\alpha)$. It is evident from the figure that L-proline and hydroxy-L-proline differ from the other α-amino acids. It appears that the values of $\delta_{ch}(C_\alpha)$ minus $\delta_{-H_2}(C_\alpha)$ decrease with increasing values of $\delta_{ch}(C_0)$ minus $\delta_{-H_2}(C_0)$, except for L-proline and hydroxy-L-proline.

Table 3 shows the chemical shifts of carboxy-carbons in chelated glycinato complexes. It is interesting that these values (187.3±1.3 ppm) were observed in a considerably narrow range, in spite of the difference of the net charge among the complex ions and the difference among the other ligands.

Chemical shift-changes of chelated β-alanine deviated largely from those of the α-amino acids. The $\delta_{ch}(C_0)$ of β-alanine was observed in higher magnetic field region than $\delta_{-H_2}(C_0)$ and $\delta_{Co}(C_0)$, while the $\delta_{ch}(C_0)$ of the α-amino acids were observed in a field lower than $\delta_{-H_2}(C_0)$ and $\delta_{Co}(C_0)$. Similar result was obtained for the $\delta_{ch}(C_\alpha)$. The factors affecting them could be as follows; size of the chelate ring of β-alanine being larger than that of the α-amino acid; carboxy-carbon and α-carbon of β-alanine being remote from the amino-group, compared with those of the α-amino acids; the absence of amino-group on α-carbon of β-alanine. Since there are insufficient data, it is not clear which factor is a most dominant one.

In summary, we obtained the following results for the Co(III) complexes. The $\Delta_{Co}(C_0)$ and $\Delta_{Co}(C_\alpha)$ values for α-amino acids were about 7 ppm and 1 ppm, respectively. On the other hand, those values for β- and γ-amino acids and fatty acids were 8—10 ppm and 2—4 ppm, respectively. The changes in chemical shifts of carboxy- and α-carbons caused by the chelation of α-amino acids, $\Delta_{ch}(C_0)$ and $\Delta_{ch}(C_\alpha)$, were 14—15 ppm and 4—6 ppm, respectively. The $\Delta_{ch}(C_0)$ and $\Delta_{ch}(C_\alpha)$ values of β-alanine were different from those of the α-amino acids and were 5.8 ppm and 2.2 ppm, respectively.

References

1) Part VIII of this series; T. Yasui and T. Ama, This Bulletin, **48**, 3171 (1975).
2) J. B. Stothers, "Carbon-13 NMR Spectroscopy,"

Academic Press, New York (1972).
3) G. C. Levy and G. L. Nelson, "Carbon-13 Nuclear Magnetic Resonance for Organic Chemists," John Wiley & Sons, New York (1972).
4) M. Hirota, Y. Koike, H. Ishizuka, K. Yamasaki, and S. Fujiwara, *Chem. Lett.*, **1973**, 853.
5) O. W. Howarth, P. Moore, and N. Winterton, *J. Chem. Soc., Dalton*, **1974**, 2771; **1975**, 360.
6) K. D. Gailey, K. Igi, and B. E. Douglas, *Inorg. Chem.*, **14**, 2965 (1975).
7) G. L. Blackmer and T. M. Vickrey, *J. Coord. Chem.*, **3**, 225 (1974).
8) D. A. House and J. W. Blunt, *Inorg. Nucl. Chem. Lett.*, **11**, 219 (1975).
9) T. Yasui, H. Kawaguchi, Z. Kanda, and T. Ama, This Bulletin, **47**, 2393 (1974).
10) T. Yasui, *ibid.*, **48**, 454 (1975).
11) T. Ama and T. Yasui, *Chem. Lett.*, **1974**, 1295.
12) T. Yasui, J. Hidaka, and Y. Shimura, This Bulletin, **39**, 2417 (1966).
13) T. Yasui, T. Ama, H. Morio, M. Okabayashi, and Y. Shimura, This Bulletin, **47**, 2801 (1974).
14) M. Linhard and G. Stirn, *Z. Anorg. Allg. Chem.*, **268**, 105 (1952).
15) T. Yasui and B. E. Douglas, *Inorg. Chem.*, **10**, 97 (1971).
16) A. R. Quirt, J. R. Lyerla, Jr., I. R. Peat, J. S. Cohen, W. F. Reynolds, and M. H. Freedman, *J. Amer. Chem. Soc.*, **96**, 570 (1974).
17) R. Hagen and J. Roberts, *ibid.*, **91**, 4504 (1969).
18) N. Matsuoka, J. Hidaka, and Y. Shimura, This Bulletin, **40**, 1868 (1967).

Selective Activation of Methylene or Methine Groups of Tripeptide-Schiff Bases Coordinated around Nickel(II)

Mamoru FUJIOKA, Yasuo NAKAO, and Akitsugu NAKAHARA

Institute of Chemistry, College of General Education, Osaka University, Toyonaka, Osaka 560

(Received October 16, 1975)

Nickel(II) chelates of the Schiff bases derived from salicylaldehyde and tripeptides such as glycylglycylglycine, glycyl-DL-α-alanylglycine, glycylglycyl-DL-α-alanine, and DL-α-alanylglycylglycine have newly been prepared. The reactivity of methylene or methine groups in the tripeptide moieties of those Schiff base chelates has been studied by PMR spectra in D_2O. It has been found that the methylene or methine protons of the N-terminal amino acid residues are most effectively activated by the coordination around nickel(II) as compared with those of the C-terminal and central amino acid residues.

It is well known that the coordination of amino acids or oligopeptides to metal ions results in activations of their methylene or methine protons of the α-positions.[1,2] In a previous paper,[3] we reported that deuteration of the methylene or methine groups in tripeptides coordinated around nickel(II) occurred most easily for those of the C-terminal as compared with those of the N-terminal and central amino acid residues.

The present paper deals with the preparation of nickel(II) chelates of the Schiff bases derived from salicylaldehyde and tripeptides containing glycine and/or DL-α-alanine, and the results of PMR study of those chelates in view of the selective activation of methylene or methine protons in coordinated tripeptide moieties. The general discussions on the relative reactivity of the methylene or methine protons of oligopeptides and amino acids in coordination are also described on the basis of our recent findings as well as the present investigation.

Experimental

Glycylglycylglycine was purchased from the Protein Research Foundation. Tripeptides[3] containing DL-α-alanine residue and bis(salicylaldehydato)nickel(II)[4] were prepared according to the directions described previously.

Preparation of Nickel(II) Chelates of the Schiff Bases Derived from Salicylaldehyde and Tripeptides. To a mixture of 0.004 mol of each tripeptide and 20 ml of water was added 0.004 mol of bis(salicylaldehydato)nickel(II). The reaction mixture was adjusted to pH 8—10 with concentrated potassium hydroxide solution. After it had been stirred at 30—40 °C for about half an hour, the reaction mixture was filtered. The *N*-salicylidene-glycylglycylglycinato- and -DL-α-alanylglycylglycinato-nickelate(II) were deposited respectively as orange crystals from the filtrate upon the addition of a large quantity of ethanol with vigorous stirring, and were recrystallized from water–ethanol. The *N*-salicylidene-glycyl-DL-α-alanylglycinato- and -glycylglycyl-DL-α-alaninato-nickelate(II) were isolated as orange crystalline products by adding a mixture of ethanol and ether(1 : 1 by volume) with constant stirring. The products were dissolved in a small quantity of water, and then recrystallized by dropwise addition of a mixture of ethanol and ether(1 : 1 by volume). For elemental analysis the products were dried at 70 °C over P_4O_{10}. The results of elemental analysis are shown in Table 1.

Measurements. The visible and ultraviolet absorption spectra were obtained with a Union Giken SM-401 high-sensitivity recording spectrophotometer. The PMR spectra were recorded with a JEOL MH-100 spectrometer and Varian EM-360 60 MHz NMR spectrometer and deuterium oxide was used as a solvent. The chemical shift was measured relative to the sodium salt of trimethylsilylpropane sulfonic acid taken as an internal standard. The pD-adjustment was carried out by the addition of concentrated NaOD–heavy water solution. A Hitachi-Horiba M-5 pH meter equipped with a No. 6026 combined electrode was used after standardization with a Nakarai standard buffer solution (pH 6.86 and 9.18 at 25 °C).

Results and Discussion

We have newly prepared four nickel(II) complexes of the Schiff bases obtained from salicylaldehyde and glycylglycylglycine, glycyl-DL-α-alanylglycine, glycylglycyl-DL-α-alanine, and DL-α-alanylglycylglycine. The complexes were prepared by reactions of each tripeptides with bis(salicylaldehydato)nickel(II) in the pH range 8—10. The visible and ultraviolet absorption spectrum for potassium *N*-salicylideneglycylglycylglycinatonickelate(II) in aqueous solution is shown in Fig. 1. Similar absorption spectra were found also for the nickel(II) complexes of *N*-salicylidene-glycyl-DL-α-alanylglycine, -glycylglycyl-DL-α-alanine, and -DL-α-alanylglycylglycine. Their absorption curves resemble those observed for the nickel(II) complexes which are considered to have the square planar structure.[4,5] On the basis of this finding as well as the results of the elemental analyses (Table 1), it is inferred that the

TABLE 1. ANALYTICAL DATA FOR $K_2[Ni(Sal=tripeptide)]\cdot nH_2O$

Complex	C, %		H, %		N, %	
	Found	Calcd	Found	Calcd	Found	Calcd
$K_2[Ni(Sal=Gly\cdot Gly\cdot Gly)]\cdot 2.5H_2O$	33.02	33.13	3.01	3.43	9.06	8.91
$K_2[Ni(Sal=Gly\cdot Gly\cdot DL\text{-}\alpha\text{-}Ala)]\cdot H_2O$	36.58	36.69	3.57	3.31	9.21	9.17
$K_2[Ni(Sal=Gly\cdot DL\text{-}\alpha\text{-}Ala\cdot Gly)]\cdot 3H_2O$	34.06	34.02	3.68	3.88	8.50	8.51
$K_2[Ni(Sal=DL\text{-}\alpha\text{-}Ala\cdot Gly\cdot Gly)]\cdot H_2O$	36.79	36.69	3.41	3.31	9.18	9.17

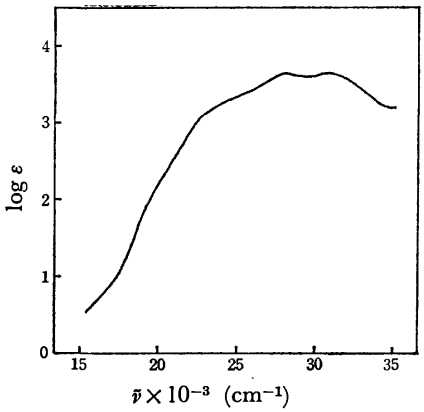

Fig. 1. Visible and ultraviolet absorption spectrum of K_2[Ni(Sal=Gly·Gly·Gly)] in aqueous solution.

structural formulas of nickel(II) complexes produced from salicylaldehyde and each tripeptide can be represented as **1**, in which the symbols (A), (B) and (C)

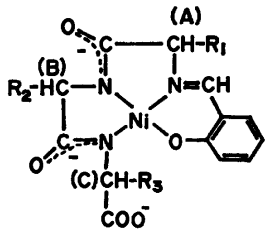

1

indicate methylene or methine protons in the N-terminal, central and C-terminal amino acid residue, respectively.

The PMR spectra at 1—4 ppm of those nickel(II) chelates in deuterium oxide under various conditions are illustrated in Figs. 2—5. The peak identification of the methylene or methine protons for the four chelates, [Ni(Sal=Gly·Gly·Gly)]$^{2-}$, [Ni(Sal=DL-α-Ala·Gly·Gly)]$^{2-}$, [Ni(Sal=Gly·Gly·DL-α-Ala)]$^{2-}$ and [Ni(Sal=Gly·DL-α-Ala·Gly)]$^{2-}$, were carried out on the basis of a comparative inspection of Figs. 2-, 3-, 4- and 5-(a), which were recorded within an hour after preparing each solution. The results of peak assignment necessary for the discussion are inserted in each figure. It is interesting to note that the assignment

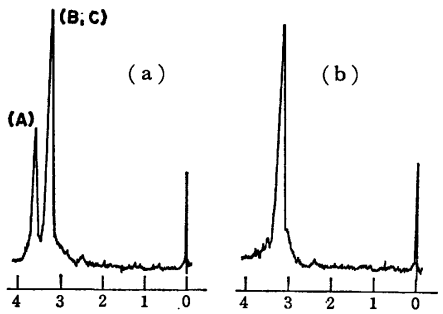

Fig. 2. PMR spectra of [Ni(Sal=Gly·Gly·Gly)]$^{2-}$: (a) pD 11.0, room temp., after 1 h; (b) pD 13.5, 40 °C, after 7 days.

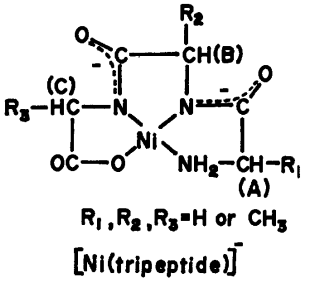

2

for the (A)- and (C)-methylene peaks of the coordinated tripeptide-Schiff bases **1** is the inverse of that for the same peaks of the coordinated simple tripeptides **2**.[3]

It is clearly shown from a comparison of Figs. 2(a) and (b) that the peak at 3.50 ppm arising from the N-terminal methylene protons of triglycine moiety for nickel(II) chelate **1**($R_1=R_2=R_3=H$) almost disappears on allowing the solution to stand at 40 °C, pD 13.5 for 7 days. On the other hand, the peak (3.12 ppm) for the central and C-terminal methylene protons were unchanged under the same condition, though the decrease of the peak(3.12 ppm) was observed in a more severe condition (40 °C, pD 13.5, after 22 days).

In case of [Ni(Sal=DL-α-Ala·Gly·Gly)]$^{2-}$, the doublet methyl signals (1.22 and 1.30 ppm) collapsed on allowing the solution to stand at 40 °C, pD 13.7 for a day, producing a singlet on account of the deuteration of the methine proton of (A), whereas the signals due to the methylene protons of (B) and (C) were almost unchanged (Fig. 3(b)).

Fig. 4(b) illustrates the PMR spectrum of [Ni(Sal=Gly·Gly·DL-α-Ala)]$^{2-}$ recorded after standing the solution at 40 °C and at pD 13.3 for a day, which indi-

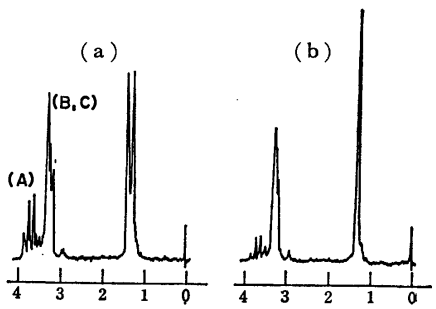

Fig. 3. PMR spectra of [Ni(Sal=DL-α-Ala·Gly·Gly)]$^{2-}$: (a) pD 11.2, room temp., after 1 hr; (b) pD 13.7, 40 °C, after 1 day.

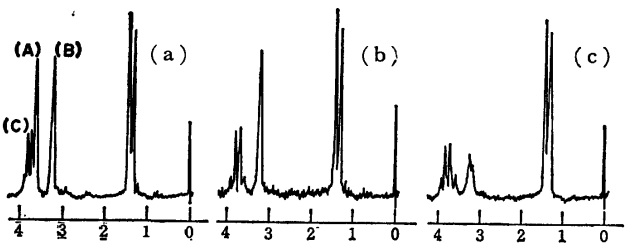

Fig. 4. PMR spectra of [Ni(Sal=Gly·Gly·DL-α-Ala)]$^{2-}$: (a) pD 11.5, room temp., after 1 h; (b) pD 13.3, 40 °C, after 1 day; (c) pD 13.1, 40 °C, after 12 days.

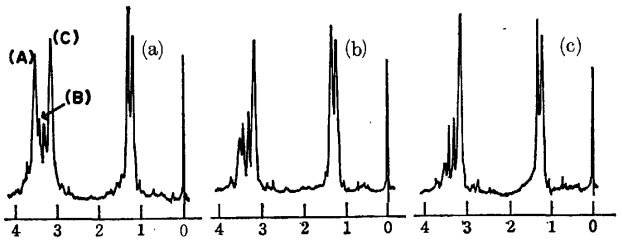

Fig. 5. PMR spectra of [Ni(Sal=Gly·DL-α-Ala·Gly)]$^{2-}$: (a) pD 11.3, room temp., after 1 h; (b) pD 12.5, 40 °C, after 1 day; (c) pD 10.7, 40 °C, after 31 days.

cates that the deuteration is going on (A) methylene groups, whereas the (B) methylene protons do not show any tendency of activation under the condition. However, at 40 °C and at pD 13.1 after 12 days the signal (3.20 ppm) for the (B) methylene group almost disappeared. Even under this condition the methyl doublet at 1.37 ppm remains unchanged, as is seen from a comparison of Fig. 4(a)—(c). The fact suggests that the exchange reaction does not occur at (C) methine group in the *N*-salicylideneglycylglycyl-DL-α-alaninatonickelate(II).

Figure 5(a) shows the PMR spectrum of [Ni(Sal=Gly·DL-α-Ala·Gly)]$^{2-}$, which was recorded within an hour after the preparation of the solution. In this spectrum the signals for the methylene or methine protons of (A), (B) and (C) are not well-separated. The resonance signals at 3.55 ppm and 3.17 ppm are supposed to arise from the methylene protons of (A) and (C), respectively. The signals at 3.33 ppm and 3.43 ppm are attributed to the (B) methine proton, and the remaining two peaks for the (B) methine proton are possibly considered as overlapping with peaks for the (A) and (C) methylene protons. After a day at 40 °C (pD 12.5), the signal at 3.55 ppm due to the (A) methylene proton decreased, but not that at 3.17 ppm (Fig. 5(b)). The methyl doublet at 1.23 ppm and 1.33 ppm remained unchanged under the same condition. Further deuteration of the (A) methylene proton could also be observed, on allowing the solution to stand at 40 °C and pD 10.7 for 31 days. Here the doublet methyl signals exhibited an indication of collapsing to give a singlet, indicating that deuteration began to occur at the (B) methine proton.

The foregoing description on the results of PMR study of nickel(II) chelates of Schiff bases derived from salicylaldehyde and tripeptides can be summarized as follows: (i) the N-terminal methylene or methine protons are more easily activated than the others; (ii) the C-terminal methylene or methine protons cannot be activated in the range of our experimental condition. The former, (i), can be explained by taking into consideration the electron-withdrawing effect of nickel(II) through the azomethine nitrogen atom. And the latter, (ii), may be interpreted as resulting from the absence of the electron-withdrawing effect of nickel(II) through the terminal carboxylate group.

Of interest is the fact that the preferential activation of the methylene or methine protons of tripeptides occurs in the different position (N-, C-terminal or central amino acid residue, respectively) depending upon the modes of tripeptides (chelate **1**, **2** or uncoordinated triglycinate **3**,[6] respectively).

$$\underset{(A)}{NH_2CH_2}CONH\underset{(B)}{CH_2}CONH\underset{(C)}{CH_2}COO^-$$

3

The results of our series of investigations on the selective activation of dipeptides[2,8] and tripeptides[9] in different structures can be summarized as follows: (i) in order to activate the C-methylene or -methine protons of oligopeptides, the coordination of the terminal carboxylate groups of peptides to metal ions is necessary; (ii) in order to activate the N-methylene or -methine groups, the terminal nitrogens of peptides have to be coordinated to metal ions in the form of Schiff bases.

The validity for the foregoing conclusion is also demonstrated by the fact that all the methylene protons in the tetraglycine-nickel(II) chelate **4** shows no tendency of activation after 4 days at 40 °C (pD 13.0).[10]

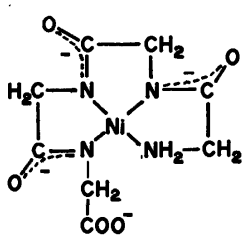

[Ni(Gly·Gly·Gly·Gly)]$^{2-}$

4

This work was supported in part by a grant from the Ministry of Education.

References

1) D. H. Williams and D. H. Busch, *J. Amer. Chem. Soc.*, **87**, 4644 (1965).
2) R. D. Gillard, P. R. Mitchell, and N. C. Payne, *Chem. Commun.*, **1968**, 1150.
3) Y. Nakao, O. Uyama, and A. Nakahara, *J. Inorg. Nucl. Chem.*, **36**, 685 (1974).
4) Y. Nakao and A. Nakahara, This Bulletin, **46**, 187 (1973).
5) S. Yamada and H. Nishikawa, *ibid.*, **36**, 755 (1963).
6) In this mode the central methylene protons (B) are most easily deuterated, see Ref. 7.
7) R. Mathur and R. B. Martin, *J. Phys. Chem.*, **69**, 668 (1965).
8) O. Uyama, Y. Nakao, and A. Nakahara, This Bulletin, **46**, 496 (1973).
9) Ref. 3 and this paper.
10) The solution of the nickel(II)-tetraglycine complex **4** was prepared by the method of Kim *et al.*: M. K. Kim and A. E. Martell, *J. Amer. Chem. Soc.*, **91**, 872 (1969).

An INDO Molecular Orbital Approach to the Proton Affinity of Oxygenated Compounds

Katsutoshi OHKUBO, Kohji TSUCHIHASHI, Toshiaki YOSHIDA, and Masahide OKADA

Department of Synthetic Chemistry, Faculty of Engineering, Kumamoto University, Kurokami, Kumamoto 860

(Received June 19, 1975)

The correlation between the gas-phase proton affinities of aliphatic oxygenated compounds (alcohols, acids, and esters and their electronic structures was investigated by means of an INDO-MO theory. There appears to be a satisfactory linear-dependence of the proton affinities with the energy difference between the parent molecule and the energetically most stable protonated species and with the bond energy of the oxygen-proton bond, although the above energies are overestimated in comparison with the proton affinities. The proton affinities are also predicted with a sufficient accuracy using the first ionization potential and the electron density of the oxygen atom (especially, the % p-character in the oxygen lone-pairs) of the parent molecule.

Mass spectroscopic investigations of ion-molecule reactions have recently centered around the determination of the relative proton affinities (Brønsted base strengths) of nitrogenated[1–5] and oxygenated[6–12] compounds, with a particular view to the dependence of the proton affinities on their molecular structures, especially on their substituents and functional groups.[2,5,12] From the trends observed experimentally for a correlation between the proton affinity and the molecular structure, it has already been noted that the proton affinities for similar molecules depend directly on the ionization potentials of the parent molecules.[13]

There have also appeared the extended Hückel[14] and *ab initio*[15–17] MO-theoretical treatments of the proton affinities of small molecules; the former MO-calculations gave energies which are of the correct order of magnitude but are too small, while the latter MO-calculations indicated appreciable percentage errors of estimated proton affinities with respect to the experimental values. Very recently, a potential model based on the Hellmann-Feynman theorem[18] combined with CNDO/2 wave functions has been proposed by Davis and Rabalais[19] for relating the proton affinities to inner-shell electron binding energies.

Recently, the authors began a semi-empirical INDO-MO study on the gas-phase proton affinities of several oxygenated compounds (aliphatic alcohols, acids, and esters) to investigates how the proton affinities depend on the electronic properties of the molecule. In this paper, the calculated results are reported with particular reference to the correlations between the proton affinities and various calculated energies such as theoretical proton affinities, bond energies for the oxygen-proton bond, ionization potentials, *etc.*

Method of Calculation

The gas-phase proton affinities (*PA*) of the following five series of aliphatic oxygenated compounds were investigated in this work: (a) formates, HCO_2R (R= H, CH_3, CH_3CH_2, and $CH_3CH_2CH_2$), (b) methyl esters, RCO_2CH_3 (R=H, CH_3, and CH_3CH_2), (c) acetates, CH_3CO_2R (R=H, CH_3, CH_3CH_2, and $CH_3CH_2CH_2$), (d) acids, RCO_2H (R=H, CF_3, CH_3, and CH_3CH_2), and (e) alcohols, ROH (R=H, CH_3, CH_3CH_2, and $CH_3CH_2CH_2$) (see Table 1). All calculations for the above compounds and their protonated species were performed using the INDO-MO method[20] which is relatively reliable for bond angles, although less so for bond lengths.[21] The approximations involved in the INDO are not repeated here, because they have been described in detail in Ref. 20.

The energy, ΔE, for the calculated proton affinity was obtained from the energy difference between the protonated species (BOH^+) and the parent molecule (BO):

$$BO + H^+ \longrightarrow BOH^+ \quad (1)$$

Since the energy of the proton is zero, the ΔE value can be given by:

$$\Delta E = E(BO) - E(BOH^+) \quad (2)$$

where the ΔE value is positive because $E(BOH^+)$ is normally a larger negative number than $E(BO)$.

The bond index of E_{OH^+} for the oxygen-proton bond of the protonated species was evaluated by means of a method of energy partitioning:[22]

$$E_{OH^+} = E^R_{OH^+} + E^V_{OH^+} + E^J_{OH^+} + E^K_{OH^+} + E^N_{OH^+} \quad (3)$$

where each energy term represents, respectively, the resonance, potential, electronic repulsion, electronic exchange interaction, and nuclear repulsion energies, which can be obtained by the usual manner described in detail in Ref. 22.

Results and Discussion

Geometries of Parent Molecule and Protonated Species. First, the geometries used for the parent molecules are discussed by comparing calculated dipole moments (μ_{calcd}) and first ionization potentials (I_{calcd})[23] with measured experimentally (μ_{obsd} and I_{obsd}). The dipole moments and ionization potentials are summarized in Table 2. Although exact agreements were not found between calculated and experimental dipole moments and ionization potentials, the approximate agreement between the calculated and observed dipole moments suggests that the charge distributions in the parent molecules appear to be plausible, while an almost constant ratio of I_{obsd}/I_{calcd} (around 0.8) indicates a systematic deviation of the calculated results from the experimental results. The deviations found for the dipole moments and ionization potentials may not be due to an inadequacy of the geometries but to the approximations involved in the INDO method, because it is well known that the INDO calculation trends to give an incomplete evaluation of the dipole

TABLE 1. ASSUMED BOND LENGTHS AND ANGLES FOR OXYGENATED COMPOUNDS AND THEIR PROTONATED SPECIES[a)]

Series	No.	Molecule	$R_{C=O}$	R_{CO}	R_{OH}	∠OCO	∠COC	∠COH
Formates	1	$HCO_2H(H^+)$	1.245	1.312	0.95	124°18'		107°48'
	2	$HCO_2CH_3(H^+)$	1.200	1.334	(0.96)	125°52'	114°47'	(114°47')
	3	$HCO_2C_2H_5(H^+)$	1.200	1.334	(0.96)	125°52'	114°47'	(114°47')
	4	$HCO_2C_3H_7(H^+)$	1.200	1.334	(0.96)	125°52'	114°47'	(114°47')
Acetates	5	$CH_3CO_2H(H^+)$	1.240	1.430	0.95	130°		107°48'
	6	$CH_3CO_2CH_3(H^+)$	1.220	1.360	(0.96)	124°	113°	(116°)
	7	$CH_3CO_2C_2H_5(H^+)$	1.200	1.334	(0.96)	125°52'	114°47'	(114°47')
	8	$CH_3CO_2C_3H_7(H^+)$	1.200	1.334	(0.96)	125°52'	114°47'	(114°47')
Methyl esters	1	$HCO_2H(H^+)$	1.245	1.312	0.95	124°18'		107°48'
	2	$HCO_2CH_3(H^+)$	1.200	1.334	(0.96)	125°52'	114°47'	(114°47')
	6	$CH_3CO_2CH_3(H^+)$	1.220	1.360	(0.96)	124°	113°	(116°)
	9	$C_2H_5CO_2CH_3(H^+)$	1.220	1.360	(0.96)	124°	113°	(114°47')
Acids	10	$CF_3CO_2H(H^+)$	1.240	1.430	0.95	130°		107°48'
	1	$HCO_2H(H^+)$	1.245	1.312	0.95	124°18'		107°48'
	5	$CH_3CO_2H(H^+)$	1.240	1.430	0.95	130°		107°48'
	11	$C_2H_5CO_2H(H^+)$	1.240	1.430	0.95	130°		107°48'
Alcohols	12	$H_2O(H^+)$			0.9572			
	13	$CH_3OH(H^+)$		1.421	0.958			110°15'
	14	$C_2H_5OH(H^+)$		1.480	0.958			110°15'
	15	$C_3H_7OH(H^+)$		1.480	0.958			110°15'

a) All values except those in parentheses were commonly used for the parent and protonated compounds, but the values in the parentheses were given only for the protonated species.

moments and an overestimation of the ionization potentials.

With regard to the geometries of the protonated compounds, it is noteworthy that the C=O bond length of the parent molecule is lengthened by the protonation so that it is nearly equal to the single C–O bond length,[16,17,24)] while the O–C–O bond angle is not so different for the parent molecule and the protonated species. For protonated formic acid, R_{CO}=1.31 Å ($R_{OH}=R_{OH^+}$=0.979 Å) and ∠OCO=124 ° have been given by Ros,[24)] and R_{CO}=1.279 Å ($R_{OH}=R_{OH^+}$= 0.96 Å) have been assumed by Csizmadia *et al.*[16)] The INDO optimization of the geometry for the above compound gave R_{CO}=1.30 Å and ∠OCO=118 °, together with ∠COH=∠COH$^+$=120 °, R_{CH}=1.12 Å, and $R_{OH}=R_{OH^+}$=1.04 Å. For simplicity of computation in the present work, the bond lengths and angles for the protonated compounds were taken to be the same as those (supplied by a standard compendium[25)]) for the parent molecules, as shown in Table 1. Regarding the values of R_{CO}, R_{OH^+}, and ∠COH$^+$, for the protonated species, they were taken to be as follows on the basis of the R_{CO}, R_{OH}, and ∠COH (or ∠COR) values of the parent molecules: R_{CO} of C–OH$^+$=R_{CO} of C–OH or C–OR, $R_{OH^+}=R_{OH}$, and ∠COH$^+$= ∠COH or ∠COR. If we assume the geometries listed in Table 1 to be equilibrium geometries, the force constants (K_{AB})[26)] for the protonated compounds are evaluated to be K_{CO}=4.04–6.65 mdyn/Å and K_{OH}=7.62 mdyn/Å; the former value is somewhat small in comparison with K_{CO}=8.11 mdyn/Å given by Ros[24)] for protonated formaldehyde. Furthermore, the INDO calculations gave the following relative stabilities of the protonated conformers in the case of R=H, although the difference in the total energies of the isomers is very small: I(−43.834 a.u.)>II (−43.830 a.u.)>III(−43.827 a.u.) in the protonated formates; IV(−52.238 a.u.)>V(−52.225 a.u.) in the protonated acetates; VI(−52.285 a.u.)>VII(−52.284 a.u.)>VIII(−52.283 a.u.)>IX(−52.278 a.u.) in the protonated methyl esters. The INDO calculation tends to underestimate the electron-electron repulsions,[20,27)] so that the *trans-trans* isomer, VII, was calculated to be more stable than the *cis-cis* isomers such as IX. As a matter of fact, alkoxy-protonated isomers such as X and XI are less stable than such keto-protonated isomers as I, II, and III. For example,

Protonated formates

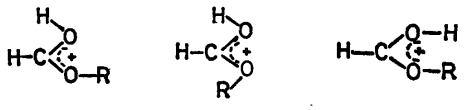

cis-trans I *cis-cis* II *trans-trans* III

Protonated acetates

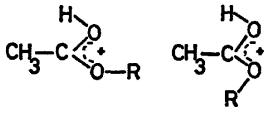

IV V

Protonated methyl esters

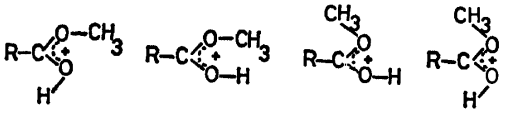

VI VII VIII IX

Table 2. Dipole moments and first ionization potentials for oxygenated compounds

Compound No.	μ_{calcd}/D	μ_{obsd}/D	I_{calcd}/eV	I_{obsd}/eV
1	1.441	1.415[a]	13.74	11.05[j]
2	1.333	1.52[b]	13.52	10.92[k]
3	1.436	1.81[c]	13.33	10.5[l]
4	1.487		13.28	
5	1.053	1.50[d]	13.25	10.35[j]
6	1.343	1.67[e]	12.95	10.92[k]
7	1.353	1.82[f]	12.62	10.09[j]
8	1.365		12.60	
9	1.362		12.60	10.5[l]
10	2.283	2.28[g]	14.12	
11	1.089	1.74[g]	12.84	10.47[m]
12	2.182	1.846[h]	16.30	12.69[n]
13	1.979	1.83[i]	14.42	10.85[j]
14	1.919	1.80[i]	14.26	10.50[j]
15	1.906	1.79[i]	14.20	10.15[o]

a) H. Kim, R. Keller, and W. D. Gwinn, *J. Chem. Phys.*, **37**, 2748 (1962). b) E. Bock, *Can. J. Chem.*, **45**, 2761 (1967). c) J. M. Rineros and F. B. Wilson, *J. Chem. Phys.*, **46**, 4605 (1967). d) J. O. Jenkins and J. W. Smith, *J. Chem. Soc., B*, **1970**, 1538. e) C. H. Townes and A. L. Schawlow, "Microwave Spectroscopy," McGraw-Hill, New York (1955). f) Y. Koga, H. Takahashi, and K. Higasi, This Bulletin, **47**, 84 (1974). g) S. S. Krishnamurthy and S. S. Soundarajan, *Tetrahedron*, **24**, 167 (1968). h) G. Birnbaum and S. K. Chatterijie, *J. Appl. Phys.*, **23**, 220 (1952). i) D. A. Ibbitson and L. F. Moore, *J. Chem. Soc., B*, **1967**, 80. j) K. Watanabe, *J. Chem. Phys.*, **26**, 542 (1957). k) C. J. Varsel, F. A. Morrell, F. E. Resnik, and W. A. Powell, *Anal. Chem.*, **32**, 182 (1960). l) A. B. King and F. A. Long, *J. Chem. Phys.*, **29**, 374 (1958). m) J. D. Morrison and A. J. C. Nicholson, *ibid.*, **20**, 1021 (1952). n) L. P. Lindeman and J. G. Guffy, *ibid.*, **29**, 247 (1958). o) A. J. Harrison, B. J. Cedesholm, and M. A. Terwillger, *ibid.*, **30**, 355 (1959).

in the case of R=H (the bond lengths and angles of X and XI were taken to be the same to those of I, II, or III), the planar species, X, is less stable than I by 8.79 kcal/mol, and the nonplanar species, XI, is

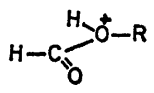

planar

X

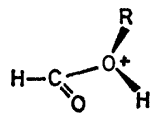

nonplanar

(H-OH plane perpendicular to O-C=O plane)

XI

12.55 kcal/mol higher than I. Although the relative stabilities of the protonated isomers on the basis of the INDO calculation results produce some discrepancies in connection with those determined by NMR observations,[28] the energetically most stable *cis-trans* conformers, I, IV, and VI which were predominantly detected by NMR spectroscopy[28] will be used in the discussions developed below.

Ionization Potential vs. *Proton Affinity.* The calculated first ionization potentials (I_{calcd}) for the protonated compounds in Table 1 were evaluated to be higher by 0.25—0.43 a.u. than those for their parent molecules. This trend can be well explained by the decrease in the electron densities of the oxygen lone-pair orbitals due to the protonation, which causes a lowering of the HOMO (the highest-occupied MO) localized by the so-called lone-pairs. If the nonbonding lone-pair orbitals play a predominant role in the protonation, the I_{calcd} values for the parent molecules may directly correlated with the proton affinities (*PA*). This consideration is related to the fact that the proton affinity corresponds to the Brønsted base strength which is inversely proportional to the ionization potential. As shown in Fig. 1, the *PA* values are satisfactorily linearly dependent on the reciprocal values of I_{calcd} ($1/I_{calcd}$) throughout the series investigated:

$$PA = a_1/I_{calcd} + b_1 \quad (4)$$

where a_1 and b_1 are constants specified by a least squares error analysis, and are listed in Fig. 1.

Equation (4) is particularly useful, because it predicts the proton affinities within a relative error of 2% of the experimental values.

We should here mention the limit of the linear cor-

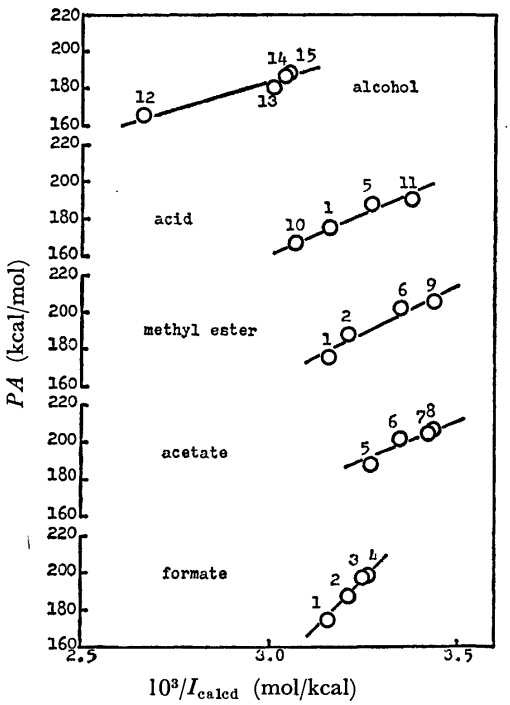

Fig. 1. Plots of *PA vs.* $1/I_{calcd}$.

Series	$10^{-5}\,a_1$	$10^{-2}\,b_1$
Formate	2.17	5.09
Acetate	1.01	1.40
Methyl ester	1.01	1.38
Acid	0.79	0.75
Alcohol	0.56	0.15

Table 3. Proton affinities and electronic properties of oxygenated compounds

Series and compound No.	PA[a] kcal/mol	M_O	M_O^{HO}	N_p	$N(s)_{lp}$	$N(p)_{lp}$	$N(p)_{lp}^{HO}$	M_H	ΔE kcal/mol
Formates									
1	175	6.367	1.476	4.581	1.786	1.912	1.467	0.700	293.0
2	188	6.347	1.316	4.583	1.764	1.894	1.298	0.702	310.6
3	198	6.351	1.272	4.587	1.764	1.894	1.248	0.706	315.0
4	198	6.354	1.208	4.590	1.764	1.894	1.174	0.708	316.9
Acetates									
5	188	6.347	1.277	4.562	1.785	1.911	1.253	0.727	276.1
6	202	6.373	1.312	4.598	1.775	1.910	1.287	0.722	320.6
7	205	6.380	1.248	4.798	1.766	1.907	1.207	0.724	335.1
8	207	6.382	1.231	4.616	1.766	1.908	1.189	0.725	337.0
Methyl esters									
1	175	6.367	1.476	4.581	1.786	1.912	1.467	0.700	293.0
2	188	6.347	1.316	4.583	1.764	1.894	1.298	0.702	310.6
6	202	6.373	1.312	4.598	1.775	1.910	1.287	0.722	320.6
9	205	6.381	1.148	4.605	1.776	1.909	1.104	0.725	324.4
Acids									
10	167	6.261	0.917	4.478	1.783	1.904	0.879	0.706	239.7
1	175	6.367	1.476	4.581	1.786	1.912	1.467	0.700	293.0
5	188	6.347	1.277	4.562	1.785	1.911	1.253	0.727	276.1
11	190	6.351	1.114	4.566	1.785	1.904	1.077	0.730	280.5
Alcohols									
12	165	6.335	2.000	4.611	1.724	2.000	2.000	0.629	255.4
13	180	6.298	1.433	4.603	1.695	1.970	1.433	0.635	261.7
14	187	6.315	1.247	4.604	1.711	1.977	1.247	0.652	276.7
15	189	6.318	1.211	4.606	1.712	1.976	1.211	0.654	279.2

a) From Ref. 12.

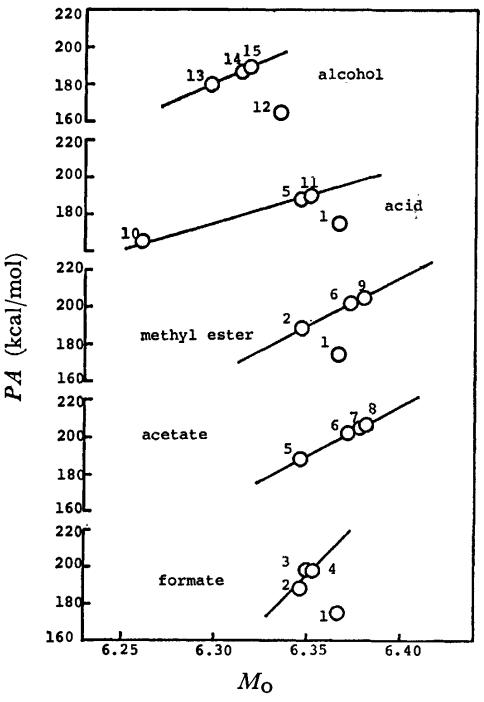

Fig. 2. Plots of PA *vs.* M_O.

relation between the PA and I_{calcd} values. The approach to a constant PA or I_{calcd} value with increasing chain length of R was observed for all the series investigated, especially for the formates, acetates, and alcohols. This may coincide with the fact that oxygenated compounds with a chain length greater than C_3 have a limited proton affinity.[12]

Electron Density of the Oxygen Atom vs. *Proton Affinity.* The electron density of the oxygen atom of BO in reaction(1), M_O, should be a measure of the proton affinity, because the electron density of such hetero-atoms as nitrogen and oxygen relates directly to the base strength.[29] As expected, the M_O values for the parent molecules are in satisfactory agreement with their PA values with some exceptions (H_2O and HCO_2H). A similar correlation with almost the same degree of accuracy as that in Eq. (4) can be seen from Fig. 2.

In connection with the linear correlation between the M_O and PA values, the electron densities of the oxygen p-orbitals (denoted as N_p; $N_p=N_{p_x}+N_{p_y}+N_{p_z}$) may correlate more directly with the proton affinities. In this respect, the linear correlations between the PA and N_p values throughout the series are found to be more satisfactorily established than those between the PA and M_O values, as may be seen from Table 3.

It is of interest here to notice the contributions of the electron densities of the oxygen s and p lone-pairs in the parent molecule to the proton affinity: the nonbonding lone-pair p-orbital expands perpendicularly to the C–O bond axis in the direction of the plane on which almost all the atoms (except the H atoms of the substituent R) are located. Although the electron densities of the lone-pair s-orbital ($N(s)_{lp}$)

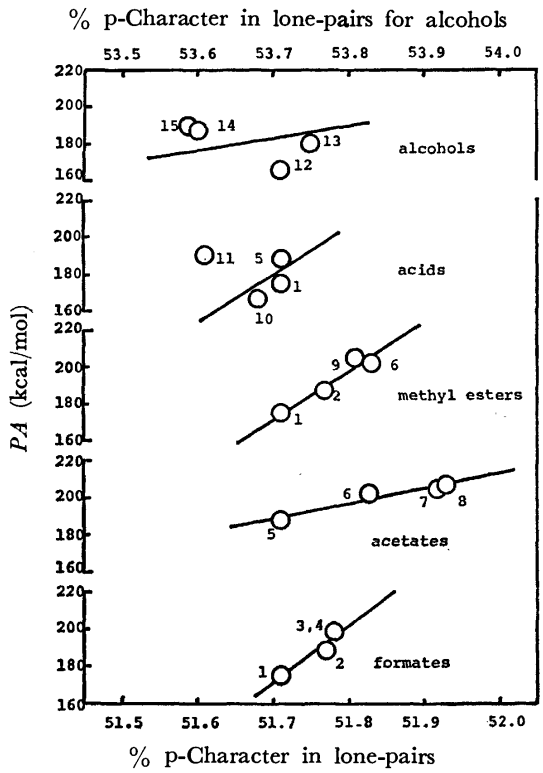

Fig. 3. Plots of % p-character in lone-pairs of parent molecule *vs.* proton affinity.

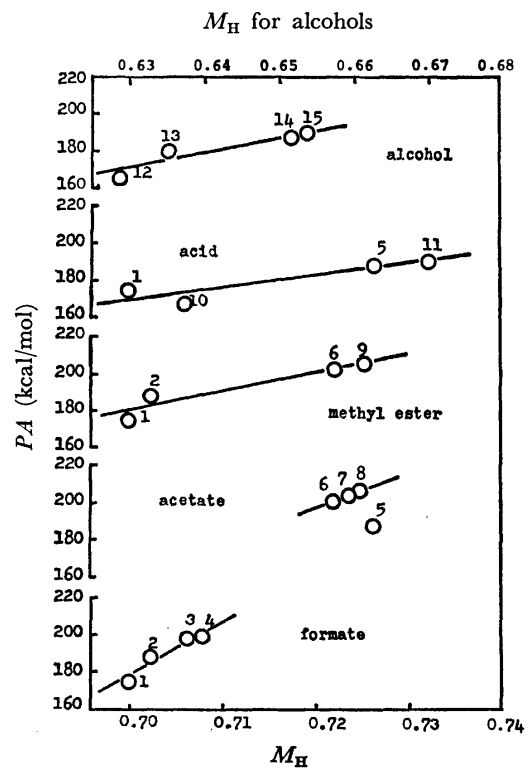

Fig. 4. Plots of *PA vs.* M_H.

and of the lone-pair p-orbital ($N(p)_{lp}$) are not linearly well related to the *PA* values (see Table 3), the % p-character in the lone-pairs, which is defined by $10^2N(p)_{lp}/(N(s)_{lp}+N(p)_{lp})$, correlates directly with the proton affinity, as shown by Fig. 3. Unfortunately, the % p-character of the lone-pairs of the alcohols, which are not completely accurate because of an unsufficient estimation of the $N(p)_{lp}$ values, showed marked deviations from the straight line. This linear relationship between the % p-character of the lone-pairs and the *PA* value coincides with the fact that nitrogen and oxygen bases with a high s-character of their lone-pairs have small *PA* values.[30]

Bearing in mind that the *PA* values correlate well with the I_{calcd} values, the electron density of the oxygen atom or of the nonbonding lone-pair p-orbital at the HOMO (denoted respectively as M_0^{HO} and $N(p)_{lp}^{HO}$) may correlate directly with the *PA* values. However, as may be seen from Table 3, the *PA* values depend inversely on the M_0^{HO} values which correspond roughly to the $N(p)_{lp}^{HO}$ values. This suggests that the proton affinity cannot be explained simply by the electron density at the HOMO of the parent molecule, that is, electrons at lower MOs (next to the HOMO, *etc.*) may participate in the protonation reaction.

We will now examine the possibility of a correlation between the proton affinities and the electron densities about the proton of the protonated compounds, M_H. As can be seen from Fig. 4, there exists a sufficiently linear correlation between them throughout the series. This is well explained by the following reasons: (a) the proton affinity correlates with the proton 1s chemical shift,[19] and (b) the proton chemical shift has also a correlation with the M_H values, as has been found in the NMR results for halomethanes.[31]

Calculated Proton Affinity. As shown in Table 3, the calculated proton affinities, ΔE, obtained from Eq. (2) are larger than the experimental proton affinities and increase with an increase in the chain length of the alkyl substituent (R). The *PA* values of all the oxygenated compounds investigated are roughly linearly correlated with the ΔE values:

$$PA = 0.388\Delta E + 75.65 \text{ kcal/mol} \quad (5)$$

However, Eq. (5) is incomplete, because a least-squares error analysis of the relation expressed by Eq. (5) has a maximum relative error of 8.2%. As shown in Fig. 5, completely linear lines can be obtained from the plots of *PA vs.* ΔE for each series and can be expressed by the following equation with a maximum error of 3%:

$$PA = a_2\Delta E + b_2 \text{ kcal/mol} \quad (6)$$

where a_2 and b_2 are constants specified in Fig. 5. The slopes of the straight lines are almost unity for the formates, methyl esters, and alcohols but are smaller than unity for the acids and acetates. In the latter two compounds, an overestimation can be seen for the effect of the substituents (R) on the calculated proton affinities, that is, a change in the ΔE values with an increase in the carbon number of the substituents is more significant than that in the corresponding *PA* values, while, in the other series, the difference between the ΔE values corresponds almost exactly to that between the *PA* values (see Table 3). Therefore, in the acids and acetates, the settled geometries, especially for those of the substituents, appear incomplete in the approximate INDO-MO method.

Bond Index of E_{OH^+} vs. Proton Affinity. Now, we examine the total bond energy (E_{OH^+}) and the resonance

TABLE 4. TOTAL BOND ENERGIES AND THEIR PARTITIONING TERMS FOR THE OXYGEN-PROTON BONDS IN THE PROTONATED COMPOUNDS

Series and compound No.	$-E_{OH^+}$/eV	% O(p)$-$H$^+$(s)[a] overlap population	$-E^R_{OH^+}$/eV	$-E^K_{OH^+}$/eV	$E^V_{OH^+}+E^J_{OH^+}+E^N_{OH^+}$/eV
Formates					
1	19.363	60.53	21.326	6.101	8.065
2	19.698	50.49	21.299	6.078	7.678
3	19.738	59.58	21.311	6.094	7.667
4	19.752	59.62	21.317	6.099	7.664
Acetates					
5	19.756	60.59	21.529	6.233	8.006
6	19.964	59.64	21.396	6.153	7.584
7	19.930	59.85	21.371	6.152	7.593
8	19.936	59.88	21.374	6.156	7.594
Methyl esters					
1	19.363	60.53	21.326	6.101	8.065
2	19.698	59.49	21.299	6.078	7.678
6	19.964	59.64	21.396	6.153	7.584
9	19.988	59.69	21.404	6.163	7.997
Acids					
10	19.445	60.12	21.460	6.149	7.580
1	19.363	60.53	21.326	6.101	8.065
5	19.756	60.59	21.529	6.233	8.006
11	19.788	60.65	21.540	6.244	7.834
Alcohols					
12	19.432	55.98	21.420	5.845	7.793
13	19.374	52.73	21.618	5.749	7.881
14	19.542	53.59	21.612	5.811	7.863
15	19.568	53.62	21.614	5.818	8.165

a) Defined by % O(p)-H$^+$(s) overlap population = oxygen-p and hydrogen-s overlap populations in the O–H$^+$ bond $\times 10^2$/total overlap population in the O–H$^+$ bond.

energy ($E^R_{OH^+}$), which indicates the covalent bond strength, for the O–H$^+$ bond of the protonated species, in connection with the relation to the proton affinity. It can be seen from Table 4 that the absolute values of E_{OH^+}, which correspond to the bond strength of O–H$^+$, are about twice as large as the proton affinities. This may be mainly attributed to the approximations in the INDO-MO method. It is also noteworthy that index of E_{AB} indicates a static property of the A–B bond and cannot be directly compared with experimental energies such as the dissociation energy.[22] However, good correlations are observed in each series with some exceptions (H_3O^+ and $HCO_2H_2^+$) if both the kinds of energies, *PA* and E_{OH^+}, are plotted against each other. In this respect, it is also noticeable that the % O(p)-H$^+$(s) overlap population defined in Table 4 correlates well with the *PA* values with some exceptions (H_3O^+ and $HCO_2H_2^+$). This coincides with the fact that the % p-character in the oxygen lone-pairs of the parent molecule plays a predominant role in the proton affinity.

In regard to the $E^R_{OH^+}$ values, the slopes of the straight lines obtained from the plots of *PA vs.* $E^R_{OH^+}$ were not constantly positive throughout the series. This may be due to the fact that the resonance energy $E^R_{OH^+}$ is not meaningful for such an ionic oxygen-proton bond in the protonated species. In this respect, the contributions of the electronic exchange term ($E^K_{OH^+}$) and the repulsive electrostatic interactions ($E^V_{OH^+}+E^J_{OH^+}+E^N_{OH^+}$) to the proton affinity are here noted. As may be seen from Table 4, the negative $E^K_{OH^+}$ values become more negative with an increase in the *PA* values, while the positive values of the repulsive terms ($E^V_{OH^+}+E^J_{OH^+}+E^N_{OH^+}$) decrease with an increase in the *PA* values. These observations are in harmony with the fact that the more negative the $E^K_{OH^+}$ value becomes (or the smaller the above sum of the repulsion terms becomes), the stronger becomes the O–H$^+$ bond. There exists on approximate relation between them with some exceptions (H_3O^+ and $HCO_2H_2^+$). Then, we can say that the above exchange and repulsion terms can also be useful as a measure of the *PA* value.

In conclusion, it is worthy of emphasis that the experimental gas-phase proton affinities for the oxygenated compounds investigated cannot be compared directly with the calculated proton affinities or the bond energies obtained by the INDO calculations, but are in satisfactory agreement with them. The proton affinities can also be predicted with a sufficient accuracy from the first ionization potentials and the electron densities of the oxygen atoms of the parent molecules.

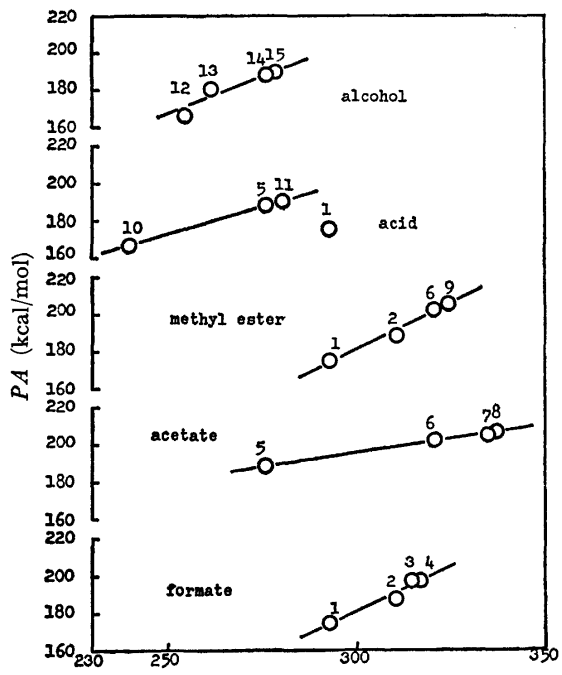

Fig. 5. Plots of *PA vs.* ΔE.

Series	a_2	$10^{-2}\ b_2$
Formate	0.98	−1.12
Acetate	0.30	1.05
Methyl ester	0.98	−1.12
Acid	0.57	0.32
Alcohol	0.88	−0.54

References

1) M. S. B. Munson, *J. Amer. Chem. Soc.*, **87**, 2332 (1965).
2) J. I. Brauman, J. M. Riveros, and L. K. Blair, *ibid.*, **93**, 3914 (1971).
3) D. H. Aue, H. M. Webb, and M. T. Bowers, *ibid.*, **94**, 4726 (1972).
4) W. G. Henderson, M. Taagerpera, D. Holtz, R. T. Mclver, Jr., J. L. Beauchamp, and R. W. Taft, *ibid.*, **94**, 4728 (1972).
5) M. Taagepera, W. G. Henderson, R. T. C. Brownlee, J. L. Beauchamp, D. Holtz, and R. W. Taft, *ibid.*, **94**, 1369 (1972).
6) M. S. B. Munson and J. L. Franklin, *J. Phys. Chem.*, **68**, 3191 (1964).
7) M. A. Haney and J. L. Franklin, *Trans. Farady Soc.*, **65**, 1974 (1969).
8) M. A. Haney and J. L. Franklin, *J. Phys. Chem.*, **73**, 4328 (1969).
9) J. L. Beauchamp and R. C. Dunbar, *J. Amer. Chem. Soc.*, **92**, 1477 (1970).
10) J. L. Beauchamp, *Annu. Rev. Phys. Chem.*, **22**, 527 (1971).
11) J. L. Beauchamp and M. C. Caserio, *J. Amer. Chem. Soc.*, **94**, 2638 (1972).
12) J. Long and B. Munson, *ibid.*, **95**, 2427 (1973).
13) J. L. Franklin, J. G. Dillard, H. M. Rosenstock, J. T. Heron, K. Draxl, and F. H. Field, "Ionization Potentials, Appearance Potentials, and Heats of Formation of Gaseous Ions," NSRDA-NBS 26, U.S. Government Printing Office, Washington, D. C. (1969).
14) A. C. Hopkinson, R. A. McClelland, K. Yates, and I. G. Csizmadia, *Theoret. Chim. Acta*, **13**, 65 (1969).
15) A. C. Hopkinson, N. K. Holbrook, K. Yates, and I. G. Csizmadia, *J. Chem. Phys.*, **49**, 3596 (1968).
16) A. C. Hopkinson, K. Yates, and I. G. Csizmadia, *ibid.*, **52**, 1784 (1970).
17) A. C. Hopkinson and I. G. Csizmadia, *Can. J. Chem.*, **52**, 546 (1974).
18) H. Hellmann, "Einfuhrung in die Quantenchemie," Franz Deuticke and Co., Leipzig (1937); R. P. Feynman, *Phys. Rev.*, **56**, 340 (1939).
19) D. W. Davis and J. W. Rabalais, *J. Amer. Chem. Soc.*, **96**, 5305 (1974).
20) J. A. Pople and D. L. Beveridge, "Approximate Molecular Orbital Theory," McGraw-Hill, New York, N.Y. (1970).
21) M. D. Newton, W. A. Lathan, W. J. Hehre, and J. A. Pople, *J. Chem. Phys.*, **52**, 4064 (1970).
22) H. Fischer and H. Kollmar, *Theoret. Chim. Acta*, **16**, 163 (1970); M. S. Gordon, *J. Amer. Chem. Soc.*, **91**, 3122 (1969).
23) The first ionization potentials were obtained as positive numbers from the energy levels of the highest-occupied orbital, according to T. Koopmans, *Physica*, **1**, 104 (1933).
24) P. Ros, *J. Chem. Phys.*, **49**, 4902 (1968).
25) L. E. Sutton, Ed., "Interatomic Distances," The Chemical Society, London, Special Publications No. 11 (1958) and No. 18 (1965).
26) The K_{AB} values were calculated by the use of the Badger formula (R. M. Badger, *J. Chem. Phys.*, **2**, 128 (1934)) with the parameters of Cossee and Schachtschneider (P. Cossee and J. H. Schachtschneider, *ibid.*, **44**, 97 (1966)): $K_{CO}=1.86/(R_{CO}-0.658)^3$ and $K_{OH}=1.86/(R_{OH}-0.335)^3$ mdyn/Å.
27) H. Fischer, H. Kollmar, and H. O. Smith, *Tetrahedron Lett.*, **1968**, 5821.
28) G. Fraenkel, *J. Chem. Phys.*, **34**, 1466 (1961); G. A. Olah and M. White, *J. Amer. Chem. Soc.*, **89**, 3591, 7072 (1967); G. A. Olah, D. H. O'Brien, and A. M. White, *ibid.*, **89**, 5694 (1967); M. Brookhart, G. C. Levy, and S. Winstein, *ibid.*, **89**, 1735 (1967).
29) In regard to the correlation between the pK_a value of a molecule and the electron density of its hetero-atom, see H. C. Longuet-Higgins, *J. Chem. Phys.*, **18**, 275 (1950); A. Kende, *Advan. Chem. Phys.*, **8**, 133 (1965).
30) D. H. Aue, H. M. Webb, and M. T. Bowers, *J. Amer. Chem. Soc.*, **97**, 4137 (1975).
31) T. Yonezawa, H. Kato, H. Saito, and K. Fukui, This Bulletin, **34**, 1814 (1963).

The Reactions of 2-Substituted 4-Chloro-6-(2-hydroxy-1-naphthyl)-1,3,5-triazines with Several Nucleophiles

Shigeo TSUNODA, Yoji HASHIDA, Shizen SEKIGUCHI, and Kohji MATSUI

Department of Chemistry, Faculty of Engineering, Gunma University, Tenjincho, Kiryu, Gunma 376

(Received July 8, 1975)

The nucleophilic substitution reactions of 2-methoxy- and 2-diethylamino-4-chloro-6-(2-hydroxy-1-naphthyl)-1,3,5-triazines (**1**) with aniline, diethylamine, sodium azide, and sodium methoxide were carried out and compared with the reactions of the corresponding derivatives of 4-chloro-6-(4-hydroxy-1-naphthyl)-1,3,5-triazine (**2**) and 4-chloro-6-(1-naphthyl)-1,3,5-triazine (**3**). Compound **1** was found to be more reactive than the corresponding (**2**) and (**3**), not only in the reactions of a neutral molecule, but also in those of anionic species. The results of the reactions of neutral species are interpreted in terms of the difference in solvation toward the substrates; however, the loss of coplanarity between the naphthalene and triazine nuclei may be responsible for the high reactivity of Compound **1** in the reactions of anionic species.

It is well known that, in nitrogen heteroaromatic compounds possessing an *O*-hydroxyaryl group in the 2-position, an intramolecular hydrogen-bond formation between the ring nitrogen and the hydroxyl group takes place.[1] In these cases, the reactivity of the heteroaromatic compound is expected to be affected more or less by the chelate formation. If the compound has an active halogen atom in the heteroaromatic nucleus, its reactivity towards nucleophiles will be different from that of the corresponding non-chelated compound. However, no such effect of chelation upon the reactivity has yet been revealed. This paper will report on the nucleophilic substitution reactions of 2-substituted 4-chloro-6-(2-hydroxy-1-naththyl)-1,3,5-triazines with some nucleophiles as examples; the experiments were undertaken in order to reveal the effect of chelate formation on the reactivity of nitrogen heteroaromatic compounds.

Results and Discussion

Preparation of Triazine Derivatives. The nucleophilic substitution reactions of 2-methoxy- and 2-diethylamino-4-chloro-6-(2-hydroxy-1-naphthyl)-1,3,5-triazines (**1**) were carried out and compared with the reactions of the corresponding derivatives of 4-chloro-6-(4-hydroxy-1-naphthyl)-1,3,5-triazine (**2**) and 4-chloro-6-(1-naphthyl)-1,3,5-triazine (**3**).

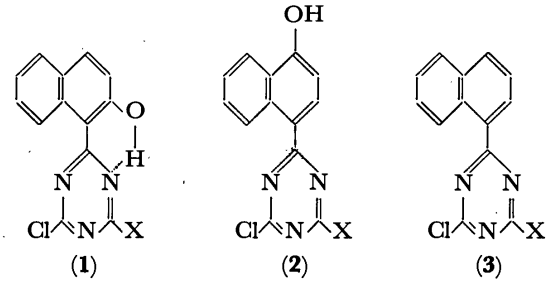

(**1**) (**2**) (**3**)

X: $-OCH_3$, $-NEt_2$

Compounds **1** and **2**, containing the methoxy group in the triazine nucleus, were prepared by the Friedel-Crafts reaction of 2,4-dichloro-6-methoxy-1,3,5-triazine with 1- and 2-naphthol in the presence of aluminium chloride, while compounds containing the diethylamino group were obtained by the condensation of cyanuric chloride with 1- and 2-naphthol in the presence of aluminium chloride,[2] followed by treatment with diethylamine. (1-Naphthyl)-1,3,5-triazine derivatives (**3**) were obtained by the reaction of cyanuric chloride with 1-naphthylmagnesium bromide, followed by treatment with methanol in combination with sodium carbonate. Table 1 lists the compounds thus obtained.

In order to estimate the structural effects upon the reactivity, kinetic measurements of the reactions of Compounds **1**, **2**, and **3** with some nucleophilic reagents were carried out. Diethylamine and aniline were used as the neutral nucleophilic reagents, while sodium azide and sodium methoxide were used as the anionic ones.

It is well known that the ordinary reactions of chloro-1,3,5-triazines with such nucleophilic reagents as amines[3] and alkoxides[4] take place very readily. The reactions in this paper were also found to take place without any appreciable side reactions by checking the reaction mixtures by tlc after the reactions had been completed; in every case, the substitution product was obtained in an almost quantitative yield, showing that these reactions are well suited to kinetic measurements. Table 2 lists the substitution products thus obtained.

Kinetics of the Reactions of 2-Substituted 4-Chloro-6-(2-hydroxy-1-naphthyl)-1,3,5-triazines with Diethylamine, Aniline, and Sodium Azide. In this study, only the derivatives of α-naphthyl-1,3,5-triazine were investigated, because the effect of the α-naphthyl group upon the reactivity of the chlorine atom is assumed to differ appreciably from that of the β-naphthyl group.[5] However, some structural differences which would affect the reactivities of these compounds can be seen between Compounds **1** and **2**. For example, there is a difference in the position of the naphthalene nucleus where the hydroxyl group is attached, and a chelate ring is formed in Compound **1**, but not in the case of Compound **2**.

In 6-substituted 2-aryl-4-chloro-1,3,5-triazines, it is generally considered that the strong electron-donating hydroxyl group in the aryl group lowers the reactivity of the active chlorine atom, not only in the *para* but also in the *ortho* position, by increasing the electron density of the triazine nucleus. Thus, if the chelation were ineffective with regard to the reactivity of the chlorine atom, both 2-hydroxy-1-naphthyl- and 4-hydroxy-1-naphthyl groups would lower the reactivity in a similar manner and the difference in substituent

Table 1. Derivatives of 1-naphthyl-1,3,5-triazine

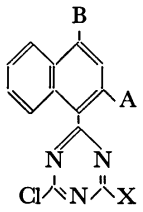

Compound	X	A	B	Mp (°C)	Solvent for recryst.	Anal. (%) Found C	Found H	Found N	Calcd C	Calcd H	Calcd N
1-1	-Cl	-OH	-H	214—215 (215—216)[a]	Dioxane	—	—	—	—	—	—
1-2	-OMe	-OH	-H	168—169	Ligroin	58.64	3.49	14.62	58.44	3.50	14.82
1-3	$-NEt_2$	-OH	-H	104.5—105.5	Ligroin	62.14	5.22	17.07	62.10	5.21	17.03
2-1	-Cl	-H	-OH	239 (decompn)	——[b]	53.71	2.47	14.24	53.45	2.41	14.38
2-2	-OMe	-H	-OH	>300	Dioxane	58.87	3.54	14.71	58.44	3.50	14.82
2-3	$-NEt_2$	-H	-OH	124 (decompn)	——[c]	62.48	5.27	17.15	62.10	5.21	17.03
3-1	-Cl	-H	-H	171—172	Benzene	56.15	2.55	15.20	56.54	2.55	15.21
3-2	-OMe	-H	-H	119—120	Ligroin	62.23	3.70	15.61	61.88	3.70	15.46

a) CIBa, Brit. P., 914798 (1963). b) Purified by column chromatography on silica gel, using a mixture of benzene and acetone (10 : 1 by volume) as the developing solvent. c) Purified by column chromatography on silica gel, using a mixture of benzene and acetone (20 : 1 by volume) as the developing solvent.

Table 2. Derivatives of 1-naphthyl-1,3,5-triazine

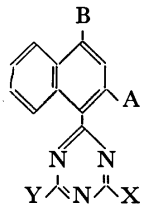

X	Y	A	B	Mp (°C)	Solvent for recryst.	Anal. (%) Found C	Found H	Found N	Calcd C	Calcd H	Calcd N
-OMe	$-NHC_6H_5$	-OH	-H	200—201	Ligroin	69.50	4.68	16.20	69.75	4.68	16.27
-OMe	$-NHC_6H_5$	-H	-OH	194—195	Benzene	70.10	4.74	16.28	69.75	4.68	16.27
$-NEt_2$	$-NEt_2$	-OH	-H	126—127	Ligroin	69.08	7.34	19.47	69.01	7.45	19.16
$-NEt_2$	$-NEt_2$	-H	-OH	118—119	Benzene	69.07	7.55	19.36	69.01	7.45	19.16
$-NEt_2$	$-N_3$	-OH	-H	93—94	Ligroin	60.89	5.25	28.95	60.88	5.11	29.24
$-NEt_2$	$-N_3$	-H	-OH	102—103	Benzene-Petroleum ether	60.78	5.47	28.88	60.88	5.11	29.24
-OMe	$-N_3$	-OH	-H	163—164	Benzene	57.25	3.44	28.45	57.14	3.43	28.56
-OMe	$-N_3$	-H	-OH	198—199	Benzene	57.24	3.44	28.62	57.14	3.43	28.56
-OMe	$-N_3$	-H	-H	98—99	Ligroin	60.75	3.64	30.87	60.42	3.62	30.20
-OMe	-OMe	-OH	-H	146—147	Ligroin	63.73	4.35	—	63.59	4.63	—
-OMe	-OMe	-H	-OH	203.5—204.5	Benzene	63.48	4.45	—	63.59	4.63	—
$-NEt_2$	-OMe	-OH	-H	87—88	Ligroin	66.86	6.30	17.21	66.65	6.22	17.27
$-NEt_2$	-OMe	-H	-OH	137—138	Benzene	66.50	6.22	17.29	66.65	6.22	17.27

Table 3. Rate constants for the nucleophilic reactions of 2-substituted 4-chloro-6-(hydroxy-1-naphthyl)-1,3,5-triazines

Compound	k_2 ($l \cdot mol^{-1} \cdot s^{-1}$)
With aniline at 35 °C	
1-2	4.28×10^{-3}
2-2	2.28×10^{-5}
With diethylamine at 20 °C	
1-3	2.36×10^{-2}
2-3	2.12×10^{-4}

effect between the two groups would not be large. However, as is apparent from Tables 3 and 4, the hydroxyl group was found to affect the reactivity of chloro-triazinyl-naphthalene in very different manners depending upon its position in the naphthalene nucleus. As compared with the case of Compound **3**, it is apparent that the hydroxyl group in the *para* position lowered the reactivity, as was to be anticipated. The hydroxyl group in the *ortho* position, on the contrary, raised the reactivity in spite of its powerful electron-donating character; in every case, the reactivity varied in the following order:

Compound **1** > **3** > **2**

Therefore, it may be reasonable to assume that the high reactivity of *O*-hydroxy compounds is mainly ascribable to the presence of the chelate ring in these compounds.

The hydroxyl group of these compounds can dissociate into anions whose reactivities should be different from those of the neutral species. Therefore, it may be necessary to ascertain the actual species in the above reactions. As the absorption spectra of these compounds are different from those of their anions, the dissociation can be checked spectrophotometrically to determine that Compounds **1** and **2** react practically like the neutral molecule in every case under the present reaction conditions.

The activation by the intramolecular hydrogen bond seems in this case to be a phenomenon similar to the acid catalysis in the reactions of chloro-triazines.[6]

However, from the activation parameters for the reactions with sodium azide, it is clear that the high reactivity of Compound **1** does not depend on the energy of activation, but results mainly from the difference in the entropy of activation. Thus, even if the chelation raised the reactivity by reducing the electron density of the triazine nucleus in a manner similar to the acid catalysis, this would not be the major reason for the high reactivity of the *O*-hydroxy compound; the assumption may also be supported by the fact that the differences in rate constant were rather larger in the cases of the derivatives containing the methoxyl group than in those of the derivatives having the diethylamino group, in spite of the fact that the order of the stability of chelation is known to be **1-2**<**1-4**.[7] In these derivatives, the two types of chelate-ring formation shown below are possible. Although it is obscure at present which is the true chemical species in the actual reactions under the present experimental conditions, the results can be reasonably explained as follows.

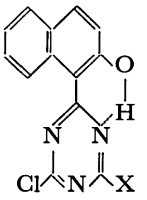

(1)′

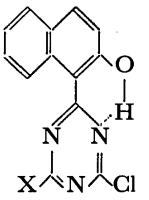

(1)″

In these cases, a difference in solvation between two compounds is assumed to be responsible for the difference in reactivity.

In the initial state of the reaction (in the reaction with sodium azide, a mixture of dioxane and water was used as the solvent), the hydroxyl group and the ring nitrogen atoms of the substrates would be the principal centers for solvation. Thus, in the case of Compound **1** the solvation may be hindered by the chelate formation, because by the chelate formation the two centers for solvation should partially negate each others abilities to solvate.

In the transition state, a negative charge poured into the triazine nucleus from the reagent (N_3^-) would spread over the three ring nitrogen atoms, and the solvation would increase with an increase in the electron density of the triazine nucleus. However, in the transition state of Compound **1** the chelation would become stronger; thus, the increase in solvation in this case would be inferior to that of the case of Compound **2**.

Table 4. Rate constants for the reactions of 2-substituted 4-chloro-6-(1-naphthyl)-1,3,5-triazines with sodium azide

Compound	k_2 ($l \cdot mol^{-1} \cdot s^{-1}$)			Activation parameters	
	35 °C	45 °C	55 °C	ΔE kcal/mol	$\Delta S^{\neq}$ cal/deg·mol (35 °C)
1-3	0.85×10^{-4}	1.77×10^{-4}	4.70×10^{-4}	16.7	−25.3
2-3	1.39×10^{-5}	2.26×10^{-5}	5.59×10^{-5}	13.5	−39.1

Compound	k_2 ($l \cdot mol^{-1} \cdot s^{-1}$)				Activation parameters	
	15 °C	25 °C	35 °C	45 °C	ΔE kcal/mol	$\Delta S^{\neq}$ cal/deg·mol (25 °C)
1-2	1.29×10^{-2}	2.77×10^{-2}	7.03×10^{-2}	——	15.3	−15.7
2-2	——	0.77×10^{-3}	1.94×10^{-3}	4.20×10^{-3}	15.4	−23.1
3-2	——	4.38×10^{-3}	9.15×10^{-3}	2.05×10^{-2}	14.5	−22.5

In other words, although Compound **2** would solvate water more strongly than Compound **1** during the full course of the reaction, the difference in solvation degree between the two would be larger in the transition state than in the initial one.

Thus, in spite of the advantage in the energy of activation, Compound **2** was less reactive because of the disadvantage in the entropy term, as can be seen by comparing the reactions of **1–3** and **2–3**. A similar relation is also seen in the reactions of **1–2** and **2–2**.

Kinetics of the Reactions with Sodium Methoxide. The reactions of Compounds **1** and **2** with sodium methoxide were carried out in a mixture of methanol and acetone (1 : 1, by volume); the rate constants for the reactions are listed in Table 5.

Table 5. Rate constants for the reactions of 2-substituted 4-chloro-6-(hydroxy-1-naphthyl)-1,3,5-triazines with sodium methoxide

Compound	k_2 ($l \cdot mol^{-1} \cdot s^{-1}$) at 20 °C	Compound	k_2 ($l \cdot mol^{-1} \cdot s^{-1}$) at 30 °C
1–2	2.03	**1–3**	4.85×10^{-3}
2–2	4.55×10^{-2}	**2–3**	4.46×10^{-4}

In these reactions, Compound **1** was again found to be more reactive than **2**. In the reactions with sodium methoxide, the substrates are assumed to dissociate into their anions. In fact, most of the substrates were found to react practically as their anions, as can be seen in Table 6.[8] It is obvious from Table 6 that the rate constants of the two compounds are of an anionic species, regardless of the substituent in the triazine nucleus. However, in the case of Compound **1–3** about 3% of the substrate was found to remain as an undissociate form in the solution. Thus, the rate constant of Compound **1–2** was practically that of the anionic species; however, when the substituent is $-NEt_2$ the rate constant probably results from the reactions of anionic and neutral substrates. Therefore, the apparent rate constant may vary with the concentration of sodium methoxide. In fact, when the apparent rate constants were plotted against the concentration of sodium methoxide, a curve converging to a constant value with an increase in the concentration of the base was obtained, as is shown in Fig. 1.

Table 6. Ratios of anion to neutral molecule of 2-substituted 4-chloro-6-(hydroxy-1-naphthyl)-1,3,5-triazines in methanol

Compound	C^-/C	Compound	C^-/C
1–3	32	**1–2**	120
2–3	1000	**2–2**	3900

C^-: Concentration of ionized molecule.
C: Concentration of non-ionized molecule.

The results indicate that the anion is less reactive than the neutral substrate, and that the converged value (about 2.9×10^{-3} l/mol·s) in the high-base-concentration region is the true rate constant of the anionic species. Thus, in the reaction of anionic species, Compound **1** was also more reactive than the corresponding Compound **2**; it may be of interest that Compound **1** is more reactive even in the absence of an intramolecular hydrogen bond.

Table 7. Effect of concentration of $NaOCH_3$ on apparent rate constant of compound **1–3**

$[NaOCH_3]$ (mol/l)	k_2' ($l \cdot mol^{-1} \cdot s^{-1}$) at 30 °C
18.67×10^{-2}	2.90×10^{-3}
14.58×10^{-2}	3.14×10^{-3}
9.65×10^{-2}	4.07×10^{-3}
9.14×10^{-2}	4.85×10^{-3}
7.18×10^{-2}	6.04×10^{-3}
4.96×10^{-2}	1.08×10^{-2}

[Substrate] : 2×10^{-2} mol/l.

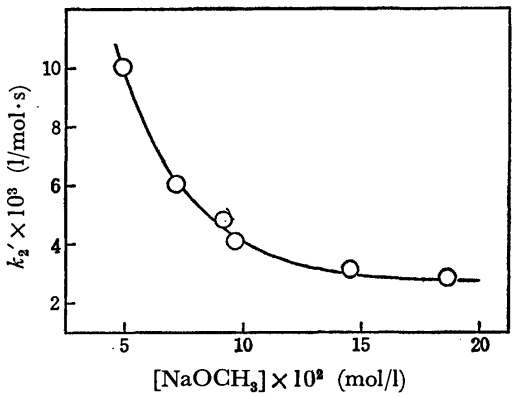

Fig. 1. Dependence of apparent rate constants of Compound **1–3** on concentration of sodium methoxide.

In the case of Compound **1**, one of the ring nitrogen atoms and one of the naphthoxide oxygen atom are assumed to be located very close to each other. Therefore, in the transition state there should be a repulsion between two atoms of same kinds of negative charge, leading to a loss of coplanarity between the naphthalene and triazine nuclei.

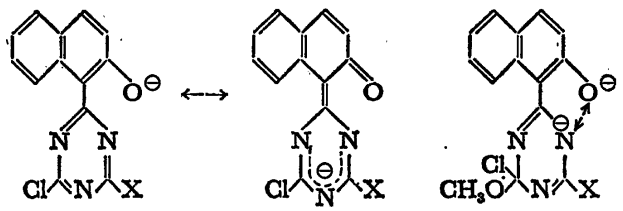

In the reaction of anionic species, the negative charge poured into the triazine nucleus from the naphthoxide anion should lower the reactivity of the substrate, regardless of the type of compound. However, in the case of Compound **1**, this lowering of reactivity should be prevented in some degree by the loss of copolanarity between the aromatic rings. Thus, Compound **1** would be more reactive than Compound **2** even in the reaction with sodium methoxide. As a whole, in the reactions with nucleophiles, Compound **1** was more reactive than the corresponding Compound **2**, regardless of the nucleophile used. The chelation

TABLE 8. pK_a VALUES OF (HYDROXY-1-NAPHTHYL)-1,3,5-TRIAZINES IN METHANOL AT 20 °C

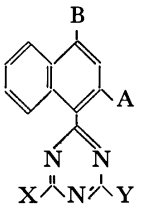

X	Y	A	B	pK_a' [a]	Indicator[c]	Buffer
-OMe	-Cl	-OH	-H	13.2[b]	——	——
-OMe	-OMe	-OH	-H	14.0	Thymol Blue	SBA
$-NEt_2$	-Cl	-OH	-H	14.2	Thymol Blue	SBA
$-NEt_2$	$-NEt_2$	-OH	-H	16.2	*O-t*-Butylphenol	$NaOCH_3$
-OMe	-Cl	-H	-OH	11.7	Bromocresol Purple	SBA+SBE
-OMe	-OMe	-H	-OH	12.4	Bromothymol Blue	SBA+SBE
$-NEt_2$	-Cl	-H	-OH	12.7	Bromothymol Blue	SBA+SBE
$-NEt_2$	$-NEt_2$	-H	-OH	13.6	Phenol Red	SBA+SBE

SBA=Sodium barbiturate. SBE=Sodium benzoate.

a) pK_a' denotes the ionization constant of (hydroxy-1-naphthyl)-1,3,5-triazine in methanol. b) Calculated using a linear relation between pK_a' and $\sum\sigma_m$ values of two substituents in the 1,3,5-triazine nucleus [Y. Ohto, Y. Hashida, S. Sekiguchi, and K. Matsui, *Bull. Chem. Soc. Japan*, **47**, 1301 (1974)], because the compound was found to be too unstable to measure an accurate pK_a' value in an alkaline solution; in this calculation the substituent constant of $-NMe_2$ was substituted for that of $-NEt_2$. c) Indicator employed for the measurement of pK_a' of triazines as the primary standard.

in Compound **1** surely plays an important role in the high reactivity; however, it has become apparent that the function of chelation is not a mere lowering of the electron density of the triazine nucleus.

Experimental

All melting points are uncorrected.

Materials. *2,4-Dichloro-6-(2-hydroxy-1-naphthyl)-1,3,5-triazine (**1-1**)*: Compound **1-1** was prepared by the reaction of cyanuric chloride with 2-naphthol in the presence of aluminium chloride in benzene.[2)]

*2,4-Dichloro-6-(4-hydroxy-1-naphthyl)-1,3,5-triazine (**2-1**)*: A solution of 40.6 g (0.22 mol) of cyanuric chloride and 32.1 g (0.22 mol) of 1-naphthol in 350 ml of benzene was added, drop by drop, into a mixture of 30.7 g (0.23 mol) of aluminium chloride in 200 ml of benzene at room temperature. After stirring for 2 h under reflux, the mixture was poured into 1 l of ice water containing 200 ml of a concd hydrochloric acid solution. The precipitate thus formed was filtered, dried, and purified by column chromatography on silica gel using a mixture of benzene and acetone (10 : 1 by volume) to give an analytical sample. Mp 239 °C (decompn.). This product gave 2,4-dimethoxy(4-hydroxy-1-naphtnyl)-1,3,5-triazine (mp 204—205 °C)[2)] upon treatment with an excess of sodium methoxide in methanol.

*2-Diethylamino-4-chloro-6-(2-hydroxy-1-naphthyl)-1,3,5-triazine (**1-3**) and 2-Diethylamino-4-chloro-6-(4-hydroxy-1-naphthyl)-1,3,5-triazine (**2-3**)*: A typical preparation is shown in the case of Compound **1-3**. A solution of 7.5 g (0.1 mol) of diethylamine in 100 ml of acetone was added, drop by drop, into a solution of 14.6 g (0.05 mol) of Compound **1-1** in 250 ml of acetone at 0 °C. After stirring for 3 h at 0—5 °C, the reaction mixture was poured into 1 l of ice water. The precipitate was then filtered and dried to give a crude product in an almost quantitative yield. The recrystallization of the product from ligroin gave an analytical sample of Compound **1-3**. Mp 104.5—105.5 °C.

*2-Methoxy-4-chloro-6-(2-hydroxy-1-naphthyl)-1,3,5-triazine (**1-2**) and 2-Methoxy-4-chloro-6-(4-hydroxy-1-naphthyl)-1,3,5-triazine (**2-2**)*: A typical preparation is shown in the case of Compound **1-2**. A solution of 10.5 g (0.073 mol) of 2-naphthol in 200 ml of benzene was added, drop by drop, into a mixture of 13.1 g (0.073 mol) of 2,4-dichloro-6-methoxy-1,3,5-triazine and 9.7 g (0.073 mol) of aluminium chloride at room temperature. After stirring at 40—50 °C for 8 h, the mixture was poured into ice water containing hydrochloric acid as has been described above. The precipitate thus formed was filtered and washed with dilute hydrochloric acid, with cold water, and then with a small amount of acetone to give a crude product in a yield of 80%. The recrystallization of the product from ligroin gave an analytical sample. Mp 168—169 °C.

*2,4-Dichloro-6-(1-naphthyl)-1,3,5-triazine (**3-1**) and 2-Methoxy-4-chloro-6-(1-naphthyl)-1,3,5-triazine (**2-3**)*: A solution of 36.9 g (0.2 mol) of cyanuric chloride in 300 ml of dry ether was added all at once into a mixture of Grignard reagent prepared from 41.4 g (0.2 mol) of 1-bromonaphthalene and 5.0 g (0.2 mol) of magnesium in 200 ml of dry ether. After the mixture had been stirred overnight at room temperature, the precipitate was filtered and washed with cold dilute hydrochloric acid and then with water to give a crude product of Compound **3-1** in a 55% yield.

A solution obtained by dissolving 1.2 g (0.05 mol) of sodium in 150 ml of methanol was added, drop by drop, into a solution of 13.8 g (0.05 mol) of Compound **3-1** in a mixture of 450 ml of dioxane and 200 ml of methanol at 0 °C. After stirring for 3 h, the solution was poured into 1.5 l of ice water. The precipitate was filtered and dried to give Compound **3-2** in an almost quantitative yield.

Kinetic Measurements. Runs were carried out with an excess of the nucleophile (the substrate and the nucleophile were used in a molar ratio of about 1 : 5; the initial concentration of the former was about 0.02 mol/l). In the reaction with aniline, acetone was used as the solvent; the reaction in aliquot portions was stopped by dilution with

cold acetone (−20 °C), followed by a titration of the hydrochloric acid with a standard acetone solution of triethylamine, using Neutral Red as the indicator.

In the reaction with diethylamine (solvent : acetone), the reaction in aliquote portions was stopped by pouring in an excess of an acetone solution of hydrochloric acid of a known concentration; the reagent consumed was estimated by back-titration with a standard acetone solution of triethylamine, using Neutral Red as the indicator.

In the reaction with sodium azide (solvent: a mixture of dioxane and water in a ratio of 4 : 1 by volume), reaction in aliquot portions was stopped by pouring in a mixture of carbon tetrachloride and water; the chloride in the water layer was estimated by titration with silver nitrate by the Volhard method in the presence of a small amount of nitrobenzene.[9]

In the reaction with sodium methoxide (solvent: a mixture of acetone and methanol in a ratio of 6 : 4 by volume), reaction in aliquot portions was stopped by pouring in an excess of a hydrochloric acid solution of a known concentration, followed by back-titration with a standard sodium hydroxide solution, using Methyl Red as the indicator. For the reactions with aniline and diethylamine, the rate constants were calculated from Eq. (1):

$$k_2t = 2.303/b-2a \cdot \log a(b-2x)/b(a-x) \quad (1)$$

where a and b are the initial concentrations of the substrate and the nucleophile respectively, and where x is the concentration of the product at time t. On the other hand, in the cases of sodium azide and sodium methoxide Eq. (2) was used:

$$k_2t = 2.303/b-a \cdot \log a(b-x)/b(a-x) \quad (2)$$

However, in the reactions of Compounds **1** and **2** with sodium methoxide, the rate constants were calculated using b-a as the initial concentration of nucleophile, because equimolar proportions of the substrate and the nucleophile should combine to form an anion of the substrate prior to the substitution reaction.

The mean values of not less than four separately determined values of k_2, which agreed within 5%, were taken as the rate constants for these reactions; they are listed in Tables 3, 4, 5, and 7.

*p*K$_a$ *Measurements.* The pK_a values of naphthol derivatives in methanol were determined by the indicator method using Eq. (3);[10] the ratio of the acidic to the basic form of an indicator and naphthol derivatives was determined spectrophotometrically:

$$pK_a' = pK_I + \log C_{Ib} \times C_{Na}/C_{Ia} \times C_{Nb} \quad (3)$$

where pK_a'=pK_a value of naphthol derivative, pK_I=the pK_a value of an indicator; C_{Ia} and C_{Ib} are the concentrations of the acidic and basic forms of an indicator respectively, and C_{Na} and C_{Nb} are the concentrations of the acidic and dissociated forms of the naphthol derivative respectively. The results obtained are summarized in Table 8.

References

1) For example, Richard Pater, *J. Heterocycl. Chem.*, **7**, 1113 (1970); J. Durmis, M. Karvas, and Z. Manasek, *Coll. Czech. Chem. Commun.*, **38**, 215 (1973); H. Shizuka, T. Kanai, T. Morita, Y. Ohto, and K. Matsui, *Tetrahedron*, **27**, 4021 (1971).

2) Y. Horikoshi, Y. Ohto, S. Sekiguchi, and K. Matsui, *Nippon Kagaku Zasshi*, **1974**, 530; H. E. Fierz-David, M. Matter, *J. Soc. Dyers Col.*, **53**, 424 (1937); CIBA, Brit. P. 914798 (1963); Eastman Kodak, Fr. P. 1573509 (1969).

3) For example, J. Thurston, J. Dudley, D. Kaiser, I. Hechenbleikner, F. Schaefer, D. Holm-Hansen, *J. Amer. Chem. Soc.*, **73**, 2981 (1951); D. Kaiser, J. Thurston, J. Dudley, F. Schaefer, I. Hechenbleikner, D. Holm-Hansen, *ibid.*, **73**, 2984 (1951); H. Schroeder and C. Grundmann, *ibid.*, **78**, 2447 (1956); B. Bitter and H. Zollinger, *Angew. Chem.*, **70**, 246 (1958); K. Matsui, K. Hagiwara, A. Hayashi, and Y. Soeda, *Yuki Gosei Kagaku Kyokai Shi*, **18**, 58, 184 (1960); B. Bitter and H. Zollinger, *Helv. Chim. Acta*, **44**, 812 (1961); H. Zollinger, *Angew. Chem.*, **73**, 125 (1961).

4) For example, J. Dudley, J. Thurston, F. Schaefer, D. Holm-Hansen, C. Hull, and P. Adams, *J. Amer. Chem. Soc.*, **73**, 2986 (1951).

5) E. Imoto, "Advances in Organic Reaction Mechanisms," ed. by M. Murakami, Vol. 2, Maki-Shoten (1960), p. 24.

6) For example, Banks, *J. Amer. Chem. Soc.*, **66**, 1127 (1944); H. Zollinger, *Angew. Chem.*, **73**, 125 (1961); T. Shiojima, Y. Hashida, K. Matsui, This Bulletin, **46**, 2914 (1973).

7) Y. Ohto, Y. Hashida, S. Sekiguchi, and K. Matsui, This Bulletin, **47**, 1301 (1974).

8) The kinetic measurements were carried out in a mixture of methanol and acetone, however the data in Table 5 were obtained on the basis of measurement in methanol, because in the presence of acetone the spectrophotometric determination of the accurate ratios of anion to neutral molecule was found to be impossible by the UV absorption band of acetone.

9) J. R. Caldwell and H. V. Moyer, *Ind. Eng. Chem., Anal. Ed.*, **7**, 38 (1935); R. F. Hudson and M. Green, *J. Chem. Soc.*, **1962**, 1055.

10) Y. Hashida, H. Ishida, S. Sekiguchi, and K. Matsui, This Bulletin, **47**, 1224 (1974).

The Metal-Ion-Catalyzed Alcoholysis of β-Dicarbonyl Compounds[1]

Kaku UEHARA, Fujio KITAMURA, and Makoto TANAKA

Department of Applied Chemistry, College of Engineering, University of Osaka Prefecture, Sakai-shi, Osaka 591

(Received July 11, 1975)

The alcoholysis of β-dicarbonyl compounds of the type $CH_3COCHRCOR'$ is catalyzed by a variety of metal ions. In the presence of a large excess of β-diketone compared with metal ions, the rate is given by the expression: rate$=k_{obsd}[M^{2+}][ROH]$. The values of k_{obsd} decrease with M^{2+} in the order $Zn^{2+}>Co^{2+}>Ni^{2+}>Cu^{2+}$. The reaction rate is remarkably affected by the substituents (R,R'), the kinds of alcohol and solvent used, the addition of a chelating agent, and also by the counter anion of the metal ion. The alcoholysis proceeds more slowly in CH_3OD than in CH_3OH by a factor of 1.4. These are interpreted in terms of a mechanism in which the β-dicarbonyl compound coordinated to a metal ion is attacked by the alcohol which is also coordinated to the metal ion to cleave the C^2–C^3 or C^3–C^4 bond of the dicarbonyl compound. A convenient method for the preparation of β,γ-unsaturated ketones and esters is provided by the alcoholysis of alkenyl substituted β-dicarbonyl compounds in the presence of zinc acetate.

Acid- and base-catalyzed cleavages of β-diketones and ketoesters are well known.[2] Alkaline alcoholysis of acetylacetone has been previously studied by Kutz and Adkins,[2d] and Pearson and Sandy.[2h] Recently, we have found that certain metal salts and chelates catalyze the alcoholysis of 3-(1-alkenyl)-2,4-pentanediones to give β,γ-unsaturated ketones.[3]

It has been shown that the β-diketo compounds react with a metal ion to form a certain type of chelate and consequently are activated toward the electrophilic attack of various reagents.[4–9] On the other hand, it has been reported that metal complexes containing both methoxy and β-dicarbonylate ions as ligands, [M(acac) (CH_3O) $(CH_3OH)_x$],[10–12] effectively catalyze the ester exchange reactions of ethyl picolinate, ethyl 2-pyridylacetate, and ethyl esters of α-amino acids.[13]

In this paper, the metal-ion-catalyzed alcoholysis of 3-substituted β-dicarbonyl compounds will be discussed in more detail; we will propose a possible mechanism involving an intermediate in which both β-dicarbonyl compound and alcohol are coordinated to a metal ion.

Results and Discussion

Kinetic Studies. The dependences of the reaction rate on the concentration of zinc acetate, 3-(1-butenyl)-2,4-pentanedione, and methanol have been investigated. The results are shown in Table 1 and Fig. 1. It is seen that the metal-ion-catalyzed alcoholysis of 3-substituted β-diketones follows the rate equation: rate$=k_{obsd}$ [Metal ion] [Alcohol]. The rate of alcoholysis is independent of [β-diketone] under the present condition of [β-diketone]≫[metal ion]. This may be due to the fact that the metal ion exists only as a metal chelate of β-diketone and the reaction species is not the metal ion itself but the metal chelate. The band of 3-(1-butenyl)-2,4-pentanedione at 288 nm was found to shift to 303 nm by the addition of $Zn(OAc)_2$, as shown in Fig. 2. The large red shift should be ascribed to the zinc enolate formation.

TABLE 1. ALCOHOLYSIS OF 3-(1-BUTENYL)-2,4-PENTANEDIONE BY ZINC ACETATE IN METHANOL AT 70 °C (reflux)

Run No.	$[Zn(OAc)_2]\times10^3$ (M)	[β-Diketone]×10 (M)	Rate×10^3 (M s^{-1})
1	20.8	13.1	4.41
2	20.1	13.1	4.76
3	13.9	13.1	3.48
4	7.33	13.1	1.79
5	4.54	13.1	1.16
6	0	13.1	0
7	7.33	6.50	1.55
8	7.33	9.75	1.62
9	7.33	19.5	1.70

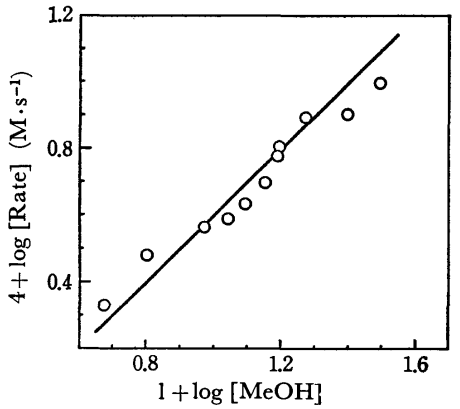

Fig. 1. Plot of log (Rate) *vs.* log [CH_3OH] in dioxane at 70 °C [$Zn(OAc)_2$]$=7.0\times10^{-3}$ M, [β-Diketone]$=$ 1.31 M.

Effect of 3-Substituent. The effect of the substituent at the 3-position of acetylacetone is shown in Table 2. The rate of alcoholysis of 3-substituted 2,4-pentanediones was found to be markedly affected by the property of the substituent. 3-(1-Butenyl)-2,4-pentanedione showed the highest reactivity and 3-benzyl- or 3-butyl-2,4-pentanedione showed a moderate reactivity. Acetylacetone, however, was inactive toward the alcoholysis. The rate of reaction increases with decrease in activation energy E_a. 3,3-Dimethyl-, 3-benzylidene-, and 3-furfurylidene-2,4-pentanedione which have no labile hydrogen to form the metal enolate showed less or no reactivity in the metal-ion-catalyzed alcoholysis, in contrast to the very high reactivity in alkaline alcoholysis of the 3,3-dialkyl

TABLE 2. EFFECTS OF SUBSTITUENTS ON THE METHANOLYSIS OF 3-SUBSTITUTED 2,4-PENTANEDIONE BY ZINC ACETATE IN DIOXANE

3-Substituent	k_{obsd} (70 °C) $\times 10^5$ ($M^{-1} s^{-1}$)	E_a (kcal mol^{-1})
1-Butenyl	83.8	12.8
Benzyl	12.6	19.4
Butyl	5.25	24.0
Dimethyl	0.32	—
Benzylidene	0	—
Furfurylidene	0	—
None (Acetylacetone)	0	—

TABLE 3. SOLVENT EFFECTS ON THE ALCOHOLYSIS OF 3-(1-BUTENYL)-2,4-PENTANEDIONE

[β-Diketone] = 1.30 M, $[Zn(OAc)_2] = 6.86 \times 10^{-3}$ M
$[CH_3OH] = 1.40$ M

Solvent	k_{obsd} (70 °C) $\times 10^4$ ($M^{-1} s^{-1}$)	E_a (kcal mol^{-1})
Benzene	14.81	16.8
Ethyl acetate	10.73	—
Dioxane	8.38	12.8
Dioxane(+Trien)[a]	3.57	—
Acetonitrile	6.39	11.0

a) 1.58×10^{-2} M of triethylenetetramine was added.

substituted β-diketone.[2d]

Solvent Effects. The methanolysis of 3-(1-butenyl)-2,4-pentanedione by zinc acetate was carried out using benzene, ethyl acetate, dioxane, and acetonitrile as diluents. The solvent effects on the reaction are summarized in Table 3. It is clear that the rate is much greater in a nonpolar solvent than in a polar solvent, in spite of the unfavorable activation energy for the former. The reaction cannot be facilitated in a nonpolar solvent. In fact, from the data of Table 1, k_{obsd} in methanol is calculated to be 9.5×10^{-3} $M^{-1} s^{-1}$, which is larger than in benzene. The solvent effect in Table 3 may be explained as follows: The polar solvent should compete with the alcohol for the occupation of the coordination site of the metal chelate so as to depress the formation of the intermediate (c) as described below.

Effect of Chelating Agent. Addition of a small amount of triethylenetetramine (Trien), which is known as a more effective chelating agent than β-diketone, induces a marked decrease in the reaction rate, as shown in Table 3. This effect may be accounted for by a reduction of the net concentration of the metal ion acting as catalyst.

Effect of Alcohol. As shown in Table 4, the rates of alcoholysis varied with the kind of alcohol used. The order of the reactivity was anti-parallel to that of the basicity as follows: methanol>ethanol>propan-2-ol>*t*-butyl alcohol. The observed reactivity order of the alcohols is attributable to the steric effect rather than the activation energy. This effect and the data of Table 3 seem to suggest that the reaction proceeds *via* the coordination of alcohol to the metal of the β-diketone complex.

TABLE 4. EFFECTS OF ALCOHOL ON THE ALCOHOLYSIS OF 3-(1-BUTENYL)-2,4-PENTANEDIONE IN DIOXANE

[β-Diketone] = 1.30 M, $[Zn(OAc)_2] = 7.0 \times 10^{-3}$ M

Alcohol	k_{obsd} (70 °C) $\times 10^4$ ($M^{-1} s^{-1}$)	E_a (kcal mol^{-1})
Methanol	8.38	12.8
Ethanol	4.37	10.7
Propan-2-ol	0.86	—
t-Butyl alcohol	0.00	—

TABLE 5. EFFECTS OF METAL SALTS ON THE ALCOHOLYSIS OF 3-(1-BUTENYL)-2,4-PENTANEDIONE IN METHANOL

[β-Diketone] = 3.25×10^{-1} M, at 70 °C (reflux)

Metal salt	$k_{obsd} \times 10^4$ (s^{-1})
Cu(OAc)	1.02
$Ni(OAc)_2$	1.93
$Co(OAc)_2$	7.44
$Zn(OAc)_2$	48.7
$Zn(acac)_2$	33.4
$ZnSO_4$	1.83
$ZnCl_2$	1.19

Deuterium Isotope Effect. The alcoholysis of 3-(1-butenyl)-2,4-pentanedione in a large amount of monodeuteriomethanol (CH_3OD) by zinc acetate gave 3,3-dideuterio-4-hepten-2-one, which was identified by means of mass spectra (parent peak, *m/e* 114) and NMR spectra (a practical disappearance of the signal of 4-hepten-2-one at 6.98 τ(2H, d, $-C\underline{H}_2COCH_3$)). The alcoholysis proceeds more slowly in CH_3OD than in CH_3OH by a factor of $k_H/k_D = 1.4$. The isotope effect may be caused by a rapid and reversible reaction, which involves breakage of the O–H (or O–D) bond and is followed by the slow rate-determining step.[15] The catalysis of divalent metallic ions for the exchange of alcohol hydroxyl protons has been reported.[16]

Effects of Metal Salts. The activities of metal salts used as the catalyst of the alcoholysis are shown in Table 5. The order of the activity of metal acetates ($M(OAc)_2$) was as follows: Zn(II)>Co(II)>Ni(II)>Cu(II). The observed activity order of $M(OAc)_2$ was anti-parallel with the stability constants[14] of metal acetylacetonates ($M(acac)_2$). The catalytic activity of a metal ion is altered by its counter anion. The rate constant of $Zn(OAc)_2$ is 40-fold larger than that of $ZnCl_2$. The lower activity of $ZnCl_2$ may be attributed to a reluctance to form metal enolate(A). Kawaguchi *et al.*[17] reported the presence of a zinc(II) complex, $ZnCl_2(acacH)$, which has a tetrahedral structure containing a ketonic molecule of acetylacetone (B). As already shown in Fig. 2, the small change in the absorption spectra of 3-(1-butenyl)-2,4-pentanedione by the addition of $ZnCl_2$ also gives evidence for the reluctance of $ZnCl_2$ to form metal enolate (A). The higher activity of $Zn(OAc)_2$ compared with that of $ZnCl_2$ or $ZnSO_4$ seems to be because the HOAc liberated by chelation is a much weaker acid than HCl or H_2SO_4 and consequently $Zn(OAc)_2$ is more likely to form the metal enolate(A).

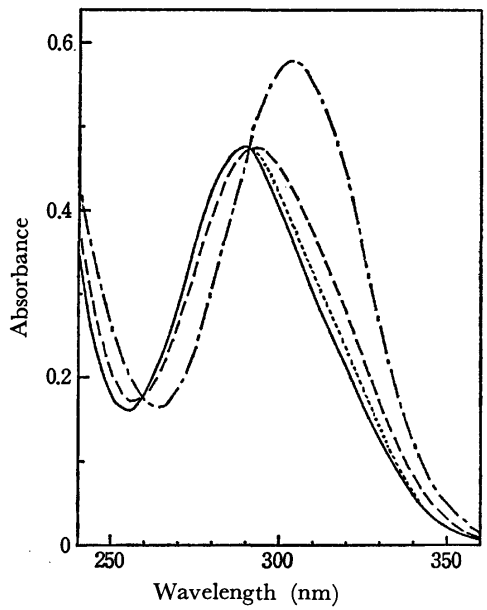

Fig. 2. Absorption spectra of 3-(1-butenyl)-2,4-pentanedione (1.03×10^{-4} M) in the absence and presence of zinc salt in methanol.
——: Absence of zinc salt,
— — —: $[Zn(OAc)_2]=5.11\times10^{-4}$ M,
— — —: $[ZnSO_4]=5.18\times10^{-4}$ M,
……: $[ZnCl_2]=6.31\times10^{-4}$ M.

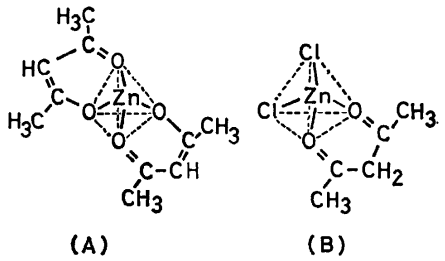

Fig. 3.

The observed effects of metal salts suggest that the formation of metal enolate is essential for a high catalytic activity. However, an extremely stable O–M bond is unfavorable, because the present catalysis presumably proceeds *via* the dissociation of the O–M bond followed by the protonation to carbonyl oxygen to form the intermediate(d) as described below.

Alcoholysis of Unsymmetrical β-Diketones. Unsymmetrical β-diketones, RCO-CHR'-COR", can be cleaved in either of two ways.[2a,2c,2e] Metal-ion-catalyzed alcoholysis of several 3-(1-butenyl)-4-substituted-2,4-butanediones was carried out in order to find the direction of the cleavage. The results are shown in Table 6, where k_1 is the rate constant of the alcoholysis of the C–$COCH_3$ bond (deacetylation) and k_2 is that of the C–COR bond (deacylation).

An electron-donating substituent increases the rate ratio k_1/k_2. Except for 3-(1-butenyl)-4-phenyl-2,4-butanedione, the direction of cleavage is found to be determined by the strength of the carboxylic acid of the two possible esters: the stronger acid is formed in a larger proportion as in the alkaline hydrolysis reported by Bradley and Robinson.[2a] The effect of

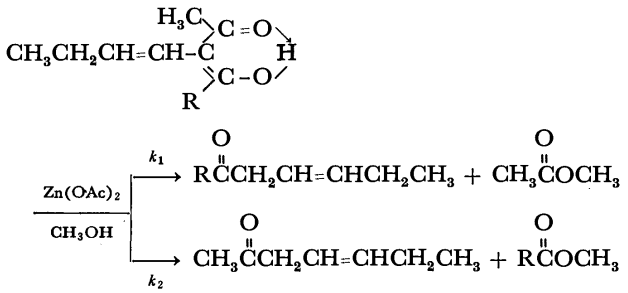

Table 6. Effects of 4-substituent in the methanolysis of 3-(1-butenyl)-4-substituted-2,4-butanedione by $Zn(OAc)_2$

4-Substituent	k_1 (70 °C)$\times10^5$ ($M^{-1}s^{-1}$)	k_2 (70 °C)$\times10^5$ ($M^{-1}s^{-}$)	k_1/k_2
CH_3-	41.9	41.9	1.0
$(CH_3)_2CH$-	27.1	4.09	6.63
	36.3	14.2	2.56
CH_3O-	6.14	0.414	14.8

phenyl substitution resulting in the k_1/k_2 value of 2.56 may be explained from the viewpoint of steric hindrance.

Mechanism. On the basis of the experimental results described above, a possible mechanism for the metal-ion-catalyzed alcoholysis of β-diketone may be proposed as follows:

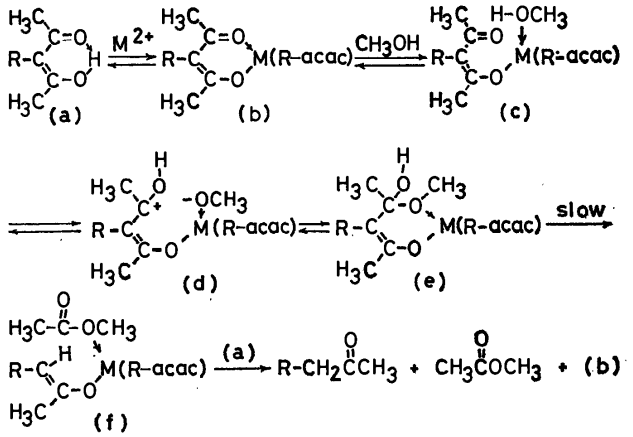

Fig. 4.

The mechanism is consistent with the observed kinetic results and the reaction products. The independence of the rate of alcoholysis from β-diketone concentration, the small or absent reactivity of 3,3-disubstituted-2,4-pentanedione, and the lower activity of zinc chloride suggest that the metal enolate(b) is the reactive species in the present alcoholysis. The presence of a pre-equilibrium (b)$+CH_3OH\rightleftarrows$(e) is supported by the observed kinetic isotope effect and the effects of the kinds of solvent and alcohol on the rate of the alcoholysis. The effects of 3-substituents and solvents on the activation energy E_a may be explained in terms of the stabilization of the intermediate in the transition state of the rate-determining step (e)→(f). The effect of 4-substituents on the rate

ratio k_1/k_2 in unsymmetrical β-diketones shows that the cleavage occurs at the more electron-deficient C–C bond. Monoketone and acetate are liberated from the coordinated site by the ligand exchange with another β-diketone(a) to re-form the metal chelate of β-diketone (b) and the cycle recurs many times.

Alcoholysis of 1-Alkenyl Substituted β-Ketoesters. It was found that in the presence of metal acetate 1-alkenyl substituted β-ketoesters underwent alcoholysis involving an ester exchange to give esters of β,γ-unsaturated carboxylic acid. For example:

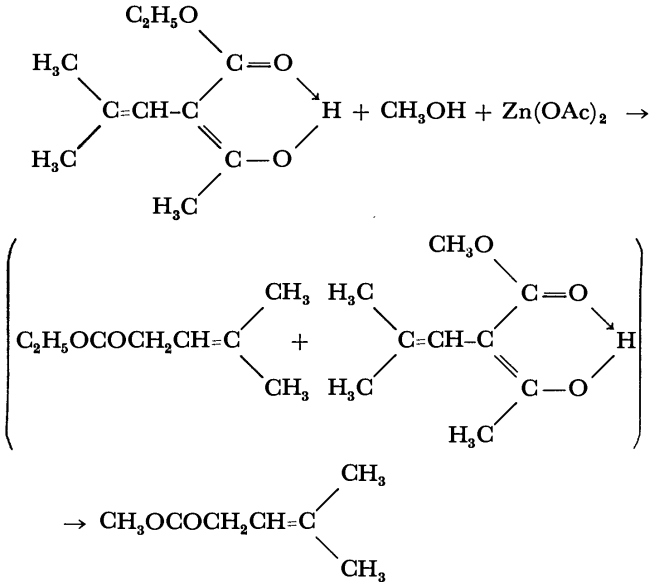

The metal-ion-catalyzed ester exchange of β,γ-unsaturated carboxylates formed by the deacetylation was found to proceed much more slowly than that of the parent β-ketoesters. Thus, in the initial stage of the methanolysis, ethyl esters of 1-alkenylacetic acid were formed predominantly as the alcoholysis product. The initial rate of the deacetylation of ethyl (2-methyl-1-propenyl)acetoacetate by the various metal acetates is shown in Table 7.

The order of the activities of metal acetates used as the catalyst is as follows: Mn(II)>Cd(II)>Zn(II)>Co(II)>Ni(II)>Cu(II). The observed activity order of $M(OAc)_2$ was again anti-parallel to the stability constants of $M(acac)_2$.

Synthesis of β,γ-Unsaturated Ketones and Esters. It has been known that β,γ-unsaturated ketones are prepared by the steam distillation of an aqueous acidic solution of 3-alkene-2,5-diols,[18] by the acid catalyzed isomerization of α,β-unsaturated ketones,[19] and by several other methods.[20–23] The present reaction seems to be interesting as a general synthetic method of β,γ-unsaturated ketones of the type $RR'C{=}CHCH_2COCH_3$ starting from aldehyde and acetylacetone, because of the ease of isolation of the β,γ-unsaturated ketone from its reaction mixture by fractional distillation with high purity and a fair yield. Zinc acetate is an efficient catalyst for the alcoholysis of 3-(1-alkenyl)-2,4-pentanediones without catalyzing side reactions such as rearrangements of double bond and alcohol additions.

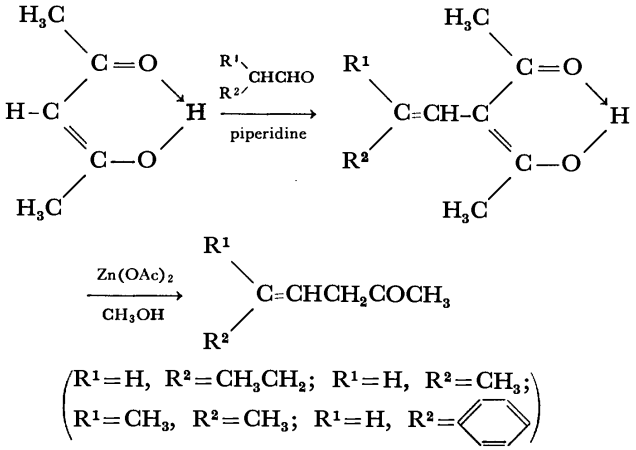

It is known that β,γ-unsaturated carboxylic acids are prepared by the condensation of malonic acid with aldehyde followed by decarboxylation[24] and that the esterification of β,γ-unsaturated carboxylic acids is carried out by the reaction of its Ag salt with alkyl iodide.[25] The present reaction seems to provide a more convenient route to the ester of β,γ-unsaturated carboxylic acid in spite of its lower yield.

Table 7. Effects of metal ion on the deacetylation of ethyl (2-methyl-1-propenyl)acetoacetate in methanol

[β-Ketoester] = 2.73×10^{-1} M, [$M(OAc)_2$] = 7.00×10^{-3} M

Metal acetate	k_{obsd} (70 °C) $\times 10^5$ (s^{-1})
$Mn(OAc)_2$	19.1
$Cd(OAc)_2$	9.42
$Zn(OAc)_2$	7.20
$Co(OAc)_2$	2.80
$Ni(OAc)_2$	0.535
$Cu(OAc)_2$	<0.1

Experimental

Materials. 3-Substituted-2,4-pentanedione was prepared by the method described in the previous paper.[26] 3,3-Dimethyl-2,4-pentanedione was prepared by the method of Pearson:[2g] bp 68—68.5 °C/18 mmHg, n_D^{23} 1.4283 (lit,[2g] bp 170—173 °C, n_D^{25} 1.4330). Benzoylacetone,[27] isobutyrylacetone,[28] and *p*-methoxybenzoylacetone[29] were allowed to react with butyraldehyde in the presence of piperidine to give Knoevenagel condensates: 3-(1-butenyl)-4-phenyl-2,4-butanedione, bp 107—110 °C/1 mmHg, n_D^{18} 1.5487, yield 52.5%; 3-(1-butenyl)-4-isopropyl-2,4-butanedione, bp 106—117 °C/16 mmHg, n_D^{17} 1.4724, yield 54%: Copper chelate, Found: C, 61.59; H, 7.99%. Calcd for $C_{22}H_{34}O_4Cu$: C, 62.02; H, 8.04%. 3-(1-Butenyl)-4-*p*-methoxyphenyl-2,4-butanedione, bp 133—141 °C/1 mmHg.

The Knoevenagel condensates of ethyl acetoacetate with aldehydes were prepared by a similar method. Ethyl (1-butenyl)acetoacetate, bp 117—120 °C, yield 41%. Ethyl (2-methyl-1-propenyl)acetoacetate, bp 115—117 °C/20 mmHg, yield 33%. Ethyl (1-propenyl)acetoacetate, bp 110—115 °C/20 mmHg, yield 21%.

Metal acetates and other metal salts were G. R. -grade reagents. Alcohols and solvents were purified by the ordinary methods and were distilled before use. Monodeuteriomethanol was supplied by E. Merck Co. and used without

further purification.

Kinetic Measurements. An alcoholic solution of β-dicarbonyl compound was allowed to undergo alcoholysis in the presence of a metal salt at the desired temperature. Aliquots of the reaction mixture were withdrawn at regular intervals and analyzed by means of gas-liquid chromatography on a column packed with Apiezone grease L (30%) on chromosorb. A Shimadzu GC-4APT gas chromatograph equipped with an integrator, model ITG-2A, was used as the analyzer. Toluene was usually employed as an internal standard, but in some experiments, cumene, ethyl benzoate, propyl benzoate, or diethyl phthalate was also used. The increase of products was measured as a function of time for various β-dicarbonyl compounds.

Spectral Measurements. The IR spectra were measured as a liquid film by means of a Hitachi Model EPI-G2 infrared spectrometer. The UV spectra were measured using a Shimadzu recording spectrophotometer model UV-200. The NMR spectra were determined by means of a Hitachi Model R-20 spectrometer. Tetramethylsilane was used as the internal standard, and carbon tetrachloride was used as the solvent. The mass spectra were recorded on a Hitachi Model RMU-6E mass spectrometer under the following conditions: chamber voltage 80 V, total emission current 80 μA, vacuum 2×10^{-6} mmHg, sample temp. 160 °C.

Synthesis of β,γ-Unsaturated Ketones. 80 g (0.52 mol) of 3-(1-butenyl)-2,4-pentanedione[26] and 0.8 g (0.0036 mol) of zinc acetate in 150 ml of methanol were heated under reflux at 70 °C for 16 h. The reaction mixture was subjected to fractional distillation. The volatile fraction is a mixture of methanol, methyl acetate, and a small amount of acetic acid. From the second fraction (bp 60—62 °C/25 mmHg), 4-hepten-2-one[30] was obtained in a yield of 64% (37 g); its purity was found to be above 99% from glc-analysis by double fractional distillation.

The following 4-alken-2-ones were obtained by the Zn-$(OAc)_2$-catalyzed methanolysis of the Knoevenagel condensates of acetylacetone with propionaldehyde, isobutyraldehyde, and phenylacetaldehyde in a similar manner to that described above (yield 60—80%): 4-Hexen-2-one, bp 61—62 °C/52 mmHg (lit,[18] 45 °C/29 mmHg). n_D^{21} 1.4265. IR spectrum (liquid film): $\nu_{C=O}$ 1710 cm^{-1}. λ_{max}^{MeOH}(C=O) 275 nm. Mass spectrum: *m/e* 98, 83, 55, 43. Semicarbazone (mp 142—143 °C), Found: C, 54.53; H, 8.31; N, 27.32%. Calcd for $C_7H_{13}ON_3$: C, 54.17; H, 8.44; N, 27.07%. 5-Methyl-4-hexen-2-one: bp 61—62 °C/25 mmHg, n_D^{28} 1.4384. IR spectrum(liquid film): $\nu_{C=O}$ 1705 cm^{-1}. λ_{max}^{MeOH} (C=O) 278 nm. Semicarbazone (mp 155—156 °C), Found: C, 56.17; H, 8.65; N, 25.28%. Calcd for $C_8H_{15}ON_3$: C, 56.17, H, 8.65; N, 25.28%. Calcd for $C_8H_{15}ON_3$: C, 56.78; H, 8.93; N, 24.83%. 5-Phenyl-4-penten-2-one: bp 85—87 °C/1 mmHg. n_D^{27} 1.5472. IR spectrum(liquid film); $\nu_{C=O}$ 1708 cm^{-1}. Semicarbazone (mp 151—152 °C), Found: C, 66.97; H, 6.97; N, 19.66%. Calcd for $C_{12}H_{15}ON_3$: C, 66.35; H, 6.91; N, 19.35%.

Synthesis of Esters of β,γ-Unsaturated Carboxylic Acids. The following 1-alkenylacetates were obtained by the $Zn(OAc)_2$-catalyzed ethanolysis or methanolysis of the Knoevenagel condensates of ethyl acetoacetate with butyraldehyde, isobutyraldehyde, and propionaldehyde in a similar manner to that described above: Ethyl 1-butenylacetate, bp 71—72 °C/20 mmHg, yield 14%. n_D^{24} 1.4228. IR spectrum ($\nu_{C=O}$), 1735 cm^{-1}. NMR spectrum (δ, ppm): 1.0 (3H,t), 1.2 (3H, t), 2.0 (2H, m), 2.9 (2H, t), 4.1 (2H, m), 5.5 (2H, m). Benzyl amide (mp 251—252 °C), Found: C, 77.15; H, 8.14; N, 7.03%. Calcd for $C_{13}H_{17}ON$: C, 76.85; H, 8.37; N, 6.90%. Methyl 1-butenylacetate, bp 61—62 °C/20 mmHg, yield 46%. Ethyl (2-methyl-1-propenyl)acetate, bp 67.5—68 °C/18 mmHg, yield 24%. n_D^{24} 1.4286. IR spectrum ($\nu_{C=O}$): 1730 cm^{-1}. NMR spectrum (δ, ppm): 1.2 (3H, t), 1.7 (6H, t), 2.9 (2H, t), 4.1 (2H, m), 5.2 (1H, m). Methyl (2-methyl-1-propenyl)acetate: bp 62—63 °C/18 mmHg, yield 40%. Ethyl propenylacetate: bp 64—66 °C/20 mmHg, yield 6%. n_D^{24} 1.4209. IR spectrum ($\nu_{C=O}$): 1735 cm^{-1}. NMR spectrum (δ, ppm): 1.2 (3H, t), 1.7 (3H, t), 2.9 (2H, t), 4.1 (2H, m), 5.5 (2H, m). Mass spectrum: *m/e* 128, 85, 55, 45.

The authers wish to thank Mr. Tetsuo Akutsu for his assistance in carrying out a part of the reported experiments.

References

1) Part XX in a series of "Catalytic Behavior of Metal Chelate Compounds." Part XIX, K. Uehara, Y. Ohashi, and M. Tanaka, *Chem. Lett.*, **1974**, 827.
2) a) W. Bradley and R. Robinson, *J. Chem. Soc.*, **128**, 2356 (1926). b) H. Adkins, W. M. Kutz, and D. D. Coffmann, *J. Amer. Chem. Soc.*, **52**, 3212 (1930). c) W. M. Kutz and H. Adkins, *ibid.*, **52**, 4036 (1930). d) W. M. Kutz and H. Adkins, *ibid.*, **52**, 4391 (1930). e) C. L. Bickel, *ibid.*, **67**, 2204 (1945). f) C. R. Hauser, F. W. Swamer, and B. I. Ringler, *ibid.*, **70**, 4023 (1948). g) R. G. Pearson and E. A. Mayerle, *ibid.*, **73**, 926 (1954). h) R. G. Pearson and A. C. Sandy, *ibid.*, **73**, 931 (1954). i) J. -P. Calmon and P. Maroni, *Bull. Soc. Chim. Fr.*, **1968**, 3761, 3772.
3) K. Uehara, F. Kitamura, and M. Tanaka, *Chem. Lett.*, **1973**, 279.
4) R. W. Kluiber, *J. Amer. Chem. Soc.*, **82**, 4839 (1960).
5) J. P. Collmann, *Angew. Chem. Int. Ed., Engl.*, **4**, 132 (1965).
6) D. C. Nonhebel and J. Smith, *J. Chem. Soc. C*, **1967**, 1919.
7) H. D. Murdoch and D. C. Nonhebel, *ibid.*, **1968**, 2298.
8) D. A. Johnson, *Inorg. Chem.*, **5**, 1289 (1966).
9) K. Matsui, M. Motoi, and T. Nojiri, This Bulletin, **46**, 562, 565 (1973).
10) R. M. Klein and J. C. Bailar, Jr., *Inorg. Chem.*, **2**, 1187 (1963).
11) J. A. Bertrand and D. Caine, *J. Amer. Chem. Soc.*, **86**, 2298 (1964).
12) J. A. Bertrand and R. I. Kaplan, *Inorg. Chem.*, **4**, 1657 (1965).
13) P. H. Chapman, R. P. Houghton, and C. S. Williams, *J. Chem. Soc. C*, **1970**, 1183.
14) J. A. Dean, "Lange's Handbook of Chemistry," eleventh ed., McGraw-Hill, New York (1973), pp, 5—51.
15) E. S. Gould, "Mechanism and Structure in Organic Chemistry," Henry Holt (1959), p. 193.
16) A. H. Hunt and M. E. Hobbs, *J. Phys. Chem.*, **75**, 1994 (1971).
17) Y. Nakamura, K. Isobe, H. Morita, S. Yamazaki, and S. Kawaguchi, *Inorg. Chem.*, **11**, 1573 (1972).
18) H. Morrison, *Tetrahedron Lett.*, **1964**, 3653.
19) F. H. Stross, J. M. Monger, and H. de V. Finch, *J. Amer. Chem. Soc.*, **69**, 1627 (1947).
20) R. Heilmann, G. de Gandemaris, and K. Noack, *Bull. Soc. Chim. Fr.*, **1954**, 992.
21) L. A. Paquette, R. F. Eizember, and O. Cox, *J. Amer. Chem. Soc.*, **90**, 5153 (1968).
22) D. D. Faulk and A. Fry, *J. Org. Chem.*, **35**, 364 (1970).

23) D. D. Faulk, W. H. Corkern, I. Ookuni, and A. Fry, *ibid.*, **35**, 1518 (1970).
24) R. P. Linstead, E. G. Noble, and E. J. Boorman, *J. Chem. Soc.*, **1933**, 557.
25) E. J. Boorman, R. P. Linstead, and H. N. Rydon, *ibid.*, **1933**, 568.
26) K. Uehara, M. Ito, and M. Tanaka, This Bulletin, **46**, 1566 (1973). K. Uehara, T. Matsumura, Y. Murata, M. Tanaka, and N. Murata, *Kogyo Kagaku Zasshi*, **72**, 1825 (1969).
27) W. M. Muir, P. D. Ritchie, and D. J. Lyman, *J. Org. Chem.*, **31**, 3790 (1966).
28) R. Levine, J. A. Conroy, J. T. Adams, and C. R. Hauser, *J. Amer. Chem. Soc.*, **67**, 1510 (1945).
29) S. S. Sabnis, K. D. Kulkarni, and C. D. Deliwala, *J. Sci. Ind. Research*, **17A**, 421 (1958). *Chem. Abstr.*, **53**, 12228 (1959).
30) K. Uehara, S. Shionoiri, M. Tanaka, and N. Murata, This Bulletin, **45**, 1570 (1972).

Photooxygenation of α,β- and β,γ-Unsaturated Enamines in 17-(1-Formylethyl)etiojervanes[1]

Akio MURAI, Chizuko SATO, Hiroshi SASAMORI, and Tadashi MASAMUNE

Department of Chemistry, Faculty of Science, Hokkaido University, Sapporo 060

(Received July 11, 1975)

Photooxygenation of α,β(13,17)- and β,γ(12,13)-unsaturated morpholine enamines (I and II) in 17-(1-formylethyl)etiojervanes by singlet oxygen was carried out under irradiation with fluorescent bulbs. Oxidation of the former (I) afforded the corresponding α,β-unsaturated ketone (III) as the only product which could be isolated, while that of the latter gave two products, one (IV) being a normally oxidized β,γ-unsaturated ketone and the other (VIII) an α,β-unsaturated ketone with the D-ring contracted. Compound (VIII) was not obtained by treatment of IV under the same photooxygenation conditions as for II, indicating that the formation of VIII would not involve IV as an intermediate.

The photooxygenation of enamines by singlet oxygen has been demonstrated to be useful for synthesis.[2] We describe further examples which involve transformation of the enamines (I) and (II) into the corresponding unsaturated ketones. These α,β-[3] and β,γ-unsaturated ketones[4] (III and IV) are not readily obtainable by the standard chemical procedures.[5]

The enamines (I) and (II) were prepared as follows. 17-(1-Formylethyl)-5α,12α-etiojerv-13(17)-en-3β-ol[3] (V) was converted into the acetate (Va), oil, which was treated with morpholine[6] to give the α,β-unsaturated morpholine enamine (I), oil, in good yield; NMR, δ 1.68 and 1.74 (each 3H, s, 21- and 18-$C_3\underline{H}$ or *vice versa*). On the other hand, 17α-(1-formylethyl)etiojerva-5,12-dien-3β-ol[4] (VI) was transformed *via* a three-step process (acetalization of the formyl group, the Oppenauer oxidation and deacetalization) into the corresponding Δ^4-3-ketone (VII), oil, in good yield; UV, λ_{max} 238 nm (ε 10500), which smoothly formed the morpholine 20-enamine (II), oil, in the same manner as Va; NMR, δ 1.46 and 1.50 (each 3H, s, 18- and 21-$C\underline{H}_3$ or *vice versa*).

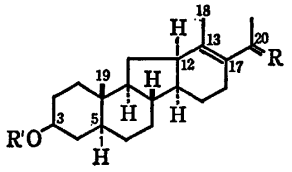

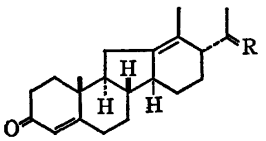

I R=CH(NC_4H_8O), R'=Ac
III R=O, R'=Ac
V R=H, CHO, R'=H
Va R=H, CHO, R'=Ac

II R=CH(NC_4H_8O)
IV R=O
VII R=H, CHO

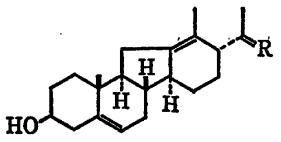

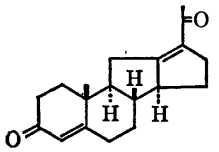

VI R=H, CHO
IX R=O

VIII

Photooxygenation of the α,β-unsaturated enamine (I) in benzene with Rose Bengal as a sensitizer was carried out in a Pyrex tube irradiated externally with four 15-watt fluorescent bulbs at room temperature for 7.5 h, when all the starting enamine had been brought to reaction. The resulting tarry product was purified by preparative tlc to give 13, 17-unsaturated 20-ketone (III), oil, in 40% yield as the only main product which could be isolated; Mass, 358 (M^+) and 255; UV, λ_{max} 249 nm (ε 13000); IR, ν_{max} 1730, 1674, 1612, 1255, and 1210 cm^{-1}; NMR, δ 0.78, 1.89, 2.04, and 2.25 (each 3H, s, 19-, 18-, acetoxy, and 21-$C\underline{H}_3$), and 4.71 (1H, br W_H=21 Hz, $\underline{H}$ at C_3). Since α,β-unsaturated enamines have been reported to undergo autooxidation and form the cooresponding 1,4-diones,[7] photooxygenation is practicable, since ketone (III) had not been obtained by hydrolysis of the corresponding oxime[3] even under mild conditions. The α,β-(13,17)-unsaturated 20-ketone (III) was found to be very unstable as compared with the other α,β-(16,17)-unsaturated 20-ketone.[6] Double bond migration[4,8] followed by hydrooxygenation probably takes place under the conditions.

Photooxygenation of β,γ-unsaturated enamine (II) under the comparable conditions (22 h) afforded a tarry mixture, from which two products (IV) and (VIII) were isolated by preparative tlc in 11 and 22% yields, respectively. (IV), mp 131—133 °C and $[\alpha]_D$ +198°, showed the following spectra: Mass, *m/e* 312 (M^+) and 269; UV, λ_{max} 238 nm (ε 11500); IR, ν_{max} 1700, 1655, and 1603 cm^{-1}; NMR, δ 1.18, 1.57, and 2.14 (each 3H, s, 19-, 18-, and 21-$C\underline{H}_3$) and 5.78 (1H, s, $\underline{H}$ at C_4). The assigned structure of (IV) was consistent with these spectra and confirmed by the Oppenauer oxidation of the corresponding etiojerv-5-en-3β-ol[4] (IX) to IV. On the other hand, (VIII), mp 196—198 °C and $[\alpha]_D$ +110°, was identified on the basis of the spectral data to be α,β-unsaturated ketone with the D-ring contracted: Mass, *m/e* 284 (M^+), 269(M^+–CH_3), 241 (M^+–$COCH_3$), and 161 (base); UV, λ_{max} 247 nm (ε 20000); IR, ν_{max} 1654 and 1614 cm^{-1}; NMR, δ 1.22 and 2.28 (each 3H, s, 19-$C\underline{H}_3$ and $COC\underline{H}_3$) and 5.79 (1H, s, $\underline{H}$ at C_4). This ring-contracted product (VIII) was not obtained by treatment of IV under the same oxygenation conditions, most of the starting material being recovered unchanged. Its formation might involve initial oxygenation of the isolated 12,13-double bond[9] followed by the usual oxidation of the enamine double bond[10] and subsequent deacetylation (Norrish Type I and/or II). The same reaction of II in methanol resulted in the predominant formation of IV. Compounds IV and VIII were isolated in 24 and 3% yields. This result was in good accord with the solvent dependency

with respect to product formation in the photooxygenation of enamines.[11]

Experimental

All the mps were uncorrected. The homogenity of each compound was always checked by tlc on silica gel (Wakogel B-5), various solvent systems being used, and the spots were developed with ceric sulfate in dil sulfuric acid and/or iodine. The optical rotations and UV, IR and NMR spectra were measured in chloroform, ethanol, chloroform, and deuteriochloroform, respectively. The abbreviations "s, d, br, and m" in the NMR spectra denote "singlet, doublet, broad, and multiplet," respectively.

α,β-Unsaturated Enamine (I). 17-(1-Formylethyl)-5α, 12α-etiojerv-13(17)-en-3β-ol[3a] (V, 240 mg) was treated with acetic anhydride (5 ml) and pyridine (5 ml) at room temperature overnight. The mixture was diluted with chloroform, washed with 1 M hydrochloric acid and 5% aqueous sodium bicarbonate, dried, and evaporated to leave an oily residue (255 mg), which was purified by column chromatography (cc) over silica gel to give the 3β-acetate (Va, 180 mg), oil; Mass *m/e* 372 (M^+) and 343 (M^+—CHO); IR, ν_{max} 1728, 1252, and 1208 cm^{-1}; NMR, δ 0.76, 1.72, and 2.05 (each 3H, s, 19-, 18-, and acetoxy-C$\underline{H}_3$), 1.14 (3H, d J= 7 Hz, 21-C$\underline{H}_3$), and 3.44 (1H, br W_H=21 Hz, $\underline{H}$ at C_3), and 9.52 (1H, s, C$\underline{H}$O). This was used for the next reaction without further purification.

A solution of Va (108 mg) in a mixture of benzene (20 ml) and morpholine (0.1 ml) containing *p*-toluenesulfonic acid (PTS, 1 mg) was refluxed under nitrogen for 6 h, water being removed by means of a Dean-Stark apparatus. After removal of the solvents below 30 °C, the residue was worked up as usual to give α,β-unsaturated enamine (I, 119 mg), oil; Mass, *m/e* 441 (M^+), 426 (M^+–CH_3), and 398 (M^+—$COCH_3$); IR, ν_{max} 1720, 1644, 1256, and 1115 cm^{-1}; NMR, δ 0.81 (3H, s, 19-C$\underline{H}_3$), 2.05 (3H, s, OCOC$\underline{H}_3$), and 2.84 and 3.70 (each 4H, m W_H=13 Hz, N$C_2\underline{H}_4C_2\underline{H}_4$O), and 4.70 (1H, br W_H=21 Hz, $\underline{H}$ at C_3).

Oxygenation of I. A solution of I (108 mg) in benzene (15 ml) containing Rose Bengal (5 mg) in a Pyrex tube was bubbled with oxygen at room temperature under external irradiation with four 15-watt fluorescent bulbs (standard desk lamps) for 7.5 hr, when the starting material had disappeared on tlc. After removal of benzene, the residue was treated with water and chloroform. The chloroform extracts were worked up as usual to leave tarry material (100 mg), which was purified by preparative tlc over silica gel (Wakogel B-5) with a 1 : 1 mixture of benzene and ether to give α,β-unsaturated ketone (III, 40 mg), oil, showing a single spot; Mass, UV, IR and NMR are given in the text.

β,γ-Unsaturated Enamine (II). To a methanol solution (54 ml) of 17α-(1-formylethyl)etiojerva-5,12-dien-3β-ol[4] (VI, 605 mg) was added boron trifluoride etherate (2.0 ml) under cooling with ice, and the mixture was stirred at room temperature for 62 h under nitrogen. The solution was neutralized with 5% aqueous sodium bicarbonate and evaporated to leave an oily residue, which was worked up as usual to give the 20-aldehyde dimethyl acetal (585 mg), oil; Mass, *m/e* 342 (M^+—CH_3OH), 310 (M^+—$2CH_3OH$), and 270 [base, M^+—$CH(CH_3)CH(OCH_3)_2$]; NMR, δ 0.68 (3H, d J=7 Hz, 21-C$\underline{H}_3$) 0.98 and 1.53 (each 3H, s, 19- and 18-C$\underline{H}_3$), 3.34 (6H, s, OC$\underline{H}_3$), 4.24 (1H, d J=8 Hz, $\underline{H}$ at C_{22}), and 5.40 (1H, br W_H=9 Hz, $\underline{H}$ at C_6).

The acetal (575 mg) was dissolved in a mixture of toluene (72 ml) and cyclohexanone (3.9 ml); 30 ml of the toluene was then distilled off to remove water. Aluminium isopropoxide (530 mg) was added and, after removal of 10 ml of the toluene by distillation, the mixture was refluxed for 2.5 h and then distilled with steam to remove the organic solvents. The residue was extracted with chloroform, and the chloroform solution was washed with water, dried, and evaporated to give the corresponding Δ^4-3-ketone (569 mg), oil; UV, λ_{max} 238 nm (ε 10500); IR, ν_{max} 1666 and 1616 cm^{-1}; NMR, δ 0.69 (3H, d J=7 Hz, 21-C$\underline{H}_3$), 1.16, 1.54 (each 3H, s, 19- and 18-C$\underline{H}_3$), 3.35 (6H, s, 2OC$\underline{H}_3$), 4.22 (1H, d J= 8 Hz, $\underline{H}$ at C_{22}), and 5.80 (1H, s, $\underline{H}$ at C_4).

A solution of the α,β-unsaturated ketone (569 mg) in a mixture of acetone (170 ml) and water (30 ml) was refluxed with PTS (117 mg) for 4 h under stirring. After removal of most of the acetone, the residue was extracted with chloroform, washed with water, dried and evaporated to give 20-formyl-Δ^4-3-ketone (500 mg), oil; IR, ν_{max} 1721, 1656, and 1609 cm^{-1}; NMR, δ 0.90 (3H, d J=7 Hz, 21-C$\underline{H}_3$) 1.16 and 1.60 (3H, s, 19- and 18-C$\underline{H}_3$), 5.78 (1H, s, $\underline{H}$ at C_4), 9.68 and 9.73 (total 1H, each s, C$\underline{H}$O).

The 20-formyl-Δ^{12}-3-ketone (84 mg) in benzene (10 ml) and morpholine (0.1 ml) was treated with PTS (1 mg) in the same manner as for Va to give the 20-morpholine enamine (II, 99 mg), oil; Mass, *m/e* 395 (M^+), 380 (M^+—CH_3), 268 [M^+—(H+17-side chain)], and 127 [base, (H+17-side chain)]; IR, ν_{max} 1660, 1616, and 1116 cm^{-1}; NMR, δ 1.16 (3H, s, 19-C$\underline{H}_3$), 2.66 and 3.76 (each 4H, m, W_H=12 Hz, N$C_2\underline{H}_4C_2\underline{H}_4$O), and 5.49 and 5.82 (each 1H, s, 2$\underline{H}$ at C_{22} and C_4).

Oxygenation of II. A solution of II (337 mg) in benzene (20 ml) was oxygenated in the same manner (60 watt, 22 h, and room temperature) as for I. The reaction mixture was worked up as usual to leave an oily residue (250 mg), showing two main spots on tlc, which was separated by cc over silica gel with a 1 : 1 mixture of benzene and ether to give two crystalline compounds (IV and VIII). The former (IV, 27 mg), mp 131—133 °C on recrystallization from acetone–isopropyl ether, showed the spectra as described. The compound (IV) was also obtained by treatment of the corresponding etiojerv-5-en-3β-ol[4] (IX) under the same Oppenauer conditions as the acetal of VI. Found: C, 80.90; H, 9.15%. Calcd for $C_{21}H_{28}O_2$: C, 80.73; H, 9.03%. The latter (VIII, 52 mg) had mp 196—198 °C (acetone–isopropyl ether); Mass, UV, IR, and NMR in the text. Found: C, 80.36; H, 8.52%. Calcd for $C_{19}H_{24}O_2$: C, 80.24; H, 8.51%.

Compound II (330 mg) was oxygenated in methanol (20 ml) under almost the same conditions (60 watt, 3.5 h, and room temperature) as for benzene and gave IV (63 mg), mp 129—131 °C, and VIII (15 mg), mp 189—191 °C.

References

1) Part XXII of "C-Nor-D-homosteroids and Related Alkaloids;" Part XXI, M. Takasugi, V. H. Castro-Araya, T. Masamune, A. Furusaki, and T. Matsumoto, *Chem. Lett.*, **1974**, 1477.

2) For examples, K. Miyano, Y. Ohfune, S. Azuma, and T. Matsumoto, *Tetrahedron Lett.*, **1974**, 1545; J. E. Huber, *ibid.*, **1968**, 3271; C. S. Foote and J. Wei-Ping Lin, *ibid.*, **1968**, 3267.

3) a) T. Masamune, K. Orito, and A. Murai, This Bulletin, **39**, 2503 (1966). b) S. M. Kupchan, T. Masamune, and G. W. A. Milne, *J. Org. Chem.*, **29**, 755 (1964).

4) A. Murai, K. Arita, and T. Masamune, This Bulletin, **46**, 3536 (1973).

5) a) R. W. Franck, G. P. Rizzi, and W. S. Johnson, *Steroids*, **4**, 463 (1964). b) S. H. Pines, J. M. Chemerda,

and M. A. Kozlowski, *J. Org. Chem.*, **31**, 3446 (1966).

6) T. Masamune, A. Murai, K. Orito, H. Ono, S. Numata, and H. Suginome, *Tetrahedron*, **25**, 4853 (1969); H. Suginome, N. Sato, and T. Masamune, *Tetrahedron Lett.*, **1969**, 3353; S. M. Kupchan and M. J. A. El-Haj, *J. Org. Chem.*, **33**, 647 (1968); W. F. Johns and I. Laos, *ibid.*, **30**, 123 (1965); W. F. Johns, *ibid.*, **29**, 2545 (1964).

7) S. K. Malhotra, J. J. Hostynek, and A. F. Lundin, *J. Amer. Chem. Soc.*, **90**, 6565 (1968).

8) *Cf.*, T. Masamune, H. Matsue, and M. Fujii, This Bulletin, **45**, 1812 (1972); K. G. Lewis and G. J. Williams, *Tetrahedron Lett.*, **1965**, 4573.

9) S. Mazur and C. S. Foote, *J. Amer. Chem. Soc.*, **92**, 3225 (1970); P. D. Bartlett and A. P. Schaap, *ibid.*, **92**, 3223 (1970); A. Nickon and J. F. Bagli, *ibid.*, **83**, 1498 (1961).

10) *Cf.*, H. H. Wasserman and S. Terao, *Tetrahedron Lett.*, **1975**, 1735; I. Saito, M. Imuta, and T. Matsuura, *Chem. Lett.*, **1972**, 1173; A. Jerusei, *J. Org. Chem.*, **34**, 3648 (1969); V. V. Rheenen, *Chem. Commun.*, **1969**, 314.

11) C. S. Foote, A. A. Dzakpasn, and J. W. -P. Lin, *Tetrahedron Lett.*, **1975**, 1247. *Cf.*, A. G. Schultz and R. H. Schlessinger, *ibid.*, **1970**, 2731.

The Reactions of the Dimers of Hexafluoropropene with *O*-Nucleophiles

Nobuo ISHIKAWA and Akira NAGASHIMA

Department of Chemical Engineering, Tokyo Institute of Technology, Meguro-ku, Tokyo 152

(Received July 14, 1975)

The reactions of the dimers of hexafluoropropene with alcohols and phenol in the presence of triethylamine, and with sodium alkoxides and phenolate were carried out. Of the two dimers, perfluoro-2-methyl-2-pentene (Dimer **2**) was much more reactive than perfluoro-4-methyl-2-pentene (Dimer **1**). While the dimer **2** and *O*-nucleophiles gave various addition and substitution products very easily, the dimer **1** reacted only with sodium alkoxides to give trialkoxylated products.

Hexafluoropropene is known to oligomerize readily in the presence of a base or a fluoride ion, giving a mixture of its dimers and trimers.[1-4] The dimers are composed of perfluoro-4-methyl-2-pentene (**1**) and perfluoro-2-methyl-2-pentene (**2**), the former being predominant. However, because of the negative hyperconjugation and the electron-withdrawing inductive effect of the trifluoromethyl groups adjacent to the double bond, **2** is thermodynamically more stable than **1**, and the latter is converted into **2** by heating with potassium fluoride.[2-5] Further, **2** is likely to be more susceptible to the nucleophilic attack than **1**, because the supposed anionic intermediate, **4**, must be more stable than another intermediate, **3**.

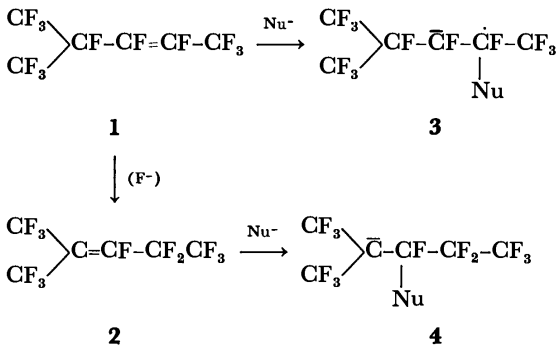

We wish to report several results derived from the reactions of these dimers with alcohols and phenol.

Results and Discussion

Reactions with Alcohols and Phenol in the Presence of Triethylamine. While the dimer **1** was unsusceptible to methanol under basic conditions, even when heated for a prolonged time, the dimer **2** and methanol in the presence of an equimolar amount of triethylamine reacted readily at −10—0 °C. They gave a mixture of addition and substitution products [**5** : **6** (R=Me) = 1 : 1; total, 44%], together with highly boiling products. These by-products seem to have resulted from further reactions of **6**. For example, a reactive terminal olefin, **7**, or a dealkylated ambident anion, **8**, might be formed[6] and might then react further with alcohol to give other products.

When a catalytic amount of triethylamine was used in the above reaction, the adduct, **5**, was obtained in a good yield (69%), together with a trace of the substituted product, **6**.

Ethanol reacted with the dimer **2** more moderately. In the presence of an equimolar amount of triethylamine, they gave a mixture of addition and substitution products, **5** and **6** (R=Et), in a ratio of 2 : 5; the total yield was rather good (71%). When the mixture was treated with aqueous potassium hydroxide, **6** was obtained as a pure product.

With a catalytic amount of triethylamine, ethanol and the dimer **2** did not react at low temperatures. At room temperature, however, they gave the substitution product (**6**) and that alone. The prevailing formation of **6** in this case is presumed to be due to the bulky OEt group, which prefers the sp^2 carbon of **6** rather than the sp^3 carbon of **5**.

This was supported by the results of the reaction between the dimer **2** and phenol. This weak and bulky nucleophile, in the presence of triethylamine, also reacted readily with **2** in diethyl ether, thus giving the substitution product, **6** (R=Ph), exclusively (65%).

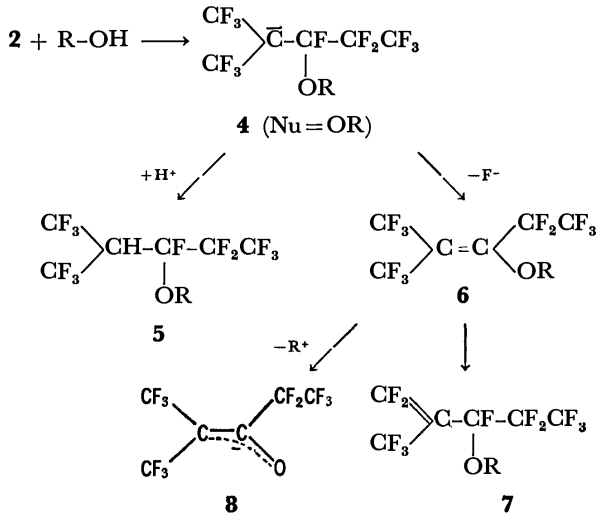

The structures of the products described above were established from various spectral data, especially the ^{19}F NMR. The chemical shifts and some of the coupling constants were as follows:*

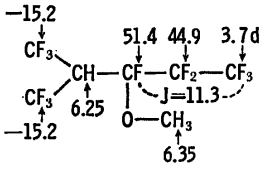

5 (R=Me)

* All the ^{19}F NMR chemical shifts throughout this article are given in δ ppm from external trifluoroacetic acid. The PMR chemical shifts and the coupling constants are given in τ and Hz, as usual. All were taken in neat.

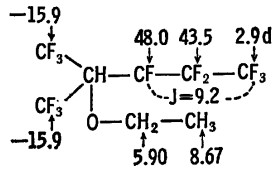

5 (R=Et)

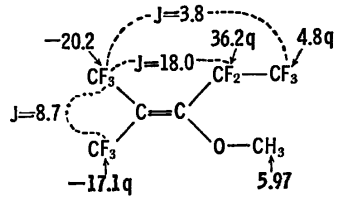

6 (R=Me)

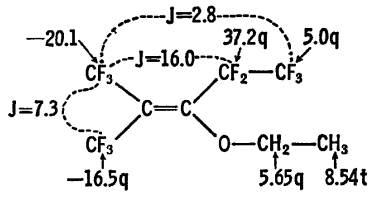

6 (R=Et)

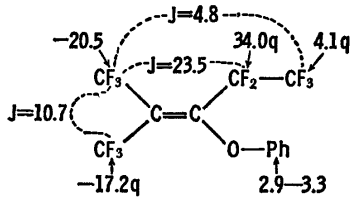

6 (R=Ph)

The Reactions with Sodium Alkoxides and Phenoxide. Althouth the dimer **1** did not react with alcohols in the presence of a base, it was readily attacked by sodium alkoxides at low temperatures from −10 to 0 °C. When three moles of sodium ethoxide in ethanol were used, a triethoxy-substituted product, **9**, was obtained. The reaction seemed to proceed according to an S_N2'-like mechanism as follows:

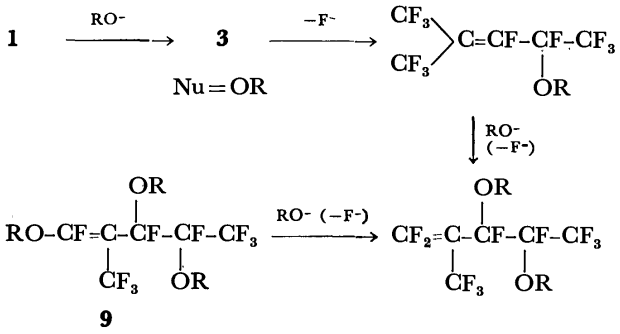

9

The crude product of this reaction partly decomposed on distillation *in vacuo*, probably because it contains a small amount of an addition product containing the EtO–CF_2–CH< group, which is hydrolyzed easily to an ester, EtO–C(=O)–CH<.

The crude product was then treated with an aqueous potassium hydroxide solution prior to distillation. The yield of the purified product thus obtained was 32%. This triethoxylated product was composed of two isomers in a ratio of 2 : 3; they were separated by means of a preparative gas chromatography. These isomers gave almost identical patterns in their IR, ^{19}F, and ^1H NMR and mass spectra. In the IR spectra, both compounds gave a strong absorption band at 1675 cm^{-1} due to the C=C double bond. In the mass spectra, strong peaks at *m/e* 333 (M^+—OEt), 233 (M^+—CF(OEt)–CF_3), and 137 ($O{=}\overset{+}{C}$–C(CF_3)=C=O)were observed for each isomer. The ^{19}F NMR chemical shifts are shown below. From these results, we assigned for the *E* and *Z* isomers to them, though we could not ascertain which was which.

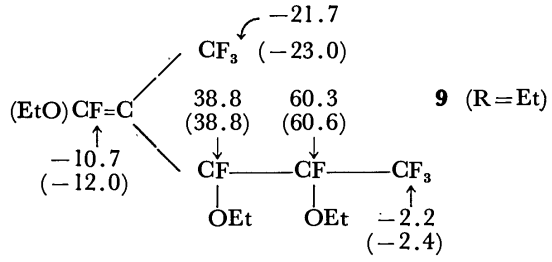

9 (R=Et)

(The values in parentheses are of the minor component)

Even when the reaction was carried out using an equimolecular amount of sodium ethoxide, the triethoxy compound was formed. This means that the second and the third steps of the above scheme proceed very fast, and that the first alkoxylation is the rate-determining step.

In the same manner, the dimer **1** and sodium methoxide gave similar trimethoxylated products, also composed of two isomers. Although the attempt to separate them from each other was unsuccessful, even by means of preparative gas chromatography, the IR and NMR spectra of the mixture supported the structure **9** (R=Me).

The dimer **2**, in contrast with **1**, gave dialkoxy compounds in a reaction with sodium alkoxide. The dimer **2** with a 2.2-molar amount of sodium ethoxide in ethanol below 0 °C yielded a diethoxy substituted product, **10** (R=Et). Vacuum distillation after treatment with an aqueous sodium hydroxide solution gave a pure compound in a 52% yield. The reaction path seemed to be as follows:

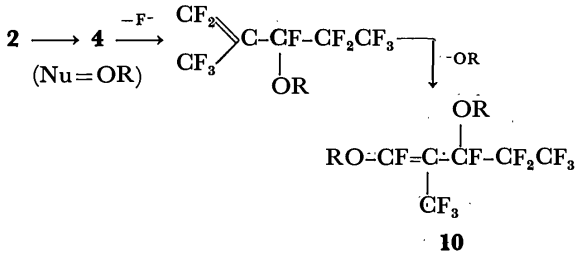

10

This ethoxylated product was also a mixture of two isomers in a ratio of 1 : 3. Since the IR, NMR and mass spectra of the mixture strongly supported the structure **10**, these two compounds are also presumed to be *E* and *Z* isomers. Sodium methoxide gave a similar dimethoxy substituted product in a 51% yield. This was also a mixture of two isomers (1 : 3). The

^{19}F NMR spectra for these products are shown below.

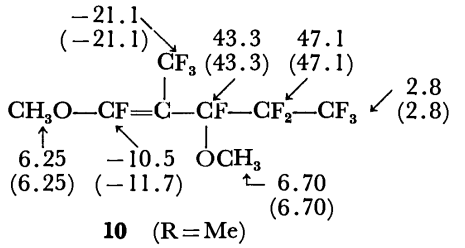

10 (R=Me)

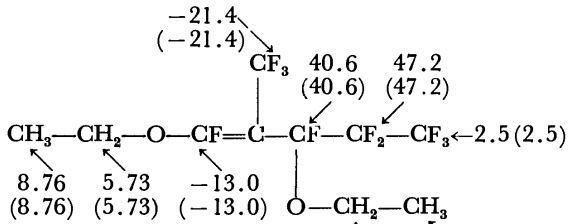

10 (R=Et)

(The values in parentheses are of the minor component)

Sodium phenoxide, a weaker nucleophile than sodium alkoxide, was unreactive to the dimer **1**. However, the dimer **2** in diethyl ether reacted even below 0 °C, giving a mixture of monophenoxylated internal and terminal olefins, **6**(R=Ph) and **11**(2 : 11), in a total yield of 70%.

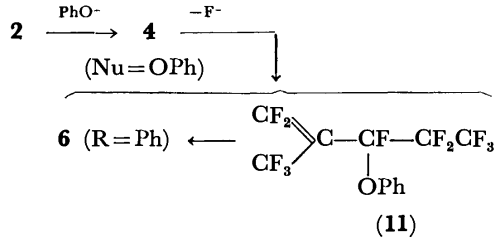

(**11**)

These phenoxylated olefins were separated from each other by means of preparative gas chromatography, and their structures were elucidated from their IR and ^{19}F NMR spectra. The IR spectrum for **11** revealed the presence of the terminal double bond by its absorption at 1725 cm^{-1}, whereas that for **6** (R=Ph) showed the absorption due to the internal double bond at 1647 cm^{-1}. As for the ^{19}F NMR spectra, **11** gave the characteristic signals for CF_2=, which appeared at −15.0 and −17.7 ppm.

When a mixture of these two isomers (**6** : **11**= 3 : 1) was treated with a catalytic amount of triethylamine in diethyl ether at room temperature, only **6** (R=Ph) was obtained. This means that the internal olefin (**6**) is thermodynamically more stable than the terminal olefin (**11**), as was previously known, and that the latter is easily converted into the former.

Experimental

Reaction of Perfluoro-2-methyl-2-pentene (Dimer 2) with Methanol in the Presence of Triethylamine. Into a mixture of the dimer **2** (9.0 g, 0.03 mol) and methanol (15 ml), was added dropwise a solution of triethylamine (3.03 g, 0.03 mol) in methanol (15 ml) at −10—0 °C. After 10 min of stirring at 0 °C, the reaction mixture was poured into dilute hydrochloric acid; the oily matter thus separated was washed with water and dried over magnesium sulfate. Distillation at an ordinary pressure gave an oil (4.2 g, 44%), bp 96—102 °C, which was a mixture of 2-trifluoromethyl-3-methoxy-1,1,1,3,4,4,5,5,5-nonafluoropentane (**5**, R=Me) and 2-trifluoromethyl-3-methoxy-1,1,1,4,4,5,5,5-octafluoro-2-pentene (**6**, R=Me) in a ratio of 1 : 1, based on the ^{19}F NMR spectrum.

When a catalytic amount of triethylamine (0.5 g, 0.005 mol) was used in this procedure, the addition product **5** (6.8 g, 69%), bp 98—99 °C, was obtained exclusively.

Found: F, 68.4%. Calcd for $C_7H_4F_{12}O$: F, 68.7%. IR: 2980 (C-H), 1150—1300 (C-F) cm^{-1}. MS: *m/e* 313 (M^+-F), 293 (M^+-HF_2), 259 ($M^+-CH_4F_3$), 213 ($M^+-C_2F_5$), 193 ($M^+-C_2HF_6$).

Reaction of the Dimer 2 with Ethanol in the Presence of Triethylamine. When ethanol instead of methanol was used in the procedure described above, it gave a mixture of 2-trifluoromethyl-3-ethoxy-1,1,1,3,4,4,5,5,5-nonafluoropentane (**5**, R=Et) and 2-trifluoromethyl-3-ethoxy-1,1,1,4,4,5,5,5-octafluoro-2-pentene (**6**, R=Et) (2 : 5), bp 110—115 °C (71%).

After the mixture (6.11 g, **5** : **6**=2 : 3) had been stirred with diethyl ether (20 ml) and a 30% aqueous potassium hydroxide solution (7 ml) for 5.5 h at room temperature, the ethereal layer was separated and washed with dilute hydrochloric acid and water successively. After being dried over magnesium sulfate, the solvent was removed and the residue was subjected to distillation, giving pure **6** (R=Et), bp 113—116 °C, in a yield of 58% (3.5 g).

Found: F, 64.2%. Calcd for $C_8H_5F_{11}O$: F, 64.1%. IR: 1635 (C=C), 1100—1400 (C-F) cm^{-1}.

Reaction of the Dimer 2 with Phenol in the Presence of Triethylamine. Into a solution of the dimer **2** (6.0 g, 0.02 mol) in diethyl ether (15 ml) was added portionwise a solution of phenol (1.88 g, 0.02 mol) and triethylamine (2.23 g, 0.022 mol) in diethyl ether (15 ml) at 0 °C. After 3 h of stirring at room temperature, the reaction mixture was washed with dilute hydrochloric acid, and then with water, and dried over magnesium sulfate. The solvent was then removed, and the residue was subjected to distillation *in vacuo*, giving 2-trifluoromethyl-3-phenoxy-1,1,1,4,4,5,5,5-octafluoro-2-pentene (**6**, R=Ph) (4.8 g, 65%); bp 69—71 °C/19 mmHg.

Found: F, 56.3%. Calcd for $C_{12}H_5F_{11}O$: F, 55.9%. IR: 1647 (C=C), 1100—1400 (C-F) cm^{-1}. MS: *m/e* 374 (M^+), 305 (M^+-CF_3), 186 (305−C_2F_5), 77 (C_6H_5).

Reaction of Perfluoro-2-methyl-2-pentene (Dimer 1) with Sodium Alkoxides. Into a mixture of the dimer **1** (9.0 g, 0.03 mol) and ethanol (15 ml), an ethanolic solution of sodium ethoxide (Na, 2.3 g, 0.01 mol and EtOH, 30 ml) was added dropwise, in a course of 1 h, while the temperature was kept at −10—0 °C. After stirring at 0 °C and then at room temperature, both times for 0.5 h, the resulting precipitate of sodium fluoride was filtered off, and the filtrate was poured into water. The separated oily matter was washed with water and refluxed for 16 h with a 15% aqueous potassium hydroxide solution in order to complete the elimination of HF from the contaminated addition product. The oily matter was separated, washed with water, and then dried over magnesium sulfate. Vacuum distillation gave a mixture of two isomers (3 : 2) of 1,3,4-triethoxy-2-trifluoromethyl-1,3,4,5,5,5-hexafluoro-1-pentene (**9**, R=Et) (3.6 g, 32%); bp 111—114 °C/16 mmHg.

Found: F, 45.2%. Calcd for $C_{12}H_{15}F_9O_3$: F, 45.2%. IR: 1675 (C=C), 1000—1400 (C-F) cm^{-1}.

A similar reaction with sodium methoxide in methanol gave an oil, bp 94—97 °C/17 mmHg, in a 57% yield. This was also a mixture of two isomers (3 : 1) of 1,3,4-trimethoxy-

2-trifluoromethyl-1,3,4,5,5,5-hexafluoro-1-pentene (**9**, R=Me). In this case, no treatment with an aqueous alkali solution was necessary.

Found: F, 50.7%. Calcd for $C_9H_9F_9O_3$: F, 50.9%. IR: 1675 (C=C), 1100—1400 (C-F) cm^{-1}.

Reaction of the Dimer 2 with Sodium Ethoxide. An ethanolic solution of sodium ethoxide (Na, 1.0 g, in EtOH, 20 ml) was vigorously stirred into the dimer **2** (6.0 g, 0.02 mol), the temperature being kept at −10—0 °C. After 30 min of stirring at 0 °C, the reaction mixture was poured into water; the resulting oily matter was separated, washed with water, and then subjected to refluxing with a 15% aqueous potassium hydroxide solution for 16 h. After washing and drying, distillation *in vacuo* gave a mixture of two isomers (3 : 1) of 1,3-diethoxy-2-trifluoromethyl-1,3,4,4,5,5,5-heptafluoro-1-pentene (**10**. R=Et), bp 81—82 °C/20 mmHg, in a yield of 52%.

Found: F, 54.0%. Calcd for $C_{10}H_{10}F_{10}O_2$: F, 54.0%. MS: *m/e* 352 (M^+), 307 ($M^+-OC_2H_5$), 233 ($M^+-C_2F_5$), 205 ($233-C_2H_4$).

The reaction with methanolic sodium methoxide was carried out in a similar manner. A mixture of two isomers of 1,3-dimethoxy-2-trifluoromethyl-1,3,4,4,5,5,5-heptafluoro-1-pentene (**10**, R=Me), bp 66—68 °C/20 mmHg, was obtained in a 51% yield.

Found: F, 59.9%. Calcd for $C_8H_6F_{10}O_2$: F, 58.6%.

Reaction of the Dimer 2 with Sodium Phenoxide. Sodium phenoxide (2.55 g, 0.02 mol) was added portionwise to a solution of the dimer **2** (6.0 g, 0.02 mol) in diethyl ether (30 ml), while the temperature was kept between −15 and 5 °C. Stirring was continued at 0 °C for 30 min and then at room temperature for 1 h. The sodium fluoride thus precipitated was removed by filtration, and the filtrate was distilled *in vacuo*. A mixture, bp 59—61 °C/15 mmHg (5.3 g, 70%), of 3-phenoxy-2-trifluoromethyl-1,1,1,4,4,5,5,5-octafluoropentene-2 (**6**, R=Ph) and 3-phenoxy-2-trifluoromethyl-1,1,3,4,4,5,5,5-octafluoro-1-pentene (**11**) (2 : 11) was thus obtained. These components were separated from each other by means of preparative gas chromatography.

(**11**): Found: F, 56.6%. Calcd for $C_{12}H_5F_{11}O$: F, 55.9%. IR: 1725 (C=O), 1100—1400 (C-F) cm^{-1}. MS: *m/e* 374 (M^+), 305 (M^+-CF_3), 281 (M^+-OPh), 255 ($M^+-C_2H_5$).

References

1) R. D. Dresdner, F. N. Tlumac, and J. A. Young, *J. Org. Chem.*, **30**, 3524 (1965).

2) W. Brunskill, W. T. Flowers, R. Gregory, and R. N. Haszeldine, *Chem. Commun.*, **1970**, 1444.

3) N. Ishikawa and A. Sekiya, *Nippon Kagaku Kaishi*, **1972**, 2214.

4) T. Martini and G. P. von Halasz, *Tetrahedron Lett.*, **1974**, 2129.

5) N. Ishikawa and A. Nagashima, *Nippon Kagaku Kaishi*, **1975**, 1439.

6) M. V. Urushadge, Yo. G. Abduganiye, Ye. M. Roxlin, and I. L. Knunyants, *Izv. Akad. Nauk SSSR*, **185**, 1347 (1972).

Palladium-catalyzed Decomposition of Azides. I. Formation of Nitriles

Hiroshi HAYASHI, Atsuyoshi OHNO, and Shinzaburo OKA
Institute for Chemical Research, Kyoto University, Uji, Kyoto-Fu 611

(Received July 16, 1975)

Palladium metal catalyzes the decomposition of benzyl azide affording benzonitrile, benzylamine, and *N*-benzylidenebenzylamine. The presence of a suitable hydrogen-acceptor improves the yield of benzonitrile at the sacrifice of benzylamine, whereas the yield of *N*-benzylidenebenzylamine remains constant. The reaction is applied to the preparation of other nitriles.

Azide group possesses many qualities that enable it an excellent starting group for organic synthesis. It can be introduced into an organic moiety by several convenient methods, even in the presence of various other functional groups.[1] The dipolar character and the reactivity (or instability) of the azide group make it react in a variety of fashions.[2] However, surprisingly little is known on its application to organic syntheses except for the syntheses of amines by reduction, carbonyl compounds by acid-catalyzed decomposition, and heterocyclic compounds by 1,3-dipolar addition. Some other transformations are restricted to azides of limited structures.[2]

In the course of our studies on the chemistry of the azide group,[3] we have found that a primary azide can be transformed into the corresponding nitrile by catalysis of palladium metal under such a mild condition as below 80 °C in neutral solutions. In this paper will be reported the procedure, scope, and limitation of the reaction.

It should be emphasized that the present procedure provides a method to obtain various nitriles *without* elongating the skeletal carbon-chain.

Results and Discussion

When a mixture of benzyl azide (**1**) and a catalytic amount of palladium black in benzene was refluxed for 30 min, benzonitrile (**2**), benzylamine (**3**), dibenzylamine (**4**), and *N*-benzilidenebenzylamine (**5**) were obtained in 43, 29, 2, and 27% yields, respectively.

$$\underset{\mathbf{1}}{PhCH_2N_3} \xrightarrow[PhH]{Pd^0} \underset{\mathbf{2}}{PhCN} + \underset{\mathbf{3}}{PhCH_2NH_2} + \underset{\mathbf{4}}{(PhCH_2)_2NH} + \underset{\mathbf{5}}{PhCH{=}NCH_2Ph}$$

The same, but a little bit slower, reaction took place at temperatures as low as 40 °C provided the mixture was set under an atmosphere of nitrogen. Ethanol could be replaced for benzene, whereas amines retarded the reaction appreciably. High-dilution technique, employed to avoid unnecessary bimolecular reaction of **1**, did not alter the yields of products. The results are summarized in Table 1.

Contrary, in the presence of a suitable compound such as 2,5-dimethyl-3-hexyne-2,5-diol or diphenylacetylene increased the yield of the nitrile greatly at the sacrifice of that of the amine (Table 2). Apparently these compounds play a role of a hydrogen-acceptor. Table 2 also shows that the high-dilution technique is effective when the reaction is run in the presence of a hydrogen-acceptor. Although in order to extend the scope of the reaction, one has to deal with azides of various types, some (especially low-molecular-weight aliphatic) azides are, unfortunately,

TABLE 1. PALLADIUM-CATALYZED DECOMPOSITION OF BENZYL AZIDE[a]

Solvent	Temp. °C	Reaction Time, h	Conv. %[b]	Yield of products, %[c]			
				2	**3**	**4**	**5**
Benzene	40	1.5	100	43	26	—	26
Benzene	reflux	0.5	100	43	29	2	27
Benzene[d]	reflux	0.25	100	45	29	3	22
Ethanol[e]	reflux	0.5	100	45	19	—	27
Diethylamine	reflux	2.0	96	42	15	—	22
Butylamine	reflux	2.0	84	29	11	—	0.4

a) Method A. b) Consumed **1**. c) Based on **1** used. d) Method B. e) 99.5%.

TABLE 2. EFFECTS OF HYDROGEN-ACCEPTORS

Acceptor	Method	Conv. %[a]	Yield of products, %[b]			
			2	**3**	**5**	AH_2[c]
$HOC(CH_3)_2C{\equiv}CC(CH_3)_2OH$ (**9**)	A	100	63	9	23	35(2)
$HOC(CH_3)_2C{\equiv}CC(CH_3)_2OH$	B	100	76	0	22	57(3)
PhC≡CPh (**10**)	A	99	69	0	24	49(4)
PhC≡CPh	B	97	75	0	24	59(4)

a) Consumed **1**. b) Based on **1** used. c) Numbers out of and in parentheses are yields of *cis*- and *trans*-isomers, respectively. AH_2 denotes the reduced acceptor.

Table 3. Preparation of aryl and aralkyl nitriles

Halide	Azide-formation[a] Temp °C	Time, h	Nitrile-formation Method	Acceptor[b]	Conv %[c]	Nitrile %[d]
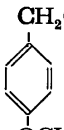	70	2	B	**9**	100	74
			B	**10**	100	73
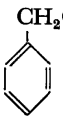	70	2	B	**9**	100	70
			B	**10**	100	68
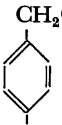	70	2	B	**9**	100	65
			B	**10**	100	65
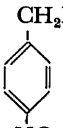	20	2	A[e]	**9**	99	57
			A[e]	**10**	82	52
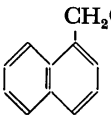	70	2.5	B	**9**	90	70
			A[f]	**10**	98	65
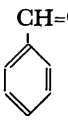	40	2	B	**9**	99	56 (2)[g]
			B	**10**	96	56 (1)[g]
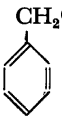	70	15	B	**9**	100	72
			B	**10**	100	68
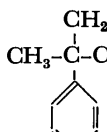	140[h]	18	A[i,j]	—	100	47
			A[j]	**9**	21	7
			A[i,j]	**9**	15	3
			A[j]	—	18	3
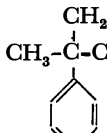	—	—	A[i,l]	—	99	47
			A[m]	**9**	87	77

a) Reaction in DMF. b) **9**; $HOC(CH_3)_2C{\equiv}CC(CH_3)_2OH$. **10**; $PhC{\equiv}CPh$. c) Azide consumed, assuming 100% conversion of the halide into the azide. d) Based on the halide used. e) Reacted for 2 h with the catalysis of palladium on charcoal. f) Reacted for 2 h. g) Numbers in parentheses are the yields of 3-phenylpropionitrile. h) Reaction in HMPA. i) Reaction with 100 mg of palladium on charcoal. j) Reacted for 12 h. k) A controlled experiment. l) Reacted for 2.5 h. m) Reacted for 16 h.

explosive and hazardous to be isolated.[4] Therefore, we have investigated a procedure to transform a halide into the corresponding nitrile without isolating the intermediate azide. Namely, benzyl chloride was reacted with sodium azide in dimethylformamide (DMF) at 70 °C for 2 h and the benzene-extract of the reaction mixture was subjected to the palladium-catalyzed decomposition. The results are listed in Table 3 together with those from substituted benzyl halides. Since the maximum yield of benzonitrile from benzyl azide was 75—76%, the present result is satisfactory. The distribution of the yield for *p*-methoxy-, *p*-chloro-, and unsubstituted benzonitrile may be accounted for by the different yields of the corresponding azides. The situation of *p*-nitrobenzonitrile is somewhat different: the reaction of *p*-nitrobenzyl bromide with sodium azide takes place more smoothly than those of other benzyl halides.

TABLE 4. PREPARATION OF ALIPHATIC NITRILES

Azide-formation[a]			Nitrile-formation				
Halide	Temp °C	Time, h	Method	Time, h	Acceptor[b]	Conv %[c]	Nitrile %[d]
n-C_4H_9Br	50	15	B	—	**9**	100	71
			B	—	**10**	100	70
n-$C_8H_{17}Cl$	70	15	B	—	**9**	100	81
			B	—	**10**	100	79
n-$C_{14}H_{29}Br$	70	15	B	—	**9**	100	76
			B	—	**10**	100	74
n-$C_{18}H_{37}Br$	50	15	B	—	**9**	100	88
			B	—	**10**	100	84
$CH_3CH(CH_3)CH_2Br$	50	15	A	1.5	**9**	98	57
n-$C_4H_9CH(C_2H_5)CH_2Br$	70	15	A	2	**9**	84	61
n-$C_4H_9CH(C_2H_5)CH_2N_3$	—[e]	—	A	2	**9**	80	66
$HO(CH_2)_3Br$	75[f]	16	A	8	**9**	98	36
$AcO(CH_2)_3Br$	50	14	A	1	**9**	99	53
			A	5	**10**	78	54
$(C_2H_5)_2NCH_2CH_2Cl$	70[f]	15	A	60	**9**	95	38
			A	60	**10**	69	37
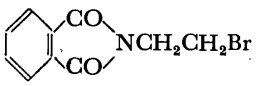	50	15	A	2	—	100	44
			A[g]	5	**9**	97	47

a) Reaction in DMF. b) See footnote (b) in Table 3. c) See footnote (c) in Table 3. d) See footnote (d) in Table 3. e) A controlled experiment. f) Reaction in water. g) Reaction with 100 mg of palladium on charcoal.

However, the *p*-nitro group behaves as a hydrogen-acceptor, which has been confirmed by a controlled experiment with benzyl azide and nitrobenzene, yielding a complex mixture of products. Palladium on charcoal was more effective catalyst than palladium black for this particular compound.

In Table 3 are also listed results on the reaction of phenethyl chloride and its analogs. It is interesting to note that the reaction of 3-azido-1-phenyl-1-propene proceeded without appreciable reduction of the internal double bond, whereas about 30% of styrene, *cis*- or *trans*-stilbene was reduced to the corresponding alkylbenzene when used as a hydrogen-acceptor for the decomposition of benzyl azide. This fact suggests that, unlike the nitro group, nonpolar carbon-carbon double bond has less facility to coordinate onto palladium than the polar azido group.

The decomposition of neophyl (2-methyl-2-phenylpropyl) azide is quite normal in the sense that it affords 2-phenyl-2-propyl cyanide in 47 and 77% yields in the absence and presence of a hydrogen-acceptor, respectively, whereas neophyl chloride gives the corresponding result only when it is subjected to the decomposition catalyzed by palladium on charcoal in the absence of a hydrogen-acceptor. Pre-treatment of the benzene extract by activated charcoal did not improve the yield when palladium black was used as a catalyst. The yield of neophyl azide from neophyl chloride was found to be 92%. Thus the factor(s) which affects the reaction starting from neophyl chloride is unpredictable.

The procedure has also been applied to aliphatic halides and the results are summarized in Table 4. Halides that have *n*-alkyl chain gave satisfactory results, whereas these branched at the β-position reacted less readily. Since neophyl azide reacts normally, the present result cannot be accounted for by steric effect, which is proposed for explaining the difference in reactivity of primary and secondary alkyl halides toward palladium.[5]

When a halide is substituted by a polar functional group, the reaction is greatly retarded and the yield of nitrile is reduced. The most extreme example can be seen in the reaction of *vic*-diazides: in spite of an expectation that the reaction of *vic*-diazides might afford α-amino nitriles, no decomposition of the azido group took place. This fact may be interpreted by the coordination of the functional group onto palladium (**6**) preventing the bidentate coordination of the azido group (**7**).[6] The latter coordination is necessary to loose the nitrogen-nitrogen bond to form an active species **8**.

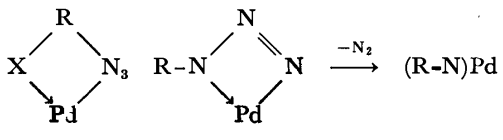

6 **7** **8**

Experimental

Materials. Benzyl azide (bp 86—87 °C/20 mmHg (*lit*,[7] 82.5 °C/16.5 mmHg), n_D^{14} 1.5407), *p*-chlorobenzyl azide (bp 80—82 °C/1.5 mmHg, n_D^{15} 1.5600),[8] and diphenylacetylene (mp 60—61 °C (*lit*,[9] mp 60—61 °C)) were prepared according to the literature, respectively. Halides, obtained from commercial sources or by well known methods, were purified by distillation or recrystallization prior to use. Solvents were distilled and kept over Molecular Sieves 4A. Other reagent-grade chemicals were used without further purification unless otherwise indicated.

2-Ethylhexyl Azide. A mixture of 2-ethylhexyl bromide (9.7 g, 0.05 mol) and sodium azide (6.5 g, 0.1 mol) in DMF (25 ml) was stirred at 70 °C for 15 h. The reaction mixture was poured into 250 ml of water and organic materials were extracted with one 100 ml portion of ether. The extract was washed with three 50 ml portions of water, dried over anhydrous sodium sulfate, and evaporated *in vacuo*. The residual oil was distilled yielding 5.8 g (74% yield) of 2-ethylhexyl azide: bp 81—82 °C/20 mmHg; n_D^{16} 1.4430; ν_{N_3} 2100 cm^{-1}. Found: C, 62.11; H, 11.10; N, 27.02%. Calcd for $C_8H_{17}N_3$: C, 61.89; H, 11.04; N, 27.07%.

Neophyl Azide. Starting from 8.4 g (0.05 mol) of neophyl chloride, 6.5 g (0.1 mol) of sodium azide, and 35 ml of hexamethylphosphoric triamide (HMPA), 6.1 g (70% yield) of neophyl azide was obtained: bp 90—91 °C/3 mmHg; n_D^{22} 1.5266; ν_{N_3} 2100 cm^{-1}. Found: C, 68.34; H, 7.73; N, 24.18%. Calcd for $C_{10}H_{13}N_3$: C, 68.54; H, 7.48; N, 23.98%.

Procedure. Method A. A mixture of benzyl azide (2.0 mmol) and palladium black (10 mg) in benzene (4.0 ml) was refluxed for 30 min or stirred for 1.5 h at 40 °C under an atmosphere of nitrogen. It was necessary to exclude air from the system when the reaction was carried out without refluxing, otherwise no reaction took place even after 12 h.

To the reaction mixture were added 200 mg of biphenyl as an internal standard, 4 ml of ether, and 10 ml of water.

The ether extract was subjected to vpc analyses on Yanagimoto G1800 with a column of Silicon DC-200 (1 m, 150 °C, H_2 0.4 kg/cm^2) or BDS (1 m, 120 °C, H_2 0.2 kg/cm^2).

Method B. Into a refluxing mixture of palladium black (10 mg) and benzene (4.0 ml) was infused benzyl azide (2.0 mmol) over a period of 2 h. The whole mixture was refluxed for additional 15 min and the products were analysed as described above.

In some experiments 100 mg of palladium on charcoal (5%) was employed in place of palladium black yielding similar results. Ethanol could be substituted for benzene, but amines were not good solvents for the reaction (Table 1).

Method C. In a typical run, 20 mmol of a halide and 40 mmol of sodium azide in 10 ml of a solvent were stirred. The solvent, reaction temperature, and reaction period are shown in Tables 3 and 4. The reaction mixture was poured into water (100 ml) and 2.0 g of biphenyl (an internal standard for vpc analyses) was added. The organic materials were extracted with one 20 ml portion of benzene. The extract was washed with three 25 ml portions of water and dried over anhydrous sodium sulfate. A 2.0 ml aliquot of the benzene solution was subjected to palladium-catalysis with the Method A or B and the products were analyzed on vpc as described above. When the reaction required more than an hour, only the Method A was employed.

Identification of Products. In a typical run 3.3 g (0.02 mol) of *p*-chlorobenzyl azide was added to a refluxing mixture of 2,5-dimethyl-3-hexyne-2,5-diol (2.8 g, 0.02 mol) and palladium black (0.1 g) in benzene (20 ml) over a period of 1 h and the whole mixture was refluxed for additional 10 min. The reaction mixture was filtered and the filtrate was washed with four 25 ml portions of water. The organic layer was dried over $CaCl_2$ and the solvent was evaporated *in vacuo* The residue was distilled at a bath temperature of 95 °C under a pressure of 20 mmHg.

The distillate was recrystallized from cyclohexane giving 1.6 g (60% yield) of *p*-chlorobenzonitrile: mp 91—93 °C (*lit*,[10] mp 89—91 °C).

The nonvolatile substance was recrystallized from hexane giving 0.5 g (20% yield) of *N*-(*p*-chlorobenzyliden)-*p*-chlorobenzylamine: mp 58—60 °C (*lit*,[11] mp 62—65 °C).

The aqueous layers were combined and extracted with 50 ml of ether. The ether layer was washed with three 25 ml portions of water and dried over $CaCl_2$. The solvent was evaporated *in vacuo* and the residue was recrystallized from benzene yielding 1.0 g (40% yield) of *cis*-2,5-dimethyl-3-hexene-2,5-diol: mp 68—69 °C (*lit*,[12] mp 68—69 °C).

References

1) M. E. C. Biffin, J. Miller, and D. B. Paul, "Introduction of the Azide Group," in "The Chemistry of the Azide Group," ed. by S. Patai, Interscience Pub., New York, N. Y. (1971), Chapter 2, pp. 57—190.

2) T. Sheradsky, "Azides as Synthetic Starting Materials," Chapter 6, pp. 331—395 in Ref. 1.

3) H. Hayashi and S. Oka, *Bull Inst. Chem. Res., Kyoto Univ.*, **52**(3), 514 (1974).

4) pp 61—63 of Ref. 1.

5) A. V. Kramer, J. A. Labinger, J. S. Bradley, and J. A. Osborn, *J. Amer. Chem. Soc.*, **96**, 7145 (1974).

6) (a) G. L'abbe, *Chem. Rev.*, **69**, 345 (1969); (b) H. Kwart and A. A. Kahn, *J. Amer. Chem. Soc.*, **89**, 1950, 1951 (1967).

7) T. Curtius and G. Ehrhart, *Chem. Ber.*, **55**, 1559 (1922).

8) A. J. Hubert, *Bull. Soc. Chim. Belg.*, **79**, 195 (1970); *Chem. Abstr.*, **73**, 3865d (1970).

9) L. I. Smith and M. M. Falkof, "Organic Syntheses," Vol. III, (1955), p. 350.

10) C. R. Hauser and G. Vermillion, *J. Amer. Chem. Soc.*, **63**, 1224 (1941).

11) Y. Sasaki and F. P. Olsen, *Can. J. Chem.*, **49**, 271 (1971).

12) I. N. Nazarov, L. D. Bergel'son, L. P. Badenkova, and B. V. Lopatin, *Zh. Obshch. Khim.*, **28**, 1132 (1958); *Chem. Abstr.*, **52**, 19925f (1958).

Stereoselective and Stereospecific Reactions. III.[1] Benzoylation, Cyclization, and Epimerization of Diols

Oyo MITSUNOBU, Junji KIMURA, Ken-ichi IIZUMI, and Noboru YANAGIDA

Department of Chemistry, College of Science and Engineering, Aoyama Gakuin University, Chitosedai, Setagaya-ku, Tokyo 157

(Received July 19, 1975)

The benzoylation of various classes of diols by means of diethyl azodicarboxylate (**1**) and triphenylphosphine (**2**) was carried out at room temperature. When primary-secondary diols were treated with an equimolar amount of benzoic acid (**3**) in the presence of 1.5 molar equivalents of **1** and **2**, reaction mainly occurred at their primary hydroxyl functions. Secondary-secondary diols gave mono- and dibenzoylated products or cyclic ethers. The course of the reactions depends on the structure of diols used. Thus, intermolecular displacement giving benzoates is a favorable process for 1,3-butanediol, 2,4-pentanediol and *trans*-1,2-indanediol, while 2,5-hexanediol and *trans*-1,2-cyclohexanediol afford the cyclized products.

For the past several years studies have been carried out on the intermolecular dehydration between alcohols and active hydrogen compounds by means of diethyl azodicarboxylate (**1**) and triphenylphosphine (**2**). The reaction of nucleosides with dibenzyl hydrogen phosphate and with benzoic acid (**3**) in the presence of **1** and **2** predominantly gave 5'-*O*-phosphorylated and 5'-*O*-benzoylated products, respectively.[2] Stereospecificity and functional selectivity were also observed in the alkylation of imides.[3] Bose *et al.*[4] reported that the present system could be utilized in the inversion of unhindered sterol configuration. In this paper, we wish to report the benzoylation of simple diols by the use of **1** and **2**.

Primary, Secondary-Diols. When 1,3-butanediol was allowed to react with an equimolar amount of **3** in the presence of 1.5 molar equivalents of **1** and **2** at room temperature, 3-hydroxybutyl benzoate was formed in a 70% yield. A small amount (7%) of dibenzoylated product was also isolated. Similarly, 1-phenyl-1,2-ethanediol or 3-chloro-1,2-propanediol predominantly gave monobenzoate. When 1.5 molar equivalent of **3** was used in the benzoylation of 1,3-butanediol, the yields of 3-hydroxybuthyl benzoate and 1,3-bis(benzoyloxy)butane increased to 80% and 10%, respectively. The results are summarized in Table 1.

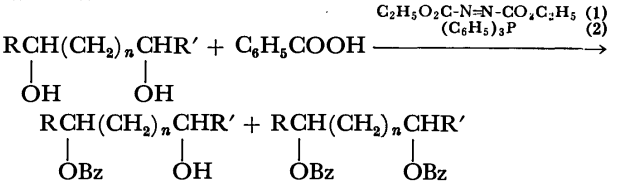

Scheme 1

TABLE 1. BENZOYLATION OF PRIMARY-SECONDARY DIOLS AND MONOBENZOATES

Diol or monobenzoate	Product	Yield %	Tlc[a] I	Tlc[a] II	NMR chemical shift (δ) in CCl_4 at 60 MHz
$CH_3CHCH_2CH_2OH$ (OH)	$CH_3CHCH_2CH_2OBz$ (OH)	70		B-M (10 : 1)	CH_3(1.22 d), $\rangle C-CH_2-C\langle$ (1.82 q) $\rangle CH$(3.93 m), $-CH_2O-$(4.40 t)
	$CH_3CHCH_2CH_2OBz$ (OBz)	7	E-PE (1 : 1)		CH_3(1.45 d), $\rangle C-CH_2-C\langle$ (2.15 q) $-CH_2-O-$(4.43 t), $\rangle CH$(5.35 sextet)
$CH_3CHCH_2CH_2OBz$ (OH)	$CH_3CHCH_2CH_2OBz$ (OBz)	63	E	B-M (5 : 1)	
$ClCH_2CHCH_2OH$ (OH)	$ClCH_2CHCH_2OBz$ (OH)	47			Cl-CH_2-(3.6 two lines, AB_2), $\rangle CH$ (3.5—4.3 m), $-CH_2-O-$(4.35 two lines, AB_2)
	$ClCH_2CHCH_2OBz$ (OBz)	5	B-EA (10 : 1)		Cl-CH_2-(3.88 d), $-CH_2-O-$(4.66 d) $\rangle CH$(5.55 quintet)
$ClCH_2CHCH_2OBz$ (OH)	$ClCH_2CHCH_2OBz$ (OBz)	81	B-EA (5 : 1)	C	
$C_6H_5CHCH_2OH$ (OH)	$C_6H_5CHCH_2OBz$ (OH)	47			$\rangle CH_2$(3.75 d, broad), $\rangle CH$(5.95 t, broad)
	$C_6H_5CHCH_2OBz$ (OBz)	5	B-E (1 : 2)		$\rangle CH_2$(4.57 d), $\rangle CH$(6.30 t)

a) I=Solvent system used for separation. II=Solvent system used for purification. Solvents are benzene (B), ether (E), petroleum ether (PE), ethyl acetate (EA), methanol (M), and chloroform (C).

Table 2. Benzoylation of secondary–secondary diols and monobenzoates

Diol or monobenzoate	Product	Yield %	Tlc[a]	NMR chemical shift (δ) in CCl_4 at 60 MHz
$CH_3CH(OH)CH(OH)CH_3$	$CH_3CH(OH)CH(OBz)CH_3$	8	E-PA (1 : 1)	CH_3CHOH(1.17 d), CH_3CHOBz(1.30 d), $>CHOH$(3.8 quintet), $>CHOBz$(4.85 quintet)
$CH_3CH(OH)CH_2CH(OH)CH_3$	$CH_3CH(OH)CH_2CH(OBz)CH_3$	57	E-PA (1 : 1)	CH_3CHOH(1.25 d), CH_3CHOBz(1.38 d), $>CHOH$(3.73 sextet), $>CHOBz$(5.35 sextet)
	$CH_3CH(OBz)CH_2CH(OBz)CH_3$	20		CH_3(1.39 d), $>CH_2$(2.03 t), $>CHO-$(5.27 sextet)
$CH_3CH(OBz)(CH_2)_2CH(OH)CH_3$	$CH_3CH(OBz)(CH_2)_2CH(OBz)CH_3$	75	E-PA (1 : 5)	CH_3(1.33 d), $-(CH_2)_2-$(1.6—1.9 m), $>CHO-$(4.8—5.4 m)
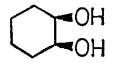	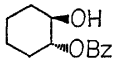	22	E-PA (2 : 3)	$-(CH_2)_4-$(1.0—2.3 m), $>CHOH$(3.7—4.1 m), $>CHOBz$(4.8—5.2 m)
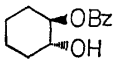	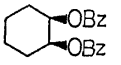	60	E-PA (1 : 1)	$-(CH_2)_4-$(1.2—2.5 m), $>CHO-$(5.15—5.5 m)
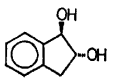	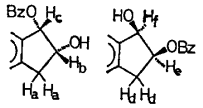	50[b]	B	H_a(2.95 d), H_b(4.48 q), H_c(5.95 d) H_d(3.05 d), H_e(5.42 q), H_f(5.04 d)

a) Solvent systems used for separation of products. See Table 1. b) The ratio of the 1-benzoylated and 2-benzoylated products is 1.4 : 1.

3-Hydroxybutyl benzoate and 3-chloro-2-hydroxypropyl benzoate reacted smoothly with **3** under the above conditions to give 1,3-bis(benzoyloxy)butane and 1,2-bis(benzoyloxy)-3-chloropropane in good yields.

Primary, Primary-Diols and Secondary, Secondary-Diols. Under the same conditions as for the reaction of primary–secondary diols, 1,3-propanediol gave 3-hydroxypropyl benzoate and 1,3-bis(benzoyloxy)propane in 65% and 12% yields, respectively. 1,4-Butanediol afforded monobenzoate and dibenzoate in 66% and 15% yields, respectively.

The benzoylation of secondary–secondary diols was then attempted. The reaction of 2,4-pentanediol with 1.5 molar equivalents of **1**, **2** and **3** proceeded with ease giving 4-hydroxy-2-pentyl benzoate and bis(benzoyloxy)pentane in 57% and 20% yields, respectively. *trans*-1,2-Indanediol gave a mixture of 1-hydroxy-2-benzoyloxy- and 1-benzoyloxy-2-hydroxyindanes in a 50% yield. 2,3-Butanediol, 2,5-hexanediol or *trans*-1,2-cyclohexanediol hardly gave benzoylated products. On the other hand, 5-benzoyloxy-2-hexanol and *trans*-2-benzoyloxycyclohexanol reacted smoothly with **3** in the presence of **1** and **2** to give 2,5-bis(benzoyloxy)hexane and 1,2-bis(benzoyloxy)cyclohexane in good yields. The results are summarized in Table 2.

Secondary–secondary 1,2- and 1,4-diols gave no corresponding benzoates, while monobenzoates of these diols were converted into dibenzoates. The contrast between these reactions can therefore be explained by assuming the facile formation of three- and five-membered cyclic ethers. In order to confirm cyclization, the mixture resulting from the reaction of *trans*-1,2-cyclohexanediol with **1**, **2** and **3** was subjected to gas chromatography(glc). The resulting chromatogram revealed the formation of cyclohexene oxide in an 82% yield.

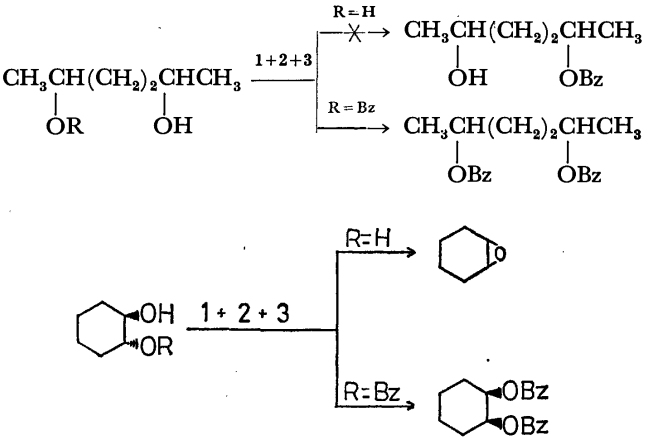

Scheme 2

The cyclization reaction would be rationalized in terms of intramolecular participation by a neighboring hydroxyl group in the initial alkoxyphosphonium salt (**4**) presumed as an intermediate of the present reaction.[5] If steric crowding renders intermolecular displacement slow and the hydroxyl group in the substrate molecule is at a suitable distance from the carbon site of substitution, three- or five- membered ring formation takes place predominantly. Somewhat related cases of cyclization have been observed in the reaction of

nucleosides.[6]

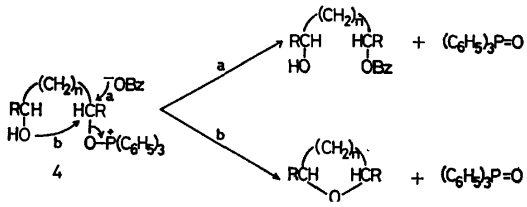

Scheme 3.

When 2,5-hexanediol was allowed to react with **1** and **2** in the absence of **3** at room temperature, 2,5-dimethyloxolane was formed in a 48% yield as determined by glc. The 2,5-dimethyloxolane was isolated by preparative glc and identified by comparison of its NMR spectrum with that of an authentic sample. Similarly, *trans*-1,2-cyclohexanediol and 1-phenyl-1,2-ethanediol were converted into the corresponding oxiranes.

Compared with the benzoylation of acyclic diols, *cis*-1,2-cyclohexanediol gave the benzoate in low yield (22%). The difference would be ascribed in part to conformational strain.[7] Although no direct evidence could be obtained, the formation of 1,2-*O*-(triphenyl)-phosphoranylcyclohexane (**5**) can not be ruled out.[8]

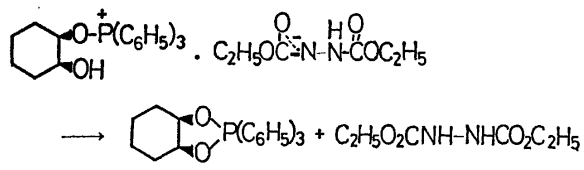

5

Scheme 4.

In some cases, for example in the benzoylation of *trans*-2-benzoyloxycyclohexanol, a small amount of *N,N'*-dibenzoyl-*N,N'*-bis(ethoxycarbonyl)hydrazine (**7**) was isolated. The formation of **7** would be explained as follows. Intermolecular dehydration between alcohols and carboxylic acids by means of **1** and **2** proceeds through initial activation of the alcohol.[5] In the reaction using sterically crowded alcohols, however, it is most likely that activation of carboxylic acid occurs to some extent giving the corresponding acid anhydride.[9] The anhydride fomed in turn reacts with the phosphonium salt (**6**) to afford **7**. In order to confirm this process, **1** was allowed to react with **2** in the presence of benzoic anhydride, **7** being isolated in an 80% yield.

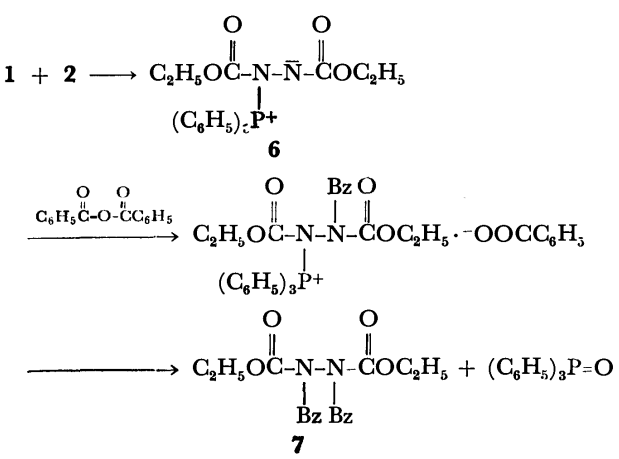

6

7

Scheme 5.

Stereochemistry. In order to examine the stereochemistry of the benzoylation of diols using a combination of **1** and **2**, a mixture of 1-hydroxy-2-benzoyloxy- and 1-benzoyloxy-2-hydroxyindanes, prepared from *trans*-1,2-indanediol, was treated with ammonia saturated in methanol affording *cis*-1,2-indanediol in a 60% yield. That 2-benzoyloxycyclohexanol derived from *cis*-1,2-cyclohexanediol by the present procedure has *trans*-configuration was proved by comparison of its NMR and IR spectra with those of an authentic sample.

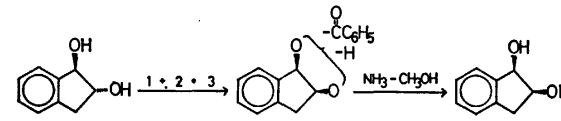

Scheme 6.

Experimental

Nuclear magnetic resonance spectra were measured on a Hitachi R-20 spectrometer using tetramethylsilane as an internal standard. Mass spectra were obtained at 70 eV on a Hitachi 6M-GC gas-chromatogram-mass spectrometer, infrared spectra on a JASCO-IRG. Gas-chromatographic analyses were performed on a Hitachi 063 instrument with a flame ionization detector, and 1 m×3 mm column of 20% SE-30 on Celite 545 (60—80 mesh). Preparative separation of cyclic ethers was made on a Shimadzu GC-1C gas chromatograph with a 1.82 m×1 cm column of 20% SE-30 on Celite 545 (60—80 mesh). Thin layer separation was carried out on silica gel PF_{254} (Merck: 20 cm×20 cm or 20 cm×30 cm) and visualization was by UV light.

Diethyl azodicarboxylate,[10] 2,4-pentanediol,[11] 1-chloro-3-benzoyloxy-2-propanol,[12] *cis*- and *trans*-1,2-cyclohexanediols,[13,14] and *trans*-1,2-indanediol[15] were prepared by procedures in literature. *cis*-2-Benzoyloxycyclohexanol was prepared in a yield of 54% by the reaction of *cis*-1,2-cyclohexanediol (348 mg, 3 mmol) with benzoic anhydride (678 mg, 3 mmol) in pyridine for 12 hr. The product was isolated by preparative tlc (ether–petroleum ether 1 : 1). Similarly, *trans*-2-benzoyloxycyclohexanol was prepared in a 63% yield. 5-Benzoyloxy-2-hexanol was prepared in a 33% yield by the reaction of 2,5-hexanediol (354 mg, 3 mmol) with benzoic anhydride (678 mg, 3 mmol) in pyridine at room temperature for 4 hr, followed by tlc separation (ether–petroleum ether 1 : 5).

General Procedure of Benzoylation of Diols and their Monobenzoates. A solution of **1** (261 mg, 1.5 mmol) in tetrahydrofurane (THF, 2 ml) was added dropwise over a period of 1 hr to a solution of primary-primary diol or primary-secondary-diol (1 mmol), **2** (393 mg, 1.5 mmol) and **3** (122 mg, 1 mmol) in THF (2 ml) with stirring at room temperature. After 12—14 hr, the mixture was fractionated by preparative tlc.

In the case of benzoylation of secondary-secondary diols, 1.5 molar equivalent of **3** was used.

Benzoylation of trans-*1,2-Indanediol.* A solution of **1** (261 mg, 1.5 mmol) in 2 ml of THF was added dropwise to a solution of *trans*-1,2-indanediol (150 mg, 1 mmol), **2** (393 mg,

1.5 mmol) and **3** (183 mg, 1.5 mmol) in THF (3 ml) under reflux. After the solution had been refluxed for 5 hr, a mixture of 1-benzoyloxy-2-hydroxyindane and 1-hydroxy-2-benzoyloxyindane was isolated by tlc (benzene) in a 50% yield. The ratio was calculated to be 1.4 : 1 from the integration of NMR absorption. When the reaction was carried out at room temperature, the yield of the mixture of the monobenzoates decreased to 30%.

cis-*1,2-Indanediol.* The mixture of monobenzoates obtained by the reaction of *trans*-1,2-indanediol with **1, 2** and **3** was treated with methanol saturated with ammonia at room temperature for 24 hr. After removal of the solvent, *cis*-1,2-indanediol was isolated in a 60% yield by preparative tlc. The *cis*-diol was recrystallized from ethyl acetate–petroleum ether, mp 94—96 °C (lit.[15] mp 98 °C).

Cyclization of Diols. Cyclohexene Oxide. A solution of **1** (1.74 g, 10 mmol) in ether (8 ml) was added dropwise over a period of 2 hr at room temperature to a solution of *trans*-1,2-cyclohexanediol (1.16 g, 10 mmol) and **2** (2.62 g, 10 mmol) in ether (12 ml). After the mixture had been kept stirring overnight, white precipitates were removed by filtration (1.40 g). The filtrate was distilled and the fraction boiling at 80—130 °C was collected. The distillate was then subjected to preparative glc to yield pure cyclohexene oxide. Cyclohexene oxide isolated was identical (IR, NMR and mass spectra) with that prepared by independent synthesis.

By a separate experiment, the yield of the cyclohexene oxide was determined to be 68% by glc analysis using tetraline as an internal standard. Similarly, 2,5-hexanediol and 1-phenyl-1,2-ethanediol were converted into 2,5-dimethyloxolane and 2-phenyloxirane in 48% and 27% yields, respectively.

Reaction of Benzoic Anhydride with 1 and 2. To a solution of benzoic anhydride (226 mg, 1 mmol) and **2** (262 mg, 1 mmol) in THF (2 ml) was added dropwise over a period of 1 hr at room temperature a solution of **1** (174 mg, 1 mmol) in THF (1 ml). After the solution had been kept stirring overnight, **7** was isolated in an 80% yield by preparative tlc (ether–petroleum ether 1 : 1). The material was recrystallized from ether–petroleum ether, mp 82—83 °C: IR (KBr) cm^{-1} 1750, 1710 (C=O); NMR (CCl_4) δ 1.05 (t, 6H), 4.13 (q, 4H), 7.1—8.0 (m, 10 H).

References

1) Part II: M. Wada, T. Sano, and O. Mitsunobu, This Bulletin, **46**, 2833 (1973).

2) a) O. Mitsunobu, K. Kato, and J. Kimura, *J. Amer. Chem. Soc.*, **91**, 6510 (1969). b) O. Mitsunobu, J. Kimura, and Y. Fujisawa, This Bulletin, **45**, 245 (1972).

3) a) O. Mitsunobu, M. Wada, and T. Sano, *J. Amer. Chem. Soc.*, **94**, 679 (1972). b) H. Morimoto, T. Furukawa, K. Miyajima, and O. Mitsunobu, *Chem. Lett.*, **1973**, 821.

4) A. K. Bose, B. Lal, W. A. Hoffman III, and M. S. Manhas, *Tetrahedron Lett.*, **1973**, 1619.

5) O. Mitsunobu and M. Eguchi, This Bulletin, **44**, 3427 (1971).

6) a) J. P. H. Verheyden and J. G. Moffatt, *J. Org. Chem.*, **35**, 2319, 2868 (1970); **37**, 2289 (1972). b) M. Wada and O. Mitsunobu, *Tetrahedron Lett.*, **1972**, 1279.

7) E. L. Eliel in "Steric Effects in Organic Chemistry," ed. by M. S. Newman, John Willey & Sons, Inc.; Maruzen Co. Ltd., Tokyo, (1956), p. 61.

8) Recently, stable phosphoranes were prepared by the reaction of **2** with uridine and **1**, or with tetramethyl-1,2-dioxetane. J. Kimura, Y. Fujisawa, T. Sawada, and O. Mitsunobu, *Chem. Lett.*, **1974**, 691: P. D. Bartlett, A. L. Baumstark, and M. E. Landis, *J. Amer. Chem. Soc.*, **95**, 6486 (1973).

9) I. Kuwajima and T. Mukaiyama, *J. Org. Chem.*, **29**, 1385 (1964).

10) J. C. Kauer, "Organic Syntheses," Coll. Vol. IV, p. 411 (1963).

11) J. M. Sprague and H. Adkins, *J. Amer. Chem. Soc.*, **56**, 2669 (1934).

12) E. Katzschmann, G. P. 1198342; *Chem. Abstr.*, **63**, 13162 (1965).

13) L. F. Fieser and M. Fieser, "Advanced Organic Chemistry," Reinhold Publishing Co., New York, (1961), p. 191.

14) A. Roebuck and H. Adkins, "Organic Syntheses," Coll. Vol., III p. 217 (1955).

15) A. Gagis, A. Fusco, and J. T. Benedict, *J. Org. Chem.*, **37**, 3181 (1972).

Anisotropy of Needle Cokes

Isao MOCHIDA, Masashi OGAWA, and Kenjiro TAKESHITA
Research Institute of Industrial Science, Kyushu University, Fukuoka 812
(Received July 30, 1975)

The anisotropic properties of several lump needle cokes were studied by means of a X-ray diffractometer, a dilatometer, and a reflected microscope in order to evaluate the anisotropic factors of the needle cokes and to discuss the relations among them. Among them several relations were found, which were well understood on the basis of the structure of the uniaxial arrangement of the crystallites. The change in these factors upon heat treatment was also investigated in order to find how these factors depended on the crystal-growth of the needle coke. Some anisotropic properties of the extruded sample were compared with those of the filler coke, which were observed in a lump shape. The results indicate that the extruded sample had its anisotropic properties considerably lowered. The structure and crystal-growth of the needle cokes are discussed based on these observations.

The carbons used for the ultra-high-power electrodes have been required to be so-called needle-like cokes, which should have not only a good crystallinity but also a highly oriented structure.[1] It is recognized that the needle cokes exhibit high anisotropy in various properties, such as thermal expansion, thermal and electric conductivity, and Hall current.[2]

Mrozowski[3] and other researchers[4] described the structure of the needle cokes. The anisotropic properties of needle cokes in extruded or molded samples have been extensively studied, and the relations among them have been discussed.[2,5] However, some problems regarding the nature and structure of the needle cokes seem to be still open. A study of lump cokes may help us to understand the needle cokes, because there is no disturbance brought about by binder cokes and different degree of preferred orientation at the shaping.

In the present study, the anisotropy of lump needle cokes has been observed by means of microscopic observation, CTE measurement, and X-ray diffraction,[6-8] and the relations among the anisotropy factors have been studied on cokes heat-treated at graphitizing temperatures. The methods of measuring the anisotropy of powdered cokes have also been surveyed because the small batch reactors often give powdered cokes, even though they are needle-like. We also intend to discuss the structure of needle cokes on the basis of these data.

Experimental

Sample Cokes. Five kinds of filler cokes (A, B, C, D, E) and three kinds of extruded samples (B, F, G) were used in the present study. They were all commercially available; some of their properties are summarized in Table 1.

TABLE 1. DESCRIPTION OF COKES USED IN THE PRESENT STUDY

Sample	Source	Starting pitch	Structure	Shape
A	Petro Cokes Ltd.	petroleum	needle	lump
B	GLW	petroleum	mosaic	lump, extruded
C	Koa Petro Co.	petroleum	needle	lump
D	Nittetsu Chem Co.	coal tar	mosaic	lump
E	Nittetsu Chem Co.	coal tar	needle	lump
F	Petro Cokes Ltd.	petroleum	needle	extruded
G	Petro Cokes Ltd.	petroleum	needle	extruded

Experimental Procedure. Calcination and Graphitization: Cokes were calcined at 1300 °C under a nitrogen flow. The calcined cokes were further graphitized at 2000 °C or 2500 °C for 0.5 hr under an argon flow. The heating rates were 20 °C/min up to 2000 °C and 10 °C/min up to 2500 °C.

Microscopic Observation and Measurement of Thermal Expansion: The optical structure of cokes and the graphites were observed using a Leitz Ortholux microscope with reflected polarized light under crossed nicols. The cokes were cut both parallel and perpendicular to the direction of the needle. They were then mounted in a cylinder of epoxy resin in order for the desired plane to be fixed on the surface of the cylinder, and were ground with several grades of alumina. As for mosaic cokes, the direction of cutting made no difference in the value of CTE or the features of microscopic observation, so each specimen was cut arbitrarily.

Thermal expansion was measured between 350° and 450 °C with a specimen heated at the rate of 10 °C/min in a vacuum. A dilatometer of a comparative type referring to the standard sample of silica (Shinku-Riko DL-1500H) was used. A cylindrical specimen 8 mm in diameter and 20 mm long was cut both parallel and perpendicular to the direction of the needle-like texture in order to obtain values of CTE parallel and perpendicular to the texture.

X-Ray Diffraction Analysis. Measurement of Crystallographic Parameters:[9] The calcined cokes and graphitized carbons were analyzed by X-ray powder diffraction Cu$K\alpha$ produced at 30 KV and 15 mA being used. The lattice constant (C_0) and the average crystallite thickness (L_c) were determined from the (002) diffraction peak. Silicon was used as the internal standard.

Measurement of Degree of Preferred Orientation: 1) Bacon Anisotropy Factor (BAF): The preferred orientation of both filler and extruded samples was measured by transmission X-ray diffraction according to the method proposed by Bacon.[6] A rectangular specimen 1 mm thick and 1 cm square was cut parallel to the direction of the needle-texture of the cokes. The intensity of the (002) reflection, $I(\phi)$, was observed at angles of every ten degrees from the normal direction of the texture. The area which was exposed to the X-ray was a circle 3 mm in diameter. BAF was calculated by the numerical integration of $I(\phi)$ based on the following equation:[6]

$$\mathrm{BAF} = \frac{1}{2}\frac{\int_0^{\pi/2} I(\phi)\sin^3\phi\,\mathrm{d}\phi}{\int_0^{\pi/2} I(\phi)\cos^2\phi\sin\phi\,\mathrm{d}\phi}$$

A random distribution of the crystallites will give equal intensities of (002) peaks against every ϕ, so that BAF is unity.

2) Method proposed by Noda and Inagaki[7] and Walker

et al.[8]: The following equation of the anisotropy factor (γ_1) was used in the present study:

$$\gamma_1 = \frac{I(002)_{/\!/}}{I(002)_{/\!/}+K\{I(100)_{/\!/}+I(101)_{/\!/}\}} \Big/ \frac{I(002)_{\perp}}{I(002)_{\perp}+K\{I(100)_{\perp}+I(101)_{\perp}\}}$$

where $I_{/\!/}$, and $I_{\perp}$ represent the intensities from the (002), (100) and (101) diffraction peaks in the planes parallel and perpendicular to the direction of the needle texture respectively. The constant, K, was fixed at 5.56 so as to set the γ_1 of the completely non-oriented sample as unity. Because the intensities of the (004) and (110) peaks were as weak as for cokes calcined below 2000 °C, the (002), (101), and (100) peaks were used instead, modifying the equation proposed by Noda and Inagaki.[7] The area exposed to X-ray in the reflection method was roughly 1 cm square.

Results

Comparison of Filler Cokes. The reflected micrographs and physical and structural properties of five cokes calcined at 1300 °C are shown in Photo 1 and Table 2 respectively. Cokes A, C, and E consisted of a flow-pattern structure, small values of CTE parallel to the direction of the texture, and large values of the anisotropic factors of both BAF and γ_1. In contrast, Cokes B and D, which showed a disordered mosaic unit-structure of several ten microns, have large CTE values and anisotropic factors near unity. The CTE values seem related to the anisotropy factors, although CTE should depend not solely on the anisotropy factor. The similar values of L_c and C_0, regardless of the kind of coke, might play some roles for such a relation, because Engle,[5a] Matsumoto and Sasaki[10] showed a slight dependence of CTE on *Lc*. Closed porosity should also be taken into account, as has been pointed by several researchers.[11] Thus, the microscopic observations and the values of BAF, γ_1, and CTE may be considered to be indications of the needle-like structure of the cokes.

Dependence of Properties of the Needle Coke on the Calcination Temperatures. Because Table 2 indicates that A coke is the best needle coke in regard to CTE, BAF, and γ_1, the dependence of its properties on the calcination temperatures was investigated in order to clarify the relation among these properties. The reflected microscopic photographs of the plane parallel or perpendicular to the direction of the needle texture are shown in Photo 2. The preferred orientation of the crystallites is clearly observed on the parallel plane, whereas a disordered mosaic structure is shown on the perpendicular plane. No essential change in the visible structure was observed upon further heat treatment up to 2500 °C, except for the development of cracks along the needle texture on the parallel plane at higher calcination temperatures. The orientation of the cracks was not observed at all on the perpendicular plane, although they run along the anisotropic boundary.

The CTE values of the cokes calcined at 600 °C were still very large on both the parallel and perpendicular planes, as is shown in Table 3, although the anisotropic nature ($\alpha_{\perp}/\alpha_{/\!/}>1$) had previously been observed. As the shrinkage of the needle texture and cracks parallel to the texture appeared at the calcination temperature of 1300 °C, the CTE value

Table 2. Properties of some cokes[a]

	A coke	B coke	C coke	D coke	E coke
CTE[b] ($\times 10^{-6}$/°C)	0.4	2.6	1.1	4.8	1.7
BAF	3.0	1.2	3.0	1.0	2.9
γ_1	4.8	1.2	6.0	1.0	7.1
C_0(002) (Å)	6.838	6.884	6.884	6.891	6.884
L_c(002) (Å)	21	28	47	27	41

a) Calcined at 1300 °C. b) Parallel to the axis of the needle if the samples are needle-like cokes.

Table 3. Properties of A cokes calcined at various temperatures

HTT	600 °C	1300 °C	2000 °C	2500 °C
CTE ($\times 10^{-6}$/°C) $\alpha_{/\!/}$	10.9	0.4	0.3	0.5
$\alpha_{\perp}$	24.6	2.6	2.4	2.1
B. A. F.	2.7	3.0	5.6	5.1
γ_1	—	4.8	12.7	10.4
C_0(002) (Å)	6.885	6.835	6.842	6.732
L_c(002) (Å)	35	21	290	990

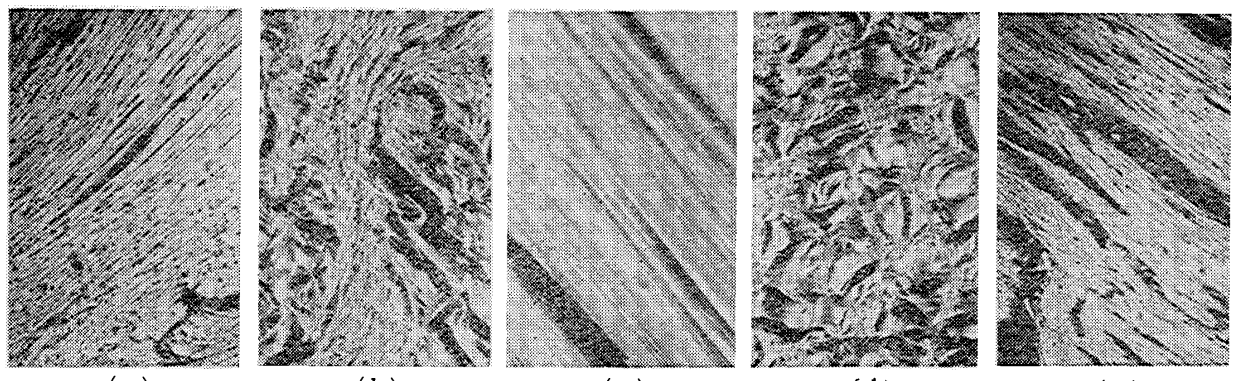

(a) (b) (c) (d) (e)

Photo. 1. Optical micrographs (crossed nicols, ×200) of various cokes calcined at 1300 °C. (a) A coke, (b) B coke, (c) C coke, (d) D coke, (e) E coke.
As for A, C and E cokes, photographs were taken parallel to the axis of the needle-texture.

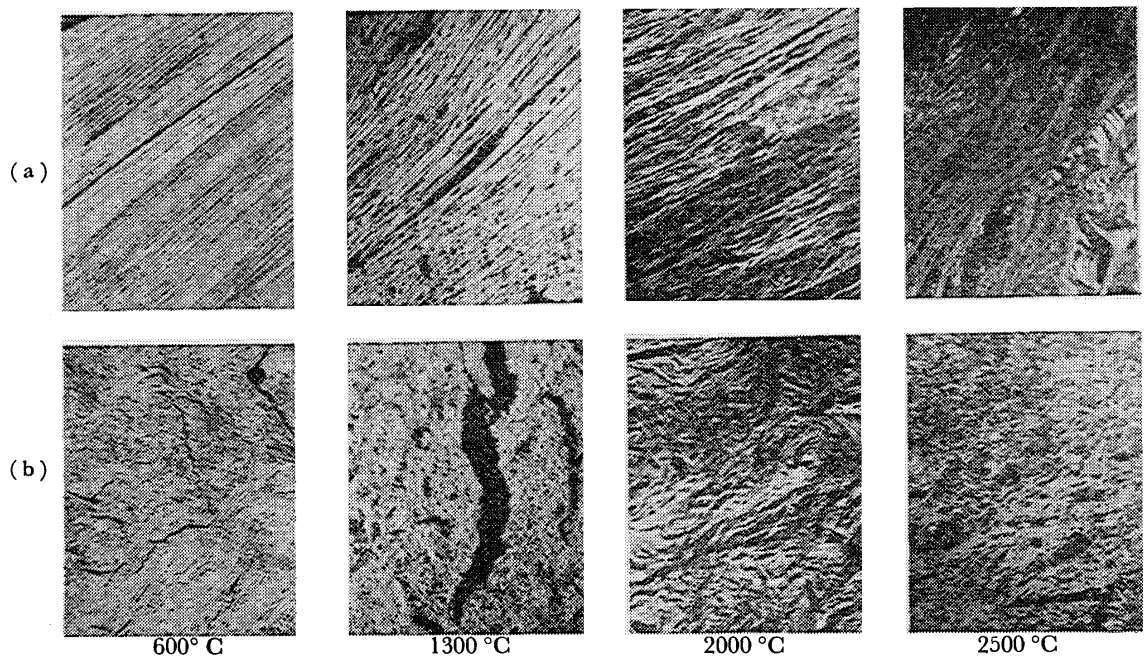

Photo. 2. Optical Micrographs (crossed nicols, ×200) of A cokes calcined at various temperatures. (a) Planes parallel to the axis of the needle texture. (b) Planes perpendicular to the axis of the needle-texture.

decreased. The value, however, did not decrease appreciably upon further heat treatment. Although the ratios of $\alpha_\perp/\alpha_{//}$ had a rather poor accuracy because of the difficulty of accurately measuring small $\alpha_{//}$ values of cokes calcined at higher temperatures, a significant increase in $\alpha_\perp/\alpha_{//}$ was observed at 1300 °C as the marked decreases of $\alpha_\perp$ and $\alpha_{//}$ occurred. In contrast, only slight changes were observable in the values of C_0, L_c, and BAF between 600 °C and 1300 °C, as is shown in Table 3. However, the background around 23°(2θ) in the X-ray diffraction pattern decreased for the sample calcined at 1300 °C, indicating that the amorphous part decreased upon heat treatment at this temperature. No more evolution of gas was observed above 1300 °C.

TABLE 4. DEGREE OF PREFERRED ORIENTATION AND GRAPHITIZATION OF WELL-ORIENTED COKES

HTT	C coke		E coke	
	1300 °C	2500 °C	1300 °C	2500 °C
BAF	3.0	4.9	2.9	3.5
γ_1	6.0	6.6	7.1	8.1
C_0 (Å)	6.884	6.739	6.884	6.743
L_c (Å)	47	750	41	570

TABLE 5. DEGREE OF PREFERRED ORIENTATION AND GRAPHITIZATION OF BADLY-ORIENTED COKES

HTT	B coke			D coke	
	1300 °C	2500 °C	3000 °C	1300 °C	2500 C
BAF	1.2	1.2	1.2	1.0	1.0
γ_1	1.2	1.2	1.1	1.0	1.2
C_0 (Å)	6.884	6.762	6.725	6.891	6.747
L_c (Å)	28	540	810	27	655

The two anisotropy factors obtained in turn by X-ray diffraction changed considerably between 1300 and 2000 °C, and both settled above 2000 °C. The crystal growth of the carbon continued up to 2500 °C, as is indicated by the increasing $L_c(002)$ value and the decreasing $C_0(002)$ value. The relation among these properties of cokes calcined at different temperatures will be discussed later.

The needle-like cokes, C and E, showed increases in the anisotropic factor and the crystal growth similar to those of the A coke (Table 4), although their starting pitches were different. In contrast, mosaic cokes showed no improvement in anisotropic factors at all up to 3000 °C, at which point a significant crystal growth was observed much as with needle-like cokes (Table 5).

The X-ray observations indicate that the anisotropy, one of important qualities of the needle-like cokes, is a property connected with the preferred orientation of the crystallites as well as with the crystallographic nature of the simple crystallite. Such a conclusion

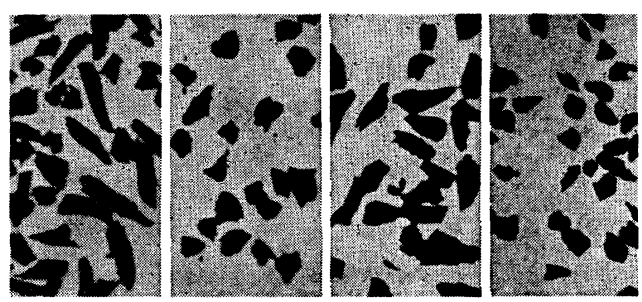

Photo. 3. Optical micrographs (×60) of the ground cokes calcined at 1300 °C. Particle size; 65—100 mesh. (a) A coke, (b) B coke, (c) C coke, (d) D coke.

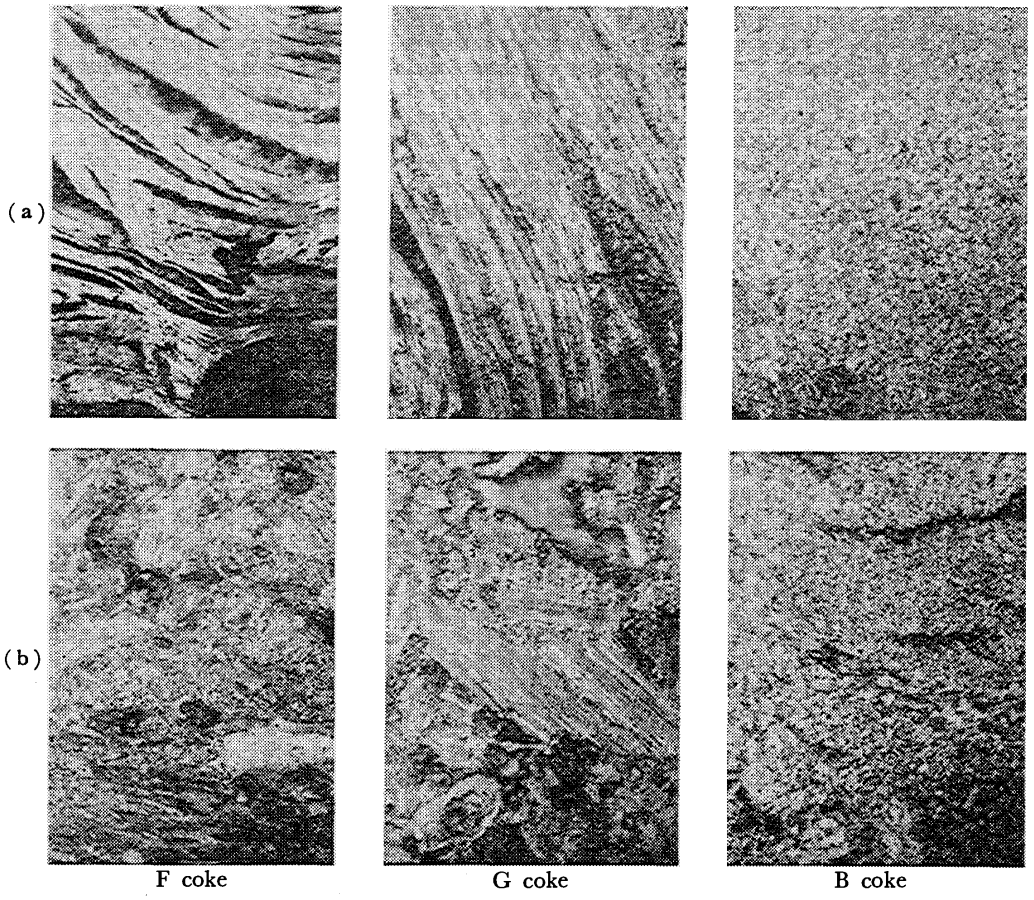

Photo. 4. Optical micrographs (crossed nicols, ×200) of F, G, B cokes, and their extruded samples. (a) Filler cokes, (b) Extruded samples.

has also been obtained in the discussion of the carbonized products from naphthalene and pyrene.[12]

Shape Factors of Ground Cokes. Microscopic photographs of ground samples from A, B, C, and D cokes are shown in Photo 3. Obviously, the needle cokes A and C were broken into elongated pieces in which the needle-textures ran lengthwise, as Mrozowski[3] and Walker *et al.*[8] recongnized. In contrast, the B and D cokes with the mosaic structure, gave rather spherical pieces. Walker *et al.*[8] proposed to define the shape factor, k, by the following equation;

$$k = S_v \mu$$

where S_v is the geometric surface area per unit of value and where μ is the arithmetic-average sieve-size diameter of the sample; they reported the relation between the shape factor and the anisotropic factors. Because their factors seem to have some ambiguity concerning the pore surface area, the ratios of the shortest and longest lengths of the particles were averaged for one hundred particles in the present study. We could not find any clear difference in the averaged ratios of ground cokes of A, B, C, and D, although distinct difference in shapes could be recognized at a glance.

Comparison of Anisotropic Factors between Filler Cokes and Their Extruded Products. The anisotropy factors of filler cokes and their extruded products were compared in an attempt to discuss how well the extrusion aligned the particles of needle cokes parallel to the axis of extrusion, and whether or not the anisotropy factor of the extruded products could represent that of filler cokes, because the elongated pieces of the needle cokes were expected to be arranged parallel to the direction of extrusion. The anisotropy factors measured by two ways of X-ray diffraction are summarized in Table 6. As for the needle cokes (F and G), a decreased anisotropy upon the extrusion was shown by both methods, although the extent of decrease was a little smaller by the reflected method (γ_1) than in the Bacon method(BAF). The arrangement of the needle coke particles in the extrusion products is shown by the micrograph[Photo 4]. When compared with the photographs of the fillers themselves, they could be easily distinguished from the binder cokes in the extrusion products, however, this arrangement was far from an uniaxial one along the extrusion axis. The disordered arrangement probably brings about the decrease in the anisotropic facors. Thus,

Table 6. Comparison of anisotropic factors between filler and extruded cokes

	B coke[a]		F coke[b]		G coke[c]	
	Filler	Ext.	Filler	Ext.	Filler	Ext.
BAF	1.2	1.1	2.5	1.4	2.2	1.4
γ_1	1.1	1.2	3.4	2.0	2.6	2.3

a) Calcined at 3000 °C. b) Calcined at 1300 °C.
c) Calcined at 3000 °C.

the usual extrusion could not be expected to be sufficient to reproduce the anisotropic factors of filler cokes. The extrusion which forces the uniaxial arrangement of filler cokes more strictly is required for this purpose. In the case of cokes of the mosaic structure, the filler cokes were difficult to distinguish by the microscopic observation, and the X-ray data shown in Table 6[B Coke] indicate the unchanged isotropic natures of both filler and extruded cokes.

The different degree of decrease in the anisotropic factors observed by the two ways of X-ray diffraction measurement may be explained as follows. The values of BAF fluctuated with the exposed location, and sometimes the plots of $I(\phi)$ *vs.* ϕ gave a quite unsymmetrical curve. These facts may be the result of the small area exposed to X-rays, and may mean that the Bacon method is not suitable for the measurement of the extruded sample the fillers of which are not uniformally arranged. In contrast, the reflection method gave constant and reproducible values, perhaps because of the larger exposed area, as has been pointed out by Noda and Inagaki.[6] This method may give the averaged anisotropic factor against the filler cokes distributed in the area exposed to the X-rays.

Discussion

There have been several proposals with regard to the structures of the needle cokes. Franklin[13] considered the needle coke to be a platelet-like arrangement of crystallites with the crystallites parallel on a large plate. Mrozowski[3] defined the needle-coke in which the crystallites of carbon were well aligned with normals to the planes distributed in all directions, but approximately parallel to the axis of the needle, so that the crystallites were not at all parallel to each other. Photo 2 clearly supports such a structure. This structure can be compared to a paper-roll.[4b] On the basis of this structure, the fact that the profiles of Bacon plots are equal in two planes perpendicular to each other, but parallel to the axis of the needle, is understandable.

The data shown in Table 3 are of value in a discussion because they seem to indicate interesting relations among crystal growth, the orientation of the crystallites, and the physical properties of the needle coke. The significant decrease of CTE value between the calcination temperatures of 600 °C and 1300 °C is considered to be the result of the crystal growth of the incorporation of the disorganized phase,[3] as is indicated by the marked decrease in the amorphous part in the X-ray diffraction, although no real crystal growth such as is shown by L_c or C_0 was observed. The disappearance of amorphous carbon may improve the CTE of the carbon.

Above 1300 °C no amorphous part was present any more, but real crystal growth may occur, as is indicated by the significantly increased L_c and C_0. The small gas evolution or the small decrease in the H/C ratio may also indicate the crystal growth in this region at the expense of other crystallites, as was mentioned by Mrozowski.[3]

Microcrystallites of carbon calcined at 1300 °C (their average L_c was as small as 21 Å) may have a CTE value similar to that of complete graphite (L_c is several hundred Å) if the chemical bonds are the most important factor in the thermal expansion, because microcrystallines already consist exclusively of carbon–carbon bonds, as does complete graphite. This might indeed be the case, although many other factors should be considered to play some role in the thermal expansion. Several researchers have studied the relation of CTE or other anisotropic properties to the crystal size, as in shaped cokes. Engle[5a] claimed the dependence of CTE and its anisotropic ratio on the mean apparent crystallite size L_c. Matsumoto and Sasaki[10] investigated similar relations. The latter authors claimed a slight dependence of CTE on the crystal size (the size has no effect on the CTE value over 700 Å) and a linear relation between the CTE anisotropic ratio and the crystal size. According to the opinion of the present authors, however, there are some problems in the study of extruded or molded samples because shaped cokes may not always represent the filler cokes and because the factor brought about at the shaping probably often has significant effects. Furthermore, the mechanism how the crystal size influences the CTE is worth further study.

Although the CTE values did not change at the calcination of 2000 °C, where essential crystal growth was also noticed, a significant increase in anisotropic factors as measured by X-ray diffraction was observed. The anisotropic factor showed no increase at 2500 °C in spite of the marked crystal growth. These facts may mean that a critical value of the crystal size may be necessary to give the leveled anisotropy factor observed for the cokes calcined at 2000 or 2500 °C, because the intensity of the (002) diffraction is influenced very much by the crystal size. It is evident from Photo 2 that the alignment of the crystallites is already formed at the temperature of the solidification of the cokes and that is persists essentially unchanged up to the highest-temperature. In this sense, the anisotropy factor may be constant regardless of the later heat treatment; however, other anisotropy factors based on the other physical properties of cokes seem to change because of the dependence of the property on characteristics of the cokes other than alignment of crystallites.

The needle cokes produced by the reactor of an experimental size are often pulverized so that their anisotropic properties are difficult to measure, although the measurement is important in evaluating the quality of the needle cokes. There are two possible ways of measurement. First, an attempt is made to measure the anisotropic properties of a particle itself. Second, powdered cokes are molded or extruded into a lump of a suitable size with binders, and the properties of the filler cokes are estimated from those of the shaped sample. The first approach is possible by the use of a strong X-ray source and an automatic full-circle goniometer; however, it is still difficult to set the sample in the right direction, parallel to the needle-axis. The reflective index, as measured by a polarized light microscope, may also give the anisotropic factor of powdered cokes.[14]

In the second method, filler cokes should be arranged in the shaped sample, with the same symmetry as the filler cokes themselves have. The needle cokes are in an uniaxial arrangement in which the axis of the powdered needle is within a plate; however, this symmetry is completely different from the uniaxial one. Although the extrusion is considered a possible way to achieve this arrangement, the results shown in Table 6 and Photo 4 indicate that the present extrusion is not sufficient to arrange the powdered needle cokes in an uniaxial direction to the same extent as was observed in an original lump coke. Ubbelohde[15] succeeded in obtaining a highly anisotropic arrangement of cokes by applying compression and sherring forces to the cokes in a shaped binder-polymer at the same time. An extrusion with a large compression ratio seems to be an expedient way to obtain a lump composed of uniaxially arranged cokes which can represent the individual coke-particle; furthermore, it is interesting because anisotropic properties superior to those of original cokes can be realized in such a way.

Our thanks are due to Professor Ryohei Takahashi of our University and Mr. Juji Furumi, The Nittetsu Chemical Industrial Co., for providing the experimental facilities. The authors are also gratefull to the Japan Securities Scholarship Foundation for its financial support.

References

1) E. Kurami, *J. Japan Petro. Inst.*, **16**, 366 (1973).
2) W. N. Reynolds, *Carbon*, **6**, 277 (1968).
3) S. Mrozowski, Proc. 1st and 2nd Conf. on Carbon, p. 31 (1956).
4) a) E. A. Kmetko, *ibid.*, p. 21. b) R. Takahashi and K. Takeshita, *J. Fuel Soc. Japan*, **53**, 1044 (1974).
5) a) G. B. Engle, *Carbon*, **8**, 485 (1970), **12**, 291 (1974). b) F. G. Vitovec and Z. H. Stachurski, *ibid.*, **10**, 417 (1972).
6) G. E. Bacon, *J. Appl. Chem.*, **6**, 477 (1956).
7) I. Noda and M. Inagaki, *Kogyo Kagaku Zasshi*, **62**, 1300 (1959).
8) P. L. Walker, Jr., R. P. Gardner, M. A. Short, and L. G. Austin, Proc. 5th Conf. Carbon, p. 483 (1963).
9) Standard Method Prescribed by Japan Society for the Promotion of Science.
10) H. Matsumoto and Y. Sasaki, *Carbon*, **12**, 351 (1974).
11) J. M. Hutcheon and M. S. T. Price, Proc. 4th Carbon Conf., Pergamon Press Oxford, p. 645 (1960): L. D. Loch and A. E. Austin, Proc. 1st and 2nd Carbon Conf., University of Buffalo, Buffalo, N.Y. (1956), p. 65.
12) I. Mochida, N. Fukuda, K. Kudo, and K. Takeshita, *Carbon*, **13**, 135 (1975).
13) R. Franklin, *Proc. Roy. Soc.* (London), **209**, 196 (1951).
14) S. Kimura, H. Tanaka, E. Yasuda, and H. Suzuki, *Tanso*, No. 76, 7 (1974).
15) A. R. Ubbelohde, *Nature*, **220**, 434 (1968), Third S.C.I., Conference on Industrial Carbon and Graphite, (1970).

Photochemical Cycloaddition Reactions of α,β-Unsaturated Lactones with Olefins, and Application to Synthesis of Natural Products[1]

Hiroshi KOSUGI, Shizuo SEKIGUCHI, Ryû-ichi SEKITA, and Hisashi UDA

Chemical Research Institute of Non-Aqueous Solutions, Tohoku University, Katahira-2, Sendai 980

(Received August 18, 1975)

The photochemical cycloaddition reactions of five- and six-membered α,β-unsaturated lactone derivatives with unsaturated substrates (ethylene, acetylene, 1,1-dimethoxyethylene *etc.*) have been studied. The parent α,β-unsaturated lactone (γ-crotonolactone) and the β-,γ-, or δ-alkyl substituted derivatives add to ethylene and acetylene in the acetone solutions and to 1,1-dimethoxyethylene in the benzene solutions in so good yields as to utilize them practically for synthesis. α-Phenyl-γ-crotonolactone and β-phenyl-γ-crotonolactone also add to ethylene and acetylene, whereas, α-methyl, β-hydroxy, and β-methoxy derivatives do not. As the synthetic applications of the reactions, the synthesis of (±)-grandisol has been achieved, and the synthetic approach to (±)-canadensolide has also been described.

Despite many examples of the photochemical cycloaddition reactions of cyclic α,β-unsaturated ketones with a variety of unsaturated substances[2,3] and of the fruitful applications in total syntheses of natural products,[4] the use of α,β-unsaturated lactones such as **1** and **2** has so far been very limited.[5-7] Tada

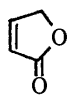

1

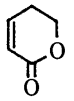

2

and his co-workers[6] reported, in mechanistic points of view, that γ-crotonolactone (**1**) underwent photocycloaddition reaction with cyclopentene or cyclohexene to give the cycloadduct in 36—42% yield and that the reaction was sensitized by acetone and quenched by 1,3-pentadiene and, therefore, the reaction proceeded through the triplet excited state of **1**. Furthermore, it is one of the most significant findings in their work that 1,1-dimethoxyethylene, which is one of the most reactive olefins in the photocycloaddition of cyclic enones,[2] did not give the cycloadduct with **1**, but quenched the photocycloaddition reaction between **1** and cyclopentene in acetonitrile. As the example of a six-membered α,β-unsaturated lactone, the acetophenone-sensitized cycloaddition of 5,6-dihydro-4-methyl-2*H*-pyran-2-one (**2b**), β-methyl derivative of **2**, to ethylene has been successfully applied to the stereoselective synthesis of (±)-grandisol by Gueldner and his co-workers.[7] We have simultaneously and independently investigated the photochemical cycloaddition reactions of **1** and the simply substituted derivatives of **1** and **2** with unsaturated substrates, especially ethylene, acetylene, and 1,1-dimethoxyethylene, for the actual synthetic purpose including the synthesis of (±)-grandisol, rather than the mechanistic view points. This work was undertaken with several goals in mind: (1) to clarify and generalize the reaction conditions and the effects of the substituents in both lactone and olefin components, (2) to elucidate the structures, including orientations, of the products obtained, (3) to apply the cycloaddition reaction to the synthesis of natural products, (4) to compare the photochemical reactivities of unsaturated lactones with those of enones.

Results and Discussion

Photochemical results are described first, followed by synthetic applications.

Photochemical Cycloadditions. All of the photochemical reactions described herein were conducted in ordinary solvents and with a 500-W high pressure mercury arc lamp fitted with or without a filter (Vycor or Pyrex cooling jacket of a lamp), in contrast with the peculiar conditions (in acetonitrile, 10-W low pressure mercury arc lamp) employed by Tada, *et al.*[6] Described below are studies on the photochemical cycloaddition reactions of γ-crotonolactone (**1a**) and the following derivatives: β-methyl (**1b**), β-phenyl (**1c**), α-methyl (**1d**), α-phenyl (**1e**), and γ-methyl (**1f**), and 5,6-dihydro-6-methyl-2*H*-pyran-2-one, parasorbic acid (**2a**).

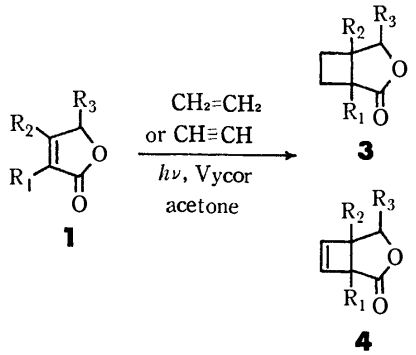

a : $R_1=R_2=R_3=H$
b : $R_1=R_3=H$, $R_2=Me$
c : $R_1=R_3=H$, $R_2=Ph$
d : $R_1=Me$, $R_2=R_3=H$ (no reaction)
e : $R_1=Ph$, $R_2=R_3=H$
f : $R_1=R_2=H$, $R_3=Me$

The photocycloaddition of **1a** to ethylene in acetone (Vycor) proceeded readily and cleanly, and afforded the cycloadduct **3a** in high yield (70% at room temperature; >80% at −50 °C). The analytical and spectral data indicate that **3a** is the expected 1 : 1 cycloadduct. Acetone was the best solvent among other solvents examined in the photocycloaddition of **1a** to ethylene and appears to play a role as the sensitizer, as suggested by Tada, *et al.*[6] For example,

the photocycloaddition of **1a** to ethylene in ether or in ether–acetone (fivefold molar excess amount of **1a**) resulted in lowering remarkably the yield of **3a**, 22 and 6%, respectively. In this case, the major product was a mixture of the diastereomers of the ether addition product **5**. This result suggests that the excited species of **1a** abstracts preferentially a hydrogen atom from ether rather than the photocycloaddition to ethylene, being quite different from the feature of the excited species of enones since enones added satisfactorily to ethylene and other olefins by irradiation in ether without the formation of the ether addition product.[8] However, the abstraction of a hydrogen atom from ether was not always the preferential pathway in the photocycloaddition of **1a** in ether; **5** was obtained as the minor component in

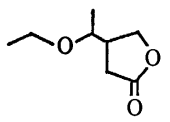

5

the photocycloaddition with cyclohexene (see below). Propyl bromide–acetone (−50 °C) was also not a suitable solvent system for the photocycloaddition of **1a** to ethylene, giving **3a** in 53% yield. Also, benzene, which is one of the very common solvents for the photocycloaddition of enones,[9] was unsatisfactory for the present reaction due to the relatively low solubility of **1a**: a solution of **1a** in benzene (the same concentration as in acetone) became emulsion by the saturation of ethylene, and in fact, no reaction occurred even in prolonged irradiation.

Similarly, the photocycloaddition of **1b**, **1c**, **1e**, and **1f** to ethylene in acetone afforded products, **3b**, **3c**, **3e**, and **3f** (44, 49, 52, and 35%) whose analytical and spectral data indicated they were the expected cycloadducts. The adduct **3f** and others derived from **1f** were obtained always as a *ca.* 1 : 1 mixture of the stereoisomers. From these experiments, although the reactions proceeded smoothly under the conditions examined (acetone, −50 °C for **1b** and **1f**; room temperature for **1c** and **1e**, Vycor filter for **1b** and **1c**; Pyrex filter for **1e**; no filter for **1f**), it was observed that prolonged irradiation caused to increase the amount of by-products which presumably arose from the participation of acetone, and therefore, in practice for preparation of the adducts it would be better to conduct the photocycloaddition reaction without a filter, resulting in making the reaction much faster. It should be noted that α-methyl derivative **1d**, contrary to the phenyl analog **1e**, did not undergo the photocycloaddition to ethylene, being similar to the observation on the photocycloaddition of 2-methyl-2-cyclohexenone.[2] On the photoeffectiveness of **1e**, the electronic effect of the conjugated phenyl group may play an important role in the reaction.

Contrary to the photochemical unreactivity of 2-cyclohexenone with acetylene (in acetone at −70 °C) observed by Owsley and Bloomfield,[10] we have found that the unsaturated lactones **1a-f** except **1d** underwent actually the photocycloaddition with acetylene under the standard conditions (acetone, −50 °C, Vycor filter for **1a-c**; Pyrex filter for **1e**; no filter for **1f**). The noteworthy features of the reactions are the slowness relative to the cases with ethylene and the formation of a large amount of by-products at the end of the reaction periods. Consequently, for the actual isolation of the desired adducts the progress of the reactions should be carefully followed by glpc or tlc analysis and intermitted at appropriate reaction periods. Thus, the corresponding acetylene adducts **4a**, **4b**, **4c**, **4e**, and **4f** were obtained in 54, 29, 8, 23, and 14% yields, respectively. Again, no reaction was observed in **1d**. The structures of the adducts were established on the basis of analytical and spectral grounds, and among them **4e** was further identified by comparison with the authentic sample obtained from the photocyclization of 3-phenyl-2(7*H*)-oxepinone (**6**).[11] In the case of **1c**, the yield of adduct **4c** was extremely low and the major product (35%) was found to be the dimer **7** which was quantitatively formed by irradiation of **1c** alone. The structure of **7** was assigned on the basis of the analytical and spectral results but the *syn*/*anti* and *cis*/*trans* natures could not be determined.

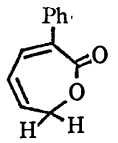

6

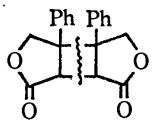

7

It should be noteworthy that the compound **1a** as well as **1c** effectively adds to 1,1-dimethoxyethylene, contrary to the observation by Tada, *et al.*[6] Thus, irradiation of **1a** or **1c** in the presence of excess 1,1-dimethoxyethylene in the benzene solution without a filter gave the cycloadducts **8** or **9** in 62 or 37% yield, respectively. Acetone was not used as a solvent in these reactions because of the easy formation of the oxetane derivative with 1,1-dimethoxyethylene.[6,12] The presence of excess 1,1-dimethoxyethylene increased the solubility of **1a** in benzene, and now the reaction proceeded smoothly. Furthermore, it was observed that the photoaddition proceeded very slowly by irradiation through a Vycor filter and that a large amount of by-products arising from 1,1-dimethoxyethylene (dimethyl succinate *etc.*) were produced by prolonged irradiation. For example, the ratio of **1a** and **8** reached to about 7 : 2 after 19 hr irradiation through a Vycor filter and did not change considerably on further irradiation, despite of a remarkable consumption of 1,1-dimethoxyethylene. The product **8** was apparently single, being *cis* fused, and the 6,6-dimethoxy structure follows from 100 MHz NMR coupling multiplicity of the methine proton (H-1) at the ring juncture; that is, the signal of H-1 appears as eight lines with the following coupling constants: J_{1-5}= 8.4, J_{1-7}^{trans}=5.1, J_{1-7}^{cis}=9.0. The coupling patterns of the protons in **9** also support the position of the dimethyl acetal grouping, and furthermore, the orientation of the photoaddition of 1,1-dimethoxyethylene was confirmed by chemical transformation of another adduct **24** described in the later section. Hence,

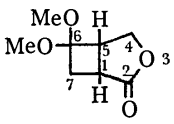

8

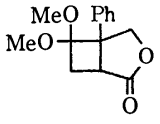

9

the orientational mode of the photocycloaddition of α,β-unsaturated lactones to 1,1-dimethoxyethylene is apparently the same as the case of cyclic enones.[2,8a] Interestingly, **1e**, which added effectively to ethylene and acetylene as mentioned above, was found to be photochemically unreactive to 1,1-dimethoxyethylene.

In order to gain more informations on the effect of an olefin-solvent combination in these photochemical processes, the reaction of cyclohexene with **1a** was performed in an ether solution. The reaction proceeded well to afford the expected product **10**[6] in 72% yield. This product appears to be a mixture of stereoisomers; however, the aspect of stereochemistry was not investigated further. In this case the by-product **5** was a minor component in a yield of less than 10%.

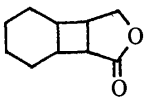

10

Furthermore, parasorbic acid (**2a**) was selected for study as an example of a six-membered α,β-unsaturated lactone. The photocycloadditions of **2a** to ethylene and acetylene in acetone and to 1,1-dimethoxyethylene in ether equally proceeded readily and gave the adducts, **11** (70%), **12** (66%), and **13** (64%), each of which was a mixture of stereoisomers, and the analytical and spectral data were consistent with the assigned structures.

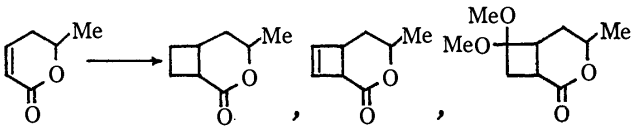

2a **11** **12** **13**

Finally, we also examined the photoreactions using acrylonitrile as an olefinic substrate and tetronic acid as an unsaturated lactonic one. It has been known that acrylonitrile is one of the good olefinic substrates for the photocycloaddition of enones and actually adds to 2-cyclohexenones;[2,8a] however, any of α,β-unsaturated lactones examined in the present work did not give the photocycloadduct with acrylonitrile.

Furthermore, in contrast with the successful photoadditions of 3-hydroxy-[13] and 3-methoxy-[8a] cyclohexenones to olefins, the photoreactions of tetronic acid (**14**) with ethylene or cyclohexene and of the methyl ether **15** with ethylene under the various conditions (solvent, Vycor or no filter *etc.*) did not entirely give the cycloadducts, resulting in recovery of the starting materials **14** and **15** or formation of an intractable mixture.

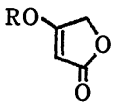

14, R=H
15, R=Me

Any of the mechanistic, sensitized, or competitive studies concerning the feature and reactivity of the

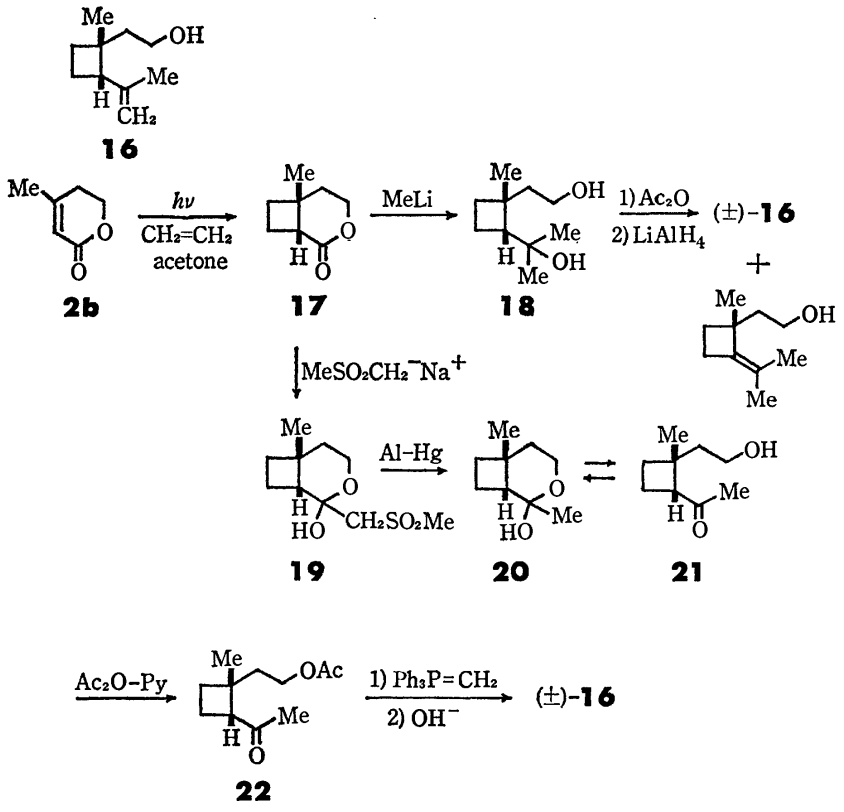

16

2b **17** **18** **19** **20** **21**

22

Scheme 1.

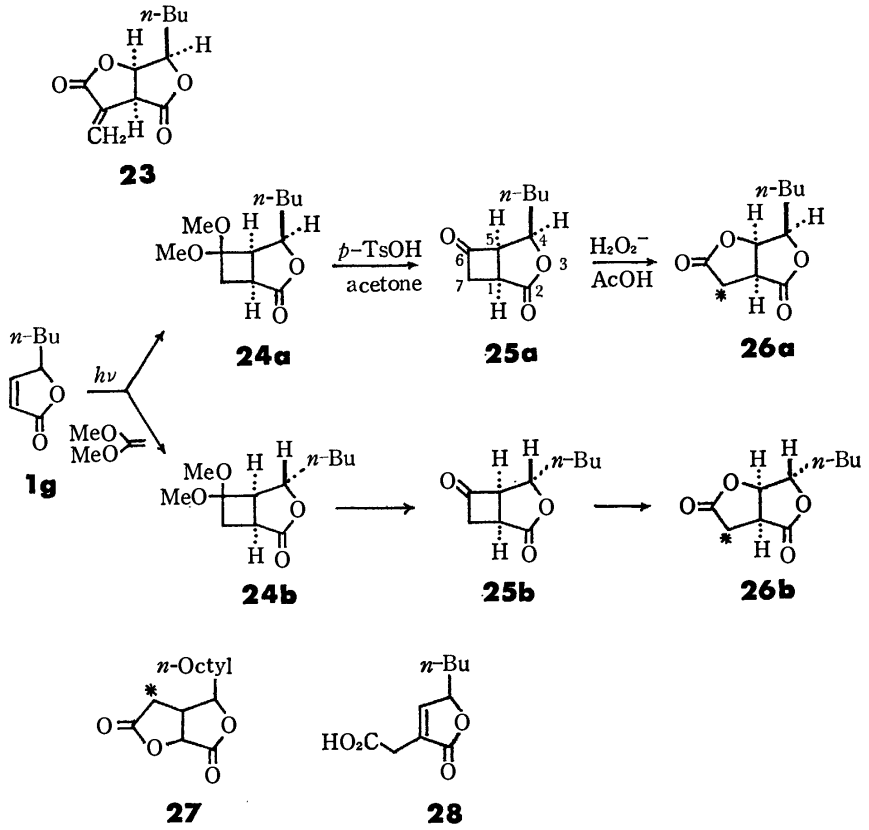

Scheme 2.

excited species o. α,β-unsaturated lactones has not been investigated precisely in the present work. However, from the experimental results, it could be pointed out that there are apparently the several different features of the excited species of unsaturated lactones from those of enones; that is, hydrogen abstraction from ether, photoaddition to acetylene, inertness for the photoaddition to acrylonitrile, and unreactive effect of 3-hydroxy and alkoxy groups.

As is clear from the several examples cited above the photocycloaddition reactions of α,β-unsaturated lactones with olefins, especially ethylene, acetylene and 1,1-dimethoxyethylene, should be of considerable utilities for the preparation of a wide variety of four-membered ring fused γ- and δ-lactone derivatives.

Synthetic Applications. (±)-Grandisol. Grandisol (**16**), one of the four components of the male boll weevil sex pheromone,[14] has been previously synthesized in racemic form,[7,9e,14] and additionally, three alternative synthetic courses have very recently been reported.[15] Among these reported synthetic sequences, the photocycloaddition reaction of 5,6-dihydro-4-methyl-2*H*-pyran-2-one (**2b**) with ethylene has been successfully applied as the initial step by Gueldner, *et al.* (**2b**→**17**→**18**→**16** in the scheme 1).[7] In this section we will describe briefly our independent synthetic work of (±)-**16** starting from **2b** and the reaction sequence is outlined in the scheme 1.

Irradiation of a solution of **2b** in acetone at room temperature through a Vycor filter with moderately rapid introduction of ethylene gave a 70% yield of the cycloadduct **17** (the reported conditions:[7] benzene, acetophenone as a sensitizer, a medium-pressure mercury-vapor lamp, no filter, yield of **17**: 56%).

The addition of **17** to excess sodium methylsulfonylcarbanion[16] at 55 °C resulted in the formation of the acetal **19**, mp 103.5—104.5 °C, (75%). For the introduction of one carbon unit the use of sodium methylsulfinylcarbanion[16,17] was unsatisfactory, affording a low yield of non-crystalline product. Reduction of **19** with aluminum amalgam in aqueous tetrahydrofuran gave an equilibrium mixture of the acetal **20** and the methyl ketone **21**, which were apparently separable on silica gel tlc but not obtained in pure form.

Acetylation of the mixture of **20** and **21** with acetic anhydride–pyridine at room temperature afforded in a 40% yield (based on **19**) of the single acetate **22** which is transformed by the Wittig process, methylenetriphenylphosphorane–dimethyl sulfoxide,[18] followed by alkaline hydrolysis to (±)-grandisol (**16**) identical with an authentic sample prepared by Zurflüh, *et al.*[9e]

(±)-Canadensolide. Canadensolide (**23**) is a mould metabolite produced by *Penicillium canadense*[19] and the total synthesis in racemic form and the revision of the stereochemistry has been reported by Yoshikoshi, *et al.*[20] The orientation of the dimethyl acetal grouping in the photocycloadduct **8** from **1a** and 1,1-dimethoxyethylene as mentioned earlier is well suited for the construction of the second lactone ring in the canadensolide bislactone ring system, and hence, the photo-

cycloaddition of γ-butyl-γ-crotonolactone (**1g**) to 1,1-dimethoxyethylene would appear to provide an alternative synthetic route leading to (±)-**23**. This part deals with this synthetic approach to (±)-**23** from **1g** (Scheme 2).

Irradiation of **1g** in the presence of excess 1,1-dimethoxyethylene in benzene gave a mixture of the stereoisomers of the adduct which were easily separated by column chromatography on silica gel into *endo* and *exo* isomers, **24a** and **24b**, in respect of the butyl side chain in 30 and 40% yields, respectively. The orientation of the dimethyl acetal grouping and the configuration of the butyl group were rigorously established on the basis of the NMR coupling pattern of H-5 in the hydrolysis product **25**.

Treatment of each isomer **24a** and **24b** with *p*-toluenesulfonic acid in acetone afforded the corresponding keto lactone **25a** and **25b**. The signals of H-5 in both isomers appear as a doublet of doublets, suggesting the position of the keto group at C-6, with the following coupling constants: $J_{4-5}=7.0$ in **25a** (assignable to *cis* coupling), $J_{4-5}=1.7$ in **25b** (assignable to *trans* coupling) respectively. Thus, the configuration of the butyl group is *endo* in the **a**-series compounds, while *exo* in the **b**-series, as shown in Scheme 2. On treatment with hydrogen peroxide–acetic acid **25a** and **25b** were transformed into the bislactone derivatives **26a** and **26b** which were identified by direct comparison with the authentic samples prepared by Yoshikoshi, *et al.*[20]

Unfortunately, however, in this bislactone ring system the introduction of a carboxylic group (or its equivalent) at the α-methylene position (asterisked) of the newly formed lactone ring failed, in contrast to the successful introduction in the case of the avenaciolide bislactone ring system **27**.[21] All attempts to introduce one carbon unit at the α-methylene position in both **26a** and **26b** under a wide variety of conditions (MMC–DMF–dioxane, *iso*-Pr_2NLi–CO_2–THF, Et_2NH–aq HCHO *etc.*) were unsuccessful; the abstraction of a proton from C-1 occurred exclusively to produce the ring opened product **28**. This problem is still unresolved.

Experimental

All melting points were determined in an oil bath and are uncorrected. Distillation of the liquid products was usually carried out evaporatively using a modified sublimation apparatus and the oil bath temperatures were recorded. IR spectra were taken on a Hitachi EPI-S2 or G2 spectrometer. NMR spectra were obtained on a JEOL Model C-60HL (60 MHz) or PS-100 (100 MHz) instrument using TMS as an internal standard and CCl_4 as the solvent unless otherwise indicated. Reported values are on the cm^{-1} in IR and δ scales in NMR, respectively. Coupling constants are given in Hz. Glpc analyses were performed on a JEOL Model JGC-750 or 1100 instrument using the following columns: A (20% Carbowax 20 M on Chromosorb W, 2 m×3 mm), B (20% Carbowax 20 M on Chromosorb W, 3 m×3 mm), and C (20% SE-30 silicone rubber on Chromosorb W, 2 m×3 mm). Elemental analyses were performed in the microanalytical laboratory of this institute.

General Procedure for Irradiation. The apparatus consisted of an irradiation vessel fitted with a Vycor, Pyrex or quartz (for experiments without a filter) immersion type cooling jacket for a lamp serving a filter as well, a rubber stopple in one side arm, and a gas inlet tube or a three-way stopcock on the other side arm. In the cases of small scale experiments, a quartz reaction tube (3×30 cm) having a glass sponge gas inlet part at the bottom was employed and irradiated externally. The entire apparatus was immersed in a dry-ice—methanol or a running water bath (for room temperature experiments). The gaseous olefinic substrates, ethylene and acetylene, were saturated at appropriate temperatures and continuously bubbled through the solutions as a finely dispersed state throughout irradiation. For the other olefins the irradiations were performed under the nitrogen atmosphere. The solutions were irradiated by a Taika immersion type 500-W high pressure mercury arc lamp and the progress of the reactions was generally monitored by removing aliquots with a syringe and examination by glpc or tlc means. The yields of the photoadducts are based on the starting unsaturated lactones.

*Photoadditions of γ-Crotonolactone (**1a**).* *(a) To Ethylene in Acetone*: A solution of γ-crotonolactone (**1a**)[22] (1.02 g) in freshly distilled acetone (400 ml) was irradiated at −50 °C for 2.5 hr through Vycor with introduction of ethylene. Evaporation of the solvent under reduced pressure and distillation (110—120 °C/15 mmHg) of the residual liquid gave 1.10 g (80%) of the single product, 3-oxabicyclo[3.2.0]-heptan-2-one (**3a**)[23], with a retention time of 24 min on column B (200 °C, He 2.0 kg/cm²). IR (CCl_4) 1780, 1150; NMR 1.90—2.70 (m, 4H), 2.88—3.34 (m, 2H), 4.12 (dd, J=10 and 2, 1H), 4.29 (dd, J=10 and 6, 1H). Found: C, 64.71; H, 7.19%. Calcd for $C_6H_8O_2$: C, 64.27; H, 7.19%.

When the reaction was carried out at room temperature, **3a** was isolated in 70% yield.

(b) To Ethylene in Ether: A solution of **1a** (0.94 g) in dry ether (500 ml) was irradiated at room temperature for 2.5 hr through Vycor with introduction of ethylene. Glpc analysis (column A, 180 °C) of the crude photolysate indicated the product contained two components with the retention times of 10.8 min (*ca.* 22% of area) and 18.8 min (*ca.* 54% of area). Pure sample of each component was collected by preparative glpc. The faster moving component was identified to be **3a** and the slower moving one was found to be the ether addition product, β-(1-ethoxyethyl)-γ-butyrolactone (**5**): IR (CCl_4) 1780; NMR around 1.13 (d, J=7, 3H), around 1.16 (t, J=7, 3H) (these are splitted small due to a mixture of diastereomers), 2.20—2.60 (m, 3H), 3.20—3.70 (m, 3H), 4.20 (m, 2H). Found: C, 60.38; H, 8.70%. Calcd for $C_8H_{14}O_3$: C, 60.78; H, 8.92%.

(c) To Acetylene: A solution of **1a** (1.58 g) in acetone (500 ml) was irradiated at −50 °C through Vycor with introduction of acetylene. After 5 hr the amount of by-products gradually increased, presumably arising from photoreaction of acetylene and/or acetone, and therefore, the reaction was stopped after 5 hr irradiation. At this stage the ratio of **1a** (retention time of 2.6 min) and the main product (4.6 min) was about 31% and 54%, in addition to 15% of by-products, respectively, determined from glpc on column C (150 °C, He 1.0 kg/cm²). After removal of the solvent under reduced pressure, the gas-chromatographically homogeneous product, 3-oxabicyclo[3.2.0]hept-6-en-2-one (**4a**), (470 mg, 23%) was collected by column chromatography on silica gel (70 g) using 7 : 3 petroleum ether–ether as eluent. The analytical sample was purified by distillation (110—125 °C/10 mmHg). IR (CCl_4) 3020, 1780, 1160; NMR 3.50—3.70 (m, 2H), 4.20—4.40 (m, 2H), 6.32 (s, 2H). Found: C, 65.79;

H, 5.49%. Calcd for $C_6H_6O_2$: C, 65.44; H, 5.49%.

(d) To Cyclohexene: A solution of **1a** (1.02 g, 12 mmol) and cyclohexene (10.5 g, 116 mmol) in dry ether (500 ml) was irradiated at room temperature for 5 hr through Vycor. Analysis of the crude photolysate by glpc (column C, 190 °C, He 1.5 kg/cm²) indicated the photoproduct consisted of three components eluted at 3.1 min, 5.7 min, and 6.8 min in the area ratio of about 1 : 1.5 : 3, respectively. After removal of the solvent under reduced pressure, the residual liquid was separated into 72 fractions of *ca.* 50 ml portion by chromatography on silica gel (60 g) using initially petroleum ether alone and then a mixture of petroleum ether and ether (gradually increasing the amount of ether, the final ratio of petroleum ether and ether was about 7 : 3) as eluting agent. Fractions 32—39, consisting of the single compoment corresponding to 6.8 min eluate on glpc, were combined and concentrated under reduced pressure to give 302 mg of one stereoisomer of 4-oxatricyclo[5.4.0.$0^{2,6}$]undecan-3-one (**10**). Purified sample by distillation (125—130 °C/6 mmHg) was gradually crystallized on standing, mp 41—45 °C. IR (CCl_4) 1775, 1150; NMR 0.90—3.20 (m, 12H), 4.20—4.40 (m, 2H). Found: C, 72.58; H, 8.75%. Calcd for $C_{10}H_{14}O_2$: C, 72.26; H, 8.49%. Fractions 40—49 amounting 452 mg were found to be a mixture of the 5.7 min and 6.8 min eluates, and the IR and NMR spectra were almost identical with those of the above mentioned pure sample. Therefore, the 5.7 min eluate was another stereoisomer of **10**. Total yield was *ca.* 50%.

The product obtained from the fractions 55—65, which was the 3.1 min eluate, was identified to be **5** (132 mg, 7%).

(e) To 1,1-Dimethoxyethylene: A solution of **1a** (0.84 g, 10 mmol) and freshly distilled 1,1-dimethoxyethylene (8.8 g, 0.1 mol) in dry benzene (50 ml) was irradiated at room temperature for 15 hr without a filter. Evaporation of the solvent under reduced pressure left 2.69 g of oily residue. From the glpc analysis (column A, 230 °C, He 2.3 kg/cm²) the starting material **1a** (retention time of 2.5 min) still remained and the ratio of **1a** and the photoproduct (retention time of 8.8 min) was about 1 : 3. Many other peaks due to by-products (totally comparable area with **1a** and the product) were also observed around 1—3 min and 4—6 min. The crude mixture was chromatographed on silica gel (75 g) using initially hexane and then a mixture of hexane and ether (gradually increasing the amount of ether, the final ratio of hexane and ether was about 7 : 3) as eluting agent to give 435 mg (26% based on **1a** used) of 6,6-dimethoxy-3-oxabicyclo[3.2.0]heptan-2-one (**8**), which was purified by distillation (95 °C/3 mmHg). IR(CCl_4) 2810, 1778; NMR (100 MHz) 2.29 (dd, J= 13.0 and 5.1, 1H), 2.50 (ddd, J= 13.0, 9.0, and 2.0, 1H), 2.83 (ddd, J=9.0, 8.4, and 5.1, 1H), 3.09 (s, 3H), 3.15 (s, 3H and m, 1H), 4.22 (dd, J=9.3 and 7.8, 1H), 4.48 (dd, J=9.3 and 2.6, 1H). Found: C, 55.79; H, 6.88%. Calcd for $C_8H_{12}O_4$: C, 55.84: H, 7.08%.

Photoadditions of β-Methyl-γ-crotonolactone (1b). *(a) To Ethylene*: A solution of β-methyl-γ-crotonolactone (**1b**)[24] (250 mg) in freshly distilled acetone (600 ml) was irradiated at −50 °C for 8 hr through Vycor with introduction of ethylene. Evaporation of the solvent under reduced pressure and chromatography of the residual liquid on silica gel (30 g) using 5 : 1 petroleum ether–ether as eluent gave 150 mg (48%) of 5-methyl-3-oxabicyclo[3.2.0]heptan-2-one (**3b**), which was homogeneous on glpc (column A, 200 °C, He 1.6 kg/cm²). Analytical sample was purified by distillation (80—120 °C/12 mmHg). IR (CCl_4) 1780, 1150; NMR 1.35 (s, 3H), 1.70—2.70 (m, 5H), 3.86 and 4.14 (AB type q, J=9.0, 1H each). Found: C, 66.42; H, 7.84%. Calcd for $C_7H_{10}O_2$: C, 66.64; H, 7.99%.

(b) To Acetylene: A solution of **1b** (600 mg) in acetone (800 ml) was irradiated at −50 °C through Vycor with introduction of acetylene. After 9 hr glpc analysis (column A, 200 °C, He 1.5 kg/cm²) indicated the ratio of **1b** (retention time of 6.2 min) and the photoadduct (4.2 min) was about 3 : 1. After an additional 1 hr irradiation the ratio reached to 1 : 1 but the amount of by-products considerably increased. Therefore, for convenience of the isolation of the product, the reaction was intermitted at 9 hr irradiation. Removal of the solvent under reduced pressure and chromatography of the residual liquid (1.1 g) on silica gel (50 g) using 5 : 1 petroleum ether–ether as eluting agent gave 86 mg (29%) of homogeneous 5-methyl-3-oxabicyclo-[3.2.0]hept-6-en-2-one (**4b**). Analytical sample was purified by distillation (80—83 °C/15 mmHg). IR (CCl_4) 1785, 1770, 1160; NMR 1.42 (s, 3H), 3.10 (s, 1H), 3.89 and 4.19 (AB type q, J=9.7, 1H each), 6.27 and 6.38 (AB type q, J=2.8, 1H each). Found: C, 67.56; H, 6.42%. Calcd for $C_7H_8O_2$: C, 67.73; H, 6.50%.

Photoadditions of β-Phenyl-γ-crotonolactone (1c). *(a) To Ethylene*. A solution of β-phenyl-γ-crotonolactone (**1c**)[25] (500 mg) in acetone (800 ml) was irradiated at room temperature for 3 hr through Vycor with introduction of ethylene. In this case the progress of the reaction was monitored by tlc instead of glpc. Removal of the solvent under reduced pressure and chromatography of the residue (972 mg) on silica gel (50 g) using 4 : 1 petroleum ether–ether as eluent gave 250 mg (50%) of 5-phenyl-3-oxabicyclo[3.2.0]heptan-2-one (**3c**). Analytical sample was purified by distillation (120—140 °C/3 mmHg). IR (CCl_4)1785, 1170; NMR 1.80—2.80 (m, 4H), 3.10—3.40 (m, 1H), 4.05 and 4.40 (AB type q, J=9.0, 1H each), 7.22 (s, 5H). Found: C, 76.42; H, 6.73%. Calcd for $C_{12}H_{12}O_2$: C, 76.57; H, 6.43%.

(b) To Acetylene: A solution of **1c** (500 mg) in acetone (800 ml) was irradiated at −50 °C through Vycor with introduction of acetylene. After 2 hr **1c** was completely consumed. Evaporation of the solvent and chromatography of the residue (806 mg) on silica gel (40 g) using 5 : 1 petroleum ether–ether as eluent gave two products. The faster moving minor product (46 mg, 8%) was purified by distillation (140—150 °C/3 mmHg) and identified to be the expected photoadduct, 5-phenyl-3-oxabicyclo[3.2.0]hept-6-en-2-one (**4c**): IR ($CHCl_3$) 1765, 1180; NMR 3.50 (br. s, 1H), 4.27 and 4.48 (AB type q, J=9.4, 1H each), 6.47 and 6.77 (AB type q, J=2.8, 1H each), 7.30 (s, 5H). Found: C, 77.08; H, 5.41%. Calcd for $C_{12}H_{10}O_2$: C, 77.40; H, 5.41%.

The crystalline major product (173 mg, 35%) isolated from the slower eluted fractions was recrystallized from hexane–chloroform, mp 192—194 °C, and found to be the dimer **7** of the starting lactone **1c**: IR ($CHCl_3$) 1790, 1180; NMR ($CDCl_3$) 3.82 (s), 4.10 (s), 7.00—7.60 (m) with area ratio of 1 : 2 : 5. Found: C, 74.86; H, 5.17%. Calcd for $(C_{10}H_8O_2)_n$: C, 74.99; H, 5.03%.

The almost identical result was obtained when a Pyrex filter instead of a Vycor one was employed. After 4 hr irradiation, the yields of **4c** and the diner **7** was 8% and 55%, in addition to 10% recovery of **1c**, respectively.

The dimer **7** was quantitatively obtained by irradiation of **1c** in acetone without introduction of acetylene.

(c) To 1,1-Dimethoxyethylene. A solution of **1c** (300 mg, 1.9 mmol) and 1,1-dimethoxyethylene (2.5 g, 28 mmol) in dry benzene was irradiated at room temperature for 21 hr through quartz. After removal of the solvent and excess olefin under reduced pressure, the residue (600 mg) was chromatographed on preparative thin layer of silica gel using 1 : 1 petroleum ether–ether as developing agent to give 172 mg (37%) of 6,6-dimethoxy-5-phenyl-3-oxabicyclo-

[3.2.0]heptan-2-one (**9**). Analytical sample was purified by distillation (110—120 °C/1 mmHg). IR ($CHCl_3$) 2810, 1765; NMR (100 MHz, $CDCl_3$) 2.52 (dd, J=13.0 and 5.0, 1H), 2.87 (dd, J=13.0 and 10.0, 1H), 2.84 (s, 3H), 3.28 (s, 3H), around 3.28 (m, 1H), 4.55 and 5.18 (AB type q, J=9.0, 1H each), 7.20—7.40 (m, 5H). Found: C, 67.43; H, 6.56%. Calcd for $C_{14}H_{16}O_4$: C, 67.73; H, 6.50%.

*Photoadditions of α-Phenyl-γ-crotonolactone (**1e**).* *(a) To Ethylene*: α-Phenyl-γ-crotonolactone (**1e**) was prepared essentially according to Swain's procedure[26] and the yield was somewhat improved by slightly modified operations. A solution of **1e** (500 mg) in acetone (700 ml) was irradiated at room temperature through Pyrex with introduction of ethylene. After 3.5 hr of the irradiation period, the solvent was removed under reduced pressure and the residue (673 mg) was chromatographed on silica gel (40 g) using 4 : 1 petroleum ether–ether as eluent to yield 305 mg (52%) of 1-phenyl-3-oxabicyclo[3.2.0]heptan-2-one (**3e**), in addition to the recovery of **1e** (100 mg, 20%). Analytical sample was purified by distillation (105—110 °C/2 mmHg). IR ($CHCl_3$) 1765, 1160; NMR ($CDCl_3$) 1.70—2.68 (m, 4H), 3.41 (m, 1H), 4.27 (dd, J=9.8 and 1.5, 1H), 4.49 (dd, J=9.8 and 5.8, 1H), 7.38 (s, 5H). Found: C, 76.66, H, 6.38%. Calcd for $C_{12}H_{12}O_2$: C, 76.57; H, 6.43%.

(b) To Acetylene: A solution of **1e** (500 mg) in acetone (700 ml) was irradiated at −50 °C for 4.5 hr through Pyrex with introduction of acetylene. After removal of the solvent under reduced pressure, the resulting oily residue (814 mg) was chromatographed on silica gel (50 g) using 4 : 1 petroleum ether–ether as eluent to give 131 mg (23%) of 1-phenyl-3-oxabicyclo[3.2.0]hept-6-en-2-one (**4e**). The IR and NMR spectra were identical with those of the authentic specimen[11] in every respect.

*Photoadditions of γ-Methyl-γ-crotonolactone, β-Angelica Lactone (**1f**).* *(a) To Ethylene*: A solution of γ-methyl-γ-crotonolactone (**1f**)[27] (1.0 g) in acetone (700 ml) was irradiated at −50 °C for 2 hr through quartz with introduction of ethylene. Glpc analysis (column A, 210 °C, He 1.4 kg/cm²) of the reaction mixture indicated the photoproduct consisted of two components eluted at 4.2 min and 4.9 min with the area ratio of about 1 : 1. After evaporation of the solvent under reduced pressure, the residual liquid (1.7 g) was chromatographed on silica gel (60 g) using 4 : 1 petrolum ether–ether as eluent. From the rapidly eluted fractions, 266 mg (21%) of *exo*-4-methyl-3-oxabicyclo[3.2.0]heptan-2-one (**3f**), corresponding to the 4.2 min eluate on glpc, was obtained. Analytical sample was purified by distillation (90—100 °C/20 mmHg). IR (CCl_4) 1775, 1155; NMR 1.25 (d, J=6.3, 3H), 1.90—2.60 (m, 4H), 2.65—3.50 (m, 2H), 4.47 (dq, J=6.3 and 1.0, 1H). Found: C, 66.76; H, 8.12%. Calcd for $C_7H_{10}O_2$: C, 66.64; H, 7.99%.

From the slowly eluted fractions, 183 mg (14%) of the *endo*-methyl isomer, corresponding to the 4.9 min eluate on glpc, was isolated. Analytical sample was purified by distillation (90—100 °C/20 mmHg). IR (CCl_4) 1775, 1170; NMR 1.32 (d, J=6.1, 3H), 1.70—2.70 (m, 4H), 2.80—3.30 (m, 2H), 4.56 (dq, J=6.1 and 5.6, 1H). Found: C, 66.75; H, 8.15%. Calcd for $C_7H_{10}O_2$: C, 66.64; H, 7.99%.

(b) To Acetylene: A solution of **1f** (1.5 g) in acetone (800 ml) was irradiated at −50 °C through quartz with introduction of acetylene. At the reaction period of 4.5 hr, the ratio of **1f** and the product to 9 : 11 as determined by glpc on column A (210 °C, He 1.4 kg/cm²) and the product consisted of the *exo*- and *endo*-methyl isomers with the ratio of 6 : 5 (retention times of 3.3 min and 4.1 min, respectively) similar to the case of the ethylene adduct **3f**. At this stage, the reaction was intermitted and the mixture was evaporated *in vacuo*. The residual liquid (2.7 g) was chromatographed on silica gel (60 g) using 9 : 1 petroleum ether–ether as eluent to give the homogeneous *exo*-methyl (134 mg, 7%) and *endo*-methyl (130 mg, 7%) isomers of 4-methyl-3-oxabicyclo[3.2.0]hept-6-en-2-one (**4f**), and the analytical samples were purified by distillation (80—90 °C/20 mmHg). *Exo*-**4f**: IR (CCl_4) 1775, 1170; NMR 1.30 (d, J=6.7, 3H), 3.17 (dd, J=1.7 and 3.5, 1H), 3.61 (d, J=3.5, 1H), 4.50 (dq, J=6.7 and 1.7, 1H), 6.39 (br. s, 2H). Found: C, 67.79; H, 6.65%. Calcd for $C_7H_8O_2$: C, 67.73; H, 6.50%. *Endo*-**4f**: IR (CCl_4) 1770, 1170; NMR 1.38 (d, J=6.2, 3H), 3.20—3.70 (m, 2H), 4.55 (quint, J=6.2 and 6.2, 1H), 6.37 (br. s, 2H). Found: C, 67.27; H, 6.65%.

*Photoaddition of γ-Butyl-γ-crotonolactone (**1g**) to 1,1-Dimethoxyethylene.* A solution of γ-butyl-γ-crotonolactone (**1g**)[27] (1.46 g, 10 mmol) and 1,1-dimethoxyethylene (9.4 g, 107 mmol) in dry benzene (25 ml) was irradiated for 19 hr at room temperature through quartz. The solvent and excess olefin were evaporated under reduced pressure to give 3.5 g of brown liquid which consisted mainly of two components in a ratio of about 1 : 1 as determined by glpc analysis (column B, 218 °C He 2.4 kg/cm²). Chromatography of the residue on silica gel (80 g) using 7 : 3 hexane–ether as eluent gave 650 mg (28%) of *endo*-4-butyl-6,6-dimethoxy-3-oxabicyclo-[3.2.0]heptan-2-one (**24a**) and 900 mg (38%) of the *exo*-butyl isomer (**24b**), in addition to a small amount of the unreacted lactone. The analytical samples were purified by distillation (70—90 °C/3 mmHg). *Endo*-**24a**: IR (CCl_4) 2850, 2820, 1760; NMR (100 MHz) 0.93 (t, J=6.0, 3H), 1.20—1.80 (m, 6H), 2.10—2.50 (m, 2H), 2.70—3.00 (m, 2H), 3.10 (s, 3H), 3.12 (s, 3H), 4.26 (m, 1H). Found: C, 63.26; H, 8.88%. Calcd for $C_{12}H_{20}O_4$: C, 63.13; H, 8.83%. *Exo*-**24b**: IR (CCl_4) 2850, 2820, 1760; NMR (100 MHz) 0.96 (t, J=6.0, 3H), 1.20—1.80 (m, 6H), 2.20—2.50 (m, 2H), 2.70—2.95 (m, 2H), 3.12 (s, 3H), 3.17 (s, 3H), 4.68 (br. t, J=6.0, 1H). Found: C, 63.26; H, 8.58%.

*Photoadditions of Parasorbic Acid (**2a**).* *(a) To Ethylene*: A solution of parasorbic acid (**2a**)[28] (1.06 g) in acetone (500 ml) was irradiated at room temperature for 3 hr through quartz with introduction of ethylene. Evaporation of the solvent under reduced pressure, followed by chromatography of the residue on silica gel (60 g) using chloroform as eluent gave 260 mg of a mixture of the stereoisomers (at least two isomers) of 4-methyl-3-oxabicyclo[4.2.0]octan-2-one (**11**) as indicated by glpc on column C (170 °C, He 0.65 kg/cm²) Analytical sample was purified by distillation (120—130 °C/10 mmHg). IR (CCl_4) 1740, 1080; NMR 1.29—1.35 (two pairs of doublet, 3H), 1.50—3.20 (m, 8H), 4.00—4.30 (m, 1H). Found: C, 68.97; H, 8.79%. Calcd for $C_8H_{12}O_2$: C, 68.54; H, 8.63%.

(b) To Acetylene: A solution of **2a** (0.5 g) in acetone (250 ml) was irradiated at room temperature for 5 hr through quartz with introduction of acetylene. Analysis of the reaction mixture by glpc (column C, 180 °C, He 1.1 kg/cm²) apparently indicated a single peak due to the photoadduct eluted at 3.5 min with about 66% of area. Spectral sample of the product, 4-methyl-3-oxabicyclo[4.2.0]oct-7-en-2-one (**12**), was collected by preparative glpc using an SE-30 column (3 m×6 mm) at 230 °C. IR (CCl_4) 1740, 1060; NMR 1.29 (d, J=6.0, 3H), 1.60—2.40 (m, 2H), 3.40—3.70 (m, 2H), 4.20—4.40 (m, 1H), 6.00—6.20 (m, 2H).

(c) To 1,1-Dimethoxyethylene: A solution of **2a** (240 mg, 2.1 mmol) and 1,1-dimethoxyethylene (1.15 g, 13.1 mmol) in dry ether (80 ml) was irradiated at room temperature for

10 hr through Vycor. Analysis of the photolysate by glpc (column A, 155 °C, He 1.2 kg/cm²) indicated a main peak eluted at 3.0 min (*ca.* 66% of area) due to the photoproduct, along with the peaks of **2a** and by-products. Spectral sample of the product, 7,7-dimethoxy-4-methyl-3-oxabicyclo-[4.2.0]octan-2-one (**13**), was collected by glpc using a preparative SE-30 column (3 m×6 mm) at 230 °C and then passed through a short column of silica gel with anhydrous ether. IR (CCl_4) 2850, 1740, 1250; NMR 1.34 (d, J= 6.8, 3H), 1.50—3.00 (m, 5H), 3.10 (s, 3H), 3.15 (s, 3H), 3.60—3.80 (m, 1H), 4.20—4.40 (m, 1H).

*Photoaddition of 5,6-Dihydro-4-methyl-2H-pyran-2-one (**2b**) to Ethylene.* A solution of 5,6-dihydro-4-methyl-2*H*-pyran-2-one (**2b**) (344 mg), prepared by dehydration of mevalonic acid lactone with potassium bisulfate, in acetone (600 ml) was irradiated at room temperature for 3 hr through Vycor with introduction of ethylene. At the end of the irradiation period the solvent was removed by distillation under reduced pressure. The residue (770 mg) was chromatographed on preparative layer of silica gel using 1 : 2 petroleum ether–ether as developing agent to give 300 mg (70%) of 6-methyl-3-oxabicyclo[4.2.0]octan-2-one (**17**). Analytical sample was purified by distillation (85—95 °C/4 mmHg). IR (CCl_4) 1740, 1075; NMR (100 MHz) 1.26 (s, 3H), 1.50—3.00 (m, 7H), 4.20—4.60 (m, 2H). Found: C, 68.35; H, 8.45%. Calcd for $C_8H_{12}O_2$: C, 68.54; H, 8.63%.

*2-Hydroxy-6-methyl-2-methylsulfonyl-3-oxabicyclo[4.2.0]octane (**19**).* Sodium methylsulfonyl carbanion was prepared according to the reported manner[16] from sodium hydride (100 mg, 4.2 mmol), dimethylsulfone (495 mg, 4.2 mmol), and dimethyl sulfoxide (3 ml), and diluted with anhydrous tetrahydrofuran (3 ml). Then, a solution of **17** (270 mg, 2.0 mmol) in anhydrous tetrahydrofuran (3 ml) was added at room temperature with stirring and under nitrogen; the mixture turned immediately to deep red, and then heated at 50—60 °C for 1 hr. After cooling, the resulting solution was poured into ice-water, neutralized to pH 4—5, and extracted with chloroform five times. The combined extracts were successively washed with water and saturated salt solution, dried over anhydrous sodium sulfate, and freed from solvent to give 450 mg of crude product. Purification by chromatography on silica gel (15 g) using chloroform afforded 270 mg (76%) of crystalline **19**. Analytical sample was recrystallized from 1 : 1 petroleum ether–ether, mp 103.5—104.5 °C. IR (KBr) 3520, 1315, 1300; NMR ($CDCl_3$) 1.20 (s, 3H), 1.90—2.30 (m, 7H), 2.92 (finely splitted d, J=15.0, 1H), 3.32 (d, J=15.0, 1H), 3.40 (finely splitted s, 3H), 3.65 (ddd, J=11.8, 5.0, and 2.5, 1H), 4.03 (dt, J=11.8, 11.8, and 3.0, 1H). Found: C, 51.62; H, 8.11%. Calcd for $C_{10}H_{18}O_4S$: C, 51.27; H, 7.75%.

*cis-2-(β-Acetoxyethyl)-2-methylcyclobutyl Methyl Ketone (**22**).* To a solution of **19** (770 mg, 3.3 mmol) in 10% aqueous tetrahydrofuran (70 ml) was added aluminum amalgam prepared from 1.0 g of aluminum foil, and the mixture was refluxed for 8 hr. After removal of the insoluble material by filtration, the filtrate was concentrated under reduced pressure and extracted with ether twice. The combined extracts were washed with water and then saturated salt solution, and dried over anhydrous sodium sulfate. Evaporation of the solvent gave 500 mg (96%) of the equilibrium mixture of the methyl ketone **20** and the acetal **21** as indicated by tlc and NMR analyses. The mixture, without further purification, was treated with a mixture of pyridine (3 ml) and acetic anhydride (3 ml) at room temperature overnight. The reaction mixture was poured into ice-water and extracted with ether three times. The combined extracts were washed successively with dilute hydrochloric acid, sodium bicarbonate solution, water, and saturated salt solution, dried over anhydrous sodium sulfate and concentrated. The crude product (500 mg) was purified by passing through a silica gel column (20 g) with 1 : 4 petroleum ether–ether and distilled (100—105 °C/10 mmHg) to give 255 mg (40%) of **22** as a sole product. IR (CCl_4) 1740, 1708, 1235; NMR 1.32 (s, 3H), 1.95 (s, 3H), 2.00 (s, 3H), 2.97 (t, J=7.5, 1H), 1.40—2.40 (m, 6H), 4.00 (t, J=7.5, 2H). Found: C, 66.71; H, 9.47%. Calcd for $C_{11}H_{18}O_3$: C, 66.64; H, 9.15%.

*cis-2-Isopropenyl-1-methylcyclobutaneethanol = (±)-grandisol (**16**).* The Wittig reagent, methylenetriphenylphosphorane, was prepared in dimethyl sulfoxide as reported in the literature[18] and this solution (1.5 equiv, *ca.* 4 ml) was added dropwise to a solution of **22** (100 mg, 0.5 mmol) in anhydrous tetrahydrofuran (3 ml) at room temperature. The resulting mixture was stirred at room temperature for 3 hr under nitrogen and poured into a separatory funnel containing ice-water. The resulting yellow solution was extracted with petroleum ether three times. The combined extracts were washed successively with 1 : 1 dimethyl sulfoxide–water, water, and then saturated salt solution, dried, and concentrated under reduced pressure to give crude product (125 mg) which consisted of two components, being presumably **16** and the acetate. The mixture was dissolved in methanol (2 ml) containing five drops of 1M sodium hydroxide solution and heated at 60—70 °C for 3 hr. The cooled reaction mixture was diluted with water and extracted with ether three times. Evaporation of the solvent, followed by distillation (100—110 °C/17 mmHg) of the residual liquid gave 67 mg (87%) of (±)—**16**, the IR and NMR spectra of which were completely indistinguishable from those of the authentic (±)-grandisol synthesized through an alternative route.[9e] Found : C, 78.02; H, 11.93%. Calcd for $C_{10}H_{18}O$: C, 77.86; H, 11.76%.

*Hydrolysis of **24a** and **24b**.* A solution of **24a** (400 mg) in acetone (14 ml) containing a catalytic amount of *p*-toluenesulfonic acid was stirred at 60 °C overnight. Usual work-up gave 330 mg of oily product. Chromatography on silica gel (10 g) using 3 : 7 petroleum ether–ether afforded 261 mg (82%) of *endo*-4-butyl-3-oxabicyclo[3.2.0]heptane-2,6-dione (**25a**).

In the same manner *exo*-isomer **25b** was obtained in 94% yield (76 mg) from 100 mg of **24b**. Analytical samples were purified by distillation (110—120 °C/1 mmHg). **25a**: IR (CCl_4) 1790, 1780; NMR 0.95 (t, J=6.0, 3H), 1.20—1.90 (m, 6H) 3.00—3.80 (m, 3H), 4.00 (m, 1H), 4.54 (dq, J= 8.0 and 7.0, 1H). Found: C, 65.62; H, 7.81%. Calcd for $C_{10}H_{14}O_3$: C, 65.91; H, 7.74%. **25b**: IR (CCl_4) 1790, 1780, 1170; NMR 0.95 (t, J=6.0, 3H), 1.20—1.80 (m, 6H), 3.10—3.80 (m, 4H), 4.58 (dt, J=6.0 and 1.7, 1H). Found: C, 65.66; H, 7.81%.

*Baeyer-Villiger Oxidation of **25a** and **25b**.* To a solution of **25a** (217 mg, 1.19 mmol) in acetic acid (4 ml) was added 30% aqueous hydrogen peroxide (520 mg), and the reaction mixture was allowed to stand at room temperature overnight. The mixture was neutralized with saturated sodium carbonate solution and extracted with ether three times. The combined extracts were washed with water and saturated salt solution and evaporated to dryness to give 216 mg (92%) of crystalline residue. Recrystallization from petroleum ether–ether–chloroform (2 : 2 : 1) gave colorless needles of *endo*-4-butyl-3,6-dioxabicyclo[3.3.0]octane-2,7-dione (**26a**), mp 85.0—85.5 °C:[20] IR (KBr) 1770, 1200, 1150; NMR ($CDCl_3$) 0.96 (t, J=6.5, 3H), 1.20—1.70 (m, 4H), 1.70—2.10 (m, 2H), 2.93 (d, J=6.0, 2H), 3.53 (q, J=6.0, 1H), 4.59 (dt, J=7.0 and 4.0, 1H), 5.10 (dd, J=6.0 and 4.0, 1H). Found: C, 60.26; H, 7.26%. Calcd for $C_{10}H_{14}O_4$: C, 60.59; H,

7.12%.

According to the identical manner using 112 mg of **25b**, crystalline *exo*-isomer **26b** was obtained in 88% yield (106 mg). Recrystallized sample from carbon tetrachloride had mp 85.0—85.5 °C.[20,29] IR (KBr) 1775, 1200; NMR ($CDCl_3$) 0.96 (t, J=6.5, 3H), 1.20—1.90 (m, 6H), 2.94 (d, J=6.2, 2H), 3.47 (q, J=6.4, 1H), 4.70 (t, J=6.5, 1H), 4.88 (d, J=6.4, 1H). Found: C, 60.53; H, 6.77%. The structures of **26a** and **26b** were further confirmed by comparison of the IR and NMR spectra with those of the samples provided by Professor Yoshikoshi.

The authors are grateful to Drs. C. A. Henrick and J. B. Siddall, Zoecon Corporation, for providing the copies of IR and NMR spectra of (±)-grandisol and to Professor A. Yoshikoshi, our Institute, for the identification of bislactones **26a** and **26b**. The authors also thank Miss Shukuko Suzuki for her technical assistance in part. Financial support from the Ministry of Education of Japan and Asahi Glass Foundation is gratefully acknowledged.

References

1) Parts of this work were presented at the 28th Annual Meeting of the Chemical Society of Japan, Tokyo, April 1, 1973 (Abstracts of Papers, Vol. 3, p. 1530) and at the 30th Annual Meeting of the Chemical Society of Japan, Higashi-Osaka, April 2, 1974 (Abstracts of Papers, Vol. 3, p. 1385).

2) E. J. Corey, J. D. Bass, R. LeMahieu, and R. B. Mitra, *J. Amer. Chem. Soc.*, **86**, 5570 (1964).

3) For the critical reviews see P. E. Eaton, *Accounts Chem. Res.*, **1**, 50 (1968); P. de Mayo, *ibid.*, **4**, 41 (1971); P. G. Bauslaugh, *Synthesis*, **1970**, 287.

4) P. G. Sammes, *Quart. Rev.*, **24**, 37 (1970).

5) Dimerization of γ-crotonolactone (**1a**): K. Ohga and T. Matsuo, This Bulletin, **43**, 3505 (1970).

6) Photocycloaddition of γ-crotonolactone (**1a**) to cycloalkenes: M. Tada, T. Kokubo, and T. Sato, *Tetrahedron*, **28**, 2121 (1972).

7) Photocycloaddition of 5,6-dihydro-4-methyl-2*H*-pyran-2-one (**2b**) to ethylene: R. C. Gueldner, A. C. Thompson, and P. A. Hedin, *J. Org. Chem.*, **37**, 1854 (1972).

8) For the examples see (a) T. S. Cantrell, W. S. Haller, and J. L. Williams, *ibid.*, **34**, 509 (1969); (b) P. E. Eaton and K. Nyi, *J. Amer. Chem. Soc.*, **93**, 2786 (1971).

9) For the examples see (a) R. L. Cargill, J. R. Damewood, and M. M. Cooper, *ibid.*, **88**, 1330 (1966); (b) Y. Yamada, H. Uda, and K. Nakanishi, *Chem. Commun.*, **1966**, 423; (c) C. M. Cimarusti and J. Wolinsky, *J. Amer. Chem. Soc.*, **90**, 113 (1968); (d) W. C. Agosta and W. W. Lowrans, Jr., *Tetrahedron Lett.*, **1969**, 3053; *J. Org. Chem.*, **35**, 3851 (1970); (e) R. Zurflüh, L. L. Dunham, V. L. Spain, and J. B. Siddall, *J. Amer. Chem. Soc.*, **92**, 425 (1970).

10) D. C. Owsley and J. J. Bloomfield, *J. Chem. Soc., (C)*, **1971**, 3445.

11) A. Kawamoto, H. Kosugi, and H. Uda, *Chem. Lett.*, **1972**, 807.

12) N. J. Turro and P. Wriede, *J. Amer. Chem. Soc.*, **90**, 6863 (1968).

13) H. Hikino and P. de Mayo, *ibid.*, **86**, 3582 (1964); B. D. Challand, H. Hikino, G. Kornis, G. Lange, and P. de Mayo, *J. Org. Chem.*, **34**, 794 (1969).

14) J. H. Tumlinson, D. D. Hardee, R. C. Gueldner, A. C. Thompson, P. A. Hedin, and J. P. Minyard, *Science*, **166**, 1010 (1969); *J. Org. Chem.*, **36**, 2616 (1971).

15) W. E. Billups, J. H. Cross, and C. V. Smith, *J. Amer. Chem. Soc.*, **95**, 3438 (1973); G. Stork and J. F. Cohen, *ibid.*, **96**, 5270 (1974); R. C. Cargill and B. Wright, *J. Org. Chem.*, **40**, 120 (1975).

16) H. O. House and J. K. Larson, *ibid.*, **33**, 61 (1968).

17) H. Nozaki, T. Mori, and M. Kawanishi, *Can. J. Chem.*, **46**, 3767 (1968).

18) R. Greenwald, M. Chaykovsky, and E. J. Corey, *J. Org. Chem.*, **28**, 1128 (1963).

19) N. J. McCorkindale, J. L. C. Wright, P. W. Brian, S. M. Clarke, and S. A. Hutchinson, *Tetrahedron Lett.*, **1968**, 727.

20) M. Kato, R. Tanaka, and A. Yoshikoshi, *Chem. Commun.*, **1971** 1561.

21) W. L. Parker and F. Johnson, *J. Amer. Chem. Soc.*, **91**, 7208 (1969).

22) C. C. Price and J. M. Judge, "Organic Syntheses," Coll. Vol. V, p. 255 (1973).

23) J. J. Bloomfield and S. L. Lee, *J. Org. Chem.*, **32**, 3919 (1967).

24) F. Fleck and H. Sching, *Helv. Chim. Acta*, **33**, 146 (1950); K. Iwai, H. Kosugi, and H. Uda, *Chem. Lett.*, **1974**, 1237.

25) G. W. Perld and H. K. L. Hundt, *J. Chem. Soc.*, **1966**, i924.

26) G. Swain, A. R. Todd, and W. S. Waring, *ibid.*, **1944**, 548.

27) K. Iwai, M. Kawai, H. Kosugi, and H. Uda, *Chem. Lett.*, **1974**, 385.

28) R. Kuhn and D. Jerchel, *Ber.*, **76**, 413 (1943).

29) T. Mukaiyama, K. Hagio, H. Takei, and K. Saigo, This Bulletin, **44**, 161 (1971).

Preparations and Properties of Some Derivatives of Pseudo-Geminal Ketone of Tris[2.2.2]paraxylylene

Fumio IMASHIRO, Zen-ichi YOSHIDA, and Iwao TABUSHI*

Department of Synthetic Chemistry, Kyoto University, Yoshida, Kyoto 606

**Department of Pharmaceutical Science, Kyushu University, Higashi-ku, Fukuoka 812*

(Received September 12, 1975)

Some derivatives of pseudo-geminal ketone of tris[2.2.2]paraxylylene (I) were prepared and their spectral properties were investigated in connection with their structural characteristics. The stereochemistry of two isomers of pseudo-geminal carbinols of tris[2.2.2]paraxylylene (III and V) was determined on the basis of chemical shifts of benzhydryl protons and H_o protons in NMR spectra and also of ν_{O-H} bands in IR spectra. The difference in chemical shifts of H_p protons of the two alcohols was explained in terms of the change in electron densities of *para* carbon atoms.

In the preceding paper,[1] the authors reported the high yield preparation of pseudo-geminal ketone of tris[2.2.2]paraxylylene (I) and its spectral properties in connection with its structure. The remarkable high frequency shift of $\nu_{C=O}$ band in the IR spectrum and the large hypochromic effect of intramolecular charge-transfer absorption on the electronic spectrum of I compared with the corresponding spectral characteristics of 5*H*-10,11-dihydrodibenzo[*a*,*d*]cycloheptene-5-one [VI] indicate the lack of coplanarity between carbonyl and benzene planes, and the presence of angle strain about the carbonyl.

Taking these characteristics into consideration, some derivatives of I were prepared in order to elucidate relationships between structures and spectral properties. In this paper, the authors describe some interesting NMR spectral characteristics in the pseudo-geminal tris[2.2.2]paraxylylene derivatives.

Results and Discussion

Preparation. Pseudo-geminal ketone (I) was prepared from tris[2.2.2]paraxylylene by acetylation, bromoform reaction and intramolecular Friedel-Crafts acylation.[1] Reduction of I with sodium tetrahydroborate(−1) in dioxane or with zinc powder in alkaline aqueous ethanol gave 92% or 71% yield, respectively, of "equatorial" alcohol (III), mp 181.0 °C, exclusively. The Wolff-Kishner reduction of I with aqueous hydrazine and sodium hydroxide at 195 °C yielded 44% of pseudo-geminal methanotris[2.2.2]paraxylylene (II) and 46% of III. III was converted into the corresponding trifluoromethanesulfonate (IV) on treatment with butyllithium and trifluoromethanesulfonyl chloride in ether. IV was hydrolyzed in aqueous dioxane to give the stereoisomeric "axial" alcohol (V), mp>300 °C, in quantitative yield.

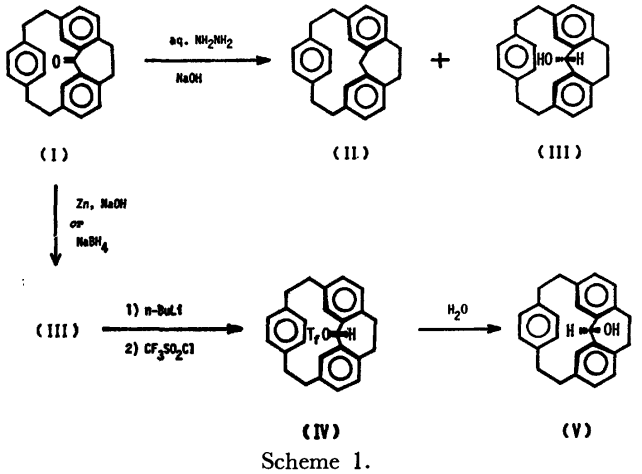

Scheme 1.

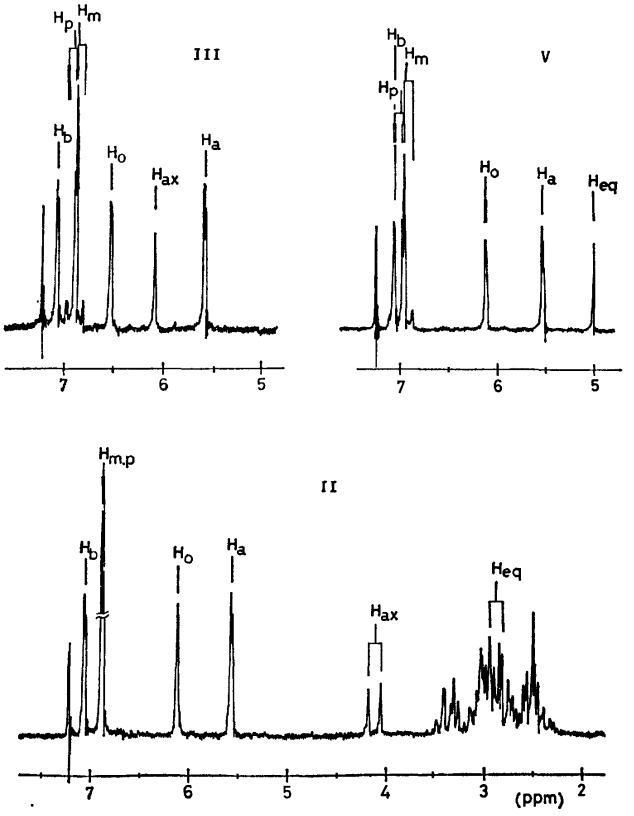

Fig 1. Aromatic and benzhydryl regions of NMR spectra of II, III and V.

Determination of Stereochemistry of Pseudo-Geminal Carbinols of Tris[2.2.2]paraxylylene. Based on molecular model (Dreiding and CPK), the pseudo-geminal bridged tris[2.2.2]paraxylylenes are regarded to have appreciably rigid structures, where conformation change between "equatorial" and "axial" positions about pseudo-geminal bridge carbon seems to be difficult and environments of these positions seem to differ remarkably. The stereochemistry of the two isomeric

* To whom correspondence should be addressed.

Table 1. The NMR chemical shifts of pseudo-geminal bridged tris[2.2.2]paraxylylenes and related compounds in $CDCl_3$ at 31.5° (δ from internal TMS).

Compound	H_o	H_m	H_p	H_a	H_b	H_{ax}	H_{eq}	$-CH_2-$	OH
I[a]	6.21	7.00	7.16	5.51	7.03			2.3—3.4	
II	6.12	6.88	5.57	5.57	7.07	4.12	2.88	2.4—3.5	
III	6.52	6.87	6.91	5.56	7.07	6.07		2.3—3.4	1.60
V	6.11	6.94	6.97	5.52	7.05		5.01	2.3—3.2	2.00
								3.7—3.9	
VI[a]	8.0	7.1—7.4						3.10	
VII		7.09					4.10	3.16	
VIII		7.0—7.5					5.91	2.9—3.4	2.22

a) Ref. 1.

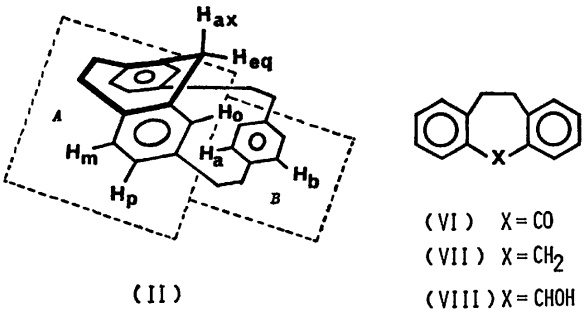

Fig. 2

alcohols (III and V) was investigated mostly by means of NMR spectra. The NMR spectral data of the two alcohols are given in Table 1 along with those of the related compounds. Absorptions of the aromatic and benzhydryl protons are shown in Fig. 1.

The seven membered ring of II (bold line, Fig. 2) is forced to be in a boat conformation due to the remarkably large barrier to the expected conformation change, as shown by the NMR spectra of II in hexachlorobutadiene which shows no substantial temperature dependence up to 180 °C. Irradiation at δ 2.88 caused increase in area intensity of the H_o signal (δ 6.12) of II by 22±1%, while only a very small increase (2.7±0.1%) was observed upon irradiation at δ 4.12. From this nuclear Overhauser effect[2] the higher field signal (δ 2.88) was determined to be H_{eq}, "equatorial" about pseudo-geminal carbon, and the lower (δ 4.12) to be H_{ax}, "axial". Since the chemical shift of a proton α to hydroxyl was reported to be not remarkably affected by the change in stereochemistry of the group,[3] assignments of stereochemistry of the present carbinols are made as shown in Fig. 1. Deshielding of the H_o protons of III (by 0.41 ppm lower field than those of V) is, thus, mainly attributed to anisotropic effect of the "equatorial" oxygen atom in a close proximity.

The low field absorption of the "axial" proton in the present system is consistent with those reported for the 3,4-homotropylidenes,[4] dihydropleiadenes[5] or dihydroanthracenes.[6]

A marked difference between observed ν_{O-H} of these two isomeric alcohols in also in line with the present stereochemistry. The ν_{O-H} values of III, V and VIII (dilute solutions in carbon tetrachloride)

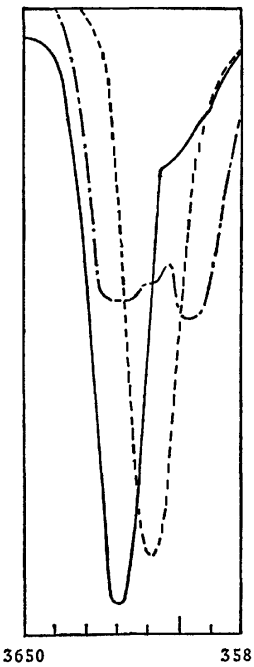

Fig. 3. ν_{O-H} absorptions of III (——), V (- - -) and VIII (— - —) in CCl_4. Concentration 5×10^{-4} M, cell thickness 2.5 cm.

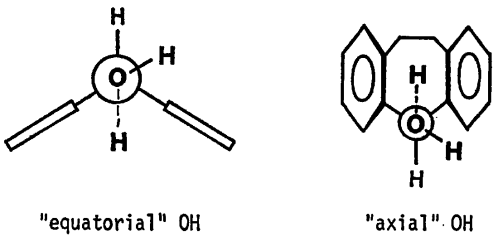

Fig. 4.

are shown in Fig. 3. The "axial" hydroxyl group is expected to interact with a phenyl group (Fig. 4), known as the π-hydrogen bonding,[7] shifting the ν_{O-H} of V to a relatively low frequency, 3608 cm^{-1}. On the other hand, the ν_{O-H} of III appears at relatively high frequency, 3619 cm^{-1}, again in line with the sterochemistry, where the "equatorial" hydroxyl group does not seem to interact with phenyl group. The above consideration is supported by IR spectra of structurally related compounds, 9-fluorenol (3591

cm^{-1}, only the "axial" conformation is allowed) and VIII (3620, 3609^{sh} and 3597 cm^{-1}, more than two conformations are allowed due to its flexible structure). The stereochemistry of the alcohols (III and V), therefore, suggests highly stereoselective attacks (*anti* to the *B* benzene ring) of nucleophiles such as hydride or hydroxide, toward the carbonyl carbon.

Chemical Shift of Pseudo-Geminal Bridged Tris[2.2.2]-*paraxylylene.* A remarkable characteristic appearing in the NMR chemical shifts (Table 1) of the pseudo-geminal bridged tris[2.2.2]paraxylylenes is the absorption of H_o and H_a protons at a considerably high field. All of the H_a protons of the four derivatives (I, II, III and V) are observed by 1.5 ppm upfield (δ from 5.51 to 5.57) than *p*-xylene. We come across a similar situation in the aromatic protons of 4,5 : 7,8-dibenzo[2.2]paracyclophane (IX, Fig. 5)[8] showing absorption at δ 5.50, which is located just above (*ca.* 3.0 Å) the aromatic ring. Thus, for the H_a protons of our present compounds, considered to be located just above (3.1 Å) the "face"[1] benzene rings (*A*) judging from molecular models, the observed high field shifts are attributed to a transannular shielding effect of the *A* rings (see II).

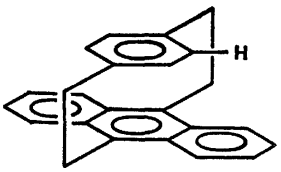

Fig. 5.

Since the absorption of the H_o protons of II appears at δ 6.12, a field higher than the corresponding noncyclic VII by 0.97 ppm, the transannular shielding of the *B* ring is estimated to be 0.82 ppm assuming a 0.15 ppm[9] upfield shift due to the inductive effect of the *meta* methylene bridges. This reduced transannular shielding is responsible for deviation (1.6 Å by the model) of location of the H_o proton from the center of the *B* ring.

The H_p protons of II appear at a field only 0.21 ppm higher than VII. This relatively small shift is mostly attributable to the *meta* methylene bridges. Only a negligibly small transannular shielding seems to be present at this position.

An interesting difference (0.06 ppm) between the chemical shifts of the H_p protons is seen for V as compared with III.[10] Since the distance between the H_p hydrogen and the hydroxyl oxygen atoms is estimated to be 6.0—6.1 Å, at most a 0.2 ppm difference is responsible for the change in the chemical shift due to anisotropic shielding and electrostatic field effect.[11,12] The main part of the difference is, therefore, interpreted in terms of the change in electron densities of the *para* carbon atoms. Linear correlations of chemical shifts of aromatic protons with electron densities of ring carbon atoms have been well established.[13] The CNDO/2[14] calculations were carried out for two conformations, where the hydroxyl was perpendicular or coplanar to the phenyl plane, of benzyl alcohol taken as a model compound. The calculated electron density of the *para* carbon was lower (by 0.003 *e*, which caused by 0.04 ppm down field shift according to the equation[13b]) for the perpendicular form. This is clearly in line with the observed lower chemical shift in V.

Experimental

Measurements and Calculations. All the melting points were uncorrected. NMR spectra were recorded with a Varian HA-100 or a Varian EM-360 spectrometer. The former was also employed for the variable-temperature and the nuclear Overhauser experiments. The sample for the latter experiment was degassed. Mass spectra were determined with a Hitachi RMU-6C mass spectrometer with ionization current 70 eV. Electronic spectra were measured with a Hitachi EPS-3T recording spectrophotometer, the IR spectra being taken on a Hitachi EPI-G3 grating infrared spectrophotometer. Theoretical calculations were carried out by use of the FACOM 230-75 computer at the Data Processing Center of Kyoto University.

Pseudo-Geminal "Equatorial" Carbinol of Tris[*2.2.2*]*paraxylylene (III).* *a) Zinc Reduction*: To a hot solution of 520 mg of I in 70 ml of ethanol was added a mixture of 7 g of zinc powder, 7 g of sodium hydroxide and 10 ml of water. The mixture was refluxed for 2 hr and concentrated to half volume. After being cooled to room temperature, the mixture was filtered. The filtrate was extracted six times with ether. The combined ether extract was washed with saturated aqueous sodium chloride, dried over anhydrous magnesium sulfate, and the solvent was evaporated. The residual solids were recrystallized with benzene-dichloromethane (6/1 vol/vol) to give 370 mg (71%) of III as colorless prisms; mp 181.0 °C. MS *m/e* (rel intensity): 340 (M^+, 88), 322 (36), 311 (54), 218 (100), 205 (31), 193 (32), 133 (47), and 104 (36). IR (KBr): 3470, 3000, 2930, 2840, 1495, 1440, 1155, 1045, 1040, 805, 620, and 455 cm^{-1}. UV (cyclohexane) λ_{max}: 279^{sh} (ε 800), 265 (900), 272^{sh} (930), 274 (1000), and 281 nm (910). Found: C, 88.48; H, 7.05%. Calcd for $C_{25}H_{24}O$: C, 88.19; H, 7.11%.

b) Sodium Tetrahydroborate (−1) Reduction: To a stirred solution of 430 mg (1.27 mmol) of I and 0.5 ml of 0.1 M aqueous sodium hydroxide in 10 ml of dioxane was added 242 mg (6.35 mmol) of sodium tetrahydroborate (−1) at room temperature, stirring being continued for 3 hr. Excess tetrahydroborate (−1) was removed by boiling the solution for 5 min. The solution was then cooled and extracted three times with chloroform. The combined chloroform extract was washed with saturated aqueous sodium chloride and dried over anhydrous sodium sulfate, the solvent being evaporated. The residual solids were chromatographed on a silica gel column with benzene to give 397 mg (92%) of III.

Pseudo-Geminal Methanotris[*2.2.2*]*paraxylylene (II).* A mixture of 50 mg of I, 200 mg of sodium hydroxide, 10 drops of hydrazine hydrate (abt. 80%) and 4 ml of diethylene glycol was refluxed for 40 min. After being cooled, the mixture was extracted with ether. The extract was washed with aqueous sodium chloride and dried over anhydrous magnesium sulfate. The solvent was evaporated and the residue was chromatographed on a silica gel column with hexane-dichloromethane (1 : 1) and then dichloromethane. The first fraction gave 21 mg (44%) of II, and the second fraction gave 23 mg (46%) of III which was identified with an authentic III by NMR and IR spectra. Recrystallization of II from hexane-chloroform gave colorless plates; mp 189.5—190.5 °C. MS *m/e* (rel intensity): 324 (M^+, 100), 220

(26), 219 (40), 205 (61), 129 (26), 104 (21), and 83 (28). IR (KBr): 3000, 2930, 2850, 1500, 1440, 1100, 810, 590, and 460 cm^{-1}. UV (cyclohexane) λ_{max}: 258^{sh} (ε 650), 261^{sh} (690), 266 (860), 274 (1060), 279 (830), and 282 nm (1070). Found: C, 92.42; H, 7.48%. Calcd for $C_{25}H_{24}$: C, 92.54; H, 7.46%.

The Trifluoromethanesulfonate of III (IV). To a stirred solution of 190 mg of III in 5 ml of dry ether was added 0.3 ml of abt. 20% butyllithium in hexane at room temperature, stirring being continued for 10 min. A few drops of trifluoromethanesulfonyl chloride were then added, and stirring was continued for 10 min at room temperature. The solvent was removed under reduced pressure and the residue was chromatographed on a silica gel column with benzene. The crystals from the major fraction were recrystallized from petroleum ether to give 180 mg (68%) of IV as colorless needles; mp 158.5—159.0 °C (dec). IR (KBr): 2930, 1415, 1250, 1215, 1200, 950, 890, 805, 635, 605, 580, 515, and 460 cm^{-1}. NMR ($CDCl_3$): δ 2.0—3.5 (m, 12H, $-CH_2-$), 5.56 (m, 2H, H_a), 6.39 (m, 2H, H_0), 6.93 (d, 2H, J=8.0 Hz, H_m), 7.00 (s, 1H, H_{ax}), 7.01 (dd, 2H, J=8.0 Hz, J=1.5 Hz, H_p), and 7.12 (m, 2H, H_b). Found: C, 66.18; H, 5.19%. Calcd for $C_{26}H_{23}F_3O_3S$: C, 66.09; H, 4.91%.

Pseudo-Geminal "Axial" Carbinol of Tris[2.2.2]paraxylylene (V). A solution of 52 mg of IV in 9 ml of dioxane and 6 ml of water in a sealed tube was placed in a bath kept at 110.6±0.1 °C for 23 hr. After being cooled, the reaction mixture was diluted with water and extracted with ether–benzene (1 : 1). The ether–benzene extract was washed with aqueous sodium hydrogencarbonate and then with saturated aqueous sodium chloride, and dried over anhydrous sodium sulfate. The solvent was evaporated to yield 39 mg (100 %) of colorless crystals of V, which was recrystallized from benzene to give colorless needles; mp> 300 °C. MS *m/e* (rel intensity): 340 (M^+, 6), 322 (45), 218 (46), 202 (19), 104 (100), 103 (27), and 78 (32). IR (KBr): 3430, 3000, 2930, 2840, 1500, 1440, 1045, 1030, 810, 630, 580, and 460 cm^{-1}. UV (cyclohexane) λ_{max}: 244^{sh} (ε 4940), 265^{sh} (1240), 274 (1320), and 284 nm (1110). Found: C, 88.42; H, 7.26%. Calcd for $C_{25}H_{24}O$: C, 88.19; H, 7.11%.

References

1) I. Tabushi, Z. Yoshida, and F. Imashiro, *Tetrahedron*, **31**, 1883 (1975).
2) F. A. L. Anet and A. J. R. Bourn. *J. Amer. Chem. Soc.*, **87**, 5250 (1965).
3) L. M. Jackman and S. Sternhill, "Applications of Nuclear Magnetic Resonance Spectroscopy in Organic Chemistry," 2nd ed., Pergamon Press, Oxford (1969), p. 239.
4) R. F. Childs, M. A. Brown, F. A. L. Anet, and S. Winstein, *J. Amer. Chem. Soc.*, **94**, 2175 (1972).
5) P. T. Lansbury, *Accounts Chem. Res.*, **2**, 210 (1969).
6) A. W. Brinkman, M. Gordon, R. G. Harvey, P. W. Rabideau, J. B. Stothers, and A. L. Temay, Jr., *J. Amer. Chem. Soc.*, **92**, 5192 (1970).
7) M. Oki and H. Iwamura, This Bulletin, **32**, 950 and 955 (1959).
8) D. J. Cram, C. K. Dalton, and G. R. Knox, *J. Amer. Chem. Soc.*, **85**, 1088 (1967).
9) Aromatic protons of 1,2,4-trimethylbenzene are absorbed at a field 0.15 ppm higher than those of *p*-xylene; H. A. Szymanski and R. E. Yieln, "NMR Band Handbook," IFI/Plenum, New York, N.Y., p. 95 and 98 (1968).
10) A similar difference (0.08 ppm) was observed between the corresponding *p*-nitrobenzoates.
11) Ref. 3), p. 61.
12) a) R. F. Zurcher, *Helv. Chim. Acta*, **44**, 1380 (1961); *ibid.*, **46**, 2054 (1963), b) K. Tori and K. Aono, *Ann. Rept. Shionogi Res. Lab.*, **14**, 136 (1964).
13) a) Ref. 3), p. 201, b) P. Lazzeretti and F. Taddie, *Org. Magn. Resonance*, **3**, 283 (1971).
14) J. A. Pople and D. L. Beveridge, "Approximate Molecular Orbital Theory," McGraw-Hill, New York, N. Y. (1970).

Chemical Synthesis of *N*-Acetylmuramyl Peptides with Partial Structures of Bacterial Cell Wall and Their Analogs in Relation to Immunoadjuvant Activities[1)]

Shoichi KUSUMOTO, Yuzo TARUMI, Kazuhiro IKENAKA and Tetsuo SHIBA

Department of Chemistry, Faculty of Science, Osaka University, Toyonaka, Osaka 560

(Received September 16, 1975)

N-Acetylmuramyl peptides of successive length corresponding to the partial structures of cell wall in *Staphylococcus aureus* were synthesized in order to elucidate the minimum effective structure responsible for immunoadjuvant activity of bacterial cell walls. In view of the finding that *N*-acetylmuramyl-L-alanyl-D-isoglutamine was the least structure moiety for exhibition of the activity, nine analogs of either *N*-acetylmuramyl amino acid or *N*-acetylmuramyl dipeptide were also synthesized.

The fact that mycobacterium cell exhibits the immunoadjuvant activity had been first described by Freund in 1956.[2)] He observed the significant stimulation of both humoral and cellular immune responses to a protein antigen, when the antigen was administered together with killed cell of this bacterium. Successive investigations have revealed that this activity is not restricted to mycobacterium cells but manifests in many other bacterial cells commonly, and that water soluble fragments involving peptidoglycan are responsible for the activity.[3)] Meanwhile, the chemical structure of such bacterial peptidoglycan was clarified by many investigators.[4)] For example, the main chain of peptidoglycan in *Staphylococcus aureus* is composed of *N*-acetylglucosamines and *N*-acetylmuramic acids alternately, and tetrapeptide subunits of L-alanyl-D-isoglutaminyl-L-lysyl-D-alanine are linked to the carboxyl groups of *N*-acetylmuramic acids. The carboxyl group of *C*-terminal D-alanine in one peptide subunit is connected to the ε-amino group of L-lysine in the another unit through a pentaglycine bridge, thus completing the network structure of cell wall. The peptidoglycans of many other bacteria have fundamentally similar structures, though the lysine residue is often replaced with α,ε-diaminopimelic acid and glycine residue in the bridge also with other amino acids.

Recently, Kotani *et al.*[1,5)] found the fact that *N*-acetylmuramyl peptides obtained by enzymatic digestion of cell wall, *i.e.*, N^{α}-(*N*-acetylmuramyl-L-alanyl-D-isoglutaminyl)-N^{ε}-(glycyl-glycyl)-L-lysyl-D-alanine from *S. aureus* and *N*-acetylmuramyl-L-alanyl-D-isoglutaminyl-*meso*-diaminopimelyl-D-alanine and/or *N*-acetylmuramyl-L-alanyl-D-isoglutaminyl-*meso*-diaminopimelic acid from *Lactobacillus plantarum*, showed definite adjuvant activities. These muramyl peptides seemed to be the smallest chemical entities possessing adjuvant activity in the cell wall structure. Lederer *et al.*[6)] as well as Fleck *et al.*[7)] also reported that the monomeric subunit is enough essential for the adjuvant activities of peptidoglycan from their result of enzymatic degradations.

However, there seemed to remain still some ambiguity on possible disturbance by inevitable impurities which contaminated the enzymatic digests and caused the adjuvant activity. Furthermore, the method of enzymatic degradation has a limitation for the determination of the minimal structure for exhibition of the activity. In view of the above situation, the chemical synthesis would be expected to have obvious advantage particularly in this case, as one can prepare not only a satisfactory pure substance of natural structure but also tailor-made analogs to investigate a relation between the structure and the activity. We therefore synthesized several *N*-acetylmuramyl peptides corresponding to the partial structures of peptidoglycan in *S. aureus*, and could thus demonstrate clearly that *N*-acetylmuramyl-L-alanyl-D-isoglutamine is the least structure required for the adjuvant activity.[8)] The experimental results on the biological tests of these synthetic substances were already reported.[1,9)] In the present paper, we report the full details of the synthesis of the muramyl peptides.

As muramyl peptides of natural type structure involved in the *S. aureus* peptidoglycan, the following four compounds of successive length were prepared by total synthesis, *i.e.*, *N*-acetylmuramyl-L-alanine (**1d**), *N*-acetylmuramyl-L-alanyl-D-isoglutamine (**2d**), *N*-acetylmuramyl-L-alanyl-D-isoglutaminyl-L-lysine (**3d**) and *N*-acetylmuramyl-L-alanyl-D-isoglutaminyl-L-lysyl-D-alanine (**4d**).

These compounds were all preprared in principle by coupling of a protected *N*-acetylmuramic acid, *i.e.*, benzyl 2-acetamido-4,6-*O*-benzylidene-3-*O*-(D-1′-carboxyethyl)-2-deoxy-α-D-glucopyranoside (**5**)[10)] with suitably protected peptide portions followed by deprotection. The all protecting groups were so selected as to be removed simultaneously by mild hydrogenolysis at the final synthetic step.

Each peptide portion was synthesized by conventional method using *t*-butoxycarbonyl (Boc) and benzyloxycarbonyl (Z) groups for α- and ε-amino protections respectively and benzyl ester for carboxyl protection. Although the synthesis of Boc-L-alanyl-D-isoglutamine benzyl ester (**2a**) and N^{α}-(Boc-L-alanyl-D-isoglutaminyl)-N^{ε}-Z-L-lysyl-D-alanine benzyl ester (**4a**) had been already described by Bricas *et al.*,[11)] synthetic procedure and yield of the products were eventually improved in this investigation. Thus, the dipeptide (**2a**) was prepared by coupling of Boc-L-alanine with *D*-isoglutamine benzyl ester using dicyclohexylcarbodiimide–*N*-hydroxysuccinimide. Hydrogenolysis of **2a** gave Boc-L-alanyl-D-isoglutamine, which was then coupled with benzyl N^{ε}-Z-L-lysinate or N^{ε}-Z-lysyl-L-D-alanine benzyl ester by means of mixed anhydride method to afford the protected tripeptide (**3a**) or

TABLE 1. LIST OF *N*-ACETYLMURAMYL AMINO ACIDS AND PEPTIDES SYNTHESIZED (**1d**—**4d** AND **6d**—**14d**) AND THEIR INTERMEDIATES

1 R^1-L-Ala-OR^2

2 R^1-L-Ala-D-Glu(OR^2)-NH_2

3 R^1-L-Ala-D-Glu(L-Lys(R^3)-OR^2)-NH_2

4 R^1-L-Ala-D-Glu(L-Lys(R^3)-D-Ala-OR^2)-NH_2

6 R^1-D-Ala-OR^2

7 R^1-D-Glu(OR^2)-NH_2

8 R^1-L-Ala-L-Glu(OR^2)-NH_2

9 R^1-L-Ala-D-Glu(NH_2)-OR^2

10 R^1-L-Ala-L-Glu(NH_2)-OR^2

11 R^1-L-Ala-D-Glu(OR^2)-OR^2

12 R^1-L-Ala-L-Glu(OR^2)-OR^2

13 R^1-L-Ala-D-Asp(OR^2)-NH_2

14 R^1-L-Ala-D-Ala-NH_2

a : R^1=Boc, R^2=Bzl, R^3=Z

b : R^1=H, R^2=Bzl, R^3=Z

c : R^1= 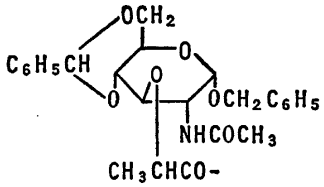 =1-α-*O*-benzyl-4,6-*O*-benzylidene-*N*-acetylmuramyl, R^2=Bzl, R^3=Z

d : R^1= 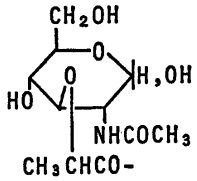 =*N*-acetylmuramyl, R^2=R^3=H

e : R^1=R^2=R^3=H

Boc=*t*-butoxycarbonyl, Bzl=benzyl, Z=benzyloxycarbonyl

TABLE 2. PHYSICAL PROPERTIES OF PROTECTED DIPEPTIDES (**8a**—**14a**)

Compd	Yield (%)	Mp (°C)	$[\alpha]_D$[a]	Molecular formula	Anal. Found (Calcd) C%	H%	N%
8a	77	133.5—134.5	−21.8°[b]	$C_{20}H_{29}O_6N_3$	59.12 (58.95	7.28 7.17	10.34 10.31)
9a	71	143.5—145.5	−7.5°	$C_{20}H_{29}O_6N_3$	58.90 (58.95	7.14 7.17	10.33 10.31)
10a	74	136 —136.5	−1.9°	$C_{20}H_{29}O_6N_3$	59.06 (58.95	7.15 7.17	10.47 10.31)
11a	83	106.5—107.0	−8.2°	$C_{27}H_{34}O_7N_2$	64.82 (65.04	6.91 6.87	5.56 5.62)
12a	78	52.5— 53.5	−14.2°[c]	$C_{27}H_{34}O_7N_2$	65.01 (65.04	6.87 6.87	5.65 5.62)
13a	76	125.5—126.5	+12.2°[d]	$C_{19}H_{27}O_6N_3$	57.81 (58.00	6.89 6.92	10.69 10.68)
14a	70	128.0—128.5	+ 2.6°[e]	$C_{11}H_{21}O_4N_3$	50.93 (50.95	8.19 8.16	16.05 16.21)

a) *c* 2.0 in ethyl acetate at 20—22 °C unless otherwise noted. b) at 28 °C. c) *c* 2.2 at 23 °C. d) *c* 0.5 at 15 °C. e) *c* 1.0 at 17 °C.

tetrapeptide (**4a**). The Boc group in **2a** was removed with hydrogen chloride in acetic acid, while trifluoroacetic acid was employed for deprotection of those in **3a** and **4a**. The di-, tri- and tetrapeptides (**2b**, **3b**, and **4b**) with free amino terminals were thus obtained and then subjected to condensation with the muramic acid moiety (**5**).

Synthesis of muramyl peptides was first reported by Lanzilotti *et al.*[12] who prepared *N*-acetylmuramyl-L-alanyl-D-α- and γ-glutamyl-L-lysyl-D-alanyl-D-alanine by the same strategy mentioned above. They used Woodward's reagent K for coupling of **5** with peptides

TABLE 3. PHYSICAL PROPERTIES OF PROTECTED *N*-ACETYLMURAMYL AMINO ACIDS AND PEPTIDES (**6c**—**14c**)

Compd.	Method of coupling[a]	Yield (%)	Mp (°C)	$[\alpha]_D^{20}$ in DMF	Molecular formula	Anal. Found (Calcd) C%	H%	N%
6c	A	76	211—213	+105° (*c* 2.3)[c]	$C_{35}H_{40}O_9N_2$	66.55 (66.44	6.36 6.37	4.43 4.43)
7c	B	80	243—245[b]	+80.2° (*c* 1.2)	$C_{37}H_{43}O_{10}N_3$	64.14 (64.43	6.26 6.28	6.18 6.09)
8c	A	83	243—245[b]	+79.0° (*c* 1.9)	$C_{40}H_{48}O_{11}N_4 \cdot 1/2H_2O$	62.58 (62.40	6.26 6.42	7.28 7.28)
9c	A	87	246—248[b]	+88.2° (*c* 1.0)	$C_{40}H_{48}O_{11}N_4 \cdot 1/4H_2O$	62.70 (62.77	6.30 6.39	7.46 7.32)
10c	A	98	240[b]	+7.8° (*c* 1.0)	$C_{40}H_{48}O_{11}N_4 \cdot 1/2H_2O$	62.41 (62.40	6.37 6.42	7.42 7.28)
11c	A	70	211	+79.1° (*c* 1.0)	$C_{47}H_{53}O_{12}N_3 \cdot 1/2H_2O$	65.58 (65.57	6.28 6.32	4.91 4.88)
12c	A	75	208	+67.4° (*c* 0.9)	$C_{47}H_{53}O_{12}N_3$	66.00 (66.26	6.32 6.27	4.85 4.93)
13c	A	69	222—223[b]	+98.9° (*c* 1.0)[c]	$C_{39}H_{46}O_{11}N_4 \cdot 1/2H_2O$	62.00 (61.97	6.20 6.27	7.45 7.41)
14c	B	83	284.5[b]	+108° (*c* 0.55)[d]	$C_{31}H_{40}O_9N_4$	60.68 (60.77	6.52 6.58	8.84 9.15)

a) A : dicyclohexylcarbodiimide—*N*-hydroxysuccinimide, B : ethyl chloroformate. b) decomposition. c) at 25 °C. d) at 17 °C.

TABLE 4. *N*-ACETYLMURAMYL AMINO ACIDS AND PEPTIDES OF UNNATURAL STRUCTURES (**6a**—**14d**)

Compd[a]	Yield (%)	$[\alpha]_D$[c] after 3 min	after 24 hr	Molecular formula	Anal. Found (Calcd) C%	H%	N%
6d	82	+63.5°	+56.7°	$C_{14}H_{24}O_9N_2 \cdot 1/4H_2O$	45.75 (45.58	6.61 6.70	7.75 7.60)
7d	92	+52.7°	+47.4°	$C_{16}H_{27}O_{10}N_3$	45.44 (45.60	6.53 6.46	9.84 9.97)
8d	94	+16.5°	+12.2°	$C_{19}H_{32}O_{11}N_4 \cdot 1/2H_2O$	45.48 (45.50	6.58 6.63	11.35 11.17)
9d	85	+36.9°	+33.1°	$C_{19}H_{32}O_{11}N_4 \cdot 1/4H_2O$	45.96 (45.92	6.63 6.59	11.11 11.27)
10d	86	+42.4°	+38.5°	$C_{19}H_{32}O_{11}N_4$	46.05 (46.33	6.62 6.55	11.33 11.38)
11d	93	+35.5°	+32.4°	$C_{19}H_{31}O_{12}N_3 \cdot 1/2H_2O$	45.70 (45.41	6.35 6.42	8.26 8.36)
12d	95	+15.5°	+11.7°	$C_{19}H_{31}O_{12}N_3 \cdot 1/2H_2O$	45.58 (45.41	6.37 6.42	8.37 8.36)
13d[b]	81	+43.7°	+34.8°	$C_{18}H_{30}O_{11}N_4 \cdot 1/3H_2O$	44.73 (44.62	6.34 6.38	11.28 11.57)
14d	90	+50.0°	+43.3°	$C_{17}H_{30}O_9N_4 \cdot 1/2H_2O$	46.30 (46.04	6.94 7.05	12.76 12.64)

a) All these compounds except **13d** are colorless hygroscopic powder and do not show definite melting points. b) This compound was recrystallized from water—methanol—ether; mp 198 °C (decomp.). c) *c* 0.5 in H_2O at 15—17 °C.

without mention of the yield of the reaction. Thereafter, Chaturvedi *et al.*[13] reported the synthesis of *N*-acetylmuramyl-L-alanine, *N*-acetylmuramyl-L-alanyl-D-glutamic acid and several their analogs again by the same procedures and reagents. In our study, more convenient and simple methods generally applicable to the synthesis of muramyl peptides were investigated for this coupling.[14] Coupling of **5** with peptides by the active ester method was first examined using benzyl L-alaninate (**1b**). When the 1-succinimidyl ester of **5** was prepared using dicyclohexylcarbodiimide and allowed to react with **1b**, the fully protected *N*-acetylmuramyl-L-alanine (**1c**) was obtained in a fairly good yield. Its structure was confirmed by elemental analysis and NMR spectrum, in which two doublet signals of methyl groups attributed to the alanine and the muramic acid residues were clearly observed. The protected *N*-acetylmuramyl peptides **2c**, **3c** and **4c** were also obtained using the similar procedure by coupling of **5** with **2b**, **3b** and **4b**. In the latter two cases, 1-succinimidyl ester of **5** was isolated and recrystallized before the coupling.

Furthermore, it was found that this coupling proceeds also by the mixed anhydride method in a comparable yield.

The hydrogenolytic removal of the protecting groups in **1c** was carried out with palladium black in acetic acid. Although addition of hydrochloric acid increased the reaction rate considerably, it caused a formation of several by-products and removal of them required laborious process. Thus, **2c** was hydrogenolyzed in acetic acid without hydrochloric acid to afford pure **2d**. However, complete deprotections of **3c** and **4c** were only accomplished by addition of 0.5 equivalent of hydrochloric acid forming **3d** and **4d** in pure states, and use of 1 equivalent or more of the acid resulted in a formation of much amount of a by-product in each case. All the free *N*-acetylmuramyl peptides (**1d**—**4d**) precipitated as hygroscopic powder on addition of anhydrous ether to their ethanol or methanol solution. The powders thus obtained were found to contain considerable amount of the solvent alcohol from the results of elemental analyses and NMR spectra. The alcohol-free compounds adequate to biological tests and elemental analyses were prepared by lyophilization.

The *N*-acetylmuramyl amino acids and peptides of unnatural structures (**6d**—**14d**) were also synthesized by the similar procedures. The peptide portions were prepared by dicyclohexylcarbodiimide–*N*-hydroxysuccinimide method using Boc and benzyl groups for protections. After removal of Boc group, the products (**6b**—**14b**) were coupled with **5** by means of either the active ester or the mixed anhydride method, and the final hydrogenolysis afforded each *N*-acetylmuramyl peptide (**6d**—**14d**).

The free di-, tri- and tetrapeptides without sugar part, *i.e.*, L-alanyl-D-isoglutamine (**2e**), L-alanyl-D-isoglutaminyl-L-lysine (**3e**) and L-alanyl-D-isoglutaminyl-L-lysyl-D-alanine (**4e**) were also prepared in order to know the significance of *N*-acetylmuramyl moiety for the adjuvant activity. The dipeptide (**2e**) was obtained by hydrogenolysis of **2a** followed by removal of Boc group with trifluoroacetic acid. Dihydrochloride and bistrifluoroacetate of **3e** and bistrifluoroacetate of **4e**[11] were also prepared similarly from **3a** and **4a**, respectively.

Experimental

All melting points are uncorrected. Silica gel G according to Stahl, Merck, was used for thin-layer chromatography (tlc). Paper electrophoresis (PEP) was carried out using Toyo filter paper No. 51 in a pyridine–acetic acid–water (30 : 4 : 966 v/v/v) buffer solution.

1-α-O-Benzyl-4,6-O-benzylidene-N-acetylmuramyl-L-alanine Benzyl Ester (1c). Dicyclohexylcarbodiimide (0.82 g, 4.0 mmol) was added to an ice-cooled solution of benzyl 2-acetamido-4,6-*O*-benzylidene-3-*O*-(D-1'-carboxyethyl)-2-deoxy-α-D-glucopyranoside (**5**)[10] (1.88 g, 4.0 mmol) and *N*-hydroxysuccinimide (0.57 g, 5.0 mmol) in tetrahydrofuran (40 ml). The mixture was stirred in an ice bath for 3 hr and then at room temperature for 1 hr. Dicyclohexylurea formed was filtered off and washed with tetrahydrofuran. The combined filtrate and washings were again cooled in an ice bath and there were added benzyl L-alaninate *p*-toluenesulfonate (1.54 g, 4.4 mmol) and triethylamine (0.62 ml, 4.4 mmol). The mixture was stirred overnight at room temperature. After evaporation of the solvent, the residue was dissolved in chloroform, worked up as usual and the product was recrystallized from ethanol; yield, 1.89 g (75%); mp 211.5—216.5 °C. A sample for elemental analysis was recrystallized again from ethanol; mp 215.5—217 °C; $[\alpha]_D^{20}+85.6°$ (*c* 2.1, *N*,*N*-dimethylformamide). NMR (in $CDCl_3$): δ1.37 and 1.44 (each 3H, d, $J=7$ Hz), 1.90 (3H, s; CH_3CO) and 7.2—7.5 (15H; aromatic).

Found: C, 66.47; H, 6.42; N, 4.65%. Calcd for $C_{35}H_{40}O_9N_2$: C, 66.44; H, 6.37; N, 4.43%.

N-Acetylmuramyl-L-alanine (1d). A solution of **1c** (1.26 g, 2.0 mmol) in acetic acid (100 ml) containing 6M hydrochloric acid (1 ml) was hydrogenolyzed in the presence of palladium black at room temperature for 31 hr. The solvent was removed *in vacuo*, the syrupy residue was dissolved in water and subjected to column chromatography on a mixture of Darco G-60 active charcoal (30 g) and Hyflo Super-Cel (90 g). Elution with water–ethanol (9 : 1) afforded a fairly pure product, which was passed through a column of Dowex 50×8 (H^+ form) to remove the ninhydrin-positive impurity. The eluate was evaporated *in vacuo* and the residue was dissolved in absolute ethanol. Hygroscopic solid was formed on addition of absolute ether; yield, 0.490 g (67%). This product was dissolved in water and lyophilized to give colorless hygroscopic solid, which was subjected to biological test and elemental analysis. $[\alpha]_D^{17}+35.6°$ (after 3 min), +30.9 ° (after 19 hr) (*c* 0.51, H_2O).

Found: C, 46.08; H, 6.76; N, 7.54%. Calcd for $C_{14}H_{24}O_9N_2$: C, 46.15; H, 6.64; N, 7.69%.

t-Butoxycarbonyl-L-alanyl-D-isoglutamine Benzyl Ester (2a). *N*-Hydroxysuccinimide (2.25 g, 19.6 mmol) and dicyclohexylcarbodiimide (4.04 g, 19.6 mmol) were added to an ice-cooled solution of Boc-L-alanine (3.71 g, 19.6 mmol) in tetrahydrofuran (70 ml). After stirring for 10 min, there was added a cold mixture of benzyl D-isoglutaminate hydrochloride (5.33 g, 19.6 mmol) and triethylamine (2.70 ml, 19.6 mmol) in tetrahydrofuran (100 ml), and the mixture was stirred in an ice bath. Stirring was continued overnight, allowing the temperature of the mixture to reach to room temperature. Triethylamine hydrochloride and dicyclohexylurea formed were filtered off and the filtrate was worked up as usual. Recrystallization was effected from ethyl acetate–hexane; yield, 7.28 g (91%); mp 137.5—138.5 °C (lit,[11] 133—134 °C); $[\alpha]_D^{28}-8.1°$ (*c* 1.0, methanol).

Found: C, 58.64; H, 7.15; N, 10.41%. Calcd for $C_{20}H_{29}O_6N_3$: C, 58.95; H, 7.17; N, 10.31%.

L-Alanyl-D-isoglutamine Benzyl Ester (2b) Hydrochloride. Dry hydrogen chloride was passed through a solution of **2a** (3.70 g, 9.1 mmol) in acetic acid (50 ml) for 1 hr. After evaporation of the solvent *in vacuo*, the syrupy residue crystallized on trituration with ether. Recrystallization was effected from ethanol–ether; yield, 2.76 g (89%); mp 149.5—151 °C; $[\alpha]_D^{23}+10.8°$ (*c* 2.1, ethanol).

Found: C, 51.68; H, 6.41; N, 11.91; Cl, 9.97%. Calcd for $C_{15}H_{21}O_4N_3Cl\cdot 1/4H_2O$: C, 51.87; H, 6.24; N, 12.10; Cl, 10.21%.

1-α-O-Benzyl-4,6-O-benzylidene-N-acetylmuramyl-L-alanyl-D-isoglutamine Benzyl Ester (2c). i) *Dicyclohexylcarbodiimide–N-hydroxysuccinimide Method*: The procedure is similar to that described above for **1c**. Compound **5** (2.83 g, 6.0 mmol) was converted into its 1-succinimidyl ester with dicyclohexylcarbodiimide (1.24 g, 6.0 mmol) and *N*-hydroxysuccinimide (0.69 g, 6.0 mmol) in tetrahydrofuran (80 ml) and then treated with **2b** hydrochloride (2.06 g, 6.0 mmol) and triethylamine (0.85 ml, 6.0 mmol). The insoluble material

was collected by filtration, and dissolved in *N,N*-dimethylformamide. After filtration of insoluble triethylamine hydrochloride, the product was precipitated on addition of ether; yield, 3.43 g (75%). Recrystallization was effected from *N,N*-dimethylformamide–95% ethanol; mp 226.5—227.5 °C (decomp.); $[\alpha]_D^{25}$ +88.5 ° (*c* 2.1, *N,N*-dimethylformamide).

Found: C, 62.36; H, 6.39; N, 7.23%. Calcd for $C_{40}H_{48}O_{11}N_4 \cdot 1/2H_2O$: C, 62.40; H, 6.42; N, 7.28%.

ii) *Mixed Anhydride Method*: Compound **2a** (408 mg, 1.0 mmol) was dissolved in trifluoroacetic acid (2 ml). After standing at room temperature for 15 min, excess trifluoroacetic acid was removed *in vacuo*, and the remaining **2b** trifluoroacetate was dried over potassium hydroxide *in vacuo*. Ethyl chloroformate (0.10 ml, 1.0 mmol) and *N*-methylmorpholine (0.11 ml, 1.0 mmol) were added to a solution of **5** (472 mg, 1.0 mmol) in tetrahydrofuran (10 ml) at −19 °C. The mixture was stirred at this temperature for 15 min, then a cold solution of **2b** trifluoroacetate above obtained and *N*-methylmorpholine (0.11 ml, 1.0 mmol) in tetrahydrofuran (10 ml) was added. The mixture was stirred at room temperature for 22 hr. Then, water (100 ml) was added and the product was collected by filtration; yield, 600 mg (79%). It was reprecipitated from *N,N*-dimethylformamide–ether; mp 224—225 °C (decomp.); $[\alpha]_D^{15}$ + 83.4 ° (*c* 2.5, *N,N*-dimethylformamide). The IR spectrum of this compound was identical with that of the product in (i).

N-Acetylmuramyl-L-alanyl-D-isogultamine (2d). A solution of **2c** (1.52 g, 2.0 mmol) in acetic acid (50 ml) was hydrogenolyzed in the presence of palladium black at room temperature for 2 days. After removal of the catalyst by filtration, the filtrate was diluted with water (300 ml) and then evaporated *in vacuo* at 35 °C. After the residue was dissolved in methanol and the solvent was evaporated *in vacuo*, the final residue was dissolved in a small amount of absolute ethanol. Addition of absolute ether afforded colorless hygroscopic powder; yield, 918 mg (94%). This substance was further subjected to lyophilization. $[\alpha]_D^{15}$ +36.9° (after 3 min), +33.1° (after 25 hr) (*c* 0.51, H_2O).

Found: C, 45.73; H, 6.81; N, 11.36%. Calcd for $C_{19}H_{32}O_{11}N_4 \cdot 1/4H_2O$: C, 45.92; H, 6.59; N, 11.27%.

t-Butoxycarbonyl-L-alanyl-D-isoglutamine. This compound was prepared by hydrogenolysis from **2a** (7.34 g, 18.0 mmol) according to Bricas *et al.*[11]; yield, 6.87 g (94%); mp 99.5—101 °C (lit,[11] 94—98 °C); $[\alpha]_D^{28}$ −8.2° (*c* 1.0, methanol).

Found: C, 49.97; H, 7.70; N, 10.11%. Calcd for $C_{13}H_{23}O_6N_3 \cdot CH_3CO_2C_2H_5$: C, 50.36; H, 7.71; N, 10.37%.

Nα-(t-Butoxycarbonyl-L-alanyl-D-isoglutaminyl)-Nε-benzyloxycarbonyl-L-lysine Benzyl Ester (3a). Triethylamine (0.82 ml, 5.8 mmol) and ethyl chloroformate (0.56 ml, 5.8 mmol) were added to a solution of Boc-L-alanyl-D-isoglutamine (2.35 g, 5.8 mmol) in *N,N*-dimethylformamide (15 ml) at −23 °C. After the mixture was stirred at this temperature for 15 min, a cooled solution of benzyl *Nε*-Z-L-lysinate *p*-toluenesulfonate (3.15 g, 5.8 mmol) and triethylamine (0.82 ml, 5.8 mmol) in *N,N*-dimethylformamide (15 ml) was added and the mixture was stirred at room temperature for 15 hr. The precipitate of triethylamine hydrochloride was filtered off, the solvent was evaporated *in vacuo*. The residue was then dissolved in ethyl acetate and worked up as usual. The product was recrystallized from 99% ethanol–hexane; yield, 3.13 g (81%); mp 130—137 °C; $[\alpha]_D^{25}$ −13.8° (*c* 1.8, *N,N*-dimethylformamide).

Found: C, 60.53; H, 7.04; N, 10.06%. Calcd for $C_{34}H_{47}O_9N_5 \cdot 1/2C_2H_5OH$: C, 60.67; H, 7.27; N, 10.11%.

1-α-O-Benzyl-4,6-O-benzylidene-N-acetylmuramic Acid 1-Succinimidyl Ester. To an ice-cooled solution of **5** (4.72 g, 10 mmol) in tetrahydrofuran (60 ml) were added *N*-hydroxysuccinimide (1.38 g, 12 mmol) and dicyclohexylcarbodiimide (2.06 g, 10 mmol). After stirring in an ice bath for 3 hr, the mixture was worked up as usual and the product was recrystallized from ethyl acetate–hexane; yield, 4.52 g (79%); mp 178—179 °C.

Nα-(1-α-O-Benzyl-4,6-O-benzylidene-N-acetylmuramyl-L-alanyl-D-isoglutaminyl)-Nε-benzyloxycarbonyl-L-lysine Benzyl Ester (3c). Trifluoroacetic acid (4 ml) was added to **3a** (1.34 g, 2.0 mmol) and the mixture was stirred at room temperature. After 10 min, absolute ether was added to the resulting solution and the precipitate of free amino tripeptide derivative (**3b**) trifluoroacetate was collected by filtration (1.24 g). 1-Succinimidyl ester of **5** (1.14 g, 2.0 mmol) was added to an ice-cooled solution of **3b** trifluoroacetate thus obtained and triethylamine (0.28 ml, 2.0 mmol) in a mixture of tetrahydrofuran (20 ml) and *N,N*-dimethylformamide (20 ml). The mixture was stirred at room temperature for 15 hr. The gelatinous solid was collected by filtration, washed with ethyl acetate and dried (1.00 g). By addition of ether to the mother liquor followed by recrystallization from *N,N*-dimethylformamide–water, further amount of the product was recovered (0.46 g); total yield, 1.46 g (79%); 221—224 °C (decomp.); $[\alpha]_D^{25}$ +53.9 ° (*c* 1.9, *N,N*-dimethylformamide).

Found: C, 62.00; H, 6.51; N, 8.36%. Calcd for $C_{54}H_{66}O_{14}N_6 \cdot H_2O$: C, 62.29; H, 6.58; N, 8.07%.

N-Acetylmuramyl-L-alanyl-D-isogultaminyl-L-lysine (3d). A solution of **3c** (256 mg, 0.25 mmol) in acetic acid (15 ml) was hydrogenolyzed in the presence of 1 M hydrochloric acid (0.12 ml, 0.12 mmol) and palladium black. After the catalyst was removed, the mixture was diluted with water (100 ml) and evaporated *in vacuo* at 35 °C. After this procedure had been repeated, the aqueous solution was passed through a column of Amberlite IR-45 (OH^- form) to remove hydrogen chloride. The eluate was evaporated *in vacuo* and the residue was dissolved in absolute methanol. Colorless hygroscopic powder was obtained on addition of absolute ether; yield, 134 mg (86%). It was reprecipitated from absolute methanol–absolute ethanol and then lyophilized. $[\alpha]_D^{28}$ +18.3 ° (after 3 min), +14.7° (after 19 hr) (*c* 1.0, H_2O).

Found: C, 47.23; H, 7.12; N, 13.27%. Calcd for $C_{25}H_{44}O_{12}N_6 \cdot H_2O$: C, 47.01; H, 7.26; N, 13.16%.

Nα-t-Butoxycarbonyl-Nε-benzyloxycarbonyl-L-lysyl-D-alanine Benzyl Ester. To an ice-cooled solution of *Nα*-Boc-*Nε*-Z-L-lysine (2.89 g, 7.6 mmol) in tetrahydrofuran (10 ml), there were added dicyclohexylcarbodiimide (1.56 g, 7.6 mmol) and then a solution of triethylamine (1.07 ml, 7.6 mmol) and benzyl D-alaninate *p*-toluenesulfonate (2.66 g, 7.6 mmol) in tetrahydrofuran (10 ml). The mixture was allowed to stand at room temperature for 20 hr. The product was recrystallized from ethyl acetate–hexane; yield, 2.91 g (71%); mp 103.5—104.5 °C (lit,[11] 96—100 °C); $[\alpha]_D^{28}$ +6.4 ° (*c* 1.1, methanol).

Found: C, 64.33; H, 7.26; N, 7.68%. Calcd for $C_{29}H_{39}O_7N_3$: C, 64.30; H, 7.26; N, 7.76%.

Nε-Benzyloxycarbonyl-L-lysyl-D-alanine Benzyl Ester p-Toluenesulfonate. This compound was prepared from *Nα*-Boc-*Nε*-Z-L-lysyl-D-alanine benzyl ester according to Bricas[11]; yield, 13.0 g (98%); mp 122—123 °C (lit,[11] 122—124 °C).

Nα-(t-Butoxycarbonyl-L-alanyl-D-isoglutaminyl)-Nε-benzyloxycarbonyl-L-lysyl-D-alanine Benzyl Ester (4a). Ethyl chloroformate (0.77 ml, 8.0 mmol) and triethylamine (1.13 ml, 8.0 mmol) were added to a solution of Boc-L-alanyl-D-isoglutamine (3.24 g, 8.0 mmol) in *N,N*-dimethylformamide (20 ml) at −18 °C. After stirring at −18 °C for 15 min,

a cold solution of N^{ε}-Z-L-lysyl-D-alanine benzyl ester *p*-toluenesulfonate (4.91 g, 8.0 mmol) and triethylamine (1.13 ml, 8.0 mmol) in *N,N*-dimethylformamide (20 ml) was added and the mixture was stirred at room temperature for 15 hr. Triethylamine hydrochloride was filtered off and the solvent was evaporated *in vacuo*. The residue was dissolved in ethyl acetate saturated with water, worked up as usual, and the product was recrystallized from *N,N*-dimethylformamide–ether; yield, 4.65 g (78%), mp 191—194.5 °C (lit,[11] 196—198 °C); $[\alpha]_D^{26}$ −10.8° (*c* 2.2, acetic acid).

Found: C, 60.11; H, 7.11; N, 11.08%. Calcd for $C_{37}H_{52}O_{10}N_6$: C, 59.98; H, 7.08; N, 11.35%.

*N^{α}-(1-α-O-Benzyl-4,6-O-benzylidene-N-acetylmuramyl-L-alanyl-D-isogultaminyl)-N^{ε}-benzyloxycarbonyl-L-lysyl-D-alanine Benzyl Ester (**4c**).* This compound was prepared in a similar way to that described for **3c**. Trifluoroacetic acid salt of **4b**, obtained from **4a** (1.41 g, 1.9 mmol), was neutralized with triethylamine (0.26 ml, 1.9 mmol) and treated with 1-succinimidyl ester of **5** (1.02 g, 1.8 mmol) in a mixture of tetrahydrofuran (40 ml) and *N,N*-dimethylformamide (20 ml). The product was recrystallized from *N,N*-dimethylformamide–water, then from *N,N*-dimethylformamide–ether; yield, 1.24 g (63%); mp 221 °C (decomp.); $[\alpha]_D^{25}$ +50.4° (*c* 2.1, *N,N*-dimethylformamide).

Found: C, 61.64; H, 6.56; N, 8.74%. Calcd for $C_{57}H_{71}O_{15}N_7 \cdot H_2O$: C, 61.55; H, 6.62; N, 8.82%.

*N-Acetylmuramyl-L-alanyl-D-isoglutaminyl-L-lysyl-D-alanine (**4d**).* This compound was prepared from **4c** (547 mg, 0.50 mmol) by the same procedure described for **3d**. The final product was precipitated from absolute methanol–absolute ether; yield, 295 mg (85%). A sample after lyophilization showed the following data: $[\alpha]_D^{15}$ +14.9° (after 3 min), +15.4° (after 25 hr) (*c* 0.51, H_2O).

Found: C, 47.42; H, 7.13; N, 13.75%. Calcd for $C_{28}H_{49}O_{13}N_7 \cdot H_2O$: C, 47.38; H, 7.24; N, 13.82%.

*t-Butoxycarbonyl-L-alanyl-L-isoglutamine Benzyl Ester (**8a**) and the Analogous Protected Dipeptides (**9a—14a**).* These compounds as shown in Table 1 were all prepared in similar manners to that described for **2a**. The yields and physical constants are summarized in Table 2.

*Protected N-Acetylmuramyl Amino Acids (**6c** and **7c**) and N-Acetylmuramyl Dipeptides (**8c—14c**).* These compounds were prepared by coupling of **5** with the corresponding amino acid benzyl esters (**6b** or **7b**) or dipeptides having free amino groups (**8b—14b**) using either dicyclohexylcarbodiimide—*N*-hydroxysuccinimide or ethyl chloroformate as described for **2c**. While **8b** hydrochloride was prepared from **8a**[15] just as described for **2b**, compounds **9b—14b** were obtained as their trifluoroacetic acid salt by treating **9a—14a** with trifluoroacetic acid at room temperature. The yields and the physical constants of the products (**6c—14c**) are summarized in Table 3.

*N-Acetylmuramyl Amino Acids (**6d** and **7d**) and N-Acetylmuramyl Dipeptides (**8d—14d**).* Compounds **6c—14c** were hydrogenolyzed in acetic acid in the presence of palladium black at room temperature. The product was isolated as described for **2d** and lyophilized. The yields, $[\alpha]_D$ and the results of elemental analyses are summarized in Table 4.

*L-Alanyl-D-isoglutamine (**2e**).* Boc-L-alanyl-D-isoglutamine (300 mg, 0.74 mmol) was dissolved in trifluoroacetic acid (1.5 ml), and the solution was set aside at room temperature for 30 min. On addition of absolute ether to the solution, trifluoroacetate of **2e** precipitated as hygroscopic powder. Removal of trifluoroacetic acid with a column of Amberlite IR-45 (OH^- form) followed by lyophilization afforded hygroscopic solid; yield, 132 mg (81%).

Found: C, 43.40; H, 7.01; N, 19.14%. Calcd for $C_8H_{15}O_4N_3 \cdot 1/4H_2O$: C, 43.33; H, 7.05; N, 18.95%. It was recrystallized from water–ethanol; mp 83 °C (decomp); $[\alpha]_D^{28}$ +14.4° (*c* 0.96, H_2O).

*L-Alanyl-D-isoglutaminyl-L-lysine (**3e**).* i) *Dihydrochloride*: Compound **3a** (0.50 g, 0.75 mmol) was dissolved in ethanol (50 ml) and hydrogenolyzed in the presence of palladium black. After removal of the solvent *in vacuo*, the residue was dissolved in methanol. Addition of ether afforded Boc-L-alanyl-D-isoglutaminyl-L-lysine (0.33 g, 99%). To a solution of this compound (190 mg) in acetic acid (6 ml) was added acetic acid (10 ml) previously saturated with dry hydrogen chloride. After standing at room temperature for 15 min, absolute ether was added to the mixture and the precipitate was collected and dried over phosphorus pentaoxide and potassium hydroxide *in vacuo*. Reprecipitation from absolute methanol–absolute ether afforded very hygroscopic powder; yield, 136 mg (76% from **3a**). This was further purified by treatment with charcoal and lyophilized for elemental analysis. $[\alpha]_D^{28}$ +2.06° (*c* 4.5, H_2O).

Found: C, 39.90; H, 7.08; N, 16.34; Cl, 16.95%. Calcd for $C_{14}H_{29}O_5N_5Cl_2$: C, 40.19; H, 6.99; N, 16.74; Cl, 16.95%.

ii) *Bistrifluoroacetate*: Compound **3a** (67 mg, 0.1 mmol) was hydrogenolyzed in acetic acid (5 ml) in the presence of palladium black. After evaporation of the solvent *in vacuo*, the residue was treated with trifluoroacetic acid (2 ml) at room temperature for 60 min. Addition of absolute ether to the mixture afforded hygroscopic powder, yield, 45 mg (76%). This compound showed a single ninhydrin-positive spot identical with the product obtained in (i) on tlc (1-butanol–acetic acid–water, 4 : 1 : 2) and PEP.

*L-Alanyl-D-isoglutaminyl-L-lysyl-D-alanine (**4e**) Bistrifluoroacetate.* This compound was prepared from **4a** (185 mg, 0.25 mmol) according to Bricas *et al.*[11] The procedure is similar to that described for **3e** (ii). Yield, 155 mg (96%); $[\alpha]_D^{19}$ +2.24° (*c* 0.45, H_2O) (lit,[11] $[\alpha]_D^{25}$ +1.6±0.5° (*c* 0.45, H_2O).

Found: C, 39.35; H, 5.60; N, 12.85%. Calcd for $C_{21}H_{34}O_{10}N_6F_6$: C, 39.13; H, 5.32; N, 13.04%.

The authors wish to express their sincere thanks to Professor Shozo Kotani and his collaborators of Osaka University Dental School for their cooperations and invaluable discussions.

References

1) This work including the biological tests was partly presented at the International Workshop on the Immunological and Biological Properties of the Peptidoglycan and Related Bacterial Cell Wall Polymers, München, July 1974. The synthetic study in this work was also reported at the 12th Symposium on Peptide Chemistry, Kyoto, Japan, November, 1974.

2) J. Freund, *Adv. Tuberc. Res.*, **7**, 130 (1956).

3) A. Adam, R. Ciorbaru, J. F. Petit, and E. Lederer, *Proc. Nat. Acad. Sci. U.S.A.*, **69**, 851 (1972).

4) J. -M. Ghuysen, *Bacteriol. Rev.*, **32**, 425 (1968).

5) S. Kotani, Y. Watanabe, T. Shimono, F. Kinoshita, T. Narita, K. Kato, D. E. S. Stewart-Tull, I. Morisaki, K. Yokogawa, and S. Kawata, *Biken J.*, **18**, 93 (1975).

6) A. Adam, R. Ciorbaru, F. Ellouz, J. F. Petit, and E. Lederer, *Biochem. Biophys. Res. Commun.*, **56**, 561 (1974).

7) G. Nauciel, J. Fleck, M. Mock, and J. P. Martin, *C. R. Acad. Sci. Paris*, **277 D**, 2841 (1974).

8) Quite independently to our work, Lederer *et al.* also reached to the same conclusion by their synthetic study. F. Ellouz, A. Adam, R. Ciorbaru, and E. Lederer, *Biochem. Biophys. Res. Commun.*, **59**, 1317 (1974).

9) S. Kotani, Y. Watanabe, F. Kinoshita, T. Shimono, I. Morisaki, T. Shiba, S. Kusumoto, Y. Tarumi, and K. Ikenaka, *Biken J.*, **18**, 105 (1975).

10) H. M. Flowers and R. W. Jeanloz, *J. Org. Chem.*, **28**, 2983 (1963).

11) P. Lefrancier and E. Bricas, *Bull. Soc. Chim. Biol.*, **49**, 1257 (1967).

12) A. E. Lanzilotti, E. Benz, and L. Goldman, *J. Amer. Chem. Soc.*, **86**, 1880 (1964).

13) N. C. Chaturvedi, M. C. Kohsla, and N. Anand, *J. Med. Chem.*, **9**, 971 (1966).

14) After we presented our preliminary communication,[1] Arendt *et al.* also reported the synthesis of **1c** by coupling of **5** with benzyl L-alaninate using *N*-ethoxycarbonyl-2-ethoxy-1,2-dihydroquinoline (EEDQ); A. Arendt, A. Kolodziejczyk, and T. Sokolowska, *Roczniki Chem.*, **48**, 1707 (1974). They removed the benzyl ester group in **1c** by alkaline hydrolysis with the intention of use of the resultant 1-*O*-benzyl-4,6-*O*-benzylidene-*N*-acetylmuramyl-L-alanine for their further synthetic program of more complex mucopeptides. Indeed, they reported more recently the synthesis of *N*-acetylmuramyl pentapeptide containing diaminopimelic acid; *ibid.*, **48**, 1921 (1974). On the contrary, our approach differs from theirs in the strategy that the peptide chains were stepwise elongated from *C*-terminal except at γ-glutamyl linkage, thus minimizing the possibility of racemization of each amino acid residue in the molecule.

15) **8b** hydrochloride: yield, 87% from **8a**; mp 112.5—114 °C; $[\alpha]_D^{20}+7.30$ (*c* 2.0, ethanol). Found: C, 52.85; H, 6.74; N, 11.76; Cl, 9.99%. Calcd for $C_{15}H_{22}O_4N_3Cl \cdot 1/2\text{-}C_2H_5OH$: C, 52.38; H, 6.87; N, 11.46; Cl, 9.66%.

Nucleophilic Ion Pairs. I. Enhanced Esterolytic Reactivity of Hydrophobic Ion Pairs in Micellar Systems*

Toyoki KUNITAKE, Seiji SHINKAI, and Yoshio OKAHATA

Department of Organic Synthesis, Faculty of Engineering, Kyushu University, Fukuoka 812

(Received September 22, 1975)

The reaction of the dodecyl(2-hydroxyimidophenethyl)dimethylammonium bromide(DHDB) and *N*-methylmyristohydroxamate (MMHA) anion with *p*-nitrophenyl acetate was studied mostly in the presence of aqueous nonionic micelles. Addition of a hydrophobic ammonium ion, TMAC, considerably enhanced the reactivity of MMHA but not that of DHDB (a zwitterion). The rate enhancement for MMHA-TMAC and DHDB in nonionic micelles were almost comparable to those in cationic(CTAB) micelles. It was proposed that the large enhancement observed for some anionic nucleophiles in cationic micelles is to a great extent caused by the formation of hydrophobic, desolvated ion pairs.

The importance of micellar catalyses which influence rates and equilibria of organic reactions and yield data pertinent to enzyme-catalyzed reactions has been reported.[1,2] Anionic nucleophiles such as alkoxide,[3,4] oximate,[5,6] hydroxamate,[7-10] thiolate[11,12] and imidazole anions[13,14] are considerably activated in the presence of cationic micelles and cationic polysoaps. The reactions studied involve nucleophilic attack toward phenyl esters,[1-8, 10, 11, 13, 14] nucleophilic substitution of 2,4-dinitrofluorobenzene[12] and hydrogen abstraction from carbon acids.[9] The nucleophilicity of some hydroxamate anions toward *p*-nitrophenyl acetate(PNPA) is enhanced by two or three orders of magnitude as compared with those predicted from the Brönsted relationship, the reaction rate exceeding even that of α-chymotrypsin and PNPA.[7,8] In contrast, the activation does not occur in anionic micelles,[15] and neutral nucleophiles such as amines and imidazoles are not subjected to activation by cationic micelles.[16]

In an attempt to elucidate the mechanism of these micellar effects, we investigated the reaction of *N*-methylmyristohydroxamic acid(MMHA) and dodecyl-(2-hydroxyimidophenethyl)dimethylammonium bromide (DHDB) with PNPA in nonionic micelles. The latter nucleophile was specially designed to allow ready formation of the intramolecular ion pair between the oximate anion and the ammonium moiety on the basis of the CPK model building. The use of nonionic micelles as the reaction environment can avoid complicating influences of the high charge density at the surface of cationic micelles.

MMHA: $CH_3(CH_2)_{12}CONOH$
$\quad\quad\quad

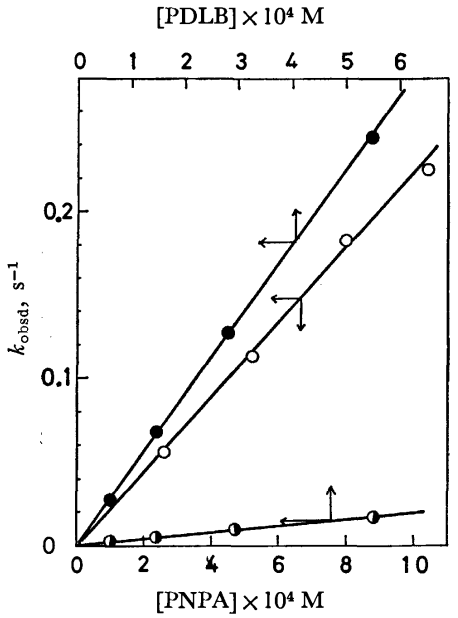

Fig. 1. Reaction of MMHA+TMAC and DHDB with PNPA in the presence of a nonionic micelle (POOA). 30 °C, μ=0.01 with KCl, 3 v/v% ethanol, [POOA]=1.0×10⁻³ M.
○; [MMHA]=1.0×10⁻⁵ M, [TMAC]=1.02×10⁻⁴ M, pH=8.56±0.05 with 0.01 M borate. ●; [PNPA]=2.13×10⁻⁵ M, pH=9.10±0.04 with 0.01 M borate ◑; POOA was not added. [PNPA]=2.13×10⁻⁵ M, pH=9.10±0.04 with 0.01 M borate.

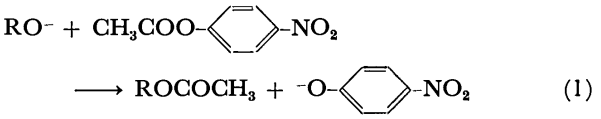

(1)

Reaction of MMHA with PNPA. The reaction of MMHA and PNPA was first carried out in the presence of nonionic micelles (Tween 80, Triton X-100, POOA**, Brij-35) above their cmc.[1] The influence of addition of quaternary ammnoium salts was also evaluated. If the $k_{a,obsd}$ value of MMHA in the absence of a nonionic micelle is approximated by that of aqueous *N*-methylisobutyrohydroxamic acid,[18] the presence of nonionic micelles results in a 2—9 time increase of $k_{a,obsd}$ (Table 1). The rate enhancement is much greater in cetyltrimethylammonium bromide(CTAB) micelle (more than 200 fold)[7]. In contrast, anionic sodium dodecyl sulfate(SDS) suppressed the reactivity of MMHA. The reactivity of MMHA can be further enhanced in nonionic micelles by addition of trioctylmethylammonium chloride(TMAC) (Fig. 2). The reaction rates increased almost linearly with increasing TMAC and then gradually levelled off. Maximal augmentation of 18-fold was brought about by addition of TMAC. Addition of $Et_4N^+Br^-$ and $Bu_4N^+Br^-$ caused no effect. TMAC, typical phase transfer catalyst, is much more hydrophobic than the latter two, but cannot form a micelle by itself. In fact, it exists as an oily suspension in as aqueous medium without nonionic micelles. Thus, TMAC should be trapped in and/or on the nonionic micelles. The micelle consisting of a nonionic surfactant plus TMAC can be envisioned as an analogue of cationic micelles which possesses a much lower positive-charge density. On the contrary, addition of an inorganic salt inhibited the reaction (*vide post*). It is noteworthy that a minute amount of TMAC caused the rate enhancement of more than one-order of magnitude and that only the hydrophobic ammonium salt was effective.

The $k_{a,obsd}$ values at a constant surfactant concentration are recorded for comparison in Table 1. The reactivity of MMHA in the presence of nonionic micelles which contain TMAC is enhanced up to

** Polyoxyethylene(n=10) oleyl alcohol.

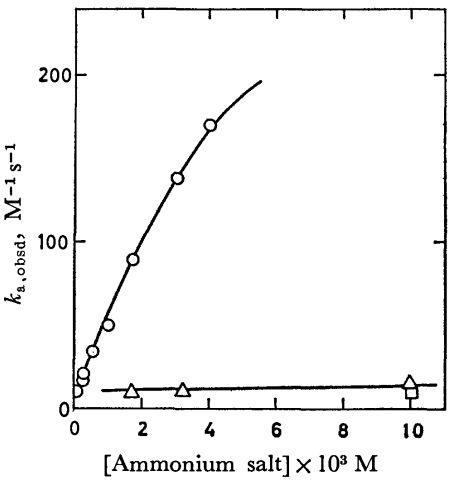

Fig. 2. Infiuence of quaternary ammonium salts on the reaction of MMHA and PNPA in the presence of a nonionic micelle (POOA).
30 °C, μ=0.01 with KCl, 3 v/v% ethanol, pH=8.35±0.04 with 0.01 M borate, [POOA]=0.01 M, [MMHA]=4.39×10⁻⁵ M, [PNPA]=1.17×10⁻³ M.
○; TMAC, □; $Et_4N^+Br^-$, △; $Bu_4N^+Br^-$.

Table 1. Apparent second-order rate constants for the reaction of MMHA and DHDB with PNPA[a]

Additives	$k_{a,obsd}$ ($M^{-1}s^{-1}$)		
	MMHA	MMHA +TMAC	DHDB
None	*ca.* 4[b]		5.3
SDS	1.38		0.7
CTAB	821		1030
Tween 80	19.0	83.6	71.6
Triton X-100	34.2	280	55.6
POOA	36.8	210	306(311)[d]
POOA[c]	9.82		
Brij-35	19.1	117	92.3
Poly(*N*-vinylpyrrolidone)			6.39
β-cyclodextrin			2.63
Poly(ethyleneimine)			5.53

a) 30°C, μ=0.01 with KCl, pH=8.5±0.1 for MMHA and 8.1±0.1 for DHDB with 0.01 M borate. [MMHA]=1.0×10⁻⁵ M, [DHDB]=1.4×10⁻⁴ M, [TMAC]=1.0×10⁻⁴ M, [additives]=1.02×10⁻³ M. b) Estimated with *N*-methylisobutyrohydroxamic acid.[18] c) [POOA]=0.01 M. d) DHDB+TMAC (1.0×10⁻⁴ M).

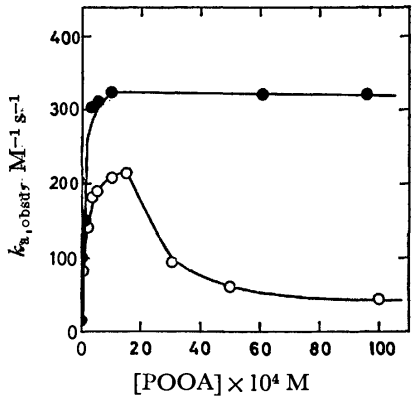

Fig. 3. Apparent second-order rate constants for the reactions of MMHA+TMAC and DHDB with PNPA as a function of the concentration of a nonionic surfactant (POOA).
30 °C, μ=0.01 with KCl, 3 v/v% ethanol.
○; [MMHA]=1.0×10^{-5} M, [PNPA]=2.62×10^{-4} M, [TMAC]=1.02×10^{-4} M, pH=8.60±0.04 with 0.01 M borate. ●; [DHDB]=1.40×10^{-4} M, [PNPA]=2.13×10^{-5} M, pH=8.87±0.04 with 0.01 M borate.

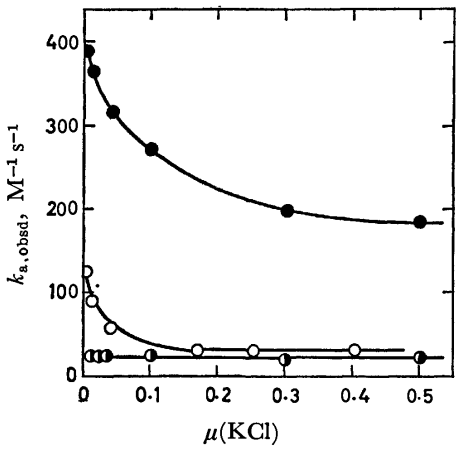

Fig. 4. Apparent second-order rate constants for the reactions of the MMHA+TMAC and DHDB with PNPA as a function of ionic strength.
30 °C, 3 v/v% ethanol.
○; [MMHA]=4.39×10^{-5} M, [PNPA]=1.17×10^{-3} M, [TMAC]=1.67×10^{-3} M, [POOA]=0.01 M, pH=8.35±0.04 with 0.01 M borate. ●; [DHDB]=1.40×10^{-4} M, [PNPA]=2.19×10^{-5} M, [POOA]=1.0×10^{-3} M, pH=8.90±0.02 with 0.02 with 0.01 M borate. ◑; [DHDB]=1.40×10^{-4} M, [PNPA]=2.19×10^{-5} M, pH=8.8±0.1 with 0.01 M borate. POOA was not added.

20—70 times as compared with that for the nonmicellar system, the maximum value (280 M^{-1} s^{-1} in Triton X-100) amounting to one-third of that in CTAB.

Reaction of DHDB with PNPA. Similar experiments were carried out for a zwitterionic nucleophile. The reaction was quenched by SDS micelle and enhanced in the presence of CTAB micelle(*ca.* 200 times), as is the case for the reaction of MMHA and PNPA. On the other hand, considerable rate enhancements (10—60 times) were readily achieved

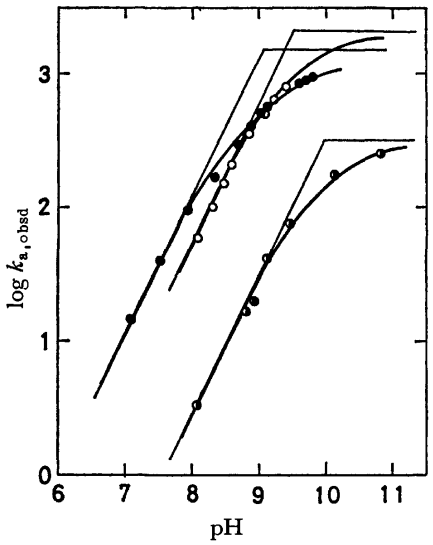

Fig. 5. pH Dependence.
30 °C, μ=0.01 with KCl, 3 v/v% ethanol, [POOA]=1.0×10^{-3} M.
○; [MMHA]=1.0×10^{-5} M, [PNPA]=2.62×10^{-4} M, [TMAC]=1.0×10^{-4} M. ●; [DHDB]=(0.8—5.6)$\times10^{-4}$ M, [PNPA]=(1.7—8.5)$\times10^{-5}$ M. ◑; POOA was not added. [DHDB]=(2.8—5.6)$\times10^{-4}$ M, [PNPA]=(4.3—8.5)$\times10^{-5}$ M.

in the presence of nonionic micelles alone. Addition of TMAC caused no increase in the reaction rate. The maximum rate constant observed for DHDB (306 M^{-1} s^{-1} in POOA) is about one-third of the value in the CTAB micelle. Other additives such as poly(ethyleneimine), β-cyclodextrin and poly(*N*-vinylpyrrolidone) were found to be ineffective.

Influence of Surfactant Concentration and Ionic Strength. The dependence of the reactivities of MMHA-TMAC and DHDB on the concentration of POOA is given in Fig. 3. The cmc of POOA is estimated to be 10^{-6} M.[1] The $k_{a,obsd}$ value for the MMHA-TMAC system first increased and then decreased gradually with increasing POOA concentrations, the maximum $k_{a,obsd}$ value being observed at [POOA]=1.5×10^{-3} M. On the other hand, the reactivity of zwitterionic nucleophile rapidly increased and reached a constant value. The difference reflects the intermolecular *vs.* intramolecular nature of these ion pairs.

The reactivities of MMHA-TMAC and DHDB toward PNPA were also examined at different ionic strength (Fig. 4). The $k_{a,obsd}$ value for DHDB in the nonmicellar system was hardly affected by the salt(KCl) concentration. On the other hand, the enhanced reactivities of these catalytic systems attained in the presence of nonionic micelles were gradually lost with increasing salt concentrations. The largest rate decrease was about 4-fold. Similar results are frequently obtained in micellar catalysis.[1]

pH Dependence. The micellar reaction of MMHA-TMAC and DHDB with PNPA was carried out in the pH range 7—10. The log $k_{a,obsd}$ values are plotted against pH, which show linear increase with slope 1.0 followed by gradual saturation in the high pH region (Fig. 5). The reaction rates were found to

be too great to be measured in the pH region higher than that in Fig. 5. The acid dissociation constants (K_a) and the true second-order rate constants (k_a) were determined by two methods: (a) fitting of the theoretical curves (Eq. (2)) to the experimental plots, and (b) finding pK_a values which give straight lines for α(degree of dissociation$=K_a/(K_a+a_H)$) *vs.* $k_{a,obsd}$ plots by trial-and-error computation. The values of K_a and k_a calculated by both methods were found to be agree within 5%.

$$k_{a,obsd} = k_a \frac{K_a}{K_a + a_H} \quad (2)$$

The results are given in Table 2, together with data we obtained recently.

Table 2. Second-order rate constants for the reactions of hydroxamates and oximates with PNPA at 30 °C

Catalyst		pK_a	k_a $M^{-1}s^{-1}$
1.	MMHA+POOA	9.5	2310
1.′	MMHA+POOA+TMAC	9.5	4900[a]
2.	DHDB+POOA	9.1	1150
3.	MMHA+CTAB	*ca.* 10.3	26800
4.[b]	DBHA+CTAB	9.72	6000
5.	DHDB	10.0	300
6.[c]	*N*-methylisobutyrohydroxamic acid	9.05	32.6
7.[c]	*N*-phenylisobutyrohydroxamic acid	8.81	25.1
8.[c]	*N*-methylnaphthohydroxamic acid	8.23	10.5

a) k''_a (the true second-order rate constant for MMHA paired with TMAC). b) DBHA (N-dodecylbenzohydroxamic acid)[10]; 3 v/v% ethanol, μ=0.5 (KCl). c) 1.4 v/v% CH_3CN, μ=0.1 (KCl).[18]

Discussion

Reactions performed in the presence of ionic micelles are influenced by various micellar effects.[1,2] Straightforward kinetic analysis is often difficult because of complications characteristic of ionic micelles. One may simplify this situation by appropriate use of nonionic micelles, as independently shown by Brown *et al.* for a general-base catalyzed reaction toward phenyl phosphate.[19] The nucleophilicity of some anions such as hydroxamates and oximates is highly enhanced in cationic micelles. We have attempted to elucidate the mechanism of these rate enhancement. We assumed that the rate enhancement of anionic nucleophiles in cationic micelles could be reduced to the problem of nucleophilic ion pairs. An anionic nucleophile forms an ion pair with a cationic surfactant molecule in a highly hydrophobic environment of micelles, the high charge density at the surface of cationic micelles playing only a secondary role. Nonionic micelles are convenient systems for testing the hypothesis, since nucleophilic ion pairs can be studied as species isolated from other charged species.

The nucleophilicity of MMHA anion as expressed by the $k_{a,obsd}$ value (Table 1) is enhanced in cationic and nonionic micelles relative to the nonmicellar system. Although the observed rate enhancement is much greater in the cationic(CTAB) micelle than in nonionic micelles, the difference can be made smaller by adding 1.0×10^{-4} M of TMAC, which is highly hydrophobic and not much soluble in water. Thus, the highly increased nucleophilicity of MMHA can be related to the formation of hydrophobic ion pairs solubilized in nonionic micelles. The absence of rate increase upon addition of less hydrophobic $Et_4N^+Br^-$ and $Bu_4N^+Br^-$ supports this view.

The apparent rate constant showed a maximum when the POOA concentration was varied. Supposedly, the hydrophobicity of POOA micelles increases with increasing POOA concentrations, and the formation of hydrophobic ion pairs becomes increasingly favorable. Further increase in the POOA concentration causes dissociation of MMHA-TMAC, resulting in rate decrease. This is consistent with the fact that no rate decrease was observed with increasing POOA concentrations in the case of intramolecular ion pair DHDB.

$k_{a,obsd}$ in the POOA micelle simply increased with increasing TMAC concentration (Fig. 2). This kinetic situation can be quantitatively treated by the following equation, provided that MMHA anion and TMAC cation form a 1 : 1 ion pair only, and that addition of TMAC does not change the micellar structure such as to affect the reaction rate.

$$\text{MMHA} + \text{TMAC} \overset{K}{\rightleftharpoons} \text{MMHA-TMAC} \quad (3)$$

$$\text{MMHA} \xrightarrow{k'_{a,obsd}\cdot[\text{PNPA}]} \text{products} \quad (4)$$

$$\text{MMHA-TMAC} \xrightarrow{k''_{a,obsd}\cdot[\text{PNPA}]} \text{products} \quad (5)$$

where K is the association constant for MMHA–TMAC, $k'_{a,obs}$ is the apparent second-order rate constant for MMHA which is not paired with TMAC and $k''_{a,obs}$ is that for MMHA paired with TMAC.

According to Mollica and Connors,[20] the following equation is derived for [MMHA]$\ll$[TMAC].

$$\frac{k'_{a,obsd}}{k_{a,obsd}-k'_{a,obsd}} = \frac{1}{q\cdot K[\text{TMAC}]} + \frac{1}{q} \quad (6)$$

where $k_{a,obsd}$ is the rate constant obtained at a given TMAC concentration and $q=(k''_{a,obsd}/k_{a,obsd})-1$.

K and q were determined by plotting $k'_{a,obsd}/(k_{a,obsd}-k'_{a,obsd})$ against 1/[TMAC], which gives a straight line (r=0.99) for [TMAC]$>1.0\times10^{-3}$ M: K=104 M^{-1} and q=0.0225. The $k''_{a,obsd}$ value thus determined (447 $M^{-1}s^{-1}$) is more than 50% of the corresponding value in the CTAB micelle (821 $M^{-1}s^{-1}$, Table 1). The reactivity of MMHA increased from 36.8 to 447 $M^{-1}s^{-1}$ upon pairing with TMAC, if the other changes which may be caused by the addition of TMAC (*e.g.* micellar structure) are negligible.

The rate-enhancing effect of a countercation trapped in the hydrophobic environment is more clearly shown by using a zwitterionic nucleophile with a long alkyl group, DHDB. The $k_{a,obsd}$ value of DHDB in a nonmicellar system does not differ much from that expected from Brönsted relationship (see below), but it is enhanced in nonionic micelles (Table 1 and Fig. 3) more effectively than that of MMHA. This means that the presence of an intramolecular countercation

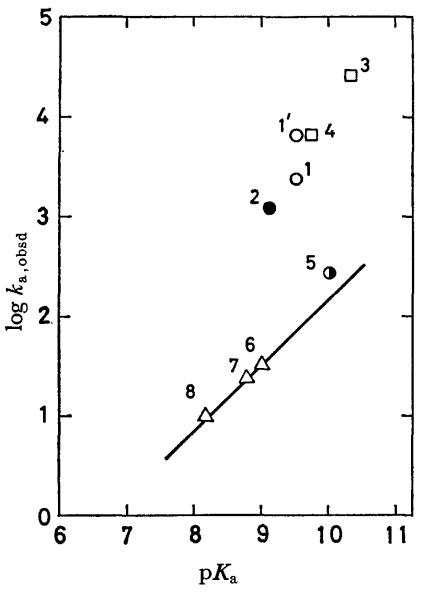

Fig. 6. Brönsted plots.
Numbers indicate those recorded in Table 2.

does not result in the increased reactivity of anionic nucleophiles unless they are placed in a hydrophobic environment. The addition of TMAC did not affect the reactivity of DHDB, reflecting the fact that DHDB forms a stable intramolecular ion pairs, as also inferred from the CPK model building.

It is thus concluded that the reactivity of an anionic nucleophile (hydroxamate and oximate) undergoes considerable augmentation in the presence of a hydrophobic countercation in a hydrophobic environment.

Figure 6 shows the Brönsted relationship for the data of Table 2. The plot for nonmicellar DHDB is located fairly close to the relationship obtained for simple hydroxamic acids. The data obtained in the CTAB micelle are placed above the Brönsted line by two orders of magnitude, though they are scattered due to varying reaction conditions. The polts for MMHA and DHDB in the nonionic micellar system are placed not far below those in the CTAB micelle.

The data (Tables 1 and 2) clearly indicate that the reactivity enhancement for intermolecular(MMHA–TMAC) and intramolecular(DHDB) ion pairs in nonionic micelles is almost comparable to those in cationic micelles. The remarkable rate enhancement in the cationic micelles has been attributed to concentration effect, proximity effect, peculiar environments of the micellar surface, desolvation of nucleophiles and to other factors, in the absence of definitive experimental evidence.

The entropic factors such as concentration effect and proximity effect cannot contribute to the large enhancement, since this has been observed not only in cationic micelles but also in anionic and conventional noninoic micelles. Characteristics peculiar to cationic micelles such as high charge density at the micellar surface do not appear to be a prerequisite for the rate enhancement, since the present investigation showed that the presence of a single countercation causes a sufficiently large enhancement. Thus, it is proposed that the rate acceleration observed for anionic nucleophiles in cationic micelles is largely derived from the formation of hydrophobic ion pairs between anionic nucleophile and cationic surfactant in a highly hydrophobic environment. The anion included in a hydrophobic ion pair will attain its high reactivity from desolvation, as already known for other nucleophilic reactions.[9,12]

The importance of hydrophobic (dehydrated) ion pairs in the nucleophilic attack is also suggested by other data obtained recently. The reaction rate of the MMHA anion and PNPA in an aqueous system increased by 100-fold in the presence of partially benzylated poly(4-vinylpyridine).[21] The polymer can provide a hydrophobic environment but cannot form a micellar structure. Kirsh *et al.*[22] reported that the reactivity of the *N*-(2-hydroxyimidophenethyl)-pyridinium unit anchored to poly(4-vinylpyridine) is higher by a factor of 100 than for the monomeric analog. The micellar structure is not required for the activation of anionic nucleophiles in these cases.

We have found that tetraethylammonium *N*-methylmyristohydroxamate(MMHA–NEt_4) shows very large reactivities toward PNPA in dry, aprotic solvents, the reaction being efficiently suppressed (*ca.* 100 times rate decrease) by the addition of 10^{-3}—10^{-4} M of H_2O.[23] The result shows the importance of the hydration term in considering the nucleophilic reactivity of some anions.

In conclusion, a remarkable rate enhancement of some anionic nucleophiles observed in cationic micelles arises from the formation of hydrophobic ion pairs (both intermolecular and intramolecular) in highly hydrophobic environments. The reactivity of these ion pairs is enhanced probably by desolvation of the anion. The micellar effect would constitute a part of a more general microenvironment effect, which is conceivably a major source of enzymatic efficiency.

We wish to express our appreciation to Miss R. Ando for her technical assistance. The present research was financially supported by the Ministry of Education.

References

1) E. J. Fendler and J. H. Fendler, *Advan. Phys. Org. Chem.*, **8**, 271 (1970).
2) E. H. Cordes and C. Gitler, *Prog. Bioorg. Chem.*, **2**, 1 (1973).
3) C. A. Bunton and L. G. Ionescu, *J. Amer. Chem. Soc.*, **95**, 2912 (1973).
4) K. Martinek, A. V. Levashov, and I. V. Berezin, *Tetrahedron Lett.*, **1975**, 1275.
5) A. K. Yatsimirski, K. Martinek, and I. V. Berezin, *Tetrahedron*, **27**, 2855 (1971).
6) W. Tagaki, I. Takahara, and D. Fukushima, paper presented at the 32nd annual meeting of the Chemical Society of Japan, III, p. 1308, Tokyo, April, 1975.
7) I. Tabushi, Y. Kuroda, and S. Kita, *Tetrahedron Lett.*, **1974**, 643; I. Tabushi and Y. Kuroda, *ibid.*, **1974**, 3613.
8) T. Kunitake, S. Shinkai, and S. Hirotsu, *J. Polymer Sci., Polymer Lett. Ed.*, **13**, 377 (1975).
9) S. Shinkai and T. Kunitake, *J. Chem. Soc., Perkin Trans. II*, in press.

10) T. Kunitake, Y. Okahata, and T. Sakamoto, *Chem. Lett.*, **1975**, 459.
11) W. Tagaki, T. Amada, Y. Yamashita, and Y. Yano, *Chem. Commun.*, **1972**, 1131.
12) H. Chaimovich, A. Blanco, L. Chayet, L. M. Costa, P. M. Monteiro, C. A. Bunton, and C. Paik, *Tetrahedron*, **31**, 1139 (1975).
13) K. Martinek, A. P. Osipov, A. K. Yatsimirski, V. A. Dadolt, and I. V. Berezin, *Tetrahedron Lett.*, **1975**, 1279.
14) *N*-Dodecylimidazole-4-carboxamide in CTAB is *ca.* 100 times more reactive than *N,N*-dimethylimidazole-4-carboxamide in an aqueous system(pH 10) toward PNPA; T. Kunitake and Y. Okahata, unpublished result.
15) T. Kunitake, S. Shinkai, and S. Hirotsu, unpublished result.
16) M. T. A. Behme and E. H. Cordes, *J. Amer. Chem. Soc.*, **87**, 260 (1965).
17) I. Heilbron and H. M. Bunbury, "Dictionary of Organic Compounds," Oxford Univ. Press, New York, N.Y. (1953).
18) T. Kunitake, Y. Okahata, and R. Ando, This Bulletin, **47**, 1509 (1974).
19) J. M. Brown, C. A. Bunton, and S. Diaz, *J. Chem. Soc., Chem. Commun.*, **1974**, 971.
20) J. A. Mollica, Jr. and K. A. Connors, *J. Amer. Chem. Soc.*, **89**, 308 (1967).
21) T. Kunitake, S. Shinkai, and S. Hirotsu, paper presented at the 24th annual meeting of the Society of Polymer Science, I, p. 46, Tokyo, May, 1975.
22) Yu. E. Kirsh, A. A. Rahnanskaya, G. M. Lukovkin, and V. A. Kabanov, *Eur. Polymer J.*, **10**, 393 (1974).
23) S. Shinkai and T. Kunitake, *Chem. Lett.*, **1976**, 109.

Reversible CO Insertion into an Ni-C Bond of Alkyl(acetylacetonato)-(triphenylphosphine)nickel(II)

Toshio SARUYAMA, Takakazu YAMAMOTO, and Akio YAMAMOTO*

Research Laboratory of Resources Utilization, Tokyo Institute of Technology, O-okayama, Tokyo 152

(Received October 23, 1975)

Reaction of alkyl(acetylacetonato)(triphenylphosphine)nickel(II), RNi(acac)(PPh_3)n (R=C_2H_5, n=1 (**1a**); R=CH_3, n=2 (**1b**)) with carbon monoxide gives acyl(acetylacetonato)(triphenylphosphine)nickel(II) RCONi(acac)(PPh_3) (R=C_2H_5 (**2a**); R=CH_3 (**2b**)). Elemental analysis, IR and NMR spectra, and chemical properties of the acylnickel complexes support the structure. A variable temperature NMR spectroscopic study has revealed that the acac ligand in the acyl complexes exchanges rapidly in solution on NMR time scale. The acylnickel complexes **2a** and **2b** tend to decarbonylate at room temperature, the decarbonylation tendency of **2b** being greater than **2a**. They undergo further disproportionation according to the stoichiometry: 3RCONi(acac)(PPh_3)→ RCOR+Ni(CO)$_2$(PPh_3)$_2$+Ni(acac)$_2$+RNi(acac)(PPh_3). The mechanism involving the cross coupling of the acylnickel complex with the alkylnickel complex is proposed for the reaction on the basis of formation of $CH_3COC_2H_5$ on reaction of **2a** with **1b**.

Insertion of carbon monoxide into a transition metal-carbon bond to give an acyltransition metal complex and its reverse process, decarbonylation from an acyltransition metal complex to an alkyl complex, consitute crucial elementary steps in industrially important processes such as carbonylations of olefins[1] and methanol[2] and in synthetically important decarbonylation reactions.[3] However, studies of the carbonylation and decarbonylation processes dealing with well characterized complexes are relatively limited.[4] Particularly, the study with an acylnickel complex has received less attention because of its unstable nature,[5] and only recently the first stable acylnickel complex $CH_3CONiCl(PMe_3)_2$ has been isolated by Klein.[6]

We report here the preparation of new stable acylnickel complexes RCONi(acac)(PPh_3) from the corresponding alkylnickel complexes and describe their properties in solutions including facile decarbonylation and ketone formation.

Results and Discussion

Preparation of Acyl(acetylacetonato)(triphenylphosphine)-nickel 2a and 2b. Bubbling of carbon monoxide through a toluene solution of ethyl(acetylacetonato)-bis(triphenylphosphine)nickel(II)[7,8] (**1a**) below 0 °C gives its CO insertion product (**2a**). A similar reaction of methyl(acetylacetonato)bis(triphenylphosphine)nickel(II) (**1b**),[7] at 20 °C gives the corresponding acetylnickel complex (**2b**).

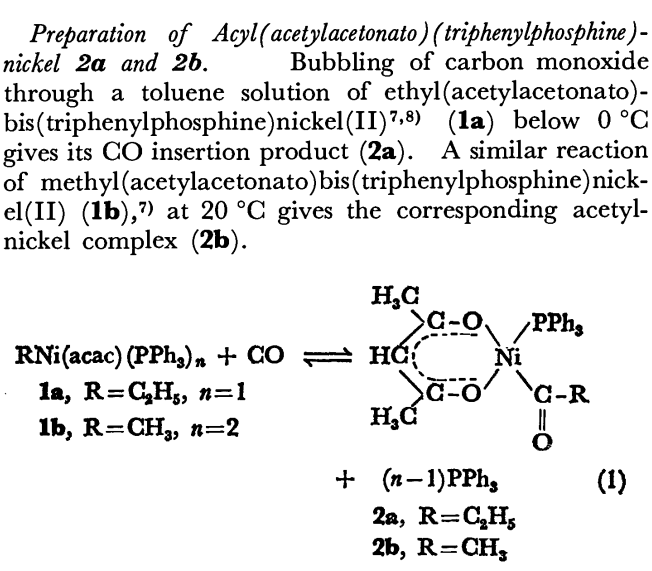

It is necessary to carry out the reaction at the low temperature for obtaining the propionyl complex **2a**, since **2a** is thermally unstable and the reaction at room temperature readily gives its decomposition products, Ni(CO)$_2$(PPh_3)$_2$ and diethyl ketone (*vide infra*).

Although the acylnickel complexes are unstable in solution, they are stable in the solid state once it is isolated. The IR spectrum of **2a** shows a ν(C=O) band of the nickel-bonded acyl group at 1665 and that of **2b** at 1680 cm^{-1} which may be compared with the ν(C=O) bands of acylplatinum, palladium and nickel complexes in the region of 1610 to 1675 cm^{-1}.[6,9] The IR bands due to the acetylacetonato and triphenylphosphine ligands in **2a** and **2b** are similar to those of the starting alkylnickel complexes **1a** and **1b**.

NMR Spectrum and Chemical Properties of 2a. The NMR spectrum of **2a** in toluene-d_8 at 20 °C (Fig. 1A) shows a triplet at δ 0.70 (3H, CH_3 of the propionyl group), a quartet at δ 2.85 (2H, CH_2 of the propionyl

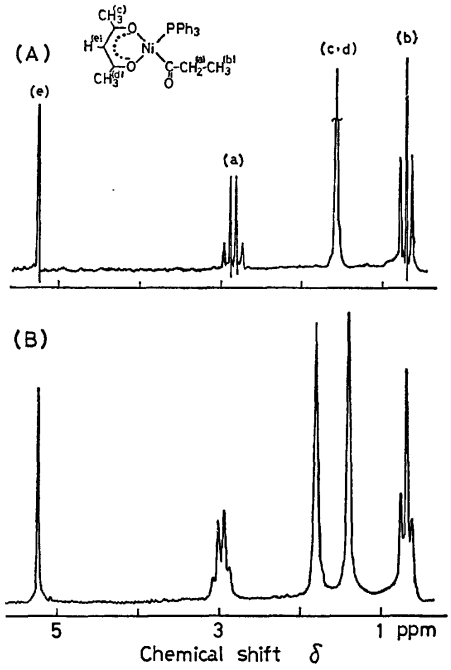

Fig. 1. NMR spectra of $C_2H_5CONi(acac)(PPh_3)$ in toluene-d_8 at (A) 20 °C and (B) −40 °C.

Table 1. The rate constants of the acac interchange in **2a** in toluene-d_8

Temp (°C)	Rate constant (s^{-1})
−40	7±2
−30	16±2
−20	70
−10	140
0	500

group), a singlet at δ 1.56 (6H, two CH_3 groups of acac) and a singlet at δ 5.25 (1H, CH of acac). Although the two CH_3 groups of the acac ligand in **2a** give a sharp singlet peak at room temperature, the singlet peak becomes broad on cooling the toluene-d_8 solution of **2a** and then separates on further cooling into two peaks indicating a rapid exchange of the acac ligand in the square planar nickel complex at room temperature on NMR time scale. Figure 1B shows the NMR spectrum of **2a** at −40°C, where the exchange is very slow. The rate constants of the exchange of the acac ligand calculated from the temperature variation of the NMR spectrum are tabulated in Table 1.

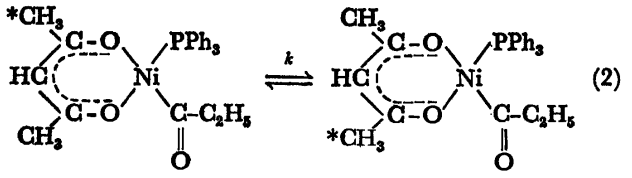

(2)

The rate constant of the acac exchange is expressed as,

$$k = 2.5 \times 10^{13} \exp(-13400/RT) \quad (3)$$

In the parent ethylnickel complexes **1a**, on the other hand, the exchange of the acac ligand is much slower in benzene, toluene, acetone and tetrahydrofuran. The methyl protons of the acac ligand in **1a** are observed as magnetically non-equivalent signals at room temperature which coalesce at elevated temperatures (~−70 °C). The higher exchange rate of the acac ligand in the propionylnickel complex may be due to the electron-withdrawing effect of the acyl group bonded to nickel.

When **2a** was allowed to stand in solution for 1 week at room temperature, it underwent disproportionation reaction to give $C_2H_5COC_2H_5$ (24 mol % per **2a**), **1a**, $Ni(CO)_2(PPh_3)_2$ and $Ni(acac)_2$. Figure 2 shows the NMR spectrum of the solution of **2a** observed after the disproportionation reaction. Each of peaks with an arrow (a,c,e, and g) is due to **1a**.[7] The ethyl group of **1a** gives rise to a singlet peak as previously reported.[7] The amount of **1a** formed is about 30 mol % per **2a**. The triplet and quartet peaks in Fig. 2 (b, d) are assigned to the methyl and methylene groups of $C_2H_5COC_2H_5$ by comparison of the spectrum with that of the authentic sample. Formation of $Ni(CO)_2(PPh_3)_2$ and $Ni(acac)_2$ was confirmed by elemental analyses and IR spectra of the complexes isolated from the reaction mixture. Heating the reaction solution further for 6 hr at 70 °C caused a slight increase in the amount of $C_2H_5COC_2H_5$ (29 mol % per **2a**) with a partial thermal decomposition of

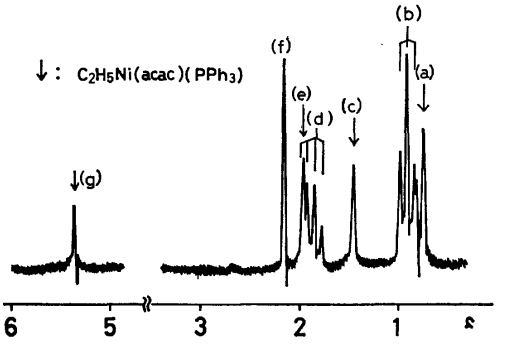

Fig. 2. NMR spetrum of the disproportionation products of **2a** in benzene. A peak (f) at δ 2.10 is due to toluene contained in C_6H_6. For assignment of the peaks (a~g) see the text.

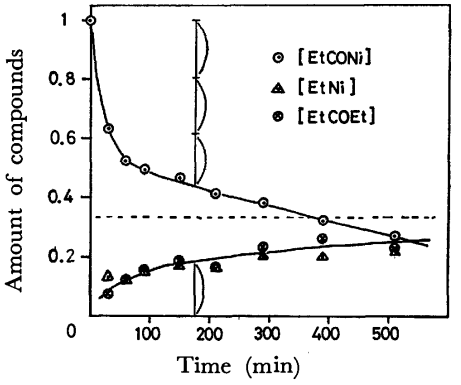

Fig. 3. Time curves for disappearance of **2a** and formation of **1a** and diethylketone during the disproportionation of **2a**. Units of the amounts of the compounds are arbitrary (calculated from areas in the NMR spectrum).

1a to give ethane (7 mol % per **2a**) and ethylene (23 mol % per **2a**).

The decrease of **2a** and the accompanying increases of $C_2H_5COC_2H_5$ and **1a** with time were followed by the NMR spectroscopy. Figure 3 shows the time curves of the amounts of **2a**, $C_2H_5COC_2H_5$ and **1a**. It is seen in Fig. 3 that the amount of **1a** produced is equal to that of $C_2H_5COC_2H_5$ produced within experimental error and 1 mol equivalent of C_2H_5-COC_2H_5 is formed with the consumption of 3 mol of **2a**. These facts suggest that the following reaction is taking place in the solution.

$$3Ni(COC_2H_5)(acac)(PPh_3) \rightarrow \underset{\textbf{2a}}{C_2H_5COC_2H_5} + \underset{\textbf{1a}}{NiC_2H_5(acac)(PPh_3)} + Ni(CO)_2(PPh_3)_2 + Ni(acac)_2 \quad (4)$$

A detailed kinetic analysis of the reaction has been unsuccessful due to the complexity of the reaction process. However, the following disproportionation mechanism seems to be most probable. (1) The first step of the reaction is the decarbonylation of **2a** to give **1a**.

$$Ni(COC_2H_5)(acac)(PPh_3) \rightarrow Ni(C_2H_5)(acac)(PPh_3) + CO \quad (5)$$

(2) The second step is the formation of $C_2H_5COC_2H_5$,

$Ni(acac)_2$ and $Ni(PPh_3)_2$ from **2a** and **1a** presumably *via* a binuclear interaction between **2a** and **1a**.

$$Ni(COC_2H_5)(acac)(PPh_3) + Ni(C_2H_5)(acac)(PPh_3) \rightarrow C_2H_5COC_2H_5 + Ni(acac)_2 + Ni(PPh_3)_2 \quad (6)$$

$Ni(PPh_3)_2$ produced will immediately accept carbon monoxide liberated from **2a** by equation 5, thus completing Eq. 4.

In order to test the assumption that the ketone is formed by interaction of the acylnickel complex with alkylnickel complex the reaction of the propionyl complex **2a** with the ethyl complex **1a** in a 1 : 1 molar ratio was examined. The amount of $C_2H_5COC_2H_5$ produced increased to 47 mol % per **2a** compared with 24 mol % produced in the absence of **2a**. The reaction was accompanied by the evolution of ethane (22 mol % per **2a**) and ethylene (22 mol % per **2a**) which may be formed from an intermediate unstable ethylnickel complex produced in the process of the disproportionation reaction.

Assumption of coupling of the acylnickel complex with the alkyl complex was further supported by formation of $CH_3COC_2H_5$ in the reaction of the propionyl complex **2a** with the methyl complex **1b**. The reaction was accompanied by formation of $C_2H_5COC_2H_5$ probably produced by coupling of the propionyl group in **2a** with the ethyl complex **1a** generated by decarbonylation of **2a**. Some methane, ethylene and ethane were also formed, which may be produced by decomposition of unstable intermediate methyl and ethynickel complexes generated during the disproportionation process as in the reaction of **2a** with **1a**.

In relation to Eq. 6 a somewhat analogous disproportionation of $NiC_2H_5(acac)(PPh_3)$ in pyridine producing $Ni(acac)_2$, $Ni(C_2H_4)(PPh_3)_2$ and ethane according to a second-order reaction kinetics has been observed.[7]

NMR Spectrum and Chemical Properties of 2b. Although **2b** is stable in the solid state and the IR spectrum of **2b** in the solid state indicates that the compound is not contaminated with **1b**, the NMR spectrum of **2b** (Fig. 4) shows not only the peaks assignable to **2a** (δ 2.23 (3H, CH_3 of CH_3CO), δ 1.60 (6H, CH_3 of acac), δ 5.26 (1H, CH of acac)) but also peaks of **1b**[7] (shown with an arrow) which is formed by the decarbonylation of **2b**. This fact suggests that **2b** readily liberates CO in solution reverting itself to **1b** in a greater decarbonylation tendency than **2a** and that **1b** and **2b** are in equilibrium in the solution. The presence of equilibrium in solution accounts for the experimental fact that **2b** was isolable from solution only under an atmosphere of CO. Attempts to isolate **2b** under an atmosphere of nitrogen were unsuccessful and **1b** was recovered from the solution.

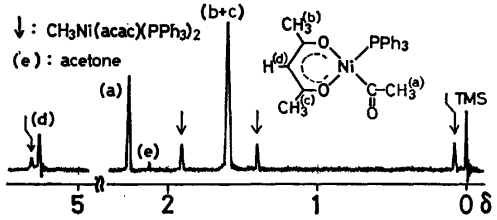

Fig. 4. NMR spectrum of $CH_3CONi(acac)(PPh_3)$ in benzene at 25 °C. The assignment of each signal (a—d) is indicated on the spectrum with reference to the formula of **2b**. Each of peaks with an arrow is due to $CH_3Ni(acac)(PPh_3)$.[7] Formation of a small amount of acetone by the disproportionation of **2b** is seen (peak e).

When the reaction of CO with **1b** in toluene was carried out at room temperature in a closed system, 0.7 mol equivalent of CO was absorbed per mol of **1b** but the complex recovered from the solution turned out to be **1b**.

As in the propionyl complex **2a**, the NMR spectrum of the acetyl complex **2b** shows that the acac ligand exchanges rapidly at room temperature in benzene as indicated by appearance of the methyl signal of the acac ligand as a sharp singlet which splits on lowering the temperature. An accurate value of the rate constant of the acac exchange in **2b** could not be obtained, since the split peaks of CH_3(acac) group in **2b** were overlapped with the CH_3(acac) peaks of **1b** at the low temperatures. Roughly estimated values for the rate constants were of the same magnitude as those obtained for **2a**. When the benzene solution of **2b** was allowed to stand at room temperature for 1 week, **2b** underwent the disproportionation reaction to give CH_3COCH_3 (20 mol % per **2b**), $Ni(CO)_2(PPh_3)_2$, **1b** and $Ni(acac)_2$. The products of the disproportionation reaction suggest that a similar reaction expressed by Eq. 4 takes place with **2b**.

It is known that some acyltransition metal complexes give biacyls.[4e,5,11] However, no biacyl has been detected in the disproportionation of **2a** and **2b**.

The work was supported by a Scientific Research Grant from the Ministry of Education Japan.

Experimental

Materials. $C_2H_5Ni(acac)(PPh_3)$, **1a**, and $CH_3Ni(acac)(PPh_3)_2$, **1b**, were prepared as described in our previous paper.[7] Solvents were dehydrated, purified and stored under nitrogen.

Preparation of $C_2H_5CONi(acac)(PPh_3)$ 2a. Dehydrated carbon monoxide was bubbled into a toluene solution (6 ml) of **1a** (0.98 g, 2.2 mmol) for an hour at −20 °C. Hexane (25 ml) was added to the red solution under an atmosphere of CO at −78 °C and the orange crystals which separated were collected by filtration to yield 0.91 g (85%) of **2a**. Found: C, 65.4; H, 6.1%. Calcd for $C_{26}H_{27}NiO_3P$: C, 65.6; H, 5.8%. IR(KBr): 1665 cm^{-1} (C=O), 595 cm^{-1} (tentatively assigned to Ni–C). NMR(benzene, 25 °C): δ: 0.77 (3H, CH_3 of propionyl, t, J=7 Hz), 2.92 (2H, CH_2 of propionyl, q, J=7 Hz), 1.60 (6H, CH_3 of acac, s), 5.38 (1H, CH of acac, s).

The same product was obtained in a closed system by the reaction of **1a** (0.43 g, 0.96 mmol) with carbon monoxide (*ca.* 60 ml, 2.5 mmol) in toluene (10 ml) at 0 °C for 1 hr; yield=70%. However, bubbling of CO into a toluene solution of **1a** at room temperature for 3 hr did not give **2a** but yellow crystals and $C_2H_5COC_2H_5$. The yellow crystals were identified as $Ni(CO)_2(PPh_3)_2$ by the IR spectrum (2000 and 1935 cm^{-1}, ν(CO))[5] and elemental analysis. Found: C, 71.8; H, 4.8%. Calcd for $C_{38}H_{30}NiO_2P_2$: C, 71.4;

H, 4.7%.

Preparation of $CH_3CONi(acac)(PPh_3)$ 2b. Dehydrated carbon monoxide was bubbled into a toluene (50 ml) solution of **1b** (1.7 g, 2.4 mmol) for an hour at 20 °C. Hexane (50 ml) was added slowly to the red solution under an atmosphere of CO at −78 °C and the orange crystals which separated were collected by filtration to give 0.98 g (55%) of **2b**. Found: C, 65.3; H, 5.4%. Calcd. for $C_{25}H_{25}NiO_3P$: C, 64.9; H, 5.4%. IR(KBr): 1680 cm^{-1} (C=O), 580 cm^{-1} (tentatively assigned to Ni–C). Since an absorption peak of **1b** at 605 cm^{-1} (tentatively assigned to Ni–C) was not observed in the IR spectrum, the product is considered not contaminated with **1b**. Prolonged bubbling of CO into the toluene solution of **1b** resulted in the formation of $Ni(CO)_2(PPh_3)_2$ (confirmed by IR and elemental analysis) and acetone, but **2b** was not obtained.

Reaction of 2a with Methyl Iodide. CH_3I (1.33 g, 9.3 mmol) was added to a flask containing 0.145 g (0.30 mmol) of **2a** by a trap-to-trap distillation in vacuum. The mixture was allowed to stand for 1.5 days at room temperature. $CH_3COC_2H_5$ (0.130 mmol), ethylene (0.062 mmol), methane (0.018 mmol) and a trace amount of C_2H_6 were obtained from the reaction mixture. When the reaction time was shorter (4 hr), a smaller amount of $CH_3COC_2H_5$ (20 mmol % per **2a**) was formed.

Disproportionation Reaction of 2a and 2b. On allowing **2a** (0.42 g, 0.87 mmol) to stand in benzene for 1 week at room temperature, the color of the solution changed from red to yellow. The gas-chromatographic analysis of the solution indicated the formation of $C_2H_5COC_2H_5$ (0.20 mmol. Trace amounts of C_2H_6 and C_2H_4 were detected. Heating the obtained solution at 70 °C for 6 hr caused an increase in the amount of $C_2H_5COC_2H_5$ (0.25 mmol) with a thermal decomposition of **1a** to give ethane and ethylene.

On adding hexane to the reaction mixture a mixture of a yellow precipitate and a green precipitate was obtained. IR spectrum of the mixture indicated that it was a mixture of $Ni(CO)_2(PPh_3)_2$[5] and $Ni(acac)_2$. $Ni(CO)_2(PPh_3)_2$ was isolated by recrystallization from hexane. Similar results were obtained from the disproportionation of **2b**.

Reaction of **2a** (0.15 g, 0.32 mmol) with **1a** (0.13 g, 0.29 mmol) was carried out in benzene (1.5 ml). After allowing the mixture to stand at room temperature for 3 days 0.13 mmol of $C_2H_5COC_2H_5$, 0.07 mmol of ethane and 0.07 mmol of ethylene were obtained. Heating the reaction mixture further at 70 °C for 5 hr caused an increase in the amount of $C_2H_5COC_2H_5$ (0.15 mmol, 47 mol % per **2a**).

Reaction of **2a** (0.14 g, 0.29 mmol) with **1b** (0.23 g, 0.33 mmol) was carried out in benzene-d_6 (1.70 g) at 50 °C. After 5 hr 0.08 mmol of $CH_3COC_2H_5$, 0.09 mmol of $C_2H_5COC_2H_5$, 0.07 mmol of CH_4, 0.13 mmol of ethylene and 0.04 mmol of ethane were obtained. When the molar ratio of **1b** to **2a** was smaller (1 : 1.8), the molar ratio of $CH_3COC_2H_5$ to $C_2H_5COC_2H_5$ decreased to 1 : 2.5.

Spectral Measurements and Analysis. The IR spectra were obtained by using Hitachi Model EPI-G3 spectrometer. NMR spectra were measured by Mr. Y. Nakamura of our laboratory with a Japan Electron Optics Laboratory PS-100 spectrometer. Solvent and TMS were added by a trap-to-trap distillation in vacuum into an NMR tube containing **2a** or **2b** and the NMR tube was sealed. Chemical shifts are referred to internal TMS (down field positive).

The microanalysis of carbon and hydrogen was performed by Mr. T. Saito of our laboratory with a Yanagimoto CHN Autocorder Type Mr-2. The amounts of gases and ketones formed by the reactions of **2a** and **2b** were measured by gas chromatography with Shimadzu GC-3B gas chromatograph.

References

1) (a) R. F. Heck, "Organotransition Metal Chemistry, a Mechanistic Approach," Academic Press, New York, 1974; (b) F. Basolo and R. G. Pearson, "Mechanisms of Inorganic Reactions," Second Edition, John Wiley and Sons, Inc. (1967) Chapter 7; (c) F. Calderazzo and K. Noack, *Coord. Chem. Rev.*, **1**, 118 (1966).

2) (a) J. F. Roth, J. H. Craddock, A. Hershman, and F. E. Paulik *Chem. Tech.*, **1971**, 600; (b) K. K. Robinson, A. Hershman, J. H. Craddock, and J. F. Roth, *J. Catal.*, **27**, 389 (1972).

3) (a) K. Ohno and J. Tsuji, *J. Amer. Chem. Soc.*, **90**, 99 (1968); (b) J. Tsuji and K. Ohno, *Synthesis*, **1969**, 157.

4) (a) T. H. Coffield, J. Kozikowski, and R. N. Closson, *J. Org. Chem.*, **22**, 598 (1957); (b) K. A. Keblys and A. H. Filbey, *J. Amer. Chem. Soc.*, **82**, 4204 (1960); (c) R. J. Mawby, F. Basolo, and R. G. Pearson, *ibid.*, **86**, 3994 (1964); (d) F. Calderazzo and F. A. Cotton, *Inorg. Chem.*, **1**, 30 (1962); (e) G. Booth and J. Chatt, *J. Chem. Soc., A*, **1966**, 634; (f) R. F. Heck, *J. Amer. Chem. Soc.*, **85**, 1220 (1963).

5) P. W. Jolly and G. Wilke, "The Organic Chemistry of Nickel," Vol. 1, Academic Press, New York, (1974), pp. 33, 166, 170, and references cited therein.

6) H. F. Klein, *Angew, Chem.*, **85**, 403 (1973).

7) (a) A. Yamamoto, T. Yamamoto, T. Saruyama, and Y. Nakamura, *J. Amer. Chem. Soc.*, **95**, 4073 (1973); (b) T. Yamamoto, T. Saruyama, Y. Nakamura, and A. Yamamoto, accepted for publication in This Bulletin.

8) F. A. Cotton, B. A. Frenz, and D. L. Hunter, *J. Amer. Chem. Soc.*, **96**, 4820 (1974).

9) D. M. Adam and G. Booth, *J. Chem. Soc.*, **1962**, 1112.

10) (a) A. C. Adams and E. N. Larsen, *Inorg. Chem.*, **5**, 814 (1966); (b) G. E. Glass and R. S. Tobias, *J. Organometal. Chem.*, **15**, 481 (1968); (c) N. Serpone and R. Ishayek, *Inorg. Chem.*, **13**, 52 (1974); (d) G. M. Tanner, D. G. Tuck and E. J. Wells, *Can. J. Chem.*, **50**, 3950 (1972).

11) (a) A. Miyashita, Ph. D. thesis, Tokyo Institute of Technology (1975); (b) O. S. Mills and E. F. Paulus, *J. Chem. Soc. Chem. Commun.*, **1966**, 738.

Chemistry of Nitrosoimines. XIV.[1] Photolysis of 5-Nitrosoimino-4-phenyl-3-phenylimino-1,2,4-thiadiazolidine

Kin-ya AKIBA, Tohru TSUCHIYA, Isaburo FUKAWA, and Naoki INAMOTO
Department of Chemistry, Faculty of Science, The University of Tokyo, Hongo, Tokyo 113
(Received October 29, 1975)

Photolysis of 5-nitrosoimino-4-phenyl-3-phenylimino-1,2,4-thiadiazolidine proceeded through π-π^* excitation and gave phenylcyanamide and 5-imino-4-phenyl-3-phenylimino-1,2,4-thiadiazolidine as primary products. It was found that other products were produced by the reactions of the primary products. The formation mechanisms have been discussed briefly.

In a previous paper,[2] we reported that photolysis of 2-nitrosoimino-2,3-dihydro-1,3-thiazoles gave the corresponding disulfides *via* π-π^* excitation.

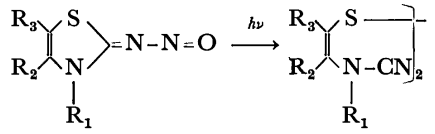

As the extention of these works, this paper describes photolysis of 4-methyl-5-nitrosoimino-3-phenyl-1,2,4-thiadiazoline (**1**) and 5-nitrosoimino-4-phenyl-3-phenylimino-1,2,4-thiadiazolidine (**2**).

Similarly to other nitrosoimines,[3] the nitrosoimines **1** and **2** decomposed thermally to give 4-methyl-3-phenyl-1,2,4-thiadiazolin-5-one (**3**) and 4-phenyl-3-phenylimino-1,2,4-thiadiazolidin-5-one (**4**), respectively, in almost quantitative yields.

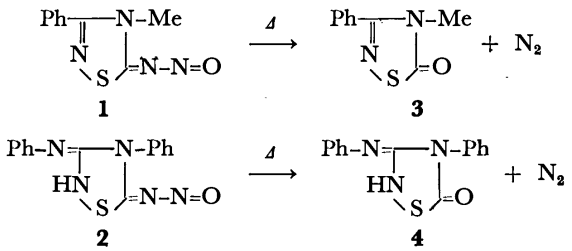

Photolysis of **1** was very slow in benzene or dichloromethane–acetone under an irradiation with a 100 W medium-pressure mercury lamp and gave a lot of products in small quantities, some of them containing cyano group (determined by IR). Therefore, the further investigation was given up, but this fact presumably supports that the photolyses of the nitrosoimino substituted heterocycles proceed through the π-π^* excitation, because the π-π^* absorption (317.5 nm) of **1** does not overlap effectively with 334.1 nm of the mercury arc.

The photolysis of **2** was carried out under several conditions. The results are summarized in Table 1.

The reaction products were **5**—**11** and phenylcyanamide, depending on the reaction conditions. The compound **5** was identical with 5-imino-4-phenyl-3-phenylimino-1,2,4-thiadiazolidine, the denitrosation product of **2**. The compound **6** was the same as the 1 : 1 adduct of **5** and phenylcyanamide.[4] The compound **7** was determined to be 3,5-dianilino-1,2,4-thiadiazole by comparison with an authentic sample.[5] The compound **8** was identical with the reaction product of **5** with cyanic acid, 5-carbamoylimino-4-phenyl-3-phenylimino-1,2,4-thiadiazolidine. The compounds **9** and **10** were determined to be phenylurea and phenylisomelamine, respectively. The structure of **11** remains

Table 1. Photolyses of **2**

Run	1[a]	2	3	4[b]
Reaction condition				
2 (mmol)	6.1	34.4	20.4	29.8
Solv. (ml)	CH_2Cl_2 (900)	PhH-DMF (2 : 1) (1400)	PhH-*i*-PrOH-DMF (5 : 5 : 7) (850)	*i*-PrOH-DMF (1 : 1) (1100)
Lamp (W)	100	100	100	400
Filter	Pyrex	Pyrex	filter soln.[c]	filter soln.[c]
Reac. Time (hr)	6	40	20	3
Reac. Temp. (°C)	20—25	5—10	5—10	10—15
Product, mmol (%)				
5	0.3(5)			
6	0.7(17.2)	4.4(19.2)	1.1 (8.1)	2.0(10.1)
7		3.7(10.8)	0.45(2.2)	
8		1.9(11.0)		
9		6.0(8.8)	2.8 (6.8)	4.3(7.2)
10			0.28(2.1)	
11		1.1(3.3)	2.8(13.7)	+
PhNHCN				12.0(20.2)

a) Other products were not identified. b) About 5 mmol of **2** was recovered (16.8%). c) For 340—360 nm. See Ref. 2.

unknown.

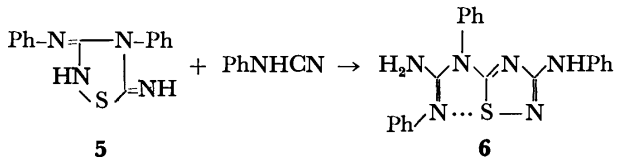

5 6

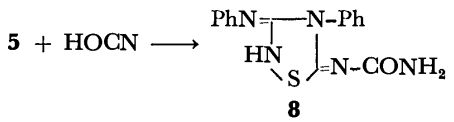

8

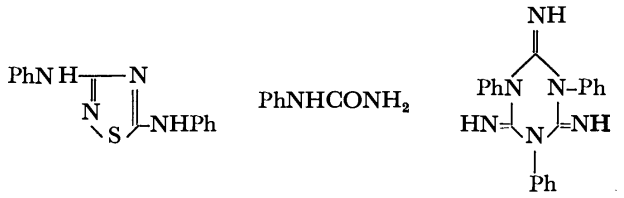

7 9 10

Since the isolation of pure reaction products was difficult, the material balance was not sufficient for quantitative discussion. However, as seen in Table 1, the reaction in a shorter irradiation time gave **5** in a considerable amount and the amount of **6** increased as a reaction time became longer (Runs 1 and 2). Moreover, a shorter irradiation time with a stronger arc gave phenylcyanamide in a fairly good yield (Run 4). Thus, the initial products are **5** and phenylcyanamide and the others are considered to be secondary products. Although **7** is an isomer of **5**, **5** could not be isomerized to **7** by acid or adsorption on silica gel. **9** is the photolysis product of phenylcyanamide with water, being contained in the solvent.

Furthermore, it is shown by experiments using a filter solution that the photolysis of **2** proceeds through π-π^* excitation, similarly to the previous results[2] (see Runs 3 and 4). Therefore, the photolysis is considered to proceed as follows.

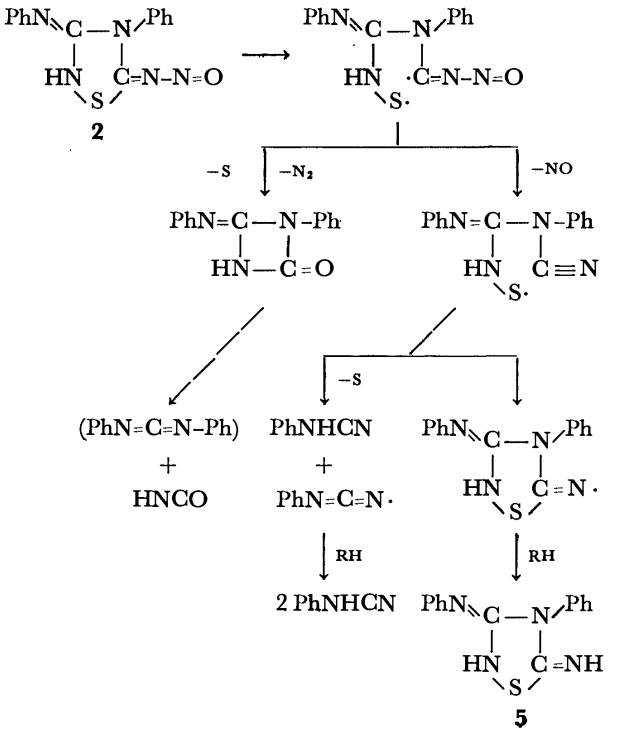

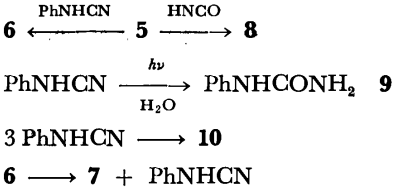

Thus, photolysis of **2** is apparently more complicated than that of 2-nitrosoimino-2,3-dihydro-1,3-thiazoles due to the character of the ring.

Experimental

Materials. 4-Methyl-5-nitrosoimino-3-phenyl-1,2,4-thiadiazoline was prepared according to the method of Goerdeler *et al.*,[6] mp 157—158 °C (dec), λ_{max} (C_6H_6): 317.5 (ε 9.08×10^3) and 429 nm (100). 5-Nitrosoimino-4-phenyl-3-phenylimino-1,2,4-thiadiazolidine was prepared from 5-imino-4-phenyl-3-phenylimino-1,2,4-thiadiazolidine according to the Hector's method,[7] mp 183.3 °C (dec), λ_{max} (C_6H_6): 359 (ε 4.0×10^3) and 433 nm (200).

Thermal Decomposition of 4-Methyl-5-nitrosoimino-3-phenyl-1,2,4-thiadiazoline (1). A suspension of 4.0 g (18.1 mmol) of **1** in 200 ml of toluene was refluxed under stirring for 7 hr. After removal of toluene, the residue was chromatographed on silica gel. Elution with benzene–chloroform gave 2.8 g (80%) of 4-methyl-3-phenyl-1,2,4-thiadiazolin-5-one (**3**), mp 76.0—76.5 °C, IR (KBr): 1680 cm^{-1} (C=O).

Found: C, 56.09; H, 4.21; N, 14.43%. Calcd for $C_9H_8N_2OS$: C, 56.23; H, 4.19; N, 14.57%.

Thermal Decomposition of 5-Nitrosoimino-4-phenyl-3-phenylimino-1,2,4-thiadiazolidine (2). The decomposition was carried out qualitatively. A suspension of **2** in xylene was refluxed for 5 hr. After removal of the solvent and addition of petroleum ether to the residue, the resulting crystals were recrystallized from ethanol to give 4-phenyl-3-phenylimino-1,2,4-thiadiazolidin-5-one (**4**) as white needles, mp 165.0—165.3 °C (lit,[8] 162 °C); IR(KBr): 3330 (NH) and 1670 cm^{-1} (C=O). The compound was identical with a sample prepared by nitric acid-catalyzed hydrolysis of 5-imino-4-phenyl-3-phenylimino-1,2,4-thiadiazolidine.

Photolysis of 2. The reactions were carried out under nitrogen.

1) A solution of 1.80 g (6.1 mmol) of **2** in 900 ml of dichloromethane was irradiated through Pyrex filter with a 100 W medium pressure mercury lamp at 20—25 °C for 6 hr, and the solvent was removed. The residue was chromatographed on alumina. Elution with benzene–ether and ether afforded 0.27 g (0.7 mmol, 17.2%) of **6**, mp 192—194 °C (lit,[4] 196—198 °C). IR(KBr): 3480, 3420, 3380, 1660, 1560, and 1535 cm^{-1}; MS: *m/e* 386 (M^+, trace). The spectral data were in agreement with those of an authentic sample[4] (see below).

Elution with ether gave 80 mg (0.3 mmol, 5%) of 5-imino-4-phenyl-3-phenylimino-1,2,4-thiadiazolidine (**5**), mp 179—180 °C (lit,[7] 180—181 °C).

2) A solution of 10.22 g (34.4 mmol) of **2** in 1400 ml of benzene-*N*,*N*-dimethylformamide (DMF) (2 : 1) was irradiated through pyrex filter with the same lamp at 5—10 °C for 40 hr. After the solvent was removed *in vacuo* at 90 °C, the residue was chromatographed on silica gel. Fractions eluted with benzene–dichloromethane (3 : 1—1 : 1) and dichloromethane were evaporated. The residue was dissolved in benzene and addition of hexane gave 1.71 g (4.4 mmol, 19.2%) of **6**, mp 183—185 °C, as precipitates. Fractions eluted with dichloromethane–ether (3 : 1) were evaporat-

ed and rechromatographed on a silica gel dry column with dichloromethane to afford **7** (0.74 g), mp 218—219 °C (from chloroform) (lit,[9] 220—222 °C). Eluate with dichloromethane–ether (1 : 1–1 : 3) was rechromatographed on silica gel to afford 0.26 g of **7** (1.00 g, 3.7 mmol, 10.8% in total) with benzene and chloroform and 0.60 g (1.9 mmol, 11.0%) of **8** with chloroform and ether–ethyl acetate, mp 208—209 °C; IR (KBr): 3480, 3400, 3320 (NH), 1760, 1640, 1610, and 1590 cm^{-1}. The spectral data of **8** were in agreement with those of an authentic sample prepared by another route (see below).

Fractions eluted with acetone and acetone–methanol (1 : 1) were rechromatographed on silica gel. Elution with dichloromethane gave 0.42 g (1.1 mmol, 3.3%) of **11**, mp 201—202 °C (from acetone), and elution with chloroform and ethyl acetate gave 1.02 g of crystalline material. The soluble part in ethyl acetate gave 0.82 g (6.0 mmol, 8.8%) of **9**, mp 148—149 °C (from ethyl acetate) (lit,[10] 148—149 °C). The insoluble part was unidentified.

11 : IR (KBr) : 3420, 3360, 3280, 3100 (NH), 1630, and 1590 cm^{-1}; MS: *m/e* 373 (0.7%), 347 (11), 311 (49), 295 (55), 293 (25), 268 (48), 195 ($PhNHCNPh^+$, 28), 150 (100), 122 (44), 119 (59), and 118 (58). The structure of **11** was unidentified.

3) As a filter solution for 340–360 nm and a coolant, a solution of 490 g of $CoSO_4 \cdot 7H_2O$ and 100 g of $CuSO_4 \cdot 5H_2O$ in 900 ml of water was used.[2] A solution of 6.09 g (20.5 mmol) in 850 ml of benzene–DMF–2-propanol (5 : 7 : 5) was irradiated with the same lamp through the filter solution at 5—10 °C for 20 hr. After evaporation of the solvent, the residue was chromatographed on silica gel. Eluates with benzene–dichloromethane (1 : 1) were treated with dichloromethane and water to afford 0.10 g (0.28 mmol, 2.1%) of **10**, mp 202.5—203.5 °C (lit,[11] 210 °C); IR (KBr): 3330 (NH), 1620, and 1590 cm^{-1}, NMR ($CDCl_3$): δ 5.4 (s, 3H, NH) and 7.35 (s, 15H, Ph); MS: *m/e* 354 (M^+), 236, and 118. Evaporation of the organic layer and washing with dichloromethane gave 0.10 g of **7**. The filtrate was treated with preparative thin layer chromatography (tlc) on silica gel with dichloromethane–ether to give 0.44 g (1.1 mmol, 8.1%) of **6**.

Eluates with benzene–dichloromethane (1 : 1) and dichloromethane were rechromatographed on silica gel. Elution with dichloromethane–ether gave 0.64 g of a mixture, which was separated by preparative tlc with ether to give 20 mg of **7** (in total, 0.12 g, 0.45 mmol, 2.2%). Elution of dichloromethane gave 1.04 g (2.8 mmol. 13.7%) of **11**. Elution of ethyl acetate afforded 0.38 g (2.8 mmol, 6.8%) of **9**.

The products were identified by the melting points and spectral data.

4) A solution of 8.84 g (29.8 mmol) of **2** in 1100 ml of DMF–2-propanol (1 : 1) was irradiated with a 400 W medium-pressure mercury lamp at 10—15 °C using the same filter solution for 3 hr. The UV spectrum of the solution indicated that about 5 mmol of **2** remained unchanged. The solvent was removed below 40 °C *in vacuo* and the residue was chromatographed on silica gel.

Elution with dichloromethane and dichloromethane–ether gave 1.42 g (12 mmol, 20.2%) of phenylcyanamide (identified by IR) and other materials which were rechromatographed on alumina. The fractions eluted with benzene–chloroform (3 : 2—2 : 3) was again chromatographed on silica gel dry column with chloroform to give 90 mg of **6**.

Fractions eluted with dichloromethane–ether and ether were purified by preparative tlc with ethyl acetate–ether to give 0.70 g of **6** (in total, 0.79 g, 2 mmol, 10.1%). Elution with ethyl acetate gave 0.59 g of **9** (4.3 mmol, 7.2%). Other fractions could not be identified.

Preparation of ***7***. Ammonia gas was bubbled to 3.0 g (11 mmol) of **5** in 40 ml of ethanol for 2 min and the mixture was heated at 135—140 °C for 3 hr in a sealed tube. After evaporation of the solvent, a small amount of dichloromethane was added to dissolve the residue and ether was added to the solution to precipitate 1.0 g (33%) of **7**, mp 220—221 °C (from ethanol) (lit,[5] 220—222 °C).

Reaction of ***5*** *and Phenylcyanamide.* A mixture of 5.0 g (18.7 mmol) of **5** and 2.0 g (17 mmol) of phenylcyanamide in 50 ml of chloroform was refluxed for 3 hr. After removal of the solvent, the residue was washed with a small amount of dichloromethane to obtain **6**. The washing was allowed to stand after addition of benzene to precipitate **6**. The total amount was 6.0 g (92%), mp 196—198 °C.

Found: C, 65.09; H, 4.56; N, 21.73; S, 8.10%. Calcd for $C_{21}H_{18}N_6S$: C, 65.25; H, 4.70; N, 21.75; S, 8.29%.

Reaction of ***5*** *and Cyanic Acid.* A mixture of 3.0 g (11.2 mmol) of **5**, 5 ml of 10% sulfuric acid, and 1.0 g (15.4 mmol) of sodium cyanate was stirred at 120 °C for 20 min to precipitate 2.5 g (72%) of **8**, mp 208—209 °C (from acetone). MS: *m/e* 311 (M^+, 100%), 295 ($M^+ - NH_2$, 16), and 268 ($M^+ - HOCN$, 63).

Found: C, 57.97; H, 4.19; N, 22.51; S, 9.93%. Calcd for $C_{15}H_{13}N_5OS$: C, 57.85; H, 4.22; N, 22.50; S, 10.30%.

This work was supported in part by a grant-in-aid from the Ministry of Education.

References

1) For part XIII see: M. Hisaoka, K. Akiba, and N. Inamoto, This Bulletin, **48**, 3274 (1975).

2) K. Akiba, I. Fukawa, N. Nomura, and N. Inamoto, This Bulletin, **45**, 1867 (1972).

3) K. Akiba, S. Matsunami, C. Eguchi, and N. Inamoto, This Bulletin, **47**, 935 (1974), and references cited therein.

4) K. Akiba, T. Tsuchiya, M. Ochiumi, and N. Inamoto, *Tetrahedron Lett.*, **1975**, 455. Recently, we have investigated the crystal structure of the tri-*p*-bromophenyl derivative of **6** by X-ray diffraction method. From the result, the structure of **6** should be revised as shown in the text, but the revised structure is consistent with the previous experimental results. This result will be reported soon.

5) C. P. Joshua, V. K. Verma, and K. S. Suresh, *Tetrahedron Lett.*, **1961**, 663; F. Kurzer, "Advances in Heterocyclic Chemistry," Vol. 5, Academic Press, New York (1965), p. 126.

6) J. Goerdeler, A. Huppertz, and K. Wember, *Chem. Ber.*, **87**, 69 (1954).

7) D. S. Hector, *Ber.*, **22**, 1176 (1889); *ibid.*, **23**, 357 (1890); *ibid.*, **25**, 799 (1892).

8) K. Dost, *Ber.*, **39**, 863 (1906); F. Kurzer and P. M. Sanderson, *J. Chem. Soc.*, **1963**, 3336.

9) F. Kurzer and P. M. Sanderson, *J. Chem. Soc.*, **1963**, 3333.

10) A. Steiner, *Ber.*, **8**, 519 (1875).

11) F. Arndt, *Ann. Chem.*, **384**, 350 (1911).

2-Chloro-1,3,5-trithiane and 2-Chloro-1,3-dithiane. Their Ionic Dissociation and Reactions with Nucleophiles

Kazutaka Arai and Michinori Ōki

Department of Chemistry, Faculty of Science, The University of Tokyo, Tokyo 113

(Received October 29, 1975)

2-Chloro-1,3,5-trithiane and 2-chloro-1,3-dithiane have been prepared by chlorination of the corresponding polythianes with *N*-chlorosuccinimide. These chlorides afford various substitution products when treated with nucleophiles, whereas nuclear substitution of the aromatic ring occurs when the chlorides are treated with phenol or *N*,*N*-dimethylaniline. ^{1}H NMR spectra of these chlorides show remarkable solvent dependence which is explained by assuming ionic dissociation of the chlorides to produce polythianyl cation and chloride anion. Free energies of activation for the dissociation in various solvents indicate that the dissociation of 2-chloro-1,3,5-trithiane is more sluggish than that of 2-chloro-1,3-dithiane. The results are attributed to the difference in availability of electrons on the sulfur atoms in two systems.

Derivatives of 1,3,5-trithiane and 1,3-dithiane have been found to show interesting stereoselectivities in reactions.[2-5] 2-Benzoyloxy-1,3,5-trithiane derivatives exhibited strong preference for the axial attack of nucleophiles and solvent-dependence of the stereoselectivity was partially attributed to the intermediacy of ion pairs.[3] Chloride ion, being a more effective leaving group than benzoate ion, may modify the reactivity and stereoselectivity of the trithiane and dithiane derivatives. And, if the reactivity is enhanced, there is a chance that an unusual phenomenon is observed.

Thus, 2-chloro-1,3,5-trithiane (**1**) and 2-chloro-1,3-dithiane (**2**) were prepared and their reactivities were examined. This paper describes the results of such studies together with a study on anomeric effect in these compounds as an extension of previous works[6-8] with the polythiane derivatives.

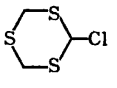

(**1**)

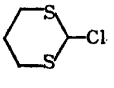

(**2**)

Experimental

NMR Measurement. The ^{1}H NMR spectra were recorded on a Hitachi R 20B spectrometer, operating at 60 MHz, with a temperature variation accessory. Temperature was read by the chemical shift differences between protons of methanol for lower temperatures and by those of ethylene glycol protons for higher temperatures than 34 °C. ^{13}C NMR spectra were obtained on a Varian CFT-20 spectrometer with a temperature variation accessory.

Kinetic Parameters. The rate constants of the exchange processes at the coalescence temperature were obtained by applying the following equation[9]

$$k_c = \frac{\pi}{\sqrt{2}}\sqrt{6J_{AB}^2+\nu_{AB}^2}$$

where J_{AB} is the coupling constant of the AB protons in positions 4 and 6 and ν_{AB} the chemical shift difference of those protons. The coalescence of the AB type signals was observed for compound **2** by irradiating the signals due to protons in position 5. Free energies of activation were obtained by the usual method.

Chlorination. To a suspension or solution of 0.5 g of 1,3,5-trithiane or 1,3-dithiane in 10 ml of benzene, which had been dried over sodium, powdered *N*-chlorosuccinimide (1.1 equivalents) was added during a 15 min period at 20 °C with stirring under a nitrogen atmosphere. Stirring was continued for 15 min after completion of the addition. The reaction mixture was filtered to remove insoluble materials, contact with moisture being avoided as completely as possible. Since attempted isolation of the resulting chlorides failed because of their high reactivities, the filtrate was directly submitted to some reactions. Spectra of chlorides in other solvents were obtained after evaporation of the filtrate *in vacuo* followed by dissolving the residue in appropriate solvents.

Benzenethiolysis. The benzene solution was treated with 2—3 equivalents of benzenethiol at room temperature for 2—3 hr and the resulted mixture was evaporated *in vacuo*. Recrystallization from hexane gave 2-phenylthio-1,3,5-trithiane (**3**), mp 122—123 °C (lit. 123.0—123.5 °C)[6] and 2-phenylthio-1,3-dithiane (**4**), mp 58—59 °C (lit. 59 °C),[10] in 80 and 90% yields, respectively.

Reaction with Imidazole. The benzene solution of the chloride was treated with 2 equivalents of imidazole and the mixture was allowed to stand overnight. The whole was washed with water, and the benzene layer dried over magnesium sulfate. Chromatography on silica gel afforded 2-(1-imidazolyl)-1,3,5-trithiane (**5**), mp 174.5—175.5 °C, and 2-(1-imidazolyl)-1,3-dithiane (**6**), mp 139.5—140.5 °C, in 75 and 90% yields, respectively.

5. Found: C, 35.22; H, 3.99; N, 13.79; S, 47.10%. Calcd for $C_6H_8N_2S_3$: C, 35.27; H, 3.95; N, 13.71; S, 47.07%. ^{1}H NMR (δ $CDCl_3$); 4.17 and 4.25 (4H, q, J=15.5 Hz), 6.27 (1H, s), 7.14 (1H, m), 7.27 (1H, m), 7.86 (1H, m).

6. Found: C, 45.42; H, 5.41; N, 15.00; S, 34.68%. Calcd for $C_7H_{10}N_2S_2$: C, 45.13; H, 5.41; N, 15.04; S, 34.42%. ^{1}H NMR (δ, $CDCl_3$): 1.8—2.3 (2H, m), 2.8—3.0 (4H, m), 5.98 (1H, s), 7.14 (1H, m), 7.35 (1H, m), 7.94 (1H, m).

Reaction with Succinimide. To a reaction mixture obtained by treating polythianes with *N*-chlorosuccinimide as above, was added 3—5 equivalents of triethylamine and the whole was allowed to stand overnight. The mixture was washed with water and the benzene layer separated. The solution was dried over magnesium sulfate and evaporated *in vacuo*. Chromatography of the residue on silica gel afforded 2-(*N*-succinimidyl)-1,3-5,trithiane (**7**), mp 148—149 °C, and 2-(*N*-succinimidyl)-1,3-dithiane (**8**), mp 101—101.5 °C, in 70 and 75% yields, respectively.

7. Found: C, 35.78; H, 3.95; N, 5.65; S, 40.74%. Calcd for $C_7H_9NO_2S_3$ C, 35.74; H, 3.86; N, 5.95; S, 40.83%. ^{1}H NMR (δ, $CDCl_3$): 2.79 (4H, s), 4.02 and 4.76 (4H, q, J=14 Hz), 6.24 (1H, s).

8. Found: C, 44.08; H, 4.94; N, 6.43; S, 29.45%. Calcd for $C_8H_{17}NO_2S_2$: C, 44.22; H, 5.10; N, 6.45; S, 29.51%. ^{1}H NMR (δ, $CDCl_3$): 1.8—2.3 (2H, m), 2.6—3.0 (2H, m), 2.74 (4H, m), 3.24—3.7 (2H, m), 6.06 (1H, s).

Reaction with Phenol. The benzene solution of the crude chloride was mixed with 7 ml of phenol at 41 °C and allowed to stand at room temperature overnight. The volatile materials were removed by distillation *in vacuo* and the residue was recrystallized from chloroform or acetone to give 2-(*p*-hydroxyphenyl)-1,3,5-trithiane (**9**), mp 183—184 °C, and 2-(*p*-hydroxyphenyl)-1,3-dithiane (**10**), mp 149—150 °C, in 50 and 75% yields, respectively.

9. Found; C, 46.87; H, 4.58%. Calcd for $C_9H_{10}OS_3$: C, 46.93; H, 4.38%. ^{1}H NMR (δ, $CDCl_3$): 4.00 and 4.51 (4H, q, J=15.5 Hz), *ca.* 4.8 (1H, s), 5.22 (1H, s), 6.82 and 7.31 (4H, q, J=9 Hz).

10. Found: C, 56.49; H, 5.60; S, 29.92%. Calcd for $C_{10}H_{12}OS_2$: C, 56.57; H, 5.70; S, 30.20%. ^{1}H NMR (δ, $CDCl_3$): 1.7—2.3 (2H, m), 2.85—3.1 (4H, m), 5.11 (1H, s), *ca.* 5.2 (1H, s), 6.76 and 7.32 (4H, q, J=8.5 Hz).

Reaction with N,N-*Dimethylaniline.* The benzene solution of crude **2** was mixed with 2.5 ml of *N,N*-dimethylaniline and the mixture was allowed to stand at room temperature overnight. The volatile materials were distilled off *in vacuo* and the residue was recrystallized from acetone to give 2-(*p*-*N,N*-dimethylaminophenyl)-1,3-dithiane (**11**), mp 115.5—116.5 °C, in 30% yield. Found: C, 59.99; H, 6.86; N, 5.95; S, 26.89%. Calcd for $C_{12}H_{17}NS_2$: C, 60.21; H, 7.16; N, 5.85; S, 26.78%. ^{1}H NMR (δ, $CDCl_3$): 1.7—2.3 (2H, m), 2.85—3.1 (4H, m), 2.92 (6H, s), 5.11 (1H, s), 6.77 and 7.32 (4H, q, J=8.5 Hz).

Results

Preparation and Conformation of Chloropolythianes. Chlorinations of 1,3,5-trithiane and 1,3-dithiane were carried out with the use of *N*-chlorosuccinimide in benzene under the conditions of α-chlorination of sulfides.[11] Since **1** and **2** were found to react readily with the atmospheric moisture, the reaction mixture was used after filtration of succinimide for spectral measurement and for reactions. The purity of **1** and **2** was checked by ^{1}H NMR spectra and found to be 90—95%. The yield was estimated to be 90—95% from the ^{1}H NMR spectra. The following ^{1}H NMR data were recorded at room temperature (δ, C_6H_6): **1**, 5.52 (1H, s), 2.91 and 4.56 (4H, q, J=15.0 Hz); **2**, 5.76 (1H, s), 2.64 (4H, m), 1.58 (2H, m).

The ^{1}H NMR spectra of these chlorides were obtained at −80 °C to avoid possible complexity of various origins. A carbon disulfide solution of **1** exhibited signals at δ 6.21 (1H, s) and 5.08 and 3.72 (4H, q, J=15 Hz), whereas that of **2** complex signals

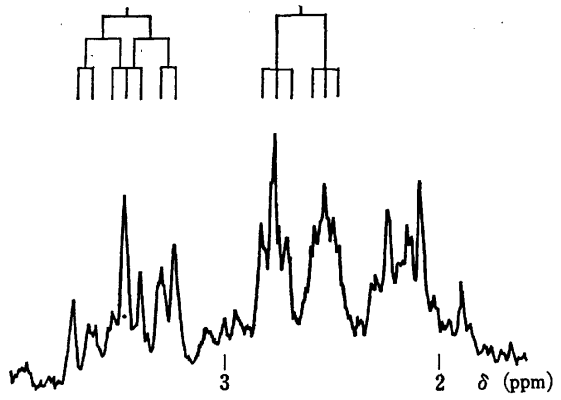

Fig. 1. First-order analysis of ^{1}H NMR signals due to 4,6-protons of **2** in carbon disulfide at −80 °C.

Table 1. ^{1}H NMR data of **2** in carbon disulfide at −80 °C, as analyzed in Fig. 1.

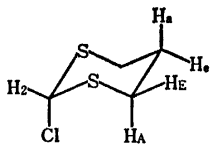

2

Coupling constants		Chemical Shifts	
Assignment	Hz	Assignment	δ
J_{aE}	3	H_E	2.66
J_{eE}	3	H_A	3.49
J_{aA}	10.5∼11		
J_{eA}	3.5		
J_{AE}	14		

(Fig. 1) and a singlet at δ 6.02 (1H, position 2). The coupling constants and chemical shifts involving the protons in 4 and 6 positions obtained by the first order analysis are given in Table 1. The spectra of **1** and **2** in carbon disulfide at −30 °C were essentially the same with those at −80 °C.

Solvent and Temperature Dependence of NMR Spectra. ^{1}H NMR spectra of **1** and **2** were remarkably affected by the solvent. Some of the typical results are shown in Fig. 2. With sulfur dioxide solutions of **2**, the following NMR data were obtained at −50 °C: ^{1}H NMR (ppm from external TMS), 2.27 (2H, m),

Table 2. ^{1}H NMR data and thermodynamic parameters for the ionic dissociation of **1** and **2**

Compound	Solvent	J_{AB}(Hz)	$\Delta\nu_{AB}$(Hz)	T_c(°C)	k_c(s^{-1})	$\Delta G_c^{\ddagger}$(kc al/mol)
1	C_6H_6	15	98	>80	1.9×10^2	>17.1
	o-$Cl_2C_6H_4$	15	78	106	1.9×10^2	18.5
	$CDCl_3$	14.5	74	>60[a]	$1.7_5\times10^2$	>16.2
	$C_6H_5NO_2$	14	72	40	1.8×10^2	15.1
	$(CH_3)_2SO$	—	—	<20	—	<14.2[b]
2	CS_2	14	51	33±3	$1.3_0\times10^2$	15.0
	C_6H_6	—	—	≤ 0	—	≤13.5[b]

a) From the line-broadening, the coalescence temperature was roughly estimated to be 85 °C. Then $\Delta G_c^{\ddagger}$ becomes *ca.* 17 kcal/mol. b) These values are derived by using coupling constants and chemical shifts in other solvents: the data used for **1** are those obtained with *o*-dichlorobenzene solution.

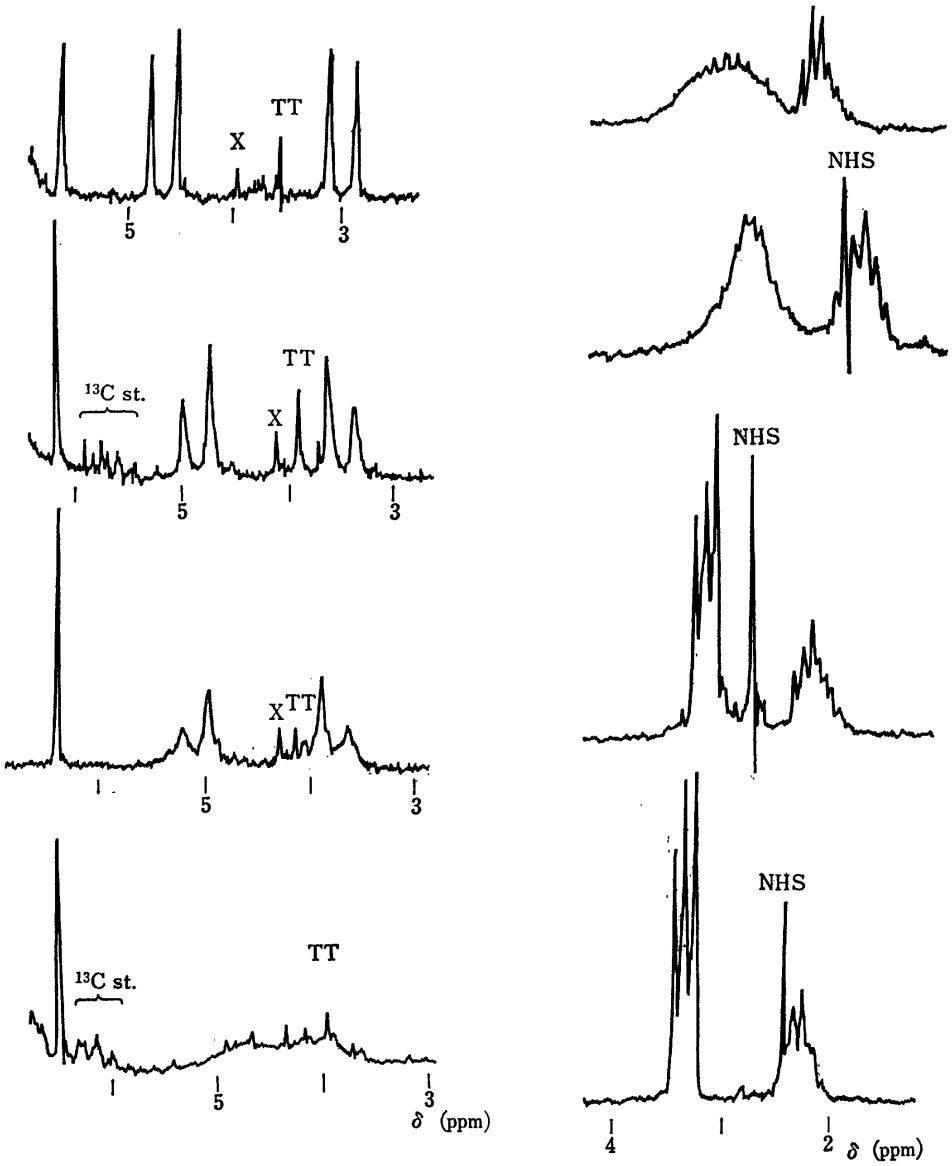

a) **1** at 35 °C. From top to bottom: in C_6H_6, in o-$Cl_2C_6H_4$, in $CDCl_3$, and in $C_6H_5NO_2$. Signals marked X and TT are due to impurities and 1,3,5-trithiane, respectively, and ^{13}C st signals are carbon-13 satellites of the solvents.

b) **2** at 32 °C, except for sulfur dioxide solution (at −40 °C). From top to bottom: in CS_2, in C_6D_6, in $CDCl_3$, and in SO_2. The signals marked NHS are due to succinimide.

Fig. 2. Solvent dependence of ^1H NMR spectra.

3.30 (4H, m), 10.65 (1H, s); ^{13}C NMR (ppm from external TMS), 16.0 (5-C), 30.5 (4, 6-C), 184.5 (2-C). The ^{13}C NMR spectra were essentially the same within the temperature range of −50∼0 °C.

In general, there seems to be an exchange process for both compounds and the process is faster in more polar solvents.

On raising the temperature, we observe spectra to become simplified (see Fig. 3), although decomposition takes place to some extent and lines due to impurities appear. The spectra at low temperatures are roughly reproducible when the temperature is lowered again. The results suggest that the exchange process becomes fast at the higher temperature. The coalescence temperatures (T_c), exchange rate constants at T_c (k_c) and the free energies of activation at T_c ($\Delta G_c^{\neq}$) obtained with various solvents are given in Table 2.

The process is unimolecular because the spectra were little affected by concentration in the range of 0.08—0.65 M. The process is not quenched by addition of potassium carbonate to remove a minute amount of hydrogen chloride which is produced by hydrolysis of **1** or **2** by moisture.

Reactions. Since the chlorides **1** and **2** were not stable, these were treated with nucleophiles and the products were analyzed and characterized. As expected, reaction with benzenethiol led to the formation of 2-phenylthio derivatives and those with imidazole and succininimide afforded the corresponding 1-

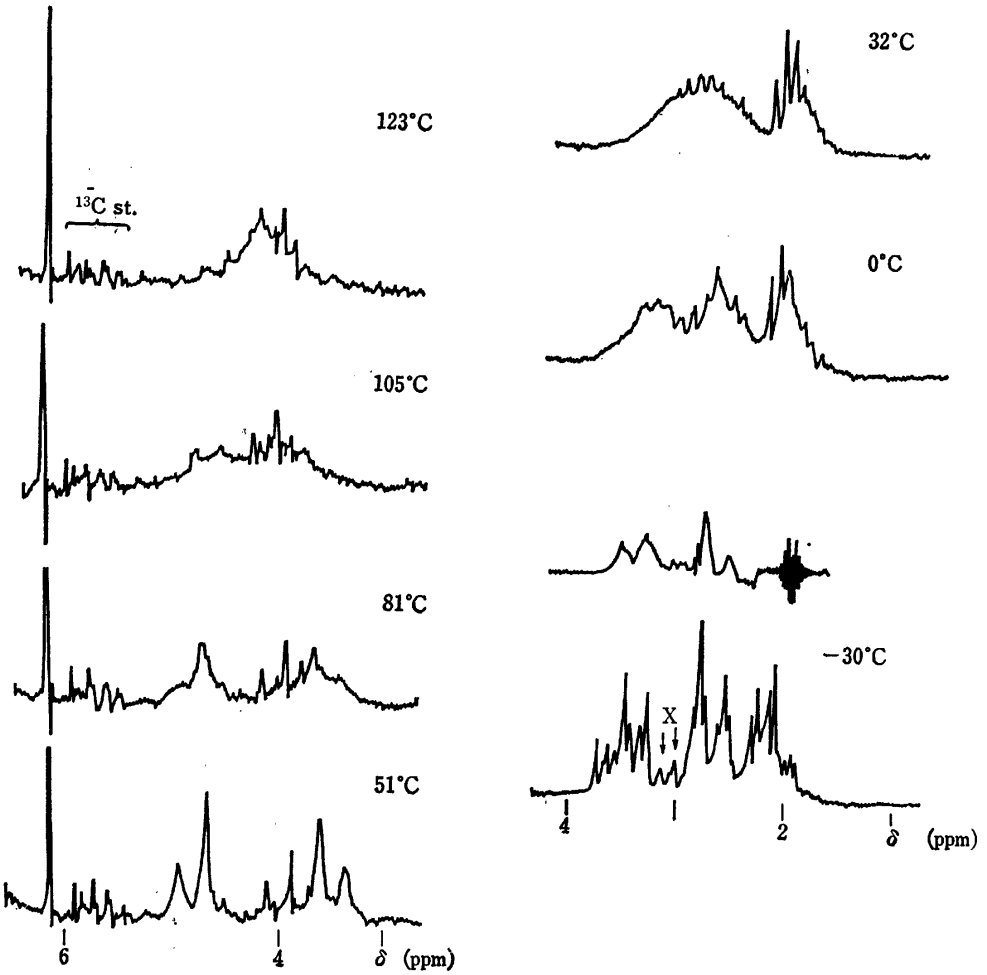

a) **1** in *o*-dichlorobenzene. Signals marked X and TT are due to impurities and 1,3,5-trithiane, respectively, and those marked ^{13}C st are carbon-13 satellites of the solvent.

b) **2** in carbon disulfide. Signals marked X are due to impurities. The second spectrum from the bottom is obtained by irradiating signals due to 5-methylene protons at −30 °C.

Fig. 3. Temperature dependence of ^{1}H NMR spectra.

imidazolyl and succinimidyl derivatives respectively.

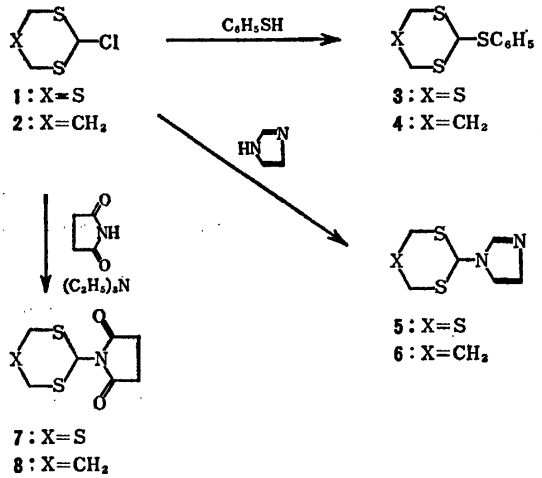

Of interest were the reactions with aromatic compounds which are rich in electron densities. Reactions with phenol and *N*,*N*-dimethylaniline in benzene afforded nuclear substitution products: polythianyl group entered in the *para* position of the electron-donating groups.

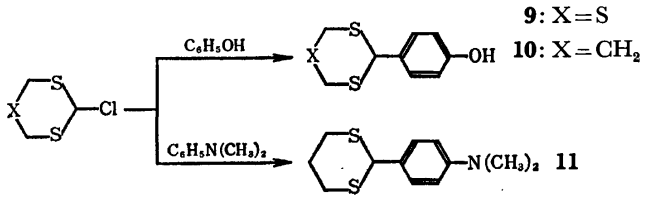

Discussion

Observed solvent and temperature effect on the ^{1}H NMR spectra might be explained by the normal ring inversion leading to an equilibrium (Eq. 1) between equatorial and axial isomers of the chloro compounds. Thus it is necessary to discuss the conformation of these compounds.

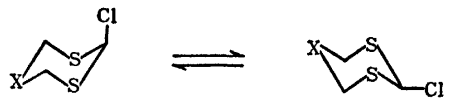

(1)

Inspection of the ^1H NMR spectral data of **1** and **2** in carbon disulfide at −80 °C reveals that there is only one stable conformer for each compound under the conditions: although the temperature of −80 °C is usually low enough to freeze the ring inversion of the trithiane ring,[12] no signals attributable to another conformer are found. The complex spectrum of **2** is the reflection of freezing of the inversion of the dithiane ring. The conformer can either be equatorial or axial, in principle. However, for the following reasons, the conformer will best be assigned to the axial.

Firstly, it is known that strong anomeric effect operates in trithianes.[6,7] 2-Benzoyloxy-1,3,5-trithiane exists as an axial conformer exclusively. The chloro group, being more effective in giving anomeric effect than the benzoyloxy,[13] must destablize the equatorial form to a greater extent. Secondly, assuming the axial conformer explains the ^1H NMR data better.[14] In 1,3,5-trithianes, an equatorial proton in 2-position, where a substituent is borne, is known to give a signal height of 0.8—1.2 if an average height of the AB quartet signals due to protons in 4- and 6-positions is taken as unity. The relative height of a signal due to an axial form, on the other hand, is 1.4—1.6. This owes to the presence of the long-range W-letter coupling by which the equatorial proton gives a broader signal. The observed relative signal height of 0.8 for the 2-proton of **1** is consistent with the conformation which has the proton equatorially and the chloro group axially. It is also known that, in 1,3,5-trithiane series, if a substituent in 2-position is axially oriented, the axial protons in 4- and 6-positions are deshielded by the anisotropy effect of the axial bond and the difference in chemical shifts of the AB protons in 4- and 6-positions amounts to 1.20 ppm or more. On the other hand, the equatorial substituent gives little effect to the chemical shifts of 4- and 6-protons. As a result, the difference in chemical shifts of AB protons in the equatorial conformer is less than 0.65 ppm. The observed difference of 1.36 ppm must be an indication that the conformation is axial.

^1H NMR spectrum of **2** showed complex signals but could be analyzed by the first order approximation. It must have been impossible to analyze by a conventional method if the two conformers coexisted. The chemical shifts of the axial and equatorial protons in 4- and 6-positions listed in Table 1 are consistent with the presence of the axial conformer, the difference being 0.83 ppm. It is also more plausible to assume the overwhelming presence of the axial isomer from the analogy of the trithiane compound **1**.

Since raising the temperature did not give any sign of the presence of the equatorial isomer but causes sudden broadening of the signals in NMR spectra, the conformational equilibrium may be taken to be one-sided in favor of the axial isomer. That essentially the same ^1H NMR spectra were obtained at −80 °C and at −30 °C is a support for the presence of one isomer only because the ring inversion of 1,3,5-trithianes usually causes coalescence of signals at about −60∼−40 °C. Since the equatorial isomer is not detected by the present technique, the free energy difference between the axial and the equatorial conformations must be over 1.7 kcal/mol at −50 °C.

Then it becomes necessary that the cause for the line-broadening of the ^1H NMR signals be sought in other processes than the ring inversion (Eq. 1). The exchange is not a kind of ionic process catalyzed by proton since the addition of potassium carbonate to the system did not affect the rate. Yet, the solvent effect that the rate of exchange is larger in polar solvents strongly suggests the process is of ionic nature. Two possibilities arise to account for the phenomenon. The first is the dissociation of the chloride into the polythianyl cation (**12**) and chloride ion (Eq. 2) and the second is that into the chloropolythianide anion (**13**) and proton (Eq. 3). The second possibility cannot be ruled out without convincing evidence because the anion (**13**) must be stable due to delocalization of the negative charge over chlorine and two sulfur atoms.[15]

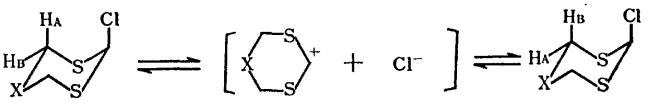

12

(2)

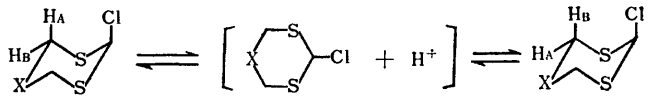

13

(3)

NMR spectra of the ionic species, if we could generate it to, at least, a significant extent, should shed light on this problem. Sulfur dioxide was chosen as a solvent, because it is strongly ionizing. Both the ^1H NMR and ^{13}C NMR spectra of **2** at −50 °C exhibited a signal at a very low field, 10.65 and 184.5 ppm from external TMS, respectively. The results unambiguously indicate that the dissociation according to Eq. 2 takes place in sulfur dioxide solution at −50 °C. As to the extent of the dissociation, we feel it is almost complete because the spectra are essentially the same although the temperature was varied between −50 °C and 0 °C and the features of the ^1H NMR spectra are very similar to those reported for 1,3-dithian-2-yl tetrafluoroborate in nitromethane-d_3.[16] The situation is reminiscent of the case of triphenylmethyl chloride[17] which is known to show first-order kinetics for chloride exchange in benzene solution.[18]

The conclusion drawn from the spectral data is also supported by the chemical properties. Substitution of aromatic rings of high electron density with an easily ionizing halides such as triphenylmethyl chloride is known.[19] Formation of phenol and dimethylaniline derivatives (**9**—**11**) can therefore be taken as an indication that the polythianyl chloride dissociates easily according to Eq. 2.

As auxiliary evidence, the behavior of polythianes bearing a methoxycarbonyl group may be cited. Although the methoxycarbonyl group is a more anion-stabilizing group than the chloro group, the barriers to proton exchange of 2-methoxycarbonyl-1,3-dithiane

and -1,3,5-trithaine were too large to be detected by the dynamic NMR technique.

The kinetic data of the benzene solutions in Table 2 indicate that the free energies of activation for the ionic dissociation of **1** is smaller than those of **2**. It generally appears that the more polar solvent is needed to effect the dissociation of **1** to a similar extent with **2**. The results are in harmony with the facts that anomeric effect is larger in 1,3-dithanes than in 1,3,5-trithianes[6-8] and benzenethiolysis of 2-benzoyloxy-1,3-dithiane is much faster than that of 2-benzoyloxy-1,3,5-trithiane.[10] Since the level of highest occupied molecular orbital of the trithiane system is more effectively lowered than the dithiane system because of the delocalization over the three sulfur atoms,[20] stabilization of the cation in question will be less effective. It seems a general tendency that the phenomenon concerned with the donation of electrons from sulfur atoms is more favored in the 1,3-dithiane system than in the 1,3,5-trithiane system. To the contraty, a phenomenon concerned with acceptance of electrons to these systems is expected to be more facilitated in the latter than in the former, although the comparison has not been made.

We wish to thank Ministry of Education for Grant in Aid for Fundamental Research which supported this work. We are also indebted to Mr. Kiyoshi Aoki of Nippon Electric-Varian Ltd. for the measurement of the ^{13}C NMR spectra.

References

1) A preliminary report has been published: K. Arai and M. Ōki, *Tetrahedron Lett.*, **1975**, 2183.
2) M. Fukunaga, K. Arai, H. Iwamura, and M. Ōki, This Bulletin, **45**, 302 (1972).
3) T. Sugawara, H. Iwamura, and M. Ōki, *Tetrahedron Lett.*, **1975**, 879.
4) K. Arai, H. Iwamura, and M. Ōki, *Chem. Lett.*, **1975**, 1181.
5) A. A. Hartmann and E. L. Eliel, *J. Amer. Chem. Soc.*, **93**, 2572 (1972).
6) T. Sugawara, H. Iwamura, and M. Ōki, This Bulletin, **47**, 1496 (1974).
7) M. Ōki, T. Sugawara, and H. Iwamura, This Bulletin, **47**, 2457 (1974).
8) K. Arai, H. Iwamura, and M. Ōki, This Bulletin, **48**, 3319 (1975).
9) J. A. Pople, W. G. Schneider, and H. J. Bernstein, "High Resolution Nuclear Magnetic Resonance," McGraw-Hill Book Co., Inc., New York (1959), p. 218: J. W. Emsley, J. Feeney, and C. H. Sutcliff, "High Resolution Nuclear Magnetic Resonance Spectroscopy," Pergamon Press, Oxford (1965), p. 481.
10) T. Sugawara, Ph. D. Thesis, The University of Tokyo (1974).
11) D. L. Tuleen and R. H. Bennett, *J. Heterocyclic Chem.*, **6**, 115 (1969).
12) J. E. Anderson, *J. Chem. Soc., B*, **1971**, 2030. See also Ref. 7.
13) D. Horton and W. N. Turner, *Chem. Commun.*, **1965**, 113; *J. Org. Chem.*, **30**, 3387 (1965); P. L. Durette and D. Horton, *Carbohydrate Res.*, **18**, 389, 403 (1971), *J. Org. Chem.*, **36**, 2685 (1971).
14) The data discussed in the following sentences are commonly found in all compounds in Refs. 5—8.
15) Acidities of 1,3-dithiane derivatives were discussed in the following paper: A. Streitwieser and S. P. Ewing, *J. Amer. Chem. Soc.*, **97**, 190 (1975).
16) E. J. Corey and S. W. Walinsky, *J. Amer. Chem. Soc.*, **94**, 8932 (1972).
17) N. N. Lichtin and P. D. Bartlett, *J. Amer. Chem. Soc.*, **73**, 5530 (1951).
18) C. G. Swain and M. M. Kreevoy, *J. Amer. Chem. Soc.*, **77**, 1122 (1955).
19) A. Baeyer, *Ber.*, **42**, 2624 (1909); B. Fohlisch and P. Burgle, *Tetrahedron Lett.*, **1965**, 2661; K. Hiratani, T. Nakai, and M. Okawara, This Bulletin, **46**, 3510 (1973).
20) J. Barret and M. J. Hitch, *Spectrochim. Acta*, **25A**, 407 (1969); L. K. Dyall and S. Winstein, *Spectrochim. Acta*, **27A**, 1619 (1971).

Hydroquinone and Quinone Derivatives of the (*Z*)- and (*E*)-β-Thiocrotonates[1]

E. CAMPAIGNE and Yasuo ABE[2]

Chemistry Laboratories, Indiana University, Bloomington, Indiana 47401, U.S.A.

(Received November 4, 1975)

Addition of ethyl thioacetoacetate to *p*-benzoquinone and 1,4-naphthoquinone gave satisfactory yields of the expected ethyl(*Z*)-β-(2,5-dihydroxyphenylthio)crotonate and ethyl(*Z*)-β-(1,4-dihydroxynaphthyl-2-thio)crotonate respectively. In the latter case, at higher temperatures the isomeric ethyl(*E*)-β-(1,4-dihydroxynaphthyl-2-thio)-crotonate was the major product. Oxidation of these compounds with chromic acid gave the corresponding *Z*- and *E*-isomeric quinone derivatives, but oxidation of the *Z*-isomer of the phenyl compound at higher temperatures gave the (*E*)-quinone derivative. All eight isomers in these two series have been isolated, characterized and identified by NMR assignment.

The addition of thiols to *p*-quinones is complicated by the oxidizing power of the quinones, which can oxidize the thiols to disulfides, and oxidize the product hydroquinone to quinone derivatives. This reaction has been discussed in some detail by Snell and Weissberger[3] who found that by deliberately using an excess of quinone, the product could be isolated as the alkyl or arylthioquinone in satisfactory yields from an alcohol solution without added catalyst. Grinev, *et al.*[4] attempted the addition of ethyl thioacetoacetate to *p*-benzoquinone, using zinc chloride as a catalyst, and obtained the desired ethyl β-(2,5-dihydroxyphenylthio)crotonate, in low yield, melting at 176—177 °C. No attempt was made by the authors to assign steric structure to this product. We have reinvestigated the addition of ethyl thioacetoacetate to both *p*-benzoquinone and 1,4-naphthoquinone, and examined the steric structure of products, and also that of the quinones obtained by further oxidation.

Results and Discussion

In Schemes 1 and 2 the reactions and products are outlined. When ethyl thioacetoacetate was mixed with one equivalent of *p*-benzoquinone in ethanol at room temperature a good yield (58%) of ethyl β-(2,5-dihydroxyphenylthio)crotonate of the same melting point as reported by Grinev, *et al.*[4] was obtained. However, concentration of the mother liquors led to the isolation of second isomer, melting at 139—140 °C, in low yield. These two compounds must have the structures shown in Scheme 1 as **1** and **4**. The higher melting compound was assigned the *Z*-configuration **1** on the basis of NMR (see later).

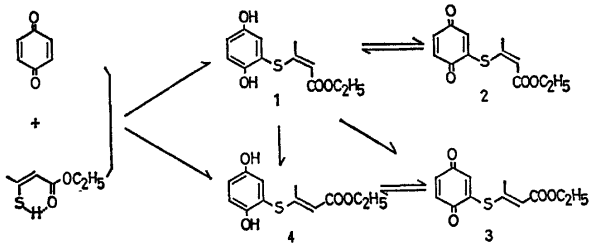

Scheme 1.

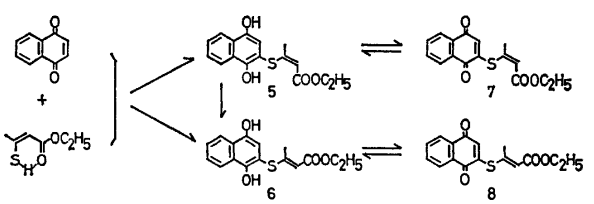

Scheme 2.

Oxidation of **1** with chromic acid at 60 °C gave a quinone **2**, whose NMR was consistent with the *Z*-configuration also. The structural relationship of **1** and **2** was confirmed by reduction of **2** with zinc and acetic acid, giving the higher melting isomer **1** again. Surprisingly, oxidation of **1** with chromic acid at 75 °C led to the formation of a mixture which contained a different, higher melting isomeric quinone, the NMR of which indicated the *E*-configuration **3**. This compound was reduced to the lower melting isomeric ethyl β-(2,5-dihydroxyphenylthio)crotonate, assigned the *E*-configuration **4**, consistent with its NMR spectrum. Oxidation of **4** gave a nearly quantitative yield of **3**.

Finally, heating **1** in acetic acid containing a catalytic amount of hydrochloric acid produced a mixture of **1** and **4**. The reverse isomerization did not occur under these conditions, nor was **2** converted to **3** under these conditions. Nevertheless, it seems reasonable to assume that **1** is the kinetically favored product of the addition of the (*Z*)-thioacetoacetic ester (stabilized by hydrogen bonding) to the quinone, but that the *E*-form, **4**, is thermodynamically favored.

Similar observations were made when ethyl thioacetoacetate was allowed to react with 1,4-naphthoquinone in alcohol solution. If care was taken to keep the solution below 40 °C, even during concentration, the crystalline product, melting at 172.5—173 °C, obtained in satisfactory yield, had the *Z*-configuration (**5**) by NMR (Scheme 2). The configuration of pure **5** was maintained at the reflux condition in alcohol. Alternatively, if a similar solution was heated with steam during work-up, and recrystallized from alcohol then a different product melting at 170—171 °C, assigned the *E*-configuration **6** was obtained as a major product. The nearness of melting points of these two isomers complicated the experimental work. However, NMR characteristics are distinctive, and the melting points of the oxidation products are quite different.

Oxidation of **5** with chromic acid at 60 °C gave the corresponding naphthoquinone **7**, also having the *Z*-configuration, and melting at 97—98 °C, while similar treatment of **6** gave a nearly quantitative yield of

TABLE 1. NMR δ VALUES FOR SELECTED PROTONS OF (*Z*)- AND (*E*)-β-THIOCROTONATES

A. β-Arylthio Derivatives

		R=benzyl[a]	R=2,5-dihydroxyphenyl	R=1,4-dihydroxynaphthyl
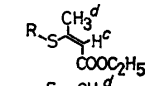	*d*	2.15 (d, 3H, J=1.0)	1.86 (d, 3H, J=1.0)	1.85 (d, 3H, J=1.4)
	c	5.72 (q, 1H, J=1.0)	5.83 (q, 1H, J=1.0)	6.01 (q, 1H, J=1.4)
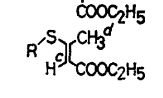	*d*	2.39 (d, 3H, J=0.9)	2.34 (d, 3H, J=1.0)	2.43 (d, 3H, J=1.1)
	c	5.61 (broad)	5.17 (q, 1H, J=1.0)	5.23 (q, 1H, J=1.1)

B. p-Quinone Derivatives

		benzoquinone	naphthoquinone
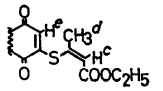	*d*	2.09 (d, 3H, J=1.0)	2.19 (d, 3H, J=1.3)
	c	6.16 (q, 1H, J=1.0)	6.37 (q, 1H, J=1.3)
	e	6.73 (d, 1H, J=2.5)	7.01 (s, 1H)
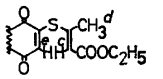	*d*	2.45 (d, 3H, J=0.9)	2.55 (d, 3H, J=1.1)
	c	6.23 (q, 1H, J=0.9)	6.42 (q, 1H, J=1.1)
	e	6.45 (d, 1H, J=2.8)[b]	6.73 (s, 1H)

a) Values from Ref. 5. b) Isopropylthiobenzoquinone shows this proton (*e*) at δ 6.36 (d, 1H, J=2.1 Hz). See Experimental.

ethyl(*E*)-β-(1,4-naphthoquinonyl-2-thio)crotonate, **8**, melting at 119—120 °C. Oxidation of **5** at 75—85 °C gave **7**, but did not give **8** in contrast with the reaction of **1** at the same condition. The reduction of **7** to **5** with zinc dust was quantitative, and **8** did produce **6**, but the reduction was much less facile than with the other quinones. Finally, heating **5** in acetic acid with added hydrochloric acid gave a mixture of isomers, in which **6** predominated, by NMR spectra.

Z- and *E*-isomers of *S*-alkyl derivatives of thioacetoacetic ester, have been examined by Hedegaard, Mortensen, and Lawesson.[5] Alkylation of ethyl thioacetoacetate gave a mixture of the (*Z*)- and (*E*)-β-alkylthiocrotonates, separable by distillation, in a ratio of about 3 to 1. The NMR chemical shifts for the vinyl methyl and vinyl protons of the *Z*- and *E*-isomers of the benzyl derivatives, as assigned by these authors, are shown in Table 1 as reference points. The values are consistent with values assigned to the *cis* and *trans* methyl groups in β,β-dimethylacrylic acid by Anet and Bourn[6] using Nuclear Overhauser effects. These authors assigned the upfield doublet (δ 1.42) to the methyl group *cis* to hydrogen, and the downfield doublet (δ 1.97) to the methyl group *cis* to carboxyl, as predicted by deshielding effects of the carboxyl group.

We have tabulated the significant δ values for our compounds in Table 1. The chemical shifts for the vinylic methyl groups and protons for the arylthio derivatives are shown in part A. Note that the deshielding effect of the *cis*-carboxyl group shows quite well, as the *E*-isomers both show chemical downfield shifts of approximately 0.50 ppm for the vinyl methyl group. On the other hand, a strong shielding effect of the arylthio group on the vinylic protons is observed in the *E*-isomers, which show upfield chemical shifts of about 0.70 ppm over values for this proton in the *Z*-series.

The *p*-quinone derivatives are compared in part B of Table 1. The chemical shifts for the vinylic methyl groups are consistent with the expected deshielding effect of a *cis* carboxyl group over that of a *trans* carboxyl, equal to about 0.36 ppm in each pair of isomers. However, in this case the vinylic hydrogens in the *E*-isomers show a weak deshielding, (0.06±0.01 ppm) probably the effect of the adjacent *p*-quinone, held partially coplanar by conjugation through the sulfur atom. The adjacent thiocrotonic ester exerts an interesting effect on the protons at the 3-position of the quinone (labeled *e* on Table 1B). These protons in the *Z*-isomers appear consistently 0.28 ppm downfield from the absorption of their counterparts in the *E*-isomers, due, apparently, to a deshielding of this proton by the carboxylic ester group in the *Z*-structures, not possible in the *E*-configuration. To confirm our identification of this proton, a sample of isopropylthiobenzoquinone, previously reported[3] was synthesized and its NMR spectra determined. The ring proton at the upfield position at δ 6.36 is clearly the 3-proton, shielded by the adjacent alkylthio group. The assignment of the 3-proton in the naphthoquinone series is simpler, since it is the only possible singlet.

Experimental

Melting points were obtained on a Mel-Temp capillary melting point apparatus and are uncorrected. NMR spectra were determined on a Varian Associates EM 360 spectrometer (60 MHz) using TMS as an internal standard, and mass spectra on a Varian Associates MAT CH-7 spectrometer. IR spectra were determined on a Perkin-Elmer Model 137-B Infracord Spectrometer using potassium bromide disks. Elemental analyses were performed by Midwest Microlabs, Inc., Indianapolis, Indiana, U.S.A.

Ethyl (Z)-β-(2,5-Dihydroxyphenylthio)crotonate (1). *a)* To a solution of 15.0 g (0.14 mol) of *p*-benzoquinone in 200 ml of ethanol was gradually added, with stirring, an ethanol solution of 22.8 g (0.16 mol) of ethyl thioacetoacetate, prepared by the method of Mitra.[7] The reaction mixture turned red and became warm, but after 30 min the color faded to pale brown or tan. Ethanol was removed on a flash evaporator, and the residual oil taken up in warm ethyl acetate. Addition of warm benzene to cloudness and

cooling produced 20.4 g (58%) of **1** as white crystals, mp 174—175 °C (lit,[4] 176—177 °C). NMR (Acetone-d_6): δ 1.23 (t, 3H, J=7 Hz), 1.86 (d, 3H, J=1 Hz), 4.10 (q, 2H, J=7 Hz), 5.83 (q, 1H, J=1 Hz), 6.81—6.89 (m, 3H), 7.84 (s, 2H).

Concentration of the mother liquor gave 5.4 g of crude oily solid which NMR analysis showed was a mixture of **1** and the corresponding *E*-isomer **4**, in a ratio of 1 : 4. This was then taken up in hot benzene and recrystallized, giving 2.1 g (6%) of **4**, mp 138—139 °C (see later).

b) A solution of 1.0 g of ethyl (*Z*)-β-(*p*-benzoquinonylthio)-crotonate (**2**, see later) in 25 ml of glacial acetic acid was stirred while 1.0 g of zinc dust was added in portions. After 45 min the colorless solution was concentrated to a syrup and water added. The white precipitate was collected and recrystallized from benzene–ethyl acetate, giving 1.0 g (98%), of crystals melting at 171—173 °C, shown to be identical to **1**, above, by congruent IR and NMR spectra.

Ethyl (Z)-β-(p-Benzoquinonylthio)crotonate (2). Chromic acid (1.0 g, 10 mmol) was added all at once to a stirred solution of 2.54 g (10 mmol) of **1** in 50 ml of glacial acetic acid at 60 °C. The temperature was maintained at 60 °C for 10 min, after which the orange solution was poured over 300 g of ice. The precipitate was collected and washed with water, then taken up in benzene and washed again. The benzene extract was dried ($MgSO_4$), evaporated, and the solid recrystallized from ethanol to give 1.1 g (44%) of **2**, mp 71—71.5 °C. IR: 1680, 1653, 1640 (C=O), 1567, 1587 (C=C), 1189 cm^{-1} (C–O). NMR: ($CDCl_3$): δ 1.25 (t, 3H, J=7 Hz), 2.09 (d, 3H, J=1 Hz), 4.14 (q, 2H, J=7 Hz), 6.16 (q, 1H, J=1 Hz), 6.70 (dd, 1H, J=2.5, 10.5 Hz), 6.73 (d, 1H, J=2.5 Hz), 6.82 (d, 1H, J=10.5 Hz). MS (*m/e*): 252 (M^+). Found: C, 57.36; H, 4.92; S, 12.94%. Calcd for $C_{12}H_{12}O_4S$: C, 57.13; H, 4.79; S, 12.71%.

Ethyl(E)-β-(p-Benzoquinonylthio)crotonate (3). *a)* Chromic acid (2.0 g, 20 mmol) was added all at once to a stirred solution of 5.1 g (20 mmol) of **1** in 100 ml of glacial acetic acid maintained at 70—75 °C. After 10 min the hot solution was poured directly over ice and the orange precipitate collected and washed with water. The crude product was chromatographed on acidic alumina (Giulini activity Grade 1) eluted with benzene, forming two orange bands. The first fraction gave **3** (0.8 g, 16%) recrystallized from ethanol, mp 83.5—84 °C. IR: 1709, 1645, 1629 (C=O), 1555 (C=C), 1186 cm^{-1} (C–O). NMR ($CDCl_3$): δ 1.28 (t, 3H, J=6.9 Hz), 2.45 (d, 3H, J=0.9 Hz), 4.16 (q, 2H, J=6.9 Hz), 6.23 (q, 1H, J=0.9 Hz), 6.45 (d, 1H, J=2.8 Hz), 6.67 (dd, 1H, J=9.5, 2.8 Hz), 6.81 (d, 1H, J=9.5 Hz). MS (*m/e*): 252 (M^+). Found: C, 57.37; H, 4.88; S, 12.92%. Calcd for $C_{12}H_{12}O_4S$: C, 57.13; H, 4.79; S, 12.71%.

The second fraction from the column worked up in the same way, gave 1.5 g (30% of **2**, identical by melting point and congruent NMR spectra. A mixture melting point of **2** and **3** was depressed.

b) When 0.37 g (1.45 mmol) of ethyl (*E*)-β-(2,5-dihydroxyphenylthio)crotonate (**4**, see later) was oxidized with an equivalent of chromic acid at 60 °C, as described above for the preparation of **2**, the orange precipitate was collected and recrystallized once from ethanol to give 0.31 g (84%) of **3**, mp 80—81 °C, identical with the authentic sample of **3** by IR and NMR spectra without further purification.

Ethyl (E)-β-(2,5-Dihydroxyphenylthio)crotonate (4). Reduction of 1 g (4 mmol) of **3** with zinc dust in glacial acetic acid, as described for the preparation of **1** (*b*) gave 0.97 g (96%) of white crystals from benzene, mp 139—140 °C. IR: 3356 (OH), 1686 (C=O), 1603 cm^{-1} (C=C). NMR (Acetone-d_6): δ 1.13 (t, 3H, J=7 Hz), 2.34 (d, 3H, J=1 Hz), 3.98 (q, 2H, J=7 Hz), 5.17 (q, 1H, J=1 Hz), 6.83 (m, 3H), 7.80 (s, broad, 1H), 7.99 (s, broad, 1H). MS (*m/e*): 254 (M^+). Found: C, 56.50; H, 5.68; S, 12.88%. Calcd for $C_{12}H_{14}O_4S$: C, 56.32; H, 5.58; S, 12.67%.

Ethyl (Z)-β-(1,4-Dihydroxynaphthyl-2-thio)crotonate (5). To a solution of 20 g (137 mmol) of ethyl thioacetoacetate in 100 ml of ethanol was added 15.0 g (91 mmol) of finely ground 1,4-naphthoquinone all at once with stirring at room temperature. The deep red solution was let stand three days, then evaporated under reduced pressure, taking care to keep the temperature below 40 °C. Cold benzene was added, and the slurry so obtained was filtered, washed with cold benzene, and dried under reduced pressure, recrystallization of the product from ethanol gave 18 g (63%) of white crystals, mp 172.5—173 °C. IR: 3322 (OH), 1667 (C=O), 1590 (C=C), 1198 cm^{-1} (C–O). NMR (Acetone-d_6): δ 1.26 (t, 3H, J=7.2 Hz), 1.85 (d, 3H, J=1.4 Hz), 4.20 (q, 2H, J=7.2 Hz), 6.01 (q, 1H, J=1.4 Hz), 6.96 (s, 1H), 7.65 (m, 2H), 8.33 (m, 3H), 8.77 (s, broad, 1H). MS (*m/e*): 304 (M^+). Found: C, 63.12; H, 5.33; S, 10.34%. Calcd for $C_{16}H_{16}O_4S$: C, 63.14; H, 5.30; S, 10.53%.

Ethyl (E)-β-(1,4-Dihydroxynaphthyl-2-thio)crotonate (6). The above experiment was repeated, except that after all of the naphthoquinone had dissolved, the red solution was refluxed on a steam bath for an hour, then the ethanol evaporated on a steam bath and the residue crystallized by the addition of benzene. On cooling, the white crystals were collected and recrystallized from ethanol, giving 13.2 g (46%) of **6**, mp 170—171 °C. IR: 3333 (OH), 1686 (C=O), 1603 (C=C), 1200 cm^{-1} (C–O). NMR (Acetone-d_6): δ 1.08 (t, 3H, J=7.3 Hz), 2.43 (d, 3H, J=1.1 Hz), 4.00 (q, 2H, J=7.3 Hz), 5.23 (q, 1H, J=1.1 Hz), 6.90 (s, 1H), 7.57 (m, 2H), 8.22 (m, 3H), 8.28 (s, broad, 1H). MS (*m/e*): 304 (M^+). Found: C, 62.86; H, 5.00; S, 10.79%. Calcd for $C_{16}H_{16}O_4S$: C, 63.14; H, 5.30; S, 10.53%.

Ethyl(Z)-β-(1,4-Naphthoquinonyl-2-thio)crotonate (7). Oxidation of 3.1 g (10 mmol) of **5** with an equivalent of chromic acid below 60 °C, as previously described for the conversion of **1** to **2**, gave 2.8 g (94%) of orange crystals (from ethanol), mp 97—98 °C. IR: 1698, 1656 (C=O), 1592, 1565 (C=C), 1200 cm^{-1} (C–O). NMR ($CDCl_3$): δ 1.28 (t, 3H, J=7.1 Hz), 2.19 (d, 3H, J=1.3 Hz), 4.23 (q, 2H, J=7.1 Hz), 6.37 (q, 1H, J=1.3 Hz), 7.01 (s, 1H), 7.85 (m, 2H), 8.15 (m, 2H). MS (*m/e*): 302 (M^+). Found: C, 63.25; H, 4.76; S, 10.32%. Calcd for $C_{16}H_{14}O_4S$: C, 63.56; H, 4.67; S, 10.61%.

Oxidation of **5** at 75—85 °C gave orange crystals **7** in 60% yield. The NMR spectra of mother liquor did not show the presence of *E*-isomer **8**.

Reduction of 7. The zinc dust reduction mixture of 1.0 g of **7** in acetic acid (25 ml) was stirred for 40 min, and worked up in the usual manner to give 0.8 g (80%) of **5**, mp 169—171 °C, identified by congruent NMR spectra.

Ethyl (E)-β-(1,4-Naphthoquinonyl-2-thio)crotonate (8). Oxidation of 1.0 g (2.9 mmol) of **6** with an equivalent of chromic acid in glacial acetic acid at 60 °C, as previously described, gave 0.92 g (92%) of yellow crystals after one recrystallization from ethanol, mp 119—120 °C. IR: 1710, 1658 (C=O), 1592, 1563 (C=C), 1198 cm^{-1} (C–O). NMR ($CDCl_3$): δ 1.33 (t, 3H, J=7.2 Hz), 2.55 (d, 3H, J=1.1 Hz), 4.27 (q, 2H, J=7.2 Hz), 6.42 (q, 1H, J=1.1 Hz), 6.73 (s, 1H), 7.83 (m, 2H), 8.32 (m, 2H). MS (*m/e*): 302 (M^+). Found: C, 63.77; H, 4.76; S, 10.33%. Calcd for $C_{16}H_{14}O_4S$: C, 63.56; H, 4.67; S, 10.61%.

Reduction of 8. The zinc dust reduction mixture of 1.0 g of **8** in acetic acid was stirred for several hours, and worked up in the usual manner to give 0.30 g (30%) of **6**,

mp 169—170 °C, identified by congruent NMR spectra. Concentration of the benzene mother liquors gave 0.63 g (63%) of recovered **8**.

Isomerization of Z-Isomers in Acid Solution. A solution of 1.0 g of **1** in 20 ml of glacial acetic acid, to which 0.5 ml of 1 M HCl had been added, was heated to 75 °C for 10 min, then diluted with water and extracted with ether. After drying and concentrating, the residue was subjected to thin layer chromatography on Silica gel G, using chloroform. The R_f range of 0.18—0.37 was collected and extracted with ether, giving 280 mg of crude **4**, mp 130—133 °C. Recrystallization from benzene gave **4**, mp 138—139 °C, identical to an authentic sample by congruent IR and NMR spectra. Extraction of the R_f 0.37—0.59 range gave approximately 500 mg of crude **1**, having a distinct thiolic odor, indicating some decomposition had occurred.

Similar treatment of **4** resulted only in recovery of 95% of **4** unchanged. Likewise, similar treatment of **2** and **3** led to recovery of starting materials in nearly quantitative yields.

A solution of 1.0 g of **5** was heated to 75 °C in 20 ml of glacial acetic acid containing 0.5 ml of 6 M HCl. After 10 min the mixture was poured over 100 g of ice, the precipitate collected, washed with water and dried, giving 0.60 g of crude solid with a definite thiolic odor. Several recrystallizations from ethanol gave a white solid melting at 167—169 °C which by NMR showed the spectrum of **6**, with traces of **5** still present.

Isopropylthiobenzoquinone. Following the procedure of Snell and Weissberger[3] a mixture of isopropylthiol and two equivalents of *p*-benzoquinone were stirred in ethanol at room temperature for 30 min, and worked up as described to yield 32% of yellow crystals, mp 74—76 °C. NMR ($CDCl_3$): δ 1.39 (d, 6H, J=6.6 Hz), 3.27 (m, 1H, J=6.6 Hz), 6.36 (d, 1H, J=2.1 Hz), 6.63 (dd, 1H, J=10, 2.1 Hz), 6.75 (d, 1H, J=10 Hz).

References

1) Contribution No. 2665, Supported by Public Health Service Research Grant GM-10366-12, to Indiana University.

2) On leave from Radiation Center of Osaka Prefecture, Sakai, Osaka, 593 Japan, 1974—1975.

3) J. M. Snell and A. Weissberger, *J. Amer. Chem. Soc.*, **61**, 450 (1939).

4) A. N. Grinev, G. Y. Uretskaya, E. S. Krichevskii, and T. F. Vlasova, *J. Org. Chem. USSR*, **7**, 862 (1971).

5) B. Hedegaard, J. Z. Mortensen, and S. O. Lawesson, *Tetrahedron*, **27**, 3853 (1971).

6) F. A. L. Anet and A. J. R. Bourn, *J. Amer. Chem. Soc.*, **87**, 5250 (1965).

7) S. K. Mitra, *J. Indian Chem. Soc.*, **10**, 71 (1933).

NOTES

BULLETIN OF THE CHEMICAL SOCIETY OF JAPAN, VOL. 49(2), 563—564 (1976)

Epoxide Rearrangement. IV.[1] Isomerization of Cyclohexene and 1-Methylcyclohexene Oxides over Solid Acids and Bases in Gas Phase

Kazushi ARATA, Kiyoshi KATO, and Kozo TANABE*

Hokkaido University of Education, 1-2 Hachiman-cho, Hakodate 040

**Department of Chemistry, Faculty of Science, Hokkaido University, Sapporo 060*

(Received May 29, 1975)

Synopsis. A large amount of diene compounds was found to form in the isomerizations of cyclohexene and 1-methylcyclohexene oxides catalyzed by solid acids and bases in gas phase. The catalysts which were quite inactive in liquid phase showed unexpectedly high activities in gas phase, indicating the different catalytic actions.

We have recently studied the isomerization of 1-methylcyclohexene oxide catalyzed by solid acids and bases in a heterogeneous solid-liquid system and observed the markedly different selectivities which depended on the type of catalysts.[1-3] In order to elucidate the electronic and steric effects of methyl group of the oxide on the reactivity and selectivity, the isomerization of cyclohexene oxide together with 1-methylcyclohexene oxide was studied in a solid-gas system in the present work, since the reaction rate of cyclohexene oxide was extremely low in a solid-liquid system.[3] The catalytic action of solid acids and bases in a solid-gas system was also compared with that in a solid-liquid system.

Experimental

Catalysts and Materials. Cyclohexene and 1-methylcyclohexene oxides, supplied from Takasago Perfumery Co., were fractionally distilled to purify to more than 98%. $NiSO_4$ and $FeSO_4$ were prepared by calcining their heptahydrates (G. R.). Al_2O_3, KAT6 of Nishio Chemical Co., was calcined at 500 °C. TiO_2, TiO_2·ZrO_2, ZrO_2, and ZnO were prepared by thermal decompositions of H_4TiO_4, H_4TiO_4·$Zr(OH)_4$, $Zr(OH)_4$ and $Zn(OH)_2$, respectively, which were produced by the same procedure as that described previously.[1,3] The preparations of $LiClO_4$ and $NaOH/SiO_2$ were also followed by the previous experiment.[3] CaO and MgO were prepared by calcining their hydroxides at 550 °C. All the catalysts were heat-treated in air and stored in sealed ampoules until use.

Procedures. The isomerization of oxides was carried out at 150 °C in a conventional pulse reactor in N_2 carrier. The catalysts (40 mg, 100—200 mesh) were heat-treated again in the reactor at their preparation temperatures in air for 3 hr before reaction. The amount of reactant injected was 0.3—0.4 μl. The products were analyzed and identified by gc comparison with the authentic samples using a 3 m column of 20% polyethylene glycol 20 M on Celite 545 SK (150 °C; N_2, 27 cc/min; FID).

Results and Discussion

The catalytic activity and selectivity for the isomerization of cyclohexene oxide are summarized in Table 1. The main products were cyclohexanone, cyclohexenol and 1,3-cyclohexadiene. Cyclohexanol and cyclohexenone, which are formed by hydrogenation and dehydrogenation of cyclohexene oxide, respectively, were almost negligible or not produced at all, though those corresponding compounds were considerably produced in the rearrangement of 1-methylcyclohexene oxide in the heterogeneous liquid phase.[1-3]

Table 1. Catalytic activity and selectivity for isomerization of cyclohexene oxide

Catalyst[a]	Conversion %	Products (%)[b]		
$NiSO_4$ (250 °C)	58.9	42.0	7.2	7.2
$NiSO_4$ (400 °C)	25.8	11.5	3.3	7.5
$FeSO_4$ (200 °C)	24.5	8.5	2.7	8.6
$FeSO_4$ (400 °C)	49.1	25.6	6.3	13.0
Al_2O_3	79.1	56.4	9.1	9.2
TiO_2	36.8	21.8	2.2	8.2
TiO_2-ZrO_2[c]	59.5	43.7	2.2	9.0
ZrO_2	22.4	5.2	2.0	8.3
ZnO (400 °C)	18.7	5.5	1.5	7.0
$LiClO_4$ (150 °C)	16.0	4.3	1.5	6.4
$NaOH/SiO_2$	18.7	5.1	1.5	6.7
MgO (550 °C)	19.3	5.2	1.8	7.4

a) Calcined at 500 °C unless noted. b) About 3% of an unidentified compound was found right before the epoxide in glc in every reaction. c) Molar ratio= 1 : 1.

The relative activities of $NiSO_4$, Al_2O_3, TiO_2, TiO_2–ZrO_2 and ZrO_2 were similar to those for 1-methylcyclohexene oxide in a liquid phase;[1-3] namely, (1) the activities were higher when calcined at low temperature for $NiSO_4$ and at high temperature for $FeSO_4$, (2) the activity of Al_2O_3 was highest, which gave the outstanding activity for the allyl alcohol formation in the liquid phase reaction, and (3) the activity of TiO_2–ZrO_2 was higher than that of TiO_2 or ZrO_2 due to its higher acidity created by combining both oxides.

Comparatively high activities were shown by ZnO, $NaOH/SiO_2$ and MgO, which were quite inactive in our previous work,[3] where it was considered that basic catalysts such as $NaOH/SiO_2$,[4] CaO and MgO[5] did not cause the rearrangement of 1-methylcyclohexene oxide. ZnO and CaO showed unexpectedly high activities for 1-methylcyclohexene oxide (Table 2). These high activities in the present investigation are considered to be due to the different reaction condi-

Table 2. Catalytic activity and selectivity for isomerization of 1-methylcyclohexene oxide

Catalyst[a]	Conversion %	Products (%)[b]		
		Dienes		Allyl[c] alcohols
$NiSO_4$ (250 °C)	72.4	35.2	35.2	0
Al_2O_3	74.2	44.8	27.3	0
TiO_2	62.9	32.1	12.6	16.3
TiO_2-ZrO_2[d]	71.3	43.3	15.3	7.0
ZrO_2	46.2	12.9	14.4	15.0
ZnO (400 °C)	45.0	12.0	16.5	14.3
CaO (550 °C)	43.6	11.0	14.9	15.5

a) Calcined at 500 °C unless noted. b) The amounts of 1-methylcyclohexanol and 2-methyl-2-cyclohexene-1-one produced in the liquid phase reaction were almost negligible. c) 2-Methyl-2-cyclohexene-1-ol and 2-methylenecyclohexanol. d) Molar ratio=1 : 1.

tions; 40 °C higher in reaction temperature, absence of solvent and gas phase.

The activity of $LiClO_4$, which was surprisingly active for the formation of ketone in the liquid phase reaction,[3] was relatively low. The fact seems to support our previous conclusion that the high activity of $LiClO_4$ in a solid-liquid system is due to the partial dissolution of the catalyst or the complex formation with the epoxide.[3]

The most unexpected observation was the formation of a large amount of the diene compound, 1,3-cyclohexadiene, which was probably formed by the dehydration of cyclohexenol, though the amounts of the corresponding dienes were almost negligible in the liquid phase reaction.[1-3] Since there is a report that cyclohexene oxide is pyrolyzed to form cyclohexanone and cyclohexenol with the negligible amount of 1,3-cyclohexadiene at 407—467 °C,[6] the readsorption of cyclohexenol on the catalyst surface is supposed to cause the dehydration. This interpretation is also supported from another experimental fact that the conversion of cyclohexenol into 1,3-cyclohexadiene was 80% over $NiSO_4$ (400 °C) under the present reaction conditions.

The similar conversion to dienes was also observed for the isomerization of 1-methylcyclohexene oxide as shown in Table 2. The dienes were not identified by comparison with the authentic samples, but the identification is unquestionable from the quite similar selectivities to those of cyclohexene oxide and the additional experimental results: that is, (1) allyl alcohols (a mixture of 2-methylenecyclohexanol and 2-methyl-2-cyclohexene-1-ol in 1 : 1.5) converted into their dienes over $NiSO_4$ (250 °C) in almost 100% under th esame reaction conditions, (2) the oxide isomerized to form 18.8% of dienes, 11.9% of ketone and 25.5% of allyl alcohols over TiO_2 (500 °C, 23 mg) in faster carrier gas (twice as fast as the flow rate in general runs), indicating the decrease of dienes from allyl alcohols and (3) relative retention time in glc between the oxide and dienes was quite close to that in the case of cyclohexene oxide.

There have not been reports concerning the considerable diene formation by the catalyzed isomerization of epoxides, with the exception of the 1,3-cycloheptadiene formation from cycloheptene oxide catalyzed by lithium diethylamide.[7] The conversion of propylene[8,9] and ethylethylene oxides[10,11] over solid acids or bases in gas phase were also not reported to yield their dienes.

We are grateful to Dr. Tadashi Nakamura for his offering a sample of cyclohexenol.

References

1) Part III: K. Arata, S. Akutagawa, and K. Tanabe, This Bulletin, **49**, 380 (1976).
2) K. Arata and K. Tanabe, *Chem. Lett.*, **1974**, 923.
3) K. Arata, S. Akutagawa, and K. Tanabe, This Bulletin, **48**, 1097 (1975).
4) S. Malinowski and S. Szczepanska, *J. Catal.*, **2**, 310 (1963).
5) T. Iizuka, H. Hattori, Y. Ohno, J. Sohma, and K. Tanabe, *ibid.*, **22**, 130 (1971).
6) M. C. Flowers, D. E. Penny, and J. C. Pommclet, *Int. J. Chem. Kinet.*, **5**, 353 (1973).
7) J. K. Crandall and L. C. Chang, *J. Org. Chem.* **32**, 435 (1967).
8) T. Imanaka, Y. Hayashi, and S. Teranishi, *Nippon Kagaku Kaishi*, **1973**, 889.
9) Y. Okamoto, T. Imanaka, and S. Teranishi, This Bulletin, **46**, 4 (1973).
10) M. Nitta, S. Matsumoto, and K. Aomura, *Nippon Kagaku Kaishi*, **1973**, 1839.
11) S. Matsumoto, M. Nitta, and K. Aomura, *ibid.*, **1973**, 2082.

BULLETIN OF THE CHEMICAL SOCIETY OF JAPAN, VOL. 49(2), 565—566 (1976)

ESR Spectra of Nitric Oxide Adsorbed on ZrO_2, CeO_2, and ThO_2

Miki NIWA, Takashi MINAMI, and Yuichi MURAKAMI

Department of Synthetic Chemistry, Faculty of Engineering, Nagoya University, Chikusa-ku, Nagoya 464

(Received June 9, 1975)

Synopsis. ESR spectra of nitric oxide adsorbed on ZrO_2, CeO_2, and ThO_2 were measured at -196 °C, and $g_\perp$, $g_{//}$ and splitting constants were determined.

Nitric oxide is a rare paramagnetic compound stable in the gas phase. However, the ESR spectrum of gaseous NO is not observed with an ordinary X-band spectrometer. Adsorption of NO allows us to observe the adsorbed radical, since the orbital momentum is quenched by the surface fields. The spectra of radicals formed by NO adsorption have been reported only for MgO, ZnO, Al_2O_3, zeolite, Molecular Sieve 4A, TiO_2, SnO_2, and Cr_2O_3–Al_2O_3.[1-10] These spectra have hyperfine structures owing to the nuclear spin of nitrogen, and are easily removed by evacuation for a short time, except for that on Cr_2O_3–Al_2O_3.[10] Lunsford determined the anisotropy of NO radical by utilizing ^{14}NO and ^{15}NO, and discussed its relationship to catalytic activity.[1-5] In the present work, an attempt was made to observe the hyperfine structure for the system of NO on ZrO_2, CeO_2, and ThO_2.

Experimental

Samples. The ZrO_2 sample was prepared by calcination of the powder in air stream at 450 °C for 2 hr. The CeO_2 and ThO_2 samples were made by thermal decomposition of nitrates at 500 °C for 4 hr. Nitric oxide (Takachiho Chemical Ind. Co. Ltd.) was used without further purification.

Measurements. The samples were placed in Pyrex glass ampules for ESR measurements, and dehydrated at 250 °C during a period of 1 hr in a vacuum of 10^{-6} Torr. Nitric oxide was adsorbed at a pressure of *ca.* 5 Torr. ESR measurements were carried out at -196 °C with a JEOL Spectrometer (JES-ME-1X). *g*-Values and hyperfine splitting constants were calculated by comparison with the value for the Mn^{2+} impurity in MgO.

Results and Discussion

The obtained spectra on ZrO_2, CeO_2, and ThO_2 are shown in Figs. 1, 2, and 3, respectively. These spectra were easily removed by evacuation for a short time. They are similar to those obtained for ZnS by Lunsford[2] and TiO_2 by Imelik *et al.*[9] This corresponds to the case in which an unpaired electron of NO (nuclear spin of nitrogen = 1) lies in a crystal field such that $g_\perp > g_{//}$. The anisotropy of spectrum is thus determined

TABLE 1. *g*-VALUES AND HYPERFINE SPLITTING CONSTANTS

Material	$g_\perp$	$g_{//}$	a (G)	Δ (eV)
ZrO_2	2.000	1.92	27.5±0.3	0.36
CeO_2	1.993	1.90	28.4±0.3	0.29
ThO_2	1.991	1.95, 1.93	27.6±0.3	0.57, 0.42

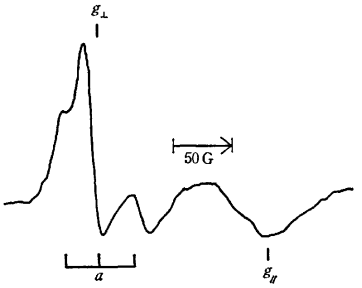

Fig. 1. ESR spectrum of NO adsorbed on ZrO_2.

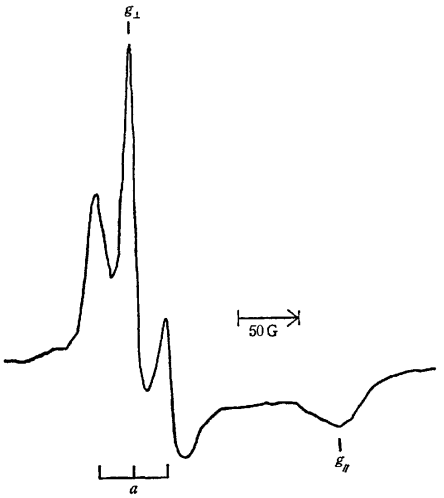

Fig. 2. ESR spectrum of NO adsorbed on CeO_2.

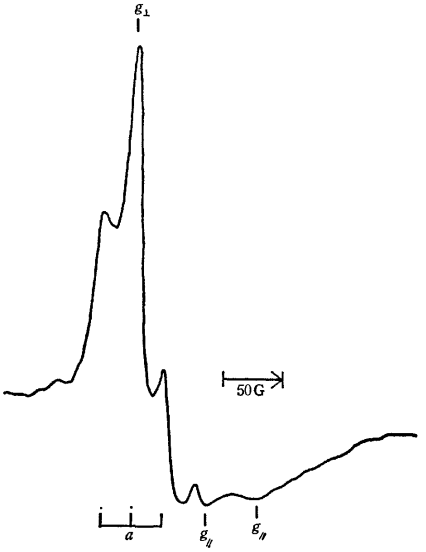

Fig. 3. ESR spectrum of NO adsorbed on ThO_2.

as shown in Table 1.

The spectrum on ThO_2 has two high-field minima as observed on silica-magnesia.[4] The anisotropy of this spectrum remained unchanged when the sample was evacuated at 665 °C under 10^{-6} torr or at 450 °C under 10^{-3} torr. It seems that two types of sites contribute to the adsorption of NO.

The splitting (Δ) of $2p\pi^*$ orbital of NO by the crystal field given by Kanzig and Cohen[11] is as follows,

$$\Delta = \frac{2\lambda}{g_e - g_{//}}$$

where λ is the spin-orbit coupling constant (0.015 eV for NO), and g_e is the g-value of free electron (2.003). The values of Δ for ZrO_2, CeO_2, and ThO_2 are given in Table 1.

References

1) J. H. Lunsford, *J. Chem. Phys.*, **46**, 4347 (1967).
2) J. H. Lunsford, *J. Phys. Chem.*, **72**, 2141 (1968).
3) J. H. Lunsford, *ibid.*, **72**, 4163 (1968).
4) J. H. Lunsford, *J. Catal.*, **14**, 379 (1969).
5) J. H. Lunsford, *J. Phys. Chem.*, **74**, 1518 (1970).
6) C. L. Gardner and M. A. Weinberger, *Can. J. Chem.*, **48**, 1317 (1970).
7) P. H. Kasai and R. J. Bishop, Jr., *J. Amer. Chem. Soc.*, **94**, 5560 (1972).
8) B. M. Hoffman and N. J. Nelson, *J. Chem. Phys.*, **50**, 2598 (1969).
9) M. Primet, M. Che, C. Naccache, M. Mathieu, and B. Imelik, *J. Chim. Phys. Physicochim. Biol.*, **67**, 1629 (1970).
10) M. Shelef, *J. Catal.*, **15**, 289 (1969).
11) W. Kanzig and M. H. Cohen, *Phys. Rev. Lett.*, **3**, 509 (1959).

BULLETIN OF THE CHEMICAL SOCIETY OF JAPAN, VOL. 49(2), 567—568 (1976)

A Study of Catalysis by Metal Phosphate. III.[1] The Dehydrogenation of Alcohols over Cadmium Phosphate and the Influence of CCl_4 Addition on the Catalytic Reaction

Fumio NOZAKI and Yutaka IIMORI

Department of Industrial Chemistry, Faculty of Engineering, Chiba University, Yayoi-cho, Chiba 280

(Received June 28, 1975)

Synopsis. Various alcohols were selectively dehydrogenated over the $Cd_3(PO_4)_2$ catalyst. The addition of CCl_4 during the reaction resulted in a rapid decrease in dehydrogenation activity and in an increase in dehydration activity, accompanied by an evolution of CO_2.

In a previous paper,[1] we have reported a kinetic study of the dehydrogenation of 2-propanol over $Cd_3(PO_4)_2$ and an investigation of the acid-base character of the catalyst. In this paper, we will describe an additional result concerning the relative reactivities of various alcohols. In addition, the results of the influence of CCl_4 addition upon the catalytic reaction will be reported and the observations will be discussed.

Experimental

The catalyst was prepared by the same method as has been described in the previous paper[1]. Before use in the tests, the catalyst was calcined at 400 °C for 2 hr in an air stream. The six kinds of alcohols, C_4H_9OH (to be subsequently referred to as *n*-BtOH), $(CH_3)_2CHCH_2OH$ (*i*-BtOH), $CH_3CH_2CH(OH)CH_3$ (*s*-BtOH), C_3H_7OH (*n*-PrOH), $CH_3CH(OH)CH_3$ (*i*-PrOH), and C_2H_5OH (EtOH), were used after they had been dehydrated and distilled in a routine manner.

The procedures for the catalytic tests and for analyzing the reaction products were practically the same as those described in the previous paper[1], except that a 12-m gas-chromatographic column of 30% DMS-chromosorb operating at room temperature was additionally used in this work for the separation and determination of CO_2, 1-butene, *trans*-2-butene, and *cis*-2-butene.

Results and Discussion

For the cases of all alcohols in so far as we have investigated, the catalyst exceeded 95% in selectivity for dehydrogenation and olefine formation attributable to the dehydration was very slight. The conversion data of alcohols were found to be approximately expressed in the zero-th order kinetics. Arrhenius plots for the rate constants are shown in Fig. 1.

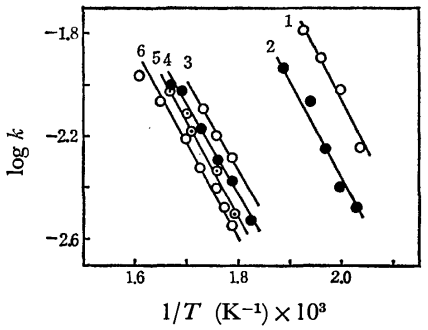

Fig. 1. Arrhenius plots for the rate constants.
1: *s*-BtOH, 2: *i*-PrOH, 3: *i*-BtOH, 4: *n*-BtOH, 5: *n*-PrOH, 6: EtOH.

Figure 1 indicates that the reactivities of the alcohols decrease in this order: *s*-BtOH>*i*-PrOH>*i*-BtOH>*n*-BtOH>*n*-PrOH>EtOH and that the apparent activation energy is about 20 kcal/mol for all the alcohols. The secondary alcohols are much more reactive than the primary alcohols. The observed sequence and regularity in reactivity are similar to that reported in the paper in which the dehydrogenation of alcohols was investigated over metallic catalysts.[2] This fact leads to the speculation that the rate-determining step of the dehydrogenation reaction is an α-hydrogen elimination process.

The changes in catalytic activity upon the addition of CCl_4 are illustrated in Fig. 2, with *i*-PrOH as the example. As CCl_4 had been placed on the catalyst surface, the dehydrogenation to acetone was rapidly retarded and was almost eliminated after the reaction had been continued for about 20 min. In contrast, a dehydration to propylene was generated, with some time-lag. The lag in the appearance of dehydration activity might be a slow response to the acidic sites generated by the reaction of the catalyst with CCl_4. As is shown by Curve 3 in Fig. 2, CO_2 was gradually produced by the addition of CCl_4, although the amount of evolution was so slight that it was difficult to make a quantitative determination. As has previously been reported,[1] the organic acid without a Cl atom, *e.g.*,

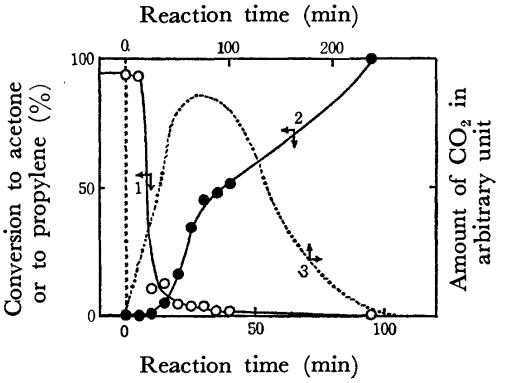

Fig. 2. Influence of CCl_4 addition on the reaction of *i*-PrOH.
1: conversion to acetone, 2: conversion to propylene, 3: relative amount of CO_2.
Reaction temperature: 300 °C, Catalyst weight: 2.0 g, Feed rate of *i*-PrOH and N_2: 0.229 mol/hr, Mol-fraction of *i*-PrOH in feed: 0.24, CCl_4 concentration in the feed: 0.1 mol/l of *i*-PrOH.

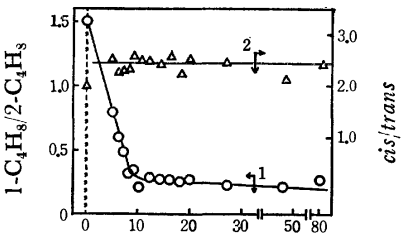

Fig. 3. Changes in the selectivity for dehydration of *s*-BtOH to butene isomers during the course of CCl_4 addition.
1: 1-butene/2-butenes ratio, 2: *cis/trans* ratio in 2-butenes. Reaction conditions are the same as for Fig. 2.

C_6H_5COOH, also retarded the dehydrogenation activity of the catalyst, but there was no enhancement of the dehydration activity. In the case of C_6H_5COOH addition, there was absolutely no such evolution of CO_2 as was observed upon the addition of CCl_4.

The influence of CCl_4 addition upon the reaction of *s*-BtOH was quite similar to that shown in Fig. 2; the dehydrogenation to 2-butanone was rapidly retarded, while the dehydration to butene isomers was much enhanced. A characteristic aspect of the behavior to be noted here is that the distribution of butene isomers changes appreciably upon the addition of CCl_4, as is shown in Fig. 3. Before the addition of CCl_4, the 1-butene/2-butenes ratio in butene isomers was about 1.5. In contrast, as CCl_4 is added the ratio decreases rapidly and leads to a value of about 0.25, a value which is quite close to the value of 0.24 in an equilibrium state.[3] The *cis/trans* ratio in 2-butenes remains almost unaltered and is kept nearly constant in the range from 2.0 to 2.5. In other words, the most abundant isomer varied from 1-butene to *cis*-2-butene upon the addition of CCl_4. Both the 1-butene/2-butenes and *cis/trans* ratios were almost independent of the *s*-BtOH conversion. This indicates that no further isomerization of the butene isomers produced by dehydration is involved.

According to the paper reported by Tanabe *et al*,[3] the change in the 1-butene/2-butenes ratio during the course of CCl_4 addition suggests that the reaction pathway of the dehydration has been altered from an acid-base bifunctional mechanism to an *E*-1 mechanism *via* the carbonium-ion intermediate.

The exact mechanism of the CO_2 formation directly attributable to the admission of CCl_4 is still not yet completely elucidated, but we have speculated that the following reaction is involved:

$$CCl_4 + 2OH^- \longrightarrow CCl_2(OH)_2 + 2Cl^- \longrightarrow 2HCl + CO_2 + 2Cl^-$$

where OH^- is the basic site of the catalyst and plays an important role in the dehydrogenation of alcohol. The acidic action of HCl is a likely cause of the appearance and enhancement of the dehydration activity upon the addition of CCl_4. None of the catalyst poisoned with CCl_4 regained its activity for dehydrogenation when the catalytic reaction of alcohol without CCl_4 was continued or when it was passed through N_2 at 300 °C. By a long period of heating in contact with a N_2 stream containing H_2O at 300 °C, the dehydrogenation activity was substantially regenerated. The introduction of CO_2 had no effect on the reaction. A definite correlation between the loss of the dehydrogenation activity upon the addition of CCl_4 and the formation of CO_2 gives a basis for speculation that OH^- is the active site for the dehydrogenation; however, further experimental evidence is necessary to clarify this postulation.

References

1) Part II of this series: F. Nozaki and H. Ohta, This Bulletin, **47**, 1307 (1974).
2) W. G. Palmer and F. H. Constable, *Proc. Roy. Soc. Ser. A*, **107**, 255 (1925); S. Kudo, "Shokubai Kogaku Koza," Vol. 7, ed. by Catalysis Soc. of Japan, Chijin Shokan, Tokyo (1964), p. 212.
3) T. Yamaguchi, T. Kobayashi, and K. Tanabe, *Nippon Kagaku Zasshi*, **92**, 1076 (1971).

BULLETIN OF THE CHEMICAL SOCIETY OF JAPAN, VOL. 49(2), 569—570 (1976)

Preparation and Properties of Cobalt(II) and -(III) Complexes of (2-Aminoethylthio)acetic Acid

Kiichi Hori

Department of Chemistry, Faculty of Science, Yamagata University, Yamagata 990

(Received April 21, 1975)

Synopsis. The cobalt(II) and -(III) complexes of (2-aminoethylthio)acetic acid (HL), $[CoL_2]\cdot H_2O$, *trans*-(*N*)-$[CoL_2]Cl$ and *cis*(*N*)-$[CoL_2]Cl\cdot 2H_2O$ were prepared and characterized. These complexes are octahedral in which the ligand is coordinated through the N, S and O atoms as a terdentate ligand.

As a part of a study on the cobalt(III) complexes containing sulfides as a ligand, the complexes of bis-(2-aminoethyl)sulfide[1] and 2,2'-thiodiacetic acid[2] have been reported. For the former ligand, only tri-valent complexes were obtained, while for the latter, di-valent complexes were generally obtained. This work was undertaken to prepare cobalt(III) complexes of (2-aminoethylthio)acetic acid and to compare the results with the previous ones.

Experimental

Preparation. *Bis[(2-aminoethylthio)acetato]cobalt(II) monohydrate,* $[Co(NH_2CH_2CH_2SCH_2COO)_2]\cdot H_2O$ ***(1)***. A solution of 4.05 g (0.03 mol) of (2-aminoethylthio)acetic acid in 50 ml of water was adjusted to about pH 11.5 with a sodium hydroxide solution. 2.67 g (0.01 mol) of hexaamminecobalt(III) chloride was added to the solution. The solution was heated at 70—75 °C until ammonia gas evolution ceased, and was filtered. On standing, pinkish crystals were precipitated. Recrystallization was carried out from water.

Found: C, 27.67; H, 5.02; N, 8.06; Co, 17.02%. Calcd for $C_8H_{18}O_5N_2Co$: C, 27.82; H, 5.26; N, 8.11; Co, 17.06%.

trans(N)- *and* cis(N)-*bis[(2-aminoethylthio)acetato]cobalt(III) chloride,* trans(N)-$[Co(NH_2CH_2CH_2SCH_2COO)_2]Cl$ ***(2)*** *and* cis(N)-$[Co(NH_2CH_2CH_2SCH_2COO)_2]Cl\cdot 2H_2O$ ***(3)***. To an aqueous solution of 3.37 g (0.025 mol) of (2-aminoethylthio)-acetic acid adjusted to about pH 9 was added 2.38 g (0.01 mol) of cobalt(II) chloride hexahydrate. The solution was gradually concentrated at 70 °C until it became sticky. Adding 2 ml of 30% hydrogen peroxide, the color of the solution turned to red-purple. The solution was allowed to stand for several days to precipitate the mixture of complexes **2** and **3**. In order to separate the two complexes, a part of the mixture was dissolved in a small volume of warm water and filtered. When the filtrate was cooled, purple crystals of complex **3** were precipitated. The remaining portion of the mixture was dissolved in warm water, and the same volume of ethanol was added. On cooling, red-purple crystals of complex **2** were precipitated. Both of the complexes **2** and **3** were recrystallized from a small amount of water by adding ethanol.

Found for (**2**): C, 26.52; H, 4.64; N, 7.83; Co, 15.67%. Calcd for $C_8H_{16}O_4N_2S_2ClCo$: C, 26.49; H, 4.45; N, 7.72; Co, 16.24%. Found for (**3**): C, 24.05; H, 5.39; N, 7.11; Co, 14.75%. Calcd for $C_8H_{20}O_6N_2S_2ClCo$: C, 24.09; H, 5.06; N, 7.03; Co, 14.78%.

Apparatus. The same instruments as those described previously were used.[1,2]

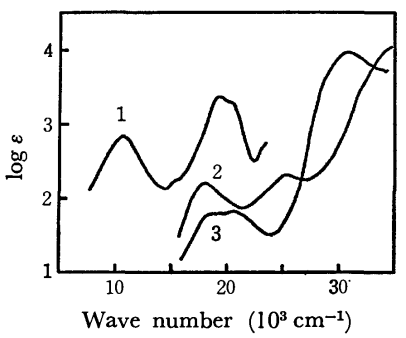

Fig. 1. Electronic spectra of complexes.
1: Reflection spectrm of (**1**) (arbitrary scale), 2: Absorption spectrum of (**2**), 3: Absorption spectrum of (**3**).

Results and Discussion

The reflectance spectrum of complex **1** is similar to those of well-known octahedral cobalt(II) complexes such as $[Co(H_2O)_6]^{2+}$ in the near-infrared and visible regions (Fig. 1).[3] Furthermore, the magnetic moment value of 5.18 B.M. obtained falls within the range of 4.7—5.2 B.M. usually found for regular high-spin octahedral complexes.[4] Therefore, complex **1** is concluded to be a high-spin octahedral cobalt(II) complex.

From the infrared spectral data, it is proven directly that both amino and carboxylate groups are coordinated in the ligand. When the S atom with both N and O terminals is present in a straight chain ligand molecule around the central cobalt(II) ion, it will be useful to promote the coordinating effect of the sulfur. Finally, since all N, O and S atoms in the ligand can be coordinated potentially on chelation, it seems more practical to consider the existence of a terdentate ligand in this case.

On the other hand, both complexes **2** and **3** are diamagnetic and their molar extinction coefficients are appropriate for the cobalt(III) complexes (Fig. 1). Therefore, they are concluded to be octahedral cobalt-(III) complexes. The ligand in these complexes is concluded to function as a terdentate ligand from a consideration analogous to the case of complex **1**.

The absorption spectrum of complex **2** shows a splitting in the first band while that of complex **3** does not. The patterns of the absorption spectra of complexes **2** and **3** are similar to those of *trans*- and *cis*-$K[Co(ida)_2]$,[5] respectively, in the visible region. Such a similarity indicates that these complexes of the $N_2S_2O_2$ type may be similar to cobalt(III) complexes of iminoacetic acid of the N_2O_4 type in the strength of crystal field splitting. It is, therefore, suggested that complex **2** which has a splitting in the first band is the

Table 1. The main bands of infrared spectra of the complexes (cm^{-1})

(1)	NiL_2[a)]	CuL_2[a)]	(2)	(3)	Complex
3248(s)	3260(s)	3220(s)	3200(s)	3270(s)	ν(N-H)
3140(s)	3130(s)	3120(s)	3080(s)	3220(m)	
				3200(m)	
1630(s)	1636(s)	1628(s)	1630(s)	1638(s)	ν_a(COO)
1565(s)	1570(s)	1570(s)	1586(s)	1563(s)	δ(N-H)
1366(s)	1368(s)	1365(s)	1318(s)	1320(s)	ν_s(COO)
370(m)	381(m)	418(m)	537(m)	528(m)	ν(M-N)
265(m)	278(m)	340(w)	374(m)	375(m)	ν(M-O)
240(w)	254(w)	260(w)	270(w)	265(w)	ν(M-S)

a) $L=NH_2CH_2CH_2SCH_2COO^-$. s: strong, m: medium, w: weak.

trans form with respect to the nitrogen atoms and complex **3** which shows no splitting is the *cis* form, as in the case of $K[Co(ida)_2]$. For these cobalt(III) complexes, six geometrical forms are possible: two species with a *trans(N)-fac* configuration, one with a *cis(N)-mer* configuration and three with a *cis(N)-fac* configuration. However, the detailed coordination structures is not known because no NMR data are available, owing to the poor solubility of the complexes. Considering the reduced yield of the *mer* configuration in the complexes with iminodiacetic acid or the related ligand,[5,6] the *mer* configuration does not seem to be contained in these complexes.

The infrared spectral data of the complexes are summerized in Table 1, together with those of nickel(II) and copper(II) complexes of (2-aminoethylthio)-acetic acid. The assignments of the bands are tentative and were made with reference to the spectra of related complexes,[7] considering deuteration effects. The ν(Co(III)–N) bands for complexes **2** and **3** were assigned to slightly higher wave numbers, because no corresponding bands could be found the bands appearing in the 480—520 cm^{-1} region. In the complexes containing the bond of thioether-type sulfur and metal, the ν(M–S) bands have been assigned to the 210—260 cm^{-1} region for the cobalt(II), nickel(II) and copper(II) complexes with (alkylthio)acetic acid,[8] and to 307 and 316 cm^{-1} for the palladium(II) and platinum(II) complexes with dimethyl sulfide, respectively.[9] It was therefore expected that the ν(Co(II)–S) and ν(Co(III)–S) bands for the present complexes would appear in the 210—250 cm^{-1} and 250—300 cm^{-1} regions, respectively. The appropriate bands appearing in this region and corresponding to the nickel and copper complexes shown in Table 1 are unique for each of the complexes **1**, **2** and **3**. These were assigned to the ν(Co(II)–S) and ν(Co(III)–S) bands, respectively.

References

1) K. Hori, *Nippon Kagaku Zasshi*, **91**, 62 (1970).
2) K. Hori, *Bull. Yamagata Univ. (Nut. Sci)*, **8**, 533 (1975).
3) A.B.P. Lever, "Inorganic Electronic Spectroscopy," Elsevier, Amsterdam (1968), p. 318.
4) E. K. Barefield, D. H. Busch, and S. M. Nelson, *Quart. Rev.*, **22**, 457 (1968).
5) J. Hidaka, Y. Shimura, and R. Tsuchida, This Bulletin, **35**, 567 (1962).
6) J. I. Legg and D. W. Cooke, *Inorg. Chem.*, **5**, 594 (1966); A. Uehara, E. Kyuno, and R. Tsuchiya, This Bulletin, **43**, 1394 (1970).
7) K. Nakamoto, "Infrared Spectra of Inorganic and Coordination Compounds," John Wiley & Son, New York (1970); R. A. Condrate and K. Nakamoto, *J. Chem. Phys.*, **42**, 2590 (1965); G. Watt and J. F. Knifton, *Inorg. Chem.*, **6**, 1010 (1967); C. V. Berney and J. H. Weber, *ibid.*, **7**, 283 (1968); B. F. G. Johnson and R. A. Walton, *Spectrochim. Acta*, **22**, 1853 (1966).
8) A. Ouchi, T. Takeuchi, and Y. Ohashi, This Bulletin, **44**, 731 (1971).
9) J. R. Allkins and P. J. Hendra, *J. Chem. Soc., A*, **1967**, 1325.

BULLETIN OF THE CHEMICAL SOCIETY OF JAPAN, VOL. 49(2), 571—572 (1976)

The Spectrophotometric Determination of Beryllium with Chromazurol S and Polyoxyethylenedodecylamine

Hiroshi NISHIDA, Taeko NISHIDA, and Hiroshi OHTOMO
Faculty of Engineering, Iwate University, Ueda, Morioka 020

(Received August 23, 1975)

Synopsis. A sensitive and selective method for the spectrophotometric determination of beryllium with Chromazurol S (CAS) and polyoxyethylenedodecylamine(POEDA) in the presence of EDTA and perchlorate is proposed.

Sensitive methods for the spectrophotometric determination of beryllium with several triphenylmethane dyestuffs and cationic surfactants have been developed.[1-5] These methods are, however, subject to interferences from large anions, such as nitrate (above 4×10^{-2} mol/l) and perchlorate (above 4×10^{-4} mol/l), which precipitate easily by forming ion-pairs with the cationic surfactant.[2] In the present work, it is found that the effects of these anions can be appreciably eliminated by the use of a surfactant with a large polarity, such as polyoxyethylenedodecylamine {*N,N*-bis-(polyethylene glycol)-dodecylamine, abbreviated as POEDA}, and perchlorate in the spectrophotometric determination of beryllium with Chromazurol S(abbreviated as CAS).

Reagents and Apparatus. The standard beryllium solution (Be 1.00 mg/ml), the CAS solution (0.25%), the ethylenediaminetetraacetic acid disodium salt (abbreviated as EDTA) solution (1%), and the sodium acetate solution (1 mol/l) used in this work were the same as those described in previous papers.[2-4] POEDA solution (0.5%): the reagent (0.5 g) was dissolved in water containing 0.5 ml of 2 mol/l hydrochloric acid. The solution was adjusted to pH 4.5 with the sodium acetate solution and diluted to 100 ml with water. All the other chemicals used were of an analytical reagent grade. A Hitachi 139 spectrophotometer and 10-mm cells were used to measure the absorbance.

Recommended Procedure. A solution containing less than about 2 μg of beryllium was transferred into a beaker, there after 1 ml of the EDTA solution and 5 ml of a sodium perchlorate solution (5 mol/l) were added. The pH was adjusted to 4.5 with the sodium acetate solution, and the solution was evaporated to 5—10 ml.[3] By this procedure, interference from aluminum can be avoided by the easy complexing with EDTA. After cooling to room temperature, 1 ml of the CAS solution and 2 ml of the POEDA solution were added. The solution was transferred into a 25-ml volumetric flask and made up to volume with water. After the solution had then stood for 15 minutes, its absorbance was measured in a 10-mm cell at 605 nm against a reagent blank.

Effects of pH and Reagent Concentrations. The absorption maximum of the beryllium–CAS complex in the presence of POEDA is at 605 nm. The maximum absorbance is about four times higher than that in the absence of POEDA. The absorbance of the complex is almost constant over the pH range from 4.2 to 4.9.

A constant absorbance is obtained by the addition of more than 0.8 ml of the CAS solution (in the presence of 2 ml of the POEDA solution) and more than 1.5 ml of the POEDA solution (in the presence of 1 ml of the CAS solution). The addition of 1 ml of the CAS solution and 2 ml of the POEDA solution at pH 4.5 is, therefore, recommended.

A constant absorbance is also obtained by the addition of more than 0.8 ml of the EDTA solution. The maximum absorbance is obtained within 10 minutes after the color development and then remains constant for at least 10 hours.

Effect of the Concentration of the Perchlorate. A turbidity does not appear in the CAS–POEDA solution, even when 10 ml of a 5 mol/l sodium perchlorate solution are added. In the previous work, since the absorbance of the CAS–zephiramine solution increases with an increase in the ionic strength in the sample solution, the concentration of anions in the sample solution has to be held constant.[4] The effect of the concentration of anions on the absorbance of the CAS–POEDA solution is, therefore, examined. The effect of the concentration of perchlorate on the absorbance of the solution at pH 4.5 is shown in Table 1. The absorbance does not vary with the variation

TABLE 1. EFFECT OF THE CONCENTRATION OF SODIUM PERCHLORATE ON THE ABSORBANCE OF CAS-POEDA SOLUTION AT pH 4.5

	Concentration of sodium perchlorate (mol/l)			
	0	0.5	1.0	2.0
Absorbance at 605 nm	0.228	0.230	0.230	0.234
	0.375[b]	0.250[a]	0.230[a]	0.230[e]
	0.425[d]	0.270[b]	0.232[b]	0.241[f]
	0.339[e]	0.276[c]	0.232[c]	0.232[g]
	0.350[h]	0.302[d]	0.248[d]	0.253[h]

Reference: water, Diverse anion added: a) nitrate (1 mol/l), b) nitrate (2 mol/l), c) chloride (1 mol/l), d) chloride (2 mol/l), e) sulfate (0.2 mol/l), f) sulfate (0.4 mol/l), g) acetate (0.1 mol/l), h) acetate (0.3 mol/l).

TABLE 2. EFFECT OF THE CONCENTRATION OF SODIUM PERCHLORATE ON THE ABSORBANCE OF THE COMPLEX

	Concentration of sodum perchlorate (mol/l)				
	0	0.5	1.0	2.0	4.0
Absorbance at 605 nm	0.400	0.399	0.398	0.395	0.361

Reference: reagent blank, Be taken: 1.00 μg.

in the concentration of perchlorate. Up to 2 mol/l of nitrate and up to 1 mol/l of chloride in the presence of 1 mol/l of perchlorate also have no effect on the absorbance of the solution. The effect of the concentration of perchlorate on the absorbance of the complex is shown in Table 2. A constant absorbance is obtained by the addition of less than 10 ml of a 5 mol/l sodium perchlorate solution. The addition of 5 ml of the sodium perchlorate solution is, therefore, recommended.

Table 3. Effects of anions

Ion added (g)		Added as	Be found (μg)	Error (μg)
ClO_4^-	2.5	$NaClO_4$	0.99	−0.01
	7.5		0.90	−0.10
NO_3^-	1.5		0.99	−0.01
	3.0	$NaNO_3$	0.99	−0.01
	4.0		0.96	−0.04
Cl^-	1.0	NH_4Cl	0.99	−0.01
	2.0		0.97	−0.03
SO_4^{2-}	0.5		1.00	0
	0.7	Na_2SO_4	1.00	0
	1.0		1.09	+0.09
CH_3COO^-	0.10		1.00	0
	0.30	CH_3COONa	0.95	−0.05
F^-	0.003	NH_4F	0.95	−0.05

Be taken: 1.00 μg.

Table 4. Effect of cations

Ion added (mg)		Added as	Be found (μg)	Error (μg)
Ca^{2+}	1	$CaCl_2$	0.99	−0.01
Ba^{2+}	1	$BaCl_2$	0.99	−0.01
Mn^{2+}	1	$MnSO_4$	1.02	+0.02
Zn^{2+}	1	$ZnSO_4$	1.02	+0.02
Cd^{2+}	1	$CdSO_4$	0.98	−0.02
Pb^{2+}	1	$Pb(NO_3)_2$	1.00	0
Cu^{2+}	0.5	$CuSO_4$	1.03	+0.03
Ni^{2+}	0.5	$NiSO_4$	1.03	+0.03
Al^{3+}	0.2	$KAl(SO_4)_2$	1.01	+0.01
	0.5		1.10	+0.10
Fe^{3+}	0.3	$Fe(NO_3)_3$	1.03	+0.03
Mo^{6+}	0.1	$(NH_4)_6Mo_7O_{24}$	1.03	+0.03
V^{5+}	0.1	NH_4VO_4	1.03	+0.03

Be taken: 1.00 μg.

Effects of Diverse Ions. The effect of anions on the beryllium determination is shown in Table 3. Up to 2.5 g of perchlorate, 3 g of nitrate, 2 g of chloride, 0.7 g of sulfate, and 0.1 g of acetate do not interfere, but fluoride interferes seriously. The effect of cations on the beryllium determination is shown in Table 4. One mg of calcium, barium, manganese, zinc, cadmium and lead, 0.5 mg of nickel and copper, 0.3 mg of iron, 0.2 mg of aluminum, and 0.1 mg of molybdemum(VI) and vanadium(V) can be tolerated for the determination of 1 μg of beryllium, with a relative error of 3%.

Calibration Curve. As a result of the examinations described above, a procedure for the beryllium determination may be proposed. In the calibration curve obtained by the recommended procedure, Beer's law is obeyed over a concentration range up to at least 0.08 μg/ml and the apparent molar absorptivity at 605 nm is 9.0×10^4 l mol^{-1} cm^{-1}, which is 12% lower than that in the CAS–zephiramine method.[4]

The proposed method has the following merits compare with the CAS–zephiramine method:[4] it is adaptable to the beryllium determination in the sample solution containing perchlorate and nitrate as well as chloride, and it is unnecessary to hold the concentration of these anions constant within the range of concentrations described above.

References

1) H. Kohara, N. Ishibashi and K. Fukamachi, *Bunseki Kagaku*, **17**, 1400 (1968).
2) Y. Horiuchi and H. Nishida, *ibid.*, **18**, 180 (1969).
3) Y. Horiuchi and H. Nishida, *ibid.*, **18**, 1401 (1969).
4) H. Nishida, *ibid*, **20**, 1080 (1971).
5) Y. Shijo and T. Takeuchi, *ibid.*, **20**, 137 (1971).

BULLETIN OF THE CHEMICAL SOCIETY OF JAPAN, VOL. 49(2), 573—574 (1976)

Synthetic Reacions by Complex Catalysts. XXXVIII. A New Preparation of Copper(I) Isocyanate(Alkyl Isocyanide) and Its Reactions

Yoshihiko Ito, Yoshinori Inubushi, Shun-ichi Matsumura, and Takeo Saegusa
Department of Synthetic Chemistry, Faculty of Engineering, Kyoto University, Kyoto 606

(Received June 23, 1975)

Synopsis. Reaction of ethyl carbamate with Cu_2O in the presence of *t*-butyl isocyanide produces copper(I) isocyanate(*t*-butyl isocyanide) complex, $Cu(NCO)(t\text{-}C_4H_9NC)_{2.5}$ (**1**), in 93% yield. Complex **1** is also produced in high yield by the reaction of ethyl *N*-trimethylsilylcarbamate with Cu_2O in the presence of *t*-butyl isocyanide. Complex **1** reacts with alkyl halides in alcohols and with acyl chlorides to afford *N*-alkylcarbamate (**2**) and acyl isocyanate (**3**), respectively, in moderate yields.

It was already reported that organocopper(I)(alkyl isocyanide) complexes[1] and copper(I) carboxylate (alkyl isocyanide) complexes[2] have been successfully prepared by the reactions of Cu_2O/RNC system with carbon acids such as cyclopentadiene, acetylacetone, and malonate (Eq. (1)), and with carboxylic acid (Eq. (2)).

$$\begin{matrix}X\\Y\end{matrix}\!\!>CH_2 + Cu_2O/RNC \xrightarrow{-H_2O} \begin{matrix}X\\Y\end{matrix}\!\!>CHCu(RNC)_n \qquad (1)$$

$$RCO_2H + Cu_2O/RNC \xrightarrow{-H_2O} RCO_2Cu(RNC)_n \qquad (2)$$

We have now found that the treatment of ethyl carbamate with Cu_2O/RNC produces copper(I) isocyanate (alkyl isocyanide) complex in high yields. This reaction presents a convenient one-step preparative method of Cu(I) isocyanate complex(**1**)[3]

$$NH_2CO_2C_2H_5 + Cu_2O/RNC \xrightarrow[-H_2O]{-C_2H_5OH} \underset{\mathbf{1}}{Cu(I)(NCO)(RNC)_n} \qquad (3)$$

The preparation of Cu(I)isocyanate(*t*-butyl isocyanide) complex (**1a**) was carried out as follows. Under nitrogen, a mixture of ethyl carbamate, Cu_2O, and *t*-butyl isocyanide in benzene was refluxed for 6 hr, water and ethyl alcohol produced being removed by azeotropic distillation. The complex of Cu(I)(NCO)-$(t\text{-}C_4H_9NC)_{2.5}$ (**1a**) was obtained as a white crystalline solid in 93% yield based upon the starting carbamate. Complex **1a** is not very sensitive to air in solid form, but is readily oxidized in solution. The identity of **1a** has been established by elemental analysis, IR and NMR spectra, and a chemical transformation. Complex **1a** was treated with ethyl alcohol containing dry HCl to produce ethyl carbamate and Cu(I)Cl(t-C_4H_9-NC) complex. It is of interest that complex **1** was also produced in high yields by the reaction of ethyl *N*-trimethylsilylcarbamate[4] with Cu_2O/RNC.

$$(CH_3)_3SiNHCO_2C_2H_5 + Cu_2O/RNC \longrightarrow \underset{\mathbf{1}}{Cu(I)(NCO)(RNC)_n} \qquad (4)$$

A detailed understanding of the reaction mechanism for the formation of copper(I)isocyanate complex **1** must await further studies.

Complex **1a**, which is soluble in most organic solvents, is conveniently utilized for the preparation of urethane derivatives and acyl isocyanates. Complex **1a** did not react with any alkyl halides but reacted with the halides in the presence of alcohol to afford *N*-alkylcarbamate (**2**) in moderate yields (Eq. (5)). Also, complex **1a** reacted with acyl chlorides to produce acyl isocyanates (**3**) in good yields (Eq. (6)). Results are summarized in Table 1.

$$\mathbf{1a} + RBr + R'OH \longrightarrow \underset{\mathbf{2}}{RNHCO_2R'} \qquad (5)$$

$$\mathbf{1a} + RCOCl \longrightarrow \underset{\mathbf{3}}{RCONCO} \qquad (6)$$

Experimental

*Preparation of Copper(I) Isocyanate(t-Butyl Isocyanide) Complex Cu(I)(NCO)(t-$C_4H_9NC)_{2.5}$ (**1a**).* Under nitrogen, a mixture of ethyl carbamate (6 mmol), Cu_2O (4 mmol),

Table 1. Reaction of complex **1a** with alkyl halide–alcohol and with acyl chloride

Halide	Alcohol	Reaction[a] °C	Reaction[a] hr	Product (%)	
n-C_3H_7Br	C_2H_5OH	80	2	n-$C_3H_7NHCO_2C_2H_5$	(83)
n-C_4H_9Br	t-C_4H_9OH	75	5	n-$C_4H_9NHCO_2(t\text{-}C_4H_9)$	(61)
n-C_3H_7Br	i-C_3H_7OH	80	2	n-$C_3H_7NHCO_2(i\text{-}C_3H_7)$	(73)
i-C_3H_7Br	C_2H_5OH	80	8	i-$C_3H_7NHCO_2C_2H_5$	(74)
$CH_3CH(Br)CO_2C_2H_5$	C_2H_5OH	80	9	$CH_3CH(CO_2C_2H_5)NHCO_2C_2H_5$	(90)
$BrCH_2CH_2CH_2OH$		100	21	$\lfloor CH_2CH_2CH_2NHCO_2 \rfloor$	(77)
PhCOCl	—	50	5	PhCONCO	(76)
n-$C_7H_{15}COCl$	—	25	3	n-$C_7H_{15}CONCO$	(85)

a) Reaction conditions: **1a** (1 mmol), halide (1.5 mmol), alcohol (1.7 mmol).

t-butyl isocyanide (30 mmol), and benzene (20 ml) was refluxed for 6 hr, water and ethyl alcohol produced being removed by azeotropic distillation. Then, the solvents were removed *in vacuo*, and the residue was recrystallized from benzene to give complex **1a** as a white crystalline solid (mp 103 °C) in 93% yield based upon the carbamate. [**1a**: Found: C, 51.68; H, 7.40; N, 15.78%. Calcd for $Cu(NCO)(C_4H_9NC)_{2.5}$: C, 51.74; H, 7.24; N, 15.64%. IR(KBr) 2220, 2200, 2180, 2140, 1200 cm^{-1}. NMR($CDCl_3$) δ 1.20 (s).]

Complex **1a** was also prepared in 90% yield by the reaction of ethyl *N*-trimethylsilylcarbamate (10 mmol)[4] with Cu_2O (12 mmol) and *t*-butyl isocyanide (50 mmol) at 80 °C for 2 hr. Hexamethyldisiloxane was also isolated.

Reaction of ***1a*** *with Alkyl Halide and Alcohol.* A mixture of **1a** (1 mmol), butyl bromide (1.5 mmol), and *t*-butyl alcohol (1.7 mmol) was heated at 75 °C for 5 hr under nitrogen. The reaction mixture was triturated with ether, and filtered to remove copper(I) bromide (*t*-butyl isocyanide) complex. The filtrate was subjected to distillation *in vacuo*. The product was identified as *t*-butyl *N*-butylcarbamate (61%) by comparison of its IR and NMR spectra with those of an authentic sample.

Reaction of ***1a*** *with Acyl Halide.* To a solution of **1a** (10 mmol) in benzene (10 ml), benzoyl chloride (10 mmol) was added dropwise with stirring, and then heated at 50 °C for 5 hr. The reaction mixture was triturated with hexane and filtered. The filtrate was subjected to distillation. The product was identified as benzoyl isocyanate (bp 95 °C/21 mmHg) by comparison of its IR spectrum with that of an authentic sample[5].

References

1) a) T. Saegusa, Y. Ito, and S. Tomita, *J. Amer. Chem. Soc.*, **93**, 5656 (1971); b) Y. Ito, T. Konoike, and T. Saegusa, *J. Organometal. Chem.*, **85**, 395 (1975).

2) T. Saegusa, I. Murase, and Y. Ito, *J. Org. Chem.*, **38**, 1753 (1973).

3) E. Soderbak, *Acta Chem. Scand.*, **11**, 1622 (1957).

4) N. Y. Derkach and N. P. Smetankina, *Zh, Obshch. Khim.*, **34**, 3613 (1964).

5) A. J. Hill and W. M. Degman, *J. Amer. Chem. Soc.*, **62**, 1595 (1940).

BULLETIN OF THE CHEMICAL SOCIETY OF JAPAN, VOL. 49(2), 575—576 (1976)

The Acidities of Substituted α-Phenylsulfinylacetophenones

Norio KUNIEDA, Yoichi FUJIWARA, Junzo NOKAMI, and Masayoshi KINOSHITA

Department of Applied Chemistry, Faculty of Engineering, Osaka City University, Sumiyoshi-ku, Osaka 558

(Received June 26, 1975)

Synopsis. The acidities of eleven *meta*- and *para*-substituted α-phenylsulfinylacetophenones (**1**) were determined potentiometrically in a 50% ethanol solution. pK_a values (10.22—12.01) which can be nicely correlated with Hammett's σ-values were obtained.

In recent years, many chemists have examined β-keto sulfoxides as key synthetic intermediates. During the course of our research concerned with the reactions of β-keto sulfoxides and their derivatives at the α-carbon atom with electrophiles in the presence of a base,[1] we became interested in the acidities of β-keto sulfoxides, synthesized eleven substituted α-phenylsulfinylacetophenones (**1**), and determined their acidities, which may shed light on the problem of their reactivity.

The β-keto sulfoxides (**1**) were prepared by treating *meta*- or *para*-substituted ethyl benzoates with α-sulfinylcarbanions derived from the corresponding *meta*- or *para*-substituted methyl phenyl sulfoxides;[2] their pK_a values were measured potentiometrically with 0.1 M potassium hydroxide in a 50% ethanol solution. The pK_a values thus obtained are listed in Table 1. The data reveal that the β-keto sulfoxides possess rather strong acidities.

Recently, Amel and Marek[3] determined the acidities of substituted phenyl phenacyl sulfones in a 95% ethanol solution, and gave pK_a values which can be correlated with Hammett's σ-values. Furthermore, the basicities of phenacyl-substituted phosphonium,[4,9a] sulfonium,[5,9a] and pyridinium[6] ylides have been determined in order to confirm the stability and reactivity of these ylides in terms of the substituent effect.

The pK_a values of the phenacyl-substituted active methylene compounds hitherto reported are summarized in Table 2, together with our results for comparison. One finds in Table 2 that the β-keto sulfoxides(**1**) are less acidic than the other active methylene compounds. This fact is compatible with the relatively weak electron-withdrawing character of sulfinyl group in comparison with those of the sulfonyl, sulfonium, and ammonium groups.[7]

When the pK_a values for the β-keto sulfoxides (**1**) thus obtained were plotted against Hammett's σ-values, a good straight line was obtained. For the substituents (X) on the phenylsulfinyl aromatic ring, $\rho=1.32$, and for the substituents (Y) on the phenacyl aromatic ring, $\rho=2.68$. The electron-withdrawing substituents on both the aromatic rings increase the acidity of **1**. As is revealed in Table 2, the magnitude of the ρ-value for the phenacyl substituents, Y, closely resembles those of phenacyl sulfones(**2**), arylmethylphenacylsulfonium salts(**3**), dimethylphenacylsulfonium

TABLE 1. α-PHENYLSULFINYLACETOPHENONES (**1**) (X-C_6H_4-SO-CH_2-CO-C_6H_4-Y)

X	Y	pK_a[a]	Mp (°C)	NMR chemical shifts ($CDCl_3$), δ(multiplicity)[b]	Anal. Found, % C	Found, % H	Calcd, % C	Calcd, % H
H	*m*-Cl	10.22	101—103	4.45 (q, J=13.8 Hz, 2H, -CH_2-) 7.20—8.10 (m, 9H)	60.81	3.84	60.32	3.98
H	*p*-Cl	10.55	119—120	4.42 (q, J=14 Hz, 2H, -CH_2-), 7.25—8.05 (m, 9H)	60.32	3.77	60.32	3.98
H	*m*-CH_3	11.13	70— 72	4.40 (q, J=13.7 Hz, 2H, -CH_2-), 7.20—8.00 (m, 9H), 2.42 (s, 3H, CH_3)	69.98	5.32	69.74	5.46
H	*p*-CH_3	11.59	92— 93	4.45 (q, J=14 Hz, 2H, -CH_2-), 7.10—8.00 (m, 9H), 2.42 (s, 3H, CH_3)	69.39	5.42	69.74	5.46
H	*p*-OCH_3	12.01	95— 96	4.43 (q, J=14 Hz, 2H, -CH_2-), 6.75—8.15 (m, 9H), 3.90 (s, 3H, OCH_3)	65.45	4.96	65.67	5.14
H	H	11.06	70— 71	4.47 (q, J=14 Hz, 2H, -CH_2-), 7.20—8.15 (m, 10H)	68.65	4.97	68.83	4.95
p-OCH_3	H	11.37	79— 80	4.48 (q, J=14 Hz, 2H, -CH_2-), 6.90—8.20 (m, 9H), 3.87 (s, 3H, OCH_3)	65.19	4.92	65.67	5.14
p-CH_3	H	11.25	82— 85	4.48 (q, J=14 Hz, 2H, -CH_2-), 7.10—8.25 (m, 9H), 2.43 (s, 3H, CH_3)	69.99	5.41	69.74	5.46
m-CH_3	H	11.14	65— 66	4.44 (q, J=13.8 Hz, 2H, -CH_2-), 6.97—8.10 (m, 9H), 2.41 (s, 3H, CH_3)	69.23	5.62	69.74	5.46
p-Cl	H[c]	10.63	99—101	4.47 (q, J=14 Hz, 2H, -CH_2-), 7.15—8.25 (m, 9H)				
m-Cl	H[c]	10.61	94.5—95	4.49 (q, J=14 Hz, 2H, -CH_2-), 7.17—8.09 (m, 9H)				

a) The average experimental error was ±0.04 pK_a unit. b) Tetramethylsilane was used as an internal reference.
c) These compounds are very unstable.

TABLE 2. THE pK_a VALUES OF PHENACYL-SUBSTITUTED ACTIVE METHYLENES ($Z-CH_2-CO-C_6H_4-Y$) AND THEIR σ-CORRELATIONS

Z	pK_a[a]	ρ(X)	ρ(Y)	Ref.
$X-C_6H_4-SO-$ (**1**)	11.06[b]	1.32	2.68	This work
$X-C_6H_4-SO_2-$ (**2**)	10.97[c]	2.01	2.35	3
$X-C_6H_4S^+(CH_3)-$ (**3**)	7.06[c]	1.13—1.23	2.63—2.68	5 a
	6.66[c]			9 a
$(CH_3)_2S^+-$ (**4**)	8.0[c]		2.1	5 b
	7.68[c]			9 a
$(C_6H_5)_3P^+-$ (**5**)	5.60[d]		2.3	4
	5.60[c]			9 a
$X-C_5H_5N^+-$ (**6**)	9.7[c]	2.6 —3.1	2.2 —2.3	6

a) This column shows the pK_a values of unsubstituted compounds (X=Y=H). The pK_a value was determined in ethanol-water mixture: b) in 50% ethanol, c) in 95—100% ethanol, d) in 80% ethanol.

salts(**4**), triphenylphenacylphosphonium salts(**5**), and phenacyl pyridinium salts(**6**), suggesting that the carbanions generated from these compounds, 1—6, are stabilized by a $p_\pi-p_\pi$ delocalization system with a carbonyl group (such as: $-CH=\overset{\ominus}{C}-\overset{O}{\overset{\|}{C}}-C_6H_4-Y$) with the same tendency. On the other hand, the magnitude of ρ-values for the phenylsulfinyl substituents, X, is considerably small in comparison with that for phenacyl sulfones(**2**) and is comparable with that for phenacylsulfonium salts(**3**). The σ-correlation for X suggests that the demand for the resonance effect of the substituent would be negligible; hence, the inductive effect of X can cause a change in electronegativity only at the sulfinyl sulfur. In addition, since the sulfur atom can expand its valence shell beyond an octet using 3d orbitals,[8] perhaps a substantial $p_\pi-d_\pi$ interaction may operate between the sulfinyl sulfur and the carbanion carbon to stabilize the carbanion of **1**, in a fashion analogous to the cases of phosphonium and sulfonium ylides and sulfones.[3,5,6,9] Of course, this interaction should result in a large inductive effect of the substituent, together with an increase in the acidity. However, the smaller ρ-value for **1**, as well as the higher pK_a values, seems to suggest that the $p_\pi-d_\pi$ interaction in the β-keto sulfoxide system stabilizes the carbanion to a less extent than in the phenacyl sulfone system(**2**).

Experimental

Preparation of α-Phenylsulfinylacetophenones (1). The β-keto sulfoxides (**1**) were prepared according to a method analogous to that developed by Russell *et al.* and by Corey *et al.*[2]

A *meta-* or *para*-substituted ethyl benzoate was treated with 2 equiv of an α-sulfinylcarbanion, derived from the corresponding *meta-* or *para*-substituted methyl phenyl sulfoxide and lithium diethylamide(prepared from 0.1 g/ml solution of butyl lithium in hexane and diethylamine in tetrahydrofuran), at 0 °C. The reaction mixture was then stirred for 1 hr. After the addition of water, the solution was acidified with 10% hydrochloric acid (*ca.* pH 3) and extracted with chloroform. The concentration of the chloroform layer, followed by the crystallization of the residue from carbon tetrachloride or ether, yielded the β-keto sulfoxide in sufficient yields. Satisfactory IR, NMR, and elemental analyses were obtained for all the β-keto sulfoxides described here. Table 1 summarizes their melting points and NMR data.

Measurement of pK_a. The pK_a value of the β-keto sulfoxides(**1**) in a 50% ethanol solution was determined potentiometrically by the titration of 0.100 M potassium hydroxide in 50% ethanol at 25 °C, according to the usual method.[10]

References

1) N. Kunieda, J. Nokami, and M. Kinoshita, *Tetrahedron Lett.*, **1974**, 3997; J. Nokami, N. Kunieda, and M. Kinoshita, *ibid.*, **1975**, 2179; N. Kunieda, J. Nokami, and M. Kinoshita, *Chem. Lett.*, **1974**, 369.

2) H. -D. Becker, G. J. Mikol, and G. A. Russell, *J. Amer. Chem. Soc.*, **85**, 3410 (1963); E. J. Corey and M. Chaykovsky, *ibid.*, **86**, 1639 (1964); E. J. Corey and M. Chaykovsky, *ibid.*, **87**, 1345 (1965).

3) R. T. Amel and P. J. Marek, *J. Org. Chem.*, **38**, 3513 (1973).

4) S. Fliszar, R. F. Hudson, and G. Salvadori, *Helv. Chim. Acta*, **46**, 1580 (1963).

5) a) K. W. Ratts, *J. Org. Chem.*, **37**, 848 (1972); b) K. W. Ratts and A. N. Yao, *ibid.*, **31**, 1185 (1966).

6) W. G. Phillips and K. W. Ratts, *ibid.*, **35**, 3144 (1970).

7) J. E. Leffler and E. Grunwald, "Rates and Equilibria of Organic Reactions," John Wiley and Sons, New York, N. Y. (1963), p. 173; H. H. Szmant and G. Suld, *J. Amer. Chem. Soc.*, **78**, 3400 (1956); F. G. Bordwell and P. J. Boutan, *ibid.*, **78**, 87 (1956); S. Oae and C. C. Price, *ibid.*, **80**, 3425 (1958). So far as our knowledge, the σ-value for the phosphonium group has never been determined.

8) C. C. Price and S. Oae, "Sulfur Bonding," Chapter 4, Ronald Press Co., New York, N. Y. (1962), and references cited therein; S. Oae, M. Yoshihara, and W. Tagaki, This Bulletin, **40**, 951 (1967).

9) a) A. W. Johnson and R. T. Amel, *Can. J. Chem.*, **46**, 461 (1968); b) A. W. Johnson, S. Y. Lee, R. A. Swor, and L. D. Royer, *J. Amer. Chem. Soc.*, **88**, 1953 (1966).

10) A. Albert and E. P. Serjeant, "Inoization Constants of Acids and Bases," Methuen & Co. London (1962), p. 16.

BULLETIN OF THE CHEMICAL SOCIETY OF JAPAN, VOL. 49(2), 577—578 (1976)

Photochemical Ligand Substitution in Hexakis(aryl isocyanide)-chromium(0)–Olefin Systems

Kazuhito IUCHI, Shintaro ASADA, Takashi KINUGASA, Koji KANAMORI, and Akira SUGIMORI

Department of Chemistry, Faculty of Science and Technology, Sophia University, Kioi-cho 7, Chiyoda-ku, Tokyo 102

(Received August 8, 1975)

Synopsis. Isocyanide chromium(0) complexes coordinated by dimethyl fumarate, fumaronitrile and maleic anhydride were prepared photochemically by the irradiation of hexakis(aryl isocyanide)chromium(0) with the corresponding olefin. Tetracyanoethylene reacts with hexakis(aryl isocyanide)chromium(0) thermally without illumination, while acrylonitrile and dimethyl maleate do not react even with irradiation.

The chemistry of isocyanide metal complexes coordinated by olefins is a newly developing field. Otsuka *et al.* studied the thermal ligand substitution of *t*-butyl isocyanide metal complexes and prepared nickel and palladium isocyanide complexes coordinated by electron poor olefins.[1] They presumed that the reaction proceeds by S_N1 mechanism. Kawakami *et al.* concluded that tetrakis(aryl isocyanide)rhodium-(I) perchlorates form TCNE adducts of square pyramidal structure, in which TCNE rotates freely.[2]

Although the photochemical ligand substitution of metal carbonyls has been extensively investigated,[3] the photochemical method has rarely been applied to the preparation of isocyanide metal complexes. We found that some aryl isocyanide chromium(0) complexes coordinated by electron poor olefins are formed under irradiation.[4]

Experimental

Materials. Aryl isocyanides were prepared by the carbylamine reaction according to Weber *et al.*[5] Phenyl isocyanide; bp 64 °C/20 mmHg. *p*-Tolyl isocyanide; bp 70 °C/8 mmHg. *p*-Anisyl isocyanide; bp 80 °C/20 mmHg. Hexakis(aryl isocyanide)chromium(0) (**1**) were synthesized by the reaction of aryl isocyanide and chromium(II) salt according to Malatesta *et al.*[6]

Commercial GR grade dimethyl fumarate, dimethyl maleate, fumalonitrile, maleic anhydride and EP grade TCNE were used.

Irradiation. **1** ($7—8\times10^{-5}$ mol) and olefin ($7—10\times10^{-5}$ mol) were irradiated in benzene (in the case of NMR measurement in benzene-d_6) or THF solutions (10 ml) in quartz vessels with a high pressure mercury lamp under a nitrogen atmosphere. The color of the solution changed from red to dark brown during the course of irradiation.

Product. Some of the photo-products were stable and isolated by means of alumina chromatography. They were identified as pentakis(aryl isocyanide)(olefin)chromium-(0). Spectral data and the results used for identification are listed in Table 1. Some of the photo-products could not be isolated, but the IR and NMR spectra of the reaction mixtures showed characteristic absorption due to the complex coordinated by olefin. IR and NMR spectra assigned to the olefin-coordinated complexes are shown in Table 1.

Results and Discussion

Hexakis(aryl isocyanide)chromium(0) (**1**) undergoes ligand exchange with electron-poor olefins either thermally or photochemically. Fumaronitrile, dimethyl fumarate and maleic anhydride react with [Cr-(ArNC)$_6$] (Ar=phenyl, *p*-tolyl, and *p*-anisyl) photochemically, affording the corresponding [Cr(ArNC)$_5$-(olefin)]. Among them three complexes are stable enough to be isolated by means of alumina chromatography in the air. Other complexes were identified spectroscopically in the irradiated reaction mixture.

$$[Cr(ArNC)_6] + \text{olefin} \xrightarrow{h\nu} [Cr(ArNC)_5(\text{olefin})] + ArNC$$

The reactivity of olefins for the ligand substitution depends principally on the electron affinities of the olefins and secondarily on the steric factor. Acrylonitrile, a weaker electron acceptor, does not undergo photochemical ligand substitution. TCNE, a stronger electron acceptor, reacts with **1** without illumination to give pentakis(aryl isocyanide) (TCNE)chromium(0).

The difference between the reactivities of dimethyl fumarate and dimethyl maleate can not be explained in terms of their electronic character. The electron affinity values are similar: E_a for dimethyl maleate, 0.60 eV; E_a for dimethyl fumarate, 0.59 eV.[7] Dimethyl fumarate reacts photochemically with **1**, whereas dimethyl maleate undergoes no ligand substitution, but isomerization to the *trans* isomer. In the photoreaction of hexakis(phenyl isocyanide)chromium(0)–dimethyl fumarate system, no *trans-cis* isomerization was observed.

UV-irradiation of **1** with dimethyl acetylenedicarboxylate and phenylacetylene gave decomposition products, but no substitution products.

IR and NMR spectra of the isocyanide–chromium(0) complexes coordinated by olefins clearly show electron transfer from the central metal to the olefins. A similar phenomenon is observed in nickel and palladium complexes.[1] NC-stretching frequencies of the chromium complexes increase with the introduction of olefins. On the other hand, the CN-stretching frequencies of coordinated TCNE and fumaronitrile are lower than those of free TCNE and fumaronitrile. Analogous shift was observed for the CO-stretching vibration of dimethyl fumarate and maleic anhydride. NMR peaks due to olefinic protons of coordinated olefins are found in a lower δ region than those of free olefins.

The photochemical ligand substitution occurs also with solar light in a glass vessel.

For the ligand substitution of metal carbonyls, the

TABLE 1. PHOTO-PRODUCTS OF HEXAKIS(ARYL ISOCYANIDE)CHROMIUM(0)–OLEFIN SYSTEMS
MF=dimethyl fumarate, FN=fumaronitrile, MA=maleic anhydride

Compound	Formation		Spectral properties			
	Irradiation time (h)	Yield (%)	IR (cm^{-1})[d] ν_{NC}	IR (cm^{-1})[d] ν_{CN}	IR (cm^{-1})[d] ν_{CO}	NMR (δ) olefin H
$[Cr(NC\langle\bigcirc\rangle)_5(MF)]$[a]	2	24	2030 1970		1680	4.85
$[Cr(NC\langle\bigcirc\rangle CH_3)_5(MF)]$		not isolated	2040 1990		1680	4.88
$[Cr(NC\langle\bigcirc\rangle OCH_3)_5(MF)]$		not isolated	2040 1995		1675	
$[Cr(NC\langle\bigcirc\rangle)_5(FN)]$[b]	2	25	2045 1980	2190		3.30
$[Cr(NC\langle\bigcirc\rangle CH_3)_5(FN)]$	0.5	38	2045 1995	2180		3.37
$[Cr(NC\langle\bigcirc\rangle OCH_3)_5(FN)]$		not isolated	2050 1980	2180		
$[Cr(NC\langle\bigcirc\rangle)_5(MA)]$		not isolated	2040 1985			4.73
$[Cr(NC\langle\bigcirc\rangle CH_3)_5(MA)]$		not isolated	2040 1990			4.88
$[Cr(NC\langle\bigcirc\rangle OCH_3)_5(MA)]$		not isolated	2040 1985			4.78
$[Cr(NC\langle\bigcirc\rangle)_5(TCNE)]$[c]	thermal	48	2145 2045	2180 2170		
$[Cr(NC\langle\bigcirc\rangle CH_3)_5(TCNE)]$	thermal	80	2125 2050 2005	2190 2155		
$[Cr(NC\langle\bigcirc\rangle OCH_3)_5(TCNE)]$	thermal	88	2125 2050 2000	2190 2170		
$[Cr(NC\langle\bigcirc\rangle)_6]$			2050 2000 1940			
$[Cr(NC\langle\bigcirc\rangle CH_3)_6]$			2040 1955 1920			
$[Cr(NC\langle\bigcirc\rangle OCH_3)_6]$			2030 1955 1920			

Elemental analysis. a) Found: C, 68.89; H, 4.54; N, 9.87%. Calcd for $C_{41}H_{33}N_5O_4Cr$: C, 69.20; H, 4.64; N, 9.85%. b) Found: C, 72.13; H, 4.14; N, 15.23%. Calcd for $C_{39}H_{27}N_7Cr$: C, 72.56; H, 4.19; N, 15.19%. c) Found: C, 69.58; H, 3.52; N, 16.08%. Calcd for $C_{41}H_{25}N_9Cr$: C, 70.78; H, 3.63; N, 18.12%. d) IR spectra of stable complexes were measured by means of KBr disk, those of unstable ones in benzene-d_6 solutions.

S_N1 mechanism has been established. S_N1 mechanism was kinetically confirmed for the exchange reaction between hexakis(phenyl isocyanide)chromium(0) and ^{14}C-labeled phenyl isocyanide.[8] However, the substitution of aryl isocyanide by TCNE is much faster (the reaction is completed immediately after the chromium complex and TCNE are mixed) than what would be expected for a S_N1 mechanism. The first order rate of the ligand exchange by ^{14}C-labeled phenyl isocyanide is very small; $\tau_{1/2}$, the half life of the reaction, is reported to be hundred hours at 20 °C. This indicates that the substitution of aryl isocyanide by TCNE can not proceed by a simple S_N1 mechanism. The fact that electron-poor olefins are reactive both in thermal and in photochemical substitution suggests that charge transfer interaction between olefins and **1**, in either the ground or the excited state, plays an important role in the ligand substitution reaction.

References

1) S. Otsuka, T. Yoshida, and Y. Tatsuno, *J. Amer. Chem. Soc.*, **93**, 6462 (1971).
2) K. Kawakami, T. Kaneshima, and T. Tanaka, *J. Organometal. Chem.*, **34**, C21 (1972).
3) V. Balzani and V. Carassiti, "Photochemistry of Coordination Compounds," Academic Press, London and New York (1970), p. 323.
4) Preliminary report; K. Iuchi, S. Asada, and A. Sugimori, *Chem. Lett.*, **1974**, 801.
5) W. P. Weber, G. W. Gokel, and I. Ugi, *Angew. Chem.*, **84**, 581 (1972).
6) L. Malatesta, A. Sacco, and S. Ghielmi, *Gazz. Chim. Ital.*, **82**, 516 (1952).
7) G. Briegleb, *Angew. Chem.*, **76**, 326 (1964).
8) G. Cetini and O. Gambino, *Ann. Chim. (Italy)*, **53**, 236 (1963).

The Mercury-photosensitized Reaction of Hydrogen with Nitric Oxide

Kohji TADASA,* Naomi IMAI, and Tetsuo INABA

Faculty of Liberal Arts and Sciences, University of Osaka Prefecture, Sakai, Osaka 591

(Received June 9, 1975)

The Hg-photosensitized reaction of a mixture of H_2 and NO has been studied mainly at room temperature. The quantum yield of the H_2O formation is nearly unity, independent of the pressures of both H_2 and NO. The quantum yield of the N_2 formation is proportional to the NO pressure, while that of N_2O decreases with the NO pressure; both of them are independent of the H_2 pressure. In order to interpret the results concerning the H_2O formation, the following process is proposed:

(i) $NO_3 + NO \longrightarrow 2NO_2$

$NO_2 + HNO \longrightarrow OH + 2NO$

$OH + HNO \longrightarrow H_2O + NO$

in addition to the well-established H_2O-forming process:

(ii) $2HNO \longrightarrow H_2O + N_2O$

NO_2, one of the reactants in Process (i), is formed by the chain process proposed by Arden and Phillips:

(iii) $H + NO + M \longrightarrow HNO + M$

$HNO + 2NO \longrightarrow N_2 + H + NO_3$

The (ii) and (iii) processes also coincide with the results of the N_2O and N_2 formations respectively.

In this laboratory, the effect of nitric oxide on the photochemical decomposition of formaldehyde has been studied.[1] The photolysis of formaldehyde has been known to proceed by means of the free-radical-chain mechanism, where the hydrogen atom is one of the chain carriers. The addition of nitric oxide to the photolysis was found to cause an inhibition of the chain decomposition of formaldehyde. In order to elucidate the kinetics of the inhibited photolysis, it is desirable to study reactions containing the hydrogen atom and nitric oxide. Thus, in this work, the mercury-photosensitized reaction of a mixture of hydrogen and nitric oxide was investigated. This photosensitized reaction has already been studied by several workers,[2-5] but no satisfactory interpretation has been given for the kinetics of the overall reaction.

Experimental

Materials. The nitric oxide and hydrogen used were obtained from the Takachiho Kagaku Co., Ltd.; they had research-grade purities of 99.6% and 99.95% respectively. They were used without further purification.

Apparatus. A cylindrical reaction cell of quartz was used; it had a volume of 262 ml. The lamp used was a 2537-source of a spiral type.

Procedure. The reactants, H_2 and NO, were successively expanded into the reaction vessel, in which they were then kept for more than two hours in order to reach the diffusion equilibration and then saturated with mercury for the same period at room temperature. Most runs were carried out at room temperature with 15-min irradiation (0.2—2% conversion). One series of runs, however, was carried out at various temperatures up to 250 °C. For all the experiments, the absorbed light intensity was approximately the same. Its value was determined to be 8.3×10^{-7} einstein l^{-1} min^{-1} by propane actinometry, assuming the quantum yield of hydrogen to be unity at a low intensity, a low temperature, a high propane pressure, and a very low conversion.[6]

Analysis. The mixture of decomposition was then separated and collected by means of cold traps (at −78 °C, for H_2O and −196 °C for N_2O) and a Toepler gauge (N_2), and analyzed quantitatively by means of a gas-chromatograph. The water, one of the products, was converted to hydrogen by treating it with the sodium evaporated as a thin layer onto the surface of a glass trap; then its amount was determined (though the measurement was not very accurate). The hydrogen and nitrogen were analyzed on a 2 m Molecular Sieve 5A column at room temperature, and the nitrous oxide, on a 4 m Porapak Q column at room temperature. Identification was achieved by using IR and a mass spectrometer.

Results

The products of the Hg-photosensitized reactions were N_2, N_2O, H_2O, and unidentified nitrogen oxides

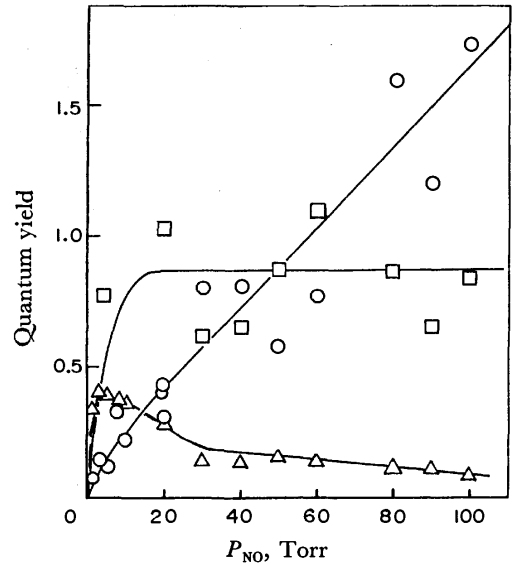

Fig. 1. Plot of quantum yield *vs.* NO pressure.
T=room temperature, P_{H_2}=20 Torr, irradiation time=15 min.
○: N_2, △: N_2O, □: H_2O.

* Present address: Department of Agricultural Chemistry Faculty of Agriculture, University of Shinshu, Ina City, Nagano-ken 396.

TABLE I. Hg-PHOTOSENSITIZED REACTION OF H_2 WITH NO
$I_a = 8.3 \times 10^{-7}$ Einsteins l^{-1} min^{-1}

Temp (°C)	Reactant (Torr)[a]		Irr. time (min)	Product (Torr)[a]			Quantum Yield		
	H_2	NO		H_2O	N_2	N_2O	ϕ_{H_2O}	ϕ_{N_2}	ϕ_{N_2O}
25	20	1	15	—	0.018	0.082	—	0.078	0.36
	20	3	15	0.18	0.034	0.092	0.78	0.148	0.40
	20	5	15	—	0.030	0.090	—	0.130	0.39
	20	8	15	—	0.072	0.088	—	0.31	0.38
	20	10	15	—	0.052	0.086	—	0.23	0.37
	20	20	15	0.24	0.066	0.063	1.04	0.29	0.27
	20	20	15	—	0.092	—	—	0.40	—
	20	20	15	—	0.099	—	—	0.43	—
	20	30	15	0.14	0.19	0.029	0.61	0.83	0.126
	20	40	15	0.15	0.19	0.027	0.65	0.83	0.117
	20	50	15	0.20	0.13	0.030	0.87	0.58	0.130
	20	60	15	0.25	0.18	0.029	1.09	0.78	0.126
	20	80	15	0.20	0.37	0.018	0.87	1.61	0.078
	20	90	15	0.15	0.28	0.018	0.65	1.22	0.078
	20	100	15	0.19	0.40	0.010	0.83	1.74	0.044
25	10	20	15	0.24	0.12	0.045	1.04	0.52	0.20
	20	20	15	0.26	0.13	0.045	1.13	0.57	0.20
	50	20	15	0.27	0.12	0.065	1.17	0.52	0.28
	80	20	15	0.22	0.08	0.060	0.97	0.35	0.26
	100	20	15	0.29	0.10	0.070	1.26	0.44	0.30
50	20	20	20	0.16	0.095	0.075	0.93	0.55	0.44
	20	20	20	0.14	0.065	0.070	0.81	0.38	0.41
75	20	20	20	0.15	0.055	0.075	0.84	0.32	0.44
100	20	20	20	0.17	0.080	0.085	1.00	0.46	0.49
	20	20	20	0.15	—	0.075	0.86	—	0.44
150	20	20	20	0.16	0.087	0.080	0.96	0.50	0.46
	20	20	20	0.15	0.055	0.073	0.84	0.32	0.42
200	20	20	20	0.17	0.050	0.070	0.96	0.29	0.41
	20	20	20	0.14	—	0.063	0.84	—	0.37
250	20	20	20	0.15	0.050	0.060	0.87	0.29	0.35

a) Pressure in the cell at room temperature.

which might react with mercury in the system. After some runs, some of a white solid was found trapped in the cold U tube. On heating *in vacuo*, it turned yellow and released mercury. Strausz *et al.*[3] found a similar substance in their experiment and identified it as predominantly $Hg_2(NO_2)_2$. Because of the reaction of NO_2 with Hg both in the reaction cell and in the analysis part, the amount of NO_2 could not be measured.

The experimental results are listed in Table 1.

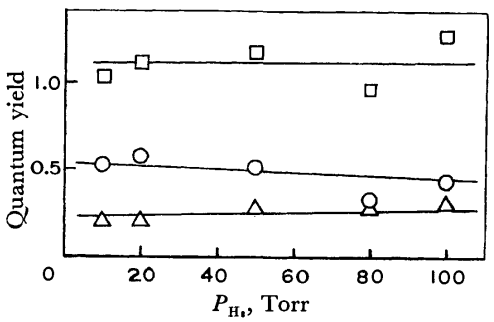

Fig. 2. Plot of quantum yield *vs* H_2 pressure.
T=room temperature, P_{NO}=20 Torr, irradiation time=15 min.
○: N_2, △: N_2O, □: H_2O.

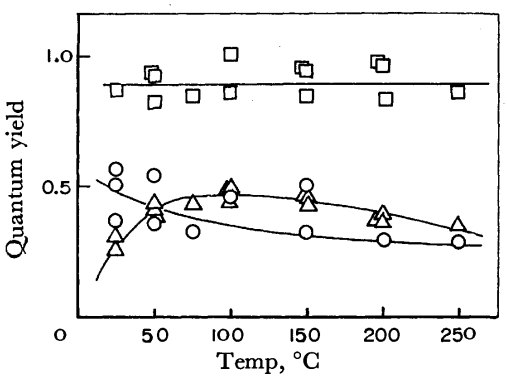

Fig. 3. Temperature dependencies of quantum yield.
P_{NO}=20 Torr, P_{H_2}=20 Torr, irradiation time=20 min.
○: N_2, △: N_2O, □: H_2O.

Figure 1 shows the effect of the NO pressure on each product formation, while Fig. 2 shows that of the H_2 pressure. These figures indicate the quantum yield of H_2O formation to be nearly unity over wide pressure ranges of reactants except for the low NO pressure range, though the accuracy of the quantitative analysis of H_2O is very low. Figure 3 shows the temperature dependencies of the yields of the products.

Discussion

The mercury-photosensitized reaction of H_2 has been studied by many workers. The primary reactions of the photosensitization were found to be as follows:[7]

$$Hg + h\nu(2537\,Å) \longrightarrow Hg^* \quad (1)$$

$$Hg^* + H_2 \longrightarrow HgH + H \quad (2)$$

$$\longrightarrow Hg + 2H \quad (3)$$

where $Hg^*=Hg(6^3P_1)$. In the presence of NO, Hg^* should be largely quenched by NO, because of its high quenching cross section[8]:

$$Hg^* + NO \longrightarrow NO^* \quad (4)$$

where $NO^*=NO(^4\Pi)$.[9]

Since the formation of H_2O, which is a measure of the rate of the primary steps, as will be described later, is constant against the amount of H_2 and NO, the following step should occur:

$$NO^* + H_2 \longrightarrow HNO + H \quad (5)$$

The hydrogen atoms formed by (2), (3) or (5) should combine with NO as:

$$H + NO + M \longrightarrow HNO + M \quad (6)^{10}$$

The HgH radicals were shown to react with NO very rapidly[5]:

$$HgH + NO \longrightarrow Hg + HNO \quad (7)$$

One Hg^* atom, therefore, leads to the formation of two HNO species.

It is well known that the HNO species combine with each other as:

$$2HNO \longrightarrow N_2O + H_2O \quad (8)^{2,3,10,11}$$

This reaction, however, is probably not the main reaction of HNO under the present conditions, since the N_2O yield is quite low compared with that of H_2O.

In the study of the H_2–NO pyrolysis at 500 °C carried out in this laboratory,[12] it was suggested that most of the HNO species react as:

$$2HNO \longrightarrow 2OH + N_2$$

and that the OH radicals thus formed react as:

$$OH + H_2 \longrightarrow H_2O + H$$

resulting in the H_2O–N_2 ratio in the product of 2: 1. In this study at room temperature, however, the N_2 formation is of the first order in NO pressure and the H_2O formation is of the zeroth order in NO pressure, showing that they are formed by reactions different from those in the pyrolysis.

Since the H_2O quantum yield equals unity within the limits of experimental error over wide pressure ranges of the reactant gases, the rate of H_2O formation seems to exhibit that of the primary process. On the other hand, N_2 may be supposed to be formed by the chain reaction containing NO, because its quantum yield exceeds unity and its formattion is of the first-order with respect to NO.

Arden and Phillips have proposed that HNO induces the chain disproportionation of NO to N_2 and NO_2.[13]

$$HNO + 2NO \longrightarrow N_2 + H + NO_3 \quad (9)$$

$$NO_3 + NO \longrightarrow 2NO_2 \quad (10)$$

These reactions do not consume the HNO, however, since H atoms formed by (9) regenerate the HNO by means of (6). Thus, N_2 is formed by the chain reaction carried out by means of (6) and (9). Strausz and Gunning[3] has proposed a HNO–NO reaction scheme alternative to (9):

$$HNO + 2NO \longrightarrow N_2 + HNO_3\dagger$$

If it is followed by this reaction:

$$HNO_3 + NO \longrightarrow HNO + NO_3$$

it leads to the same results as (9).

As the mechanism of H_2O formation, when the NO pressure is not low, the following reactions may be proposed in addition to (8):

$$NO_2 + HNO \longrightarrow OH + 2NO \quad (11)$$

$$OH + HNO \longrightarrow H_2O + NO \quad (12)$$

Thus, one H_2O molecule is formed by consuming two HNO species by means of (11) and (12) as well as (8). The rate of the H_2O formation should equal that of the absorption of the light quanta:

$$R_{H_2O} = I_a \quad (I)$$

This has been clearly proved by the results, $\phi_{H_2O}=1$, shown in Figs. 1 and 2. This equation is not affected by the occurence of the chain disproportionation of NO carried out by means of (6) and (9).

The H_2O formation by this reaction:

$$OH + H_2 \longrightarrow H_2O + H$$

instead of (12) seems to be improbable at low temperature, since its activation energy is 5.2 kcal mole^{-1} ($E_{12}\sim0$).[14] If this reaction, nevertheless, occurrs appreciable, the H atom would be regenerated and (6) and (11) would follow it. In this case, H_2O would be formed by the chain reaction, and, accordingly, ϕ_{H_2O} should depend on the H_2 pressure; this is not consistent with the results shown in Fig. 2.

Accepting the reaction scheme (1)—(12), the rates of N_2 and N_2O formations in the steady state may be expressed as:

$$R_{N_2} = k_9[HNO][NO]^2 \quad (II)$$

and:

$$R_{N_2O} = k_8[HNO]^2 \quad (III)$$

where [HNO] can be obtained from this equation:

$$I_a = k_8[HNO]^2 + k_{11}[NO_2][HNO] \quad (IV)$$

From Rate Equations (II) and (III), we obtain:

$$\phi_{N_2}^{1/2}/\phi_{N_2O}^{1/4} = k_9^{1/2}[NO]/I_a^{1/4}k_8^{1/4} \quad (V)$$

This equation is tested in Fig. 4, which shows that this relation holds, although the plots do not fall on a straight line very clearly.

If $R_8 \ll R_{12}(=R_{11})$ (this reaction holds when [NO] is not low), the first term on the right-hand side of Eq. (IV) can be neglected. Thus,

$$\phi_{N_2} = k_9[NO]^2/k_{11}[NO_2] \quad (VI)$$

and

† This reaction was shown experimentally to be of the first order with respect to both HNO and NO, while (9) is of the first order with respect to HNO and of the second order with respect to NO.

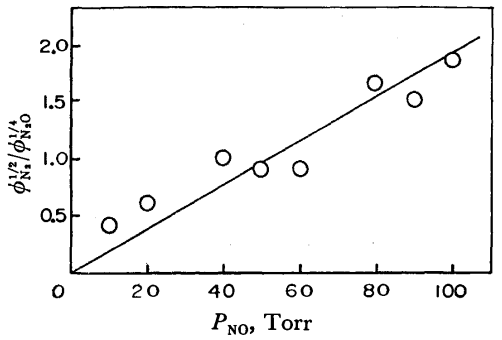

Fig. 4. Plot of $(\phi_{N_2}^{1/2}/\phi_{N_2O}^{1/4})$ value *vs.* NO pressure.
T=room temperature, P_{H_2}=20 Torr

$$\phi_{N_2O} = k_8 I_a / k_{11}^2 [NO_2]^2 \qquad \text{(VII)}$$

As NO_2 is consumed by the reaction with Hg,

$$NO_2 + Hg \longrightarrow (1/2)Hg_2(NO_2)_2$$

its concentration could not be measured. If $[NO_2]$ is assumed to be proportional to the added NO pressure, $\phi_{N_2} \propto [NO]$ and $\phi_{N_2O} \propto I_a/[NO]^2$. Figures 1 and 2 seem to indicate these relations to hold, even though very roughly.

Figure 3 shows that ϕ_{H_2O} does not vary, while ϕ_{N_2} decreases and ϕ_{N_2O} reaches a maximum, with the rise in the temperature to 250 °C. These tendencies are quite the same of those in the CH_2O–NO photolysis.[1] The decrease in the rate of the termolecular reaction (9) is supposed to cause the decrease of ϕ_{N_2} at higher temperatures. The increase of ϕ_{N_2O} with the temperature up to 100°C may be attributed to the occurence of Reaction (13):

$$HNO + NO \longrightarrow N_2O + OH \qquad (13)$$

in addition to (8). At temperatures higher than 100°C, Reaction (14) takes place:

$$2HNO \longrightarrow 2OH + N_2 \qquad (14)$$

Thus, HNO is consumed by (14) and (12) to a great extent, so that the rate of the N_2O formation by (8) and (13) should decrease above 100°C. It was suggested that these reactions occur in the H_2–NO[12] and CH_2O–NO[15] pyrolyses. The latter reaction, especially, was indicated to be predominant compared with (8) at 400 and 500 °C in these experiments. The occurence of these reactions, however, does not affect the (I) relation. Consequently, ϕ_{H_2O} holds constant over the temperature range examined.

References

1) K. Tadasa, N. Imai, and T. Inaba, to be published.
2) H. A. Taylor and C. Tanford, *J. Chem. Phys.*, **12**, 47 (1944). M. Z. Hoffman and R. B. Bernstein, *J. Phys. Chem.*, **64**, 1753 (1960). R. Atkinson and R. J. Cvetanović, *Can. J. Chem.*, **51**, 370 (1973).
3) O. P. Strausz and H. E. Gunning, *Trans. Faraday Soc.*, **60**, 347 (1964).
4) A. B. Callear and P. M. Wood, *J. Chem. Soc., Faraday II*, **68**, 302 (1972).
5) A. B. Callear and P. M. Wood, *Trans. Faraday Soc.*, **67**, 3399 (1971).
6) R. A. Back, *Can. J. Chem.*, **37**, 1834 (1959).
7) A. B. Callear and R. E. M. Hedges, *Trans. Faraday Soc.*, **66**, 605, 615 (1970).
8) J. R. Bates, *J. Amer. Chem. Soc.*, **54**, 569 (1932).
9) R. J. Fallon, J. T. Vanderslice, and E. A. Mason, *J. Phys. Chem.*, **63**, 2082, (1959). M. Z. Hoffman and R. B. Bernstein, *ibid.*, **64**, 1769 (1960). O. P. Strausz and H. E. Gunning, *Can. J. Chem.*, **39**, 2549 (1961). G. Karl, P. Kraus, J. C. Polanyi, and L. W. M. Smith, *J. Chem. Phys.*, **46**, 244 (1967).
10) P. Harteck, *Ber.*, **66**, 423 (1933).
11) L. Phillips, *J. Chem. Soc.*, **1961**, 3082. K. A. Wilde, *Combust. and Flame*, **13**, 173 (1969).
12) K. Tadasa, N. Imai, and T. Inaba, This Bulletin, **47**, 2979 (1974).
13) E. A. Arden and L. Phillips, *J. Chem. Soc.*, **1964**, 5118.
14) J. L. Franklin, *Ann. Rev. Phys. Chem.*, **18**, 261 (1967).
15) K. Tadasa, N. Imai, and T. Inaba, This Bulletin, **47**, 548 (1974).

Magnetic Two-dimensionality and Antiferromagnetism in the DANO Crystal

Osamu TAKIZAWA

Department of Chemistry, Faculty of Science, Kyoto University, Kyoto 606

(Received August 13, 1975)

An organic free radical crystal, the di-*p*-anisyl nitric oxide (DANO) crystal, was found to exhibit the characteristics of the two-dimensional Heisenberg spin system in its magnetic susceptibility at low temperatures and in its angular dependence of the ESR line width at room temperature. A distinct minimum of magnetic susceptibility due to a phase transition to antiferromagnetic spin ordering was observed at 1.67 K; this is consistent with the results of the NMR measurements, while another unexplainable anomaly was found near 2.7 K. The magnetic anisotropy field, H_A, along the a-axis, perpendicular to the magnetic easy-plane, was determined to be $(3\pm1)\times10^2$ Oe at 0 K from the analysis of the antiferromagnetic resonance; it was attributed to the magnetic field originating from the spin magnetic dipoles distributed over the radical molecules. The ratio of the anisotropy field to the exchange field within the magnetic two-dimensional plane, H_A/H_E, and that of the Néel temperature to the Weiss temperature, T_N/θ, were found to be 5×10^{-3} and 0.34 respectively. The ratio of the inter-plane exchange interaction to the intra-plane one, J'/J, was estimated therefrom to be of the order of 10^{-3}.

Recently, a number of magnetic studies of organic free radical crystals have been performed in spite of difficulties in the purification of the samples and the complexity of the structure; these studies have revealed the magnetic-ordering phenomena at low temperatures in some typical crystals.[1-4] Above the magnetic-ordering temperatures they generally exhibit the characteristics of low-dimensional magnetic systems.[5-8] The low-dimensional characteristics of these organic radical crystals are a consequence of the crystal structures with a pile of plane radical molecules. The magnetic moment originates from an unpaired electron spin in a 2pπ-orbital stretched perpendicularly to the molecular plane. When each molecule is stacked plane-to-plane in the crystal, an unpaired electron spin interacts magnetically with those of only a few neighboring molecules through an overlapping of the 2pπ-orbitals; this causes the low-dimensional magnetic characters of these organic radical crystals.

The magnetically one-dimensional systems[5-8] have been extensively studied in organic radical crystals. Radical crystals with a two-dimensional character can be formed only under favorable conditions with regard to the crystal structure. These crystals, if ideal, can be expected to show interesting magnetic behavior; that is, as is well known, the ideal two-dimensional Heisenberg spin system cannot exhibit a long-range ordered state. In the real systems, a small deviation from the ideal system, such as the existence of a weak anisotropy and/or of interlayer interaction, gives rise to three-dimensional ordering at a finite temperature.[9]

The crystal of the di-*p*-anisyl nitric oxide radical, $(CH_3OC_6H_4)_1NO$ (hereafter abbreviated to DANO), may be possibly regarded as a two-dimensional magnetic system, judging from its crystal structure[10] and from thermal and magnetic properties of the powdered sample studied by Duffy *et al.*[11] However, they found a weak anomaly around 2.7 K and ascribed it to the three-dimensional magnetic ordering. Recently, we also found that the DANO crystal undergoes the antiferromagnetic transition at 1.67 K from the results of NMR measurements of its single crystal.[12] The cause of the magnetic phase transition in this crystal was not clarified in the previous study.

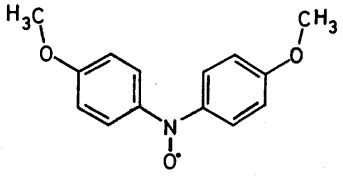

Fig. 1. DANO.

This paper will deal with the results of magnetic susceptibility and ESR measurements of powdered and single crystal of DANO. The measurements were undertaken in order to examine the magnetic two-dimensionality and to study the magnetic ordering of this crystal.

Structural Consideration

The DANO radical shown in Fig. 1 is a nitroxide radical. The ESR[13] and ENDOR[14] spectra of the DANO in solution revealed that the unpaired electron is distributed mainly on a 2pπ-orbital of the N–O group and partially on 2pπ-orbitals of the two phenyl rings. The 2pπ-orbital of the N–O group is stretched perpendicularly to the plane made of the –C–NȮ–C– group.

An X-ray analysis of the DANO crystal by Hanson[10] showed that the crystal structure belongs to the orthorhombic space group Aba2 and that a unit cell with four molecules has dimensions of $a=7.33$ Å, $b=26.8$ Å, and $c=6.25$ Å. Ignoring the twist of the two phenyl rings, it can be said that all the molecules in the unit cell occupy crystallographically equivalent sites and make the plane formed by the –C–NȮ–C– group parallel to the bc-plane and the axis of the N–O bond to the c-axis, resulting in the 2pπ-orbital of the N–O group being stretched along the a-axis. The distances from an N-atom to the first, second, and third nearest neighboring molecules in the ac-plane are 4.8 Å, and 6.2 Å, and 7.3 Å respectively. The layer of the molecules parallel to the ac-plane is separated from the adjacent one by 13.4 Å. Figure 2 is a schematic drawing of the crystal structure, which is simply assumed to be face-

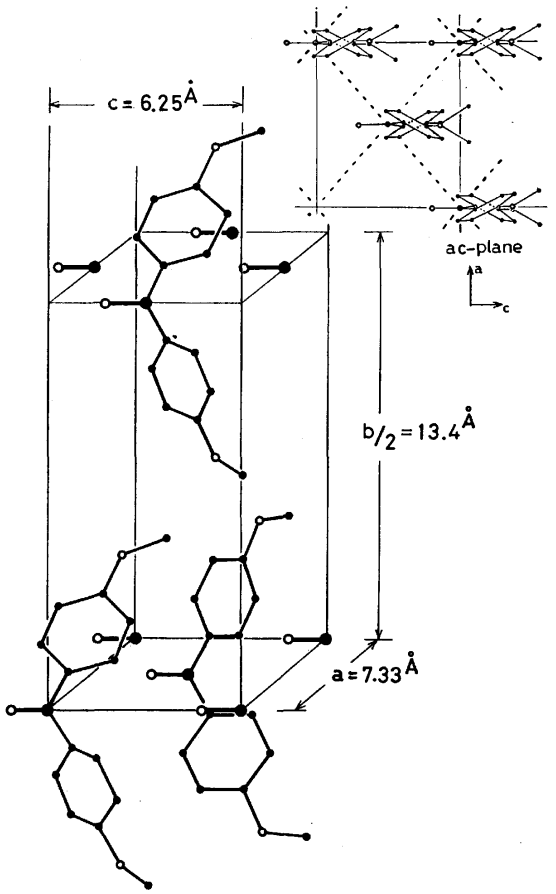

Fig. 2. Crystal structure of DANO crystal. The inset shows the projection to (010) plane.

centered orthorhombic.

Generally, the overlapping of the orbitals of magnetic electrons gives a measure of the magnitude of the exchange interaction. One can assume from the above-mentioned directional configuration of the 2pπ-orbital of the N–O group that the magnitude of the exchange interaction with nearest neighbors much exceed those with the second and the third nearest neighbors in the ac-plane, while the exchange interaction between the ac-planes is much weaker than those in the ac-plane. As a consequence, the DANO crystal may be regarded as forming a two-dimensional magnetic lattice with a nearly quadratic network.

Experimental

Fine copper-colored powder of the DANO crystal was synthesized by the method of Meyer *et al.*[15] After it has been recrystallized several times from ethanol, dark brown platelets with (010) crystal faces were obtained. Elementary analysis gave these values: C, 68.92; H, 5.79; N, 5.75% (calcd: C, 68.84; H, 5.79; N, 5.73%). Its crystallographic axes were determined with a polarized microscope.

The magnetic susceptibility was measured from 1.55 K to 300 K by means of a magnetic torsion balance[16] under magnetic fields of 8 kOe to 11 kOe, calibrated with that of Mn–Tutton salt. The ESR absorptions were observed by means of a conventional spectrometer with operating frequencies of 9.5 GHz and 35.5 GHz. The magnetic field was calibrated using Mn^{2+} doped in MgO (1/2000) after correction by DPPH recrystallized from ether ($g=2.0036$).

Results

Magnetic Susceptibility. At high temperatures, the magnetic susceptibility of a powdered sample obeys the Curie–Weiss law $\chi=C/(T-\theta)$, with $\theta=-4.9\pm0.3$ K and $C=0.377$,* determined in the temperature range between 300 and 63 K; from these results the radical concentration was evaluated to be more than 97%. The diamagnetic correction, -1.35×10^{-4} emu/mol, estimated from Pascal's law[17] was used in this evaluation.

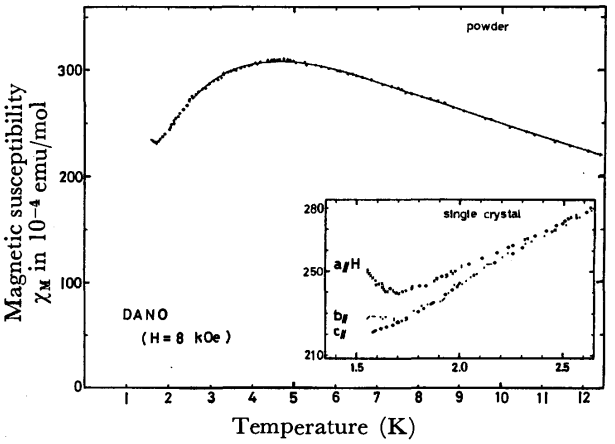

Fig. 3. Temperature dependence of the magnetic susceptibility of DANO crystal. Solid line indicates the results of the HTS calculation for $J/k=-2.45$ K.

With a lowering of the temperature, a broad maximum of the magnetic susceptibility, $\chi_{max}=304\times10^{-4}$ emu/mol, appears at 4.6 ± 0.2 K, as is shown in Fig. 3. Besides a vague anomaly near 2.7 K, reported by Duffy *et al.*,[11] a distinct minimum of the magnetic susceptibility was observed at 1.67 ± 0.02 K.

The inserted figure in Fig. 3 shows the magnetic susceptibility of a single crystal along three crystallographic axes. On account of inaccuracy in the sample weight, the observed values were scaled to that of the powdered sample at 4.2 K; the correction for the diamagnetic anisotropy, less than -1.1×10^{-4} emu/mol, was neglected. The susceptibility is clearly anisotropic below about 2.5 K, and only the susceptibility along the a-axis exhibits a distinct minimum at 1.67 K. This minimum in susceptibility of the single crystal can not be attributed to the origin in impurity but is attributable to the existence of the magnetic ordering of spins.

ESR Absorption. The ESR absorption of a single crystal was measured in order to study variations in the g-value and in the linewidth between 1.3 K and 300 K. Only a single absorption line was observed in the field from 0.5 kOe to 13.0 kOe at all temperatures. At room temperature the g-tensor coincides with that of the isolated radical,[18] and its principal

* The small disagreement between the θ, C, and χ_{max} values in the present work and those in Ref. 11 is probably due to the existence of an impurity, judging from the fact that, in the latter, the authors used a fitting parameter of magnetic susceptibility; $p=0.93$ or 0.95.

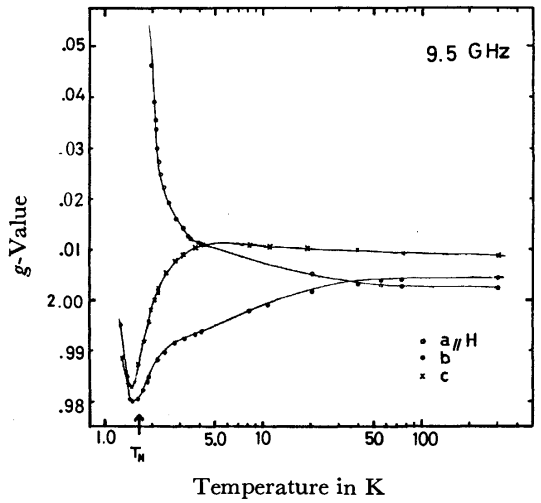

Fig. 4. Temperature dependence of g-values.

axes are parallel to the crystal ones. The g-value shown in Fig. 4 is strongly dependent on the temperature but not on the sample size. Above 2 K, the g-values observed at 9.5 GHz and 34.4 GHz are in agreement with each other within an error of ± 0.0002, and they shift monotonically with the temperature. Below 2 K, but above T_N, a marked shift of the g-value was observed; this is attributable to the shortr-ange magnetic ordering, as has been demonstrated for typical one-dimensional antiferromagnets.[19]

At room temperature the line width shows its maximum when the external field, H_0, is applied parallel to the b-axis and shows its second extremum when H_0 is applied parallel to the a- or c-axes, while it has its minimum value when H_0 and the b-axis make an angle of about 55°, as is indicated in Fig. 5.

Figure 6 shows the temperature dependence of the line width. The line width observed at 9.5 GHz is anomalously broadened up to more than 500 Oe at 1.3 K as compared with the width of less than 20 Oe

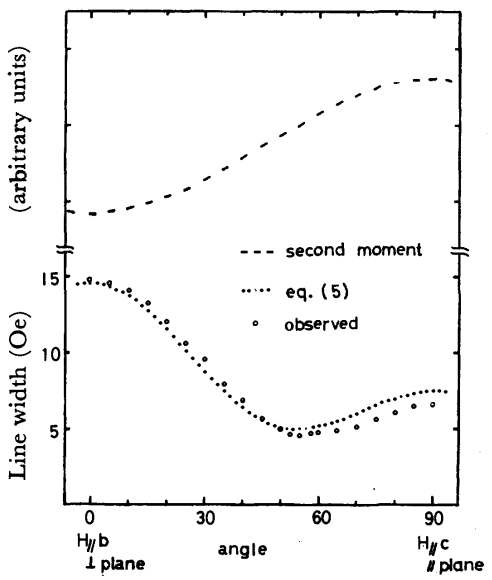

Fig. 5. Angular dependence of ESR line width at room temperature in the bc-plane.

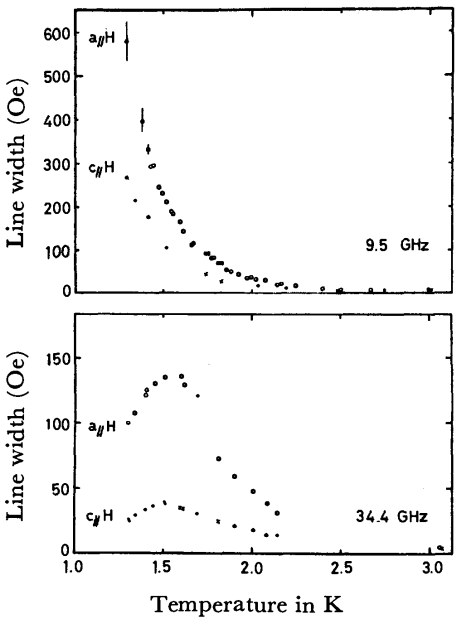

Fig. 6. Temperature dependence of ESR line width at low temperatures measured at a) 9.5 GHz and b) 34.4 GHz.

at 3 K. On the other hand, the linewidth observed at 34.4 GHz shows its maximum at about 1.6 K. With a lowering of the temperature, the absorption line can be observed continuously across the transition temperature, accompanied by a gradual shift of the resonance field although the paramagnetic resonance switches over to the antiferromagnetic resonance (AFMR) at T_N; below this temperature, the resonance position is determined by the AFMR condition.

Discussion

Magnetic Two-dimensionality. The DANO crystal can be expected to be an isotropic two-dimensional antiferromagnetic spin system, with $S=1/2$, coupled with four nearest neighboring spins, on the following grounds: 1) The unpaired electron distributed in the $2p\pi$-orbital has a spin with $S=1/2$. 2) As the observed g-tensor is almost isotropic and is nearly equal to that of the free electron, the magnetic exchange interaction is considered to be approximately isotropic, that is, of the Heisenberg type. 3) From structural considerations, the radical spins may be supposed to interact predominantly with those in the two-dimensional plane. 4) The dominant exchange interaction, J, within the two-dimensional plane is considered to be negative, judging from the negative Weiss temperature.

According to the high-temperature-series expansion (HTS) method applied to the two-dimensional Heisenberg spin system, the magnetic susceptibility is expanded as a function of $x=kT/2JS(S+1)$ as;

$$Ng^2\mu_B^2/\chi\cdot|J| = 3x + \sum_n C_n/x^{n-1} \quad (n=1, 2, \cdots) \qquad (1)$$

where C_n are the HTS coefficients.[20,21] By utilizing the first ten terms for the $S=1/2$ system, the broad maximum in the curve of the magnetic susceptibility *versus* the temperature can be reproduced. The

temperature of the susceptibility maximum, T_{max}, and the maximum value of the susceptibility, χ_{max}, are, respectively, given as;[22]

$$\left.\begin{aligned} kT_{max}/|J| \cdot S(S+1) &= 2.53 \pm 00.5 \text{ for } S = 1/2 \\ \chi_{max} \cdot |J|/Ng^2\mu_B^2 &= 0.0469 \pm 0.0001. \end{aligned}\right\} \quad (2)$$

The combination of these two equations gives a parameter independent of J;

$$\chi_{max} \cdot T_{max}/C = 0.356. \quad (3)$$

The observed values, $\chi_{max}=304\times10^{-4}$ emu/mol and $T_{max}=4.6\pm0.2$ K, yield $\chi_{max} \cdot T_{max}/C=0.36\pm0.01$, which is consistent with the two-dimensional character of the DANO crystal. The solid line in method for Fig. 3 shows the susceptibility calculated by the HTS $J/k=-2.45$ K. In the temperature range of $T>0.9 \cdot S(S+1) \cdot |J|/k$, where the HTS method is valid, the present model explains satisfactorily the magnetic susceptibility of the DANO crystal. In the molecular-field theory, the Weiss temperature is given by;

$$\theta = (2/3) \cdot z \cdot S(S+1) \cdot J/k, \quad (4)$$

which yields $J/k=-2.45\pm0.1$ K, in excellent agreement with the value obtained by the HTS method.

In the recent ESR studies, the effects of magnetic low-dimensionality on the line width have been the topics of great interest.[23] Experimental studies have revealed that, in the two-dimensional system, the angular dependence of the ESR line width, ΔH, at high temperatures cannot be explained by either the three-dimensional-exchange narrowing theory or the dipolar width obtained by the second moment, but is roughly of the form:[24]

$$\Delta H = A(3\cos^2\varphi - 1)^2 + B. \quad (5)$$

Here φ is the angle of the external magnetic field with respect to the normal direction of the two-dimensional plane. The angular dependence of this form was interpreted successfully by the theory taking into account the spin diffusion in the plane.[25] The theory predicts that the angular dependence observed in the two-dimensional system is different from both that in the one-dimensional system and that in the three-dimensional system. In Fig. 5 the angular dependence calculated from Eq. (5) and the dipolar width obtained by the second moment are compared with the line width in the ab-plane observed at 9.5 GHz. Hence, the angular dependence of the line width observed here indicates the two-dimensional characteristics of the magnetic system.

Antiferromagnetism and Magnetic Anisotropy. To investigate the ordered state of the DANO crystal, the results of ESR measurements in 34.4 GHz at 1.39 K ($T/T_N=0.83$) are discussed in terms of the antiferromagnetic resonance (AFMR).[26] The AFMR in an organic free radical crystal was recently reported with regard to the *p*-Cl-BDPA crystal,[27] in which the AFMR was observed in the vicinity of the paramagnetic resonance field because of the very small magnetic anisotropy in contrast with the cases of the antiferromagnets of ionic crystals.[26] In the case of the DANO crystal, the resonance field begins to shift remarkably around 2 K and finally shifts to almost 1 kOe at 1.3 K,

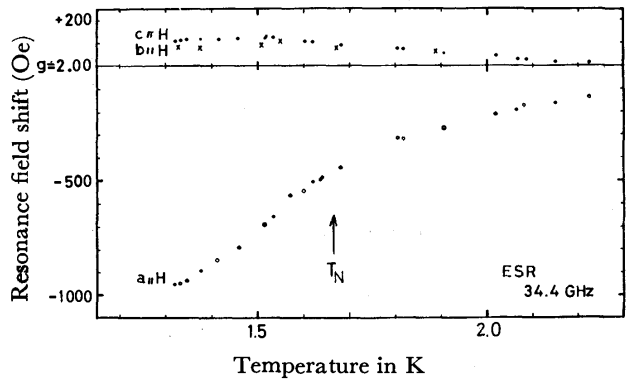

Fig. 7. Temperature dependence of the resonance field at 1.39 K measured at 34.4 GHz.

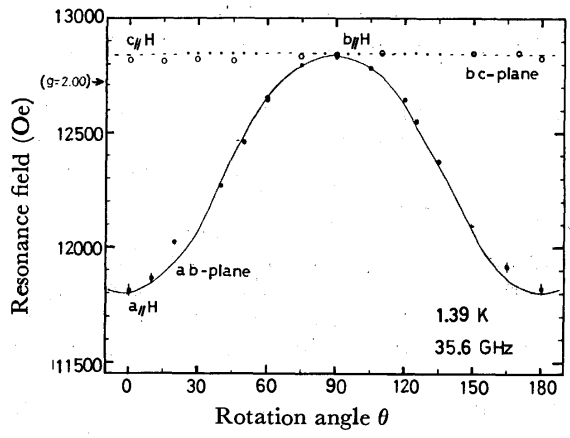

Fig. 8. Angular dependence of AFMR line field at 1.39 K measured at 34.4 GHz.

but no indication of anomaly appears at $T_N=1.67$ K, as is shown in Fig. 7. Fig. 8 shows that the resonance field at 1.39 K has predominantly a uniaxial symmetry around the a-axis and takes the minimum field along the a-axis. The downward shift of the resonance field in the a-axis suggests that this axis is perpendicular to the spin-easy axis.[26] The most remarkable feature of the DANO crystal is the following; its AFMR is observed continuously on the rotation of the external field from the spin-easy axis to the spin-hard axis, indicating the absence of spin flipping; this is confirmed by magnetic torque measurements.[28] These results can be understood reasonably by the model that the DANO crystal is a collinear antiferromagnet with a spin-easy plane perpendicular to the a-axis.[29] It must be noted here that the spin-easy plane (bc-plane) is prependicular to the two-dimensional plane (ac-plane). When the external field, H_0, is applied along the a-axis nearly perpendicular to the sublattice magnetization, the resonance condition is given by:[29]

$$H_0^2 = (\omega/\gamma)^2 - C, \quad C = 2H_AH_E, \quad (6)$$

where H_A and H_E are the anisotropy field along the hard axis and the effective exchange field respectively, ω and γ are calculated from the resonance frequency, 34.4 GHz, and $g=2.0055$ as usual.

According to the molecular field theory, $\sqrt{C}$ is in proportion to the sublattice magnetization, M, which is given by the Brillouin function as a function of the

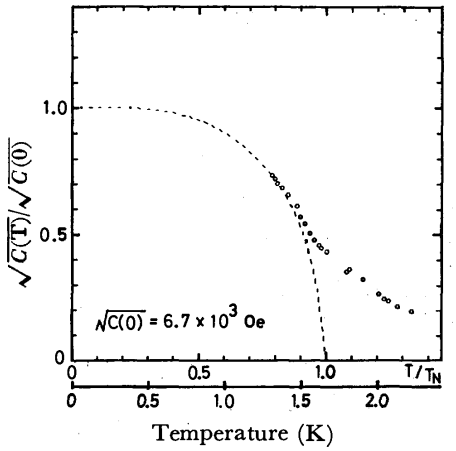

Fig. 9. Temperature dependence of $\sqrt{C}$.

temperature. Figure 9 shows the observed temperature dependence of $\sqrt{C}$ fitted to the Brillouin function for $S=1/2$ at 1.3 K. By the extrapolation of $\sqrt{C}$ along the Brillouin function to $T=0$ K, $\sqrt{C}(0)=(6.7\pm1.0)\times 10^3$ Oe is obtained. In the molecular-field theory, the exchange field is expressed by

$$H_E = 2z|J|\cdot S_z/g\mu_B. \quad (7)$$

Numerical calculations for $z=4$ and $J/k=-2.45$ K yield $H_E=7\times10^4$ Oe at 0 K. From this value, together with $\sqrt{C}(0)$, $H_A=(3\pm1)\times10^2$ Oe at 0 K is obtained.

In the orthorhombic crystals, the magnetic anisotropy energy, F_A, can be generally expressed by the following formula:

$$F_A = (1/2)(K_a\cos\theta_a + K_c\cos\theta_c) \quad (8)$$

where K_a and K_c are the anisotropy constants in the direction of the a-axis and the c-axis respectively with reference to the b-axis. θ_a and θ_c are the angles which the sublattice magnetization makes with the a-axis and the c-axis respectively. Then the effective anisotropy field in each direction, H_A^i, is derived by means of the following equation:

$$H_A^i = K_i/M \quad (i=a, c).$$

In an $S=1/2$ spin system with isotropic-g such as the DANO crystal, the magnetic anisotropy is mainly caused by the magnetic dipolar interaction. The magnitude of the classical magnetic dipolar anisotropy energy was calculated by the direct sum method, taking into account the magnetic dipoles within a diameter of 60 Å. For the examination of the effect of the spin delocalization in the molecule, numerical calculations were performed for the following two cases: 1) the case where the whole magnetic moment ($1\,\mu_B$) is localized at the center of the N–O bond, and 2) the case where the magnetic moment is delocalized over the molecular frame according to the spin density distribution, as calculated by a simple Hückel molecular orbital theory, as is shown in Table 1. In the course of the calculation of the magnetic dipole field, a collinear two-sublattice antiferromagnetic ordering was assumed. The contribution from the spins in the neighboring two-dimensional plane was found to be negligibly small for any spin configuration.

Table 1 summarizes the numerical values of H_A^i.

Table 1. Observed and calculated anisotropy fields with reference to the b-axis in the antiferromagnetic state

	Anisotropy observed from AFMR (Oe)	Dipolar field anisotropy (Oe)	
		Case 1	Case 2
H_A^a	300	216	195
H_A^c	0	106	10

Case 1: spin localized at the center of the N–O bond, Case 2: spin density 0.42 at N, 0.22 at O, 0.06 at *ortho*-C and 0.06 at *para*-C.

In the case 1, the anisotropy field, H_A^c, which should be equal to H_A^a in the case of an ideal quadratic lattice, becomes about 1/2 of H_A^a in the actual lattice shown in Fig. 2. When the delocalization of the spin over the entire molecule is taken into consideration, H_A^a becomes about 1/20 of H_A^a, and the a-axis becomes a unique spin-hard axis (case 2). This corresponds to the experimental result that the system is almost isotropic around the a-axis; *i.e.*, $H_A^c=0$. The observed anisotropies, $H_A=H_A^a=300$ Oe and $H_A^c=0$ Oe, can be approximately explained by the contribution from the magnetic dipoles delocalized over the DANO molecule.

Magnetic Phase Transition. The temperature of the magnetic phase transition of the DANO crystal was determined to be $T_N=1.67$ K from the magnetic susceptibilities of the single crystal and the powdered samples; this value is compatible with the results of the NMR experiments. The resonance-field shift of the ESR spectra, however, shows no anomaly at the transition temperature; thus, no clear distinction was found between the paramagnetic and the antiferromagnetic resonances. This unusual result may be attributed to the well-developed short-range magnetic ordering near T_N. No anomaly was observed either at T_N in the specific heat measurements reported by Duffy *et al.*[11] Bloembergen *et al.* showed that, in the two-dimensional system, the specific heat anomaly is expected to be vanishingly small even if a magnetic ordering occurs as a result of a deviation from the ideal system.[30] The absence of any anomaly at the magnetic-phase-transition temperature in the specific heat and the ESR spectra suggests that the two-dimensionality of the DANO crystal is nearly ideal.

The phase-transition temperature of the two-dimensional system is greatly raised by the interplane exchange interaction, J', and the magnetic anisotropy field, H_A.[9] As a result, J'/J can be evaluated from T_N/θ and H_A/H_E. Table 2 lists the H_A/H_E, T_N/θ, and J'/J

Table 2. Magnetic properties in some two-dimensional magnetic systems with $S=1/2$.

Sample	T_N/θ	H_A/H_E	J'/J
DANO	0.34	5×10^{-3}	10^{-3} a)
Rb_2CuCl_4	0.37	10^{-4}	8×10^{-3}
$Rb_2CuBrCl_3$	0.43	10^{-4}	1.6×10^{-2}

a) Estimated from the data T_N/θ and H_A/H_E of DANO in comparison with those of other samples in this table.

values of some typical two-dimensional magnets with $S=1/2$ listed in a review paper by De Jongh *et al.*,[9] together with those of the DANO crystal. From a comparison of these data, a plausible J'/J value for the DANO crystal is less than 10^{-3}. The three-dimensional magnetic ordering at 1.67 K of the DANO crystal is, therefore, caused by deviations from the ideal two-dimensionality, the existence of J' or H_A, even though these are very small.

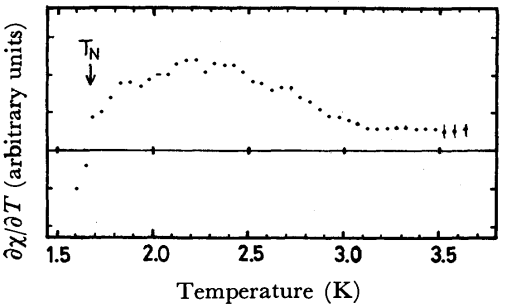

Fig. 10. Temperature derivative of magnetic susceptibility of powdered sample.

Duffy *et al.*[11] assigned weak anomalies in both the magnetic susceptibility and the specific heat near 2.7 K to a three-dimensional magnetic phase transition. In the present experiment, a slight anomaly in the $\partial\chi/\partial T$ spread in the temperature range between 2.4 and 2.9 K was found, as is shown in Fig. 10, while, by the measurements of single crystals, we could hardly detect the anomaly since the accuracy of the measurements is poor for the small single-crystal. In the ESR absorption, nothing anomalous—only a gradual change—was observed at 2.7 K. The shift of the proton-NMR lines also changes gradually and loses its proportionality to the magnetic susceptibility below about 2.7 K. These results do not support the model of the three-dimensional magnetic phase transition at 2.7 K, but they indicate the occurrence of some change, in the short-range magnetic ordering. Further study is necessary to clarify this phenomenon around 2.7 K.

In conclusion, 1) the DANO crystal is an isotropic, nearly two-dimensional spin system with a 10^{-3} ratio of the interplane exchange interaction to the intraplane interaction, 2) the absence of the anomaly in the ESR spectra at T_N is the direct consequence of the short-range magnetic ordering, and 3) the magnetic dipoles distributed over the molecule mainly yield the anisotropy in the ordered state, which orientates the magnetic moment perpendicularly to the a-axis.

The author would like to express his appreciation to Professors Hideo Takaki, Ikuji Tsujikawa, and Yasuo Deguchi for their continual encouragements. He also wishes to thank Drs. Mamoru Mekata, Hiroaki Ohya-Nishiguchi, Yoshitami Ajiro, and Jun Yamauchi for their illuminating discussions. The numerical calculations have partly been done at the Data Processing Center of Kyoto University.

References

1) W. Duffy, Jr., J. F. Dubach, P. A. Pianetta, J. F. Deck, D. L. Strandburg, and A. R. Miedema, *J. Chem. Phys.*, **56**, 2555 (1972).
2) J. Yamauchi, K. Adachi, and Y. Deguchi, *Chem. Lett.*, **1972**, 733; *J. Phys. Soc. Japan*, **35**, 443 (1973).
3) J. P. Boucher, M. Nechtschein, and M. Saint-Paul, *Phys. Lett.*, **42A**, 397 (1973).
4) M. Saint-Paul and C. Veyret, *Phys. Lett.*, **45A**, 362 (1973).
5) J. Yamauchi, T. Fujito, E. Ando, H. Nishiguchi, and Y. Deguchi, *J. Phys. Soc. Japan*, **25**, 1558 (1968).
6) J. Yamauchi, This Bulletin, **44**, 2301 (1971).
7) O. Takizawa, J. Yamauchi, H. Ohya-Nishiguchi, and Y. Deguchi, *ibid.*, **44**, 3188 (1971).
8) Y. Barjhoux, F. Devreux, J. P. Boucher, F. Ferrieu, M. Nechtschein, and M. Plaindoux, *Proceedings 18th AMPERE Congress, Nottingham*, **1974**, 89.
9) L. J. De Jongh and A. R. Miedema, *Adv. Phys.*, **23**, 1 (1974).
10) A. W. Hanson, *Acta Crystallogr.*, **6**, 32 (1953).
11) W. Duffy, Jr., D. L. Strandburg, and J. P. Deck, *Phys. Rev.*, **183**, 567 (1969).
12) O. Takizawa, T. Yoshioka, H. Ohya-Nishiguchi, and Y. Deguchi, *Chem. Lett.*, **1976**, 223.
13) B. H. H. Fisher and F. A. Neugebauer, *Z. Naturforsch.*, **19a**, 1514 (1964).
14) R. D. Allendoerfer and J. H. Englemann, *Mol. Phys.*, **20**, 569 (1971).
15) K. H. Meyer, H. Gottlieb Bierloth, *Chem. Ber.*, **52B**, 1476 (1919).
16) M. Mekata, *J. Phys. Soc. Japan*, **17**, 796 (1962).
17) Landort-Boernstein I. Band 3. Teil 1951. Springer Verlag.
18) O. Takizawa, J. Yamauchi, H. Ohya-Nishiguchi, and Y. Deguchi, This Bulletin, **46**, 1991 (1973).
19) K. Nagata and Y. Tazuke, *J, Phys. Soc. Japan*, **32**, 337 (1972).
20) M. E. Lines, *J. Phys. Chem. Solid*, **31**, 101 (1970).
21) G. A. Baker, Jr., H. E. Gilbert, J. Eve, and G. S. Rushbrooke, *Phys. Lett.*, **25A**, 207 (1967).
22) L. J. De Jongh, *Proc. 18th Ann. Conf. Magnetism and Magnetic Materials, Denver*, **10**, 561 (1972).
23) R. E. Dietz, F. R. Merritt, R. Dingle, D. Hone, B. G. Silbernagel, and P. M. Richards, *Phys. Rev. Lett.*, **26**, 1186 (1971).
24) H. R. Boesh, U. Schmocker, F. Waldner, K. Emerson, and Drumheller, *Phys. Lett.*, **36A**, 461 (1971).
25) P. M. Richards and M. B. Salamon, *Phys. Rev.*, **B9**, 32 (1974).
26) T. Nagamiya, K. Yoshida, and R. Kubo, *Adv. Phys.*, **4**, 1 (1955).
27) J. Yamauchi, *Chem. Lett.*, **1974**, 1031.
28) H. Ozaki, O. Takizawa, J. Yamauchi, H. Ohya-Nishiguchi, and Y. Deguchi, in preparation.
29) E. A. Turov, "Physical Properties of Magnetic Ordered Crystals," Academic Press, New York (1965), p. 53.
30) P. Bloembergen, *J. Physique*, **32**, Suppl. C-1, 879 (1972).

Dynamic Behavior of Acetylacetonato, Triphenylphosphine and Alkyl Ligands in NiR(acac)$(PPh_3)_n$ (R=C_2H_5, CH_3) in Solution and Disproportionation of the Alkylnickel Complexes in Pyridine

Takakazu YAMAMOTO, Toshio SARUYAMA, Yoshiyuki NAKAMURA, and Akio YAMAMOTO*

Research Laboratory of Resources Utilization, Tokyo Institute of Technology, Ookayama, Meguro, Tokyo 152

(Received August 18, 1975)

Dynamic behavior of acetylacetonato (acac), triphenylphosphine (PPh_3) and ethyl (in the case of **1**) ligands of NiR(acac)$(PPh_3)_n$ (R=C_2H_5, n=1 (**1**); R=CH_3, n=2 (**2**)) in solution has been studied. PPh_3 ligand(s) in **1** and **2** exchange rapidly on NMR time scale with free PPh_3 in solution. Addition of excess PPh_3 makes the exchange rate much faster and an S_N2 mechanism is proposed to explain the acceleration effect. ^{31}P-NMR spectrum of **1** in pyridine shows that the PPh_3 ligand is replaced by the solvent molecule. Acac ligands in **1** and **2** also undergo rapid interchange on NMR time scale. The activation energy for the acac interchange is about 10 kcal/mol. On standing a specifically deuterated ethylnickel complex, Ni(CH_2CD_3)(acac)(PPh_3) **1**-d_3 in solution, the hydrogens and deuteriums in the ethyl group were scrambled. Appearance of the methyl proton signals in the ^{1}H-NMR spectrum of the deuterated ethylnickel complex after the treatment in solution demonstrates the occurrence of the H–D scrambling in solution. Both **1** and **2** undergo disproportionation reactions in pyridine. The rate of the disproportionation is second-order with respect to the concentration of **2**.

Ethyl(acetylacetonato)(triphenylphosphine)nickel(II), **1**, provides an interesting object for study of its dynamic behavior in solution. The preliminary NMR study of this complex has led us to suggest that all the ligands including ethyl, acetylacetonato and triphenylphosphine may have dynamic properties in solution.[1] The prime attention was focussed on the NMR spectrum of the ethyl group which appeared as a singlet in benzene, toluene, tetrahydrofuran and acetone and as a pair of a triplet and a quartet in pyridine (at 220 MHz). The observation of the nickel-bound ethyl group as a singlet in particular solvents appeared to suggest that this complex might afford a unique example that the ethyl group undergoes rapid reversible processes involving β-elimination and its reverse reaction such as:

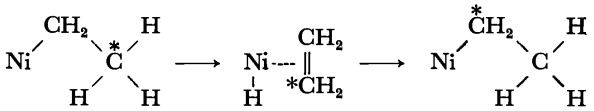

or an alternative process such as:

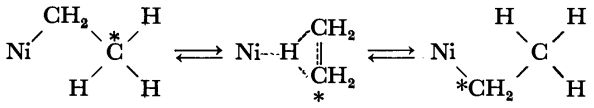

where the intermediacy of the ethylene-coordinated nickel hydride of any significant life time is not involved but the abstracted hydrogen is rapidly transferred in a concerted manner back and forth between two carbon atoms bonded to nickel.[12] If this should be the case the complex may be regarded as a model system for the active species of catalysts promoting various olefin catalyses such as isomerization and oligomerization. The particular feature of the complex has immediately caught attention of Cotton and coworkers who refuted the non-rigid nature of the ethyl group on the basis of ^{13}C-NMR study as well as X-ray examination of **1** which was shown to possess a normal molecular structure with a square planar configuration of the ethyl group, bidentate acetylacetonato and triphenylphosphine ligands around nickel.[2]

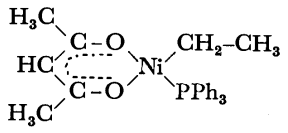

1

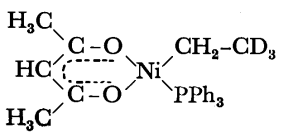

1-d_3

Our subsequent ^{13}C-NMR study of the complex also confirmed the normal ^{13}C-NMR spectrum for the ethyl group. The observation of the normal ^{13}C-ethyl signal recorded by a PFT method, however, does not warrant the complete exclusion of the possibility of proton scrambling of the ethyl group. If the chemical shift difference between CH_2 and CH_3 groups in ^{13}C-NMR is much larger than that in ^{1}H-NMR, and the relaxation of ^{13}C's of the ethyl group should be much faster than the rate of scrambling, the non-decoupled ^{13}C-NMR may still exhibit the triplet and quartet feature with the concomitant scrambling process taking place. In order to get an unequivocal information regarding the suspected proton scrambling process we prepared a specifically deuterated ethylnickel complex Ni(CH_2CD_3)(acac)(PPh_3) **1**-d_3 and examined its behavior by spectroscopic as well as chemical means. The NMR examination of **1**-d_3 revealed that the H–D scrambling is not taking place on NMR time scale but a chemical study of **1**-d_3 in solution indicated that slow scrambling process does occur.

In addition to the ethyl group, other ligands coordinated to nickel in **1** including the acetylacetonato and triphenylphosphine ligands show dynamic behavior amenable to NMR study. We describe here the detailed study of the dynamic behavior of **1** in solution and compare it with its methyl analog, NiCH_3(acac)$(PPh_3)_2$, **2**.

These alkylnickel complexes behave differently in pyridine and undergo a disproportionation reaction. This paper includes the kinetic study of the reaction in pyridine as followed by ^{1}H-NMR spectroscopy.

Experimental

Materials. $NiC_2H_5(acac)(PPh_3)$ **1**[1] was prepared by stirring 15 g (58 mmol) of $Ni(acac)_2$, 18.6 g (71 mmol) of PPh_3 and 36 ml (240 mmol) of $Al(C_2H_5)_2(OC_2H_5)$ in 90 ml of deoxygenated and dehydrated toluene at −40 °C for 40 hr under nitrogen. The yellow-brown complex can be recrystallized from toluene, benzene, acetone or ether. Yield: about 65%; mp 93 °C (decomp.). Found: C, 66.9; H, 6.1%. Calcd for $NiC_2H_5(acac)(PPh_3)$: C, 66.9; H, 6.0%; mol wt, 449; mol wt, (cryoscopic in benzene), 450.

$NiCH_3(acac)(PPh_3)_2$ **2**[1] was prepared and recrystallized in a similar manner by using $Ni(acac)_2$, PPh_3 and $Al(CH_3)_2(OC_2H_5)$ in a molar ratio of 1:2:4: mp 102—103 °C. Found: C, 72.5; H, 6.0%. Calcd for $NiCH_3(acac)(PPh_3)_2$: C, 72.3; H, 5.8%.

Deuterated triethylaluminum $Al(CH_2CD_3)_3$ was prepared by using commercially available CD_3COOD (150 g, 2.38 mol) as the starting material for the preparation of $Ni(CH_2CD_3)(acac)(PPh_3)$ **1**-d_3. CD_3COOD was reduced to CD_3CH_2OH by $LiAlH_4$, and the deuterated ethanol was converted to CD_3CH_2Br by treatment with PBr_3. Deuterated triethylaluminum etherate, $Al(CH_2CD_3)_3(O(C_2H_5)_2)$, was prepared and purified by distillation (91—93 °C/10 mmHg) by the method described in literature.[3] Yield, 10.3 g (0.16 mmol, 6.6%). $Al(CH_2CD_3)_2(O(C_2H_5)_2)$ was prepared from the deuterated triethylaluminum and ethyl alcohol (1:1) and used without purification. Acidolysis of the deuterated triethylaluminum by H_2SO_4 gave 92% of CH_3CD_3 and 8% of CH_2DCHD_2 as analyzed by mass spectroscopy, suggesting a slight H–D scrambling took place during the preparation (presumably during the distillation of $Al(CH_2CD_3)_3(O(C_2H_5)_2)$. The deuterated ethylnickel complex $NiCH_2CD_3(acac)(PPh_3)$ was prepared both in toluene, as described above, and in diethyl ether by the method described by Cotton and coworkers.[2] Cotton's method, in which the reaction was carried out at room temperature, was modified for avoiding the possible scrambling of the ethyl group and the reaction temperature was kept below —10 °C throughout the preparation of **1**-d_3.

The mass spectrum of the ethane released by acidolysis of the deuterated ethylnickel complex with H_2SO_4 and the ^{1}H-NMR spectrum of **1**-d_3 in pyridine indicated that the H–D scrambling of the ethyl group during the preparation was negligible (see the results and discussion). The IR spectrum (KBr) of the deuterated ethylnickel complex showed ν_{C-D} at 2190, 2160, 2100, and 2040 cm^{-1}. When the preparation was carried out at room temperature (in toluene, 1 day), hydrogens and deuteriums of the ethyl group were scrambled during the preparation as proved by the evolution of CH_3CD_3 and CH_2DCHD_2 in a ratio of about 1:1 on acidolysis of the complex by H_2SO_4.

Reaction of **1** *with Deuterium.* On treating **1** (0.75 mmol) with D_2 (2.1 mmol) in toluene (18 °C, 3 days) variously deuterated ethanes (4 mol % per **1**) were formed, whose mass spectrum (70 eV) showed the following pattern: m/e=36 (relative peak height=37), 35 (51), 34 (108), 33(143), 32(670), 31 (635), 30 (819), 29 (643), 28 (890), 27 (265), 26 (127). The isotopic purity of the deuterium gas employed decreased from 0.995 to 0.966 after the treatment of **1** with the deuterium gas.

Spectral Measurements and Analysis. The IR spectra of complexes were obtained by using Hitachi Model EPI-G3 spectrometer. IR spectra of deuterated ethylene evolved on standing **1**-d_3 in pyridine were recorded on Perkin Elmer Model 125. The IR spectra of specifically deuterated ethylene are given in literature.[11] ^{1}H-, ^{31}P-, and ^{13}C-NMR spectra were measured with a Japan Electron Optics Laboratory PS-100 spectrometer. ^{31}P- and ^{13}C-NMR were obtained in the pulsed Fourier transform mode at 40.50 and 25.15 MHz, respectively. Measuring temperature of the NMR spectra was not corrected. Deuterated solvents were used as purchased from Merck and Co., Inc. The solvent and tetramethylsilane were added to an NMR tube containing $NiR(acac)(PPh_3)_n$ by a trap-to-trap distillation in vacuum and the NMR tube was sealed. ^{1}H- and ^{13}C-NMR chemical shifts are referred to internal TMS (downfield positive) and ^{31}P-NMR signals to external triphenylphosphine (downfield positive).

Mass spectra of gases were obtained with a Hitachi type RMU-5B Spectrometer. The distribution of deuterated ethanes evolved on acidolysis of the deuterated ethylnickel complex was calculated from the mass spectra. The mass spectra of specifically deuterated ethanes are given in literature.[4]

The microanalysis of carbon and hydrogen was performed by Mr. T. Saito of our laboratory with a Yanagimoto CHN Autocorder Type Mt-2.

Results and Discussion

Dynamic Behavior of Ligands in $NiC_2H_5(acac)(PPh_3)$ **1** *and* $NiCH_3(acac)(PPh_3)_2$ **2**. *Triphenylphosphine (PPh_3) Ligand*: ^{31}P-NMR spectra of **1** in toluene and pyridine with and without addition of excess triphenylphosphine are shown in Fig. 1. In toluene, without excess PPh_3, a sharp singlet peak due to the coordinated PPh_3 ligand is observed at 44 ppm downfield from external free PPh_3 at −60 °C. At higher temperatures the singlet becomes broad with slight shift to higher field. With excess PPh_3 ([**1**]/[PPh_3]=1) the ^{31}P-NMR spectrum at −80 °C shows two broad signals at 44 ppm and at the position of free PPh_3 in an area ratio of *ca.* 1:1. These results indicate that liberation of PPh_3 from **1** at −60 °C is negligible whereas raising the temperature enhances the liberation of PPh_3 from **1** and

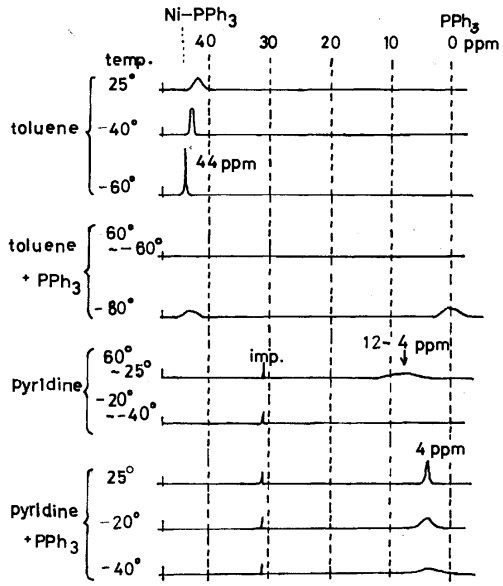

Fig. 1. ^{31}P-NMR spectra of $NiC_2H_5(acac)(PPh_3)$ under various conditions. A peak near 30 ppm which appears in pyridine is due to $Ni(C_2H_4)(PPh_3)_2$ formed by the disproportionation of **1** in pyridine (see the text).

accelerates the PPh_3 exchange of **1** with the liberated PPh_3, although the degree of dissociation is not extensive even at room temperature as revealed by the ^{31}P-NMR in toluene and molecular weight measurement of **1** in benzene. In the presence of added PPh_3, ligand exchange takes place more rapidly even at −80 °C suggesting an S_N2 mechanism, although no definite sign for the formation of $NiC_2H_5(acac)(PPh_3)_2$ corresponding to the methyl analog **2** was observed. The more rapid ligand exchange between **1** and the added PPh_3 at higher temperatures than −60 °C causes collapse of the separated two peaks.

The rate constants of the dissociation of PPh_3 from **1** (the reciprocal of the life time of PPh_3 in **1**, $1/\tau_{Ni-p}=k$ in Eq. 1) calculated

$$Ni(C_2H_5)(acac)(PPh_3) \underset{k'}{\overset{k}{\rightleftharpoons}} Ni(C_2H_5)(acac) + PPh_3 \quad (1)$$

from the half widths of the ^{31}P-NMR signals are summarized in Table 1, which includes the rate constants of dissociation of PPh_3 from **1** in acetone and pyridine and those from **2** in toluene.

Table 1. The rate constants of dissociation of PPh_3 from $NiR(acac)(PPh_3)_n$

Compound	Solvent	[Added PPh_3]/[1]	Temp (°C)	Rate constant (s^{-1})
1	Toluene	0	25	1.6×10^2
	Toluene	0	−40	4.0×10
	Toluene	1	−80	4.2×10^2
	Acetone	0	25	2.2×10^2
	Pyridine	3.4	25	1.0×10^5
	Pyridine	3.4	−20	2.6×10^4
	Pyridine	3.4	−40	1.9×10^4
			E_a=4 kcal/mol	
2	Toluene	0	25	2.8×10^3
	Toluene	0	−60	2.1×10^2

In pyridine the dissociation of **1** to liberate the coordinated triphenylphosphine ligand is more extensive as shown in Fig. 1. The exchange rate seems to be also high and only a broad signal was observed at 25 °C and above at a position between the coordinated PPh_3 and free PPh_3, but much closer to that of free PPh_3. Decrease of the temperature obscured the spectrum and no distinct signal was observed at −20∼ −40 °C. Addition of PPh_3 to the pyridine solution containing **1** gives rise to a somewhat sharp singlet observed at 25 °C downfield from that of free PPh_3. Suppression of the exchange by lowering the temperature from 25 °C down to −40 °C makes the signal broader.

If one assumes that the chemical shift of the coordinated PPh_3 ligand of **1** in pyridine does not differ so markedly from that in toluene, the ratio of undissociated complex to the completely dissociated complex solvated with pyridine can be computed from the chemical shift of the broad signal observed in the absence of added PPh_3 as 1/10 to 1/4 in the temperature range of 60 °C to 25 °C.

The ^{31}P-NMR spectrum of the pentacoordinated methylnickel complex **2** shows somewhat different temperature dependence pattern from that of the ethyl

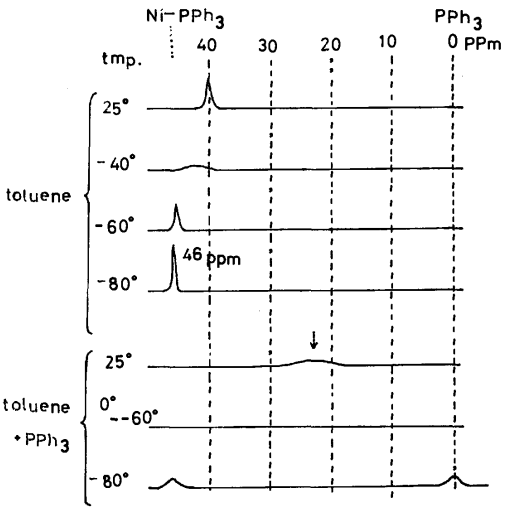

Fig. 2. ^{31}P-NMR spectra of **2** in toluene with and without addition of PPh_3.

analog **1** (Fig. 2). The single resonance which is observed as a reasonably sharp signal at −80 °C in toluene at 46 ppm downfield from free PPh_3 may be ascribed to the coordinated PPh_3 ligands in **2**. With raising the temperature to −40 °C the signal broadens and shifts to higher field indicating the exchange of the coordinated PPh_3 ligands with PPh_3 liberated from **2**. At 25 °C the signal shifts further upfield and sharpens indicating the more rapid exchange taking place. ^{31}P-NMR spectrum of the mixture of **2** and added PPh_3 in a 1 : 0.6 ratio in toluene is similar to the system of (**1**+PPh_3) showing broad peaks of the coordinated PPh_3 and free PPh_3 exchanging each other even at −80 °C. Raising the temperature causes collapse of the peaks and at 25 °C building up of a broad single peak can be noticed as an indication that exchange rate is enhanced by raising the temperature.

The activation energies for dissociation of PPh_3 from **1** and **2**, roughly estimated from the data in Table 1 are in the range of 4—6 kcal/mol which are much less than the values reported for dissociation of tertiary phosphines from nickel complexes.[5]

Acetylacetonato(acac) Ligand: The ^1H-NMR spectra of **1** and **2** have been summarized in our preliminary report.[1] The ^1H-NMR spectra of **1** in acetone-d_6 and benzene-d_6 at various temperatures have been also observed by Cotton, *et al.*[2] At room temperature or below the ^1H-NMR shows two acac(CH_3) peaks. On heating **1** in the solvents these peaks undergo a continued broadening, coalescence, and then sharpening as a result of a time averaging of the two CH_3 groups. A similar temperature dependence of ^1H-NMR spectra is observed in toluene-d_8 and tetrahydrofuran-d_8. In pyridine, however, only one sharp acac(CH_3) peak appears at room temperature. On cooling the pyridine solution the peak becomes broad and then separates into two broad peaks.

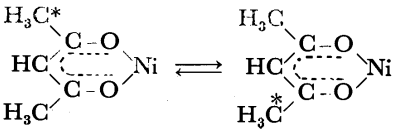

(2)

TABLE 2. THE RATE CONSTANTS OF THE acac INTERCHANGE IN **1**

Solvent	Additive	[Additive]/[1]	Temp (°C)	Rate Constant (s^{-1})
Toluene	—	—	60	1.3×10^{2}
Toluene	—	—	40	1.1×10
Toluene	PPh_3	4.3	70	2.1×10^{2}
Toluene	PPh_3	4.3	60	1.3×10^{2}
Toluene	PPh_3	4.3	40	1.1×10
Benzene	Ethylene	2.0	60	4.3×10^{2}
Benzene	Ethylene	2.0	40	9.3×10
Benzene	Ethylene	2.0	25	6.8×10
Pyridine	—	—	20	3.9×10^{3}
Pyridine	—	—	0	1.0×10^{3}
Pyridine	—	—	−20	3.0×10^{2}
Pyridine	—	—	−40	1.4×10^{2}
Pyridine	PPh_3	1.7	25	5.0×10^{3}
Pyridine	PPh_3	1.7	0	9.0×10^{2}
Pyridine	PPh_3	1.7	−20	2.1×10^{2}
Pyridine	PPh_3	1.7	−40	1.3×10^{2}

The rate constants of the acac interchange in **1** (Eq. 2) under various conditions are summarized in Table 2.

Since the addition of excess PPh_3 does not affect the rate constant, the acac interchange is independent of the exchange of PPh_3 whose exchange rate depends on the excess PPh_3 in the solutions. The mechanism for the interchange is not clear at the moment. However, a mechanism involving M–O bond rupture to form a monodentate acac complex has been proposed for the mechanism of the exchange of acac ligand in some acetylacetonato complexes,[6] and the rupture of Ni–O bond followed by a rotation of the monodentate acac around the Ni–O bond and formation of a new Ni–O bond will be one of the most probable mechanisms for the present acac interchange.

Replacement of PPh_3 in **1** by pyridine and addition of ethylene cause the acceleration of the interchange. Since attempts to obtain an ethylene-coordinated complex from a mixture of **1** and ethylene failed, the interaction between **1** and ethylene seems to be weak. However, such a weak interaction (presumably π-type interaction) makes the rate faster by a factor of 4—9. A similar acceleration effect was observed when one added stryrene or acrylonitrile into the solution of **1**.

The activation energy for the acac interchange (about 10 kcal/mol) is of the same magnitude as those obtained for various acac complexes.[6]

The ^{1}H-NMR spectra of **2** at room temperature show two separate peaks for the acac CH_3 groups in toluene-d_8 and a single peak in pyridine-d_5, similarly to the ^{1}H-NMR spectra of **1** in these solvents. On cooling the pyridine solution the singlet becomes broad. However, since the acac interchange of **2** in pyridine is faster than that of **1**, separation of the peak was not observed even at the low temperatures, in contrast to the case of **1**.

Ethyl Group in **1**: We prepared deuterated ethylnickel complexes from $Ni(acac)_2$, PPh_3 and $Al(CH_2CD_3)_2(OC_2H_5)(O(C_2H_5)_2)$ at −40~−10 °C. The following three facts indicate that the H–D scrambling did not take place during the preparation. (1) The acidolysis of the complex by H_2SO_4 gives 91% of CH_3CD_3 and 9% of CH_2DCHD_2 which coincides, within experimental

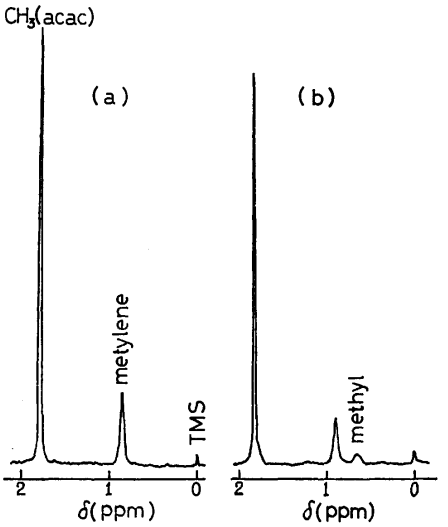

Fig. 3. ^{1}H-NMR spectra of the deuterated ethylnickel complex in pyridine (a) without treatment in solution and (b) after treatment in toluene (Room temp., 2 hr).

error, with the composition of ethane released on the acidolysis of the deuterated triethylaluminum used for the preparation. (2) The ^{1}H-NMR of the deuterated ethylnickel complex in pyridine shows a strong methylene peak, and methyl peak is not observable (Fig. 3a). (3) The ^{1}H-NMR spectrum of propionyl(acetylacetonato)(triphenylphosphine)nickel[7] prepared by the reaction of the deuterated ethylnickel complex with CO clearly demonstrates that it is composed mainly of $NiCOCH_2CD_3$ (Fig. 4a).

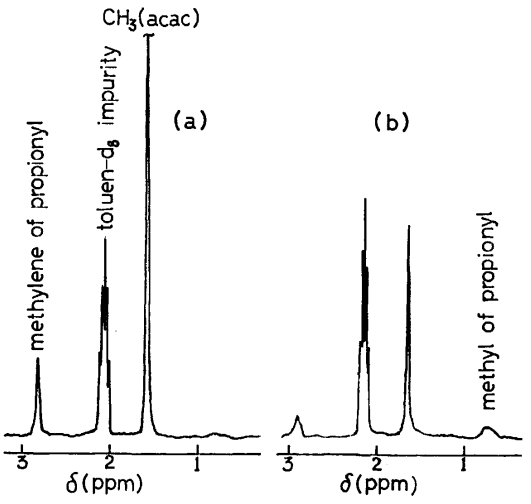

Fig. 4. ^{1}H-NMR spectra of the propionyl (acetylacetonato)(triphenylphosphine)nickel in toluene-d_8 prepared by the reaction of **1**-d_3 and CO. (a) Without treatment of **1**-d_3 in solution. (b) After treatment of **1**-d_3 in acetone (Room temp., 1.5 days).

Since the preparation of $Ni(CH_2CD_3)(acac)(PPh_3)$ **1**-d_3 was carried out at −40~−10 °C where the ethyl signal appears as a sharp singlet in less basic solvents, the H–D scrambling should have taken place during the preparation if the rapid scrambling on NMR time scale should occur and, consequently, we can completely rule out the rapid proton scrambling on NMR time

TABLE 3. COMPOSITION OF THE DEUTERATED ETHANES EVOLVED ON ACIDOLYSIS OF THE DEUTERATED ETHYLNICKEL COMPLEX

No	H–D Scrabling conditions			Composition of deuterated ethanes formed on acidolysis					
	Solvent	Temp (°C)	Time	C_2HD_5	$C_2H_2D_4$	CH_3CD_3	CH_2DCHD_2	$C_2H_4D_2$[a]	C_2H_5D[a]
1	Without treatment					91	9		
2	Toluene	25.6	7.5 min			86.5	13.5		
3	Toluene	25.6	16 min			83	17		
4	Toluene	25.6	31 min			78	22		
5	Toluene	25.6	82 min			71	29		
6	Acetone	24.4	47 min		1	74	24	1	
7	Acetone	24.4	111 min	1	16	22	42	16	1
8	Acetone	Room temp.	a few hrs	2	16	12	52	16	2
9	Pyridine	Room temp.	2.5 days		3	38	56	3	

a) The following relation was assumed: the amounts of $C_2H_4D_2$ and C_2H_5D are equal to the amounts of $C_2H_2D_4$ and C_2HD_5, respectively.

scale based on the facts described above.

Although the rapid scrambling on NMR time scale does not take place, a slow H–D scrambling does occur when one allows the deuterated ethylnickel complex to stand in solutions.

Table 3 summarizes the composition of ethane evolved on acidolysis of the deuterated ethylnickel complex with H_2SO_4 after treatments in solutions.

Through an intramolecular H–D scrambling the specifically deuterated ethylnickel complex is expected to become a mixture of Ni–CH_2CD_3, Ni–$CHDCHD_2$ and Ni–CD_2CH_2D complexes; the first one will evolve CH_3CD_3 on acidolysis with H_2SO_4 and the last two CH_2DCHD_2. Therefore, an increase of CH_2DCHD_2 fraction in Table 3 is regarded as an indication of increase of the degree of internal H–D scrambling.

The random distribution of H and D without isotope effect will result in the formation of Ni–CH_2CD_3, Ni–$CHDCHD_2$ and Ni–CD_2CH_2D complexes in a ratio of 1 : 6 : 3. Such a mixture of the Ni–$C_2H_2D_3$ complexes will evolve CH_3CD_3 and CH_2DCHD_2 in a ratio of 1 : 9 on the acidolysis.

It is shown in Table 3 that the degree of the H–D scrambling increases with time. In toluene formation of Ni-ethyl-d_4 and Ni-ethyl-d_5 species is negligible and the CH_2DCHD_2 fraction increases linearly with time in the early stage (7.5—31 min). In the case of the treatments in acetone the degree of the H–D scrambling at 47 min is of the same extent as that achieved in toluene. However, after allowing the solution containing **1**-d_3 to stand for 111 min or more, considerable amounts of Ni-ethyl-d_4 and Ni-ethyl-d_5 species were formed as proved by evolution of $C_2H_2D_4$ and C_2HD_5 on acidolysis with H_2SO_4. Since the Ni-ethyl-d_4 and Ni-ethyl-d_5 species are not formed at the early stage, they may be formed through a intermolecular interaction of the deuterated ethylnickel complex catalyzed by an unknown compound which is formed during standing the complex in acetone. The H–D scrambling in pyridine is somewhat slower than in acetone and in toluene. In pyridine the ethylnickel complex undergoes disproportionation reaction (*vide infra*) and more than half of the ethylnickel complex is decomposed in a day at room temperature. Therefore most of the Ni–$C_2H_2D_3$ bond had been cleaved before the acidolysis and the data given in Table 3 (No. 9) is for the remaining ethylnickel-d_3 complex resistant to the disproportionation.

Further evidence for the H–D scrambling was provided as follows. (1) The ^{1}H-NMR spectrum of the toluene-treated (Room temp., 2 hr) ethylnickel-d_3 complex in pyridine shows methylene and methyl peaks in an area ratio of 1 : 0.35 (Fig. 3b). (2) The ^{1}H-NMR spectra of propionyl(acetylacetonato)(triphenylphosphine)nickel prepared by the reaction of the acetone-treated (room temp, 1.5 days) ethylnickel-d_3 complex with CO shows methylene and methyl peaks of the propionyl group in an area ratio of 1 : 1.3 (Fig. 4b).

Although it has been known that the H–D scrambling in some deuterated alkylplatinum complexes occurs during their thermal decomposition,[8] this is the first report concerning the H–D scrambling in deuterated alkyltransition metal complex without its decomposition.[12]

Another feature of a dynamic behavior of hydrogens in the ethyl group was demonstrated when **1** was treated with D_2. Although the ethylnickel complex **1** reacts very slowly with D_2 at room temperature, mass spectroscopic examination of ethane gas formed revealed that it contained considerable amounts of C_2D_6, C_2D_5H, $C_2D_4H_2$, $C_2D_3H_3$ and $C_2D_2H_4$ in addition to C_2H_5D which was expected as the sole product in the absence of H–D exchange during the reaction of **1** by D_2 (see the experimental section).[9] Since the ethyl group in the remaining ethylnickel complex **1** was not deuterated at all, this type of H–D exchange is considered to take place only at the moment when the ethyl-nickel bond is cleaved by the reaction with D_2.

Disproportionation of NiR(acac)$(PPh_3)_n$ in Pyridine.

Although **1** and **2** are stable in less basic solvents (benzene, toluene, acetone, *etc.*), the complexes undergo an intermolecular reaction in pyridine. The NMR spectral change of **1** and **2** in pyridine is shown in Fig. 5. The ethyl signals of the ethylnickel complex **1** decrease with time and signals assignable to C_2H_6 and Ni$(C_2H_4)(PPh_3)_2$ increase (the molar ratio of C_2H_6 : Ni$(C_2H_4)(PPh_3)_2 \fallingdotseq 1 : 1$), although the signal of the ethylene in Ni$(C_2H_4)(PPh_3)_2$ is somewhat broadened due to exchange with uncoordinated ethylene in the solution.[10]

In the methyl complex, the methyl signal decreases and peaks assignable to CH_4 and C_2H_6 increase with time. After completion of the reaction one can isolate

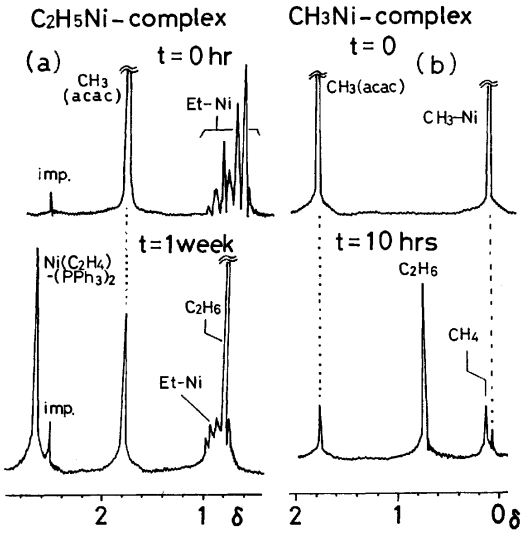

Fig. 5. Changes of ^{1}H-NMR spectra of **1** and **2** with time in pyridine. (a) $NiC_2H_5(acac)(PPh_3)$; (b) $NiCH_3(acac)(PPh_3)_2$.

$Ni(acac)_2(pyridine)_2$ from the both systems. These results suggest that the following disproportionation reaction *via* formation of an unstable dialkylnickel complex may be taking place in pyridine.

$$2NiR(acac)(PPh_3)_n \xrightarrow{2Py} Ni(acac)_2\cdot 2Py + [(PPh_3)_2NiR_2]$$

$$R=C_2H_5 \swarrow \qquad \downarrow R=CH_3$$

$$Ni(C_2H_4)(PPh_3)_2 + C_2H_6 \qquad Ni(PPh_3)_n' + CH_4 + C_2H_6 \ (1:2)$$

Although the rate of the disproportionation of **1** is very slow, that of **2** is reasonably fast and the disproportionation reaction of **2** was followed by NMR spectroscopy. Figure 6 shows the decrease of **2** with time and the second-order plot for the reaction. If we take into account the kinetic result as well as the observation of the fluxionality of the acac ligand, a partial dissociation of acac ligand from nickel and a following coordination of the partially dissociated acac ligand with another alkylnickel complex to form a binuclear complex seem to be the most probable process for the disproportionation reaction.

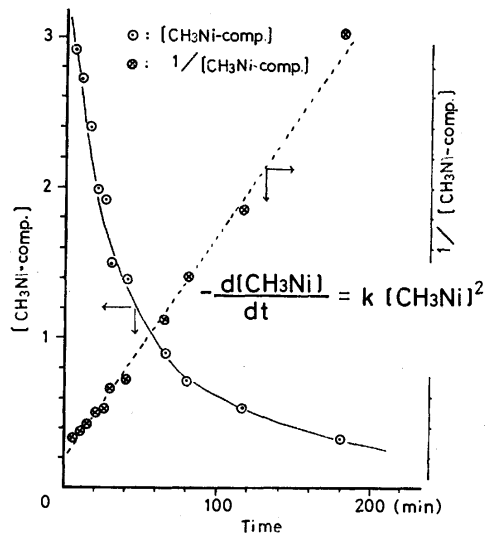

Fig. 6. Disproportionation of $NiCH_3(acac)(PPh_3)_2$ in pyridine followed by ^{1}H-NMR spectroscopy. The unit of the concentration of **2** is arbitrary (peak area).

When **1**-d_3 was employed for the disproportionation reaction in pyridine, the ethylene evolved in a day at room temperature was $CH_2=CD_2$ and other deuterated ethylene was not detected (IR spectrum). This suggests that the scission of the Ni–C_2H_5 bonds in the supposed unstable diethylnickel complex proceeds through a β-elimination mechanism.

We are grateful for the grant support of this work by Research Grants in Basic Chemistry administered through Japan Society for Promotion of Science.

References

1) A. Yamamoto, T. Yamamoto, T. Saruyama, and Y. Nakamura, *J. Amer. Chem. Soc.*, **95**, 4073 (1973).

2) F. A. Cotton, B. A. Frenz, and D. L. Hunter, *ibid*, **96**, 4820 (1974). In the literature they claimed that the ethylene ligand formed by the β-elimination of the ethyl group should have rotated about the axis from Ni to the center of the ethylene in order to lead to scrambling of hydrogens. However, we think that the rotation of ethylene is not necessary and the reversible processes involving the β-elimination and its reverse reaction is enough to lead to scrambling of hydrogen.

3) E. Krause and B. Wendt, *Chem. Ber.*, **B56**, 466 (1923).

4) Y. Amenomiya and R. F. Pottie, *Can. J. Chem.*, **46**, 1741 (1968).

5) a) C. A. Tolman, W. C. Seidel, and L. W. Gosser, *J. Amer. Chem. Soc.*, **96**, 53 (1974); b) M. Meier, F. Basolo, and R. G. Pearson, *Inorg. Chem.*, **8**, 795 (1969); c) R. D. Johnston, F. Basolo, and R. G. Pearson, *ibid.*, **10**, 247 (1971); d) C. H. Bamford and E. O. Hughes, *Proc. Roy. Soc. Ser. A*, **326**, 469 (1972).

6) a) A. C. Adams and E. N. Larsen, *Inorg. Chem.*, **5**, 814 (1966); b) G. E. Glass and R. S. Tobias, *J. Organometal. Chem.*, **15**, 481 (1968); c) N. Serpone and R. Ishayek, *Inorg. Chem.*, **13**, 52, (1974); d) G. M. Tanner, D. G. Tuck, and E. J. Wells, *Can. J. Chem.*, **50**, 3950 (1972).

7) T. Saruyama, T. Yamamoto, and A. Yamamoto, *Bull. Chem. Soc. Jpn.*, **49**, 546 (1976).

8) a) J. Chatt, R. S. Coffey, A. Gough, and D. T. Thompson, *J. Chem. Soc., A* **1968**, 190; b) G. M. Whitesides, J. F. Gaasch and E. R. Stedronsky, *J. Amer. Chem. Soc.*, **94**, 5258 (1972).

9) A. Yamamoto, T. Yamamoto, M. Takamatsu, T. Saruyama, and Y. Nakamura, 'Organotransition-metal Chemistry,' Eds. Y. Ishii and M. Tsutsui, Plenum Publishing Coorporation, New York (1975), p. 281.

10) P. T. Cheng, C. D. Cook, S. C. Nyburg, and K. Y. Wan, *Inorg. Chem.*, **10**, 2210 (1971).

11) R. L. Arnett and B. L. Crawford, Jr., *J. Chem. Phys.*, **18**, 118 (1950).

12) After having submitted this paper we noted Osborn and coworkers' paper in which they described that hydrogen of Mo–H in $MoH(C_2H_4)_2$ (diphenylphosphinoethane)$_2$(CF_3-COO) exchanged rapidly and reversibly with the half of the bound ethylene protons on NMR time scale (J. W. Byrne, H. U. Blaser, and J. A. Osborn, *J. Amer. Chem. Soc.*, **97**, 3872 (1975)). They proposed that the rapid exchange proceeded *via* the insertion of ethylene into the Mo–H bond and its reverse reaction.

The Crystal and Molecular Structure of Zinc Complex of 2-Chlorobenzoic Acid. II. The Crystal and Molecular Structure of μ_3-Hydroxo-tri-μ-(2-chlorobenzoato)dizinc(II) Dihydrate

Yoshifumi NAKACHO, Takeshi MISAWA, Takaji FUJIWARA,* Akio WAKAHARA,* and Ken-ichi TOMITA*

Otsuka Chemical Co., Ltd., Satoura, Naruto, Tokushima 772

* *Faculty of Pharmaceutical Sciences, Osaka University, Yamada-kami, Suita, Osaka 565*

(Received August 22, 1975)

$C_{21}H_{12}O_6Cl_3Zn_2OH \cdot 2H_2O$ crystallizes in the monoclinic space group $P2_1/c$: $a=12.779$, $b=23.732$, $c=14.749$ Å, $\beta=147.98°$, and $Z=4$. The structure was determined by the usual heavy atom method and refined to $R=0.039$. The complex forms polymeric complex chains in the crystalline state. The ligands around two independent zinc atoms form an unusual trigonal bipyramid and an octahedron, respectively; the coordination geometry apparently differs from that found in the crystal structure of bis(2-chlorobenzoato) zinc(II). The correlation between coordination geometry and catalytic action of zinc atom is also discussed.

Two different forms of zinc complex of 2-chlorobenzoic acid were found.[1] In this paper, we report the detailed crystal and molecular structure of the second crystal, a reactive form, as regards the coordination around central zinc atom differing from that in the first crystal, an inactive form. From the results, a mechanism for complex formation and catalytic reactivity of zinc atom is discussed.

Experimental

The complex was prepared by mixing three-molar sodium 2-chlorobenzoate and two-molar zinc chloride in aqueous or acetone-aqueous solution at room temperature. By recrystallization from a mixed solvent of acetone and water 9: 1 ratio, a hexagonal pillar-shaped single crystal was obtained, which was cut to approximately $0.12\times0.11\times0.55$ mm for X-ray study. The density was measured by the flotation method in a carbon tetrachloride and ethylene dibromide mixture. The cell dimensions were obtained on a Rigaku-Denki four-circle diffractometer with Cu$K\alpha$ radiation (Table 1). From the systematic absence of reflections ($h0l$: $l=2n+1$, $0k0$: $k=2n+1$), the space group was determined to be $P2_1/c$. The intensity data were collected on the diffractometer with Cu$K\alpha$ radiation

TABLE 1. CRYSTAL DATA OF μ_3-HYDROXO-TRI-μ-(2-CHLOROBENZOATO)DIZINC DIHYDRATE

$C_{21}H_{17}O_9Cl_3Zn_2$: M.W.=650.5

Crystal system:	monoclinic
Cell constants:	$a=12.779\pm0.004$ Å
	$b=23.732\pm0.006$ Å
	$c=14.749\pm0.006$ Å
	$\beta=147.98\pm0.04°$
	$U=2371.40$ Å^3
Space group:	$P2_1/c$
Z :	4
Density (obsd):	$D_m=1.825\pm0.002$ g/cm^3
(calcd):	$D_x=1.830$ g/cm^3

TABLE 2. THE FINAL FRACTIONAL COORDINATES WITH THEIR STANDARD DEVIATIONS IN PARENTHESES

Atom	x	y	z	Atom	x	y	z
Zn 1	0.0724(1)	0.0610(0)	0.0472(1)	C B5	0.3453(11)	0.0658(3)	−0.0438(9)
Zn 2	0.5506(1)	0.0217(0)	0.6373(1)	C B6	0.4770(10)	0.0585(3)	0.1207(8)
ClA	0.3172(3)	0.2286(1)	0.3674(3)	C B7	0.3825(10)	0.0455(3)	0.1409(8)
ClB	0.8671(3)	0.0597(1)	0.4674(2)	C C1	0.4718(10)	0.2065(3)	0.7276(8)
ClC	0.2814(3)	0.1599(1)	0.6225(3)	C C2	0.4431(12)	0.2648(3)	0.7239(10)
O A1	0.2949(6)	0.1155(2)	0.2583(5)	C C3	0.5971(13)	0.3021(3)	0.8103(10)
O A2	0.5078(6)	0.0550(2)	0.4755(5)	C C4	0.7669(14)	0.2849(2)	0.9014(12)
O B1	0.4845(7)	0.0162(2)	0.2671(6)	C C5	0.8023(11)	0.2276(3)	0.9103(10)
O B2	0.2029(6)	0.0651(2)	0.0293(5)	C C6	0.6506(9)	0.1879(3)	0.8194(8)
O C1	0.5524(6)	0.1010(2)	0.6874(5)	C C7	0.6924(10)	0.1285(3)	0.8216(8)
O C2	0.8741(6)	0.1110(2)	0.9654(5)	H A1	0.686 (12)	0.288 (4)	0.622 (11)
OW1	0.2178(6)	0.0219(2)	0.4091(5)	H A2	1.052 (11)	0.264 (3)	0.860 (10)
OW2	0.1497(6)	−0.0091(2)	0.1689(5)	H A3	1.126 (12)	0.168 (3)	0.881 (10)
OW3	0.0486(8)	0.1240(2)	0.2614(7)	H A4	0.844 (11)	0.102 (3)	0.668 (9)
C A1	0.5623(10)	0.2064(3)	0.5179(8)	H B1	0.920 (10)	0.085 (3)	0.334 (9)
C A2	0.7147(12)	0.2483(3)	0.6269(10)	H B2	0.654 (12)	0.099 (3)	0.016 (10)
C A3	0.9121(12)	0.2338(3)	0.7513(10)	H B3	0.314 (12)	0.082 (3)	−0.202 (10)
C A4	0.9661(11)	0.1781(3)	0.7774(10)	H B4	0.207 (11)	0.056 (3)	−0.124 (9)
C A5	0.8135(10)	0.1374(3)	0.6682(9)	H C1	0.307 (12)	0.280 (3)	0.654 (10)
C A6	0.6105(9)	0.1505(3)	0.5355(8)	H C2	0.584 (13)	0.348 (4)	0.823 (12)
C A7	0.4555(9)	0.1045(2)	0.4122(8)	H C3	0.876 (14)	0.316 (4)	0.963 (12)
C B1	0.6834(10)	0.0648(3)	0.2517(8)	H C4	0.919 (11)	0.219 (3)	0.979 (10)
C B2	0.7565(11)	0.0778(3)	0.2233(10)	HW1	0.171 (11)	0.047 (3)	0.377 (10)
C B3	0.6214(13)	0.0839(4)	0.0572(12)	HW2	0.167 (12)	−0.012 (4)	0.235 (11)
C B4	0.4148(12)	0.0775(4)	−0.0777(10)	HW3	0.044 (13)	0.126 (4)	0.216 (11)

using the ω-2θ scan technique. A total of 2472 independent reflections were collected in the range $\sin\theta/\lambda \leqq 0.55$ Å^{-1}. A Wilson plot was then made to place the observed intensities on an absolute scale. No correction was made for absorption.

Structure Determination and Refinement

The structure was solved by application of the usual heavy atom method. Except for three water molecules, all the positions of thirty-two nonhydrogen atoms were determined by the first Fourier synthesis with phases based on zinc and chlorine atoms. The coordinates of oxygen atoms in three water molecules were then found (R=0.26). After several cycles of block-diagonal least-squares refinement, a difference Fourier synthesis was carried out in order to determine the location of hydrogen atoms. Twelve hydrogen atoms bound to carbon atoms and three hydrogen atoms (HW1, HW2, and HW3, see Fig. 1) attached to water molecules were satisfactorily located at proper positions with reasonable peak heights. Only one hydrogen atom peak was found around the water oxygen atom OW2, almost on the line connecting OW1 and OW2 to form a hydrogen bond. However, the positions of the remaining two hydrogen atoms bound to the oxygen atoms (OW1 and OW3) were obscure, and were omitted in further refinement. The final least-squares refinement including fifteen hydrogen atoms with isotropic temperature factors (B=2.0~7.0 Å^2) reduced the R-value to 0.041. The final atomic parameters with their estimated standard deviations except those for the two undetectable hydrogen atoms are given in Tables 2 and 3. The observed and calculated structure factors are listed in Table 4.[2] The atomic scattering factors and all the numerical calculation procedures were the same as given previously.[1]

TABLE 3. THE FINAL TEMPERATURE FACTORS AND THEIR STANDARD DEVIATIONS ($\times 10^4$)

The anisotropic temperature factors are in the form of $\exp[-(\beta_{11}h^2+\beta_{22}k^2+\beta_{33}l^2+\beta_{12}hk+\beta_{13}hl+\beta_{23}kl)]$

Atom	β_{11}	β_{22}	β_{33}	β_{12}	β_{13}	β_{23}
Zn 1	107(2)	6(0)	81(1)	0(1)	148(3)	0(1)
Zn 2	113(2)	7(0)	76(1)	0(1)	147(3)	1(1)
ClA	270(6)	10(0)	222(4)	15(2)	411(9)	2(2)
ClB	161(5)	24(0)	129(3)	−12(2)	220(8)	1(2)
ClC	194(5)	22(0)	196(4)	6(2)	333(9)	2(2)
O A1	119(11)	7(1)	70(7)	−3(5)	122(17)	2(4)
O A2	153(11)	6(1)	73(7)	−8(5)	178(17)	−5(4)
O B1	193(13)	15(1)	148(9)	16(6)	301(21)	25(5)
O B2	114(11)	16(1)	94(8)	11(5)	167(18)	17(5)
O C1	182(12)	7(1)	104(8)	3(5)	255(19)	−10(4)
O C2	144(12)	12(1)	107(9)	30(5)	181(19)	−1(5)
OW1	142(12)	13(1)	104(8)	8(5)	191(18)	4(5)
OW2	110(10)	7(1)	55(7)	−4(4)	123(16)	0(4)
OW3	289(16)	18(1)	216(11)	27(7)	457(25)	22(6)
C A1	196(19)	11(1)	106(13)	−13(8)	237(30)	−7(7)
C A2	321(25)	9(1)	168(16)	−40(10)	387(38)	−22(8)
C A3	236(23)	15(2)	140(15)	64(10)	264(35)	−34(8)
C A4	183(21)	16(2)	143(15)	−39(10)	228(33)	−15(8)
C A5	160(19)	12(1)	120(13)	−18(8)	211(30)	−6(7)
C A6	142(17)	8(1)	92(12)	−16(7)	191(27)	−6(6)
C A7	144(17)	7(1)	107(12)	−7(7)	216(27)	−7(6)
C B1	153(18)	13(1)	106(13)	0(8)	216(28)	−2(7)
C B2	209(21)	19(2)	180(16)	−17(10)	348(35)	−10(8)
C B3	354(28)	22(2)	291(21)	−21(12)	601(47)	−3(10)
C B4	268(24)	30(2)	180(17)	−13(12)	391(38)	8(10)
C B5	203(20)	21(2)	148(15)	−18(10)	308(33)	−2(8)
C B6	176(18)	10(1)	111(12)	0(8)	249(28)	0(7)
C B7	178(18)	9(1)	114(13)	−27(8)	250(29)	−18(6)
C C1	175(19)	11(1)	110(13)	25(8)	233(29)	11(7)
C C2	271(24)	21(2)	158(15)	59(11)	366(37)	31(9)
C C3	350(27)	10(2)	210(18)	21(10)	472(41)	9(8)
C C4	374(29)	11(2)	272(21)	−13(11)	550(46)	−19(9)
C C5	227(22)	12(2)	188(16)	−1(9)	348(36)	−11(8)
C C6	147(17)	9(1)	93(12)	10(7)	191(27)	2(6)
C C7	172(18)	8(1)	132(13)	8(8)	270(29)	2(7)

Results and Discussion

Numbering of molecule is made by use of two letters and two numbers. The first letter corresponds to the kind of atom, and the second to one of the three independent 2-chlorobenzoic acid ligands (A, B and C) or water molecule (W). The first number corresponds to the

TABLE 5. BONDLENGTHS WITH ESTIMATED STANDARD DEVIATIONS IN PARENTHESES

(a) Zn–O lengths

From	To	Unit[a]	Length	From	To	Unit[a]	Length
Zn1–O	A1	1	2.110(9) Å	Zn2–O	A2	1	2.113(9) Å
Zn1–O	B1	1	1.998(9)	Zn2–O	A2	2	2.138(9)
Zn1–O	C2	3	2.013(10)	Zn2–O	B2	2	2·007(10)
Zn1–O	W2	1	1.986(8)	Zn2–O	C1	1	2.011(10)
Zn1–O	W2	4	2.093(8)	Zn2–O	W1	1	2.266(9)
				Zn2–O	W2	2	2.101(8)

(b) Other lengths

From	To	Length	From	To	Length
Cl A–C	A1	1.793(14) Å	C lB–C	B1	1.727(13) Å
O A1–C	A7	1.238(14)	O B1–C	B7	1.238(15)
O A2–C	A7	1.279(14)	O B2–C	B7	1.283(14)
C A1–C	A2	1.427(20)	C B1–C	B2	1.343(19)
C A1–C	A6	1.400(18)	C B1–C	B6	1.439(17)
C A2–C	A3	1.414(22)	C B2–C	B3	1.353(22)
C A3–C	A4	1.384(21)	C B3–C	B4	1.428(23)
C A4–C	A5	1.416(19)	C B4–C	B5	1.367(21)
C A5–C	A6	1.430(17)	C B5–C	B6	1.352(19)
C A6–C	A7	1.521(17)	C B6–C	B7	1.500(17)
C A2–H	A1	1.01 (16)	C B2–H	B1	1.13 (13)
C A3–H	A2	1.19 (15)	C B3–H	B2	1.04 (15)
C A4–H	A3	1.13 (15)	C B4–H	B3	1.02 (15)
C A5–H	A4	0.91 (14)	C B5–H	B4	1.01 (13)
OW1–H	W1	0.68 (14)	OW2–H	W2	0.81 (16)
Cl C–C	C1	1.775(13)	C C5–C	C6	1.426(19)
O C1–C	C7	1.240(15)	C C6–C	C7	1.498(17)
O C2–C	C7	1.308(15)	C C2–H	C1	1.08 (13)
C C1–C	C2	1.420(20)	C C3–H	C2	1.14 (17)
C C1–C	C6	1.414(17)	C C4–H	C3	1.08 (18)
C C2–C	C3	1.380(22)	C C5–H	C4	0.86 (14)
C C3–C	C4	1.375(24)	OW3–H	W3	0.63 (16)
C C4–C	C5	1.405(23)			

a) *cf.* Unit No. in Table 7.

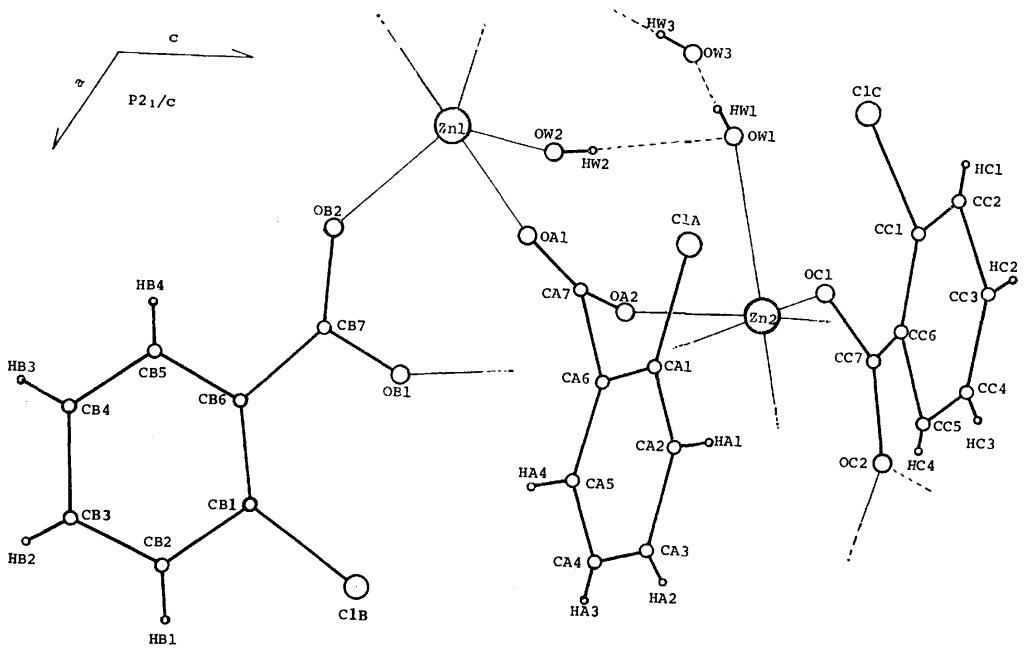

Fig. 1. Schematic drawing around two kinds of zinc ions.

TABLE 6. BOND ANGLES WITH ESTIMATED STANDARD DEVIATIONS IN PARENTHESES.

	Angle		Angle		Angle
ClA–CA1–CA2	118.5(10)°	ClB–CB1–CB2	111.9(10)°	ClC–CC1–CC2	117.1(10)°
ClA–CA1–CA6	122.5(10)	ClB–CB1–CB6	123.1(9)	ClC–CC1–CC6	123.1(10)
CA2–CA1–CA6	119.0(12)	CB2–CB1–CB6	125.0(12)	CC2–CC1–CC6	119.7(12)
CA1–CA2–CA3	121.5(14)	CB1–CB2–CB3	115.6(14)	CC1–CC2–CC3	118.8(14)
CA2–CA3–CA4	120.9(14)	CB2–CB3–CB4	121.6(15)	CC2–CC3–CC4	122.5(15)
CA3–CA4–CA5	117.0(13)	CB3–CB4–CB5	121.2(14)	CC3–CC4–CC5	120.5(15)
CA4–CA5–CA6	124.0(12)	CB4–CB5–CB6	118.5(13)	CC4–CC5–CC6	118.6(13)
CA1–CA6–CA5	117.6(11)	CB1–CB6–CB5	118.0(12)	CC1–CC6–CC5	119.9(11)
CA1–CA6–CA7	122.8(11)	CB1–CB6–CB7	128.6(11)	CC1–CC6–CC7	124.8(11)
CA5–CA6–CA7	119.4(10)	CB5–CB6–CB7	113.4(11)	CC5–CC6–CC7	115.2(11)
OA1–CA7–OA2	124.0(11)	OB1–CB7–OB2	127.1(11)	OC1–CC7–OC2	126.6(11)
OA1–CA7–CA6	119.6(10)	OB1–CB7–CB6	114.5(11)	OC1–CC7–CC6	117.0(11)
OA2–CA7–CA6	116.2(10)	OB2–CB7–CB6	118.4(10)	OC2–CC7–CC6	116.4(10)
CA1–CA2–HA1	121(9)	CB1–CB2–HB1	120(7)	CC1–CC2–HC1	121(9)
CA3–CA2–HA1	118(9)	CB3–CB2–HB1	124(7)	CC3–CC2–HC1	120(9)
CA2–CA3–HA2	126(7)	CB2–CB3–HB2	124(8)	CC2–CC3–HC2	122(9)
CA4–CA3–HA2	112(7)	CB4–CB3–HB2	114(8)	CC4–CC3–HC2	115(9)
CA3–CA4–HA3	118(8)	CB3–CB4–HB3	120(9)	CC3–CC4–HC3	119(9)
CA5–CA4–HA3	125(8)	CB5–CB4–HB3	118(9)	CC5–CC4–HC3	120(9)
CA4–CA5–HA4	116(9)	CB4–CB5–HB4	130(8)	CC4–CC5–HC4	116(10)
CA6–CA5–HA4	118(9)	CB6–CB5–HB4	111(8)	CC6–CC5–HC4	125(10)

individual atom number in a ligand and the second one to the unit number (Table 7), those corresponding to unit No. 1 being omitted (Fig. 1).

The bond lengths and angles are listed in Tables 5 and 6 with their estimated standard deviations. Two of the exocyclic bond angles increase from the normal value of 120° to 122.5° and 122.8° for A, to 123.1° and 128.6° for B, and to 123.1° and 124.8° for C. This might be due to repulsion between the adjacent chlorine atom and carboxyl group. The dihedral angles between carboxyl plane and benzene-ring plane in three independent 2-chlorobenzoic acid ligands are 35° for A, 30° for B and 35° for C, whereas the values in bis(2-chlorobenzoato)zinc(II) are 9° and 41°,[1] and 23° in 2-chloro-5-nitrobenzoic acid.[3]

The coordination geometry around two independent zinc atoms is of interest. Znl is surrounded by five ligands to form a distorted trigonal bipyramid, and Zn2 by six ligands to form a distorted octahedron (Fig. 2 and Table 7). Znl shifts by 0.015 Å toward OA1 from the trigonal plane formed by OC2, OB1 and OW2, and the directions of two bonds, Znl–OW2-4 and Znl–OA1, deviate by 9.2° and 6.6° from the normal to the trigonal plane, respectively. Similarly, the bonds, Zn2–OW1

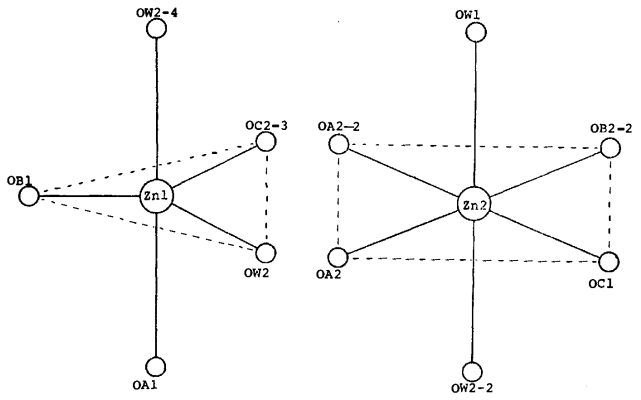

Fig. 2. The coordinations of zinc atoms.

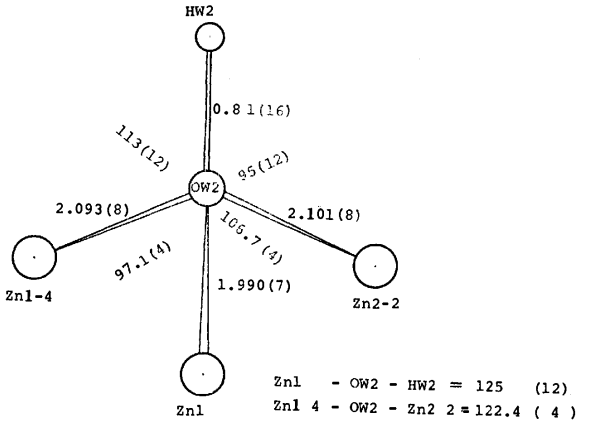

Fig. 3. The coordination of the hydroxyl oxygen atom. Bond distances are in Å and angles are in degree.

TABLE 7. BOND ANGLES AROUND TWO INDEPENDENT ZINC ATOMS

Atom Unit	Atom Unit	Angle
O B1 1	Zn1	O W2 4	91.6(3)°
O W2 4	Zn1	O C2 3	92.8(4)
O C2 3	Zn1	O W2 1	116.8(4)
O B1 1	Zn1	O C2 3	133.4(4)
O W2 4	Zn1	O W2 1	83.0(3)
O A1 1	Zn1	O C2 3	88.0(4)
O A1 1	Zn1	O W2 4	176.8(3)
O B1 1	Zn1	O W2 1	109.6(4)
O A1 1	Zn1	O B1 1	85.7(4)
O A1 1	Zn1	O W2 1	99.4(3)
O W1 1	Zn2	O W2 2	170.5(3)
O W1 1	Zn2	O A2 2	82.8(3)
O W1 1	Zn2	O B2 2	78.2(4)
O W1 1	Zn2	O A2 1	87.8(3)
O W1 1	Zn2	O C1 1	88.3(4)
O W2 2	Zn2	O A2 2	87.7(3)
O W2 2	Zn2	O B2 2	102.5(4)
O W2 2	Zn2	O C1 1	101.1(4)
O W2 2	Zn2	O A2 1	90.5(3)
O C1 1	Zn2	O B2 2	96.3(4)
O C1 1	Zn2	O A2 1	88.3(4)
O A2 2	Zn2	O A2 1	81.5(3)
O A2 2	Zn2	O B2 2	91.5(4)

The coordinates of Zn1 and Zn2 are those belongoing to unit No. 1

Unit No. 1 ($0.0+x, 0.0+y, 0.0+z$)
Unit No. 2 ($1.0-x, 0.0-y, 1.0-z$)
Unit No. 3 ($-1.0+x, 0.0+y, -1.0+z$)
Unit No. 4 ($0.0-x, 0.0-y, 0.0-z$)

and Zn2-OW2-2, deviate by 5.5° and 8.8° from the least-squares plane consisting of OA2, OA2-2, OB2-2, and OCl. These unusual coordinations, especially a distorted trigonal bipyramidal coordination, which is probably the first case in zinc complexes,** might give important information on catalytic function of the zinc atom. The interatomic distances between adjacent zinc atoms are 3.06 Å for Zn1 to Zn1-4, 3.22 Å for Zn2 to Zn2-2, and 3.28 Å for Zn1 to Zn2-2. The values are much smaller than those in bis(2-chlorobenzoato)-zinc(II), 3.77 Å.[1] From density measurement, it seems that three water molecules are involved in an asymmetric unit. However, the difference Fourier map indicates that one of these water molecules should be of anionic form, OH^-, that is, only one peak for hydrogen atom around OW2 was found. This is reasonable for the balance of charge in crystal, provided that four units of positive charge are supplied by $2Zn^{2+}$ and four units of negative charge by three $C_6H_4ClCOO^-$ and one OH^- ions. This was confirmed by counting the number of OH-proton in NMR spectra. As shown in Fig. 3, OW2 coordinates to three neighboring zinc atoms, Zn1, Zn1-4 and Zn2-2, and the OH^- (*i.e.*, OW2-HW2) bond directs to one remaining apex of tetrahedron to form a hydrogen bond with OW1 (2.94 Å). Two water molecules participate in hydrogen bonding of OW1-HW1···OW3 (2.70 Å) and OW3-HW3 ···OC2 (2.77 Å), but the remaining two hydrogen atoms bound to OW1 and OW3 do not take part in hydrogen-bond formation, their positions being obscure. The molecular arrangements projected along the a- and b-axes are given in Figs. 4(a) and 4(b), respectively. They show the formation of a complicated infinite chain through coordinations and hydrogen bonds.

In comparison with the coordination geometry around two independent zinc atoms, the infrared spectra reported previously and herewith were measured by KBr disk technique. As in the case of metal complex of acetic acid, the zinc complex of 2-chlorobenzoic acid has characteristic strong absorption bands associated with the stretching of carboxyl group; for this complex, the bands appear at 1610 cm^{-1} and 1545 cm^{-1} for ν_{as} (OCO), and 1410 cm^{-1} and 1375 cm^{-1} for ν_s(OCO), while the corresponding bands of bis(2-chlorobenzoato)-zinc(II) appear at 1540 cm^{-1} for ν_{as}(OCO) and at 1410 cm^{-1} for ν_s(OCO). The splitting of bands in this complex supports the X-ray evidence of the antisymmetrical chelation around two independent zinc atoms, Zn1 and Zn2.

The difference in the coordination geometry of the two zinc complexes of 2-chlorobenzoic acid described in the present and previous papers might be strongly

** M. Bonamico *et al.* report that the coordination geometry around the zinc atom is considered to be a distorted trigonal bipyramidal in the crystal structure of zinc diethyldithiocarbamate.[4]

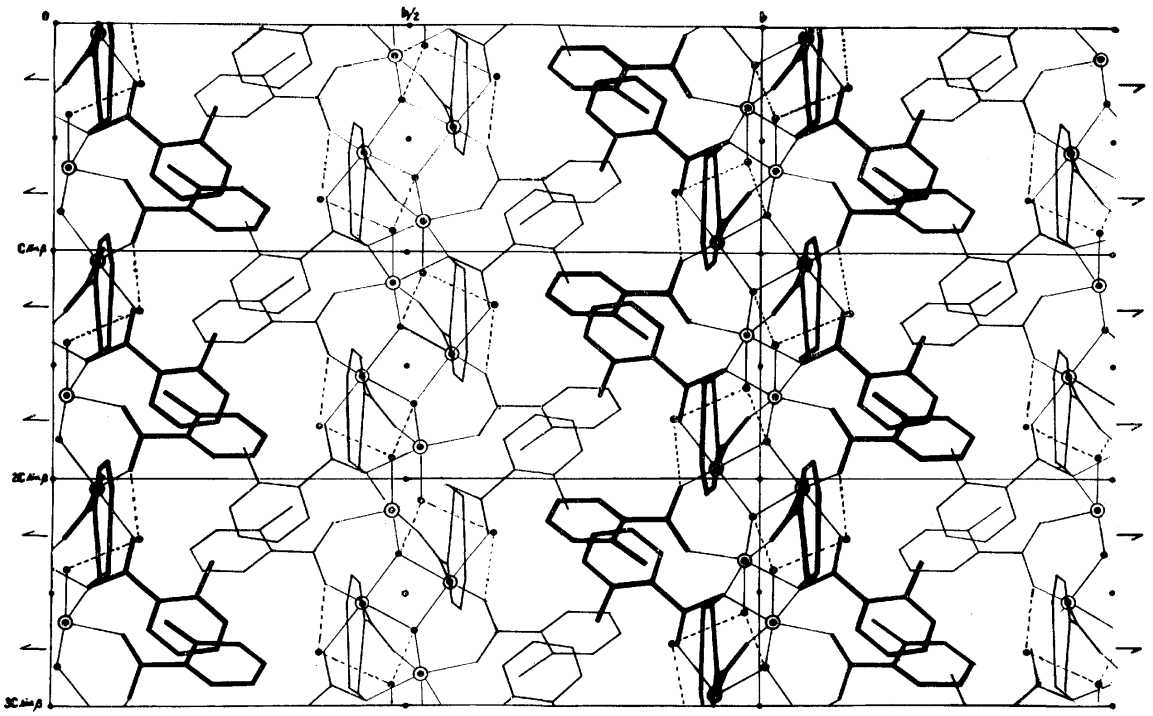

Fig. 4(a). The view of the structure looking down the a-axis.

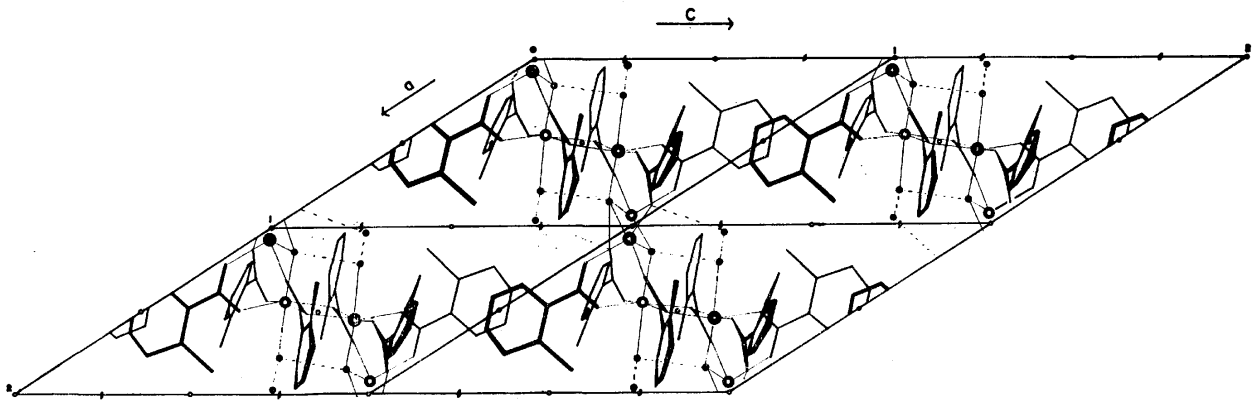

Fig. 4(b). The view of the structure looking down the b-axis.

correlated with the difference in their catalytic actions, *i.e.*, the former is active but the latter is inactive for the following condensation reaction with 2,3-xylidine. The distorted trigonal bipramidal coordination around the zinc atom found in this crystal is probably the first example as a zinc complex so far determined by the X-ray method. By the difference thermal analysis, it was confirmed that two water molecules disappeared at 60—70 °C and 140 °C, respectively, but the remaining OH^- ion was tightly bound to zinc atoms even at the condensation reaction temperature, 170—180 °C (Fig. 3). The overall coordination geometry might be retained at the condensation reaction except two water molecules. At the first step of the condensation reaction, it seems that a reactive group, the amino group of 2,3-xylidine, is fixed by coordination to the zinc atom, and the other reactive atom, the chlorine atom attached at C-2 position of benzoic acid, adjoins the amino group as much as possible. Let us suppose that the amino-nitogen of 2,3-xylidine coordinates to Zn2 in place of OW1 on addition of 2,3-xylidine to the non-aqueous solution of this complex. The nearest chlorine atom to OW1 is ClB-2 in the molecule B of 2-chlorobenzoic acid coordinated to Zn1-2 with a distance of 3.42 Å. The reaction mechanism is still obscure, but probably these amino groups and the chlorine atom react to synthesize mefenamic acid.

References

1) Y. Nakacho, T. Misawa, T. Fujiwara, A. Wakahara, and K. Tomita, This Bulletin, **49**, 58 (1976).

2) Table 4 has been deposited at the Chemical Society of Japan (Document No. 7608).

3) G. Ferguson and G. A. Sim, *J. Chem. Soc.*, **1962**, 1767.

4) M. Bonamico, G. Mazzone, A. Vaciago, and L. Zambonelli, *Acta Crystallogr.*, **19**, 898 (1965).

The Radiolysis of Anthraquinone Dye in Aqueous Solutions

Nobutake SUZUKI, Takeshi NAGAI, Hiroshi HOTTA, and Masamitsu WASHINO

Japan Atomic Energy Research Institute, Takasaki Radiation Chemistry Research Establishment, Takasaki, Gunma 370-12

(Received September 5, 1975)

The decoloration yields of an Acid Blue 40 neutral aqueous solution, G(-Dye), obtained from the optical density at 610 nm for the nitrogen-, oxygen-, and N_2O-saturated solutions, equaled 0.18, 0.29, and 0.51 in the respective early stages. In view of the effects of NCS^- and NO_3^- on the G(-Dye), the decoloration is attributable to the attacks of the OH radicals and hydrated electrons on the dye. The rate constants for the reactions of the OH radical and the hydrated electron with Acid Blue 40, obtained from competition reactions with various additives, were $(6.6\pm1.2)\times10^9$ $M^{-1}s^{-1}$ and 1.5×10^{10} $M^{-1}s^{-1}$ respectively. In the nitrogen-saturated solutions, the G(-Dye) increased markedly upon the addition of alcohols-for example, up to 1.25 upon the addition of 2 mM butyl alcohol. In this case, at the same time, a new absorption band which is attributable to the formation of the reduction products by the attacks of the hydrated electrons and alcohol radicals on the dye appeared at 460—490 nm. This new absorption band disappeared slowly in the presence of oxygen; the rate of this disappearance was 2.8×10^{-5} s^{-1}. On the other hand, in the oxygen-saturated solutions, the G(-Dye) decreased markeld upon the addition of even a small amount of alcohol.

In a preceding paper,[1] we studied the radiation-induced decoloration of azo dye (Acid Red 265) in aqueous solutions and found that the decoloration is attributable to the attack of OH radicals and is promoted markedly by the addition of alcohols in the nitrogen-saturated solutions. On the other hand, it is known that quinones react easily with hydrated electrons as well as with OH radicals.[2,3] The radiolysis of quinones in aqueous solutions is also interesting from the point of view of biochemistry.[4-6]

In this paper, a study of anthraquinone dye (Acid Blue 40) was carried out as part of a series of radiolysis of dyes in aqueous solutions. This dye was not only decolored at 610 nm, but also gave a new absorption band at 460—490 nm as a result of the reduction reactions with the hydrated electrons and alcohol radicals. The behavior of the new absorption band will be clarified in this study.

Experimental

The experimental procedures were the same as in the preceding work[1] except for those described below.

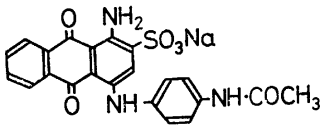

Fig. 1. Schematic diagram of the sodium salt of Acid Blue 40.

The Acid Blue 40 (Kayacyl Blue AGG, see Fig. 1), obtained from the Nippon Kayaku Co., Ltd., was further purified by recrystallization from a methyl alcohol–ethyl alcohol mixture.

When the irradiation was continued over 1 hr without any bubbling of oxygen, the dye solution began to lack oxygen. Therefore, in the case of an irradiation for over 1 hr, oxygen was bubbled in during the irradiation through a porous plate at the bottom of a Pyrex reaction vessel (5 cm in diameter and 16 cm in height).

The absorption spectra were measured with a Shimadzu spectrophotometer, UV-200. The decoloration yield was determined by the measurement of the optical density at 610 nm.

Results

Decoloration of Acid Blue 40 in Aqueous Solutions. The absorption spectra, shown in Fig. 2 as measured for the oxygen-saturated 0.1 mM Acid Blue 40 solution, indicate that the absorption bands at 250, 285, and 610 nm disappeared with the dose, and that these bands almost disappeared at 1.1×10^6 rad (Curve 7). The number of the curves is in common in Figs. 2 and 3 for the same dose.

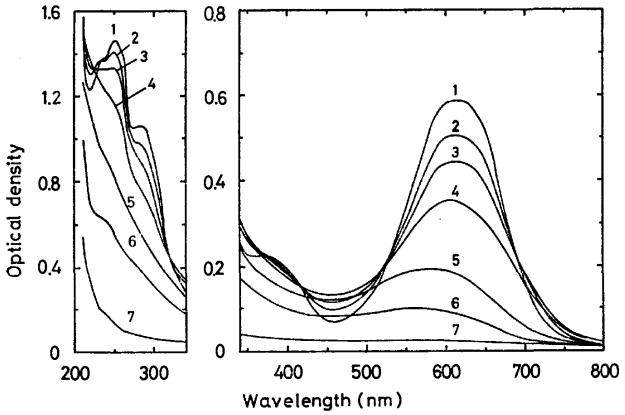

Fig. 2. Absorption spectra of irradiated oxygen-saturated Acid Blue 40 aqueous solutions.
Dye concentration: 0.1 mM. Dose (rad): 0 (Curve 1), 3.7×10^4 (Curve 2), 7.4×10^4 (Curve 3), 1.7×10^5 (Curve 4), 3.9×10^5 (Curve 5), 5.5×10^5 (Curve 6), and 1.1×10^6 (Curve 7).

The absorption spectra for the nitrogen-saturated solution are shown in Fig. 3. The absorption bands at 250 and 285 nm did not disappear with the dose so much as that at 610 nm. An interesting fact is that a new absorption band appears at 460—490 nm at 5.5×10^5 rad (Curve 6). This new absorption band hardly appeared for the N_2O-saturated solution, and the optical density at 250 and 285 nm decreased more efficiently for the N_2O-saturated solution than for the nitrogen-saturated solution.

Since the Acid Blue 40 solutions have a strong absorption band at 610 nm (Figs. 2 and 3), the degrees

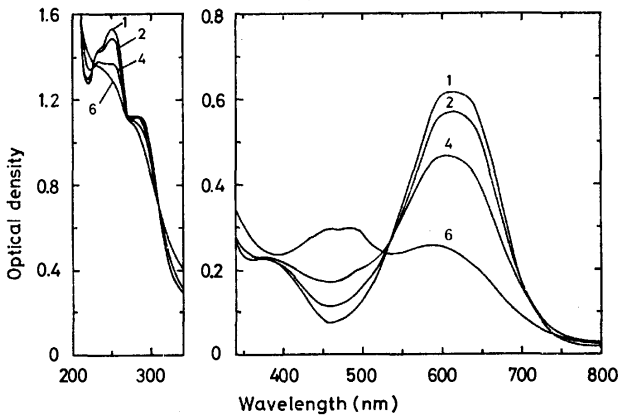

Fig. 3. Absorption spectra of irradiated nitrogen-saturated Acid Blue 40 aqueous solutions.
Dye concentration: 0.1 mM. The number of the curves is the same with Fig. 2.

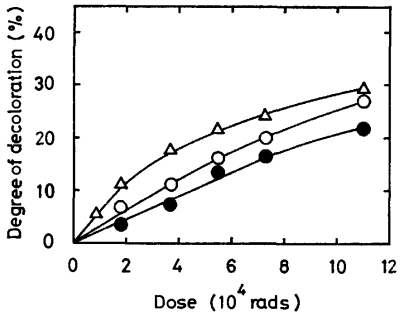

Fig. 4. Effects of inorganic gases on degree of decoloration.
Dye concentration: 0.1 mM. ●: N_2 saturation, ○: O_2 saturation, and △: N_2O saturation.

of decoloration were estimated from the reduction of the optical density. As may be seen in Fig. 4, the degrees of decoloration for the nitrogen-, oxygen-, and N_2O-saturated 0.1 mM Acid Blue 40 solutions increased with the dose. The decoloration yields, G(-Dye), obtained from the linear part in the early stage, are 0.18, 0.29, and 0.51 for the nitrogen-, oxygen-, and N_2O-saturated solutions respectively. These values were independent of the dose rate in the range from 5.3×10^4 to 1.9×10^5 rad/hr and of the initial dye concentration from 0.05 to 0.4 mM.

When the initial pH of the solutions was changed by the addition of sulfuric acid, the G(-Dye) was independent of the initial pH between 6.3 and 5.1; it increased from 0.29 to 0.35 for the oxygen-saturated solution and from 0.18 to 0.24 for the nitrogen-saturated solution at initial pH values between 5.1 and 2.4. This tendency may be attributable to the pH dependence of the yields of the primary species formed from the radiolysis of water.[7] The pH of the nitrogen- and oxygen-saturated solutions used in the present study changed from 6.3 to 6.0 and to 5.1 at 6.7×10^4 rad respectively. Therefore, the G(-Dye) is hardly affected by this pH change during irradiation.

Effects of NCS^- and NO_3^-. The G(-Dye) for the nitrogen-saturated 0.1 mM Acid Blue 40 solution containing NCS^- at 5.5×10^4 rad is shown as a function

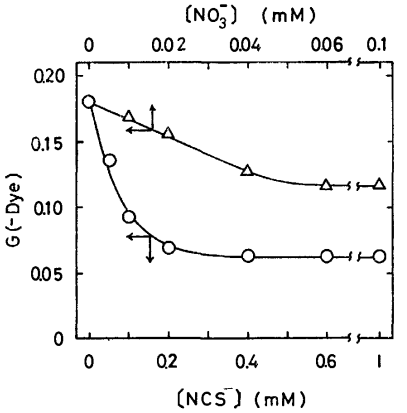

Fig. 5. Effects of NCS^- and NO_3^- on G(-Dye).
Dye concentration: 0.1 mM. Dose: 5.5×10^4 rad.
Additives: NCS^-(○) and NO_3^-(△).

of the NCS^- concentration in Fig. 5. The G(-Dye) decreased to 0.06 upon the addition of NCS^- and became constant above 0.4 mM. The reduction upon the addition of NCS^- was G(-Dye)=0.12 above 0.4 mM. On the other hand, the G(-Dye) decreased to 0.12 upon the addition of NO_3^- and became constant above 0.06 mM. The reduction upon the addition of NO_3^- was G(-Dye)=0.06 above 0.06 mM. The sum of the two reductions equals the original G(-Dye)=0.18 without these solutes.

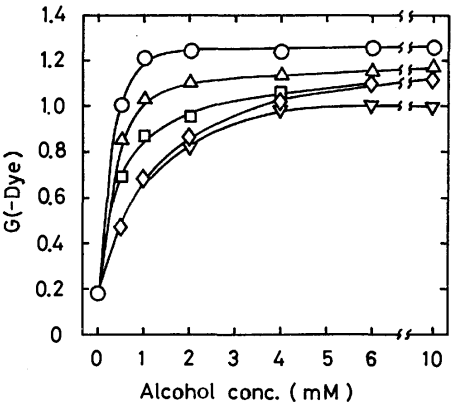

Fig. 6. Effects of alcohols on G(-Dye) in the nitrogen-saturated solutions.
Dye concentration: 0.1 mM. Dose: 5.5×10^4 rad.
◇: methyl alcohol, □: ethyl alcohol, △: propyl alcohol, ○: butyl alcohol, and ▽: *t*-butyl alcohol.

Effects of Alcohols. The G(-Dye) for the nitrogen-saturated 0.1 mM Acid Blue 40 solutions containing normal alcohols (C_1—C_4) and *t*-butyl alcohol at 5.5×10^4 rad is shown as a function of the alcohol concentration in Fig. 6. The G(-Dye) increased steeply with an increase in the alcohol concentration to 2 mM. The G(-Dye) at 2 mM alcohols is shown in Table 1. The increase in the G(-Dye) upon the addition of alcohols was in the order of:

butyl alcohol > propyl alcohol > ethyl alcohol > methyl alcohol > *t*-butyl alcohol (1)

The G(-Dye) increased to 1.25 upon the addition of

TABLE 1. G(-Dye) FOR THE AQUEOUS SOLUTIONS CONTAINING ALCOHOLS

Alcohols	Alcohol conc. (mM)	G(-Dye)
a) Nitrogen-saturated solutions.		
None	0	0.18
Methyl alcohol	2	0.86
Ethyl alcohol	2	0.95
Propyl alcohol	2	1.10
Butyl alcohol	2	1.25
t-Butyl alcohol	2	0.82
b) Oxygen-saturated solutions.		
None	0	0.29
Methyl alcohol	2	0.10
Ethyl alcohol	2	0.07
Propyl alcohol	2	0.06
Butyl alcohol	2	0.04
t-Butyl alcohol	2	0.14

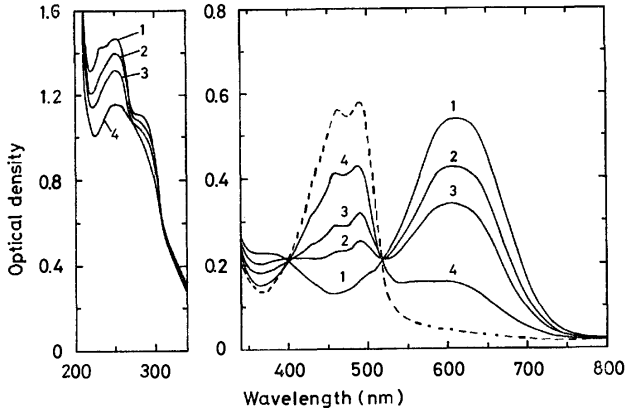

Fig. 7. Absorption spectra of irradiated nitrogen-saturated Acid Blue 40 aqueous solution containing methyl alcohol.
Dye concentration: 0.1 mM. Dose: 5.5×10^4 rad. Methyl alcohol concentration (mM): 0 (Curve 1), 0.5 (Curve 2), 1 (Curve 3), and 10 (Curve 4). Dotted curve represents the spectrum of the irradiated solution containing 10 mM butyl alcohol.

2 mM butyl alcohol from 0.18 for the non-alcoholic solution.

The absorption spectra, shown in Fig. 7 as measured for the nitrogen-saturated solution containing methyl alcohol, indicate that the absorption band at 610 nm disappears with an increase in the alcohol concentration, while, at the same time, the new absorption band at 460—490 nm appears more clearly than that for the non-alcoholic solution (Fig. 3). Similar results were obtained for the solutions containing other alcohols. In Fig. 7, the spectrum of the irradiated solution containing 10 mM butyl alcohol is shown by the dotted curve as a typical result. The intensity in the new absorption bands at 490 nm was in the same order (1) as the increase in the G(-Dye) for the nitrogen-saturated solutions for the same dose.

On the other hand, the G(-Dye) for the oxygen-saturated solutions containing normal alcohols (C_1—C_4) and *t*-butyl alcohol at 5.5×10^4 rad decreased with an increase in the alcohol concentration, in contrast with that for the nitrogen-saturated solutions, much like the curves in Fig. 5 in the preceding paper.[1] The decrease in the G(-Dye) upon the addition of 2 mM alcohol, as is shown in Table 1, was in the same order (1) as the increase in the G(-Dye) for the nitrogen-saturated solutions.

Discussion

The Nitrogen-saturated Solutions. As may be seen in Fig. 5, the G(-Dye) in the nitrogen-saturated solution decreased from 0.18 to 0.06 upon the addition of NCS^-, which is an efficient scavenger of OH radicals.[8] This means that the reduction (0.12) in the G(-Dye) is due to the contribution of the OH radical to the decoloration. On the other hand, the G(-Dye) decreased from 0.18 to 0.12 upon the addition of NO_3^-, which is an efficient scavenger of hydrated electrons.[9,10]

$$e_{aq}^- + NO_3^- \xrightarrow{k_2} NO_2 + 2OH^- \qquad (2)$$

This means that the reduction (0.06) in the G(-Dye) is due to the contribution of the hydrated electron to the decoloration. The sum of the two contributions equals the original G(-Dye) (0.18) without these solutes. It may be concluded from these results that the decoloration reaction of Acid Blue 40 in the nitrogen-saturated solution is mainly attributable to the attacks of the OH radicals and hydrated electrons, and that the contribution of the H atom to the decoloration reaction is minor.

The primary yields[11] of the OH radical and the hydrated electron formed from the radiolysis of water are 2.74 and 2.76 respectively for neutral water. These primary yields are much larger than the above G(-Dye) value. This fact indicates that the most of the primary species are consumed by reactions other than the decoloration reaction.

On the basis of these results, as postulated previously for azo dye,[1] the radiation-induced decoloration reaction of Acid Blue 40 at 610 nm in the nitrogen-saturated solutions may be represented as follows:

$$AB + OH \xrightarrow{k_3} ABOH \text{ (decolored product)} \qquad (3)$$

$$AB + OH \longrightarrow ABOH' \text{ (colored product)} \qquad (4)$$

$$AB + e_{aq}^- \xrightarrow{k_5} AB_{red} \text{ (decolored product)} \qquad (5)$$

$$AB + e_{aq}^- \longrightarrow AB'_{red} \text{ (colored product)} \qquad (6)$$

where AB, ABOH, and AB_{red} are Acid Blue 40, its OH adduct, and its reduction product by the hydrated electron respectively.

The dye molecule has three kinds of reaction sites for Reactions 3—6: (a) the anthraquinone ring, (b) the carbonyl group in the anthraquinone ring, and (c) the substituted benzene ring, not conjugated to the carbonyl group in the anthraquinone ring. The attacks of the OH radical and hydrated electron on Site c are independent of the decoloration reaction and cause little change in the absorption spectrum at 610 nm. This is represented by Reactions 4 and 6.

In Fig. 3, the absorption band at 285 nm is attributable to the carbonyl group, and that at 610 nm, to an auxochromic effect on the anthraquinone.[12,13] The

absorption band near 250 nm is attributable to substituted aromatic rings.[12,13] The optical density at 250 nm does not decrease with the dose so much as does that at 610 nm. This suggests that the decoloration reaction is not necessarily accompanied by the destruction of the skeleton of the dye molecule.

According to Broadbent and Newton,[14] the reaction of sodium 9,10-anthraquinone-2-sulfonate with Fenton's reagent gives the hydroxylation products. In this case, the OH radical does not react with the carbonyl group, but with the anthraquinone ring. This rate constant is 5.6×10^9 $M^{-1}s^{-1}$.[3] On the other hand, according to Hulme *et al.*,[3] the pulse radiolysis of sodium 9,10-anthraquinone-2-sulfonate in an aqueous solution gives its radical anion. This means that the hydrated electron reacts with the carbonyl group. The rate constant of the reduction is 2.8×10^{10} $M^{-1}s^{-1}$.[3]

Therefore, it may be concluded that Site a is attacked by the OH radical, and Site b, by the hydrated electron. These processes reduce the absorption band at 610 nm. The OH radical and the hydrated electron also react with the part (Site c) not conjugated to Site b. Furthermore, since the ABOH and the AB_{red} from Reaction 3 and 5 can react with the OH radicals and hydrated electrons, the dye molecule is degraded to the lower molecular weight compounds by consuming many primary species formed from the radiolysis of water. Therefore, the G(-Dye) is much less than the primary yields of the OH radical and the hydrated electron.

The absorption band at 460—490 nm is attributable to the reaction of the dye with the hydrated electron (Reaction 5), which will be interpreted in detail after discussing Reaction 3.

The Oxygen-saturated Solutions. As may be seen in Fig. 2, the absorption bands at 250, 285, and 610 nm in the oxygen-saturated solution decrease more efficiently than in the nitrogen-saturated solution. Curve 7 in Fig. 2 suggests that the skeleton of the dye molecule in the oxygen-saturated solution is almost destroyed at 1.1×10^6 rad. The G(-Dye) (0.29) in the oxygen-saturated solution is higher than that (0.18) in the nitrogen-saturated solution. This may be attributable to the contribution of the HO_2 radical, which is formed from the reaction of oxygen with the hydrogen atom. Peroxides formed by the degradation of the dye molecule may also accelerate the decoloration reaction.

The N_2O-saturated Solutions. The $G(\text{-Dye})_{N_2O}$ (0.51) for the N_2O-saturated solution is larger than that (0.18) for the nitrogen-saturated solution. N_2O reacts rapidly with the hydrated electron to form the OH radical:[10]

$$e^-_{aq} + N_2O \longrightarrow OH + OH^- + N_2 \qquad (7)$$

Therefore, such a large G(-Dye) is attributable to an increase in the OH radical.

As has been already described, the absorption band at 250 nm in the N_2O-saturated solution disappears more efficiently than in the nitrogen-saturated solution. This suggests that the skeleton of the dye molecule is mainly destroyed by the attack of the OH radical.

The Solutions Containing Alcohols. The increase in the G(-Dye) upon the addition of alcohols in the nitrogen-saturated solution (Fig. 6) means that the alcohol radical ($R\dot{C}HOH$) destroys the dye chromophore more efficiently than the OH radical does.[1]

$$RCH_2OH + OH \xrightarrow{k_3} R\dot{C}HOH + H_2O \qquad (8)$$

The values of the G(-Dye) in Table 1 correspond to the order of the rate constants for the reaction of alcohols with OH radicals, as measured by the pulse-radiolysis technique; these rate constants are listed in Table 2.[8,15]

Table 2. Rate constants for reactions 3 and 8

Additives	k_3[a] ($M^{-1}s^{-1}$)	k_8[b] ($M^{-1}s^{-1}$)
Methyl alcohol	5.5×10^9	4.8×10^8
Ethyl alcohol	6.6×10^9	1.1×10^9
Propyl alcohol	6.7×10^9	1.5×10^9
Butyl alcohol	7.4×10^9	2.2×10^9
t-Butyl alcohol	5.3×10^9	2.5×10^8
NCS^-	7.8×10^9	6.6×10^9

a) Initial pH 6.3. b) Rate constants for reaction of OH radical with additives from Ref. 8 and 15.

On the basis of these results, the radiation-induced decoloration reaction of Acid Blue 40 at 610 nm in the nitrogen-saturated solution containing alcohols may be represented as follows:

$$AB + R\dot{C}HOH \longrightarrow ABH\ (\text{decolored product}) + RCHO \qquad (9)$$

where AB and ABH are Acid Blue 40 and its reduction product respectively. It is known that quinones are reduced by alcohol radicals, leading to the formation of reduction products.[6,16]

On the other hand, in the oxygen-saturated solution, the alcohol radicals react rapidly with oxygen prior to Reaction 9 and are degraded to lower molecular weight compounds.[1] Therefore, the G(-Dye) for the oxygen-saturated solution decreased upon the addition of alcohols, in contrast with that for the nitrogen-saturated solution.

Rate Constant for Reaction 3. The rate constant for Reaction 3 can be determined by using a competition reaction method with additives from the following equation:[1]

$$\frac{1}{G(\text{-Dye})} = \frac{1}{G_r}\left(1+\frac{k_8[RCH_2OH]}{k_3[AB]}\right) \qquad (10)$$

where G_r is the yield of the OH radicals consumed by Reactions 3 and 8, and where [AB] and [RCH_2OH] are the initial concentrations of Acid Blue 40 and alcohols respectively.

The plots of $1/G$(-Dye) are linear against the alcohol concentration, in good agreement with Eq. (10). From Eq. (10), the slope of the curve gives the k_8/k_3 ratio and the intercept gives the G_r value by means of the least-squares method. The k_3 values listed in Table 2 were obtained from the observed k_8/k_3 ratio by using the corresponding k_8 values in Table 2. The average k_3 value is $(6.6\pm1.2)\times10^9$ $M^{-1}s^{-1}$. This value is in good agreement with the rate constant of the additional reaction of the OH radical with sodium 9,10-anthraquinone-2-sulfonate (5.6×10^9 $M^{-1}s^{-1}$),[3] as obtained by the pulse-radiolysis technique. The k_3 value is

also near to the rate constant of the similar reaction with Acid Red 265 (azo dye, 9.3×10^9 $M^{-1}s^{-1}$).[1] The rate constant, obtained by using a competition reaction with NCS^-, is listed in Table 2.

Rate Constant for Reaction 5. Similarly, the rate constant for Reaction 5 (k_5) can be determined from the results shown in Fig. 5.

The plots of $1/G$(-Dye) are linear against the NO_3^- concentration. The k_5 value can be obtained from the observed k_2/k_5 ratio by using the k_2 value (1.1×10^{10} $M^{-1}s^{-1}$).[9] The k_5 value is 1.5×10^{10} $M^{-1}s^{-1}$. This value is near to the rate constant of the reduction reaction of the hydrated electron with sodium 9,10-anthraquinone-2-sulfonate (2.8×10^{10} $M^{-1}s^{-1}$).[3]

Appearance of Absorption Band at 490 *nm.* As may be seen in Fig. 3, in the nitrogen-saturated solution a new absorption band appears clearly at 460—490 nm at 5.5×10^5 rad (Curve 6). This new absorption band appears hardly at all in the presence of oxygen and N_2O, which react rapidly with hydrated electrons, leading to the formation of the O_2^- and OH radicals (Reaction 7) respectively. Furthermore, as may be seen in Figs. 3 and 7, this new absorption band appears more clearly for the solution containing alcohols than for the non-alcoholic solution, while the absorption band at 610 nm disappears more efficiently in the presence of alcohols as a consequence of Reaction 9.

It may be concluded from these facts that the formation of the reduction product from Reactions 5 and 9 reduces the absorption band at 610 nm; at the same time, it causes new absorption bands with maxima at about 460 and 490 nm, and also with a shoulder at about 430 nm, to appear, as may be seen in Fig. 7.

The final reduction product through Reactions 5 and 9, whose half-life is about 7 hr, as will be discussed in the next section, is appreciably stable. Therefore, this product is considered to be a permanent product even if it is unstable chemically. Then, the final reduction product is assumed to be the hydroquinone of AB. In fact, the Acid Blue 40 solution was immediately reduced to the leuco-form with alkaline sodium dithionite, and then recovered by oxygen. The leuco-base solution at pH 8.2 had two bands with maxima at about 460 and 485 nm, while the solution at pH 13.2 had two bands with maxima at about 430 and 480 nm. These bands are in good agreement with those in Fig. 7.

According to Phillips *et al.*,[16] the flash photolysis of the sodium 9,10-anthraquinone-2-sulfonate (A) alcoholic aqueous solution gives absorption bands at 275 and 385 nm for the semiquinone radical (AH·), and at 395 and 505 nm for the semiquinone radical anion ($A\cdot^-$). Both transients are long-lived (several millisec.). On the other hand, sodium 9,10-anthrahydroquinone-2-sulfonate (AH_2), a permanent reduction product of A, has two bands with maxima at about 265 and 385 nm, and the corresponding dianion (A^{2-}) has two bands with maxima at about 435 and 505 nm. The AH_2 and A^{2-} are produced through the disproportionation reaction from the semiquinone radical (AH·) and from the semiquinone radical anion ($A\cdot^-$) respectively.[16]

The reduction product may be dissociated in the aqueous solution as follows:

$$ABH\cdot \rightleftarrows AB\cdot^- + H^+ \qquad (11)$$

where ABH· is the semiquinone radical of AB. The pK values of the semiquinone radical are 4 for benzoquinone,[2] 4.5 for menaquinone,[6] and 3.25 for sodium 9,10-anthraquinone-2-sulfonate.[16] Since the pH is about 5—6 for the present experiments, as has been already described, ABH· may be rather dissociated to the right side. Since the pH values of the above leuco-base solutions are higher than the pH of the solution shown in Fig. 7, the spectra at the high pH must correspond to the dianion, and the spectra in Fig. 7 must contain the spectra of the undissociated form.

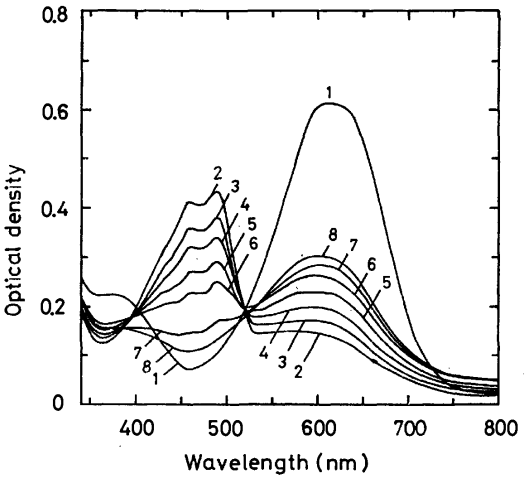

Fig. 8. Effect of oxygen on the spectra of the nitrogen-saturated Acid Blue 40 aqueous solution containing 10 mM methyl alcohol after irradiation of 5.5×10^4 rad. Dye concentration: 0.1 mM. Bubbling time of oxygen (hr): 0 (Curve 2), 1 (Curve 3), 2 (Curve 4), 4 (Curve 5), 7 (Curve 6), 24 (Curve 7), and 45 (Curve 8). Curve 1 represents the spectrum of the solution before irradiation.

Disappearance of Absorption Band at 490 *nm by Oxygen.* As may be seen in Fig. 8, the absorption spectra for the irradiated nitrogen-saturated solution containing methyl alcohol changed gradually upon the bubbling-in of oxygen after irradiation. The spectrum after 70 hr was almost identical with the curve after 45 hr. At the same time, about one-half of the intensity of the original absorption band at 610 nm was recovered finally. The other half of the intensity is attributable to the degradation of the dye by, for example, through Reaction 3. This recovery of the absorption band at 610 nm may be represented as follows:

$$AB_{red,f} + O_2 \xrightarrow{k_{12}} AB \text{ (colored product at 610 nm)} + O_2^- \text{ (or } HO_2) \qquad (12)$$

where $AB_{red,f}$ is the final reduction product.

Thus, the rate of Reaction 12 can be represented in terms of the rate constant, k_{12}, as follows:

$$-\frac{d[AB_{red,f}]}{dt} = k_{12}[O_2][AB_{red,f}] \qquad (13)$$

When the oxygen concentration dissolved is assumed to be constant, Eq. (13) can be rewritten by using the rate of the disappearance of the absorption band at 490 nm (k_{12}') as follows:

$$-\frac{dx}{dt} = k_{12}'(a-x) \quad (14)$$

that is;

$$-k_{12}'t = \ln\frac{(a-x)}{a} \quad (15)$$

where a is the initial intensity of the absorption band at 490 nm, and where x is the intensity of the absorption band which disappears in time t. The plots of $\ln(a-x)/a$ are linear against the time, in good agreement with Eq. (15). From the slope of the curve, the k_{12}' value is 2.8×10^{-5} s^{-1}. Then, the half-life of $AB_{red,f}$ is 6.8 hr. Similarly, the rate of the recovery of the absorption band at 610 nm, k_{12}'', can be estimated. When the intensity of the absorption band at 610 nm for the dye solution after 45 hr is assumed as the initial concentration, the k_{12}'' value is 2.6×10^{-5} s^{-1}. Since the value of $[O_2]$ is 1.2×10^{-3} M in the oxygen-saturated solution,[17] the k_{12} value becomes 2.3×10^{-2} M^{-1} s^{-1}.

References

1) N. Suzuki, T. Nagai, H. Hotta, and M. Washino, This Bulletin, **48**, 2158 (1975).
2) G. E. Adams and B. D. Michael, *Trans. Faraday Soc.*, **63**, 1171 (1967).
3) B.E. Hulme, E.J. Land, and G. O. Phillips, *J. Chem. Soc., D*, **1969**, 518.
4) P. C. Shragge and J. W. Hunt, *Radiat. Res.*, **60**, 233 (1974).
5) P. C. Shragge, A. J. Varghese, J. W. Hunt, and C. L. Greenstock, *Radiat. Res.*, **60**, 250 (1974).
6) E. Hayon and M. Simic, *J. Amer. Chem. Soc.*, **95**, 1029 (1973).
7) E. Hayon, *Trans. Faraday Soc.*, **61**, 734 (1965).
8) G. E. Adams, J. W. Boag, J. Currant, and B. D. Michael, "Pulse Radiolysis," Proceedings of the International Symposium held at Manchester, April, 1965, Academic Press, London (1965), pp. 131—143.
9) S. Gordon, E. J. Hart, M. S. Matheson, J. Rabani, and J. K. Thomas, *Discuss. Faraday Soc.*, **36**, 193 (1963).
10) F. S. Dainton and S. R. Logan, *Trans. Faraday Soc.*, **61**, 715 (1965).
11) B. H. J. Bielski and A. O. Allen, *Int. J. Radiat. Phys. Chem.*, **1**, 153 (1969).
12) A. E. Gillam and E. S. Stern, "An Introduction to Electronic Absorption Spectroscopy in Organic Chemistry," Edward Arnold Ltd., London (1960).
13) J. R. Dyer, "Applications of Absorption Spectroscopy of Organic Compounds," Prentice-Hall, Inc., New Jersey (1965).
14) A. D. Broadbent and R. P. Newton, *Can. J. Chem.*, **50**, 381 (1972).
15) M. Anbar and P. Neta, *Int. J. Appl. Radiat. Isotopes*, **18**, 493 (1967).
16) G. O. Phillips, N. W. Worthington, J. F. Mckellar, and R. R. Sharpe, *J. Chem. Soc., A*, **1969**, 767.
17) H. Hotta, A. Terakawa, and S. Ohno, This Bulletin, **33**, 442 (1960).

Spectroscopic Study of Concentration Fluctuation and Intermolecular Interaction in Liquid

Tsunetake FUJIYAMA, Masao KAKIMOTO,* and Tetsuo SUZUKI

Department of Chemistry, Faculty of Science, Tokyo Metropolitan University, Setagaya-ku, Tokyo 158

** Department of Chemistry, Faculty of Science, The University of Tokyo, Bunkyo-ku, Tokyo 113*

(Received September 19, 1975)

The band widths of the infrared absorption spectra were observed for binary solutions of methyl iodide, methyl cyanide, chloroform, and carbon disulfide. The observed bands are: the ν_1 fundamental of chloroform in carbon disulfide and in carbon tetrachloride; the ν_2 fundamental of methyl iodide in methyl cyanide, nitromethane, benzene, carbon disulfide, and carbon tetrachloride; the $2\nu_2$ band of methyl iodide in methyl cyanide, and the ν_8 and $2\nu_8$ bands of methyl cyanide in methyl iodide. The concentration dependence of a band width was explained in terms of the concentration fluctuation. The theory was compared with the observed band widths, together with the light-scattering data. A fluctuation volume was related with the intermolecular interactions in these binary solutions.

Gordon[1] and Shimizu[2] have shown that a shape of an infrared absorption band of a liquid or a solution can be interpreted as the Fourier transform of a time-correlation function of a transition dipole moment. The time-correlation function of a transition dipole moment is considered to be determined mainly by the reorientational motion of molecules. Many reports have been published which have determined the rate of molecular reorientation in liquids or solutions from measurements of the shapes of infrared-absorption bands.[3–6] However, the time-correlation function of a transition moment may be affected by many other factors than the reorientational motion of molecules. Among these factors, two important factors, namely, the vibrational relaxation and the vibration-rotation interaction, have been shown to affect the observed band shape considerably in some cases.[7,8] The former of the two factors is concerned with the decay of an excited vibrational level, and the latter, with the fact that a transition moment is not fixed to a molecular frame in the case of a degenerate-type vibration of a symmetric top molecule. Taking into account the effects of these factors, the present authors have succeeded in explaining the abnormal behavior of the half-band width of carbon disulfide[7] and of methyl cyanide[8] in liquid and in solutions. Recently, Bondarev and Mardaeva[9] have suggested that the concentration fluctuation affects the half-band width of the spectra of solutions.

The present report will be concerned with the observation of the half-band widths of the infrared-absorption spectra for a few binary solutions and with the introduction of concentration fluctuation to the explanation of the band widths. A consideration of the nature of the concentration fluctuation observed from the infrared spectra will be given, together with a detailed description of the relation between the half-band width of the infrared absorption spectra and the concentration fluctuation.

Experimental

All the chemicals used in the present study were commercial products. The methyl iodide was distilled just before the observation to remove its pale yellowish color. The other samples were used without further purification, although the infrared spectra of methyl cyanide showed a small amount (about 0.5 wt %) of water in it, the presence of water in methyl cyanide seems to cause no serious error.

The binary solutions were prepared just before the observation in order to attain the appropriate concentration by measuring the weight of each component. The mole percentage was calculated by the use of the density data.[10]

The infrared absorption spectra were measured with a Perkin-Elmer 112G single-beam infrared spectrometer (the ν_1 band of chloroform, and the ν_2 and $2\nu_2$ bands of methyl iodide). A Perkin-Elmer 12C single-beam infrared spectrometer mounted with a CsBr prism was used to measure the ν_8 band of methyl cyanide in a methyl iodide solution. A Hitachi EPI-G2 double-beam infrared spectrometer was used to measure the $2\nu_8$ band of methyl cyanide in a methyl iodide solution.

The spectrometers were operated under a resolution of about 1 cm^{-1} except for the case of the ν_8 and $2\nu_8$ bands of methyl cyanide, where the resolution was about 2—3 cm^{-1}. The effect of the finite slit width on the observed spectra was found to be very small. All the measurements were carried out at room temperature (25 °C). The frequencies were calibrated by the use of atmospheric water-vapor or carbon dioxide lines for the 112G spectrometer, and by the use of atmospheric water-vapor or methanol-vapor lines for the 12C spectrometer.

The observed spectra were reduced to the absorption index curve, $k(\nu)$. We fitted a Lorentzian curve to the observed $k(\nu)$ curve by the method of least-squares. The half-width and peak frequency of a band were determined as the parameters of the Lorentzian curve.

Results and Discussion

Half-band Width and Concentration Fluctuation. Consider the case where a peak frequency of a spectral line varies according to the concentration variation. We will confine our discussion to a binary solution. The two components of a binary solution will be denoted hereafter as 1 and 2. All the symbols suffixed by 1 and 2 correspond to the 1 or 2 component, respectively. When a sample of the binary solution is prepared to give a mole fraction of one component, x_1°, the actual mole fraction, x_1, is not always the same as x_1°, but has a distribution around x_1°. The difference between x_1 and x_1° is denoted as Δx_1:

$$x_1 = x_1^\circ + \Delta x_1 \tag{1}$$

Corresponding to the distribution of x_1, the peak frequency, ν_1, also has a distribution:

$$\nu_1 = \nu_1^\circ + \Delta\nu_1 \tag{2}$$

where ν_1° corresponds to a peak frequency at a mole fraction of x_1°, and where $\Delta\nu_1$ is expressed as:

$$\Delta\nu_1 = \frac{\partial\nu_1}{\partial x_1}\Delta x_1 \tag{3}$$

A spectral band of a 1 component directly reflects the distribution of $\Delta\nu_1$. If there is no broadening factor for the spectral band other than the concentration fluctuation, and if a Gaussian distribution is assumed to be the distribution of $\Delta\nu_1$, a normalized intensity distribution, $I(\Delta\nu_1)$, of the band may be expressed as:

$$I(\Delta\nu_1) = \frac{1}{\sqrt{2\pi\langle\Delta\nu_1^2\rangle}}\exp\left[-\frac{\Delta\nu_1^2}{2\langle\Delta\nu_1^2\rangle}\right] \tag{4}$$

where $\langle\ \rangle$ means a statistical average. Then, a half-band width, $\Delta\nu_{1/2}$, of the band is:

$$\Delta\nu_{1/2} = 2\sqrt{2\ln 2}\sqrt{\langle\Delta\nu_1^2\rangle} = 2\sqrt{2\ln 2}\left|\frac{\partial\nu_1}{\partial x_1}\right|\sqrt{\langle\Delta x_1^2\rangle} \tag{5}$$

Let the N_1 and N_2 molecules of the components be contained in a volume in which the concentration fluctuation takes place. We call this volume the "fluctuation volume." Then, we can write:

$$x_1 = \frac{N_1}{N_1+N_2} \tag{6}$$

and:

$$\Delta x_1 = \frac{N_2}{(N_1+N_2)^2}\Delta N_1 \tag{7}$$

It is derived by the method of statistical mechanics that

$$\langle\Delta N_1^2\rangle = kT\Big/\left(\frac{\partial\mu_1}{\partial N_1}\right)_{T,P} \tag{8}$$

where k is the Boltzmann constant; T, the absolute temperature; P, the pressure, and μ_1, the chemical potential. The chemical potential is expressed as:

$$\mu_1 = kT\ln x_1 \tag{9}$$

if the solution is considered to be an ideal solution. A straightforward calculation using Eqs. (6) through (9) leads to:

$$\langle\Delta x_1^2\rangle = \frac{x_1(1-x_1)}{N_1+N_2} \tag{10}$$

which, combined with Eq. (5), gives:

$$\Delta\nu_{1/2} = \sqrt{2\ln 2}\left|\frac{\partial\nu_1}{\partial x_1}\right|\sqrt{\frac{x_1(1-x_1)}{N}} \tag{11}$$

where:

$$N = N_1 + N_2 \tag{12}$$

is the number of molecules contained in the fluctuation volume. Equation (11) tells us that the necessary conditions for the appearance of the broadening of this type are a large change in a peak frequency and a small number of molecules in the fluctuation volume. When these conditions are satisfied, the broadening appears to a measurable extent; the maximum width occurs at $x_1=0.5$.

Comparison with Observed Data. Figure 1 shows the half widths, γ's, of the infrared absorption band of the ν_1 fundamental of chloroform observed in the carbon disulfide and carbon tetrachloride solutions. It may be seen from the figure that the concentration dependence of γ is quite different in the two solutions. In the carbon disulfide solution, γ increases in magnitude as the concentration decreases down to 50 mole percent, and then it decreases as the concentration decreases. This is just the same as what the factor, $\sqrt{x_1(1-x_1)}$, of Eq. (11) predicts. In the carbon tetrachloride solution, on the other hand, γ takes an almost constant value over the whole concentration range. As is shown in Fig. 2, the concentration dependence of the peak frequency of the ν_1 band of chloroform has a strong dependency on the concentration in the carbon disulfide solution at all the concentrations. This fact is consistent with the result of Eq. (11) namely, the line broadening due to the concentration fluctuation is proportional to the magnitude of the change in the peak frequency

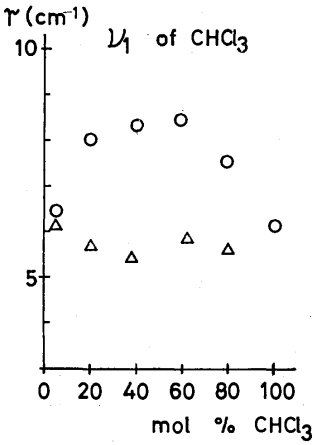

Fig. 1. Concentration dependence of the half width, γ, of the infrared absorption band of the ν_1 fundamental of chloroform. The circles and triangles correspond to those observed in carbon disulfide solutions and in carbon tetrachloride solutions, respectively.

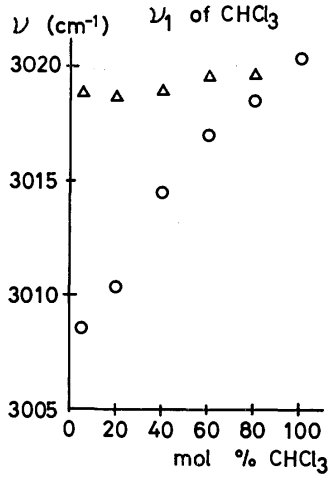

Fig. 2. Concentration dependence of the peak frequency of the infrared absorption band of the ν_1 fundamental of chloroform. The circles and triangles correspond to those observed in carbon disulfide solution and in carbon tetrachloride solution, respectively.

against the concentration. Similar phenomena were observed for the ν_2 band of methyl iodide in nitromethane, methyl cyanide, carbon tetrachloride, benzene, and carbon disulfide solutions. The results are given in Figs. 3 and 4. It may be seen from the figures that a broadening of this type is observed for the ν_2 band in methyl cyanide or nitromethane solutions, and that the shifts of the peak frequencies are very large in these solutions. Figure 4 shows that the frequency shift of the $2\nu_2$ band is about two times that of the ν_2 band in methyl cyanide solutions. In Eq. (11), all the factors except $|\partial\nu_1/\partial x_1|$ should be the same for these two absorption bands. Thence, the broadening of the $2\nu_2$ band should be about two times that of the ν_2 band, which is seen to be true in Fig. 3.

The observed band widths are composed not only

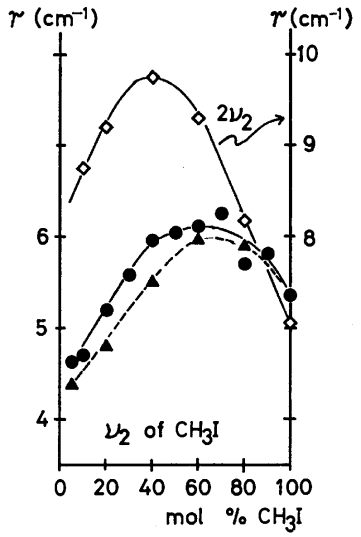

Fig. 3-a. Concentration dependence of the half width, γ, of the infrared absorption band of the ν_2 and $2\nu_2$ of methyl iodide. The open squares correspond to the $2\nu_2$ band observed in methyl cyanide solutions. The closed circles and closed triangles correspond to the ν_2 band observed in methyl cyanide solutions and in nitromethane solutions, respectively.

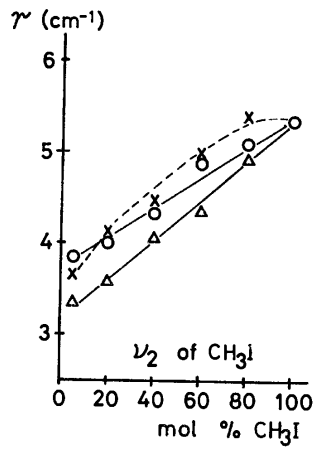

Fig. 3-b. Concentration dependence of the half-width, γ, of the infrared absorption band of the ν_2 band of methyl iodide. Used solvents are: ×; benzene, ○; carbon disulfide, △; carbon tetrachloride.

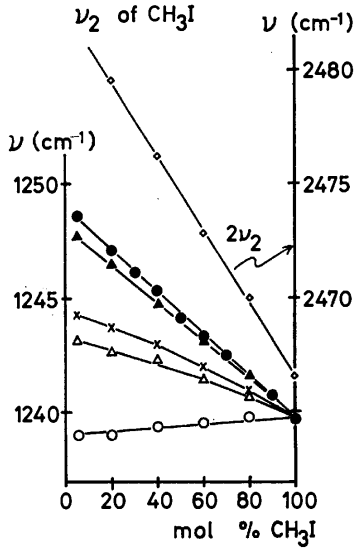

Fig. 4. Concentration dependence of the peak frequencies of the ν_2 and $2\nu_2$ infrared absorption bands of methyl iodide. The open squares correspond to the $2\nu_2$ band in methyl cyanide solutions. Used solvents are: ●; methyl cyanide, ▲; nitromethane, ×; benzene, △; carbon tetrachloride, ○; carbon disulfide.

of the width due to concentration fluctuation, but also of those due to the other factors the reorientational motion of molecules, vibrational relaxations, and so on. When $|\partial\nu/\partial x|$ is small, an observed band width is thought to be independent of the concentration; an example of this is the ν_1 band of chloroform in the carbon tetrachloride solution (see Fig. 2).[11] Therefore, the part of the band-width caused by the concentration fluctuation, γ_f, is expressed as:

$$\gamma_f = \gamma - \gamma' \tag{13}$$

where γ is an observed band width, and where γ' is a width caused by the other factors. We consider that γ' is expressed as:

$$\gamma' = \gamma_0 + x(\gamma_1 - \gamma_0), \tag{14}$$

where x is a mole fraction; γ_1 and γ_0 are the observed band widths at $x=1$ and $x=0$ respectively. Thus, $\Delta\nu_{1/2}$ of Eq. (11) is defined as:

$$\Delta\nu_{1/2} = 2\gamma_f. \tag{15}$$

In the case of the $2\nu_8$ band of methyl cyanide, which is shown in Fig. 5, no reliable change in the half-band width due to concentration fluctuation was observed, although the peak-frequency change due to concentration is considerably large. This can probably be explained by the fact that the width of the band is very broad, while the width can be explained by γ' of Eq. (13). The accuracy of the band-width measurement was not satisfactory enough to detect the width change due to concentration fluctuation from γ. Fig. 5 shows the results obtained for the ν_8 and $2\nu_8$ bands of methyl cyanide in the methyl iodide solution. The $|\partial\nu/\partial x|$ values for the ν_8 and $2\nu_8$ bands are 6 and 11 cm^{-1} respectively.

Comparison with Light-scattering Data. So far the relation between the concentration fluctuation and the

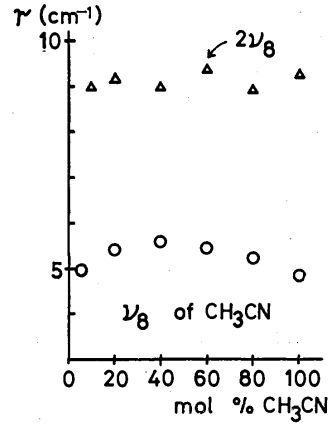

Fig. 5. Concentration dependence of the half width, γ, of the ν_8 and $2\nu_8$ infrared absorption bands of methyl cyanide observed in methyl iodide solutions.

band widths of the infrared spectra has been discussed. A light-scattering measurement is also an useful method to determine the concentration fluctuation. We cannot, however, compare the results obtained by these two methods directly. A band width affords information about the concentration fluctuation in the $\langle \Delta x^2 \rangle$ form. On the other hand, an intensity measurement of the Rayleigh scattering affords information about the concentration fluctuation in the form of $\langle \Delta x^2 \rangle \times V^*$, where V^* is the fluctuation volume, that is, the volume in which the concentration fluctuation is observed. We call this product, $\langle \Delta x^2 \rangle \times V^*$, the "fluctuation ability."[12]

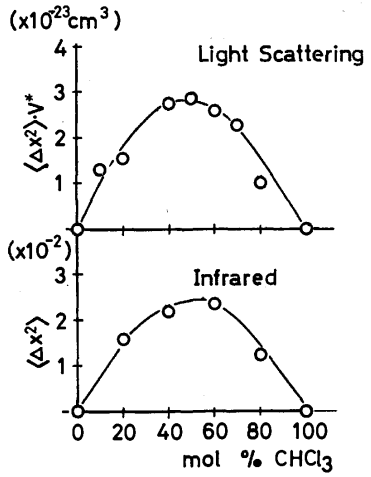

Fig. 6. Comparison of the concentration fluctuation obtained from infrared absorption spectra with that from light scattering data (chloroform–carbon disulfide system).

For the chloroform–carbon disulfide system, a fluctuation ability was observed by the intensity measurement of the Rayleigh scattering.[12] Figure 6 shows a comparison of the $\langle \Delta x^2 \rangle_{IR}$ obtained from the infrared data with the $[\langle \Delta x^2 \rangle \times V^*]_{LS}$ obtained from the light-scattering data. They show quite an analogous dependency on the change in concentration, indicating a qualitative consistency between the two sets of experimental results.

Attention should be paid to the fact that the $\langle \Delta x^2 \rangle_{IR}$ values are obtained, in the case of the infrared spectra, regardless of the dimensions of the fluctuation volume. It is important, therefore, to examine the dimensions of the fluctuation volume from which a band width of the infrared spectrum receives information about the concentration fluctuation. In order to examine the fluctuation volume quantitatively, the number of molecules contained in a fluctuation volume, N, was calculated in two ways. One was to calculate N directly from Eq. (11), using the observed spectral data, $\Delta\nu_{1/2}$ and $|\partial\nu_1/\partial x_1|$. In this procedure, the system was assumed to be an ideal solution. The other way was to calculate N from the observed scattering data, $[\langle \Delta x^2 \rangle \times V^*]_{LS}$, and the absorption spectral data, $\langle \Delta x^2 \rangle_{IR}$, as:

$$N = \frac{[\langle \Delta x^2 \rangle \times V^*]_{LS}}{\langle \Delta x^2 \rangle_{IR}} \times \frac{N_a}{x_1\left(\frac{M_1}{\rho_1}\right) + x_2\left(\frac{M_2}{\rho_2}\right)} \qquad (16)$$

where M was the molecular weight; ρ, the density, and N_a, the Avogardro number. The additivity of volumes on mixing is assumed in the procedure. If the infrared data correctly reflect the concentration fluctuation of the binary solution, and if the binary solution can be regarded as an ideal solution, the N values calculated by the two different ways should be identical. The calculated results are summarized in Table 1. The agreement between these two sets of N values is quite good; this in turn indicates that the proposed mechanism of line broadening as being due to concentration fluctuation is quite reasonable.

Table 1. Comparison of N and $\langle \Delta x^2 \rangle$ obtained from infrared absorption data with those from infrared and light scattering data, for chloroform–carbon disulfide system

Mole fraction of $CHCl_3$	Infrared		Light scattering	
	$\langle \Delta x^2 \rangle$	N	$\langle \Delta x^2 \rangle \times V^* \times 10^{23}$ (cm³)	N
0.0	0		0	
0.1			1.32	
0.2	0.0160	10.0	1.55	9.0
0.3				
0.4	0.0213	11.3	2.76	11.3
0.5			2.84	
0.6	0.0234	10.3	2.57	9.1
0.7			2.28	
0.8	0.0126	12.7	1.0	6.2
0.9				
1.0	0		0	

Fluctuation Volume and Intermolecular Interaction. The problem of spectral-line broadening due to concentration fluctuation has now been reduced to the problem of the shift of the peak frequency in the solutions. It is necessary, for a complete understanding of the spectral-line broadening due to concentration fluctuation, to understand why a peak frequency changes its magnitude according to the concentration variation. This is a quite difficult problem indeed, and no satisfactory answer has yet been given. The deter-

mination of the N values, however, seems to give some useful information regarding this problem.

Considering the mechanism through which the concentration fluctuation causes broadening in a spectral line, the N value or the dimensions of the fluctuation volume corresponding to $\langle \Delta x^2 \rangle_{IR}$ indicates the region in which the surrounding molecules are confined, which can affect the peak frequency of a central molecule through intermolecular interactions.

It is established in the preceding paragraph that N can reasonably be estimated using only the infrared spectral data and Eq. (11), if the solution can be considered to be an ideal solution. Now, let us proceed further in the calculation of N through Eq. (11) for the other absorption bands observed. The results are summarized in Table 2. It may be seen from Table 2 that the N values are almost the same for the three bands observed in the methyl iodide–methyl cyanide system. If we compare the results of Table 2 with those of Table 1, we see, however, a difference between these two sets of N values; that is the N value is larger for the methyl iodide–methyl cyanide system than for the chloroform–carbon disulfide system. The N values of Table 1 are around 10. This may indicate that the intermolecular interaction, which effectively affects the peak frequency of the ν_1 band of chloroform in the carbon disulfide solution, arises from about 10 surrounding molecules. In other words, the peak-frequency change reflects the intermolecular interaction between a given molecule and the nearest neighbor molecules. The larger N values for methyl iodide–methyl cyanide system indicate the existence of a different type of intermolecular interaction. The peak-frequency change or the band-width change, in this case, may afford information about the intermolecular interaction between a given central molecule and the nearest and next nearest neighbour molecles.

TABLE 2. N AND $\langle \Delta x^2 \rangle$ CALCULATED FROM INFRARED ABSORPTION SPECTRA

Mole Fraction of CH_3I	$\nu_2(CH_3I)$[a]		$2_2\nu(CH_3I)$[a]		$\nu_8(CH_3CN)$[a]		$\nu_2(CH_3I)$[b]	
	$\langle \Delta x^2 \rangle$	N	$\langle \Delta x^2 \rangle$	N	$\langle \Delta x^2 \rangle$	N	$\langle \Delta x^2 \rangle$	N
0.0	0		0		0		0	
0.2	0.0038		0.0022		0.0030		0.0017	
0.4	0.0118	20	0.0086	28	0.0068	35	0.0087	28
0.6	0.0129	19	0.0086	28	0.0106	23	0.0130	18
0.8	0.0027		0.0022		0.0057		0.0069	
1.0	0		0		0		0	

a) CH_3I–CH_3CN. b) CH_3I–CH_3NO_2.

A part of the experimental work has been done in the Department of Chemistry, the University of Tokyo. The authors of this report are grateful to all the members of the Shimanouchi Laboratory for their helpful correspondence about this work.

References

1) R. G. Gordon, *J. Chem. Phys.*, **43**, 1307 (1965).
2) H. Shimizu, *J. Chem. Phys.*, **43**, 2453 (1965).
3) T. Fujiyama and B. Crawford, Jr., *J. Phys. Chem.*, **72**, 2174 (1968); **73**, 4040 (1969); B. Crawford, Jr., A. C. Gilby, A. A. Clifford, and T. Fujiyama, *Pure Appl. Chem.*, **18**, 373 (1969).
4) W. G. Rothschild, *J. Chem. Phys.*, **49**, 2250 (1968), **51**, 5187 (1969), **53**, 990, 6453 (1970); *Chem. Phys. Lett.*, **9**, 149 (1971); *J. Chem. Phys.*, **55**, 1402 (1971), **56**, 4722 (1972), **57**, 991 (1972), **59**, 2498 (1973).
5) Marsault-Herail, Jean-Pierre Marsault, Maurice Chalaye, Lean-Louis Saulnier, and Georges Levi, *C. R. Acad. Sci. Paris*, **B275**, 307 (1972).
6) K. Klier, *J. Chem. Phys.*, **58**, 737 (1973).
7) M. Kakimoto and T. Fujiyama, *Bull. Chem. Soc. Jpn*, **45**, 2970 (1972).
8) M. Kakimoto and T. Fujiyama, *Bull. Chem. Soc. Jpn*, **45**, 3021 (1972).
9) A. F. Bondarev and A. I. Mardaeva, *Opt. Spectrosc.*, **35**, 167 (1973).
10) "International Critical Tables," National Research Council, McGraw-Hill, New York (1928).
11) As the intensity values of these bands are small in magnitude, band widths due to vibrational relaxation are comparatively small. Therefore, the term of vibrational relaxation is thought to be negligible, so far as the concentration dependence of band widths is considered (see Ref. 7).
12) K. Iwasaki, M. Tanaka, and T. Fujiyama, to be published.

Conformation of Thymidine 3′,5′-Cyclic Phosphate in Aqueous Solution. Compatibility of the Information from the Lanthanide-Ion Probe and the Spin-Coupling Constants

Fuyuhiko INAGAKI, Seizo TAKAHASHI, Mitsuo TASUMI, and Tatsuo MIYAZAWA

Department of Biophysics and Biochemistry, Faculty of Science, The University of Tokyo, Bunkyo-ku, Tokyo 113

(Received October 4, 1975)

The Pr(III)- and Eu(III)-induced shifts of ^{1}H nuclear magnetic resonances of thymidine 3′,5′-cyclic phosphate were observed in D_2O solution. The results indicated that the induced shifts were primarily of dipolar origin and that the magnetic susceptibility tensor had effective axial symmetry. The ratios of shifts intrinsic to the lanthanide-substrate 1:1 complex were determined after correcting for the contributions of the complex formation shifts (diamagnetic terms). The Gd(III)-induced perturbations of the spin-lattice relaxation times were also observed, and the ratios of relaxation rates were obtained. A computer search was then performed to find out the molecular conformation of this cyclic nucleotide which best fitted the shift and relaxation ratios. As a result the phosphate-ring part was found to have a typical chair conformation. The effective symmetry axis of the magnetic susceptibility tensor coincided with the bisector of the OPO angle almost completely. It was rather difficult, however, to establish the conformation of the deoxyribose ring from the shift and relaxation ratios alone. The use of the additional information from the vicinal ^{1}H—^{1}H coupling constants ($J_{1'2'}$ and $J_{1'2''}$) was necessary for obtaining a reasonable conformation of the entire molecule. The compatibility of the information from the lanthanide-ion probe and the spin coupling constants ($^3J_{HH}$ other than $J_{1'2'}$ and $J_{1'2''}$ and $^3J_{HP}$) is discussed along with the limitations of both methods.

The chemical shift and relaxation perturbations induced by paramagnetic lanthanide cations[1–6] have been increasingly utilized for the determination of conformations of biologically important molecules.[7,8] The advantage of this lanthanide-ion probe method lies in its potentiality of yielding information on relative arrangements of nuclei located within a relatively long distance (approximately 10 Å) and in various directions from the bound lanthanide cation. The information obtainable by this method is particularly valuable when the molecule under study has a portion for which neither vicinal nor long-range spin-coupling data are available. For the phosphodiester linkage in dinucleoside monophosphates no spin coupling is present and accordingly, no information is obtainable as to the torsional angles about the P–O bonds. It seems therefore interesting to apply the lanthanide-ion probe method to conformation studies of this class of molecules. However, such flexible molecules should be treated with caution. For 5′-nucleotides the results obtained by this method[9–11] are not quite consistent with the conclusions derived from the spin-coupling constants.[12–14] Therefore, it is important to check the compatibility of these two methods with an appropriate molecule related to dinucleoside monophosphates. For such a purpose it has been found that thymidine 3′,5′-cyclic phosphate (3′,5′-cTMP) is particularly suited on the following grounds. (a) The binding of the lanthanide cation to 3′,5′-cTMP and to a dinucleoside monophosphate would be similar, since either has a phosphodiester linkage as the binding site. (b) Unlike other 3′,5′-cyclic nucleotides, the analysis of ^{1}H and ^{13}C NMR spectra of 3′,5′-cTMP has given an exceptionally complete set of the ^{1}H–^{1}H, ^{1}H–^{31}P, and ^{13}C–^{31}P coupling constants.[15,16] From the analysis of these coupling constants it has been concluded that the deoxyribose and cyclic phosphate rings of 3′,5′-cTMP are locked in a rigid conformation. Consequently, the result from the lanthanide-ion probe may be compared easily with that from the spin-coupling constants.

Experimental

Materials and Preparation of Sample Solutions. Thymidine 3′,5′-cyclic phosphate (3′,5′-cTMP) was purchased from Sigma Chemical Co. and was used without further purification. The nitrates of Eu(III), Pr(III), Gd(III), and La(III) (purity better than 99.9%) obtained from Nakarai Chemical Co. were used for measuring the induced shifts or the relaxation-time perturbations.

The shifts induced by Pr(III) and the "complex formation" shifts induced by La(III)[17,18] were observed in D_2O solutions by the successive dilution method.[19,20] The concentrations of 3′,5′-cTMP in the initial solutions were 0.307 and 0.253 M for the measurements with Pr(III) and La(III), respectively. The molar ratio of a lanthanide ion to the substrate was kept constant [1.186 for Pr(III) and 1.185 for La(III)] throughout a series of dilution measurements. The shifts induced by Eu(III) were also observed but unfortunately the resonance peaks due to $H_{5'}$ and $H_{5''}$ were overlapped with the HDO peak as a result of the shift and the peaks arising from $H_{2'}$ and $H_{2''}$ could not be separated clearly. The "pH" (uncorrected pH meter reading) was adjusted to about 2.0. Precipitation occurred at higher pH. A Radiometer PHM 26 pH meter was used with a long thin Ingold combination electrode (Catalog No. 6030—04). For the measurements of Gd(III)-perturbed proton relaxation times, a small amount of Gd(III) nitrate solution was added successively to the 0.19 M solution of 3′,5′-cTMP. Thus the concentration of Gd(III) was varied from 20 to 140 μM in steps of 20 μM.

NMR Measurements. The NMR spectra were obtained with a Hitachi R-22/FT spectrometer operating at 90 MHz for ^{1}H. The probe temperature was kept at 37 °C. The chemical shifts were determined by a frequency counter using a frequency-sweep mode. Sodium 4,4-dimethyl-4-silapentane-1-sulfonate (DSS) was used as an internal standard. Spin-lattice relaxation times (T_1) were obtained by means of a standard 180°—τ—90° pulse sequence.

Data Analysis. Computer programs were developed to derive a conformation which best fitted not only the chemical

shift and relaxation perturbations induced by lanthanide ions but also the conformation-dependent coupling constants. The main features of the programs are described in the Appendix. Computations were carried out with a HITAC 8800/8700 system at the Computer Centre of the University of Tokyo.

Results and Discussion

Lanthanide-Induced Shifts. The induced chemical shifts of all the protons of 3',5'-cTMP could be observed only with Pr(III), whereas the results with Eu(III), Nd(III), and Yb(III) were incomplete because of unfavorable line overlappings and/or line broadenings. The Pr(III)-induced shifts observed by the successive dilution method were corrected for the complex formation shifts which were determined using diamagnetic La(III). Next the ratios of the Pr(III)-induced shifts of protons $H_{5'}$, $H_{5''}$, $H_{4'}$, $H_{2'}$, $H_{2''}$, $H_{1'}$, H_6, and H_{Methyl} relative to that of H_3, were calculated and extrapolated to zero substrate concentration [as for the numbering of protons, see Fig. 1(a)]. Such a procedure was previously shown to be appropriate for obtaining experimentally the shift ratios intrinsic to the 1:1 complex between the substrate molecule and the lanthanide ion.[19,20] The shift ratios thus obtained with Pr(III) are listed in Table 1, together with the results with Eu(III). Although the Eu(III)-induced shifts were observed only for $H_{3'}$, $H_{5'}$, $H_{4'}$, $H_{1'}$, H_6, and H_{Methyl} the shift ratios derived from them were not much different from the corresponding ones obtained with Pr(III). This means that the induced shifts for these protons are mainly of dipolar origin and that the susceptibility tensor has effective axial symmetry. Therefore, the shift ratios for the above six protons could be used for conformation

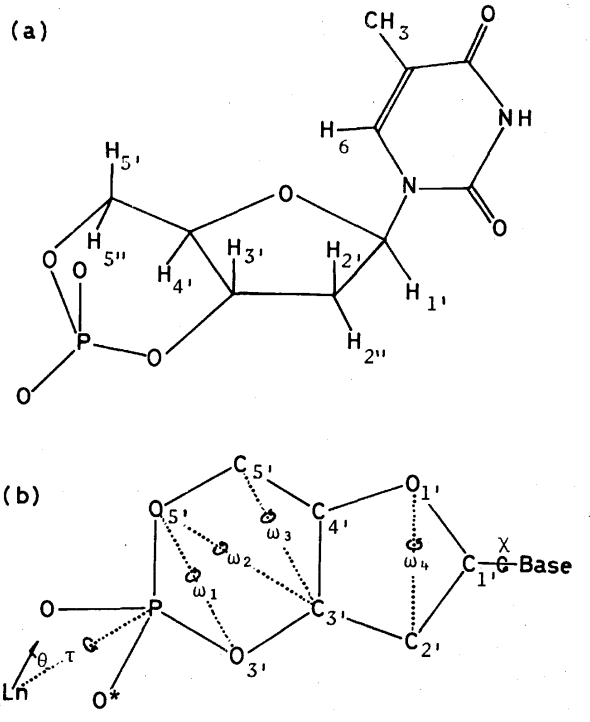

Fig. 1. Schematic representation of the structure of thymidine 3',5'-cyclic phosphate. (a), Numbering of the protons; (b), ring-puckering and torsional coordinates.

TABLE 1. THE OBSERVED AND CALCULATED SHIFT AND RELAXATION RATIOS FOR THYMIDINE 3',5'-CYCLIC PHOSPHATE

^1H[a]	Shift Ratio			
	Obsd		Calcd[b]	
	Pr(III)	Eu(III)	A	B
3'	1.000	1.000	1.000	1.000
5'	0.798	0.831	0.825	0.813
4'	0.623	0.642	0.634	0.643
5''	0.581[c]	—	0.556	0.569
2''	0.322[c]	—	0.350	0.369
2'	0.235[c]	—	0.249	0.252
1'	0.167	0.206	0.206	0.251
6	0.073	0.075	0.096	0.107
CH_3	−0.060	−0.018	−0.068[d]	−0.028[d]

^1H[a]	Relaxation Ratio		
	Obsd	Calcd[b]	
		A	B
3'	1.000	1.000	1.000
5'	0.561	0.555	0.557
4'	0.186	0.152	0.133
5''	0.161	0.169	0.164
2''	0.101	0.078	0.082
2'	0.101	0.106	0.101
1'	0.080	0.028	0.028
6	0.091	0.083	0.073
CH_3	0.046	0.030[d]	0.015[d]

a) As for the notations of the protons, see Fig. 1(a). b) The values in the columns A and B were obtained, respectively, from Conformations A and B of Table 2. c) The weights for these values were 1/10 of those for the other data. d) An average position of the methyl protons was assumed to be the center of the triangle formed by them.

studies with the McConnel-Robertson equation.[21] Since only the Pr(III)-induced shifts were obtained for $H_{5''}$, $H_{2''}$, and $H_{2'}$, the shift ratios for these three protons were used in the conformation search with a weight factor of 1/10 relative to the other protons.

Gd(III)-Induced Relaxation Rate Enhancement. The relaxation rates for the nuclei of a Gd(III)-bound molecule are to a good approximation proportional to $\langle r_i^{-6} \rangle$, where r_i refers to the distance between Gd(III) and the ith nucleus.[7,9] In the present study the change of the spin-lattice relaxation time (T_1) with successive addition of a small amount of Gd(III) was followed. The observed spin-lattice relaxation rates ($1/T_1^{obsd}$) are plotted against the concentrations of Gd(III) in Fig. 2. As shown in a previous paper,[22] the slope of each plot is proportional to the relaxation rate of each nucleus in the Gd(III)-bound molecule. Using the data thus obtained, the relaxation ratios were calculated as listed in Table 1, where the relaxation rate for $H_{3'}$ was chosen as a reference.

Spin-Coupling Constants. The ^1H–^1H and ^1H–^{31}P coupling constants of 3',5'-cTMP at pD 7.2 were obtained by Blackburn *et al.*[15] No appreciable varia-

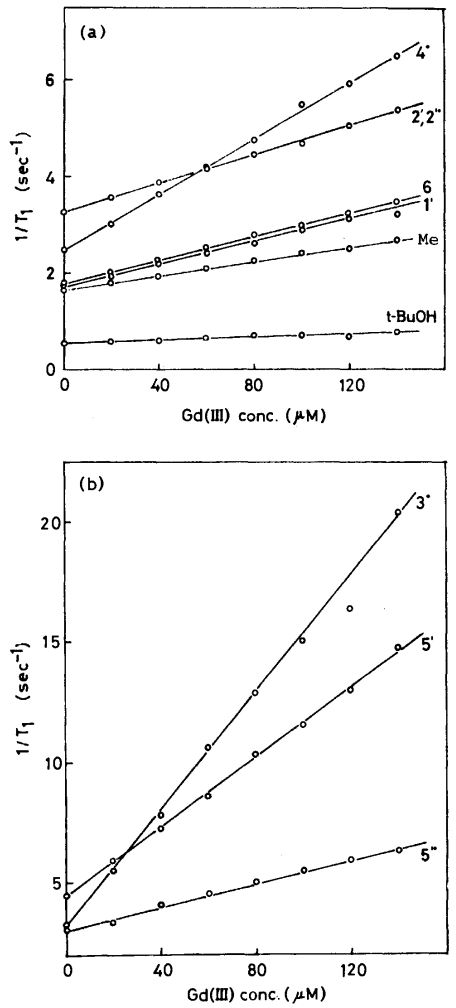

Fig. 2. Dependence of the spin-lattice relaxation rate ($1/T_1^{obsd}$) on the concentration of Gd(III). (a), $H_{1'}$, $H_{2'}$, $H_{2''}$, $H_{4'}$, $H_{6'}$, and H_{Methyl}; (b), $H_{3'}$, $H_{5'}$, and $H_{5''}$. The concentration of 3',5'-cTMP was 0.19 M. *t*-BuOH (*ca.* 20 mM) was used as an internal standard.

tions of the spin-coupling constants from these values were found with the addition of approximately equimolar La(III) at pD 2.0. This indicated that the conformation of 3',5'-cTMP remained unchanged upon complex formation with the lanthanide cation. It is also known that for 3',5'-cTMP no protonation occurs between pH 2.0 and 7.2. Therefore, the spin-coupling constants given by Blackburn *et al.* will be used in the following discussion.

Conformation Search. A search for the conformation of 3',5'-cTMP which best fitted all the observed data was carried out in the following way. A conformation based on the structure of uridine 3',5'-cyclic phosphate in a crystal was assumed at first. This model was employed because no crystallographic data were available for 3',5'-cTMP itself. By modifying this initial model a conformation was obtained which gave the best fit between the observed and calculated values of the shift and relaxation ratios. Finally a further adjustment of molecular parameters was performed by taking a few key spin-coupling constants into consideration. Such a process and the results obtained will be described below in more detail.

From the crystal data of uridine 3',5'-cyclic phosphate (molecule A)[23] all the necessary parameters, *viz.*, bond lengths, bond angles, ring-puckering angles, and the torsional angle around the glycosidic bond, were obtained and transferred to 3',5'-cTMP. The four ring-puckering angles $\omega_1-\omega_4$ [shown in Fig. 1(b)] as well as the torsional angle around the glycosidic bond were chosen as variable parameters[24] in the iteration process of fitting the calculated shift and relaxation ratios to the observed values. These are defined as the dihedral angles between the two planes, each of which is indicated below by the three atoms in a parenthesis: ω_1 ($PO_{5'}O_{3'}$) and ($O_{5'}O_{3'}C_{3'}$); ω_2 ($O_{3'}O_{5'}C_{3'}$) and ($O_{5'}C_{3'}C_{5'}$); ω_3 ($O_{5'}C_{3'}C_{5'}$) and ($C_{2'}C_{5'}C_{4'}$); ω_4 ($C_{4'}C_{2'}$-$O_{1'}$) and ($C_{2'}O_{1'}C_{1'}$). Since each dihedral angle is equivalent to the torsional angle around the imaginary bond XY in the atomic sequence A–X–Y–B as given in Table 2, its sign was given according to the IUPAC-IUB conventions on the definition of a torsional angle.[25] The torsional angle χ around the glycosidic bond is defined with respect to the sequence $O_{1'}$–$C_{1'}$–N_1–C_6. To describe the conformation of a five-membered ring two puckering angles are generally needed. However, only one (ω_4) was sufficient for the deoxyribose ring of 3',5'-cTMP because of the interlocking of this and the phosphate rings. In Table 2 the initial values of $\omega_1-\omega_4$ and χ are given as Conformation I.

Table 2. Molecular parameters of thymidine 3',5'-cyclic phosphate

Molecular Parameter[a]	Conformation		
	I	A	B
ω_1(P–$O_{5'}$–$O_{3'}$–$C_{3'}$)	−135°	−116°	−114°
ω_2($O_{3'}$–$O_{5'}$–$C_{3'}$–$C_{5'}$)	−179°	−189°	−189°
ω_3($O_{5'}$–$C_{3'}$–$C_{5'}$–$C_{4'}$)	−121°	−121°	−126°
ω_4($C_{4'}$–$C_{2'}$–$O_{1'}$–$C_{1'}$)	−160°	−187°	−152°
χ($O_{1'}$–$C_{1'}$–N_1–C_6)	77°	135°	84°
θ		4°	4°
τ		−101°	−66°

a) As for the definitions of ω, χ, θ, and τ, see the text and Fig. 1(b).

The shift and relaxation ratios were calculated on the assumption that the lanthanide cation was located on the bisector of the OPO angle. This assumption was substantiated by previous studies,[9-11,24,26] particularly for the early members of the series of lanthanide cations like Pr(III) and Eu(III).[27] The direction of the symmetry axis of susceptibility tensor was made variable. Two parameters θ and τ were used to specify this direction, the former being the angle between the symmetry axis and the OPO bisector and the latter the dihedral angle between the plane involving the symmetry axis and the P atom and the plane defined by Ln, P, and O* [see Fig. 1(b)]. The angle τ could be regarded as the torsional angle around the Ln–P linkage in the sequence formed by a point on the symmetry axis–Ln–P–O* and, therefore, its sign was given in the same way as for ω's and χ. The distance between Ln(III) and P was fixed to 3.0 Å (corresponding

to the Ln–O distance of 2.6 Å) which is in the range generally accepted.

The agreement factor (R_1)[28] defined below is a useful measure for evaluating the degree of fit between the observed and the calculated values.

$$R_1 = \left\{ \frac{\sum_i v_i (p_i^{\text{obsd}} - p_i^{\text{calcd}})^2 + \sum_i w_i (q_i^{\text{obsd}} - q_i^{\text{calcd}})^2}{\sum_i v_i (p_i^{\text{obsd}})^2 + \sum_i w_i (q_i^{\text{obsd}})^2} \right\}^{1/2} \quad (1)$$

Here p_i and q_i refer to the shift ratio and the relaxation ratio for the ith nucleus, respectively, and v_i and w_i are the corresponding weights (both set to unity unless otherwise mentioned). After minimizing the R_1 value by varying ω_1–ω_4, χ, θ, and τ, Conformation A of Table 2 was obtained as the best-fit model. The shift and relaxation ratios calculated for Conformation A are listed in Table 1 as Calcd A. The R_1 value for Calcd A was 0.048 [using the shift ratios observed by Pr(III)], which is comparable with the value (0.037) obtained for hydroxy-L-proline.[22] The R_1 value was found rather insensitive to ω_4 since it is related only to $H_{1'}$, H_6, and H_{Methyl} which have small shift and relaxation ratios. Therefore, the two spin-coupling constants $J_{1'2'}$ and $J_{1'2''}$ were included in the conformational search in order to add further information for determining ω_4. The Karplus-type equation derived by Altona and Sundaralingam[29] was used for this purpose. The agreement factor (R_2) defined below was used in this search.

$$R_2 = \left\{ \frac{\left(\sum_i v_i (p_i^{\text{obsd}} - p_i^{\text{calcd}})^2 + \sum_i w_i (q_i^{\text{obsd}} - q_i^{\text{calcd}})^2 \right) + \sum_k u_k (J_k^{\text{obsd}} - J_k^{\text{calcd}})^2}{\sum_i v_i (p_i^{\text{obsd}})^2 + \sum_i w_i (q_i^{\text{obsd}})^2 + \sum_k u_k (J_k^{\text{obsd}})^2} \right\}^{1/2} \quad (2)$$

In this equation p_i, q_i, v_i, and w_i are the same as in Eq. (1), and J_k and u_k refer to the coupling constant and the corresponding weight, respectively. The ratio of u_k to v_i (except those for $H_{5''}$, $H_{2''}$, and $H_{2'}$ as indicated in Table 1) or w_i was set to 0.004 somewhat arbitrarily. With this value, shift ratios, relaxation ratios, and coupling constants contributed almost equally to the structure determination. The resultant best-fit conformation is indicated as Conformation B in Table 2, and the shift and relaxation ratios calculated for this model are listed in the column Calcd B of Table 1. The R_1 value (*not* R_2) for Calcd B was 0.070. A stereoscopic drawing of Conformation B is shown in Fig. 3.

The following points may be noted from the results described above. (1) The conformation of the phosphate ring could be determined by the lanthanide-ion probe method. There is no significant difference between phosphate-ring conformation determined here (Conformations A and B) and that of 3′,5′-cUMP in a crystal. Both may be called a chair form (see Fig. 3). (2) The small value of θ as determined for either Conformation A or B indicates the virtual coincidence of the symmetry axis of susceptibility tensor with the bisector of the OPO angle. Such a result ensures the validity of assuming this coincidence in the studies of other molecules having a phosphodiester bond. (3) It was difficult to obtain definite information on the positions of $H_{1'}$, H_6, and H_{Methyl} by the lanthanide-ion probe method alone. This is mainly because the distances between the lanthanide cation and these protons are relatively long (8.1, 7.0, and 9.0 Å for $H_{1'}$, H_6, and H_{Methyl}, respectively). (4) A reasonable conformation of the entire molecule could be obtained by the use of $J_{1'2'}$ and $J_{1'2''}$ in addition to the shift and relaxation data. The conformation of the deoxyribose ring may be described as 4′-*exo* (Fig. 3) in agreement with the conclusion of Blackburn *et al.*[15] However, it should be remembered that the parameters in the Karplus-type equation used here were based on the data of ribosylnucleosides and ribosylnucleotides.[29] If a different set of parameters is found to hold for the deoxyribose ring of 3′,5′-cyclic phosphates, the deoxyribose part of Conformation B should be modified accordingly. The conformation of the phosphate and deoxyribose rings determined here is roughly similar to the corresponding one of adenosine 3′,5′-cyclic phosphate reported by Barry *et al.*[24] According to these authors, the distance between Ln and $H_{4'}$ calculated from the relaxation data was not consistent with the structure determined from the shift ratios. Such discrepancy was not encountered in our case, since both the shift and relaxation ratios were used simultaneously. (5) In Conformation B the torsional angle around the glycosidic bond χ is close to that of molecule A of 3′,5′-cUMP in a crystal[23] and is in the anti range.[30] The value of χ in Conformation A seems less reliable. (6) If R_1 has a shallow minimum with respect to a variable parameter (*e.g.*, ω_4), a minor decrease in R_1 does not necessarily reflect a closer approach to the true conformation. Therefore, such

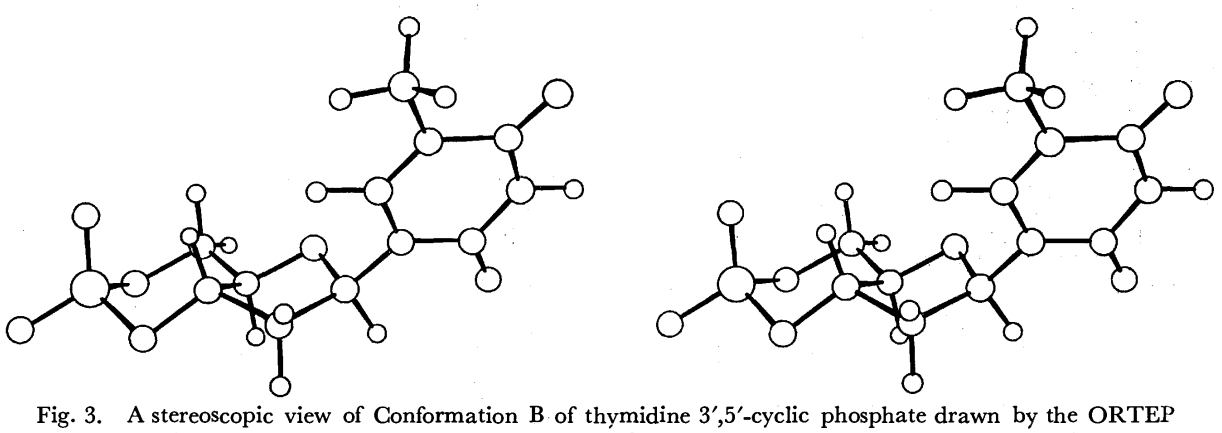

Fig. 3. A stereoscopic view of Conformation B of thymidine 3′,5′-cyclic phosphate drawn by the ORTEP program [C. K. Johnson, ORTEP. Report ORNL-3794, Oak Ridge National Laboratory (1965)].

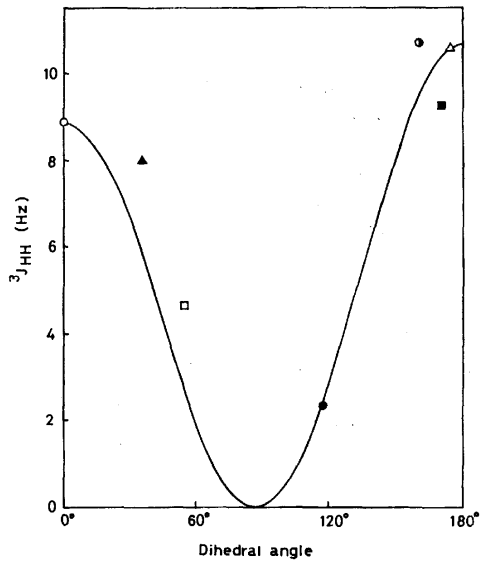

Fig. 4. The vicinal ^1H—^1H coupling constants $^3J_{HH}$ of thymidine 3',5'-cyclic phosphate plotted against the corresponding H–C–C–H dihedral angles in Conformation B. ○, $J_{1'2''}$; ▲, $J_{2'3'}$; □, $J_{4'5'}$; ●, $J_{1'2'}$; ◑, $J_{2''3'}$; ■, $J_{3'4'}$; △, $J_{4'5''}$. The solid curve indicates the variation of $^3J_{HH}$ with the dihedral angle as expressed by the Karplus-type equation with the coefficients of Altona and Sundaralingam.[29]

a case should be treated with caution.

In Fig. 4 the vicinal ^1H–^1H coupling constants ($^3J_{HH}$) are plotted against the H–C–C–H dihedral angles in Conformation B. Although the observed $^3J_{HH}$'s qualitatively follow the trend expressed by the Karplus-type equation (solid curve), there are considerable deviations of $J_{2'3'}$ and $J_{4'5'}$ from the curve. It is likely that these deviations reflect the limitations of the semi-empirical Karplus-type equation rather than the errors in the dihedral angles of Conformation B. Any possible torsional angle about the $C_{2'}$–$C_{3'}$ bond cannot give good fits of both $J_{2'3'}$ and $J_{2''3'}$ with the curve in Fig. 4. Blackburn *et al.* also noted using another Karplus-type expression that the observed $^3J_{HH}$ values were not in satisfactory agreement with the values calculated for a 4'-*exo* conformation, though it gave better fits than the other conformations.

Blackburn *et al.* determined three vicinal ^1H–^{31}P coupling constants ($^3J_{HP}$), namely $J_{3'P}$, $J_{5'P}$, and $J_{5''P}$, to be 1.7, 2.2, and 20.4 Hz, respectively.[15] The corresponding H–C–O–P dihedral angles (ϕ_{HP}) in Conformation B are 46°, 63°, and 179°, respectively. Such a relationship between $^3J_{HP}$ and ϕ_{HP} is in agreement with the results obtained earlier by Tsuboi and coworkers,[31–33] White and Verkade,[34] and Hall and Malcolm[35] from the spectral studies of some molecules containing the H–C–O–PO_2^- system. This gives another support to the use of the $^3J_{HP}$–ϕ_{HP} relationship to structural studies of dinucleoside monophosphates.[36]

Conclusion

The lanthanide-ion probe method is useful for determining the conformation of the phosphate ring of thymidine 3',5'-cyclic phosphate. The resultant phosphate ring conformation is compatible with what is expected from the vicinal ^1H–^1H and ^1H–^{31}P coupling constant. The direction of the symmetry axis of magnetic susceptibility tensor virtually coincides with the bisector of the OPO angle. If two ^1H–^1H coupling constants $J_{1'2'}$ and $J_{1'2''}$ are used in the conformation search to supplement the shift and relaxation data, a reasonable conformation of the entire molecule (Conformation B depicted in Fig. 3) is obtained.

Appendix

Conformation search based on the shift and relaxation ratios requires a considerable amount of computation when the molecule under study has many degrees of internal freedom, *e.g.*, the internal rotation around a single bond and the puckering of a ring. Although the outlines of computer programs developed by other workers have been published,[6,9,28] it would be still worth while to describe the main procedure of our program which we believe has some unique aspects.

Our program consists of two parts, namely, PCS-I and PCS-II. PCS-I is used to compute internal coordinates from atomic coordinates when the latter data are available from a crystallographic analysis. The bond length, bond angle, internal-rotation (torsional) angle, and ring-puckering angle are adopted as internal coordinates. As described in the text, the latter two angles are defined in accord with the IUPAC-IUB conventions. The internal coordinates thus obtained are used as an initial set of parameters for the conformation search by PCS-II. If no crystal data are available, an initial set of internal coordinates is assumed appropriately by referring to the data of analogous molecules.

PCS-II has the functions of computing (1) the space-fixed Cartesian coordinates of atoms from the internal coordinates (the reversal of the process carried out by PCS-I), (2) the shift and relaxation ratios using the McConnel-Robertson equation and the first term in the Solomon-Bloembergen equation, respectively, and (3) the agreement factor (R). It is also possible to calculate the spin-coupling constants from the Karplus equation (or its modification) and to include the spin-coupling terms in the agreement factor. PSC-II is also used to minimize the R value by varying the internal coordinates. This is performed in the following manner.

(a) According to user's instructions the internal coordinates are divided into two groups, variable and invariable. The former usually includes the position of the lanthanide ion and the direction of the principal axis of magnetic susceptibility tensor in addition to internal-rotation and ring-puckering angles. Bond lengths are almost always invariable (fixed to the initial values), and bond angles are varied only in some special cases.

(b) The R values are computed for the conformation with the initial set of variable parameters (ϕ_1^0, ϕ_2^0, ···, and ϕ_n^0) and the $2n$ conformations with the new sets ($\phi_1^0 \pm h_1$, ϕ_2^0, ···, and ϕ_n^0), ···, and (ϕ_1^0, ϕ_2^0, ···, and $\phi_n^0 \pm h_n$). Here, h_1, h_2, ···, and h_n are the variable increments which should be set appropriately by the user. If the smallest one among the R values for the new conformations is smaller than that for the initial conformation, the initial set is replaced by the set corresponding to the smallest. The same process is repeated until no further variations of internal coordinates reduce the R value. In order to gain fast convergence it is advantageous to use large h_i values in the first

search and to make h_i values smaller and smaller in the subsequent searches. This can be performed either automatically or stepwise at user's option.

Recently we extended PCS-II to treat the flexible molecules which exist in two or more conformers with various populations. The application of such a function of PCS-II will be reported separately.

References

1) R. E. Sievers, Ed., "Nuclear Magnetic Resonance Shift Reagents," Academic Press, New York, N. Y. (1973).
2) G. N. La Mar, W. D. Horrocks, Jr., and R. H. Holm, Eds., "NMR in Paramagnetic Molecules: Principles and Applications," Academic Press, New York, N. Y. (1973).
3) J. Reuben, "Progress in N. M. R. Spectroscopy," ed. by J. W. Emsley, J. Feeney, and L. H. Sutcliffe, Pergamon Press, Oxford (1973).
4) A. F. Cockerill, G. L. O. Davies, R. C. Harden, and D. M. Rackham, *Chem. Rev.*, **73**, 553 (1973).
5) B. C. Mayo, *Chem. Soc. Rev.*, **2**, 49 (1973).
6) J. D. Roberts, G. E. Hawkes, J. Husar, A. W. Roberts, and D. W. Roberts, *Tetrahedron*, **30**, 1833 (1974).
7) R. A. Dwek, "Nuclear Magnetic Resonance (N. M. R.) in Biochemistry," Clarendon Press, Oxford (1973).
8) B. A. Levine and R. J. P. Williams, *Proc. Roy. Soc. London A*, **345**, 5 (1975).
9) C. D. Barry, J. A. Glasel, R. J. P. Williams, and A. V. Xavier, *J. Mol. Biol.*, **84**, 471 (1974).
10) C. M. Dobson, R. J. P. Williams, and A. V. Xavier, *J. Chem. Soc., Dalton*, **1974**, 1762.
11) C. D. Barry, C. M. Dobson, R. J. P. Williams, and A. V. Xavier, *J. Chem. Soc., Dalton*, **1974**, 1765.
12) C. Altona and M. Sundaralingam, *J. Amer. Chem. Soc.*, **95**, 2333 (1973).
13) F. E. Evans and R. H. Sarma, *J. Biol. Chem.*, **249**, 4754 (1974).
14) D. B. Davies and S. S. Danyluk, *Biochemistry*, **13**, 4417 (1974).
15) B. J. Blackburn, R. D. Lapper, and I. C. P. Smith, *J. Amer. Chem. Soc.*, **95**, 2873 (1973).
16) R. D. Lapper, H. H. Mantsch, and I. C. P. Smith, *J. Amer. Chem. Soc.*, **95**, 2878 (1973).
17) K. Tori and Y. Yoshimura, *Tetrahedron Lett.*, **1973**, 3127.
18) D. J. Chadwick and D. H. Williams, *J. Chem. Soc., Perkin II*, **1974**, 1202.
19) F. Inagaki, S. Takahashi, M. Tasumi, and T. Miyazawa, This Bulletin, **48**, 853 (1975).
20) F. Inagaki, M. Tasumi, and T. Miyazawa, This Bulletin, **48**, 1427 (1975).
21) H. M. McConnel and R. E. Robertson, *J. Chem. Phys.*, **29**, 1361 (1958).
22) F. Inagaki, M. Tasumi, and T. Miyazawa, *J. Chem. Soc., Perkin II*, **1976**, 167.
23) C. L. Coulter, *Acta Crystallogr.*, **B25**, 2055 (1969).
24) C. D. Barry, D. R. Martin, R. J. P. Williams, and A. V. Xavier, *J. Mol. Biol.*, **84**, 491 (1974).
25) IUPAC-IUB Commission on Biochemical Nomenclature, *J. Mol. Biol.*, **52**, 1 (1970).
26) D. K. Lavallee and A. H. Zeltmann, *J. Amer. Chem. Soc.*, **96**, 5552 (1974).
27) R. J. P. Williams, private communication.
28) M. R. Willcott, III, R. E. Lenkinski, and R. E. Davis, *J. Amer. Chem. Soc.*, **94**, 1742 (1972); R. E. Davis and M. R. Willcott, III, *ibid*, **94**, 1944 (1972).
29) C. Altona and M. Sundaralingam, *J. Amer. Chem. Soc.*, **95**, 2333 (1973).
30) J. Donohue and K. N. Trueblood, *J. Mol. Biol.*, **2**, 363 (1960).
31) M. Tsuboi, F. Kuriyagawa, K. Matsuo, and Y. Kyogoku, This Bulletin, **40**, 1813 (1967).
32) M. Tsuboi, M. Kainosho, and A. Nakamura, "Recent Developments of Magnetic Resonance in Biological Systems," ed. by S. Fujiwara and I. H. Piette, Hirokawa, Tokyo (1968), p. 43.
33) M. Kainosho, A. Nakamura, and M. Tsuboi, This Bulletin, **42**, 1713 (1969).
34) D. W. White and J. G. Verkade, *J. Magn. Resonance*, **3**, 111 (1970).
35) L. D. Hall and R. B. Malcolm, *Can. J. Chem.*, **50**, 2092 (1972).
36) M. Tsuboi, S. Takahashi, Y. Kyogoku, H. Hayatsu, T. Ukita, and M. Kainosho, *Science*, **166**, 1504 (1969).

Optical Activity of Biphenyl Derivatives: The π-π^* and n-π^* Transitions of *o,o'*-Dinitrobiphenyls

Ichiro HANAZAKI

Department of Chemistry, Faculty of Science, Osaka University, Toyonaka, Osaka 560

(Received October 20, 1975)

The optical rotatory power for the lower electronic transitions of several *o,o'*-dinitrobiphenyl derivatives is examined on the basis of a theoretical method previously developed and applied to metal chelate compounds and binaphthyl derivatives. The theoretical energy, absorption intensity, and rotational strength are shown to be in reasonable agreement with the observed absorption and circular dichroism spectra, confirming the applicability of the theory to the optical activity of this simple type of dissymmetric molecules. In addition, the origin of the rotational strength for the n-π^* transition is examined in detail. The results indicate that the n-π^* transition gains its intensity and rotatory power through the interaction of the nonbonding electrons in a nitro group with the π electron system in the other nitrobenzene ring.

The optical rotatory dispersion (ORD) and circular dichroism (CD) of organic compounds and of metal complexes have been a subject of increasing interest in relation to their importance in biology as well as in the fundamental theory of molecular electronic structure. Although the general theory for the phenomenon has been established,[1-3] a more extensive study of the electronic origin of the optical activity for each optically active molecule seems to be necessary. It is also desirable to examine in more detail the reliability of the approximations employed in the calculation of the optical activity.

Some years ago, we first tried to use semiempirical electronic wave functions in the calculation of the rotatory strength accompanying the lower electronic transitions in transition-metal chelate compounds and in some binaphthyl derivatives.[4,5] For these two typical types of optically active molecules, the method was revealed to be satisfactory in explaining the observed CD spectra. It was also noticed that the method is capable of treating the rotational strength fully for the "charge-transfer" transition between two chromophors, as well as for the "locally excited" transition in each chromophor, which may be related to the well-known polarizability theory of Kirkwood.[6]

Recently, the optical activity of the biphenyl derivatives, one of the simplest optically active molecules, has been studied in our laboratory in order to clarify the origin of the interaction responsible for the optical activity and in order to examine the applicability of the theoretical method more extensively. Two difficulties have been found in the case of weakly substituted biphenyls (*e.g.*, alkyl- or halogeno-substituted ones); one of them is the vibrationally enhanced electric and magnetic transition moments, which seem to be responsible predominantly for some CD bands. The other is the interaction between the σ and π electrons in a benzene chromophor induced through the interaction with the other. In view of these results, it seems to be desirable to study a biphenyl compound with a strong substituent, for which the above-mentioned effects do not contribute predominantly to the rotational strength.

In the present paper, a theoretical study is presented for *o,o'*-dinitrobiphenyl, and the results are compared with the experimental CD spectra of its derivatives.[7] It is also interesting to study the origin of the CD band accompanying the n-π^* transition since, in this type of compounds, it is not clear whether the n-π^* transition gains its intensity through the vibronic interactions, as in the case of nitrobenzene, or through a purely electronic interaction.

Method of Calculation

The π-π Interaction. Details of the theoretical treatment were given in previous papers.[4,5] Here we will give only an outline of the method and some parameter values characteristic of the compound studied.

The electronic structure of the π electron system of nitrobenzene is calculated by means of the Pariser-Parr-Pople SCFCI method[8] for the geometry given by Trotter.[9] Since there are some ambiguities in the choice of parameter values concerning the nitro group, several choices of the core resonance integrals between nitrogen and oxygen and between nitrogen and carbon are examined in order to determine the best values (see Results and Discussion). The wave functions are then used in the composite-molecule calculation[10] of *o,o'*-dinitrobiphenyl with various dihedral angles (θ). The geometry and coordinate system employed are shown in Figs. 1 and 2. The core resonance integral over the 2pπ AO's (atomic orbitals), $\chi_1{}^a$ and $\chi_1{}^b$ is expressed as a function of θ:

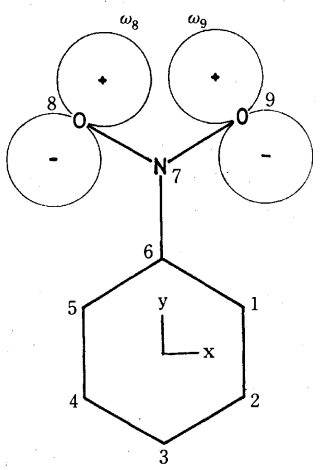

Fig. 1. Numbering of atomic orbitals in nitrobenzene.

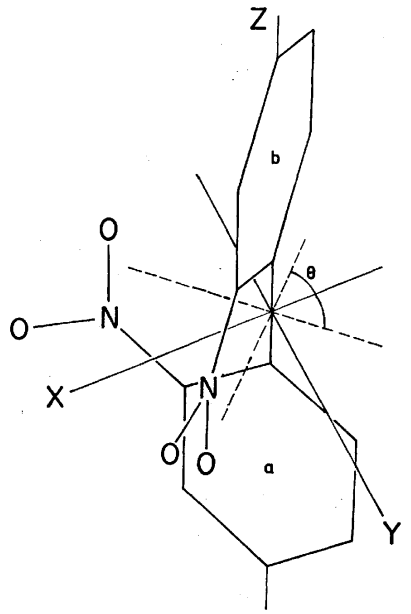

Fig. 2. Numbering and coordinate system for *S-o,o'*-dinitrobiphenyl.

$$\beta(\chi_1^a, \chi_1^b) = -\beta_0 \cos\theta \quad (1)$$

Assuming 1.50 Å for the distance between atoms 1a and 1b, β_0 is calculated to be -1.99 eV by means of its proportionality to the benzene value.[8]

The composite-molecule calculation is performed with 14 LE(locally excited) electron configurations in the electron system of each nitrobenzene fragment and 24 CT (charge transfer) configurations between two π electron systems. The effect of the σ electron in each fragment is neglected.[11]

The rotational strength[1,2] for the n-th excited state is given by the following formula:

$$R_{0-n} = -1.187\times 10^{2}\bar{\nu}^{-1}\langle 0|\boldsymbol{\nabla}|n\rangle\cdot\langle n|\boldsymbol{\lambda}|0\rangle \ (\text{Å}^2) \quad (2)$$

assuming real wave functions. Here, $\boldsymbol{\lambda}=\mathbf{r}\times\boldsymbol{\nabla}$, and the gradient, $\boldsymbol{\nabla}$ and the excitation energy, $\bar{\nu}$, are expressed in units of Å^{-1} and cm^{-1} respectively. The integrals, $\langle 0|\boldsymbol{\nabla}|n\rangle$ and $\langle n|\boldsymbol{\lambda}|0\rangle$, are reduced to the integrals over AO's (only the nearest neighbour integrals are retained), the latter being evaluated for nitrobenzene to be[12]:

$$\nabla_{CC} = -0.417,\ \nabla_{CN} = -0.314 \text{ and}$$
$$\nabla_{NO} = -0.412\ (\text{Å}^{-1}) \quad (3)$$

The integral of $\boldsymbol{\lambda}$ over AO's χ_p and χ_q can also be expressed by ∇_{pq}:

$$\begin{aligned}\langle p|\boldsymbol{\lambda}|q\rangle &= \langle\chi_p|\mathbf{r}\times\boldsymbol{\nabla}|\chi_q\rangle \\ &= \langle\chi_p|\mathbf{R}_q\times\boldsymbol{\nabla}|\chi_q\rangle + \langle\chi_p|\mathbf{r}_q\times\boldsymbol{\nabla}|\chi_q\rangle \\ &= \mathbf{R}_q\times\langle\chi_q|\boldsymbol{\nabla}|\chi_p\rangle \\ &= \nabla_{pq}\cdot(\mathbf{R}_q\times\boldsymbol{\sigma}_{pq}) \end{aligned} \quad (4)$$

where $\mathbf{r}$ and $\mathbf{r}_q$ are the position vectors of an electron measured from a common origin, O, and atom q respectively. $\mathbf{R}_q$ is a vector directed from O to q.

The integrals between two fragments are expressed as:

$$\langle\chi_1^b|\nabla_z|\chi_1^a\rangle = -\nabla_0\cos\theta,$$
$$\langle\chi_1^b|\lambda_z|\chi_1^a\rangle = S_0\sin\theta \text{ (for } S \text{ configuration)}, \quad (5)$$

where the X and Y components are all vanishing. The quantity ∇_0 is calculated to be -0.359 Å^{-1} by means of the Slater AO.

The n-π Transition.* In the calculation of the rotational strength accompanying the n-π* transition, it is assumed that the non-bonding AO's (ω_8 and ω_9) are the 2p AO's of oxygen lying in the molecular plane and with their axes perpendicular to the N–O bond. They are taken as their positive directions towards one another (Fig. 1). Taking the symmetry orbitals as:

$$\omega_S = \frac{1}{2}(\omega_8+\omega_9)$$
$$\omega_A = \frac{1}{2}(\omega_8-\omega_9), \quad (6)$$

one obtains two n-π* states in nitrobenzene corresponding to the transitions from ω_S and ω_A to the lowest vacant MO(molecular orbital) φ_6. Thus, the following four n-π* wavefunctions can be constructed for dinitrobiphenyl:

$$\Psi_\tau^{\pm} = (2)^{-1/2}(\Psi_\tau^a \pm \Psi_\tau^b) \quad (\tau = \text{S or A})$$

where Ψ_τ^μ corresponds to transition $\omega_\tau\rightarrow\varphi_6$ in the μ-th fragment. The average transition energy for these n-π* transitions is evaluated to be 3.2 eV on the basis of the ionization potential of the oxygen non-bonding AO, the semiempirical two-center repulsions, and the calculated orbital energy of φ_6. This value is in reasonable agreement with the observation (3.6 eV).[13]

The n-π* transitions have an intrinsic (one-center) transition magnetic moment in a direction parallel with the N–O bond. On the basis of ω_S and ω_A, theyare calculated to be:

$$\langle\varphi_6|\lambda_x|\omega_S\rangle = -(3/2)^{1/2}C_{68}$$
$$\langle\varphi_6|\lambda_y|\omega_A\rangle = (2)^{-1/2}C_{68} \quad (7)$$

where the coordinates, x and y, correspond to those in Fig. 1, and where C_{68} is the coefficient of 2pπ AO χ_8 in MO φ_6. The effect of the mixing of the π-π* transition on λ can safely be neglected since the one-center magnetic moment is very large. On the other hand, the n-π* transition may gain ∇ from the π-π* transition. In the present work, it is proposed that the n-π* state gains ∇ through the mixing with the π-π* CT states. In fact, the n-π* state, $\omega_9^a\rightarrow\varphi_6^a$, interacts appreciably with the CT state, $\varphi_i^b\rightarrow\varphi_6^a$, through the resonance interaction between ω_9^a and φ_i^b (i=1, 2,···,5). The

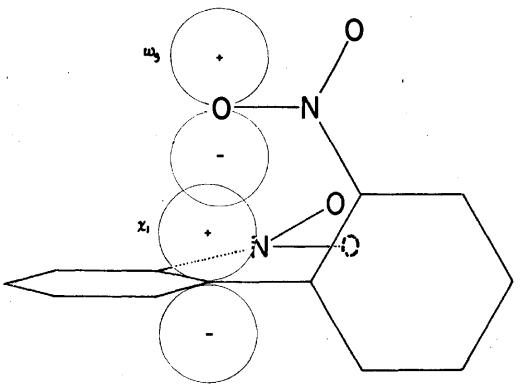

Fig. 3. Interaction of the nonbonding orbital with the 2pπ orbital.

Table 1. Core resonance integral between ω_9^a and χ_p^b (eV)[a]

p	(deg.)[b] 60	80	91	100
1	0.71	0.30	0.11	0.07
2	0.57	0.65	0.66	0.65
3	0.03	0.07	0.12	0.30

a) $\beta(\omega_9^b, \chi_p^a)=\beta(\omega_9^a, \chi_p^b)$. b) Dihedral angle.

same holds for the interaction between $\omega_9^b \rightarrow \varphi_6^b$ and $\varphi_i^a \rightarrow \varphi_6^b$. The schematic drawing of the interaction is given in Fig. 3. The core resonance integrals between ω_9^a and the $2p\pi$ AO's, χ_1^b, χ_2^b, and χ_6^b, and those between ω_9^b and χ_1^a, χ_2^a and χ_6^a, are evaluated on the basis of their proportionality to the overlap integral and the valence-state ionization potential.[14,15] They are summarized in Table 1 for several dihedral angles. The effects of the mixing are calculated by the first-order perturbation treatment.

Results and Discussion

Nitrobenzene. The transition energies and oscillator strengths for some lower electronic transitions of nitrobenzene calculated by means of the SCFCI method are given in Table 2, together with the observed values obtained by Nagakura and his coworkers[16] and by Labhart.[17] The theoretical results given in the table are calculated with $\beta_{CN}=-2.4$ and $\beta_{NO}=-2.7$ eV, which seem to give a reasonable agreement with the experimental results. It should be noted that the oscillator strength for nitrobenzene shown in Table 2 is calculated on the basis of the transition dipole moment:

$$f_m = 1.085\times 10^{-5}\bar{\nu}|\langle 0|\mathbf{r}|n\rangle|^2 \quad (8)$$

whereas the f value for the dinitrobiphenyls given below (Tables 4, 5, and 6) is calculated by means of the dipole velocity:

$$f_v = 4.16\times 10^{4}\bar{\nu}^{-1}|\langle 0|\boldsymbol{\nabla}|n\rangle|^2 \quad (9)$$

It has been pointed out that f_m generally gives a considerably larger value, whereas f_v gives a favorable agreement with the experimental results.[18] In view of this, the present result for nitrobenzene is fairly satisfactory.

Table 2. Calculated and observed transitions for nitrobenzene

Transition Energy (10^3 cm^{-1}) Obsd[a]	Calcd[b]	Oscillator Strength Obsd[a]	Calcd[b]
30[c]	—	0.004[d]	—
35.3	35.6	0.01	0.04
41.2	37.8	0.17	0.37
51.8	44.9	0.38	0.17
	48.4		0.25
	48.5		0.40
61.0	57.8	0.87	0.61
	57.8		1.11

a) Ref. 16 except for the n-π^* transition. b) Calculated on the basis of the transition dipole moment; Eq. (8). c) The n-π^* transition. Taken from Ref. 17. The oscillator strength is estimated from the spectrum given in the reference.

o,o'-Dinitrobiphenyl (Type I). There are two types of *o,o'*-dinitrobiphenyl derivatives for which the CD spectra have been measured by Mislow *et al.*;[7] one has a bridge between the 2 and 2′ positions (Type I), and the other has substituents at the 2 and 2′ positions (Type II). The compounds for which the CD measurement was made are summarized in Table 3. The dihedral angle for the latter compounds is not known and may fluctuate around a stable position. On the other hand, the former compounds have a well-defined dihedral angle. It seems reasonable to take $\theta\approx 60°$ for the compounds studied here.[19]

Table 3. *o,o'*-Dinitrobiphenyls

Type	Compound	X
I	Ia	$=C(COOC_2H_5)_2$
	Ib	=CHOH
	Ic	$=N^+\cdot Br^-$
II	IIa	CH_3
	IIb	CH_2Br
	IIc	CH_2OH
	IId	COOH
	IIe	$COOCH_3$

The calculated results for the *S*-isomer with $\theta=60°$ are summarized in Table 4, together with the CD and absorption spectra observed by Mislow *et al.* for Ia. Since the methylene bridge is expected to work as a very weak substituent, the experimental results for this compound can be compared with the theoretical results in which the effect of bridge is not taken into account. This conclusion is also supported by the fact that the CD spectra for the related compounds with different X are almost the same in their shape, indicating that the rotational strength is predominantly determined by the nitrobenzene groups and their relative orientation.

Except for the n-π^* transition, which will be discussed below, the characteristic features of the CD spectrum seem to be explained by the present calculation—that is, a positive Cotton effect around 35000 cm^{-1} and a stronger negative one in the higher-energy region. The experimental rotational strength for the latter is -2.7×10^{-4} (Å^2), whereas the calculated one is -5.62×10^{-4} (Å^2). The calculated rotational strength for the lower-energy transition is correct in its sign. It is, however, too large compared with the corresponding CD band, although the mixing with the n-π^* transition reduces the theoretical rotational strength to some extent (see below). One reason for this inconsistency may lie in the fact that the nitro group twists to some extent. The first LE state in nitrobenzene is of a CT character (benzene to the nitro group). The first three calculated rotational strengths for dinitrobiphenyl, which have the LE_1 state as main components, are sensitive to the twist. In fact, the X-ray crystal analysis of nitromesitylene[20] shows that the nitro group twists by 66° from the

TABLE 4. RESULTS FOR (*S*)-*o,o'*-DINITROBIPHENYL WITH $\theta=60°$

Calcd				Obsd[a]				
				Absorption		CD		
E (cm^{-1})[b]	f[c]	R (Å^2)[d]	Remarks	E(cm^{-1})[b]	ε	E(cm^{-1})[b]	$\Delta\varepsilon$	R(Å^2)[d]
—	—	—	n-π^*			30.3×10^3	17	1.7×10^{-4}
34.72×10^3	0.05	3.82×10^{-4}	LE_1, LE_2					
36.28	0.01	0.27	LE_1			34.6	5	0.2
36.40	0.12	3.37	LE_2, LE_1					
37.95	0.18	−5.62	LE_2	38×10^3	7100	39.1	−32	−2.5
41.57	0.03	0.49	CT_{46}					
41.71	0.00	−0.25	CT_{46}					
43.25	0.00	−0.07	CT_{56}					
43.91	0.06	1.75	CT_{56}	43.5	17000			
46.00	0.00	0.12	CT_{36}					
46.03	0.00	−0.05	CT_{36}					
47.61	0.02	1.42	LE_3					
47.84	0.09	−0.45	LE_5, LE_3, LE_4					
48.56	0.24	10.62	LE_3, LE_5					

a) Observed for Ia; Ref. 7. b) Transition energy or peak energy. c) Oscillator strength calculated on the basis of dipole velocity; Eq. (9). d) Rotational strength.

benzene plane. The angle of twist must be much smaller in the present case, since the steric hindrance due to the *ortho* substituent (in the present case, a phenyl group) is expected to be much weaker than that for nitromesitylene.

Another point to be discussed here is the origin of the peak at 43500 cm^{-1} in the absorption spectrum. The band is very intense ($f\approx0.6$) if it is considered as a single transition. The strong transitions predicted to appear between 47000—50000 cm^{-1} are unlikely to be responsible for the observed peak; they are mainly composed of LE_3, LE_4, and LE_5 in nitrobenzene (see Table 2), the calculated energies of which are somewhat lower than the observed one. Since we have calculated the electronic structure of dinitrobiphenyl on the basis of the calculated energies for nitrobenzene, the predicted energies (47000—49000 cm^{-1}) for the LE transitions must be somewhat lower than the actual energies. The most reasonable interpretation is that the peak is due to the CT transition predicted to appear at 43910 cm^{-1} overlapping on the tail of the strong absorption bands in the higher-energy region. It is desirable to extend the absorption and (especially) CD measurements to a higher-energy region in order to clarify this point.

o,o'-Dinitrobiphenyl (Type II). The calculated results for the (*S*)-*o,o'*-dinitrobiphenyl with $\theta=91°$ are summarized in Table 5, together with the observed results[7] for (*S*)-2,2'-dimethyl-6,6'-dinitrobiphenyl (IIa). Again, the lowest CD band at 29000 cm^{-1} is the n-π^*

TABLE 5. RESULTS FOR (*S*)-*o,o'*-DINITROBIPHENYL WITH $\theta=91°$

Calcd				Obsd[a]				
				Absorption		CD		
E (cm^{-1})[b]	f[c]	R (Å^2)[d]	Remarks	E(cm^{-1})[b]	ε	E(cm^{-1})[b]	$\Delta\varepsilon$	R(Å^2)[d]
—	—	—	n-π^*	29×10^3	(500)[e]	28.6×10^3	−0.7	-0.8×10^{-5}
34.30×10^3	0.07	0.10×10^{-4}	LE_1	33	(4000)[e]			
34.87	0.00	0.30	LE_1					
35.75	0.13	−10.01	LE_2			33.6	−2.7	−4.4
36.64	0.18	7.25	LE_2	38.6	10000	40.0	4.9	3.8
38.86	0.00	0.00	CT_{56}					
38.86	0.00	−0.01	CT_{56}					
42.03	0.00	0.00	CT_{46}					
42.03	0.00	0.00	CT_{46}					
44.33	0.01	1.66	LE_3					
46.50	0.05	0.11	LE_4, LE_3					
46.87	0.30	−2.13	LE_3, LE_4					
47.79	0.01	0.28	LE_4					
48.11	0.10	−5.28	LE_5					
48.40	0.26	8.64	LE_5					

a) Observed for IIa; Ref. 7). b) Transition energy or peak energy. c) Oscillator strength calculated on the basis of dipole velocity; Eq. (9). d) Rotational strength. e) Shoulder.

transition, and the remaining two CD bands with opposite signs are qualitatively consistent with the theoretical third and fourth transitions, which are of an LE_2 character. The sum of the theoretical oscillator strengths for the first four transitions ($f \approx 0.38$) is also in reasonable agreement with the observed one ($f \approx 0.3$). However, the magnitude of the two CD bands ($R = -1.00 \times 10^{-3}$ and 7.25×10^{-4} Å^2) are too large compared with the corresponding observed CD bands ($R \approx -4.4 \times 10^{-5}$ and 3.8×10^{-5} Å^2 respectively). In view of the agreement between the theoretical and experimental f values, the most probable reason for this discrepancy is the mutual cancellation of the positive and negative CD bands. The effect of the cancellation should be remarkable for the dihedral angle of ~90°, since the energy separation becomes smaller. This viewpoint may also be supported by the fact that the rotational strength of the n-π^* transition, in which the algebraic sum of R's for four transitions is responsible for the observed single peak, is in reasonable agreement with the observation (see below).

The n-π^* Transition. Before discussing the rotational strength of the n-π^* transition, it is necessary to consider the splitting of the n-π^* excited states. McEwen[21] has calculated the n-π^* states of nitromethane by taking account of the interaction of two nonbonding AO's (ω_8 and ω_9) with the nitrogen σ AO's. The results show that the orbital energy of ω_S is higher than that of ω_A by about 400 cm^{-1}. The result of configuration interaction predicts that the n-π^* state in which an electron has been removed from ω_S will lie at an energy lower by 1200 cm^{-1}. In view of these results, it may be reasonable to assume that the energies of these n-π^* transitions are very close to each other. The remarkable asymmetry observed by Labhart[17] for the n-π^* band of nitrobenzene may be taken as an indication of the overlapping of these two bands.[22] The splitting into the Ψ_τ^+ and Ψ_τ^- states (τ=S or A) in dinitrobiphenyls is very small and can safely be neglected for the present purposes.

The rotational strengths and oscillator strengths for the n-π^* transitions are summarized in Table 6 for several dihedral angles. In view of the calculated R values for four n-π^* transitions, the observed single CD band is predominantly accounted for by the transition to Ψ_S^-, while those to Ψ_A^+ and Ψ_A^- must give small negative contributions on the longer-wavelength tail of the spectrum. The calculated total rotational strength for $\theta = 60°$ is 2.85×10^{-4} Å^2, which is in reasonable agreement with the observation, 1.8×10^{-4} Å^2, given in Table 4.

Table 6. Calculated results for the n-π^* transitions of (*S*)-*o*,*o*'-dinitrobiphenyl

	n-π^* State	θ (deg.)[a] 60	80	91	100
R[b] $\times 10^4$ (Å^2)	Ψ_S^+	0.50	0.19	−0.019	−0.020
	Ψ_S^-	2.62	0.98	−0.12	−1.48
	Ψ_A^+	−0.50	−0.19	0.019	0.020
	Ψ_A^-	0.23	−0.005	−0.006	−0.11
	total	2.85	0.98	−0.13	−1.59
f[c] $\times 10^3$	Ψ_S^+	0.97	0.18	0.0022	0.27
	Ψ_S^-	7.10	0.95	0.013	1.78
	Ψ_A^+	0.97	0.18	0.0022	0.27
	Ψ_A^-	7.10	0.95	0.013	1.78
	total	16.2	2.3	0.03	4.1

a) Dihedral angle. b) Rotational strength. c) Oscillator strength calculated from Eq. (9).

The calculated total oscillator strength for $\theta = 60°$ is 0.016. Comparing this value with that of nitrobenzene ($f \approx 0.004$[17]; presumably of vibronic origin), one can conclude that the present mechanism of the interaction between the nonbonding AO and the π electron system determines predominantly the intensity of the n-π^* transition for this compound, although the vibronic intensity borrowing may give rise to an additional effect. Unfortunately, the n-π^* band is much weaker than the nearby π-π^* transitions and cannot be observed as distinct peaks in the absorption spectrum. However, the very long tail on the longer-wavelength side of the absorption spectrum of Ia can be taken as an indication of the overlapping of absorption bands with $\varepsilon \approx 10^3$, which is in order-of-magnitude agreement with the calculated intensity (f=0.016).

The observed n-π^* rotational strength for Compound IIa is -7.9×10^{-6} Å^2. If one supposes that the observation corresponds to a pure optical isomer, this result indicates that the dihedral angle for this compound is only slightly larger than 90°. In fact, the calculated result, $R = -1.3 \times 10^{-5}$ Å^2 for $\theta = 91°$, is in reasonable agreement with the observation.[23] This conclusion is also consistent with the above discussion of the π-π^* transition bands.

In view of these results, it can be concluded that the rotational strength and oscillator strength for the n-π^* transition are due to direct interaction between the non-bonding AO of the nitro group and the π electrons in the adjacent benzene ring.

The rotational strength of the π-π^* type transition is also affected by the interaction with the n-π^* states. This is caused by the mixing of the intrinsic transition magnetic moment of the n-π^* transition into the π-π^* transition. For instance, the rotational strengths for the first, third, and fifth transitions for Compound Ia change from 3.82, 3.37, and 0.49×10^{-4} Å^2 to 1.93, 4.20, and -0.19×10^{-4} Å^2 respectively, while the second and fourth transitions remain unchanged. This brings the theoretical results in Table 4 into better agreement with the observed CD spectrum, although the effect of the twisting of nitro groups mentioned above may also be responsible.

The unoccupied orbitals, φ_7 and φ_8, of nitrobenzene lie at higher energies than φ_6 by 1.82 and 2.35 eV respectively. Hence, the second and third n-π^* transitions to these π^* orbitals may appear in the 45000—50000 cm^{-1} region. Although, in the present treatment, we focus on the lowest n-π^* transition at 30000 cm^{-1}, these higher n-π^* transitions may have some effect on the calculated rotational strengths.

Related Compounds. The CD spectra of two additional compounds of Type I (Ib and Ic) have been recorded by Mislow *et al.*[7] Their spectra resemble that of Ia quite well, so their electronic structures can

be regarded as almost the same as that of Ia. The result also indicates that the substituent on the bridge does not bring about any significant effect on the optical activity. Among the Type II compounds (IIb—IIe), IIb and IIc show CD spectra similar to that of IIa, while a remarkable deformation is observed for IId and IIe. The latter is undoubtedly due to the strong substituent effect of carboxyl groups at the 2 and 2′ positions. Finally, the present theoretical results for the *S* configuration are consistent with the observed CD spectra for the optical isomers, determined to have the same absolute configuration on the basis of the chemical correlation.[7,24] This confirms the reliability of the present theoretical treatment in determining the absolute configuration in this type of compound.

References

1) E. U. Condon, *Rev. Mod. Phys.*, **9**, 432 (1937).
2) W. Moffitt and A. Moscowitz, *J. Chem. Phys.*, **30**, 648 (1959).
3) S. F. Mason, *Quart. Rev.*, **17**, 20 (1963).
4) I. Hanazaki and S. Nagakura, *Inorg. Chem.*, **8**, 654 (1969).
5) I. Hanazaki and H. Akimoto, *J. Amer. Chem. Soc.*, **94**, 4102 (1972).
6) J. G. Kirkwood, *J. Chem. Phys.*, **5**, 479 (1937).
7) K. Mislow, E. Bunnenberg, R. Records, K. Wellman, and C. Djerassi, *J. Amer. Chem. Soc.*, **85**, 1342 (1963).
8) R. Pariser and R. G. Parr, *J. Chem. Phys.*, **21**, 466, 767 (1953); J. A. Pople, *Trans. Faraday Soc.*, **49**, 1375 (1953); H. Kon, *Bull. Chem. Soc. Jpn.*, **28**, 275 (1955).
9) J. Trotter, *Acta Crystallogr.*, **12**, 884 (1959).
10) S. Nagakura and J. Tanaka, *J. Chem. Phys.*, **22**, 236 (1954); S. Nagakura, *ibid.*, **23**, 1441 (1954); *Mol. Phys.*, **3**, 105 (1960); J. N. Murrell, *Quart. Rev.*, **15**, 191 (1960).
11) The effect of the σ-π^* and π-σ^* excited states in the benzene chromophor will be discussed in a forthcoming paper.
12) The quantity V_{pq} is defined by:

$$\langle \chi_p | \nabla | \chi_q \rangle = V_{pq} \boldsymbol{\sigma}_{pq}$$

where $\boldsymbol{\sigma}_{pq}$ is the unit vector directed from atom q to atom p. It is calculated nonempirically for the Slater AO's (see Eq. (3) of Ref. 5).
13) The other type of n-π^* transition which may take part in the interaction between the n-π^* and π-π^* states is the transition from ω_8 or ω_9 of one nitrobenzene to the lowest vacant MO of the other. Its transition energy is estimated in a similar manner to be about 8 eV. Hence, its effect is ignored in the present treatment.
14) The interactions between ω_9 and χ_3, χ_4, and χ_5 are ignored.
15) G. Pilcher and H. A. Skinner, *J. Inorg. Nucl. Chem.*, **24**, 937 (1962).
16) S. Nagakura, M. Kojima, and Y. Maruyama, *J. Mol. Spectrosc.*, **13**, 174 (1964).
17) H. Labhart, *Tetrahedron*, **19**, Suppl. 2, 223 (1963).
18) D. P. Chong, *Mol. Phys.*, **14**, 275 (1968).
19) A calculation based on the molecular model indicates θ=55—60°, whereas the estimation based on the electronic absorption spectra indicates θ=46° for bridged biphenyls with no substituent at the 2,2′ positions (H. Suzuki, This Bulletin, **32**, 1357 (1959)). In the present calculation, we assume θ=60° taking account of the repulsive interaction between two nitro groups.
20) J. Trotter, *Acta Crystallogr.*, **12**, 605 (1959).
21) K. L. McEwen, *J. Chem. Phys.*, **32**, 1801 (1960).
22) On the other hand, a recent photoelectron study [T. Kobayashi and S. Nagakura, *Chem. Lett.*, **1972**, 903; *Bull. Chem. Soc. Jpn.*, **47**, 2563 (1974)] shows that the third peak at 11.01 eV for nitrobenzene corresponds to the ionization from ω_S, whereas the energy of the ionization from ω_A is not lower than 12.65 eV Since the splitting between the n-π^* excited states is not the same as that between the non-bonding orbitals, this result cannot be taken as definite evidence for a large separation between the n-π^* states. Even if the splitting is large, our conclusion will not be altered essentially, since the main contribution to the rotational strength arises from Ψ_S^-, one of the lower n-π^* states.
23) Since two benzene rings are not fixed in this compounds, the dihedral angle may fluctuate over a considerably wide range. The estimated value of θ corresponds to a weighted mean value.
24) When the actual spectrum is shown for the *R* optical isomer, the same spectrum with a reversed sign is taken for the *S* isomer.

Hydration of Pyridine Bases in Benzene

Katsumi HIROSE and Motoharu TANAKA*

Laboratory of Analytical Chemistry, Faculty of Science, Nagoya University, Nagoya 464

(Received October 30, 1975)

Hydration of pyridine bases in benzene has been studied by partition at 25 °C, the total concentration of pyridine bases being less than 1.0 M in benzene. The studied pyridine bases include pyridine, 2-methylpyridine, 4-methylpyridine, 2,6-dimethylpyridine, 3,5-dimethylpyridine, 2,4,6-trimethylpyridine, 2-chloropyridine, 2-bromopyridine, 3-bromopyridine and 2,6-dibromopyridine. Hydrated species with different composition are formed: the composition of the hydrated species (base to water ratio) is as follows: (1:2) for 2,6-dibromopyridine, (1:1) and (1:2) for 2-chloro- and 2-bromopyridine, (1:1) and (2:1) for 3-bromopyridine, (1:1), (1:2) and (2:1) for 4-methylpyridine and pyridine itself, and (1:1), (1:2), (2:1) and (2:2) or (2:3) for the other methyl derivatives. A linear free energy relationship has been observed between the hydration in benzene for the monomer monohydrate and the protonation in water of the corresponding base.

There have been numerous investigations on the hydrogen-bonded complex of polar organic compounds in nonpolar solvents. Studies on hydration are of importance among them because of the unique ability of water to act as a bridge binding two base molecules. Christian *et al.* have studied the hydration of various organic compounds in nonpolar solvents[1–4] and reviewed on the interaction of polar solutes with water.[5]

In order to study in detail the extraction mechanism, it should be important to determine the hydration equilibrium of extractants and/or synergists in the organic solvents. A study along this line has been carried out by Li *et al.*,[6] who determined the hydration of TBP in the organic solvent. In many cases, however, little attention has been paid to the hydration of extractants and synergists in the organic solvents.

Among various organic bases the hydration of pyridine in nonpolar solvents has been extensively studied by infrared spectroscopy and partition technique.[7–10] An analysis of pyridine water hydrogen-bonded system using Hückel theory has been published recently by Adam *et al.*[11] In the present paper, we shall describe the hydration of several pyridine bases with special reference to the effect of substituents.

Experimental

Materials. All pyridine bases, *i.e.* pyridine, 2-methylpyridine, 4-methylpyridine, 2,6-dimethylpyridine, 3,5-dimethylpyridine, 2,4,6-trimethylpyridine 2-chloropyridine, 2-bromopyridine, 3-bromopyridine and 2,6-dibromopyridine, were of G. R. grade. Pyridine bases except for 2,6-dibromopyridine were purified by distilling and by collecting a fraction distilled at constant temperature. 2,6-Dibromopyridine was purified by twice recrystallization in alcohol. Benzene (G. R.) washed successively with sodium hydroxide, sulfuric acid and water was finally distilled. Calcium chloride of G. R. grade was purified by recrystallization.

Procedure. The method of Christian *et al.*[12] was used for equilibrating the organic phase with solutions of known water activity. 50 ml Centrifuge tubes were utilized for the partition. Equilibrium is known to be reached within less than 12 h.[12] The water activity was controlled by $CaCl_2$–H_2O mixtures of known water activity.[13] It was confirmed that no calcium ion was extracted in the organic phase: 15 ml of 1 M solution of a pyridine base in benzene was equilibrated with the same volume of 5.5 M aqueous calcium chloride. The organic phase was separated and then shaken with 10 ml of distilled water, in which we were not able to detect calcium ion with 3,3′-bis[*N*,*N*-di(carboxymethyl)aminomethyl]-*o*-cresolphthalein. The partition was carried out at 25±0.1 °C. After standing for at least 24 h for complete phase separation, the total concentration of water in the organic phase was determined by the Karl-Fischer method with the Coulometric generation of iodine. The method allows to determine the water content with an error of less than 1%. The total concentration of pyridine base in the organic phase was determined by the colorimetry for the halogen derivatives of pyridine, while for the other pyridine bases it was determined by the acid-base titration in glacial acetic acid with Crystal Violet as an indicator.

Results and Discussion

Equilibrium Treatment. Hydrates of pyridine base, $B_m(H_2O)_n$, being assumed to be formed in benzene, the hydration equilibrium of a pyridine base B is written as follows:

$$mB_o + n(H_2O)_o \rightleftarrows (B_m(H_2O)_n)_o \qquad (1)$$

where the subscript o denotes the organic phase. Under the experimental conditions, Henry's law is assumed to be valid for both hydrated and non-hydrated species. The vapor pressure measurement has revealed the ideal behavior of non-hydrated pyridine and 2-methylpyridine in benzene at least up to 0.1 mole fraction (1 M).[14] The concentration equilibrium constant, $\beta_{m,n}$, for hydrated species $(B_m(H_2O)_n)_o$ remains constant.

$$\beta_{m,n} = [B_m(H_2O)_n]_o/[B]_o^m[H_2O]_o^n \qquad (2)$$

Water in the organic solvent may be present as monomeric and/or polymeric species, such as dimer, trimer and so on.[15–18] It is known, however, that only monomeric water is present in benzene. Therefore, the partition equilibrium of water is given as follows:

$$(H_2O)_w \rightleftarrows (H_2O)_o$$

$$K_{D,H_2O} = [H_2O]_o/a_w$$

where a_w is the activity of water in the aqueous phase and the subscript w denotes the aqueous phase.

When a pyridine base is partitioned between the aqueous and organic phases, the total concentration

* To whom correspondence should be addressed.

of the pyridine base in the organic phase, $C_{B,o}$, is given as follows:

$$C_{B,o} = \sum_{m=0} \sum_{n=1} m[B_m(H_2O)_n]_o \quad (3)$$

Since the increase in the formal solubility of water in the presence of the pyridine base in the organic phase at a given water activity is due to the formation of hydrated pyridine bases, the total concentration of water in the organic phase, $C_{H_2O,o}$, is given as follows:

$$C_{H_2O,o} = \sum_{m=0} \sum_{n=1} n[B_m(H_2O)_n]_o \quad (4)$$

The composition of the hydrated species and the hydration equilibrium are determined on the basis of Eqs. (2), (3), and (4).

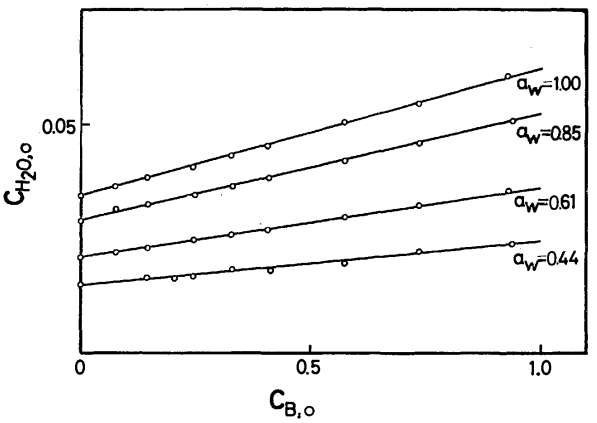

Fig. 1. The total concentration of water as a function of the total concentration of pyridine base in benzene for 2-bromopyridine. Curves are calculated with the constants given in Table 1.

Determination of the Composition of the Hydrated Species. In order to determine the composition of the hydrated species, the total concentration of water, $C_{H_2O,o}$, was plotted against the total concentration of pyridine base $C_{B,o}$ at various water activities. The result for 2-bromopyridine is shown in Fig. 1 as an example. Similar plots were obtained for 2-chloropyridine and 2,6-dibromopyridine. The linear relationship between $C_{B,o}$ and $C_{H_2O,o}$ points to the fact that the hydrated species are monomeric in the organic phase. Then the following expression is obtained from Eqs. (2), (3), and (4).

$$C_{H_2O,o} = (\sum_{n=1} n\beta_{1,n}[H_2O]_o^n)(1+\sum_{n=1} \beta_{1,n}[H_2O]_o^n)^{-1}C_{B,o} + [H_2O]_o \quad (5)$$

The composition of the hydrated species is determined from the relation between the water concentration in benzene and the slope of the plot of $C_{B,o}$ *vs.* $C_{H_2O,o}$. Monomer monohydrate and monomer dihydrate are both present in benzene for 2-chloropyridine and 2-bromopyridine, while monomer monohydrate was hardly detected for 2,6-dibromopyridine, that is, $\beta_{1,1}<0.1$. The hydration constants thus obtained are given in Table 1. The plot of $C_{H_2O,o}$ against $C_{B,o}$ for pyridine is different from these halogen derivatives as shown in Fig. 2. Similar plots were obtained for the other pyridine bases. Non-linearity of the plot points to the presence of the hydrated species involving

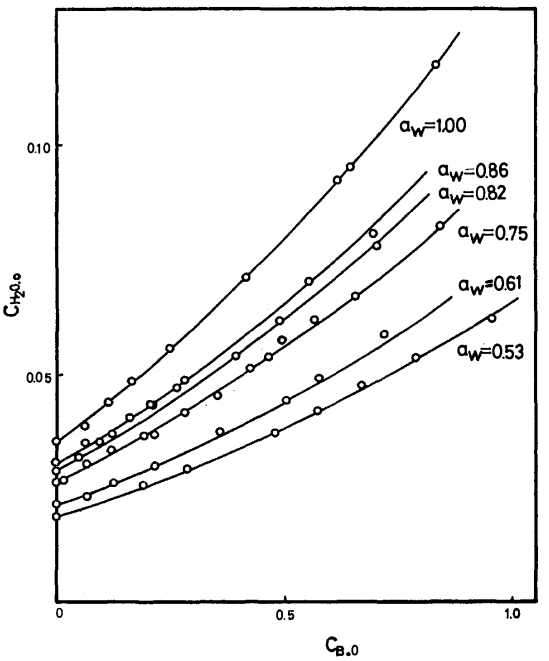

Fig. 2. The total concentration of water as a function of the total concentration of pyridine base in benzene for pyridine. Curves are calculated with the constants given in Table 1.

more than one molecule of pyridine base in benzene for 3-bromopyridine, pyridine and its methyl derivatives. If the number of pyridines involved in the hydrated species is two or less, the total concentration of the pyridine base is given by Eq. (6) and the increment of water in the organic phase due to the presence of the pyridine base, $\Delta C_{H_2O,o}$, is given by Eq. (7).

$$C_{B,o} = \alpha_1[B]_o + \alpha_2[B]_o^2 \quad (6)$$

$$\Delta C_{H_2O,o} = \alpha_3[B]_o + \alpha_4[B]_o^2 \quad (7)$$

with

$$\alpha_1 = 1 + \sum_{n=1} \beta_{1,n}[H_2O]_o^n$$

$$\alpha_2 = \sum_{n=1} 2\beta_{2,n}[H_2O]_o^n$$

$$\alpha_3 = \sum_{n=1} n\beta_{1,n}[H_2O]_o^n$$

$$\alpha_4 = \sum_{n=1} n\beta_{2,n}[H_2O]_o^n$$

where $\Delta C_{H_2O,o}=C_{H_2O,o}-[H_2O]_o$, and α_1, α_2, α_3 and α_4 are constant when the activity of water is kept constant. The composition of hydrated species and these hydration constants are determined from Eqs. (6) and (7). This calculation was carried out on a computer, FACOM 230-60, by use of the least squares method. The result is given in Table 1. For 3-bromopyridine we have monomer monohydrate and dimer monohydrate, although we have hardly detected monomer dihydrate. For pyridine and 4-methylpyridine we have monomer monohydrate, dimer monohydrate and monomer dihydrate, while for the other methyl derivatives we should take into account dimer dihydrate or dimer trihydrate in addition. Thus the following equilibria are relevant to the hydration of pyridine bases in benzene:

$$B_o + (H_2O)_o \rightleftarrows (BH_2O)_o$$

$$B_o + 2(H_2O)_o \rightleftarrows (B(H_2O)_2)_o$$

Table 1. Hydration constants of pyridine derivatives in benzene

Pyridine derivatives	$\beta_{1,1}$ M^{-1}	$\beta_{1,2}$ M^{-2}	$\beta_{2,1}$ M^{-2}	$\beta_{2,2}$ M^{-3}	$\beta_{2,3}$ M^{-4}	sd[a]
Pyridine	1.0_1	19	1.1			0.0008
	1.2[b]	6.4[b]	1.6[b]			
2-Methylpyridine[c]	1.9_4	7.7	0.4_5	19		0.0011
	2.0_4	8.6	0.7_3		2.7×10^2	0.0019
4-Methylpyridine	1.6_3	17	1.6			0.0012
3,5-Dimethylpyridine	1.5_9	17	0.7_0	24		0.0011
	1.5_9	17	1.3		3.2×10^2	0.0011
2,6-Dimethylpyridine[c]	1.0_7	26	1.1	12		0.0009
	1.8_5	13	0.7_7		3.7×10^2	0.0008
2,4,6-Trimethylpyridine[c]	1.8_6	33	1.3	17		0.0010
	1.9_5	33	1.8		2.3×10^2	0.0010
2-Chloropyridine	0.39	9.0				0.0003
2-Bromopyridine	0.51	4.3				0.0003
3-Bromopyridine	1.1_1		0.4_0			0.0006
2,6-Dibromopyridine		5.1				0.0003

a) Standard deviation. b) Ref. 10. c) Dimer dihydrate and dimer trihydrate interpret the experimental results equally well.

$$2B_o + (H_2O)_o \rightleftarrows (B_2(H_2O))_o$$
$$2B_o + n(H_2O)_o \rightleftarrows (B_2(H_2O)_n)_o$$
$$n = 2 \text{ or } 3$$

The hydrated species obtained for pyridine are in accord with the results reported by Christian *et al.*[10] except for monomer trihydrate which was not found in our case. The presence of the monomer monohydrate and dimer monohydrate are consistent with the results by the infrared spectroscopy for pyridine.[7-9] On the basis of our results and others, the fundamental types of the hydrated organic base are the monomer monohydrate B···H–O–H and thedime r monohydrate B···H–O–H···B in a nonpolar solvent as pointed out by Josien[19] when any specific effect such as steric hindrance is not present. Monomer dihydrate and dimer monohydrate are formed as a result of a competition of water with pyridine base for the monomer monohydrate.

For the *o*-halogen derivatives of pyridine, dimer monohydrate cannot be detected under the experimental conditions, and the sequence of the hydration constant for monomer dihydrate is not parallel with the basicity of pyridine bases. Very low basicity and the steric effect of the *o*-halogen should prevent the formation of dimer monohydrate, whereas the hydogen-bond formation with *o*-halogen favors the formation of monomer dihydrate.

The hydration of pyridine bases is considered as an acid-base reaction in benzene. Recently the formation of molecular complexes involving phenol, alcohol, and so on, in inert solvents has been reported.[20-22] The formation constant of the hydrogen-bonded complex is linearly related with the basicity of bases involved. In Fig. 3 the hydration constant $\beta_{1,1}$ for monomer monohydrate is plotted against pK_a of corresponding pyridinium. This figure includes the plot of the hydration constant of triethylamine in benzene.[4] The correlation is obviously good: the stronger the base, the more extensive the hydration. The following two Hammett equations (8) and (9) may be written[23] for the hydration of pyridines in benzene and the dissociation of pyridinium ion in water, respectively:

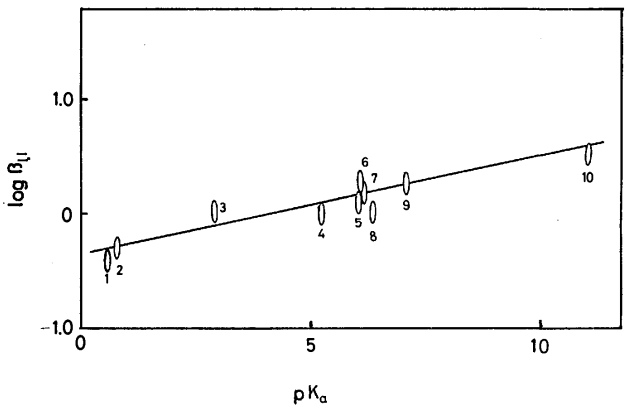

Fig. 3. Correlation of hydration constant $\beta_{1,1}$ with the basicity. 1) 2-chloropyridine, 2) 2-bromopyridine, 3) 3-bromopyridine, 4) pyridine, 5) 4-methylpyridine, 6) 2-methylpyridine, 7) 3,5-dimethylpyridine, 8) 2,6-dimethylpyridine, 9) 2,4,6-trimethylpyridine, 10) triethylamine. Data of pK_a's taken from Refs. 24 and 25.

$$\log \beta_{1,1} = \log \beta^\circ_{1,1} + \rho\Sigma\sigma_x \quad (8)$$
$$pK_a = pK_a^\circ + \rho'\Sigma\sigma_x \quad (9)$$

where $\beta_{1,1}$ and $\beta^\circ_{1,1}$ refer to the formation constants of the 1:1 hydrates of substituted and non-substituted pyridines, respectively, pK_a and pK_a° denote the acid dissociation constants of the substituted and non-substituted pyridiniums, respectively. σ_x is the substituent constant for x in pyridines and ρ and ρ' are the reaction constants for the hydration and the acid dissociation, respectively. From Eq. (8) and (9), we have immediately

$$\log \beta_{1,1} = \frac{\rho}{\rho'} pK_a + \text{constant.} \quad (10)$$

This is a linear free energy relationship as shown in Fig. 3. Water, being a very week acid, discriminates the basicity of these pyridines to an extent much smaller than proton does: ρ' is much greater than ρ. Thus the hydration constant is not very sensitive to the basicity as seen from Fig. 3.

References

1) S. D. Christian, H. E. Affsprung, and S. A. Taylor, *J. Phys. Chem.*, **67**, 187 (1963).
2) J. R. Johnson, S. D. Christian, and H. E. Affsprung, *J. Chem. Soc.*, **1965**, 1.
3) R. D. Grigsby, S. D. Christian, and H. E. Affsprung, *J. Phys. Chem.*, **72**, 2465 (1968).
4) M. D. Gregory, S. D. Christian, and H. E. Affsprung, *ibid.*, **71**, 2283 (1967).
5) S. D. Christian, A. A. Taha, and B. W. Gash, *Quart. Rev.*, **24**, 20 (1970).
6) F. Takahashi, C. H. Ke, and N. C. Li, *J. Amer. Chem. Soc.*, **90**, 234 (1968).
7) A. N. Sidrov, *Opt. Spectrosc.*, **8**, 24 (1960).
8) W. K. Thompson, *J. Chem. Soc.*, **1964**, 4028.
9) S. C. Mohr, W. D. Wilk, and G. M. Barrow, *J. Amer. Chem. Soc.*, **87**, 3048 (1965).
10) J. R. Johnson, P. L. Kilpatrick, S. D. Christian, and H. E. Affsprung, *J. Phys. Chem.*, **72**, 3223 (1968).
11) W. Adam, A. Grimison, R. Hoffmann, and C. Z. de Ortiz, *J. Amer. Chem. Soc.*, **90**, 1509 (1968).
12) S. D. Christian, H. E. Affsprung, J. R. Johnson, and J. D. Worley, *J. Chem. Educ.*, **40**, 419 (1963).
13) R. A. Robinson and R. H. Stokes, "Electrolyte Solution," Butterworths, London (1959), p. 491.
14) G. N. Vriens and E. C. Medcalf, *Ind. Eng. Chem.*, **45**, 1098 (1953).
15) W. L. Masterton and M. C. Gendrano, *J. Phys. Chem.*, **70**, 2895 (1966).
16) J. R. Johnson, S. D. Christian, and H. E. Affsprung, *J. Chem. Soc., A*, **1966**, 77; **1967**, 1924.
17) L. Ödberg and E. Högfeldt, *Acta Chem. Scand.*, **23**, 1330 (1969).
18) L. Ödberg, A. Löfvenberg, E. Högfeldt, and F. Fredlung, *J. Inorg. Nucl. Chem.*, **34**, 2605 (1972).
19) P. Saumagne and M. L. Josien, *Discuss. Faraday Soc.* **43**, 142 (1967).
20) L. Joris and P. von R. Schleyer, *Tetrahedron*, **24**, 5991 (1968).
21) T. Kitao and C. H. Jarboe, *J. Org. Chem.*, **32**, 407 (1967).
22) R. W. Taft, D. Gurka, L. Joris, P. von R. Schleyer, and J. W. Rakshys, *J. Amer. Chem. Soc.*, **91**, 4801 (1969).
23) L. P. Hammett, "Physical Organic Chemistry," McGraw-Hill Book Company, New York (1940), p. 186.
24) D. D. Perrin, "Dissociation Constants of Organic Bases in Aqueous Solution," Butterworths, London (1965).
25) K. Kahmann, H. Sigel, and H. Erlenmeyer, *Helv. Chim. Acta*, **47**, 1754 (1964).

Stereochemical Studies of Elimination Reactions of 2-Bromobutane and 2,3-Dibromobutane over Alkali-Ion Exchanged Silica Gels

Makoto Misono, Yukio Aoki, and Yukio Yoneda

Department of Synthetic Chemistry, Faculty of Engineering, The University of Tokyo, Hongo, Bunkyo-ku, Tokyo 113

(Received November 6, 1975)

The stereochemistry (*anti* or *syn* mode) of elimination reactions of 2-bromobutane and 2,3-dibromobutane over alkali-ion exchanged silica gels (Li, Na, K, and Cs) was determined at 100—300 °C from the products of the diastereomeric isomers of each alkyl bromide. They were *erythro*- and *threo*-2-bromobutanes-3-d_1 and *meso*- and *dl*-2,3-dibromobutanes. The steric course of dehydrobromination of 2-bromobutane changed nearly reversibly between *syn* and *anti* mode by the partial exchange of a surface proton with K^+ or Cs^+ ion, although the surface structure seemed to remain unchanged by the exchange procedure. On the other hand, the exchange with Na^+ or Li^+ ion did not change the steric course. Dehydrobromination of 2,3-dibromobutane proceeded by *anti* mode over Na–, K–, and Cs–SiO_2, while SiO_2 and Li–SiO_2 were not active. The poisoning effect of acidic and basic reagents as well as the indicator test revealed that basic sites played important roles over K– and Cs–SiO_2 where *anti* elimination prevailed, and that weakly acidic sites were responsible for *syn* elimination.

Study of the stereochemistry of reactions over solid catalysts is a useful tool for the elucidation of reaction mechanisms and for the characterization of surface active sites. The knowledge of the stereochemistry of liquid-phase elimination reactions seems well accumulated.[1,2] However, relatively few studies have been reported for heterogeneous systems. Although various factors such as the steric effect, the timing of bond breakings, and the shape of the transition state have been suggested,[3–7] the problem of what is the essential factor controlling the steric course of a reaction still remains unsettled.

We reported previously that the steric course of dehydrohalogenation of 2-bromobutane over silica gels varied markedly by the alkali-treatment, and proposed a postulate that the prime factor determining the stereochemistry is not the surface geometry but the acid-base properties of both catalyst and reactant in these systems; *syn* elimination prevalied over an acidic surface and *anti* over a basic one, regardless of the wide variation of surface area. This postulate was applicable to other basic solids such as alkaline-earth metal oxides, which are known to be strongly basic and to have substantially different surface structures.[8] We further suggested that the elimination reaction proceeded by a concerted mechanism over a basic surface and *via* a carbonium-ion like intermediate over an acidic surface.

In the present work, we studied the stereochemistry of dehydrobromination over silica gels containing different cations, since the previous results indicated that the cation species played important roles. For example, similar *anti*-selectivity was observed for KOH–SiO_2 and for K_2CO_3–SiO_2.[6] If the surface structure remains unchanged, it is expected that only the role of the acid-base properties of the surface would be important, as we reported preliminarily.[9] The silica gels studied were prepared carefully by means of ion-exchange, so as to keep the surface structure as constant as possible.

The acid-base properties of these silica gels were clarified from the indicator test and the poisoning effect of acidic and basic reagents. The correlations of these properties with the stereochemistry and the reaction mechanism are discussed.

Experimental

Apparatus and Procedure. A conventional pulse technique described previously was utilized.[6] The carrier gas was hydrogen or helium, which was deoxygenated and dried by a "DEOXO" column and a molecular-sieve trap kept at liquid N_2 temperature. Catalysts (100—500 mg) were ordinarily preheated at 300 °C for 1 h in the stream of carrier gas. After they were cooled to the reaction temperature, 1 or 2 μl of alkyl halide was injected into the gas stream with aid of a microsyringe. All the reactants submitted for elimination reactions in this study gave different stereoisomeric products depending on the steric course of reaction (*anti* or *syn*, *cf.* Scheme I). The stereochemistry of each reaction was determined from the product distribution. No isomerization of butenes of 2-bromo-2-butenes took place under the present reaction conditions.

The analysis of products followed the same procedure as before.[6] The deuterium content of each butene isomer was determined by use of a mass spectrometer (Hitachi, RMU-S) after gas chromatographic separation.

Catalysts. Silica gel was prepared from the hydrolysis of tetraethoxysilane, as before.[6] Ordinarily it was used after being calcined at 500 °C for 6 h and washed with dilute HCl aqueous solution and then with water. Alkali-exchanged silica gels, M–SiO_2 (M=Li, Na, K, or Cs), were prepared by soaking SiO_2 three times in an aqueous solution (N/20) of alkali chloride and carbonate (*ca.* 2: 1) with vigorous shaking for several hours each time at room temperature. The initial pH of the solutions was adjusted every time to 8.0 or 10.0 (low or high alkali content, respectively) by the addition of a small amount of hydrochloric acid. They were then washed and dried at 110 °C. Decationized M–SiO_2 was prepared by repeated washing with aqueous HCl solution (pH=4). The alkali ion contents were determined by flame photometry.

Reagents. 2-Bromobutane (C_4Br), 2-bromobutane-3-d_1 and *meso*- and *dl*-2,3-dibromobutanes (C_4Br_2) were prepared and purified as described previously.[6] The purity of 2-bromobutane-3-d_1 was determined more strictly in the present work, as described in the following section.

Results

Determination of Diastereoisomeric Purity of 2-Bromobutane-3-d_1. Two kinds of 2-bromobutane-3-d_1 which differed in the compositions of *erythro*-d_1, *threo*-d_1, and d_0 species were prepared from *trans*- and *cis*-2-butene as

described above. The compositions were determined by the following method from the butene compositions and the contents of d_1-species in each butene isomer formed from the stereospecific dehydrobromination in liquid phase. The rates of *trans*- and *cis*-2-butene formation from 2-bromobutane-d_0 can be represented as (*cf.* Refs. 4 and 6)

$$v_t^0 = k_t^a + k_t^s \quad (1)$$

$$v_c^0 = k_c^a + k_c^s \quad (2)$$

normalizing the rate of 1-butene formation to unity. Then, since 1-butene formation is little affected by the deuterium atom at C-3 position, the rates of butene formation from 2-bromobutane-3-d_1 (*erythro*: *threo*: d_0= x: y: $1-x-y$) are, referring to Scheme I,

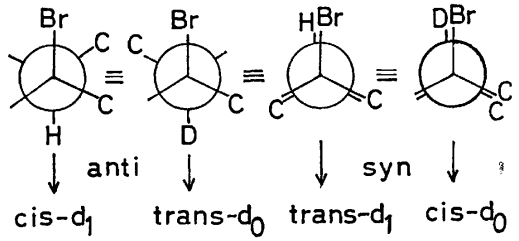

Scheme 1. Stereochemistry and butenes produced in the dehydrobromination of *erythro*-2-bromobutane-3-d_1.

$$v_t(d_0) = xR_t^a k_t^a + yR_t^s k_t^s + (1-x-y)(k_t^a + k_t^s) \quad (3)$$

$$v_t(d_1) = xr_t k_t^s + yr_t k_t^a \quad (4)$$

$$v_c(d_0) = xR_c^s k_c^s + yR_c^a k_c^a + (1-x-y)(k_c^a + k_c^s) \quad (5)$$

$$v_c(d_1) = xr_c k_c^a + yr_c k_c^s \quad (6)$$

where $v_i(d_m)$ is the relative rate of formation of butene i (*trans* or *cis*) with d_m (m=0, 1), R_i^j and k_i^j are the reciprocals of the primary deuterium isotope effect and the relative rate of formation of butene i by j mode (*anti* or *syn*), and r_i is the reciprocal of the secondary isotope effect for butene i formation. Since the reaction utilized for analysis is known to be 100% *anti* elimination (k_t^s, k_c^s=0),[11] the composition (x and y) of 2-bromobutane-3-d_1 can be determined from these equations. The compositions of butenes and their deuterium contents obtained from the reaction in EtOK–EtOH and KOH–ethylene glycol systems at 70 °C are given in Table 1. The content of d_1 species ($x+y$) was 94%, as seen from the d_1 content of 1-butene and confirmed by NMR. The position of deuterium atom was exclusively at 3-position, as evidenced by the microwave spectroscopic analysis of the 1-butene-d_1 formed.[10] Values of x and y are determined for each system by the method of least squares* using Eqs. (1) to (6) as given in the same table. The butene compositions in the case of the EtOK–EtOH system almost agreed with those in the literature, so that 100% *anti* elimination was reasonably assumed in the calculation (k_t^s=k_c^s=0). The compositions of two bromobutane-3-d_1 (**A** and **B**) are as follows, by taking the average of the values from the two systems.

	erythro	*threo*	d_0	
A	77%	17%	6%	(*erythro* rich)
B	28	66	6	(*threo* rich)

The primary isotope effects ($1/R$) for *trans*- and *cis*-2-butene formations were respectively 3.7 and 4.0 (EtOK–EtOH), and 3.0 and 3.5 (KOH–ethylene glycol).

Dehydrobromination of 2-Bromobutane over Silica Gels. Dehydrobromination of 2-bromobutane over Na– and Li–SiO_2 as well as SiO_2 seemed to proceed catalytically, as indicated by the small change in the rate from the repeated pulses. On the other hand, Cs– and K–SiO_2 showed rapid deactivation, and the reaction seemed stoichiometric at the initial stage, as in KOH–SiO_2.[6] However, catalytic elimination by *anti* mode at a stationary rate was possible also over Cs–SiO_2 in the later stage (Fig. 1). The butene compositions changed little in most cases from pulse to pulse. They were

Table 1. Butenes from the dehydrobromination of 2-bromobutanes in alcoholic KOH solutions and the isomeric compositions of 2-bromobutane-3-d_1 (**A** and **B**)

2-Bromobutane	Solvent	Butene composition (d_1% in parentheses)			Composition (%)	
		1-	*trans*	*cis*	*erythro*	*threo*
d_0	Ethanol	1.0	2.65	0.88		
	Ethylene glycol	1.0	2.74	1.06		
3-d_1[b] (**A**)	Ethanol	1.0 (96)	1.17 (36)	0.74 (91)	78	16
	Ethylene glycol	1.0 (93)	1.37 (36)	0.92 (85)	76	18
3-d_1[b] (**B**)	Ethanol	1.0 (95)	2.01 (85)	0.47 (59)	29	65
	Ethylene glycol	1.0 (93)	2.35 (83)	0.65 (58)	26	68

a) Contents of d_0 species in 2-bromobutane-3-d_1 (**A**) and (**B**) are 6%. b) 2-Bromobutane-3-d_1 (**A**) and (**B**) were prepared by DBr addition of *trans*- and *cis*-2-butene, respectively.

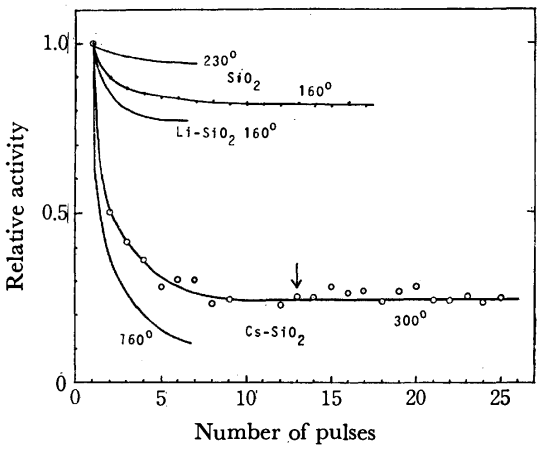

Fig. 1. Variation of activity for the dehydrobromination of 2-bromobutane by repeated pulses.
Arrow indicates that the amount of 2-bromobutane which reacted in repeated pulses was equivalent to that of Cs ion.

* A library program (C7/TC/POWl) of the Computer Center of the University of Tokyo written by Y. Oyanagi, by use of the Powell's method.

Table 2. Variation of stereochemistry of dehydrobromination of 2-bromobutane over silica gel by K exchange

Catalyst	K content (mg-ion/g)	Surface area (m^2/g)	Relative activity[a]	d_1 content of 2-butene (%)[b]		$\frac{(trans/cis)_0}{(trans/cis)_1}$[c]	Stereochemistry
				trans	*cis*		
SiO_2[d]	0.0	425	3.3	76	42	0.82	81% *syn*
K–SiO_2[e]	0.12	400	11.0	47	70	1.42	71% *anti*
H–SiO_2[f]	0.01	390	2.3	68	46	0.79	70% *syn*
SiO_2[g]	0.0	472	6.9	—	—	0.86	*syn*
K–SiO_2[h]	—	380	5.9	—	—	1.33	*anti*
H–SiO_2[i]	—	380	1.8	—	—	0.86	*syn*

a) Normalized to % conversion over 100 mg of catalyst at 160°C. b) From 2-bromobutane-3-d_1 (**A**; *erythro* rich). c) See text. d) Calcined at 800°C. e) SiO_2[d] was treated with KCl–K_2CO_3 aq solution (N/20, pH=8). See text. f) K–SiO_2[e] was decationized by washing with aq HCl solution (pH=4). g) Calcined at 500°C. h) and i) SiO_2[g] was treated as e) and f), respectively.

Table 3. Stereochemistry of dehydrobromination of 2-bromobutane over alkali-ion exchanged silica gels at 160°C

Alkali (pH)[a]	Alkali content (mg-ion/g)	Surface area (m^2/g)	Relative[b] activity	Butene compositions[c] (d_1% in parentheses)			$\frac{(trans/cis)_0}{(trans/cis)_1}$[d]	Stereochemistry
				1-	*trans*	*cis*		
Li(8)	0.04	285	5.1	1.0(92)	2.5(67)	2.5(53)	0.92	62% *syn*
Li(10)	*ca.* 0.4	280	10.8	1.0(95)	2.1(78)	2.4(49)	0.87	77% *syn*
Na(8)	0.07	—	2.6	1.0(92)	1.9(75)	1.8(48)	0.88	74% *syn*
Na(10)	—	—	3.1	1.0	1.3	1.2	0.95	*syn*
K(8)	*ca.* 0.1	260	2.4	1.0	2.3	1.8	1.23	*anti*
Cs(8)	0.08	250	3.4	1.0(—)	2.9(38)	1.8(74)	1.49	80% *anti*
Cs(8)[e]	0.08	250	2.8	1.0	2.7	1.7	1.50	*anti*
Cs(10)[f]	0.41	92	12.6	1.0(96)	3.7(25)	2.8(87)	1.82	100% *anti*
Cs(10)	*ca.* 0.5	180	37	1.0	2.8	1.7	1.54	*anti*
SiO_2	0	470	3—8[g]	1.0	2.6—3.2[g]	2.5—3.2[g]	0.81—0.84[g]	*syn*

a) pH of ion exchange. b) See Table 2. c) Butene compositions from 2-bromobutane-d_0 and contents of d_1 species in butenes from 2-bromobutane-3-d_1 (**A**). d) See text. e) Preheated at 400 °C for 1.5 h. f) Reaction temperature was 100 °C. g) Rate and butene composition varied depending on pH of HCl solution used for SiO_2 washing.

determined from the first four pulses. It was ascertained that the conversion increased proportionally to the amount of catalyst, while the butene composition remained constant.

The absence of butene isomerization** and of d_2 species in butenes from 2-bromobutane-3-d_1, together with the agreement of the d_1 content of 1-butene to that of the starting 2-bromobutane-3-d_1, makes possible a reasonable application of Eqs. (1) to (6) for the determination of the stereochemistry. In practice, it was mostly determined only from the reaction of 2-bromobutane-3-d_1 (**A**), with the approximation that *anti*-selectivity is the same for *trans*- and *cis*-2-butene formations, as well as $r=1$ and $R_t=R_c$. These approximations may be rationalized by the results obtained in the cases of SiO_2 and KOH–SiO_2.[6]

The ratio $(trans/cis)_0/(trans/cis)_1$, which is the ratio of the *trans*-/*cis*-2-butene from 2-bromobutane-d_0 to that from 2-bromobutane-3-d_1 (**A**, *erythro* rich), is also a measure of the stereochemistry. This ratio becomes larger than unity for *anti* mode and smaller than unity for *syn* mode, since one of the 2-butene formations decreases substantially by the introduction of deuterium atom at 3-position, owing to the primary isotope effect.[6]

The effect of K exchange is given in Table 2. *Syn* elimination was favored over SiO_2, as reported previously.[6] The favored steric course of the reaction changed to *anti* mode by the partial exchange of surface protons with K^+ ion. When K^+ ion was reexchanged with H^+ by washing with dilute acid, the steric course returned to *syn* mode almost reversibly. During this exchange procedure the surface area changed little (particularly in the $K^+ \rightarrow H^+$ treatment). The same change in the stereochemistry was observed with Cs exchange, as well as the K exchange of SiO_2 calcined at 1000 °C, which had surface area of 100 m^2/g.***

The effect of alkali-ion species is demonstrated by the results given in Table 3. *Syn* elimination was favored over Li– and Na–SiO_2 and *anti* over K– and Cs–SiO_2,

** Besides the absence of reaction of butenes before and after the pulse of 2-bromobutane, it was also confirmed that pentenes pulsed together with 2-bromobutane did not isomerize.

*** SiO_2 calcined at 1000 °C showed appreciable activity after being washed with dilute HCl solution.

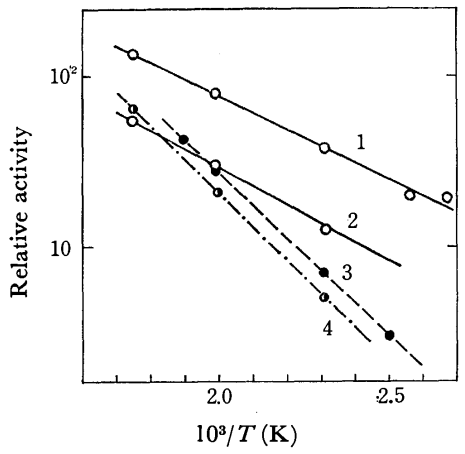

Fig. 2. Arrhenius plots of dehydrobromination of 2-bromobutane over several silica gels.
1. Cs-SiO_2 (*ca.* 0.5 mg-ion/g): E_A=4.4 kcal/mol,
2. Cs-SiO_2 (0.41 mg-ion/g): E_A=4.8 kcal/mol,
3. SiO_2: E_A=8.6 kcal/mol,
4. Li-SiO_2 (0.04 mg-ion/g): E_A=8.7 kcal/mol.

with *anti*-selectivity in the order of Cs>K>Na~Li. It is worthwhile to note that nearly 100% *anti* elimination was observed over the solid surface. The 2-/1-butene ratio was in the order of Cs>K>Na<Li and the *trans/cis* ratio of 2-butene formed increased as Li≦Na<K<Cs.

The dependences of the reaction rates on the reaction temperature are shown in Fig. 2. The predominant steric course did not change for each silica gel at the temperature range studied, as far as judged from the $(trans/cis)_0/(trans/cis)_1$ ratio. The apparent activation energy for Cs-SiO_2 (*anti*) was smaller by about 4 kcal/mol than those for SiO_2 and Li-SiO_2 (*syn*), but the frequency factor for *anti* elimination was about 50 times less favorable.

Dehydrobromination of 2,3-Dibromobutanes over Silica Gels. 2-Bromo-2-butenes formed from dehydrobromination at 2,3-position were the only products over K- and Cs-SiO_2. This reaction proceeded very stereospecifically by *anti* mode; *e.g.*, *meso* isomer produced almost exclusively *cis*-2-bromo-2-butene (Table 4). Over Na-SiO_2, debromination took place besides the dehydrobromination. This debromination proceeded also by *anti* mode. Li-SiO_2 and SiO_2 were almost inactive for the dehydrobromination at this temperature.

Table 4. Products from the reactions of 2,3-dibromobutanes over alkali-ion exchanged silica gels at 160 °C

Alkali (pH)[a]	Relative activity[b]	Pulse no.	Dibromobutane	Products (yield, %) 2-Bromo-2-butene *trans*	2-Bromo-2-butene *cis*	2-Butene *trans*	2-Butene *cis*
Cs(8)	11.2	(1)	*meso*	1.0	23.0	0	0
		(2)	*dl*	7.3	0	0	0
K(8)	5.9	(1)	*meso*	1.8	17.1	0	0
		(2)	*dl*	6.7	0	0	0
Na(8)	1.5	(1)	*meso*	tr	2.4	1.2	0
		(2)	*dl*	0.5	0	0	1.7

a) pH of ion exchange. b) See Table 2. Amounts of catalysts were 213, 316, and 255 mg for Cs-, K-, and Na-SiO_2, respectively.

Table 5. Effect of preadsorbed pyridine on the activity of alkali-ion exchanged silica gels for dehydrobromination of 2-bromobutane

Catalyst	Alkali content (mg-ion/g)	Amount of pyridine added (mmol/g)	Relative activity[a]
Cs-SiO_2	0.41	0	12.6
		0.13	13.0
Cs-SiO_2	*ca.* 0.5	0	37
		0.23	42
		0.98	39
Li-SiO_2	0.04	0	5.1
		0.04	2.6
Li-SiO_2	*ca.* 0.4	0	10.8
		0.25	5.6

a) See Table 2.

Acid-Base Properties of Alkali-Ion Exchanged Silica Gels. The effect of preadsorbed pyridine (a basic reagent which will poison the acidic sites) on the activity was investigated. As the typical results given in Table 5 show, the rate remained unchanged or increased slightly with Cs-SiO_2, while it decreased significantly with Li-SiO_2 and SiO_2. The deactivation by the repeated pulses, which is probably due to HBr (an acidic reagent) formed by the reaction, and, therefore, reflects the basicity of the active sites, was large with Cs- and K-SiO_2, but small with the others. Although these silicas were not as strongly basic as the alkaline-earth oxides nor as strongly acidic as silica alumina, observation of the color changes of indicators (methyl red, bromothymol blue, and cresol red) shows that the acidity increases (or basicity decreases) in agreement with the order of the electronegativity, as Cs<Na<Li (Table 6). The acid strength of silica was comparable with or a little less than Li-SiO_2. Methyl red turned to pink over SiO_2. All of these results demonstrate that the basic sites play important roles over *anti*-prevailing Cs- and K-SiO_2, and the acidic sites over *syn*-prevailing ones.

Table 6. Indicator test of alkali-ion exchanged silica gels[a]

Indicator	Li-SiO_2	Na-SiO_2	Cs-SiO_2
Methyl red	red	yellow	yellow
Bromothymol blue	(bluish) yellow	yellowish blue	blue
Cresol red	yellow (-red)	red	red

a) Ion-exchanged at pH 10. Pretreated at 300 °C for 2 h.

The results of thermogravimetric analysis (TGA) of SiO_2, Li- and Cs-SiO_2 are given in Fig. 3. Prior to TGA analysis, samples were equilibrated with water vapor for 3 days in a desiccator which contained 50% sulfuric acid. The rate of temperature increase was 10 °C/min.

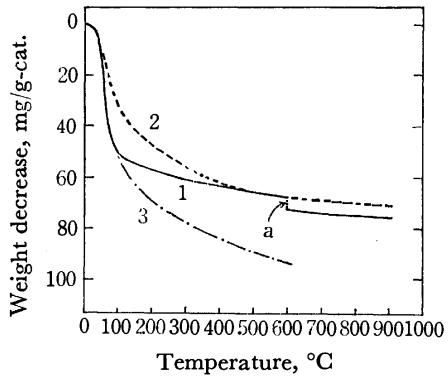

Fig. 3. Thermogravimetric analysis of silica gels.
1. SiO_2 (472 m^2/g),
2. Cs–SiO_2 (*ca.* 0.5 mg-ion/g, 180 m^2/g),
3. Li–SiO_2 (*ca.* 0.4 mg-ion/g, 280 m^2/g).
a. Temperature was kept at 600 °C for 1 h.

Discussion

Stereochemistry of Dehydrobromination and Acid-Base Properties. The present results obviously show that a close correspondence exists between the prevailing steric course of dehydrobromination and the acid-base properties of the catalyst surface. In the case of 2-bromobutane, *anti* mode prevailed over basic surface (Cs– and K–SiO_2) and *syn* mode over acidic surface (SiO_2, Na– and Li–SiO_2).

The steric effect or the geometry of the surface must influence the steric course, in the general case. In *anti* elimination, the two leaving groups or atoms must be released from the opposite sides of a reactant molecule. Therefore, the number of active sites and/or the shape of transition state for *anti* mode may be more restricted by geometrical reasons than those for *syn* elimination. The apparent frequency factor of Cs–SiO_2 was actually much smaller than that over SiO_2 or Li–SiO_2, while activation energy was favorable for *anti* elimination. Thus, it may be expected that *anti* elimination is more sensitive to the surface structure. However, as far as the present systems are concerned, the surface structure is not important from the following reasons in addition to those described before.[6,8]

(i) By the exchange of a small portion of surface silanols by K^+ or Cs^+ ion and then by H^+ (SiOH→SiOM→SiOH), the stereochemistry changed reversibly between *syn* and *anti* mode. During this exchange procedure (particularly in the $K^+ \rightarrow H^+$ treatment), the surface seemed to remain unchanged except for the cation species, as indicated by the small change in the surface area.

(ii) A marked effect of the alkali-ion species on the stereochemistry was observed, although it is unlikely that the surface structures were much different among the four alkali-ion exchanged silicas.

It is difficult to clarify the reason why the stereochemistry seems insensitive to the surface structure and how H and Br can be moved onto the surface from the opposite sides of a reactant molecule. Probably the surface of the silica gel is rough and irregular enough in the dimension of a reactant molecule so as to satisfy the geometrical requirements both for *anti* and *syn* elimination. Therefore, either mode can occur depending on the acid-base properties of surface and reactant. Possible explanations are also found in the proposals by Kibby, Lande, and Hall[4] and Knözinger, Bühl, and Kochloefl.[12]

Acidic and Basic Centers Created by Alkali-ion Exchange of Surface Silanols. The results of many investigations by various methods agree in general as regards the density of silanol groups on the silica surface.[13,14] Adsorbed water on silica gel is desorbed by the evacuation at room temperature. Water adsorbed by hydrogen bonding to silanols is also desorbed by the evacuation at as low as 150 °C. The surface density of silanols after evacuation at 150—300 °C is *ca.* 5/100 $Å^2$. Heating at higher temperature causes surface dehydroxylation, and "free" silanols of 1/100—2/100 $Å^2$ remain after evacuation at 600—800 °C. TGA of SiO_2 (Fig. 3) agreed in general with those reported.[14f]

The introduction of alkali ions increased the amount of adsorbed water, which was retained on the surface more tightly, as indicated by the TGA curves in the range of 100—300 °C. However, there was little difference between Cs and Li, if one takes into account the difference in surface area. It has been reported that Na-doped silica retained no water after evacuation at 170 °C, as evidenced by the absence of the combination mode of stretching and bending of water in the IR spectrum.[14e] Therefore, heating at 300 °C probably eliminated almost all of the adsorbed water on the alkali-ion exchanged silica gels. Then it may be irrational to assume the existence of a liquid water phase only on the surface of Cs–SiO_2 for the explanation of the *anti* elimination. In conformity with this, Cs–SiO_2 preheated at 400 °C and 300 °C showed no significant difference in *anti*-selectivity and butene composition (Table 3).

Surface silanol exchanges its proton with alkali ion as

$$\geqslant SiOH + M^+ \rightleftarrows \geqslant SiOM + H^+ \qquad (7)^{15}$$

According to Boehm,[13] the extent of the exchange with Na^+ ion increases with pH and almost 100% exchange is attained at pH 9—10. However, surface siloxane bonds open and silica starts to dissolve at high pH. In fact, the surface area considerably decreased by the exchange at pH 10, but the decrease was small at pH 8 and negligible at pH 4 (Table 2). In support of Eq. (7), the pH changes during exchange at lower pH were in good agreement with those expected from Eq. (7) and the alkali content determined by flame photometry. If one takes 5/100 $Å^2$ as the density of surface silanols, the extents of exchange in the present work are, for example, 4% for Cs–SiO_2 (Cs: 0.08 mg-ion/g) and *ca.* 50% for Cs–SiO_2 (Cs: 0.41 mg-ion/g).

Usually alkali-ion exchange acts as a poison to the surface acidity and catalytic activity in the case of strongly acidic silica alumina or zeolite. Cs exchange decreased the activity for dehydrobromination of 2-bromobutane at low Cs content, but further exchange increased the activity. Since the stereochemistry was opposite to SiO_2, even for Cs– and K–SiO_2 with low activity, it is obvious that the exchange with these alkali ions created new active sites, besides acting as a

poison. An increase in the activity with the extent of exchange was observed also in the case of Li–SiO_2. However, the change was small in this case and was negligible for Na–SiO_2. Therefore, it is not certain whether or not the exchange created new sites in these cases, besides acting as a poison. From the indicator test and the catalytic activity, the weak acidity or basicity of the sites of the original silica surface and those created by the exchange seems sufficient for the reaction to occur.

The electronegativity or the acid strength of alkali ions increases in the order of Cs<K<Na<Li.[16] The active sites responsible mainly for *syn* elimination, which is acidic, may be the alkali ion and/or the protonic sites of silica. The *anti*-selectively increased in the reverse order. The basic strength of the oxide ion will increase by the coordination of the alkali ion in the decreasing order of the electronegativity (OCs>OK>ONa>OLi), so that this oxide ion may play essential roles in *anti* elimination. As a result, the activity order including both steric modes becomes Cs>K~Na<Li, as observed. The active basic sites on Cs–SiO_2 which was deactivated quickly in the initial stage was roughly 20—40% of the total Cs ions. It has been suggested by Imanaka, Hayashi, and Teranishi that K or Cs exchange of porous glass creates basic sites.[17] Yashima *et al.*[18] reported that K- or Cs-exchanged zeolites exhibit a basic character, although Li-zeolite is acidic. Malinowski and coworkers[19] have measured acidic and basic sites on NaOH-treated SiO_2 and correlated its catalytic activity with them.

The marked change in the catalytic action from one alkali ion to another seems to be one of the remarkable characteristics of the solid surface. In aqueous solutions, there is little difference expected among alkali ions owing to the levelling effect of water. Even in aprotic solvent, although the rate changed, the selectivity remained essentially the same in the isomerization of an olefin.[20]

Reaction Mechanisms, Stereoselectivity, and Stereochemistry. In the dehydrobromination, the surface acts as an acid-base bifunctional catalyst; the acid site abstracts a bromide ion and the basic center a β-proton. The reaction mechanism, therefore, may be classified by the timing of the C–H and C–Br bond breaking,

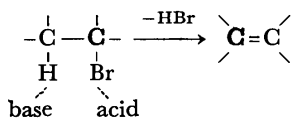

although it is very difficult to determine strictly whether the two bonds break simultaneously or not.[21]

A carbanion mechanism in which the C–H bond breaks (or becomes loose) in the first step seems unlikely because of the observed relative reactivity (*sec*-butyl>isopropyl>ethyl) and the butene composition from C_4Br (2->1-butene). The primary isotope effect and the stereospecificity observed suggest a concerted mechanism where two bonds break in a single concerted step. A carbonium-ion mechanism may also be applied in some cases, if the turnover of the ion on the surface is restricted.

The present results are reasonably explained as in the previous papers by the application of the extended Bunnett's hypothesis of the variable transition state,[2] which was originally proposed for concerted elimination reactions in the liquid phase. The reaction mechanism of elimination varies from an ideally concerted to a carbonium-ion like mechanism, as a reagent attacking the C–H bond becomes less basic or that attacking the C–Br bond becomes more acidic. A variation of the mechanism of the elimination reaction consistent with this idea has been reported also in solid catalysis.[5,22]

When the surface basicity decreases as in Li– and Na–SiO_2, it will become difficult for the surface to abstract a β-proton. But it may be removed to a bromide ion which is already or nearly released, so that *syn* elimination results.[6] The opposite stereochemistry observed with Na–SiO_2 between C_4Br and C_4Br_2 is attributed to a similar variation of mechanism caused by the much higher tendency of β-proton of dihalide to dissociate as a proton, which enables *anti* elimination even over a weak base like Na–SiO_2. The higher reactivity of dibromide than of monobromide (C_4Br_2>C_4Br), as well as the elimination of HBr exclusively from 2,3-position (not from 1,2-position), is explained similarly by the strong acidity of β-proton of dihalide. These trends are well recognized in the liquid-phase elimination.[2,23,24] The C–Br bond breaking, on the contrary, is retarded by β-halogen. These effects explain the reversed reactivity of alkyl bromide over Li–SiO_2 (C_4Br>C_4Br_2) and the activity order for C_4Br_2 of Cs>K>Na>Li.

The fact that the relative reactivity of C_4Br to isopropyl bromide was about 4 over Cs–SiO_2 but about 10 over Li–SiO_2 also supports the idea that the transition state exhibits a more carbonium-ion character in the latter surface. Changes in the rate and butene composition with acid-base properties are also consistent with the mechanisms described here. For example, increases in 2-/1- and *trans*/*cis* ratios from Li to Cs are expected, when the mechanism becomes more concerted[2,25] and the stability of the transition state reflects more that of the products.

The authors are indebted to Prof. Y. Saito and Dr. J. Take for helpful discussions and to Dr. H. Matsumoto for analysis of alkali content. They also gratefully acknowledge Prof. M. Tsuchiya and Dr. S. Saito for mass spectrometric and microwave spectroscopic analyses, respectively.

References

1) C. K. Ingold, "Structure and Mechanism in Organic Chemistry," 2nd ed., Cornell Univ. Press, Ithaca and London (1969).
2) J. F. Bunnett, *Surv. Progr. Chem.*, **5**, 53 (1969).
3) H. Pines and J. Manassen, *Advan. Catal.*, **16**, 49 (1966).
4) C. L. Kibby, S. S. Lande, and W. K. Hall, *J. Amer. Chem. Soc.*, **94**, 214 (1972).
5) H. Noller, P. Andreu, and M. Hunger, *Angew. Chem. Intern. Ed.*, **10**, 172 (1971).
6) M. Misono, *J. Catal.*, **30**, 226 (1973); M. Misono and Y. Yoneda, *Chem. Lett.*, **1972**, 551.

7) K. Thomke and H. Noller, *Proc. 5th Intern. Congr. Catal.*, 1972, **2**, 1183 (1973).
8) M. Misono and Y. Yoneda, *J. Catal.*, **33**, 474 (1974).
9) M. Misono, Y. Aoki, and Y. Yoneda, *Chem. Lett.*, **1974**, 535.
10) Y. Sakurai, Y. Kaneda, S. Kondo, E. Hirota, T. Onishi, and K. Tamaru, *Trans. Faraday Soc.*, **67**, 3275 (1971).
11) P. S. Skell and R. G. Allen, *J. Amer. Chem. Soc.*, **81**, 5383 (1959); R. A. Bartsch, *ibid.*, **93**, 3683 (1971).
12) H. Knözinger, H. Bühl, and K. Kochloefl, *J. Catal.*, **24**, 57 (1972).
13) H. P. Boehm, *Advan. Catal.*, **16**, 179 (1966).
14) a) L. H. Little, "Infrared Spectra of Adsorbed Species," Academic Press, New York (1966). b) M. L. Hair, "Infrared Spectroscopy in Surface Chemistry," Marcel Dekker, New York (1967). c) J. B. Peri and A. L. Hensley, Jr., *J. Phys. Chem.*, **72**, 2926 (1968). d) A. V. Kiselev, *Disc. Faraday Soc.*, **52**, 14 (1971). e) A. C. Zettlemoyer and L. Klier, *ibid.*, **52**, 46 (1971). f) S. Kondo and M. Muroya, *Bull. Chem. Soc. Jpn.*, **43**, 2657 (1970).
15) D. L. Dugger, J. H. Stanton, B. N. Irby, B. L. McConnell, W. W. Cummings, and R. W. Maatman, *J. Phys. Chem.*, **68**, 757 (1964).
16) M. Misono, E. Ochiai, Y. Saito, and Y. Yoneda, *J. Inorg. Nucl. Chem.*, **29**, 2685 (1967).
17) T. Imanaka, Y. Hayashi, and S. Teranishi, *Nippon Kagaku Kaishi*, **1973**, 889.
18) T. Yashima, K. Sato, T. Hayasaka, and N. Hara, *J. Catal.*, **26**, 303 (1972).
19) S. Malinowski and S. Szczepanska, *J. Catal.*, **2**, 310 (1963).
20) S. Bank, A. Schriesheim, and C. A. Rowe, *J. Amer. Chem. Soc.*, **87**, 3244 (1965).
21) S. Oae, *Kagaku*, **27**, 432 (1972).
22) I. Mochida, Y. Anju, H. Yamamoto, A. Kato, and T. Seiyama, *Bull. Chem. Soc. Jpn.*, **44**, 3305 (1971); T. Seiyama and I. Mochida, *Kagaku Sosetsu*, No. 3 (1973), p. 131.
23) S. Oae, "Elimination Reactions," Tokyo Kagaku Dojin, Tokyo (1965).
24) G. Biale, D. Cook, D. J. Lloyde, A. J. Parker, I. D. R. Stevens, J. Takahashi, and S. Winstein, *J. Amer. Chem. Soc.*, **93**, 4735 (1971).
25) R. A. Bartsch, *J. Org. Chem.*, **35**, 1334 (1970); R. A. Bartsch, G. M. Pruss, D. M. Cook, R. L. Buswell, B. A. Bushaw, and K. E. Wiegers, *J. Amer. Chem. Soc.*, **95**, 3405, 6745 (1973); **96**, 430 (1974).

Acidic Nature of Chemisorption Sites on Silica-Alumina and Alumina Catalysts. Characterization by UV Spectra of Adsorbed *p*-Nitroaniline

Koichi MIZUNO, Jun-ichiro TAKE, Yukio YONEDA

Department of Synthetic Chemistry, Faculty of Engineering, The University of Tokyo, Hongo, Bunkyo-ku, Tokyo 113

(Received November 12, 1975)

Chemisorbed *p*-nitroaniline (PNA) gives two bands at 245 and 445 nm on silica-alumina and one band at 450 nm on alumina. The present paper deals with the nature of these chemisobed species and of the chemisorption sites. Kinetic studies of PNA chemisorption onto silica-alumina from cyclohexane solution revealed that the chemisorbed species responsible for the 245 nm band was formed with an activation energy by 0.9 kcal/mol smaller than that responsible for the 445 nm band. The two bands on silica-alumina are due conclusively to two different chemisorbed species. Comparison among UV absorption spectra of PNA in various solutions and on various solid surfaces led to the conclusion that the 245 nm band is ascribable to PNA chemisorbed on Brønsted acid sites and the 445 and 450 nm bands to PNA chemisorbed on Lewis acid sites (*i.e.* surface Al^{3+} ions).

The characterization of the surface acid sites of solid catalysts has provided information useful for the clarification of solid acid catalysis. A variety of techniques have been proposed for determining acid properties.[1] Most of them, however, scarcely give information on the type of surface acid sites (Brønsted or Lewis acid). Such information must also be required for the elucidation of reaction mechanism. In recent years, the distinguishment between both types of surface acid sites has been attempted in IR spectroscopic studies of chemisorbed bases. Ammonia,[2] pyridine,[3] and 2,6-dimethylpyridine[4] were employed successfully because their protonated species exhibit IR absorption bands definitely different from those of the species coordinated to Lewis acid sites.

If an indicator is available which shows UV absorption bands distinct from each other when it interacts with Brønsted and Lewis acids, all of the acid strength of acid sites, their content, and their type are possibly determined as an extension of the butylamine titration method. In a previous study,[5] we found that *p*-nitroaniline (PNA) shows two bands at 245 and 445 nm upon chemisorption on silica-alumina catalyst and concluded that these two bands may be due to two different chemisorbed species.

The present study was undertaken in order to confirm further the previous conclusion and to understand the nature of the chemisorbed species and hence of the chemisorption sites. Kinetic studies of PNA chemisorption onto silica-alumina from cyclohexane solution revealed that the chemisorbed species responsible for the 245 nm band was formed with an activation energy by 0.9 kcal/mol smaller than that responsible for the 445 nm band, demonstrating that these two bands are due unambiguously to two different chemisorbed species. Comparison among UV absorption spectra of PNA in various systems (*i.e.*, in solutions and on surfaces) led to the conclusion that the 245 and 445 nm bands are ascribable to PNA coordinated to Brønsted acid sites and to Lewis acid sites (*i.e.* surface Al^{3+} ions), respectively.

Experimental

Materials. The silica-alumina (SA-1, 13% Al_2O_3) and the silica gel (S-3) were used earlier.[6] Alumina (A-1) was prepared by the neutral hydrolysis of aluminum isopropoxide distilled twice immediately before use.[7] Its surface area was 170 m^2/g. Silica gel impregnated with sulfuric acid (SS-3) was prepared by soaking a thin S-3 wafer calcined in air at 550 °C for 4 h in a diluted aqueous solution of sulfuric acid (20%) and then dried in air at about 80 °C overnight. *p*-Nitroaniline (PNA) was a GR grade reagent and dissolved in cyclohexane without further purification. Cyclohexane used was exhaustively dried and degassed as previously described.[6]

Kinetic Adsorption and UV Studies. Procedures were essentially the same as in a previous study,[6] except that a single wafer was used in all experiments.

A wafer of SA-1, after mounted on the rectangular quartz cage, was treated in a dry oxygen stream at 550 °C for 2.5 h and then in a wet oxygen stream at 150 °C for 0.5 h. The wafer was activated at 450 °C and 10^{-4} mmHg for 2 h in the specially designed UV-cell which is transparent in all sides. Back-ground spectra were determined for both the wafer and the solvent, after introduction of cyclohexane (about 3 ml) followed by that of dry nitrogen. A small amount of PNA (2×10^{-7} mol) was added in a dry nitrogen stream onto frozen cyclohexane in the cell kept at 0 °C, in order to prevent the chemisorption of PNA onto the wafer during the course of addition. The capped cell was rapidly warmed on a water bath thermostatted at temperatures of 10 to 80 °C under stirring with a magnetic stirrer. Separate experiments proved that the frozen PNA almost instantaneously reached adsorption temperature with this procedure. The change of PNA concentration with time was followed by UV spectrophotometry for both the wafer and the solvent.

Wafers of A-1 and S-3 were treated in a dry oxygen stream at 500 °C for 2 h and then activated *in situ* under identical conditions with those employed for SA-1 wafers. A wafer of SS-3 was evacuated briefly *in situ* at room temperature immediately after preparation.

UV spectra over the range of 220 to 600 nm were recorded on a Shimadzu multipurpose recording spectrometer Model MPS-50L at room temperature with a control of atmospheric air.

ESR Studies. A 494 mg sample of powdered SA-1 was activated in an adsorption vessel equipped with a conventional ESR-tube. Experimental conditions for oxygen-treatment and activation were the same as employed in kinetic studies. After addition of cyclohexane and PNA (3.9×10^{-6} mol), the vessel was kept at 62 °C for 2 h. The solvent was removed by evaporation under a vacuum, and then the catalyst was trans-

ferred into the ESR-tube. ESR spectra were recorded on a JES-3BS-X spectrometer at room temperature.

Results and Discussion

UV Spectra of PNA. UV absorption spectra of PNA on various solid surfaces are shown in Fig. 1 and, together with those in various solutions, are summarized in Table 1. PNA chemisorbed on SA-1 shows two bands at 245 (Band I) and 445 nm (Band II), whereas PNA adsorbed on A-1, S-3 and SS-3 gives a single band.

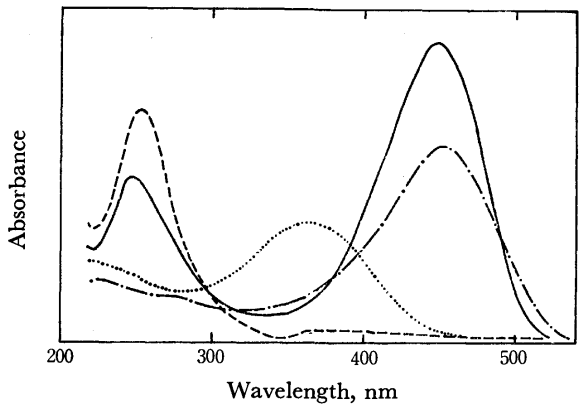

Fig. 1. UV spectra of PNA adsorbed on SA-1 (——), A-1 (-·-), SS-3 (------), and S-3 (·····).

Table 1. UV absorption spectra of PNA on various catalysts and in various solutions (nm)

System		Species		
	Acidic nature	Protonated	Neutral	Coordinated to Al^{3+} ion
on SA-1	L[a] and B[a]	245 (Band I)		445 (Band II)
on A-1	L			450
in $AlBr_3$–$(C_2H_5)_2O$	L			440[b]
in $AlCl_3$–$(C_2H_5)_2O$	L			440[c]
on SS-3	B	252		
in aq H_2SO_4 (20%)	B	255		
on S-3	Nonacidic		365	
in C_2H_5OH	Nonacidic		370	
in cyclo-C_6H_{12}	Nonacidic		322	

a) L and B stand for Lewis and Brønsted acidity, respectively. b) Ref. 8. c) Ref. 9.

Chemisorption of PNA onto SA-1 from Cyclohexane. Chemisorption of PNA onto SA-1 from cyclohexane solution was kinetically investigated in order to determine whether Bands I and II over SA-1 are due to two different chemisorbed species. Figure 2 shows an example of the change of PNA concentration with time. Both Bands I and II increased in intensity with decreasing intensity of the 322 nm band due to PNA in cyclohexane. After initial 2—3 h the 322 nm band completely disappeared and both Bands I and II reached stationary intensities, indicating that the chemisorption was completed. The disappearance of PNA from cyclohexane solution obeyed well a first-order kinetics with

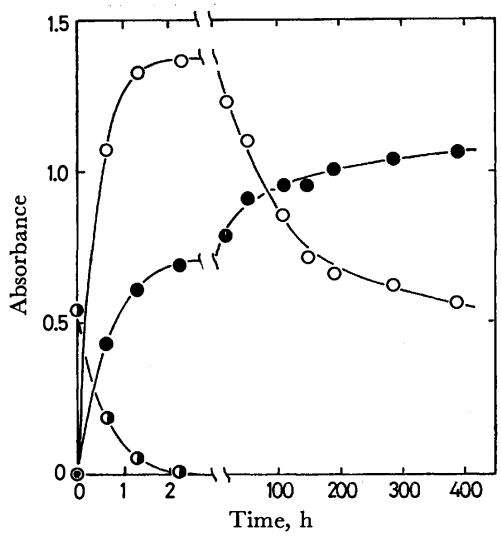

Fig. 2. Change of absorption intensity during chemisorption at 70 °C.
245 (●), 322 (◑), and 445 nm (○) band.

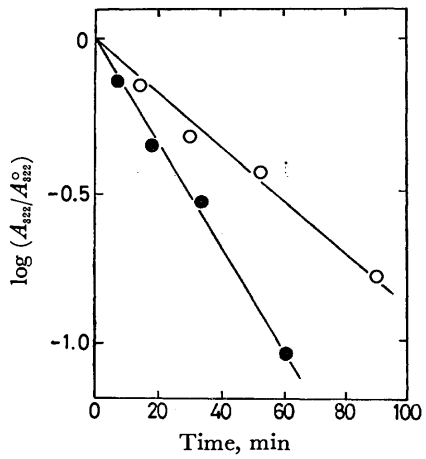

Fig. 3. Disappearance rates of PNA from cyclohexane at 10 (○) and 65 °C (●).

respect to the concentration of PNA, as shown in Fig. 3. From the temperature dependence of rate constants for the disappearance of PNA, the overall activation energy was evaluated to be 1.4 kcal/mol for the chemisorption from cyclohexane.

At every temperature, linear correlations were observed between the increment in intensity of both Bands I and II and the decrement in intensity of the 322 nm band: *i.e.*, $\Delta A_{\mathrm{I}} = -\alpha_{\mathrm{I}} \Delta A_{322}$ and $\Delta A_{\mathrm{II}} = -\alpha_{\mathrm{II}} \Delta A_{322}$, where ΔA_i is the increment in absorbance of Band I, α_i its proportionality constant, as exemplified in Fig. 4. The ratio of the proportionality constants ($\alpha_{\mathrm{II}}/\alpha_{\mathrm{I}}$) *i.e.*, the ratio of the increments in intensity of Bands I and II ($\Delta A_{\mathrm{II}}/\Delta A_{\mathrm{I}}$) at a given time, however, changed depending upon adsorption temperature, as is shown in Fig. 5. If Bands I and II were ascribed to identical chemisorbed species, this ratio would correspond simply to the ratio of the molar extinction coefficients of Bands I and II independent of adsorption temperature. Therefore, the temperature dependence observed demonstrates that Bands I and II are ascribable unambiguously to two different chemisorbed species. As will be described in

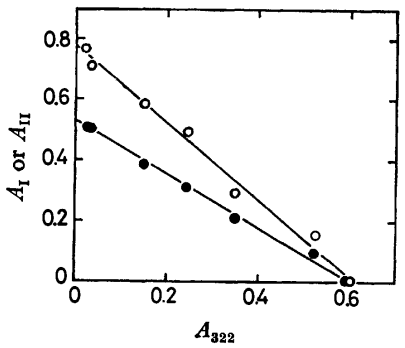

Fig. 4. Ratio of increment in absorbance of Band I (●) or II (○) over decrement in absorbance of 322 nm band (40 °C).

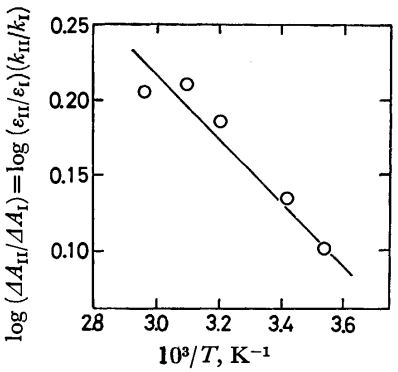

Fig. 5. Difference between activation energies for chemisorption of PNA onto Brønsted acid sites and onto Lewis acid sites.

detail later, these two chemisorbed species correspond to PNA chemisorbed on two types of acid sites different in nature (Sites I and II).

After the completion of chemisorption above 40 °C, the intensity of Band II decreased very slowly with an accompanying increase in intensity of Band I (see Fig. 2), indicating that Band II was just replaced by Band I. This observation provides additional evidence supporting the conclusion that there exist two different chemisorbed species. The observed slow replacement of Band II by Band I is best explained by the following postulation: because the apparent stationary state is far from an equilibrium, the system gradually approaches a true adsorption equilibrium by the migration of less stable chemisorbed species on Site II (responsible for Band II) onto Site I, producing more stable chemisorbed species responsible for Band I. This explanation is in line with the expectation by Polanyi's rule that less stable species become less unfavorable at kinetically controlled stage than at equilibrium. Also, the explanation is consistent with our previous conclusion that the establishment of an adsorption equilibrium of indicators and *n*-butylamine is seriously difficult under the ordinary conditions employed in the butylamine titration method.[10]

Accordingly, the ordinate of Fig. 5 corresponds to the product of the ratio not of equilibrium constants but of the rate constants for chemisorption onto Sites I and II (k_{II}/k_I) and the ratio of molar extinction coefficients for Bands I and II ($\varepsilon_{II}/\varepsilon_I$). The temperature dependence in Fig. 5 thus indicates that the activation energy of the chemisorption of PNA is by 0.9 kcal/mol higher for Site II than for Site I.

Nature of Chemisorption Sites. Inspection of Table 1 will provide interesting information on the nature of the chemisorbed species on SA-1 and hence of the chemisorption sites. The solutions and solid acids employed in the present study can be devided into four groups according to their acidic nature.

As regards the solutions, it has been well established that the acidity of a diluted aqueous solution of sulfuric acid is of the Brønsted type, whereas aluminum bromide and chloride in diethyl ether behave as Lewis acids, and also that ethanol having hydrogen-bonding ability and cyclohexane are both nonacidic. With regard to the solid except for SS-3, the characterization of the surface acidity by means of the IR spectra of adsorbed pyridine indicated that SA-1 has both Lewis and Brønsted acid sites while on A-1 only Lewis acid sites are present, and that S-3 is nonacidic though it has hydrogen-bonding ability,[12] in accord with the results in the literature.[3] SS-3 probably has Brønsted acidity alone.

A noteworthy feature in UV absorption spectra of PNA is that maximal absorption takes place in one or two of three different wavelength regions, depending upon the acidic nature of environments: the first region (240—260 nm), the second (320—370 nm), and the third (440—450 nm) are characteristic for environments of Brønsted acidity, for nonacidic environments, and for environments containing Al^{3+} ions as a Lewis acid, respectively. The second region can be further classified in two subregions: one is the 370 nm region characteristic for environments having hydrogen-bonding ability and the other the 320 nm region characteristic for nonpolar environments.

These considerations lead reasonably to the conclusion that Bands I and II on SA-1 are due to PNA chemisorbed on the Brønsted acid sites and Lewis acid sites (surface Al^{3+} ions), respectively. The 450 nm band on A-1 is ascribed, of course, to PNA chemisorbed on the Lewis acid sites. Reportedly the bathochromic shift from 322 nm in cyclohexane to 370 nm in ethanol is due to the formation of intermolecular hydrogen bonds with the solvents.[12] The 365 nm band on S-3 is therefore ascribed to PNA hydrogen-bonded with the surface, probably with surface hydroxyl groups and oxide ions.

From spectral and reaction-mechanistic evidence, it has been established that besides acidic sites, various sites such as an oxidizing, reducing, and basic site coexist on silica-alumina and alumina surfaces.[13–16] On oxidizing and reducing sites PNA may be converted to radical cations and anions, respectively, by one-electron transfer. In strongly basic media, PNA which is a weak acid of $pK_a=18.9$ is ionized with the loss of a proton from the amino group to produce an anion giving rise to absorption at 467 nm.[17] This wavelength is close to that of Band II or of the 450 nm band on A-1. Such an ionization may also take place over basic sites on SA-1 and A-1. However, we ruled out the formation of either ionic radicals or anions as a main chemisorbed species responsible for Band II on the

following grounds: (a) the presumption that a system of $AlBr_3$ (or $AlCl_3$)–$(C_2H_5)_2O$ has neither a strong basicity nor the ability of oxidation or reduction is quite reasonable, (b) Band II, as well as Band I, was unaffected by the introduction of gaseous oxygen, which enhances the ability of oxidation of silica-alumina and alumina,[18] (c) the surface concentration of the chemisorbed species responsible for Band II on SA-1 was estimated to amount to about 500 times that of reducing sites of silica-alumina with an alumina content of 13%,[14] (d) the ESR spectrum of PNA chemisorbed on SA-1 (g-value=2.00) indicates that the surface concentration of radical species amounts to 5×10^{15} spins/g and corresponds to about one thousandth of that of chemisorbed PNA, and (e) the surface basicities of SA-1 and A-1 are both too weak to ionize PNA, as evidenced by the experimental fact that both catalysts exhibited no absorption peaks around 500 nm upon adsorption of 2,4-dinitroaniline,[19] which is a less weak acid of $pK_a=15.0$ and produces in strongly basic media an anion giving rise to absorption at 388 and 535 nm.[20] This statement is also applicable to Band I characteristic of an anilinium-ion type of species.

Mohammad and Satchell[8] have attributed the 440 nm band observed in their system, PNA–$AlBr_3$ (or $AlCl_3$)–$(C_2H_5)_2O$, to a charge-transfer type of absorption by the complex, and proposed a structural model in which the aluminum ion coordinates weakly to the amino nitrogen atom of PNA. Consistent with this model is our interpretation that the chemisorbed species on Lewis acid sites (*i.e.*, surface Al^{3+} ions) is less stable than that on Brønsted acid sites. It is not obvious why Lewis acid sites of SA-1 should interact less strongly with PNA than do Brønsted acid sites, in contrast with the fact that pyridine coordinates more strongly to Lewis acid sites than to Brønsted acid sites of SA-1.[11]

The authors are indebted to Drs. Yasukazu Saito, and Toshio Uchijima for valuable discussions, to Dr. Makoto Misono for helpful discussion and ESR data, and to Mr. Haruyuki Kawai for kind assistance in the preliminary stage of this work.

References

1) L. Forni, "Catalysis Review," Vol. 8, ed. by H. Heinemann, Marcel Dekker, New York (1974), p. 65.
2) J. E. Mapes and R. P. Eischens, *J. Phys. Chem.*, **58**, 1059 (1954).
3) E. P. Parry, *J. Catal.*, **2**, 371 (1963).
4) P. A. Jacobs and C. F. Heylen, *ibid.*, **34**, 267 (1974).
5) J. Take, K. Mizuno, and Y. Yoneda, *ibid.*, in press.
6) J. Take, H. Kawai, and Y. Yoneda, *ibid.*, **36**, 356 (1975).
7) H. Arai, Y. Saito, and Y. Yoneda, This Bulletin, **40**, 312 (1967).
8) A. Mohammad and D. P. N. Satchell, *J. Chem. Soc., B*, **1967**, 726.
9) A. Mohammad and D. P. N. Satchell, *ibid.*, **1968**, 331.
10) H. A. Benesi, *J. Phys. Chem.*, **61**, 970 (1957).
11) J. Take, T. Ueda, and Y. Yoneda, presented at the 28th Annual Meeting of Chem. Soc. of Japan, Tokyo, April, 1973.
12) B. D. Pearson, *Proc. Chem. Soc.*, **1962**, 78.
13) B. D. Flockhart, J. A. N. Scott, and R. C. Pink, *Trans. Faraday Soc.*, **62**, 730 (1966).
14) B. D. Flockhart, I. R. Leith, and R. C. Pink, *ibid.*, **66**, 469 (1970).
15) J. B. Peri, *J. Phys. Chem.*, **70**, 3168 (1966).
16) J. W. Hightower and W. K. Hall, *Trans. Faraday Soc.*, **66**, 477 (1970).
17) D. Dolman and R. Stewart, *Can. J. Chem.*, **45**, 911 (1967).
18) W. K. Hall, *J. Catal.*, **1**, 53 (1962).
19) J. Take, H. Kawai, and Y. Yoneda, unpublished data.
20) R. Stewart and J. P. O'Donnell, *Can. J. Chem.*, **42**, 1681 (1964).

Molecular Structures of 5-Thiabicyclo[2.1.1]hexane and 7-Thianorbornane as Studied by Gas Electron Diffraction

Tsutomu FUKUYAMA, Kazuko OYANAGI, and Kozo KUCHITSU

Department of Chemistry, Faculty of Science, The University of Tokyo, Bunkyo-ku, Tokyo 113

(Received November 22, 1975)

Molecular structures of 5-thiabicyclo[2.1.1]hexane and 7-thianorbornane (7-thiabicyclo[2.2.1]heptane) were studied by gas electron diffraction. For 7-thianorbornane the rotational constants obtained by Hirota *et al.* by microwave spectroscopy were also taken into account. Least-squares analyses gave the following r_g bond distances and valence angles (r_a for 5-thiabicyclo[2.1.1]hexane and r_{av} for 7-thianorbornane): for 5-thiabicyclo[2.1.1]-hexane, $(C_1-C_2,\ C_2-C_3)_{av}=1.539\pm0.016$ Å, $C_1-C_6=1.564\pm0.024$ Å, $C-S=1.865\pm0.004$ Å, $(C-H)_{av}=1.110\pm0.008$ Å, $\angle C-S-C=69.5\pm0.6°$ and the dihedral angles (C_1SC_4)-$(C_1C_2C_3C_4)=115.2\pm1.7°$ and $(C_1C_6C_4)$-$(C_1C_2C_3C_4)=116.1\pm2.4°$; for 7-thianorbornane, $C_1-C_2=1.538\pm0.006$ Å, $C_2-C_3=1.561\pm0.015$ Å, $C-S=1.837\pm0.004$ Å, $(C-H)_{av}=1.115\pm0.008$ Å, $\angle C-S-C=80.2\pm0.8°$, the dihedral angle $(C_1C_2C_3C_4)$-$(C_4C_5C_6C_1)=115.0\pm1.2°$ and $\angle H-C-H=106\pm5°$. The uncertainties represent the estimated limits of experimental error. The C–S bond length in 5-thiabicyclo[2.1.1]hexane is longer than that in dimethyl sulfide by 0.06 Å and that in 7-thianorbornane by 0.03 Å. The C–S–C angle in 5-thiabicyclo[2.1.1]hexane is smaller than that in dimethyl sulfide by about 30° and that in 7-thianorbornane by about 11°. The C_1-C_6 bond in 5-thiabicyclo[2.1.1]hexane is longer than the weighted average of the C_1-C_2 and C_2-C_3 bond lengths. The C_1-C_2 bond in 7-thianorbornane is longer than the C_2-C_3 bond.

Bicyclic compounds provide important clues for understanding the relationship between the geometry of molecules and intramolecular forces, since their bond lengths and angles are often very different from the corresponding values in open-chain molecules. When a heteroatom is introduced into a bicyclic system, the system is further distorted. As one of such systems, the structure of 7-oxanorbornane[1] was recently studied. The present paper is concerned with the structures of two thiabicyclic compounds, 5-thiabicyclo[2.1.1]hexane (TBH) and 7-thianorbornane (TN) (Fig. 1). After our

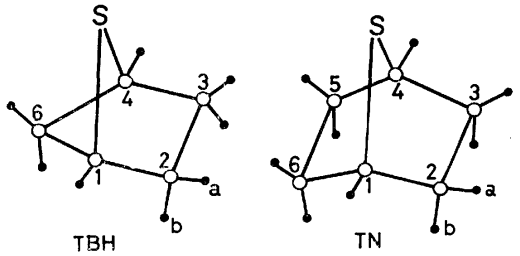

Fig. 1. 5-Thiabicyclo[2.1.1]hexane (TBH) and 7-thianorbornane (TN).

preliminary report on their structures[2] was published, a further refinement was made, particularly for the latter molecule, since a set of rotational constants for TN became available.[3] By means of a joint analysis of electron diffraction and spectroscopic data the two non-equivalent C–C distances, C_1-C_2 and C_2-C_3 have been determined independently.

Experimental

The samples were prepared by the procedures described in the literature[4] and were purified by sublimation and recrystallization. By using a high-temperature nozzle[5] the samples were vaporized at about 60 °C (TBH) and 105 °C (TN), and diffraction photographs were taken with nozzle-to-plate distances of about 249.07 and 114.39 mm. The accelerating voltage of the electrons, about 40 kV, was stabilized within ±0.01% during the experiment.

The scale factors of the diffraction patterns taken with the short camera length were calibrated with reference to the r_a(C=O) distance[6] of carbon dioxide measured under essentially the same experimental conditions as those for the sample gases. In the experiment with the long camera length, nitrogen was used as a reference gas. Other experimental details are described in Refs. 6 and 7.

Three photographic plates taken with each camera length were selected for the analysis, and their optical densities were measured by means of a microphotometer and an integrating digital voltmeter.[8] After correction for imperfection in the r^3-sector and drawing smooth background curves,[7] molecular scattering intensities were obtained in the ranges $s=2.8$—20.1 Å^{-1} and $s=7.9$—34.6 Å^{-1} from the long distance and the short distance data, respectively, at intervals of $s=$

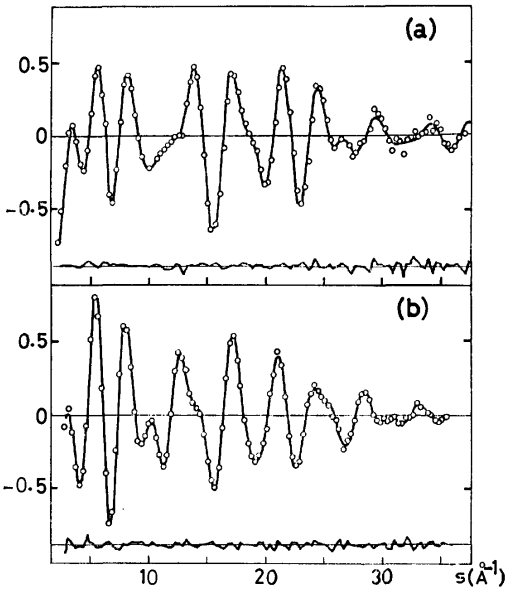

Fig. 2. Molecular intensities. a) 5-Thiabicyclo[2.1.1]-hexane. b) Thianorbornane. Observed values are shown as open circles, and the solid curves represent the best-fit theoretical intensities. The lower solid curves represent the residuals.

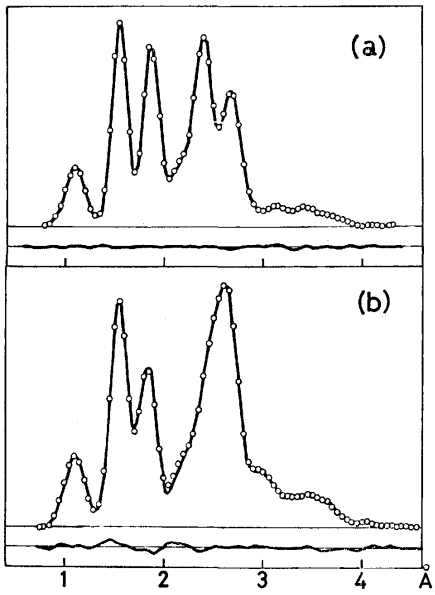

Fig. 3. Experimental (open circles) and the theoretical radial distribution curves. a) 5-Thiabicyclo[2.1.1]-hexane. b) 7-Thianorbornane. Damping factors, $\exp(-0.0016s^2)$ for a) and $\exp(-0.0018s^2)$ for b), were used. The residuals are shown below in the same scale.

$\pi/10$. Since the intensities from the two camera lengths agreed in their overlapping region, they were joined at $s=$ 11.9 Å^{-1}. The elastic and inelastic scattering factors and the phase shifts used for correction of the non-nuclear scattering were taken from the tables prepared by Schäfer *et al.*[9] Typical molecular intensity curves are shown in Fig. 2,[10] and the corresponding radial distribution curves are shown in Fig. 3. Most of the calculations were carried out on a HITAC 8800/8700 in the Computer Center of the University of Tokyo.

Analysis

Analysis of Electron Diffraction Data. The molecular intensities were analyzed by a least-squares method. In order to limit the variable parameters to a tractable number, the following assumptions were made.

1) TBH and TN have C_s and C_{2v} symmetry, respectively.

2) The H–C–H plane in the methylene group is perpendicular to the C–C–C plane, and bisectors of the C–C–C angle and the H–C–H angle are colinear.

3) The C–C–H angles and the S–C–H angle at the bridgehead are equal to one another, *i.e.*, $\angle C_2$–C_1–H$=$ $\angle$S–C_1–H$=\angle C_6$–C_1–H.

4) All the C–H bond lengths are equal.

5) All the H–C–H bond angles are equal. For TBH the angles are assumed to be 110° and are not varied in the analysis.

6) The C_1–C_2 and C_2–C_3 bond lengths are equal. With these assumptions, the structure of TBH is defined by seven parameters: the weighted average of C_1–C_2 and C_2–C_3 bond lengths, the C_1–C_6, and C–S bond lengths, the weighted average C–H bond lengths, the C–S–C angle and the two dihedral angles: $\angle(C_1SC_4)$-$(C_1C_2C_5C_4)$ and $\angle(C_1C_6C_4)$-$(C_1C_2C_3C_4)$. TN For the following six parameters are taken as variables: the weighted average C–C and C–H bond lengths, C–S–C and the weighted average H–C–H angles, and the dihedral angle $\angle(C_1C_2C_3C_4)$-$(C_4C_5C_6C_1)$. In the analysis of the TN structure the last assumption 6) was released by the joint use of diffraction and spectroscopic data, whereas the other constraints were maintained throughout.

Table 1. Estimated force constants for 5-thiabicyclo[2.1.1]hexane and 7-thianorbornane[a]

K(C–C)	2.30	H(S–C–C)	0.07	F(S–C–C)	0.70
K(C–S)	1.75	H(C–C–C)	0.32	F(C–C–C)	0.20
K(C–H)	4.25	H(C–S–C)	0.24	F(C–S–C)	0.21
Y(C–C)$_g$	0.15[b]	H(S–C–H)	0.17	F(S–C–H)	0.39
Y(C–C)$_c$	0.11[b]	H(C–C–H)	0.21	F(C–C–H)	0.47
Y(C–S)	0.05	H(H–C–H)	0.40	F(H–C–H)	0.18

a) Estimated force constants taken from cyclohexane[11] and ethyl methyl sulfide.[12] The torsional force constants (Y) are in mdyn·Å and the others are in mdyn/Å units. b) Symbols g and c represent the C–C axes which have *gauche* and *cis* C···C atom pairs, respectively.

In addition to the geometrical parameters, a number of mean amplitudes were determined by the least-squares analysis: the average C–H, bonded C–S and nonbonded C_2–S and C_6–S amplitudes for TBH, and the average C–C, C–H amplitudes, bonded C–S and nonbonded C_2–S amplitudes for TN. The rest of the mean amplitudes were fixed to values calculated by the use of Urey-Bradley force constants. Since the vibrational spectra of TBH and TN have not been observed, the force constants transferred from cyclohexane[11] and ethyl methyl sulfide[12] were used without further refinement. They are given in Table 1. In order to apply assumption 1), corrections for the shrinkage effects, r_a–r_α,[13,14] were also calculated on the basis of this force field for all the internuclear distances. The calculated mean amplitudes and the shrinkage corrections are shown in Tables 2 and 3. The asymmetry parameter κ for the C–H bond was estimated to be 1.2×10^{-5} Å^3 by a diatomic approximation.[15] The κ parameters for the other atom pairs were assumed to be zero.

Table 2. Mean amplitudes (l_{ij}) and shrinkage corrections (r_a-r_α) for 5-thiabicyclo-[2.1.1]hexane[a] (in 10^{-4} Å)

	l_{ij}	r_a-r_α		l_{ij}	r_a-r_α
C_1–C_2	529	15	$C_2\cdots H_1$	1014	33
C_2–C_3	526	25	$C_2\cdots H_3$	1059	128
C_1–C_6	534	8	$C_2\cdots H_4$	958	19
C_1–S	549	0	$C_2\cdots H_{6a}$	1017	27
C–H	777	86	$C_2\cdots H_{6b}$	1468	−20
$C_1\cdots C_3$	613	0	$C_6\cdots H_1$	1029	25
$C_1\cdots C_4$	588	1	$C_6\cdots H_{2a}$	1202	56
$C_2\cdots C_6$	727	−5	$C_6\cdots H_{2b}$	2029	−62
$C_2\cdots$S	686	−8	S$\cdots H_1$	1058	14
$C_6\cdots$S	574	−1	S$\cdots H_{2a}$	2143	−91
$C_1\cdots H_2$	1420	63	S$\cdots H_{2b}$	1125	53
$C_1\cdots H_6$	1049	37	S$\cdots H_{6a}$	1331	−8
$C_1\cdots H_3$	1383	36	S$\cdots H_{6b}$	916	31
$C_1\cdots H_4$	935	23	$H_{2a}\cdots H_{2b}$	1246	364

a) Calculated at 60 °C.

TABLE 3. MEAN AMPLITUDES (l_{ij}) AND SHRINKAGE CORRECTIONS ($r_a - r_\alpha$) FOR 7-THIANORBORNANE[a] (in 10^{-4} Å)

	l_{ij}	$r_a - r_\alpha$		l_{ij}	$r_a - r_\alpha$
C_1–C_2	538	16	$C_1 \cdots H_{3a}$	1204	25
C_2–C_3	531	30	$C_1 \cdots H_{3b}$	1204	25
C–S	555	3	$C_2 \cdots H_4$	1008	19
C–H	780	86	$C_2 \cdots H_{6a}$	1077	43
C_1–C_3	657	2	$C_2 \cdots H_{6b}$	1594	−12
$C_2 \cdots C_6$	777	2	$C_1 \cdots H_4$	987	18
$C_1 \cdots C_4$	665	−4	$C_2 \cdots H_{5a}$	1096	24
$C_2 \cdots C_5$	896	−14	$C_2 \cdots H_{5b}$	1784	−44
$C_2 \cdots S$	677	−3	$S \cdots H_1$	1089	14
$C_1 \cdots H_2$	1069	61	$S \cdots H_{2a}$	1547	−19
$C_2 \cdots H_1$	1046	32	$S \cdots H_{2b}$	999	37
$C_2 \cdots H_3$	1068	78	$H_{2a} \cdots H_{2b}$	1251	144

a) Calculated at 105 °C.

The r_α structures were determined by a least-squares analysis of the molecular intensities. A conventional diagonal weight matrix[16] with unit elements in the range $6.3 \leq s \leq 26.7$ and smaller for smaller and larger scattering angles was used. The results are listed in Tables 4 and 5. The r_g bond lengths derived from the r_α structure are also shown.

The error limits quoted in Tables 4 and 5 were estimated from random and systematic errors from various sources,[1,17] including those originating from preceding assumptions. The structure of TBH given in Table 4 is regarded as the final result of the present study. The corresponding error matrix is listed in Table 6.

Joint Analysis of Electron Diffraction Intensities and Rotational Constants for TN. The rotational constants for the normal species of TN were reported by Hirota *et al.* from microwave spectroscopy.[3] Their rotational constants for the ground vibrational state, A_0, B_0, and C_0, were transformed into A_z, B_z and C_z by making vibrational corrections.[18] The electronic and centrifugal corrections were ignored. The uncertainties in the vibrational corrections were tentatively assumed to be 20%, and the uncertainties in the A_0, B_0, and C_0 constants were also taken into account in the total uncertainties in A_z, B_z and C_z.

In order to check the consistency of the diffraction data with the spectroscopic data, the r_α structure determined from the diffraction data was extrapolated to zero kelvin[13,14] by calculating the difference $r_\alpha^0 - r_\alpha$. The anharmonic contribution to the difference was estimated on the basis of a diatomic approximation,[15] while the harmonic contribution was derived from the force constants mentioned in the preceding subsection. The temperature effect on the bond angles was ignored.

As shown in Table 7, the rotational constants, A_α^0, B_α^0 and C_α^0 calculated from the r_α^0 structure agreed with their spectroscopic equivalents, A_z, B_z and C_z within their uncertainties. In general, if two bonds in a molecule with nearly equal distances are approximately parallel to different principal axes, the rotational constants with respect to these axes can be used for discriminating these bond lengths. For 7-thianorbornane, like 7-oxanorbornane,[1] the rotational constants A_z and B_z are sensitive to the C_2–C_3 and C_1–C_2 bond lengths, respectively. Therefore, the rotational constants were taken into the least-squares analysis to complement the

TABLE 4. STRUCTURE AND MEAN AMPLITUDES OF 5-THIABICYCLO[2.1.1]HEXANE DERIVED FROM ELECTRON DIFFRACTION DATA[a] (in Å and degrees)

	r_α	r_g	ε[b]		r_α[c]	ε[b,c]		l	ε[b,c]
$(C_1$–C_2, C_2–$C_3)_{av}$	1.535	1.539	0.016	$\angle C_1$–C_6–C_4	85.4	1.6	C–S	0.057	0.006
C_1–C_6	1.562	1.564	0.024	$\angle C_1$–C_2–C_3	101.1	0.6	C–H	0.074	0.023
C–S	1.863	1.865	0.004	$\angle C_2$–C_1–C_6	101.2	1.8	$C_2 \cdots S$	0.071	0.007
C–H	1.096	1.110	0.008	$\angle C_2$–C_1–S	103.6	1.2	$C_6 \cdots S$	0.050	0.011
∠C–S–C	69.5		0.6	$\angle C_6$–C_1–S	89.1	1.4			
$\angle(C_1SC_4)$-$(C_1C_2C_3C_4)$[d]	115.2		1.7	$\angle C_2$–C_1–H	119.2	0.5			
				$\angle C_1$–C_2–H_2	111.4	2.3			
$\angle(C_1C_6C_4)$-$(C_1C_2C_3C_4)$[d]	116.1		2.4	$\angle C_1$–C_6–H_6	114.9	1.1			

a) Final result of the present study. b) Estimated limits of error. c) Calculated from the independent parameters. Uncertainties are estimated from those in the independent parameters. d) Dihedral angle.

TABLE 5. STRUCTURE AND MEAN AMPLITUDES OF 7-THIANORBORNANE DERIVED FROM ELECTRON DIFFRACTION[a] (in Å and degrees)

	r_α	r_g	ε[b]		l	ε[b]
C–C	1.541	1.545	0.004	C–C	0.058	0.009
C–S	1.834	1.836	0.007	C–S	0.064	0.008
C–H	1.098	1.112	0.008	C–H	0.087	0.013
∠C–S–C	79.8		0.8	C ··· S	0.077	0.006
$\angle(C_1C_2C_3C_4)$-$(C_4C_5C_6C_1)$[c]	115.5		1.5			
∠H–C–H	108		7			

a) Intermediate result. See Table 8 for the final result of the present study. b) Estimated limits of error. c) Dihedral angle.

Table 6. Error matrix for 5-thiabicyclo[2.1.1]hexane[a)]

	k_1	k_2	x_1	x_2	x_3	x_4	x_5	x_6	x_7	l_1	l_2	l_3	l_4
k_1	157	20	−26	21	13	15	−27	40	−11	−10	23	−19	18
k_2		275	−84	113	−29	−43	56	102	39	63	56	56	34
x_1			31	−39	9	14	−18	−37	−20	−19	17	−17	−4
x_2				53	−12	−19	27	49	26	26	23	23	14
x_3					10	5	−5	−13	9	−7	−6	−6	4
x_4						25	−12	−17	−11	−10	−11	−10	−3
x_5							25	24	−32	13	11	13	10
x_6								50	−17	23	21	20	6
x_7									108	8	9	14	41
l_1										17	13	13	7
l_2											26	11	8
l_3												19	4
l_4													28

a) k_1, k_2=indices of resolution for the long and short camera length data (0.99±0.06, 0.92±0.08), respectively, x_1=the weighted average of $r(C_1-C_2)$ and $r(C_2-C_3)$, $x_2=r(C_1-C_6)$, $x_3=r$(C–S), $x_4=r$(C–H), $x_5=\angle$C–S–C, $x_6=\angle(C_1SC_4)$-$(C_1C_2C_3C_4)$, $x_7=\angle(C_1C_6C_4)$-$(C_1C_2C_3C_4)$, $l_1=l$(C–S), $l_2=l$(C–H), $l_3=l(C_2-S)$ and $l_4=l(C_6-S)$. Units ($\times 10^{-4}$) for the distances and mean amplitudes are Å, those for the angles are rad, and those for the indices are dimensionless.

Table 7. Observed and calculated rotational constants for 7-thianorbornane[a)] (in cm^{-1})

	B_0[b)]	B_z[c)]	B_α^0[d)]	B_{av}[e)]
A	0.091741(6)	0.091702(10)	0.0919(5)	0.091702(10)
B	0.088194(2)	0.088169(5)	0.0887(6)	0.088169(5)
C	0.081402(2)	0.081388(3)	0.0810(4)	0.081388(3)

a) Uncertainties attached to the last significant digits are given in parentheses. b) Observed rotational constants for the ground vibrational state. Ref. 3. c) Zero-point average rotational constants calculated from A_0, B_0 and C_0 with corrections for vibrational effects. d) Rotational constants calculated from r_α^0 parameters given in Table 5 determined in the analysis of electron diffraction intensities. Uncertainties are estimated from those in the r_α^0 parameters. e) Best-fit rotational constants corresponding to the r_{av} structure, listed in Table 8, derived from the combined analysis of diffraction and microwave data. Uncertainties represent 2.5 times the estimated standard deviations.

diffraction data.

For each least-squares calculation the standard deviations in the rotational constants were estimated from those in the r_α^0 parameters by using the law of propagation of errors. The relative weights for the rotational constants were then adjusted in such a way that 2.5 times their standard deviations were approximately equal to their estimated uncertainties. The weights assigned in this way were 4×10^8, 1×10^9 and 3×10^9 for A_z, B_z and C_z respectively, in comparison with unit weights assigned to the molecular intensities from s=6.3 to 26.7 $Å^{-1}$. It was possible to release the constraint 6) on the C–C bond lengths by the joint use of the rotational constants and the electron diffraction

Table 9. Observed mean amplitudes for 7-thianorbornane[a)] (in Å)

	l_{obsd}[a)]	l_{calcd}[a,b)]
C–C[c)]	0.054(9)	0.054(5)
C–S	0.061(8)	0.056(6)
C–H	0.081(13)	0.078(8)
$C_2\cdots S$	0.075(5)	0.068(14)

a) Uncertainties attached to the last significant digits are given in parentheses. b) Taken from Table 2. Uncertainties are tentatively estimated to be about ±10% for C–C, C–S and C–H and about ±20% for $C_2\cdots S$. c) $l(C_1-C_2)$ and $l(C_2-C_3)$ are assumed to be equal to each other.

Table 8. Structure of 7-thianorbornane derivived from electron diffraction and microwave data[a)] (in Å and degrees)

	r_{av}	r_g	ε[b)]		r_{av}[c)]	ε[b,c)]
C_1-C_2	1.535	1.538	0.006	$\angle C_1-C_2-C_3$	105.2	0.5
C_2-C_3	1.557	1.561	0.015	$\angle C_2-C_1-C_6$	109.0	1.1
C–S	1.834	1.837	0.004	$\angle C_2-C_1-S$	103.1	0.7
C–H	1.101	1.115	0.008	$\angle H_1-C_1-S$	113.5	0.6
∠C–S–C	80.2		0.8	$\angle C_1-C_2-H_2$	111.5	1.2
$\angle(C_1C_2C_3C_4)$-$(C_4C_5C_6C_1)$[d)]	115.0		1.2			
∠H–C–H	106		5			

a) Final result of the present study. b) Estimated limits of error. c) Calculated from the independent parameters. Uncertainties are estimated from those in the independent parameters. d) Dihedral angle.

Table 10. Error matrix for 7-thianorbornane[a]

	k_1	k_2	x_1	x_2	x_3	x_4	x_5	x_6	x_7	l_1	l_2	l_3	l_4
k_1	150	78	−44	64	24	21	−60	58	116	5	13	18	25
k_2		321	−16	46	−39	−29	−29	−29	−42	59	61	76	44
x_1			20	−28	−9	−11	27	−25	−46	7	−3	−2	−9
x_2				43	8	15	−39	35	75	−7	8	11	14
x_3					12	3	−12	15	27	−7	−8	−9	−3
x_4						24	−14	16	50	−7	−4	−9	4
x_5							37	−34	−64	8	−5	−6	−12
x_6								34	67	−10	−6	−7	10
x_7									177	−21	−8	−13	23
l_1										13	11	14	8
l_2											16	14	8
l_3												28	8
l_4													12

a) k_1, k_2=indices of resolution for the long and short camera length data (1.03±0.08, 1.03±0.09), respectively, $x_1=r(C_1-C_2)$, $x_2=r(C_2-C_3)$, $x_3=r(C-S)$, $x_4=r(C-H)$, $x_5=\angle C-S-C$, $x_6=\angle(C_1C_2C_3C_4)$-$(C_4C_5C_6C_1)$, $x_7=\angle H-C-H$, $l_1=l(C-C)$, $l_2=l(C-S)$, $l_3=l(C-H)$ and $l_4=l(C\cdots S)$. Units ($\times 10^{-4}$) for the distances and mean amplitudes are Å, those for the angles are rad, and those for the indices are dimensionless.

intensities. Including the indices of resolution for the long and short distance data, thirteen parameters were refined. The final structural parameters and mean amplitudes with estimated error limits are shown in Tables 8 and 9. The observed mean amplitudes for TBH and TN agree with the calculated mean amplitudes to within the limits of their uncertainties. The corresponding error matrix is given in Table 10.

Discussion

The final structures of TBH and TN are compared with the structures of bicyclo[2.1.1]hexane,[19,20] norbornane,[21] 7-oxanorbornane,[1] tetrahydrothiophene[22] and dimethyl sulfide[23] in Table 11.

C–S Bond Lengths and Sulfur Valence Angles. The present study demonstrates unusual bond lengths and

Table 11. Comparison of the structures of related molecules[a] (in Å and degrees)

	$(C_1-C_2, C_2-C_3)_{av}$	C_1-C_2	C_2-C_3	C_1-C_6	C–S	∠C–S–C	$\angle C_1-C_6-C_4$[i]	$\angle C_1-C_2-C_3$[i]	θ[j]
b)	1.539(16)			1.564(24)	1.865(4)	69.5(6)	85.4(16)	101.1(6)	116.1(24)
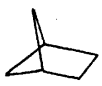 c)	1.538(8)[k,l]			1.548(10)[k,l]			85.4(28)[l]	100.5(10)[l]	115.3(39)[l]
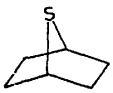 d)	1.546(4)	1.538(6)	1.561(15)		1.837(4)	80.2(8)		105.2(5)	115.0(12)
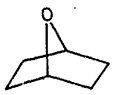 e)	1.546(4)	1.538(14)	1.571(15)					100.3(6)	113.5(8)
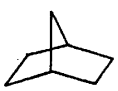 f)	1.545(10)	1.539(12)	1.557(25)	1.560(24)[m]				103.3(7)	113.1(18)
g)					1.841(2)[n]	93.4(5)			
h)					1.808(3)	99.0(3)			

a) Distances in r_g and angles in r_{av} (r_α for b and f, r_a for c and g). Uncertainties represent estimated limits of error attached to the last significant digits. b) 7-Thiabicyclo[2.1.1]hexane, the present study. c) Bicyclo[2.1.1]hexane, Ref. 19. See also Ref. 20. d) 7-Thianorbornane, the present study. e) 7-Oxanorbornane, Ref. 1. f) Norbornane, Ref. 21. g) Tetrahydrothiophene, Ref. 22. h) Dimethyl sulfide, Ref. 23. i) Calculated from the independent parameters. j) Dihedral angles, $\angle(C_1C_6C_4)$-$(C_1C_2C_3C_4)$ for b and c, and $\angle(C_1C_2C_3C_4)$-$(C_4C_5C_6C_1)$ for d, e and f. k) Estimated from the r_a distance reported in the literature by addition of l^2/r_a. l) Uncertainties have been re-estimated. m) The C_1-C_7 bond length in norbornane. n) Ref. 24.

angles in bicyclic compounds. The C–S bond length in TBH is longer than that in dimethyl sulfide[23] by 0.06 Å, and the C–S–C angle is smaller by about 30°. On the other hand, the C–S bond length and the C–S–C angle in TN are shorter by about 0.03 Å and larger by about 11°, respectively, than the corresponding values in TBH. This trend implies that intramolecular strain is much greater in TBH than in TN.

The present study also demonstrates a systematic decrease in the C–S–C angle in a series of sulfur substituted hydrocarbons: (a) acyclic, (b) five-membered ring and (c) bicyclic. The corresponding series of unsubstituted and oxygen substituted hydrocarbons showed a similar systematic trend in the C–C–C and C–O–C angles.[1] The C–S lengths do not show regular increases in the series of sulfur substituted hydrocarbons,[24] as do the C–C and C–O lengths in the series of unsubstituted and oxygen substituted hydrocarbons.[1] (See Table 11.)

C–C Bond Lengths. The essential features regarding the C–C bond lengths are the following:

1) The C_1–C_6 bond in TBH is longer than the weighted average of the C_1–C_2 and C_2–C_3 bond lengths. Similar trends were reported for norbornane.[21]

2) The average values of the C_1–C_2 and C_2–C_3 distances in TN, 7-oxanorbornane and norbornane are equal to one another to within their limits of error and about 0.01 Å longer than the normal single C–C bond length, whereas the corresponding average C–C bond length in TBH seems to be shorter and approximately equal to the normal C–C bond length.

3) For TN and 7-oxanorbornane the C_1–C_2 and C_2–C_3 bonds were separated by use of the rotational constants. The corresponding distances in these molecules are essentially equal to each other. The C_1–C_2 distances are similar to the normal single bond length, while the C_2–C_3 distances are about 0.02 Å longer and close to the C_1–C_6 distance in TBH or the C_1–C_7 distance in norbornane. The trend that the C_2–C_3 bond is longer than the C_1–C_2 bond has also been suggested for norbornane and bicyclo[2.2.2]octane.[25]

4) The C–C bond lengths in the six-membered rings in norbornane, 7-oxanorbornane and TN are remarkably similar in spite of the very different bond lengths and valence angles in the C–C–C, C–O–C and C–S–C bridges.

Angles in the Rings. The dihedral angles in norbornane and 7-oxanorbornane are nearly equal to each other and are about 2° smaller than that in TN. The C_1–C_6–C_4 angle in TBH seems to be essentially equal to that in bicyclo[2.1.1]hexane.[19] The C_1–C_2–C_3 angle in TN is about 5° larger than that in 7-oxanorbornane and about 3° larger than that in norbornane.

The authors are indebted to Professor Zen-ichi Yoshida, Professor Iwao Tabushi, and Dr. Yoshinao Tamaru for preparation of the samples and to Professor Robert K. Bohn and Dr. Ken-ichi Karakida for their helpful comments.

References

1) K. Oyanagi, T. Fukuyama, K. Kuchitsu, R. K. Bohn, and S. Li, This Bulletin, **48**, 751 (1975).
2) T. Fukuyama, K. Kuchitsu, Y. Tamaru, Z. Yoshida, and I. Tabushi, *J. Amer. Chem. Soc.*, **93**, 2799 (1971).
3) K. Irie, T. Tanaka, E. Hirota, Y. Tamaru, I. Tabushi, and Z. Yoshida, 27th Annual Meeting of the Chemical Society of Japan, Nagoya (1972), 1M02.
4) TBH: I. Tabushi, Y. Tamaru, and Z. Yoshida, *Tetrahedron Lett.*, **1970**, 2931. TN: E. J. Corey and E. Block, *J. Org. Chem.*, **31**, 1663 (1966).
5) A. Yokozeki and K. Kuchitsu, This Bulletin, **44**, 72 (1971).
6) Y. Murata, K. Kuchitsu, and M. Kimura, *Japan. J. Appl. Phys.*, **9**, 591 (1970).
7) M. Tanimoto, K. Kuchitsu, and Y. Morino, This Bulletin, **43**, 2776 (1970).
8) Y. Morino, K. Kuchitsu, and T. Fukuyama, *ibid.*, **40**, 423 (1967).
9) L. Schäfer, A. C. Yates, and R. A. Bonham, *J. Chem. Phys.*, **55**, 3055 (1971).
10) Numerical experimental data of the leveled total intensity and the background have been deposited with the Chemical Society of Japan (Document No. 7609).
11) H. Takahashi and T. Shimanouchi, *J. Mol. Spectrosc.*, **13**, 43 (1964).
12) M. Ohsaku, Y. Shiro, and H. Murata, This Bulletin, **46**, 1399 (1973).
13) K. Kuchitsu and S. Konaka, *J. Chem. Phys.*, **45**, 4342 (1966).
14) K. Kuchitsu and S. J. Cyvin, "Molecular Structures and Vibrations," ed. by S. J. Cyvin, Elsevier, Amsterdam (1972), Chapter 12.
15) K. Kuchitsu, This Bulletin, **40**, 505 (1967).
16) Y. Morino, K. Kuchitsu, and Y. Murata, *Acta Crystallogr.*, **18**, 549 (1965).
17) K. Kuchitsu, "Molecular Structures and Vibrations," ed. by S. J. Cyvin, Elsevier, Amsterdam (1972), Chapter 10.
18) M. Toyama, T. Oka, and Y. Morino, *J. Mol. Spectrosc.*, **13**, 193 (1964).
19) G. Dallinga and L. H. Toneman, *Rec. Trav. Chim.*, **86**, 171 (1967).
20) J. F. Chiang, *J. Amer. Chem. Soc.*, **93**, 5044 (1971). The structure of bicyclo[2.1.1]hexane reported in this reference is in significant discrepancy with that in Ref. 19. The analysis of Ref. 20 in which highly correlated structural parameters are claimed to be determined uniquely seems to be questionable.
21) A. Yokozeki and K. Kuchitsu, This Bulletin, **44**, 2356 (1971).
22) Z. Náhlovska, B. Náhlovsky, and H. M. Seip, *Acta Chem. Scand.*, **23**, 3534 (1969).
23) T. Iijima, private communication.
24) The C–S bond length reported in Ref. 22 seems to be slightly too long. K. Takemura, T. Fukuyama, and K. Kuchitsu, unpublished data (1975).
25) A. Yokozeki, K. Kuchitsu, and Y. Morino, This Bulletin, **43**, 2017 (1970).

The Crystal and Molecular Structure of Tris-(2,2,6,6-tetramethylheptane-3,5-dionato)lutetium(III)

Shigeki ONUMA, Hironao INOUE,* and Shuzo SHIBATA
Department of Chemistry, Shizuoka University, Oya, Shizuoka 422
(Received December 22, 1975)

The crystal and molecular structure of tris-(2,2,6,6-tetramethylheptane-3,5-dionato)lutetium(III) has been determined by X-ray diffraction method. The space group is $Pmn2_1$, and the unit cell is orthorhombic with $a=17.713(4)$, $b=10.638(2)$, $c=9.973(3)$ Å, and $Z=2$. The structure is isomorphous with the erbium analogue. The atomic parameters of the molecule (except for hydrogen atoms) were refined by the block-diagonal least-squares method to an R of 0.053. Three chelate rings are planar. One of them lies in the crystallographic mirror plane, and the other two rings are symmetrically related to each other with respect to this mirror plane. Six oxygen atoms of the three β-diketones form a distorted trigonal prism around the central lutetium ion, the average Lu–O distance being 2.19 Å.

The anhydrous lanthanide complexes of 2,2,6,6-tetramethylheptane-3,5-dione, H(thd), are volatile.[1] Among them the complexes of La to Dy are monoclinic and those of Ho to Lu are orthorhombic.[2,3] Crystal structure analyses were carried out on the tris-thd chelates of praseodymium[3] and erbium;[4] the praseodymium chelate is dimeric and each Pr atom is surrounded by seven oxygen atoms in a monocapped trigonal prism, while the erbium chelate is monomeric and the coordination polyhedron is approximately trigonal prismatic, giving a sixfold coordination. The present study was undertaken to determine the crystal and molecular structure of the anhydrous tris-thd chelate of the most heavy element of lanthanides.

Experimental

Single-crystals of anhydrous tris-thd chelate of lutetium were prepared by sublimation. They are transparent prisms. It was, however, noticed that the crystals become opaque and amorphous slowly when exposed to X-rays in the atmosphere. The crystal was, therefore, sealed in a glass capillary tube to avoid such changes.

Approximate cell constants were determined from Weissenberg photographs, and they were refined by a least-squares method using 23 higher angle reflections measured on a Rigaku Denki automatic four-circle single-crystal diffractometer with Mo$K\alpha_1$ radiation ($\lambda=0.70926$ Å). They are given in Table 1 with other crystal data.

The intensity data were collected on a single-crystal diffractometer using Zr-filtered Mo$K\alpha$ radiation at room temperature. The ω–2θ scan technique was employed at a speed of 2°/min in 2θ. The intensities of three reflections (002, 010 and 400) were checked every 50 reflection measurements. The fluctuations were less than 1%, and no appreciable decomposition of crystal was observed. A total of 2360 accessible reflections with $2\theta<55°$ were measured. The data were corrected for the Lorentz and polarization factors, but not corrected for absorption. Reflections whose amplitude $|F|$ were less than three times their standard deviations were not included in the subsequent calculations. The number of observed reflections was 1731.

TABLE 1. CRYSTAL DATA

$Lu(thd)_3$, $LuC_{33}H_{57}O_6$
Molecular weight 724.8
Orthorhombic
$a=17.713(4)$
$b=10.638(2)$
$c=9.973(3)$ Å
Space group $Pmn2_1$
Volume of a unit cell 1879.2(8) Å^3
Density, calculated for $Z=2$: 1.286 g cm^{-3}
Number of electrons per unit cell $F(000)=634$ (without hydrogen atoms)

Structure Determination and Refinement

The crystal structure of $Lu(thd)_3$ was supposed to be isomorphous with that of $Er(thd)_3$[4] because the cell constants and systematic absences are similar. Therefore, the atomic parameters of $Er(thd)_3$ were used as initial values and they were refined by a block-diagonal least-squares method. The quantity minimized was $\sum w(|F_o|-|F_c|)^2$, where the weighting function w was unity. Positional and anisotropic thermal parameters

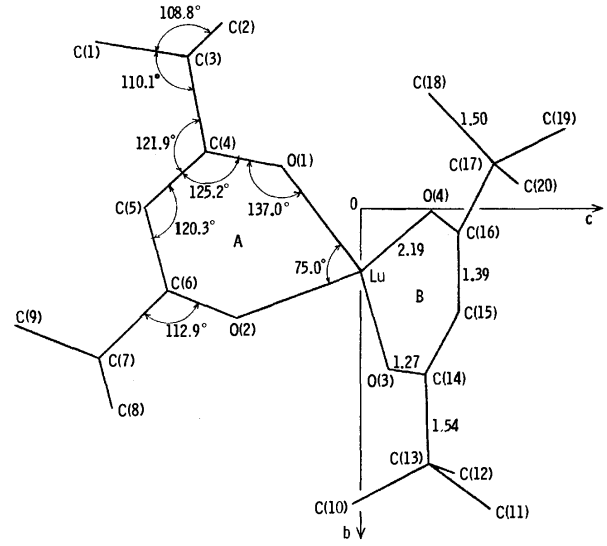

Fig. 1. Projection of the molecular skeleton along the a-axis.
The numbering system of atoms and average bond lengths (l/Å) and angles (φ/°) are also indicated.

* Rigaku Denki Company, Ltd., Matsubaracho, Akishima, Tokyo 196.

TABLE 2. THE FINAL ATOMIC PARAMETERS AND THEIR ESTIMATED STANDARD DEVIATIONS IN PARENTHESES ($\times 10^4$)
Anisotropic temperature factors are of the form: $\exp[-(B_{11}h^2+B_{22}k^2+B_{33}l^2+B_{12}hk+B_{13}hl+B_{23}kl)]$

	x	y	z	B_{11}	B_{22}	B_{33}	B_{12}	B_{13}	B_{23}
Lu	0	977(1)	0	39(0)	72(1)	116(1)	0	0	26(4)
O(1)	0	−675(13)	−1284(16)	65(7)	93(15)	123(19)	0	0	19(28)
O(2)	0	1708(13)	−2039(16)	63(7)	77(13)	138(21)	0	0	10(28)
C(1)	0	−2567(31)	−4359(34)	335(58)	134(36)	120(39)	0	0	−84(65)
C(2)	−674(16)	−2874(22)	−2312(42)	129(18)	166(28)	779(119)	201(39)	−401(80)	−346(99)
C(3)	0	−2337(16)	−2845(28)	55(10)	43(15)	198(38)	0	0	−15(41)
C(4)	0	−908(20)	−2547(23)	30(6)	100(19)	137(27)	0	0	−64(46)
C(5)	0	−26(20)	−3552(25)	55(10)	84(20)	156(31)	0	0	55(46)
C(6)	0	1282(20)	−3229(22)	29(7)	115(23)	125(27)	0	0	−16(42)
C(7)	0	2303(22)	−4315(27)	49(10)	120(25)	183(36)	0	0	124(53)
C(8)	687(13)	3107(21)	−4116(24)	69(10)	222(30)	265(37)	−101(31)	−38(33)	246(60)
C(9)	0	1792(23)	−5725(23)	147(22)	110(25)	75(26)	0	0	76(45)
O(3)	800(7)	2477(9)	443(12)	62(5)	93(9)	201(24)	−11(11)	−85(17)	41(21)
O(4)	920(6)	55(9)	1141(12)	51(5)	82(9)	168(15)	−7(11)	−7(15)	21(21)
C(10)	1647(21)	4542(19)	−173(55)	306(32)	190(26)	288(59)	−376(51)	54(150)	−14(125)
C(11)	1203(21)	4637(21)	2088(38)	197(27)	137(26)	615(91)	−139(46)	429(89)	−360(85)
C(12)	2512(17)	4070(21)	1527(50)	95(14)	142(26)	1156(139)	−91(37)	−395(79)	81(122)
C(13)	1709(10)	3971(14)	1106(19)	60(8)	78(13)	197(24)	−16(19)	−34(24)	11(36)
C(14)	1413(10)	2581(13)	1056(15)	59(8)	86(13)	109(17)	−14(17)	−12(20)	3(27)
C(15)	1840(9)	1578(13)	1604(17)	50(7)	74(12)	147(21)	−22(16)	2(21)	19(28)
C(16)	1568(8)	382(14)	1584(16)	32(5)	110(15)	141(20)	6(15)	−24(17)	29(30)
C(17)	1994(9)	−699(13)	2192(18)	46(6)	101(16)	163(23)	14(17)	−37(22)	44(33)
C(18)	2061(12)	−1780(16)	1104(24)	74(10)	106(17)	281(37)	50(23)	−76(34)	−46(46)
C(19)	1546(14)	−1216(24)	3382(26)	84(12)	305(41)	254(39)	95(39)	75(38)	414(71)
C(20)	2808(11)	−362(19)	2614(29)	64(10)	144(24)	343(49)	32(25)	−107(41)	79(60)

of atoms except hydrogen were refined until all the parameter shifts became less than one tenth of the estimated standard deviations. The conventional R was 0.053 for the observed reflections.** At this final stage of refinement the difference Fourier map was flat and unreasonable electron density regions were not found, though no evidence of the hydrogen atoms were obtained.

The atomic scattering factors for carbon and oxygen atoms were taken from Ref. 5, and those for lutetium ion were from the table of Cromer and Waber.[6] The calculations were carried out using UNICS programs[7] at the Computer Center of the University of Tokyo. The refined parameters of atoms, the numbering of which is indicated in Fig. 1, are listed in Table 2.

Results and Discussion

The crystal consists of monomeric Lu(thd)$_3$ units, and in this unit there are two crystallographically independent chelate rings A and B. All the atoms of the forming the ligand A lie in the crystallographic mirror plane except two methyl carbon atoms of C(2) and C(8), which are accompanied with symmetrically related methyl carbon atoms. Projection of the unit along the a-axis (on the mirror plane) was shown in Fig. 1. The other two chelate rings of B are symmetrically related to each other. The angle between the A and B planes is about 117°. The chelate ring is nearly planar as indicated in Table 3 and the folding is about 3.5°. The interatomic distances and angles are listed in Table 4 and the average values are shown in Fig. 1. A comparison of the average values with those for other lanthanide complexes (Table 5) seems to indicate that the structure of the skeleton remains unchanged independent of the atomic number of the central atom and that the structure of the acetylacetonato ring is nearly the same as that reported by Lingafelter and Braun.[8]

TABLE 3. LEAST-SQUARES PLANE BY 8 ATOMS OF THE CHELATE RING B AND THEIR DEVIATIONS FROM THE PLANE (d/Å)

$0.4542x'-0.1571y'-0.8769z'+0.2095=0$
(x', y' and z' are in Ångstrom units)

Lu	0.046	C(15)	0.023
O(3)	0.052	C(16)	0.022
O(4)	−0.057	C(13)	−0.046
C(14)	−0.009	C(17)	0.014
C(10)	0.927	C(18)	1.200
C(11)	−1.424	C(19)	−1.301
C(12)	0.215	C(20)	0.243

The oxygen atoms coordinated to the central lutetium ion form a distorted trigonal prism as shown in Fig. 2, and this coordination polyhedron is the same as that found in Er(thd)$_3$. Metal-oxygen and oxygen-oxygen (bite) distances of β-diketone lanthanide complexes are summarized in Table 6. A constant bite cannot be found. The oxygen-oxygen distances widely range in these complexes probably because of the molecular

** The table of the observed and calculated structure factors ($\times 10$) is kept as Document No. 7610 at the Chemical Society of Japan.

Table 4. Distances (l/Å) and angles (φ/°) with their estimated standard deviations in parentheses

Lu -O(1)	2.174(16)	Lu -O(3)	2.179(12)	O(1)-Lu -O(2)	74.9(0.6)	O(3)-Lu -O(4)	75.0(0.4)
Lu -O(2)	2.177(16)	Lu -O(4)	2.216(12)	Lu -O(1)-C(4)	137.2(1.5)	Lu -O(3)-C(14)	136.7(1.1)
O(1)-C(4)	1.284(28)	O(3)-C(14)	1.251(21)	Lu -O(2)-C(6)	138.2(1.5)	Lu -O(4)-C(16)	135.8(1.1)
O(2)-C(6)	1.270(28)	O(4)-C(16)	1.278(20)	O(1)-C(4)-C(5)	125.8(2.2)	O(3)-C(14)-C(15)	125.8(1.6)
C(4)-C(5)	1.373(34)	C(14)-C(15)	1.417(24)	O(2)-C(6)-C(5)	123.9(2.1)	O(4)-C(16)-C(15)	125.3(1.5)
C(5)-C(6)	1.428(34)	C(15)-C(16)	1.361(23)	C(4)-C(5)-C(6)	120.1(2.2)	C(14)-C(15)-C(16)	120.6(1.6)
C(3)-C(4)	1.549(36)	C(13)-C(14)	1.570(26)	O(1)-C(4)-C(3)	112.2(2.0)	O(3)-C(14)-C(13)	112.9(1.5)
C(6)-C(7)	1.534(35)	C(16)-C(17)	1.503(24)	C(5)-C(4)-C(3)	122.1(2.1)	C(15)-C(14)-C(13)	121.2(1.5)
C(1)-C(3)	1.530(44)	C(10)-C(13)	1.417(58)	C(5)-C(6)-C(7)	122.0(2.1)	C(15)-C(16)-C(17)	122.1(1.5)
C(2)-C(3)	1.426(50)	C(11)-C(13)	1.505(42)	O(2)-C(6)-C(7)	114.0(2.0)	O(4)-C(16)-C(17)	112.5(1.4)
C(7)-C(8)	1.501(36)	C(12)-C(13)	1.487(53)	C(4)-C(3)-C(1)	110.3(2.3)	C(14)-C(13)-C(10)	110.4(2.6)
C(7)-C(9)	1.508(36)	C(17)-C(18)	1.586(30)	C(4)-C(3)-C(2)	108.8(2.6)	C(14)-C(13)-C(11)	105.4(1.9)
		C(17)-C(19)	1.530(31)			C(14)-C(13)-C(12)	113.3(2.3)
		C(17)-C(20)	1.544(34)	C(6)-C(7)-C(8)	108.1(2.0)	C(16)-C(17)-C(18)	108.4(1.5)
O(1)-O(2)	2.644(23)	O(3)-O(4)	2.677(17)	C(6)-C(7)-C(9)	113.8(2.1)	C(16)-C(17)-C(19)	109.1(1.6)
						C(16)-C(17)-C(20)	113.6(1.7)
				C(1)-C(3)-C(2)	107.7(2.7)	C(10)-C(13)-C(11)	109.7(2.9)
				C(8)-C(7)-C(9)	109.2(2.1)	C(10)-C(13)-C(12)	107.3(3.2)
						C(11)-C(13)-C(12)	110.7(2.7)
				O(1)-Lu -O(4)	86.8(0.5)	C(18)-C(17)-C(19)	108.0(1.7)
				O(2)-Lu -O(3)	85.9(0.5)	C(18)-C(17)-C(20)	106.6(1.7)
				O(1)-Lu -O(3)	135.3(0.5)	C(19)-C(17)-C(20)	110.9(1.8)
				O(2)-Lu -O(4)	129.6(0.5)		

Table 5. Average bond lengths and angles of the chelates

	Pr[3]	Er[4]	Lu[a]
C_c–O	1.28 Å	1.27 Å	1.27 Å
C_c–C_s	1.42	1.40	1.39
C_c–C_t	1.56	1.56	1.54
C_t–C_m	1.53	1.52	1.50
$C_cC_sC_c$	124.1°	122.6°	120.3°
$C_cC_tC_m$	109.4	110.0	110.1
$C_sC_cC_t$	121.1	122.3	121.9

The subscripts c, s, t and m mean carbonyl, secondary, tertiary and methyl, respectively. a) Present study.

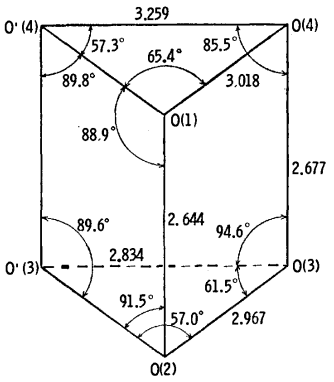

Fig. 2. Distorted trigonal prism formed by oxygen ligand atoms.
Primed and unprimed atoms of the same number are related by the mirror plane.

constraints. The metal-oxygen distances, however, remarkably correlate with the atomic number of the metal. The distances are nearly equal to the sum of the ionic radii[9] of the metal (+3 for six coordination) and oxygen. The deviations are probably dependent on the kind of ligands (acac, thd and fod), and the coordination number of the metal (6 to 9). For example, the M–O lengths in fod complexes are generally smaller than those in thd complexes and the M–O lengths in six coordination complexes are smaller than those for seven coordination complexes (monohydrate or anhydrous dimer).

The four crystallographically independent *t*-butyl groups of the chelate rings A and B have nearly the same orientation with respect to the corresponding chelate rings. It is interesting to note that this orientation is the same as that in $Ni(thd)_2$[10] but is the opposite of $Zn(thd)_2$[11] (180° rotation about the C_3 axis of *t*-butyl group). To check the rotational configuration of the *t*-butyl group, the least-squares calculations were examined using the same structural parameters as listed

Table 6. Average metal-oxygen[a] and oxygen-oxygen (bite) distances for lanthanide chelates[b]

	M–O	O–O		Ref.
La	2.47 Å	2.78 Å	$La(acac)_32(H_2O)$	12)
Pr	2.42	2.78	$Pr_2(fod)_62(H_2O)$	13)
Pr	2.45	2.83	$Pr_2(thd)_6$	3)
Eu	2.35	2.81	$Eu(thd)_3(py)_2$	14)
Dy	2.28	2.74	$Dy(thd)_3H_2O$	15)
Ho	2.29	2.79	$Ho(dpp)_3H_2O$	16)
Er	2.21	2.67	$Er(thd)_3$	4)
Yb	2.23	2.76	$Yb(acac)_3H_2O$	17)
Yb	2.25	2.75	$Yb(acac)_3H_2O$ $0.5(C_6H_6)$	18)
Lu	2.17	2.57	$Lu(fod)_3H_2O$	19)
Lu	2.19	2.66	$Lu(thd)_3$	Present study

a) Oxygen atoms of M–O and O–O means carbonyl oxygen atoms. b) fod: 1,1,1,2,2,3,3-heptafluoro-7,7-dimethyl-4,6-octanedione, dpp:1,3-diphenyl-1,3-propanedione.

in Table 2 except 180° rotation of *t*-butyl groups of the ring A and/or B. In these cases the *R* values did not increase significantly (~0.07), but the C_t–C_m lengths became unreasonably small (1.0—1.3 Å). However, uncertainty concerning the positions of the methyl groups may remain, if the high temperature factors observed for the methyl carbon atoms are interpreted as static disorder rather than as thermal motion.[3)]

All the intermolecular distances are about twice the van der Waals radius for a methyl group or longer, except a distance of 3.65 Å between C(12)(x,y,z) and C(2)$(0.5-x, -y, 0.5+z)$.

We are indebted to Dr. R. E. Sievers for providing the crystals of $Lu(thd)_3$.

References

1) K. J. Eisentraut, R. E. Sievers, *J. Amer. Chem. Soc.*, **87**, 5254 (1965).
2) V. A. Mode and G. S. Smith, *J. Inorg. Nucl. Chem.*, **31**, 1857 (1969).
3) C. S. Erasmus and J. C. A. Boeyens, *Acta Crystallogr.*, **B26**, 1843 (1970).
4) J. P. R. de Villiers and J. C. A. Boeyens, *ibid.*, **B27**, 2335 (1971).
5) "International Tables for X-ray Crystallography," Vol. III, Kynoch Press, Birmingham (1962), p. 202.
6) D. T. Cromer and J. T. Waber, *Acta Crystallogr.*, **18**, 104 (1965).
7) "The Universal Crystallographic Computation Program System," ed. by T. Sakurai, The Crystallographic Society of Japan, Tokyo (1967).
8) E. C. Lingafelter and R. L. Braun, *J. Amer. Chem. Soc.*, **88**, 2951 (1966).
9) L. H. Ahrens, *Geochim. Cosmochim. Acta*, **2**, 155 (1952).
10) F. A. Cotton and J. J. Wise, *Inorg. Chem.*, **5**, 1200 (1966).
11) F. A. Cotton and J. S. Wood, *ibid.*, **3**, 245 (1964).
12) T. Phillips, D. E. Sands, and W. F. Wagner, *ibid.*, **7**, 2295 (1968).
13) J. P. R. de Villiers, and J. C. A. Boeyens, *Acta Crystallogr.*, **B27**, 692 (1971).
14) R. E. Cramer and K. Seff, *ibid.*, **B28**, 3281 (1972).
15) C. S. Erasmus and J. C. A. Boeyens, *J. Cryst. Mol. Struct.*, **1**, 83 (1971).
16) A. Zalkin, D. H. Templeton, and D. G. Karraker, *Inorg. Chem.*, **8**, 2680 (1969).
17) J. A. Cunningham, D. E. Sands, W. F. Wagner, and M. F. Richardson, *ibid.*, **8**, 22 (1969).
18) E. D. Watkins, J. A. Cunningham, T. Phillips, D. E. Sands, and W. F. Wagner, *ibid.*, **8**, 29 (1969).
19) J. C. A. Boeyens and J. P. R. de Villiers, *J. Cryst. Mol. Struct.*, **1**, 297 (1971).

A High-Resolution Vacuum Spectrometer for the Infrared

Tsunetake FUJIYAMA,*1 Jun NAKAGAWA,*2 Isao SUZUKI,*3 Ichiro NAKAGAWA,*4 and Takehiko SHIMANOUCHI

*1 *Department of Chemistry, Faculty of Science, Tokyo Metropolitan University, Setagaya-ku, Tokyo 158*
*2 *Department of Chemistry, Faculty of Science, Hiroshima University, Higashi-Sendamachi, Hiroshima 730*
*3 *Educational Computer Cenret, The University of Tokyo, Bunkyo-ku, Tokyo 113*
*4 *Department of Chemistry, Faculty of Science, Tohoku University, Aoba, Aramaki, Sendai 980*
Department of Chemistry, Faculty of Science, The University of Tokyo, Bunkyo-ku, Tokyo 113

(Received November 20, 1975)

A high-resolution vacuum spectrometer for the near and medium infrared has been designed and built with capability of resolving 0.03 cm^{-1}. The spectrometer consists of the fore-optics with a built-in White cell, a 2.5 m Littrow-McCubbin type monochromator which utilizes a 31.6 lines/mm echelle grating with the ruled area of 102 mm × 206 mm, and an order-sorter which is essentially a prism spectrometer of Wadsworth mount. Details of the design, construction, and performance of the instrument are described.

There are three types of method available for a construction of a high-resolution infrared spectrometer at present. They are dispersion type infrared spectrometer with a large grating, a Michelson type Fourier spectrometer and a spectroscopy using a laser source.

Recently, laser sources have been introduced to infrared spectroscopy and recognized to be very useful sources to obtain magnificient resolution. However, observable spectral regions are confined to the frequency ranges very close to particular laser lines. In order to correlate laser lines to molecular absorption lines, the laser frequencies must be tuned by appropriate methods, *e.g.*, a Zeeman shift technique, or the molecular absorption lines must be moved to the laser frequencies using a Stark effect, a spin-magnetic resonance effect, and so on. These methods can cover very narrow frequency regions, say, ± 1 cm^{-1} from laser frequencies. In the case where a molecule has no dipole moment or electric spin moment, it is impossible to move molecular absorption lines by the above techniques. Although recent developments of dye lasers and semiconductor lasers make it possible to extend the tunable regions considerably, it is not wide enough to use the laser elements in a system for general purposes.

In principle, Fourier spectrometer using Michelson interferometer is the most preferable spectrometer in the respects of a resolution and of observable spectral regions. A resolution which has been actually obtained by the method is about 0.005 cm^{-1} and an observable spectral region 2830—10000 cm^{-1} with a PbS detector.[1] Since a resolution of an interferometer is inversely proportional to a path difference of two interfering beams, one must translate one of the plane mirrors over a long distance with a high accuracy. Suppose the mirror is translated 200 cm, a resolution obtained is 0.005 cm^{-1} so long as an apodization procedure is perfect. During the translation of the mirror, the path differences must be measured with a high accuracy and the direction of the mirror must be kept definitely constant. The other difficulty is a treatment of interferograms. In order to transform an interferogram to a usual spectrum, a computer with large memories must be used, because a number of observed points of a interferogram is numerous.

On the other hand, a large grating high-resolution spectrometer is the most general method and its construction is comparatively easier than the other two methods. Though a resolution obtainable by a large grating spectrometer is much lower than those of the other two methods, this type of spectrometer is more convenient to use than the others in the respect of its construction and its operation. A wide frequency region can be covered by the use of suitable gratings and detectors. Therefore, we decided to construct a large grating spectrometer. Our wishes to study rotational fine structures of vibrational transitions for usual interesting molecules dictated the basic design requirements. Briefly, these were that the instrument should cover the spectral region 600 to 4000 cm^{-1}, that the resolution should be the order of 0.03 cm^{-1} at all wave numbers, that we should be able to handle samples of ordinary interests conveniently, and that the operation and calibration of the instrument should be relatively straightforward. The following items have been mainly taken into account in the design and construction of the present spectrometer, *viz.*,

(1) the resolution is better than 0.04 cm^{-1},

(2) the frequency region covers from 600 to 4000 cm^{-1},

(3) the accuracy of frequency measurement is better than 0.001 cm^{-1},

(4) the accuracy of intensity measurement is better than $\pm 1\%$,

(5) the whole spectrometer system is stable enough to do continuous measurements, and

(6) the lines of atmospheric carbon dioxide and water vapour should be eliminated sufficiently.

A resolution, $\Delta\nu$, of a spectrometer is expressed as

$$\Delta\nu = \frac{d\cdot\cos\theta}{p\cdot n}\cdot\frac{s_1+s_2}{f}\nu^2+\frac{1}{p\cdot 2W\cdot\sin\theta} \qquad (1)$$

where d is a grating constant, p a number of optical paths to the grating, s_1 and s_2 mechanical slit widths of entrance and exit slits, respectively, f a focal length of a collimating mirror, and W a ruled width of the grating. On the other hand, radiant power which arrives at a detector for a particular frequency and a slit width is given by

$$E = \frac{BThAD}{f}\cdot(\Delta\nu)^2 \qquad (2)$$

where B denotes source radiance, T transmittance of a whole spectrometer, h a slit height, A an effective area of a collimating mirror which usually corresponds to a ruled area of a grating, and D angular dispersion of a grating. Equations (1) and (2) show that a resolution is higher as a focal length increases, while energy arrives at a detector decreases as a focal length increases. In order to increase a focal length to realize the required resolution without losing too much energy, an effective area of a collimating mirror, A, and a slit height, h, should be increased at the same time, which leads to the increase of the whole dimensions of a spectrometer.

Most of the large grating spectrometers reported so far have been designed for special uses in the regions above 2800 cm^{-1} and have been used for the observations of the C–H stretching fundamental bands and other summation bands. We referred to the spectrometer constructed in the University of Minnesota,[2] because it satisfies most of the required items for our spectrometer.

Removal of atmospheric carbon dioxide and water vapor was essentially important, because their existence makes it impossible to measure absorption spectra in the regions where these molecules show strong absorption lines, *e.g.*, 2200—2400 cm^{-1} region, 1300—1800 cm^{-1} region, and so on. Therefore a vacuum spectrometer has been considered and the problem of vacuum has been one of the most troublesome problems at all stages in the building.

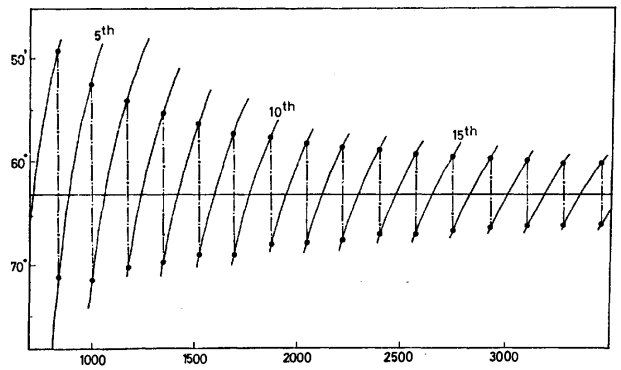

Fig. 1. Relation between angle of incidence on grating and frequency for various grating orders. Actual frequency scanning is performed along the real lines.

A grating is the most important component of an optical system, so we must decide a desirable grating at first to construct the spectrometer. A grating finally chosen is an echelle type plane replica grating made by Bausch and Lomb Co., Ltd. The grating has a ruled area of dimensions 206 mm × 102 mm with 31.6 lines per mm and a blaze angle of 63°26′. This type of grating is superior, in the respect of linear dispersion and brightness, to that of fine echellette, because the latter has a small grating constant, d, and a small blaze angle of about 30°. By the use of the above grating of echelle type, the frequency region of 600—4000 cm^{-1} can be covered by changing a grating order. Figure 1 shows relations between an angle of incidence on the grating and frequencies for various grating orders. The horizontal line corresponds to the blaze angle and, therefore, an actual frequency scanning is performed along the real lines of the figure. It is seen from the figure that the lower a grating order the more angular change is necessary for scanning of the same frequency interval.

Optical Systems

The main part of the monochromator is of Littrow-McCubbin type with an optical system of 2500 mm focal length as shown in Fig. 2. The whole optical system may be classified into three parts, namely, fore-optics with a sampling system, a grating monochromator, and an order sorter.

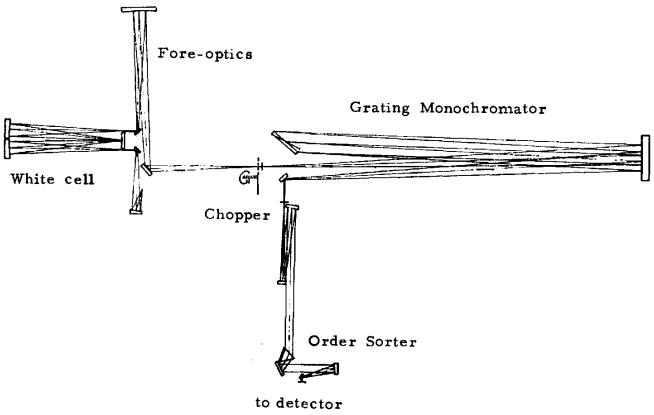

Fig. 2. Optical layout of spectrometer.

Grating Monochromator. A grating monochromator is the most essential of all, because it governs a resolution and an accuracy of frequency measurement. According to Eq. (1), the theoretical resolution for the grating described in the preceding section is 0.027 cm^{-1}

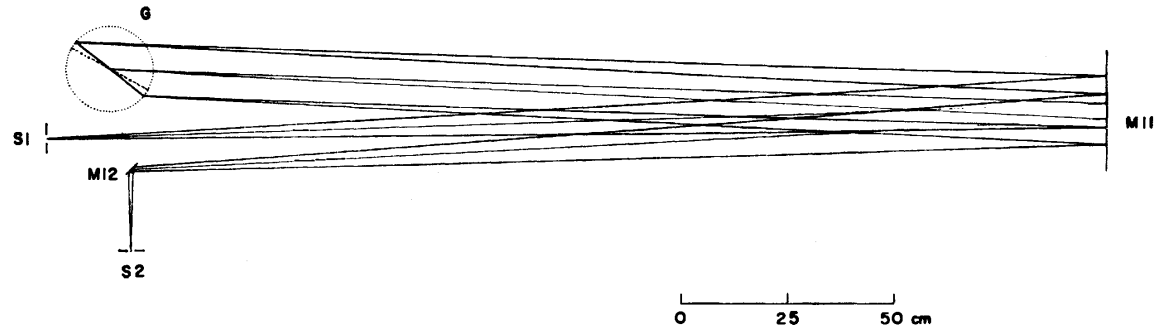

Fig. 3. Optical layout of grating monochromator for single pass operation.

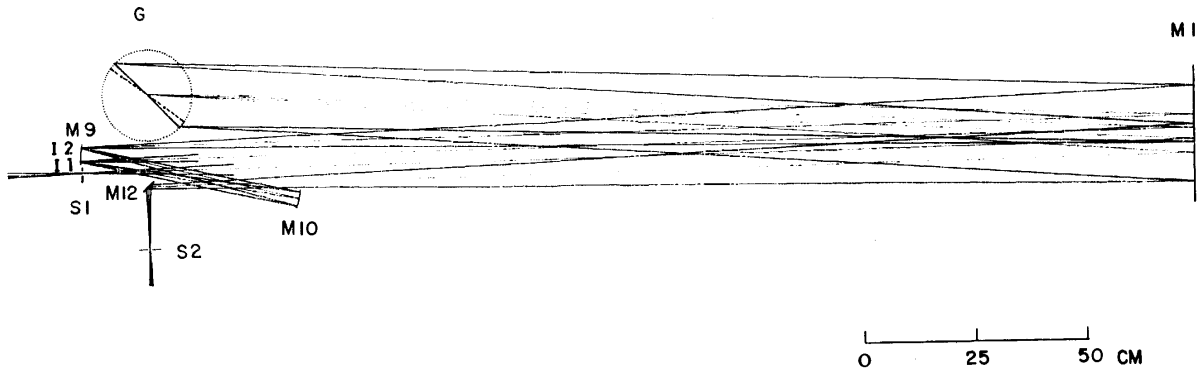

Fig. 4. Optical layout of grating monochromator for double pass operation.

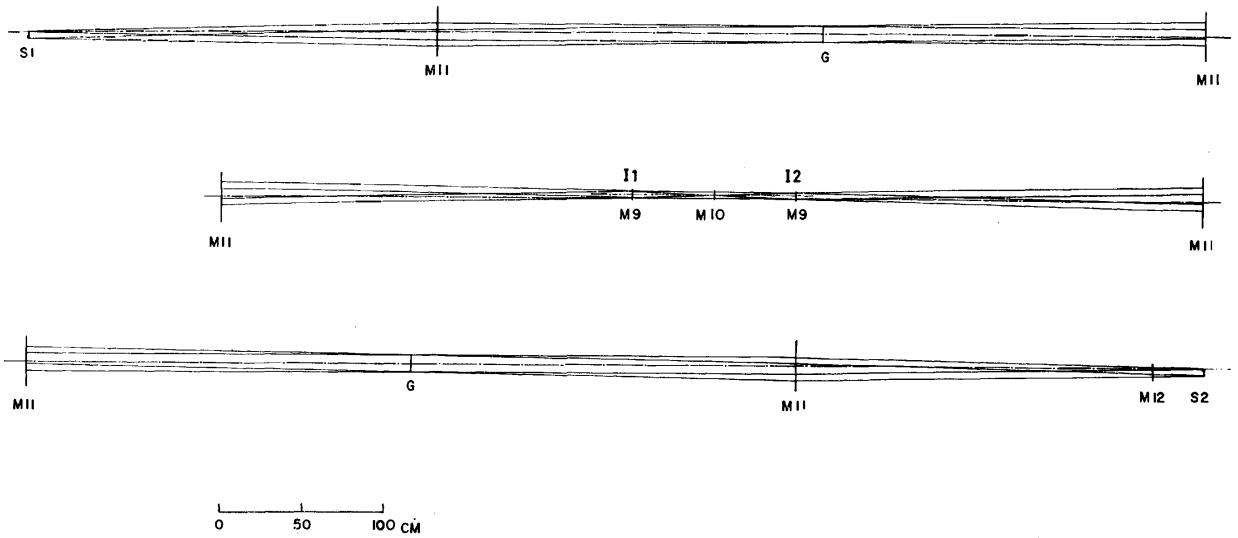

Fig. 5. Vertical tracing of monochromator optics for double pass operation. Single pass component is separated by masking upper halves of entrance and exit slits.

and 0.014 cm^{-1} at the blaze angle with single path ($p=1$) and double path ($p=2$) operations, respectively. The optical layouts are shown in Fig. 3 for a single path operation and in Figs. 4 and 5 for a double path operation. The collimating mirror M11 has a focal length of 2500 mm and a diameter of 300 mm. The f-number of the monochromator is about 25. For the double path operation, the light beam from the entrance slit S1 illuminates the grating G, after being collimated by the mirror M11. The reflected light from G is focused upon the spherical mirror M9 ($R=1000$ mm) at I1. The image at I1 is transformed to I2 by the spherical mirror M10 ($R=500$ mm). After being collimated and reflected by M11 and G once more, the light beam is finally focused upon the exit slit S2 (see Figs. 4 and 5).

Since the light beam is chopped just before the entrance slit S1, the single-pass radiation and the double-pass radiation must be separated optically. If the upper half of the entrance slit is masked, the image at S1 is transferred to the lower half of S2 with respect to the optical axis in the case of double pass operation. For the case of single pass operation, on the other hand, the upper half image at S1 is transferred to the lower half image at S2. Therefore, a double pass component can be definitely separated from a single pass component by masking either upper or lower halves of the entrance and exit slits. The situation is illustrated in Fig. 5, where the dotted line corresponds to the optical axis and the image I1 of double pass operation corresponds to the image S2 of single pass operation. The points at I1 and I2 are conjugated with respect to M10, while the points at S1 and S2 are conjugated with respect to M10. The grating pupil is focused upon the field mirror M10 and, therefore, M10 can be as small as 20×20 mm^2.

The slits S1 and S2 have the heights of 80 mm, but only the lower halves of about 30 mm are used for a double path operation. For the double path operation, both entrance and exit slits[3] have a radius of curvature of 640 mm. For the single path operation, S1 is a straight slit and S2 has a curvature. The curvature of 640 mm is based upon the sagittal curvature calculated at the blaze angle. Although the curvature is slightly different at the other angles, the difference is negligible because relatively small range of angle is used for the actual scanning (see Fig. 1). Moreover, if half of the slit is masked, effect of the different angles becomes much smaller.

The aberration which arises from the use of a spherical mirror for M11 is examined carefully by the beam tracing method using a large electronic computer. A few results are illustrated in Figs. 6a and 6b. In this

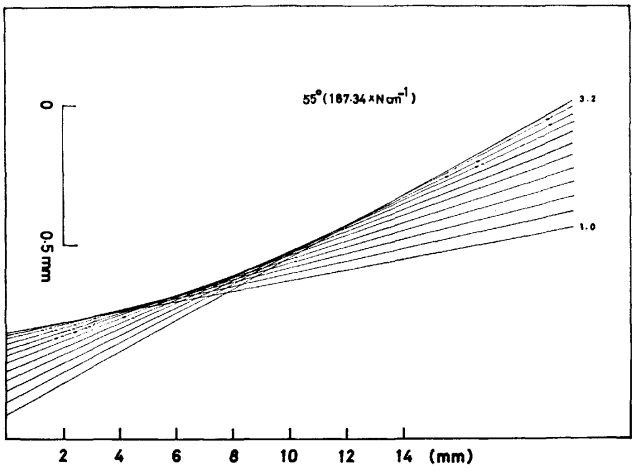

6a. Incident angle to the grating is 55°.

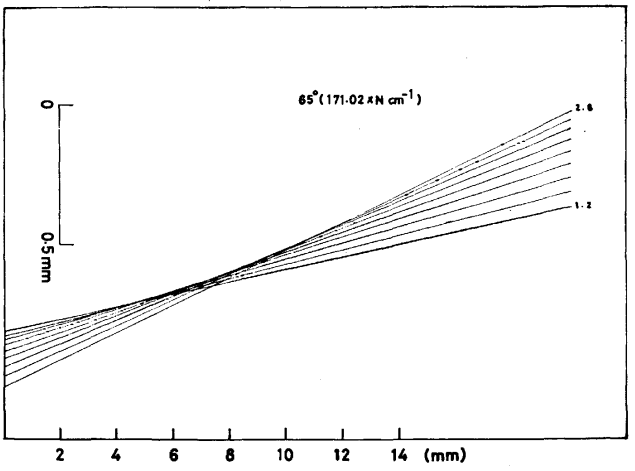

6b. Incident angle to the grating is 65°.

Fig. 6. Results of beam tracing by computer. The entrance slit is put at the origin which is 2500 mm apart from the collimating mirror. Spindle axis parallel to optical axis. Small figures of the right side show angles of the ray at entrance slit. Note that scales of the spindle and cross axes are different.

calculation, the entrance slit is put at the origin which is 2500 mm apart from M11. The diffuseness at the focal point is about 0.06 or 0.04 mm for the incidental angle of 55° or 65°, respectively. Because the mechanical slit width used for the ordinary spectral measurements is 0.4—0.2 mm, the effect of the aberration is negligibly small. Figure 6 shows that the focal point at the exit slit is about 8 mm forward. Therefore, the entrance and exit slits are simultaneously moved about 4 mm forward along the optical axis, because S1 and S2 must be optically conjugated.

Fore-optics and White Cell. For a measurement of high-resolution infrared spectrum, it is necessary to use a long path cell, for the line width due to pressure broadening often exceeds the spectral width of a monochromator even under low sample pressure. Thus, we designed the fore-optics with a long-path cell of White type[4] optically matched to the monochromator.

Figure 7 shows the optical layout of the fore-optics with a White cell. The light from the source S0 is focused by an ellipsoidal mirror M1 at the point very

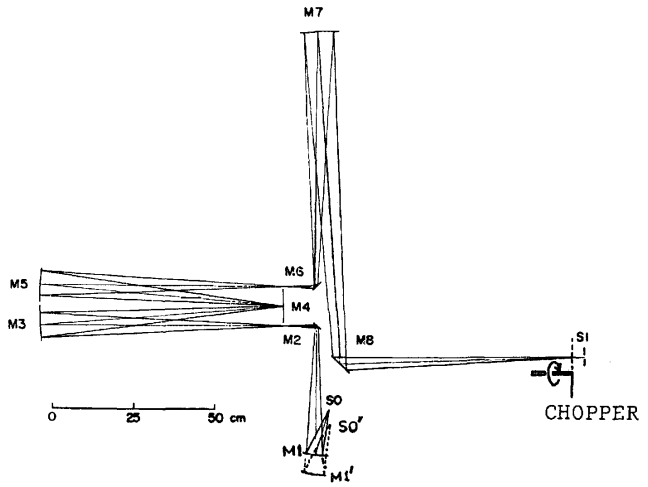

Fig. 7. Optical layout of fore-optics with White cell.

close to the KBr window of the White cell. After being reflected multiple times in the White cell between the spherical mirrors M3, M4, and M5, the light beams are focused on the entrance slit S1. The *f*-number is matched to 25 which is the same with that of the grating monochromator. As the *f*-number at the source S0 is about 3.75, the source image is magnified by about 6.6 at S1. The ellipsoidal mirror M1 and the spherical mirror M7 are used for the *f*-number matching.

The White type long-path cell has three spherical mirrors with a focal length of 757.9 mm and has two KBr windows with diameters of 70 mm. This cell is optically matched with the spectrometer. The light beam is guided into the cell by the plane mirror M2. The White cell has a physical length of about 75 cm between the mirrors M3 and M4, or M5 and M4, giving path length up to 30 m. The sampling system of a vacuum line is always combined with the White cell, which guarantees the vacuum of about 10^{-5} Torr when there is no sample in the system.

The White cell can be removed and mirrors M2 and M6 are used to bring the radiation out to an external sampling device and return it to the vacuum instrument. Mirrors M2 and M6 can be removed, giving a sample space for a short cell use. In this case, it is necessary to translate a mirror M1 and a source S0 to the positions M1' and S0'. Both components are mounted on a single plate which slides along the rail parallel to the optical axis.

The source S0 is a Nernst glower purchased from Perkin-Elmer with an active length of 20 mm. The source is covered with a brass mantle. The electric circuit involves a 60 W balast lamp. The conditions of the source operation are 0.3—0.45 A and 80—100 V. The stability of the light source is quite satisfactory in the vacuum, because there is no convection of air in the vacuum.

Order Sorter. The optical layout of the order sorter is shown in Fig. 8. The order sorter is essentially a prism spectrometer of Wadsworth mount and separates the order of a grating. The prism P and the Wadsworth mirror M15 are mounted on a single plate and is rotated so as to keep the angle of minimum deviation.

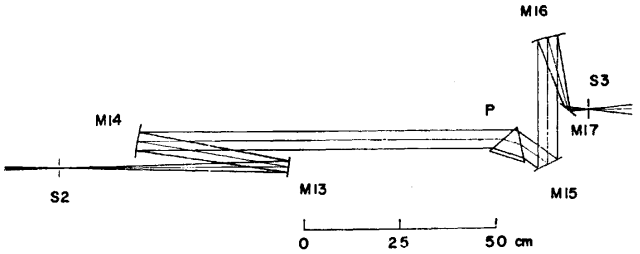

Fig. 8. Optical layout of order sorter.

Three different prisms of KBr, NaCl, and CaF_2 are used for the different frequency ranges. They are 60° prisms with 70 mm in height and with 100 mm base length.

The light beam from the exit slit S2 of the grating monochromator is collimated by the parabolic mirror M14 which has a focal length of 1000 mm. After being separated into grating orders by the prism P, the light beam is focused on the exit slit S3 of the order sorter by the parabolic mirror M16 of a focal length of 250 mm. Therefore, the image at S3 is one fourth of the image at S2. A straight slit is used for S3, because the prism P is oriented so that the curved image at S2 is changed into the straight image at S3. The position of P is at an exit pupil of the grating. The mirror M16 is positioned to give another exit pupil of the grating at about 300 mm behind the exit slit S3.

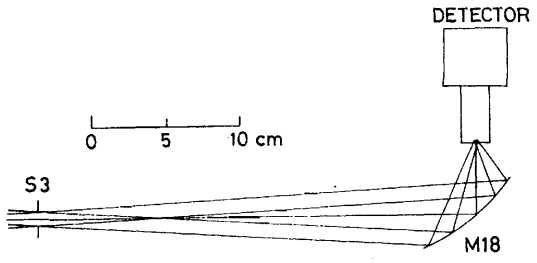

Fig. 9. Optical layout between exit slit and detector (vertical).

In order to collect the radiation to the detector, we used an ellipsoidal mirror M18 by which the light beam is vertically reflected and focused upon the detector element (see Fig. 9). The exit slit S2 is finally imaged upon the detector with a magnification of about one twenty-fourth. The detector is positioned out of the vacuum tank and the distance from the exit window of

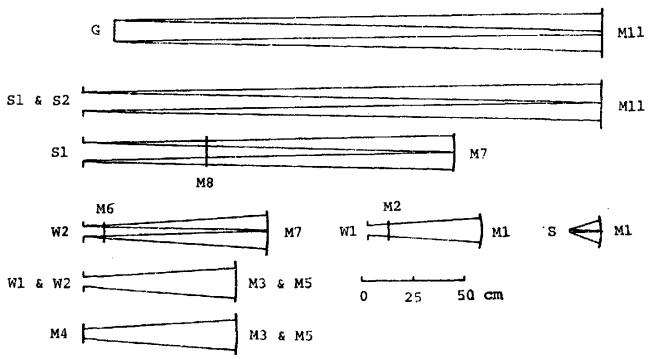

Fig. 10. Vertical tracing for grating monochromator (for single pass) and fore-optics.

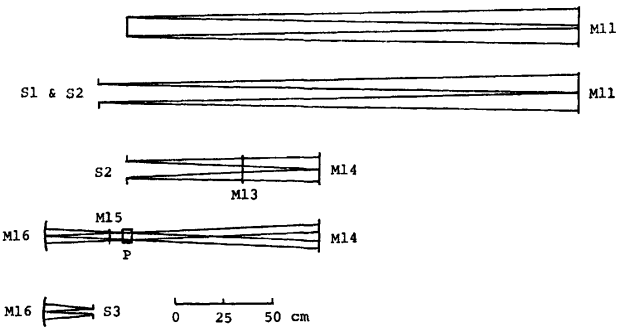

Fig. 11. Vertical tracing for grating monochromator and order sorter.

TABLE 1. DETAILS OF MIRRORS

Name	Type	Dimension (mm)	Remarks
M1	ellipsoidal	150×78	a=325.0, b=269.5, α=22°
M2, M6	plane	80×50	
M3, M5	spherical	160×125	R=757.9
M4	spherical	60×110	R=757.9
M7	spherical	230 ϕ	R=1207.43
M8	plane	150×90	
M9	spherical	55×55	R=1000
M10	spherical	40×40	R=500
M11	spherical	300 ϕ	R=5000
M12	plane	80×25	
M13	plane	180×50	
M14	parabolic	150×80	f=1000, α=6°
M15	plane	100×90	
M16	parabolic	100×70	f=250, α=15°
M17	plane	80×35	
M18	ellipsoidal	80×70	a=175.0, b=86.6, α=19°

R: Radius of spherical mirror (mm), f: focal length of parabolic mirror (mm), a: a half of longer axis of ellipsoidal mirror (mm), b: a half of shorter axis of ellipsoidal mirror (mm), α: off-axis angle.

the vacuum spectrometer to the mirror M18 is about 15 cm. One can use this space to put a short path gas cell for the calibration purpose or the usual spectral measurement.

Mirrors. All the mirrors used are made on BK7 glasses and the thickness is greater than one fifth a diameter. Aliminum surface is coated with silicon monoxide. An accuracy of a surface is better than $\lambda/2$ (λ=546 nm). The dimensions of the mirrors are determined by drawing the plane figures (see Figs. 2, 3, 4, 7, and 8) and the vertical figures (see Figs. 5, 9, 10, and 11) of the optical layout. In Table 1, the mirrors used are summarized with the types and dimensions.

Detection System

The detection system adopted in this spectrometer is a phase sensitive detection system. The schematic diagram of the whole system is shown in Fig. 12. A mechanical chopper of a rotating circle is positioned just in front of the entrance slit S1 and chops the signal and reference signal beams simultaneously. The rotating circle has six wings made of a pasteboard and is jointed to the direct current vacuum motor[6] which rotates

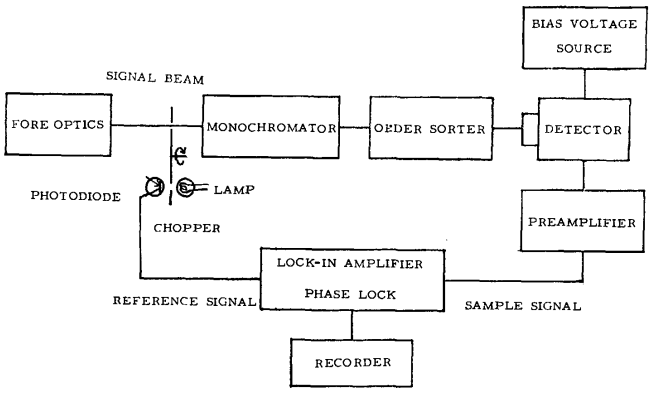

Fig. 12. Detection system (schematic).

about 100 Hz in vacuum. Therefore, the light beams arrive at the detector is a 600 Hz alternating pulse signal. After being amplified by a preamplifier,[7] the signal from the detector is put into the lock-in amplifer[8] and compared with the reference signal. The 6.3 V midget lamp is used as the reference light source and the light energy is transformed into electric current by the phototransistor OS14. The final output from the lock-in amplifier is direct current and is sent to recorder.[9]

Detector and Preamplifier. As an actual resolution of a spectrometer is governed by a signal to noise ratio, detectivity of a detector is the most important problem for the construction of a spectrometer. In our spectrometer, an InSb semiconductor detector is used for the region around 2000 cm^{-1}, a Ge: Au detector below 1800 cm^{-1} region, and a PbS detector above 3000 cm^{-1} region. The detectivity of InSb detector is higher than that of Ge: Au detector about one order of magnitude at 2300 cm^{-1} region. The ν_2 band of carbon dioxide is measured by use of these two different types of detectors under the same instrumental conditions. The S/N ratio of the spectra for InSb detector is about ten times better than that for Ge: Au detector. Although at the longer wavelength region, there are a few detectors which are superior in detectivity to Ge: Au detector, they must be cooled by liquid helium. At the present situation of our laboratory, it is rather inconvenient and troublesome to use liquid helium. Thus we decided to use a Ge: Au detector for the longer wavelength region.

The preamplifiers suitably designed to the individual detectors are made by ourselves. The amplification factors are limited to 20—50 dB.

The InSb detector was purchased from JEOL, Ltd.,[10] with the sensitive area of 1×1 mm^2. The preamplifier and the bias voltage supplier were constructed according to the data sheet, the amplification degree being about 30 dB.

The Ge: Au detector was purchased from Barnes Co.,[11] with the sensitive area of 2×2 mm^2. The magnitudes of bias voltage and load registor are adjusted to the recommended values from the detector manufacturer. The preamplifier was made by the use of an operational amplifier of Burr-Brown model 3503A.[12] The amplification degree is about 50 dB.

The PbS detector was purchased from Infrared Industries[13] with the sensitive area of 2×2 mm^2.

Vacuum System and Room

The elimination of atmospheric carbon dioxide and water vapor is essentially important, because they have strong absorption bands in the infrared regions. Since the optical pathlength of the entire system is about 30 m long, it is desired to build a spectrometer in vacuum.

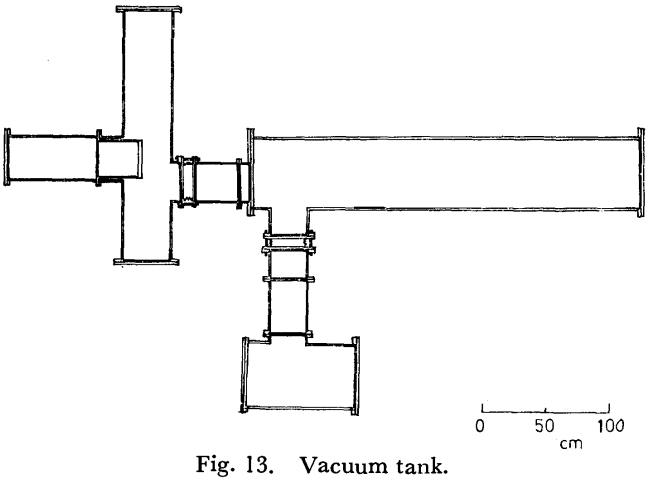

Fig. 13. Vacuum tank.

Figure. 13 shows a plane tracing of a vacuum tank system. The tank system is conveniently separated into three parts in accordance with the optical system, *i.e.*, a main tank, a fore-optics tank, and an order sorter tank. These three parts are connected with each other by bellows flanges which can be collapsed and removed without disturbing the optical system, since there are no internal optical benches inside of the bellows sections. This system is beneficial to avoid the spread of distortions of the individual tank due to temperature changes and to evacuation. All the flanges and end covers are sealed with O-rings. Removing these covers and bellows sections, we can set and adjust all the necessary optical elements effectively.

A rotary pump[15] is used to evacuate the vacuum tank with evacuation speeds of 3000 l/min. As the total volume of the tank is about 1000 l, we can reach pressures of about 10^{-3} torr within a few minutes. Using an oil diffusion pump,[16] we have actually reached pressures of 10^{-4} Torr, although it is not always necessary to operate the spectrometer under such low pressure. In order to avoid the mechanical vibration transferred from the main rotary pump, we can use a supplementary pump of 450 l/min evacuation speed[17] after the spectrometer is evacuated by the main pump.

The detector system is placed out of the vacuum tank and, therefore, nitrogen gas is flashed to remove atmospheric carbon dioxide and water vapour. Actually the detector system is confined in an aluminum box. The disturbing absorption lines of these molecules were reduced to about one twentieth by flashing dry nitrogen gas inside of the box.

In order to avoid the effect of mechanical vibrations of room floors, the spectrometer base is fixed rather loosely to the floor by the use of sand and mortar as illustrated in Fig. 14. In addition, optical benches

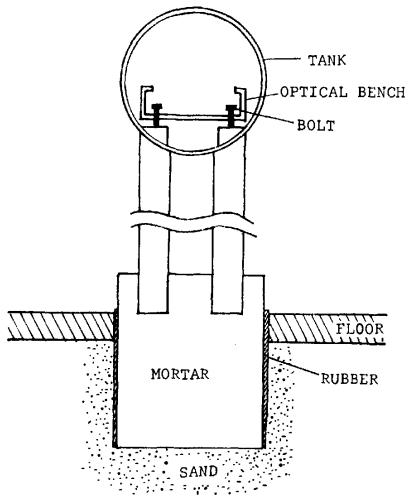

Fig. 14. Schematic figure for spectrometer base. Optical bench is mounted on vacuum tank kinematically.

are kinematically mounted so that the distortion and vibration of the tanks would not directly disturb the optical set-up.

The room is airconditioned,[18] which keeps the temperature and humidity of the room within 23±0.5 °C and 45±5%. The variation of the temperature will cause the thermal expansions of optical benches and vacuum tanks, which will disturb the optical alignment of the spectrometer.

Mechanical System[19]

Driving Mechanism of Grating. The most principal part of all the mechanisms is a driving mechanism of a grating, because it governs an accuracy of frequency measurements. Figure 15 shows the plane figure for the grating drive mechanism. Figure 16 is the cross section of the rotatory shaft of the grating drive. The mechanism is arranged to give both fine and coarse drives. The former is used for the precise measurements under optimum resolution, while the latter is used for the survey works and for setting the instrument to a suitable wavelength range. The coarse driving mechanism is extremely convenient and indispensable for actual measurements.

As shown in Figs. 15 and 16, the rotatory shaft is composed of three coaxial cylinders made of stainless steel. The outer cylinder is fixed to the optical bench. The intermediate cylinder is equipped with a 400 mm tangent arm and rotates inside the outer cylinder. The weight of this cylinder is supported by a ball bearing which is set upon the outer cylinder. Since the cylinder faces are carefully polished, the rotation is very smooth. The tangent arm is pushed by a stainless steel rod which is connected to a 50 mm micrometer head.[20] The micrometer is driven through a gear box external to the vacuum tank. The rotatory rod which connects the micrometer and the gear box is sealed by O-rings as shown in Fig. 17. The gear box is designed to give six scanning speeds from about $(5n/2)$ to $(5n/64)$ cm^{-1}/h, where n is the grating order.

The inner cylinder, upon which the grating is mounted, is rotated by a worm and wheel of about 160 mm diameter. This part is placed upon the tangent arm and is designed for coarse driving purpose. The inner cylinder is driven by a second gear box which is set out of the vacuum tank. Scanning speed is changeable from $20n$ to $640n$ cm^{-1}/h, where n is the grating order. The diameters of these three cylinders are 120, 80, and 40 mm.

In order to determine the frequencies with the

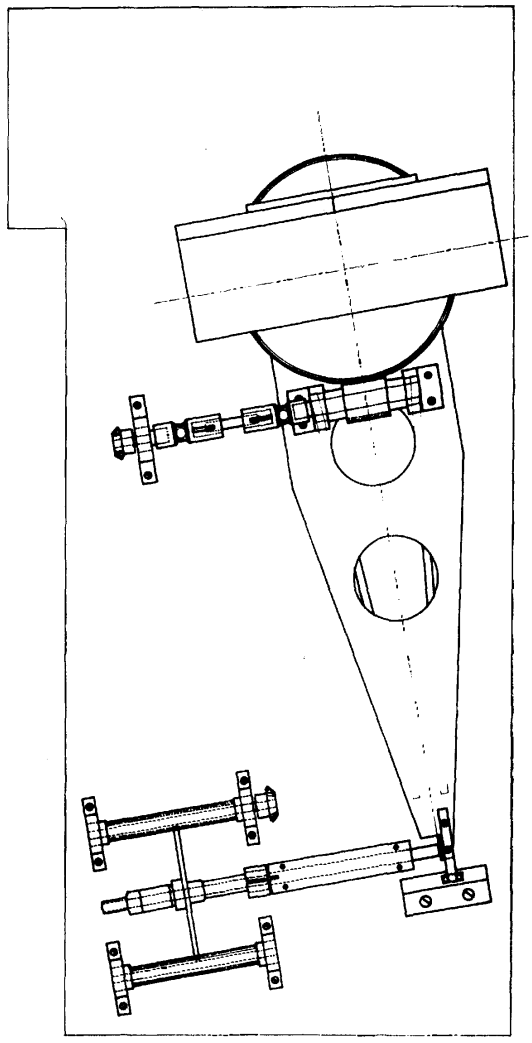

Fig. 15. Plane figure of grating drive mechanism.

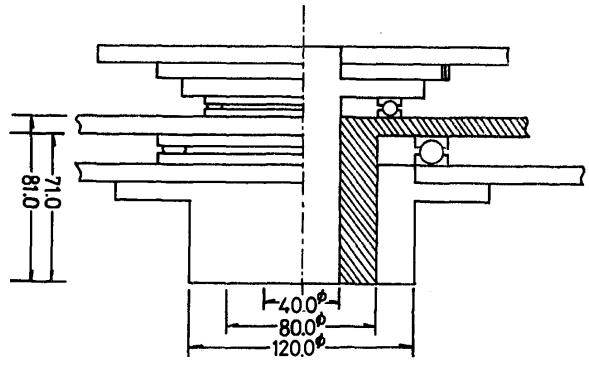

Fig. 16. Cross section of rotating shaft of grating drive mechanism.

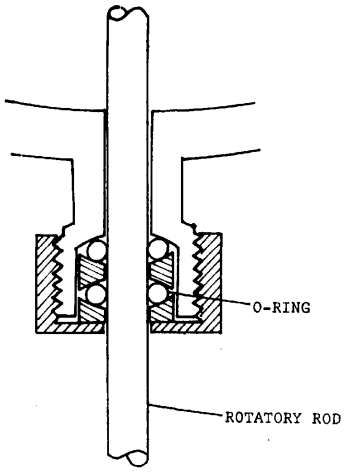

Fig. 17. Sealing of rotatory rod.

accuracy of 0.002 cm^{-1}, the grating must be rotated with the accuracy of 1 second of arc. As mentioned above, the fine drive mechanism consists of a 400 mm tangent arm and a 50 mm micrometer head. The required accuracy can be satisfied, because the accuracy of the micrometer drive is ascertained to be better than 0.01 mm.

Driving Mechanism of Prism. The prism drive mechanism is essentially the same as that of grating drive. A bearing of 30 mm diameter is connected to the nut which, in turn, slides along the screw. We manually drive the screw from outside the vacuum tank. No provision is made for coupling the prism rotation with that of the grating mechanically, because the setting of prism rotation must be changed only about once an hour under normal running conditions.

Mirror Holders. Modified Perkin-Elmer mount has been applied for the design of all the mirror holders, except for the spherical mirrors, M7 and M11. The holders for M7 and M11 can slide along a guiding rod by a screw and a nut which is fixed to the mirror mount (see Fig. 28). We can accurately adjust the position of the mirror by driving the screw.

Performance

As mentioned earlier, a particular order of an echelle type grating has a narrow frequency region. Using a few orders, however, we can cover the wider frequency region (see Fig. 1). Firstly we have to know the relation between the grating order and the rotating angle of a prism. The grating is fixed at a particular position and the prism is rotated slowly by hand. As shown in Fig. 18, we can observe the successive intensity maxima along the angle of prism rotation. The grating order can be determined from the cut off frequency of the detector and the atmospheric CO_2 absorption. The 4.5 μ absorption band of carbon dioxide is observed in the 13-th order.

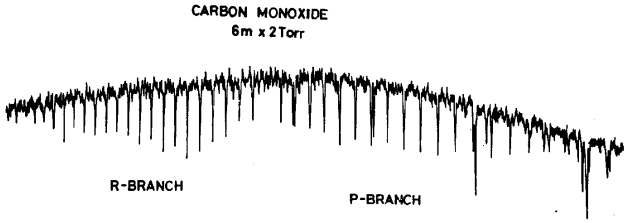

Fig. 19. Rapidly scanned spectra for CO.

Next procedure is to determine the relation between the coarse drive counter and the frequency. The carbon monoxide has absorption lines in fairly wide region with regular spacing. Fixing the prism angle at 12-th order of the grating, we scan the coarse driving mechanism without moving the fine drive. We obtain the CO spectrum as shown in Fig. 19. As the frequencies of CO lines are accurately known,[21] the calibration diagram for the coarse drive can be obtained.

It is necessary to know the relation between the mechanical slit width and the counter number of slit drive mechanism. The entrance slit S1 is fixed about 4 mm wide, and the width of exit slit S2 is changed from 2.00 mm to zero. Since the energy which reaches at the detector is proportional to the width of S2, we can calibrate the mechanical slit width against the counter number of the slit S2. The same method is applied to the entrance slit S1.

The resolving power of the spectrometer is checked by observing the ν_3 band of NNO, $2\nu_3$ band of CH_3F, 10 μm CO_2 laser lines and so on. The line width of CO_2 laser line is about 0.002 cm^{-1} for the multimode operation, which corresponds to a Doppler breadth. Since the diffraction limit of the grating of this spectrometer is about 0.027 cm^{-1} for single pass operation, the line width of the CO_2 laser is negligibly small. In Fig. 20 shows the observed spectrum of CO_2 laser

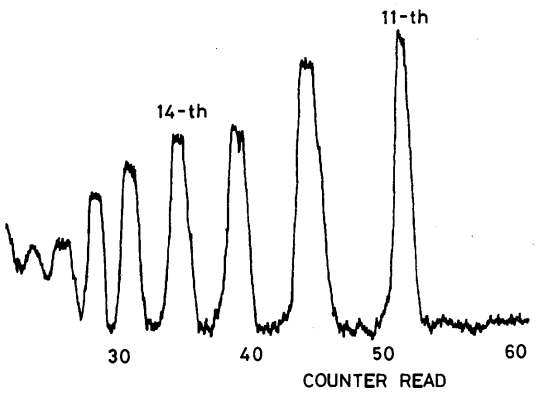

Fig. 18. Grating orders and prism counter.

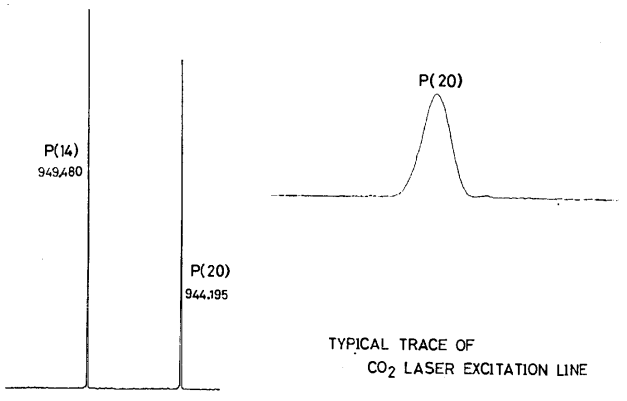

Fig. 20. Typical trace of CO_2 laser line.

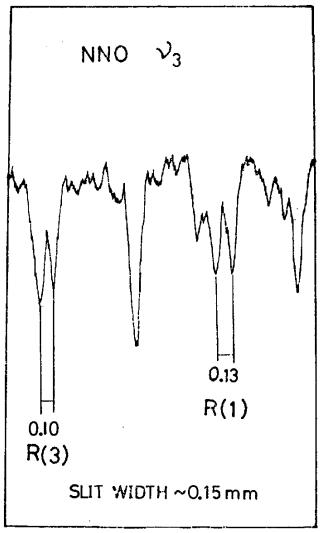

Fig. 21. Resolution check by ν_3 band of NNO. Single pass operation, InSb detector.

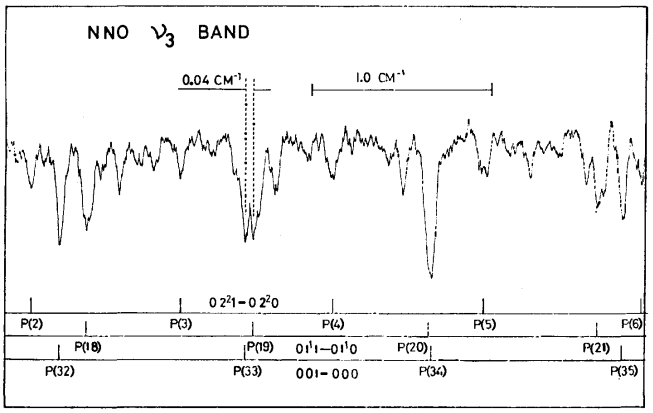

Fig. 22. Resolution check by ν_3 band of NNO. Double pass operation, InSb detector.

line. The half width of the observed line is about 0.03 cm^{-1}, which corresponds to the resolution limit for the single pass operation.

For usual measurements, the resolution is limited by a signal to noise ratio which is governed by the detectivity of a detector. As the ν_3 band of NNO has a number of hot band series, the absorption lines have various separation. Figure 28 shows the observed spectra of the ν_3 band of NNO with a single pass operation using an InSb detector. The resolution is better than 0.07 cm^{-1}, although this region is far from the blaze angle of the grating. In Fig. 22, the spectra of ν_3 band of NNO observed with a double pass operation is shown with their assignments. These lines are seen to be measured with good S/N ratio and the resolution is ascertained to be better than 0.04 cm^{-1}.

The ^QQ-branch of $2\nu_3$ band of CH_3F is completely resolved into its J-components and the individual J-component is resolved into a lot of K-components. From the spacing of the resolved lines, the resolution is ascertained to be better than 0.04 cm^{-1}. The detailed analysis of the band has been given in elsewhere.[22]

An accuracy of a frequency measurement is estimated from the standard deviation of the CO calibration lines fitted with the quartic equation. The standard deviation of the actually observed CO lines is about 0.005 cm^{-1}. The value of 0.005 is obtained from a single measurement and the error arises mainly from the reading ambiguity of the line positions.

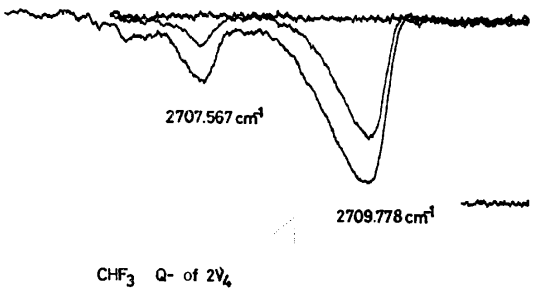

Fig. 23. Q branch of $2\nu_4$ and related hot bands of CHF_3.

The intensity accuracy is checked by observing relative intensities of the Q branch of the $2\nu_3$ band of CHF_3, the observed result of which is shown in Fig. 23. The three Q branches are assigned to one main band and two hot bands. As the intensity of the Q branch is proportional to the Boltzmann factor, we can ascertain the accuracy of the intensity measurements by comparing the theoretical and observed intensity ratios of the three Q branches. The result indicates that the accuracy along an intensity axis is better than $\pm 3\%$ of the full-scale disregarding to the effect of the S/N ratio.

Photographs of the Spectrometer

Photographs of the spectrometer are summarized in Figs. 24—29. In Fig. 24 a part of the monochromator tank is seen at the right hand side and the order sorter tank at the lower left. These two tanks are combined with bellows flanges. The fore-optics tank is seen at the middle of the picture. The vacuum lines which is seen at the upper side is the sampling system. Figure 25 shows the fore-optics with a long path cell of White type. Behind the fore-optics tank, the flange of the monochromator is seen. The U-pipe leads to the vacuum pump. Figure 26 shows the top view of the grating monochromator. The grating and the coarse driving mechanism are clearly seen. At the upper left we see the entrance slit S1 and double pass mirror M9.

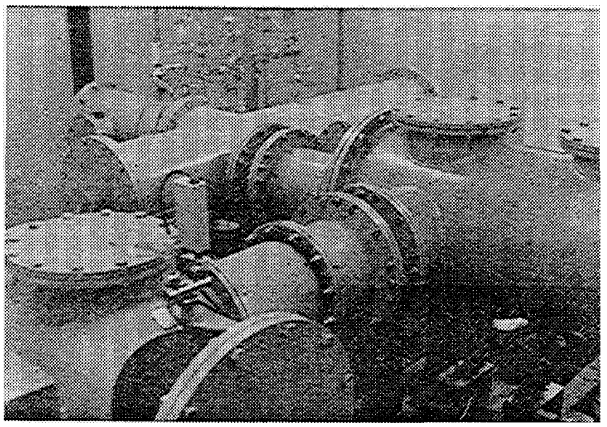

Fig. 24. Vacuum tank (whole view).

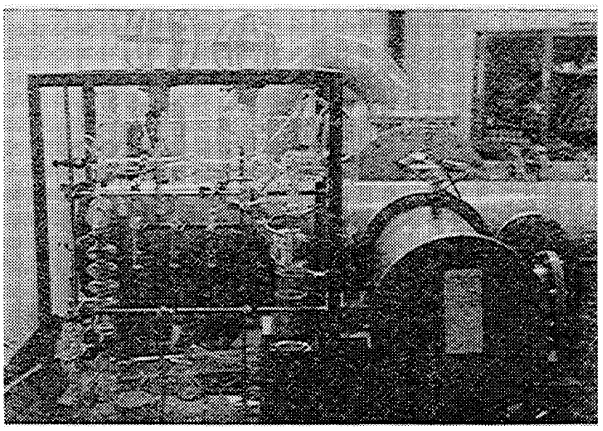

Fig. 25. Sampling system.

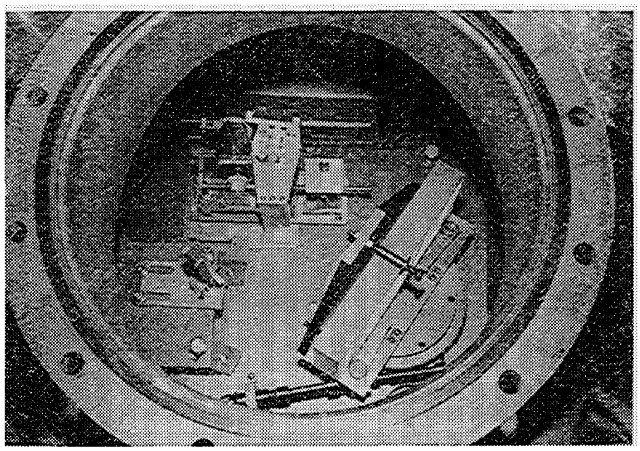

Fig. 26. Top view of grating monochromator.

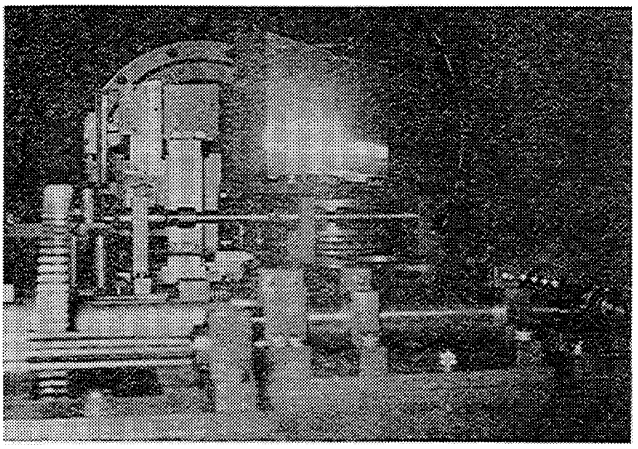

Fig. 27. Side view of grating monochromator.

The coarse driving mechanism consists of a worm and wheel. The side view of this part seen from the direction of the collimator mirror is shown in Fig. 27. The grating strongly reflects the flash-lamp light. Behind the grating, the entrance slit and double pass mirror M9 are seen. The fine drive mechanism which consists of the micrometer and the tangent arm is seen before the grating. In Fig. 28, we can see the optical bench and the mirror holder inside the main tank. Note that the optical bench is supported by bolts and is not fixed to the tank directly. The order sorter part is

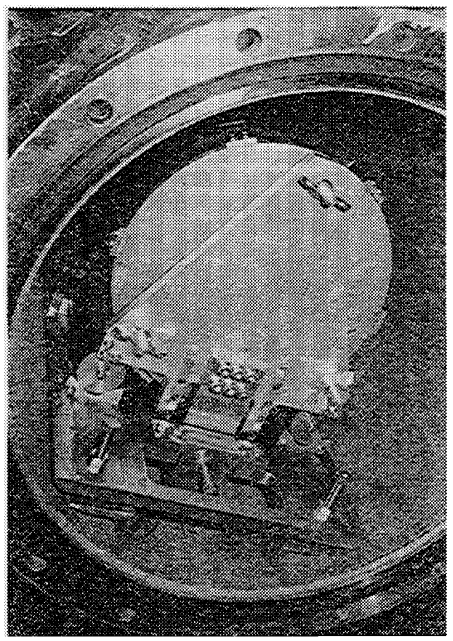

Fig. 28. Collimating mirror.

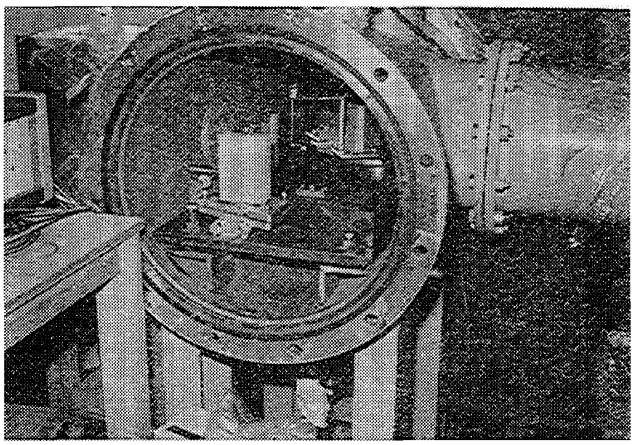

Fig. 29. Order sorter.

seen in Fig. 29. The prism and M15 are placed on the same rotatory holder.

References

1) J. Connes, and P. Connes, *J. Opt. Soc. Am.*, **56**, 896 (1966); P. Jacquinot, *Appl. Opt.*, **8**, 497 (1969); J. Connes, H. Delonis, P. Connes, G. Guelachuili, J. P. Maillard, and G. Michel, *Nouv. Rev. Optique Appliquee*, **1**, 3 (1970).

2) J. Overend, A. C. Gilby, J. W. Russel, C. W. Brown, J. Beutel, C. W. Bjork, and H. G. Paulat, *Appl. Opt.*, **6**, 475 (1967); see also T. K. McCubbin, Jr., R. P. Grosso, and J. D. Mangus, *Appl. Opt.*, **1**, 431 (1962); T. K. McCubbin, Jr., J. A. Lowenthal, and H. R. Gordon, *Appl. Opt.*, **4**, 711 (1965).

3) J. U. White, *J. Opt. Soc. Am.*, **32**, 285 (1942).

4) The slit jaws were made of flat stainless steel by ourselves. After roughly making the shape of slit jaws, we accomplished the jaw to a final shape by an oilstone and oil.

5) Mizojiri Kogaku Kogyosho, Tokyo, Japan.

6) Olympus Precision Co., Ltd., Tokyo, Japan, Model CL-4B, 24V, 2.2W.

7) We made a preamplifier to match the detector.

8) NF Circuit Design Block Co., Ltd., Tokyo, Japan, Model LI-572B.
9) Hitachi Co., Ltd., Tokyo, Japan, Model 1001.
10) JEOL, Ltd., Tokyo, Japan, Model 101S and 501S.
11) Barns Engineering Company, Connecticut, USA, Model A-200 series.
12) Burr-Brown Research Corporation, Arizona, USA, Model 3503A.
13) Infrared Industries, Inc., Mass., USA, Type B3 with a liquid nitrogen 4-hour hold Dewar.
14) Sanwa Ulvac Co., Ltd., Tokyo, Japan.
15) Nihon Shinku Co., Ltd., Tokyo, Japan.
16) Nihon Shinku Co., Ltd., Tokyo, Japan.
17) Nihon Shinku Co., Ltd., Tokyo, Japan.
18) Ohnishi Netsugaku Co., Ltd., Tokyo, Japan.
19) The design of all the mechanisms is performed by ourselves. The construction is done by Shotoku Mfg. Co., Ltd., Kawasaki, Japan.
20) Mitsutoyo Mfg. Co., Ltd., Tokyo, Japan, Model 151-256, MHHI-50.
21) K. N. Rao, C. J. Humphreys, and D. H. Rank, "Wavelength Standard in the Infrared," Academic Press, New York (1966).
22) J. Nakagawa, I. Suzuki, T. Shimanouchi, and T. Fujiyama, This Bulletin **46**, 3399 (1973).

Effect of Temperature on the Infrared Spectroscopic Parameters of Hydrogen Bonds between Some Phenols and Nitriles

Inam JAWED*

Department of Physical Chemistry, Peshawar University, Peshawar, Pakistan

(Received March 18, 1975)

The effect of temperature on the infrared spectroscopic parameters of hydrogen bonds between a number of phenol-nitrile systems has been studied. The infrared frequency shift always decreases with increase in temperature. The variation of half width of the hydrogen bonded band, however, is not regular and is within the error of measurement. The intensity of the bonded band shows a general decrease with rise in temperature. All these variations are interpreted as being indicative of the weakening of the hydrogen bond with increase in temperature.

The effect of temperature on the infrared spectroscopic parameters of hydrogen bonds has long been recognized.[1] The present study was undertaken to investigate this effect for some hydrogen bonded systems of phenols and nitriles in the temperature range 20—60 °C and is concerned with stretching vibration of the hydroxyl group, ν(OH), involved in the hydrogen bond. The phenols and nitriles were chosen so as to give a rather wide range of acidities and basicities respectively as shown by the pK_a values and Hammett substituent constants of phenols and Taft substituent factors of nitriles (Table 1). Taft factor, being a measure of the inductive effect of the substituent group, can be conveniently considered to be directly related to the basicity of the nitrile group. Para-substituted phenols were preferred to avoid any complications arising from intramolecular associations and steric effects.

Experimental

The spectra were recorded on a Perkin-Elmer Model 125 infrared spectrophotometer using an expanded scale (1 cm=5 wave nos.). Tetrachloroethylene was used as the solvent which was dried carefully and fractionally distilled. The phenols and nitriles were also purified by the usual methods of drying, recrystallization and fractional distillation. Quartz cells, 20 mm long, were used.

The use of rather large cells enabled us to use very dilute solutions which is very desirable, but, on the other hand, required a special heating arrangement. Hence a special heating jacket was designed for the cells. It consisted of two solid brass pieces carefully cut from inside so that when the two pieces were brought into contact with each other by means of a screw, they formed a round hole in the centre of which the cell fitted almost exactly. The brass pieces were fitted, through an asbestos insulator, onto a brass backing plate. Copper tubes were soldered round the brass pieces through which water could be circulated continuously from a thermostat maintaining the cells at any desired temperature. Both the sample and reference cells were heated or cooled simultaneously to avoid any base line error due to differences in the background spectra which appear when only the sample cell is heated or cooled. The temperature of the solution in the cell was measured by means of an iron-constantan thermocouple.

* Present Address: Department of Inorganic Materials, Tokyo Institute of Technology, O-okayama, Meguro-ku, Tokyo, Japan,

Results and Discussion

In fact, both the free and bonded ν(OH) stretching frequencies have been found to be temperature dependent and shift towards higher values with increase in temperature. However, the frequency of the bonded band changes much more markedly than that of the free band with the result that the frequency shift, $\Delta\nu$, decreases with rise in temperature. This variation of $\Delta\nu$ with temperature is generally linear (Fig. 1). Tables 2 and 3 give some of the results from our present study.

Finch and Lippincott,[2] on the basis of a potential function for hydrogen bond suggested by Lippincott and Schroeder,[3] have predicted the temperature coefficient of the bonded frequency, $d\nu_b/dt$, to fall within the range 0.20—0.64. However, vapour phase measurements of the bonded ν(OH) have shown that the bonded frequency remains virtually unchanged over a wide range of temperature.[4,5] Jones and Watkinson,[6] from their studies of hydrogen bonds between substituted phenols and heptyl halides in solvent tetrachloroethylene, conclude that, since both the free as well as bonded frequencies behave similarly with regard to temperature effect, the 'free' ν(OH)

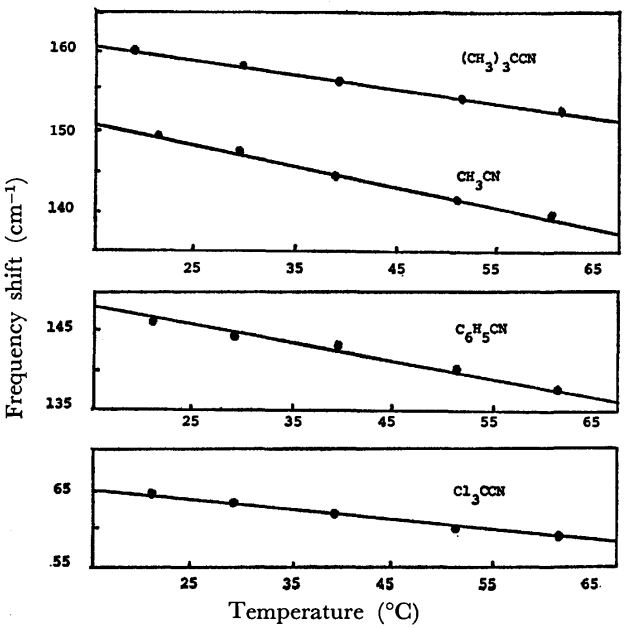

Fig. 1. Frequency shift *vs.* temperature.
Proton donor: *p*-methoxyphenol.

TABLE 1. SUBSTITUENT CONSTANTS OF PHENOLS AND NITRILES

Phenol	*p*-Methoxy phenol	Phenol	*p*-Chloro-phenol	*p*-Cyano-phenol	*p*-Nitro-phenol
pK_a	10.20	9.99	9.42	7.95	7.15
Hammett σ	−0.268	0.000	0.227	1.000	1.270
Nitrile	**Trichloro-acetonitrile**	**Benzonitrile**		**Acetonitrile**	***t*-Butyl cyanide**
Taft $\sigma^{a)}$	+2.65	0.60		0.00	−0.30

a) Refs. 15—17.

TABLE 2. CHANGE OF FREQUENCY SHIFT WITH TEMPERATURE

Proton donor	Proton Acceptor	Temp (°C)	$\nu(OH)_{free}$ (cm^{-1})	$\nu(OH)_{bonded}$ (cm^{-1})	Frequency shift (cm^{-1})
p-Chloro-phenol	Cl_3CCN	21.0	3604.0	3530.0	74.0
		59.0	3607.5	3540.0	67.5
	C_6H_5CN	21.0	3605.5	3437.0	168.5
		61.0	3608.5	3449.0	159.5
	CH_3CN	20.0	3605.5	3436.0	169.5
		60.0	3609.5	3450.0	159.5
	$(CH_3)_3CCN$	20.0	3605.5	3422.0	183.5
		60.0	3609.0	3432.0	177.0
p-Nitro-phenol	Cl_3CCN	21.0	3589.5	3490.5	99.0
		61.0	3593.5	3501.5	92.0
	C_6H_5CN	21.0	3589.5	3380.5	209.0
		60.0	3594.5	3393.0	201.5
	CH_3CN	21.0	3589.5	3378.0	211.5
		60.0	3594.5	3394.5	200.0
	$(CH_3)_3CCN$	21.0	3589.5	3360.5	229.0
		61.0	3593.5	3371.0	222.5

Accuracy of measurement of the values of frequencies: $\pm 0.5\ cm^{-1}$. All measurements were made using quartz cells, 20 mm long. Solvent: Tetrachloroethylene.

TABLE 3. TEMPERATURE COEFFICIENTS FOR THE FREE AND BONDED (OH) FREQUENCIES AND FOR THE FREQUENCY SHIFTS

Phenol	Nitrile	$\frac{d\nu(OH)_{free}}{dt}$	$\frac{d\nu(OH)_{bonded}}{dt}$	$\frac{d(\Delta\nu)}{dt}$
p-Methoxy-phenol	Cl_3CCN	0.081	0.23	−0.15
	C_6H_5CN	0.070	0.27	−0.21
	CH_3CN	0.069	0.27	−0.27
	$(CH_3)_3CCN$	0.071	0.25	−0.18
Phenol	Cl_3CCN	0.085	0.25	−0.16
	C_6H_5CN	0.071	0.22	−0.17
	CH_3CN	0.071	0.36	−0.29
	$(CH_3)_3CCN$	0.071	0.23	−0.17
p-Chloro-phenol	Cl_3CCN	0.091	0.25	−0.16
	C_6H_5CN	0.083	0.29	−0.21
	CH_3CN	0.088	0.35	−0.27
	$(CH_3)_3CCN$	0.089	0.25	−0.17
p-Cyano-phenol	Cl_3CCN	0.110	0.27	−0.15
	C_6H_5CN	0.096	0.28	−0.20
	CH_3CN	0.110	0.29	−0.20
	$(CH_3)_3CCN$	0.110	0.29	−0.23
p-Nitro-phenol	Cl_3CCN	0.120	0.25	−0.15
	C_6H_5CN	0.110	0.30	−0.21
	CH_3CN	0.120	0.39	−0.27
	$(CH_3)_3CCN$	0.130	0.29	−0.15

Solvent: Tetrachloroethylene. (Quartz cells, 20 mm long).

TABLE 4. EFFECT OF TEMPERATURE ON HALF WIDTH OF THE BONDED BAND

Phenol	Nitrile	Half width of the bonded band (in cm^{-1}) At 21 °C	At 60 °C	$\frac{d(\Delta\nu_{1/2})_b}{dt}$
p-Methoxyphenol	Cl_3CCN	49.0	47.0	−0.10
	C_6H_5CN	79.0	75.0	−0.10
	CH_3CN	85.0	79.0	−0.18
	$(CH_3)_3CCN$	85.0	88.0	+0.10
Phenol	Cl_3CCN	52.0	49.0	−0.08
	C_6H_5CN	82.0	84.0	+0.06
	CH_3CN	86.5	87.5	+0.03
	$(CH_3)_3CCN$	83.0	89.0	+0.17
p-Chlorophenol	Cl_3CCN	50.5	45.0	−0.14
	C_6H_5CN	80.0	89.0	+0.25
	CH_3CN	87.0	91.0	+0.12
	$(CH_3)_3CCN$	82.5	88.0	+0.14
p-Cyanophenol	Cl_3CCN	60.5	65.0	+0.12
	C_6H_5CN	84.0	91.0	+0.18
	CH_3CN	86.5	90.5	+0.11
	$(CH_3)_3CCN$	90.0	97.0	+0.19
p-Nitrophenol	Cl_3CCN	66.5	63.0	−0.11
	C_6H_5CN	85.0	95.0	+0.26
	CH_3CN	84.5	89.5	+0.14
	$(CH_3)_3CCN$	91.0	99.0	+0.20

Solvent: Tetrachloroethylene (Quartz cells, 20 mm long).

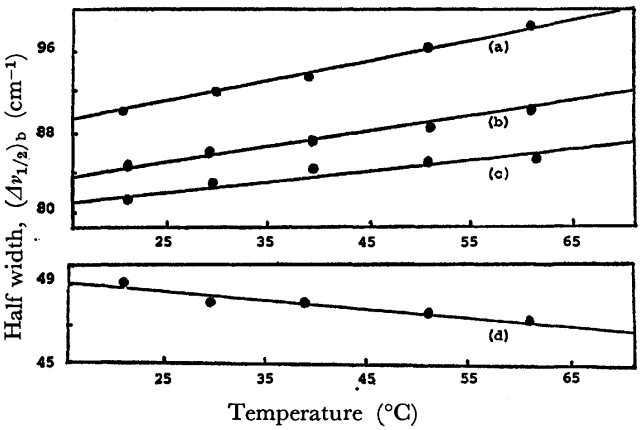

Fig. 2. Half width of the bonded band *vs.* temperature. (a): *p*-Cyanophenol + $(CH_3)_3CCN$, (b): *p*-nitrophenol + CH_3CN, (c): phenol + C_6H_5CN, (d): *p*-methoxyphenol + Cl_3CCN.

band arises from phenol molecules bonded to solvent tetrachloroethylene. The difference in behaviour of the two frequencies is only in magnitude but there is no qualitative difference as both result from the same type of interaction, namely, hydrogen bonding. In other words, two types of hydrogen bonded species, phenol–solvent and phenol–heptyl halides, are present in the solution both of which are weakened with a rise in temperature. Present results for the temperature coefficients of the bonded frequency, $d\nu_b/dt$, are seen to fall within the range predicted by Finch and Lippincott.[2] However, an examination of our data for temperature coefficients of free ν(OH) band, $d\nu(OH)_f/dt$, for a series of phenols reveals that this coefficient for *p*-nitrophenol and *p*-cyanophenol is somewhat larger than that for *p*-methoxyphenol or phenol. This could mean that the more acidic the phenol, the stronger is its interaction with the solvent, thus supporting the conclusions of Jones and Watkinson.[6]

The effect of temperature on the half width of the bonded band is not straightforward. (Fig. 2) Some systems show an increase in the half width, $(\Delta\nu_{1/2})_b$, with temperature, others a decrease while some hardly any change. In any case, the variation is only slightly larger than the experimental error. Similar results have been reported by other workers.[7–9] A theoretical treatment by Buckingham[10] shows a linear relationship between $(\Delta\nu_{1/2})_b$ and $\sqrt{T}$. This is, however, not verified by our results. Moreover, Buckingham's treatment does not explain the change of sign of the slopes as our results show. Table 4 summarises our results for the effect of temperature on $(\Delta\nu_{1/2})_b$.

It is not quite clear whether absence of any definite trend is due to the differences in the proton acceptor concentrations employed. The half-width seems to have a positive coefficient for the complexes of *t*-butyl cyanide where much less cyanide concentration was required for measurements, while the complexes of trichloroacetonitrile have generally a negative temperature coefficient where much higher concentration was necessary.

The product $(\varepsilon_{max}\cdot\Delta\nu_{1/2})_b$ has been taken, for convenience, as a measure of intensity of the bonded band. This quantity was first used by Gramsted and Askenes[11] as a relative measure of intensity. Table 5 shows our results. There is a general decrease in the intensity parameter $(\varepsilon\cdot\Delta\nu_{1/2})_b$ with temperature (Fig. 3). ε_b is found to decrease with increase in temperature, while $(\Delta\nu_{1/2})_b$ shows no definite pattern. However, the product decreases to some extent with increased temperature. This observation is consistent with the previous findings that for absorption bands in liquids

TABLE 5. EFFECT OF TEMPERATURE ON THE INTENSITY PARAMETERS OF THE HYDROGEN BONDED BAND

Phenol	Nitrile	Absorption coefficient, (ε_{max}) At 21 °C (l mol^{-1} cm^{-1})	Absorption coefficient, (ε_{max}) At 60 °C (l mol^{-1} cm^{-1})	Band intensity $(\varepsilon \cdot \Delta\nu_{1/2})_b \times 10^{-4}$ (25 °C)	$\frac{d(\varepsilon \cdot \Delta\nu_{1/2})_b}{dt}$
	Cl_3CCN	163.0	138.0	0.78	−0.38
p-Methoxy-	C_6H_5CN	242.0	220.0	1.88	−0.60
phenol	CH_3CN	240.0	228.0	2.03	−0.67
	$(CH_3)_3CCN$	231.0	220.0	1.98	−0.33
	Cl_3CCN	143.0	123.0	0.74	−0.36
	C_6H_5CN	248.0	227.0	2.04	−0.37
Phenol	CH_3CN	175.0	133.0	1.46	−0.83
	$(CH_3)_3CCN$	199.0	174.0	1.63	−0.18
	Cl_3CCN	128.0	102.0	0.62	−0.45
p-Chloro-	C_6H_5CN	277.0	239.0	2.21	−0.19
phenol	CH_3CN	274.0	263.0	2.42	−0.15
	$(CH_3)_3CCN$	250.0	222.0	2.07	−0.40
	Cl_3CCN	166.0	155.0	1.00	—
p-Cyano-	C_6H_5CN	358.0	305.0	2.99	−0.54
phenol	CH_3CN	251.0	223.0	2.16	−0.47
	$(CH_3)_3CCN$	294.0	244.0	2.63	−0.66
	Cl_3CCN	231.0	218.0	1.50	−0.45
p-Nitro-	C_6H_5CN	365.0	338.0	3.13	−0.17
phenol	CH_3CN	289.0	270.0	2.44	−0.27
	$(CH_3)_3CCN$	317.0	297.0	2.87	−0.17

Solvent: Tetrachloroethylene. (All measurements were made using quartz cells, 20 mm long.)

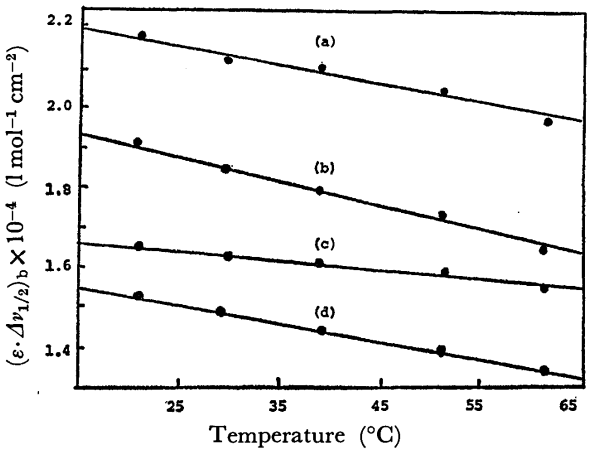

Fig. 3. Intensity of the bonded band *vs.* temperature. (a): *p*-Cyanophenol + CH_3CN, (b): *p*-methoxyphenol + C_6H_5CN, (c): phenol + $(CH_3)_3CCN$, (d): *p*-nitrophenol + Cl_3CCN.

and solutions, ε_{max} decreases more rapidly than the integrated intensity with increase in temperature. Similar results have been reported by other workers also.[1,12,13]

If the intensity of the bonded band is related to the strength of the hydrogen bond, then the observed decrease with temperature is indicative of the weakening of the bond. Satisfactory explanations of the decrease of intensity with temperature have been suggested by various authors. Finch and Lippincot's explanation,[2] based on the charge transfer model of the hydrogen bond suggested by Tsubomura[14] seems most satisfactory.

The author is grateful to Professor Sir Harold Thompson for helpful advice and to Dr. R. J. L. Popplewell for constructing the cell heating jacket. An award of a research fellowship by the Ministry of Education, Government of Pakistan, is also gratefully acknowledged.

References

1) G. C. Pimentel and A. L. McClellan, "The Hydrogen Bond," W. H. Freeman & Co., San Francisco (1960).
2) J. N. Finch and E. R. Lippincott, *J. Phys. Chem.*, **61**, 894 (1957).
3) E. R. Lippincott and R. Schroeder, *J. Chem. Phys.*, **23**, 1131 (1955).
4) E. Fishman and T. L. Chen, *Spectrochim. Acta*, **25A**, 1231 (1969).
5) E. Osawa and Z. Yoshida, *ibid.*, **23A**, 2029 (1967).
6) D. A. K. Jones and G. G. Watkinson, *J. Chem. Soc.*, **1964**, 2366.
7) A. W. Baker, H. O. Kerlinger, and A. T. Shulgin, *Spectrochim. Acta*, **20A**, 1467, 1477 (1964).
8) M. S. C. Lopes, Ph. D. Thesis, Oxford (1967).
9) M. van Thiel, E. D. Becker, and G. C. Pimentel, *J. Chem. Phys.*, **27**, 95 (1957).
10) A. D. Buckingham, *Proc. Roy. Soc., Ser A*, **255**, 32 (1960).
11) A. G. Askenes and T. Gramstad, *Acta Chem. Scand.*, **14**, 1485 (1960).
12) E. D. Becker, *Spectrochim. Acta*, **17A**, 436 (1961).
13) M. S. C. Lopes and H. W. Thompson, *Spectrochim. Acta*, **24A**, 1367 (1968).
14) H. Tsubomura, *J. Chem. Phys.*, **24**, 927 (1956).
15) R. W. Taft, "Steric Effects in Organic Chemistry", ed. by M. S. Newman, John Wiley and Sons, New York (1956), Chap. 13.
16) "Dissociation Constants of Organic Acids," (I.U.P.-A.C.), Butterworths, London (1961).
17) H. H. Jaffé, *Chem. Rev.*, **53**, 191 (1953).

Dielectric Relaxation in *p*-Substituted Thiophenols in the Liquid State

Subir K. Roy, Kamalendu Sengupta, and S. B. Roy

Optics Department, Indian Association for the Cultivation of Science, Calcutta-32, India

(Received April 21, 1975)

The dielectric absorption in 4-methylthiophenol and 4-chlorothiophenol in the liquid state has been studied in 0.8, 1.25, 1.62 and 3.49 cm microwave regions. Molecular and intramolecular relaxation times, their relative weight factors and the heats of activation have been determined. The results have been discussed and compared with other related molecules.

Intramolecular rotation of various polar groups in aromatic molecules[1-3] in dilute solutions and in pure liquids has been studied extensively. Such studies of intramolecular rotation of SH group in organic molecules are rather few. Fong and Smyth[4] reported the intramolecular rotation of SH group in naphthalenethiol in dilute benzene solution. Recently, Hasan *et al.*,[5] from studies of dielectric relaxation in benzenethiol and benzylthiol in the liquid state reported that intramolecular rotation of the SH group was the main relaxation process in both the thiophenols. From a comparison of the values of SH group relaxation time τ_2 and its weight factor C_2 in the thiophenols, with the corresponding τ_2 and C_2 values for OH group rotation in phenols and substituted phenols reported by Aihara and Davies,[6] Hasan *et al.*[5] concluded that the intermolecular hydrogen bonding S–H···S are negligible in the thiophenols even in the liquid state.

The object of the present investigations was to extend similar studies in the case of *p*-substituted thiophenols in the liquid state and compare the results with the corresponding *p*-substituted phenols. The results obtained in the case of 4-methylthiophenol and 4-chlorothiophenol are presented and discussed in this paper.

Experimental

The apparatus for the measurements of dielectric permittivity ε', dielectric loss ε'' in the region 0.8, 1.25, 1.62 and 3.49 cm microwaves were described earlier.[7] The static dielectric constant ε_0 was measured at 1 MHz, the refractive index n_D was determined with an Abbe refractometer, the viscosity η was measured with an Ostwald viscometer and the density d with a pycnometer. The temperature in each experiment was kept constant within ± 1 °C by means of a thermostat. The estimated errors in ε' and ε'' are about 2% and 4% respectively.

Results

The experimental values of ε' and ε'' at different microwave frequencies together with the values of ε_0 at different temperatures are given in Table 1. These data were then fitted in Cole-Cole arc plots (Fig. 1). The high frequency dielectric constant $\varepsilon\infty$ and the distribution parameter α were obtained as usual from the arc plots. The values of $\varepsilon\infty$ in each case was found much higher than that of n_D^2. The values of the distribution parameter were appreciably high at all temperatures, indicating the presence of more than one relaxation process. This was confirmed by the non linear plots of ε' vs $\varepsilon''\omega$. The dielectric data were

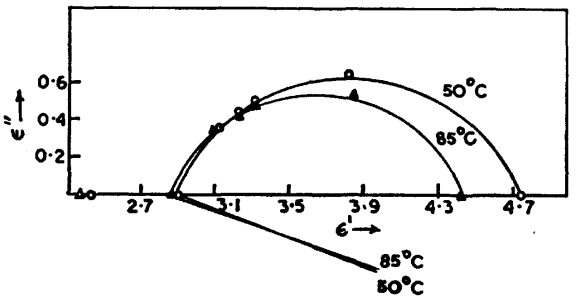

Fig. 1. Cole-Cole arc plot of 4-thiocresol.

then analysed in terms of two relaxation processes following the equations of Bergmann *et al.*[8] and as simplified by Bhattacharyya *et al.*[9] for straightforward calculations.

Bergmann's equations are

$$a = \frac{\varepsilon' - \varepsilon_\infty}{\varepsilon_0 - \varepsilon_\infty} = \frac{C_1}{1+\omega^2\tau_1^2} + \frac{(1-C_1)}{1+\omega^2\tau_2^2} \tag{1}$$

and

$$b = \frac{\varepsilon''}{\varepsilon_0 - \varepsilon_\infty} = \frac{C_1\omega\tau_1}{1+\omega^2\tau_1^2} + \frac{(1-C_1)\omega\tau_2}{1+\omega^2\tau_2^2} \tag{2}$$

The simplified equation[9] is

$$\frac{1-a}{b\omega} = \tau_1 + \tau_2 - \frac{a\omega}{b}\tau_1\tau_2 \tag{3}$$

which can be written in the form

$$\sum_{i=1}^{n} Sx_i - Py_i - 1 = 0 \tag{4}$$

where

$$S = \tau_1 + \tau_2,\ P = \tau_1\tau_2,\ x = \frac{b\omega}{1-a} \text{ and } y = \frac{a\omega^2}{1-a}$$

Eq. (4) is a linear equation and can be solved by the method of least squares. From the principle of least square, it can be easily shown from Eq. (4) that

$$S = \frac{\sum_{i=1}^{n} y_i \sum_{i=1}^{n} x_i y_i - \sum_{i=1}^{n} x_i \sum_{i=1}^{n} y_i^2}{\left(\sum_{i=1}^{n} x_i y_i\right)^2 - \sum_{i=1}^{n} x_i^2 \sum_{i=1}^{n} y_i^2} \tag{5}$$

$$P = \frac{\sum_{i=1}^{n} y_i \sum_{i=1}^{n} x_i^2 - \sum_{i=1}^{n} x_i \sum_{i=1}^{n} x_i y_i}{\left(\sum_{i=1}^{n} x_i y_i\right)^2 - \sum_{i=1}^{n} x_i^2 \sum_{i=1}^{n} y_i^2}. \tag{6}$$

Solving Eqs. (5) and (6), τ_1 and τ_2 can be calculated. The value of C_1 is then determined from the equation given below, obtained from Eqs. (1) and (2) by applying the least square principle.

Table 1. Observed and calculated values of dielectric permittivity ε' and dielectric loss ε''

T °C	Freq.=8.60 GHz				Freq.=18.50 GHz				Freq.=24.03 GHz				Freq.=35.13 GHz				1MHz
	ε'_{obsd}	ε'_{calcd}	ε''_{obsd}	ε''_{calcd}	ε'_{obsd}	ε'_{calcd}	ε''_{obsd}	ε''_{calcd}	ε'_{obsd}	ε'_{calcd}	ε''_{obsd}	ε''_{calcd}	ε'_{obsd}	ε'_{calcd}	ε''_{obsd}	ε''_{calcd}	ε_0
4-Methylthiophenol																	
50	3.83	3.68	0.66	0.70	3.32	3.35	0.50	0.51	3.24	3.28	0.44	0.45	3.13	3.20	0.36	0.39	4.74
70	3.85	3.68	0.59	0.66	3.31	3.34	0.48	0.50	3.23	3.27	0.42	0.43	3.12	3.19	0.34	0.36	4.56
85	3.85	3.70	0.54	0.63	3.32	3.37	0.47	0.47	3.24	3.25	0.41	0.41	3.09	3.19	0.32	0.33	4.43
4-Chlorothiophenol																	
65	3.43	3.40	0.20	0.22	3.27	3.27	0.21	0.21	3.22	3.23	0.20	0.20	3.16	3.18	0.18	0.18	3.59
85	3.40	3.39	0.18	0.18	3.26	3.27	0.20	0.20	3.23	3.23	0.19	0.19	3.18	3.18	0.18	0.18	3.52

Table 2. Values of α, ε_∞, τ_1, τ_2, $\Delta H\tau_1$, $\Delta H\eta$ and μ

T °C	α	n_D^2	ε_∞	$\tau_1\times10^{12}$ s	$\tau_2\times10^{12}$ s	C_1	$\Delta H\tau_1$ kcal/mol	$\Delta H\eta$ kcal/mol	μ_D
4-methylthiophenol									
50	0.23	2.43	2.91	29.7	3.1	0.79	1.31	2.03	1.4
70	0.22	2.40	2.92	25.8	2.6	0.79			
85	0.22	2.38	2.92	22.2	1.9	0.82			
4-Chlorothiophenol									
65	0.21	2.50	3.00	17.7	2.8	0.63	2.00	—	—
85	0.19	2.47	2.99	14.2	2.4	0.62			

$$C_1 = \frac{\sum_{i=1}^{n} a_i f_i + \sum_{i=1}^{n} b_i g_i - \sum_{i=1}^{n} f_i f_i' - \sum_{i=1}^{n} g_i g_i'}{\sum_{i=1}^{n} f_i^2 + \sum_{i=1}^{n} g_i^2} \qquad (7)$$

where

$$f_i = (f_1 - f'),\ f_1 = \frac{1}{1+\omega^2\tau_1^2},\ f' = \frac{1}{1+\omega^2\tau_2^2}$$

$$g_i = (g_1 - g'),\ g_1 = \frac{\omega\tau_1}{1+\omega^2\tau_1^2},\ g' = \frac{\omega\tau_2}{1+\omega^2\tau_2^2}.$$

The value of ε_∞ as obtained from Cole-Cole plot may not coincide with the actual value in Eqs. (1) and (2), but it will lie between the n_D^2-value and ε'-value obtained at the highest microwave frequency used. So, to start with, any value for ε_∞ within the above limit is assumed and τ_1, τ_2 and C_1 values are determined. With these values of τ_1, τ_2 and C_1, the values of ε' and ε'' are calculated from Eqs. (1) and (2). The value of ε_∞ is then varied and the process is repeated till the mean square deviation A, from the relation

$$A = \sum (\varepsilon''_{obsd} - \varepsilon''_{calcd})^2 + \left\{\frac{\varepsilon'_{obsd} - \varepsilon'_{calcd}}{n}\right\}^2,$$

is found to be minimum. The 'n' is a scaling factor to reduce the error in ε', to the same magnitude of the error in ε''. A value of $n=3$ is used in the present case. The values of ε_∞, τ_1, τ_2 and C_1 are given in Table 2. All the calculations were carried on the IBM Computer 1130. The calculated values of ε' and ε'' are included in Table 1.

The activation energies for dielectric relaxation and viscous flow were obtained from the straight line plots of $\log \tau T$ *vs.* $1/T$ and $\log \eta$ *vs.* $1/T$ respectively. The dipole moment in the case of 4-methylthiophenol was calculated from ε_0 and density d using Onsager's equation. The values of α, n_D^2, $\Delta H\tau_1$, $\Delta H\eta$ and μ are included in Table 2.

Discussion

It can be seen from Table 2 that the molecular and intramolecular relaxation times in both the *para* substituted thiophenols, decrease with increase in temperature as is generally observed in polar liquids, so also the distribution parameter α decreases with increase of temperature.

The intramolecular relaxation time τ_2 for SH group rotation in both the liquids are of the same order ($\approx$3ps) and compares well with the τ_2-values in thiophenol (2.6 ps) and in benzylthiol (3.1 ps) in the liquid state reported earlier[5] as also in naphthalenethiol (2.5 ps) in dilute solution in benzene reported by Fong and Smyth.[4] Thus it is found that the SH group relaxation times in pure liquids as also in dilute benzene solution are almost the same, showing thereby that the intermolecular hydrogen bondings S–H···S of the type hydroxyl hydrogen bonding, observed in phenol and substituted phenols,[10] are negligible in the thiophenols even in the liquid state.

It would be interesting to compare the τ_1 and τ_2 values of the present liquids, with those of *p*-substituted phenols reported by Magee and Walker.[10] Though the molecular relaxation time τ_1 of 29.7 ps at 50 °C in 4-methylthiophenol compares well with the value of $\tau_1=32$ ps at 25 °C in 4-methylphenol in *p*-xylene solution, the SH group relaxation time of 2.85 ps in the former, is definitely much smaller than the OH group relaxation time $\tau_2=8.4$ ps in the latter. The molecular relaxation time $\tau_1=17.7$ ps at 65 °C in 4-chlorothiophenol in the liquid state is almost half the value of $\tau_1=39$ ps in 4-chlorophenol in *p*-xylene solution and the τ_2-value of 2.8 ps for SH group rotation in the former is about our fourth the τ_2-value of 12.7 ps

for OH group rotation in the latter. The unusual lengthing of the OH group relaxation of *p*-substituted phenols in *p*-xylene solution was attributed by Magee and Walker[10] to association among the solute molecules, in addition to the effects of solvents. The lengthing of molecular relaxation time (τ_1=39 ps) in 4-chlorophenol in dilute *p*-xylene solution to double the τ_1-value of 17.7 ps in 4-chlorothiophenol, seems to suggest that a dimer has been formed in *p*-chlorophenol molecule by association with other solute molecule probably through H-Cl hydrogen bond. Similar bond formation is not observed in 4-methylphenol in the *p*-xylene solution.

Weight factors: It is seen from Table 2 that the weight factor C_1 for 4-methylthiophenol and 4-chlorothiophenol are about 0.79 and 0.63 respectively. An estimate for the weight factors for both the thiophenols can be made from consideration of bond moments. Assuming the moments of μ_{CH_3}=0.37D, μ_{C-S}=0.9D, μ_{H-S}=0.7D, μ_{C-Cl}=1.5D and $\angle$CSH=135°,[11] and remembering that the CH_3 group moment is directed towards the benzene ring, the moment components responsible for SH group rotation are μ_2=0.49D in both the molecules, while the moment components responsible for molecular reorientations are μ_1=0.8 D in methyl thiophenol and μ_1=1.1D in 4-chlorothiophenol. From the above values of μ_1 and μ_2, the ratio of the weight factors in the two cases are,

$$\frac{C_2}{C_1}=\left(\frac{0.49}{0.8}\right)^2=\frac{0.24}{0.64} \text{ or } C_1=0.73$$

in 4-methylthiophenol and

$$\frac{C_2}{C_1}=\left(\frac{0.49}{1.1}\right)^2=\frac{0.24}{1.21} \text{ or } C_1=0.83$$

in 4-chlorothiophenol. Thus the weight factors C_1 for molecular reorientation in both the liquids are larger than that for group rotation. The is in conformity with the values obtained experimentally. It may be noted here that some uncertainty may arise in the calculated value of the dipole moment in 4-chlorothiophenol, due to appreciable mesomeric charge shift occurring across the molecule.[12]

The activation energy $\Delta H\tau_1$ for molecular relaxation in 4-methylthiophenol is about 1.3 kcal/mol which, as usual, is less than the corresponding activation energy of $\Delta H\eta$=2 kcal/mol for viscous flow. In the case of 4-chlorothiophenol, the dielectric data could be taken only for two temperatures and therefore activation energy $\Delta H\tau_1$ may not be reliable in this case.

The values of ε_∞ in both the *p*-substituted thiophenols are appreciably larger than the value of n_D^2 at all temperatures. This indicates the presence of a third dispersion region of the 'Poley type' in the high frequency region.

The dipole moment of 4-methylthiophenol has been determined from ε_0 and density *d*, using Onsager's equation and is found to be 1.4D, which agrees well with the value of 1.46D obtained from bond moment calculation of the CH_3 group in the *para* postition of thiophenol (μ=1.22D).

The authors express their sincere thanks to Professor G. S. Kastha for helpful discussions and to Mr. D. Bhowmic for his help in making the computer programme.

References

1) C. P. Smyth, "Molecular Relaxation processes," Academic Press, London (1966), p. 1.
2) K. H. Illinger, "Progress in Dielectrics," (Ed. Birk and Hart), Vol 4, (1962).
3) K. Higasi, "Dielectric Relaxation and Molecular Structurer," Res. Inst. Appl. Electricity, Tokyo, Japan (1961).
4) K. F. Fong and C. P. Smyth, *J. Phys. Chem.*, **67**, 226 (1963).
5) A. Hasan, A. Das and A. Ghatak. *Indian J. Phys.*, **48**, 246 (1974).
6) A. Aihara and M. Daries, *J. Colloid Sci.*, **11**, 671 (1956).
7) A. Das, A. Chatak, and A. Hasan, This Bulletin, **46**, 1354 (1973).
8) K. Bergmann, D. Roberti, and C. P. Smyth *J. Phys. Chem.*, **64**, 665 (1960).
9) J. Bhattacharyya, A. Hasan, S. B. Roy, and G. S. Kastha, *J. Phys. Soc. Japan*, **28**, 204 (1970).
10) M. D. Magee and S. Walker, *J. Phys. Chem.*, **74**, 2378 (1970).
11) V. I. Minkin, O. A. Osipov, and Y. Zhdanov, "Dipole Moments in Organic Chemistry," Plenum Press, New York (1970).
12) J. W. Smith, "Electric Dipole Moments," Butterworth & Co., London (1955).

Potassium μ-(*trans*-Hyponitrito-*N,N'*)-bis{pentacyanocobaltate(III)} and Potassium μ-(*Trans*-Hyponitrito-*O,O'*)-Bis-{Pentacyanocobaltate(III)}

Hiromichi OKAMURA,* Eiichi MIKI,** Kunihiko MIZUMACHI, and Tatsujiro ISHIMORI

Department of Chemistry, College of Science, Rikkyo University, Nishi-Ikebukuro, Toshima-ku, Tokyo 171

(Received July 28 1975)

$K_6[Co_2(CN)_{10}(N_2O_2)]\cdot 2H_2O$ (orange salt) was prepared by reaction of $[Co(NO)(NH_3)_5]Cl_2$ with an aqueous solution of potassium cyanide. $K_6[Co_2(CN)_{10}(N_2O_2)]\cdot 4H_2O$ (yellow salt) was obtained by adding an aqueous solution of the orange salt to methanol. On the basis of IR and Raman spectra for their ^{14}NO- and ^{15}NO-salts, and of IR spectra for their gaseous decomposition products, the orange salt is considered to be a linkage isomer of the yellow salt with respect to the *trans*-hyponitrito bridge. It is presumed that the orange salt is potassium μ-(*trans*-hyponitrito-*N,N'*)-bis{pentacyanocobaltate(III)}, the yellow salt being potassium μ-(*trans*-hyponitrito-*O,O'*)-bis{pentacyanocobaltate(III)}.

Toyuki[1] and Jezowska-Trzebiatowska *et al.*[2] prepared $K_6[Co_2(CN)_{10}(N_2O_2)]\cdot 4H_2O$ with a *cis*- or *skew*-hyponitrito bridge by the method given by Nast and Rohmer.[3] On the other hand, Raynor[4] prepared $K_6[Co_2(CN)_{10}(N_2O_2)]\cdot 4H_2O$ with a *trans*-hyponitrito group, according to the method given by Nast, Mesche and Neubauer.[5] While investigating the method of Nast and Rohmer,[3] we prepared two new isomers with a *trans*-hyponitrito group, $K_6[Co_2(CN)_{10}(N_2O_2)]\cdot nH_2O$ (n=2 or 4 for orange and yellow salts, respectively).[6]

This paper describes studies on the two isomers with respect to IR and Raman spectra, UV spectra, and thermal decomposion. The product prepared according to the method of Nast and Rohmer[3] is also discussed by comparing its IR absorption bands with those of the two isomers.

Experimental

Preparation. Synthetic procedures and elementary analyses for the orange and the yellow salts were reported in detail.[6] From 1 to 3 g of $[Co(NO)(NH_3)_5]Cl_2$ was used for preparing the orange salt. Powdered $[Co(NO)(NH_3)_5]Cl_2$ was added little by little to a 30% aqueous solution of potassium cyanide with stirring in order to keep the reaction vessel at constant temperature (−10 °C). The procedure differs from that reported by Nast and Rohmer.[3] Yield, 0.6—2 g. χ_g (at 293K) $=-0.45\times 10^{-6}$ (c.g.s.). One gram of the orange salt was used for preparing the yellow salt. Yield, 0.8 g. χ_g (at 293K) $=-0.36\times 10^{-6}$ (c.g.s.).

Thermal Decomposition and Decomposition with 10% Potassium Cyanide Aqueous Solution. Decomposition was carried out in a vacuum line. A reaction vessel containing the salt (*ca.* 0.5 g) was heated *in vacuo* in an electric furnace at a rate of *ca.* 1—2 °C min^{-1}. Both the orange and the yellow salts decomposed violently at *ca.* 155 and 116 °C, respectively, to give gray powders. About 0.5 g of the salt was added in a reaction vessel containing 5 ml of 10% KCN solution frozen with the aid of liquid nitrogen, and the reaction vessel was evacuated. When the frozen solution was melted, both the salts decomposed by contact with the aqueous solution. The gaseous products thus obtained were dehydrated with P_4O_{10} and transferred to a gas cell with windows of calcium difluoride.

Measurements. The magnetic susceptibility was measured by the Gouy method. The IR spectra of the salts were measured as Nujol and hexachlorobutadiene mulls in the region 200—4000 cm^{-1} on JASCO 402G and JASCO model IR-F spectrometers. The Raman spectra of the powdered samples were recorded in the region 100—1500 cm^{-1} on a JASCO R-300 spectrometer equipped with He–Ne laser. The gaseous products were identified by means of their IR spectra.[7] The mole ratio of the liberated NO to N_2O was determined.[8] The diffuse reflection spectra of the salts were measured with a Hitachi EPS-3T spectrometer. The UV spectra in aqueous solution were recorded with a Hitachi 124 spectrometer.

Results and Discussion

Raman and IR Spectra for the Orange and Yellow Salts. Wave numbers of the IR and Raman bands and their assignments are summarized in Table 1.

Raman Spectra: Upon ^{15}NO-substitution (^{15}N atom% =95), the bands at 1257 and 1165 cm^{-1} for the orange salt shifted downwards by 31 and 39 cm^{-1}, respectively and, the bands at 1412 and 1070 cm^{-1} for the yellow salt shifted downwards by 43 and 18 cm^{-1}, respectively. Upon ^{15}NO-substitution (^{15}N atom %=50), the 1257 cm^{-1} band for the orange salt shifted and split into three peaks at 1253, 1242, and 1226 cm^{-1} (their intensity ratio 1:2:1). The same phenomenon was observed with the yellow salt; the 1412 cm^{-1} band shifted and split into three peaks, 1414, 1392, and 1369 cm^{-1} (their intensity ratio 1:2:1). This indicates that N–N bond is present in both the orange and yellow salts. For other bands, no isotopic shifts upon ^{15}NO-substitution could be observed. The bands in the region *ca.* 400—550 cm^{-1} are considered to be due to the $Co(CN)_5$ group.[9]

IR Spectra: The bands at 1157, 609, and 299 cm^{-1} for the orange salt shifted downwards by 21, 14, and 2 cm^{-1} upon ^{15}NO-substitution (^{15}N atom %=95), respectively, while the bands at 987, 630, and 329 cm^{-1} for the yellow salt shifted downwards by 15, 6, and 6 cm^{-1}, respectively.

The 1630 and 3580 cm^{-1} bands for the orange salt

* Present address: Synthetic Chemistry Laboratory, Nisso Chemicals Co., Ltd., 12-8, Goi-Minamikaigan, Ichihara, Chiba 290

** Present address: Department of Chemistry, The University of Texas at Austin, Austin, Texas 78712

Table 1. Wave numbers and assignments of Raman and IR bands for the orange and yellow salts

Orange salt		Yellow salt		Assignments
IR	Raman	IR	Raman	
3580 m		3620 s		O–H str
2140 sh, 2127 vs, 2090 sh		2147 sh, 2127 vs, 2092 sh		C–N str
1630 w		1643 s		H–O–H def
	1257 (31) [a]		1412 (43)	N–N sym str
1157 (21) vs		987 (15) vs		N–O asym str
	1165 (39)		1070 (18)	N–O sym str
			830	
	704		760, 650	in-plane NNO sym def
609 (14) s		630 (6) s		out-of-plane ONNO distortion
	550		550	Co–C–N bend
544 s, 536 s		538 s		
			500	
474 s	473		480	
466 s		462 s	468	
453 s				
440 vs				
423 sh, 412 vs, 404 sh	422	421 vs	422	Co–CN str
			403	
	370	373 s		
365 s				
353 sh				
338 sh				
299 (2) s		329 (6) s		in-plane NNO asym def
	286		288	
200 s		200 s	203	
	182		166	

a) The value in parentheses indicates observed isotopic shift. Abbreviations; str=stretching, bend=bending, asym=antisymmetric, sym=symmetric, def=deformation, vs=very strong, s=strong, m=medium, w=weak, sh=shoulder.

and the 1643 and 3620 cm^{-1} bands for the yellow salt are considered to be due to the water of crystallization. The sharp bands at 2127 cm^{-1} with two shoulders for the orange and yellow salts are assigned to the C–N stretching vibrations. Many absorption bands were observed in the region 200—600 cm^{-1}. Some of them in the region *ca.* 400—550 cm^{-1} are considered to be due to the skeletal vibrations between the cobalt atom and the CN group.[9]

Assignments of the Bands due to the Bridged Hyponitrito Group: The Raman and IR bands for the orange and yellow salts can be explained on the basis of the bands due to the hyponitrito group. Raman and IR studies on $M_2N_2O_2$ (M=Na and K) containing a *cis*- or *trans*-hyponitrite ion show that one band at 1380—1420 cm^{-1} is assigned to the N–N stretching and two bands at 830—1120 cm^{-1} to the N–O stretching vibrations.[10-14]

Of the three bands in the region 990—1400 cm^{-1} observed on the IR and Raman Spectra for the orange and yellow salts, two bands are Raman active, and one band is IR active. The mutual exclusion rule holds for the set of the three bands as observed on the *trans*-hyponitrite ion.[11] It can be considered that both the orange and yellow salts contain a *trans*-hyponitrite ion but not a *cis*-one. On the basis of the mutual exclusion rule and the ^{15}N-isotopic shifts, the 1257 cm^{-1} band for the orange salt and the 1412 cm^{-1} band for the yellow salt can be assigned to the N–N symmetric stretching vibrations, the 1165 cm^{-1} band for the orange salt and the 1070 cm^{-1} one for the yellow salt to the N–O symmetric stretching, and the 1157 cm^{-1} band for the orange salt and the 987 cm^{-1} band for the yellow salt to the N–O antisymmetric stretching vibrations.

For the bands in the region 200—800 cm^{-1} for *trans*-hyponitrite ion, Millen *et al.*[11] and McGraw *et al.*[12] assigned the Raman band at 485 or 698 cm^{-1} to the in-plane NNO symmetric deformation, the IR band at *ca.* 370 cm^{-1} to the in-plane NNO antisymmetric one, and the IR band at *ca.* 500 cm^{-1} to the out-of-plane ONNO distortion. McGraw *et al.*[12] also reported that the bands due to both the in-plane NNO antisym-

metric deformation and the out-of-plane ONNO distortion shifted downwards by *ca.* 10 cm^{-1}, but the band due to the in-plane NNO symmetric deformation hardly shifted upon ^{15}NO-substitution (^{15}N atom %= 95).

As for complexes other than the cyano complexes with hyponitrito group, $[(C_6H_5)_3M]_2(N_2O_2)$ (M=Sn and Pb),[15] $\{[MoCl_2(NO)(das)]_2N_2O_2\}Cl_2$ (das=*o*-phenylene-bis(dimethylarsine)),[16] $[Co_2(N_2O_2)(NH_3)_{10}](NO_3)_4 \cdot H_2O$,[17] and $Pt(N_2O_2)(PPh_3)_2$ (PPh_3=triphenylphosphine)[18] have been reported. IR study on *μ*-(*trans*-hyponitrito-*O,O'*)-bis{triphenyltin(II)} and its lead(II) analog has shown that the band at 580—620 cm^{-1} is due to the metal–O antisymmetric stretching, the band at 370—380 cm^{-1} to the out-of-plane ONNO distortion, and the band at 310—360 cm^{-1} to the in-plane NNO antisymmetric deformation.[15] IR study on *μ*-(*cis*-hyponitrito-*N,O*)-bis{pentaamminecobalt(III)} nitrate has shown that the band at 616 cm^{-1} is due to the NNO bending, the band at 577 cm^{-1} to the Co–NO stretching, the band at 536 cm^{-1} to the ONNO out-of-plane bending, the band at 374 cm^{-1} to another NNO bending, and the band at 247 cm^{-1} to the O_2N_2–Co–NH_3 bending vibrations.[17] On the other hand, IR study on $K_6[Co_2(CN)_{10}(N_2O_2)] \cdot 4H_2O$ with a *cis*- or *skew*-hyponitrito bridge has shown that the bands at 599, 537, 450, and 281 cm^{-1} are assigned to the Co–N stretching, the NNO bending, the Co–O stretching, and the N–Co–C or the Co–NO bending vibrations, respectively.[2] However, the bands other than the N–N and N–O stretching vibrations due to the hyponitrito bridge have not yet been definitely assigned.

From studies by means of IR and nitrogen-15, the 299 cm^{-1} band for the orange salt and the 329 cm^{-1} band for the yellow salt can probably be assigned to the in-plane NNO antisymmetric deformation, and the 609 cm^{-1} band for the orange salt and the 630 cm^{-1} band for the yellow salt to the out-of-plane ONNO distortion. The bands are considered to be coupled with the skeletal vibrations between the cobalt atom and the hyponitrito group. The Raman bands at 704 cm^{-1} for the orange salt and at 760 or 650 cm^{-1} for the yellow salt can be assigned to the in-plane NNO symmetric deformation.

N_2O and NO Liberated by the Decompositions of the Orange and Yellow Salts. The results are shown in Table 2. The IR spectra of the gaseous products show that NO and N_2O were liberated as major products by the thermal decomposition, while the decomposition, with 10% KCN aqueous solution, milder than the thermal decomposition, gave N_2O only. The amount of the N_2O formed in the thermal decomposition was greater than that of the NO for both the orange and the yellow salts. The mole ratio of the NO to N_2O from the orange salt was greater than that from the yellow one. The results obtained by isotopic analyses of the N_2O suggest that the hyponitrito group is present in both the orange and yellow salts, and that the N_2O is formed without a cleavage of the N–N bond in the hyponitrite group.

UV Spectra for the Orange and Yellow Salts. The diffuse reflection spectrum for the yellow salt was the same as the spectrum for its fresh aqueous solution (Fig. 1). On the other hand, the diffuse reflection spectrum for the orange salt was different from that

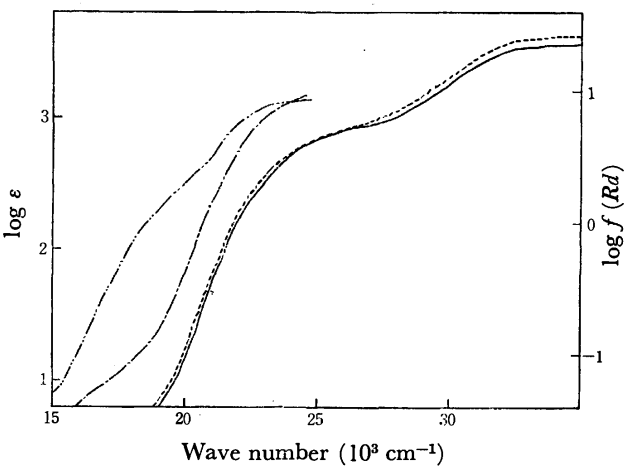

Fig. 1. Diffuse reflection spectra and spectra in an aqueous solution for the orange and yellow salts. —, the orange salt in an aqueous solution freshly prepared; ---, the yellow salt in an aqueous solution freshly prepared; –·–·–, the orange salt in solid state; –·–, the yellow salt in solid state.

Table 2. NO and N_2O from thermal decomposition and decomposition with 10% KCN aqueous solution of the orange and yellow salts

Compounds		Method	Gaseous products
Orange salt	^{14}NO-complex	Thermal	^{14}NO(0.67)[a] $^{14}N^{14}NO$(1)
	^{15}NO-complex (^{15}N atom%=95)	Thermal	^{15}NO(0.67) $^{15}N^{15}NO$(1)
	Mixture of ^{14}NO- and ^{15}NO-complexes (^{15}N atom%=95)	Thermal	^{14}NO(0.67) ^{15}NO(0.67) $^{14}N^{14}NO$(1) $^{15}N^{14}NO$(0.13) $^{14}N^{15}NO$(0.2) $^{15}N^{15}NO$(0.67)
	^{14}NO-complex	10% KCN aq. soln.	$^{14}N^{14}NO$
Yellow salt	^{14}NO-complex	Thermal	^{14}NO(0.43) $^{14}N^{14}NO$(1)
	^{15}NO-complex (^{15}N atom%=95)	Thermal	^{15}NO(0.43) $^{15}N^{15}NO$(1)
	^{14}NO-complex	10% KCN aq. soln.	$^{14}N^{14}NO$

a) The values in parentheses indicate the relative mole ratio.

for the yellow one. The spectrum for the fresh aqueous solution of the orange salt was almost equal to that for the yellow one. The orange species is considered to change rapidly to the yellow one on dissolution as expected from the synthetic method of the yellow salt.[6] The aqueous solution of the yellow salt was unstable; intensity of a shoulder at *ca.* 24 Kcm^{-1} due to the yellow species decreased to give a peak at 26 Kcm^{-1} after the solution had been allowed to stand for 2 weeks at room temperature. UV study on $K_3[Co(CN)_5(OH)]$ in an aqueous solution has shown that the $[Co(CN)_5(OH)]^{3-}$ decomposes to give $[Co(CN)_4(OH)_2]^{3-}$ and $[Co(CN)_6]^{3-}$ upon standing.[19] The spectrum obtained for the yellow salt solution which had been allowed to stand was the same as that for the solution of the mixture of $[Co(CN)_4(OH)_2]^{3-}$ and $[Co(CN)_6]^{3-}$. It is suggested that the complex anion of the yellow salt decomposes in water to give $[Co(CN)_4(OH)_2]^{3-}$ and $[Co(CN)_6]^{3-}$ through $[Co(CN)_5(OH)]^{3-}$:

$$[Co_2(CN)_{10}(N_2O_2)]^{6-} + H_2O \longrightarrow 2[Co(CN)_5(OH)]^{3-} + N_2O$$

$$2[Co(CN)_5(OH)]^{3-} \longrightarrow [Co(CN)_4(OH)_2]^{3-} + [Co(CN)_6]^{3-}.$$

Comparison of Compounds Prepared by the Method of Nast and Rohmer with the Orange and the Yellow Salts. For the compound with a *cis*- or *skew*-hyponitrito bridge reported by Jezowska-Trzebiatowska *et al.*, IR bands at 1340—1400 (the N–N stretching vibration), 1043 (the N–O one), and 831 cm^{-1} (the N–O one) have been observed.[2] IR spectra in the region 800—1400 cm^{-1} for the "yellow product," prepared by the authors according to the method of Nast and Rohmer[3] on *ca.* 1/10 scale, gave broad bands at 1393(s), 1373(s), 1155(m), 1054 (m), 982(m), and 910(s) cm^{-1}, which shifted downwards by 31, 31, 25, 32, 13, and 17 cm^{-1}, respectively, upon ^{15}NO-substitution (^{15}N atom %=95). On the other hand, the IR spectra for the compound reported by Toyuki gave the bands at 1389(sh), 1333(w), 1158(w), 1058(w), and 984(w) cm^{-1}.[1] The bands at *ca.* 1160 and 980 cm^{-1} for the "yellow product" might correspond to the N–O antisymmetric stretching vibrations due to the orange and yellow salts, respectively. The residual three components at 1393—1373, 1054, and 910 cm^{-1} for the "yellow product" might be due to a new linkage isomer of the compounds with a *cis*-hyponitrito group since wave numbers of these residual bands observed on the "yellow product" are different from those of the bands observed on the compounds with the *cis*-hyponitrito group reported by Toyuki[1] and Jezowska-Trzebiatowska *et al.*,[2] and also since all the N–N and the N–O stretching vibrations due to the *cis*-hyponitrito bridge are IR active. The IR study by Raynor on the compound prepared according to the method of Nast, Mesche and Neubauer[5] has shown that the N–O stretching vibration is observed at 1120 cm^{-1}.[4] However, it seems that this compound has not yet been well characterized.

The "yellow product" might be a mixture of the yellow salt, the orange salt, and an unknown compound with a *cis*-hyponitrito group. New linkage isomers with a *cis*-hyponitrito group can be expected to be isolated by subtle changes in the preparative conditions.

The yellow salt can be considered to be a linkage isomer of the orange salt. The N–N bond strength for the orange salt might be weaker than that for the yellow one. On the other hand, the N–O bond strength for the orange salt might be stronger than that for the yellow one. The mole ratio of NO to N_2O formed in the thermal decomposition for the orange salt is greater than that for the yellow one. This suggests that the N–N bond strength for the orange salt is weaker than for the yellow one as expected from the Raman spectra. Thus, it is presumed that the anion of the orange salt is μ-(*trans*-hyponitrito-*N,N'*)-bis{pentacyanocobaltate(III)} (A), that of the yellow salt being μ-(*trans*-hyponitrito-*O,O'*)-bis{pentacyanocobaltate(III)} (B) as shown in Fig. 2.

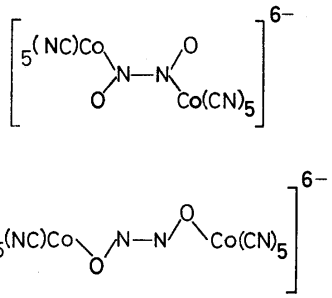

Fig. 2. Probable structures of the orange (A) and yellow (B) salts.

The authors are indebted to Mr. M. Arita and Mr. T. Takakuwa of the Japan Spectroscopic Co., Ltd., for the measurements of the Raman spectra. The present work was supported in part by a Grant for Scientific Research from the Ministry of Education.

References

1) H. Toyuki, *Spectrochim. Acta*, **27A**, 985 (1971).
2) B. Jezowska-Trzebiatowska, J. Hanuza, M. Ostern, and J. Ziolkowski, *Inorg. Chim. Acta*, **6**, 141 (1972).
3) R. Nast and M. Rohmer, *Z. Anorg. Allg. Chem.*, **285**, 271 (1956).
4) J. B. Raynor, *J. Chem. Soc. Inorg. Phys. Theor.*, **1966**, 997.
5) R. Nast, H. R. Mesche, and M. H. Neubauer, *Z. Anorg. Allg. Chem.*, **312**, 314 (1961).
6) H. Okamura, E. Miki, K. Mizumachi, and T. Ishimori, *Chem. Lett.*, **1974**, 103.
7) K. Nakamoto, "Infrared Spectra of Inorganic and Coordination Compounds," 2nd Ed., Wiley-Interscience, New York, N. Y. (1970).
8) E. L. Sailer and A. Pozefsky, *Anal. Chem.*, **26**, 1079 (1954).
9) D. M. Adams, "Metal-Ligand and Related Vibrations," E. Arnold, London (1967).
10) L. Kuhn and E. R. Lipincott, *J. Amer. Chem. Soc.*, **78**, 1820 (1956).
11) D. J. Millen, C. N. Polydoropoulos, and D. Watson, *J. Chem. Soc.*, **1960**, 687.
12) G. E. McGraw, D. L. Bernitt, and I. C. Hisatsune, *Spectrochim. Acta*, **23A**, 25 (1967).
13) J. Goubeau and K. Leitenberger, *Z. Anorg. Allg. Chem.*, **320**, 78 (1963).

14) N. Gee, D. Nicholls, and V. Vincent, *J. Chem. Soc. Supplement 1*, **1964**, 5897.
15) W. Beck, H. Engelmann, and H. S. Smedal, *Z. Anorg. Allg. Chem.*, **357**, 134 (1968).
16) R. D. Feltham, W. Silverthorn, and G. McPherson, *Inorg. Chem.*, **8**, 344 (1969).
17) E. E. Mercer, W. A. McAllister, and J. R. Durig, *ibid.*, **6**, 1816 (1967).
18) S. Cenini, R. Ugo, G. LaMonica, and S. D. Robinson, *Inorg. Chim. Acta*, **6**, 182 (1972).
19) L. C. Smith, J. Kleinberg, and E. Criswold, *J. Amer. Chem. Soc.*, **75**, 449 (1953).

Formation of Oxygen Deficient Pyrochlore Solid Solutions $Pb_2Ta_{2-2x}M_{2x}O_{7-x}$(M=Ti, Sn and Zr) and Their Optical and Dielectric Properties

Yasuyoshi TORII and Hideo MATSUMOTO*

Government Industrial Research Institute, Nagoya, Hirate-machi, Kita-ku, Nagoya 462

(Received July 29, 1975)

It was found that oxygen deficient pyrochlore solid solutions $Pb_2Ta_{2-2x}M_{2x}O_{7-x}$ with M=Ti, Sn, and Zr exist over wide ranges. The formation of oxygen deficient pyrochlore structure results from the occupancy of Pb^{2+} ions in the A position, which have a high polarizability. Their reflectance and infrared absorption spectra, and dielectric constants were measured. With the increase of M^{4+} ions, the color turned lemon yellow to reddish yellow, and the dielectric constants increased. The infrared absorption spectra in their pyrochlore solid solutions were similar to those in $PbTiO_3$ and $PbZrO_3$. The infrared properties of two strong absorption bands observed were discussed in comparison with those in the perovskites.

Pyrochlore type compounds are represented by the general formula $A_2B_2O_7$ and exhibit interesting physical properties such as ferroelectricity in $Cd_2Nb_2O_7$[1,2] and electrooptic effect in $Ca_2Nb_2O_7$.[3] Compounds of this type have a face-centered cubic structure with a unit cell of *ca.* 10 Å. The structural framework is a three-dimensional array of BO_6 octahedra, all sharing corners, and the framework thus has the composition $(B_2O_6)_\infty$. The seventh set of oxygen ions and the A ions occupy open spaces in the framework as the large ions do in the perovskite structure. The mixed oxides consisting only of oxygen octahedra can generally yield a large internal field for ferroelectricity to occur. Both perovskite and pyrochlore are furnished with such a structural condition. There are, however, essential differences between the two structure types. In the ABO_3 perovskite, the O–B–O chains lie on straight lines parallel to the cubic axis. In the pyrochlore structure the configuration of the BO_6 octahedra is much more complicated, the O–B–O chains lying on zig-zag lines along the <110> directions. The zig-zag structure of O–B–O chains seems to be unfavorable for the occurrence of ferroelectricity since few[4,5] have been found to be ferroelectric among pyrochlores. Nikiforov *et al.*[6,7] concluded that oxygen deficient pyrochlores with more loose structure than pyrochlores of the type $A_2B_2O_7$ are favorable for its occurrence from a crystallochemical analysis of the conditions for a spontaneously polarized state in pyrochlores. Among perovskites, a number of ferroelectric substances have been found.[8] $PbTiO_3$ is ferroelectric with a Curie point of 490 °C and $PbZrO_3$ is antiferroelectric below 230 °C. It is of interest to see if a binary system consisting of pyrochlore and perovskite as end members exists in the form of oxygen deficient pyrochlore. In the present study, the formation of solid solutions $Pb_2Ta_{2-2x}M_{2x}O_{7-x}$ with M=Ti, Sn and Zr was examined and their optical and dielectric properties were investigated.

Experimental

Specimens were prepared from PbO, Ta_2O_5, TiO_2, SnO_2, and ZrO_2 of high purity. In particular, an electronic grade sample (>99.99%) was used for SnO_2. Mixtures of various compositions were ground together in an agated mortar, pressed into a disk and then ignited on platinum foil in the air at *ca.* 1050 °C. The resulting materials were reground, repressed and re-ignited at 1100—1200 °C for 3 h. They were then left to cool in the furnace.

Phase identification was carried out by X-ray diffraction technique using a X-ray diffractometer with nickel filtered Cu $K\alpha$ radiation. Calibration of goniometer was made using high purity silicon as a standard. Their lattice constants were determined from the reflection line of (662). The spectral reflectance between 400—760 nm was recorded with a spectrophotometer to pursue the displacement of absorption. Infrared absorption measurements between 4000—250 cm^{-1} were made for powder specimens dispersed in a pressed KBr disk, using a Perkin-Elmer infrared spectrophotometer model 457. The dielectric constants were measured on a capacitance bridge employing a frequency of 1000 cps. Fired-on silver electrodes were used for the measurements. No correction was made as regards the porosity of specimen.

Results and Discussion

Formation of Oxygen Deficient Pyrochlore Solid Solutions.

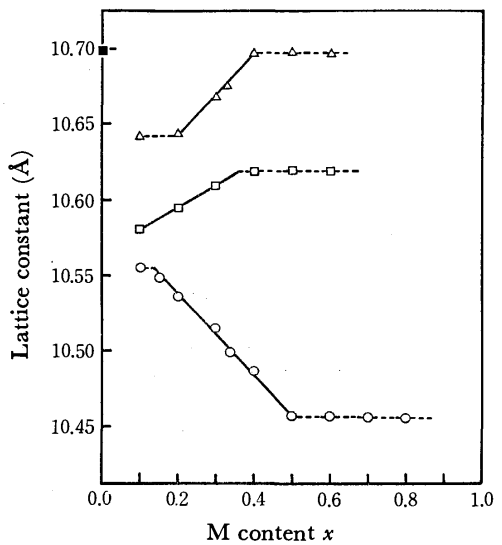

Fig. 1. Lattice constants for the solid solutions of pyrochlore $Pb_2Ta_{2-2x}M_{2x}O_{7-x}$ (M=Ti, Sn, and Zr).
○: Ti-containing system, □: Sn-containing system, △: Zr-containing system, ■: rhombohedral $Pb_2Ta_2O_7$($\sqrt[3]{V}$).

* Present Address: Yamatsu China Mfg. Co., Ltd.

Powder X-ray diffraction analyses show that cubic pyrochlore solid solutions exist in wide ranges. The variation of lattice constants for the solid solutions $Pb_2Ta_{2-2x}M_{2x}O_{7-x}$ with M=Ti, Sn and Zr are shown in Fig. 1. The part drawn by solid line represents the compositional range in which a single phase of cubic pyrochlore is observed in the powder X-ray patterns. $Pb_2Ta_2O_7$ is known to be rhombohedrally distorted pyrochlore with the unit cell with dimensions, $a=10.700$ Å and $\alpha=88°25'$. Partial substitution of M^{4+} ions for Ta^{5+} ions makes it possible for the cubic pyrochlore to form. In the case of Ti-containing system, the crystal distortion disappears when $x=0.15$. The unit cell dimension of cubic pyrochlore phase becomes smaller with a further increase in x, but remains much the same when the value of x, exceeds *ca.* 0.50. From the result, the substitutional limitation of Ti^{4+} ions to form the cubic pyrochlore phase is *ca.* $x=0.50$. According to Ahrens's radii,[9] the ionic size of Ti^{4+} ion is 0.68 Å and is the same as that of Ta^{5+} ion. The unit cell dimension in this system, however, decreases with the increase of x in the substitutional range of Ti^{4+} ions. This affords an experimental proof for the formation of pyrochlore structure with oxygen deficiencies.

In the case of Sn- and Zr-containing systems, similar series of solid solutions exist in the form of cubic oxygen deficient pyrochlore. Their unit cell dimensions, however, increased with the increase of x in the compositional ranges in which cubic oxygen deficient pyrochlore is formed as a single phase. The regions of their solid solutions were narrower than that in the Ti-containing system. This is because the ionic sizes of Sn^{4+} ion (0.71 Å) and Zr^{4+} ion (0.79 Å) are larger than that of Ta^{5+} ion.

When Ta^{5+} ions were substituted partially with Ti^{4+} ions in cubic pyrochlore $Ca_2Ta_2O_7$, a series of oxygen deficient pyrochlore solid solution was not formed as in the case of the pyrochlore with Pb^{2+} ions in the A position. The partial substitution of Y^{3+} ions plus Ti^{4+} ions for Ca^{2+} ions plus Ta^{5+} ions gave a pyrochlore. The formation of the oxygen deficient pyrochlore structure seems to be related with the occupancy of Pb^{2+} ions in the A position. The structure with oxygen deficiency is derived from the pyrochlore structure by the removal of oxygen ions located in the tetrahedral interstices of the cationic array of Pb ions.[10] The oxygen ions removed do not contribute to the framework structure even though they are necessary in the structure. Pb^{2+} ion has an eigthfold coordination (nearly an hexagonal bipyramid) in the pyrochlore structure. However, Pb^{2+} ion has a coordination less than eightfold in the oxygen dificient pyrochlore structure. The removal of oxygen ions located in the tetrahedral interstices results in an increase in the oxygen polarization. Since Pb^{2+} ion has a high polarizability due to its electronic configuration ($6s^2$), the occupancy of Pb^{2+} ions in the A position is favorable for the formation of oxygen deficient pyrochlore structure. It is understandable that oxygen deficient pyrochlores have often been formed, as in the examples of $Pb_2Ti_{1.5}W_{0.5}O_{6.5}$[11] and $Bi_2Zn_{4/3}Ta_{2/3}O_6$,[6] when Pb^{2+} or Bi^{3+} ion occupies the A position. Consequently the occupancy of Ca^{2+} ions in the A position seems unfavorable for the formation of oxygen deficient pyrochlore structure.

Reflectance Spectra. Samples of cubic oxygen deficient pyrochlore prepared were yellowish powder, a slight difference in the tone of color being found. Figure 2 shows the reflectance spectra in the range 400—760 nm for the Ti-containing system. The curves show strong absorption extending over violet and blue parts of visible light. The strong absorption is responsible for the yellowish color development. $Pb_2Ta_2O_7$ is white powder. With the increase in the amount of substituted Ti^{4+} ions, the reflectance curve shifts towards higher wavelength side, the color changing from lemon yellow to reddish yellow. Similar results were obtained for Sn- and Zr-containing systems. Each reflectance in the vicinity of the blue part increased in the order of Sn-, Ti-, and Zr-containing oxygen deficient pyrochlores under the condition of equimolecular substitution of M^{4+} ions. It seems that the color development can be ascribed to a significant contribution of covalent character in the Pb-O bond of these oxygen deficient pyrochlores. The Pb-O distances in $Pb_2Ta_{1.4}Ti_{0.6}O_{6.7}$ were calculated as an example, using its lattice constant ($a=10.518$ Å) and atomic coordinate parameters of cubic pyrochlore structure[12] (oxygen parameter $u=5/16$). It was found that each Pb atom has two close oxygen neighbors at 2.28 Å and six close oxygen neighbors at 2.69 Å. Of the two kinds of Pb-O distance, the former is a little smaller than that in tetragonal PbO, which is a reddish color. The latter distance is nearly the same as that (2.70 Å) in $Pb(NO_3)_2$ with a typical ionic character. Pb^{2+}, Ta^{5+}, Ti^{4+}, or O^{2-} alone causes no visible absorption, but the combination gave a yellowish color. In the shorter Pb-O distance, consideration must be given to the fact that the outer electron orbits and energy levels are affected by the neighboring ions of oxygen. This is the electron band in which color-producing transition occurs as known in Cu_2O (red) and tetragonal PbO (reddish).[13] The development of yellowish color is attributed to visible absorption in the vicinity of the violet part, by which the nonbonding electrons of O^{2-} ions are transferred to the outer orbits of Pb^{2+} ions. The volume of rhombohedral $Pb_2Ta_2O_7$ was larger by 2.8% than that of cubic $Pb_2Ta_2O_7$ (actually not existing at room temperature) estimated from the curve of lattice constant *vs.* composition in the solid solution $Pb_2Ta_{2-2x}Ti_{2x}O_{7-x}$. The atomic coordinates of each atom in rhombohedral $Pb_2Ta_2O_7$ have not been determined yet. The crystal distortion would cause the shorter Pb-O distance to enlarge, since rhombohedral $Pb_2Ta_2O_7$ is colorless.

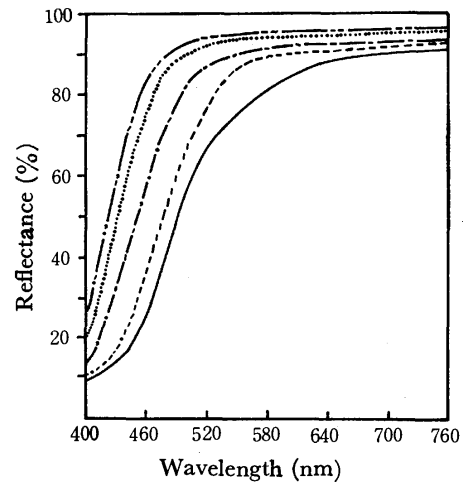

Fig. 2. Reflectance spectra of pyrochlore solid solution $Pb_2Ta_{2-2x}Ti_{2x}O_{7-x}$.
-·-·-: $x=0.1$, ·····: $x=0.2$, -·-; $x=0.3$, ----: $x=0.4$, ——: $x=0.5$.

The pyrochlores were stable without dissolution in the lead glaze and the yellowish color remained unchanged when about 5% of them by weight were well dispersed in the lead glaze and their mixtures were ignited at 900 °C. These pyrochlore solid solutions might be used as a pigment in ceramics.

Infrared Absorption Spectra. Figure 3 shows infrared spectra of the solid solution $Pb_2Ta_{2-2x}Ti_{2x}O_{7-x}$. Two strong absorption bands were observed in all the specimens. Their

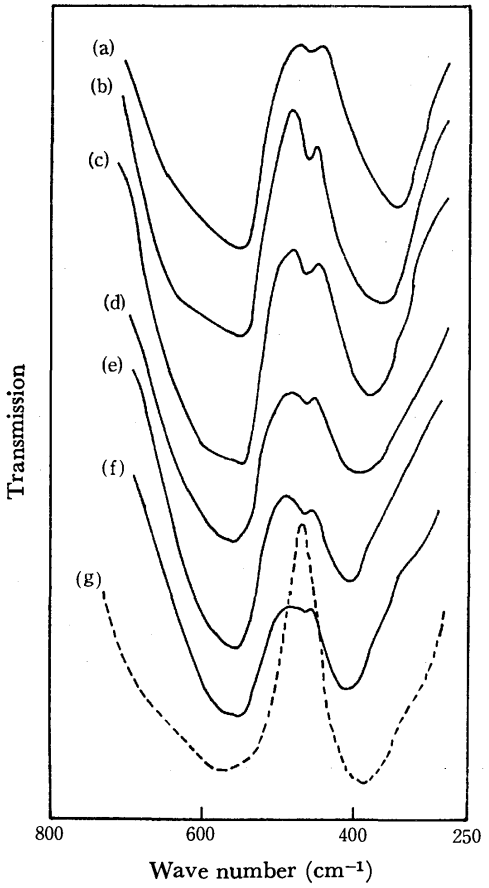

Fig. 3. Infrared absorption spectra of pyrochlore solid solution $Pb_2Ta_{2-x}Ti_{2x}O_{7-x}$ and $PbTiO_2$.
(a): $x=0.0$, (b): $x=0.1$, (c): $x=0.2$, (d): $x=0.3$, (e); $x=0.4$, (f): $x=0.5$, (g): $PbTiO_3$ ($x=1.0$).

spectra were all similar in general features. The higher frequency bands, ν_1, extend from *ca.* 800 to 490 cm^{-1}, with a peak of *ca.* 550 cm^{-1}. They are asymmetric, with a high-frequency tail. The lower frequency bands, ν_2, extend from *ca.* 490 cm^{-1} to the limit of the experimental range at 250 cm^{-1}, with a peak of 350—400 cm^{-1}. With the increse of Ti^{4+} ions, band locations of ν_1 remained nearly unchanged, these bands becoming slightly sharper. The band locations of ν_2 shifted towards high frequency side. Except two strong absorption bands, a weak absorption band was observed at *ca.* 460 cm^{-1}. The infrared spectra of pyrochlore solid solution were similar to that of $PbTiO_3$ except for the band locations (Fig. 3). The two absorption band peaks ν_1 and ν_2 observed in $PbTiO_3$ are 585 and 390 cm^{-1}. These values are in good agreement with Last's data.[14] Similar absorption spectra were obtained for two series of Sn- and Zr-containing systems. Assignment of infrared spectrum has been done on perovskite,[15-17], but not on pyrochlore. It should be noted that the infrared absorption spectra observed in these pyrochlore solid solutions were similar to those of the perovskites. The infrared absorption spectra between metastable pyrochlore $K_{1.5}(Ta_{0.65}Nb_{0.35})_2O_{5.75}$ and perovskite $K(Ta, Nb)O_3$ are similar.[18] Thus it is of significance to compare the infrared absorption spectra of pyrochlore with those of perovskite, since they have analogous structural frameworks. According to the study by Perry *et al.*,[15,16] the vibrations ν_1 and ν_2 observed in the ABO_3 perovskite are assigned to the B–O stretching mode and the B–O_3 torsional mode, respectively. Figures 4 and 5 show the compositional dependence of ν_1 and ν_2 for three series of oxygen deficient pyrochlore solid solutions.

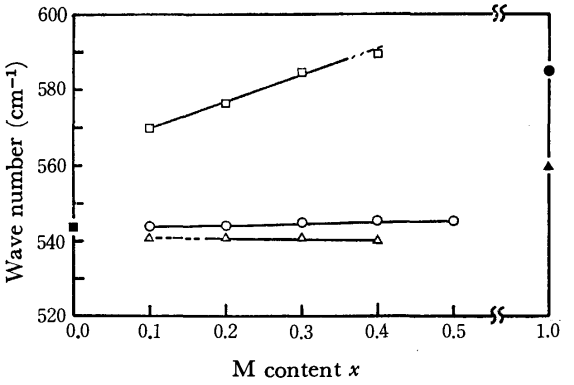

Fig. 4. Compositional dependence of ν_1 for the solid solutions of pyrochlore $Pb_2Ta_{2-2x}M_{2x}O_{7-x}$ (M=Ti, Sn, and Zr).
○: Ti-containing system, □: Sn-containing system, △: Zr-containing system, ■: rhombohedral $Pb_2Ta_2O_7$, ●: perovskite $PbTiO_3$, ▲: perovskite $PbZrO_3$.

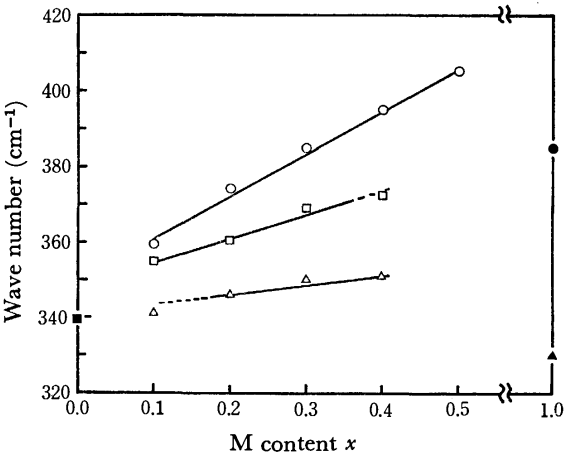

Fig. 5. Compositional dependence of ν_2 for the solid solutions of pyrochlore $Pb_2Ta_{2-2x}M_{2x}O_{7-x}$ (M=Ti, Sn, and Zr).
○: Ti-containing system, □: Sn-containing system, △: Zr-containing system, ■: rhombohedral $Pb_2Ta_2O_7$, ●: perovskite $PbTiO_3$, ▲: perovskite $PbZrO_3$.

The band locations of ν_1 remain nearly unchanged, except for Sn-containing system. On the other hand, all the band locations of ν_2 for three systems shift linearly towards high frequency side with the increase of M^{4+} ions. The values and slopes for ν_2 increase in the order of Ti-, Sn-, and Zr-containing systems. The observed band locations of ν_2 seem to have an inverse relationship between atomic masses and vibrational frequencies. Such a tendency appeared in the perovskites with the same cation in the A position. For example, the band locations of ν_1 for $BaTiO_3$, $BaSnO_3$, and $BaZrO_3$ are 578, 635, and 573 cm^{-1}, respectively, and the band locations of ν_2 for $BaTiO_3$, $BaSnO_3$, and $BaZrO_3$ are 410, 400, and 420 cm^{-1}, respectively.[19] Similar results were obtained for $PbTiO_3$ and $PbZrO_3$ (Figs. 4 and 5). That the vibrational frequencies of ν_1 for Ti- and Zr-containing systems remain nearly unchanged is probably because both effects of reduced mass and force constant on them are cancelled out. The band locations of ν_1 for Sn-containing system, however, shift towards high frequency side, the values being larger than those observed in Ti- and Zr-containing systems. It will be attributed to larger force constants of ν_1 in Sn-containing

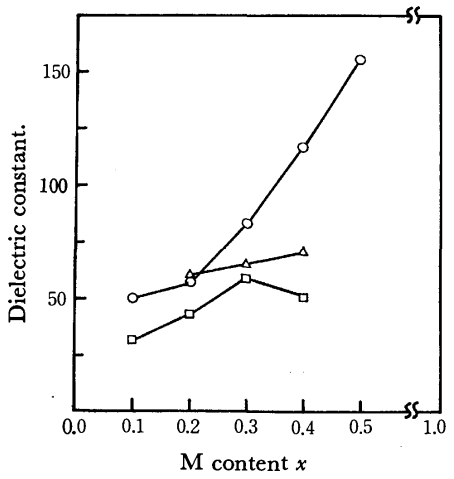

Fig. 6. Compositional dependence of dielectric constant for the solid solutions of pyrochlore $Pb_2Ta_{2-2x}M_{2x}O_{7-x}$ (M=Ti, Sn, and Zr).
○: Ti-containing system, □: Sn-containing system, △: Zr-containing system.

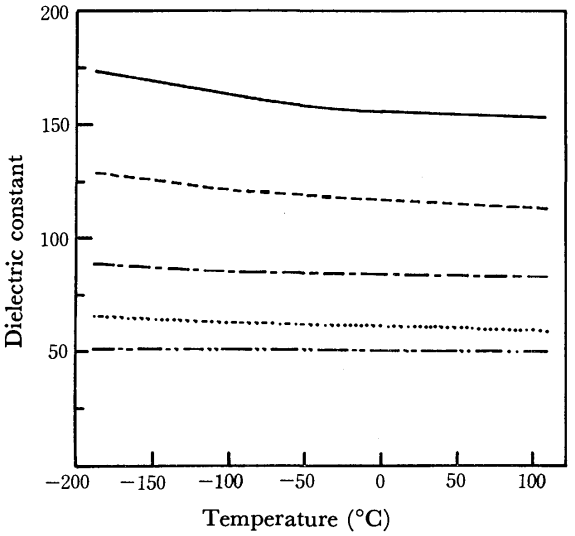

Fig. 7. Temperature dependence of dielectric constant for the pyrochlore solid solution $Pb_2Ta_{2-2x}Ti_{2x}O_{7-x}$. -·-·-: $x=0.1$, ·····: $x=0.2$, -·-: $x=0.3$, ——: $x=0.4$, ——: $x=0.5$.

system than in Ti- and Zr-containing ones. The band locations of ν_1 for pyrochlores of compositions $PbTiO_3$ and $PbZrO_3$ (actually not existing), estimated from the compositional dependence of frequency (Fig. 4), are larger than those observed in the perovskites of $PbTiO_3$ and $PbZrO_3$. This is because force constants of ν_1 in these pyrochlores are larger than those in the perovskites, assuming that the higher frequency ν_1 observed in these pyrochlore solid solutions corresponds to the perovskite B–O stretching mode. The weak absorption band located at 460 cm^{-1} would result from the splitting of degeneracy in the vibrational mode of ν_2. The qualitative similarity of infrared absorption spectra between pyrochlore and perovskite can be expected in view of the assignment based on the vibrations of oxygen octahedron, since they have an analogous structural framework. Further investigation is necessary to confirm whether two absorption bands ν_1 and ν_2 observed in pyrochlores correspond to the B–O stretching mode and the $B–O_3$ torsional mode, respectively, or not.

Dielectric Constant. The compositional dependence of dielectric constant for the solid solutions at room temperature is shown in Fig. 6. The dielectric constants are relatively high, but small as compared with those of titanates or zirconates of typical perovskite. They increase with the increase of M^{4+} ions. In particular, a marked increase of dielectric constant was observed in the Ti-containing system. The temperature dependence of dielectric constant for the Ti-containing system from −190 to 110 °C is shown in Fig. 7. The dielectric constants tend to increase slightly with the decrease in temperature. Such a tendency also appeared in Sn- and Zr-containing systems. If ferroelectric phases occur among these oxygen deficient pyrochlores, the dielectric anomalies would be below liquid nitrogen temperature.

The authors wish to thank Dr. Tetsuo Noguchi of this Institute for his discussions and encouragement.

References

1) W. R. Cook, Jr. and H. Jaffé, *Phys. Rev.*, **88**, 1426 (1952).
2) F. Jona, G. Shirane, and R. Pepinsky, *ibid.*, **98**, 903 (1955).
3) C. H. Hokmes, E. G. Spencer, A. A. Ballman, and P. V. Lenzo, *Appl. Opt.*, **4**, 551 (1965).
4) J. K. Hulm, *Phys. Rev.*, **92**, 504 (1953).
5) G. A. Smolenskii, V. A. Isupov, and A. I. Agranovskaya, *Soviet Phys. -Dokl.*, **1**, 300 (1957).
6) L. G. Nikiforov, V. V. Ivonova, Yu. N. Venevtsev, and G. S. Zhdanov, *Izv. Akad. Nauk SSSR, Ser. Neorg. Mater.*, **4**, 381 (1968).
7) L. G. Nikiforov, Dissertation, Moscow, 1969.
8) F. S. Galasso, "Structure, Properties and Preparation of Perovskite-type Compounds," Pergamon Press, New York (1969), p. 79.
9) L. H. Ahrens, *Geochim. Cosmchim. Acta*, **2**, 155 (1952).
10) E. Aleshin and R. Roy, *J. Amer. Ceram. Soc.*, **45**, 18 (1962).
11) I. N. Belyaev, L. N. Aver'yanova, and I. I. Belyaeva, *Kristallografiya*, **9**, 280 (1964).
12) "International Tables for X-ray Crystallography," Vol. 1, Kynoch Press, Birmingham (1965), p. 341.
13) M. Nakahara, *Kagaku Kyoiku*, **14**, 262 (1966).
14) J. T. Last, *Phys. Rev.*, **105**, 1740 (1957).
15) C. H. Perry and B. N. Khanna, *ibid.*, **135**, A408 (1964).
16) C. H. Perry and D. J. McCarthy, *ibid.*, **138**, A1537 (1965).
17) A. F. Corsmit, H. E. Hoefdraad, and G. Blasse, *J. Inorg. Nucl. Chem.*, **34**, 3401 (1972).
18) S. Ito, T. Kokubo, and M. Tashiro, *Yogyo-Kyokai-Shi*, **81**, 327 (1973).
19) A. F. Yatsenko, *Izv. Akad. Nauk SSSR, Ser. Fiz.*, **22**, 1456 (1958).

Fundamental Research into the Treatment of the Chromic Plating Rinse by Reverse Osmosis

Hitoshi MASUDA, Chiyoshi KAMIZAWA, Masazi MATSUDA, Takashi NAKANE, and Tsuyoshi OHIRA*

National Chemical Laboratory for Industry, Hon-machi, Shibuya-ku, Tokyo 151

** Niigata Prefectural Center of Industrial Science and Technology, Abumi, Niigata 950*

(Received August 8, 1975)

Fundamental research into the treatment of the chromic plating rinse by reverse osmosis were carried out with Loeb-type skinned membranes. The effect of the pH on the transport of chromic acid was quantitatively investigated. With the increase in pH, chromic acid dissociates to form a divalent ion, CrO_4^{2-}, and the rejection by the membrane increases. For example, the rejection of 0.01 M chromic acid at pH 3 was 83%, while it was 96% at pH 7.25, both at 40 atm. The permeation behavior of additives such as sodium hexafluorosilicate and chromium (III) sulfate was also examined, mainly in connection with their dissociation in the solution. In the case of the concentration of chromic acid, the rejection remained constant up to about 15000 ppm, while the flux decreased considerably with an increase in the concentration.

In Japan as well as other developed countries, concern with pollution has been growing remarkably, and legislative restrictions on discharged harmful effluents are becoming stricter. In addition to national regulations, some more restrictions have been imposed in some local communities. At the same time, it is well recognized among the people concerned that pure water can no longer be treated as limitless natural resource.

The plating rinse effluents are regarded as among the most harmful wastes which contain numerous toxic constituents. In these circumstances, some studies[1,2] have been made on the application of reverse osmosis to the treatment of plating rinses with a view to the recovery of harmful substances and the reuse of the water. These experimental data give us much information for practical use. However, there have been few reports describing the relation between the state of the species in the solution and their permeation behavior. It may be necessary to consider even such a basic problem for a feasibility study. Therefore, simulated chromic plating rinse was chosen here and fundamental experiments were performed in order to clarify the relation mentioned above.

These fundamental experiments were carried out under the following conditions; a three-stage countercurrent rinse system had been chosen in which the concentration of the total dissolved solid in the first stage rinse was 2000 ppm. The concentrated solution (15000 ppm) of the first-stage rinse was returned to the plating bath for balance and the permeated water was used as the rinse. Golomb reported a scheme for the rinse system and the mass-balance of the Watts nickel plating rinse and should be referred to for the details.

Experimental

The modified cellulose acetate (E-398-3) membranes were prepared by the method reported by Loeb and Manjikian.[3] The casting solution was composed of 25 wt. % cellulose acetate, 65 wt. % acetone, and 10 wt. % phosphoric acid. The annealing temperatures of the Loeb-type membranes were 60, 65, 70, 75, and 78 °C. The evaporation temperature was 20±1 °C and the evaporation time was 40 s for all Loeb-type membranes. The membranes thus prepared had approximately 20% more fluxes, with the same rejections, as compared with standard (formamide-type) membranes. The effective membrane area in the desalination cell was 12.6 cm^2. The pressurized (40 atm) solution was circulated along the surface of the membrane at 1.2 l/min to reduce the concentration polarization.

Aqueous solutions of 0.01 M—0.2 M chromic acid, 0.005 M sodium-hexafluorosilicate, and 0.004 M chromic (III) sulfate were tested. Their pH was controlled by adding a suitable amount of 0.1 M NaOH or 0.1 M HCl to the solution. In all the experiments the permeated water was collected one hour after the beginning of the operation. The analysis of the chromic acid was performed by photo-absorption at 274 nm after adjusting the pH of the solution to 8. Sodium hexafluorosilicate was supposed to dissociate in the solution to form various species, so sodium, fluorine, and silicon were analyzed individually.

The sodium was determined by flame photo-absorption at 589 nm. The fluorine was measured by photo-absorption at 620 nm after color developing by a Dotite reagent, "Alfusone." The silicone was also analyzed by photo-absorption at 334 nm after treatment with ammonium molybdate. The properties of the membrane were shown by water flux ($m^3/m^2 \cdot day$) and salt rejection. The salt rejection is shown by;

$$R_e = (1 - C_p/C_f) \times 100 \quad (1)$$

where C_p and C_f are the salt concentrations of the product and feed solutions respectively.

Results

Rejection of Chromic Acid. It is well known[4,5] that, in the case of electrolytes, fluxes of a given solute through the membrane are closely related to the charged state of the molecules in the solution. Since chromic acid dissociates in the solution, chromic acid solutions with pHs of 2, 3, 5, 6, and 7 were tested in order to clarify the effect of pH on the permeation of chromic acid. The rejection of chromic acid was considerably influenced by the pH of the solution, as had been expected. For instance, the rejection of chromic acid was 83% and 96% at pH 3 and 7.25 respectively for the membrane annealed at 70 °C, as is shown in Fig. 1. As it is known that the cellulose acetate membrane is deteriorated rapidly, with a loss

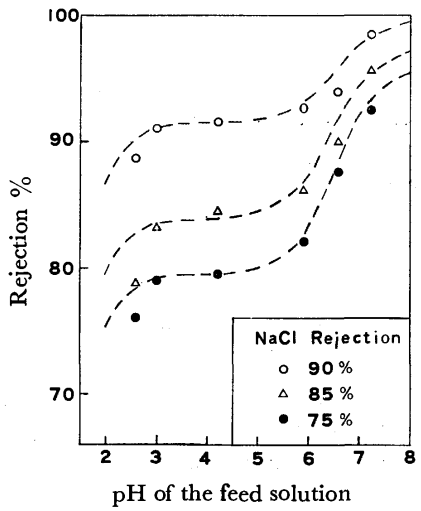

Fig. 1. The effect of pH on the rejection of chromic acid.

of performance, by a strong acidic solution,[6] experiments were carried out as rapidly as possible. That there was no loss of performance of the membrane during the experiment was verified by the fact that there was no change in the water flux or NaCl rejection between before and after the experiment, as is shown in Table 1.

Table 1. Membrane performance before and after experiment

	Memb. ●[a] NaCl rej. %	● Water flux m³/m²·day	△ NaCl rej. %	△ Water flux m³/m²·day	○ NaCl rej. %	○ Water flux m³/m²·day
Before	74.0	1.55	85.3	1.14	90.0	1.07
Intermediate	76.2	1.55	84.1	1.18	90.6	1.09
After	76.8	1.52	84.4	1.18	90.5	1.09

a) Symbols in Table 1 correspond to those in Fig. 1.

Rejection of Additives. The permeation behavior of chromium(III) sulfate and sodium hexafluorosilicate as additives was also examined.

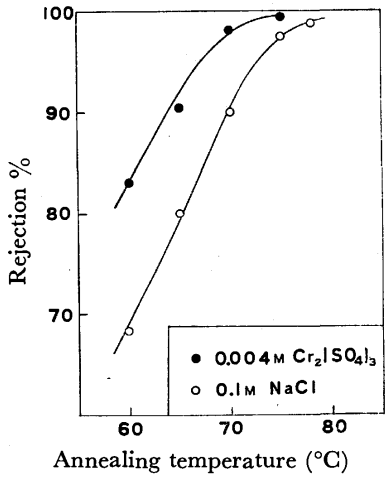

Fig. 2. Rejections of $Cr_2(SO_4)_3$.

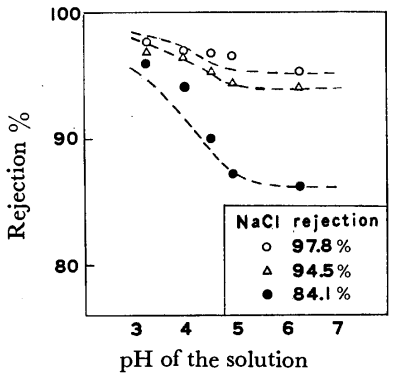

Fig. 3. Rejection of Si in Na_2SiF_6.
------: Calculated rejection.

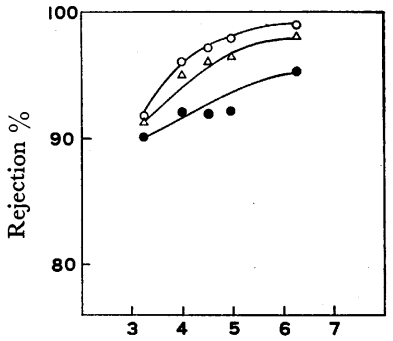

Fig. 4. Rejections of F in Na_2SiF_6.

In the case of inorganic salts, the order of separation is usually consistent with the order of the lyotropic property.[7] In that sense, the rejection of chromium (III) sulfate, which is composed of cations and anions with a high valency, was remarkably higher than that of NaCl, as is shwon in Fig. 2. Since sodium hexafluorosilicate was supposed to dissociate to form various type of species, the rejection was calculated by taking into account the existence of each species.

The analytical data of silicon and fluorine indicate that the rejection of species which contain silicon decreased with the increase in pH, while in the case of species which contain fluorine the opposite is true, as is shown in Figs. 3 and 4.

Discussion

Rejection of Chromic Acid. Chromic acid dissociates in an aqueous solution as follows.

$$H_2CrO_4 \overset{K_1}{\rightleftharpoons} H^+ + HCrO_4^- \quad (2)$$

$$HCrO_4^- \overset{K_2}{\rightleftharpoons} H^+ + CrO_4^{2-} \quad (3)$$

The literature values[7] of the dissociation constants K_1 and K_2 are 1.8×10^{-1} and 3.2×10^{-7} respectively.

The amounts of H_2CrO_4, $HCrO_4^-$, and CrO_4^{2-} in 0.01 M chromic acid solution were calculated using the values of K_1 and K_2. The calculation indicated that at pH 3, most of the chromic acid exists in the solution in the form of $HCrO_4^-$, while at pH 7.25, $HCrO_4^-$ and CrO_4^{2-} exist in the solution in portions of 14.8% and 85.2% respectively. Over the pH range from 2 to

7, the amount of H_2CrO_4 is too small to affect the rejection of chromic acid. Based on the calculation, the expected values of rejection were calculated in the following manner:

(1) The rejection of chromic acid at pH 3 was supposed to be the rejection of $HCrO_4^-$.

(2) Taking into account the existence ratio of CrO_4^{2-} and $HCrO_4^-$, the rejection of CrO_4^{2-} was calculated from the observed rejection at pH 7.25 by using the calculated rejection of $HCrO_4^-$.

(3) The rejection at pH values from 2 to 8 was expressed by the following equation:

$$R = \frac{a(H_2CrO_4) + b(HCrO_4^-) + c(CrO_4^{2-})}{(H_2CrO_4) + (HCrO_4^-) + (CrO_4^{2-})} \quad (4)$$

where a, b, and c are the expected rejections of H_2CrO_4, $HCrO_4^-$, and CrO_4^{2-} respectively. As the amount of H_2CrO_4 was insignificantly small, the value of a is not very important and is supposed to be zero here.

The calculated values of a, b, and c for each membrane are shown in Table 2.

Table 2. Calculated values of a,b, and c

Membrane		a[a)]	b	c
NaCl Rej.	75%	0	79.5	96.0
	85%	0	84.0	97.6
	90%	0	91.5	99.7

a) Not calculated but determined in advance.

The calculated rejections are thus in fair agreement with the experimental values, as is shown in Fig. 1.

At pH 2.5 the observed rejections were several percent lower than the ones expected for each membrane. It can be considered that the amount of species with no charge, H_2CrO_4, became richer at the surface of the membrane, when the concentration of chromic acid increased there due to concentration polarization thereby displacing the equilibrium.

Rejection of Sodium Hexafluorosilicate. The dissociation of sodium hexafluorosilicate is expressed as follows:

$$Na_2SiF_6 \rightleftarrows 2Na^+ + SiF_6^{2-} \quad (5)$$

$$SiF_6^{2-} \overset{K_1}{\rightleftarrows} SiF_4 + 2F^- \quad (6)$$

$$SiF_4 + 2H_2O \overset{K_2}{\rightleftarrows} SiO_2 + 4HF \quad (7)$$

$$HF \overset{K_3}{\rightleftarrows} H^+ + F^- \quad (8)$$

where K_1, K_2, and K_3 are the dissociation constants; their literature values[9] are 1.0×10^{-6}, 1.0×10^{-8}, and 4×10^{-4} respectively.

In this case, the dissociation is so complex that it is very difficult to explain the rejction of each species. The species were, therefore, classified into three groups, containing sodium, fluorine, and silicon respectively.

There are numerous reports[7] seeking to explain the permeation behavior of sodium ions, and so nothing will be mentioned about it here. The species which contain silicon are SiF_6^{2-}, SiF_4, and SiO_2. Calculations based on Eqs. (6), (7), and (8) suggest that at pH 6, the amounts of SiF_6^{2-} and SiF_4 are vanishingly small, while at pH 3 suggests that SiO_2 and SiF_6^{2-} exist in the solution in portions of 30.0 mol.% and 66.6 mol.%. Considering the charged state of the species, SiF_6^{2-} seems to have a much higher rejection rate than the other two species. Just as in the previous section, the rejection of SiO_2 was calculated assuming the amount of SiO_2 to be 5×10^{-3} M at pH 6.25.

Then the rejections of SiF_6^{2-} were calculated considering the existence ratio of each species at pH 3.15. In calculating, it was assumed that the rejection of SiF_4 was almost the same as that of SiO_2, since both of them are the same type of nonelectrolyte. The rejections thus calculated are shown by dotted lines in Fig. 3, and they agree with experimental values. In the case of the separation of the species containing fluorine, it is very difficult to describe the permeation behavior of each species, since there are too many species in the solution.

It may be said, however, that, with an increase in the pH of the solution, HF was enhanced to produce charged species, H^+ and F^-, and that the rejection of the fluorine-containing species became higher, as is shown in Fig. 4. As is shown in this case, the species in the permeated solution are sometimes different from those in the feed solution.

Particular attention should be paid to the cases when species with small solubilities are concentrated or produced in the feed or permeated solution.

Concentration of Chromic Acid. Experiments on the concentration were carried out using a batched-type cell with an effective membrane area of 12.6 cm^2. To avoid concentration polarization, an impeller was rotated over the membrane at 300 r.p.m. The cell was initially charged with 4 l of a chromic acid solution; then it was pressurized with nitrogen gas, which was maintained at 40 atm during the experiment. The permeated solution was collected every hour by using a fraction collector. The initial concentrations of the chromic acid solutions were 0.01—0.05, and each solution was concentrated by a factor of 3—4.

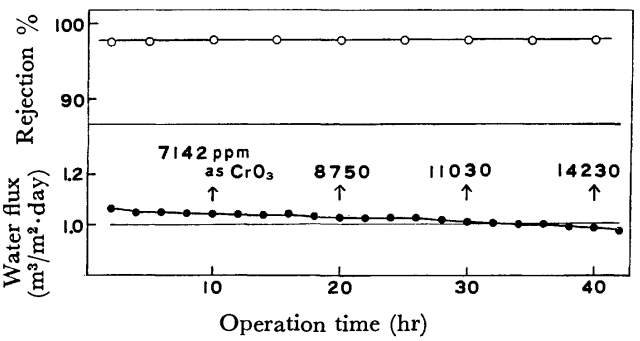

Fig. 5. Concentration of chromic acid. Initial concentration of the feed; 4560 ppm, pH of the feed; 7.1.

Results obtained with an initial concentration of 0.05 M are shown in Fig. 5. Figure 5 indicates that water flux decreased with the increase in the concentration of the feed, while the rejection of chromic acid remained approximately constant. According to those results, the concentration of the permeate was in linear propor-

tion to that of the feed.

When the rejection remains constant, the extent of the concentration can be calculated from the following equation,[10] which corresponds to the concentration process by evaporation:

$$C/C_0 = (V_0/V)^R \quad (9)$$

where C is the concentration of the feed and V is the residual volume of the feed. C_0 and V_0 indicate the initial concentration and volume of the feed.

Later, hexavalent chromium in the permeate should be removed by a method such as ion-exchange resin if the permeate is to be drained off.

The addition of NaOH to control the pH of the feed may be troublesome in that the concentrated solution must be returned to the plating bath. A new type of membrane which has a high resistance to chemicals is expected to be developed.

References

1) A. Golomb, *Plating*, **10**, 1001 (1970).
2) R. G. Donnelly, R. L. Goldsmith, K. J. McNulty, and M. Tan, *Plating*, **5**, 432 (1974).
3) S. Manjikian, S. Loeb, and J. W. McCutchan, First Symposium on Water Desalination, Washington, D. C. (1965), SWD/12.
4) T. Matsuura and S. Sourirajan, *J. Appl. Polym. Sci.*, **15**, 2905 (1971).
5) C. Kamizawa, H. Masuda, and S. Ishizaka, This Bulletin, **45**, 2964 (1972).
6) U. Merten, Ed., "Desalination by Reverse Osmosis," (1966), p. 151.
7) S. Sourirajan "Reverse Osmosis," (1970), p. 29.
8) Gmelin, system-number 52, p. 107.
9) Gmelin, system-number 21, p. 1533.
10) E. S. Perry, Ed., "Progress in Separation and Purification," (1968), p. 323.

Influence of Added Alcohols on the Pfeiffer Effect of Tris-(1,10-phenanthroline)zinc(II)-*l*-Malic Acid and -*d*-Tartaric Acid Systems in Water

Katsuhiko MIYOSHI, Yasushige KURODA, Yuji ISOE, and Hayami YONEDA

Department of Chemistry, Faculty of Science, Hiroshima University, Higashi-senda-machi, Hiroshima 730

(Received August 15, 1975)

Influence of lower alcohols (methanol to butanol) was examined on the Pfeiffer effect of the $[Zn(phen)_3]^{2+}$-*l*-malic acid and -*d*-tartaric acid systems in water at 25 °C (phen=1,10-phenanthroline). It was found that the Pfeiffer rotation α_p decreases linearly with molar concentration C_A of added alcohols for both systems, and that the logarithm of the rate of the decrease in α_p with C_A is a linear function of the number of methylene groups in added alcohol molecules. This is well interpreted on the assumption that added alcohol molecules adhere to $[Zn(phen)_3]^{2+}$ ion, thereby preventing the complex and chiral acid from coming into contact with each other. The enthalpy change per methylene group on passing from the alcohol environment to the complex environment was estimated to be *ca.* 0.7 *RT*.

When a racemic mixture of a certain labile complex is added to a solution containing a chiral compound which is not subject to usual racemization, additional optical activity is developed. This phenomenon is called the Pfeiffer effect[1] and is usually ascribed to spontaneous enantiomerization of the complex in favor of either the *dextro-* or *levo*-form, depending on the spacial demand of the chiral compound present.[2] Partial resolution of some complexes was successfully performed by utilizing this phenomenon,[3] which provides so far the strongest evidence for the occurrence of the enantiomerization in the Pfeiffer-active systems.[4] However, little is known yet as regards the nature of the interaction of the complex with the chiral environment compound.[1]

The Pfeiffer systems are classified into three groups according to their charge types: (1) systems of the same charge, *e.g.*, $[Zn(phen)_3]^{2+}$-*l*-stryH$^+$ and -cinchoH$^+$ systems in water (phen=1,10-phenanthroline, *l*-stryH$^+$ =*l*-strychninium, and cinchoH$^+$=cinchoninium), (2) systems of the opposite charge, *e.g.*, $[Zn(phen)_3]^{2+}$-*d*-BCS$^-$ system in water (*d*-BCS$^-$=*d*-α'-bromocamphor-9-sulfonate), and (3) systems containing nonelectrolytes, *e.g.*, $[Zn(phen)_3]^{2+}$-*l*-malic acid and -*d*-tartaric acid systems in water.[5] The influence of some additives was examined on the systems of the first group and the hydrophobic bonding was proposed as one of the essential driving forces by which $[Zn(phen)_3]^{2+}$ cation could associate with cationic environment compounds such as *l*-stryH$^+$ and cinchoH$^+$ against mutual electrostatic repulsion.[6] In this paper, we report the results of an investigation of the influence of some lower alcohols, dioxane, and urea on the systems of group (3). Zinc-complex systems were chosen since they exhibit an instantaneous Pfeiffer rotation.

Experimental

A stock solution of $[Zn(phen)_3]SO_4$ was prepared by dissolving $ZnSO_4 \cdot 7H_2O$ and phen$\cdot H_2O$ in water in a mole ratio of 1:3. Sample solutions containing $[Zn(phen)_3]SO_4$ and *l*-malic acid or *d*-tartaric acid were prepared by diluting respective stock solutions appropriately in volmetric flasks (25 ml). To these solutions were added methanol, ethanol, 1- and 2-propanol, 1- and 2-butanol, *iso-* and *tert*-butyl alcohol, dioxane, and urea, all of which were of reagent grade. Optical rotations were measured in a 5-cm cell at 405 nm with a Union-Giken PM-71 polarimeter kept at 25±0.1 °C.

Results and Discussion

In Table 1 are listed the observed optical rotations of the $[Zn(phen)_3]^{2+}$-*l*-malic acid and -*d*-tartaric acid systems without additives, where code numbers are attached to identify the systems. In Figs. 1—4 is plotted the Pfeiffer rotation α_p, defined as the observed rotation of the Pfeiffer system minus that of the chiral environment compound α_e, as a function of molar concentration

Table 1. Observed rotations in degrees at 405 nm of the Pfeiffer systems[a]

System	Racemic complex	Chiral compd	Rotation of chiral compd, α_e	Obsd Rotation, α_{obsd}	Pfeiffer Rotation, α_p
	$[Zn(phen)_3]SO_4$				
		l-malic acid			
1a	0.02M	0.02M	−0.002	−0.219	−0.217
1b	0.02M	0.03M	−0.003	−0.335	−0.332
	$[Zn(phen)_3]SO_4$				
		d-tartaric acid			
2a	0.02M	0.02M	+0.034	+0.453	+0.419
2b	0.01M	0.03M	+0.049	+0.379	+0.330

a) In a 5 cm cell at 25 °C.

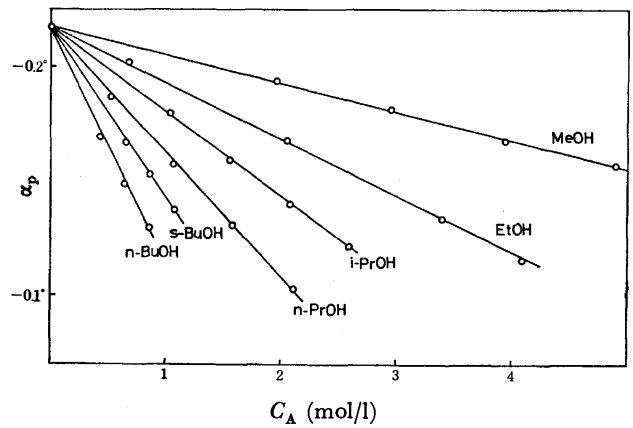

Fig. 1. Plots of α_p as a function of molar alcohol concentration C_A for the $[Zn(phen)_3]^{2+}$ (0.02 M)-*l*-malic acid (0.02 M) system (system 1a).

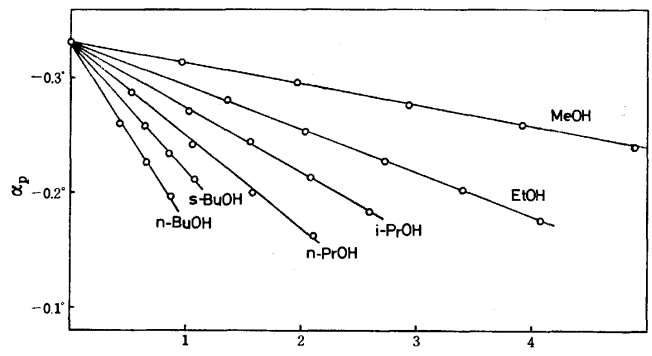

Fig. 2. Plots of α_p as a function of molar alcohol concentration C_A for the $[Zn(phen)_3]^{2+}$ (0.02 M)-*l*-malic acid (0.03 M) system (system 1b).

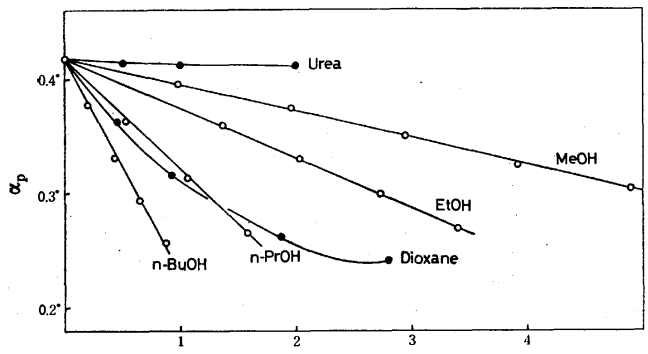

Fig. 3. Plots of α_p as a function of molar concentration of additives C_A for the $[Zn(phen)_3]^{2+}$ (0.02 M)-*d*-tartaric acid (0.02 M) system (system 2a).

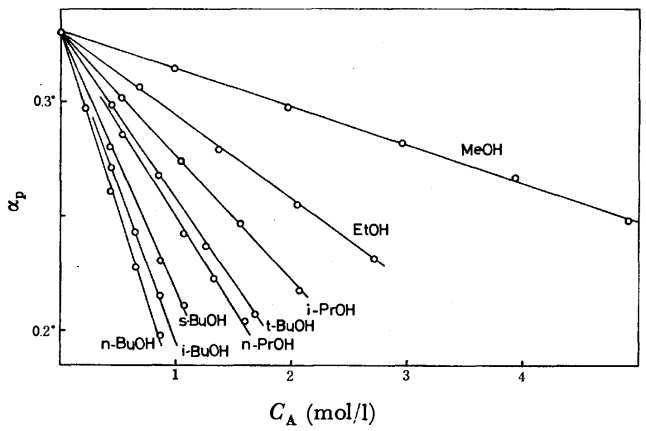

Fig. 4. Plots of α_p as a function of molar alcohol concentration C_A for the $[Zn(phen)_3]^{2+}$ (0.01 M)-*d*-tartaric acid (0.03 M) system (system 2b).

of additives. Since α_e was somewhat affected by the additives, all the α_p's plotted are corrected values as regards small changes in α_e. It is seen that α_p decreases linearly with molar alcohol concentration C_A for both systems, and that the longer the carbon chain of the alcohol molecules, and the greater the Pfeiffer rotation, the steeper the slopes. We are thus led to suppose that added alcohol molecules intervene between the complex and chiral acid, thereby preventing them from coming into contact with each other. In other words, it is assumed that added alcohol molecules are distributed between aqueous phase and the aggregate composed of the complex and chiral acid, the latter being called the Pfeiffer aggregate.[7]

According to the regular solution theory,[8] the chemical potential of the alcohol transferred to water, μ_w, is given by

$$\mu_w = \mu^\circ + RT\ln x_w + m\omega_w^{CH_2} + \omega_w^{OH} \quad (1)$$

where x_w is mole fraction of the alcohol in water, $\omega_w^{CH_2}$ and ω_w^{OH} represent the enthalpy change of CH_2- and OH-groups, respectively on passing from the alcohol environment to water, and m is the number of CH_2-groups in the alcohol molecule.[9] The corresponding chemical potential in the Pfeiffer aggregate, μ_p, is given in a similar manner by

$$\mu_p = \mu^\circ + RT\ln x_p + m\omega_p^{CH_2} + \omega_p^{OH} \quad (2)$$

where x_p is mole fraction of the alcohol in the Pfeiffer aggregate, and $\omega_p^{CH_2}$ and ω_p^{OH} represent the corresponding enthalpy changes from the alcohol environment to the Pfeiffer aggregate. In distribution equilibrium, μ_w must be equal to μ_p. Then, from Eqs. (1) and (2),

$$\ln(x_p/x_w) = m(\omega_p^{CH_2}-\omega_p^{CH_2})/RT + (\omega_w^{OH}-\omega_p^{OH})/RT \quad (3)$$

It seems reasonable to assume that α_p is proportional to the concentration of the Pfeiffer aggregate, and its decrease upon the addition of alcohols is in turn proportional to that of the alcohols in the Pfeiffer aggregate. Then, x_p is expressed as

$$x_p = K_i d\alpha_p/\alpha_p \quad (4)$$

where K_i is a proportionality constant and $d\alpha_p$ is the decrease in α_p when added alcohol concentration is dC_A. On the other hand, x_w is approximated to $C_A/55.5$, since C_A is sufficiently low and the amount of the alcohol transferred to the Pfeiffer aggregate is at most equal to or less than that of the complex or chiral acid present. Substituting the above relations, Eq. (3) is rearranged into

$$\ln(d\alpha_p/\alpha_p dC_A) = m(\omega_w^{CH_2}-\omega_p^{CH_2})/RT + (\omega_w^{OH}-\omega_p^{OH})/RT + C_i \quad (5)$$

where C_i is a constant for a given Pfeiffer system. Equation (5) indicates that a linear relationship holds between $\ln(d\alpha_p/\alpha_p dC_A)$ and m.

Table 2. Derived values of $(d\alpha_p/\alpha_p dC_A)$ and $(\omega_w^{CH_2}-\omega_p^{CH_2})$

Added alcohol	1a	1b	2a	2b
MeOH	5.87×10^{-2}	5.70×10^{-2}	5.83×10^{-2}	5.16×10^{-2} a)
EtOH	1.13×10^{-1}	1.16×10^{-1}	1.06×10^{-1}	1.09×10^{-1}
n-PrOH	2.44×10^{-1}	2.45×10^{-1}	2.40×10^{-1}	2.41×10^{-1}
i-PrOH	1.70×10^{-1}	1.72×10^{-1}		1.65×10^{-1}
n-BuOH	4.89×10^{-1}	4.83×10^{-1}	4.65×10^{-1}	4.67×10^{-1}
s-BuOH	3.44×10^{-1}	3.44×10^{-1}		3.43×10^{-1}
i-BuOH				4.16×10^{-1}
t-BuOH				2.23×10^{-1}
$(\omega_w^{CH_2}-\omega_p^{CH_2})$ b)	$0.714RT$	$0.716RT$	$0.705RT$	$0.728RT$

a) Omitted in the calculation because of somewhat large deviation. b) Calculated using the values for normal alcohols only.

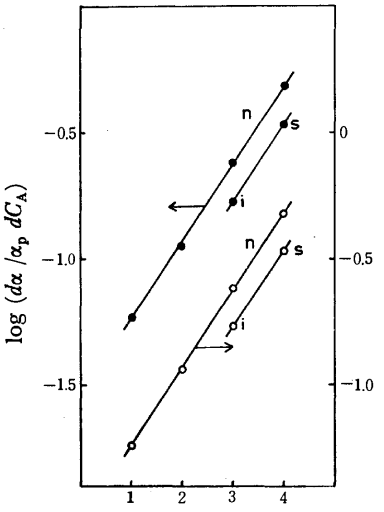

Fig. 5. Plots of $\log(d\alpha_p/\alpha_p dC_A)$ *vs.* m for the $[Zn(phen)_3]^{2+}$-*l*-malic acid system. Filled circles (system 1a) and open circles (system 1b) correspond to left- and right-hand scales, respectively.

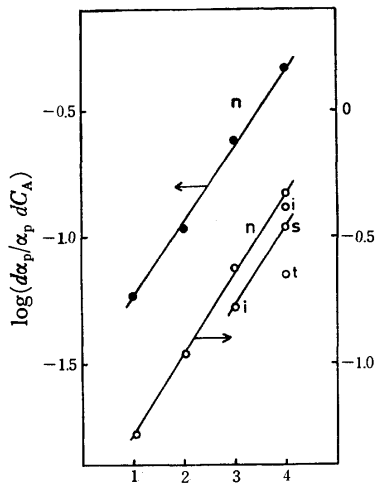

Fig. 6. Plots of $\log(d\alpha_p/\alpha_p dC_A)$ *vs.* m for the $[Zn(phen)_3]^{2+}$-*d*-tartaric acid system. Filled circles (system 2a) and open circles (system 2b) correspond to left- and right-hand scales, respectively.

In Table 2 are listed the values of $(d\alpha_p/\alpha_p dC_A)$, where code numbers correspond to those in Table 1. It is seen that for a given alcohol, these values are almost constant for a given system irrespective of the magnitude of its Pfeiffer rotation. This supports the validity of Eq. (5). In Figs. 5 and 6 is plotted log $(d\alpha_p/\alpha_p dC_A)$ *vs.* m for the $[Zn(phen)_3]^{2+}$-*l*-malic acid and -*d*-tartaric acid systems, respectively. We see that a good linearity holds, as expected from Eq. (5), and that the slope for *n*-alcohols is nearly equal to that for 2-propanol and 2-butanol. The α_p-decreasing order of butanol isomers is found to follow the order of their solubility in water. From these figures, the value of $(\omega_w^{CH_2}-\omega_p^{CH_2})$ corresponding to the enthalpy change per CH_2-group of the alcohol molecule on passing from the Pfeiffer aggregate to water, was estimated by the least squares method

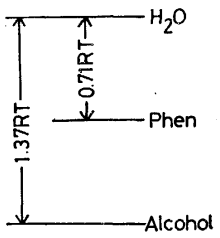

Fig. 7. Energy diagram for the CH_2-group in different environments.

and is included in Table 2.

The value of $\omega_w^{CH_2}$ was estimated by Kinoshita *et al.*[10] to be 1.37 RT from the solubility measurement of higher alcohols in water. The energy diagram for the CH_2-group in different environments is established as shown in Fig. 7. The value of $(\omega_w^{CH_2}-\omega_p^{CH_2})$ for the $[Zn(phen)_3]^{2+}$-*l*-malic acid and -*d*-tartaric acid systems is nearly equal to the value (0.67 RT) found for the $[Zn(phen)_3]^{2+}$-*l*-stryH$^+$ and -cinchoH$^+$ systems, but somewhat different from that (0.57 RT) for the $[Zn(bipy)_3]^{2+}$-cinchoH$^+$ systems (bipy=2,2'-bipyridine).[6,11] The value depends on the kind of racemic complexes but not the chiral environment compound. This suggests that added alcohol molecules adhere to the complex, rather than being distributed between the Pfeiffer aggregate and aqueous phase, thereby diminishing the Pfeiffer effect. It seems necessary for the complex and chiral acid to come into direct contact with each other in order to exhibit additional optical activity.

The influence of dioxane and urea on the $[Zn(phen)_3]^{2+}$-*d*-tartaric acid system is shown in Fig. 3. The striking feature is that the system is considerably affected by dioxane but not appreciably by urea, though both additives diminish the Pfeiffer effect of the first group greatly.[6] This implies that the driving force in developing the Pfeiffer effect in the third group differs from that in the first group[6] for which we have proposed the hydrophobic bonding.[1b,13] For the system of the third group Kirschner[2,12] proposed the hydrogen bonding between the hydrogen in the –COOH and –OH groups of the environment substance and the complex's pi electrons of the aromatic rings. The present result in which addition of urea has little influence on the Pfeiffer effect clealy contradicts the hydrophobic bonding mechanism. We are inclined to assume the hydrogen bonding as the probable cause of the Pfeiffer effect in the system of the third group.

The authors wish to thank the Ministry of Education for the financial support granted for this research.

References

1) a) S. Kirschner and N. Ahmad, "Coordination Chemistry," Ed. by S. Kirschner, Plenum Press, New York, N. Y. (1969), p. 42; b) R. C. Brasted, V. J. Landis, E. J. Kuhajek, P. E. Nordquist, and L. Mayer, *ibid.*, p. 64.
2) S. Kirschner, *J. Indian Chem. Soc.*, **51**, 28 (1974).
3) S. Kirschner and N. Ahmad, *J. Amer. Chem. Soc.*, **90**,

1910 (1968).

4) Even symmetrical complexes sometimes exhibit anomalous optical activity when they are mixed with or dissolved into some chiral compounds. This phenomenon is attributed to an outer-sphere association of these complexes with chiral compounds and involves no enantiomerization of the complexes.

5) The Pfeiffer effect is observed also in some nonaqueous solvents. See, S. Kirschner, N. Ahmad, and K. R. Magnell, *Coord. Chem. Rev.*, **3**, 201 (1968).

6) K. Miyoshi, K. Sakata, and H. Yoneda, *J. Phys. Chem.*, **79**, 1622 (1975).

7) The structure of the aggregate has not been clarified yet. However, it is certain that the complex behaves as if it is aware of the optical activity of the chiral acid.

8) J. H. Hildebrand and R. L. Scott, "The solubility of Nonelectrolytes," 3rd ed., Reinhold Publishing Corp., New York, N. Y. (1950).

9) Strictly speaking, the interaction of the CH_3-group with water, alcohol, and the Pfeiffer aggregate differs from that of the CH_2-group. However, the difference was not detected under our experimental conditions. Therefore, m is put equal to the number of all carbon atoms in the alcohol molecule. For the group additivity of enthalpy changes, see, C. V. Krishnan and H. L. Friedman, *J. Phys. Chem.*, **73**, 1572 (1969); *ibid.*, **75**, 3598 (1971).

10) K. Kinoshita, H. Ishikawa, and K. Shinoda, This Bulletin, **31**, 1081 (1958).

11) Though the values of $(\omega_w^{CH_2}-\omega_p^{CH_2})$ for the $[Zn(phen)_3]^{2+}$-*l*-stryH$^+$ and -*d*-cinchoH$^+$ systems are not given in Ref. 6, they are derived from the data listed in Table 2 of Ref. 6. The value for the $[Zn(bipy)_3]^{2+}$-cinchoH$^+$ system is from our unpublished data.

12) R. Pollock, Ph. D. Dissertation, Wayne State University (1972).

13) G. Némethy, *Angew. Chem., Int. Ed. Engl.*, **6**, 195 (1967)

Transition-metal Complexes of Pyrrole Pigments. XIII. Reduction and Coordination Behaviors of the Cobalt(II) Complexes of 1,19-Disubstituted Tetradehydrocorrins as Demonstrated by the Presence of Various Bases*

Yukito MURAKAMI and Yasuhiro AOYAMA

Department of Organic Synthesis, Faculty of Engineering, Kyushu University, Hakozaki, Higashi-ku, Fukuoka 812

(Received August 27, 1975)

The interaction of various bases with the cobalt(II) complexes of 1,19-disubstituted tetradehydrocorrins (Co(II)-TDHC) was investigated. The parent cobalt(II) complexes were shown to undergo ready reduction at the nuclear cobalt(II) with the unsolvated hydroxide ion as well as with bulky triethylamine. A relatively large positive reduction potential of Co(II)-TDHC is responsible for these novel electron transfer reactions. Less hindered amines (B), on the other hand, failed to show such electron transfer reactions with the cobalt(II) complexes and Co(II)-TDHC became the pentacoordinated complex by taking up an amine base in the axial position: Co(II)-TDHC+B$\rightleftharpoons$B-Co(II)-TDHC. For the interaction of 4-substituted pyridines with the cobalt(II) complex, the general behavior of the equilibrium constants was interpreted in terms of the amine basicity and the Hammett equation by referring to the corresponding behavior of the porphyrin complexes. The weaker coordination tendency of some aliphatic amines and hindered pyridines toward Co(II)-TDHC was attributed to their electronic and steric effects in the coordination process. The intrinsic correlation between electronic and stereochemical characteristics pertaining to the tetradehydrocorrin skeleton and the nature of nuclear cobalt(II) was discussed on the basis of these observations.

In order to provide the chemical basis for the enzymatic functions of naturally occurring macrocyclic complexes such as metal corrinoids and porphyrins, extensive investigations have been carried out on the redox properties of a series of synthetic macrocyclic complexes of various electronic characters.[1-4] Among the biological redox systems, vitamin B_{12}, which involves a corrin framework (**1**), has attracted particular attention from the viewpoint of its unique ability to form a Co(III)-C σ bond.[5,6] The cobalt(I) species has been widely recognized as the key intermediate in the alkylation of vitamin B_{12} and a number of synthetic cobalt complexes have been shown to undergo alkylation *via* nucleophilic reactions of the cobalt(I) intermediates generated by reduction of the parent cobalt(II) or cobalt(III) complexes.[6-12] The redox property of a cobalt complex would be controlled by several factors, such as the cavity size provided by a macrocyclic skeleton which incorporates a cobalt ion, the electronic structure of a macrocyclic ligand, and so on. Attempts have been made to clarify the structural characteristics of these macrocycles which lead to the formation of stable Co(III)-C bonds,[1,11,12] but no satisfactory explanation has been given so far for the significance of the corrinoid structure. In connection with the chemistry of corrinoids, the tetradehydrocorrins (**2**), which have a macrocyclic framework closely related to the corrins (**1**), have been prepared and their metal complexes have been investigated from several structural viewpoints.[13-15] On the basis of these structural studies, the interaction of the hydroxide ion and various organic bases with the cobalt(II) complexes of 1,19-disubstituted tetradehydrocorrins was investigated in the present study. This work, therefore, may elucidate the effects of electronic and stereochemical structures pertaining to the tetradehydrocorrin skeleton on the reactivity of nuclear cobalt(II).

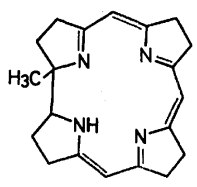

1

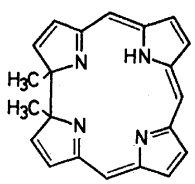

2

* Contribution No. 378 from this Department. Part XII: Y. Murakami, K. Sakata, Y. Tanaka, and T. Matsuo, This Bulletin, **48**, 3622 (1975).

Experimental

Electronic spectra were taken on a Hitachi EPS-2 recording spectrophotometer. NMR spectra were recorded on a Varian A-60 spectrometer. Solvents for spectroscopic measurements were prepared by the standard procedures.[16] Sodium hydroxide and potassium hydroxide of analytical grade were obtained from commercial sources. Diethylammonium chloride was recrystallized twice from ethanol–ether and dehydrochlorinated with sodium hydroxide. Free diethylamine was recovered by fractional distillation after being dried over potassium hydroxide. Similarly, triethylamine was obtained from triethylammonium chloride recrystallized twice from ethanol. Other liquid amines (pyridine, 2-methyl- and 4-methylpyridine, 2,4,6-trimethylpyridine, butylamine, and piperidine) were refluxed with potassium hydroxide and then fractionally distilled. Commercially available 4-cyanopyridine and imidazole were recrystallized from aqueous ethanol and benzene, respectively. 4-Aminopyridine was prepared by ammonolysis of (4-pyridyl)pyridinium dichloride[17] and recrystallized twice from benzene. The purity of these organic amines was checked by gas chromatographic analysis. Dibenzo-18-crown-6 and its potassium hydroxide complex were prepared after Pedersen.[18]

*Tetradehydrocorrinatocobalt(II) Perchlorates (**7a** and **7b**).* 8,12-Diethyl-1,2,3,7,13,17,18,19-octamethyltetradehydrocorrinatocobalt(II) perchlorate (**7a**) was prepared after Johnson *et al.*[19,20] with slight modifications. First, 2,4-dimethyl-3-

acetyl-5-ethoxycarbonylpyrrole was converted to 2,4-dimethyl-3-ethyl-5-ethoxycarbonylpyrrole (**3**, yield 90%) by essentially the same procedure as applied for the synthesis of 2,3,4-triethyl-5-ethoxycarbonylpyrrole.[21] Then, **3** was brominated at the 2-methyl group and further converted to 3,3′-diethyl-4,4′-dimethyl-5,5′-diethoxycarbonyldipyrromethane (**4**, yield 87%) *via* solvolytic coupling of the resulting 2-bromomethyl derivative.[22] The dipyrromethane (**4**) was recrystallized from aqueous ethanol (mp 123.5—125 °C; lit,[23] 126 °C) and hydrolyzed quantitatively with sodium hydroxide to give 3,3′-diethyl-4,4′-dimethyl-5,5′-dicarboxydipyrromethane (**5**). 2-Formyl-3,4,5-trimethylpyrrole underwent condensation with **5** in the presence of hydrogen bromide to afford 1,19-dideoxy-8,12-diethyl-1,2,3,7,13,17,18,19-octamethylbiladiene-ac dihydrobromide (**6**) according to the general procedure of Johnson *et al.*[19] (yield 30—65%). Aeration of a mixture of biladiene-ac dihydrobromide **6** and cobalt acetate tetrahydrate in ethanol followed by addition of sodium perchlorate afforded the tetradehydrocorrinatocobalt(II) perchlorate (yield 35—40%); recrystallized from acetone–benzene. The preparation of 2,8,12,18-tetrakis(2-ethoxycarbonylethyl)-1,3,7,13,17,-19-hexamethyltetradehydrocorrinatocobalt(II) perchlorate (**7b**) has been described previously.[15]

NMR Spectrum of Tetradehydrocorrinatocobalt(I) (8b). To a dichloromethane solution (5 ml) of **7b** (50 mg) was added solid sodium hydroxide (1.0 g) under nitrogen atmosphere, and the mixture was stirred for 2 hr at room temperature. Sodium hydroxide was then removed by filtration. The electronic spectrum of the filtrate indicated the complete conversion of **7b** to **8b**. Most of the solvent was carefully removed under dry nitrogen. The NMR spectrum of the residue (**8b**): δ 1.49 (6H, s, 1,19-C$\underline{H}_3$), 1.85 and 2.45 (both 6H, s, 3,7,13,17-C$\underline{H}_3$), 9.78 (2H, s, 5-$\underline{H}$ and 15-$\underline{H}$), 10.82 (1H, s, 10-$\underline{H}$), 1.27 (12H, t, $CO_2CH_2C\underline{H}_3$), 3.6—4.5 (16H, multi, $CH_2C\underline{H}_2CO_2C\underline{H}_2CH_3$) and 2.9—3.4 (8H, multi, $C\underline{H}_2CH_2$-$CO_2CH_2CH_3$).

Reduction of 7a with the Potassium Hydroxide Complex of Dibenzo-18-crown-6. Into a benzene solution of **7a** (1×10^{-5} M) was added the potassium hydroxide complex of dibenzo-18-crown-6 in an excess amount. The mixture was stirred for 5 min under nitrogen. The electronic spectrum of the mixture showed that **7a** was completely converted to the tetradehydrocorrinatocobalt(I) (**8a**). Controlled experiments were carried out by addition of a calculated amount of a benzene solution of the potassium hydroxide complex (1.5×10^{-2} M).

Determination of Equilibrium Constants for the Complex Formation Between 7a and Amine Bases. The interaction of **7a** with an amine base was investigated by measuring the visible spectra of a series of solutions in which the concentration of an amine was varied in about 10^2-fold range on one side and that of **7a** maintained constant (3×10^{-5} M) on the other. According to the Benesi-Hildebrand relationship, the equilibrium constant for the complex formation between **7a** and an amine base was determined on the basis of spectral changes observed upon addition of an amine.

Results and Discussion

Reduction of Tetradehydrocorrinatocobalt(II) Perchlorates with Hydroxide Ion. The reaction of tetradehydrocorrinatocobalt(II) perchlorates (**7a** and **7b**, Co(II)–TDHC hereafter) with sodium hydroxide was investigated at room temperature. When the reaction was carried out in an aprotic solvent (dichloromethane, THF, acetonitrile, or pyridine) with solid sodium

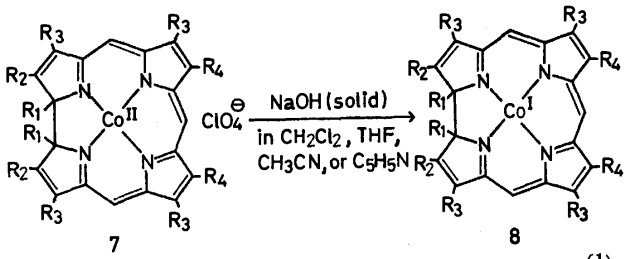

hydroxide, the product was identified as the tetradehydrocorrinatocobalt(I) complex (**8a** or **8b**, Co(I)–TDHC hereafter, refer to Eq. (1)) due to the following facts: (1) the electronic spectrum of the product (**8a**) was almost identical with that of 1,19-diethoxycarbonyl-8,12-diethyl-2,3,7,13,17,18-hexamethyltetradehydrocorrinatocobalt(I) (**8c**) obtained by reduction of the corresponding cobalt(II) complex with sodium film[13] (Fig. 1); (2) the product (**8b**) was diamagnetic and showed a sharp NMR spectrum, suggesting the d^8 configuration of cobalt(I); and (3) the product was oxidized by oxygen only slowly back to the parent cobalt(II) complex, but instantaneously upon treating with iron(III) chloride, as observed for **8c**.[13]

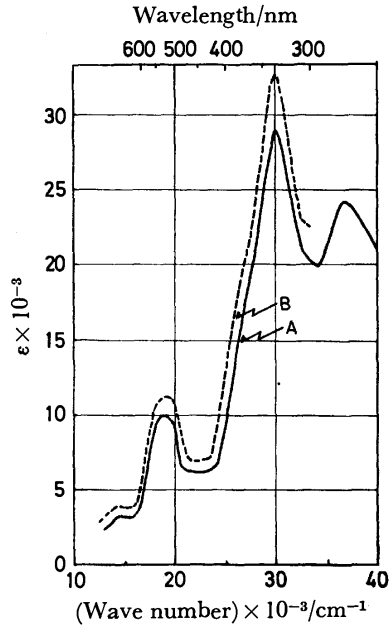

Fug. 1. Electronic spectra of 8,12-diethyl-1,2,3,7,13,17,-18,19-octamethyltetradehydrocorrinatocobalt(I) (**8a**) at room temperature: A, in dichloromethane; B, in pyridine.

As shown in Fig. 2, the electronic spectrum of the parent cobalt(II) complex (**7a**) shows an appreciable solvent dependence. This spectral behavior seems to indicate a further coordination of one pyridine molecule at the axial position of the complex, which is consistent with the corresponding ESR data.[13,15] In contrast, the electronic spectrum of the cobalt(I) species (**8a**) does not show any significant change upon changing the solvent from dichloromethane to pyridine. This fact

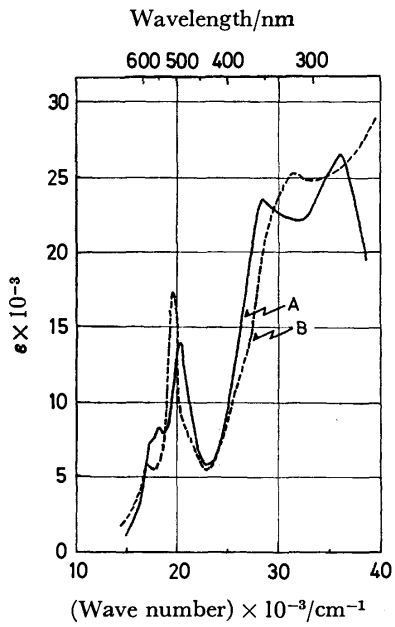

Fig. 2. Electronic spectra of 8,12-diethyl-1,2,3,7,13,17,-18,19-octamethyltetradehydrocorrinatocobalt(II) perchlorate (**7a**) at room temperature: A, in dichloromethane; B, in pyridine.

indicates that the reduced complex has no further ability to coordinate with an organic base. The reduction of Co(II)–TDHC failed in both dichloromethane and methanol solutions, even though the saturation level of sodium hydroxide concentration was maintained. These results indicate that the novel electron transfer from sodium hydroxide to Co(II)–TDHC takes place on the solid surface of the base. In marked contrast, the ready reduction of Co(II)–TDHC was again observed in an aprotic solvent (acetonitrile, THF, or benzene) with potassium hydroxide solubilized *via* complex formation with a cyclic polyether, dibenzo-18-crown-6 (**9**). Controlled experiments showed that Co(II)–TDHC was completely reduced to Co(I)–TDHC with less than 3 equivalents of the crown complex, indicating that the active reducing reagent was certainly the hydroxide ion and not any impurity which may exist in alkaline hydroxide. The observed successful reduction of Co(II)–TDHC may be attributed to the absence of any solvation effects for the hydroxide ion. The hydroxide ion at the solid surface or in an aprotic solvent may exist in a naked state without any significant solvation, and is consequently active enough to transfer an electron to an appropriate acceptor, *i.e.* Co(II)–TDHC. The activation of inorganic anions through the complex formation with crown polyethers has been reported for some nucleophilic and oxidation reactions.[24–26]

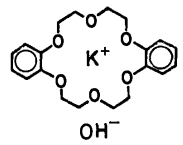

9

The electron-transfer mechanism for the hydroxide–Co(II)–TDHC system is not fully understood. Gillard has suggested that an unstable intermediate cobalt(II) species is present in the ligand substitution of a cobalt(III) complex, as promoted with a hydroxide ion (Eq. (2)).[27]

$$L_5Co(III)\text{-}Br + OH^- \longrightarrow (L_5Co(II)\cdot OH) + Br^- \longrightarrow L_5Co(III)\text{-}OH + Br^- \quad (2)$$

Cobalt(II) corrinoids[28,29] as well as bis(dimethylglyoximato)cobalt(II)[28,30] have been known to undergo disproportionation in alkaline solutions to the corresponding cobalt(I) and cobalt(III) complexes. A mechanistic distinction, however, should be made between those reactions and the present novel reduction of Co(II)–TDHC. The hydroxide ion transfers an electron to the cobalt(II) complex in the present reaction without its final coordination to or causing disproportionation of Co(II)–TDHC. Such a strong oxidizing power of Co(II)–TDHC is consistent with its higher positive reduction potential relative to other analogous cobalt complexes (Table 1).

There are a number of papers which have reported the successful preparation of coordination compounds containing Co(III)–C σ bonds.[6–12] The nucleophilic attack of a cobalt(I) species on an appropriate alkyl donor seems to provide the most suitable method for such preparative purposes. The present Co(I)–TDHC appears to be an exception for this kind of reaction. Addition of methyl iodide to a solution of Co(I)–TDHC did not result in the formation of a Co(III)–C bond, and no other reaction was detected as proceeding in the system. This result can be understood in the light of the electrochemical data listed in Table 1. The nucleophilicity of various cobalt(I) complexes seems to follow the order of the Co(II)–Co(I) reduction potential.[6,31] The Co(I)–Bae complex, among the complexes listed in Table 1, reacts even with bromobenzene, while Co(I)[(DO)(DOH)pn]P(C_6H_5)$_3$ does not show any reactivity toward propyl bromide even after a prolonged time.[9] Thus, the lack of any nucleophilicity of Co(I)–TDHC appears to be reasonable on the basis of its reduction-oxidation trend, as listed in Table 1. In conclusion, the effects of the corrin and tetradehydrocorrin rings on the reduction-oxidation

Table 1. Co(II)–Co(I) reduction potentials for the $Co^{II}L$ complexes

L[a]	Bae	Salen	Saloph	$(DH)_2$	B_{12r}	(DO)(DOH)pn	**7a**	**7c**
$E_{1/2}$ (V *vs.* S.C.E.)	−1.50	−1.38	−1.35	−1.24	−1.02	−0.85	−0.25	−0.16
Ref.	9	42	42	42	9	9	43	13

a) Bae, *N,N'*-ethylenebis(acetylacetoniminato); Salen, *N,N'*-bis(salicylidene)ethylenediamino; Saloph, *N,N'*-bis(salicylidene)-*o*-phenylenediamino; $(DH)_2$, bis(dimethylglyoximato); (DO)(DOH)pn, 1-(diacetylmonoximato-imino)-3-(diacetylmonoximeimino)propane; B_{12r}, vitamin B_{12r}.

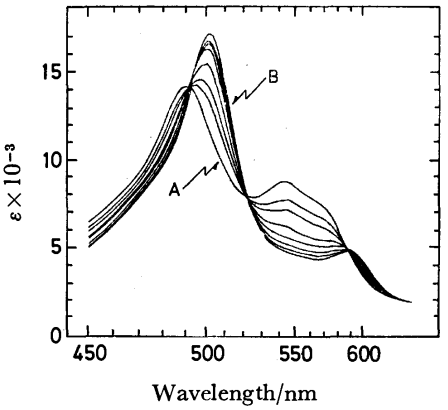

Fig. 3. Electronic spectra of the tetradehydrocorrinatocobalt(II) perchlorate (**7a**) (3.47×10^{-5}M) in dichloromethane at various concentrations of 4-methylpyridine: 0, 7.93×10^{-5}, 1.59×10^{-4}, 3.97×10^{-4}, 7.93×10^{-4}, 1.59×10^{-3}, and 3.02×10^{-3} M (read from A to B).

behavior of the nuclear cobalt are not so alike as would be judged from the similarity in their skeletal structures.

Interaction of Tetradehydrocorrinatocobalt(II) Perchlorates with Amine Bases. The electronic spectrum of Co(II)–TDHC dissolved in dichloromethane underwent variation upon addition of any of the following amine bases: substituted pyridines (4-NH_2, 4-CH_3, 4-CN, 2-CH_3, and 2,4,6-$(CH_3)_3$), imidazole, and aliphatic amines (butyl, diethyl, and piperidine). Since the spectral feature is almost identical with that for the pyridine adduct shown in Fig. 2, the cobalt(II) ion becomes pentacoordinated by having an amine base in the axial position as the fifth ligand. The spectral variations upon addition of 4-methylpyridine are shown in Fig. 3 as an example. The effect of amine concentration on the spectral change was consistent with the following solution equilibrium:

$$\text{Co(II)-TDHC} + \text{B} \overset{K}{\rightleftharpoons} \text{B-Co(II)-TDHC} \qquad (3)$$

where B stands for an amine base. The observations of isosbestic points at 491, 523, and 590 nm and the unit slope for the plots of log([B–Co(II)–TDHC]/[Co(II)–TDHC]) *vs.* log[B] are further evidence for the 1 : 1 complex formation for each of the amine ligands treated, in contrast to the case of the cobalt(II) porphyrin system for which the ESR data suggested the formation of 1 : 2 (metal complex to base) complexes.[32] The equilibrium constants (K) were obtained from the intensity change at 502 nm by adopting the Benesi-Hildebrand-type relation[33] (Eq. (4)).

$$\frac{[\text{Co(II)-TDHC}][\text{B}]}{\Delta A} = \frac{1}{\Delta\varepsilon \cdot K} + \frac{[\text{B}]}{\Delta\varepsilon} \qquad (4)$$

In this equation, [Co(II)–TDHC] and [B] stand for the total concentrations of **7a** and amine, respectively, $\Delta\varepsilon$ is the difference in molar extinction coefficient between Co(II)–TDHC and B–Co(II)–TDHC, and ΔA represents the extent of the absorbance change upon addition of amine bases. A good linear correlation based on Eq. (4) is observed, as shown in Fig. 4 for the Co(II)–

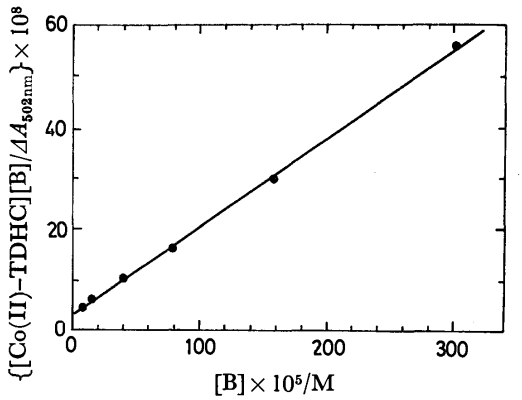

Fig. 4. Benesi-Hildebrand plot for the complex-forming equilibrium between 4-methylpyridine (B) and Co(II)–TDHC (**7a**).

TDHC–4-methylpyridine system: $K=5.90\times10^3\,M^{-1}$ and $\Delta\varepsilon=0.578\times10^4$. This $\Delta\varepsilon$ value is in good agreement with that obtained upon addition of a large excess of 4-methylpyridine (0.584×10^4). Equilibrium constants for other amines were obtained in a similar manner, and are summarized in Table 2.

Table 2. Formation constants for the amine complexes of Co(II)–TDHC (**7a**)[a]

Amine[b]	$pK_a(BH^+)$	K, M^{-1}
Py	5.19	1.95×10^3
4-NH_2Py	9.11	1.60×10^4
4-MePy	6.02	5.90×10^3
4-CNPy	1.90	3.00×10^2
2-MePy	5.97	5.16
2,4,6-Me_3Py	7.48	4.11
Im	7.25[c]	9.85×10^3
n-$BuNH_2$	10.59	1.85×10^3
Et_2NH	10.98	*ca.* 1.5×10[d]
Pip	11.22	1.15×10^3

a) Measured in dichloromethane at 15 °C. b) Py, pyridine; 4-MePy, 4-methylpyridine; 4-NH_2Py, 4-aminopyridine; 4-CNPy, 4-cyanopyridine; 2-MePy, 2-methylpyridine; 2,4,6-Me_3Py, 2,4,6-trimethylpyridine; Im, imidazole; n-$BuNH_2$, butylamine; Et_2NH, diethylamine; Pip, piperidine. c) Statistically corrected for two hydrogens in ImH^+. d) Determined at low concentrations of diethylamine: see Ref. 41.

The equilibrium constants for the formation of pyridine and imidazole adducts of **7a** are comparable in magnitude to those for the porphyrin complexes, but significantly larger than those for the Schiff base complexes, as shown in Table 3. This is consistent with the prediction based on the electrochemical data, *i.e.*, the more negative the cobalt(II)-cobalt(I) reduction potential the smaller the equilibrium constant. Apparently, there exists no systematic correlation between log K and amine basicity, as shown in Fig. 5, without considering the structural characteristics of the amine bases. However, if the 4-substituted pyridines are taken up, the following correlation is established by a least squares analysis, where $a=0.24$ and $b=2.1$:

$$\log K = apK_a + b \qquad (5)$$

Table 3. Formation constants for the $Co^{II}LB$ complexes[a]

L[b]	B[b] Py	B[b] Im	B[b] MeIm	Ref.
TDHC (**7a**)[c]	1.95×10^3	9.85×10^3		This work
PP(IX)DME[d]	6.0×10^3	4.4×10^3	5.0×10^3	38
		4.5×10^3	5.1×10^3	36
p-MeOTPP[e]	4.85×10^2	1.40×10^3	2.37×10^3	37
Saloph[f]	2.0×10^2	1.2×10^3		44
Salen			2.3×10	44
			2.6×10	45

a) Formation constants are given in M^{-1}. b) Py, pyridine; Im, imidazole; MeIm, 1-methylimidazole; TDHC, tetradehydrocorrin; PP(IX)DME, protoporphyrin IX dimethyl ester; *p*-MeOTPP, α,β,γ,δ-tetrakis(*p*-methoxyphenyl)porphyrin; Saloph, *N*,*N*′-bis(salicylidene)-*o*-phenylenediamino; Salen, *N*,*N*′-bis(salicylidene)ethylenediamino. c) In dichloromethane at 15 °C. d) In toluene at 23 °C. e) In toluene at 25 °C. f) In dichloromethane at 25 °C.

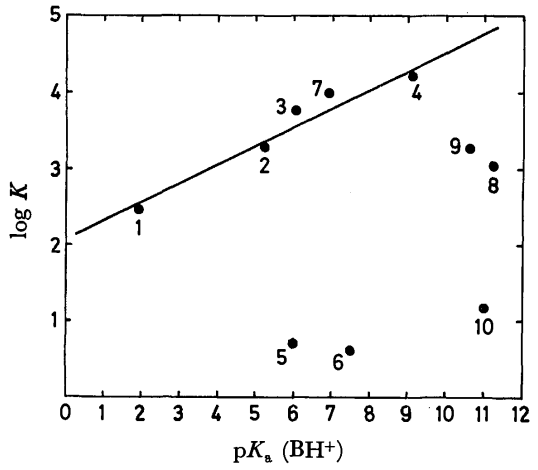

Fig. 5. Correlation between log *K* and amine basicity. Amines: 1) 4-cyanopyridine; 2) pyridine; 3) 4-methylpyridine; 4) 4-aminopyridine; 5) 2-methylpyridine; 6) 2,4,6-trimethylpyridine; 7) imidazole; 8) piperidine; 9) butylamine; 10) diethylamine.

This is due to the fact that these 4-substituted pyridines exert the least and a constant steric effect on Co(II)–TDHC among the amine bases. The equilibrium data for the present set of 4-substituted pyridines can be referred to the Hammett equation with $\rho=1.6$ (Eq. (6)):

$$-\log K/K_0 = \rho\sigma \qquad (6)$$

where K is for a substituted pyridine and K_0 for pyridine, and σ is the Hammett substituent constant. Such a linear free energy relationship has been reported for the complex-forming equilibria between 4-substituted pyridines and metalloporphyrins.[34-38] It is interesting to note that both *a* and ρ values for the present Co(II)–TDHC (**7a**) system are considerably larger than the corresponding values for the cobalt(II) complexes of protoporphyrin ($a=0.09$, $\rho=0.6$)[38] and tetrakis(*p*-methoxyphenyl)porphyrin ($a=0.19$, $\rho=1.0$).[37] The current interpretation of *a*[39] and ρ values may lead to an important conclusion that the nuclear cobalt in Co(II)–TDHC is more electronegative than in cobalt(II) porphyrins, and the pyridine nitrogen in X–C_5H_4N–Co(II)–TDHC is much more electron deficient than in the corresponding cobalt(II) porphyrin complexes. This is again what might be expected from the extremely positive cobalt(II)–cobalt(I) reduction potential of Co(II)–TDHC (Table 1).

A large decrease in K value was observed for some hindered pyridines, such as 2-methylpyridine and 2,4,6-trimethylpyridine (Fig. 5). This may be attributed to the front strain exerted between these amines and Co(II)–TDHC in the coordination process. The coordination of pyridines to metalloporphyrins is also subject to a similar steric effect.[34,35,37] The formation constant of the 2,4,6-trimethylpyridine complex of cobalt(II) tetrakis(*p*-methoxyphenyl)porphyrin is 1.5 log unit less than that expected from the basicity of the amine.[37] This effect is even larger in the present system and the formation constants for 2-methyl- and 2,4,6-trimethylpyridine are reduced by 3 log units more than expected (Fig. 5). In addition to the repulsion between the in-plane π-electron system of the macrocyclic ligand and the 2- and/or 6-methyl groups of the substituted pyridines, another steric interaction seems to interfere greatly with the coordination of 2-methyl- and 2,6-dimethylpyridines to Co(II)–TDHC. This other significant steric effect may arise from the interaction of the angular methyl groups placed at the 1- and 19-positions of the macrocyclic ligand and the substituted pyridines.

Aliphatic amines form complexes with Co(II)–TDHC which are less stable than those derived from substituted pyridines, on the basis of the basicity scale shown in Fig. 5. The extra stabilization observed for the pyridine complexes may be attributed to the π-back bonding from the nuclear cobalt to the pyridine moiety. It is interesting to note that imidazole has an affinity toward Co(II)–TDHC which falls relatively well on the $\log K - pK_a$ correlation line for the 4-substituted pyridines. It has been generally realized, on the other hand, that imidazole behaves as a better π-electron acceptor relative to pyridine.[37] The present result indicates, therefore, that π-back donation from the nuclear cobalt to the π*-orbital of the fifth ligand such as imidazole and pyridine derivatives would not be so marked as predicted for the porphyrin complexes,[40] due to the significant electronegative character of cobalt in Co(II)–TDHC.

Because of the bulkiness of triethylamine, it demonstrates the least coordination tendency toward Co(II)–TDHC among the amine bases used in this work. The spectrum of Co(II)–TDHC (**7a**) (2×10^{-5}M in dichloromethane) remained unchanged upon addition of triethylamine (up to 10^{-2} M.) However, when the concentration of the amine was adjusted to the 10^{-1} to 1 M range, the reduction of **7a** took place to afford Co(I)–TDHC (**8a**). The reduction product gave a spectrum identical with that observed for the cobalt(I) complex obtained upon treating with sodium hydroxide. The observed electron transfer from triethylamine to Co(II)–TDHC is of considerable interest since the less hindered amines resulted not in electron transfer but

in coordination to Co(II)–TDHC.[41] These results may be interpreted in a consistent manner as follows: (1) the electron transfer takes place appreciably in a long range scheme (outer sphere mechanism), since triethylamine has the least tendency of coordination toward Co(II)–TDHC due to its sterically hindered structure; (2) less hindered amines donate two electrons in a stepwise manner to Co(II)–TDHC microscopically and the first electron is transferred to the Co(II)–TDHC through the outer sphere mechanism. The resulting Co(I)–TDHC intermediate and the electron defficient amine may couple together to give the corresponding coordination compound. The entire mechanistic scheme is given by Eq. (7).

$$\begin{array}{c} \text{Co(II)-TDHC} + \text{NR}^1\text{R}^2\text{R}^3 \\ \Updownarrow \\ [\text{Co(I)-TDHC} + \cdot\overset{+}{\text{N}}\text{R}^1\text{R}^2\text{R}^3] \qquad (7) \\ \swarrow \qquad\qquad \searrow \\ \begin{array}{ll} \text{Co(I)-TDHC} + \cdot\overset{+}{\text{N}}\text{R}^1\text{R}^2\text{R}^3 & \text{R}^1\text{R}^2\text{R}^3\text{N-Co(II)-TDHC} \\ (\text{R}^1, \text{R}^2, \text{R}^3\text{: alkyl}) & (\text{R}^1\text{: H and} \\ & \text{R}^2, \text{R}^3\text{: H or alkyl}) \end{array} \end{array}$$

References

1) D. H. Busch, K. Farmery, V. Goedken, V. Katovic, A. C. Melnyk, C. R. Sperati, and N. Tokel, "Bioinorganic Chemistry," ed. by R. F. Gould, Advan. Chem. Ser. No. 100, Amer. Chem. Soc., (1971), p. 44.

2) F. V. Lovecchio, E. S. Gore, and D. H. Busch, *J. Amer. Chem. Soc.*, **96**, 3109 (1974), and references therein.

3) J. C. Dabrowiak, F. V. Lovecchio, V. L. Goedken, and D. H. Busch, *ibid.*, **94**, 5502 (1972).

4) N. Takvoryan, K. Farmery, V. Katovic, F. L. Lovecchio, E. S. Gore, L. B. Anderson, and D. H. Busch, *ibid.*, **96**, 731 (1974).

5) Reviews: (a) H. A. O. Hill, "Inorganic Biochemistry," Vol. 2, ed. by G. L. Eichhorn, Elsevier Scientific Publishing Co., Amsterdam (1973), Chapter 30. (b) J. M. Pratt, "Inorganic Chemistry of Vitamin B_{12}," Academic Press, London (1972). (c) S. Fukui and T. Toraya, *Kagaku*, **28**, 570, 676, and 786 (1973).

6) Reviews: (a) G. N. Schrauzer, *Acc. Chem. Res.*, **1**, 97 (1968). (b) G. Costa, *Coord. Chem. Rev.*, **8**, 63 (1972). (c) A. Biggotto, G. Costa, G. Mestroni, G. Pellizer, A. Puxeddu, E. Reisenhofer, L. Stefani, and G. Tauzher, *Inorg. Chim. Acta Rev.*, **4**, 41 (1970). (d) Y. Murakami, *Kagaku*, **28**, 12 (1973). (e) D. Dodd and M. D. Johnson, *Organometal. Chem. Rev.*, **52**, 1 (1973).

7) G. Costa, G. Mestroni, and L. Stefani, *J. Organometal. Chem.*, **7**, 493 (1967).

8) G. Costa, G. Mestroni, G. Tauzher, and L. Stefani, *ibid.*, **6**, 181 (1966).

9) G. Costa, G. Mestroni, and E. de Savorgnani, *Inorg. Chim. Acta*, **3**, 323 (1969).

10) D. A. Clark, R. Grigg, and A. W. Johnson, *Chem. Commun.*, **1966**, 208.

11) E. Ochiai, K. M. Long, C. R. Sperati, and D. H. Busch, *J. Amer. Chem. Soc.*, **91**, 3201 (1969).

12) K. Farmery and D. H. Busch, *Inorg. Chem.*, **11**, 2901 (1972).

13) N. S. Hush and I. S. Woolsey, *J. Amer. Chem. Soc.*, **94**, 4107 (1972).

14) N. S. Hush and I. S. Woolsey, *J. Chem. Soc., Dalton*, **1974**, 24.

15) Y. Murakami, K. Sakata, Y. Tanaka, and T. Matsuo, This Bulletin, **48**, 3622 (1975).

16) J. A. Riddick and W. B. Bunger, "Organic Solvents," Wiley Interscience, New York, N. Y. (1970).

17) A. Albert, *J. Chem. Soc.*, **1951**, 1376.

18) C. J. Pedersen, *J. Amer. Chem. Soc.*, **89**, 7017 (1967).

19) D. Dolphin, R. L. N. Harris, J. L. Huppatz, A. W. Johnson, and I. T. Kay, *J. Chem. Soc. C*, **1966**, 30.

20) A. W. Johnson and I. T. Kay, *J. Chem. Soc.*, **1961**, 2418.

21) H. W. Whitlock and R. Hanauer, *J. Org. Chem.*, **33**, 2169 (1968).

22) For example: G. P. Ansenault, E. Bullock, and S. F. MacDonald, *J. Amer. Chem. Soc.*, **82**, 4384 (1960).

23) H. Fischer and P. Halbig, *Justus Liebigs Ann. Chem.*, **447**, 123 (1926).

24) D. J. Sam and H. E. Simmons, *J. Amer. Chem. Soc.*, **94**, 4024 (1972).

25) C. L. Liotta, H. P. Harris, M. McDermott, T. Gonzalez, and K. Smith, *Tetrahedron Lett.*, **1974**, 2417.

26) H. D. Durst, *ibid.*, **1974**, 2421.

27) R. D. Gillard, *J. Chem. Soc. A*, **1967**, 917.

28) G. N. Schrauzer and R. J. Windgassen, *Chem. Ber.*, **99**, 602 (1966).

29) R. Yamada, S. Shimizu, and S. Fukui, *Biochemistry*, **7**, 1713 (1968).

30) M. G. Swanwick and W. A. Waters, *J. Chem. Soc. B*, **1971**, 1059.

31) G. N. Schrauzer and E. Deutsch, *J. Amer. Chem. Soc.* **91**, 3341 (1969).

32) F. A. Walker, *ibid.*, **92**, 4235 (1970).

33) H. A. Benesi and J. H. Hildebrand, *ibid.*, **71**, 2703 (1949).

34) C. H. Kirksey, P. Hambright, and C. B. Storm, *Inorg. Chem.*, **8**, 2141 (1969).

35) C. H. Kirksey and P. Hambright, *ibid.*, **9**, 958 (1970).

36) D. V. Stynes, H. C. Stynes, J. A. Ibers, and B. R. James, *J. Amer. Chem. Soc.*, **95**, 1142 (1973).

37) F. A. Walker, *ibid.*, **95**, 1150 (1973).

38) D. V. Stynes, H. C. Stynes, B. R. James, and J. A. Ibers, *ibid.*, **95**, 1796 (1973).

39) J. G. Jones, J. B. Poole, J. C. Tomkinson, and R. J. P. Williams, *J. Chem. Soc.*, **1958**, 2001.

40) (a) J. E. Falk, "Porphyrins and Metalloporphyrins," Elsevier Publishing Co., Amsterdam (1964), Chapter 3. (b) S. J. Cole, G. C. Curthoys, and E. A. Magnusson, *J. Amer. Chem. Soc.*, **92**, 2991 (1970).

41) In the presence of diethylamine at very high concentrations ($>$0.1 M), the spectrum of Co(II)–TDHC (**7a**) indicated the existence of both Co(I)–TDHC and (diethylamine)–Co(II)–TDHC, suggesting that some electron transfer from diethylamine to Co(II)–TDHC took place.

42) G. Costa, G. Mestroni, A. Puxeddu, and E. Reisenhofer. *J. Chem. Soc. A*, **1970**, 2870.

43) C. M. Elson, A. Hamilton, and A. W. Johnson, *J, Chem. Soc., Perkin I*, **1973**, 775.

44) L. G. Marzilli, P. A. Marzilli, and J. Halpern, *J. Amer. Chem. Soc.*, **93**, 1374 (1971).

45) L. G. Marzilli, P. A. Marzilli, and J. Halpern, *ibid.*, **92**, 5752 (1970).

Determination of Oxygen in Zinc Compounds[1)]

Kazuo IMAEDA, Takeo KURIKI,* and Keiko OHSAWA

Hoshi College of Pharmacy, Ebara, Shinagawa-ku, Tokyo 141

* *Pharmaceutical Laboratory, Hoechst Japan Limited, Minamidai, Kawagoe-shi, Saitama 350*

(Received August 28, 1975)

Oxygen in zinc compounds was determined by a modification of the method of Schütze. Oxygen in some zinc compounds such as zinc oxide, zinc acetate and zinc oxalate could not be determined by the usual method. The carrier gas method of adding carbon was employed for the determination of total oxygen. Total oxygen could be determined by the addition of 5 mg of carbon to a sample boat and heating at 1000 °C. The determination was also carried out by the carrier gas method by addition of 2 mg naphthalene. As a result, total oxygen could be determined by the addition of 2 mg of naphthalene.

Determination of oxygen in zinc compounds was first reported by Schütze in 1939.[2)] Carbon was placed in a sample boat in an atmosphere of nitrogen, the boat was heated at 1000 °C, and determination of oxygen in zinc oxide was carried out. Oxygen determination in zinc oxide by the method of inert gas fusion was reported by Engelsman *et al.*,[3)] who employed a platinum bath, heating being carried out at 2000 °C. Merz[4)] reported that oxygen in zinc oxide could be determined by the addition of ammonium chloride or an indulin base.

In spite of the publication of several reports, little is known about the determination of oxygen in zinc compounds other than zinc oxide.

We have studied oxygen determination in compounds containing metals such as silver, arsenic, mercury, tin and copper. The present paper deals with the determination of oxygen in zinc compounds.

Experimental

Samples. The following samples were employed for the experiments: zinc oxide, ZnO; zinc acetate, $Zn(CH_3COO)_2 \cdot 2H_2O$; ammonium zinc sulfate, $(NH_4)_2Zn(SO_4)_2$; zinc anthranilate, $Zn(C_7H_6NO_2)_2$; zinc benzoate, $Zn(C_7H_5O_2)_2$; zinc 4-cyclohexylbutyrate, $Zn(C_{10}H_{17}O_2)_2$; zinc formate, $Zn(CHO_2) \cdot 2H_2O$; zinc lactate, $Zn(C_3H_5O_3)_2 \cdot 3H_2O$; zinc nitrate, $Zn(NO_3)_2 \cdot 6H_2O$; zinc oxalate, $ZnC_2O_4 \cdot 2H_2O$; zinc perchlorate, $Zn(ClO_4)_2 \cdot 6H_2O$; zinc *p*-phenolsulfonate, $Zn(C_6H_5O_4S)_2 \cdot 8H_2O$; zinc stearate, $Zn(C_{18}H_{35}O_2)_2$; zinc salicylate, $Zn(C_7H_5O_3)_2$; zinc sulfate, $ZnSO_4 \cdot 7H_2O$; zinc tartrate, $ZnC_4H_4O_6$; bis[bis(2-hydroxyethyl)dithiocarbamato]zinc, $Zn(C_5H_{10}NO_2S_2)_2$; bis(2,4-pentanedionato)zinc, $Zn(C_5H_7O_2)_2$; bis(2-quinolinecarboxylato)zinc, $Zn(C_{10}H_6NO_2)_2 \cdot H_2O$; bis(8-quinolinolato)zinc, $Zn(C_9H_6NO)_2$; *p*-[N-ethyl(2-hydroxyethyl)amino]benzenediazonium tetrachlorozincate, $C_{20}H_{28}Cl_4N_6O_2Zn$. The results of the determination of carbon and hydrogen are given in Table 1. They are in fair agreement with the corresponding calculated values.

Reagents and Apparatus. The reagents and apparatus used were the same as those previously reported.[5)]

Procedure. *(1) Usual Method of Oxygen Determination in Organic Compounds:* Nitrogen was passed throughout the apparatus as a carrier gas at a rate of 10—15 ml/min. Nitrogen was purified by passing through a silica gel drying tube, a deoxidation tube filled with porous copper heated at 550 °C and two tubes one containing sodium hydroxide and the other magnesium perchlorate. The temperatures of the combustion furnace, desulfurization furnace and heating furnace were maintained at 900, 550, and 150 °C, respec-

TABLE 1. ANALYTICAL RESULTS OF CARBON AND HYDROGEN IN ZINC COMPOUNDS

Sample	Carbon(%)		Hydrogen(%)	
	Found	Calcd	Found	Calcd
Zinc oxide ZnO	0.05	0.00	0.02	0.00
Zinc acetate $Zn(CH_3COO)_2 \cdot 2H_2O$	21.94	21.89	4.60	4.59
Ammonium zinc sulfate $(NH_4)_2Zn(SO_4)_2$	0.12	0.00	2.89	2.75
Zinc anthranilate $Zn(C_7H_6NO_2)_2$	49.80	49.80	3.48	3.58
Zinc benzoate $Zn(C_7H_5O_2)_2$	54.62	54.66	3.28	3.28
Zinc 4-cyclohexylbutyrate $Zn(C_{10}H_{17}O_2)_2$	59.40	59.48	8.34	8.49
Zinc formate $Zn(CH_2)_2 \cdot 2H_2O$	12.72	12.55	3.28	3.16
Zinc lactate $Zn(C_3H_5O_3)_2 \cdot 3H_2O$	24.32	24.22	5.38	5.42
Zinc nitrate $Zn(NO_3)_2 \cdot 6H_2O$	0.18	0.00	4.13	4.07
Zinc oxalate $ZnC_2O_4 \cdot 2H_2O$	12.56	12.68	2.24	2.13
Zinc perchlorate $Zn(ClO_4)_2 \cdot 6H_2O$	0.15	0.00	3.42	3.25
Zinc *p*-phenolsulfonate $Zn(C_6H_5O_4S)_2 \cdot 8H_2O$	26.06	25.93	4.70	4.72
Zinc stearate $Zn(C_{18}H_{35}O_2)_2$	68.39	68.38	11.12	11.16
Zinc salicylate $Zn(C_7H_5O_3)_2$	49.56	49.59	3.09	2.97
Zinc sulfate $ZnSO_4 \cdot 7H_2O$	0.03	0.00	4.94	4.90
Zinc tartrate $ZnC_4H_4O_6$	22.34	22.51	2.00	1.89
Bis[bis(2-hydroxyethyl)dithiocarbamato]zinc $Zn(C_5H_{10}NO_2S_2)_2$	28.03	28.20	4.81	4.73
Bis(2,4-pentanedionato)zinc $Zn(C_5H_7O_2)_2$	45.69	45.56	5.38	5.35
Bis(2-quinolinecarboxylato)-zinc $Zn(C_{10}H_6NO_2)_2 \cdot H_2O$	56.01	56.16	3.45	3.30
Bis(8-quinolinolato)zinc $Zn(C_9H_6NO)_2$	61.17	61.13	3.54	3.42
p-[*N*-Ethyl(2-hydroxyethyl)-amino]benzenediazonium tetrachlorozincate $C_{20}H_{28}Cl_4N_6O_2Zn$	40.73	40.60	4.51	4.77

tively. A boat containing a weighed sample was put into a pyrolysis tube through a sample inlet, nitrogen being flushed at the sample inlet lest air should come into the pyrolysis tube. The boat was moved up to a sample heated by means of an iron ball and a magnet, and the sample was pyrolized over a period of 15 min. Oxygen contained in the sample was completely converted into carbon monoxide by means of platinum-carbon heated at 900 °C. The carbon monoxide was oxidized to carbon dioxide by iodine petaoxide, and the resulting carbon dioxide was allowed to be absorbed into an absorption tube packed with sodium hydroxide. Thirty minutes after the beginning of pyrolysis, the absorption tube of carbon dioxide was disconnected from the apparatus and weighed. The content of oxygen in the sample was calculated as follows:

$$\text{The content of oxygen (\%)} = \frac{0.3636\times(a-b)}{s}\times 100$$

where s=sample weight (mg); a=increase in weight of the absorption tube of carbon dioxide (mg); and b=blank value (mg). The determination took *ca.* 40 min.

(2) Determination by Means of a Solid Reaction Agent: This method was approximately the same as that described in (1) except that carbon powder was sprinkled on the sample boat prior to and after placement of the sample.

(3) Determination by Addition of a Reaction Agent: Purification of the carrier gas and the procedure after oxygen in a sample had been converted into carbon monoxide were the same as those described in (1), except for insertion of the sample boat and pyrolysis of the sample which were carried out as follows. A weighed sample was placed in the sample boat which was then put in the sample inlet after the apparatus was ventilated reversely. An iron ball and then a boat with a weighed reaction agent (2 mg of naphthalene) were inserted into the apparatus, and the apparatus was ventilated reversely for 3—5 min. The direction of the ventilation was then changed and the sample boat was moved up to a sample heater by means of the iron ball and a magnet. During the course of pyrolysis, the iron ball was brought back to the boat with the reaction agent and the boat was moved up to a place about 2—3 cm from the sample heater. The reaction agent was gasified by the heat from the sample heater and the gas was allowed to flow along with the carrier gas toward the sample heater. The sample or oxidation products remaining in the sample boat were allowed to react directly with the gas or the pyrolysis products of the reaction agent. The oxygen compounds resulting from the reaction of the pyrolysis gas produced by the heating of the sample or of the oxygen remaining in the sample boat with the reaction agent were allowed to react with platinum carbon heated at 900 °C in order to convent the oxygen in the sample into carbon monoxide.

Results and Discussion

Determination of Oxygen in Zinc Compounds by the Usual Method. Oxygen in zinc compounds was determined according to the method for determination of oxygen in organic compounds. The results are shown in Table 2. Heating was carried out at 900 °C. The values for oxygen in zinc oxide, zinc acetate, zinc ammonium sulfate, zinc formate, zinc nitrate, zinc oxalate, zinc perchlorate and zinc sulfate was 3—18% lower than the corresponding calculated values. Oxygen in the other 13 compounds, however, could be determined more accurately. Since zinc oxide has a high

TABLE 2. ANALYTICAL RESULTS OF OXYGEN IN ZINC COMPOUNDS

Sample	Sample taken (mg)	CO_2 (mg)	O-found (%)	O-calcd (%)	Δ%
Zinc oxide ZnO	3.913	0.136	1.26	19.66	−18.40
	3.895	0.119	1.11		−18.55
	4.720	0.186	1.43		−18.23
Zinc acetate $Zn(CH_3COO)_2\cdot 2H_2O$	3.857	4.286	40.40	43.74	−3.34
	3.441	3.851	40.69		−3.05
	3.918	4.303	39.93		−3.81
Ammonium zincsulfate $(NH_4)_2Zn(SO_4)_2$	4.111	4.469	39.53	43.60	−4.07
	4.053	4.422	39.67		−3.93
	3.538	3.877	39.84		−3.76
Zi nc anthranilate $Zn(C_7H_6NO_2)_2$	4.212	2.185	18.86	18.96	−0.10
	4.425	2.314	19.01		+0.05
	3.633	1.892	18.94		−0.02
Zinc benzoate $Zn(C_7H_5O_2)_2$	3.501	1.979	20.55	20.81	−0.26
	3.129	1.784	20.73		−0.08
	3.676	2.093	20.70		−0.11
Zinc 4-cyclohexyl-butyrate $Zn(C_{10}H_{17}O_2)_2$	3.958	1.728	15.87	15.85	+0.02
	3.846	1.679	15.87		+0.02
	4.128	1.801	15.86		+0.01
Zinc formate $Zn(CHO_2)_2\cdot 2H_2O$	3.417	4.109	43.72	50.15	−6.43
	3.587	4.284	43.43		−6.72
	4.170	4.945	43.12		−7.03
Zinc lactate $Zn(C_3H_5O_3)_2\cdot 3H_2O$	3.907	5.189	48.29	48.39	−0.10
	3.299	4.374	48.21		−0.18
	3.961	5.282	48.49		+0.10
Zinc nitrate $Zn(NO_3)_2\cdot 6H_2O$	4.661	7.628	59.51	64.54	−5.03
	3.279	5.374	59.59		−4.95
	4.668	7.622	59.37		−5.17
Zinc oxalate $ZnC_2O_4\cdot 2H_2O$	4.431	5.275	43.29	50.68	−7.39
	4.592	5.415	42.88		−7.80
	3.898	4.608	42.98		−7.70
Zinc perchlorate $Zn(ClO_4)_2\cdot 6H_2O$	3.905	6.107	56.86	60.15	−3.29
	3.527	5.488	56.58		−3.57
	3.367	5.219	56.36		−3.79
Zinc *p*-phenol-sulfonate $Zn(C_6H_5O_4S_2)_2\cdot 8H_2O$	4.490	5.701	46.17	46.06	+0.11
	3.259	4.135	46.13		+0.07
	3.828	4.872	46.28		+0.22
Zinc stearate $Zn(C_{18}H_{35}O_2)_2$	4.419	1.262	10.38	10.12	+0.26
	3.142	0.876	10.14		+0.02
	3.327	0.950	10.38		+0.26
Zinc salicylate $Zn(C_7H_5O_3)_2$	4.202	3.286	28.43	28.27	+0.16
	3.776	2.944	28.35		+0.08
	3.563	2.763	28.20		−0.07
Zinc sulfate $ZnSO_4\cdot 7H_2O$	3.222	4.863	54.88	61.21	−6.33
	3.361	5.064	54.78		−6.43
	3.318	5.063	55.48		−5.73
Zinc tartrate $ZnC_4H_4O_6$	4.140	5.092	44.72	44.98	−0.26
	3.282	4.024	44.58		−0.40
	3.295	4.049	44.68		−0.30
Bis[bis(2-hydroxy-ethyl)dithiocarba-mato]zinc $Zn(C_5H_{10}NO_2S_2)_2$	4.128	1.729	15.23	15.03	+0.20
	3.988	1.680	15.32		+0.29
	3.332	1.397	15.24		+0.21
Bis(2,4-pentane-dionato)zinc $Zn(C_5H_7O_2)_2$	3.723	2.459	24.02	24.28	−0.26
	4.101	2.763	24.50		+0.22
	3.912	2.640	24.54		+0.26

Table 2. (Continued)

Sample	Sample taken (mg)	CO_2 (mg)	O-found (%)	O-calcd (%)	Δ%
Bis(2-quinoline-carboxylato)zinc	4.437	2.272	18.62		−0.08
	4.223	2.144	18.46	18.70	−0.24
$Zn(C_{10}H_6NO_2)_2 \cdot H_2O$	3.512	1.812	18.76		+0.06
Bis(8-quinolinolato)-zinc	3.402	0.864	9.23		+0.18
	3.422	0.881	9.36	9.05	+0.31
$Zn(C_9H_6NO)_2$	3.610	0.906	9.13		+0.08
p-[*N*-Ethyl(2-hydro-xyethyl)amino]ben-zenediazonium	3.521	0.535	5.52		+0.11
	3.631	0.554	5.55	5.41	+0.14
tetrachlorozincate	4.103	0.634	5.62		+0.21
$C_{20}H_{28}Cl_4N_6O_2Zn$					

Table 3. Influence of temperature on the determination of oxygen in zinc oxide by addition of solid reaction agent (About 5 mg of Carbon)

Sample	Temperature of sample heater (°C)	Sample taken (mg)	CO_2 (mg)	O-found (%)	O-calcd (%)	Δ%
Zinc oxide	850	3.802	0.099	0.95		−18.71
	900	3.148	0.696	8.04		−11.62
	950	3.105	1.484	17.38	19.66	−2.28
	1000	3.042	1.661	19.85		+0.19
	1050	3.639	1.975	19.73		+0.07

Table 4. Analytical results of oxygen in zinc compounds by addition of solid reaction agent (About 5 mg of Carbon)
Heating temperature of sample: 1000 °C

Sample	Sample taken (mg)	CO_2 (mg)	O-found (%)	O-calcd (%)	Δ%
Zinc oxide	3.042	1.661	19.85		+0.19
	3.509	1.911	19.80	19.66	+0.14
	3.256	1.787	19.96		+0.30
Zinc acetate	3.315	3.974	43.59		−0.15
	3.173	3.828	43.87	43.74	+0.13
	3.443	4.116	43.47		−0.30
Ammonium zinc sulfate	4.590	5.527	43.78		+0.18
	4.383	5.262	43.65	43.60	+0.05
	4.295	5.147	43.57		−0.03
Zinc formate	3.884	5.337	49.96		−0.19
	3.281	4.534	50.25	50.15	+0.10
	3.643	5.038	50.28		+0.13
Zinc nitrate	3.882	6.879	64.43		−0.11
	3.590	6.402	64.84	64.54	+0.30
	4.418	7.838	64.51		−0.03
Zinc oxalate	3.799	5.300	50.73		+0.05
	3.466	4.843	50.81	50.68	+0.13
	4.185	5.817	50.54		−0.14
Zinc perchlorate	3.324	5.516	60.34		+0.19
	4.323	7.180	60.39	60.15	+0.24
	4.210	7.005	60.50		+0.35
Zinc sulfate	3.161	5.315	61.14		−0.07
	3.895	6.563	61.27	61.21	+0.06
	4.056	6.810	61.05		−0.16

melting point, we supposed that oxygen in zinc oxide could not be determined at all by the method for determination of oxygen in organic compounds. However, we have found that heating of zinc oxide at 900 °C in an atmosphere of nitrogen is likely to lead to the dissociation of zinc oxide, and we were able to determine about 1% of oxygen in this compound although the calculated content of oxygen was 19.66%. The residue left in the sample boat after determination of oxygen in zinc acetate was white and seemed to be zinc oxide. We see from the analytical results that 5.5 oxygen atoms out of 6 in zinc acetate could be determined. The residue in the sample boat after determination of oxygen in zinc ammonium sulfate, zinc formate, zinc nitrate, zinc oxalate, zinc perchlorate or zinc sulfate was white and seemed to be zinc oxide. The analytical results show that the value found was approximately the same as the calculated value obtained by subtracting one oxygen atom left as zinc oxide from all the oxygen atoms in each sample.

Determination of Total Oxygen in Zinc Compounds by the Carrier Gas Method with a Solid Reaction Agent. Total oxygen in some of the zinc compounds can not be determined by the usual method. We therefore used the carrier gas method with carbon as a solid reaction agent. In order to examine the influence of temperature on oxygen determination, 5 mg of carbon was placed in a sample boat and the temperature was measured according to the carrier gas method with a solid reaction agent. Zinc oxide was used as the

Table 5. Analytical results of oxygen in zinc compounds by addition of reaction agent (About 2 mg of Naphthalene)

Sample	Sample taken (mg)	CO_2 (mg)	O-found (%)	O-calcd (%)	Δ%
Zinc oxide	3.550	1.923	19.70		+0.04
	4.177	2.233	19.44	19.66	−0.22
	3.736	2.006	19.52		−0.14
Zinc acetate	3.495	4.187	43.56		−0.18
	4.319	5.171	43.53	43.74	−0.21
	3.852	4.623	43.64		−0.10
Ammonium zinc sulfate	4.062	4.857	43.48		−0.22
	4.221	5.080	43.76	43.60	+0.16
	3.613	4.326	43.54		−0.06
Zinc formate	3.441	4.750	50.19		+0.04
	3.734	5.161	50.26	50.15	+0.11
	4.118	5.702	50.35		+0.20
Zinc nitrate	3.968	7.048	64.58		+0.14
	3.800	6.768	64.76	64.54	+0.22
	4.168	7.397	64.53		−0.01
Zinc oxalate	4.134	5.778	50.82		+0.14
	3.791	5.264	50.49	50.68	−0.19
	3.955	5.507	50.63		−0.05
Zinc perchlorate	3.020	5.007	60.28		+0.13
	3.615	5.951	59.86	60.15	−0.19
	4.231	6.997	60.13		−0.02
Zinc sulfate	3.291	5.551	61.33		+0.12
	4.155	7.006	61.31	61.21	+0.10
	4.445	7.491	61.28		+0.07

sample. The analytical results are given in Table 3. It was found that oxygen in zinc oxide can be determined fairly accurately when the sample is heated at 1000 °C or above. With compounds the oxygen of which can not be determined by the usual method, determination of oxygen was also carried out at 1000 °C. The results are given in Table 4. We see that oxygen in zinc compounds can be determined quite accurately by the addition of carbon to a sample boat.

Determination of Total Oxygen in Zinc Compounds by the Carrier Gas Method with a Reaction Agent. The total oxygen in zinc compounds can be determined by the addition of carbon to a sample boat and by heating at 1000 °C. We also attempted the addition of naphthalene (2 mg) instead of carbon. The results are given in Table 5. It was found that total oxygen in the zinc compounds can be determined accurately even in the presence of naphthalene.

The authors are indebted to Dr. Nobuo Suzuki of Pharmaceutical Laboratory, Hoechst Japan Limited, for his encouragement. Thanks are also due to Miss Motoko Kanda for her assistance in the early stage of the present experiments.

References

1) Studies on oxygen determination by carrier gas methods, XI, part X of this series: K. Imaeda, T. Kuriki, and K. Ohsawa, *Bunseki Kagaku*, **24**, 725 (1975).
2) M. Schütze, *Z. Anal. Chem.*, **118**, 241 (1939).
3) J. J. Engelsman, A. Meyer, and J. Visser, *Talanta*, **13**, 409 (1966).
4) W. Merz, *Anal. Chim. Acta*, **50**, 305 (1970).
5) K. Imaeda and T. Kuriki, *Bunseki Kagaku*, **23**, 47 (1974).

Preparative Thin-Layer Chromatography of Semi-Xylenol Orange and Xylenol Orange by Development with Solvents Giving Discrete pH Change on the Plate*

Mutsuo YAMADA and Masatoshi FUJIMOTO

Department of Chemistry, Faculty of Science, Hokkaido University, Sapporo 060

(Received September 1, 1975)

A new procedure is proposed to obtain pure Semi-Xylenol Orange (SXO) and Xylenol Orange (XO) from *ca.* 100 mg of synthetic mixture using preparative thin-layer chromatography on cellulose layer *ca.* 2 mm thick. Development with a composite solvent, 55—60 ml of 1-butanol saturated with 25% aqueous acetic acid-0.6—0.8 ml of 28% aqueous ammonia, forms two discrete zones of different pH values on the layer. The zones favor a sharp separation of polybasic Brønsted acids with structures similar to those of SXO and XO.[1] SXO and XO are in the protonated forms corresponding to the pH values of the given zones. XO is located near the starting line in the lower zone of higher pH and SXO migrates through the layer in the upper part of the same zone. Both SXO and XO constitute the compact and concentrated bands. Each run takes only 3 hr. 18 mg of SXO and 36 mg of XO are obtained as sodium salts from 100 mg of the synthetic mixture.

Semi-Xylenol Orange, 3-[*N*,*N*-bis(carboxymethyl)-aminomethyl]-*o*-cresolsulfonphthalein, is an appropriate chelating agent for spectrophotometric determination of zirconium(IV)[2] and for interpreting the kinetic behavior for the metal complex formation in a strongly acid medium.[3]

Xylenol Orange, 3,3′-bis[*N*,*N*-bis(carboxymethyl)-aminomethyl]-*o*-cresolsulfonphthalein, is a well-known metallochromic indicator.[4] However, there has been considerable disagreement in the results obtained by different authors on the solution chemistry of the metal complex formation.[5] The disagreement is caused by the use of "*impure*" XO containing iminodiacetic acid (IDA) and SXO with complexing properties and the lack of attention to the existence of metal complex species other than mononuclear 1 : 1 complex.[6]

Two methods have been reported for the purification of XO and/or SXO: (1) Selective precipitation of XO with ethanol from a saturated aqueous sodium acetate solution containing the mixture,[7] and (2) column chromatography on cellulose powder with the eluent, 1-butanol–acetic acid–water.[2,8] By the former, XO is partly decomposed[2,8] and cannot sufficiently be separated from SXO and IDA.[8] The latter causes serious tailing and cross-contamination of XO and SXO.

In the present paper we propose a new procedure to obtain "*pure*"[9] SXO and XO from a synthetic mixture. The procedure is preparative thin-layer chromatography with a developing solvent, 55—60 ml of 1-butanol saturated with 25% aqueous acetic acid-0.6—0.8 ml of 28% aqueous ammonia. The solvent yields on the cellulose layer two distinct zones I and II with stepwise different pH values. Zones I and II correspond to the regions of lower and higher pH values, respectively. Development with the composite solvent satisfactorily separates SXO, XO and *o*-Cresol Red (*o*-CR). SXO is thus concentrated in the upper part of zone II, while XO near the starting line in the same zone. *o*-CR moves much faster than both SXO and XO and is located in zone I at the top of the plate. The band of XO partly overlaps that of IDA and further separation is required. Development with the solvent, acetone–water–1 M hydrochloric acid (160/59/1, v/v/v), is found to be very effective for this purpose. "*Pure*" specimens of SXO and XO in the forms of free acid are prepared by cation exchange.

Experimental

Materials. Reagents: All the chemicals used were of analytical grade, unless otherwise specified. Water was deionized and distilled. *n*-BuOH was distilled.

SXO and XO: These compounds were synthesized by Mannich condensation.[4] 1.91 g (0.5×10^{-2} mol) of *o*-CR, 1.33 g (1.0×10^{-2} mol) of IDA and 1 g of NaOH were dissolved in 50 ml of glacial acetic acid followed by dropping 1 ml of 37% HCHO and kept at 65 °C for 10 h with stirring. The solvent was distilled off under reduced pressure to give a dry sample.

Cellulose Powder: Toyo-Roshi cellulose powder (300 or 200—300 mesh) was suspended in 0.5 M HCl and left to stand overnight. The suspension was sucked off, washed with water until washings became free from chloride, washed with acetone and dried in an oven at 80 °C for 2 h.

Ion Exchanger: A macroreticular strongly acid cation-exchange resin of low cross-linkage, Diaion PK-204 (Mitsubishi Kasei, Ltd.), was treated with HCl to remove trace of metal impurities and used in the hydrogen-form.

Preparative Thin-Layer Chromatography. Adsorbent Layer: A slurry was prepared by adding 90 ml of water to 30 g of the pretreated cellulose powder. A layer was obtained by the pouring procedure:[10] The slurry was rapidly poured on the middle of a glass plate (20×20 cm) and uniformly distributed over the plate by gentle tilting and shaking. The layer was sufficiently dried in the air at room temperature to avoid cracking during the course of heating. The plates were heated in an oven at 110 °C for 80 to 100 min, and stored in a desiccator over silica gel. Fairly uniform layers *ca.* 2 mm thick were usually prepared.

Chromatographic Chamber: A sandwich chamber ($20\times20\times$ 0.3 or 0.6 cm) was used. The terminal edge of the chamber was kept open during the development in order to allow free evaporation of the solvent at the top of the plate.[10]

Application of the Sample: About 100 mg sample powder was dissolved in 0.36 ml of water and successively applied with a 0.06 ml band-pipet (2.6 cm wide) in a line *ca.* 15 cm wide on

* Presented in part at the IUPAC International Congress on Analytical Chemistry, Kyoto, April 7, 1972, Abstracts, p. 183.

the layer 1.5 cm apart from the solvent surface in a sandwich chamber trough. After the application of the sample the plate was stored in a desiccator over silica gel until the water of the sample solution evaporated.

Developing Solvents: *Fifty-five* to *sixty* milliliters — a volume sufficient for one run — of *n*-BuOH saturated with 10, 20, or 25% aqueous HOAc was poured into a sandwich chamber trough (19×207×23 mm), and 0.6—0.8 ml of 28% aqueous NH_3 was added drop by drop so as to form an emulsion as uniformly as possible. Developing was started immediately after the preparation of the emulsion.

Identification of Each Band on the Chromatogram: The bands of *o*-CR, SXO and XO were readily identified by their intense coloration on the plate. It was necessary to confirm a position of the colorless band of IDA under similar experimental conditions beforehand, otherwise the band was inevitably covered with the intense coloration of XO. The band of IDA was detected by spraying a copper(II) acetate solution on the layer.

Transfer of SXO and XO from the Adsorbent to Solutions: The bands of SXO and XO on the layer were carefully scraped off with a glass rod, extracted with a small amount of water and dried *in vacuo*.

Ion Exchange. The extracts of SXO and XO were subjected to cation exchange to yield their free acids.

H_4SXO: About 50 mg of the sodium salt of purified SXO was dissolved in 25 ml of water, passed through a column containing 4 ml of pretreated cation-exchange resin, and eluted with 25 ml of water. A small part of SXO remaining on the resin phase was thoroughly washed out with a small amount of *n*-BuOH saturated with water.

H_6XO: About 50 mg of the sodium salt of purified XO was dissolved in 25 ml of water, passed through a column containing 9.5 ml of resin, and eluted with 75 ml of water. A small part of XO retained on the resin was washed out with a small amount of *n*-BuOH saturated with water.

Each effluent was evaporated to dryness at room temperature under reduced pressure and further kept *in vacuo* for 3 days to yield a dried sample. For the XO portion a further separation from IDA was required.

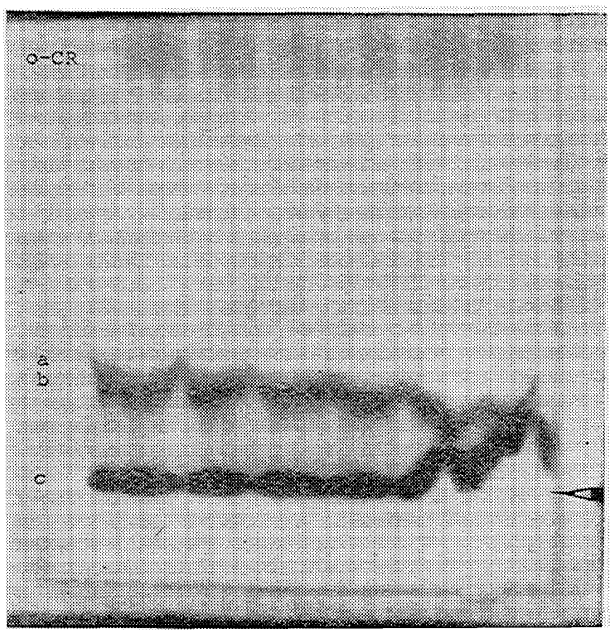

Fig. 1. Chromatogram developed for 3 hr with 60 ml of *n*-BuOH satd. with 10% HOAc–0.6 ml of 28% NH_3. a) NH_4-front, b) SXO, and c) XO.

Results

Separation of SXO and XO. Figure 1 shows a chromatogram with the developing solvent, 60 ml of *n*-BuOH saturated with 10% HOAc–0.6 ml of 28% NH_3.

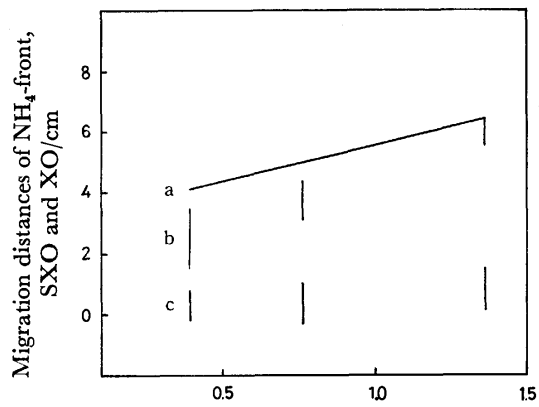

Fig. 2. Dependence of the migration distances of SXO, XO, and NH_4-front on the concentrations of HOAc contained in the *n*-BuOH satd. with 10, 20, and 25% HOAc.
The developing solvents used are 60 ml of *n*-BuOH saturated with 10, 20, and 25% HOAc–0.6—0.8 ml of 28% NH_3. a) NH_4-front, b) SXO, and c) XO.

Figure 2 shows the dependence of the migration distances of SXO, XO and NH_4-front on the concentrations of HOAc contained in *n*-BuOH saturated with 10, 20 and 25% HOAc. The developing solvents are 60 ml of *n*-BuOH saturated with 10, 20 and 25% HOAc–0.6—0.8 ml of 28% NH_3. It is found that as far as the experimental conditions are concerned the greater the concentration of HOAc, the better the

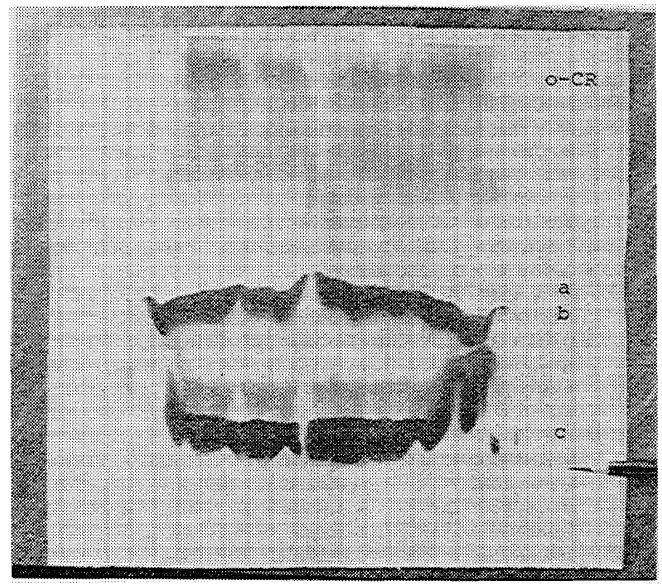

Fig. 3. Chromatogram developed for 3 hr with 60 ml of *n*-BuOH satd. with 25% HOAc–0.8 ml of 28% NH_3. a) NH_4-front, b) SXO, and c) XO.

separation of SXO and XO. Figure 3 gives the chromatogram obtained in the case of 25% HOAc and 0.8 ml of 28% NH_3 added.

SXO is finely separated from XO under the following conditions: The sample is applied on the layer 1.5 cm apart from the solvent surface in the trough, and developed with an emulsion freshly prepared in the trough by adding 0.6—0.8 ml of 28% NH_3 drop by drop to 55—60 ml of *n*-BuOH saturated with 25% HOAc.

The solvent, 55—60 ml of *n*-BuOH saturated with 10, 20 and 25% HOAc–0.6—0.8 ml of 28% NH_3 forms zones I and II with discrete different pH values, the zones being divided by a distinct boundary. After 3 hr development using 60 ml of *n*-BuOH saturated with 25% HOAc–0.8 ml of 28% NH_3 without the sample applied, three acid-base indicators, Bromophenol Blue, Bromocresol Green and Bromothymol Blue, are sprayed on the layer. They exhibit uniform visible colorations on the layer corresponding to the pH value of both zones I and II as shown in Table 1.

Table 1. The coloration of the layer sprayed with acid-base indicators

Zone	Acid-base indicators		
	BPB[a)]	BCG[b)]	BTB[c)]
I	Yellow	Yellow	Yellow
II	Blue	Blue	Bluish green

a) Bromophenol Blue. b) Bromocresol Green.
c) Bromothymol Blue.

Uniformity of the sensitive coloration indicates that the given solvent forms two distinct zones of discrete pH values as defined by the acid-base indicators. The pH of zone I is estimated to be lower than 3.0 and that of zone II between 5.4 and 6.0.

Separation of XO and IDA. In this stage of separation the band of XO is inevitably contaminated with IDA. Acetone–water (8/2, v/v) is useful for the separation of the sodium salts of aminopolycarboxylic acids by paper chromatography.[11] *Seventy* milliliters of a solvent, acetone–water–1 M HCl (160/59/1, v/v/v) was found to be effective to separate 5 mg mixture a band-pipet. The mixture contains *ca.* 90% XO and *ca.* 10% IDA in free acid form. It is necessary to confirm a position of the band of IDA under similar experimental conditions beforehand. In Fig. 4 the band of IDA is schematically reproduced by d, where 10 mg of pure IDA in the acid form is applied. *Thirty* milligrams of the mixture in the free acid form was applied on the layer (prepared from cellulose powder of 200—300 mesh) 1.0 cm apart from the solvent surface in a trough and developed with 70 ml of the solvent, acetone–water–1 M HCl (160/59/1, v/v/v) (Fig. 4), each run taking 1 hr. A sandwich trough (34×205×29 mm) was used.

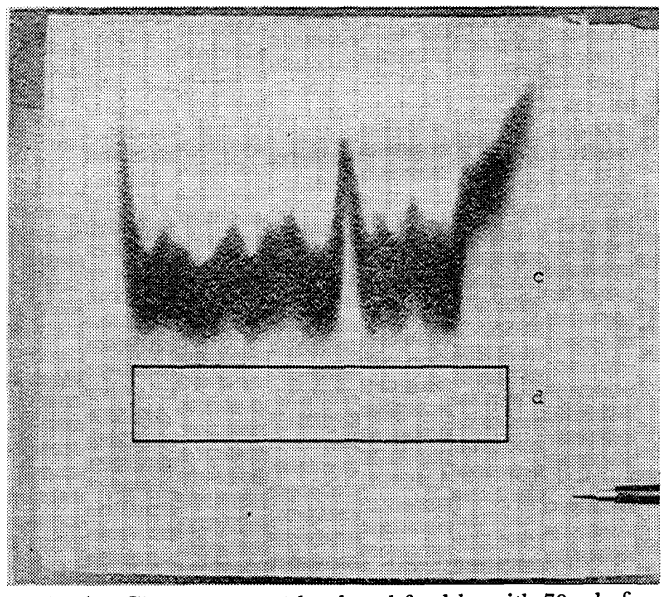

Fig. 4. Chromatogram developed for 1 hr with 70 ml of acetone–water–1M HCl (160/59/1, v/v/v).
c) XO and d) IDA.

Elemental Analysis. Table 2 gives the results of elemental analyses together with the decomposition points for the purified specimens of SXO and XO in free acid form, which have no melting points. The decomposition points were determined by a Rigaku Denki Differential Scanning Calorimeter Model 8001 SL/C. The temperature was calibrated with anthracene (216 °C) and anthraquinone (286 °C).

Discussion

The solvent *n*-BuOH–HOAc–H_2O–NH_3 forms on the layer two zones I and II with stepwise different pH values. Zone I consists of *n*-BuOH–HOAc–H_2O system which primarily acts as an organic phase for the solute species. Zone II consists of NH_4OAc–HOAc–*n*-BuOH–H_2O system which primarily acts as an aqueous phase for solutes.

The polybasic Brønsted acids SXO and XO dissociate to the species corresponding to the pH of zone II. They dissociate in aqueous solution with acid dissociation constants, pK_a,[8] as follows.

Table 2. Analytical data of the purified specimens of SXO and XO

Compound	Formula	Dp (°C)		Elemental analyses				
				C, %	H, %	N, %	S, %	C/N
SXO	$C_{26}H_{25}O_9NS \cdot H_2O$	201	Calcd	57.24	4.99	2.57	5.87	22.3
			Found	56.05	4.97	2.53	5.68	22.2
XO	$C_{31}H_{32}O_{13}N_2S \cdot 2H_2O$	281	Calcd	52.54	5.12	3.95	4.52	13.3
			Found	52.40	4.93	3.95	4.20	13.3

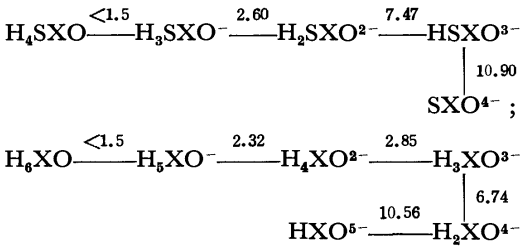

Since there is a discrete change in pH value between zones I and II, SXO exists only as a diprotonated species H_2SXO^{2-} in zone II, and cannot migrate through zone I; it constitutes a concentrated "*one*" band completely separated from the band of *o*-CR. XO is concentrated near the starting line as H_3XO^{3-} and H_2XO^{4-} in zone II. Thus SXO is satisfactorily separated from XO and *o*-CR.

In the chromatography using *n*-BuOH saturated with 10% aqueous HOAc without aqueous NH_3, the band of SXO lengthens due to the increasing number of species in protolytic equilibria and causes serious cross-contamination with XO and *o*-CR.[1)]

The best conditions for the separation of SXO and XO in preparative thin-layer chromatography (p-tlc) differ from those in thin-layer chromatography (tlc).[1)] In tlc, XO migrates through zone II beneath the NH_4-front and SXO migrates through zone I. In p-tlc, both XO and SXO migrate through zone II. The difference is due to the fact that the amount of NH_4OAc formed in zone II is in large excess relative to that of the solute species applied. Thus NH_4OAc forms a saturated adsorption band in zone II and XO migrates through zone II beneath the NH_4-front. In p-tlc, however, the NH_4OAc cannot form a saturated adsorption band in zone II under the conditions mentioned above owing to the increased amount of the solutes applied. Therefore, both SXO and XO remain in zone II. With increase in the amount of NH_3 added the chromatographic behavior of p-tlc approaches that of tlc.

However, in the deeper portion of the layer the band of SXO becomes considerably overlapped with that of XO.

With a thick layer some substances show different rates of migration in the surface and the deeper portion of the layer.[12)] We observed that the band of SXO moves faster in the surface of the layer than in the deeper layer, but this is not the case for XO. Under the given conditions, the band of SXO is not contaminated with XO and IDA either in the surface or in the deeper layer.

The authors wish to thank Professor Y. Matsunaga for aid in the DSC measurements. They also thank Miss H. Kakizaki, Faculty of Pharmacology, for elemental analysis.

One of the authors (M. Y.) is indebted to Professor S. Abe, Tokyo University of Agriculture and Technology, for instruction in tlc.

References

1) M. Yamada and M. Fujimoto, This Bulletin, **44**, 294 (1971).
2) D. C. Olson and D. W. Margerum, *Anal. Chem.*, **34**, 1299 (1962).
3) Y. Kawai, T. Takahashi, K. Hayashi, T. Imamura, H. Nakayama, and M. Fujimoto, This Bulletin, **45**, 1417 (1972).
4) J. Körbl and R. Přibil, *Chem. and Ind.*, **1957**, 233.
5) B. Buděšínský, "Chelates in Analytical Chemistry," Vol. 1, ed. by H. A. Flaschka and J. A. Barnard, Jr., Marcel Dekker, New York, N. Y. (1967), pp. 15—47.
6) B. Buděšínský, *Z. Anal. Chem.*, **206**, 262 (1964).
7) J. Körbl, *Collection Czech. Chem. Commun.*, **22**, 1789 (1957).
8) M. Murakami, T. Yoshino, and S. Harasawa, *Talanta*, **14**, 1293 (1967).
9) H. Eyring, *Anal. Chem.*, **20**, 98 (1948).
10) E. Stahl, "Dünnschicht-Chromatographie," ed. by E. Stahl, Springer-Verlag Berlin-Heidelberg-New York (1967).
11) J. Sykora and V. Eybl, *Československ. Farm.*, **17**, 92 (1968).
12) C. G. Honegger, *Helv. Chim. Acta*, **45**, 1409 (1962); **46**, 1772 (1963).

Mössbauer Studies of the Thermal Decomposition of Tris(2,2'-bipyridine)iron(II) Chloride and the Structures of the Isomers of 2,2'-Bipyridineiron(II) Chloride

Haruo SATO and Takeshi TOMINAGA*

Department of Chemistry, Faculty of Science, The University of Tokyo, Bunkyo-ku, Tokyo 113

(Received September 30, 1975)

The thermal decomposition of $[Fe(bipy)_3]Cl_2 \cdot 5H_2O$ in nitrogen was investigated by means of Mössbauer spectroscopy. Two isomers of $Fe(bipy)Cl_2$ were found to occur in the decomposition sequence; one of them appears to be identical with the rose-red form of $Fe(bipy)Cl_2$ prepared by the wet process. The structures of the two isomers were determined on the basis of the Mössbauer spectra, the infrared and Raman spectra, the powder X-ray patterns, and the magnetic moments of these compounds. It has been concluded that tris(2,2'-bipyridine)-iron(II) chloride presumably decomposes in the following sequence:

$[Fe(bipy)_3]Cl_2 \cdot 5H_2O \longrightarrow Fe(bipy)_2Cl_2 \longrightarrow$ orange $Fe(bipy)Cl_2$ (monomeric, tetrahedral) $\longrightarrow$ rose-red $Fe(bipy)Cl_2$ (polymeric, octahedral) $\longrightarrow FeCl_2$

Earlier papers of this series[1-3] have demonstrated that the structural changes during the step-by-step pyrolysis of iron(II) pyridine complexes and the ^{57}Co-labeled cobalt(II) pyridine complex can be monitored by Mössbauer spectroscopy. As a part of the Mössbauer studies of iron complexes with multidentate ligands, we have recently investigated the thermal decomposition of tris(2,2'-bipyridine)iron(II) chloride in nitrogen and found that two isomers of 2,2'-bipyridineiron(II) chloride arise in the pyrolysis sequence.[4] Since the structures of these isomers have not been known, however, we have now attempted to determine their structures by means of Mössbauer spectroscopy, together with other physicochemical methods.

The object of the present article is to give a more complete report on our work concerning the thermal decomposition process of tris(2,2'-bipyridine)iron(II) chloride and the structures of the two isomers of 2,2'-bipyridineiron(II) chloride obtainable as decomposition products.

Experimental

Materials. *Tris(2,2'-bipyridine)iron(II) Chloride*: A concentrated aqueous NaCl solution was added to an aqueous solution containing a 1:3 mixture (mole ratio) of iron (II) sulfate and 2,2'-bipyridine, and the separated crystals were washed and stored over P_2O_5 in a desiccator. The compound thus prepared was pentahydrate.[5] Found: C, 52.5; H, 4.7; N, 12.4%. Calcd for $[Fe(bipy)_3]Cl_2 \cdot 5H_2O$: C, 52.6; H, 5.0; N, 12.3%.

2,2'-Bipyridineiron(II) Chloride (Rose-red Form): This compound was prepared from iron(II) chloride and 2,2'-bipyridine in an aqueous HCl solution in the manner described by Broomhead and Dwyer.[6] Found: C, 42.5; H, 2.9; N, 10.1%. Calcd for $Fe(bipy)Cl_2$: C, 42.5; H, 2.9; N, 9.9%.

Measurements. The thermogravimetric analysis and differential thermal analysis were performed in a nitrogen stream at a heating rate of 1, 2 or 5 °C/min. The powder X-ray patterns of the isomers of $Fe(bipy)Cl_2$ and $Co(bipy)Cl_2$ were made using a Rigaku Denki Geigerflex and Fe-$K\alpha$ radiation. The infrared spectra of $Fe(bipy)Cl_2$ isomers were recorded on a Hitachi EPI-L Spectrophotometer (for the 200—700 cm^{-1} region) or on a Hitachi EPI-G2 Spectrophotometer (for the 400—4000 cm^{-1} region). The Raman spectra were measured by means of a Spectra Physics 166-01 Spectrophotometer using the 6471 Å exciting line of a Kr-ion laser. The magnetic susceptibilities were determined at room temperature by the Faraday method.

The Mössbauer spectra of the parent complex, the decomposition products (including those obtained at intermediate stages), and the 2,2'-bipyridineiron(II) chloride prepared by the wet method (rose-red form) were taken at 78, 195, and 293 K by using a Shimadzu MEG-2 Mössbauer Spectrometer with a ^{57}Co source diffused into copper foil.

* To whom all correspondence should be addressed.

Results and Discussion

Thermal Decomposition of $[Fe(bipy)_3]Cl_2 \cdot 5H_2O$.

In Fig. 1 are represented the TGA and DTA curves for tris(2,2'-bipyridine)iron(II) chloride, $[Fe(bipy)_3]Cl_2 \cdot 5H_2O$. Three phases, II, III, and IV, can be observed distinctly during the thermal decomposition of this compound (Phase I). Based on the TGA curve, the II, III, and IV phases were assumed to indicate the products which were obtainable by the loss of all the water and one molecule of 2,2'-bipyridine from the parent complex in the first step, and then by the successive loss of an additional molecule each of 2,2'-bipyridine: the II, III, and IV phases correspond to $Fe(bipy)_2Cl_2$, $Fe(bipy)Cl_2$, and $FeCl_2$ respectively. The results of elementary analysis were also in good agreement with the values expected for the assumed compounds. Found for the product at Phase II: C, 54.7; H, 3.7; N, 12.7%. Calcd for $Fe(bipy)_2Cl_2$: C, 54.7; H,

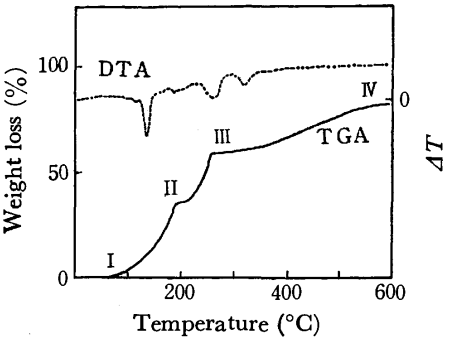

Fig. 1. TGA and DTA curves of $[Fe(bipy)_3]Cl_2 \cdot 5H_2O$ (heating rate: 2 °C/min).

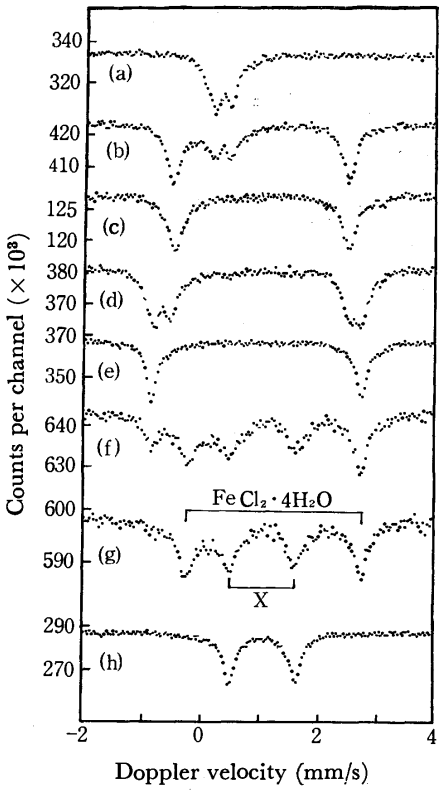

Fig. 2. Mössbauer spectra at 293 K of $[Fe(bipy)_3]Cl_2 \cdot 5H_2O$ and thermal decomposition products: (a) phase I ($[Fe(bipy)_3]Cl_2 \cdot 5H_2O$); (b) intermediate stage, phase I→phase II; (c) phase II ($Fe(bipy)_2Cl_2$); (d) intermediate stage, phase II→phase III; (e) phase III (orange $Fe(bipy)Cl_2$); (f) intermediate stage obtained at about 400 °C, phase III→phase IV; (g) intermediate stage obtained at 460 °C, phase III→phase IV; (h) rose-red $Fe(bipy)Cl_2$ prepared by the wet process.

3.7; N, 12.8%. Found for the product at Phase III: C, 42.5; H, 2.8; N, 9.9%. Calcd for $Fe(bipy)Cl_2$: C, 42.5; H, 2.9; N, 9.9%.

Figure 2 reveals some typical Mössbauer spectra at 293 K of $[Fe(bipy)_3]Cl_2 \cdot 5H_2O$, the products at the II and III phases, and the products (mixtures) obtained at intermediate stages between the distinct phases. The Mössbauer parameters of tris-, bis-, and mono-(2,2′-bipyridine)iron(II) chloride are summarized in Table 1. The detailed process of thermal decomposition can be elucidated by comparing the Mössbauer spectra taken at various stages of the reactions, as will be done below.

Phase I: The Mössbauer spectrum of $[Fe(bipy)_3]Cl_2 \cdot 5H_2O$ (Phase I) consists of a doublet with δ and ΔE_Q values indicating low-spin iron(II) (Fig. 2a). The anhydrous salt, $[Fe(bipy)_3]Cl_2$, prepared by dehydration in an Abderhalden's dryer, reveals a spectrum identical with the pentahydrate's.

Intermediate Stages between Phases I and II: The intermediate products obtained at 140 °C between Phases I and II indicate a composite spectrum composed of the Mössbauer peaks of $[Fe(bipy)_3]Cl_2 \cdot 5H_2O$ (Phase I) and $Fe(bipy)_2Cl_2$ (Phase II), as is shown in Fig. 2b. However, the spectrum of the products obtained at 130 °C was identical with that of Phase I, while the spectrum of the products obtained at 150 °C was identical with that of Phase II. While Phase II is attained at about 200 °C on the TGA curve, the large endothermic peak due to the *Phase I→Phase II* transition appears at 140 °C on the DTA curve. No plateau for the anhydrous $[Fe(bipy)_3]Cl_2$ phase was detectable on the TGA curve. These observations imply that the dissociation of one 2,2′-bipyridine molecule occurs quickly at about 140 °C before dehydration is completed, but that the volatilization of the dissociated 2,2′-bipyridine molecules from crystals proceeds rather slowly below 200 °C.

Phase II: The Mössbauer spectrum of $Fe(bipy)_2Cl_2$ (Phase II) consists of a doublet with large δ and ΔE_Q values corresponding to high-spin iron(II) (Fig. 2c). The Mössbauer parameters of this compound at room temperature were reported by König *et al.*;[7] they are in agreement with the values obtained in the present work.

Intermediate Stages between Phases II and III: In the stages between Phases II and III, mixtures of the absorption peaks of $Fe(bipy)_2Cl_2$ (Phase II) and $Fe(bipy)Cl_2$ in the orange form (Phase III) were observed (Fig. 2d); the intensity of the $Fe(bipy)Cl_2$ peaks relative to that of the $Fe(bipy)_2Cl_2$ peaks increased with the increase in the reaction temperature.

Phase III: The spectrum of $Fe(bipy)Cl_2$ in the orange form (Phase III) is composed of a doublet with an even larger quadrupole splitting than that of $Fe(bipy)_2Cl_2$, characteristic of high-spin iron(II) (Fig. 2e).

Intermediate Stages between Phases III and IV: The Mössbauer spectrum of the intermediate products obtained between Phases III and VI indicates a new doublet of high-spin iron(II) in addition to the peaks ascribable to known products expected at Phases III and IV (Figs. 2f and 2g). In the meantime, the color of the mixture of products changes from orange to dark red upon the formation of the new compound. Since the new rose-red compound (hereafter designated as X)

TABLE 1. MÖSSBAUER PARAMETERS OF TRIS(2,2′-BIPYRIDINE)IRON(II) CHLORIDE, THERMAL DECOMPOSITION PRODUCTS AND ROSE-RED FORM OF 2,2′-BIPYRIDINEIRON(II) CHLORIDE PREPARED BY THE WET PROCESS

Compound	Isomer shift[a] δ(Fe) (mm/s)			Quadrupole splitting[a] ΔE_Q (mm/s)		
	78K	195K	293K	78K	195K	293K
$[Fe(bipy)_3]Cl_2 \cdot 5H_2O$	0.39	0.36	0.33	0.34	0.31	0.28
$Fe(bipy)_2Cl_2$	1.11	1.04	1.01	3.40	3.29	2.98
$Fe(bipy)Cl_2$ (orange form)	1.08	1.00	0.93	3.71	3.65	3.58
Compound X[b]	1.1_8	1.0_7	1.0_4	1.7_8	1.4_4	1.0_9
$Fe(bipy)Cl_2$ (rose-red form)	1.18	1.09	1.07	1.76	1.38	1.14

a) Errors: ±0.02 mm/s. b) Because of the uncertainty due to the complexity of overlapping peaks and to the counting statistics, parameters of compound X involve relatively large errors of ± 0.06 mm/s.

could not be isolated as a pure product, but was usually found as mixtures with the other decomposition products corresponding to Phases III and IV (*i.e.*, $Fe(bipy)Cl_2$ in the orange form, $FeCl_2$, and its hydrates),[8] it was not readily identified by ordinary physicochemical methods of analysis. Although Compound X was observed distinctly in the Mössbauer spectra of the reaction products obtained above the temperature range of Phase III, the weight loss was negligible and its formation was not detectable on the TGA curve. Therefore, it is unlikely that Compound X is a product formed by the further decomposition of $Fe(bipy)Cl_2$ (orange form).[9] The Mössbauer parameters at 78, 195, and 293 K of the rose-red Compound X are entirely different from those of the orange-form $Fe(bipy)Cl_2$ obtained by thermal decomposition, whereas they are in agreement with those of the rose-red form of $Fe(bipy)Cl_2$ prepared by the wet process in hydrochloric acid (Table 1 and Fig. 2h). Thus, we may presume that the rose-red Compound X formed in the intermediate stages between Phases III and IV is identical with the rose-red form of $Fe(bipy)Cl_2$ prepared by the wet process, which appears to be isomeric with the orange form of $Fe(bipy)Cl_2$ obtained by the thermal decomposition (Phase III).

Phase IV: In the Mössbauer spectra of the products at Phase IV we often observed the hydrates of iron(II) chloride, $FeCl_2 \cdot 2H_2O$, and $FeCl_2 \cdot 4H_2O$, since anhydrous iron(II) chloride is so hygroscopic that it is partially hydrated before the Mössbauer measurements.

Structures of $Fe(bipy)Cl_2$ Isomers. Both $[Fe(bipy)_3]Cl_2 \cdot 5H_2O$ (Phase I) and $Fe(bipy)_2Cl_2$ (Phase II) are octahedral monomers. Although a marked discrepancy has been reported between the magnetic moments of $Fe(bipy)Cl_2$ samples prepared by different methods,[6,10] the structures of the two isomers of $Fe(bipy)Cl_2$ have never been studied before. According to the following data of the Mössbauer spectra, powder X-ray patterns, infrared and Raman spectra, and magnetic moments of the orange $Fe(bipy)Cl_2$ obtained by the thermal decomposition and the rose-red $Fe(bipy)Cl_2$ prepared by the wet process, we may conclude that the orange-form $Fe(bipy)Cl_2$ is monomeric and tetrahedral, while the rose-red form $Fe(bipy)Cl_2$ (or the compound, X, obtained between Phases III and IV) is polymeric and octahedral, with chloride bridges.

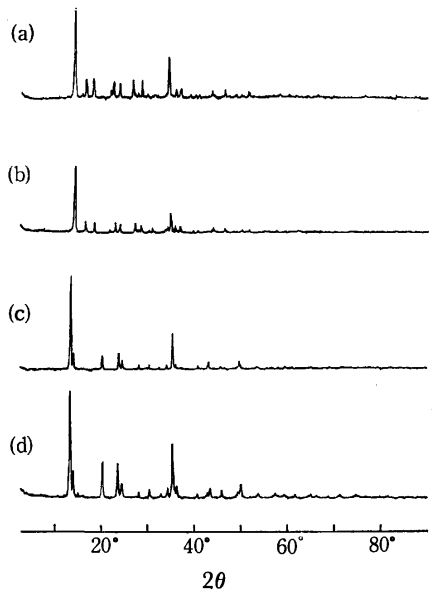

Fig. 3. Powder X-ray patterns of (a) orange $Fe(bipy)Cl_2$, (b) β-$Co(bipy)Cl_2$, (c) rose-red $Fe(bipy)Cl_2$, and (d) α-$Co(bipy)Cl_2$.

Mössbauer Spectra: It has been found for high-spin iron(II) complexes that a tetrahedral complex generally gives a smaller isomer shift as compared with the octahedral complex containing similar ligands.[11-13] Since the isomer shift of the rose-red $Fe(bipy)Cl_2$ is larger than that of $Fe(bipy)_2Cl_2$, which is octahedral, the former may not be tetrahedral, but octahedral (Table 1). Accordingly, the orange form of $Fe(bipy)Cl_2$, with a smaller isomer shift, is probably tetrahedral.

Powder X-Ray Patterns: The structures of the α and β isomers of $Co(bipy)Cl_2$ have been reported as an octahedral polymer and a tetrahedral monomer respectively on the basis of their electronic and infrared spectra.[14,15] As is shown in Fig. 3, the two isomers of $Fe(bipy)Cl_2$ (or $Co(bipy)Cl_2$) give different powder X-ray patterns, while the pattern of each isomer of $Fe(bipy)Cl_2$ is quite similar to that of the corresponding analogue of $Co(bipy)Cl_2$. Hence, a comparison of their powder X-ray patterns reveals that the orange $Fe(bipy)Cl_2$ and β-$Co(bipy)Cl_2$ are isomorphous and tetrahedral, while the rose-red $Fe(bipy)Cl_2$ and α-$Co(bipy)Cl_2$, octahedral: these results confirm the conclusion derived from the Mössbauer data.

Infrared and Raman Spectra: In a number of transition-metal complexes, the metal-halogen stretching vibrations are affected by whether or not the halogen is bridging.[16-18] Hence, the region of iron-chlorine stretching vibrations of FeL_2Cl_2 (L=py, 1/2bipy, *etc.*) can be expected to shift to lower frequencies in the polymeric octahedral isomer (in the vicinity of 200 cm^{-1}),[18,19] as compared with the region for the monomeric tetrahedral isomer (in the vicinity of 300 cm^{-1}).[20] In the infrared and Raman spectra of the orange form of $Fe(bipy)Cl_2$ we observed a band at 360 cm^{-1} (Fig. 4) which can be ascribed to the Fe–Cl stretching vibrations, in accordance with the assignment by Strukl *et al.* of the 361/369 cm^{-1} region of this compound as such.[21] In the case of the rose-red $Fe(bipy)Cl_2$, no strong band was observed in the 270—340 cm^{-1} region, while the

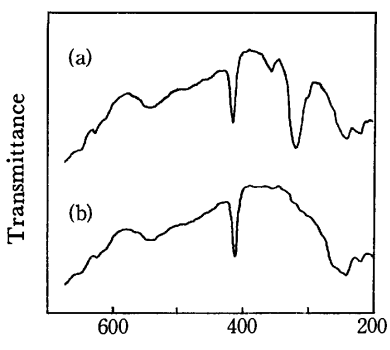

Fig. 4. Infrared spectra of (a) orange $Fe(bipy)Cl_2$, and (b) rose-red $Fe(bipy)Cl_2$.

band occurring at 152 or 187 cm^{-1} in the Raman spectrum may possibly correspond to the Fe–Cl streching vibrations. Therefore, the infrared and Raman spectra of these isomers also support the structures presumed on the basis of the Mössbauer and powder X-ray data.

Magnetic Moments: There has been a considerable disagreement among the reported values of the magnetic moments of Fe(bipy)Cl_2: 1.8 B.M.[10] and 4.8 B.M.[6] for the Fe(bipy)Cl_2 samples prepared by decomposition in a vacuum, and 5.72 B.M.[6] for the Fe(bipy)Cl_2 prepared by the wet process. The magnetic moments obtained in the present work are 4.9 ± 0.1 B.M. for the orange Fe(bipy)Cl_2 and 5.3 ± 0.1 B.M. for the rose-red Fe(bipy)-Cl_2. Hence, it may be concluded that the low value of 1.8 B.M. reported by Basolo *et al.*[10] is in error, as has been suggested.[6] This is further confirmed by the fact that no low-spin iron(II) was observed in the Mössbauer spectra of the products from the pyrolysis of [Fe(bipy)$_3$]$Cl_2\cdot5H_2O$ in nitrogen or a vacuum. The observation that the magnetic moment of the rose-red Fe(bipy)Cl_2 is larger than that of the orange Fe(bipy)Cl_2 is compatible with the assignment of the rose-red isomer as octahedral and the orange isomer as tetrahedral.[22]

In conclusion, we can say that the thermal decomposition of tris(2,2'-bipyridine)iron(II) chloride in nitrogen presumably proceeds as follows:

$$[Fe(bipy)_3]Cl_2\cdot5H_2O \longrightarrow Fe(bipy)_2Cl_2 \longrightarrow$$
orange Fe(bipy)Cl_2 (monomeric, tetrahedral) $\longrightarrow$
rose-red Fe(bipy)Cl_2 (polymeric, octahedral) $\longrightarrow$
$FeCl_2$

The authors wish to express their thanks to Professor Nobufusa Saito for his encouragement and support. They are also indebted to Dr. Hiroo Hamaguchi for the measurements of the Raman spectra, and to Dr. Toshiaki Ohta and Mr. Tadashi Sugano for the measurements of the magnetic susceptibilities.

References

1) T. Tominaga, T. Morimoto, M. Takeda, and N. Saito, *Inorg. Nucl. Chem. Lett.*, **2**, 193 (1966).
2) T. Tominaga, M. Takeda, T. Morimoto, and N. Saito, This Bulletin, **43**, 1093 (1970).
3) N. Saito, M. Takeda, and T. Tominaga, *Radiochem. Radioanal. Lett.*, **6**, 169 (1971).
4) H. Sato and T. Tominaga, *Radiochem. Radioanal. Lett.*, **22**, 3 (1975).
5) Heptahydrate or hexahydrate is obtainable when the separated crystals are dried in air.
6) J. A. Broomhead and F. P. Dwyer, *Aust. J. Chem.*, **14**, 250 (1960).
7) E. König, S. Hüfner, E. Steichele, and K. Madeja, *Z. Naturforsch.*, **22a**, 1543 (1967); **23a**, 632 (1968).
8) The Mössbauer peaks of Compound X, orange Fe(bipy)Cl_2, and hydrates of $FeCl_2$ were observed in the spectrum of the reaction products obtained at about 400 °C (Fig. 2f), while the peaks of the orange Fe(bipy)Cl_2 disappeared in the products obtained at 460 °C (Fig. 2g).
9) The small endothermic peak at 330 °C on the DTA curve may not be related to the conversion of the orange Fe(bipy)Cl_2 into the rose-red isomer, since a similar endothermic peak is also observable on the thermal decomposition of the rose-red form and an exothermic peak appears at about the same temperature on the cooling of the orange form. The Mössbauer spectra indicate the presence of mixtures of both forms over a fairly wide temperature range between Phases III and IV.
10) F. Basolo and F. P. Dwyer, *J. Amer. Chem. Soc.*, **76**, 1454 (1954).
11) C. D. Burbridge and D. M. L. Goodgame, *J. Chem. Soc. A*, **1967**, 694.
12) T. C. Gibb and N. N. Greenwood, *J. Chem. Soc.*, **1965**, 6989.
13) G. M. Bancroft, A. G. Maddock, W. K. Ong, and R. H. Prince, *J. Chem. Soc. A*, **1966**, 723.
14) R. H. Lee, E. Griswold, and J. Kleinberg, *Inorg. Chem.*, **3**, 1278 (1964).
15) R. J. H. Clark and C. S. Williams, *Spectrochim. Acta*, **23A**, 1055 (1967).
16) R. J. H. Clark and C. S. Williams, *Inorg. Chem.*, **4**, 350 (1965).
17) C. Postmus, J. R. Ferraro, A. Quattrochi, K. Shobatake and K. Nakamoto, *Inorg. Chem.*, **8**, 1851 (1969).
18) M. Goldstein and W. D. Unsworth, *Inorg. Chim. Acta*, **4**, 342 (1970).
19) T. Birchall and M. F. Morris, *Can. J. Chem.*, **50**, 201 (1972).
20) T. Birchall and M. F. Morris, *Can. J. Chem.*, **50**, 211 (1972).
21) J. S. Strukl and J. L. Walter, *Spectrochim. Acta*, **27A**, 223 (1971).
22) N. S. Gill and R. S. Nyholm, *J. Inorg. Nucl. Chem.*, **18**, 88 (1961).

X-Ray Diffraction Studies of the Structures of Hydrated Divalent Transition-Metal Ions in Aqueous Solution*

Hitoshi OHTAKI, Toshio YAMAGUCHI, and Masunobu MAEDA

Laboratory of Solution Chemistry, Department of Electronic Chemistry, Tokyo Institute of Technology, O-okayama, Meguro, Tokyo 152

(Received October 21, 1975)

X-ray scattering measurements have been carried out for concentrated aqueous solutions of divalent transition-metal perchlorates of manganese(II) to zinc(II). The radial distribution curves showed that each central metal ion was octahedrally surrounded by six water molecules at the distances of 2.20 Å for Mn^{2+}–OH_2, 2.12 Å for Fe^{2+}–OH_2, 2.08 Å for Co^{2+}–OH_2, 2.04 Å for Ni^{2+}–OH_2, and 2.08 Å for Zn^{2+}–OH_2. The results from the radial distribution curves were confirmed by the direct analysis of reduced intensities. Concentrated aqueous solutions of copper(II) and zinc(II) sulfates have also been measured. The bond distances of 1.94 Å for the Cu^{2+}–OH_2 (equatorial), 2.38 Å for the Cu^{2+}–OH_2 (axial) and 2.08 Å for Zn^{2+}–OH_2 were consistent with those obtained for the perchlorate solutions. No evidence for the contact ion pairs of metal and sulfate ions was found by the present X-ray measurements. The bond energies between metal ions including copper ion[26] were discussed by application of the Garrick model with a slight modification.

In crystals, divalent transition-metals of various salts are coordinated by 2 to 6 water molecules and the vacant apices of the octahedral structure of the metal ions are occupied by other ligands. The bond distance between a central metal ion and a water molecule is affected by counter-anions.

The manganese(II) ion in the $Mn(NH_4)_2(SO_4)_2 \cdot 6H_2O$ crystal combined with water molecules at the distance of 2.18 Å.[1] For iron(II) salts the Fe^{2+}–OH_2 distance varied from 1.96 Å to 2.15 Å[2-6] depending on anions in salts. The Co^{2+}–OH_2 distance in crystals changed over the range of 2.08 Å to 2.23 Å,[7-10] which was longer than the Ni^{2+}–OH_2 distance; the latter was found to be 2.04—2.07 Å.[10-14] In copper salts were found two different Cu^{2+}–OH_2 bond lengths due to the Jahn–Teller distortion. The shorter bond length was in the order of 1.97 Å[15-19] except the bond within $Cu(H_2O)_6(ClO_4)_2$ in which the length was 2.125 Å,[20] and the longer one was about 2.3—2.8 Å.[15-20] The zinc(II) ion had a regular octahedral structure and the Zn^{2+}–OH_2 distance was about 2.08—2.10 Å.[10,21,22]

In contrast to a number of crystallographic studies of divalent transition-metal salts, only a few studies by X-ray diffraction have been reported on the structures of hydrated divalent transition-metal ions in solution. According to Shapovalov *et al.* who measured X-ray scatterings of sulfate solutions,[23,24] divalent transition-metals were hydrated with six water molecules and the bond lengths were about 2.15 Å independent of the metal ions except the Mn^{2+}–OH_2 distance of 2.20 Å and the longer Cu^{2+}–OH_2 distance of 2.5 Å. Bol *et al.* reported shorter bond lengths for hydrated Co^{2+}, Ni^{2+}, and Zn^{2+} ions in nitrate solutions[25] than those by Shapovalov *et al.* Our previous results for a copper perchlorate solution[26] showed that the Cu^{2+}–OH_2 distance in the equatorial position was 1.94 Å and that in the axial position was 2.43 Å, both of them being shorter than the distances reported by Shapovalov and Radchenko[23] in a sulfate solution.

In the present investigation we aim at determining the structures of a series of divalent transition-metal ions from Mn^{2+} to Zn^{2+} in aqueous perchlorate solutions by means of X-ray diffraction and discussing the change in the M^{2+}–OH_2 bond length with varying metal ions. The structures of hydrated copper(II) and zinc(II) ions in sulfate solutions are also determined in order to examine if the bond distances of metal and water molecules would really be affected by anions even in solutions.

Preparation and Analysis of Sample Solutions

Mn(II), Co(II), and Ni(II) Perchlorate Solutions. Manganese, cobalt, and nickel perchlorates were prepared by dissolving the metal chlorides (Wako reagent grade), which had been recrystallized twice from water, in dilute perchloric acids. Hydrochloric acid formed in solution was removed by repeated evaporation. After recrystallizing twice from water, crystals thus obtained were dissolved in water to prepare sample solutions. The concentrations of these metal ions were determined by two different methods; gravimetry as pyrophosphate $Mn_2P_2O_7$ and titration with EDTA for Mn^{2+}, electrogravimetry and titration with EDTA for Co^{2+}, and electrogravimetry and gravimetry as the dimethylglyoximate for Ni^{2+} ions.

Fe(II) Perchlorate Solution. A stoichiometric amount of $Ba(ClO_4)_2$ crystals (Wako reagent grade) was dissolved into an aqueous solution of $FeSO_4 \cdot 7H_2O$ (Wako reagent grade) containing perchloric acid and then either $Ba(ClO_4)_2$ or sulfuric acid solution was added dropwise from burets to attain the exact stoichiometric ratio of Ba^{2+} to SO_4^{2-} ions in the mixture. The equivalent point was detected by the naked eye. A solution of iron (II) perchlorate was obtained by removing the $BaSO_4$ precipitates through G4 glass filters and No. 5C filter papers. All the treatments were performed under an atmosphere of nitrogen gas. The sample solution thus prepared was tested for Ba^{2+} and SO_4^{2-} ions by the addition of drops of sulfuric acid and a $Ba(ClO_4)_2$ solution, respectively. A check for Fe^{3+} ion with a KSCN aqueous solution was negative. The content of Fe^{2+} was determined by titration with a $KMnO_4$ solution.

Zn(II) Perchlorate Solution. Zinc perchlorate crystals were prepared by dissolving zinc oxide (Wako reagent grade)

* A part of the work has been submitted to The Prof. Ringbom Memorial Volume, to be published from Pergamon Press.

Table 1. Compositions of the sample solutions (in g-atoms·dm^{-3})

	$Mn(ClO_4)_2$	$Fe(ClO_4)_2$	$Co(ClO_4)_2$	$Ni(ClO_4)_2$	$Cu(ClO_4)_2$[26]	$Zn(ClO_4)_2$	$CuSO_4$	$ZnSO_4$
M	2.612	2.173	2.672	2.491	3.550	2.886	1.368	2.797
S	—	—	—	—	—	—	1.371	2.809
Cl	5.818	4.499	5.710	5.430	7.357	6.179	—	—
O	65.93	64.10	66.66	66.61	69.86	67.65	60.51	64.87
H	85.48	92.36	88.00	90.23	81.12	86.27	110.1	107.1

in a hot perchloric acid and recrystallizing twice from water. A solution of the zinc perchlorate was prepared by dissolving the crystals in water. The content of Zn^{2+} was determined both by gravimetry as $ZnHg(SCN)_4$ and by titration with EDTA.

The amounts of perchlorate and hydrogen ions in the solutions were determined as described in the previous papers.[26,27]

Cu(II) and Zn(II) Sulfate Solutions. Copper and zinc sulfate crystals (Wako reagent grade) were recrystallized once from water. The content of Cu^{2+} in the copper sulfate sample solution was determined by electrogravimetric analysis and by titration with EDTA. The concentration of zinc in the sample was analyzed by the same method as used for the zinc perchlorate solution. The content of SO_4^{2-} ions in the solutions was determined gravimetrically as $BaSO_4$.

The results of analysis for metal ions made by two different methods agreed each other within 0.2%. A small amount of perchloric or sulfuric acid was added to all the sample solutions in order to prevent the hydrolysis of the metal ions.

The density of the solutions was determined pychnometrically.

The compositions of the solutions investigated are given in Table 1, together with that of the $Cu(ClO_4)_2$ solution previously reported.[26]

X-Ray Scattering Measurements

X-Ray scattering measurements were carried out on a θ–θ X-ray diffractometer (JEOL Co., Tokyo) in a room thermostated at 25±1 °C. In the case of the iron(II) perchlorate solution, the measurements were carried out under an atmosphere of nitrogen gas in order to prevent the oxidation of the iron(II) ion by air.

Mo$K\alpha$ radiation (λ=0.7107 Å) was diffracted at the sample solution and then monochromatized by reflection on a curved surface of an LiF crystal. A Philips PW 210500 X-ray tube was employed. The observed range of scattering angles (2θ) was 2° to 140°, corresponding to the range 0.31 Å^{-1}<s<16.6 Å^{-1} ($s=4\pi\sin\theta/\lambda$). Times required to accumulate 40000 counts at each angle were recorded. The whole angle range was scanned twice. The details of the measurements are described elsewhere.[26,27]

Symbols

$D(r)$	The radial distribution function
ρ_0	The bulk electron density in the stoichiometric unit volume
s_{max}	The maximum value of s accessible in the experiments
$i(s)$	The reduced intensity
$M(s)$	The modification function
$I(s)$	The scaled intensities after correction for background, polarization, and absorption in the sample
n_i	The number of atom "i" in the stoichiometric volume containing one metal atom
$f_i(s)$	The scattering factor for atom "i" corrected for the real part of the anomalous dispersion
$\Delta f_i''$	The imaginary part of the anomalous dispersion correction for atom "i"
$\Phi(s)$	The fraction of the total incoherent scattering reaching the counter
$I_i^{inco}(s)$	The incoherent scattering of atom "i"
k	The damping factor
r_{ij}	The distance between the atoms "i" and "j"
b_{ij}	The temperature factor of the atoms "i" and "j"

Treatment of Intensity Data

The measured intensities were corrected for background, polarization,[28] and absorption in the sample,[28] and then scaled to absolute intensities by the conventional methods.[26,29,30] The coherent scattering factors used for Mn, Fe, Co, Ni, Cu, Zn, Cl, S, and O were those given by Cromer and Waber.[31] The values for H were those given by Stewart *et al.*[32] The incoherent scattering factors cited from Cromer[33] for Fe, Co, Ni, O, S, and Cl, from Cromer and Mann[34] for Mn, Cu, and Zn, and from Compton and Allison[35] for H were corrected for the Breit–Dirac factors. Values of anomalous dispersion corrections for all atoms were taken from Cromer and Lieberman.[36]

The radial distribution functions $D(r)$ were calculated by means of the Fourier transform according to Eq. 1:

$$D(r) = 4\pi r^2\rho_0 + 2r\pi^{-1}\int_0^{s_{max}} si(s)M(s)\sin(rs)ds \qquad (1)$$

where the reduced intensities $i(s)$ are written as[26,27]

$$i(s) = I(s) - \sum_i n_i(f_i^2(s) + (\Delta f_i'')^2 + \Phi(s)I_i^{inco}(s)) \qquad (2)$$

and the modification function $M(s)$ used in this study was $(\sum_i n_i f_i^2(0)/\sum_i n_i f_i^2(s))\exp(-ks^2)$ with the damping factor k of 0.015 Å^2 except the $CuSO_4$ case for which k=0.01 Å^2 was used.

Spurious peaks below 1 Å which appeared in the $D(r)$ curve were corrected since these spurious peaks did not correspond to any interatomic distances.[26,27] The reduced intensities $i(s)$ multiplied by s and the $D(r)$ curves thus deduced are shown in Figs. 1 and 2, respectively, for all the solutions, those for $Cu(ClO_4)_2$ solution previously reported[26] being also included.

Theoretical intensities due to interatomic interactions were calculated according to Eq. 3:

$$i(s)_{calc} = \sum_i\sum_j n_i f_i(s) f_j(s)\frac{\sin(r_{ij}s)}{r_{ij}s}\exp(-b_{ij}s^2) \qquad (3)$$

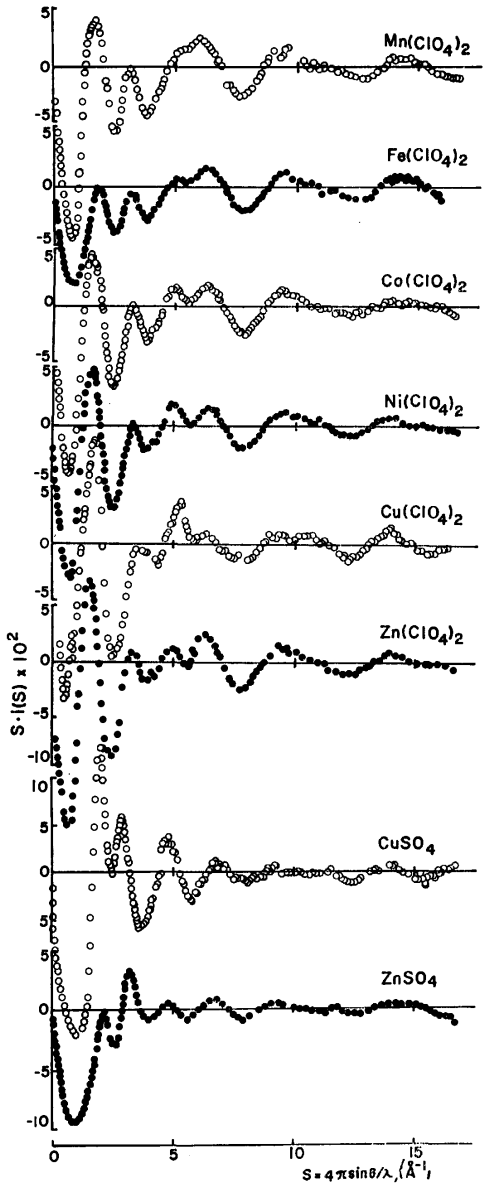

Fig. 1. Observed $s \cdot i(s)$ values of the solutions.

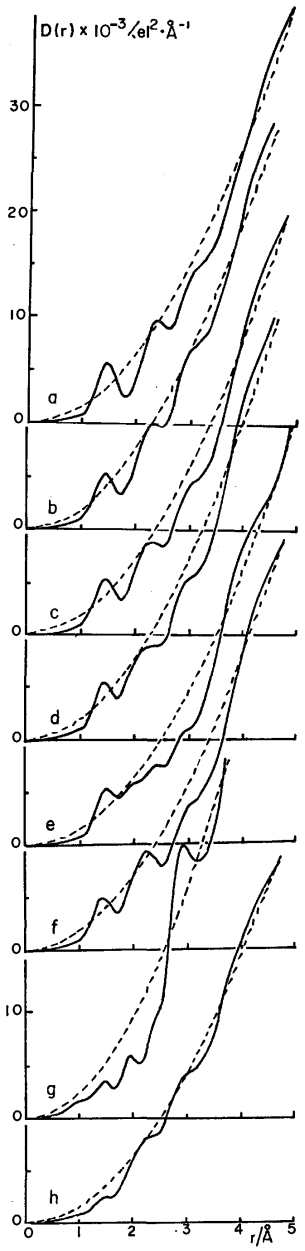

Fig. 2. Radial distribution curves $D(r)$'s (solid line) and $4\pi r^2\rho^0$ (dashed line) for the solutions. a. $Mn(ClO_4)_2$, b. $Fe(ClO_4)_2$, c. $Co(ClO_4)_2$, d. $Ni(ClO_4)_2$, e. $Cu(ClO_4)_2$, f. $Zn(ClO_4)_2$, g. $CuSO_4$, h. $ZnSO_4$.

All calculations were carried out on a HITAC 8700 computer at the Computer Center of our Institute by means of the KURVLR program.[37]

Analysis of Intensity Data and Results

a) Solutions of Manganese, Iron, Cobalt, Nickel, and Zinc Perchlorates. The $D(r)$ curves for these solutions are shown in Fig. 2 (a, b, c, d, and f); the $D(r)$ curve (Fig. 2e) for the $Cu(ClO_4)_2$ solution reported in the previous paper[26] being also contained for comparison. The $D(r)$ curves represented the first peak at around 1.4 Å, which corresponded to the Cl–O distance within the ClO_4^- ion according to previous investigations.[26,27] The second peak appeared in the region 2.0—2.2 Å which was expected to correspond to both the distance between the metal ions and neighboring water molecules and the O–O distance ($\simeq 1.4$ Å $\times\sqrt{8/3}=2.3$ Å) within the ClO_4^- ion which is known to form a regular tetrahedron. In order to deduce the peaks corresponding to the distances between metal ions and water molecules, the contributions from the Cl–O bond and the O–O

Table 2. Parameter values for the Cl–O, O–O atom pairs within ClO_4^-, the S–O, O–O atom pairs within SO_4^{2-}, and the O–H atom pair within H_2O

		r_{ij}/Å	b_{ij}/Å²	n_{ij}
ClO_4^-	Cl–O	1.43	0.001	4
	O–O	2.34	0.002	6
SO_4^{2-}	S–O	1.47	0.001	4
	O–O	2.40	0.002	6
H_2O	O–H	1.01	0.001	2

interactions within the ClO_4^- ion were theoretically subtracted from the $D(r)$ curves. Calculations of these contributions were carried out according to Eqs. 1 and 3. Values of parameters attributed to the structure of the ClO_4^- ion used for the calculations are listed in Table 2.[38] Theoretical peak shapes thus calculated are shown in Fig. 3 with a special reference to the zinc perchlorate solution. The distance between the metal ion and water molecules was obtained from the residual peak shown in Fig. 3a. The number of water molecules bonded to the metal ion was roughly estimated from the peak area (shown by the dotted line in Fig. 3a) according to procedures described in a previous paper.[27] Final values for the structure of the aqua complex were determined by the method of trial and error so that the subtraction of the calculated peak due to the M–OH_2 bond from the $D(r)$ curve led to a smooth background curve with no indication of residual intramolecular interaction. (Fig. 3b).

The distances between metal ions and water molecules were found to be 2.20 Å for Mn^{2+}, 2.12 Å for Fe^{2+}, 2.08 Å for Co^{2+}, 2.04 Å for Ni^{2+}, and 2.08 Å for Zn^{2+}, and the numbers of water molecules in the first hydration sphere and the temperature factors were about 6 and 0.004 $Å^2$, respectively, for all the solutions.

In order to confirm the results obtained by the analysis of $D(r)$ curves, the distances, the temperature factors, and the frequency factors for the hydrated metal ions as well as for the perchlorate ions were refined by a least squares method in which the minimum of the function $U=\sum s^2(i(s)-i(s)_{calc})^2$ was sought. Various subsets of the reduced intensities from different s regions were used in order to check experimental errors in the data and errors in the parameter values introduced by contributions from intermolecular interactions which largely contribute to the reduced intensities at low s regions. The calculations were carried out by the use of the program NLPLSQ, which is a modified program of the algorithm described by Marquardt.[39]

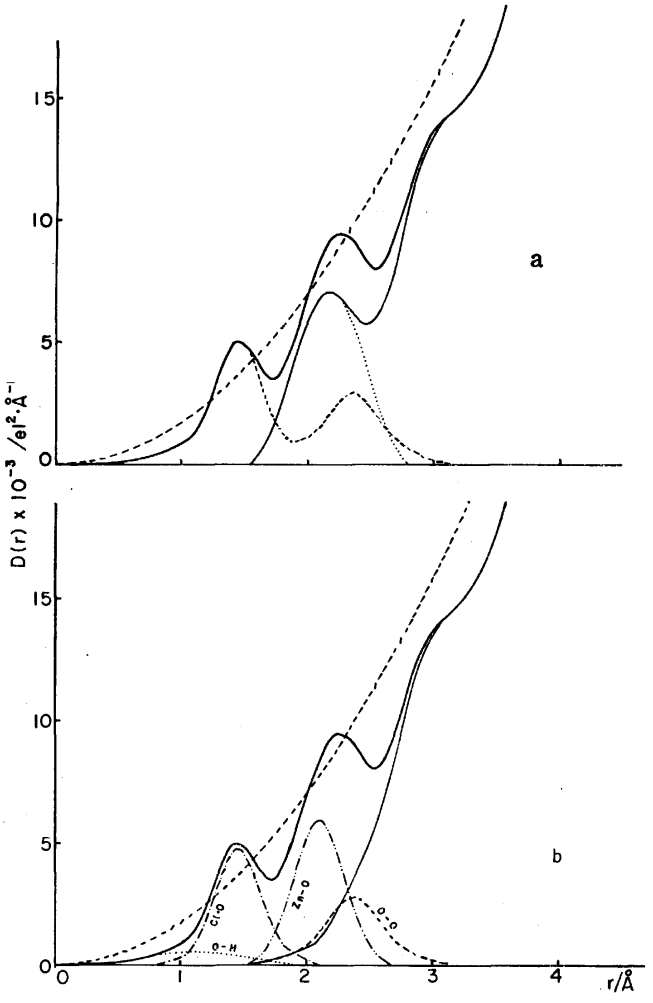

Fig. 3. a. The fine solid line gives the difference between $D(r)$ and the theoretical peaks (broken line) for the Cl–O and O–O atom pairs wrthin ClO_4^-.
b. The smooth curve (fine solid line) gives the residual distribution function obtained after subtraction of the peak shapes of the O–H, Cl–O, O–O, and Zn–OH_2 atom pairs from the $D(r)$ curve.

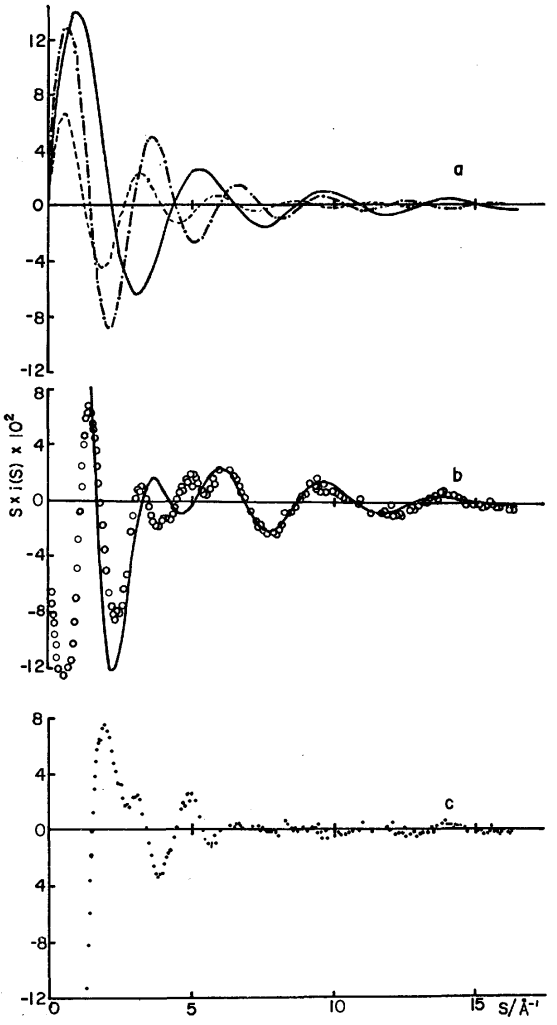

Fig. 4. Observed and calculated $s \cdot i(s)$ values for the $Zn(ClO_4)_2$ solution.
a. Each contribution of the Cl–O(—), O–O (···), and Zn–OH_2 (-·-) atom pairs.
b. Comparison between observed $s \cdot i(s)$ (circle) and the calculated $s \cdot i(s)$ (solid line) for the atom pairs considered using the refined parameter values given in Table 3.
c. Difference between observed and calculated $s \cdot i(s)$ values.

Table 3. The results of least squares refinements of the $Zn(ClO_4)_2$ solution by program NLPLSQ. The units of r and b are Å and Å^2, respectively. Standard deviations are listed in parentheses.

	$3.22<s/Å^{-1}<14.95$	$6.01<s/Å^{-1}<14.95$	$10.70<s/Å^{-1}<14.95$
r_{Zn-O}	2.083(4)	2.081(2)	2.080(6)
b_{Zn-O}	0.0047(3)	0.0042(1)	0.0043(2)
n_{Zn-O}	5.84(4)	5.92(6)	5.7(2)
r_{Cl-O}	1.427(2)	1.430(1)	1.428(2)
b_{Cl-O}	0.0008(2)	0.0010(1)	0.0010(1)
n_{Cl-O}	4.06(3)	3.98(3)	4.07(7)
r_{O-O}	2.376(1)	2.339(7)	2.338(1)
b_{O-O}	0.0025(7)	0.0013(3)	0.0013(4)
n_{O-O}	5.97(1)	6.3(2)	6.8(4)
U	0.126×10^7	0.101×10^6	0.409×10^5

The results calculated in various s ranges are shown in Table 3 with a reference to the $Zn(ClO_4)_2$ solution. The refined parameter values of a given hydrated metal ion were almost the same for different s regions, and did not differ significantly from the values estimated from the $D(r)$ curve. The $s\cdot i(s)_{calc}$ values are compared with the values of $s\cdot i(s)$ in Fig. 4 for the $Zn(ClO_4)_2$ solution as an example. From Fig. 4 it is seen that the agreement is good except at a low s region where various interactions including intermolecular interactions, which are not taken into account in the present refinements, significantly contribute to the $s\cdot i(s)$values.

b) Copper Sulfate Solution. The $D(r)$ curve for the copper sulfate solution (Fig. 2g) showed three peaks at 1.5 Å, 1.95 Å, and 2.9 Å and shoulders at about 1 Å and 2.4 Å. The shoulder at 1 Å was ascribed to the intramolecular O–H interaction within H_2O. The peak at 1.5 Å could be identified as being due to the S–O bond within the SO_4^{2-} ion.[40–42]

Table 4. Parameter values of the hydrated copper ion

	r_{ij}/Å	b_{ij}/Å^2	n_{ij}
$Cu-O_{eq}$	1.94	0.002	4
$Cu-O_{ax}$	2.38	0.004	2
cis-$O_{eq}-O_{eq}$	2.70	0.01	4
$O_{eq}-O_{ax}$	3.05	0.01	8

The distances and the numbers of equatorial and axial Cu^{2+}–OH_2 bonds were determined by the same procedures as those made for the copper perchlorate solution[26] after subtraction of interactions of the S–O and O–O bonds within the SO_4^{2-} ion and the O–H bond of H_2O from $D(r)$. Calculations are illustrated in Fig. 5a. Figure 5b shows the difference curve $(D(r)-4\pi r^2\rho_0)$ on which the peaks are better distinguishable. Values for the structure of the SO_4^{2-} ion given in Table 2 were used.[38] From the peak positions of the residual curve (Fig. 5a, b), it was found that the distance of the equatorial Cu^{2+}–OH_2 bond was 1.94 Å and that of the axial Cu^{2+}–OH_2 bond was 2.38 Å. The area for Cu^{2+}–OH_2 interaction in the equatorial position was found to correspond to four Cu^{2+}–OH_2 bonds by an analogous calculation to that in the perchlorate systems. Interactions within the hydrated

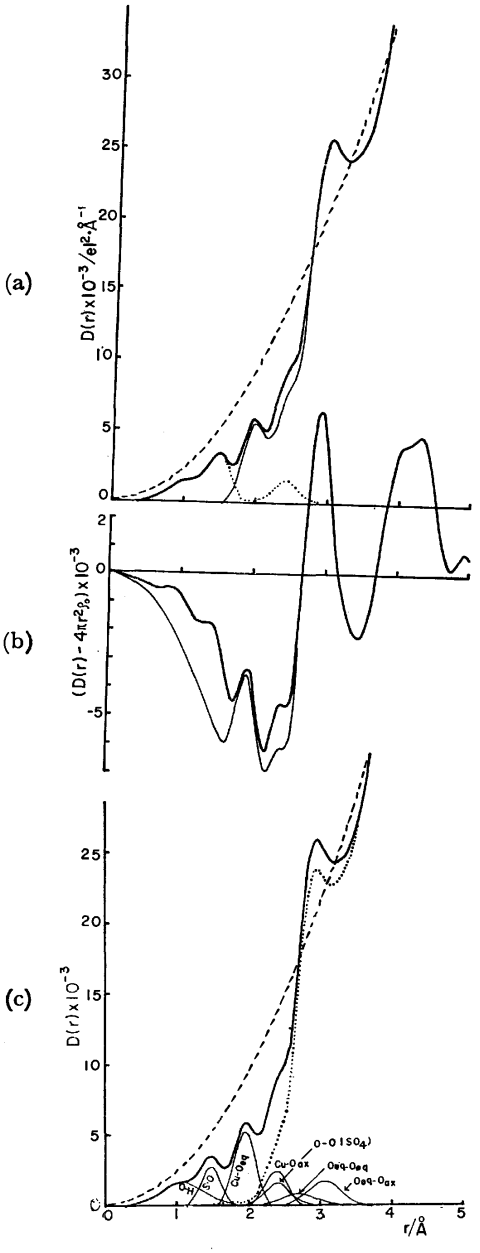

Fig. 5. a. The residual curve (fine solid line) obtained after subtraction of the theoretical peak(dotted line) of the S–O, O–O atom pairs within SO_4^{2-} and the O–H atom pair within H_2O from $D(r)$.
b. $D(r)-4\pi r^2\rho_0$ curve (upper) and the residual curve given in $a-4\pi r^2\rho_0$ (lower).
c. The smooth curve (dotted line) obtained by subtraction of theoretical peak shapes from $D(r)$.

copper ion which formed a distorted octahedron were calculated using the values listed in Table 4 and are shown in Fig. 5a. The subtraction of these interactions from the residual curve in Fig. 5a led to a smooth curve, which showed no dominant peak in the region below 2.8 Å (Fig. 5c). The sharp peak at 2.9 Å may be due to both adjacent O–O interactions of bulk water[43] and the interaction between water molecules and the oxygen atom of the SO_4^{2-} ion.[41]

c) Zinc Sulfate Solution. The $D(r)$ curve in Fig. 2h showed three peaks at around 1.5 Å, 2.1 Å, and 3 Å.

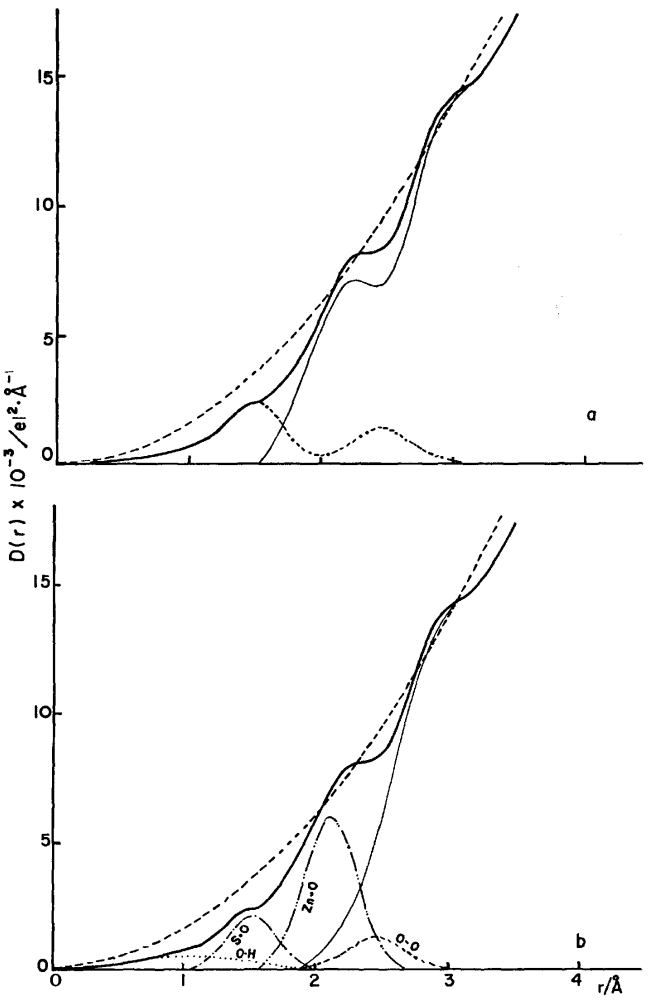

Fig. 6. a. The residual curve (fine solid line) obtained by subtraction of the theoretical peak (broken line) of the S–O and O–O atom pairs within SO_4^{2-} from $D(r)$. b. The smooth curve(fine solid line) gives the residual distribution function obtained after subtraction of the S–O, O–O, and Zn–OH_2 atom pairs from $D(r)$.

The peak at 1.5 Å corresponded to the S–O distance within the SO_4^{2-} ion. The second peak at around 2.1 Å was due to both Zn^{2+}–OH_2 and O–O interactions within the SO_4^{2-} ion. Parameter values for the Zn^{2+}–OH_2 bond within the hydrated Zn^{2+} ion were estimated according to the same procedures as those in the perchlorate system after subtraction of the contributions from the S–O and O–O interactions within the SO_4^{2-} ion from the $D(r)$ curve. These procedures are illustrated in Fig. 6. From the analysis, the Zn^{2+}–OH_2 distance was found to be 2.08 Å, and the number of the Zn^{2+}–OH_2 bonds was about 6, and the corresponding temperature factor was estimated to be 0.004 Å^2.

Discussion

In the aqueous perchlorate solutions of divalent transition-metal ions, Mn^{2+}, Fe^{2+}, Co^{2+}, Ni^{2+}, and Zn^{2+}, the M–OH_2 bond distances were found to be 2.20 Å, 2.12 Å, 2.08 Å, 2.04 Å, and 2.08 Å, respectively, and all the metal ions were octahedrally hydrated with six water molecules. The measurements for interatomic distances of zinc and copper sulfate solutions resulted in the same values as those obtained in the perchlorate solutions. Values of the cation–water distances obtained in this study are summarized in Table 5, along with those reported in the literature.[23–25] As is seen in Table 5, the present results were in excellent agreement with those found by Bol *et al.* in the metal nitrate solutions.[25] The distance of the longer Cu^{2+}–OH_2 bond in the copper sulfate solution differed slightly from that in the copper perchlorate solution, but this difference in the distance could not be significant in view of uncertainties in the present investigation. From the results obtained in this work and those reported by Bol *et al.*,[25] we concluded that the anions cause no change in the bond distances between cation and water molecules. This conclusion agreed with that obtained by Andreev *et al.*[44] and by Holmes and McClure[45] from the visible and ultraviolet spectra of the transition-metals in aqueous solution, who reported that the atmosphere around central metal ions was not affected by anions such as sulfate and nitrate ions. Values by Shapovalov *et al.*[23,24] are too large for the distances between transition-metal ions and neighboring water molecules.

In metal sulfate solutions, metal ions tend to form complexes with the sulfate ion. From infrared spectrophotometric measurements of divalent transition-metal ions in aqueous sulfate solutions, Larsson[46] estimated that the degree of inner-sphere complexity was about 10%. On the contrary, Hester and Plane[47] reported, using the Raman spectroscopy, that there was no evidence for the contact ion-association between transition-metal ions and sulfate ions in aqueous solution. According to the association constants reported in aqueous solution[48] of as high an ionic strength as of the sample solution, about 50% of the sulfate ions in our sample solutions were estimated to be bound as complexes. If 50% of the sulfate ions were directly coordinated to the metal ions through the M–OSO_3

Table 5. The distances between the metal ions and water molecules

	Anion	Mn^{2+}	Fe^{2+}	Co^{2+}	Ni^{2+}	Cu^{2+}	Zn^{2+}	
r_{M-OH_2}/Å	Perchlorate	2.20	2.12	2.08	2.04	1.94 2.43	2.08	This work
	Sulfate	—	—	—	—	1.94 2.38	2.08	This work
	Sulfate	2.20	—	2.15	2.15	2.15 2.50	2.15	Shapovalov *et al.*[23,24]
	Nitrate	—	—	2.06	2.06	—	2.09	Bol *et al.*[25]

bond, the peaks ascribed to the M–O bond in the sulfate solutions would become broader and more or less asymmetrical compared with those in the perchlorate solutions, because it is expected that the M–OSO_3 bond within metal sulfate compounds is a little shorter than the M–OH_2 bond.[49] However, such evidence could not be observed in both copper and zinc sulfate solutions. Therefore, we concluded that the association of copper and zinc ions with sulfate ions was solvent-separated and the hydration sphere of the ions was not affected by the associated sulfate ions in the outer-sphere.

Estimation of the M–OH_2 Bond Energies. Bond energies for aqua complexes with the regularly symmetric configuration have so far been calculated on the basis of several models.[50–52] However, no calculation for the hydrated copper(II) ion has been carried out, because of its asymmetric structure due to the Jahn–Teller effect.

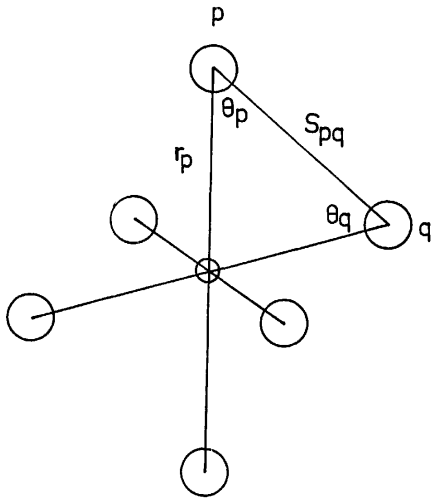

Fig. 7. The model of octahedral hydration.

We calculated the bond energies for the hydrated divalent transition-metal ions by application of the electrostatic model proposed by Garrick[52] and Basolo and Pearson[53] with a modification for a distorted octahedral structure. The bond energy in vacuum $-\Delta H_{\text{bond}}$ for a model of the octahedral hydration (Fig. 7) may be written as follows.

$$-\Delta H_{\text{bond}} = U_{\text{ed}} + U_{\text{dd}} + U_{\text{id}} + U_{\text{vw}} \quad (4)$$

Here subscripts ed, dd, id, and vw refer to the interaction between the ion and the dipole, that between the dipole and dipole, polarization of ligands to form induced dipoles, and the van der Waals repulsion. Each energy term is given as follows.

$$U_{\text{ed}} = -\sum_{p=1}^{N}(ze)(\mu_0+\mu_{\text{i}.p})/r_p^2 \quad (5)$$

$$U_{\text{dd}} = 1/2\sum_{p=1}^{N}\sum_{q=1}^{N}(\mu_0+\mu_{\text{i}.p})(\mu_0+\mu_{\text{i}.q}) \times(\sin\theta_p\sin\theta_q+2\cos\theta_p\cos\theta_q)/s_{pq}^3 \quad (6)$$

$$U_{\text{id}} = \sum_{p=1}^{N}\mu_{\text{i}.p}^2/2\alpha \quad (7)$$

$$U_{\text{vw}} = \sum_{p=1}^{N}B_p/r_p^9 \quad (8)$$

where r_p denotes the distance between a central metal ion and a water molecule p, ze the charge of the central metal ion, μ_0 the permanent dipole moment of the water molecule (1.85×10^{-18} esu·cm), $\mu_{\text{i}.p}$ and $\mu_{\text{i}.q}$ the induced dipole moments of the water molecules p and q at a distance s_{pq}, α the polarizability of water (1.48 Å^3), and N the hydration number which is 6 in this case. The dipole moment of the water molecule p induced by another water molecule q was calculated by Eq. 9.

$$\mu_{\text{i}.p} = \frac{\mu_0+(ze)/r_p}{1+\sum_{q=1}^{N-1}\alpha s_{pq}^{-3}(\sin\theta_p\sin\theta_q+2\cos\theta_p\cos\theta_q)} - \mu_0 \quad (9)$$

The constant B_p in the repulsion term was estimated according to the procedures proposed by Basolo and Pearson[53] on the assumption of spherical hydrated ions. For a copper ion both $B_{p\cdot\text{eq}}$ and $B_{p\cdot\text{ax}}$ were estimated on the assumption of spherically hydrated ions having radii of $r_{p\cdot\text{eq}}$ and $r_{p\cdot\text{ax}}$. This approximation may be acceptable in calculating the interaction energies because of the relatively small value of van der Waals repulsion energies.

Each interaction energy calculated by the use of Eqs. 4—9 is tabulated in Table 6 and the total bond energies for the hydrated metal ions ($-\Delta H_{\text{bond}}$) thus calculated are graphically represented in Fig. 8, together with the experimental values of the enthalpy change of hydration ($-\Delta H_{\text{h}}$) of these ions in solution.[54]

The curves of $-\Delta H_{\text{bond}}$ and $-\Delta H_{\text{h}}$ were parallel and the maxima of both curves appeared at Cu^{2+}. The differences between the two curves were about 150 kcal·mol^{-1} independent of the ions, which was approximately equal to the sum of the free energy change in transfer of one mole of a hydrated divalent ion with an ionic radius of about 3.5 Å ($\simeq$ an average $r_{\text{M–OH}_2}+$ the radius of a water molecule) and the energy change of vaporization of six moles of water. The dotted lines show the enthalpy change expected after the correction

Table 6. The bond energies ($-\Delta H_{\text{bond}}$) calculated by the use of the Garrick model[52] and the enthalpy change of hydration ($-\Delta H_{\text{h}}$)[54] for the hydrated divalent transition-metal ions (in kcal·mol^{-1})

Ion	$r_{\text{M–OH}_2}$/Å	U_{ed}	U_{dd}	U_{id}	U_{vw}	$-\Delta H_{\text{bond}}$	$-\Delta H_{\text{h}}$
Mn^{2+}	2.20	+617.4	−124.8	−89.4	−95.4	+307.8	+459.0
Fe^{2+}	2.12	+676.2	−144.0	−96.0	−102.0	+334.2	+480.0
Co^{2+}	2.08	+708.6	−155.4	−99.6	−105.6	+348.0	+503.1
Ni^{2+}	2.04	+743.4	−167.4	−102.6	−109.2	+364.2	+518.6
Cu^{2+}	1.94 2.43	+586.8 +151.8	−157.2	−89.2 −18.8	−79.6 −27.2	+366.6	+519.5
Zn^{2+}	2.08	+708.6	−155.4	−99.6	−105.6	+348.0	+506.6

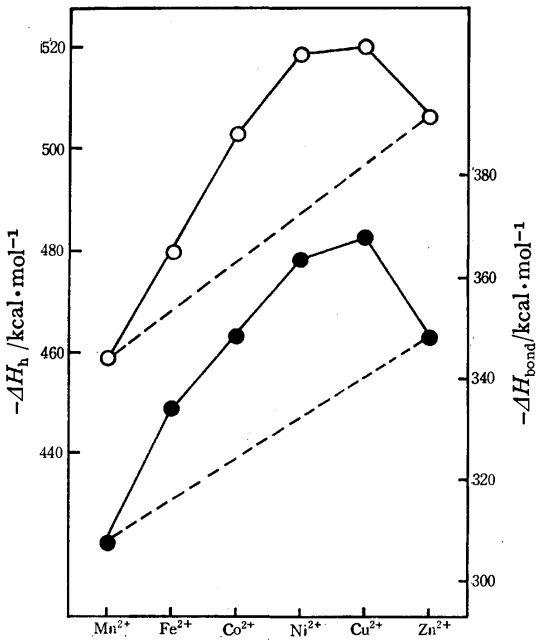

Fig. 8. $-\Delta H_{bond}$ (full circle) and $-\Delta H_h$ (open circle) for Mn^{2+}, Fe^{2+}, Co^{2+}, Ni^{2+}, Cu^{2+}, and Zn^{2+}. The dashed line shows the enthalpy change expected after correction of the crystal field stabilization.

for the effect of the crystal field. From these results we see that the crystal field largely contributes to the bond distances between a central metal ion and ligands in complexes.

References

1) H. Montgomery, *Acta Crystallogr.*, **20**, 731 (1966).
2) B. R. Penfold and M. R. Taylor, *ibid.*, **13**, 953 (1960).
3) B. R. Penfold and J. A. Grigor, *ibid.*, **12**, 850 (1959).
4) W. C. Hamilton, *ibid.*, **15**, 353 (1962).
5) P. S. Caric, *Bull. Soc. Franc. Miner. Crist.*, **82**, 50 (1959).
6) W. H. Baur, *Acta Crystallogr.*, **15**, 815 (1962).
7) A. Zalkin, H. Ruben, and D. H. Templeton, *ibid.*, **15**, 1210 (1962).
8) H. Montgomery, R. V. Dhastain, J. J. Natt, A. M. Witkowska, and E. C. Lingafelter, *ibid.*, **22**, 775 (1967).
9) G. J. Bullen, *ibid.*, **12**, 70 (1959).
10) S. Ray, A. Zalkin, and D. H. Templeton, *ibid.*, **B29**, 2741 (1973).
11) S. Baggit and L. N. Becka, *ibid.*, **B25**, 1150 (1969).
12) B. H. O'Connor and D. H. Dale, *ibid.*, **21**, 705 (1966).
13) N. W. Grimes, H. F. Kay, and M. W. Webb, *ibid.*, **16**, 823 (1963).
14) P. Gallezot, D. Weigel, and M. Prettre, *ibid.*, **22**, 699 (1967).
15) S. Ray, A. Dalkin, and D. H. Templeton, *ibid.*, **B29**, 2748 (1973).
16) P. J. Fisher and R. Weiss, *ibid.*, **B29**, 1963 (1973).
17) E. Dubler, P. Korber, and H. R. Oswald, *ibid.*, **B29**, 1929 (1973).
18) C. A. Beevers and H. Lipson, *Proc. Roy. Soc. (London)*, **A146**, 570 (1934).
19) R. F. Zahrobsky and W. H. Baur, *Acta Crystallogr.*, **B24**, 508 (1968).
20) N. V. Mani and S. Ramaseshan, *Z. Kristallogr.*, **115**, 97 (1961).
21) A. Ferrari, A. Braibanti, and A. N. Lanfredi, *Acta Crystallogr.*, **22**, 240 (1967).
22) T. Doyne, R. Pepinsky, and T. Watanabe, *ibid.*, **11**, 438 (1957).
23) I. M. Shapovalov and I. V. Radchenko, *Russ. J. Struct. Chem.*, **12**, 769 (1971).
24) I. M. Shapovalov, I. V. Radchenko, and M. K. Lesoristskaya, *ibid.*, **13**, 140 (1972).
25) W. Bol, G. J. A. Gerrits, and C. L. van Panthaleon van Eck, *J. Appl. Cryst.*, **3**, 486 (1970).
26) H. Ohtaki and M. Maeda, This Bulletin, **47**, 2197 (1974).
27) H. Ohtaki, M. Maeda, and S. Ito, This Bulletin, **47**, 2217 (1974).
28) H. A. Levy, M. D. Danford, and A. H. Narten, "Data Collection and Evaluation with an X-Ray Diffractometer Designed for the Study of Liquid Structure," ORNL-3960 (1966).
29) N. Norman, *Acta Crystallogr.*, **10**, 370 (1957).
30) J. Krogh-Moe, *ibid.*, **9**, 951 (1956).
31) D. T. Cromer and J. T. Waber, *ibid.*, **18**, 104 (1965).
32) R. F. Stewart, E. R. Davidson, and W. T. Simpson, *J. Chem. Phys.*, **42**, 3175 (1964).
33) D. T. Cromer, *ibid.*, **50**, 4857 (1969).
34) D. T. Cromer and J. B. Mann, *ibid.*, **47**, 1892 (1967).
35) A. H. Compton and S. K. Allison, "X-Rays in Theory and Experiment," Van Nostrand, New York (1935).
36) D. T. Cromer and D. Lieberman, *J. Chem. Phys.*, **53**, 1891 (1970).
37) G. Johansson and M. Sandström, *Chem. Scripta*, **4**, 195 (1973).
38) L. E. Sutton, Ed., "Tables for Interatomic Distances and Configurations in Molecules and Ions," Special Publication No. 18, The Chemical Society, London (1965).
39) D. W. Marquardt, *J. Soc. Industr. Appl. Math.*, **11**, 431 (1963).
40) C. Finbak, O. Rönning, and H. Viervoll, *Tidsskr. Kjemi. Bergves. Metallurgi*, **75**, 800 (1969).
41) I. M. Shapovalov and I. V. Radchenko, *Russ. J. Struct. Chem.*, **10**, 921 (1969).
42) J. U. Weidner, H. Beisenfelder, and H. Zimmermann, *Ber. Bunsenges. Phys. Chem.*, **75**, 800 (1971).
43) A. H. Narten, "X-Ray Diffraction Data on Liquid Water in the Temperature Range 4 °C—200 °C," ORNL-4578 (1970).
44) A. N. Andreev, V. G. Khaldin, and E. V. Stroganov, *Russ. J. Struct. Chem.*, **2**, 4 (1961).
45) O. G. Holmes and D. S. McClure, *J. Chem. Phys.*, **26**, 1686 (1957).
46) R. Larsson, *Acta Chem. Scand.*, **18**, 923 (1964).
47) R. E. Hester and R. A. Plane, *Inorg. Chem.*, **3**, 769 (1964).
48) R. Näsänen, *Suomen Kem.*, **B26**, 67 (1957).
49) R. F. Zahrobsky and W. H. Baur, *Acta Crystallogr.*, **B24**, 508 (1968).
50) A. D. Buckingham, *Discuss. Faraday Soc.*, **24**, 151 (1957).
51) F. S. Muirhead-Gould and K. J. Laidler, "The Thermodynamic Properties of Charge Bearing Systems in Aqueous Solution; A Discontinuous Model for Octahedral Hydration" in "Chemical Physics of Ionic Solutions," ed. by B. E. Conway and R. G. Barrada, John Wiley & Sons, (1966), p. 75.
52) F. J. Garrick, *Phil. Mag.*, **9**, 131 (1930); **10**, 71 (1930).
53) G. Basoro and R. G. Pearson, "Mechanisms of Inorganic Reactions," 2nd ed., John Wiley & Sons (1967).
54) D. R. Rosseinsky, *Chem. Rev.*, **65**, 467 (1967); The Japan Society of Analytical Chemistry, Ed., "Saku-keisei-Hanno," Maruzen, Tokyo (1974), p. 519.

The Polymorphic Crystallization of TiO_2 under Hydrothermal Conditions. I. The Effect of Phosphate Ions on the Selective Crystallization of Anatase[1)]

Fujio IZUMI and Yoshinori FUJIKI

National Institute for Researches in Inorganic Materials, Sakura-mura, Niihari-gun, Ibaraki 300-31

(Received October 30, 1975)

The hydrothermal growth of anatase has been investigated at 480—650 °C and 500—1000 atm. Only rutile was formed in KF solutions. On the other hand, anatase was found to crystallize in solutions containing 5 wt% KF+0.1—10 wt% K_2HPO_4 at temperatures up to 600 °C, accompanied by small amounts of $K_2Ti_6O_{13}$ on the addition of 5—10 wt% of K_2HPO_4. The optimum growth conditions were: mineralizer solution, 5 wt% KF+1—2.5 wt% K_2HPO_4; temperature, 550—600 °C; pressure, 1000 atm. Anatase crystals were found as irregular aggregates of dipyramidal grains, blue and transparent. Individual crystals grown at a low supersaturation were characterized by well-developed {101} and {103} faces. The observed habit agrees with the expectations based on Hartman's PBC theory. The presence of phosphate ions favored anatase formation in NH_4F solutions as well, and the retrograde solubility of TiO_2 was observed. The reaction scheme for anatase formation has been proposed. The polymorphic crystallization of TiO_2 under hydrothermal conditions has been shown to be greatly affected by the complexing anions, such as fluoride or phosphate, in mineralizer solutions.

Natural TiO_2 exhibits three structural modifications, the rutile(tetragonal), brookite(orthorhombic), and anatase(tetragonal) minerals. In each of these, the Ti^{4+} ion is surrounded by an irregular octahedron of O^{2-} ions. The number of edges shared by other octahedra increases, from two in rutile to three in brookite and four in anatase, which implies that the free energies of the three forms increase in the above order.[2)] In nature rutile is much more common than brookite and anatase, being formed as a rule at high temperatures. Brookite and anatase transform, exothermally and irreversibly, to rutile over a wide range of temperatures. The rate and activation energy of the anatase–rutile transformation are greatly affected by the concentration of oxygen vacancies or interstitials.[3)] Navrotsky and Kleppa[4)] have demonstrated that anatase is metastable with respect to rutile under all conditions of temperature and pressure.

It is well known that the polymorphic crystallization of TiO_2 from aqueous solutions is influenced by some inorganic anions.[5)] The crystallization of amorphous TiO_2 under hydrothermal conditions leads to brookite in the presence of Na^+ ions.[6,7)] As for natural minerals,[8)] rutile formation is facilitated by the presence of Fe. A lack or deficiency in Fe leads to anatase formation, whereas brookite is preponderantly formed in the presence of Nb.

The only practical method for growing single crystals of rutile in large sizes is that of Verneuil. Other means include solution growth from molten salts,[9–11)] vapor-phase growth by chemical-transport reactions,[9,12)] and the hydrothermal method.[13–16)] Single crystals of brookite can be prepared hydrothermally in NaOH[6)] and NaF[7)] solutions. On the other hand, no authenticated reports have been published on the crystal growth of anatase.

The present study was undertaken in order to establish the optimum conditions for the hydrothermal growth of anatase on a small scale. The hydrothermal method should provide the highest probability of growing large crystals of anatase, since it combines a low temperature and a reasonable solubility. However, it may suffer from the defect that the temperature of the conversion of anatase to rutile is markedly lowered under hydrothermal conditions.[17)] It has now been shown that spectroscopically pure anatase crystals can be successfully grown in KF–K_2HPO_4 solutions. The reaction scheme for anatase formation, as well as some properties and morphology of crystals, has now been investigated.

Experimental

The TiO_2 (rutile) used was obtained commercially and was 99.99% pure. All the other materials used were of a guaranteed reagent grade. The hydrothermal reactions were carried out in sealed Au capsules in cold-seal-type pressure vessels with a capacity of 5.5 cm^3 and an inner diameter of 1/4 inch. About 0.1 g of TiO_2 was packed into a nutrient capsule 4 mm in diameter and 15 mm long, with a small hole. This was then placed, together with 0.5 ml of a mineralizer solution, in a larger capsule 5 mm in diameter and 70 mm in length, and sealed by crimping and welding one end shut. This double capsule was placed in the pressure vessel set horizontally with a temperature gradient between the dissolution and crystallization zones. The TiO_2 in the nutrient capsule fixed at one end of the larger one was dissolved, transported by convection to the other end, and recrystallized spontaneously through supersaturation. The nutrient capsule serves as both a container of the starting material and a baffle controlling the growth rate. The reaction temperature was measured by means of a chromel–alumel thermocouple on the outside of the vessel,[18)] while the pressure was measured with a Bourdon gauge. The experiments were conducted at temperatures between 480 and 650 °C and at pressures between 500 and 1000 atm. The temperature difference between the hot and cold zones was 40—90 °C. The duration of the runs was 4—15 days in most cases, but some lasted 25 days.

The reaction products were identified by the X-ray powder diffraction technique. The directions of the crystallographic axes of anatase crystals were found by means of the Wissenberg method. The Miller indices of the crystal faces were determined by use of a reflecting goniometer. The pH values before and after the hydrothermal reactions were measured by Toyo Roshi pH test papers.

Results and Discussion

The experimental conditions and the products of the hydrothermal reactions are summarized in Table 1. In these runs, KF and NH_4F solutions were used with or without additives. Keesmann[6] has suggested that anatase formation under hydrothermal conditions requires both a pH value around neutrality and a temperature below *ca.* 600 °C. The pH values of the 5 wt % solutions of KF and NH_4F were 8.6 and 6.3 respectively, and the hydrothermal solubilities of TiO_2 in these solutions are large enough to effect its crystal growth.[14,15] Therefore, each solution is expected to be advantageous for the hydrothermal growth of anatase.

Effect of Inorganic Ions on the Selective Crystallization of Anatase. The starting material was transported from the hot to the cold zone of the large capsule in KF solutions. Only rutile was formed in 10 wt % KF solutions at 500 °C and 800 atm. Kuznetzov[14,16] also prepared rutile crystals hydrothermally from NaF and KF solutions at 470—585 °C. Judging from the previous finding that, in the presence of F^- ions, rutile crystals grow at the expense of anatase at temperatures as low as 250 °C,[17] anatase would not be formed even if the reaction temperature was lowered to below 500 °C.

It is generally recognized that when TiO_2 is precipitated from an aqueous solution, the presence of a large amount of sulfate or phosphate ions favors anatase formation very strongly.[5] We, therefore, performed hydrothermal reactions in which several materials were added to the KF solution, expecting a similar effect under supercritical conditions (Runs No. 3—No. 7). However, only the addition of K_2HPO_4 proved to be effective in crystallizing anatase. It is worth noting that the presence of Na_2SO_4 did not aid anatase formation; this will be discussed later.

Hydrothermal Reactions in KF–K_2HPO_4 Solutions. Anatase was found to crystallize by adding 0.1—10 wt% of K_2HPO_4 at temperatures up to 600 °C. However, the rate of the transport of TiO_2 fell sharply when only 0.1 wt% of K_2HPO_4 was added. The highest temperature that allows the exclusive formation of anatase lies between 600 and 650 °C because rutile was formed in Runs No. 12 and No. 14. This corresponds well to the temperature of anatase–rutile conversion under hydrothermal conditions.[17]

Small amounts of needle or filamentary crystals, though not more than the minimum detection limit of X-ray powder diffraction analysis, were observed under a microscope in the products formed in solutions containing 5—10 wt% of K_2HPO_4. X-Ray diffraction study showed these crystals to be $K_2Ti_6O_{13}$ elongated along the b axis. The crystallization of the titanate was enhanced by a higher pH value as well as by a higher concentration of K^+. For instance, the addition of 5 wt% of $K_3PO_4 \cdot nH_2O$ (n=2—4) resulted in the formation of only $K_2Ti_6O_{13}$ (Fig. 1). The initial pH of this solution was 12.8. After the hydrothermal reaction, however, the pH was reduced to 6.6. These results can be explained in terms of the following reaction:

$$6TiO_2 + 2K^+ + OH^- \longrightarrow K_2Ti_6O_{13} + H^+$$

As is shown in Table 1, the pH values of KF–K_2HPO_4

Table 1. Transport of TiO_2 in fluoride solutions

Run No.	Mineralizer solution (wt %)	Temperature (°C)	Pressure (atm)	Duration (h)	Change in pH	Products[a]
1	5% KF	525	875	238		Ru
2	10% KF	500	800	453	8.6→8.4	Ru
3	5% KF+5% $K_2B_4O_7 \cdot 5H_2O$	550	1000	190		Ru
4	5% KF+5% Na_2SO_4	550	1000	168		Ru
5	5% KF+5% K_2WO_4	550	800	261		Ru
6	5% KF+7% $Na_2HAsO_4 \cdot 7H_2O$	550	800	213		Ru
7	5% KF+5% K_2HPO_4	550	1000	185		An
8	5% KF+0.01% K_2HPO_4	550	900	449		Ru
9	5% KF+0.1% K_2HPO_4	550	1000	593		An>Ru
10	5% KF+1% K_2HPO_4	550	1000	263		An
11	5% KF+2.5% K_2HPO_4	600	1000	267	8.6→8.2	An
12	5% KF+2.5% K_2HPO_4	650	1000	305	8.6→6.4	Ru
13	5% KF+5% K_2HPO_4	600	1000	256	8.6→6.6	An≫Ti
14	5% KF+5% K_2HPO_4	650	1000	74		An>Ru≫Ti
15	5% KF+10% K_2HPO_4	550	900	234	8.5→8.6	An≫Ti
16	5% KF+10% K_2HPO_4	600	900	210		An≫Ti
17	5% KF+5% $K_3PO_4 \cdot nH_2O$	600	1000	144	12.8→6.6	Ti
18	5% KF+ {0.5% KH_2PO_4, 4.5% Na_2HPO_4}	560	950	356		An≫Ti
19	5% KF+ {3% KH_2PO_4, 4% K_2HPO_4}	600	1000	474	6.6→6.5	An
20	5% NH_4F	480	500	95	6.3→8.0	Ru
21	5% NH_4F	370	500	89		b)
22	5% NH_4F+2% $(NH_4)_2HPO_4$	480	500	89	6.6→8.8	An>?

a) Ru, rutile; An, anatase; Ti, $K_2Ti_6O_{13}$. b) No transport of TiO_2 occurred.

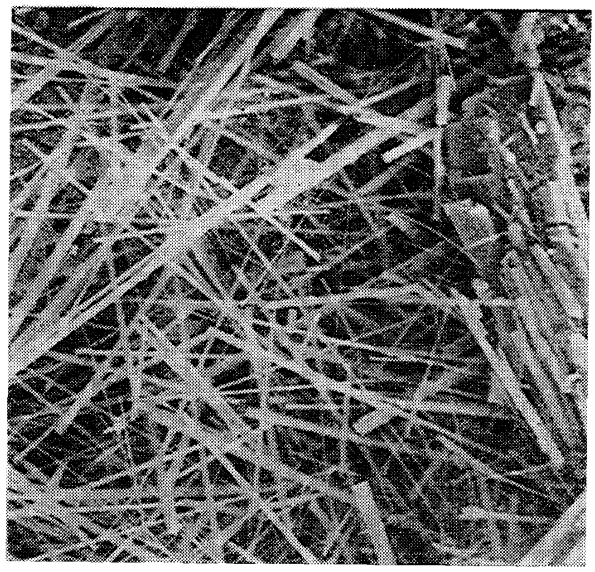

Fig. 1. Needle crystals of $K_2Ti_6O_{13}$.

solutions before and after the hydrothermal reactions did not deviate much from neutrality, since dissolution–crystallization reactions of TiO_2 occurred almost exclusively in these solutions.

In conclusion, the best growth of anatase is achieved under the following conditions: mineralizer solution, 5 wt% KF+1—2.5 wt% K_2HPO_4; temperature, 550—600 °C; pressure, 1000 atm.

Characterization of Anatase Crystals Grown in KF–K_2HPO_4 Solutions. Anatase crystals grown in KF–K_2HPO_4 solutions were usually found as irregular aggregates of dipyramidal grains, blue and transparent (Fig. 2). Upon continued heating at 1000 °C in air, these crystals turned opaque brown.

Individual crystals with maximum dimensions of 1 mm were mostly subhedral, although those grown at a low supersaturation were characterized by well-developed {101} and {103} faces. Hartman's PBC theory[19] predicts the (101) face in anatase to be an F-face and all the other (*h*0*l*) faces to be of the S type. The S-face in the zone [010] with the longest d_{hkl} value is (103). In view of these structural features, the appearance of the {101} and {103} faces on the anatase crystals grown hydrothermally seems to be quite reasonable. The observed habit of the synthetic anatase is in accord with expectations based on the description in the literature[20] that natural anatase occurs in crystals usually showing a simple dipyramid of the second order {101} or, less commonly, {103}.

No impurities could be detected by either the emission spectral analysis or the EPMA analysis of the anatase crystals. The tetragonal unit-cell constants determined by the powder technique are: $a=3.783\pm0.001$ Å; $c=9.508\pm0.002$ Å, which are in good agreement with the data published for anatase. The temperature of the anatase–rutile transformation was measured to be 975 °C by the high-temperature X-ray diffraction method.

Hydrothermal Reactions in NH_4F Solutions. TiO_2 showed retrograde solubility in NH_4F solutions; that is, the transport of the starting material proceeded from the cold to the hot zone of the capsule. From 5 wt% NH_4F solution, only rutile crystallized at 480 °C, and hardly any transport of TiO_2 was observed at 370 °C. On the other hand, anatase was obtained in the presence of 2 wt% of $(NH_4)_2HPO_4$, accompanied by unknown by-products which were found as brownish and translucent solids that formed an aggregate with anatase crystals (Fig. 3) and as a white powder dispersed throughout the whole capsule. The EPMA analysis of the former showed the main constituents to be Ti and P, indicating that it is a kind of titanium phosphate. However, no further effort was devoted to examining this phase in detail. The anatase crystals obtained

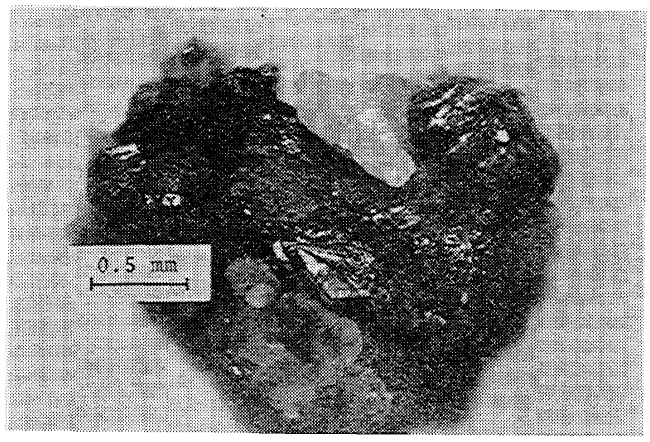

Fig. 3. Anatase crystals accompanied by an unknown phosphate.

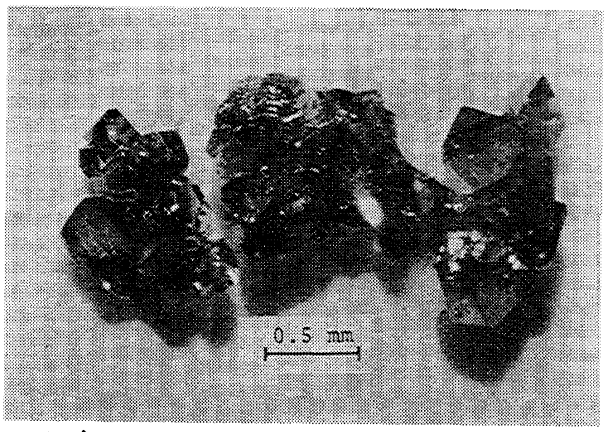

Fig. 2. Aggregates of anatase crystals (Run No. 19).

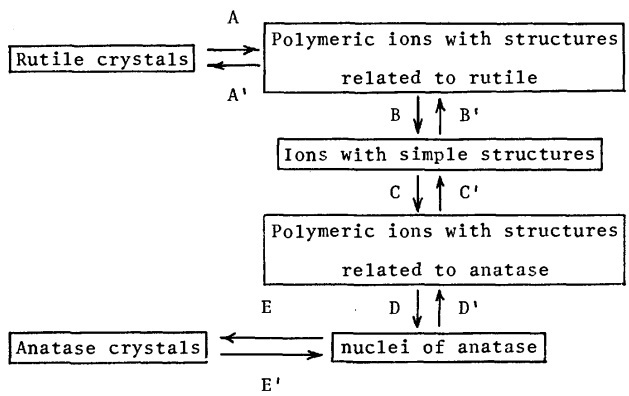

Fig. 4. The reaction scheme for anatase formation under hydrothermal conditions.

were in the form of opaque black grains with an average size of 0.3 mm. These results revealed that the presence of phosphate ions favors anatase formation in NH_4F solutions as well.

The Reaction Scheme for Anatase Formation under Hydrothermal Conditions. The reaction scheme for anatase formation assumed on the basis of the work by Yamaguchi *et al.*[21,22] is illustrated schematically in Fig. 4. The starting material (rutile) reacts with F^-, H_2O, and other species to form polymeric ions with structures related to the lattice of rutile; these ions undergo further cleavage and form ions with simple structures. The resulting ions are unstable under supersaturated conditions; they are hydrolyzed to give polymeric ions with structures related to anatase. Further hydrolysis leads to the formation of the nuclei of anatase, which grow into anatase crystals. Processes A and B should take place in the dissolution zone, whereas Processes C and D are predominant in the crystallization zone.

Caglioti *et al.*[23] have revealed that the $TiOF^+$, $TiOF_2$, $TiOF_3^-$, and $TiOF_4^{2-}$ species exist in aqueous solutions of Ti^{4+} and F^- ions. These mononuclear and/or polynuclear oxyfluoro-complexes are probably formed in the hydrothermal solutions of KF and NH_4F as well, which leads to the selective formation of rutile-like polymeric ions through Process B'. On the other hand, the above species are assumed to be further complexed by phosphate ions in the presence of K_2HPO_4 or $(NH_4)_2HPO_4$, with the result that only polymeric ions with structures related to anatase can be formed through Process C. Complexing between Ti^{4+} and phosphate is quite likely to occur since Ti^{4+}, one of the hardest acids, has a very strong affinity for the oxygen donor.[24] The decrease in the concentration of K_2HPO_4 lowers the rate of Process C, but favors Process B' (Runs No. 8 and No. 9). Above 600 °C, polymeric ions and/or nuclei with the anatase structure are partially transformed into the denser rutile-type structures.

The emission spectral analysis of the anatase crystals grown in KF–K_2HPO_4 solutions indicates that the phosphorus content does not exceed 10 ppm, which supports the idea that phosphate ions do not enter the crystal lattice of anatase, but are released almost completely into an aqueous environment during Processes C, D, and E. This is understandable in view of the large difference in ionic radius between Ti^{4+} and P^{5+} (Ti^{4+}, 0.69 Å; P^{5+}, 0.25 Å).[25] The failure to crystallize anatase in the presence of Na_2SO_4 may be ascribed to the weaker complexing ability of the sulfate ion compared with that of the phosphate ion.[26]

The detailed mechanism by which the nucleation of anatase occurs in the presence of phosphate ions is still a matter of speculation. However, the data presented in this paper suggest that the polymorphic crystallization of TiO_2 under hydrothermal conditions is greatly affected by the complexing anions, such as fluoride or phosphate, in mineralizer solutions. Work is now under way to investigate this problem in detail.

The authors wish to thank Drs. Mamoru Watanabe and Takefumi Mitsuhashi for helpful discussions and technical assistance during this work. Thanks are also due to Dr. Hiroshi Kawamoto, Faculty of Technology, Gunma University, for the emission spectral analysis.

References

1) A part of this paper was briefly reported in F. Izumi and Y. Fujiki, *Chem. Lett.*, **1975**, 77.
2) L. Pauling, *J. Amer. Chem. Soc.*, **51**, 1010 (1929).
3) R. D. Shannon and J. A. Pask, *J. Amer. Ceram. Soc.*, **48**, 391 (1965).
4) A. Navrotsky and O. J. Kleppa, *ibid.*, **50**, 626 (1967).
5) "Gmelins Handbuch der Anorganischen Chemie," Titan (1951), pp. 227, 228.
6) I. Keesmann, *Z. Anorg. Allg. Chem.*, **346**, 30 (1966).
7) E. Schwarzmann and K. H. Ognibeni, *Z. Naturforsch.*, B, **29**, 435 (1974).
8) I. Kostov, "Mineralogy," Oliver & Boyd, Edinburgh, (1968), p. 242.
9) I. N. Anikin, I. I. Naumova, and G. V. Rumyantseva, *Kristallografiya*, **10**, 230 (1965).
10) J. S. Berkes, W. B. White, and R. Roy, *J. Appl. Phys.*, **36**, 3276 (1965).
11) T. Sugai and S. Hasegawa, *Yogyo Kyokai Shi*, **77**, 65 (1969).
12) T. Niemyski and W. Piekarczyk, *J. Cryst. Growth*, **1**, 177 (1967).
13) M. L. Harvill and R. Roy, *J. Phys. Chem. Solid, Suppl.*, 563 (1967).
14) V. A. Kuznetzov, *J. Cryst. Growth*, **3**, **4**, 405 (1968).
15) M. Passaret, Y. Toudic, A. Regreny, R. Aumont, and J. F. Bayon, *ibid.*, **13**, **14**, 524 (1972).
16) V. A. Kuznetzov, "Crystallization Process under Hydrothermal Conditions," ed. by A. N. Lobachev, Consultants Bureau, New York, N. Y. (1973), pp. 43—55.
17) E. F. Osborn, *J. Amer. Ceram. Soc.*, **36**, 147 (1953).
18) Attention should be called to the fact that the temperatures described in this paper refer to those of the dissolution zones in the case of Runs No. 1—No. 19 and those of the crystallization zones in Runs No. 19—No. 21.
19) P. Hartman, "Crystal Growth: An Introduction," ed. by P. Hartman, North-Holland Publishing Co., Amsterdam (1973), pp. 398—401.
20) C. Palache, H. Berman, and C. Frondel, "Dana's System of Mineralogy," 7th ed., Vol. I, John Wiley & Sons, New York, N. Y. (1963), p. 583.
21) G. Yamaguchi and H. Yanagida, This Bulletin, **36**, 1155 (1963).
22) G. Yamaguchi, H. Yanagida, and T. Fujimaru, *ibid.*, **38**, 54 (1965).
23) V. Caglioti, L. Ciavatta, and A. Liberti, *J. Inorg. Nucl. Chem.*, **15**, 115 (1960).
24) C. F. Bell and K. A. K. Lott, "Modern Approach to Inorganic Chemistry," 2nd ed., Butterworth & Co., London (1966), p. 207.
25) This seems to exclude the possibility for P^{5+} to substitute Ti^{4+} in the anatase structure.[3]
26) For example, when concentrated H_3PO_4 was added to the solution of titanium sulfate, a white precipitate of titanium phosphate was immediately formed.

The Photo-Enolization of β-Disubstituted αβ-Unsaturated Ketone

Masaru TADA and Kyo MIURA

Department of Chemistry, School of Science and Engineering, Waseda University, Shinjuku, Tokyo 160

(Received May 27, 1975)

γ-Methyl groups of mesityl oxide (I), dypnone (II), 2-isopropylidenecyclopentanone (III), and pulegone (IV) were deuterated by ultra-violet irradiation in methanol-*d*. It has been claimed that these ketones are not enolized by photo-excitation, but the formation of enol by irradiation was proved by infrared spectroscopy at a low temperature and was correlated to the photo-deuteration. The photo-enolization was deduced to occur from an n–π* singlet excited state.

It has previously been reported that several β-disubstituted α,β-unsaturated ketones such as mesityl oxide(I) do not isomerize to β,γ-unsaturated ketones upon ultraviolet irradiation;[1-4] Yang and Jorgensen[1] attributed the photo-stability of mesityl oxide (I) to the π–π* nature of the lowest triplet excited state, which was proposed to have no ability to abstract γ-hydrogen.[5] This conclusion was drawn on the basis of a comparison with the behavior of the *ortho*-alkylated aromatic ketone, in which an n–π* triplet state has been proved to be responsible for photo-enolization by flush photolysis.[6] This deduction does not, however, seem proper since the nature of the excited state is very different between aliphatic and aromatic ketones, especially in the efficiency of intersystem crossing. A recent publication by Turro *et al.*[7] has demonstrated that the n–π* singlet and triplet excited states of adamantanone have the same degree of reactivity toward intermolecular hydrogen abstraction and that the lower effectiveness of the singlet excited state is attributable to its short life-time.

In this paper we wish to report on the general photo-enolization of β-disubstituted α,β-unsaturated ketones, which have no tendency to isomerize to β,γ-unsaturated ketones; an n–π* singlet state is responsible for the hydrogen transfer.

Experimental

Materials. Commercially available mesityl oxide (I) (bp 130 °C) and pulegone (IV) (bp 103 °C/17 mmHg) were purified by distillation. Dypnone (II) (bp 141—144 °C/0.3 mmHg) was prepared by the base-catalyzed condensation of acetophenone.[8] 2-Isopropylidenecyclopentanone (III) (bp 90—91 °C/14 mmHg) was prepared by the condensation of acetone with cyclopentanone.[9] The purity of these materials was checked by glc analysis (SE-30 and Carbowax 20 M on Chromosorb W, N_2) before use. UV λ nm (ε): I, 252 (3600), 314 (60); II, 295 (15800); III, 252 (3650), 325 (68); IV, 252 (6450), 324 (40). NMR (JEOL ps-100 spectrometer) of ketones (I, III, and IV) in MeOD show two signals due to *syn* and *anti*-methyls at 1.83 and 2.05 ppm for I, at 1.78 and 2.12 ppm for III, and at 1.72 and 1.98 ppm for IV, respectively, by using TMS as an internal reference. Dypnone (II) originally showed one signal at 2.53 ppm due to the methyl group of the *E*-form, but rapid photo-equilibration between *E* and *Z*-forms occurred upon irradiation and another signal appeared at 2.25 ppm.

Deuterium Exchange. Each ketone (I, II, III, or IV) was dissolved (2%) in MeOD containing 1% of TMS as an internal reference for the chemical shift and the signal intensity. The solution was then sealed in a Pyrex NMR sample tube and irradiated by a 450-W medium-pressure Hg lamp—the distance between lamp and tube was *ca.* 1 cm. The NMR spectrum of the irradiated sample was inspected periodically. The relative intensities of the signals of the methyl groups to that of TMS were decreased by irradiation, as is shown by Figs. 1 and 2 in the text. Another sample tube wrapped with aluminum foil was placed in the irradiation apparatus as a reference. The reference sample did not show any change in its NMR spectrum. The solutions of the ketones in MeOH instead of MeOD were also irradiated under the same conditions, but their NMR spectra were identical with those of the non-irradiated solutions. Glc analyses of the samples also showed a quantitative recovery of the starting ketones.

Acid-catalyzed Deuteration. A solution of a ketone (I, II, III, or IV) in MeOD containing HCl (0.01 mol/l) was sealed in an NMR sample tube and kept under the same conditions as in photodeuteration, but without irradiation; the NMR spectra were taken periodically. The spectra showed no decrease in the signal intensities of the γ-methyl groups, but the signal intensities of the α-methyl group of mesityl oxide (I) at 2.05 ppm and of the α-methylene groups of the III and IV ketones at around 2.5 ppm were decreased—a 50% decrease within 15 hr for the I ketone.

Triplet Quenching of the Photo-deuteration. The solutions (2%) of dypnone (II) and pulegone (IV) in MeOD containing 0.0 and 0.1 mol/l of 3,3,4,4,-tetramethyl-1,2-diazetine 1,2-dioxide[10] were placed in a merry-go-round-type irradiation apparatus and were irradiated by means of a 450-W medium-pressure Hg lamp—the distance between lamp and tube was 5 cm—for 35 min (II) and 5 hr (IV). The irradiation caused the deuteration of γ-methyl groups (*ca.* 15% for II and *ca.* 30% for IV), and the quencher did not show any effect on the rate of deuteration of the γ-methyl groups.

Low Temperature Infrared Spectra. Pulegone (IV) dissolved in the mixed solvent of methyl cyclohexane and 2-methyltetrahydrofuran (2: 1) was placed in an infrared cell of CaF_2 plate, and the cell was mounted in the ditch of a brass block connected to a container of liquid nitrogen. The sample was hang in a glass case with a window of CaF_2 and was cooled by liquid nitrogen, with an occasional evacuation of the system. After a tight matrix of the sample has been obtained, the system was evacuated continuously (*ca.* 10^{-3} mm Hg). Pulegone (IV) in the cold matrix showed the absorptions at 1675 and 1615 cm^{-1} due to the carbonyl group and the carbon-carbon double bond respectively. An external irradiation of the matrix through the window was carried out by means of a 500-W high-pressure Hg lamp mounted in a lamp house equipped with an optical system of a quartz lens and a Pyrex filter. Irradiation caused a diminuation of the original absorptions, with a concomitant increase in new absorptions at 1664 and 1596 cm^{-1} due to the enol form of IV (see Fig. 3); the photo-equilibrated state was attained after 2 hr.

In the case of mesityl oxide (I), the solvent system of methyl-

cyclohexane-2-methyltetrahydrofuran-isopentane (1 : 1 : 2) was superior to the system used for pulegone (IV). The original absorptions at 1695 and 1622 cm^{-1} due to the *s-cis* form of ketone I, and at 1690 and 1645 cm^{-1} due to the *s-trans* form of I, decreased, with a concomitant increase in the absorptions at 1655 and 1602 cm^{-1} due to the enol form of I. The spectral change in mesityl oxide (I) was slower than that of pulegone (IV); it required irradiation for 10 hr to reach the photo-equilibrated state. The samples were warmed slowly after irradiation, and the spectral measurements were repeated during the period of warming up. Only the original absorptions were observed in the infrared spectrum of the warmed sample; the absorptions due to the enol form disappeared completely.

Results and Discussion

We found that, upon ultraviolet irradiation, β-disubstituted α,β-unsaturated ketone enolizes to dienol, and that the lack of the isomerization of the dienol to a β,γ-unsaturated ketone accounted for the nominal inertness of such a ketone. This result was established by the following experimental results. Each solution of mesityl oxide (I), dypnone (II), 2-isopropylidenecyclopentanone (III), and pulegone (IV) in methanol-*d* was irradiated, and the photo-deuteration of the γ-methyl groups was examined by NMR. The relative intensities of the signals *versus* irradiation period are shown in Figs. 1 and 2 A reference experiment in the dark did not show deuteration to any detectable extent, and the irradiations of I—IV the ketones in methanol resulted in a quantitative recovery of the starting materials. There is a possibility that a kind of acidic compound formed by the irradiation of methanol-*d* containing a trace amount of oxygen[11] would catalyze the deuteration of γ-methyl groups. The addition of hydrochloric acid (0.01 mol/l) to the solution, however, caused only the deuteration of the α-methylene or α-methyl groups; no deuteration of γ-methyl groups was observerd.

The photo-enolization was proved more directly by the infrared spectrum the dienol isolated in a cold matrix.

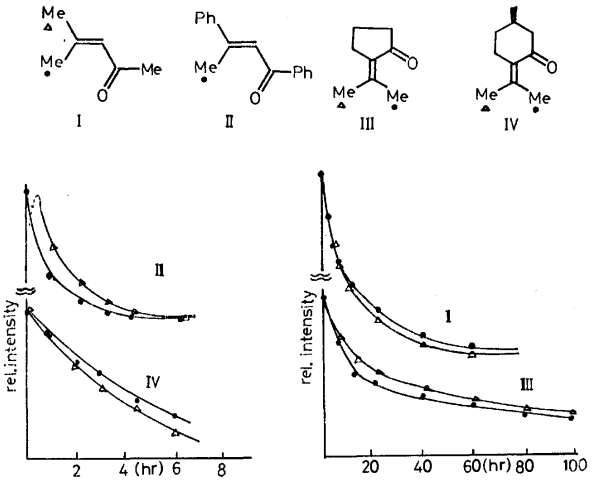

Fig. 1 Fig. 2

Fig. 1 and 2. Decrease of NMR signal-intensities of α-methyls *versus* irradiation period.

Pulegone (IV) dissolved in methylcyclohexane-2-methyltetrahydrofuran (2: 1) was solidified to a clear matrix under cooling by liquid nitrogen. The irradiation of the matrix caused a distinct change in its infrared spectrum, as is shown in Fig. 3. The absorptions due to the starting pulegone (IV) at 1675 ($\nu_{C=O}$) and 1615 cm^{-1} ($\nu_{C=C}$) decreased, with a concomitant increase in the absorptions at 1664 ($\nu_{C=O}$) and 1596 cm^{-1} ($\nu_{C=C}$, strong) due to the enol form of pulegone. The same spectroscopic behavior was observed with mesityl oxide (I), in which the absorptions at 1655 ($\nu_{C=O}$) and 1602 cm^{-1} ($\nu_{C=C}$, strong) increased, with a concomitant decrease in the absorptions at 1695 ($\nu_{C=O}$) and 1622 cm^{-1} ($\nu_{C=C}$) for the *s-cis* form of I and at 1690 ($\nu_{C=O}$) and 1645 cm^{-1} ($\nu_{C=C}$) for the *s-trans* form of I.[12] In accordance with the difference in the rate of photo-deuteration between the I and IV ketones, the photo-equilibrium state of IV was attained after 2 hr, whereas that of I required 10 hr. The original absorptions for I and IV were regenerated by warming up the sample after the termination of the irradiation.

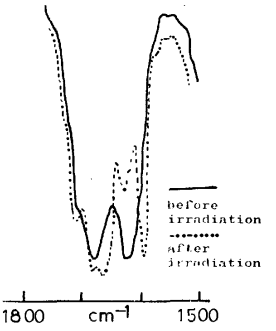

Fig. 3. Infrared spectra.

These experimental findings are compatible with Scheme 1. The deuterium exchange of the hydroxy group of the enol and the hydrogen return to the γ-carbon explain the photo-stability in the non-deuterated methanol and the deuterium exchange of the γ-methyl groups of these ketones. It is worthwhile to point out that the prototropy in these ketones, upon ketonization, takes the 1,5-migration instead of the 1,3-migration path to give β,γ-unsaturated ketone. This behavior can be explained by considering that the prototropy is completely intramolecular and that the 1,5-transfer is more favorable in the energy surface of the reaction. Dypnone (II) and pulegone (IV) isomerize to β,γ-unsaturated isomers upon irradiation in the presence of hydrochloric acid[13]; this feature can be accounted for by the intermolecular prototropy

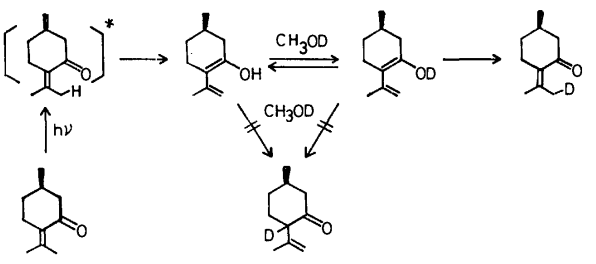

Scheme 1

placing a proton at the α-position of the enol.[14,15]

We deduced the excited state responsible for the photo-enolization to be the n–π^* singlet. This conclusion is based on a consideration of the relation between the rate of enolization and the geometry of the ground state of these ketones, and by triplet-quenching experiments. The deuterations of dypnone (II) and pulegone (IV) are much faster than those of mesityl oxide (I) and 2-isopropylidenecyclopentanone (III); this property is considered to be a reflection of the geometry of the ground state.[16,17] Judging from the Dreiding molecular model, the shortest distance between carbonyl oxygen and one of the hydrogens of γ-methyl is 1.9 Å for the III ketone and 1.5 Å for the IV ketone when the conjugate system takes a planar conformation. The influence of the ground-state geometry on the reaction rate can be expected only in the singlet state immediately after excitation. In the case of acyclic ketone, we propose that the difference in the rates of the deuteration of the I and II ketones is a reflection of the coplanarity of the enone system. The II ketone is more coplanar than the I ketone due to the conjugate effect of the aromatic ring. Another possibility is the consequence of the difference in absorbance (ε: I, 60 at 314 nm; II, 15800 at 295 nm). The large absorption coefficient of the II ketone indicates that both the lowest singlet and triplet states are π–π^* in nature, but the efficiency for hydrogen abstraction by the π–π^* state is, in general, very low. Therefore, we feel that the higher-lying n–π^* state instead of the π–π^* state is responsible for the photo-enolization of II, and that the coplanarity of the system is more crucial.

The photo-deuterations of dypnone (II) and pulegone (IV) were not quenched by a triplet quencher, 3,3,4,4-tetramethyl-1,2-diazetine 1,2-dioxide (E_T=*ca.* 40 kcal/mol);[10] therefore, the photo-deuteration *via* photo-enolization must be a singlet or an extremely fast triplet process. It has been established that an n–π^* singlet state abstracts hydrogen as fast as an n–π^* triplet state does.[7] The fast formation of a photo-equiliblium mixture of the *E* and *Z* forms of dypnone (II), as well as the deuteration of both methyl groups of the I, III, and IV ketones at a similar rate, shows the existence of fast geometrical isomerization from the excited state with a triplet manifold. This free rotor effect[18-20] must be responsible for the dissipation of the triplet excited energy, and the present phot-deuteration must be a singlet process.

In conclusion, it follows from the present results that the isomerization of an α,β-unsaturated ketone into a β,γ-unsaturated ketone is not a definite guide for the usefulness of photo-enolization, as has previously been reported, and that the γ-hydrogen abstraction in the I—IV ketones is a fast process from the singlet n–π^* state, retaining the geometry of the ground state.

The authors are indebted to Professor T. Sato of Waseda University for disclosing his unpublished data to them and for his discussions. Financial support by the Matsunaga Science Foundation is also acknowledged.

References

1) N. C. Yang and M. J. Jorgensen, *Tetrahedron Lett.*, **1964**, 1203.
2) P. J. Wagner and G. S. Hammond, *J. Amer. Chem. Soc.*, **88**, 1245 (1966).
3) L. F. Friedrich and G. B. Schuster, *ibid.*, **91**, 7204 (1969).
4) D. R. Morton and N. J. Turro, *ibid.*, **95**, 3947 (1973).
5) N. C. Yang, "Reactivity of the Excited State Organic Molecule," Interscience Publishers, London (1967), p. 145.
6) E. F. Zwicker, L. I. Grossweiner, and N. C. Yang, *J. Amer. Chem. Soc.*, **85**, 2671 (1963).
7) D. R. Chorney, J. C. Dalton, R. R. Hantala, J. J. Snyder, and N. J. Turro, *ibid.*, **96**, 1407 (1974).
8) N. O. Calloway and L. D. Green, *ibid.*, **59**, 809 (1937).
9) G. Vovon and A. Apchie, *Bull. Soc. Chim. Fr.*, **43**, 667 (1928).
10) E. F. Ullman and P. Singh, *J. Amer. Chem. Soc.*, **94**, 5077 (1972).
11) S. J. Crist, G. A. Lee, and A. L. Noreen, *Tetrahedron Lett.*, **1971**, 4175.
12) L. J. Bellamy, "Advances in Infrared Group Frequencies," Methuen and Co., London (1968), p. 34.
13) Private communication from Prof. T. Sato of Waseda University.
14) D. Bellus, D. R. Kerns, and K. Schaffner, *Helv. Chim. Acta*, **52**, 97 (1969).
15) P. Margaretha and K. Schaffner, *ibid.*, **56**, 2884 (1973).
16) F. D. Lewis and B. W. Johnson, *J. Amer. Chem. Soc.*, **94**, 8914 (1972).
17) F. D. Lewis and B. W. Johnson, *Tetrahedron Lett.*, **1973**, 2557.
18) J. S. Swenton, A. R. Crumrine, and T. J. Walker, *J. Amer. Chem. Soc.*, **92**, 1406 (1970).
19) H. E. Zimmerman and A. C. Pratt, *ibid.*, **92**, 1407 (1970).
20) K. G. Hancock and R. O. Grider, *Tetrahedron Lett.*, **1972**, 1367.

The Air Oxidation of Catecholamines by Flavin Mononucleotide

Fujio TAKAHASHI, M. B. RAHMAN,* and Hirotoshi MAEDA

Research Laboratory of Resources Utilization, Tokyo Institute of Technology, Ookayama, Meguro-ku, Tokyo 152

** Department of Chemistry, University of Rajshahi, Raishahi, Bangladesh*

(Received June 7, 1975)

Polarographic studies of the aerobic oxidation of catecholamines under the influence of FMN in various concentrations, and spectrophotometric investigations of the formation of FMN–catecholamine complexes, have been carried out. By following the course of the oxidation reaction polarographically, the rate constants have been found. The oxidation of catecholamines by air was found to be disturbed through complex formation and to be facilitated by light illumination. The equilibrium constants for the formation of some catecholamine complexes with FMN have been calculated.

It has been established that such flavins as flavin mononucleotide (FMN) and flavin adenine dinucleotide can form charge transfer (CT) complexes with tryptophane, purines, and catechol.[1] These flavins act as catalysts for the redox reactions in flavin enzymes. The oxidation of ethylenediamine tetraacetate or reduced nicotinamide adenine dinucleotide (NADH) in the presence of flavins has been reported to be facilitated by light exposure.[2] This oxidation reaction is inhibited if the donor compounds coexist in the systems.[3] Such acceptors as methyl viologen do not inhibit the reaction. Menadiol diphosphate is oxidized by oxygen in the presence of riboflavin with light exposure.[4]

It was expected that such catecholamines as 3,4-dihydroxyphenylalanine (DOPA), 3-hydroxytyramine (dopamine), and adrenaline, which are susceptible to be oxidized by oxygen,[5] might form the CT complex as donors. No papers on the study of the flavin-sensitized photooxidation of catecholamines have yet been found, however. Both catecholamines and flavins are biochemicals utilized as medicines. Therefore, it is important to clarify the interaction between flavins and catecholamines. For this purpose, we studied the formation of CT complexes in FMN-catecholamine systems and the oxidation of catecholamines in the presence of FMN. In this paper we will present the results obtained by the polarographic and spectrophotometric methods.

Experimental

The determination of FMN was carried out by spectrophotometry at 450 nm. L-DOPA, dopamine hydrochloride, and L-adrenaline bitartrate were used as catecholamines. All the sample solutions were prepared in a 0.1 mol/l phosphate buffer (pH 7.0).

Anode polarograms were obtained by using a Yanaco platinum rotating electrode equipped with a Hokuto Denko linear scanning unit LS-1D and potentiostat HA101, and a Toa Electronics Ltd. X-Y recorder SYR-1A. The platinum rotating electrode used was 1 cm long, with a diameter of 0.1 cm, and had a rotation of 600 rpm. The sweep speed for recording polarograms was set at 3 V/min. The accuracy of the half-wave potentials obtained was estimated to be within ± 0.01 V. The intensity of the illumination and the dissolved oxygen were measured by means of a Tokyo Koden illumination meter ANA-300 and an Anal Instrument Co DO meter respectively. The absorption spectra were determined with a Shimadzu UV-200 spectrophotometer.

Results

Polarography. In several 50 ml beakers, 40 ml portions of solutions containing FMN and catecholamines were prepared and shaken under the air at 30 °C with illumination (400—3000 lx). Polarograms were measured at desired intervals. Some results are shown in Fig. 1. In the case of adrenaline, the half-wave potential, $E_{1/2}$, of the anodic wave was found to shift from +0.14 to +0.16 V *vs.* SCE with an increase in the FMN concentration from 2.5 to 20 mmol/l. Towards the end of the oxidation process, the waveheight at each $E_{1/2}$ gradually reduced and finally disappeared overnight, but another anodic wave became predominant, its $E_{1/2}$ value being clearly determined to be at +0.28 V *vs.* SCE. The waveheight at the first $E_{1/2}$ changed with the lapse of time. It increased measurably during the first 30 min and then decreased. After that, the oxidation seemed to occur in the first order

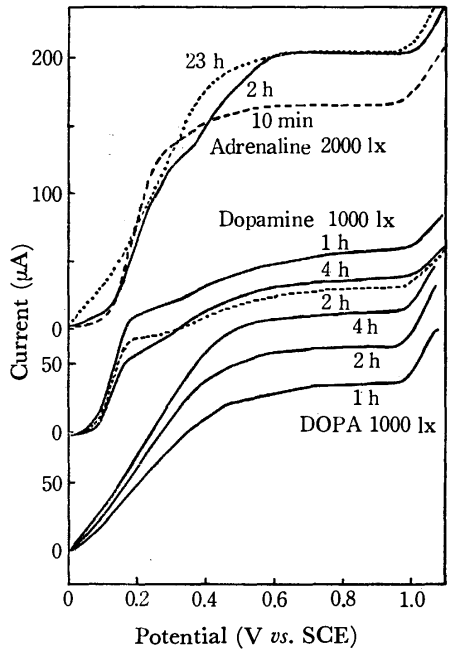

Fig. 1. Polarograms of catecholamine–FMN systems.
Catecholamine: 1 mmol/l
FMN: 20 mmol/l (Adrenaline)
5 mmol/l (Dopamine or DOPA)
pH 7.0, 30 °C

Table 1. Equilibrium constants and velocity constants

	Equilibrium Constant (1/mol)	Velocity Constant (h^{-1})			
		400 lx	1000 lx	2000 lx	3000lx
Adrenaline	19±4	0.12	0.18	0.25	0.24
DOPA	11±4	—	—	—	—
Dopamine	89±10	—	0.14	0.068	—

with respect to adrenaline. The reaction velocity was found to be independent of the FMN concentration and to be influenced by illumination. The velocity constants were obtained from the slopes in Fig. 2; they have been summarized in Table 1.

The reaction velocity in the case of dopamine was smaller than that in adrenaline and was also independent of the FMN concentration. The value of the first $E_{1/2}$ of dopamine fell on +0.12 V *vs.* SCE when the FMN concentration varied from 2.5 to 20 mmol/l. The second $E_{1/2}$ was apparent in the region between 0.38 and 0.43 V, but the exact value could not be obtained because the waveheight at the first $E_{1/2}$ still remained after 22 h. The velocity constant obtained from the slope in Fig. 2 is recorded in Table 1.

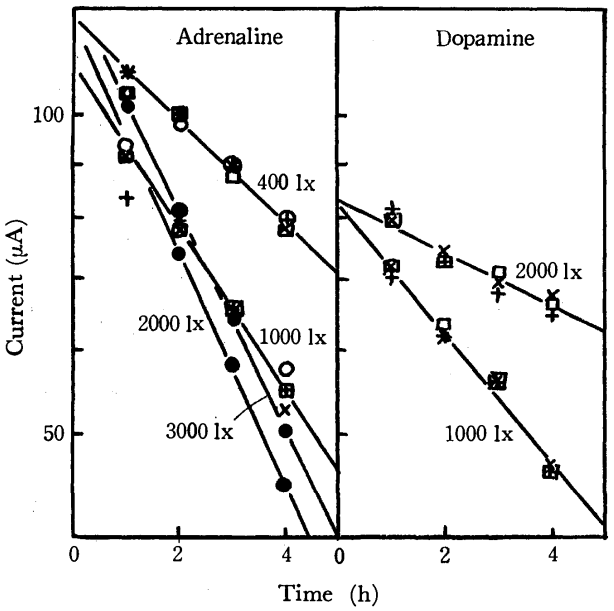

Fig. 2. Air oxidation of catecholamines.
Adrenaline or dopamine: 1 mmol/l, FMN: +; 2.5, ■; 5, ×; 10, ○; 20 mmol/l ●; average in each concentration of 2.5—10 mmol/l.

In the case of DOPA, $E_{1/2}$ was found to be centered in the region of 0.2—0.3 V. However, the definite position of $E_{1/2}$ and the waveheight at $E_{1/2}$ could not be obtained. The waveheight at about 0.6 V was found to increase considerably with the lapse of time (Fig. 1).

Spectrophotometry. The absorbances of the FMN–catecholamine systems at 505 nm were measured in a way similar to that described in a previous paper.[6] Dissolved oxygen from the sample solutions was removed by bubbling in nitrogen gas. The results plotted according to Benesi–Hildebrand's equation are shown in

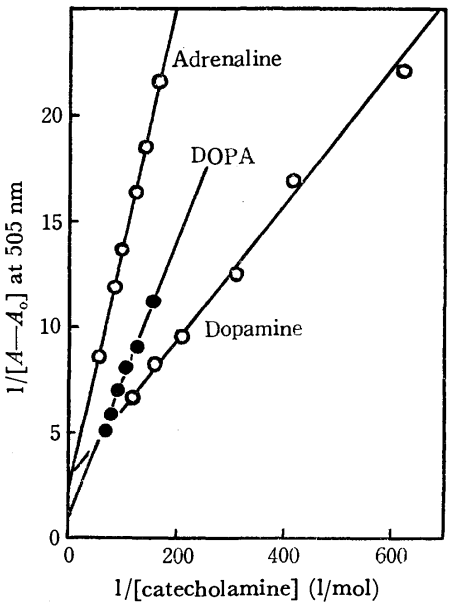

Fig. 3. Benesi–Hildebrand's plots of FMN–catecholamine systems.
FMN: 8.0×10^{-4} mol/l Oxygen free, pH 7.0, 25 °C

Fig. 3. The equilibrium constants calculated from the results in Fig. 3. are summarized in Table 1.

In a 100-ml beaker a 20 ml solution containing 3.2 mmol/l DOPA with or without 8.0×10^{-2} mmol/l FMN was prepared and stirred on a waterbath at 25 °C with illumination. The absorbance change at 340 nm was determined[7] and found to increase linearly with the lapse of time within an hour. The initial velocities (v_0's) were calculated from the absorbance change (340 nm)-time curves. The v_0's of DOPA oxidation were compared with different strengths of illumination (Figs. 4 and 5). DOPA oxidation was found to be facilitated in the presence of FMN and with stronger illumination. The plots of $1/v_0$–1/DOPA concentration fall on a straight line. Its oxidation was very slow without light exposure, even when FMN was present in the solution. In another experiment, when nitrogen gas was bubbled through a solution, the absorbance at 450 nm diminished to 82% after illuminating for 16

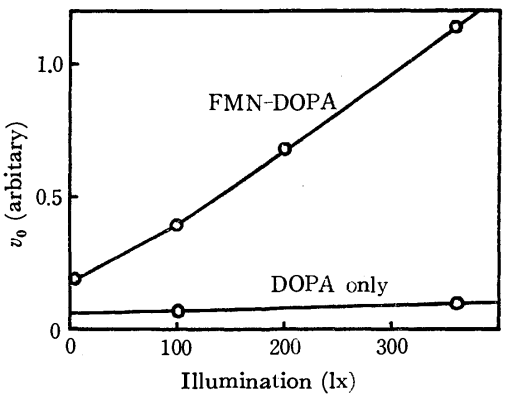

Fig. 4. Influence of illumination to the initial velocity of DOPA oxidation reaction.
FMN: 8.0×10^{-5} mol/l, DOPA: 3.2×10^{-3} mol/l, Oxygen: 2.7×10^{-4} mol/l, pH 7.0, 25 °C.

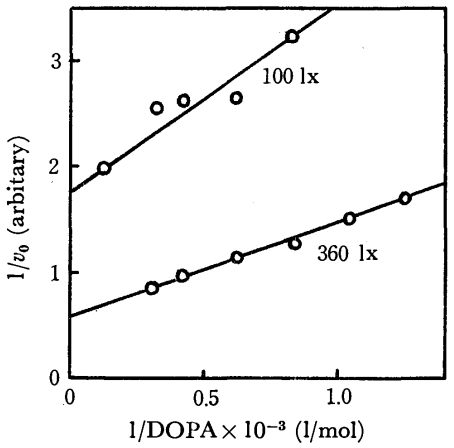

Fig. 5. Plots of 1/DOPA *vs.* $1/v_0$. FMN: 8.0×10^{-5} mol/l, Oxygen: $2{,}7 \times 10^{-4}$ mol/l, pH 7.0, 25 °C.

h at 1300 lx. Similar results were obtained when dopamine and adrenaline were used in place of DOPA. The ratios of the absorbance change of dopamine and adrenaline against DOPA were 0.4 and 1.2 respectively at 360 lx.

Discussion

It seemed that the complex formation might disturb the oxidation, as the velocity constant in the FMN–dopamine system was smaller than that in the FMN–adrenaline system. The illumination was found to enhance the air oxidation reaction in the case of adrenaline.

The reaction by which FMN oxidized NADH to form NAD, which has been reported by Radda and Calvin,[2] is a downhill reaction, because the redox potentials of NADH/NAD and $FMNH_2$/FMN are −0.32 and −0.22 V *vs.* NHE, respectively. The redox potential of adrenaline is known to be +0.80 V *vs.* NHE.[8] It is not probable that adrenaline or other catecholamines can be oxidized directly by FMN. Moore and Song[4] have reported that the energy transfer occurred from a photoexcited FMN to oxygen to attain a singlet state and that, in turn, the oxygen in the singlet state oxidized menadiol diphosphate. This oxidation reaction seems similar as that in the case of catecholamines.

It has been recently reported that a preequilibrium complex must react directly with oxygen in the process of lumiflavin reduction by *N*-methyl-1,4-dihydronicotinamide.[9] A similar reaction was observed in the FMN–DOPA reaction in Fig. 5, which showed the following Michaelis–Menten-type reaction:

$$\begin{array}{ccccc} F + D & \rightleftharpoons & FD & \rightleftharpoons & FH_2 + \text{Product} \\ & & \downarrow O_2 & & \downarrow O_2 \\ & & \text{Product} + F + H_2O_2 & & F + H_2 \end{array} \quad (1)$$

F: FMN D: Catecholamine

The fact that the reaction proceeded without illumination (Fig. 4) might be explained as a result of the oxidation of a trace amount of FH_2 produced in the equilibrium. The reduced flavin is known to be easily oxidized by oxygen.[10] It is plausible that the light reaction and the dark reaction proceed together.

It is known that catecholamine-oxidized can form a cyclic compound, III,[5] which may accumulate through the reaction if the velocity constant, k_1, is larger than k_2. This assumption is considered to be justified, because the reaction proceeds by the first order with respect to catecholamines. The half-wave potential of leucoadrenochrome is known to be +0.44 V *vs.* NHE at pH 7.[8] This is almost in accord with the second half-wave potential in adrenaline (+0.28 V *vs.* SCE) if some interaction between FMN and adrenaline is considered. Therefore, the second half-wave potentials in adrenaline and dopamine solutions can be assigned to III. Then the fact of the waveheight increase Fig. 1 seems reasonable because III is oxidized faster than I at the anode to limiting currents of the III and I of adrenaline, as shown in Fig. 1, are 205 and 165 μA respectively.

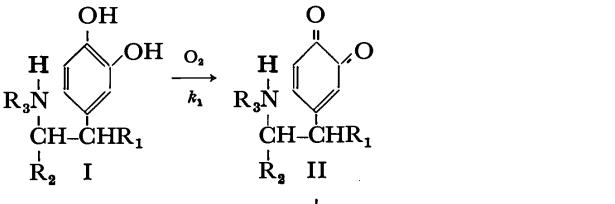

	R_1	R_2	R_3
Adrenaline	OH	H	CH_3
DOPA	H	COOH	H
Dopamine	H	H	H

The authors express their sincere thanks to Professor Shuichi Suzuki of Tokyo Institute of Technology for his encouragement. Thanks are due to the Ministry of Eduction, Japan through the Japanese National Commission for UNESCO for a fellowship (to M.B.R.).

References

1) M. A. Slifkin, "Charge Transfer Interactions of Biomolecules," Academic Press, London and New York (1971), p. 132.
2) G. K. Radda and M. Calvin, *Biochemistry*, **3**, 184 (1964).
3) G. K. Radda, *Biochim. Biophys. Acta*, **112**, 448 (1966).
4) T. A. Moore and P. S. Song, *Photochem. Photobiol.*, **10**, 13 (1969).
5) R. A. Heacock, *Chem. Rev.*, **59**, 181 (1959). G. Cilento and K. Zinner, *Biochim. Biophys. Acta*, **143**, 88 (1967).
6) F. Takahashi and H. Maeda, This Bulletin, **47**, 488 (1974).
7) M. Hatano, T. Nozawa, S. Ikeda, and T. Yamamoto, *Makromol. Chem.*, **141**, 11 (1971).
8) W. M. Clark, "Oxidation-Reduction Potentials of Organic Systems," The Williams & Wilkins, Baltimore (1960), pp. 373, 514.
9) D. J. T. Porter, G. Blankenhorn, and L. L. Ingraham, *Biochem. Biophys., Res. Comm.*, **52**, 447 (1973).
10) V. Massey, G. Palmer, and D. Ballou, "Flavins and Flavoproteins," University Park Press, Butterworths (1971), p. 349.

The Catalytic Action of a Mixed Micelle of Lauroylamino Acid and a Detergent

Tohru INOUE,* Kazuo NOMURA,** and Hideo KIMIZUKA

Department of Chemistry, Faculty of Science, Kyushu University, Fukuoka 812

(Received June 12, 1975)

The catalytic effect of the mixed micelles of lauroylamino acids (LauAm) and detergents on the hydrolysis of *p*-nitrophenyl acetate has been studied. The amino acids used for the synthesis of LauAm were glycine, serine, histidine, tyrosine, lysine, and arginine. Cetyltrimethylammonium bromide (CTAB), polyoxyethylene dodecyl ether ($C_{12}E_6$) and sodium dodecyl sulfate (SDS) were used for the preparation of the mixed micelles with LauAm. Among the detergents used, only CTAB remarkably enhanced the catalytic activity of LauAm. A reaction scheme was proposed, and the rate constant for the catalytic activity of LauAm was estimated from the kinetic data. The effect of pH was also studied. Discussions were given of the mechanism of the catalytic action on the basis of the present study.

In general, it is thought that the detergent micelle is roughly spherical and that the hydrophilic groups occupy the micellar surface and are exposed to the solvent phase, while the hydrophobic groups occupy the interior and form the hydrophobic region. In this respect, micelles resemble globular proteins, which have a structure in which the nonpolar amino acid residues are inside and the polar ones are outside. On the other hand, it has been known that several organic reactions are accelerated or inhibited when they occur in solutions containing detergent micelles and that this catalytic action shows a pattern similar to that of the Michaelis–Menten type. For these reasons, the study of the reaction rates in micellar system is useful as a model of enzymatic reaction, and recently many investigations in this area have been carried out.[1,2]

Gitler *et al.* found that the mixed micelle of N^{α}-myristoyl-L-histidine and cetyltrimethylammonium bromide (CTAB) remarkably enhanced the rate of the liberation of *p*-nitrophenol by the hydrolysis of *p*-nitrophenyl acetate (PNPA).[3] Heitman observed a similar enhancement of the reaction rate in the presence of sodium dodecanoylcysteinate in the micelle.[4] It has been regarded that the acylation reaction accompanies the liberation of *p*-nitrophenol in these systems.

When amino-acid side chains are in the vicinity of the micellar surface or the boundary between apolar and polar regions, their properties might be different from those in an aqueous environment. Thus, it is interesting to investigate the catalytic action of amino-acid residues in micelles in comparison with that of the enzyme. Thus, the effect of the mixed micelle of *N*-long chain acylamino acid and a detergent on the rate of the hydrolysis of PNPA has been studied.

Experimental

Materials. N^{α}-lauroylamino acid (LauAm) was prepared by the method of Lapidot *et al.*[5] The amino acids used for the synthesis of LauAm were glycine, serine, histidine, tyrosine, lysine, and arginine. To a solution of amino acid (20 mmol) and sodium hydrogencarbonate (20 mmol) in 200 ml of water we added a solution of the *N*-hydroxysuccimid ester of lauric acid (20 mmol) in 200 ml of tetrahydrofuran. The mixture was stirred for 16 h at room temperature and then acidified with 1 M HCl to pH 2—3, and the organic solvent was removed *in vacuo*. After the addition of 100 ml of water, the precipitate was filtered and recrystallized from the methanol–water mixture three times. In the cases of N^{α}-lauroyllysine (LauLys) and N^{α}-lauroylarginine (LauArg), two protective groups were removed by the catalytic hydrogenation of palladium black after the coupling of ε-benzyloxycarbonyl-L-lysine (or N^{ω}-nitro-L-arginine) with lauric acid. The products were recrystallized from the methanol–ether mixture or ethanol. Each compound moved as a single spot on a thin-layer chromatogram. The results of the elementary analysis of LauAm are given in Table 1.

The cetyltrimethylammonium bromide (CTAB), *p*-nitrophenyl acetate (PNPA), tris(hydroxymethyl)aminomethane (Tris), 2-amino-2-methyl-1,3-propanediol, potassium hydrogenphosphate, and disodium hydrogenphosphate were of a guaranteed grade and were used without further purification. A purified specimen of polyoxyethylene dodecyl ether, $C_{12}H_{25}O(CH_2CH_2O)_6H$, ($C_{12}E_6$), was obtained from the Kao Soap Co., Ltd. The sodium dodecyl sulfate (SDS) was purified by recrystallization from 95% ethanol.

The experiments were carried out at detergent concentrations well above the critical micelle concentration (CMC) of the detergent. Gitler *et al.* reported that N^{α}-myristoyl-L-histidine and CTAB formed a mixed micelle.[3] Although LauAm is insoluble in water at a neutral pH, it is easily solubilized by detergent micelles. In this study, sample solutions were prepared by solubilizing LauAm into the detergents in a buffer solution where the molar ratio of LauAm to detergents was less than 1/5. The micellar solutions were transparent for a long time at room temperature. The pH of the sample solution was adjusted with a 1/20 M Tris buffer unless otherwise stated.

Kinetic Measurements. An absorption cell was filled with 3.0 ml of a sample solution containing a mixed micelle of LauAm and a detergent, and was then placed in the thermostated chamber (25 °C) of a HITACHI 124 spectrophotometer. 15 min later, 20 μl of an acetonitrile solution of PNPA was added to the sample solution, and the two were mixed by stirring. The initial concentration of PNPA in the system was maintained at 10^{-5} M throughout. Then, the increase with time in the absorbance at 400 nm (at pH 6 and above) or 317 nm (below pH 6) due to the liberated *p*-nitrophenol was recorded. The pseudo-first-order kinetics were

* Present address: Department of Chemistry, Faculty of Science, Fukuoka University, Fukuoka.

** Present address: Laboratory of Chemistry, College of General Education, Kyushu University, Ropponmatsu, Fukuoka.

TABLE 1. RESULTS OF ELEMENTARY ANALYSIS

Compound Molecular Formula (mol wt)	Calculated			Found			Mp °C
	C	H	N	C	H	N	
	percentage						
LauGly $C_{14}H_{27}O_3N$ (257.2)	65.31	10.58	5.44	65.16	10.50	5.45	117—119 (117)[a]
LauSer $C_{15}H_{29}O_4N$ (287.2)	62.69	10.17	4.87	62.33	10.21	4.66	89—90 (87)[a]
LauHis $C_{18}H_{31}O_3N_3$ (337.5)	64.07	9.26	12.45	63.94	9.35	12.41	160—161 (158—159)[b]
LauTyr $C_{21}H_{33}O_4N$ (363.3)	69.39	9.15	3.85	68.97	9.20	3.80	126—127 (127—128)[b]
LauLys $C_{18}H_{36}O_3N_2$ (328.5)	65.81	11.05	8.53	65.54	11.11	8.65	
LauArg $C_{18}H_{36}O_3N_4$ (356.5)	60.64	10.18	15.72	60.37	10.17	15.85	

a) Ref. 5). b) Ref. 6).

observed under the present experimental condition: [detergent]>[LauAm]≫[PNPA]. The pseudo-first-order rate constants, k_ψ, were calculated from $(1/t)\cdot\ln a/(a-x)$, where a and x are the absorbances at an infinite time (about ten half-lives) and at time t respectively. The duplicate values of k_ψ agreed within 4%.

Results and Discussion

Effect of Detergent on the Rate of Hydrolysis of PNPA. The rate constant, k_ψ, was measured with detergent solutions at pH 8.7, 25 °C. SDS and $C_{12}E_6$ did not appreciably alter k_ψ as compared with the non-micellar system, whereas in the presence of CTAB greater values of k_ψ were observed.

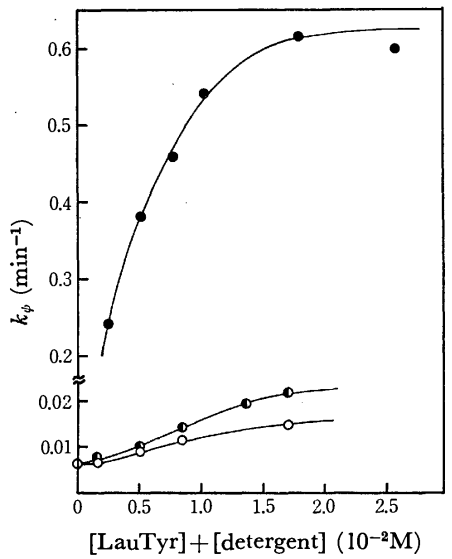

Fig. 1. Catalytic action of LauTyr.
●: CTAB, ◐: SDS, ○: $C_{12}E_6$. The molar ratio of LauTyr to detergent is 1: 16. $[PNPA]_0=10^{-5}$ M.

A series of experiments were carried out with a constant molar ratio of LauAm to the detergent. The results for LauTyr are shown in Fig. 1. This figure indicates that CTAB remarkably accelerates the rate of the hydrolysis of PNPA and that SDS causes a small increase in the reaction rate. However, in the presence of SDS the reaction rate is somewhat lower than that in the absence of SDS or in the presence of LauTyr alone. This indicates that SDS suppresses the reaction rate to some extent. Similar effects of CTAB and SDS were observed with LauHis, LauLys, LauSer, and LauArg. It may be noted that the acceleration by CTAB is small for mixed micelles with LauSer and LauArg. $C_{12}E_6$ tends to decrease the catalytic activity of LauAm except in the case of LauHis.

On the other hand, the mixed micelle of LauGly and a detergent showed a smaller catalytic activity than the detergent solution itself.

Change in the Reaction Rate with the Detergent Concentration. The catalytic effect of the mixed micelles of CTAB and LauAm has been studied as a function of the concentration with a fixed molar ratio of LauAm to CTAB. It may be seen, *e.g.*, in Fig. 1, that the rate constant, k_ψ, increases with the concentration and approaches a saturation value. The concentration dependence showed a similar pattern regardless of the composition of the mixed micelle. However, the saturation value becomes greater as the fraction of LauTyr becomes larger. This can be attributed to the increase in the number of the active sites of a mixed micelle. Similar results were obtained with LauHis, LauLys, LauArg, and LauSer.

Kinetics. The micellar concentration dependence of the rate constant can be explained by assuming the following reaction scheme:

$$S \xrightarrow{k_b} P$$

$$S + M \underset{}{\overset{K}{\rightleftharpoons}} MS \xrightarrow{k} P \qquad (1)$$

where S denotes the substrate (PNPA); M, the micelle; MS, the micelle–substrate complex and P, the product (*p*-nitrophenol); k_b and k are the rate constants of the product formation in the bulk and at the micellar surface respectively; K represents the dissociation constant of the micelle–substrate complex.

This scheme differs from that proposed by Gitler *et al.*[3] in the catalytic action of the mixed micelle of N^{α}-myristoyl-L-histidine and CTAB. The application of their theory to the results of present study showed that the dissociation constant of the inactive micelle-substrate complex changed appreciably with the kind of LauAm in the mixed micelle. This disagrees with their assumption that the dissociation constant is independent of the kind of LauAm.

In the present study, the experiments were carried out under these conditions: [detergent]≫CMC, and [detergent]>[LauAm]≫[PNPA]. According to Scheme (1), the pseudo-first-order rate constant, k_ϕ, is given by:

$$k_\phi = \frac{k_b + k \cdot \frac{[M]}{K}}{1 + \frac{[M]}{K}} \qquad (2)$$

where [M] denotes the sum of the initial concentrations of detergent and LauAm. By rearranging Eq. (2) we obtain:

$$\frac{1}{k_\phi - k_b} = \frac{K}{(k-k_b)[M]} + \frac{1}{k-k_b} \qquad (3)$$

Thus, $(k-k_b)$ and K can be evaluated from the plot according to Eq. (3); an example is shown in Fig. 2. For estimating k and K, the value of k_b is necessary. It was found that k_b increased with the pH. The values of k_b at pH's, 7.5, 8.7, and 9.7 were found to be 7.02×10^{-4}, 6.55×10^{-3}, and 2.23×10^{-2} min^{-1} respectively.

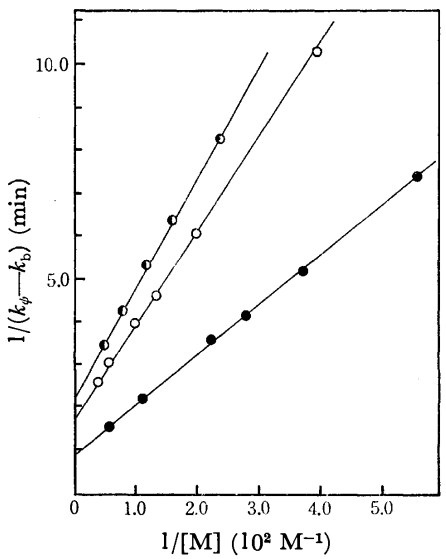

Fig. 2. $1/(k_\phi - k_b)$ *vs.* 1/[M]. The molar ratios of LauHis to CTAB are 1:8 (●), 1:16 (○), and 1:20 (◐), respectively. [M]=[LauHis]+[CTAB].

Table 2. Kinetic data for the hydrolysis of PNPA catalyzed by mixed micelles (25 °C)

System	pH	[LauAm]/[CTAB]	K (10^{-2}M)	k (min^{-1})	k_a (min^{-1})	k_c (min^{-1})
CTAB	7.5[a]	0/1	0.26	5.8×10^{-3}		5.8×10^{-3}
	8.7	0/1	0.45	2.7×10^{-2}		2.7×10^{-2}
	9.7[b]	0/1	0.45	2.3×10^{-1}		2.3×10^{-1}
LauHis -CTAB	8.7	1/8	1.30	1.12	10.1	
		1/16	1.24	0.572	9.72	
		1/20	1.15	0.451	9.47	
		av.	1.23		9.76	
LauTyr -CTAB	8.7	1/8	0.724	1.73	15.6	
		1/16	0.693	0.884	15.0	
		1/20	0.659	0.748	15.7	
		av.	0.692		15.4	
LauLys -CTAB	7.5[a]	1/5	0.882	0.292	1.75	
		3/20	0.984	0.271	1.81	
		1/10	1.09	0.187	2.05	
		1/20	0.981	0.0975	2.05	
		av.	0.984		1.92	
LauArg -CTAB	9.7[b]	1/8	0.483	0.361	1.39	
		1/10	0.418	0.333	1.39	
		3/40	0.383	0.309	1.39	
		1/20	0.375	0.291	1.39	

a) in phosphate buffer. b) in 2-amino-2-methyl-1,3-propanediol–HCl buffer.

The k and K values for mixed micelles are summarized in Table 2, together with those for CTAB micelle. It may be seen in this table that the mixed micelles consisting of the same components yield almost a constant K, regardless of the molar ratio of LauAm to CTAB. This may imply that the micelle–substrate complex formation takes place without electrical processes, since changes in the molar ratio of LauAm to CTAB should alter the micellar charge. This may be attributed to the fact that the substrate, PNPA, is electrically neutral.

It may also be seen in this table that the K value is a characteristic constant for each LauAm. If the micelle-substrate complex formation is regarded as a solubilization of PNPA into the interior of the micellar hydrocarbon phase, the K value should be a constant, regardless of the kind of LauAm in the mixed micelle. Thus, it is likely that the complex formation takes place near the micellar surface or the palisade layer of the micelle.

The treatment given in the present paper assumes that the molar ratio of the micellar substance to the substrate is 1:1. When n molecules bind with a substrate molecule, K in Eqs. (2) and (3) should be replaced by nK. However, no information on n could be obtained from the present data.

On the other hand, k increases as the fraction of LauAm increases, as is shown in Table 2. Since the surface layer of mixed micelles consists of CTAB and LauAm, the rate constant, k, may be expressed as:

$$k = k_a \frac{[\text{LauAm}]}{[M]} + k_c \frac{[\text{CTAB}]}{[M]} \qquad (4)$$

or:

$$k = (k_a - k_c)\frac{[\text{LauAm}]}{[M]} + k_c$$

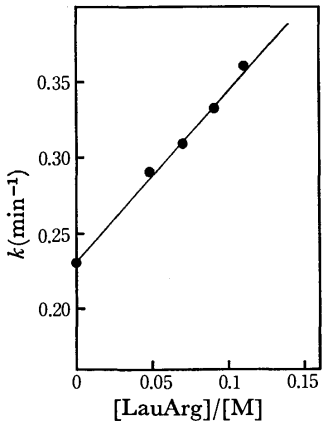

Fig. 3. Plot of k *vs.* [LauArg]/[M]. [M]=[LauArg]+[CTAB]

where k_a denotes the rate constant for the active site (LauAm), and k_c, that for the nonspecific site (CTAB).

For the LauArg–CTAB system, the variation in k with the molar ratio of LauArg to CTAB obeys Eq. (4), as is shown in Fig. 3. The intercept of the ordinate agrees well with the value of k for the CTAB micelle. It may be seen in Table 2 that the k's are much greater in mixed micelles than in the CTAB micelle and that k_c may be ignored as compared with k except in the case of LauArg. Thus, the k_a values for the other systems were estimated according to this relation:

$$k_a = k[\mathrm{M}]/[\mathrm{LauAm}]$$

which is found to be almost independent of the composition of the mixed micelles, as is shown in Table 2.

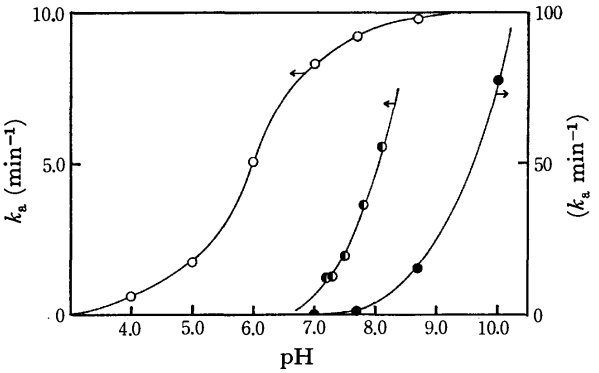

Fig. 4. pH dependence of k_a.
○: LauHis, ◐: LauLys, ●: LauTyr.
Buffer; 1/30 M phosphate (for LauLys), 1/20 M acetate pH 4—6 (for LauHis), 1/20 M Tris pH 7—8.7 (for LauHis and LauTyr), 1/20 M sodium carbonate-sodium hydrogencarbonate (for LauTyr).

The pH Dependence of k_a. The pH dependence of the catalytic activity has been measured; the results are shown in Fig. 4. The values of k_a varied with the pH to a great extent, in contrast to the small change in K. In mixed micelles of LauHis and CTAB, a sigmoidal curve was obtained. This suggests that k_a is proportional to the concentration of the dissociated form of the group with a pK_a value of *ca.* 6.0. Since the pK_a value of the imidazolium group of histidine in protein is 5.6—7.0,[7] the catalytic activity may be ascribed to the imidazolium group of LauHis.

For the mixed micelle of LauTyr and CTAB, it can be predicted from Fig. 4 that phenolate ions, the dissociated form of the side group of tyrosine, possess catalytic activity. The UV spectra of LauTyr were observed in order to find out evidence of dissociation. Two absorptions are found around 245 nm and 300 nm at pH 8.7; they are more enhanced at pH 10.0, while at pH 7.7 they disappear. These two absorptions correspond to those of tyrosine in an alkaline solution.[8] Therefore, it can be concluded that the dissociation of the *p*-hydroxyphenyl group of tyrosine is small at pH 7.7 and that it becomes appreciable at pH 8.7. Thus, it is evident that the catalytic activity of LauTyr is ascribable to the dissociated form of the *p*-hydroxyphenyl group. However, in the mixed micelles of LauTyr and SDS or $C_{12}E_6$ as well as the LauTyr solution without a detergent, the catalytic effect was very small, even at pH 8.7, where the absorption spectra associated with the phenolate ion were not observed. The dissociation of the *p*-hydroxyphenyl group of LauTyr incorporated into the micelle may be promoted by a positive charge at the surface of the CTAB micelle. Probably, the actual pH is higher in the vicinity of the surface of the mixed micelle than in the bulk phase because of an accumulation of hydroxide ions, which are responsible for the dissociation of the *p*-hydroxyphenyl group.

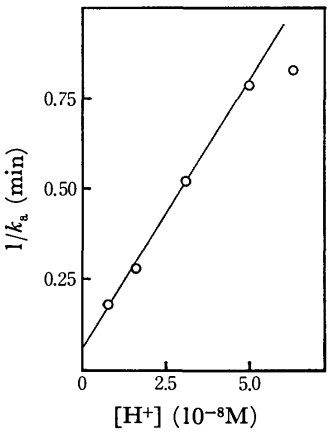

Fig. 5. $1/k_a$ *vs.* [H$^+$] for the mixed micelle of LauLys and CTAB.

From Fig. 4, it can be presumed that the dissociated form of the ε-amino group of N^{α}-lauroyllysine (LauLys) possesses catalytic activity. On this assumption, k_a is expressed by:

$$k_a = k_a^* \cdot \frac{K_a}{[\mathrm{H}^+]+K_a} \tag{6}$$

where k_a^* denotes the rate constant, which is independent of the pH, and K_a, the apparent dissociation constant of the functional group in the mixed micelle. By rearranging Eq. (6) we obtain:

$$\frac{1}{k_a} = \frac{[\mathrm{H}^+]}{k_a^* \cdot K_a} + \frac{1}{k_a^*} \tag{7}$$

The results for the mixed micelle of LauLys and CTAB obey Eq. (7), as is shown in Fig. 5. From the slope and

intercept of the plot, pK_a and k_a* were found to be 8.8 and 37 (min^{-1}) respectively. The value of pK_a determined from the kinetic data is somewhat smaller than that of the ε-amino group of lysine in an aqueous solution.[9] However, it may be thought that this smaller value of pK_a is caused by electrostatic interaction with a positive charge at the surface of the mixed micelle. Such an effect has already been shown in the mixed micellar system of N^{α}-myristoyl-L-histidine and CTAB.[3] A detailed study of the effect of the pH will be required in order to elucidate the mechanism underlying the catalytic action of the functional groups in mixed micelles.

References

1) E. H. Cordes and R. B. Dunlap, *Accounts Chem. Res.*, **2**, 329 (1969).
2) E. J. Fendler and E. H. Fendler, *Advan. Phys. Org. Chem.*, **8**, 271 (1970).
3) C. Gitler and A. Ochoa-Solano, *J. Amer. Chem. Soc.*, **90**, 5004 (1968).
4) P. Heitman, *Eur. J. Biochem.*, **5**, 305 (1968).
5) Y. Lapidot, S. Rappoport, and Y. Wolman, *J. Lip. Res.*, **8**, 142 (1967).
6) *Chem. Abstr.*, **52**, 14669 g (1968).
7) M. Dixon and E. C. Webb, "Enzymes," 2nd ed., Academic Press, New York, (1964), p. 144.
8) G. H. Beaven and E. R. Holiday, "Advances in Protein Chemistry," Academic Press, New York, (1952), Vol. VII, p. 319.
9) C. Tanford, *Advan. Protein Chem.*, **17**, 69 (1962).

Substituent Effects in the Ionization of *trans*-2-Substituted Cyclopropanecarboxylic Acids

Yoshiaki KUSUYAMA and Yoshitsugu IKEDA

Department of Chemistry, Wakayama University, Masagocho, Wakayama 640

(Received July 16, 1975)

The ionization constants of *trans*-2-substituted cyclopropanecarboxylic acids were determined in water and 50% aqueous ethanol at 25 °C. The substituent effects thus obtained were interpreted by the use of the four parameter equations presented by Yukawa and Tsuno. The transmitting resonance effect of *trans*-cyclopropylene is about a quarter that of *trans*-vinylene and a half that of *p*-phenylene.

There have been a number of reports on the analogy between a cyclopropane ring and a double bond. Previous investigations based on linear free-energy relationships (LFER) have suggested almost exclusively the possibility of the transmission of a resonance effect through a cyclopropane ring.[1] However, the degree of transmission of the resonance effect is still uncertain because of the use of limited data and the variety of treatments of the LFER. In connection with the previous study of the estimation of the electronic effects of the cyclopropane ring,[2] a definite answer has been sought concerning the degree of the transmission of conjugation through a *trans*-cyclopropylene. The ionization constants of *trans*-2-substituted cyclopropanecarboxylic acids have been determined in water and in 50% ethanol at 25 °C, and the substituent effects thus obtained have been interpreted in terms of the LFER reported by Yukawa and Tsuno.[3]

Results and Discussion

The pK_a values measured are listed in Table 1. The effects of the substituents in the two solvents were in the usual order and were correlated with each other, as is illustrated in the figure. The plot of the ΔpK_a values against the substituent constants, σ', σ^0, σ_p, σ^-, or σ^+, fails to give a linear relationship. The correlation coefficients proved to be from 0.885 to 0.94. However, an excellent correlation with a ρ value of 1.99 was obtained by means of σ_m with the correlation coefficient of 0.999 (in water), while the ionization of acrylic acids was correlated with the σ_p constants.[4] In the case of ionization in 50% ethanol, ρ and the correlation coefficient for σ_m were 2.92 and 0.998 respectively.

Yukawa and Tsuno successfully separated the polar effects of the substituent into inductive and resonance effects,[3] they expressed σ_m and σ_p as $0.87\sigma'+0.21\Delta\bar{\sigma}_R$ and $0.74\sigma'+0.685\Delta\bar{\sigma}_R$ respectively, where σ' is a polar substituent constant presented by Roberts[5] and where $\Delta\bar{\sigma}_R$ measures the capacities of the substituents to supply electrons by resonance.[3] Thus, the substituent effects (ΔpK_a) for the ionization of *trans*-2-substituted cyclopropanecarboxylic, *trans*-β-substituted acrylic, β-substituted propionic, and *p*-substituted benzoic acids are expressed by the equations given in Table 2. In the sets of the same structural type, such as XZCOOH, it seemed reasonable to assume that the ratio (*fr*) of the coefficient of $\Delta\bar{\sigma}_R$ to that of $\Delta\bar{\sigma}_R$ of the reference system is a measure of the ability of the Z group to transmit the resonance effect to the reaction site, *i.e.*, COOH, under the same reaction conditions. The *fr* values of (1) and (2) to (4) were 0.62 and 2.7 respectively. Thus,

TABLE 1. pK_a VALUES OF *trans*-2-SUBSTITUTED CYCLOPROPANE CARBOXYLIC ACIDS IN WATER AT 25°.

Substituent	pK_a (±0.01)	
	In water	In 50% ethanol
H	4.84, 4.83[a]	6.44
CH_3	4.98	6.62
Br	4.09	5.41
C_2H_5O	4.46	
CH_3O		5.76
CH_3CO	4.08	5.36
C_2H_5OCO	4.10	5.35
CH_3OCO	4.09	
CN	3.73	4.63

a) M. Kilpatric and J. O. Morse, *J. Am. Chem. Soc.*, **75**, 1854 (1953).

TABLE 2. SUBSTITUENT EFFECTS FOR THE DISSOCIATION OF CARBOXYLIC ACIDS IN WATER(a) AND IN 50% ETHANOL(b)

				fi	*fr*
(a)					
	(1)	*trans*-2-XC_3H_4COOH	$1.73\sigma'+0.42\Delta\bar{\sigma}_R$	1.08	0.62
	(2)	*trans*-β-XC_2H_2COOH	$1.63\sigma'+1.86\Delta\bar{\sigma}_R$[a]	1.02	2.71
	(3)	XC_2H_4COOH	$1.60\sigma'$[b]	1.00	0.00
	(4)	*p*-XC_6H_4COOH	$0.743\sigma'+0.685\Delta\bar{\sigma}_R$		1.00
(b)					
	(1)	*trans*-2-XC_3H_4COOH	$2.54\sigma'+0.61\Delta\bar{\sigma}_R$		0.57
	(4)	*p*-XC_6H_4COOH	$1.06\sigma'+1.08\Delta\bar{\sigma}_R$		1.00

a) ρ value is 2.19: K. Bowden, *Can. J. Chem.*, **43**, 3354 (1965). b) ρ was calculated by the ionization constants appeared in "Lange's Handbook of Chemistry," ed. by J.A. Dean, eleventh edition, Mcgraw-Hill (1973).

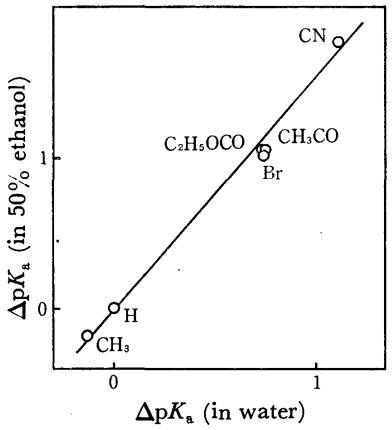

Fig. 1. Linear free energy relation for dissociation of *trans*-2-substituted cyclopropanecarboxylic acids at 25 °C.

the transmitting-resonance effect of *trans*-cyclopropylene is about a quarter that of *trans*-vinylene and a half that of *p*-phenylene.[6] Three models (a trigonally hybridized model,[7] a bent-bond model,[8] and a molecular orbital model[9]) for the bonding in cyclopropane, previously presented, have led to a prediction of the *p* orbital character of C–C bonds. Since there is no steric interaction between the substituent and the carboxy group in *trans*-2-substituted cyclopropanecarboxylic acids, the substituent and the carboxy group can both overlap with the cyclopropane ring. Thus, it is revealed that cyclopropylene is a transmitter of the resonance effect, although its action is rather poor.

The ratios(f_i) of the coefficients of σ' of (1) and (2) to that of σ' of (3) were 1.0 and 1.1 respectively, indicating that the transmission of the inductive effect was practically equal in all three series.

Experimental

The materials were identified on the basis of spectroscopic and gas-chromatographic measurements and elemental analysis. The NMR spectra were measured on a JEOL JNM-C-60HL (60 MHz) spectrometer, with tetramethylsilane employed as the internal standard. The structure assignments for the geometrical isomers were made by means of the NMR spectra of ring protons by means of shift reagents based on a generalization that the tendency of the shift of the signal of the *cis* proton to ethoxycarbonyl is larger than that of the shift of the *trans* protons.[10] Unsubstituted,[11] *trans*-2-methyl,[12] ethoxycarbonyl,[13] methoxycarbonyl[13] and bromocyclopropanecarboxylic[13] acids were synthesized by the methods described in the literature. The syntheses of other substituted cyclopropanecarboxylic acids will be described below.

Ethyl trans-2-*Ethoxycyclopropanecarboxylate.* To a mixture of commercial ethyl vinyl ether (100 g) and an anhydrous copper (I) sulfate catalyst (1 g), ethyl diazoacetate was added over a period of 1 h with rapid stirring. The mixture was then cooled to room temperature, and the catalyst was removed by filtration. The remaining ethyl vinyl ether was removed *in vacuo*, and the residue was distilled to give a main fraction boiling at 95—105 °C at 35 mmHg. Yield, 75 g. Pure ethyl *trans*-2-ethoxycyclopropanecarboxylate was obtained by fractional distillation; bp 66 °C/9 mmHg. NMR (CCl_4) δ 0.72—1.86 (3H, m, ring), 1.24 (3H, t, J=7 Hz, CH_3), 1.16 (3H, t, J=7 Hz, CH_3), 3.16—3.5 (1H, m, ring), 3.54 (2H, q, J=7 Hz, $COCH_2$), 4.06 (2H, q, J=7 Hz, ester CO_2CH_2), Found: C, 59.56; H, 9.04%. Calcd: C, 60.74; H, 8.92%.

trans-2-*Ethoxycyclopropanecarboxylic Acid.* Ethyl *trans*-2-ethoxycyclopropanecarboxylate (20 g) was saponified by refluxing with 6 g of sodium hydroxide in 40% ethanol to yield, after acidification, extraction with 50 ml of ether, and distillation *in vacuo*, 13 g of *trans*-2-ethoxycyclopropanecarboxylic acid; bp 119 °C/10 mmHg. NMR (CCl_4) δ 1.0—1.4 (2H, m, ring), 1.16 (3H, t, J=7 Hz, CH_3), 1.49—1.82 (1H, m, ring), 3.35—3.6 (1H, m, ring), 3.35—3.75 (2H, q, (J=7 Hz); neut. equiv. Found 132, Calcd 130.

Ethyl trans-2-*Methoxycyclopropanecarboxylate.* To a stirred mixture of 100 g of methyl vinyl ether and 1 g of anhydrous copper (I) sulfate in 100 ml of hexane at 35 °C, we added, drop by drop, 110 g of ethyl diazoacetate. After the reaction has been completed, the catalyst was removed by filtration. The solvent and unreacted methyl vinyl ether were removed *in vacuo*, and the residue was distilled to give 65 g of crude products; bp 75—100 °C/15 mmHg. The fractional distillation afforded 5 g of pure ethyl *trans*-2-methoxycyclopropanecarboxylate; bp 61—63 °C/15 mmHg. NMR (CCl_4) δ 0.80—1.80 (3H, m, ring), 1.23 (3H, t, J=7 Hz, CCH_3), 3.32 (3H, s, OCH_3), 4.6 (2H, q, J=7 Hz, CO_2CH_2C). Found: C, 56.36; H, 8.40%. Calcd: C, 58.31; H, 8.39%.

trans-2-*Methoxycyclopropanecarboxylic Acid.* Ethyl *trans*-2-methoxycyclopropanecarboxylate (6 g) was hydrolyzed by refluxing with sodium hydroxide (2.6 g) in 70 ml of water to yield, after a routine treatment, *trans*-2-methoxy-cyclopropanecarboxylic acid (2 g); bp 116 °C/16 mmHg. NMR ($CDCl_3$) δ 1.16—1.45 (2H, m, ring), 1.60—1.90 (1H, m, ring), 3.41 (3H, s, CH_3), 3.3—3.8 (1H, m, ring). neut. equiv: Found 117, Calcd 116.

trans-2-*Cyanocyclopropanecarboxylic Acid.* The saponification of ethyl *trans*-2-cyanocyclopropanecarboxylate (8 g)[14] with potassium carbonate (4 g) in water (20 ml) gave crude *trans*-2-cyanocyclopropanecarboxylic acid (1.5 g). Pure acid was obtained by recrystalization from benzene; mp 127—128 °C. NMR ($CDCl_3$) δ 1.80—2.45 (2H, m), 0.92—1.70 (2H, m). neut. equiv: Found 112, Calcd 111.

Ethyl trans-2-*Acetylcyclopropanecarboxylate.* This ester was obtained by the reaction of *trans*-2-ethoxycarbonylcyclopropanecarbonyl chloride (25 g) with dimethyl cadmium in benzene prepared by the treatment of methyl magnesium bromide (about 0.17 mol) with cadmium chloride (20 g); bp 105 °C/19 mmHg. IR (in CS_2) 1730 cm^{-1} (C=O, ketone), 1710 cm^{-1} (C=O, ester), NMR (CCl_4) δ 1.25 (3H, t, J=7 Hz, $OCCH_3$), 1.25—1.45 (2H, m, ring), 1.8—2.15 (1H, m, ring), 2.16—2.6 (1H, m, ring), 2.23 (3H, s, $COCH_3$), 4.05 (2H, q, J=7 Hz, CO_2CH_2C). Found: C, 60.72; H, 8.07%, Calcd: C, 61.51; H, 7.74%.

trans-2-*Acetylcyclopropanecarboxylic Acid.* Ethyl *trans*-2-acetylcyclopropanecarboxylate (6.2 g) was hydrolyzed with sodium hydroxide (1.6 g) in 80% ethanol (35 ml) to yield *trans*-2-acetylcyclopropanecarboxylic acid (4 g); bp 122—124 °C/3 mmHg, mp 56—57 °C. NMR (CCl_4) δ 1.88—2.60 (2H, m, ring), 1.20—1.55 (2H, t, J=6 Hz, ring), 2.26 (3H, s, CH_3). neut. equiv: Found 128, Calcd 128.

The ionization constants were determined by a potentiometric titration of substituted cyclopropanecarboxylic acids (0.005 M) with sodium hydroxide (0.02 M) according to the previously outlined procedure.[2]

The authors wish to thank Professor Yasuhide Yukawa and Professor Yuho Tsuno for their many helpful discussions and suggestions during this work.

References

1) R. Fuchs and J. J. Bloomfield, *J. Am. Chem. Soc.*, **81**, 3158 (1959); J. J. Bloomfield and R. Fuchs, *J. Org. Chem.*, **26**, 2991 (1961); R. Fuchs, C. A. Kaplan, J. J. Bloomfield, and L. F. Hatch, *ibid.*, **27**, 733 (1962); R. Fuchs and J. J. Bloomfield, *ibid.*, **28**, 910 (1963); A. B. Thigpen, Jr., and R. Fuchs, *ibid.*, **34**, 505 (1969); M. Charton, *J. Am. Chem. Soc.*, **91**, 5769 (1969); M. Charton, "The Chemistry of Alkens," ed. by J. Zabicky, Wiley-Interscience (1970), Vol. 2, Chap. 10, p. 566.

2) Y. Kusuyama and Y. Ikeda, This Bulletin, **46**, 204 (1973).

3) Y. Yukawa and Y. Tsuno, *Nippon Kagaku Zasshi*, **86**, 783 (1965).

4) K. Bowden, *Can. J. Chem.*, **43**, 3354 (1965).

5) J. D. Roberts and W. T. Moreland, Jr., *J. Am. Chem. Soc.*, **75**, 2167 (1953).

6) During the course of this investigation, Charton (Ref. 1) suggested by means of Taft's equation, that the *trans*-cyclopropylene group is about as effective in transmitting resonance effects as is the *p*-phenylene group. As has been mentioned by Yukawa and Tsuno (Ref. 3), however, Taft's parameter, σ_R, does not evaluate the resonance effect strictly.

7) A. D. Walsh, *Trans. Faraday Soc.*, **45**, 179 (1949).

8) C. A. Coulson and W. E. Moffit, *J. Chem. Phys.*, **15**, 151 (1947).

9) R. Hoffman, *J. Chem. Phys.*, **49**, 2480 (1964); N. C. Baird and M. J. S. Dewar, *J. Am. Chem. Soc.*, **89**, 3960 (1967).

10) Y. Kusuyama and Y. Ikeda, *Bull. Fac. Edu. Wakayama Univ.*, Natural Science, **24**, 13 (1974).

11) C. M. McClosky and G. H. Coleman "Organic Syntheses," Coll. Vol. III, (1955), p. 221.

12) J. E. Cloke, E. Stehr, T. R. Steadman, and L. C. Westcott, *J. Am. Chem. Soc.*, **67**, 1587 (1958).

13) K. B. Wiberg, R. K. Barnes, and J. Albin, *ibid.*, **79**, 4994 (1957).

The Reaction of Tris(diethylamino)bismuthine with Carbonyl Compounds and the Reactivity Comparison of Several Metal Amides

Fumio ANDO, Kumao OHASHI, and Jugo KOKETSU

Department of Chemistry, Chubu Institute of Technology, 1200 Matsumoto, Kasugai, Aichi 487

(Received July 28, 1975)

Tris(diethylamino)bismuthine (I) reacted with the sterically unhindered carbonyl compounds to give the corresponding enamines. The reactivity of the metal amides $M(NR_2)_n$ (M=As, Sb, Bi, and Ti; R=Me and Et) toward the carbonyl compounds was examined. The order of reactivity: Bi>Sb>Ti>As was observed for the addition reaction that took place as the first step in the reaction. On the other hand, the order of enamine formation was Sb>Ti>As>Bi. The effectiveness of the amination reaction depends both on the reactivity of metal amides to carbonyl groups and also on the affinity for oxygen of metal atoms. Although bismuth amide gives the addition product very rapidly, because of its poor affinity for oxygen, the addition products decompose thermally on prolonged standing or on distillation giving large amounts of starting carbonyl compounds along with small amounts of enamines.

The preparation and reactions of tris(dialkylamino)-bismuthines with heterocumulenes have been reported.[1] The reactions of these reagents with acetic anhydride and heterocumulenes were found to be much easier than those of arsine amide or stibine amide, and the reagents could be expected to be useful for aminating carbonyl compounds. The reactions of various carbonyl compounds with the following organometallic compounds have been reported: tributylmethylaminotin,[2-4] tris-(dimethylamino)borane,[5,6] tris(dimethylamino)-arsine,[7-9] tetrakis(dimethylamino)titanium,[4,7,10-13] and tris(dimethylamino)stibine.[14,15] The amination ability order of metal amides, $M(NR_2)_n$, towards carbonyl compounds has been found to be Ti>As>B>Sn.[7] Tris(dimethylamino)stibine was proved to have an amination ability towards carbonyl compounds comparable to that of tetrakis(dimethylamino)titanium.[14,15] Amination of carbonyl compounds by metal amides is known to be a very easy way for obtaining the versatile synthetic intermediate enamines, because the reaction is very fast and the by-product (metal oxide) can be separated easily. Therefore it is of significance to find out the factors which control the amination reactions. This paper reports the reaction of tris(diethylamino)bismuthine (I) with carbonyl compounds along with a comparison of the reactivity of various metal amides.

Experimental

General Remarks. All reactions were carried out under argon. IR and NMR spectra were taken on a JASCO A-1 spectrometer and a JEOL-C 60 HL spectrometer respectively. Glc analyses were carried out on a Shimadzu GC 6A apparatus, using PEG 6000 (10%) on Shimalite W-301 (1.0 m) and helium as a carrier gas.

Reagent. The preparation of tris(diethylamino)bismuthine (I), was reported previously.[1] Tris(diethylamino)-arsine (II), -stibine (III), and tetrakis(diethylamino)titanium (IV) were prepared by the same method reported in the preparation of their dimethylamino derivatives; II: bp, 47—50 °C/0.08 mmHg; yield, 72%, III: bp, 59—62 °C/0.02 mmHg; yield, 82% and IV: bp, 96—98 °C/0.12 mmHg; yield, 64%.

The other commercial reagents were dried over calcium hydride and distilled before use.

Reaction of I with Benzaldehyde. To a solution of I (3.0 g, 7.07 mmol) in 10 ml of ether, benzaldehyde (0.74 g, 7.00 mmol) was added slowly with stirring. A slightly exothermic reaction took place giving a yellowish solution. After removal of the solvent, a viscous yellowish liquid remained. IR spectra of the liquid showed no absorption of carbonyl group and a new absorption at 1060 cm^{-1} (ν_{C-O}). NMR also showed no reasonance of aldehyde-proton but a new reasonance of -OCH-N moiety at δ 4.10. On distillation of the liquid under reduced pressure, benzaldehyde was recovered almost completely (0.65 g). The distillation residue was a dark black solid whose structure was not identified. Hydrolysis of the reaction mixture, and the following extraction with ether gave mostly (90%) benzaldehyde with several materials detected on a TLC. These materials was not identified.

Reaction of I with Reactive Carbonyl Compounds. A typical

Table 1. Bp and yield of the amination products by means of $Bi(NEt_2)_3$

	Carbonyl compounds	Aminated products	Bp (°C/mmHg)	Yield (%)
V			60.5—62.0/10	29
VI			74.0—75.0/10	49
VII	$Et_2C=O$	$Et-\underset{\displaystyle NEt_2}{\overset{}{C}}=CHCH_3$	68.0—69.0/35	28
VIII	PhCOMe	$PhC(NEt_2)=CH_2$	60.0—61.0/1.0	4

Table 2. Relevant IR frequencies and NMR absorptions of the aminated products

	IR (C=C) cm^{-1} [a]	NMR (δ) ppm [b]		
V	1615	4.19(m, 1H)	3.04(q, 4H)	2.35(m, 4H)
		1.97(m, 2H)	1.03(t, 6H)	
VI	1630	4.49(m, 1H)	2.92(q, 4H)	2.04(m, 4H)
		1.59(m, 4H)	0.97(t, 6H)	
VII	1635	4.26(q, 1H)	2.91(q, 4H)	2.14(q, 2H)
		1.61(d, 3H)	0.99(t, 3H)	0.97(t, 6H)
VIII	1635	7.37—7.90(m, 5H)	4.14(s, 1H)	
		4.04(s, 1H)	2.96(q, 4H)	1.01(t, 6H)

a) Coated on NaCl Crystal. b) In $CHCl_3$ (V, VI and VII), in $CDCl_3$ (VIII).

reaction (with cyclohexanone) is described.

Details are given in Tables 1 and 2. To a solution of (I) (2.82 g, 5.92 mmol) in 10 ml of ether, cyclohexanone (0.87 g, 8.4 mmol) was added slowly with stirring. A slightly exothermic reaction took place giving a small amount of a yellowish grey precipitate. The precipitate was removed by filtration and the filtrate was condensed on a rotary evaporator. Distillation of the remaining viscous liquid which showed no carbonyl absorption on its IR spectra gave a large amount (0.44 g, 50% recovery) of cyclohexanone and the aminated product; *N,N*-diethylcyclohex-1-enylamine in 49% yield (0.39 g); bp, 74.0—75.0 °C/10 mmHg, NMR (in $CHCl_3$) δ 4.49 (m, 1H), 2.92 (q, 4H), 2.04 (m, 4H), 1.59 (m, 4H) and 0.37 (t, 6H), IR 1630 cm^{-1} ($\nu_{C=O}$). These spectroscopic data coincide with those of the reaction product of cyclohexanone with III[14,15] or IV.[4,7,10-13]

Reaction of Acetophenone with Various Metal Amides. The reactions of acetophenone with I—IV as well as with their dimethyl amino homologues were carried out under the same reaction conditions. To a solution of metal amide (5 mmol) in 10 ml of ether, acetophenone (0.9 g, 7.5 mmol) was added slowly with stirring. The reaction mixture was kept at 20 °C for 24 hr. The same treatment as above gave α-dimethylaminostyrene or α-diethylaminostyrene. The yields of the substituted styrenes are given in Table 3.

Measurements of the Rate of Carbonyl Compounds Consumption on the Reactions with I—IV. An equimolar (0.05 mol/l) reaction between metal amide and carbonyl compounds at an appropriate temperature was started by mixing each reagent dissolved in chlorobenzene containing a constant amount of *o*-dichlorobenzene as an internal standard. Aliquots of the reaction mixture were withdrawn at appropriate time intervals and the remaining amounts of the carbonyl compounds were determined by GLC analyses. The results are shown in Figs. 1 and 2.

Table 3. Yield (%) of the enamine in the reaction of $M(NR_2)_n$ with PhCOMe

R	M			
	As	Sb	Ti	Bi
Me	41	86	65	0
Et	12	78	38	4

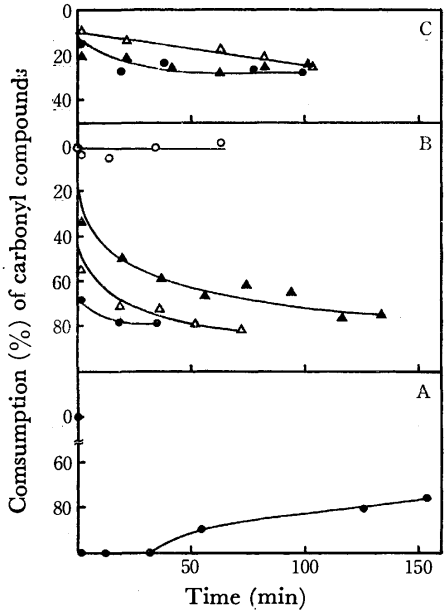

Fig. 1. Consumption (%) curves of the reactions between reactive carbonyl compounds and various metal amides.
A: Benzaldehyde, 100 °C; B: Acetophenone, 40 °C; C: Di-isopropyl ketone, 40 °C.
○: with As–N; △: with Sb–N; ●: with Bi–N; ▲: with Ti–N.

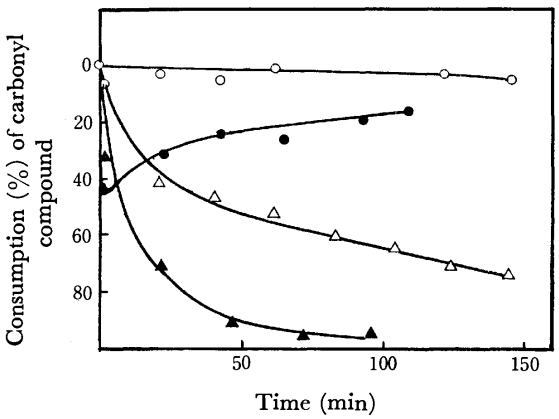

Fig. 2. Consumption (%) curves of the reactions between *N,N*-Dimethylformamide and various metal amides.
○: with As–N; △: with Sb–N; ●: with Bi–N; ▲: with Ti–N.

Results and Discussion

The amination of various carbonyl compounds with tris(dimethylamino)stibine has been studied,[14] and the amination ability is found to be comparable to that of tetrakis(dimethylamino)titanium which has been known as the most effective amination reagent so far.[7] Bismuth amide has labile bonds and could be expected to be an effective amination reagent. In fact bismuth amides are very reactive towards acetic anhydride and heterocumulenes and also towards moisture and oxygen in air.[1] Contrary to expectation, I gave only poor yields of amination products even in the reactions with reactive carbonyl compounds such as cyclohexanone, cyclopentanone, diethyl ketone and acetophenone (Table 1). The structures of the amination products were determined by comparison of their IR and NMR spectra with those of the reaction products obtained in the reaction between III or IV and the corresponding carbonyl compounds.[4,7,10-15] The reaction mixture of I with these carbonyl compounds shows no carbonyl absorption on their IR spectra. This result together with that of the reaction of I with benzaldehyde indicate that I could react with such carbonyl compounds quantitatively. Distillation of the reaction mixture under reduced pressure, however, gave only small amounts of aminated product and large amounts of starting carbonyl compounds (Table 1). Table 2 shows the yields of the enamines in the reaction of acetophenone with various metal amides. Bismuth amides gave the least amounts of the enamines among the metal amides examined. These unexpected observations prompted us to compare the reactivity of several

metal amides. Figure 1 shows the consumption curves of benzaldehyde (A), acetophenone (B), and di-isopropyl ketone (C), in the reaction with compounds I—IV. The corresponding consumption curves of DMF with the same metal amides are shown in Fig. 2. They show only the consumption of the carbonyl compounds and not the formation of aminated products. It has been proposed that the reaction mechanism includes an addition step of metal–nitrogen bond to carbonyl groups (step A), followed by a deoxygenation step of carbonyl oxygen by metal moieties forming metal oxides (step B).[7,14] The results (Figs. 1 and 2) reveal that the bismuth amide has the highest reactivity in the addition step (step A) and reactivity order of $M(NEt_2)_n$ ($n=3$ or 4) is Bi>Sb>Ti>As in this step. The effectiveness of amination reaction is Sb>Ti>As>Bi based on the yield of the amination products (Table 3). This result can be explained in terms of the affinity for oxygen of the metal atoms. The properties of group Va metals have not been compared, but they could be parallel to factors such as the metal–oxygen bond energies, and the tendency of the quarternary onium salt formation. The σ-bond energies for the phosphorus–, arsenic–, and stibine–oxygen bonds have been reported to be 86,[16] 72 and 71 kcal/mol,[17] respectively. There have been several observations of the fact that the stability order of quinqivalence state of group Va metal is P>As>Sb>Bi.[18] Because of the poor affinity of bismuth atom for oxygen, the addition products decomposed thermally giving mostly original carbonyl compounds and unidentified decomposition products of bismuth amide. This is shown in the reaction of I with benzaldehyde (Fig. 1-A). Reappearance of benzaldehyde from the reaction mixture was observed at a high temperature (100 °C). In the reaction with amide carbonyls, group Va metal amides are apparently inferior to titanium amide from a preparative viewpoint.[14] Figure 2 shows, however, I could add to the amide carbonyl group much faster than IV, but the thermal decomposition of the addition products occurred again easily, giving the starting amide carbonyl. The reason why titanium amide could have a large reactivity towards amide carbonyl is not known but it may be partly ascribed to the fact that the titanium atom is a transition metal and has vacant d orbitals which increase the interactions with the lone pairs of the oxygen atom.

This work was supported by a research fund of C. I. T. (1975).

References

1) F. Ando, T. Hayashi, K. Ohashi, and J. Koketsu, *J. Inorg. Nucl. Chem.*, **37**, 2011 (1975).
2) J. C. Pommier and A. Roubineau, *J. Organometal. Chem.*, **17**, 25 (1969).
3) T. A. George and M. F. Lappert, *Chem. Commun.*, **1966**, 463.
4) G. Chandra, T. A. George, and M. F. Lappert, *J. Chem. Soc., C*, **1969**, 2565.
5) P. Nelson and A. Pelter, *J. Chem. Soc.*, **1965**, 5142.
6) T. Levitt and A. Pelter, *Nature*, **211**, 299 (1966).
7) H. Weingarten and W. A. White, *J. Org. Chem.*, **31**, 4041 (1966).
8) H. V. Hirsch, *Chem. Ber.*, **100**, 1289 (1967).
9) G. Manoussakis, *J. Inorg. Nucl. Chem.*, **30**, 3100 (1968).
10) H. Weingarten and W. A. White, *J. Amer. Chem. Soc.*, **88**, 850 (1966).
11) H. Weingarten and W. A. White, *J. Org. Chem.*, **32**, 213 (1967).
12) H. Weingarten and W. A. White, *ibid.*, **33**, 1506 (1968).
13) H. Weingarten and W. A. White, *ibid.*, **31**, 2874 (1966).
14) J. Koketsu and Y. Ishii, *J. Chem. Soc., C*, **1971**, 511.
15) A. Kiennemann and R. Kieffer, *J. Organometal. Chem.*, **60**, 255 (1973).
16) S. B. Hartley, W. S. Holmes, J. K. Jacques, M. F. Mole, and J. C. McCoubrey, *Quart. Rew.*, **17**, 204 (1963).
17) F. S. Dainton, *Trans. Faraday Soc.*, **43**, 244 (1947).
18) G. O. Doak, L. D. Freedman "Organometallic Compounds of Arsenic, Antimony, and Bismuth," Wiley-Interscience (1970). pp. 214, 336.

Elimination and Nucleophilic Substitution on Nitrogen Atom. Reactions of *O*-Aroyl-*N*,*N*-di(*p*-substituted benzyl)- and *O*-Aroyl-*N*-benzoyl-*N*-benzylhydroxylamines with Various Nucleophiles in Dipolar Aprotic Solvents[1]

Shigeru OAE and Tadamitsu SAKURAI*

Department of Chemistry, The University of Tsukuba, Sakura-mura, Niihari-gun, Ibaraki 300-31

* *Department of Applied Chemistry, Faculty of Engineering, Osaka City University, Sugimoto-cho, Osaka 552*

(Received July 31, 1975)

The reactions of the title compounds with various nucleophiles were found to proceed through either elimination or nucleophilic substitution on the nitrogen atom depending on both the structure of the substrate and the nature of nucleophiles used. The effect of substituent and the primary isotope effect (k_H/k_D of 7.6 and 8.1 with NaN_3 and LiCl at 30 °C) on the elimination of *O*-(*p*-nitrobenzoyl)-*N*,*N*-dibenzylhydroxylamine revealed that the reaction is an E2 process involving the rate-determining proton abstraction by base and proceeds *via* an ionic transition state of an ideal concerted type. Nucleophilic substitution on the trivalent nitrogen atom has been inferred for the reactions with such nucleophiles as diethyl sulfide, *p*-toluenethiol and sodium cyanide on the basis of product distribution.

The nucleophilic substitution and elimination reactions on carbon atom have been studied extensively in the past and well understood.[2] However, no systematic study concerning the nature of both nucleophilic substitution and elimination reactions on the trivalent nitrogen atom has been attempted, though there have been some investigations on the nucleophilic substitution[3] and elimination[4] reactions at oxygen atom. A careful literature survery reveals that there are a few reactions which appear to be the nucleophilic substitution[5] and elimination[6] reactions on the nitrogen atom. Very recently, the occurrence of S_N2 type reaction on nitrogen atom has been well confirmed on the basis of both detailed kinetic study and product analysis by us[7b] and Krueges *et al.*[7a] However, as to the elimination reaction on the trivalent nitrogen atom giving either C–N double bond or C–N triple bond, a more critical examination would be necessary.

Thus, we have prepared *O*-aroyl-*N*,*N*-di(*p*-substituted benzyl)- and *O*-aroyl-*N*-benzoyl-*N*-benzylhydroxylamines as model compounds, and allowed them to react with various nucleophiles in dipolar aprotic solvents for studying both nucleophilic substitution and elimination reactions on the nitrogen atom.

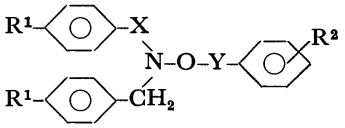

(I)

R^1=CH_3, H, Cl
R^2=3,5-$(NO_2)_2$, *p*-$(NO_2)_2$, *p*-Cl, *p*-OCH_3, 2,4,6-$(CH_3)_3$
X=CH_2, CO Y=CO, SO_2

Results and Discussion

Reactions of (I) (X=CH_2; Y=CO; R^1=CH_3, H, Cl; R^2=p-NO_2, 3,5-$(NO_2)_2$) with Charged Nucleophiles. The reactions of (I) with charged nucleophiles in dimethyl sulfoxide (DMSO) gave substituted benzaldehydes, substitutted benzylamines and substituted benzoate ions in good yields respectively, as indicated in Table 1. There are two conceivable mechanisms to explain the product distribution. Although the formation of substituted benzaldehydes could be interpreted as a modification of the Kornblum reaction,[8] this mechanism may be ruled out since benzaldehyde (R^1=H) was also obtained (85% yield) when *N*,*N*-dimethylformamide (DMF) was used as a solvent. Formation of the aldehyde and the amine can be explained by assuming the imine (IV) as the precursor of which intermediacy was confirmed by direct hydrolysis of the authentic imine (IV) in the presence of HCl in DMSO.

Moreover, the imine (IV, R^1=H) was actually isolated from the reaction with NaOH as a nucleophile probably because of lower acidity of HNu (Nu=OH) than other HNu (Nu=N_3, Cl, I). Interestingly, the

Path A

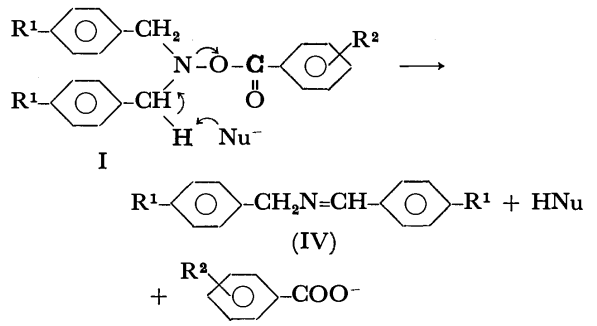

Path B

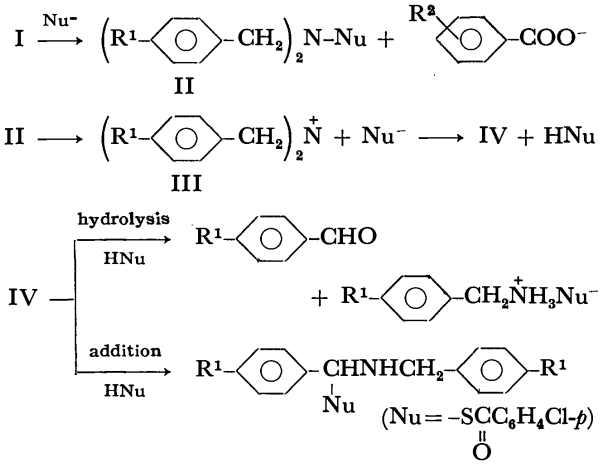

TABLE 1. THE PRODUCTS OF THE REACTION OF 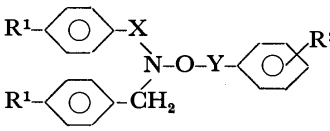 WITH NUCLEOPHILES IN DMSO AT ROOM TEMPERATURE

							Producst (% Yield)				
R^1	X	Y	R^2	Nu or M–Nu	Time (hr)	Re-cov.	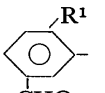	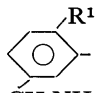	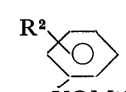	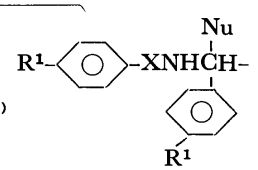	Others
H	CH_2	CO	*p*-NO_2	NaN_3	24	—	76	73	quant.	—	—
H	CH_2	CO	*p*-NO_2	LiCl	25	—	70	67	72	—	—
H	CH_2	CO	*p*-NO_2	NaBr	24	78	19	18	22	—	—
H	CH_2	CO	*p*-NO_2	NaI	50	67	24	28	33	—	—
H	CH_2	CO	*p*-NO_2	NaOH	26	—	22	20	70	—	$PhCH_2N{=}CHPh$ (51)
H	CH_2	CO	*p*-NO_2	$NaSC(=O)C_6H_4Cl$-*p*	40	—	57	29	58	35	—
H	CH_2	CO	3,5-$(NO_2)_2$	NaN_3	15	—	75	68	75	—	—
H	CH_2	CO	*p*-OCH_3	NaN_3	36	63	20	18	18	—	—
CH_3	CH_2	CO	*p*-NO_2	NaN_3	15	—	82	75	80	—	—
Cl	CH_2	CO	*p*-NO_2	NaN_3	20	—	64	60	76	—	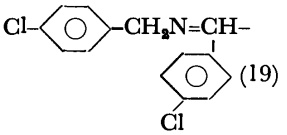 (19)
H	CH_2	CO	*p*-NO_2	NaCN	15	—	7	8	87	22	$(PhCH_2)_2NH$ (58)
H	CH_2	CO	3,5-$(NO_2)_2$	NaCN	15	—	25	20	small amount	—	—
H	CO	CO	*p*-NO_2	NaCN	15	—	—	—	27	58	—
H	CO	CO	*p*-NO_2	NaCN[b]	10	—	—	—	82	39	PhC(=O)–N(OH)–CH_2Ph (41)
H	CO	SO_2	2,4,6-$(CH_3)_3$	NaCN	20	—	—	—	72[c]	65	—
H	CH_2	CO	*p*-NO_2	$(C_2H_5)_2S$	48	28	49	33	38	—	—
H	CH_2	CO	3,5-$(NO_2)_2$	$(C_2H_5)_2S$	36	13	66	62	46	—	—
H	CH_2	CO	*p*-NO_2	*p*-$CH_3C_6H_4SH$[b]	25	13	51	40	52	—	$CH_3C_6H_4SH$ (31), $(p\text{-}CH_3C_6H_4S)_2$ (46)
H	CH_2	CO	*p*-Cl	NaCN	20	—	8	d)	72	79	—
H	CH_2	CO	*p*-OCH_3	NaCN	20	—	8	d)	87	65	—
H	CH_2	CO	*p*-OCH_3	KCN[b]	15	53	trace	d)	30	22	—

a) as carboxylic acid. b) Reaction was carried out in DMF. c) as *S*-benzylthiuronium salt. d) Isolation was not carried out.

reaction of I (R^1=H; R^2=*p*-NO_2) with sodium *p*-chlorobenzenecarbothioate gave the addition product along with the expected products, indicating clearly that the imine (IV) is involved during these reactions.

On the other hand, there are two conceivable processes to give the imine (IV). The one is the base-catalyzed elimination of the carboxylate ion from the starting material (Path A) and the other, the decomposition of the initial product (II), which was formed by the nucleophilic substitution on the nitrogen atom, due to the instability of the N–Nu bond of II and then the nitrenium ion (III) will easily decompose to afford the imine (IV).[9]

Isolation of the imine (IV) in the reaction of I (R^1=Cl; *p*-R^2=NO_2) with NaN_3 may be due to the increased stability of the imine (IV) intermediate, bearing electron-withdrawing *p*-chloro substituent.

Kinetics of the Reactions of I (X=CH_2; Y=CO; R^1=CH_3, H, Cl; R^2=p-NO_2, 3,5-$(NO_2)_2$) with NaN_3 and LiCl in DMSO. In order to make a choice between the two mechanisms (Path A and B) and to know the nature of these reactions in detail, we carried out the kinetic experiments using some substituted hydroxylamines (I) under pseudo-first order conditions with a large excess of nucleophiles. The over-all reaction rate was measured spectrophotometrically by following the increase in absorbance of *p*-nitro- and 3,5-dinitrobenzoate ions at 290 nm. Hydrogen–deuterium kinetic

TABLE 2. RATE CONSTANTS AND ACTIVATION PARAMETERS FOR THE REACTIONS OF THE HYDROXYL AMINES, $(R^1\text{-}C_6H_4\text{-}X)_2N\text{-}OC\text{-}C_6H_4\text{-}R^2$ (O) WITH NUCLEOPHILES IN DMSO

Nu[a)]	R^1	X	R^2	Temp (°C)	10^5k (s^{-1})[b)]	$\Delta H^{\ddagger}$ (kcal/mol)	$\Delta S^{\ddagger}$ (e.u.)	k_H/k_D
NaN_3	CH_3	CH_2	p-NO_2	30.0±0.1	6.46 ±0.50			
NaN_3	H	CH_2	p-NO_2	30.0	6.47 ±0.30	17.4	−20.2	
NaN_3	H	CD_2	p-NO_2	30.0	0.85 ±0.05			7.6
NaN_3	H	CH_2	p-NO_2	36.1	12.1 ±0.7			
NaN_3	H	CH_2	p-NO_2	42.0	20.2 ±0.9			
NaN_3	Cl	CH_2	p-NO_2	30.0	21.6 ±1.1			
NaN_3	H	CH_2	3,5-$(NO_2)_2$	30.0	75.0 ±2.0			
LiCl	H	CH_2	p-NO_2	30.0	1.41 ±0.12			
LiCl	H	CD_2	p-NO_2	30.0	0.173±0.018			8.1

a) Concentration of nucleophiles is 12 times excess, *i.e.*, [Substrates]$=6.9\times10^{-3}$ mol/l, [Nucleophiles] $=8.3\times10^{-2}$ mol/l. b) Pseudo-first order rate constants and error limits are standard deviation.

isotope effect was measured using the substrate which was labeled with D at the benzylic position of I under the same condition.

Good pseudo-first order kinetic behaviors were observed and the kinetic results are summarized in Table 2. As seen from Table 2, the isotope effects are 7.6 and 8.1 for the reactions of I (R^1=H; R^2=p-NO_2) with NaN_3 and LiCl as nucleophiles at 30 °C, respectively.

On the other hand, it has been generally known that secondary hydrogen isotope effects are $k_H/k_D=1.00$ for S_N2 reaction and $k_H/k_D=1.15$ for S_N1 reaction.[10] The isotope effect, thus, clearly indicates that the reaction is of base-catalyzed elimination (Path A). The order of the reactivities of the halide ions, $Cl^->Br^->I^-$, deduced from the recovered amounts of the starting material and the reaction times, also support that the reaction involves the rate-determining proton abstraction by the base.

The substituent effect (R^1) gave hardly any correlation with Hammett σ value. Apparently, an electron-withdrawing substituent such as Cl accelerated the reaction, while an electron-donating substituent (CH_3) could not retard it. On the other hand, the substituent effect (R^2) indicates the reaction rate to increase with the increase in electron-withdrawing ability of the substituent. This is also supported by the observation that the staring material was recovered in 63% yield for the reaction of I (R^1=H; R^2=p-OCH_3) with NaN_3, while no starting material was recovered in the reaction of I (R^1=H; R^2=p-NO_2) under the same condition. The activation parameters for the reaction of I (R^1=H; R^2=p-NO_2) with NaN_3 in DMSO are $\Delta H^{\ddagger}$, 17.4 kcal/mol and $\Delta S^{\ddagger}$, −20.2 *e.u.* respectively.

On the basis of these experimental observations, one can assume that the elimination reaction on the trivalent nitrogen atom involves the ionic transition state of an ideal concerted type like in the carbonyl-forming

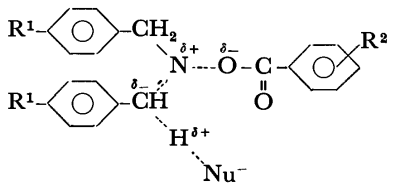

elimination reaction of benzyl and 9-fluorenyl nitrates where primary hydrogen isotope effects are 5.94 for the former nitrate and 4.3 for the latter nitrate at 30 °C.[4b]

Reactions of I (X=CH_2, CO; Y=CO, SO_2; R^1=H; R^2=p-NO_2, p-Cl, p-OCH_3, 2,4,6-$(CH_3)_3$) with NaCN and KCN. The reaction of (I) (X=CH_2; Y=CO; R^2=p-NO_2) with NaCN in DMSO unexpectedly gave the dibenzylamine which may be formed *via* *N,N*-dibenzylcyanamide as the precursor in a substantial yield along with the products which were produced by the elimination (Path A). Among these products, the α-aminonitrile must be formed by the addition of HCN to the imine (IV). Although in a previous experiment[1] we have reported that the above reaction yields the *N,N*-dibenzylcyanamide, a careful reexamination revealed the cyanamide to be a mixture of dibenzylamine and an unidentified product bearing cyano group, which could not be separated from the other.

Meanwhile, a mechanism involving the nucleophilic attack of cyanide ion upon oxygen atom of the N-O bond in (I) seems to be unlikely since the anion of dibenzylamine is a very poor leaving group in DMSO.

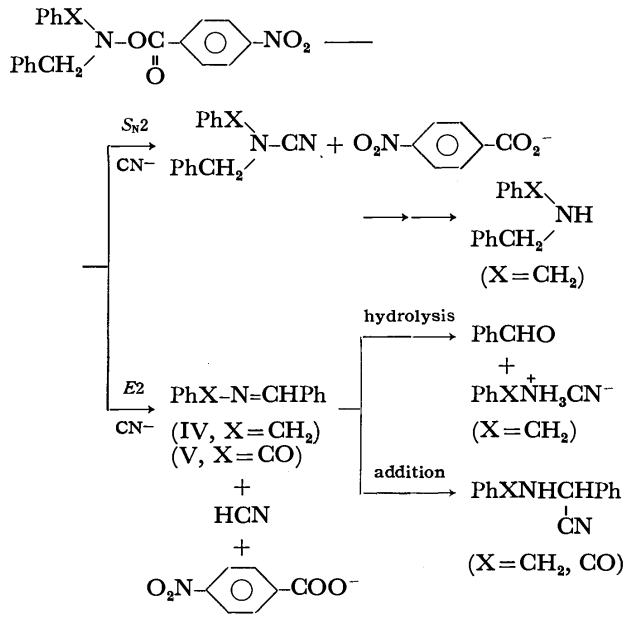

Therefore, the scheme of the reaction with cyanide ion is depicted as follows.

Neither α-aminonitrile nor dibenzylamine was found among the products when the leaving group changes from *p*-nitrobenzoyloxy to 3,5-dinitrobenzoyloxy groups as seen in Table 1. In this reaction, a Meisenheimer-type complex would be formed in the main route like in the reaction of *O*-(3,5-dinitrobenzoyl)-*N*-aroyl-*N*-arylhydroxylamines with cyanide ion in DMSO[11] since a strong absorption band appeared at 602 nm immediately upon addition of NaCN. Furthermore, the final products were those which are expected by a minor path, *i.e.*, Path A.

Here, it is interesting to examine the effect of substituents X, Y and R^2 on the product distribution, namely, the Substitution/Elimination ratio, since only the reaction with cyanide ion affords both substitution and elimination products on the nitrogen atom. The elimination-addition product, *i.e.*, α-benzoylamino-α-phenylacetonitrile, was obtained in a good yield by replacing a methylene group by a carbonyl group for the substituent X when substituents Y and R^2 are carbonyl and *p*-nitro groups. The yield of α-aminonitrile is better in DMSO than in DMF.

A similar tendency was observed in the reaction with I (X=CO; Y=SO_2; R^2=2,4,6-$(CH_3)_3$). Further inspection of the results in Table 1 reveals that introduction of more electron-donating substituents such as Cl and OCH_3 for R^2 in place of NO_2 group resulted in a predominant elimination according to Path A. Thus, the substitution product was shown to be obtained only when the substituents X, Y and R^2 are methylene, carbonyl and *p*-nitro groups, respectively. No formation of benzaldehyde in the reaction of I (X=CO; Y=CO; R^2=*p*-NO_2) with NaCN may be ascribed to the difference in stabilities of either the imine (IV) and (V) or the addition products which are obtained by the addition of HCN to the imine (IV) and (V). Accordingly, in the reaction with cyanide ion, the product distribution seems to be sensitive to the substituents R^2, X and Y.

Reactions of I (X=CH_2; Y=CO; R^1=H; R^2=p-NO_2, 3,5-$(NO_2)_2$) with Diethyl Sulfide and p-*Toluenethiol.* The reaction of I with nucleophiles such as sulfide and thiol is expected to proceed *via* nucleophilic substitution on the nitrogen atom at the initial step due to the very low proton affinity of these nucleophiles because the occurrence of elimination requires a high proton affinity of nucleophiles.

As indicated in Table 1, the reactions of I (R^2=*p*-NO_2, 3,5-$(NO_2)_2$) with an excess of diethyl sulfide were found to give the products which are same as those in

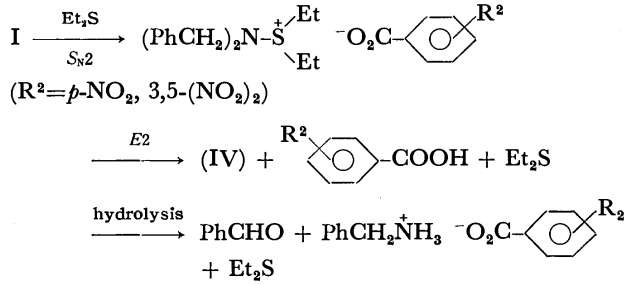

the reaction with NaN_3. Therefore, the following mechanism involving the initial nucleophilic substitution and the subsequent elimination appears to be the most plausible, judging from the nature of the nucleophile used.

These results suggest the initial step of the reaction to proceed *via* a S_N2 path on the nitrogen atom like in the reaction of *O*-2,4-dinitrophenylhydroxylamine with phenyl methyl sulfide.[7a] One can also assume that these reactions proceed through the S_N1 path, namely, by forming dibenzylnitrenium ion as an intermediate because of the bulky benzyl groups, as shown below. If the ion-pair intermediate (VI) would exist, this very

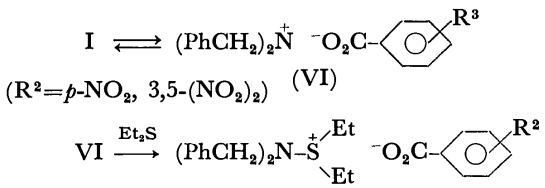

reactive nitrenium ion must yield benzaldehyde and benzylamine *via* the imine (IV). The starting material, however, was recovered nearly quantitatively when it was allowed to stand for 50 hr at room temperature in the absence of any nucleophile. Therefore, the S_N1 path seems to be unlikely, though no detailed mechanism for this reaction can be elucidated at present.

In the reaction with *p*-toluenethiol, a same reaction scheme as above may be applied on the basis of product distribution in Table 1. The sulfenamide (VII) which was produced by a S_N2 reaction on the trivalent

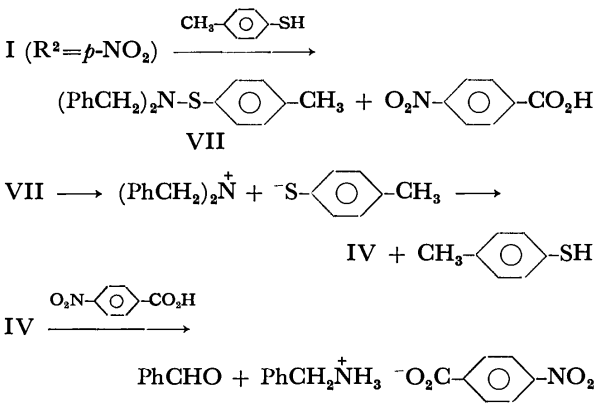

nitrogen atom at the initial step will decompose to give the nitrenium ion and *p*-toluenethiolate ion. No formation of dibenzylamine excludes the following two possibilities, namely, the nucleophilic attack of the thiol upon the sulfur atom of the sulfenamide (VII) giving dibenzylamine and the disulfide, and the addition of the thiol to the imine affording dibenzylamine and the disulfide as shown below. The

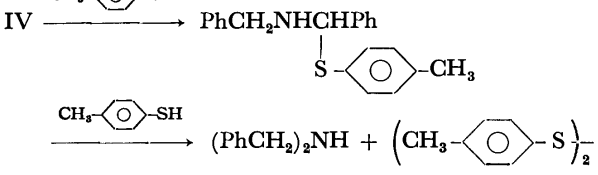

disulfide obtained may be formed by the oxidation of the thiol in DMF. This is confirmed by the control experiment independently.

Recently, Krueger *et al.*[7b] have shown that for substitution on the trivalent nitrogen atom polarizability of the nucleophile plays a major role, with basicity making a minor contribution. Their results support the earlier prediction by Edwards and Pearson.[12]

In the reactions of (I) (X=CH_2; Y=CO; R^1=H; R^2=*p*-NO_2) with various nucleophiles in DMSO, proton affinity (basicity) of the nucleophiles plays an important role, since the elimination can compete with the nucleophilic substitution on the nitrogen atom in this model compound (I). Thus, reactions with charged nucleophiles such as N_3^-, X^- (X=Cl, Br, I) and OH^- underwent elimination reaction, while reactions with sulfide and thiol underwent nucleophilic substitution at the initial step despite the presence of a bulky benzyl group.

Experimental

Materials. *N,N*-Dibenzylhydroxylamine was prepared according to the method of L. W. Jones and C. N. Sneed, mp 123—124 °C (lit, 124 °C).[13] *N*-Benzoyl-*N*-benzylhydroxylamine was prepared by the reaction between benzoyl chloride (1 mol) and *N*-benzylhydroxylamine (2 mol), which was synthesized according to the method of L. W. Jones and C. N. Sneed, in dry ether at 0 °C. Recrystallization from ethanol–water gave white needles, mp 107—108 °C. *O*-Aroyl-*N,N*-di(*p*-substituted benzyl)- and *O*-aroyl-*N*-benzoyl-*N*-benzylhydroxylamines were obtained by the reactions of aroyl chlorides with *N,N*-di(*p*-substituted benzyl)hydroxylamines, and with *N*-benzoyl-*N*-benzylhydroxylamine respectively under usual Schotten-Baumann conditions. The physical properties of these hydroxylamines are listed in Table 3.

Solvents. Dichloromethane was distilled after drying over calcium chloride and acetonitrile was distilled over phosphorus pentoxide. Dimethyl sulfoxide was distilled twice over activated alumina and *N,N*-dimethylformamide was distilled under reduced pressure.

Nucleophiles. Alkali-metal azide, halides, hydroxide and cyanide were all commercial products which were used without further purification other than drying at 100—120 °C overnight *in vacuo*. Sodium *p*-chlorobenzenecarbothioate was prepared from the reaction of *p*-chlorothiobenzoic acid with sodium hydroxide and was used without further purification after drying *in vacuo*. Diethyl sulfide and *p*-toluenethiol were used after purification by distillation.

General Procedure for the Reactions of O-*Aroyl*-N,N-*di*(p-*substituted benzyl)hydroxylamines with Nucleophiles such as* NaN_3, *LiCl, NaI, NaOH, and* $NaSCOC_6H_4Cl$-p. A small excess of a nucleophile (2.3—3.0 mmol) was added into DMSO (8 ml) solution of the hydroxylamine (2.0—2.3 mmol) in a reaction vessel and the whole solution was stirred with magnetic stirrer at room temperature for 15—50 h. After the reaction had subsided, the reaction mixture was poured into water (120 ml) and then products were extracted twice with dichloromethane (40 ml). The dichloromethane solution was washed with water several times and dried over anhydrous sodium sulfate. Evaporation of the solvent afforded the residual oil, which was then chromatographed on silica gel, eluting with dichloromethane. The aqueous layer was acidified slightly with dil-HCl aqueous solution and extracted twice with chloroform (60 ml), which was then washed with water several times. After drying over anhydrous sodium sulfate, evaporation of chloroform gave the crude *p*-nitro- and 3,5-dinitrobenzoic acids. Next, the acidic aqueous solution was made alkaline with sodium carbonate and extracted twice with dichloromethane (40 ml), and dried over anhydrous sodium sulfate. Removal of solvent *in vacuo* gave *p*-substituted benzylamines.

TABLE 3. PHYSICAL PROPERTIES OF HYDROXYLAMINES,

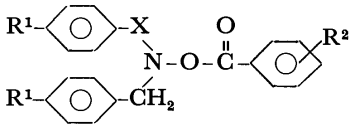

R^1	X	R^2	mp (°C)	Anal. %, Found (Calcd) C	H	N	IR (KBr) ν_{CO}, cm^{-1}	NMR ($CDCl_3$), δ
H	CO	*p*-NO_2	112.5—114.5	66.82 (67.01)	4.30 (4.29)	7.48 (7.44)	1780, 1670	5.03 (s, 2H), 7.12—7.72 (m, 10H), 8.01 (dd, 4H)
H	CH_2	*p*-OCH_3	83—84	75.90 (76.06)	6.05 (6.09)	3.90 (4.03)	1725	3.73 (s, 3H), 4.18 (s, 4H), 6.81 (dd, 4H), 7.10—7.60 (m, 10H)
H	CH_2	*p*-Cl	82—83	71.43 (71.69)	5.19 (5.16)	3.80 (3.98)	1740	4.20 (s, 4H), 7.15—7.95 (m, 14H)
H	CH_2	*p*-NO_2	108—109	69.71 (69.60)	5.08 (5.01)	7.64 (7.73)	1750	4.20 (s, 4H), 7.03—7.55 (m, 10H), 7.84 (dd, 4H)
H	CH_2	3,5-$(NO_2)_2$	148—149	62.03 (61.91)	4.30 (4.21)	10.19 (10.31)	1755	4.32 s(, 4H), 7.13—7.61 (m, 10H), 8.79—8.90 (m, 2H), 9.03—9.17 (m, 1H)
CH_3	CH_2	*p*-NO_2	111—113	70.78 (70.75)	5.83 (5.68)	6.98 (7.17)	1740	2.24 (s, 6H), 4.13 (s, 4H), 7.45 (dd, 8H), 7.91 (dd, 4H)
Cl	CH_2	*p*-NO_2	133—134	58.46 (58.48)	3.82 (3.74)	6.44 (6.49)	1740	4.20 (s, 4H), 7.08—7.50 (m, 8H), 7.99 (dd, 4H)
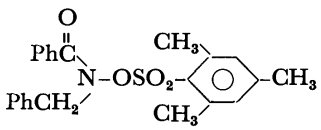			129—130	67.83 (67.46)	5.69 (5.66)	3.23 (3.42)	1670	2.26 (s, 3H), 2.55 (s, 6H), 5.06 (s, 2H), 6.83 (s, 2H), 7.02—7.45 (m, 10H)

Structures of the products isolated were identified by comparing their physical properties with those of the authentic compounds.

N-Benzylidenebenzylamine, which was obtained in the reaction with NaOH, was hydrolyzed to give benzaldehyde and benzylamine when the imine obtained was passed through silica gel column. Therefore, yields of the imine and benzaldehyde were determined before separation by means of NMR spectroscopy.

Addition product, i.e., α-benzylaminobenzyl p-chlorobenzenecarbothioate, which was isolated in the reaction with sodium *p*-chlorobenzenecarbothioate, was recrystallized from benzene–hexane to give colorless needles, mp 162—163 °C; IR (KBr) 3300, 1640 cm^{-1}; NMR ($CDCl_3$) δ 4.51 (s, 1H), 4.61 (s, 2H), 6.86 (broad s, 1H), 7.13—7.90 (m, 14H); Anal. Found: C, 68.60; H, 4.77%. Calcd for $C_{21}H_{18}NOSCl$: C, 68.56; H, 4.93%.

Reactions of O-(p-Substituted Benzoyl)-N,N-dibenzylhydroxylamines with Cyanide Ion. A typical run was as follows: to the *O*-(*p*-nitrobenzoyl)-*N,N*-dibenzylhydroxylamine (2.6 mmol) in DMSO (7 ml) was added NaCN (2.7 mmol) at room temperature. After 15 h, the reaction mixture was poured into water (120 ml) and then products were extracted twice with dichloromethane (40 ml). After drying over anhydrous sodium sulfate, solvent was evaporated *in vacuo*. The resulting residue was subjected to column chromatography packed with silica gel using dichloromethane as eluent, and three fractions, benzaldehyde (7%), α-benzylamino-α-phenylacetonitrile (22%) and dibenzylamine (58%) were obtained respectively. *p*-Nitrobenzoic acid (87%) and benzylamine (8%) were isolated by similar work-up as above. Structures of the products were determined in comparison with authentic samples. The α-aminonitrile was colorless oily liquid; IR (neat) 3330, 2225 cm^{-1}; NMR ($CDCl_3$) δ 1.80 (s, 1H), 3.83 (s, 2H), 4.58 (s, 1H), 7.09—7.63 (m, 10H). This α-aminonitrile was allowed to react with an equimolar amount of *p*-nitrobenzoyl chloride to afford α-*p*-nitrobenzoylbenzyl-α-phenylacetonitrile in 87% yield, which was recrystallized from benzene to give pale yellow needles, mp 148—149 °C; IR (KBr) 1645, 1525, 1350 cm^{-1}, ν_{CN} was too weak to detect; NMR ($CDCl_3$) δ 4.52 (dd, 2H), 6.73 (s, 1H), 6.86—7.42 (m, 5H), 7.47 (s, 5H), 7.92 (dd, 4H); Anal. Found: C, 71.76; H, 4.56; N, 11.24%. Calcd for $C_{22}H_{17}N_3O_3$: C, 71.15; H, 4.61; N, 11.31%.

Reactions of O-Aroyl-N-benzylhydroxylamines with Cyanide Ion. For a typical run, a mixture of *O*-(*p*-nitrobenzoyl-*N*-benzoyl-*N*-benzylhydroxylamine (2.2 mmol) and NaCN (2.7 mmol) was dissolved in DMSO (8 ml) in a reaction vessel, and the mixture was stirred for 15 h at room temperature. The contents were then poured into water (120 ml), the solution was extracted, and the products were separated by column chromatography through silica gel using dichloromethane as eluent. The product obtained was α-benzoylamino-α-phenylacetonitrile (58%) which was recrystallized from benzene–hexane, mp 147.5—148.5 °C; IR (KBr) 3250, 2220, 1640 cm^{-1}; NMR ($CDCl_3$) δ 6.32 (d, 1H), 7.24—8.04 (m, 11H); Mass spectrum *m/e* 236 (parent); Anal. Found: C, 76.46; H, 5.06; N, 11.84%. Calcd for $C_{15}H_{12}N_2O$: C, 76.25; H, 5.12; N, 11.86%. Acid-catalyzed methanolysis of this product in refluxing methanol–HCl gave methyl α-benzoylamino-α-phenylacetate (90%) which had mp 113.5—114.5 °C; IR (KBr) 3280, 1760, 1635 cm^{-1}; NMR ($CDCl_3$) δ 3.76 (s, 3H), 5.80 (d, 1H), 7.05—7.98 (m, 11H). The aqueous layer was acidified with dil-HCl aqueous solution and extracted twice with chloroform (60 ml). The chloroform solution was dried over anhydrous sodium sulfate after washing with water several times, followed by evaporation of chloroform afforded crude *p*-nitrobenzoic acid in 27% yield, identical with the authentic sample.

Reactions of O-(p-Nitrobenzoyl)- and O-(3,5-Dinitrobenzoyl)-N,N-dibenzylhydroxylamines with Diethyl Sulfide and p-Toluenethiol. A typical run was as follows: to *O*-(*p*-nitrobenzoyl)-*N,N*-dibenzylhydroxylamine (2.2 mmol) in DMSO (7 ml) was added diethyl sulfide (3.0 mmol) at room temperature and the whole solution was allowed to stand for 48 h. A similar work-up as in the above experiment gave recovered starting material (28%), benzaldehyde (49%), *p*-nitrobenzoic acid (38%) and benzylamine (33%).

In the reaction with *p*-toluenethiol, two molar amount of *p*-toluenethiol was allowed to react with the hydroxylamine in DMF at room temperature. Separation and identification of the products obtained were carried out similarly.

O-(p-*Nitrobenzoyl*)-N,N-*di(benzyl-α-d_2)hydroxylamine* was prepared according to the following reaction steps.

$$PhCOC_2H_5 \xrightarrow[\text{in dry ether}]{LiAlD_4} PhCD_2OH \xrightarrow[\text{in dry ether}]{SOCl_2,\ \text{pyridine}} PhCD_2Cl \xrightarrow[\text{in } C_2H_5OH\text{–}H_2O]{NH_2OH\cdot HCl,\ Na_2CO_3} (PhCD_2)_2N\text{–}OH \xrightarrow[\text{Pyridine in } CH_2Cl_2]{p\text{-}NO_2C_6H_4COCl} (PhCD_2)_2N\text{–}OCC_6H_4NO_2\text{-}p$$

O-(*p*-Nitrobenzoyl)-*N,N*-di(benzyl-α-d_2)hydroxylamine obtained was recrystallized twice from benzene–hexane to give pale yellow needles, 700 mg (total yield, 11%) which had mp 108—109 °C. The NMR showed no proton of the methylene groups.

Procedure for Kinetic Runs. Each kinetic run was carried out by monitoring the UV absorbance of *p*-nitro- and 3,5-dinitrobenzoate ions liberated during the reaction at 290 nm. At first the solution of *O*-aroyl-*N,N*-di(*p*-substituted benzyl) hydroxylamines in 10 ml of DMSO (13.8×10^{-3} mol/l) was placed in a reaction vessel and immersed in a constant temperature bath which was kept at 30.0±0.1 °C. The solution of a nucleophile such as NaN_3 or LiCl in 10 ml of DMSO (16.6×10^{-2} mol/l), which was previously kept at 30.0±0.1 °C in a same constant temperature bath, was added to the DMSO solution of the hydroxylamine. The reaction was followed by taking out 0.5 ml aliquot at suitable time intervals, diluting the aliquot with 50 ml of acetonitrile–water (2:1 in volume), and finally subjecting the solution for measurement of the optical density of the resulting solution at 290 nm. All the pseudo-first order rate constants were determined from following rate equation and the extent of reaction studied was *ca.* half-life.

$$\log(a_\infty - a_0) - \log(a_\infty - a_t) = (k/2.303)t$$

a_∞; the final absorbance at 290 nm,
a_0; the initial absorbance at 290 nm,
a_t; the absorbance at 290 nm after t.

For a typical run, molar extinction coefficients of *O*-(*p*-nitrobenzoyl)-*N,N*-dibenzylhydroxylamine, sodium *p*-nitrobenzoate, benzaldehyde, *N*-benzylidenebenzylamine and benzylamine in acetonitrile–water (2:1 in volume) were 4400, 7200, 1000, 400 and 0 at 290 nm respectively. Effect of the absorbance of benzaldehyde seems to be negligibly small since a good pseudo-first order kinetic behavior was observed in each case.

References

1) A preliminary report has been published: S. Oae, T.

Sakurai, and S. Kozuka, *Chem. Lett.*, **1974**, 621.

2) C. K. Ingold, "Structure and Mechanism in Organic Chemistry," 2nd ed., Cornell University Press (1969), Chapter 7 and 9; W. H. Saunders, Jr. and A. F. Cockerill, "Mechanism of Elimination Reactions," John Wiley & Sons, New York, N. Y. (1973), Chapter 2.

3) J. O. Edwards, "Peroxide Reaction Mechanism," ed. by J. O. Edwards, Wiley-Interscience, New York (1962), pp. 67—106.

4) a) J. W. Baker and D. M. Easty, *J. Chem. Soc.*, **1952**, 1193, 1208. b) P. J. Smith and A. N. Bourns, *Can. J. Chem.*, **44**, 2553 (1966).

5) F. N. Collier, Jr., W. W. Horner, P. M. Dickens, J. G. Hull, and W. T. Layton, *J. Amer. Chem. Soc.*, **83**, 2235 (1961); M. Anbar and G. Yagil, *ibid.*, **84**, 1790 (1962); B. A. S. Smith, H. R. Alul, and R. L. Baumgarten, *ibid.*, **86**, 1139 (1964); R. E. Corbett, W. S. Metcalf, and F. G. Soper, *J. Chem. Soc.*, **1953**, 1927; R. E. McCoy, *J. Amer. Chem. Soc.*, **76**, 2829 (1954); S. Oae, N. Tsujimoto, and A. Nakanishi, This Bulletin, **46**, 535 (1973); T. Sheradsky, *J. Heterocycl. Chem.*, **4**, 413 (1967); *Tetrahedron Lett.*, **1968**, 1909; T. Sheradsky and Z. Nir, *ibid.*, **1969**, 77.

6) C. R. Hauser, J. W. LeMaistre, and A. E. Rainsford, *J. Amer. Chem. Soc.*, **57**, 1956 (1935); M. J. Miller and G. M. Loudon, *J. Org. Chem.*, **40**, 126 (1975).

7) a) S. Oae and F. Yamamoto, *Tetrahedron Lett.*, **1973**, 5143; This Bulletin, **48**, 77 (1975). b) J. H. Krueger, B. A. Sudbury, and P. F. Blanchet, *J. Amer. Chem. Soc.*, **96**, 5773 (1974).

8) N. Kornblum, J. W. Powers, G. J. Anderson, W. J. Jones, H. O. Larson, O. Levand, and W. M. Weaver, *ibid.*, **79**, 6562 (1957).

9) P. G. Gassman and G. D. Hartman, *ibid.*, **95**, 449 (1973); P. G. Gassman, *Accounts Chem. Res.*, **3**, 26 (1970).

10) L. Melander, "Isotope Effects on Reaction Rates," The Ronald Press Company, New York (1960), Chapter 5.

11) S. Oae and T. Sakurai, This Bulletin, **48**, 1075 (1975).

12) J. O. Edwards and R. G. Pearson, *J. Amer. Chem. Soc.*, **84**, 16 (1962).

13) L. W. Jones and C. N. Sneed, *ibid.*, **39**, 674 (1917).

Furan Derivatives. II. The Cyclization of 3-(Benzofuran-3-yl)-propionic Acid Derivatives

Takaaki HORAGUCHI, Takahachi SHIMIZU, and Teishiro ABE*

Department of Chemistry, Faculty of Science, Niigata University, Ikarashi, Niigata 950-21

** Department of General Education, Niigata University, Ikarashi, Niigata 950-21*

(Received August 4, 1975)

A compound, 6-methoxy-2a,3,4,5-tetrahydro-2*H*-naphtho[1,8-*bc*]furan-5-one (XX), was prepared in a 72% yield by heating 3-(5-methoxy-2,3-dihydrobenzofuran-3-yl)propionic acid (XIX) with polyphosphoric acid. However, when 3-(5-methoxybenzofuran-3-yl)propionic acid (IX) or 3-(2-benzoyl-5-methoxybenzofuran-3-yl)-propionic acid (XIII) were treated with polyphosphoric acid, the product was 7-methoxy-2,3-dihydro-1*H*-cyclopenta[*b*]benzofuran-3-one (XI) rather than the corresponding naphtho[1,8-*bc*]furan derivatives, Also, neither naphtho[1,8-*bc*]furan nor cyclopenta[*b*]benzofuran derivatives were obtained from 3-(2-benzyl-5-methoxybenzofuran-3-yl)propionic acid (XIV) or 3-(2-ethyl-5-methoxybenzofuran-3-yl)propionic acid (XVII).

Naphtho[1,8-*bc*]furans (IV) have been prepared[1] by the two methods shown in Scheme 1. The yields of carboxylic acids (II) based on tetralones (I) were almost the same as one another (40—50%), regardless of the kind of the substituents (R_1 and R_2) on the benzene ring. The yields of naphtho[1,8-*bc*]furans (IV) based on carboxylic acids (III) were found in the region of 40—70%, according to kind of substituent (R_1 and R_2). We attempted to devise a novel method to synthesize naphtho[1,8-*bc*]furans from 3-(5-methoxybenzofuran-3-yl)propionic acid (IX), as the yields of II or IV (based on I or III respectively) were not very good.

Results and Discussion

The important intermediate compound 3-(5-methoxybenzofuran-3-yl)propionic acid (IX) was obtained, as is shown in Scheme 2, according to the method of Hallmann *et al.*[2] It was expected that the naphtho-[1,8-*bc*]furan derivative (X) would be produced from IX by intramolecular cyclization. When IX was treated with polyphosphoric acid, cyclization took place[3] to give a crystalline product. However, the product was 7-methoxy-2,3-dihydro-1*H*-cyclopenta[*b*]-benzofuran-3-one (XI) rather than X. This result suggests that the furan ring is more reactive than the benzene ring. The structure of XI was determined from the spectral properties. The IR and UV spectra showed absorptions due to a conjugated-carbonyl group at 1698 cm^{-1} and at 284 (ε 24600) and 289 nm (24000) respectively. The NMR spectrum exhibited no peak corresponding to a hydrogen atom on the furan ring. The structure of XI was also supported by the catalytic hydrogenation of XI with 5% palladium–charcoal to give 7-methoxy-2,3,3a,8b-tetrahydro-1*H*-cyclopenta[*b*]benzofuran-3-ol (XII).

The formation of XI rather than X in the cyclization mentioned above required us to make further attempts to prepare such benzofuran derivatives as XIII, XIV, and XVII, all of which have substituents on the 2-position of the furan ring. For this reason, the XIII compound 3-(2-benzoyl-5-methoxybenzofuran-3-yl)-propionic acid was prepared from VII and phenacyl bromide.[1] When XIII was treated with polyphos-

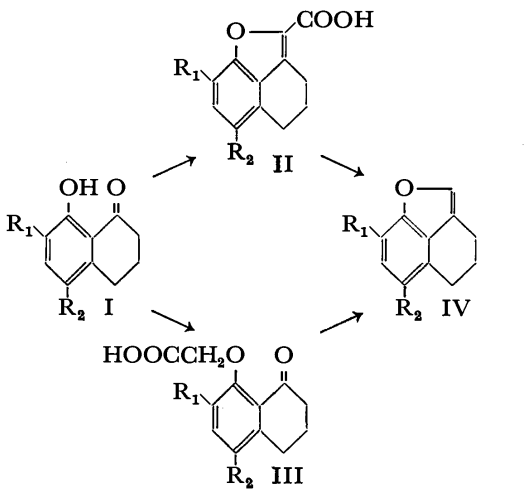

a) R_1=H, R_2=H b) R_1=H, R_2=OCH_3
c) R_1=OCH_3, R_2=H d) R_1=OCH_3, R_2=Cl

Scheme 1.

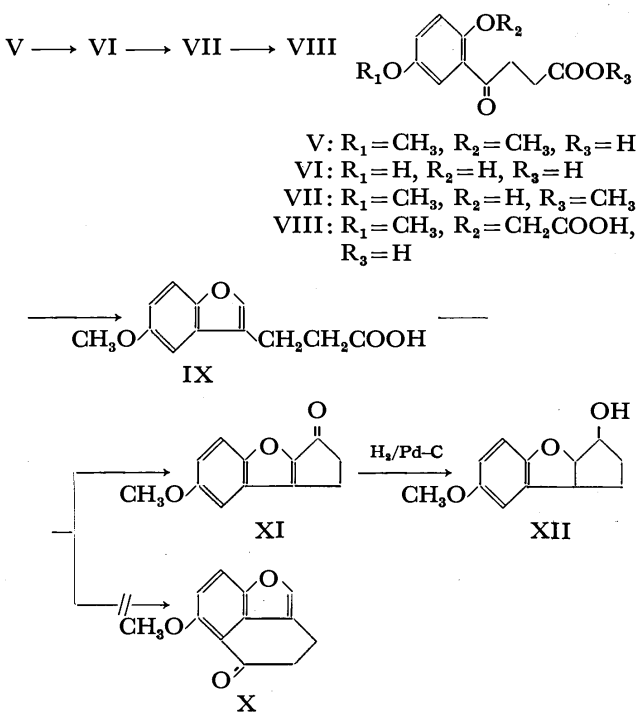

Scheme 2.

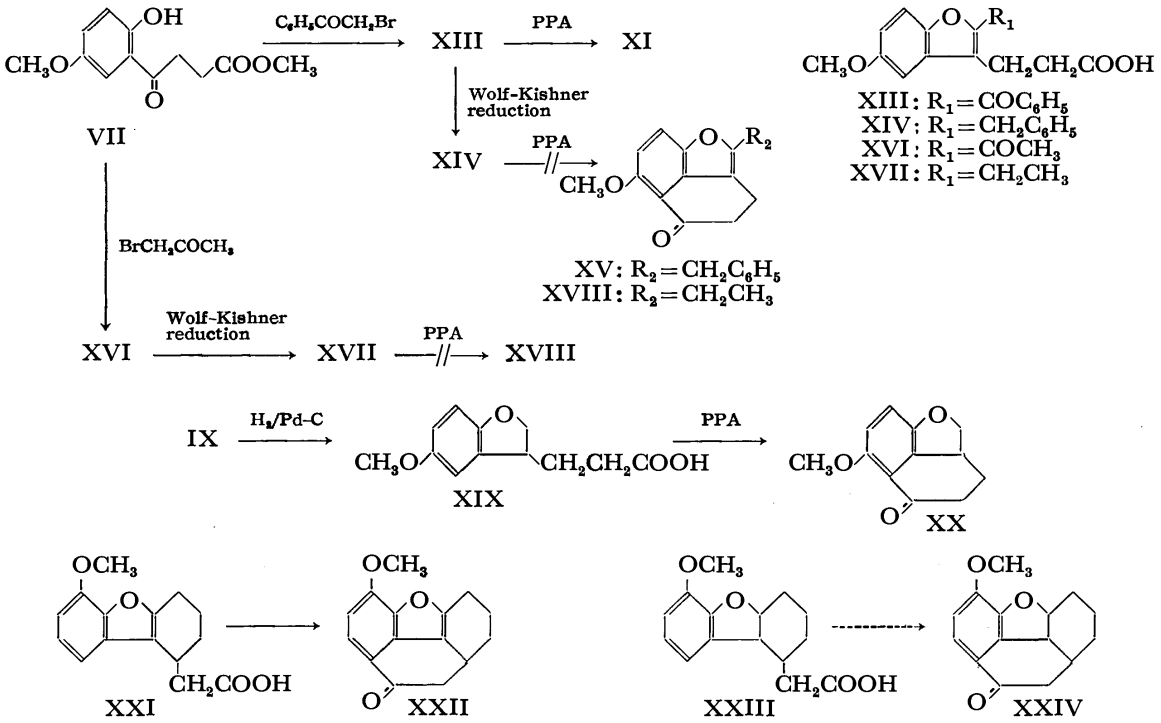

Scheme 3.

phoric acid, a carbonyl compound was produced along with benzoic acid. The carbonyl compound was identical in its IR spectra with the product (XI) obtained from the reaction between IX and polyphosphoric acid. Therefore, XIII was converted to 3-(2-benzyl-5-methoxybenzofuran-3-yl)propionic acid(XIV) by a Wolf-Kishner reduction,[4] as the benzoyl group tended to be eliminated under acidic reaction conditions and so XIV was treated with polyphosphoric acid. Nevertheless, only a tarry material was produced; the desired naphtho[1,8-*bc*]furan derivative (XV) was not obtained. Similarly, 3-(2-acetyl-5-methoxybenzofuran-3-yl)propionic acid (XVI) was prepared by the reaction between VII and bromoacetone and was reduced to 3-(2-ethyl-5-methoxybenzofuran-3-yl)propionic acid (XVII). Also, the corresponding naphtho[1,8-*bc*]furan derivative (XVIII) was not obtained by the treatment of XVII with polyphosphoric acid.

From these results, it appears difficult to convert benzofuran derivatives (IX, XIII, XIV, and XVII) where furan rings remained fully unsaturated to naphtho[1,8-*bc*]furan derivatives by intramolecular cyclization. We made a further examination of a partially saturated benzofuran derivative. The IX compound was reduced to 3-(5-methoxy-2,3-dihydrobenzofuran-3-yl)propionic acid (XIX) by catalytic hydrogenation with 10% palladium–charcoal. When XIX was treated with polyphosphoric acid,[5] the desired 6-methoxy-2a,3,4,5-tetrahydro-2*H*-naphtho[1,8-*bc*]furan-5-one (XX) was obtained in a 72% yield. Compound XX showed an absorption corresponding to the carbonyl group at 1670 cm^{-1} in the IR spectrum and peaks corresponding to two adjacent aromatic hydrogen atoms on the benzene ring at δ 6.90 (d, 1H, J=8 Hz) and 6.68 (d, 1H, J=8 Hz) in the NMR spectrum.

These results suggest that the presence of the carbon–carbon double bond of the furan ring hinders intramolecular cyclization because of the formation of by-products, but partially saturated benzofuran derivatives readily undergo cyclization to the corresponding naphtho[1,8-*bc*]furan derivatives. Dendy *et al.*[6] obtained a phenanthro[4,5-*bcd*]furan derivative (XXII) in a very poor yield from a benzofuran derivative (XXI). They ascribed this difficulty of cyclization to a strain in the fused-ring system. However, the above results suggest that the dihydrobenzofuran derivative (XXIII) may be converted to a phenanthro[4,5-*bcd*]furan derivative (XXIV) in a good yield. The reactivities of naphtho[1,8-*bc*]furans will be further investigated.

Experimental

All the melting points are uncorrected. The column chromatography was performed on silica gel (WAKOGEL C-200). The polyphosphoric acid (PPA) was prepared from 85% phosphoric acid (100 ml) and phosphorus pentoxide (125 g) by heating them at 160—165 °C for 5 h. Unless otherwise stated, anhydrous sodium sulfate was employed as the drying agent. The infrared absorption spectra were determined with a JASCO Model DS 402 G infrared spectrophotometer. The ultraviolet absorption spectra were determined with a Shimadzu Model UV-200 spectrophotometer. The nuclear magnetic resonance spectra were determined at 100 MHz with a JEOL Model 4H-100 NMR spectrometer, using tetramethylsilane as the internal standard.

3-(2,5-Dihydroxybenzoyl)propionic Acid (VI). A mixture of 3-(2,5-dimethoxybenzoyl)propionic acid (V, 20 g)[7] and pyridinium chloride (100 g) was heated for 40 min at 200 °C.[8] After cooling, the mixture was poured into dilute hydrochloric acid and extracted with ether. The ethereal layer was washed with 1M hydrochloric acid and water, dried, and then evaporated. The residue was recrystallized from 35% aqueous

methanol to give 11.1 g (63%) of VI as orange prisms; mp 181—182 °C. IR(KBr): 3200 (OH), 1700 (COOH), 1635 (C=O), 1175 (OH), and 830 cm^{-1} (two adjacent aromatic hydrogen atoms). Found: C, 57.03; H, 4.80%. Calcd for $C_{10}H_{10}O_5$: C, 57.14; H, 4.80%.

Methyl 3-(2-Hydroxy-5-methoxybenzoyl)propionate (VII). A mixture of VI (15.0 g), dimethyl sulfate (13.0 g), potassium carbonate (17.0 g), and acetone (50 ml) was refluxed for 2.5 hr at 62 °C.[9] After the decomposition of the dimethyl sulfate with water, the reaction mixture was extracted with ether. The ethereal layer was washed with a 1M potassium carbonate solution and water, dried, and then evaporated. The residue was chromatographed over silica gel and eluted with benzene (95)–ether (5); the first fraction gave 16.5 g (48%) of crystals. Recrystallization from ether–hexane gave yellow plates of VII; mp 41—42 °C. IR (KBr): 1726 ($COOCH_3$), 1642 (C=O), 1042 cm^{-1} (OCH_3). NMR ($CDCl_3$): δ 2.75 (t, 2H, J=7 Hz, $-CH_2-$), 3.35 (t, 2H, J=7 Hz, $-CH_2-$), 3.72 (s, 3H, OCH_3), 3.80 (s, 3H, OCH_3), 6.90 (d, 1H, J=9 Hz, Ar–H), 7.10 (d, d, 1H, J=3 Hz and 9 Hz, Ar–H), 7.20 (d, 1H, J=3 Hz, Ar–H), 11.60 (s, 1H, OH). Found: C, 60.66; H, 6.06%. Calcd for $C_{12}H_{14}O_5$: C, 60.50; H, 5.92%.

The yield of VII was not good because of the formation of methyl 3-(2,5-dimethoxybenzoyl)propionate and methyl 3-(2,5-dihydroxybenzoyl)propionate.

3-(2-Carboxymethoxy-5-methoxybenzoyl)propionic Acid (VIII). Compound VIII was prepared (84%) according to the method of Hallmann *et al.* Colorless prisms (from tetrahydrofuran–benzene); mp 188—189 °C. (lit,[2] mp 189—190 °C)

3-(5-Methoxybenzofuran-3-yl)propionic Acid (IX). Compound IX was also prepared (67%) according to the method of Hallmann *et al.* Colorless plates (from benzene–hexane); mp 124—125 °C. (lit,[2] mp 126—127 °C) IR (KBr): 1681 (COOH), 1620 (C=C), 792 cm^{-1} (two adjacent aromatic hydrogen atoms). NMR (CD_3COCD_3): δ 2.73 (t, 2H, J=7 Hz, $-CH_2-$), 2.98 (t, 2H, J=7 Hz, $-CH_2-$), 3.85 (s, 3H, OCH_3), 6.90 (d, d, 1H, J=3 Hz and 8 Hz, Ar–H), 7.19 (d, 1H, J=3 Hz, Ar–H), 7.35 (d, 1H, J=8 Hz, Ar–H), 7.60 (s, 1H, furan H). UV (EtOH): λ_{max} 210 (ε 23800), 252 (8300), 304 (4100), 302 nm (3700). Though a mixture of VIII (200 mg), sodium acetate (500 mg), and acetic anhydride (7 ml) was heated for 1 h at 145 °C and for 10 min at 160 °C, only a tarry material was produced.

7-Methoxy-2,3-dihydro-1H-cyclopenta[b]benzofuran-3-one (XI). A mixture of IX (0.5 g) and polyphosphoric acid (70 g) was heated for 4 h at 80 °C with stirring. The reaction mixture was decomposed with ice–water, and the resulting precipitates were extracted with ether. The ethereal layer was washed with a 1M potassium carbonate solution and water, dried, and then evaporated. The residue was chromatographed over silica gel and eluted with benzene(92)–ether(8) to give 0.2 g (43%) of crystals; mp 136—138 °C. Recrystallization from benzene–hexane gave colorless needles of XI; mp 138—139 °C. IR (KBr): 1695 (C=O), 810 cm^{-1} (two adjacent aromatic hydrogen atoms). NMR (CD_3COCD_3): δ 3.87 (s, 3H, OCH_3), 7.12 (d, d, 1H, J=2 Hz and 9 Hz, Ar–H), 7.28 (d, 1H, J=2 Hz, Ar–H), 7.52 (d, 1H, J=9 Hz, Ar–H). UV (EtOH): λ_{max} 219 (ε 14400), 284 (24600), 289 (24000), 325 nm (5600). Found: C, 71.09; H, 4.92%. Calcd for $C_{12}H_{10}O_3$: C, 71.28; H, 4.99%.

7-Methoxy-2, 3, 3a, 8b-tetrahydro-1H-cyclopenta[b]benzofuran-3-ol (XII). A mixture of XI (200 mg), palladium chloride (50 mg) in 0.1 M hydrochloric acid (5 ml), charcoal (100 mg), and ethanol (60 ml) was shaken under a hydrogen atmosphere for 1.5 h at room temperature. After the removal of the catalyst, the ethanol was evaporated. The residue was chromatographed over silica gel and eluted with benzene (9)–ether (1) to give 150 mg (74%) of crystals; mp 66—67 °C. Recrystallization from methanol gave XII as colorless plates; mp 68—69 °C. IR (KBr): 3530 (OH), 1100 (C–OH), 1030 cm^{-1} (OCH_3). NMR (CCl_4): δ 1.20—1.95 (m, 4H, $-CH_2-$+ $-CH_2-$), 2.35 (s, 1H, OH), 3.67 (s, 3H, OCH_3), 3.70 (m, 1H, =CH–), 4.87 (d, d, 1H, J=5 Hz and 7 Hz, a hydrogen atom on the 3a carbon atom), 6.53 (s, 3H, Ar–H). UV (EtOH): λ_{max} 204 (ε 14300), 230 (4200), 300 nm (2900). Found: C, 69.73; H, 6.74%. Calcd for $C_{12}H_{14}O_3$: C, 69.89; H, 6.84%.

3-(2-Benzoyl-5-methoxybenzofuran-3-yl)propionic Acid (XIII). A mixture of VII (1.5 g), phenacyl bromide (6.1 g), and potassium carbonate (4.4 g) was heated for 3 h at 140 °C. The reaction mixture was then extracted with acetone, and the acetone was evaporated. The residue was dissolved in a small amount of ethanol and hydrolyzed with a 3M potassium hydroxide solution. The alkaline solution was acidified with 6M hydrochloric acid, and the resulting precipitates were extracted with ether. The ethereal layer was then extracted with a 1M potassium carbonate solution, and the alkaline solution was acidified with 6M hydrochloric acid. The resulting precipitates were extracted with ether, and the ethereal layer was washed with water, and then evaporated. The residue was triturated with benzene to give 0.8 g (57%) of crystals; mp 169—170 °C. Recrystallization from methanol gave colorless needles of XIII; mp 171—172 °C. IR (KBr): 1720 (COOH), 1637 (C=O), 1027 (OCH_3), 810 cm^{-1} (two adjacent aromatic hydrogen atoms). UV(EtOH): λ_{max} 207 (ε 33000), 257 (9300), 317 nm (20900). Found: C, 70.39; H, 5.13%. Calcd for $C_{19}H_{16}O_5$: C, 70.36; H, 4.98%.

The Formation of XI from XIII. A mixture of XIII (100 mg) and polyphosphoric acid (10 g) was heated with stirring for 4 hr at 90 °C. The reaction mixture was then decomposed with ice–water and extracted with ether. The ethereal layer was washed with a 1M potassium carbonate solution and water, dried, and then evaporated. The residue was chromatographed over silica gel and eluted with benzene (92)–ether (8) to give 20 mg (33%) of crystals; mp 135—136 °C. Recrystallization from benzene–hexane gave colorless needles of XI; mp 138—139 °C. The compound was identical in its IR spectra with the sample prepared from IX and polyphosphoric acid.

3-(2-Benzyl-5-methoxybenzofuran-3-yl)propionic Acid (XIV). A mixture of XIII (500 mg), 80% hydrazine hydrate (2.5 g), potassium hydroxide (7.0 g), and triethylene glycol (25 ml) was heated for 1 h at 140 °C; the temperature was thereafter gradually raised to 190 °C, after which the mixture was kept for 4 h at that temperature. The reaction mixture was poured into ice–water, acidified with 6M hydrochloric acid, and then extracted with ether. The ethereal layer was washed with water, dried, and then evaporated. The residue was chromatographed on silica gel and eluted with benzene (9)–ether (1) to give 220 mg (46%) of crystals; mp 116—117 °C. Recrystallization from ether–hexane gave colorless needles of XIV; mp 117—118 °C. IR (KBr): 1700 (COOH), 1624 (C=C), 803cm^{-1} (two adjacent aromatic hydrogen atoms). NMR ($CDCl_3$): δ 2.66 (d, 2H, J=7 Hz, $-CH_2-$), 2.92 (d, 2H, J=7 Hz, $-CH_2-$), 3.80 (s, 3H, OCH_3), 4.06 (s, 2H, $-CH_2-$), 6.79 (d, d, 1H, J=2 Hz and 8 Hz, Ar–H), 6.93 (d, 1H, J=2 Hz, Ar–H), 7.22 (s, 5H, Ar–H), 7.25 (d, d, 1H, J=1 Hz and 8 Hz, Ar–H), 9.66 (broad s, 1H, COOH). UV (EtOH): λ_{max} 210 (ε 31400), 255 (14000), 292 (5600), 302 nm (5000). Found: C, 73.51; H, 5.85%. Calcd for $C_{19}H_{18}O_4$: C, 73.53; H, 5.85%. Though a mixture of XIV (100 mg) and polyphosphoric acid (14 g) was heated with stirring for 4 h at 90 °C, XV was not obtained.

3-(2-Acetyl-5-methoxybenzofuran-3-yl)propionic Acid (XVI).

A mixture of VII (2.0 g), bromoacetone (7.0 g), and potassium carbonate (7.0 g) was refluxed for 4 h at 120 °C. The reaction mixture was then extracted with acetone, and the acetone was evaporated. The residue was dissolved in a small amount of ethanol and hydrolyzed with a 3M potassium hydroxide solution. The alkaline solution was acidified with 6M hydrochloric acid, and the resulting precipitates were extracted with ether. The ethereal layer was washed with water, dried, and then evaporated. The residue was chromatographed on silica gel and eluted with benzene (8)–ether (2) to give 1.0 g (44%) of crystals; mp 124—126 °C. Recrystallization from aqueous methanol gave colorless needles of XVI; mp 124—126 °C. IR (KBr): 1710 (COOH), 1675 (C=O), 800 cm^{-1} (two adjacent aromatic hydrogen atoms). UV (EtOH): λ_{max} 205 (ε 21500), 296 nm (17800). Found: C, 63.90; H, 5.31%. Calcd for $C_{14}H_{14}O_5$: C, 64.11; H, 5.38%.

3-(2-Ethyl-5-methoxybenzofuran-3-yl)propionic Acid (XVII). Compound XVII was obtained (54%) by a method similar to the preparation of XIV from XIII. Recrystallization from ether–hexane gave colorless prisms; mp 86—87 °C. IR (KBr): 1713 (COOH) and 813 cm^{-1} (two adjacent aromatic hydrogen atoms). NMR ($CDCl_3$): δ 1.25 (t, 3H, J=7 Hz, CH_3), 2.50—3.00 (m, 6H, $-CH_2-$), 3.82 (s, 3H, OCH_3), 6.80 (d, d, 1H, J=2 Hz and 8 Hz, Ar-H), 6.92 (d, 1H, J=2 Hz, Ar-H), 7.26 (d, d, 1H, J=1 Hz and 8 Hz, Ar-H), 9.91 (broad s, 1H, COOH). Found: C, 67.79; H, 6.50%. Calcd for $C_{14}H_{16}O_4$: C, 67.73; H, 6.50%. Though a mixture of XVII (100 mg) and polyphosphoric acid (8 g) was heated with stirring for 6 h at 90 °C, XVIII was not obtained.

3-(5-Methoxy-2,3-dihydrobenzofuran-3-yl)propionic Acid (XIX). A mixture of IX (300 mg), 10% palladium–charcoal (200 mg), and ethanol (70 ml) was shaken under a hydrogen atmosphere for 20 h at room temperature. After the subsequent removal of the catalyst, the ethanol was evaporated to give 280 mg (92%) of crystals; mp 94—96 °C. Recrystallization from benzene–hexane gave colorless plates of XIX; mp 96—97 °C. IR (KBr): 1692 (COOH), 1033 (OCH_3), 800 cm^{-1} (two adjacent aromatic hydrogen atoms). NMR ($CDCl_3$): δ 2.00 (m, 2H, $-CH_2-$), 2.42 (t, 2H, J=6 Hz, $-CH_2-$), 3.47 (m, 1H, =CH–), 3.77 (s, 3H, OCH_3), 4.20 (d, d, 1H, J=5 Hz and 9 Hz, $-CH_2-$), 4.60 (t, 1H, J=9 Hz, –OCH–), 6.70 (s, 2H, Ar-H), 6.76 (s, 1H, Ar-H), 10.90 (broad s, 1H, COOH). UV (EtOH): λ_{max} 204 (ε 16400), 230 (6300), 299 nm (4800). Found: C, 64.66; H, 6.22%. Calcd for $C_{12}H_{14}O_4$: C, 64.85; H, 6.35%.

6-Methoxy-2a,3,4,5-tetrahydro-2H-naphtho[1,8-bc]furan-5-one (XX). A mixture of XIX (300 mg) and polyphosphoric acid (30 g) was heated with stirring for 4 h at 80 °C. The reaction mixture was then decomposed with ice–water, and the resulting precipitates were extracted with ether. The ethereal layer was washed with a 1M potassium carbonate solution and water, dried, and then evaporated to give 200 mg (72%) of crystals; mp 102—103 °C. Recrystallization from benzene–hexane gave colorless prisms of XX; mp 104—105 °C. IR (KBr): 1670 (C=O), 832 cm^{-1} (two adjacent aromatic hydrogen atoms). NMR ($CDCl_3$): δ 3.72 (m, 1H, =CH–), 3.88 (s, 3H, OCH_3), 4.10 (d, d, 1H, J=9 Hz and 10 Hz, –OCH–), 4.84 (t, 1H, J=9 Hz, –OCH–), 6.80 (d, 1H, J=8 Hz, Ar-H), 6.91 (d, 1H, J=8 Hz, Ar-H). Found: C, 70.37; H, 6.05%. Calcd for $C_{12}H_{12}O_3$: C, 70.57; H, 5.92%.

The authors wish to thank Mr. Yoshiaki Takahashi for the elemental analyses, Mr. Hideo Saisu for the infrared analyses, and Mr. Takao Ono for the nuclear magnetic resonance analyses.

References

1) T. Horaguchi, T. Shimizu, and T. Suzuki, This Bulletin, **48**, 1249 (1975).
2) G. Hallmann and K. Haegeke, *Ann. Chem.*, **662**, 147 (1963).
3) H. Gilman and L. C. Cheney, *J. Amer. Chem. Soc.*, **61**, 4149 (1938).
4) Huang-Minlon, *ibid.*, **68**, 2487 (1946).
5) T. Shimizu, T. Horaguchi, and A. Watanabe, This Bulletin, **46**, 1772 (1973).
6) A. V. Dendy, J. H. P. Tyman, and W. B. Whalley, *J. Chem. Soc.*, **1963**, 4040.
7) L. F. Fieser and E. B. Hershburg, *J. Amer. Chem. Soc.*, **58**, 2314 (1936).
8) M. S. Newman and R. L. Childers, *J. Org. Chem.*, **32**, 62 (1967).
9) G. N. Vyas and N. M. Shah, "Organic Syntheses," Coll. Vol. IV, p. 836 (1963).

Effect of Spiro Ring Size on the Photochemical Ring Expansion of Dispiro Substituted Cyclobutane-1,3-diones

Koji KIMURA, Masakazu TAKAMURA, Shigeru KOSHIBE, Masayoshi JURO, Yoshihiro FUKUDA, and Yoshinobu ODAIRA

Department of Petroleum Chemistry, Faculty of Engineering, Osaka University, Suita-shi, Osaka 565

(Received August 5, 1975)

The photochemical ring expansion of dispiro substituted cyclobutane-1,3-diones in methanol has been investigated. The formation of ring expansion product was strongly dependent on the spiro ring size of dispiro substituent. The ring expanded acetal was obtained in a low yield when the spiro ring of dispiro substituted cyclobutane-1,3-diones was a five- or seven-membered ring. This is the first example of photochemical ring expansion from cyclobutane-1,3-diones. A mechanism is postulated.

Three primary photochemical processes, (**a**) decarbonylation (α-cleavage) (**b**) cycloelimination(β-cleavage) and (**c**) ring expansion, are usually observed in the photochemistry of simple cycloalkanones such as cyclobutanones[1] and cyclopentanones.

Recently extensive studies have been carried out from an interest in photochemical ring expansion *via* an oxacarbene intermediate(**c**).[1a,b,2,3] However, in the photochemistry of cyclobutane-1,3-diones,[4] no photochemical ring expansion seems to have been found.[1c,d] In a previous communication,[5] a report was given on the first example of ring expansion in the photochemical reaction of dispiro[4.1.4.1]dodecane-6,12-dione. We now report the effect of the ring size on the photochemical ring expansion of spiro substituted cyclobutanones and cyclobutane-1,3-diones in methanol, and suggest a plausible mechanism.

Results and Discussion

The photochemical reaction of cyclobutanone derivatives substituted by a spiro five-membered ring has been carried out to clarify the effect of spiro ring substituent on the photochemical processes. When dispiro[4.1.4.1]-dodecane-6-one (**1**) was irradiated in methanol at —70 °C for 10 hr with a Pyrex filter, a photochemical ring expansion *via* an oxacarbene intermediate took place smoothly to give ring expanded acetal (**2**) predominantly.

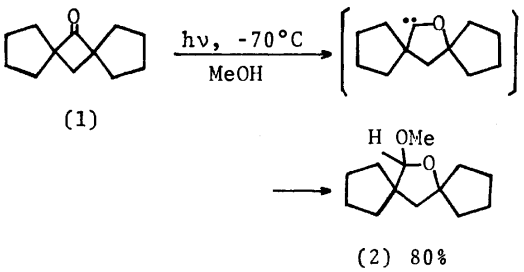

(1) (2) 80%

When 7-tetramethylene-bicyclo[3.2.0]hept-2-en-6-one (**3**) was irradiated in methanol, α-cleavage into only one of two possible directions occurred preferentially to yield a large quantity of ring expanded acetal (**4**) and an ester (**5**) without any formation of β-cleavage product.

In both cases, the ring expanded acetals were obtained predominantly. This is of great interest as compared with the cases of bicyclo[3.2.0]hept-2-en-6-one[6] and

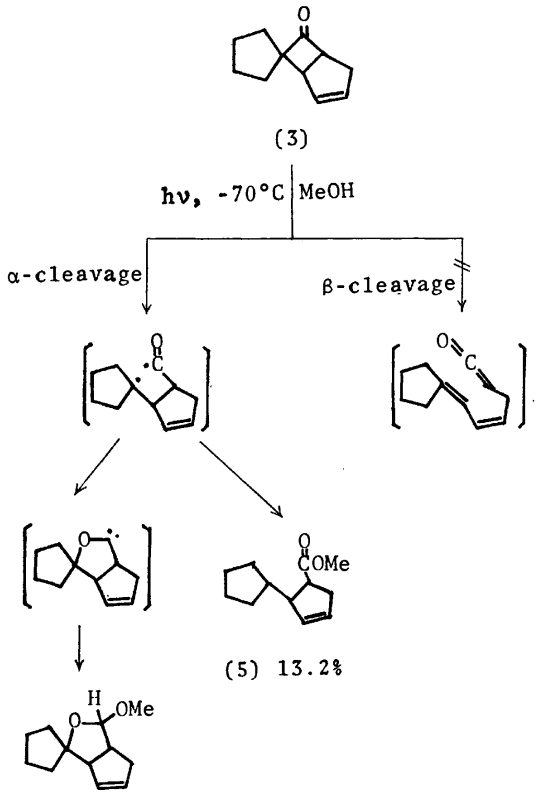

(5) 13.2%

(4) 68.3%

its 7,7-dimethyl derivative,[7] accompanied by comparable amounts of β-cleavage. This enhancement of ring expansion in **1** and **3** may be interpreted in terms of the nucleophilicity and stability of the carbon atom migrated to electron defficient oxygen atom. In connection with the stability of migratory carbon atom, it is not unreasonable to presume that the spiro five-membered ring substituent affects the stability of 1,4-biradical derived from initial α-cleavage in a striking manner. It can be anticipated that photo ring expansion would occur depending upon the selection of certain spiro substituents, even in the photochemical reaction of dispiro substituted cyclobutane-1,3-diones. A spiro five-membered ring substituent was chosen as a suitable substituent. As expected, irradiation of degassed methanolic solution of dispiro[4.1.4.1]dodecane-6,12-dione (**6a**) at —70 °C for 2 h through a Pyrex filter gave ring expanded acetal (**7a**) in 6.1% yield.[5] The formation of **7a** represents the first example of photo-

TABLE 1. PER CENT YIELDS OF PRODUCTS DERIVED FROM PHOTOLYSES OF CYCLOBUTANE-1,3-DIONES IN METHANOL

Compd	Irrad Temp	Acetal(%)	Other Products(%)			
6a	−70°C	**7a** (6.1)	**8a** (55.5)	**9a** (3.9)	**10a**[a] (1.1)	**11a** (3.6)
	0°C	(2.0)	(4.2)	(45.5)	(2.3)	(4.2)
	30°C	(1.4)	(1.6)	(54.6)	(3.8)	(3.6)
6b	−70°C		**8b** (3.4)		**10b'** (12.5)[b]	**11b** (41.7)
6c	−70°C		**8c** (54.9)		**10c** (5.6)	**11c** (4.9)

Besides the above products, cyclopentanone and cyclohexanone were obtained for both **6a** and **6b**, but not quantified. a) Compound (**10a**) was also produced by further irradiation of isolated compound(**8a**) in methanol. b) Methyl 1-(1-cyclohexenyl)cyclohexanecarboxylate.

chemical ring expansion from cyclobutane-1,3-diones. In analogy with cyclobutanones, the formation of **7a** from **6a** can be satisfactorily explained by a photochemical ring expansion reaction by way of an oxacarbene intermediate. As the major nongaseous product other than **7a**, methyl 1-(cyclopentylcarbonyl)cyclopentanecarboxylate (**8a**) was obtained in 55.5% yield, together with small amounts of α-methoxy dicyclopentyl ketone (**9a**), methyl 1-(cyclopentyl)cyclopentanecarboxylate (**10a**) and methyl cyclopentanecarboxylate (**11a**).

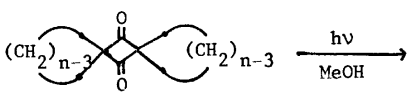

(6) a n=5
b n=6
c n=4

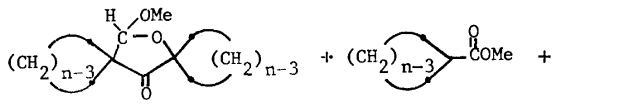

(7) (11)

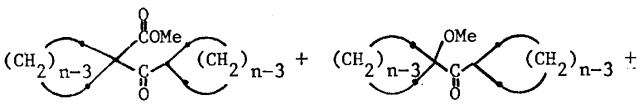

(8) (9)

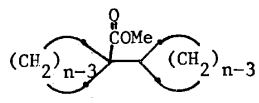

(10)

On the other hand, in a similar irradiation of dispiro-[5.1.5.1]tetradecane-7,14-dione (**6b**) and dispiro[3.1.3.-1]decane-5,10-dione (**6c**), no ring expansion product could be detected by vapor phase chromatography. In these reactions, either β- or α-cleavage took place predominantly and, as the major products in each case, methyl cyclohexanecarboxylate (**11b**) and methyl 1-(cyclobutylcarbonyl)cyclobutanecarboxylate (**8c**) were obtained in 41.7% and 54.9% yields, respectively. It has been confirmed, however, that all or most of keto ester (**8c**) is easily formed by the dark reaction. This is perhaps due to the release of internal ring strain. The yields of photolysis products are given in Table 1.[8]

The effect of spiro ring size on the photochemical processes of cyclobutane-1,3-diones is remarkable. With the increase in temperature in the case of **6a**, the formation of **7a** and **8a** decreases and that of **9a**, which appears to be derived from intermediary unstable dispirocyclopropanone, increases markedly (Table 1). 1,3-Pentadiene is ineffective for the formation of **7a**, an attempt to sensitize with benzophenone being unsuccessful. It is thus assumed that a reactive species of **6a** is an n–π* singlet (or unquenchable triplet). From this excited state, the molecule undergoes α-cleavage to give a spin-conserved singlet biradical (1,4-acyl cycloalkyl biradical) (**A**). In these photochemical reactions, there are three primary photoprocesses (decarbonylation, β-cleavage, and ring expansion) which compete for the short-lived 1,4-acyl cycloalkyl biradical.[9] We would like to postulate that the stability of 1,4-acyl cycloalkyl biradical intermediate (**A**) is of importance in determining the subsequent path, though there is little evidence for the existence of 1,4-acyl cycloalkyl biradical. Increasing stability of intermediary biradical might increase the efficiency of ring expansion. The main path which describes the photochemical transformation of dispiro cyclobutane-1,3-diones is given in the Scheme.

Since cycloalkyl radicals are stable in the sequence $\cdot C_5 \sim \cdot C_7 > \cdot C_6 > \cdot C_4$,[10] it may be reasonable to consider that an acyl cyclopentyl biradical derived from initial α-cleavage of excited **6a** is stable enough to undergo electronic rearrangement, and that the bonding between the carbonyl oxygen atom and cyclopentyl radical center in the biradical intermediate produces the oxacarbene intermediate. Dispiro[6.1.6.1]hexadecane-8,16-dione (**6d**) would undergo photochemical ring expansion, since the stability of an acyl cycloheptyl radical intermediate derived from initial α-cleavage may be comparable to that of an acyl cyclopentyl radical. As expected, ring expanded acetal (**7d**) was

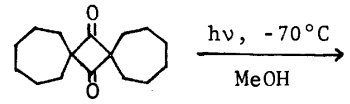

(6d)

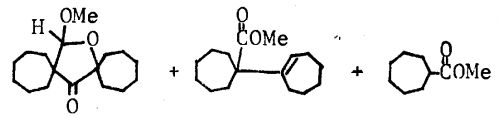

(7d) 3.8% (10d') 21.1% (11d) 9.3%

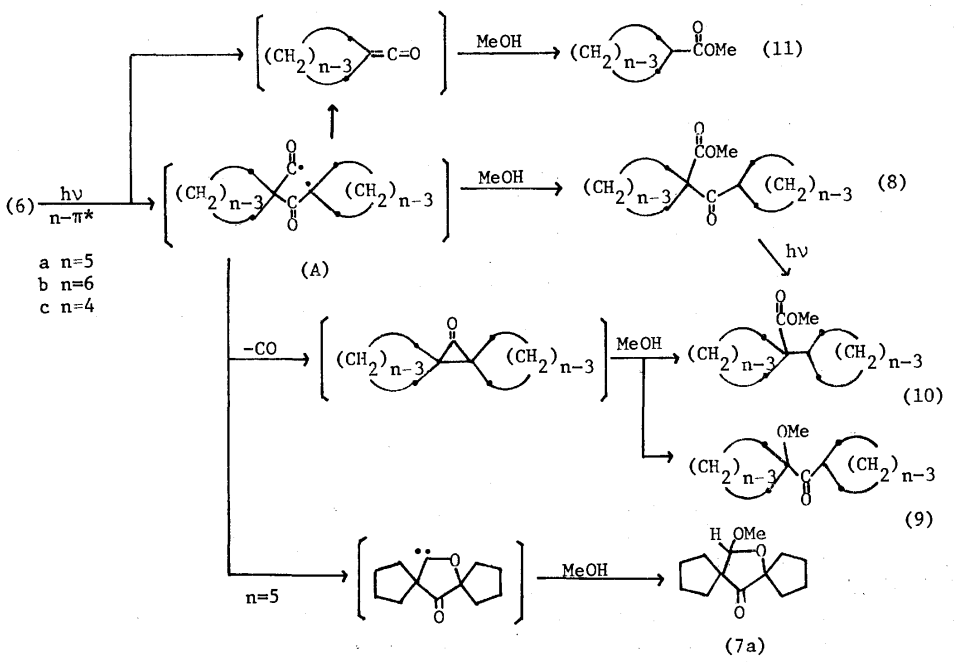

Scheme

obtained in 3.8% yield.

In order to obtain precise information on the effect of two different spiro ring sizes on the photochemical processes and, in particular, the direction of initial α-cleavage, the photolysis of dispiro[4.1.5.1]tridecane-6,13-dione (**6e**) in methanol has been examined.

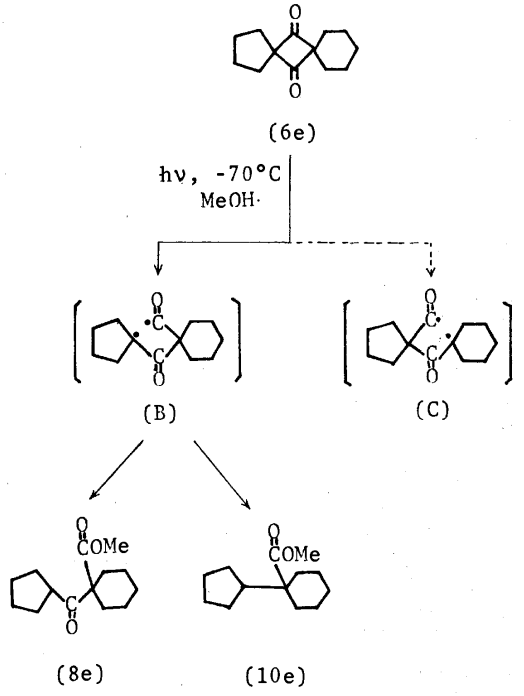

The above reaction led to the preferential formation of methyl 1-(cyclopentylcarbonyl)cyclohexanecarboxylate (**8e**). The result can be explained by the difference in the stability of two 1,4-acyl cycloalkyl biradical intermediates (**B**) and (**C**) derived from the different directions of α-cleavage.

Experimental

All the melting points and boiling points are uncorrected. Infrared spectra were measured with a JASCO IR-G spectrometer, UV spectra with a Hitachi Two-wavelength Double Beam Spectrophotometer 356, and NMR spectra with a JEOL JNM-3H-60 or JEOL JNM-PS-100 spectrometer, tetramethylsilane being used as an internal standard. Mass spectra were taken on a Hitachi RMU-6E spectrometer. Gas chromatography was carried out on a Hitachi gas chromatograph 063 and on a Varian aerograph model 90-P.

Dispiro Substituted Cyclobutane-1,3-dione. Dispiro cyclobutane-1,3-diones (**6a,b,c,d**) were prepared by the procedure given by Erickson *et al.*[11] Dispiro[4.1.5.1]tridecane-6,13-dione (**6e**) was synthesized by the following procedure. To a stirred solution of cyclopentanecarbonyl chloride (7.6 mmol) and cyclohexanecarbonyl chloride (23.2 mmol) in 50 ml of ether under nitrogen was added triethylamine (46.5 mmol) over a period of 0.5 hr. The reaction mixture was stirred and refluxed for 24 hr, then worked up as usual to give dione (**6e**) in 37.7% yield, together with **6a** and **6b**. After diones had been chromatographed on silica gel, recrystallization from pentane gave white needles (**6e**). Dione (**6e**) was obtained in maximum yield, when the molar ratio of cyclopentanecarbonyl chloride to cyclohexanecarbonyl chloride was 1 : 3. The

Table 2. Properties and spectral data for the dispiro cyclobutane-1,3-diones

	Mp °C	Mass (*m/e*)	IR (C=O)cm^{-1}	UV(in CH_2Cl_2) nm(ε)
6a	75	192 (M^+)	1727	347 (24), 306 (27)
6b	164—165	220 (M^+)	1721	342 (22), 313 (43), 302 (49)
6c	86— 87	164 (M^+)	1730	359 (25), 312 (81)
6d	145—146	248 (M^+)	1730	333 (27), 312 (57)
6e[a)]	91— 92	206 (M^+)	1736	345 (20), 309 (35)

a) Found: C, 75.56; H, 9.01%. Calcd for $C_{13}H_{18}O_2$: C, 75.69; H, 8.80%.

properties and spectral data for these dispiro cyclobutane-1,3-diones are given in Table 2. The ultraviolet absorption of the dispiro cyclobutane-1,3-diones showed two distinct n-π^* transitions due to 1,3 π interactions in the excited states and a small, regular increase in each absorption maximum with decreasing spiro ring size.

General Irradiation Procedure. A solution degassed by bubbling nitrogen slowly for 30 min was irradiated through a Pyrex filter using 500W high pressure mercury lamp. The reaction progress was monitored periodically by glpc analysis. Upon termination of the irradiation, the solvent was evaporated and the residue was purified by glpc. The yields were determined by glpc analysis (Poly Ethylene Glycol 20-M).

Synthesis of Dispiro[4.1.4.1]dodecane-6-one (1). A mixture of Raney nickel (80 g), ethanol (200 ml) and 12,12-di-(ethylthio)dispiro[4.1.4.1]dodecane-6-one (2.5 g, 8.4 mmol)[12] was refluxed for 8 hr. Distillation of the residue gave **1** (753 mg, 50%), bp 81—82 °C/3 Torr; IR (neat) 2950, 2900, 1760, 1440, 1110, 1015 cm^{-1}; NMR (CCl_4) δ 1.32—1.90 (m, 16H), 1.98 (s, 2H); Mass *m/e* 178 (M^+), 150, 96, 83, 68. Found: C, 80.62; H, 10.38%. Calcd for $C_{12}H_{18}O$: C, 80.85; H, 10.18%.

Photolysis of Dispiro[4.1.4.1]dodecane-6-one (1) in Methanol. A degassed solution of (**1**) (537 mg, 3.0 mmol) in 250 ml of methanol was irradiated at −70 °C for 10 hr. Preparative glpc afforded cyclic acetal (**2**) (80%): IR (neat) 2980, 2910, 1450, 1330, 1190, 1160, 1095, 1030, 960 cm^{-1}; NMR (CCl_4) δ 1.35—2.00 (m, 16H), 2.02 (s, 2H), 3.25 (s, 3H), 4.28 (s, 1H); Mass *m/e* 210 (M^+), 178, 160, 149, 137, 96, 81, 67.

Synthesis of 7-Tetramethylene-bicyclo[3.2.0]hept-2-en-6-one (3). Triethylamine (0.12 mol) was added to a solution of cyclopentanecarbonyl chloride (0.1 mol) and cyclopentadiene (0.7 mol) in 200 ml of dry ether under an atmosphere of nitrogen, and the resulting suspension was stirred and refluxed for 20 hr. The amine salt was removed by filtration. After distillation of the residue three times, spiro ketone (**4**) was obtained in 74.4% yield, bp 68—69 °C/9.5 Torr; IR (neat) 1775, 1600 cm^{-1}; NMR (neat) δ 1.60 (m, 8H), 2.38 (m, 2H), 3.19 (d, 1H), 3.58—4.00 (three d or two t, 1H), 5.80 (m, 2H); Mass *m/e* 162 (M^+), 134, 119, 105, 96, 91, 68, 66. Found: C, 81.24; H, 8.78%. Calcd for $C_{11}H_{14}O$: C, 81.44; H, 8.70%.

Photolysis of Spiro Ketone (3) in Methanol. A solution of **3** (18.5 mmol) in 300 ml of methanol was irradiated at −70 °C for 10 hr. Preparative glpc afforded acetal (**4**) in 68.4% yield, together with methyl 2-(cyclopentyl)-3-cyclopentene-1-carboxylate (**5**) (13.2%). For **4**, IR (neat) 3075, 2900, 1615, 1445, 1190 cm^{-1}; NMR (neat) δ 1.60 (m, 8H), 2.48—2.80 (m, 2H), 3.08 (m, 1H), 3.20 (s, 3H), 4.30 (m, 1H), 4.50 (s, 1H), 5.60 (m, 2H); Mass *m/e* 194 (M^+), 162, 144, 133, 110, 105, 91, 79, 77, 67, 55. Found: C, 74.17; H, 9.32%. Calcd for $C_{12}H_{18}O_2$: C, 74.10; H, 9.34%. For **5**, IR (neat) 3075, 2900, 1725, 1615, 1445, 1360, 1190, 1100 cm^{-1}; NMR (CCl_4) δ 1.40—2.10 (m, 8H), 2.20—2.80 (m, 4H), 3.10 (m, 1H), 3.25 (s, 3H), 5.60 (m, 2H); Mass *m/e* 194 (M^+), 163, 134, 120, 106, 91, 79.

Photolysis of Dispiro[4.1.4.1]dodecane-6,12-dione (6a) in Methanol. A degassed solution of **6a** (18 mmol) in 200 ml of methanol was irradiated using a Pyrex filter at −70 °C for 2 hr. Analysis of the photolysate by glpc revealed the following products: ring expanded acetal (**7a**, 6.1%), methyl 1-(cyclopentylcarbonyl)cyclopentanecarboxylate (**8a**, 55.5%). In addition, α-methoxydicyclopentyl ketone (**9a**, 3.9%), methyl 1-(cyclopentyl)cyclopentanecarboxylate (**10a**, 1.1%) and methyl cyclopentanecarboxylate(**11a**, 3.6%) were detected. Methyl cyclopentanecarboxylate (**11a**) was identified by comparison of glpc retention time with that of an authentic sample. For **7a**, IR (neat) 2950, 2890, 1742, 1445, 1090, 1015, 975 cm^{-1}; NMR (CCl_4) δ 1.77 (b, 16H), 3.35 (s, 3H), 4.60 (s, 1H); Mass *m/e* 224 (M^+), 193, 165, 112, 96, 84, 67, 55, 41. Found: C, 69.34; H, 9.01%. Calcd for $C_{13}H_{20}O_3$: C, 69.61; H, 8.99%. For **8a**, IR (neat) 2960, 2890, 1740, 1707, 1447, 1435, 1335, 1230, 1160, 1120, 1080, 1010 cm^{-1}; NMR (CCl_4) δ 1.30—2.30 (m, 16H), 2.50—3.30 (b, 1H), 3.68 (s, 3H); Mass *m/e* 224 (M^+), 193, 165, 128, 97, 69, 41. The structure of **8a** was confirmed also by its identity with an authentic sample prepared by treating **6a** with methanol containing a catalytic amount of sodium methoxide. For **9a**, IR (neat) 2950, 2870, 1700, 1440, 1360, 1070 cm^{-1}; NMR (CCl_4) δ 1.70—2.00 (m, 16H), 2.50 (m, 1H), 3.05 (s, 3H); Mass *m/e* 196 (M^+), 164, 149, 135, 99, 67. For **10a**, IR (neat) 2950, 2890, 1724, 1440, 1155 cm^{-1}; NMR (CCl_4) δ 1.40—2.30 (m, 17H), 3.60 (s, 3H); Mass *m/e* 196 (M^+), 194, 166, 137, 111, 97, 81, 69. Irradiation of **6a** at 0 °C and 30 °C gave the same photoproducts in somewhat different yields (Table 1).

Quenching with 1,3-Pentadiene. Three samples were prepared, each containing 250 ml of methanol solution of **6a** (18 mmol). One also contained 1,3-pentadiene (0.1 mol) and another contained 1,3-pentadiene (0.01 mol). All the samples were irradiated at −70 °C for 2 hr. 1,3-Pentadiene has no quenching effect on the formation of cyclic acetal (**7a**).

Photolysis of Dispiro[5.1.5.1]tetradecane-7,14-dione (6b) in Methanol. A solution of **6b** (41 mmol) in 300 ml of methanol was irradiated at −70 °C for 5 hr. Isolation of products by preparative glpc afforded methyl cyclohexanecarboxylate (**11b**, 41.7%), dimethyl (bicyclohexyl)-1,1′-dicarboxylate (**12**, 15.4%), methyl 1-(1-cyclohexenyl)cyclohexanecarboxylate (**10b′**, 12.5%), and methyl 1-(cyclohexylcarbonyl)cyclohexanecarboxylate (**8b**, 3.4%). Methyl cyclohexanecarboxylate (**11b**) was identified by comparison of glpc retention time with that of an authentic sample. For **12**, mp 117—118 °C (lit,[13] 116 °C); IR (KBr) 3030, 2970, 2900, 1720, 1450, 1435, 1350, 1300, 1210, 1130, 1060, 1030, 985 cm^{-1}; NMR (CCl_4) δ 1.0—2.2 (m, 20H), 3.60 (mc, 6H); Mass *m/e* 282 (M^+), 251, 223, 169, 163, 142, 113, 109, 81. For **10b′**, IR (neat) 2950, 2890, 2700, 1728, 1450, 1298, 1260, 1212, 1200, 1175, 1155, 1130, 995 cm^{-1}; NMR (CCl_4) δ 0.9—2.0 (m, 14H), 2.07 (m, 4H), 3.58 (s, 3H), 5.50 (m, 1H); Mass *m/e* 222 (M^+), 190, 163, 142, 95, 83, 81. For **8b**, IR (neat) 2940, 2820, 1730, 1703, 1445, 1365, 1210, 1130, 1110, 980 cm^{-1}; NMR (CCl_4) δ 1.0—2.1 (m, 20H), 2.2—2.6 (b, 1H), 3.65 (s, 3H); Mass *m/e* 252 (M^+), 221, 193, 142, 111, 83, 55. The structure of **8b** was confirmed also by its identity with an authentic sample.

Photolysis of Dispiro[3.1.3.1]decane-5,10-dione (6c) in Methanol. A solution of **6c** (8.2 mmol) in 250 ml of methanol was irradiated at −70 °C for 2 hr. Preparative glpc gave methyl 1-(cyclobutylcarbonyl)cyclobutanecarboxylate (**8c**, 54.9%), dimethyl (bicyclobutyl)-1,1′-dicarboxylate (**14**, 17.1%), methyl 1-(cyclobutyl)cyclobutanecarboxylate (**10c**, 5.6%) and methyl cyclobutanecarboxylate (**11c**, 4.9%). For **8c**, IR (neat) 2950, 1734, 1700, 1430, 1350, 1273, 1245, 1220, 1118, 968 cm^{-1}; NMR(CCl_4) δ 1.5—2.6 (m, 12H), 3.30 (m, 1H), 3.68 (s, 3H); Mass *m/e* 196 (M^+), 165, 141, 113, 83, 55. For **14**, IR (neat) 2970, 1728, 1430, 1283, 1215, 1195, 1120, 1070, 970 cm^{-1}; NMR (CCl_4) δ 1.6—2.6 (m, 12H), 3.58 (mc, 6H); Mass *m/e* 226 (M^+), 194, 170, 166, 153, 139, 114, 107, 83, 79, 59, 55. Methyl cyclobutanecarboxylate (**11c**) was identified by comparison of glpc retention time with that of an authentic sample. However, when a solution of dione (**6c**) (100 mg) in methanol (20 ml) was allowed to stand at room temperature for 5 hr, **6c** underwent a facile ring opening to produce **8c** quantitatively. On the other hand, diones (**6a**, **b**,**d**,**e**) were stable in refluxing methanol.

Photolysis of Dispiro[6.1.6.1]hexadecane-8,16-dione (6d) in Methanol. A solution of dione (**6d**) (5.1 mmol) in 250 ml

of methanol was irradiated using a Pyrex filter at −70 °C for 2 hr. Analysis of the photolysate by glpc revealed the following products: ring expanded acetal (**7d**, 3.8%), methyl 1-(1-cycloheptenyl)cycloheptanecarboxylate (**10d'**, 21,1%) and methyl cycloheptanecarboxylate (**11d**, 9.3%). Methyl cycloheptanecarboxylate (**11d**) was identified by comparison of glpc retention time with that of an authentic sample. For **7d**, IR (neat) 2930, 2850, 1725, 1440, 1100, 970 cm^{-1}; NMR (CCl_4) δ 1.50—1.90 (m, 24H), 3.36 (s, 3H), 4.62 (s, 1H); Mass *m/e* 280 (M^+), 220, 140, 124, 108, 95. For **10d'**, IR (neat) 2930, 2850, 1725, 1440, 1240, 1190, 1170, 1060 cm^{-1}; NMR (CCl_4) δ 1.30—1.80 (m, 18H), 1.94—2.20 (m, 4H), 3.56 (s, 3H), 5.62 (t, 1H); Mass *m/e* 250 (M^+), 191, 180, 156, 109, 95.

Photolysis of Dispiro[4.1.5.1]tridecane-6,13-dione (6e) in Methanol. A solution of **6e** (1.84 mmol) in 300 ml of methanol was irradiated at −70 °C for 1 hr. Preparative glpc afforded keto ester (**8e**) and methyl 1-(cyclopentyl)cyclohexanecarboxylate (**10e**) in 20.5% and 15.2% yields, respectively. For **8e**, IR (neat) 2950, 2900, 1730, 1705, 1445, 1295, 1220, 1120 cm^{-1}; NMR (CCl_4) δ 1.27—2.30 (m, 18H), 2.50—2.78 (b, 1H), 3.66 (s, 3H); Mass *m/e* 238 (M^+), 206, 195, 178, 142 (vs), 110, 96, 85, 67. For **10e**, IR (neat) 2950, 2900, 1725, 1450, 1200, 1170, 1130, 1000 cm^{-1}; NMR (CCl_4) δ 1.20—2.65 (m, 19H), 3.64 (s, 3H); Mass *m/e* 210 (M^+), 208, 176, 151, 149, 142, 128, 95, 87, 83, 81, 69.

References

1) (a) D. R. Morton and N. J. Turro, *J. Amer. Chem. Soc.*, **95**, 3947 (1973) and references therein; (b) G. Quinkert, P. Jacobs, K. H. Kaiser, G. Weich, and W. -D. Stohrer, *Angew. Chem. Intern. Edt.*, **13**, 197, 198, 199, 200 (1974); (c) O. L. Chapman and O. S. Weiss, "Organic Photochemistry," Vol. III, ed. by O. L. Chapman, Marcel Dekker, New York, N. Y. (1973), pp. 197—280; (d) G. Quinkert, "Topics in Current Chemistry," Vol. 46, "Photochemistry," Springer-Verlag, Berlin, Heiderberg, New York (1974).

2) P. M. Collins, N. N. Oparaeche, and B. R. Whitton, *Chem. Commun.*, **1974**, 292.

3) It has been shown that some cyclobutane-1,2-diones also undergo the photochemical ring expansion. J. M. Conia and J. M. Denis, *Tetrahedron Lett.*, **1973**, 461.

4) (a) N. J. Turro, P. A. Leermakers, H. R. Wilson, D. C. Neckers, G. W. Byers, and G. F. Vesley, *J. Amer. Chem. Soc.*, **87**, 2613 (1965); (b) R. C. Cookson, M. J. Nye, and Subrahamanyam, *Proc. Chem. Soc., London*, **1964**, 144; (c) H. G. Richey, J. M. Richey, and D. C. Clagett, *J. Amer. Chem. Soc.*, **86**, 3906 (1964); (d) I. Haller and R. Srinivasan, *ibid.*, **87**, 1144 (1965); (e) N. J. Turro, G. W. Byers, and P. A. Leermakers, *ibid.*, **86**, 955 (1964); (f) P. A. Leermakers, G. F. Vesley, N. J. Turro, and D. C. Neckers, *ibid.*, **86**, 4213 (1964); (g) N. J. Turro, D. C. Neckers, P. A. Leermakers, D. Seldner, and P. D'Angelo, *ibid.*, **87**, 4097 (1965); (h) A. P. Krapcho and F. J. Waller, *J. Org. Chem.*, **37**, 1079 (1972); (i) A. P. Krapcho and B. Abegaz, *ibid.*, **39**, 2251 (1974).

5) K. Kimura, M. Takamura, A. Kunai, and Y. Odaira, *Chem. Comm.*, **1974**, 685.

6) G. Jones II and S. A. Zalk, *Tetrahedron Lett.*, **1973**, 4095.

7) H. U. Hostettler, *ibid.*, **1965**, 687.

8) No ring expansion reaction is mentioned by Krapcho and Abegaz in their report on the photochemistry of cyclobutane-1,3-diones.[4i]

9) As an alternative mechanism, there is one involving concerted reaction from excited S_1. In the photolysis of some 3-methylene cyclobutanones, Quinkert *et al.*[1b] recently reported that the oxacarbene intermediate is formed directly from the electronic excited state but not *via* 1,4-acyl alkyl biradical intermediate.

10) (a) C. G. Overberger, A. B. Finestone, H. Biletch, J. Lilker, and J. Herbert, *J. Amer. Chem. Soc.*, **75**, 2078 (1953); (b) C. Rüchardt, *Angew. Chem. Intern. Edt.*, **9**, 830 (1970).

11) J. L. Erickson, F. E. Collins, Jr., and B. L. Owen, *J. Org. Chem.*, **31**, 480 (1966).

12) H. M. Walborsky and E. R. Buchman, *J. Amer. Chem. Soc.*, **75**, 6339 (1953).

13) M. Kitabatake and M. Ogawa, *Nippon Kagaku Zasshi*, **85**, 450 (1964).

The Catalytic Effect of Crown Ethers on Benzoin Condensation

Sadatoshi AKABORI,* Michiko OHTOMI, and Katsuhiko ARAI

Department of Chemistry, Faculty of Science, Tōho University, Funabashi, Chiba 275

(Received August 9, 1975)

Aromatic aldehydes were treated with potassium cyanide in the presence of a crown ether in water or in aprotic solvents to give benzoins in high yields, although similar reactions in the absence of the crown ether proceeded sluggishly in general. The catalysis is believed to be due to the ability of the crown ether to bring anions into the organic phase.

In recent years there have been reported several synthetic applications of crown ethers, such as 18-crown-6 (I) and dibenzo-18-crown-6 (II), which possess the ability to form complexes with a variety of inorganic salts and also the ability to solubilize these salts in aprotic solvents. The following reactions are reported to be enhanced by the crown ether: substitution reactions,[1-6] elimination reactions,[7,8] a condensation reaction,[9] oxidation reactions,[3,10] a reduction reaction,[3] and an addition reaction.[11]

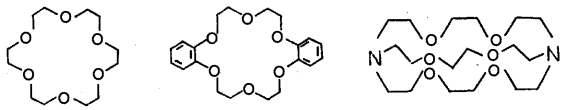

(I) (II) (III)

In a previous paper,[12] we have reported on the reaction of potassium alkanoate with alkyl halide in an aprotic solvent. Although the reaction of potassium alkanoate with alkyl halide does not proceed in aprotic solvents such as benzene, the reaction with the same starting materials in the presence of catalytic amounts of a bicyclopolyether such as III affords alkyl esters in high yields. As an extension of our previous work, we have been interested in seeking examples of the enhancement of the reaction by crown ethers in the field of condensation, which has been little studied.[9] Benzoin condensation was taken as our target. Generally benzoins are generated by the action of sodium cyanide or potassium cyanide on aromatic aldehydes in aqueous ethanol.[13] We now wish to report that dramatic results can be achieved by the addition of crown ethers (I and II) to benzoin condensations in water and in aprotic solvents at appropriate temperatures.

Results and Discussion

Benzoin Condensation in Water. The condensation reactions represented by Eq. 1 were run in heterogeneous systems by the use of crown ethers (I and II) as anion-transfer catalysts:

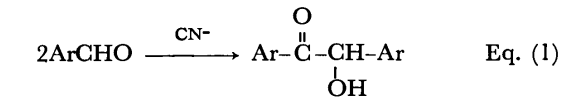

$$2\mathrm{ArCHO} \xrightarrow{\mathrm{CN^-}} \mathrm{Ar{-}C(=O){-}CH(OH){-}Ar} \qquad \text{Eq. (1)}$$

IV: Ar=C_6H_5–, V: Ar=*p*-CH_3-C_6H_4–,
VI: Ar=furyl

The reagent is prepared by dissolving potassium cyanide in water and by then adding 18-crown-6. After the mixture has been stirred for 30 min, the organic substrate is added and the resulting heterogeneous mixture is stirred for 15 min to 6 hr at appropriate temperatures. The results are shown in Table 1. The reaction conditions are relatively mild (at 25 or 60 °C), and the conversions are high at 60 °C; in the presence of *ca.* 7% of crown ether, benzoin was obtained in more than 78% yields within 15 min from benzaldehyde, *p*-toluoin (99%) in 3 hr from *p*-tolualdehyde, and furoin (66%) in 15 min from 2-furaldehyde.

Table 1. Reactions of aromatic aldehydes with potassium cyanide

Substrate	Solvent[a]	Reaction temp (°C)	Reaction time (hr)	Product[b]	Yield(%)[c] Crown ether present	Yield(%)[c] Crown ether absent
IV	H_2O	25	1.5	Benzoin	73.9	3.1
IV	H_2O	60	0.25	Benzoin	78.0	3.3
V	H_2O	25	6.0	*p*-Toluoin	44.3	0.0
V	H_2O	60	3.0	*p*-Toluoin	99.0	1.9
VI	H_2O	25	1.5	Furoin	35.6	24.4
VI	H_2O	60	0.25	Furoin	66.2	48.0
IV	CH_3CN	25	3.0	Benzoin	78.4	1.1
IV	CH_3CN	60	1.5	Benzoin	73.6	9.0
IV	C_6H_6	25	3.0	Benzoin	70.9	0.1
IV	C_6H_6	60	3.0	Benzoin	95.9	0.5
V	CH_3CN	25	6.0	*p*-Toluoin	56.4	2.7
V	CH_3CN	60	3.0	*p*-Toluoin	99.0	6.0
V	C_6H_6	25	6.0	*p*-Toluoin	29.1	0.0
V	C_6H_6	60	3.0	*p*-Toluoin	90.8	0.0
VI	CH_3CN	25	3.0	Furoin	65.0	3.7
VI	CH_3CN	60	0.25	Furoin	43.6	3.6
VI	C_6H_6	25	3.0	Furoin	52.7	0.3
VI	C_6H_6	60	3.0	Furoin	53.0	0.0

a) 2.7 ml of water or 9.0 ml of aprotic solvents were used. b) All product show the same retention time with authentic sample and mass spectra were consistent with the proposed structure. c) The values are those obtained by GLC.

In sharp contrast, benzoin and *p*-toluoin were obtained in less than 3% yields in the absence of the crown ether, although furoin was obtained in a good yield from 2-furaldehyde under similar conditions. These results can be accounted for in terms of the solubility of aldehydes in water; 2-furaldehyde is fairly soluble in water, whereas benzaldehyde and *p*-tolualdehyde are soluble in water to only a limited extent. Generally a reaction between two substrates located in different phases of a mixture is often inhibited because of the inability of reagents to come together. However, this reaction is brought about by the use

of small quantities of a reagent, which transfers one reactant across the interface into the other phase. Although potassium cyanide is an excellent catalyst for benzoin condensation at 90 °C in 95% ethanol,[14] it exhibits hardly any catalytic ability in water at room temperature.[15] However, as is shown in Table 1, complexes of crown ether with potassium cyanide afford benzoin in high yields even when the reaction was run at room temperature. Thus, in the benzoin condensation of aromatic aldehydes, it is most likely that crown ethers transport cyanide into the organic phase, although the possibility of transforming the aromatic aldehyde into the aqueous phase can not be ruled out.

Benzoin Condensation in Aprotic Solvents. The crown ethers are known to form complexes with alkali and other metal salts to increase the solubility and to increase the reactivity of anions in aprotic solvents. The potassium cyanide complex of 18-crown-6 was prepared *in situ* by dissolving a catalytic amount of 18-crown-6 in *ca.* 9 ml of a dry aprotic solvent (benzene or acetonitrile) and by then adding appropriate amounts of potassium cyanide, most of which remained insoluble. After the heterogeneous system had been stirred for 30 min, the aromatic aldehyde was added at once; the resulting mixture was stirred for from 15 min to 6 hr at 25 or 60 °C. In the absence of the crown ether, potassium cyanide does not have any detectable solubility in benzene and hardly no reaction occurs; benzaldehyde gives less than a 0.5% yield of benzoin after 3 hr at 60 °C when it is treated with potassium cyanide in the absence of 18-crown-6, whereas benzoin is formed in a 95.9% yield within 3 hr when a trace amount of 18-crown-6 is present. The reaction was found to be faster in acetonitrile than benzene.

In summary, these experimental results in water indicate that crown ethers may be at least as useful as onium salts in reactions which proceed by means of phase-transfer. It has been shown that crown ether (I) effectively solubilizes potassium cyanide in aprotic solvents and that the reagent produces benzoins in high yields from a variety of organic substrates. The catalytic activity of dibenzo-18-crown-6 is almost the same as that of 18-crown-6.

Experimental

Analysis. The products were analyzed by gas chromatography. The gas chromatograms were obtained on a Hitachi 023 gas chromatograph, using 10% FFAP on Chromosorb W AW/DMCS 1 m×3 mm. The mass spectra were recorded on a Shimadzu LKB 9000 gas-chromatograph-mass-spectrometer at an ionizing voltage of 70 eV.

Materials. 18-Crown-6[16] and dibenzo-18-crown-6[17] were prepared according to the procedures described in the literature. Authentic samples (benzoin[14], *p*-toluoin[18] and furoin[19]) were also prepared according to the procedures described in the literature. Potassium cyanide of Koso Co., Ltd., and aromatic aldehydes of the Tokyo Kasei kogyo Co., Ltd., were used without further purification. The solvents used were purified by distillation.

Benzoin Condensation of Benzaldehyde in Water. The following procedure for the preparation of benzoins is representative. A mixture of potassium cyanide (20.0 mmol), 18-crowm-6 (1.22 mmol), and 2.7 ml of water was stirred for 30 min at 60 °C. Benzaldehyde (41.7 mmol) was then added at once, and the mixture was stirred for a further 15 min. A yellow precipitate, which gradually formed, was collected by filtration, and the filtrate was extracted with chloroform. The yellowish solid was dissolved in the chloroform extract, and then the solution was subjected to gas-chromatographic analysis.

Benzoin Condensation of Benzaldehyde in Aprotic Solvents. A mixture of potassium cyanide (20.7 mmol), 18-crown-6 (1.40 mmol), and *ca.* 9 ml of benzene was stirred for 30 min at 25 °C. Benzaldehyde (49.9 mmol) was then added at once, and the mixture was stirred for a further 3 hr. The work-up and analysis were performed analogously with the case cited above.

Benzoin Condensation with the Aid of Dibenzo-18-crown-6. The reaction was carried out similarly. The results were usually quite similar, although results a little inferior were sometimes obtained.

The authors wish to express their gratitude to Professor Michinori Ōki, the University of Tokyo, for his valuable discussions and suggestions.

References

1) C. L. Liotta and H. P. Harris, *J. Amer. Chem. Soc.*, **96**, 2250 (1974).
2) D. J. Sam and H. E. Simmons, *J. Amer. Chem. Soc.*, **96**, 2252 (1974).
3) D. Landini and F. Montanari, *Chem. Commun.*, **1974**, 879.
4) C. L. Liotta, H. P. Harris, M. McDermott, Tom Gonzalez, and K. Smith, *Tetrahedron Lett.*, **1974**, 2417.
5) H. D. Durst, *Tetrahedron Lett.*, **1974**, 2421.
6) F. L. Cook, C. W. Bowers, and C. L. Liotta, *J. Org. Chem.*, **30**, 3416 (1974).
7) M. Svoboda, J. Hapala, and J. Závada, *Tetrahedron Lett.*, **1972**, 265.
8) R. A. Bartsch and K. E. Wiegers, *Tetrahedron Lett.*, **1972**, 3819.
9) M. Makosza and M. Ludwikow, *Angew. Chem.*, **86**, 744 (1974).
10) D. J. Sam and H. E. Simmons, *J. Amer. Chem. Soc.*, **94**, 4024 (1972).
11) T. Mastuda and K. Koida, This Bulletin, **46**, 2259 (1973).
12) S. Akabori and M. Ohtomi, *ibid.*, **48**, 2991 (1975).
13) W. S. Ide and J. S. Buck, "Organic Reactions," Vol. IV, p. 269 (1957).
14) Adams and Marvel, "Organic Syntheses," Coll. Vol. I, p. 94 (1956).
15) J. Solodar, *Tetrahedron Lett.*, **1971**, 287.
16) G. W. Gokel, D. J. Cram, C. L. Liotta, H. P. Harris, and F. L. Cook, *J. Org. Chem.*, **39**, 2445 (1974).
17) C. J. Pedersen, *J. Amer. Chem. Soc.*, **89**, 7017 (1967).
18) M. Stirelin, *Ber.*, 380 (1889).
19) W. W. Hartman and J. B. Dickey, *J. Amer. Chem. Soc.*, **55**, 1228 (1933).

Double 1,3-Dipolar Cycloaddition Reaction of 3-Phenylsydnone with 1,3-Dienes

Akira HANEDA, Takeshi IMAGAWA, and Mituyosi KAWANISI

Department of Industrial Chemistry, Faculty of Engineering, Kyoto University, Sakyo-ku, Kyoto 606

(Received August 14, 1975)

Thermal reaction of 3-phenylsydnone with isoprene or 2,3-dimethylbutadiene gave 2-methyl- or 2,6-dimethyl-7-phenyl-1,7-diazatricyclo [2.2.1.$0^{2,6}$]heptane, together with 3-isopropenyl-1-phenylpyrazole. The former is the product of the double 1,3-dipolar cycloaddition. A similar reaction with 1,3-butadiene gave only 3-vinyl-1-phenylpyrazole.

3-Phenylsydnone (**1**) and other sydnone derivatives have been found by Huisgen and his co-workers[1] to undergo 1,3-dipolar cycloaddition with both electron-deficient and -abundant olefins and acetylenes.

Of the many reactions reported by Huisgen, there is only one case in which one molecule of **1** adds to two molecules of dipolarophile, *i.e.*, acenaphthylene. The intermediate of this reaction is thought to be the azomethine-imine (**2**), which has been known to behave as a 1,3-dipole.

Recently, the intramolecular case of this double 1,3-dipolar cycloaddition reaction has been reported by Weintraub[2]; he used 1,5-cyclooctadiene as the dipolarophile. The tetracyclic product (**3**) is composed of four rings, two of which are formed by the two 1,3-dipolar cycloadditions; the other two, indicated by the bold lines, may be considered to be due to the concomitant cyclization reactions.

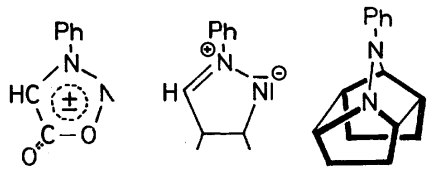

(1) (2) (3)

Formulas.

The formation of alicyclic rings has been discussed in terms of two kinetic factors: energy (strain) and entropy (probability) factors.[3] The above-mentioned cyclization forming the five-membered rings is governed mainly by energy factor.[4] The other factor contributes to the case of cyclopropane-ring formation. Therefore, if we utilize 1,3-dienes as the diene component, the intramolecular capture of the reactive intermediate can be expected to be easily done by the concomitant cyclopropane-ring formation. This prediction[5] was substantiated in the case of the Diels-Alder reactions of 2-pyrone derivatives with 1,3-dienes.[6]

The aim of the present study is to apply this principle to the 1,3-dipolar cycloaddition reaction and to obtain the diazanortricyclenes.

Heating of a solution of **1** and isoprene (**4a**) in ethyl acetate at 150 °C for 24 hr, followed by flash distillation, gave an oily mixture which was shown by GLC analysis to consist of two components present in the ratio of about 1: 1. Preparative GLC separation allowed their isolation.

The faster-moving fraction (**5a**) gave the correct

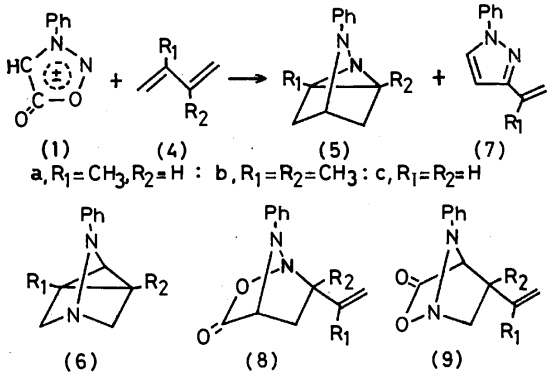

(1) (4) (5) (7)

a, R_1=CH_3, R_2=H : b, R_1=R_2=CH_3 : c, R_1=R_2=H

(6) (8) (9)

Scheme.

analysis for $C_{12}H_{14}N_2$. In the NMR spectrum, the absence of any signal of olefinic protons except those of aromatic protons indicates the tricyclic structure, while the absence of any prominent coupling pattern indicates the diazanortricyclyl system, since the reported coupling constants in the nortricyclyl system[7] are small (1.5 Hz at most). The two methine protons adjacent to nitrogen atom clearly exclude the alternative structure, **6a**.

The slower-moving fraction (**7a**) showed the NMR signals of only aromatic and olefinic protons, except for the methyl protons. The magnitude of the coupling constants and the chemical shifts of the pyrazole ring protons revealed the 3-substituted 1-phenylpyrazole structure.[8] The isopropenyl substituent could be derived from the olefinic proton signals, exhibiting patterns characteristic of *exo*-methylene signals.[9]

A similar reaction of **1** and 2,3-dimethylbutadiene (**4b**) at 150 °C for 6.5 hr gave, after distillation, an oily mixture consisting of two components in the ratio of 4: 1.

The isolation of the major component by preparative GLC revealed the major component to be identical with the pyrazole, **7a**, obtained in the reaction with **4a**. The formation of **10a** in the present reaction is explained by the elimination of a methane molecule after the first decarboxylation. This apparently unusual reaction is not without precedent in the 1,3-dipolar cycloaddition reaction.[10]

The minor product was proved to have a tricyclic structure (**5b**).

In the reaction of **1** with butadiene (**4c**), prepared *in situ* from sulfolene, at 150 °C for 47 hr, we could not obtain the tricyclic product (**5c**); only 1-phenyl-3-vinylpyrazole (**7c**) could be isolated.

From these structures of the products, it was concluded

that the first 1,3-dipolar addition step gave, regioselectively, the adduct (**8**) and that no product originating from an alternative intermediate (**9**) was found. This regioselectivity is in the same line as the 1,3-dipolar cycloaddition reaction of **1** with stilbene[1] and is not in conflict with the prediction made by the perturbation molecular orbital methods of Bastide[11] and of Houk.[12]

Our initial attempt has been successful, although the yield is far from satisfactory. In these reactions it was not possible to by-pass the formation of tarry material, and no optimization of the yield of the tricyclic products was undertaken.

Experimental

The NMR spectra were measured in CCl_4 solution, using TMS as the internal standard. The mass spectra (MS) were obtained at 70 eV. GLC was performed at the column temperature of 130 °C with a Shimadzu GC-4AIT apparatus with a 3 mm × 1 m column packed with 10% High Vacuum Silicone Grease on Chromosorb W (80—100 mesh).

Reaction of 1 with Isoprene (4a). A solution of 1.00 g (6.18 mmol) of **1** and 0.48 g (12.4 mmol) of isoprene (**4a**) in ethyl acetate (10 ml) was heated in a pressure bottle at 150 °C for 24 hr. After evaporation of the solvent, bulb-to-bulb distillation (oven temperature 150—180 °C, 3 mm) gave an oily mixture (1.15 g) which consisted of two components in the ratio of about 1: 1. These substances were separated by preparative GLC.

The first eluate (**5a**); IR: 1601, 1500, 752, and 690 cm^{-1}. NMR: δ 7.0 (m, 5H, Ph), 1.48 (s, 3H, CH_3), 1.4 (m, 4H, 2× CH_2). 2.24 (s, 1H, CH–N), and 3.83 (broad s, 1H, CH–N); MS: *m/e* 186 (M^+, 31), 105 (57), 81 (67), 79 (36), 77 (100%). Found: C, 77.34; H, 7.56; N, 14.84%. Calcd for $C_{12}H_{14}N_2$: C, 77.38; H, 7.58; N, 15.04%.

The second eluate (**7a**): IR; 1516, 1500, 1341, 1280, 1146, 942, 891, 750, 692 cm^{-1}; UV: λ_{max}^{MeOH} 276 nm (ε 18000); MS: *m/e* 185 (M^++1, 21), 184 (M^+, 100), 183 (43), 169 (23), 81 (20), 77 (38); NMR: δ 7.77 (d, 2.5 Hz, 1H), 6.47 (d, 1H, 2.5 Hz) (pyrazole), 7.0—7.9 (m, 5H, Ph–), 5.47 (m, 1H), 5.05 (m, 1H) (CH_2=), and 2.20 (s, 3H, CH_3) ppm. Found: C, 78.15; H, 6.72; N, 15.14%. Calcd for $C_{12}H_{12}N_2$: C, 78.23; H, 6.57; N, 15.21%.

Reaction of 1 with 2,3-Dimethylbutadiene (4b). A solution of 1.00 g of **1** (6.18 mmol) and 1.01 g (12.4 mmol) of **4b** in ethyl acetate (10 ml) was heated in a pressure bottle at 150 °C for 6.5 hr. Distillation gave an oily mixture (441 mg) which consisted of two components in the ratio of 4: 1. These substances were separated by preparative GLC.

The major substance was identified as **7a**, by comparison of its IR, NMR, MS, and the retention time of GLC with those of the afore-mentioned product.

The minor substance, **5b**: MS: *m/e* 200 (M^+, 33), 105 (35), 95 (100), 77 (83), 67 (40%); NMR: δ 7.0 (m, 5H, Ph–), 3.80 (m, 1H), 1.4 (m, 4H, 2× CH_2), 1.42 (s, 6H, 2× CH_3) ppm. Found: C, 77.67; H, 7.91; N, 13.71%. Calcd for $C_{13}H_{16}N_2$: C, 77.96; H, 8.05; N, 13.99%.

Reaction of 1 with Butadiene (4c). A solution of 231 mg (1.42 mmol) of **1**, 252 mg (2.14 mmol) of 3-sulfolene and a trace of hydroquinone in ethyl acetate was heated in a pressure bottle at 150 °C for 47 hr. Distillation gave an oily mixture (102 mg; 1: 1). One components was **7c**. The other was an unidentified hydrocarbon, probably originating from **4c**.

7c; MS: *m/e* 170 (M^+, 100), 169 (78), 152 (27), 149 (45), 77 (36%); NMR: δ 7.1—7.7 (m, 5H, Ph–), 7.80 (d, 3.1 Hz, 1H) and 6.48 (d, 3.1 Hz, 1H) (pyrazole), 6.76 (q, 11.0 and 17.8 Hz, 1H), 5.70 (q, 17.8 and 1.6 Hz, 1H), 5.30 (q, 11.0 and 1.6 Hz, 1H). Found: C, 77.66; H, 5.78; N, 16.70%. Calcd for $C_{11}H_{10}N_2$; C, 77.62; H, 5.92; N, 16.46%.

References

1) (a) R. Huisgen, R. Grashey, and J. Sauer, "The Chemistry of Alkenes," S. Patai, Ed., Interscience Publishers, London (1964), p. 739; (b) R. Huisgen, H. Gotthardt, and R. Grashey, *Chem. Ber.*, **101**, 536 (1968); (c) H. Gotthardt and R. Huisgen, *ibid.*, **101**, 552 (1968); (d) R. Huisgen and H. Gotthardt, *ibid.*, **1059** (1968).

2) P. M. Weintraub, *Chem. Commun.*, **1970**, 760.

3) For a pertinent reference, see M. Smith, "Rodd's Chemistry of Carbon Compounds," 2nd ed., Vol. II, Part A, ed. by S. Coffey, Elsevier Publishing, Amsterdam (1967), p. 1.

4) The genuine energy factor should be considered only in the case of 1,5-hexadiene, since 1,5-cyclooctadiene is considered to be controlled by both energy and entropy factors due to the ethylene bridging of 1,5-hexadiene.

5) See also A. Kranz and C. Y. Lin, *J. Amer. Chem. Soc.*, **95**, 5562 (1973).

6) T. Imagawa, M. Kawanisi, and K. Sisido, *Chem. Commun.*, **1971**, 1292; T. Imagawa, N. Sueda, and M. Kawanisi, *Chem. Lett.*, **1973**, 417; T. Imagawa, N. Sueda, and M. Kawanisi, *Tetrahedron*, **30**, 2227 (1974).

7) B. Franzus, S. Wu, W. C. Baird, Jr., and M. L. Scheinbaum, *J. Org. Chem.*, **37**, 2759 (1972).

8) L. G. Tensmeyer and C. Ainsworth, *ibid.*, **31**, 1878 (1966).

9) O. Yamamoto and H. Tomita, "Selected Spectra of Nuclear Magnetic Resonance, Olefinic Protons," Physico-Chemical Data Association Ltd., Tokyo (1972).

10) See Ref. 1a.

11) J. Bastide, N. El Ghandour, and O. Henri-Rousseau, *Bull. Soc. Chim. Fr.*, **1973**, 2290.

12) K. N. Houk, J. Sims, C. R. Watts, and L. J. Luskus, *J. Amer. Chem. Soc.*, **95**, 7301 (1973).

Cyclopentadienylsodium and Phenylethynylsodium as Cocatalysts in Olefin Metathesis

Kazuaki ICHIKAWA, Toru TAKAGI,* and Kazuo FUKUZUMI

Department of Applied Chemistry, Faculty of Engineering, Nagoya University, Furo-cho, Chikusa, Nagoya 464

(Received August 29, 1975)

Cyclopentadienylsodium and phenylethynylsodium are effective cocatalysts with WCl_6 in the homogeneous olefin metathesis. The optimum mole ratios of C_5H_5Na and $PhC{\equiv}CNa$ to WCl_6 ranged more widely—from 1.5 to 3.0 and from 1.5 to 2.5 respectively—than that of BuLi to WCl_6. The formation of the Friedel-Crafts products was extremely small—such as 1—%, if the cocatalyst/WCl_6 ratio was about 2. The new catalyst systems were less poisoned by ether than the other catalyst systems and were hardly deactivated in the course of the reaction. The characteristics of these catalyst systems were discussed.

In olefin metathesis, the alkylidene moieties of olefins are redistributed as follows:

$$\begin{matrix} R_1CH{=}CHR_2 \\ + \\ R_3CH{=}CHR_4 \end{matrix} \rightleftharpoons \begin{matrix} R_1CH \\ \| \\ R_3CH \end{matrix} + \begin{matrix} HCR_2 \\ \| \\ HCR_4 \end{matrix}$$

For the homogeneous metathesis, binary catalyst systems, such as WCl_6, $MoCl_5$ or $ReCl_5$–R_4Sn,[1] RMgX,[2] RLi,[3] or $R_{3-n}AlCl_n$,[4] in which R is an alkyl or an aryl group, have been used *in situ*. Also, hydridic agents, such as lithium aluminum hydride and sodium borohydride, have been used as cocatalysts with WCl_6.[5] This reaction is unique and useful, but it has the faults that the catalysts are unstable and easily deactivated.

This study of cyclopentadienylsodium and phenylethynylsodium as cocatalysts was carried out in order to improve these faults and in order to investigate the scope and the limitations of the cocatalysts.

Results and Discussion

Dependence of Conversion on the Cocatalyst/WCl_6 Ratio. The dependence of the conversion on the Na/W mole ratio in the metathesis with catalyst systems of WCl_6–C_5H_5Na and WCl_6–$PhC{\equiv}CNa$ is shown in Table 1. Good conversions were obtained at a Na/W ratio near 2 in both cases. Wang and Menapace have reported that the optimization at Li/W=2 strongly suggests a W^{IV} catalytic intermediate in the metathesis with a binary catalytic system of WCl_6 and *n*-BuLi.[3]

In the WCl_6–$PhC{\equiv}CNa$ system the formation of diphenyldiacetylene was confirmed by GLC analysis. This fact suggests that the active catalyst species, $W^{IV}Cl_4$, forms as follows:

$$WCl_6 + 2PhC{\equiv}CNa \xrightarrow{-2NaCl} (PhC{\equiv}C)_2WCl_4 \longrightarrow WCl_4 + PhC{\equiv}C\text{-}C{\equiv}CPh$$

In the NMR study, when WCl_6 was added to the C_5H_5Na benzene solution, the proton signal of $C_5H_5^-$ (1.7 ppm to high fields of the benzene reference, a singlet) disappeared and a new peak assignable to the vinyl protons of cyclopentadiene (about 0.85 ppm to high fields of the benzene reference, a multiplet) appeared. Also, in the WCl_6–C_5H_5Na system, it is speculated that the catalyst formation proceeds by a mechanism similar to that of the WCl_6–$PhC{\equiv}CNa$ system.

Table 1. Effect of cocatalyst/WCl_6 ratio[a]

Cocatalyst (M)	M/W ratio	Products, mol%[b]			
		C_4	C_7	C_{10}	F.C.[c]
C_5H_5Na	0.5	3	93	3	1
	1	11	76	12	1
	1.5	18	63	18	1
	2	25	49	25	1
	3	20	59	20	1
	4	12	76	12	0
$PhC{\equiv}CNa$	0.5	3	61	3	33
	1	6	84	6	4
	1.5	18	62	18	2
	2	20	58	21	1
	3	10	76	11	3
	4	2	95	3	0
BuLi	0.5	1	78	1	20
	1	4	87	4	5
	1.5	10	77	11	2
	2	20	59	20	1
	3	4	91	4	1
	4	0	100	0	0

a) The reactions of 2-heptene (1.2 mol/l) with WCl_6 (2.4×10^{-2} mol/l) and the listed cocatalysts were carried out in benzene at room temperature for 15 h. b) Mol% of each product to the total amounts of 2-butene, 2-heptene, 5-decene, and Friedel-Crafts products. c) Friedel-Crafts products.

In Fig. 1 the conversions are plotted against the cocatalyst/WCl_6 mole ratio. The optimum ranges of the cocatalyst/WCl_6 ratio decreased as follows:

C_5H_5Na, 1.5—3.0 > $PhC{\equiv}CNa$, 1.5—2.5 > BuLi, 2

In the WCl_6–BuLi system, the sharp decrease in the conversion at Li/W>2 suggests that the Bu^- from BuLi easily displaces more than two Cl^- on WCl_6 because of the strong nucleophilicity of the carbanion, that is, the $W^{IV}Cl_4$ formed is easily attacked further by the excess BuLi to be destroyed. On the other hand, the wide optimum range of the Na/W ratio in the WCl_6–C_5H_5Na system suggests that $C_5H_5^-$ from C_5H_5Na does not destroy the active W^{IV} species to any considerable extent, because of the weaker nucleophilicity of the carbanion. As the optimum range of the Na/W ratio

* Present address: Faculty of Fisheries, Hokkaido University, Minato-cho, Hakodate 040.

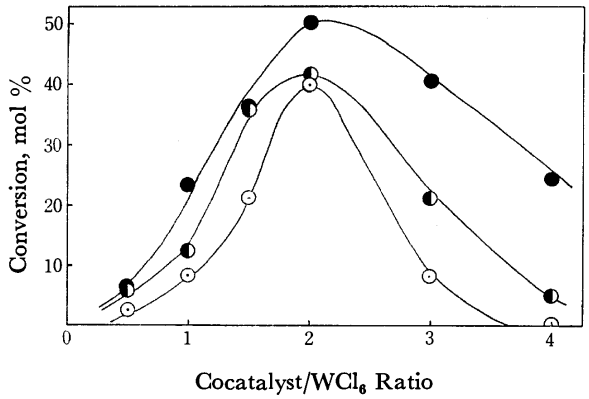

Fig. 1. Plot of conversion *vs.* cocatalyst/WCl_6 ratio.
Cocatalyst: ● C_5H_5Na, ◐ PhC≡CNa, ○ BuLi.
Conversion is mol % to 2-butene+5-decene.

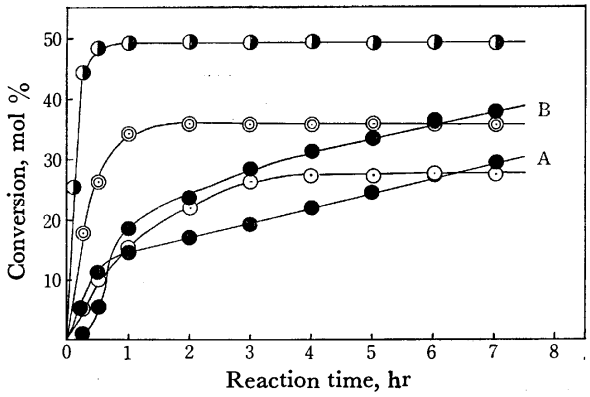

Fig. 2. Plot of conversion *vs.* reaction time. The reactions of 2-heptene (0.6 mol/l) with WCl_6 (2.4×10^{-2} mol/l) and cocatalysts were carried out in 1,2,4-trichlorobenzene at room temperature.
Cocatalyst: ● C_5H_5Na,Na/W=2, A: Preformed system, B: *In situ* system, ○ BuLi, Li/W=2, ◎ Bu_4Sn,Sn/W=1, ◑ Et_3Al,Al/W=1.
Conversion is mol % to 2-butene+5-decene.

in the WCl_6–PhC≡CNa system lies in between that in WCl_6–C_5H_5Na and that in WCl_6–BuLi, the nucleophilicity of $PhC{\equiv}C^-$ may be stronger than that of $C_5H_5^-$ and weaker than that of Bu^-. These cocatalysts are different from any other cocatalyst reported in that, in C_5H_5Na, the negative charge of the cyclopentadienide anion is delocalized on all the five carbon atoms, while in PhC≡CNa the anion is composed of the carbon atoms of the sp hybridization. The weak nucleophilicity may be attributable to this unique character.

The higher activity of the WCl_6–C_5H_5Na and WCl_6–PhC≡CNa systems than the WCl_6–BuLi system in the region of cocatalyst/$WCl_6<2$ may be explained by either one or both of the following reasons: (1) the slower deactivation of the WCl_6–C_5H_5Na and WCl_6–PhC≡CNa systems than the WCl_6–BuLi system, as will be described later, and (2) BuLi reacts completely and irreversibly with water, but C_5H_5Na and PhC≡CNa do so only reversibly and incompletely. Moreover, the hydroxide anion resulting from the reactions may be a more powerful inhibitor than water itself. Water is presumed to be the main inhibitor, since the deactivation of the metathesis catalyst was observed upon the addition of water and trace amounts of water are inferred to exist in the solvent and olefin, and on the wall of the reaction tube, though it was excluded as much as possible. Similarly, the higher activity of these catalyst systems than that of the WCl_6–BuLi system in the cocatalyst/$WCl_6\geqq2$ region may be attributable to the slower deactivation of these catalyst systems and the weaker nucleophilicity of the carbanions of the cocatalysts.

Because of the highly acidic character of the hydrogens of the cyclopentadiene and phenylacetylene, these cocatalysts are easily synthesized. Moreover, they are less hazardous and more stable than most other cocatalysts and less toxic than R_4Sn.

Phenylsodium and 1-hexynylsodium were also effective as cocatalysts of metathesis. However, triphenylmethylsodium and diphenylmethylsodium were not effective. These facts can be explained by the difficulties of the displacement of Cl in WCl_6 with the carbanions from triphenylmethylsodium and diphenylmethylsodium due to their weak nucleophilicity, itself attributable to the steric hindrance and the electronic effect.

Dependence of Conversion on the Reaction time.

Figure 2 shows the dependence of the conversion on the reaction time in the metathesis of 2-heptene with a catalyst system of WCl_6–C_5H_5Na, together with the reaction by the WCl_6–BuLi, WCl_6–Bu_4Sn, or WCl_6–Et_3Al system. The catalyst from WCl_6–C_5H_5Na required preformation periods to reach its maximum activity toward metathesis. In Curve A of Fig. 2, WCl_6 and C_5H_5Na had been allowed to stand for half an hour at room temperature before the olefin was added. The two reactions of A and B were identical in all other respects. The S shape of Curve B may be attributed to the incompleteness of the formation of active species at the initial stage of the reaction without standing, whereas the catalysts from WCl_6–BuLi, WCl_6–Bu_4Sn, and WCl_6–Et_3Al do not require the preformation periods. These facts suggest that, in the WCl_6–C_5H_5Na system, the catalyst formation, that is, the nucleophilic attack of carbanion on WCl_6 and/or the reductive elimination of carbanion from R_2WCl_4, proceeded more slowly than in WCl_6–BuLi, WCl_6–Bu_4Sn, or WCl_6–Et_3Al. Moreover, Fig. 2 shows that the initial rates increased in the following order:

$$C_5H_5Na \sim BuLi < Bu_4Sn < Et_3Al.$$

The fact that alkali salts of carbanions afford the active metathesis catalysts with WCl_6 suggests that the central metals of the cocatalysts need not be Lewis acids. However, the order of the initial rates suggests that the reduced tungsten component was activated by the presence of acidic aluminum and tin species. Aluminum capable of binding to tungsten through Cl bridges might be a constituent of the catalyst and might modify the distribution of the electron density of the reduced tungsten component and/or might accelerate the formation of an active *cis* intermediate, *cis*-WCl_4-$(Olefin)_2$.[6] Also, the possibility of Sn–W coordination bond formation in the WCl_6–Bu_4Sn system can not be denied, since several compounds containing tin-transition metal bonds have been reported.[7] Tin might function as the electron modifier of the reduced tungsten component.

Table 2. Friedel-Crafts products[a]

Cocatalyst (M)	M/W ratio	Olefin/W ratio	Products, mol%[b]			
			C_4	C_7	C_{10}	F.C.[c]
C_5H_5Na	2	100	25	49	25	1
PhC≡CNa	2	100	25	49	25	1
Bu_4Sn	1	100	20	52	21	7
Et_3Al	1	100	23	46	23	8

a) The reactions of 2-heptene with WCl_6 (2.4×10^{-2} mol/l) and the listed cocatalysts were carried out in benzene at room temperature for 15 h. b) Mol% of each product to the total amounts of 2-butene, 2-heptene, 5-decene and Friedel-Crafts products. c) Friedel-Crafts products.

Friedel-Crafts Products. The yield of the Friedel-Crafts products was 1% in the metathesis of 2-heptene by WCl_6–C_5H_5Na and by WCl_6–PhC≡CNa, whereas it was 7—8% in the metathesis reaction of 2-heptene by WCl_6–Bu_4Sn and by WCl_6–Et_3Al, as is shown in Table 2. These facts, that the WCl_6–acidic cocatalyst system favors the Friedel-Crafts reaction more than the WCl_6-basic cocatalyst system, may be attributable to the influence of aluminum and tin on the reduced tungsten component through the W–Cl–Al or W–Sn bond.

Stability of Catalysts. In the olefin metathesis, the conversion of olefin should attain the equilibrium conversion, 50%. The failure to reach the equilibrium value results from catalytic deactivation, as has been described in our previous paper.[1,2] As is shown in Fig. 2, when BuLi or Bu_4Sn was used as a cocatalyst, the conversion leveled off within 3 h. On the other hand, in the WCl_6–C_5H_5Na system, the increase in conversion continued and the equilibrium conversion was reached. This result and those shown in Table 3 show that the deactivation of the WCl_6–C_5H_5Na system proceeded more slowly than those of the WCl_6–BuLi and WCl_6–Bu_4Sn systems.

The deactivation of the metathesis catalyst not only has been reported in the literature but has also been observed in our laboratory by the addition of heteroatom compounds, such as water, alcohols, ethers, carbonyl compounds, carboxylic acids, esters, amines, nitriles, amides, phosphines, thiophene and thiophenol, as has previously been reported.

Table 3. Stability of catalyst[a]

Cocatalyst (M)	M/W ratio		Products, mol%[b]		
			C_4	C_7	C_{10}
C_5H_5Na	2	*In situ*	25	50	25
		Preformed	16	68	16
Bu_4Sn	1	*In situ*	25	50	25
		Preformed	3	94	3

a) The reactions of 2-heptene (0.6 mol/l) with WCl_6 (2.4×10^{-2} mol/l) and the listed cocatalysts were carried out in 1,2,4-trichlorobenzene at room temperature for 15 h. In the *in situ* system, 2-heptene, WCl_6 and the listed cocatalyst were added successively. In the preformed system, 2-heptene was added 1 h later after WCl_6 and the listed cocatalyst were mixed. b) Mol% of each product to the total amounts of 2-butene, 2-heptene and 5-decene.

Table 4. Effect of ether addition to system[a]

Cocatalyst (M)	M/W ratio	Et_2O/W ratio	Products, mol%[b]			
			C_4	C_7	C_{10}	F.C.[c]
C_5H_5Na	2	0	25	49	25	1
		1	21	56	22	1
		2	15	68	16	1
		4	8	83	8	1
PhC≡CNa	2	0	24	50	25	1
		1	20	58	21	1
		2	14	70	15	1
		4	7	86	7	0
BuLi	2	0	21	55	22	2
		1	9	80	10	1
		2	2	95	2	1
		4	0	100	0	0
Bu_4Sn	1	0	23	47	23	7
		1	22	53	22	3
		2	11	76	12	1
		4	4	92	4	0

a) The reactions of 2-heptene (1.2 mol/l) with WCl_6 (2.4×10^{-2} mol/l) and the listed cocatalysts were carried out in benzene at room temperature for 15 h. b) Mol% of each product to the total amounts of 2-butene, 2-heptene, 5-decene and Friedel-Crafts products. c) Friedel-Crafts products.

In the metathesis using C_5H_5Na or PhC≡CNa with WCl_6, also, the effect of ether on the conversion was investigated; the results are shown in Table 4. The fact that the WCl_6–C_5H_5Na and WCl_6–PhC≡CNa systems were less poisoned by ether than the WCl_6–BuLi and WCl_6–Bu_4Sn systems suggests that the former systems are less deactivated by the water present in the reaction systems. The deactivation of the catalysts by ether may be explained by the following inferences: (1) the coordination of the inhibitor at its heteroatom to tungsten, which interrupts the formation of active intermediates, such as diolefin complexes; (2) the decomposition of the bimetallic catalyst system by the coordination of the basic inhibitor to the cocatalyst metal,[6] though no evidence for the formation of the tungsten-lithium or sodium binary complex has been reported in the olefin metathesis, and (3) the decomposition of the cocatalysts by a reaction with ether, such as a Wittig rearrangement.

The WCl_6–Bu_4Sn and WCl_6–BuLi systems showed the optimum conversion when 2—3 equivalent moles of dicyclopentadiene, cyclopentadiene, or phenylacetylene to WCl_6 were added. This suggests that the stability of the catalyst from the WCl_6–C_5H_5Na or PhC≡CNa system is also attributable to the organogroups from the cocatalysts, which may interrupt the coordination of the inhibitor, water, to tungsten by means of the coordination at the cyclopentadienyl ring or the triple bond.

Experimental

Materials. The cyclopentadienylsodium was prepared according to a modification of the method given in the literature.[8] Sodium-dried benzene and a sodium–naphthalene

dispersion containing 15 wt% sodium were used instead of xylene and sodium metal. The supernatant solution was stored in a sealed Schlenk tube. The concentration of the reagent was determined by titration with aqueous sodium hydroxide after the addition of excess hydrochloric acid to the reagent. The preparation and the analysis of phenylethynylsodium were carried out in a similar way.[9] The triethylaluminum and butyllithium (both 15 w/v % hexane solutions) and tetrabutyltin (extra pure reagent) were purchased and used without further purification. The tungsten hexachloride was purified by the sublimation of the more volatile contaminants, WO_2Cl_2 and $WOCl_4$, under nitrogen at about 200 °C, leaving a residue of pure tungsten hexachloride. The benzene was distilled over sodium wire under nitrogen. After having been dried over anhydrous calcium sulfate (Drielite), 1,2,4-trichlorobenzene was distilled under nitrogen. The mixed 2-heptene (*cis* content, 75%; Tokyo Kasei; extra pure reagent) was dried by sodium wire and distilled over sodium hydrogensulfite under nitrogen.

Procedure. A typical procedure for the metathesis of 2-heptene will now be described. To a dried glass tube sealed with a neopren rubber cap, 2-heptene (0.28 ml, 2.4×10^{-3} mol, 1.2 mol/l), a benzene solution of WCl_6 (4.8×10^{-5} mol, 2.4×10^{-2} mol/l), and a benzene solution of C_5H_5Na (9.6×10^{-5} mol, 4.8×10^{-2} mol/l) were injected, in this order, by means of hypodermic syringes. The total volume of the reaction mixture was 2.0 ml. The reaction mixture was oscillated vigorously at room temperature for 15 h, and then analyzed by gas-liquid chromatography, which was performed with a Shimadzu-GC-4APF or a JEOL-GC-1100 chromatograph, using an 1 m×3 mm column packed with 10% SE30 on 80—100 mesh Chromosorb W.

The Friedel-Crafts products were identified by gas-liquid chromatography using authentic samples which had been prepared by the alkylation of benzene with olefin catalyzed by sulfuric acid and aluminum chloride respectively. The identity of diphenyldiacetylene was determined by gas-liquid chromatography using an authentic sample prepared according to the method given in the literature.[10]

The NMR spectra were obtained by means of a Japan Electron Optics Lab. JEOL 60 HL apparatus operating at 60 MHz.

References

1) J. A. Moulijin and C. Boelhouwer, *Chem. Commun.*, **1971**, 1170; P. B. van Dam, M. C. Mittelmeijer, and C. Boelhouwer, *ibid.*, **1972**, 1221; *Fette Seifen Anstrichmittel*, **76**, 264 (1974); T. Takagi, K. Ichikawa, T. Hamaguchi, K. Fukuzumi, and M. Aoyama, *Yukagaku*, **24**, 377 (1975).

2) T. Takagi, T. Hamaguchi, K. Fukuzumi, and M. Aoyama, *Chem. Commun.*, **1972**, 839; P. A. Raven and E. J. Warton, *Chem. Ind.*, **1972**, 292; T. Takagi, K. Ichikawa, K. Fukuzumi, and T. Hamaguchi, *Yukagaku*, **24**, 518 (1975).

3) J. L. Wang and H. R. Menapace, *J. Org. Chem.*, **33**, 3794 (1968).

4) N. Calderon, H. Y. Chen, and K. W. Scott, *Tetrahedron Lett.*, 3327 (1967); N. Calderon, E. A. Ofstead, J. P. Ward, W. A. Judy, and K. W. Scott, *J. Amer. Chem. Soc.*, **90**, 4133 (1968); E. A. Zuech, W. B. Hughes, D. H. Kubicek, and E. T. Kittleman, *J. Amer. Chem. Soc.*, **92**, 528 (1970); N. Calderon, *Accounts Chem. Res.*, **5**, 127 (1972); A. Uchida, Y. Mukai, Y. Hamano, and S. Matsuda, *Ind. Eng. Chem. Prod. Res. Develop.*, **10**, 369 (1971).

5) J. Chatt, R. J. Haines, and G. J. Leigh, *Chem. Comm.*, **1972**, 1202; S. A. Matlin and P. G. Sammes, *ibid.*, **1974**, 173.

6) L. Bencze and L. Marko, *J. Organometal. Chem.*, **69**, C19 (1974); J. L. Wang, H. R. Menapace, and M. Brown, *J. Catal.*, **26**, 455 (1972); M. Hidai, T. Tatsumi, and Y. Uchida, This Bulletin, **47**, 3177 (1974).

7) N. A. D. Carey and H. C. Clark, *Inorg. Chem.*, **7**, 94 (1968).

8) G. Wilkinson, "Organic Syntheses," Coll. Vol. IV, p. 473 (1973); R. B. Moffett, "Organic Syntheses," Coll. Vol. IV, p. 238 (1963).

9) T. F. Rutledge, *J. Org. Chem.*, **22**, 649 (1957); H. Gilman and R. V. Young, *ibid.*, **1**, 315 (1936).

10) I. D. Campbell and G. Eglinton, "Organic Syntheses," Coll. Vol. V, p. 517 (1973).

The Thermal Reaction of Azoxybenzenes

Ichiro SHIMAO and Hirokazu HASHIDZUME

Department of Industrial Chemistry, Faculty of Engineering, Toyama University, Takaoka-shi, Toyama 933

(Received September 1, 1975)

Azoxybenzenes (**1**) were heated at 245—250 °C to give azobenzenes (**2**), 2-hydroxyazobenzenes (**3**), 2-hydroxyazoxybenzenes (**4**), 4-hydroxyazobenzenes (**5**), and 4-hydroxyazoxybenzenes (**6**). Compounds **4** and **6** were mostly composed of α-isomers. In the reaction of azoxytoluenes, their methyl groups were oxidized to formyl groups. It was proposed that **4** and **6** were the intermediates of the thermal rearrangement of **1** to **3** and **5**.

The Wallach rearrangement[1] and photorearrangement[2] of azoxybenzenes (**1**) have been extensively investigated, and it is well known that azobenzenes (**2**) can be prepared by a dry distillation of **1**. Recently, Feinstein and Fields[3] have investigated the reaction of azoxybenzene with benzene at elevated temperatures. However, only one work on the thermal rearrangement has been done. About seventy years ago, Knipscheer[4] reported that **1** decomposed thermally to give **2**, 2-hydroxyazobenzenes (**3**), and 4-hydroxyazobenzenes (**5**) at 240—250 °C in a carbon dioxide atmosphere. Azoxybenzenes gave mostly **5** in a Wallach rearrangement, and exclusively **3** in a photorearrangement, but they gave **3** and **5** in a thermal reaction. Consequently, it seemed that the thermal rearrangement may proceed by a mechanism different from those presented for the other rearrangements of **1**. In this paper, we will deal in detail with the thermal reaction of unsubstituted, 4-bromo-, 3,3′-, and 4,4′-disubstituted azoxybenzenes.

Results and Discussion

It was found by the differential thermal analysis that the exothermic reaction occurred when **1** was heated at 245—250 °C. The thermal decomposition of **1** at 245—250 °C gave **2**, **3**, 2-hydroxyazoxybenzenes (**4**), **5**, and 4-hydroxyazoxybenzenes (**6**), while the formation of **2**, **3**, and **5** has previously been reported by Knipscheer.[4] The results are shown in Table 1.

TABLE 1. THERMAL REACTION OF AZOXYBENZENES

$RC_6H_4N^+=NC_6H_4R'$ (O$^-$)

R	R′	Time (min)	**1** (%)	**2** (%)	**3** (%)	**4** (%)	**5** (%)	**6** (%)
H [a]	H	60	27	25.9	4.1	1.2	1.2[b]	
4-Cl	4-Cl	30	70	7.5	1.3	1.1		
3-Cl	3-Cl	30	50	14.5	3.6[c]	0.8[c]	0.9	1.8
4-CH_3	4-CH_3	60	15	36.9	1.2	0.5		d)
3-CH_3	3-CH_3	30	38	20.4			0.4	d)
4-OCH_3	4-OCH_3	60	12	23.9	1.0			
3-OCH_3	3-OCH_3	30	45	14.8	3.1[c]	0.5[c]	0.5	1.5
H	4-Br	30	52	16.0	2.3[e]	1.1		
4-Br	H	30	8	38.4	2.7[e]	trace		

a) Reaction temperature, 245—250 °C. b) Crude product, mixture of **5** and **6**. c) Mixture of 2-hydroxy compound and 6-hydroxy compound. d) Tolylazobenzaldehyde was obtained. e) Mixture of 5-bromo-2-(phenylazo)phenol and 2-(4-bromophenylazo)phenol.

Significant amounts of black resinous substances were also formed as by-products.

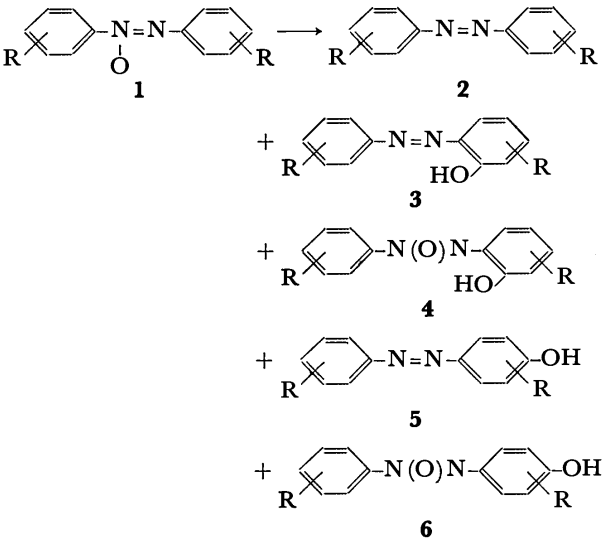

After long heating **4** and **6** were not isolated, because of their lability under these conditions. Figure 1 shows the influence of the heating time on the yields of **2**, **3**, and **4** for the thermal reaction of azoxybenzene. The 2-hydroxyazoxybenzenes obtained by the thermal reaction were exclusively 2-(phenyl-ONN-azoxy)phenols (α-isomers). The α- and β-isomers of **4** were easily distinguished by their NMR spectra. The OH proton signal of the β-isomer appeared in a lower magnetic field than that of the α-isomer (2-hydroxyazoxybenzene: β-isomer, δ 11.73 ppm; α-isomer, δ 7.66 ppm). This may be attributed to the formation of an intramolecular hydrogen bond between the hydroxyl group and the

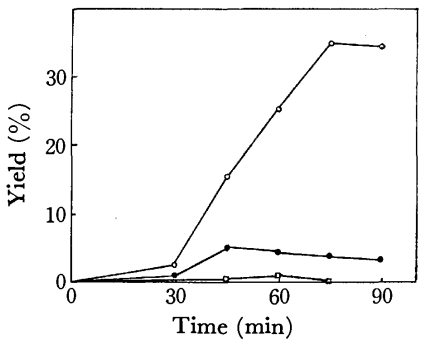

Fig. 1. The effect of the heating time on the yield of products, **2**, **3**, and **4**, for thermal reaction of azoxybenzene. At 245—250 °C.
○: **2**, ●: **3**, □: **4**.

oxygen atom of the azoxy group in the β-isomer. On the other hand, in the α-isomer the formation of the analogous intramolecular hydrogen bond is impossible, because of a steric strain present in its coplanar seven-membered ring. Those results agreed with those postulated by Digiavi[5] from the fact that the α-isomer is more liable to undergo oxidation with a potassium permanganate solution than is the β-isomer. In addition, the presence of the intramolecular hydrogen bond in the β-isomer was also shown by an absorption near 3400 cm^{-1} in its IR spectrum and by a higher R_f value in TLC on silica gel.

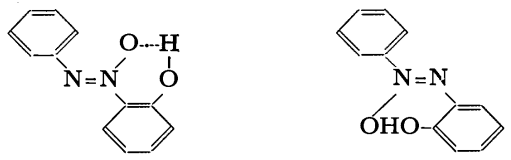

β-isomer α-isomer

The ratio of 2-(3-chlorophenylazo)-4-chlorophenol to 2-(3-chlorophenylazo)-6-chlorophenol was determined by gas chromatography to be 1:1. 2-(3-Methoxyphenylazo)-4-methoxyphenol and 2-(3-methoxyphenylazo)-6-methoxyphenol were separated by column chromatography on silica gel, and the ratio of the 4-methoxy isomer to the 6-methoxy isomer was 1:2.1. Those ratios were analogous to that in the photorearrangement of the corresponding **1**. Tanikaga[6] reported that the substituents on 3,3'-positions do not have a steric effect on the isomer ratios upon the photorearrangement. Interestingly, it was found that, on the irradiation of an ethanolic solution of 3,3'-dimethoxyazoxybenzene, the oxygen atom rearranged preferentially to the *o*-position of methoxy group (4-methoxy isomer: 6-methoxy isomer=1:2.5).

The 2-hydroxyazoxybenzenes obtained from 3,3'-dichloro- and 3,3'-dimethoxyazoxybenzenes were a mixture of the α-isomers; however, because of difficulties in the separation, the ratios of the 2-hydroxy isomer to the 6-hydroxy isomer could not be determined. The mixture of 3,3'-dichloro-**4** was reduced with lithium aluminum hydride in ethyl ether to give the corresponding **2** and a mixture of the corresponding substances **3**. It was presumed, by a comparison of the retention time in high-speed liquid chromatography with that of the authentic samples,[7] that 4-hydroxyazoxybenzene was composed mostly of α-isomers.

The thermal reactions of 3,3'- and 4,4'-azoxytoluenes gave 3-(*m*-tolylazo)benzaldehyde (yield, 2.1%) and 4-(*p*-tolylazo)benzaldehyde (yield, 2.5%) respectively. The methyl group was oxidized to only the formyl group, and the hydroxymethyl and carboxyl groups have not been found in the reaction products, which did not show a characteristic absorption of the carboxyl group in the IR spectra or a signal of the benzyl methylene proton in the NMR spectra.

The ratios of 2-phenylazo-5-bromophenol to 2-(4-bromophenylazo)phenol obtained from 4-bromo-ONN- and 4-bromo-NNO-azoxybenzenes were 2.5:1 and 1:3 respectively. These ratios were determined by means of the strength of the OH proton signal of the mixture on the NMR spectra (2-phenylazo-3-bromophenol, δ 13.30 ppm; 2-(4-bromophenylazo)phenol, δ 12.88 ppm). The hydroxyl group was preferentially introduced in the benzene ring remote from the oxygen atom of the azoxy group; however, the selectivity was significantly lower than that in the photorearrangement. 4-Bromo-ONN-azoxybenzene reacted faster than the NNO-isomer, and the **1** was recovered from the reaction mixture without isomerization to the other azoxy isomer.

In order to examine the pathway of the formation of **4** and **6**, mixtures of **1** and **3**, or **5** (1:1), were heated at 245—250 °C for 30 min. If **3** or **5** were oxidized to **4** or **6**, a large quantity of **4** or **6** should be formed in this condition. Azobenzene was formed in a larger quantity than when azoxybenzene was heated alone (yield of azobenzene: azoxybenzene+2-hydroxyazobenzene, 44%; azoxybenzene+4-hydroxyazobenzene, 53%; azoxybenzene alone, 2.6%); however, **4** or **6** were not isolated. These results show that **4** or **6** is not formed by the oxidation of **3** or **5** with **1**. The absence of **4** or **6** may be attributed to the fact that **1** was readily reduced with **3** or **5** to give **2**. This is reflected by the increasing yield of **2**. On the other hand, azoxybenzene was easily reduced to azobenzene on heating with phenols, such as naphthols; the resinous material and water were then formed.

Since **1** served as oxidizing agent at high temperatures and was converted to **2**, the *o*- or *p*-position of **1** was oxidized to the hydroxyl group. The formation of **4** or **6** is a novel reaction in which the aromatic nucleus is directly oxidized to phenols. The formation of the α-isomer of **4** or **6** is due to the ready oxidation of the benzene ring apart from the oxygen atom of the azoxy group. This may be explained in terms of the resonance of **1** and the nucleophilic attack.

In addition, 2-hydroxyazoxybenzene and 3,3'-dichloro-4-hydroxyazoxybenzene gave 2-hydroxyazobenzene (yield, 17%) and 3,3'-dichloro-4-hydroxyazobenzene (yield, 18%) respectively on heating at 245—250 °C for 5 min. Thus, we may conclude that the thermal rearrangement of **1** to **3** or **5** involves the disproportionation of **1** to **2** and **4** or **6** (oxidation and reduction), and then the reduction of **4** or **6** to **3** or **5**:

$$2C_6H_5N(O)NC_6H_5 \longrightarrow C_6H_5N_2C_6H_5 + C_6H_5N(O)NC_6H_4(OH)\ (o\text{- or } p\text{-})$$

$$C_6H_5N(O)NC_6H_4(OH) \xrightarrow{\text{Reduction}} C_6H_5N_2C_6H_4(OH)\ (o\text{- or } p\text{-})$$

However, it is possible that the thermal rearrangement proceeds partly by the pathway[8] proposed for the Wallach rearrangement, which includes protonation and a symmetrical intermediate ion, or by the intramolecular pathway[9] proposed for the photorearrangement.

Experimental

The IR spectra were recorded with a JASCO IRA-1 spectrometer. The NMR spectra were obtained with a JEOL MH-100 spectrometer, using TMS as the internal standard. The gas-chromatographic analysis was carried out using a Shimadzu GC-2C apparatus on a 1.5 m×3 mm column packed with 5% SE-52. The high-speed liquid-chromato-

graphic analysis was carried out using a JASCO-FLC 150 apparatus on a 0.5 m×2.1 mm column packed with JASCO-DAC SV-02 (solvent: methanol–water). The differential thermal analysis was carried out using a Mitamura-Riken 2-100 DTA-S apparatus with a sample packed as a layer in α-alumina. The melting points are uncorrected.

The azoxybenzenes were prepared by the methods described in the literature.[10-12]

Thermal Reaction of 1. General Procedure: About a 0.2 g portion of **1** was placed in a small glass tube and heated at 245—250 °C in a silicone oil bath. After cooling, the reaction mixture was extracted with benzene, and then the extract was further extracted with a dilute sodium hydroxide solution. The alkali extract was acidified with hydrochloric acid, and the resulting precipitate was collected and chromatographed on silica gel by the use of chloroform as the solvent. The elution was in the following order: **3**, **4**, **5**, and **6**.

The alkali-insoluble material was chromatographed on alumina by the use of benzene as the solvent; the elution was in the following order: **2** and **1**.

Each eluent was evaporated and recrystallized from hexane or ehanol. These products were identified by a comparison of their mp and their IR and NMR spectra with those of the corresponding authentic samples, or by chromatographic analysis.

Tolylazobenzaldehydes: These compounds were obtained as second fractions in chromatography, on silica gel, of the alkali-insoluble parts in the reaction of azoxytoluenes. 4-(*p*-Tolylazo)benzaldehyde was recrystallized from acetone and sublimed under reduced pressure; mp 177—178 °C (lit,[13] 177.5 °C). 3-(*m*-Tolylazo)benzaldehyde, obtained as an oil (IR: 1700 cm^{-1}, NMR: δ 9.82 ppm (COH)), was oxidized with silver oxide to the carboxylic acid. The acid was esterified with methanol in the presence of sulfuric acid; subsequent recrystallization from petroleum ether gave methyl 3-(*m*-tolylazo)benzoate; mp 66.5—68 °C; Found: C, 70.85; H, 5.40; N, 10.97%. Calcd for $C_{15}H_{14}N_2O_2$: C, 70.85; H, 5.55; N, 11.02%.

Preparation of the Authentic Samples. The compounds **3**, except for 2-(3-chlorophenylazo)-6-chlorophenol, were synthesized by the photorearrangement of **1**, or by the coupling of the corresponding phenols and diazonium salts. 2-(3-Methoxyphenylazo)-4-methoxyphenol; mp 80.5—81.5 °C. Found: C, 64.82; H, 5.25; N, 11.08%. Calcd for $C_{14}H_{14}N_2O_3$: C, 65.10; H, 5.46; N, 10.85%. 2-(3-Methoxyphenylazo)-6-methoxyphenol, mp 128.5—129.5 °C. Found: C, 65.07; H, 5.31; N, 10.68%. Calcd for $C_{14}H_{14}N_2O_3$: C, 65.10; H, 5.46; N, 10.85%.

The compounds **5** were prepared by diazo-coupling in the usual method. 4-(3-Chlorophenylazo)-2-chlorophenol, mp 127—128 °C. Found: C, 54.17; H, 2.81; N, 10.67%. Calcd for $C_{12}H_8Cl_2N_2O$: C, 53.95; H, 3.02; N, 10.49%. 4-(3-Methoxyphenylazo)-2-methoxyphenol, mp 88—89 °C. Found: C, 64.91; H, 5.24; N, 10.88%. Calcd for $C_{14}H_{14}N_2O_3$: C, 65.10; H, 5.46; N, 10.85%.

2-(3-Chlorophenylazo)-6-chlorophenol: This compound was formed during the irradiation of 3,3′-dichloroazoxybenzene; however, its separation from its isomer was difficult. Consequently, the following synthesis was carried out. A mixture of 2-chloro-6-nitrophenol (9.1 g), benzyl chloride (13.3 g), and 3% sodium hydroxide solution (186 ml) was stirred for 4 hr at 50—60 °C. A subsequent recrystallization of the oily substance from methanol gave *benzyl 2-chloro-6-nitrophenyl ether*; mp 49 °C (yield, 17%). Found: C, 59.66; H, 3.85; N, 5.35%. Calcd for $C_{13}H_{10}ClNO_3$: C, 59.50; H, 3.70; N, 5.39%.

The catalytic hydrogenation of the benzyl ether (2.4 g) in ethanol using the Pt catalyst gave *3-chloro-2-benzyloxyaniline*. The treatment of the aniline with hydrochloric acid gave the amine hydrochloride (yield, 83%). The *acetanilide*; mp 84—85 °C. Found: C, 69.20; H, 5.27; N, 5.13%. Calcd for $C_{15}H_{14}ClNO_2$: C, 69.36; H, 5.43; N, 5.39%.

A mixture of the amine hydrochloride (2.4 g), 3-chloronitrosobenzene (1.1 g), and anhydrous sodium acetate (0.1 g) in acetic acid (11 ml) and benzene (10 ml) was stirred for 15 hr at room temperature. The reaction mixture was then steam-distilled, and the residue was collected. After purification by column chromatography on alumina, recrystallization from ethanol gave *3-chloro-2-benzyloxy-(3-chlorophenylazo)-benzene*; mp 74—75 °C (yield, 21%). Found: C, 63.63; H, 3.79; N, 7.86%. Calcd for $C_{19}H_{14}Cl_2N_2O$: C, 63.88; H, 3.95; N, 7.84%.

A mixture of the benzyloxyazobenzene (0.6 g), acetic acid (3.7 ml), and 47% hydrobromic acid (3.7 ml) was stirred for 8 hr at 45 °C. The mixture was then poured into cold water. The recrystallization of the resulting precipitate from ethanol gave 6-chloro-2(3-chlorophenylazo)phenol; mp 143.5—145 °C (yield, 74%); lit,[6] mp 144 °C.

α-2-Hydroxyazoxybenzenes: The 2-hydroxyazobenzenes were oxidized by 30% hydrogen peroxide in acetic acid according to the usual method.[14] The product was chromatographed on silica gel, using petroleum benzine–benzene as the developing solvent, to separate the α-isomer from the β-isomer and the unchanged azo compound, and then recrystallized from petroleum benzine. The results are shown in Table 2.

TABLE2. PREPARATION OF α-2-HYDROXYAZOXYBENZENES,

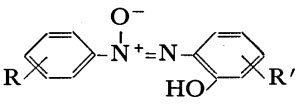

R	R′	Yield (%)	Mp (°C)	Found (Calcd) C %	H %	N %
4-Cl	4′-Cl	16	145.5—147	50.69	2.60	9.64
				(50.91	2.85	9.89)
5-Cl	3′-Cl	31	172 —173	50.76	2.65	9.61
				(50.91	2.85	9.89)
3-Cl	3′-Cl	31	128.5—129.5	51.00	3.01	10.00
				(50.91	2.85	9.89)
4-CH_3	4′-CH_3	9	107.5—108	69.57	5.64	11.39
				(69.40	5.83	11.56)
4-OCH_3	4′-OCH_3	2.5	114.5—116	61.18	4.93	10.06
				(61.31	5.15	10.21)
5-OCH_3	3′-OCH_3	3.5	84.5—86	61.10	5.10	10.05
				(61.31	5.15	10.21)
3-OCH_3	3′-OCH_3	8	69 — 71	61.04	5.13	10.12
				(61.31	5.15	10.21)
4-Br	H	33	101.5—102	49.32	3.08	9.85
				(49.17	3.09	9.56)
H	4′-Br	21	127 —128	49.35	3.12	9.85
				(49.17	3.09	9.56)

We wish to express our thanks to Professor Syuzi Hirooka for his valuable suggestions.

References

1) O. Wallach and E. Belli, *Chem. Ber.*, **13**, 525 (1880).
2) W. M. Cumming and G. S. Ferrier, *J. Chem. Soc.*, **127**,

2374 (1925).
3) A. I. Feinstein and E. K. Fields, *J. Org. Chem.*, **36**, 3878 (1971).
4) H. M. Knipscheer, *Recl. Trav. Chim. Pays-Bas*, **22**, 1 (1903).
5) D. Bigiavi, *Atti. accad. Lincei*, [6] **5**, 446 (1927).
6) R. Tanikaga, This Bulletin, **41**, 2151 (1968).
7) D. Bigiavi and S. Stefanic, *Atti accad. Lincei*, [6] **9**, 326 (1929).
8) R. A. Cox, *J. Amer. Chem. Soc.*, **96**, 1059 (1974), and the references cited therein.
9) D. J. W. Goon, N. G. Murray, J-P. Schoch, and N. J. Bunce, *Can. J. Chem.*, **51**, 3827 (1972), and the references cited therein.
10) I. Shimao, *Nippon Kagaku Kaishi*, **1974**, 515.
11) H. W. Galbaith, F. Degering, and E. F. Hitch, *J. Amer. Chem. Soc.*, **73**, 1323 (1951).
12) L. C. Behr, *ibid.*, **76**, 3672 (1954).
13) F. J. Alway, *Chem. Ber.*, **36**, 2311 (1903).
14) B. T. Newbold, *J. Org. Chem.*, **27**, 3919 (1962).

Role of Amine in Arylation of Ethylene with Iodobenzene Catalyzed by Rhodium Trichloride

Kunio Mori, Tsutomu Mizoroki, and Atsumu Ozaki

Research Laboratory of Resources Utilization, Tokyo Institute of Technology, Ohokayama, Meguro-ku, Tokyo 152

(Received September 5, 1975)

Rhodium trichloride effectively catalyzes the arylation of ethylene with iodobenzene in the presence of an amine to give styrene, although neither rhodium-powder nor chlorotris(triphenylphosphine)rhodium(I) is effective. The efficacy of the amine in increasing the yield of styrene is remarkable with tertiary and secondary amines but negligible with a primary amine. The difference among these amines in their interaction with rhodium trichloride is explained by their steric hindrance based on the isolation of the Rh(III)–amine complex only with primary amine.

The oxidative addition of an organic halide to Rh(I) complexes is well known. Alkyl, allyl, or acyl halide, for example, can be added to chlorotris(triphenylphosphine)rhodium(I) to give the corresponding σ-organorhodium(III) complex.[1] One of the well-known catalytic reactions using oxidative addition of an organic halide to Rh(I) complex is the acetic acid synthesis from methanol and carbon monoxide, of which the rate determining step is admittedly the oxidative addition of methyl iodide to Rh(I).[2] The oxidative addition of an aryl halide to Rh(I), however, is rarely found, except that iodobenzene reacts with methyltris(triphenylphosphine)rhodium(I) to give toluene.[3]

In the preceding paper, it was reported that, in the presence of a base, palladium-black effectively catalyzes the arylation of olefins with iodobenzene[4] as well as the carbonylation of iodobenzene.[5] These reactions are considered to take place *via* σ-arylpalladium(II) intermediate formed by the oxidative addition of iodobenzene to Pd(0) complex. As an extention of these studies, the oxidative addition of an aryl halide to rhodium has been examined. It has been found that the arylation of ethylene takes place smoothly in toluene when rhodium trichloride, $RhCl_3 \cdot 3H_2O$, is used as the catalyst together with a tertiary amine, whereas the primary amine is not very effective. The present paper is mainly concerned with the effect of the amine, and an interpretation is given for the reason why a tertiary amine is most effective in this catalytic reaction.

Experimental

Reaction Procedure. Rhodium trichloride ($RhCl_3 \cdot 3H_2O$, 0.5 mmol), iodobenzene (30 mmol), amine (0~30 mmol), and toluene (30 ml) were placed in a titanium-alloy autoclave (100 ml) equipped with a magnetic stirrer. Ethylene was introduced up to 20 kg/cm² at room temperature. The temperature was then raised up to 120 °C within 20 min, and kept constant for 3 hr. The autoclave was then cooled to room temperature with water, and the gaseous materials were discharged. The liquid products were quantitatively determined by gas chromatography, using a DC-550 column and bromobenzene as an internal standard.

Preparation of Rhodium Complexes. (a) Wilkinson's complex. $RhCl(P\phi_3)_3$ was prepared according to the literature[6] (Found: C, 70.46; H, 5.01; Cl, 4.23%. Calcd: C, 70.1; H, 4.9; Cl, 3.8%). (b) Penta(butylamine)chlororhodium(III)dichloride, $[RhCl(C_4H_7NH_2)_5]Cl_2$. $RhCl_3 \cdot 3H_2O$ (0.5 mmol) and butylamine (15 mmol) were placed in toluene (30 ml), and the solution was heated under reflux for 1 h. The solution turned yellow, giving a pale-yellow crystalline precipitate, which was recrystallized from methanol–water, and dried *in vacuo* (Found: C, 42.1; H, 10.0; N, 12.1; Cl, 19.3%. Calcd: C, 41.8; H, 9.58; N, 12.2; Cl 18.5%). (c) Tetra(butylamine)dichlororhodium(III)chloride, $[RhCl_2(C_4H_7NH_2)_4]Cl$. $[RhCl(C_4H_7NH_2)_5]Cl_2$ was treated with iodobenzene in the presence of butylamine under the conditions (Table 2) employed in the arylation of ethylene. No iodobenzene was consumed, while a precipitate was formed after the reaction. The precipitate was recrystallized from methanol and water (Found: C, 39.2; H, 9.6; N, 11.3; Cl, 19.0%. Calcd: C, 38.2; H, 8.8; N, 11.2; Cl 21.2%). (d) Tetra(benzylamine)dichlororhodium(III)chloride, $[RhCl_2(C_6H_5CH_2NH_2)_4]Cl$. The treatment of $RhCl_3 \cdot 3H_2O$ with benzylamine under the conditions employed in the arylation (Table 2) gave a crystalline yellow complex which was recrystallized from methanol and water (Found: C, 51.6, H, 5.9, N, 8.5, Cl, 17.5%. Calcd: C, 52.7, H, 5.7, N, 8.9, Cl, 16.7%). In this reaction, no arylation was observed, as in (c). (e) Phenyl rhodium(III) complex, $C_6H_5Rh(P\phi_3)_2(Cl)$(I). $RhCl(P\phi_3)_3$ (1 mmol) and iodobenzene (30 mmol) were placed in dried and degassed toluene (40 ml) under nitrogen. The solution was heated under reflux for 4 h. $RhCl(P\phi_3)_3$ was gradually dissolved, and the solution changed from reddish brown to dark brown, giving a dark brown crystalline precipitate on cooling. The precipitate was washed with hexane and dried *in vacuo* (Found: C, 57.9; H, 4.3; Halogen, 17.6%. Calcd: C, 58.1; H, 4.0; Halogen 18.7%). By treating a toluene solution of this complex with atmospheric hydrogen at room temperature for 3 h, benzene was quantitatively obtained. $RhCl(P\phi_3)_3$, however, was practically inactive for the formation of styrene. (f) Phenylrhodium(III)carbonyl complex, $C_6H_5Rh(P\phi_3)_2(CO)(Cl)$(I). A greenish yellow precipitate was obtained by treatment of iodobenzene (30ml) with a methanol solution (30 ml) of $RhCl_3 \cdot 3H_2O$ (0.5 mmol) in the presence of $P\phi_3$ (1.5 mmol) and butylamine (15 mmol) under ethylene pressure (20 kg/cm²) at 120 °C for 3 h, although no styrene was detected. The precipitate was recrystallized from benzene and methanol, and a yellow crystal was obtained(Found: C, 57.2; H, 3.9; Halogen, 18.0%. Calcd: C, 57.8; H, 4.0; Halogen, 17.2%. ν_{CO} 1965 cm^{-1}). Treatment of a chlorobenzene solution of this complex with dry hydrogen chloride at room temperature gave benzene quantitatively.

Results

General Features of the Reaction. From the reaction of iodobenzene (30 mmol) with ethylene (20 kg/cm²) at 120 °C for 3 h in methanol (30 ml) using $RhCl_3 \cdot 3H_2O$ (0.5 mmol) as the catalyst in the presence of butylamine (15 mmol) or tributylamine (15 mmol), a

small amount of styrene (8.0 and 0.96 mmol, respectively) was obtained; most of the catalyst was found in the form of metallic rhodium after the run. The addition of triphenylphosphine (1.5 mmol, $P\phi_3/Rh=3$ in mol) to this catalyst system completely inhibited the formation of styrene, and no iodobenzene was consumed. From the reaction mixture, σ-phenylrhodium(III)-carbonyl complex, $C_6H_5Rh(P\phi_3)_2(CO)(Cl)$(I), as described in the experimental section, was isolated. Carbon monoxide seems to be supplied from methanol.

Table 1. Arylation of ethylene catalyzed by Rh-catalyst

Catalyst 0.5 mmol, Iodobenzene 30 mmol, Tributylamine 15 mmol, Toluene 30 ml, P_{C_2}' 20 kg/cm² at room temp, Temp, 120 °C, and Time 3 h.

Rh-Catalyst	$P\phi_3$ (mmol)	Conv[a)] (%)	Select (%)
Rh-powder	0	0	0
$RhCl(P\phi_3)_3$	0	61	4
$RhCl_3\cdot 3H_2O$	0	86	80
$RhCl_3\cdot 3H_2O$	0.75	72	78
$RhCl_3\cdot 3H_2O$	1.5	7	0
$RhCl_3\cdot 3H_2O$	3	5	0

a) Based on iodobenzene.

The yield of styrene, however, was considerably increased by using a toluene–tributylamine mixture instead of methanol as the solvent. The results are summarized in Table 1. Rh-powder[7] showed no activity, and $RhCl(P\phi_3)_3$ gave only a small amount of styrene in spite of a considerable consumption of iodobenzene. Even in the case of $RhCl_3\cdot 3H_2O$, which proved to be effective for the arylation, the addition of triphenylphosphine($P\phi_3/Rh\geq 3$ in mol) also inhibited almost completely the formation of styrene.

The Effect of Amine. The effect of the amount of tertiary amines on the conversion of iodobenzene and selectivity to styrene is shown in Fig. 1. In the absence of tertiary amine, no styrene was formed and a substantial amount of metallic rhodium was found after the run. It is clear in Fig. 1 that the conversion of iodobenzene increases with increase in the amount of tertiary amine, while the selectivity to styrene decreases when a larger amount of the amine is added. Neither stilbene nor 1,1-diphenylethylene was detected.

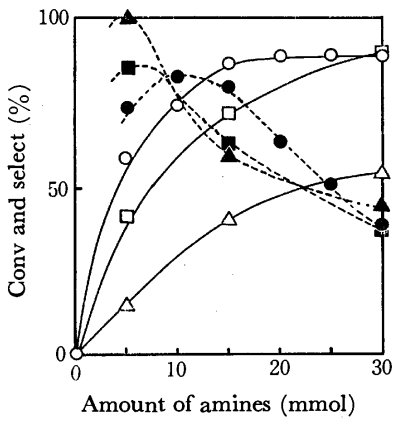

Fig. 1. Effect of the amount of tertiary amines. $RhCl_3\cdot 3H_2O$ 0.5 mmol, toluene 30 ml, iodobenzene 30 mmol, P_{C_2}' 20 kg/cm², Temp. 118 °C, and Time 3 h.
— Conv and --- Select
○ Tributylamine, □ Tripropylamine, and △ Triethylamine.

Separate experiments showed that iodobenzene remained unchanged in the absence of $RhCl_3\cdot 3H_2O$ under the condition specified in Fig. 1, while a considerable amount of iodobenzene was consumed even in the absence of ethylene when $RhCl_3\cdot 3H_2O$ was added. Although the reaction products were unidentified, this suggests that the rhodium catalyst catalyzes also a reaction of iodobenzene with the tertiary amine.

The effects of primary, secondary, and tertiary amines are summarized in Table 2. The yield of styrene decreases in the order, tertiary≥secondary≫primary amine. Practically no arylation takes place when primary amine or pyridine is added. The steric effect of primary amine was examined under the same

Table 2. Effect of amines (1)

$RhCl_3\cdot 3H_2O$ 0.5 mmol, Iodobenzene 30 mmol, Toluene 30 ml, P_{C_2}' 20 kg/cm² at room temp, Amine 15 mmol, Temp 120 °C, and Time 3 h.

Amine	pK_b	Conv[a)] (%)	Select (%)
None	—	0	0
Diethylamine	3.02	42	89
Triethylamine	3.35	40	60
Propylamine	3.47	0	—
Dipropylamine	3.00	53	90
Tripropylamine	3.35	71	63
Butylamine	3.41	0	—
Dibutylamine	2.75	58	86
Tributylamine	3.11	86	80
Octylamine		0	—
Dioctylamine		47	93
Trioctylamine		92	84
Aniline	9.42	23	29
Pyridine	8.85	0	—

a) Based on iodobenzene.

Table 3. Effect of amine (2)

$RhCl_3\cdot 3H_2O$ 0.5 mmol, Iodobenzene 30 mmol, Toluene 30 ml, P_{C_2}' 20 kg/cm$_2$ at room temp, Temp 120 °C, and Time 3 h.

Tributylamine (mmol)	Butylamine (mmol)	Conv.[d)] (%)	Select. (%)
15	0	86	80
15	3.75	38	95
15	5	12	100
15	7.5	0	—
15	15	0	—
5[a)]	0	51	88
5[a),b)]	0	38	84
5[a)]	30[c)]	36	71

a) $RhCl_3\cdot 3H_2O$ was used 0.75 mmol. b) Reaction time is 1 h. c) Butylamine was injected after 1 h and the temperature was kept constant furthermore for 2 h. d) Based on iodobenzene.

reaction condition. Monotertiarybutylamine and 1,1,3,-3-tetramethylbutylamine selectively gave styrene, although the conversions were low (9 and 10% respectively). The arylations in the presence of both tributylamine and butylamine were carried out to define their effects more clearly. The results are described in Table 3. It is clear that even when a large amount of tributylamine is present, the addition of butylamine remarkably decreases the yield of styrene. When butylamine was added through a high pressure injector during the course of arylation in the presence of tributylamine, it also terminated the formation of styrene (the last line of Table 3).

The isolation of rhodium–amine complex was carried out as described in the experimental section. The treatment of $RhCl_3 \cdot 3H_2O$ with butylamine gave $[RhCl(C_4H_9NH_2)_5)_5]Cl_2$, which changed into another complex, $[RhCl_2(C_4H_9NH_2)_4]Cl$, under the arylation condition. The treatment of $RhCl_3 \cdot 3H_2O$ with benzylamine under the arylation condition gave $[RhCl_2(C_6H_5CH_2NH_2)_4]Cl$, which has an analogy with the Rh(III)–butylamine complex. The primary amine is known to give stable Rh(III) complexes.[8] Practically no metallic rhodium was formed after the arylation in the presence of tertiary amine; all attempts to isolate a rhodium–tertiary amine complex, however, were unsuccessful.

Discussion

The treatment of $RhCl(P\phi_3)_3$ with iodobenzene in toluene under reflux gives a stable σ-phenylrhodium(III) complex, $C_6H_5Rh(P\phi_3)_2(Cl)(I)$, as described in the experimental section. $RhCl(P\phi_3)_3$ is catalytically inactive for the arylation of ethylene in spite of a considerable consumption of iodobenzene by the reaction with amine, as shown in Table 1. This suggests that the oxidative addition of iodobenzene to Rh(I) takes place readily, while $P\phi_3$ prevents the coordination of ethylene. When $RhCl_3 \cdot 3H_2O$ is used as the catalyst, the addition of a catalytic amount of $P\phi_3$ prevents not only the formation of styrene, but also the consumption of iodobenzene, as shown in Table 1. In this case, $P\phi_3$ presumably stabilizes the Rh(III) complex as $RhCl_3(P\phi_3)_3$,[6] because, if Rh(I) were formed during the reaction, iodobenzene should be consumed, as observed with $RhCl(P\phi_3)_3$. In the absence of $P\phi_3$, however, $RhCl_3 \cdot 3H_2O$ is fairly active for the arylation of ethylene with iodobenzene in the presence of tertiary amine. From the above consideration, it is postulated that the arylation reaction proceeds *via* a Rh(I) complex which is formed by reduction of a Rh(III) complex, although all attempts to isolate the Rh(I) complex in the absence of $P\phi_3$ were unsuccessful. Possible reducing agents were separately examined for their effectiveness under relevant conditions. Practically no reduction of Rh(III) was observed with amine or toluene. The treatment of $RhCl_3 \cdot 3H_2O$ with ethylene in the absence of iodobenzene, however, gave a black precipitate, presumably metallic rhodium, demonstrating some reducing ability for ethylene. Accodingly, it seems likely that Rh(III) is reduced by ethylene[9] during the course of arylation.

A question arises why the primary amines are almost ineffective for the arylation in spite of the fact that their basicities are almost the same as those of the secondary and tertiay amines, as shown in Table 2. The most plausible explanation may be a steric hindrance of the amine, because a bulky primary amine, for example, monotertiarybutylamine or 1,1,3,3-tetramethylbutylamine, gave styrene selectively, although the conversion was low. The less crowded primary amine tightly coordinates to Rh(III) to give a highly stable Rh(III)–primary amine complex, thus stabilizing the Rh(III) state. On the other hand, tertiary amines, which are sterically more crowded, are likely to coordinate weakly to Rh(III), giving rise to only slight inhibition of the reduction from Rh(III) to Rh(I). In fact, no Rh(III)–tertiary amine complexes have been isolated.

The active species may be a weakly bonded Rh(I)–tertiary amine complex, to which iodobenzene is oxidatively added to give σ-phenylrhodium(III) complex, followed by insertion of ethylene and elimination of β-hydrogen to give styrene as follows:

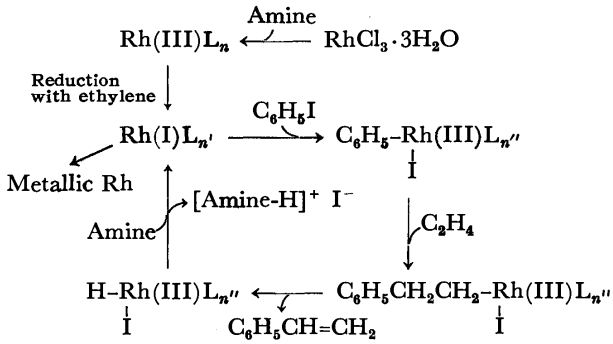

L: Hologen, Amine, Olefin, and Solvent.

Scheme.

The more tight coordination of the primary amine to Rh(III) than of the tertiary amine is also supported by the result that the formation of styrene is almost completely inhibited by the injection of butylamine during the course of the arylation described in Table 3. This means that the primary amine stabilizes the Rh(III) intermediate, resulting in a lack of regeneration of Rh(I) complex.

Since iodobenzene is consumed in the interaction with $RhCl_3 \cdot 3H_2O$–tributylamine mixture even in the absence of ethylene, σ-phenylrhodium(III) complex seems to react with tributylamine to give $[C_6H_5N(C_4H_9)_3]^+I^-$, although its isolation was unsuccessful. This may be the reason why the selectivity to styrene decreases with the increase in the amount of tributylamine, as shown in Fig. 1.

References

1) (a) D. N. Lawson, J. A. Osborn, and G. Wilkinson, *J. Chem. Soc. A*, **1966**, 1733. (b) M. C. Baird, J. A. Osborn, and G. Wilkinson, *ibid.*, **1967**, 1347.

2) (a) J. F. Roth, J. H. Craddock, A. Hershman, and F. E. Paulik, *Chem. Tech.*, **1971**, 600. (b) K. K. Robinson, A, Hershman, J. H. Craddock, and J. F. Roth, *J. Catal.*, **27**, 389 (1972).

3) M. F. Semmelhack and L. Ryono, *Tetrahedron Lett.* **1973**, 2967.
4) K. Mori, T. Mizoroki, and A. Ozaki, This Bulletin, **46**, 1505 (1973).
5) T. Ito, K. Mori, T. Mizoroki, and A. Ozaki, *ibid.*, **48**, 2091 (1975).
6) J. A. Osborn, F. H. Jardine, J. F. Young, and G. Wilkinson, *J. Chem. Soc. A*, **1966**, 1711.
7) Obtained from commercial sources (Wako Pure Chemical Industries, Ltd.).
8) H. Sawai and H. Hirai, *Inorg. Chem.*, **10**, 2068 (1971).
9) R. Cramer, *ibid.*, **1**, 722 (1962).

Synthesis of 2,5-Diaryltetrazoles from *N*-Phenylsulfonylbenzhydrazidoyl Chlorides and Arylhydrazines[1]

Suketaka Ito, Yumo Tanaka, and Akikazu Kakehi

Department of Industrial Chemistry, Faculty of Engineering, Shinshu University, Wakasato, Nagano 380

(Received September 11, 1975)

A new synthesis of 2,5-diaryltetrazoles is given by the reaction of *N*-phenylsulfonylbenzhydrazidoyl chlorides with arylhydrazines and the action of potassium carbonate on the intermediate product formed in the initial reaction. Thirty tetrazoles carrying H, CH_3, Cl, Br, or NO_2 as the *para*-substituent of the 2-phenyl group, and H, CH_3, Cl, CH_3O, CN, or NO_2 as that of the 5-phenyl group, were synthesized in 70—16% yields, respectively. The reaction may proceed *via* the concerted elimination of benzenesulfinate ion from the intermediate 1,3-diaryl-5-phenylsulfonylformazanide anion taking a quasi-aromatic configuration.

N-Phenylsulfonylbenzonitrilimine derived from the corresponding hydrazidoyl halide does not undergo 1,3-dipolar cyclo-addition but dimerizes easily to 1,4-dihydro-3,6-diphenyl-1,4-bis(phenylsulfonyl)-1,2,4,5-tetrazine.[2] This behavior which differs from that of *N*-phenylbenzonitrilimine should be attributed to the strong electron-withdrawing nature of the arylsulfonyl group. Since arylsulfonyl groups can be eliminated[3] and hydrazidoyl halides are a kind of imidoyl halide, the parent *N*-phenylsulfonylbenzhydrazidoyl halides can be utilized as a starting material for the synthesis of heterocycles.

The present paper gives a new synthesis of 2,5-diaryltetrazoles[4] by the reaction of *N*-phenylsulfonylbenzhydrazidoyl chlorides with arylhydrazines and the action of base such as potassium carbonate on the intermediate product formed in the initial reaction. Previously we described an alternative procedure for the synthesis of 2,5-disubstituted tetrazoles from phenylsulfonylhydrazones of aromatic aldehydes and benzenediazonium salt, in which formazan was postulated as an intermediate.[5]

Results and Discussion

The reactions were carried out without isolation of intermediates. *N*-Phenylsulfonylbenzhydrazidoyl chlorides, prepared from the corresponding hydrazides and thionyl chloride,[2,6] were allowed to react with two equivalents of an arylhydrazine in tetrahydrofuran. In cases of reactants carrying a nitro group, it was necessary to reflux or warm the mixture of the reactant materials in the solvent. After removal of the precipitated arylhydrazine hydrochloride by filtration,[7] the tetrahydrofuran solution was stirred with excess potassium carbonate for 24 h at room temperature. From the reaction mixture, 2,5-diaryltetrazole was isolated by extraction with chloroform–water and by subsequent chromatographic treatment of the chloroform extract. The results are summarized in Table 1.

The use of a tertiary amine such as triethylamine or pyridine with one equivalent of arylhydrazine in the first step of reaction caused the predominant formation of 1,4-dihydro-3,6-diaryl-1,4-bis(phenylsulfonyl)-1,2,4,5-tetrazine, and it was therefore unsuitable as the trapping agent of hydrogen chloride. Tetrahydrofuran was the most suitable solvent in this reaction; the use of benzene, chloroform, or diethyl ether as the solvent reduced the yields of the tetrazoles. Prolonged stirring with potassium carbonate brought about an increase in yield. Pyridine could serve as a substitute for potassium carbonate, giving tetrazoles in slightly lower yields. After removal of arylhydrazine hydrochloride from the reaction mixture, the filtrate was concentrated under reduced pressure below 30 °C. The resulting oily residue was stirred for 24 h at room temperature with the same volume of pyridine as that of the tetrahydrofuran removed to afford tetrazoles (Table 2). Stirring without a base in the second step of reaction gave a small amount of tetrazoles (7%, in the case of 2,5-diphenyltetrazole).

From the water layer in the chloroform–water extraction, benzenesulfinic acid was extracted with dichloromethane and confirmed to be phenyl benzhydryl sulfone.

Identification of tetrazoles was carried out by their analytical and spectral data and, in the case of known compounds, by comparison with authentic specimens. The spectral data of the products are listed in Table 3.

In the IR spectra, the absorptions due to the *para*-substituted phenyl groups at 2- and 5-position of the tetrazoles were additive and constitutive with minor changes. The absorption at 1260—1290 cm^{-1} may be assigned to the cyclic N–N=N group in analogy with other tetrazoles and triazoles.[8] The absorptions at near 1070, 1010, and 990 cm^{-1} can be attributed also to the tetrazole ring system: absorptions in the 1100 to 990 cm^{-1} region observed in tetrazole,[9a] 5-substituted tetrazoles,[9a] and 1,5-disubstituted tetrazoles[9b,c] have been assigned to the tetrazole ring system.

The reaction route can be illustrated as follows:

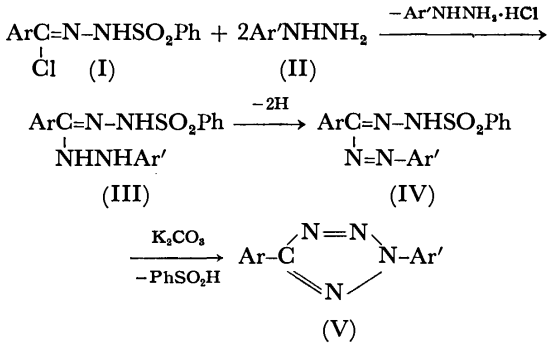

It is known that the reaction of *N*-arylbenzhydrazidoyl halide with phenylhydrazines yields formazans.[10]

TABLE 1. 2,5-DIARYLTETRAZOLES, 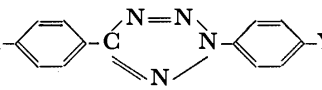 , FROM *N*-PHENYLSULFONYL-BENZHYDRAZIDOYL CHLORIDES AND ARYLHYDRAZINES

No.	Tetrazole[a,b] X	Y	Yield[c] (%)	Mp[d] (°C)	Molecular formula	Calcd(%) C	H	N	Found(%) C	H	N
1	H	H	65	101—102[e]	$C_{13}H_{10}N_4$						
2	H	CH_3	56	104—105[f]	$C_{14}H_{12}N_4$						
3	H	Cl	66	120—121[g]	$C_{13}H_9N_4Cl$						
4	H	Br	70	121—122[h]	$C_{13}H_9N_4Br$						
5	H	NO_2	49	187—188(dec.)	$C_{13}H_9N_5O_2$	58.43	3.39	26.21	58.33	3.44	26.20
6	CH_3	H	65	94—95[i]	$C_{14}H_{12}N_4$						
7	CH_3	CH_3	46	139—140	$C_{15}H_{14}N_4$	71.98	5.64	22.38	71.94	5.71	22.25
8	CH_3	Cl	55	143—144	$C_{14}H_{11}N_4Cl$	62.11	4.10	20.70	61.87	4.14	20.52
9	CH_3	Br	62	142—143	$C_{14}H_{11}N_4Br$	53.35	3.52	17.78	53.33	3.53	17.90
10	CH_3	NO_2	25	172—173(dec.)	$C_{14}H_{11}N_5O_2$	59.78	3.94	24.90	59.67	3.95	24.83
11	Cl	H	54	109—110[j]	$C_{13}H_9N_4Cl$						
12	Cl	CH_3	49	141—142	$C_{14}H_{11}N_4Cl$	62.11	4.10	20.70	62.17	4.14	20.65
13	Cl	Cl	58	177—178	$C_{13}H_8N_4Cl_2$	53.63	2.77	19.24	53.54	2.77	19.39
14	Cl	Br	56	176—177(dec.)	$C_{13}H_8N_4ClBr$	46.53	2.40	16.70	46.56	2.42	16.68
15	Cl	NO_2	39	185—186(dec.)	$C_{13}H_8N_5ClO_2$	51.76	2.67	23.21	51.61	2.69	22.89
16	CH_3O	H	47	107—108[k]	$C_{14}H_{12}N_4O$						
17	CH_3O	CH_3	40	111—112	$C_{15}H_{14}N_4O$	67.65	5.30	21.04	67.72	5.34	21.10
18	CH_3O	Cl	42	140—141	$C_{14}H_{11}N_4ClO$	58.65	3.87	19.54	58.73	3.89	19.66
19	CH_3O	Br	52	143—144	$C_{14}H_{11}N_4BrO$	50.78	3.35	16.92	50.88	3.34	16.91
20	CH_3O	NO_2	36	183—185(dec.)	$C_{14}H_{11}N_5O_3$	56.57	3.73	23.56	56.77	3.75	23.64
21	CN	H	50	170—171	$C_{14}H_9N_5$	68.01	3.67	28.32	67.79	3.71	28.19
22	CN	CH_3	50	173—174	$C_{15}H_{11}N_5$	68.95	4.24	26.80	68.85	4.24	26.76
23	CN	Cl	40	197—198(dec.)	$C_{14}H_8N_5Cl$	59.69	2.86	24.86	59.80	2.95	24.59
24	CN	Br	54	194—196(dec.)	$C_{14}H_8N_5Br$	51.56	2.47	21.47	51.42	2.47	21.57
25	CN	NO_2	16	205—207(dec.)	$C_{14}H_8N_6O_2$	57.54	2.76	28.76	57.79	2.83	28.49
26	NO_2	H	39	201—203(dec.)[l]	$C_{13}H_9N_5O_2$						
27	NO_2	CH_3	30	174—175	$C_{14}H_{11}N_5O_2$	59.78	3.94	24.90	59.84	3.99	24.73
28	NO_2	Cl	40	191—192(dec.)	$C_{13}H_8N_5ClO_2$	51.76	2.67	23.21	51.92	2.81	23.34
29	NO_2	Br	35	197—198(dec.)	$C_{13}H_8N_5BrO_2$	45.11	2.33	20.23	45.24	2.38	20.13
30	NO_2	NO_2	16	204—205(dec.)	$C_{13}H_8N_6O_4$	50.01	2.58	26.91	50.21	2.63	26.59

a) Satisfactory analytical data (±0.3% for C, H, N) were also obtained for all known compounds in the table. b) Tetrazole 5, 10, 15, 20, 25, and 30 were pale yellow to yellow crystals, and the others were colorless or almost colorless crystals. c) Calculated as mole per cent of total amounts obtained after column chromatography. d) Solvent for recrystallization: Tetrazole 1—4, ethanol; 5, 25, 29, and 30, benzene; the others, ethanol–benzene. e) Lit. mp 101.5—102.0°C: O. Dimroth and S. Merzbacher *Ber.*, **40**, 2402 (1907). f) Lit. mp 103°C: D. Jercher and H. Fischer, *Chem. Ber.*, **89**, 563 (1956). g) Lit. mp 120.5—121.5°C: Soon-Yung Hong and J.E. Baldwin, *Tetrahedron*, **24**, 3787 (1968). h) Lit. mp 122°C: O. Dimroth and S. Merzbacher, *Ber.*, **40**, 2402 (1907). i) Lit. mp 92.0—93.0°C: Soon-Yung Hong and J.E. Baldwin, *Tetrahedron*, **24**, 3787 (1968). j) Lit. mp 108.0—108.5°C: Soon-Yong Hong and J. E. Baldwin, *ibid.*, **24**, 3787 (1968). k) Lit. mp 105.0—105.5°C: Soon-Yung Hong and J. E. Baldwin, *ibid.*, **24**, 3737 (1968). l) Lit. mp 199.0—200.0°C: E. Wedekind, *Ber.*, **31**, 478 (1898).

TABLE 2. 2,5-DIARYLTETRAZOLES BY THE USE OF PYRIDINE

Tetrazole	Yield(%)
1	48
6	52
11	50
16	40
21	43
26	33

Although no reaction intermediates were isolated in this study,[11] the intermediacy of formazan in this reaction is undoubted from the reaction process and our other tetrazole synthesis.[5] The process, hydrazidine to formazan(III→IV), should be an autoxidation by air.

As a possible mechanism for the formation of tetrazole from formazan(IV→V), the following three can be given:

(1) Mechanism involving the Bamford-Stevens type α-elimination of benzenesulfinic acid followed by 1,5-dipolar cyclization[12] of the resultant arylazoaryldiazomethane:

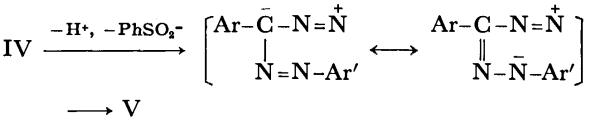

Scheme 1.

Table 3. Spectral data of the 2,5-diaryltetrazoles

Tetrazole	UV spectra (ethanol) λ_{max} nm($\varepsilon \times 10^4$)		IR spectra(KBr),[a] cm^{-1}					Tetrazole ring system[b]			
			CN	NO_2		Ar–O–CH_3	Ar–Cl				
1	240 (1.38)	272 (1.80)						1276	1071	1015	994
2	242 (1.27)	273 (2.00)						1274	1070	1011	996
3	241 (1.47)	274 (2.08)					1090	1275	1072	1010	994
4	240 (1.52)	275 (2.28)						1274	1063	1008	993
5	241 (1.85)	304 (2.30)		1517	1336			1280	1069	1011	998
6	244 (1.68)	275 (1.88)						1272	1068	1011	989
7	246 (1.69)	275 (2.17)						1275	1071	1010	994
8	244 (1.90)	276 (2.15)					1091	1271	1069	1008	990
9	245 (1.85)	277 (2.14)						1272	1069	1008	990
10	247 (2.09)	312 (2.02)		1529	1338			1272	1065	1011	985
11		276 (2.39)					1087	1269	1067	1008	992
12		277 (2.37)					1090	1268	1071[c]	1009	991
13		277 (2.64)					1093	1268	1064	1006	990
14		278 (2.59)					1090	1266	1063	1006	990
15	258 (1.72)	300 (2.77)		1521	1336		1090	1266	1065	1010	986
16	256 (1.84)	279 (2.00)				1250 1017		1286	1068	1006	990
17	257 (1.90)	279 (2.16)				1247 1022		1284	1077	1008	995
18	254 (2.17)	281 (2.19)				1246 1022	1096	1285	1070	1008	991
19	255 (2.16)	282 (2.19)				1244 1019		1285	1062	1005	986
20	259 (2.48)	326 (1.65)		1510[c]	1331	1240 1016		1285	1068	1005	983
21		279 (2.96)	2245					1273	1067	1013	996
22		281 (2.99)	2245					1272	1069	1010	995
23		281 (1.57)	2255				1091	1273	1068	1008	993
24		282 (2.97)	2260					1270	1065	1008	995
25	257 (1.69)	300 (2.78)	2255	1525	1348			1274	1067	1012	991
26	212 (2.05)	294 (2.63)		1512	1337			1279	1070	1010	999
27		299 (2.74)		1511	1337			1276	1071	1009	998
28		296 (2.95)		1525	1350		1094	1277	1071	1009	997
29	213 (2.19)	298 (3.05)		1523	1342			1278	1065	1007	997
30	213 (2.18)	304 (3.44)		1528	1348			1282	1068	1008	991

a) Absorptions other than those given in the table are omitted. b) The two peaks at 1266—1286 and 1062—1077 cm^{-1} are weak, and the others are strong to medium. c) Shoulder.

(2) Concerted elimination of benzenesulfinate ion from the intermediate formazanide anion taking a quasi-aromatic configuration:

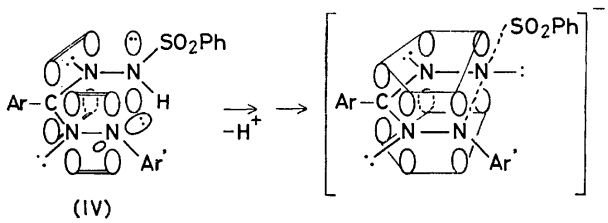

$\longrightarrow$ V + $PhSO_2^-$

Scheme 2.

(3) Polar cyclization of formazanide anion to tetrazolinide anion and its subsequent release of benzenesulfinate ion:

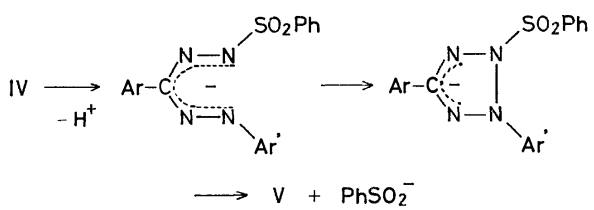

$\longrightarrow$ V + $PhSO_2^-$

Scheme 3.

The elimination of arenesulfinic acid occurs far more readily in the present reaction as compared with that in the Bamford-Stevens reaction[13] and in the pyrazole synthesis from α,β-unsaturated aldehydes tosylhydrazones.[14] Thus, the second mechanism (Scheme 2) is most probable: the greater facility of eliminating of benzenesulfinate ion may be due to the increased delocalization of π-electrons and the participation of a lone-pair orbital of nitrogen in the transition state.

Formazan and formazanide anion are isoelectronic with pentadienyl anion, and their most favored configuration would therefore be the planar U-shaped form.[15,16] The U-shaped form may possess some quasi-aromatic character.[17,18] Thus, keeping the U-shaped quasi-aromatic configuration, the formazanide anion might pass into the transition state, in which a three-center four-electron orbital-interaction arises between 1-*N*, 5-*N*, and the phenylsulfonyl group (analogous to S_N2 reaction) with a more stabilized 6π-electron structure (Scheme 2).

Arylazoaryldiazomethane can also cyclize easily to tetrazole, keeping its quasi-aromatic configuration by participation of the lone-pair orbital of the nitrogen atom adjacent to aryl group.[19] No matter how the azodiazomethane is involved in the reaction, it should be merely

a transition species.

The third mechanism may be improbable, since tetrazolinide ions lack the aromatic stabilization.

The lower yields of the tetrazoles with *para*-nitro-substituent, especially in the *N*-phenyl group, should be correlated to the electron-withdrawing nature of the substituent. *p*-Nitrophenylhydrazine reacted with the hydrazidoyl chlorides with difficulty because of its weak nucleophilicity, and 2,4-dinitrophenylhydrazine did not react with them. The nitro group in the *N*-phenyl group, and presumably in the *C*-phenyl group, may stabilize the hydrazidine to prevent oxidation to formazan.

The present method is comparable to others[4] as regards yield and utility for preparative purpose.

Experimental

Melting points were determined with a Yanagimoto micro-melting point apparatus Model MP-S3 and are uncorrected. The microanalysis was performed on a Perkin-Elmer elemental analyzer Model 240. Molecular weights were determined with a Hitachi Perkin-Elmer molecular weight apparatus Model 115. The IR and UV spectra were recorded with a JASCO DS-301 spectrometer and a Hitachi EPS-3 spectrometer, respectively.

1-Aroyl-2-phenylsulfonylhydrazines. General Procedure: Benzenesulfonyl chloride (0.1 mol) was added dropwise to a solution of an aroylhydrazine[20] (0.1 mol) in pyridine (50 ml)[21] with stirring and external cooling. The reaction mixture was allowed to stand at room temperature for 30 min and then poured into cold water. The resulting precipitates were collected by filtration, washed with dilute hydrochloric acid and water in succession, and dried; yield: almost quantitative. The product was purified by crystallization from methanol. The results are summarized in Table 4.

N-Phenylsulfonylbenzhydrazidoyl Chlorides. Typical Procedure: A mixture of 1-benzoyl-2-phenylsulfonylhydrazine (5.5 g, 0.02 mol) and thionyl chloride (10 ml) was refluxed for 1.5 h. After removal of excess thionyl chloride *in vacuo*, the resulting residue was crystallized from benzene to give colorless prisms; yield: 4.2 g (71%). The results are summarized in Tables 5 and 6.

2,5-Diaryltetrazoles. General Procedure: A solution of an arylhydrazine[22] (0.01 mol) in tetrahydrofuran (15 ml) was added dropwise to a solution of a *N*-phenylsulfonylbenzhydrazidoyl chloride (0.005 mol) in tetrahydrofuran (15 ml) at room temperature. With reactants carrying a nitro group, the mixture was warmed or refluxed for 10—60 min. The separated arylhydrazine hydrochloride was filtered and washed with tetrahydrofuran (20—30 ml). The filtrate combined with the washings was then stirred with potassium carbonate (2.5 g) for 24 h at room temperature using a magnetic instrument. The reaction mixture was concentrated and extracted with chloroform and water. After removal of the solvent from the chloroform extract, the resulting residue was chromatographed on a silica gel column using benzene as the eluent to give the corresponding tetrazole, which was purified by recrystallization from an appropriate solvent (ethanol,

Table 4. 1-Aroyl-2-phenylsulfonylhydrazines, X-C$_6$H$_4$-CONHNHSO$_2$Ph

Hydrazine X	Mp (°C)	Appearance	IR (KBr, cm^{-1}) NH	CO	SO$_2$	Other
H	198—199[d]	Columns	3270, 3120	1665	1340, 1167	
CH_3[a]	162—164	Needles	3300, 3080	1685	1330, 1160	
Cl[b]	184—185	Needles	3300, 3150	1645	1345, 1170	1094 (Ar-Cl)
CH_3O	186—188[e]	Prisms	3240, 3100	1650	1330, 1160	1250, 1020 (Ar-O-CH_3)
CN[c]	211—213	Needles	3220, 3080	1680	1355, 1170	2280 (CN)
NO_2	196—197[f]	Fine needles[g]	3280, 3060	1670	1340,[h] 1160	1525, 1340[h] (NO_2)

a) Found: C, 57.81; H, 4.87; N, 9.54%; mol wt(chloroform), 281. Calcd for $C_{14}H_{14}N_2O_3S$: C, 57.92; H, 4.86; N, 9.65%; mol wt, 290. b) Found: C, 50.11; H, 3.62; N, 9.17%; mol wt(acetone), 316. Calcd for $C_{13}H_{11}N_2O_3SCl$: C, 50.25; H, 3.57; N, 9.01%; mol wt, 311. c) Found: C, 55.46; H, 3.69; N, 13.80%; mol wt(acetone), 296. Calcd for $C_{14}H_{11}N_3O_3S$: C, 55.81; H, 3.68; N, 13.95%; mol wt, 301. d) Lit. mp 199°C: P. Grammaticakis, *Bull. Soc. Chim. Fr.*, **1953**, 86. e) Lit. mp 187—189°C: J. S. McFadyen and T. S. Stevens, *J. Chem. Soc.*, **1936**, 584. f) Lit. mp 201—202°C: C. Niemann and J.T. Hays, *J. Amer. Chem. Soc.*, **65**, 482 (1943). g) Pale yellow. h) Overlapped.

Table 5. Preparation of *N*-phenylsulfonylbenzhydrazidoyl chlorides, X-C$_6$H$_4$-C(Cl)=N-NHSO$_2$Ph

Hydrazidoyl chloride X	Yield (%)	Mp[a] (°C)	Appearance	IR (KBr, cm^{-1}) NH	C=N	SO$_2$	Other
H	71	121—122	Prisms	3150	1603	1344, 1170	
CH_3	79	153—154	Columns	3160	1610	1351, 1175	
Cl	85	156—158	Prisms	3170	1608	1351, 1180	1095 (Ar-Cl)
CH_3O	75	132—134	Plates	3170	1605	1346, 1170	1245, 1030 (Ar-O-CH_3)
CN	65	191—193	Plates	3080	1581	1353, 1168	2250 (CN)
NO_2	78	194—198	Prisms[b]	3160	1590	1340,[c] 1175	1515, 1340[c] (NO_2)

a) Solvent for recrystallization: X=H, CH_3, Cl, CH_3O....benzene; X=CN, NO_2....tetrahydrofuran.
b) Pale yellow. c) Overlapped.

Table 6. Analytical data of *N*-phenylsulfonylbenzhydrazidoyl chlorides, X-C(Cl)=N-NHSO$_2$Ph

Hydrazidoyl Chloride X	Molecular formula	Calcd(%) C	Calcd(%) H	Calcd(%) N	Found(%) C	Found(%) H	Found(%) N	Mol wt Calcd	Mol wt Found
H	$C_{13}H_{11}N_2O_2SCl$	52.97	3.76	9.50	53.02	3.75	9.56	295	295(benzene)
CH_3	$C_{14}H_{13}N_2O_2SCl$	54.46	4.24	9.07	54.45	4.29	9.12	309	317(benzene)
Cl	$C_{13}H_{10}N_2O_2SCl_2$	47.43	3.06	8.51	47.48	3.09	8.44	329	334(benzene)
CH_3O	$C_{14}H_{13}N_2O_3SCl$	51.77	4.03	8.63	51.71	4.05	8.61	325	323(benzene)
CN	$C_{14}H_{10}N_3O_2SCl$	52.59	3.15	13.14	52.35	3.14	13.14	320	318(acetone)
NO_2	$C_{13}H_{10}N_3O_4SCl$	45.96	2.97	12.37	45.77	2.99	12.47	340	331(chloroform)

benzene, or ethanol–benzene). The results are summarized in Tables 1 and 3.

The aqueous layer in the chloroform–water extraction was acidified, saturated with sodium chloride, and then extracted with dichloromethane. The dichloromethane extract was dried over sodium sulfate and treated with diphenyldiazomethane to give phenyl benzhydryl sulfone,[23] mp 189—190 °C (Ref. [24] mp 188 °C).

References

1) Presented in part at the 30th Annual Meeting of the Chemical Society of Japan, Osaka, April, 1974.

2) S. Ito, Y. Tanaka, and K. Yoshida, Abstracts of the Meeting of the Tokai Branch of the Chemical Society of Japan, Matsumoto, November, 1972, p. 1; Abstracts of the 28th Annual Meeting of the Chemical Society of Japan, Tokyo, April, 1973, Vol. III, p. 1371.

3) A typical example of α-elimination of arylsulfonyl group is the Bamford-Stevens reaction. Concerning β-elimination of arylsulfonyl group, see W. Paterson and G. R. Proctor, *J. Chem. Soc.*, **1965**, 485.

4) Concerning this subject, see F. R. Benson, "Heterocyclic Compounds," Vol. 8, Chapter 1, ed. by R. C. Elderfield, John Wiley & Sons, Inc., New York (1967).

5) S. Ito, Y. Tanaka, A. Kakehi, and K. Kondo, *Chem. Lett.*, **1973**, 1071.

6) S. Wawzonek and J. N. Kellen also prepared *N*-*p*-tolylsulfonylbenzhydrazidoyl chloride in a similar way, see *J. Org. Chem.*, **33**, 3627 (1973).

7) Except in the case of *p*-nitrophenylhydrazine, arylhydrazine hydrochloride was recovered almost quantitatively.

8) (a) E. Lieber and T. Enkoji, *J. Org. Chem.*, **26**, 4472 (1961); (b) E. Lieber, C. N. R. Rao, T. S. Chao, and H. Rubinstein, *Can. J. Chem.*, **36**, 1441 (1958).

9) (a) E. Lieber, D. R. Leverring, and L. J. Patterson, *Anal. Chem.*, **23**, 1594 (1951); (b) C. W. Roberts, G. F. Fanta, and J. D. Martin, *J. Org. Chem.*, **24**, 654 (1959); (c) C. W. Roberts and M. L. Maskaleris, *ibid.*, **24**, 926 (1959).

10) (a) H. von Pechmann, *Ber.*, **27**, 320 (1894); (b) F. D. Chattaway and A. J. Walker, *J. Chem. Soc.*, **127**, 975 (1925).

11) Attempts to separate formazan were unsuccessful. The tetrahydrofuran solution of hydrazidoyl chloride turned red gradually when mixed with arylhydrazine; the red color faded by stirring with potassium carbonate.

12) H. Reimlinger, *Chem. Ber.*, **103**, 1900 (1970).

13) W. R. Bamford and T. S. Stevens, *J. Chem. Soc.*, **1952**, 4735.

14) R. K. Bartlett and T. S. Stevens, *J. Chem. Soc., C*, **1967**, 1964.

15) R. Hoffmann and R. A. Olofson, *J. Amer. Chem. Soc.*, **88**, 943 (1966).

16) In the case of formazan, the hydrogen bond should also be taken into account.

17) Lloyd defined the term "quasi-aromatic" or "-aromaticity." In the present paper, the term "quasi-aromatic…" is used in the usual sense. *Cf. Angew. Chem. Intern. Ed. Engl.*, **11**, 404 (1972).

18) Hoffmann and Olofson interpreted the favored U-shaped form of pentadienyl anion in terms of the phase of the terminals of the HOMO. *Cf.* Ref. 15. A concept analogous to the quasi-aromaticity is applicable to the rationalization of the favored U-shaped configuration of pentadienyl anion.

19) The possibility of such participation of lone-pair orbital of hetero-atom was mentioned by Woodward and Hoffmann. *Cf.* R. B. Woodward and R. Hoffmann, "The Conservation of Orbital Symmetry," Academic Press, New York (1969), p. 32.

20) Aroylhydrazine was prepared from the corresponding ethyl aroate and hydrazine hydrate in the usual way.

21) In the cases of *p*-nitro-, *p*-cyano-, and *p*-chlorobenzoylhydrazine, a mixture of 25 ml each of pyridine and *N*,*N*-dimethylformamide was used.

22) Arylhydrazines, except phenyl- and *p*-nitrophenylhydrazine, were prepared from their corresponding hydrochlorides.

23) M. Kobayashi, H. Minato, and H. Fukuda, This Bulletin, **46**, 1266 (1973).

24) R. Knoll, *J. Prakt. Chem.*, **113**, 40 (1926); *Chem. Abstr.*, **20**, 2669 (1926).

Structure of C-2801X, a New Cephamycin-type Antibiotic

Hiroshi FUKASE and Hidesuke IWASAKI

Medicinal Research Laboratories, Central Research Division, Takeda Chemical Industries, Ltd. Jūso, Yodogawa-ku, Osaka 532

(Received September 29, 1975)

The C-3 side chain moiety of C-2801X, a new cephamycin-type antibiotic, was almost quantitatively obtained by Dowex 50-catalyzed hydrolysis, and its structure was established as 3,4-dihydroxy-α-methoxycinnamic acid (I) by spectroscopic analyses and synthesis. The full structure of C-2801X was also assumed to be XIII by NMR analysis.

In the course of screening for new antibiotics, two new species of *Streptomyces*, *S. heteromorphus* and *S. panayensis*, were found to produce a new cephamycin-type antibiotic C-2801X[1] together with cephamycins A and B.[2,3]

As described in detail in the paper[1] on characterization, C-2801X (Na salt: $C_{25}H_{28}N_3O_{12}SNa$) was regarded as a 7-(5-amino-5-carboxyvaleramido)-7-methoxycephem (cephamycin-type) antibiotic from the following facts: (1) C-2801X was inactivated by cephalosporinase; (2) it exhibits an IR absorption at 1760 cm^{-1} due to β-lactam, as shown in Fig. 1; (3) a signal corresponding to C-7 methoxyl group was observed in the NMR spectrum; and (4) glycine and α-aminoadipic acid in the hydrolyzate of C-2801X were determined to be 1:2 in molar ratio, as reported in cephamycin-type antibiotics.[3,4] The IR (Fig. 1) and UV [$\lambda_{max}^{H_2O}$ 234 nm (ε 12800), 318 (16900), $\lambda_{sh}^{H_2O}$ 295(15700)] spectra and paper chromatography indicated that C-2801X is a new antibiotic differing from known cephem antibiotics.

This paper describes first the elucidation of structure of the C-3 side chain moiety, and then presents evidence for the full structure for C-2801X.

Structure of C-3 Side Chain Moiety

C-2801X was almost quantitatively hydrolyzed at the C-3 side chain by treatment with Dowex 50 W×8 in methanolic solution. The hydrolysis products having amino groups were separated by adsorption on Dowex 50, and the methanolic solution containing a neutral or acidic substance was concentrated *in vacuo* to give I. The UV absorption (Table 2) was similar to that of C-2801X. Therefore, I was assumed to be the C-3 side chain moiety. The IR spectrum (Fig. 2) shows the presence of hydroxyl (3450, 1190 cm^{-1}), α,β-unsaturated carboxylic acid (1660, 1630) and aromatic ring (1605, 1510, 905). A phenolic hydroxyl group is probably present, as judged by the IR absorption and a positive color reaction with $FeCl_3$–$K_3Fe(CN)_6$ reagent.[5] The NMR spectrum in CD_3OD shows the signals of 1,2,4-*tri*-substituted benzene (δ, ppm: 7.35, 1H, d, J=1.5 Hz; 7.03, 1H, dd, J=1.5, 8 Hz; 6.75, 1H, d, J=8 Hz), a single vinylic proton (6.90, 1H, s), and methoxyl protons (3.70, 3H, s). These spectroscopic analyses suggest that I is a cinnamic acid derivative having two hydroxyl (at least one hydroxyl group is phenolic) and one methoxyl group.

Mass spectral fragmentations of I are shown in Table 1 and compared with those of *p*-hydroxy-α-methoxycinnamic acid (II) obtained from cephamycin B by hydrolysis in a similar manner. Peaks corresponding to M^+, M−15, M−32, M−43, M−60, M−87, M−88, and M−89 were observed in both mass spectra of I and II at a difference of *m/e* 16. As the peaks at *m/e* 107, 106, and 105 of II are due to fragments IIIa, IVa, and Va, the corresponding peaks at *m/e* 123, 122, and 121 of I were assigned to IIIb, IVb, and Vb, respectively. This fact indicates that I has two phenolic hydroxyl groups and that the methoxyl group is located at the α-position. A characteristic peak at M−33, observed

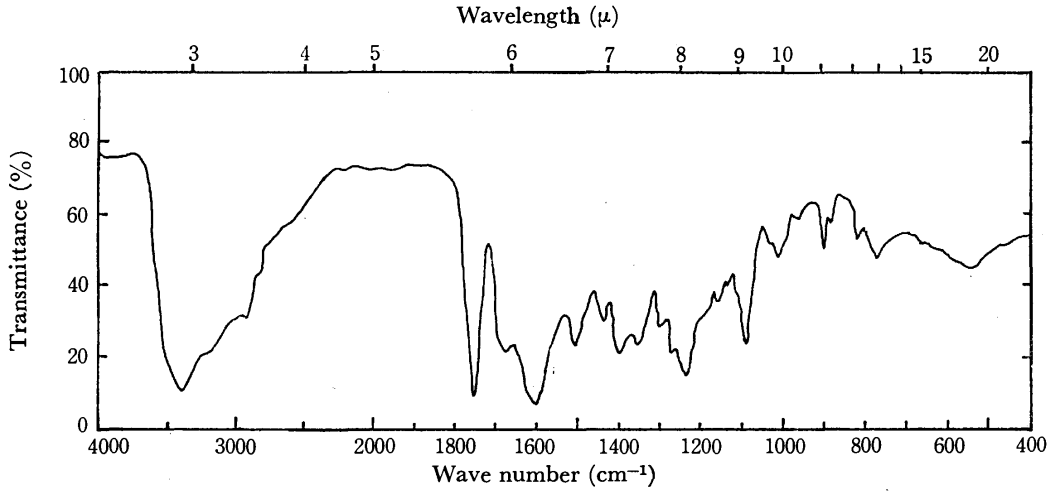

Fig. 1. IR spectrum of C-2801X mono-Na salt (KBr).

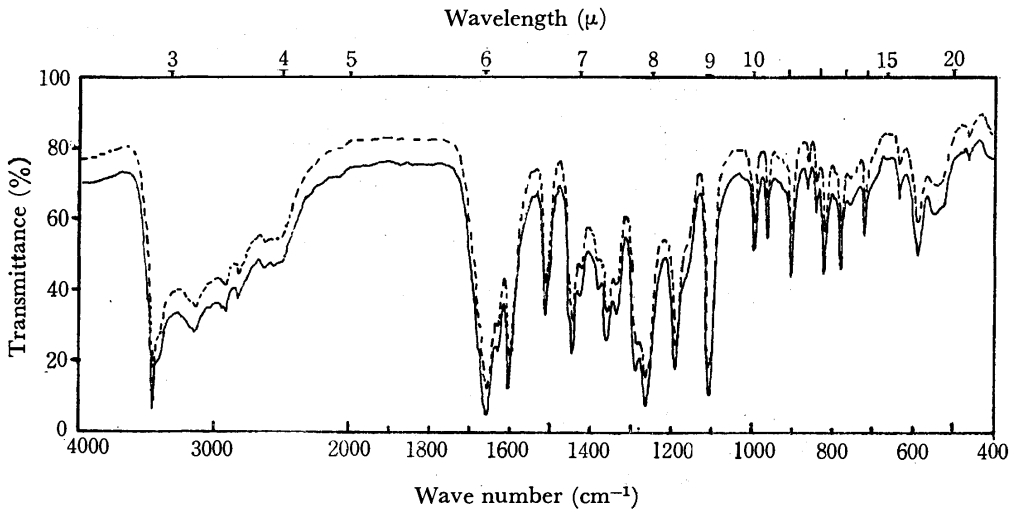

Fig. 2. IR spectra of natural and synthetic 3,4-dihydroxy-α-methoxycinnamic acid (I) (KBr).

—: Natural, —: synthetic.

TABLE 1. MASS SPECTRAL FRAGMENTATIONS OF I AND *p*-HYDROXY-α-METHOXYCINNAMIC ACID (II)

Fragments	I	II
M+	210 *m/e*	194 *m/e*
M−15 (CH_3)	195	179
M−32 (OCH_3+H)	178	162
M−33 (OCH_3+2H)	177	—
M−43 (CH_3+CO)	167	151
M−60 (CO_2H+CH_3)	150	134
M−87	123	107
M−88	122	106
M−89	121	105

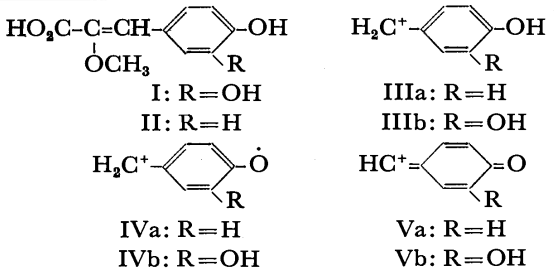

I: R=OH
II: R=H

IIIa: R=H
IIIb: R=OH

IVa: R=H
IVb: R=OH

Va: R=H
Vb: R=OH

TABLE 2. COMPARISON OF UV ABSORPTION MAXIMA OF I WITH THOSE OF DIHYDROXYCINNAMIC ACIDS[a] (VI)

Dihydroxycinnamic acid	λ_{max}^{MeOH} nm	$\lambda_{max}^{MeOH-NaOH}$ nm
3, 4-	230, 290, 320	240, 305, 345
2, 4-	225, 280	
2, 5-	248, 258	
3, 5-	225, 279	
2, 6-	227, 290	
2, 3-	225, 279	
I	218, 294, 318	250sh, 300, 335

a) Data taken from Ref. 6.

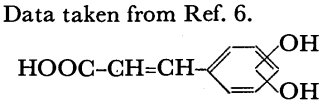

VI

only in the spectrum of I, is consistent with the structure having two hydroxyl groups.

To confirm the positions of the two hydroxyl groups on the benzene nucleus, UV absorption maxima[6] of six isomers of dihydroxycinnamic acid (VI) were compared with that of I (Table 2). The absorption maxima of I are obviously similar to that of 3,4-dihydroxycinnamic acid (caffeic acid).

From these data the chemical structure of I was assumed to be 3,4-dihydroxy-α-methoxycinnamic acid (I).

Since I is a hitherto unreported compound, 3,4-dihydroxy-α-methoxycinnamic acid was synthesized from protocatechualdehyde (VII) and ethyl methoxyacetate (X) as shown in the Scheme. As I is considerably labile in an alkaline solution, the two hydroxyl groups of VII were protectedby converting into hemiacetals which revert easily to hydroxyl by mild acidic hydrolysis. The addition reaction of dihydropyran[7] and ethyl vinyl

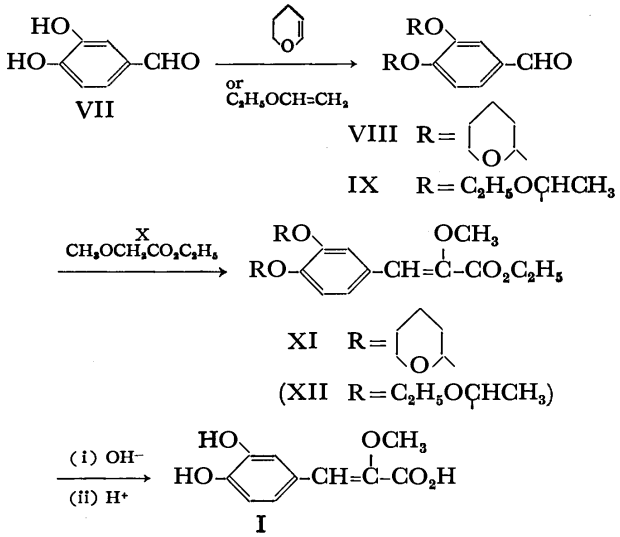

Scheme. Synthesis of 3,4-dihydroxy-α-methoxycinnamic acid.

ether[8] onto VII in the presence of phosphoric acid yielded VIII and IX, respectively. Condensation of VIII and IX with ethyl methoxyacetate (X) was carried out in toluene in the presence of metallic sodium to give XI and XII (not isolated), respectively.

Saponification of ester XI or XII and subsequent acid hydrolysis of the acetals gave 3,4-dihydroxy-α-methoxycinnamic acid (I). NMR, Mass, UV, and IR spectra (Fig. 2) of the synthetic compound were identical with those of the natural specimen (I).

Full Structure of C-2801X

In the Dowex 50-catalyzed hydrolysis described above, compounds adsorbed on the resin were eluted with 1 M sodium acetate. The investigation by paper chromatography of the eluate revealed that it contains α-aminoadipic acid and 7-methoxycephem moieties showing the same R_f values as those of hydrolysis products obtained by the same treatment of cephamycin B.

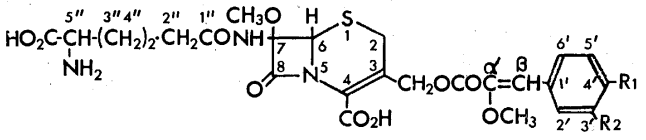

C-2801-X (XIII) $R_1 = R_2 = OH$

cephamycin A $R_1 = OSO_3H$ $R_2 = H$

cephamycin B $R_1 = OH$ $R_2 = H$

Table 3. NMR assignments of monosodium salts of C-2801X, cephamycin A and B
NMR (in D_2O) δ, ppm Mono-Na salt

Proton	C-2801X	Cephamycin A	Cephamycin B
2-C**H**$_2$	3.72, 3.34 (dd, J=18 Hz)	3.74, 3.35 (dd, J=18)	3.64, 3.31 (dd, J=18)
6-C**H**	5.21 (s)	5.15 (s)	5.10 (s)
7-OC**H**$_3$	3.60 (s)[a]	3.57 (s)[a]	3.59 (s)[a]
α-OC**H**$_3$	3.70 (s)[a]	3.65 (s)[a]	3.62 (s)[a]
β-C**H**	6.90 (s)	6.92 (s)	6.83 (s)
2′-C**H**	7.35 (d, 1.5)	7.68 (d, 8)[a]	7.52 (d, 8)[a]
3′-C**H**	—	7.32 (d, 8)[a]	6.85 (d, 8)[a]
5′-C**H**	6.90 (d, 8)	7.32 (d, 8)[a]	6.85 (d, 8)[a]
6′-C**H**	7.15 (dd, 1.5, 8)	7.68 (d, 8)[a]	7.52 (d, 8)[a]
2″-C**H**$_2$	2.4—2.7 (m)	2.4—2.7 (m)	2.4—2.7 (m)
3″,4″-(C**H**$_2$)$_2$	1.7—2.2 (m)	1.6—2.2 (m)	1.7—2.3 (m)
5″-C**H**	4.0—4.2 (m)	4.0—4.2 (m)	4.0—4.3 (m)

a) Tentative assignment. The figures in parentheses are coupling constants. s=singlet, d=doublet, dd=double doublet, m=multiplet

The NMR assignments of C-2801X are shown in Table 3, for comparison with those of cephamycin A and B. The chemical shifts, multiplicity, and coupling constants of each proton of C-2801X except the aromatic protons of the C-3 side chain were in fair agreement with those of cephamycin A and cephamycin B; *i.e.* 7-OC**H**$_3$, 6-C**H**, and 2-C**H**$_2$ of methoxycephem nucleus, α-OC**H**$_3$ of the C-3 side chain, and 2″-C**H**$_2$, 3″,4″-(C**H**$_2$)$_2$, and 5″-C**H** of the C-7 aminoadipoyl moiety. The chemical shifts of the aromatic protons of the C-3 side chain were assigned as shown in Table 3, in comparison with the NMR of I. The C-3′ of C-2801X has no proton, so the 2′-benzene proton does not show any *ortho*-coupling in J=8 Hz, but has a *meta*-coupling with the 6′-benzene proton in J=1.5 Hz. As the chemical shifts of the 2′-C**H**, 5′-C**H**, and 6′-C**H** are closer to those of cephamycin B than to those of cephamycin A, the two phenolic hydroxyl groups were supposed to be free. UV absorption and phenolic color reaction[5] of C-2801X also support this structure. Consequently, C-2801X was assumed to have the chemical structure shown as XIII.

Among C-2801X, cephamycin A, and cephamycin B, C-2801X (having two phenolic hydroxyl groups) shows the strongest activity against gram-negative bacteria, although their activities against gram-positive bacteria are almost indistinguishable.[1] This phenomenon is very interesting from the viewpoint of the structure-activity relationship.

Experimental

Hydrolysis of C-2801X. In a suspension of Dowex 50W×8 (H^+) (1 ml) in methanol (3 ml), the sodium salt (3 mg) of C-2801X was dissolved and the mixture was stirred at room temperature for 3 h. After filtration, the resin was washed with methanol (10 ml). The filtrate and the washings were combined and concentrated *in vacuo* to dryness. Addition of benzene to the residue, followed by standing at 10 °C overnight, afforded colorless prisms (1.1 mg) of I, mp 215 °C (dec.).

Found: C, 57.22; H, 4.67%; (M^+) *m/e* 210. Calcd for $C_{10}H_{10}O_5$: C, 57.14; H, 4.80%; mol wt, 210.18.

To Dowex resin separated by filtration was added 1M sodium acetate solution (5 ml), and the mixture was stirred for 30 min. The mixture was poured into a glass column (0.9×10 cm) and additional 1M sodium acetate solution (3 ml) was passed over the resin. The resulting eluates were combined and concentrated to *ca.* 1 ml. Ascending paper chromatography of the concentrate was carried out using 1-butanol–acetic acid–water (4: 1: 5) as a developing solvent. By spraying ninhydrin reagent, spots corresponding to α-aminoadipic acid and 7-methoxycephem moieties were observed, showing the same R_f values as those of the hydrolysis products of cephamycin B.

3,4-Bis(tetrahydropyranyloxy)benzaldehyde (VIII). A few drops of 80% phosphoric acid was added to a suspension of VII (2.7 g) in dihydropyran (10 ml) and the mixture was stirred at room temperature until in solution. After stirring at room temperature for an additional 3 h, the reaction mixture was poured into ice water (500 ml). The oily substance which separated out was extracted with ether, and after washing with 5% sodium hydrogencarbonate solution, the ether extracts were dried over anhydrous sodium sulfate and concentrated *in vacuo* to dryness. The residue was dissolved in ethyl acetate–benzene (1: 1) (10 ml) and charged to a column containing Merck's silica gel (250 ml). The column was developed with ethyl acetate–benzene (1: 1) and the eluate was evaporated *in vacuo* to give VIII (4.3 g) as an oil (yield: (72%).

Found: C, 66.79; H, 7.28%. Calcd for $C_{17}H_{22}O_5$: C, 66.65; H, 7.24%.

3,4-Bis(α-ethoxyethyloxy)benzaldehyde (IX). A few drops of 80% phosphoric acid was added with stirring and cooling

below 5 °C to a suspension of VII (2.7 g) in ethyl vinyl ether (10 ml). The suspension was stirred below 10 °C overnight and the resulting clear reaction mixture was poured into ice water (500 ml). The mixture was extracted with ether and the extracts, after washing with 5% sodium hydrogencarbonate solution, were dried over anhydrous sodium sulfate and concentrated *in vacuo*. The oily residue was purified by vacuum distillation, bp 134—137 °C/1 mmHg, to give IX (3.0 g) as a colorless oil (yield: 43%).

Found: C, 63.71; H, 7.86%. Calcd for $C_{15}H_{22}O_5$: C, 63.81; H, 7.85%.

Ethyl 3,4-Bis(tetrahydropyranyloxy)-α-methoxycinnamate (XI). To a mixture of metallic sodium (2.5 g), anhydrous toluene (50 ml), and VIII (3.0 g), anhydrous ethanol (0.1 ml) was added with stirring. Under cooling with ice and stirring, X (3.6 g) was added dropwise to the mixture. The condensation reaction was performed by stirring the whole mixture under ice-cooling for 2 h and then at room temperature for an additional 6 h. The reaction mixture was poured into ice water (200 ml) and the product was extracted with benzene. After washing with 0.1 M hydrochloric acid and 5% sodium hydrogencarbonate solution, the benzene extracts were dried over anhydrous sodium sulfate and concentrated *in vacuo* to dryness. The residue was purified by column chromatography using Merck's silica gel (250 ml) as adsorbent and ethyl acetate–benzene (1: 9) as developer to obtain XI (1.8 g) as a colorless oil (yield: 43%).

Found: C, 64.94; H, 7.57%. Calcd for $C_{22}H_{30}O_7$: C, 65.01; H, 7.44%.

3,4-Dihydroxy-α-methoxycinnamic Acid (I). (i) Aqueous 1 M sodium hydroxide solution (50 ml) was added to a solution of XI (1.0 g) in methanol (50 ml) and the mixture was stirred overnight at room temperature. The reaction mixture was concentrated (*ca.* 20 ml) under reduced pressure. After acidification of the concentrate with 1 M hydrochloric acid, the resulting oil was extracted with ethyl acetate, and the extracts were concentrated *in vacuo*. The residue obtained was dissolved in methanol (20 ml) and, after addition of 0.2 M hydrochloric acid (20 ml), the mixture was warmed at 60 °C for 15 min. The reaction mixture was adjusted to pH 4 with 0.1 M sodium hydroxide solution on cooling with ice-water, and concentrated to dryness under reduced pressure. The residue was extracted with ethanol and the ethanol extracts were concentrated to dryness. The residue was crystallized from water to yield I (310 mg) as colorless prisms (yield: 60%), mp 215 °C (dec.).

Found: C, 57.40; H, 4.78%. Calcd for $C_{10}H_{10}O_5$: C, 57.14; H, 4.80%.

(ii) The condensation reaction of IX with X was carried out in a similar manner to that described in the preparation of XI to obtain XII (*ca.* 3.5 g) in a crude oil. Without further purification, a mixture of a solution of XII in methanol (100 ml) and aqueous 1M sodium hydroxide solution (100 ml) was stirred overnight at room temperature. The reaction mixture was concentrated (30 ml) *in vacuo*, neutralized with hydrochloric acid, and evaporated to dryness. The residue was dissolved in acetic acid (50 ml) and the solution was warmed at 60 °C for 10 min. The reaction mixture was concentrated to dryness and the residue was extracted with ethanol. The ethanol extracts were evaporated to dryness, and the residue was crystallized from water to obtain I (1.0 g) as colorless prisms (yield 48%), mp 215 °C (dec.).

Found: C, 56.88; H, 4.74%. Calcd for $C_{10}H_{10}O_5$: C, 57.14; H, 4.80%.

We are indebted to Drs. R. Takeda, A. Miyake, K. Mizuno, and M. Yoneda for their encouragement and advice throughout this work. Thanks are also due to Drs. T. Yamano, T. Hasegawa, and their co-workers for fermentation and to the members in charge of elemental analysis and physicochemical measurements.

References

1) H. Fukase, T. Hasegawa, K. Hatano, H. Iwasaki, and M. Yoneda, *J. Antibiotics*, **29**, 113 (1976).

2) G. Albers-Schönberg, B. H. Arison, and J. L. Smith, *Tetrahedron Lett.*, **1972**, 2911.

3) T. W. Miller, R. T. Goegelman, R. F. Weston, I. Putter, and F. J. Wolf, *Antimicrob. Ag. Chemother.*, **2**, 132 (1972).

4) D. R. Brannon, J. A. Mabe, R. Ellis, J. G. Whitney, and R. Nagarajan, *Antimicrob. Ag. Chemother.*, **1**, 242 (1972).

5) G. M. Barton, R. S. Evans, and J. A. F. Gardner, *Nature*, **170**, 249 (1952).

6) J. Méendez and M. J. Lojo, *Microchem. J.*, **13**, 232 (1968).

7) W. E. Parham and E. L. Anderson, *J. Am. Chem. Soc.*, **70**, 4187 (1948).

8) S. Chládek and J. Smrt, *Chem. Ind.* (London), **1964**, 1719.

The Synthesis of Cubebol from (−)-Carvone by Introducing the Electrochemical Acetoxylation Reaction

Sigeru Torii and Tsutomu Okamoto

Department of Industrial Chemistry, School of Engineering, Okayama University, Tsushima, Okayama 700

(Received October 2, 1975)

The synthesis of cubebol and the related compounds from (−)-carvone is described. In the preparation of the key intermediate, 7,10-*trans*-2,6-epi-2-acetoxy-7-isopropyl-10-methyltricyclo[4.4.0.0^{1,5}]decan-4-one (**10**) the electrochemical acetoxylation reaction could be used as an effective method for introducing the acetoxy group at C-2 carbon atom instead of the carboxy function of 7,10-*trans*-2,6-epi-4-oxo-7-isopropenyl-10-methyltricyclo-[4.4.0.0^{1,5}]decan-2-carboxylic acid (**6a**). The condensation of (+)-*p*-menth-8-en-2-one (**2a**) prepared from (−)-carvone with dimethyl succinate afforded Stobbe half-ester **3**, which provided the diazoketone **4** smoothly. Thermal decomposition of **4** in benzene gave intramolecular adducts **5a** and **5b** (4: 1). Hydrolysis of **5a** afforded **6a** in *ca.* 40% yield. Electrolysis of **6a** in AcOH–*t*-BuOH–Et_3N (2: 1: 0.1) using platinum electrodes gave **10** in 72% yield. Elimination of acetic acid gave two isomers **11a** and **11b** (3: 1) in 87% yield and subsequent methylation of **11a** afforded 7-isopropyl-4,10-dimethyltricyclo[4.4.0.0^{1,5}]deca-2-en-4-ol (**12**) in 82% yield, which on hydrogenation gave the desired product **1a** (36.5%) along with the epimer **1b** (36.5%).

For the synthesis of complex sesquiterpenes, principal components in essential oils, cubebol (**1a**) and its related compounds, α- and β-cubebenes, isolated from the essential oil of the fruits of cubeb (*Piper cubeba* L.)[1] and citrus oils[2] are of interest as regards their synthesis.

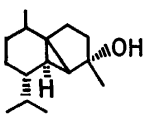

1a

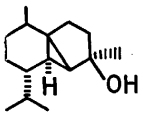

1b

Recently, Yoshikoshi *et. al.*,[1c] reported the preparation of **1a**, elucidating the stereochemistry of the related sesquiterpenoids. The present work deals with a convenient synthesis of **1a** from (−)-carvone by means of an electrochemical method. An electrochemical procedure for the replacement of carboxyl function to acetoxy group at the C-2 carbon atom of tricyclo[4.4.0.0^{1,5}]-decan-4-one system was reported.[3] In order to utilize electrochemical acetoxylation in cubebol synthesis it is desirable to find an intermediate which is easily prepared and stable during the course of electrolysis. We chose 7,10-*trans*-2,6-epi-7-isopropenyl-10-methyl-4-oxo-tricyclo[4.4.0.0^{1,5}]decan-2-carboxylic acid (**6a**) for the present synthesis.

The Stobbe condensation of (+)-8-*p*-methen-2-one (**2a**), contaminated with 24% of 8-*p*-isomenthen-2-one (**2b**),[4] with dimethyl succinate afforded the starting material **3** in 92% yield. In order to obtain the tricyclo[4.4.0.0^{1,5}]decan-4-one skeleton, intramolecular addition of keto-carbene to the double bond of **3** was attempted.[5] The diazoketone **4** obtained by the reaction of acid chloride of **3** with diazomethane was subjected to thermal decomposition in benzene at 80—81 °C using bis(*N*-propylsalicylideneaminato)copper(II) as a soluble catalyst.[6] This afforded 51% yield (based on **3**) of a C-10 isomeric mixture of the adducts **5a** and **5b**, which was separated by column chromatography over alumina to afford 40% of **5a** and 11% of **5b**. Hydrolysis of **5a** in 5% aqueous methanolic potassium hydroxide afforded **6a** quantitatively.

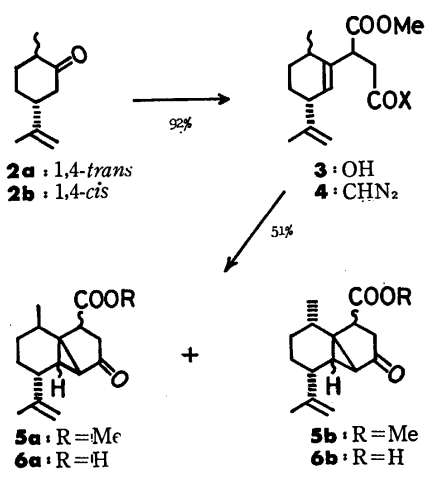

Mc Murry and Blaszczak[7] reported a new method for the synthesis of the cyclic enones from β-carboxy ketones by oxidative decarboxylation with lead tetraacetate in the presence of cupric ion. However, the method could only be applied to γ-methyl-β-carboxy ketones. It seems that application of stepwise reactions and mild reaction conditions is particularly suitable for the complex acid **6a**. We have encountered some difficulties in obtaining the enones **7** selectively from

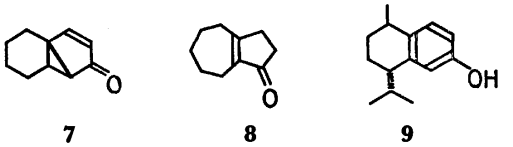

7 **8** **9**

4-oxotricyclo[4.4.0.0^{1,5}]decan-2-carboxylic acid by electrolytic decarboxylation directly, a mixture of **7** and **8** being obtained.[3] Under similar electrolysis conditions, the acid **6a** afforded a mixture of the enone **11** and the aromatic compound **9**. The synthesis of the enone **11** was successfully accomplished on treatment of the acetate **10** with triphenylmethylenephosphorane.[8] Thus, electrolytic acetoxylation of **6a** in a mixed solvent of acetic acid-*t*-butyl alcohol-trimethylamine (2:1:0.1) using platinum electrodes with a constant current of 0.08 A/cm^2, applied voltage *ca.* 20 V (1.6—1.7 *vs.* SCE) at 10 °C for 20 h afforded 72% of the acetate **10** as the sole product.[3] Under these electrolytic conditions,

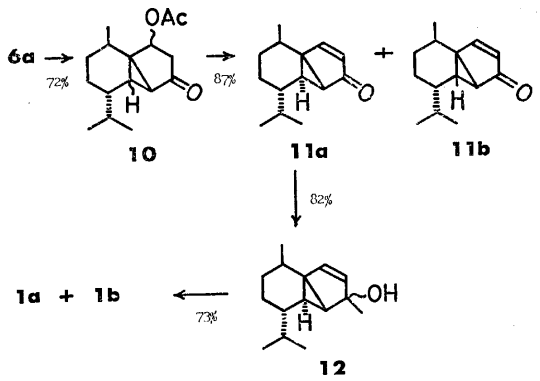

hydrogenation to the isopropenyl function of **6a** occurred spontaneously. The conversion of **10** into an epimeric mixture of α,β-unsaturated ketones **11a** and **11b** (3: 1) was accomplished in 87% yield on treatment with a benzene solution containing a slightly excess amount of triphenylmethylenephosphorane at 0—4 °C. Separation of the epimers **11a** and **11b** was carried out by preparative glpc to afford the desired **11a** in 65% yield (based on **10**). The Grignard reaction of **11a** with methyl magnesium iodide resulted in the formation of C-4 isomeric mixtures **12** in 82% yield. Without separation of the isomers, **12** was hydrogenated over platinum oxide to afford cubebols **1a** and **1b** (1: 1) in 73% yield. Separation of the isomers could be achieved by column chromatography over silica gel.

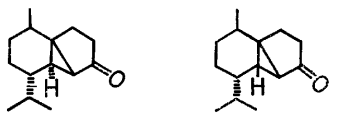

13a **13b**

Norcubebanone **13a**[9] prepared from hydrogenation of **11a** could be used for the preparation of **1a** by the reaction with methylmagnesium iodide.[1c] The coupling of alkylmetals with the carbonyl group of the bicyclo[3.1.0]hexan-2-ones occurred mainly on the side opposite the cyclopropane ring.[1c,10] However, the Grignard reactions of **11a** and/or **13a** with methyl magnesium iodide provided a small amount of the epimer **1b** together with **1a**.

Experimental

Melting points and boiling points are uncorrected. NMR spectra were determined with a Hitachi R-24 instrument. IR spectra were recorded on a Hitachi EPI-S2, only the major absorptions being cited. Mass spectra were obtained on a Hitachi RMS-4 mass spectrometer at 70 eV, the molecular and major fragment ions being cited: *m/e* (relative intensity).

Electrolysis Apparatus. The electrolytic vessel was a water-jacketed beaker, diam. 2.5 cm, height 10 cm, fitted with a gas lead pipe, thermometer and magnetic stirrer, two smooth platinum electrodes (3 cm^2) being placed parallel to each other 3 mm apart. The current was controlled by adjusting the voltage. The direction of current was changed every 30 s by means of a commutator.

Preparation of Stobbe Half-ester (3). A solution of (+)-8-*p*-menthen-2-one (**2**), $[\alpha]_D^{14}$ +18.8° (*c* 3.03, $CHCl_3$)[4] (500 mg, 3.3 mmol) and dimethyl succinate (720 mg, 4.9 mmol) was treated with *t*-BuOK (from 200 mg of K metal) in 5 ml of dry *t*-BuOH. The mixture was heated at *ca.* 90 °C for 3 h with stirring. After being cooled to 0 °C the mixture was acidified with ice-cold 10% HCl. The organic phase was extracted with ether–benzene (1: 1). The extracts were washed with water, dried (Na_2SO_4), and concentrated. The residue (920 mg) was chromatographed over silica gel. Elution with 70 ml of hexane–ether (9: 1, monitored by TLC) gave a fraction of R_f 0.26—0.62. Subsequent elution with *ca.* 60 ml of acetone gave 805 mg (92%) of **3** (R_f 0.19): IR (neat) 3400—2500 (COOH), 1740 (ester), 1715 (COOH), 1645 (C=C), and 892 cm^{-1}; NMR ($CDCl_3$) δ 0.95—1.14 (m, 3H, CH_3), 1.68 (s, 3H, CH_3C=C), 3.64 (s, 3H, CH_3O), 4.45—4.80 (m, 2H, H_2C=C), and 5.41 (m, 1H, HC=C); $[\alpha]_D^{13}$ +54.75° (*c* 2.56, $CHCl_3$).

Found: C, 67.48; H, 8.29%. Calcd for $C_{15}H_{22}O_4$: C, 67.65; H, 8.33%.

2,6,10-Epi-2-methoxycarbonyl-7-isopropenyl-10-methyltricyclo-[4.4.0.0^{1,5}]decan-4-ones (5a and 5b). To a stirred suspension of 72 mg of NaH (50% mineral oil dispersion, washed with anhydrous hexane before use) in 10 ml of dry benzene, was added dropwise 266 mg (1 mmol) of **3** in 3 ml of dry benzene. The mixture was stirred for 1 h at room temperature and 0.2 ml of oxalyl chloride was added at 5 °C. Stirring was continued for 1 h at room temperature and the mixture was filtered under N_2. The residual acid chloride was dissolved in 2 ml of dry benzene. The benzene solution was treated with excess diazomethane at 0 °C. The mixture was stirred overnight at 0—5 °C. Removal of the solvent under reduced pressure at 10 °C and subsequent chromatography over alumina with CH_2Cl_2 gave 210 mg of the diazo ketone **4**, a yellow oil: IR (neat) 2075 (CN_2), 1737 (ester), and 1645 cm^{-1} (diazo ketone); NMR ($CDCl_3$) δ 0.95—1.18 (m, 3H, CH_3), 1.67 (s, 3H, CH_3C=C), 3.43 (s, 3H, CH_3O), 4.45—4.80 (broad d, 2H, H_2C=C), 5.20 (s, 1H, $COCHN_2$), and 5.38 (m, 1H, HC=C). Without further purification, the diazo ketone (210 mg, 0.72 mmol) was added to a mixture of 40 ml of benzene and 20 ml of bis(*N*-propylsalicylideneaminato)-copper(II), dried in an oven at 80—100 °C for 10 min before use, and dissolved in 5 ml of dry benzene with vigorous stirring at 80—81 °C for 4 hr. The solvent was then removed on a rotoevaporator and the residue was chromatographed over alumina. Elution with 20 ml of hexane–ether (2: 1, monitored by tlc) gave 105 mg (40%) of **5a** (R_f 0.77) and subsequent elution with 20 ml of hexane–ether (1: 1) gave 29.1 mg (11%) of **5b** (R_f 0.53). The spectral data along with elemental analyses are as follows: *7,10-trans-2,6-epi-2-methoxycarbonyl-7-isopropenyl-10-methyltricyclo[4.4.0.0^{1,5}]decan-4-one (5a)*: IR (neat) 3080, 1732 (C=O), and 1648 cm^{-1} (C=C); NMR ($CDCl_3$) δ 0.95—1.18 (m, 3H, CH_3), 1.75 (s, 3H, CH_3C=C), 3.72 (s, 3H, CH_3O), and 4.86 (broad, 2H, H_2C=C); mass spectrum (*m/e*) 262 (M^+, 14), 247 (14), 234 (15), 203 (22), 181 (21), 175 (20), 161 (25), 159 (29), 147 (39), and 135 (100); $[\alpha]_D^{24}$ +6.1° (*c* 3.68, $CHCl_3$).

Found: C, 73.13; H, 8.51%. Calcd for $C_{16}H_{22}O_3$: C, 73.25; H, 8.45%.

7,10-cis-2,6-Epi-2-methoxycarbonyl-7-isopropenyl-10-methyltricyclo[4.4.0.0^{1,5}]decan-4-one (5b): IR (neat) 3080, 1737 (C=O), and 1647 cm^{-1} (C=C); NMR ($CDCl_3$) δ 0.47—1.18 (m, 3H, CH_3), 1.78 (broad, 3H, CH_3C=C), 3.66 (s, 3H, CH_3O), and 4.75 (m, 2H, H_2C=C); mass spectrum (*m/e*) 262 (M^+, 9), 247 (13), 234 (8), 203 (26), 181 (13), 175 (19), 161 (26), 159 (22), 147 (44), and 135 (100); $[\alpha]_D^{24}$ −8.5° (*c* 2.64, $CHCl_3$).

Found: C, 73.08; H, 8.60%. Calcd for $C_{16}H_{22}O_3$: C, 73.25; H, 8.45%.

7,10-trans-2,6-Epi-7-isopropenyl-10-methyl-4-oxotricyclo-[4.4.0.0^{1,5}]decene-2-carboxylic Acid (6a). A mixture of

330 mg (1.26 mmol) of **5a** and 700 mg (12.5 mmol) of KOH in 20 ml of 5% aqueous MeOH was stirred at room temperature overnight. The solvent was removed on a rotoevaporator. The residual alkaline solution was washed with hexane–benzene and neutralized with aqueous tartaric acid under cooling with an ice-water bath and then extracted with ether. The combined extracts were washed with water, dried (Na_2SO_4), and concentrated. The residue (312 mg) was chromatographed over silica gel using hexane–ether (1: 1) to give 305 mg (98%) of **6a**: IR (neat) 3500—2500 (COOH), 1728 (C=O), 1705 (COOH), and 1645 cm^{-1}; NMR ($CDCl_3$) δ 1.02—1.19 (d, J=6.5 Hz, 3H, CH_3), 1.74 (s, 3H, CH_3C=C), 3.15—3.60 (m, 1H, HCC=O), 4.73 (broad, 2H, H_2C=C), and 10.63 (broad, 1H, COOH); $[\alpha]_D^{24}$ +7.7° (*c* 2.92, $CHCl_3$).

Found: C, 72.44; H, 8.38%. Calcd for $C_{15}H_{20}O_3$: C, 72.55; H, 8.12%.

Electrolytic Acetoxylation of ***6a***. The acid **6a** (150 mg, 0.61 mmol) was dissolved in a mixed solution of AcOH (6 ml), *t*-BuOH (3 ml), and Et_3N (20 mg). The mixture was electrolyzed at a constant current of *ca.* 0.25 A (*ca.* 20 V) at 10 °C for 20 h. The solvent was removed on a rotoevaporator and the residue was taken up in benzene–ether (1: 1). The organic phase was washed with water and saturated $NaHCO_3$ and dried (Na_2SO_4), and concentrated. The residue was chromatographed over silica gel using hexane–ether (2: 1) to give 115 mg (72%) of **10**, bp 129—130 °C (0.005 mmHg).[3]

7,10-trans-*6-Epi-7-isopropyl-10-methyltricyclo*[*4. 4. 0. 0*^{1,5}]-2-*decen-4-ones* (***11a and 11b***). A salt free benzene solution (10 ml) of triphenylmethylenephosphorane prepared from triphenylmethylphosphonium bromide (210 mg, 0.59 mmol) was added dropwise with cooling in an ice-water bath to a stirred solution of **10** (119 mg, 0.45 mmol) in 2 ml of benzene. The mixture was diluted with 20 ml of hexane and the precipitate was filtered off. The filtrate was concentrated. The residual oil was chromatographed over silica gel tlc plate (Merck PF-254, hexane–ether, 1: 1) to give 80 mg (87%) of **11a** and **11b** (R_t 0.64—0.72). Separation of the epimers was carried out by preparative glpc to give **11a** and **11b** in a 3: 1 ratio (polyneopentyl glycol succinate, 10% coated on Chromosorb W, 4 mm×2 m column, carrier gas H_2 32 ml/min, 169 °C, R_t (min) **11a** (11.00), **11b** (15.00).

6,7-cis-*7,10*-trans-*7-Isopropyl-10-methyltricyclo*[*4. 4. 0. 0*^{1,5}]-2-*decen-4-one* (***11a***): IR (neat) 3020, 1702 (C=O), and 1571 cm^{-1} (C=C); NMR ($CDCl_3$) δ 0.60—1.07 (10H, $3CH_3$, CH), 1.10—2.40 (m, 8H, CH_2, CH), 5.55 (d, J=9 Hz, 1H, CH=C), and 7.46 (d, J=9 Hz, 1H, HC=C); mass spectrum (*m/e*) 204 (M^+, 39), 189 (50), 161 (100), 149 (56), 148(53), 147 (57), 133 (84), 121 (50), 109 (62), 105 (75), and 91 (94); $[\alpha]_D^{24}$ −136.7° (*c* 1.88, $CHCl_3$).

Found: C, 82.15; H, 10.02%. Calcd for $C_{14}H_{20}O$; C, 82.30; H, 9.87%.

6,7-trans-*7,10*-trans-*7-Isopropyl-10-methyltricyclo*[*4. 4. 0. 0*^{1,5}]-*decene-4-one* (***11b***): IR (neat) 3080, 1706 (C=O), and 1568 cm^{-1} (C=C); NMR ($CDCl_3$) δ 0.60—1.10 (10H), 1.10—2.40 (8H), 5.48 (d, J=9 Hz, 1H, HC=C), and 7.62 (d, J=9 Hz, 1H, HC=C); mass spectrum (*m/e*) 204 (M^+, 39), 189 (38), 161 (83), 149 (54), 148 (25), 147 (48), 133 (56), 121 (46), 109 (34), 105 (58), and 91 (100); $[\alpha]_D^{24}$ +77.4° (*c* 0.23, $CHCl_3$).

Found: C, 82.26; H, 9.82%. Calcd for $C_{14}H_{20}O$: C, 82.30; H, 9.87%.

7-Isopropyl-4,10-dimethyltricyclo[*4. 4. 0. 0*^{1,5}]*deca-2-en-4-ol* (***12***). A solution of **11a** (26 mg, 0.13 mmol) in ether (3 ml) was added for 10 min to a stirred solution of MeMgI prepared from MeI (50 mg, 0.35 mmol) and Mg metal (5 mg, 0.21 mg atom) under N_2 and cooling with ice. The solution was gently refluxed for 2 h. After being cooled to room temperature the mixture was poured into aqueous 20% NH_4Cl (5 ml) and extracted with benzene. The extracts were washed with water, dried (Na_2SO_4), and concentrated *in vacuo*. The residue was chromatographed over silica gel with benzene to give **12** (23.0 mg, 82%): IR (neat) 3400 (OH), 3050 (shoulder), 1370, 1027, 917, and 756 cm^{-1}; NMR (CCl_4) δ 0.60—1.20 (m, 14H, $3CH_3$, CH_2, CH), 1.40 (d, 3H, CH_3), 1.40—1.80 (m, 5H, CH_2, CH), 5.00—5.24 (m, 1H, HC=C), and 5.52—5.76 (m, 1H, HC=C); mass spectrum (*m/e*) 220 (M^+, 7), 207 (32), 202 (28), 177 (56), 161 (53), 159 (78), 145 (29), 135 (43), 131 (58), 121 (58), 119 (57), 118 (100), 117 (58), 105 (63); $[\alpha]_D^{24}$ −91.5° (*c* 0.87, $CHCl_3$).

Found: C, 81.50; H, 11.04%. Calcd for $C_{15}H_{24}O$: C, 81.76; H, 10.98%.

Hydrogenation of ***12***. To a solution of **12** (34.0 mg, 0.15 mmol) in 5 ml of AcOEt was added 5 mg of platinum dioxide. The mixture was flushed with H_2 gas and stirred efficiently under H_2. After 1 h the theoretical amount of H_2 was absorbed. The mixture was filtered and the solvent was rotoevaporated to afford a residue which was immediately chromatographed over silica gel (2.5 g). Careful elution with benzene gave 4-epicubebol (**1b**, 12.5 mg, 36.5%) as an oil contaminated with a small amount of **1a**. The following elution with benzene gave cubebol (**1a**) (12.5 mg, 36.5%) as crystals. Repeated chromatography of the products over silica gel using benzene gave analytical samples: cubebol (**1a**), mp 58—59 °C (lit,[1a,1c] 61—62 °C, 64 °C); IR (Nujol) 3300 (OH), 1385, 1370, 1300, 1223, 1155, 1134, 1080, 1032, 980, 970, 928, and 890 cm^{-1}; NMR ($CDCl_3$) δ 0.89 (d, J=7 Hz, 6H, CH_3), 0.95 (d, J=6.5 Hz, 3H, CH_3), and 1.27 (s, 3H, CH_3); mass spectrum (*m/e*) 222 (M+,2), 207 (39), 204 (29), 189 (4), 179 (8), 161 (100), 121 (32), 119 (58), 105 (72), and 91 (55); $[\alpha]_D^{15}$ −44.7° (*c* 0.85, $CHCl_3$) (lit,[1c,1a] −48.3 °, −61.6 °).

4-Epicubebol (***1b***): IR (neat) 3400 (OH), 1370, 1321, 1152, 1123, 1040, 1008, 980, and 915 cm^{-1}; NMR (CCl_4) δ 0.87—1.05 (m, $3CH_3$), and 1.25 (s, 3H, CH_3); mass spectrum (*m/e*) 222 (M^+, 3), 207 (53), 204 (26), 189 (6), 179 (21), 161 (100), 121 (54), 120 (55), 119 (58), 105 (67), and 91 (64); $[\alpha]_D^{14}$ −4.0° (*c* 1.25, $CHCl_3$).

7,10-trans-*7-Isopropyl-10-methyltricyclo*[*4.4.0.0*^{1,5}]*decan-4-one* (*norcubenbanone*) (***13a***). Hydrogenation of 44 mg (0.22 mmol) of **11a** was carried out in 3 ml of absolute EtOH with 40 mg of 10% Pd-carbon until 4.8 ml of H_2 gas was absorbed. The mixture was filtered and the solvent was evaporated to afford an oil. The crude product was chromatographed on silica gel, eluted with benzene, to give 44 mg (99%) of **13a**, mp 57.0—57.5 °C (lit,[1c] mp 57—58 °C); mass spectrum (*m/e*) 206 (M^+, 42), 191 (10), 164 (78), 163 (45), 149 (32), 134 (31), 122 (100), 93 (77), and 79 (92); $[\alpha]_D^{24}$ −22.8 ° (*c* 0.12, MeOH). (lit,[1c] $[\alpha]_D^{24}$ −23.9° (*c* 0.16, MeOH)). IR and NMR spectra of **11a** were identical with those of an authentic sample.[9]

Cubebol (***1a***) *from Norcubebanone* (***13a***). To an ether solution of MeMgI, prepared from MeI (80 mg, 0.56 mmol) and Mg metal (10 mg, 0.42 mg atom), was added 33 mg (0.16 mmol) of **13a** in 5 ml of ether over a period of 5 min. The stirred mixture was refluxed for 2 h and poured into ice-cold aqueous 20% NH_4Cl (5 ml). The organic phase was extracted with ether. The extracts were washed with brine, dried (Na_2SO_4), and concentrated. The residue was chromatographed over silica gel using benzene to give **1a** (17.3 mg, 49%). Compound **1a** melted at 58—59 °C. IR and NMR spectral data were identical with those of an authentic sample.

We gratefully acknowledge financial support from the

Ministry of Education for the Grant-in-aid for Scientific Research, General Research (B) 047086 (1975).

References

1) Isolation and elucidation: (a) F. Vanasek, V. Herout, and F. Sorm, *Collect. Czech. Chem. Commum.*, **25**, 919 (1960); (b) Y. Ohta, T. Sakai, and Y. Hirose, *Tetrahedron Lett.*, **1966**, 6365. Synthesis: (c) A. Tanaka, R. Tanaka, H. Uda, and and A. Yoshikoshi, *Chem. Commun.*, **1969**, 308; *J. Chem. Soc., Perkin 1*, **1972**, 1721.

2) M. K. Veldhuis and G. L. K. Hunter, *J. Food Sci.*, **32**, 697 (1967).

3) S. Torii, T. Okamoto, G. Tanida, H. Hino, and Y. Kitsuya, *J. Org. Chem.*, **41**, 166 (1976).

4) J. C. Fairlie, G. L. Hodgson, and T. Money, *J. Chem. Soc. Perkin I*, **1973**, 2109.

5) The construction of the bicyclo[3.1.0]hexane-2-one system of α- and β-cubebenes has been carried out by the intramolecular addition of keto-carbene to double bond. (a) O. P. Vig, M. S. Bhatia, A. K. Verma, and K. L. Matta, *J. Indian Chem. Soc.*, **47**, 277 (1970); (b) E. Piers, R. W. Britton, and W. de Waal, *Can. J. Chem.*, **49**, 12 (1971).

6) J. D. White, S. Torii, and J. Nogami, *Tetrahedron Lett.*, **1974**, 2879.

7) J. E. McMurry and L. C. Blaszczak, *J. Org. Chem.*, **39**, 2217 (1974).

8) F. Sondheimer and R. Mechoulam, *J. Amer. Chem. Soc.*, **80**, 3087 (1958).

9) We are grateful to Professor A. Yoshikoshi, Tohoku University, for providing NMR and IR spectra of norcubebanones (**13a** and **13b**).

10) W. I. Fanta and W. F. Erman, *J. Org. Chem.*, **33**, 1656 (1968).

The Bromination and Mercuration of bis-Dimethylglyoxymato-(alkyl)pyridinecobalt(III), Alkyl Cobaloxime[1]

Hiraku SHINOZAKI, Hiroki OGAWA, and Masaru TADA

Department of Chemistry, School of Science and Engineering, Waseda University, Shinjuku, Tokyo 160

(Received October 2, 1975)

The bromination and mercuration of *cis*-2-methoxycyclohexyl(pyridine)cobaloxime (I) gave *trans*-1-bromo-2-methoxycyclohexane (V) and *trans*-2-methoxycyclohexylmercury(II) chloride (VII), along with other by-products derived from the cyclohexene formed by β-elimination. β-Elimination is an exclusive degradation path with *trans*-2-hydroxycyclohexyl(pyridine)cobaloxime(II). The reaction of *cis* and *trans*-4-*t*-butylcyclohexyl(pyridine)cobaloximes (III and IV) gave *trans* and *cis*-1-bromo-4-*t*-butylcyclohexanes (X and XI), and *trans* and *cis*-4-*t*-butylcyclohexylmercury(II) chloride, with an exculsive or preferential inversion at the reaction center. These results show that the S_E2 reaction of alkyl cobaloxime takes a stereochemical course of inversion.

The electrophilic rupture of the alkyl group from cobalamine, the coenzyme B_{12} derivative,[2] is considered to be a simple metabolic pathway to produce methane, acetic acid, and methyl mercurial. Especially, methyl cobalamine has been recognized to be responsible for the transformation of mercury(II) ion into dimethylmercury in the sludge of river and sea, which causes a serious pollution problem.[3] Schrauzer[4] demonstrated that bis-dimethylglyoxymato(alkyl)pyridinecobalt(III) (the conventional name, alkyl cobaloxime, will be used hereafter) constituted a superior model system for the alkyl derivative of the B_{12} coenzyme. Much attention has been paid to the stereochemistry of the electrophilic displacement of alkyl σ-metal complexes, and the steric courses of both retention and inversion have been reported.[1,5-12] Kinetic studies have established the nature of these electrophilic reactions of alkyl cobaloximes to be a bimolecular substitution, a S_E2 reaction.[13,14] We reported in preliminary form about the steric consequence of the bromination and mercuration of alkyl cobaloxime;[1] in this paper we wish to report the details of our study.

Experimental

Preparation of cis-*2-Methoxycyclohexyl(pyridine)cobaloxime (I) and* trans-*2-Hydroxycyclohexyl(pyridine)cobaloxime (II).* Cobaloxime I was synthesized by the reaction of *trans*-1-bromo-2-methoxycyclohexane (5.0 g) with the cobaloxime anion prepared *in situ* from $CoCl_2 \cdot 6H_2O$ (5.95 g), dimethylglyoxime (5.80 g), sodium hydroxide (2.0 g), pyridine (2.0 g), and sodium tetrahydroborate (200 mg)under nitrogen in methanol (90 ml) at 0 °C for 1 h and at room temperature for 12 h. The reaction mixture was condensed to *ca.* 30 ml under reduced pressure, and the residue was extracted with chloroform (30 ml×3) after the addition of water (30 ml). The condensation of the extract after drying over sodium sulfate gave a residue containing cobaloxime I. The separation of I from the residue was achieved by column-chromatography on Florisil (30 g), eluting with benzene (unreacted 1-bromo-2-methoxycyclohexane) and chloroform (cobaloxime I). The repeated chromatography of the latter fraction on Florisil gave 3.85 g (32%) of the pure I.

The cobaloxime, II, was synthesized from cyclohexene oxide by a similar method, but using hydrogen as the reducing agent, in a 24% yield. Spectroscopic data showed the I and II cobaloximes to be identical with the compounds described by Jensen *et al.*[15]

I, NMR ($CDCl_3$): 8.7—7.1 (5H, pyridine), 3.30 (broad singlet, $W_{1/2}$=9 Hz, 1H), 3.15 (singlet, 3H), 2.10 (singlet, 12H), and 2.1—0.9 ppm (δ) (multiplet, 9H).

II, NMR ($CDCl_3$): 8.7—7.1 (5H, pyridine), 3.05—2.70 (sextet, $W_{1/2}$=19 Hz, 1H), 2.07 (singlet, 6H), 2.13 (singlet, 6H), and 2.1—0.8 ppm (δ) (multiplet, 9H).

Preparation of cis-*4-t-Butylcyclohexyl(pyridine)cobaloxime (III) and* trans-*4-t-Butylcyclohexyl(pyridine)cobaloxime (IV).* Cobaloxime III was synthesized in essentially the same way as cobaloxime I, using *trans*-4-*t*-butylcyclohexyl tosylate. The reaction period was prolonged to 21 h, and the crude product was chromatographed on Florisil to give the unreacted tosylate in a benzene eluate and the cobaloxime III in a chloroform eluate. The yield was poor (7.7%), but it was fruitless to continue the reaction further because of the deterioration of the cobaloxime anion. The reaction of *cis*-4-*t*-butylcyclohexyl tosylate with the cobaloxime anion in the same manner for 13 h gave the cobaloxime IV in a higher yield (40.7%).

III, mp 110—120 °C (dec.). Found: C, 54.47; H, 7.40; N, 13.59%. Calcd for $C_{23}H_{38}N_5O_4Co$: C, 54.43; H, 7.55; N, 13.80%. IR(KBr): 2690, 1600, 1550, 1448, 1365, 1232, 1090, and 520 cm^{-1}. NMR ($CDCl_3$): 8.5—7.0 (5H, pyridine), 2.10 (singlet, 12H), 1.9—0.8 (10H), and 0.77 ppm (δ) (singlet, 9H).

IV, mp 150—160 °C (dec.). Found: C, 54.34; H, 7.48; N, 13.92%. Calcd for $C_{23}H_{38}N_5O_4Co$: C, 54.43; H, 7.55; N, 13.80%. IR (KBr): 2940, 1595, 1550, 1445, 1360, 1230, 1082, and 515 cm^{-1}. NMR ($CDCl_3$): 8.4—7.0 (5H, pyridine), 2.10 (singlet, 12H), 1.9—0.8 (10H), and 0.76 ppm (δ) (singlet, 9H).

Bromination of the Cobaloximes (I and II). To a solution of the I cobaloxime (120 mg) in dichloromethane (50 ml) we added, drop by drop, a solution of bromine (42 mg, 1.0 equivalent) in benzene (3 ml) under cooling to −70 °C. After stirring for 3 h under argon, the reaction mixture was passed through a column of Florisil (20 g) to remove the inorganic complex formed. The subsequent evaporation of the eluate gave a mixture (11 mg) of *trans*-1-bromo-2-methoxycyclohexane (V), *trans*-1,2-dibromocyclohexane (VI), and cyclohexanone, whose GLC analysis (OV-17 on Chromosorb W, N_2) showed signal intensities of *ca.* 2:1:2 respectively. The treatment of the II cobaloxime (500 mg) under the same reaction conditions, but at the reaction temperature of 0 °C, gave the VI dibromide (169 mg, 65%).

Bromination of the Cobaloximes (III and IV). The III cobaloxime (25 mg) in dichloromethane (1 ml) was cooled in an ice-water bath to −5 °C and then treated with 22 mg of bromine (2.6 equivalents) in dichloromethane. The reaction mixture was subsequently stirred for 6 h under nitrogen.

After the careful evaporation of the solvent, the product was chromatographed on Florisil (1 g), using hexane as the eluent. The careful evaporation of the eluate yielded *ca.* 10 mg of a product (*ca.* 92%). GLC analysis (Carbowax 20 M on Chromosorb W, N_2) showed the product to be a 1:3 mixture of *cis* and *trans*-1-bromo-4-*t*-butylcyclohexanes, XI and X, which were identical with authentic samples. The same treatment of the IV cobaloxime gave exclusively the XI bromide in a *ca.* 90% yield.

Mercuration of the Cobaloximes (I and II). To a solution of the I cobaloxime (360 mg) in ethanol (30 ml) containing acetic acid (0.02 mol/l), we added solid mercuric acetate (360 mg, 1.48 equivalents), after which the reaction mixture was refluxed for 2.5 h under nitrogen. Excess sodium chloride was added to the cooled mixture, which was then further stirred for 2.5 h at room temperature. The filtrate of the mixture was condensed and extracted with chloroform after the addition of water to the condensate. The passing of the extract through Florisil gave products in benzene eluate, while the I cobaloxime (73 mg) was recovered in the chloroform eluate. The chromatography of the products on silica gel eluted with dichloromethane gave a mixture of *trans*-2-methoxycyclohexylmercury(II) chloride (VII) and *trans*-2-ethoxycyclohexylmercury(II) chloride (VIII) (77 mg, 36% based on the I cobaloxime consumed). The ratio of VII to VIII was determined by the transformation of these mercurials into *trans*-1-bromo-2-methoxycyclohexane (V) and *trans*-1-bromo-2-ethoxycyclohexane (IX) by bromine in pyridine at −20 °C. The V and IX bromides, obtained in 40 mg after chromatography on alumina eluted by hexane, were found by analysis to exist in the ratio of 3:2.

The treatment of the II cobaloxime (467 mg) with mercuric acetate in methanol under essentially the same reaction conditions, but at the reaction temperature of 20 °C, gave *trans*-2-methoxycyclohexylmercury(II) chloride (VIII) in a 70% yield; this substance was identified with an authentic sample obtained by the methoxymercuration of cyclohexene.

Mercuration of the Cobaloximes (III and IV). To a solution of cobaloxime III (204 mg) in methanol (20 ml) we added powdered mercuric nitrate hydrate (274 mg), after which the solution was stirred for 120 h under nitrogen at room temperature. The reaction mixture was further stirred for 2.5 h after the addition of excess sodium chloride. The product was extracted with chloroform after the evaporation of methanol under reduced pressure and the addition of water to the condensed mixture. The extract was chromatographed on Florisil (6 g) to give the product as a benzene eluate and the recovered cobaloxime as a chloroform–methanol (9:1) eluate. The chromatography of the product on silica gel (2 g) gave *trans*-4-*t*-butylcyclohexylmercury(II) chloride, XII (3 mg, 2.0%), in a benzene eluate; this substance was identified with an anthentic sample synthesized from *trans*-4-*t*-butylcyclohexylmagnesium(II) bromide[16] and, further, by the transformation of XII into *trans*-1-bromo-4-t-butylcyclohexane (X) in the same way as was used for the transformation of mercurial VII and VIII into the V and IX bromides.

The mercuration of the IV cobaloxime (127 mg) was carried out in the same manner, but for 5 h at 50 °C. The chromatography of the products on Florisil (5 g) gave the products as the benzene eluate and the recovered IV cobaloxime (66 mg) as the chloroform eluate. Repeated chromatography of the products on silica gel (6 g) gave a mixture of *cis* and *trans*-4-*t*-butylcyclohexylmercury(II) chloride. The structure and ratio of the isomers were determined, by the transformation of the mercurials into bromides as has been described above, to be *cis*(XI): *trans*(X)=3:2.

Results and Discussion

cis-2-Methoxycyclohexyl(pyridine)cobaloxime (I) was synthesized by the substitution of *trans*-1-bromo-2-methoxycyclohexane with the cobaloxime anion, $(Co)^-$, prepared *in situ* by the sodium tetrahydroborate reduction of the complex from dimethylglyoxime, cobalt(II) chloride, and pyridine. The steric course of this reaction has been proved to proceed with an inversion at the reaction center, and the *trans* arrangement of the methoxy group and the cobaloxime moiety was confirmed by the NMR spectrum of I. The signal due to the hydrogen attached to the carbon bearing methoxy group is at 3.30 ppm (δ), with a half-band width of 9 Hz, which shows a lack of diaxial coupling and the axial conformation of the methoxy group. This feature unequivocally limits the stereochemistry of the I cobaloxime to *cis*, since the large steric requirement of the ligand enforces the cobaloxime group to take an equatorial conformation.[15] *trans*-2-Hydroxycyclohexyl(pyridine)cobaloxime (II), prepared from cyclohexene oxide and the cobaloxime anion, $(Co)^-$, has an NMR signal at 3.05—2.70 ppm as a diffused sextet with a half-band width of 19 Hz (J=10, 10, and 5 Hz), indicating the presence of two diaxial coupling and one axial-equatorial coupling. *Cis* and *trans*-4-*t*-butylcyclohexyl(pyridine)cobaloxime (III and IV) were prepared by the S_N2 displacement of *trans* and *cis*-4-*t*-butylcyclohexyl tosylate respectively. The reaction of the *trans* tosylate to give the *cis*-cobaloxime (III) was sluggish, and the yield was poor, 7.7%, even after a prolonged reaction period. This behavior can be accounted for by the steric hindrance on the approach of the cobaloxime anion from the axial direction when the S_N2 mechanism operates.[17] The large substituents at the 1,4-position of the cyclohexane ring suggest that the conformation of III is a boat form. The spectroscopic data do not discriminate the stereochemistry of III and IV, but the S_N2 nature of the reaction suggests the stereochemistry of the cobaloximes to be *cis* and *trans* respectively.[15] This reasoning was proved by the bromination of III and IV giving different products, as will be described below.

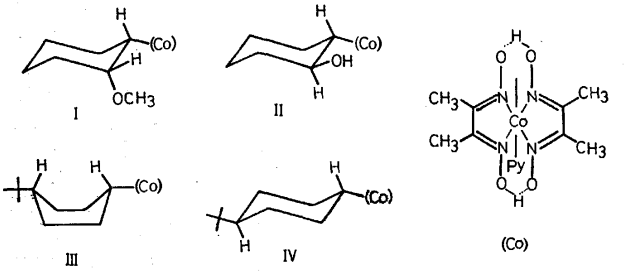

The bromination of *cis*-2-methoxycyclohexyl(pyridine)cobaloxime (I) in dichloromethane gave a complex mixture at an ambient temperature, but the reaction at a lower temperature (−70 °C) yielded *trans*-1-bromo-2-methoxycyclohexane (V) in a poor yield, besides *trans*-1,2-dibromocyclohexane (VI) and cyclohexanone (Eq. 1). The formation of V, in spite of the low yield, clearly shows that the reaction proceeds

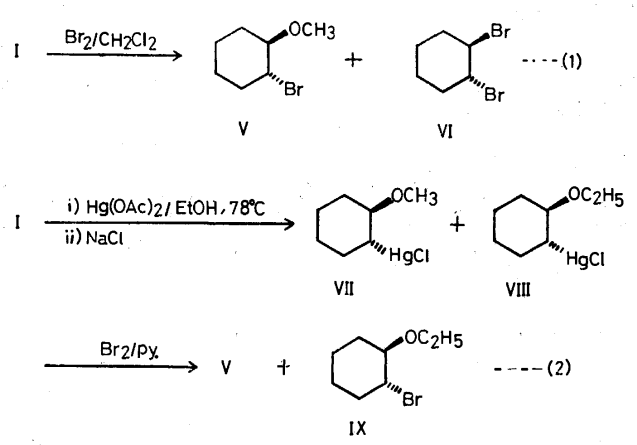

with an inversion of the configuration, though the formation of VI indicates the side reaction *via* cyclohexene as an intermediate. The mercuration of I with mercuric acetate was attempted under the conditions in which Schrauzer *et al.*, determined the kinetic property of the reaction to be second order.[13] In our preliminary report, we errornously recorded the formation of *trans*-2-methoxycyclohexylmercury(II) chloride (VII) when *cis*-2-hydroxycyclohexyl(pyridine)cobaloxime was treated with mercuric acetate in methanol; we attributed this result to a mercury-assisted corbonium ion. A detailed analysis of the NMR spectrum, however, clarified that the cobaloxime in some synthetic lots contained varying amounts of II due to the intervention by cyclohexene oxide when *cis*-2-hydroxycyclohexyl-(pyridine)cobaloxime was prepared under the basic conditions. The mercuration of the I cobaloxime was sluggish at an ambient temperature, but gave a mixture of *trans*-2-methoxycyclohexylmercury(II) chloride (VII) and *trans*-2-ethoxycyclohexylmercury(II) chloride (VIII) when the ethanol solution of I and mercuric acetate was refluxed. The bromination of the resulting mixture in pyridine gave a mixture of *trans*-1-bromo-2-methoxyhexane (V) and *trans*-1-bromo-2-ethoxyclohexane (IX) in the ratio of 3: 2—the yield of the mixture from I was 36% (Eq. 2). The bromination of organo-mercurial in pyridine has been determined to proceed with a retention of the configuration;[18] hence, the mercuration of *cis*-2-methoxycyclohexyl(pyridine)-cobaloxime (I) clearly proceeds with inversion. The formation of the by-product, 1-bromo-2-ethoxycyclohexane, must be accounted for by the intermediate formation of cyclohexene upon mercuration as in the case of bromination.

The bromination and mercuration of *trans*-2-hydroxycyclohexyl(pyridine)cobaloxime (II), under the same reaction conditions as were used for the reaction of the I cobaloxime, gave *trans*-1,2-dibromocyclohexane (VI)

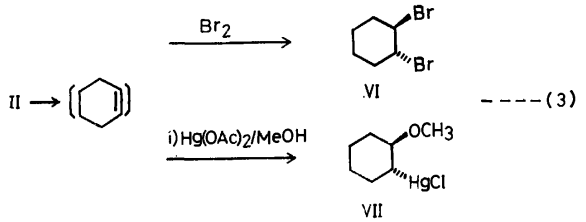

(65%) and *trans*-2-methoxycyclohexylmercury(II) chloride (VII) (70%) (Eq. 3). This implies that the *trans* arrangement of the hydroxy and cobaloxime groups in II brings about a facile β-elimination to give cyclohexene, and that the bromination or mercuration of the resulting cyclohexene takes place efficiently.

The bromination of *cis*-4-*t*-butylcyclohexyl(pyridine)cobaloxime (III) in dichloromethane at −5 °C gave a mixture of *trans*-1-bromo-4-*t*-butylcyclohexane (X) and its *cis* isomer, XI, in the ratio of 3: 1 and in a 92% yield (Eq. 4). The same treatment of *trans*-cobaloxime IV gave exclusively the XI *cis* isomer in a 90% yield (Eq. 5). The incompleteness of the stereospecificity in the bromination of III may arise from the intrusion of the radical process, since the back-side attack of III, in boat-like conformation, by bromine is hardly allowed. The mercuration of III and IV with mercuric acetate is sluggish, so the reaction was attempted by using the more reactive mercuric nitrate in methanol (Eqs. 6 and 7). The product from the reaction of III was identified with authentic *trans*-4-*t*-butylcyclohexylmercury(II) chloride (XII) prepared from the corresponding Grignard reagent.[16] The mercuration itself was a rather smooth process and the complete disappearance of III and IV was observed by the thin-layer chromatography of the reaction mixture. The addition of sodium chloride to convert the resulting organo-mercurial into the more stable organo-mercuric chloride, or the condensation of the reaction solution for isolation reverted the reaction and regenerated the III and IV cobaloximes.[19] This behavior was also suggested by observing the NMR spectrum of the reaction solution of IV. The signal at 2.17 ppm (δ) in methanol due to the four methyl groups of the dimethylglyoxymato-ligand of IV was displaced to 2.22 ppm by the addition of the mercuric ion. The addition of powdered sodium chloride to this solution regenerated the original signal. Several efforts to isolate the resulting mercurial in a practical yield from III and IV were unsuccessful in this situation. The stereochemistry of

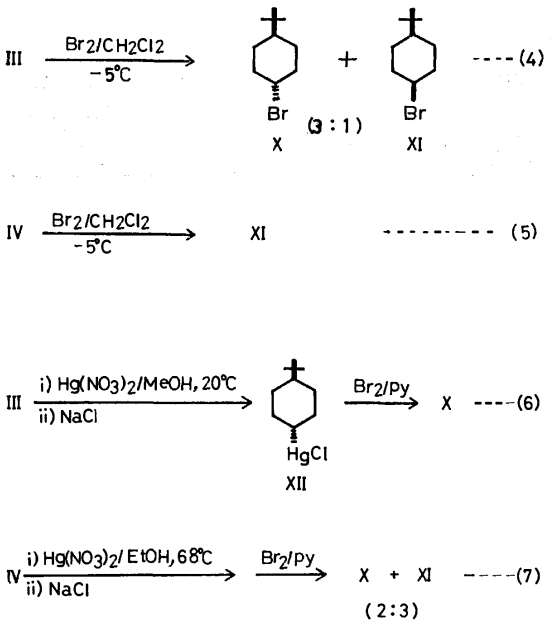

the mercurials thus obtained in poor yields was determined by the transformation of these mercurials into bromides by the action of bromine in pyridine. GLC analyses of the resulting bromides revealed that the bromide from III was exclusively *trans*-1-bromo-4-*t*-butylcyclohexane (X), while the bromide from IV was a 3:2 mixture of *cis* and *trans*-1-bromo-4-*t*-butylcyclohexanes. The latter result may be due to the incomplete stereospecificity upon the bromination of the *cis*-4-*t*-butylcyclohexylmercury(II) chloride derived from IV, since the *cis* mercurial can be expected to have a mercuric chloride group in the axial conformation;[20] the bromination with retention may not be favored.

In general, the S_E2 reaction is known to proceed with retention at the reaction center.[21] Reactions with inversion, however, have been reported in several instances, such as the brominations of tri-norbornyl borane in the presence of sodium methoxide,[22] alkyl tin,[23] and the alkyl iron complex.[5] Jensen *et al.*,[24] and Johnson *et al.*,[25] showed in preliminary reports, independently from ours, that the bromination of cobaloxime took a reaction path with an inversion at the reaction center; our results described in the preliminary report[1] and in the present paper are in good accordance with the results by those authors.

The bromination and mercuration of the II cobaloxime were found not to be suitable for the test of stereospecificity because of the reaction path of β-elimination. The equilibrium between 4-*t*-butylcyclohexyl(pyridine)cobaloxime and the mercuric ion, as proved by TLC and NMR analyses, may confuse the stereochemical course of the mercuration, but the reverse reaction must take the same stereochemical course as that of mercuration since the transition state is common to both the reactions in the equilibrium (Eq. 8).

$$Hg^{2+} + \rangle R\text{-}(Co) \rightleftharpoons [Hg\cdots C\text{-}(Co)]^{2+} \rightleftharpoons Hg\text{-}R + (Co)^{+} \cdots (8)$$

transition state

The discussions in this paper define the stereochemical nature of the bromination and mercuration as involving inversion, despite some incomplete stereospecificity in the systems with difficult geometries to take a penta valent transition state for the S_E2 reaction.

References

1) The major part of this work was previously reported as a preliminary report; M. Tada and H. Ogawa, *Tetrahedron Lett.*, **1973**, 2639.

2) E. L. Smith, "Vitamine B_{12}," 3rd ed., Methuen and Co., London (1965).

3) See for example a) J. M. Wood, F. S. Kennedy, and C. G. Rosen, *Nature*, **220**, 173 (1968). b) N. Imura, E. Sukegawa, S-K. Pan, K. Nagao, J-Y. Kim, T. Kwan, and T. Ukita, *Sciences*, **172**, 1248 (1971).

4) G. N. Schrauzer, *Acc. Chem. Res.*, **1**, 97 (1968).

5) P. L. Bock, D. J. Boschetto, J. R. Rosmussen, J. P. Demers, and G. M. Whitesides, *J. Amer. Chem. Soc.*, **96**, 2814 (1974).

6) D. R. Coulson, *ibid.*, **91**, 200 (1969).

7) R. W. Johnson and R. G. Pearson, *Chem. Commun.*, **1970**, 986.

8) D. Slack and M. C. Baird, *ibid.*, **701** (1971).

9) P. L. Bock and G. M. Whitesides, *J. Amer. Chem. Soc.*, **96**, 2826 (1974).

10) J-E. Bäckvall and B. Åkermark, *Chem. Commun.*, **1975**, 82.

11) H. L. Fritz, J. H. Espenson, D. A. Williams, and G. A. Molander, *J. Amer. Chem. Soc.*, **96**, 2378 (1974).

12) L. J. Dizikes and A. Wojcicki, *ibid.*, **97**, 2540 (1975).

13) G. N. Schrauzer, J. H. Weber, T. M. Beckham, and R. K. Ho, *Tetrahedron Lett.*, **1971**, 275.

14) V. E. Magnusson and J. H. Weber, *J. Organometal. Chem.*, **74**, 135 (1974).

15) F. R. Jensen, V. Madan, and D. H. Buchanan, *J. Amer. Chem. Soc.*, **92**, 1414 (1970).

16) F. R. Jensen and K. L. Nakamaye, *ibid.*, **90**, 3248 (1968).

17) E. L. Eliel and R. S. Ro, *ibid.*, **79**, 5992 (1957).

18) R. F. Jensen, L. D. Wipple, D. K. Wedegaertner, J. A. Landgrebe, *ibid.*, **82**, 2468 (1960).

19) G. N. Schrauzer and G. Kratel, *Chem. Ber.*, **102**, 2392 (1969).

20) F. A. L. Annet and J. Krane, *Tetrahedron Lett.*, **1975**, 3255.

21) J. March, "Advanced Organic Chemistry: Reactions, Mechanism, and Structure," McGraw-Hill, New York (1968), p. 442.

22) H. C. Brown and C. F. Lane, *Chem. Commun.*, **1971**, 521.

23) F. R. Jensen and D. D. Davis, *J. Amer. Chem. Soc.*, **93**, 4047 (1971).

24) F. R. Jensen, V. Madan, and D. H. Buchanan, *ibid.*, **93**, 5283 (1971).

25) S. N. Anderson, D. H. Ballard, J. Z. Chrzastowski, D. Dodd, and M. D. Johnson, *Chem. Commun.*, **1972**, 685.

The Michael Reaction of Silyl Enol Ethers with α,β-Unsaturated Ketones and Acetals in the Presence of Titanium Tetraalkoxide and Titanium Tetrachloride

Koichi NARASAKA, Kenso SOAI, Yukiko AIKAWA, and Teruaki MUKAIYAMA

Department of Chemistry, Faculty of Science, The University of Tokyo, Hongo, Bunkyo-ku, Tokyo 113

(Received November 4, 1975)

Silyl enol ethers react with α,β-unsaturated ketones and esters in the presence of $TiCl_4$ or in the coexistence of $TiCl_4$ and $Ti(O^i\text{-}Pr)_4$ to give 1,5-dicarbonyl compounds in good yields. The reactions of acetals derived from α,β-unsaturated ketones with silyl enol ethers in the coexistence of $TiCl_4$ and $Ti(O^i\text{-}Pr)_4$, followed by successive addition of 1,2-ethanedithiol, give the Michael products, δ-keto ethylene thioacetal, in good yields. The reaction of silyl enol ethers with acetals derived from α,β-unsaturated aldehydes also gives the Michael products when $Ti(OCEt_3)_4$ is employed instead of $Ti(O^i\text{-}Pr)_4$ in the above experiment and is successfully applied to the simple synthesis of dihydro rose oxide.

The Michael reaction of silyl enol ethers with various α,β-unsaturated ketones was briefly reported in the previous paper.[1] In this report, the reaction is explained in detail with additional results.

During the investigation on the cross-aldol reaction of silyl enol ethers with carbonyl compounds,[2] it was found that $TiCl_4$-promoted reaction of α,β-unsaturated ketones with silyl enol ethers results in the formation of 1,5-dicarbonyl compounds (the Michael products) instead of aldol products. For example, equimolar amounts of mesityl oxide (IIa) and α-trimethylsiloxystyrene (Ia) were treated with an equimolar amount of $TiCl_4$ in methylene chloride at −78 °C, and the mixture was quenched with aqueous K_2CO_3 after 2 min. Following purification by preparative tlc(silica gel), the Michael product, 3,3-dimethyl-1-phenyl-1,5-hexanedione (IIIa), was isolated in 76% yield.

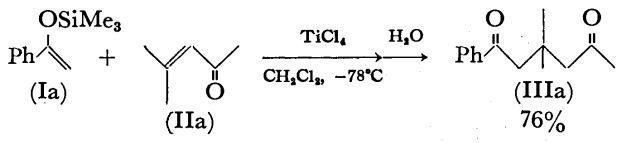

The reactions of various silyl enol ethers with a variety of α,β-unsaturated carbonyl compounds were tried in the presence of an equimolar amount of $TiCl_4$ and the corresponding Michael products were obtained in good yields as shown in the following equations.

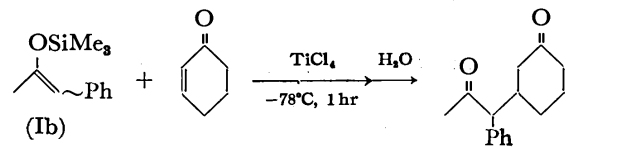

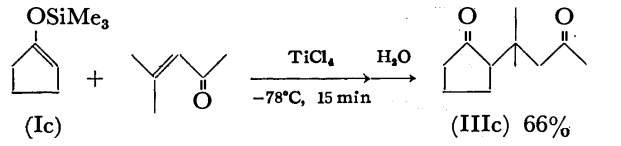

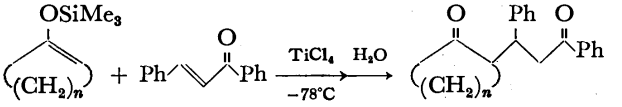

n=2 (Ic) n=2, 45 min 85% (IIId)
n=3 (Id) n=3, 60 min 95% (IIIe)

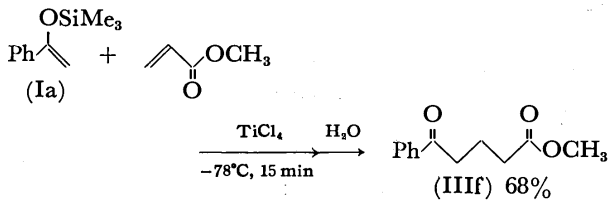

As shown in the above equations, 1,5-dicarbonyl compounds were generally obtained in good yields by the $TiCl_4$-promoted reaction of silyl enol ethers with α,β-unsaturated ketones. When $TiCl_4$-sensitive compounds such as isopropenyl trimethylsilyl ether (Ie) or 2-cyclohexen-1-one and isopropenyl methyl ketone were employed as a nucleophile or the Michael acceptors, the yields of the products became vary low. However, when the same reaction was carried out at —78 °C in the coexistence of $TiCl_4$ and $Ti(O^iPr)_4$, 1,5-diketones (IIIg, h, i) were obtained in fairly good yields.

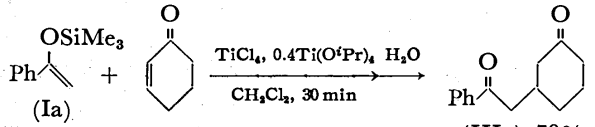

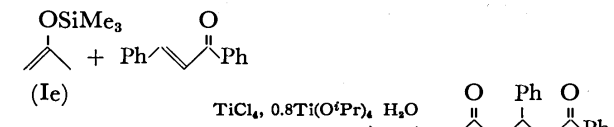

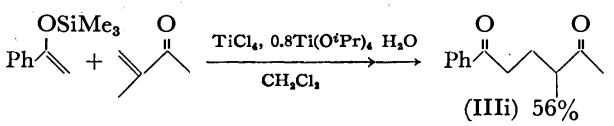

In general, the Michael reaction of an α,β-unsaturated carbonyl compound with a ketone is carried out under basic conditions and the product, a 1,5-dicarbonyl compound, frequently tends to undergo further transformation in the presence of a base.[3] Furthermore, when α,β-unsaturated ketones are used as the Michael acceptors, there are many possibilities leading to a variety of side reactions such as self-condensation reactions and the Michael reaction followed by aldol reaction.[4] On the other hand, a few examples are known concerning the acid catalyzed Michael reaction,

but in these cases, none of the 1,5-dicarbonyl compounds can be isolated bacause of further transformations of initially formed 1,5-dicarbonyl compounds.[5] In contrast to these known methods, the present Michael reaction proceeds under a very mild condition (−78 °C) to afford 1,5-dicarbonyl compounds exclusively without accompanying any by-product.

In addition, an advantage of this acid catalyzed Michael reaction is that an α,β-unsaturated acetal is able to be used as the Michael acceptor. When methyl vinyl ketone ethylene acetal (IVa)[6] was treated with α-trimethylsiloxystyrene (Ia) in the presence of equimolar amounts of $TiCl_4$ and $Ti(O^iPr)_4$ in methylene chloride at −78 °C, 1-phenyl-1,5-hexanedione (IIIj) and its monoacetal (IIIk) were isolated in 37% and 38% yields, respectively, after hydrolysis with aqueous K_2CO_3.

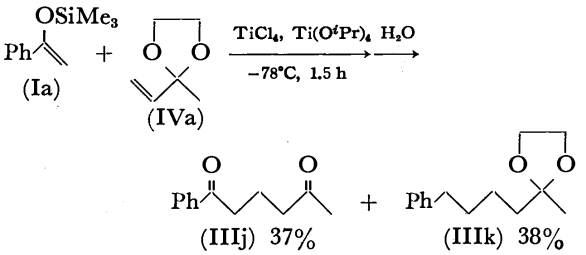

However, it was found that the subsequent treatment of the reaction mixture with 1,2-ethanedithiol gives the corresponding δ-keto thioacetal as the Michael product. For example, dropwise addition of a methylene chloride solution of equimolar amounts of Ia and IVa to a mixture of equimolar amounts of $TiCl_4$ and $Ti(O^iPr)_4$ in methylene chloride at −78 °C followed by stirring at −78 °C for 1 h. After addition of 1,2-ethanedithiol (1.1 molar amount) to the mixture, it was allowed to stand overnight at room temperature. δ-Keto thioacetal (Va) was isolated in 78% yield by preparative tlc (silica gel). Similarly, several δ-keto thioacetals were prepared and, in all cases, the carbonyl group originated from the starting acetal was selectively protected as an ethylene thioacetal.

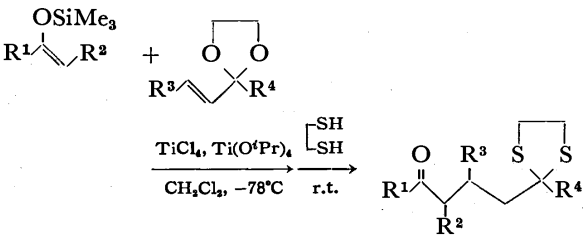

Va: R^1=Ph, R^2=H, R^3=H, R^4=Me 78%
Vb: R^1=Me, R^2=Ph, R^3=H, R^4=Me 61%
Vc: R^1=Ph, R^2=H, R^3, R^4=$-(CH_2)_3-$ 70%
Vd: R^1=Me, R^2=Ph, R^3, R^4=$-(CH_2)_3-$ 58%

Acetals derived from α,β-unsaturated aldehydes were also used as the Michael acceptors in order to prepare δ-ketoaldehyde derivatives. The reaction of crotonaldehyde dimethyl acetal (IVb) with α-trimethylsiloxystyrene (Ia) was carried out by using equimolar amounts of $TiCl_4$ and $Ti(O^iPr)_4$, but the desired Michael product (VIa) was not obtained and the β-alkoxyketones (VIIa, VIIb R=^{i}Pr) were isolated in 83% yield in total after quenching with methanol.

The preferential formation of β-alkoxyketones (VIIa, b) may be attributable to the decrease of steric hindrance around the acetal group as compared with that derived from ketones. According to this assumption, the formation of β-alkoxyketones (VIIa, b) may be suppressed by the use of aldehyde acetal having sterically large alkoxy groups instead of the methoxy group to result in the predominant formation of the Michael product (VIa).

On the other hand, it was found in our laboratory that on treatment with $Ti(O^iPr)_4$ and $TiCl_4$, 3-phenylpropionaldehyde dimethyl acetal is readily converted into the corresponding diisopropyl acetal at low tem-

Table 1. Effect of titanium alkoxides

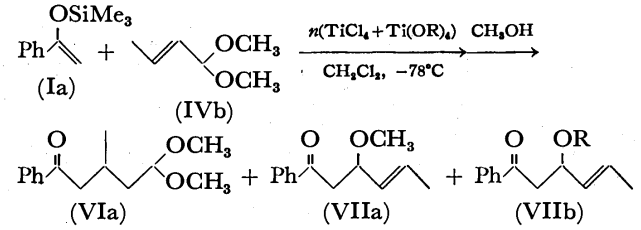

$Ti(OR)_4$	n	Yield (%) VIa[a]	VIIa	VIIb
$Ti(O^iPr)_4$	1	0	33	50
$Ti(O^tAm)_4$	1	46	28	18
	3	59	10	19
$Ti(OCEt_3)_4$	3	70	—	—

a) The Michael product was isolated as dimethyl acetal since the resulted mixture was quenched with a large amount of methanol.

Table 2. The reaction of silyl enol ethers with aldehyde acetals

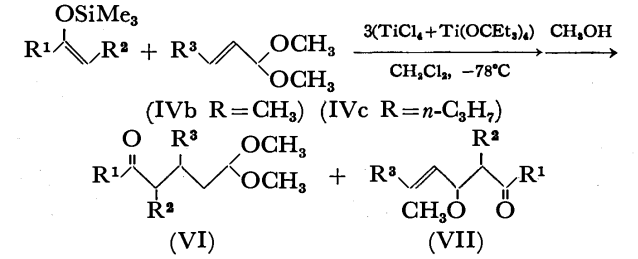

	Silyl enol ether	Acetal R^3	Yield (%) VI	VII
b		CH_3	46	trace
c		CH_3	42	trace
d		n-C_3H_7	52	9
e	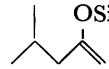	n-C_3H_7	47[a]	trace

a) In this case, the reaction mixture was quenched with water instead of methanol, and the product was isolated as aldehyde.

perature,[7] and this fact indicates that an acetal having sterically hindered alkoxy group would be readily prepared *in situ* by the reaction of the corresponding dimethyl acetal with titanium alkoxides such as $Ti(OCEt_3)_4$ and $Ti(O^tAm)_4$[8] derived from sterically hindered alcohols.

Based on this assumption, crotonaldehyde dimethyl acetal (IVb) was treated at −78 °C with $Ti(OCEt_3)_4$ or $Ti(O^tAm)_4$ and $TiCl_4$ prior to the addition of the silyl enol ether (Ia) in order to replace at least one of the methoxy group with sterically hindered alkoxy group originated in $Ti(OCEt_3)_4$ or $Ti(O^tAm)_4$. In fact, it was found that when Ia was added to the above reaction mixture, the Michael product (VIa) predominated over the formation of β-alkoxyketones (VIIa, b) as the steric hindrance of the alkoxy group increased. Especially, when 3 molar amounts of $Ti(OCEt_3)_4$ and $TiCl_4$ were employed, the Michael product (VIa) was isolated almost exclusively as summarized in Table 1.

The reactions of crotonaldehyde dimethyl acetal (IVb) and (*E*)-2-hexenal dimethyl acetal (IVc) with several silyl enol ethers were tried using 3 molar amounts of $Ti(OCEt_3)_4$ and $TiCl_4$, and the results are shown in the Table 2.

The present method for the synthesis of δ-keto aldehyde acetal was successfully applied to the simple syn-

Table 3. Physical properties and analytical data of the products

Product	Physical property Mp, °C	IR, cm^{-1}	NMR, δ	*Anal.* (%) Found, (Calcd) C	H
IIIa		1680 (C=O) 1715 (C=O)	8.00—7.10 (m, 5H, arylCH), 3.09 (s, 2H, CH_2), 2.63 (s, 2H, CH_2), 1.97 (s, 3H, CH_3CO), 1.08 (s, 6H, CH_3)		
IIIb		1715 (C=O)	7.25 (s, 5H, arylCH), 3.52 (d, 1H, CH), J=9.0 Hz		
IIIc		1715 (C=O) 1735 (C=O)	2.91 (d, 1H, CH_2CO), J=18.0 Hz, 2.33 (d, 1H, CH_2CO), J=18.0 Hz, 1.00 (s, 3H, CH_3), 0.93 (s, 3H, CH_3)	72.38 (72.49)	10.24 (9.96)
IIId	85	1680 (C=O) 1735 (C=O)	8.09—7.00 (m, 10H, arylCH)	82.36 (82.15)	6.89 (6.89)
IIIe	128—132	1680 (C=O) 1710 (C=O)	8.10—7.10 (m, 10H, arylCH)	82.52 (82.32)	7.42 (7.24)
IIIf		1685 (C=O) 1735 (C=O)	8.12—7.00 (m, 5H, arylCH), 3.60 (s, 3H, OCH_3), 2.94 (t, 2H, CH_2CO), J=6.0 Hz, 2.55—1.55 (m, 4H, CH_2)		
IIIg	75—76	1680 (C=O) 1720 (C=O)	8.00—7.40 (m, 5H, arylCH), 2.90 (d, 2H, CHCO), J=5.4 Hz	77.64 (77.75)	7.56 (7.46)
IIIh	81—82	1690 (C=O) 1715 (C=O)	8.00—6.80 (m, 10H, arylCH), 3.80 (m, 1H, CH), 2.00 (s, 3H, CH_3), 3.26 (d, 2H, CH_2), J=6.0 Hz, 2.90 (d, 2H, CH_2), J=6.0 Hz	81.27 (81.17)	7.01 (6.81)
IIIi		1685 (C=O) 1710 (C=O)	8.00—7.15 (m, 5H, arylCH), 2.08 (s, 3H, CH_3CO), 1.08 (d, 3H, CH_3), J=6.6 Hz		
IIIj		1680 (C=O) 1715 (C=O)	8.00—7.10 (m, 5H, arylCH), 2.90 (t, 2H, CH_2CO), J=6.0 Hz, 2.05 (s, 3H, CH_3)		
IIIk		1680 (C=O)	8.00—7.10 (m, 5H, arylCH), 3.85 (s, 4H, OCH_2CH_2O), 1.25 (s, 3H, CH_3)		
Va	60—61	1690 (C=O)	8.07—7.30 (m, 5H, arylCH), 3.32 (s, 4H), 1.78 (s, 3H)		
Vb		1715 (C=O)	7.20 (s, 5H, arylCH), 3.20 (s, 4H, SCH_2CH_2S), 2.05 (s, 3H, CH_3CO)		
Vc		1690 (C=O)	8.30—7.20 (m, 5H, arylCH), 3.30 (s, 4H, CH_2CH_2)		
Vd		1715 (C=O)	7.18 (s, 5H, arylCH), 2.00 (s, 3H, CH_3)		
VIb		1735 (C=O) 2820	4.35 (m, 1H, CH), 3.22—3.14 (m, 6H, OCH_3)	66.19 (65.97)	10.20 (10.07)
VIc		1710 (C=O) 2820	7.22 (s, 5H, arylCH), 4.40 (t, 1H, CH), 3.25 (s, 6H, OCH_3), 1.97 (s, 3H, CH_3CO), 0.65 (d, 3H, CH_3), J=7.2 Hz		
VId		1685 (C=O) 2820	8.01—7.08 (m, 5H, arylCH), 4.38 (t, 1H, CH), J=6.0 Hz, 3.18 (s, 3H, OCH_3), 3.12 (s, 3H, OCH_3), 2.86 (dd, 2H, $COCH_2$)		
VIe		1720 (C=O) 2715	9.67 (t, 1H, CHO)		

thesis of dihydro rose oxide (VIII). The reaction of 4-methyl-2-trimethylsiloxy-1-pentene (If) with crotonaldehyde dimethyl acetal (IVb) was carried out using 3 molar amounts of $TiCl_4$ and $Ti(OCEt_3)_4$ at −78 °C in methylene chloride. After hydrolysis, the ketoaldehyde (IX) was obtained in 57% yield (83% when 2 molar amounts of If was employed). Reduction of IX with $LiAlH_4$ in ether readily afforded the corresponding diol (X) in 88% yield and the dehydration of the diol (X) according to literature[9] gave a *cis* and *trans* mixture of dihydro rose oxide (VIII), which was identical by glc analysis with the authentic sample prepared by the hydrogenation of a *cis* and *trans* mixture of rose oxide over palladium.

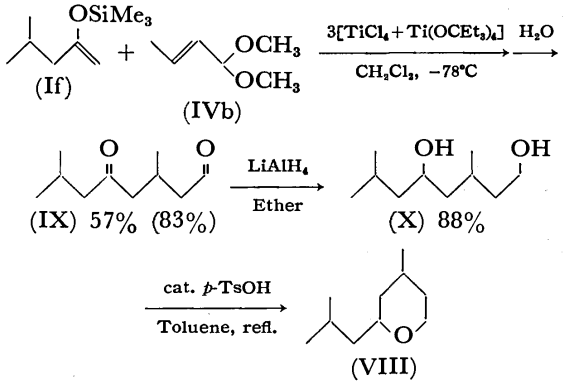

Experimental

Materials. Commercially available $TiCl_4$ and $Ti(O^iPr)_4$ were distilled under an argon atmosphere before use. Trimethylsilyl enol ethers of carbonyl compounds, α-trimethylsiloxystyrene (Ia), 1-phenyl-2-trimethylsiloxy-1-propene (Ib), 1-trimethylsiloxy-1-cyclopentene (Ic), 1-trimethylsiloxy-1-cyclohexene (Id), were prepared according to the procedures described in the literature[10] and purified by distillation: Ia, bp 89—91 °C/12 mmHg (lit, bp 89—91 °C/12 mmHg); Ib, bp 103 °C/8 mmHg (lit, bp 106 °C/10 mmHg); Ic, bp 155 °C/760 mmHg (lit, bp 158—159 °C/760 mmHg); Id, bp 97—99 °C/65 mmHg (lit, 74—75 °C/20 mmHg). In a similar manner, isopropenyl trimethylsilyl ether (Ie) was prepared from acetone, trimethylsilyl chloride and triethylamine and 4-methyl-2-trimethylsiloxy-1-pentene (If) was prepared from the corresponding ketone, trimethylsilyl chloride and lithium diisopropylamide: Ie, bp 94.5—95.5 °C, NMR(CCl_4); δ 3.96 (s, 2H, vinyl CH_2), δ 1.75 (s, 3H, CH_3), δ 0.19 (s, 9H, $Si(CH_3)_3$); If, bp 58—60 °C/35 mmHg, NMR(CCl_4); δ 3.97(s, 2H, vinyl CH_2), δ 0.19(s, 9H, $Si(CH_3)_3$).

Reaction of α-Trimethylsiloxystyrene (Ia) with Mesityl Oxide (IIa) in the Presence of $TiCl_4$. A solution of $TiCl_4$ (2 mmol) in 8 ml of CH_2Cl_2 was cooled to −78 °C and stirred under an argon atmosphere. A solution of mesityl oxide (IIa, 2 mmol) in CH_2Cl_2 (3 ml) and a solution of α-trimethylsiloxystyrene (Ia, 2 mmol) in CH_2Cl_2 (3 ml) were added successively to the above solution. After stirring for 2 min at −78 °C, the mixture was quenched with aqueous K_2CO_3 (0.7 g in 15 ml of water), and resulting precipitate was filtered off. The filtrate was extracted with ether and the extract was washed with water and brine. After removal of the solvent, 3,3-dimethyl-1-phenyl-1,5-hexanedione (IIIa, 76%) was separated by preparative tlc (silica gel) using hexane–ether 2: 1) as eluent.

Reaction of α-Trimethylsiloxystyrene (Ia) with 2-Cyclohexen-1-one in the Presence of $TiCl_4$ and $Ti(O^iPr)_4$. To a CH_2Cl_2 (4 ml) solution of $TiCl_4$ (1.0 mmol) and $Ti(O^iPr)_4$ (0.4 mmol) [$TiCl_4$ and $Ti(O^iPr)_4$ must be mixed at −78 °C] was added a mixture of α-trimethylsiloxystyrene (Ia, 1.0 mmol) and 2-cyclohexen-1-one (1.0 mmol) in CH_2Cl_2 (6 ml) at −78 °C with stirring under an argon atmosphere. After being stirred for 30 min, the mixture was hydrolyzed with 12 ml of aqueous K_2CO_3 (0.75 g) and extracted with ether. The extract was washed with brine, dried over anhydrous Na_2SO_4 and condensed under reduced pressure. By preparative tlc (silica gel), 3-phenacylcyclohexan-1-one (IIIg) was isolated in 70% yield.

Reaction of α-Trimethylsiloxystyrene (Ia) with Methyl Vinyl Ketone Ethylene Acetal (IVa). To a CH_2Cl_2 (4 ml) solution of $TiCl_4$ (1.0 mmol) and $Ti(O^iPr)_4$ (1.0 mmol) was added a mixture of α-trimethylsiloxystyrene (Ia, 1.0 mmol) and methyl vinyl ketone ethylene acetal (IVa, 1.0 mmol) in CH_2Cl_2 (6 ml) at −78 °C with stirring under an argon atmosphere. After stirring the mixture for 1 h, 1,2-ethanedithiol (1.1 molar amounts) was added to the mixture. After being allowed to stand overnight at room temperature, the mixture was quenched with aq. K_2CO_3 (0.7 g in 15 ml of water) and the resulting precipitate was filtered off. The filtrate was extracted with ether and the extract was washed with water and brine, dried over anhydrous Na_2SO_4. After removal of the solvent δ-keto thioacetal (Va, 78%) was isolated by preparative tlc (silica gel) using hexane–ether (2: 1) as eluent. The structure was also established by hydrolysis in the presence of $CuCl_2$[11] to 1-phenylhexane-1,5-dione.

Reaction of α-Trimethylsiloxystyrene (Ia) with Crotonaldehyde Dimethyl Acetal (IVb). To a mixture of $Ti(OCEt_3)_4$(3 mmol) and crotonaldehyde dimethyl acetal (1 mmol) in CH_2Cl_2 (6 ml) was added $TiCl_4$ (3 mmol) in 2 ml of CH_2Cl_2 under an argon atmosphere. After stirring the mixture for 6 min, α-trimethylsiloxystyrene (Ia, 1 mmol in 3 ml of CH_2Cl_2) was added. The mixture was stirred for 1 h, treated with 3 ml of MeOH at 0 °C for 30 min and worked-up in the usual manner. After separation by preparative TLC (silica gel), 5,5-dimethoxy-3-methyl-1-phenylpentan-1-one (VIa) was isolated in 70% yield. (VIa: NMR(CCl_4): δ 0.98 (d, 3H), δ 3.17 (s, 3H), δ 3.20 (s, 3H), δ 4.41 (t, 1H): IR; 2820, 1685 cm^{-1}).

3,5-Dimethyl-5-oxooctanal (IX). To a mixture of 3 mmol of $Ti(OCEt_3)_4$ and crotonaldehyde dimethyl acetal (1 mmol) in CH_2Cl_2 (6 ml) was added $TiCl_4$ (3 mmol) in 2 ml of CH_2Cl_2 at −78 °C under an argon atmosphere. After stirring the mixture for 6 min 4-methyl-2-trimethylsiloxy-1-pentene (If, 1 mmol in 3 ml CH_2Cl_2) was added. The mixture was stirred for 1 h, followed by hydrolysis with aq. K_2CO_3 (0.75 g in 12 ml of water), and extracted with ether. The extract was washed with brine, dried over anhydrous Na_2SO_4 and condensed under reduced pressure. 3,7-Dimethyl-5-oxooctanal (IX) was isolated in 57% (83% when 2 equimolar amounts of If was employed) by preparative tlc (silica gel) using hexane–ether (2: 1) as eluent. (IX: NMR (CCl_4); δ 9.72 (t, 1H): IR; 2725, 1725, 1715 cm^{-1}).

3,7-Dimethyl-1,5-octanediol (X). To a suspension of $LiAlH_4$ (2.4 mmol) in Et_2O (16 ml) was added a Et_2O (12 ml) solution of 3,7-dimethyl-5-oxooctanal (IX, 1.19 mmol) in 7 min at 0 °C. After stirring the mixture for 1 h at room temperature, saturated aqueous solution of Na_2SO_4 was added into the mixture. The resulted precipitate was washed with THF (5 ml×3) by decantation. The THF-Et_2O solution was dried over anhydrous Na_2SO_4. Distillation under reduced pressure gave 3,7-dimethyl-1,5-octanediol (X, 88%). (X: NMR (CCl_4); δ 4.49 (s (broad), 2H), δ 3.40—4.40 (m, 3H), δ 0.79—2.20 (m, 15H): IR; 3330, 1370, 1380 cm^{-1}).

Dihydro Rose Oxide (VIII). Dehydration of 3,7-dimethyl-1,5-octanediol (X) according to literature[9] method gave a *cis* and *trans* mixture of dihydro rose oxide (VIII), which was identical by glc analysis with the authentic sample prepared by the hydrogenation of a *cis* and *trans* mixture of rose oxide over palladium catalyst.

References

1) K. Narasaka, K. Soai, and T. Mukaiyama, *Chem. Lett.* **1974**, 1223.

2) T. Mukaiyama, K. Narasaka, and K. Banno, *Chem, Lett.*, **1973**, 1011; T. Mukaiyama, K. Banno, and K. Narasaka. *J. Amer. Chem. Soc.*, **96**, 7503 (1974).

3) E. D. Bergann, K. Ginsburg, and R. Pappo, "Org. Reactions," Vol. 10, p. 179 (1959).

4) G. Kabas and H. C. Rutz, *Tetrahedron*, **22**, 1219 (1966); D. W. Theobald, *ibid.*, **23**, 2767 (1967); J. Grimshaw and D. W. Jennings, *J. Chem. Soc., C*, **1970**, 817; N. J. Leonard and W. J. Muslinger, *J. Org. Chem.*, **31**, 639 (1966); G. Büchi, J. H. Hansen, K. Knutson, and E. Koller, *J. Amer. Chem. Soc.*, **80**, 5517 (1958).

5) J. A. van Allan and G. A. Reynolds, *J. Org. Chem.*, **33**, 1102 (1968); J. D. Surmatis, A. Walser, J. Gibas, and R. Thommen, *ibid.*, **35**, 1053 (1970).

6) E. F. Hahn, *J. Org. Chem.*, **38**, 2092 (1973).

7) T. Mukaiyama and A. Ishida, *Chem. Lett.*, **1975**, 319.

8) D. C. Bradley, R. C. Mehrotra, and W. Wardlaw, *J. Chem. Soc.*, **1952**, 4204.

9) K. C. Brannock and H. E. Davis, *J. Org. Chem.*, **31**, 980 (1966).

10) H. O. House, L. J. Czuba, M. Gall, and H. D. Olmstead, *J. Org. Chem.*, **34**, 2324 (1969).

11) K. Narasaka, T. Sakashita, T. Mukaiyama, This Bulletin, **45**, 3724 (1972).

Reactions of Dihydridotetrakis(tertiary phosphine)ruthenium(II) Complexes with Carbon Dioxide, Carbon Disulfide and Sulfur Dioxide

Sanshiro KOMIYA and Akio YAMAMOTO

Research Laboratory of Resources Utilization, Tokyo Institute of Technology, O-okayama, Meguro-ku, Tokyo 152

(Received November 7, 1975)

Carbon dioxide reacts with $RuH_2(PPh_3)_4$ to give its insertion product, hydridoformatotris(triphenylphosphine)-ruthenium(II). The reversibility of the CO_2 insertion has been demonstrated. Insertion products of carbon disulfide and adducts of sulfur dioxide with ruthenium also have been obtained by the reactions of carbon disulfide and sulfur dioxide with various ruthenium dihydride complexes, RuH_2L_4 (L=PPh_3, PPh_2H, PPh_2Me, $PPhMe_2$). These compounds were characterized by IR and NMR spectroscopy, elemental analysis and chemical reactions.

Since the first reports on the reactions of a hydrido-(dinitrogen)cobalt complex with carbon dioxide to yield a cobalt formate complex[1,2] the reactions of CO_2 with transition metal alkyls and hydrides have been attracting increasing attention.[3] As an extension of our preliminary communication[4] we now report the reactions of tertiary phosphine-coordinated ruthenium dihydride complexes (RuH_2L_4) with carbon dioxide and its analogs, carbon disulfide and sulfur dioxide.

Results and Discussion

Reaction of Dihydridotetrakis(phosphine)ruthenium(II) with Carbon Dioxide. The reaction of $RuH_2(PPh_3)_4$ (I) with carbon dioxide in toluene proceeds readily at room temperature to give a diamagnetic complex $RuH(O_2CH)(PPh_3)_3$(toluene) (II) in a high yield.[a]

$$\underset{\text{(I)}}{RuH_2(PPh_3)_4} + CO_2 \xrightarrow{\text{toluene}} \underset{\text{(II)}}{RuH(O_2CH)(PPh_3)_3(\text{toluene})} + PPh_3$$

Complex II is an air-sensitive yellow solid which is stable in a nitrogen atmosphere but decomposes in air in about 1 day releasing 1 mol of carbon dioxide per ruthenium. The IR spectrum of II is in agreement with its formulation as a hydrido-formato complex. Table 1 tabulates relevant IR absorption bands of the hydridoformato complex II with assignments based on comparison with IR spectra of other known formates, $Rb(O_2CH)$[6] and $Co(O_2CH)(PPh_3)_3$.[1]

The reactions of CO_2 with other phosphine-coordinated complexes of a general formula RuH_2L_4 (L=PPh_2H,[7] PPh_2Me,[8] $PPhMe_2$[9]) also have been examined. However, none of these complexes other than I reacted with CO_2 in toluene even at 110 °C and only starting dihydrido complexes were recovered. Presumably, a predissociation of one of the four phosphine ligands from the coordinatively saturated complexes is required for accommodating a coordination site for the reactant to enter into the reaction. Examination of $^{31}P\{^1H\}$-NMR of RuH_2L_4 complexes in polar solvents such as pyridine revealed that complex I is completely dissociated to $RuH_2(PPh_3)_3$(solvent) and PPh_3 whereas other phosphine-coordinated complexes are not dissociated in the polar solvents.[10] In non-polar solvents the dissociation of PPh_3 from I is much less extensive and the dissociative process may constitute a rate determining step as we previously observed in polymerization of vinyl compounds by PPh_3-coordinated complexes.[11,12]

Acidolysis of II in the solid state with sulfuric acid liberated carbon monoxide and hydrogen in addition to carbon dioxide. Complex II readily loses CO_2 on various chemical treatments. Reaction of II with alkyl halides released carbon dioxide and alkanes and gave a quantitative yield of hydridohalotris(triphenylphosphine)ruthenium.[13]

$$\underset{\text{(II)}}{(HCOO)RuH(PPh_3)_3(\text{toluene})} + RX \longrightarrow HRuX(PPh_3)_3 + RH + CO_2 + \text{toluene}$$

(RX=MeI, EtBr, EtI)

Table 1. Main IR bands of formato complexes

Assignment	IR bands (cm^{-1})		
	$Rb(O_2CH)$[6]	$(HCO_2)RuH(PPh_3)_3$	$(HCO_2)Co(PPh_3)_3$[1]
C–H stretch	2801 w	2895 w, 2805 w	2795 w, 2700 w
asym OCO stretch	1592 s	1553 s	1620 s
asym OCO deformation	1381	1365 m, 1347 m	
sym OCO stretch	1370 s	1310 s	1300 s
sym OCO deformation	774 s	795 s	
out of plane deformation	1066 vw		
M–H stretch		1996 m	

a) Vol'pin *et al.* first reported the reaction claiming that $Ru(OMe)H(PPh_3)_3 \cdot CO_2$ was obtained.[3a] However, subsequent to our communication[4] the complex was reformulated as $RuH(OOCH)(PPh_3)_3$ and its molecular structure with an octahedral configuration containing the formato group as a bidentate ligand has been established by X-ray analysis.[5]

Complex II is thermally fairly stable, and thermolysis of II takes place in two steps. At *ca.* 140 °C II releases about one mol of CO_2 per II leaving a ruthenium hydride complex having a ν(Ru-H) band at 2080 cm^{-1}. The second decomposition takes place at 200 °C, which is very close to the decomposition point of $RuH_2(PPh_3)_4$, and at the temperature hydrogen and a small amount of carbon monoxide are liberated.

The formate Complex II can be also obtained by reactions of carbon dioxide with $RuH_4(PPh_3)_3$ and $RuH_2(N_2)(PPh_3)_3$.[14,15]

A salient feature of the formate complex is the ready release of carbon dioxide in solution. Bubbling of H_2 and N_2 through benzene solutions containing II displaces readily carbon dioxide giving $RuH_4(PPh_3)_3$ and $RuH_2(N_2)(PPh_3)_3$, respectively. Addition of PPh_3 to the benzene solution containing II also liberated CO_2 giving Complex I.

$$RuH(OOCH)(PPh_3)_3 + H_2 \rightleftarrows RuH_4(PPh_3)_3 + CO_2$$

$$RuH(OOCH)(PPh_3)_3 + N_2 \rightleftarrows RuH_2(N_2)(PPh_3)_3 + CO_2$$

$$RuH(OOCH)(PPh_3)_3 + PPh_3 \rightleftarrows RuH_2(PPh_3)_4 + CO_2$$

(I)

Addition of triphenylphosphite and tributylphosphine to II also led to liberation of CO_2 and toluene. The reversibility of the reactions among $RuH_2(PPh_3)_4$, $RuH_4(PPh_3)_3$ and $RuH_2(N_2)(PPh_3)_3$ have been previously demonstrated.[14,15]

Reaction of RuH_2L_4 with Carbon Disulfide. As extension of the reaction of RuH_2L_4 with carbon dioxide the reaction with its isoelectronic compound toward RuH_2L_4 have been examined. Insertion reactions of CS_2 into transition metal-alkyl bonds are known;[16] several examples of CS_2 insertion into transition metal-hydrogen bond have been reported.[16d,17]

In the interium since we started this line of work the reactions of I and $RuH_4(PPh_3)_3$ with CS_2 to afford $Ru(S_2CH)_2(PPh_3)_2$ have been reported by Harris *et al.*[18] We describe here the reactions of CS_2 with RuH_2L_4 including other phosphine ligands (L=PPh_3, PPh_2H, PPh_2Me, $PPhMe_2$).

In contrast to the reaction of CO_2 with RuH_2L_4, where the CO_2 insertion into only one of the two Ru–H bonds in I was observed, the CS_2 insertion into both of the Ru–H bonds proceeds smoothly at room temperature in all of the RuH_2L_4 type complexes examined to afford bis(dithioformato) type complexes. Negligible amounts of hydrogen were evolved in the reactions. One might observe the formation of HCSSH if one molecule of CS_2 should be inserted into one of the two Ru–H bonds to be followed by abstraction of hydrogen from the remaining Ru–H bond. Examination of the volatile reaction products by NMR excluded the formation of HCSSH in the reaction. This was further supported by failure of the formation of silver dithioformate by treating the volatile matters with silver nitrate.

Table 2 shows yields, physical and chemical properties, and analytical data of the isolated bis(dithioformato) complexes obtained by the reactions of RuH_2L_4 with CS_2.

The thermal stability of the dithioformate complex appears to depend on the phosphine ligand. Less basic ligands such as triphenylphosphine and diphenylphosphine gave more stable complexes than more basic ligands such as diphenylmethylphosphine and phenyldimethylphosphine. Pyrolysis of the dithioformate complex containing triphenylphosphine releases carbon disulfide and triphenylphosphine sulfide. Liberation of CS_2 was observed in the pyrolysis of other phosphine-coordinated complexes and the release of a small amount of hydrogen was noted in the pyrolysis of $Ru(S_2CH)_2(PPh_2H)_4$.

Acidolysis of $Ru(S_2CH)_2(PPh_3)_2$ (III) with concentrated sulfuric acid released CS_2 and SO_2. Hydrogen chloride and methyl iodide did not react with (III) at room temperature.

Table 2 includes IR bands which are not observed in the RuH_2L_4 type complexes. Known dithioformate and dithiobenzoate complexes[16] show ν (CS_2) bands in the range of 900—1100 cm^{-1} whereas CS_2-coordinated complexes and carbon-bonded metal dithio acid type (M-CSSR) complexes have $\nu(CS_2)$ bands at much higher frequencies. Therefore the strong new bands in the range of 900—1100 cm^{-1} may be assigned to $\nu(CS_2)$ bands of the dithio formate group. The dithioformate group can act as a bidentate as well as a monodentate ligand. In $Ru(S_2CH)_2(PPh_3)_2$ the $\nu(CS_2)$ band appears at the lowest frequency among the four dithioformate complexes shown in Table 2. This may well arise from its octahedral configuration having two bidentate

Table 2. Reactions of RuH_2L_4 with CS_2

Reactant	$RuH_2(PPh_3)_4$	$RuH_2(PPh_2H)_4$	$RuH_2(PPh_2Me)_4$	$RuH_2(PPhMe_2)_4$
Product	$Ru(S_2CH)_2(PPh_3)_2$	$Ru(S_2CH)_2(PPh_2H)_4$	$Ru(S_2CH)_2(PPh_2Me)_3$	$Ru(S_2CH)_2(PPhMe_2)_3$
Color	red-orange	yellow	brown	red
Yield	*ca.* 80%	*ca.* 80%	*ca.* 20%	*ca.* 20%
Dec.pt.	196—200°C	200—203°C	138°C	140°C
Pyrolysis product	CS_2	$CS_2+(H_2)$	CS_2	CS_2
Analysis	Found (Calcd)	Found (Calcd)	Found (Calcd)	Found (Calcd)
	C, 59.2(58.5)	C, 60.3(60.0)	C, 57.8(57.5)	C, 45.4(46.6)
	H, 4.0(4.1)	H, 4.6(4.7)	H, 4.8(4.8)	H, 5.5(5.3)
	S, 17.3(16.4)	S, 12.2(12.8)	S, 15.9(15.0)	S, 20.7(19.2)
IR	910 cm^{-1}(s)	1016 cm^{-1}(s)	1090 cm^{-1}(w)	990 cm^{-1}(s)
(new peaks)	918(sh)	950(sh)	1022(s)	960(s)
	786(m)		995(s)	

dithioformate groups. Conversely the strong $\nu(CS_2)$ absorption band at 1016 cm^{-1} in $Ru(S_2CH)_2(PPh_2H)_4$ may be ascribed to the monodentate dithioformate group in the octahedral complex, and the strong bands in $Ru(S_2CH)_2(PPh_2Me)_3$ and $Ru(S_2CH)_2(PPhMe_2)_3$ may be due to the presence of two modes of coordination of the two dithioformate ligands in these complexes. All the dithioformate complexes showed a weak band at 1510 cm^{-1} which disappears on drying them in vacuum for a long period. This band may be due to the presence of an S-bonded CS_2 molecule which has a weak interaction with the ruthenium complex. A similar band has been observed in the IR spectrum of $PtMe(I)(CS_2)(PPh_3)_2$.[16d]

Reaction of RuH_2L_4 with Sulfur Dioxide. We have examined further the reactions of RuH_2L_4 type complexes with sulfur dioxide. The reactions of SO_2 with various organometallic compounds have been recently reviewed.[19] The reactions of SO_2 with $RuH_2(PPh_2H)_4$ and $RuH_2(PPh_2Me)_4$ in toluene gave light yellow complexes without evolution of hydrogen, whereas a considerable amount of hydrogen was evolved in the reactions of SO_2 with $RuH_2(PPh_3)_4$ and $RuH_2(PPhMe_2)_4$. We tentatively formulate the sulfinate structures $Ru(SO_2H)(PPh_2H)_3$ and $Ru(SO_2H)(PPh_2Me)_3$ for the products obtained without evolution of hydrogen and SO_2-coordinated structures $Ru(SO_2)_2(PPh_3)_2$ and $Ru(SO_2)(PPhMe_2)_3$ for those obtained with evolution of hydrogen. The latter complexes liberated only SO_2 on acidolysis and pyrolysis whereas the PPh_2H-coordinated complex released H_2 in addition to SO_2 on pyrolysis. No infrared band due to ν(Ru–H) was observed in these complexes. The complexes which may have the sulfinate structure showed a broad NMR signal in the region of δ 5. Formulation of the reaction product of $RuH_2(PPh_3)_4$ with SO_2 as $Ru(SO_2)_2(PPh_3)_2$ has been previously proposed by Eliades *et al.*[18a]

Experimental

All the reactions were carried out under nitrogen or in a vacuum. Infrared spectra were recorded as KBr disks on a Hitachi model EPI-G3 spectrometer. NMR spectra were measured on JNM-PS-100 and JNM-MH-60. Elemental analyses were performed with Yanagimoto CHN Autocorder Type MT2. Gas chromatograms were recorded by using Shimadzu type GC-5A. Solvents were purified by usual methods under nitrogen. Carbon dioxide gas was dried by passing it through a $CaCl_2$ column and carbon disulfide was dried with CaH_2. Sulfur dioxide was obtained on reaction of Cu with concd H_2SO_4 and dried by passing through a concd H_2SO_4 bubbler. RuH_2L_4 (L=PPh_3,[18] PPh_2H,[7] PPh_2Me,[8] and $PPhMe_2$[9]) were synthesized by the methods previously reported.

Hydrido(formato)tris(triphenylphosphine)(toluene)ruthenium(II) (II), $RuH(O_2CH)(PPh_3)_3$(toluene). When carbon dioxide was brought in contact with or bubbled into the toluene solution of I at room temperature, a yellow precipitate was formed in about 1 day. The precipitate was washed with hexane a few times and dried in a vacuum; yield, *ca.* 80%. Anal. Calcd for $RuH(O_2CH)(PPh_3)_3$(toluene): C, 72.6; H, 5.4%. Found: C, 72.8; H, 5.2%.

Attempts of recrystallization led only to decomposition of the formate complex with liberation of CO_2. Reactions of $RuH_2(N_2)(PPh_3)_3$ or $RuH_4(PPh_3)_3$ with carbon dioxide gave the same product.

Reaction of $RuH(O_2CH)(PPh_3)_3$(toluene) (II). i) Acidolysis. Acidolysis of II (159.0 mg, 0.155 mmol) by *ca.* 5 ml of concd sulfuric acid released carbon monoxide (0.08 mmol) and hydrogen (0.03 mmol) at room temperature.

ii) Reaction of II with Alkyl Halide. The reaction of II (162.6 mg, 0.158 mmol) with methyl iodide (*ca.* 2 ml) gave methane (0.15 mmol) and carbon dioxide (0.13 mmol). The resultant complex is considered to be hydridoiodotris(triphenylphosphine)ruthenium $RuHI(PPh_3)_3$ on the basis of IR spectrum showing a ruthenium-hydrogen stretching band at 2020 cm^{-1}. Because a quaternary salt of triphenylphosphine with methyl iodide was also produced in this reaction, the complete purification was not feasible, but in case of the reaction of II with ethyl bromide $RuHBr(PPh_3)_3$ was isolated. Pyrolysis of II (148.5 mg, 0.145 mmol) liberated carbon dioxide (0.15 mmol) at *ca.* 200 °C. Formation of a small amount of benzene was observed.

iv) Reaction of II with Triphenylphosphite. When complex (II) (625.7 mg, 0.610 mmol) was treated with triphenylphosphite (*ca.* 2 ml), toluene was released as identified by gas chromatography in a yield of 52 mg (0.56 mmol, 93%). Hydrogen and carbon dioxide were also evolved. By the reaction of II with tributylphosphine CO_2 and toluene were released.

v) Reaction of II with Hydrogen, Nitrogen and Triphenylphosphine. An excess of hydrogen was brought in contact with a benzene solution of II to precipitate white needles in a few hours. Carbon dioxide was detected in the gas phase. The white needles were washed with hexane a few times and dried in a vacuum, dec. pt. 135°; ν(Ru–H) 1950 cm^{-1}.[14] No particular attempt was made for purification of the complex by recrystallization, but the analytical value was close to that of $RuH_4(PPh_3)_3$. Found: C, 71.8; H, 5.2%. Calcd for $RuH_4(PPh_3)_3$: C, 72.8; H, 5.5%.

Bubbling of nitrogen into the heterogeneous solution of II gave $RuH_2(N_2)(PPh_3)_3$ with the liberation of CO_2; the formation of the dinitrogen complex was confirmed on the basis of its IR spectrum with a $\nu(N_2)$ band at 2143 cm^{-1}. Addition of excess triphenylphosphine into the benzene solution of II liberated carbon dioxide at room temperature forming $RuH_2(PPh_3)_4$. The formation of $RuH_2(PPh_3)_4$ was confirmed by its infrared spectrum with a ν(Ru–H) band at 2080 cm^{-1}.

Reactions of RuH_2L_4 with Carbon Disulfide. The reactions of CS_2 with RuH_2L_4 type complexes were carried out in a similar manner. Excess CS_2 was introduced by a trap-to-trap distillation method to a flask containing RuH_2L_4. The suspension became homogeneous in an hour at room temperature and a yellow or red precipitate was deposited which was washed with hexane a few times and dried *in vacuo* (yield 50—80%). No detectable amount of gas was evolved in the reaction. The product was recrystallized from dichloromethane and ether, or from toluene except for $Ru(S_2CH)_2(PPh_3)_2$ which reacted with dichloromethane.

Pyrolysis of $Ru(S_2CH)_2(PPh_3)_2$ (0.1954 g, 0.251 mmol) at 200 °C liberated carbon disulfide (0.023 mmol, 9%) and triphenylphosphine sulfide. The carbon disulfide was identified by IR and mass spectroscopy and gas chromatography. Triphenylphosphine sulfide was identified on the basis of IR spectrum, ν(P=S) 1105 cm^{-1}, and elemental analysis (Calcd for $C_{18}H_{15}PS$: S, 10.9%; Found: S, 10.8%).

Reactions of RuH_2L_4 with SO_2. The reactions of SO_2 with RuH_2L_4 type complexes were performed by allowing SO_2 gas to contact with toluene solutions containing the hydrido complexes at room temperature. In the reactions of RuH_2-

$(PPh_3)_4$ and $RuH_2(PPhMe_2)_4$ hydrogen evolution (30—40%) was observed. The precipitate was washed with hexane and dried *in vacuo*, and recrystallized from dichloromethane and ether.

$Ru(SO_2)_2(PPh_3)_2$, mp (dec.) 243—251 °C; new IR (KBr disc) peaks not present in $RuH_2(PPh_3)_4$: 1270 (s), 1138 (s), 650 (w), 570 cm^{-1} (w). Found: C, 57.2; H, 4.3; S. 7.4%. Calcd for $Ru(SO_2)_2(PPh_3)_2$: C, 57.4; H, 4.0; S, 7.4%.

$Ru(SO_2)(PPhMe_2)_3$ (tentative formula), mp (dec.) 270—280 °C; new IR (KBr disc) peaks not present in $RuH_2(PPhMe_2)_4$: 1210 (s), 1140 (s), 1010 (m), 652 (m), 610 (w), 455 cm^{-1} (w). Considerable difficulty was encountered in purification due to the formation of $PPhMe_2$–SO_2 adduct. Found: C, 45.7; H, 5.5; S, 5.1%. Calcd for $Ru(SO_2)(PPhMe_2)_3$: C, 49.7; H, 5.7; S. 5.5%.

$Ru(SO_2H)(PPh_2Me)_3$ (tentative formula), mp (dec.) 212—215 °C; IR (KBr disc) not present in $RuH_2(PPh_2Me)_4$: 1260 (m), 1138 (s), 1122 (s), 640 (m), 565 cm^{-1} (w). Found: C, 56.0; H, 4.8; S, 6.8%. Calcd for $Ru(SO_2H)_2(PPh_2Me)_3$: C, 56.3; H, 5.0; S, 7.7%.

$Ru(SO_2H)_2(PPh_2H)_3$ (tentative formula), mp, 146 °C; dec. 226 °C; new IR (KBr) peaks not present in $RuH_2(PPh_2H)_4$: 1238 (m), 1130 (s), 650 (m), 545 cm^{-1} (sh). Found: S, 8.0%. Calcd for $Ru(SO_2H)_2(PPh_2H)_3$: S, 8.1%.

We are very grateful for the support of this work by the Asahi Glass Foundation for the Contribution to Industrial Technology.

References

1) L. S. Pu, A. Yamamoto, and S. Ikeda, *J. Amer. Chem. Soc.*, **90**, 3896 (1968).

2) A. Misono, Y. Uchida, M. Hidai, and T. Kuse, *Chem. Commun.*, **1968**, 981.

3) (a) M. E. Vol'pin and I. S. Kolomnikov, *Pure and Appl. Chem.*, **30**, 607 (1972); (b) M. E. Vol'pin and I. S. Kolomnikov, *ibid.*, **33**, 567 (1973) and references cited therein; (c) I. S. Kolomnikov, T. S. Lobeeva, and M. E. Vol'pin, *Izv. Akad. Nauk SSSR., Ser. Khim.*, **211** (1972); (d) V. D. Bianco, S. Dronzo, and M. Rossi, *J. Organometal. Chem.*, **35**, 337 (1972); (e) I. S. Kolomnikov, A. O. Gusev, T. S. Belopotapova, M. Kh. Grigoryan, T. V. Lysyak, Yu. T. Struchkov, and M. E. Vol'pin, *ibid.*, **69**, C10 (1974); (f) B. Jezowska-Trzebiatowska and P. Sobota, *ibid*,. **76**, 43 (1974); (g) B. Jezowska-Trzebiatowska and P. Sobota, *ibid.*, **80**, C27 (1974).

4) S. Komiya and A. Yamamoto, *J. Organometal. Chem.*, **46**, C58 (1972).

5) I. S. Kolomnikov, A. I. Gusev, G. G. Aleksandrov, T. S. Lobeeva, Yu. T. Struchkov, and M. E. Vol'pin, *J. Organometal. Chem.*, **59**, 349 (1973).

6) J. D. Donaldson, J. F. Knifton, and S. D. Ross, *Spectrochim. Acta*, **20**, 847 (1964).

7) J. R. Sanders, *J. Chem. Soc., A*, **1972**, 1333.

8) K. C. Dewhirst, W. Keim, and C. A. Reilly, *Inorg. Chem.*, **7**, 546 (1968).

9) D. G. Gerlach, W. G. Peet, and E. L. Muetterties, *J. Amer. Chem. Soc.*, **94**, 4545 (1972).

10) S. Komiya and A. Yamamoto, to be submitted to *J. Mol. Catal.*

11) (a) Y. Kubo, A. Yamamoto, and S. Ikeda, *J. Organometal. Chem.*, **60**, 165 (1973); (b) Y. Kubo, A. Yamamoto, and S. Ikeda, This Bulletin, **47**, 393 (1974); (c) A. Yamamoto, *Annal. N. Y. Acad. Sci.*, **239**, 60 (1974).

12) S. Komiya, A. Yamamoto, and S. Ikeda, This Bulletin **48**, 101 (1975).

13) P. S. Hallman, B. R. McGarvey, and G. Wilkinson, *J. Chem. Soc., A*, **1968**, 3143.

14) W. H. Knoth, *J. Amer. Chem. Soc.*, **94**, 104 (1972).

15) T. Ito, S. Kitazume, A. Yamamoto, and S. Ikeda, *J. Amer. Chem. Soc.*, **91**, 3011 (1970).

16) For example: (a) E. Lindner, R. Grimmer, and H. Weber, *Angew. Chem.*, **82**, 639 (1970); (b) E. Lindner, R. Grimmer, and H. Weber, *J. Organometal. Chem.*, **23**, 209 (1970); (c) *ibid.*, **25**, 493 (1970); (d) D. Commereuc, I. Douek, and G. Wilkinson, *J. Chem. Soc., A*, **1970**, 1711; (e) I. S. Butler and A. E. Fenster, *J. Organometal. Chem.*, **66**, 161 (1974).

17) (a) A. Pallazzi, L, Busetto, and M. Graziani, *J. Organometal. Chem.*, **30**, 273 (1971); (b) V. G. Albano, P. L. Bellon, and G. Ciani, *ibid.*, **31**, 75 (1971); (c) M. Maltese, *J. Chem. Soc., A*, **1972**, 2664.

18) (a) T. I. Eliades, R. O. Harris, and M. C. Zia, *Chem. Commun.*, **1970**, 1709; (b) R. O. Harris, N. K. Hota, L. Sadavoy, and J. M. C. Yuen, *J. Organometal. Chem.*, **54**, 259 (1973).

19) (a) A. Wojcicki, *Adv. Organometal. Chem.*, **12**, 31 (1974); (b) S. Otsuka and M. Tatsuno, *Yuki Gosei Kagaku Kyokai Shi*, **28**, 902 (1970); (c) W. Kitching and C. W. Fong, *Organometal. Chem., Rev.*, **A5**, 281 (1970).

Branched-chain Sugars V. Stereoselective Synthesis of 3-*C*- and 5-*C*-Methyl-D-glucoses, and 5-*C*-Methyl-L-idose Derivatives[1]

Masuo FUNABASHI, Haruo SATO, and Juji YOSHIMURA

Laboratory of Chemistry for Natural Products, Faculty of Science, Tokyo Institute of Technology, Meguro-ku, Tokyo

(Received November 18, 1975)

The title compounds were prepared stereoselectively from 1,2: 5,6-di-*O*-isopropylidene-3-*C*-methylene-α-D-*ribo*-hexofuranose (**1**) and 3-*O*-benzyl-1,2-*O*-isopropylidene-5-*C*-methylene-6-*O*-trityl-α-D-*xylo*-hexofuranose (**5b**) by the successive epoxidation and reduction, and from 3-*O*-benzyl-1,2-*O*-isopropylidene-6-*O*-trityl-α-D-*xylo*-hexofuranos-5-ulose (**5a**) by the Grignard reaction, respectively.

The high stereoselectivity of nucleophilic reaction to 2-,[2] 3-,[3] 4-,[4] and 5-[5] keto-sugars has generally been recognized in the synthesis of branched-chain sugars, and as a matter of fact, most of such stereoselectivities (sometimes stereospecificities) have been interpreted in terms of the intrinsic conformational and configurational characters of each keto-sugars.

If this is the case applicable to addition reactions to 2-, 3-, 4-, and 5-*C*-methylene-sugars, which could be obtained from the corresponding uloses by the Wittig reaction, the reversal of the configuration by the similar stereochemical process would be possible to give the desired diastereomeric *C*-substituted sugars not accessible in the conventional manner.

The present paper, therefore, describes the model system applying the above idea to a couple of compounds such as 1,2: 5,6-di-*O*-isopropylidene-3-*C*-methylene-α-D-*ribo*-hexofuranose (**1**)[6] and 3-*O*-benzyl-1,2-*O*-isopropylidene-5-*C*-methylene-6-*O*-trityl-α-D-*xylo*-hexofuranose (**5b**) in order to obtain 3-*C*-methyl-D-glucose and 5-*C*-methyl-L-idose derivatives. A part of which was reported in the preliminary communication.[7]

Results and Discussions

The principle of this experiment is to apply epoxidation followed by reduction to compounds **1** and **5b** to get 3-*C*-methyl-D-glucose and 5-*C*-methyl-L-idose derivatives stereoselectively, and we selected as references 1,2: 5,6-di-*O*-isopropylidene-3-*C*-methyl-α-D-allofuranose[8] and newly prepared 3-*O*-benzyl-1,2-isopropylidene-5-*C*-methyl-6-*O*-trityl-α-D-glucofuranose (**7b**) in order to confirm the reversal of the configuration at the branched carbon.

The preparation of 1,2: 5,6-di-*O*-isopropylidene-3-*C*-methyl-α-D-gluco-furanose (**3**) was done in a following way. 3-*C*-Methylene derivative (**1**) obtained from 1,2: 5,6-di-*O*-isopropylidene-α-D-*ribo*-hexofuranos-3-ulose[9] by a modified procedure using butyllithium in tetrahydrofuran in place of sodium amide–liquid ammonia[6a] or sodium hydride–dimethyl sulfoxide[6b] was oxidized with *m*-chloroperbenzoic acid in 1,2-dichloroethane at room temperature to D-*gluco*-epoxide (**2**) in an excellent yield. Compound **2** was also isolated from reaction between **1** and diazomethane in *ca.* 20% yield.[3c] NMR spectrum showed the typical terminal epoxide-methylene protons at δ 3.08 as AB quartet (J=5.0 Hz). The epoxide was then reduced with lithium aluminum hydride in ether to yield a crystalline 1,2; 5,6-*di*-*O*-isopropylidene-3-*C*-methyl-α-D-glucofuranose (**3**) in 85% yield.

Compound **3** was completely differentiated from the corresponding D-allose isomer.

Removal of isopropylidene group of **3**, followed by acetylation gave 1,3,4,6-tetra-*O*-acetyl-3-*C*-methyl-β-D-glucopyranose (**4**) as a major product.

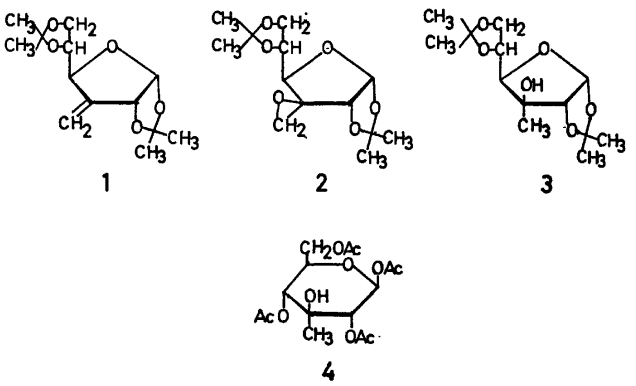

Scheme 1.

The same techniques were also applied to the compound **5b**, which was newly prepared from 3-*O*-benzyl-1,2-*O*-isopropylidene-5-*O*-trityl-α-D-*xylo*-hexofuranos-5-ulose (**5a**) and methylenetriphenylphosphorane in tetrahydrofuran in 80% yield. **5b** was then oxidized in the same way as in the case of the compound **1** in 1,2-dichloroethane to a mixture of epoxide (**6**: L-*ido* and D-*gluco*), quantitatively. Reduction of **6** with lithium aluminum hydride in ether gave 5-*C*-methyl-hexofuranose derivatives (**7a** and **7b**). The ratio of **7a** to **7b** was estimated to be *ca.* 2: 1 by comparing the intensity of

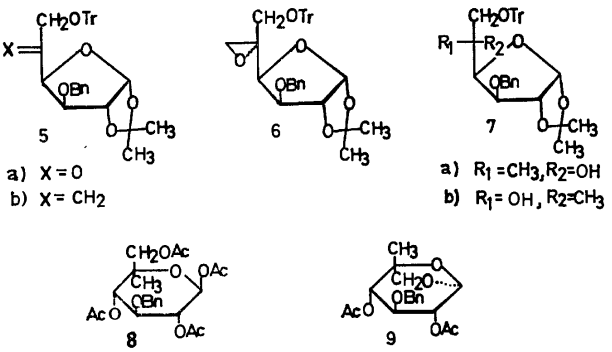

Scheme 2.

H-6 and H-6′ protons of both compounds in NMR spectrum.

On the other hand, the reference compound, 3-*O*-benzyl-1,2-*O*-isopropylidene-5-*C*-methyl-6-*O*-trityl-α-D-glucofuranose (**7b**) was exclucively prepared by reacting **5a** with an excess amount of methylmagnesium iodide in ether. This stereospecificity must be explained if such a cyclic intermediate (scheme 3) could be possible; the attack of methyl group should take place from the less-hindered site opposite to benzyl group at C-3 to give only D-gluco configuration as was suggested in the case of 3-*O*-benzyl-6-deoxy-1,2-*O*-isopropylidene-α-D-xylohexofuranos-5-ulose with phenylmagnesium bromide.[5] The situation would be almost same in the epoxidation of **5b** since the attack by peracid could preferentially from the less-hindered site mentioned above to give L-*ido* configuration predominantly if bulkier trityloxymethyl group situated rather rigidly.

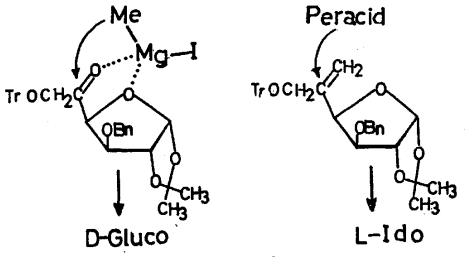

Scheme 3.

As a matter of fact, the configuration of both compounds (**7a** and **7b**) was unambiguously established in the following way. When the compounds **7a** and **7b** were hydrolyzed in hot acetic acid (70%) and followed by acetylation with acetic anhydride in pyridine, 2,4-di-*O*-acetyl-1,6-anhydro-3-*O*-benzyl-5-*C*-methyl-β-L-idopyranose (**9**) from **7a** and 1,2,4,6-tetra-*O*-acetyl-3-*O*-benzyl-5-*C*-methyl-β-D-glucopyranose (**8**) from **7b** were isolated respectively in good yields.

The structure of both compounds (**8** and **9**) was easily established by NMR (see experimental section), comparing the intensity between acetoxy methyl and methyl signals, $J_{1,2}$ (**8**; 7.5 Hz, **9**; 1.5 Hz) and by elemental analysis. It may be noted that similar intramolecular condensation occurrs in a solvolytic process of 3-*O*-benzyl-1,2-*O*-isopropylidene-β-L-idofuranose[10] to yield 1,6-anhydro-3-*O*-benzyl-β-L-idopyranose.

Experimental

Melting points were determined on a Yanagimoto micro-melting point apparatus and uncorrected. NMR spectra were measured with JNM-4H-100 spectrometer in chloroform-*d* using tetramethylsilane as the internal reference. Specific rotations were measured in a 0.5-dm tube with a Carl Zeis photoelectric polarimeter. IR spectra were taken with a Hitachi Model EPI-G2 spectrophotometer. Tlc and preparative tlc was effected on a silica-gel (Merk type 60) plate using solvent systems such as (A) benzene/methanol (25/3), (B) benzene/ether (10/1), (C) benzene/ethyl acetate (8/1), and (D) benzene/ethyl acetate (1/1) respectively by detecting compounds with iodine vapor or with 5% methanolic sulfuric acid spray followed by heating on a hot plate.

1,2: 5,6-Di-O-isopropylidene-3-C-methylene-α-D-ribo-hexofuranose (1b). To an ice-cooled suspension of methyltriphenylphosphonium bromide (25 g, 0.07 mol) in dry THF (150 ml) was added a solution of butyllithium in hexane (15%, w/v, 35 ml) with stirring under a nitrogen atmosphere. A solution of 1,2:5,6-di-*O*-isopropylidene-α-D-*ribo*-hexofuranos-3-ulose (**1a**) (10 g, 0.04 mol) in THF (50 ml) was then gradually added to the above yellow suspension with keeping cold in an ice-water bath. The stirring was continued for 10 min and the precipitate was filtered off. The filtrate and ether washings were concentrated *in vacuo* to a crude syrup, which was further chromatographed on silica gel column (Wakogel C-200, 150 g), and eluted with ether. Concentration of ether elutes gave a clear oil (6.5 g) pure enough for the next step. A part of which was further purified by preparative tlc, $[\alpha]_D^{22}$ 93° (*c* 2.0, $CHCl_3$) [lit,[5a]); $[\alpha]_D^{23}$ +104° (c, 2, $CHCl_3$), lit,[5b]); $[\alpha]_D^{23}$ +75° (*c* 1.0, $CHCl_3$)] NMR; 1.34, 1.40, 1.43 (6-H, 3-H, 3-H, s, isopropyl methyl), 4.0 (3-H, m, H_5, H_6, H_6'), 4.60 (1-H, m, H_4), 4.89 (1-H, m, H_2), 5.06 (2-H, m, exomethylene), 5.80 ppm. (1-H, d, H_1, $J_{1,2}$=3.8 Hz). (Found: C, 61.12; H, 7.65%)

1,2: 5,6-Di-O-isopropylidene-3-C-hydroxymethyl-3,3′-anhydro-α-D-glucofuranose (2). A solution of **1** (3.5 g, 0.014 mol) and *m*-chloroperbenzoic acid (3.5 g, 85% purity) in dry 1,2-dichloroethane (40 ml) was stirred at room temperature for 18 h. The precipitate was filtered off, and the filtrate was concentrated *in vacuo* to a syrup, which was redissolved in hexane or ether, washed with aqueous sodium hydrogen carbonate and water, dried over anhydrous magnesium sulfate, and concentrated to a clear syrup (3.2 g), $[\alpha]_D^{23}$ +55° (*c* 1.7, methanol). NMR; 1.31, 1.38, 1.54 (3-H, 6-H, 3-H, s, isopropyl methyl), 3.08 (1-H, q, J=5.0 Hz, epoxymethylene), 4.0 (3-H, m, H_5, H_6, H_6'), 4.25 (1-H, d, H_2, $J_{1,2}$=3.8 Hz), 4.3 (1-H, m, H_4), 5.92 ppm. (1-H, d, H_1).

Found: C, 57.26; H, 7.37%. Calcd for $C_{13}H_{20}O_6$: C, 57.34; H, 7.40%.

1,2: 5,6-Di-O-isopropylidene-3-C-methyl-α-D-glucofuranose (3). A mixture of **2** (0.17 g, 0.63 mmol) and lithium aluminium hydride (30 mg) in dry ether (5 ml) was allowed to stand at room temperature for 10 min and refluxed for 30 min. After usual work-up, the filtrate was extracted with ether (10 ml×3), washed with aqueous sodium chloride, dried over anhydrous magnesium sulfate, and concentrated *in vacuo* to a crystalline residue (0.14 g), which was recrystallized from hexane; mp 66—67 °C, $[\alpha]_D^{23}$ +23 °C (*c* 1.0, acetone). NMR; 1.30, 1.34, 1.42, 1.44, 1.50 (3-H×5, CH_3 at C-3 and isopropyl), 2.48 (1-H, broad, OH), 3.75—4.38 (5-H, m, H_2, H_4, H_5, H_6, H_6'), 5.86 ppm. (1-H, d, H_1, $J_{1,2}$=3.7 Hz). Found: C, 56.67; H, 7.99%. Calcd for $C_{13}H_{22}O_6$: C, 56.92; H, 8.08%.

1,2,4,6-Tetra-O-acetyl-3-C-methyl-β-D-glucopyranose (4a). A solution of **3a** (155 mg) in 70% acetic acid (6 ml) was heated at 95 °C for 2 h, and concentrated *in vacuo* to a dry syrup, which was then treated with acetic anhydride (2 ml) and pyridine (3 ml) for 3 h. The crude syrup (180 mg) obtained by the usual work-up was subjected to a preparative tlc (solvent D) to give an amorphous powder (120 mg), $[\alpha]_D^{22}$ −23 °C (*c* 2.34, $CHCl_3$). NMR; 1.29 (3-H, CH_3 at C_3), 2.05, 2.08, 2.09, 2.11 (3-H×4, acetyl), 3.01 (1-H, broad, OH), 3.80 (1-H, o, H_5, $J_{5,6}$=5.0, $J_{5,6'}$=2.5 Hz), 4.10 (1-H, H_6, q, $J_{6,6'}$=12.5 Hz), 4.30 (1-H, q, H_6), 5.03 (1-H, d, H_2, $J_{1,2}$=8.5 Hz), 5.05 (1-H, d, H_4), 5.68 ppm (1-H, d, H_1).

Found: C, 49.43; H, 6.09%. Calcd for $C_{15}H_{22}O_{10}$: C, 49.72; H, 6.12%.

3-O-Benzyl-1,2-O-isopropylidene-5-C-methylene-6-O-trityl-α-D-xylohexofuranose (5b). A solution of **5a** (0.5 g, 1.1 mmol) in dry THF (5 ml) was added to a yellow solution of methylenetriphenylphosphorane prepared from methyltriphenyl-

phosphonium bromide (0.7 g, 2.2 mmol) and butyllithium (15% w/v, 1 ml) in dry THF (10 ml). The stirring was continued at room temperature for 30 min. The precipitate was filtered off and filtrate and ether washings were concentrated *in vacuo* to a crude syrup, which was further subjected to preparative tlc (solvent B) to give a crystalline residue. Recrystallization from ethanol gave fine crystals having mp 113—114 °C, $[\alpha]_D^{23}$ −33 °C (*c* 1.0, $CHCl_3$). NMR: 1.28, 1.48 (3-H×2, isopropylidene), 3.48—3.81 (3-H, m, H_6 and $H_{6'}$), 4.25 (2-H, q, J_{AB}=12.0 Hz, benzyl methylene), 4.50 ppm (1-H, d, $J_{1,2}$=3.8 Hz).

Found: C, 78.91; H, 6.69%. Calcd for $C_{36}H_{36}O_5$; C, 78.80; H, 6.61%.

Oxidation of ***5b*** *with* m-*Chloroperbenzoic Acid.* A solution of **5b** (0.55 g, 1 mmol) and *m*-chloroperbenzoic acid (0.31 g, 1.8 mmol) in dry 1,2-dichloroethane (10 ml) was allowed to stand at room temperature for 24 h. After filtration of the precipitate, the filtrate was washed with dilute sodium hydroxide solution (0.7%, 10 ml) and water, dried over anhydrous magnessium sulfate and concentrated *in vacuo* to a crystalline residue, which was recrystallized from ethanol to give a mixture of 3-*O*-benzyl-1,2-*O*-isopropylidene-5-*C*-hydroxymethyl-5,6′-anhydro-6-*O*-trityl-α-D-gluco- and β-L-idofuranose, mp 179—180 °C, $[\alpha]_D^{23}$ −22.4 °C (*c* 1.0, $CHCl_3$).

Found: C, 76.32; H, 6.45%. Calcd for $C_{36}H_{36}O_6$: C, 76.57; H, 6.43%.

3-O-Benzyl-1,2-O-isopropylidene-5-C-methyl-6-O-trityl-β-L-idofuranose (7a). A mixture of **6** (0.41 g, 0.73 mmol) and lithium aluminum hydride (30 mg) was refluxed in dry THF (5 ml) for 2 h. After the usual work-up, the filtrate was extracted with ether, washed with aqueous sodium chloride, dried over anhydrous magnesium sulfate, and concentrated to a crystalline residue, which was subjected to a preparative tlc (solvent B) to give prismatic crystals (0.2 g) having mp 150—151 °C, $[\alpha]_D^{23}$ −54 °C (*c* 1.37, acetone). NMR: 1.20, 1.34, 1.50 (3-H×3, CH_3 at C-5 and isopropyl methyl), 2.75, 3.45 (1-H ×2, H_6, $H_{6'}$, $J_{6,6'}$=8.7 Hz), 3.64 (1-H, s, OH), 4.15 (1-H, d, H_3, $J_{3,4}$=3.0 Hz), 5.40, 4.60 (1-H×2, dd, benzyl methylene), 4.54 (1-H, d, H_4), 4.60 (1-H, d, H_2, $J_{1,2}$=3.8 Hz), 6.03 ppm (1-H, d, H_1).

Found: C, 76.25; H, 6.88%. Calcd for $C_{36}H_{38}O_6$: C, 76.30; H, 6.76%.

3-O-Benzyl-1,2-O-isopropylidene-5-C-methyl-6-O-trityl-α-D-glucofuranose (7b). A solution of **5a** (0.5 g, 0.9 mmol) in dry tetrahydrofuran (5 ml) was gradually added to a solution of methylmagnessium iodide prepared from magnesium (0.245 g, 10 mmol) and methyl iodide (2 ml, 17 mmol) in dry ether (10 ml). The reaction mixture was then refluxed for 30 min, poured into ice-water containing ammonium chloride (0.535 g, 10 mmol), extracted with ether (20 ml×2), washed with aqueous sodium chloride, dried over anhydrous magnesium sulfate, evaporated to a crystalline residue, which was recrystallized from ethanol, mp 182—183 °C, $[\alpha]_D^{23}$ −5.7 °C (*c* 1.0, $CHCl_3$). NMR: 1.28, 1.52, 1.55 (3-H×3, s, CH_3 at C-5 and isopropyl methyl), 2.93, 3.32 (1-H×2, d, H_6, $H_{6'}$, $J_{6,6'}$=8.5 Hz), 3.05 (1-H, d, H_3, $J_{3,4}$=3.3 Hz), 3.65, 4.20 (1-H×2, d, $C\underline{H}_2Ph$), 4.38 (1-H, d, H_4), 4.43 (1-H, d, H_2, $J_{1,2}$=4.0 Hz), 5.99 ppm (1-H, d, H_1).

Found: C, 76.49; H, 6.65%. Calcd for $C_{36}H_{38}O_6$: C, 76.30; H, 6.76%.

1,2,4,6-Tetra-O-acetyl-3-O-benzyl-5-C-methyl-β-D-gluco-pyranose (8). A suspension of **7b** (300 mg) in 70% acetic acid (10 ml) was refluxed for 2 h, and concentrated *in vacuo* to a syrup, which was then allowed to stand at room temperature in a mixture of acetic anhydride (2 ml) and pyridine (5 ml) for 8 h. The reaction solution was then treated with ice-water containing sodium hydrogen carbonate, extracted with chloroform, washed with aqueous sodium chloride and water, and dried over anhydrous magnesium sulfate. Concentration of the solvent gave fine needles, which was recrystalized from hexane; mp 128—129 °C (100 mg), $[\alpha]_D^{23}$ −18 °C (*c* 1.08, acetone). NMR: 1.34 (3-H, s, CH_3 at C-5), 1.85, 1.97, 2.08 (3-H×2, 3-H×2, s, acetyl methyl), 3.85 (1-H×2, d, H_6, $H_{6'}$, $J_{6,6'}$=12.0 Hz), 4.61 (2-H, s, $C\underline{H}_2Ph$), 5.14 (1-H, q, H_2, $J_{1,2}$=7.5 Hz), 5.33 (1-H, d, H_4), 5.89 ppm (1-H, d, H_1).

Found: C, 58.48; H, 6.26%. Calcd for $C_{22}H_{28}O_{10}$: C, 58.40; H, 6.24%.

1,6-Anhydro-2,4-di-O-acetyl-3-O-benzyl-5-C-methyl-β-L-idopyranose (9). A suspension of **7a** (200 mg) was treated as described above. Fine needles from hexane; mp 118—119 °C, $[\alpha]_D^{23}$ +67 °C (*c* 1.0, acetone). NMR: 1.30 (3-H, s, CH_3 at C-5), 1.98, 2.02 (3-H×2, s, acetyl methyl), 3.35 (1-H, q, $H_{6'}$, $J_{6,6'}$=8.7, $J_{1,6'}$=1.5 Hz), 3.83 (1-H, q, H_3, $J_{2,3}$=7.5, $J_{3,4}$=8.7 Hz), 4.08 (1-H, d, H_6), 4.60 (2-H, s, $C\underline{H}_2Ph$), 4.86 (1-H, q, H_2, $J_{1,2}$=1.5 Hz), 5.13 (1-H, q, H_4, $J_{4,6'}$=1.0 Hz), 5.42 ppm (1-H, H_1).

Found: C, 61.63; H, 6.24%. Calcd for $C_{18}H_{22}O_7$: C, 61.70; H, 6.33%.

References

1) Part IV. This Bulletin, **46**, 3207 (1973).

2) J. S. Burton, W. G. Overland, and N. R. Williams, *J. Chem. Soc.*, **1965**, 3433.

3) a) R. D. Rees, K. Jonnes, A. R. Tachell, and R. H. Williams, *ibid.*, *C* **1968**, 2716 and references cited therein; b) A. Rosenthal, K-S. Ong, and D. Baker, *Carbohyd. Res.*, **13**, 113 (1970); c) J. Yoshimura, K. Kobayashi, S. Sato, and M. Funabashi, this Bulletin, **45**, 1806 (1972); d) J. Yoshimura, K. Sato, K. Kobayashi, and C. Shin, *ibid.*, **46**, 1515 (1973).

4) M. Miljkovic, M. Gligorijevic, T. Sato, and D. Miljkovic, *J. Org. Chem.*, **39**, 1379 (1974).

5) T. D. Inch, R. V. Ley, and P. Rich, *J. Chem. Soc. C*, **1968**, 1683.

6) a) A. Rosenthal and M. Sprinzl, *Can. J. Chem.*, **47**, 3941 (1969); b) W. A. Szarek, J. S. Jewell, I. Szczerek, and J. K. N. Jones, *ibid.*, **47**, 4473 (1969).

7) M. Funabashi, H. Sato, and J. Yoshimura, *Chem. Lett.*, **1974**, 803.

8) a) A-M. Sepulchre, G. Vass, and S. D. Gero, *C. R. Acad. Sci., Paris, Ser. C*, **274**, 1077 (1972); b) H. Paulsen, V. Sinnwell, and P. Stadler, *Chem. Ber.*, **105**, 1978 (1972); c) J. S. Brimacombe, S. Mahmood, and A. J. Kollins, *Carbohyd. Res.*, **38**, C7 (1974).

9) W. Sowa and G. H. S. Thomas, *Can. J. Chem.*, **44**, 836 (1966); K. Onodera, S. Hirano, and N. Kashimura, *Carbohyd. Res.*, **6**, 276 (1968).

10) J. Kiss and P. C. Wyss, *Carbohyd. Res.*, **27**, 282 (1973).

Photochemical Reaction of 9,10-Phenanthrenequinone with Hydrogen Donors.[1] Behavior of Radicals in Solution as Studied by CIDNP

Kazuhiro MARUYAMA, Tetsuo OTSUKI, and Yoshinori NARUTA

Department of Chemistry, Faculty of Science, Kyoto University, Kyoto 606

(Received July 15, 1975)

Behavior of radicals produced in the photochemical reaction of 9,10-phenanthrenequinone was investigated by use of CIDNP and ESR technique. By comparison of the sign of CIDNP signals in formation of and in decomposition (photochemical or thermal) of adducts, the rearrangement of adducts, *e.g.*, from the 1,2-adduct to 1,4-adduct and *vice versa*, was proposed. Although the adducts are stable enough to isolate in general, they decomposed photochemically or thermally to give the mixture of 9,10-phenanthrenediol (or its quinhydrone), the dehydrogenated dimer of hydrogen donor, and others as minor product.

Photochemical reactions of 9,10-phenanthrenequinone with hydrogen donors were reinvestigated by means of CIDNP technique.[2] Although the results are rather qualitative, investigation by means of CIDNP technique is quite informative for study of the radical reaction mechanism.

Results and Discussion

The photochemical reaction of 9,10-phenanthrenequinone with hydrogen donors in preparative scale can be classified in the following three types on the basis of the resulting major products. The inspection of the CIDNP spectra, however, reveals that the formation of both 1,2- and 1,4-photoadducts is essential but their stabilities are dependent on the nature of hydrogen donors, solvents used, and reaction temperature. Polarized PMR signals of the protons indicated by Gothic letter were the indices of formations of 1,2- and 1,4-photoadducts. The assignments of polarized signals were straightforward by comparison of the chemical shifts with those of isolated products, and the results

Photochemical Reaction of 9,10-phenanthrenequinone with Hydrogen Donors at 15—20°C.

Type 1

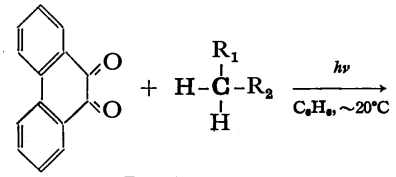

R_1: Aryl
R_2: Aryl or Alkyl

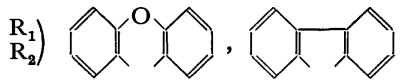

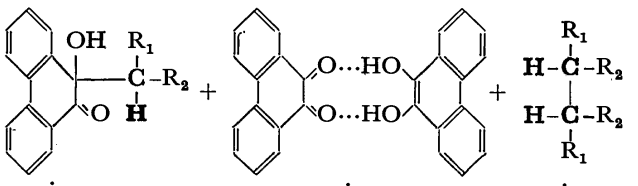

major
"1,2-adduct"
ν_{OH}: 3510 cm^{-1} (sharp)
$\nu_{C=O}$: 1690 cm^{-1}

minor

minor

Type 2

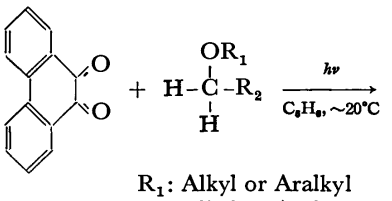

R_1: Alkyl or Aralkyl
R_2: Alkyl or Aryl

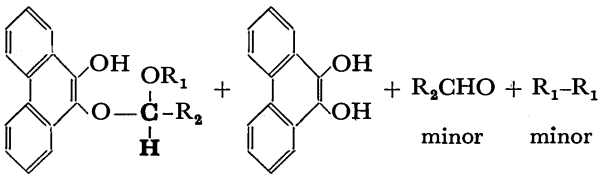

major
"1,4-adduct"
ν_{OH}: 3280 cm^{-1}
$\nu_{C=O}$: none

minor

minor

minor

Type 3

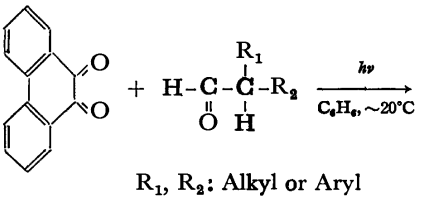

R_1, R_2: Alkyl or Aryl

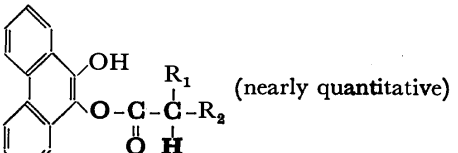

(nearly quantitative)

"1,4-adduct"
ν_{OH}: 3380 cm^{-1}
$\nu_{C=O}$: 1730 cm^{-1} (ester)

could be substantiated by reaction of 9,10-phenanthrenequinone with the corresponding deuterated hydrogen donors.

According to the accepted simple rule for the polarized signal by Kaptein,[3] the absorption polarized signal of methine proton of xanthyl moiety (or methine proton of diphenylmethyl moiety) due to the 1,2-photoadduct (Fig. 1) is reasonable (see Eq. (1)). By the same reason the emission polarized signal due to methyl protons of acetyl moiety of 1,2-adduct (Fig. 2) is con-

$$PQ \xrightarrow{h\nu} PQ^T \xrightarrow{RH} \overline{PQH\cdot\ \cdot R}^T \longrightarrow 1,2\text{-photoadduct} \quad (1)$$

PQ: 9,10-phenanthrenequinone
RH: hydrogen donor
$\overline{PQH\cdot\ \cdot R}^T$: radical pair derived from triplet precursor

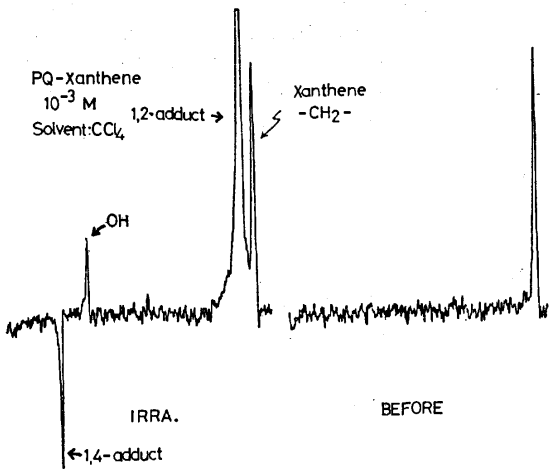

Fig. 1. Polarized PMR spectra observed in the course of the photochemical reaction of PQ with xanthene (Solvent: CCl_4 at room temperature).

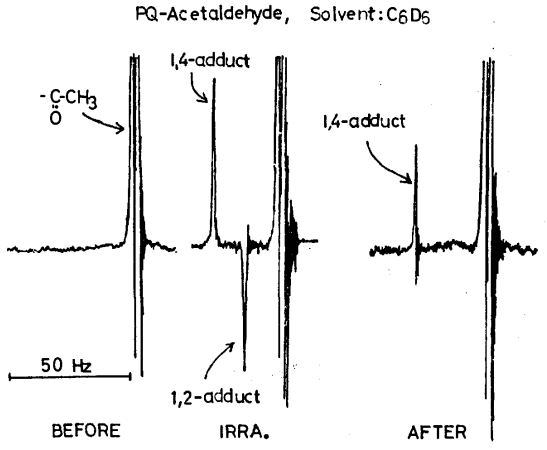

Fig. 2. Polarized PMR spectra observed in the course of the photochemical reaction of PQ with acetaldehyde (Solvent: C_6D_6 at room temperature).

vincible according to the following considerations.

$$\Gamma = \Delta g \varepsilon \mu \alpha \quad (2)$$

if $\Gamma = +$, then absorption polarized signal,
$\Gamma = -$, then emission polarized signal

These parameters have their usual meaning.[3] In the case of the reaction of 9,10-phenanthrenequinone with alkyl aromatics, $\Delta g = -$,[4] $\varepsilon = +$, $\mu = +$, and $\alpha = -$[5] are to be considered on the basis of the preceding reaction mechanism for methine-H and then, $\Gamma = -++-=+$, that is, the absorption polarized signal is expected.

In the case of the reaction of 9,10-phenanthrenequinone with acetaldehyde, for acetyl-H $\Gamma = -+++=-$, then the emission polarized signal is expected. However, the reversely polarized signals due to 1,4-photoadducts compared to those of 1,2-adducts are hard to be explained by the simple route given in Eq. (1) (see Figs. 1 and 2). Since the radical components of the pair for 1,2- and 1,4-adducts are the same, Δg, ε, and α for the formation of 1,4-adducts have the same sign for those of 1,2-adduct. If we postulate the preceding formation of a radical pair which may result from vibrationally excited but singlet molecule of 1,2-adduct in advance of the formation of 1,4-adduct, all of the observed polarized signals for 1,4-adducts may be explicable, because the sign of μ is to be reverse. Further, we can explain the polarized signals due to methine-H of 1,2- and 1,4-adducts (Fig. 3) observed during the course of photochemical reaction of 9,10-phenanthrenequinone with dibenzyl ether (in general, with ethers) taking into consideration of the similar concept described above.

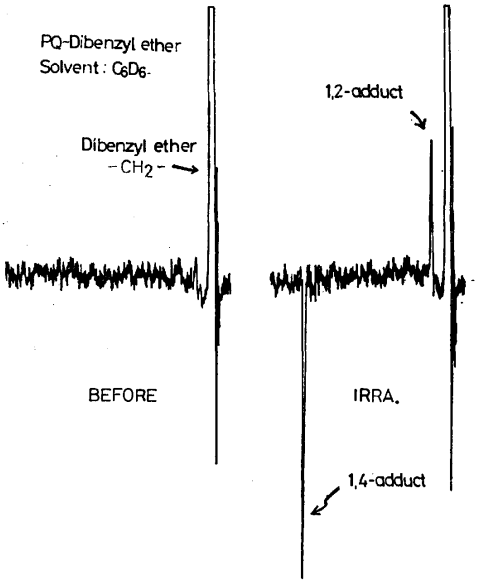

Fig. 3. Polarized PMR spectra observed in the course of the photochemical reaction of PQ with dibenzyl ether (Solvent: C_6D_6 at room temperature).

In fact, the concept was confirmed experimentally. Thermal and/or photo-induced decomposition of the purely isolated 1,2-adducts in suitable solvents was inspected by means of CIDNP. When at slightly elevated temperature (32 °C) isolated pure 1,2-adduct from 9,10-phenanthrenequinone (PQ) and an alkyl aromatic (PQ–*p*-xylene, PQ–*m*-xylene, PQ–*o*-xylene, PQ–mesitylene, PQ–diphenylmethane and PQ–xanthene system), was activated in carbon tetrachloride or benzene-d_6 by light of high pressure mercury arc lamp, two polarized signals due to methine or methylene proton corresponding to 1,2-(absorption in region of δ: 4.0) and 1,4-adducts (emission in region of δ: 6.0) are observed. Although the 1,4-adduct thus derived is too unstable to be isolated in this condition, this is the unambiguous evidence for the rearrangement from 1,2-adduct to 1,4-adduct *via* the radical pair derived from singlet precursor (Fig. 4). ESR inspection of the decomposing system at the same condition in the region of *g*-value=2.00 reveals the presence of no appreciable

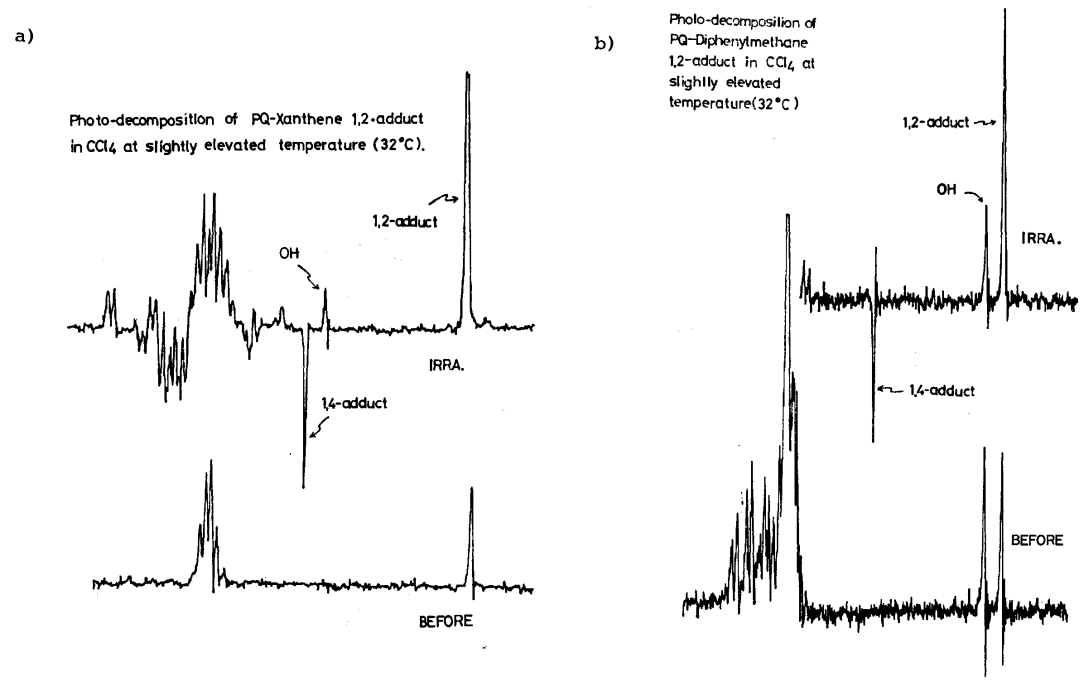

Fig. 4. Polarized PMR spectra observed in the course of the photodecomposition of a) PQ–xanthene 1,2-adduct, b) PQ–diphenylmethane 1,2-adduct (Solvent: CCl_4 32 °C).

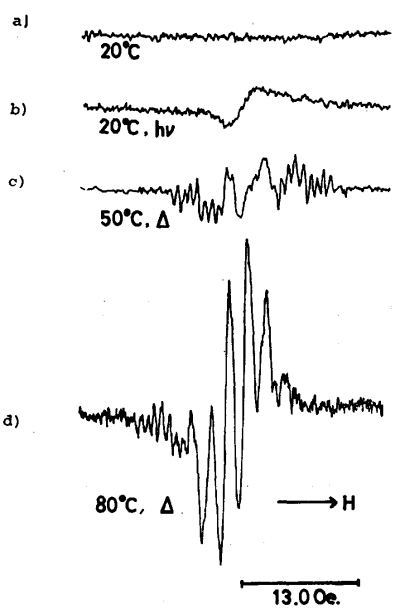

Fig. 5. ESR signals observed in the course of the decomposition of PQ–xanthene 1,2-adduct, a) 20 °C, b) 20 °C, *hν*, c) 50 °C, d) 80 °C (Solvent: CCl_4). Non symmetry of signals indicates that signals are composed of a mixture of radicals.

free radical in solution (Fig. 5). On the other hand, when we decomposed 1,2-adduct (from PQ–xanthene and PQ–diphenylmethane) at 80 °C or higher temperature, an absorption polarized and an emission polarized signal each corresponding to 1,4- and 1,2-adducts were observed (Fig. 6). In the decomposing systems of 1,2-adduct at these temperatures were observed, in actual, strong ESR.signals indicating the appearence of *free radicals* in solution (see Fig. 5). We can recognize the polarized signals which were observed during the course of decompositions taking into consideration of the following reaction scheme;

Photodecomposition at lower temperature:

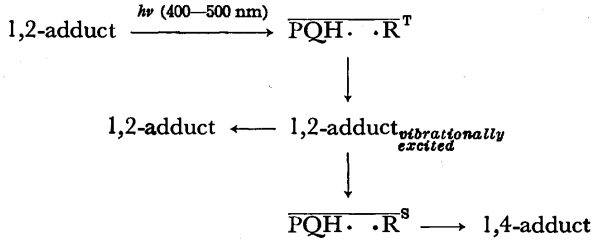

Thermal decomposition at higher temperature:

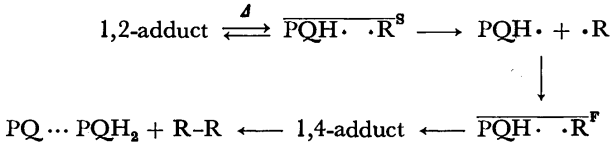

$\overline{PQH\cdot\ \cdot R^T}$: radical pair derived from triplet precursor
$\overline{PQH\cdot\ \cdot R^S}$: radical pair derived from singlet precursor
$\overline{PQH\cdot\ \cdot R^F}$: radical pair derived from free radical precursor

Thus, the absorption polarized PMR signal corresponding to 1,4-adduct observed in thermally decomposing system of 1,2-adduct at the higher temperature indicates the recombination of the two component radicals *via free radical* state.

On irradiation of 9,10-phenanthrenequinone with ethers by visible light in benzene-d_6 or carbon tetrachloride at about 20 °C, 1,4-adducts (methine-H: in region of δ: 5.7—6.4, emission polarized) are accumu-

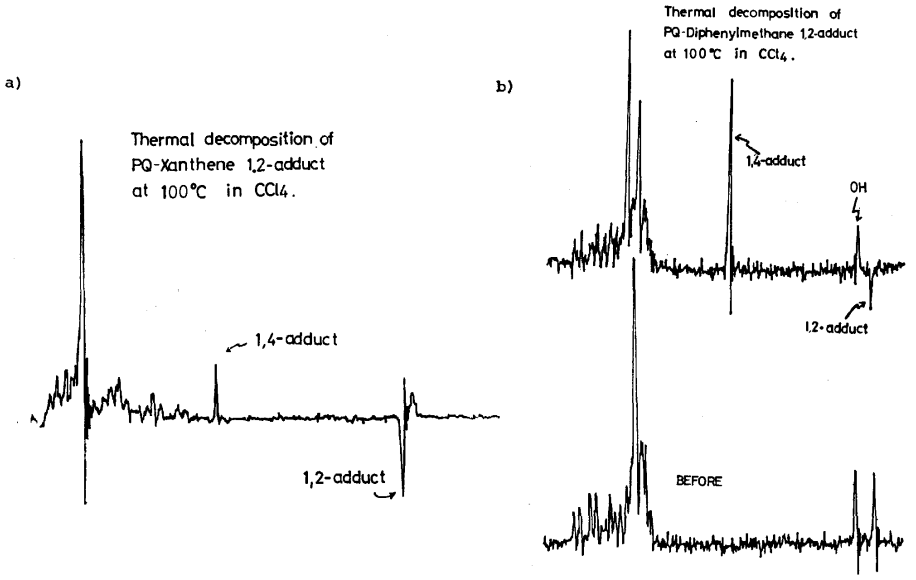

Fig. 6. Polarized PMR spectra observed in the course of the thermal decomposition of a) PQ–xanthene 1,2-adduct, b) PQ–diphenylmethane 1,2-adduct (Solvent: CCl_4 at 100 °C).

lated products in spite that the CIDNP signals indicate the transient formation of 1,2-adducts (methine-H: in region of δ: 4.4—5.1, absorption polarized) accompanying with 1,4-adducts. Irradiation of a 1,4-adduct, for example, 1,4-adduct derived from 9,10-phenanthrenequinone and dibenzyl ether, by UV-light[6] *in situ* exhibits an absorption polarization of methine-H (δ: 5.8) due to 1,4-adduct and an absorption polarization of methine-H (δ: 4.6) due to 1,2-adduct[7] (Fig. 7). This is an indication of rearrangement from 1,4-adduct to 1,2-adduct *via* radical pair produced from triplet precursor. It may be formularized as the followings;

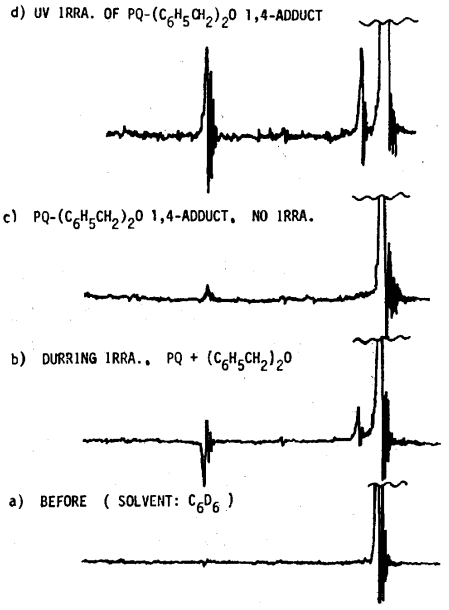

Fig. 7. Polarized PMR spectra observed in the course of the photodecomposition reaction of PQ–dibenzyl ether (Solvent: C_6D_6 at room temperature).

$$PQ^T + R'H \longrightarrow \overline{PQH\cdot\ \cdot R'}^T$$

$$\overline{PQH\cdot\ \cdot R'}^T \longrightarrow 1,2\text{-adduct}_{\substack{vibrationally\\ excited}} \longrightarrow 1,2\text{-adduct (H-A)}$$

$$\overline{PQH\cdot\ \cdot R'}^S \longrightarrow 1,4\text{-adduct (H-E)} \qquad (3)$$

$$1,4\text{-adduct} \xrightarrow{\text{UV-light}} \overline{PQH\cdot\ \cdot R'}^T \begin{cases} \nearrow\ 1,4\text{-adduct (H-A)} \\ \searrow\ 1,2\text{-adduct (H-A)} \end{cases} \qquad (4)$$

H-A: polarized absorption signal of methine-H
H-E: polarized emission signal of methine-H

Similarly, the absorption polarized PMR signal due to acyl proton of stable 1,4-adduct (9-acyloxy-10-hydroxyphenanthrene) is comprehensive by assuming the preceding formation of unstable 1,2-adduct, and the subsequent rearrangement to 1,4-adduct *via* singlet radical pair. This is obviously confirmed in the photo-

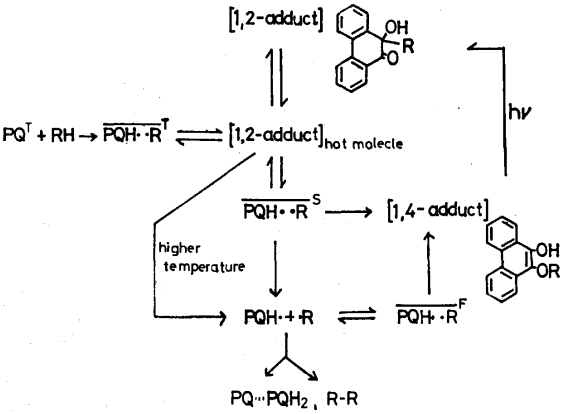

Reaction scheme.

chemical reaction of PQ with acetaldehyde in benzene-d_6 by use of CIDNP technique (Fig. 2).

Summarizing the behavior of radicals in photochemical reaction of 9,10-phenanthrenequinone we may write schematically the whole reaction as in the preceding reaction scheme.

Experimental

1,2-Adducts. 1,2-Adducts were obtained in preparative scale on irradiation of mixtures of 9,10-phenanthrenequinone and suitable hydrogen donors in neat or in benzene solution. The reaction mixture was kept in a usual glass tube dipped into cool water, and irradiated by high pressure Hg-arc lamp from outside. All the 1,2-adducts of 9,10-phenanthrenequinone with alkyl aromatics have characteristic IR bands due to carbonyl and hydroxyl groups; $\nu_{C=O}$: 1690 cm^{-1}, and ν_{OH}: 3510 cm^{-1} (sharp). Their compositions were confirmed by elemental analysis. PQ–xanthene: mp 103 °C (decomp.), PQ–diphenylmethane: mp 129—132 °C (decomp.), PQ–fluorene: mp 165—167 °C (decomp.), PQ–mesitylene: mp 165—167 °C (decomp.), PQ–*p*-xylene: mp 128—128.5 °C (decomp.), PQ–*m*-xylene: mp 93—94 °C (decomp.), PQ–*o*-xylene: mp 146 °C (decomp.), PQ–anisole: mp 109—111 °C (decomp.). (PQ: 9,10-phenanthrenequinone)

1,4-Adducts. 1,4-Adducts were obtained by procedures analogous to those of 1,2-adducts. They show characteristic IR band due to hydroxyl group; ν_{OH}: 3280 cm^{-1}, and no carbonyl band. PQ–1,4-dioxane: mp 92—94 °C (decomp.), PQ–1,4-dibenzyloxybenzene: mp 143—144 °C (decomp.). Their compositions were confirmed by elemental analysis.

CIDNP. PS-100 type and MH-100 type NMR instruments equipped with PMR probe for irradiation (manufactured by JEOL) were used in CIDNP examinations. For irradiation 1 kW and 500 W high pressure Hg-arc lamps were applied with or without use of filter (Toshiba VY-42).

ESR. ME-3 type ESR machine manufactured by JEOL (X-band) was used in this experiment.

References

1) This work was presented at Magnetic Conference on CIDNP and CIDEP which was held at Grenoble, May 21—23, 1975.

2) K. Maruyama, H. Shindo, and T. Maruyama; This Bulletin, **44**, 585 (1971), K. Maruyama, T. Otsuki, H. Shindo, and T. Maruyama; *ibid.*, **44**, 2000, 2756, 2789 (1971), K. Maruyama, and T. Otsuki; *ibid.*, **44**, 2885 (1971), K. Maruyama, A. Takuwa, T. Otsuki, and S. Kako; *Bull. Inst. for Chem. Res., Kyoto Univ.*, **50**, 348 (1971), and references cited therein.

3) R. Kaptein; *Chem. Commun.*, **1971**, 732; *J. Amer. Chem. Soc.*, **94**, 6251 (1972).

4) *g*-Value of semiquinone radical is in general larger than that of carbon radical without exception.

5) Sign of hyperfine coupling constant (α) of α-hydrogen of carbon radicals is assumed to be negative. *cf.* H. Fischer; "Structure of Free Radicals by ESR Spectroscopy" (J. K. Kochi Ed., "Free Radicals") Vol. 2, p. 435, Wiley Interscience, New York (1973).

6) For decomposition of 1,4-adduct visible light in the region of 400—500 nm is not effective, but UV-light is only effective. The decomposition may be induced by π-π^* excitation of 1,4-adduct, because the adduct has no carbonyl group.

7) K. Maruyama and T. Otsuki; This Bulletin, **44**, 2885 (1971).

Preparation of Reinforcing Fillers from Japanese Acid Clays with Lime and by Calcination. IV. Investigation on the Structure, Physicochemical Properties and Morphology of M Hard Clay in Relation to the Reinforcing Effect

Hideki Rai and Junkichi Yamada*

The Institute of Industrial Science, The University of Tokyo, 22-1, Roppongi 7 chome, Minato-ku, Tokyo 106

(Received May 21, 1975)

In order to find the optimum conditions for the preparation of satisfactory reinforcing filler from Matsune (**M**) acid clay, two series of fillers of **M** hard clay (CaO 0—9%: drying 110 °C, 5 hr for M-1 series; calcination 600 °C, 1.5 hr for M-2 series: wet ball-milling 6—24 hr) were investigated with respect to their structure, physicochemical properties and morphology. Treatment with hydrated lime (CaO 3%), followed by calcination (600 °C, 1.5 hr) and mechanical disintegration (wet ball-milling 18 hr) was found to give good results. Calcination after the lime treatment gives rise to adequate dehydroxylation as well as dehydration of the montmorillonite, calcium silicate hydrates (CSH) and excess silica remaining. This process helps to restrain the great surface activity of acid clay and facilitate pulverization of the final products combined with the effect of inhibiting polycondensation of the montmorillonite and α-cristobalite due to an even formation of the CSH distributed on the interlayer surfaces and the interfaces of the minute crystallites.

In previous papers we reported on the availability of Nakajo (**N**) and Matsune (**M**) acid clays for preparing a reinforcing filler of elastomers,[1] the optimum conditions of preparation and evaluation of their reinforcing properties.[2] An investigation of the changes in the structure, morphology and physicochemical properties of **N** hard clay derived from **N** with relation to the reinforcement was carried out.[3]

The same treatment as in **N** hard clay (CaO 3—60%; calcination 400—800 °C, 1.5 hr; wet ball-milling 18 hr) revealed that the optimum conditions for preparing a good hard clay from **M** were very close to those of **N**; the requisite amount of alkali less than 10% and calcination at 600 °C for 1.5 hr. The patterns of structural changes in **M** hard clay investigated by X-ray diffraction and IR spectroscopy were found to be similar to those of **N** hard clay. However, a deviation was accompanied by the optimum amount of alkali; 3% for **M** and 6% for **N**.

For the purpose of confirming the optimum conditions, **M** was treated with a less amount of hydrated lime (CaO 0—9%) and then either calcined at 600 °C for 1.5 hr or dried at 110 °C for 5 hr to remove the moisture. Changes in the structure, morphology and physicochemical properties of the fillers were examined as well.

Evidences are given to show the merit of the treatment with alkali followed by calcination and mechanical disintegration for the preparation of a satisfactory reinforcing filler from **M**.

Experimental

Materials. Two series of fillers of **M** hard clay (M-1 and M-2) were used; they were derived from Matsune acid clay with hydrated lime (CaO 0, 1.25, 3, 6 or 9%) followed by thermal treatment (drying 110 °C, 5 hr for M-1; calcination 600 °C, 1.5 hr for M-2) and mechanical disintegration (wet ball-milling 18 hr).[2]

Dixie Clay, Silene EF and the original acid clay **M** which had been ground under 200 mesh and dried at 110 °C for 2 hr without the lime treatment and mechanical disintegration beforehand were utilized as references.

Investigation on Structure, Physicochemical Properties and Morphology. The structure of **M** hard clay was investigated by X-ray diffraction, IR spectroscopy and thermal analyses, DTA and TG. The physicochemical properties were determined by means of hygroscopicity, pH, DPG adsorption, specific gravity and bulk density. The shape, size and particle distribution of the prepared fillers were studied by electron microscopy. The methods, apparatus and conditions of measurement are summarized in Table 1.

The structural feature of the best **M** hard clay (CaO 3%; calcination 600 °C, 1.5 hr; wet ball-milling 18 hr) was studied by selected area electron diffraction (SAD) technique in comparison with that of the best **N** hard clay (CaO 6%; calcination 600 °C, 1.5 hr; wet ball-milling 18 hr).

Results and Discussion

Investigation of Structural Changes. (1) X-ray Diffraction Patterns. Figures 1 (a) and 1 (b) give the X-ray diffraction diagrams showing the difference of structural changes between the M-1 and M-2 fillers, respectively.

(i) M-1 fillers: As the amount of alkali increased, normal montmorillonite, the principal constituent of **M**, still retained its basal reflection[4] (15.37 Å) with a little diminution (less than 5%) in the intensity and a slight, constant shift (1.68 Å) towards a lower spacing (Fig. 1 (a) curves 1—5). The basal shift is smaller than in the case of **N** (about 2 Å) and attributable mainly to the formation of Ca-montmorillonite.

The intensity of α-cristobalite[5] (4.05 Å (101), the most prominent reflection characteristic of **M**, decreased in proportion to the amount of alkali. New but feeble reflections ascribable to tobermolite-like calcium silicate hydrates[6,7] (CSH, 2.97 and 2.81 Å) and calcite[8] (2.45 Å) appeared even in the filler treated with the least amount of alkali, 1.25% CaO. Those prepared with more than 3% CaO showed some weak peaks of unknown significance around 4.85—4.91, 3.20 and 2.65 Å.

The results indicate that the M-1 fillers substantially

* Present address: AA Chemical Co., Ltd., 3-4, Shibakoen 2 chome, Minato-ku, Tokyo 105.

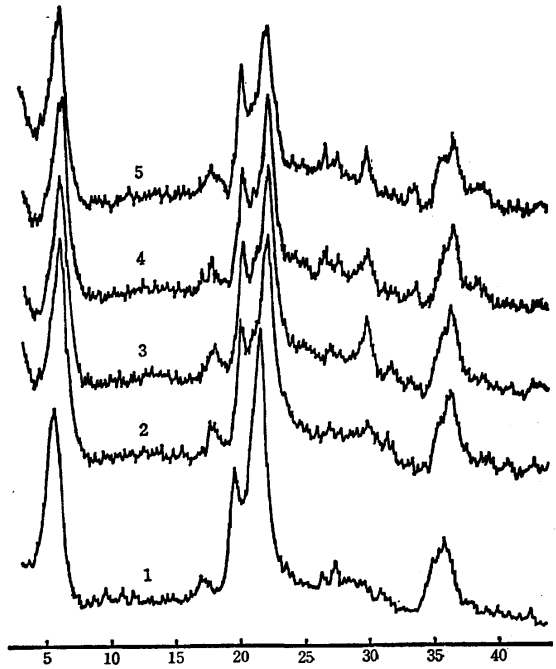

Fig. 1(a). X-Ray powder diagrams of M-1 series fillers in comparison with that of the original acid clay. (Cu$K\alpha$ radiation).
Curve 1: Matsune acid clay pulverized under 200 mesh and dried at 110 °C for 2 hr without lime treatment and calcination beforehand.
Curves 2—5: M-1 series fillers treated with hydrated lime (1.25, 3, 6 or 9% CaO, respectively), disintegrated by wet ball-milling for 18 hr and dried at 110 °C for 5 hr without calcination.

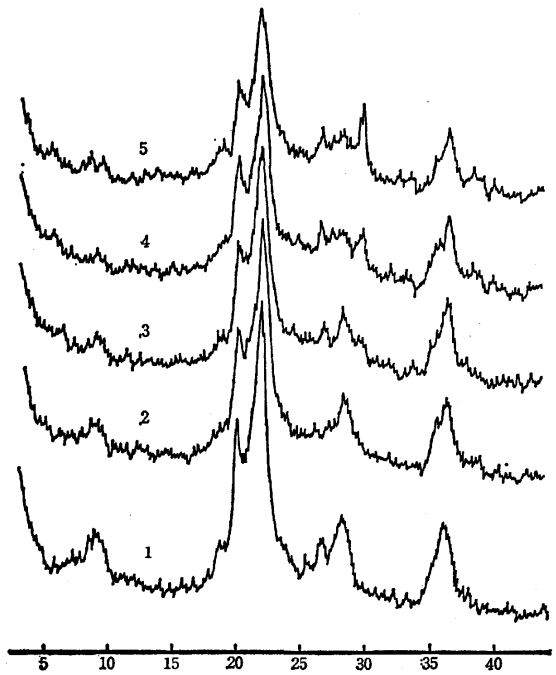

Fig. 1(b). X-Ray powder diagrams of M-2 series fillers. Curves 1—5 show the fillers prepared with or without hydrated lime (0, 1.25, 3, 6 or 9% CaO, respectively) followed by calcination (600 °C, 1.5 hr) and mechanical disintegration (wet ball-milling 18 hr).

retain the montmorillonite lattices with no significant structural changes though the conversion of the crystallite into Ca-montmorillonite, the consumption of the excess silica with alkali and the formation of small amounts of CSH, calcite and unknown crystalline materials were observed.

(ii) M-2 fillers: The basal reflection of montmorillonite almost disappeared. The remaining portion shifted towards lower spacings in the range 1.01—6.12 Å, in which the greatest shift occurred in the filler treated with 3% CaO (Fig. 1 (b) curves 1—5). A close relationship can be suggested with the reinforcing properties of the best **M** hard clay.

The most prominent reflection of α-cristobalite also decreased in proportion to the increase in the amount of alkali. New reflections analogous to those of the M-1 fillers appeared with relatively less intensity. They showed in sharpened mode as the reflections of the distinguished α-cristobalite and remaining montmorillonite.

Consequently, more structural changes occurred in the M-2 fillers than in the M-1 fillers. However, the minute crystallites still retained the montmorillonite lattices with no serious collapse though the capability

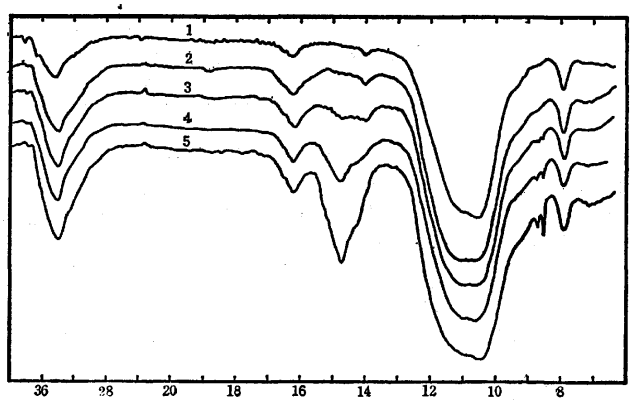

Fig. 2(a). Infrared spectra of M-1 series fillers in comparison with that of the original acid clay.
The respective curve corresponds to that of the same number shown in Fig. 1(a).

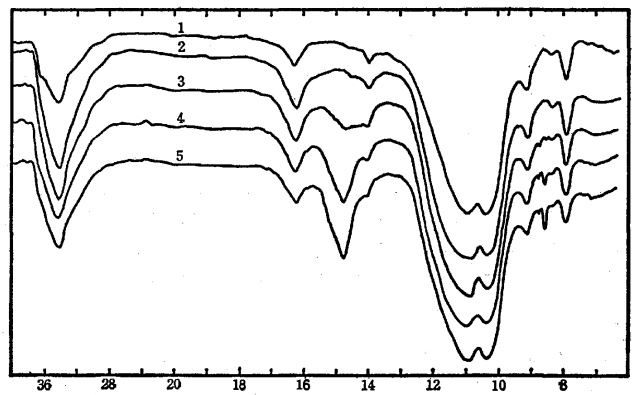

Fig. 2(b). Infrared spectra of M-2 series fillers. The respective curve corresponds to that of the same number shown in Fig. 1(b).

Table 1. Investigation of structure, morphology and physicochemical properties

	Methods	Apparatus	Conditions
Structure and morphology	X-ray diffraction	Rigaku Denki Geigerflex diffractometer	Nickel filtered Cu$K\alpha$ radiation, 30 kV, 12 mA, rate meter 16, multiplier 1, time constant 4 sec, slits 1°—1°—0.2 mm, scanning speed 2° (2θ)/min, chart speed 1 cm/min
	IR spectroscopy	JASCO Model DS-403G spectrophotometer	Through a KBr disk and Nujol mull in the regions 4000—200 and 4000—2800 cm^{-1}
	DTA and TG	Rigaku Denki Thermoflex differential thermogravimetric analyzer	From room temperature up to 1300 °C with a heating rate 10 °C/min
	Electron microscopy	JEOL JEM-6AS electron microscopy	Operated at 50 kV
Physicochemical properties	Hygroscopicity	Weighing bottle (10 ml), electric oven, desiccator and chemical balance	Expose a specimen (1 g) to the air for 24 hr, dry at 110 °C in an oven to constant weight and weigh the loss (wt%) before and after drying
	pH	pH meter with glass electrode	JIS K 6221-60 (1960); ASTM D 1512-57T (1957)
	DPG adsorption	Conical flask (200 ml) with stopper, centrifugal and titration apparatus	A modification[1] of the W. B. Wiegand and J. W. Snyder method, *I. E. C.*, **23**, 646 (1931). Adsorbate, 0.01 N DPG ethanol solution; indicator, 0.1% BPB ethanol solution
	Specific gravity	Pycnometer (10 ml), exhauster and chemical balance	ASTM D 153—39 (1939). Immersion liquid, kerosene (bp 70—100°C/2 mmHg, d_4^{30} 0.7811)
	Bulk density	Graduated, thick-walled test tube (20 ml) and rubber plate as a cushion	S. Kurabayashi, "Methods of Examination for Rubber and Relating Materials," ed. by S. Kunisawa, Soc. Rubber Ind. Japan (1963), p. 651.

of rehydration and rehydroxylation[9–11] disappeared almost completely as in the case of **N** hard clay (CaO less than 10%, calcination 600 °C, 1—1.5 hr; mechanical disintegration 18 hr).

(2) Infrared Spectra. Figures 2(a) and 2(b) illustrate the infrared spectra giving the difference of structural changes between the M-1 and M-2 fillers, respectively.

(i) M-1 Fillers: The diagnostic bands[12] of montmorillonite in the dried **M** varied with the treatment with alkali followed by mechanical disintegration and drying without calcination (Fig. 2(a) curves 1—5).

As the amount of alkali increased, the bands at 3640 (νO–H, free), 3430 (νO–H, hydrogen bonded) and 1630 cm^{-1} (δO–H) in curve 1 first increased and then decreased as a result of the formation of Ca-montmorillonite and CSH (curves 2—5). The latter two bands slightly shifted towards lower frequencies at 3410 and 1620 cm^{-1}, respectively. The bands at 915 (δAl^{3+}–O–H)[13–15] and 853 cm^{-1} (δFe^{3+}–O–H)[13–15] decreased in proportion to the amount of alkali. The uptake of Ca^{2+} ion seems to take place in the outer edges of octahedrons of the montmorillonite. Of the bands characteristic of layer-lattice silicates in the regions 950—1250 (νSi–O) and 400—650 cm^{-1} (not shown), the band at 1100 cm^{-1} related to colloidal silica[16–18] became broad, the intensity considerably increasing, suggesting the progress of ion saturation.[19] However, the bands at 1035 and 472 cm^{-1} (δSi–O)[13–15] related to the skeletal vibrations of the tetrahedrons of montmorillonite and the band at 519 cm^{-1} (Si–O–Al^{VI})[13–15] remained unchanged.

New distinct bands at 1460—1475 and 855 cm^{-1} ascribable to CSH[20,21] increased in proportion to the decrease of the band at 794 cm^{-1} related to hydrated amorphous silica[16–18] with an increase in the amount of alkali. Only feeble bands at 1420, 876 and 715 cm^{-1} attributable to calcite,[22,23] which appeared in the fillers prepared with more than 3% CaO, hardly changed with the variation in the amount of alkali.

The results indicate that no significant alternation occurred in the montmorillonite lattices except for the formation of Ca-montmorillonite, CSH and calcite and the uptake of Ca^{2+} ion in the octahedrons.

(ii) M-2 Fillers: More changes appeared in the diagnostic bands of the montmorillonite than in the case of the M-1 fillers (Fig. 2(b) curves 1—5).

Irrespective of calcination (600 °C, 1.5 hr) for the fillers, the bands at 3430 and 1630 cm^{-1} increased in proportion to the amount of alkali. In view of the abrupt loss and noticeable shift in the basal reflections of calcined fillers, the increase can be attributed mainly to the water of crystallization of CSH. The bands were partially retained after calcination indicating rehydrated during the course of mechanical disintegration. The bands at 1035 and 472 cm^{-1} gradually shifted towards higher frequencies overlapping the adjacent bands at 1100 and 519 cm^{-1}, giving one stronger and broader band around 1060 and 485 cm^{-1}. Some irreversible contraction or condensation might take place in the montmorillonite lattices.

The band at 794 cm^{-1} decreased in intensity and became broader. This suggests the consumption of hydrated amorphous silica and the occurrence of partial polycondensation. The new bands ascribed to CSH and calcite appeared more distinctly than the

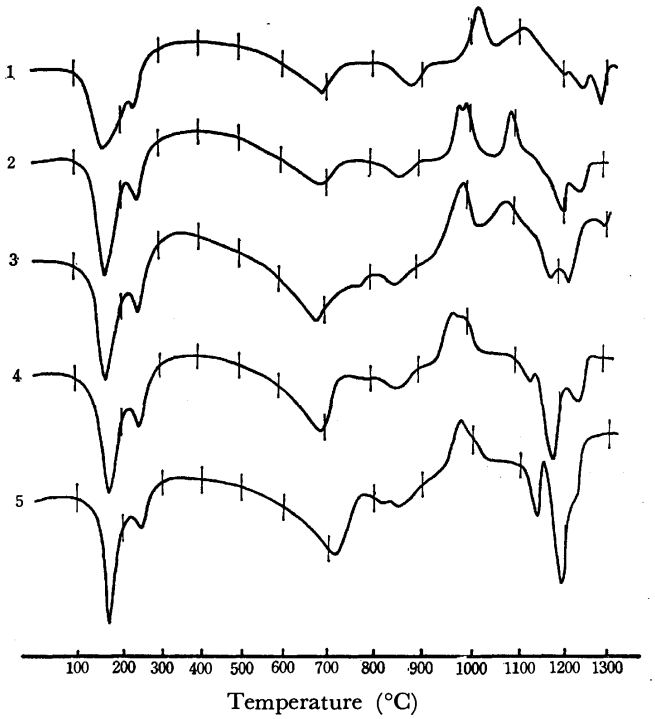

Fig. 3(a). DTA thermograms of M-1 series fillers in comparison with that of the original acid clay.
The respective curve corresponds to that of the same number shown in Fig. 1(a).

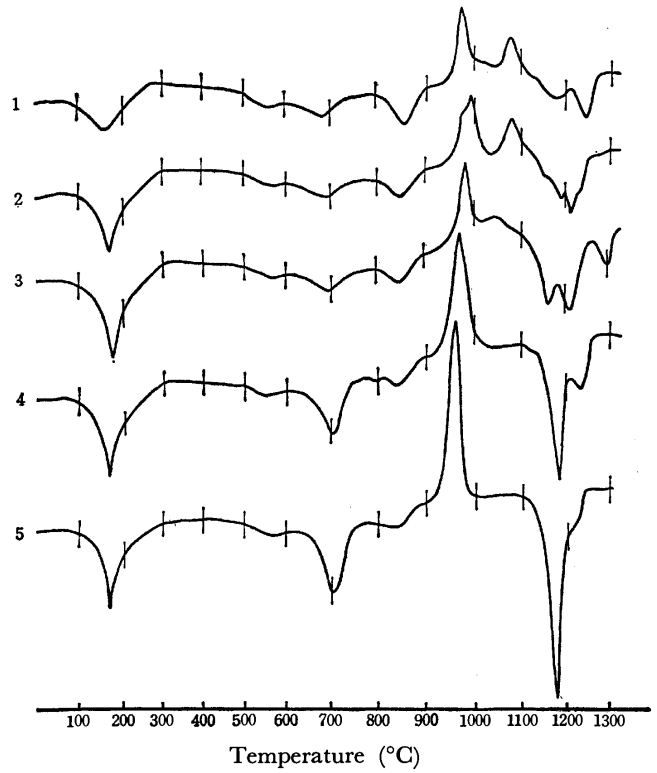

Fig. 3(b). DTA thermograms of M-2 series fillers.
The respective curve corresponds to that of the same number shown in Fig. 1(b).

corresponding bands of the M-1 fillers with an increase in the amount of alkali.

The fillers thus prepared still retained the minute crystallites of montmorillonite structure involving some irreversible contraction in the layer lattices. The consumption of α-cristobalite with alkali and partial polycondensation of the excess silica remained and the formation of new crystalline minerals such as CSH and calcite were observed in the matrix as well. The results agree with those of X-ray investigation.

(3) DTA Thermograms. Figures 3(a) and 3(b) show the DTA thermograms demonstrating the difference of structural changes between the M-1 and M-2 fillers, respectively.

(i) M-1 Fillers: The diagnostic peaks of montmorillonite[24-26] changed with the treatment as follows (Fig. 3(a) curves 1—5).

Endothermic Reactions: With an increase in the amount of alkali, the first two endotherms (152 °C, strong and broad; 225 °C, a medium shoulder) in the dried **M** (curve 1) became greater and gradually shifted towards higher temperatures; the filler treated with 9% CaO gave the endotherms at 173 and 243 °C (curve 5). The major endotherm in curve 1 is ascribable to dehydration[25,26] (100—300 °C) of the water adsorbed on the surfaces and among the interfaces of the minute crystallites of the montmorillonite and α-cristobalite, and the minor one to the water hydrated with the exchangeable cations interposed between the interlayers. With an increase in the amount of alkali, the major endotherm showed increase in the peak temperature, sharpness and symmetry of the profile (curves 2—5). This suggests that the dehydration can be explained in terms of the loss of the water of crystallization due to newly formed minerals CSH besides the adsorbed one.

The endotherm (685 °C, medium and broad) attributable to the dehydroxylation[25,26] (500—780 °C) of the normal montmorillonite and excess silica of the dried **M** showed a considerable rise in temperature around 9% CaO; the endotherm of the filler prepared with 1.25, 3, 6 or 9% CaO appeared at 683, 681, 685 or 709 °C, respectively. It was accompanied by a gradual increase in the area of profile. The results verify the formation of Ca-montmorillonite[25] and CSH[27] together with the appearance of the exotherm (around 970 °C) and endotherms (around 1130 and 1180 °C).

The endotherm (872 °C, medium and broad) due to the phase transition[25,26] (820—920 °C) of montmorillonite in the dried **M** gradually shifted towards lower temperatures, accompanied by a decrease in the area of profile; the filler prepared with 9% CaO gave the endotherm at 848 °C. An appreciable amount of Ca^{2+} ion should have been taken into the octahedrons of montmorillonite during the course of treatment.

The remaining endotherms at 1197 (a weak shoulder), 1237 (small and broad) and 1280 °C (medium and sharp) changed to 1132 (medium and sharp), 1185 (very strong and sharp) and 1222 °C (a medium shoulder), respectively.

The fusion point of the dried **M** (over 1300 °C) is lowered noticeably with the increase in the amount of

alkali; the filler treated with 9% CaO melted at 1185 °C.

No endotherm ascribable to the dehydroxylation of calcium hydroxide (about 570 °C, strong),[27] which would take place during the course of mixing raw materials and subsequent mechanical disintegration, was found in both fillers. However, a weak one (around 772—812 °C) attributable to calcite[28] appeared in almost the same area for the fillers prepared with more than 3% CaO. This indicates that a nearly equal amount of calcite was produced in the fillers; the amount was estimated to be less than 3% from the area of endotherm. The formation resulted from the carbonation of liberated alkali $Ca(OH)_2$ during the course of preparation.

Exothermic Reactions: The exotherms due to β-quartz[24] or spinel[24] (1009 °C, medium and sharp) and β-cristobalite[24] (1102 °C, medium and broad) in the dried **M** showed splitting and sharpening, decreasing in the peak temperatures (979, 993 and 1085 °C) for the filler treated with the least amount of alkali, 1.25% CaO. With an increase in the amount of alkali, the exotherms gradually decreased in the temperatures and overlapped the adjacent peaks. The filler prepared with 9% CaO gave a medium and broad exotherm (972 °C) containing a weak shoulder (998 °C). The formation of some CSH gel in combination with alumina might be suggested.[27]

(ii) M-2 Fillers: The calcined **M** without the lime treatment showed a change in the diagnostic peaks of montmorillonite as follows (Fig. 3(b) curve 1).

Endothermic Reactions: The first two prominent endotherms (152 and 225 °C) in the dried **M** disappeared completely by calcination (600 °C, 1 hr). A medium and broad one (165 °C) appeared by subsequent mechanical disintegration (wet ball-milling 18 hr) and drying (110 °C, 5 hr). The first endotherm is ascribed to the dehydration of the water rehydrated during the course of the wet ball-milling. Disappearance of the minor one (225 °C) indicates that fixation[25] of the exchangeable cations interposed between the interlayers of the montmorillonite took place during the course of calcination.

The endotherm at 685 °C in the dried **M** diminished noticeably just after the calcination, and showed two peaks at 575 °C (small and broad) and 686°C (medium and broad) by the subsequent mechanical disintegration and drying. The endotherms are attributed to the dehydroxylation of the structural water rehydroxylated during the course of the wet ball-milling; the former (575 °C) corresponds to the disorder[10,25] of the montmorillonite lattices resulting from the calcination and mechanical disintegration, and the latter (686 °C) to the residual normal montmorillonite.

The endotherm (872 °C) due to the phase transition of montmorillonite in the dried **M** shifted towards a lower temperature (860 °C) with a slight increase in the area. During the course of calcination, some substitution[25] occurred in the octahedrons of the montmorillonite with the exchangeable cations originally interposed between the interlayers.

The remaining endotherms (1197, 1237 and 1280 °C) in the dried **M** moved to considerably lower temperatures (1130, 1193 and 1251 °C, respectively) with appreciable broadening in the calcined **M**.

Exothermic reactions: The exotherms due to β-quartz (1009 °C) and β-cristobalite (1102 °C) in the dried **M** also shifted towards lower temperatures (983 and 1080 °C, respectively), accompanied by appreciable sharpening in the calcined **M**. A pronounced crystallization would proceed by calcination without previous lime treatment. Additional treatment with hydrated lime caused noticeable changes in the DTA thermograms of the M-2 fillers (Fig. 3(b) curves 2—5).

Endothermic Reactions: As the amount of alkali increased, the first endotherm (165 °C) in the calcined **M** appeared around 180 °C. The endotherm gradually increased in the area and sharpness of profile. This can be attributed to the dehydration of the water of crystallization of CSH rehydrated during the course of wet ball-milling besides the readsorbed water distributed on the surfaces and among the interfaces of the minute crystallites.

The endotherm (575 °C) ascribed to the disorder of the montmorillonite lattices in the calcined **M** moved in succession towards a lower temperature (around 560 °C) with no change in the area of profile. However, the adjacent endotherm (686 °C) attributed to the dehydroxylation of the residual normal montmorillonite of the calcined **M** increased in the area, temperature and sharpness of the profile in proportion to the amount of alkali. This indicates a linear formation of CSH with an increase in the amount of alkali in accordance with the increase in the area and sharpness of the peaks observed around 180, 960 and 1180 °C. The filler prepared with 9% CaO gave the endotherm at 708 °C with more than three times area as compared with that of the calcined **M**.

An endotherm (795 °C) ascribable to calcite, easily observable by means of X-ray diffraction and IR spectroscopy, appeared only in the filler treated with 6% CaO.

The endotherm (860 °C) attributed to the phase transition of montmorillonite in the calcined **M** showed a gradual decrease in temperature (835 °C for 9% CaO) and the area (less than 1/3 for 9% CaO) of the profile. This suggests that the consumption of alumina proceeded in the octahedrons of the montmorillonite, resulting in the formation of CSH gel incorporated with alumina.

The endotherms appearing at 1193 and 1251 °C in the calcined **M** varied complicatedly with an increase in the amount of alkali. New peaks accompanied by an increase or a decrease in the area, shifting or overlapping adjacent peaks were observed.

Exothermic Reactions: The exotherm (983 °C) due to β-quartz in the calcined **M** showed a shoulder (975 °C) in the filler treated with the least amount of alkali, 1.25% CaO. The exotherm increased in the area and sharpness of profile, gradually decreased in the peak temperature in proportion to the amount of alkali and finally became one single peak. This suggests the formation of a considerable amount of CSH gel incorporated with alumina. The adjacent exotherm (1080 °C) ascribed to β-cristobalite in the calcined **M** decreased in the temperature and disappeared in the fillers treated with more than 6% CaO.

The greater the amount of alkali, the more advanced the formation of CSH (I, II and gel) and the greater the lowering of the fusion point; the one treated with 9% CaO melted at 1179 °C, about 120 °C lower than that of the dried **M**. Depression in the fusion point due to excess alkali over the optimum amount (CaO 3%) caused agglomeration, sintering or hardening of the minute crystallites of acid clay as in the case of polycondensation observed in the calcined **M** without previous lime treatment or in the fillers treated with alkali less than 3% followed by calcination. The calcined products became too hard to be sufficiently disintegrated. The reinforcing properties were reduced noticeably.

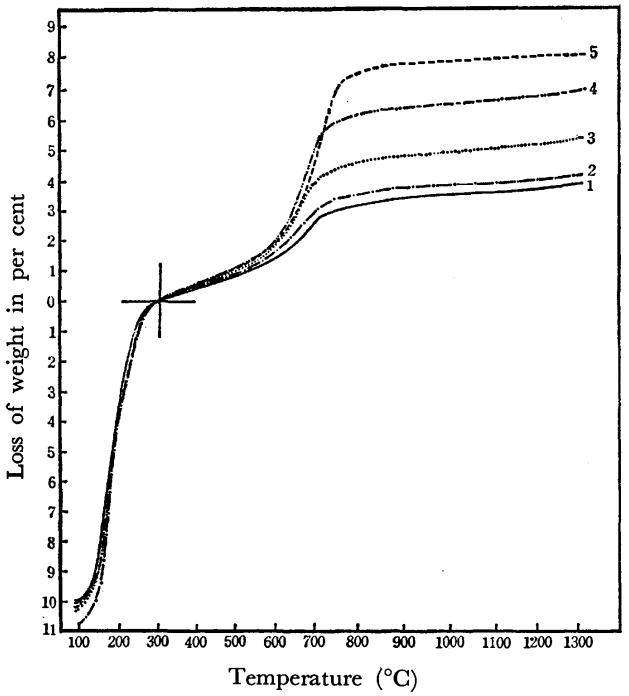

Fig. 4(a). TG thermograms of M-1 series fillers in comparison with that of the original acid clay.
The respective curve corresponds to that of the same number shown in Fig. 1(a).

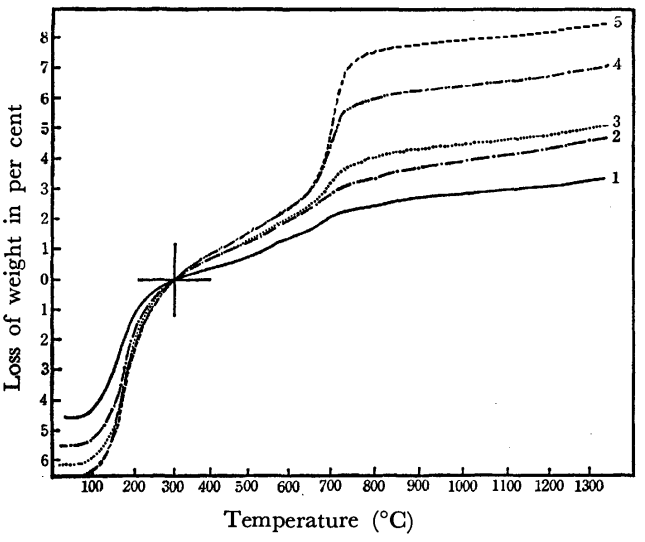

Fig. 4(b). TG thermograms of M-2 series fillers.
The respective curve corresponds to that of the same number shown in Fig. 1(b).

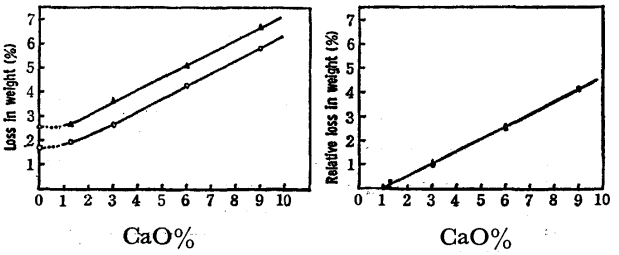

Fig. 4(c). A linear formation of CSH with an increase in the amount of CaO.
The relative loss in weight corresponds to the net weight loss related to the dehydroxylation of newly formed minerals.
△——△ M-1 series fillers; ○——○ M-2 series fillers.

(4) TG Thermograms. Figures 4(a) and 4(b) illustrate the TG thermograms of the M-1 and M-2 fillers, respectively. Four fractions, *viz.*, dehydration (up to 300 °C), oxidation (300—500 °C), dehydroxylation (500—780 °C) and phase transition (780—1300 °C), can be deduced with reference to the characteristic peaks of corresponding DTA thermograms.

Dehydration caused remarkable changes in weight; 7.8—11.9% and 4.3—6.2% for the M-1 and M-2 fillers, respectively.

Oxidation of adsorbed organic matter and/or the partial dehydration of newly formed minerals CSH (I, II and gel) resulted in a linear loss in weight; the loss varied within the ranges 0.76—1.11% and 0.71—1.57% for the M-1 and M-2 fillers, respectively.

A proportional increase in weight loss due to the dehydroxylation of the prepared fillers took place with an increase in the amount of alkali. The weight loss amounted to 2.59—6.66% and 1.67—5.77% for the M-1 and M-2 fillers, respectively.

The phase transition accompanied by or not by the fusion of specimen showed a linear loss in weight; it changed in the ranges of 0.90—1.39% and 0.74—1.77% for the M-1 and M-2 fillers, respectively.

The total loss in weight, consequently, increased with an increase in the amount of alkali; the M-1 fillers varied from 12.07 (CaO 0%) to 18.38% (CaO 9%) and the M-2 fillers from 7.56 (CaO 0%) to 14.22% (CaO 9%). Irrespective of calcination, the net loss in weight attributable to the dehydroxylation of the new minerals CSH was found to be accurately in proportion to an increase in the amount of alkali (Fig. 4(c)). The value can be estimated from TG thermogram by reducing the weight loss of a corresponding reference specimen, dried or calcined **M**, from that of a M-1 or M-2 filler, respectively. This indicates that the amounts of CSH produced in the fillers are proportional to those of the alkali. This is in line with the results obtained by X-ray diffraction, IR spectroscopy and DTA.

Determination of Physicochemical Properties. Changes in the physicochemical properties such as hygroscopicity, pH, DPG adsorption, specific gravity and bulk density are demonstrated in comparison with those of Dixie Clay, Silene EF and **M**, dried and calcined (Figs. 5(a)—

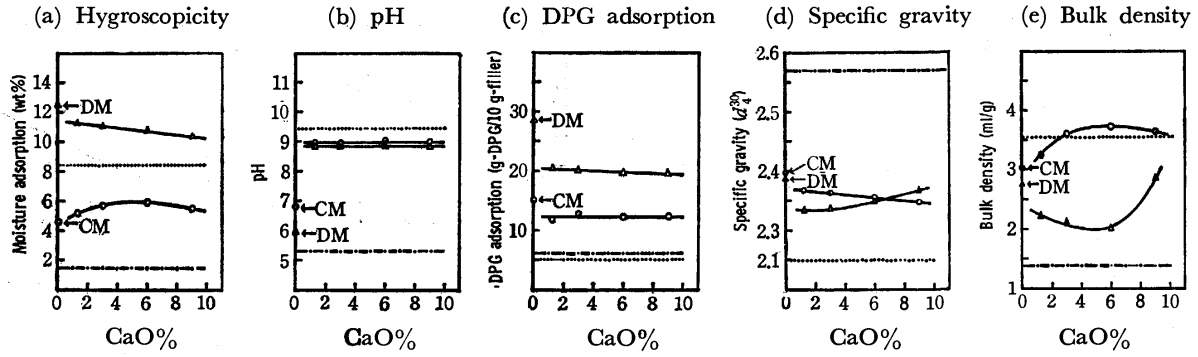

Fig. 5. Changes in the physicochemical properties of **M** hard clay with alkali (CaO 0—9%) and by thermal treatment (110 °C, 5 hr for M-1 series fillers; 600 °C, 1.5 hr for M-2 series fillers) in comparison with those of references, Dixie Clay, Silene EF and the original acid clay **M**, dried (110 °C, 2 hr) and calcined (600 °C, 1.5 hr).
Inscriptions are as follows: (a): Hygroscopicity (wt%), (b): pH, (c): DPG adsorption (g DPG/10^4 g filler), (d): Specific gravity (d_4^{30}), (e): Bulk density (ml/g), DM: Dried **M**, CM: Calcined **M**.
△——△ M-1 series fillers; ○——○ M-2 series fillers, —·—· Dixie Clay; ····· Silene EF.

(e)).

(1) Hygroscopicity: The hygroscopicity of the dried and calcined **M** without lime treatment were found to be 12.44 and 4.53%, respectively (Fig. 5 (a)). The former (12.44%) is much greater than the value of Dixie Clay (1.46%) or Silene EF (8.41%), and the latter (4.53%) is less than the mean value of the reference fillers.

By the lime treatment (CaO 1.25—9%) without subsequent calcination, the hygroscopicity of the M-1 fillers decreased in proportion to an increase in the amount of alkali. However, the value was still greater than that of Silene EF.

The hygroscopicity of the M-2 fillers decreased noticeably by the subsequent calcination (600 °C, 1.5 hr). The hygroscopicity was comparable to the mean value of the reference fillers, accompanied by a maximum around 6% CaO.

(2) pH: The pH of the dried and calcined **M** without previous lime treatment were found to be 5.95 and 6.77, respectively (Fig. 5 (b)). The values are smaller than the value of Silene EF (9.45) but close to that of Dixie Clay (5.30).

Treatment with hydrated lime and without subsequent clacination resulted in a noticeable increase in the pH of the M-1 fillers; a constant value as high as 8.84 was obtained.

Subsequent calcination gave rise to only a small increase (0.12) in the pH values of the M-2 fillers. They were comparable to the pH of Silene EF, deviating from that of Dixie Clay.

(3) DPG Adsorption: The DPG adsorption of **M** (dried 28.57 g DPG/10^4 g filler; calcined 15.03 g DPG/10^4 g filler) was found to be much greater than that of the reference fillers (Dixie Clay 6.05 g DPG/10^4 g filler; Silene EF 5.08 g DPG/10^4 g filler) (Fig. 5 (c)).

The DPG adsorption of the M-1 fillers decreased to a 70% value of the dried **M** by treatment with hydrated lime without subsequent calcination. Irrespective of the variation in the amount of alkali (CaO 1.25—9%), the value remained almost unchanged.

Subsequent calcination caused a further, constant diminution (7.73 g DPG/10^4 g filler) in the DPG adsorption of the M-2 fillers. A reduction to a 57% value of the dried **M**, twice as much as the value of Dixie Clay was observed.

(4) Specific Gravity: The specific gravity of the calcined **M** (2.3957) was found to be a little greater than that of the dried **M** (2.3891) (Fig. 5 (d)). The value of **M**, dried or calcined, is smaller than that of Dixie Clay (2.5684) but greater than that of Silene EF (2.0984).

Treatment with hydrated lime without subsequent calcination caused a noticeable decrease in the specific gravity of the M-1 fillers. The value, however, gradually increased with an increase in the amount of alkali.

Subsequent calcination resulted in a decrease in the specific gravity of the M-2 fillers in proportion to the amount of alkali. Consequently an intersection with the former plots appeared around 7% CaO.

The variation of the specific gravity of the M-1 and M-2 fillers with the amount of alkali remained in the ranges 0.0331 and 0.0203, respectively.

(5) Bulk Density: The bulk density of dried and calcined **M** was found to be 3.02 and 2.75 ml/g, respectively (Fig. 5(e)). The latter (2.75 cc/g) is comparable to the mean value of Dixie Clay (1.38 ml/g) and Silene EF (4.05 ml/g)

Treatment with hydrated lime less than 6% CaO without subsequent calcination caused a gradual decrease in the bulk density of the M-1 fillers. More alkali, however, gave rise to a rapid increase. Consequently a minimum value of the bulk density appeared around 4—6% CaO.

Subsequent calcination afforded a further increase in the bulk density of the M-2 fillers. A maximum exceeding the value of Silene EF was obtained with 5—7% CaO.

The results indicate that not only reduction in the hygroscopicity, DPG adsorption and specific gravity of the original acid clay **M**, but also increase in the pH and bulk density of the fillers can be attained by treatment with hydrated lime (CaO 1.25—9%) followed by calcination (600 °C, 1.5 hr) as compared with a single treatment with alkali or by calcination alone.

Morphological Study by Electron Microscopy and SAD

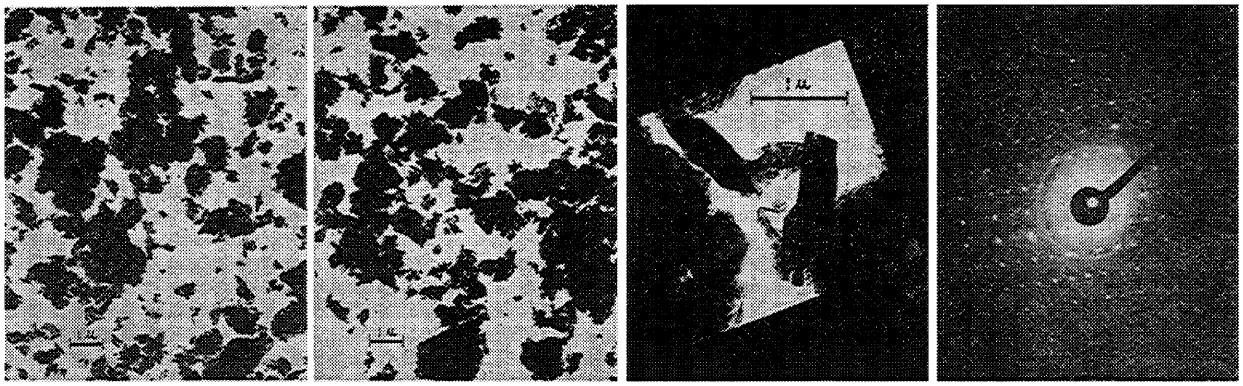

1 2 3A 3B

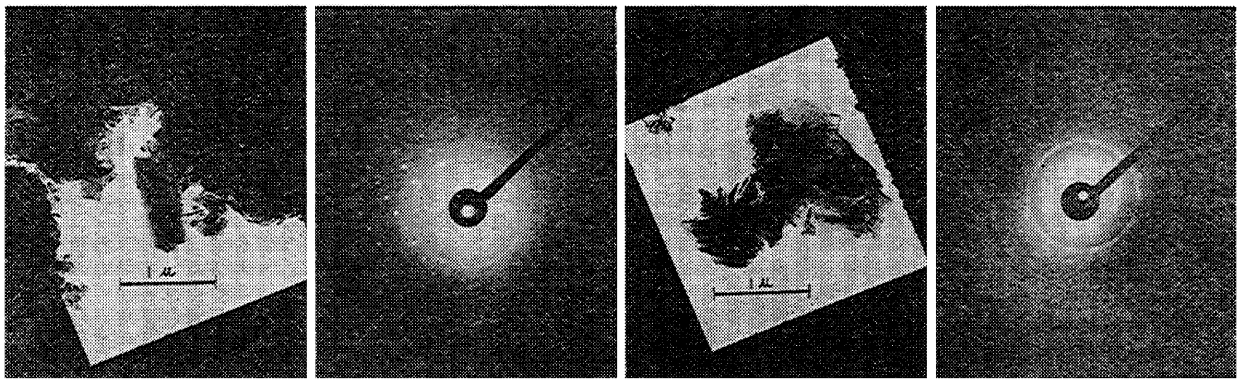

4A 4B 5A 5B

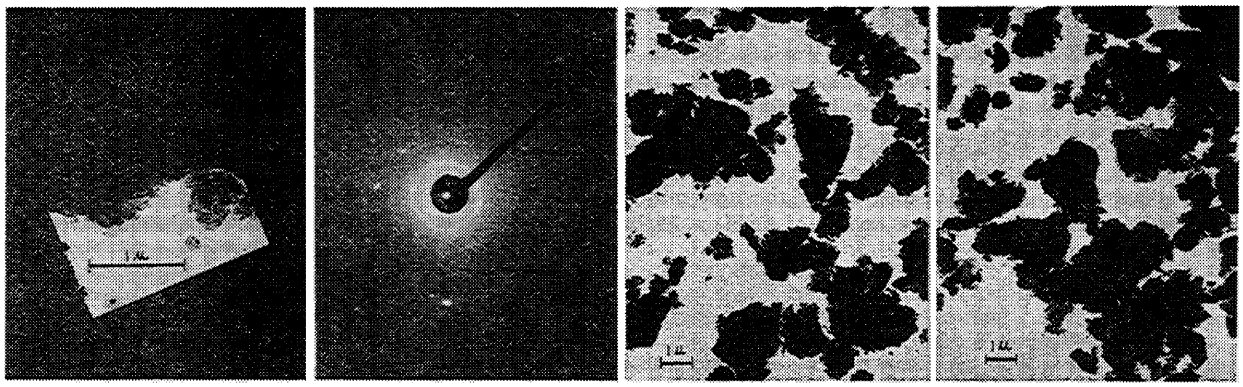

6A 6B 7 8

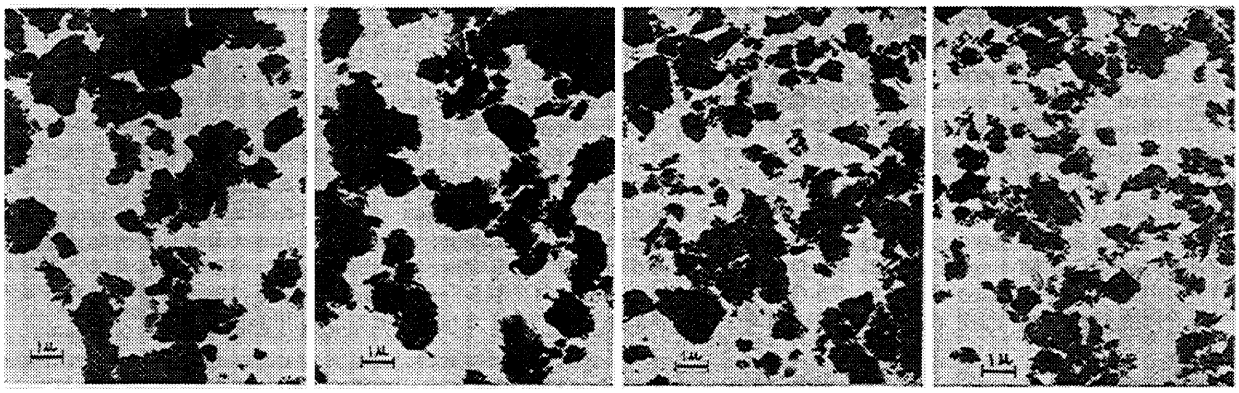

9 10 11 12

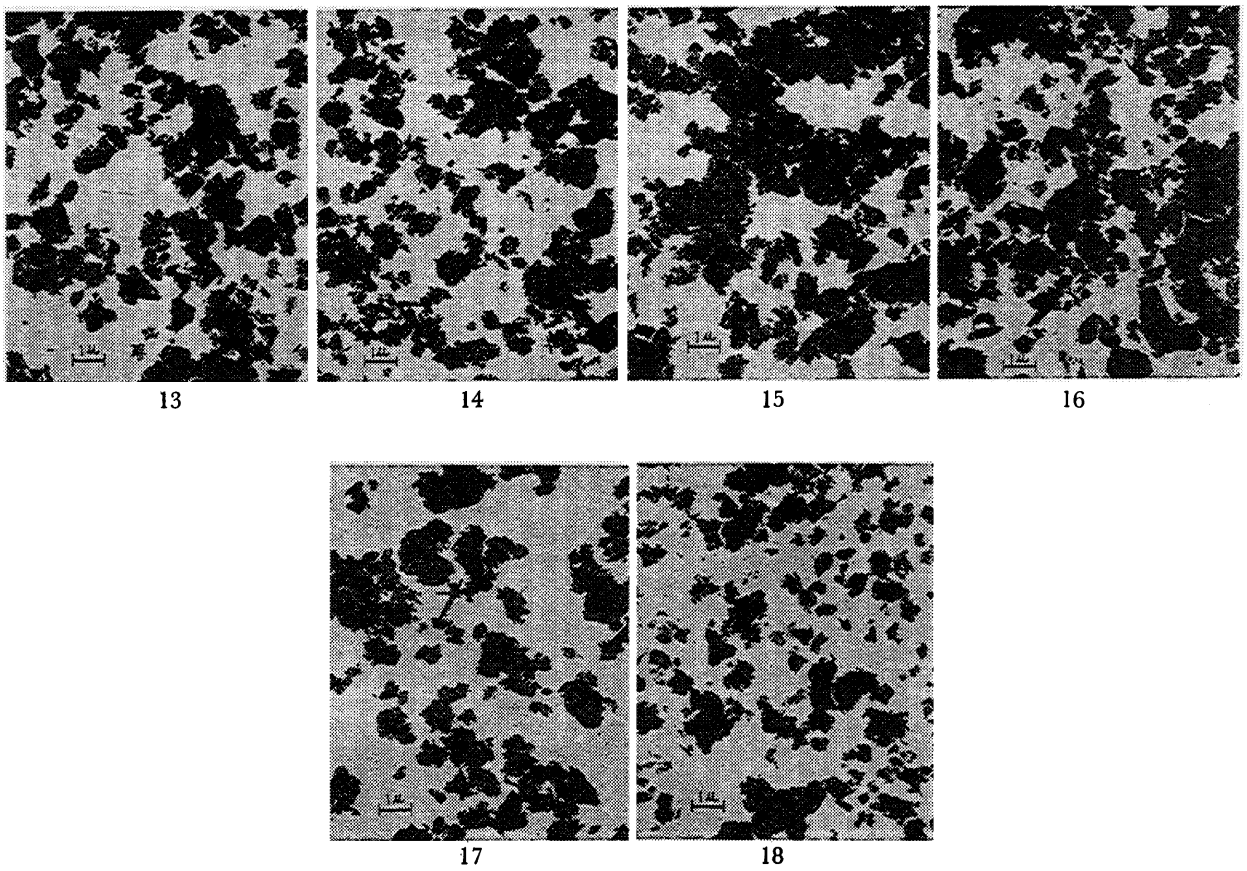

Fig. 6. Electron micrographs and SAD diagrams of **M** hard clay with magnifications of 9000 and 26000, respectively in comparison with those of **N** hard clay.

Plate 1: **M** hard clay (CaO 6%; calcination 600 °C, 1 hr; wet ball-milling 18 hr).
Plate 2: **N** hard clay (CaO 6%; calcination 600 °C, 1 hr; wet ball-milling 18 hr).
Plate 3A: Well crystallized CSH in **M** hard clay (CaO 6%; calcination 600 °C, 1 hr; wet ball-milling 18 hr).
Plate 3B: The SAD diagram of the new mineral in Plate 3A.
Plate 4A: Thin, platey crystal of CSH in **M** hard clay (CaO 3%; calcination 600 °C, 1.5 hr; wet ball-milling 18 hr).
Plate 4B: The SAD diagram of the new mineral in Plate 4A.
Plate 5A: Poorly crystallized aggregate in **N** hard clay (CaO 6%; calcination 600 °C, 1.5 hr; wet ball-milling 18 hr).
Plate 5B: The SAD diagram of the aggregate in Plate 5A.
Plate 6A: Cluster of globular-shaped CSH in **M** hard clay (CaO 3%; wet ball-milling 18 hr; drying 110 °C, 5 hr).
Plate 6B: The SAD diagram of the cluster in Plate 6A.
Plate 7: M-1 series filler (a) (CaO 1.25%; wet ball-milling 18 hr; drying 110 °C, 5 hr).
Plate 8: M-1 series filler (b) (CaO 3%; wet ball-milling 18 hr; drying 110 °C, 5 hr).
Plate 9: M-1 series filler (c) (CaO 6%; wet ball-milling 18 hr; drying 110 °C, 5 hr).
Plate 10: M-1 series filler (d) (CaO 9%; wet ball-milling 18 hr; drying 110 °C, 5 hr).
Plate 11: M-2 series filler (a) (CaO 1.25%; calcination 600 °C, 1.5 hr; wet ball-milling 18 hr).
Plate 12: M-2 series filler (b) (CaO 3%; calcination 600 °C, 1.5 hr; wet ball-milling 18 hr).
Plate 13: M-2 series filler (c) (CaO 6%; calcination 600 °C, 1.5 hr; wet ball-milling 18 hr).
Plate 14: M-2 series filler (d) (CaO 9%; calcination 600 °C, 1.5 hr; wet ball-milling 18 hr).
Plate 15: **M** hard clay (1) (CaO 6%; calcination 600 °C, 1.5 hr; wet ball-milling 6 hr).
Plate 16: **M** hard clay (2) (CaO 6%; calcination 600 °C, 1.5 hr; wet ball-milling 12 hr).
Plate 17: **M** hard clay (3) (CaO 6%; calcination 600 °C, 1.5 hr; wet ball-milling 18 hr).
PlBte 18: **M** hard clay (4) (CaO 6%; calcination 600 °C, 1.5 hr; wet ball-milling 24 hr).

Technique. **M** hard clay gave a greater amount and smaller size of particle than **N** hard clay under the same conditions of preparation (Fig. 6, Plate 1 *cf.* Plate 2). This can be attributed mainly to the difference of mineralogical constituents between the original acid clays, **M** and **N**, *viz.*, the amounts of normal and abnormal montmorillonites as well as excess silica α-cristobalite.

The deviation in the optimum amount of hydrated lime in the best reinforcing fillers (CaO 3% for **M**, 6% for **N**; calcination 600 °C, 1.5 hr; wet ball-milling 18 hr) can be interpreted in the same way. The SAD technique applied to the best reinforcing fillers and others revealed that a distinct diffraction pattern of CSH appeared in **M** hard clay but only a feeble one in **N** hard clay besides the diagnostic reflections of montmorillonite (Plates 3-A, 3-B, 4-A and 4-B *cf.* 5-A and 5-B), and that subsequent calcination affected the formation of CSH noticeably (Plates 4-A and 4-B *cf.* Plates 6-A and 6-B).

The fact that the greater part of hydrated lime added to **N** is combined with the montmorillonite lattices is interpreted as follows: (i) **N** consists of abnormal montmorillonite in a greater amount than normal montmorillonite,[1] (ii) the former reacts with alkali more easily than the latter, (iii) the amount of excess silica involved in **N** (13%) is much less than in **M** (34%),[1] (iv) α-cristobalite contained in the interior of montmorillonite lamellae reacts with alkali with more difficulty than the one distributed on the surface of crystallite or in an isolated state.

The less the content of excess silica involved in the original acid clay, the less the formation of CSH in the fillers prepared with the same amount of alkali. However, the formation of CAH and calcite increased with an increase in the amount of alkali. This agrees with the results obtained by X-ray diffraction and IR spectroscopy.

The indispensability of thermal treatment at an appropriate temperature for the preparation was proved by comparing the morphology of the M-1 and M-2 fillers (Plates 7—10 *cf.* Plates 11—14). After mechanical disintegration in wet state for 18 hr, the particle size and its distribution range of the M-1 fillers were found to be even smaller than those of the corresponding M-2 fillers. During the course of drying, however, the active silanol groups, originally contained and mechanochemically[29,30] generated in the wet ball-milling, and alkali liberated in the matrix cause the recombination of minute crystallites of the fillers, resulting in the formation of much greater and harder agglomerates. Subsequent pulverization with an atomizer to minimize the agglomerates is so difficult that the reinforcing effect of the M-1 fillers on SBR-1502 compounds decreased noticeably.[2]

In the case of the M-2 fillers, calcination (600 °C, 1.5 hr) after lime treatment gives rise to adequate dehydroxylation as well as dehydration of the montmorillonite, CSH and excess silica remaining. This process helps to facilitate the pulverization of the final products and also has the effect of inhibiting polycondensation of montmorillonite and α-cristobalite due to an even formation of the CSH distributed on the interlayer surfaces and the interfaces of the minute crystallites. Thus the great surface activity inducing agglomeration during the course of drying and the great adsorption encountered in compounding can be restrained properly.

The reduction of the particle size and its distribution range of the same-series fillers was found to be proportional to the time of mechanical disintegration up to 18 hr (Plates 15—18).

Conclusion

In spite of the similarity in the constitutional units, fineness and functional groups of montmorillonite and kaolinite, acid clays, hitherto, could not be utilized as a material for reinforcing fillers due to structural factors[31,32] such as substitutions in the tetrahedral and/or octahedral sheet, nonconformity in the layers and lattice defects of montmorillonite which cause too great adsorption, cation exchange, swelling and catalytic activity.

It has been found that treatment with hydrated lime followed by calcination and mechanical disintegration can suppress the great surface activity of acid clay and maintain the fineness and available functional groups of the crystallites properly, turning acid clays into a reinforcing filler.

The reinforcing effect on SBR-1502 compounds was found to be in line with the reduction in both the particle size and its distribution range. The average particle size and its distribution are closely related to the mineralogical constituents of the original acid clays, **K**, **M** and **N**, as well as the conditions of preparation as in the case of the contents of remaining functional groups and newly formed minerals, CSH, CAH and calcite.[1-3] The optimum conditions for the preparation were found to be as follows: Raw materials consist of normal and/or abnormal montmorillonite involving excess silica α-cristobalite as principal constituents. Treatment with hydrated lime (CaO 3% for **M**, 6% for **N**) followed by calcination (600 °C, 1.5 hr) and mechanical disintegration (wet ball-milling 18 hr).

The precise mechanism of the reinforcing effects caused by the prepared fillers has not been clarified. However, it is certain that surface energy, especially the interaction between the hydroxyl radicals distributed on the outer surfaces of filler particles and compounded elastomer molecules play the most important role.[33,34]

The encouragement and support of the late Prof. T. Kuwata, the University of Tokyo, are gratefully acknowledged. Thanks are also due to Prof. J. Kumanotani, the University of Tokyo, for his valuable discussions and Mr. Y. Sugawara, President of Mizusawa Industrial Chemicals Co., Ltd., for the supply of acid clays.

References

1) H. Rai and J. Yamada, This Bulletin, **45**, 1540 (1972).
2) H. Rai and J. Yamada, *ibid.*, **46**, 3555 (1973).
3) H. Rai and J. Yamada, *ibid.*, **48**, 1621 (1975).

4) D. M. C. MacEwan, "The X-Ray Identification and Crystal Structures of Clay Minerals," ed. by G. Brown, Miner. Soc. London (1961), p. 143, 200.
5) H. E. Swanson and E. Tatge, *NBS Circular* 539, **I**, 39 (1953).
6) G. R. Glenn, *J. Amer. Ceram. Soc.*, **50**, 312 (1967).
7) H. F. W. Taylor, "Progress in Ceramic Science," Vol. 1, ed. by J. E. Burke, Pergamon Press (1961), p. 89.
8) H. E. Swanson and R. K. Fuyat, *NBS Circular* 539, **II**, 51 (1953); ASTM, X-Ray Powder Data File Card 5-0586.
9) L. Heller, V. C. Farmer, R. C. Mackenzie, B. D. Mitchell, and H. F. W. Taylor, *Clay Mineral Bull.*, **5**, 56 (1962).
10) E. C. Jonas, *Nat. Acad. Sci. Publ.*, **395**, 66 (1955).
11) R. E. Grim and W. F. Bradley, *Amer. Mineral.*, **33**, 50 (1948).
12) I. Oinuma and H. Kodama, "Clay Science Handbook," ed. by S. Iwao, Clay Sci. Soc. Japan, Gihodo, Tokyo (1967), pp. 65—75.
13) V. Stubičan and R. Roy, *Amer. Mineral.*, **46**, 32 (1961).
14) V. Stubičan and R. Roy, *Z. Krist.* **115**, 200 (1961).
15) V. Stubičan and R. Roy, *J. Amer. Ceram. Soc.*, **44**, 625 (1961).
16) B. D. Mitchell, V. C. Farmer, and W. J. MacHardy, *Advan. Agr.*, **16**, 349 (1964).
17) E. R. Lippincott, A. V. Valkenburg, C. E. Weir, and E. N. Bunting, *J. Res. Nat. Bur. Stand.*, **61**. 61 (1958).
18) M. Field, I. K. Walker, and P. P. Williams, *New Zealand J. Sci. Tech.*, **38**, 31 (1956).
19) V. C. Farmer and J. D. Russel, *Spectrochim. Acta*, **20**, 1149 (1964).
20) K. Fukui, *J. Soc. Rubber Ind. Japan*, **37**, 858 (1964).
21) E. Suito and M. Arakawa, *ibid.*, **34**, 885 (1961).
22) E. E. Angino, *Amer. Mineral.*, **52**, 137 (1967).
23) C. E. Weir and E. R. Lippincott, *J. Res. Nat. Bur. Stand.*, **65A**, 175 (1961).
24) R. E. Grim and Kulbicki, *Amer. Mineral.*, **46**, 1333 (1961).
25) R. G. Kelly, "The Differential Thermal Investigation of Clays," ed. by R. C. Mackenzie, Miner. Soc. London (1957), p. 140.
26) K. Nagasawa, Ref. 12, p. 36.
27) S. Diamond, J. L. White, and W. L. Dolch, "Clay and Clay Minerals, Proc. 12th Nat. Conf.," Pergamon Press, New York (1964), p. 359.
28) a) S. Iwao, Ed., Ref. 12, p. 40, 395; b) R. C. Mackenzie, Ed., Ref. 25, p. 331.
29) H. Takahashi, Ref. 12, p. 339, 346 and 364.
30) T. Kubo, "An Introduction to Mechanochemistry," Tokyo Kagakudojin, Tokyo (1972), pp. 30—50; 107—138.
31) Y. Otsubo, *Kagaku To Kogyo*, **4**, 229 (1951).
32) R. E. Grim, "Clay Mineralogy," 2nd ed., MacGrow-Hill Book Co., New York (1968), p. 77.
33) E. Suito and M. Arakawa, *J. Soc. Rubber Ind. Japan*, **36**, 704 (1963); *Kogyo Kagaku Zasshi*, **66**, 1616 (1963).
34) E. M. Dannenberg, *Rubber Chem. Technol.* **48**, 410 (1975).

NOTES

BULLETIN OF THE CHEMICAL SOCIETY OF JAPAN, VOL. 49(3), 807—808 (1976)

The Many-body Effects in $(N_2)_n$ Systems

Masao HASHIMOTO

The Chemical Research Institute of Tohoku University, Sendai, 980

(Received July 14, 1975)

Synopsis. Many-body effects in $(N_2)_n$ systems are discussed on the basis of CNDO/2-Clementi SCF calculations of the deviation from the pairwise additivity. The many-body effects cancel each other out, and this makes the deviation from the pairwise additivity only a small percentage of the pairwise interaction in the rather high n-mers.

The total energy of an interacting n-molecular system can be described as follows (the so-called multibody expansion[1]):

$$E = \sum_r E_r + \sum_{r<s} E_{rs} + \sum_{r<s<t} E_{rst} + \cdots + \sum_{r<s<t<\cdots<n} E_{rst\cdots n} \quad (1)$$

The first term of Eq. (1) is the summation of the self-energies of individual molecules. The second term is the summation of the two-body interaction energies, the third term is that of the three-body interaction energies, and so on. Rewriting Eq. (1) in terms of the (2) and (3) defintitions, we obtain the defintition for the deviation from the pairwise additivity, $\sigma(n)$:

$$\Delta E_n = E - \sum_r E_r \quad (2)$$

$$\Delta E_2 = \sum_{r<s} E_{rs} \quad (3)$$

$$\sigma(n) = \Delta E_n - \Delta E_2 = \sum E_{rst} + \cdots + \sum E_{rst\cdots n} \quad (4)$$

It is expected that the three-body effects contribute most significantly to $\sigma(n)$.

Recently, there have appeared several papers on SCF calculations of $\sigma(n)$ in various configrations of rare gas trimers and, in a few cases, tetramers.[2] Novaro and Beltran-Lopez made a calculation of the system of $(He)_4$ and found that the four-body effects were not small compared with the three-body effects. Therefore, the superiority of three-body effects in Eq. (4) may be questionable in general.

TABLE 1. MANY-BODY EFFECT IN α-N_2, IN ELECTRON VOLTS

n	Species	ΔE_n	ΔE_2	$\sigma(n)$	n-Body effect
2	(2, 5)	0.00000			
	(1, 2)	−0.01072			
	(1, 10)	−0.01894			
	(2, 3)	−0.00004			
3	(1, 2, 3)	−0.02754	−0.02148	−0.00606	−0.00606
	(2, 1, 5)	−0.02284	−0.02144	−0.00140	−0.00140
	(2, 3, 5)	−0.00010	−0.00008	−0.00002	−0.00002
4	(1, 2, 3, 5)	−0.03404	−0.03224	−0.00180	0.01174
	(2, 3, 4, 5)	−0.00018	−0.00016	−0.00002	0.00006
	(7, 10, 6, 11)	−0.04588	−0.04296	−0.00292	0.02132
5	(1, 2, 3, 4, 5)	−0.04700	−0.04304	−0.00396	−0.02386
	(1, 7, 10, 6, 11)	−0.12111	−0.08584	−0.03527	0.00401
7	(1····· 7)	−0.14232	−0.15040	0.00808	
9	(1····· 9)	−0.25089	−0.25784	0.00691	
13	(1·····13)	−0.53288	−0.56472	0.03184	

TABLE 2. MANY-BODY EFFECT IN γ-N_2 CRYSTAL, IN ELECTRON VOLTS

n	Species	ΔE_n	ΔE_2	$\sigma(n)$	n-Body effect
2	(1, 2)	−0.02898			
	(3, 4)	−0.00281			
	(2, 4)	−0.03734			
	(2, 5)	−0.00243			
3	(2, 3, 5)	−0.07421	−0.07711	0.00290	0.00290
	(2, 3, 4)	−0.08068	−0.07749	−0.00319	−0.00319
	(1, 3, 5)	−0.09460	−0.09530	0.00070	0.00070
	(1, 3, 4)	−0.05731	−0.06077	0.00346	0.00346
	(1, 2, 5)	−0.05419	−0.06039	0.00620	0.00620
4	(2, 3, 4, 5)	−0.15722	−0.13788	−0.01934	−0.01876
	(1, 3, 2, 4)	−0.15856	−0.16443	0.00587	0.00420
	(1, 2, 4, 5)	−0.14807	−0.16405	0.01598	0.00548
5	(1·····5)	−0.25773	−0.27052	0.00279	−0.00897
7	(1·····7)	−0.34965	−0.36582	0.01617	
9	(1·····9)	−0.51269	−0.53580	0.02311	

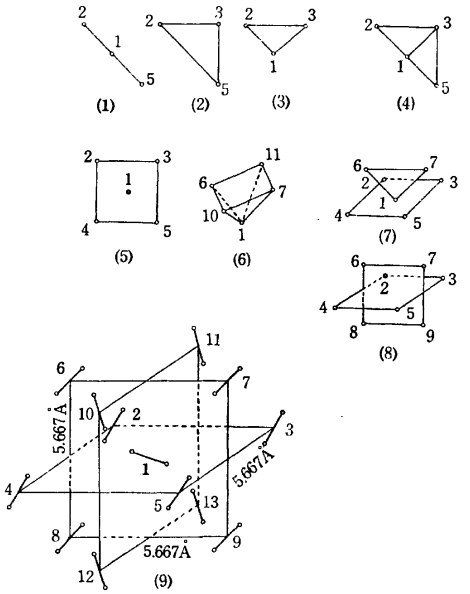

Fig. 1. The configurations of n-mers in α-N_2 crystal. (1), (2), (3): 3-mer; (4): 4-mer; (5), (6): 5-mer; (7): 7-mer; (8): 9-mer; (9): 13-mer. In (1)—(8), only the positions of the centers of N_2 molecules are indicated.

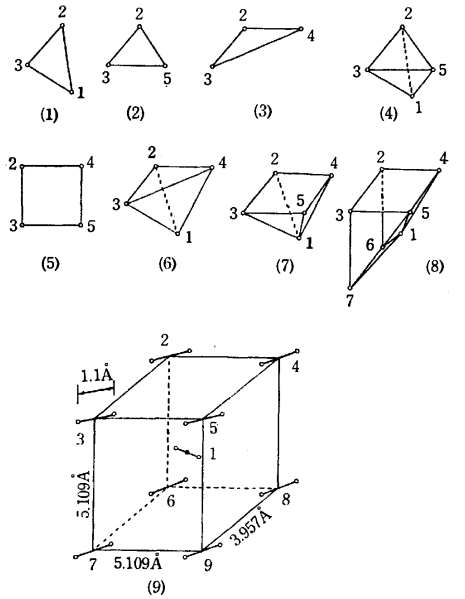

Fig. 2. The configurations of n-mers in γ-N_2 crystal. (1),(2),(3),: 3-mer; (4),(5),(6): 4-mer; (7): 5-mer; (8): 7-mer; (9): 9-mer. In (1)—(8) only the positions of the centers of N_2 molecules are indicated.

In the case of polyatomic molecular n-mer, there have not been any papers reported concerning this point.

In the present paper, we calculate $\sigma(n)$ for $(N_2)_n$ systems in the way previously used[3] for the calculation of $\sigma(3)$ in $(N_2)_3$ systems, and discuss the many-body effects higher than the three-body.

In Tables 1 and 2 the CNDO/2-Clementi SCF LCAO MO results are shown. The configurations of the molecules in n-mers in these Tables correspond to a part of the configurations of molecules in the real crystals, α- and γ-N_2 (see Figs. 1 and 2).[4] The four-body effect in Fig. 1 (4) is calculated as the difference between $\sigma(4)$ and four three-body effects, which can be calculated easily:

$$\begin{aligned} E_{1235} &= \sigma(4) - \sum E_{rst} \\ &= \sigma(4) - (E_{215}+E_{235}+E_{123}+E_{135}) \\ &= -0.00180 - (-0.00140-0.00002 \\ &\quad -0.00606-0.00606) \\ &= 0.01174 \end{aligned} \tag{5}$$

The other four-body effects in Figs. 1 and 2 were calculated in the same way. The five-body effect in Fig. 1(5) was calculated using the four-body effects thus calculated:

$$\begin{aligned} E_{12345} &= \sigma(5) - (E_{2345}+E_{1235}\times 4+E_{123}\times 4+E_{235}\times 4 \\ &\quad +E_{215}\times 2) \\ &= -0.00396 - (0.00006+0.01174\times 4 \\ &\quad -0.00606\times 4-0.00002\times 4-0.00140\times 2) \\ &= -0.02386 \end{aligned} \tag{6}$$

The other five-body and higher-body effects could be calculated in the same way, but the effects higher than five-body were not evaluated since their calculations are rather time-consuming.

The n-body effects obtained throw doubt on the rapid convergence of multibody expansions shown in Eq. (1). However, because the signs of the components in Eq. (4) can be either positive or negative (as may be seen from Tables 1 and 2), there may occur cancellations between them. As a result, the deviations from the pairwise additivity, $\sigma(n)$'s, are of the order of a few percent of ΔE_2 in the n-mers higher than the pentamers. This is another confirmation of the pairwise additivity in molecular crystals.

These discussions are, of course, justified only with respect to the intermolecular distance corresponding to the van der Waals minimum: at larger or smaller distances they are questionable. However, we are not interested in the latter region of distance, because we are concerned exclusively with molecular crystals.

All the numerical calculations were made by means of the NEAC-2200 model 700 computer system at the Computer Center of Tohoku University.

References

1) H. Margenau and J. Stamper, *Advan. Quantum Chem.*, **3**, 129 (1969).
2) O. A. Novaro and V. Beltran-Lopez, *J. Chem. Phys.*, **56**, 815 (1972).
3) M. Hashimoto and T. Isobe, This Bulletin, **47**, 40 (1974).
4) A. Zunger and E. Huler, *J. Chem. Phys.*, **62**, 3010 (1975).

BULLETIN OF THE CHEMICAL SOCIETY OF JAPAN, VOL. 49(3), 809—810 (1976)

The Sensitization of Rare Earth Ion Luminescence in Dilute Solutions by [1]Benzopyrano[3,4-*c*]pyridine-4,5(3*H*)-dione Derivatives

Akira FUJIMOTO, Akio SAKURAI* and Eiichi IWASE

Tokyo Electrical Engineering College, Kanda, Chiyoda-ku, Tokyo 101
**The Institute of Physical and Chemical Research, Wako-shi, Saitama 351*

(Received April 5, 1975)

Synopsis. Luminescence spectra and lifetimes are presented for the rare earth ions sensitized by [1]benzopyrano-[3,4-*c*]pyridine-4,5(3*H*)-dione derivatives in dilute solutions. It is to be noted that, among the benzopyranopyridine derivatives investigated, 2-phenyl-[1]benzopyrano[3,4-*c*]pyridine-4,5(3*H*)-dione brings about the most efficient sensitization for the luminescence of europium and terbium ions. Some discussions are made of the energy-transfer processes from these excited benzopyranopyridine derivatives to terbium ions.

Although the phenomenon of intramolecular energy transfer in β-diketone chelates of rare earth ions is well known,[1] the process of intermolecular energy transfer between organic compounds and rare earths has been discussed only recently.[2] This note will give the luminescence characteristics of europium and terbium ions sensitized by 2-phenyl-[1]benzopyrano[3,4-*c*]pyridine-4,5(3*H*)-dione (PBPP), 2-*p*-methoxyphenyl-[1]-benzopyrano[3,4-*c*]pyridine-4,5(3*H*)-dione (*p*-MBPP), and 7-methoxy-2-phenyl-[1]benzopyrano[3,4-*c*]pyridine-4,5(3*H*)-dione (MPBPP) in 1:1 (v/v) ethanol–methanol solutions.

Experimental

Three benzopyranopyridine derivatives, europium nitrate hexahydrate and gadolinium nitrate hexahydrate, and terbium acetate hemihydrate and gadolinium acetate anhydrate were prepared by the methods described by Sakurai *et al.*,[3] Dawson *et al.*,[4] and Witt *et al.*[5] respectively. The luminescence and excitation spectra were measured using the Hitachi Model MPF-2A fluorescence spectrophotometer. Measurements of the lifetimes of the rare earth ion luminescence sensitized by benzopyranopyridine derivatives were made with a photomultiplier located at a 90° angle from the exciting intense ultraviolet beam from a xenon lamp. The flash light given by this lamp had a life-duration of less than 50 μs.

Results and Discussion

The spectra observed at room temperature are presented in Fig. 1. The degree of enhancement in the rare earth ion luminescence at a certain fixed wavelength, *i.e.*, 613 nm for europium and 544 nm for terbium ions, sensitized by donors (benzopyranopyridine derivatives), are shown in Table 1 in terms of the enhancement factor obtained by dividing the relative intensity of the luminescence of the rare earth ions in the presence of the donors by that in their absence, the concentration of the donors being 2.0×10^{-4} M, and that of the acceptors (rare earth salts), 4.5×10^{-3} M. It should be noted that, among the donors investigated, PBPP brings about the most efficient sensitization for the luminescence of europium and terbium ions.

The presence of an acceptor causes a blue shift to the fluorescence and excitation bands of a benzopyranopyridine derivative (Figs. 1 and 2). This result indicates that there is a weak interaction between benzopyranopyridine derivatives and the rare earth ions. Since the excitation spectrum of the rare earth luminescence overlaps appreciably with that of the benzopyranopyridine derivative–rare earth mixed system, a direct excitation of the rare earth should also occur (Fig. 2). However, such an excitation would be

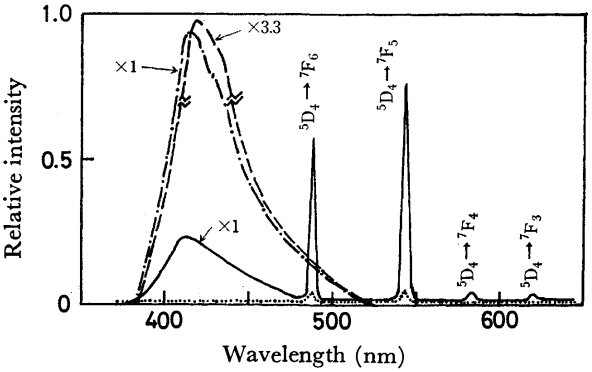

Fig. 1. Luminescence spectra of PBPP (8×10^{-5} M) alone (—), PBPP (8×10^{-5} M)–gadolinium acetate (9×10^{-4} M) system (-·-), PBPP (8×10^{-5} M)–terbium acetate (9×10^{-4} M) system (—), and terbium acetate (9×10^{-4} M) alone (···).

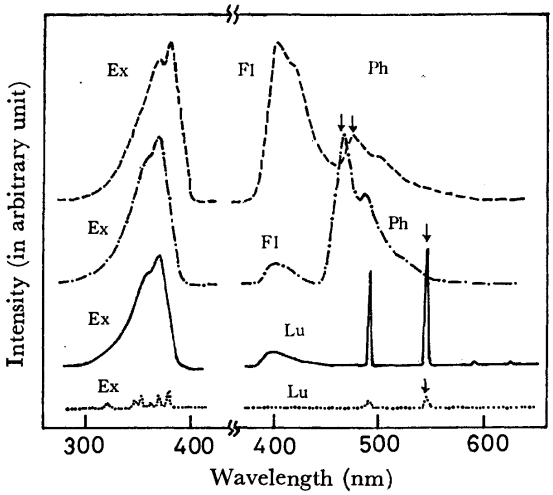

Fig. 2. Excitation (Ex), fluorescence (Fl), and phosphorescence (Ph) spectra of PBPP alone (—) and PBPP–gadolinium acetate system (-·-) at 77 K and Ex and luminescence (Lu) spectra of PBPP–terbium acetate system (—) at 77 K and terbium acetate alone (···) at room temperature. Ex spectra; for the emissions as indicated by arrows. Fl, Ph, and Lu spectra; excitation at 370 nm.

Table 1. Enhancement factors for various rare earth ion systems and triplet energy levels[a] of the donors alone and the donor–gadolinium nitrate mixed systems

Donor	Excitation wavelength (nm)	Enhancement factor		Triplet level[a]	
		Eu^{3+} (613 nm)	Tb^{3+} (544 nm)	Donor alone (cm^{-1})	Gd^{3+} (cm^{-1})
PBPP	370	40	70	21300	21500
p-MBPP	370	27	32	21200	21400
MPBPP	370	20	55	21100	21600

a) The phosphorescence maxima of the donors.

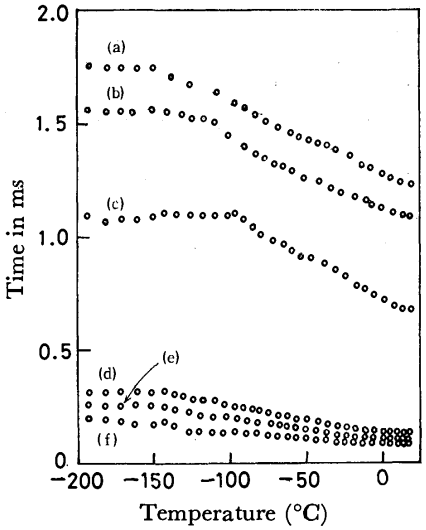

Fig. 3. The lifetimes of terbium $^5D_4$—$^7F_5$ for the *p*-MBPP–Tb (a), PBPP–Tb (b), and MPBPP–Tb (c) systems, and those of the europium $^5D_0$—$^7F_2$ for the *p*-MBPP–Eu (d), PBPP–Eu (e), and MPBPP–Eu (f) systems.

inefficient, because the excitation bands for the luminescence of rare earth ions are weak and very narrow.

As is shown in Fig. 1, the fluorescence intensity of PBPP at room temperature decreases when rare earth ions are present. It is impossible to excite gadolinium ions by energy transfer from either the lowest excited singlet or triplet state of the PBPP, since no transitions in the visible or near-infrared regions exist in the case of gadolinium ions. It can be seen from Fig. 2 that the intensity ratio of the phosphorescence to the fluorescence of the donor at 77 K is much increased by the presence of gadolinium ions. Accordingly, the decrease (about 70%) in fluorescence intensity in the presence of gadolinium ions at room temperature is due to the enhancement in the intersystem crossing (from the lowest excited singlet state to the lowest excited triplet state) of the donor caused by gadolinium ions. The fact that the fluorescence intensity of the donor at room temperature is weakened to about 10% by the presence of terbium (III) ions must be due to the combined effect of the increase in the intersystem crossing of the PBPP caused by terbium ions, with that of the energy transfer from the PBPP to the terbium ions. The excitation of terbium ions by the direct transfer of energy from the lowest excited singlet states of the donors is energetically feasible, but this process would be inefficient because the intersystem crossing of the donors would be enhanced by terbium ions in almost the same degree as by gadolinium ions.

The triplet energy levels of the donors alone and those of the donor–Gd systems at 77 K are listed in Table 1. When the gadolinium ions are present, the triplet levels show a blue shift. The triplet levels of all the donor–Gd systems are nearly 21500 cm^{-1} above the ground energy levels of the donors. The resonance level ($^5D_4$)[6] of terbium ions is 20430 cm^{-1} above the ground level ($^7F_6$). The $^5D_4$ level of terbium ions is, therefore, readily populated by the energy transfer from the triplet state of the donor. Consequently, the luminescence is due to the transition to the ^7F manifold levels from the $^5D_4$ levels of terbium ions. In addition, the intensity ratio of the phosphorescence to the fluorescence decreases with an increase in the concentration of terbium when the donor concentration is kept constant at 77 K, until finally it becomes impossible to observe the phosphorescence spectra of the donors (Fig. 2). From the facts described above, it may be concluded that an energy transfer can be expected from the lowest triplet energy levels to terbium ion levels.

The line emissions due to the transitions from the $^5D_0$ levels of europium and the $^5D_4$ levels of terbium ions sensitized in the mixed systems were so intense that measurements of the lifetimes could be made easily. The observed lifetimes are presented in Fig. 3. Among the mixed systems of the [1]benzopyrano[3,4-*c*]pyridine-4,5(3*H*)-dione derivatives and rare earth ions so far investigated, the duration of the luminescence of the *p*-MBPP–Tb system was found to be the longest.

This work was supported by grants from the Tokyo Electrical Engineering College (T.E.E.C.) Research Fund. The authors wish to express their thanks to Dr. Hiroshi Midorikawa and Dr. Kozo Inuzuka for their kind advice during this study.

References

1) a) W. R. Dawson, J. L. Kropp, and M. W. Windsor, *J. Chem. Phys.*, **45**, 2410 (1966). b) M. L. Bhaumik and L. J. Nugent, *ibid.*, **43**, 1680 (1965).

2) a) S. P. Tanner and D. L. Thomas, *J. Amer. Chem. Soc.*, **96**, 706 (1974). b) A. Heller and E. Wasserman, *J. Chem. Phys.*, **42**, 949 (1965).

3) A. Sakurai, H. Midorikawa, and Y. Hashimoto, This Bulletin, **43**, 2925 (1970).

4) W. R. Dawson and J. L. Kropp, *J. Opt. Soc. Am.*, **55**, 822 (1965).

5) J. R. Witt and E. I. Onstott, *J. Inorg. Nucl. Chem.*, **24**, 637 (1962).

6) G. A. Crosby, R. E. Whan, and R. M. Alire, *J. Chem. Phys.*, **34**, 743 (1961).

BULLETIN OF THE CHEMICAL SOCIETY OF JAPAN, VOL. 49(3), 811—812 (1976)

The Molecular Motion of Phenyl Groups in Toluene, Diphenylmethane and Triphenylmethane in Solutions of Carbon Tetrachloride by Raman Line Shape Analysis

Hiroyasu NOMURA, Yutaka MIYAHARA, and Shinobu KODA*

Department of Chemical Engineering, Faculty of Engineering, Nagoya University, Chikusa-ku, Nagoya-shi 464
**Department of Synthetic Chemistry, Faculty of Engineering, Nagoya University, Chikusa-ku, Nagoya-shi 464*

(Received August 12, 1975)

Synopsis. The reorientational correlation times of phenyl groups in the molecules of toluene, diphenylmethane, and triphenylmethane in carbon tetrachloride solutions were measured by the Raman-line-shape analysis. The reorientational relaxation times of the phenyl groups obtained increased in this order: toluene<diphenylmethane<triphenylmethane as a result of the increase in the mutual interaction among phenyl groups themselves in the molecule.

In the Raman spectroscopic study of the molecular dynamics in the liquid state, the most important model-independent quantity obtainable is the reorientational correlation time, τ(OR). When a molecule has a symmetric top, the analysis of the isotropic and anisotropic Raman-line shapes of the nondegenerate vibrations uniquely determines the reorientational correlation time for the tumbling motion of the molecule.

In our previous papers[1-3] it has been shown that the reorientational correlation time of a molecule obtained is an important quantity intimately related to the inter- and intramolecular interaction.

In the present note, the reorientational correlation times of phenyl groups in the molecules of toluene, diphenylmethane, and triphenylmethane dissolved in carbon tetrachloride were determined by Raman-line shape analysis, and the mutual interaction among phenyl groups in the molecule was discussed.

The apparatus used consisted of an argon ion laser (800 mW at 4880 Å) produced by the Coherent Radiation Co. Ltd., and a laser Raman spectrometer of the JRS-Ul type of JEOL, Ltd., Japan. The toluene and carbon tetrachloride used were commercial products of spectra-grade reagents, while the diphenylmethane and triphenylmethane were extra-pure-grade reagents supplied by the Tokyo Kasei (Chemical) Industrial Co., Ltd. The solutions used for the measurements contained such amounts of the solutes that the concentration of phenyl groups was 2 mol per liter of solution.

In order to obtain the orientational correlation times, the Raman-line shape of the ν_2 fundamental of the phenyl group was analyzed. The Raman spectrum was observed at 90 °C with respect to the linearly polarized incident light. With $I_{\parallel}(\omega)$ and $I_{\perp}(\omega)$ representing the strong and weak components of the scattered light, one can write,

$$I_{\parallel}(\omega) = I_{\mathrm{isot}}(\omega) + 4/3 I_{\mathrm{anis}}(\omega) \quad (1)$$

$$I_{\perp}(\omega) = I_{\mathrm{anis}}(\omega) \quad (2)$$

$$\rho_s = \frac{I_{\perp}(\omega)}{I_{\parallel}(\omega)} \quad (3)$$

where ρ_s is the depolarization ratio. $I_{\mathrm{isot}}(\omega)$ represents the intrinsic vibrational line shape, and $I_{\mathrm{anis}}(\omega)$, a convolution of the vibrational line shape and the orientational spectrum.

The line shape of $I_{\parallel}(\omega)$ and $I_{\perp}(\omega)$ of the ν_2 (a_{1g}) fundamental (1002 cm^{-1}) obtained showed Lorentz-type cruves. This fact shows that the vibrational and the rotational motions of the phenyl group are not coupled. We can write;

$$\omega_{1/2}(\mathrm{anis}) = \omega_{1/2}(\mathrm{isot}) + \omega(\mathrm{or}) \quad (4)$$

where the $\omega_{1/2}$ terms are the half-width of the respective line shapes.

In order to eliminate the effect of the slit-width on the shape of the spectrum, the half-width of the spectrum was plotted against the slit-width, the true half-width was then obtained by extrapolating to zero slit-width.

The reorientational correlation time is obtained by means of;

$$\tau(\mathrm{OR})^{-1} = 2\pi c\omega(\mathrm{or}) \quad (5)$$

where τ(OR) is the reorientational correlation time, and c, the velocity of light. The details of the experimental procedures and the data reductions have been reported previously.[1-2]

Table 1.

	$\rho_s \times 10^{-2}$	$\omega_{1/2}$ (isot) cm^{-1}	$\omega_{1/2}$ (anis) cm^{-1}	ω (or) cm^{-1}	τ (OR) $\times 10^{-12} s^{-1}$
Toluene	1.13	1.72	3.56	1.84	2.88
Diphenylmethane	2.32	1.52	2.47	0.95	5.58
Triphenylmethane	3.15	2.37	2.66	0.29	18.6

The experimental results obtained are summarized in Table 1, where the half-width and the correlation time of the reorientational motion are listed in the last two columns. As may be seen in Table 1, the reorientational correlation time increase with an increase in the number of phenyl groups in a molecule; one in toluene, two in diphenylmethane, and three in triphenylmethane. Since the concentration of phenyl groups in the solutions was kept constant, this change in correlation time can be ascribed to the change in the degree of mutual interaction among phenyl groups themselves in a molecule.

The reorientational correlation time of phenyl groups in the dibenzyl molecules dissolved in carbon tetrachloride was 3.80×10^{-12} s^{-1},[2] as has been reported previously. The reorientational correlation time of the phenyl groups in the diphenylmethane molecules is a little larger than that in the dibenzyl molecules. This shows the existence of some interaction between the

phenyl groups themselves in the diphenylmethane molecules, which hinders the orientational motion of the phenyl groups to some extent.

In the triphenylmethane molecules, the rotational motion of phenyl groups are much more strongly hindered by the strong interaction among phenyl groups themselves, such as the steric hinderance and π-coupling. For this reason, the value of the reorientational correlation time of triphenylmethane increased to as much as three times that of free toluene molecules in the solution.

References

1) H. Nomura and Y. Miyahara, This Bulletin, **48**, 2779 (1975).
2) H. Nomura and Y. Miyahara, *Polmer J.*, **8**, 30 (1976).
3) H. Nomura, S. Koda, and Y. Miyahara, *J. Chem. Phys.*, in printing.

BULLETIN OF THE CHEMICAL SOCIETY OF JAPAN, VOL. 49(3), 813—814 (1976)

Lumiflavin-sensitized Photooxygenation Accelerated by Adenine. II. The Photolysis of ^{14}C-labeled Reactants

Akio YOSHIMURA and Shunji KATO

Institute of Chemistry, College of General Education, Osaka University, Toyonaka, Osaka 560

(Received August 26, 1975)

Synopsis. Radioactive tryptophan, histidine, methionine, and guanine were photolyzed in the presence of lumiflavin either with or without adenine, and the reaction products were compared chromatographically. Adenine accelerated these lumiflavin-sensitized photooxygenation reactions, and no effect of adenine on the reaction products was shown.

In a previous paper,[1] it was reported that the lumiflavin-sensitized photooxygenation of indoles is greatly accelerated by the addition of adenine when the reactants are present in very low concentrations. At that time, fluorometry was succesfully used as a highly sensitive method to follow the reaction; however, there remained an open question of whether or not adenine simply accelerates the oxygenation of indoles without altering the basic pattern of the reaction. In the present work, the effects of adenine on the lumiflavin-sensitized photooxygenations of tryptophan, histidine, methionine, and guanine, and on the reaction products have been examined by the use of ^{14}C-labeled reactants.

Experimental

The lumiflavin was prepared as has previously been described.[1] *dl*-Tryptophan-3-^{14}C (3.76 mCi/mmol), *l*-histidine-^{14}C (U) (216 mCi/mmol), and *l*-methionine-1-^{14}C (5.81 mCi/mmol) were purchased from the Daiichi Pure Chemicals Co., While guanine-8-^{14}C hydrochloride (5.4 mCi/mmol) was obtained from the New England Nuclear Co.

The photolysis was carried out as has previously been described (at 435.8 nm and 30 °C).[1] After the paper chromatography of the reaction mixtures on Toyo Roshi No. 51A paper, the autoradiograms were prepared by exposing Sakura Industrial X-ray film (type N) (8.4×30.5 cm) for several weeks. The radiochemical counting was carried out using a liquid-scintillation counter (Beckman LS-250) for sections of the paper-chromatograms in 5-ml solutions of 2,5-diphenyloxazole in toluene (4 g/l), or conventionally using a gas-flow counter (Aloka TRM-1) with a paper-chromatogram scanner for each strip of the chromatograms. The initial concentration of tryptophan-3-^{14}*C* was determined by fluorometry,[1] while the other ^{14}C-labeled reactants were measured by the use of the liquid-scintillation counter.

Results and Discussion

The reaction mixtures of the lumiflavin-sensitized photooxygenation of 10 μM tryptophan-3-^{14}*C* in the absence and in the presence of adenine were developed on filter paper with 1-butanol–acetic acid–water (4:1:2). The autoradiograms for the samples at different reaction periods (from 20% to more than 90% decomposition) showed that tryptophan decomposed to several reaction products and that the patterns of the products were not changed with the degree of the decomposition. Therefore, Fig. 1 shows the autoradiograms for the reaction mixtures in which the photolysis was almost completed in the presence and in the absence of adenine. In both chromatograms, six spots of the reaction products were observed; no difference was detected between the patterns of these reaction products with and without adenine. Similar results were obtained when 1-butanol saturated with water was used as the developing solvent. Thus, it was concluded that adenine does not alter the final products in spite of its great accelerating effect on the reaction rate. At pH 8.0, where the reaction quantum yield was about twice as much as that at pH 7.2, the photoproducts also consisted of plural species which were not altered whether adenine was present or not.

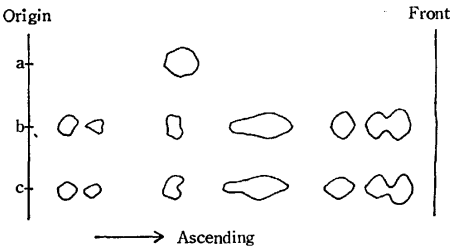

Fig. 1. Autoradiograms for the photoproducts of 10 μM tryptophan-3-^{14}*C* sensitized by 2.5 μM lumiflavin in the absence and presence of adenine.
a) Adenine 0. Before irradiation.
b) Adenine 0. Irradiation 280 min (92% decomp.).
c) Adenine 0.2 mM. Irradiation 82 min (98% decomp.).

In the previous work,[1] the reactions were followed by fluorometry, by which indoles were analyzed with high accuracy even in micromolar concentrations without any interference from adenine. The radioactive-iso-

TABLE 1. ACCELERATING EFFECT OF ADENINE ON THE LUMIFLAVIN-SENSITIZED PHOTOOXYGENATION OF SEVERAL ^{14}C-LABELED REACTANTS

Reactant	Reaction time (min)	Fraction of reactant remaining	
		without adenine	with adenine[a]
Tryptophan	27	0.81	0.25
(10 μM)	82	0.53	0.02
Histidine	75	—	0.56
(0.8 μM)	165	0.88	0.24
Methionine	21	—	0.6
(1.0 μM)	64	0.9	0.2
Guanine[b]	90	0.72	0.16
(8.0 μM)	150	0.56	0.05

Lumiflavin 2.5 μM, phosphate buffer 0.05M, at pH 7.2.
a) Adenine 0.2 mM. b) At pH 6.9.

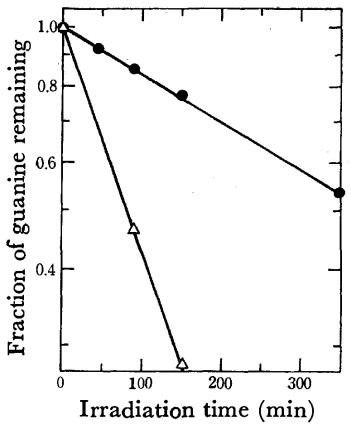

Fig. 2. First order plots for the photooxygenation of 8.0 μM guanine-8-^{14}C sensitized by 2.5 μM lumiflavin in 0.05 M phosphate buffer at pH 6.9.
Adenine: ● 0 mM and △ 0.2 mM.

tope-tracer method is good for the kinetical treatment of the reaction as well as for the product analysis. Therefore, the effect of adenine on the photolysis of nonfluorescent ^{14}C-labeled reactants under dilute conditions was examined. Among the nonfluorescent amino acids which undergo photodynamic action, histidine and methionine were chosen; the effect of the addition of adenine on the lumiflavin-sensitized photooxygenation of these reactants was investigated. The results are summarized in Table 1. The accelerating effect of adenine was observed as in the case of tryptophan.

Besides several amino acids, guanine also undergoes photodynamic action.[2] It was similarly examined whether or not the photodecomposition of this purine derivative, adenine. Since guanine is hard to dissolve in water (5 mg/l), guanine-8-^{14}C hydrochloride was first dissolved in 0.1 M hydrochloric acid and then diluted. The pH value of the sample solution containing 8.0 μM guanine and 2.5 μM lumiflavin was adjusted to 6.9 with a 0.05 M phosphate buffer. The accelerating effect of the addition of 0.2 mM adenine on the photosensitized decomposition of guanine was also observed on the autoradiograms, as is shown in Fig. 2 and Table 1. When guanine was decomposed by equal quantities of both solutions with and without adenine, the effect of adenine on the reaction products was also examined. Successive reactions were observed to occur, but the identity of the products was observed at every stage of the reaction.

On the basis of the results mentioned above, it was concluded that the addition of adenine accelerates the lumiflavin-sensitized photooxygenation of not only tryptophan, but also of many reactants, and that it does not alter the reaction type. Similarly, the enhancement of photodynamic action may take place *in vivo*, because flavin dyes and adenine are general substances in bioorganisms.

The authors wish to express their gratitude to Dr. Sadaaki Komura for his help in the measurements of the radioactivity using the apparatus of the Institute for Protein Research, Osaka University.

References

1) A. Yoshimura and S. Kato, This Bulletin, **46**, 1141 (1973).
2) A. D. McLaren and D. Shugar, "Photochemistry of Proteins and Nucleic Acids," Pergamon Press, Oxford (1964), p. 162.

BULLETIN OF THE CHEMICAL SOCIETY OF JAPAN, VOL. 46(3), 815—816 (1976)

Chromatography of Inorganic Ions on TEAE-cellulose Layers in Hydrochloric Acid Media

Rokuro KURODA, Toshiaki TAKAHASHI, and Koichi OGUMA

Laboratory for Analytical Chemistry, Faculty of Engineering, University of Chiba, Yayoi-cho, Chiba 280

(Received August 13, 1975)

Synopsis. The ion-exchange behavior of inorganic ions on TEAE-cellulose was investigated in hydrochloric acid media with and without methanol. Adsorbabilities are low relative to those on strongly basic ion-exchange resin, varying with acid concentration in line with gradual building-up of chlorocomplexes.

Only fragmentary information is available on paper-[1–8] and thin-layer[9]-chromatography of inorganic ions on a strongly basic anion-exchange cellulose with a quarternary ammonium group. Recently we have investigated the adsorption behavior of about 15 metal ions on TEAE-cellulose columns[10] in hydrochloric acid media, revealing markedly weak preference of metal ions to TEAE-cellulose relative to a strongly basic ion-exchange resin. The work was extended in order to obtain individual adsorption characteristics of a number of metal ions on TEAE-cellulose in hydrochloric acid as well as methanol–hydrochloric acid media. The thin-layer-chromatographic method was used throughout, which served to distinguish small differences in weak adsorption among metal ions.

Experimental

Triethylaminoethylcellulose (Serva, Heidelberg, G. F. R., 0.68 meq/g, for column use), a strong base anion-exchange cellulose, was used in the chloride form. Twenty g of swollen TEAE-cellulose was made into a slurry with 65 ml of deionized water, and spread over five 20×20 cm glass plates 500 μm thick. After being dried at 40 °C for several hr it was stored in a desiccator over a saturated potassium bromide solution. Metal ions[11] (1 μl of solution) were developed by the ascending technique for a distance of 15 cm in a rectangular glass tank with ground glass lid, after 1 hr equilibration. They were detected as described previously.[12]

Results and Discussion

In Fig. 1 are illustrated the R_f values of 43 metal ions as a function of hydrochloric acid concentration. The R_f trends against hydrochloric acid concentration are similar to those reported by Lederer and Ossicini[13] for DEAE- and AE-cellulose papers. Chlorocomplexes of noble metals and oxyacids including V(V), Se(IV), Cr(VI), Mo(VI), W(VI), and Re(VII) are adsorbed on a TEAE-cellulose column to a great extent from 0.001 M HCl, showing that K_d(weight distribution coefficient)>100.[10] However, because of the strong preference of chloride ions to ion-exchange sites, the adsorbabilities decreased rapidly with increasing concentration of hydrochloric acid; K_d values for several ions in 0.1 M HCl were Se(IV)<2, Mo(VI) 20, Pd(II) 160, Re(VII) 20, Ir(IV)>100, Pt(IV)>100 and 25 (two bands appeared), Au(III) 80, Hg(II) 90, being mostly insufficient to allow effective column separation. From 6 M HCl these metals were adsorbed with $K_d \leq 10$, being eluted from a 1 g TEAE-cellulose column actually with no adsorption. The column elution study based on the 1 g TEAE-cellulose column[10] did not distinguish the difference in adsorption among *e.g.* Ni(II), Se(IV), Zn(II), and Te(IV) over the 0.10—6 M HCl concentration range, but the tlc chromatograms clearly demonstrate their differences (Fig. 1).

The adsorption of Zn(II), Ga(III), Cd(II), In(III), Sn(IV), and Te(IV) increases with increasing concentration of hydrochloric acid. These metals exhibit a maximum adsorption on a strongly basic resin in the range ~2 to ~8 M HCl.[14] On the other hand, Pd(II), Ag(I), Re(VII), Pt(IV), Au(III), Hg(II), and Bi(III) are adsorbed tightly on the strongly basic resin,

TABLE 1. R_f VALUES OF METAL IONS IN METHANOL–HCl (1:1) ON TEAE-CELLULOSE LAYER (500 μm)

HCl (M)	1.0	6.0	11.2
Be (II)	1.00	0.99	0.85
Mg (II)	0.96	0.91	0.79
Al (III)	0.99	0.99	0.76
Ca (II)	0.91	0.69	0.52
Sc (III)	0.94	0.82	0.65
Ti (IV)	0.94	0.89	0.68
V (IV)	0.94	0.88	0.66
Cr (III)	0.95	0.98	0.65
Mn (II)	0.93	0.86	0.65
Fe (III)	0.91	0.79	0.51
Co (II)	0.94	0.85	0.50
Ni (II)	0.94	0.84	0.68
Cu (II)	0.87	0.65	0.53
Zn (II)	0.37	0.42	0.48
Ga (III)	0.98	0.57	0.55
Se (IV)	0.77	0.84	0.85
Y (III)	0.93	0.68	0.49
Zr (IV)	0.0—0.44	0.0—0.67	0.0—0.38
Mo (VI)	0.0, 0.56	0.50	0.53
Pd (II)	0.08	0.32	0.40
Ag (I)	0.00	0.0—0.53	0.18—0.64
Cd (II)	0.20	0.40	0.49
In (III)	0.67	0.56	0.54
Sn (IV)	0.52	0.32	0.25
Sb (III)	0.38	0.47	0.51
Te (IV)	0.63	0.34	0.24
Ba (II)	0.78	0.34	0.00
La (III)	0.92	0.64	0.44
Sm (III)	0.92	0.62	0.43
Yb (III)	0.92	0.64	0.44
Hf (IV)	trail	trail	trail
W (VI)	0.00	0.00	trail
Re (VII)	0.33	0.54	0.59
Ir (IV)	0.08, 0.34	0.0—0.51	0.0, 0.57
Pt (IV)	0.05	0.21	0.30
Au (III)	0.23	0.37	0.42
Hg (II)	0.09	0.32	0.38
Pb (II)	0.0—0.39	0.06—0.46	0.46
Bi (III)	0.09	0.27	0.38
Th (IV)	0.92	0.33—0.73	0.29
U (VI)	0.94	0.54	0.33

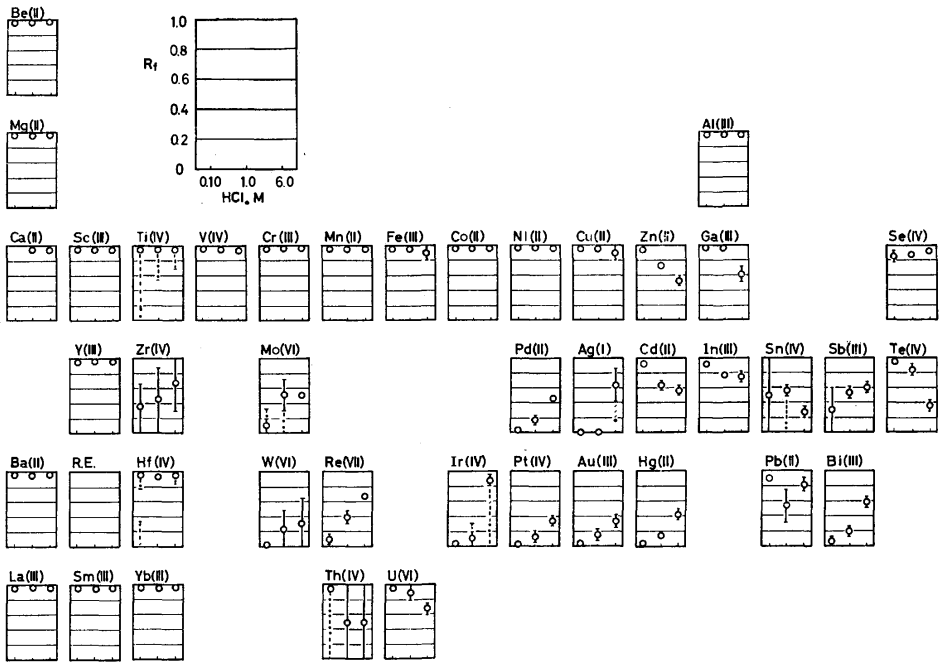

Fig. 1. R_f values of metals on TEAE-cellulose layer (500 μm) in hydrochloric acid media.

showing decreasing adsorption with increasing hydrochloric acid concentration.[14] All these metals show a similar decrease in their adsorption on TEAE-cellulose with increasing hydrochloric acid concentration. In hydrochloric acid media the distribution curve of metals on the strongly basic resin can be described in terms of the gradual building-up of cationic, neutral, and anionic chlorocomplexes with increasing hydrochloric acid concentration, corresponding to positive, zero, and negative slopes of the adsorption curve (log distribution coefficient *vs.* HCl concentration), respectively.[15,16] Closely related adsorption trends, observed in the TEAE-cellulose–hydrochloric acid system, suggest that the dominant factor controlling the R_f values is ion-exchange, but not the partition, which sometimes dominates to control the distribution of metals in chromatography involving the ion-exchange cellulose.[17]

We have also examined the adsorption behavior of metals in methanol–hydrochloric acid media (1 : 1) as a function of hydrochloric acid concentration (1.0, 6.0, and 11.2 M). The R_f values of the metals are summarized in Table 1. Adsorption trends do not change except for Zn(II) and Cd(II), which indicate the decrease in adsorption with increasing concentration of hydrochloric acid. Actually, polar methanol considerably enhances the formation of anionic chlorocomplexes of these metals.

Analytical separation in aqueous hydrochloric acid and mixed methanol–hydrochloric acid media is quite feasible. With 1 M HCl the following separation was accomplished: Hg(8—17)-Cd(58—64)-Zn(69—75); Bi(15—24)-Sb(52—59)-In(72—81)/or Se(77—92); Au(11—16)-Cd(55—65)-Cu(90—100). With 6 M HCl elution the separations Te(35—43)-Cd(56—63)-In(69—78); Sn(26—33)-Cd(57—67)/or Sb(53—63)-In(76—79); Pt(31—43)-Mo(45—51)-Re(65—71); U(57—70)-La(90—100)/or Hf(94—100) were successful. By elution with methanol–6 M HCl (1 : 1) Ba(30—41)-Ca(64—79)-Be(100); Pd(16—27)-Cu(57—66)-Ni(72—100); Pt(12—21)-Au(28—34)-Cu(57—64)-Ni(72—100); Hg(21—28)-Zn(31—40)-Cu(58—66)-Ni(74—100) were separated, respectively. Pt(15—32)-Au(35—43)-Co(46—55)-Ni(69—83); Zr(7—33)-Y(45—58)-Sc(58—71); U(20—30)-Y(43—58)-Ti(58—76); Zr(7—31)/or Th(17—46)-Ti(48—77); Co(46—57)-Mn(69—86) were separated by elution with methanol–11.2 M HCl (1 : 1). The oxidation states of metals separated are the same as listed in Table 1. The values in parentheses indicates the range of R_f ($\times 100$).

References

1) G. Bagliano, G. Grassini, M. Lederer, and L. Ossicini, *J. Chromatogr.*, **14**, 238 (1964).
2) S. K. Shukla, *J. Chromatogr.*, **21**, 92 (1966).
3) G. Bagliano, L. Ossicini, and M. Lederer, *J. Chromatogr.*, **21**, 471 (1966).
4) G. Bagliano and L. Ossicini, *J. Chromatogr.*, **21**, 499(1966).
5) J. Sherma, *Anal. Chem.*, **39**, 1497 (1967).
6) L. Ossicini and M. Lederer, *J. Chromatogr.*, **34**, 292(1968).
7) M. Pavlova, *J. Chromatogr.*, **51**, 346 (1970).
8) M. Lederer and M. Sinibaldi, *J. Chromatogr.*, **60**, 275 (1971).
9) T. Yamabe, S. Ishii, and N. Takai, *Seisan-Kenkyu*, **22**, 283 (1970).
10) R. Kuroda, K. Oguma, M. Suzuki, and Y. Fuchu, *Bunseki Kagaku*, **24**, 1 (1975).
11) R. Kuroda, K. Oguma, and M. Otani, *J. Chromatogr.*, **96**, 233 (1974).
12) R. Kuroda, K. Oguma, and H. Watanabe, *J. Chromatogr.*, **86**, 167 (1973).
13) M. Lederer and L. Ossicini, *J. Chromatogr.*, **13**, 188(1964).
14) K. A. Kraus and F. Nelson, *Proc., Intern. Conf. Peaceful Uses Atomic Energy*, **7**, 113 (1956), United Nations.
15) Y. Marcus and C. D. Coryell, *Bull. Res. Counc. Isr., Sect. A*, **8**, 1 (1959).
16) S. K. Jha, F. de Corte, and J. Hoste, *J. Chromatogr.*, **102**, 217 (1974).
17) R. Kuroda, N. Yoshikuni, and K. Kawabuchi, *J. Chromatogr.*, **47**, 453 (1970).

BULLETIN OF THE CHEMICAL SOCIETY OF JAPAN, VOL. 49(3), 817—818 (1976)

The Preparation and Properties of Some Triorgano-(oxinato)antimony Hydroxides

Yoshikane KAWASAKI

Department of Petroleum Chemistry, Osaka University, Yamadakami, Suita, Osaka 565

(Received September 25, 1975)

Synopsis. Some new triorgano(oxinato)antimony hydroxides, $R_3Sb(L)OH$ (R=CH_3, C_6H_5 and *p*-$CH_3C_6H_4$: L=Ox, 2-Me-Ox, and 5-Cl-Ox), have been prepared, and the UV, IR, and NMR spectra of these compounds have been measured. These compounds have a hexa-coordinate configuration around antimony. The effects of the hydroxyl group on the IR and NMR spectra are discussed.

The preparation of the $R_3Sb(OH)X$ type of compounds have been reported by several workers.[1-8] These compounds, however, have been characterized only by chemical analysis, and no IR spectral data such as the O–H stretching band have been reported. Many authors[9-14] have reported that triorganoantimony dihalides, on hydrolysis or on treatment with appropriate silver salts, form stable oxybistriorganoantimony compounds of the $(R_3SbX)_2O$ type. Therefore, there is considerable confusion in the literature regarding the structure of these oxy compounds in the solid state *i.e.*, as to whether they should be regarded as hydroxy compounds, $R_3Sb(OH)X$, or as oxides, $(R_3SbX)_2O$. Doak *et al.*[12] have concluded that compound of the $R_3Sb(OH)X$ type probably do not exist in the solid state.

In the present paper we wish to report on the preparation and spectral data of some new triorgano(oxinato)-antimony hydroxides, $R_3Sb(L)OH$.

Experimental

Preparation of $R_3Sb(L)OH$ (R=CH_3, C_6H_5, and p-$CH_3C_6H_4$; *L=Ox, 2-Me-Ox* and 5-Cl-Ox**).* All of these complexes were prepared in an essentially identical manner, so that only one typical procedure will be given. A benzene solution (70 ml) of trimethylantimony dibromide (10 mmol) was added to sodium methoxide (20 mmol) in methanol (about 10 ml), and the mixture was heated at reflux for 30 min. After distilling off a portion of the solvent, the precipitated sodium bromide was removed by filtration. To the filtrate we then added 8-quinolinol (10 mmol) in benzene (50 ml), and the mixture was heated at reflux for 1 h; the solvent was then removed by distillation under reduced pressure. A mixture of acetone (20 ml) and water (5 ml) was added to the residual, highly viscous yellow liquid. A yellow solid product was obtained by scratching the vessel with a glass rod. The complex was purified by recrystallization from acetone. The analytical data for this and similar compounds are shown in Table 1.

TABLE 1. ANALYTICAL DATA OF TRIORGANO-(OXINATO)ANTIMONY HYDROXIDE

$R_3Sb(L)OH$ R	L	Mp (°C)	Analysis Found (Calcd) (%) C	H	N
CH_3	Ox	110—111	43.87 (43.94)	5.01 (4.92)	4.40 (4.27)
C_6H_5	Ox	108—109	63.00 (63.07)	4.68 (4.31)	2.65 (2.72)
C_6H_5	2-Me-Ox	129—131	63.49 (63.66)	4.66 (4.58)	2.61 (2.65)
C_6H_5	5-Cl-Ox	161—163	59.38 (59.12)	3.84 (3.86)	2.80 (2.55)
p-$CH_3C_6H_4$	Ox	170—171	64.56 (64.77)	5.10 (5.07)	2.67 (2.52)

* 2-Methyloxine.
** 5-Chlorooxine.

Spectral Measurements and Analysis of the NMR Spectra. The UV spectra were recorded on a Hitachi model 124 spectrometer with 1-mm quartz cells. The absorption maxima measured in methylene chloride are shown in Table 2. The IR spectra were measured on a Hitachi model 225 grating spectrometer in Nujol mulls or a 5 wt% methylene chloride solution. The NMR measurements were made with a JEOL model JNM-PS-100 spectrometer operating at 100 MHz. The chemical shifts were measured relative to tetramethylsilane as the internal standard. Methylene chloride was used as the solvent. The spectra for the 2-, 3-, and 4-protons of the oxinato ligand were analyzed as a first-order system, and those for the 5-, 6-, and 7-protons as an ABC system by using the method reported by Reilly *et al.*[16] The calculations were carried out on a NEAC 2200 model 700 computer at the Computer Center of Osaka University.

Results and Discussion

The absorption maxima of the longest wavelength for the triorgano(oxinato)antimony hydroxides are found in the region where the chelation of the oxinato ligand is expected.[17-19] From these result, it seems almost certain that the antimony atom is hexacoordinate, as has been reported for triorgano(oxinato)antimony halides.[20,21] The absorption maxima for the triaryl(oxinato)antimony hydroxides appear at longer wavelengths than those for the trimethylantimony analogs. Similar bathochromic shifts upon the substitution of methyl group by aryl groups have been noted for triorgano-(oxinato)antimony halides.[15,20,21]

As has been shown in Table 2, in the solid state all the triorgano(oxinato)antimony hydroxides gave one very broad band, in some cases there was also an additional sharp band in the O–H stretching region. The broad band indicates a hydrogen-bonded hydroxyl group, and the sharp one, a free hydroxyl group. Two similar O–H stretching bands, one sharp and one broad, have been reported for tetraphenylantimony hydroxide.[22] In a methylene chloride solution, triorgano(oxinato)antimony hydroxides show only one sharp O–H stretching band at a somewhat higher wave number than is found for these compounds in the solid state. This result may be attributed to the absence of hydrogen bonding in the methylene chloride solution.

TABLE 2. UV AND IR DATA OF TRIORGANO(OXINATO)ANTIMONY HYDROXIDE

$R_3Sb(L)OH$ R	L	λ_{max}[a] (nm)	ν (O–H) CH_2Cl_2	ν (O–H) solid	ν (Sb–O) solid	ν (Sb–O)(Ox) solid
CH_3	Ox	350 (2380)	3627 sh[b]	3240 br[c]	540	508
C_6H_5	Ox	376 (2200)	3608 sh	3555 br	561	512
C_6H_5	2-Me-Ox	352 (2430)	3613 sh	3605 sh 3350 br	558	506
C_6H_5	5-Cl-Ox	386 (3030)	3609 sh	3595 sh 3380 br	568	514
p-$CH_3C_6H_4$	Ox	375 (1900)	3605 sh	3580 br 3370 br	562	515

a) Value in parentheses is extinction coefficient. b) sh: Sharp. c) br: Broad.

TABLE 3. PROTON CHEMICAL SHIFTS OF $(CH_3)_3Sb(Ox)X$[a] (δ value)

X	NO_3	Cl	Br	OAc	OH	Ox^-[b]	H_2Ox^+[c]
2-H	8.86	8.74	8.76	9.05	8.69	8.47	9.26
3-H	7.52	7.43	7.39	7.39	7.39	7.12	8.12
4-H	8.28	8.19	8.22	8.12	8.18	7.90	9.19
5-H	7.31	7.22	7.24	7.15	7.14	6.56	7.66
6-H	7.49	7.44	7.44	7.41	7.46	7.00	7.75
7-H	7.11	7.02	7.04	6.96	6.93	6.37	7.66
CH_3–Sb	1.84[d]	1.91[d]	2.07[d]	1.64[d]	1.42	—	—

a) Coupling constants, J_{23}, J_{24}, J_{34}, J_{56}, J_{57} and J_{67}, were found to be 4.2±0.2, 1.5±0.2, 8.0±0.2, 8.1±0.2, 1.1±0.2 and 7.6±0.2 Hz, respectively. b) Sodium oxinate in HMPA (Ref. 26). c) 8-Quinolinol hydrochlordie in HMPA (Ref. 26). d) Ref. 15.

The frequency of the O–H stretching band for triorgano(oxinato)antimony hydroxides is not affected to a large extent by the substituent on the oxinato ligand, but the value is somewhat small for trimethyl(oxinato)antimony hydroxide.

A strong but somewhat broad band in the region of 540—570 cm^{-1} is assigned to the Sb–O stretching band between the hydroxyl group and the antimony atom, because triorgano(oxinato)antimony complexes, $R_3Sb(Ox)X$, X=NO_3, Cl, Br, and OAc show no band in the region. The frequencies observed are almost the same as those assigned to the Sb–O stretching bands in trialkyl-bis(ethoxy)antimony,[23] $R_3Sb(OC_2H_5)_2$ (562, 547, 545, and 540 cm^{-1} for R=CH_3, C_2H_5, n-C_3H_7, and n-C_4H_9 respectively), and $(SbF_5OH)^-(NR_4)^+$ (560 and 554 cm^{-1} for R=C_2H_5 and n-C_4H_9 respectively,[24] but the values are larger than that reported for tetraphenylantimony hydroxide (528 cm^{-1}). [22]Zingaro *et al.*[25] estimated the Sb–O stretching frequency to be 550 cm^{-1} by using Gody's rule.

The Sb–O stretching bands between the oxinato group and the antimony atom for some trimethyl(oxinato)antimony complexes, $(CH_3)_3Sb(Ox)X$, are found to be 525, 520, 520, 516, and 508 cm^{-1} for X=NO_3, Cl, Br, OAc, and OH respectively. The corresponding value for tetramethyl(oxinato)antimony has been reported to be 497 cm^{-1}.[20] The Sb–O bond in the hydroxide complex, therefore, is weaker than those in the nitrate and halide complexes.

Except for the 2-proton of trimethyl(oxinato)antimony acetate, the chemical shifts of the ring protons show a general drift of the low-field shift in the order: NO_3> Cl≳Br>OAc>OH. This order is the same as that for the high-frequency shifts of the Sb–O stretching band between the oxinato group and the antimony atom. These results may indicate that the electron-withdrawing effect of the hydroxyl group is smaller than that of the nitrato group and the halogens.

We wish to express our hearty thanks to Professor Rokuro Okawara for his continuous encouragement throughout this study.

References

1) G. T. Morgan, F. M. G. Micklethwait, and G. S. Whitby, *J. Chem. Soc.*, **97**, 34 (1910).
2) G. T. Morgan and F. M. G. Micklethwait, *J. Chem. Soc.*, **99**, 2286 (1911).
3) G. T. Morgan and V. E. Yarsley, *Proc. Roy. Soc., A*, **110**, 534 (1926).
4) F. Challenger and A. T. Peters, *J. Chem. Soc.*, **1929**, 2610.
5) K. A. Jensen, *Z. Anorg. Allgem. Chem.*, **250**, 268 (1943).
6) G. Wittig and K. Clauss, *Ann.*, **577**, 26 (1952).
7) H. Hartmann and G. Kühl, *Z. Anorg. Allgem. Chem.*, **312**, 186 (1961).
8) O. A. Ptitsyna, O. A. Reutov, and G. Ertel, *Izv. Akad. Nauk. SSSR, Otd. Khim. Nauk*, **1961**, 265.
9) H. Landolt, *J. Prak. Chem.*, **84**, 328 (1861).
10) A. Hantzsch and H. Hibbert, *Ber.*, **40**, 1508 (1907).
11) L. Kolditz, M. Gitter, and E. Risel, *Z. Anorg. Allgem. Chem.*, **316**, 270 (1962).
12) G. G. Long, G. O. Doak, and L. D. Freedman, *J. Amer. Chem. Soc.*, **86**, 209 (1964).
13) G. O. Doak, G. G. Long, and L. D. Freedman, *J. Organometal. Chem.*, **4**, 82 (1965).
14) M. Shindo and R. Okawara, *J. Organometal. Chem.*, **5**, 537 (1966).
15) Y. Kawasaki and K. Hashimoto, *J. Organometal. Chem.*, **99**, 107 (1975).
16) C. A. Reilly and R. S. Swallen, *J. Chem. Phys.*, **32**, 1378 (1960).
17) T. Moeller and A. J. Cohen, *J. Amer. Chem. Soc.*, **72**, 3546 (1950).
18) T. Moeller and F. L Pundsack, *J. Amer. Chem. Soc.*, **76**, 617 (1954).
19) K. Sone, *J. Amer. Chem. Soc.*, **75**, 5207 (1953).
20) H. A. Meinema, E. Rivarola, and J. G. Noltes, *J. Organometal. Chem.*, **17**, 71 (1969).
21) Y. Kawasaki, *Inorg. Nucl. Chem. Lett.*, **5**, 805 (1969).
22) A. L. Beachamp, M. J. Bennett, and F. A. Cotton, *J. Amer. Chem. Soc.*, **91**, 297 (1969).
23) Y. Matsumura, private communication.
24) L. Kolditz and B. Nussucker, *Z. Anorg. Allgem. Chem.*, **337**, 191 (1965).
25) G. N. Chremos and R. A. Zingaro, *J. Organometal. Chem.* **22**, 637 (1970).
26) M. Aritomi and Y. Kawasaki, *J. Organometal. Chem.*, **81**, 363 (1974).

BULLETIN OF THE CHEMICAL SOCIETY OF JAPAN, VOL. 49(3), 819—820 (1976)

Ligand Isotopic Exchange Kinetics of Tris(acetylacetonato)-titanium(IV) Perchlorate in Acetonitrile

Masato NISHIZAWA, Hiroaki KIDO, Isamu KINOSHITA, Yoshikuni SOMA,* and Kazuo SAITO

Chemistry Department, Faculty of Science, Tohoku University, Aoba, Aramaki, Sendai, 980

(Received December 9, 1975)

Synopsis. The rate of isotopic exchange between tris(acetylacetonato)titanium(IV) ions and acetylacetone-$^{14}C_3$ in enol form is measurable at −20 °C in acetonitrile. Water, free ligand and a strong acid catalyse the exchange.

The tris(acetylacetonato)titanium(IV) ion $[Ti(acac)_3]^+$ has been known as salts of various anions[1-3] and the absorption spectrum examined.[4,5] Its dynamic behavior is, however, not known.[6] We have examined the isotopic exchange of this complex ion with free acetylacetone (Hacac) labelled with ^{14}C in acetonitrile and obtained some information concerning the kinetics.

Experimental

Materials. *The Complex Perchlorate*: Dichlorobis(acetylacetonato)titanium(IV)[7] (3.9 g) was dissolved in chloroform (20 ml), mixed with ethanol (10 ml), concentrated to *ca.* 10 ml, and trented with barium perchlorate trihydrate (4.8 g) in ethanol (15 ml). The precipitate was filtered off, washed with chloroform (60 ml) and the filtrate and washings were concentrated to 20 ml together with Hacac (15 ml) at 30 °C and 50 mmHg. Addition of hexane (10 ml) gave $[Ti(acac)_3]ClO_4$, which was recrystallized by dissolving in chloroform and Hacac, and adding hexane. The orange needles decomposed at 180 °C. Anal. Found: C, 40.62; H, 4.83%; Calcd for $C_{15}H_{21}O_{10}ClTi$: C, 40.51; H, 4.76%. IR spectrum in Nujol mull gave a very similar pattern to those of $[Si(acac)_3]ClO_4$[8] and $[Ge(acac)_3]ClO_4$.[9] NMR pattern in deuterochloroform coincided with that in literature.[10] This method gives a higher yield (*ca.* 60%) and a purer product than solvent extraction[3] and direct synthesis from titanium (IV) sulfate and Hacac.[10]

Other Reagents: Acetylacetone-$^{14}C_3$(2,4-pentenedione-1,3,5-$^{14}C_3$) was prepared as in literature.[11] Acetonitrile (AN) was refluxed with phosphorus pentoxide and distilled. The water content was 3 to 5×10^{-3} M. Hexane was washed with sulfuric acid and alkali solution, dried with phosphorus pentoxide and distilled.

Measurements. The UV spectrum was recorded with a Hitachi 323 Spectrometer in the presence of varying amounts of water ($\leq$0.1 M). The radioactivity was recorded with a Unilux IIA of Nuclear Chicago Co., in anisole containing 0.4% *p*-terphenyl and 0.01% POPOP. The enol/keto ratio of free Hacac was determined from UV absorption at 273 nm.[12]

Kinetic Runs. The complex solution ($\simeq10^{-2}$ M) in AN (5 ml) and Hacac-^{14}C ($\simeq10^{-2}$ M) in AN (5 ml) were placed in the two sections of a glass-stoppered test tube with a branched side bottom. The tube was kept in a thermostat at −21.3 °C and both solutions mixed. One ml portions were taken out at appropriate time intervals and poured into chilled hexane (5 ml, −50 °C) in a thin test tube within 10 s. (The UV spectra showed that only the enol tautomer of free Hacac was extracted into the hexane layer while the AN solution flows down.). After 30 s 2 ml portions were pipetted out of the middle part of hexane layer. One ml was dissolved in the anisole scintillator (14 ml) for β-activity counting. The other one ml was diluted with hexane (9 ml) and the extinction measured at 273 nm to find the concentration of Hacac. The water content of the AN solution was determined in the reaction tube by Karl Fischer titration.

Results and Discussion

Absorption Spectrum. The complex perchlorate has three absorption peaks in AN at 364, 257, and 225 nm with log ε values 3.91, 4.34, and 4.30, respectively. When the water content in the solution was $\simeq10^{-3}$ M (the same order as the complex in a 0.1 mm thick cell), the peak heights decreased little (by *ca.* 2% within 30 min.). When the water concentration was $\simeq10^{-1}$ M in $\simeq10^{-5}$ M complex solution, the absorbancy at 364 and 225 nm decreased rapidly, and after several minutes two shoulders were observed with log ε *ca.* 3.4 and 3.6, respectively. Simultaneously a new shoulder appeared at $\simeq$270 nm with log ε *ca.* 3.9, which seemed to be due to free Hacac. The peak at 257 nm gave only a small shift to 259 nm and a very little decrease in absorbancy. When a large excess of Hacac ($\simeq10^{-1}$ M) was added, the log ε at 364 nm increased and the pattern gradually approached that of freshly prepared solution. It seems the change in absorption in the presence of overwhelming amount of water is caused by partial hydrolysis of the complex. The absorption data given in literatures[4,5] may represent those of partially hydrolysed products.

Isotopic Exchange. The experimental results were calculated by McKay's formula,

$$R = -2.3[3ab/(3a+b)][\log(1-F)/t] \quad (1)$$

where a and b are the concentrations of the complex and free Hacac, respectively, and t is the lapse of time. F is the fraction of reaction and is known from $(x_0-x_i)/(x_0-x_\infty)$, where x_0, x_i, and x_∞ are the specific counting rates at time 0, t and infinity, respectively.

Acetylacetone is in tautomeric equilibrium and *ca.* 67% is in enol form in AN at −10 °C. The interchange between keto and enol form is much slower (*ca.* $10^{-5}s^{-1}$) than the present isotopic exchange. The R can be calculated in two ways by considering the participation of either the enol tautomer or total Hacac in the exchange. The experimental x_∞ values come in between the values calculated in the two ways. The x_i *vs.* t diagrams are simulated by considering that the keto tautomer exchanges with the ligand at a much smaller

* Present address: Research Institute, Mitsui Petrochemical Co. Ltd., Iwakuni Yamaguchi-ken.

rate than the enol does (*e.g.* in 0.02 M complex solution containing 0.03 M water and 0.015 M Hacac, the ratio R_{enol}/R_{keto} is *ca.* 30.). Hence the following discussion is made on the assumption that only the enol form exchanges with the ligand. McKay plots made in this way gave straight lines at the initial stage of exchange ($F<$*ca.* 0.5). The UV absorption of the reaction mixture remained unchanged for at least 100 min. These facts indicate that the R values thus calculated give rates of the following isotopic exchange.

$$[Ti(acac)_3]^+ + Hacac(enol)^* \rightleftharpoons [Ti(acac^*)(acac)_2]^+ + Hacac(enol) \quad (2)$$

Attempts have been made to elucidate the influence of various factors upon R. However, only limited information was obtained because of experimental difficulty, especially in adjusting the water concentration, and the discussion is very much limited.

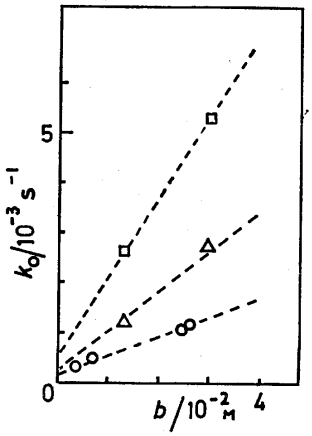

Fig. 1. Dependence of the exchange rate constant on the concentration of Hacac in enol form.
$[H_2O]$=○ 0.016, △ 0.037, □ 0.079 M.

When a was changed as 1.0, 2.0, and 3.4×10^{-2} M at given concentrations of Hacac (0.029 ± 0.001 M) and water (0.016 ± 0.001 M), R increased linearly, and the quotient R/a was almost equal, *i.e.* 1.6, 1.5, and 1.3×10^{-3} s^{-1}, respectively. The quotient k_0 can be the measure of exchange rate. Figure 1 shows the plot R *vs.* b at given concentrations of water. At a water concentration 0.016 ± 0.001 M, the plot is linear. Not many plots were obtained at higher concentrations of water, but both the gradient and the intercept seem to increase. Hence a kinetic formula, Eq. 3 may be appropriate,

$$R = k_0 a = a(k_1+k_2[H_2O]+k_3 b+k_3'b[H_2O]) \quad (3)$$

where b is the concentration of free Hacac in enol form. The dotted lines in Fig. 1 are those calculated on best fitted k values in Eq. 3; *i.e.* $k_1=(1.4\pm0.6)\times10^{-4}$ s^{-1}, $k_2=(5.0\pm1.5)\times10^{-3}$ M^{-1}s^{-1}, $k_3=(7.9\pm2.6)\times10^{-3}$ M^{-1}·s^{-1} and $k_3'=(1.9\pm0.1)$ M^{-2}s^{-1} at −21.3 °C. They do not deviate much from the observed plots, and Eq. 3 can be an adequate expression of the kinetics.

The exchange was catalysed by a strong acid (Fig. 2). As the concentration of trichloroacetic acid increases, k_0 increases and then approaches constant.

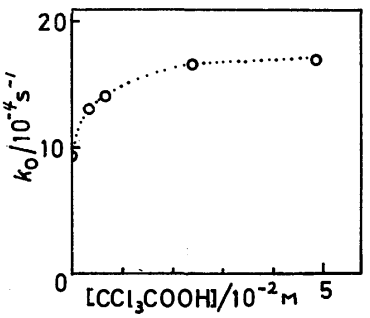

Fig. 2. Influence of the concentration of trichloroacetic acid upon the exchange rate constant.
b=0.024 M $[H_2O]$=0.012 M at −21.4 °C.

Further increase in water and acid concentration caused decomposition of the complex. The saturation may be due to limited formation of H_3O^+ from the acid and water (0.012 M) rather than to the saturation of protonation of complex cation. Weak acids fail to give such a catalytic action, and the influence of Hacac concentration in Eq. 3 cannot be acid catalysis.

It is seen that the isotopic exchange can proceed through several reaction routes. The hydrolysis of $[Ti(acac)_3]^+$ under the given experimental conditions is much slower ($\simeq10^{-5}$ s^{-1} at +20 °C) than the isotopic exchange and the reaction paths should be different. In the k_3 and k_3' path, an associative contribution of enolic Hacac is feasible in the rate-determining step, whereas k_1, k_2 and acid-catalyzed reaction path may involve dissociative rate-determining step. Further elucidation of the reaction mechanism, however, requires more detailed kinetic studies by more sophisticated methods.

The results, however, provides the first example of kinetic studies of intermolecular substitution reaction of titanium(IV) compounds, and it was made clear that $[Ti(acac)_3]^+$ undergoes isotopic exchange much faster than $[Si(acac)_3]^+$ and $[Ge(acac)_3]^+$ do, and the rate is similar to that of $[Sn(acac)_3]^+$.[13]

References

1) W. Dilthey, *Ber.*, **37**, 588 (1904).
2) M. Cox, J. Lewis, and R. S. Nyholm, *J. Chem. Soc.*, **1964**, 6113.
3) M. L. Reynolds, *J. Inorg. Nucl. Chem.*, **26**, 667 (1964).
4) R. J. Woodruff, J. L. Marini, and J. P. Fackler, *Inorg. Chem.*, **3**, 687 (1964).
5) G. M. Bancroft, A. G. Maddock, W. K. Ong, and R. H. Prince, *J. Chem. Soc., A*, **1966**, 723.
6) Kinetic studies have been made only with dihalobis(acetylacetonato)titanium(IV) by NMR; R. C. Fay and R. N. Lowry, *Inorg. Chem.*, **9**, 2048 (1970); also see Ref. 7.
7) R. C. Fay and R. N. Lowry, *Inorg. Chem.*, **6**, 1512 (1967).
8) T. Inoue and K. Saito, This Bulletin, **46**, 2417 (1973).
9) A. Nagasawa and K. Saito, *ibid.*, **47**, 131 (1974).
10) R. C. Fay, and N. Serpone, *J. Amer. Chem. Soc.*, **90**, 5701 (1968).
11) K. Saito and K. Masuda, This Bulletin, **41**, 384 (1968).
12) H. Watarai and N. Suzuki, *J. Inorg. Nucl. Chem.*, **36**, 1815 (1974).
13) K. Saito, *Pure Appl. Chem.*, **38**, 325 (1974).

BULLETIN OF THE CHEMICAL SOCIETY OF JAPAN, VOL. 49(3), 821—822 (1976)

The Photo-induced Diels-Alder Reaction of 2-Cycloocten-1-one and 2-Cyclohepten-1-one

Hiraku SHINOZAKI, Susumu ARAI, and Masaru TADA

Department of Chemistry, School of Science and Engineering, Waseda University, Shinjuku, Tokyo 160

(Received September 24, 1974)

Synopsis. *trans*-2-Cycloocten-1-one and *trans*-2-cyclohepten-1-one, which are supposed to be formed by the ultra-violet irradiation of *cis*-2-cycloocten-1-one and *cis*-2-cyclohepten-1-one, give Diels-Alder addition products with cyclopentadiene and isoprene.

It is well established that the irradiation of a medium ring cycloalkenone, such as 2-cycloocten-1-one and 2-cyclohepten-1-one, induces a *cis-trans* isomerization.[1-3] The *trans* isomer of these enones is highly strained and has been reported to enter into a Diels-Alder addition with some dienes. This facile cycloaddition provides a promising method of constracting a carbocyclic system with a medium ring. Previously *trans*-2-cyclohepten-1-one was found to undergo a photochemically-induced cycloaddition with cyclopentadiene.[1] In this paper we wish to extend the scope of the photo-induced Diels-Alder addition of *trans*-2-cycloocten-1-one and *trans*-2-cyclohepten-1-one with dienes.

The irradiation of a mixture of *cis*-2-cycloocten-1-one and an excess amount of cyclopentadiene or isoprene gave two adducts, I and II, in yields of 66 and 58% respectively. In these runs a large excess of dienes was used to suppress the dimerization of the enone. In the same manner, *cis*-2-cyclohepten-1-one gave the Diels-Alder adducts, III with cyclopentadiene[1,4] and IV with isoprene, in yields of 95%. The 2-cyclohepten-1-one disappeared within 1 hr, while 2-cycloocten-1-one required a longer reaction period—2 hr with cyclopentadiene and 4.5 hr with isoprene. This difference in the reactivity must be a reflection of the strain energy in *trans*-2-cyclohepten-1-one and *trans*-2-cycloocten-1-one.

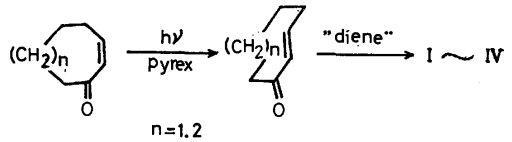

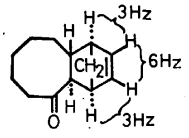

I

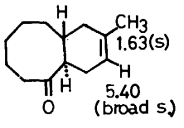

II

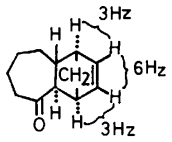

III

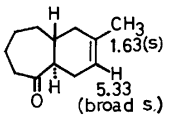

IV

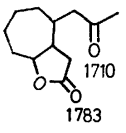

V

The adducts with 2-cycloocten-1-one were difficult to purify so as to give satisfactory results on elemental analysis due to the *retro*-Diels-Alder reaction which occurred on distillation or gas chromatography. High resolution mass spectrometry, however, defined the molecular formula of the adducts. The mass spectra of these adducts showed base peaks at $m/e=110$ and 124 due to 2-cyclohepten-1-one and 2-cycloocten-1-one cations formed by the fragmentation of the *retro*-Diels-Alder type. The structure of the I adduct, including its stereochemistry, was deduced from a comparison of the spectral data with those of the III adduct between *trans*-2-cyclohepten-1-one with cyclopentadiene. The proton magnetic resonance of the olefinic hydrogens of the I adduct and that of the III adduct show the same signal pattern with the same coupling constants, as is shown in the figures, and the structure of the latter was unambiguously established by chemical degradation.[1] The structures of II and IV adducts were deduced from their spectroscopic data and from their chemical degradation. These two adducts show almost identical NMR signals; the position of the methyl group was assigned by the transformation of the IV adduct into the ketolactone, V. The transformation was achieved by the hydride reduction of the IV adduct, the hydroxylation of the resulting alcohol at the double bond by osmium tetraoxide in pyridine, and successive oxidations by lead tetraacetate and chromic anhydride in acetic acid. The ketolactone, V, had infrared absorptions at 1783 and 1710 cm^{-1} due to γ-lactone and methyl ketone. The *trans*-fusion of the ring system in the II and IV adducts was deduced from its innertness to acid or base treatment and from mechanistic considerations.[5]

Experimental

General Precedure of the Photo-Diels-Alder Reaction. *cis*-2-Cycloocten-1-one or *cis*-2-cyclohepten-1-one (500 mg) and a 20-fold amount of a diene dissolved in 100 ml of hexane were placed in a reaction vessel, after which the mixture was internally irradiated by a 100-W medium-pressure mercury lamp in a Pyrex immersion jacket under an atomosphere of nitrogen. In the case of cyclopentadiene, the mixture was cooled in an ice-salt bath during irradiation. The reaction was monitored by the disappearance of the infrared absorptions due to the conjugate carbonyl groups. After the complete disappearance of the starting ketone–after 2 hr for I adduct, 4.5 hr for the II adduct, and 1 hr for the IV adduct–the solvent and the excess of diene were removed by distillation. The residues were distilled under reduced pressure by using a short-path distillation apparatus, Kugelrohr, to give the adducts in yields of 66% (I), 58% (II), and 95% (IV).

The photo-dimer of 2-cycloocten-1-one contaminated in the fraction with a higher boiling point was removed by chromatography on silica gel eluted with hexane–ether (1: 1); the products were found to be essentially pure by gas-chromatographic analysis (5% SE-30 on Chromosorb W and 5% Carbowax 20M on Chromosorb W).

Adduct I. Bp 75—80 °C/0.7 mmHg. Mass: M^+= 190.138. Calcd for $C_{13}H_{18}O$ m/e=190.135. IR (neat): 1685 and 720 cm^{-1}. NMR (CCl_4): δ=6.34—5.93 (2H, octet, J=3 and 6 Hz), 2.93 (1H, diffused singlet), and 2.7—1.4 ppm (15 H).

Adduct II. Bp 77—82 °C/0.5 mmHg. Mass: M^+= 192.150. Calcd for $C_{13}H_{20}O$ m/e=192.151. IR(neat): 1685, 795, and 780 cm^{-1}. NMR (CCl_4): δ=5.40 (1H, diffused singlet), 1.63 (3H, singlet), and 2.6—1.3 ppm (16 H).

Adduct IV. Bp 90—95 °C/0.2 mmHg. Found: C, 80.80; H, 10.18%. Calcd for $C_{12}H_{18}O$: C, 80.85; H, 10.18%. IR (neat): 1701 and 785 cm^{-1}. NMR (CCl_4): δ=5.33 (1H, diffused singlet), 1.63 (3H, singlet), and 2.6—1.3 ppm (14H).

Ketolactone V. A solution of the IV adduct (1.10 g) in 20 ml of ethanol was treated with 500 mg of sodium borohydride, after which the mixture was allowed to stand for 14 hr at room temperature (*ca.* 27 °C). After the evaporation of the solvent *in vacuo*, the residue was treated with 10 ml of the saturated solution of tartaric acid to destroy the excess of the hydride. The subsequent ethereal extraction of the mixture gave 1.18 g of crude alcohol. IR (neat): 3470, 1637, 1033, and 785 cm^{-1}. NMR (CCl_4): δ=5.25 (1H, diffused singlet) and 3.87 ppm (1H, diffused doublet, J=5 Hz). The alcohol (450 mg) obtained above in 2 ml of pyridine was treated with 600 mg of osmium tetraoxide in 1 ml of pyridine under cooling in an ice-bath, and the reaction mixture was stirred at room temperature for 12 hr under nitrogen. After the destruction of the osmium complex by adding 20 g of sodium hydrogensulfite in 40 ml of water, the product was extracted with ether to give 171 mg of the triol. IR(neat): 3500, 1117, and 1042 cm^{-1}. The triol (171 mg) in 10 ml of benzene was treated with lead tetraacetate (480 mg) in acetic acid, and the mixture was stirred for 5 hr in a nitrogen atmosphere. The reaction mixture was condensed *in vacuo*, and the condensate was extracted with ether after the addition of a saturated solution of sodium hydrogencarbonate to give a crude oil. The oil in 4 ml of acetic acid was treated with 100 mg of chromic trioxide in 1 ml of water over a 10-min period with cooling, after which the reaction mixture was stirred for 12 hr at room temperature. The product was extracted with ether after the destruction of the excess chromic trioxide by sodium hydrogensulfite to give 71 mg of crude ketolactone. The recrystallization of the product from carbon tetrachloride gave pure V. Mp 68—69 °C. Mass: M^+=210.129. Calcd for $C_{12}H_{18}O_3$ m/e=210.126. IR (neat): 1783, 1710, 1178, and 1010 cm^{-1}.

The authors are indebted to Professor Yasuji Yamada of the Tokyo Colledge of Pharmacy for the measurement of the high-resolution mass spectra.

References

1) E. J. Corey, M. Tada, R. LeMahieu, and L. Libit, *J. Amer. Chem. Soc.*, **87**, 2051 (1965).
2) P. E. Eaton and K. Lin, *ibid.*, **87**, 2052 (1965).
3) P. E. Eaton and K. Lin, *ibid.*, **86**, 2087 (1964).
4) This reaction was previously reported in Reference 1, but the NMR data is now reported for the first time.
5) 2-Cyclohepten-1-one gave the photo-induced adducts with butadiene (79%) and 2,3-dimethylbutadiene (37%), though a detailed description is omitted in the present report.

BULLETIN OF THE CHEMICAL SOCIETY OF JAPAN, VOL. 49(3), 823—824 (1976)

Heterogeneous Asymmetric Hydrogenation of Benzil Using Bis-(dimethylglyoximato)cobalt Complexes as Catalysts

Hideaki FUJIKOSHI, Riichiro NAKAJIMA, and Tadashi HARA

Department of Chemical Engineering, Faculty of Engineering, Doshisha University, Kamikyo-ku, Kyoto 602

(Received March 19, 1975)

Synopsis. The asymmetric hydrogenation of benzil in the heterogeneous system was found to proceed not only in the presence of quinine soluble in benzene phase, but also of an optically active amino or ascorbic acids soluble in aqueous phase.

Although the asymmetric hydrogenation of benzil using the complexes of bis(dimethylglyoximato)cobalt and optically active amine(abbreviated to $Co(DMG)_2$–amine) as catalysts was exclusively carried out by Yoshimura *et al.*[1] in the homogeneous system, it was further extended by the authors to the heterogeneous system, which consists of the benzene phase containing benzil and the aqueous phase containing $Co(DMG)_2$–amine complex. The asymmetric hydrogenation of benzil was found to proceed not only in the presence of quinine soluble in benzene phase, but also of an optically active amino or ascorbic acids soluble in aqueous phase. This made possible the use of an optically active and water-soluble base as well as ascorbic acid, which did not react with ammonia and glycine under the experimental conditions,[2] instead of benzene-soluble quinine.

For the hydrogenation of benzil under atmospheric pressure, the conventional apparatus[3] was modified and used. All the reagents used were of guaranteed or purified in advance. Optical rotations were measured in a 1-dm cell with a Union PM-71 polarimeter. The method was as follows unless otherwise stated. In a 100-ml vessel of the hydrogenation apparatus, $CoCl_2 \cdot 6H_2O$ (0.238 g, 0.001 mol) and dimethylglyoxime (0.232 g, 0.002 mol) were placed. The vessel was replaced by nitrogen and added with 10 ml of ethanol solution containing quinine hydrochloride (0.397 g, 0.001 mol) which was previously deaerated by nitrogen, followed by stirring for 5 min. To this solution was added 30 ml of deaerated aqueous solution containing sodium hydroxide (0.004 mol) and base (0.001 mol)

Table 1. Asymmetric induction by optically active compounds in the hydrogenation of benzil to benzoin[a]

Run	Optically active compound	Amine	$[\alpha]_D$	Optical yield (%)	Conf[b]
1	Quinine	Ammonia	+42.8	36.1	*S*
2	Quinine	Glycine	+20.7	17.5	*S*
3	L-Ascorbic acid	Ammonia	−5.81	4.9	*R*
4	L-Ascorbic acid	Glycine	−3.74	3.2	*R*
5	L-Tyrosine	L-Tyrosine	−1.64	1.4	*R*
6	L-Lysine	L-Lysine	−0.89	0.8	*R*
7	L-Glutamic acid	L-Glutamic acid	−0.62	0.5	*R*
8	L-Aspartic acid	L-Aspartic acid	−0.37	0.3	*R*

a) In every case, chemicaly yield was almost quantitative. b) Configuration of predominant isomer.

Table 2. Effect of the pre-absorption of hydrogen by $Co(DMG)_2$–NH_3 complex on the asymmetric hydrogenation of benzil[a]

Run	A[b] (ml)	Optical yield (%)	Conf[c]	IH[d] (10^{-3} s^{-1})	Time[e] (min)
1	0.00	36.1	*S*	2.27	240
2	6.90	44.2	*S*	2.06	310
3	12.90	46.2	*S*	1.46	330
4	18.80	47.7	*S*	1.03	370
5	25.30	50.4	*S*	0.94	390
6	30.05	51.4	*S*	0.54	480

a) In every case, quinine was used as an optically active compound and chemical yield was almost quantitative. Initial pH was approximately 7.3—7.9. b) Amount of the hydrogen pre-absorbed by $Co(DMG)_2$–NH_3 complex at 20 °C. c) Configuration of predominant isomer. d) Initial rate of hydrogen absorption in the presence of benzil (H_2-mol consumed/s/mol of catalyst). e) Time necessary for the completion of hydrogenation.

Table 3. Effect of the amount of added NaOH on the asymmetric hydrogenation of benzil catalyzed by $Co(DMG)_2$–amine[a]

Run	Optically active compound (mmol)	Amine	Amount of added NaOH (mmol)	pH[b]	Optcal yield (%)	Time[c] (min)
1	Quinine	Ammonia	3.00	6.6	54.5	540
2	(0.25)		3.25	7.9	43.5	340
3			3.50	8.7	33.5	510
4			3.75	9.5	25.4	720
5	L-Ascorbic acid	Ammonia	3.00	5.3	1.5	550
6	(1.0)		3.50	6.5	2.8	520
7			4.00	7.4	4.9	370
8			4.50	8.3	4.3	450

a) In every case, chemical yield was almost quantitative. b) Initial pH of an aqueous phase. c) Time necessary for the completion of hydrogenation.

Table 4. Relationship between optical yield of benzoin and mole ratio of quinine or L-ascorbic acid to the cobalt complex[a)]

Run	Amine	Optically active compound	A/Co[b)]	Optical yield (%)	Conf[c)]	Time[d)] (min)
1	Ammonia	Quinine	0	0.0	—	220
2			1/16	46.3	*S*	320
3			1/8	42.7	*S*	300
4			1/4	43.5	*S*	340
5			1/2	39.1	*S*	360
6			1	36.1	*S*	240
7			2	26.6	*S*	380
8	Ammonia	L-Ascorbic acid	0	0.0	—	220
9			1/8	0.9	*R*	480
10			1/4	2.5	*R*	470
11			1/2	3.7	*R*	480
12			1	4.9	*R*	370
13			2	6.2	*R*	270

a) In every case, chemical yield was almost quantitative, and initial pH was approximately 7.3—7.9. b) Mole ratio of quinine or L-ascorbic acid to the cobalt. c) Configuration of predominant isomer. d) Time necessary for the completion of hydrogenation.

such as ammonia and amino acid, and then 30 ml of deaerated benzene solution containing benzil (0.420 g, 0.002 mol). The vessel was replaced by hydrogen and the solution was stirred under atmospheric pressure of hydrogen at room temperature. The amount of hydrogen absorbed was measured by a gas burette every definite interval. The amount of sodium hydroxide added was controlled, if necessary, so as to give a desired pH.

After absorption of the theoretical amount of hydrogen, the reaction mixture was transferred into a 100-ml separatory funnel and shaken with 30 ml of benzene, followed by separating the aqueous layer. The residual benzene layer was washed with each 50 ml of water, 2M-HCl and water in that order, one, three and four times, respectively. The benzene layer was concentrated *in vacuo*. The resulting product was dried overnight in a desiccator and obtained as white needles, followed by measuring the optical rotation of its acetone solution (c=0.8—1.2). The optical yield was calculated from the specific rotation of the product and that of the optically pure benzoin.[4)] Based on the additional data of melting point and mass spectrum, the above product was identified as (*S*)-benzoin.

As seen from Table 1, the asymmetric hydrogenation of benzil proceeded more or less only if an optically active compound was present in either a benzene phase or aqueous phase. The optical yield depended on the amount of the hydrogen pre-absorbed by $Co(DMG)_2$–NH_3 (Table 2), pH of the aqueous phase (Table 3) and the mole ratio of quinine or L-ascorbic acid to the cobalt complex (Table 4). Though the relationships between the optical yield and the above mentioned factors are interesting, their reasons still remain unknown.

References

1) Y. Ohashi, Y. Sasada, Y. Tashiro, Y. Ohgo, S. Takeuchi, and J. Yoshimura, This Bulletin, **44**, 583 (1971); *ibid.*, **46**, 2589 (1973); *Chem. Lett.*, **1973**, 265; *ibid.*, **1974**, 33, 709, 1327.

2) For example, T. Ozawa and Y. Nakamura, *Yakugaku Zasshi*, **90**, 933 (1970). This was also confirmed experimentally.

3) T. Takaya, T. Koga, and T. Hara, This Bulletin, **39**, 654 (1966).

4) I. V. Hopper and F. J. Wilson, *J. Chem. Soc.*, **1928**, 2483.

BULLETIN OF THE CHEMICAL SOCIETY OF JAPAN, VOL. 49(3), 825—826 (1976)

Rearrangement of 4,5-Benzo-3-thiatricyclo[4.1.0.0^{2,7}]heptenes Promoted by Butyllithium: A New Synthetic Route to 3,4-Benzo-2-thiabicyclo[3.2.0]hepta-3,6-dienes

Toshio TATSUOKA and Ichiro MURATA*

Department of Chemistry, Faculty of Science, Osaka University, Toyonaka, Osaka 560

(Received August 18, 1975)

Synopsis. The reaction of 4,5-benzo-3-thiatricyclo-[4.1.0.0^{2,7}]heptenes (**1a—d**) with butyllithium followed by quenching with water or methyl iodide at −60 °C gives the expected bridgehead substituted products, whereas the same reaction conducted at somewhat higher temperature gives the skeletal rearrangement products, 3,4-benzo-2-thiabicyclo-[3.2.0]hepta-3,6-dienes (**2a—f**), almost quantitatively. A mechanism in line with the results is proposed.

The well-known bridgehead deuteration and alkylation of the bicyclo[1.1.0]butanes involve an anion intermediate and electrophilic attack of the corresponding reagents.[1] During the course of our study on 4,5-benzo-3-thiatricyclo[4.1.0.0^{2,7}]heptene (**1a**)[2-6] we found that the deuteration of **1a** with *n*-BuLi/D_2O at 0 °C gives the skeletal rearrangement product, 3,4-benzo-2-thiabicyclo[3.2.0]hepta-3,6-diene-6-*d* (**2a**), exclusively.[3] We report on the generality of this type of rearrangement of **1**.

When 4,5-benzo-3-thiatricyclo[4.1.0.0^{2,7}]heptene (**1a**) was lithiated with *n*-BuLi in ether at −60 °C and then methylated with excess methyl iodide at −30 °C, the expected bridgehead methyl derivative (**1b**)[6] was obtained quantitatively. However, when lithiation was performed at 0 °C in ether, the rearrangement product (**2b**) was obtained quantitatively after methyl iodide quenching at 0 °C. Definite proof of the structure of the product is obtained from its NMR spectrum and synthesis from 4-methyl-1-benzothiepin (**3a**)[6] by photoisomerization. The rearrangement usually took place at 0 °C. However, a lower temperature, −20 °C, also sufficed in the case of methyl substituted substrates, **1b**[6] and **1c**[6] which afforded 1,6-dimethyl-3,4-benzo-2-thiabicyclo[3.2.0]hepta-3,6-diene (**2e**) and 5,6-dimethyl-3,4-benzo-2-thiabicyclo[3.2.0]hepta-3,6-diene (**2f**), respectively. Assignment of structures **2e** and **2f** was based on their spectral data. In addition, **2f** was available from photoisomerization of 4,5-dimethyl-1-benzothiepin (**3b**).[6]

Other examples were also found in the case of water quenching experiments. On treatment with *n*-BuLi/H_2O, **1b** afforded 1-methyl-3,4-benzo-2-thiabicyclo-[3.2.0]hepta-3,6-diene (**2c**). The structure assigned to **2c** follows from its spectral data coupled with an independent synthesis. Thus, dechlorination of the photoadduct (**4**),[7] obtained from irradiation of a mixture of 2-methylbenzo[*b*]thiophene and *cis*-dichloroethylene in the presence of benzophenone as sensitizer, with sodium phenanthrene[8] in THF at 0 °C afforded **2c** in 40% yield.

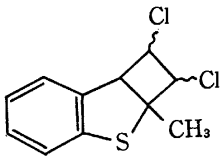

(**4**)

Furthermore, dimethyl derivative (**1d**) gave 1,5-dimethyl-3,4-benzo-2-thiabicyclo[3.2.0]hepta-3,6-diene (**2d**) on treatment with *n*-BuLi/H_2O at ambient temperature. The NMR spectrum of **2d** was in complete accord with the proposed structure.

In all the cases, we found that the newly introduced methyl or hydrogen is always bonded at C-6 position of **2**. The complete regiospecificity of this rearrangement was interpreted by assuming the intermediacy of a carbene type species (**B**), derived from an initially formed bridgehead anion (**A**), which is subsequently converted into the vinyl anion (**C**). Electrophilic attack of methyl iodide or water would give the observed products. Since **1a** is readily accessible,[1,2] the present reactions provide a useful synthetic route to the substituted 3,4-benzo-2-thiabicyclo[3.2.0]hepta-3,6-dienes (**2**).

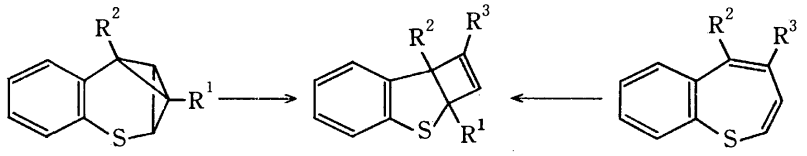

(**1**)
a: $R^1=R^2=H$
b: $R^1=CH_3$, $R^2=H$
c: $R^1=H$, $R^2=CH_3$
d: $R^1=R^2=CH_3$

(**2**)
a: $R^1=R^2=H$, $R^3=D$
b: $R^1=R^2=H$, $R^3=CH_3$
c: $R^1=CH_3$, $R^2=R^3=H$
d: $R^1=R^2=CH_3$, $R^3=H$
e: $R^1=R^3=CH_3$, $R^2=H$
f: $R^1=H$, $R^2=R^3=CH_3$

(**3**)
a: $R^2=H$, $R^3=CH_3$
b: $R_2=R_3=CH_3$

* To whom all correspondence should be addressed.

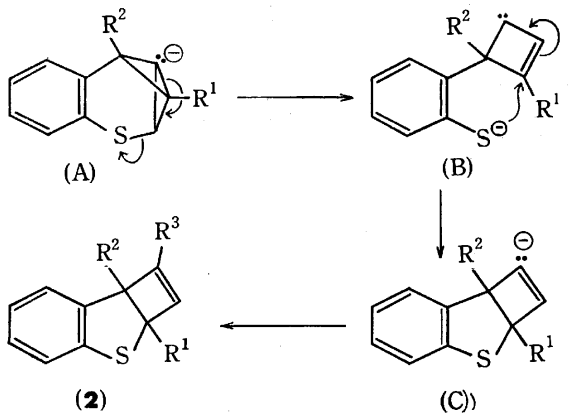

Experimental

Generals. The UV spectra were measured with a Hitachi Model 124 spectrophotometer. All the absorptions are given in nm with log ε in parentheses. The NMR spectra were recorded on a Varian XL-100-15 spectrometer with tetramethylsilane as an internal standard.

General Procedure for Rearrangement of 1. To a stirred solution of **1** (0.25 mmol) in 2—5 ml of dry ether was added dropwise a solution of *n*-BuLi (0.25 mmol) in hexane at temperatures indicated in the text [**1a**→**2b**: 0 °C; **1b**→**2e**: −20 °C; **1c**→**2f**: −20 °C; **1d**→**2d**: room temp] under nitrogen atmosphere. The mixture was stirred for 15 min at the specified temperature and treated with 20 fold excess of methyl iodide or water. Excess water was added and the aqueous iayer was washed with water and dried over anhydrous magnesium sulfate. Removal of the solvent afforded **2** quantitatively. Analytically pure compounds were obtained by column chromatography on a deactivated (with 5% of water) alumina with light petroleum ether.

2b: Colorless liquid, Found: C, 75.58; H, 5.99%. Calcd for $C_{11}H_{10}S$: C, 75.82; H, 5.78%. NMR (CCl_4) δ 1.73 (3H, d, J=1.8 Hz, CH_3), 4.52 (2H, s, H-1,5), 5.73 (1H, q, J=1.8 Hz, H-7), 6.90—7.17 (4H, m, arom.); UV (cyclohexane) (λ_{max} (log ε)) 217 (4.26), 255 (sh, 3.89), 257 (3.92), 263 (sh, 3.83), 297 (3.29), 305 nm (3.22).

2c: Colorless liquid, Found: C, 75.94; H, 5.75%. Calcd for $C_{11}H_{10}S$: C, 75.82; H, 5.78%. NMR (CCl_4) δ 1.68 (3H, s, CH_3), 4.10 (1H, bs, H-5), 5.96 (1H, dd, J=2.8, 0.7 Hz, H-7), 6.13 (1H, dd, J=2.8, 0.5 Hz, H-6), 6.85—7.17 (4H, m, arom.); UV (cyclohexane) (λ_{max} (log ε)) 218 (4.24), 223 (sh, 4.06), 254 (3.95), 258 (3.96), 296 (3.29), 298 (3.27), 305 (3.23).

2d: Colorless liquid, Found: C, 76.55; H, 6.45%. Calcd for $C_{12}H_{12}S$: C, 76.55; H, 6.42%. NMR (CCl_4) δ 1.43 (3H, s, 5-CH_3), 1.53 (3H, s, 1-CH_3), 5.93 (1H, d, J=2.6 Hz, H-7), 6.00 (1H, d, J=2.6 Hz, H-6), 6.90—7.15 (4H, m, arom.); UV (cyclohexane) (λ_{max} (log ε)) 216 (4.21), 236 (3.70), 255 (3.96), 293 (3.30), 302 (3.25).

2e: Colorless liquid, Found: C, 76.29; H, 6.36%. Calcd for $C_{12}H_{12}S$: C, 76.55; H, 6.42%. NMR (CCl_4) δ 1.67 (6H, m, 1- and 6-CH_3), 3.95 (1H, m, H-5), 5.84 (1H, dq, J=1.7, 0.5 Hz, H-7), 6.88—7.14 (4H, m, arom.); UV (cyclohexane) (λ_{max} (log ε)) 218 (4.23), 255 (sh, 3.91), 258 (3.92), 297 (3.32), 305 (3.27).

2f: Colorless liquid, Found: C, 76.72; H, 6.48%. Calcd for $C_{12}H_{12}S$: C, 76.55; H, 6.42%. NMR (CCl_4) δ 1.56 (3H, s, 5-CH_3), 1.65 (3H, dd, J=1.7, 1.6 Hz, 6-CH_3), 4.11 (1H, q, J=1.6 Hz, H-1), 5.61 (1H, q, J=1.7 Hz, H-7), 6.93—7.10 (4H, m, arom.); UV (cyclohexane) (λ_{max} (log ε)) 214 (4.31), 235 (sh, 3.79), 256 (3.95), 263 (sh, 3.89), 294 (3.30), 303 (3.25).

*Photoisomerization of **3a**, and **3b** to **2b** and **2f**.* A solution of **3** (0.25 mmol) in 0.5 ml of dry THF was irradiated through a pyrex filter with a 450w high-pressure mercury arc lamp at 0 °C for 4—5 hr. Removal of the solvent afforded **2** (*ca.* 90%) along with a small amount of the corresponding naphthalene (sulfur extrusion product).

*Independent Synthesis of **2c**.* A solution of sodium phenanthrene (4 ml) prepared from 310 mg of sodium metal and 2.67 g phenanthrene in 30 ml of dry THF, was added to 245 mg of 6,7-dichloro-1-methyl-3,4-benzo-2-thiabicyclo-[3.2.0]heptene-3 (**4**) in 5 ml of dry THF. The color of the reagent solution rapidly vanished at the beginning but returned at the end of the addition. After 10 min, one drop of water was added to quench the excess of the reagent. The solvent was evaporated and the residue was chromatographed on a silver nitrate impregnated silica gel column with hexane. Removal of the solvent gave 70 mg (40%) of 1-methyl-3,4-benzo-2-thiabicyclo[3.2.0]hepta-3,6-diene which was identical in all respects with **2c**.

References

1) *Cf.* G. L. Closs and L. E. Closs, *J. Amer. Chem. Soc.*, **85**, 2022 (1963); L. A. Paquette and E. Zon, *ibid.*, **96**, 203 (1974).

2) I. Murata, T. Tatsuoka, and Y. Sugihara, *Tetrahedron Lett.*, **1973**, 4261.

3) I. Murata, T. Tatsuoka, and Y. Sugihara, *Tetrahedron Lett.*, **1974**, 199.

4) I. Murata, T. Tatsuoka, and Y. Sugihara, *Angew. Chem. Int., Ed. Engl.*, **13**, 142 (1974).

5) C. Kabuto, T. Tatsuoka, I. Murata, and Y. Kitahara, *Angew. Chem. Int. Ed. Engl.*, **13**, 669 (1974).

6) I. Murata and T. Tatsuoka, *Tetrahedron Lett.*, **1975**, 2697.

7) D. C. Neckers, J. H. Dopper, and H. Wynberg, *J. Org. Chem.*, **35**, 1582 (1970).

8) L. A. Paquette and J. C. Stowell, *J. Amer. Chem. Soc.*, **93**, 5735 (1971).

BULLETIN OF THE CHEMICAL SOCIETY OF JAPAN, VOL. 49(3), 827—828 (1976)

Tri(hetero)substituted Carbonium Ions. XI. A Novel Synthetic Route to 2-Dialkylamino-4-alkyl-1,3-dithiolium Salts

Takeshi NAKAI,* Kazuhisa HIRATANI,[1] and Makoto OKAWARA

Research Laboratory of Resources Utilization, Tokyo Institute of Technology, Ookayama, Meguro-ku, Tokyo 152

(Received August 30, 1975)

Synopsis. Pyrolysis of 2-dialkylamino-4-(α-bromoalkyl)-1,3-dithiolanylium bromides (**2**) readily prepared by bromination of the β,γ-unsaturated dithiocarbamates (**1**) affords 2-dialkylamino-4-alkyl-1,3-dithiolium salts (**3**) in good yields, providing a useful way to prepare dithiolium salts.

We have shown that bromination of β,γ-unsaturated dithiocarbamates (**1**) results in the quantitative formation of the corresponding 2-dialkylamino-4-(α-bromoalkyl)-1,3-dithiolanylium bromides (**2**) *via* regiospecific (S-5) participation by the dithiocarbamate function.[2] In this Note we wish to report an intriguing thermal transformation of **2** into 2-dialkylamino-4-alkyl-1,3-dithiolium salts (**3**) in good yields. The simple ring transformation is of interest since the dithiolium salt **3** has been an important class of synthetic intermediates[3] for the synthesis of tetrathiofulvalene derivatives which attracted attention in view of the interesting electroconductivity[4] of their charge transfer complexes. The new synthetic route to 4-alkyl-1,3-dithiolium salts is more advantageous than the recently developed methods[3c,5] in view of the operational simplicity and accessibility[6] of the starting materials.

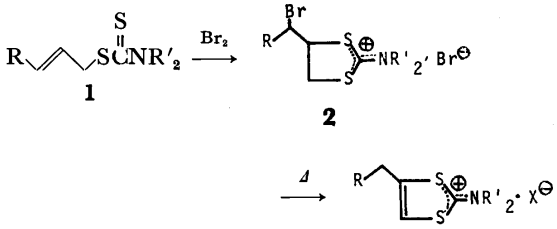

1 **2** **3**

a, R=H, R′=CH_3
b, R=H, R′=C_2H_5
c, R=CH_3, R′=CH_3

When 1,3-dithiolanylium salt (**2**) was heated in bulk at melting point (160—190 °C) in nitrogen under reduced pressure (*ca.* 5—10 mmHg), decomposition took place with the evolution of hydrogen bromide gas which was trapped in an ethanolic solution of triethylamine. The gas evolution ceased after 10—20 min. The resulting bromides, **3b** and **3c**, were converted, on treatment with an aqueous solution of sodium tetraphenylborate, into the tetraphenylborates which were then purified and characterized. The dithiolium salts thus obtained were identified by spectroscopic methods (NMR and UV) and elemental analyses, and/or by spectral comparison with authentic samples. Yields and physical properties of **3** are summarized in Table 1.

From the results it appears that the novel ring transformation involves an initial 1,2-dehydrobromination of **2** giving 4-alkylidene-1,3-dithiolanylium bromides (**4**) which further undergo 1,3-hydrogen shift, ultimately yielding the dithiolium salt **3**.

4 **5**

(1) A similar pyrolysis of 4-bromomethyl-4-methyl-1,3-dithiolanylium bromide (**5**) which does not undergo 1,2-dehydrobromination gave no dithiolium salt, a ring expansion taking place.[7] This indicates that the transformation is initiated by the thermal 1,2-dehydrobromination.

(2) 4-Vinylidene-1,3-dithiolanylium bromide (**4a**; R=H, R′=CH_3) was isolated by the reaction of **2a** with triethylamine (Table 1). When **4a** thus obtained was

TABLE 1. 1,3-DITHIOLIUM SALTS (**3**) AND THE RELATED SALT

Salt (Anion)	Yield %	Mp °C	N, % Found/Calcd	NMR (DMSO-d_6)[a] (δ ppm from TMS)	UV (EtOH)[b] (λ_{max}, nm)
3a	91	178—180[c]		2.54(s, 3H), 3.57(s, 6H)	247.5
(X=Br)				7.58(s, 1H)	303.5
3b	~100	147—150	2.73/2.76	1.23(t, 6H), 2.32(s, 3H)	249
(X=BPh_4)				3.63(q, 4H), 6.5—7.5(m, 21H)	308.5
3c	~100	183—187	2.88/2.84	1.40(t, 3H), 2.92(q, 2H)	248
(X=BPh_4)				3.65(s, 6H), 7.08(s, 1H)[a]	304.5
4a	83	189—190.5	5.97/5.83	3.62(s, 6H), 4.95(spl.s, 2H)	253.5
(X=Br)				5.80—6.10(m, 2H)	

a) All NMR spectra are those of the bromides except for **3b** (X=BPh_4). b) The molar extinction coefficients were not determined. Absorbances of the longer wavelength bands were greater than those of the shorter ones for all the dithiolium salts. c) Lit,[5b] mp 178—180 °C.

* To whom inquiries should be addressed: Department of Chemical Engineering, Tokyo Institute of Technology, Meguro-ku, Tokyo 152.

heated under the same conditions as in the pyrolysis of **2a**, the dithiolium salt **3a** was obtained quantitatively, thus providing convincing evidence for occurrence of the 1,3-hydrogen shift of the intermediate **4**. A similar thermal 1,3-hydrogen shift was observed elsewhere.[8]

Experimental

All the melting points are uncorrected. NMR and UV spectra were recorded on Japan Electron Optics spectrometers (PS-100 or MH-60) and a Hitachi EPS-2 spectrometer, respectively.

4-Bromoalkyl-1,3-dithiolanylium Bromides (**2**) were prepared from the corresponding β,γ-unsaturated dithiocarbamates (**1**) following the procedure described previously[2]; **2a**, mp 193—195 °C (lit,[2] 193—195 °C); **2b**, mp 115—116 °C (Found: N, 4.10%. Calcd for $C_8H_{15}NS_2Br_2$: N, 4.01%); **2c**, mp 162—164 °C (lit,[2] 162—164 °C).

Pyrolysis of 2. Bromide **2a** (0.65 g, 2.0 mmol) was placed in a 30-ml distilling flask equipped with a nitrogen balloon. The flask was then connected with a vacuum pump through a trapping tube containing an ethanolic solution of triethylamine placed in a Dry Ice–acetone bath. When the flask was gradually heated up to 190 °C under reduced pressure (5—10 mmHg), the bromide gradually melted, evolution of hydrogen bromide being observed. After heating at 180—190 °C for 10 min, the gas evolution ceased. The flask was then cooled and the solid residue was recrystallized from a mixture of acetone and acetonitrile giving 0.44 g (91%) of the dithiolium bromide (**3a**). The physical data of **3a** (Table 1) are in agreement with the reported values.[5b]

Pyrolysis of **2b** at *ca.* 160 °C for 20 min gave the crude bromide which was further converted, on treatment with a saturated aqueous solution of sodium tetraphenylborate, into the dithiolium salt (**3b**, X=BPh_4); the salt was recrystallized from an aqueous acetone. Similarly, pyrolysis of **2c** at *ca.* 170 °C for 20 min followed by the anion exchange gave **3c** (X=BPh_4) which was then recrystallized from a mixture of acetone and acetonitrile.

Reaction of 2a with Triethylamine. Triethylamine (0.13 g, 1.3 mmol) was added to a solution of **2a** (0.40 g, 1.2 mmol) in dimethylformamide (6 ml) at 0 °C, and the mixture was stirred at room temperature for 1 hr. The solvent was then distilled off under reduced pressure below room temperature giving a white solid. The solid was washed five times with cooled acetone and recrystallized from a mixture of acetone and ethanol to give 0.25 g (83%) of **4a**. The physical properties and the nitrogen analysis of **4a** are given in Table 1. Found: C, 30.32; H, 4.27%. Calcd for $C_6H_{10}NS_2Br$: C, 30.0; H, 4.17%.

Dithiolium bromide **3a** was obtained quantitatively when **4a** was heated in bulk at *ca.* 180 °C for 10 min.

References

1) Present address: Industrial Products Research Institute, Ohta-ku, Tokyo 144.

2) K. Hiratani, T. Nakai, and M. Okawara, *Chem. Lett.*, **1974**, 1041.

3) (a) A. Takamizawa and K. Hirai, *Chem. Pharm. Bull.*, **17**, 193 (1969); (b) J. P. Ferraris, *Tetrahedron Lett.*, **1973**, 2553; (c) Y. Ueno, A. Nakayama, and M. Okawara, *Synthesis*, **1975**, 277.

4) For example, F. Wudl, D. Wobschall, and E. J. Hufnagel, *J. Amer. Chem. Soc.*, **94**, 670 (1972).

5) (a) E. Campaign and N. W. Jacobsen, *J. Org. Chem.*, **29**, 1703 (1964); (b) K. Hiratani, H. Shiono, and M. Okawara, *Chem. Lett.*, **1973**, 867.

6) It should be noted that the starting γ-alkyl-substituted β,γ-unsaturated dithiocarbamates (**1**) are easily derived from the S-allyl derivative (**1a**) and alkyl halides (RX) *via* α-alkylation of the lithium salt of **1a** with RX followed by thermal [3,3]-sigmatropic rearrangement: T. Hayashi, *Tetrahedron Lett.*, **1974**, 339; T. Nakai, H. Shiono, and M. Okawara, *ibid.*, **1974**, 3625.

7) T. Nakai, *et al.*, Unpublished results; K. Hiratani, Dissertation, Tokyo Institute of Technology, 1974.

8) K. Tomita and M. Nagano, Jap. Patent, 69—30501; *Chem. Abstr.*, **72**, 90436 (1970).

BULLETIN OF THE CHEMICAL SOCIETY OF JAPAN, VOL. 49(3), 829—830 (1976)

The Reaction of Organic *gem*-Dihalides with Zerovalent Transition Metal Complexes. An Approach to Organic Synthesis

Junji FURUKAWA, Akira MATSUMURA, Yoshihito MATSUOKA, and Jitsuo KIJI

Department of Synthetic Chemistry, Kyoto University, Kyoto 606

(Received September 11, 1975)

Synopsis. The reaction of ω,ω-dibromoacetophenone with $Ni(COD)_2$ (COD=1,5-cyclooctadiene), $Fe(CO)_5$, or $Co_2(CO)_8$ gave *trans*-1,2,3-tribenzoylcyclopropane, while the reaction with $Pd[P(C_6H_5)_3]_4$ or $Ni[P(OC_2H_5)_3]_4$ gave *trans*-1,2-dibenzoylethylene. Phenyl isocyanide dichloride was dechlorinated by metal carbonyls to give phenyl isocyanide-substituted metal carbonyls.

Carbon-carbon bond formation by means of low-valent transition metal complexes is of current interest, and a variety of regio- or stereospecific reactions have been developed.[1] Reactions of *gem*-dihalides with iron carbonyls are known; in them a transiently formed carbenoid is assumed to be the intermediate.[2,3] To find versatile applications of organotransition metals to organic synthesis, several organic dihalides were allowed to react with metal complexes.

Results and Discussion

It has been reported that the reaction of ω,ω-dibromoacetophenone (I) with zinc-copper gives 1,3-diphenyl-2-buten-1-one.[4] The reaction of I with $Ni(COD)_2$, $Fe(CO)_5$, or $Co_2(CO)_8$ in benzene at 80 °C was found to afford *trans*-1,2,3-tribenzoylcyclopropane (II) as the sole organic product. Bis(cyclooctadiene)-nickel, $Ni(COD)_2$, was superior to the metal carbonyls, because $NiBr_2$ was more easily separated from the product by filtration. On the other hand, when dimethyl maleate or methyl sorbate was added to the system, these olefinic compounds did not participate in the reaction, and II was formed. This is a rare example of cyclopropane formation by the dehalogenation of an organic halide by transition metals.

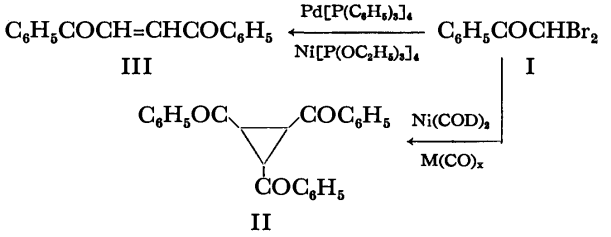

If the debromination occurs by a step-by-step mechanism, an intermediate oxo-allyl complex might be isolated. In fact, the reaction of α-haloketones with $Fe_2(CO)_9$ affords the oxo-allyl complex (IVa).[5] A similar complex (IVb) has been prepared by the reaction of diazoacetophenone with bis(benzonitrile)palladium dichloride.[6] The isolation of the oxo-allyl complex from the reaction of I with tetrakis(triphenylphosphine)palladium $Pd[P(C_6H_5)_3]_4$ was not achieved even at 0 °C, but *trans*-1,2-dibenzoylethylene (III) was obtained in a high yield. The palladium was recovered

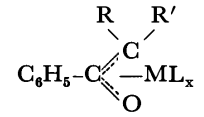

IV a; R=R′=H, M=Fe
b; R=H, R′=Cl, M=Pd

as bis(triphenylphosphine)palladium dibromide $PdBr_2[P(C_6H_5)_3]_2$. The reaction with tetrakis(triethyl phosphite)nickel $Ni[P(OC_2H_5)_3]_4$ gave similar results. The presence of donor ligands such as phosphine or phosphite appears to suppress the formation of the cyclopropane. The ligands seem to alter the nature of the intermediate (presumably "carbenoid") electronically or sterically.

In relation to the above reaction, dimethyl dibromosuccinate was treated with $Fe(CO)_5$ with the expectation of gaining insight into the stereochemistry of the dehalogenation, because there is a possibility that II or III is formed by a step-by-step dehalogenation after the coupling of the bromoacetophenone moiety. This debromination proceeded smoothly in benzene at 80 °C. The *dl*(*racemic*)-, and *meso*-isomers gave dimethyl fumarate predominately. Under these conditions, the isomerization of the double bond occurs.[7] Therefore, the specificity, if any, is obscured by the *cis-trans* isomerization.

Contrary to the case with the reaction with I, ethyl dichloroacetate was difficult to be dechlorinated under similar conditions. No appreciable organic product was formed. The dechlorination of phenyl isocyanide dichloride $C_6H_5NCCl_2$ (V) required a higher temperature. On refluxing in toluene, the reaction with 2 mol of $Fe(CO)_5$ gave $(C_6H_5NC)Fe(CO)_4$ in a 67% yield. The reaction with $Ni(CO)_4$ gave pale-yellow solid with IR absorptions at 2040 and 1990 cm^{-1},[8] they are assigned to ν_{NC} of $Ni(C_6H_5NC)_4$.

Experimental

ω,ω-Dibromoacetophenone,[9] *dl*- and *meso*-dimethyl dibromosuccinate,[10] phenyl isocyanide dichloride,[11] $Ni(COD)_2$,[1] $Pd[P(C_6H_5)_3]_4$,[12] and $Ni[P(OC_2H_5)_3]_4$[13] were prepared by the known methods. Commercially available $Fe(CO)_5$, $Co_2(CO)_8$, and $Cr(CO)_6$ were used without further purification. Benzene and toluene were purified by distillation in the presence of sodium ketyl under an atmosphere of argon.

The following procedures are typical examples of the reactions. The amounts of material used are shown in Table 1.

Reaction of I with $Fe(CO)_5$. A test tube fitted with a three-way stopcock was filled with argon by evacuating and filling it with argon several times. To a benzene solution (3 ml) of I (1.0 mmol) was added $Fe(CO)_5$ (1.2 mmol) and the solution was heated at 80 °C with stirring. The precipitate was separated by filtration, and the filtrate was percolated

Table 1. Reactions of *gem*-dihalides with zerovalent metal complexes

Dihalide mmol		Complex mmol		Conditions Solv.[a]	°C	hr	Product[b],	Yield[c] %
$C_6H_5COCHBr_2$,	1	$Ni(COD)_2$,	1.2	B,	80	10	II,	66
$C_6H_5COCHBr_2$,	1	$Co_2(CO)_8$,	1.2	B,	80	10	II,	51
$C_6H_5COCHBr_2$,	1	$Fe(CO)_5$,	1.2	B,	80	10	II,	28
$C_6H_5COCHBr_2$,	1	Pd-black,	1.2	B,	80	10	No reaction	
$C_6H_5COCHBr_2$,	1	$Pd(PPh_3)_4$,	1.2	B,	80	10	III,	77
$C_6H_5COCHBr_2$,	1	$Pd(PPh_3)_4$,	1.2	B,	0	24	III,	53
$C_6H_5COCHBr_2$,	1	$Ni[P(OEt)_3]_4$,	1.2	B,	80	10	III,	n.d.
$C_6H_5NCCl_2$,	10	$Fe(CO)_5$,	20	T,	110	10	$Fe(CO)_4L$[d],	67
$C_6H_5NCCl_2$,	5	$Cr(CO)_6$,	10	T,	110	10	$Cr(CO)_5L$[d],	55
$C_6H_5NCCl_2$,	8	$Ni(CO)_4$,	10	B[e],	80	10	Not isolated	

a) B, In benzene (3 ml); T, in toluene (30 ml). b) II, *trans*-1,2,3-Tribenzoylcyclopropane; III, *trans*-1,2-dibenzoylethylene. c) Based on the dihalides used. d) L, C_6H_5NC. e) In benzene (30 ml).

through a thin layer of alumina. The concentrated solution was poured into petroleum ether. A colorless compound, II, was thus obtained in a 28% yield. It was identified by comparing its spectral data with those of an authentic sample.[14]

Reaction of I with $Pd[P(C_6H_5)_3]_4$. To a benzene solution (3 ml) of I (1.0 mmol) was added $Pd[P(C_6H_5)_3]_4$ (1.2 mmol) under an atmosphere of argon. The reaction mixture was kept at 80 °C with stirring. The precipitate was identified as $PdBr_2[P(C_6H_5)_3]_2$ by comparing its infrared spectrum with that of the reported substance.[15]

The filtrate was concentrated, and the formation of III (in 77% yield) was confirmed by comparing its infrared spectrum with that of an authentic sample.[14]

Reaction of V with Metal Carbonyls. Phenyl isocyanide dichloride (V) was allowed to react with metal carbonyls under the conditions summarized in Table 1. After the reaction, the metal chloride thus precipitate was separated by filtration. The evaporation of the solvent gave isocyanide-substituted metal carbonyls.

References

1) M. F. Semmelhack, "Organic Reactions," Vol. 19, John Wiley Sons, Inc., New York (1972), p. 115 and references cited therein.
2) C. E. Coffey, *J. Amer. Chem. Soc.*, **83**, 1623 (1961).
3) K. K. Joshi, *J. Chem. Soc. A*, **1966**, 594.
4) M. Charpentier-Morize and J. Sausoulet, *C. R. Acad. Sci. Paris*, **267**, 1060 (1968).
5) H. Alper and E. C. H. Keunz, *J. Org. Chem.*, **37**, 2566 (1972).
6) N. Yoshimura, S-I. Murahashi, and I. Moritani, *J. Organometal. Chem.*, **52**, C58 (1973).
7) In a separated experiment it was confirmed that $Fe(CO)_5$ isomerized dimethyl maleate into fumarate rapidly.
8) F. A. Cotton and F. Zingales, *J. Amer. Chem. Soc.*, **83**, 351 (1961).
9) W. Taylor, *J. Chem. Soc.*, **1937**, 304.
10) H. R. Ing and W. H. Perkin, *J. Chem. Soc., Transactions*, **125**, 1814 (1924).
11) E. Kühle, B. Anders, and G. Zumach, *Angew. Chem.*, **79**, 663 (1967).
12) E. O. Greaves, C. J. L. Lock, and P. M. Maitlis, *Can. J. Chem.*, **46**, 3879 (1968).
13) W. C. Drinkard, D. R. Eaton, J. P. Jesson, and R. V. Lindsey, Jr., *Inorg. Chem.*, **9**, 392 (1970).
14) B. M. Trost, *J. Amer. Chem. Soc.*, **88**, 1587 (1966).
15) K. Shobatake and K. Nakamoto, *ibid.*, **92**, 3332 (1970).

BULLETIN OF THE CHEMICAL SOCIETY OF JAPAN, VOL. 49(3), 831—832 (1976)

The Syntheses of 4- and 5-(α- and β-Naphthyl)tropolones[1]

Josuke TSUNETSUGU, Masaru SATO, and Seiji EBINE

Department of Chemistry, Faculty of Science and Engineering, Saitama University, Urawa, Saitama 338

(Received September 16, 1975)

Synopsis. 4- And 5-(α- and β-naphthyl)tropolones have been synthesized *via* naphthyl-tropilidenes, -tropones, and -aminotropones.

Only 3-(α- and β-naphthyl)tropolones in a series of naphthyl-substituted tropolones have ever been reported.[2] This paper describes the syntheses of 4- and 5-(α- and β-naphthyl)tropolones by the successive reactions: tropenylations of naphthalene, transformation of naphthyltropilidenes to naphthyltropones and then to (naphthyl)aminotropones, and hydrolysis to naphthyltropolones.

7-Ethoxytropilidene was allowed to react with α-naphthylmagnesium bromide[3] to produce a mixture of isomeric α-naphthyltropilidenes (Iα, 44%), which was treated with phosphorus pentachloride in carbon tetrachloride, alkali, and acid successively to yield a mixture of isomeric α-naphthyltropones (IIα and IIIα, 85%).[4] Separation of them by chromatography or by fractional recrystallization of their picrates was unsuccessful. The mixture of IIα and IIIα was treated with 80% hydrazine in ethanol to afford three aminonaphthyltropones (IVα, Vα, and VIα; 3.4, 55, and 16%). The position of the amino group on these tropones became partially evident only after independent hydrolysis of each aminotropone with alkali.[5] IVα and VIα were hydrolyzed respectively to yield the same α-naphthyltropolone (VIIα, 86%), while Vα afforded α-naphthyltropolone (VIIIα, 80%). From these results, it is found that VIIα is 4-(α-naphthyl)tropolone and therefore IVα or VIα is 2-amino-4- or 2-amino-6-(α-naphthyl)tropone, although which is which remains unknown, and VIIIα is 5-(α-naphthyl)tropolone and Vα is 2-amino-5-(α-naphthyl)tropone.

For the β-naphthyl series, a mixture of β-naphthyltropilidenes (Iβ, 30%), a mixture of isomeric β-naph-

TABLE 1. α- AND β-NAPHTHYL-SUBSTITUTED TROPILIDENES, TROPONES, AMINOTROPONES, AND TROPOLONES

Compound	Appearance, Mp or Bp (°C)	Molecular formula	Analytical data[a]		
			C(%)	H(%)	N(%)
Iα	A pale yellow oil, 148.0—169.5/2 mmHg	$C_{17}H_{14}$	93.32	6.68	
			(93.53)	(6.47)	
Iβ	A pale yellow oil, 163.0—168.0/1.5 mmHg	$C_{17}H_{14}$	93.23	6.52	
IIα and IIIα (mixture)	Yellow oily crystals	$C_{17}H_{12}O_2$	87.95	5.11	
			(87.90)	(5.21)	
IIβ and IIIβ (mixture)	Yellow crystals, 132.5—135.0	$C_{17}H_{12}O_2$	87.77	5.19	
Picrates of IIα and IIIα	Yellow needles, 108.0—109.0	$C_{23}H_{15}O_8N_3$	60.05	3.34	9.11
			(59.87)	(3.28)	(9.11)
Picrates of IIβ and IIIβ	Brown needles, 128.5—129.5	$C_{23}H_{15}O_8N_3$	60.14	3.40	9.03
2,4-DNP of IIα and IIIα	Dark brown crystals, 162.0—164.0	$C_{23}H_{16}O_4N_4$	66.66	4.06	13.86
			(66.98)	(3.91)	(13.59)
2,4-DNP of IIβ and IIIβ	Black powder, 210.0—212.0	$C_{23}H_{16}O_4N_4$	66.68	3.85	13.26
IVα	Yellow plates, 162.0—163.0	$C_{17}H_{13}ON$	82.64	5.49	5.89
			(82.57)	(5.30)	(5.66)
IVβ	Yellow needles, 195.5—196.5	$C_{17}H_{13}ON$	82.66	5.28	5.77
Vα	Yellow plates, 201.0—202.0	$C_{17}H_{13}ON$	82.91	5.32	5.70
Vβ	Yellow leaflets, 200.5—201.5	$C_{17}H_{13}ON$	82.48	5.46	5.75
VIα	Yellow pyramids, 188.0—189.0	$C_{17}H_{13}ON$	82.70	5.25	5.53
VIβ	Yellow needles, 141.0—142.0	$C_{17}H_{13}ON$	82.40	5.30	5.51
Acetate of IVα	Pale yellow needles, 135.0—136.0	$C_{19}H_{15}O_2N$	78.80	5.24	4.73
			(78.87)	(5.23)	(4.84)
Acetate of IVβ	Yellow leaflets, 170.0—172.0	$C_{19}H_{15}O_2N$	78.71	5.26	4.93
Acetate of Vα	Yellow pyramids, 168.0—169.0	$C_{19}H_{15}O_2N$	79.02	5.37	4.75
Acetate of Vβ	Yellow leaflets, 166.5—167.5	$C_{19}H_{15}O_2N$	78.46	5.26	4.90
Acetate of VIα	Yellow plates, 189.5—190.5	$C_{19}H_{15}O_2N$	79.25	5.42	4.77
Acetate of VIβ	Yellow crystals, 174.0—176.0	$C_{19}H_{15}O_2N$	78.60	5.23	4.73
VIIα	Pale yellow needles, 117.0—118.0	$C_{17}H_{12}O_2$	82.31	4.78	
			(82.24)	(4.87)	
VIIβ	Pale yellow leaflets, 149.5—150.5	$C_{17}H_{12}O_2$	82.34	4.69	
VIIIα	Yellow pyramids, 138.5—139.0	$C_{17}H_{12}O_2$	82.13	4.84	
VIIIβ	Pale yellow needles, 201.0—202.0	$C_{17}H_{12}O_2$	82.30	4.78	

a) Numerals in parentheses indicate calculated values.

thyltropones (IIβ and IIIβ, 61%), three isomeric amino-β-naphthyltropones (IVβ, Vβ, and VIβ; 31, 41, and 18%), of which IVβ or VIβ is 2-amino-4- or 2-amino-6-(β-naphthyl)tropone, and two β-naphthyltropolones (VIIβ and VIIIβ, 41%) were obtained successively in a similar manner.

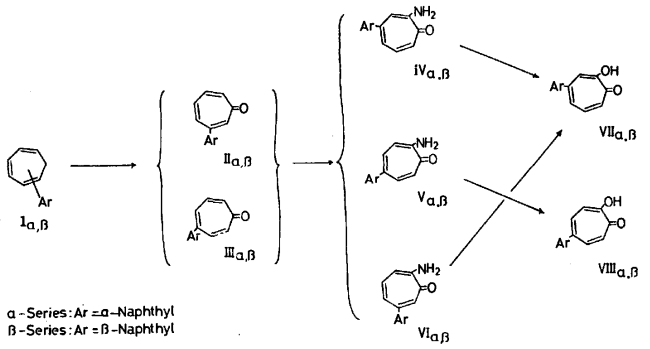

Experimental

α-Naphthyltropilidenes (Iα). 7-Ethoxytropilidene (55 g) was added to the Grignard reagent, prepared from α-bromonaphthalene (84.1 g) and magnesium (10.8 g) in dry ether (240 ml), and the ether was evaporated. The reaction mixture was heated for 3 hr at about 130 °C to yield naphthalene (5.6 g) and Iα (37.4 g); δ (CCl_4): 2.15 (t, J=6.8 Hz), 2.19 (t, J=6.8 Hz), 2.69 (d, J=6.8 Hz) and the peak areas of these methylene protons of the tropenyl groups suggest that the ratio between 3-, 2-, and 1-(α-naphthyl)tropilidenes is 3 to 10 to 13; 5.17 (1.65 H, m, tropyl), 6.07 (1.65 H, m, tropyl), 6.42 (1.65 H, m, tropyl), 6.88—8.12 (7H, m, naphthyl).

3- And 4-(α-naphthyl)tropones (IIα and IIIα, mixture). A mixture of phosphorus pentachloride (12.5 g), dry carbon tetrachloride (120 ml), and Iα (6.54 g) was stirred at room temperature overnight. The extraction of the mixture with cold water, neutralization of the water layer and extraction of it with ether afforded a yellow oil (4.55 g). This was hydrolyzed with concentrated hydrochloric acid to give recovered Iα (2.7 g) and a mixture of IIα and IIIα (2.27 g); ν (neat); 1630, 1575 cm^{-1}.

Amino-α-naphthyltropones (IVα, Vα, and VIα). A mixture of IIα and IIIα (590 mg), 80% hydrazine (0.5 ml), and ethanol (10 ml) was refluxed for 6 hr. The reaction mixture was separated through a silica-gel column with benzene–ether to afford three products: VIα (21 mg), IVα (345 mg), and Vα (98 mg), successively.

Acetate of VIα; λ_{max}^{MeOH}, nm (log ε): 220.5 (4.83), 261 (4.33), 290 (3.98 sh), 326 (4.14 sh), 370 (3.97 sh). ν(Nujol): 3230, 1693, 1616, 1220, 837, 808, 783, 730 cm^{-1}.

Acetate of IVα; λ_{max}^{MeOH}, nm (log ε): 221 (4.84), 250—255 (4.34), 324 (4.17), 368 (3.97), 3.88 (3.81 sh). ν(Nujol): 3235, 1692, 1617, 1225, 918, 793, 780, 726 cm^{-1}.

Acetate of Vα; λ_{max}^{MeOH}, nm (log ε): 219 (4.80), 253 (4.31), 280 (4.00 sh), 344 (4.20), 390 (4.01 sh). ν (KBr): 3240, 1693, 1618, 1248, 1220, 1203, 875, 869, 861, 808, 783, 743 cm^{-1}.

4-(α-Naphthyl)tropolone (VIIα). A mixture of IVα (600 mg), potassium hydroxide (660 mg), water (1.5 ml), and ethanol (4 ml) was refluxed for 12 hr and the solvent was evaporated off. The residue was acidified with 3 M sulfuric acid and extracted with chloroform (50 ml) to afford a brown solid of VIIα (518 mg, which was purified from cyclohexane); λ_{max}^{MeOH}, nm (log ε): 220.5 (4.79), 248 (4.42), 319 (4.16), 386 (3.83). ν (KBr): 3200, 1610, 1550, 915, 830, 800, 795, 775 cm^{-1}.

5-(α-Naphthyl)tropolone (VIIIα). This was prepared from Vα (purified from methanol) in a similar manner. λ_{max}^{MeOH}, nm (log ε): 219 (4.80), 346 (4.24). ν (KBr): 3400, 1615, 1550, 862, 805, 785 cm^{-1}.

The compounds of β-naphthyl series were prepared by practically the same treatment as in the α-naphthyl series described above.

References

1) Presented at the 23 rd Annual Meeting of the Chemical Society of Japan, Tokyo, April, 1970.

2) K. Kikuchi, *Nippon Kagaku Zasshi*, **77**, 1439 (1956).

3) C. M. Hill, R. A. Walker, and M. E. Hill, *J. Amer. Chem. Soc.*, **73**, 1663 (1951); C. M. Hill, L. Hayness, D. E. Simmons, and M. E. Hill, *ibid.*, **75**, 5408 (1953).

4) D. N. Kursanov and M. E. Volpin, *C. R. Acad. Sci. U. R. S. S.*, **113**, 339 (1957); T. Ikemi, T. Nozoe, and H. Sugiyama, *Chem. Ind.* (London), **1960**, 932.

5) T. Nozoe, S. Seto, H. Takeda, S. Morosawa, and K. Matsumoto, *Sci. Repts. Tohoku Univ.*, **I**, **36**, 126 (1952).

BULLETIN OF THE CHEMICAL SOCIETY OF JAPAN, VOL. 49(3), 833—834 (1976)

The Acid-Catalyzed Rearrangement of 1-Allylindoles. A Hypothesis for the Biogenesis of Echinulin-Type Compounds

Seisaku INADA, Kunio NAGAI, Yasuo TAKAYANAGI, and Mitsuo OKAZAKI

Department of Chemical Engineering, Faculty of Engineering, Tokyo Institute of Technology, Ohokayama, Meguro-ku, Tokyo 152

(Received September 18, 1975)

Synopsis. The aluminum chloride-catalyzed rearrangement of 1-allyl- (**1a**) and 1-(*trans*-2-butenyl)indole (**1b**) produced 3-allyl-(**3a**) and 3-(1-methylallyl)indole (**3b**) in 58 and 43% yields, respectively. Based on this, a hypothesis for the biogenetic mechanism of echinulin is proposed.

Recently, Patterson *et al.* showed that the pyrolysis of a mixture of 1-(*trans*- and *cis*-2-butenyl)indole at 450—470 °C gave 3-(1-methylallyl)indole and indole as the major primary reaction products.[1] We wish to report here the exclusive charge-induced [3,3]-shift of 1-allylindoles in connection with our interest in the biogenesis of the mould metabolite echinulin.

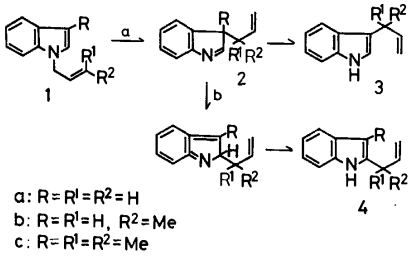

The experimental results for the rearrangement of 1-allylindole (**1a**) are summarized in Table 1. The $ZnCl_2$-catalyzed reaction of **1a** afforded an isolable amount of 3-allylindole (**3a**)[2] together with indole and 3-*n*-propyl-1-allylindole (**5**) only under the rather drastic conditions where the reaction was carried out in boiling tetralin. They were separated by preparative GLC and identified, based on analytical and/or spectral data, respectively. In the NMR spectrum of **5**, the presence of absorptions at 6.71 δ (s, 1H) due to 2-H in the indole nucleus and 4.48—4.62 δ (m, 2H) due to the α hydrogens of $N\text{-}CH_2CH{=}CH_2$ indicates the probable location of the propyl group at the 3-position, which may originate from the allyl group of **1a**.

Although the reaction under $SbCl_5$ catalysis formed a fair amount of tarry matter, the $AlCl_3$- and $TiCl_4$-catalyzed reactions were found to give **3a** exclusively, with the exception of a slight formation of tarry matter. The former proceeds with higher reactivity and less formation of tarry products than the latter. Thus, when **1a** and $AlCl_3$ (equimolar amounts) were refluxed in benzene for 4 hr, **3a** was obtained in 58% yield. This was confirmed by GLC to contain no detectable amount of by-products.

TABLE 1. ACID-CATALYZED REACTION OF **1a**

Acid	Solvent	Reaction time(hr)	Relative compositions (glc area %)
$ZnCl_2$	Benzene	24	**1a**, >99; **3a**, trace.
$ZnCl_2$	Tetralin	20	**1a**, 68; **3a**, 14; indole, 4; **5**, 9; unidentified, 5.
$SbCl_5$	Benzene	0.5	
$AlCl_3$	Benzene	1	**1a**, 15; **3a**, 85.
$TiCl_4$	Benzene	3	**1a**, 74; **3a**, 26.

The rearrangement of 1-(*trans*-2-butenyl)indole (**1b**) was similarly performed; heating of **1b** with $AlCl_3$ for 2 hr (**1b** seems more reactive than **1a**) gave 3-(1-methylallyl)indole (**3b**)[1] in 43% yield. This demonstrates that the isomerization is presumably a [3,3]-sigmatropic reaction followed by enamination.

The biogenesis of the mould metabolite echinulin (**6**) and the formally related alkaloids, which involve a

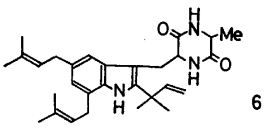

1,1-dimethylallyl group at the 2-position of the indole nucleus, has been of interest.[3] In particular, different biogenetic mechanisms for the process through which the reversed isoprene unit is inserted at the 2-position have been suggested.[4,5] Recently, Casnati *et al.* have found that 3-methyl-1-(3-methyl-2-butenyl)indole (**1c**) rearranged under acid catalysis to give 2-(1,1-dimethylallyl)3-methylindole (**4c**) and 3-methyl-2-(3-methyl-2-butenyl)indole with partial inversion of the migrating group, and stated that this represented a hitherto unobserved type of rearrangement, which might have a biogenetic implication for echinulin-type compounds.[6] However, in view of our experimental results, it seems possible to assume that the reaction affording **4c** (and consequently the process of the biogenesis for echinulin-type compounds also) involves a charge-induced [3,3]-shift to form an intermediate, 3-alkyl-3-allylindolenines (**2**),[7] followed by a [1,5]-shift and subsequent enamination to give 3-alkyl-2-allylindoles (**4**).

It is well-known that 3,3-dialkylindolenines isomerize readily to 2,3-dialkylindoles in an acidic medium, especially when one of the alkyl groups is an allylic group (route b).[5,8] On the other hand, the [3,3]-shift of 1-allylindoles (route a) has not been reported, except for the experiment which was carried out under the rather drastic conditions described above.[1] Our experimental results may be one of primary pieces of evidence supporting the proposed hypothesis.

Experimental

Gas chromatographic analyses were made on a Shimadzu GC 3AH gas chromatograph using a 3 mm×2 m column packed with 25% Apiezon L on Chromosorb W at 220 °C.

For preparative GLC, a Schimadzu GC 1B gas chromatograph having a 6 mm × 1.5 m column packed similarly was employed. 1-Allylindole (**1a**)[9] and 3-allylindole (**2a**)[2] were prepared according to the methods reported in the literature.

1-(trans-2-Butenyl)indole (1b). According to the method of Cardillo *et al.* for preparing **1a**,[9] **1b** (34.5 g, bp 116 °C/2 mmHg) also was prepared from indole (30.0 g, 0.256 mol), sodium hydride (50% dispersion, 12.6 g, 0.262 mol), and *trans*-1-chloro-2-butene (23.2 g, 0.256 mol) in DMF. This was contaminated with a by-product which could not be excluded by distillation. This was treated with picric acid (46.6 g) in methanol (300 ml) and the picrate obtained (51 g) was repeatedly recrystallized from methanol to give red needles (20.4 g) which melted at 73.5—74.5 °C. IR (KBr, cm^{-1}) 3125, 1635, 970. Found: N, 13.76%. Calcd for $C_{18}H_{16}N_4O_7$: N, 13.99%.

The purified picrate was added to 5% aqueous NaOH and extracted with ethyl acetate. The organic solution was washed with water and dried over $MgSO_4$. After removal of the solvent the residue was distilled *in vacuo* and a fraction of bp 91 °C/1.5 mmHg was collected. Yield, 5.0 g (11.4%). The GLC analysis denoted that this fraction consisted of a single product. IR (neat film, cm^{-1}) 3050, 1455, 1320, 970. NMR ($CDCl_3$, δ) 1.59 (br. d, 3H), 4.42 (br. d, 2H), 5.20—5.64 (m, 2H), 6.30 (d, 1H), 6.80 (d, 1H), 6.88—7.14 (m, 3H), 7.36—7.52 (m, 1H). Found: N, 8.10%. Calcd for $C_{12}H_{13}N$: N, 8.18%.

Acid-catalyzed Reaction of 1a. A mixture of **1a** (0.5 g) and a Lewis acid (equimolar amounts) in a solvent (4 ml) was refluxed for an appropriate time. The reaction mixture was poured into 10% aqueous NaOH and extracted with ethyl acetate. The organic layer was washed with water and provided for GLC analysis. The results are shown in Table 1.

1-Allyl-3-n-propylindole (5). Pale yellow oil. IR (neat film, cm^{-1}) 3050, 1465, 990, 920. NMR ($CDCl_3$, δ) 1.00 (t, 3H), 1.44—1.90 (m, 2H), 2.70 (t, 2H), 4.48—4.62 (m, 2H), 4.78—5.08 (m, 2H), 5.60—6.20 (m, 1H), 6.71 (s, 1H), 6.80—7.15 (m, 3H), 7.35 —7.55 (m, 1H). Found: N, 7.00%. Calcd for $C_{14}H_{17}N$: N, 7.03%.

$AlCl_3$-catalyzed Rearrangement. Synthesis of 2a: A solution of **1a** (5.0 g, 32 mmol) and $AlCl_3$ (4.3 g, 32 mmol) in benzene (80 ml) was refluxed for 4 hr. To the cooled solution 2% HCl (100 ml) was added and the organic solution was separated, washed with water, and dried over $MgSO_4$. After removal of the solvent, the residue (4.6 g) was distilled *in vacuo*; a fraction of bp 105 °C/2 mmHg was collected. Yield, 2.9 g (58%). The IR and NMR spectra were completely in accord with those of an authentic sample prepared according to the method of Brown *et al.*[2]

Synthesis of 2b: A mixture of **1b** (3.0 g, 18 mmol) and $AlCl_3$ (2.3 g, 18 mmol) was refluxed in benzene (60 ml) for 2 hr. The reaction mixture was treated similarly and a fraction of bp 111—112 °C/1.5 mmHg was collected. Yield, 1.3 g (43%). The IR and NMR spectra corresponded to those described by Patterson *et al.*[1] This sample was 98% pure (GLC area %), but sensitive to the air; it darkened after standing for a few days.

References

1) J. M. Patterson, A. Wu, C. Kook, and W. T. Smith, Jr., *J. Org. Chem.*, **39**, 486 (1974).

2) J. B. Brown, H. B. Henbest, and E. R. H. Jones, *J. Chem. Soc.*, **1952**, 3172.

3) A. J. Birch, G. E. Blance, S. Davis, and H. Smith, *ibid.*, **1961**, 3128.

4) B. W. Bycroft and W. Landon, *Chem. Commun.*, **1970**, 967; A. H. Jackson and A. E. Smith, *Tetrahedron*, **21**, 989 (1965); A. J. Birch and K. R. Farrar, *J. Chem. Soc.*, **1963**, 4277.

5) G. Casnati, M. Francioni, A. Guareschi, and A. Pochini, *Tetrahedron Lett.*, **1969**, 2485.

6) G. Casnati, R. Marchelli, and A. Pochini, *J. Chem. Soc., Perkin I*, **1974**, 754. See also G. Casnati and A. Pochini, *Chem. Commun.*, **1970**, 1328.

7) Schmid *et al.* also pointed out a similar intermediacy for this migration. M. Schmid, H. -J. Hansen, and H. Schmid, *Helv. Chim. Acta*, **56**, 105 (1973).

8) A. H. Jackson and P. Smith, *Tetrahedron*, **24**, 2227 (1968).

9) B. Cardillo, G. Casnati, A. Pochini, and A. Ricca, *Tetrahedron*, **23**, 3771 (1967).

BULLETIN OF THE CHEMICAL SOCIETY OF JAPAN, VOL. 49(3), 835—836 (1976)

New A-*nor*-B-*homo*-*ent*-Kauranoids (Grayanotoxin XVI and XVII) from *Leucothoe Grayana Max.*

Shinsei GASA, Ryūzō IKEDA, Nobuyuki HAMANAKA, and Takeshi MATSUMOTO
Department of Chemistry, Faculty of Science, Hokkaido University, Sapporo 060

(Received September 18, 1975)

Synopsis. Two physiologically active diterpenoids, grayanotoxin XVI and XVII, have been isolated from *Leucothoe grayana Max.*, and the structures have been determined to be 6-*O*-acetylgrayanotoxin II and 3,6-didehydrograyanotoxin III respectively on the basis of spectral and chemical evidence.

The structures of a number of diterpenoids with an A-*nor*-B-*homo*-*ent*-kaurane skeleton have been elucidated by several groups.[1] In this paper we wish to report on the isolation and characterization of two physiologically active diterpenoids of this type from *L. grayana Max.* These toxic substances, grayanotoxins (hereafter G) XVI and XVII, were obtained as minor constituents by the careful chromatography of alcohol extracts of dried leaves, together with G I,[1] II,[1] III,[1] IV,[2] V,[2] XIV,[3], XV,[3] as well as leucothols A, [4a] B[4b] and C.[4b]

The first compound, G XVI ($C_{22}H_{34}O_6$, mp 116—118 °C, $[\alpha]_D$ +2.8 ° (*c* 1, MeOH) was obtained in a 5×10^{-6}% yield from dried leaves. The IR and NMR spectra indicated the presence of the following groups: two tertiary methyls (δ 0.92 and 1.20), a tertiary methyl on a carbon bearing a hydroxyl group (δ 1.33), two secondary hydroxyls (3511 cm^{-1}, δ 3.57, 1H, q, J_{AX+BX}=3+6 Hz and 4.44, 1H, s), a secondary acetoxyl (1719 cm^{-1}, δ 2.12, 3H, s, and 4.77, 1H, q, J_{AX+BX}= 2+10 Hz), and an exocyclic methylene group (1634 cm^{-1}, δ 5.00 and 5.16, each 1H, s). Since the treatment of this compound with sodium hydroxide in ethanol afforded G II **1**, the new toxin must be either 3-*O*- or 6-*O*-acetyl G III. In order to clarify the position of the acetoxyl group, the toxin was next oxidized with chromium trioxide in pyridine to give an amorphous diketone **7**, whose NMR spectrum indicated a quartet (J_{AX+BX}=4+9 Hz) due to the acetoxyl-bearing methine proton at δ 6.39. The extraordinary large downfield shift of the quartet indicates the steric closeness of the methine proton and the newly-formed carbonyl group (s). Since, on the other hand, **7** seemingly takes a G I-like conformation, **8**,[5] the 6-*O*-acetyl structure was concluded for the diketone and, accordingly, for G XVI also. Supporting evidence for the **2** structure was obtained by means of the INDOR technique. On monitoring the four lines due to the C-6 proton under INDOR conditions, only eight INDOR peaks altogether were observed at δ 2.76. 2.59, 2.52, 2.35, 2.12, 2.08, 1.88, and 1.84, indicating the presence of a **9** moiety (δ_A2.01, δ_B2.53, J_{AB}=−14.4 Hz, J_{AX}= 2.4 Hz, J_{BX}=10.2 Hz) in **7**. Several 6-*O*-acylated grayanoids have been isolated from *Lyonia ovalifolia* D. *elliptica* Hand. -Mazz.,[7a] *Pieris japonica* D. Don,[7b] and *Rhododendron japonicum* Suringer.[7c] However, the new grayanotoxin is the first 6-*O*-acylate to be isolated from *Leucothoe grayana Max.* It causes skin inflammation upon contact.

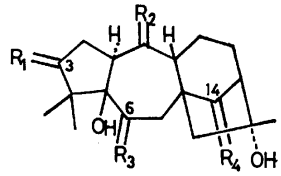

	1	2	3	4	5	6	7
R_1	OH H	OH H	OH H	OH H	=O	=O	=O
R_2	$=CH_2$	$=CH_2$	CH$_3$ OH	CH$_3$ OH	CH$_3$ OH	CH$_3$ OH	$=CH_2$
R_3	OH H	OAc H	OH H	OH H	=O	=O	OAc H
R_4	OH H	OH H	OH H	OAc H	OAc H	OH H	=O

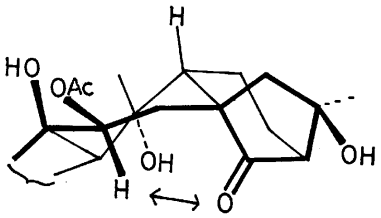

8 Partial conformation of diketone **7**

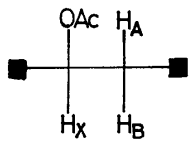

9

■ denotes a quaternary carbon atom

The second compound, G XVII ($C_{20}H_{30}O_6$, mp 268—270 °C (dec.), $[\alpha]_D$ −157.3 ° (*c* 1, MeOH)), was obtained in a 2.9×10^{-6}% yield from dried leaves and has the following spectral proterties: IR (cm^{-1}, Nujol) 3470 (OH), 1731 and 1712 (C=O); NMR (C_5D_5N, TMS) δ 1.02, 1.19, 1.42, 1.62 (each 3H, s, four tert. methyls), 2.92 (2H, bd, J=~11 Hz, C-2[8]), 3.90 (1H, q, J_{AX+BX}=9+12 Hz, C-1[8]), 2.84 (1H, d, J_{AB}=−13 Hz, C-7Hax), 4.22 (1H, d, J_{AB}=—13 Hz, C-7Heq), 5.27 (1H, s, C-14); ORD *a*=−463 (MeOH). The analytical and mass spectral data indicated that the compound corresponds to a bisdehydro derivative of G III (**3**). A comparison of the above spectral data with those of G III[1] suggested the presence of the C-14 hydroxyl group and two carbonyl groups as well as the absence of C-3 and C-6 protons. Moreover, the appreciable downfield shift of the C-14 proton of G XVII as compared to that of G III (δ 5.10, in C_5D_5N) also suggested the spatial closeness of the C-14 proton and a carbonyl group in G XVII (see **8**). Therefore, the 3,6-didehydro G III structure seemed suitable for G XVII.

This reasoning was proved correct by leading G I (**4**) with chromium trioxide in pyridine to 3,6-didehydro G I[6] (**5**) and by hydrolyzing the diketone with potassium carbonate in ethanol to give a product, which

was, in all respects, (IR, MS, NMR, and tlc) identical with G XVII. The new toxin was, therefore, formulated as 3,6-didehydro G III (**6**).

Two monoketo grayanoids, G V[2] and XIV,[3] were previously isolated and shown to possess no appreciable physiological activity. G XVII is the first grayanoid containing two carbonyl groups, and, in contrast to the monoketo grayanoids, it shows the sneeze-causing activity characteristic of polyhydroxylated grayanoids. The conformation of the central cycloheptane rings of G XVI and G XVII seems quite similar to that of G I on the basis of the NMR evidence presented above.

Experimental

All the mps are uncorrected. The NMR spectra were obtained on a Hitachi R-20B spectrometer, modified for INDOR experiments, in $CDCl_3$ or C_5D_5N, containing TMS as the internal reference. The chemical shifts are reported on the δ scale (s=singlet, q=quartet, d=doublet, bd=broad doublet). The IR spectra were measured on a JASCO Model IR-S spectrophotometer. The ORD curves were obtained on a JASCO ORD/UV-5 spectrometer. The specific rotations were measured in methanol at room temperature.

Isolation of G XVI and XVII. The powder (41 kg) of the leaves, which had been collected on Mt. Tarumae, Hokkaido, in July and dried, was extracted with hot water (*ca.* 4×10^3 l) for 3 days. The extracts were then concentrated under reduced pressure to *ca.* 70 l. An excess sat. lead acetate solution was added to the concentrate, and the ppt. was filtered off. An ammonium hydroxide solution was then added to the filtrate until the solution became alkaline (pH 8), after which the ppt. was filtered off again. H_2S gas was next bubbled through the filtrate to remove the Pb. After filtration and concentration, the solution was extracted with ethyl acetate. The organic phase was then dried over anhydrous sodium sulfate and concentrated under reduced pressure to give a crude mixture consisting mainly of G I and III (368 g). After the removal of the solid material, the mother liquor was chromatographed on silica gel (2 kg, Wako, 100 mesh) and was roughly fractionated into A, B, and C. The first fraction, A (154 g), eluted with ethanol–chloroform (3:97, 2 l), was a mixture of several components and was rechromatographed on silica gel (600 g). A mixture containing G XVII (3 g, subfraction A_1) was first eluted with ethanol–chloroform (3:97, 0.8 l). Further elution with ethanol–chloroform gave, successively, G I, IV, V, and II (85, 13, 3, and 25 g respectively). The second fraction, B (252 g), a semicrystalline solid, was obtained by elution with ethanol–chloroform (5:95, 2 l). After the removal of the crystalline mixture of G I and II (125 g) with ethyl acetate, the filtrate was concentrated and the residue (126 g) was chromatographed on silica gel (800 g). Elution with ethanol–chloroform (3:97, 0.5 l) yielded a mixture (0.7 g, subfraction B_1) of leucothol A, C, and G XVII. Further elution with the same solvent afforded a mixture (5.8 g) of G I and XV, while elution with a more polar solvent system (7:93, 1.8 l) gave a mixture (119 g) of G I, II and V. Later fractions eluted with ethanol–chloroform (7:93, 3 l) contained, altogether, 282 g of G I, II, III, and V.

The above-described subfractions, A_1 and B_1, were then combined, and the mixture (3.7 g) was chromatographed on silica gel (400 g). Elution with ethanol–chloroform (2:98, 0.5 l) gave unknown compounds (268 mg). Further elution with the above solvent (3:97, 0.8 l) afforded leucothol C (53 mg) and then G XVII (118 mg): needles from methanol; mp 268—270 °C (dec.), $[\alpha]_D$ −157.3° (*c* 1, MeOH); ORD $[\phi]^{320nm}_{min}$ −20532 °C, $[\phi]^{275nm}_{max}$ +25752 °C; MS *m/e* 366 (M^+).

Found: C, 65.78; H, 8.27%. Calcd for $C_{20}H_{30}O_6$: C, 65.55; H, 8.25%.

Further elution with the same solvent system (4:96, 0.8 l) gave a mixture of leucothol A and B (390 mg), while elution with the 5:95 solvent system (1.5 l) afforded, successively, crystals of GV (380 mg), XV (185 mg), and XVI (210 mg). The last compound was recrystallized from ether to give plates; mp 116—118 °C, $[\alpha]_D$ +2.8° (*c* 1, MeOH); MS *m/e* 394 (M^+).

Found: C, 66.88; H, 8.69%. Calcd for $C_{22}H_{34}O_6$: C, 66.78; H, 8.44%.

Hydrolysis of G XVI. G XVI (37 mg) was dissolved in a mixture of aqueous sodium hydroxide (5%, 0.5 ml) and ethanol (2 ml), and the solution was heated under reflux for 1 hr. After cooling, the solution was diluted with excess ethyl acetate, washed with water and brine, and dried over anhydrous sodium sulfate. The evaporation of the solvent gave crystals (34 mg) identical (IR, NMR, and tlc) with those of G II.

Oxidation of G XVI. To a chromium trioxide–pyridine complex solution prepared from 90 mg of chromium trioxide and 1 ml of pyridine, a solution of G XVI (30 mg) in pyridine (2 ml) was added, after which the whole solution was left to stand for 1 day at room temperature. An usual work-up gave an amorphous solid (26 mg) which was purified from ethyl acetate. IR (cm^{-1}, film) 3480, 1745 (C=O), 1720 (O_2CCH_3), 1630 (C=C); NMR ($CDCl_3$) 1.08, 1.11, 1.42 (each 3H, s, C–CH_3), 2.06 (3H, s, O_2CCH_3), 5.00, 5.19 (each 1H, bs, C=CH_2), 6.39 (1H, q, J_{AX+BX}=4+9 Hz, C-6); MS *m/e* 390 (M^+).

Hydrolysis of 3,6-Didehydro G I (5).[6] A mixture of **5** (111 mg) and potassium carbonate (17 mg) in ethanol (5 ml) was stirred for 20 min at room temperature. After the evaporation of ethanol under reduced pressure, the residue was dissolved in ethyl acetate and the solution was washed with water and brine and dried over anhydrous sodium sulfate. The subsequent removal of the solvent gave crude crystals which were purified with ethyl acetate to afford prisms (85 mg). The crystalline product was identical with G XVII in all respects (IR, NMR, MS, and tlc).

References

1) S. Miyajima and S. Takei, *J. Agr. Chem. Japan*, **10**, 1093 (1934); H. Kakisawa, M. Kurono, S. Takahashi, and H. Hirata, *ibid.*, **1961**, 59; J. Iwasa and Y. Nakamura, *Tetrahedron Lett.*, **1969**, 3937; H. Hikino, M. Ogura, T. Ohta, and T. Takemoto, *Chem. Pharm. Bull.*, **18**, 1072 (1970).

2) T. Okuno, N. Hamanaka, H. Miyakoshi, and T. Matsumoto, *Tetrahedron*, **26**, 4765 (1970).

3) N. Hamanaka, H. Miyakoshi, A. Furusaki, and T. Matsumoto, *Chem. Lett.*, **1972**, 779.

4) (a) A. Furusaki, N. Hamanaka, H. Miyakoshi, and T. Matsumoto, *Chem. Lett.*, **1972**, 783; (b) idem, *ibid.*, **1972**, 787.

5) X-ray analysis of G I; P. Narayanan, M. Rohl, K. Zechmeister and W. Hoppe, *Tetrahedron Lett.*, **1970**, 3943.

6) T. Matsumoto and M. Watanabe, *Tetrahedron Lett.*, **1968**, 6019.

7) (a) M. Yasue, Y. Kato, T. Kishida, and H. Ohta, *Chem. Pharm. Bull.*, **9**, 171 (1961); (b) H. Hikino, K. Ito, and T. Takemoto, *ibid.*, **17**, 854 (1969); (c) H. Hikino, M. Ogura, T. Ohta and T. Takemoto, *ibid.*, **18**, 1071 (1970).

8) Tentative assignment. It appears that in general, C-1 and C-2 protons of Gs resonate at unusually low field in pyridine and exhibit unusually large coupling constants S). Gasa and T. Matsumoto, unpublished observations).

BULLETIN OF THE CHEMICAL SOCIETY OF JAPAN, VOL. 49(3), 837—838 (1976)

Substituted Tetrahydropyridine and Dihydropyridobenzoxazine Ring Syntheses

Akio SAKURAI and Hiroshi MIDORIKAWA*

The Institute of Physical and Chemical Research, Wako, Saitama 351

**Department of Domestic Science, Showa Women's University, Setagaya, Tokyo 154*

(Received September 25, 1975)

Synopsis. The ternary condensation of ethyl acetoacetate, 3-methoxysalicylaldehyde, and substituted benzaldehydes in the presence of ammonium acetate gave 1,2,5,6-tetrahydropyridine (**1**) and 6*H*-8,9-dihidropyrido[1,2-*c*][1,3]-benzoxazine (**2**) derivatives.

We have previously shown[1] that the reaction of ethyl acetoacetate with substituted salicylaldehydes gives heterocyclic products which contain two salicylaldehyde residues. However, the ternary condensation of ethyl acetoacetate, 3-methoxysalicylaldehyde, and benzaldehyde derivatives was found to produce compounds containing salicylaldehyde and benzaldehyde residues. In this reaction, the use of *m*-nitrobenzaldehyde as the aldehyde reactant afforded a mixture of **1** and **2** or exclusively **2**, depending on the conditions. Attempts to isolate an intermediate from the reaction of 3-methoxysalicylaldehyde with 2,4-dichlorobenzaldehyde in ethanol gave a yellow crystalline solid. The elemental analysis and NMR spectral data of this substance are compatible with the structure **3** (R_1=R_3=Cl, R_2=H).

The mode of formation of the compound **1** can be concluded as follows. Two molecules of 3-methoxysalicylaldehyde and one of substituted benzaldehyde condense with ammonia to yield **3**. Then, **3** (which undergoes C–N bond cleavage) reacts to ethyl acetoacetate to form **1**. In support of this, treatment of ethyl acetoacetate with **3** (R_1=R_3=Cl, R_2=H) in the presence of ammonium acetate gave the compound **1e**. The compound **2** could be formed by further condensation of **1a** with another molecule of *m*-nitrobenzaldehyde.

Experimental

4-Amino-6-aryl-3-ethoxycarbonyl-2-(2-hydroxy-3-methoxyphenyl)-1,2,5,6-tetrahydropyridines (1). To a mixture of ethyl acetoacetate (0.05 mol), 3-methoxysalicylaldehyde (0.05 mol), and substituted benzaldehyde (0.05 mol) in ethanol (15 ml), ammonium acetate (0.05—0.06 mol) was added and the mixture was refluxed for 1—2 hr. The solid that separated on cooling was recrystallized from ethanol–dimethyl sulfoxide.

10-Amino-11-ethoxycarbonyl-4-methoxy-6,8-bis(3-nitrophenyl)-6H-8,9-dihydropyrido[1,2-c][1,3]benzoxazine (2). Ammo-

Table 1. Compounds **1a-e** and **2**

Compound	R_1	R_2	R_3	Yield (%)	Mp (°C) (dec)	Formula	Analysis % Found C	Found H	Found N	Calcd C	Calcd H	Calcd N
1a[a]	H	NO_2	H	13[a]	189—190	$C_{21}H_{23}N_3O_6$	61.18	5.62	10.12	61.01	5.61	10.16
1b	H	H	NO_2	46	197—198	$C_{21}H_{23}N_3O_6$	60.84	5.60	10.30	61.01	5.61	10.16
1c	H	H	Br	12	205—206	$C_{21}H_{23}N_2O_4Br$	56.45	5.13	6.30	56.37	5.14	6.26
1d	H	H	CN	8	209—210	$C_{22}H_{23}N_3O_4$	67.35	5.93	10.52	67.16	5.89	10.68
1e	Cl	H	Cl	19	187—189	$C_{21}H_{22}Cl_2N_2O_4$	57.59	5.04	6.61	57.67	5.03	6.41
2				30	211—212	$C_{28}H_{26}N_4O_8$	61.33	4.86	10.22	61.53	4.80	10.25

a) This substance was obtained along with 2 (13.5% yield).

Table 2. IR and NMR data for the compounds **1a**, **1e**, and **2**

Compound	IR[a] (ν_{max}, cm^{-1})	NMR[b] δ, (ppm)
1a	3440, 3330 (NH_2), 3280 (NH), 1665 (C=O)	0.92 (t, 3H, ester CH_3), 2.78 (d, 2H, $-C\underline{H}_2-CH\langle$), 3.76 (s, 3H, OCH_3), 4.0 (q, 2H, ester CH_2), 4.24 (t, 1H, $-CH_2C\underline{H}\langle$), 5.24 (s, 1H, $-NH-C\underline{H}\langle$), 6.6—6.9 (m, 3H, aromatic), 7.4—8.3 (m, 6H, aromatic and NH_2)
1e	3410, 3310 (NH_2), 3280 (NH), 1665 (C=O)	0.88 (t, 3H, ester CH_3), 3.0 (d, 2H, $-C\underline{H}_2-CH\langle$), 3.66 (s, 3H, OCH_3), 4.0 (q, 2H, ester CH_2), 4.56 (t, 1H, $-CH_2-C\underline{H}\langle$), 5.83 (s, 1H, $-NH-C\underline{H}\langle$), 6.8—7.5 (m, 6H, aromatic), 7.7—8.4 (b, 2H, NH_2)
2	3470, 3350 (NH_2), 1670 (C=O)	0.88 (t, 3H, ester CH_3), 3.0 (d, 2H, $-C\underline{H}_2-CH\langle$), 3.8 (q, 2H, ester CH_2), 3.86 (s, 3H, OCH_3), 4.15 (t, 1H, $-CH_2-C\underline{H}\langle$), 4.82 (s, 1H, $\rangle N-CH\langle$), 6.1 (s, 1H, $\rangle N-\dot{C}H-O-$), 6.6—7.0 (m, 3H, aromatic), 7.6—8.3 (m, 10H, aromatic and NH_2)

a) IR spectra were recorded for KBr disks. b) NMR spectra were determined in deuteriopyridine with tetramethylsilane as internal reference; s, singlet; d, doublet; t, triplet; q, quartet; b, broad; m, multiplet.

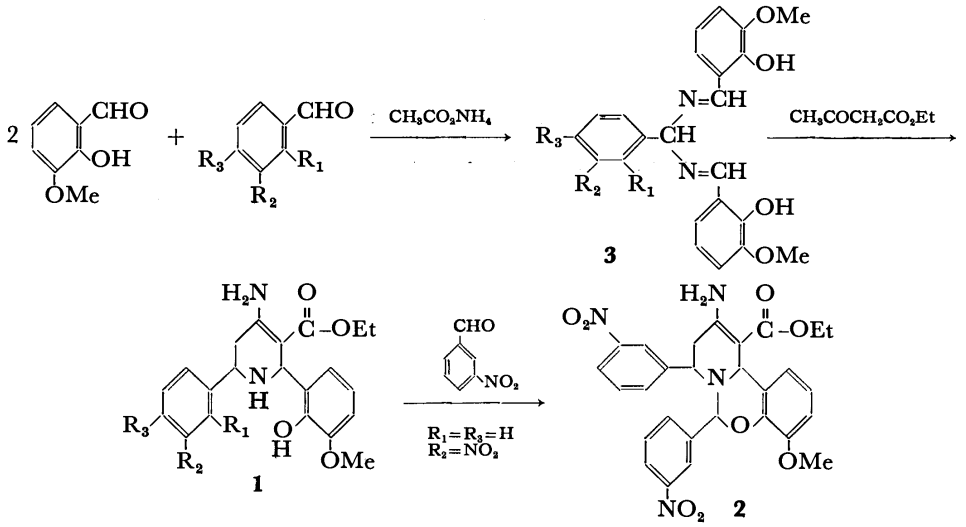

nium acetate (0.06 mol) was added to a mixture of ethyl acetoacetate (0.05 mol), 3-methoxysalicylaldehyde (0.05 mol), and *m*-nitrobenzaldehyde (0.05 mol) in ethanol (10 ml) and the mixture was heated under reflux for 2 hr. The reaction mixture was left at room temperature for several days, when yellow crystals were formed. The same reaction under reflux for 1 hr afforded a mixture of **1a** (13%) and **2** (13.5%). **2** was also prepared in 60% yield from the reaction of **1a** and *m*-nitrobenzaldehyde by refluxing with ammonium acetate in ethanol.

α,α-Bis(3-methoxysalicyclideneamino)-2,4-dichlorotoluene (3, R_1=R_3=Cl, R_2=H). To a mixture of 3-methoxysalicylaldehyde (2.0 g) and 2,4-dichlorobenzaldehyde (2.3 g) in ethanol (15 ml), ammonium acetate (1.0 g) was added and the mixture was heated under reflux for 0.5 hr. After cooling, water (3 ml) was added to the reaction mixture and the solution was left to cool for several days, a crystalline yellow solid separated; yield: 1.0 g; mp 135—136 °C (from ethanol).

Found: C, 59.93; H, 4.74; Cl, 15.26; N, 5.87%. Calcd for $C_{23}H_{20}Cl_2N_2O_4$: C, 60.13; H, 4.35; Cl, 15.45; N, 6.10%. NMR ($CDCl_3$): δ 3.88 (s, 6H, 2 OCH_3), 6.38 (s, 1H, =N-CH-N=), 6.8—7.1 (m, 6H, aromatic), 7.2—7.4 (m, 3H, aromatic), 8.56 (s, 2H, 2 -N=CH-), 12.84—13.24 (broad, 2H, 2 OH).

Heating this product with ethyl acetoacetate and ammonium acetate in ethanol for 1 hr gave the compound **1e** in 42% yield.

Reference

1) A. Sakurai and H. Midorikawa, *J. Chem. Soc., Perkin I*, **1975**, 2025.

BULLETIN OF THE CHEMICAL SOCIETY OF JAPAN, VOL. 49(3), 839 (1976)

A Zwitterionic Alkaloid from *Daphniphyllum Teijsmanni* Zollinger

Shosuke YAMAMURA, Masaaki TODA,* and Yoshimasa HIRATA*

Faculty of Pharmacy, Meijo University, Showa-ku, Nagoya 468
**Chemical Institute, Nagoya University, Chikusa-ku, Nagoya 464*

(Received November 12, 1975)

Synopsis. A zwitterionic alkaloid, the hydration product of daphnilactone-B, has been isolated from the fruits of the plant *Daphniphyllum teijsmanni* Zollinger, and its structure also been determined on the basis of its spectral and chemical properties.

Many alkaloids have been isolated from the bark and leaves of the plant *Daphniphyllum macropodum* Miquel.[1] Further examination of the alkaloidal components in the fruits of the plant *Daphniphyllum teijsmanni* Zollinger led to the isolation of several alkaloids including daphnilactone-B (**1**) as a major product.[1,2] The present paper deals with the zwitterionic alkaloid related with daphnilactone-B.

As described in the previous paper,[2] an oily material containing alkaloidal components was chromatographed on alumina, and eluted successively with hexane, hexane–benzene (1: 1), benzene, benzene–$CHCl_3$ (1: 1) and $CHCl_3$ to give six alkaloids. Further elution with EtOAc–MeOH (9: 1) afforded colorless plates of a new alkaloid (**2**) in 0.00042% overall yield.

This alkaloid (**2**) has a molecular formula [$C_{22}H_{33}O_3N$ (*m/e* 359 (M^+)); mp (decomp) 247—248 °C] with the following spectral data: ν_{max} (Nujol) 3300, 1595, and 1575 sh.cm^{-1}; δ (CD_3OD–D_2O) 1.09 (3H, d, J=6.0 Hz), 3.40—4.05 (5H, complex), 3.70 (1H, d, J=10.5 Hz), 4.27 (1H, d, J=10.5 Hz) and 5.74 ppm (1H, br.s, $W_h \simeq 5$ Hz). The IR and NMR spectra of **2** indicate the presence of a hydroxymethyl group (ν_{max} 3300 cm^{-1}; δ 3.70 and 4.29 ppm). Furthermore, the IR absorption band at 1595 and 1575 sh.cm^{-1} may be due to the CO group of a carboxylate. This is confirmed by the following chemical evidence.

When treated with anhydrous MeOH containing HCl gas (room temp., 5 hr), this alkaloid was readily converted into a mixture of two compounds. The major product was proved to be identical with daphnilactone-B (**1**) (mp, mass and IR spectra), and the remaining one was the expected methyl ester (**3**) which had been already obtained on treatment of **1** with NaOMe.[2] Action of 90% HCOOH on **2** also converted it to daphnilactone-B.

Biogenetically, this zwitterionic alkaloid (**2**) may be regarded as a precursor of daphnilactone-B (**1**), although we can not rule out a possibility, in which the former is produced from **1** in the course of isolation.

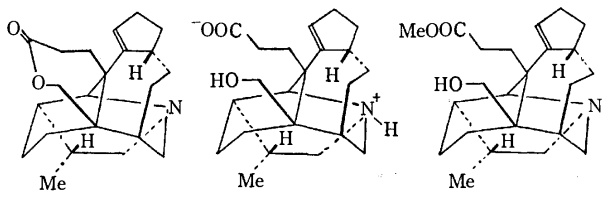

1 **2** **3**

Experimental

All mps are uncorrected. The IR and mass spectra were recorded on a JASCO Model IR-S and on a Hitachi RMU 6C mass spectrometer, respectively. The NMR spectra were obtained on a Nihondenshi JNM-PS 100. Chemical shifts are given in ppm from TMS as an internal standard. Only prominent peaks are cited.

Isolation of the Zwitterionic Alkaloid (2). The fruits of the plant *Daphniphyllum teijsmanni* Zollinger (10 kg) were extracted with MeOH (10 l) at room temperature for 2 weeks and treated according to the procedure described in Ref. 2 to give an oil (12 g), which was chromatographed on alumina (Nakarai Chemical Co. Ltd., *ca.* 300 mesh) (60 g) and eluted with hexane, hexane–benzene (1: 1), benzene, benzene–$CHCl_3$ (1: 1) and $CHCl_3$ to afford methyl homodaphniphyllate, daphnilactone-B, daphniphylline, yuzurimine, methyl homosecodaphniphyllate and yuzurimine-B.[2] Further elution with EtOAc–MeOH (9: 1) afforded a crystalline solid, which was recrystallized from water–acetone to give colorless plates of **2**, mp (decomp) 247—248 °C (Found: *m/e* 359.24395. Calcd for $C_{22}H_{33}O_3N$: *m/e* 359.24603).

Formation of Daphnilactone-B (1) and the Methyl Ester (3). To a solution of **2** (50 mg) in anhydrous MeOH (2 ml) was added one drop of ether saturated with HCl gas. The reaction solution was stirred at room temp. for 5 h, and then concentrated under reduced pressure below 5 °C to leave a solid which was dissolved in $CHCl_3$ containing small amounts of $NaHCO_3$ and subjected to preparative tlc (Kieselgel 60 PF_{254}: hexane–Et_2O–Et_2NH (10: 10: 1)]. From the less polar fraction daphnilactone-B (**1**) (30 mg) was isolated (mp, IR and mass spectra), and the methyl ester (**3**) (5 mg) was obtained from the more polar fraction (IR and mass spectra).[2]

Conversion of 2 to Daphnilactone-B (2). A solution of **2** (73 mg) in 90% aq. HCOOH (1 ml) was stirred at 85 °C overnight, and then diluted with small amounts of water. The aqueous solution was made basic with Na_2CO_3 and extracted with $CHCl_3$. The extract was washed with sat. NaCl aq., and then dried over Na_2SO_4. Removal of the solvent gave a colorless oil, which was chromatographed on basic alumina (2 g) and eluted with $CHCl_3$ to afford daphnilactone-B (28 mg) (mp, and IR spectrum).[2]

References

1) S. Yamamura and Y. Hirata, "The Alkaloids," Vol. XV, ed. by R. H. F. Manske, Academic Press, New York (1975), p. 41.

2) M. Toda, H. Niwa, H. Irikawa, Y. Hirata, and S. Yamamura, *Tetrahedron*, **30**, 2683 (1974).

The Initiation Reaction of Electro-initiated Polymerization of Acrylamide in the Kolbe Electrolysis System*

Zempachi OGUMI, Isao TARI**, Zenichiro TAKEHARA, and Shiro YOSHIZAWA

Department of Industrial Chemistry, Faculty of Engineering, Kyoto University, Yoshida, Sakyo-ku, Kyoto 606

(Received May 10, 1975)

The mechanism of electro-initiated polymerization of acrylamide in the Kolbe electrolysis system was investigated in detail and the reaction path of the intermediate radicals was clarified by product analysis and a measurement of the consumption rate of the monomer. The Kolbe intermediate radical, $CF_3\cdot$, reacts first preferentially with the monomer. Next, the radical thus formed reacts with other species to produce $CF_3CH_2CH_2CONH_2$, $CF_3CH_2CH(CF_3COO)CONH_2$ and $CF_3CH_2CH(CONH_2)CH(CF_3CH_2)CONH_2$. The first reaction is fast, but the reaction of $CF_3COO\cdot$ with the monomer appears to be unreasonable. These reactions proceed on the electrode surface and in the layers below the diffusion layer, *i.e.*, in layers of the same order as the depth of unevenness on the platinized platinum electrode.

A few papers have been published concerning the utilization of Kolbe electrolysis as a source of free radicals for initiating polymerization and papers explaining the process of initiating polymerization are very few. The authors have also investigated the production of an oligomer[1,2] and a high polymer[3,4] of acrylamide utilizing the Kolbe reaction in a system of acetate and trifluoroacetate solutions. In a preceding paper[2], they have proposed the following reaction path as the most probable process of initiating polymerization of acrylamide in an aqueous solution of trifluoroacetic acid and potassium trifluoroacetate.

$$R\cdot + M \longrightarrow RM\cdot \quad (1)$$

$$RM\cdot + X \longrightarrow RMX \quad (2)$$

$$2RM\cdot \longrightarrow RMMR \quad (3)$$

$$RM\cdot + R\cdot \longrightarrow RMR \quad (4)$$

$$RM\cdot + M \longrightarrow RMM\cdot \xrightarrow{M} \text{oligomer} \quad (5)$$

where R· represents Kolbe intermediate radical, $CF_3COO\cdot$ and/or $CF_3\cdot$. Reaction (1) was assumed to be very fast. If this assumption is correct, one mol of the monomer will be consumed for every Farady of electricity in addition to that required for oligomer formation. The low current efficiency of oligomer production was ascribed to the fact that reaction (5), which leads to the formation of the oligomer, competes with reactions (2)—(4) which are considered to be fast. Therefore, it is expected that the products with low molecular weight represented by RMX, RMR and RMMR are formed during the oligomer formation. These compounds are examined in this paper in order to verify the above reaction path which was proposed by the authors. Also the kind of radicals taking part in initiating reactions and the manner by which the reactions of the intermediate radicals proceeds are discussed. Furthermore, the site of the polymerization reaction is examined. This is very important from the standpoint of improving of the current efficiency of the oligomer formation and of reaction system for the production of high polymers. This problem may concern the state of the Kolbe intermediate radicals.[5]

The experiments were conducted using a rotating cylindrical electrode and platinized platinum electrodes.

Experimental

The same equipment as that used in previous work was used for the electrolysis[2]. A cylindrical platinum electrode (1.3 cm in diameter, 10 cm^2 in area) was used in the rotating electrode experiment. Platinized platinum electrodes having various degrees of roughness were used. Besides a TFA and TFK 4M solution***, a 2M acetate solution was used, which includes 1 mol acetic acid and 1 mol potassium acetate in 1 liter. The measurement of the acrylamide content in the solution was carried out following the bromate-bromide method, which was modified so that the addition of bromide was performed in a nitrogen atmosphere and in the dark to eliminate the effect of oxygen.

Results

Low Molecular Weight Products. As shown in a preceding paper[2], neither normal Kolbe coupling products nor other gaseous products are formed in a system of electro-initiated polymerization in spite of the low current efficiency of oligomer formation. This fact and the above reaction path imply the existence of products such as RMX, RMR and RMMR in the electrolyte. On the basis of this prediction, the electrolyte was analysed after electrolysis. After electrolysis of a TFA and TFK 4 M solution containing 20 g/100 ml of acrylamide at 400 mA on a platinum electrode (3×3 cm^2), the electrolyte was analyzed using the gel filtration chromatographic technique. Peak b of curve A in Fig. 1 indicates the existence of products with low molecular weight. Peaks a, c and d correspond to products with high molecular weight, monomeric acrylamide and trifluoroacetate, respectively. Curve B corresponds to an aqueous solution of the acrylamide monomer. The following low molecular weight products were detected. $CF_3CH_2CH(CF_3COO)CONH_2$, $CF_3CH_2CH_2CONH_2$ and $CF_3CH_2CH(CONH_2)CH(CF_3CH_2)CONH_2$. These were isolated using the gas-chromatographic technique and identified using mass and infrared spectrophotometric techniques. The gas chromatogram also exhibited traces of products with

* Studies of Electro-Initiated Polymerization. (Part 4).

** Present address: Department of Synthetic Chemistry, Faculty of Engineering, Okayama University, Tsushima, Okayama 700.

*** This is an aqueous solution of 2 mol trifluoroacetic acid and 2 mol potassium trifluoroacetate in 1 liter.

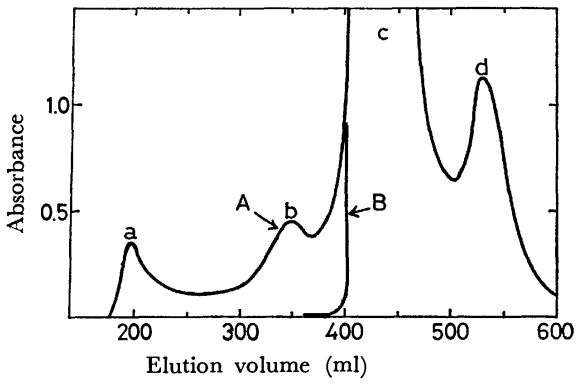

Fig. 1. Gel filtration chromatograms.
Column: Sephadex G-10, 4 cmϕ, 40 cm hight, V_v=195 ml
A: Electrolyte after electrolysis, B: an aqueous solution of monomeric acrylamide.

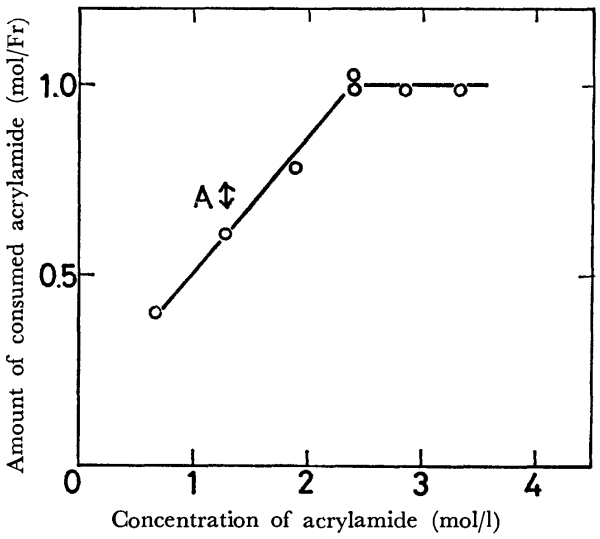

Fig. 2. Relationship between the amount of consumed monomer and monomer concentration.
Electrolyte: TFA+TFK 4 M, Electrode: Smooth platinum (3×3 cm²), Current: 400 mA.

molecular weights higher than the above three compounds.

The Amount of Consumed Acrylamide. In order to confirm the participation of the intermediate radical R· in the Kolbe reaction with the monomer forming RM·, the amount of consumed monomeric acrylamide was measured based on the modified bromate-bromide method. The amount of the monomer consumed and of the polymer produced were measured. From these measurements, the amount of monomer consumed for reactions other than oligomer formation was calculated. This value per Faraday is illustrated in Fig. 2. The higher the concentration of acrylamide up to 2.4 M, the more acrylamide is consumed. At concentrations above 2.4 M, about one mol of monomer is consumed per Faraday. At concentrations lower than 2.4 M, the Kolbe dimer, ethane, is formed. In this case, R· produced by charge transfer on the electrode reacts to form the oligomer, ethane and other products. The amount of R· consumed other than that for oligomer

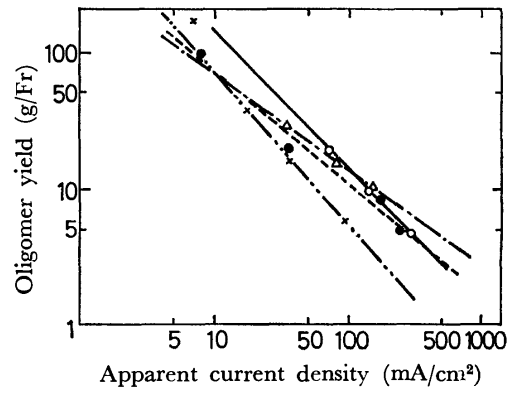

Fig. 3. The effect of surface roughness on the oligomer yield.
Electrolyte: 2 M acetate solution 100 ml+acrylamide 20 g, Electrode: Platinized platinum (1.5×3×2 cm²) r; ○: 1300, △: 175, ●: 60, ×: 45.

and ethane formation were calculated in order to obtain the amount of consumed acrylamide per mol of R· which resulted in products in the electrolyte with lower molecular weight. This amount is illustrated by A in Fig. 2.

The Effect of Electrode Surface Unevenness. The effect of electrode surface roughness was examined in order to obtain information about the area where the oligomer formation occurred. Platinum electrodes (1×2 cm²), coated on one side with silicon resin, were plated with platinum black in a solution of chloroplatinic acid so as to produce a surface of different roughness. The real surface area (A_1) was calculated from the amount of adsorbed hydrogen measured based on the charging curve method in 0.5 M H_2SO_4. The ratio of A_1 to the apparent surface area is designated the roughness factor (r). The relationship between the oligomer yield and the apparent current density on electrodes with different roughness factors was examined. As shown in Fig. 3, the yield increases with roughness factor in the region of relatively high current densities. The effect of roughness, however, is not great. The apparent current density at a given potential increases with r in a 2 M acetate solution without acrylamide but this increase is not great in comparison with the increase of r, and is less than in a solution containing acrylamide. This fact implies that only a part of the surface measured by the hydrogen adsorption method is effective for charge transfer on the electrode.

The Effect of Electrode Rotation. The relation between the area where the polymerization occurs and the thickness of the diffusion layer and the effect of the mass transfer rate to the electrode on oligomer formation were examined using the rotating cylindrical electrode in a 2 M acetate solution. As shown in Fig. 4, below 1500 rpm and above 2000 rpm only a small effect is observed, but there exists a marked increase between 1500 and 2000 rpm. This jump may be ascribed to a change from laminar to turbulent flow.

The Effects of Monomer Concentration and Current Density. The effect of current density was examined at different monomer concentrations in a 2 M acetate solution

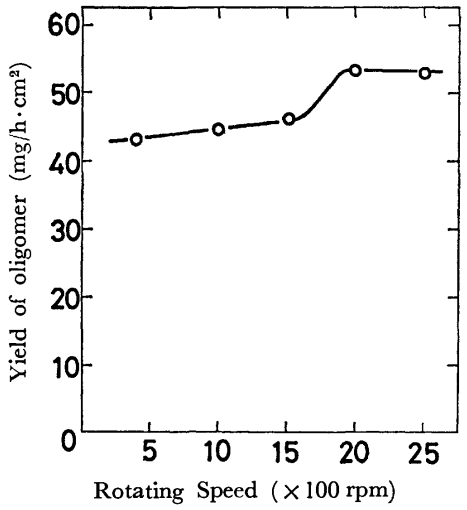

Fig. 4. Dependence of oligomer yield on rotating speed. Electrolyte: 2 M acetate solution 100 ml+acrylamide 20 g, Electrode: Cylinder electrode (10 cm²), Current: 200 mA.

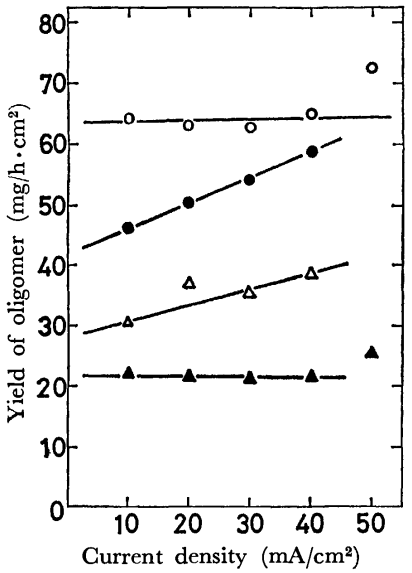

Fig. 5. Dependence of oligomer yield on current density and monomer concentration. Electrode: Cylinder electrode (10 cm²), Rotating speed: 1450 rpm, Electrolyte: 2 M acetate solution 100 ml+acrylamide, Acrylamide; ▲: 10 g, △: 15 g, ●: 20 g, ○: 25 g.

using a cylindrical electrode. Figure 5 shows that at the acrylamide concentrations of 25 g/100 ml and 10 g/100 ml, the yield does not depend on the current density, in agreement with the case of the TFA and TFK 4 M solution[2]. As concentrations of 15 g/100 ml and 20 g/100 ml, however, the yield increases linearly with current density but does not exceed the value at 25 g/100 ml.

Discussion

Three compounds, $CF_3CH_2CH_2CONH_2$, $CF_3CH_2CH(CF_3COO)CONH_2$ and $CF_3CH_2CH(CONH_2)CH(CF_3CH_2)CONH_2$ were detected as products with low molecular weight, RMX, RMR and RMMR. These products indicate the occurrence of reactions (1)—(4). It was observed that 1 mol of the monomer was consumed per Faraday in addition to the consumption required for oligomer formation at high monomer concentrations. This fact supports the assumption that reaction (1) is so fast that almost all of the Kolbe intermediate radicals react with the monomer. In this consideration the current efficiency of the acetate discharge can be considered to be 100%. There exist two kinds of radical species, $CF_3\cdot$ and $CF_3COO\cdot$, as Kolbe intermediates. The fact that $CF_3COOCH_2CH_2CONH_2$ and $CF_3COOCH_2CH(CONH_2)CH(CF_3COOCH_2)CONH_2$ were not detected, but that $CF_3CH_2CH_2CONH_2$ and $CF_3CH_2CH(CONH_2)CH(CF_3CH_2)CONH_2$ were produced clearly shows that $CH_3\cdot$ reacts first with the monomer and the RM· thus formed produces farther reactions. This indicates that the reaction of the radical with the monomer is not as fast as the decarboxylation reaction of $CF_3COO\cdot$. Radical RM· is more active than the monomer and it can react fast with $CF_3COO\cdot$ or RM·, or it can extract hydrogen from other species. From these results we can deduce the reaction path of intermediate radicals as shown in Fig. 6. We have considered that the region where polymerization occurs is just in the vicinity of electrode, but it is still a question as to how far from the electrode this region extends. Some investigators have considered that it occurs on the electrode surface.[6]

The correlation between the height of the rough surface and the thickness of the reaction region in the experiment with the platinized platinum electrode is schematically shown in Fig. 7. In case A, where the thickness is small and the reaction layer is parallel to

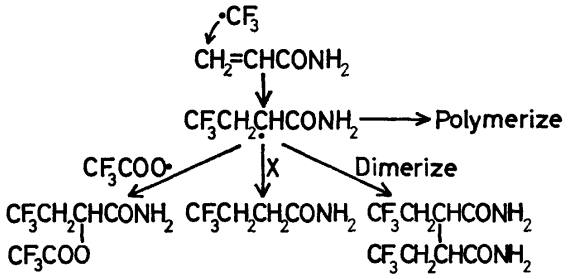

Fig. 6. Reaction path of intermediates.

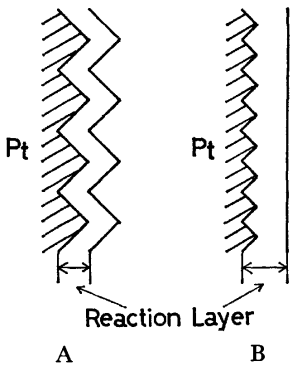

Fig. 7. The relation between surface unevenness and polymerization region.

the uneven surface of the electrode, the volume of the reaction region increases proportionally with an increase of the electrode surface on which the electrode reactions proceed. Thus the radical concentration is this region changes with the surface roughness at the same apparent current density. This causes an increase in the current efficiency of oligomer formation with an increase in surface roughness, because the current efficient of oligomer formation decreases with an increase in current density. In case B, where the reaction layer is thick enough so that the unevenness of the surface does not affect the deepest surface of the layer, the volume of the reaction layer does not increase even if the surface roughness increases. Accordingly, no change in oligomer yield will be caused by a change in the surface roughness. As is shown in Fig. 3, only a slight effect of surface roughness was observed at high current densities, while none was observed at low current densities. This indicates a state between A and B in Fig. 7, *i.e.*, the reaction layer is very thin and that of the same order of thickness as the unevenness of the platinized platinum electrode. Furthermore, this consideration is supported by the results using the rotating cylindrical electrode in which only a slight effect of the rotational speed was observed above 2000 rpm and below 1500 rpm. Namely, the reaction layer is very thin and does not extend into the diffusion layer which is influenced by the electrode rotational speed.

References

1) S. Yoshizawa, I. Tari, and M. Suhara, *Denki Kagaku*, **40**, 650 (1972).
2) Z. Ogumi, I. Tari, Z. Takehara, and S. Yoshizawa, *Bull. Chem. Soc. Jpn.*, **47**, 1843 (1974).
3) S. Yoshizawa, Z. Takehara, Z. Ogumi, and C. Nagai, *Denki Kagaku*, **40**, 724 (1972).
4) S. Yoshizawa, Z. Takehara, Z. Ogumi, and C. Nagai, *J. Appl. Electrochem.*, **6**, No. 2 (1976) to be published.
5) L. Eberson, *Electrochim. Acta*, **12**, 1473 (1967).
6) I. Izumi, Ph. D. Thesis, Osaka City University (1971).

C-13 NMR Chemical Shifts and Charge Densities of Substituted Thiophenes—The Effect of Vacant d^{π} Orbitals

Yoshihiro OSAMURA, Osamu SAYANAGI, and Kichisuke NISHIMOTO
Department of Chemistry, Osaka City University, Sumiyoshi-ku, Osaka 558

(Received June 11, 1975)

The effect of vacant d^{π} orbitals on the charge distributions of heteroatomic systems containing sulfur and halogens is discussed. From an appropriate estimation of the Coulomb and resonance integrals associated with the vacant d^{π} orbitals, a linear relationship is obtained between charge density and C-13 chemical shift. For a discussion of the reactivity for electrophilic substitution of thiophene, the contribution of d^{π} orbitals of sulfur atom should be taken into account.

The C-13 NMR chemical shift can be empirically correlated with the charge density on a given carbon atom in a molecule.[1] Since charge density is an important quantity for the study of the chemical reactivity of molecule, an investigation of a relationship between the C-13 chemical shift and the charge density will greatly contribute to theoretical organic chemistry. For aromatic hydrocarbons, substituted benzenes and aromatic heterocyclic compounds containing oxygen or nitrogen atoms, π-electron densities calculated by the MO method have a nearly linear relationship with the C-13 chemical shifts.[1] However, such linear correlation has not yet been obtained for the organic compounds containing halogen and sulfur atoms. The reason for this may be due to the contribution of the vacant d-orbitals to the electronic structure of these compounds. In order to elucidate the effect of vacant d-orbitals of sulfur, chlorine, and bromine atoms on the charge distributions, we carried out a MO calculation based on the σ-included ω-HMO method.[2] We have studied the relationship between C-13 NMR chemical shifts and charge densities for pyrrole, furan, thiophene, and its derivatives.

Theoretical

NMR Chemical Shift and Local Charge Density. The quantum theory of NMR chemical shift was developed by Ramsey.[3] He calculated the shielding parameter σ by means of the second order perturbation theory. However, it is difficult to apply his equation to large molecules. The total shielding constant can be expressed by a sum of local contributions. The expression of shielding constant is divided into the following three terms: 1) The diamagnetic contribution or Lamb term for the atom being considered, σ_d. 2) The paramagnetic term for the same atom, σ_p. 3) The contribution from other atoms, σ'. Thus

$$\sigma = \sigma_d + \sigma_p + \sigma' \tag{1}$$

The diamagnetic term, σ_d, can be given by

$$\sigma_d = \frac{e}{3mc^2}\sum_i \langle r_i^{-1} \rangle \tag{2}$$

where $\langle r_i^{-1} \rangle$ is the mean inverse distance of electron i from the nucleous, and the summation is taken over the electrons in the atom considered.

Karplus and Pople[4] pointed out that in a C-13 NMR chemical shift, σ_d makes no significant contribution. The neighbor atom term, σ', is also very small. Thus, the main contribution to the C-13 chemical shift arises from the paramagnetic term, σ_p. Since the NMR measurement in liquid sample deals with a rotational average, σ_p^A associated with a given atom A can be represented by

$$\sigma_p^A = -\frac{e^2h^2}{2m^2c^2\Delta E}\langle r^{-3} \rangle_{2p} \sum_B Q_{AB} \tag{3}$$

where

$$Q_{AB} = \frac{4}{3}\delta_{AB}(P_{x_Ax_B} + P_{y_Ay_B} + P_{z_Az_B}) - \frac{2}{3}(P_{y_Ay_B}P_{z_Az_B} + P_{z_Az_B}P_{x_Ax_B} + P_{x_Ax_B}P_{y_Ay_B}) + \frac{2}{3}(P_{y_Az_B}P_{z_Ay_B} + P_{z_Ax_B}P_{x_Az_B} + P_{x_Ay_B}P_{y_Ax_B}). \tag{4}$$

ΔE is a mean excitation energy, and $\langle r^{-3} \rangle_{2p}$ is the mean cube inverse distance of a 2p electron from the nucleous. $\sum$ extends over the atom considered and the neighboring atoms, P_{ab} being the element of charge density and bond order matrix in the unperturbed molecule.

For the sake of simplicity, we make the following approximations; 1) σ-AO of carbon atom can be represented by a sp^2 hybridization. Thus, each σ-AO can be expressed as follows.

$$\left.\begin{aligned} \sigma_1 &= \frac{1}{\sqrt{3}}\phi(2s) + \frac{2}{\sqrt{6}}\phi(2p_x) \\ \sigma_2 &= \frac{1}{\sqrt{3}}\phi(2s) - \frac{1}{\sqrt{6}}\phi(2p_x) + \frac{1}{\sqrt{2}}\phi(2p_y) \\ \sigma_3 &= \frac{1}{\sqrt{3}}\phi(2s) - \frac{1}{\sqrt{6}}\phi(2p_x) - \frac{1}{\sqrt{2}}\phi(2p_y) \end{aligned}\right\} \tag{5}$$

2) ΔE is assumed to be constant for each molecule. The assumption does not seem to be unreliable, since the C-13 NMR chemical shifts of aromatic hydrocarbons are almost constant, in spite of the fact that the average excitation energy changes considerably with the size of molecule. 3) Bond order dependence of the chemical shift is neglected. The C-13 chemical shifts should depend on the bond orders. However, Olah and Mateescu[5] showed that in a series of stable carbonium ions the C-13 chemical shifts can be fairly well correlated with only the charge densities, in spite of the fact that their bond orders vary considerably. Let us assign the charge densities q_1, q_2 and q_3 to each σ-AO's, σ_1, σ_2, and σ_3 of a given carbon atom and q^{π} to the π-AO, respectively.

If we use the expression

Table 1. Parameters associated with π and σ AO's

Atom	δ_μ^π	ω	Bond	$k_{\mu\nu}^\pi$	Atom	δ_μ^σ	ω
C·	0.0	0.5	C≡C	1.0	C(sp^2)	0.0	0.25
N·	0.5	0.5	C=C	1.1	C(sp^3)	−0.05	0.25
N:	0.8	0.5	C-C	0.9	O	0.5	0.25
O·	1.0	0.5	C-NO_2	0.9	N	0.25	0.25
O:	1.4	0.5	N≡O	1.1	H	−0.1	0.43
S:	1.0	0.5	C=O	1.2	S	−0.06	0.17
Cl:	1.7	0.5	C-O	0.7	Cl	0.0	0.17
Br:	1.3	0.5	C-S	0.5	Br	−0.2	0.12
			C-Cl	0.6			
			C-Br	0.5		$\beta_{\mu\nu}^\sigma = \beta$	

$$\Delta q_i = q_i - 1 \tag{6}$$

we obtain

$$\left.\begin{aligned} \Delta P_{xx} &= \frac{1}{6}(\Delta q_1 + 4\Delta q_2 + \Delta q_3) \\ \Delta P_{yy} &= \frac{1}{2}(\Delta q_1 + \Delta q_3) \\ \Delta P_{zz} &= \Delta q^\pi \end{aligned}\right\} \tag{7}$$

$$P_{xy}P_{yx} = \frac{(q_3 - q_1)^2}{12}.$$

Assuming Slater's rule, the integral $\langle r^{-3}\rangle_{2p}$ can be easily represented by

$$\langle r^{-3}\rangle_{2p} = \frac{1}{24a_0^3}(3.25 - 0.35\Delta Q)^3 \tag{8}$$

where

$$\Delta Q = \Delta q_1 + \Delta q_2 + \Delta q_3 + \Delta q^\pi$$

a_0 means the Bohr radius. Substituting Eqs. (4), (7), and (8) into Eq. (3), we obtain

$$\sigma_p^A = -K(1 - 0.108\Delta Q)^3\{9 - \Delta q^\pi(\Delta q_1 + \Delta q_2 + \Delta q_3) - (\Delta q_1\Delta q_2 + \Delta q_2\Delta q_3 + \Delta q_3\Delta q_1)\} \tag{9}$$

where

$$K = \frac{e^2h^2}{m^2c^2\Delta E}\frac{3.25^3}{216a_0^3}$$

Since Δq_t is usually very small, we can, to a first approximation, neglect higher terms. Consequently, Eq. (9) can be rewritten as

$$\sigma_p^A = -9K(1 - 0.324\Delta Q) \tag{10}$$

showing a linear relationship between C-13 NMR chemical shift and charge density. The present expression is the same as that obtained by Yonezawa *et al.*[6] for saturated hydrocarbon systems. As Alger *et al.*[7] pointed out, when orbital contraction of σ-AO is considered, Eq. (10) is modified as follows:

$$\sigma_{C^{13}} = a\Delta q^\pi + b\Delta Q - c\Delta P \quad (a = b) \tag{11}$$

B. MO calculation

In the present study, the charge densities were calculated by the σ-included ω-HMO method which is summarized as follows: As σ-bonds are almost localized between two atoms, we can approximately describe them by means of the two center MO. ω-Technique is used in order to take so-called inductive effect of a heteroatom through bonds into account. Thus, the polarized σ-framework is determined by the two center ω-HMO method. The π-electrons are regarded as moving over this σ-framework. The π-densities, then are dependent on the σ- and π-charge densities. We neglect the effect of π-charge densities on the σ-bonds. The net charge ΔQ_μ on the atom μ is given by

$$\Delta Q_\mu = \Delta Q_\mu^\sigma + \Delta q_\mu^\pi. \tag{12}$$

The Coulomb integrals associated with the σ- and π-AO's of the μ-th atom, α_μ^σ and α_μ^π are expressed as follows:

$$\alpha_\mu^\sigma = \alpha_c^\sigma + \delta_\mu^\sigma\beta + \omega^\sigma\Delta Q_\mu^\sigma$$
$$\alpha_\mu^\pi = \alpha_c^\pi + \delta_\mu^\pi\beta + \omega^\pi\Delta Q_\mu$$

The resonance integral for the μ-ν bond, $\beta_{\mu\nu}$, is represented by

$$\beta_{\mu\nu}^\sigma = k_{\mu\nu}^\sigma\beta, \qquad \beta_{\mu\nu}^\pi = k_{\mu\nu}^\pi\beta.$$

The values of ω's, δ_μ's and $k_{\mu\nu}$'s, used are summarized in Table 1.

Since the compounds we considered include sulfur and halogen atoms, the contribution of d-orbitals should be taken into account. We consider only the vacant d^πAO's in our MO calculation. The Coulomb and resonance integrals associated with d^πAO's are estimated with use of atomic energy levels[8] and overlap integrals between $2p\pi$ and $3d\pi$ AO's. Their values are given in Table 2.

Table 2. Parameters associated with d^π orbitals

Atom	$\delta_{\mu d}^\pi$	ω	Bond	$k_{\mu\nu}$
S	−1.0	0.4	C-S	0.5
Cl	−0.8	0.4	C-Cl	0.5
Br	−0.7	0.4	C-Br	0.5

Results and Discussion

Charge Density and C-13 *NMR Chemical Shift.* The effect of substitution on the electron distribution is quite important for discussing the chemical reactivity of a substituted compound. The influence of the heteroatoms on the charge density of a given carbon atom can be described in terms of mesomeric and inductive effects. Takahashi *et al.*[9] reported the C-13 NMR chemical shifts of thiophene and its derivatives and presented some interesting results. However,

they could not obtain inter-relationship between the charge density and the chemical shift. In this paper, the experimental data are quoted from their work. From the NMR measurements, it is expected that in pyrrole and furan the charge densities of C_2 positions are smaller than those of C_3 positions, because of the lower chemical shifts. However, in thiophene the chemical shifts of both positions are almost the same.

In Fig. 1, the charge densities of substituted thiophenes calculated by σ-included ω-HMO method are plotted against the chemical shifts, neglecting the contribution of d-orbitals. The plots deviate considerably from lineality. This might be caused by the neglect of contribution of vacant d-orbitals. The results of thiophene derivatives calculated by CNDO/2 method are shown in Fig. 2. The CNDO/2 method takes explicitly the contribution of d-orbitals into account. However, no improvement could be obtained. This could be attributed to an overestimation of the contribution of d-orbitals at C_3 and C_4 positions. The failure is due to the estimation of parameters associated with d-orbitals.

In our calculations, the resonance integrals between $d\pi$ and $2p\pi$ AO's of non-neighbors are completely neglected. In thiophene, the C–S–C bond angle is known to be almost 90°.[10] We, therefore, assumed σ AO's of sulfur atom are not hybridized but are pure $3p_x$ or $3p_y$ AO's. Thus, $3d_{xz}$ and $3d_{yz}$ should be directed toward each C-S bonds as shown in Fig. 3. We considered only one $d\pi$ AO in a halogen atom, Cl or Br. In Figs. 4 and 5, the charge densities calculated by σ-included ω-HMO method, including

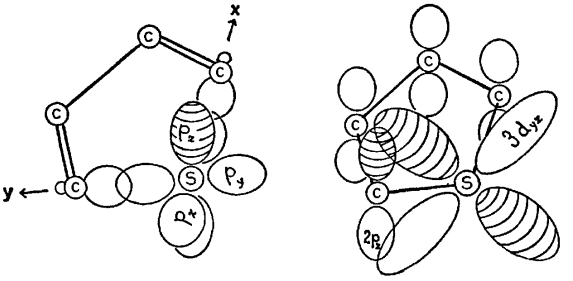

(a) (b)

Fig. 3. p and d orbital profile for thiophene. (a) 3p-sp^3 overlap, (b) $3d_{yz}$-$2p^\pi$ overlap.

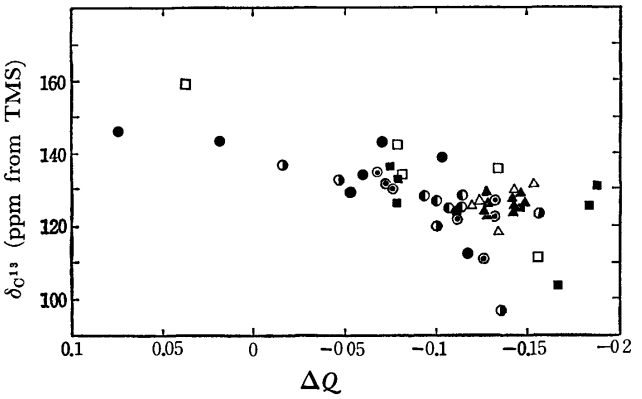

Fig. 1. C-13 NMR chemical shifts *vs.* charge densities of substituted thiophenes (σ-included ω-HMO method without d orbitals).
● C_2 of 2-substituted thiophene, ■ C_3 of 2-substituted thiophene, ▲ C_4 of 2-substituted thiophene, ⊙ C_5 of 2-substituted thiophene, ◑ C_2 of 3-substituted thiophene, □ C_3 of 3-substituted thiophene, △ C_4 of 3-substituted thiophene, ◐ C_5 of 3-substituted thiophene.

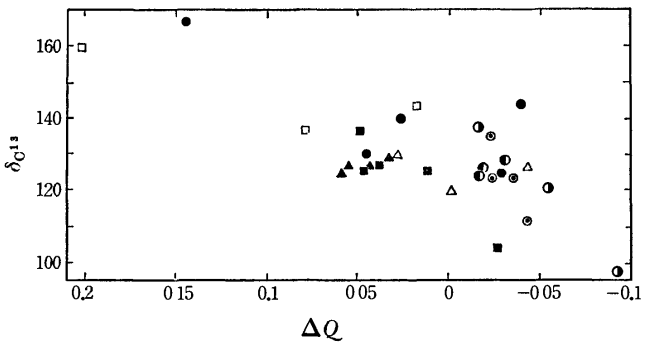

Fig. 2. C-13 NMR chemical shifts *vs.* charge densities of substituted thiophenes (CNDO/2 method).

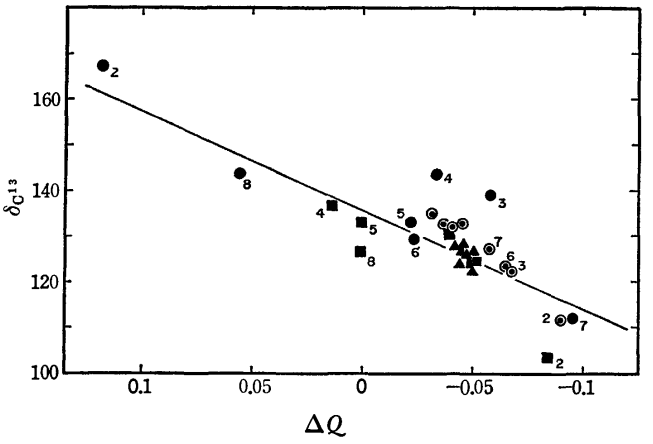

Fig. 4. C-13 NMR chemical shifts *vs.* charge densities of 2-substituted thiophenes (σ-included ω-HMO method considering d^π orbitals). 1; H, 2; OCH_3, 3; CH_3, 4; CHO, 5; $COOCH_3$, 6; Cl, 7; Br, 8; NO_2.

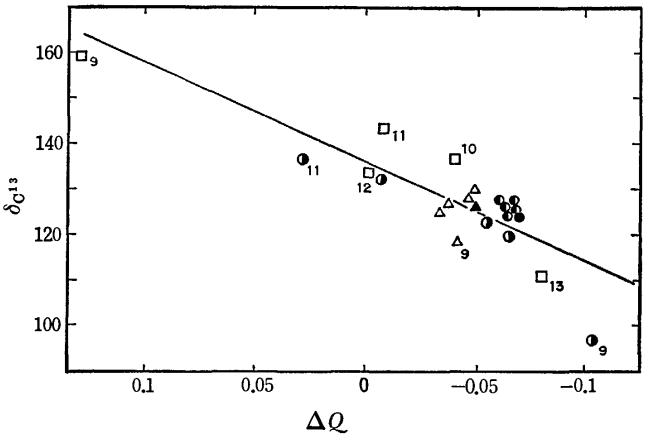

Fig. 5. C-13 NMR chemical shifts *vs.* charge densities of 3-substituted thiophenes (σ-included ω-HMO method considering d^π orbitals). 9; OCH_3, 10; CH_3, 11; CHO, 12; $COOCH_3$, 13; Br.

$d\pi$ orbitals, are plotted against the chemical shifts. We see a better correlation than the results without $d\pi$ orbitals. The plots of α-positions of methyl, carbonyl, and cyano derivatives deviated considerably. This deviation may be caused by another factor, such as anisotropy effect.

The mesomeric effect of a substituent on the charge distribution is an important problem in theoretical organic chemistry. The resonance structure of thiophene derivative having an electron donating group can be written as follows:

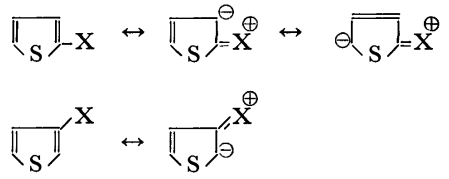

Thus, the π-electron densities on the β and δ carbons vary a great deal with mesomeric effect of substituent. In the case of δ-carbon of 2-substituted thiophene, a plot of π-electron density against the corresponding C-13 NMR chemical shift has distinct lineality, as shown in Fig. 6. A similar plot shows no lineality, when the contribution of $d\pi$ orbitals is neglected. This fact suggests us that, in order to investigate the mesomeric effect in a heteroatomic system containing S, P, Cl, or Br atoms, the contribution of the vacant $d\pi$ orbitals should be taken into consideration. When we take $d\pi$ orbitals of sulfur atom into consideration, the plots of pyrrole, furan, and thiophene show a better lineality.

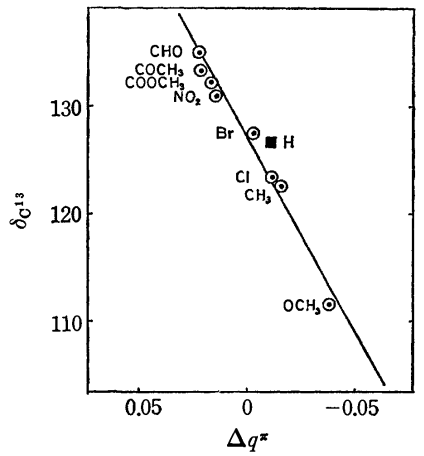

Fig. 6. C-13 NMR chemical shifts *vs.* π-charge densities on δ-carbons in substituted thiophenes.

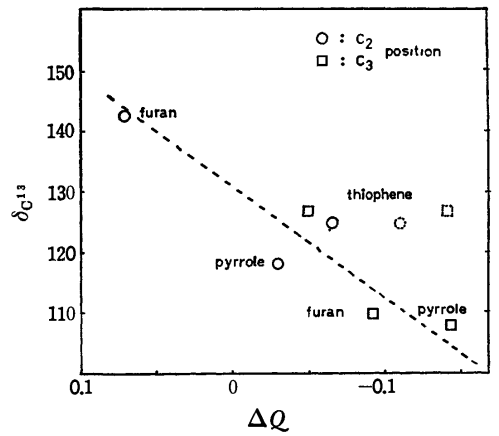

Fig. 7. C-13 NMR chemical shifts *vs.* charge densities of pyrrole, furan, and thiophene. ○ and □ represent the results of thiophene, neglecting d^π orbitals.

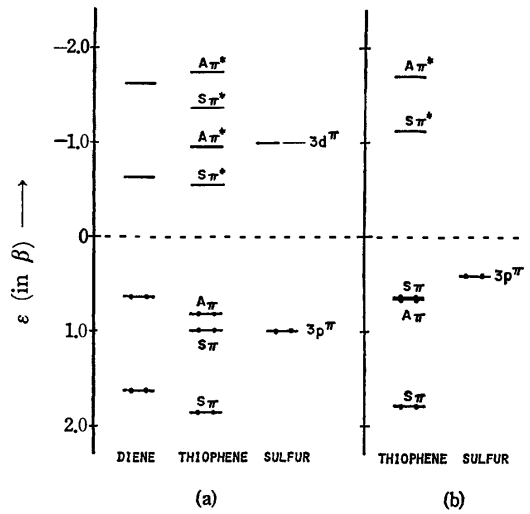

Fig. 8. Correlation diagram of π-MO's of diene fragment, sulfur atom, and thiophene. (a) With d^π orbitals, (b) without d^π orbitals.

Table 3. MO and MO energies of thiophene

			Case i); without d^π orbitals				
MO energy	$\alpha+1.793\beta$	$\alpha+0.678\beta$	$\alpha+0.668\beta$	$\alpha-1.107\beta$	$\alpha-1.705\beta$		
Symmetry	S	A	S	S	A		
S	0.419	0.0	0.815	0.401	0.0		
C_2	0.423	0.588	0.059	−0.563	0.392		
C_3	0.483	0.392	−0.405	0.320	−0.588		
			Case ii); with d^π orbitals				
MO energy	$\alpha+1.872\beta$	$\alpha+0.992\beta$	$\alpha+0.806\beta$	$\alpha-0.563\beta$	$\alpha-0.958\beta$	$\alpha-1.379\beta$	$\alpha-1.772\beta$
Symmetry	S	S	A	S	A	S	A
$S(p^\pi)$	0.495	−0.816	0.0	−0.241	0.0	0.175	0.0
C_2	0.410	0.043	0.581	0.388	0.009	−0.424	−0.404
C_3	0.452	0.406	0.369	−0.296	−0.299	0.207	0.524
$S(d^\pi)$	0.072	0.011	0.164	0.483	0.641	0.512	0.250

Contribution of dπ Orbital to Frontier MO's. The chemical reactivity of conjugated system can be interpreted, to a first approximation, by the frontier MO's, HOMO and LUMO.[11] The MO's and their energies of thiophene are summarized in Table 3. MO spacings are shown in Fig. 8. We see that if dπ orbitals are neglected, ψ_2 and ψ_3 are almost degenerate each other. The frontier electron densities at C_2 and C_3 are calculated to be 0.350 and 0.318, respectively. It is known experimentally that the C_2 position is most reactive. Thus, this tendency can not be interpreted by the calculation of case i) in Table 3. On the other hand, in the calculation of case ii), the orbital degeneracy of HOMO's is removed by the contribution of vacant dπ orbitals. The frontier electron density at C_2 becomes much larger than that at C_3. This shows that in order to explain the reactivity of electrophilic substitution of thiophene, we should consider vacant dπ orbitals. In the discussion of the Diels-Alder reaction, Lert and Trindle[12] pointed out the importance of the contribution of dπ orbitals in thiophene.

References

1) For example, J. B. Stothers, "Carbon-13 NMR Spectroscopy," Academic, New York, (1972); G. C. Levy, "Topics in Carbon-13 NMR Spectroscopy," Vol. 1, Wiley, New York (1974).

2) K. Nishimoto, 23rd Annual Meeting of the Chemical Society of Japan, Tokyo (1970).

3) N. F. Ramsey, *Phys. Rev.*, **78**, 699 (1950); **86**, 243 (1952).

4) M. Karplus and J. A. Pople, *J. Chem. Phys.*, **38**, 2803 (1963).

5) G. A. Olah and G. D. Mateescu, *J. Am. Chem. Soc.*, **92**, 1430 (1970).

6) T. Yonezawa, I. Morishima, and H. Kato, *Bull. Chem. Soc. Jpn.*, **39**, 1398 (1966).

7) T. P. Alger, D. M. Grant, and E. G. Paul, *J. Am. Chem. Soc.*, **88**, 5397 (1966).

8) C. E. Moore, "Atomic Energy Levels," Vols 1 and 2, Circular of the National Bureau of Standards, No. 467 (1949), (1952), Washington D. C.

9) K. Takahashi, T. Sone, and K. Fujieda, *J. Phys. Chem.*, **74**, 2765 (1970).

10) B. Bak, D. Christensen, J. Rastrup-Anderson, and E. Tannenbaum, *J. Chem. Phys.*, **25**, 892 (1956).

11) K. Fukui, "Molecular Orbitals in Chemistry, Physics, and Biology," ed. by P. O. Lowdin and B. Pullman, Academic Press, New York (1964).

12) P. W. Lert and C. Trindle, *J. Am. Chem. Soc.*, **93**, 6392 (1971).

ESR Study of Cationic Radicals in Aromatic Compound–Cu–$AlCl_3$ Systems

Sei-ichiro IMAMURA, Kumao HAMANOUE, Seiji FUKUDA, Hiroshi TERANISHI, and Yoshihisa WATANABE*

Department of Chemistry, Kyoto Institute of Technology, Matsugasaki, Sakyo-ku, Kyoto 606

**Department of Hydrocarbon Chemistry, Kyoto University, Yoshida, Sakyo-ku, Kyoto 606*

(Received June 12, 1975)

The electron spin resonance spectra of several aromatic compound–Cu–$AlCl_3$ systems were observed. When benzene, toluene, and ethylbenzene were used as the aromatic compounds, a singlet with a *g*-value of 2.003 was obtained. In the case of the *o*-, *m*-, and *p*-xylene systems, spectra with well-resolved hfs's resulted. It was suggested that cationic radicals were formed by a transfer of an electron from the benzene ring to Cu(II)–$AlCl_3$.

It has been reported that copper(I) chloride, aluminium chloride, and benzene form a ternary complex, and its structure has been determined by an X-ray diffraction technique.[1] The copper(I) ion has a distorted tetrahedral environment and is located above one of the C–C bonds of the benzene ring by means of a π-type interaction. The distances between the copper(I) ion and the two nearest adjacent carbon atoms are not equivalent; they are 2.15 and 2.30 Å respectively.

When the complex was used in the Friedel-Crafts reaction as a catalyst, the product distribution differed from that in the reaction catalyzed by aluminium chloride alone.[2] For example, in the synthesis of cymene from toluene and isopropyl chloride, the selectivity in *o*- and *m*-products was highly increased by use of the complex. However, the catalytic action of the complex has not been discussed in detail, and it seemed that it would be interesting to study the nature of the aromatic compound–Cu–$AlCl_3$ system (ArH–Cu–$AlCl_3$) by means of the ESR technique from the viewpoint of the interaction of copper with a benzene ring.

Experimental

Materials. The aromatic compounds were carefully purified by the usual method. The anhydrous copper(I) chloride and copper(II) chloride were prepared by the reduction of, and by the dehydration of copper(II) chloride dihydrate respectively. Commercial G. R. grade copper(I) oxide, copper(II) oxide, and aluminium bromide were used without further purification. The aluminium chloride was purified by the sublimation of a commercial G. R. grade reagent.

Preparation of the Samples. The samples were prepared in the following two ways.

Method A: In a 50-ml reaction flask, a mixture of known amounts of copper salt, aluminium salt, and a 5-ml portion of an aromatic compound was stirred under a nitrogen atmosphere at room temperature. The upper layer was put into an ESR sample tube by means of a syringe, and the tube was sealed.

Method B: In a 10-ml reaction vessel equipped with an ESR sample tube, known amounts of copper salt and aluminium salt were placed, and then the vessel was evacuated. About a 5-ml portion of a degassed aromatic compound was distilled into the vessel by the use of a vacuum line, after which the mixture was stirred. An upper layer was decanted into the sample tube and sealed. The concentration of copper salts was 0.1—0.2 mol/l.

ESR Spectra. The electron spin resonance spectra were usually recorded at room temperature with a JEOL-JESPE spectrometer, while the *g*-values were determined by the use of Mn^{2+} as a standard marker. When the measurements at an elevated temperature were necessary, the temperature was maintained by passing hot air through the cavity.

Results and Discussion

ESR Spectra of the Samples Prepared by Method A. While copper salts were insoluble in aromatic compounds, such as benzene or toluene, they were easily dissolved by the addition of aluminium chloride to form brown, purple, yellow, or green homogeneous solution. The rate of the dissolution of copper salts in the aromatic compounds increased in the order of benzene, toluene, ethylbenzene, and *p*-xylene. Copper(II) chloride was the most soluble among the copper salts used.

From Table 1 one can see that all the spectra of ArH–Cu–$AlCl_3$ consist of a singlet with a *g*-value of 2.003 and a ΔH_{msl} value smaller than 10 G, indicating the presence of organic radicals. However, the aluminium bromide systems investigated showed no signal or, if any, a very weak one. In all cases, no spectrum due to the copper(II) ion was observed; this suggests that copper is in the copper(I) state.

TABLE 1. ESR SPECTRA OF AROMATIC COMPOUND–Cu–Al SYSTEMS PREPARED BY METHOD A

Aromatic compound	Al-salt	Cu-salt	ΔH_{msl}/G	*g*-Vlaue
Benzene	$AlCl_3$	CuCl	9.00	2.003
		Cu_2O	9.45	2.003
		$CuCl_2$	7·17	2.003
		CuO	9.46	2.003
	$AlBr_3$	CuCl		2.003[a]
		CuO	—	—
Toluene	$AlCl_3$	CuCl	8.00	2.003
		Cu_2O	8.80	2.003
		$CuCl_2$	7.80	2.003
		CuO	7.50	2.003
	$AlBr_3$	CuCl	—	—
p-Xylene	$AlCl_3$	CuCl	8.10	2.003
	$AlBr_3$	CuCl	—	—
		CuO	—	—
Ethylbenzene	$AlCl_3$	CuCl	5.00	2.003

a) very weak

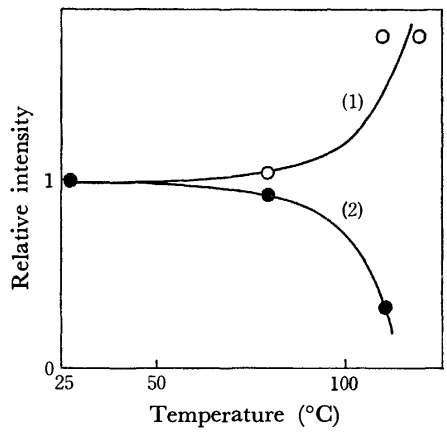

Fig. 1. Temperature dependence of the spectra of (1) toluene-CuCl-$AlCl_3$ and of (2) *p*-xylene-CuCl-$AlCl_3$.

Figure 1 shows an effect of the temperature on the intensities of the signals of ArH-Cu-$AlCl_3$. The ordinate indicates the intensity relative to that of the Mn^{2+} marker. The intensity of the signals of *p*-xylene system does not decrease up to 80 °C, while that of the toluene system increases by heating up to 120 °C. These facts indicate that the radicals are thermally stable to a considerable extent.

They were also found to be stable toward oxygen, and the radical nature still remained under an atmospheric condition when the unreacted aromatic compound was excluded. For example, when excess *p*-xylene was removed by the evaporation from the *p*-xylene-CuCl-$AlCl_3$ system, the spectrum of the residual solid material was observed to be as is shown in Fig. 2.[3] A sharp singlet with a *g*-value of 2.003 is superimposed upon the broad spectrum of the copper(II) ion. It seems that the copper(II) ion was formed by the oxidation of the copper(I) ion by air during the procedure.

ESR Spectra of the Samples Prepared by Method B. As has been mentioned above, the spectra of ArH-Cu-$AlCl_3$ prepared by Method A had no hfs. This may be due to dissolved oxygen, which causes the line broadening of the spectrum. Dissolved oxygen may also affect the valence state of copper; the copper(I) ion may be oxidized to the copper(II) state during the preparation of the samples. Therefore, the effect of oxygen was excluded by preparing the samples under a vacuum. The aromatic compounds used were toluene, *o*-, *m*-, and *p*-xylene, while the copper salts used were copper(I) chloride, copper(II) chloride, and copper(II) oxide.

Copper(I) chloride, although dissolved rapidly in these organic solvents to form brown homogeneous solutions, showed no spectrum. On the other hand, spectra were obtained in all cases where copper(II) salts were used. However, the spectra of the samples prepared in toluene consisted of only a singlet; the same result was obtained in the case of *p*-xylene-$CuCl_2$-$AlCl_3$.

The *p*-xylene-CuO-$AlCl_3$ system gave a dark purple solution; its ESR spectrum, consisting of about eighty lines spaced over thirty gauss, is shown in Fig. 3. As has been mentioned before, Turner has reported that the benzene-CuCl-$AlCl_3$ complex has a π-type copper-benzene ring interaction and that the copper is located above one of the C-C bonds.[1] Taking this into consideration, it appears that the spectrum shown in Fig. 3 is due to a cationic or an anionic radical of Turner's type. If the radical has a symmetrical configuration, and if all the protons on the benzene ring are equivalent, its spectrum will consist of thirty-five lines. An alternate explanation for the unusual complex spectrum may be that there exists a dimer of the ionic radical, as has been reported for a cationic radical of naphthalene.[4] However, the exact assignment of the observed spectrum has not yet been done. This radical was stable in the presence of oxygen. Though line broadening occurred after air was introduced, the hfs could still be observed. The line broadening may be explained by the dipole-dipole interaction with oxygen and/or with the copper(II) ion formed by the oxidation of the copper(I) ion.

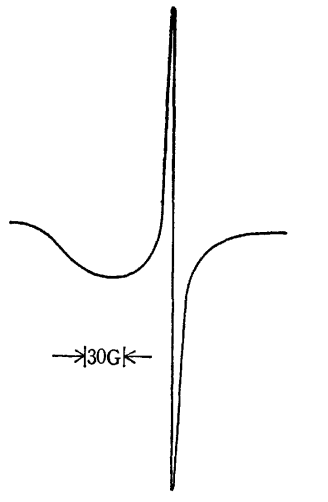

Fig. 2. ESR spectrum of *p*-xylene-CuCl-$AlCl_3$ after evaporation of excess *p*-xylene,

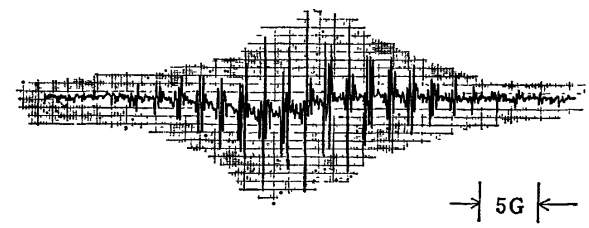

Fig. 3. ESR spectrum of *p*-xylene-CuO-$AlCl_3$.

Figures 4 and 5 show the spectra of *o*-xylene-CuO-$AlCl_3$ and *m*-xylene-CuO-$AlCl_3$ respectively. They are different from that of *p*-xylene-CuO-$AlCl_3$; each consists of about one hundred and fifty lines. It is expected that the hfs of the toluene system as well as of the other systems listed in Table 1 can be obtained by choosing optimum conditions for the preparation of these samples.

The copper(I) systems prepared by Method B yielded no signal. However a signal began to appear when air was introduced into *p*-xylene-CuCl-$AlCl_3$,

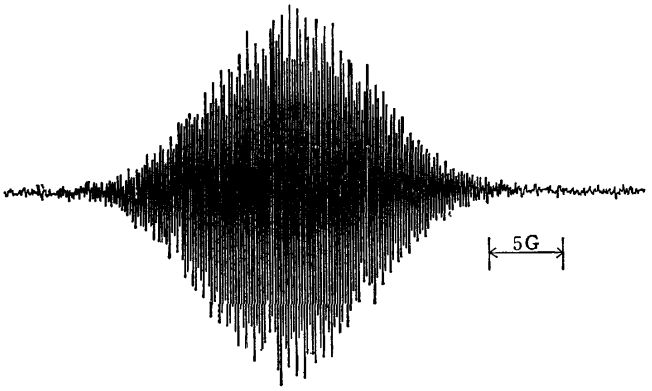

Fig. 4. ESR spectra of *o*-xylene–CuO–$AlCl_3$.

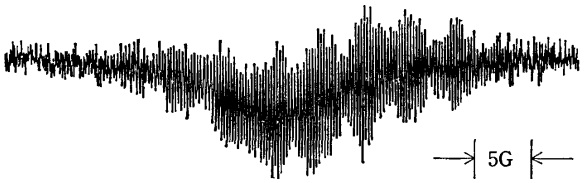

Fig. 5. ESR spectrum of *m*-xylene–CuO–$AlCl_3$.

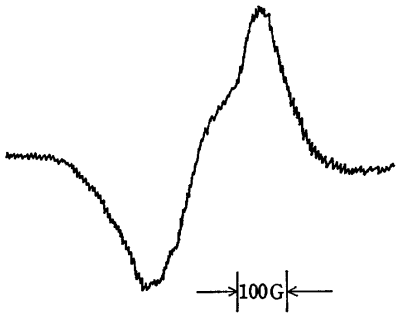

Fig. 6. ESR spectrum of *p*-xylene–CuCl–$AlCl_3$ after an introduction of air and successive addition of tetrahydrofuran.

and, in the presence of an optimum amount of air, a spectrum exactly identical with that shown in Fig. 3 was observed. On the addition of tetrahydrofuran to the system, a precipitate appeared. As is shown in Fig. 6, the spectrum of this precipitate had no signal due to an organic radical; instead, an absorption due to the copper(II) ion was observed. These results suggest that the copper ion in the system is in the copper(I) state and that the copper(II) ion is necessary to produce the organic radical. Therefore, it appears that a transfer of an electron from the benzene ring to the copper(II) ion occurs and that, as a result, the copper(I) ion and an aromatic cationic radical are formed.

It has been known that aluminium halides form complexes with aromatic hydrocarbons.[5-7] Therefore, aluminium chloride alone was dissolved in *p*-xylene under the conditions described in Method B; the spectrum of the resultant pale yellow solution was observed to be as is shown in Fig. 7. The spectrum consists of about sixteen lines, with a hyperfine coupling constant of 1.7 G. The ESR spectra of cationic

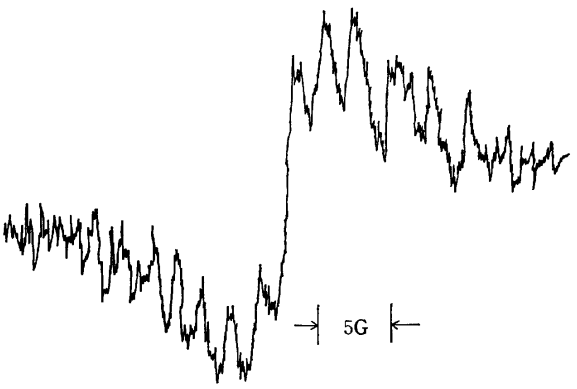

Fig. 7. ESR spectrum of *p*-xylene–$AlCl_3$.

radicals in the complexes of aluminium chloride with aromatic compounds (–anthracene, chrysene, and perylene–) were observed by Rooney *et al.*[8]; our result is very similar to theirs. Therefore, the radical shown in Fig. 7 seems to be a cationic radical produced from *p*-xylene. There is a possibility that the spectra of ArH–Cu–$AlCl_3$ obtained are formed merely by an interaction of aromatic compounds with aluminium chloride. However, this can be excluded on the basis of the following facts: (1) Both the colour and the ESR spectra of ArH–Cu–$AlCl_3$ are different from those of the aromatic compound–$AlCl_3$ systems. (2) The copper(I) ion does not produce any radical species under a vacuum even in the presence of aluminium chloride. Therefore, the cationic radicals in ArH–Cu–$AlCl_3$ are essentially different from those in aromatic compound–$AlCl_3$ systems.

Summary. From the results obtained so far, it can be concluded that a transfer of an electron from the benzene ring to Cu(II)–$AlCl_3$ occurs and that a cationic radical is formed. In this process, the copper(II) ion is reduced to the copper(I) state. The cationic radical thus formed is stabilized by an interaction with Cu(I)–$AlCl_3$:

$$ArH + Cu(II) + AlCl_3 \longrightarrow ArH^+\cdots Cu(I)\cdots AlCl_3$$

However, it is not yet known whether the cationic radical is in a monomer or a dimerized form.

The copper(I) ion produces no cationic radical, although it reacts readily with aluminium chloride and aromatic compounds. On the addition of oxygen to the system, the copper(I) ion is oxidized to the copper(II) ion, which removes a π-electron from the benzene ring and produces the cationic radical:

$$ArH + Cu(I) + AlCl_3 \longrightarrow ArH\cdots Cu(I)\cdots AlCl_3 \xrightarrow{O_2}$$

$$[ArH\cdots Cu(II)\cdots AlCl_3] \longrightarrow ArH^+\cdots Cu(I)\cdots AlCl_3$$

A complete assignment of the hfs of the spectra could not be achieved; a detailed investigation is, therefore, now under way using the ENDOR technique.

References

1) R. W. Turner and E. L. Amma, *J. Am. Chem. Soc.*, **88**, 1877 (1966).

2) Y. Takegami, Y. Watanabe, and T. Suzuki, Jpn Pat. 28977 (1972).
3) This residual solid material was decomposed by adding tetrahydrofuran, and the *p*-xylene content was determined roughly as 23 wt% by the use of a gas chromatograph.
4) I. C. Lewis and L. S. Singer, *J. Chem. Phys.*, **43**, 2712 (1965).
5) R. E. V. Dyke, *J. Am. Chem. Soc.*, **72**, 3619 (1950).
6) H. C. Brown and W. J. Walace, *J. Am. Chem. Soc.*, **75**, 6265 (1953); **75**, 6268 (1953).
7) S. U. Choi and H. C. Brown, *J. Am. Chem. Soc.*, **88**, 903 (1966).
8) J. J. Rooney and R. C. Pink, *Proc. Chem. Soc.* (*London*), **1961**, 142.

Picosecond Flash Spectroscopy of Solvent-Induced Intramolecular Electron Transfer in the Excited 9,9′-Bianthryl[1)]

Nobuaki NAKASHIMA, Masamichi MURAKAWA, and Noboru MATAGA

Department of Chemistry, Faculty of Engineering Science, Osaka University, Toyonaka, Osaka 560

(Received June 21, 1975)

$S_n \leftarrow S_1$ absorption spectra of 9,9′-bianthryl in the visible and near infrared regions have been measured by means of picosecond flash spectroscopy. The $S_n \leftarrow S_1$ spectra in hexane measured at 500 ps after the exciting pulse were similar to those of anthracene while those in acetone were similar to the superposition of spectra of anthracene anion and cation. The results of the $S_n \leftarrow S_1$ spectral measurements together with those of the solvent effects upon the fluorescence yield and lifetime indicate an intramolecular electron transfer induced by the interaction with polar solvents in the excited state of 9,9′-bianthryl.

Solvent-induced changes of electronic structures are observed in the excited state of various systems[1–6)] such as *p*-(*N*,*N*-dimethylamino)-benzonitrile,[2)] 9,9′-bianthryl[3)] and some intramolecular heteroexcimer systems.[4–6)] Of these, 9,9′-bianthryl is one of the most important molecules investigated by various methods.

The fact that the two anthracene chromophores of 9,9′-bianthryl in the ground state as well as Franck-Condon(FC) excited state scarcely interact with each other has been shown by the measurements of polarizability,[7)] dipole moment,[7)] half reduction potential,[8)] molecular refraction,[9)] combustion energy,[10)] absorption, and fluorescence spectra.[3)] Moreover, the absorption spectra show no dependence upon the solvent polarity. The fluorescence spectra in rigid matrices and the absorption spectra in rigid as well as fluid solutions remain well structured as in the case of anthracene. Fluorescence spectra in solvents of low viscosity are diffuse compared with those of anthracene, although a slight vibrational structure can be observed in a nonpolar solvent. In polar solvents, the fluorescence spectra are composed of two bands; one shows a slight vibrational structure and is placed at the same wavelength region as in the nonpolar solvent and the other is structureless and shifted towards red.[3,11)] The results indicate a change of the electronic structure of 9,9′-bianthryl in the relaxation process from the FC excited state to the relaxed fluorescent state.[3)] We call the structured band E band and its emitting state E state, and the structureless band P band and its emitting state P state.

The red shift of the fluorescence in a polar solvent indicates that the relaxed fluorescent state has a dipole moment.[3)] It has been concluded on the basis of this fact as well as some quantum chemical calculations that the intramolecular charge transfer from one anthracene nucleus to another caused by the interaction with polar solvent molecules occurs in the excited state.[3,12)] If this is correct, the above result seems to indicate the phenomenon of solvent-induced "broken symmetry,"[13)] *i.e.* the lowering of the symmetry of the solute molecule due to the interaction with polar solvent molecules, resulting in the charge transfer state even if the molecule is composed of two identical chromophores. One of the most direct experimental methods to confirm this would be the measurement of $S_n \leftarrow S_1$ absorption spectra in various solvents of different polarities.

A method of picosecond flash spectroscopy has recently been developed by use of picosecond continuum (pc) as a monitoring light.[14)] We have also established a method of transient absorption measurement by picosecond flash spectroscopy in the visible, near infrared, and uv regions.[1,15,16)] Our method has a resolution of 50 ps in time and 2 nm in wavelength, and can be used for the transient absorption measurement even in the wavelength region of a strong fluorescence. By means of this method, we have measured the $S_n \leftarrow S_1$ absorption spectra of 9,9′-bianthryl in several solvents and have tried to demonstrate that the solvent-induced change of electronic structure is due to the intramolecular charge transfer from one anthracene nucleus to another.

In addition to the $S_n \leftarrow S_1$ absorption measurements, we have investigated the solvent effects upon the fluorescence yield and lifetime of 9,9′-bianthryl. The results seem to give some evidence for the solvent-induced change of electronic structure. Measurements of $T_n \leftarrow T_1$ spectra have also been carried out.

Experimental

Picosecond Flash Apparatus. The details of the method of picosecond flash photolysis and transient spectral measurements used in the present study have been described elsewhere.[1,15,16)] A summary is given herewith.

The sample was pumped with a frequency doubled single picosecond pulse at 347 nm from a mode-locked ruby laser system of JEOL and the transient spectra were monitored by a pc which was generated by collimating a single picosecond pulse at 694 nm into a cell of length 2—20 cm containing polyphosphoric acid (PPA) or water. A single pulse at 694 nm, which was selected from a mode-locked pulse train by a Pockels cell and amplified through a ruby rod, has an energy of *ca.* 100 mJ and a pulse width of 28 ps, and a pulse at 347 nm frequency doubled with KDP an energy of *ca.* 1 mJ. It was first reported by Nakashima and Mataga that the pc from PPA extends from 350 nm to 920 nm and can be used as the most suitable monitoring light in the spectral range 350—650 nm.[16)] The pc probe pulse with *ca.* 50 ps width, determined by an optical Kerr gate, was optically delayed with respect to the exciting pulse (delay time 0—20000 ps).

The 347 nm pump pulse entered the sample cell through one of the two 0.5 mm apertures at the front of the cell. The pc pulse passed through the sample cell from the opposite side was separated into two beams by the apertures. One beam passed through the part of the sample where the mole-

cules were excited. The other passed through the part where the molecules are in the ground state, and was used for correction of shot to shot power variations. The two beams were photographed simultaneously with a Shimadzu GE 100 spectrograph on a Kodak tri-X pan film in the UV~visible wavelength region and on a Kodak high speed infrared 2481 film in the visible near infrared region. We have confirmed that the usual relationship between the photographic density and exposure holds even in the case of the picosecond pulse excitation. Thus, the difference in the photographic densities for the two beams in the spectral range where the ground state absorption is not strong gives transient absorption spectra.

Even in the presence of a strong fluorescence in the same wavelength region as the transient absorption, we can obtain the absorption spectra since the sample cell was set 3 m apart from the spectrograph and the beam divergence of pc is very small (almost the same as that of laser light) in contrast to the fluorescence which becomes very weak after passing the long distance, spreading out in all direction. Our picosecond laser photolysis system was checked by measuring $S_n \leftarrow S_1$ spectra which had been established by the nanosecond laser photolysis method, for example, those of 1,2,4,5-tetracyanobenzene-toluene complex.[17]

Fluorescence Decay Curve Measurements. A 300 kW N_2 gas laser with a half width of 5.5 ns at 337 nm and a Q-switched ruby laser (JEOL, JLR-02A) with an output of *ca.* 100 mJ and a half width of 15 ns at 347 nm were used as the exciting light sources. The fluorescence decay curves were detected through a Nalumi R21 monochrometor with an RCA 1P28 photomultiplier and displayed on a Tektronix 475 oscilloscope. The circuit response time was *ca.* 5 ns. The picosecond pulse at 347 nm from the mode-locked ruby laser was also used for the excitation and the fluorescence was detected with an HTV R617 photodiode and a Tektronix 7912 transient digitizer (0.5 ns time resolution).

Measurements of $T_n \leftarrow T_1$ *Absorption Spectra.* $T_n \leftarrow T_1$ absorption spectra were measured with a conventional μ second flash photolysis apparatus.[18] Both the exciting and monitoring flash lights had a half width of 4 μs. The spectra were photographed with a Shimadzu GE 100 spectrograph.

Measurements of Fluorescence Quantum Spectra. A calibrated Amino-Bowman spectrophotometer was used for the measurements of fluorescence quantum spectra. Fluorescence quantum yields were determined by numerically integrating the areas under the emission curves of both the standard and the sample solutions. Anthracene dissolved in ethanol (2.5×10^{-5} M) was used as a standard, its quantum yield being taken as 0.27.[19]

Synthesis of 9,9'-Bianthryl. 9,9'-Bianthryl was prepared by reduction of anthraquinone in glacial acetic acid with zinc powder.[10] The product was recrystallized from chlorobenzene, washed with ethanol, chromatographed on activated alumina using benzene for elution, and recrystallized twice from glacial acetic acid, mp 312 °C. Found: C, 95.07; H, 4.99%. Calcd for $C_{28}H_{18}$: C, 94.88; H, 5.12%. The absorption and emission spectra in various solvents were identical with those reported.[3]

Solvents. Hexane (Wako, spectrograde), 2-propanol (Wako, spectrograde), diethyl ether (Wako, analytical grade), acetone (Nakarai, spectrograde), ethanol (Wako, analytical grade), methanol (Wako, analytical grade) and acetonitrile (Merck, spectrograde) were used without further purification. Decalin (Wako, analytical grade) was distilled under reduced pressure before use. All samples were deaerated by repeated freeze-pump-thaw cycles.

Results and Discussion

Picosecond Flash Photolysis. Photographs of pc are shown in Fig. 1, and the transient absorption spectra of 9,9'-bianthryl in Figs. 2 and 3. Each point in the visible region of the spectra (Fig. 2c and Fig. 3a) was obtained by taking an average of several measurements and contains an error of only ± 0.05 in the relative optical density unit. The base line of the spectra has an error of $+0.1$ since two beams through the apertures do not always have equal intensities.

(1) $S_n \leftarrow S_1$ *Spectra in Hexane Solution*: The $S_n \leftarrow S_1$ absorption spectra of 9,9'-bianthryl in hexane obtained

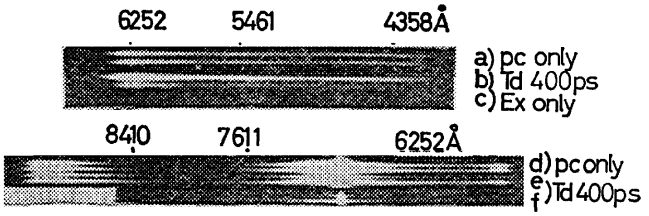

Fig. 1. A photographic display of time-resolved absorption spectra of 9,9'-bianthryl in acetone (5.1×10^{-4} M). a, d; pc without exciting pulse, b; with exciting pulse (lower one) and at 400 ps delay time in the visible region, c; exciting pulse without pc, e; with exciting pulse (upper one) and at 400 ps delay time in the infrared region (over exposure due to exciting Xe flash lamp and ruby fluorescence is observed around 694 nm). f; the same as e except that only the monitoring light intensity was reduced to 1/16. Vertical lines are reference spectra of Hg. The near UV cut off is due to the ground state absorption, and the red or near infrared cut off is due to the low sensitivity of the photographic film.

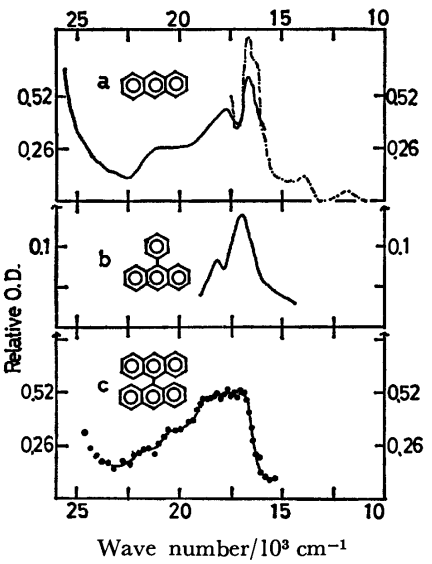

Fig. 2. $S_n \leftarrow S_1$ absorption spectra of anthracene, 9-phenylanthracene and 9,9'-bianthryl. a: Anthracene in hexane, 1.9×10^{-3} M. ——, at 250 ps delay time. —·—, at 300 ps delay time. b: 9-Phenylanthracene in methylcyclohexane. Taken from Ref. 5. c: 9,9'-bianthryl in hexane, 5.1×10^{-4} M. Measured at 500 ps delay time.

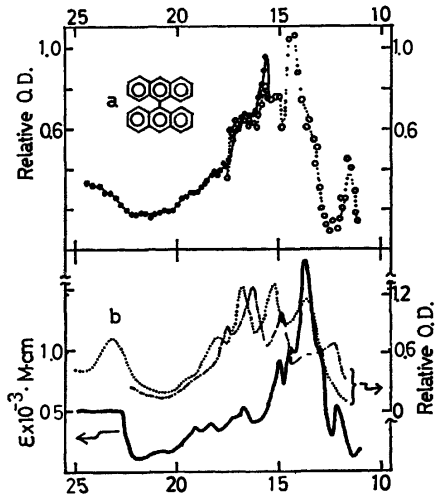

Fig. 3. $S_n \leftarrow S_1$ absorption spectra of 9,9'-bianthryl. a: -●-●-, Transient spectra at 500 ps delay time. An average of several measurements. -○-○-, Spectra at 400 ps delay time obtained by scanning the photographs of Fig. 1 e and f. b: ——, The superposition of the absorption bands of anthracene anion and cation. Each spectra are quoted from Ref. 23 and the extinction coefficients at 13.8 kcm^{-1} are taken from Ref. 24. -·-·-, The spectra of 9.10-diphenylanthracene anion.[25] ----, The spectra of 9,10-diphenylanthracene cation.[25]

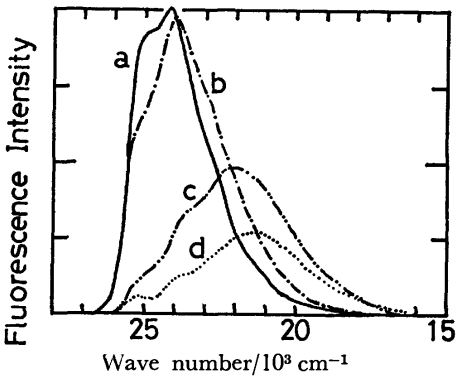

Fig. 4. Fluorescence quantum spectra of 9,9'-bianthryl (2.5×10^{-5} M) in several different solvents. a: ——, hexane. b: -·-·-, diethyl ether. c: -·-·-, acetone. d: ----, acetonitrile.

at the delay time of 500 ps are shown in Fig. 2c. Since only the E band is observed in this solvent, the spectra contain no contribution from the P state. At a delay time of 500 ps, the formation of the triplet state of 9,9'-bianthryl may be negligible since the fluorescence lifetime and quantum yield are 8 ns and 0.55, respectively. We have confirmed by means of μs flash photolysis that 9,9'-bianthryl shows T_n—T_1 absorption at approximately the same position as that of anthracene. Thus, the spectra (Fig. 2c) contain no contribution from the T_n—T_1 spectra. No strong absorption band was observed in the near infrared regions of 15—11 kcm^{-1}. The S_n—S_1 spectra of anthracene in hexane at 250—300 ps delay time[15] as well as those of 9-phenylanthracene in methylcyclohexane measured by the ns laser photolysis method[5] are also given in Fig. 2 for the sake of comparison.

The characteristic band of anthracene at 16.7 kcm^{-1} has been assigned to the $^1A_{1g}^- \leftarrow {}^1B_{2u}^+$ transition and that at 18 kcm^{-1} may be assigned partly to the $^1B_{1g}^- \leftarrow {}^1B_{2u}^+$ transition and partly to the vibrational structure of the $^1A_{1g}^- \leftarrow {}^1B_{2u}^+$ transition.[20] We can see these characteristic bands in the spectra of 9-phenylanthracene although they are a little shifted towards blue. The spectra of 9,9'-bianthryl are also similar to those of anthracene and 9-phenylanthracene, though the former spectra are somewhat broad and further shifted towards blue as compared with the latter. The results suggest that the E fluorescence state with a slight vibrational structure is the locally excited state or exciton resonance state.

(2) *Formation of P State and Estimation of the Equilibrium Constant between E and P States*: We see from Fig. 4 that, with increasing solvent polarity, the intensity of the E band decreases and is accompanied by the appearance of the P band. Schneider and Lippert[3] has shown that the lower the temperature, the stronger the P fluorescence when the viscosity of the solvent is not so high. The results indicate that the P state is formed from the E state. However, it was possible only to observe the single exponential decay of the P as well as E fluorescence. Their lifetimes were almost the same. The result indicates that the P and E states are in equilibrium within 500 ps after the excitation with a picosecond pulse.

Chuang *et al.*[21] showed by the picosecond laser technique that the rise of the intramolecular heteroexcimer formation of *N*,*N*-dimethyl-4-[3-(9-anthryl)-propyl]-aniline in hexane is *ca.* 900 ps. Though there seems to be orientational requirement for the heteroexcimer formation, the rise time becomes much shorter (~60 ps) in the anthracene-DEA(*N*,*N*-diethylaniline) two component system.[22]

In the case of the present system, our results suggest that orientational requirement for the formation of the P state, if any, is slight. The electron transfer would occur far more rapidly than the above intramolecular heteroexcimer formation, presumably competing with the solvent reorientational relaxation.

From the values of fluorescence quantum yields and lifetimes given in Table 1, we can estimate approximately the equilibrium constant between E and P. The yield of the E fluorescence, η_E, can be given by

$$\eta_E = \frac{q_E}{1+(\tau_E/\tau_P)K_e} \qquad (1)$$

where q_E is the fluorescence quantum yield when there is only the E state, τ_E ans τ_P are intrinsic lifetimes of the E and P states, respectively, and $K_e=[P]/[E]$. The value of (η_E/q_E) in acetone was estimated from the spectra (Fig. 4) using the η_E value in hexane for q_E. From the observed values in hexane and acetone for τ_E and τ_P, and the estimated (η_E/q_E) value, K_e was evaluated to be approximately 40.

(3) $S_n \leftarrow S_1$ *Spectra in Acetone Solution*: The $S_n \leftarrow S_1$ spectra of 9,9'-bianthryl in acetone obtained at the delay time of 500 ps are given in Fig. 3a. We have

confirmed that the rise time of the P fluorescence in acetone is shorter than 500 ps, and that the P state is populated predominantly in the excited state.

The $T_n \leftarrow T_1$ spectra of 9,9'-bianthryl in acetonitrile are similar to those in hexane. This indicates that $T_n - T_1$ spectra do not depend on solvent polarity. Thus, the spectra in Fig. 3a contain no contribution from the $T_n \leftarrow T_1$ spectra.

The spectra in acetone differ considerably from those in hexane (Fig. 3). Although the spectra in acetone are a little broad and shifted towards blue as compared with the superposition of those[23,24] of anthracene anion and cation (Fig. 3b), both spectra are rather similar. Considering that the reference spectra were taken for the anthracene ions produced by γ-ray irradiation and measured at 77 K,[23] the observed broadening and blue shift can be ascribed to the effects of counter ions (a charged anthryl group in the present case), substituent, and the temperature of the system. This is supported by the fact that the absorption spectra of 9,9'-bianthryl anion and its dianion are similar to those of Fig. 3a,[25] *i.e.* they are somewhat broad and shifted towards blue as compared with those of anthracene anion and that the spectra of 9,10-diphenylanthracene ions are also broad and shifted towards blue as compared with those of anthracene (Fig. 3b).[26] Similar effects of the spectra of ion radicals of aromatic hydrocarbons being affected by the existence of counterions, *etc.* have been observed in the case of ion radicals of naphthalene[23] and fluorene.[27]

The observed shoulder at 16.7×10^3 cm^{-1} (Fig. 3a) might be assigned to the back CT transition to the same S_n state as that for the transition corresponding to the 17.5×10^3 cm^{-1} band in hexane. However, considering that the fluorescent state of 9,9'-bianthryl in acetone is stabilized due to the reorientation of solvents, the back CT transition in $S_n \leftarrow S_1$ spectra, if any, should be shifted towards blue as compared with the corresponding transition of 9,9'-bianthryl in hexane solution. Therefore, the shoulder at 16.7×10^3 cm^{-1} should be assigned to the ion band at *ca.* 17×10^3 cm^{-1}. Thus, the spectra in acetone can be assigned to the transitions localized in anthryl ions.

The electronic structure of the relaxed S_1 state in acetone as well as in more polar solvents seems to be close to the ion-pair with negligibly small delocalization interaction between the pair. This can be possible if the two anthracene planes are almost perpendicular to each other in the relaxed S_1 state in those polar solvents.

Solvent Effects upon Fluorescence Yields and Lifetimes

(1) *The Structural Change of E State*: We have measured fluorescence quantum yields and lifetimes. The results are listed in Table 1. From these values we can examine the effect of structural change on the radiative lifetime. The value in hexane was obtained as $\tau_f^\circ \simeq 14.5$ ns from the observed fluorescence quantum yield and lifetime. On the other hand, the radiative lifetime evaluated from the absorption spectra by using Strickler-Berg's equation[28] is $\tau_f^\circ \sim 6$ ns. This indicates that, due to the structural change in the relaxation process from the FC excited state to the relaxed fluorescent state, the radiative transition probability is decreased. Namely, two π-electronic systems of 9,9'-bianthryl are oriented perpendicular to each other because of a strong steric hindrance in the relaxed ground state as well as the FC excited state. However, the stable conformation in the excited state may not be the perpendicular one but the oblique one as suggested by Schneider and Lippert.[3] This structural change in the excited state seems to result in the decrease of the radiative transition probability.

Table 1. Fluorescence quantum yields and lifetimes of 9,9'-bianthryl in various solvents[a]

Solvent	ε[b]	$\tilde{\nu}_{a,max}$[c]/ 10^3 cm^{-1}	$\tilde{\nu}_{f,max}$[d]/ 10^3 cm^{-1}	$\phi_{f,rel}$[e]	τ_f/ns[f]
Hexane	1.88	25.7	24.2	1.00 (0.55±0.05)	8
Decalin	2.15	25.5	24.0	1.07	
Benzene	2.28	25.3	23.7[g]		11.8[g]
Diethyl ether	4.34	25.7	23.9	1.08	15
2-Propanol	17.9	25.7	22.8	0.91	
Acetone	20.7	25.6	22.1	0.71	32
Ethanol	24.6	25.7	22.6	0.71	33
Methanol	32.7	25.8	22.0	0.60	
Aceto-nitrile	37.5	25.6	21.3	0.41	35

a) All measurements were carried out at room temperature, the concentration of 9,9'-bianthryl being 2.4 10^{-5} M for all the solutions. b) Dielectric constant of the solvent at room temperature. c) Wave numbers of the absorption maxima quoted from Ref. 3. d) Wave numbers of fluorescence maxima measured in the present work. These values are essentially the same as those of Ref. 3. e) The relative fluorescence quantum yield. The value in parentheses is the absolute value determined by using anthracene as a standard. f) Fluorescence lifetimes were measured at 20×10^3 cm^{-1} through a monochromator except the value of hexane solution. The latter was obtained with the use of Toshiba color filters VV40 and UV39. g) I. B. Berlman, "Handbook of Fluorescence Spectra of Aromatic Molecules", Academic Press, New York, N. Y. (1971), p. 366.

(2) *Solvent-Induced Change of Electronic Structure of P State*: The fluorescence spectra observed in highly polar solvents such as acetone, ethanol, and acetonitrile are almost exclusively due to the P state. We see from Table 1 that the fluorescence lifetimes in these polar solvents are considerably longer than those in nonpolar solvents. Moreover, the lifetime in the polar solvent shows a slight increase with an increase in solvent dielectric constant. However, the fluorescence quantum yield decreases considerably in the strongly polar solvents such as methanol and acetonitrile. In alcoholic solutions, in contrast to the case of aprotic polar solution, specific behaviors in the excited solute-solvent interactions are observed. As has been pointed out already by Schneider and Lippert,[3] as well as by Kosower and Tanizawa,[11] the fluorescence wave number in an alcohol solution is large as compared with the value in an aprotic solvent with almost the same dielectric constant. The fluorescence quantum

yield η_P in alcohol is not smaller than that in acetone though the dielectric constant of the former is larger than that of the latter. Similar effects of solvent polarity as well as alcohol on the behavior of excited molecular composite system are found in the case of aromatic hydrocarbon–amine heteroexcimer.[5,29]

The above results concerning the effects of the solvent dielectric constant upon the fluorescence quantum yield and lifetime of 9,9'-bianthryl indicate the decrease of the radiative transition probability with the increase in the solvent polarity, which can be ascribed to the solvent-induced change in the electronic structure of the P state, just as in the case of some intramolecular heteroexcimers.[5,6]

References

1) Preliminary results have been published in: N. Mataga, "The Exciplex" (Proceeding of International Exciplex Conference, held at Western Ontario, Canada, May 28—31, 1974), ed. by M. Gordon and W. R. Ware, Academic Press, New York (1975), p. 57.

2) E. Lippert, W. Lüder, and H. Boos, "Advances in Molecular Spectroscopy", Pergamon Press, 1962, p. 443; N. Nakashima, E. Inoue, N. Mataga, and C. Yamanaka, *Bull. Chem. Soc. Jpn.*, **46**, 2288 (1973); N. Nakashima and N. Mataga, *ibid.*, **46**, 3016 (1973); W. S. Struve, P. M. Rentzepis, and J. Jortner, *J. Chem. Phys.*, **59**, 5014 (1973); W. S. Struve and P. M. Rentzepis, *ibid.*, **60**, 1533 (1974).

3) F. Schneider and E. Lippert, *Ber. Bunsenges. Phys. Chem.*, **72**, 1155 (1968); *ibid.*, **74**, 624 (1970).

4) E. A. Chandross and H. T. Thomas, *Chem. Phys. Lett.*, **9**, 393 (1971); E. A. Chandross and C. J. Dempster, *J. Am. Chem. Soc.*, **92**, 3586 (1970).

5) T. Okada, T. Fujita, M. Kubota, S. Masaki, N. Mataga, R. Ide, Y. Sakata, and S. Misumi, *Chem. Phys. Lett.*, **14**, 563 (1972); T. Okada, T. Fujita, and N. Mataga, *Z. Phys. Chem. N. F.*, to be published. Intramolecular Charge Transfer Interactions and Dynamic Behaviors of Excited *p*-(9'-Anthryl)-*N*,*N*-dimethylaniline.

6) N. Mataga, T. Okada, H. Masuhara, N. Nakashima, Y. Sakata, and S. Misumi, *J. Lumin.*, to be published. Electronic Structures and Dynamical Behaviors of Some Intramolecular Exciplexes.

7) W. Liptay, G. Walz, W. Baumann, H. Schlosser, H. Deckers, and N. Detzer, *Z. Naturforsch.*, **26a**, 2020 (1971).

8) G. J. Hoijtink, *Rec. Trav. Chim. Pays-Bas*, **74**, 1525 (1955).

9) J. A. Bigot and D. W. Van Krevelen, *Trans. Faraday Soc.*, **56**, 322 (1960).

10) A. Magnus, H. Hartmann, and F. Becker, *Z. Phys. Chem.*, **197**, 75 (1951).

11) E. M. Kosower and K. Tanizawa, *Chem. Phys. Lett.*, **16**, 419 (1972); *ibid.*, **26**, 545 (1974).

12) H. Beens and A. Weller, *Chem. Phys. Lett.*, **3**, 666 (1969).

13) See for example, P. W. Anderson, *Science*, **177**, 393 (1972).

14) P. M. Rentzepis, R. P. Jones, and J. Jortner, *J. Chem. Phys.*, **59**, 766 (1973); H. Kuroda and S. Shionoya, *Opt. Commun.*, **10**, 74 (1974); H. Tashiro and T. Yajima, *Chem. Phys. Lett.*, **25**, 582 (1974); D. Magde and M. W. Windsor, *ibid.*, **27**, 31 (1974).

15) N. Mataga and N. Nakashima, *Spectrosc. Lett.*, **8**, 275 (1975).

16) N. Nakashima and N. Mataga, *Chem. Phys. Lett.*, **35**, 487 (1975).

17) H. Masuhara and N. Mataga, *Chem. Phys. Lett.*, **6**, 608 (1970); *Bull. Chem. Soc. Jpn.*, **45**, 43 (1972); R. Potashnik and M. Ottolenghi, *Chem. Phys. Lett.*, **6**, 525 (1970).

18) N. Yamamoto, Y. Nakato, and H. Tsubomura, *Bull. Chem. Soc. Jpn.*, **39**, 2603 (1966).

19) W. H. Melhuish, *J. Phys. Chem.*, **65**, 229 (1961).

20) C. R. Goldschmidt and M. Ottolenghi, *Chem. Phys. Lett.*, **4**, 570 (1970); D. Bebelaar, *Chem. Phys.*, **3**, 205 (1974).

21) T. J. Chuang, R. J. Cox, and K. B. Eisenthal, *J. Am. Chem. Soc.*, **96**, 6828 (1974).

22) T. J. Chuang and K. B. Eisenthal, *J. Chem. Phys.*, **59**, 2140 (1973).

23) T. Shida and S. Iwata, *J. Am. Chem. Soc.*, **95**, 3473 (1973).

24) P. Balk, G. J. Hoijtink, and J. W. Schreurs, *Rec. Trav. Chim.*, **76**, 813 (1957); W. Ij. Aalbersberg, G. J. Hoijtink, G. L. Mackor, and W. P. Weijland, *J. Chem. Soc.*, **1959**, 3055.

25) W. H. Hamill, "Radical Ions", ed. by E. T. Kaiser and L. Kevan, John Wiley & Sons, New York (1968), p. 321.

26) M. Hoshino, K. Kimura, and M. Imamura, *Chem. Phys. Lett.*, **20**, 193 (1973).

27) T. E. Hogen-Esch and J. Smid, *J. Am. Chem. Soc.*, **88**, 307 (1966).

28) S. J. Strickler and R. A. Berg, *J. Chem. Phys.*, **37**, 814 (1962).

29) N. Mataga, T. Okada, and N. Yamamoto *Chem. Phys. Lett.*, **1**, 119 (1967); H. Knibbe, K. Rollig, F. P. Schafer, and A. Weller, *J. Chem. Phys.*, **47**, 1184 (1967); H. Knibbe, Thesis, Free University, Amsterdam, 1969; N. Orbach and M. Ottolenghi, Private Communication.

X-Ray Photoelectron Spectroscopic Studies of Catalysts —Chromia–Alumina Catalysts—

Yasuaki OKAMOTO, Masaki FUJII, Toshinobu IMANAKA, and Shiichiro TERANISHI

Department of Chemical Engineering, Faculty of Engineering Science, Osaka University, Toyonaka, Osaka 560

(Received June 30, 1975)

The XPS studies of chromia–alumina catalysts were carried out to elucidate the surface of these catalysts. Photoreduction was found to occur during the XPS measurements. Therefore, all spectra were measured rapidly to prevent any photoreduction. It was found that the information about the spin-orbit splitting of the Cr2P level is very useful for determining the valence state of chromium. The surface state of chromium in chromia–alumina catalysts calcined at 500 °C for 5 h is predominantly Cr^{6+} at low chromia concentration catalysts. However, the Cr^{3+} phase appears in catalysts of higher chromium content, and the surface concentration of Cr^{3+} increases with increasing content of supported chromia. The XPS spectra due to Cr^{5+} were observed after mild reduction of the catalysts. Moreover, it was found that almost all surface chromium is present as Cr^{5+} at low chromia content catalysts after mild reductions. Qualitatively, the results obtained by the XPS technique, which gives information about the surface of catalysts, agree well with the results obtained by ESR and other techniques, which gives information about the bulk of catalysts, especially low chromium concentration catalysts. These findings indicate a high dispersion of chromium on γ-Al_2O_3 for low chromium content catalysts.

Since the X-ray photoelectron spectroscopy (XPS or ESCA) measurements reveal both the chemical composition and state of the surface atoms of solids, they provide a new probe for studying the properties of catalysts.[1] From XPS measurements of catalysts, we can obtain three important pieces of information—that is, information about the binding energy, the satellite structure, and the relative intensities of some levels. The information about the binding energy and the satellite structure reveals the chemical and magnetic state of the atom concerned. Recently, the information about the spin-orbit splitting of the 2p level for some transition metals was emphasized to be useful in determining the magnetic state or valence state of the transition metal ions.[2–4] By comparing the XPS peak intensities of different levels, we can obtain knowledge about the surface composition of a catalyst or the surface coverage of supported catalysts on a carrier.

Chromia-alumina catalysts have been studied by many workers[5] using ESR and other techniques, since chromia–alumina catalysts are active in a great variety of reactions such as dehydrocyclization, dehydrogenation, and the polymerization of olefins. On the basis of the results obtained by means of ESR, magnetic susceptibility measurements, titration method, NMR, X-ray diffraction, and optical reflectance spectroscopy, it is revealed that various valence states of chromium are present on chromia–alumina catalysts.[5] However, from these techniques we can only obtain information about the bulk catalysts or thick surface layer of the catalysts.

The advantages of XPS over these techniques are that, in principle, it is capable both of determining the valencies of metal ions on the thin surface layer (~10 Å) of supported oxide and simultaneously of detecting the interaction between catalyst and support.

In this paper, on the basis of the information obtained by XPS measurements for chromia–alumina catalysts, the surface properties of the catalysts will be discussed and compared with the results obtained by other techniques. XPS spectra of some chromium compounds were measured and the spin-orbit splitting of the Cr2p level was emphasized as being very useful for discriminating the valence states of chromium. The first XPS spectra of Cr^{5+} were, to our knowledge, observed in this study. Moreover, it was pointed out that photoreduction phenomena during XPS measurements must be considered in the case of chromia–alumina catalysts.

Experimental

Materials. Chromia–alumina catalysts supported on γ-Al_2O_3 with different compositions were prepared by a conventional impregnation technique using chromium nitrate or chromic oxide. After drying at 120 °C, catalysts were calcined at 500 °C for 5 h in air. In the case of 2 wt% catalysts, the catalysts calcined at 900 °C for 3 h were also investigated. The surface area of γ-Al_2O_3 used in our experiments was 235 m^2/g.

Procedure. Photoelectron spectra were measured on a Hitachi 507 photoelectron spectrometer using Al$K\alpha$ radiation. The power of X-ray radiation was 500 W (10 kV, 50 mA) in all measurements. The spectrometer was linked to a multichannel analyser in the multiscaler mode, which was useful for the study of time dependent spectra. Powdered samples were mounted on a sample holder made of stainless steel mounted with mesh. The spectrometer operating pressure was *ca.* 1×10^{-6} Torr. After the samples were pretreated in a pretreatment chamber (*ca.* 5×10^{-5} Torr), they were introduced into the analyser.

Binding energies were corrected by using the value of 285.0 eV for the ClS level resulting from the contaminated carbon. The reproducibilities of the values thus obtained were within +0.2 eV; the energy differences were determined with an accuracy of ±0.1 eV.

The reduction of the catalysts was carried out in the pretreatment chamber using hydrogen with a pressure of about 10 Torr. The severe reductions were accomplished with a conventional flow system using atmospheric hydrogen.

Results and Discussion

1) XPS Spectra of Chromium Compounds. There have been several reports of X-ray photoelectron spectroscopic measurements of chromium compounds.[6–11] The binding energies of the Cr2p level

for the chromium compounds examined in this study are listed in Table 1. It is clear from Table 1 that Cr^{6+}, Cr^{3+}, and Cr metal can be distinguished by the binding energy alone. However, recently the XPS spectra of Cr^{4+} compounds have been reported by Ikemoto *et at.*[12] According to their results, the binding energies of CrO_2 and CrOOH are 576.3 and 577.0 eV respectively. They also reported the $Cr2p_{3/2}$ binding energies for Cr_2O_3 and $K_2Cr_2O_7$; their values agree very well with our data in Table 1. These values for Cr^{4+} compounds are located around Cr_2O_3. In the case of CrO_2, its binding energy is even lower than that of Cr_2O_3. These facts will be explained in terms of the solid effects which cancel chemical shifts, as has been discussed by Kim and Winograd.[13] The chemical shift data, therefore, are not considered to be useful for determining the valence state of chromium, as in the case of Co,[2] Ni,[14] Pb,[15] and Cu.[16] As for Cr^{5+}, there have been no reports about XPS spectra in spite of its importance in catalysis.

The XPS spectra of the Cr2p level for Cr^{3+} compounds have weak satellites and their satellite splittings ($\Delta\varepsilon$) of the $Cr2p_{1/2}$ level were shown in Table 1, but the Cr^{6+} compounds give no such satellite peak. The $\Delta\varepsilon$ values and satellite intensities agree well with those reported by many workers.[17,18]

Helmer[9] reported that the spin-orbit intensity of the Cr2p doublet of Cr^{6+} is 0.33, instead of the theoretical value of 0.50. Also in our measurements it was found that the intensity ratios (I) ($Cr2p_{1/2}/2p_{3/2}$) for Cr^{6+} compounds are about 0.40, which are samller than 0.50: these are shown in Table 1. The discrepancy between the theoretical value and the observed values may be due to solid effects. In the case of Cr^{3+} compounds, I values are larger than those of Cr^{6+} compounds. This fact can be well understood by recognizing that the satellite peak of $Cr2p_{3/2}$ overlaps with the main peak of $Cr2p_{1/2}$.

The spin-orbit splittings of Cr^{3+} compounds are larger than those of Cr^{6+} compounds, as has been reported.[2,9] The difference of the spin-orbit splitting between Cr^{3+} and Cr^{6+} compounds can be explained in terms of the exchange interaction between 2p electrons and unpaired 3d electrons.[2-4] Such an interaction makes the 2p level spectra broad, as is shown in the last column of Table 1. Similar but larger effects of unpaired 3d electrons on the XPS spectra of 2p levels have been found for cobalt compounds.[2-4]

From these facts, Cr^{3+} and Cr^{6+} compounds and Cr-metal can be distinguished in terms of the binding energy, the satellite structure, the spin-orbit intensity ratio, and the spin-orbit splitting. However, in the studies of supported catalysts, the spectra obtained are usually weak, especially when the concentration of the catalytic component is low. The information about the satellite is sometimes ambiguous for supported transition metals, especially for supported chromium catalysts, since the satellite intensities are rather weak for chromium compounds. Moreover, the measurements of spin-orbit intensity ratios are considered to be difficult because of the uncertainties in the estimation of the base line. Therefore, we use the information about the binding energy and the spin-orbit splitting in order to distinguish the valence states of chromium supported on the carrier. In the case of the XPS studies of the supported cobalt catalysts,[2] such information has been found to be very useful to discriminate Co^{2+} and Co^{3+} species.

2) XPS Spectra of Chromia–Alumina Catalysts. 2—1 Photoreduction of Chromium on Chromia–Alumina Catalysts: The XPS spectra of chromium on the chromia–alumina catalysts were found to be time-dependent. The Cr2p spectra for a 2 wt% chromia–alumina catalyst, which was prepared by impregnation with chromium nitrate and calcined at 500 °C for 5 h, are shown at various irradiation times in Fig. 1. No change in the spectrum was observed within the irradiation time of 12.5 min. But, after 37.5 min-irradiation, an additional peak appeared at the lower binding energy of *ca.* 578 eV. After 80 min-exposure to X-ray flux, the additional and original peaks became comparable. An additional predominant peak appeared after 300 min irradiation, while a peak at 577.8 eV appeared by further irradiation. The peak obtained by the photoreduction has the spin-orbit splitting (ΔE) of 9.0 eV. Therefore, this chromium compound cannot be attributed to a Cr^{3+} compound, which has larger spin-orbit splitting values, as is shown in Table 1. The valence state this chromium compound will be discussed later. In the case of other chromia–alumina catalysts, similar phenomena were observed; the chromium states obtained were: B. E., 577.7 eV and ΔE, 9.5 eV for 5 wt%; B. E., 577.8 eV and ΔE, 9.7 eV for 10 wt%; and B. E., 577.2 eV and ΔE, 9.9 eV for 20 wt% after several hours irradiation. In the 20 wt% catalyst, the final state of chromium can be attributed to Cr^{3+} compound, because it has a energy of 577.2 eV and the ΔE value of 9.9 eV.

Such a pronounced surface reduction of some 3d transition metal compounds has been observed during XPS measurements. Particularly strong effects were found in copper(II) fluoride and potassium hexa-

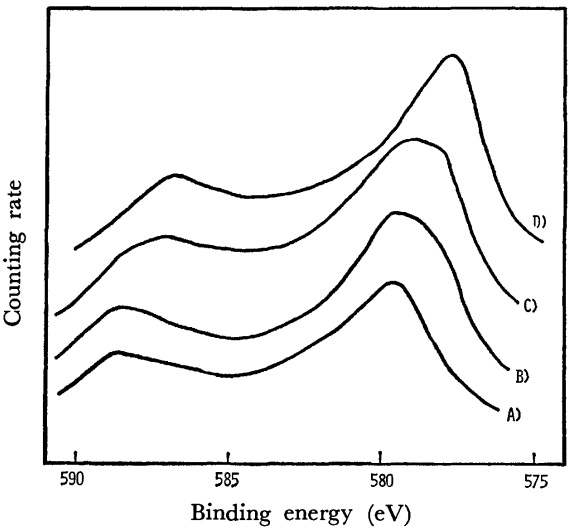

Fig. 1. Time-dependence of Cr2P XPS spectra for a 2 wt% chromia–alumina catalyst.
A) 12.5 min, B) 37.5 min, C) 80 min, D) 300 min-irradiation.

TABLE 1. BINDING ENERGY OF $Cr2p_{1/2}$ AND $2p_{3/2}$, SATELLITE SPLITTING, SPIN-ORBIT SPLITTING OF Cr2p LEVEL, INTENSITY RATIO OF $Cr2p_{1/2}$ and $2p_{3/2}$, AND FULL WIDTH AT HALF MAXIMUM OF $Cr2p_{3/2}$

	Compound	Binding energy[a]		ΔE[b]	I[c]	Δe[d]	FWHM[e]
		$Cr2p_{1/2}$	$Cr2p_{3/2}$				
1	CrO_3	589.4	580.3	9.1	0.43	—	2.8
2	K_2CrO_4	589.3	580.2	9.1	0.40	—	2.1
3	$K_2Cr_2O_7$	589.1	579.9	9.2	0.40	—	1.9
4	CrF_3	589.1	579.2	9.9	0.67	11.4	3.6
5	$Cr(NO_3)_3$	588.2	578.4	9.8	0.64	9.4	3.2
6	$CrPO_4$	587.9	578.3	9.6	0.56	11.5	4.1
7	$CrCl_3$	587.8	577.8	9.6	0.54	9.5	3.4
8	Cr_2O_3	586.4	576.6	9.8	0.63	10.9	3.6
9	Cr-metal[f]	583.6	574.5	9.1	nd[g]	—	nd[g]

a) eV. b) Spin-orbit splitting (eV). c) Intensity ratio: $Cr2p_{1/2}/Cr2p_{3/2}$. d) Satellite splitting of $Cr2p_{1/2}$ (eV). e) Full width at half maximum (eV). f) Not reduced. g) Not determined.

cyanoferrate (III).[19] No photoreduction phenomena, however, were observed in the chromium compounds examined in our study. These facts indicate that the chromium on the chromia–alumina catalysts can be easily reduced.

2—2 Surface State of Chromium on Chromia–Alumina Catalysts: As has been discussed above, the surface reduction of the catalyst during XPS measurements was found to be negligible within 12.5 min irradiation. Therefore, all spectra were measured within 4—12.5 min exposure to X-ray flux. In Fig. 2, the XPS spectra of the Cr2p level for 1, 2, 5, 10, and 20 wt% chromia–alumina catalysts (impregnated with chromium nitrate and calcined) are shown. The binding energies of the $Cr2p_{3/2}$ level and the spin-orbit splitting (ΔE) for the Cr2p level for these catalysts are listed in Table 2. In the case of 1 and 2 wt% catalyst, the valence state of surface chromium is considered to be almost entirely Cr^{6+} (B. E, 579.7 eV and ΔE, 9.0 eV), whereas the spectrum for a 5 wt% catalyst has a weak shoulder at the lower binding energy side. The shoulder intensity increases with increasing the supported amount of chromia. According to Table 2, the valence state of chromium with lower binding energy can be assigned to Cr^{3+} (B. E., 577.7 eV and ΔE, 9.8 eV). Then, the amount of the Cr^{3+} on the catalyst surface increases with increasing the chromia concentration. This tendency was also ascertained in the bulk analysis of the catalysts examined in our studies† by means of ESR (Cr^{3+}) and chemical analysis (Cr^{6+}; Bunsen-Rupp method). It has been reported by Matsunaga[20] that essentially all of the chromium ions were oxidized at 450 °C to the Cr^{6+} state for low chromia concentration catalysts, which were prepared by impregnation with chromic oxide and reduced in a stream of hydrogen for 5 h at 360 °C after calcination at 350 °C. Poole and MacIver[21] suggested, based on their optical measurements, that the Cr^{6+} detected is probably present on the catalyst surface and not in the catalyst bulk. The surface compositions obtained by XPS techniques support their results for low concentration catalysts. At higher chromium content catalysts, the Cr^{6+} content on the catalyst surface seems to be a little larger than that in a bulk catalyst. For example, in the case of a 20 wt% catalyst about half of chromium was found to be present as Cr^{6+}, according to chemical analysis by Bunsen-Rupp method, whereas the Cr^{3+} peak, as is shown in Fig. 2, is observed only as a shoulder of the Cr^{6+} one.

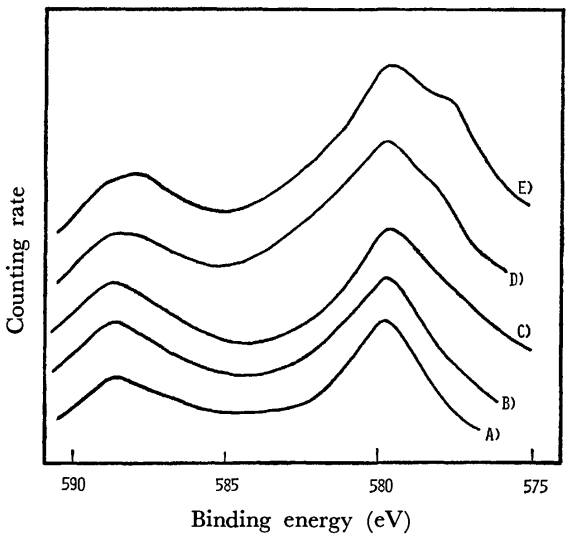

Fig. 2. XPS spectra of Cr2p level for impregnated chromia–alumina catalysts with chromium nitrate, which are calcined at 500 °C for 5 h.
A) 1 wt%, B) 2 wt%, C) 5 wt%, D) 10 wt%, E) 20 wt% catalyst.

Regarding the chromia–alumina catalysts prepared by impregnation with chromic oxide, the spectra were the same as those in Fig. 2 at low concentration of chromia, that is, almost all of the chromium are Cr^{6+}, while in the case of a 20 wt% catalyst the amount of Cr^{6+} is a little larger than that on the 20 wt% catalyst impregnated with chromium nitrate.

The Cr^{6+} binding energies are essentially the same among the calcined catalysts impregnated with different

† The ESR signal intensity of Cr^{5+} decreases with increasing the amount of supported chromium, indicating the maximum at 1 wt% catalyst. This fact suggests that the main valence state of chromium in the bulk is Cr^{5+}, but that the surface of the catalyst calcined in air is covered with Cr^{6+}.

starting compounds and uncalcined catalysts impregnated with chromium(III) oxide. They are slightly lower compared with that of CrO_3. The small changes in the binding energy may be attributed to charging effects, differences in crystal structure, or interactions between chromium and γ-Al_2O_3. Therefore, we cannot determine precisely the chemical state of the Cr^{6+} compound on γ-Al_2O_3 after calcination. However, the binding energies of Cr^{3+} on the surface of chromia–alumina catalysts are considerably increased (1.0—1.4 eV), comparing with that for Cr_2O_3. This fact is considered to indicate the presence of the interaction between small crystallines of Cr_2O_3[5] and γ-Al_2O_3, that is, the electron flow from Cr_2O_3 to γ-Al_2O_3 and be expected.

Before calcination, the valence states of chromium were Cr^{3+} (B. E., 578.0 eV and ΔE, 9.8 eV) for the catalysts prepared from chromium nitrate. This result coincides with that obtained by Poole *et al.*[22] using reflectance spectroscopy. In the case of the catalysts prepared from chromium(III) oxide, the chromium is Cr^{6+} (B. E., 579.8 eV and ΔE, 9.0 eV) before calcination.

The changes in the Cr2p spectra for chromia–alumina catalysts were observed by evacuation at elevated temperature or by reduction with hydrogen. These results are summarized in Table 2. In the case of a 2 wt% catalyst, the binding energy of $Cr2p_{3/2}$ become lower (1.9 eV), while the spin-orbit splitting was invariant (9.0 eV) even after evacuation at 230 °C for 20 min or at 350 °C for 1 h. The binding energy of 577.8 eV is close to that of Cr^{3+} compound, but the ΔE value of 9.0 eV is much smaller than that of Cr^{3+} compound. The XPS spectrum of this chromium was the same as that in Fig. 1 (D), which was observed by photoreduction. We cannot attribute this chromium to Cr^{3+} or Cr^{6+}.

The catalysts are considerably reduced by heating them in a pretreatment vacuum chamber. For example, the pronounced reduction of molybdena–alumina catalysts (Mo^{6+}—Mo^{5+}, Mo^{4+}) were observed by evacuation at 300—400 °C in our sample pretreatment chamber, which is evacuated with a cryogenic pump.[23] Therefore, the sexivalent chromium in the original catalyst is considered to be reduced to the chromium with the binding energy of 577.8 eV and the ΔE of 9.0 eV. In fact, the treatment of the catalyst with hydrogen at the pressure of 7.8 Torr gave the same valence state of chromium produced by the treatment of the evacuation or the photoreduction, as is shown in Table 2.

To determine the state of chromium observed after the evacuation at high temperature or the mild reduction with hydrogen, we consider the correlation between spin-orbit splitting (ΔE) and the number of the 3d unpaired electrons. In Table 3, these correlations are listed. When the number of unpaired 3d electron is one, no or only a small change in ΔE was observed, as for the cases of V, Co, and Cu. But when the unpaired 3d electron number is larger than two, a considerable change in ΔE was observed. The fact that ΔE values increase with increasing the number of 3d unpaired electrons can be explained qualitatively in terms of the exchange interaction between 2p electrons and 3d unpaired electrons.[2] From these facts, we can conclude that the number of 3d unpaired electrons in chromium obtained by the reduction is one or zero. The initial state of chromium is Cr^{6+}, as has been discussed. Therefore, the valence state of chromium is considered to be Cr^{5+}, which has one 3d unpaired electron. As discussed above, the chemical shifts data are not useful for determining the valence

Table 2. Binding energy of $Cr2p_{3/2}$ and spin-orbit splitting of Cr2p level for various chromia–alumina catalysts[a] prepared by impregnation with chromium nitrate

Catalyst (wt%)	Treatment	Binding energy of $Cr2p_{3/2}$ (eV)	ΔE (eV)	Assignment[c]
1	no treatment	579.7	9.0	6+
2	no treatment	579.7	8.9	6+
	evac. at 320 °C for 20 min	577.8	9.0	5+
	evac. at 350 °C for 1 h.	577.8	9.0	5+
	reduced with H_2 (7.8 Torr) at 300 °C for 5 min	577.8	9.1	5+
	reduced with atmospheric H_2 at 440 °C for 2 h	577.8	9.4	5+, (3+)
	reduced with atmospheric H_2 at 440 °C for 10 h	557.8	9.6	3+, (5+)
2[b]	no treatment	579.5	8.5	6+, (3+)
	evac. at 300 °C for 15 min	578.0	9.9	3+
5	no treatment	579.8[d]	9.0	6+, (3+)
	evac. at 340 °C for 15 min	577.5	9.4	5+, (3+)
10	no treatment	579.8	9.0	6+
		ca. 578.0	nd[e]	3+
	evac. at 330 °C for 50 min	577.5	9.6	3+, (5+)
20	no treatment	579.0	9.0	6+
		577.7	9.8	3+
	evac. at 340 °C for 30 min	577.5	9.6	3+, (5+)
	reduced with H_2 (10 Torr) at 200 °C for 10 min	577.6	9.8	3+

a) Calcined at 500 °C for 5 h in air. b) Calcined at 900 °C for 3 h. c) Valence state in parentheses indicates minor one. d) This peak has a weak shoulder at lower binding energy side. e) Not determined.

Table 3. Dependence of ΔE value on the number of unpaired 3d electrons for some transition metals

Metal	Valence state	Number of unpaired 3d electrons	ΔE (eV)	Compound
V	5+	0	7.5	NH_4VO_3
	4+	1	7.6	$VOSO_4$
Cr	6+	0	9.1	Table 1
	4+	2	9.8	CrO_2,[a] CrOOH
	3+	3	9.8	Table 1
	0	—	9.1	Table 1
Ni	2+	2	17.6	NiO, $Ni(HCOO)_2$
	0	—	17.2	Ni-metal
Co[b]	3+	0	15.0	
	2+	3	16.0	
		1	15.0	
	0	—	15.0	
Cu	2+	1	20.1	CuO
	1+	0	20.0	Cu_2O
	0	—	20.0	Cu-metal

a) Ikemoto *et al.* Ref. 12. b) Okamoto *et al.* Ref. 2.

state of chromium, and ΔE values are considered to be more powerful and reliable in discriminating the valence state of chromium. Therefore, the valence state of chromium obtained by the mild reduction of Cr^{6+} is concluded to be Cr^{5+}, though the binding energy is lower than expected. The low binding energy of Cr^{5+} will be explained in terms of solid effects,[13] as in the case of Cr^{4+}. Moreover, it is considered, based on our assignment, that almost all chromium is present as the Cr^{5+} state after such mild reduction at low chromia concentration catalysts. According to Cossee *et al.*,[24] the mild reductions of chromia–alumina catalysts produce over 95% Cr^{5+} in total chromium in the case of low concentration of chromium. Our XPS results coincide with their ESR results. These facts show that our assignment is reasonable. However, it is not easy to define the chemical state of Cr^{5+} precisely, since there have been no reports, to our knowledge, about the XPS spectrum for Cr^{5+}.

In the case of the high chromia concentration catalysts, the binding energy and ΔE value of the surface state of chromium were 577.5 eV and 9.4—9.6 eV respectively after evacuation at high temperature. The XPS spectra for these chromiums were similar to that in Fig. 1 (D) except for the ΔE value. The spectra containing both Cr^{3+} and Cr^{5+} are deduced to have ΔE of a intermediate value between 9.0 and 9.9 eV, when the spectra of Cr^{3+} and Cr^{5+}, whose binding energies are almost the same, overlap each other. After the evacuation the ΔE values were 9.4, 9.6, and 9.6 eV for 5, 10, and 20 wt% catalysts, respectively. Therefore, it is concluded that these high chromia content catalysts contain both Cr^{3+} and Cr^{5+} after evacuation and that the higher the chromia content is, the larger is the amount of Cr^{3+} produced.

On the basis of a discussion similar to the above, it is considered that the Cr^{3+} phase can be produced at first by severe reductions at low chromia concentration catalysts, as is shown in Table 2. Accordingly, it is concluded that at lower chromia content catalysts, such as a 2 wt% catalyst, Cr^{5+} phase is rather stable, while at higher chromia content catalysts Cr^{3+} phase can be easily produced.

In the case of a 2 wt% catalyst calcined at 900 °C for 3 h, however, chromium was easily reduced by the mild reduction and gave almost entirely Cr^{3+} state, as is listed in Table 2. These findings seem to correlate with the fact that the catalysts calcined at high temperature give a weaker γ-phase intensity in ESR spectra than the catalysts calcined at 500 °C.[5]

On the basis of these results, the assignments for the valence states of surface chromium before and after the treatments were accomplished and listed in the last column of Table 2. Qualitatively, these surface properties of chromia–alumina catalysts obtained by XPS technique agree very well with the results obtained by ESR or other techniques, especially at low chromium concentration catalysts. These facts indicate the good dispersion of chromium on γ-Al_2O_3 at low chromium content catalysts.

References

1) W. N. Delgass, T. R. Hughes, and C. S. Fadley, *Catal. Rev.*, **4**, 179 (1970).
2) Y. Okamoto, H. Nakano, T. Imanaka, and S. Teranishi, *Bull. Chem. Soc. Jpn.*, **48**, 1163 (1975).
3) D. C. Frost, C. A. MacDowell, and I. S. Woolsey, *Chem. Phys. Lett.*, **17**, 320 (1972).
4) D. C. Frost, C. A. MacDowell, and I. S. Woolsey, *Mol. Phys.*, **27**, 1473 (1974).
5) C. P. Pool and D. S. MacIver, *Advan. Catal.*, **17**, 224 (1967).
6) D. N. Hendrickson, J. M. Hollandar, and W. L. Jolly, *Inorg. Chem.*, **9**, 612 (1970).
7) M. V. Zeller and R. G. Hayes, *Chem. Phys. Lett.*, **10**, 610 (1971).
8) J. C. Carver, G. K. Schweitzer, and T. A. Carlson, *J. Chem. Phys.*, **57**, 973 (1972).
9) J. C. Helmer, *J. Electron Spectrosc.*, **1**, 259 (1972/73).
10) G. C. Allen, M. T. Curtis, A. J. Hooper, and P. M. Ticler, *J. Chem. Soc., Dalton*, **1973**, 1675.
11) Y. Okamoto, K. Adachi, T. Imanaka, and S. Teranishi, *Chem. Lett.*, **1974**, 241.
12) I. Ikemoto, K. Ishii, S. Kinoshita, H. Kuroda, M. A. Franco, and J. M. Thomas, Preprint for the 32nd Annual Meeting of Chemical Society of Japan, Tokyo, April, 1975.
13) K. S. Kim and N. Winograd, *Chem. Phys. Lett.*, **30**, 91 (1975).
14) L. J. Matienzo, L. I. Yin, S. O. Grim, and W. E. Swartz, *Inorg. Chem.*, **12**, 2762 (1973).
15) K. S. Kim, T. J. O'Leary, and N. Winograd, *Anal. Chem.*, **45**, 2213 (1973).
16) P. E. Larson, *J. Electron Spectrosc.*, **4**, 213 (1974).
17) T. A. Carlson, J. C. Carver, L. J. Saethre, F. G. Santibanez, and G. A. Vernon, *J. Electron Spectrosc*, **5**, 247 (1974).
18) B. Wallbank, I. G. Main, and C. E. Johnson, *J. Electron Spectrosc.*, **5**, 259 (1974).
19) B. Wallbank, C. E. Johnson, and I. G. Main, *J. Electron Spectrosc.*, **4**, 263 (1974).
20) Y. Matsunaga, *Bull. Chem. Soc. Jpn.*, **30**, 868 (1957).
21) C. P. Poole and D. S. MacIver, *J. Chem. Phys.*, **41**, 1500 (1964).
22) C.P. Poole and J.F. Itzel, *J. Chem. Phys.*, **39**, 3445 (1963).
23) Y. Okamoto, H. Nakano, T. Imanaka, and S. Teranishi, unpublished.
24) P. Cossee and L. L. Reigen, Proc. 2nd Int. Congr. Cat., Paris (1960).

Concentration Depolarization of the Fluorescence and Phosphorescence of Acridine Orange Cations

Tomoko KOMIYAMA* and Yuji MORI

Department of Chemistry, Tokyo Institute of Technology, Ohokayama, Meguro-ku, Tokyo 152

(Received July 15, 1975)

Concentration depolarization of fluorescence and phosphorescence has been studied for Acridine Orange cations in PVA films. Depolarization can be observed with concentrations above 10^{-6} M. For concentrations ranging from 10^{-6} M to 10^{-4} M both depolarization of fluorescence and of phosphorescence obey the Weber equation. The results indicate that singlet-singlet energy transfer is responsible for depolarization of fluorescence, as well as of phosphorescence. Above 10^{-4} M, the effect of the exchange interaction cannot be ignored due to the formation of higher aggregates.

Acridine dyes have a common notable characteristic of readily aggregating. Acridine Orange, a typical acridine dye undergoes many interesting phenomena that remain yet to be studied, although a number of investigations have dealt with the concentration dependence of absorption spectra and the equilibrium between monomers and aggregates.[1,2] Schmidt[3] and Chambers *et al.*[4] have studied the behavior of the triplet state as a function of the dye concentration. It was found that dye molecules aggregate to form a complex in which the molecules are orientated in a fixed direction.

It is the purpose of this paper to demonstrate the favorable energy transfer process in a system of dye molecules embedded in a polymer matrix by means of depolarization of the fluorescence and phosphorescence as a function of the dye concentration.

Experimental

The techniques used to prepare poly vinyl alcohol (PVA) films are similar to those employed by Tanizaki *et al.*[5] PVA solutions were prepared by mixing 20 g of PVA powder with 150 ml of redistilled water, followed by vigorous stirring in a boiling water-bath for 2 h. To this solutions was added 50 ml of a hydrochloric acidified ethanol solution of chromatographically purified Acridine Orange. After careful mixing, the solutions were poured over a glass plate (20× 20 cm) and were spread out to a uniform thickness. The solutions were dried in a dust-free box for a few days at room temperature. The hard films obtained have a typical thickness of about 0.2 mm.

Absorption spectra were measured with a Shimadzu MPS-50L spectrophotometer. A 150 W xenon lamp combined with various interference filters was used to excite the samples. A Nikon G-250 grating monochromator was used for the emission spectra. The exciting light beam falls on the film surface at an angle of 60° and the fluorescence was observed in the direction at right angles with the exciting light beam. For the measurement of polarization, two rotatable film polarizers ("Polaroid" HN-22) were used. A quartz depolarizer was inserted in front of the photomultiplior (HTV-R636). The transmittance of the monochromater for the polarized light was independent of the polarization of the incident light for all wavelengths. To obtain phosphorescence spectra, a cylindrical sector was rotated around the cylindrical Dewar flask in which the films were immersed in liquid nitrogen. Absorption spectra were corrected for the transmittance of the neat PVA film without the dye. The degree of polarization P was corrected for the self-polarization of the apparatus.[6] P was determined by $P=(I_{\parallel}-I_{\perp}f)/(I_{\parallel}+I_{\perp}f)$, where f[7] is a correction factor. $I_{\parallel}$ and $I_{\perp}$ are the observed intensities of vertical and horizontal components of the fluorescence with respect to the vertically polarized exciting light.

Results and Discussion

Figure 1 shows the absorption and fluorescence spectra of Acridine Orange cations in PVA films at 77 K. The room temperature absorption spectra in PVA are essentially identical with those in ethanol solutions. At 77 K, however, there is a remarkable difference between the absorption spectra in ethanol solutions and those in PVA films due to the aggregation of dyes in liquid solutions. The first absorption band with the peak at 495 nm is attributed to the $S_1 \leftarrow S_0$ transition of the dye monomers. The second band around 465 nm appears as a shoulder and becomes more prominent relative to the first band, as the concentration of dye cations increases. It is interesting to note that Acridine Orange cations form dimers in PVA films. In studies by Tanizaki *et al.*,[5] the formation of dimers in PVA films was not observed.

To account for the effect of concentration on the absorption spectra in PVA films, the monomer-dimer equilibrium of dye molecules is assumed and an ap-

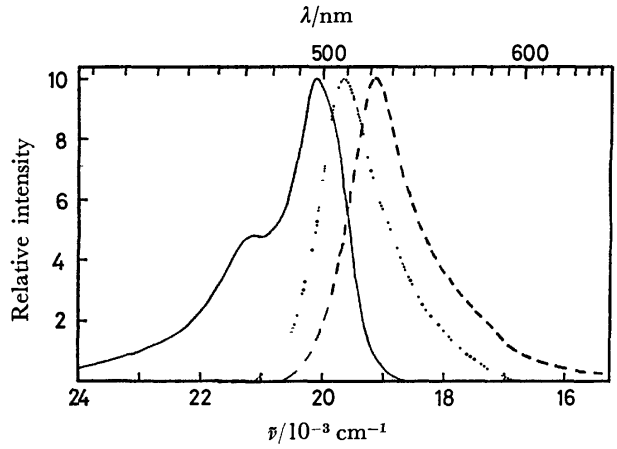

Fig. 1. Absorption and fluorescence spectra of Acridine Orange cations in PVA at 77 K. Absorption; ——: 2.64×10^{-5} M. Fluorescence; ····: 1.32×10^{-6} M. ----: 2.64×10^{-5} M.

* Present address: Department of Industrial Chemistry, College of Technology, Seikei University, Kichijojikitamachi, Musashino-shi, Tokyo 180, Japan.

propriate K value, 1.3×10^4 M^{-1}, is obtained for concentrations ranging from 10^{-4} to 10^{-6} M. In the case of ethanol solutions at 10^{-4}—10^{-6} M, a value of 1.4×10^4 M^{-1} is obtained for the association constant. The equilibrium constant, 1.3×10^4 M^{-1}, can be attributed to that in the film before it hardens and not to that in the hard film. Spectra derived from this dimerization equilibrium display a shoulder at 470 nm in agreement with the results of Zanker.[1] The 495 nm peak and the 470 nm shoulder have been assigned by Sheppard[8] to the 0–0 and 0–1 vibrational transitions, respectively. The association constant in PVA films is independent of the temperature. Therefore, the dimerization equilibrium is the same as that at room temperature.

The fluorescence spectra show good mirror image relationships with the absorption spectra. In all the experiments, no excitation spectra indicate that the samples contain any free base of the dye. The spectra in PVA are rather diffuse, compared with those of ethanol solutions, as well as the absorption spectra. The change of the fluorescence profile with increasing dye concentration is remarkable on the longer wavelength side of the broad emission band, this change appearing to be due to dimer formation. The peak of the broad emission band at 510 nm shifts toward the red by 490 cm^{-1} for a change in the dye concentration from 10^{-6} to 10^{-3} M. The red shift of the fluorescence peak cannot be interpreted in terms of reabsorption, which is negligible in the present optical system.

In ethanol glasses at 77 K, the fluorescence shows three sharp peaks at 510, 535 and 570 nm. In combination with the concentration change of the fluorescence spectra, these bands are assigned as follows. The first is the monomer band and the second that of the dimer. The third band is attributed to the oligomer band because of the appearance of the same peak for the polycrystalline dye films on a glass plate obtained by solvent evaporation from dye cation solutions. Compared with these complex features of solution fluorescence at 77 K, PVA matrix fluorescence spectra appear to be rather simple. The first sharp band is attributed to the monomer band and the second is a weak, but detectable, broad dimer band mixed with that of the oligomer.

In the highest concentration range, the broad intense phosphorescence at 655 nm is observed with a swift decay rate at room temperature. It is expected that the phosphorescence states are established in PVA films because of the slow quenching reaction of the phosphorescence by oxygen. As shown in Fig. 2, phosphorescence spectra in PVA at 77 K give the main peak at 610 nm and the second peak at 655 nm. The lifetime of the phosphorescence is 2.0 s at 10^{-3} M in PVA films at 77 K. If the dimer band is excited at 465 nm, the intensity of the second phosphorescence band is stronger than the first. In addition to the consistency with the excitation spectra, the intensity of the second phosphorescence band becomes stronger as the dye concentration is increased. On the basis of these spectral changes, the second phosphorescence band is attributed to the triplet state

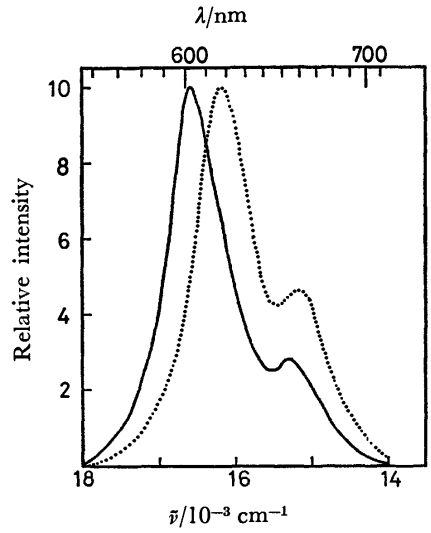

Fig. 2. Phosphorescence spectra of Acridine Orange cations in PVA at 77 K.
——: 7.92×10^{-5} M. ····: 6.12×10^{-4} M.

of the dimer.[4]

However, the energy gap between the triplet states of the monomer and dimer appears to be much larger than the generally accepted values for dimers. The peaks of phosphorescence spectra show a red shift of 600 cm^{-1}, which is larger than that for fluorescence, when the dye concentration increases above 6×10^{-4} M. The energy gap may be interpreted on the basis of the lowering of the triplet state by the formation of complicated aggregates rather than simple dimers.

The second phosphorescence band is shifted makedly toward the red, and is accompanied by an extension of the excitation spectra into the red at concentrations greater than 6×10^{-4} M. Consistent with the present observation, Schmidt[3] and Yamaoka[9] *et al.* have reported the appearance of a broad absorption band with a peak around 570 nm at a high dye concentration above 6×10^{-4} M.

Polarization measurements were made for their fluorescence, phosphorescence and excitation spectra

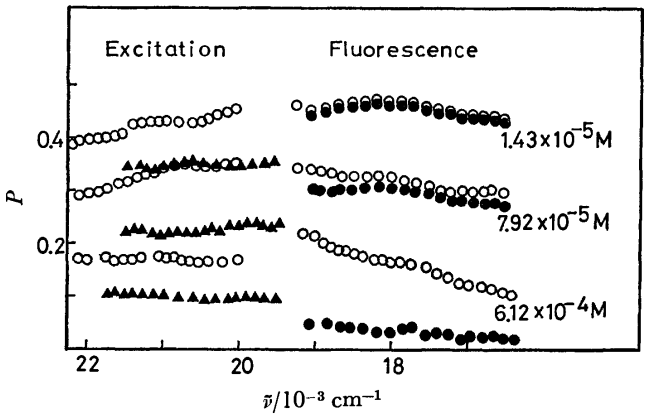

Fig. 3. Polarization degrees of fluorescence and excitation spectra. Fluorescence; ○: excited at 495 nm, ●: excited at 465 nm. Excitation; ○: observed at 525 nm, ▲: observed at 655 nm.

in PVA films. In Fig. 3, the variation of the degree of polarization of excitation as a function of the fluorescence observed at 525 nm is shown. At medium concentrations of 10^{-4}—10^{-6} M, there is a slight, but detectable, difference between the degree of polarization of the monomer at 495 nm and that of the dimer band at 465 nm. The excitation of the dimer band results in a higher depolarization than that of the monomer band. In Fig. 3, fluorescence also exhibits similar differences in the degree of polarization of the monomer, dimer and oligomer bands. Thus, it seems probable that each electronic transition exhibits a certain degree of polarization, but that the separation of each fluorescence band is poor due to the broad emission bands in polymer films. At low concentrations, below 10^{-6} M, it is difficult to obtain a degree of polarization with good reproducibility. At these concentrations, however, the degree of polarization remains constant independent of the fluorescence spectral range. At high concentrations, above 4×10^{-4} M, the structure of the fluorescence spectra disappears in parallel with the fluorescence depolarization.

The fluorescence depolarization indicates energy transfer in PVA films which inhibit molecular diffusion. The plots of $1/P$ *versus* concentration are linear regardless of the exciting or observed wavelengths over the concentration range of 10^{-4}—10^{-6} M, where P is the degree of polarization. Fig. 4 serves to illustrate the linear relation for the case of the monomer-band excitation and observation. For concentrations above 10^{-4} M, $1/P$ at a given concentration is remarkably dependent of the excitation wavelength and the fluorescence wavelength.

The limiting polarization P_0, the degree of polarization in the absence of energy transfer is obtained by extrapolation to zero concentration. Weber[10] derived an equation describing the intermolecular energy transfer as revealed by fluorescence depolarization measurements as follows:

$$\frac{1}{P}-\frac{1}{3}=\left(\frac{1}{P_0}-\frac{1}{3}\right)\left(1+\frac{4\pi NR^6\times 10^{-3}}{15(2a)^3}C\right) \qquad (1)$$

in which N is Avogadro's number, C is the concentration in M, R is the critical distance for two oscillators and a is the effective molecular radius. Assuming a value for $2a$ of 10 Å and utilizing the slope of the straight line in Fig. 4, R was calculated under several conditions and is listed in Table 1.

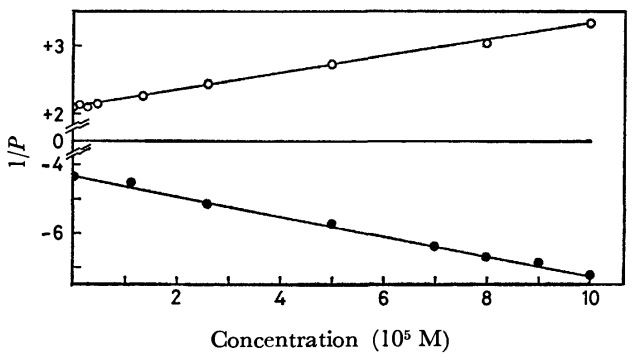

Fig. 4. $1/P$ plots *versus* concentration for fluorescence and phosphorescence spectra. ○; Fluorescence, excited at 495 nm, observed at 525 nm. ●; Phosphorescence, excited at 495 nm, observed at 610 nm.

TABLE 1. CRITICAL DISTANCES OBTAINED FROM FLUORESCENCE DEPOLARIZATION ($10^{-6}-10^{-4}$ M)

Excitation spectra		
Fluorescence	Excitation	
	at 495 nm	465 nm
535 nm	47.5	50.4
570 nm	49.5	52.0
Fluorescence spectra		
Exciting wavelength	Fluorescence	
	at 510—535 nm	570 nm
465	48.3	48.9
500	47.7	48.3

Furthermore, the degree of polarization of the phosphorescence is measured as a function of the concentration at 77 K for two peaks located at 610 and 655 nm. Room temperature phosphorescence is too weak to measure the degree of polarization accurately. The phosphorescence spectra are negatively polarized in contrast with the fluorescence spectra. The degree of polarization around 610 nm is higher than that around 655 nm. The concentration depolarization of phosphorescence is measured for two excitations at 465 and 495 nm while monitoring the phosphorescence peaks. The 465-nm excitation gives a higher depolarization than that at 495 nm.

The results give the relation between the phosphorescence depolarization and the dye concentration as in the case of fluorescence depolarization. A linear relationship between $1/P$ and the concentration is obtained in the concentration range of 10^{-4}—10^{-6} M. Selecting the phosphorescence observed at 610 nm and excited at 495 nm, a linear relation is shown in Fig. 4, for the degree of phosphorescence polarization. Using the slope of Fig. 4, the value of the critical distance R=47.3 Å is obtained from Eq. 1 for the phosphorescence depolarization on the assumption that it is possible to extend the previously mentioned treatment to the case of phosphorescence. This result indicates that the phosphorescence depolarization is also governed by singlet-singlet energy transfer. Above 10^{-4} M, somewhat more complicated features, such as triplet-triplet energy transfer, should be taken into consideration to account for the concentration depolarization of phosphorescence.

The concentration depolarization of phosphorescence has been studied by Chaudhuri and El-Sayed[11] and Iwao *et al.*[12] using the aromatic compounds such as naphthalene and its halogenated or deuterated derivatives. Concerning the primary process of phosphorescence depolarization, the present observations are in agreement with the conclusion obtained by Iwao *et al.*

One of the present authors (T. K.) is greatly indebted to Professor Y. Tanizaki for helpful discussions and suggestions.

References

1) V. Zanker, M. Held and H. Rammensee, *Z. Naturforsch.*, **14b**, 789 (1959).
2) M. E. Lamm and D. M. Neville, Jr., *J. Phys. Chem.*, **69**, 3872 (1965).
3) H. Schmidt, *Z. Physik. Chem. Neue Folge*, **80**, 44 (1972).
4) R. W. Chambers, T. Kajiwara, and D. R. Kearns, *J. Phys. Chem.*, **78**, 380 (1974).
5) Y. Tanizaki, T. Kobayashi, and N. Ando, *Bull. Chem. Soc. Jpn.*, **32**, 119 (1959).
6) T. Azumi and S. P. McGlynn, *J. Chem. Phys.*, **37**, 2413 (1962).
7) $f=I'_{\perp}/I'_{\parallel}$, where $I'_{\perp}$ and $I'_{\parallel}$ are the observed intensities of vertical and horizontal components of fluorescence with respect to the horizontally polarized exciting light.
8) S. E. Sheppart, *Rev. Mod. Phys.*, **14**, 303 (1942).
9) K. Yamaoka, Y. Matsuoka, and M. Miura, *J. Phys. Chem.*, **78** 1040 (1974).
10) G. Weber, *Trans. Faraday Soc.*, **50**, 552 (1954).
11) N. K. Chaudhuri and M. A. El-Sayed, *J. Chem. Phys.*, **42**, 1946 (1965).
12) T. Iwao, Y. Gondo, and Y. Kanda, *Chem. Lett.*, **1975**, 463.

Adsorption and Desorption of Molecular Oxygen in Solid State of Polymeric Hemochrome

Kenji HONDA, Seiji HATA, and Eishun TSUCHIDA
Department of Polymer Chemistry, Waseda University, Tokyo 160
(Received July 16, 1975)

The oxygenation of a pyridine-hemochrome bound to a polymer ligand has been studied in solid state. The oxygenation rate and the amount of oxygen adsorbed were determined by volumetry. The rate of adsorption of oxygen depends upon the structure of polymer matrix. Pyridine hemochrome included in a polyion complex takes up oxygen more rapidly than others. The rate of adsorption depends a great deal upon the surface condition of polymer matrix in case of oxygen binding in solid state. The degree of oxygenation was nearly equal in all cases. The difference in the rate of adsorption of oxygen may be due to the difference in gas permeability of the polymer matrix. This was supported by the fact that the hemochrome bound to a porous polymer matrix adsorbs oxygen more rapidly than the hemochrome bound to a non-porous polymer matrix. The surface condition of the polymer matrix greatly affects the reversibility of oxygenation.

An artificial oxygen carrier which can reversibly take up and release molecular oxygen with a relatively small difference in the partial pressure of oxygen in solution or solid state would meet extensive requirements.

Pfeiffer *et al.*[1] found the reversible binding of molecular oxygen of *N,N'*-ethylene bis(salicylideneiminato)-cobalt(II) complex (salcomin) in crystalline state. Calvin *et al.*[2] developed reversible oxygenation systematically for a series of salcomin derivatives in solid state. Studies on a reversible oxygen complex have actively been made in various fields. However, no metal complex which can reversibly take up oxygen in a neutral aqueous solution at room temperature has been synthesized. The failure in synthesizing a stable oxygen complex is due to the rapid irreversible autoxidation of a central metal ion. Wang *et al.*[3] synthesized the imidazole-hemochrome as a hemoglobin model included in polystyrene film and examined the stability and reversibility of the oxygen complex imbedded in the film in the presence of water.

The present authors[4-9] have found that oxygen complex can exist in a stable form even in aqueous dimethylformamide solution at room temperature by modification of a polymer ligand of heme-iron. Recent studies on oxygen complex have been made mainly in organic solvents.[10-15] In contrast, few studies in solid state have been carried out except for the series of Calvin's studies. In this paper, the oxygenation of the polymer-heme complex in solid state will be discussed. The correlation of the oxygenation reactivity to the surface condition of the polymer matrices has been studied.

Experimental

Materials. Poly(4-vinylpyridine) (PVP; $\overline{P}_n=49$) and partially-quaternized poly(4-vinylpyridine) (QPVP: $\overline{P}_n=49$, 24% of quaternization by benzyl chloride) were prepared and purified according to the conventional method.[4,9] Polystyrene sulfonic acid (PSS; $\overline{P}_n=321$, sulfonation=77%), polyglutamic acid (PGA; $\overline{P}_n=331$) and alginic acid (Alg) were purified according to directions reported in previous papers.[16,17] Isolation of chlorohemin from blood was carried out by Willstatter's method.[18] Sodium dithionite ($Na_2S_2O_4$) of a reagent grade was used without purification and α,α'-azobisisobutyronitrile(AIBN)was recrystallized from methanol.

Preparation of Powdery Polymer Matrix Including Hemochrome. A powdery sample of a polymer-bound hemochrome was prepared as follows. Chlorohemin (150 mg) was dissolved in 150 ml of an aqueous solution (pH=12). An aqueous solution (20 ml) containing 4.0 g of $Na_2S_2O_4$ was added, and then 150 ml of an aqueous solution containing 0.6 g of QPVP was added immediately in an atmosphere of nitrogen. The complex formation between heme and QPVP was accompanied by a color change from black brown to reddish brown. Another component of polyion such as PSS, PGA, and Alg was added in order to form a polyion complex; An aqueous solution (80 ml) containing PSS (0.38 g), PGA (0.35 g) or Alg (0.38 g) was slowly added to the above solution. The resulting precipitate was filtered off and dried completely *in vacuo* at 70—80 °C. This type of polymer-heme complex is called "complexed-type hemochrome".

Another type of polymer-heme complex "single-type hemochrome" was also prepared. PVP (1.06 g) and chlorohemin (68 mg) were dissolved in 150 ml of methanol. Methanol (140 ml) containing 0.9 g of L-ascorbic acid was then slowly added with vigorous stirring in an atmosphere of nitrogen. The resulting reddish solution was evaporated and dried at 50 °C *in vacuo*.

The content of heme of the polymer complex was determined by spectrometry to be 5.0×10^{-5} mole per unit gram of the polymer matrix. The powdery sample used for oxygenation analysis was ground to particles under 48 mesh.

Measurement of Magnetic Susceptibility. Metal complexes used were the monomeric and polymeric pyridine hemichromes. The measurement of magnetic susceptibility of powdery samples was carried out by the Faraday method. A magnetic torsion balance was operated at a field strength of 10000 G over the temperature range from liquid nitrogen temperature to room temperature. Gd_2O_3 was used as a standard sample. The magnetic susceptibility was recorded automatically and continuously as a function of temperature on an X-Y recorder. The apparatus used for the measurement is the same as that reported by Kohn.[19] The errors inherent in this method of analysis are of the order of ten per cent.

Manometric Measurement of Oxygen Uptake in Solid State. The time-conversion curves of oxygenation in solid state of polymer-bound hemochrome were obtained by use of a Warburg apparatus. Heme (1.0×10^{-5} mole) imbedded in 0.2 g of the matrix was put into a cuvette in an atmospheric oxygen pressure, the amount of oxygen adsorbed by the powdery sample being checked by use of a manometer. The amount of oxygen adsorbed by the hemochrome was corrected with a small quantity of oxygen adsorbed by the

powdery polymer and an excess of the reductant.

Results and Discussion

Coordination Structure of the Polymer-Heme Complex. The coordination numbers ($\bar{n}$) of the axial ligand and the equilibrium constants (K) of the hemichrome and hemochrome were determined by the method of Miller and Dorough.[20] The parameters $\bar{n}$ and K were calculated on the basis of the analysis of the spectrophotometrical titration for the complexation between hemin or heme and various bases. Application of this method to polymer ligands was reported previously[4,9]

The results given in Table 1 show that the axial 5th site of heme-iron is occupied by the pyridine molecule of PVP or QPVP. Another axial site of heme-iron might be either occupied by water or vacant. However, all the coordination numbers ($\bar{n}$) of the axial ligands were intermediate between 1.0 and 2.0 in both cases of the hemichrome and hemochrome. It is reasonable to consider that the six-coordinate pyridine hemichrome or hemochrome, whose axial sites are both occupied by two pyridine molecules, is mixed with the five-coordinate complex. The result of magnetic susceptibility also suggests that the high spin complex and the low spin complex are in equilibrium, because the molar magnetic susceptibility (X_M) of the pyridine hemichrome was intermediate between the calculated values of the high spin and low spin states (Table 1). From the temperature dependence of the magnetic susceptibility (Fig. 1), it was found that the high spin complex and the low spin complex are in spin equilibrium at the iron(III) state.[21] On the other hand, the equilibrium constant of spin exchange between the high spin state and the low spin state of the heme-ion(II) does not depend upon temperature. The observed value of the magnetic susceptibility was nearly equal to the calculated one of the high spin complex. Thus, in the case of the hemochrome, the six-coordinate complex can hardly be mixed with the five-coordinate complex.

Table 1. Axial coordination numbers ($\bar{n}$) and magnetic susceptibility of hemichrome and hemochrome bonded to polymer ligand

Axial base	$\bar{n}$		λ_{max} (nm)		$\chi_M \times 10^6$ (e.m.u.)
	Fe^{3+}	Fe^{2+}	Fe^{3+}	Fe^{2+}	Fe^{3+} at 0°C
Py	1.02	1.11	424	418	13900
PVP	0.95	1.32	424	418	7900
QPVP	1.30	1.25	397	419	14200
QPVP-PSS	—	—	397	422	9900

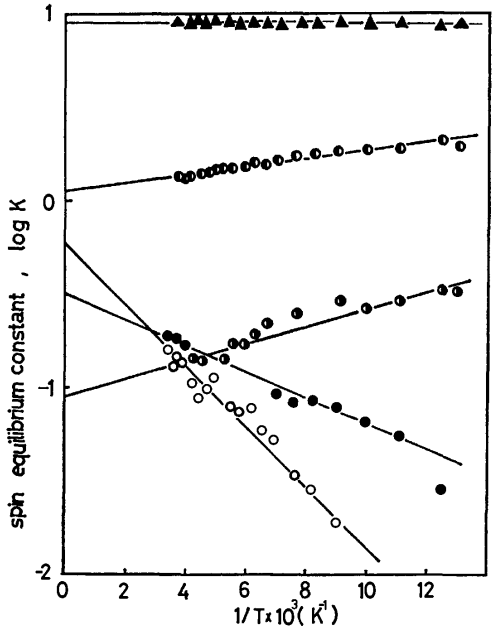

Fig. 1. Correlation of the spin equilibrium constant to inverse temperature for various types of polymer-hemin complexes.
◐ QPVP, ◑ QPVP-PSS, ● Py, ○ PVP, ▲ QPVP-PSS-Heme.

Correlation of the Reactivity of Oxygenation to the Surface Condition of the Polymer Matrix. The oxygen adsorption curves of the complexed-type and the single-type polymeric hemochromes are shown in Fig. 2. Table 2 gives the initial rate, the half-saturation time and the degree of oxygen-saturation for the various types of polymer matrices. We see that the initial rate of the complexed-type system was appreciably larger than that of the single-type system. In general, the rate of adsorption of oxygen in solid state is affected by the diffusion of oxygen in solid matrix.[2b] The difference in the rate of adsorption between the complexed-type and single-type hemochromes may be due to the difference in the rate of diffusion of oxygen in the polymer matrices.

In order to clarify the correlation of the reactivity of oxygenation to gas permeability in the polymer matrix, the rate of adsorption of oxygen was checked for a porous polymer-bound hemochrome prepared by treatment of the matrix with a foaming agent such as

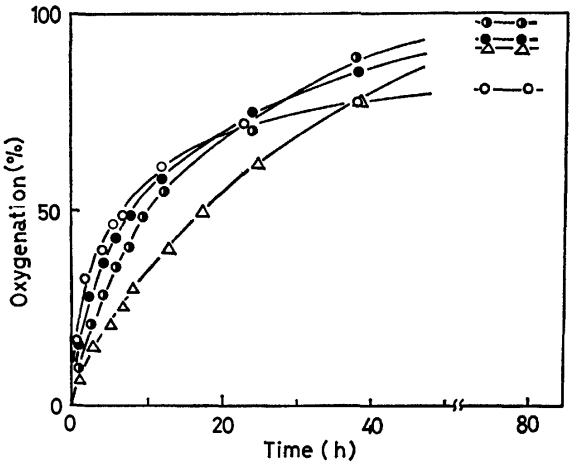

Fig. 2. Time conversion curve of oxygenation of polymer-bound hemochromes in solid state.
Matrix: ○ QPVPP-GA, ◑ QPVP-Alg, ● QPVP-PSS, △ PVP.
Heme: 1.0×10^{-5} mol/0.2 g polymer, at 30° C.

Table 2. Oxygenation of polymeric hemochrome in polymer matrix

System	Matrix	V_1 (μl/mol)[a]		T_{50} (h)[b]		D_s (%)[c]	
		solid	dispersion[d]	solid	dispersion[d]	solid	dispersion[d]
Complexed	QPVP-PSS	3.00	65.8	7.5	0.58	93	92
	QPVP-PGA	3.80	96.5	6.6	0.50	80	90
	QPVP-Alg	1.40	60.1	9.7	0.60	100	95
Single	PVP	0.78	53.2	17.1	0.67	93	92

PVP-Heme dissolved in DMF/MeOH=1/1; V_1=280, D_s=92.
a) V_1: initial rate of oxygenation, b) T_{50}: time for half-saturation of oxygen, c) D: degree of saturation of oxygenation, d) dispersed in H_2O (pH=6.0), Heme=1×10^{-5} mol/0.2 g polymer matrix, at 30 °C.

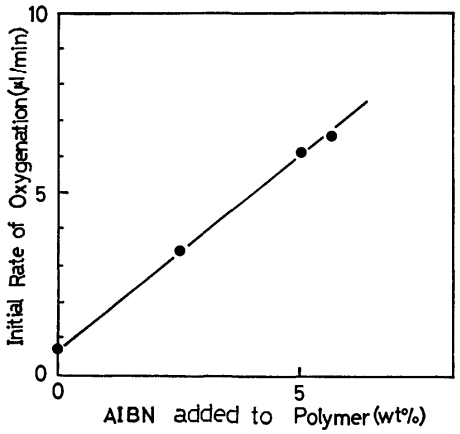

Fig. 3. Effect of porosity of polymer matrix on the oxygenation rate.
Heme: 1.0×10^{-5} mol/0.2 g polymer, at 30 °C.

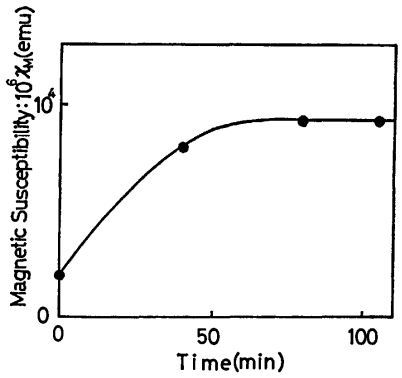

Fig. 4. Time conversion curve of magnetic susceptibility due to deoxygenation of a poly(vinylpyridine)-hemochrome.
X_M: Measured at 25 °C, deoxygenation: atmospheric, at 90 °C. Heme: 1.0×10^{-5} mol/0.2 g polymer.

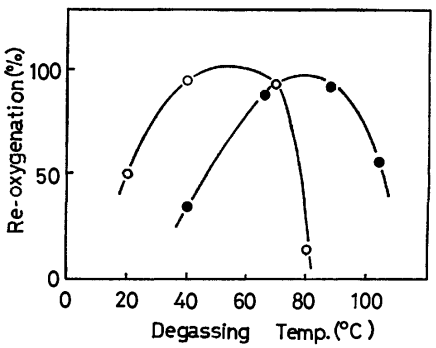

Fig. 5. Temperature effect on deoxygenation of a polymer-bound hemochrome.
Deoxygenation: 3 mmHg, for 1 h.

azobisisobutyronitrile (AIBN). Figure 3 shows the relationship between the initial rate of oxygen uptake and the amount of AIBN added. The adsorption rate is linearly proportional to the amount of AIBN. This might be due to the increase in porosity of the polymer matrix. The porosity of matrix is of importance for oxygen uptake in solid state.

Table 2 also gives the corresponding parameters of oxygenation of the dispersion system in water. The gas permeability calculated by the Fick's Law becomes very large in the presence of water owing to the formation of water-bridge.[2b] We found that the oxygenation rate of the dispersion system is much larger than that of the solid system. This may also be due to the difference in gas permeability between the solid system and the dispersion system. However, the rate of the dispersion system in water was still much smaller than that of the homogeneous solution system.

Reversible Desorption of the Oxygen Complex Bound to Polymer Matrix. The oxygen complex can reversibly desorb molecular oxygen under reduced pressure, by heating or in a nitrogen stream. When the PVP-heme complex was heated at 90 °C, molecular oxygen bonded to heme-iron(II) was reversibly dissociated from heme-iron(II) with increasing magnetic susceptibility (Fig. 4). The spin state of heme-iron(II) of the pyridine hemochrome changed from the low spin state to the high spin state with deoxygenation.

The reversibility of oxygen binding was affected by the temperature of degassing. Figure 5 shows a plot of the degree of re-oxygenation against the temperature. Deoxygenation is complete in heating above 40 °C for one hour. However, at much higher temperatures, the degree of deoxygenation decreases owing to the irreversible autoxidation. Figure 6 shows the reversibility of oxygenation for the solid system and the dispersion system of the PVP-heme and QPVP/PSS-heme complexes. It is due to the irreversible autoxidation that the degree of oxygenation gradually decreases with the number of cycles of deoxygenation. The autoxidation of the complexed-type hemochrome proceeded more rapidly than that of the single-type hemochrome and the autoxidation of the dispersion system in water proceeded much more rapidly.

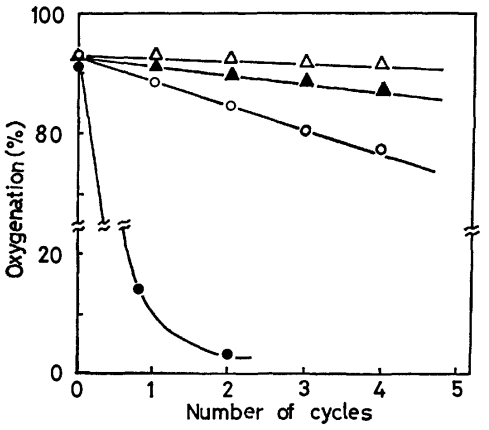

Fig. 6. Reversibility of oxygenation of some types of polymer-bound hemochrome.
PVP: △ solid, ▲ dispersion in H_2O.
QPVP-PSS: ○ solid, ● dispersion in H_2O.

In conclusion, oxygenation in solid state differs from that in solution in the following points: (1) The rate of oxygenation in solid state is smaller than that in solution. (2) Irreversible autoxidation scarcely occurs at room temperature in solid state. (3) The oxygen complex in solid state is much more stable than in solution, especially in comparison with the oxygen complex in an aqueous solution.

This work was partially supported by a Grant-in-Aid for Scientific Research from the Ministry of Education, Japan (No. 085203). The authors wish to thank Prof. Kay Kohn, Waseda University, for his help in the measurement of magnetic susceptibility.

References

1) P. Pfeiffer, E. Breith, E. Lubbe, and T. Tsumaki, *Ann.*, **503**, 84 (1933).
2) (a) M. Calvin, R. H. Bailes, and W. K. Wilmarth, *J. Am. Chem. Soc.*, **68**, 2254 (1946); (b) C. H. Barklew and M. Calvin, *ibid.*, **68**, 2257 (1946); (c) W. K. Wilmarth, S. Aranff, and M. Calvin, *ibid.*, **68**, 2263 (1946); (d) O. L. Harle and M. Calvin, *ibid.*, **68**, 2612 (1946); (e) R. H. Bailes and M. Calvin, *ibid.*, **69**, 1886 (1947).
3) J. H. Wang, A. Nakahara, and E. B. Fleischer, *J. Am. Chem. Soc.*, **80**, 1109 (1958); J. H. Wang, *Acc. Chem. Res.*, **3**, 90 (1970).
4) E. Tsuchida, K. Honda, and H. Sata, *Biopolymers*, **13**, 2147 (1974).
5) E. Tsuchida and K. Honda, *Chem. Lett.*, **1975**, 119.
6) K. Honda, H. Sata, and E. Tsuchida, *Nippon Kagaku Kaishi*, **1975**, 915.
7) E. Tsuchida and K. Honda, *Polym. J.*, **7**, 498 (1975).
8) E. Tsuchida, K. Honda, and H. Sata, *Makromol. Chem.*, **176**, 2251 (1975).
9) E. Tsuchida, K. Honda, and E. Hasegawa, *Biochim. Biophys. Acta*, **393**, 384 (1975).
10) (a) J. P. Collman and C. A. Reed, *J. Am. Chem. Soc.*, **95**, 2048 (1973); (b) J. P. Collman, R. R. Gagne, T. R. Harbert, J. C. Marchon, and C. A. Reed, *ibid.*, **95**, 7868 (1973); (c) J. P. Collman, R. R. Gagne, C. A. Reed, T. R. Harbert, G. Lang, and W. T. Robinson, *ibid.*, **97**, 1427 (1975).
11) (a) J. E. Baldwin and J. Huff, *J. Am. Chem. Soc.*, **96**, 5600 (1974); (b) J. Almog, J. E. Baldwin, R. L. Dyer, and M. Peters, *ibid.*, **97**, 226 (1975).
12) C. K. Chang and T. G. Traylor, *J. Am. Chem. Soc.*, **96**, 5595 (1974).
13) (a) M. J. Carter, D. P. Rillena, and F. Basolo, *J. Am. Chem. Soc.*, **96**, 392 (1974); (b) D. L. Anderson, C. J. Weschler, and F. Basolo, *ibid.*, **96**, 5599 (1974).
14) (a) H. C. Stynes and J. A. Ibers, *J. Am. Chem. Soc.*, **94**, 1559, 5125 (1972); (b) D. V. Stynes, H. C. Stynes, J. A. Ibers, and B. R. James, *ibid.*, **95**, 1142, 1796 (1973).
15) F. A. Walker, *J. Am. Chem. Soc.*, **95**, 1150, 1154 (1973).
16) Y. Osada, K. Abe, and E. Tsuchida, *Nippon Kagaku Kaishi*, **1973**, 2222.
17) T. Ikawa, K. Abe, K. Honda, and E. Tsuchida, *J. Polym. Sci., Polym. Chem.* Ed., **13**, 1505 (1975).
18) R. Willstätter, *Liebigs Ann. Chem.*, **365**, 197 (1950).
19) M. Haida and K. Kohn, *Kotai Butsuri*, **9**, 43 (1974).
20) J. R. Miller and G. D. Dorough, *J. Am. Chem. Soc.*, **74**, 3977 (1952).
21) E. Tsuchida, K. Honda, S. Hata, H. Suwa, and K. Kohn, *Chem. Lett.*, **1975**, 761.

The Crystal Structure of 1-(2-Thiazolylazo)-6-bromo-2-naphthol

Masayasu KURAHASHI*, Makoto FUKUYO, Akira SHIMADA†, and Akira KAWASE**

Faculty of Science, Osaka City University, Sumiyoshi-ku, Osaka 558

***National Chemical Laboratory for Industry, Honmachi, Shibuya-ku, Tokyo 151*

(Received July 21, 1975)

The crystals of 1-(2-thiazolylazo)-6-bromo-2-naphthol are orthorhombic, with a space group of $P2_12_12_1$, and with unit-cell dimensions of $a=19.044(3)$, $b=31.996(9)$, $c=4.221(1)$ Å, and $z=8$. The crystal structure was solved by the heavy-atom method and refined by the least-squares technique to give an R value of 0.064 for 1608 observed reflections. Both of the two crystallographically independent molecules show a generally similar shape and size. The phenolic oxygen atom is linked to the azo nitrogen atom adjacent to the thiazole ring by intramolecular hydrogen bonding, the O···N distances being 2.54 Å.

1-(2-Thiazolylazo)-2-naphthol(hereafter abbreviated as H-TAN) is a useful analytical reagent for metals. The crystal structures of H-TAN[1] and its metal chelates[2-5] have been determined in order to elucidate the structural change on chelate-ring formation; however, it is possible that the observed conformation for H-TAN is affected by the packing forces. Accordingly, it was desirable to determine the structures of several H-TAN derivatives. The title compound (H-TANBr shown in Fig. 1) was selected. A preliminary communication of this work based on the photographic data has been reported.[6] We will now present a refined structure of H-TANBr based on the newly collected diffractometer data.

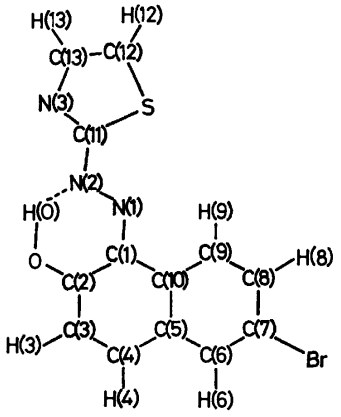

Fig. 1. Numbering of atoms.

Experimental

Red needle crystals of H-TANBr were grown by the sublimation of crude materials. The crystal data are summarized in Table 1. Both the determination of the cell constants and the collection of the intensity data were carried out on a Rigaku automatic four-circle diffractometer, using Cu$K\alpha$ radiation monochromatized with a graphite plate. The density was measured by floatation in an aqueous solution of sodium iodide.

Using the ω-2θ scan technique at a scan rate of 4 °/min, the integrated intensities were measured up to $2\theta=120$ °. The scan ranges were determined according to this formula: $1.5\,°+0.6\,°\times\tan\theta$. The background counts were taken on both sides of each peak for 10 s. The net counts were corrected for Lorentz and polarization effects; no absorption correction was made. The intensities of three standard reflections measured at every 50 reflections showed no significant variations during data collection. From this data set, 1608 reflections with $F\geq 3\sigma(F)$ were used for the subsequent calculations.

Table 1. Crystal data

$C_{13}H_8N_3OSBr$	$V=2572.2$Å^3
F. W.$=334.2$	$Z=8$
Orthorhombic	$D_m=1.72$ g·cm^{-3}
Space group: $P2_12_12_1$	$D_x=1.72$ g·cm^{-3}
$a=19.044(3)$Å	$\mu=61.9$ cm^{-1} (for Cu$K\alpha$)
$b=31.996(9)$Å	
$c=4.221(1)$Å	

Structure Determination and Refinement

The structure was solved by the heavy-atom method and refined by the block-diagonal least-squares method on the basis of a set of photographic data ($hk0$~$hk3$ and $0kl$).[6] The R value was 0.12 for 2074 reflections ($R=0.105$ for 1570 non-zero reflections).

Refinement was continued using the data collected on the diffractometer. Anisotropic thermal parameters were employed for the bromine and sulfur atoms, R being reduced to 0.086. A difference synthesis calculated at this stage did not show any significant hydrogen peaks. The hydrogen atoms attached to the ring systems, whose positions were assumed from the suitable geometry and B's to be 5.5 Å^2, were included in the structure-factor calculations in subsequent refinements, but they were not refined. The final R value was 0.064 for the 1608 observed reflections. A unit weight was given to each reflection. The atomic scattering factors were taken from International Tables for X-ray Crystallography.[7] The least-squares calculations were performed using the HBLS-4 program.[8] The final coordinates and thermal parameters are given in Table 2. The observed and calculated structure amplitudes are listed in Table 3.***

* Present address: National Research Institute for Metals, Nakameguro, Meguro-ku, Tokyo 153.

† Deceased August 5, 1973.

*** Table 3 is kept as Document No. 7611 at the Chemical Society of Japan, 1-5, Kanda, Surugadai, Chiyoda-ku, Tokyo 101.

TABLE 2. ATOMIC PARAMETERS AND THEIR e.s.d.'s[a]

Atom	x/a	y/b	z/c	B	Atom	x/a	y/b	y/c	B
Br	0.6621(1)	0.5604(1)	−0.6985(5)		C(12)	0.3249(8)	0.3702(4)	0.5852(43)	4.7(3)
Br′	0.2727(1)	0.2239(1)	0.0949(6)		C(13)	0.3450(8)	0.3311(4)	0.5919(42)	4.6(3)
S	0.3811(2)	0.4001(1)	0.3579(12)		O′	0.6920(5)	0.1654(3)	−0.0488(30)	5.3(3)
S′	0.5596(2)	0.5132(1)	−0.7121(12)		N(1′)	0.5743(6)	0.1235(3)	−0.3261(33)	3.8(2)
O	0.5809(5)	0.3155(3)	−0.2267(28)	4.4(2)	N(2′)	0.6368(6)	0.1087(3)	−0.3873(33)	4.1(3)
N(1)	0.5058(6)	0.3898(3)	−0.0167(29)	3.4(2)	N(3′)	0.6937(6)	0.0533(4)	−0.6548(36)	5.0(3)
N(2)	0.4870(6)	0.3541(3)	0.0867(32)	3.7(2)	C(1′)	0.5692(7)	0.1571(4)	−0.1407(39)	3.5(3)
N(3)	0.4046(6)	0.3212(4)	0.4145(36)	4.7(3)	C(2′)	0.6278(8)	0.1792(5)	−0.0021(43)	4.8(4)
C(1)	0.5631(6)	0.3896(4)	−0.2209(36)	3.1(3)	C(3′)	0.6150(9)	0.2144(5)	0.1854(51)	6.2(4)
C(2)	0.6001(7)	0.3532(4)	−0.3190(41)	3.9(3)	C(4′)	0.5487(8)	0.2295(5)	0.2358(46)	5.2(4)
C(3)	0.6585(8)	0.3575(4)	−0.5236(40)	4.4(3)	C(5′)	0.4888(7)	0.2088(4)	0.0924(42)	4.3(3)
C(4)	0.6794(7)	0.3960(4)	−0.6255(42)	4.4(3)	C(6′)	0.4207(7)	0.2246(4)	0.1563(42)	4.4(3)
C(5)	0.6437(7)	0.4330(4)	−0.5393(36)	3.7(3)	C(7′)	0.3655(7)	0.2027(4)	0.0123(41)	4.3(3)
C(6)	0.6674(7)	0.4716(4)	−0.6411(38)	3.7(3)	C(8′)	0.3725(8)	0.1676(4)	−0.1559(44)	4.7(3)
C(7)	0.6334(7)	0.5072(4)	−0.5515(40)	4.0(3)	C(9′)	0.4398(7)	0.1521(4)	−0.2088(40)	3.8(3)
C(8)	0.5751(6)	0.5057(4)	−0.3459(38)	3.4(3)	C(10′)	0.4995(7)	0.1723(4)	−0.0846(39)	3.6(3)
C(9)	0.5505(7)	0.4675(4)	−0.2398(39)	3.5(3)	C(11′)	0.6372(7)	0.0745(4)	−0.5723(39)	3.8(3)
C(10)	0.5852(6)	0.4299(4)	−0.3298(36)	3.0(3)	C(12′)	0.6084(8)	0.0132(5)	−0.8888(46)	5.2(4)
C(11)	0.4274(7)	0.3548(4)	0.2855(43)	4.1(3)	C(13′)	0.6764(8)	0.0188(5)	−0.8333(47)	5.4(4)

Anisotropic temperature factors[b] ($\times 10^4$)

Atom	B_{11}	B_{22}	B_{33}	B_{12}	B_{13}	B_{23}
Br	30(1)	11(1)	699(12)	−6(1)	−10(5)	15(3)
Br′	45(1)	14(1)	983(18)	15(1)	79(7)	9(4)
S	33(1)	10(1)	741(34)	5(1)	−22(13)	−29(7)
S′	24(1)	10(1)	755(33)	−1(1)	−17(12)	14(7)

a) E.s.d.'s in parentheses are in units of least significant digit. b) The anisotropic temperature factors are of the form: $\exp[-(B_{11}h^2+B_{22}k^2+B_{33}l^2+B_{12}hk+B_{13}hl+B_{23}kl)]$

	x/a	y/b	z/c		x/a	y/b	z/c
H(3)	0.6845	0.3313	−0.5961	H(3′)	0.6575	0.2280	0.3036
H(4)	0.7235	0.3983	−0.7646	H(4′)	0.5416	0.2561	0.3713
H(6)	0.7116	0.4742	−0.7791	H(6′)	0.4129	0.2505	0.3051
H(8)	0.5516	0.5331	−0.2775	H(8′)	0.3290	0.1526	−0.2497
H(9)	0.5082	0.4665	−0.0853	H(9′)	0.4473	0.1252	−0.3470
H(12)	0.2820	0.3815	0.7076	H(12′)	0.5862	−0.0112	−0.0179
H(13)	0.3173	0.3082	0.7089	H(13′)	0.7141	−0.0011	−0.9210

Description of the Structures and Discussion

The structure consists of two crystallographically independent H-TANBr molecules (referred to as A and B). Figure 2 shows their conformations projected on the naphthalene plane. As can be seen in the figure, the A and B molecules show generally similar shapes. Each azo group adopts a *trans* conformation,

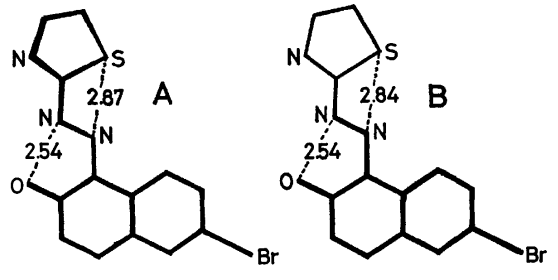

Fig. 2. Conformation of H-TANBr molecules. Views are perpendicular to the naphthalene plane.

and the oxygen atom is linked to the azo nitrogen atom adjacent to the thiazole ring by intramolecular hydrogen bonding, the O···N(2) distances being 2.54 Å.

Molecules A and B are nearly planar, with maximum deviations of 0.15 and 0.07 Å respectively. The A molecule is twisted along the N(1)–C(1) bond, and the naphthol ring makes an angle of 6.7° with the thiazole ring, whereas the B molecule is slightly folded at N(2), and the angle between the thiazole and naphthol rings is 1°. Similar features were observed in the crystals of H-TAN.[1]

It seems that there is no definite reason to restrict the rotation around the C(11)–N(2) bond. In all four crystallographically independent molecules, two in noncentrosymmetric H-TANBr crystals and two in centrosymmetric H-TAN crystals, however, N(1) and N(3) are in the *trans* position. This indicates that the observed conformation is the most stable one. There is no evidence for the strong intermolecular interaction which dominates the molecular conformation. Short intramolecular non-bonded distances of 2.87 Å in A and 2.84 Å in B are found between S and N(1) (Fig. 2).

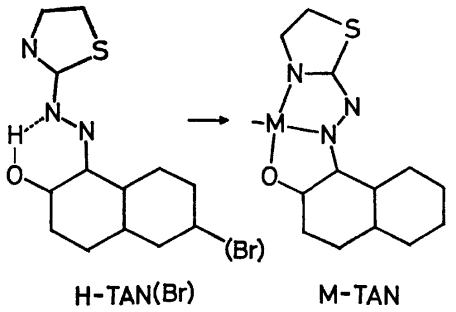

Fig. 3. A comparison of the structures between H-TAN(Br) and M-TAN.

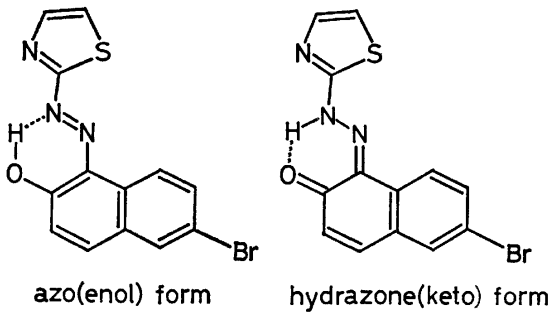

Fig. 4. Two possible tautomers for H-TANBr.

Figure 3 compares the structures of H-TAN(Br) and its metal chelate(M-TAN). If, in solution, the H-TAN(Br) molecules exist in the same conformation as in a solid, it is apparent that both of the two ring systems attached to the central azo group are rotated by 180° upon chelate-ring formation.

The bond lengths and angles are shown in Table 4, along with their estimated standard deviations. All the distances except for that of C(7)-Br agree with the values observed in the crystal of H-TAN, within the range of experimental error. The coexistance of azo and hydrazone tautomers in the crystalline state of H-TAN has been reported[1] previously on the basis of the difference in the electron density map and the examination of the relevant bond lengths. The good agreement in the distances of N(1)-N(2), C(2)-O between H-TANBr and H-TAN may, therefore, indicate that, in the present crystal also, there are the azo and hydrazone tautomers shown in Fig. 4.

The crystal structure projected along the c-axis is shown in Fig. 5. Intermolecular distances less than 3.5 Å are given in Table 5. The molecular planes of both A and B are inclined by about 45° from the (001) plane. This stacking scheme of the molecules along the c-axis is very similar to that of H-TAN. The molecular arrangements in the ab-plane, however, differ considerably from each other as a result of the large effective volume of bromine atoms.

TABLE 4. BOND LENGTHS AND ANGLES WITH e.s.d.'s IN PARENTHESES

	A	B		A	B
Bond lengths (Å)					
S-C(11)	1.72(2)	1.76(2)	C(3)-C(4)	1.36(2)	1.37(3)
S-C(12)	1.73(2)	1.71(2)	C(4)-C(5)	1.41(2)	1.45(3)
O-C(2)	1.32(2)	1.31(2)	C(5)-C(6)	1.38(2)	1.42(3)
N(1)-N(2)	1.28(2)	1.31(2)	C(5)-C(10)	1.43(2)	1.40(2)
N(1)-C(1)	1.39(2)	1.33(2)	C(6)-C(7)	1.36(2)	1.40(3)
N(2)-C(11)	1.41(2)	1.35(2)	C(7)-C(8)	1.41(2)	1.34(3)
N(3)-C(11)	1.28(2)	1.32(2)	C(8)-C(9)	1.38(2)	1.39(3)
N(3)-C(13)	1.40(2)	1.38(3)	C(9)-C(10)	1.42(2)	1.41(2)
C(1)-C(2)	1.42(3)	1.45(2)	C(12)-C(13)	1.31(3)	1.33(3)
C(1)-C(10)	1.43(2)	1.43(3)	Br-C(7)	1.89(2)	1.93(2)
C(2)-C(3)	1.42(2)	1.40(3)			
Bond angles (°)					
C(11)-S-C(12)	87(1)	89(1)	C(5)-C(6)-C(7)	120(2)	115(2)
N(2)-N(1)-C(1)	115(1)	118(1)	C(6)-C(7)-C(8)	121(2)	125(2)
N(1)-N(2)-C(11)	114(1)	114(1)	C(6)-C(7)-Br	117(1)	116(1)
C(11)-N(3)-C(13)	108(2)	111(2)	C(8)-C(7)-Br	122(1)	119(1)
N(1)-C(1)-C(2)	125(1)	125(2)	C(7)-C(8)-C(9)	120(2)	118(2)
N(1)-C(1)-C(10)	115(1)	116(1)	C(8)-C(9)-C(10)	120(1)	121(2)
C(2)-C(1)-C(10)	120(1)	119(1)	C(1)-C(10)-C(5)	119(1)	120(2)
O-C(2)-C(1)	122(2)	120(2)	C(1)-C(10)-C(9)	123(1)	122(2)
O-C(2)-C(3)	119(2)	121(2)	C(5)-C(10)-C(9)	118(1)	117(2)
C(1)-C(2)-C(3)	119(2)	119(2)	S-C(11)-N(2)	122(1)	122(1)
C(2)-C(3)-C(4)	121(2)	122(2)	S-C(11)-N(3)	117(1)	112(1)
C(3)-C(4)-C(5)	122(2)	120(2)	N(2)-C(11)-N(3)	121(2)	125(2)
C(4)-C(5)-C(6)	121(1)	119(2)	S-C(12)-C(13)	111(1)	111(2)
C(4)-C(5)-C(10)	119(1)	119(2)	N(3)-C(13)-C(12)	116(2)	116(2)
C(6)-C(5)-C(10)	121(1)	122(2)			

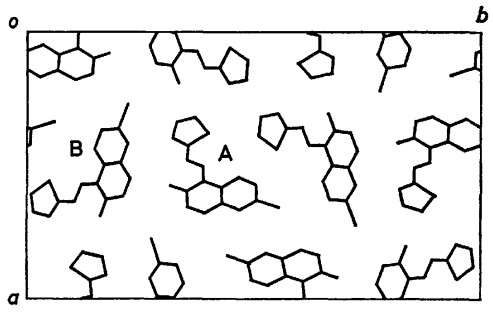

Fig. 5. The crystal structure projected along the c-axis.

Calculations were carried out on a FACOM 270-30 computer at the Computer Center of Osaka City University, and on a HITAC 8800/8700 computer at the Computer Centre of the University of Tokyo.

The authors wish to express their deep thanks to Dr. E. Asada and Mrs. M. Goto of the National Chemical Laboratory for Industry, who kindly allowed them to use the X-ray diffractometer.

Table 5. Intermolecular distances less than 3.5Å

		Symmetry operation	Distance (Å)
S	C(12)	2	3.48
O	C(4′)	1	3.41
N(1)	C(11)	2	3.48
N(2)	N(3)	2	3.40
N(2)	C(1)	3	3.45
N(2)	C(2)	3	3.25
N(3)	C(6′)	1	3.32
C(6)	C(9)	2	3.36
C(1)	C(4)	3	3.33
C(11)	C(13)	2	3.38
C(12)	O′	4	3.13
C(13)	O′	4	3.27
S′	N(1′)	2	3.45

Symmetry operations

1 $(x \quad y \quad z)$ 3 $(x \quad y \quad 1+z)$

2 $(x \quad y \quad -1+z)$ 4 $(\frac{1}{2}+x \quad \frac{1}{2}-y \quad 1+z)$

References

1) M. Kurahashi, *Chem. Lett.*, **1974**, 181.
2) M. Kurahashi, *Bull. Chem. Soc. Jpn.*, **47**, 2045 (1974).
3) M. Kurahashi, *Bull. Chem. Soc. Jpn.*, **47**, 2067 (1974).
4) M. Kurahashi, *Chem. Lett.*, **1974**, 63.
5) M. Kurahashi, *Chem. Lett.*, **1974**, 1271.
6) M. Kurahashi, A. Kawase, K. Hirotsu, M. Fukuyo and A. Shimada, *Bull. Chem. Soc. Jpn.*, **45**, 1940 (1972).
7) "International Tables for X-Ray Crystallography," vol. III, Kynoch Press, Birmingham, England (1962).
8) "The Universal Crystallographic Computing System (I)," Japanese Crystallographic Association (1967).

Partial Molal Volumes of Surfactants in Methanol–Water Mixtures

Shoji KANESHINA, Masahiro MANABE,* Gohsuke SUGIHARA,** and Mitsuru TANAKA**

College of General Education, Kyushu University, Ropponmatsu, Chūō-ku, Fukuoka 810

**Department of Technical Chemistry, Niihama Technical College, Niihama, Ehime 792*

***Department of Chemistry, Faculty of Science, Fukuoka University, Nanakuma, Nishi-ku, Fukuoka 814*

(Received August 11, 1975)

The partial molal volumes of surfactants in the micellar state ($\bar{V}_m$) and in the singly dispersed state ($\bar{V}_s$) have been determined at 25 °C in methanol–water mixtures up to the composition of 25 mol% methanol. The $\bar{V}_m$ of sodium dodecyl sulfate (SDS) increases gradually with the addition of methanol across the plateau region (3—15 mol% methanol). On the other hand, the $\bar{V}_s$ values of SDS and its homologous salts containing the alkyl chain of carbon numbers from 6 to 10 decrease initially with the addition of methanol and then increase up to 25 mol% methanol *via* the minimum at 3 mol% methanol. The value of $\bar{V}_m - \bar{V}_s$ reaches its maximum at 3 mol% methanol and then approaches zero at about 30 mol% methanol. The latter behavior is an indication of the lack of any micelle formation. In order to elucidate the solute-solvent interactions, the split of $\bar{V}_s$ into the contributions of the ionic and the hydrophobic part was attempted. Consequently, the variation in $\bar{V}_s$ with the solvent composition can primarily be attributed to the behavior of the hydrophobic group in solutions. On the basis of these results, the interactions between the hydrophobic part of the solute and the binary solvent were discussed.

The micelle formation of surfactants in solutions has been known to be affected by the temperature, the pressure, and various kinds of additives. Studies of the effect of organic additives on the critical micelle concentration (CMC) have led to an understanding of the part played by the solvent in the micelle formation.[1–6]

The thermodynamic quantity known as the partial molal volume has proved to be a very useful tool in elucidating the interactions occurring in solutions. Studies of the partial molal volume of surfactants have been used to examine the behavior of surfactant solutions.[7–12] They have also proved useful in determining the effect of the pressure on the micelle formation.[7,13,14] With regard to the partial molal volume in a mixed solvent, Lee and Hyne[15] have determined the partial molal volumes of tetraalkylammonium chlorides in ethanol–water mixtures in order to examine ion–solvent interactions in aqueous solvent mixtures. They also discussed the structural changes accompanying the addition of ethanol to water.

In this study, the partial molal volume of sodium dodecyl sulfate (SDS) has been determined above and below the CMC as a function of the cosolvent composition. Methanol was chosen as the cosolvent because it penetrates the micelle only slightly and chiefly changes the solvent property of water. The partial molal volumes of a homologous series of sodium alkyl sulfates have also been determined in the range of concentrations below the CMC in methanol–water mixtures. On the basis of these results, the interactions among water, methanol, and the hydrocarbon chain of a surfactant have been discussed.

Experimental

The SDS and its homologous salts used in this study were synthesized and purified by a method described previously.[16] The water was redistilled from an alkaline permanganate solution. The methanol was distilled before use.

The partial molal volume was determined partly by a density method and also partly by a direct dilatometric method.[7] The values of the partial molal volumes obtained by the two methods were in good agreement with each other. The densities of a series of solutions were simultaneously measured by using seven pycnometers with a capacity of about 20 ml; the errors in measurement was within $\pm 1 \times 10^{-5}$ g/cm^3. The thermostatted bath was controlled to 25($\pm$0.005) °C. The volume of solution per 1000 g of the solvent (water+methanol) was plotted against the molality of the surfactant, resulting in a straight line in the ranges of concentration below and above the CMC, as is shown in Fig. 1. The partial molal volume of the surfactant in aqueous methanol solutions was taken as the slope of the line; it was determined by the least-squares method on the basis of the 7—14 density data. Since the partial molal volume is almost independent of the surfactant concentration over the concentration ranges studied here,[7,8] the experimental values thus obtained have been assumed to be identical with those corresponding to an infinite dilution. The values of the partial molal volume in a pure aqueous solution were 237.5 for SDS below the CMC, 247.0 for SDS above the CMC, and 203.6 for sodium decyl sulfate (SDeS), 172.6 for sodium octyl sulfate (SOS), and 141.3 for sodium

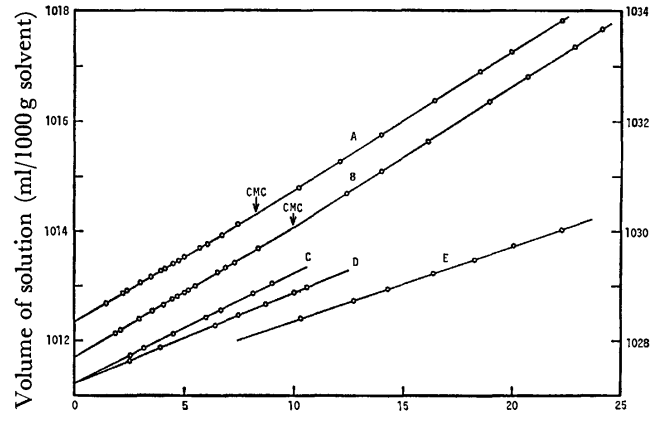

Fig. 1. Representative plots of the volume of solution per 1000 g solvent against the concentration of surfactant. A: SDS(3.31), B: SDS (9.04), C: SDeS (2.94), D: SOS (2.94), and E: SHS (2.87). The numerical values in parentheses indicate mol% of methanol in solvent. (Right scale shown is for B only).

hexyl sulfate (SHS) below the respective CMC's. These values are comparable to those of the literature.[7,8,16]

Results and Discussion

The partial molal volumes of four surfactants in the singly dispersed state and that of SDS in the micellar state are shown in Fig. 2 as functions of the solvent composition. The partial molal volume of the singly dispersed state ($\overline{V}_s$) for any surfactant decreases initially upon the addition of methanol and then increases up to 25 mol% methanol *via* a minimum at about 3 mol% methanol. On the other hand, the partial molal volume of the micellar state ($\overline{V}_m$) increases gradually upon the addition of methanol across the plateau region (3—15 mol% methanol). The $\overline{V}_m$ is slightly affected by the addition of both methanol and urea,[17] whereas the $\overline{V}_s$ is sensitive to such additives as urea[17-19] and alcohols.[15,20] This can reasonably be expected in view of the fact that the solute-solvent interaction, containing structural changes in water around the hydrophobic part of the surfactant, is included in $\overline{V}_s$.

The change in the partial molal volume on micellization, $\Delta\overline{V}_m(=\overline{V}_m-\overline{V}_s)$, was calculated from the results shown in Fig. 2; it is shown in Fig. 3 as a function of the methanol content. The $\Delta\overline{V}_m$ in water is in good agreement with that of the literature.[7,8] As may be seem from Fig. 3, $\Delta\overline{V}_m$ initially increases upon the addition of methanol, and then it decreases *via* the maximum at 3 mol% methanol. The $\Delta\overline{V}_m$ is thermodynamically related to the pressure dependence of the

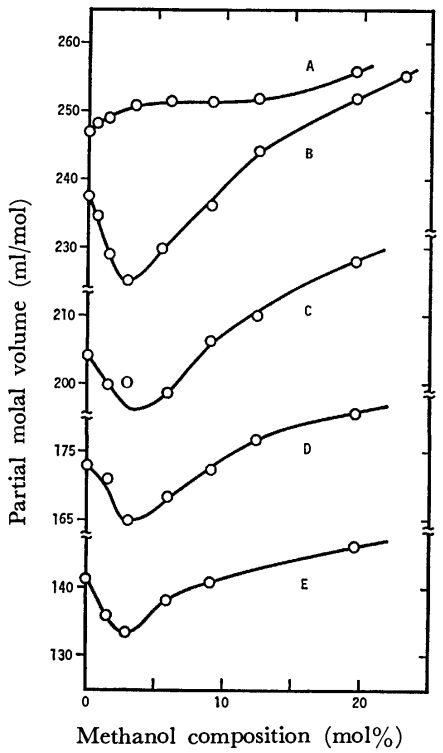

Fig. 2. Partial molal volumes of a homologous series of sodium alkyl sulfate in methanol-water mixtures at 25 °C.
Micellar state; A: SDS. Singly dispersed state; B: SDS, C: SDeS, D: SOS, and E: SHS.

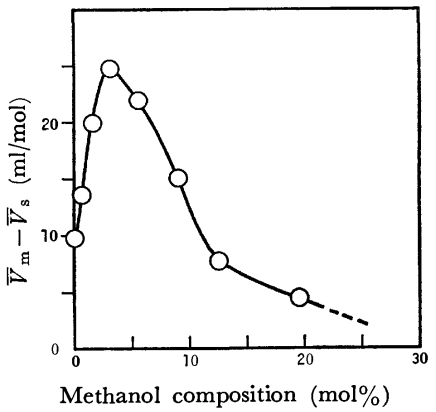

Fig. 3. The change of partial molal volume on micellization as a function of methanol content.

CMC by the following expression, as has been described previously:[21]

$$\Delta\overline{V}_m = (1+\beta)\,RT\left(\frac{\partial \ln \mathrm{CMC}}{\partial P}\right)_{T,\Delta\overline{G}_m} \quad (1)$$

where β is the constant which indicates the ratio of the number of the counterion to that of the surfactant ion in micelles. The results shown in Fig. 3 suggest that the CMC-increasing effect by compression reaches its maximum at 3 mol% methanol. In practice, the results of CMC measurements under high pressures in methanol–water mixtures have substantiated the above suggestion,[22] although the effect of added methanol on β has still not been elucidated. It can be seen from Fig. 3 that the extrapolation of $\Delta\overline{V}_m$ to a higher methanol content approaches zero at about 30 mol% methanol. This seems to indicate whether $\overline{V}_m$ is merely equal to $\overline{V}_s$ or whether no micelles are formed in about a 30 mol% methanol–water mixture. The latter is more likely from the facts that the CMC increases with the addition of methanol and is ultimately undeterminable at about 30 mol% methanol,[23] that the micellar weight decreases with the increase in the methanol content, and that at about 27 mol% methanol there is no evidence of micelle formation.[2,23]

It is generally known that, in alcohol–water mixtures, compounds containing the hydrophobic chain show a minimal partial molal volume at a water-rich composition and a maximal partial molal volume at a moderate composition of the solvent.[15,20] As may be seen from Fig. 2, the minimum of $\overline{V}_s$ for a homologous series of sodium alkyl sulfates was observed at a definite solvent composition (3 mol% methanol). The value of the minimal $\overline{V}_s$ is smaller by *ca.* 5% than the $\overline{V}_s$ in pure water. This contraction and the following expansion in $\overline{V}_s$ show the solute–solvent interaction characteristic of a system with methanol–water solvent mixtures. Since a surfactant molecule is composed of two parts with opposing properties, a hydrophobic and a hydrophilic group, the interactions between each part of the solute and the solvent should be discussed separately. Therefore, the split of $\overline{V}_s$ into the contributions of the ionic and the hydrophobic part was attempted as follows. By plotting $\overline{V}_s$ against the length of alkyl chain N, straight lines were obtained at various compositions of the solvent, as is shown in

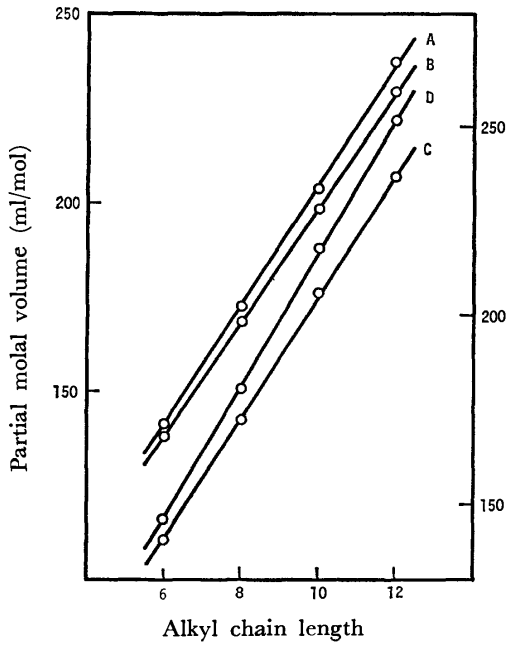

Fig. 4. Partial molal volumes of surfactants as a function of alkyl chain length. A linear relationship between $\overline{V}_s$ and N in mixed solvents of various compositions is typically shown. Methanol composition in mol%; A: 0, B: 5.87, C: 9.05, and D: 19.40. (Left scale shown is for lines A, B, and right scale for C, D.)

Fig. 4. Then the relation between $\overline{V}_s$ and N can be satisfactorily represented by the following expression.

$$\overline{V}_s = \overline{V}_1 + \overline{V}_{me}N \quad (2)$$

where $\overline{V}_{me}$ is the partial molal volume per methylene group and where $\overline{V}_1$ may be assumed to be the contribution of the ionic part, which is obtained by extrapolating N to zero in a linear plot of $\overline{V}_s$ *vs.* N. The value of $\overline{V}_1$ in water (47.0 ml/mol) is in fair agreement with the value estimated by Mukerjee for $NaHSO_4$ (47.5 ml/mol).[24] The value of $\overline{V}_1$ tends to decrease monotonously with an increase in the methanol content. This reduction of $\overline{V}_1$ may be qualitatively explained on the basis of the electrostrictive solvation effect, as was mentioned by Lee and Hyne.[15]

The $\overline{V}_{me}$ has its minimum at 3 mol % methanol, as is shown in Fig. 5. Thus, the variation in $\overline{V}_s$ with the solvent composition can be attributed to the behavior of the hydrophobic group in solutions. It is known that the transfer of hydrocarbons from a nonpolar environment to water results in a negative volume change,[25] which is considered to reflect the ordering of water molecules around the hydrocarbon chains or the "iceberg" formation.[26] Actually, the value of $\overline{V}_{me}$ in water, 15.7 ml/mol CH_2, is smaller than the contribution of the methylene group to the molal volume of normal alkanes at the C_8–C_{12} chain lengths, 16.7 ml/mol CH_2.[27] In an aqueous mixture of 3 mol % methanol, the $\overline{V}_{me}$ is more reduced than in water. This may be explained on the basis of the variation in the structure of the binary solvent with the composition.

Using the multilayer hydration models by Gurney,[28] Frank and Wen,[29] and Eigen and Wicke[30] for ion–water interactions, the partial molal volume of an ion at an infinite dilution, $\overline{V}^0_{ion}$, can be attributed to the following components:[31]

$$\overline{V}^0_{ion} = \overline{V}^0_{int} + \overline{V}^0_{elect} + \overline{V}^0_{disord} + \overline{V}^0_{caged} \quad (3)$$

where $\overline{V}^0_{ion}$ is the intrinsic partial molal volume, $\overline{V}^0_{elect}$ is the electrostriction partial molal volume, $\overline{V}^0_{disord}$ is the disordered partial molal volume, and $\overline{V}^0_{caged}$ is the caged or structured partial molal volume. Here, the $\overline{V}_{me}$ under consideration may be taken to contain only the contributions of $\overline{V}^0_{int}$ and $\overline{V}^0_{caged}$, and can be expressed by the following relation:

$$\overline{V}_{me} = \overline{V}^{int}_{me} + n_h(\overline{V}^h_0 - V_0) \quad (4)$$

where $\overline{V}^{int}_{me}$ is the intrinsic partial molal volume for the methylene group, $\overline{V}^h_0$ is the partial molal volume of structured water around the hydrocarbon chain, V_0 is the molal volume of bulk water, and n_h is the number of hydrated or structured water molecules and is taken as 2 or 3.[26] As has been mentioned above, $\overline{V}^h_0 < V_0$ for structured water around the hydrocarbon chains. We assume that Eq. (4) is applicable to the $\overline{V}_{me}$ values in the aqueous solvent mixtures containing a small amount of methanol. In this case, V_0 should be taken as the mean molal volume of a mixture, and $\overline{V}^h_0$, as the mean partial molal volume of the solvent mixture around the hydrocarbon chain. The value of V_0 increases monotonously with an increase in the methanol content. Of course, $\overline{V}^h_0$ may be affected by the methanol added. The results shown in Fig. 5, however, show that the difference between $\overline{V}^h_0$ and V_0 reaches its maximum at the mixture of about 3 mol % methanol provided that n_h (the number of solvent molecules affected by one methylene group) changes only slightly and monotonously with the methanol content. This means that the initial addition of methanol is likely to be attributable to the structure-promotion of the solvent. By the addition more than 3 mol% of methanol, the difference between $\overline{V}^h_0$ and V_0 decreases gradually; that is, the increase in $\overline{V}^h_0$ with the increase in the methanol content overcomes that of V_0. This indicates that the addition more than 3 mol% of methanol will begin to break down the characteristic water structure.

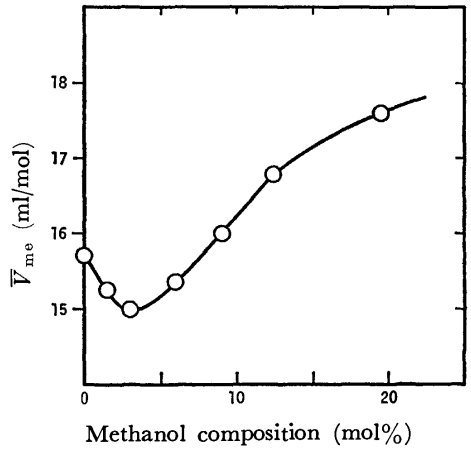

Fig. 5. The partial molal volume per one methylene group as a function of methanol content.

There is an alternative explanation for the minimal $\overline{V}_{me}$ at 3 mol % methanol. We assume that methanol is unaffected by the hydrocarbon chain; *i.e.*, the partial molal volume of methanol around the hydrocarbon chain is the same as that of methanol in the bulk binary solvent. Thus, in Eq. (4), V_0 should be taken as the partial molal volume of water in the binary mixed solvent, and n_h, as the number of water molecules affected by one methylene group, which number probably varies in proportion to the volume fraction of water in the binary solvent. It is well known that, in the methanol–water binary system, the partial molal volume of water increases slightly with the initial addition of methanol and then decreases with an increase in the methanol content *via* a maximum at about 10 mol% methanol; on the other hand, the partial molal volume of methanol has its minimum at the corresponding composition in the binary system.[32] Therefore, it can be seen from Fig. 5 that the methanol composition at which the $\overline{V}_{me}$ has its minimum is not consistent with the composition of the minimal partial molal volume of methanol in the binary system; it is rather low. The results shown in Fig. 5 indicate that the second term of the right-hand side of Eq. (4) reaches its minimum at 3 mol% methanol. This probably means that the decrease in $\overline{V}_0^h$, together with the increase in V_0, is responsible for the initial decrease in $\overline{V}_{me}$ upon the addition of methanol. Thus, it may be concluded that the solvent structure is maximally promoted around the hydrocarbon chain of surfactant ions in the aqueous solvent mixture of 3 mol% methanol.

References

1) M. F. Emerson and A. Holtzer, *J. Phys. Chem.*, **71**, 3320 (1967).
2) G. D. Parfitt and J. A. Wood, *Kolloid-Z. Z. Polym.*, **229**, 55 (1969).
3) K. Shirahama and T. Kashiwabara, *J. Colloid Interface Sci.*, **36**, 65 (1971).
4) K. Deguchi, T. Mizuno, and K. Meguro, *J. Colloid Interface Sci.*, **48**, 474 (1974).
5) J. W. Larsen and L. B. Tepley, *J. Colloid Interface Sci.*, **49**, 113 (1974).
6) N. Nishikido, Y. Moroi, H. Uehara, and R. Matuura, *Bull. Chem. Soc. Jpn.*, **47**, 2634 (1974).
7) K. Shinoda and T. Soda, *J. Phys. Chem.*, **67**, 2072 (1963).
8) J. M. Corkill, J. F. Goodman, and T. Walker, *Trans. Faraday Soc.*, **63**, 768 (1967).
9) J. E. Desnoyers and M. Arel, *Can. J. Chem.*, **45**, 359 (1967).
10) G. M. Brown, P. Dubreuil, F. M. Ichhaporia, and J. E. Desnoyers, *Can. J. Chem.*, **48**, 2525 (1970).
11) G. M. Musbally, G. Perron, and J. E. Desnoyers, *J. Colloid Interface Sci.*, **48**, 494 (1974).
12) P. -A. Leduc, J. -L. Fortier, and J. E. Desnoyers, *J. Phys. Chem.*, **78**, 1217 (1974).
13) S. D. Hamann, *J. Phys. Chem.*, **66**, 1359 (1962).
14) M. Tanaka, S. Keneshina, K. Shinno, T. Okajima, and T. Tomida, *J. Colloid Interface Sci.*, **46**, 132 (1974).
15) I. Lee and J. B. Hyne, *Can. J. Chem.*, **46**, 2333 (1968).
16) M. Tanaka, S. Kaneshina, W. Nishimoto, and H. Takabatake, *Bull. Chem. Soc. Jpn.*, **46**, 364 (1973).
17) M. Tanaka, S. Kaneshina, S. Kuramoto, and R. Matuura, *Bull. Chem. Soc. Jpn.*, **48**, 432 (1975).
18) W. A. Hargraves and G. C. Kresheck, *J. Phys. Chem.*, **73**, 3249 (1969).
19) P. R. Philip, J. E. Desnoyers, and A. Hade, *Can. J. Chem.*, **51**, 187 (1973).
20) M. Manabe and M. Koda *Bull. Chem. Soc. Jpn.*, **48**, 2367 (1975).
21) S. Kaneshina, M. Tanaka, T. Tomida, and R. Matuura, *J. Colloid Interface Sci.*, **48**, 450 (1974).
22) S. Kaneshina, M. Tanaka, and R. Matuura, *Mem. Fac. Sci. Kyushu Univ., C*, **9**, 71 (1974).
23) H. Uehara, M. Manabe, and R. Matuura, *Mem. Fac. Sci. Kyushu Univ.*, **8**, 55 (1972).
24) P. Mukerjee, *J. Phys. Chem.*, **65**, 740 (1961).
25) W. L. Masterton, *J. Chem. Phys.*, **22**, 1830 (1954).
26) G. Nemethy and H. A. Scheraga, *J. Chem. Phys.*, **36**, 3401 (1962).
27) M. L. Huggins, *J. Am. Chem. Soc.*, **63**, 116 (1941).
28) R. M. Gurney, "Ionic Processes in Solution," McGraw-Hill, New York (1953).
29) H. Frank and W. -Y. Wen, *Discuss. Faraday Soc.*, **24**, 133 (1957).
30) M. Eigen and E. Wicke, *J. Phys. Chem.*, **58**, 702 (1954).
31) F. J. Millero, "Water and Aqueous Solutions, Structure, Thermodynamics, and Transport Processes," (R. A. Horne, ed.) John-Wiley & Sons, New York (1972).
32) R. E. Gibson, *J. Am. Chem. Soc.*, **57**, 1551 (1935). K. Nakanishi, *Bull. Chem. Soc. Jpn.*, **33**, 793 (1960).

The Two-step Collapse of Mixed Monolayers of Cholesterol and Its Esters

Masayuki NAKAGAKI and Tetsurou HANDA

Faculty of Pharmaceutical Sciences, Kyoto University, Sakyo-ku, Kyoto 606

(Received August 28, 1975)

Mixed monolayers of two insoluble components out of cholesterol and its acetate and propionate were spread on a dilute aqueous solution of disodium hexadecyl phosphate. The curves of the surface pressure against the molecular area were found to have two kink points, collapse points, although the curves of each component, and also that of the "concollapse" mixture, had only one collapse point. The diagram showing the relation between these two collapse pressures and the composition was entirely analogous to the phase diagrams of bulk mixtures which have an eutectic point. It has, therefore, been concluded that the mixed monolayer of two mutually immisible substances undergoes a two-step collapse. At the lower collapse point, one of the two components, *i*, starts separating from the monolayer. The lower collapse pressure, F_{Ci}' varies with the mole fraction, X_i, according to $F_{Ci}'=F_{oi}'-(kT/A_{oi})\ln X_i$. At the higher collapse point, the other component starts separating as well. Upon further compression, the surface pressure remains unchanged at the higher collapse pressure, which is equal to the equilibrium-spreading pressure and is independent of the composition.

In studies of insoluble monolayers it has sometimes been noticed that there is a disagreement between the collapse pressure, F_c, and the equilibrium-spreading pressure, F_s. Here, F_c is obtained as the kink point on a curve of the surface pressure, F, against the molecular area, A, when an insoluble monolayer is compressed, while F_s is observed when small particles or droplets of an insoluble substance are placed on a clean aqueous surface. Two reasons can be pointed out for this disagreement: (1) When the insoluble components have large hydrophobic groups, the molecules are oriented completely at the aqueous surface and the cohesion between the hydrophobic groups resists collapse, so that the monolayer is readily supercompressed. (2) For multicomponent monolayers, the disagreement can be explained thermodynamically. It must be emphasized here, however, that the thermodynamic discussion is significant only when the effect of the supercompression has been eliminated completely.

In the case of one-component monolayers, F_c, is greater than or equal to F_s. For example,[1] the monolayers of tristearin, tripalmitin, and trimyristin were supercompressed so that $F_c>F_s$, while the monolayer of trilaurin was in equilibrium with the bulk phase so that $F_c=F_s$.

In the case of a mixed monolayer, however, F_c may be either greater or smaller than F_s. The mixed monolayer of tristealin and trilaurin was supercompressed so that $F_c>F_s$, while that of cholesterol and trilaurin was in thermodynamic equilibrium with the bulk phase so that $F_c<F_s$.[2] For a mixed monolayer of triolein and tricaprylin, which belongs to the latter case with $F_c<F_s$, it has been verified experimentally that at $A\to 0$ agrees with F_s, and that on the phase diagram expressing F against the mole fraction, X, at a fixed temperature, the curve of F_s against X reveals an arc and that of F_s against X reveals another arc, indicating that these two components mix with each other at all proportions.[3]

If the components, on the contrary, do not mix at all in the bulk phase, a phase diagram analogous to that which has an eutectic point would be expected. In this paper, mixed monolayer of two components out of cholesterol(CH) and its acetate (CA) and propionate (CP) will be discussed. For this effect, the following two experimental devices were needed:

1: As the substrate, an aqueous solution of disodium hexadecyl phosphate (SHP) was used at 0.5 mM instead of water because the mixed monolayers studied here were leaky on the water surface; the addition of as much SHP as this concentration made the monolayers stable enough for us to measure the collapse pressures without changing the essential features of the phase diagram. 2: The F—A relation is usually studied by the compression of a monolayer. In order to avoid the supercompression, however, the method of insoluble-component addition to a constant surface area was used, particularly for the monolayers containing CP.

Experimental

Materials. The specimen of CH used was from the Sigma Chemical Co., the CP was from The Aldrich Chemical Co., and the CA, from the Nakarai Chemical Co. was recrystallized from acetone. The specimen of SHP was the same as used in the previous paper,[4] which had been synthesized and dissolved in water as has been reported elsewhere.[5]

Monolayer Spreading. The insoluble components to be spread as a monolayer were dissolved in benzene and supplied from an Agla Micrometer Syringe onto the surface of water or an aqueous SHP solution in a trough ($60\times 20\times 1$ cm) made of methacryl-resin, coated with paraffin, and sectioned by paraffinized glass barriers.[6]

The occupied area per molecule of insoluble components, A(Å^2/molec.), can be calculated by the following equation:

$$A = S/nN_A \qquad (1)$$

where S is the area of the aqueous surface between barriers, where n is the sum of the moles of insoluble components spread in this area, and where N_A is the Avogadro number. Therefore, A can be decreased either by decreasing S (SAD method) or by increasing n (ICA method). In the latter method, n was increased by dropping additional benzene solution without changing the S.

Surface Pressure. The surface pressure, F (dyn/cm), was measured by Wilhelmy's plate method. A ground plate of quartz was used after it had been cleaned by immersion in fuming nitric acid for more than one night and washing well with distilled water. The torsion balance used was Shimadzu T-NR, modified and equipped with mirror in order to magnify the movement of the plate by a lump and scale. The temperature was kept at 25±0.2 °C

by circulating thermostated water through glass tubing immersed in the trough.

The surface pressure-area curve of the cholesterol monolayer thus obtained was in good agreement with that reported in the literature,[7] and the collapse pressure of the monolayer of cholesterol and its ester on the SHP solution were reproducible and stable for a few hours. Therefore, the possiblity of air oxidation[8] will not be considered here, following many papers which have been published without referring to air oxidation.[7]

Equilibrium-spreading Pressure. The equilibrium-spreading pressure, F_s (dyn/cm), was measured by Wilhelmy's plate method, taking the reading at the equilibrium reached when powder of CH, CA, or CP, or of their mixture was sprinkled on the surface of water or a SHP solution contained in a Petri dish 10 cm in diameter. In case of a mixture, its components were dissolved in ethyl ether at a given composition, the solvent was evaporated, and the residue dried in a vacuum was mixed well with a spatula before use.

Results

Monolayer of CA. Prior to the study of mixed monolayers of CH and CA, the monolayers of each component were studied. The results on the CH monolayer have been reported already.[2] On the other hand, the CA monolayer was found to be difficult to study on water, but easier on an aqueous SHP solution.

Figure 1 shows the F—A curves of CA at various values of the SHP concentration, c_2 (mM), the solution of the latter containing $c'=10$ mM of NaOH in order to prevent the binding of the proton to SHP. Figure 1 indicates the following: 1: The CA monolayer is not supercompressed, since the agreement between the data obtained by the SAD method and by the ICA method is good. 2: Each curve has one kink point, to be called the collapse point, with a collapse pressure, F_c, and a collapse area, A_c. 3: The value of F remains constant at F_c when the monolayer is compressed further beyond the collapse point. 4: The F–A curves move toward higher F values when c_2 is larger. Results similar to these have been obtained for CH as well.

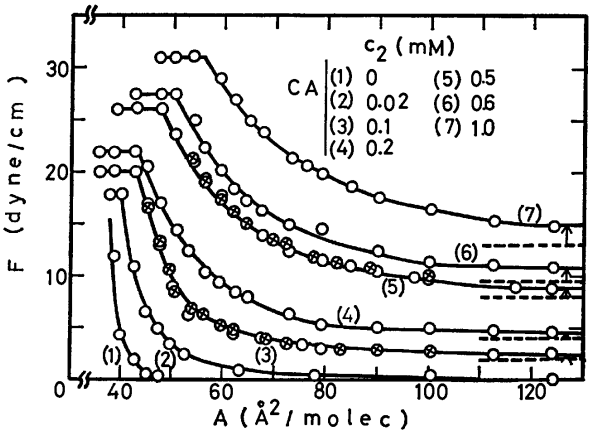

Fig. 1. Relation between the surface pressure, F, and molecular area, A, of CA monolayer at various SHP concentrations, c_2, and at fixed concentration of added NaOH, $c'=10$ mM, at 25 °C, by SAD-method (○) and ICA-method (⊗).

The surface pressure, F, is defined ,as usual, on the basis of the surface tension of pure water, γ_w, by means of the following equation:

$$F = \gamma_w - \gamma \quad (2)$$

where γ is the surface tension of the surface covered with a monolayer. If there is no insoluble monolayer, the surface pressure of the adsorption monolayer of SHP, F_{SHP}, is given by:

$$F_{SHP} = \gamma_w - \gamma_{SHP} \quad (3)$$

where γ_{SHP} is the surface tension of the SHP solution. Each F–A curve on a SHP solution shown in Fig. 1 approaches, when A becomes sufficiently large, a horizontal broken line which represents the F_{SHP}-value. Therefore, the shift of the F–A curves with c_2 toward higher F-values is mainly due to the increase in F_{SHP}. To eliminate this, the practical surface pressure, F', is introduced; it is defined on the basis of the surface tension of the substrate instead of that of pure water:

$$F' = \gamma_{SHP} - \gamma = F - F_{SHP} \quad (4)$$

According to this equation, Fig. 1 is redrawn as Fig. 2, in which the practical collapse pressure, F_c', has turned out to be independent of c_2, at least within the range examined here. On the other hand, the molecular area increases with c_2. This will be discussed in detail in a separate paper.

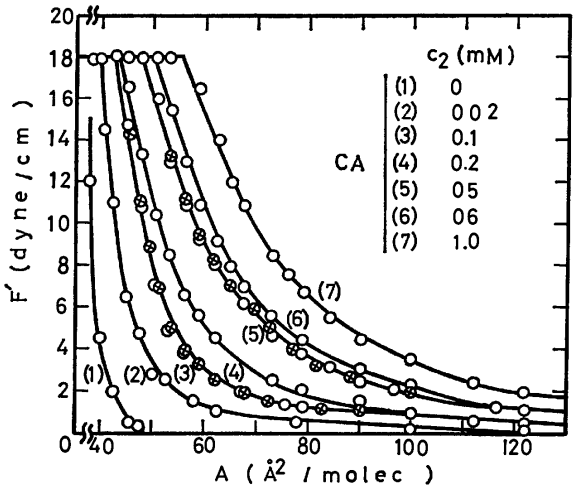

Fig. 2. Relation between the practical surface pressure, F', and molecular area, A, of CA obtained from the data shown in Fig. 1.

Mixed Monolayer of CH and CA. In this case of mixed monolayers, too, the practical surface pressure, F', is adopted: the results obtained for the mixed monolayer of CH and CA on the SHP solution of $c_2=0.5$ mM are shown in Fig. 3. It may be seen in this figure that each F'–A curve of the CH–CA mixed monolayer has, in general, two kind points, in contradistinction to the CH and CA monolayers which had only one kind point. Both of the two kink points of each F'–A curve are collapse points, as will be discussed in detail later on. The mixed monolayer, therefore, undergoes a two-step collapse.

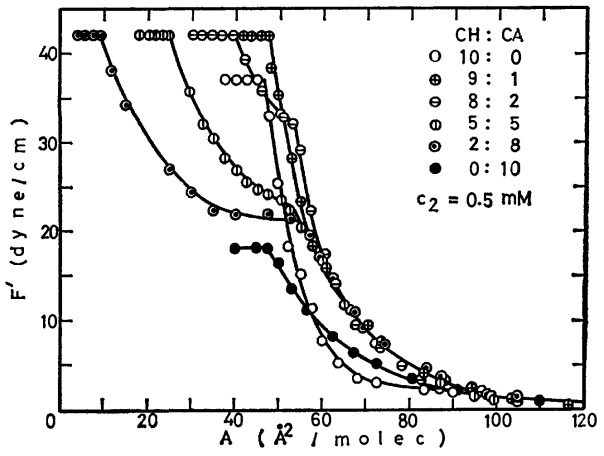

Fig. 3. Variation of F'–A curves of CH–CA monolayers with the composition, at $c_2=0.5$ mM, $c'=10$ mM and at 25 °C.

The collapse pressure and the collapse area at the lower collapse point, which is one located at the lower surface pressure, are designated by F'_{c1} and A'_{c1}, while those at the higher collapse point are designated by F'_{ch} and A_{ch}. Therefore, as may be seen from Fig. 3, F'_{c1} depends on the composition of the mixed monolayer, whereas F'_{ch} is independent of the composition of the mixed monolayer and F' remains unchanged at F'_{ch} when the monolayer is compressed further. Two other points particularly noteworthy in Fig. 3 are that the mixed monolayer at the mole ratio of CH : CA =9 : 1 has only one collapse point, while the F'_c of this monolayer coincides with F'_{ch} at other compositions.

Mixed Monolayer of CA and CP. Before studying the mixed monolayer, the monolayer of CP was examined; it is shown in Fig. 4. The data obtained by the SAD method show that the F'_c of CP increased with c_2 even when the value is expressed as the practical surface pressure, in contradistinction to the cases of CH and CA mentioned above. This is verified to be due to the supercompression on the basis of the observation of the change with time and measurements by the ICA method as follows: 1: The values of F'_c decrease with the time as is shown by the vertical arrows in Fig. 4, and stop decreasing at $F'_c=7.5$ dyn/cm, the value at $c_2=0$ (pure water). 2: The F'—A curves obtained by means of the ICA method showed no change with time, agreed well with the curves obtained by means of the SAD method in the region of low F' values, and gave the value of $F'_c=7.2$ dyn/cm, which is practically equal to the above-mentioned value of the "equilibrium" collapse pressure obtained by means of the SAD method. In Fig. 4, an example obtained by means of the ICA method is shown for $c_2=0.5$ mM.

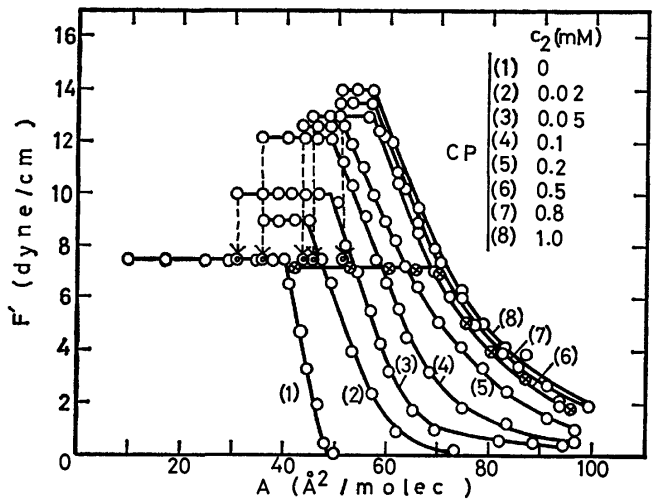

Fig. 4. The F'–A curves of CP monolayer at various c_2 values ($c'=10$ mM) at 25 °C. SAD-method (○), its equilibrium values (◎), and ICA-method (⊗).

The mixed monolayer of CA and CP at $c_2=0.5$ mM gave the F'–A curves shown in Fig. 5, obtained by means of the SAD method. The general features of the CA–CP system are identical with those of the CH–CA system described in the preceding section, since each F'–A curve has, in general, two collapse points except

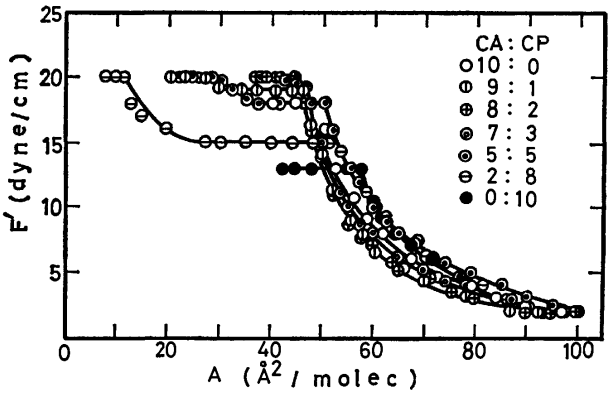

Fig. 5. Variation of F'–A curves of CA–CP monolayers with the composition, at $c_2=0.5$ mM, $c'=10$ mM and at 25 °C.

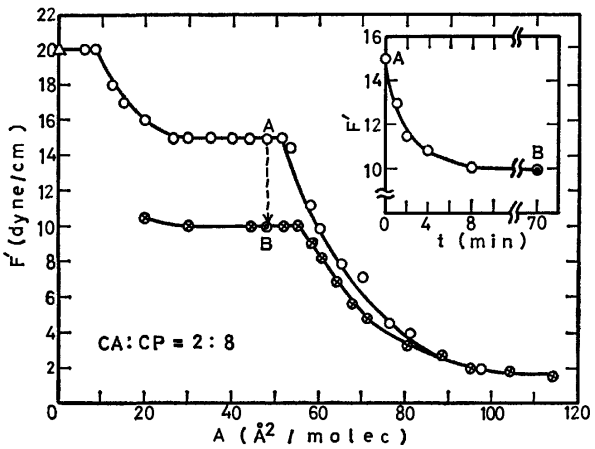

Fig. 6. Comparison of the practical surface pressure, F', obtained by SAD- and ICA-method and the variation with time, t, of the mixed monolayer at the mole ratio of CA : CP=2 : 8, at $c_2=0.5$ mM, $c'=10$ mM and at 25 °C.
SAD-method (○), its equilibrium values (◎), ICA-method (⊗), and the equilibrium spreading pressure, F'_s (△).

for CA : CP=8 : 2, the F'_{ch} is independent of the composition and is in agreement with F'_s, and F'_{cl} depends on the monolayer composition. In contradistinction to the CH–CP system, however, the value of F'_{cl} of this CA–CP system was not steady, but decreased with the time.

As example, the case of a mixed monolayer with the mole ratio of CA : CP=2 : 8 is shown in Fig. 6. The data were obtained by means of the SAD method. Moreover, the vertical arrow in Fig. 6 shows that F' decreased, while the surface area was kept constant, from A to B with the time, t (min), as is shown in the insert; the "equilibrium" collapse pressure at B coincides with the F'_{cl} obtained by means of the ICA method. The same result was also obtained from the experiments at other compositions of the CA–CP system.

Mixed Monolayer of CP and CH. The F'–A curves of CP–CH systems at c_2=0.5 mM are given in Fig. 7. As for the CH monolayer, the agreement between the data obtained by means of the SAD method and ICA method is shown. All the others were obtained by means of the ICA method, becase the time dependence of F' was expected for the monolayers containing CP. The broken lines were drawn according to the calculated value of F'_{ch} and by extrapolation from lower F'-values in order to estimate the A_{ch} values, which will be discussed later on.

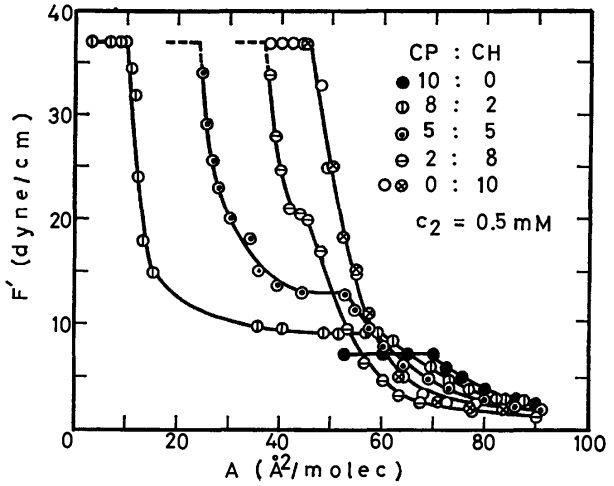

Fig. 7. Variation of F'–A curves of CP–CH monolayers with the composition, at c_2=0.5 mM, c'= 10 mM and at 25 °C, by DAD-method (○) and ICA-method (all others).

Discussion

Two-step Collapse. According to the experimental results shown in Figs. 3, 5, and 7, each F'–A curve of the mixed monolayer consisting of two components out of CH, CA and CP has, in general, two collapse points, indicating that the mixed monolayers undergo a two-step collapse when they are compressed.

The dependence of F_c of the monolayer composition is shown in Fig. 8, taking ,on the abscissa, the mole fraction in the insoluble components, X_4, as defined by:

$$X_4 = n_4/(n_3+n_4) \quad (5)$$

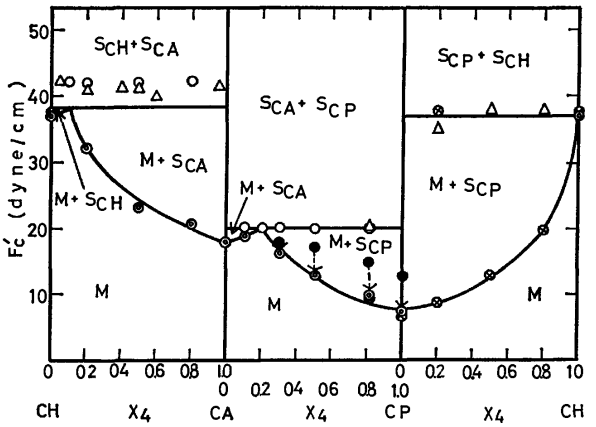

Fig. 8. Relation between the collapse pressure, F'_c, and mole fraction X_4, for CH–CA, CA–CP, and CP–CH systems at c_2=0.5 mM, c'=10 mM and at 25 °C. Solid lines are theoretical by Eq. (15). F'_{ch} (○), F'_{cl} by SAD-method (●), and its equilibrium values (◎), F'_c by ICA-method (⊗), and F'_s (△).

Here, n is the moles and the 3 and 4 suffixes indicate the respective insoluble components, reserving the 1 and 2 suffixes for water and SHP respectively. It has been confirmed here as well as experimentally that the shift of curves with c_2 is mostly cancelled by taking F' instead of F. In Fig. 8, the values of the equilibrium-spreading pressure, which is measured on the same SHP solution and expressed in terms of the practical surface pressure, F'_s, are also plotted to show that the values are independent of X_4 and agree well with F'_{ch}.

Figure 8 shows the dependence of the practical surface pressure at these two collapse points, F_{cl} and F'_{ch}, on the mole fraction in the insoluble components, X_4, indicating that F'_{ch} is independent of X_4 and agrees with F'_s, while F'_{cl} varies with X_4 and its curves merge with F'_{ch} at one point, which can be called a "concollapse point". As a result, the two mixed monolayers of CH : CA=9 : 1 (Fig. 3) and CA : CP= 8 : 2 (Fig. 5) have only one collapse point, whose collapse pressure agrees with the F'_{ch} values of the monolayers at other X_4 values. Thus, Fig. 8 is completely analogous to the ordinary-phase diagram representing the pressure-composition relation, at a given temperature, of a solid-liquid equilibrium of mixtures which have an eutectic point[9] and may be considered to be a phase diagram representing the equilibrium between the monolayer and the bulk phase separated from the monolayer due to the collapse.

Therefore, the following conclusions may be drawn: When a mixed monolayer is compressed, one of the components, which is presented in more than the concollapse composition, starts separating at F'_{cl}. This separation continues during the further compression, accompanying the increase in F' and the approach of the value of X_4 to that of the concollapse monolayer. When the F' reaches F'_{ch}, the other component starts separating simultaneously, but this second deposit does not mix with the first one. Under a given pressure, temperature, and SHP concentration, the freedom of the system become zero when the two

bulk phases have been separated.[2,3,10] Therefore, further compression beyond the higher collapse point does not change F' from $F'_{c\,h}$, the latter being independent of the composition of the starting monolayer, X_4, and being equal to F'_s. Thus, in the regions designated by M, M+S and S_3+S_4 in Fig. 8, there exist the monolayer, the monolayer and a bulk phase, and two bulk phases respectively.

In the CP–CH system, both the $F'_{c\,h}$ and F'_s of the mixed monolayers agree with those of pure CH. This is because the F'_c of CP is much lower than that of CH, that means CP is far easier to collapse than CH, so that the component remaining in the concollapse monolayer is mostly CH.

Collapse Pressure and Composition. The monolayer to be studied here has three components, because the mixed monolayer of two insoluble components, 3 and 4, contains also the soluble component 2 (SHP in our case), which has penetrated from the substrate: The chemical potential of the j component in the monolayer, μ_j^m, is written:[10]

$$d\mu_j^m = kT\,d\ln\xi_j + \omega_j dF \qquad (j=2, 3 \text{ or } 4) \qquad (6)$$

or, if the SHP concentration c_2 is constant so that F_{SHP} is also constant:

$$d\mu_j^m = kT\,d\ln\xi_j + \omega_j dF' \qquad (j=2, 3 \text{ or } 4) \qquad (6a)$$

Here, ξ_j is the mole fraction of the j component in the monolayer:

$$\xi_j = n_j/(n_2+n_3+n_4) \qquad (7)$$

which is different from the mole fraction to X_j, defined by Eq. (5), and ω_j is the partial molecular area of the j component and is related to the (average) molecule area of the insoluble components, A, by:

$$A = \nu_2\omega_2 + X_3\omega_3 + X_4\omega_4 \qquad (8)$$

where ν_2 is the mole of the penetrated component, 2. per mole of insoluble components:

$$\nu_2 = n_2/(_3 + n_4) \qquad (9)$$

The mole fraction which can be assigned experimentally is not ξ_i, but X_i. Therefore, by using the relation:

$$d\ln\xi_i = d\ln X_i - [\xi_i/(1-\xi_i)]\,d\ln\xi_i \qquad (i=3 \text{ or } 4) \qquad (10)$$

Equation (6a) can be rewritten when c_2 is constant and $d\mu_2^m=0$:

$$d\mu_i^m = kT\,d\ln X_i + A_{0i}dF' \qquad (i=3 \text{ or } 4) \qquad (11)$$

where;

$$A_{0i} = \omega_i + \nu_2\omega_2 \qquad (i=3 \text{ or } 4) \qquad (12)$$

This equation may then be used to determine the penetration amount of the 2 component, as will be discussed in a separate paper to be published later. The quantity, A_{0i}, defined by Eq. (12) is a kind of partial molecular area of the i component on the surface of the solution of the 2 component; it is related to the average molecular area of the insoluble components, A, by:

$$A = X_3A_{03} + X_4A_{04} \qquad (13)$$

When a mixed monolayer is in equilibrium with the bulk phase, i, separated from the monolayer at the lower collapse point, the chemical potential of the i component in the monolayer, μ_i^m, is equal to that in the bulk phase, μ_i^b, and the latter is independent of the monolayer composition, X_i, because the other insoluble component is not separated at the lower collapse point. Integrating Eq. (11) with $d\mu_i^m = d\mu_i^b = 0$, the following is obtained for the lower collapse pressure:

$$F'_{c\,i} = F'_{0\,i} - (kT/A_{0i})\ln X_i \qquad (i=3 \text{ or } 4) \qquad (14)$$

Here, $F'_{0\,i}$ is introduced to determine the integration constant on condition that $F'_{c\,i}=F'_{0\,i}$ at $X_i=1$; it is the collapse pressure of the monolayer of the i component on the aqueous SHP solution. To obtain Eq. (14), it has been assumed that A_{0i} is a constant. This is acceptable because the molecular area at the lower collapse point, $A_{c\,l}$, does not change much with the composition, X_i, at a given c_2.

According to Eq. (14), the theoretical values of $F'_{c\,i}$ shown in Fig. 8 by solid curves as a function of X_4 are calculated by using the parameter values, $F'_{0\,i}$ and A_{0i}, obtained experimentally from the collapse point of the one-component monolayer on the aqueous SHP solution; these values are given in Table 1. The agreement between the theoretical curves and the experimental plots in Fig. 8 is good. The intersection of two curves is the concollapse point. For this point, the practical surface pressure, F'_e, and the mole fraction, X_e, are calculated; they are given in Table II. The concollapse pressure, F'_e, is, as has been stated before, equal to the higher collapse pressure, $F'_{c\,h}$, shown by the horizontal solid line in Fig. 8. The agreement between the theoretical value and the experimental plot is, again, fairly good.

TABLE 1. EXPERIMENTAL VALUES OF THE PARACTICAL COLLAPSE PRESSURE, $F'_{0\,i}$, AND COLLAPSE AREA, A_{0i}, AT $c_2=0.5$ mM AND $c'=10$ mM AT 25 °C

Component i	F_{0i} (dyn/cm)	A_{0i} (Å²/molec.)
CH	36.9	46.5
CA	18.0	47.0
CP	7.5	55.0

TABLE 2. CALCULATED VALUES OF CONCOLLAPSE PRESSURE, F'_e, AND CONCOLLAPSE MOLE FRACTION, X_e, AT $c_2=0.5$ mM AND $c'=10$ mM AT 25 °C

Components 3—4	F_c (dyn/cm)	$X_{e,4}$
CH-CA	38.2	0.11
CA-CP	20.0	0.20
CP-CA	37.0	0.98

Collapse Area and Composition. The relation between the collapse area, A_c, and X_4 at $c_2=0.5$ mM is shown in Fig. 9. The molecular area at the higher collapse point, A_{ch}, is, of course, smaller than that at the lower collapse point, A_{cl}. The latter does not depend much on the composition, as has been mentioned before, while the former varies almost linearly with X_4,

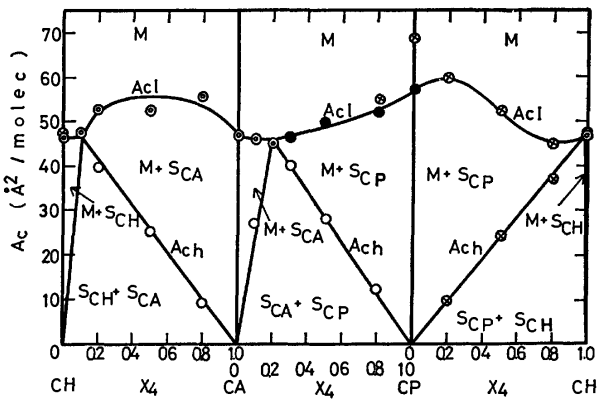

Fig. 9. Relation between the collapse area, A_c, and the mole fraction, X_4, for CH-CA, CA-CP, and CP-CH systems at $c_2=0.5$ mM, $c'=10$ mM and at 25 °C. Symbols are same as in Fig. 8.

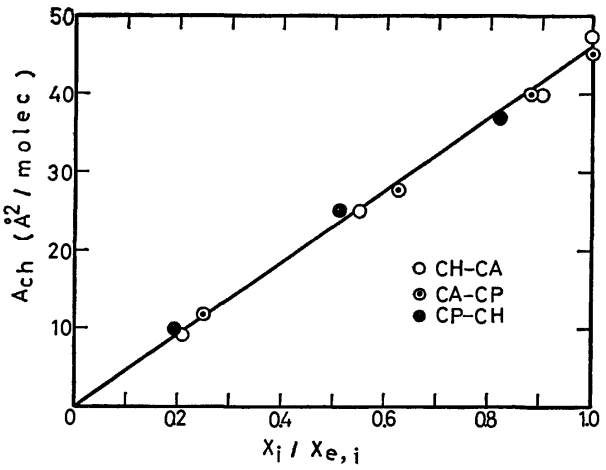

Fig. 10. The proportionality of A_{ch} to $(x_i/X_{e,i})$ expected by Eq. (15), for CH-CA (○), Ca-CP (◎), and CP-CH(●).

describing a triangle, the top of which is the concollapse point with the molecular area of A_e and the mole fraction of X_i.

When a mixed monolayer, consisting of n_3 and n_4 moles of two insoluble components, 3 and 4, respectively, is compressed beyond the lower collapse point, the 4 component (if $X_4>X_{e,4}$) is separated from the monolayer, resulting in a marked decrease in the surface area, S. Therefore, the molecular area, A, calculated on the basis of the initial moles of the insoluble components (n_3+n_4):

$$A = S/[(n_3+n_4)N_A] \quad (1a)$$

decreases remarkably at the lower collapse point.

When the monolayer reachs the higher collapse point upon further compression, the mole fraction in the monolayer becomes equal to that of the concollapse monolayer, X_e, and the total area is expressed as $S=A_e\ (n_3/X_{e,3})N_A$, because n_3 does not change in the process. Therefore, after the introduction of this into Eq. (1a),

$$A_{ch} = A_e X_3/X_{e,3} \quad (X_4>X_{e,4}) \quad (15)$$

or:

$$A_{ch} = A_e X_4/X_{e,4} \quad (X_4<X_{e,4}) \quad (16)$$

These equation are tested in Fig. 10 and proved to be satisfactory, since the experimental A_{ch} value is found to be proportional to $(X_i/X_{e,i})$, the proportionality coefficient being $A_e=46.0$ (Å²/molec.) if the $X_{e,i}$ values given in Table II are used. The straight line in Fig. 9, drawn by using this value of A_e and the values of $X_{e,4}$ given in Table 2, agree well with the experimental plots.

References

1) M. Nakagaki, N. Funasaki, and K. Fujita, *Nippon Kagaku Zasshi*, **92**, 243 (1972).
2) M. Nakagaki, and N. Funasaki, *Bull. Chem. Soc. Jpn.*, **47**, 2094 (1974).
3) M. Nakagaki and N. Funasaki *Bull. Chem. Soc. Jpn.*, **47**, 2482 (1974).
4) M. Nakagaki, T. Handa, and S. Shimabayashi, *J. Colloid Interface Sci.*, **43**, 521 (1973).
5) M. Nakagaki and T. Handa, *Yakugaku Zasshi*, **92**, 611 (1972).
6) M. Nakagaki, N. Funasaki, and M. Nishino, *Yakugaku Zasshi*, **90**, 1088 (1970).
7) For examples, a) D. O. Shah, and J. H. Shulman, *J. Lipid Res.*, **8**, 215 (1967); b) D. Parahadjopolos, M. Cower, and H. Kimelberg, *Biochem. Biophys. Acta*, **330**, 7 (1973); c) N. L. Gershfeld, and R. E. Pagano, *J. Phys. Chem.*, **76**, 1244 (1972).
8) A. M. Kamel, N. D. Weiner, and A. F. Felmeister, *J. Colloid Interface Sci.*, **35**, 163 (1971).
9) J. G. Kirkwood and I. Oppenheim, "Chemical Thermodynamics," McGraw-Hill, New York (1962), Chapter 6.
10) R. Defay, I. Prigogine, A. Bellmans, and D. H. Everett, "Surface Tension and Adsorption," Longmans, London (1966), p. 165.

Dipolar Interaction in TEMPAD Biradical. II[1)]

Akira NAKAJIMA, Jun YAMAUCHI,* Hiroaki OHYA-NISHIGUCHI,** and Yasuo DEGUCHI***

Medical College of Miyazaki, Kiyotake, Miyazaki 889-16

**The Institute for Chemical Research, Kyoto University, Uji 611*

***Faculty of Science, Kyoto Universtiy, Kyoto 606*

****College of Liberal Arts and Science, Kyoto University, Kyoto 606*

(Received September 5, 1975)

The EPR of TEMPAD single crystals diluted in diamagnetic matrices was studied. The results of the 10% TEMPAD were almost the same as those of the very dilute one studied previously. In the case of the 25% TEMPAD, the spectra are composed of three parts. The central broad line, whose linewidth was analyzed in comparison with the pure TEMPAD case using the three-dimensional Anderson-Weiss formula, is the spectrum of clusters constructed by the free radicals. The side lines with the hyperfine splitting are the spectrum of the isolated TEMPAD molecule, and the outer broad lines are from the molecules coupled in pairs along the a-axis. The EPR spectra of the pure TEMPAD at very low temperature were also measured in order to have information concerning the dipolar interaction in the pure crystal. These spectra are the superposition of the spectra caused by the intra-molecular dipolar interaction and of the spectra due to impurities. All the results were explained with the suitable molecular stack model and the triplet exciton theory.

There have been a number of investigations regarding the magnetic properties of organic stable free radical solids.[2-4)] In these works, the magnetic ordering effects caused by some magnetic interactions between unpaired electrons have been of special interest. When the unpaired electrons couple with each other three-dimensionally, the long-range ordering effect can occur.[2,3)] On the other hand, the low-dimensionally coupled spins or clustering spins induce the short-range ordering effect.[3,4)]

To clarify these magnetic ordering effects, one must study the magnetic interactions, especially the exchange interaction and the dipolar interaction between unpaired electrons. EPR spectroscopy is a powerful technique for the study of these magnetic interactions, because it gives much information about the microscopic magnetic structure and the dynamical behavior of the magnetic system.

Previous magnetic studies of 2,2,6,6-tetramethyl-4-piperidone azine 1,1'-dioxyl (TEMPAD) revealed three kinds of exchange interactions (see Fig. 1):[5-7)] one of them is the stronger inter-molecular exchange interaction along the a-axis (J_1;$J_1/k=-12.8$ K) which produces the broad maximum in the magnetic susceptibility (χ_M) of the pure TEMPAD at the temperature of 16.5 K and the large Weiss constant in the χ_M-T curves of the diluted crystals.[5,7)] The second kind is the weaker inter-molecular exchange interaction (J_1'; $|J_1'|/k\sim 1$ K) in the inter-molecular alternating chain, and the third is the weaker intra-molecular one (J_2; $|J_2|/k\sim 2\times 10^{-2}$ K)which affects the hyperfine structure in the EPR spectrum in solution[6)]; both contribute to the small Weiss constant in the χ_M-T curves of the diluted TEMPAD crystals.[7)]

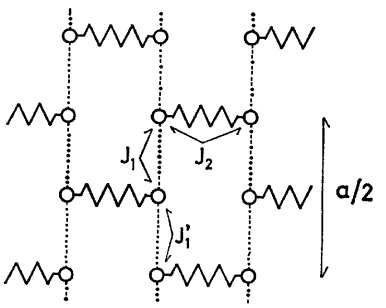

Fig. 1. Exchange interactions in TEMPAD biradical.

The EPR of the diluted TEMPAD in the diamine host was also studied and the principal values and the direction cosines of the inter- and the intra-molecular dipolar interactions were determined.[8)] The angular dependence of the EPR linewidth of the pure TEMPAD could be well explained using the three-dimensional Anderson-Weiss formula, which indicates that the inter-molecular dipolar interaction and the weak exchange interactions (J'_1 and J_2) are very important for the dynamical behavior in our case.[8)] The EPR spectrum of the powdered TEMPAD at room temperature shows one symmetrical line, and new lines appear on both sides of the central line at very low temperatures. They have been explained in terms of the intra-molecular dipolar interaction on the basis of the triplet exciton theory.[1)]

In this paper, the authors will report on their EPR studies of the pure TEMPAD at very low temperature and of the diluted TEMPAD in the diamine host at room temperature. Some discussion is given on the inter- and intra-molecular exchange and dipolar interactions in the biradical crystal by comparison with the data published elsewhere.

Experimental

TEMPAD and 2,2,6,6-tetramethyl-4-piperidone azine (the diamine), whose molecular structures are shown in Figs. 2(a) and 2(b), respectively, were prepared from 2,2,6,6-tetramethyl-4-piperidone supplied by the Aldrich Chemicals Co. in accordance with the method described by Rassat *et al.*[9)] The single crystals of the pure TEMPAD and the 25% and 10% TEMPAD in the diamine host were crystallized from their ethereal solutions.

The EPR spectra were measured using X-band (9.5 GHz) spectrometers, JEOLCO JES-ME-3X equipped with an 80 Hz field modulation at low temperatures and JEOLCO JES-PE-3X equipped with a 100 kHz field modulation at room temperature. In the low temperature measurements, the temperature was determined by measuring the vapor

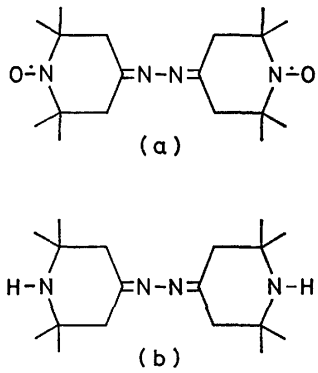

Fig. 2. Molecular structures of the TEMPAD biradical (a) and the corresponding diamine (b).

pressures of liquid helium. The magnetic field was calibrated with 0.1% Mn^{2+} in MgO (the hyperfine coupling constant between central two lines is 86.2×10^{-4} T and $g=2.00641$) and peroxylamine disulfonate, $[\cdot ON(SO_3)_2]^{2-}$ ($A_N=13.0\times10^{-4}$T and $g=2.00550$). The error in the measurements of angles was estimated to be about two degrees.

Results and Discussion

Crystal Structure. The crystal structures of the TEMPAD and the diamine crystals are the monoclinic system with the parameter β of nearly 90° (see Table 1); thus we can adopt the a, b, and c-axes as the rectangular coordinate system for the pure and the diluted single crystals (see Figs. 3(a) and 3(b)). It should be noted here that the molecular stack model presumed from the EPR results[8] indicates that the electron spins form a linear chain along the a-axis. This means that the direction of the largest exchange and dipolar interactions is along the a-axis, as is shown in Fig. 1.

Table 1. The space groups and the lattice constants for the diamine and TEMPAD biradical

	Diamine	TEMPAD
Space group	Monoclinic C_c	Monoclinic C_c or $C_{2/c}$
a	29.0 Å	29.1 Å
b	12.6 Å	12.8 Å
c	10.4 Å	10.5 Å
β	~90°	~90°
z	8	8

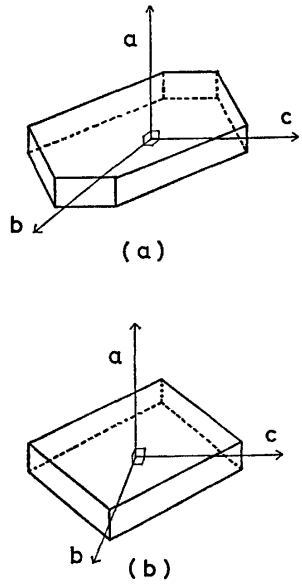

Fig. 3. Coordinate systems of the diamine host (a) and the TEMPAD crystal (b).

Exciton Density. If the electron spins form an alternate linear chain, in which the spins couple with each other through exchange interactions, a short-range ordering will occur at low temperature and then some triplet excitons will be produced. The triplet exciton plays an important role in the dynamic behavior of the unpaired electrons of the TEMPAD biradical at low temperature. The density of the triplet exciton is given by

$$\rho = 1/[1+(1/3)\exp(\delta/kT)] \quad (1)$$

where $\delta=2|J_1|$[10]. From the χ_M-T curve, J_1/k is equal to -12.8 K for the TEMPAD biradial and the density of the triplet exciton at 4.2 K is about 0.5%. Even in a pure TEMPAD crystal, this low density of the triplet exciton makes it possible to observe the EPR spectra modified by the intra-molecular dipolar interaction at low temperature.

Diluted Crystal. The interactions between biradicals in a diamagnetic host crystal may be divided into three types of interaction; that is, an isolated biradical, a dimer, and a cluster which contains three or more interacting biradical molecules. These are shown in Fig. 4. Type I contains only intra-molecular exchange and dipolar interactions; in Type II there are inter-molecular exchange and dipolar interactions in addition to the intra-molecular interactions. "Cluster" has a very complicated interaction mechanism and may exhibit rather exchange-narrowed EPR absorptions.

The EPR results of the 10% TEMPAD single crystal are the same as those of the very diluted case (2% in concentration)[8] except for showing EPR spectra of a low resolution at some orientations. The spectra consist of two parts of the absorption lines, the one due to the intra-molecular interactions (Type I) and

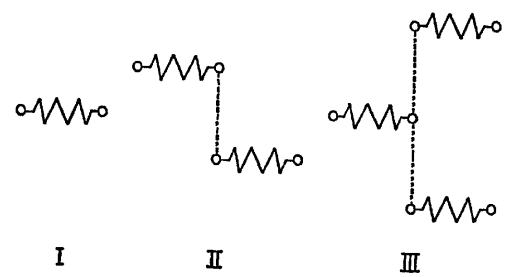

Fig. 4. TEMPAD biradicals in a diamine host crystal. Type I represents an isolated TEMPAD biradical surrounded by diamagnetic host molecules. Type II represents a pair interaction scheme. Type III represents one of the interaction schemes in which three or more TEMPAD molecules interact each other. Type III is called "cluster".

the other due to the inter-molecular interactions (Type II). The former has a doublet splitting due to intra-molecular dipole-dipole interaction and each of the doublet absorptions shows hyperfine splittings attributable to exchange-coupled nitrogen nuclei. It is the exchange interaction, J_2 in Fig. 1, that couples two nitrogen nuclei in the same molecule. The latter spectrum, which is outside of the former spectrum and has an apparently broad linewidth, comes from the inter-molecular dipole-dipole interaction. The angular dependence of these spectra can be obtained and then the principal values of the intra-molecular dipole-dipole interaction tensor and their direction cosines can be determined. These results are quite the same as in the case of the 2% TEMPAD crystal within the accuracy of the experimental error. The results of the direction cosines show that in the 10% TEMPAD crystal the biradical molecules in a unit cell occupy two different sites, the p- and q-sites, as reported in Ref. 8. The principal values and the crystal field parameters are listed in Table 2 and the splitting constants of the spectra at some orientations are summarized in Table 3. The EPR spectra of the 25% and 100% TEMPAD crystals can be analyzed on the basis of these values. The good agreement between the results of 10% and 2% TEMPAD crystals may indicate that the biradical concentration of 10% TEMPAD is not high enough to affect the EPR spectra through the inter-molecular interaction. In other words, there are in the EPR spectra mainly contributions from Types I and II and no appreciable contributions from the cluster in Fig. 4.

The results of the 25% TEMPAD are quite different from those of the 10% or 2% TEMPAD crystals.

TABLE 2. THE PRINCIPAL VALUES OF THE TENSORS OF THE INTRA-MOLECULAR AND INTER-MOLECULAR DIPOLE-DIPOLE INTERACTIONS WITH REGARD TO THE abc-SYSTEM AND THE CRYSTAL FIELD PARAMETERS

Principal values	Crystal field parameters
Intra-molecular dipole-dipole interaction	
D_{xx} $\pm(18.7\pm0.5)\times10^{-4}$T	$\lvert D\rvert/g\mu_B$ $51.0\pm1.5\times10^{-4}$T
D_{yy} $\pm(15.3\pm0.4)$	$\lvert E\rvert/g\mu_B$ 3.4 ± 0.9
D_{zz} $\mp(34.0\pm1.0)$	
Inter-molecular dipole-dipole interaction	
D'_{xx} $\pm13\times10^{-4}$T	$\lvert D'\rvert/g\mu_B$ 130×10^{-4}T
D'_{yy} ±73	$\lvert E'\rvert/g\mu_B$ 30
D'_{zz} ∓86	

TABLE 3. DIPOLAR INTERACTIONS IN TEMPAD BIRADICAL AS THE SPLITTING OF THE SPECTRUM AT EACH ORIENTATION

Axis (//H)	a	b	c
2% D'	264×10^{-4}T	172×10^{-4}T	208×10^{-4}T
10% D	55	40	106
25% D'	263	—	—
25% D	—	—	106
100% D (4.2 K)	—	—	60
100% D (1.7 K)	—	65	73

D': Inter-molecular dipolar coupling
D : Intra-molecular dipolar coupling

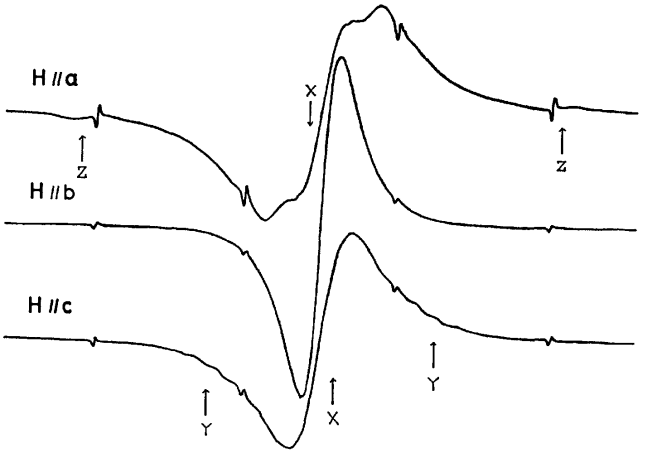

Fig. 5. Typical EPR spectra of the 25% TEMPAD crystal with the static magnetic field parallel to a, b, and c-axes. Small sharp peaks are the spectra of Mn^{2+} in MgO.

This fact indicates that an exchange narrowing effect becomes large in the 25% TEMPAD crystals. The EPR spectra of the 25% TEMPAD single crystal at some orientations are shown in Fig. 5. These spectra are composed of three kinds of spectral lines; one of them is a central broad line (X), the second is the side lines with the hyperfine splitting (Y), and the last is the broad side lines (Z). From comparing these spectra with those of the 10% or 2% TEMPAD case it follows that the contributions from Types I and II are rather decreased and that the contribution from Type III is much more increased. The central broad line can be considered to be the spectrum of the inter-molecular clusters (Type III in Fig. 4). The angular dependence of the linewidth of X is shown in Fig. 6 in comparison with that of the pure TEMPAD. The linewidth of X in the 25% TEMPAD is broader than that of the pure TEMPAD for all orientations of the crystal in the magnetic field H except for the orientation where the linewidth takes a minimum value, and the spectra of X splits into three lines for the case of H//a-axis. For the comparison with the pure TEMPAD

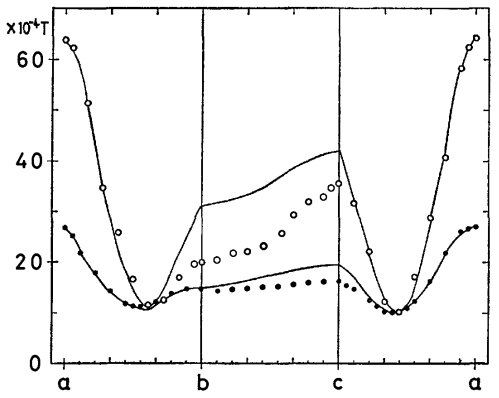

Fig. 6. Peak-to-peak linewidths of the 25% and the pure TEMPAD spectra. The solid curves are the calculated results using the three-dimensional Anderson-Weiss model. ●: Pure TEMPAD, ○: center line X of 25% TEMPAD.

case, we can consider the three-dimensional Anderson-Weiss formula for a Lorenzian line:[11]

$$\Delta H_{pp} = \Delta H_d^2/\sqrt{3}H_{ex} + C \qquad (2)$$

where ΔH_{pp} is the peak-to-peak linewidth, ΔH_d^2 the second moment of the dipolar interaction, H_{ex} an effective exchange field, and C the residual linewidth. The secular part of the second moment ΔH_d^2 was calculated using the term of the inter-molecular dipolar interaction (D') obtained from the 10% or 2% TEMPAD crystal. Thus H_{ex} and C were estimated to be $\sim$0.2 T ($\sim$2000 G or 0.3 K) and $\sim 10^{-3}$ T ($\sim$10 G), respectively. These values reproduce quite well the angular dependence of the linewidth. If we take into account H_{ex}=0.43 T (4300 G) and C=9.5$\times 10^{-4}$ T (9.5 G) in the pure TEMPAD crystal, the averaged inter-molecular exchange interaction in the cluster is weaker than that in the pure TEMPAD and the residual linewidth C is nearly equal to that of the pure TEMPAD. It may be reasonable that the effect of the exchange narrowing in the cluster is reduced by a diamagnetic dilution and that there is no noticeable change in the residual linewidth C because it represents the broadening mechanisms which come mainly from the nuclear hyperfine interaction and the non-secular part of the inter-molecular dipole-dipole interaction.

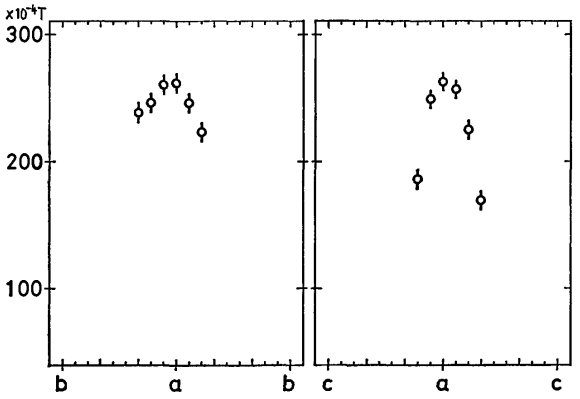

Fig. 7. Dipolar splitting of the line Z of the 25% TEMPAD crystal.

The side doublet line Y with a hyperfine structure can easily be assigned to the line of the isolated TEMPAD biradical (Type I) and corresponds to the intra-molecular dipolar interaction (D), because this spectrum has a hyperfine structure and a maximum separation 106×10^{-4} T at the H//c-axis. The angular dependence of the line separation of the side line Z is shown in Fig. 7. These lines, whose maximum separation is about 264×10^{-4} T at the H//a-axis, are caused by the pair (Type II) and correspond to the inter-molecular dipolar interaction (D') in the 10% or 2% diluted system (see Tables 2 and 3). The angular dependence of Fig. 7 is also in good agreement with that of D'. As the last two groups, Y and Z, are very much weaker than the central line X, the TEMPAD molecules are distributed homogeneously in the diamine host.

Pure Crystal. In the pure crystal, the exchange narrowing effect is so large that we can not obtain much information about any dipolar interactions in the TEMPAD biradical at room temperature. In order to reduce its effect we measured EPR spectra in the liquid helium temperature region, where the triplet exciton density becomes small enough for us to observe the dipolar splitting in EPR spectra. The EPR spectra of the pure TEMPAD single crystal at very low temperature are shown in Fig. 8. These spectra are the superposition of one central line and two side lines. The angular dependence of the two side lines are shown in Fig. 9. These lines have a maximum splitting at an orientation of the H//c-axis with its magnitude of about 60×10^{-4} T. The dipolar splittings of the 2%, 10%, and 25% TEMPAD crystals at room temperature and the pure TEMPAD at low temperature are listed in Table 3. From these results, the two side lines can be determined to be due to the intra-molecular dipolar interaction, which is also consistent with the powder results of 100% TEMPAD.[1] The fact that there is no hyperfine splitting may be caused by the weak inter-molecular exchange inter-

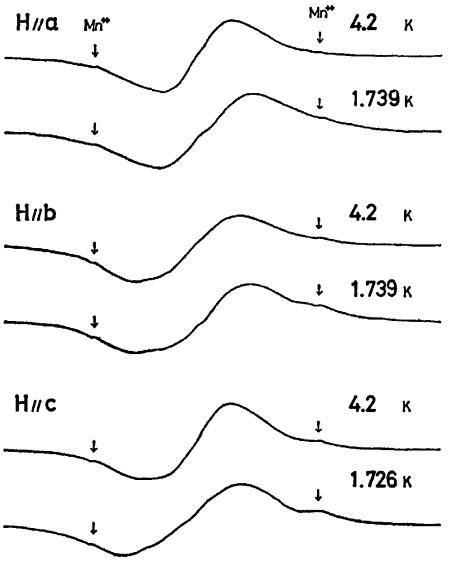

Fig. 8. Low temperature EPR spectra of the pure TEMPAD crystal at some orientations.

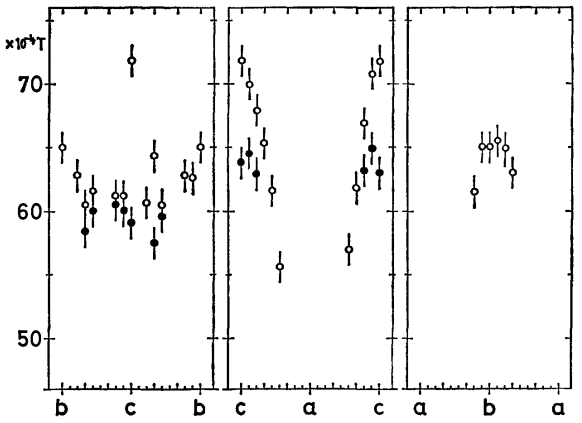

Fig. 9. Dipolar splitting of the outer peak of the pure TEMPAD spectra at low temperature. ●: 4.2 K, ○: 1.73 K.

action.

For the central line there are four possible interpretations; one of them is that it is attributable to the spectrum of the triplet exciton along the a-axis narrowed by the exciton motion, the second is that it is the spectrum of the isolated cluster, the third is due to that of the non-interacting TEMPAD molecule, and the last is that of the monoradicals derived from the TEMPAD biradical by decomposition. As the density of the triplet exciton at 4.2 K is about 0.5%, the EPR spectrum of the triplet exciton at 4.2 K must be very weak and should have a well-resolved fine structure. The spectrum of the non-interacting TEMPAD molecule shows the hyperfine splitting, as we can see in the 25% TEMPAD spectrum. Zvarykina *et al.* showed the typical spectra of a non-interacting adipate biradical at the temperature of the short-range ordering region,[12] but in our case we cannot observe the hyperfine splitting in all the directions. The *g*-value of the central line is slightly different from that of the two side lines; thus the central line may possibly correspond to the last case. This is also ascertained by the angular dependence of the linewidth of the central line, which is shown in Fig. 10. The dotted line(·····) shows the angular dependence of 100% TEMPAD at room temperature. This angular dependence is well explained on the basis of the three-dimensional Anderson-Weiss model, as was already discussed,

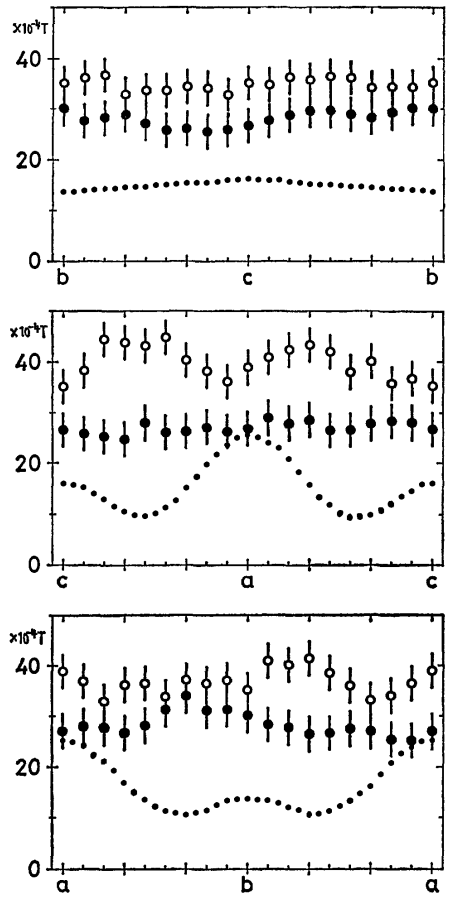

Fig. 10. Peak-to-peak linewidths of the TEMPAD spectra. ●: center line at 4.2 K, ○: center line at 1.74 K, ●: at room temperature.

that is, it depends exclusively on the angular variation of the inter-molecular dipole-dipole interaction parameter, D'. The angular dependence of the linewidth clearly changes as the temperature is lowered, and at 1.73 K it can neither be explained in terms of the inter-molecular dipole-dipole interaction (D') nor the intra-molecular dipole-dipole interaction (D). Thus, we presume that the central line is due to the monoradicals. However, we do not have any reasonable explanation for the broadening mechanism of the linewidth.

As for the dipolar interaction between molecules which have exchange interaction J_1 in Fig. 1, we tried to find some absorptions in a wider magnetic field region, but could not obtain any information, possibly because of the low triplet exciton density.

References

1) J. Yamauchi, T. Fujito, A. Nakajima, H. Ohya-Nishiguchi, and Y. Deguchi, *Bull. Chem. Soc. Jpn.*, **44**, 2263 (1971).

2) J. P. Boucher, M. Nechtschein, and M. Saint-Paul, *Phys. Lett.*, **42A**, 379 (1973); S. Saito and T. Sato, *ibid.*, **44A**, 347 (1973); M. Saint-Paul and C. Veyret, *ibid.*, **45A**, 362 (1973).

3) W. O. Hamilton and G. E. Pake, *J. Chem. Phys.*, **39**, 2694 (1963); J. Yamauchi, *Bull. Chem. Soc. Jpn.*, **44**, 2301 (1971); W. Duffy, Jr., J. F. Dubach, P. A. Pianetta, J. F. Deck, D. L. Strandburg, and A. R. Miedema, *J. Chem. Phys.*, **56**, 2555 (1972); J. Yamauchi, K. Adachi, and Y. Deguchi, *Chem. Lett.*, **1972**, 733; J. Yamauchi, K. Adachi, and Y. Deguchi, *J. Phys. Soc. Jpn.*, **35**, 443 (1973); C. Veyret and A. Blaise, *Molecular Phys.*, **25**, 873 (1973).

4) Yu. S. Karimov, *Soviet Physics-JETP Lett.*, **8**, 239 (1968); H. Lemaire, P. Rey, A. Combarieu, and J. C. Michel, *Molecular Phys.*, **14**, 201 (1968); J. Yamauchi, T. Fujito, E. Ando, H. Nishiguchi, and Y. Deguchi, *J. Phys. Soc. Jpn.*, **25**, 1558 (1968); Yu. S. Karimov, *Soviet Physics-JETP*, **30**, 1062 (1969); D. Fedutin and V. B. Strukov, *Zh. Strukt., Khim.*, **11**, 854 (1970); A. Nakajima, H. Ohya-Nishiguchi, and Y. Deguchi, *Bull. Chem. Soc. Jpn.*, **44**, 2120 (1971); A. Blaise, H. Lemaire, J. Pilon, and C. Veyret, *C. R. Acad. Sci. Compt. Rend.*, **274B**, 157 (1972); J. Lajzerowicz-Bonneteau, B. S. Fr., *Mineral Crystallogr.*, **95**, 202 (1972); V. B. Strukov, S. Ya. Umansky, and A. V. Zvorikina, *Chem. Phys. Lett.*, **18**, 240 (1973); K. Yamamoto, T. Enoki, T. Fujito, A. Nakajima, H. Ohya-Nishiguchi, and Y. Deguchi, *Chem. Lett.*, **1974**, 457; A. M. Prokhorov and V. B. Fedrov, *Soviet Physics-JETP*, **16**, 1489 (1962); H. J. Gerritsen, R. Okkes, H. M. Gijsman, and J. Van den Handel, *Physica*, **20**, 13 (1954); W. Duffy, Jr. and D. L. Strandburg, *J. Chem. Phys.*, **46**, 456 (1967); P. A. Fedders and J. Kommandeur, *ibid.*, **52**, 2014 (1970); T. Fujito, T. Enoki, H. Ohya-Nishiguchi, and Y. Deguchi, *Chem. Lett.*, **1972**, 557.

5) A. Nakajima, H. Nishiguchi, and Y. Deguchi, *J. Phys. Soc. Jpn.*, **24**, 1175 (1968).

6) A. Nakajima, H. Ohya-Nishiguchi, and Y. Deguchi, *Bull. Chem. Soc. Jpn.*, **45**, 713 (1972).

7) A. Nakajima, *Bull. Chem. Soc. Jpn.*, **46**, 779 (1973).

8) A. Nakajima, *Bull. Chem. Soc. Jpn.*, **46**, 1129 (1973).

9) R. Briere, R. M. Dupeyre, H. Lemaire, C. Morat, A. Rassat, and P. Ray, *Bull. Soc. Chim. Fr.*, **1965**, 3290.

10) R. C. Hughes and Z. G. Soos, *J. Chem. Phys.*, **48**, 1066 (1968).

11) T. Z. Huang, R. P. Tayler, and Z. G. Soos, *Phys. Rev. Lett.*, **28**, 1054 (1972); P. W. Anderson and P. R. Weiss, *Rev. Mod. Phys.*, **25**, 269 (1953).

12) A. V. Zvarykina, V. B. Strukov, D. N. Fedutin, and A. B. Shapiro, *Soviet Physics-JETP Lett.*, **19**, 1 (1974).

Microwave Spectrum of *syn*-Acetaldehyde Oxime-*d*

Osamu OHASHI, Ryoji ISHIHARA, Kakuji MURAKAMI, Takeshi SAKAIZUMI, Masao ONDA, and Ichiro YAMAGUCHI

Department of Chemistry, Faculty of Science and Technology, Sophia University, Chiyoda-ku, Tokyo 102

(Received September 23, 1975)

The microwave spectrum of *syn*-acetaldehyde oxime-*d* was investigated in the frequency region 7.5~35 GHz. Several a-type R-branch transitions were identified and the following rotational constants in MHz were obtained: $A=45682$, $B=4057.21$, $C=3806.13$. The transitions of *syn*-acetaldehyde oxime-*d* are split into the A and E species by tunneling of the methyl group through the potential barrier hindering the internal rotation. From these separations the height of the barrier was determined to be 1948 cal mol^{-1}. The dipole moment of the molecule was determined to be 0.938 D from the Stark effect.

It has been found that acetaldehyde oxime has α- and β-modifications, which melt at 46.5 °C and 12 °C, respectively.[1] This molecule also has the two geometrical isomers whose conformations are *syn*- and *anti*-forms. The infrared spectrum of acetaldehyde oxime was investigated with attention to the effects of the geometrical isomerism.[2] The nuclear magnetic resonance study has revealed that the conformation change from one isomer to another is made easily.[3] Rogowski and Schwendeman studied the microwave spectrum of acetaldehyde oxime and have shown that the potential barrier hindering the internal rotation of the methyl group is abnormally low in the *anti*-form.[4]

We examined the microwave spectrum of *syn*-acetaldehyde oxime-*d* ($CH_3CH{=}NOD$) and determined the rotational constants, the potential barrier hindering the internal rotation of the methyl group, and the dipole moment. The orientation of the OH bond and the direction of the dipole moment of the molecule have been discussed, in conjunction with Rogowski's results for the normal species ($CH_3CH{=}NOH$).[4]

Experimental

Sample of acetaldehyde oxime obtained commercially (Tokyo Kasei Kogyo Co., Ltd.) was purified by trap-to-trap distillations several times *in vacuo*. No attempt was made to separate the *syn* and *anti* species; all the measurements were, consequently, made with the equilibrium mixture of the isomers. The deuterated species was prepared in the absorption cell as follows. First, the cell was filled with D_2O vapor at room temperature. It was then evacuated by vacuum pump for about half an hour. At the end of this time the sample of acetaldehyde oxime purified beforehand was admitted into the cell.

The spectrometer used was a conventional 100 kHz sinusoidal and square wave Stark modulation type with a phase sensitive detector. Because the sample apparently decomposed slowly at room temperature in the sample cell, the spectrum was observed at 0~−10 °C and the sample was renewed about every half an hour.

Results and Discussion

Observed Spectrum and Assignment. The structure of *syn*-acetaldehyde oxime-*d* was assumed to be the same as that of *syn*-acetaldehyde oxime (normal species) which has been considered to be a planar molecule. This assumption was based on the structural parameters for formaldehyde oxime determined by Levine[5] and the parameters fitted to the rotational constants B and C of the normal species.[4] The bond angles and bond distances assumed are given in Table 1. The projection of the molecule in its plane of symmetry is shown in Fig. 1(a). Although there are two possible orientations of the OH bond in this molecule, as shown in Figs. 1(a) and 1(b), the same orientation as that of formaldehyde oxime was assumed: that is, the OH bond is at the *trans* position relative to the C=N double bond. The assumed orientation of the OH bond will be discussed later. Frequencies of the rotational transitions were predicted from the moments of inertia calculated from the assumed structure. Substitution of a deuterium atom for the hydrogen atom of the hydroxyl group of *syn*-acetaldehyde oxime makes only a small change of the directions of the principal axes of the moment of inertia. Therefore, it was expected that the a-type R-branch transitions would be the most intense, as observed for the normal species.[4] In fact, only the a-type R-branch transitions have been observed and assigned. They were identified by their Stark effects. The b-type transitions were searched for, but there was no absorption line to be assigned as a b-type transition. This may suggest that the b-type transitions are quite weak because of

Table 1. Structural parameters assumed for *syn*-acetaldehyde oxime-d

$r(C_2{=}N)$	1.276 Å	∠N-O-D	102.68°
r(N-O)	1.408	$\angle C_2{=}N{-}O$	110.20°
r(O-D)	0.956	$\angle H{-}C_2{=}N$	121.77°
$r(C_2{-}H)$	1.085	$\angle H{-}C_1{-}H$	108.80°
$r(C_1{-}H)$	1.094	$\angle C_1{-}C_2{=}N$	119.34° [b]
$r(C_1{-}C_2)$	1.506[b]		

a) C_1=methyl carbon. b) Fitted to the rotational constants B and C of the normal species.[4]

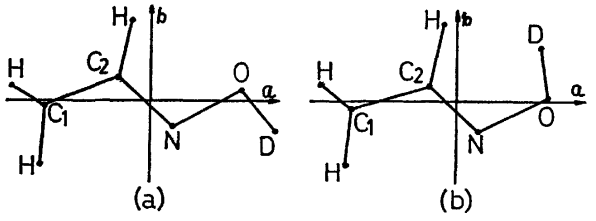

Fig. 1. Projection of *syn*-acetaldehyde oxime-*d* in its plane of symmetry.

Table 2. Observed transitions for *syn*-acetaldethyde oxime-*d* (A species)

$J \rightarrow J'$	ν_{obsd} (MHz)	$\Delta\nu$[a] (MHz)
$0_{00} \rightarrow 1_{01}$	7863.36	+0.03
$1_{11} \rightarrow 2_{12}$	15475.71	+0.13
$1_{01} \rightarrow 2_{02}$	15725.69	+0.16
$1_{10} \rightarrow 2_{11}$	15977.28	−0.45
$2_{12} \rightarrow 3_{13}$	23212.37	−0.30
$2_{02} \rightarrow 3_{03}$	23585.68	+0.22
$2_{11} \rightarrow 3_{12}$	23966.40	+0.51
$3_{13} \rightarrow 4_{14}$	30948.86	−0.05
$3_{03} \leftarrow 4_{04}$	31441.96	−0.03
$3_{12} \rightarrow 4_{13}$	31952.82	−0.37

a) $\Delta\nu = \nu_{obsd} - \nu_{calcd}$

Table 3. Observed and calculated rotational constants of *syn*-acetaldehyde oxime

	Observed (MHz)	Calculated I[a] (MHz)	Calculated II[b] (MHz)
Deuterated species			
A	45682±500	44281	44908
B	4057.20±0.04	4055.56	4334.09
C	3806.13±0.04	3804.51	3952.62
Normal species			
A	44613±385[c]	45511	42661
B	4237.73±0.03[c]	4236.84	4360.06
C	3973.81±0.03[c]	3973.20	4057.06

a) Calculated from the structure in Fig. 1(a).
b) Calculated from the structure in Fig. 1(b).
c) Ref. 4.

their small μ_b components, as described later.

The $K_{-1}=1$ absorption lines were split into A and E members by the internal rotation of the methyl group. The absorption lines of the A member showed the second-order Stark effect, while those of the E member showed the first-order Stark effect. Assuming the rigid rotor Hamiltonian, the rotational constants were fitted to the frequencies of the transitions belonging to the A symmetry species. A comparison of the observed and calculated frequencies is given in Table 2. The effective rotational constants obtained from the rigid rotor fit are in Table 3, together with the rotational constants calculated from the assumed structures.

Splittings of the lines due to the nuclear quadrupole moment of the ^{14}N nucleus were observed in the $1_{10} \rightarrow 2_{11}$ and $1_{11} \rightarrow 2_{12}$ transitions of the A member. Only one quadrupole coupling constant, $\chi_{aa}=3.5\pm0.7$ MHz, could be determined.

Barrier to Internal Rotation. The spectra of the A and E species can be treated with the Hamiltonian given by Herschbach.[6] *syn*-Acetaldehyde oxime-*d* is a near prolate symmetric top molecule with the axis of the internal rotation of the methyl group close to the principal a-axis. Therefore, the Hamiltonian for this molecule can be simplified.[4] Using the Hamiltonian including the perturbation terms up to third-order, the A-E splittings of the low J transitions can be fitted to a barrier-dependent parameter from which the barrier height V_3 may be obtained.[4,7]

The A-E splittings of the $K_{-1}=1$ lines were about 1 MHz for $J=2\rightarrow3$ transitions and about 4 MHz for $J=1\rightarrow2$ transitions. A value of the barrier height, 1948±100 cal mol^{-1}, was obtained by averaging the values of V_3 determined from each of the splittings of the $K_{-1}=1$ lines of the $J=1\rightarrow2$ and $J=2\rightarrow3$ transitions given in Table 4. The uncertainty, 100 cal mol^{-1}, was estimated by taking account of the uncertainties of the assumed parameters λ_a and I_α. But, because we took no account of the uncertainty of the moment of inertia I_a, the uncertainty obtained may have been underestimated. The barrier height of the deuterated species obtained in this work is higher by about 100 cal mol^{-1} than that of the normal species.

Principal Axis Coordinates of Hydroxyl Hydrogen Atom. The absolute values of the principal axis coordinates of the hydroxyl hydrogen atom were calculated from the moments of inertia of *syn*-acetaldehyde oxime and its deuterated species, using the expressions given by Kraitchman.[8] The conversion factor used was 505376 MHz·amu·Å^2. The value obtained for the a-coordinate is fairly good, while the value for the b-coordinate has a large error. In particular the c-coordinate could not be determined because of the negative square value of the c-coordinate. This may be attributed to the large uncertainty of the rotational constant A. The uncertainties given in Table 5 were calculated from the standard deviations of the rotational constants fitted to the observed frequencies.

From the results given in Tables 3 and 5, it seems reasonable to be led to the following conclusion: The plausible orientation of the OH bond is as shown in Fig. 1(a). The *trans* form as shown in Fig. 1(a) is consistent with the orientation of the OH bond in formalde-

Table 4. Internal-rotation splittings and barrier height for *syn*-acetaldehyde oxime-*d*

$J \rightarrow J'$	$(\nu_A-\nu_E)_{obsd}$ (MHz)	$(\nu_A-\nu_E)_{calcd}$ (MHz)	V_3 (cal mol^{-1})
$1_{11} \rightarrow 2_{12}$	−3.79	−3.73	1944.7
$1_{10} \rightarrow 2_{11}$	3.83	3.81	1945.8
$2_{12} \rightarrow 3_{13}$	−0.97	−0.94	1941.7
$2_{11} \rightarrow 3_{12}$	0.98	1.04	1958.2

Assumed internal-rotation parameters: $\lambda_a=0.9473$, $\lambda_c=0$, $I_\alpha=3.18$ amu·Å^2.

Table 5. Principal axis coordinates of the H atom of the hydroxyl group

	r_s-Coordinate	Assumed structure III[a]	Assumed structure IV[b]
a	2.379±0.016 Å	2.318 Å	1.515 Å
b	−0.13±0.32	−0.572	1.017
c	——	0	0

Uncertainties were estimated from the standard deviations of the rotational constants. See text.
a) Structure shown in Fig. 1(a). b) Structure shown in Fig. 1(b).

hyde oxime determined by Levine.[5]

Dipole Moment. The dipole moment was determined by measurements of the Stark shifts of the $0_{00}\rightarrow 1_{01}$, $1_{01}\rightarrow 2_{02}$, $2_{02}\rightarrow 3_{03}$, and $3_{03}\rightarrow 4_{04}$ absorption lines. The electric field in the absorption cell was calibrated by measurements of the Stark shifts of the $J=0\rightarrow 1$ and $J=1\rightarrow 2$ absorption lines of OCS. The dipole moment of OCS is 0.71521 D.[9]

The observed and calculated Stark coefficients are given in Table 6. Assuming that the molecule has a plane of symmetry and the component of the dipole moment along the axis perpendicular to the plane of symmetry is zero, we obtained $\mu_a=0.865\pm0.004$ D, $\mu_b=0.363\pm0.015$ D, and $\mu_{total}=0.938\pm0.009$ D. The uncertainties are the standard deviations obtained by the least square fit. The value of μ_{total} obtained in this work is in good agreement with that of *syn*-acetaldehyde oxime.[4]

If it is assumed that the structure of the deuterated species is exactly the same as that of the normal species and its structural parameters are as given in Table 1,

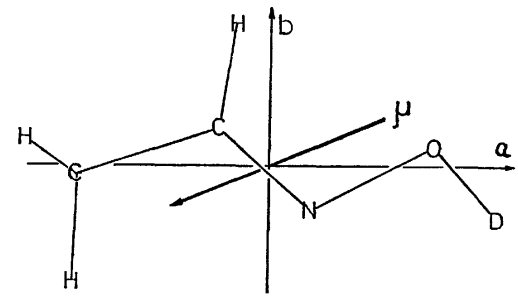

Fig. 2. Orientation of the dipole moment in *syn*-acetaldehyde oxime-*d* molecule.

the orientation of the dipole moment in the molecule can be determined. From the compositions of the dipole moments of normal and deuterated species along the principal axes, the direction of the dipole moment in the molecule was determined as shown with a thick line in Fig. 2. The angle between the dipole moment and the NO bond is 8.09°.

Table 6. Stark effect and dipole moment of *syn*-acetaldehyde oxime-*d*

$J\rightarrow J'$	|M|	$(\partial\nu/\partial E^2)_{obsd}$[a] MHz(V cm^{-1})$^{-2}$	$(\partial\nu/\partial E^2)_{calcd}$[b] MHz(V cm^{-1})$^{-2}$
$0_{00}\rightarrow 1_{01}$	0	12.97×10^{-6}	12.97×10^{-6}
$1_{01}\rightarrow 2_{02}$	0	−3.665	−3.645
	1	3.130	3.142
$2_{02}\rightarrow 3_{03}$	0	−0.480	−0.689
	1		−0.219
	2	1.147	1.191
$3_{03}\rightarrow 4_{04}$	1	0.222	0.296

a) Based on $\mu(OCS)=0.71521$ D.[9] b) Calculated assuming $|\mu_a|=0.865$ D, $|\mu_b|=0.363$ D, and $|\mu_c|=0$.

References

1) W. R. Dunstan and T. S. Dymond, *J. Chem. Soc.*, **61**, 470 (1892).
2) D. Hadži and L. Premru, *Spectrochimica Acta*, **23A**, **35** (1967).
3) G. J. Karabatsos and R. A. Taller, *Tetrahedron*, **24**, 3347 (1968).
4) R. S. Rogowski and R. H. Schwendeman, *J. Chem. Phys.*, **50**, 397 (1969).
5) I. N. Levine, *J. Chem. Phys.*, **38**, 2326 (1963).
6) D. R. Herschbach, *J. Chem. Phys.*, **31**, 91 (1959).
7) R. W. Kilb and L. Pierce, *J. Chem. Phys.*, **27**, 108 (1957).
8) J. Kraitchman, *Am. J. Phys.*, **21**, 17 (1953).
9) D. Muenter, *J. Chem. Phys.*, **48**, 4544 (1968).

Activity Coefficients of Hydrochloric Acid in Hydrogen Chloride-Metal Perchlorate-Water Systems

Kiichi TERUYA, Kikuo SHIRAOGAWA, and Issei NAKAMORI

Department of Chemical Engineering, Faculty of Engineering, Kyushu University, Hakozaki, Fukuoka 812

(Received September 30, 1975)

In the HCl–$LiClO_4$–H_2O, HCl–$NaClO_4$–H_2O, HCl–$Mg(ClO_4)_2$–H_2O, HCl–$Ba(ClO_4)_2$–H_2O, HCl–$LiClO_4$–$NaClO_4$–H_2O, HCl–$NaClO_4$–$Ba(ClO_4)_2$–H_2O, and HCl–$LiClO_4$–$NaClO_4$–$Ba(ClO_4)_2$–H_2O systems, the mean activity coefficients of hydrochloric acid, $\gamma_{\pm HCl}$, have been obtained at 25 °C by emf measuremts of the cell:

$$H_2(Pt)/HCl,\ MClO_4,\ M'(ClO_4)_2,\cdots/AgCl,\ Ag \quad (M=Li,\ Na;\ M'=Mg,\ Ba)$$

Moreover, the following relation has been examined with the experimental results:

$$\log \gamma_{\pm HCl} = \log \gamma^{\circ}_{\pm HCl} + \sum_i a_{i(HCl)} m_i \qquad (i \neq H, Cl)$$

where $\gamma^{\circ}_{\pm HCl}$ is the mean activity coefficient of hydrochloric acid in a solution containing only hydrochloric acid at the same ionic strength as the mixture; m_i is the molality of the i ion, and $a_{i(HCl)}$ is the parameter assigned to the three-ion system of hydrogen, chloride, and i ions, but is independent of the ionic strength. The results of the examination with $a_{M(HCl)}$ determined in our previous paper showed that $a_{ClO_4(HCl)}$ may be about zero regardless of the kind of metal ion coexisting in the solution. The activity coefficients calculated by the above relationship with the determined parameters agree, with deviation of only about 5%, with the experimental results for all the systems.

While a considerable amount of information is available about the activity coefficients in single electrolyte solutions,[1,2] experimental data on the activity coefficients in multicomponent electrolyte solutions are difficult to obtain and relatively few direct measurements have been reported. The activity coefficients in multicomponent electrolyte solutions are, however, important as fundamental data for the treatment of chemical processes, since most electrolyte solutions commonly encountered in chemical industry are multicomponent electrolyte solutions. Most of the direct measurements in the past have been limited to the hydrogen chloride–metal chloride–water systems.[3] Data on hydrogen chloride–metal perchlorate–water systems have been reported only by Bates and Urmston,[4] Prue and Read,[5] Stokes and Stokes,[6] and Weeks,[7] and most of these data are within the limits of low concentrations of hydrochloric acid.

Although many theoretical treatments of the properties of multicomponent electrolyte solutions have been proposed by various authors,[3,8–10] the principal object in these treatments has been the consideration of the interionic forces. As a result, the expressions for the activity and osmotic coefficients in multicomponent electrolyte solutions are complicated in form and contain a number of parameters which are functions of the ionic strength and so are cumbersome for engineering calculations.

In their previous papers, therefore, the present authors proposed a simple and convenient method of estimating the activity coefficients in multicomponent electrolyte solutions for use in engineering calculations[11] and showed that satisfactory results could be obtained when the method was applied to examinations of the activity coefficients of hydrochloric acid in hydrogen chloride–metal chloride–water systems.[12] The object here is to obtain the mean activity coefficients of hydrochloric acid at 25 °C by emf measurements in aqueous solutions containing one or more perchlorates of metal (lithium, sodium, magnesium, or barium) over a wide range of concentrations of hydrochloric acid and to a high total ionic strength, and to examine the method of estimation in these systems containing perchlorate ions on the basis of the experimental results.

Theoretical

The total excess Gibbs energy of an electrolyte solution may be dominated by the effect of the long-range electrostatic forces of the Debye-Hückel type, and the contributions due to the short-range forces resulting from ion–ion and ion–solvent interactions may be added to it with the increase in the concentrations of the solute species. In a previous paper,[11] by assuming that the short-range forces may be independent of the ionic strength, the following method was obtained for the estimation of the activity coefficients of a strong electrolyte 12, $\gamma_{\pm 12}$, in a solution containing 1, 2, ···, i (odd : cation, even : anion) ions:

$$\log \gamma_{\pm 12} = \log \gamma^{\circ}_{\pm 12} + \sum_i a_{i(12)} m_i \qquad (i \neq 1, 2) \qquad (1)$$

where $\gamma^{\circ}_{\pm 12}$ is the mean activity coefficient of the electrolyte 12 in a solution containing only 12 at the same ionic strength as the mixture; m_i is the molality of the i ion and $a_{i(12)}$ is the parameter assigned to the three-ion system of the 1, 2, and i ions. As a result of the assumption used in the derivation of Eq. (1), this parameter may be independent of the ionic strength and the ions coexisting in the solution other than 1, 2 and i. In this treatment, molality scales are used for the concentrations of the ion and the electrolyte and the activity coefficients of the electrolyte.

In the hydrogen chloride (HCl)–metal perchlorate ($M(ClO_4)_n$)–water systems, the activity coefficients of hydrochloric acid, $\gamma_{\pm HCl}$, are given by Eq. (1) as 1=H, 2=Cl, 3=M, and 4=ClO_4 as follows:

$$\log \gamma_{\pm HCl} = \log \gamma^{\circ}_{\pm HCl} + a_{M(HCl)} m_{M^{n+}} + a_{ClO_4(HCl)} m_{ClO_4^-} \qquad (2)$$

or:

$$\log (\gamma_{\pm HCl}/\gamma^{\circ}_{\pm HCl}) = [a_{M(HCl)} + n a_{ClO_4(HCl)}] m_{M(ClO_4)_n} \qquad (3)$$

A considerable amount of information is available about the activity coefficients of hydrochloric acid in the solutions containing only hydrochloric acid, $\gamma^{\circ}_{\pm HCl}$,

required in this treatment.[1,2] If this treatment is appropriate, $\log(\gamma_{\pm HCl}/\gamma^{\circ}_{\pm HCl})$ may be expected to vary linearly with $m_{M(ClO_4)_n}$.

On the other hand, $a_{M(HCl)}$ has been determined for various metal ions in investigations of the hydrogen chloride–metal chloride–water systems at 25 °C. The values are shown in Table 1.[12] It is, therefore, convenient to rewrite Eq. (2) as follows:

$$[\log(\gamma_{\pm HCl}/\gamma^{\circ}_{\pm HCl}) - a_{M(HCl)}m_{M^{n+}}] = a_{ClO_4(HCl)}m_{ClO_4^-} \quad (4)$$

Thus, if the parameter for the perchlorate ion, $a_{ClO_4(HCl)}$, may be independent of the ionic strength and the coexisting metal ion, M^{n+}, a straight line may be obtained by the plots of the left-hand side of Eq. (4) against $m_{ClO_4^-}$ and $a_{ClO_4(HCl)}$ can be determined from the slope of the resultant straight line. Therefore, the activity coefficients of hydrochloric acid in aqueous solutions containing more than one metal perchlorate may be evaluated by means of Eq. (1) using the $a_{M(HCl)}$ and $a_{ClO_4(HCl)}$ values determined in this work and the previous one.[12]

Experimental

The activity coefficients of hydrochloric acid in the hydrogen chloride–metal perchlorate–water systems were obtained by means of emf measurements of the following cell:

$$Pt(H_2)/HCl(m_1), MClO_4(m_2), M'(ClO_4)_2(m_3),\cdots/AgCl, Ag$$
$$(M=Li, Na; M'=Mg, Ba)$$

The techniques and equipment used for the emf measurements were the same as has been described in detail previously.[13] The emf measurements were made at 25.00±0.05 °C. The emf values were reproducible to within about ±0.05 mV. The following systems were investigated: HCl–$LiClO_4$–H_2O, HCl–$NaClO_4$–H_2O, HCl–$Mg(ClO_4)_2$–H_2O, HCl–$Ba(ClO_4)_2$–H_2O, HCl–$LiClO_4$–$NaClO_4$–H_2O, HCl–$NaClO_4$–$Ba(ClO_4)_2$–H_2O, and HCl–$LiClO_4$–$NaClO_4$–$Ba(ClO_4)_2$–H_2O. The reagents used in this work were special-grade and were used without further purification.

In the above-mentioned cell, the emf values corrected to 1.00 atm of hydrogen pressure, E, are expressed by the Nernst equation as follows:

$$E = E^{\circ} - (2RT/F)\ln(m_1\gamma_{\pm HCl}) \quad (5)$$

where E° is the standard potential of the Ag–AgCl electrode and where m_1 is the molality of hydrochloric acid, while T is the absolute temperature; R, the gas constant and F, the Faraday. 0.22234 (V) has been given as the value of E° by Bates and Bower;[14] this value was used in this work. The emf values shown as the results are corrected to a hydrogen pressure of 1.00 atm. Using Eq. (5), the activity coefficients of hydrochloric acid, $\gamma_{\pm HCl}$ (exp), were obtained.

Results and Discussion

The outlines of experimental conditions in the past[4–7] and in this work on the hydrogen chloride–metal perchlorate–water systems at 25 °C are summarized in Table 2. While the data in the past were obtained at low concentrations of hydrochloric acid from 0.01 to 0.1 mol kg^{-1}, these data were used also for the examinations of Eq. (3) or (4).

The experimental data and the calculated results in the three-component systems, HCl–$LiClO_4$–H_2O, HCl–$NaClO_4$–H_2O, HCl–$Mg(ClO_4)_2$–H_2O, and HCl–$Ba(ClO_4)_2$–H_2O, are shown in Table 3. The data in these systems are plotted in Figs. 1 and 2 on the basis of Eq. (3). The literature values are also plotted in these figures. Figures 1 and 2 show that a straight line is obtained by these plots for each system and that the parameters, $a_{M(HCl)}$ and $a_{ClO_4(HCl)}$, may be regarded as approximately independent of the ionic strength; therefore, the treatments on the basis of Eq. (1) may be approximately appropriate.

Plots drawn on the basis of Eq. (4) are shown in Fig. 3. All the data are scattered on the zero axis. It shows that $a_{ClO_4(HCl)}$ seems to be about zero, regardless of the kind of metal ion coexisting in the solution.

The values calculated by Eq. (2) with $a_{M(HCl)}$ in Table 1 and the $a_{ClO_4(HCl)}$ determined above, and the percentage deviations between the experimental and the

Table 1. Parameters, $a_{M(HCl)}$, assigned to the three-ion systems at 25 °C[12]

Metal ion, M	Li^+	Na^+	K^+	Rb^+	Cs^+	Mg^{2+}	Ca^{2+}	Sr^{2+}	Ba^{2+}	Al^{3+}	La^{3+}	Ce^{3+}
$-a_{M(HCl)}$/mol^{-1} kg	0.003	0.030	0.061	0.090	0.100	0.126	0.157	0.170	0.200	0.374	0.499	0.559

Table 2. Systems investigated for the correlation (25 °C)

No.	System	Number of Data	m_{HCl} / mol kg^{-1}	$m_{M(ClO_4)_n}$ / mol kg^{-1}	I_T[a] / mol kg^{-1}	Reference
1	HCl-$LiClO_4$-H_2O	5	0.4454—0.9162	0.4612—2.3845	0.9492—3.2284	This work
2	HCl-$NaClO_4$-H_2O	16	0.0481—1.9553	0.0504—5.0697	0.0989—5.5789	This work
		12	0.05—0.25	0.05—0.95	0.10—1.00	Bates, *el al.*[4]
		16	0.0041—0.2124	2.4621—2.8545	2.8543—3.0543	Prue, *et al.*[5]
3	HCl-$KClO_4$-H_2O	5	0.0994	0.0132—0.1219	0.1126—0.2213	Bates, *et al.*[4]
4	HCl-$Mg(ClO_4)_2$-H_2O	11	0.4543—0.9596	0.0850—1.7331	0.7381—6.0923	This work
5	HCl-$Ca(ClO_4)_2$-H_2O	7	0.0108	0.0369—1.1063	0.1215—3.3297	Stokes, *et al.*[6]
6	HCl-$Sr(ClO_4)_2$-H_2O	8	0.0101	0.0237—1.145	0.0812—3.4451	Weeks[7]
7	HCl-$Ba(ClO_4)_2$-H_2O	11	0.4793—1.4630	0.2096—3.0325	1.9383—10.108	This work
		12	0.0101	0.0138—1.3169	0.0515—3.9608	Weeks[7]

a) Total ionic strength.

Table 3. Activity coefficients of hydrochloric acid in the three-component systems at 25 °C

m_1 / mol kg^{-1}	m_2 / mol kg^{-1}	I_T[a] / mol kg^{-1}	E / mV	$\gamma_{\pm HCl}$ (exptl)	$\gamma^0_{\pm HCl}$	$\gamma_{\pm HCl}$ (calcd)	Dev. / %
		(A)	$HCl(1)-LiClO_4(2)-H_2O$ System				
0.4880	0.4612	0.9492	271.15	0.792	0.802	0.799	0.9
0.4617	1.4312	1.8929	263.18	0.978	0.983	0.973	−0.5
0.4454	2.0309	2.4763	257.00	1.144	1.140	1.124	−1.7
0.9162	1.0093	1.9255	226.71	1.002	0.991	0.984	−1.8
0.8439	2.3845	3.2284	212.21	1.443	1.408	1.385	−4.0
		(B)	$HCl(1)-NaClO_4(2)-H_2O$ System				
0.0485	0.0504	0.0989	389.42	0.799	0.797	0.794	−0.6
0.0485	0.4778	0.5263	392.88	0.747	0.759	0.734	−1.7
0.0485	0.9832	1.0317	391.18	0.772	0.814	0.760	−1.6
0.0485	2.0970	2.1455	381.63	0.929	1.049	0.908	−2.3
0.0481	3.4488	3.4969	368.62	1.206	1.517	1.195	−0.9
0.0481	4.9907	5.0388	351.26	1.691	2.410	1.707	0.9
0.5092	0.5117	1.0209	268.90	0.793	0.812	0.784	−1.1
0.5092	1.0127	1.5219	264.27	0.868	0.900	0.840	−3.2
0.5092	2,5993	3.1085	249,20	1.134	1.360	1.136	−0.2
0.5092	3.8091	4.3183	236.47	1.491	1.939	1.490	−0.1
0.5092	5.0697	5.5789	221.23	2.006	2.841	2.002	−0.2
0.9300	3.5785	4.5085	200.81	1.634	2.093	1.635	0.1
0.9300	3.6673	4.5973	199.44	1.679	2.102	1.632	−2.8
1.9553	1.0342	2.9895	176.00	1.261	1.313	1.222	−3.1
1.9553	2.2952	4.2505	161.17	1.682	1.901	1.623	−3.5
1.9553	3.6216	5.5769	145.75	2.271	2.839	2.211	−2.6
		(C)	$HCl(1)-Mg(ClO_4)_2-H_2O$ System				
0.4545	1.4158	4.7017	243.33	1.463	2.177	1.444	−1.3
0.4646	0.9124	3.2018	258.42	1.067	1.398	1.073	0.6
0.4739	0.4348	1.7783	269.32	0.846	0.955	0.842	−0.5
0.4831	0.0850	0.7381	274.16	0.755	0.776	0.757	−0.3
0.8779	1.1836	4.4287	212.66	1.375	2.006	1.423	3.5
0.8930	1.7331	6.0923	190.28	2.090	3.312	2.003	−4.2
0.9012	0.6601	2.8815	225.44	1.045	1.274	1.052	0.7
0.9128	0.3915	2.0873	230.48	0.935	1.032	0.921	−1.5
0.9179	1.2168	4.5683	205.91	1.500	2.096	1.473	−1.8
0.9355	0.7302	3.1262	220.05	1.118	1.367	1.060	−1.1
0.9596	0.2623	1.7465	230.75	0.885	0.948	0.879	−0.7
		(D)	$HCl(1)-Ba(ClO_4)_2-H_2O$ System				
0.4793	0.7701	2.7896	266.62	0.875	1.245	0.873	−0.2
0.4793	1.7334	5.6795	247.86	1.269	2.920	1.314	3.5
1.0101	0.3094	1.9383	228.81	0.873	0.994	0.862	−1.3
1.0101	0.8047	3.4242	220.40	1.028	1.487	1.027	−0.1
1.0101	1.3142	4.9527	210.91	1.237	2.348	1.287	3.6
1.0101	1.8327	6.5082	197.79	1.597	3.804	1.636	2.4
1.0101	2.5450	8.6451	181.65	2.186	7.216	2.235	2.2
1.0101	3.0325	10.108	174.41	2.517	10.70	2.648	5.2
1.4630	0.2096	2.0918	205.02	0.958	1.034	0.939	−2.0
1.4630	1.1614	4.9472	186.05	1.386	2.344	1.373	−0.9
1.4630	1.8091	6.8903	172.40	1.807	4.230	1.839	1.8

a) Total ionic steength.

calculated values are shown in Table 3 as $\gamma_{\pm HCl}$(calcd) and Dev. %($=100[\gamma_{\pm HCl}(\text{calcd})-\gamma_{\pm HCl}(\text{exptl})]/\gamma_{\pm HCl}$ (exptl)). The Dev.% in these systems are within about 5% over a wide range of ionic strengths, similar results were obtained for the data in the past.[4-7]

The experimental data and calculated results in the four-component systems, $HCl-LiClO_4-NaClO_4-H_2O$, and $HCl-NaClO_4-Ba(ClO_4)_2-H_2O$, are shown in Table 4, while the results in the five-component system, $HCl-LiClO_4-NaClO_4-Ba(ClO_4)_2-H_2O$, are given in Table 5. In the four- and five-component systems, the values calculated by means of Eq. (1)

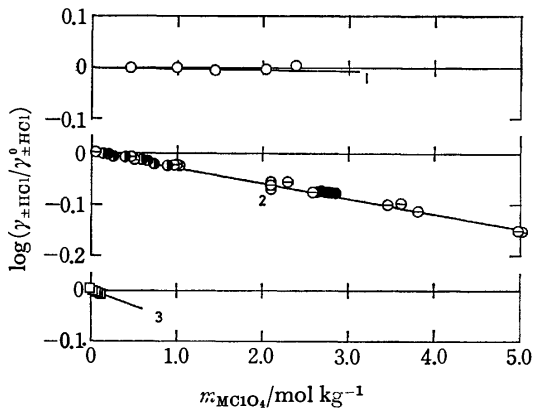

Fig. 1. Activity coefficients of hydrochloric acid in the hydrogen chloride-alkali metal perchlorate-water systems at 25 °C.
1: HCl-$LiClO_4$-H_2O System (○: This work).
2: HCl-$NaClO_4$-H_2O System (⊖: This work, ◑: Bates, *et al.*,[4] ●: Prue, *et al.*[5]).
3: HCl-$KClO_4$-H_2O System (□: Bates, *et al.*[4]).

with the parameters mentioned also agree with the experimental results within about 5%.

In the treatments of the activity coefficients in the three-component systems, *i.e.*, in the solutions containing two electrolytes, the method based on Eq. (1) is similar to the Harned-rule[15] in form. However, the Harned-rule is restricted to the treatments of the three-component systems; furthermore, its parameters are treated as the functions of the ionic strength, while the parameters, $a_{i(12)}$, in Eq. (1) may be treated independently of the ionic strength and the coexisting ions other than 1, 2, and i ions because Eq. (1) has been derived on the assumption that the short-range forces may be independent of the ionic strength. As a result, this method may be expanded to treatments of solutions containing more than two electrolytes.

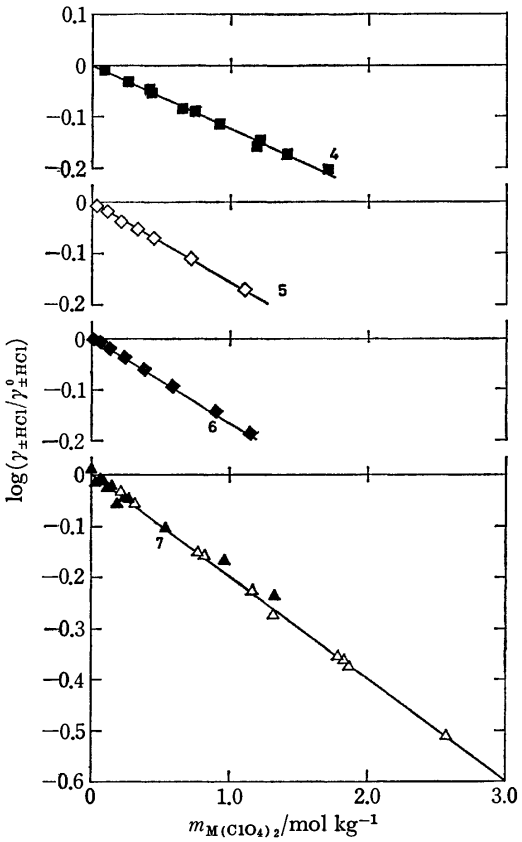

Fig. 2. Activity coefficients of hydrochloric acid in the hydrogen chloride-alkaline earth metal perchlorate-water systems at 25 °C.
4: HCl-$Mg(ClO_4)_2$-H_2O System (■: This work).
5: HCl-$Ca(ClO_4)_2$-H_2O System (◇: Stokes, *et al.*[6]).
6: HCl-$Sr(ClO_4)_2$-H_2O System (◆: Weeks[7]).
7: HCl-$Ba(ClO_4)_2$-H_2O System (△: This work, ▲: Weeks[7]).

TABLE 4. ACTIVITY COEFFICIENTS OF HYDROCHLORIC ACID IN THE FOUR-COMPONENT SYSTEMS AT 25 °C

m_1 / mol kg^{-1}	m_2 / mol kg^{-1}	m_3 / mol kg^{-1}	I_T[a] / mol kg^{-1}	E / mV	$\gamma_{\pm HCl}$ (exptl)	$\gamma^0_{\pm HCl}$	$\gamma_{\pm HCl}$ (calcd)	Dev. / %
		(A)	HCl(1)-$LiClO_4$(2)-$NaClO_4$(3)-H_2O System					
0.4503	1.4143	0.5396	2.4042	258.92	1.090	1.121	1.069	−1.9
0.4610	1.0096	1.0523	2.5229	258.20	1.079	1.155	1.067	−1.1
0.4730	0.5560	1.5887	2.6177	257.12	1.074	1.187	1.060	−1.3
0.9756	1.4395	0.4940	2.9091	212.13	1.250	1.285	1.230	−1.6
1.0107	0.8278	0.8728	2.7113	215.20	1.137	1.218	1.140	0.3
1.0293	0.5035	1.6568	3.1896	208.99	1.260	1.393	1.238	−1.7
		(B)	HCl(1)-$NaClO_4$(2)-$Ba(ClO_4)_2$(3)-H_2O System					
0.4793	1.8108	0.5100	3.8201	252.04	1.170	1.674	1.168	−0.2
0.4793	0.4118	1.0126	3.9289	258.01	1.042	1.727	1.053	1.1
0.4793	1.5257	1.0062	5.0236	245.55	1.328	2.397	1.357	2.2
0.9692	0.5231	0.5121	3.0286	222.43	1.030	1.328	1.012	−1.7
0.9692	1.4651	0.4226	3.7021	213.90	1.216	1.617	1.203	−1.1
0.9692	0.3969	0.9096	4.0949	216.40	1.158	1.815	1.162	0.3
1.4630	0.8105	0.2170	2.9245	195.63	1.149	1.290	1.104	−3.9
1.4630	0.5189	0.5134	3.5221	193.08	1.208	1.529	1.165	−3.6
1.4630	0.4479	0.9292	4.6985	185.68	1.395	2.175	1.375	−1.4

a) Total ionic strength.

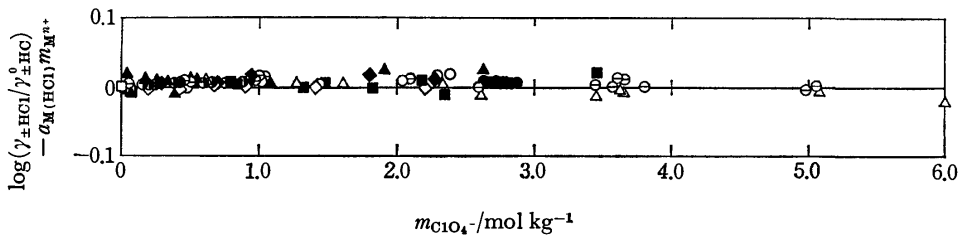

Fig. 3. Determination of parameter for perchlorate ion, $a_{ClO_4(HCl)}$. Symbols are identical with those in Figs. 1 and 2.

Table 5. Activity coefficients of hydrochloric acid in the five-component system, HCl(1)-$LiClO_4$(2)-$NaClO_4$(3)-$Ba(ClO_4)_2$(4)-H_2O, at 25 °C

m_1 / mol kg^{-1}	m_2 / mol kg^{-1}	m_3 / mol kg^{-1}	m_4 / mol kg^{-1}	I_T[a] / mol kg^{-1}	E / mV	$\gamma_{\pm HCl}$ (exptl)	$\gamma^0_{\pm HCl}$	$\gamma_{\pm HCl}$ (calcd)	Dev. / %
0.4626	0.8731	0.9302	0.2815	3.1104	254.78	1.150	1.357	1.111	−3.4
0.4636	0.8290	1.2928	0.1870	3.1464	252.91	1.190	1.371	1.143	−3.9
0.4690	0.5701	0.7797	0.7994	4.2170	249.35	1.260	1.881	1.229	−2.5
0.4791	0.2283	0.5967	0.5687	3.0102	259.57	1.011	1.320	0.973	−3.8
1.0286	0.5151	0.4827	0.4922	3.5030	212.52	1.177	1.519	1.167	−0.8
1.0324	0.4490	0.8280	0.2967	3.1995	213.68	1.146	1.397	1.147	0.1

a) Total ionic strength.

As a matter of course, it seems that the short-range forces may be independent of the ionic strength; the results in a previous[12] and in this one show that indeed the $a_{i(12)}$ values are approximately independent of the ionic strength over a wide range and that the effects on $a_{i(12)}$ of the coexisting ions other than 1, 2, and i ions can generally be ignored. Moreover, the parameters which can be determined easily in the simpler systems containing three or four ions may be applied to the more complicated systems. It should also be noted that this method may be used, with errors in estimation within about 5%, over a wide range of ionic strengths. Although the examinations using this method in this work were made only on the activity coefficients of hydrochloric acid, yet this method may be useful in evaluating that of the other strong electrolytes in multicomponent electrolyte solutions. The method based on Eq. (1) may, therefore, be a convenient one for evaluating the activity coefficients in multicomponent electrolyte solutions for use in engineering calculations.

References

1) H. S. Harned and B. B. Owen, "The Physical Chemistry of Electrolytic Solutions," 3rd ed., Reinhold, New York (1958).
2) R. A. Robinson and R. H. Stokes, "Electrolyte Solutions," 2nd ed. (revised), Butterworths, London (1968).
3) H. S. Harned and R. A. Robinson, "Multicomponent Electrolyte Solutions," Pergamon Press, London (1968).
4) S. J. Bates and J. W. Urmston, *J. Am. Chem. Soc.*, **55**, 4058 (1933).
5) J. E. Prue and A. J. Read, *J. Chem. Soc., A*, **1966**, 1812.
6) J. M. Stokes and R. H. Stokes, *J. Phys. Chem.*, **67**, 2242 (1963).
7) I. A. Weeks, *Aust. J. Chem.*, **20**, 2367 (1967).
8) G. Scatchard, R. M. Rush, and J. S. Johnson, *J. Phys. Chem.*, **74**, 3876 (1970).
9) P. J. Reilly, R. H. Wood, and R. A. Robinson, *J. Phys. Chem.*, **75**, 1305 (1971).
10) K. S. Pitzer, *J. Phys. Chem.*, **77**, 268 (1973).
11) K. Teruya and I. Nakamori, *Technol. Rep. Kyushu Univ.*, **48**, 267 (1975).
12) K. Teruya, T. Mori, and I. Nakamori, *Kagaku Kogaku Ronbunshu*, **2**, 91 (1976).
13) K. Teruya, T. Mori, K. Shiraogawa, F. Noguchi, and I. Nakamori, *Technol. Rep. Kyushu Univ.*, **48**, 507 (1975).
14) R. G. Bates and V. E. Vower, *J. Res. Nat. Bur. Stand.*, **53**, 283 (1954).
15) H. S. Harned, *J. Am. Chem. Soc.*, **57**, 1865 (1935).

Properties of Water Solubilized in Reversed Micellar Systems of Dodecylammonium Propionate in Nonpolar Solvents

Manabu SENŌ, Koji ARAKI, and Shinsaku SHIRAISHI

Institute of Industrial Science, University of Tokyo, Roppongi 7-22, Minato-ku, Tokyo 106

(Received October 4, 1975)

The properties of the reversed micelles of dodecylammonium propionate(DAP) and of solubilized water were examined for systems with hexane, chloroform and benzene as a nonpolar component. The aggregation number of DAP, the conductivity, the heat of solution of water, IR and NMR spectra, and near infrared spectra of solubilized water were measured. From the results the properties of the reversed micellar system were analyzed, the following conclusion being obtained. The aggregation state of DAP is scarcely affected by the addition of water. Water is first dispersed in the nonpolar organic phase, and then solubilized in the cores of the reversed micelles. The former is free or weakly bonded water, while the latter is bonded water like that in the bulk phase. The catalytic effect of DAP reversed micellar system is discussed.

Surfactant micelle catalyzes various reactions and serves as a model for the enzyme action. Fendler *et al.* observed that reversed micelles in nonpolar solvents significantly catalyze several reactions, and suggested that this could provide a favorable model for a microenvironment of enzyme active sites.[1] They also suggested that the water solubilized in the polar cavities of reversed micelles is less polar than the water in the bulk phase, which is closely related to the catalytic effect of the reversed micellar systems.[2,3]

We investigated the hydrolysis of adenosine 5'-triphosphate (ATP) in a reversed micellar system where an aqueous ATP phase is solubilized in hexane by dodecylammonium propionate (DAP), and found that the hydrolysis rate in this system is enhanced several times as compared with that in an aqueous system.[4] This reversed micellar system shows an enzyme-like behavior such that the addition of Mg^{2+} or Ca^{2+} enhances markedly the hydrolysis rate, suggesting that the rate enhancement is closely related to the polarity of the water solubilized in the reversed micelles. It is of interest to investigate by more direct methods the properties of the DAP reversed micelles and the solubilized water in relation to the catalytic activities of these systems.

Experimental

Materials. The preparation and purification of dodecylammonium propionate (DAP) were described previously;[4] mp 55—56 °C (Lit, 54—56 °C[5]); Found (Calcd), C, 69.68(69.44); H, 12.38 (12.82); N, 5.32 (5.40)%. Dodecyltrimethylammonium acetate (DTAA) was prepared by the anion exchange reaction of dodecyltrimethylammonium chloride with silver acetate in a 1-propanol-water mixed solvent, and was purified and dried three times by freeze-drying from its benzene solution. The structure and purity were confirmed by IR and NMR spectra and elementary analysis; Found (Calcd): C, 70.24 (71.02); H, 13.10 (12.97), N, 4.75 (4.87)%. Distilled water with conductivity below 10^{-7} mho·cm^{-1}, was used.

Measurements. Conductivity of solutions was measured with a Toa conductmeter model CM-2A equipped with a CG-7001PL cell, the sensitivity being 10^{-7} mho·cm^{-1}. The sample solution was stirred and maintained at 35.0 °C. Vapor pressure osmometric measurements (VPO) were made at 37.0 and 50.0 °C with a Hewlett-Packard vapor pressure osmometer model 302B.

Infrared spectra were recorded with a Jasco IRA-2 spectrometer at room temperature using a pair of cells of 0.05 mm in path length. The reference cell was filled with solvent in order to record spectra of DAP micellar solutions. Near infrared spectra were recorded with a Hitachi spectrophotometer model EPS-3T. The absorption cells were 10 mm in light path and thermostatted at 35.0 °C. A solution containing DAP of the same concentration as that of the sample solution was used as a reference, in order to record the spectra of water solubilized in the reversed micellar system.

The 90 MHz proton nuclear magnetic resonance spectra were taken with a Hitachi R-22 high-resolution spectrometer at 35 °C. The chemical shifts were recorded by using TMS as an internal standard. A coaxial double tube was used for measurements of spectra of water in DTAA reversed micellar system; pure water was contained in the inner tube as an external standard, and the sample solution in the outer tube.

The heat of solution was measured with a Tokyo Riko twin-isothermal calorimeter at 35.0 °C. The water was sealed in a glass ampoule, and after attaining thermal equilibrium the ampoule was crushed into the sample solution. The temperature difference between the sample cell and reference cell was detected by a thermocouple, and calibrated against a standard electric heater.

Results and Discussion

Conductivity of the Systems. Conductivity of DAP reversed micellar systems with hexane, chloroform, and benzene as a nonpolar component was measured at 35.0 °C. The results are shown in Fig. 1 as a function of water concentration. A break point observed in each conductivity curve coincides with

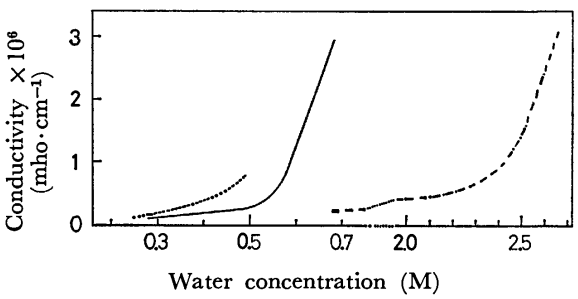

Fig. 1. Conductivities of the DAP (0.2 M) reversed micellar systems at 35.0 °C in hexane (——), chloroform (----), and benzene (-·-·).

the water concentration where a homogeneous solution becomes heterogeneous. At water concentrations below the break point this curve gives the conductivity of homogeneous DAP reversed micellar solution, the values lying within *ca.* 10^{-7}—10^{-6} mho·cm^{-1}. When an aqueous electrolyte solution (0.1 M sodium acetate) was used instead of pure water, the conductivity of the system remained nearly the same. It is thus evident that the conductivity in this concentration range is due to DAP in the system. Increase in water content scarcely affects the association state of DAP. However, the conductivity increases abruptly at water concentrations above the break point. By considering the large values of conductivity, this increase is thought to be caused by the dissociation of DAP salt in water phase which is not solubilized.

The amount of water that could be solubilized in each solution determined from the conductivity measurement is given in Table 1. The value for the benzene solution is almost the same as that reported by Kitahara[5] and Kon-no and Kitahara.[6]

Aggregation Numbers of DAP. Aggregation numbers of DAP in the reversed micellar systems were estimated from the average molecular weights of micelles determined by VPO. In these measurements, it was assumed that the vaporization of water solubilized in DAP reversed micelles is neglected in the range where the amount of water is comparable to that of DAP. The results are shown as a function of water concentration (Fig. 2). The values obtained are nearly the same as those determined by Seoud *et al.* through the NMR method for the systems in benzene, chloroform and carbon tetrachloride in the absence of water.[7] The aggregation number of DAP in the reversed micellar system is much smaller than that in aqueous micelles, the amount of water added scarcely affecting the value. This would mean that the addition of water does not alter significantly the aggregation state of DAP.

Infrared Spectra and Near Infrared Spectra. The effect of water concentration on IR spectra of DAP in the reversed micellar system was examined. It was found that the absorption band of asymmetric stretching of carboxylate anion shifts to a lower wave number side with an increase in water concentration (Table 2). This would indicate that the solubilized water interacts with the carboxylate group of DAP. No further information could be obtained as to the ammonium group of DAP and water, since the absorption bands of these groups are broad.

The near infrared spectra of water in various systems were recorded in the range 1800—2000 nm (5000—5556 cm^{-1}), where water exhibits a strong absorption band due to the $\nu_2+\nu_3$ combination mode. The spectra of the systems with various solvents and various concentrations of water and DAP are shown in Figs. 3, 4, and 5. The water solubilized in the reversed micellar systems in chloroform and benzene has a sharp band at about 1890 nm and a broad band at 1920—1950 nm, while in hexane the former band is observed as a shoulder of the broad band. These bands could be separated into two parts on figures by assuming that the sharp band is of a Gaussian type, and the areas of

Table 1. Solubility of water in DAP (0.2 M) reversed micellar solutions (5 ml) at 35.0 °C

	Water	
	Amount (μl)	Concentration (M)
Hexane	54.1	0.599
Chloroform	42.5	0.472
Benzene	230	2.55

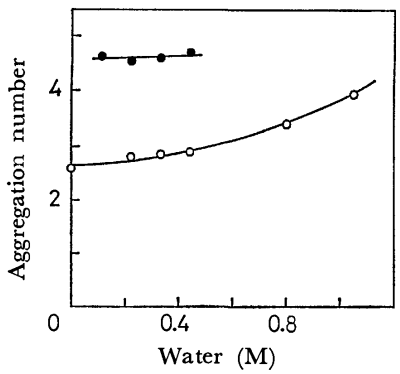

Fig. 2. Aggregation numbers of DAP (0.2 M) in hexane at 37.0 °C (-●-), and in benzene at 50.0 °C (-○-).

Table 2. IR spectra of carboxylate anion of DAP in reversed micellar systems

Water concentration (M)	Wave number (cm^{-1})	
	In chloroform	In hexane
0	1569	—
0.111	1565	1566
0.167	1560	—
0.222	1554	1562
0.278	1553	—
0.333	1551	1560
0.389	1551	—
0.444	—	1557

DAP: 0.2 M.

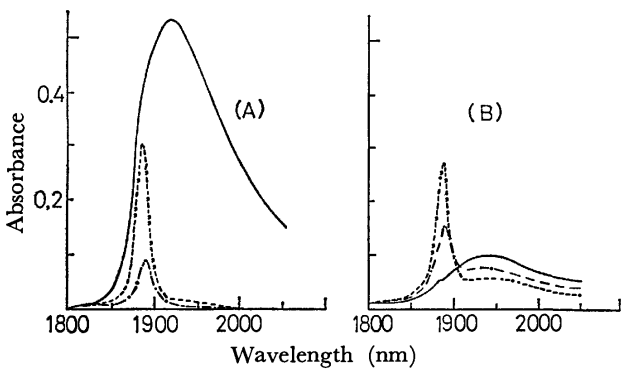

Fig. 3. Near infrared spectra of water at 35.0 °C: (A) water in the following solvents in the absence of DAP; water (——), chloroform (----), and benzene (-·-·); (B) water solubilized in the DAP (0.2 M) reversed micellar systems in hexane (——), chloroform (----), and benzene (-·-·).

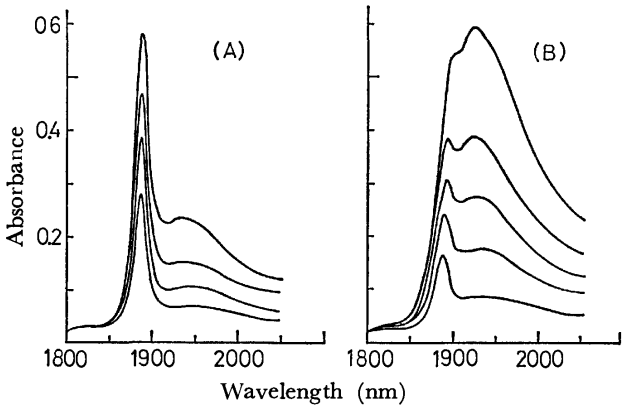

Fig. 4. Effect of water concentration on the near infrared spectra of solubilized water at 35.0 °C in chloroform (A), and benzene (B). DAP concentration is kept constant (0.2 M), and water concentration is varied as follows; (A): 0.111 M, 0.167 M 0.278 M, and 0.389 M; (B): 0.111 M, 0.222 M, 0.333 M, 0.444 M, and 0.666 M.

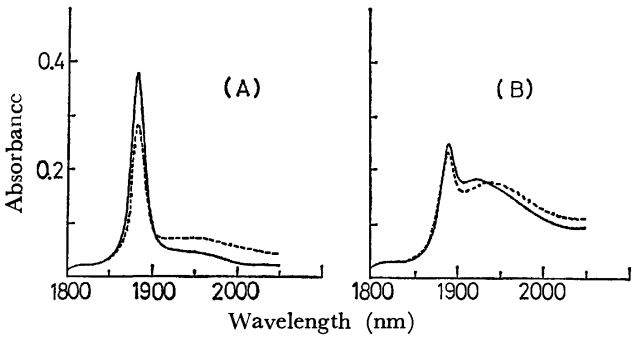

Fig. 5. Effect of DAP concentration on the near infrared spectra of solubilized water at 35.0 °C in chloroform (A), and benzene (B). Water concentration is kept constant ((A): 0.111 M, (B): 0.167 M), and DAP concentration is varied as follows; (A): 0.05 M (——), and 0.2 M (----); (B): 0.05 M (——), and 0.2 M (----).

these two parts is given in Fig. 6 as a function of water concentration in chloroform. The sharp band at 1890—1900 nm is ascribed to free or extremely weakly bonded water.[8] This assignment suggests that in the present system the sharp band at about 1890 nm is not due to the water solubilized in the polar region of reversed micelles, but to the water dispersed in the nonpolar organic phase. The interpretation is based as follows: 1) This band coincides in position and shape with that of water dissolved in pure solvents in the absence of surfactants (Fig. 3); 2) The increase in DAP concentration does not increase the intensity of this band (Fig. 5); 3) The increasing order of the intensity of this band, chloroform>benzene≫hexane, agrees with that of the solubility of water in these solvents.

The band occurring at wave lengths greater than 1900 nm is thought to be due to the bonded water, usually hydrogen bonded water.[8] The broad band observed at 1920—1950 nm in Fig. 3 is thus ascribed to the water solubilized in the reversed micelles be-

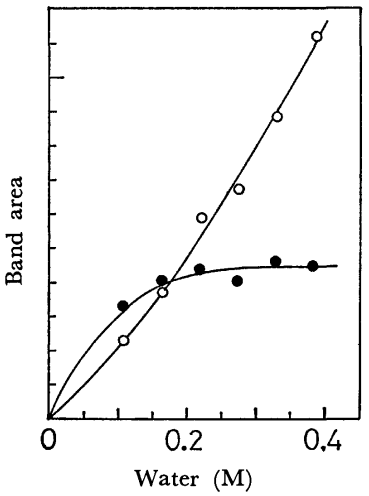

Fig. 6. Band areas of near infrared spectra of water in chloroform at 35.0 °C; one is the sharp band at 1890 nm (●); and the other is the broad band above 1900 nm (○).

cause of the following reasons: 1) The band resembles that of pure water in shape, and water solubilized in micelles could be supposed to form a water phase, while it is hard to suppose that water dispersed in the organic phase forms a water phase; 2) The increase in DAP concentration increases the intensity of this band (Fig. 5); 3) The increase in the amount of water beyond the solubility of water in the organic solvent results exclusively in the increase in intensity of this absorption band. Furthermore, the position of this band (λ_{max}: 1921—1953 nm) shifts a little to a greater wavelength side as compared with that of pure water (λ_{max}: 1919 nm), the increase in water concentration diminishing the extent of this shift. The greater wavelength shift could be caused by the interaction between the water solubilized in the reversed micelles and polar groups of DAP.

These results could be summarized as follows: 1) Two types of water exist in the reversed micellar solution; one is the water dispersed in the organic phase which shows a sharp band at about 1890 nm, and the other is the water solubilized in the reversed micelles which shows a broad band at 1920—1950 nm. 2) In chloroform a considerable amount of water is dispersed in the organic phase, while in hexane almost all the water is solubilized in the reversed micelles. 3) As seen from Fig. 6, water added is at first dispersed in the organic phase and then solubilized in the reversed micelles. 4) The water solubilized in the reversed micelles is bonded to the head groups of DAP or to each other a little more strongly as compared with the case of pure water.

NMR Spectra. The effect of water concentration on chemical shifts of DAP protons in the reversed micellar system in deuterochloroform at 35 °C is shown in Table 3. As the ammonium protons of DAP and water protons gave only a single peak because of the rapid proton exchange between them, we could not observe the dependence of the chemical shift of ammonium protons on water concentration. The dependence of the chemical shift of these protons on solubilizate

Table 3. Chemical shifts, $\delta_{(PPM)}$, of DAP in deuterochloroform at 35 °C

	Water concentration (M)					in D_2O
	0	0.07	0.14	0.28	0.30	
CH_3-$(CH_2)_{10}$-$CH_2\overset{+}{N}H_3$	1.23	1.24	1.24	1.24	1.24	1.26
$CH_3(CH_2)_{10}$-CH_2-$\overset{+}{N}H_3$	2.73	2.74	2.76	2.77	2.78	2.89
CH_3-CH_2-COO^-	2.16	2.15	2.15	2.15	2.15	2.14
$C_{12}H_{25}$-$\overset{+}{N}H_3$+H_2O	7.97	6.94	6.54	5.99	5.97	—

DAP: 0.2 M.

Table 4. Chemical shifts, $\delta_{(PPM)}$, of DTAA in deuterochloroform at 35 °C

	Water concentration (M)			
	0	0.12	0.24	0.36
CH_3-$(CH_2)_{11}\overset{+}{N}(CH_3)_3$	0.86	0.86	0.87	0.87
CH_3-$(CH_2)_{10}$-$CH_2\overset{+}{N}(CH_3)_3$	1.24	1.24	1.24	1.24
$CH_3(CH_2)_{11}\overset{+}{N}$-$(CH_3)_3$	3.36	3.31	3.26	3.23
CH_3-COO^-	1.88	1.87	1.85	1.83
H_2O	—	4.36	4.57	4.73

DTAA: 0.2 M.

concentration is reported for other solubilizates such as dimethyl sulfoxide or methanol.[9] We have carried out a similar measurement on the reversed micellar system of DTAA which has no ammonium protons exchangeable with water protons. The result is given in Table 4. Both the NMR spectra of DAP and DTAA in the reversed micellar system show a similar feature; the extent of chemical shifts of methylene and methyl protons adjacent to the cationic or anionic group depends somewhat on water concentration, while those of the other protons are not dependent on water content. A similar behavior was observed for other solubilizates.[9] This indicates that the water solubilized in reversed micelles exists near the polar head groups and, in other words, in the cores of reversed micelles.

The water protons give only a sharp single peak, and not a broad one or two peaks as in the case of near infrared spectra. This shows that the lifetime of water of each type is below the NMR time scale. The δ value of water protons in the DTAA reversed micellar system is smaller than that of pure water (δ=4.66) at lower water concentration, but a little greater than that of pure water at higher water concentration. Water dissolved in deuterochloroform without any surfactant gives a peak at δ=1.54. The observed peak position is said to be an average of the two peak positions, one of which is due to the water dispersed in the nonpolar organic phase which gives a high-field shift as compared with that of pure water, and the other to the water solubilized in the core of reversed micelles which gives a small low-field shift.

Calorimetric Measurements. The heat of solution of water in a DAP (0.05 M) reversed micellar system in hexane (100 ml) at 35.0 °C was measured. The results given as an integral heat of solution, ΔH_{soln} (cal/100 ml of hexane), and a differential heat of solution, Δh_{soln} (kcal/mol of water), are shown in Fig. 7. Since the addition of water does not cause a pronounced change in the state of micelles, the values show the enthalpy change between pure water and the water solubilized in the reversed micellar system. The initial step of addition of water is endothermic, while the subsequent steps are exothermic. By the addition of more than 0.03 M water, the differential heat of solution becomes nearly constant, Δh_{soln}= −450 cal/mol of water. When water is dispersed in the nonpolar organic phase, the enthalpy change is thought to be positive because of destruction of water structure in the bulk phase. On the other hand, when water is solubilized in the reversed micelles the enthalpy change is thought to be negative, since water interacts with the polar groups of DAP as elucidated from IR and NMR spectra. Thus the calorimetric measurement provides results which coincide with other results.

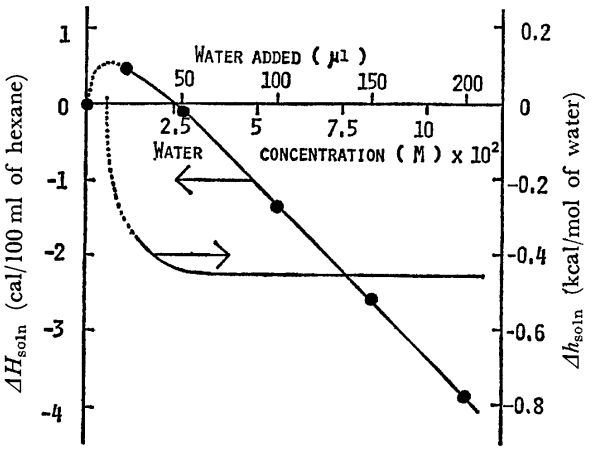

Fig. 7. Integral (ΔH_{soln}) and differential (Δh_{soln}) heats of solution of water in DAP (0.05 M) reversed micellar system in hexane (100 ml) at 35.0 °C.

Catalytic Effect of the DAP Reversed Micellar System. The hydrolysis rate of ATP in the DAP reversed micellar system in hexane is proportional to the DAP concentration and inversely proportional to the concentration of solubilized water.[4] The polarity of the core of DAP micelles in hexane, which was measured by the absorption band shift of pyridine 1-oxide solubilized in the reversed micelles, depends on the [water]/[DAP] ratio, and is less polar than pure water. The catalytic effect of this system would be closely related to this polarity.

The effect of water content on this system could be discussed from the following three related aspects: (a) the effect on the aggregation state of DAP, (b) the effect on the property of solubilized water, and (c) the effect on the substrate in the reversed micelles. In this paper we have discussed the system from (a) and (b), and in the preceding paper from (c).[4] Since the water content scarcely affects the aggregation states of reversed micelles, the micro-environment of the substrate is closely related to the property of water solubilized in the reversed micellar system. As almost all portions of the water added exist in the cores of DAP reversed micelles in hexane, it could be said that the catalytic effect of this system depends greatly on the property of the water solubilized in the reversed micelles,

which is bonded a little more strongly than the water in the bulk phase.

References

1) E. J. Fendler, S. A. Chang, J. H. Fendler, R. T. Medary, O. A. El Seoud, and V. A. Woods, "Reaction Kinetics in Micelles," ed. by E. H. Cordes, Plenum Press, New York, N. Y. (1973), p. 127.
2) J. H. Fendler, F. Nome, and H. C. Van Woert, *J. Am. Chem. Soc.*, **96**, 6745 (1974).
3) J. H. Fendler, and L. Liu, *J. Am. Chem. Soc.*, **97**, 999 (1975).
4) M. Senō, S. Shiraishi, K. Araki, and H. Kise, *Bull. Chem. Soc. Jpn.*, **48**, 3678 (1975).
5) A. Kitahara, *Bull. Chem. Soc. Jpn.*, **28**, 234 (1955).
6) K. Kon-no and A. Kitahara, *J. Colloid Interface Sci.*, **33**, 124 (1970).
7) O. A. El Seoud, E. J. Fendler, J. H. Fendler, and R. T. Medary, *J. Phys. Chem.*, **77**, 1876 (1973).
8) O. D. Bonner, and Y. S. Choi, *J. Phys. Chem.*, **78**, 1723 (1974).
9) O. A. El Seoud, E. J. Fendler, and J. H. Fendler, *J. Chem. Soc., Faraday I*, **70**, 450 (1974).

Photoemission from Polycyclic Aromatic Crystals in the Vacuum-Ultraviolet Region. V.† Photoelectron Spectroscopy by the Rare Gas Resonance Lines and Vacuum-Ultraviolet Absorption Spectra

Kazuhiko SEKI, Tomohiko HIROOKA*, Yusuke KAMURA,†† and Hiroo INOKUCHI†††

The Institute for Solid State Physics, The University of Tokyo, Roppongi, Minato-ku, Tokyo 106

**Department of Chemistry, Faculty of Science, The University of Tokyo, Hongo, Bunkyo-ku, Tokyo 113*

(Received October 6, 1975)

The photoelectron spectra (energy distribution curves, ECDs) of naphthacene, pentacene, perylene, coronene, and *p*-terphenyl by He(I), Ne(I), and Ar(I) resonance lines (photon energies, 11.62—21.22 eV**) and the absorption spectra of naphthacene, pentacene, perylene, and coronene at 4—9.5 eV are measured for evaporated polycrystal films. The absorption spectra are compared with the spectral dependence of the quantum yield (SDQY) of photoemission. A similar comparison is also made for *p*-terphenyl and anthracene. The origin of the structures in SDQY curves is discussed. The analysis reveals that: (1) the MOs of a molecule are preserved even in crystals; (2) the large peak at a low kinetic energy of the photoelectron spectra is due to secondary electrons, and (3) at least for naphthacene, pentacene, and coronene, autoionization takes place with a considerable efficiency.

Photoemission has now become a powerful tool for the study of the electronic properties of solids.[1)]

Polycyclic aromatic hydrocarbons form a major branch of organic semiconductors, and many studies have been made of their electronic properties.[2)] Experiments on photoemission from these compounds in the solid state have also been carried out since the beginning of the 1960s.[2,3)]

Usually two quantities are measured in photoemission experiments: the spectral dependence of its quantum yield (SDQY), and the energy distribution curves of photoelectrons (EDCs, photoelectron spectra) at each photon energy.

SDQY for photoemission from the aromatic hydrocarbons has been studied by many workers.[2,3)] Particular efforts have been made to explain the shape of SDQY around the threshold region in order to make an accurate extrapolation for determining the photoemission thresholds from SDQY.

The photoelectron spectroscopic study of organic solids was first made by Vilesov and his co-workers[4)] in the vacuum-ultraviolet (vacuum-UV) region. They measured the EDCs and discussed the energetics and mechanism of the photoemission. Related studies were also made by Kochi *et al.*,[5)] Hirooka *et al.*[6,7)] and Zagrubskii and Vilesov[8)] in the vacuum-UV region and by Belkind *et al.*[3)] in the region near to and below the threshold. Further, the introduction of the windowless monochromator[8a)] and the use of rare gas resonance lines[9,10)] extended the photon energies, and a high resolution was obtained by the use of a deflector-type analyzer.[10,11)]

These efforts clarified many points about the microscopic mechanism of the photoemission. However, the understanding of the mechanism for aromatic hydrocarbons seems still to be incomplete (for a review, see the article by Belkind *et al.*[3)]). This is partly due to the lack of experimental data. For example, almost all the optical studies of solid aromatics in the vacuum-UV region have been restricted to small molecules.[12)] On the other hand, Schechtman and Spicer[13)] made an extensive study of phthalocyanines and showed that the comparison of the optical spectra with the SDQYs of the photoemission is very useful for the analysis of SDQY. Although several electron energy-loss experiments have been carried out for large aromatics,[12,14)] Kramers-Kronig analysis must be carried out in order to obtain the absorption spectra. This was carried out only by Hinz and Venghaus[14)] for a few compounds. Due to the lack of experimental data on the optical spectra, no comparison between SDQY and the optical spectrum can be made for compounds such as naphthacene, which has been most frequently studied in photoemission work.

Further, almost all the investigations have been restricted to the photon energies of the LiF window cutoff (11.5 eV), with some recent exceptions. The extension of measurements to higher photon energies can be expected to give more useful information. For example, the effect of electron scattering will become clear with the increase in the photon energy. Further, deeper valence levels and upper conduction bands can be investigated by means of higher photon energies.

In this paper, we wish to report: (1) the photoelectron spectra of polycrystals of naphthacene, perylene, pentacene, coronene, and *p*-terphenyl by rare gas resonance lines with photon energies up to 21.22 eV, and (2) a comparison of SDQY with the optical spectra for these compounds and anthracene in the region of 5—11.5 eV. The results will be discussed in order to clarify the energy structures of these compounds and the nature and role of several processes in the photoemission. The results of the photoelectron spectra in the range of 5—11.5 eV have been reported elsewhere.[7)] Particular attention is paid to the characteristic properties of these compounds as molecular crystals; these properties distinguish them from other classes of substances. Information on these points will also be useful in other areas, such as the photoconduction and radiation physics of these substances. Some of the experimental results have already been

† Part IV: Ref. 5b.

†† Present address: Hatano Research Institute, F. D. S. C., Ochiai, Hatano-City 257.

††† Present address: Institute for Molecular Science, Okazaki 444.

** The electron volt is not coherent with the SI units. One electron volt $\cong 1.6022 \times 10^{-19}$ J.

reported in other periodicals.[9,15,16]

Experimental

Samples. The materials used in this study were purified by zone refining, recrystallization, and sublimation. X-Ray diffraction measurements revealed that the evaporated samples are oriented polycrystals, with their c-axes perpendicular to the substrates,[15,17] both for the photoemission and for the optical spectra measurements. The crystal structure of perylene is known to be the α-form, in which molecules form dimers.[18]

Photoelectron Spectra. The rare gas discharge lamp was of the π-type. He(I)(21.22 eV), Ne(I)(16.85 and and 16.67 eV), and Ar(I)(11.83 and 11.62 eV) resonance lines were used. For the He(I) discharge, $1—5\times10^{-2}$ Pa of helium was supplied through a liquid nitrogen-cooled charcoal trap. For the Ne(I) and Ar(I) discharges, a small amount of neon and argon was added to the helium gas.[19] An a.c. voltage of 5—8 kV was applied from a neon-sign transformer. The photoelectron energy analyzer was of the retarding-potential type. A gold-plated collector 150 mm in diameter was used, with the emitter located at its center.

The samples were evaportaed onto a polished copper emitter substrate 12—20 mm in diameter in a separate evaporation vessel under a vacuum of $10^{-3}—10^{-4}$ Pa. Measurements were made under a vacuum of $1—3\times10^{-4}$ Pa. The continuous slow sublimation of the organic specimen helped to maintain a clean surface and enabled satisfactory measurements to be made without the use of an ultrahigh vacuum. The sample thickness was monitored with a quartz crystal oscillator (Toyo Tsushinki TVF-1). Considering several factors (the charging of the sample, the effect of the substrate, and the loss of the sample due to sublimation), thin film specimens 30—200 nm thick were employed.

The photoelectron-energy distribution curves were measured by means of an a.c. modulation technique which has been reported previously.[6,7] A Cary-31 vibrating-reed electrometer and a PAR-128 lock-in amplifier were used, with an a.c. modulation of 200 mV_{P-P}, 4 Hz. The total photocurrents were of the order of 10^{-10} to 10^{-11} A. The resolution of the spectrometer was estimated to be about 0.3 eV.

Optical Spectra. The method of the measurement of the absorption spectra of films evaporated onto LiF plates has already been reported.[15]

The measurement of the normal incidence reflection spectra of evaporated films was also attempted; it gave useful preliminary results for perylene and pentacene for $h\nu<7.7$ eV. The experimental details have been reported elsewhere.[20]

Results

Photoelectron Spectra. Figures 1—5 show the EDCs of naphthacene, perylene, pentacene, coronene, and *p*-terphenyl as functions of the retarding potential, *RP*. *RP* is related to the kinetic energy of the electron, *KE*, thus:

$$KE = e(RP+V_S), \quad (1)$$

where V_S is the saturation voltage defined as the negative of the value of *RP* at the right-hand cutoff point of the EDCs. If the electrical contact between the sample and substrate is good enough, the value of V_S is the contact potential difference between the sample and the collector. Further, the ionization

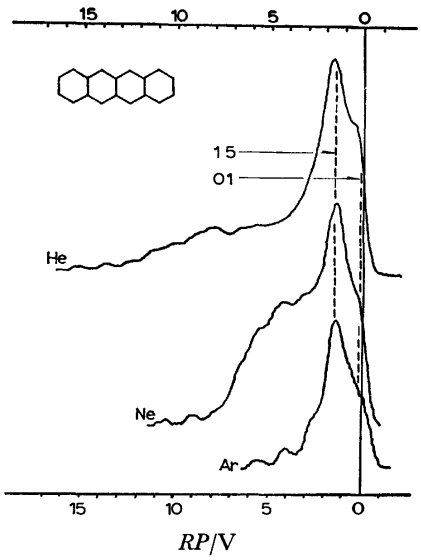

Fig. 1. EDCs of naphthacene in retarding potential scale.

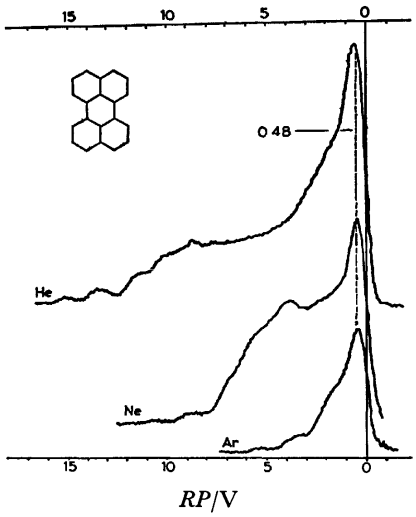

Fig. 2. EDCs of perylene in retarding potential scale.

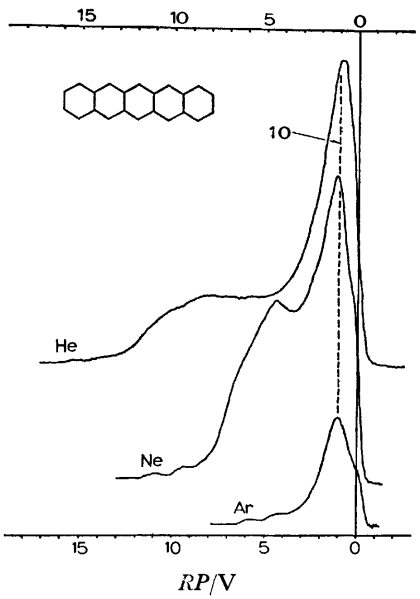

Fig. 3. EDCs of pentacene in retarding potential scale.

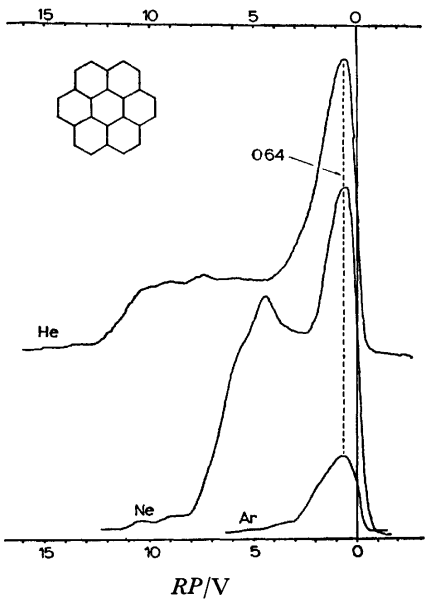

Fig. 4. EDCs of coronene in retarding potential scale.

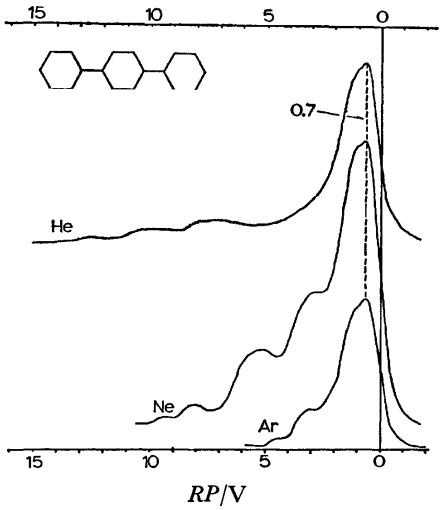

Fig. 5. EDCs of *p*-terphenyl in retarding potential scale.

potential, *IP* (binding energy measured from the vacuum level) is derived from the Einstein relation:

$$IP = h\nu - KE. \quad (2)$$

When $h\nu$ is changed, small moving structures in the higher *RP* region and large non-moving structures in the lower *RP* region were observed in all the spectra.

The non-moving structures can be classified into two groups: (1) the shoulders observed near zero *RP* for naphthacene and pentacene (whose spectral shapes and intensities were sensitive to the sample condition) and (2) the peaks observed in all compounds in the *RP*=0.5—1.5 V region (their peak intensities increased rapidly with the photon energy). These two groups of structures were also found by Hirooka[7] at lower photon energies. We shall refer to these structures as "lower energy non-moving structures" (LNMSs) and as "high energy non-moving peaks" (HNMPs) respectively. In Hirooka's work,[7] LNMSs were found for all the compounds, while HNMPs were found only for naphthacene, pentacene, and perylene. A recent report by Hino *et al.*[16] shows that LNMS does not appear in *p*-terphenyl, even at lower photon energies.

A weak charging effect was observed for some samples, due to fairly large photoemission currents. This caused a scatter of the observed values of V_S of 0.2 V. Therefore, the minimum value of V_S obtained was used to calculate the *IP*s. This gave a good agreement with the *IP*s obtained by Hirooka[7] and Hino *et al.*[16] The values of V_S and *KE* for the non-moving structures are listed in Table 1.

Figures 6—10 show the EDCs as functions of *IP*. It may be seen that the *IP*s of the moving structures have nearly constant values, independent of the photon energies. For comparison, the results of molecular photoelectron spectroscopy[21] are also shown in the figures. The *IP*s obtained are listed in Tables 2—6, together with the results of other photoemission studies[5-8,10] and of molecular photoelectron spectroscopy. In the tables, *P* is the polarization energy,[22] defined here as the difference in the *IP* values between the solid and gas phases.

TABLE 1. SATURATION VOLTAGES AND KINETIC ENERGIES OF NON-MOVING STRUCTURES

Compound	V_S/V	*KE*/eV
Naphthacene	0.4	0.5 1.9
Pentacene	0.3$_5$	1.4 0.6
Perylene	0.3	0.8
Coronene	0.4	1.0
p-Terphenyl	0.4	1.1

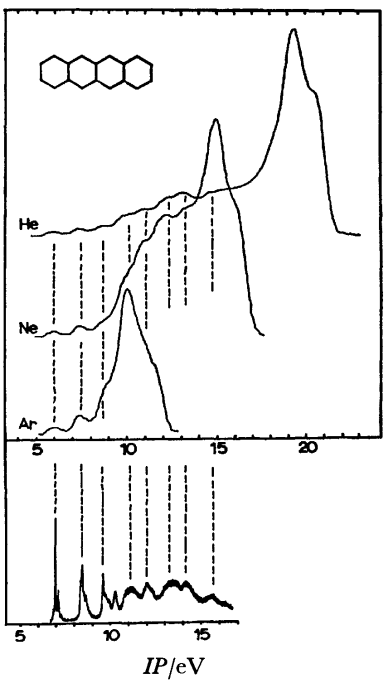

Fig. 6. EDCs of naphthacene in ionization potential scale (upper). Photoelectron spectrum of a free molecule is also shown (lower, Ref. 21a).

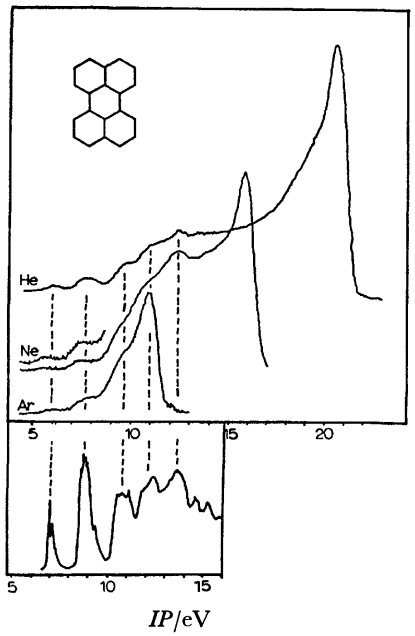

Fig. 7. EDCs of perylene in ionization potential scale (upper). Photoelectron spectrum of a free molecule is also shown (lower, Ref. 21c).

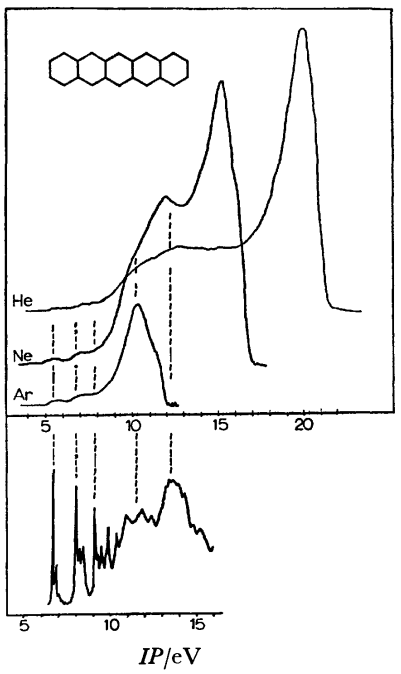

Fig. 8. EDCs of pentacene in ionization potential scale (upper). Photoelectron spectrum of a free molecule is also shown (lower, Ref. 21d).

On the whole, the agreement with the other photoemission studies and the correspondence with the gas-phase data are satisfactory. However, the *IP* values of 15.3 and 16.2 eV for naphthacene, which we reported in the preliminary communication,[9] seem dubious in the light of this work and the recent photoelectron spectrum obtained by Ueno *et al.*[10b] using a He(II) (40.8 eV) resonance line.

Recently, Shibata *et al.*[23] measured the Penning emission from naphthacene by means of rare gas metastable atoms. Their results for the location of valence levels agree with the present results very well.

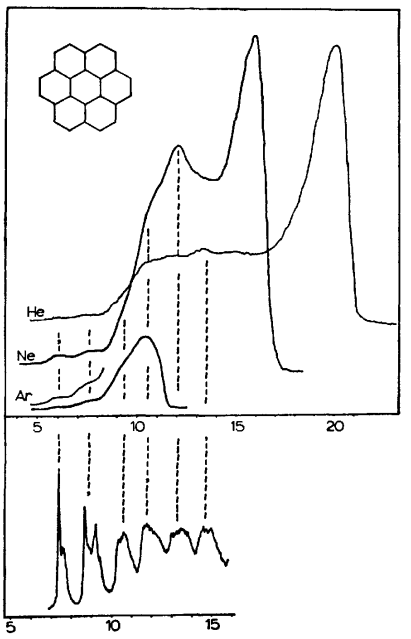

Fig. 9. EDCs of coronene in ionization potential scale (upper). Photoelectron spectrum of a free molecule is also shown (lower, Ref. 21d).

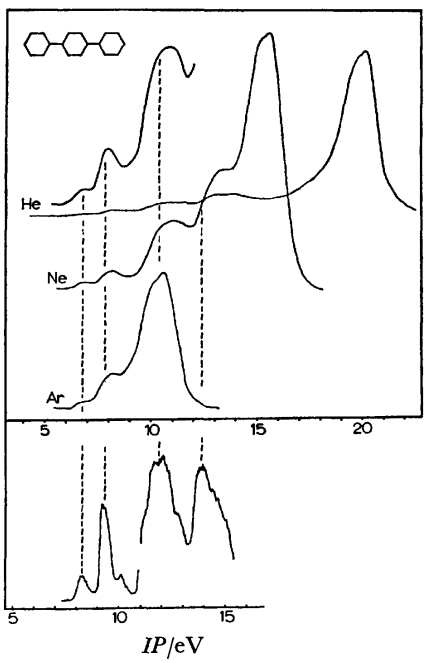

Fig. 10. EDCs of *p*-terphenyl in ionization potential scale (upper). Photoelectron spectrum of a free molecule is also shown (lower, Ref. 16).

The spectra for perylene are much clearer than the preliminary ones reported previously.[9] The sharpness of the structures of coronene depended on the sample preparation. A similar but weaker effect was also found for perylene; its origin is not understood. The structures of the spectra for pentacene are not very

Table 2. Ionization potentials/eV of naphthacene in solid and gaseous states

Crystal		Gas[21a]		Polarization energy[b]	HTFIHK[6]		ZV[8]		KUH[10a]	
IP	ΔE[a]	*IP*	ΔE	(*P*)	*IP*	ΔE	*IP*	ΔE	*IP*	ΔE
5.3[c]					5.28[c]		5.2[c]			
5.9	0.0	7.01	0.0	1.1	5.83	0.0	5.76	0.0	5.75	0.0
7.3	1.4	8.41	1.41	1.1	7.28	1.45	7.15	1.39	7.27	1.52
		(8.6)	(1.5_9)							
8.7	2.8	9.56	2.55	1.0	8.29	2.46	8.25	2.49	8.64	2.89
		(9.7)	(2.6_9)		8.70	2.87	8.6	2.8_4		
(9.2)	3.2	10.25	3.24	1.1	9.40	3.57	9.5	3.7_4		
10.0	4.1	11.1	4.1	1.1					9.8	4.07
10.9	5.1	12.0	5.0	1.1	10.7		10.7	4.9_4	10.7	4.95
12.3	6.4	13.4	6.4	1.1			11.9	6.1_4	12.1	6.35
13.2	7.3	14.1	7.1	0.9					13.1	7.35
14.4	8.5	15.7	8.7	1.3					14.4	8.65
									15.0	9.25

a) Energy difference from the first peak. b) Defined as $IP(\text{gas}) - IP(\text{crystal})$. c) Photoemission threshold.

Table 3. Ionization potentials/eV of perylene in solid and gaseous states

Crystal		Gas[21c]		Polarization energy	Hirooka[7]		ZV[8]
IP	ΔE	*IP*	ΔE	(*P*)	*IP*	ΔE	ΔE
5.2[a]					5.37[a]		
5.8	0.0	7.00	0.0	1.1	5.88	0.0	0.0
		8.55	1.55		(7.15)	(1.27)	
7.7	1.9	8.68	1.68	1.0	7.48	1.60	1.75
		8.9	1.9		7.95	2.07	
		9.34	2.34				
9.7	3.9	10.4	3.4	(1.0_5)	9.10	3.22	
		11.1	4.1				
10.7	4.9	11.7	4.7	(1.3)			
		12.3	5.3				
12.3	6.5	13.6	6.6	1.3			
13.8	8.0	14.5	7.5				
		15.2	8.2				
(15.3)	(9.5)						

a) Photoemission threshold.

Table 4. Ionization potentials/eV of pentacene in solid and gaseous states

Crystal		Gas[21c]		Polarization energy	Hirooka[7]	
IP	ΔE	*IP*	ΔE	(*P*)	*IP*	ΔE
4.9_5[a]					4.85[a]	
5.6	0.0	6.64	0.0	1.1	5.51	0.0
		7.93	1.29		6.61	1.10
7.2	1.6	8.35	1.71	1.1	7.13	1.62
		9.00	2.36		7.65	2.14
		9.39	2.75		(8.1)	(2.5_9)
		9.80	3.16			
9.7	4.1	10.26	3.62	0.6		
12.3	6.7					

a) Photoemission threshold.

clear. This might be partly due to the fact that the separations between the levels are rather small, as can be seen from the gas-phase photoelectron spectrum.

For *p*-terphenyl, although the molecular structures in the solid and gaseous phases might differ a little, as a result of the rotation of phenyl groups, the correspondence seems to be good. Its details were reported elsewhere.[16]

Optical Spectra. The results of the absorption and reflection spectra for naphthacene, pentacene, perylene, and coronene are shown in Figs. 11—14(c). Further, the absorption spectra of anthracene and *p*-terphenyl obtained from the data by Clark[24] and Venghaus[14] are shown in Figs. 15 and 16(c).

The peaks observed in the absorption spectra are due to molecular excitons. Their interpretation has been discussed in another periodical.[15] The rising baselines may correspond to the direct ionization in solids. Some other workers have also suggested the occurrence of direct ionization.[20,24]

For comparison, the results of SDQY measurements of naphthacene, pentacene, perylene, coronene, and anthracene by Hirooka[7] are shown in Figs. 11—15(b). The result for *p*-terphenyl by Hino *et al.*[16] is also shown in Fig. 16(b). The quantum yield is defined here as

Table 5. Ionization potentials/eV of coronene in solid and gaseous states

Crystal		Gas[21d]		Polarization energy	Hirooka[7]		ZV[8]
IP	ΔE	*IP*	ΔE	(*P*)	*IP*	ΔE	ΔE
5.3[a]					5.52[a]		−0.8
6.1	0.0	7.34	0.0	1.2	6.20	0.0	0.0
7.7	1.6	8.64 9.15	1.30 1.81	1.2	7.85	1.65	1.6
9.5	3.4	10.4 10.55	3.0_6 3.21	1.0	9.40	3.20	2.8
10.7	4.6	11.6	4.2_4	0.9			
12.0	5.9						
13.5_5	7.4_5						

a) Photoemission threshold.

Table 6. Ionization potentials/eV of *p*-terphenyl in solid and gaseous states

Crystal		Gas[16]		Polarization energy	Hino[16]		ZV[8]
IP	ΔE	*IP*	ΔE	(*P*)	*IP*	ΔE	ΔE
6.2[a]					6.1[a]		−0.55
6.9	0.0	8.20	0.0	1.3	6.6	0.0	0.0
8.1	1.3	9.17	0.97	1.1	7.6 7.8_5	1.0 1.2_5	1.05 1.27
		10.10	1.90		8.7	2.1	2.09
		11.2 11.4 11.6	3.0 3.2 3.4		9.7	3.1	
11.0	4.1	12.1	3.9	1.1			
		12.7 13.1	4.5 4.9				
13.3	6.4	13.9	5.7	0.6			

a) Photoemission threshold.

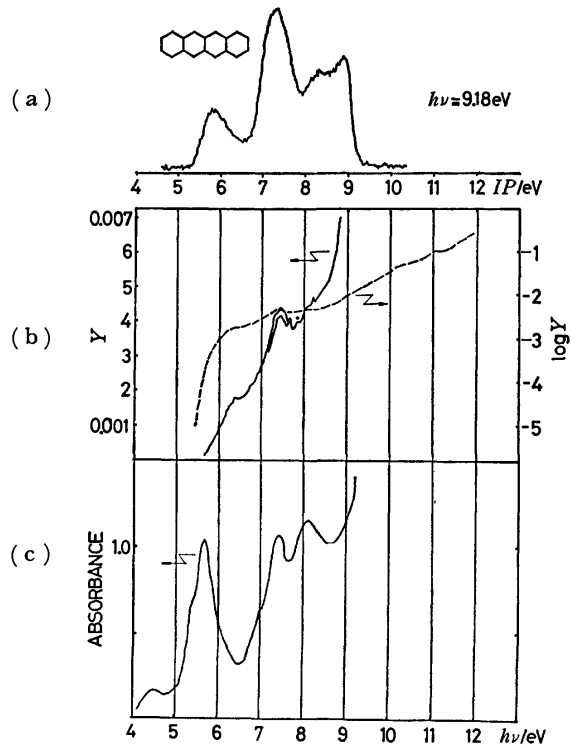

Fig. 11. Comparison of (c) the absorption spectrum of naphthacene with (a) EDC[7] and (b) SDQY[7] of photoemission.

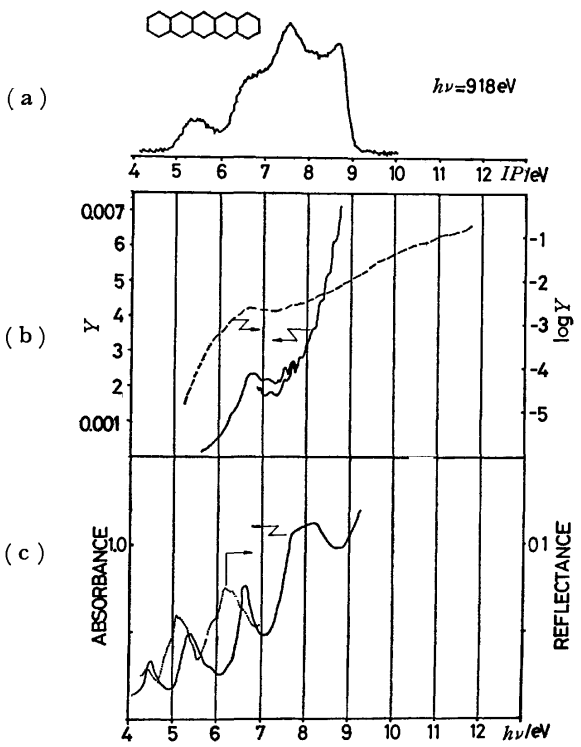

Fig. 12. Comparison of (c) the absorption and reflection spectra of pentacene with (a) EDC[7] and (b) SDQY[7] of photoemission.

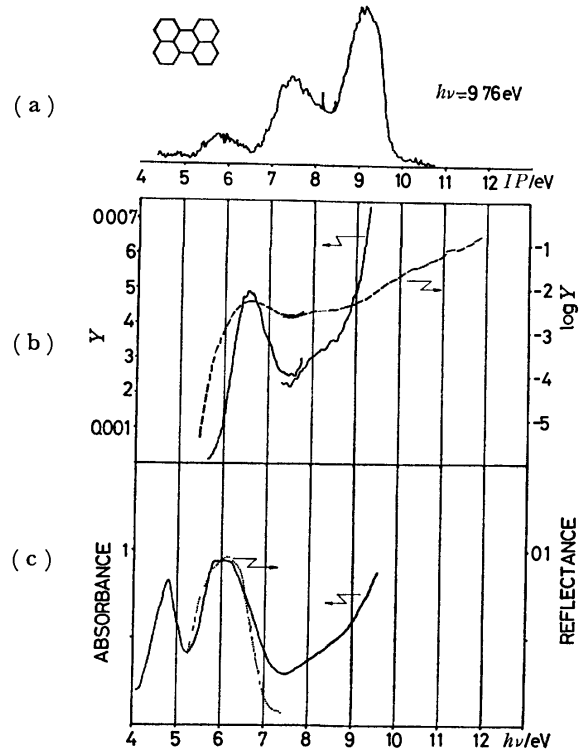

Fig. 13. Comparison of (c) the absorption and reflection spectra of perylene with (a) EDC[7] and (b) SDQY[7] of photoemission.

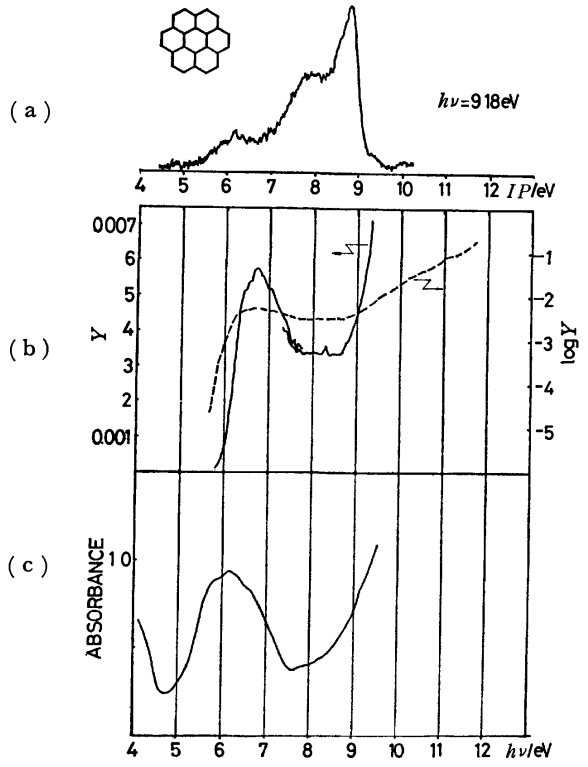

Fig. 14. Comparison of (c) the absorption spectrum of coronene with (a) EDC[7] and (b) SDQY[7] of photoemission.

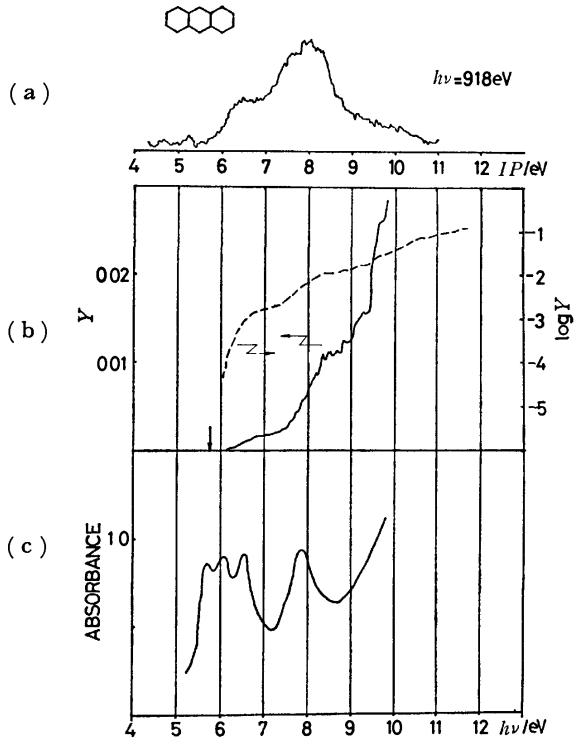

Fig. 15. Comparison of (c) the absorption spectrum of anthracene with (a) EDC[7] and (b) SDQY[7] of photoemission. Absorption spectrum is taken from Ref. 24, by averaging of the a- and b-axes components of ab-plane spectrum.

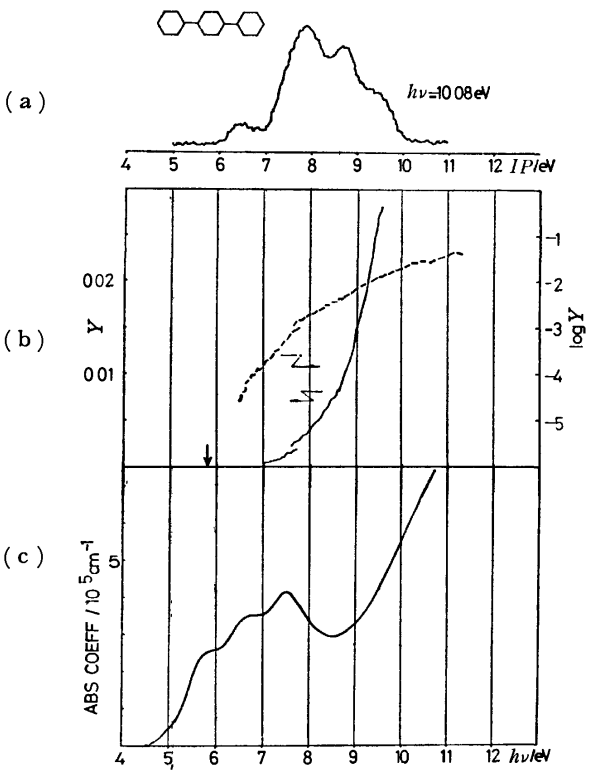

Fig. 16. Comparison of (c) the absorption spectrum of *p*-terphenyl with (a) EDC[16] and (b) SDQY[16] of photoemission. Absorption spectrum is obtained from the data of Ref. 14, by averaging the spectra for z and y axes of anisotropic dielectric tensor which roughly correspond to ab plane.

the number of photoelectrons per incident photon, and no correction of reflection is made. However, as will be seen later, the neglect of reflection has no significant effect. The discrepancies in the SDQY curves at 7—8 eV are due to the use of a quartz filter at low photon energies. The small ripples in the SDQYs are due to the experimental uncertainty caused by the use of a many-line hydrogen light source.

For perylene and pentacene, the results for SDQY agree well with those of other works.[5] For anthracene and naphthacene, however, some discrepancies from the findings of other works[5,25] were found. For the time being we shall rely on Hirooka's data,[7] although a more accurate measurement of SDQY should be attempted. For coronene and *p*-terphenyl, no other work is available on the vacuum-UV region.

Further, the EDCs at appropriate photon energies[7,16] are also shown in Figs. 11—16(a) to show the location of the valence-band levels.

Discussion

We adopted the phenomelogical three-step treatment.[1] The three steps are: (1) the formation of a quasi-free electron by photon absorption, (2) transport process to the surface, and (3) transmission through the surface. The characteristic aspects of these processes in molecular crystals are:[3,26] (a) not only direct ionization (DI) but also autoionization through a highly excited molecular exciton (AI) might take place; (b) on ionization, *k*-vector conservation is not an effective selection rule, because of the localization of the hole;[1] (c) quasi-free electrons must escape from geminate recombination in the Coulomb field formed by the hole, and (d) electrons can suffer energy loss due to the excitation of the exciton or the intramolecular vibration of other molecules, in addition to the other processes observed in inorganic solids.

The theory of photoemission for organic solids has already been discussed by several workers.[3,13,27]

I. Moving Structures of EDCs. The moving structures in EDCs are considered to be closely associated with the valence bands of the organic crystals. According to Koopmans' theorem, their *IP*s correspond to the energy of the valence levels. All the results show that the agreement of these levels between the gaseous and crystalline states is fairly good, if the polarization energy is assumed to be constant for a compound. This shows that the MOs of a molecule are preserved even in the solid because of the weak intermolecular interactions.

This result was predicted on the basis of a comparison with MO calculations[4,7] and was verified experimentally for π-levels.[7] Molecular photoelectron spectroscopy studies[21e] report that the onset of the ionization from σ levels is at about 10.6—11.0 eV for aromatic hydrocarbons. Assuming a polarization energy of about 1 eV, the emission from σ levels begins at the solid ionization potential of 9.5—10.0 eV. This should correspond to the observed sharp rise of EDCs at about 9 eV. Therefore, the good correspondence between the gas and solid phases extends into the σ electrons. This confirms the validity of the concept of polarization energy proposed by Lyons.[22]

The origin of the peak width of the photoelectron spectra for a solid was discussed previously.[11] We will not compare the peak intensities of the gaseous and solid phases because of the lack of information about the angular distributions of photoelectrons for gaseous samples. Further, the effect of scattering in the solid state makes comparison difficult for such high photon energies (see II).

II. Non-moving Structures in EDCs. Kochi *et al.*[5c] found the HNMPs for some compounds at $h\nu < 11.5$ eV and ascribed them to secondary electrons. The nature of the secondary electrons for organic crystals has been discussed by them and by Schechtman.[13] Their conclusions are: (1) the EDCs of secondary electrons show a peak at a small kinetic energy, and its position does not move significantly with the change in $h\nu$. (2) Secondary electrons contribute to photoemission only in the higher photon energy region, and their contribution grows rapidly with $h\nu$. Although the assumptions they used to derive these conclusions need some re-examination, these criteria are still valid for distinguishing the effect of secondary electrons (see Appendix).

Zagrubskii and Vilesov[8] also observed HNMP and LNMS for several compounds. However, they argued that they are not due to secondary electrons, for their quantum yields (for naphthacene) remain roughly constant at the photon energy of 12—13 eV before decreasing abruptly. They assigned this phenomenon to autoionization, with a preliminary energy loss (AIPL):

$$\begin{aligned} M &\xrightarrow{h\nu} M_I{}^{**} \\ M_I{}^{**} &\longrightarrow M_J{}^{*} \\ M_J{}^{*} &\longrightarrow M^{+} + e^{-} \\ &\searrow M^{+*} + e^{-}, \end{aligned} \qquad (3)$$

where M is the ground state of a molecule, $M_I{}^{**}$ is a high-energy exciton state, $M_J{}^{*}$ is the autoionizing state, and M^+ and M^{+*} are the ground and excited states of an ion respectively. On the basis of this model, they attributed the structures of naphthacene at $KE=0.4$ and 1.8 eV to autoionization to the M^+ state at 5.68 eV and the M^{+*} state at 7.15 eV. They also atrributed the HNMPs of EDCs for perylene and *p*-terphenyl to this mechanism.

They[8c] further attributed the peaks in the SDQY of naphthacene and perylene to the direct optical excitation of the autoionizing state, M^*_J. The energy values of $M_J{}^{*}$ thus obtained are: 7.56 eV for naphthacene, 6.75 and 8.5 eV for perylene, and 7.13 eV for *p*-terphenyl. Further, they identified these autoionizing levels as plasma oscillations of π electrons on the basis of the coincidence of the reflection spectra of graphite, naphthacene, and *p*-terphenyl.

However, their conclusions are dubious for the following reasons; therefore, we assign HNMP to secondary electrons.

(1) The results obtained here for the high-photon-energy region satisfy the criteria described above. The HNMPs are not observed at lower photon energies. Hirooka[7] examined the ratio of the peak height to

the peak of the maximum *KE* and estimated that these peaks begin to appear at photon energies of 8.5—9.3 eV for naphthacene, pentacene, and perylene. In the present experiment also, this ratio increases monotonically with the photon energy. Further, their peak positions are roughly independent of the photon energy, as is shown in Table 1.

(2) The peak positions of HNMP agree with those of secondary electrons formed by slow electron impact.[10,32]

(3) At least for naphthacene, pentacene, and coronene, the small values of the scattering length, *L*, of the order of 10 nm or less[28b] suggest that scattering does occur in these crystals.

(4) The fact that the peak at $RP \cong 0$ V (LNMS) appears even at lower photon energies, while HNMP appears only at higher photon energies, cannot be explained by the AIPL model.

(5) The peak intervals between the LNMS and HNMP in pentacene do not agree with the interval between M^+ and M^{+*} (see Tables 1 and 4).

(6) At least for naphthacene, pentacene, and coronene, the structures of SDQY can be explained by ordinary autoionization, as will be described in III. Further, no structure is found in the SDQY of *p*-terphenyl at the predicted value, $h\nu = 7.13$ eV.

(7) According to Robin,[12] it is useful for the identification of plasmon to compare the optical absorption and the electron energy-loss spectra. Plasma oscillation is intense in the energy-loss spectra, but it should be much weaker in the absorption spectra. For *p*-terphenyl and naphthacene, the absorption coefficient is fairly large at the predicted photon energies, 7.13 eV and 7.56 eV (Figs. 1 and 6). For perylene, there is a peak in the energy-loss spectrum (calculated from the data by Fuke *et al.*[20]) at about 7 eV, but this can be attributed to the one-electron excitation at 6 eV in optical absorption. Therefore, the possibility of the existence of plasma oscillations at these energies is also dubious.

(8) Further confirmation is afforded by the recent experiment of Penning emission from naphthacene by rare gas metastable atoms.[23] That experiment showed that two nonmoving structures also appear in the Penning-emission spectra at the positions of HNMP and the LNMSs. However, their relative intensities were reversed from those in the photoelectron spectra presented here. Considering the nature of the metastable atom, which cannot penetrate into the solid, the Penning-emitted electrons should be less affected than photoelectrons by bulk properties such as electronic scattering. Therefore, HNMP will become weaker in Penning emission, as was observed in the experiment. It is hard to explain this result by the AIPL model, although the detailed mechanism of Penning emission is not yet clear.

From these considerations, it seems certain that the HNMPs are due to secondary electrons. However, the abrupt decrease in the quantum yield for the HNMP of naphthacene above 13 eV reported by Zagrubskii and Vilesov[8] remains unexplained. Furhter investigations are necessary for this point.

The small shoulders (LMNSs) observed in naphthacene and pentacene at $RP \cong 0$ V probably have a different cause from that of the HNMPs. The other compounds except *p*-terphenyl also show similar structures at lower photon energies, but they seem to be covered by the large peaks for perylene and coronene at the higher photon energies used here. The shapes and intensities of these structures are sensitive to the method of sample preparation. This fact was also found by Hirooka[7] and by Schechtman.[13] Therefore, it could be an effect due to some peculiarity of the transmission probability through the surface or to the effect of surface contamination.[7,13]

III. Spectral Dependence of Quantum Yield (SDQY) and the Absorption spectra. As may be seen from Figs. 11—16(b), three regions can be distinguished in the SDQYs, except for the case of *p*-terphenyl: (a) near the threshold region (up to about 1 eV above the threshold): here a sharp increase in the quantum yield, *Y*, is observed; (b) the intermediate region (from 1 eV above the threshold to about 9.5 eV): here there is a rather gradual increase in *Y*, with several structures, and (c) far beyond the threshold region (above 9.5 eV): here there is a monotonic increase in *Y*.

In the region where the data of reflectance $R(h\nu)$ are available (anthracene,[29] perylene,[20] pentacene, *p*-terphenyl,[8] and naphthacene[8]), $R(h\nu)$ is smaller than 0.15 and the $1-R(h\nu)$ factor does not correspond with SDQY. Therefore, the reflection of the incident light has no significant effect on SDQY.

As has been stated in II, the contributions of secondary electrons are small in the low-energy regions, (a) and (b).

(a) *Near the Threshold Region*: No correspondence is found between *Y* and the total absorption coeffecient, a_t, in this region. This has previously been noted by Lyons and his co-workers.[25,27] Kochi *et al.*[5] assumed that *Y* is determined by the energy distribution of photoelectrons arriving at the surface and by the transmission probability $T(E)$ through the surface. With this assumption, they could derive the cube root law which can explain the experimental results: $Y^{1/3} \sim a(h\nu - E_{th})$, where *a* is a constant and where E_{th} is the threshold of photoemission. This sharp increase in *Y* is sufficient to smear out the effect of the variation in a_t. Therefore, it is not surprising that no correspondence exists in this region.

(b) *Intermediate Region*: Vilesov *et al.*[4] and Kochi *et al.*[5] ascribed the structures of SDQY to the occurrence of the photoemission from deeper levels. As may be seen from the comparison of SDQY and EDC in Figs. 11—16(b) and (a), this theory can be applied to polyacenes. However, the distinct minima in SDQY for perylene and coronene (Figs. 13(b) and 14(b)) cannot be explained in this way. Kochi *et al.*[5c] ascribed the decrease in *Y* in perylene to the abrupt decrease in the escape depth, $L(E)$, casued by the occurrence of pair-production, where *E* is the energy of the quasi-free electron measured from the top of the valence band. However, Zagrubskii and Vilesov[8c] examined the EDC of perylene and concluded that $L(E)$ does not change so much with *E*. Further, it was shown that pair-production is not the main

mechanism of the scattering of electrons (see Appendix).

On the other hand, there is another possible explanation, one based on the change in the absorption coefficient.[13,27] If $L(E)$ is much shorter than the extinction length of the incident light ($a_tL \ll 1$), only light absorbed in a thin layer, L, from the surface can contribute to photoemission. The number of photons absorbed in this layer is determined by the absorption coefficient. Then, if all the photons absorbed in this layer contribute to photoemission, and if the average escape depth does not change significantly with the photon energy, the quantym yield should be proportional to the absorption coefficient, a_t.

Of course, we must note that not all the absorbed photons might contribute to photoemission, unless autoionization occurs with a high probability. Batley[27] analyzed the expected behavior of Y under various conditions (whether scattering is severe and which, AI or DI, dominates ionization) in a way similar to that used by Pope[30a] for photoconduction. His results can be summarized as in Table 7. In Table 7, $a_{DI}(h\nu, E)$ is the effective absorption coefficient to form quasi-free electrons with the E energy, a_{AI} is the absorption coefficient of the autoionizing exciton, $k(h\nu, E)$ is the autoionizing probability to form quasi-free electrons with the E energy, and A_t includes all factors other than the change in a_{DI}, a_{AI}, and a_t. In the last column of Table 7, it is assumed that $\int a_{DI}\,dE$ gradually increases with the photon energy.[13] Note that $a_t \sim a_{AI}$ when autoionization dominates ionization. As may be seen from Table 7, a comparison of the absorption coefficient and SDQY will be useful in determining whether or not autoionization occurs with a high probability.

A comparison of the SDQY and a_t in Figs. 11—15(b) and (c) shows that a good symbatic correspondence exists between them for perylene and coronene and a fairly good one for polyacenes. *p*-Terphenyl seems to be an exception to this. However, as may be seen in Fig. 16(a), the intensity ratio of the first and other peaks of EDC is very large for this compound. Therefore this can be interpreted as ionization from deeper levels overwhelming other changes.

As may be seen from Table 7, the comparison of a_t and Y strongly suggests that $a_tL \ll 1$ and that autoionization takes place with considerable efficience.

Table 7. Expected behavior of quantum yield $Y(h\nu)$

Scattering condition	Dominant mechanism of ionization		Expected behavior of $Y(h\nu)$ when a_t decreases
$a_tL \gg 1$	DI	$Y \sim A_1 \int \frac{a_{DI}}{a_t} dE$	increases
	AI	$Y \sim A_2 \int \frac{a_{AI}k}{a_t} dE$	nearly constant
$a_tL \ll 1$	DI	$Y \sim A_3 \int a_{DI} L\, dE$	gradully increases
	AI	$Y \sim A_4 \cdot a_{AI} kL$ $\sim A_4 \cdot a_t kL$	decreases

The occurence of autoionization has also been suggested by other workers.[30] A similar correspondence between Y and a_t was found for phthalocyanines[13] and several inorganic materials.[31] In the case of polyacenes, the photoemission from deeper levels may also affect the shape of SDQY.

Recently several measurements of L have been made for organic solids.[28] Hino *et al.*[28b,c] showed that $a_tL < 1$ is satisfied for naphthacene, pentacene, and coronene. This confirms the present suggestion. For perylene, however, they reported that $a_tL = 1.3$ ($L = 80$ nm) for electrons injected from CuI by the illumination of light with a photon energy of 7.75 eV. When this is the case, the mechanism described above is not very effective for perylene. On the other hand, the other cases in Table 7 cannot explain the minimum of Y for perylene. One possible explanation involves a combination of the change in a_t and an abrupt decrease in $L(E)$. Such an abrupt decrease in $L(E)$ could occur when the probability of exciton formation increases sharply above a certain energy value, but Zagrubskii and Vilesov[8c] discounted such a possibility. We will not discuss this point in detail because no direct experimental data are available about the E dependence of $L(E)$. Further studies will be necessary for perylene.

Another mechanism to explain the shape of SDQY was proposed by Zagrubskii and Vilesov.[8] Their explanation, however, seems to be dubious, as has been described in II.

(c) *Far-beyond Threshold Region*: The sharp rise in Y in this region corresponds either to the photoemission from a deeper level or to the onset of the large peak in EDC (HNMP). The latter is due to secondary electrons, as has been described in II.

The authors wish to thank Professor Yoshiyo Harada for his constant interest and many helpful discussions. They are also grateful to Mr. Kiyoo Tsuji and Mr. Tatsuo Takeda of their Institute for the preparation of the experimental apparatuses. Thanks are also due to Dr. Kiyokazu Fuke for the measurement of the reflection spectra and his helpful discussions, to Mr. Shojun Hino for his colaboration in the study of *p*-terphenyl, to Dr. J. N. A. Ridyard of Perkin-Elmer Ltd., for the measurement of the molecular photoelectron spectrum of *p*-terphenyl by means of a PS-18 photoelectron spectrometer, and to Professors Satoshi Iwashima and Masahiro Kotani and Dr. Kentaro Murano for the gift of samples. They also wish to thank Professors W. Schmidt and H. Venghaus and Dr. Nobuo Ueno for their communications of experimental results.

PAPENDIX. Remarks on Electron Scattering

In their discussion of the effect of secondary electrons, Schechtman[13] and Kochi *et al.*[5] assumed that pair-production is the main electronic-energy-loss processes of electrons. However, recent results on the energy loss of slow electrons[10,28,33] show that exciton excitation (including triplet excitons) makes a greater contribution to scattering than does pair-production, partic-

Table 8. Energy parameters/eV of aromatic hydrocarbons

	I_g[a]	E_{th}[b]	E_c(calc)[c]	E_T[d]	E_S[e]	E_T+E_c(calcd)	E_S+E_c(calcd)
Anthracene	7.47	5.70	3.93	1.85	3.11 3.16	5.8	7.1
Naphthacene	7.01	5.28	3.55	1.27	2.38 2.46	4.7	7.1
Pentacene	6.64	4.85	3.06	0.95	1.85	4.0	4.9
Perylene	7.00	5.37	3.74	1.56	2.65	5.2	6.4
Coronene	7.34	5.52	3.70	2.37	3.44	6.1	7.1
p-Terphenyl	8.20	6.1	4.0	2.55	4.48	6.6	8.5

a) The first ionization potential of a free molecule; from Refs. 16 and 21. b) Threshold energy of photoemission; from Refs. 7 and 16. c) The energy of the bottom of the broad conduction band calculated from Eq. 5. d) The energy of the lowest triplet state; from Refs. 2 and 34. e) The energy of the lowest singlet state; from Refs. 2 and 34.

ularly at a small energy loss. However, from a comparison of the results of Merkel and Hamill[33] and that of Schechtman, it seems that the conclusion such as that (1) the scattering length $L(E)$ decreases monotonically with E, or that (2) secondary electrons tend to have only a small kinetic energy are also valid for the exciton-excitation process. Therefore, the conclusions described in the discussion should also be valid. The main change in going from pair-production to exciton excitation will be the change in the threshold for scattering: from $2E_g$ for pair-production to E_g+E_x for exciton excitation, where E_g is the band gap and where E_x is the energy of the lowest exciton.

It is somewhat difficult to determine the effective value of E_g for organic crystals. When energy loss occurs, the electron must fall into a lower conduction band. However, the lowest conduction band, at[2,26]

$$E_c' = 2E_{th} - I_g - A_g \quad (4)$$

(where E_{th} is the threshold of photoemission and where I_g and A_g are the ionization potential and the electron affinity of a free molecule), is very narrow, and there may be band gaps between the conduction bands. Therefore, electrons cannot fall into this gap. There seems to be no definite experimental information about the threshold above which an electron with any given energy can undergo inelastic scattering. However, considering the breadth of the exciton bands and the fact that the intermolecular interaction increases with the electron energy, we may use the energy of the bottom of the 'broad conduction band', E_c, evaluated by[2,26]

$$E_c = 2E_{th} - I_g \quad (5)$$

as a guide for the energy of the effective bottom of the continuous band, E_g. The quantities mentioned above are shown in Table 8 for both the lowest triplet and singlet excitons. The results shown in Table 8 demonstrate that almost all the electrons above the threshold can suffer inelastic scattering if triplet excitons are excited. However, no detailed information on the E dependence of $L(E)$ is available at present.

There are other mechanisms of energy loss in organic solids: the excitation and absorption of the phonon and intramolecular vibration, and the excitation of plasmon. The former two do not affect the quantum yield so much, and so we will not discuss them in detail. Plasmon was considered in the discussion of HNMP.

References

1) a) W. E. Spicer, *J. Res. Nat. Bur. Stand.*, **74A**, 397 (1970); b) W. E. Spicer, in "Optical Properties of Solids," ed. by F. Abelès, North-Holland, Amsterdam (1972).

2) F. Gutmann and L. E. Lyons, "Organic Semiconductors," John Wiley and Sons, N. Y. (1967).

3) A. I. Belkind, S. B. Aleksandrov, V. V. Aleksandrov, and V. V. Grechov, "Preprints of Electrical Properties of Organic Solids Conference," Karpacz, Poland (1974) and references therein.

4) F. I. Vilesov, A. A. Zagrubskii, and D. Z. Garbuzov, *Fiz. Tverd. Tela*, **5**, 2000 (1963); *Sov. Phys. Sol. State*, **5**, 1460 (1964).

5) a) M. Kochi, Y. Harada, and H. Inokuchi, *Bull. Chem. Soc. Jpn.*, **40**, 531 (1967); b) M. Kochi, Y. Harada, T. Hirooka, and H. Inokuchi, *ibid.*, **43**, 2690 (1970).

6) T. Hirooka, K. Tanaka, M. Fujihira, H. Inokuchi, Y. Harada, and K. Kuchitsu, *Chem. Phys. Lett.*, **18**, 930 (1973).

7) T. Hirooka, Ph. D. Thesis, Univ. of Tokyo, Tokyo, 1973.

8) a) A. A. Zagrubskii and F. I. Vilesov, *Fiz. Tverd. Tela*, **13**, 2300 (1971); *Sov. Phys. Sol. State*, **13**, 1927 (1972); b) A. A. Zagrubskii and F. I. Vilesov, "Uspechi Fotoniki," Vol. 3, ed. by F. I. Vilesov, Izd. Leningrad Univ., Leningrad (1973), p. 98; c) A. A. Zagrubskii and F. I. Vilesov, "Uspechi Fotoniki," Vol. 4, ed. by F. I. Vilesov, Izd. Leningrad Univ., Leningrad (1974), p. 109.

9) K. Seki, H. Inokuchi, and Y. Harada, *Chem. Phys. Lett.*, **20**, 197 (1973).

10) a) S. Kiyono, N. Ueno, and Y. Hayasi, *Tech. Rep. Tohoku Univ.*, **38**, 173 (1973); b) N. Ueno, Y. Hayasi, and S. Kiyono, *Chem. Phys. Lett.*, **35**, 31 (1975); c) N. Ueno, Y. Hayasi, and S. Kiyono, 30th Annual Meeting of the Physical Society of Japan, Kyoto (1975).

11) K. Seki, Y. Harada, K. Ohno, and H. Inokuchi, *Bull. Chem. Soc. Jpn.*, **47**, 1608 (1974).

12) M. B. Robin, "Higher Excited States of Polyatomic Molecules," Academic Press, N. Y. (1974).

13) a) B. H. Schechtman and W. E. Spicer, *Chem. Phys. Lett.*, **2**, 207 (1970); b) B. H. Schechtman and W. E. Spicer, *J. Mol. Spectrosc.*, **33**, 28 (1970); c) B. H. Schechtman, Ph. D. Thesis, Stanford Univ., Stanford, Calif. U.S.A., 1968.

14) H. -J. Hinz and H. Venghaus, *J. Chem. Phys.*, **62**, 4937 (1975) and references therein; H. Venghaus, private communication.

15) Y. Kamura, K. Seki, and H. Inokuchi, *Chem. Phys Lett.*, **30**, 35 (1975).

16) S. Hino, K. Seki, and H. Inokuchi, *Chem. Phys. Lett.*, **36**, 335 (1975).

17) H. Inokuchi, H. Kuroda, and H. Akamatu, *Bull.*

Chem. Soc. Jpn., **34**, 749 (1961).
18) J. Tanaka, *Bull. Chem. Soc. Jpn.*, **36**, 1237 (1963).
19) A. D. Baker, C. R. Brundle, and D. W. Turner, *Int. J. Mass Spectrom. Ion Phys.*, **1**, 443 (1968).
20) K. Fuke, K. Kaya, T. Kajiwara, and S. Nagakura, *J. Mol. Spectrosc.*, in press.
21) a) P. A. Clark, F. Brogli, and E. Heilbronner, *Helv. Chim. Acta*, **55**, 1415 (1972); b) F. Brogli and E. Heilbronner, *Angew. Chem.*, **84**, 551 (1972); c) R. Boschi, J. N. Murrell, and W. Schmidt, *Discuss. Faraday Soc.*, **54**, 116 (1972); d) R. Boschi and W. Schmidt, *Tetrahedron Lett.*, **1972**, 2557; W. Schmidt, private communication; e) R. Boschi, E. Clar, and W. Schmidt, *J. Chem. Phys.*, **60**, 4406 (1974).
22) a) L. E. Lyons, *J. Chem. Soc.*, **1957** 5001; b) L. E. Lyons and J. C. Mackie, *Proc. Chem. Soc.*, **1962**, 71; c) M. Batley, L. J. Johnstone, and L. E. Lyons, *Aust. J. Chem.*, **23**, 2397 (1970); d) A. Jurgis and E. A. Silinsh, *Phys. Stat. Sol.*, **b53**, 735 (1972).
23) T. Shibata, T. Hirooka, and K. Kuchitsu, *Chem. Phys. Lett.*, **30**, 241 (1975).
24) L. B. Clark, *J. Chem. Phys.*, **53**, 4092 (1970).
25) L. E. Lyons and G. C. Morris, *J. Chem. Soc.*, **1960** 5192.
26) D. M. Hanson, *Crit. Rev. Sol. State Sci.*, **3**, 243 (1973).
27) M. Batley, Ph. D. Thesis, Univ. of Sydney, Sydney, Australia, 1966.
28) a) W. Pong and J. A. Smith, *J. Appl. Phys.*, **44**, 174 (1973); b) S. Hino, N. Sato, and H. Inokuchi, submitted to *Chem. Phys. Lett.*, and references therein; c) S. Hino and N. Sato, private communication.
29) B. E. Cook and P. G. Le Combre, *J. Phys. Chem. Solids*, **32**, 1321 (1971).
30) a) N. Geacintov and M. Pope, *J. Chem. Phys.*, **50**, 814 (1969). b) C. Fuchs and R. Voltz, *Chem. Phys. Lett.*, **18**, 394 (1973).
31) W. Gudat and C. Kunz, *Phys. Rev. Lett.*, **29**, 169 (1972).
32) a) L. Ya. Bubnov, E. L. Frankevich, and B. S. Yakoviev, *Fiz. Tverd. Tela*, **15**, 3415 (1973); *Sov. Phys. Sol. State*, **15**, 2274 (1974); b) L. Ya Bubnov and E. L. Frankevich, *Phys. Stat. Sol.*, **b62**, 281 (1974).
33) P. B. Merkel and W. H. Hamill, *J. Chem. Phys.*, **55**, 1409 (1971).
34) S. P. McGlynn, T. Azumi, and M. Kinoshita, "Molecular Spectroscopy of the Triplet State," Prentice Hall, New Jersey (1969).

The Microwave Spectrum of Thiirane in Excited Vibrational States

Chiaki HIROSE, Kazuhiro OKIYE, and Shiro MAEDA

Research Laboratory of Resources Utilization, Tokyo Institute of Technology, O-okayama, Meguro-ku, Tokyo 152

(Received October 13, 1975)

The microwave spectra in the ground and five low-lying vibrational states of $^{12}C_2H_4{}^{32}S$ and in the ground state of $^{12}C^{13}CH_4{}^{32}S$ and $^{12}C_2H_4{}^{34}S$ have been assigned to high-J transitions. The rotational and centrifugal distortion constants were derived. Four of the five vibrational states were found to be in Coriolis interaction in pairs; one of the pairs was identified as the symmetric and antisymmetric ring deformation modes, $\nu_5(A_1)$ and $\nu_{12}(B_1)$, but another pair was unexplicable from any of the previously reported vibrational assignments. The infrared and Raman spectra in the liquid and gas phases were examined, and the latter pair of vibrations was interpreted as $\nu_{14}(B_2)$ at 945 cm^{-1} and $\nu_8(A_2)$ at about 970 cm^{-1}. This novel assignment of ν_8 around 970 cm^{-1} was based on not only the results of microwave spectroscopy, but also on the observation of an unsymmetric band contour in the infrared spectrum of the gaseous sample.

The vibrational spectrum of thiirane has been studied by several authors;[1-7] Thompson and Dupré[1], who reported in 1940 their observation of the infrared spectrum in the gas phase and the Raman spectrum of the liquid state, proposed a molecular symmetry of C_{2v}, along with an assignment of the vibrational modes. The study by Thompson and Cave[2] revised the assignment on the grounds that the band at 711 cm^{-1} which had been assigned to ν_{12} (ring deformation) in the previous paper was due to the impurity hydrogen cyanide, and that the polarization data from the Raman spectrum also reported in the previous paper were questionable because of the background haze introduced by the formation of a solid polymer during the measurement. Guthrie *et al.*[3] reported the observation of the infrared spectra of the liquid thiirane and of the solid polymer which was deposited on the window of the cell, in addition to the calculation of thermodynamic quantities; they proposed an assignment which was different from the previous ones in the ordering of three pairs of modes. Brumant observed the Raman spectrum of liquid thiirane and the infrared spectrum of the solid polymer,[4a] the Raman spectrum of the solid at 85 K,[4b] and the infrared spectrum of the molecule in an argon matrix at 10 K.[4c] The assignment given by Brumant[4a] puts ν_7 and ν_8, which are of an infrared-inactive A_2 symmetry, at 1172 cm^{-1} and 900 cm^{-1} respectively. Venkatesuwarlu and Joseph calculated the force constants and mean-square amplitude of vibrations,[5] and also the Coriolis coupling constants[6] of ethylene oxide and thiirane on the basis of yet another assignment, one differing from those of the previous reports. A recent study by Hirokawa *et al.*[7] of the infrared spectrum and the force field of ethylene oxide and thiirane deduced essentially the same assignment as that given by Thompson and Cave, except for the vibrations of A_2 symmetry. The assignments given thus far are compared in Table 1; it can be easily seen that the assignments are not conclusive for the ν_7 and ν_8 modes, as has been pointed out by Hirokawa *et al.* In most of the above studies, the assignment of ethylene oxide is referred to; one of them also refers to the assignment of aziridine.

The observation of the microwave spectrum in excited vibrational states is known to provide complementary information on the vibrational assignment. A recent study of the microwave spectrum of ethylene oxide,[8] for instance, cast doubt on the previous assignments which place the ν_8 mode (CH_2 twisting of A_2 symmetry) at about 800 cm^{-1}, because it identified but one vibrational state of symmetric (with respect to C_2 operation) species around 800 cm^{-1} which was assigned to the ν_5 mode (ring deformation of A_1 symmetry) on the basis of the analysis of vibration-rotation interaction. The study concluded that the lowest possible state of A_2 symmetry, ν_8, of ethylene oxide is at about 1000 cm^{-1}.

Table 1. Comparison of vibrational assignments (cm^{-1})

Mode		Set 1[a]	Set 2[a]	Set 3[a]	Set 4[a]	Set 5[a]
ν_1:	CH str.	3017	3000	2993	3017	3012
ν_2:	CH_2 sci.	1471	1446	1450	1471	1454
ν_3:	CH_2 wag.	1101	1025	1027	(1040)	1109
ν_4:	ring breath.	—	1112	1115	(1107)	1024
ν_5:	ring def.	626	625	616	626	624
ν_6:	CH str.	3089	3080	3070	3089	3088
ν_7:	CH_2 rock.	—	875	1172	(971)	891
ν_8:	CH_2 twist.	660	1100	900	660	800
ν_9:	CH str.	(3017)	3000	2993	3017	3012
ν_{10}:	CH_2 sci.	1440	1427	1432	1440	1434
ν_{11}:	CH_2 wag.	1050	1051	1050	1050	1050
ν_{12}:	ring def.	685	660	655	685	660
ν_{13}:	CH str.	(3089)	3080	3070	3089	3088
ν_{14}:	CH_2 rock.	945	824	946	945	945
ν_{15}:	CH_2 twist.	825	943	822	825	824

a) 1; Ref. 2, 2; Ref. 3, 3; Ref. 4, 4; Ref. 5, 5; Ref. 7.

This paper will report on the microwave spectrum in the ground and five vibrational states of thiirane. The symmetry properties with respect to the C_2 operation of the respective vibrations were determined from the measurement of the relative intensities, and the effect of Coriolis interaction was observed as a vibrational dependence of the centrifugal distortion. The infrared spectrum of the gas phase and the Raman spectra of the liquid and gas phases were also studied, and the existence of strong interactions among sets of vibrational modes was indicated by the peculiar band shape and/or polarization-depolarization character of the Raman bands. The results of the infrared and Raman spectra will be excerpted to help in the analysis of the microwave spectrum.

Experimental and Results

The sample of thiirane was a distilled fraction of the product of the reaction of ethylene carbonate with potassium thiocyanate;[9] the sample container was wrapped with aluminum foil to inhibit the photochemical decomposition. White particles precipitated slowly during storage, and the presence of ethylene was observed in the infrared spectrum of the gas when sampled without purification. The impurities were removed by evacuating a liquid sample cooled by dry ice and by a subsequent trap-to-trap transfer of the liquid. The NMR spectrum of the distilled liquid showed peaks above 6 ppm with intensities less than 0.1% of the main peak at 3 ppm; the impurities did not show up in the infrared spectrum of a gaseous sample from the outgassed liquid. The infrared spectrum of the gas showed little difference before and after letting the sample container stand for 40 hours and then placing it under sunlight for two hours. No solid deposit was observed on the KBr windows of the cell despite the previous reference to the phenomenon,[3] and all the lines disappeared when the cell was evacuated. It should be mentioned, though, that the intensity of the microwave absorption lines diminished slowly to about half their original height in a couple of hours, without any new line developing; this indicates that the decomposition of the gas is accelerated on a metal (copper and stainless steel in the present case) surfaces, along with a production of a nonpolar gaseous material.

Microwave Spectrum. The microwave spectrum was observed using a conventional Stark modulation spectrometer. The measurement was performed at room temperature of about 293 K. The assignment of the rotational transitions for $^{12}C_2H_4{}^{32}S$, $^{12}C^{13}CH_4{}^{32}S$, and $^{12}C_2H_4{}^{34}S$ from the previous reports[10,11] was extended to transitions with higher J numbers and, for $^{12}C_2H_4{}^{32}S$, to forbidden transitions. The transitions in five excited vibrational states were also assigned on the basis of the Stark effects, the relative intensities, and the spectral pattern. The five states are tentatively designated as ν_a, ν_b, ν_c, ν_d, and ν_e. The results were analyzed by a least-squares method which included centrifugal distortion to the first order. Table 2* lists the observed frequencies of the assigned transitions, along with their differences from the calculated values. The converged values of the parameters are given in Table 3, along with their reliability intervals of 2.5 times the variances. A preliminary analysis indicated that the higher-order effect of centrifugal distortion becomes significant for the transitions with J numbers exceeding 30. Because the transitions with high J numbers are of the Q branch,[12] the inclusion of higher-order effects from centrifugal distortion is not expected to result in any meaningful values to the newly included parameters. Therefore, the higher-order effects in the least-squares fit, which included centrifugal distortion to the first order, were made insignificant by appropriately weighting the larger J transitions; weighting 1 for transitions with the J values less than 20, 0.01 for the J values from 21 to 30, 0.0001 for the J values between 31 and 50, and 0.000001 for the J values of more than 51, with the exception of the forbidden transitions of the ground state of $^{12}C_2H_4{}^{32}S$, for which the intensity of each transition was taken into account.

The measurement of the spectral intensities was only semi-quantitative because of the wide spread of the transition frequencies by vibrational state, and the instrumental instability.** Nonetheless, it was possible to derive the symmetry properties of the vibrations, along with a rough estimate of the vibrational frequencies, from the measured intensities shown in Table 4. A number of lines were left unassigned, but, judging from their intensities, these lines were from vibrational states higher than those for which rotational transitions were identified. The unassigned lines included some of the $J=1\leftarrow0$ and $J=2\leftarrow1$ transitions of ^{33}S species which have been assigned by Shoemaker and Flygare.[13]

The presence of Coriolis interactions between ν_a and ν_b and between ν_c and ν_e is suggested by the large values of the vibration-rotation constants, $\alpha_v^{(c)}$'s, which exceed 1% of the rotational constant, C_0, of the ground state. This becomes evident when one compares the vibrational change in the corrections for the centrifugal distortion (Fig. 1). The assignment of the two lowest vibrational states, ν_a and ν_b, to the symmetric and antisymmetric ring deformations, ν_5 and ν_{12}, is rather straightforward. The calculation by Venkatesuwarlu and Joseph gives $\zeta_{5,12}^{(c)}=-0.882$, indicating that the Coriolis interaction between the two states should indeed be appreciable about the c-axis. The Coriolis terms in the $\alpha_5^{(c)}$ and $\alpha_{12}^{(c)}$ constants through $\zeta_{5,12}^{(c)}$ are calculated to be +279 MHz and −236 MHz respectively by taking the vibrational frequencies of $\nu_5=624\ cm^{-1}$ and $\nu_{12}=660\ cm^{-1}$. The above terms are dominant in the harmonic terms in $\alpha_5^{(c)}$ and $\alpha_{12}^{(c)}$, as the contributions from other Coriolis terms are

* Table 2 is deposited as Document No. 7612 at the office of the Editor of the Bulletin of the Chemical Society of Japan. Available from the authors on request.

** The transitions used for the measurement of the relative intensities were $1_{0,1}\leftarrow0_{0,0}$, $2_{0,2}\leftarrow1_{0,1}$, $5_{2,3}\leftarrow5_{2,4}$, $7_{2,5}\leftarrow7_{2,6}$, $2_{1,1}\leftarrow1_{1,0}$, $2_{1,2}\leftarrow1_{1,1}$, $3_{1,2}\leftarrow3_{1,3}$, $8_{3,5}\leftarrow8_{3,6}$, and $9_{3,6}\leftarrow9_{3,7}$. The spectral lines of the ^{34}S species, which has the abundance ratio of 4.22% were used as the internal standard instead of those of the normal species in order to avoid the possible saturation of lines and instrumental nonlinearity. A variable attenuator was inserted between the preamplifier and the main amplifier; the depth of attenuation was varied until the spectral line was of the same intensity as the corresponding transition of the ^{34}S species. Although the error in each measurement was from 0.5 to 1 dB, the overall error was estimated to be 2 dB because of the instrumental instability and the possible reflection of microwave power inside the cell. The latter may cause serious error with regard to the transitions of the ν_c, ν_d, and ν_e states since the rotational transitions in these states are widely separated from the corresponding lines of the ^{34}S species (see Table 2). Thus, it is quite possible that ν_d and ν_e are at 824 cm^{-1} and 945 cm^{-1} respectively, as will be estimated in the later part of this paper, despite the result derived from the measurement of the relative intensities of the rotational transitions.

Table 3. Derived rotational, vibration-rotation,

Species[b]	A (α_v^A)[c]	B (α_v^B)[c]	C (α_v^C)[c]	τ_{aaaa}
n, G. S.	21973.86±0.27	10825.11±0.13	8026.29±0.10	−0.182±0.008
^{34}S, G. S.	21972.97±0.67	10551.03±0.34	7874.58±0.22	−0.253±0.26
^{13}C, G. S.	21481.71±0.53	10653.40±0.29	7866.33±0.20	−0.417±0.20
ν_a (A)	+24.69±0.93	+42.95±0.43	+143.81±0.29	−0.509±0.27
ν_b (B)	−70.48±1.1	+79.84±0.57	−54.57±0.38	+0.300±0.33
ν_c (A)	−16.12±1.8	+34.50±0.88	−84.73±0.58	−0.407±0.57
ν_d (B)	−19.73±0.83	+45.87±0.36	+36.57±0.25	−0.123±0.21
ν_e (B)	+67.50±0.82	−0.20±0.39	+99.92±0.27	−0.211±0.23

a) τ_{aacc} was assumed to be zero in the least-squares fit. 2.5 times variances are listed as reliability intervals. state, and ν_a to ν_e: vibrational states of $^{12}C_2H_4{}^{32}S$ with their symmetry properties with respect to C_2 being indi- vibrational states.

Table 4. Symmetry and estimated frequencies of vibrations as derived from the relative intensity measurement

State	Symmetry[a]	(cm^{-1})[b]	Proposed assignment[c]
ν_a	A_1 or A_2	680 (580—890)	ν_5(624 cm^{-1})
ν_b	B_1 or B_2	710 (640—810)	ν_{12}(660 cm^{-1})
ν_c	A_1 or A_2	920[c] (850—1050)	ν_7 or ν_8(970 cm^{-1})
ν_d	B_1 or B_2	950 (860—1120)	ν_{15}(824 cm^{-1})
ν_e	B_1 or B_2	800 (700—1020)	ν_{14}(945 cm^{-1})

a) Symmetry properties with respect to the C_{2v} group are indicated. b) Statistical error limits of 2.5 times variances in the relative intensity measurement are transformed and shown in parentheses to indicate the reliability intervals of the derived frequencies. c) Values in parentheses are those reported in Ref. 7 except for that of ν_c which is estimated from the analysis of Coriolis coupling between ν_c and ν_e and the band contour of infrared spectrum of the gas sample in the present study.

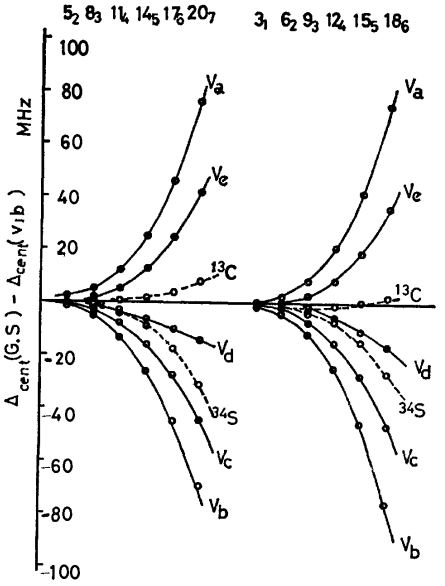

Fig. 1. Vibrational change in the corrections for the centrifugal distortion, $\Delta_{cent}(G.S.)-\Delta_{cent}(v_i)$, and the isotope change are plotted.
Solid and broken lines are drawn to identify the species.

estimated to be within a few megahertz. They are proportional to the inverse of the vibrational difference, $\nu_5-\nu_{12}$, to a good approximation. The observed values are 143.81 MHz and −54.57 MHz for $\alpha_5^{(c)}$ and $\alpha_{12}^{(c)}$ respectively; the rather large difference between the observed and the calculated values indicates that the ν_{12}-ν_5 separation is larger than 26 cm^{-1}, although the value is derived from the most recent assignment.[7] At the same time, the anharmonic terms in the α constants are expected to be of the order of 10 MHz, because when one fits the Coriolis terms in $\alpha_5^{(c)}$ to 140 MHz by putting $\nu_{12}-\nu_5$ to 52 cm^{-1}, there remains a difference of about 60 MHz between the Coriolis term and the observed value of $\alpha_{12}^{(c)}$. A similar situation was encountered in the α constants of ethylene oxide.[8]

The large departure of the centrifugal distortions of the ν_a and ν_b states, each in opposite directions from the ground state seen in Fig. 1, also distinctly shows the presence of the Coriolis interaction. The large uncertainties that accompany the converged values of the centrifugal distortion constants except for those of the ground vibrational state of normal species unfortunately restricted the analysis of the effect and made it semiquantitative.

The almost identical behavior of the pair of ν_c and ν_e to that of ν_b and ν_a in both the $\alpha^{(c)}$ constants and centrifugal-distortion effects strongly suggests another c-type Coriolis interaction between ν_c and ν_e states, with the vibrational frequency ν_c being slightly more than the ν_e. The study of the infrared and Raman spectra which will be outlined in the next section shows that the second lowest antisymmetric vibration is ν_{15} at 824 cm^{-1}; this band is assigned to the CH_2 twisting mode. Other possible candidates for ν_d and ν_c, which are antisymmetric vibrations, are ν_{14} (CH_2 rocking mode) at 945 cm^{-1} and ν_{11} (CH_2 bending mode) at 1050 cm^{-1}. Our results show that ν_c is the second lowest vibration of A symmetry, that is either $\nu_4(A_1)$ or $\nu_8(A_2)$, and we have already mentioned that no conclusive assignment has been given to the ν_7 and ν_8 modes by the study of the vibrational spectra. The values which determine the Coriolis coupling are listed in Table 5, the coupling constants used in the table being excerpted from the paper by Venkatesuwarlu and Joseph.[6] Although the values may change when

AND CENTRIFUGAL DISTORTION CONSTANTS (in MHz)[a]

	τ_{bbbb}	τ_{cccc}	τ_{aabb}	τ_{bbcc}
n, G. S.	−0.067±0.003	−0.023±0.002	−0.179±0.01	−0.048±0.003
^{34}S, G. S.	−0.016±0.14	+0.014±0.14	−0.042±0.25	+0.018±0.17
^{13}C, G. S.	−0.082±0.12	−0.055±0.12	−0.153±0.22	−0.054±0.15
ν_a (A)	−0.027±0.12	+0.031±0.12	−0.054±0.22	+0.023±0.15
ν_b (B)	−0.087±0.18	−0.069±0.18	−0.191±0.33	−0.097±0.21
ν_c (A)	−0.071±0.31	−0.063±0.31	−0.100±0.56	−0.046±0.37
ν_d (B)	−0.085±0.09	−0.049±0.09	−0.172±0.17	−0.076±0.11
ν_e (B)	−0.036±0.11	+0.016±0.11	−0.105±0.19	−0.006±0.13

b) n, G. S.: $^{12}C_2H_4{}^{32}S$ in ground state, ^{34}S, G. S.: $^{12}C_2H_4{}^{34}S$ in ground state, ^{13}C, G. S.: $^{12}C^{13}CH_4{}^{32}S$ in ground cated in parentheses. c) Vibration-rotation constants ($\alpha_v^B = X_0 - X_v$, $X = A$, B, or C) are listed for excited

TABLE 5. CONSTANTS THAT CAN PARTICIPATE IN CORIOLIS INTERACTION (in MHz)[a)]

$C\zeta^{(c)}_{3,11}$	1585		
$C\zeta^{(c)}_{3,12}$	−51	$C\zeta^{(c)}_{7,14}$	1462
$C\zeta^{(c)}_{4,11}$	1422	$C\zeta^{(c)}_{7,15}$	6175
$C\zeta^{(c)}_{4,12}$	−3186	$C\zeta^{(c)}_{8,14}$	−6154
$C\zeta^{(c)}_{5,11}$	−2015	$C\zeta^{(c)}_{8,15}$	2423
$C\zeta^{(c)}_{5,12}$	−7078		

a) As for the types of vibrations, see set 4 of Table 1. Contributions of Coriolis terms to $\alpha_v^{(x)}$ and the centrifugal distortion constants are expressed as;

$\Delta\alpha^{(x)}_{v,v'}(\text{Coriolis}) = -8c/\nu_v \cdot \nu_{v'}^2/(\nu_v^2 - \nu_{v'}^2) \cdot (X\zeta^{(x)}_{v,v'})^2$

$\Delta\tau^{v,v'}_{xxxx}(\text{Coriolis}) = c'(\nu_v + \nu_{v'})^4 (X\zeta^{(x)}_{v,v'})^4/(\nu_v - \nu_{v'})^3 \nu_v^2 \nu_{v'}^2$,

where $\Delta\alpha^{(x)}_{v,v'}$ and $\Delta\tau^{v,v'}_{xxxx}$ are the contribution to the vibration-rotation constant $\alpha_v^{(x)}$ and the centrifugal distortion constant τ_{xxxx} in the v-state, respectively, ν_v and $\nu_{v'}$ are the vibrational frequencies of ν_v and $\nu_{v'}$ modes, c and c′ are the constants to give proper units to the quantities, and X is the rotational constant A_0, B_0, or C_0 depending on the principal axis of inertia denoted by x.

other vibrational assignments are used, the changes are expected to be small, as is the case in ethylene oxide. Table 5 indicates that the two pairs, ν_7 and ν_{15}, and ν_8 and ν_{14}, are capable of similar interaction, and thus likely candidates for the ν_c and ν_e pair. The infrared spectrum of the gaseous sample shows a band contour at 945 cm^{-1} (ν_{14}) unsymmetric about the sharp Q-branch peak. The perturbation through Coriolis interaction between ν_{14} and ν_8 modes is a plausible explanation for the peculiar band shape; the assignment of ν_c and ν_e to ν_8 and ν_{14} respectively is then more likely than the other sets. The remaining state, ν_d, can then be assigned to ν_{15} at 825 cm^{-1}. Thus the present study of the microwave spectrum suggests the assignment of ν_8 at 970±5 cm^{-1}.

Infrared and Raman Spectra. The vibrational spectrum of thiirane was reexamined; the infrared spectrum in the gas phase was observed from 400 cm^{-1} to 10000 cm^{-1} using a Perkin-Elmer 125 spectrograph, while the Raman spectrum was recorded on a JEOL model JRS-SI spectrometer in both gas and liquid phases by using a 488-nm line of the Ar$^+$ laser (Coherent Radiation CR-52G) as the exciting source. The sample was outgassed prior to each measurement to get rid of the ethylene impurity produced by decomposition. The cell used for the infrared spectrum was a 10-cm-long Pyrex tube with KBr windows. The liquid sample for the Raman spectrum was distilled and sealed in a conventional cell made of a Pyrex tube of about 8 mm i. d., while the Raman spectrum of the gas was recorded at a pressure of 148 Torr using a multipass configuration of about 30 beams.

A summary of the Raman spectrum is given in Table 6, with the previous observation by Brumant in the liquid phase being given for reference. The infrared spectrum of gaseous thiirane from 800 to 1180 cm^{-1} is shown in Fig. 2. Corresponding to a weak Q-branch peak observed in the infrared spectrum, the Raman spectrum of the liquid sample showed a depolarized band at 825 cm^{-1}, leading us to the assignment of this band to the lowest mode of B_2 symmetry, ν_{15}. The polarized Raman band at 1607 cm^{-1} can then be readily assigned to the overtone, $2\nu_{15}$. A very weak band was observed in the Raman spectrum of the liquid sample; it was also reported by Brumant[4b)] at 895 cm^{-1}. The observation of this band in the infrared spectrum too was reported by Hirokawa *et*

TABLE 6. SUMMARY OF RAMAN BANDS OF THIIRANE (in cm^{-1})

liquid[a)]		gas[b)]	liquid[a)]		gas[b)]
612*	s,P	632	1430	m	1434+
650	m	662+	1448	m,P	1454+
825	w,dP		1607	m,P	
895	vw,P?		2230*	w,P	
947	w,dP		2845	m,P	2860
1023	m,P	1028	2885	m,P	2900
1113	s,P	1115	(2904)		
(1172)			2995	vs,P	3011
1235	w,P		3076	m	3060+
1377*	w,P				

a) Bands that are not reported in Ref. 4b is indicated by * while the bands which were not observed in the present study despite the reported observation (Ref. 4b) as very weak bands are indicated in parentheses. Intensities are indicated by; vs: very strong, m: moderately strong, w: weak, and vw: very weak. Polarized bands are indicated by the letter P. b) Bands with broad contour are indicated by +.

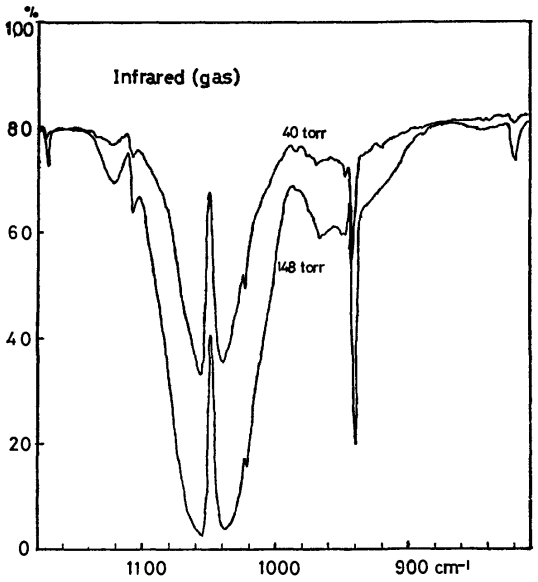

Fig. 2. Infrared spectrum of thiirane at gas phase between 810 to 1180 cm^{-1}.

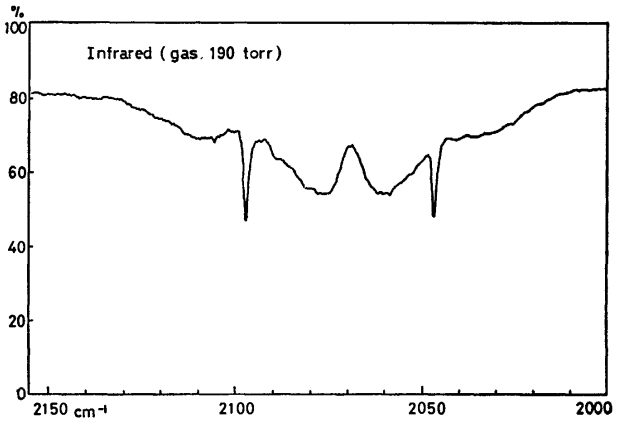

Fig. 3. Infrared spectrum of thiirane in the overtone region of 2000—2150 cm^{-1}.
A B-type band center is situated between the A-type Q-branches of overtones.

al.,[7] who assigned it to the infrared-inactive ν_7 mode, but the present study failed to detect it (see Fig. 2). Since all of the infrared-active fundamentals are found at other frequencies, the band at 895 cm^{-1} has to be interpreted either as an infrared-inactive ν_7 or ν_8 or as due to some impurity. There is no infrared band near 895 cm^{-1} which can give some intensity to an infrared-inactive mode through Coriolis interaction; thus, the assignment of ν_7 or ν_8 at 895 cm^{-1} can be ruled out if the observation by Hirokawa *et al.* is to be retained.

Four vibrational modes have been assigned in the region from 900 to 1200 cm^{-1}; two CH_2 bending modes, $\nu_3(A_1)$ at 1109 cm^{-1} and $\nu_{11}(B_1)$ at 1050 cm^{-1}, a ring breathing, $\nu_4(A_1)$ at 1024 cm^{-1}, and a CH_2 rocking mode, $\nu_{14}(B_2)$ at 945 cm^{-1}.[7] The Raman spectrum of the liquid gave one depolarized band at 947 cm^{-1} and two polarized bands at 1023 and 1113 cm^{-1}. The two polarized bands were also observed in the Raman spectrum of the gas phase. A polarized band was observed at the overtone region of 2230 cm^{-1} in the liquid phase. Although the infrared spectrum of this region is quite complicated, as may be seen from Fig. 2, the assignment of the bands is rather straightforward: $\nu_{14}(B_2)=945$ cm^{-1}, $\nu_4(A_1)=1024$ cm^{-1}, $\nu_{10}(B_1)=1050$ cm^{-1}, and $\nu_3(A_1)=1109$ cm^{-1}, when one takes the Raman results into account. The assignment of lines at 1024 and 1050 cm^{-1} is further confirmed by the appearance of two A-type bands and a B-type band center in between them in the overtone region of the infrared spectrum, as is shown in Fig. 3.

The infrared spectrum shows an anomalous shoulder on the R-branch side of ν_{14} at 945 cm^{-1}. The pressure dependence of the shoulder indicates that it originates from the sample itself. As vibrational modes of A_1, B_1, and B_2 symmetry species are identified at other frequencies, as has been mentioned before, the shoulder can be explained as resulting from the intensity borrowing of an A_2 mode through the Coriolis interaction with ν_{14}. Judging from the values of the Coriolis coupling terms listed in Table 5, the assignment of the symmetric CH_2 twisting at about 970 cm^{-1} is probably the most reasonable. Finally, the weak band observed at 1172 cm^{-1} in the infrared spectrum was explained by Hirokawa *et al.* as due to a polymer,[7] but the pressure dependence of the band (see Fig. 2) seems to indicate that the band is from the sample itself. The explanation is open to speculation at the moment, but it should be remembered that weak and polarized Raman bands were observed at 1230 and 1377 cm^{-1} which can best be explained as the $2\nu_5$ and $2\nu_{12}$ overtones respectively.

Conclusion

Of the five vibrational states for which the rotational spectrum has been identified, the lowest two states, ν_a and ν_b, are in resonance through a Coriolis term; they were assigned to ν_5 and ν_{12} (symmetric and antisymmetric ring deformation modes). Another coupling between the ν_c and ν_e, as observed in the microwave spectrum, indicates the assignment of ν_c to ν_8 (CH_2 twisting) of A_2 symmetry and ν_e to ν_{14} (CH_2 rocking) at about 970 cm^{-1} and 945 cm^{-1} respectively. The fact that ν_c is slightly more than ν_e and that the ν_4 and ν_{11} states are free from Coriolis interactions, as seen by the infrared spectrum in the overtone region (Fig. 3), excludes the assignment of ν_c and ν_e to ν_8 at 970 cm^{-1} and ν_{15} at 824 cm^{-1} or to ν_4 at 1024 cm^{-1} and ν_{11} at 1050 cm^{-1}, respectively. The complicated-looking band contour observed in the infrared spectrum around 950 cm^{-1} supports the present assignment. The remaining state, ν_d, which is antisymmetric to the C_2 operation, is assigned to ν_{15} (CH_2 twising) at 824 cm^{-1}, the lowest vibration of B_2 symmetry and the second lowest of the antisymmetric modes. The very weak Raman band at 895 cm^{-1}, which Hirokawa *et al.* claim to have observed also in the infrared spectrum of the gas phase, may be the remaining mode of A_2 symmetry, although its appearance in the infrared spectrum would present a serious contradiction to this assignment since there is no neighboring band which

can couple with and give away a part of its infrared intensity to the infrared-inactive ν_8 mode. Thus, the band at 895 cm^{-1} may well be due to an impurity. In any event, there is little chance for the ν_8 mode to be around the previously estimated 800 cm^{-1}. This conclusion is in accord with that obtained for ethylene oxide.[8)]

The present study revealed the existence of couplings among several sets of vibrations and suggests the need of further investigations to establish the vibrational assignment of thiirane.

The authors are grateful to Professor Yonezo Morino, Dr. Shuji Saito, and Dr. Charles D. LeCroix for their critical reading of the manuscript.

References

1) H. W. Thompson and D. J. Dupré, *Trans. Faraday Soc.*, **36**, 805 (1940).
2) H. W. Thompson and W. T. Cave, *ibid.* **47**, 951 (1951).
3) G. B. Guthrie, Jr., D. W. Scott, and G. Waddington, *J. Am. Chem. Soc.*, **74**, 2795 (1952).
4) a) L. LeBrumant, *C. R. Acad. Sci. Paris, Ser. B*, **266**, 283 (1968) b) J. LeBrumant, *ibid*, **268**, 486 (1969), c) J. LeBrumant, *ibid*, **270**, 801 (1970).
5) K. Venkatesuwarlu and P. A. Joseph, *J. Mol. Struct.*, **6**, 145 (1970).
6) K. Venkatesuwarlu and P. A. Joseph, *Ind. J. Pure Appl. Phys.*, **10**, 754 (1972).
7) T. Hirokawa, M. Hayashi, and H. Murata, *J. Sci. Hiroshima Univ.*, **37A**, 2831 (1973).
8) N. Yoshimizu, C. Hirose, and S. Maeda, *Bull. Chem. Soc. Jpn.*, **48**, 2529 (1975).
9) *Org. Synth.*, **42**, 59 (1962).
10) G. L. Cunningham, Jr., A. W. Boyd, R. J. Myers, W. D. Gwinn, and W. I. LeVan, *J. Chem. Phys.*, **19**, 676 (1951).
11) K. Okiye, C. Hirose, D. G. Lister, and J. Sheridan, *Chem. Phys. Lett.*, **24**, 111 (1974).
12) Q-branch transitions were classified into several sets as indicated in Table 2; successive transitions in a set have J values changing by 3 and K_{-1} by 1. This classification was of help in predicting the transitions to be measured.
13) R. L. Shoemaker and W. H. Flygare, *J. Am. Chem. Soc.*, **90**, 6263 (1968).

Electronic Structure and Spectra of Acrylic Acid in the Vapor and Condensed Phases

Hiroshi MORITA, Kiyokazu FUKE, and Saburo NAGAKURA

The Institute for Solid State Physics, The University of Tokyo, Roppongi, Minato, Tokyo 106

(Received October 27, 1975)

Near and vacuum UV absorption spectra of acrylic acid were measured at room temperature in the vapor phase and at 77 K in the condensed phase. From a comparative study of the observed spectra, a Rydberg excitation band was observed at 7.46 eV in addition to valence-shell transition bands. The estimated value of the quantum defect ($\delta=1.01$) indicates that the Rydberg orbital is 3s. A new modified CNDO-CI method applicable to planar molecules was developed and applied to acrylic acid to investigate the valence-shell transitions, the observed bands at ~5.0 and 6.71 eV being assigned to the transitions to the n-π^* and π-π^*, respectively.

Electronic absorption spectra of carboxylic acids have been studied extensively[1-3] in comparison with those of amides, acyl fluorides, and carbonyls. Concerning acetic acid, Barnes and Simpson[1] assigned the bands at 48000, 58000, 63000, and 68000 cm^{-1} to the transitions to n-π^*, n'-π^*, n-σ^*, and π-π^* states, respectively. On the other hand, from a comparison of the spectrum in the vapor phase with that in the condensed phase and also from the calculation of the electronic structure, Basch, Robin, and Kuebler[3] assigned the bands of trifluoroacetic acid observed near 48000, 62000, 68000, and 77000 cm^{-1} to the transitions to n-π^*, n-3s Rydberg, π-π^*, and n-3p Rydberg states, respectively, emphasizing the existence of Rydberg excitation bands in the vacuum ultraviolet (VUV) region.

Acrylic acid has the vinyl group conjugating with the carboxyl group. The conjugation may be expected to have some effect on both the valence-shell transition bands and the Rydberg excitation bands. According to our knowledge, the absorption spectrum of acrylic acid has scarcely been studied.[4] This is because analysis of the result may be complicated by the existence of the *s-cis-* and *s-trans*-isomers in the vapor phase at room temperature,[5] the formation of the dimer at higher pressure,[6] and the occurrence of thermal and photochemical reactions.[7]

In the present study, we have measured the near and vacuum UV absorption spectra of acrylic acid in the vapor and condensed phases, for the purpose of identifying the Rydberg excitation bands in addition to the valence-shell transition bands. Furthermore, to understand the electronic structure of acrylic acid, we have calculated the electronic structures of the *s-cis-* and *s-trans*-acrylic acids in monomeric form and also of the dimer by a new modified CNDO-CI method suitable for interpretation of electronic structures of planar molecules, σ- and π-orbitals being treated independently in estimating semi-empirical core resonance, Coulomb repulsion, and core potential integrals.

Experimental

Acrylic acid (Wako G. R. grade) was purified by vacuum distillation through a column filled with silica gel and diphosphorus pentaoxide immediately before use. Cyclohexane (Wako Spectro grade) was used without further purification.

Absorption spectra of the cyclohexane solution of acrylic acid were measured at room temperature with a Cary recording spectrophotometer model 14. Vapor-phase absorption spectra of acrylic acid at various pressures were measured at room temperature with a JASCO VUV-3 recording spectrophotometer,[8] a 10 cm cell being used. The vapor pressure of the sample was regulated with a cryogenic bath at various temperatures.

Near and vacuum UV absorption spectra in a condensed phase were measured at 77 K with a spectrophotometer constructed in our laboratory.[9] A thin film of pure acrylic acid was prepared by spraying the vapor onto a refrigerated CaF_2 window on a Dewar flask through a gas-inlet nozzle.

Theoretical

The modified CNDO-CI method (see Appendix) was applied to acrylic acid to investigate the valence-shell transitions. Since the monomeric *s-cis-* and *s-trans*-isomers and dimeric species of acrylic acid co-exist in the vapor phase,[5,6] calculations for all the species were performed by the use of the semi-empirical parameters listed in Table 1.

The geometry and molecular parameters for the monomeric and dimeric species were taken from the electron diffraction study by Ukaji.[10] The O–H bond length was assumed to be 0.96 and 1.00 Å for the monomer and dimer, respectively.

Results and Discussion

The absorption spectra measured with gaseous acrylic acid at various vapor pressures in the 43000—

TABLE 1. ONE-CENTER COULOMB REPULSION INTEGRAL ($\gamma_{\sigma_A\sigma_A}$ or $\gamma_{\pi_A\pi_A}$ (eV)) AND BONDING PARAMETER (β^0_A (eV)) FOR H, C, AND O ATOMS

	H	C		O		
		σ-AO	π-AO	σ-AO	π-AO	R-COOH[a]
γ	12.85	13.22	10.60	18.76	14.67	17.89
β^0_A	−12.0	−17.9	−12.9	−30.5	−19.8	−27.0

a) Values employed for both the σ- and π-AO's of O atom in the carboxyl group.

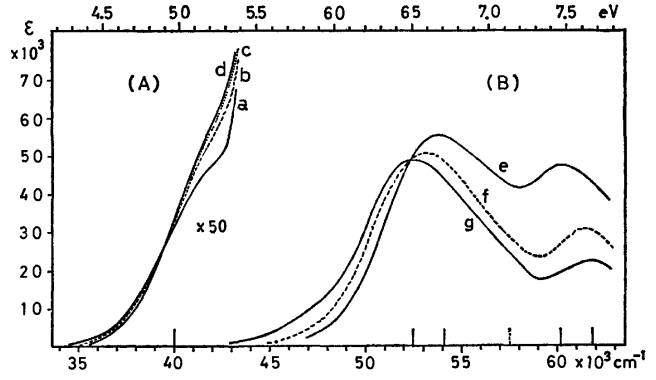

Fig. 1. Near and vacuum UV absorption spectra of acrylic acid measured at room temperature: (A) in cyclohexane (35000—43000 cm^{-1} region); (B) in the vapor phase (43000—63000 cm^{-1} region). The concentrations of acrylic acid are a, 8.9×10^{-4} M; b, 1.1×10^{-2} M; c, 2.7×10^{-2} M; d, 2.6×10^{-1} M; e, 2.3×10^{-6} M; f, 4.6×10^{-5} M; g 3.0×10^{-4} M.

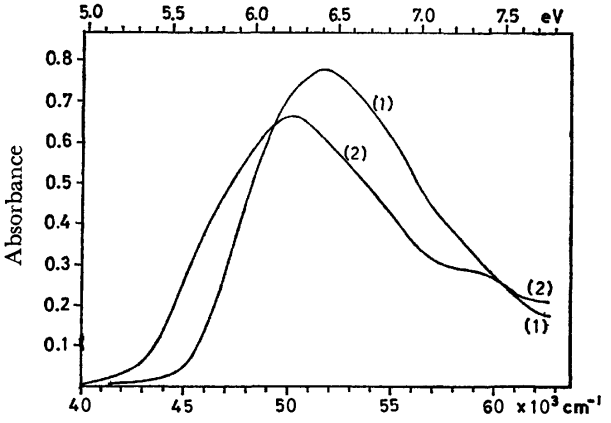

Fig. 2. Near and vacuum UV absorption spectrum observed at 77 K with a thin film of acrylic acid prepared (1) quickly (within one minute) and (2) slowly (for ten minutes).

63000 cm^{-1} region are shown in Fig. 1. This figure also shows the spectra measured for the cyclohexane solution with various concentrations of acrylic acid in the 35000—43000 cm^{-1} region. Spectral curves a and e in Fig. 1 are mainly due to the monomeric species, and curves d and g to the dimeric one. Since the *s-cis*- and *s-trans*-isomers of acrylic acid co-exist comparably,[5] we could only observe the spectrum for the mixture of both isomers. Table 2 gives transition energies and oscillator strengths calculated by the modified CNDO-CI method for the *s-cis*- and *s-trans*-isomers of acrylic acid.

From a comparison of the observed and theoretical values of the band intensity and position, the weak band near 40000 cm^{-1} (~5.0 eV) observed with the cyclohexane solution is safely ascribed to the first n-π^* transition. According to the concentration dependence of acrylic acid on the first n-π^* band (Fig. 1), the band shifts to higher frequencies by about 1000 cm^{-1} (0.12 eV) for the dimer. The result agrees well with the theoretical prediction (higher frequency shift of 0.13—0.14 eV by the dimer formation).

Let us turn to the VUV bands observed with acrylic acid. As is seen in curve e (Fig. 1), two absorption peaks appear at 54100 cm^{-1} (6.71 eV) and at 60200 cm^{-1} (7.46 eV) in the VUV absorption spectrum of gaseous acrylic acid. The band at 7.46 eV is very sensitive to the pressure of acrylic acid and decreases its intensity to a great extent with increasing pressure. This indicates that the upper state of the band is of the "big-orbit" nature. In order to check this point, we measured the VUV absorption spectrum in the condensed phase at 77 K. Actual measurements were made with thin films prepared by spraying gaseous acrylic acid on a cooled CaF_2 plate in a vacuum vessel; the result is shown in Fig. 2. Spectrum 1 was obtained for the sample prepared quickly (within one minute) and may conceivably correspond to that of anomalous solid; spectrum 2 was obtained for the sample prepared slowly (about ten minutes) and may correspond to that of the dimeric species in microcrystal. We can see that the 7.46 eV band observed with gaseous acrylic acid disappears almost completely in the condensed phase. This shows that the band is due to the transition to the upper state of "big-orbit" nature and can safely be assigned to the Rydberg transition.

The Rydberg excitation energy is expected to fit the following formula[3,11]

$$h\nu = I_p - (109737/(n-\delta)^2)$$

where $h\nu$ is the excitation energy (cm^{-1}), I_p is the ionization potential (cm^{-1}), and δ is the quantum defect which results from the penetration of Rydberg orbital into the core. By applying the equation to the observed band at 7.46 eV of acrylic acid, δ was determined to be 1.01, corresponding to $n=3$. This strongly suggests that the band is due to the transition to the 3s Rydberg orbital[11] as the first Rydberg band of CF_3COOH.[3]

The strong band at 6.71 eV in curve e (Fig. 1) is much less sensitive to the pressure of acrylic acid compared with that at 7.46 eV, although it shifts to lower frequencies with increasing pressure (by about 1600 cm^{-1} (0.20 eV)), and appears even in the condensed phase as strongly as in the vapor phase. Therefore, the band is interpreted to be a valence-shell transition band. From a comparison of the observed band position and intensity with the theoretical values given in Table 2, the 6.71 eV band can safely be assigned to the first π-π^* transition.

The spectrum of acrylic acid in the condensed phase (curve 2, Fig. 2) has a peak at 59500 cm^{-1} (7.38 eV). This may correspond to a band at 61800 cm^{-1} (7.66 eV) in the vapor-phase spectrum (curve g, Fig. 1). We interpret that the 7.66 eV band is different from the Rydberg transition band at 7.46 eV; the former is covered by the latter in the spectrum of low vapor pressure (curve e, Fig. 1). From the theoretical results (Table 2), the band at 7.66 eV in the vapor phase may tentatively be assigned to the transition to the second π-π^* state. Curves f and g (Fig. 1) show another weak band appearing as a shoulder at 57500 cm^{-1} (7.13 eV). This band may tentatively be as-

Table 2. Transition energies (ΔE (eV)) and oscillator strengths (f) observed and calculated for the monomeric and dimeric species of *s-trans*- and *s-cis*-acrylic acid

Assignment	Monomer						Dimer				
		s-cis-isomer		*s-trans*-isomer				*s-cis*-isomer		*s-trans*-isomer	
	ΔE_{obsd}[a]	ΔE_{calcd}	f_{calcd}	ΔE_{calcd}	f_{calcd}	main configuration	ΔE_{obsd}[a]	ΔE_{calcd}	f_{calcd}	ΔE_{calcd}	f_{calcd}
n-π^*	~5.0	3.91	0.000_3	3.84	0.000_6	14-15 (14-16)	~5.1	4.05[b]	0 0.000_9	3.97[b]	0 0.001
π-π^*	6.71	6.62	0.353	6.91	0.697	13-15	6.51	6.61 6.70	0.740 0	6.95 6.97	1.470 0
σ-π^*		6.91	0.002	6.92	0.000_7	11-15		6.74[b]	0 0.002	6.73[b]	0 0.000_8
n-π^*		7.73	0.007	7.57	0.004	14-16 10-15 14-15		7.65[b]	0 0.009	7.52[b]	0 0.006
π-π^*		8.27	0.268	8.12	0.014	12-15 (13-16)	7.66	8.03 8.18	0 0.650	7.86 7.97	0 0.029
π-σ^*		8.25	0.028	8.21	0.029	12-17 13-17 12-20		8.52[b]	0 0.050	8.49[b]	0.050 0
σ-π^*		8.89	0.000_6	8.78	0.005	10-15		8.72[b]	0 0.000	8.69[b]	0 0.005
n-σ^*		9.11	0.113	9.04	0.013	14-17 (13-16)		9.04 9.09	0.110 0	9.03 9.09	0.029 0

a) Observed values in the vapor phase. b) Degenerate levels.

signed to the weak σ-π^* or n-π^* transition.

Next, let us examine the nature of the valence-shell transition bands in detail. Figure 3 shows low-lying electron configurations (with in-plane transition moments) caused by valence-shell excitations and the energy levels of *s-trans*-acrylic acid evaluated by considering the configuration interaction. In this figure, *i-j* represents a singly excited configuration caused by the one-electron excitation from the *i*-th occupied orbital to the *j*-th vacant orbital. The shapes of orbitals 10 to 17 are also shown in Fig. 4. As is shown in Fig. 3, the 13-15 configuration of *s-trans*-acrylic acid contributes predominantly (87.8%) to the first allowed π-π^* state, and the 12-15 and 13-16 configurations contribute mainly (60.0% and 18.1%, respectively) to the second π-π^* state. From the shapes of orbitals 12, 13, 15, and 16 (Fig. 4), it is seen that the 6.71 eV band (*i.e.*, the first π-π^* band) is due to the π-π^* excitation within the vinyl group of acrylic

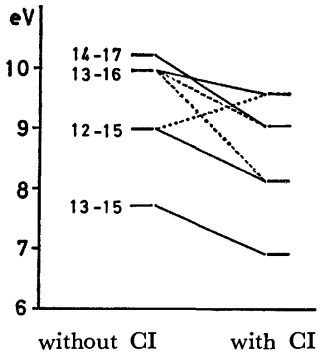

Fig. 3. Energy levels calculated with and without CI treatment for some lower π-π^* and n-σ^* excited states of *s-trans*-acrylic acid.

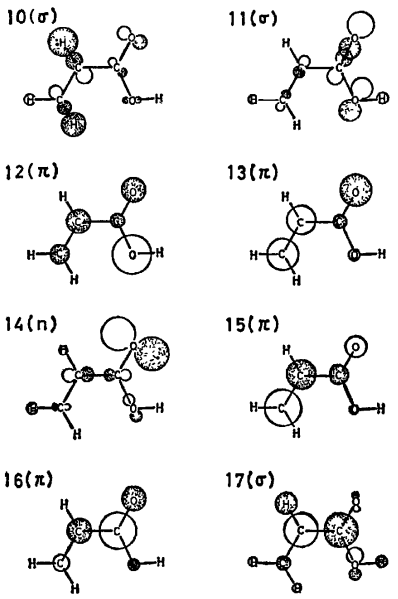

Fig. 4. Schematic shapes of some occupied and vacant MO's of *s-trans*-acrylic acid.

acid, and that the 7.66 eV band (*i.e.*, the second π-π^* band) is due to the intramolecular charge-transfer (from the carboxyl group to the vinyl group) excitation. The nature of the π-π^* transitions is different from that of formic or acetic acid.[2,3] The main configurations of other transitions are also listed in Table 2, and the characters of the transitions can easily be seen from the shapes of orbitals in Fig. 4. Essentially the same conclusion can be derived from the energy levels and wave functions calculated for *s-cis*-acrylic acid and for the dimer.

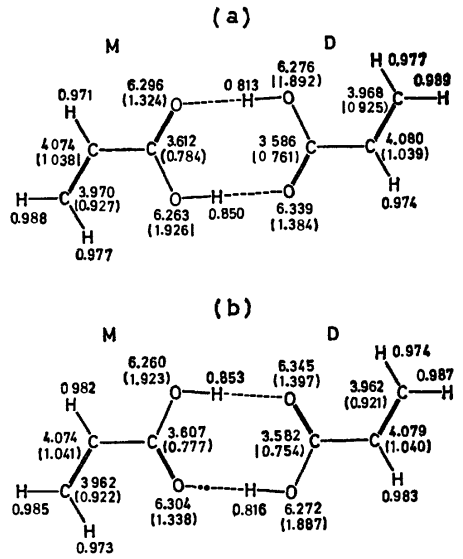

Fig. 5. The total and π- (in parentheses) electron densities calculated for monomeric and dimeric species of (a) *s-trans*-acrylic acid, and (b) *s-cis*-acrylic acid. The electron densities of the monomer and dimer are shown on the left-hand-side and right-hand-side molecules of the dimer, respectively.

Figure 5 shows electron densities for the ground states of monomeric and dimeric species of *s-cis*- and *s-trans*-acrylic acids. The dipole moment in the ground state was calculated to be 1.35 and 0.88 D for *s-trans*- and *s-cis*-acrylic acids, respectively.

The authors are greatly indebted to Dr. Akira Kuboyama, National Chemical Laboratory for Industry, for his kindness in putting a JASCO VUV-3 recording spectrophotometer at their disposal.

Appendix

Modified CNDO-CI Method Applicable to Planar Molecules. The original CNDO method by Pople, Santry, and Segal[12,13] and CNDO/S method by Bene and Jaffé[14] combined with configuration-interaction (CI) were modified to calculate the electronic structures of planar molecules.

a) Conditions for Transformation Invariance: Our guiding principle is to distinguish the σ- and π-electrons from each other in evaluating semi-empirically some kinds of integrals. Our consideration is restricted to only planar molecules. Let us fix the x-y plane as the molecular plane, and define the 2pz atomic orbital (AO) (designated as z_A) as π-orbital on atom A, π_A. Suppose that one of such operations within the molecular (x-y) plane as rotations about local axes and hybridization is designated by an orthogonal transformation matrix, **O**. In order to preserve invariance under these operations based on the assumption of zero differential overlap (ZDO) employed in the present procedure, the CNDO SCF procedure should satisfy the following transformation conditions between original atomic orbital basis functions, $\boldsymbol{\chi}$ and new ones, $\mathbf{t}(=\mathbf{O}\boldsymbol{\chi})$, concerning core Hamiltonian matrix elements (H_{mn}) and Coulomb repulsion integrals ($(mn|ls)$).

$$H_{mn} = \sum_{\mu,\nu} O_{m\mu} O_{n\nu} H_{\mu\nu} \tag{1}$$

$$(mn|ls) = \sum_{\mu}\sum_{\nu}\sum_{\lambda}\sum_{\sigma} O_{m\mu} O_{n\nu} O_{l\lambda} O_{s\sigma} (\mu\nu|\lambda\sigma) \tag{2}$$

where Greek subscripts indicate the original basis functions, and Roman subscripts the new ones. From Eq. 1 the following relations are derived concerning the bonding parameters, $\beta^0_{\sigma_A}$, of the three σ-AO's on atom A and also concerning the core potential integrals, $(\sigma_A\sigma_A|V_B)$, between the σ_A orbitals and the core potential of atom B;

$$\beta^0_{\sigma_A} \equiv \beta^0_{s_A} = \beta^0_{x_A} = \beta^0_{y_A} \tag{3}$$

$$(\sigma_A\sigma_A|V_B) \equiv (s_As_A|V_B) = (x_Ax_A|V_B) = (y_Ay_A|V_B) \tag{4}$$

On the assumption of ZDO, Eq. 2 gives the following relations:
For the one-center Coulomb repulsion integrals;

$$\gamma_{\sigma_A\sigma_A} \equiv \gamma_{s_As_A} = \gamma_{x_Ax_A} = \gamma_{y_Ay_A} = \gamma_{s_Ax_A} = \gamma_{s_Ay_A} = \gamma_{x_Ay_A} \tag{5}$$

$$\gamma_{\sigma_A\pi_A} \equiv \gamma_{s_Az_A} = \gamma_{x_Az_A} = \gamma_{y_Az_A} \tag{6}$$

For the two-center Coulomb repulsion integrals;

$$(\sigma_A\sigma_A|\nu_B\nu_B) \equiv (s_As_A|\nu_B\nu_B) = (x_Ax_A|\nu_B\nu_B) = (y_Ay_A|\nu_B\nu_B) \tag{7}$$

where ν_B is a σ- or π-orbital on atom B. Equations 3—7 are concerned only with the σ-AO's. The corresponding integrals for π-AO, *i.e.*, $\beta^0_{z_A}$, $(z_Az_A|V_B)$, $\gamma_{z_Az_A}$, and $\gamma_{z_Az_B}$ can be determined separately from the values in Eqs. 3—7.

b) Parametrizations: On the basis of the above relationships, the one-center Coulomb repulsion integral, $\gamma_{\sigma_A\sigma_A}$ and $\gamma_{\pi_A\pi_A}$, were taken to be equal to the difference[15] between the ionization potential, I, and electron affinity, A, of an appropriate valence state.[16,17] Their values employed in the present paper are listed in Table 1. The $\gamma_{\sigma_A\pi_A}$ values and two-center Coulomb repulsion integrals between all the σ- and π-AO's were evaluated from the $\gamma_{\sigma_A\sigma_A}$ and $\gamma_{\pi_A\pi_A}$ values by the use of Klopman's equation,[18] Eqs. 6 and 7 being satisfied.

The core potential integral was evaluated for σ-AO by Eq. 8 and for π-AO by Eq. 9.

$$(\sigma_A\sigma_A|V_B) = Z_B \times (\sigma_A\sigma_A|\sigma_B\sigma_B) \tag{8}$$

$$(\pi_A\pi_A|V_B) = Z_B \times (\pi_A\pi_A|\sigma_B\sigma_B) \tag{9}$$

where Z_B is the core charge of atom B. The bonding parameters for σ- and π-AO's were assumed to be proportional to each valence state ionization potential for the carbon and oxygen atoms, whereas the value for the hydrogen atom, β^0_H was fixed to be -12.0 eV. From the best fit between observed and calculated transition energies, a proportionality constant was chosen to be 1.15 in the present calculation; the values are tabulated in Table 1.

Finally, $1/2(I+A)$ values necessary to evaluate one-center core matrix elements, $U_{\mu\mu}$, were adjusted semi-empirically to give a reasonable electron density for the formaldehyde molecule. Consequently, the lower values were found to be preferable for 2s and 2p orbitals of oxygen to the original values;[13] namely, 24.390 eV for the 2s AO, and 8.111 eV for the 2px, 2py, and 2pz AO's.

c) Hartree-Fock and CI Matrix Elements: According

to the present method, the Hartree-Fock matrix elements and the CI matrix elements for the singlet and triplet manifolds are modified from the original equations[13,19] and calculated by the use of the modified semi-empirical values determined above. In the CI treatment on the ZDO approximation, exchange integrals characteristic of the singlet manifold of the CI matrix elements between the n-π^*, σ-π^*, and π-σ^* configurations vanish and the singlet CI element coincides with the corresponding triplet one. Therefore, the calculated transition energies for the singlet and triplet manifolds of n-π^*, σ-π^*, or π-σ^* excited state are equal to each other and should be compared with the observed transition energies to the triplet states.

Results for Some Planar Molecules. The modified CNDO-CI method mentioned above was applied to such planar molecules as ethylene, formaldehyde, formic acid, *s-trans*-butadiene, *s-trans*-glyoxal, and *s-trans*-acrylaldehyde to investigate their electronic structures and to check the applicability of the method. The geometrical structures of these molecules were taken from the analysis of the rotation-vibration spectrum[20,21] and from the electron diffraction studies.[22,23]

a) Orbital Energies: Tables IA and IIA give orbital energies calculated by the present authors, together with experimental values obtained by photoelectron spectroscopy.[24,25] Except for *s-trans*-glyoxal the sequences of molecular orbitals calculated by the present authors are in accordance with those determined experimentally[24,25] and calculated by the other semi-empirical[26-28] and non-empirical[29-31] methods. In the case of *s-trans*-glyoxal, the calculated splitting between the two n-orbitals was nearly twice as large (3.45 eV) as the observed value[24] ($\sim$1.6 eV). Owing to this large calculated splitting, the experimental sequence[24] (n, n, π) was not predicted by the present calculation (n, π, n)

The experimental results[1,25] of formic acid concerning both the sequence of orbitals and transition energies were found to be well reproduced by the theoretical calculation when the β^0 (−27.0 eV) and γ value (17.89 eV) are commonly used for all the 2s and 2p AO's of the two oxygen atoms in the carboxyl group. On the basis of this fact, the calculations of formic acid listed in Tables IA and IIIA and of acrylic acid discussed before were performed by the use of the above β^0 and γ values.

b) Electron Densities: Figure IA shows the electron densities of ethylene, formaldehyde, formic acid, *s-trans*-butadiene, *s-trans*-glyoxal, and *s-trans*-acrylalde-

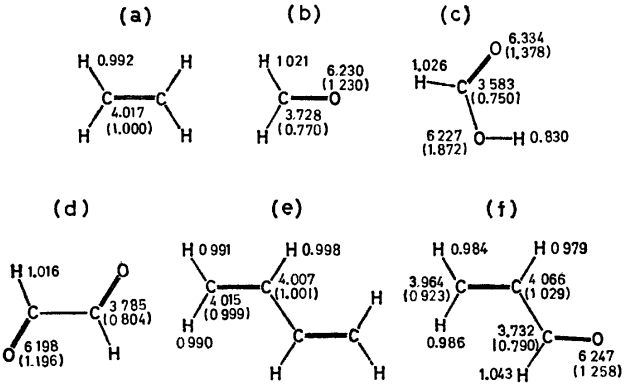

Fig. IA. The total and π- (in parentheses) electron densities of (a) ethylene, (b) formaldehyde, (c) formic acid, (d) *s-trans*-glyoxal, (e) *s-trans*-butadiene, and (f) *s-trans*-acrylaldehyde.

TABLE IA. CALCULATED ORBITAL ENERGIES OF ETHYLENE, FORMALDEHYDE, AND FORMIC ACID

C_2H_4			H_2CO			HCOOH		
Orbital	Energy (eV)	Ionization[a] potential (eV)	Orbital	Energy (eV)	Ionization[a] potential (eV)	Orbital	Energy (eV)	Ionization[b] potential (eV)
$b_{1u}(\pi)$	−13.15	10.51	$b_2(n)$	−13.17	10.88	n	−12.92	11.51
b_{1g}	−15.26	12.73	$b_1(\pi)$	−15.12	14.38	π	−13.29	12.50
a_g	−18.01	14.7	a_1	−18.57	16.0	σ	−15.37	14.78
b_{2u}	−23.76	15.82	b_2	−23.47	16.9	π	−18.64	15.76

a) Taken from Ref. 24. b) Taken from Ref. 25.

TABLE IIA. CALCULATED ORBITAL ENERGIES OF *s-trans*-BUTADIENE, *s-trans*-GLYOXAL, AND *s-trans*-ACRYLALDEHYDE

Butadiene			Glyoxal			Acrylaldehyde		
Orbital	Energy (eV)	Ionization[a] potential (eV)	Orbital	Energy (eV)	Ionization[a] potential (eV)	Orbital	Energy (eV)	Ionization[a] potential (eV)
$b_g(\pi)$	−11.49	9.07	$a_g(n)$	−12.06	10.6	n	−12.54	10.11
a_g	−14.23	11.4	$b_g(\pi)$	−14.37	14.03	π	−12.81	10.93
$a_u(\pi)$	−15.72	12.2	$b_u(n)$	−15.51	12.19	π	−16.59	13.7
a_g	−15.97		$a_u(\pi)$	−17.22	15.5	σ	−16.60	14.8
b_u	−16.89		a_g	−17.96	16.0	σ	−16.72	16.1
b_u	−21.19		b_u	−20.83	16.84	σ	−20.74	18.9

a) Taken from Ref. 24.

hyde. The C=O groups of formaldehyde, formic acid, glyoxal, and acrylaldehyde are fairly polarized. The dipole moments calculated by the present method for formaldehyde (2.25 D), formic acid (1.43 D), and acrylaldehyde (3.02 D) agree better with the experimental values (2.30, 1.4—1.7, 3.11 D, respectively)[32,33] than the theoretical values obtained by other authors.[13,26,34-38]

c) Transition Energies: Tables IIIA and IVA give some lower transition energies calculated for the planar molecules under consideration, together with the observed values. The result shows that the lowest singlet π-π^* transition energy of each molecule agrees satisfactorily with the observed value.[1,39-42]

The transition energies to the n-π^* state calculated for formaldehyde (3.19 eV) and acrylaldehyde (2.88 eV) agree well with the observed values to the triplet state (3.0 eV for both).[43,44] The calculated energy (1.87 eV) for the lowest n-π^* state of glyoxal is slightly lower than the observed triplet energy (2.38 eV).[45]

In the present calculation, the n-σ^* bands of formaldehyde, formic acid, glyoxal, and acrylaldehyde are predicted to appear at 9.46, 8.84, 8.43, and 9.16 eV, respectively, being 1—2 eV higher than the observed values assigned to the Rydberg or n-σ^* excited states.[1,40] Since the n-σ^* state of the molecules under consideration is expected to interact significantly with the Rydberg excited state, it is difficult to expect better agreement between the observed and calculated values of the n-σ^* transition energy in the present calculation in which the Rydberg 3s and 3p orbitals are disregarded.

Table IIIA. Singlet and triplet transition energies ($^1\Delta E$ and $^3\Delta E$ (eV)) and oscillator strength (f) calculated and observed for ethylene, formaldehyde, and formic acid

	Obsd		Calcd		
	$^3\Delta E$	$^1\Delta E$	$^3\Delta E$	$^1\Delta E$	f[a]
Ethylene					
π-π^*	4.6[b]	7.6[c]	5.48	7.66	0.470
σ-π^*			8.40		0
π-σ^*			9.53		0
σ-π^*			10.19		0
Formaldehyde					
n-π^*	3.0[d]	~4.3[e]	3.19		0
π-π^*	(4.2)[f]	7.94[e]	5.42	7.83	0.245
σ-π^*			8.03		0.016
n-σ^*		(7.10)[e]	8.73	9.46	0.037
Formic acid					
n-π^*		5.64[g]	4.54		0.000$_4$
π-π^*		8.3[h]	5.28	7.78	0.187
σ-π^*			7.68		0.008
n-σ^*		(7.5 or 8.7)[h]	8.46	8.84	0.009
π-σ^*			8.48		0.029

a) Calculated value for the singlet manifold. b) D. F. Evans, *J. Chem. Soc.*, **1960**, 1735. c) Taken from Ref. 41. d) Taken from Ref. 43. e) Taken from Ref. 40. f) Taken from Ref. 35. g) Taken from Ref. 3. h) Taken from Ref. 1.

Table IVA. Singlet and triplet transition energies ($^1\Delta E$ and $^3\Delta E$ (eV)) and oscillator strength (f) calculated and observed for *s-trans*-butadiene, *s-trans*-glyoxal, and *s-trans*-acrylaldehyde

	Obsd	Calcd		
	$^1\Delta E$	$^3\Delta E$	$^1\Delta E$	f[a]
s-trans-Butadiene				
π-π^*	6.0[b]	4.02	6.21	0.993
π-π^*	(7.2)[b]	5.82	8.02	0
σ-π^*		7.13		0
σ-π^*		8.38		0.002
σ-π^*		8.64		0
π-σ^*		8.66		0.001
π-σ^*		9.23		0
π-π^*		9.67	9.93	0
s-trans-Glyoxal				
n-π^*	2.72[c] (2.38)[d]	1.87		0
n-π^*	4.50[e]	3.44		0
π-π^*	7.2—7.6[f]	4.30	6.81	0.495
π-π^*		5.84	8.32	0
σ-π^*		7.14		0.017
n-π^*		7.47		0
n-σ^*	(6.0—6.7)[g]	7.49	8.43	0.069
σ-π^*		8.85		0
n-σ^*		8.94	9.58	0
s-trans-Acrylaldehyde				
n-π^*	3.76[g] (3.01—3.08)[h]	2.88		0
π-π^*	6.41[g]	4.20	6.55	0.733
π-π^*	(8.38 or 8.49)[g]	6.02	8.31	0.017
n-π^*		7.04		0
σ-π^*		7.46		0.007
n-σ^*	(7.08)[g]	8.47	9.16	0.026
σ-π^*		8.91		0.003
π-σ^*		9.31		0.004
π-π^*		9.79	10.11	0.019

a) Calculated value for the singlet manifold. b) Taken from Ref. 39. c) Taken from Ref. 45. d) Triplet transition energy taken from Ref. 45. e) H. L. McMurry, *J. Chem. Phys.*, **9**, 241 (1941). f) Taken from Ref. 42. g) Taken from Ref. 40. h) Triplet transition energy taken from Ref. 44.

In conclusion, the modified CNDO-CI method was found to be useful for the investigation of electronic structures of planar molecules, especially of lower excited π-π^* and n-π^* states.

References

1) E. E. Barnes and W. T. Simpson, *J. Chem. Phys.*, **39**, 670 (1963).
2) S. Nagakura, K. Kaya, and H. Tsubomura, *J. Mol. Spectrosc.*, **13**, 1 (1964).
3) H. Basch, M. B. Robin, and N. A. Kuebler, *J. Chem. Phys.*, **49**, 5007 (1968).
4) (a) S. S. Krishnamurthy and S. Soundararajan, *Tetrahedron*, **24**, 167 (1968): (b) M. V. Henri, *Compt. Rend.*, **178**, 846 (1924).
5) K. Bolton, N. L. Owen, and J. Sheridan, *Nature*, **218**, 266 (1968); N. L. Owen, *J. Mol. Struct.*, **6**, 37 (1970).

6) W. R. Feairheller, Jr. and J. E. Katon, *Spectrochim. Acta*, **23A**, 2225 (1967).
7) (a) J. A. Riddick and W. B. Bunger, "Organic Solvents," John Wiley and Sons, London (1970): (b) P. Hyden and H. W. Melville, *J. Polym. Sci.*, **43**, 201 (1960); *ibid.*, 215 (1960); (c) M. S. Matheson, E. E. Auer, E. B. Bevilacqua, and E. J. Hart, *J. Am. Chem. Soc.*, **73**, 5395 (1951).
8) A. Kuboyama, S. Matsuzaki, H. Takagi, and H. Arano, *Bull. Chem. Soc. Jpn.*, **47**, 1604 (1974).
9) K. Kaya and S. Nagakura, *J. Mol. Spectrosc.*, **44**, 279 (1972).
10) T. Ukaji, *Bull. Chem. Soc. Jpn.*, **32**, 1266 (1959).
11) S. R. La Paglia, *J. Mol. Spectrosc.*, **10**, 240 (1963).
12) J. A. Pople, D. P. Santry, and G. A. Segal, *J. Chem. Phys.*, **43**, S129 (1965).
13) J. A. Pople and G. A. Segal, *J. Chem. Phys.*, **43**, S136 (1965); *ibid.*, **44**, 3289 (1966).
14) J. Del Bene and H. H. Jaffé, *J. Chem. Phys.*, **48**, 1807, 4050 (1968).
15) R. Pariser, *J. Chem. Phys.*, **21**, 568 (1953); R. Pariser and R. G. Parr, *ibid.*, **21**, 767 (1953).
16) G. Pilcher and H. A. Skinner, *J. Inorg. Nucl. Chem.*, **24**, 937 (1962).
17) J. Hinze and H. H. Jaffé, *J. Am. Chem. Soc.*, **84**, 540 (1962).
18) G. Klopman, *J. Am. Chem. Soc.*, **86**, 4550 (1964); *ibid.*, **87**, 3300 (1965).
19) C. C. J. Roothaan, *Rev. Mod. Phys.*, **23**, 69 (1951).
20) H. C. Allen and E. K. Plyler, *J. Am. Chem. Soc.*, **80**, 2673 (1958).
21) R. G. Lerner, B. P. Dailey, and J. P. Friend, *J. Chem. Phys.*, **26**, 680 (1957).
22) D. P. Stevenson, J. E. LuValle, and V. Schomaker, *J. Am. Chem. Soc.*, **61**, 2508 (1939).
23) K. Kuchitsu, T. Fukuyama, and Y. Morino, *J. Mol. Struct.*, **1**, 463 (1968).
24) D. W. Turner, C. Baker, A. D. Baker, and C. R. Brundle, "Molecular Photoelectron Spectroscopy," John Wiley and Sons, London (1970).
25) K. Kimura, S. Katsumata, T. Yamazaki, and H. Wakabayashi, *J. Electron Spectrosc.*, **6**, 41 (1975).
26) F. Hirota and S. Nagakura, *Bull. Chem. Soc. Jpn.*, **43**, 1642 (1970).
27) J. M. Sichel and M. A. Whitehead, *Theor. Chim. Acta*, **11**, 254 (1968).
28) N. C. Baird and M. J. S. Dewar, *Theor. Chim. Acta*, **9**, 1 (1967).
29) J. M. Schulman, J. W. Moskowitz, and C. Hollister, *J. Chem. Phys.*, **46**, 2759 (1967).
30) M. D. Newton and W. E. Palke, *J. Chem. Phys.*, **45**, 2329 (1966).
31) M. D. Newton, F. P. Boer, and W. N. Lipscomb, *J. Am. Chem. Soc.*, **88**, 2367 (1966).
32) A. L. McClellan, "Tables of Experimental Dipole Moments," W. H. Freeman and Company, San Francisco, California (1963).
33) R. Wagner, J. Fine, J. W. Simmons, and J. H. Goldstein, *J. Chem. Phys.*, **26**, 634 (1957).
34) P. Schuster, *Internat. J. Quant. Chem.*, **3**, 851 (1969).
35) T. Yonezawa, K. Yamaguchi, and H. Kato, *Bull. Chem. Soc. Jpn.*, **40**, 536 (1967).
36) H. Kato, H. Konishi, H. Yamabe, and T. Yonezawa, *Bull. Chem. Soc. Jpn.*, **40**, 2761 (1967).
37) M. Jungen and H. Labhart, *Theor. Chim. Acta*, **9**, 345 (1968).
38) B. Tinland, *Mol. Phys.*, **16**, 413 (1969).
39) R. S. Mulliken, *Rev. Mod. Phys.*, **14**, 265 (1942).
40) A. D. Walsh, *Trans. Faraday Soc.*, **41**, 498 (1945); *ibid.*, **42**, 66 (1946).
41) P. G. Wilkinson and R. S. Mulliken, *J. Chem. Phys.*, **23**, 1895 (1955).
42) J. W. Sidman, *J. Chem. Phys.*, **27**, 429 (1957).
43) A. D. Cohen and C. Reid, *J. Chem. Phys.*, **24**, 85 (1956).
44) G. Herzberg, "Electronic Spectra and Electronic Structure of Polyatomic Molecules," van Nostrand Company, Princeton, New Jersey (1967).
45) J. C. D. Brand, *Trans. Faraday Soc.*, **50**, 431 (1954).

Modified INDO Calculations of the Electronic Structure of Transition Metal Carbonyl Compounds

Kazuyuki TATSUMI and Takayuki FUENO

Department of Chemistry, Faculty of Engineering Science, Osaka University, Toyonaka, Osaka 560

(Received November 4, 1975)

An INDO molecular-orbital method developed for the treatment of systems involving 3d orbitals have been applied to transition metal carbonyl complexes $Ni(CO)_4$, $Cr(CO)_6$, and $Fe(CO)_3$(butadiene). The Koopmans-theorem values of ionization potentials are found to be in excellent agreement with the observed photoelectron-spectroscopic data, except for the cases where a considerable reorganization in electronic distribution accompanies the ionization process. The INDO molecular orbital functions compare well with those reported on the basis of *ab initio* calculations.

There appears to be an increasing necessity of devising reliable theoretical methods for use in the investigation of chemistry of transition metal complexes. Fortunately, recent advances in the He(I) photoelectron spectroscopy provide data useful for testing the validity of theoretical calculations.

We here report the results of INDO calculations for transition metal carbonyl compounds: $Ni(CO)_4$, $Cr(CO)_6$, and $Fe(CO)_3$(butadiene). The primary aim of this work is to examine the vertical ionization potentials of these compounds and thereby to assess the semiempirical procedure here adopted. It will be shown that our method is at least as useful an approximation as *ab initio* calculations hitherto reported.

Computational Method

Since the INDO procedure has already been described in detail elsewhere,[1] we will only give a brief outline here. The basis atomic orbitals consist of 3d, 4s, and 4p functions for central metals and of 2s and 2p functions for first row atoms. Zerner's single-parameter atomic orbitals[2] have been employed for Ni and Fe atoms, Burns' function[3] for Cr atom, and Clementi's functions[4] for ligand atoms. In evaluating one-center integral parameters, we have adopted the same method as described in Ref. 1 using the data compiled by Oleari *et al.*[5-7] and by Hinze and Jaffé.[8] Table 1 summarizes the orbital exponents of the basis set and the valence-orbital ionization potentials (VOIP), together with various two-electron integral values adopted for the transition metals.

The molecular geometries used for calculations were taken from the experimental results. The interatomic distances and coordinate axes chosen are given in Figs. 1 to 3 for $Ni(CO)_4$,[9] $Cr(CO)_6$,[10] and $Fe(CO)_3$(butadiene),[11] respectively.

TABLE 1. ATOMIC PARAMETERS[a] OF THE TRANSITION METALS STUDIED

	Cr	Fe	Ni
Exponents			
3d	2.450	2.722	2.960
4s	1.300	1.370	1.473
4p	0.775	1.370	1.473
VOIP (eV)	(d^4s^2)	(d^6s^2)	(d^{10})
I_d	11.64	12.64	5.02
I_s	6.11	6.73	7.19
I_p	3.23	3.24	3.10
Two-electron integrals (eV)			
J_{sp}	5.955	6.414	6.872
$J_{pp'}$	5.233	5.500	5.768
J_{sd}	8.948	9.509	10.088
$J_{z,zx}$	7.601	8.091	8.583
J_{x,z^2}	7.404	7.867	8.331
$J_{z,xy}$	7.295	7.755	8.215
J_{z,z^2}	7.709	8.203	8.699
$J_{z^2,xy}$	12.590	13.799	15.015
$J_{z^2,xz}$	13.124	14.383	15.644
J_{xy,x^2-y^2}	13.302	14.578	15.854
$J_{xz,yz}$	12.768	13.993	15.225

a) The other parameters, $U_{\mu\mu}$ and $g_{\mu\nu}$, are tabulated in Ref. 7. The exchange integrals $K_{\mu\nu}$ can be obtained from $K_{\mu\nu}=2(J_{\mu\nu}-g_{\mu\nu})$.

Results and Discussion

$Ni(CO)_4$. The He(I) photoelectron spectrum for $Ni(CO)_4$ was recorded by Lloyd and Schlag[12]

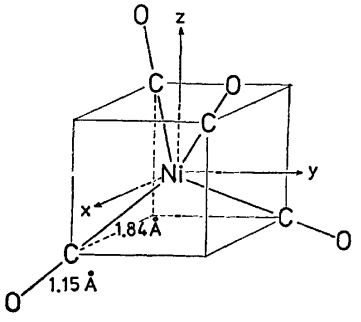

Fig. 1. Coordinate systems and structure for $Ni(CO)_4$ (T_d).

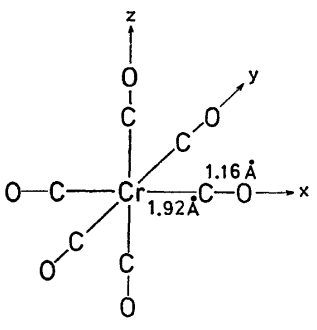

Fig. 2. Coordinate systems and structure for $Cr(CO)_6$ (O_h).

Table 2. Computed and experimental ionization potentials of $Ni(CO)_4$ (in eV)

Symmetry[a]	This calculation		*Ab initio*			SCF-X_α[e]	Expt.[f]
	$-\varepsilon$	Nature	$-\varepsilon$[b]	$-\varepsilon$[c]	⊿SCF[d]		
$^2T_2$	9.00	$d_{xz}, d_{yz}, d_{x^2-y^2}$	11.67	10.75	7.0	9.3	8.8
^2E	9.72	d_{xy}, d_{z^2}	13.49	12.82	7.8	10.7	9.7
$^2T_2$	14.09	σ(CO)	18.48	17.52		12.0(t_1) 12.2(t_2)	14.8

a) Irreducible representation of the point group T_d.
b) Ref. 15. c) Ref. 17. d) Ref. 16. e) Ref. 18. f) Refs. 12 and 13.

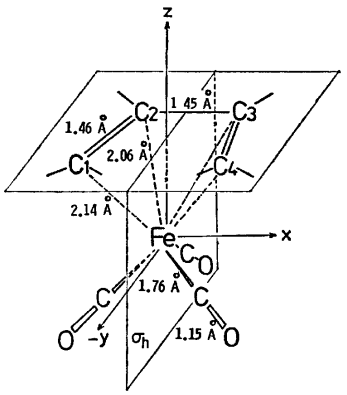

Fig. 3. Coordinate systems and structure for $Fe(CO)_3$-(butadiene)(C_s). The distances between C and H in the butadiene moiety are assumed to be 1.08 Å.

and by Green *et al.*[13] The first three bands have been assigned to the ionizations from the t_2(Ni-d), e(Ni-d), and t_2(CO) orbital sets.

Table 2 shows the lowest three vertical ionization potentials (IP) obtained by the present calculation. The first two IP's correspond to the removal of an electron from the orbitals which have mainly a metal 3d character with $5t_2$[14] (d_{xz}, d_{yz}, and $d_{x^2-y^2}$) and 2e (d_{xy} and d_{z^2}) symmetries. The third IP, on the other hand, is ascribable to the $4t_2$ orbital which is composed chiefly of the CO σ orbitals. The IP values calculated are in excellent agreement with the experimental data for ionization potential.

Also listed in Table 2 are the results of *ab initio* calculations by Hillier *et al.*[15,16] and by Demuynck and Veillard,[17] together with the IP values calculated by Johnson and Wahlgen[18] using the SCF-X_α scattered-wave method. The *ab initio* calculations predict the same ordering of ionization orbitals as does our INDO treatment. However, the numerical values of IP do not agree well with observation; the Koopmans-theorem values are 2—4 eV higher than the observed IP while the ⊿SCF values too low by *ca.* 2 eV. The SCF-X_α data are apparently more satisfactory than the results of *ab initio* calculations. They are yet no better than the IP values obtained by the present INDO approximation.

The excellent agreement of the INDO results with observation may perhaps be largely fortuitous. However, it appears that the semiempirical method used deserves credit as being a useful working tool.

$Cr(CO)_6$. The He(I) photoelectron spectrum for $Cr(CO)_6$[19] has two peaks at 8.4 and 13.3 eV and a broad band in the range 14—16 eV. The first peak has been assigned to the ionization from the predominantly metal $2t_{2g}$ orbital. The second peak, which is much separated in energy from the first, might be due to the removal of an electron from either the $3e_g$ or (and) $4t_{1u}$ orbital; the assignment has not yet been settled. The order of the highest three occupied orbitals calculated by the self-consistent-charge-and-configuration(SCCC) method[20] is $4t_{1u}<3e_g<2t_{2g}$, while *ab initio*[15] and self-consistent-charge (SCC) molecular-orbital[21] calculations result in the order $3e_g<4t_{1u}<2t_{2g}$.

In Table 3, the first three IP obtained by the INDO and *ab initio* calculations are compared with the experimental values. The assignment of the second and third IP is that predicted by Hillier and Saunders,[15] who ascribe these two ionizations together to the second peak at 13.3 eV. The INDO calculations are successful in reproducing the experimental values for IP, in contrast to the considerable errors of the *ab initio* results. Although there is a disagreement in the ordering of $3e_g$ and $4t_{1u}$ orbitals between the two treatments, they show a common feature that the two orbitals in question are mutually very closely spaced.

For a further comparison between the two theoretical methods, we show in Table 4 the atomic populations in the molecular orbitals of our concern. Strictly speaking, it will be improper to directly compare the

Table 3. Computed and experimental ionization potentials of $Cr(CO)_6$ (in eV)

Symmetry[a]	This calculation $-\varepsilon$	*Ab initio*[b] $-\varepsilon$	Expt.[c]
$^2T_{2g}$	9.10	10.7	8.4
$^2T_{1u}$	12.68	17.5	13.3
^2E_g	12.62	17.9	

a) Irreducible representation of the point group O_h.
b) Ref. 15. c) Ref. 19.

Table 4. Comparison of population analyses for $Cr(CO)_6$ (in percent)

MO	Method	$-\varepsilon$(eV)	Cr(3d)	C	O
$2t_{2g}$	INDO	9.10	63	10	27
	Ab initio	10.7	75	8	17
$4t_{1u}$	INDO	12.68	0	37	59
	Ab initio	17.5	0	54	38
$3e_g$	INDO	12.62	19	42	38
	Ab initio	17.9	18	59	23

populations derived from the orthogonal (or Löwdin) basis set (INDO) with those reduced from the Mulliken analyses (*ab initio*). Nevertheless, the comparison will still have some significance in a qualitative sense. As Table 4 shows, the populations calculated by the INDO method are uniformly in harmony with the *ab initio* results. Of the highest three levels, the $2t_{2g}$ orbital consists of 60—80% Cr 3d orbitals (d_{xy},d_{yz}, d_{xz}) with an appreciable CO π^* orbitals. The $4t_{1u}$ orbital is predominantly CO π bonds, while $3e_g$ is about 20% Cr 3d ($d_{x^2-y^2}$, d_{z^2}) and 80% CO orbitals.

Fe(CO)$_3$(butadiene). Measurement of photoelectron spectrum for Fe(CO)$_3$(butadiene) was first made by Dewar and Worley[22] using a low-resolution spectrometer. Recently, Connor *et al.*[23] have recorded a preciser spectrum to achieve assignment of the bands with the aid of *ab initio* calculations.

In Fig. 4, we compare the observed spectrum with IP calculated by the INDO and *ab initio* methods. Aside from the 16a' orbital, the sequence of the INDO orbital energies accords well with the *ab initio* results. However, neither set of these Koopmans-theorem values can rationalize the observed spectrum of Fe(CO)$_3$(butadiene). The discrepancy in height between the filled orbitals and the valence ionic states is probably due to greater orbital relaxation on ionization. The ΔSCF results[22] show that the effect of the orbital relaxation is particularly great for the molecular orbitals 17a', 15a', and 11a". For these orbitals, the breakdown of the Koopmans theorem is enormous. In this work, we have not attempted SCF calculations for the resulting ions, since our parametrization was originally aimed at best possible interpretations of the ground-state properties only.

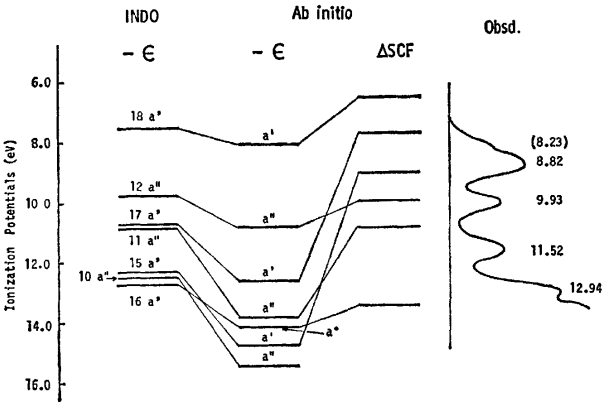

Fig. 4. Computed and experimental ionization potentials of Fe(CO)$_3$(butadiene). Symmetry designations of the molecular orbitals are based on the irreducible representation of the point group C_s.

Table 5 summarizes the results of population analysis of the molecular orbitals given in Fig. 4. It should be noted that the INDO calculation well reproduces the pattern of the *ab initio* populations. For the aforementioned three orbitals, for which the Koopmans theorem breaks down most seriously, the population on the central metal 3d orbitals is relatively large. Apparently, the orbital relaxation is most closely related with the 3d orbital population. With the orbitals

Table 5. Comparison of population analyses for Fe(CO)$_3$(butadiene) (in percent)

MO	Method	$-\varepsilon$(eV)	Fe(3d)	C_1+C_4	C_2+C_3
18a'	INDO	7.51	15	26	17
	Ab initio	8.1	33	34	9
12a"	INDO	9.75	11	45	20
	Ab initio	10.8	10	62	21
17a'	INDO	10.72	78	1	1
	Ab initio	12.6	51	12	20
11a"	INDO	10.74	84	3	2
	Ab initio	13.8	66	11	8
16a'	INDO	12.69	14	17	51
	Ab initio	14.1	34	12	48
15a'	INDO	12.31	90	2	1
	Ab initio	14.7	65	10	5
10a"	INDO	12.45	2	41	25
	Ab initio	15.4	13	32	18

12a" and 10a", the 3d orbital populations are calculated to be small. Consistently, the INDO Koopmans-theorem values of IP due to these orbitals (9.75 and 12.45 eV) are in reasonable agreement with the observed ionization potentials (9.93 and 12.94 eV).

Finally, we will briefly comment on the bonding character of the various molecular orbitals. The iron (3d)–butadiene (π) bonding is accomplished primarily through the d_{yz}–$1b_1$ and d_{xz}–$1a_2$ mixings in the orbitals 18a' and 12a", respectively. Both the orbitals 17a' and 11a" consist mainly of the iron 3d orbitals with an appreciable CO π orbitals. The orbitals 16a' and 15a' both have a slight iron–butadiene antibonding character. The 10a" orbital is predominantly butadiene σ orbitals.

Concluding Remarks

The INDO calculations combined with Koopmans' theorem are found to be successful in interpreting the photoelectron spectra of transition metal carbonyl compounds, unless the orbital relaxation upon ionization is substantial. However, the results by no means indicate that Koopmans' theorem are indeed applicable to these compounds. In fact, the available results of *ab initio* calculations show that the effects of this relaxation are not negligibly small. It seems that our semiempirical treatment is just in effect allowing favorably for the effects of electron correlation. It follows that the resulting description of the ground states is probably reliable enough to discuss the bonding properties with. One obvious merit of semiempirical theories lies in the computational economy for the quality of the results they provide. One may thus anticipate immediate, though perhaps somewhat limited, usefulness of the present method for the investigation of various chemical problems[1] associated with transition metal complexes.

References

1) K. Tatsumi, T. Fueno, A. Nakamura, and S. Otsuka, *Bull. Chem. Soc. Jpn.*, in press.

2) M. Zerner and M. Gouterman, *Theoret. Chim. Acta (Berlin)*, **4**, 44 (1966).
3) G. Burns, *J. Chem. Phys.*, **39**, 1521 (1964).
4) E. Clementi and D. L. Raimond, *J. Chem. Phys.*, **38**, 2686 (1963).
5) L. Oleari, L. Di Sipio, and G. De Michelis, *Mol. Phys.*, **10**, 97 (1966).
6) E. Tondello, G. De Michelis, L. Oleari, and L. Di Sipio, *Coord. Chem. Rev.*, **2**, 65 (1967).
7) L. Di Sipio, E. Tondello, G. De Michelis, and L. Oleari, *Chem. Phys. Lett.*, **11**, 287 (1971).
8) J. Hinze and H. H. Jaffé, *J. Chem. Phys.*, **38**, 1834 (1963).
9) J. Ladell, B. Post, and I. Faukuchen, *Acta Crystallogr.*, **5**, 795 (1952).
10) L. B. Brockway, R. V. G. Evens, and M. W. Lister, *Trans. Faraday Soc.*, **34**, 1350 (1938).
11) O. S. Mills and G. Robinson, *Acta Crystallogr.*, **16**, 758 (1963).
12) D. R. Lloyd and W. E. Schlag, *Inorg. Chem.*, **8**, 2544 (1969).
13) J. C. Green, I. D. King, and J. H. D. Eland, *J. Chem. Soc., Chem. Commun.*, **1970**, 1121.
14) The orbital numbering in this paper ignores the core electrons.
15) I. H. Hillier and V. R. Saunders, *Mol. Phys.*, **22**, 1025 (1971).
16) I. H. Hillier, M. F. Guest, B. R. Higginson, and D. R. Lloyd, *Mol. Phys.*, **27**, 215 (1974).
17) J. Demuynck and A. Veillard, *Theoret. Chim. Acta (Berlin)*, **28**, 241 (1973).
18) K. H. Johnson and U. Wahlgen, *Int. J. Quantum Chem.*, **S6**, 243 (1972).
19) D. W. Turner, A. D. Baker, C. Baker, and C. R. Brundle, "Molecular Photoelectron Spectroscopy," Wiley, New York (1970).
20) N. A. Beach and H. B. Gray, *J. Am. Chem. Soc.*, **90**, 5713 (1968).
21) I. H. Hillier, *J. Chem. Phys.*, **52**, 1948 (1970).
22) M. J. S. Dewar and S. D. Worley, *J. Chem. Phys.*, **50**, 654 (1969).
23) J. A. Connor, L. M. R. Derrick, M. B. Hall, I. H. Hillier, M. F. Guest, B. R. Higginson, and D. R. Lloyd, *Mol. Phys.*, **28**, 1193 (1974).

A Comparison of the Primary Processes of the Radiolyses Induced by α-, β-, and γ-Rays

Shin SATO, Ken-ichi KOWARI, and Kiyoshi OKAZAKI

Department of Applied Physics, Tokyo Institute of Technology, Ookayama, Meguro-ku, Tokyo 152

(Received November 22, 1975)

By using the cross sections derived by the binary encounter collision theory and the assumption of a continuous slowing down, the *G*-values for the ionization and excitation of helium gas irradiated by α-, β-, and γ-rays have been calculated. In the radiolysis by high-energy electrons, the *G*-values started to decrease at an incident electron energy of about 10^3 eV with a decrease in the energy. Calculation showed that, if the radiation energy is extremely high, the *G*-values are independent of the kind of radiation. In the radiolysis induced by α-particles, the ratio of the yield resulting from the direct interaction with α-particles to that due to the secondary electrons was calculated as a function of the energy of the incident α-particles. When the energy was 8 MeV, the ratio for ionization was calculated to be 1.31.

There are several naive questions when we consider the primary process of the radiolyses induced by different ionizing radiations.

1) In radiation chemistry, the radiolysis yield obtained by the irradiation of high-energy electrons is believed to be independent of the energy of the incident electrons if they are high in energy. Then, what eV is the threshold value for calling electrons "high-energy electrons"—10^2, 10^3, or 10^4 eV?

2) It is believed that the chemical reaction induced in such materials as organic compounds by the irradiation of γ-rays from ^{60}Co is exactly the same as the reaction induced by the irradiation of high-energy electrons except for the difference in the penetration of the two ionizing radiations. However, the energy of the secondary electrons produced by the γ-irradiation through the Compton effect distributes down to zero eV. Consequently, the yield obtained by the irradiation of monoenergetic electrons of a high energy, say 100 keV, might not agree quantitatively with the yield obtained by γ-irradiation.

3) According to the experimental data,[1] when the energy of incident radiation is extremely high, the ionization yield in a gas does not depend upon the kind of radiation. However, the interaction of high-energy electrons with a material must be different from the interaction of other particles; for example, an incident electron can replace an electron in a material, but other particles cannot. Such an effect might result in a quantitative difference in the radiolysis yield.

4) When the *W*-value of a certain gas is measured by using α-particles as the radiation source, a question may be raised—what percentage of the ionization is induced by the direct interaction with α-particles, and what percentage by the interaction with the secondary electrons produced?

In this paper, we will attempt to answer these questions by performing numerical calculations on the radiolysis of helium gas. The calculating method is classical and approximate; however, we believe that the result is not far from the truth.

Radiolysis by High-energy Electrons

Throughout this paper, we will use the following equation, derived from the classical binary encounter theory,[2] for the differential cross section of the energy loss:

$$\sigma_{E,\mathrm{dir}} = \frac{\pi e^4}{T+I_i+E_i}\left(\frac{1}{E^2}+\frac{4E_i}{3E^3}\right) \quad (1)$$

for $T \geq I_i+E$. Here, T is the energy of the incident particle; I_i and E_i are, respectively, the binding energy and the average kinetic energy of the target electron, and E is the energy loss of the incident particle. When the incident particle is an electron and when an exchange with the target electron occurs, the differential cross section ($\sigma_{E,\mathrm{exc}}$) is expressed by replacing E in Eq. 1 with $T+I_i-E$.

For the calculation of the yields of ionization and excitation, we use the concept of the degradation spectrum, $y(T)$, and calculate it on the assumption of a continuous slowing down. The details of this procedure have been discussed previously;[3] therefore, we will only briefly outline them here.

According to the assumption of a continuous slowing down, the degradation spectrum of the incident electron, $y_1(T)$, is expressed as a reciprocal of the stopping power of the incident electron in the target gas. While the degradation spectrum of the incident electron is being formed, the secondary electrons are ejected and form their degradation spectrum, $y_2(T)$. The formulation of $y_2(T)$ can easily be carried out by using the differential cross section in Eq. 1. Similarly, the degradation spectrum of the electrons ejected in later steps can be constructed. The total degradation spectrum, $y(T)$, is obviously the sum of these spectra. Once $y(T)$ is obtained, the yield of any process can be calculated by using the total cross section, $Q_s(T)$, for that process:

$$N_s = Nn_i\int_{T_s}^{T_0} y(T)Q_s(T)\mathrm{d}T \quad (2)$$

Here, N_s is the number of species produced in the s process; N is the number of the target atoms in unit volume; n_i is the number of electrons in the i-th shell; T_s is the threshold energy of the incident electron for the s process, and T_0 is the energy of the primary electron. Then, the *G*-value of the product is calculated by this equation:

$$G_s = 100\,N_s/T_0 \quad (3)$$

Figure 1 shows the *G*-values thus calculated for the

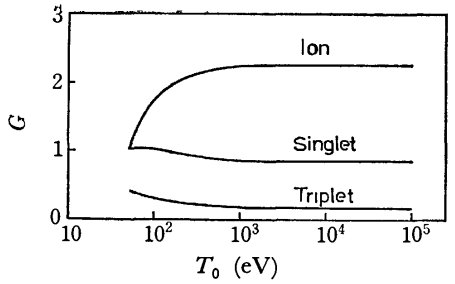

Fig. 1. The G-values for ionization and singlet and triplet excitations as functions of the energy of the primary electron.

TABLE 1. CONSTANTS USED FOR CALCULATION (eV)

Binding energy	$I_i = 24.581$
Singlet excitation energy	$E_s = 21.2$
Triplet excitation energy	$E_t = 19.8$
Average kinetic energy	$E_i = 38.74$

TABLE 2. COMPARISON OF G-VALUES FOR IONIZATION AND EXCITATIONS INDUCED BY DIFFERENT IONIZING RADIATIONS

	G_{ion}	G_{singl}	G_{tripl}
High energy electrons ($>10^3$ eV)	2.27	0.86	0.16
γ-Rays from ^{60}Co	2.30	0.86	0.16
α-Particles (8 MeV)	2.24	0.85	0.15

ionization and singlet and triplet excitations in helium gas as functions of the energy of the primary electrons. The constants used for the calculation are summarized in Table 1.[3] Obviously, the G-value of ionization tends to decrease at 10^3 eV with the decrease in the energy of the primary electrons. Above 10^3 eV, the G-values of any process are independent of the energy of the primary electrons. The values are listed in Table 2.

γ-Radiolysis

Energy Distribution of Compton Electrons. When a material consisting of atoms with low atomic numbers is irradiated by γ-rays from ^{60}Co, the primary interaction occurs mainly through the Compton effect. In order to calculate the energy distribution of the Compton electrons, Davison and Evans[1] derived this equation:

$$\frac{d\sigma(T)}{dT} = \frac{\pi r_0^2}{\alpha h\nu}\left[1+\frac{T^2}{(h\nu-T)h\nu}+\left\{1-\frac{T}{\alpha(h\nu-T)}\right\}^2\right] \quad (4)$$

from the famous Klein-Nishina formula.[5] Here, $\sigma(T)$ is the cross section for the formation of Compton electrons with the energy of T, $h\nu$ is the energy of the incident γ-rays, $\alpha=h\nu/mc^2$, and $r_0=e^2/mc^2$. m is the mass of electron, e is the charge, and c is the velocity of light.

Figure 2 shows the calculated energy distribution of the Compton electrons produced by the irradiation of ^{60}Co γ-rays, which consist of two different photons, 1.17 and 1.33 MeV. This figure is the same as that shown in the literature.[6] It is assumed in this calculation that the interaction of γ-rays with the gas occurs only once; *i.e.*, the interaction of the scattered γ-rays is not taken into account. As Fig. 2 shows, because of the momentum conservation, the maximum energy of the Compton electrons is less than the energy of incident radiation.

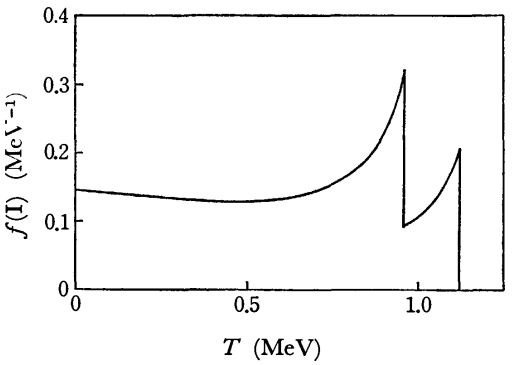

Fig. 2. The energy distribution of Compton electrons produced in helium irradiated by γ-rays from ^{60}Co.

$$T_{max} = \frac{2\alpha}{1+2\alpha}h\nu \quad (5)$$

Comparison with the Radiolysis Induced by High-energy Electrons. Since the energy distribution of the primary electrons produced by the Compton effect has been obtained, the degradation spectrum of electrons in helium irradiated by γ-rays can be calculated in a manner similar to that shown in the previous section. The degradation spectrum of the primary electrons, $y_1(T)$,[7] and the total energy, T_0, absorbed by helium in the present case are expressed as follows:

$$y_1(T) = \int_T^{T_{max}} f(T)dT/S(T) \quad (6)$$

and

$$T_0 = \int_0^{T_{max}} Tf(T)dT \quad (7)$$

Here, $f(T)$ is the fraction of the primary electrons with the energy of T, and $S(T)$ is the stopping power of helium gas for the electrons with the energy of T. $S(T)$ is formulated as follows:[8]

$$S(T) = \sum_i n_i\left\{\int_{E_{si}}^{(T+I_i)/2} E(\sigma_{E,dir}+\sigma_{E,exc})dE + \frac{1}{2}\int_{E_{ti}}^{E_{si}} E\sigma_{E,exc}dE\right\} \quad (8)$$

E_{si} and E_{ti} are the energies of the singlet and triplet excitations for the electron in the i-th shell.

Figure 3 shows the total degradation spectrum, $y(T)$, thus calculated. The calculated G-values for ionization and excitations are summarized in Table 2. Practically no difference can be seen in the G-values calculated for the γ-radiolysis and for the radiolysis by high-energy electrons. The difference of 1% in the G-value of ionization is within the limits of error of the calculation technique.

Radiolysis by α-Particles

According to the binary encounter theory, the differential cross-section for the energy loss of the incident-

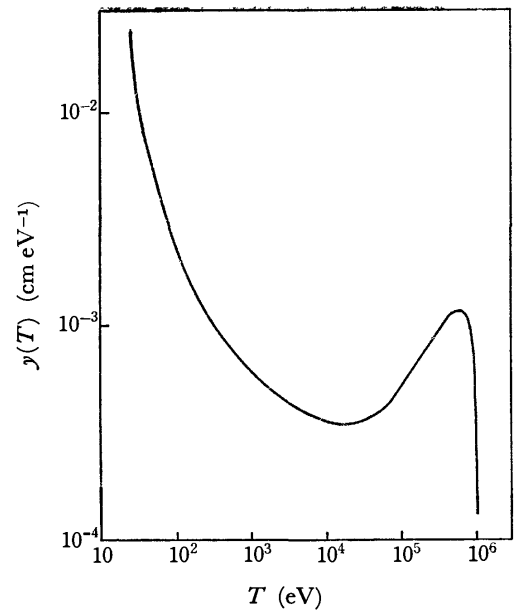

Fig. 3. The degradation spectrum of electrons in helium irradiated by γ-rays from ^{60}Co.

heavy-charged particles can be formulated in a manner similar to that used for electrons. Using the notations of Vriens,[9] the differential cross-sections are expressed as follows:

$$\sigma_1(E) = \frac{\pi Z^2 e^4}{3V_1^2 V_2 E^3}\left\{4V_1^3 - \frac{1}{2}(V_2' - V_2)^3\right\} \quad (9)$$

for $2mV_1(V_1-V_2) \leq E \leq 2mV_1(V_1+V_2)$. Here, $\sigma_1(E)$ is the differential cross section for the energy loss, E; Ze is the charge of the incident particle; V_1 is the incident velocity; V_2 is the velocity of the target electron, and V_2' is that after the collision with the heavy-charged particle. When $E \leq 2mV_1(V_1-V_2)$, the differential cross section has to be modified to this form:

$$\sigma_2(E) = \frac{2\pi Z^2 e^4}{mV_1^2}\left(\frac{1}{E^2} + \frac{2mV_2^2}{E^3}\right) \quad (10)$$

The formulation for these cross-sections has already been reported in detail.[10]

By using Eqs. 9 and 10, we can derive the total cross-sections for ionization and excitation (Q_{ion} and Q_{exc}):

$$Q_{\text{ion}} = \int_{2mV_1(V_1-V_2)}^{2mV_1(V_1+V_2)} \sigma_1(E)\mathrm{d}E + \int_{I_i}^{2mV_1(V_1-V_2)} \sigma_2(E)\mathrm{d}E \quad (11)$$

for $I_i \leq 2mV_1(V_1-V_2)$. Here, I_i is the binding energy of the target electron. When the binding energy is higher than $2mV_1(V_1-V_2)$, the term for σ_2 in Eq. 11 dissappears and Q_{ion} is expressed as follows:

$$Q_{\text{ion}} = \int_{I_i}^{2mV_1(V_1+V_2)} \sigma_1(E)\mathrm{d}E$$

for $2mV_1(V_1+V_2) \geq I_i \geq 2mV_1(V_1-V_2)$. In a similar manner, the total cross-sections for excitations can be formulated:

$$Q_{\text{exc}} = \int_{E_s}^{I_i} \sigma_2(E)\mathrm{d}E$$

for $2mV_1(V_1-V_2) \geq I_i$, and

$$Q_{\text{exc}} = \int_{2mV_1(V_1-V_2)}^{I_i} \sigma_1(E)\mathrm{d}E + \int_{E_s}^{2mV_1(V_1-V_2)} \sigma_2(E)\mathrm{d}E$$

for $2mV_1(V_1+V_2) \geq I_i \geq 2mV_1(V_1-V_2) \geq E_s$, where E_s is the threshold energy for the excitation.

$$Q_{\text{exc}} = \int_{E_s}^{I_i} \sigma_1(E)\mathrm{d}E$$

for $2mV_1(V_1+V_2) \geq I_i \geq E_s \geq 2mV_1(V_1-V_2)$, and

$$Q_{\text{exc}} = \int_{E_s}^{2mV_1(V_1+V_2)} \sigma_1(E)\mathrm{d}E$$

for $I_i \geq 2mV_1(V_1+V_2) \geq E_s \geq 2mV_1(V_1-V_2)$. In the treatment of the binary encounter theory, the excitation into the triplet state results from the exchange between the incident electron and the target electron. Therefore, in the present case, the formation of the triplet state cannot be taken into account.

In a manner similar to that used for electrons, the stopping power for heavy-charged particles is expressed in this form:

$$S(T) = N\sum_i n_i \left\{\int_{2mV_1(V_1-V_{2i})}^{2mV_1(V_1+V_{2i})} E\sigma_1\mathrm{d}E + \int_{E_{si}}^{2mV_1(V_1-V_{2i})} E\sigma_2\mathrm{d}E\right\} \quad (12)$$

Then, the degradation spectrum of the incident-heavy-charged particle may be expressed as follows:

$$y_0(T) = 1/S(T)$$

and the yield of the product formed through the s process in the collision of heavy-charged particles can be calculated by using Eq. 2.

In the radiolysis induced by the irradiation of heavy-charged particles, the secondary electrons ejected play an important role. The treatment on these electrons is similar to that for the Compton electrons produced by the γ-irradiation.

Figure 4 shows the $Ty(T)Q_s(T)$ values as a function of ln T. The incident radiation is 8 MeV α-particles. The solid lines correspond to the direct interaction of α-particles, and the dashed lines, to that of the secondary electrons. The ratio of the G-value for ionization due to the interaction with α-particles to that due to the secondary electrons is 1.31. Similar calculations can also be made for the excitation. The results are summarized in Table 3. Obviously the fraction due to the direct interaction increases with the decrease in the incident energy.

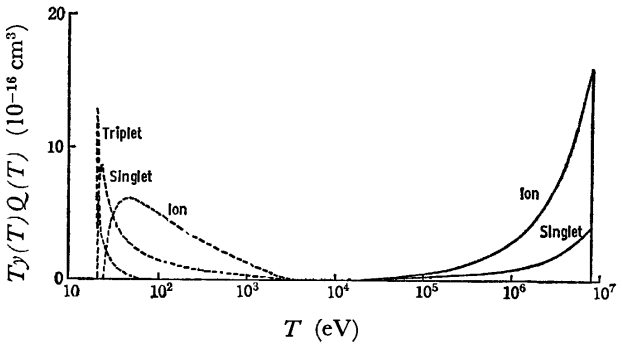

Fig. 4. Contribution of different portions of the degradation spectra of α-particles (solid) and of electrons (dashed) to the ionization and excitations in helium.

Table 3. Ionization and excitations of helium by different energy α-particles

T_0 (MeV)	G_{ion}	f_d (%)	f_s	G_{singl}	f_d (%)	f_s	G_{tripl}
0.02	1.30	100	0	1.83	100	0	0.0004
0.04	1.78	99.7	0.3	1.50	98.9	1.1	0.015
0.1	2.05	97.1	2.9	1.19	93.2	6.8	0.050
0.3	2.17	91.8	8.2	1.02	83.4	16.6	0.082
0.5	2.20	88.9	11.1	0.96	78.2	21.8	0.094
0.7	2.21	85.4	14.6	0.93	72.5	27.5	0.11
1.0	2.22	80.7	19.3	0.90	66.1	33.9	0.12
1.5	2.22	75.3	24.7	0.88	59.5	40.5	0.13
2.0	2.23	71.5	28.5	0.87	55.1	44.9	0.14
3.0	2.24	66.6	33.4	0.86	49.8	50.2	0.14
5.0	2.24	61.0	39.0	0.85	44.4	55.6	0.15
8.0	2.24	56.6	43.4	0.85	40.4	59.6	0.15

f_d: the fraction due to the direct interaction of α-particles. f_s: the fraction due to secondary electrons.

Conclusion

Let us summarize the answers to four questions proposed in the Introduction. To the first question, the answer is that, from the point of view of the radiation chemist, the lower threshold value for high-energy electrons is about 10^3 eV. The answer to the second question is that the primary process of the γ-radiolysis is certainly the same as that of the radiolysis induced by high-energy electrons. This conclusion has been widely accepted. The present calculation is another support for it. The answer to the third question, regarding the radiation-chemical difference between heavy-charged particles and electrons, is also simple; *i.e.*, if the radiation energies are extremely high, the yield of the primary process is independent of the kind of radiation which induces the reactions. If present, the difference is within a few percent. The answer to the fourth question is shown by the numbers in Table 3. These numbers may be used when discussing the effect of δ-rays on the radiolysis induced by α-particles. Similar calculations can easily be carried out for the radiolysis induced by other heavy-charged particles, such as protons and argon ions. Recently Ohno has made a few such calculations.[11]

The calculating method we have used above is based on two important assumptions, one regarding the cross section for the energy loss, and the other, the assumption of the continuous slowing down. These assumptions probably introduce serious deviations in the numbers. However, the conclusions summarized above may hold nevertheless.

References

1) D. W. Huyton and T. W. Woodward, *Radiat. Res. Rev.*, **2**, 205 (1970).
2) L. H. Thomas, *Proc. Camb. Phil. Soc.*, **23**, 829 (1927).
3) S. Sato, K. Okazaki, and S. Ohno, *Bull. Chem. Soc. Jpn.*, **47**, 2174 (1974).
4) C. M. Davison and R. D. Evans, *Rev. Mod. Phys.*, **24**, 79 (1952).
5) O. Klein and Y. Nishina, *Z. Phys.*, **52**, 853 (1929).
6) H. E. Johns, D. V. Cormack, S. A. Denesuk, and G. F. Whitmore, *Can. J. Phys.*, **30**, 556 (1952).
7) D. V. Cormack, R. W. Hummel, H. E. Johns, and T. W. Spinks, *J. Chem. Phys.*, **22**, 1 (1954).
8) S. Ohno, H. Nagayama, K. Okazaki, and S. Sato, *Bull. Chem. Soc. Jpn.*, **48**, 2153 (1975).
9) L. Vriens, "Case Studies in Atomic Collision Physics I," ed. by E. W. McDaniel *et al.*, North-Holland, Amsterdam (1969), p. 335.
10) L. Vriens, *Proc. Phys. Soc.*, **90**, 935 (1967).
11) S. Ohno, *Bull. Chem. Soc. Jpn.*, **48**, 2229 (1975).

A Photoelectron Spectroscopic Study of Thioformamide

Katsumi KIMURA, Shunji KATSUMATA, Takahiko ISHIGURO,* Akiko Y. HIRAKAWA,* and Masamichi TSUBOI*

Physical Chemistry Laboratory, Institute of Applied Electricity, Hokkaido University, Sapporo 060

**Faculty of Pharmaceutical Sciences, University of Tokyo, Hongo, Tokyo 113*

(Received November 29, 1975)

The He I photoelectron spectrum of thioformamide ($HCSNH_2$) has been measured. On the basis of spectral features, CNDO/2 calculations, and sum rule considerations, the following assignments have been concluded. 1) Six ionization bands appearing below 17 eV correspond to six-p-type MOs and two bands in the region 17—20 eV correspond to s-type MOs. 2) The first ionization band is attributed to the highest occupied (in-plane) MO constructed mainly from the sulfur lone pair which is mixed to some extent with the σ_{CN} orbital. 3) The second and fourth bands are due to the out-of-plane MOs, mainly corresponding to the nitrogen lone pair and the π_{CS} orbital, respectively. 4) The remaining p-type bands may be interpreted in terms of σ_{CS}, σ_{CN}, and π_{NH_2} (pseudo pi) orbitals.

Photoelectron spectroscopy using a He 584 Å source provides valuable information on valence orbital structure as well as vibrational structure in ionized states.[1] The He I photoelectron spectra of simple amides and carboxylic acids were studied by Brundle *et al.*,[2] who payed a special attention to the assignment of the closely overlapped bands due to the n_O (oxygen nonbonding) and π_2 (antisymmetric pi) MOs. Only a few photoelectron works has been published on thiocarbonyl compounds. Kroto *et al.* [3–5] reported the photoelectron spectra of several pyrolytically produced unstable compounds, H_2CS, CH_3CHS, $(CH_3)_2CS$, and F_2CS. No photoelectron studies have so far been published on thioformamide, which is fairly stable in the gaseous phase at room temperature. Debies and Rabalais[6] have recently published the He I and II photoelectron spectra of some amino acids, urea and thiourea. Our primary concern in the present work is to study the valence orbitals of thioformamide by means of He I photoelectron spectroscopy.

Experimental

Measurements of He I photoelectron spectra were carried out with a high-resolution photoelectron spectrometer used previously.[7,8] Calibration of the ionization energy scale was carried out using known ionization energies of Xe as an internal standard. A gaseous sample was introduced through a vacuum glass line with a Teflon needle valve. No metal tube was used to avoid decomposition. The pressure in the spectrometer tank was 1×10^{-6} Torr before the photoelectron measurements and 1 to 5×10^{-5} Torr during the measurements. The ionization chamber of cylindrical type (14 mm in diameter and 27 mm long) was used. The electron analyzer of the spectrometer was operated at ±0.2 V.

The sample of thioformamide used was prepared by a reaction of formamide and phosphorus pentasulfide,[9] and purified by a recrystallization from cold ether and then from cold (>15 °C) ethylacetate. The infrared absorption spectrum of the sample was in a perfect agreement with what Suzuki[10] observed.

Results and Discussion

The He I photoelectron spectrum of thioformamide below 20 eV is shown in Fig. 1, from which the following spectral features may be seen. 1) The first two ionization bands are well resolved with vibrational structure in the region 8.5—10 eV. 2) The third and fourth bands are considerably overlapped with each other in the region 12.5—13.5 eV, the latter being much sharper. 3) The fifth band appearing at about 14.1 eV is much weaker and the sixth band at 15.0—16.5 eV consists of three sub-bands associated with vibrational structure. 4) There are two more additional weak bands in the region 17—20 eV. The individual ionization bands in the photoelectron spectrum in Fig. 1 are indicated by vertical lines with the numbering.

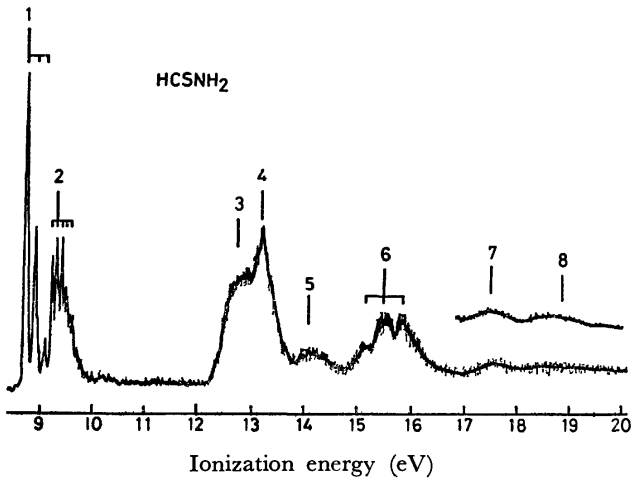

Fig. 1. He I photoelectron spectrum of thioformamide.

All the vertical ionization energies obtained from the thioformamide spectrum are summarized in Table 1.

Table 1. Vertical ionization energies (eV) and orbital assignments of thioformamide

	Vertical ionization energy	Orbital assignment Sym. (Main character)
I_1	8.70	$a'(n_S)$
I_2	9.30	$a''(n_N)-\pi_2$
I_3	12.80	$a'(\sigma_{C=S})$
I_4	13.18	$a''(\pi_{C=S})-\pi_1$
I_5	14.1_5	$a'(\pi_{NH_2})$
I_6	15.52	$a'(\sigma_{CN})$
I_7	17.7_0	$a'(s_S)$
I_8	18.9_0	$a'(s_C)$

As previously done,[7,8,11,12] we use the following p-type localized molecular orbitals (LOs) in order to represent main orbital features of the p-type bands: n_S (sulfur nonbonding), n_N (nitrogen nonbonding), π_{CS} (C=S pi bonding) σ_{CS} (C=S sigma bonding), σ_{CN} (C–N sigma bonding), and π_{NH_2} (amino-group pseudo pi). Since thioformamide has a planar molecular structure (C_s),[13] bonding and antibonding pi MOs (designated as π_1 and π_2, respectively) may be formed from the out-of-plane n_N and π_{CS} LOs. The valence orbitals of thioformamide therefore may be explained in terms of the two out-of-plane p-type LOs (n_N and π_{CS}), four in-plane p-type LOs (n_S, σ_{CS}, π_{NH_2}, and σ_{CN}) and three in-plane s-type LOs (s_C, s_S, and s_N).

In most of the saturated and unsaturated aliphatic compounds so far studied,[7,8,11,12] all p-type photoelectron bands are observed below about 18 eV. From the numbers of p- and s-type LOs, it may be reasonably considered that the six bands appearing below about 17 eV are due to the p-type LOs and the remaining two bands are due to the s-type LOs.

The third, nitrogen s-type band of thioformamide is expected to appear around 27 eV (beyond the He I region), since Potts *et al.*[14] have reported that the nitrogen s-type band of the methylamine is located at 27.5 eV. The carbon s-type bands of the C=O groups in H_2CO and CH_3CHO appear around 18—19 eV.[7] No sulfur s-type bands have so far been reported.

In the present work, we carried out CNDO/2 calculations[15] of orbital energies using a recently available geometry[13] and obtained the following orbital assignments under Koopmans' theorem:[16] $I_1 \rightarrow \varepsilon_1(a', n_S)$, $I_2 \rightarrow \varepsilon_2(a'', \pi_2)$, $I_3 \rightarrow \varepsilon_3(a', \sigma_{CS})$, $I_4 \rightarrow \varepsilon_4(a', \pi_{NH_2})$, $I_5 \rightarrow \varepsilon_5(a'', \pi_1)$, $I_6 \rightarrow \varepsilon_6(a', \sigma_{CN})$, $I_7 \rightarrow \varepsilon_7(a', s_S)$, $I_8 \rightarrow \varepsilon_8(a', s_C)$, and $I_9 \rightarrow \varepsilon_9(a', s_N)$. However, this assignment of I_4 to the π_{NH_2} seems to be incorrect, since the ionization of an electron from the pseudo π orbital always gives rise to a broad band as in methylamine. From the spectral shape, therefore, the fourth, sharp band may be assigned to the out-of-plane π_1 rather than the in-plane π_{NH_2} LO. This may also be supported by the sum rule consideration mentioned later.

The sum rule previously proposed[7,8,11,12] may approximately hold for the vertical ionization energies associated with the out-of-plane LOs of thioformamide, as summarized in Table 2. In the sum rule consideration, we used the empirical ionization energies given in Table 3 which are based on the experimental vertical ionization energies of simple molecules (I^0). The I^0 values given for the n_N and $\pi_{C=S}$ LOs in Table 3 were taken from the available photoelectron data of the first ionization energy of ammonia and the second ionization energy of thioformaldehyde, respectively. As shown in Table 2, good agreement is obtained between the experimental and calculated partial sums for thioformamide. A similar sum rule consideration is also demonstrated for formamide in Table 2, a considerably good agreement being again obtained between experiment and calculation. The orbital assignments finally concluded in the present work (Table 1) therefore differ from those of the CNDO/2 calculations in the order of the fourth and fifth inner orbitals.

TABLE 2. EXPERIMENTAL AND CALCULATED PARTIAL SUMS, $P(a'')$, FOR THE OUT-OF-PLANE LOs

Compound	$(I_s)\rightarrow$(LOs)	$-P(a'')$, eV	
		Expt.	Calcd.
$HCSNH_2$	$(I_2, I_4)\rightarrow a''(n_N, \pi_{C=S})$	22.48	22.66
$HCONH_2$	(I_2, I_4)[a] $\rightarrow a''(n_N, \pi_{C=O})$	25.27	25.38

a) $I_2 = 10.52$ eV, $I_4 = 14.75$ eV, taken from Ref. 2.

TABLE 3. EMPIRICAL ENERGIES (I^0, eV) USED FOR THE LOCALIZED MOLECULAR ORBITALS (LOs) IN THE SUM RULE CONSIDERATIONS

$I^0(n_N)$	$= 10.88$[a]
$I^0(\pi_{C=S})$	$= 11.78$[b]
$I^0(\pi_{C=O})$	$= 14.50$[c]

a) I_1 of NH_3; A. W. Potts and W. C. Price, *Proc. Roy. Soc., Ser. A*, **326**, 181 (1972). b) I_2 of H_2CS; Ref. 4. c) I_2 of H_2CO; C. R. Brundle, M. B. Robin, N. A. Kuebler, and H. Basch, *J. Am. Chem. Soc.*, **94**, 1451 (1972).

The vibrational structures of the first and second bands are shown in an expanded scale in Fig. 2. The vibrational intervals of about 1460 cm^{-1} which appear in the first band of $HCSNH_2$ are probably due to the C–N stretching (about 1450 cm^{-1} in the ground state of neutral liquid thioformamide). The second band of $HCSNH_2$ shows the vibrational intervals of about 730 cm^{-1} which are probably assigned to the C–S stretching (about 840 cm^{-1} in the ground state of neutral liquid thioformamide). These vibrational progressions seem to be closely associated with the facts that the orbital interactions exist between the n_S and σ_{CN} LOs in the highest occupied MO and between the n_N and π_{CS} LOs in the second inner MO.

The experimental orbital levels of thioformamide based on Koopmans' theorem are shown in Fig. 3, compared with those of its some related compounds. The LO levels (n_N, π_{CS}, and π_{CH_3}) are also shown in

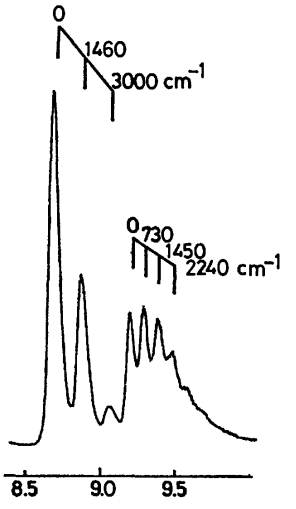

Fig. 2. The vibrational structure of the first two ionization bands of $HCSNH_2$ shown in an expanded scale.

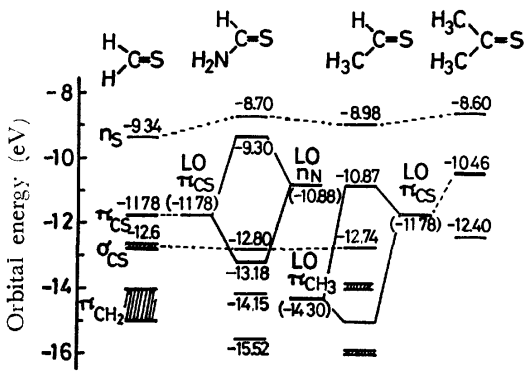

Fig. 3. Experimental (Koopmans' theorem) orbital correlation diagrams for thioformamide and its related compounds. The LO levels are based on the photoelectron data of simple compounds. Orbital energies for H_2CS, CH_3CHS, and $(CH_3)_2CS$ were taken from the literatures.[3,4] (The -12.6 eV level of H_2CS was tentatively assumed from the sharp peak of the available photoelectron spectrum.)

Fig. 3, together with their energy values in parentheses. The interaction schemes of the out-of-plane LOs are indicated by connecting the levels with solid lines. The σ_{CS} level of thioformamide is located at -12.80 eV, close to those of thioformaldehyde and thioacetaldehyde (-12.6 and -12.7 eV, respectively).

The assignment of the first band to the n_S rather than the n_N LO was also confirmed without Koopmans' theorem in the present CNDO/2 calculations by obtaining the difference in total energy between thioformamide and its cation in the ground state, a calculated ionization energy of 9.43 eV being obtained.

According to an electronic absorption study by Hosoya *et al.*,[17] the ultraviolet absorption bands of thioformamide in the regions 260—280 and 220—240 nm may be attributed to electron transitions to the $\pi^*_{C=S}$ orbital from the sulfur and nitrogen lone pair orbitals, respectively. The difference in transition energy between these absorption bands is 0.8 eV. It is interesting to note that this transition-energy difference of thioformamide is considerably close to the separation of the first two photoelectron bands (0.6 eV).

References

1) D. W. Turner, C. Baker, A. D. Baker, and C. R. Brundle, "Molecular Photoelectron Spectroscopy," Wiley, New York (1969).
2) C. R. Brundle, D. W. Turner, M. B. Robin, and H. Basch, *Chem. Phys. Lett.*, **3**, 292 (1969).
3) H. W. Kroto and R. J. Suffolk, *Chem. Phys. Lett.*, **15**, 545 (1972).
4) H. W. Kroto, B. M. Landsberg, R. J. Suffolk, and A. Vodden, *Chem. Phys. Lett.*, **29**, 265 (1974).
5) H. W. Kroto and R. J. Suffolk, *Chem. Phys. Lett.*, **17**, 213 (1972).
6) T. P. Debies and J. W. Rabalais, *J. Electron Spectrosc.*, **3**, 315 (1974).
7) K. Kimura, S. Katsumata, T. Yamazaki, and H. Wakabayashi, *J. Electron Spectrosc.*, **6**, 41 (1975).
8) S. Katsumata and K. Kimura, *J. Electron Spectrosc.*, **6**, 309 (1975).
9) R. Willstater and T. Werth, *Ber. Deut. Chem. Ges.*, **42**, 1908 (1909).
10) I. Suzuki, *Bull. Chem. Soc. Jpn.*, **35**, 1286 (1962).
11) K. Kimura, S. Katsumata, Y. Achiba, H. Matsumoto, and S. Nagakura, *Bull. Chem. Soc. Jpn.*, **46**, 373 (1973).
12) T. Yamazaki and K. Kimura, *Bull. Chem. Soc. Jpn.*, **48**, 1602 (1975).
13) R. Sugisaki, T. Tanaka, and E. Hirota, *J. Mol. Spectrosc.*, **49**, 241 (1974).
14) A. W. Potts, T. A. Williams, and W. C. Price, *Discuss. Faraday Soc.*, **54**, 104 (1972).
15) J. A. Pople and D. L. Beveridge, "Approximate Molecular Orbital Theory," McGrad-Hill, New York (1970). The present CNDO/2 calculations were carried out with a library program written by H. Itoh, K. Yoshida, and T. Nakamura of Hokkaido University.
16) T. Koopmans, *Physica*, **1**, 104 (1934).
17) H. Hosoya, J. Tanaka, and S. Nagakura, *Bull. Chem. Soc. Jpn.*, **33**, 850 (1960).

Radiative Triplet Lifetimes in Benzene and Azabenzenes with Particular Reference to Phosphorescence Mechanisms in Benzene

Hirotoshi Ito and Yasumasa J. I'Haya

Department of Materials Science, The University of Electro-Communications, Chofu-shi, Tokyo 182

(Received December 8, 1975)

Calculations of radiative triplet lifetimes of benzene and azabenzenes are carried out by making use of an INDO/S method in which the parametrization of the CNDO/S method is used, retaining the semi-empirical Slater-Condon parameters determined in the INDO/2 method. The calculated excitation energies, oscillator strengths, and radiative lifetimes are in reasonable agreement with experimental values. The possible phosphorescence mechanisms for the $^3B_{1u}$ state of benzene are discussed rather in detail, considering the first-order vibronic as well as the first-order spin-orbit and the second-order spin-vibronic couplings. It is concluded that the strong first-order vibronic coupling between the triplet manifolds, $^3B_{1u}$ and $^3E_{1u}$, is responsible for the almost purely out-of-plane polarized phosphorescence of benzene, borrowing an intensity from the $^3E_{1u}$-$^1A_{1g}$ intercombination, and that the effects of the first-order spin-orbit and the second-order spin-vibronic couplings are small. The conclusion is in accord with the analyses of the Zeeman and MIDP spectra presented by van Egmond and van der Waals.

Theoretical prediction of radiative lifetimes for triplet states of aromatic hydrocarbons not only gives an important information for intersystem crossing mechanisms in luminescence spectroscopy but also serves as a sensitive check for the validity of quantum chemical approximations. The controversy on whether a π-electron model is adequate or states of mixed σ-π electronic character should be included has been almost settled, since the former yields predicted phosphorescence spectra $T_1 \rightarrow S_0$ always to be in-plane polarized whereas observed spectra of many aromatic hydrocarbons are predominantly out-of-plane polarized.[1,2] As for the importance of σ-electrons the earlier paper by Mizushima and Koide[3] was a foresighted one, though the lifetime of the spin-forbidden phosphorescent transition of benzene was only estimated.

As for the phosphorescence mechanisms in benzene, Clementi's scheme[4] for the $^3E_{1u} \rightarrow {}^1A_{1g}$ intercombination and Albrecht's second-order perturbation treatment[5] of the vibronic coupling between the triplet manifolds $^3B_{1u}$ and $^3E_{1u}$ are at present sufficiently convincing. In fact, Veeman and van der Waals[6] calculated the lifetime of the $^3B_{1u} \rightarrow {}^1A_{1g}$ transition to be 23.2 second using those schemes. As for the molecular spin-orbit coupling intergrals, it has been shown by several authors[6-9] that when σ-electron MO's are taken into account together with π-electron MO's the approximation to retain only one-center spin-same orbit coupling integrals is good enough to describe spin-orbit interactions in aromatic hydrocarbons. It is true in general that one-center spin-same-orbit coupling integrals are much larger in their magnitude than two- and three-center ones and also one- and multi-center spin-other-orbit coupling integrals. In the usual π-electron approximation for benzene and other planar aromatic hydrocarbons, all one- and two-center spin-same-orbit integrals vanish and contribution of small three- and four-center integrals to spin-orbit coupling has to be retained to calculate the triplet lifetimes which are therefore too long to compare with the corresponding experimental results.[10]

Though it is clear that the dominant spin-orbit coupling mechanism for radiative $T_1 \rightarrow S_0$ transitions involves $\pi\sigma^*$ and/or $\sigma\pi^*$ rather than $\pi\pi^*$ coupling, what type of approximate method is adequate comes into question. When one uses the CNDO/S method, one meets with a difficulty that energy separations between the singlet and triplet levels of both $\sigma\pi^*$ and $\pi\sigma^*$ states become zero in molecules of high symmetry. It is recognized fairly generally that the original INDO method gives non-zero but too high singlet and triplet states. In order to obtain better wave functions to predict whole lower-lying singlet and triplet levels of molecules, we use in this paper a modified INDO method in which the parametrization of Bene-Jaffé-Ellis-Kuehnlenz's modified CNDO method is adopted without changing the values of the semi-empirical Slater-Condon parameters used in the original INDO/2 method. Another modification is a use of Chojnacki's approximation[13] for two-center electronic repulsion integrals. In this respect, our INDO/S method is somewhat different from those proposed by Chen and Hedges[14] and Ridley and Zerner.[15]

We first check the reliability of the present INDO/S method with regard to singlet and triplet excitation energies and their intensities in benzene and azabenzenes and calculate the radiative lifetimes of lower-lying triplet states. In order to clarify the mechanisms of the phosphorescence in benzene, we investigate the symmetry forbidden lowest triplet radiative lifetime and the phosphorescence polarization in benzene rather in detail.

Theoretical Background

With the first-order perturbation theory, the spin-contaminated wave functions for the ground state, $|S_0^c\rangle$, and ith excited triplet state, $|T_i^c\rangle$, produced by spin-orbit coupling are written down as

$$|S_0^c\rangle = |S_0\rangle + \sum_m \gamma_m |T_m\rangle \text{ with } \gamma_m = \frac{\langle T_m|H_{so}|S_0\rangle}{E(S_0)-E(T_m)} \quad (1)$$

$$|T_i^c\rangle = |T_i\rangle + \sum_n \delta_n |S_n\rangle \text{ with } \delta_n = \frac{\langle S_n|H_{so}|T_i\rangle}{E(T_i)-E(S_n)}. \quad (2)$$

Here the spin-orbit Hamiltonian has the following form in the notation of our previous paper:[16]

$$H_{so} = \alpha^2\{\sum_i \sum_N Z_N(\vec{l}_{Ni}/r_{Ni}^3)\cdot\vec{S}_i + \sum_i \sum_{j\neq i} (2\vec{p}_i - \vec{p}_i) \times (\vec{r}_{ij}/r_{ij}^3)\cdot\vec{S}_i\} \quad (3)$$

The transition moment between the states $|S_0^c\rangle$ and $|T_i^c\rangle$ is then given by

$$\langle S_0^c|\vec{M}|T_i^c\rangle = \sum_n \delta_n\langle S_0|\vec{M}|S_n\rangle + \sum_m \gamma_m^*\langle T_m|\vec{M}|T_i\rangle \quad (4)$$

where $\vec{M}$ is the electric dipole operator. The corresponding oscillator strength and lifetime are derived from

$$f(S_0-T_i) = 1.085\times10^{-5}\,\nu(S_0-T_i)|\langle S_0^c|\vec{M}|T_i^c\rangle|^2 \quad (5)$$

$$\tau(T_i-S_0) = 1.5(g_T/g_S)/[\nu^2(S_0-T_i)f(S_0-T_i)] \quad (6)$$

where $\nu(S_0-T_i)$, the frequency of the emission from the lowest triplet state, is measured in units of cm^{-1} and the transition moment in units of Å. g_S and g_T represent the degeneracies in the ground singlet and excited triplet states, respectively, being put to be $g_S=1$, $g_T=3$ for temperature higher than 4.2 K and $g_T=1$ for temperature lower than 1.34 K according to experimental evidence.[17,18] $g_T/g_S=3$ is used throughout our computation.

The singlet and triplet state functions are expressed in terms of the Slater determinantal wavefunctions ${}^{2S+1}\psi_{i\to j}(SM)$ where S and M denote the total spin angular momentum and its z-projection, as follows:

$$|S(00)\rangle = \sum_i C_{i\to j}^{(i)}\,{}^1\psi_{i\to j}(00) \quad (7)$$

$$|T(1M)\rangle = \sum_i C_{i\to j}^{(i)}\,{}^3\psi_{i\to j}(1M),\quad M=0,\ \pm1 \quad (8)$$

After obtaining CI coefficients, it is convenient for practical applications to transform the triplet state functions $|T(1\,M)\rangle$ into $|T^x\rangle$, $|T^y\rangle$ and $|T^z\rangle$ so as to belong to the same representation of the appropriate point group as the cartesian components of the spin angular momentum.[10] Namely,

$$\begin{aligned}|T^x\rangle &= \frac{1}{\sqrt{2}}\{|T(1-1)\rangle - |T(11)\rangle\} = \sum_i C_{i\to j}^{(i)}\,{}^3\psi_{i\to j}^x\\ |T^y\rangle &= \frac{i}{\sqrt{2}}\{|T(1-1)\rangle + |T(11)\rangle\} = \sum_i C_{i\to j}^{(i)}\,{}^3\psi_{i\to j}^y \quad (9)\\ |T^z\rangle &= |T(10)\rangle = \sum_i C_{i\to j}^{(i)}\,{}^3\psi_{i\to j}^z\end{aligned}$$

where

$$\begin{aligned}{}^3\psi_{i\to j}^x &= \frac{1}{\sqrt{2}}\{{}^3\psi_{i\to j}(1-1) - {}^3\psi_{i\to j}(11)\}\\ {}^3\psi_{i\to j}^y &= \frac{i}{\sqrt{2}}\{{}^3\psi_{i\to j}(1-1) + {}^3\psi_{i\to j}(11)\} \quad (10)\\ {}^3\psi_{i\to j}^z &= {}^3\psi_{i\to j}(10)\end{aligned}$$

The matrix elements over MO's for the one-electron part of H_{so} are given by [19,20]

$$\sum_{\mu=x,y,z}\langle{}^1\psi_0|H_{so}^\mu|{}^3\psi_{i\to j}^\mu\rangle = \frac{1}{\sqrt{2}}\langle i|H_{so}^x - H_{so}^y - H_{so}^z|j\rangle \quad (11)$$

$$\sum_{\mu=x,y,z}\langle{}^1\psi_{i\to j}|H_{so}^\mu|{}^3\psi_{k\to l}^\mu\rangle = \frac{1}{2}\delta_{jl}\langle i|H_{so}^x - H_{so}^y - H_{so}^z|k\rangle - \frac{1}{2}\delta_{ik}\langle j|H_{so}^x - H_{so}^y - H_{so}^z|l\rangle \quad (12)$$

which are reduced to the spin-same-orbit coupling integrals over AO's. The one-center spin-same-orbit integrals over 2p AO's are analytically given as

$$\begin{aligned}&\langle 2p_y|H_{so}^z|2p_x\rangle = -\langle 2p_x|H_{so}^z|2p_y\rangle = -\langle 2p_y|H_{so}^x|2p_z\rangle\\ &= \langle 2p_z|H_{so}^x|2p_y\rangle = \langle 2p_x|H_{so}^y|2p_z\rangle = -\langle 2p_z|H_{so}^y|2p_x\rangle\\ &= i\alpha^2(Z_N^4/24)\ (\text{Rydberg}) = 5.8437\,i\,(Z_N^4/28)\ (cm^{-1}) \quad (13)\end{aligned}$$

where the leading sign is plus when the sequence of the sub- and super-scripts μ=x, y, z on $2p_\mu$ AO's and H_{so}^μ is cyclic and it is minus when the sequence is uncyclic, and Z_N is the effective nuclear charge.

Method of Calculation and Results

We use an INDO-type method based on the parametrization of the CNDO/S method which was first presented by Del Bene and Jaffé[11] and later somewhat reparametrized by Ellis, Kuehnlenz and Jaffé[12], retaining the semi-empirical Slater-Condon parameters determined in the INDO/2 method. The method is therefore called the INDO/S method hereafter. Like the CNDO/S method, the calculation of the off-diagonal matrix elements of the Fock operator $F_{\mu\nu}$, after the notation of Pople and Beveridge,[21] is carried out through the equation

$$F_{\mu\nu} = \beta_{AB}^0 S_{\mu\nu} - \frac{1}{2}P_{\mu\nu}\gamma_{AB} \quad (\mu\in A,\ \nu\in B) \quad (14)$$

where

$$S_{\mu\nu} = K_\sigma G_\sigma S_{\mu\nu}^\sigma + K_\pi G_\pi S_{\mu\nu}^\pi \quad (15)$$

for a pair of $2p_i$ and $2p_j$ (i, j$\in$x, y, z). G_σ and G_π are geometrical factors needed to project an arbitrary pair of 2p AO's in the cartesian coordinates suitably chosen onto the local bond axis. We adopted $K_\sigma=1$ and $K_\pi=0.585$ which are the values fixed by Del Bene and Jaffé[11] in their CNDO/S method. Other authors use a little different values for parameters K_σ and K_π. We found however that these parametrization does not produce an important effect in the final result, compared with the choice of an approximation for two-center electronic repulsion integrals which will be mentioned below. The zero differential overlap approximation is relaxed by retaining one-center integrals of the type $\langle 2s|\vec{er}|2p_i\rangle$ and $\langle 2p_i|\vec{er}|2p_i\rangle$ in the computation of transition moments.[12]

We have prepared a program for the present INDO/S method by modifying the computer program QCPE 91 for the CNDO/2 method written by Segal.[22] Throughout our computation, we solve 30×30 CI matrices made up of all the excitations which are unconditionally produced from *five* MO's below the highest occupied orbital to *six* MO's above the lowest unoccupied orbital. Reduction of the matrix elements over molecular integrals into those over atomic integrals in the INDO type method is prescribed by Ho *et al.*[23]

and Ridley and Zerner.[15]

With our INDO/S method, we carried out a pilot calculation of the excitation energies and oscillator strengths of benzene using the Nishimoto-Mataga (NM)[24] and the Ohno[25] approximations for two-center electronic repulsion integrals. The NM approximation was found to produce singlet levels tolerably well but lower triplet levels too low. On the other side, when Ohno's approximation is used the low-lying triplet levels are well reproduced but the singlet levels are not, in particular the $^1B_{2u}$ and $^1B_{2u}$ levels turn out to be reversed. These features are not typical of our INDO/S method but are also the cases whenever a Pariser-Parr-Pople type scheme is adopted for a π-electron model benzene (and other aromatic hydrocarbons) with the NM and Ohno approximations.

In order to obtain better wave functions which can predict both excitation energies and oscillator strengths, we tried to find out a parameter θ in the Chojnacki-type approximation[13]

$$\gamma_{AB} = \theta\gamma_{AB}^{NM} + (1-\theta)\gamma_{AB}^{Ohno} \quad (\theta<1) \tag{16}$$

where γ_{AB} is the two-center Coulomb repulsion integral. Chojnacki obtained $\theta=0.4$ in his P-P-P type π-electron calculations,[13] the value producing both first singlet and triplet levels which are in good agreement with experimental values. In our INDO/S calculations, however, a suitable value for θ was not obtained so as to reproduce the singlet and triplet levels of benzene simultaneously well. We adopted the Chojnacki's value $\theta=0.4$ because this was found to give a best compromise in simultaneous singlet and triplet level setting in benzene.

The results of our INDO/S calculation are listed in Table 1 for benzene and in Table 2 for azabenzenes. For comparison, we calculated the lower three $\pi\pi^*$ singlet and triplet state energies with the same procedure as our INDO/S but with the NM and Ohno approximations; these are 4.84, 6.06, 6.98 eV (NM) and 4.62, 4.93, 7.41 eV (Ohno) for the singlets, and 2.41, 3.93, 4.84 eV (NM) and 3.39, 4.45, 4.94 eV (Ohno) for the triplets. In so far as these lower excitation energies are concerned, it can be safely said therefore that the Chojnacki-type approximation produces better overall agreement with observed values than the NM and Ohno approximations. The oscillator strength and the lifetime of the transition $^3E_{1u}\rightarrow{}^1A_{1g}$ in benzene are calculated from Eqs. 5 and 6 and are listed at the bottom of Table 1.

The calculated excitation energies and oscillator strengths of the lower triplet states of some azabenzenes listed in Table 2 are fairly in good agreement with experimental values. As for 1, 3, 5-triazine, though the calculated lowest triplet state $^3E''$ comes rather high, the radiative lifetime from the state is computed to be 0.323 second which compares well with the

Table 1. Calculated excitation energies (ΔE), oscillator strengths (f), and phosphorescence lifetime (τ) of benzene[a]

State No.	States	ΔE(eV)	$f(S_0\rightarrow S_i)$	State No.	States	ΔE	$f(T_1\rightarrow T_i)$	$f(T_2\rightarrow T_i)$
1	$^1B_{2u}(\pi\pi^*)$	4.90	0	1	$^3B_{1u}(\pi\pi^*)$	3.04	Ref.	
		⟪4.93⟫	⟪0.001⟫			⟪3.95⟫		
2	$^1B_{1u}(\pi\pi^*)$	5.21	0	2A, B	$^3E_{1u}(\pi\pi^*)$	4.26		Ref.
		⟪6.21⟫	⟪0.1⟫			⟪4.75⟫		
3A, B	$^1E_{1u}(\pi\pi^*)$	7.23	2.070(x, y)	3	$^3B_{2u}(\pi\pi^*)$	4.90		
		⟪6.96⟫	⟪0.690⟫			⟪5.60⟫		
4	$^1A_{2u}(\sigma\pi^*)$	7.82	0.003(z)	4A, B	$^3E_{2g}(\pi\pi^*)$	6.11	0.022(x, y)	0.052(x, y)
5A, B	$^1E_{2u}(\pi\sigma^*)$	7.88	0			⟪6.75⟫		
6A, B	$^1E_{2u}(\pi\sigma^*)$	7.94	0	5A, B	$^3E_{2u}(\pi\sigma^*)$	7.16		
7	$^1A_{1u}(\sigma\pi^*)$	8.02	0	6	$^3B_{2g}(\pi\sigma^*)$	7.65	0.052(z)	
8A, B	$^1E_{2g}(\pi\pi^*)$	8.15	0	7	$^3A_{2u}(\sigma\pi^*)$	7.70		
		⟪7.48⟫		8A, B	$^3E_{2u}(\sigma\pi^*)$	7.79		
9	$^1B_{2g}(\pi\sigma^*)$	8.99	0	9	$^3A_{1u}(\sigma\pi^*)$	7.89		
10	$^1B_{1g}(\pi\sigma^*)$	9.00	0	10A, B	$^3E_{1g}(\pi\sigma^*)$	8.61		0.097(z)
11A, B	$^1E_{1g}(\sigma\pi^*)$	9.12	0	11	$^3B_{1g}(\pi\sigma^*)$	8.93		
12A, B	$^1E_{2g}(\pi\pi^*)$	10.32	0	12A, B	$^3E_{2g}(\pi\pi^*)$	9.22	0.412(x, y)	1.983(x, y)
13A, B	$^1E_{1g}(\sigma\pi^*)$	10.64	0	13A, B	$^3E_{1g}(\sigma\pi^*)$	10.50		4×10^{-5}(z)
14A, B	$^1E_{1u}(\sigma\sigma^*)$	11.76	0.992(x, y)	14A, B	$^3E_{1u}(\sigma\sigma^*)$	10.60		
15	$^1A_{2g}(\sigma\pi^*)$	12.37	0	15	$^3A_{1g}(\sigma\pi^*)$	11.75		
16	$^1A_{1g}(\sigma\pi^*)$	12.52	0	16A, B	$^3E_{2g}(\sigma\sigma^*)$	11.84	2×10^{-5}(x, y)	3×10^{-4}(x, y)
17A, B	$^1E_{2g}(\sigma\sigma^*)$	12.71	0	17	$^3A_{2g}(\sigma\pi^*)$	11.93		2×10^{-5}(x, y)
18	$^1B_{2u}(\pi\pi^*)$	12.79	0	18	$^3B_{2u}(\pi\pi^*)$	12.36		
19A, B	$^1E_{2u}(\pi\sigma^*)$	14.00	0	19	$^3B_{2g}(\pi\sigma^*)$	12.85	0.001(z)	
				20A, B	$^3E_{2u}(\pi\sigma^*)$	13.65		

$f(^3E_{1u}\rightarrow{}^1A_{1g}) = 0.92247\times10^{-9}$

$\tau(^3E_{1u}\rightarrow{}^1A_{1g}) = 4.13$ s

a) Geometry: C-C 1.40 Å; C-H 1.10 Å.

⟪ ⟫ Obsd, J. Karwowski, *Acta Phys. Polon.*, **A37**, 417 (1970).

TABLE 2. CALCULATED TRIPLET EXCITATION ENERGIES (ΔE), OSCILLATOR STRENGTHS (f), AND PHOSPHORESCENCE LIFETIMES (τ) OF SOME AZABENZENES[a)]

States	ΔE (eV)		$f(T_i \rightarrow S)$	τ (s)	
	Calcd	Obsd[b)]		Calcd	Obsd
Pyridine (x-axis: out-of-plane)					
$^3B_1(n\pi^*)$	3.62	3.68	0.109×10^{-7} (z)	0.485	—
$^3A_1(\pi\pi^*)$	3.84		0.341×10^{-8} (x)	1.378	
$^3B_2(\pi\pi^*)$	3.93		0.602×10^{-10} (x)	73.451	
$^3A_1(\pi\pi^*)$	4.64		0.464×10^{-7} (x)	0.069	
Pyrazine (x-axis: out-of-plane)					
$^3B_{3u}(n\pi^*)$	2.52	3.32	0.199×10^{-6} (z)	0.055	0.02[c)]
$^3B_{2u}(\pi\pi^*)$	3.12		0.182×10^{-11} (z)	1.759×10^{2}	
$^3B_{1u}(\pi\pi^*)$	3.86		0.873×10^{-8} (x)	0.532	
$^3B_{2g}(n\pi^*)$	3.90		0		
Pyrimidine (x-axis: out-of-plane)					
$^3B_1(n\pi^*)$	3.68	3.63	0.462×10^{-7} (y)	0.090	0.01—0.02[c)]
			0.105×10^{-7} (z)		
$^3A_2(n\pi^*)$	4.13		0.174×10^{-6} (x)	0.016	
			0.675×10^{-7} (z)		
$^3B_2(\pi\pi^*)$	4.20		0.219×10^{-6} (x)	0.018	
$^3A_1(\pi\pi^*)$	4.40		0.268×10^{-8} (x)	1.335	
Pyridazine (x-axis: out-of-plane)					
$^3B_1(n\pi^*)$	2.89	3.01	0.135×10^{-7} (y)	0.380	0.05[d)]
			0.826×10^{-8} (z)		
$^3B_2(\pi\pi^*)$	3.50		0.667×10^{-7} (x)	0.084	
$^3A_2(n\pi^*)$	3.51		0.138×10^{-4} (x)	0.388×10^{-3}	
$^3A_1(\pi\pi^*)$	4.02		0.188×10^{-6} (x)	0.023	
1,3,5-Triazine (z-axis: out-of-plane)					
$^3E''(n\pi^*)$	4.48	3.08	0.776×10^{-8} (x)	0.323	0.4[e)]
			0.291×10^{-8} (y)		
$^3A_2''(n\pi^*)$	4.63		0.163×10^{-6} (x)	0.631×10^{-2}	
			0.162×10^{-6} (y)		
			0.187×10^{-6} (z)		
$^3A_2''(n\pi^*)$	4.70		0.110×10^{-6} (x)	0.014	
			0.110×10^{-6} (y)		
1,2,4,5-Tetrazine (x-axis: out-of-plane)					
$^3B_{3u}(n\pi^*)$	1.18	1.69	0.195×10^{-6} (y)	0.222	72×10^{-6} [f)]
					10×10^{-9} [g)]
			0.291×10^{-7} (z)		
$^3B_{1g}(n\pi^*)$	2.95		0		
$^3B_{1u}(\pi\pi^*)$	3.21		0.375×10^{-7} (x)	0.179	
$^3A_u(n\pi^*)$	3.25		0.152×10^{-7} (x)	0.039	
			0.987×10^{-7} (y)		
			0.523×10^{-7} (z)		

a) Molecular geometries are taken from K. K. Innes, J. P. Byrne and I. G. Ross, *J. Mol. Spectrosc.*, **22**, 125 (1967). b) J. Karwowski, *Acta Phys. Polon.*, **A37**, 417 (1970). c) Ref. 17, p. 217. d) R. M. Hochstrasser and C. Marzzacco, *J. Chem. Phys.*, **46**, 4155 (1967). e) J. Paris, R. Hirt, and R. Schmitt, *J. Chem. Phys.*, **34**, 1851 (1961). f) J. R. McDonald and L. E. Brus, *J. Chem. Phys.*, **59**, 4966 (1973).

observed value 0.4 second and the assignment of the excited triplet states is in reasonable agreement with the experimentally fixed order. We do not list calculated results for lower singlet states of these azabenzenes since the results are quite similar to those obtained by Ridley and Zerner.[15)] These authors used a modified NM approximation in their INDO type calculations of lower excited singlet states of azabenzenes but did not refer to their excited triplet states. The choice of CI's in the present paper is rather different from that of Ridley and Zerner. Nevertheless, this does not yield much discrepancies in the final results for the low-lying singlet states. Chen and Hedges[14)] used a rather different parametrization in their INDO type calculation and obtained fairly good results for both low-lying singlet and triplet levels. Their assignment for higher energy levels is, however, much different from those obtained in the present paper and by Ridley and Zerner.

In the next section, we use the present results as a

theoretical foundation to explain the phosphorescence mechanisms in benzene.

Phosphorescence Mechanisms in Benzene

$^3E_{1u} \rightarrow {}^1A_{1g}$ Intercombination. In the range of our choice of CI's, the $^{1,3}B_{2u}$ and $^{1,3}B_{1u}$ states of benzene are found to be almost pure $\pi\pi^*$ states, so that the matrix element $\langle {}^1B_{2u}|H_{so}^z|{}^3B_{1u}\rangle$ vanishes provided that only the one-center spin-same-orbit coupling integrals are retained. It should be noted therefore that the $^{1,3}E_{1u}$ states having considerable amount of $\sigma\sigma^*$ characters play an important role in the spin-orbit mechanism.

Our starting wave functions for the degenerate E_{1u} states are, for example, of the forms (the state numbers 3A and 3B follow after Table 1)

$$|{}^{1,3}E_{1u}\begin{Bmatrix}3A\\2A\end{Bmatrix}\rangle = \begin{Bmatrix}0.6829\\-0.4011\end{Bmatrix}({}^{1,3}\psi_{14\rightarrow16} - {}^{1,3}\psi_{15\rightarrow17}) - \begin{Bmatrix}0.0983\\0.5824\end{Bmatrix}({}^{1,3}\psi_{14\rightarrow17} + {}^{1,3}\psi_{15\rightarrow16}) + \begin{Bmatrix}0.2193\\0.0021\end{Bmatrix}{}^{1,3}\psi_{12\rightarrow18} - \begin{Bmatrix}0.0026\\0.0043\end{Bmatrix}{}^{1,3}\psi_{13\rightarrow18} \quad (17)$$

$$|{}^{1,3}E_{1u}\begin{Bmatrix}3B\\2B\end{Bmatrix}\rangle = \begin{Bmatrix}0.0983\\0.5824\end{Bmatrix}({}^{1,3}\psi_{14\rightarrow16} - {}^{1,3}\psi_{15\rightarrow17}) + \begin{Bmatrix}0.6829\\-0.4011\end{Bmatrix}({}^{1,3}\psi_{14\rightarrow17} + {}^{1,3}\psi_{15\rightarrow16}) - \begin{Bmatrix}0.0026\\0.0043\end{Bmatrix}{}^{1,3}\psi_{12\rightarrow18} - \begin{Bmatrix}0.2193\\0.0021\end{Bmatrix}{}^{1,3}\psi_{13\rightarrow18} \quad (18)$$

where the upper and lower figures in braces correspond to the singlet and triplet states, respectively, and each configurational wave function is constructed from the ground state configuration as in the following:

$$(1a_{1g})^2(2,3e_{1u})^4(4,5e_{2g})^4(6a_{1g})^2(7b_{1u})^2(8b_{2u})^2(9,10e_{1u})^4\text{-}(11\pi a_{2u})^2(12,13e_{2g})^4(14\pi,15\pi e_{1g})^4(16\pi,17\pi e_{2u})^0(18b_{2u})^0\text{-}(19\pi b_{2g})^0(20,21e_{2g})^0(22a_{1g})^0(23,24e_{1u})^0(25b_{1u})^0(26,27e_{1u})^0(28,29e_{2g})^0(30a_{1g})^0 \quad (19)$$

In the above, each figure before the symmetry designation shows the orbital number in the order of increasing energy (double numbers are used for degenerate levels) and the simbol π after each figure denotes a π-electron MO, a specification for a σ-electron MO being omitted. With this orbital numbers we designate the configurational wave functions appearing in Eqs. 17 and 18 such as $\psi_{14\rightarrow16}$.

We obtained the following spin-contaminated wave functions for the ground state $|G^c\rangle$ and the triplet E_{1u} state $|{}^3E_{1u}^c\rangle$ needed to produce the $^3E_{1u}$-$^1A_{1g}$ intercombination:

$$\begin{aligned}|G^c\rangle &= |{}^1A_{1g}\rangle + \sum_i \lambda_i^{so}|{}^3E_{1g}(\sigma\pi^*,\pi\sigma^*;\ i)\rangle + \sum_i \omega_i^{so}|{}^3A_{2g}(\sigma\pi^*,\pi\sigma^*;\ i)\rangle \\ &= |{}^1A_{1g}\rangle + 0.7059\times10^{-4}|{}^3E_{1g}^x(10A)\rangle - 0.7234\times10^{-5}|{}^3E_{1g}^y(10A)\rangle + 0.7234\times10^{-5}|{}^3E_{1g}^x(10B)\rangle + 0.7059\times10^{-4}|{}^3E_{1g}^y(10B)\rangle \\ &\quad + 0.5152\times10^{-4}|{}^3E_{1g}^x(13A)\rangle + 0.1836\times10^{-3}|{}^3E_{1g}^y(13A)\rangle - 0.1836\times10^{-3}|{}^3E_{1g}^x(13B)\rangle + 0.5152\times10^{-4}|{}^3E_{1g}^y(13B)\rangle - 0.7770\times10^{-4}|{}^3A_{2g}^z(17)\rangle \quad (20)\end{aligned}$$

where λ_i^{so} and ω_i^{so} are the mixing coefficients for the ith perturbing triplets of symmetries $^3E_{1g}$ and $^3A_{2g}$, respectively, and each figure in a parenthesis is the state number in order of increasing energy, a symbol A or B after figure showing either of the degenerate states (see Table 1): and

$$\begin{aligned}|{}^3E_{1u}^c(2A)\rangle &= |{}^3E_{1u}(\pi\pi^*,\sigma\sigma^*;\ 2A)\rangle + \sum_i \nu_i^{so}|{}^1E_{1u}(\pi\pi^*,\sigma\sigma^*;\ i)\rangle + \sum_i \mu_i^{so}|{}^1A_{2u}(\sigma\pi^*,\pi\sigma^*;\ i)\rangle \\ &= |{}^3E_{1u}(2A)\rangle + 0.3689\times10^{-6}|{}^1E_{1u}^z(3A)\rangle + 0.1828\times10^{-6}|{}^1E_{1u}^z(3B)\rangle + 0.9425\times10^{-5}|{}^1A_{2u}^x(4)\rangle - 0.1834\times10^{-4}|{}^1A_{2u}^y(4)\rangle - 0.2521\times10^{-6}|{}^1E_{1u}^z(14A)\rangle - 0.6792\times10^{-6}|{}^1E_{1u}^z(14B)\rangle \quad (21)\\ |{}^3E_{1u}^c(2B)\rangle &= |{}^3E_{1u}(2B)\rangle + 0.1828\times10^{-6}|{}^1E_{1u}^z(3A)\rangle + 0.3689\times10^{-6}|{}^1E_{1u}^z(3B)\rangle - 0.1834\times10^{-4}|{}^1A_{2u}^x(4)\rangle - 0.9424\times10^{-5}|{}^1A_{2u}^y(4)\rangle + 0.6792\times10^{-6}|{}^1E_{1u}^z(14A)\rangle - 0.2510\times10^{-6}|{}^1E_{1u}^z(14B)\rangle. \quad (22)\end{aligned}$$

This computational output is in accord with a group-theoretical consideration given by Clementi,[4] apart from the numerical factors. We have thus a hypothetical transition moment between the $^3E_{1u}$ and the ground $^1A_{1g}$ states (in a.u.):

$$\sum_{i=2A,2B}\langle G^c|\vec{M}|{}^3E_{1u}^c(i)\rangle = 2.2890\times10^{-7}\vec{e}_x - 7.1426\times10^{-7}\vec{e}_y - 9.4013\times10^{-5}\vec{e}_z. \quad (23)$$

If we assume that the main contribution to the phosphorescence polarization comes from the transition $^3E_{1u} \rightarrow {}^1A_{1g}$, the phosphorescence spectrum of benzene is predicted to be almost 100% out-of-plane polarized.

How large is the effect of many-center spin-orbit coupling integrals? Clementi,[4] after the manner of Hameka and Oosterhoff, estimated the contribution of three-center spin-same-orbit coupling integrals and three- and four-center spin-other-orbit coupling integrals to the $|{}^3E_{1u}^c(2A)\rangle$ and $|{}^3E_{1u}^c(2B)\rangle$ states of pure π character. If we use his estimated value of such contribution

$$|{}^3E_{1u}^{cm}(i)\rangle = |{}^3E_{1u}^c(i)\rangle + 2.15\times10^{-5}\sum_{i=3A,3B}|{}^1E_{1u}(i)\rangle \quad (24)$$

we have the following transition moment (in a.u.):

$$\sum_{i=2A,2B}\langle G^c|\vec{M}|{}^3E_{1u}^{cm}(i)\rangle = -5.1001\times10^{-5}\vec{e}_x + 5.0516\times10^{-5}\vec{e}_y$$

$$- 9.4013\times10^{-5}\vec{e}_z. \quad (25)$$

Thus, the ratio of the out-of-plane to the in-plane polarizations of the phosphorescence $^3E_{1u}\rightarrow{}^1A_{1g}$ turns out to be 81 : 51 which is in accord with the observation (*ca.* 3 : 2) of Russel and Albrecht.[1] However, Eq. 25 does not lead to the almost out-of-plane polarized $^3B_{1u}\rightarrow{}^1A_{1g}$ phosphorescence which is the more recent experimental result obtained by van Egmond and van der Waals[2] (*vide infra*). The value 2.15×10^{-5} in Eq. 24 seems to be overestimated, even from the fact that the contribution of the one-center integrals in CH_2[26,27] and H_2CO[16,20] is calculated to be from ten to fifty times larger than that of many-center integrals.

Vibronically Induced $^3B_{1u}\rightarrow{}^1A_{1g}$ *Emission via* $^3E_{1u}$-$^1A_{1g}$ *Intercombination.* If we take account of the vibronic coupling H_{vib} as well as the spin-orbit coupling neglecting spin-vibronic terms, spin- and vibronically-contaminated wave functions for excited triplet states might be given by the second-order perturbation theory, because of relatively large values of vibronic coupling integrals compared with spin-orbit coupling integrals.

$$\begin{aligned}|T_i^c\rangle = |T_i\rangle &+ \sum_{j\neq i}\frac{\langle T_j|H_{vib}|T_i\rangle}{E(T_i)-E(T_j)}|T_j\rangle \\ &+ \sum_j\frac{\langle S_j|H_{so}|T_i\rangle}{E(T_i)-E(S_j)}|S_j\rangle \\ &+ \sum_j\sum_{k\neq i}\frac{\langle S_j|H_{vib}|S_k\rangle\langle S_k|H_{so}|T_i\rangle}{[E(T_i)-E(S_j)][E(T_i)-E(S_k)]}|S_j\rangle \\ &+ \sum_j\sum_{k\neq i}\frac{\langle S_j|H_{so}|T_k\rangle\langle T_k|H_{vib}|T_i\rangle}{[E(T_i)-E(S_j)][E(T_i)-E(T_k)]}|S_j\rangle \quad (26)\end{aligned}$$

or in an abbreviated form

$$\begin{aligned}|T_i^c\rangle = |T_i\rangle &+ \sum_{j\neq i}\delta_j^{vib}|T_j\rangle + \sum_j\gamma_j^{so}|S_j\rangle \\ &+ \sum_j\sum_{k\neq i}\alpha(S_j|S_k|T_i)|S_j\rangle \\ &+ \sum_j\sum_{k\neq i}\beta(S_j|T_k|T_i)|S_j\rangle \quad (27)\end{aligned}$$

where in Albrecht's notation[5] we write

$$H_{vib} = \sum_a (\partial H/\partial Q_a)_0 Q_a. \quad (28)$$

If we adopt the possible phosphorescence routes suggested by Albrecht,[5] we have

$$\begin{aligned}|^3B_{1u}^c(1)\rangle = |^3B_{1u}(1)\rangle &+ \sum_{i=2A,2B}\delta_i^{vib}|^3E_{1u}^c(i)\rangle + \gamma_1^{so}|^1B_{2u}(1)\rangle \\ &+ \sum_{i=3A,3B}[\alpha(^1E_{1u}(i)|^1B_{2u}(1)|^3B_{1u}(1)) \\ &+ \sum_{j=2A,2B}\beta(^1E_{1u}(i)|^3E_{1u}(j)|^3B_{1u}(1))]|^1E_{1u}(i)\rangle \\ &+ [\sum_{i=5A,5B}\alpha(^1A_{2u}(4)|^1E_{2u}(i)|^3B_{1u}(1)) \\ &+ \sum_{i=2A,2B}\beta(^1A_{2u}(4)|^3E_{1u}(i)|^3B_{1u}(1))]|^1A_{2u}(4)\rangle \\ &+ \sum_{i=3A,3B}[\sum_{j=5A,5B}\{\alpha(^1E_{1u}(i)|^1E_{2u}(j)|^3B_{1u}(1)) \\ &+ \beta(^1E_u(i)|^3E_{2u}(j)|^3B_{1u}(1))\} \\ &+ \beta'(^1E_{1u}(i)|^3A_{2u}(7)|^3B_{1u}(1))]|^1E_{1u}(i)\rangle \quad (29)\end{aligned}$$

where

$$\delta_i^{vib} = \frac{\langle ^3E_{1u}^c(i)|H_{vib}|^3B_{1u}(1)\rangle}{E(^3B_{1u}(1))-E(^3E_{1u}^c(i))} \cong \frac{\langle ^3E_{1u}(i)|H_{vib}|^3B_{1u}(1)\rangle}{E(^3B_{1u}(1))-E(^3E_{1u}(i))} \quad (30)$$

and $|^3E_{1u}^c(i)\rangle$ corresponds to Eqs. 21 and 22. These individual contribution are schematically shown in Fig. 1, where (a), (b), (c), (d) and (e) correspond to the second, third, fourth, fifth and the last terms of Eq. 29, respectively. In order to obtain the mixing coefficients of Eq. 29, we adopt experimental values of excitation energies, if available, and otherwise use the corresponding calculated values. For vibronic integrals we use the values determined by Albrecht.[5] The last term of Eq. 29 is cut off, since the values of

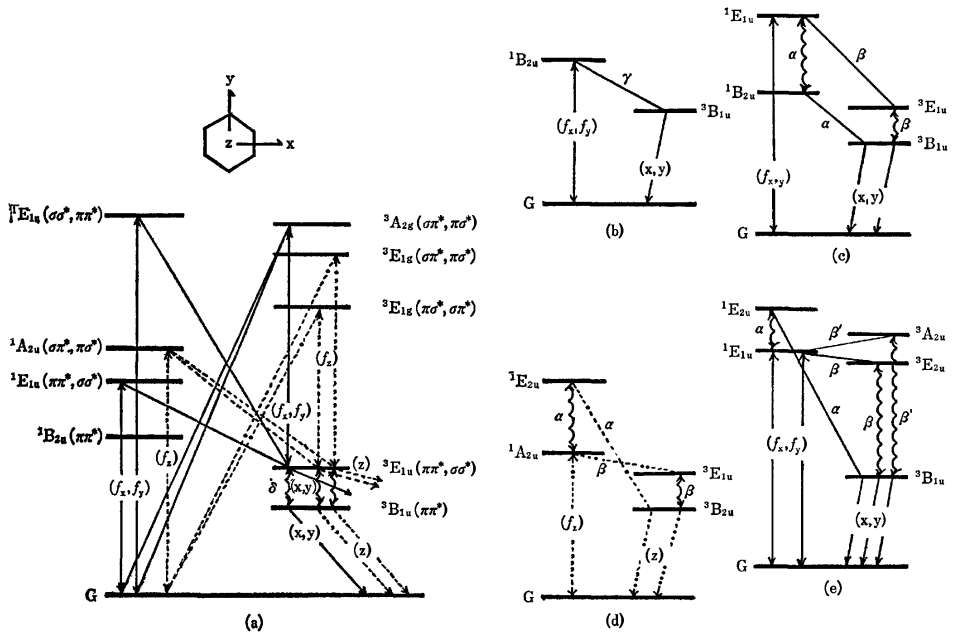

Fig. 1. Possible phosphorescence mechanisms in benzene. (a), (b), (c), (d), and (e) correspond to the 2nd, 3rd, 4th, 5th and 6th terms of Eq. 29 in the text, respectively. Solid arrow: in-plane polarized transition; dashed arrow: out-of-plane polarized transition.

these vibronic integrals are unknown. Matrix elements over many-center integrals are neglected by the reason mentioned before. Only exception is the element $\langle {}^1B_{2u}|H^z_{so}|{}^3B_{1u}\rangle$ which is included in the following in order to estimate the effect of Route (b). The forbidden transition moment $\langle {}^1A_{1g}|M_{x,y}|{}^1B_{2u}\rangle$ is estimated to be $\pm 1.013\times 10^{-2}$ atomic unit from an experimental point of view.

Equation 29 is now calculated to be[28]

$$\begin{aligned}|{}^3B^c_{1u}(1)\rangle &= 0.9025|{}^3B_{1u}(1)\rangle \\ &\quad - 0.3047[|{}^3E^c_{1u}(2A)\rangle + |{}^3E^c_{1u}(2B)\rangle] \\ &\quad + 0.1190\times 10^{-4}|{}^1B_{2u}(1)\rangle \\ &\quad + 0.1473\times 10^{-5}|{}^1E_{1u}(3A)\rangle \\ &\quad + 0.1411\times 10^{-5}|{}^1E_{1u}(3B)\rangle \\ &\quad - 0.3239\times 10^{-5}|{}^1A_{2u}(4)\rangle. \end{aligned} \tag{31}$$

Finally, we have

$$\begin{aligned}\langle G^c|\vec{M}|{}^3B^c_{1u}(1)\rangle &= -0.3047[\langle G^c|\vec{M}|{}^3E^c_{1u}(2A)\rangle \\ &\quad + \langle G^c|\vec{M}|{}^3E^c_{1u}(2B)\rangle] \\ &\quad + 0.1190\times 10^{-4}\langle {}^1A_{1g}|\vec{M}|{}^1B_{2u}(1)\rangle \\ &\quad + 0.1473\times 10^{-5}\langle {}^1A_{1g}|\vec{M}|{}^1E_{1u}(3A)\rangle \\ &\quad + 0.1411\times 10^{-5}\langle {}^1A_{1g}|\vec{M}|{}^1E_{1u}(3B)\rangle \\ &\quad - 0.3239\times 10^{-5}\langle {}^1A_{1g}|\vec{M}|{}^1A_{2u}(4)\rangle \\ &= (-3.411\pm 0.060)\times 10^{-6}\vec{e}_x \\ &\quad + (3.838\pm 0.060)\times 10^{-6}\vec{e}_y \\ &\quad + 2.825\times 10^{-5}\vec{e}_z. \end{aligned} \tag{32}$$

Fractional contributions of the four phosphorescence routes shown in Fig. 1 to the transition moment $\langle G^c|\vec{M}|{}^3B^c_{1u}(1)\rangle$ are listed in Table 3. The final result given in Eq. 32 clearly shows that the phosphorescence from the ${}^3B_{1u}(1)$ state is almost 100% out-of-plane polarized. This is in accord with the results of the Zeeman and MIDP experiments obtained by van Egmond and van der Waals.[2] If we use the observed energy separation 3.95 eV between the ${}^3B_{1u}(1)$ state and the ground state, Eqs. 5 and 6 yield the oscillator strength $f({}^3B_{1u}\rightarrow {}^1A_{1g})=0.7940\times 10^{-10}$ and the lifetime $\tau=55.8$ second.

As evident from Eq. 32, the main contribution to the phosphorescence lifetime comes from the term δ^{v1b} for which we have used Albrecht's value $\langle {}^3E^c_{1u}(i)|H_{v1b}|{}^3B_{1u}(1)\rangle=0.27$ eV, i=2A and 2B. Comparison of the calculated lifetime with the observed value 4.75 second[29,30] suggests that the value of δ^{v1b}, namely the value of $\langle {}^3E^c_{1u}|H_{v1b}|{}^3B_{1u}\rangle$, is underestimated. In fact, van der Waals *et al.*[31] estimated the value of the δ^{v1b} to be -0.4031 which yields $f({}^3B_{1u}\rightarrow {}^1A_{1g})=1.390\times 10^{-10}$ and $\tau=31.9$ second. If one wants to reproduce the observed lifetime 4.75 second by making use of the same computational scheme as above, δ^{v1b} must be taken the value 0.55 and one has

$$\begin{aligned}|{}^3B^c_{1u}(1)\rangle &= 0.63|{}^3B_{1u}(1)\rangle \\ &\quad - 0.78\frac{1}{\sqrt{2}}\{|{}^3E^c_{1u}(2A)\rangle + |{}^3E^c_{1u}(2B)\rangle\} + \cdots. \end{aligned}$$

Thus the mixing coefficients of the triplet B_{1u} and E_{1u} states come out to be absolutely improbable. On the other hand, if the value of δ^{v1b} is fixed to be around -0.4, a value of the z-component of the transition moment between the ${}^3E_{1u}$ and the ground states $-1.3\times 10^{-4}\vec{e}_z$ instead of our calculated value $-9.40\times 10^{-5}\vec{e}_z$ yields the lifetime which is in accord with the observed value. Though further studies are needed to clarify this matter, our conclusion at present is that molecular wave functions to calculate the transition moment due to the ${}^3E_{1u}$-${}^1A_{1g}$ intercombination are very sensitive to the prediction of the triplet lifetime in benzene.

Table 3. Contribution of possible phosphorescence routes to transition moment $\langle G^c|\vec{M}|{}^3B^c_{1u}(1)\rangle$

Route in Fig. 1	M_x	M_y	M_z
a	-0.6978×10^{-7}	2.1756×10^{-7}	2.8646×10^{-5}
b	$\pm 0.6027\times 10^{-7}$	$\pm 0.6027\times 10^{-7}$	0
c	-0.3341×10^{-5}	0.3612×10^{-5}	0
d	0	0	-0.0401×10^{-5}
e	—	—	—

References

1) P. G. Russel and A. C. Albrecht, *J. Chem. Phys.*, **41**, 2536 (1964).
2) J. van Egmond and J. H. van der Waals, *Mol. Phys.*, **26**, 1147 (1973).
3) M. Mizushima and S. Koide, *J. Chem. Phys.*, **20**, 765 (1952).
4) E. Clementi, *J. Mol. Spectrosc.*, **6**, 497 (1961).
5) A. C. Albrecht, *J. Chem. Phys.*, **38**, 354 (1963).
6) W. S. Veeman and J. H. van der Waals, *Mol. Phys.*, **18**, 63 (1970).
7) V. G. Krishna and W. R. Salzman, *J. Chem. Phys.*, **50**, 3875 (1969).
8) B. R. Henry and W. Siebrand, *J. Chem. Phys.*, **51**, 2396 (1969).
9) F. J. Adrian, *J. Chem. Phys.*, **52**, 622 (1970).
10) J. H. van der Waals and M. S. De Groot, "The Triplet State," Cambridge University Press (1967), p. 104.
11) J. Del Bene and M. H. Jaffé, *J. Chem. Phys.*, **48**, 1807 (1968).
12) R. L. Ellis, G. Kuehnlenz, and H. H. Jaffé, *Theor. Chim. Acta*, **26**, 131 (1972).
13) H. Chojnacki, *Theor. Chim. Acta*, **11**, 174 (1968).
14) S-Y. Chen and R. M. Hedges, *Theor. Chim. Acta*, **31**, 275 (1973).
15) J. Ridley and M. Zerner, *Theor. Chim. Acta*, **32**, 111 (1973).
16) H. Ito and Y. J. I'Haya, *Mol. Phys.* **24**, 1103 (1972).
17) S. P. McGlynn, T. Azumi, M. Kinoshita, "Molecular Spectroscopy of the Triplet State," Prentice-Hall, New York (1969), p. 18.
18) M. S. De Groot, I. A. M. Hesselmann, J. Schmidt, and J. H. van der Waals, *Mol. Phys.*, **15**, 17 (1968).
19) D. G. Carroll, L. G. Vanquickenborne, and S. P. McGlynn, *J. Chem. Phys.*, **45**, 2777 (1966).
20) J. L. Ginsburg and L. Goodman, *Mol. Phys.*, **15**, 441 (1968).
21) J. A. Pople and D. L. Beveridge, "Approximate Molecular Orbital Theory," McGraw-Hill, New York (1970), p. 67.

22) Quantum Chemistry Program Exchange, Bloomington, Indiana.
23) J. C. Ho, G. A. Segal, and H. S. Taylor, *J. Chem. Phys.*, **56**, 1520 (1972).
24) N. Mataga and K. Nishimoto, *Z. Phys. Chem. (Frankfurt)*, **13**, 140 (1957).
25) K. Ohno, *Theor. Chim. Acta*, **2**, 219 (1964).
26) S. J. Fogel and H. F. Hameka, *J. Chem. Phys.*, **42**, 132 (1965).
27) J. W. McIver and H. F. Hameka, *J. Chem. Phys.*, **45**, 767 (1966).
28) In the case that the mixing coefficient δ^{v1b} between the $^3B_{1u}^e$ and $^3E_{1u}^e$ states is calculated not from the second-order perturbation method but from the Ritz variation method, the value of δ^{v1b} comes out to be -0.3408 instead of -0.3047 in Eq. 31. This value yields $\langle G^e|\vec{M}|^3B_{1u}^e(1)\rangle = -0.0078\times10^{-5}\vec{e}_x+0.0243\times10^{-5}\vec{e}_y+3.2040\times10^{-5}\vec{e}_z$, $f(^3B_{1u}\rightarrow{}^1A_{1g})=0.9933\times10^{-10}$ and $\tau=44.6$ second.
29) T. E. Martin and A. H. Kalantar, *J. Chem. Phys.*, **48**, 4996 (1968).
30) J. W. Rabalais, H. Maria, and S. P. McGlynn, *J. Chem. Phys.*, **51**, 2259 (1969).
31) J. H. van der Waals, A. M. D. Berghuis, and M. S. De Groot, *Mol. Phys.*, **13**, 301 (1967).

Microwave Spectrum of Ethyl Isothiocyanate

Takeshi SAKAIZUMI, Osamu OHASHI, and Ichiro YAMAGUCHI

Department of Chemistry, Faculty of Science and Technology, Sophia University, Kioi-cho, Chiyoda-ku, Tokyo 102

(Received December 16, 1975)

The microwave spectrum of ethyl isothiocyanate, CH_3CH_2NCS, has been obtained in the frequency region from 8.5 to 35 GHz. The spectrum identified is attributed to the *cis* configuration, namely, the methyl group eclipses the isothiocyanato group. The rotational constants for the ground vibrational state obtained are $A=14194\pm10$, $B=1799.27\pm0.02$ and $C=1612.14\pm0.02$ MHz. The dipole moment of this rotamer is $\mu_{total}=3.33\pm0.03$ D ($\mu_a=3.33\pm0.03$ D, $\mu_b=0.07\pm0.02$ D). Two sets of vibrational satellites were observed and assigned to the modes of C–N torsion (58 ± 30 cm^{-1}) and CNC bending (107 ± 30 cm^{-1}).

Recently microwave spectroscopy has been increasingly applied to the study of the rotational isomerism of molecules. Most of these studies have, however, been made on the rotational isomerism about a C–C single bond, and less attention has been paid to that about single carbon-heteroatom bonds. It is interesting, therefore, to study the rotational isomerism of mono-substituted ethanes, having, for example, thiocyanato (–SCN), isothiocyanato (–NCS), selenocyanato (–SeCN), isoselenocyanato (–NCSe) groups, *etc.* Kniseley *et al.*[1] have investigated the structure of ethyl isothiocyanate using infrared spectroscopy and concluded that the molecule existed in two rotameric forms, presumably *trans* and *gauche*. They observed two absorption bands at 2199 and 2154 cm^{-1} at liquid nitrogen temperature and assigned them to the NCS asymmetric stretching vibration in the *gauche* and *trans* configurations. Bjørseth and Marstokk[2] have studied the microwave spectrum of ethyl thiocyanate, CH_3CH_2-SCN, and determined that the molecule exists in a single rotameric form, probably *gauche*, in gas phase, which is more stable than the *trans* form by at least 0.8 kcal·mol^{-1}.

In this paper, the spectrum of ethyl isothiocyanate in a configuration characterized by predominant absorption lines, the *cis* form, is reported and the structure and dipole moment are discussed.

Experimental

The sample of ethyl isothiocyanate was obtained commercially and purified by distillation *in vacuo*. The rotational spectrum was obtained in the frequency region from 8.5 to 35 GHz with a conventional 100-kHz sinusoidal- and square-wave Stark modulation spectrometer. The waveguide cell was cooled with dry ice in order to enhance the intensity of the absorption lines. Transition frequencies were measured with a Hewlett-Packard Model 5245 L frequency counter.

Results and Discussion

Spectrum and Assignment for the Vibrational Ground State. The observed spectrum was considerably dense in appearance, consisting of a large number of absorption lines. This feature may be ascribed to the various rotational isomers and their vibrationally-excited states. Four rotational isomers may be considered for the ethyl isothiocyanate molecule, namely, the *cis*, *gauche*, *skew*, and *trans* forms, as shown in Fig. 1. The moments of inertia calculated from the assumed structure of

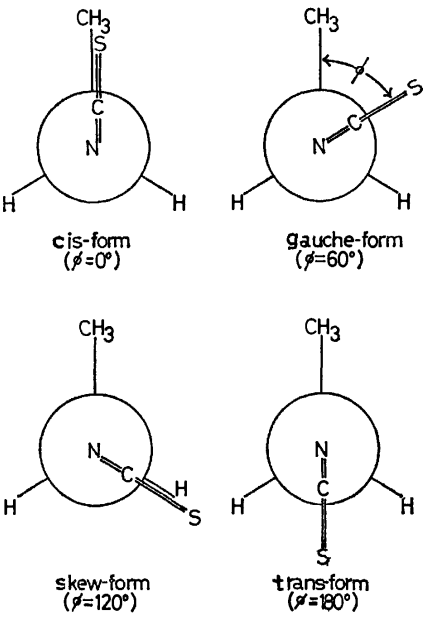

Fig. 1. Model of rotational isomers of ethyl isothiocyanate.
ϕ: dihedral angle.

these isomers indicate that all are nearly prolate symmetric top molecules (the value of the asymmetric parameter of Ray are in the region from −0.998 to −0.974). A large a-component of the dipole moment is expected for these molecules because the –N=C=S group, having a large moment, lies close to the a-axis. Consequently, strong a-type R-branch absorption lines with $K_{-1}=0$ and 1 are expected. In the vicinity of the $K_{-1}=0$ line, absorption lines for K_{-1} equal to or larger than two should appear and a large Stark effect should be observed.

The $J=4\leftarrow3$ transitions with $K_{-1}=0$ and 1 in the ground vibrational state were first observed and identified from their Stark effects. With the preliminary values of the rotational constants fitted to only the low-J transition frequencies, the high-J transition frequencies were predicted from the rigid rotor Hamiltonian. As the values of J and K_{-1} increase, the difference between the observed and calculated transition frequencies was found to become larger, in particular, for lines with values of K_{-1} larger than one as shown in Fig. 2 (obsd and calcd-I). This difference is probably attributable to the centrifugal distortion effect.

The preliminarily determined rotational constants

TABLE 1. ASSIGNED ROTATIONAL TRANSITIONS OF ETHYL ISOTHIOCYANATE (in MHz)

Transition	Ground state		Set-I CN torsion		Set-II CNC bend	
	ν_{obsd}[a]	$\Delta\nu$[b]	ν_{obsd}[a]	$\Delta\nu$[b]	ν_{obsd}[a]	$\Delta\nu$[b]
$4_{04} \leftarrow 3_{03}$	13548.86	0.30	13372.96	0.02	13303.99	−0.16
$4_{14} \leftarrow 3_{13}$	13228.17	0.16	13083.72	0.38	13016.68	−0.17
$4_{13} \leftarrow 3_{12}$	13896.66	0.21	13684.15	−0.07	13612.25	0.20
$4_{23} \leftarrow 3_{22}$	13565.29	0.13	13387.15	0.60	13317.82	0.39
$4_{22} \leftarrow 3_{21}$	13581.70	−0.18	13399.53	0.10	13329.25	−0.44
$4_{32} \leftarrow 3_{31}$ $4_{31} \leftarrow 3_{30}$	13570.90[c]	−0.35 −0.41	13392.97[c]	0.50 0.52	13323.59[c]	0.31 0.27
$5_{05} \leftarrow 4_{04}$	16922.53	−0.36	16706.15	0.10	16620.58	−0.01
$5_{15} \leftarrow 4_{14}$	16531.28	−0.37	16351.54	0.08	16267.93	−0.46
$5_{14} \leftarrow 4_{13}$	17367.34	0.27	17102.61	0.14	17012.65	0.35
$5_{24} \leftarrow 4_{23}$	16954.38	0.31	16730.86	−0.38	16645.02	0.19
$5_{23} \leftarrow 4_{22}$	16987.16	−0.32	16757.56	0.17	16669.29	−0.05
$5_{33} \leftarrow 4_{32}$ $5_{32} \leftarrow 4_{31}$	16965.41	0.13 0.13	16741.61[c]	0.61 0.46	16655.38[c]	0.59 0.46
$5_{42} \leftarrow 4_{41}$ $5_{41} \leftarrow 4_{40}$	16966.01	0.07 0.07	16742.38[c]	−0.51 −0.51	16657.90	0.22 0.22
$6_{06} \leftarrow 5_{05}$	20289.00	0.23	20032.51	0.03	19930.22	−0.44
$6_{16} \leftarrow 5_{15}$	19833.38	0.26	19617.81	0.01	19517.92	−0.26
$6_{15} \leftarrow 5_{14}$	20835.55	0.25	20518.88	0.08	20410.85	0.17
$6_{25} \leftarrow 5_{24}$	20341.28	−0.11	20074.74	0.10	19970.84	−0.10
$6_{24} \leftarrow 5_{23}$	20399.96	0.18	20120.62	0.27	20013.42	−0.36
$6_{31} \leftarrow 5_{33}$ $6_{33} \leftarrow 5_{32}$	20360.18[c]	0.12 0.46	20090.26[c]	−0.18 −0.58	19987.17[c]	0.44 0.09
$6_{43} \leftarrow 5_{42}$ $6_{42} \leftarrow 5_{41}$	20360.18	0.24 0.24	20092.20	0.22 0.22	19989.82	0.32 0.32
$6_{52} \leftarrow 5_{51}$ $6_{51} \leftarrow 5_{50}$	20363.38[c]	0.96 0.96	20096.24	0.18 0.18	19995.06	−0.01 −0.01
$7_{07} \leftarrow 6_{06}$	23644.20	−0.41	23350.87	−0.08	23233.23	0.06
$7_{17} \leftarrow 6_{16}$	23131.36	−0.67	22882.10	0.03	22765.92	0.02
$7_{16} \leftarrow 6_{15}$	24300.36	−0.24	23933.41	0.61	23806.91	0.13
$7_{26} \leftarrow 6_{25}$	23726.66	−0.16	23416.69	0.20	23295.36	−0.13
$7_{25} \leftarrow 6_{24}$	23820.11	0.13	23489.42	−0.04	23363.86	−0.04
$7_{35} \leftarrow 6_{34}$ $7_{34} \leftarrow 6_{33}$	23756.18 23756.18[c]	0.50 −0.81	23441.10[c]	0.60 −0.30	23319.83[c]	0.69 −0.11
$7_{41} \leftarrow 6_{43}$ $7_{43} \leftarrow 6_{42}$	23754.20	−0.16 −0.16	24441.10	−0.25 −0.25	23321.82	0.34 0.34
$7_{53} \leftarrow 6_{52}$ $7_{52} \leftarrow 6_{51}$	23756.18	−0.45 −0.45	23446.06	0.45 0.45	23327.87	0.38 0.38
$7_{62} \leftarrow 6_{61}$ $7_{61} \leftarrow 6_{60}$	23760.85	−0.21 −0.21	23452.15	0.02 0.02	23336.49	0.43 0.43
$8_{08} \leftarrow 7_{07}$	26988.64	−0.30	26660.09	−0.17	26526.74	−0.21
$8_{18} \leftarrow 7_{17}$	26427.64	−0.06	26144.04	0.09	26526.74	−0.21
$8_{17} \leftarrow 7_{16}$	27762.21	−0.21	27343.51	−0.50	26011.15	−0.12
$8_{27} \leftarrow 7_{26}$	27109.90	−0.13	26756.13	−0.38	26617.96	−0.27
$8_{26} \leftarrow 7_{25}$	27249.39	0.20	26865.88	0.24	26720.48	−0.06
$8_{36} \leftarrow 7_{35}$ $8_{35} \leftarrow 7_{34}$	27152.48 27155.54[c]	0.27 0.69	26791.32	0.10 0.10	26653.54[c]	1.47 −0.12
$8_{45} \leftarrow 7_{44}$ $8_{44} \leftarrow 7_{43}$	27149.30	−0.03 −0.03	26791.32	0.27 0.27	26653.54	−0.11 −0.12
$8_{54} \leftarrow 7_{53}$ $8_{53} \leftarrow 7_{52}$	27151.21	0.14 0.14	26795.38	0.12 0.12	26660.18[c]	0.28 0.28
$8_{63} \leftarrow 7_{62}$ $8_{62} \leftarrow 7_{61}$	27155.54	−0.16 −0.16	26803.15[c]	0.79 0.79	26669.54	0.16 0.16
$8_{72} \leftarrow 7_{71}$ $8_{71} \leftarrow 7_{70}$	27162.20	−0.07 −0.07	26812.02	0.41 0.41	26680.80	−0.58 −0.58
$9_{09} \leftarrow 8_{08}$	30320.20	−0.30	29959.09	−0.22	29810.67	−0.27
$9_{19} \leftarrow 8_{18}$	29720.92	0.11	29403.74	0.56	29254.56	0.55

Table 1. (Continued)

Transition	Ground state		Set-I CN torsion		Set-II CNC bend	
	ν_{obsd}[a]	$\Delta\nu$[b]	ν_{obsd}[a]	$\Delta\nu$[b]	ν_{obsd}[a]	$\Delta\nu$[b]
$9_{18} \leftarrow 8_{17}$	31219.69	−0.43	30751.20[c]	−0.78	30589.92	−0.47
$9_{28} \leftarrow 8_{27}$	30490.44	−0.27	30093.88[c]	0.79	29939.10	0.22
$9_{27} \leftarrow 8_{26}$	30688.71	0.38	30249.67	0.01	30084.29	−0.15
$9_{37} \leftarrow 8_{36}$	30550.10	0.41	30142.54	−0.18	29986.37[c]	0.85
$9_{36} \leftarrow 8_{35}$	30554.58	0.06	30145.20[c]	−0.70	29988.42	−0.01
$9_{46} \leftarrow 8_{45}$ $9_{45} \leftarrow 8_{44}$	30545.08	0.24 0.24	30141.09	0.01 0.01	29986.37	0.35 0.35
$9_{55} \leftarrow 8_{54}$ $9_{54} \leftarrow 8_{53}$	30545.68	−0.07 −0.07	30145.20	0.19 0.19	29992.87[c]	0.59 0.59
$9_{64} \leftarrow 8_{63}$ $9_{63} \leftarrow 8_{62}$	30550.10	−0.30 −0.30	30152.80	0.24 0.24	30002.89	0.36 0.36
$9_{73} \leftarrow 8_{72}$ $9_{72} \leftarrow 8_{71}$	30557.46	−0.02 −0.02	30162.83	0.12 0.12	30015.49	−0.30 −0.30
$9_{82} \leftarrow 8_{81}$ $9_{81} \leftarrow 8_{80}$	30566.30	−0.14 −0.14	30175.09	0.03 0.03	30030.86[c]	−0.82 −0.82
$10_{010} \leftarrow 9_{09}$	33637.99	−0.26	33246.63	−0.55	33084.52	0.29
$10_{110} \leftarrow 9_{19}$	33010.42	0.33	34158.35[c]	2.15	32494.95[c]	1.09
$10_{19} \leftarrow 9_{18}$	34672.84	−0.24	32660.27	0.76	33975.66[c]	−1.31
$10_{29} \leftarrow 9_{28}$	33868.42	−0.12	33429.77	−0.33	33257.35	0.14
$10_{28} \leftarrow 9_{27}$	34138.34	0.28	33641.88	−0.27	33456.24	0.04
$10_{38} \leftarrow 9_{37}$	33948.09	−0.01	33494.60	−0.12	33319.31	−0.17
$10_{37} \leftarrow 9_{36}$	33956.62	0.26	33500.05	−0.30	33324.83	0.36
$10_{47} \leftarrow 9_{46}$ $10_{46} \leftarrow 9_{45}$	33940.88	−0.13 −0.23	33491.39	−0.16 −0.22	33319.31[c]	0.69 0.69
$10_{56} \leftarrow 9_{55}$ $10_{55} \leftarrow 9_{54}$	33940.88	0.14 0.14	33494.60	−0.28 −0.28	33324.83	0.21 0.21
$10_{65} \leftarrow 9_{64}$ $10_{64} \leftarrow 9_{63}$	33945.42	0.21 0.21	33502.69	−0.04 −0.04	33335.92	0.43 0.43
$10_{74} \leftarrow 9_{73}$ $10_{73} \leftarrow 9_{72}$	33952.81	0.16 0.16	33513.58	−0.10 −0.10	33349.22[c]	−0.73 −0.73
$10_{83} \leftarrow 9_{82}$ $10_{82} \leftarrow 9_{81}$	33962.46	0.11 0.11	33526.82	−0.38 −0.38	33349.22[c]	0.62 0.62
$10_{92} \leftarrow 9_{91}$ $10_{91} \leftarrow 9_{90}$	33973.78	−0.18 −0.18	33542.86	−0.14 −0.14	33388.36[c]	0.71 0.71

a) Experimental uncertainty: ±0.20 MHz. b) $\Delta\nu = \nu_{obsd} - \nu_{calcd}$. c) Not included in the least-squares fitting.

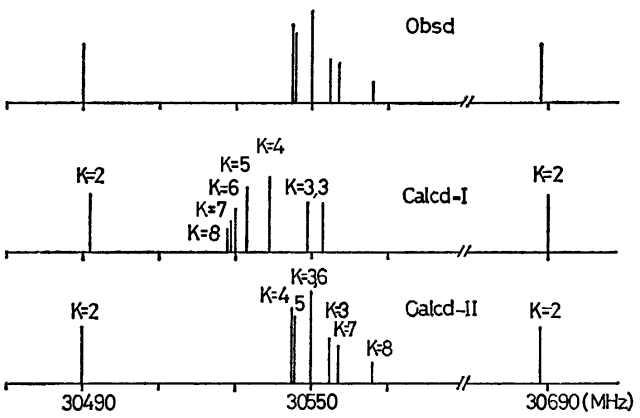

Fig. 2. Observed and calculated $J=9\leftarrow8$ transition of ethyl isothiocyanate (ground vibrational state). Calcd-I: calculated with the rigid rotor model; Calcd-II: calculated using Eq. (1), the centrifugal distortion effect included.

suggest that the molecule studied was a nearly symmetric top. Therefore, the observed transition frequencies given in Table 1 were fitted to the following equations:

$$E = E_r + E_d \quad (1)$$

$$E_d = -D_J J^2(J+1)^2 - D_{JK} J(J+1)K^2 - D_K K^4 \quad (2)$$

where E_r is the energy for a nearly symmetric rigid rotor molecule and E_d the correction for the first-order centrifugal distortion effect.

The rotational and centrifugal distortion constants were obtained by the least-squares method as given in Table 2. The observed and calculated transition frequencies are in good agreement, as is shown in the column of Table 1 with the heading "ground state". As shown in Fig. 2, the transitions with K_{-1} larger than four appear at higher frequencies as their K_{-1} increase, (obsd and calcd-II), in contrast with the rigid rotor spectrum (calcd-I). This is because of the negative value of D_{JK}.

Conformation of the Molecule. For the ground vibrational state, the value of $\Delta(I_a+I_b-I_c)$ is 6.159

Table 2. Rotational constants and moments of inertia[a] for ethyl isothiocyanate

	Ground State	Set-I C-N torsion	Set-II CNC bend
A(MHz)	14194±10	14599±10	15215±15
B(MHz)	1779.27 ±0.02	1748.42 ±0.02	1739.03 ±0.02
C(MHz)	1612.14 ±0.02	1598.18 ±0.02	1590.22 ±0.02
D_J(kHz)	1.58 ±0.02	1.70 ±0.02	2.31 ±0.02
D_{JK}(kHz)	−36.9 ±0.2	−48.6 ±0.2	−61.6 ±0.2
I_a(amu·Å^2)	35.605±0.025	34.617±0.024	33.215±0.033
I_b(amu·Å^2)	284.035±0.003	289.047±0.003	290.608±0.003
I_c(amu·Å^2)	313.481±0.004	316.219±0.004	317.803±0.004
Δ(amu·Å^2)[b]	6.159±0.032	7.445±0.031	6.020±0.040
Δ'(amu·Å^2)[c]	0.084±0.032	−1.202±0.031	0.222±0.040

a) Conversion factor $=5.05376\times10^5$ MHz·amu·Å^2. b) $\Delta=I_a+I_b-I_c$. c) $\Delta'=I_c-I_b-I_a+8m_Hc_H^2$.

amu·Å^2, as calculated from the moments of inertia given in Table 2. If the molecule studied in this work has a plane of symmetry, there are four hydrogen atoms out of this plane. Consequently, the following relation is valid if the molecule is rigid:

$$8m_Hc_H^2 = I_a + I_b - I_c \quad (3)$$

where m_H is the mass of one hydrogen atom and c_H is its distance from the plane of symmetry. There are two possible configurations for the molecule having a plane of symmetry, namely, the *cis* and *trans* forms. Using the assumed structural parameters given in Table 3, the value of $8\,m_Hc_H^2$ for the two forms was calculated to be 6.345 amu·Å^2. This is in good agreement with the value determined experimentally. This result suggests that the configurations of the molecule are the forms having plane symmetry, namely, the *cis* or *trans* form. Moreover, comparing the rotational constants determined experimentally with those calculated from the assumed structures given in Table 4, the preferred configuration is clearly the *cis* form shown in Fig. 3. Ethyl isothiocyanate molecules are in the *cis* conformation in the gas phase as one of the possible rotational isomers. This result is consistent with the fact that propionaldehyde,[3] 1-butene,[4] propionic acid,[5] and propionyl fluoride[6] exist in the *cis* and *skew* forms as rotational isomers, rather than in the *trans* form, with respect to the methyl group and the C=O or C=C double bond.

Three structural parameters, $r_{C_\alpha-N}$, $\angle C_\beta C_\alpha N$ and $\angle C_\alpha NC$, of the ethyl isothiocyanate molecule in the ground vibrational state were obtained from the observed rotational constants, A, B, and C, fixing the remaining structural parameters to the values assumed in Table 3. The results obtained are $r_{C_\alpha-N}=1.454$ Å,

Table 3. Assumed structural parameters[a]

Distances	Angles
C-H : 1.091Å	∠HCH : 108.8°
C_β-C_α : 1.522Å	$\angle HC_\beta C_\alpha$: 109.6°
C_α-N : 1.437Å	$\angle C_\beta C_\alpha H$: 110.6°
N=C : 1.210Å	$\angle C_\beta C_\alpha N$: 109.5°
C=S : 1.550Å	$\angle C_\alpha NC$: 147.5°

a) Carbon atoms at the α- and β-positions are denoted as C_α and C_β, respectively. The structural parameters are taken from mono-substituted ethanes CH_3CH_2X (X=F[9], Cl[10], Br[11], I[12], OH[13], NC[14]) for the ethyl group and from methyl isothiocyanate[15] for the isothiocyanato group.

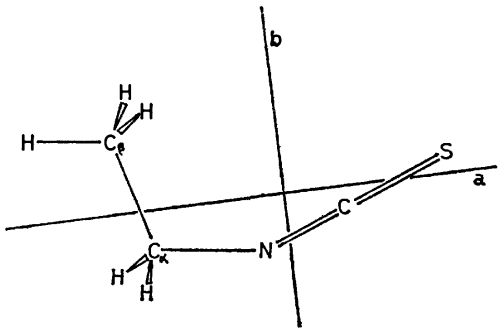

Fig. 3. Configuration of the predominant rotamer, *cis*-ethyl isothiocyanate. The c principal axis is perpendicular to the plane of paper.

Table 4. Observed and predicted rotational constants

	Obsd	Calcd			
		cis	*gauche*	*skew*	*trans*
A(MHz)	14194	14197.29	15558.54	24035.91	33364.61
B(MHz)	1779.27	1778.77	1694.55	1494.95	1427.60
C(MHz)	1612.14	1612.73	1569.60	1451.58	1392.96
κ	−0.973433	−0.973611	−0.982135	−0.996159	−0.997833
Δ(amu·Å^2)[a]	6.159	6.345	8.740	10.925	6.343
ϕ(°)[b]		0	60	120	180

a) $\Delta=I_a+I_b-I_c$. b) ϕ: dihedral angle about the C-N bond, see Fig. 1.

$\angle C_\beta C_\alpha N = 109.6°$ and $\angle C_\alpha NC = 151.0°$.

An attempt was made to assign the microwave spectrum of the other rotamers which would give rather weak absorption lines, but it was unsuccessful. This may be partly because of the overlap of the lines of the vibrationally-excited states of the *cis* form with those of the *skew* or the *trans* form.

Vibrational Satellites. Satellite lines were observed around each rotational transition of the ground vibrational state. They spread from 300 to 500 MHz and have essentially the same Stark effect behavior and K series pattern as the corresponding ground state transitions. Evidently, these satellites are due to molecules in the vibrationally-excited states for which the effective moments of inertia are different from those for the ground states. Figure 4 illustrates the typical satellite pattern of the a-type transitions of $J=4\leftarrow3$. Two sets (set-I and set-II) of vibrationally-excited lines were assigned as shown in Table 1. The

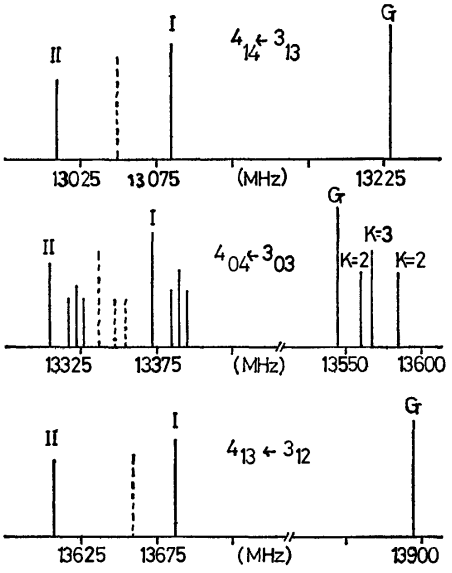

Fig. 4. Observed spectrum of $J=4\leftarrow3$ transitions showing vibrational excited satellite lines, I and II; dotted lines are unassigned lines.

Table 5. Far-infrared spectrum (cm^{-1})

CH_3NCS[a]	CH_3CH_2NCS	Assignment
(100)[b]	70(w)	C–N torsion
180.0	130(s)	CNC bend
	225(w)	C–C torsion
	380(s)	CCN bend (in-plane)[c]
440.0	450(m)	NCS bend (out-of-plane)[c]
569.0	540(s)	NCS bend (in-plane)[c]

Abbreviations: s, strong; m, medium; w, weak.
a) Ref. 15. b) Postulated value. c) Ref. 1.

effective rotational constants obtained for two vibrationally-excited states are given in Table 2.

Measurements of the relative intensities of the satellites with respect to the ground state line yielded vibrational frequencies 58±30 cm^{-1} for set-I and 107±30 cm^{-1} for set-II. Bands were observed at 70, 130 and 225 cm^{-1} in the far-infrared spectrum of ethyl isothiocyanate in the gas phase. Referring to Kniseley's assignment of the infrared spectrum[1] and to the study of methyl isothiocyanate,[15] these bands were assigned to the C–N torsion, CNC bending and C–C torsion modes, respectively, as shown in Table 5. Therefore, the vibrational satellite corresponding to 58 and 107 cm^{-1} can be ascribed to excited states of the C–N torsion and CNC bending modes, respectively. These assignments are supported by the fact that $\Delta'(I_c-I_b-I_a+8m_Hc_H^2)$ for set-I (out-of-plane vibration) has a negative value while the value of Δ' for set-II (in-plane vibration) is larger than that of the ground state[16] as shown in Table 2.

Dipole Moment. From the Stark coefficients of the transitions $4_{04}\leftarrow3_{03}$, $4_{14}\leftarrow3_{13}$, and $4_{13}\leftarrow3_{12}$, the dipole moment of the molecule was determined for both the ground and excited vibrational states. The second-order Stark coefficients determined for the eight Stark component lines and the dipole moment obtained are shown in Table 6. The electric field strength in the absorption cell was calibrated using

Table 6. Stark coefficients ($\Delta\nu/E^2$[MHz/(V/cm)^2]$\times10^{-5}$) and dipole moments

Transition	M	Ground state		Set-I CN torsion		Set-II CNC bend	
		Obsd	Calcd	Obsd	Calcd	Obsd	Calcd
$4_{13}\leftarrow3_{12}$	0	−0.440	−0.455	−0.476	−0.476	−0.485	−0.514
	1	−1.68	−1.74	−1.95	−1.97	−2.07	−2.14
$4_{04}\leftarrow3_{03}$	0	−0.758	−0.749	−0.809	−0.790	−0.881	−0.840
	1	−0.446	−0.452	−0.467	−0.478	−0.514	−0.504
	2	0.442	0.441	0.454	0.456	0.508	0.501
	3	1.91	1.93	2.06	2.01	2.27	2.18
$4_{14}\leftarrow3_{13}$	0	−0.441	−0.472	−0.396	−0.493	−0.515	−0.517
	1	1.34	1.30	1.44	1.52	1.62	1.66
μ_a(D)		3.33±0.03		3.38±0.03		3.50±0.05	
μ_b(D)		0.07±0.02		0.05±0.02		0.04±0.02	
μ_c(D)		0 (assumed)		0 (assumed)		0 (assumed)	
μ_{total}(D)		3.33±0.03		3.38±0.03		3.50±0.05	

the value of the dipole moment of OCS, 0.71521 D.[7] The dipole moment determined for the ground state was $\mu_{total}=3.33\pm0.03$ D, with $\mu_a=3.33\pm0.03$ D and $\mu_b=0.07\pm0.02$ D. The μ_c component was assumed to be zero because of the plane symmetry as discussed above. The total dipole moment μ_{total} is compared with the value of 3.31 D obtained from dielectric constant measurements in a benzene solution.[8]

The authors wish to express their thanks to Prof. Hiroaki Takahashi and Dr. Norio Kaneko of Waseda University for the use of their Hitachi FIS-3 far-infrared spectrophotometer and for helpful discussions.

References

1) R. N. Kniseley, R. P. Hirschmann, and V. A. Fassel, *Spectrochim. Acta*, **23**, 109 (1967).
2) A. Bjørseth and K. M. Marstokk, *J. Mol. Struct.*, **11**, 15 (1972)
3) S. S. Butcher and E. B. Wilson, Jr., *J. Chem. Phys.*, **40**, 1671 (1964).
4) S. Kondo, E. Hirota and Y. Morino, *J. Mol. Spectrosc.*, **28**, 471 (1968).
5) O. L. Stiefvater, *J. Chem. Phys.*, **62**, 233 (1975).
6) O. L. Stiefvater and E. B. Wilson, *J. Chem. Phys.*, **50**, 5385 (1969).
7) J. S. Muenter, *J. Chem. Phys.*, **48**, 4544 (1968).
8) E. C. E. Hunter and J. R. Partington, *J. Chem. Soc.*, **1932**, 2312.
9) B. Bak, S. Detoni, L. Hansen-Nygaard, J. T. Nielsen, and J. Rastrup-Andersen, *Spectrochim. Acta*, **16**, 376 (1960).
10) R. H. Schwendeman and G. D. Jacobs, *J. Chem. Phys.*, **36**, 1245 (1962).
11) C. Flanagan and L. Pierce, *J. Chem. Phys.*, **38**, 2963 (1963).
12) T. Kasuya and T. Oka, *J. Phys. Soc., Jpn.*, **15**, 296 (1960).
13) J. Michielsen-Effinger, *Ann. Soc. Scient., Bruxelle*, **78**, 223 (1964); **79**, 253 (1966).
14) R. J. Anderson and W. D. Gwinn, *J. Chem. Phys.*, **49**, 3988 (1968).
15) R. G. Lett and W. H. Flygare, *J. Chem. Phys.* **47**, 4730 (1967).
16) D. R. Herschbach and V. W. Laurie, *J. Chem. Phys.*, **40**, 3142 (1964).

The Crystal and Molecular Structure of *N*-Carboxy Anhydride of Glycine

Hitoshi KANAZAWA, Yoshiki MATSUURA*, Nobuo TANAKA,* Masao KAKUDO,*
Tadashi KOMOTO, and Tohru KAWAI

Department of Polymer Technology, Tokyo Institute of Technology, Ookayama, Meguro-ku, Tokyo 152
**Institute for Protein Research, Osaka University, Yamadakami, Suita, Osaka 565*

(Received December 16, 1975)

The crystal and molecular structure of *N*-carboxy anhydride(NCA) of glycine was determined from three-dimensional X-ray diffraction data. The crystals of glycine-NCA are monoclinic with space group C2/c and $Z=8$; the cell dimensions are $a=9.298(2)$, $b=5.156(2)$, $c=16.900(4)$ Å and $\beta=107.88(2)°$. A pair of molecules forms the dimer structure around a center of symmetry, with two N(1)–H(1)···O(1′) hydrogen bonds in the crystals.

Amino acid-NCA's are very often used for synthesis of polypeptides. The polymerization has been carried out not only in homogeneous system but also in heterogeneous system and crystalline state.[1-3]

Generally, it might be expected that polymers with unique structures may be produced in the crystalline state polymerization, the crystal structure of monomer affecting that of the resulted polymer.[4] There have been several studies about the crystalline state polymerization of amino acid-NCA's. Miller and his co-workers reported that *N*-benzyloxycarbonyl L-lysine-NCA could be polymerized by allowing it to stand in air.[5] Morawetz and his co-workers reported on the polymerization of some amino acid-NCA's by heating.[6] In both cases, however, the complete crystal structures of the NCA's were not determined and therefore, the investigation on the polymerization mechanism could not be done in detail.

We found that high-molecular-weight polypeptides were produced when the crystals of amino acid-NCA's were immersed in hexane (the non-solvent of both the monomer and polymer crystals) and triethylamine or *n*-butylamine was added into the system as the initiator.[7] It becomes necessary to know the crystal structures of the amino acid-NCA's to discuss their polymerizability.

In this paper, we shall report the crystal structure of the simplest amino acid-NCA, glycine-NCA.

Experimental

Powdered glycine (10 g : 0.132 mol) was dispersed in about 700 ml of purified tetrahydrofuran in a round-flask, and 9 ml (0.075 mol) of trichloromethyl chloroformate was added into it. The reaction mixture was allowed to stand at about 50 °C with stirring. After about 6 h the system changed to be clear, and subsequently the sovlent was evaporated up to about 50 ml at reduced pressure and room temperature. Hexane (about 100 ml) was added to the resultant mixture, and then crude crystalline material appeared. The crude crystals were dissovled in ethyl acetate up to saturated state at about 40 °C, and this solution was cooled down to −20 °C to obtain the purified crystals. After several times of this purification process, well-shaped crystals suitable for X-ray work were selected.

Oscillation and Weissenberg photographs taken with nickel-filtered Cu$K\alpha$ radiation indicated the crystals to be monoclinic and the possible space group C2/c or Cc (systematic absences: $h\,k\,l$, $h+k$ odd; $0\,0\,l$, l odd). The former was chosen on the basis of the E(normalized structure factor) statistics and confirmed by the structure analysis.

The density of the crystal was measured by a flotation mothod using the mixture of bromoform and hexane.

Table 1. CRYSTAL DATA OF GLYCINE-NCA

$C_3NO_3H_3$	$U=771.6(4)$ Å^3
M. W. : 101.06	Space group : C2/c
monoclinic	$Z=8$
$a=9.298(2)$ Å	$D_c=1.74$ g·cm^{-3}
$b=5.156(2)$	$D_m=1.74$ g·cm^{-3}
$c=16.900(4)$	μ(Mo$K\alpha$)$=1.940$ cm^{-1}
$\beta=107.88(2)°$	

All diffraction experiments were done within a few days after the crystallization, because the auto-polymerization took place conspicuously in two or three days, which was visible as white turbidity on the crystals.

A colorless prismatic crystal with approximate dimensions $0.4\times0.5\times0.7$ mm was mounted on a Rigaku automated four-circle diffractometer with the b axis nearly parallel to the ϕ-axis of the goniometer. Accurate cell parameters were obtained by the least-squares refinements with 29 high angle reflections. Crystal data are given in Table 1. The intensity data with 2θ less than 55° were collected by usual ω-2θ scans using Zr-filtered Mo$K\alpha$($\lambda=0.7107$ Å) radiation. A total of 887 independent reflections (783 of them were non-zero) were obtained.

Structure Determination

The position of the oxygen atom O(1) was obtained from an analysis of the Harker section (u 0 w) and the interatomic vector resulting from a center of symmetry on a three-dimensional sharpened Patterson function. Subsequently, Buerger's minimum function was calculated using the O–O vectors between four symmetry related atoms, and seven non-hydrogen atoms were located in this map, where the carbon and nitrogen atoms could not be distinguished clearly. Successive Fourier synthesis with the phases based on these seven atoms showed the position of the nitrogen atom.

Refinement by a block-diagonal least-squares method (HBLS V Program[8]) using anisotropic temperature factors was continued until the R-value ($R=\sum||F_o|-|F_c||/\sum|F_o|$) dropped to 0.0683. At this stage, a difference Fourier synthesis map revealed the position of all hydrogen atoms. Finally, all the positional parameters together with the anisotropic temperature factors for the non-hydrogen atoms and the isotropic temperature factors for the hydrogen atoms are refined, and the R-value was reduced to 0.0428. A list of observed and calculated structure factors has

TABLE 2. FINAL ATOMIC COORDINATES AND THERMAL PARAMETERS FOR GLYCINE-NCA WITH THEIR ESTIMATED STANDARD DEVIATIONS

The anisotropic thermal parameters ($\times 10^5$) are expressed in the form:
$\exp\{-(B_{11}h^2+B_{22}k^2+B_{33}l^2+B_{12}hk+B_{13}hl+B_{23}kl)\}$
The isotropic thermal parameters of the H atoms are B/Å^2.

Atom	x	y	z	B_{11}(or B)	B_{22}	B_{33}	B_{12}	B_{13}	B_{23}
C(1)	0.4166 (1)	0.2198 (4)	0.4327 (2)	214(6)	2009(66)	895(23)	− 23(35)	242(20)	−397(66)
C(2)	0.3222 (1)	0.0768 (4)	0.2181 (2)	234(7)	2129(68)	789(23)	− 75(35)	264(20)	−237(65)
C(3)	0.3605 (1)	0.3195 (4)	0.1796 (2)	291(8)	2449(74)	749(22)	−367(40)	213(21)	−100(69)
N(1)	0.4180 (1)	0.3877 (4)	0.3255 (2)	283(6)	2231(61)	830(20)	−427(34)	183(19)	−205(59)
O(1)	0.4542 (1)	0.2176 (3)	0.5667 (2)	320(6)	3238(63)	808(17)	−263(33)	135(16)	−137(56)
O(2)	0.3603 (1)	0.0226 (3)	0.3690 (1)	262(5)	1976(48)	792(16)	−215(27)	14(15)	112(48)
O(3)	0.2690 (1)	−0.0579 (3)	0.1413 (2)	336(6)	3063(61)	955(19)	−733(33)	165(17)	−514(58)
H(1)	0.4507(14)	0.5336(50)	0.3436(26)	2.1(5)					
H(2)	0.3178(14)	0.4538(48)	0.1338(25)	1.7(5)					
H(3)	0.3919(14)	0.2692(48)	0.1105(25)	1.6(5)					

been deposited with the Chemical Society of Japan (Document No. 7613).

Results and Discussion

The final atomic coordinates and the thermal parameters are shown in Table 2. The perspective view of glycine-NCA molecule is shown in Fig. 1 together with the numbering of the atoms, the bond lengths and angles. The bond length C(1)–O(1) is 1.212(3) Å, slightly longer than the usual value. This might be caused by the hydrogen bond formed between N(1)–H(1) and O(1') as will be discussed later. The bond length C(1)–N(1) (1.326 Å) is shorter than C(3)–N(1) (1.449 Å), probably due to the resonance effect between the double bond of C(1)–O(1) and the lone-pair electrons of the N(1) atom.

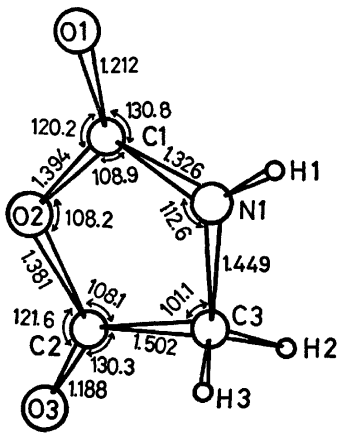

Fig. 1. A perspective view of glycine-NCA seen along the a axis with the numbering of the atoms, the bond lengths (l/Å) and angles (ϕ/°). The estimated standard deviations are 0.002—0.003Å in distances and 0.02° in angles.
The bond lengths involving hydrogen atoms are N(1)–H(1) 0.919(26), C(3)–H(2) 0.996(25) and C(3)–H(3) 0.986(25) Å.
The bond angles involving hydrogen atoms are C(1)–N(1)–H(1) 123.2(16), C(3)–N(1)–H(1) 124.2(16), N(1)–C(3)–H(3) 109.5(15), C(2)–C(3)–H(3) 107.0 (15) and H(2)–C(3)–H(3) 111.7(20)°.

TABLE 3. THE EQUATION OF THE LEAST-SQUARES PLANE THROUGH THE ATOMS IN GLYCINE-NCA

Equation	Atom	Deviation
$-0.8136X+0.5433Y+0.2071Z+3.3117=0$	C(1)	−0.002 Å
	C(2)	0.002
$X=ax+cz\cos\beta$	C(3)	−0.003
$Y=by$	N(1)	0.004
$Z=cz\sin\beta$	*O(1)	0.031
	*O(2)	−0.047
	*O(3)	0.037
	*H(1)	0.037
	*H(2)	0.770
	*H(3)	−0.864

* Atoms not included in the least-squares calculation.

Other bond lengths are normal and well agree with the corresponding values of maleic anhydride and succinic anhydride, respectively.[9,10]

The equation of the best plane through four atoms C(1), C(2), C(3) and N(1) in the five-membered ring of glycine-NCA was calculated and is shown in Table 3, together with the deviations of the atoms from the plane. The atoms C(1), C(2), C(3), and N(1) can be regarded to be coplanar, their maximum deviation from the plane being 0.004 Å. Both the exocyclic atoms O(1) and O(3) are slightly displaced out of the plane on the same side.

The packing of the molecules in the crystal viewed along the b axis are shown in Fig. 2. One can see a dimer joined together in a pair around a center of symmetry, by two N–H···O hydrogen bonds with a distance of 2.915(2) Å and the angle of N(1)–H(1)–O(1') 162(2)°.

Other intermolecular distances can be explained in terms of the packing of van der Waals type.

The authors wish to thank Professor Y. Sasada and his laboratory members at Laboratory of Chemistry for Natural Products, Tokyo Institute of Technology for their help in many facets of this work,

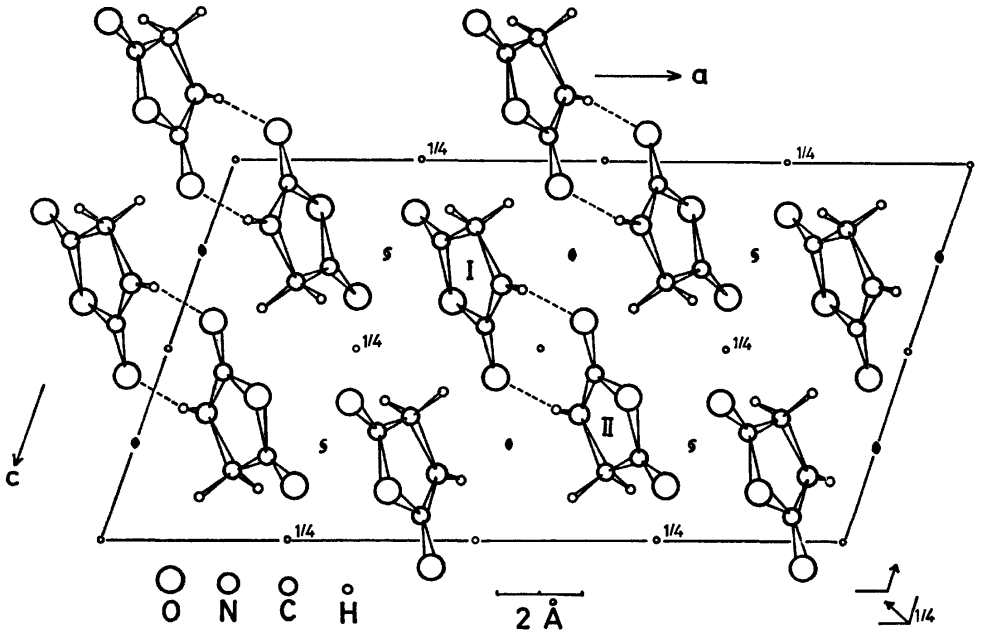

Fig. 2. Projection of the crystal structure of glycine-NCA along the b axis.
General coordinates: I, (x,y,z); II, $(1-x, 1-y, 1-z)$.
Hydrogen bonds are shown by broken lines.

References

1) C. H. Bamford, A. Elliot, W. H. Hanby, "Synthetic Polypeptides," Academic Press, New York (1956), p. 63.
2) Y. Imanishi, *Kobunshi*, **21**, 32, 92 (1972).
3) T. Kawai, T. Komoto, *Kobunshi*, **22**, 22 (1973).
4) H. Morawetz, *J. Polym. Sci., C*, **1966**, 79.
5) E. Miller, I. Fankchen, H. Mark, *J. Appl. Phys.*, **20**, 531 (1949).
6) G. Kovacs, H. Morawetz, *J. Polym. Sci., A-1*, **4**, 1553 (1966).
7) M. Ohya, The 22nd Discuss. Meeting Polymer Sci., High Polymers, Japan (1973), p. 1.
8) T. Ashida, The Universal Crystallographic Computing System, Osaka, The Computing Center, Osaka University (1973), pp 55.
9) R. E. Marsh, E. Ubell, H. E. Wilcox, *Acta Crystallogr.*, **15**, 35 (1962).
10) M. Ehrenberg, *Acta Crystallogr.*, **19**, 698 (1965).

ESR Studies of Nitrobenzene Ion-Pair Equilibria in *N,N*-Dimethylformamide

Shinobu Toshima and Kingo Itaya

Department of Applied Chemistry, Faculty of Engineering, Tohoku University, Aramaki, Sendai 980

(Received June 17, 1974)

The hyperfine splitting constants of the nitrobenzene radical anion in DMF vary with the type of the counter cations and the concentrations. The tendency of these variations is related to the shift of the half-wave reduction potential of nitrobenzene. The variation of the nitrogen ^{14}N hyperfine splitting constant is attributable to the formation of ion pairs involving the nitrobenzene radical anion and its counter cation. The ion-pair formation constants were evaluated from the changes in the hyperfine splitting and are completely consistent with those obtained from polarographic studies.

In recent years, ESR techniques have been extensively applied to studies of radical ions and ion pairs in the liquid phase, revealing detailed structure and kinetic information of the ion-pair systems.[1-3] In particular, discussions treating the equilibrium between a tight ion pair and a loose ion pair have been reported by a few workers[4,5] and the migrations of the cation in ion-pair systems have also been examined by many workers.[6-8] A large part of these investigations were carried out in solvents such as tetrahydrofuran (THF) and 1,2-dimethoxyethane (DME), in which alkali metal hyperfine splitting (hfs) might arise from ion-pair systems of alkali metal ions and hydrocarbon radical anions. In these solvents, the observed hfs under normal conditions ($\sim 10^{-4}$ M) should be equal to that of the ion-pair system because large numbers of radical ions exist in the form of ion pairs due to the large value of the ion-pair formation constant, thus the existence of a free ion was not confirmed by ESR techniques.

On the other hand, in the solvents having a high dielectric constant, such as *N,N*-dimethylformamide (DMF) and acetonitrile, generally no alkali metal hfs has been observed in the ion-pair systems composed of hydrocarbon radical anions and alkali metal cations. This suggests that the studies on pairing in these solvents based on the hfs due to alkali metal cations are invalid. Furthermore, the observed hfs of the radical ions in these solvents is very close to that for free ions, which may be due to the small value of the ion-pair formation constant. For these reasons, the ion-pairing phenomena in solvents, such as DMF, are very difficult to discuss.

Since the variation in the nitrogen ^{14}N hfs of the nitrobenzene radical anion and its derivatives is very sensitive to the type of alkali metal cation and the concentration,[9-12] many workers have attempted to discuss ion pairing and solvent effects on the basis of the variation of the nitrogen hfs. Kitagawa *et al.* have reported qualitatively on the variation of the hfs of *p*-chloronitrobenzene radical anions with various counter cations and the concentrations of these in DMF.[27] However, the authors were unable to obtain quantitative results concerning the ion-pair equilibrium from their experimental results. Therefore, we discuss more quantitatively the variation of the hfs and obtain interesting quantities such as the ion-pair formation constant, the hfs of the free ion, and that of the ion pair.

The polarographic reduction waves of nitrobenzene are also highly affected by the type of supporting electrolytes as is shown in the paper of Holleck and Becher.[13] The polarographic techniques not only offer some information concerning the ion pair but also allow the present authors to determine the ion-pair formation constant and the coordination number in such solvents.

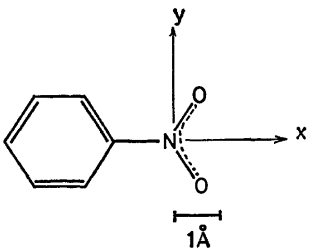

Fig. 1.

In this paper, the influence of alkali metal cations on the ESR spectra is dealt with and the structures of the ion-pair systems and the equilibrium between the free nitrobenzene radical anion and the ion pair composed of alkali metal cations is discussed. Quantitative correlations are drawn between the results obtained from the polarographic studies and those from the ESR studies.

Experimental

Materials. DMF was pre-dried with CaH_2 and was further dried over 4A and 5A molecular sieves in a vacuum. All salts, which were purified by recrystallization from aqueous solutions, were well dried in a vacuum (of less than 5×10^{-5} mmHg) for more than 24 h.

Nitrobenzene was used after additional degassing in a vacuum line and was stored in a graduated 0.5 ml pipet.

Tetrahydrofuran, which was used for the metal reduction of nitrobenzene, was refluxed over potassium metal and then distilled. The distillate was degassed five times in a vacuum and rigorously dried with the addition of sodium anthracenide to absorb trace amounts of moisture and oxygen.

The ESR spectra were measured with a Hitachi X-band ESR spectrometer model 771, employing field modulation at 100 kHz, while maintaining the room temperature at 21—23 °C.

Preparations of the Radical Anion. Electrolytic Reduction: In a solution containing 0.1 M of the supporting electrolytes, nitrobenzene radical anions were prepared by electrolytic reduction in a vacuum electrolytic cell with two Pt electrodes. The concentration of nitrobenzene was about 5×10^{-4} M in the present series of measurements, and a sample solution was electrolyzed carefully for more than 24 h to convert all nitrobenzene to its radical anion in the cavity of the ESR spectrometer. When the electrolyte was

lithium perchlorate, the selective production of the radical anion was so difficult due to the small difference between the first and the second waves in the polarogram that the preparation of the radical anions was carried out by the lithium metal reduction procedure.

Alkali-metal Reduction. Alkali-metal reduction in THF was carried out by the conventional method.[14] Sodium and potassium metals were purified in a vacuum (see Fig. 2) and the surface of the lithium metal was etched by treatment with a THF–nitrobenzene solution. The pieces were stored in a tube with a break-seal.

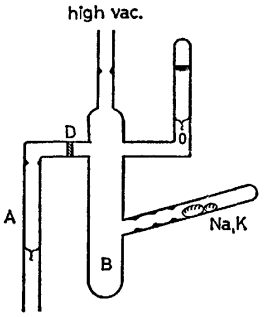

Fig. 2. The apparatus used for preparation of the radical anion.

After the preparation of the radical anion-THF solution, the solution was introduced into A through sintered glass D. The solvent was removed by distillation into a tube B using liquid nitrogen and tube B was sealed off. The solid metal nitrobenzenide was dissolved in DMF containing a given amount of salts. All experiments were carried out in a high vacuum line using break-seals.

Results

Hyperfine Splitting Constants Obtained in a Solution of 0.1 M Salt Concentration. Figure 3 shows the ESR spectra obtained in a solution of 0.1 M salt concentration. The sample solutions were prepared by the electrolytic reduction method excepting the 0.1 M lithium perchlorate solution. Lithium nitrobenzenide was prepared by the metal reduction method and was dissolved in a 0.1 M lithium perchlorate solution. A well-resolved ESR spectrum was obtained in a solution of 0.1 M TEAP, while those obtained in cesium and rubidium salts were extraordinarily broad. Table 1 shows the hfs obtained from an analysis of these spectra, which were confirmed by simulation using a JEOL spectrum computer, model JRA-5. The approximate line-widths ($\Delta H_{1/2}$) are also shown in the table. It was not possible to confirm the spectrum obtained in the solutions of cesium perchlorate and rubidium perchlorate with simulation owing to the broadening of the line-width.

In general, hfs due to the nucleus varies with the kind of salt. The variations of the nitrogen hfs ($\mathbf{a}_N$) and the proton hfs at the *para*-position ($\mathbf{a}_P$) were remarkably large. The values of $\mathbf{a}_N$ and $1/\mathbf{a}_P$ increased with decreasing radius of the cation. Thus, it is possible to compare the nitrogen hfs in the solutions of Li^+, Na^+, K^+, Cs^+ and Rb^+ in descending order (with the value for Cs^+ about the same as that for Rb^+), which is essentially the same as that obtained from the polarographic studies.

Variation of ^{14}N hfs with the Concentration of Counter Cations. Figure 4 shows the variations of the nitrogen hfs as a function of the concentration of the added salt, while maintaining the total ionic strength at 0.1 M with TEAP. The nitrobenzene radical anions were obtained by the metal reduction procedure, and were dissolved in a solution of arbitrary concentration of the added salt. The total concentration of the radical anions was less than 5×10^{-4} M for these experiments.

The variations of the nitrogen hfs show a regular shift in the concentration range of 10^{-3}—10^{-1} M for both sodium perchlorate and potassium nitrate. This behavior is the same as that for the *p*-chloronitrobenzene radical anion in DMF reported by Kitagawa *et al.*[27] However, no reports on the quantitative explanations to the change of the ^{14}N hfs, have apparently been published to date.

The origins of the curves indicate the hfs in a 0.1 M TEAP-solution containing about 5×10^{-4} M of the alkali metal cations. The values of the origins of the two curves are identical and equal to the hfs obtained in a 0.1 M TEAP-solution by the electrolytic reduction method without alkali metal cations. These results show that nitrobenzene radical ion pairs composed of sodium and potassium cations are almost dissociated in a solution of TEAP. We must also mention that the hfs in a 0.1 M TEAP-solution is completely consistent with the hfs obtained in a solution of alkali metal nitrobenzenide ($\sim5\times10^{-4}$ M) in the absence of TEAP. This result seems to indicate that the nitrobenzene radical anions are almost free in a solution of TEAP.

The variation of the nitrogen hfs is shown in Fig. 5 as a function of the concentration of lithium perchlorate.

Table 1. Proton and nitrogen hyperfine splitting constants of nitrobenzene radical anions in a solution with a 0.1 M salt concentration (in gauss)

Position[a]	$LiClO_4$	$NaClO_4$	KNO_3	$RbClO_4$[d]	$CsClO_4$[d]	TEAP
$\mathbf{a}_N$	11.36	11.12	10.50	10.0	≈10.0	9.62
$\mathbf{a}_p$	3.86	3.88	3.95	—	—	4.01
$\mathbf{a}_o$	3.40	3.38	3.35	—	—	3.36
$\mathbf{a}_m$	1.11	1.09_5	1.06	—	—	1.06
$H_{1/2}$[b]	0.68	1.10	0.45	2.5	> 2.5	0.45
r_c[c]	0.60	0.95	1.33	1.48	1.69	—

a) $\mathbf{a}_N$; nitrogen hyperfine splitting constant. $\mathbf{a}_p$, $\mathbf{a}_o$, $\mathbf{a}_m$; *para*-proton hyperfine splitting constant, *etc.* b) Line-width (in gauss). c) Pauling's cationic radius (in Å). d) Still not completely confirmed by simulation.

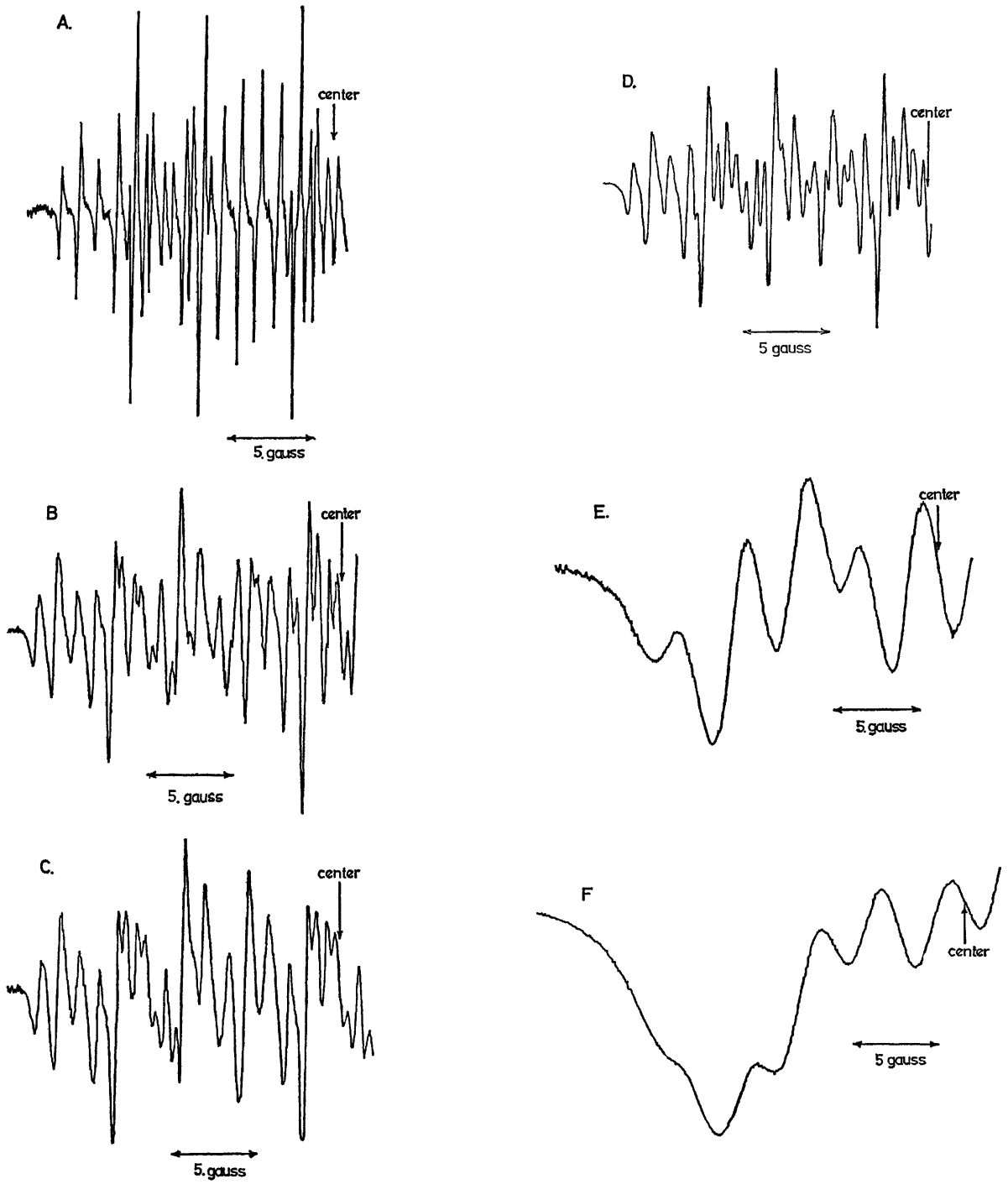

Fig. 3. The ESR spectra obtained in the solution of 0.1 M salt concentration.
A: 0.1 M TEAP, B: 0.1 M $LiClO_4$, C: 0.1 M $NaClO_4$,
D: $\approx$0.1 M (saturation) KNO_3, E: 0.1 M $RbClO_4$, F: 0.1 M $CsClO_4$.

ESR spectra obtained in the region of lower concentration of lithium perchlorate are shown in Fig. 6 and the outlined spectrum simulations are also displayed as stick diagrams. Obviously, the spectra due to two different species are superimposed in these spectra, that is, the two different species are the ion pairs and the free ions, respectively. The relative intensities due to the free ions decrease with increasing concentration of lithium perchlorate. In the region of lower concentration of the salt, the nitrogen hfs due to the ion pair decreases with increasing concentration of the salt. On the other hand, the hfs due to the free ions increases with an increase of the concentration of the salt, as shown in Fig. 5. Thereafter, the hfs increases monotonically with the concentration of sodium and potassium ion pairs, as shown in Fig. 4.

In an infinitely-dilute solution (of less than 5×10^{-4}M), the ESR spectrum consisted of the free ion and the nitrogen hfs coincided with that obtained in a solution of TEAP, as in the studies of the sodium and potassium

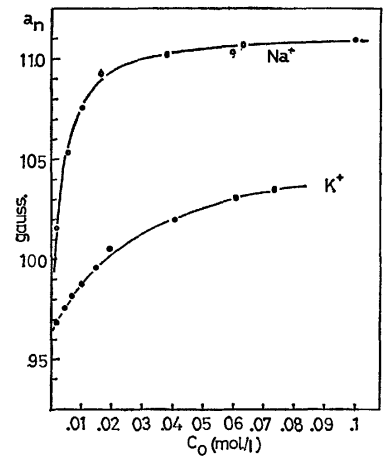

Fig. 4. Variation of the nitrogen hfs with the concentration of the metal cations. Total ionic strength kept formally at 0.1 M.
Na^+, added sodium perchlorate.
K^+, added potassium nitrate.

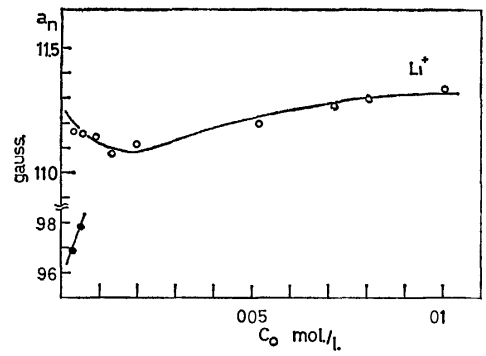

Fig. 5. Variation of the nitrogen hfs with the concentration of lithium perchlorate.
○: Nitrogen owing to ion pair.
●: That of free ion.

nitrobenzenide systems.

In the region of high concentration of lithium perchlorate, the ESR spectra also consisted of a single species, the ion pair.

Discussion

Perturbation of the Distribution of Unpaired Spin Densities. As stated above, it is possible to compare the nitrogen hfs in the solutions of Li^+, Na^+, K^+, Cs^+ and Rb^+ in descending order. It seems that the radius of the alkali metal cation may be responsible for this order.

The interactions between the radical anions and the counter cations have been formulated by Huch and Rowland,[15] and McClelland.[16] Since the McClelland theory based on the Hückel approximation is of a simple form, its application to aromatic radical anions and their derivatives has been carried out by many workers.[17–20] Takeshita and Hirota[21] modified the cationic field effects to the following effective Hamiltonian (H'_{eff}):

$$H'_{\mathrm{eff}} = H^0_{\mathrm{eff}} - \frac{Ze^2}{\varepsilon(r)r} \qquad (1)$$

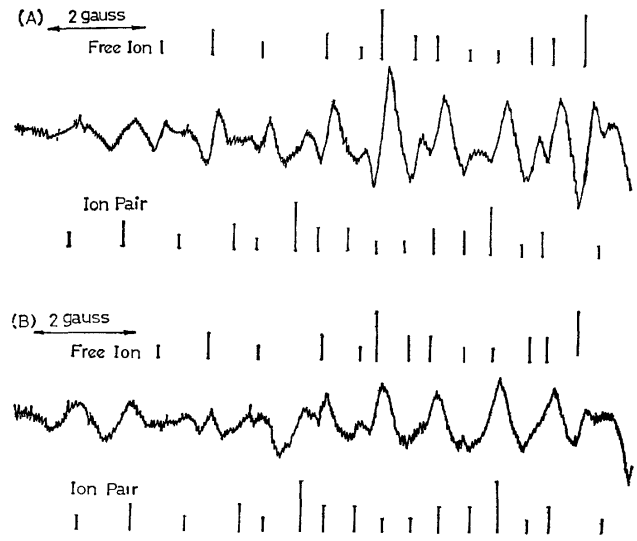

Fig. 6. ESR spectra obtained in the solution of lithium perchlorate.
The stick diagrams indicate the splittings of the ion pair and free ion.
A) In a solution of 5.1 mM lithium perchlorate.
B) In that of 8.8 mM lithium perchlorate.

where $\varepsilon(r)$ is a screening factor which accounts for the screening effects of the solvent in the cationic fields. The solvent effect on the hfs can be taken into account with this screening parameter. In the present calculations of the perturbation energy and the variations of the spin density, some values of the screening parameter have been applied.

The dimensions of the radical anion and the parameters of the Coulomb and exchange integrals were choosen to be as follows:[22]

aromatic C-C=1.39 Å	$\delta\alpha_O = 1.4\beta$
aromatic angle=120°	$\delta\alpha_N = 2.2\beta$
C-N=1.49 Å	$\beta_{NO} = 1.67\beta$
N-O=1.21 Å	$\beta_{NC} = 1.2\beta$
O-N-O=117°	

All overlap integrals were neglected in the sense of simple Hückel approximation. From the extensive calculations of the interaction energy, the time averaged position of the cation is determined on the X-axis of the coordination system as shown in Fig. 1. This conclusion agrees with the case of 4-nitropyridine *N*-oxide anion radicals in DME reported by Kawamura *et al.*[23] The interaction energy, when the dielectric constant of DMF is used as the screening factor, is less than that when the factor is equal to 1. However, the minimum points of the potential surfaces are consistent with each other.

The unpaired spin densities of each position were calculated using the method of McClelland with the McLachlan approximate configurational interaction treatment,[24] assuming the cations approach the nitrobenzene radical anions along X-axis.

The calculations of the hfs of ring protons ($\mathbf{a}_H$) were carried out using the following generally applied equation:[25]

$$\mathbf{a}_{II} = -Q \cdot \rho_C^{\pi} \quad (2)$$

where Q is taken to be 27.3

On the other hand, the nitrogen hfs were theoretically calculated using the following equation, which was given by Rieger and Fraenkel:[26]

$$\mathbf{a}_N = 99.0 \cdot \rho_N^{\pi} - 2 \times 35.8 \cdot \rho_O^{\pi} + 17 \cdot \rho_C^{\pi} \quad (3)$$

in which ρ_N^{π}, ρ_O^{π}, and ρ_C^{π} are the π-electron spin densities at the nitrogen, oxygen and adjacent carbon atoms, respectively. In the present calculations of the spin densities, the parameter λ in the procedure of McLachlan was set at 1.2.

Figure 7 shows the calculated hfs of the *para*-proton and nitrogen which are greatly affected by the distance of closest approach of the cations, assuming the screening parameter to be 37.0. The hfs of the *meta*- and *ortho*-protons are apparently not changed by the distance of closest approach of the cations. The nitrogen hfs increases with the decrease in the distance of closest approach of the cations. On the other hand, the *para*-proton hfs shows the opposite tendency. The same observations were made for the cations when the screening parameter was nearly equal to the dielectric constant of DMF. However, when the screening parameter was chosen to be 1, as has often been done by other workers,[3,20] the variations of the nitrogen hfs became extraordinarily large.

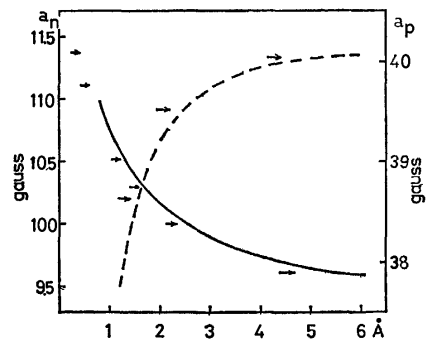

Fig. 7. The calculated hfs of the *para*-proton and nitrogen assuming $\varepsilon(r)=37.0$. The cation is on the X-axis. The arrows indicate the observed value in the solution of 0.1 M salt concentration (Table 1).

Takeshita and Hirota have concluded that the screening parameters in contact ion-pair systems are closer to the macroscopic dielectric constant than to 1.[21] Although detailed information about the ion-pair structures has not been obtained at the present stage of these investigations, it seems to be a reasonable approximation to set the value of the screening parameter in the vicinity of the dielectric constant of DMF. More detailed discussions of the structure of ion pairs will now be presented on the basis of the present research.

It can be semi-quantitatively explained from the above calculations that nitrogen hfs in solutions of Li^+, Na^+, K^+, Cs^+, Rb^+, and Et_4N^+ can be arranged in this descending order. That is, the smaller the radius of the cation, the closer the cation can approach the radical anion of nitrobenzene.

Discussion of Ion-Pair Equilibria. Sodium and Potassium Ion-Pair Equilibria: The above discussion was limited to the observed hfs obtained in solutions with a constant salt concentration (0.1 M). However, the ion-pair formations must be rigorously discussed on the basis of equilibrium considerations.

The regular shifts of the nitrogen hfs as a function of the concentration of the added salts, as shown in Fig. 4, are discussed considering the next equilibrium between the free ions and ion pairs:

$$(A^{\cdot-}, M^+)_{IP} \rightleftharpoons A_f^{\cdot-} + M^+, \quad (4)$$

where $A_f^{\cdot-}$ is the free nitrobenzene radical anion, $(A^{\cdot-}, M^+)_{IP}$ the ion pair and M^+ the counter cation.

The coordination number in the sodium nitrobenzenide ion ion-pair system has been proved to be 1 from polarographic studies. Although the number in the potassium nitrobenzenide ion-pair system was not determined exactly by means of polarography, the discussion of this system is continued assuming the coordination number to be 1.

One can expect that the ion pairs and free ions have different hfs and that the variations of the ring proton hfs are less than those for nitrogen. It is possible to interpret the regular shift of the nitrogen hfs as a function of the concentration of the added salt, based on the rapid equilibrium of reaction (4), assuming that the ring proton hfs does not change for the two different states, *the ion pair* and *the free ion.*

In general, if the forward and backward reaction rates of reaction (4) are slow, the spectrum will consist of two separate signals which are obtained in a solution of lithium perchlorate as described above. If they are rapid, only one signal will appear at an approximately averaged position. In the case of the sodium and potassium nitrobenzenides, the nitrogen hfs showed a regular increase with an increase of the concentration of the counter cation and all ESR spectra could be simulated by one species. These results indicate that the equilibrium of reaction (4) in these cases are in the limit of the rapid exchange region.

According to the two-jump model, the observed nitrogen hfs ($\mathbf{a}_{ob}$) in the limit of rapid exchange between two states is given by:[28,29]

$$\mathbf{a}_{ob} = \frac{\tau_f}{\tau_f + \tau_{IP}} \cdot \mathbf{a}_f + \frac{\tau_{IP}}{\tau_f + \tau_{IP}} \cdot \mathbf{a}_{IP}, \quad (5)$$

where τ_f and τ_{IP} are the lifetimes of the free ions and ion pairs, respectively. Using the rate constants of the forward and backward reactions, the reaction rates are given by the following equations:

for the forward reaction:

$$v_f = \frac{[(A^{\cdot-}, M^+)_{IP}]}{\tau_{IP}} = k_1 \cdot [(A^{\cdot-}, M^+)_{IP}], \quad (6)$$

for the backward reaction:

$$v_b = \frac{[A_f^{\cdot-}]}{\tau_f} = k_{-1} \cdot C_{M^+} \cdot [A_f^{\cdot-}], \quad (7)$$

where $[A_f^{\cdot-}]$, C_{M^+} and $[(A^{\cdot-}, M^+)_{IP}]$ are the concentrations of these species. The ion-pair formation constant for reaction (4) is given by

$$K_f = \frac{k_{-1}}{k_1} = \frac{\tau_{IP}}{\tau_f \cdot C_{M^+}}. \quad (8)$$

When Eq. 8 is substituted into Eq. 5, Eq. 5 can be rewritten as

$$\mathbf{a}_{ob} = \frac{1}{1+K_f \cdot C_{M^+}} \cdot \mathbf{a}_f + \frac{K_f \cdot C_{M^+}}{1+K_f \cdot C_{M^+}} \cdot \mathbf{a}_{IP}. \quad (9)$$

If $\mathbf{a}_{ob}$ is normalized as follows:

$$\mathbf{a}_{ob} = \frac{\mathbf{a}_{ob}-\mathbf{a}_f}{\mathbf{a}_{IP}-\mathbf{a}_f}, \quad (10)$$

Eq. 10 can be expressed in the simple form

$$\bar{\mathbf{a}}_{ob} = \frac{K_f \cdot C_{M^+}}{1+K_f \cdot C_{M^+}}. \quad (11)$$

On the other hand, Eq. 9 can also be transformed into:

$$\frac{1}{\mathbf{a}_{ob}} = \frac{1}{K_f \cdot \mathbf{a}_{IP}} \cdot \frac{1}{C_{M^+}}\left(1-\frac{\mathbf{a}_f}{\mathbf{a}_{ob}}\right) + \frac{1}{\mathbf{a}_{IP}}. \quad (12)$$

For exact arguments concerning the regular increase of the nitrogen hfs from Eq. 12, it is necessary to assume the following approximations.

1. The concentrations of the cation are equal to that of the salt, if the dissociation constant of the salt is large, *i.e.*, $C_{M^+}=C_o$, where C_o is concentration of the salt.

2. Nitrogen hfs of the free nitrobenzene radical anion is equal to that obtained in a 0.1 M solution of TEAP, *i.e.*, $\mathbf{a}_f=9.62$ ($\pm$0.01) gauss.

The second approximation seems to be almost correct as was discussed above.

From a plot of the inverse of the observed nitrogen hfs ($1/\mathbf{a}_{ob}$) *vs.* $1/C_{M^+}\cdot(1-\mathbf{a}_f/\mathbf{a}_{ob})$, the hfs of the ion pairs and the ion-pair formation constants can be obtained by determining the intercept and the slope of the straight-line, respectively.

Figure 8 shows the plot for the solutions of sodium perchlorate. A straight-line is found over the wide concentration range of 1×10^{-3}—10^{-1} M. The hfs of the ion pairs and the formation constant were determined from the intercept and the slope by least-squares calculations, respectively. The nitrogen hfs of the ion pair is equal to $\mathbf{a}_{IP}=11.23$ ($\pm$0.03) gauss, and the formation constant was calculated to be $K_f=220$ ($\pm$5) 1/M from the slope with $\mathbf{a}_{IP}$ obtained from the intercept. It is particularly noteworthy that the

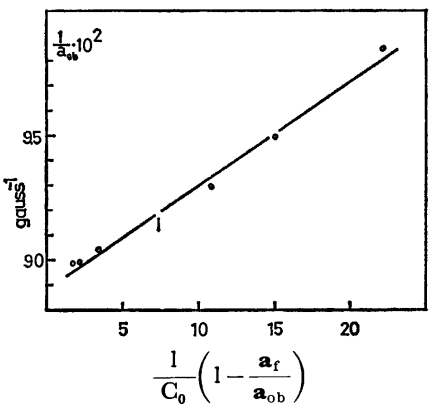

Fig. 8. Plot $1/\mathbf{a}_{ob}$ *vs.* $1/C_o(1-\mathbf{a}_f/\mathbf{a}_{ob})$ for the sodium perchlorate addition.
Slope; $4.05(0.09)\times10^{-4}$, Intercept; $8.90(0.02)\times10^{-2}$.
Standard deviations are shown in parentheses.

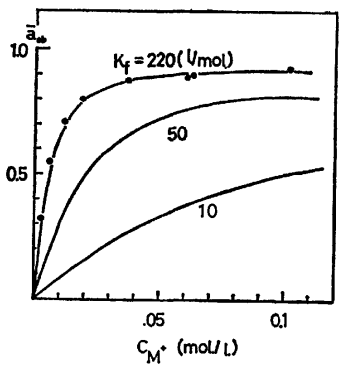

Fig. 9. Plot of Eq. 11 for the variation of the average nitrogen hfs with the concentration of the cation. The lines have been drawn for $K_f=10$, 50, 220 (l/M).
●; Experimental points in the case of sodium nitrobenzenide.

formation constant of the sodium nitrobenzenide system, as determined from the variation of the nitrogen hfs is completely compatible with that obtained from polarographic studies (200 $\pm$20 l/M) to within the experimental error. (Detailed discussions of the polarographic studies will be published elsewhere.) This coincidence seems to be most important argument in this paper. It strongly supports the approximate correctness of the present treatment of the regular increase of the nitrogen hfs. Figure 9 shows the normalized hfs $\mathbf{a}_{ob}$ as a function of the concentration of the counter cation (C_{M^+}) for the various formation constants. The curves in Fig. 9 are in qualitative accordance with the regular shifts of the nitrogen hfs as shown in Fig. 4. The experimental points obtained for the sodium nitrobenzenide system are also plotted in the same figure.

It is also important that the hfs of the ion-pair itself can be evaluated from the above discussion in solvents having a high polarity, such as DMF, because this quantity is useful for discussions of the structure of the ion pairs. The present paper is the first report in which the hfs of the ion-pair itself was determined in a high polar solvent.

Since potassium nitrate does not have a large dissociation constant in DMF, the concentrations of the potassium ions must be calculated. Although there is some question as to the validity of using the dissociation constant ($K_d=0.043$ l/M) reported by Ames and Sears[30] for this purpose, the concentrations of the ion were calculated.

Figure 10 shows the plots of $1/\mathbf{a}_{ob}$ *vs.* $1/C_{M^+}\cdot(1-\mathbf{a}_f/\mathbf{a}_{ob})$ and $1/C_o\cdot(1-\mathbf{a}_f/\mathbf{a}_{ob})$ which give straight lines. The difference in the linearity of the two lines is not significant. But the standard deviations of the slope and intercept of the plot with the potassium nitrate concentration are less than that of the plot as a function of the concentration of potassium ions. The hfs of the ion pair is equal to $\mathbf{a}_{IP}=10.99$ ($\pm$0.05) gauss, and the formation constant was determined to be $K_f=30$ ($\pm$6) 1/M, from the slope and intercept of the line with the concentration of potassium ions. On the other hand, the hfs and the formation constant can also be

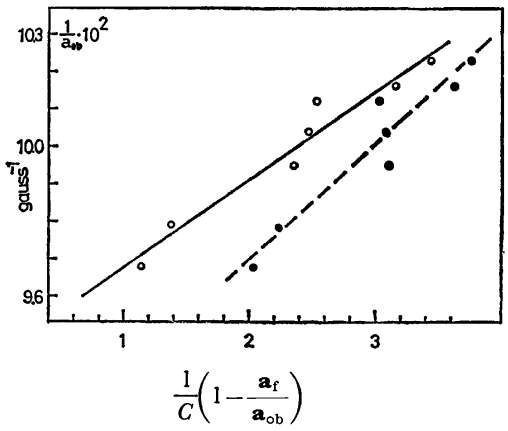

Fig. 10. Plot $1/a_{ob}$ *vs.* $1/C_M{}^+(1-a_f/a_{ob})$ and $1/C_o\cdot(1-a_f/a_{ob})$ for the potassium nitrate addition.
○; Against the salt concentration.
Slope; $2.4(0.2)\times10^{-3}$, Intercept; $9.44(0.02)\times10^{-2}$
●; Against the cation concentration calculated from the dissociation constant of potassium nitrate in DMF.
Slope; $3.0(0.4)\times10^{-3}$, Intercept; $9.1(0.1)\times10^{-2}$

determined from the plot as a function of the potassium nitrate concentration, as summarized in Table 2.

Lithium Ion-Pair Equilibrium: As shown in Fig. 6, the ESR spectra obtained in the solutions of lower concentration of lithium ions (of less than 10^{-2} M) are a superposition of the two spectra due to the free ions and ion pairs. In this region, the exchange reaction (4) is a "*slow exchange*" reaction in the sense of magnetic resonance spectroscopy. In general, the spectrum consists of two separate signals when the reaction rates for reaction (4) are small, as stated above.

From the solution of the modified Bloch equation for the two-jump model, the ratio of the separation between the positions of the two maxima (Δ) to that when the exchange between the two states does not exist (Δ_0) is given by:[31]

$$\frac{\Delta}{\Delta_0}=\left[1-\frac{1}{2\cdot\pi^2\cdot\tau^2\cdot(\nu_{IP}-\nu_f)^2}\right]^{1/2}, \qquad (13)$$

assuming that the lifetimes of ion pairs and of the free ions are equal to each other, *i.e.*, that $\tau_{IP}=\tau_f=2\cdot\tau$, and that the inverse of the transverse relaxation times are negligibly small. ν_{IP} and ν_f are the resonance frequencies of the two states, respectively.

Equation 13 means that the greater the difference between the resonance frequencies of the ion pair and the free ion, the greater the decrease in the critical lifetime at which the two signals merge into only one signal. In other words, when the difference of the resonance frequencies is large, the spectrum will consist of two separate signals, even if the exchange reaction rate is relatively large. As shown in Table 1, the nitrogen hfs is highest in the solution of lithium perchlorate. Therefore, the difference between the resonance frequencies of the ion pair composed of lithium cations and the free ions is largest in the present experiments. The exchange rates of reaction (4) are accelerated with increasing concentration of lithium perchlorate, and the resonance lines merge into a single line in the intermediate exchange region.

In the region showing a regular increase of the nitrogen hfs as in Fig. 5, the equilibrium reaction is in the range of the rapid exchange as mentioned above.

Equation 12 was examined in order to determine the ion-pair formation constant and the nitrogen hfs of the ion pair in the rapid exchange region. Figure 11 shows the plot of $1/a_{ob}$ with $1/C_M{}^+\cdot(1-a_f/a_{ob})$. The variations of the nitrogen hfs in the region of rapid exchange are not so large, and the error of the hfs becomes of importance in the accuracy of the formation constant and the hfs of the ion pair. Analyzing the linear relation using the least-squares method, the hfs of the ion pair itself and the formation constant are $a_{IP}=11.36$ (±0.03) gauss and $K_f=340$ (±40) 1/M, respectively. The formation constant determined here is somewhat larger than that determined by polarographic techniques, as shown in Table 2. The accuracy of the formation constant using ESR

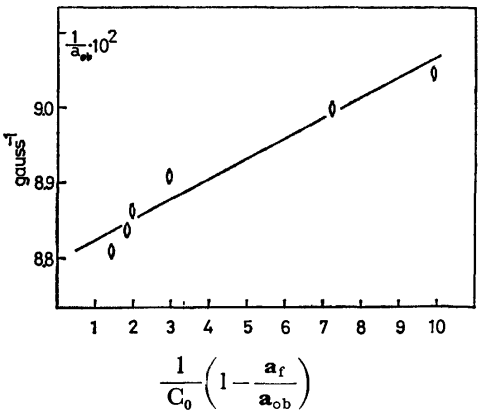

Fig. 11. Plot $1/a_{ob}$ *vs.* $1/C_o(1-a_f/a_{ob})$ for the lithium perchlorate addition.
Slope; $2.5(0.3)\times10^{-4}$, Intercept; $8.80(0.02)\times10^{-2}$

Table 2. Summary of the formation constants, the hfs of the ion pair, and the coordination numbers obtained from the ESR and Polarographic studies in DMF

Cation	Formation Constant (l/M)		Nitrogen hfs (gauss)	Coordination number	
	ESR	Polarog.[c]		ESR	Polarog.[c]
Li^+	340(±40)	150(±10)	11.36(±0.03)	1	1
Na^+	220(± 5)	200(±20)	11.23(±0.03)	1	1
K^+	41(± 3)[a]	—	10.58(±0.03)	1	—
	30(± 6)[b]	—	10.99(±0.05)		

a) Using the concentration of potassium nitrate. b) Using the concentration of potassium ions. c) Details will be reported in the near feature.

techniques is not satisfactory because the change of the nitrogen hfs in the rapid exchange region is not large enough, as shown in Fig. 5. For this reason, the formation constant determined from the variations of the hfs appears to be approximately consistent with that obtained using polarographic techniques, which will be described in detail elsewhere.

The formation constants of the ion pairs between nitrobenzene radical anions and cesium and rubidium cations could not be determined because the line-width of the spectra in the solutions of these salts were extraordinarily large, as is seen in Fig. 3.

We found that the line-widths associated with the nitrogen nuclear spin quantum number $m_z=\pm 1$ were larger than that for $m_z=0$. The line-width broadening effects in the ESR spectra are now under study, a part of the results of which will be reported in the near future.

Summary

The ion pair formation constants, the nitrogen hfs of the ion-pair itself, and the coordination numbers are summarized in Table 2.

In the case of the lithium ion pair, the variations of the nitrogen hfs in the fast exchange region are so small that the formation constant obtained by polarographic techniques seems to be more correct than that obtained using ESR.

The formation constants of the sodium ion pair system obtained from both studies are completely consistent with each other.

The authors wish to thank Professors T. Isobe and M. Matsuda, and Assistant Professors M. Iwaizumi and Y. Ikegami for their kind direction throughout the course of this work.

References

1) M. Szwarc, "Carbanions, Living Polymers and Electron-Transfer Processes," Interscience, New York (1968).
2) J. H. Sharp and M. C. R. Symons, "Ions and Ion Pairs in Organic Reactions," ed. by M. Szwarc, Interscience, New York (1972), Chapter 5.
3) M. Iwaizumi, M. Suzuki, T. Isobe, and H. Azumi, *Bull. Chem. Soc. Jpn.*, **40**, 2754 (1967).
4) N. Hirota, *J. Phys. Chem.*, **71**, 127 (1967).
5) N. Hirota, *J. Am. Chem. Soc.*, **90**, 3603 (1968).
6) A. W. Rutter and E. Warhurst, *Trans. Faraday Soc.*, **64**, 2339 (1968).
7) T. A. Claxton, W. M. Fox, and M. C. R. Symons, *Trans. Faraday Soc.*, **63**, 2570 (1967).
8) T. A. Claxton, J. Oakes, and M. C. Symons, *Trans. Faraday Soc.*, **64**, 596 (1968).
9) R. L. Ward, *J. Am. Chem. Soc.*, **83**, 1296 (1961).
10) P. Lundwig, T. Layloff, and R. N. Adams, *J. Am. Chem. Soc.*, **86**, 4568 (1964).
11) J. M. Gross, J. D. Barnes, and G. N. Pillans, *J. Chem. Soc., A*, **1969**, 109.
12) J. Oakes, J. Slater, and M. C. R. Symons, *Trans. Faraday Soc.*, **66**, 546 (1970).
13) L. Holleck and D. Becher, *J. Electroanal. Chem.*, **4**, 321 (1962).
14) D. B. Paul, L. Lipkin, and S. I. Weissmann, *J. Am. Chem. Soc.*, **78**, 116 (1956).
15) N. S. Hush and J. R. Rowland, *Mol. Phys.*, **6**, 201 (1963).
16) B. J. McClelland, *Trans. Faraday Soc.*, **57**, 1458 (1961).
17) M. Iwaizumi, M. Suzuki, T. Isobe, and H. Azumi, *Bull. Chem. Soc. Jpn.*, **40**, 1325 (1967); **41**, 732 (1968).
18) C. A. McDowell and K. F. G. Paulus, *Can. J. Chem.*, **43**, 224 (1965).
19) N. M. Atherton and A. E. Goggins, *Trans. Faraday Soc.*, **62**, 1702 (1966).
20) I. B. Goldberg and J. R. Bolton, *J. Phys. Chem.*, **74**, 1965 (1970).
21) T. Takeshita and N. Hirota, *J. Am. Chem. Soc.*, **93**, 6421 (1971).
22) D. H. Geske, J. L. Ragle, M. A. Bambenek, and A. L. Balch, *J. Am. Chem. Soc.*, **86**, 987 (1964).
23) Y. Kawamura, N. Nishikida, and T. Kubota *Bull. Chem. Soc. Jpn.*, **46**, 737 (1973).
24) A. D. McLachlan, *Mol. Phys.*, **3**, 233 (1960).
25) H. M. McConnell, *J. Chem. Phys.*, **24**, 633, 764 (1956).
26) P. H. Rieger and G. K. Fraenkel, *J. Chem. Phys.*, **39** 603 (1963).
27) T. Kitagawa, T. Layloff, and R. N. Adams, *Anal. Chem.*, **36**, 925 (1964).
28) J. A. Pople, W. G. Schneider, and H. J. Bernstein, "High Resolution Nuclear Magnetic Resonance," McGraw-Hill, New York (1959).
29) P. D. Sullivan and J. R. Bolton, "Advances in Magnetic Resonance," Vol. 4, ed. by J. S. Waugh, Academic Press, New York (1970).
30) D. P. Ames and P. G. Sears, *J. Phys. Chem.*, **56**, 16 (1955).
31) Chapter 10 in Ref. 28.

S_2 Formation during the Pyrolysis of H_2S in Shock Waves

Tetsuo HIGASHIHARA, Ko SAITO, and Hitoshi YAMAMURA

Department of Chemistry, Faculty of Science, Hiroshima University, Higashisenda-machi, Hiroshima 730

(Received April 28, 1975)

The rate of S_2 formation from shock-heated H_2S was measured by means of the UV absorption technique in the temperature range of 2380—3000 K. At all the temperatures measured, the S_2 absorption during the reaction could be represented by $(S_2)_t=(S_2)_\infty\{1-\exp(-kt)\}$, where:

$$k=10^{9.2}\exp(-72\ \text{kcal}/RT)\ \text{s}^{-1}.$$

The mechanism of the S_2 formation was proposed, and the value of the second-order rate constant, k_1, for the primary reaction, $H_2S+M\rightarrow SH+H+M$, was estimated as follows:

$$k_1 = 10^{13.1}\exp(-92\ \text{kcal}/RT)\ \text{l mol}^{-1}\ \text{s}^{-1}.$$

The effects of the addition of NO and O_2 on the rate of S_2 formation were also investigated. The results showed the validity of the proposed reaction mechanism.

The thermal decomposition of H_2S was studied by a static method by Darwent *et al.*[1] in pure H_2S at pressures between 30 and 300 Torr and in the temperature range of 720—970 K. At the temperatures above 900 K, they found that the reaction was second-order with respect to the concentration of H_2S and that its apparent activation energy was about 50 kcal/mol. The reaction was suggested to be $2H_2S\rightarrow 2H_2+S_2$. In shock waves at temperatures above 1000 K, on the other hand, the primary s.ep of the decomposition of H_2S, which is diluted in an inert gas, may be considered to be as follows:

$$H_2S + M \rightarrow SH + H + M \qquad (1)$$

such as has been reported for the other triatomic molecules. However, no data about the pyrolysis of H_2S in shock waves have been reported, although in the oxidation of H_2S Reaction (1) was recognized to be the primary step.[2] It was then stated that the difficulty in the evaluation of the kinetic data for Reaction (1) was due to the effects of oxygen and other oxidizers which could not be removed from the reactant.[3] In this work, we observe the rate of the S_2 formation from shock-heated H_2S in Ar by using a reactant purified carefully, and discuss the mechanism of the H_2S decomposition.

Experimental

The experiments were conducted in a 5-cm-diameter shock tube with a 4.3-m-long test section. The shocks were generated by high-pressure hydrogen in a 1.7-m-long driver section. The system was pumped by an oil-diffusion pump to less than 1×10^{-4} Torr before each run. All the measurements were made behind the incident shock waves. The light source used for the absorption measurements was a 300W Xe lamp (Ushio Electric Co.). The light was focused with a mirror on the entrance slit of a monochromator (Jarrell-Ash, 0.25 m) which had been placed on the side opposite the light source with respect to the shock tube. The selected light was detected by a photomultiplier (MS9SY), whose output was recorded on a single sweep of an oscilloscope. The rise time of the electronics was 2 μs or less. The concentration of S_2 was followed by observing the absorption intensity at 320 nm ($^3\Sigma_g^-\rightarrow{}^3\Sigma_u^-$ system). Although the SH absorption band lies around 320 nm, the measured absorption at this wavelength was attributed to S_2, since the absorption due to SH was negligibly small compared to the strong absorption of S_2.[4]

Hydrogen sulfide was produced by dropping a saturated NaS aqueous solution into a 10% H_2SO_4 aqueous solution and was dried by passing it through calcium chloride and phosphorus pentoxide. The gas thus obtained was solidified and degassed at −115 °C (mp of EtOH) and then purified by fractional distillations between −115 °C and −196 °C. Mixtures of 5%H_2S–95%Ar, 5%H_2S–1%NO–94%Ar, and 5%H_2S–1%O_2–94% Ar were prepared and kept in 8-l flasks for more than 12 hr before use.

The experimental conditions were as follows: P_1=8—16 Torr, P_2=300—460 Torr, T_2=2380—3000 K and ρ_2(total density)$=(3.2—6.2)\times10^{-6}$ mol/cm^3, where the subscript 2 denotes the condition just behind the shock front (chemically frozen condition).

Results and Discussion

Rate of S_2 Formation. In preliminary experiments, it was found that the rate of the S_2 formation was greatly influenced by trace amounts of oxygen. Therefore, the purification of H_2S was carefully performed in the manner described in the experimental section. For the mixture of 5%H_2S–95%Ar, no induction period of the S_2 formation was observed over the temperature range measured. A typical oscilloscopic trace of S_2 absorption is shown in Fig. 1 (a). The variation in the concentration of S_2 with the time was expressed by the following relation:

$$\ln\{(S_2)_\infty/((S_2)_\infty-(S_2)_t)\} = kt \qquad (I)$$

where $(S_2)_\infty$ denotes the concentration of S_2 at the steady state, which is reached within the observation time. In Fig. 1(b), a plot of the value of the left-hand side of Eq. I is shown as a function of the laboratory time. The experimental conditions and the values of k determined from the above relation are listed in Table 1. The Arrhenius plots of k are shown in Fig. 2, where the data obtained in preliminary experiments are also included for comparison (lines (a) and (b)). In the preliminary experiments, samples were purified by solidifying, degassing, and distilling by using liquid N_2 and were used without further purification. Therefore, it is thought that slight amounts of air were still present in the samples. From this figure, it appears that trace amounts of an impurity accelerate the rate

TABLE 1. EXPERIMENTAL CONDITIONS AND RATE CONSTANTS

Run No.	P_1 Torr	P_2 Torr	T_2 K	ρ_2 mol/cm^3	k s^{-1}	k_1 l mol^{-1} s^{-1}
274	13	419	2640	5.08×10^{-6}	1.80×10^{3}	3.54×10^{5}
276	15	432	2380	5.83	0.682	1.17
279	14	414	2440	5.45	1.09	1.99
280	11	376	2780	4.86	3.31	7.62
282	9	329	2950	3.58	7.60	21.4
283	8	300	3000	3.19	11.4	35.8
284	10.5	375	2890	4.81	5.44	11.3
285	9	321	2890	3.57	5.13	14.4
287	9.5	335	2860	3.76	5.38	14.3
289	16	460	2380	6.20	0.738	1.19
290	14	438	2570	5.48	1.04	1.89

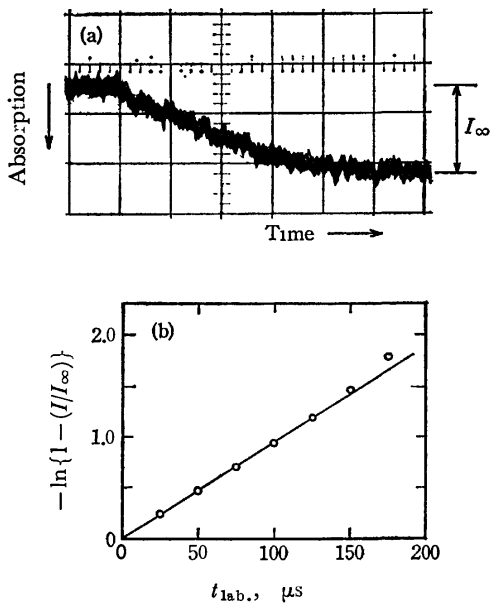

Fig. 1. (a): Sypical oscilloscopic trace of S_2 absorption at 320 nm, 5% H_2S–95% Ar; T_2=2570 K; sweep time=50 μs/cm. (b): Plot of $-\ln\{1-(I/I_\infty)\}$ *vs.* laboratory time.

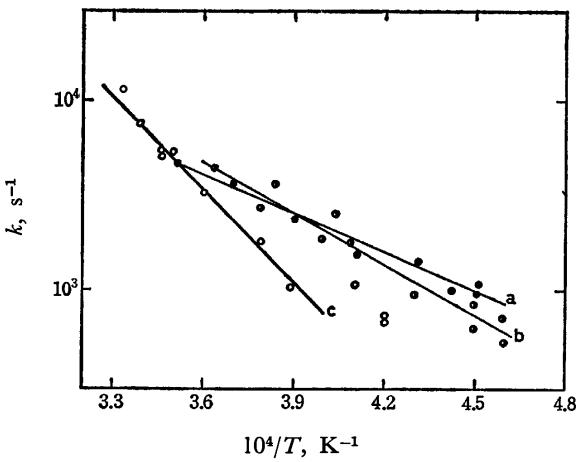

Fig. 2. Arrhenius plots of the rate constant k for S_2 formation. Data around lines (a) and (b) were obtained in preliminary experiments for 5% H_2S–95% Ar mixtures. Data around line (c) were obtained in this experiment for 5% H_2S–95% Ar mixture.

of S_2 production. The data obtained in this experiment, corresponding to the most purified H_2S, show a large temperature dependence compared with the other two sets of data, (a) and (b). The best fitting straight line (c) gives the following expression in the temperature range of 2500—3000 K:

$$k = 10^{9.2}\exp(-72\ \text{kcal}/RT)\ \text{s}^{-1}.$$

In Fig. 3, the values of $\{\ln(I_0/I_e)\}/(H_2S)_0$ are plotted as a function of T, where I_e is the light intensity at the equilibrium and where the subscript o denotes the condition just behind the shock front. Since the extinction coefficient of S_2 does not vary with the temperature,[5] it appears that the quantity of S_2 produced from the unit concentration of H_2S is almost constant over the temperature range measured. This fact means that the recombination of S atoms does not play a dominant role in the S_2 formation because the composition between S_2 and S at the equilibrium, $S_2 \rightleftarrows 2S$, varies largely with the temperature in the range considered.

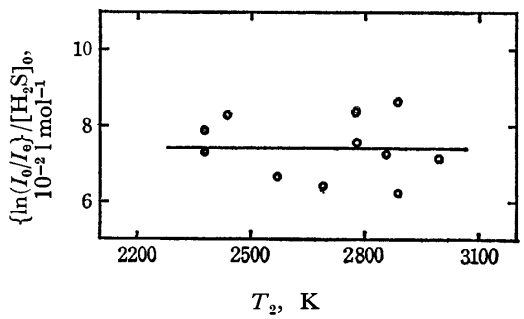

Fig. 3. Plot of $\{\ln(I_0/I_e)\}/(H_2S)_0$ against temperature, where I_0 and I_e are transmitted light intensities at shock front and at equilibrium, respectively.

A possible mechanism of the pyrolysis of H_2S accompanying the S_2 formation is considered to be as follows:

	ΔH°_{298} (kcal/mol)[6]	
$H_2S + M \rightarrow H + SH + M$	90.9	(1)
$H_2S + H \rightarrow H_2 + SH$	−13.3	(2)

$2SH \rightarrow H_2S + S$	− 6.1	(3)
$H_2S + S \rightarrow 2SH$	6.1	(−3)
$2SH \rightarrow H_2 + S_2$	−37.3	(4)
$SH + H \rightarrow H_2 + S$	−19.4	(5)
$SH + S \rightarrow H + S_2$	−17.9	(6)

From the above reaction scheme and the observed result that there existed no induction time for the S_2 formation, it is assumed that the consumption of the intermediates, H, SH, and S, is very rapid compared with their production rate through the primary reaction. Therefore, it is reasonable to use the steady-state method for these radicals. Also, we assume that $(S_2)_\infty = C(H_2S)_0$ and $(S_2)_\infty - (S_2)_t = C(H_2S)_t$, where C is a constant. With these relations, Eq. I is rewritten as:

$$\ln \{(H_2S)_0/(H_2S)_t\} = kt \qquad \text{(II)}$$

It appears that k is the first-order rate constant for the overall reaction of H_2S consumption.

For the S_2 formation in the H_2S pyrolysis, we do not have knowledge about which reaction is dominant under those experimental conditions. Reaction (4) was proposed for the flash photolysis of H_2S by Norrish *et al.*[7] On the other hand, Reaction (6) was proposed by Cullis *et al.*[8] in their review of the combustion of sulfur compounds, on the basis of the reason that the latter is much faster than the former in spite of its lower exothermicity. Also, in the discharge flow system of $H+H_2S$,[9] Reaction (6) was taken as a dominant reaction of S_2 formation. In any event, if the steady-state assumption is used for the intermediates, the following conclusion can be obtained whether Reaction (4) or (6) is taken as the main process of S_2 formation. That is, the overall rate of the H_2S decomposition becomes twice the primary reaction rate, as:

$$-\mathrm{d}(H_2S)/\mathrm{d}t = 2k_1(H_2S)(M) \qquad \text{(III)}$$

Since, in this experiment, the concentration (M) does not vary with the time behind the shock front, the second-order rate constant, k_1, can be determined from Eqs. II and III. The Arrhenius plots of k_1 are shown in Fig. 4, where the preliminary data (corresponding to Lines (a) and (b) in Fig. 2) are also included. It appears that the effects of impurities become apparent at lower temperatures and that, even for the most purified mixture, the data below 2500 K become higher than the (c) line, the one most suitable for the data above 2500 K. It has been shown in the pyrolysis of H_2O and SO_2 that, under the conditions of relatively lower temperatures and higher concentrations of the reactant, the systems involved many bimolecular reactions and that, as a result, the mechanisms were complicated. This seems to hold also for the pyrolysis of H_2S. Thus, the following expression for k_1 was evaluated from the data above 2500 K:

$$k_1 = 10^{13.1} \exp(-92 \text{ kcal}/RT) \text{ l mol}^{-1} \text{ s}^{-1}.$$

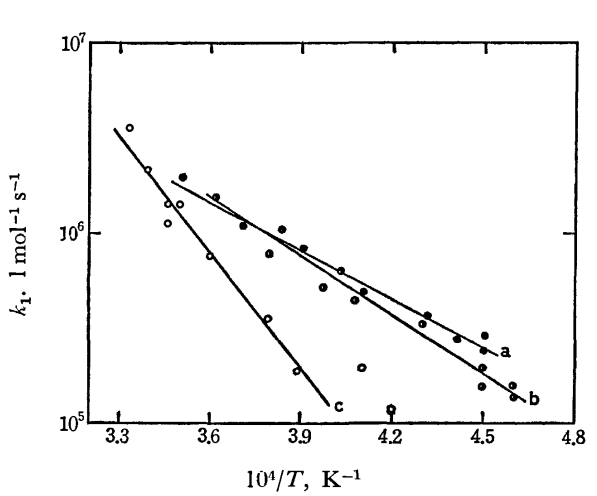

Fig. 4. Arrhenius plots of k_1. Lines (a) and (b) correspond to the preliminary experimental data for 5% H_2S–95% Ar mixtures. Line (c) corresponds to this experiment.

Effects of NO and O_2. When a mixture of 5% H_2S+1% NO+94% Ar was shock-heated, it was found that the rate of S_2 formation slowed down extremely. Because of the large effect of NO, the value of k could not be determined for this mixture. This effect suggests that NO acts as a scavenger of radicals. As has been proposed by Bradley *et al.*[10] in the experiment on the $H+H_2S$ flow system, the following reaction is thought to occur in our system also:

$$SH + NO \rightarrow (SHNO)^* \rightarrow \text{removal of SH} \qquad (7)$$

Furthermore, the following reactions may occur to eliminate H atoms from the system:

$$H + NO + M \rightarrow HNO + M \qquad (8)$$

$$H + HNO \rightarrow H_2 + NO \qquad (9)$$

much like the elimination of S atom observed in the photolysis of CS_2 and COS,[11] but at high temperatures these reactions are thought to be less important than Reaction (7).

As is shown in Figs. 2 and 4, in the presence of trace amounts of impurities the rate of S_2 formation was accelerated in the lower-temperature region. The most effective species is thought to be oxygen, which could not be removed from the sample in the usual manner. In the experiment on the 5% H_2S+1% O_2+94% Ar mixture, it was found that the rate of S_2 formation was further accelerated. This can be explained by adding the following bimolecular reactions to the above reaction Scheme 1—6:

$$H + O_2 \rightarrow OH + O \qquad (10)$$

$$H_2S + O \rightarrow SH + OH \qquad (11)$$

$$H_2S + OH \rightarrow SH + H_2O \qquad (12)$$

These reactions contribute to the formation of the SH radical. Thus, the effects of the addition of both NO and O_2 qualitatively support the above reaction scheme proposed for the decomposition of H_2S, although, from this study, it is not apparent whether the main reaction of S_2 formation is Reaction 4 or 6.

On the Value of k_1. Our experimental result for k_1 can be expressed by the equation of the collision theory: $k_1 = \{pZ(D/RT)^{s-1}/(s-1)!\}\exp(-D/RT)$, where p is the steric factor; Z, the collision frequency; s, the number of effective vibrations in the molecule, and D, the critical energy for HS–H bond dissociation. According to the absorption spectrum of H_2S[12], there

exists a continuum band with a maximum at about 51000 cm^{-1} and extending to 37000 cm^{-1}. This continuum was also observed in the experiment by Watanabe *et al.*[13] and was ascribed to a predissociation. Since, no discrete structure has been observed in the region of further low wave numbers, this continuum is thought to correspond to a nonbonding state which arises from $SH(^2\Pi)+H(^2S)$. Therefore, it may be considered that the dissociation proceeds *via* a crossing point whose potential is higher than the energy state of the products, $SH(^2\Pi)+H(^2S)$. If we take 106 kcal/mol for the critical energy, D,[14] we obtain $s=3.5$. By introducing these values into the empirical equation, $E_a=D-(s-1.5)RT$, the activation energy, E_a, is calculated to be 94 kcal/mol at 2750 K. This value is very close to the experimental value. Assuming the collision diameters for H_2S–H_2S and H_2S–Ar pairs to be 3.5 and 3.0 Å respectively, we obtain $p=0.5$, which is comparable to the value of 0.14 for the analogous molecule, H_2O.[15] The relatively large values of p for these molecules can be feasibly explained by the spin-allowed reactions.

Although, in this study, we did not consider either the temperature change during the course of the reaction behind the shock front or the boundary-layer effects, it may be thought that the results are not essentially changed by these effects.

References

1) B. De B. Darwent and R. Roberts, *Proc. Roy, Soc.*, *A*, **216**, 344 (1953).

2) J. N. Bradley and D. C. Bobson, *J. Chem. Phys.*, **46**, 2865 (1967).

3) H. H. Homan and A. Haas, "Comprehensive Chemical Kinetics," Vol. 4, ed. by C. H. Bamford and C. F. H. Tipper, Elsevier Publishing Co., New York (1972), Chap. 1.

4) R. A. Fifer, R. Moreau, and S. H. Bauer, "Proceedings of the Ninth International Shock Tube Symposium," Stanford Univ. Press, Calif. (1973), p. 731.

5) A. G. Gaydon, G. H. Kimbell, and H. B. Palmer, *Proc. Roy. Soc.*, *A*, **279**, 313 (1964).

6) S. W. Benson, "Thermochemical Kinetics," Wiley, New York (1968).

7) R. G. W. Norrish and A. P. Zeelenberg, *Proc. Roy. Soc.*, *A*, **240**, 293 (1957).

8) C. F. Cullis and M. F. R. Mulcahy, *Combust. Flame*, **18**, 255 (1972).

9) L. T. Cupitt and G. P. Glass, "Proceedings of the Symposium on Chemical Kinetics Data for the Upper and Lower Atmosphere," ed. by S. W. Benson, John Wiley & Sons, Inc., New York (1975), P. 39.

10) J. N. Bradley, S. P. Truemen, D. A. Whytock, and T. A. Zaleski, *J. Chem. Soc. Faraday*, **69**, 416 (1973).

11) N. Basco and A. E. Pearson, *Trans. Faraday Soc.*, **63**, 2684 (1967).

12) C. F. Goodeve and N. O. Stein, *Trans. Faraday Soc.*, **27**, 393 (1931).

13) K. Watanabe and A. S. Jursa, *J. Chem. Phys.*, **41**, 1956 (1964).

14) G. Herzberg, "Molecular Spectra and Molecular Structure," Vol. III, D. Van Nostrand Co., Princeton, N. J. (1967).

15) K. Kuratani and S. Tsuchiya, "Shock Waves in Chemistry and Physics," Shokabo, Tokyo (1968), Chap. III.

The Differences in Surface and Catalytic Properties of Two Magnesium Oxides Prepared from the Hydroxide and the Carbonate Hydroxide

Hideshi HATTORI, Katsuaki SHIMAZU, Naoji YOSHII, and Kozo TANABE

Department of Chemistry, Faculty of Science, Hokkaido University, Sapporo 060

(Received July 14, 1975)

Two kinds of MgO were prepared; MgO(I) from magnesium hydroxide and MgO(II) from magnesium carbonate hydroxide by evacuating at various temperatures and their surface and structural properties and catalytic actions for alkylation and isomerization reactions were examined. IR spectra of CO_2 retaining or adsorbed showed broad bands on MgO(II), but relatively sharp bands on MgO(I). In the alkylation of phenol with methanol over MgO(I), phenol was selectively alkylated at the *ortho* positions to produce *o*-cresol and 2,6-xylenol. The *ortho*-selectivity of MgO(I) was higher than 96%, while that of MgO(II) was about 75%. A low selectivity of MgO(II) was considered to be caused by a heterogeneity of surface structure of MgO(II), which was suggested by broad IR bands of CO_2 species on MgO(II). For the isomerization of 1-butene, both of MgO became active when evacuated at 450 °C and showed maximum activities when evacuated at 600 °C. The activity and the selectivity (ratio of *cis*-2-butene to *trans*-2-butene) of both catalysts were not much different. However, for the isomerization of *cis*-2-butene, the maximum activity and the selectivity (ratio of *trans*-2-butene to 1-butene) of MgO (I) were about four times higher than those of MgO(II).

The catalytic properties are generally recognized to be dependent on the preparation method. The preparation consists of various factors which determine the property of the final product. These include precipitation method, aging period, washing way, calcining condition *etc.* Among these are kind of starting material and pretreatment condition which give often large effect on catalytic property.

The catalytic properties of alkaline earth oxides are quite dependent on the starting material and the pretreatment temperature. Schächter and Pines[1] observed that CaO prepared from $Ca(OH)_2$ by calcining at 900 °C had little activity for the isomerization of 1-hexene, while CaO prepared from $CaCO_3$ by the same way showed a high activity. MgO was also reported to vary its catalytic property with the pretreatment temperature for the isomerization of 1-butene[2,3] and H_2–D_2 exchange reaction.[4]

In this study, two kinds of MgO were prepared from magnesium hydroxide and magnesium carbonate hydroxide by evacuating at various temperatures, and examined for their surface properties and catalytic actions for the isomerization of butenes and the alkylation of phenol with methanol.

Experimental

MgO(I) was obtained from magnesium hydroxide (guaranteed reagent of Kanto Chemical Co.) and MgO(II) from magnesium carbonate hydroxide (guaranteed reagent of Merck Co.) by evacuating at various temperatures. X-Ray diffraction patterns of the powder samples evacuated at different temperatures were recorded at room temperature by using CuK_α as a radiation source in air. Specific surface area was measured by applying BET equation to the adsorption isotherm of nitrogen at −196 °C.

The amount of CO_2 and H_2O evolved upon heating the starting material were measured as follows. The sample was evacuated at 100 °C, heated up to 200 °C and kept at this temperature for 2 h for MgO(I) (1 h for MgO(II)), the evolved gas being trapped by liq. N_2. The amount of gas evolved when the liq. N_2 was replaced by dry ice was taken as the amount of CO_2 and the amount still trapped by dry ice was taken as the amount of H_2O.

IR spectra of CO_2 retaining on MgO were measured by using an *in situ* cell. The sample was evacuated at a certain temperature for 2 h and a spectrum was measured at room temperature. Then, the sample was evacuated at a temperature higher than the previous evacuation temperature and a spectrum was measured again. The spectrum of CO_2 adsorbed on MgO was also measured. A sample was evacuated at 600 °C and exposed to a certain amount of CO_2 after cooling to room temperature.

The isomerization of butenes was carried out at 30 °C in a closed circulation system with a volume of about 1350 ml. In a quartz reactor, 17—25 mg of $Mg(OH)_2$ or 10—122 mg of $4MgCO_3 \cdot Mg(OH)_2 \cdot 5H_2O$ was placed and evacuated at various temperatures. The butenes were purified by passing through molecular sieves 4A kept at −78 °C. For analysis of butenes, a 5 m column packed with 30% propylene carbonate on Uniport C was operated at 0 °C.

The alkylation of phenol with methanol was carried out at 500 °C in a flow reactor. The catalyst used for the reaction was pretreated under a nitrogen stream at 530 °C or 650 °C for 3 h. The equimolar mixture of phenol and methanol was passed over the catalyst at contact time of 1.9 $g \cdot s \cdot ml^{-1}$. The products were trapped at 0 °C and subjected to gas chromatographic analysis. A 2 m column packed with polyethylene glycol 6000 on Celite-545 and thermostated at 100 °C was used.

Results

Upon heating $Mg(OH)_2$ and $4MgCO_3 \cdot Mg(OH)_2 \cdot 5H_2O$, the amounts of H_2O and CO_2 evolved are shown in Fig. 1. The evolution of CO_2 from $Mg(OH)_2$ continued over a wide range of the temperature from 200 °C to 700 °C, while the evolution of CO_2 from $4MgCO_3 \cdot Mg(OH)_2 \cdot 5H_2O$ occurred sharply around 400 °C. On the other hand, the dehydration of $Mg(OH)_2$ began at 200 °C and almost ended around 400 °C, whereas that of $4MgCO_3 \cdot Mg(OH)_2 \cdot 5H_2O$ persisted from 100 to 600 °C. The variations of the specific surface area for MgO(I) and MgO(II) are shown in Fig. 2. Decrease in a surface area was more prominent for MgO(II).

In Fig. 3 are shown the IR spectra of $Mg(OH)_2$ and $4MgCO_3 \cdot Mg(OH)_2 \cdot 5H_2O$ evacuated at different temperatures. In the case of MgO(I), the pairs of

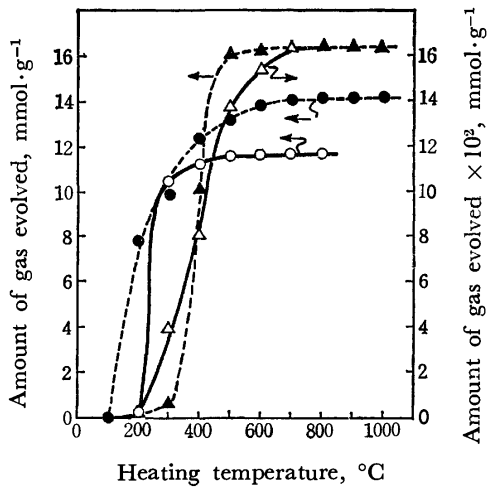

Fig. 1. Evolution of H_2O and CO_2. H_2O (-○-) and CO_2 (-△-) from $Mg(OH)_2$; H_2O (--●--) and CO_2 (--▲--) from $4MgCO_3 \cdot Mg(OH)_2 \cdot 5H_2O$.

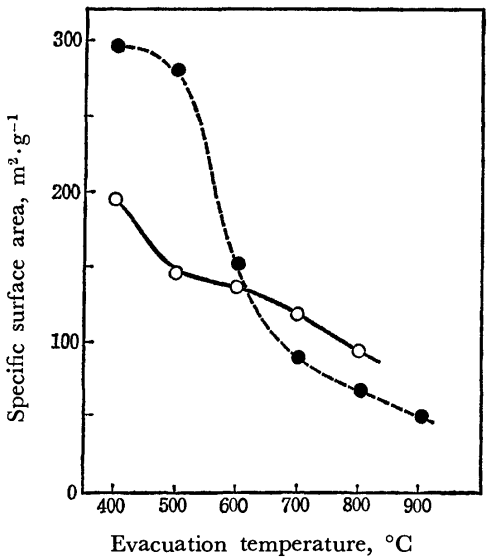

Fig. 2. The variations of specific surface areas of MgO-(I) (-○-) and MgO(II) (--●--) with evacuation temperature.

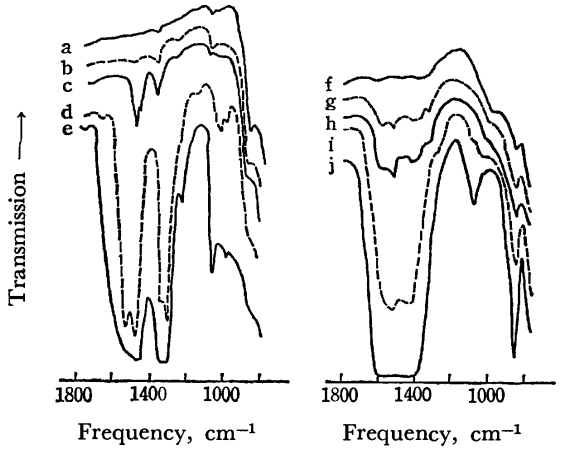

Fig. 3. IR spectra of $Mg(OH)_2$ (left) and $4MgCO_3 \cdot Mg(OH)_2 \cdot 5H_2O$ (right) after evacuating at a: 700, b: 600, c: 500, d: 400, e: 300, f: 600, g: 500, h: 480, i: 470, j: 460 °C.

the bands at 1520; 1330 cm^{-1} and 1470; 1340 cm^{-1} indicate that two kinds of CO_2 exist. The absorption bands of MgO(II) are rather broad compared with those of MgO(I). Those bands may be superposed bands of several kinds including unidentate CO_2, bidentate CO_2 and CO_3^{2-}.

Spectra of CO_2 adsorbed on MgO(I) were also different from those on MgO(II) as shown in Fig. 4. Spectrum c shows distinct separations of the bands at 1665 ; 1630 cm^{-1} and 1315 ; 1280 cm^{-1}. However, spectrum e obtained when about the same amount of CO_2 as in spectrum c was adsorbed shows indistinctly separated bands around 1650 cm^{-1} and 1300 cm^{-1}. Besides, it shows very broad shoulders around 1550 cm^{-1} and 1400 cm^{-1}.

X-Ray diffraction patterns of both MgO(I) and MgO-(II) evacuated at 400—900 °C for 2 h showed only a pattern of MgO. Half width of the peak at $2\theta =$ 42 °50' was about 1 °03' and 2 °33' for MgO(I) and MgO(II) evacuated at 400 °C, respectively, while it was about 51' and 30' for MgO(I) and MgO(II) evacuated at 900 °C, respectively.

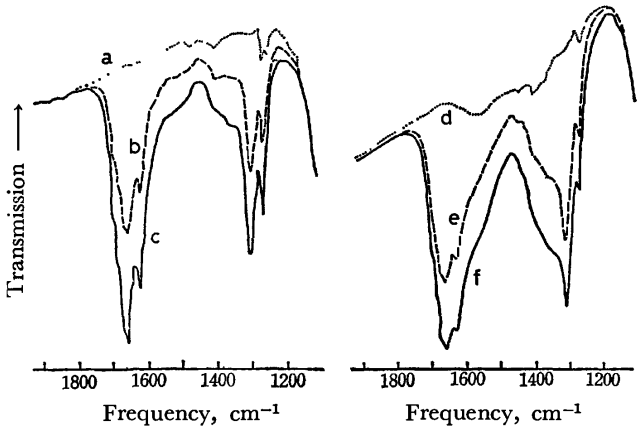

Fig. 4. IR spectra of CO_2 adsorbed on MgO(I) (left) and on MgO(II) (right). a: background of MgO(I), b: 6.5×10^{-5} mol CO_2/g, c: 13.5×10^{-5} mol CO_2/g, d: background of MgO(II), e: 15.0×10^{-5} mol CO_2/g, f: 26.8×10^{-5} mol CO_2/g.

TABLE 1. ALKYLATION OF PHENOL WITH METHANOL OVER MgO

Catalyst		MgO(I)		MgO(II)	
Pretreatment temperature, °C		529	650	533	657
Reaction temperature, °C		498	508	498	505
% Each Product	phenol	88.1	80.5	72.1	77.2
	o-cresol	10.1	16.9	18.7	15.8
	m,p-cresol	0.2	0.4	5.3	4.6
	2,6-xylenol	0.9	1.8	1.2	0.8
	2,4-xylenol	0	0.4	2.0	1.3
	2,4,6-trimethyl-phenol	0	0	0.3	0
	anisole	0	0	0.4	0.3
Activity, %·g⁻¹		11.5	18.9	26.9	22.0
ortho-Selectivity[a]		0.98	0.96	0.73	0.74

a) The ratio of (*o*-cresol+2,6-xylenol)/(*o*-cresol+*m,p*-cresol+2,6-xylenol+2,4-xylenol).

The results of the alkylation of phenol with methanol are listed in Table 1. MgO(I) was less active than MgO(II). However, the *ortho*-selectivity was more than 96% for MgO(I), while it was about 75% for MgO(II).

For the isomerization of 1-butene, the variations of the activity and the selectivity with evacuation temperature were substantially the same for two kinds of MgO as shown in Fig. 5. The maxima of the activity were observed when evacuated at 600 °C for two MgO. The ratio of *cis*-2-butene to *trans*-2-butene decreased to about 1—2 by raising the evacuation temperature to 600 °C and increased again to about 4—6 by evacuating at higher temperature.

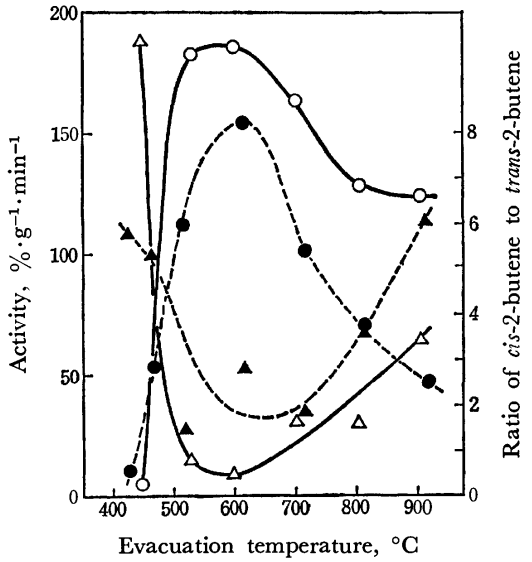

Fig. 5. Activity and selectivity for the isomerization of 1-butene. Activity (-○-) and selectivity (-△-) of MgO(I). Activity (--●--) and selectivity (--▲--) of MgO(II).

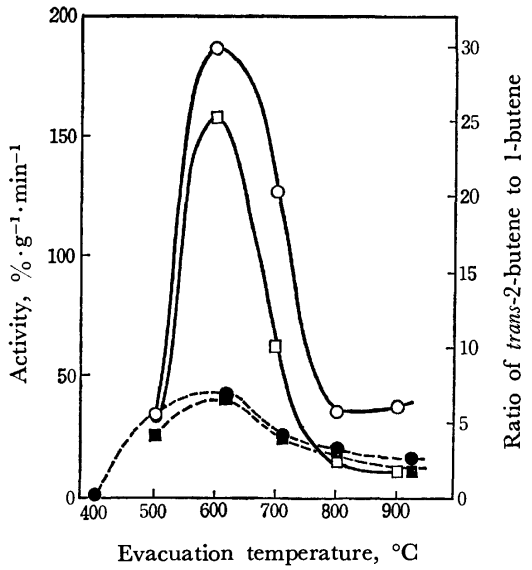

Fig. 6. Activity and selectivity for the isomerization of *cis*-2-butene. Activity (-○-) and selectivity (-□-) of MgO(I). Activity (--●--) and selectivity (--■--) of MgO(II).

Although the shapes of the change in the activity and the selectivity with evacuation temperature were about the same for the isomerization of *cis*-2-butene, the values of the activity and the selectivity were different for two MgO as shown in Fig. 6. Both the activity and the selectivity of MgO(I) at the maximum values were four times as high as those of MgO(II).

Discussion

The surface properties of two kinds of MgO which were prepared from different starting materials were not the same. Broad IR bands of adsorbed CO_2 on MgO(II) suggest that the surface structure of MgO(II) deviates from regularly ordered MgO surface and consists of several different sites for CO_2 adsorption. Rather sharp IR bands of CO_2 on MgO(I) indicates that the surface structure of MgO(I) is ordered much regularly than that of MgO(II). Since spectra of $Mg(OH)_2$ and $4MgCO_3 \cdot Mg(OH)_2 \cdot 5H_2O$ evacuated at different temperatures (Fig. 3) shows not only CO_2 on the surface but also CO_2 in the bulk, superposed bands of several kinds of CO_2 observed in MgO(II) indicate that the bulk structure of MgO(II) is also less regularly ordered than that of MgO(I). Since an irregularly ordered structure is not so stable as a regularly ordered structure, a remarkable decrease in the surface area of MgO(II) with a rise of the pretreatment temperature also suggests that MgO(II) is less regularly ordered than MgO(I).

For the alkylation of phenol with methanol, the difference between two MgO was observed in the *ortho*-selectivity. The *ortho*-selectivity was reported to be governed by the adsorption state of phenol.[5] If phenol is adsorbed in such a state that the *para* position is far from the surface, high *ortho*-selectivity is expected. Parallel adsorption of benzene ring to the surface, on the contrary, makes it easy to be alkylated at *meta* or *para* position. Since MgO(II) is considered to have several different kinds of sites, some of them might adsorb phenol in parallel, and produce *m*-, *p*-cresol and 2,4-xylenol.

These differences between MgO(I) and MgO(II), however, did not reflect on the catalytic action for the isomerization of 1-butene. As discussed in the previous paper on MgO(I),[3] the active sites for the formation of *cis*-2-butene appear by removing the carbonate having infrared absorption bands at 1520 and 1330 cm^{-1} and those for the formation of *trans*-2-butene by removing the carbonate having absorption bands at 1470 and 1340 cm^{-1}. Although the pursuit of the kind of CO_2 relevant to activity was not successful because of the existence of several kinds of CO_2 on MgO(II), a coincidence of the variation of the activity and the selectivity with evacuation temperature for two MgO suggests that the active sites of MgO(II) for the isomerization of 1-butene are generated by the same manner as those of MgO(I).

For the isomerization of *cis*-2-butene, the activity and the selectivity changed with evacuation temperature in a similar way for two MgO. The temperature at which the activity increased roughly coincided with

the temperature at which CO_2 evolved. As the variation of the activity is parallel to that of selectivity, the variation of the activity would represent the variation of the rate of the formation of *trans*-2-butene, while the rates of the formation of 1-butene are almost constant. Thus, the active sites for the formation of *trans*-2-butene from *cis*-2-butene are also considered to be generated by the evolution of CO_2. The values of the activity and the selectivity of MgO(I), however, were four times higher than those of MgO(II). The reason for this is still uncertain.

References

1) Y. Schachter and H. Pines, *J. Catal.*, **11**, 147 (1968).
2) M. J. Baird and J. H. Lunsford, *J. Catal.*, **26**, 440 (1972).
3) H. Hattori, N. Yoshii, and K. Tanabe, Proc. 5th Intern. Congr. Catalysis, Miami Beach 1972, **10**-233 (1973).
4) M. Boudart, A. Delbouille, E. G. Derouane, V. Indovina, and A. B. Walters, *J. Am. Chem. Soc.*, **94**, 6622 (1972).
5) T. Nishizaki and K. Tanabe, *Shokubai*, **15**, No. 4, 94 (1973).

Dielectric Relaxation Mechanism in Some Substituted Phenones

Neera SAHNI, J. P. SHUKLA, and M. C. SAXENA

Microwave and E.P.R. Laboratory, Department of Physics, University of Lucknow, India

(Received October 6, 1975)

Dielectric constants and losses at microwave frequency as well as static dielectric constants and refractive indices have been measured for *o*-methylacetophenone, *m*-methylacetophenone, *o*-hydroxybutyrophenone, 2′,4′-dihydroxyacetophenone and 2′,4′-dihydroxypropiophenone in dilute solutions of 1,4-dioxane. These values are used to calculate the dielectric relaxation times, distribution parameters, dipole moments and activation energies of the molecules. The results have been discussed in terms of the molecular motion of the system in the medium. Comparatively higher relaxation times and their variations irrespective of the molecular size, have been attributed to the intermolecular hydrogen bonding between the solvent and solute molecules.

Fong and Smyth[1] investigated the possibility of rotation of the polar acetyl and hydroxyl groups in molecules and the possible effects of the steric hindrance and resonance energy by determining the dielectric relaxation time of a number of organic molecules. Antony and Smyth[2] determined the dielectric relaxation and intramolecular hydrogen bonding in hydroxy- and methoxyacetophenones. In order to investigate the effect of increasing chain length in the case of hydrogen bonded molecules, Makhija *et al.*[3] have studied the dielectric relaxation of 2′-hydroxy-5′-methyl derivatives of phenones and found that whereas the relaxation time and the distribution parameter increase with increasing chain length, the dipole moment does not change significantly. With a view to study the intramolecular rotation of the polar groups and the intramolecular interaction consisting of hydrogen bonding and steric hindrance, the authors have investigated five phenone molecules of different substitutions and chain lengths.

The most probable relaxation time τ_0 and the distribution parameter α have been determined from the measurements of ε' and ε'' at a single frequency using Higasi's[4] equations. The dipole moment μ and the relaxation time τ have been determined for the same compounds by the single frequency method of Gopala Krishna[5] for dilute solutions. A comparison of the τ values obtained by the above two methods has been made.

The values of the free energy of activation for dielectric relaxation and for the viscous flow have been calculated using Eyring's[6] equations by utilising the values of τ obtained by Gopala Krishna's method at varying temperatures.

Experimental

A dipolemeter based on the principle of heterodyne beat method was used for the measurement of the static permittivity at 300 kHz. Refractive indices of all the solutions were measured by Abbe's refractometer, which in turn determined the optical permittivity ($\varepsilon_\infty = n_D^2$). The dielectric constant ε' and loss ε'' were measured at 3 cm wavelength, at four different temperatures by using the standing wave technique of Roberts and von Hippel[7] and its subsequent simplification by Dakin and Works[8]. The estimated accuracies in the measurements of ε' and ε'' are $\pm 1\%$ and $\pm 5\%$ respectively.

All the substances used were of pure quality obtained from Messers British Drug House. The purest 1,4-dioxane was distilled before use.

Results and Discussion

The values of the relaxation time and the distribution parameter, calculated by Higasi's single frequency method are given in Table 1. The τ value for *o*-methylacetophenone is found to be smaller than that of *m*-methylacetophenone, although the two are of the same molecular size. This could, perhaps, be due to the compact shape of the former molecule in contrast with the greater length of the latter molecule.

The relaxation time for *o*-methylacetophenone is less than that obtained by Antony and Smyth[2] for *o*-hydroxyacetophenone ($\tau = 31.0 \times 10^{-12}$ s) in dioxane, the differences in the molecular sizes of the two molecules being negligibly small. This may be due to the fact that the acetyl group in *o*-methylacetophenone has greater freedom of rotation than the acetyl group in *o*-hydroxyacetophenone which behaves almost as a rigid molecule because of the intramolecular hydrogen bonding between the –OH and acetyl groups.[2] The large value of distribution parameter for *o*-methylacetophenone also indicates the presence of an internal mode of relaxation, apart from the overall rotation of the molecule.

The relaxation time value for 2′,4′-dihydroxypropiophenone is greater than that for 2′,4′-dihydroxyacetophenone. This is expected because of the greater chain length of the former molecule. However, the τ value for *o*-hydroxybutyrophenone is found to be less than that of *o*-hydroxyacetophenone.[2] The nearly zero values of distribution parameters for 2′,4′-dihydroxyacetophenone and *o*-hydroxybutyrophenone indicate that the molecules relax largely due to the overall molecular rotations.

Adgonker and Kher[9] have determined the value of τ to be 38.73×10^{-12} s for 2′-hydroxy-4′-methylacetophenone in solutions of carbon tetrachloride. This value is considerably smaller than that of 2′,4′-dihydroxyacetophenone in dioxane. This may be partly due to the higher viscosity of dioxane than that of carbon tetrachloride and also because of the hydrogen bonding due to the solvent solute interaction at *para* position of the latter molecule. On comparing the τ value for 2′,4′-dihydroxypropiophenone with that obtained by Dhar *et al.*[10] of *p*-hydroxypropiophenone ($\tau = 25.4 \times 10^{-12}$ s in dioxane), it is found that the former value is more than 2½ times greater than the latter value.

Table 1. Slopes of plots of dielectric permittivity against concentration, values of relaxation time and distribution parameter (22 °C)

Compound	a_0	a'	a''	a_∞	τ_0	α
o-Methylacetophenone	4.81	2.12	1.49	0.32	23.1	0.240
m-Methylacetophenone	6.60	1.81	2.62	0.26	29.1	0.025
o-Hydroxybutyrophenone	6.82	2.05	2.88	0.27	26.0	0.002
2',4'-Dihydroxyacetophenone	8.01	1.30	2.31	0.44	46.8	0.018
2',4'-Dihydroxypropiophenone	8.73	1.29	1.90	0.36	66.4	0.139

Table 2. Relaxation times, dipole moments and thermodynamical parameters ($\lambda=3$ cm)

Compound	T K	$\tau\times10^{12}$ s	μ D	ΔF_ε kcal/mol	ΔH_ε kcal/mol	ΔS_ε cal/mol	ΔF_η kcal/mol	ΔH_η kcal/mol	ΔS_η cal/mol
o-Methyl-	287	14.6	—	2.55	1.10	−5.07	4.61	3.27	−4.67
acetophenone	295	13.5	2.03	2.59	1.10	−5.07	4.66	3.27	−4.71
	303	12.2	—	2.62	1.10	−5.01	4.70	3.27	−4.71
	311	11.7	—	2.67	1.10	−5.07	4.75	3.27	−4.75
m-Methyl-	287	19.9	—	2.73	1.24	−5.19	4.61	3.27	−4.67
acetophenone	295	18.6	2.35	2.78	1.24	−5.23	4.66	3.27	−4.71
	303	17.0	—	2.82	1.24	−5.22	4.70	3.27	−4.71
	311	15.8	—	2.86	1.24	−5.22	4.75	3.27	−4.75
o-Hydroxy-	295	16.4	2.18	2.71	0.73	−6.70	4.66	3.27	−4.71
butyrophenone	303	15.9	—	2.78	0.73	−6.75	4.70	3.27	−4.71
	311	15.1	—	2.84	0.73	−6.76	4.75	3.27	−4.75
2',4'-Dihydroxy-	287	19.0	—	2.70	1.19	−5.27	4.61	3.27	−4.67
acetophenone	295	18.1	2.19	2.77	1.19	−5.33	4.66	3.27	−4.71
	303	16.6	—	2.80	1.19	−5.32	4.70	3.27	−4.71
	311	15.4	—	2.85	1.19	−5.33	4.75	3.27	−4.75
2',4'-Dihydroxy-	287	21.6	—	2.78	0.87	−6.64	4.61	3.27	−4.67
propiophenone	295	19.1	2.68	2.80	0.87	−6.52	4.66	3.27	−4.71
	303	17.8	—	2.85	0.87	−6.52	4.70	3.27	−4.71
	311	16.7	—	2.90	0.87	−6.52	4.75	3.27	−4.75

Apart from the greater size of the molecule, the unusually high relaxation time of 2',4'-dihydroxypropiophenone can be explained as due to the hydrogen bonding between the solvent and the solute molecules, at various positions of the benzene ring.

It is significant from Table 2 that the values of relaxation times obtained by Gopala Krishna's method are invariably lower than those obtained by Higasi's method (Table 1). This may be due to the fact that unlike Higasi's method, Gopala Krishna's method is based on Debye's model of single relaxation process in which the distribution parameter is zero. Similar results were reported by Krishnaji for esters in solutions.[11]

It is evident from Table 2 that while the relaxation time decreases with increasing temperature, the free energy of activation increases. This is in line with the observation of other workers.[12] The free energy of activation ΔF_η is greater than ΔF_ε, which is quite natural because the viscosity process consists of rotational as well as translational motion of the molecule, while the dielectric relaxation is only due to rotation.

For all the molecules, the free energy of activation is greater than the molar enthalpy of activation, with the result that the entropy of activation is negative. This shows that the activated state is more ordered than the normal state.

The authors are thankful to Dr. B. G. Gokhale, Professor and Head of the Physics department, for his interest in the work. One of us (N.S.) is also grateful to the Council of Scientific and Industrial Research (New Delhi) for giving financial assistance.

References

1) F. K. Fong and C. P. Smyth, *J. Amer. Chem. Soc.*, **85**, 1565 (1963).
2) A. A. Antony and C. P. Smyth, *ibid.*, **86**, 156 (1964).
3) I. J. Makhija, A. L. Dawar, and B. N. Tripathi, *Ind. J. Pure Appl. Phys.*, **10**, 16 (1972).
4) K. Higasi, *Bull. Chem. Soc. Jpn.*, **39**, 2157 (1966).
5) K. V. Gopala Krishna, *Trans. Faraday Soc.*, **53**, 767 (1957).
6) S. Glasstone, K. J. Laidler, and H. Eyring, "The Theory of Rate Process," McGraw-Hill Book Co., New York (1941), p. 548.
7) S. Roberts and A. von Hippel, *J. Appl. Phys.*, **17**, 610 (1946).
8) T. W. Dakin and C. N. Works, *ibid.*, **18**, 610 (1947).
9) C. S. Adgonker and V. G. Kher, *Indian J. Pure Appl. Phys.*, **11**, 940 (1973).
10) R. L. Dhar, A. Mathur, J. P. Shukla, and M. C. Saxena, *Indian J. Pure Appl. Phys.*, **11**, 568 (1973).
11) Krishnaji, S. C. Srivastava, and Dina Nath, *Bull. Chem. Soc. Jpn.*, **43**, 2805 (1970).
12) F. H. Eranin, Jr. and C. P. Smyth, *J. Chem. Phys.*, **20**, 1121 (1952).

The Electronic Spectra of α,ω-Di-1- and α,ω-Di-2-naphthylpolyenes in Solution and in Solid State

Krishnagopal MANDAL and T. N. MISRA

Department of Physics, North Bengal University, Darjeeling, India, Pin 734430

(Received October 24, 1975)

The electronic absorption spectra of α,ω-di-1- and α,ω-di-2-naphthylpolyenes have been studied in solution and in the crystalline state. Both polyenes have four distinct electronic band systems. The spectral properties indicate that the terminal naphthyl group reduces the symmetry of the short-chained polyene molecules whereas long naphthylpolyenes retain the usual conjugated polyene symmetry of C_{2h}. A plot of λ^2_{max}-n gives a straight line and a nearly *all-trans* form seems to be retained by the polyene chain. Unlike that in some conjugated polyenes a good overlap between the first absorption band and the highest energy emission band is observed. This suggests that there is no low-lying forbidden state in these polyenes. Some of the absorption bands of naphthylpolyene crystal could be explained in terms of factor group split components. Two extra bands observed in α,ω-di-2-naphthylpolyenes seem to be related to naphthalene transitions.

Compared to the effort expanded in the spectral study of aromatic molecules little experimental works on the electronic spectrum of conjugated polyenes have been done. A systematic investigation of the electronic spectral properties of polyenes in different states has been undertaken in this laboratory. It has already been established[1-4] that in some linear polyenes with the general structure R_1-$(CH{=}CH)_n$-R_2, R_1 and R_2 being the end groups, there exists a low energy excited state (^1A_g) below the previously observed strongly allowed electronic state (^1B_u) and emission of polyenes originates from this state. The effect of the end groups on the electronic states of polyenes is well known.[5-8] In an earlier[9] paper it has been shown that in anthryl polyenes the lowest excited state is an allowed ^1B_u type. The terminal anthryl group interaction is such that ^1A_g is not lowered relative to ^1B_u in these polyenes. In order to study the effect of other end groups on the electronic excitation of polyacetylene chromophore, it was thought worthwhile to extend the investigation to other polyenes with terminal aromatic groups. Here we report the results of our investigation on the electronic spectra of a series of naphthylpolyenes in solution and also in the solid state.

Experimental

Highly pure, synthetic α,ω-di-1- and di-2-naphthylpolyenes were obtained from Prof. Nakagawa of Osaka University as a gift. They were used without further purification. Solvent tetrahydrofuran (THF) and haxane used were spectrograde. The electronic absorption spectra were measured with Spektromom-202 spectrophotometer of Hungarian optical works at room temperature using a well-matched pair of 1-cm cells. The fluorescence spectra were measured using a high intensity UV mercury source and a Corning C.S 7-54 filter with right angle excitation. The spectra in the solid state were obtained by making a thin crystal on the quartz plate. Five α,ω-di-1-naphthylpolyenes (I_n) and six α,ω-di-2-naphthylpolyenes (I_n') of type R-$(CH{=}CH)_n$-R where R stands for the naphthyl group and n=1—6, have been studied.

Results

Solution Spectra. *α,ω-Di-1-naphthylpolyene(I_n)*: The electronic absorption spectra of a series of I_n are reproduced in Fig. 1. Results are summarized in Table 1. Solvent hexane has been used to get the high energy bands in the region 2000—2400 Å. The spectrum from 2400 Å to the visible region has been measured in solvent THF because of better solubility of the polyenes in this solvent and the THF itself has no absorption in this spectral region.

The solution spectra show four distinct band systems. The transition to the lowest excited singlet state of the polyene is observed in the region 3000—5000 Å and this is very intense. Its intensity increases linearly with the chain length. This band has been identified

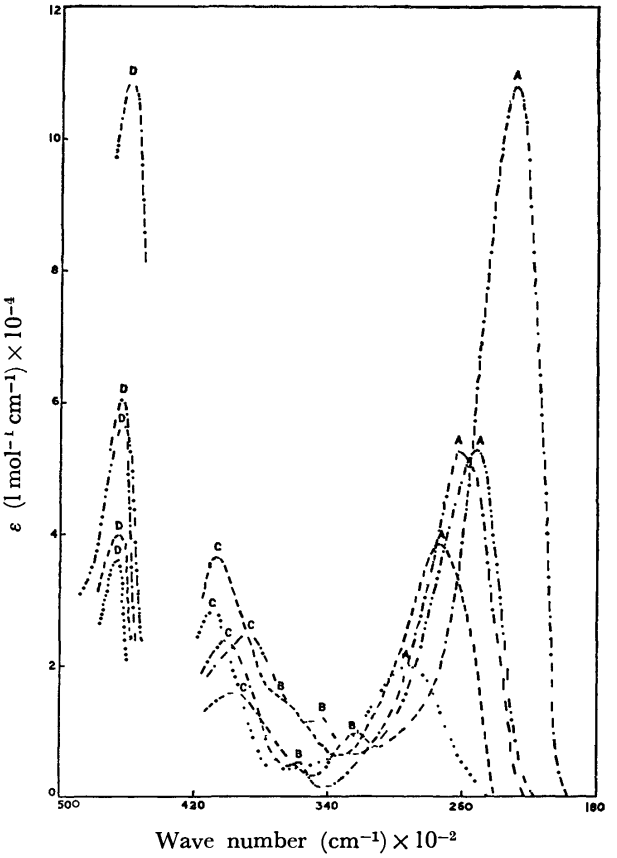

Fig. 1. ·····: Solution spectrum of I_1, ----: Solution spectrum of I_2, -·-·-: Solution spectrum of I_3, -·-·-·-: Solution spectrum of I_4, --·--·--: Solution spectrum I_6.

TABLE 1. ABSORPTION BANDS OF α,ω-DI-1-NAPHTHYLPOLYENES

No. of double bonds (n)	Bands in solution[a]		Bands in crystalline state	
	Wave number (cm^{-1})	Assignment	Wave number (cm^{-1})	Assignment
1	29200 (s)	A (O_1)	25600	A
	41000 (vs)	C (O_3)	40000	C
	46400 (vs)	D (O_4)	46300	D
2	27400 (s)	A (O_1)	26000	A
	37000 (vw)	B (O_2)		
	40600 (s)	C (O_3)	39400	C
	46300 (s)	D (O_4)	45600	D
3	26200 (s)	A (O_1)	29600	A_1
			23600	A_2
	35700 (vw)	B (O_2)		
	40000 (ms)	C (O_3)	39400	C
	46200 (s)	D (O_4)	45600	D
4	25000 (vs)	A (O_1)	29000	A_1
			24000	A_2
	34200 (w)	B (O_2)		
	38800 (ms)	C (O_3)	38500	C
	46200 (s)	D (O_4)	45500	D
6	22800 (vs)	A (O_1)	23400	A_1
			20000	A_2
	32200 (w)	B (O_2)	27800	B
	39400 (w)	C (O_3)	35600	C
	45600 (s)	D (O_4)	47200	D_1
			44000	D_2

a) Values are for THF solution for the A—C bands and for hexane for the D band.
s: strong, w: weak, v: very, m: medium.

as A in the diagram. The band in the region 2600—3200 Å identified as B, is very weak. This band becomes more and more distinct as n is increased in the polyene. An intense band C appears in the region 2400—2700 Å. Its intensity, in general, continues to decrease with the increase in polyene length. The highest energy band D is observed at about 2200 Å. This band is intense. It is observed that in long naphthylpolyenes two bands A, D are strong and B, C weak. The spectra of these polyenes in THF solution are in general agreement with that reported by Yasuhara *et al.*[10]

The fluorescence spectra of I_n have been studied in solvent hexane. The fluorescence bands of I_2 and I_4 are found to have band maxima at 22200 cm^{-1} and 21800 cm^{-1} respectively. The bands of I_2 and I_4 are shown in Fig. 2.

α,ω-Di-2-naphthylpolyene (I_n'): The electronic absorption spectra of I_n are presented in Fig. 3. For clarity the spectra of I'_{1-3} and I'_{4-6} are shown separately in the diagram. Results are given in Table 2. The spectrum, in general, consists of four band systems. One more high energy band is observed in higher members I_4', I_5' and I_6' and an extra low energy weak band is observed only in the lowest member I_1 of the polyene. Here too the high energy bands are measured in hexane and the rest part of the spectrum, in THF.

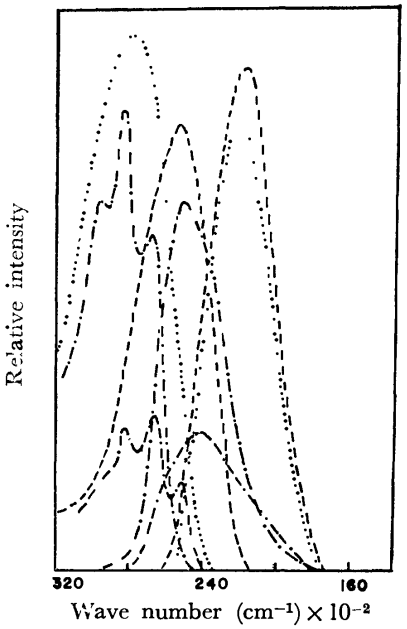

Fig. 2. ·····: First absorption band and fluorescence band of I_2, ----: First absorption band and fluorescence band of I_4, -·-·-: First absorption band and fluorescence band of I_2', --·---·--: First absorption band and fluorescence band of I_3'.

The first allowed singlet–singlet transition appears in the region 3000—5000 Å with sharp vibrational structure. The vibrational spacing is about 1400 cm^{-1}. This band system is very intense. The band in this region has been identified as A in the diagram. In the region 2400—3400 Å, there are two bands B and C in each of I_n'. This is clearly observed in I_2'. Here the band B is in the region 2700—3100 Å and the band C, in the region 2400—2700 Å. The bands B and C become weaker relative to other bands with increasing n. The band D is found to be in the region 2000—2600 Å. The band E in the region 2000—2300 Å appears only in I_4', I_5' and I_6' whereas in I_1' a very weak band is observed at about 3590 Å. The spectra of these polyenes in THF solution are similar to that reported by Yasuhara *et al.*[10]

In THF the second band (B) is much weaker than the first band A. In hexane, however, appreciable intensity enhancement of B band compared to A band is observed in I_1', I_2' and I_4', particularly in the first member.

The fluorescence spectra of I_n' have been studied in solution. The fluorescence band maxima of I_1' in THF is observed at 25000 cm^{-1}. Polyenes I_2' and I_3' (Fig. 2) are found to have fluorescence maxima at 24900 cm^{-1} and 24000 cm^{-1} respectively in hexane.

Solid Film Spectra. The crystal spectra of I_n are broad and the spectral data are summarized in Table 1. The spectra of I_1 and I_2 in the solid state are very broad and retain identity with the spectra in solution. The band B in solution of I_{2-4} is absent in crystals. The crystal spectrum of I_6 is shown in Fig. 4. For brevity crystal spectra of I_3 and I_4 are not presented, the data, however, have been shown in Table 1.

TABLE 2. ABSORPTION BANDS OF α,ω-DI-2-NAPHTHYLPOLYENES

No. of double bonds (n)	Bands in solution[a]		Bands in crystalline state	
	Wave number (cm^{-1})	Assignment	Wave number (cm^{-1})	Assignment
1	27800 (vw)	N (related to $^1A_g \rightarrow {}^1B_{3u}$ band of naphthalene)	26400	New band system
	28700 (vw)	A (O_1)	28400	A (O_1)
	30000 (s)	A (O_1+1300)	29800	A (O_1+1400)
	31300 (vw)	A ($O_1+2\times1300$)	31200	A ($O_1+2\times1400$)
	34800 (w)	B (O_2)	34600	B
	36200 (s)	B (O_2+1400)		
	37400 (vw)	C (O_3)		
	38600 (w)	C (O_3+1200)		
	48400 (s)	D (O_4)		
2	—	—	24600	New band system
	26400 (w)	A (O_1)	26300	A (O_1)
	27800 (vs)	A (O_1+1400)	27700	A (O_1+1400)
	29300 (w)	A ($O_1+2\times1400$)	29200	A ($O_1+2\times1400$)
	30600 (vw)	A ($O_1+3\times1400$)	30500	A ($O_1+3\times1400$)
	32600 (w)	B (O_2)	32600	B (O_2)
	33900 (ms)	B (O_2+1300)	33900	B (O_2+1300)
	35200 (w)	B ($O_2+2\times1300$)	35200	B ($O_2+2\times1300$)
	38100 (w)	C (O_3)	37900	C (O_3)
	39300 (w)	C (O_3+1200)		
	46800 (s)	D (O_4)	47900	D_1
3	—	—	22900	New band system
	24700 (w)	A (O_1)	24900	A (O_1)
	26200 (s)	A (O_1+1500)	26400	A (O_1+1500)
	27700 (w)	A ($O_1+2\times1500$)	27900	A ($O_1+2\times1500$)
	29200 (vw)	A ($O_1+3\times1500$)	29200	A ($O_1+3\times1500$)
	31600 (w)	B (O_2)	31500	B (O_2)
	33000 (w)	B (O_2+1400)	33000	B (O_2+1500)
	35400 (ms)	C (O_3)	35300	C
	45500 (ms)	D (O_4)	47500	D_1
			45000	D_2
4	—	—	21700	New band system
	23400 (s)	A (O_1)	23600	A (O_1)
	24800 (vs)	A (O_1+1400)	25000	A (O_1+1400)
	26200 (s)	A ($O_1+2\times1400$)	26400	A ($O_1+2\times1400$)
	27600 (vw)	A ($O_1+3\times1400$)		
	30800 (vw)	B (O_2)	33000	B
	32200 (vw)	B (O_2+1400)		
	33600 (vw)	B ($O_2+2\times1400$)		
	35600 (w)	C (O_3)	35000	C
	43600 (ms)	D (O_4)	43000	D
	48000 (ms)	E (O_5)	48000	E
5	—	—	21000	New band system
	22300 (s)	A (O_1)	22800	A (O_1)
	23700 (vs)	A (O_1+1400)	24200	A (O_1+1400)
	25100 (s)	A ($O_1+2\times1400$)	25600	A ($O_1+2\times1400$)
	26500 (vw)	A ($O_1+3\times1400$)		
	29900 (vw)	B (O_2)		
	30800 (w)	B (O_2+1000)		
	31900 (vw)	B ($O_2+2\times1000$)		
	33800 (vw)	C (O_3)		
	40400 (ms)	D (O_4)	40000	D
	47400 (ms)	E (O_5)	44000	E
6	—	—	19600	New band system
	21200 (s)	A (O_1)	21600	A (O_1)
	22800 (s)	A (O_1+1600)	23200	A (O_1+1600)
	24400 (vs)	A ($O_1+2\times1600$)	24800	A ($O_1+2\times1600$)
	26000 (s)	A ($O_1+3\times1600$)	26400	A ($O_1+3\times1600$)
	27600 (vw)	A ($O_1+4\times1600$)		

Table 2. Continued.

No. of double bonds (n)	Bands in solution[a]		Bands in crystalline state	
	Wave number (cm^{-1})	Assignment	Wave number (cm^{-1})	Assignment
6	29200 (vw)	A ($O_1+5\times1600$)		
	31600 (vw)	B (O_2)		
	33000 (vw)	B (O_2+1400)		
	35600 (w)	C (O_3)	35000	C
	40600 (ms)	D (O_4)	39000	D
	45400 (s)	E (O_5)	44800	E

a) Values are for THF solution for the A—C bands, and for hexane solution for the D—E bands.
s: strong, w: weak, v: very, m: medium.

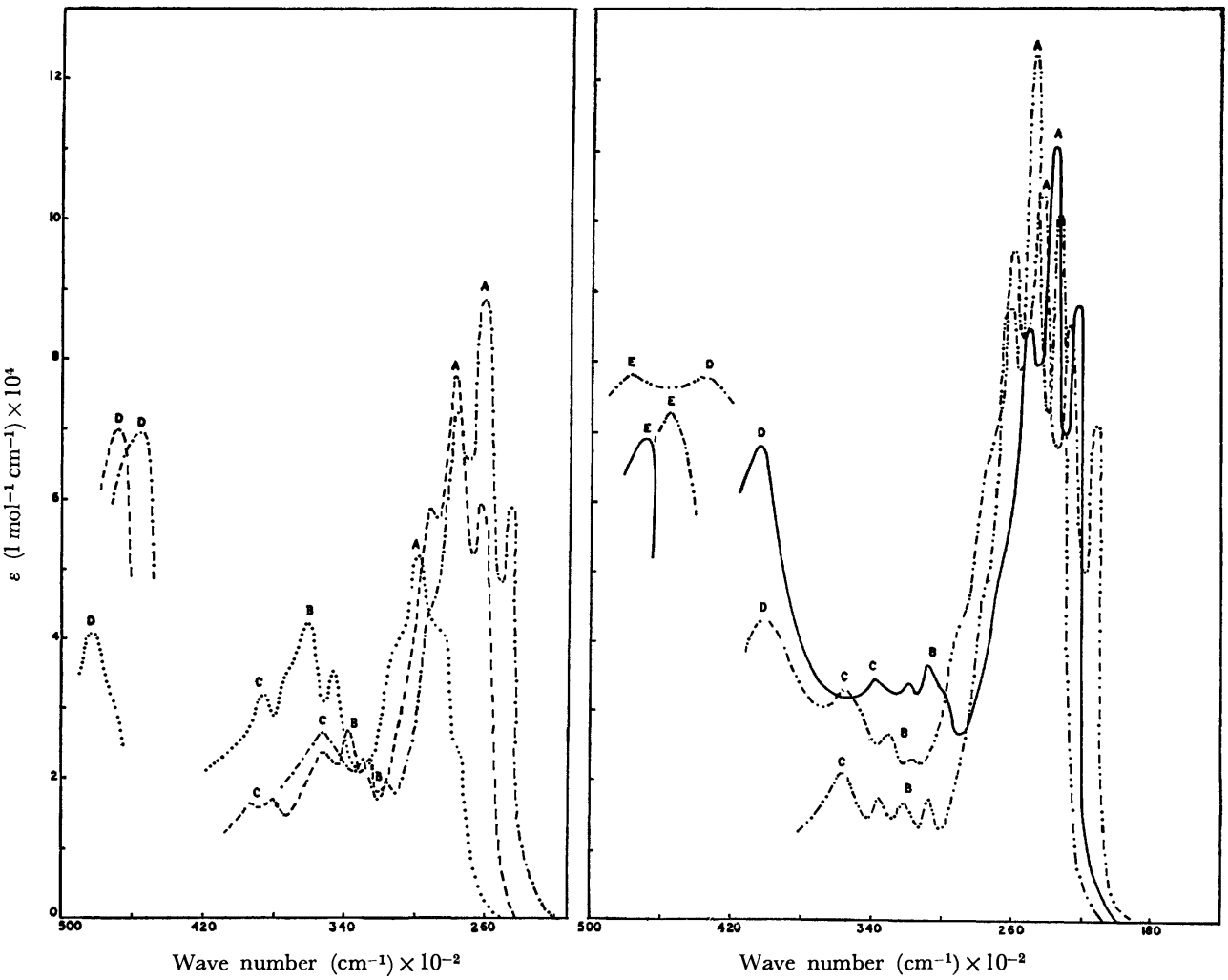

Fig. 3. ·····: Solution spectrum of I_1', ----: Solution spectrum of I_2', -·-·-: Solution spectrum of I_3', -··-··-: Solution spectrum of I_4', ——: Solution spectrum of I_5', --··--; Solution spectrum of I_6'.

The absorption spectra of I_n' in the crystalline state are shown in Fig. 5. The bands in the solid state are broad and shift little towards red or blue from their position in solution. The long wavelength band A appears with subbands. The vibrational spacing is about 1400—1600 cm^{-1}. The spacing between the longest wavelength subband and the next is found to be about 2000 cm^{-1}.

Discussion

Solution Spectra. All-*trans* conjugated polyenes belong to C_{2h} point group. The ground electronic state of these polyenes is ^1A_g and the excited states in increasing energy order are ^1B_u, ^1A_g, ^1A_g, ^1B_u according to the Pariser-Parr-Pople (PPP) method.[11] As

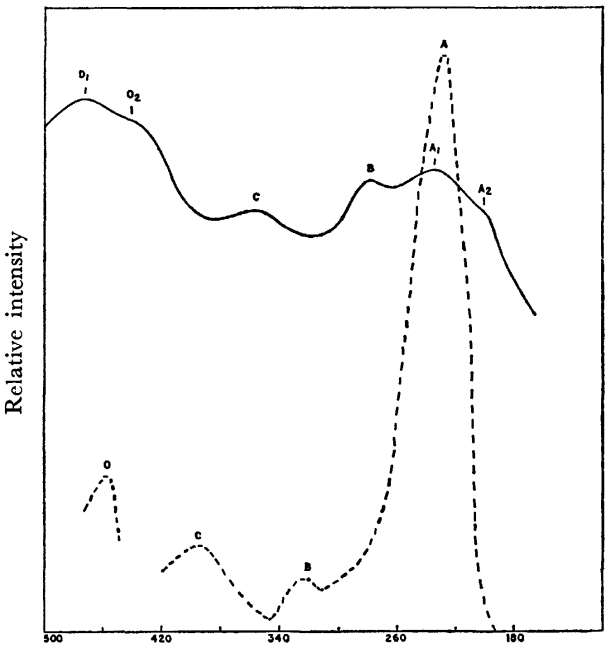

Fig. 4. —— Solid film spectrum of I_6, ----: Solution spectrum of I_6.

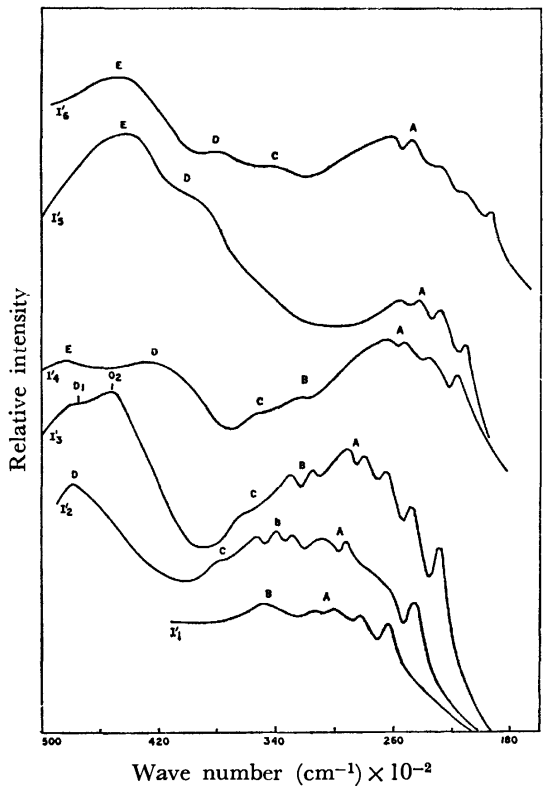

Fig. 5. Solid film spectra of I'_{1-6}.

a result the transitions $^1A_g \rightarrow {}^1B_u$, $^1A_g \rightarrow {}^1B_u$ are generally observed and are strongly allowed. Two $^1A_g \rightarrow {}^1A_g$ transitions are forbidden. From the band-intensity of I_n amd I_n' it is observed that in the higher members two transitions are strongly allowed and the other two transitions, weakly allowed. As the chain length of the polyene decreases the weakly allowed bands become

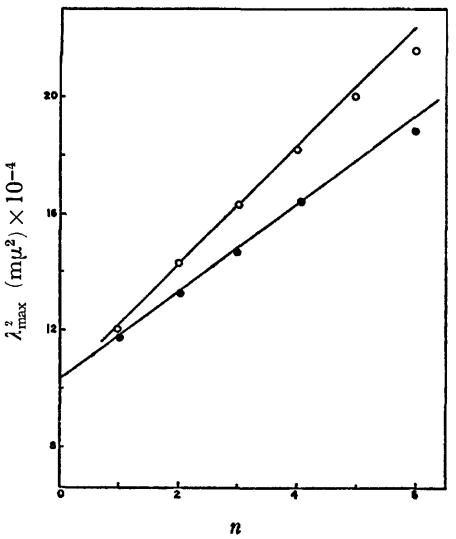

Fig. 6. -●-●-: Plot of $\lambda^2_{max} - n$ of I_n, -○-○-: Plot of $\lambda^2_{max} - n$ of I_n'.

equally intense with the allowed ones. The strong allowedness of the weak bands seems to be due to reduction in symmetry of the molecule by the presence of the terminal naphthyl group. When the polyene chain is short, the naphthyl group possibly destroys the center of symmetry and the lower members of the naphthylpolyene seem to have lower symmetry than C_{2h}. As a result one gets B and C bands as allowed in lower members of both I_n and I_n'.

In our spectra of I_n the bands in the region 3000—5000 Å (A), 2600—3200 Å (B), 2400—2700 Å (C) and 2160—2200 Å (D) possibly belong to the transitions $^1A_g \rightarrow {}^1B_u$, $^1A_g \rightarrow {}^1A_g$, $^1A_g \rightarrow {}^1A_g$ and $^1A_g \rightarrow {}^1B_u$ respectively of C_{2h} symmetry (true for higher members).

In the spectra of I_n', similarly, the bands in the region 3000—5000 Å (A), 2700—3400 Å (B), 2400—2900 Å (C) and 2000—2600 Å (D) seem to belong to transitions $^1A_g \rightarrow {}^1B_u$, $^1A_g \rightarrow {}^1A_g$, $^1A_g \rightarrow {}^1A_g$, and $^1A_g \rightarrow {}^1B_u$ respectively. The band E in the region 2000—2300 Å of I_4', I_5' and I_6' is possibly related to the $^1A_g \rightarrow {}^1B_{3u}$ (^1B_b in Platt's notation) transition of naphthalene and arises from the interaction between the ^1B_u state of the polyene chromophore and the $^1B_{3u}$ state of naphthalene. The long wavelength band at about 3590 Å of I_1' is structurally different from the lowest transition $^1A_g \rightarrow {}^1B_u$ of the polyene chromophore and may be related to the $^1A_g \rightarrow {}^1B_{3u}$ (^1L_b band in Platt's notation) of naphthalene group. In the higher members I'_{2-6} of the naphthylpolyene the band related to the lowest $^1A_g \rightarrow {}^1B_{3u}$ transition of naphthalene molecule may be hidden under the intense $^1A_g \rightarrow {}^1B_u$ band of the polyene chromophore.

As is evident from Figs. 1 and 3 and Tables 1 and 2, the longest wavelength maxima undergo red shift with increasing n. For conjugated polyenes it has generally been accepted[12] and λ^2_{max} is proportional to n, the number of conjugated double bonds. We have made such a plot of λ^2_{max} against n for both I_n and I_n' and the plot as shown in Fig. 6 is a straight line for the four lower members. I_6 and I'_{5-6} are not quite in the straight line. Further weakly allowed

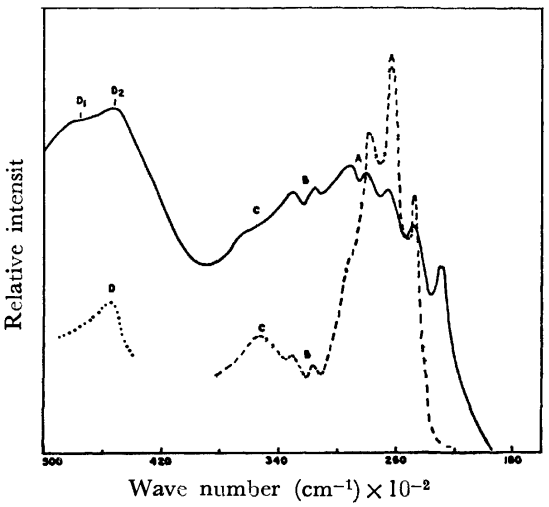

Fig. 7. —— Solid film spectrum of I_3', ----: Solution spectrum of I_3'.

transitions appear in the higher members. This suggests some deviations of the polyene chain from *all-trans* form in higher naphthylpolyenes.

In some conjugated polyenes there exists a low-lying forbidden π-electronic state.[1,4] Fluorescence originates from this state. In naphthylpolyenes four transitions have been observed. No forbidden transition is, therefore, expected. Our fluorescence and absorption spectra of naphthylpolyene I_n and I_n' show that there is a good overlap between the low energy absorption and highest energy emission bands (Fig. 7). We, therefore, conclude that in naphthylpolyenes there is no such low-lying forbidden state as is observed in some other polyenes.[1,4]

Solid Film Spectra. The crystal spectra of I_n differ somewhat from the spectra of free molecules. Identification of solution C and D bands of I_3 and I_4 in the solid state is obvious and no additional band is observed in this region. Both I_3 and I_4 in the solid state have two bands, one intense on the higher energy side and the other broad on the low-energy side of the solution band A. It seems that the band A is split into components A_1 and A_2 in the crystalline state. Free molecular bands B and C of I_6 as shown in Fig. 4 undergo red shift in the solid state. In I_6 in the region of each of the solution bands A and D there are two bands in the spectra of crystal. From these structures of the bands it seems that the band A is split into A_1 and A_2 and D into D_1 and D_2 in the solid state. In solid state the absorption bands of all these polyenes are broad and the assignment of the factor group split components in Table 1 is only tentative and numerical values of splitting are of no significance. Study of single crystal polarized spectra at liquid N_2 or liquid He temperature is required for any unequivocal identification of factor group split components.

The solid film spectra of I_n', in general, are very similar to the solution spectra. The bands D of I_2' and I_3' in solution seem to show some factor group splitting. In I_2' the band D is blue shifted in the solid state and this may be one of the factor group split components, D_1. As is obvious from the spectrum in Fig. 7 the band D of I_3' in the free molecular state has two bands on its high and low energy side in the crystalline state. Two bands are possibly the split components D_1 and D_2 of solution band D. No factor group splitting is observed in other members of I_n'. As has already been pointed out, assignment of these factor group split components is only tentative.

In the intense lowest energy band of each crystal spectrum of I_n' it is observed that the vibrational spacing between the subbands of A is 1400—1600 cm^{-1} in agreement with those observed in solution. The spacing between the longest wavelength maxima and the next, however, is about 2000 cm^{-1}. Thus it seems that this longest wavelength band is a new band system and appears in each of I_n' in the crystalline state. This band is possibly related to the $^1A_g \rightarrow {}^1B_{3u}$ band (^1L_b band in Platt's notation) of naphthalene molecule. In solution this band is found only in I_1'. In the solid state this band is separated out from the intense $^1A_g \rightarrow {}^1B_u$ band of the polyene chromophore in other I_n' polyenes.

The authors thank Prof. Nakagawa for his kind donation of the compounds studied. One of the authors (K. G. M.) expresses his thanks to University Grants Commission, India for a fellowship.

References

1) B. S. Hudson and B. E. Kohler, *Chem. Phys. Lett.*, **14**, 299 (1972).
2) K. Schulten and M. Karplus, *Chem. Phys. Lett.*, **14**, 305 (1972).
3) B. S. Hudson and B. E. Kohler, *J. Chem. Phys.*, **59**, 4988 (1973).
4) K. G. Mandal and T. N. Misra, *Chem. Phys. Lett.*, **27**, 57 (1974).
5) J. H. Pinckard, B. Wille, and L. Zechmeister, *J. Am. Chem. Soc.*, **70**, 1938 (1948).
6) L. Zechmeister and J. H. Pinckard, *J. Am. Chem. Soc.*, **76**, 4144 (1954).
7) K. Lunde and L. Zechmeister, *J. Am. Chem. Soc.*, **76**, 2308 (1954).
8) H. M. Walborsky and J. F. Pendleton, *J. Am. Chem. Soc.*, **82**, 1405 (1960).
9) K. G. Mandal and T. N. Misra, *Bull. Chem. Soc. Jpn.*, **49**, 198 (1976).
10) A. Yasuhara, S. Akiyama, and M. Nakagawa, *Bull. Chem. Soc. Jpn.*, **45**, 3638 (1972).
11) H. Suzuki, "Electronic Absorption Spectra and Geometry of Organic Molecules," Academic Press, New York (1967).
12) L. N. Ferguson, *Chem. Rev.*, **43**, 408 (1948).

Rotational Isomerism in β-Diketone *cis* and *trans* Enol Ethers. An IR and PMR Study*

Janusz DABROWSKI** and Michal TENCER

Institute of Organic Chemistry, Polish Academy of Sciences, 00-961 Warsaw, Poland

(Received March 31, 1975)

The *cis* (*Z*) isomers of β-alkoxy-α,β-unsaturated ketones, $R^1COCH{=}CR^2OR^3$, have been shown by IR spectra to exist as a mixture of *s-cis* (*ZZ*) and *s-trans* (*ZE*) rotamers, with the equilibrium shifting towards the former upon increasing the steric requirements of the R^1 substituent. The *trans* (*E*) isomers have uniformly the *s-cis* (*EZ*) structure. *O-s-trans* (or non-planar) and *O-s-cis* conformations due to rotation around the C_{sp^2}–O bond have been proposed for the *Z* and *E* isomers, respectively. Based on known structures, a rationalization of the rule governing the chemical shifts of R^1 and R^2 protons, called here the "ene-one cross shielding rule", has been offered.

While the vast majority of β-keto enols obtained to date have a *cis* configuration, obviously due to the stabilizing effect of the chelate hydrogen bond, most β-keto enol ethers have the alkoxy group in the *trans* position with respect to the carbonyl. Such was *e.g.*, the case with ethers of β-keto aldehydes studied in our previous work.[1] The *cis* β-keto enol ethers are kinetic products which spontaneously isomerize into the thermodynamically stable *trans* form. With β-diketone enol ethers, the isomerization is slow enough to enable the isolation and spectral investigation of these two isomers.

The simplest representatives of this class of compounds *viz.*, *cis* and *trans* methyl ethers of the enol of acetylacetone first obtained by Eistert *et al.*[2] have recently been investigated by Awang[3] using NMR spectroscopy. Although his assignments based on indirect data (NOE and ASIS) correctly ascribed the *trans-s-cis* structure to the isomer with a lower boiling point, the *cis* isomer was erroneously assumed to be homogeneous with respect to conformation; as shown below (see Results and Discussion section and Fig. 1) a considerable amount of the *s-cis* rotamer can directly be observed in the infrared spectra together with the *s-trans* one assigned by Awang.[3] Taking advantage of the more favorable time scale of the infrared spectroscopy we have investigated here some of the factors affecting the conformational equilibria, *viz.*, the steric requirements of the alkyl substituents and the solvent effect in a series of β-diketone enol ethers.***

While the *trans*(*E*) β-keto aldehyde enol ethers exhibited up to eight IR bands in the double bond stretching region due to rotation about both the C_{sp^2}–C_{sp^2} and C_{sp^2}–O single bonds,[1] the number of bands never exceeded four in the case of the *cis*(*Z*) and *trans*(*E*) β-diketone enol ethers reported here, which indicates that some of the rotamers are not present. The scrutiny of the IR spectra permitted us to identify the existing rotamers and to estimate their populations.

Joint utilization of the IR and NMR data allowed us to investigate the applicability of the rule[3,5–7] governing the shielding of the allylic and acylic protons in the compounds of the type studied here and to propose a rationalization of this rule.

Results and Discussion

IR Spectra. IR spectra data are given in Table 1. In order to illustrate the relationship between band intensities and steric requirements of the alkyl substituents, spectra of selected compounds are shown in Figs. 1 and 3. The dependence of the rotational equilibria upon the polarity of the solvent is illustrated by the spectra presented in Fig. 2.

In the *cis*(*Z*) series of β-diketone enol ethers, four bands are observed in most cases between 1550 and 1700 cm^{-1}. As seen from Fig. 1, one band in the $\nu_{C=O}$ region (band B) and one in the $\nu_{C=C}$ region (band C) decrease in intensity with increasing bulkiness of the substituent R^1 in going from compound **1** *Z* to **2** *Z*, **3** *Z* and **8** *Z*, while the other $\nu_{C=O}$ band (A) and $\nu_{C=C}$ band (D) increase in the same sequence.****

Since the enlargement of the alkyl group R^1 causes a stronger interaction with the alkoxy group in the *s-trans* conformation, these dramatic spectral changes can safely be interpreted as a result of the equilibrium shift towards the *s-cis* form:

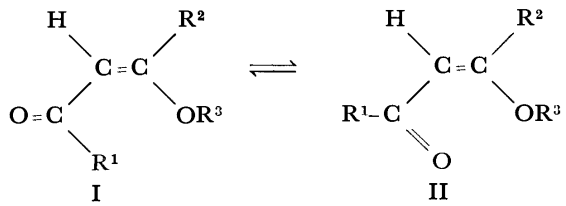

I II

ZE (*i.e.*, *cis/s-trans*) *ZZ* (*i.e.*, *cis/s-cis*)

Consequently, as with β-keto aldehyde enol ethers[1] and other α,β-unsaturated ketones,[8,9] the "inner" bands B and C are assigned to the coupled $\nu_{C=O}$ and $\nu_{C=C}$ vibrations of the *s-trans* rotamer and the "outer" ones A and D to the same vibrations of the *s-cis* rotamer.

In view of the strong non-bonded interaction between R^1 and OR^3 it might seem surprising, at first, that the *s-trans* rotamer prevails in the case of the first homologue of the series (**1** *Z*; R^1=Me) and occurs in still

* Paper XX of the series, "Infrared spectra and structure of substituted unsaturated carbonyl compounds."

** Present addres: Max-Plank-Institute for Medical Research, Jahnstrasse 29, D-6900 Heidelberg, Germany.

*** Some of the compounds investigated here have been examined IR-spectroscopically by Giza,[4] but poor resolution of the spectra and some uncertainty (and even incorrectness; see footnote of Table 3) of the configurational assignments render those results unreliable.

**** Although the vibrations of the C=O and C=C groups are undoubtedly strongly coupled, the bands will be denoted, for the sake of simplicity, $\nu_{C=O}$ and $\nu_{C=C}$.

Table 1. Wave numbers (cm^{-1}) of absorption bands and probable conformational preferences of *cis* (*Z*) and *trans* (*E*) α,β-unsaturated β-alkoxy ketones, $R^1COCH{=}CR^2OR^3$ in tetrachloroethylene

Compound	R_1	R_2	R_3	Configuration	Concentration (mol/l)	Absorption bands[a] $\nu_{C=O}$ *s-cis* A	$\nu_{C=O}$ *s-trans* B	$\nu_{C=C}$ *s-trans* C	$\nu_{C=C}$ *s-cis* D	Preferred conformation C_{sp^2}–C_{sp^2}	Preferred conformation C_{sp^2}–O
1*Z*	CH_3	CH_3	CH_3	*cis*	0.17	1685	1660	1632	1599	*s-trans*>*s-cis*	*O-s-trans*[b]
1*E*				*trans*	0.09	1689			1590	*s-cis*	*O-s-cis*
2*Z*	CH_3CH_2	CH_3CH_2	CH_3	*cis*	0.16	1684	1659	1631	1598	*s-trans*~*s-cis*	*O-s-trans*[b]
2*E*				*trans*	0.08	1688			1592	*s-cis*	*O-s-cis*
3*Z*	$(CH_3)_2CH$	$(CH_3)_2CH$	CH_3	*cis*	0.13	1684	1658	1627	1596	*s-cis*>*s-trans*	*O-s-trans*[b]
3*E*				*trans*	0.10	1684			1587	*s-cis*	*O-s-cis*
4*Z*	CH_3	CH_3	CH_3CH_2	*cis*	0.19	1683	1657	1630	1608	*s-trans*>*s-cis*	*O-s-trans*[b]
4*E*				*trans*	0.10	1688			1588	*s-cis*	*O-s-cis*
5*Z*	CH_3CH_2	CH_3CH_2	CH_3CH_2	*cis*	0.16	1683	1658	1630	1593	*s-trans*~*s-cis*	*O-s-trans*[b]
5*E*				*trans*	0.09	1686			1587	*s-cis*	*O-s-cis*
6*Z*	$(CH_3)_2CH$	$(CH_3)_2CH$	CH_3CH_2	*cis*	0.15	1683	1658	1628	1589	*s-cis*>*s-trans*	*O-s-trans*[b]
6*E*				*trans*	0.11	1683			1584	*s-cis*	*O-s-cis*
7*Z*	CH_3	CH_3	$(CH_3)_2CHCH_2$	*cis*	0.18	1683	1655	1629	1600	*s-trans*>*s-cis*	*O-s-trans*[b]
7*E*				*trans*	0.12	1687			1587	*s-cis*	*O-s-cis*
8*Z*	$(CH_3)_3C$	CH_3	CH_3	*cis*	0.19	1677			1601	*s-cis*	*O-s-trans*[b]
8*E*				*trans*	0.19	1682			1592	*s-cis*	*O-s-cis*

a) The spectra of all solutions were obtained in a standard cell of thickness 0.1 mm. b) Or non-planar.

Table 2. PMR chemical shifts of *cis* (*Z*) and *trans* (*E*) β-diketone enol ethers (ppm; in CCl_4)

Compound[a]	Acylic protons of R^1 $-\underline{C}-C=O$	$\Delta\delta_Z^E(R^1)$	Allylic protons of R^2 $-\underline{C}-C=C$	$\Delta\delta_Z^E(R^2)$	$\Delta\delta_{R^1}^{R^2}$	Vinylic protons $\underline{H}-C=C$	$\Delta\delta_Z^E$	Ether proton (R^3) $-\underline{C}-O-$	$\Delta\delta_Z^E(R^3)$	Other signals
1*Z*	2.14	−0.10	2.02	+0.17	−0.12	4.98	+0.49	3.82	−0.19	—
1*E*	2.04		2.19		+0.15	5.47		3.63		—
2*Z*	2.53(q)	−0.15	2.31(q)	+0.42	−0.12	5.06	+0.30	3.84	−0.16	0.99(t); 1.13(t)
2*E*	2.38(q)		2.73(q)		+0.35	5.36		3.68		1.03(t); 1.06(t)
3*Z*	2.58(spt)	−0.09	2.35(spt)	+1.64	−0.13	5.23	+0.04	3.80	−0.15	1.02(d); 1.09(d)
3*E*	2.49(spt)		3.99(spt)		+1.50	5.27		3.65		1.00(d); 1.02(d)
4*Z*	2.17	−0.14	2.00	+0.20	−0.17	4.98	+0.48	4.11(q)	−0.25	1.35(t)
4*E*	2.03		2.20		+0.17	5.46		3.86(q)		1.33(t)
5*Z*	2.52(q)	−0.19	2.27(q)	+0.40	−0.15	4.99	+0.27	4.04(q)	−0.22	0.96(t); 1.10(t); 1.30(t)
5*E*	2.33(q)		2.67(q)		+0.34	5.26		3.82(q)		1.04(t); 1.08(t); 1.35(t)
6*Z*	2.57(spt)	−0.13	2.34(spt)	+1.56	−0.23	5.20	+0.01	4.04(q)	−0.24	1.06(d); 1.13(d); 1.29(t)
6*E*	2.44(spt)		3.90(spt)		+1.46	5.21		3.80(q)		1.05(d)[b]; 1.05(d)[b]; 1.35(t)
7*Z*	2.21	−0.19	2.03	+0.19	−0.17	4.90	+0.50	3.81(d)	−0.29	1.05(d)~2.1 multiplet[c]
7*E*	2.02		2.22		+0.20	5.40		3.52(d)		0.97(d)~2.1 multiplet[c]
8*Z*	—	—	1.92	+0.28	—	5.36	+0.24	3.76	−0.13	1.05
8*E*	—		2.20		—	5.60		3.63		1.10

a) See Table 1. b) Two doublets completely overlapped. c) Position difficult to determine because of strong overlap with other signals.

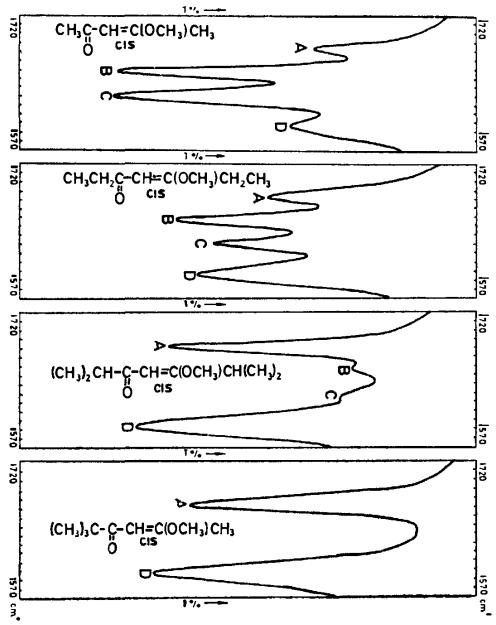

Fig. 1. Infrared spectra of compounds **1** *Z*, **2** *Z*, **3** *Z*, and **8** *Z* in tetrachloroethylene. Cell thicknesses and concentrations are given in Table 1.

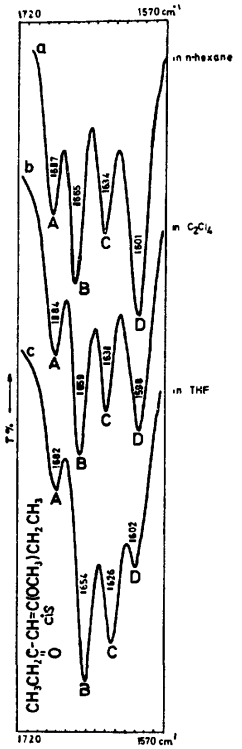

Fig. 2. Infrared spectra of compound **2** *Z*.
a in hexane;
b in tetrachloroethylene;
c in tetrahydrofuran.
Concentrations 0.16 M, cell thicknesses 0.1 mm.

considerable amounts with compound **2** *Z* (R^1=Et). This situation is in contrast with what was found for other *cis* β-substituted unsaturated ketones,[8,9] including the *trans(E)* isomers of the compounds just discussed (*vide infra*) which bear an alkyl *cis* β-substituent and exist entirely as *s-cis* rotamers. This seeming contradiction can reasonably be explained by taking into account the electrostatic repulsion between two oxygen atoms in the alternative *s-cis* conformation. The latter effect, assisted by the greater resonance energy of the *s-trans* structure, seems to account for the preponderance of the *s-trans* rotamer if R^1=Me. Now, both the electrostatic and the resonance factors are practically constant in the whole series under consideration, whereas the non-bonded R^1–OR^3 interactions in the *s-trans* rotamer obviously increase in the sequence, thus satisfactorily explaining the observed equilibrium shift.

The conformational equilibrium is apparently not affected by the size of the substituent R^3: the spectra of compounds **4** *Z*, **5** *Z*, and **6** *Z* with R^3=Et are very similar to those of **1** *Z*, **2** *Z*, and **3** *Z*, respectively, and substitution of R^3=Me by *i*-Bu (compound **7** *Z*) has practically no effect on the relative intensities of the IR bands A—D.

The solvent-induced intensity changes are in agreement with the assignments of the two $\nu_{C=O}$ and two $\nu_{C=C}$ bands: when passing from hexane to tetrachloroethylene and particularly to the considerably more polar tetrahydrofuran solutions, an increase of bands B and C of the more polar *s-trans* form at the expense of the bands A and D is observed (*e.g.*, with R^1=Et a reversal of band intensities occurs; see for **2** *Z* in Fig. 2).

With the *trans(E)* series, only one $\nu_{C=O}$ and one $\nu_{C=C}$ band are observed; their positions clearly indicate that the only observed rotamer is the *s-cis* one (see Fig. 3). This decisive equilibrium shift is obviously due to steric interactions between the R^1 and R^2 alkyl groups in the *s-trans* form:

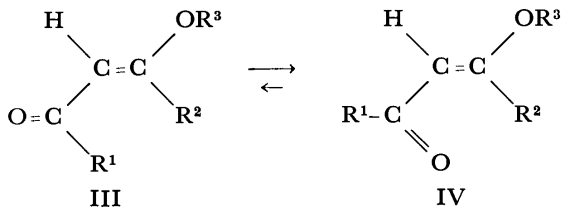

EE (*i.e.*, *trans/s-trans*) *EZ* (*i.e.*, *trans/s-cis*)

It must be noted, however, that in some of the *trans* compounds weak absorptions near wave numbers characteristic of the *s-trans* rotamer are observed (*e.g.*, see Fig. 3). Since the strain energy in the *s-trans* rotamer is extremely high, it is likely that these absorptions are due to a twisted form. In this connection we should like to mention that, in general, some non-planar deformations may occur in many structures termed here *s-cis* or *s-trans*; in this sense, the terms "*s-cis*" and "*s-trans*" have only an approximate meaning.

Unlike the β-keto aldehyde enol ethers,[1] β-diketone enol ethers exhibit no extra splitting of the $\nu_{C=O}$ or $\nu_{C=C}$ bands caused by rotation around the C_{sp^2}–O bond, obviously because of additional steric hindrance. The conformation of the =C(R^2)–OR^3 fragment, though not directly accessible, can be estimated from model considerations and the comparison of $\Delta\nu_{C=C}^{C=O}$ values obtained here with those previously[1] found for all possible *s-cis*, *s-trans*, *O-s-cis*, *O-s-trans* conformational combinations in β-keto aldehyde enol ethers.

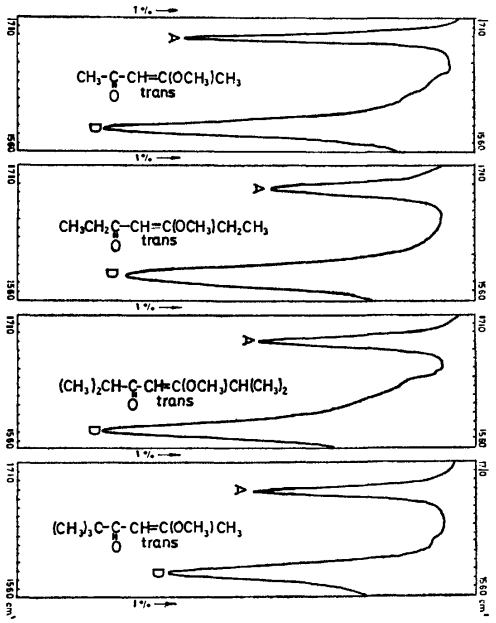

Fig. 3. Infrared spectra of compounds **1** *E*, **2** *E*, **3** *E* and **8** *E* in tetrachloroethylene. Cell thicknesses and concentrations are given in Table 1.

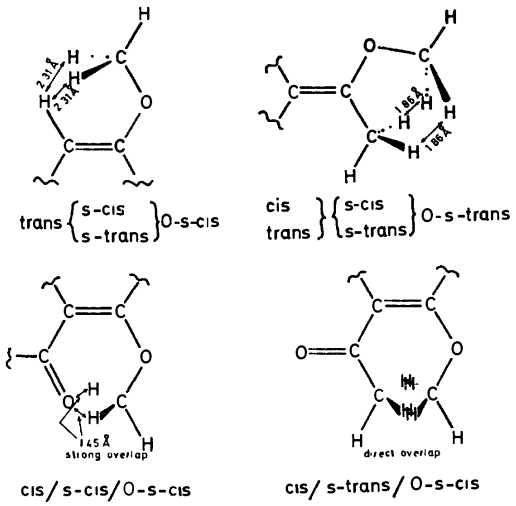

Fig. 4. Interatomic distances in assumed *O-s-cis* and *O-s-trans* conformations of β-methoxy compounds. The orientations of methyl groups were chosen to minimize the Pitzer strain energy.

Thus, there is obviously a much weaker non-bonded interaction in the *trans/s-cis/O-s-cis* isomer than in the *trans/s-cis/O-s-trans* one (see formula IV), with the alternative H–H interatomic distance amounting to 2.31 Å *vs.* 1.86 Å (see Fig. 4).† Besides, the *O-s-cis* rotamer is strongly preferred here for electronic reasons.[1,12] Correspondingly, as can be derived from the data of Table 1, the $\Delta\nu_{C=C}^{C=O}$ values lie within the limits of 90—100 cm^{-1}, in excellent agreement with the previous estimation[1] of 80—100 cm^{-1} while the alternative *O-s-trans* conformation requires 75—85 cm^{-1}.

As for the *cis* structures I and II, steric hindrance is important in both *O-s*-conformations, being particularly pronounced in the *O-s-cis* one where a direct overlap of the nearest non-bonded atoms should occur (see Fig. 4). Hence, the anticipated conformation is *O-s-trans*.†† It was of interest to clear up whether the regularities concerning the wave number differences $\Delta\nu_{C=C}^{C=O}$ in the *trans* series[1] hold also for the *cis* isomers. The agreement is again very good as far as the *s-trans* conformation is concerned: the values now found (26—31 cm^{-1}) lie almost exactly within the limits previously established[1] (20—30 cm^{-1}), whereas 35—50 cm^{-1} was found[1] for the alternative *O-s-cis* conformation. On the other hand, the results for the *s-cis* rotamers are less favorable: although the majority of the *O-s-trans* rotamers II exhibit lower $\Delta\nu_{C=C}^{C=O}$ values as compared with the *O-s-cis* rotamers IV (75—94 cm^{-1} *vs.* 90—100 cm^{-1})—a tendency already noticed for keto aldehyde enol ethers, the upper limit of the range now observed (75—94 cm^{-1}) is moved by 9 cm^{-1} above that found[1] for the latter compounds (75—85 cm^{-1}).

PMR Spectra. With the exception of compounds **8** *Z* and *E*, all the enol ethers studied here contain identical groups $R^1=R^2$, thus the assignment of their signals posed some problems. Anteunis and Schamp[5] examined several unsymmetrically substituted enol ethers ($R^1\neq R^2$) and were able to establish the "ene-one rule", from which it follows that α protons of the R^2 group resonate at lower field than α protons of the R^1 group. While Anteunis and Schamp[5] were not aware of the *trans* configuration of the compounds studied, it was shown subsequently by Gelin and Rouet[6] that the "ene-one rule" holds for the *trans* structures only, whereas an opposite assignment is true for the *cis* configuration. Assignments coinciding with those by Gelin and Rouet were made by Awang[3] for **1** *E* and *Z* and (apparently intuitively) by Elvidge and Stevens[7] for **2** *E* and *Z*.

Since the term "ene-one rule" refers to the original incomplete assignments by Anteunis and Schamp[5] and might thus be misleading, it seems appropriate to rename the rule as the "ene-one cross-shielding rule". Terminologic problems aside, it should be emphasized that no rationalization was offered for the rule in either of the papers mentioned. The eight *E*, *Z* pairs of compounds, the conformational equilibria of which were established rather reliably, permit us to propose an explanation of the observed phenomena.

Let us consider first the *trans(E)* isomers of compounds **1**—**7** which, as shown above, all have the *s-cis* conformation (see formula IV on p. 983). Compared with the usual allylic protons, the "ene-side" protons of R^2 are additionally deshielded by both the carbonyl and ether oxygens, whereas the magnetic environment of the "one-side" α-protons is practically the same as in the case of typical acylic groups. The resulting

† For details, see our previous paper;[1] the bond lengths and angles have been taken from the paper by Cahill *et al.*[10] and from the tables.[11] As before, the calculations are for $R^1=R^2=R^3=Me$.

†† It is likely that deviations from planarity may occur not only in the O=C–C=C fragment (*vide supra*) but also in the C=C–OR moiety.

lower-field absorption of R^2 *vs.* R^1 is thus readily explainable. The role of the deshielding of R^2 caused by the carbonyl group is further substantiated by the fact that the δ values increase along with the progressing branching of this substituent:

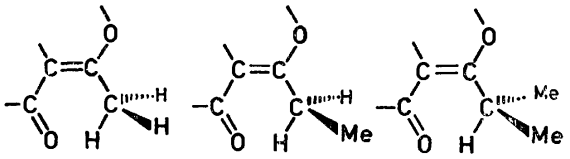

R^2=Me R^2=Et R^2=*i*-Pr

While the deshielding produced by this group, measured as $\Delta\delta_{R^1}^{R^2}$†††, is assumed to be evenly distributed between the three protons of the rotating methyl group, the average effect should be statistically 3/2 and 3 times greater with R^2=Et and R^3=*i*-Pr, respectively, the rotation of these two groups being severely restricted. The observed increase is in fact even greater, $\Delta\delta_{R^1}^{R^2}$ amounting to 0.15, 0.17 and 0.20 ppm for R^2=Me, 0.35, and 0.34 ppm for R^2=Et, and 1.50 and 1.46 ppm for R^2=*i*-Pr†††† (see Table 2). This extra increase of $\Delta\delta_{R^1}^{R^2}$ is explainable in terms of a buttressing effect resulting from the interaction between the ether oxygen and the methyls in R^2=Et and R^2=*i*-Pr.

It seems worth noticing that the deshielding of the methine protons of the isopropyl group in **3** *E* and **6** *E* is so strong as to produce a low-field shift even greater than that observed for the α protons of the R^3 group attached to the ether oxygen.

In the *cis(Z)* isomers R^2 is no longer deshielded by the carbonyl oxygen, so it is natural that the acylic protons absorb, as usual, at lower fields than the allylic ones, *i.e.*, $\Delta\delta_{R^1}^{R^2}$ values are negative. These differential shifts are expected to be more negative in the case of the *s-trans* rotamer, due to additional deshielding of R^1 by the alkoxy and olefinic groups. In this connection it might seem surprising that the branching of R_1, which was shown※ to shift the rotational equilibrium towards the *s-cis* isomer and can thus be anticipated to reduce the additional deshielding just mentioned, leaves the $\Delta\delta_{R^1}^{R^2}$ practically unaffected (see Table 2). It must be taken into account, however, that such branching simultaneously affects the shielding in the opposite direction by a mechanism similar to that discussed above for the *trans* isomer, *i.e.*, by restricting the rotation of the R^1

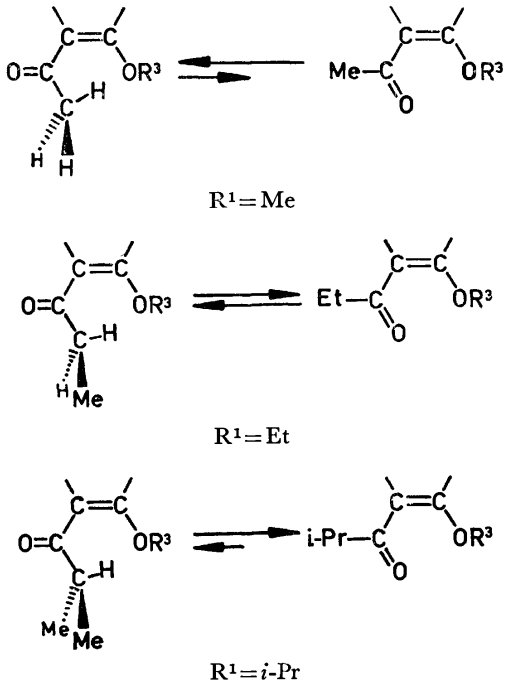

R^1=Me

R^1=Et

R^1=*i*-Pr

The two effects are apparently compensated in this way.

As for the other NMR signals, only those of the R^3 group seem to be informative. Since the branching of R^1 affects the *s-cis*⇌*s-trans* equilibrium, the constancy of the $\Delta\delta_z^E(R^3)$ values within the two series of compounds containing fixed R^3 and varying R^1 suggest that deshielding of R^3 by the carbonyl group in the *cis*/*s-cis* isomer does not play any marked role. Thus, the *cis*/*O-s-trans* or non-planar conformation proposed in the IR part of the present paper receives additional support.

Experimental

cis(Z) *Isomers*: *4-methoxy-3-penten-2-one* (*1* Z), *5-methoxy-4-hepten-3-one* (*2* Z), *and 5-methoxy-2,6-dimethyl-4-hepten-3-one* (*3* Z) were prepared from acetylacetone, dipropionylmethane[13], or diisobutyrylmethane,[14] by treatment with diazomethane as follows: to an excess of an ethereal solution of diazomethane[15] was added 0.05 M of diketone and 10 ml of methanol. The mixture was allowed to stand in dark for 16 h (with **1** *Z* and **2** *Z*) or 24 h (with **3** *Z*). The ether and the unchanged diazomethane were evaporated. Twofold vacuum distillation afforded fairly pure **1** *Z*, bp 37 °C (0.5 Torr), lit,[2] 84—86 °C (10 Torr), lit,[3] 56—58 °C (3.5 Torr), new compounds; data given in Table 3.

cis(Z) *5-Methoxy-2,2-dimethyl-4-hexen-3-one* (*8* Z): The reaction of pivaloylacetone[13] with diazomethane was carried out analogously for 24 h. The fractionate distillation *in vacuo* gave a mixture of isomers (which was not worked up) and an oil which solidified immediately. The resulting solid was pressed on porous porcelain and sublimed two times at 0.3 Torr to yield pure **8** *Z*.

The analogous reaction of diazoethane[15] with acetylacetone, dipropionylmethane, and diisobutyrylmethane in the presence of methanol (reaction time 16 h) gave after sublima-

††† Since R^1=R^2, the use of the differential shifts $\Delta\delta_{R^1}^{R^2}=\delta_R{}^2-\delta_R{}^1$ allows one to eliminate the difficulty arising from the necessity of comparing the methyl, methylene, and methine protons of R^2.

†††† In order to estimate the deshielding effect of the carbonyl group exerted upon R^2 another differential value concerning the resonance of this group only, *viz.*, $\Delta\delta_z^E$, can be used equally successfully. Indeed, the δ_Z values are good reference points for each of the homologues, as they are influenced by all the deshielding factors, the δ_E values are, except for the contribution of the carbonyl group, just now to be found. Numerically, $\Delta\delta_{R^1}^{R^2}$ and $\Delta\delta_E^Z(R^2)$ are very close.

※ See the part concerning IR spectra.

Table 3. Physical properties and analytical data

Compound	Bp (°C)	Mp (°C)	%C		%H	
			Calcd	Found	Calcd	Found
2*Z*	51 (0.8 Torr)	—	67.57	67.29	9.93	9.91
2*E*	41 (0.8 Torr)	—				
3*Z*	52 (0.8 Torr)	—	70.54	70.60	10.66	10.78
3*E*	45 (0.8 Torr)	—				
4*Z*	—	41	65.59	65.56	9.44	9.38
4*E*[a]	76 (15 Torr)	—				
5*Z*	58 (0.8 Torr)	—	69.19	69.20	10.32	10.26
5*E*	42 (0.4 Torr)	—				
6*Z*	53 (0.7 Torr)	—	71.69	71.33	10.94	10.73
6*E*	107 (15 Torr)	—				
7*Z*	53 (0.7 Torr)	—	69.19	69.19	10.32	10.46
7*E*	61 (2 Torr)	—				
8*Z*	—	64	69.19	69.01	10.32	10.30
8*E*	41 (1.3 Torr)	—				

Bp and mp were not corrected. a) This *trans*(*E*) compound was described incorrectly by Giza[4] to have a *cis*(*Z*) configuration.

tion *4-ethoxy-3-penten-2-one* (**4** *Z*) and, after distillation, *5-ethoxy-4-hepten-3-one* (**5** *Z*) and *5-ethoxy-2,6-dimethyl-4-hepten-3-one* (**6** *Z*), respectively.

A similar treatment of acetylacetone with 1-diazo-2-methylpropane[15] and methanol yielded *4-isobutoxy-3-penten-2-one* (**7** *Z*).

All the *trans*(*E*) compounds **1**—**8** *E* were prepared by isomerization of their *cis*(*Z*) isomers: the solution of a *cis*(*Z*) isomer in CCl_4 was refluxed for a few hours, then the solvent was removed and the product was distilled *in vacuo*; data given in Table 3.

The physical properties and analytical data of the new compounds and of those whose configuration was not established previously to this paper are given in Table 3.

The structures of all the compounds **1**—**8** *Z* and **1**—**8** *E* were confirmed by NMR spectra (see Table 2). The structures of the unsymmetrical compounds **8** *Z* and *E* were checked additionally by reduction with lithium aluminium hydride:[16] to a suspension of an excess of $LiAlH_4$ in ether was added **8***E* and the mixture was refluxed for 1.5 h. Water and aqueous potassium hydroxide were added and the mixture was filtered off. The ethereal layer was dried over KOH pellets and worked up in the usual manner to yield *5-methoxy-2,2-dimethyl-4-hexen-3-ol* bp 44—45 °C (0.5 Torr). NMR (δ, ppm in $CDCl_3$): 4.53, d, 1H; 3.50, s, 3H; 1.82, s, 3H; 0.90, s, 9H.

Infrared spectra were recorded on a Perkin-Elmer 325 spectrophotometer with a spectral slit width of 0.7—0.9 cm^{-1} and a scanning speed of 0.25 $cm^{-1}\,s^{-1}$. Commercial "for spectroscopy" solvents were used. The substances investigated were freshly distilled or sublimed before the measurements, and the middle fraction was used. The spectra were calibrated with polystyrene.

NMR spectra were recorded on Varian HA-60/IL and JEOL JNM-4H-100 instruments.

This work is a part of the Polish Academy of Sciences Programme for Structural Research (PAN-3).

References

1) J. Dabrowski and M. Tencer, *Bull. Chem. Soc. Jpn.*, **48**, 1310 (1975).
2) B. Eistert, F. Arndt, L. Loewe, and E. Ayca, *Chem. Ber.*, **84**, 156 (1951).
3) D. V. C. Awang, *Can. J. Chem.*, **49**, 2672 (1971).
4) V. C. Giza, Dissertation, Univ. of Massachusetts, Amherst, Univ. Microfilms, Order No. 64-7123.
5) M. Anteunis and N. Schamp, *Bull. Soc. Chim. Belges*, **76**, 330 (1967).
6) S. Gelin and J. Rouet, *Bull. Soc. Chim. Fr.*, **1971**, 2179.
7) J. A. Elvidge and R. Stevens, *J. Chem. Soc.*, **1965**, 2256.
8) (a) E. A. Braude and C. J. Timmons, *J. Chem. Soc.*, **1955**, 3766; (b) E. S. Waight and R. L. Erskine, "Steric Effects in Conjugated Systems," Butterworths, London (1958), p. 73; (c) R. L. Erskine and E. S. Waight, *J. Chem. Soc.*, **1960**, 3425; (d) R. Mecke and K. Noack, *Chem. Ber.*, **93**, 210 (1960); (e) K. Noack and R. N. Jones, *Can. J. Chem.*, **39**, 222 (1961); (f) J. Kossanyi, *Bull. Soc. Chim. Fr.*, **1965**, 704; (g) R. Barlet, M. Montagne, and P. Arnaud, *Spectrochim. Acta*, **25A**, 1081 (1969); (h) A. Bienvenue, *J. Am. Chem. Soc.*, **95**, 7345 (1973).
9) (a) J. Dabrowski and K. Kamienska-Trela, *Spectrochim. Acta*, **22**, 211 (1966); (b) J. Dabrowski and U. Dabrowska, *Chem. Ber.*, **101**, 3392 (1968); (c) J. Dabrowski and K. Kamienska-Trela, *Bull. Chem. Soc. Jpn.*, **39**, 2565 (1966); (d) J. Dabrowski and J. Terpinski, *J. Org. Chem.*, **31**, 2159 (1966); (e) J. Dabrowski, K. Kamienska-Trela, and A. J. Sadlej, *J. Mol. Struct.*, **12**, 185 (1972).
10) P. Cahill, L. P. Gold, and N. L. Owen, *J. Chem. Phys.*, **48**, 1620 (1968).
11) Landolt-Bornstein, "Zahlenwerte und Funktionen aus Physik, Chemie···," 2-Teil, Molekeln 1, Springer-Verlag, Berlin (1951), pp. 10—20.
12) B. Cadioli and M. Pinceli, *J. Chem. Soc., Faraday Trans. 2*, **1972**, 991.
13) J. T. Adams and C. R. Hauser, *J. Am. Chem. Soc.*, **66**, 1220 (1944).
14) T. Shigematsu, M. Matsui, and K. Utsunomiya, *Bull. Inst. Chem. Res., Kyoto Univ.*, **46**, 256 (1968).
15) B. Eistert, M. Regitz, G. Heck, and H. Schwall, "Methoden der Organischen Chemie," Vol. 10/4, ed. by Houben-Weyl, Georg Thieme-Verlag Stuttgart, West Germany (1968), pp. 537—540.
16) M. Stiles and A. L. Longroy, *J. Org. Chem.*, **32**, 1095 (1967).

New Red Pentaamminenitrosylcobalt(III) Complexes Obtained by the Reaction of a Cobalt(II)-ammoniacal Solution with Nitrogen Oxide

Eiichi MIKI* and Tatsujiro ISHIMORI

Department of Chemistry, College of Science, Rikkyo University, 3-Chome, Nishi Ikebukuro, Toshima-ku, Tokyo 171

(Received July 16, 1975)

New Red Pentaamminenitrosylcobalt(III) chloride and nitrate, $[Co_2(N_2O_2)(NH_3)_{10}]Cl_4\cdot 4H_2O$ and $[Co_2(N_2O_2)(NH_3)_{10}](NO_3)_4\cdot 2H_2O$ were prepared by the reaction of NO at *ca.* 0 °C with a cobalt(II)-ammoniacal solution which had been exposed to air for 20 h at *ca.* 20 °C. Data of the new red salts were compared with those of the red salt $[Co_2(N_2O_2)(NH_3)_{10}](NO_3)_4\cdot H_2O$ prepared by Sand and Genssler. The new red salt may be considered to be a linkage isomer of the red salt, a binuclear complex in which two of the $Co(NH_3)_5$ groups are bridged through a dimer of nitrosyl group, $N\text{–}O\text{–}O\text{–}N^{2-}$ ion.

Extensively studies have been carried out on the black and red series of compounds with the composition $Co(NH_3)_5(NO)X_2$ (X=Cl, Br, I, and NO_3) since they were first prepared by Sand and Genssler by the reaction of a cobalt(II)-ammoniacal solution with NO gas.[1] Recent X-ray diffraction studies have shown that the black salt $[Co(NO)(NH_3)_5]Cl_2$ is a monomer,[2] and the red one $[Co_2(N_2O_2)(NH_3)_{10}](NO_3)_4\cdot H_2O$ (Red salt I) is a binuclear complex in which two cobalt atoms are bridged through a *cis*-hyponitrite ion, one cobalt atom being bound to the oxygen atom and the other to the nitrogen atom.[3]

We prepared new red-pentaamminenitrosylcobalt(III) chloride and nitrate (Red salt II), $[Co_2(N_2O_2)(NH_3)_{10}]Cl_4\cdot 4H_2O$ and $[Co_2(N_2O_2)(NH_3)_{10}](NO_3)_4\cdot 2H_2O$ by the reaction of a ammoniacal cobalt(II)-solution with NO gas.[4] Molar conductivities, UV spectra, ^{15}N-isotopic effects on IR spectra upon ^{15}NO-substitution, and ^{15}N-NMR spectra were measured for Red salt I and II. Red salt II is considered to be a new type of compound containing a dimer of nitrosyl, $N\text{–}O\text{–}O\text{–}N^{2-}$ ion.

Experimental

Preparations. *Red Salt I (Nitrate)*: The compound was prepared according to the method of Moeller and King,[5] and could be recrystallized from a dilute ammoniacal solution and dimethyl sulfoxide (DMSO). Found: Co, 19.2; N, 36.1; H, 4.93; NH_3, 28.4%. Calcd for $[Co_2(N_2O_2)(NH_3)_{10}](NO_3)_4\cdot H_2O$: Co, 19.19; N, 36.49; H, 5.09; NH_3, 27.73%. The ^{15}NO-complexes (^{15}N atom %=50 and 99) were synthesized in a vacuum line; 4 ml of concentrated ammonia was added to a solution of cobalt (II) salt (2 g of $Co(NO_3)_2\cdot 6H_2O$/9 ml of H_2O) at room temperature. The fresh filtrate was degassed with nitrogen, evacuated, and kept at 20 °C in a reaction vessel. 5 mmol of ^{15}NO was introduced at 20 °C into the ammoniacal solution and allowed to stand for 4 hr. Resulting red precipitates were collected by filtration, washed with concentrated ammonia, methyl alcohol, and ether, succesively, and dried in air. Yield, 50—200 mg.

Red Salt I (Chloride): The compound was prepared from Red salt I (nitrate) by stirring its aqueous solution with anion exchange resins of a chloride-ion form, and then adding a large excess of ammonium chloride to the filtrate. Found: Co, 22.4; N, 31.2; H, 5.71; Cl, 24.3%. Calcd for $[Co_2(N_2O_2)(NH_3)_{10}]Cl_4\cdot 2H_2O$: Co, 22.4; N, 31.9; H, 6.52; Cl, 27.0%.

Red Salt II (Chloride and Nitrate): Red salt II was prepared by the following procedure; 15 ml of ice-cooled concentrated ammonia was added to a cobalt(II) chloride or nitrate solution (5 g of the cobalt(II) salts/20 ml of H_2O) at *ca.* 0 °C. The solution was then exposed to air for 20 h at *ca.* 20 °C. The filtrate thus obtained was poured into a reaction vessel and degassed with nitrogen. Nitrogen oxide was passed into the solution cooled with an ice-water bath to obtain red precipitates. Yield, *ca.* 1 g. Red salt II (chloride) could be recrystallized only from an ice-cooled aqueous solution, and not from an ammoniacal solution. Red salt II (nitrate) could be recrystallized from an ice-cooled aqueous solution and from DMSO. The ^{15}NO-complexes (^{15}N atom %=50 and 99) were synthesized in a vacuum line; by cooling with liquid nitrogen, 5 mmol portion of ^{15}NO was trapped in a reaction vessel containing the ammoniacal cobalt (II) solution (*ca.* 4 g of the chloride or the nitrate/*ca.* 5M ammonia) which had been exposed to air for 20 hr at *ca.* 20 °C. The reaction vessel was shaken under running water until the frozen solution thawed, and was kept at *ca.* 0 °C for 1 hr to obtain the ^{15}NO-complex. Yield, 300—400 mg. The ^{2}H-complex was prepared by use of deuterated ammonia which was obtained by the reaction of magnesium nitride with heavy water. Found: Co, 21.5; N, 30.8; H, 5.4 (± 1.0)[6]; NH_3, 32.0; Cl, 25.2%. Calcd for $[Co_2(N_2O_2)(NH_3)_{10}]Cl_4\cdot 4H_2O$: Co, 20.97; N, 29.90; H, 6.81; NH_3, 30.30; Cl, 25.23%. $\chi_g=-0.170\times 10^{-6}$ (at 117 K), -0.193×10^{-6} (at 157 K), -0.262×10^{-6} (at 244 K), and -0.276×10^{-6} (at 288 K) (c. g. s.). Preparation of the $N^{18}O$-complex of Red salt II (chloride) was attempted by the use of $N^{18}O$ prepared by a reduction of $N^{18}O_2$ (^{18}O atom %=*ca.* 50) using selenium metal. However, the isotopic labeling of the nitrosyl group with ^{18}O was unsuccessful. Found: Co, 18.9; N, 33.63; H, 4.6 (± 1.0)[6]; NH_3, 27.2%. Calcd for $[Co_2(N_2O_2)(NH_3)_{10}](NO_3)_4\cdot 2H_2O$: Co, 18.64; N, 35.44; H, 5.42; NH_3, 26.94%.

Measurements. The UV spectra in an aqueous solution and in DMSO (Dotite Spectrosol) were measured with a Hitachi 124 spectrometer and the diffuse reflection spectra with a Hitachi EPS-3T spectrometer. The molar conductivities in an aqueous solution (at 2.5 °C) and in DMSO (at 25 °C) were measured with a universal bridge (Model 4225A of Yokogawa-Hewlett-Packard Ltd.). The IR spectra of Red salt I and II were measured in the region 200—4000 cm^{-1} with JASCO DS-402G and JASCO model IR-F spectrometers as Nujol and hexachlorobutadiene mulls. The wave numbers of the observed IR bands were calibrated with polystyrene

* Present address: Department of Chemistry, The University of Texas at Austin, Austin, Texas 78712

film, 1,2,4-trichlorobenzene, and water vapor. The differential thermal analyses were performed with a DTA standard-type apparatus of Rigaku Denki Co. Ltd., Gaseous products obtained by the decomposition of Red salt I and II were trapped in a calcium difluoride gas cell with the aid of liquid nitrogen, and were identified from their IR bands.[7] Solid products obtained by dissolving Red salt II in ammonia or water and adding ammonium chloride or acetone to the solution were identified on the basis of their IR spectra[7] and elementary analyses. The Raman spectra for Red salt I (nitrate) and Red salt II (chloride) of the powdered samples and of the rotating potassium bromide disk were measured in the region 650—1700 cm^{-1} on a JASCO R-800 spectrometer equipped with an Ar ion laser, and on a Narumi 750Z-1200 double monochrometer equipped with a He-Ne laser. The magnetic susceptibility was measured by the Gouy method in the temperature range 120—290 K. ^{15}N-NMR spectra of the ^{15}NO-complex (^{15}N atom %=99) or Red salt II (nitrate) in DMSO-d^6 (*ca.* 0.2 g/2 ml) were measured on JEOL JNM-PS-100/PFT-100 FT-NMR system.

Results and Discussion

Red salt II could be prepared at *ca.* 0 °C by the reaction of nitrogen oxide with ammoniacal cobalt(II) solution which had been exposed to the air for 20 h at *ca.* 20 °C. It has been reported that when an ammonical cobalt(II) solution is exposed to the air, some binuclear cobalt(III) ammine complexes containing peroxo, superoxo, or amide groups are likely to be formed,[8] and reactions of these complexes with nitrogen oxide give μ-nitro or μ-nitrato complexes.[9] However, there was no spectroscopic evidence that the μ-nitro or μ-nitrato complexes were formed under the conditions for preparation of Red salt II. A mixture of $[Co(NO)(NH_3)_5]X_2$ and Red salt II was formed but not Red salt I when the time of exposure was less than 20 h and the temperature of the solution was kept below *ca.* 20 °C. No precipitate was obtained nor did the yield of Red salt II decrease when the time of exposure exceeded 20 h and the temperature of the ammoniacal solution was above 20 °C. A mixture of Red salt I and II was obtained when nitrogen oxide, without being fully cooled in an ice-water bath, was passed in the ammoniacal solution which had been exposed to air at 20 °C for 20 h. Red salt I seems to be prepared through the black isomer.[10] It might be possible that the black isomers dimerise to give Red salt II. Another possibility that Red salt II is formed by the reaction of nitrogen oxide with the peroxo complex formed when the cobalt(II)-ammoniacal solution has been exposed to air cannot be excluded. The temperature in the reaction of the ammoniacal cobalt solution with nitrogen oxide might control the formation of Red salt I or Red salt II.

The failure to label the nitrosyl group in Red salt II with ^{18}O is considered to be due to the fact that oxygen of the nitrosyl group is rapidly exchanged with oxygen in the ammoniacal solution.

UV Spectra and Molar Conductivities. The UV spectra for Red salts I and II in an aqueous solution were nearly the same as those in DMSO, and their spectral figures were also similar to those of the diffuse reflection spectra as shown in Table 1.

Table 1. UV spectra of red salts I and II in the solid state and in solution

Complexes	in H_2O		in DMSO		in solid state	
	position of band (in cm^{-1})	log ε	position of band (in cm^{-1})	log ε	position of band (in cm^{-1})	log $f(R)$
Red salt I (nitrate)	20700	1.50	20800	1.28	20700	2.03
	35100	4.05	a)			
	38300	4.15	a)			
Red salt II (chloride)	20300	1.28			20200	1.99
	31000	2.82				
	38000	3.48	insoluble			
	42000	4.08				
Red salt II (nitrate)	20600	1.38	20600	1.18	20500	1.51
	31200	2.91	31000	2.91		
	39000	3.74	a)			
	42000	4.30	a)			

a) These bands could not be measured due to the strong absorption of DMSO.

The molar conductivities of Red salts I and II were compared with those of 4: 1-, 3: 1-, and 2: 1-type electrolytes by the method of Feltham and Hayter.[11] In an aqueous solution at 2.5 °C, the molar conductivities at infinite dilution of Red salt I(nitrate), Red salt II(nitrate), and Red salt II(chloride) were 333, 358, and 366 $ohm^{-1}cm^2$, respectively, while those of $K_4[Fe(CN)_6]$, $[Cr(NH_3)_6](ClO_4)_3$, and $K_2[RuBr_5(NO)]$ were 386, 283, and 164 $ohm^{-1}cm^2$, respectively. The result for Red salt I supports that obtained by Feltham.[12] In DMSO at 25 °C, the molar conductivities at infinite dilution of Red salt I(nitrate) and Red salt II(nitrate) were 142 and 169 $ohm^{-1}cm^2$, and those of $[(CH_3)_4N]_4[RuCl(SnCl_3)_5]$, $[Co(phen)_3](ClO_4)_3$, and $[Ru(phen)_3](ClO_4)_2$ were 140, 115, and 77 $ohm^{-1}cm^2$, respectively.

Studies based on the UV spectra and molar conductivities show that Red salt II is a 4: 1-type electrolyte as well as Red salt I, and that the structure of the cationic ions in the solid states of Red salts I and II can be kept in aqueous and DMSO solutions.

Products Obtained by the Decomposition of Red Salts I and II. Gaseous Products Obtained by Thermal and Acid Decompositions of Red Salts I and II: Differential thermal analyses in atmosphere showed that for Red salt I(nitrate) an endothermic peak was observed at 143 °C, a violent exothermic reaction following at 180 °C. For Red salt II (chloride) an endothermic reaction began at 220 °C and a violent exothermic one followed at 260 °C, and for Red salt II(nitrate) an endothermic reaction at 150 °C and a violet exothermic one at 180 °C. These endothermic reactions are considered to correspond to the liberation of water of crystallization. Red salts I and II darkened at *ca.* 180 °C in a vacuum. Red salt II(chloride) was completely decomposed at 210 °C in a vacuum to give a blue powder, $CoCl_2$. Gaseous analyses by the IR spectra showed that NH_3, N_2O, and water vapor were liberated when Red salts I and II were heated in a vacuum up to 350 °C at a rate of *ca.* 10 °C/min in an electric furnace. A small amount of NO was also detected. However, $^{15}NH_3$ could not be identified in the gaseous decomposition

Table 2. Nitrosyl chloride and dinitrogen oxide from acid and thermal decompositions of red salts I and II

Compounds		Acid		Thermal[a]
Red salt I (nitrate)	^{14}NO-complex	6M H_2SO_4	$^{14}N^{14}NO$	$^{14}N^{14}NO$
		6M HCl	$^{14}N^{14}NO$, $^{14}NOCl$	
	^{15}NO-complex (^{15}N atom%=99)	6M H_2SO_4	$^{15}N^{15}NO$	$^{14}N^{14}NO$(1)
				$^{15}N^{15}NO$(1.5)
	^{15}NO-complex (^{15}N atom%=50)			$^{14}N^{14}NO$(1.6)
				$^{15}N^{14}NO$(1.5)
				$^{14}N^{15}NO$(1.2)
				$^{15}N^{15}NO$(1)
	Mixture of ^{14}NO-complex and ^{15}NO-one (^{15}N atom%=99) (1:1)			$^{14}N^{14}NO$(1.4)
				$^{15}N^{15}NO$(1)
Red salt II (nitrate)	^{14}NO-complex	6M H_2SO_4	$^{14}N^{14}NO$	$^{14}N^{14}NO$
		6M HCl	$^{14}NOCl$, $^{14}N^{14}NO$	
	^{15}NO-complex (^{15}N atom%=98)			$^{14}N^{14}NO$(2.3)
				$^{14}N^{15}NO$(1)
Red salt II (chloride)	^{14}NO-complex	6M H_2SO_4	$^{14}NOCl$, $^{14}N^{14}NO$	$^{14}N^{14}NO$
		6M HCl	$^{14}NOCl$, $^{14}N^{14}NO$	
	^{15}NO-complex (^{15}N atom%=99)	6M H_2SO_4	$^{15}NOCl$, $^{15}N^{15}NO$	$^{14}N^{14}NO$(0.3) $^{14}N^{15}NO$(1)
	^{15}NO-complex (^{15}N atom%=50)			$^{14}N^{14}NO$(1.5)
				$^{14}N^{15}NO$(1)
	Mixture of ^{14}NO-complex and ^{15}NO-one (^{15}N atom%=99) (1:1)			$^{14}N^{14}NO$(1.4)
				$^{14}N^{15}NO$(1)

a) The values in parentheses indicate the relative ratio of the amount of dinitrogen oxide.

product of the ^{15}NO-complexes of Red salts I and II. The results obtained are summarized in Table 2. $^{14}N^{14}NO$ and $^{14}N^{15}NO$ were derived from the ^{15}NO-complexes(^{15}N atom%=50 and 99) of Red salt II and from a mixture of the ^{14}NO- and ^{15}NO-complexes-(^{15}N atom%=99)(1:1) of Red salt II. On the other hand, $^{14}N^{14}NO$ and $^{15}N^{15}NO$ were derived from the ^{15}NO-complex(^{15}N atom%=99) of Red salt I and from a mixture of the ^{14}NO- and ^{15}NO-complexes(^{15}N atom%=99)(1:1) of Red salt I. $^{14}N^{14}NO$, $^{15}N^{14}NO$, $^{14}N^{15}NO$, and $^{15}N^{15}NO$ were observed in the ^{15}NO-complex (^{15}N atom%=50) of Red salt I.

Studies on a catalytic reaction of ^{15}NO with a large excess of $^{14}NH_3$ at 200—250 °C on platinum supported on alumina have shown that the reaction products and their relative ratios are $^{15}N^{15}NO$: $^{15}N_2$:$^{14}N^{15}N$:$^{14}N^{15}NO$ =32:6:50:13, and that a considerable amount of $^{14}N^{15}NO$ was obtained but no $^{15}N^{14}NO$ was detected.[13]

The thermal decomposition of ^{15}NO-complex(^{15}N atom%=99) of Red salt I(nitrate) gave $^{14}N^{14}NO$ and $^{15}N^{15}NO$, but not $^{14}N^{15}NO$. The $^{14}N^{14}NO$ from the ^{15}NO-complex of Red salt I(nitrate)(^{15}N atom%=99) probably arise as a by-product in the thermal decomposition; the $^{14}N^{14}NO$ contains two nitrogen atoms which come from the nitrogen of ammines and nitrate ions in this complex. The $^{14}N^{14}NO$ thus obtained occupied *ca.* 40% in all of the N_2O. The relative ratios of $^{14}N^{14}NO$: $^{15}N^{14}NO$: $^{14}N^{15}NO$: ^{15}N-^{15}NO from the hyponitrite ion in the ^{15}NO-complex (^{15}N atom%=50) of Red salt I(nitrate) became 1:1.4:1.2:1, and those of $^{14}N^{14}NO$: $^{15}N^{15}NO$ from the mixture of the ^{14}NO- and ^{15}NO-complexes(^{15}N atom%=99)(1:1) became 1:1.2. If the dinitrogen oxide exclusively comes from the hyponitrite ion in Red salt I without the N–N bond cleavage, the relative ratios of the mixture of $^{14}N^{14}NO$, $^{15}N^{14}NO$, $^{14}N^{15}NO$, and $^{15}N^{15}NO$ derived from the ^{15}NO-complex(^{15}N atom%=50) will be 1:1:1:1, and those of $^{14}N^{14}NO$ and $^{15}N^{15}NO$ from the mixture of ^{14}NO- and ^{15}NO-complexes(^{15}N atom%=99)(1:1) will be 1:1. It is hardly conceivable that the hyponitrite ion in Red salt I(nitrate) is decomposed to give nitrogen oxide, and the nitrogen oxide thus obtained reacts with NH_3.

The $^{14}N^{15}NO$ from the ^{15}NO-complex(^{15}N atom%=99) of Red salt II(chloride and nitrate) suggests the presence of the reaction of ^{15}NO with an excess of coordinated ammonia in these compounds. The ^{14}N-^{14}NO from the ^{15}NO-complex(^{15}N atom%=99) of Red salt II(chloride) seems to arise from oxidation of the $^{14}NH_3$. The $^{14}N^{14}NO$ as a by-product occupied *ca.* 20% of the total N_2O. The relative ratio of $^{14}N^{14}NO$ and $^{14}N^{15}NO$ from the nitrosyl group in the ^{15}NO-complex(^{15}N atom%=50) of Red salt II(chloride) became 1.2:1, and that of $^{14}N^{14}NO$ and $^{14}N^{15}NO$ from

the mixture of the ^{14}NO- and ^{15}NO-complexes(^{15}N atom%=99)(1:1) became 1:1. These isotopic studies suggest that the coordinated nitrosyl groups react with the NH_3 groups to give the dinitrogen oxide. The ratio, the dinitrogen oxide as the by-product to all the dinitrogen oxide derived from Red salt II(nitrate) was about 40%, showing that a considerable amount of the dinitrogen oxide is derived from the reaction of the coordinated NH_3 groups with the nitrate ions.

Table 2 also shows the gaseous products obtained by acid decomposition which is milder than the thermal one. The ^{15}NO-complex (^{15}N atom%=99) of Red salt II(chloride) was decomposed by addition of 6M sulfuric acid to give $^{15}NOCl$ and a very small amount of $^{15}N^{15}NO$, while only $^{15}N^{15}NO$ was derived from the ^{15}NO-complex(^{15}N atom%=99) of Red salt I(nitrate). The result from the addition of 6M sulfuric acid to the ^{14}NO-complex of Red salt I(nitrate) was in agreement with that obtained by Mercer *et al.*[14] The ratio of N_2O to NOCl derived from Red salt II(nitrate) was much smaller than that derived from Red salt I(nitrate) when 6M hydrochloric acid was added.

The thermal and acid decompositions of Red salts I and II suggest the following. If the hyponitrite ion were present in Red salt II, the N–N bond strength of the hyponitrite group would be smaller than that for Red salt I. However, another possibility that a small amount of $^{15}N^{15}NO$ from Red salt II is due to the contamination of Red salt II by Red salt I cannot be excluded (see IR spectra of Red salts I and II). In this case, it may be considered that the hyponitrite group is absent in Red salt II.

Solid Products Obtained by Treating Red Salt II with Ammoniacal Solution and Water: Red salt II(chloride) was completely decomposed in boiling water to give a mixture of cobalt(III) hydroxide and cobalt(III) ammine-complex with coordinated nitro group. The IR spectra of solid products precipitated by the addition of ammonium chloride or acetone to a 3M ammoniacal solution of Red salt II(0.5 g/40 ml) at *ca.* 0°C showed that Red salt II(chloride) was completely decomposed within 4 h to give an orange-yellow compound, the nitro-complex, while, in an aqueous solution of Red salt II at *ca.* 0 °C, Red salt II was stable for 9 days. The pink precipitate obtained by the addition of acetone to the aqueous solution was identified to be Red salt II with a small amount of the nitro-complex. Thus, Red salt II is considered to be stable in water at *ca.* 0 °C.

A yellow product was obtained when the ammoniacal solution of Red salt II was boiled and then cooled at *ca.* −15 °C. The IR spectra of this compound show the characteristic absorption bands of nitro-complex and of nitrate ion[7] and the corresponding bands of the ^{15}N-compound shifted downwards, but no characteristic ones of Red salt II could be observed. The IR spectra of the yellow product obtained from Red salt II(nitrate) was almost equal to that from Red salt II(chloride). Elementary analyses of the yellow salt from Red salt II(chloride) gave a Co: N: H: Cl atom ratio of 1: 7.7: 15.4: 0.2, and those from Red salt II(nitrate) gave a Co: N: H atom ratio of 1: 8.5: 16.9. The results obtained from the IR spectra and the elementary analyses show that a main component of the yellow salts is $[Co(NO_2)(NH_3)_5](NO_3)_2$.

Red salt I(nitrate) is very stable in a boiling 3M ammoniacal solution, and can be recrystallized by cooling the solution to −15 °C, and reprecipitated by addition of a large excess of ammonium nitrate to the ammoniacal solution. In boiling water, however, a part of Red salt I(nitrate) was decomposed to give cobalt(III) hydroxide.

The complex cation of Red salt II might be generally unstable with respect to the nitrosyl groups. No intermediates clearly reflecting structure for the complex cation of Red salt II could be isolated. All of the nitrosyl group in Red salt II might change into the nitro and nitrate ions.

IR Spectra of Red Salts I and II. *Red Salt I(Nitrate)*: No isotopic shifts for the bands in the region 200—700 cm^{-1} could be observed because of the broadness of the bands. Of the bands in the region 700—4000 cm^{-1}, three bands at 1137, 1048, and 930 cm^{-1} shifted to 1112, 1027, and 917 cm^{-1}, respectively, upon ^{15}NO-substitution(^{15}N atom%=99). These bands have been previously assigned to the N–N, the antisymmetric N–O, and the symmetric N–O stretching vibrations, respectively, on the basis of the oxtent of the isotopic shifts upon ^{15}NO-substitution[14] and IR studies on $M_2N_2O_2$ (M=Na and K) containing *cis*-$N_2O_2^{2-}$ ion.[15]

However, our assignments of these three bands differ from those by Mercer *et al.*[14] Five absorption bands for the ^{15}NO-complex(^{15}N atom%=50) were observed at 1137, 1112, 1048, 1027, and 924 cm^{-1}, and six absorption bands for the mixture of the ^{14}NO-complex and the ^{15}NO-complex(^{15}N atom%=99)(1:1) at 1137, 1112, 1048, 1027, 929, and 920 cm^{-1}.

For the ^{15}NO-complex(^{15}N atom%=50), the N–N stretching vibration can be expected to split into three absorption bands, the ^{14}N–^{14}N, the ^{14}N–^{15}N, and the ^{15}N–^{15}N stretching vibrations(their intensity ratio 1:2:1).[16] For the mixture of the ^{14}NO- and the ^{15}NO-complexes(^{15}N atom%=99)(1:1), the ratio of the absorption intensity for the ^{14}N–^{14}N and ^{15}N–^{15}N stretching vibrations can be expected to be 1:1. Both the 1137 cm^{-1} and the 1048 cm^{-1} bands clearly splitted into two bands upon ^{15}NO-substitution(^{15}N atom%=50), so they may not be due to the N–N stretching vibration. On the other hand, the 930 cm^{-1} band shifted to 924 cm^{-1} (this wave number lies midway between 930 cm^{-1} of the ^{14}NO-complex and 917 cm^{-1} of the ^{15}NO-complex) upon ^{15}NO-substitution(^{15}N atom%=50). The 924 cm^{-1} band is seemingly a single band, the half width of this band being larger than that of the 930 cm^{-1} band and of the 917 cm^{-1} one. The 924 cm^{-1} band might therefore consist of three absorption bands, the ^{14}N–^{14}N, the ^{14}N–^{15}N, and the ^{15}N–^{15}N stretching vibrations. The 1137 cm^{-1} and the 1048 cm^{-1} bands could be assigned to the antisymmetric and the symmetric N–O stretching vibrations, respectively, since the wave numbers of antisymmetric stretching vibration are generally larger than those of symmetric one.[7]

If the 930 cm^{-1} band corresponds to the N–N stretching vibration, the bond order of the N–N would be

about one[7] and the bond distance about 1.4 Å.[17] X-Ray diffraction study on Red salt I has shown that the N–N bond distance is 1.25 Å,[3] and the bond order about two,[17] suggesting that the N–N stretching vibration can be observed in the region *ca.* 1300 cm^{-1}. There was a possibility that the N–N stretching vibration could not be observed due to overlapping with very strong broad bands of the nitrate ions at 1360 cm^{-1}. However, this was eliminated by measurement of the IR spectra for the chloride of Red salt I; no absorption band was observed in the 1360 cm^{-1} region except for the band due to the NH_3 symmetric deformation vibration. Three bands at 1154, 1060, and 940 cm^{-1} were observed in the region 900—1200 cm^{-1}. They can be assigned to the antisymmetric N–O stretching vibration, the symmetric N–O one, and the N–N one, respectively.

The N–N stretching vibration for the *cis*-$N_2O_2^{2-}$ ion has been observed in the region 1300—1390 cm^{-1},[15] while the N–N stretching vibration due to the hyponitrite ion bridged with the $Co(NH_3)_5$ groups was observed at 930 cm^{-1}. Lowering of the wave numbers is considered to be due to the coordination of two cobalt atoms to the hyponitrite ion.

Red Salt II(Chloride and Nitrate): The IR spectra and their assignments for Red salt II(chloride) in the region 200—4000 cm^{-1} are shown in Table 3 and Fig. 1.

The absorption bands due to the water of crystallization may be overlapped with the broad bands due to the N–H stretching and the NH_3 degenerate deformation vibrations as observed on Red salt I(nitrate).

IR studies on ammine-complexes show that the NH_3 rocking vibration is sensitive to the oxidation state of the metal atom.[18,19] The wave numbers of these bands of Red salt II seem to support the view that the oxidation state of the cobalt atom for Red salt II is III as for Red salt I. Red salt II was diamagnetic as expected from the oxidation state of the cobalt atom of Red salt II.

Upon ^{15}NO-substitution(^{15}N atom%=99.3), the bands at 1481(vs),[20] 1278(vs), 804(w), and 595(s) cm^{-1} for the chloride shifted, and the bands at 1481, 1278, and 804 cm^{-1} split into two peaks upon ^{15}NO-substitution(^{15}N atom%=50). The band at 1020 cm^{-1}(m) did not shift or split, but shifted downwards by *ca.* 6 cm^{-1} upon ^2H-substitution. The spectral features for the nitrate were similar to those for the chloride except for the absorption band, *ca.* 1360 cm^{-1} due to the nitrate ions. The 1011 cm^{-1}(s) band hardly shifted upon ^{15}NO-substitution as observed on the 1020 cm^{-1} band of the chloride.

From a comparison of the IR spectra of Red salts I and II, II seems to be contaminated with a very small amount of I. I could not be removed from II by crystallization.

If the same N–N bond as in Red salt I and in $K_6[Co_2(CN)_{10}(N_2O_2)]\cdot nH_2O$,[16] is present in Red salt II, the N–N stretching and the N–N–O bending vibrations should be observed on IR and/or Raman spectra and shift and split into three peaks upon ^{15}NO-substitution (^{15}N atom%=50). However no such phenomena were observed. Such a N–N bond might not be present in the complex cation of Red salt II.

IR studies with the use of nitrogen-15 will exclude the possibility that the nitrosyl group terminally coordinates to the cobalt atom, and that two cobalt atoms are bridged through two nitrogen atoms of the two nitrosyl groups; in the former case, the stretching vibration of the terminal NO group is generally observed in the region 1530—1980 cm^{-1},[21] and in the latter case, the coordination number of the cobalt(III) ion

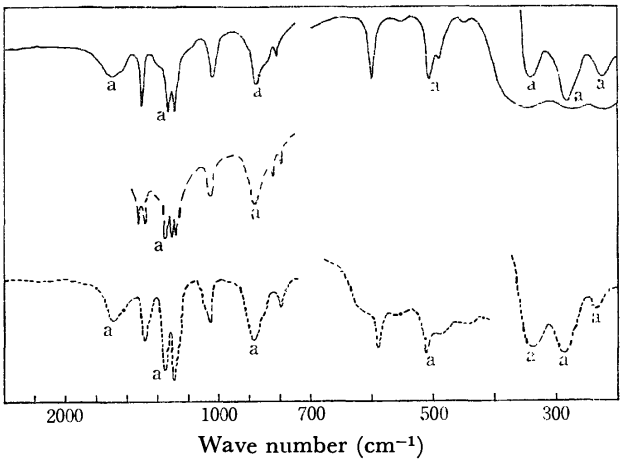

Fig. 1. IR spectra of Red salt II(chloride); —, ^{14}NO-complex; -·-, ^{15}NO-complex (^{15}N atom %=50); ---, ^{15}NO-complex (^{15}N atom %=99.3); a, characteristic bands of cobalt(III)-ammine complex.

Table 3. Wave numbers and assignments of IR bands for red salt II (chloride and nitrate)[a]

Red salt II (chloride)	Red salt II (nitrate)	Assignments
3250 vs, b 3110 vs, b	3280 vs 3200 vs, sh	O–H str and N–H str
1608 m, b	1625 m, b	H_2O bend and NH_3 deg def
1481(31)[b] vs	1491(32) s	N–O str
	1370 vs, b	N–O asym str of NO_3^{1-}
1318 vs	1320 sh	NH_3 sym def
1278(19) vs	1269(20) vs	N–O str
	1050 vw	N–O sym str of NO_3^{1-}
1020(1) m	1011(3) s	O–O str
859 s	852 s	NH_3 rock
	831 s	out-of-plane def of NO_3^{1-}
804(21) w	806(26) w	N–O–O bend
595(14) s	586(17) w	N–O–O bend or Co–N–O bend
501 s 478 m	493 w 475 sh	Co–NH_3 str
334 vs 278 vs 223 vs	325 vs, b 270 m, b	H_3N–Co–NH_3 bend

a) The bands due to Red salt I contained as impurity are excluded. b) The values in parentheses indicate the observed isotopic shift. Abbreviations: str=stretching, bend=bending, deg=degenerate, sym=symmetric, asym=asymmetric, rock=rocking, def=deformation, vs=very strong, s=strong, m=medium, w=weak, vw=very weak, b=broad, sh=shoulder.

becomes seven and the IR bands cannot be explained in terms of this skeleton. Elementary analyses and IR studies show that the number of the nitrogen atoms labeled with nitrogen-15 is two, and two of the nitrosyl groups are present in Red salt II.

The possibility that two of the $Co(NH_3)_5$ groups are bridged through an ion consist of a dimer of nitrosyl, N–O–O–N^{2-} can not be excluded. If the N–O–O–N anion is contained in the complex cation of Red salt II, the five IR bands in the region 580—1490 cm^{-1} could be explained on the basis of this anion; the 1481 and 1278 cm^{-1} bands of the chloride and the 1490 and 1269 cm^{-1} bands of the nitrate can be assigned to the N–O stretching vibrations, the 1020 cm^{-1} band of the chloride and the 1011 cm^{-1} band of the nitrate to the O–O stretching vibrations. The 804 cm^{-1} band of the chloride and the 806 cm^{-1} band of the nitrate may be assigned to the N–O–O bending vibrations. The 595 cm^{-1} band of the chloride and the 586 cm^{-1} band of the nitrate may be assigned to another N–O–O bending or the Co–N–O bending vibrations. The wave numbers of the N–O stretching vibrations for Red salt II are larger than those for the complexes with the hyponitrite ions. This seems to reflect the fact that the bond order of the N–O for Red salt II is larger than that for the complexes with the bridged hyponitrito ion. The O–O stretching vibrations of O_2^{2-} and O_2^{1-} anions are in the region 1050—1090 cm^{-1}, and 1070—1150 cm^{-1} [22] and those of μ-oxo cobalt(III)-ammine complexes and μ-superoxo ones are in the region *ca.* 830 cm^{-1} [23] and 1070—1150 cm^{-1}, respectively.[24] The band in the region 1010—1020 cm^{-1} for Red salt II may be reasonably assigned to the O–O stretching vibration. The N–N–O bending vibration of the hyponitrite ion are also observed in the region 600—860 cm^{-1}.[15,25] Thus, the bridged N–O–O–N^{2-} ion would most likely explain the results obtained.

Raman Spectra of Red Salts I and II. Since the nitrates of Red salts I and II decomposed in DMSO on irradiation with laser, their spectra could not be measured. Satisfactory Raman spectra of the powdered samples and the rotating potassium bromide disk could not be obtained because of a partial decomposition of the compounds. The bands due to nitro group and an unassignable band at 1653 cm^{-1} overlapped with the original bands for Red salt I(nitrate) and Red salt II(chloride). For Red salt II(chloride), the bands due to nitrate ion were also observed. However, all of the bands observed on IR spectra could be observed on Raman spectra for both Red salts I and II.

Nitrogen-15 NMR Spectra of Red Salt II. A preliminary ^{15}N-NMR study of the ^{15}NO-complex(^{15}N atom%=99) of Red salt II(nitrate) in DMSO-d_6 showed one peak, which is considered to support the view that two of the nitrosyl groups are in an equivalent chemical circumstance. The possibility that one cobalt atom is bound to the oxygen atom and the other to the nitrogen one in N–O–O–N^{2-} ion may be excluded.

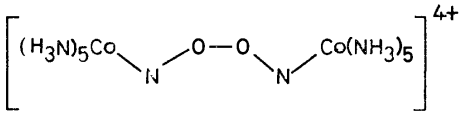

Fig. 2. Probable structure of the complex cation of Red salt II.

From the results, the structure as shown in Fig. 2 can be predicted for the complex cation of Red salt II. The coordination ability of the nitrogen of the N–O–O–N^{2-} ion to the cobalt atom may be stronger than that of the oxygen.

The authors express their appreciation to Mr. Takashi Takakuwa, Japan Spectroscopic Co. Ltd. and to Mr. Hiroshi Saito, Rikkyo University, for measurements of the Raman spectra, and to Mr. Shozo Shimizu of JEOL Ltd. for measurement of the ^{15}N-NMR spectra. The present work was supported in part by a Grant for Scientific Research from the Ministry of Education.

References

1) J. Sand and O. Genssler, *Ber.*, **36**, 2083 (1903).
2) C. S. Pratt, B. A. Coyle, and J. A. Ibers, *J. Chem. Soc. Inorg. Phys. Theor.*, **1971**, 2146.
3) B. F. Hoskins, F. D. Whillans, D. H. Dale, and D. C. Hodgkin, O. M., *Chem. Commun.*, **1969**, 69; B. F. Hoskins and F. D. Whillans, *J. Chem. Soc., Dalton*, **1973**, 607.
4) E. Miki, T. Ishimori, and H. Okuno, *Bull. Chem. Soc. Jpn.*, **42**, 3050 (1969).
5) T. Moeller and G. L. King, *Inorg. Synth.*, Vol. 4 (1953), p. 168.
6) Reprcducibility of elementary analyses of the hydrogen atom to the same samples was very poor because Red salt II was decomposed violently by heating.
7) K. Nakamoto, "Infrared Spectra of Inorganic and Coordination Compounds," 2nd ed., Wiley-Interscience, New York, N. Y. (1970).
8) R. Davies, M. Mori, A. G. Sykes, and J. A. Weil, "Inorganic Syntheses," Vol. 12 (1970), p. 197; A. G. Sykes, *Progr. Inorg. Chem.*, **13**, 1 (1970).
9) D. Yang, D. P. Keeton, and A. G. Sykes, *J. Chem. Soc. Dalton*, **1974**, 1089.
10) P. Gans, *J. Chem. Soc. Inorg. Phys. Theor.*, **1967**, 943.
11) R. D. Feltham and R. G. Hayter, *J. Chem. Soc.*, **1964**, 4587.
12) R. D. Feltham, *Inorg. Chem.*, **3**, 1038 (1964).
13) K. Otto, M. Shelef, and J. T. Kammer, *J. Phys. Chem.*, **74**, 2690 (1970); *Inorg. Chem.*, **75**, 875 (1971).
14) E. E. Mercer, W. A. McAllister, and J. R. Durig, *Inorg. Chem.*, **6**, 1816 (1967).
15) J. Goubeau and K. Laitenberger, *Z. Anorg. Allg. Chem.*, **320**, 78 (1963); N. Gee, D. Nicholls, and V. Vincent, *J. Chem. Soc. Supplement* **1**, 5897 (1964).
16) H. Okamura, E. Miki, K. Mizumachi, and T. Ishinori, *Chem. Lett.*, **1974**, 103.
17) R. C. Evans, "An Introduction to Crystal Chemistry," 2nd ed., Cambridge University Press (1964), p. 74; A. F. Wells, "Structural Inorganic Chemistry," 3rd. ed., Oxford at the Clarendon Press (1967), p. 601.
18) T. Shimanouchi and I. Nakagawa, *Inorg. Chem.*, **3**, 1805 (1964).
19) D. M. Adams, "Metal-Ligand and Related Vibrations," Edward Arnold Publishers Ltd., London (1967).
20) The signs in parentheses indicate the abbreviation of the strength and shape of the band; vs=very stong, s=strong, m=medium, w=weak, sh=shoulder, b=broad.
21) B. F. G. Johnson and J. A. McCleverty, *Progr. Inorg. Chem.*, **7**, 277 (1966); N. G. Connelly, *Inorg. Chim. Acta Rev.*,

6, 47 (1972).
22) F. J. Blunt, P. J. Hendra, and J. R. Mackenzie, *Chem. Commun.*, **1969**, 278.
23) M. Mori, J. A. Weil, and M. Ishiguro, *J. Amer. Chem. Soc.*, **90**, 615 (1968); W. P. Griffith and T. D. Wickins, *J. Chem. Soc. Inorg. Phys. Theor.*, **1968**, 397.
24) T. Shibahara and M. Mori, 1B18 at 23 rd Symposium on Coordination Compounds, Kyushu University, Japan (1973).
25) L. Kuhn and E. R. Lippincott, *J. Amer. Chem. Soc.*, **78**, 1820 (1956); D. J. Miller, C. N. Polydoropoulos, and D. Watson, *J. Chem. Soc.*, **1960**, 687; G. E. McGraw, D. L. Bernitt, and I. C. Hisatsune, *Spectrochim. Acta*, **23A**, 25 (1967).

Study of Emulsions in Molten Salts. III. The Concentration, Stability and Particle-Size Distribution of Dispersed Lithium in Molten Lithium Chloride[1)]

Tsuyoshi NAKAJIMA, Koichiro NAKANISHI, and Nobuatsu WATANABE
Department of Industrial Chemistry, Faculty of Engineering, Kyoto University, Yoshida, Sakyo-ku, Kyoto 606
(Received June 21, 1975)

The concentration, stability and particle-size distribution of lithium dispersed in molten lithium chloride were investigated. The maximum content of dispersed lithium obtained by spontaneous emulsification was 4.8×10^{-3} mol/g at 678 °C. The concentration of dispersed lithium somewhat increased with the amounts of lithium oxide and nitride added to the molten salt by the mechanical agitation of the lithium–lithium chloride solution. The concentration was about 1.7 times that obtained by spontaneous emulsification except when a large amount of lithium nitride was added. Dispersed lithium in lithium chloride was shown to be fairly stable in the liquid state, as well as against the solidification of molten lithium chloride. The particle-size distribution of dispersed lithium was obtained by means of a scanning electron microscope. The sizes of the lithium particles dispersed in lithium chloride were shown to be mostly between 0.3 and 0.9 μ.

In previous papers,[1,2)] the authors have reported that, in addition to the true (physical) dissolution, metallic lithium was found to disperse into molten lithium chloride as colloidal particles, when a certain amount of lithium oxide was added to the molten salt or a small amount of oxygen or nitrogen was present in an argon atmosphere. The total concentration of lithium found in the solution thus obtained was considerably larger than the value for physical solubility. These facts may be ascribed to the emulsifying action of lithium oxide (or nitride) which is either simply added to the molten salt or formed by the reaction of lithium with oxygen (or nitrogen) in the atmosphere.[2)] Such metallic lithium–molten salt emulsions have been observed not only in molten lithium chloride but also in LiF–KF and NaCl–$CaCl_2$ systems. Larger amounts of lithium were found to disperse in LiCl and LiCl–KCl eutectic mixture where the solubilities of lithium oxide (or nitride) were almost equal to those in liquid lithium. On the other hand, the amounts of dispersed lithium were smaller in LiF–KF, LiF–LiCl and NaCl–$CaCl_2$ systems where the solubilities of oxide (or nitride) were quite different from those in lithium.[1)] It is interesting to further investigate the various factors governing the concentration and stability of lithium emulsions. In this paper, the concentration, stability and particle-size distribution of dispersed lithium in molten lithium chloride are reported.

Experimental

The concentration of lithium (dispersed as colloidal particles and dissolved to atomic dimensions) in molten lithium chloride was determined in the following manner. Three different instruments were designed and used. A highly-concentrated lithium solution was prepared with the apparatus in Fig. 1 (a), the stability of dispersed lithium was investigated in a stainless steel container (b), and the effect of mechanical agitation on the dispersion of lithium was studied with apparatus (c). For the measurements with (a) and (b), the amount of lithium added was sufficient to completely cover the surface of the molten salt. In the case of apparatus (c), about 1.5 mol (10 g) of lithium was added into 1.5 mol (64 g) of lithium chloride. The rate of agitation of the stirrer was 300 to 1300 rpm.

The methods of chemical analysis of lithium, lithium oxide and nitride, and of the purification of argon which was used as the atmospheric gas were the same as those described previously.[1,2)]

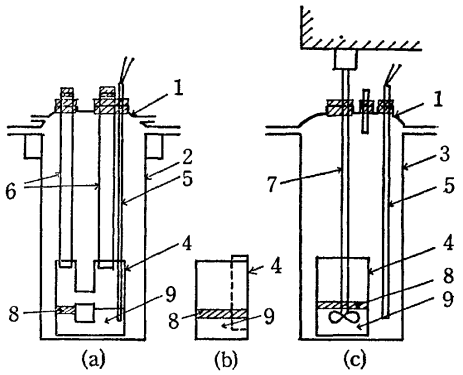

Fig. 1. Apparatus.
1: Pyrex cap, 2: stainless steel container, 3: silica container, 4: stainless steel container, 5: thermocouple, 6: stainless steel pipe, 7: stirrer, 8: molte lithium, 9: molten lithium chloride.

Furthermore, direct observations of liquid and solid samples were attempted by means of a binocular stereomicroscope and a scanning electron microscope.

Results and Discussion

Concentration of Dispersed Lithium in Emulsion. The amounts of lithium dispersed in molten lithium chloride considerably increased with time using a U-type container (a) with a by-pass in a dried argon atmosphere, as shown in Fig. 2.

Since the true solubility of lithium is about 0.7 mol% at the experimental temperature, it is obvious from the figure that a large amount of lithium was dispersed in lithium chloride. For lithium concentrations higher than 12 mol%, the sampling with a thin silica pipe was difficult owing to the considerable decrease in the surface tension of the lithium–lithium chloride solution. The maximum concentration of dispersed lithium was 17.0 mol% at 678 °C. This value is equal to 4.8×10^{-3} mol/g which is the largest in lithium–lithium chloride emulsions.

Effect of Mechanical Agitation on the Concentration of Dispersed Lithium. The effects of the agitation time, agitation speed and concentration of lithium

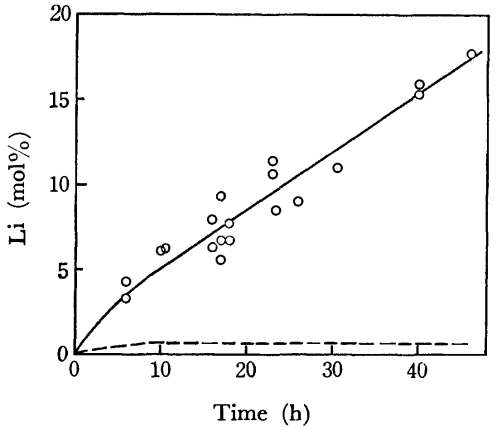

Fig. 2. Concentration of lithium in molten lithium chloride in argon atmosphere *vs.* time plot.
Temp: 678±3 °C, ----: true solubility of lithium in molten lithium chloride.

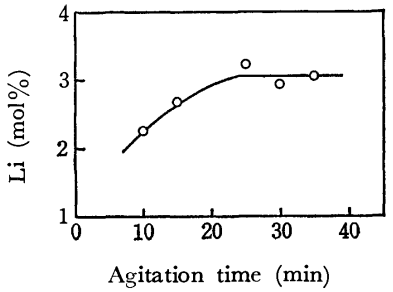

Fig. 3. Effect of agitation time on the lithium concentration.
Temp: 650 °C, agitation: 1000 rpm, added Li_2O: 1.14 mol%.

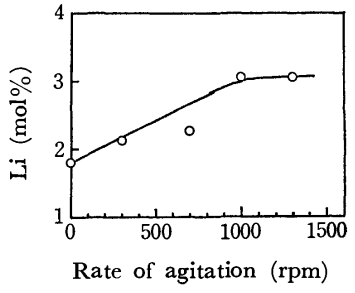

Fig. 4. Effect of rate of agitation on the lithium concentration.
Temp: 650 °C, agitation: 30 min, added Li_2O: 1.14 mol%.

oxide or nitride on the concentration of dispersed lithium were investigated and the results are shown in Figs. 3, 4 and 5, respectively. Figure 6 shows the lithium concentration *vs.* time obtained without mechanical agitation. In this condition, the lithium concentration amounted to about 1.8 to 2 mol% by spontaneous emulsification and true dissolution. As shown in Fig. 5, mechanical agitation did not cause the dispersion of lithium when no lithium oxide or nitride was added to lithium chloride. The addition of oxide and nitride to the molten salt, however, brought about an increase

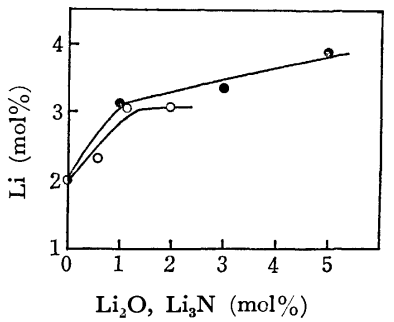

Fig. 5. Effects of lithium oxide and nitride on the lithium concentration.
○: Li_2O, ●: Li_3N.
Temp: 650 °C, agitation: 1000 rpm, 30 min.

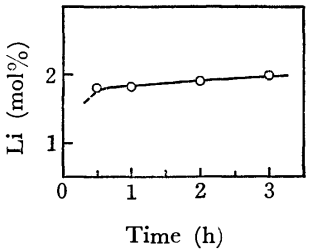

Fig. 6. Concentration of lithium *vs.* time plot in the absence of mechanical agitation.
Temp: 650 °C.

in the concentration of dispersed lithium. The increase in lithium concentration may, therefore, be attributed to the emulsifying action of lithium oxide or nitride. Furthermore, lithium oxide added in excess of its solubility[3] in lithium chloride had little effect on the concentration of dispersed lithium. This result is consistent with that obtained in the absence of mechanical agitation as described in a previous paper.[2] If solid films of lithium oxide are formed on lithium particles, the activity of oxide ions in the molten salt will decrease to some extent. Under the present conditions, the dissolution of lithium oxide to make up for the decrease in the activity of oxide ions should be accelerated by mechanical agitation. Therefore, if the decrease in the activity of oxide ions is not very small, the concentration of dispersed lithium is expected to increase by mechanical agitation in concentrations of lithium oxide higher than about 1 mol%. But this expectation is not supported by the experimental results. This means that lithium oxide acts as the emulsifying agent in an ionized state. On the other hand, the concentration of dispersed lithium increased monotonically with the addition of lithium nitride because its solubility in lithium chloride was 14.6 mol%[1] at 650 °C.

Stability of Lithium–Lithium Chloride Emulsion. The apparatus was sealed when the lithium concentration reached a certain value in a dried, deoxidized argon atmosphere and the change of lithium concentration was monitored. The results are shown in Fig. 7. Since the true solubility of lithium in molten lithium chloride is about 0.6 mol% at the experimental temperature, the amounts of lithium over the solubility

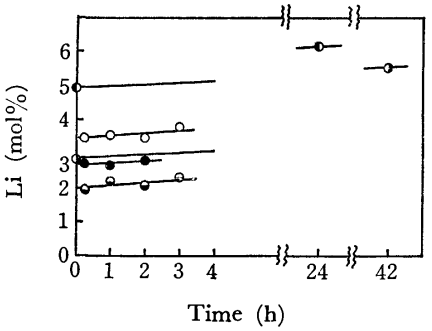

Fig. 7. Stability of dispersed lithium.
Temp: 647±2 °C.
◐: First run, ○: second run, ◑: third run, ●: fourth run, ◒: fifth run.

are those of lithium dispersed by spontaneous emulsification. The concentrations of dispersed lithium and lithium compounds[4] were both slightly larger than those obtained at the time when the apparatus was sealed. Somewhat larger increases in the concentrations were, therefore, observed in systems standing for a long time. This is probably because lithium oxide or nitride on the surface of liquid lithium was dissolved or dispersed in the molten salt, or a small amount of air entered into the apparatus. The concentration of lithium in the molten salt depends on the dispersion of lithium due to the emulsifying action of lithium oxide or nitride and the oxidation or nitridation of dispersed lithium on the surface of the molten salt. Figure 7 shows that dispersed lithium may be stable in the molten salt if it is not too oxidized or nitridized with air.

When the emulsion is solidified, it seems possible that dispersed lithium particles in the system are distorted and coalesce with each other, that is, the lithium–lithium chloride emulsion is broken. It is said that the stability of dispersed particles against the solidification of the solvent is a measure of the capability of an emulsifying agent. As shown in Table 1, the lithium concentrations after remelting of the solid samples were slightly lower than those obtained before solidification, but the differences between them are smaller than the true solubility of lithium at the experimental temperature.[5] The emulsion appears to be fairly stable upon solidification. The small decrease in the lithium concentration may be due to the phase separation of lithium physically dissolved to atomic dimensions in the molten salt.

Particle-Size Distribution of Dispersed Lithium. Direct observations of lithium particles in a molten lithium chloride–potassium chloride eutectic mixture at a certain partial pressure of nitrogen were attempted using a binocular stereomicroscope with a long focal distance (maximum magnification : 160 times), because an ordinary optical microscope was difficult to use at the high temperatures of 400 to 650 °C. If the diameter of a lithium particle was larger than 3 μ, the lithium particles could be expected to be observed, but none were found.

Table 1. Stability of dispersed lithium against the solidification of molten lithium chloride

Concentration of lithium before solidification of lithium chloride (mol%)	Concentration of lithium after remelting of lithium chloride (mol%)
2.03	1.59
6.15	5.84

Then, a cross section of a cylindrical solid sample, which was obtained by direct sampling from a salt-rich phase with a thin silica pipe, was observed by means of a scanning electron microscope. Four kinds of samples were prepared at 650 °C:

(a) Lithium chloride containing 5 mol% lithium nitride.

(b) A sample prepared by dissolving lithium physically in lithium chloride with a sealed-type cell.[2]

(c) A sample prepared by dispersing lithium in lithium chloride at a partial pressure of nitrogen of 0.02 atm.

(d) A sample prepared by dispersing lithium in lithium chloride containing 5 mol% lithium nitride by means of mechanical agitation (1000 rpm, 25 min).

No small particles were found in samples (a) and (b). In sample (b), small particles which may have been formed by phase separation of lithium dissolved to atomic dimensions could possibly be observed in solid lithium chloride, but were probably not found because they were too small to be recognized or were covered with solid lithium chloride.

In almost all cases with samples (c) and (d), the recognition of small particles was considerably difficult because granular substances on the cross section were not clearly exposed and were covered with solid salt.

Figures 8, 9 and 10 were obtained with sample (d). A large number of small particles are observed in the figures. It appears that the surface in the figures where many particles exist is not a newly prepared cross section obtained by breaking a solid sample, but is instead a cave hidden inside cylindrical sample. Perhaps for this reason, small particles are clearly observed at the places not thickly covered with solid

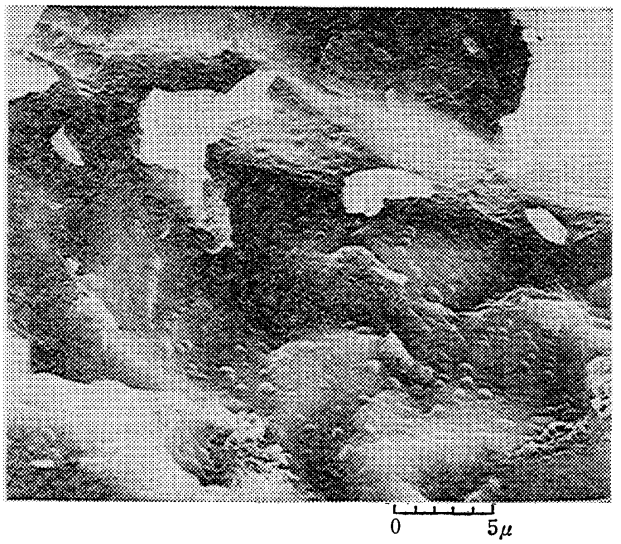

Fig. 8. Scanning electron micrograph of metallic lithium particles in lithium chloride.

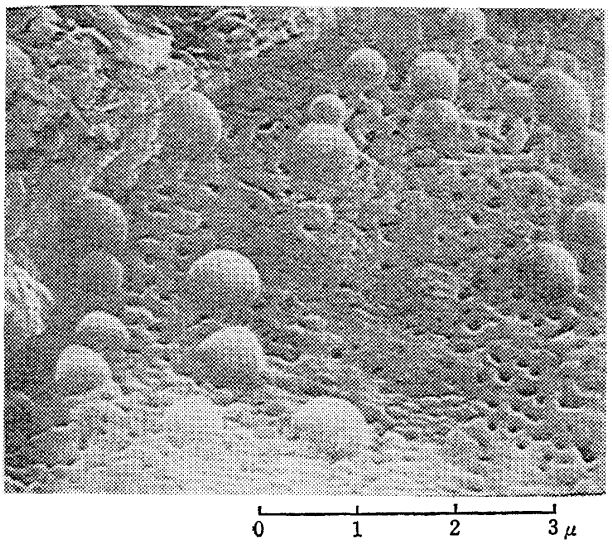

Fig. 9. Scanning electron micrograph of metallic lithium particles in lithium chloride.

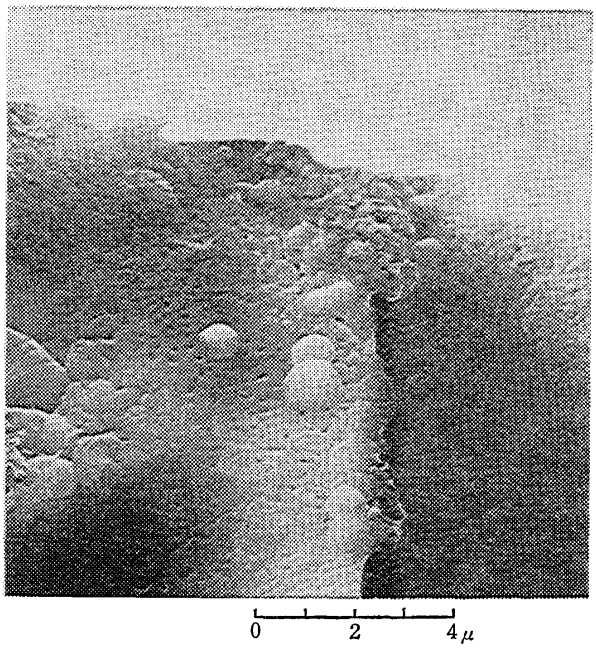

Fig. 10. Scanning electron micrograph of metallic lithium particles in lithium chloride.

salt. Elemental analysis was then carried out by means of an X-ray microanalyser in order to confirm whether these small particles were lithium metal. The distribution of lithium atoms cannot be found directly since the intensity of X-rays emitted by lithium atoms is too weak to be detected efficiently. Therefore, the X-ray intensities emitted from chlorine atoms were compared with each other by applying an electron beam to a small particle and its surroundings on as flat a surface as possible. Both the diameters of an electron beam and its transmission depth are 1 μ. Accordingly, if the diameter of a small particle is less than 1 μ or the small particle is covered with a thin film of solid salt, it is possible that chlorine atoms present around the particle or in the film of the solid salt would be detected and that the difference of both chlorine intensities would not be large. Actually the intensities for chlorine atoms obtained with small particles in the center of Fig. 10 were only slightly smaller than those obtained from their surroundings. If small particles in the figures are not lithium metal but solid salt, the chlorine intensities obtained from the projecting small particles would be considerably larger than those obtained from their surroundings because both concentrations of chlorine atoms are equal. Consequently, the small particles in the figures are regarded as lithium metal.

Now, the following situations should be taken into account when the particle sizes of dispersed lithium metal in the molten salt are evaluated from the small particles in the figures:

(1) Whether or not the coalescence of lithium particles occurred on rapid solidification of the sample.

(2) It is possible that small particles which were formed by the coalescence of lithium dissolved physically to atomic dimensions were mixed in the colloidal lithium.

(3) If lithium particles are covered with solid salt, they may be observed as particles larger than their true sizes.

(4) Since the temperature at which the sample was prepared was different from that at which a scanning electron micrograph was taken, it is necessary to correct for the contraction of the particles.

The particle-size distribution for 100 particles was obtained by taking the above problems into consideration and is given in Fig. 11. Most of the particles are distributed in the range of 0.3 to 0.9 μ and the largest particle has a diameter of 1.2 μ. The sizes of lithium particles in emulsion are then expected to be distributed in this range.

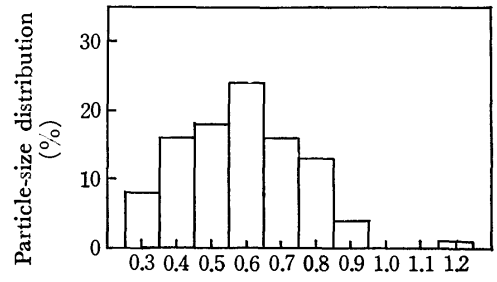

Fig. 11. Particle-size distribution of dispersed lithium in lithium chloride.

Generally, particles formed by spontaneous emulsification are smaller than those formed by mechanical agitation. In other words, it is expected that particles with larger diameters are formed by agitation, and thus the particle-size distribution also becomes slightly broader. For this reason, no lithium particles should be found by direct observation of the liquid state.

References

1) Part II of this series. T. Nakajima, K. Nakanishi, and N. Watanabe, *Nippon Kagaku Kaishi*, **1975**, 617.

2) N. Watanabe, K. Nakanishi, and T. Nakajima, *Nippon Kagaku Kaishi*, **1974**, 401.

3) 1.14 mol%. Ref. 1.

4) Lithium nitride and oxide. The amounts are not shown in Fig. 7.

5) 0.6 mol%. T. Nakajima, R. Minami, K. Nakanishi, and N. Watanabe, *Bull. Chem. Soc. Jpn.*, **47**, 2071 (1974).

Phase Equilibria in $Fe-Fe_2O_3-Ln_2O_3$ (Ln=Sm and Er) Systems at 1200 °C

Kenzo KITAYAMA and Takashi KATSURA

Department of Chemistry, Faculty of Science, Tokyo Institute of Technology, Ookayama, Meguro-ku, Tokyo 152

(Received July 7, 1975)

Phase equilibria in $Fe-Fe_2O_3-Ln_2O_3$ (Ln=Sm and Er) systems were established at 1200 °C. In the $Fe-Fe_2O_3-Sm_2O_3$ system, perovskite, garnet, magnetite, wustite, and metallic iron were stable, while in the $Fe-Fe_2O_3-Er_2O_3$ system, the $ErFe_2O_4$ phase appeared in addition to the other five phases. On the basis of the phase equilibria, the Gibbs free energy for the reaction of $LnFeO_3$, $Ln_3Fe_5O_{12}$, and $ErFe_2O_4$ from Ln_2O_3, metallic iron, and oxygen was determined to be as follows: $SmFeO_3$ -64.1 ± 0.1 kcal, $Sm_3Fe_5O_{12}$ -298.5 ± 0.5 kcal, $ErFe_2O_4$ -100.8 ± 0.1 kcal, $ErFeO_3$ -59.7 ± 0.3 kcal, and $Er_3Fe_5O_{12}$ -286.2 ± 0.7 kcal.

In previous studies, Kimizuka and Katsura,[1] Sugihara *et al.*,[2] and Kimizuka and Katsura[3,4] have established the phase equilibria in $Fe-Fe_2O_3-Ln_2O_3$ systems (Ln=La, Y, Eu, and Yb) at 1200 °C. They have also determined the standard Gibbs free energy for reaction of each ternary double oxide found in these systems from metallic iron, Ln_2O_3, and oxygen. On the basis of these studies, Kimizuka and Katsura[4] have proposed that $Fe-Fe_2O_3-Ln_2O_3$ systems (Ln=La, Nd, Sm, Eu, Gd, Tb, Dy, Ho, Er, Tm, Yb, Lu, and Y) can be classified into four groups with respect to the assemblage of ternary compounds which are in stable co-existence at 1200 °C. According to them, the $Fe-Fe_2O_3-Sm_2O_3$ system may belong to the B-type having two ternary compounds, $SmFeO_3$ and $Sm_3Fe_5O_{12}$, while the $Fe-Fe_2O_3-Er_2O_3$ system is of the C-type having the three stable ternary compounds, $ErFeO_3$, $Er_3Fe_5O_{12}$, and $ErFe_2O_4$. Preceding these studies, Schneider *et al.*[5] had studied the subsolidus binary phase equilibria for the $Fe_2O_3-Sm_2O_3$, and the $Fe_2O_3-Er_2O_3$ systems by the X-ray powder diffraction technique at various temperatures, and found the two rare-earth iron oxides of perovskite and garnet at 1200 °C. The discovers of two new compounds, $LnFe_2O_4$ (Ln=Ho, Er, Tm, and Y) and $Ln_2Fe_3O_7$ (Ln=Yb and Lu) have recently been reported by Kimizuka and Katsura,[3,4] Kimizuka *et al.*,[6,7] Kato *et al.*,[8,9] Tannieres *et al.*,[10] and Evrard *et al.*[11,12]

The objectives of the present study are, firstly, to ascertain the validity of the classification for two systems involving Sm_2O_3 and Er_2O_3 at 1200 °C, after establishing the phase equilibria in these systems, and secondly, to determine the standard Gibbs free energy for reaction of $LnFeO_3$, $LnFe_2O_4$, and $Ln_3Fe_5O_{12}$ compounds at 1200 °C from metallic iron, Ln_2O_3, and oxygen.

Experimental

Analytical grade Fe_2O_3, Sm_2O_3(99.9%), and Er_2O_3(99.9%) powder were employed as starting materials. Desired ratios of Ln_2O_3/Fe_2O_3 were obtained by mixing thoroughly in an agate mortar with ethyl alcohol. Mixtures thus obtained were treated by the same procedures as those described previously.[2-4]

Mixed gases of CO_2 and H_2 were used to obtain low oxygen partial pressures in the present experiment. The actual oxygen partial pressures of the gas phase was measured by means of a solid electrolytic cell composed of $(ZrO_2)_{0.85}$-$(CaO)_{0.15}$.[13]

Phases in quenched samples were identified by the powder X-ray diffraction method with Mn-filtered Fe$K\alpha$ radiation.

Details of the apparatus and procedures for maintaining constant temperature, methods of thermogravimetry and quenching, the criterion for equilibrium-establishment, and the method of wet chemical analysis are the same as those described in a previous paper.[2-4,14] Lattice constants were determined by the powder X-ray diffraction method with Mn-filtered Fe$K\alpha_1$ radiation and with a slow scanning speed of 0.5° per minute. Instrumental errors were calibrated by measuring the diffraction angles of a standard specimen of silicon.

Results and Discussion

Phase Equilibria. The $Fe-Fe_2O_3-Sm_2O_3$ System: Six samples with Sm_2O_3/Fe_2O_3 compositions of 0.25, 0.60, 0.724, 1, 1.222, and 1.5 were prepared. The results of the phase equilibria are illustrated in Fig. 1. The following phases were stable under the experimental conditions: samarium sesquioxide (Sm_2O_3),

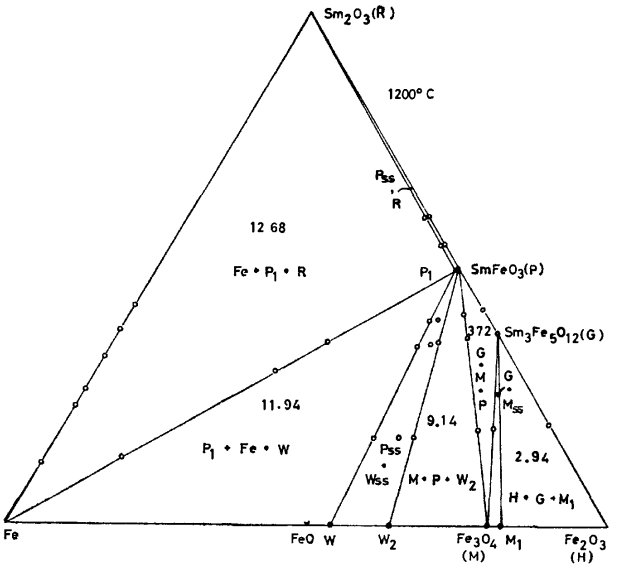

Fig. 1. Phase equilibria in the $Fe-Fe_2O_3-Sm_2O_3$ system at 1200 °C (mol%). Numbers in the figure mean values of $-\log P_{O_2}$ at which three crystalline phases are in equilibrium state. Letters R, P, G, and M represent stoichiometric compositions of Sm_2O_3, $SmFeO_3$, $Sm_3Fe_5O_{12}$, and Fe_3O_4, respectively. M_1 means the endmember of the magnetic solid solution with a chemical composition, $Fe_{2.957}O_4$. P_{ss}, W_{ss}, and M_{ss} mean the solid solution of $SmFeO_3$ from P to P_1, of FeO from W to W_2, and Fe_3O_4 from M to M_1, respectively. The other letters as for in Table 2.

Table 1. Lattice constants of ternary oxides

Composition	a (Å)	b (Å)	c (Å)	V(Å^3)
$SmFeO_3$				
$SmFeO_{3.000}$	5.398±0.002	5.598±0.002	7.708±0.002	232.9±0.2
$SmFeO_{2.982}$	5.398±0.001	5.591±0.001	7.706±0.001	232.6±0.1
(a)[15]	5.394	5.592	7.711	
$ErFeO_3$				
$ErFeO_{3.000}$	5.262±0.001	5.584±0.001	7.593±0.001	223.1±0.1
$ErFeO_{2.974}$	5.261±0.001	5.585±0.001	7.592±0.001	223.1±0.1
$Sm_3Fe_5O_{12}$				
$Sm_3Fe_5O_{12.00}$	12.519±0.002			1962.1±0.6
(b)[16]	12.524			
(c)[17]	12.529			1967.2
$Er_3Fe_5O_{12}$				
$Er_3Fe_5O_{12.00}$	12.346±0.001			1881.8±0.5
(b)[16]	12.349			
(d)[18]	12.347			1882.3
$ErFe_2O_4$ (hexagonal)				
$ErFe_2O_{3.984}$	3.489±0.001		24.929±0.004	262.8±0.2
$ErFe_2O_{3.957}$	3.494±0.001		24.927±0.004	263.6±0.2
$ErFe_2O_{3.904}$	3.500±0.001		24.948±0.005	264.6±0.3

hematite (Fe_2O_3), magnetite (Fe_3O_4), wustite (FeO), metallic iron (γ-Fe), samarium-iron-perovskite ($SmFeO_3$), and samarium-iron-garnet ($Sm_3Fe_5O_{12}$).

Sm_2O_3 was stable in oxygen partial pressures from one to $10^{-12.8}$ atm at 1200 °C, and appeared to have no significant nonstoichiometry in its composition. The deviation from the stoichiometric composition of $SmFeO_3$ extended up to $SmFeO_{2.982}$ at an oxygen partial pressure of $10^{-12.68}$ atm. The lattice constants of the $SmFeO_3$ solid solution seemed to be constant irrespective of the compositional variation. The data are given in Table 1 together with the data of Geller and Wood.[15] This is the same trend as those found for $EuFeO_3$,[2] $YFeO_3$,[3] and $YbFeO_3$.[4] $Sm_3Fe_5O_{12}$ had no compositional variation and remained stoichiometric under the experimental conditions. The lattice constants of $Sm_3Fe_5O_{12}$ were almost identical with those obtained by Bertaut and Forrat[16] and Espinosa.[17] The data are given in Table 1.

The $Fe-Fe_2O_3-Er_2O_3$ System: Seven samples with Er_2O_3/Fe_2O_3 compositions of 0.25, 0.429, 0.499, 0.6, 0.739, 1 and 1.222 were prepared. Figure 2 shows the experimental results. The following phases were stable under the experimental conditions: erbium sesquioxide (Er_2O_3), hematite (Fe_2O_3), magnetite (Fe_3O_4), wustite (FeO), metallic iron (γ-Fe), erbium-iron-perovskite ($ErFeO_3$), erbium-iron-garnet ($Er_3Fe_5O_{12}$), and $ErFe_2O_4$.

Er_2O_3 was stable in oxygen partial pressures from one to $10^{-12.0}$ atm, and appeared to have no compositional variation. The deviation from the stoichiometric composition of $ErFeO_3$ extended up to $ErFeO_{2.973}$ at an oxygen partial pressure of $10^{-11.19}$ atm. The lattice constants of the $ErFeO_3$ solid solution seemed to be constant irrespective of the compositional variations. The data are given in Table 1. $Er_3Fe_5O_{12}$ had no compositional variation under the experimental conditions, and its lattice constants were almost identical with those obtained by Bertaut and Forrat[16] and Geller *et al.*[18] The data are given in Table 1. The $ErFe_2O_4$ phase had a wide composition range from $ErFe_2O_{3.955}$ at an oxygen partial pressure of $10^{-10.00}$ atm to $ErFe_2O_{3.903}$ at an oxygen partial pressure of $10^{-11.96}$ atm. The lattice constants of the $ErFe_2O_4$ solid solution were determined on the basis of the study of the crystal structure by Kato *et al.*,[8] and these data are also given in Table 1. As shown in Table 1, the lattice constants of this solid solution increase with decreasing oxygen content.

In conclusion, from the studies of the phase equilibria of two systems, it has become clear that the $Fe-Fe_2O_3-Sm_2O_3$ system belongs to the B-type having two ternary compounds as presumed by Kimizuka and Katsura,[4] and that the $Fe-Fe_2O_3-Er_2O_3$ system belongs to the C-type having three ternary compounds, $ErFeO_3$, $Er_3Fe_5O_{12}$, and $ErFe_2O_4$.

Calculations of Standard Gibbs Free Energies of Ternary Compounds. On the basis of the phase equilibria, we can determine the standard free energy of reaction of the respective $ErFe_2O_4$, $SmFeO_3$, $Sm_3Fe_5O_{12}$, $ErFeO_3$, and $Er_3Fe_5O_{12}$ compounds, referring to the following equations:

$$Fe + 1/2Sm_2O_3 + 3/4O_2 = SmFeO_3 \quad (1)$$

$$5Fe + 3/2Sm_2O_3 + 15/4O_2 = Sm_3Fe_5O_{12} \quad (2)$$

$$2Fe + 1/2Er_2O_3 + 5/4O_2 = ErFe_2O_4 \quad (3)$$

$$Fe + 1/2Er_2O_3 + 3/4O_2 = ErFeO_3 \quad (4)$$

$$5Fe + 3/2Er_2O_3 + 15/4O_2 = Er_3Fe_5O_{12} \quad (5)$$

The standard Gibbs free energies of reaction (1) and (3) may be calculated directly by adopting each equilibrium oxygen partial pressure corresponding to the equation. Here, the activity of each component of $SmFeO_3$ and $ErFe_2O_4$ in each solid solution was set equal to one, and where the compositions were $SmFeO_{2.982}$ (P_1 in Fig. 1) and $ErFe_2O_{3.903}$ (A in Fig. 2),

both were in equilibrium with metallic iron and sesquioxide.

In order to calculate the standard Gibbs free energy of reaction (2), it is necessary to calculate the standard Gibbs free energy of the following reaction (6):

$$3SmFeO_3 + 2/3Fe_3O_4 + 1/6O_2 = Sm_3Fe_5O_{12} \quad (6)$$

This may be readily calculated on the basis of the experimental results illustrated in Fig. 1. The activity of the $SmFeO_3$ component in stoichiometric composition which was in equilibrium with both stoichiometric Fe_3O_4 and $Sm_3Fe_5O_{12}$ was calculated by means of the Gibbs-Duhem equation. The relationship between $-1/2 \log P_{O_2}$ and N_O/N_{SmFeO_3}, the fraction ratio of oxygen to $SmFeO_3$, indicating the deviation from stoichiometry, was substantially linear from the present experimental results, and the activity was calculated to be 1.125. A detailed calculation method has been described in the paper of Kimizuka and Katsura.[4] Since the standard Gibbs free energy of formation of Fe_3O_4 referred to the Eq. 7.

$$3Fe + 2O_2 = Fe_3O_4 \quad (7)$$

has been determined by Darken and Gurry,[19] the standard Gibbs free energy of $Sm_3Fe_5O_{12}$ referred to Eq. 2 may be determined by adding together $3\Delta G°(1)$, $\Delta G°(6)$, and $2/3\Delta G°(7)$.

In order to calculate the standard Gibbs free energy referred to Eq. 4, we have to invoke the following reaction (8):

$$1/4Er_2O_3 + 1/2ErFe_2O_4 + 1/8O_2 = ErFeO_3. \quad (8)$$

The standard Gibbs free energy of reaction (8) may be readily calculated on the basis of the experimental results shown in Fig. 2. Here, the activity of the $ErFeO_3$ component with composition $ErFeO_{2.973}$ (P_3 in Fig. 2) was set equal to one. The activity of the $ErFe_2O_4$ component in the $ErFe_2O_4$ solid solution from $ErFe_2O_{3.903}$ to $ErFe_2O_{3.995}$ is calculated by means of the Gibbs-Duhem equation, and the relationship between $-1/2 \log P_{O_2}$ and $N_O/N_{ErFe_2O_4}$ was substantially linear from the experimental results. After determining the activity of $ErFe_2O_4$ with a composition of $ErFe_2O_{3.942}$ (A_1 in Fig. 2), we may determine the standard Gibbs free energy referred to Eq. 4 by adding together $1/2\ \Delta G°(3)$ and $\Delta G°(8)$.

To determine the standard Gibbs free energy referred to Eq. 5, it is necessary to calculate the standard Gibbs free energy of the following reaction (9):

$$3ErFeO_3 + 2/3Fe_3O_4 + 1/6O_2 = Er_3Fe_5O_{12} \quad (9)$$

The procedure for determining the standard Gibbs free energy of reaction (9) is the same as that for reaction (6). Adding together $2/3\ \Delta G°(7)$, $3\Delta G°(4)$, and $\Delta G°(9)$, we obtain the value of $\Delta G°(5)$. The calculated activity data are summarized in Table 2, and the standard Gibbs free energies of reactions (1) to (9) are given in Table 3.

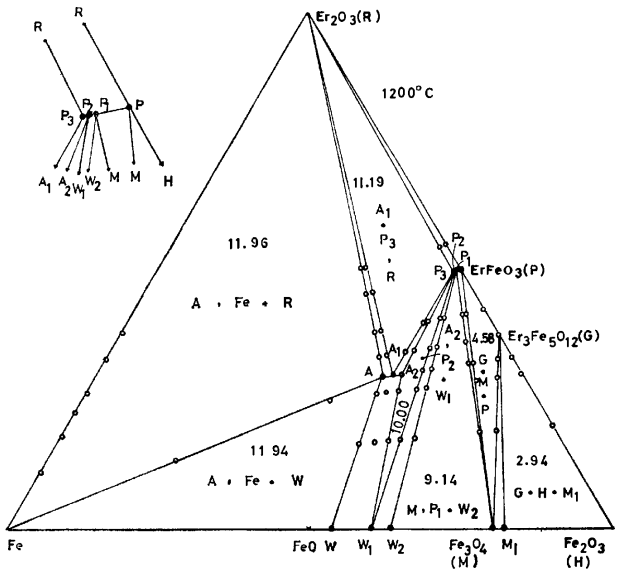

Fig. 2. Phase equilibria in the Fe–Fe_2O_3–Er_2O_3 system at 1200 °C (mol %). Numbers in the figure mean values of $-\log P_{O_2}$ at which three crystalline phases are in equilibrium state. Letters R, P, G, amd M represent stoichiometric compositions of Er_2O_3, $ErFeO_3$, $Er_3Fe_5O_{12}$, and Fe_3O_4, respectively. M_1 means the endmember of the magnetite solid solution with a chemical composition, $Fe_{2.957}O_4$. The other letters as for in Table 2.

Table 2. Composition and activity in solid solutions

Component	Composition	Symbol	$-\log P_{O_2}$	$\log a_i$
FeO	$FeO_{1.049}$	W	11.94	0
	$FeO_{1.125}$	W_1	10.00	−0.0805
	$FeO_{1.166}$	W_2	9.14	−0.150
$SmFeO_3$	$SmFeO_{2.982}$	P_1	12.68	0
	$SmFeO_{3.000}$	P	9.14	0.0512
			0.68	0.0512
$Sm_3Fe_5O_{12}$	$Sm_3Fe_5O_{12.00}$	G	3.72	0
$ErFe_2O_4$[a]	$ErFe_2O_{3.903}$	A	11.96	0
	$ErFe_2O_{3.942}$	A_1	11.19	0.0350
	$ErFe_2O_{3.995}$	A_2	10.00	0.0478
$ErFeO_3$[b]	$ErFeO_{2.973}$	P_3	11.19	0
	$ErFeO_{2.977}$	P_2	10.00	0.0213
	$ErFeO_{2.980}$	P_1	9.14	0.0240
	$ErFeO_{3.000}$	P	3.64	0.0509
$Er_3Fe_5O_{12}$	$Er_3Fe_5O_{12.00}$	G	4.58	0

a) The relationship between the composition and $\log P_{O_2}$ is, $N_O/N_{ErFe_2O_4} = 0.04494 \log P_{O_2} + 0.4447$. b) The relationship between the composition and $\log P_{O_2}$ is, $N_O/N_{ErFeO_3} = 0.03571 \log P_{O_2} + 0.0130$.

Table 3. The summary of the standard Gibbs free energy values

	Reactions	$-\Delta G°$(kcal)
(1)	$Fe + 1/2Sm_2O_3 + 3/4O_2 = SmFeO_3$	64.1±0.1
(2)	$5Fe + 3/2Sm_2O_3 + 15/4O_2 = Sm_3Fe_5O_{12}$	298.5±0.5
(3)	$2Fe + 1/2Er_2O_3 + 5/4O_2 = ErFe_2O_4$	100.8±0.1
(4)	$Fe + 1/2Er_2O_3 + 3/4O_2 = ErFeO_3$	59.7±0.3
(5)	$5Fe + 3/2Er_2O_3 + 15/4O_2 = Er_3Fe_5O_{12}$	286.2±0.7
(6)	$3SmFeO_3 + 2/3Fe_3O_4 + 1/6O_2 = Sm_3Fe_5O_{12}$	3.2±0.2
(7)	$3Fe + 2O_2 = Fe_3O_4$	154.5±0.3
(8)	$1/4Er_2O_3 + 1/2ErFe_2O_4 + 1/8O_2 = Er_2FeO_3$	9.3±0.2
(9)	$3ErFeO_3 + 2/3Fe_3O_4 + 1/6O_2 = Er_3Fe_5O_{12}$	4.1±0.3

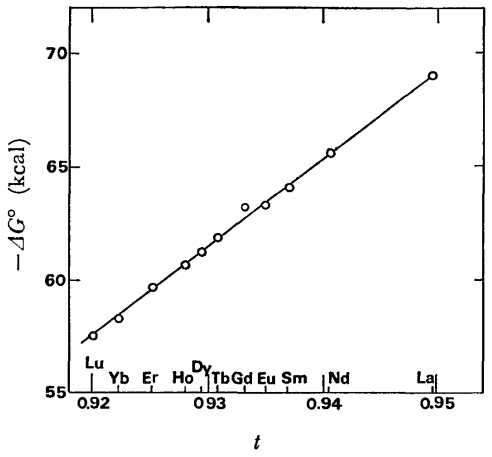

Fig. 3. The relationship between $\Delta G°$ and the tolerance factor t.

The Relationship Between the Value of $\Delta G°$ of Lanthanoid-Iron-Perovskite and the Tolerance Factor. Katsura *et al.*[20] and Kimizuka and Katsura[4] have pointed out that the standard Gibbs free energy of reactions of lanthanoid-iron-perovskite from metallic iron, lanthanoid sesquioxide, and oxygen may change proportionally with the tolerance factor defined by Goldschmidt.[21] The tolerance factor t is defined as $\gamma_A+\gamma_O=t\sqrt{2}(\gamma_B+\gamma_O)$, where γ_A, γ_B, and γ_O are the ionic radii of the A-atom, B-atom, and O-atom of the perovskite, ABO_3, respectively.

The same rule holds also for $ErFeO_3$, $HoFeO_3$,[22] and $LuFeO_3$[23] as seen in Fig. 3. The deviation from the general trend in $GdFeO_3$ is estimated to be about 400—500 cal, and is significant in considering the range of the experimental errors. A more detailed discussion will be published in the near future after the completion of the study of all the lanthanoid-iron-perovskite members.

References

1) N. Kimizuka and T. Katsura, *Bull. Chem. Soc. Jpn.*, **47**, 1801 (1974).
2) T. Sugihara, N. Kimizuka, and T. Katsura, *Bull. Chem. Soc. Jpn.*, **48**, 1806 (1975).
3) N. Kimizuka and T. Katsura, *J. Solid State Chem.*, **13**, 176 (1975).
4) N. Kimizuka and T. Katsura, *J. Solid State Chem.*, **15**, 151 (1975).
5) S. J. Schneider, R. S. Roth, and J. L. Waring, *J. Res. NBS*, **64A**, 345 (1960).
6) N. Kimizuka, A. Takenaka, Y. Sasada, and T. Katsura, *Solid State Commun.*, **15**, 1321 (1974).
7) N. Kimizuka, A. Takenaka, Y. Sasada, and T. Katsura, *Solid State Commun.*, **15**, 1199 (1974).
8) K. Kato, I. Kawada, N. Kimizuka, and T. Katsura, *Z. Krist.*, **141**, 314 (1975).
9) K. Kato, I. Kawada, N. Kimizuka, I. Shindo, and T. Katsura, *Z. Krist.*, in press (Die Kristallstruktur von $Yb_2Fe_3O_7$).
10) N. Tannieres, O. Evrard, and J. Aubry, *C. R. Acad. Sci. Paris*, **278**, 241 (1974).
11) O. Evrard, B. Malaman, F. Jeannot, N. Tannieres, and J. Aubry, *C. R. Acad. Sci. Paris*, **278**, 413 (1974).
12) O. Evrard, B. Malaman, N. Tannieres, F. Jeannot, and J. Aubry *C. R. Acad. Sci. Paris*, **279**, 1021 (1974).
13) T. Katsura and H. Hasegawa, *Bull. Chem. Soc. Jpn.*, **40**, 561 (1967).
14) I. Iwasaki, T. Katsura, M. Yoshida, and T. Tarutani, *Bunseki Kagaku*, **6**, 211 (1957).
15) S. Geller and E. A. Wood, *Acta Crystallogr.*, **9**, 563 (1956).
16) F. Bertaut and F. Forrat, *C. R. Acad. Sci. Paris*, **244**, 96 (1957).
17) G. P. Espinosa, *J. Chem. Phys.*, **37**, 2344 (1962).
18) S. Geller, H. J. Williams, and R. C. Sherwood, *Phys. Rev.*, **123**, 1962 (1961).
19) L. S. Darken and R. W. Gurry, *J. Am. Chem. Soc.*, **67**, 1398 (1945), **68**, 798 (1946).
20) T. Kastura, K. Kitayama, T. Sugihara, and N. Kimizuka, *Bull. Chem. Soc. Jpn.*, **48**, 1809 (1975).
21) V. M. Goldschmidt, T. Barth, G. Lunde, and W. H. Zachariasen, Pt. VIII Skrifter Norske Videnskaps-Akad. Oslo, I. Mat. Naturv. K I, No. 2 (1926).
22) T. Sekine and T. Katsura, unpublished data.
23) T. Sekine and T. Katsura, *J. Solid State Chem.*, **17** (1976), in press.

Table 3. NMR and IR spectra of γ-butyrolactones[a] (IIIa—f)

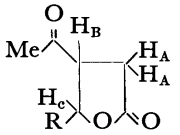

Butyrolactones	R	NMR (in $CDCl_3$) H_A(2H)	NMR (in $CDCl_3$) H_B(1H)	H_C(1H)	Me(3H)	IR (cm^{-1})[b]
IIIa	7.16(s, 5H), 1.83—2.13 (m, 5H), 2.66—3.53(m, 5H)	c)	c)	5.52 (q)	2.17 (s)	1780 1715
IIIb	7.29 (s, 5H)	2.76—2.92 (m)	3.30—3.72 (m)	5.52 (d, J=7 Hz)	2.10 (s)	1780 1715
IIIc(*trans*)	7.30(s, 5H), 5.83—6.40 (m, 1H), 6.45—6.88(m, 1H)	2.50—2.93 (m)	3.33 (q)	5.01 (t)	2.17 (s)	1785 1715
IIIc(*cis*)	7.29(s, 5H), 5.73—6.23 (m, 1H), 6.50—6.90(m, 1H)	2.53—2.97 (m)	3.78 (q)	5.39 (t)	2.10 (s)	1785 1715
IIId	3.82 (d, 2H, J=4 Hz)	2.70—2.95 (m)	3.20—3.82 (m)	4.80—5.20 (m)	2.21 (s)	1800 1680
IIIe[d]	6.00 (d, 1H, J=4 Hz)	2.40—3.02 (m)	3.20—3.82 (m)	5.00 (t)	2.21 (s)	1800 1725
IIIf	4.40(s, 1H), 4.53(d, 1H, J=3 Hz)	2.66(s, 1H) 2.80(s, 1H)	3.64 (quin)	c)	2.26 (s)	1780 1715

a) These lactones were probably composed of *cis* and *trans* isomers. b) Spectra of lactone (higher wave number) and acetyl (lower wave number) carbonyl. c) These protones were overlapped with R. d) The ratio of *cis* and *trans* isomer was *ca.* 1 : 11 by NMR spectra (the chemical shift of the methyl of *cis* isomer was 2.11). However, the other butyrolactones, except IIIc and IIIe, showed only one peak as the signal of the methyl ($CH_3C{=}O$).

Table 4. NMR spectra of δ-valerolactones[a] (IVa—f)

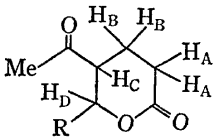

Valerolactones		H_A(2H)	H_B(2H)	H_C(1H)	H_D(1H)	Me(3H)
IVa	7.15(s, 5H), 1.53—2.27 (m, 4H), 2.77—3.10(m, 5H)	b)	b)	b)	4.33—4.75 (m)	2.18 (s)
IVb	0.97—1.15(m, 3H) 1.42—1.60(m, 2H)	2.35—2.71 (m)	1.88—2.71 (m)	2.73—3.09 (m)	4.38—4.77 (m)	2.21 (s)
IVc	3.7—3.9 (m, 2H)	2.4—2.7 (m)	1.7—2.3 (m)	2.97—3.47 (m)	4.77—5.16 (m)	2.33 (s)
IVd	7.17(s, 5H) 2.9—3.1(m, 2H)	2.33—2.67 (m)	1.9—2.3 (m)	2.6—2.9 (m)	4.7—5.1 (m)	2.10 (s)
IVe	7.33(s, 5H)	2.50—2.83 (m)	2.15 (t)	3.0—3.4 (m)	5.4 (d, J=10 Hz)	1.87 (s)
IVf	4.50(d, J=6 Hz, 2H)	2.3—2.7 (m)	2.0—2.3 (m)	3.0 (q)	b)	2.35 (s)

a) These lactones were probably composed of *cis* and *trans* isomers. b) These protones were overlapped with R.

give 1.196 g (93%) of β-acetyl-γ-butyrolactone (IIIf).

Reaction of 3,4-Dihydro-6-methyl-2H-pyran-2-one with 3-Phenylpropanal. $BF_3 \cdot OEt_2$ (0.142 g, 1 mmol) in 1 ml of methylene chloride was added into a mixture of 3,4-dihydro-6-methyl-2*H*-pyran-2-one (0.244 g, 2 mmol) and 3-phenylpropanal (0.134 g, 1 mmol) in 2 ml of methylene chloride at 0 °C. After the reaction mixture was stirred for 15 h at 0 °C, it was worked up as in the preparation of IIIf, to give 0.206 g (84%) of γ-acetyl-δ-phenethyl-δ-valerolactone (IVa).

IVb—e were obtained by the same procedure. The physical properties and analytical data of IVa—f are shown in Table 2. IR spectra of IVa—f indicated the carbonyl of lactone (1735 cm^{-1}) and acetyl (1710 cm^{-1}). NMR spectra of IVa—f are listed in Table 4.

Reaction of 3,4-Dihydro-6-methyl-2H-pyran-2-one with Formaldehyde. Formaldehyde gas, produced from paraformaldehyde (0.121 g, 4 mmol), was bubbled into a mixture of 3,4-dihydro-6-methyl-2*H*-pyran-2-one (0.224 g, 2 mmol) and $BF_3 \cdot OEt_2$ (0.284 g, 2 mmol) at 0 °C. After the reaction

The Photochemical Cycloaddition of the Enol Acetate of Dimedone to Cyclopentene

Misao UMEHARA, Tomio ODA,* Yoshinori IKEBE,** and Shinzaburo HISHIDA**

Department of Chemistry, Keio University, Hiyoshi-cho, Kohoku-ku, Yokohama 223

(Received July 19, 1975)

The photochemical cycloaddition of the enol acetate of dimedone to cyclopentene yields two stereoisomers I and II of 2-acetoxy-4,4-dimethyltricyclo[6.3.0.0^{2,7}]undecan-6-one. The NMR and IR data suggest a *cis-anti-cis* configuration for I and a *cis-anti-trans* configuration for II. The NMR and IR spectra determined on III, IV and V, the $NaBH_4$ reduction products of I and II, also support these configurations. Both of the photo adducts, I and II, lose acetic acid in the presence of an alkali to give an α,β-unsaturated ketone (VI), while it undergoes retro-aldol cleavage in the presence of an acid to give 4,4-dimethylbicyclo[6.3.0]undecane-2,6-dione (VII). A comparative study was made of the mass spectra of I, II, and VI.

The photochemical cycloaddition of the enol acetates of β-diketones to alkenes has been reported by de Mayo *et al.*[1] These photoadducts undergo retro-aldol cleavage under the basic conditions to give 1,5-diketones. Using this sequence, we undertook the photochemical cycloaddition of cyclopentene to the enolacetate of dimedone as a first step in the synthesis of terpens containing a medium-size ring. However, very few studies have been made of the stereochemistry of such photoannelation adducts. Hence, the purpose of this paper is to determine the configuration of the photo-adducts. The NMR spectral data of the photoadducts thereby obtained are difficult to analyze; hence, the configuration is not easy to determine. In the present study, the configuration was determined with the aid of an NMR-shift reagent—tris(dipivalomethanato)-europium,[2] $Eu(DPM)_3$, which has come into use in recent years.

The product, VII, resulting from the retro-aldol cleavage of the photoadducts, I and II, has a fused ring system consisting of a five-membered ring and an eight-membered ring. Compounds of such a skeleton have rarely been synthesized thus far. They constitute a partial skeleton of some sesterterpenes and are of interest in this respect.

Results and Discussion

The enol acetate of dimedone yields, upon irradiation in cyclopentene, a mixture of two stereoisomeric photoadducts, I and II, in a ratio of roughly 2 : 1. To gain some knowledge of the configuration of such photoadducts, I and II were reduced by $NaBH_4$; I gave two alcohols, III and IV, while II gave one alcohol, V.

I or II readily loses acetic acid at room temperature to yield an α,β-unsaturated ketone (VI) upon treatment with sodium methoxide or sodium hydroxide in methanol,[3] but it does not undergo retro-aldol cleavage to produce a 1,5-diketone.[1] However, I or II undergoes retro-aldol cleavage in methanol containing sulfuric acid to yield a 1,5-diketone (VII).

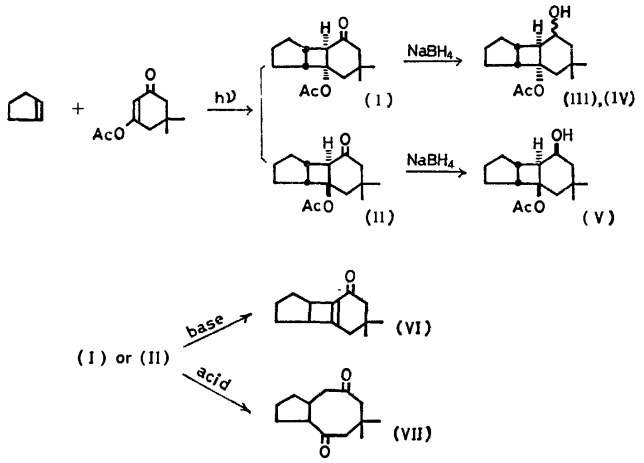

Scheme 1.

IR Spectra of I and II. As is shown in Table 1, the I photoadduct shows a ketonic carbonyl absorption at 1703 cm^{-1} which is normal for ordinary six-membered ketones. On the other hand, the II photo-adduct shows a ketonic carbonyl absorption at the unusually large wave number of 1730 cm^{-1}, which indicates the presence of a large strain in the six-membered ring of II. This finding suggests that the configuration of the ring junction between the four-membered and six-membered rings is a highly strained *trans* form in II, whereas it is *cis* in I.[4]

NMR Spectra of I and II. The NMR spectra of I and II, as measured in the usual manner, do not allow the assignment of each proton because there are not large differences in chemical shift among the protons. The NMR spectra were, therefore, measured by applying $Eu(DPM)_3$ as a shift reagent.

Figure 1(a) shows the NMR spectrum of I measured in the absence of the shift reagent, while Fig. 1(b) shows the NMR spectrum of I measured in a solution of 20 mg of I in 0.4 ml of carbon tetrachloride to which 60 mg of $Eu(DPM)_3$ had been added. Likewise, Fig. 2(a) shows the NMR spectrum of II, while Fig. 2(b) shows the NMR spectrum measured in a solution of 20 mg of II in 0.4 ml of carbon tetrachloride plus 60 mg of $Eu(DPM)_3$. In both Figs. 1 and 2, the addition of 60 mg of $Eu(DPM)_3$ caused an increase in the chemical shift and a complete separation of proton signals, and the assignment of each proton was done by

* Present address: Department of Chemistry, University of New Brunswick, Fredericton, New Brunswick, Canada.

** Present address: Naka Works, Hitachi Ltd., Ichige, Katsuta, Ibaraki 312.

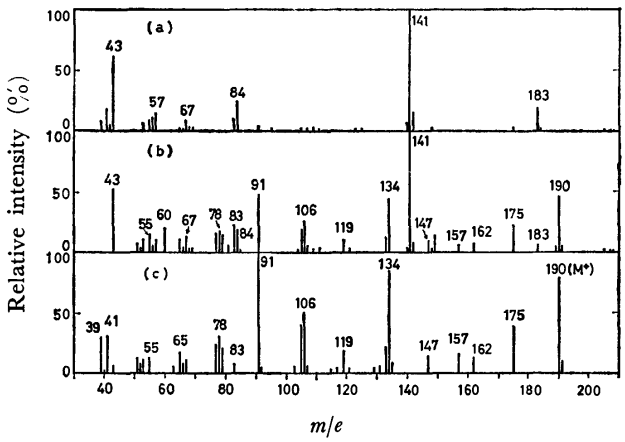

Fig. 5. Mass spectra of I, II and VI. (a) I; (b) II; (c) VI.

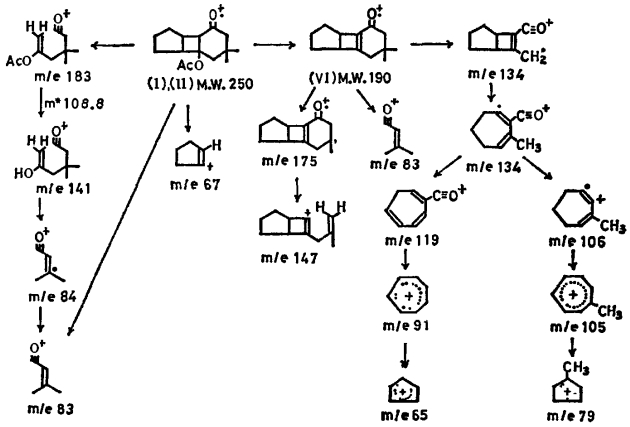

Scheme 3.

m/e=183.

Experimental

The NMR spectra were determined on a Hitachi R-22 spectrometer at 90 MHz, with TMS as the internal standard. The mass spectra measured with a Hitachi RMU-6L and RMU-7M spectrometer. The IR spectra were recorded with a JASCO IR-G spectrophotometer. The UV data were recorded with a Hitachi EPS-3 spectrophotometer. The VPC analyses were carried out on a 063 Hitachi gas chromatograph. The melting points were uncorrected.

2-Acetoxy-4,4-dimethyltricyclo[6.3.0.0^{2,7}]undecan-6-one (I and II). A solution of 16.5 g of dimedone enol acetate in 200 ml of cyclopentene was irradiated for 15 h in a Pyrex tube with a 100-W high-pressure marcury arc at 0—5 °C in a nitrogen atmosphere. The crude crystalline residue remaining after the removal of the solvent was crystallized from ether; 14.4 g were thus yielded as a mixture of I and II (65% yield). Fractional recrystallization from ether afforded 7 g of I and 3.2 g of II.

I: mp 126—127 °C. IR (see Table 1). NMR (see Fig. 1 and Table 2). Found: C, 71.76; H, 8.80%. Calcd for $C_{15}H_{22}O_3$: C, 71.97; H, 8.86%. MS (see Fig. 5(a)).

II: mp 117—118 °C. IR (see Table 1). NMR (see Fig. 2 and Table 2). Found: C, 72.04; H, 8.24%. MS (see Fig. 5(b)).

Sodium Borohydride Reduction of I. A solution of 1 g of the I adduct in 20 ml of methanol was stirred, over a 5-min period, into a solution of 0.1 g of sodium borohydride in 10 ml of methanol at 0—5 °C. The mixture was kept in an ice bath for 25 min, diluted with 150 ml of water, and extracted with ether (three times). The evaporation of the extract after drying gave an oily mixture of III and IV (1 g). VPC analysis indicated that the mixture consisted of 66% III and 34% IV. Repeated fractional crystallizations from hexane gave the pure III and IV.

III: mp 49.5—51.5 °C. IR (see Table 1). NMR ($CDCl_3$): δ 0.98 (3H, CH_3), δ 1.02 (3H, CH_3), δ 2.00 (3H, $OCOCH_3$) and δ 3.77 (m, 1H, CHOH). Found: C, 71.22; H, 9.60%. Calcd for $C_{15}H_{24}O_3$: C, 71.43; H, 9.52%

IV: mp 86—88.5 °C. IR (see Table 1). NMR ($CDCl_3$): δ 0.88 (3H, CH_3), δ 0.94 (3H, CH_3), δ 1.98 (3H, $OCOCH_3$) and δ 4.05 (m, 1H, CHOH). Found: C, 71.38; H, 9.27%.

Sodium Borohydride Reduction of II. The II adduct (1 g) was reduced by the method described above. The yielded product showed one peak in VPC and one spot in TLC. The crystallization from hexane gave 0.82 g of V (82% yield). Mp 54.5—55.5 °C (after four recrystallizations). IR (see Table 1). NMR ($CDCl_3$): δ 0.97 (3H, CH_3), δ 1.14 (3H, CH_3), δ 2.07 (3H, $OCOCH_3$) and δ 4.01 (m, 1H, CHOH). Found: C, 71.56; H, 9.34%. Calcd for $C_{15}H_{24}O_3$: C, 71.43; H, 9.52%.

4,4-Dimethyltricyclo[6.3.0.0^{2,7}]-$\Delta^{2,7}$-undecen-6-one, VI (α,β-Unsaturated Ketone). A solution of 5.9 g of photoadducts (mixture of I and II) in 65 ml of absolute methanol was stirred into a solution of sodium methoxide, prepared from 0.6 g of sodium and 50 ml of absolute methanol. The mixture was then allowed to stand at room temperature overnight. The methanol was removed under reduced pressure after neutralization with Dry Ice. The remaining oil was extracted with ether. The ethereal extract was washed with water and dried by sodium sulfate. The subsequent removal of the solvent gave 3.7 g of a pale yellow oil. After distillation. 2 g of a colourless oil was obtained (44% yield). A solution of 1.1 g of I in 50 ml of absolute methanol, in which there was dissolved 0.2 g of sodium, was allowed to stand overnight; 0.61 g of the α,β-unsaturated ketone was thus obtained (76% yield). The 0.2 g of II also produced 0.08 g of VI (53% yield); bp 136—138 °C/14 mmHg; mp 24—25 °C (after three distillations). IR: 1660 cm^{-1}, UV (ethanol): 250 nm (ε, 9250) and 322 nm (ε, 98). Found: C, 82.35; H, 9.12%. Calcd for $C_{13}H_{18}O$: C, 82.11; H, 9.47%. MS (see Fig. 5(c)). 2,4-DNP: mp 173—174 °C.

4,4-Dimethylbicyclo[6.3.0]undecane-2,6-dione, VII. A solution of 1 g of I in 50 ml of methanol containing 1.5 ml of sulfuric acid was left to stand for two weeks at room temperature. The reaction mixture was then concentrated under reduced pressure and extracted with ether. The ethereal extract was neutralized with sodium bicarbonate, washed with water, and then dried over sodium sulfate. The semicrystalline residue remaining after the removal of the ether was sublimed under reduced pressure (13 mm Hg) to give 0.46 g of the dione, VII (56% yield). Also, 1 g of II produced 0.41 g of VII (50% yield). Crystallization from hexane afforded pure crystals; mp 64—65 °C. IR (Nujol) 1695 cm^{-1}. NMR ($CDCl_3$): δ 1.11 (3H, CH_3) and δ 1.13 (3H, CH_3). Found: C, 75.14; H, 9.60%. Calcd for $C_{13}H_{20}O_2$: C, 75.00; H, 9.62%. MS: *m/e* 208 (M^+, $C_{13}H_{20}O_2$, 5%), 193 ($C_{12}H_{17}O_2$, 5), 190 ($C_{13}H_{18}O$, 11), 180 ($C_{12}H_{20}O$, 4), 152 ($C_9H_{12}O_2$, 13), 141 ($C_8H_{13}O_2$, 26), 124 ($C_8H_{12}O$, 41), 112 ($C_7H_{12}O$, 24), 95 (C_6H_7O, 43), 83 (C_5H_7O, base), 81 (C_6H_9, 23), 67 (C_5H_7, 29), 55 (C_4H_7, C_3H_3O, 24) and 41 (C_3H_5, 23).

Determination of the Rate Constants (I and II→VI). The

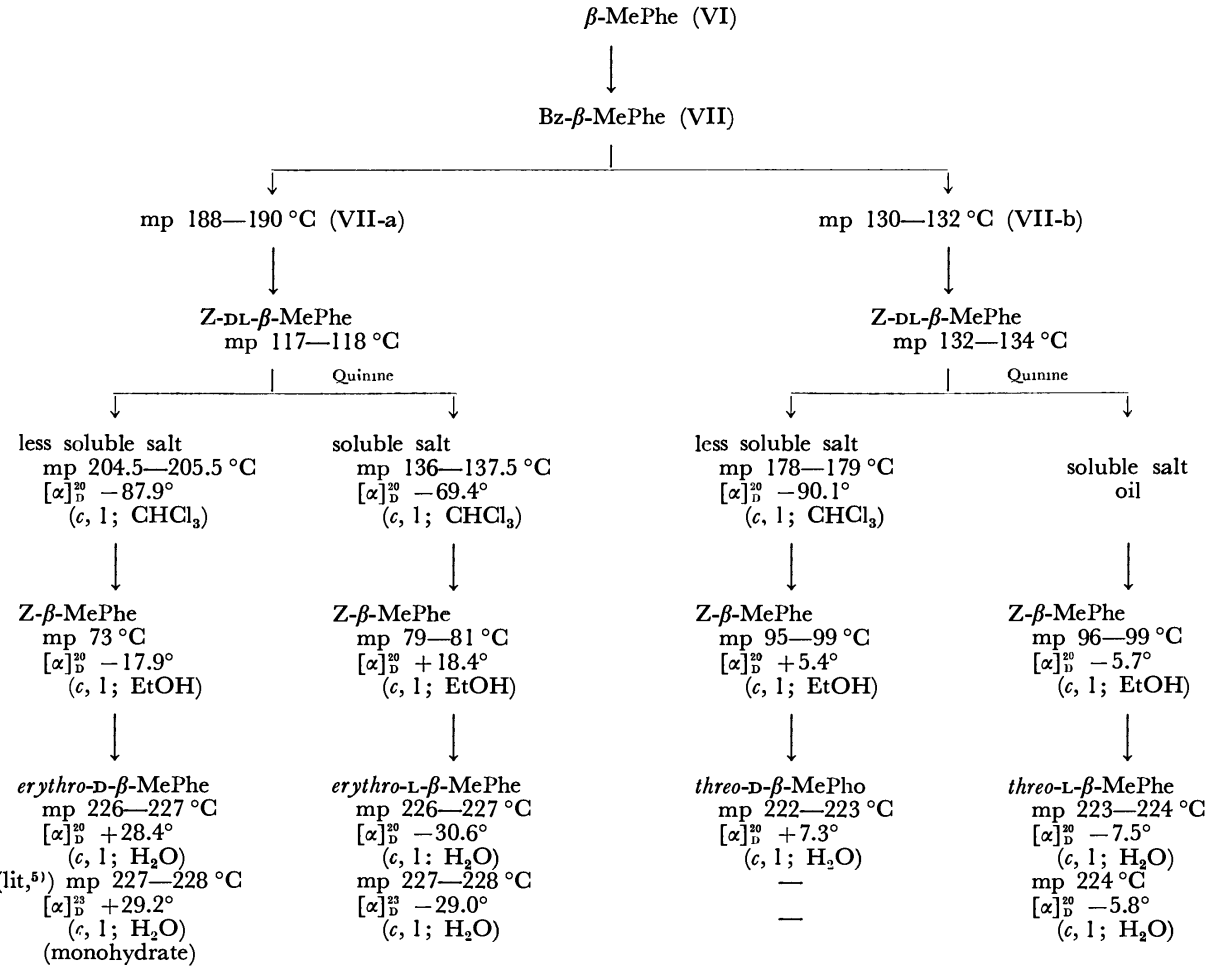

Scheme 2. Separation of β-methyl-phenylalanine (β-MePhe) into four isomers.

TABLE 1. NMR DATA OF β-METHYL-PHENYLALANINE (60 MHz, DSS)

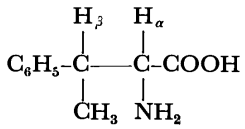

	Compound	Medium		
		D_2O	D_2O+DCl	D_2O+NaOD
$\delta_{H\alpha}$ (ppm)	VI-a	3.81	4.26	3.34
	VI-b	3.94	4.34	3.41
$\delta_{H\beta}$ (ppm)	VI-a	3.31	3.49	2.98
	VI-b	3.55	3.59	3.19
$J_{CH_3-H\beta}$ (Hz)	VI-a	6.9	7.4	6.8
	VI-b	7.2	7.5	7.2
$J_{H\alpha-H\beta}$ (Hz)	VI-a	7.5	7.2	7.5
	VI-b	4.8	6.0	5.2

It was noted that the difference in $J_{\alpha\beta}$ appeared more remarkable in a neutral medium than in an acidic or a basic condition.

In order to determine the *erythro/threo* ratio, the condensation product (III) was converted into a mixture of free amino acids (VI) by hydrolyzing it with hydrochloric acid. From the NMR spectra of the amino acids, the *erythro/threo* ratios were determined as (1.5—1.7) : 1. The benzyloxycarbonylation of the mixture of the free amino acids afforded the crystalline *threo* isomer and the oily, difficult-to-refine *erythro* derivative; the ratio of the amount of the *erythro* to that of the *threo* compounds was again found to be about 2 : 1. These results apparently indicate that the diastereoselective decarboxylation of the malonic acid derivative occurred quite similarly to Arold's observation.

To resolve each diastereomer, a diastereoselective reaction between *N*-acetyl-β-methyl-phenylalanine and hydrazine in the presence of papain was attempted, but no crystalline hydrazide was obtainable. The benzoyl derivative could not be used in this case because of its low solubility in a buffer solution of pH 5. By using 30% aqueous dioxane, it could be brought into solution, but no desired results were obtained. The resolution of the *N*-acyl derivatives by alkaloid bases was alternatively tried in various combinations; the results are shown in Table 2. The *N*-benzoyl derivative gave no definite alkaloid salt so far as we examined; with a quaternary ammonium hydroxide obtained from quinine by methylation, it gave crystalline salt, but the operations were too troublesome. As to the *erythro* derivative, the best result was obtained by treating the *N*-benzyloxycarbonyl-derivative with quinine in ethanol. *N*-Benzyloxycarbonyl-*erythro*-β-methyl-phenylalanine was mixed with equimolar quinine in ethanol, the less soluble salt was treated with hydrochloric acid to remove the quinine, and then

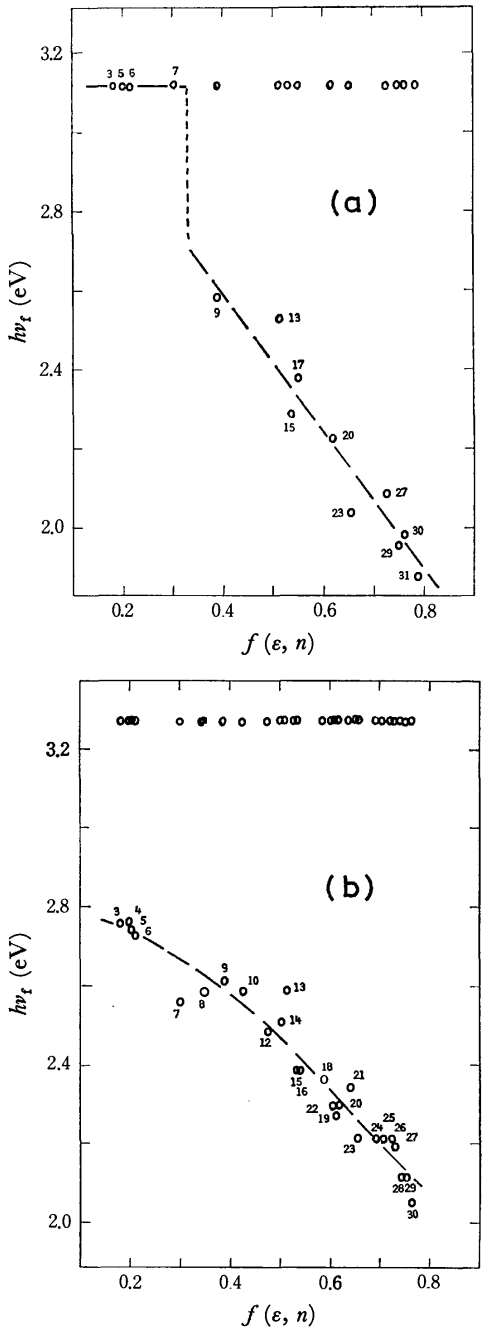

Fig. 5. Observed $h\nu_f$ *vs.* $f(\varepsilon, n)$ relations for A_2 (a) and P_2 (b).

the two moieties. Therefore, the electron transfer state is placed at higher energy than the LE state (S_1) of anthracene or pyrene and there may arise only a very weak interaction between the electron transfer configuration and the LE configuration because of the long distance between the two groups and the unfavorable geometrical configuration for the delocalization interaction. However, because their dipole moments in the CT state are much larger than those of the sandwich type exciplexes, the CT state may be stabilized rather strongly by the interaction with the polar solvent.

The energy of the CT state in solution may be given by Eq. 1, if we neglect the delocalization interaction between the two moieties.

$$\begin{aligned} E_{CT} &= I - A - C - H_s \\ &= I - A - C - (\mu_e^{eq*}/a^3)(\varepsilon - 1/2\varepsilon + 1) \\ &= I - A - C - \frac{1}{2}\mu_e^{eq*} f_\varepsilon \end{aligned} \tag{1}$$

where I and A are the ionization potential of the donor and electron affinity of the acceptor, respectively, C is the coulomb interaction energy between the donor cation and acceptor anion calculated by using the Hückel MO's putting point charges at each AO, and H_S is the solvation energy of the ion-pair. We have approximated here H_S by the interaction energy of a dipole with the surrounding dielectric continuum according to Onsager's reaction field theory. a is the cavity radius in the reaction field theory and μ_e^{eq} is the dipole moment of the excited equilibrium state. For example, the value of (μ_e^{eq*}/a^3) for S_1 was estimated to be 2.1 eV from the slope of the $h\nu_f$—$f(\varepsilon,n)$ linear relation in Fig. 3. Taking I=7.5 eV, A=0.5 eV, C= 3.2 eV, and $(\varepsilon-1/2\varepsilon+1)\approx0.26$ (the CT fluorescence appears above the value of $(\varepsilon-1/2\varepsilon+1)\approx0.26$), E_{CT} was estimated to be 3.25 eV. (For the evaluation of C, it was assumed that the long axis of anthracene is parallel with the short axis of DMA and the angle between the short axis of anthracene and the long axis of DMA is 109°28′.) Since the ground state will have no dipole moment due to CT from DMA to anthracene, the Franck-Condon (FC) ground state may be destabilized with respect to solvation. Again by using the dielectric continuum approximation, the destabilization energy amounts to

$$\begin{aligned} \delta E_g^{FC} &= (\mu_e^{eq*}/a^3)[(\varepsilon - 1/2\varepsilon+1) - (n^2 - 1/2n^2 + 1)] \\ &= (1/2)\mu_e^{eq*}(f_\varepsilon - f_n) \end{aligned} \tag{2}$$

$\delta E_g^{FC}\approx0.12$ eV at $(\varepsilon-1/2\varepsilon+1)\approx0.26$ since $(n^2-1/2n^2+1)\approx0.2$ for almost all solvents used in the present work. Therefore, $h\nu_f=E_{CT}-\delta E_g^{FC}=3.13$ eV. This $h\nu_f$ value is almost equal to that of anthracene LE fluorescence. The circumstance in the case of A_2 and P_1 seems to be quite analogous. Therefore, the solvent-induced change of the electronic structure of these compounds may be regarded as a solvent-induced reversal of two energy levels which do not interact with each other or do interact only very weakly. In other words, the solvent-induced changes of the fluorescence spectra of these compounds can be interpreted satisfactorily on the basis of the solvation of the CT state calculated with the dielectric continuum theory. However, as was pointed out in the introductory part, it may be possible that the solvation of the CT state is accompanied by some change of the geometrical structure. For example, the molecular plane of anthracene or pyrene might be perpendicular to that of DMA in the CT fluorescent state, so that the electronic delocalization interaction between the two moieties would become negligibly small.

The change of the excited electronic structure of these molecules induced by solvation can be observed also by changing the temperature of the solution, as indicated in Fig. 6 for the case of A_1 in dibutyl ether. At high temperatures, one can observe only the anthracene LE fluorescence. When the temperature is lowered,

TABLE 2. SOLVOLYSES OF **3** AND **5**.

Substrate	Reaction medium	Temp °C	Time h	Product			
				6		**4**	
				dl	*meso*	*threo*	*erythro*
erythro-**5** (0.1 M)	98% EtOH–KOAc (0.2 M)	100	1	8	trace	75	6
threo-**5** (0.2 M)	98% EtOH–KOAc (0.2 M)	100	1	—	4	2	86
erythro-**5** (1 M)	Ac_2O-KOAc (1 M)	130	1	22	78		
erythro-**5** (1 M)	HOAc[a]–Ac_2O(2 M)–KOAc (1.5 M)	115	1	8	92		
threo-**5** (1 M)	HOAc[a]–Ac_2O(2 M)–KOAc (1.5 M)	100	2	87	13		
erythro-**3** (1 M)	HOAc[a]–Ac_2O(2 M)–KOAc(1.5 M)	140	4	20	80		
threo-**3** (1 M)	HOAc[a]–Ac_2O(2 M)–KOAc(1.5 M)	140	4	70	30		
threo-**3** (0.1 M)	HOAc[b]–Ac_2O(0.2 M)–KOAc(0.2 M)	130	7	trace	30	—	70
			13	7	76	—	17

a) Dry acetic acid. b) Moist acetic acid.

(**6**) with complete inversion. Acetic anhydride–acetic acid (50: 50 by volume) mixture which was prepared without special precaution to remove the trace amount of water gave retention product of **4**. The results with acetic acid were not reproducible. From run to run, the product ratios of **4** (with retention) and **6** (with inversion) changed from 70 :30 to 30: 70. It appears that the difficulty of removing trace amount of water would be responsible for such observations. Since the acetylation of the produced **4**, which proceeds gradually under the conditions, gives **6** with retention, the product analyses after sufficient reaction times give the results as if the steric course of the direct acetolysis is affected by the presence of trace amount of water. The same change of the steric course by the presence of water reported by Winstein and his co-workers[1] may be explained by the same way. It is concluded that the reaction of **1** with water is much faster than those with other reagents and proceeds through the intermediate A or B.

Solvolyses of 4-Acetoxy-2-chloropentane (3) and 4-Acetoxy-2-pentyl tosylate (5). The steric courses of the solvolyses of **3** and **5** which are expected to proceed through AcO-6 cation have been studied by comparing with the results of the reactions of **1** mentioned above. The starting materials of *erythro*- and *threo*-**3** and -**5** were prepared by chlorination and tosylation of the half esters **4**, which were obtained by the hydrolyses of *cis*- and *trans*-**1**, respectively. The results of solvolyses are summarized in Table 2.

The reactions proceeded to give 2,4-diacetoxypentane (**6**) and **4** with no detectable amount of by-product, and were almost complete under the conditions described. By gas-chromatography, the product distributions were determined.

In 98% ethanol containing potassium acetate, *erythro*- and *threo*-**5** gave *threo*- and *erythro*-**4** as the main products with inversion, respectively. Since the solvolyses of these compounds through planar carbonium ion without participation should form the same 50: 50 mixtures of *threo*- and *erythro*-**4**, the mechanism depicted in Fig. 3 appears to be the most probable. Formations of AcO-6 cations with inversion and the subsequent reactions with water, which have been shown to give the retention products, should result in the formation of inversion products. The formations of the retention products in **4** and the inversion products in **6** appear to show the solvolysis without participation proceeded as a minor reaction.

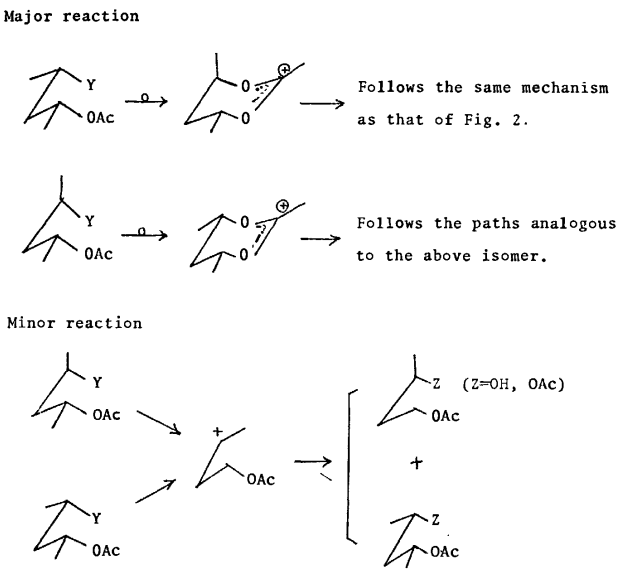

Fig. 3. Mechanism of the solvolysis of 4-acetoxy-2-pentanol derivatives.

The main products of the acetolyses of *erythro*- and *threo*-**5** in dry acetic anhydride and acetic anhydride–acetic acid mixtures containing potassium acetate were *meso*- and *dl*-**6** with retention, respectively. Double inversions in AcO-6 cation formation and the subsequent reaction of the cation with acetate ion explain the

TABLE 2. SPECTRAL DATA FOR 1-ARYL-2,5-DIMETHYLPYRROLES

Compound	IR	Aryl-H	NMR		Others
			Pyrrole-H 2H-singlet	CH_3 6H-singlet	
1	3410, 3250, 1620, 1500	7.4—6.7 (m)	5.97	1.96	3.0—3.1 (bs, 2H)
4	1605, 1505	7.4—7.0 (m)	5.66	2.00	
5	3300, 1590, 1500	7.3—6.8 (m)	5.73	1.96	4.9—5.1 (b, 1H)
6	1500	7.3—6.9 (m)	5.70	1.83	1.93 (s, 3H)
7	1590, 1490	7.9—7.6 (m, 1H) 7.4—6.9 (m, 3H)	5.67	1.90	
8	3470, 3380, 1620, 1520	7.00 6.73 (ABq, J=9)	5.85	2.02	3.75 (bs, 2H)
9	1500	7.36 7.03 (ABq, J=9)	5.66	1.97	

reaction of **1** with trifluoroacetic anhydride gave **3** (mp 42 °C) in 40% yield, together with **2**. **3** was so labile that the sample became deeply colored and melted during storage. However, its NMR spectrum in TFA did not change remarkably at 25 °C for 48 h. Therefore, this possibility can apparently be excluded.

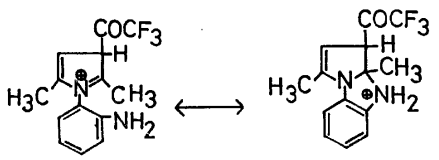

In conclusion, it has been shown that the 1,5-participation of an amino group is possible in the electrophilic substitution of a pyrrole derivative, even TFA acting as an electrophilic reagent in such a case.

Experimental

All the mps and bps are uncorrected. The NMR spectra were taken with a Varian T-60 instrument, and the chemical shift data are reported in ppm (δ) downfield from tetramethylsilane as an internal standard, with a coupling constant (J) in Hz. The mass spectra were run on a Hitachi RMU-7 apparatus with an ionizing potential of 70 eV. The IR spectra were recorded on a Hitachi 215 spectrophotometer, in Nujol, while the absorption maxima are reported in cm^{-1}. The spectral data for the pyrrole derivatives are summarized in Table 2.

The pyrrole derivatives were prepared by the following general method. Into an equimolar mixture of acetonylacetone and the aniline derivative dissolved in benzene, was added a drop of phosphoryl chloride. Then the solution was heated under reflux for 2 to 4 h, taking off the produced water as an azeotropic mixture. After washing, drying, and the evaporation of the solvent, the product was purified either by recrystallization or by distillation; yield, 75—90%.

1-Phenyl-2,5-dimethylpyrrole (4): mp 49—50 °C, lit,[5] 51—52 °C.

1-(2-Hydroxyphenyl)-2,5-dimethylpyrrole (5): mp 95—97 °C, lit,[6] 95 °C.

1-(2-Methylphenyl)-2,5-dimethylpyrrole (6): bp 78 °C (2 Torr), lit,[7] 105 °C (7.5 Torr).

1-(2-Iodophenyl)-2,5-dimethylpyrrole (7): mp 69—72 °C. Found: C, 48.57; H, 4.09; N, 4.70%. Calcd for $C_{12}H_{12}NI$: C, 48.48; H, 4.04; N, 4.52%.

1-(4-Aminophenyl)-2,5-dimethylpyrrole (8): mp 95—97 °C, lit,[7] 97.5—98 °C.

1-(4-Chlorophenyl)-2,5-dimethylpyrrole (9): mp 49—50 °C, lit,[5] 56—57 °C.

These six compounds were stable in TFA at 50 °C for 48 h and could be recovered intact.

1-(2-Aminophenyl)-2,5-dimethylpyrrole (1): mp 50—54 °C, *m/e* (M^+) 186. In addition to the general method, this compound was also prepared by the following procedure. An equimolar mixture of acetonylacetone and *o*-phenylenediamine was dissolved in an aqueous solution of citric acid and sodium hydrogenphosphate adjusted at pH 5.0, the mixture was then stirred at room temperature for 4 h. The precipitates were filtered, washed thoroughly with water, and recrystallized from cyclohexane to give **1** in a 90% yield.

Though the melting points (50—54 °C) of all samples obtained in several runs were different from that (77 °C) reported in the literature,[7] the product was obviously **1**, judging from the data given in Table 2.

1-(2-Aminophenyl)-2,5-dimethyl-3-trifluoroacetylpyrrole (2). A solution of **1** (10 g) dissolved in TFA (65 ml) was kept for 48 h in a thermostat maintained at 25 °C. During this experiment, an aliquot was subjected to NMR measurement at regular intervals in order to observe the relative ratio of the integral intensities between the signals due to the dimethyl groups of the starting **1** and that due to the product (**2**). The half-life of this reaction was 3.5 h, according to such observations. After being poured onto crushed ice, the mixture was neutralized with sodium hydrogencarbonate. The precipitates were filtered and recrystallized from light petroleum; mp 84—86 °C; purified product in a 20% yield. Found: C, 59.27; H, 4.58; N, 9.87%. Calcd for $C_{14}H_{13}N_2OF_3$ C, 59.57; H, 4.61; N, 9.93%.

Reaction of 1 with Trifluoroacetic Anhydride. A mixture of **1** (930 mg, 5 mmol) and trifluoroacetic anhydride (1.12 g, 7 mmol) dissolved in dichloroethane (10 ml) was stirred at room temperature for 1 h. After being poured into ice–water, the mixture was extracted with dichloroethane. The organic layer was washed with aqueous sodium hydrogencarbonate and then with water, after which it was dried over anhydrous sodium sulfate. After the evaporation of the solvent, the residue was separated into components by column chromatography using alumina (10 g). Four compounds were eluted in the following order by a mixture of light petroleum and benzene:

(1) 1-(2-Trifluoroacetylaminophenyl)-2,5-dimethylpyrole (**3**); mp 42 °C, (370 mg). Found: C, 60.51; H, 4.75; N, 10.22%. Calcd for $C_{14}H_{13}N_2OF_3$: C, 59.57; H, 4.61; N, 9.93%. Elementary analysis was unstatisfactory because of its high unstability. IR: 3400, 1740, 1600; NMR: 8.51,

Table 7. Intermolecular distances (l/Å) less than 3.0 Å

(1) MONa complex								
O(6′,G1)-O(W6)		2.85	O(W1)-O(W5)	(c)	2.85	O(5,G3)-O(W2)	(d)	2.93
O(6′,G2)-O(W2)		2.75	O(6′,G2)-O(6′,G3)	(c)	2.65	Na-O(W1)	(d)	2.51
O(W4)-O(W6)		2.74	Na-O(W2)	(c)	2.89	O(2,G2)-Na	(e)	2.90
O(W4)-O(W5)		2.61	O(5,G2)-Na	(d)	2.86	O(3,G1)-O(W3)	(e)	2.93
O(6′,G3)-O(W1)	(a)	2.86	O(5,G1)-O(W1)	(d)	2.85	O(2,G1)-O(W1)	(e)	2.77
O(3,G1)-O(6,G1)	(b)	2.78	O(6′,G2)-Na	(d)	2.91	O(2,G2)-O(W5)	(e)	2.93
O(3,G2)-O(6,G2)	(b)	2.79	O(W2)-O(W2)	(d)	2.68	O(2,G3)-O(W2)	(e)	2.75
O(3,G3)-O(6,G3)	(b)	2.87						
(2) MOK complex								
O(6′,G1)-O(W6)		2.77	O(6′,G2)-O(6′,G3)	(c)	2.71	O(6′,G2)-K	(d)	2.92
O(6′,G2)-O(W2)		2.74	K-O(W2)	(c)	2.78	K-O(W1)	(d)	2.69
O(W4)-O(W5)		2.75	O(W1)-O(W5)	(c)	2.80	O(2,G2)-O(W5)	(e)	2.84
O(6′,G3)-O(W1)	(a)	2.86	O(5,G2)-K	(d)	2.97	O(2,G1)-O(W1)	(e)	2.75
O(3,G1)-O(6,G1)	(b)	2.78	O(5,G3)-(W2)	(d)	2.91	O(2,G2)-K	(e)	2.80
O(3,G2)-O(6,G2)	(b)	2.74	O(W2)-O(W5)	(d)	2.69	O(2,G3)-O(W2)	(e)	2.74
O(3,G3)-O(6,G3)	(b)	2.82	O(5,G1)-O(W1)	(d)	2.82			

Symmetry code	Symmetry operator	Symmetry code	Symmetry operator
none	$x,\ y,\ z$	c	$1/2-x,\ 1/2+y,\ -z$
a	$x,\ -1+y,\ z$	d	$1/2-x,\ -1/2+y,\ z$
b	$x,\ y,\ 1+z$	e	$1/2-x,\ -1/2+y,\ 1-z$

between the anion in the channel and the cation outside the channel. A similar disorder of the "guest" molecule has been found in the 2 : 1 complex of pyromellitic dianhydrate with *trans*-4-methylstilbene.[17]

In the crystal, the hydrogen-bonding contact between primary hydroxyl groups with the *gauche-gauche* conformation is observed between O(6′, G2) and O(6′, G3) ($1/2-x$, $1/2+y$, $-z$). The space outside the channel is filled with water molecules and cations. The water molecules form a hydrogen-bonding network with each other or with hydroxyl groups of α-CDx. O(W1), O(W2), O(W3), and O(W4) are located at positions similar to those in the potassium acetate complex. In Methyl Orange complexes, a relatively small electron density peak was observed at the special position on the electron density map. We considered it that of a water molecule(O(W6)) with an occupancy of 0.25, since it has hydrogen-bonding contacts with water and a hydroxyl group of α-CDx; the distances of O(W6)···O(6′, G1) and O(W6)···O(W4) in the MONa complex are 2.85 and 2.74 Å respectively.

The author wishes to thank Dr. Hisashi Uedaira for supporting this study and for his useful discussions. The author also wishes to acknowledge the helpful discussions and critical comments on the manuscript of Professor Jiro Tanaka of Nagoya University. The computation was carried out on a HITAC 8450 computer in our laboratory.

References

1) W. Lautsch, W. Brosser, W. Biedermann, and H. Gnichtel, *J. Polym. Sci.*, **17**, 479 (1955).
2) F. Cramer, W. Saenger, and H. -Ch. Spatz, *J. Am. Chem. Soc.*, **89**, 14 (1967).
3) A. Hybl, R. E. Rundle, and D. E. Williams, *J. Am. Chem. Soc.*, **87**, 2779 (1965).
4) R. K. McMullan, W. Saenger, J. Fayos, and D. Mootz, *Carbohyd. Res.*, **31**, 211 (1973).
5) P. C. Manor and W. Saenger, *J. Am. Chem. Soc.*, **96**, 3630 (1974).
6) W. Saenger and M. Noltemeyer, *Angew. Chem.*, **86**, 594 (1974).
7) W. Saenger, R. K. McMullan, J. Fayos, and D. Mootz, *Acta Crystallogr.*, **B30**, 2019 (1974).
8) K. Harata, *Bull. Chem. Soc. Jpn.*, **48**, 2409 (1975).
9) R. K. McMullan, W. Saenger, J. Fayos, and D. Mootz, *Carbohyd. Res.*, **31**, 37 (1973).
10) A. W. Hanson, *Acta Crystallogr.*, **B29**, 454 (1973).
11) "International Tables for X-Ray Crystallography," Vol. III, Birminghan: Kynoch Press (1965), pp. 201—208.
12) C. J. Brown, *J. Chem. Soc., A*, **1966**, 927.
13) G. J. Quigley, A. Sarco, and R. H. Marchessault, *J. Am. Chem. Soc.*, **92**, 5834 (1970).
14) S. C. C. Shirley and G. A. Jeffrey, *Acta Crystallogr.*, **23**, 1038 (1967).
15) W. R. Busing and H. A. Levy, *Acta Crystallogr.*, **17**, 142 (1964).
16) H. Kim and R. D. Rosenstein, *Acta Crystallogr.*, **22**, 648 (1967).
17) T. Kodama and S. Kumakura, *Bull. Chem. Soc. Jpn.*, **47**, 2146 (1974).

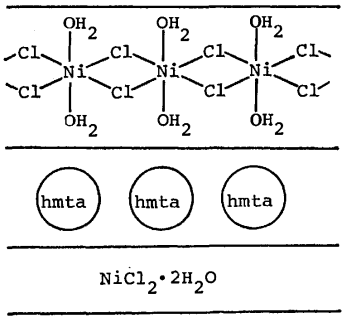

Fig. 4. Postulated structure of $NiCl_2(hmta)_2 \cdot 2H_2O$, in which hmta molecules are captured between chains of the composition of $NiCl_2 \cdot 2H_2O$.

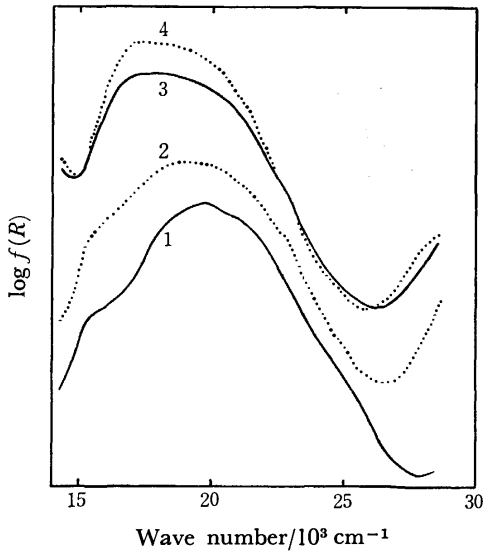

Fig. 5. Visible reflectance spectra of (1) $Co(NO_3)_2(hmta)_2 \cdot 10H_2O$, (2) $Co(NO_3)_2(hmta)_2 \cdot 4H_2O$, (3) $Co(NO_3)_2(hmta)_2 \cdot 2H_2O$ and (4) $Co(NO_3)_2(hmta)_2$.

and four bridging chlorine atoms in a distorted square plane, the dihydrate complex also seems to be composed of similar units (or chains) of $NiCl_2 \cdot 2H_2O$ and of hmta captured between them, probably by hydrogen bondings (Fig. 4).

From the reflectance and infrared spectra, the structure of $NiCl_2(hmta)_2$ and $NiBr_2(hmta)_2$ formed in the next stage was found to be identical with that of the other anhydrous halide complexes. The results of the nickel chloride complex indicate that Cl^- enters into the coordination sphere more easily than hmta.

$Co(NO_3)_2(hmta)_2 \cdot 10H_2O$ loses its water molecules in three steps. The visible reflectance spectra of the cobalt nitrate complexes in each dehydration step are shown in Fig. 5, together with that of the decahydrate. In the first step ($-6H_2O$), the octahedral structure and T_d symmetry of hmta are retained, and the tetrahydrate formed gives strong infrared bands at 1300 and 1440 cm^{-1} (curve 2, Fig. 6), which can be ascribed to the two NO stretching bands of unidentate NO_3^- ligands.[10] The tetrahydrate can thus be described as $[Co(NO_3)_2(H_2O)_4] \cdot 2hmta$.

The dihydrate formed in the second step ($-2H_2O$)

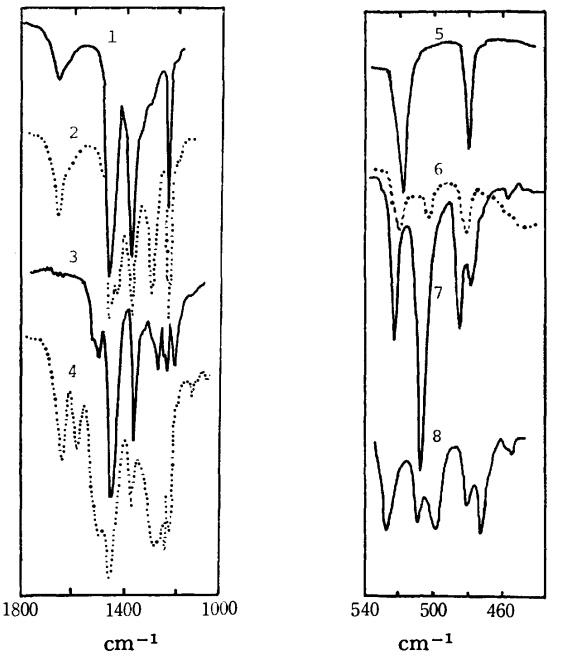

Fig. 6. Infrared spectra of (1) $Co(NO_3)_2(hmta)_2 \cdot 10H_2O$, (2) $Co(NO_3)_2(hmta)_2 \cdot 4H_2O$, (3) $Co(NO_3)_2(hmta)_2$, (4) $Ni(NO_3)_2(hmta)_2$, (5) $Co(NCS)_2(hmta)_2 \cdot 4H_2O$, (6) $Ni(NCS)_2(hmta)_2 \cdot 2.5H_2O$, (7) $Co(NCS)_2(hmta)_2$ and (8) $Ni(NCS)_2(hmta)_2$.

shows an electronic spectrum which is intermediate between the spectrum of a typically octahedral complex and that of a typically tetrahedral one. In this step, the $\bar{\nu}_{max}$ value decreases and $\log f(R)$ increases, but the changes are not so large as those observed in typical octahedral→tetrahedral changes; no definite characteristic splitting of the "*tetrahedral band*" could be observed. This suggests that the dihydrate, and the anhydrous complex which shows a similar electronic spectrum, are deformed octahedral complexes and not simple tetrahedral ones.

On the other hand, the infrared spectra of these two complexes show strong bands at 1290 and 1505 cm^{-1}, which can be ascribed to the NO stretching bands of bidentate NO_3^- ligands.[10] It was also found that the anhydrous complex shows very weak bands at *ca.* 1710 and 1760 cm^{-1}, their positions indicating the presence of bidentate NO_3^-.[11] The symmetry of hmta in the dihydrate is T_d, and that in the anhydrous complex C_{3v}.

All these data lead to the formulation of the dihydrate as $[Co(NO_3)_2(H_2O)_2] \cdot 2hmta$, and that of the anhydrous complex as $[Co(NO_3)_2(hmta)_2]$.

The nickel nitrate complex $Ni(NO_3)_2(hmta)_2 \cdot 10H_2O$ also loses its water molecules in three steps. The visible reflectance spectra indicate that the octahedral structure is retained through all the steps. The ionic NO_3^- of the original complex is transformed into unidentate NO_3^- in the first step, further change into bidentate NO_3^- occurring in the final step (curve 4, Fig. 6). The T_d symmetry of hmta was retained until the second step and changed to C_{3v} in the final step. The nickel in the anhydrous complex thus seems to be surrounded octahedrally by two bidentate

Mechanism for Light Induced Hydrogen Isotope Exchange in Benzonitrile

Masayuki YOSHIDA, Hiroyuki KANEKO, Akihide KITAMURA,** Tomiyasu ITO, Kunio OOHASHI,* Naotake MORIKAWA,* Hirochika SAKURAGI, and Katsumi TOKUMARU**

Department of Chemistry, Faculty of Science, The University of Tokyo, Bunkyo-ku, Tokyo 113

**Radioisotope Centre, The University of Tokyo, Bunkyo-ku, Tokyo 113*

***Institute of Chemistry, The University of Tsukuba, Sakura-mura, Nihari-gun, Ibaraki-ken 300-31*

(Received March 5, 1976)

Light induced tritiation of benzonitrile with diethylamine[N^{3}H] or triethylamine-tritiated water was studied with respect to quenching of benzonitrile fluorescence by the amines and the tritium distribution in the nucleus. A mechanism involving an exciplex possessing charge transfer nature was proposed.

It is well known that photolysis of thiols yields hydrogen atoms, and this method has been used to study the properties of the hydrogen atom in solution.[1,2] Thus, Pryor and his co-workers[2] have reported the aromatic substitution by tritium atoms generated by photolysis of benzenethiol[S^{3}H]. We have also studied[3] the light induced tritiation of aromatic compounds with 1-propanethiol[S^{3}H] in respect of the tritium distribution in the nucleus and the relative rate of tritiation, and found that the nuclear tritium distribution data are different from those reported by Pryor.[2] Kinetic studies[4] have shown that the rate constants for the reaction of hydrogen atoms with aromatic compounds vary only between 2.4×10^8 and 26×10^8 M^{-1} s^{-1}. Electron-donating substituents on the aromatic nucleus enhance the rate and electron-withdrawing groups retard the rate, indicating an electrophilic character of hydrogen atoms for the reaction.[4] On the contrary, our work with 1-propanethiol showed that the rate of nuclear tritiation relative to benzene, obtained in competitive methods, is extremely high in benzonitrile,[3] methyl benzoate,[3] and terephthalonitrile.[5] Furthermore, fluorescence of terephthalonitrile in benzene was quenched by 1-octanethiol with the quenching rate constant near to the diffusion-controlled value.[5] On the basis of these results a mechanism involving a reaction of singlet excited aromatic compounds with thiols was proposed for the tritiation reaction, at least in the case of benzonitrile, methyl benzoate, and terephthalonitrile.

This consideration reminds us the photoreaction of aromatic compounds with amines, in which singlet excited aromatic compounds are demonstrated to interact with amines.[6] Thus, the possibility that such interaction may be followed by hydrogen exchange led us to investigate the positional reactivity of light induced tritiation of benzonitrile with amines as well as quenching of the lowest excited singlet state of aromatic nitriles by amines. The results are interpreted in terms of a mechanism involving formation of an exciplex followed by its decay to a radical pair.

Results and Discussion

Fluorescence Quenching of Aromatic Nitriles. Fluorescence of benzonitrile, α-naphthonitrile, and terephthalonitrile was strongly quenched by diethylamine and triethylamine in benzene. The Stern-Volmer plots of the reciprocal of relative fluorescence intensities against amine concentrations were linear in all compounds investigated, and the slopes of the Stern-Volmer plots ($k_q\tau_s$) are shown in Table 1, where k_q is the rate constant of the bimolecular quenching process, and τ_s is the lifetime of the singlet state in the absence of the amines in aerated benzene. Assuming diffusion-controlled oxygen quenching (1.5×10^{10} M^{-1} s^{-1}),[7] the effect of air saturation on fluorescence intensity affords an estimate of τ_s (air) in benzene; benzonitrile, 25 ns; α-naphthonitrile, 12 ns; terephthalonitrile, 18 ns. The observed $k_q\tau_s$ values for the amines are divided by the τ_s values and the resulting k_q values are listed in Table 1. The quenching rate constants (k_q) of diethylamine are several times larger than those of triethylamine and are close to the diffusion limit. The higher efficiency of the quenching, therefore, indicates the interaction of the singlet excited aromatic compounds with the ground state amine. Furthermore,

TABLE 1. QUENCHING OF FLUORESCENCE FROM AROMATIC NITRILES BY AMINES IN AERATED BENZENE

Fluorescer	Quencher	$k_q\tau_s$, M^{-1}	$k_q\times10^{-9}$, M^{-1} s^{-1}
Benzonitrile	$HN(C_2H_5)_2$	56.9	2.3
	$N(C_2H_5)_3$	9.43	0.38
α-Naphthonitrile	$HN(C_2H_5)_2$	92.6	7.5
	$N(C_2H_5)_3$	10.5	0.85
Terephthalonitrile	$HN(C_2H_5)_2$	174	9.8
	$N(C_2H_5)_3$	18.8	1.1

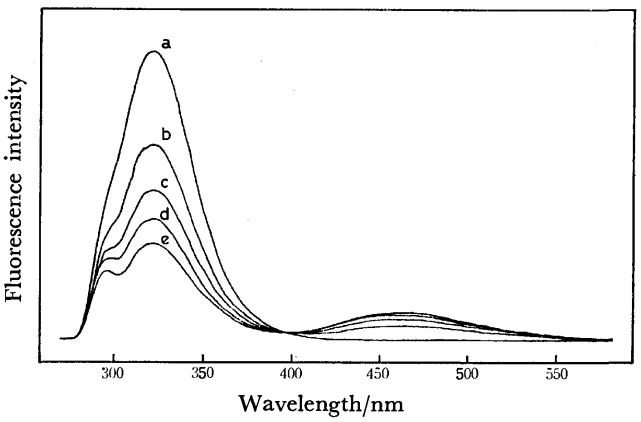

Fig. 1. Fluorescence of benzonitrile (6.14×10^{-3} M) in benzene in the presence of triethylamine. Concentration of quencher (M): a, nil; b, 5.64×10^{-3}; c, 1.13×10^{-2}; d, 1.69×10^{-2}; e, 2.26×10^{-2}.

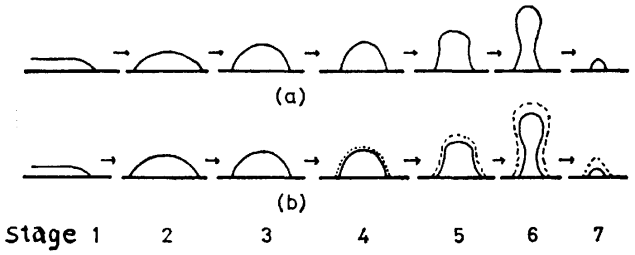

Fig. 8. Schematic diagram of the rolling up process of oily soils.
a) oleic acid or olive oil, b) lauryl alcohol.

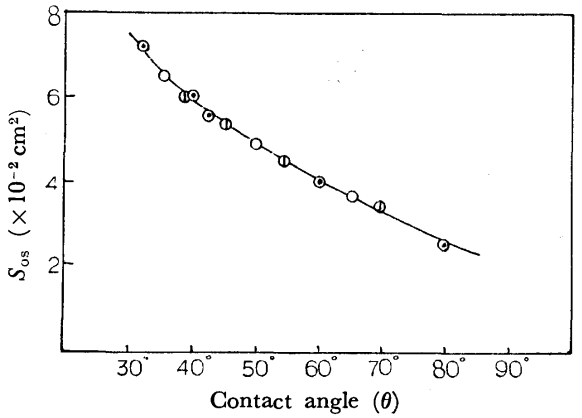

Fig. 9. The droplet/substrate interfacial area as a function of contact angle of the droplet on the substrate.
⊙: oleic acid, ◑: olive oil, ○: lauryl alcohol.

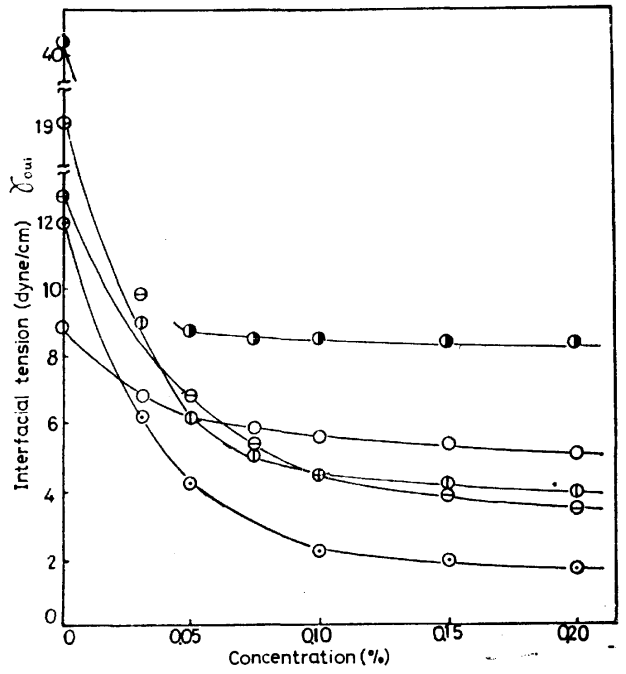

Fig. 10. The effect of NaDBS on the interfacial tension at oily soil/water interface at 30 °C.
⊙: oleic acid, ◑: olive oil, ○: lauryl alcohol, ⊖: oleyl alcohol, ◑: liquid paraffin.

containing no builders.

Discussion of the Rolling-up Phenomenon. It is well known that the rolling-up of oily soils occurs at the

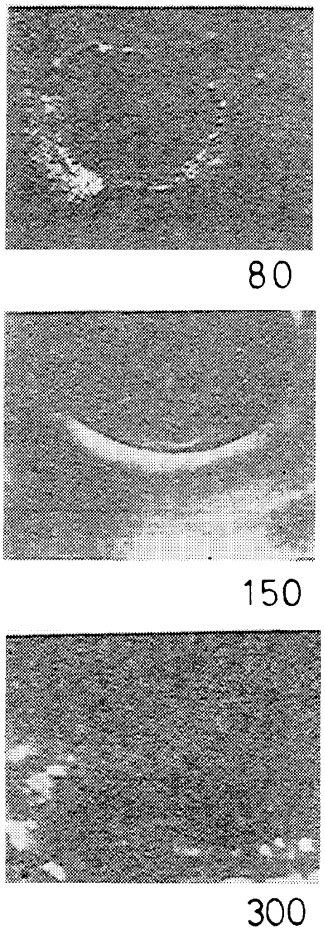

Fig. 11. The microscopic photograph of oily soils in 0.150% NaDBS solution with crossed nicols (number shows the time in minutes after immersion into the solution).
a) oleic acid, b) lauryl alcohol, c) oleyl alcohol.

contact angle (θ) of 180° on the substrates of various kinds of textile fibers.[4,6,9] However, as is shown in Fig. 1, on a low-energy surface such as PP sheet, rolling-up occurs at $0°<\theta<90°$. The process of rolling-up for oleic acid, olive oil, and lauryl alcohol is illustrated schematically in Fig. 8 (a) and (b). In the initial stages [up to Stage 4 in Fig. 8 (a) or up to Stage 3 in Fig. 8(b)], the droplet/substrate contact area (S_{os}) is plotted against the contact angle of the droplet on the substrate in Fig. 9. From these results, the area of S_{os} seems to decrease with an increase in the contact angle of the droplet. The process in Fig. 8 is believed to be caused by the reduction of interfacial tension as a result of the adsorption of surfactant molecules to soil/water and substrate/water interfaces.[3,4,6]

The interfacial tension between oily soils and the NaDBS solution are shown in Fig. 10; the interfacial tension for polar oily soils decreases remarkably with an increase in the surfactant concentration. From the results, the surfactant can be expected to be adsorbed on the surface of polar oily soils.

It seems reasonable to assume that there are three substantial forces by which a liquid oily droplet may be removed by rolling-up in a detergent solution: the

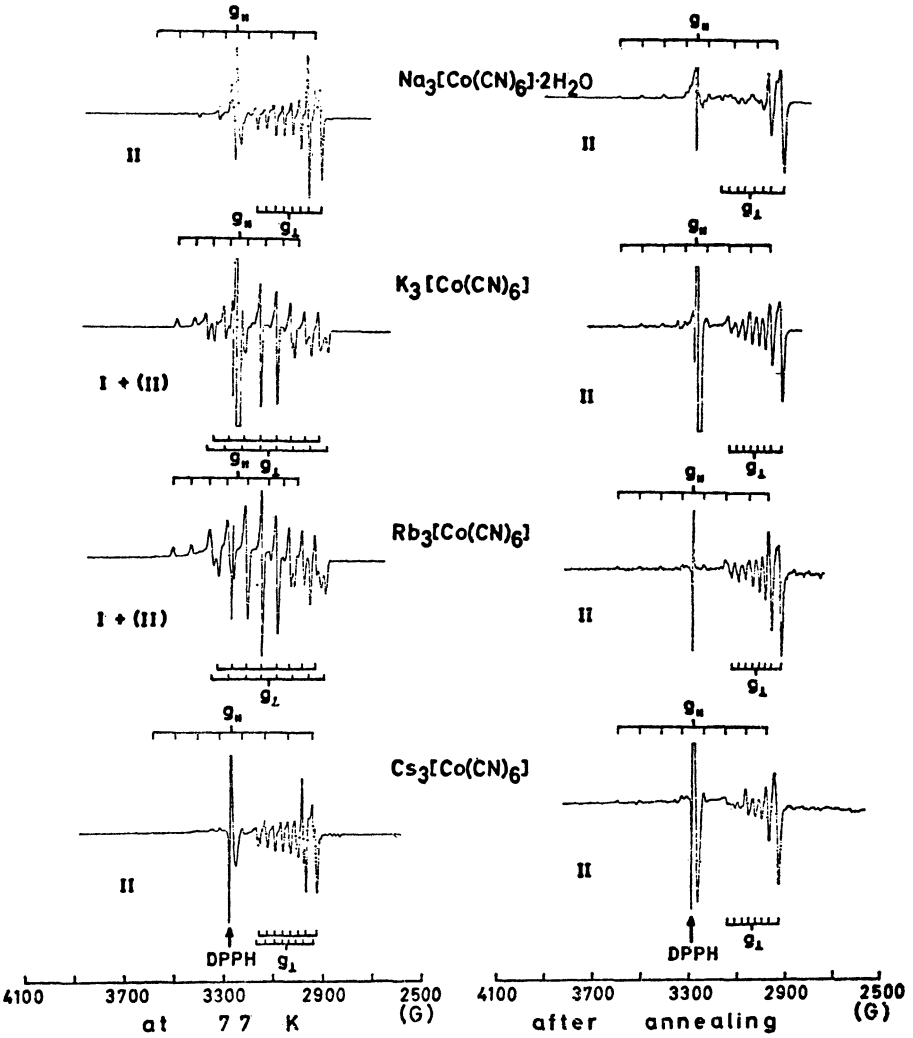

Fig. 9. ESR spectra of γ-irradiated powder of $M_3[Co(CN)_6]$ (M=Na, K, Rb, Cs).

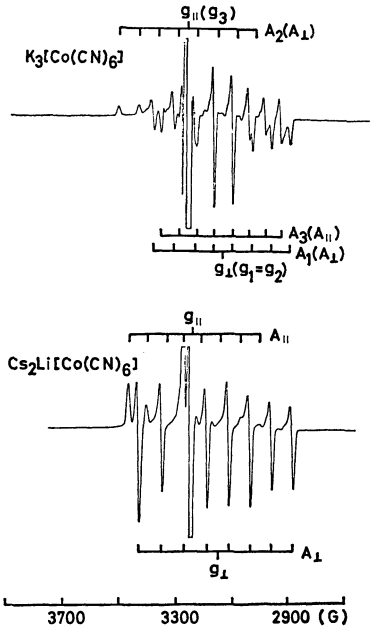

Fig. 10. ESR spectra of γ-irradiated powder of $K_3[Co(CN)_6]$ and $Cs_2Li[Co(CN)_6]$.

When the cation is changed from $3K^+$ to $2Cs^+Li^+$, the crystal system changes from orthorhombic to cubic. ESR parameters of hot ions produced in γ-irradiated $Cs_2Li[Co(CN)_6]$ at 77 K are shown in Table 7 for

TABLE 7. ESR PARAMETERS OF HOT IONS PRODUCED IN γ-IRRADIATED $K_3[Co(CN)_6]$ AND $Cs_2Li[Co(CN)_6]$.

	$g_{//}$	$A_{//}$(G)	$g_\perp$	$A_\perp$(G)
$Cs_2Li[Co(CN)_6]$	2.025	64	2.078	−78.1
$K_3[Co(CN)_6]$	2.011	61.7	2.091	−70.0

comparison with the case of $K_3[Co(CN)_6]$. In the case of $Cs_2Li[Co(CN)_6]$, no superhyperfine structures due to nitrogen atoms were observed. The $A_\perp$ can be seen at the $g_\perp$ part, and the $A_{//}$ can be seen at the $g_{//}$ part (Fig. 10). It can be concluded that the noncollinearity of the g-tensor and the A-tensor is not due to the local nature of the central metal, but to the entire nature of the mother lattice of the compound.

We wish to thank Mr. Shingo Katsura of the γ-ray irradiation center for his experimental assistance. We wish also to thank Dr. Yoji Arata and Dr. Jun-ichi Isoya for their helpful discussion.

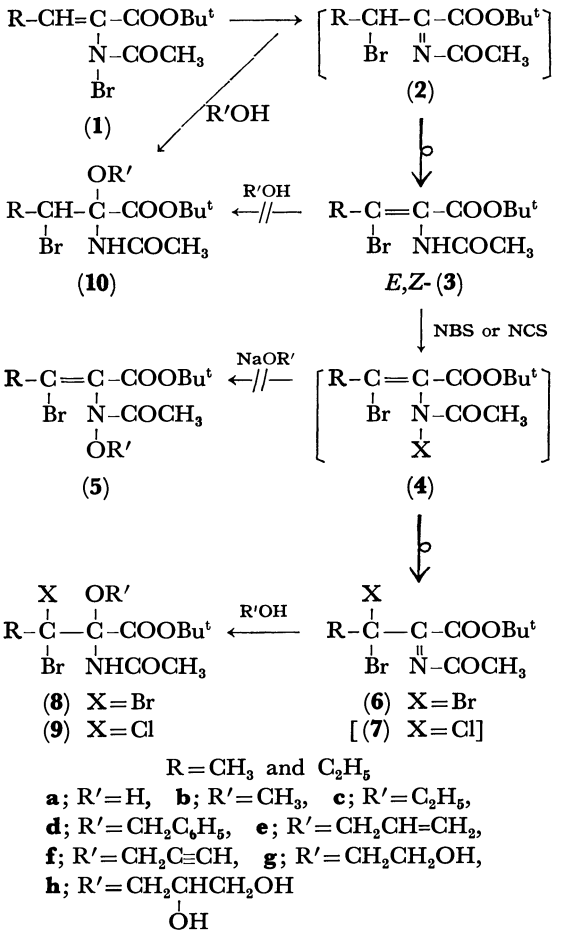

R=CH_3 and C_2H_5

a; R'=H, **b**; R'=CH_3, **c**; R'=C_2H_5,
d; R'=$CH_2C_6H_5$, **e**; R'=$CH_2CH{=}CH_2$,
f; R'=$CH_2C{\equiv}CH$, **g**; R'=CH_2CH_2OH,
h; R'=CH_2CHCH_2OH (OH)

Scheme 1.

alcohols to the imino intermediates **7** and **2**, respectively.

Experimental

All the melting points are uncorrected. The IR spectra were recorded with a Hitachi EPI-G3 Spectrometer. The NMR spectra were measured with a JNM-PS-100 Spectrometer (Japan Electron Optics Laboratory Co., Ltd.), using tetramethylsilane as the internal standard.

Materials. Compounds **1** and **3** were prepared by methods previously reported.[10]

Preparation of **6**. Into a solution of **3** (0.0036 mol) in chloroform (10 ml) was added NBS (0.004 mol) portion by portion with stirring at room temperature. After stirring for 20 min, the reaction solution was concentrated to give a yellow syrup containing succinimide. After the addition of carbon tetrachloride (10 ml) to the residue, the succinimide which had thus separated out was filtered off, and the filtrate was evaporated under reduced pressure to give a pale yellow syrup in a quantitative yield. The syrup obtained was purified on a silica gel column using benzene as an eluent. *t*-Butyl 2-acetylimino-3,3-dibromobutanoate, IR (KBr disk): 1720 (-COO), 1655 (>NCO) cm^{-1}, NMR (δ): 2.30 ($COCH_3$). Found: C; 33.80, H; 4.20, N; 3.91%. Calcd for $C_{10}H_{15}NO_3Br_2$: C; 33.64, H; 4.23, N; 3.92%. *t*-Butyl 2-acetylimino-3,3-dibromopentanoate, IR (KBr disk): 1725 (-COO), 1660 (>NCO) cm^{-1}, NMR (δ): 2.29 ($COCH_3$). Found: C, 35.49; H, 4.81; N, 3.61%. Calcd for $C_{11}H_{17}NO_3Br_2$: C, 35.61; H, 4.62; N, 3.77%.

Preparation of **8a**. Into a solution of **6** (R=CH_3, 0.0036 mol) in dry *N,N*-dimethylformamide (10 ml) was added water (3 ml) drop by drop with stirring at room temperature. After stirring for 8 h, the reaction solution was poured into water (30 ml) and then the aqueous solution was extracted twice with benzene (20 ml). The benzene extracts were washed twice with water and then dried over anhydrous sodium sulfate. The benzene layer was evaporated under reduced pressure to give colorless crystals, which were identified as *t*-butyl 2-acetylamino-3,3-dibromo-2-hydroxybutanoate.

Preparation of **8b**. A solution of **6** (R=CH_3, 0.0036 mol) in methanol (10 ml) was stirred for 6 h, and was worked up similarly to give *t*-butyl 2-acetylamino-3,3-dibromo-2-methoxybutanoate.

In a similar manner, *t*-butyl 2-acetylamino-3,3-dibromo-2-methoxypentanoate was obtained from the reaction of **6** (R=C_2H_5) with methanol, after stirring for 24 h.

Preparation of **8c**. *Procedure A*: A solution of **6** (R=CH_3, 0.0036 mol) in ethanol (10 ml) was stirred for 10 h and worked up similarly to give *t*-butyl 2-acetylamino-3,3-dibromo-2-ethoxybutanoate.

In a similar manner, *t*-butyl 2-acetylamino-3,3-dibromo-2-ethoxypentanoate was obtained from the reaction of **6** (R=C_2H_5) with ethanol, after stirring at *ca.* 50 °C for 7 h and purification of the syrup obtained on a silica gel column using benzene–ethyl acetate (20: 1 V/V) as an eluent.

Procedure B: Into a solution of **3** (R=CH_3, 0.0036 mol) in ethanol (10 ml) was added NBS (0.004 mol) portion by portion with stirring at room temperature. After stirring for 6 h, the reaction solution was concentrated under reduced pressure to give a reddish syrup containing succinimide. The residue was dissolved in benzene (30 ml) and then the benzene solution was washed three times with water. The benzene layer was dried over anhydrous sodium sulfate and then evaporated under reduced pressure to give **8c** (R=CH_3). Yield: 69.3%.

Preparation of **8d**. After treating **6** (R=CH_3, 0.0036 mol) with benzyl alcohol (3 ml) with stirring at room temperature for 2 h, a similar work up gave a colorless syrup, which gradually crystallized when allowed to stand at room temperature. The colorless crystals were identified to be *t*-butyl 2-acetylamino-2-benzyloxy-3,3-dibromobutanoate.

In a similar manner, *t*-butyl 2-acetylamino-2-benzyloxy-3,3-dibromopentanoate was obtained from the reaction of **6** (R=C_2H_5) with benzyl alcohol, after stirring for 10 h.

Preparation of **8e**. After treating **6** (R=CH_3, 0.0036 mol) with allyl alcohol (5 ml) with stirring at *ca.* 60 °C for 10 h, a similar work up gave a yellow syrup. The syrup was subsequently purified on a silica gel column using benzene–ethyl acetate (15: 1 V/V) as the eluent to give colorless crystals of *t*-butyl 2-acetylamino-2-allyloxy-3,3-dibromobutanoate.

In a similar manner, *t*-butyl 2-acetylamino-2-allyloxy-3,3-dibromopentanoate was obtained from the reaction of **6** (R=C_2H_5) with allyl alcohol, after stirring for 20 h. The syrup obtained was purified on a silica gel column using benzene–ethyl acetate (20: 1 V/V) as an eluent to give colorless crystals.

Preparation of **8f**. After treating **6** (R=CH_3, 0.0036 mol) with propargyl alcohol (3 ml) with stirring at *ca* 50 °C for 10 h, a similar work up gave a brown syrup. The syrup was subsequently purified on a silica gel column using benzene–acetone (30: 1 V/V) to give colorless crystals of *t*-butyl 2-acetylamino-3,3-dibromo-2-(2-propynyloxy)butanoate.

In a similar manner, *t*-butyl 2-acetylamino-3,3-dibromo-2-(2-propynyloxy)pentanoate was obtained from the reaction of **6** (R=C_2H_5) with propargyl alcohol, after stirring at *ca.* 60 °C for 20 h. The syrup obtained was purified on a silica

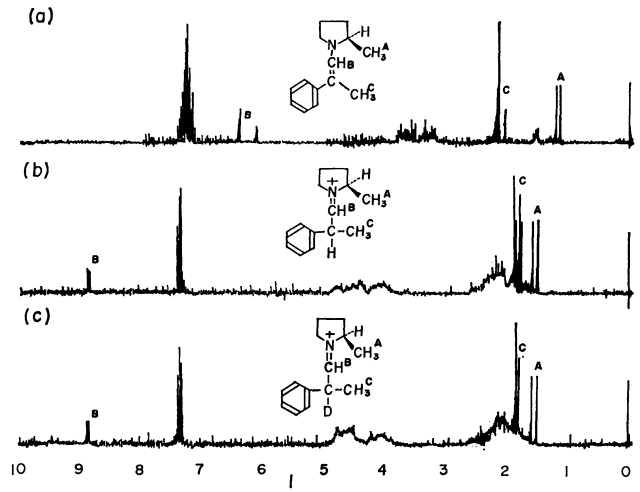

Fig. 2.

active 2-methylpyrrolidine enamine of **1** in $CDCl_3$. The solution has a color varying from initially light yellow to dark-brown at the end. The immonium salt thus prepared was confirmed by NMR spectra. Figure 2 shows NMR spectra of the enamine (a), the immonium salt with HCl (b) and the immonium salt with DCl (c). The existence of two geometrical isomers of the enamine is observed from (a). Their ratio can be obtained by the measurement of peak areas. The spectra of immonium salt, (b) and (c), showed two diastereomeric isomers. Displacement of the balance in favor of one diastereomeric immonium salt can be observed. Possibility of the existence of geometrical isomer (B) can be neglected by consideration of the steric interaction using models (Corey-Pauling-Koltum type and Dreiding type). The mechanism of the optical activation is considered to be an asymmetric, reversible protonation to the enamine and successive hydrolysis of the immonium salt.

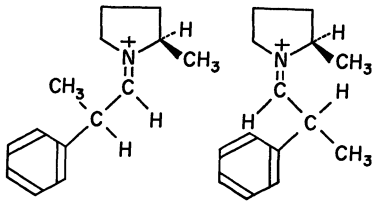

(A) (B)

References

1) K. Hiroi and S. Yamada, *Chem. Pharm. Bull.*, **23**, 1103 (1975); K. Nagasawa, H. Takahashi, K. Hiroi, and S. Yamada, *Yakugaku Zasshi*, **95**, 33 (1975).
2) J. W. Scott, R. Borer, and G. Saucy, *J. Org. Chem.*, **37**, 1659 (1972); H. Nohira and H. Miura, *Nippon Kagaku Kaishi*, **1975**, 1122; L. M. Kogan, V. E. Gulaya, and I. V. Torgov, *Tetrahedron Lett.*, **1967**, 4673.
3) G. Bredig and K. Fajas, *Chem. Ber.*, **41**, 752 (1908).
4) R. Kuhn, H. E. Driesen, and H. J. Haas, *Justus Liebigs Ann. Chem.*, **718**, 78 (1968); G. Otani and S. Yamada, *Chem. Pharm. Bull.*, **21**, 2130 (1973).
5) Marckwald and A. McKenzie, *Chem. Ber.*, **32**, 2120 (1899).
6) H. Leuchs, *Chem. Ber.*, **54**, 830 (1921).
7) H. Matsushita, M. Noguchi, M. Saburi, and S. Yoshikawa, *Bull. Chem. Soc. Jpn.*, **48**, 3715 (1975).
8) R. G. Kostyanovsky, I. M. Gella, V. I. Markov, and Z. E. Samojlova, *Tetrahedron*, **30**, 39 (1974).
9) H. L. Goering, J. N. Eikenberry, and G. S. Koermer, *J. Am. Chem. Soc.*, **93**, 5913 (1971).
10) D. J. Cram, *J. Am. Chem. Soc.*, **71**, 3883 (1949).
11) G. A. C. Gough, H. Hunter, and J. Kenyon, *J. Chem. Soc.*, **1926**, 2052.
12) H. C. Brown, J. H. Brewster, and H. Shechter, *J. Am. Chem. Soc.*, **76**, 467 (1954).
13) W. D. Gurowitz and M. A. Joseph, *J. Org. Chem.*, **32**, 3289 (1967).
14) N. J. Leonard and R. R. Sauers, *J. Am. Chem. Soc.*, **79**, 6210 (1957).
15) J. Read and A. M. McMath, *J. Chem. Soc.*, **1925**, 1572.

Table 4. NMR of substituted (chloro)ethylenes

Compound	Vinylic H (δ ppm) (J_{Hz})	Aromatic and aliphatic H (δ ppm)
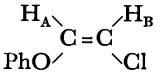	H_A 6.72 (1H, d), H_B 5.47 (1H, d), J_{AB}=4.3	6.90—7.50 (5H, m)
$(PhO)_2C=CH_2$	3.84 (2H, s)	6.90—7.45 (10H, m)
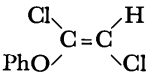	5.90 (1H, s)	6.95—7.50 (5H, m)
$PhOCCl=CCl_2$	—	6.95—7.55 (m)
$(PhO)_2C=CCl_2$	—	6.90—7.40 (m)
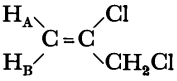	H_A 6.11 (1H, d), H_B 5.90 (1H, d), J_{AB} =1.6	4.50 (2H, s)[a]
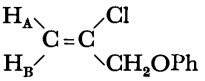	H_A 5.38 (1H, m), H_B 5.50 (1H, m)	6.80—7.40 (5H, m) 4.52 (2H, t)[a]
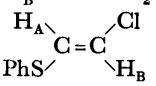	H_A 6.47 (1H, d), H_B 6.20 (1H, d), J_{AB}=13.0	7.15—7.40 (5H, m)
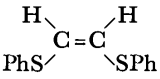	6.50 (2H, s)	7.12—7.50 (10H, m)
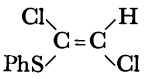	6.50 (1H, s)	7.10—7.45 (5H, m)
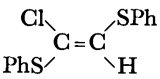	6.91 (1H, s)	7.15—7.55 (10H, m)
$(PhS)_2C=C(SPh)_2$	—	7.16—7.50 (m)
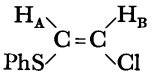	H_A 6.58 (1H, d), H_B 6.18 (1H, d), J_{AB}=6.5	7.20—7.55 (5H, m)
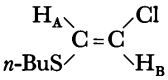	H_A 6.38 (1H, d), H_B 5.97 (1H, d), J_{AB} =13.0	2.46—2.93 (2H, m)[a] 0.73—1.94 (7H, m)
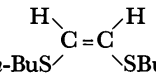	6.13 (2H, s)	2.44—2.90 (4H, m)[a] 0.72—1.88 (14H, m)

a) Aliphatic H

when X=O

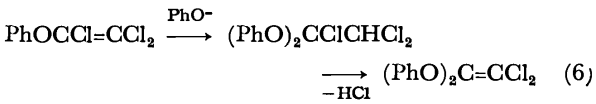

when X=S

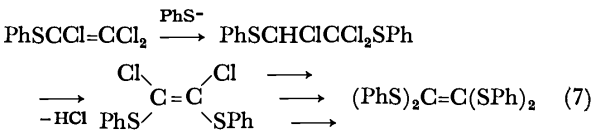

Experimental

Illustrative examples of the reactions will be given below.

a) Reaction of 1,1,2,2-Tetrachloroethane (III) with PhONa. In a three-necked flask equipped with a reflux condenser and a mechanical stirrer we placed 200 ml of DMSO, 37.6 g (0.40 mol) of phenol, and 16.0 g (0.40 mol) of NaOH. The mixture was gently warmed up to 70 °C with stirring to dissolve most of the NaOH. To the nearly homogeneous solution we then slowly added 16.8 g (0.10 mol) of III at 70 °C. The stirred mixture was then kept at 70 °C for an additional 5 h, after which the mixture was cooled, diluted with *ca.* 500 ml of water, and saturated with NaCl. The organic layer was extracted with three 100 ml portions of ether. The combined ethereal extracts were washed with water, dried over anhydrous Na_2SO_4, and then distilled to yield 17.0 g of crude *trans*-1,2-dichloro-1-phenoxyethylene; bp 72—74 °C/4 mmHg (yield, 90%).

b) Reaction of Pentachloroethane (IV) with PhSNa. In a similar way, a nearly homogeneous solution of 27.5 g (0.25 mol) of benzenethiol and 10.0 g (0.25 mol) of NaOH in 125 ml of DMF was prepared. Then a 10.1 g portion (0.05 mol) of IV was gradually added at 70 °C, after which the stirring was continued for 5 h at that temperature. All these procedures were carried out under a nitrogen atmosphere to prevent the oxidation of benzenethiol to diphenyl disulfide. The reaction mixture was cooled and diluted with *ca.* 300 ml of water. The resulting precipitate was collected and recrystallized from chloroform to afford 17.0 g of tetrakis(phenylthio)ethylene; mp 154—156 °C (yield, 74%).

The NMR spectra of all the olefinic products are summarized in Table 4.

References

1) For example, J. B. Hendrickson, D. J. Cram, and G. S. Hammond, "Organic Chemistry," 3rd ed., McGraw-Hill, New York (1959), Chapter 11.

2) J. Hine, C. H. Thomas, and S. J. Ehrenson, *J. Am. Chem. Soc.*, **77**, 3886 (1955). Relative reactivities for the reac-

Nickel-Phosphine Complex-Catalyzed Grignard Coupling. I. Cross-Coupling of Alkyl, Aryl, and Alkenyl Grignard Reagents with Aryl and Alkenyl Halides: General Scope and Limitations

Kohei TAMAO, Koji SUMITANI, Yoshihisa KISO, Michio ZEMBAYASHI, Akira FUJIOKA, Shun-ichi KODAMA, Isao NAKAJIMA, Akio MINATO, and Makoto KUMADA*

Department of Synthetic Chemistry, Faculty of Engineering, Kyoto University, Kyoto 606

(Received April 2, 1976)

It has been established that dihalodiphosphinenickel(II) complexes exhibit extremely high catalytic activity for selective cross-coupling of Grignard reagents with aryl and alkenyl halides. This catalytic reaction can be employed in synthetic practice for reasons of simple procedures, mild reaction conditions, high yields and high purity of the coupling products, and the wide applicability to reactions involving primary and secondary alkyl (regardless of the presence or absence of β-hydrogen(s)), aryl, and alkenyl Grignard reagents and nonfused, fused, and substituted aromatic halides and haloolefins. Limitations lie in sluggish reactions between alkyl Grignard reagents and dihaloethylenes. The most effective catalysts are $[Ni\{(C_6H_5)_2P(CH_2)_3P(C_6H_5)_2\}Cl_2]$ for alkyl and simple aryl Grignard reagents, $[Ni\{(CH_3)_2P(CH_2)_2P(CH_3)_2\}Cl_2]$ for alkenyl and allylic Grignard reagents and $[Ni\{P(C_6H_5)_3\}_2Cl_2]$ for sterically hindered aryl Grignard reagents and halides. Great stabilizing effects of phosphine ligands on the catalytic species are demonstrated by no effect observed after aging the catalyst. Organic chlorides are generally the most suitable halide in view of the reasonable reactivities and limited side reactions. Ether is favored over tetrahydrofuran as solvent. About sixty experimental results are presented and several features are discussed.

The metal-promoted coupling reactions of organic halides are one of the most attractive and useful procedures for formation of the carbon-carbon σ bond.[1] In recent years low valent transition metals and organotransition metallics hold an important position as coupling agents for such processes. Representatives include the Ullmann reaction,[2,3] the nickel(0)-promoted coupling reactions,[4-7] and cross-coupling using π-allylnickel complexes,[6] organocuprates,[3,8,9] or organoferrates.[10] Reactions of active organometallic reagents, such as organolithium and Grignard reagents, with transition metal salts also provide a route to the formation of the carbon–carbon bond; salts of Cu(I), Cu(II),[3,9,11] Ag(I), and various Group VIII metals[12,13] have been used successfully. These reactions, however, have the disadvantages that they require at least stoichiometric amounts of transition metals.

It has been known for thirty years that catalytic amounts of transition metal salts induce the coupling reaction of Grignard reagents with organic halides.[12] In spite of a number of mechanistic studies,[14] such catalytic reactions, "Kharasch reaction," have been seldom employed in synthetic practice, because of the formation of a complex mixture of products consisting of homo coupling products and a variety of disproportionation products in substantial amounts. Since 1971, when Tamura and Kochi reported that "soluble catalysts" consisting of silver,[15,16] iron[15,16a] or copper[15] in tetrahydrofuran were extremely effective for selective coupling of Grignard reagents with organic halides, the synthetic applicability of these catalytic reactions has received much attention.[17b,18,19] In 1972, Corriu and Masse[20] and we[21] independently reported that nickel–phosphine complexes catalyze the selective cross-coupling of Grignard reagents with aryl and alkenyl halides:

$$RMgX + R'X' \xrightarrow{[NiL_2Cl_2]} R\text{-}R' + MgXX'$$

More recently, Murahashi *et al.*[22] examined the catalytic activity of a palladium–phosphine complex for the similar Grignard cross-coupling. It was rather surprising that little attention had been paid to the catalytic activity of phosphine–modified transition metals for the Kharasch type reactions, despite extensive studies on a variety of homogeneous catalyses.

The nickel–phosphine complex-catalyzed Grignard coupling has opened up the possibility of preparing a large variety of unsaturated organic compounds from two different organic halides[23,24] and there have been reported several characteristic features of the reaction, including the alkyl group isomerization,[25] stereochemical aspects,[26] asymmetric synthesis,[27] and applications to the cyclophane synthesis[28] and to the heterocycle coupling.[29] In this paper, we report, aside from the mechanistic aspects, the general scope and limitations of the nickel–phosphine complex-catalyzed Grignard cross-coupling.

Results and Discussion

I. Design of a Catalytic Cycle. When undertaking this series of studies, we designed the catalytic process of the cross-coupling reaction as pictured in Scheme 1 by combining two important observations on the chemistry in relation to σ-organonickel complexes bearing "supporting" ligand(s): (1) two organic groups on a nickel complex L_2NiR_2 are released by the action of, for example, a halobenzene R'X' to undergo coupling, along with the formation of $L_2Ni(R')(X')$,[30,31] and (2) such a halogen–nickel bond is readily replaced by a Grignard reagent to form the corresponding organonickel bond, $L_2Ni(R')(R)$.[32]

Thus, a dihalodiphosphinenickel reacts with a Grignard reagent to form the intermediate diorganonickel complex **2** which is subsequently converted to the halo(organo)nickel complex **3** by an organic halide.

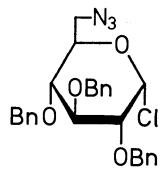

10

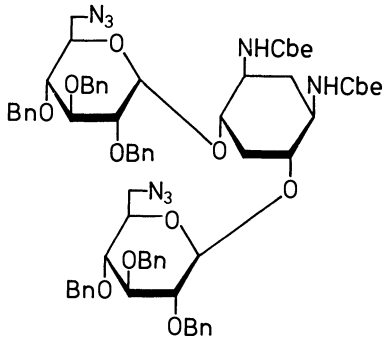

11

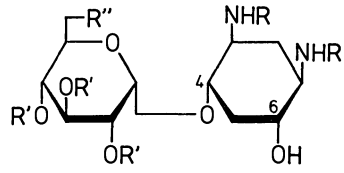

12a, 14a, 15a, 16a

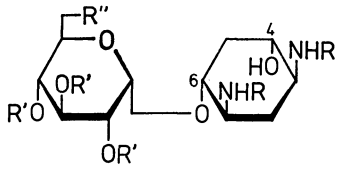

12b, 14b, 15b, 16b

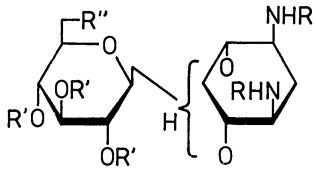

13, 17, 18

	R	R'	R''
12a,b,13	Cbe	Bn	N_3
14a,b,17	Cbe	Bn	NHCbe
15a,b,18	H	H	NH_2
16a,b	Ac	H	NHAc

2,5-dideoxystreptamine, *viz.* 5-deoxyparomamine.

In the case of a preparation of 6-amino-6-deoxy-D-glucopyranosyl-2,5-dideoxystreptamine, *N*,*N'*-diethoxycarbonyl-2,5-dideoxystreptamine (**1b**) was used instead of **1a** in order to improve solubilities of the products. Condensation of **1b** with 6-azido-2,3,4-tri-*O*-benzyl-6-deoxy-α-D-glucopyranosyl chloride (**10**)[10] was conducted in the presence of mercuric cyanide in a mixture of benzene and dioxane for two weeks at reflux temperature. A mixture of crude products thus obtained could successfully be separated by a silica gel column chromatography to give a crystalline pseudo trisaccharide derivative (**11**)[6] (25%), 6-*O*-(6'-azido-2',3',4'-tri-*O*-benzyl-6'-deoxy-α-D-glucopyranosyl)-*N*,*N'*-diethoxycarbonyl-2,5-dideoxystreptamine (**12b**) (15%), 4- or 6-*O*-β-D-glycoside (**13**) (3%), and an amorphous 4-*O*-α-D-glycoside (**12a**) being contaminated with a trace of **12b** and **13**. Catalytic reduction of the azido group of **12a** by Raney nickel T-4[11] followed by treatment with ethyl chloroformate gave a crystalline 4-*O*-(2',3',4'-tri-*O*-benzyl-6'-deoxy-6'-ethoxycarbonylamino-α-D-glucopyranosyl)-*N*, *N'*-diethoxycarbonyl-2,5-dideoxystreptamine (**14a**) in 5% yield based on **1b** used. The similar treatment of **12b** and **13** gave the corresponding tri-*N*-ethoxycarbonyl derivatives (**14b** and **17**) in 61 and 74% yields, respectively. Hydrogenolysis of **14a** and **14b** in the presence of palladium black and subsequent treatment with aqueous barium hydroxide at 120 °C gave crude free aminoglycosides, which were purified by Amberlite CG-50 (NH_4^+) column chromatography using aqueous ammonia as an eluent to afford 4- and 6-*O*-(6'-amino-6'-deoxy-α-D-glucopyranosyl)-2,5-dideoxystreptamines (**15a** and **15b**) as a homogeneous glass in 74 and 68% yields, respectively. They were further characterized by converting into the corresponding tri-*N*-acetyl derivatives (**16a** and **16b**). Compound **17** was also converted into the free aminoglycoside (**18**).

Table 1. Biological activities of synthesized aminoglycosides (**8** and **15a**)[a]

Test organisms	Zone of inhibition,[b] mm					
	8			**15a**		
	A	B	C	A	B	C
Bacillus subtilis ATCC 6633	27 (36)	24 (34)	21 (31)	30 (31)	28 (29)	24 (25)
Staphylococcus aureus 6538 p	15 (21)	11 (19)	0 (17)	22 (24)	18 (21)	15 (19)
Escherichia coli K-12	28 (35)	23 (32)	20 (29)	35 (33)	31 (30)	27 (28)
Klebsiella pneumoniae 7	—	—	—[c]	17 (0)	13 (0)	10 (0)
Mycobacterium smegmatis ATCC 607	—	—	—[c]	37 (30)	30 (24)	24 (18)

a) Determined by paper disk method (Hole method). Concentrations: A, 1000 μg/ml; B, 500 μg/ml; C, 250 μg/ml. b) Data in the parentheses were those of antibiotic neamine determined as the reference compound under the same conditions. c) Not determined.

In the PMR spectra of **15a** and **15b** in deuterium oxide, signals of the anomeric proton appeared at δ 5.14 and 5.10 as a doublet with 3 and 3.5 Hz spacings, respectively. Empirical rule[12] on difference in the chemical shift of anomeric protons of α-D-glucopyranosyl 2-deoxystreptamine between 4- and 6-glycosides might not be applied to our compounds which lacked the 5-hydroxyl group. But it seems to support the above configurational assignment that the anomeric proton of 4-*O*-α-D-glycoside resonated at relatively lower field than that of 6-*O*-α-D-glycoside. Examination on biological activities of **15a** and **15b** indicated that the

Table 3. NMR spectra of the 2-trialkylphosphonio-1,3-dithiole-4-carboxylates, **4**

Compound	Solvent	NMR Signals, δ[a]
4a	DMSO-d_6	1.96 (d, 9H, $J_{CH_3\text{-}^{31}P}$=14.4 Hz) 5.41 (s, 1H)
4a	DMSO-d+methanol-d_4	1.98 (d, $J_{CH_3\text{-}^{31}P}$=14.4 Hz) disappearance of the methine H
4b	DMSO-d_6	1.24 (d, t, 9H, J=7.2 Hz, $J_{CH_3\text{-}^{31}P}$=17.5 Hz) 2.48 (d, q, 6H. J=7.2 Hz, $J_{CH_3\text{-}^{31}P}$=14.4 Hz) 5.83 (s, 1H)
4c	DMSO-d_6	0.93 (t, 9H, methyl H), 1.3—1.8 (m, 12H, β- and γ-methylene H), 2.1—2.7 (m, 6H, α-methylene H), 5.79 (s, 1H, methine H)
4d	Methanol-d_4	1.34 (d, t, 9H, J=7.2 Hz, $J_{CH_3\text{-}^{31}P}$=17.5 Hz) 2.49 (d, q, 6H, J=7.2 Hz, $J_{CH_3\text{-}^{31}P}$=14.4 Hz) 6.74 (s, 1H, vinyl H)
4e	DMSO-d_6	0.93 (t, 9H), 1.3—1.8 (m, 12H), 2.1—2.7 (m, 6H), 6.24 (d, 1H, $J_{CH_3\text{-}^{31}P}$=2 Hz, methine H), 6.37 (s, 1H, vinyl H)
4e	DMSO-d_6+methaol	1.0 (t, 9H), 1.3—1.8 (m, 12H), 2.1—2.7 (m, 6H) 6.72 (s, 1H, vinyl H), disappearance of the methine H

a) Measured in ppm downfield from TMS as an internal standard.

was coupled with ^{31}P (J=2 Hz). Each methine proton, as expected, was readily exchanged by deuterium in the presence of methanol-d_4, and disappeared from NMR spectra. The methyl protons of **4a** and the methylene protons of **4b** and **4d**, at the α-position of alkyl group attached to phosphorous, were coupled with ^{31}P (J= 14.4 Hz). The methyl protons of **4b** and **4d** at the β-position of alkyl group attached to phosphorus were also coupled with ^{31}P. (J=17.5 Hz). These coupling constants are in reasonable accord with literature precedents.

The reaction of acetylene carboxylic acids with ylides of type **2** to give **4** adds to our growing knowledge of acetylene reactions in tetrathiafulvalene (TTF) syntheses.[8] A more detailed knowledge of the mechanism (Scheme 1) is still needed to provide the synthetic chemist insight in developing improved routes to substituted TTF derivatives, compounds of intense current interest.[8]

Experimental

Proton magnetic resonance spectra were recorded on a Hitachi Perkin-Elmer R-20 B with tetramethylsilane as an internal reference. Infrared spectra were obtained with a Beckman IR-33. THF was dried over calcium hydride and distilled prior to use. Melting points are uncorrected. The elemental analyses of sulfur and phosphorus were performed by Schwarzkopf Microanalytical Laboratory, 56—19 37th Avenue, Woodside, New York 11377.

Reaction of Acetylene Carboxylic Acids With Trialkylphosphine–Carbon Disulfide Ylides (2). Trialkylphosphine (0.05 mol) in 50 ml of tetrahydrofuran was added dropwise to a solution of 10 ml of carbon disulfide in 50 ml of tetrahydrofuran at −20——30°C under nitrogen. In the case of trimethylphosphine and triethylphosphine, the ylides, **2**, precipitated. To the deep maroon solution of **2** a solution of acetylene carboxylic acid (0.05 mol) in 50 ml of tetrahydrofuran was added dropwise. The temperature was maintained between −20 and −30 °C during addition. The system was warmed to room temperature and stirred further for 1 h. The zwitterionic products, **4**, were formed as precipitates. The precipitate was filtered and washed with acetone and/or methanol. The crude products, 2-trialkylphosphonio-1,3-dithiole-4-carboxylates, **4a**—**f**, could be recrystallized from solvents shown in Table 1. Table 1 also gives physical characteristics of the compounds prepared. IR absorption bands of **4** and **7** are summarized in Table 2.

2,6(7)-Bis(ethoxycarbonyl)tetrathiafulvalene. The procedure is the same as preparation of **4**. After addition of ethyl propiolate at −20——30 °C, instead of acetylene carboxylic acids, the system was warmed to room temperature and stirred further 3 h. Volatiles were removed under reduced pressure and excess ether was added to the residue which was refrigerated. A precipitate formed and was filtered to give 18% of the title compound. Recrystallization from glyme gave a red-orange crystalline product: mp 176—178 °C (lit,[2] 169—172 °C); NMR ($CDCl_3$) δ 1.35 (t, 3H, methyl H, J=7 Hz), 4.31 (q, 2H, methylene H), and 7.40 (s, 1H, vinyl H).

Hydrolysis of 2-Tributylphosphonio-1,3-dithiole-4-carboxylates (4c and 4e). Zwitterionic salt **4c** (4.00 g: 0.01 mol) was suspended in 40 ml of 1 M sodium hydroxide solution and stirred for 30 min. Crystals dissolved gradually, and an oily material was separated. The oily material was extracted with ether. Removal of ether gave tributylphosphine oxide. The aqueous layer was acidified with 3 M hydrochloric acid, while cooled with ice, to give 1.44 g (69%) of yellow needles of 1,3-dithiole-4,5-dicarboxylic acid hydrate, **7b** H_2O. This crude material was purified by reprecipitation from water solution by acidification with 3 M hydrochloric acid. The filtrate was concentrated under vacuum and the residue was washed with acetone. From the washings another 0.50 g (26%) 1,3-dithiole-4,5-dicarboxylic acid, **7b**, was obtained as orange crystals.

The 1,3-dithiole, **4e**, was also hydrolyzed in the same manner to give 1,3-dithiole-4-carboxylic acid, **7a**, in 90% yield.

Physical properties, elemental analyses, and IR data of 1,3-dithiole carboxylic acids were shown in Tables 1 and 2. The NMR spectrum of **7a** in acetone-d_6 consisted of singlets at δ 7.28 (1H) and 4.68 (2H), assigned to olefinic and methylene hydrogens, respectively. In DMSO-d_6, the NMR spectra of **7a** and **7b** H_2O had a singlet at δ 4.49 and δ 4.02 (methylene

BULLETIN OF THE CHEMICAL SOCIETY OF JAPAN, VOL. 49 (7), 2007—2008 (1976)

A Shock-tube Investigation of Ethylene-Oxygen-Argon Mixtures. Chemi-ionization and Apparent Activation Energy

Yoshiaki HIDAKA, Tomofumi NISHI, and Masao SUGA

Department of Chemistry, Faculty of Science, Ehime University, Bunkyo-cho, Matsuyama 790

(Received December 25, 1975)

Synopsis. The reaction of ethylene–oxygen mixtures highly diluted with argon was studied over the temperature range of 1400—1800 K behind reflected shock waves by monitoring the total ionization. A kinetic study of the chemi-ionization in the ethylene oxidation was undertaken. It was inferred that the mechanism of CHO^+ formation was dependent on the composition and the temperature, and that the rate-determining step for the chemi-ionization was $C_2H_3+O_2 \rightarrow C_2H_3O+O$.

The oxidation of ethylene has been previously studied by shock-tube techniques.[1-4] Kinetic studies have been mainly done by various optical methods[2-4] and mass spectrometric methods;[1] also, we ourselves have reported our results monitoring the emission from CH*, C_2*, and OH*.[5] The oxidation of ethylene and other hydrocarbons in the shock tube is accompanied by an intense chemi-ionization. In the present paper, we wish to report the results of our simultaneous measurements of CH* emission and chemi-ionization and to discuss the formation mechanism of ions. Another purpose of this paper is to determine the apparent activation energy of the total ionization in the ethylene oxidation.

Experimental

The shock tube and the techniques for measuring the chemiluminescence have already been described.[5] In the present experiment, the time intervals for the shock-speed measurements were determined by the use of a universal counter (Iwatsu US-6141) with a precision of ± 0.1 μs. For the measurement of the ion current, the Langmuir probe was located at the same distance as the quartz window, 1 cm from the reflected plate of the shock tube.

The compositions of the reaction mixtures used were:

(A) 0.5% C_2H_4, 1.0% O_2, 98.5% Ar

(B) 0.5% C_2H_4, 1.5% O_2, 98.0% Ar

(C) 0.5% C_2H_4, 2.0% O_2, 97.5% Ar

The ethylene, oxygen, and argon were commercial gases; then purities were 99.99%, 99.9%, and 99.99% respectively. The initial pressures of the reaction mixtures were about 100 Torr. The ion current (+6.5 V bias on the Langmuir probe) and CH* emission (4315 Å, with a half-width of 25 Å) were simultaneously measured behind reflected shock waves.

Results and Discussion

Some typical oscillograms on the oscilloscope are shown in Fig. 1 (a) and (b). The following characteristics were seen from the profiles of each run:

(1) The onset of the ion signal was earlier than that of the CH* emission signal in the (A) and (B) mixtures below 1700 K. However, in the (A) and (B) mixtures above 1700 K and the (C) mixture over the temperature range of 1400—1800 K, the reverse tendency was true.

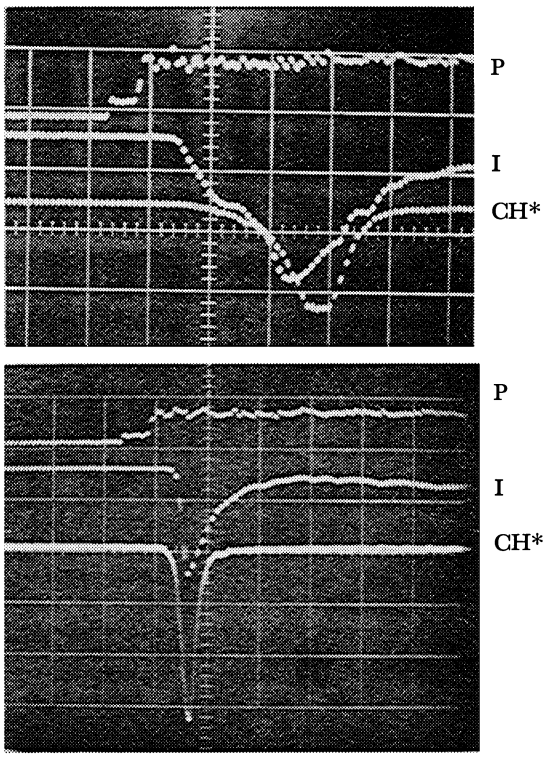

Fig. 1. Time histroy of CH* emission and ion currents.
Upper trace: Pressure signal.
Middle trace: Ion current signal.
Lower trace: CH* emission signal.
(a) $T_5=1593$ K, $P_5=4.04$ atm, Sweep=50 μs/div., 1.0% O_2+0.5% C_2H_4.
(b) $T_5=1610$ K, $P_5=4.48$ atm, Sweep=50 μs/div., 2.0% O_2+0.5% C_2H_4.

(2) In most profiles of the (A) mixture over the temperature range of 1400—1800 K, the arrival time to the peak of the ion signal was earlier than that of the CH* emission signal. In the lower-temperature regions of the (B) mixture (below 1700 K) and the (C) mixture (below 1500 K), the arrival time to the peak of the ion signal was later than that of the CH* emission. In the higher-temperature regions of the (B) and (C) mixture, they were almost identical.

The maximum intensities of the ion signals are plotted against the temperature at the C_2H_4/O_2 ratios of 1/2 (A mixture), 1/3 (B mixture), and 1/4 (C mixture) respectively in Fig. 2. These results indicate that the maximum intensity, I_{max}, increased with the increase in the temperature and the O_2 concentration over the temperature range of 1400—1800 K.

Mass-spectral analysis has shown that, in the oxidation of ethylene in a shock tube, the $C_3H_3^+$ ion is dominant

Table 2. Observed and calculated ^{13}C-NMR chemical shifts[a] for THI and MTI

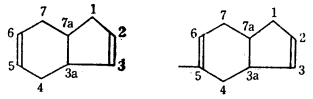

cis-THI *cis*-MTI

Compound		C-1	C-2	C-3	C-3a	C-5	C-6	C-7a	C-4 or 7		CH_3
Calcd	THI	32.3	130.0	136.0	39.5	130.3	130.3	39.5	32.0		
Obsd	THI	40.2	129.5	136.2	43.1	128.1	128.1	35.6	27.8	28.7	
		(t)	(d)	(d)	(d)	(d)	(d)	(d)	(t)	(t)	
Obsd	MTI	40.1	129.5	135.9	43.5	135.5	121.4	34.9	32.8	29.1	23.8
		(t)	(d)	(d)	(d)	(d)	(d)	(d)	(t)	(t)	(q)

( ): off-resonance a) In ppm relative to internal TMS.

The selection of a suitable structure for **A** and **B** was governed by the following three factors: (i) by comparison with the ^{13}C-NMR spectra of *endo*- and *exo*-5-vinyl-2-norbornene(VNB),[2] (ii) by matching with the calculated chemical shifts according to parameter of Lindemann[3] for alkane and that of Roberts[4] for alkene and (iii) by referring to the off-resonance decoupling information. From this evidence, **A** and **B** were identified to be the *endo*- and *exo*-5-isopropenyl-2-norbornene (MVN), respectively. The data of the ^{13}C-NMR spectra are listed in Table 1.

Structure of MTI. The following two formulae are presented as possible structures of MTI.

3 **4**

From the results of the ^{13}C-NMR spectra data (in Table 2) and the VPC analysis, it was found that the fraction of MTI consists of only a single component. The determination of the stereochemical structure of MTI contained in the fraction was performed in the following section.

Rearrangement of MVN to MTI. The rearrangement of the fraction of MVN was carried out by a method similar to that reported in a previous paper.[2] In the case of the fraction (*endo*-MVN: *exo*-MVN= 59: 41) obtained from the reaction at 170 °C for 4 h, the *endo*-MVN was rearranged to MTI, while no *exo*-MVN reacted. This fact indicates that MTI was produced along with Cope rearrangement and its structure must be **4**.

Further, the rearrangement kinetics were examined using a fraction having a high content of the *endo*-product(*endo*: *exo*=86: 14), in the temperature range from 145 to 170 °C. The rate constants and the activation parameters are listed in Table 3.

The positive value of $\Delta S^{\ddagger}$ may also support the above mechanism where by the reaction proceeds through Cope rearrangement.[5]

Table 3. Rate constants for the rearrangement of *endo*-MVN to MTI at various temperatures

Reaction temp (°C)	Rate constant ($\times 10^{-4}$ s^{-1})
145	0.22
155	0.38
165	1.13
170	2.25

$\Delta H^{\ddagger}$: 33.8 kcal/mol, $\Delta S^{\ddagger}$: 0.40 e.u. (at 150 °C) calculated from the Eyring equation.

The Diels-Alder reaction of the IP–CP equi-molar mixture gave products **2** and **4**, while neither the **1** nor the **3** compounds were obtained. The reason for the absence of **1** in the products may be illustrated by steric repulsion between the methylene protons of CP(diene) and the methyl group of IP(dienophile).

The reaction scheme is illustrated as follows:

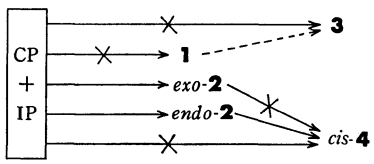

References

1) S. Tsuchida, T. Maehata, and M. Ogawa, *Sekiyu Gakkaishi*, **14**, 257 (1971).

2) T. Maeda, M. Muranaka, S. Hamanaka, and M. Ogawa, *Nippon Kagaku Kaishi*, **1974**, 1587.

3) L. P. Lindeman and J. Q. Adams, *Anal. Chem.*, **43**, 1245 (1971).

4) D. E. Dorman, M. Jautelate, and J. D. Roberts, *J. Org. Chem.*, **36** 2757 (1971).

5) The observed $\Delta S^{\ddagger}$ value differs widely in comparison with the value for the reaction of VNB with THI reported in a previous paper.[2] In that work, no explanation of this fact was presented.

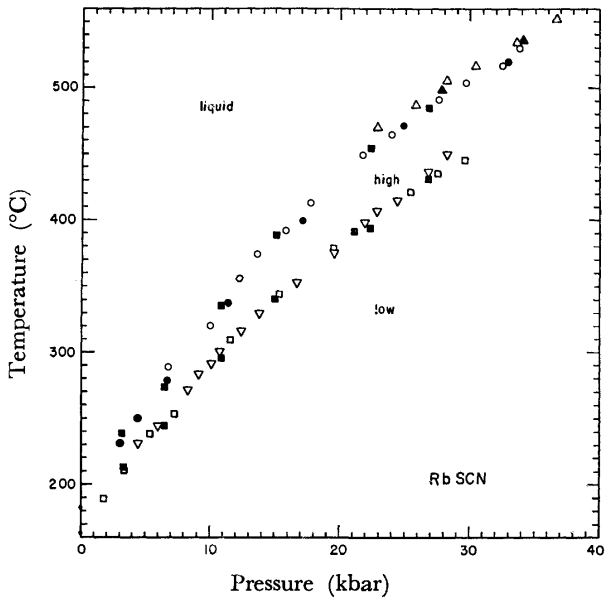

Fig. 2. Solid-solid and melting temperatures for RbSCN. Accepted 1-bar transition temperatures are indicated. Open symbols denote upstroke data; filled symbols denote downstroke data. Circles denote data from first run, triangles second and squares third run, all in aluminium capsules.

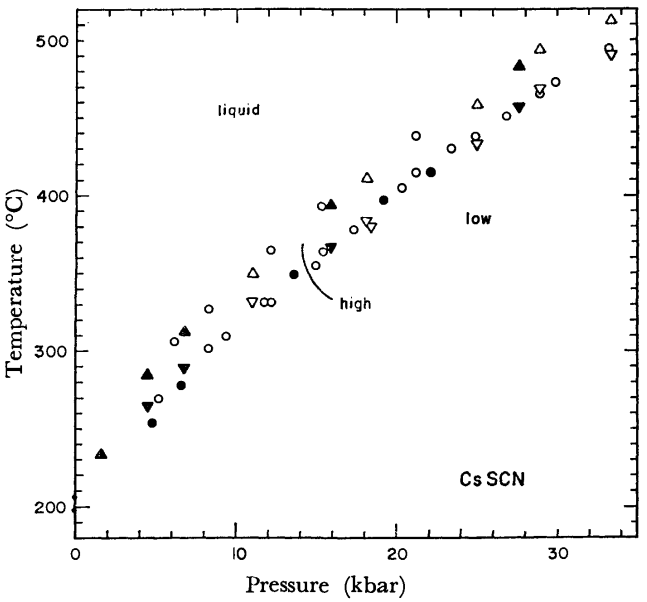

Fig. 3. Solid-solid and melting temperatures for CsSCN. Accepted 1-bar transition temperatures are indicated. Open symbols denote upstroke data; filled symbols denote downstroke data. Circles denote data from first run and triangles those from second run, both in aluminium capsules.

solid transition was observed as before and also data were obtained on decreasing pressure, which were used in the corrections for friction. A single datum was then obtained for the onset of melting, after which decomposition was indicated. The solid-solid transition data (Fig. 1) can be fitted by a straight line of slope 12.6 (±10%) deg kbar^{-1} and intercept 120±4 °C, which agrees with other 1-bar results.[9,10] Taking the 1-bar melting point to be ~146 °C, the tentative slope for the melting curve is ~20 deg kbar^{-1} (Fig. 1).

RbSCN. In all three runs, aluminium capsules were used to contain the RbSCN, which was of unknown origin (and afterwards was shown by X-ray diffraction to contain some RbCl). In the first run, the melting curve was followed on both increasing and decreasing pressure, with the onset of the DTA signal taken for the melting temperature and undercoolings of ~5 to 25 °C, roughly increasing with increasing temperature, observed for the freezing signals. In the second run, the solid-solid transition was detected as a small but distinct break in the DTA signal on heating and as a small peak on cooling, the temperatures corresponding to these features agreeing to within 2—3 °C. Some corroborative melting data were also obtained in this run and the third run provided further corroborative data for both transitions. The data (Fig. 2) for the solid-solid transition can be fitted by a power series with 1-bar intercept 166±3 °C, initial slope (dT/dp) 13.5±1.0 deg kbar^{-1} and initial curvature ($-d^2T/dp^2$) 0.3±0.1 deg kbar^{-2}. The melting data (Fig. 2) can be fitted by a power series with 1-bar intercept 184±2 °C, initial slope 15.7±0.3 deg kbar^{-1} and initial curvature 0.32±0.05 deg kbar^{-2}. Uncertainties are estimated by regression fits of individual sets of data and then of all the data taken together. It cannot be ruled out that the 'melting' curve here is actually the RbSCN-RbCl eutectic but neither the DTA signals nor the DSC results (below) indicated that the transition was spread out over a particularly large temperature range. Since RbCl melts at a much higher temperature than RbSCN and it is unlikely that there is much solid solubility of RbCl in RbSCN, the eutectic is probably 'degenerate', with composition and temperature very close to pure RbSCN and its true melting point, respectively. The present results (Fig. 2) for 'melting' are then a close lower bound to the melting of pure RbSCN.

CsSCN. In both runs, aluminium capsules were used to contain the material, which was obtained from K & K Laboratories. For the solid-solid transition, the onsets of the quite distinct DTA signals on heating and on cooling agreed to within ±1 °C and were taken for the transition temperatures. The onset of the DTA signal on heating was taken as the melting temperature. In the first run, the DTA signals became so indistinct at the higher pressures that the run was abandoned without any data obtained on decrease of pressure. In the second run, however, data were quite reproducibly obtained on both increasing and decreasing pressure. Large undercoolings were observed after melting up to 50 °C or 60 °C— and the melt crystallized directly to the low-temperature phase since only the freezing signal was seen on cooling. The data (Fig. 3) for the solid-solid transition are not fitted well by the usual power series, with intercept ≈197 °C, but there may be estimated an initial slope of $11._8$ ($\pm 1._0$) deg kbar^{-1} and an initial curvature ~0.2 deg kbar^{-2}; similarly, for the melting data (Fig. 3) with intercept ≈206 °C, there may be estimated an initial slope of 14 ($\pm 1._5$) deg kbar^{-2} and an initial curvature ~0.2—0.4 deg kbar^{-2}. The relatively poor fits afforded here by the power series to order p^2 may be due to the difficulties with the friction corrections at the lower pressures.

TlSCN. The first two runs were made with material from Electronic Space Products, in inconel and copper capsules, chronologically. No definite signals could be concluded for the solid-solid transition (see DSC results below) and only signals with rather indistinct onsets for melting; considerable undercooling was noted from the freezing signals. The next two runs were made with material from Ventron, in aluminium and then tantalum capsules. For the solid-solid transition, inflexions in the DTA signals on heating and distinct halts on cooling served to establish

TABLE 1. THE YIELDS AND THE PHYSICAL PROPERTIES OF 3-METHYL-5-(2-OXOALKYL, 2-HYDROXYALKYL, AND 2-HYDROXYALKENYL)ISOXAZOLES AND 4-(3-METHYL-5-ISOXAZOLYL)BUTANOIC ACID DERIVATIVES

Compd	Yield[a] (%)	Mp or Bp (°C) (°C/mmHg)	IR[b] (cm^{-1})	NMR (δ, ppm), J are in Hz			
				3-CH_3[c]	4-CH[d]	5-CH_2	Others
3	40	105—100/3	1725, 1612	2.24 or 2.28	6.08	3.86(s)	2.24 or 2.28(s, 3H)[e]
6	18	142—153/2	3420, 1612	2.18	6.00	3.78(s)	1.11(d, 3H, J=6.6), 1.8—2.8 (m, 4H), 3.5—4.5(m, 1H)[f]
7	22	140—145/2	3400, 1605	2.08	5.67	2.95(d, J=6.6)	3.6(br. s, 1H), 4.86(t, 1H, J=6.6), 7.18(s, 5H)[f]
9	17	130—140/2	3390, 1607	2.08	5.66	2.91(d, J=7.2)	2.30(s, 3H), 3.7(br. s, 1H), 4.80(t, 1H, J=7.2), 7.04 (s, 4H)[f]
10	41	150—165/2	3400, 1611	2.07	5.66	2.91(d, J=6.6)	3.66(s, 3H), 3.7(br. s, 1H), 4.77(t, 1H, J=6.6), 6.93(ABq, 4H, J_{AB}=8.4, $\Delta\nu_{AB}$=23.8)[f]
12	18	144—147/20	3400, 1605	2.29	5.98	2.91(s)	1.30(s, 6H), 2.39(s, 1H, exchanged with D_2O)[e]
13	35	50—60/0.001	3410, 1608	2.11	5.57	3.10(s)	1.52(s, 3H), 3.1(br. s, 1H), 7.1—7.5(m, 5H)[f]
14	27	55—60/0.001	3400, 1605	2.23	5.87	2.78(s)	1.1—1.9(m, 10H), 2.5(br. s, 1H)[f]
23	35	107—108 (CCl_4)	3390, 1600[g]	2.17	5.72	3.41(s)	2.5(br. s, 1H), 6.57(s, 2H), 7.1—7.6(m, 10H)[f]
24	11	125.5—126.5 (CCl_4)	1676, 1608[g]	2.18	5.64	3.13(d, J=6.6)	3.53(d, 2H, J=6.6), 3.5—4.1 (m, 1H), 7.2—8.0(m, 5H), 7.22(s, 5H)[f]
25	6	104—111/3	3370, 1609	2.27	5.98	2.97(s)	1.36(s, 3H), 2.85(s, 1H, exchanged with D_2O), 5.07(dd, 1H, J=2.4, 10.2), 5.25(dd, 1H, J=2.4, 17.4), 6.01(dd, 1H, J=10.2, 17.4)[e]
26	8	173—179/23	1710, 1607	2.16 or 2.26	5.88	1.5—3.0 (m)	2.16 or 2.26(s, 3H), 1.5—3.0 (m, 4H)[f]
27	38	110—125/0.01	3400, 1607	2.23	5.91	3.00(d, J=6.6)	2.6(br. s, 1H), 4.4—4.8(m, 1H), 6.14(dd, 1H, J=6.6, 15.5), 6.60(d, 1H, J=15.5), 7.25(s, 5H)[e]
28	trace	oil	1723, 1605	2.20	5.65	3.04(d, J=7.2)	2.80(dd, 2H, J=1.8, 7.2), 3.3—4.0(m, 1H), 7.0—7.5(m, 5H), 9.63(t, 1H, J=1.8)[e]
29	5	150—157/20	3410, 1610	2.27	5.95	2.95(d, J=6.6	2.72(s, 1H, exchanged with D_2O), 4.2—4.7(m, 1H, 5.16 (dd, 1H, J=1.2, 10.2), 5.27 (dd, 1H, J=1.2, 16.8), 5.6—6.3(m, 1H)[e]
30	43	170—174/21	3390, 1610	2.27	5.97	2.93(d, J=6.6)	1.71(d, 3H, J=4.8), 2.63 (s, 1H, exchanged with D_2O), 4.3—4.6(m, 1H), 5.5—5.9 (m, 2H)[e]
31	10	47.5—48.5 (hexane)	1733, 1608[g]	2.17	5.62	2.69 or 3.05(d, J=7.2)	2.69 or 3.05(d, 2H, J=7.2), 3.3—3.8(m, 1H), 3.53(s, 3H), 7.19(s, 5H)[e]
32	4	137—140/10^{-6}	3030(broad), 1720, 1609	2.18	5.65	2.70 or 3.06(d, J=7.2)	2.70 or 3.06(d, 2H, J=7.2), 3.0—3.8(m, 1H), 7.22(s, 5H), 8.9(br. s, 1H, exchanged with D_2O)[e]

a) Isolation yield. b) Neat unless otherwise stated. c) Singlet. d) Singlet. e) In $CDCl_3$. f) In CCl_4. g) KBr.

Table 2. The yields and the physical properties of 3-methyl-5-(2-alkoxyalkyl)isoxazoles

Compd	Yield[a] (%)	Mp or Bp (°C) (°C/mmHg)	IR[b] (cm^{-1})	NMR (δ, ppm), J are in Hz.			
				3-CH_3[d]	4-CH[d]	5-CH_2	Others
16	14	150—160/4	1603	2.23	5.78	2.9—3.2 (m)	3.20(s, 3H), 4.47(dd, 1H, J=6.0, 7.8), 7.28(s, 5H)[e]
17	10	117—129/3	1605	2.16	5.60	2.6—3.3 (m)	1.12(t, 3H, J=7.2), 3.29(q, 2H, J=7.2), 4.47(dd, 1H, J=6.0, 7.8), 7.17(s, 5H)
18	16	130—139/2	1608	2.18	5.63	2.6—3.4 (m)	3.6—3.9(m, 2H), 4.55(dd, 1H, J=6.0, 7.8), 4.9—5.3 (m, 2H), 5.4—6.1(m, 1H), 7.20(s, 5H)
19	23	195—199/4	1608	2.18	5.58	2.6—3.4 (m)	4.29(ABq, 2H, J_{AB}=12.0, $\Delta\nu_{AB}$=12.6), 4.58(dd, 1H, J=6.0, 7.8), 7.12(s, 5H), 7.22 (s, 5H)
20	28	137—146/4	1610	2.18 or 2.32	5.62	2.6—3.4 (m)	2.18 or 2.32(s, 3H), 3.13 (s, 3H), 4.34(dd, 1H, J=6.0, 7.8), 7.07(s, 4H)
21	13	52 (hexane)	1612[f]	2.18	5.66	2.6—3.4	3.13(s, 3H), 3.73(s, 3H), 4.34(dd, 1H, J=6.0, 7.8), 6.93(ABq, 4H, J_{AB}=8.4, $\Delta\nu_{AB}$=20.5)
22	13	98—99 (hexane)	1603[f]	2.06	5.06	3.68(s)	3.12(s, 3H), 7.0—7.3(m, 10H)

a) Isolation yield. b) Neat unless otherwise stated. c) In CCl_4 unless otherwise stated. d) Singlet. e) In $CDCl_3$. f) KBr.

Table 3. The elemental analyses of 3-methyl-5-(2-oxoalkyl, 2-hydroxyalkyl, 2-alkoxyalkyl, and 2-hydroxyalkenyl)isoxzoles and 4-(3-methyl-5-isoxazolyl)butanoic acid derivatives

Compound	Molecular formula	Found (%)			Calculated (%)		
		C	H	N	C	H	N
3	$C_7H_9NO_2$	60.19	6.47	9.87	60.42	6.52	10.07
6	$C_{10}H_{15}NO_3$	60.12	7.79	7.36	60.89	7.67	7.10
7	$C_{12}H_{13}NO_2$	70.69	6.44	7.05	70.91	6.45	6.89
9	$C_{13}H_{15}NO_2$	71.71	6.79	6.43	71.86	6.96	6.45
10	$C_{13}H_{15}NO_3$	66.78	6.41	5.79	66.93	6.48	6.01
12	$C_8H_{13}NO_2$	62.00	8.60	9.03	61.91	8.44	9.03
13	$C_{13}H_{15}NO_2$	71.70	6.94	6.28	71.68	6.96	6.45
14	$C_{11}H_{17}NO_2$	67.55	8.85	7.27	67.66	8.78	7.17
16	$C_{13}H_{15}NO_2$	71.88	7.06	6.37	71.86	6.96	6.45
17	$C_{14}H_{17}NO_2$	72.57	7.42	6.22	72.70	7.41	6.06
18	$C_{15}H_{17}NO_2$	73.88	6.90	5.71	74.05	7.04	5.76
19	$C_{19}H_{19}NO_2$	77.48	6.48	4.90	77.79	6.53	4.77
20	$C_{14}H_{17}NO_2$	72.51	7.35	5.97	72.70	7.41	6.06
21	$C_{14}H_{17}NO_3$	68.14	7.01	5.59	67.99	6.93	5.66
22	$C_{19}H_{19}NO_2$	78.13	6.53	4.64	77.79	6.53	4.77
23	$C_{20}H_{19}NO_2$	78.71	6.34	4.55	78.76	6.27	4.59
24	$C_{20}H_{19}NO_2$	78.43	6.37	4.68	78.66	6.27	4.59
25	$C_9H_{13}NO_2$	63.63	8.00	8.56	64.65	7.84	8.38
26	$C_9H_{13}NO_2$	64.02	7.90	8.33	64.65	7.84	8.38
27	$C_{14}H_{15}NO_2$	73.22	6.61	5.91	73.34	6.59	6.11
29	$C_8H_{12}NO_2$	62.55	7.52	9.01	62.72	7.24	9.14
30	$C_9H_{13}NO_2$	64.46	7.94	8.48	64.65	7.84	8.38
31	$C_{15}H_{17}NO_3$	69.43	6.66	5.43	69.48	6.61	5.40
32	$C_{14}H_{15}NO_3$	68.16	6.30	6.03	68.55	6.16	5.71

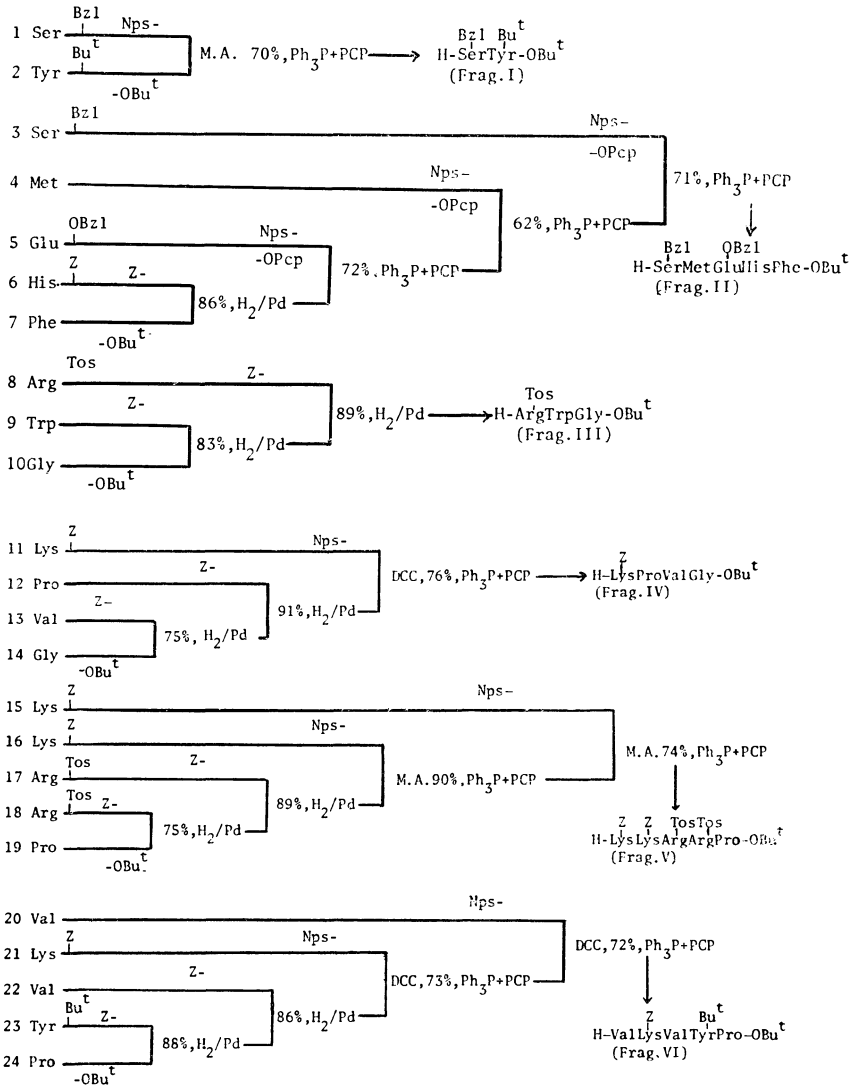

Fig. 2. The scheme for the preparation of peptide fragments.

TABLE 1. PHYSICAL PROPERTIES OF PEPTIDE FRAGMENTS

Fragment	Mp	$[\alpha]_D^{20}$ (c 1, methanol)	Amino acid ratios
Nps-Ser(Bzl)Tyr(Bu^t)-OBu^t (I)	oil	—	Ser : Tyr 0.98 1
Nps-Ser(Bzl)Met-Glu(OBzl)HisPhe-OBu^t (II)	158—160 °C	−26.3°	Ser : Met : Glu : His : Phe 1.01 0.94 0.97 1 0.99
Z-Arg(Tos)TrpGly-OBu^t (III)	137—140 °C	−24.5°	Arg : Trp : Gly 0.99 0.87 1
Nps-Lys(Z)ProValGly-OBu^t (IV)	85—86 °C	−101.5°	Lys : Pro : Val : Gly 1.05 0.96 0.96 1
Nps-Lys(Z)Lys(Z)Arg(Tos)Arg(Tos)Pro-OBu^t (V)	130—135 °C	−38.3°	Lys : Arg : Pro 2 1.96 0.96
Nps-Val-Lys(Z)Val-Tyr(Bu^t)Pro-OBu^t (VI)	206—209 °C (dec)	−105.5°	Lys : Val : Tyr : Pro 0.96 1.96 1 1.03

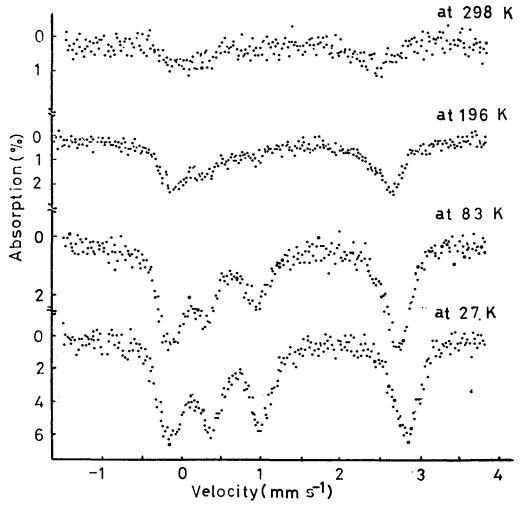

Fig. 3. Mössbauer spectra of $Fe(pot)_2(NCS)_2 \cdot 1/2CHCl_3$ a a variety of temperatures.

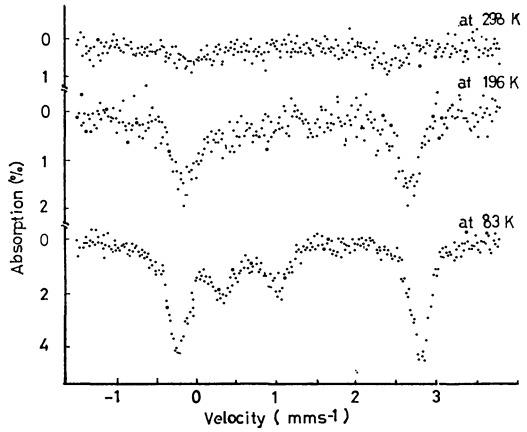

Fig. 4. Mössbauer spectra of $Fe(ppt)_2(NCS)_2$ at a variety of temperatures.

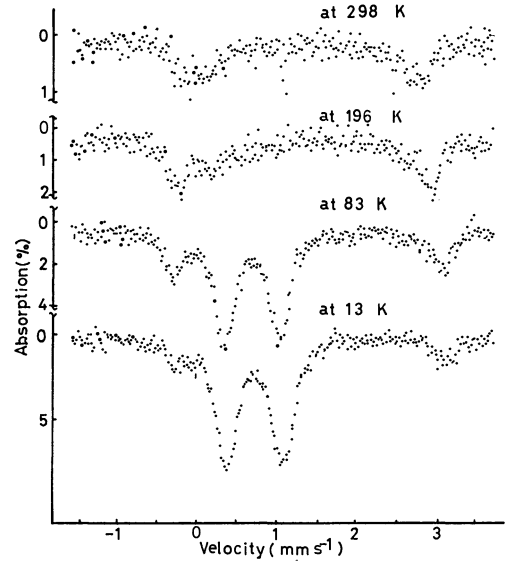

Fig. 5. Mössbauer spectra of $Fe(ppa)_2(NCS)_2$ at a variety of temperatures.

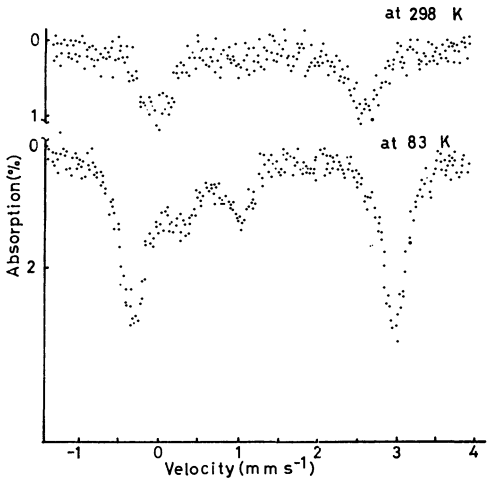

Fig. 6. Mössbauer spectra of $Fe(ppca)_2(NCS)_2$ at a variety of temperatures.

area of iron of the low-spin state to the total absorption area of the Mössbauer spectrum. Based on the general inductive effects of the substituent in the 4-position, it is anticipated that the greater the electronic density of the nitrogen, the greater the ligand-field splitting and the higher the value of Dq. An incomplete transition to the $^1A_1$ state results in a paramagnetic isomer or the existence of a $^5T_2$ excited state having a small energy separation from the $^1A_1$ state. The paramagnetic isomer has still not been observed up to the present time.

The isomer shift of $FeLCl_2$ is smaller than that of FeL_2Cl_2 (L: Schiff bases of quinolinecarbaldehyde or pyridinecarbaldehyde). This fact is interpreted in terms of a tetrahedral structure which is in accordance with the infrared spectral data. The isomer shift of the complexes having a tetrahedral structure is small, in general, because of the smaller s-character or the shielding of the core s-electrons by a larger d-electron contribution.[10]

The spectra of $Fe(qea)_2(NCS)_2$, $Fe(qba)_2(NCS)_2$, $Fe(qea)_2Cl_2 \cdot 1/2H_2O$, and $Fe(qba)_2Cl_2 \cdot 1/2H_2O$ show a pair of lines at 83 K, which is obviously typical for high-spin iron(II) compounds, although the Schiff bases of quinolinecarbaldehyde are more π-electron acceptable and appear to have a stronger field. This ligand field which is weaker than that of the Schiff bases of pyridinecarbaldehyde might be explained by assuming steric interactions, although the quinoline is a better acceptor of π-electrons than the pyridine. A weaker bond has been observed in the cobalt complexes of quinoline *N*-oxide derivatives.[11]

The spectra of the compounds, $Fe(ph)_3(NCS)_2$ and $Fe(pba)_3(NCS)_2 \cdot H_2O$, show the small doublet usually observed for low-spin iron(II) compounds.

Magnetic Properties. The temperature dependences of the magnetic moments, in the range of 77—295 K for the complexes $Fe(pipa)_2(NCS)_2$, $Fe(pa)_2(NCS)_2$, and $Fe(ppa)_2(NCS)_2$ are shown in Fig. 7. The magnetic behaviors of the compounds $Fe(pot)_2(NCS)_2 \cdot 1/2CHCl_3$, $Fe(ppt)_2(NCS)_2$, and $Fe(ppca)_2(NCS)_2$ are similar to that of $Fe(pa)_2(NCS)_2$. At low temperatures, the magnetic moment of $Fe(pipa)_2(NCS)_2$ has values

Table 4. Spectral data of vinyl halides (**4**)—(**7**)

Compd	NMR (CCl_4, δ)	λ_{max} (cyclohexane) nm (ε)	MASS (m/e)
4	3.46 (s, 3H, OCH_3)	285 (13400)	426, 424 (M^+)
	3.65 (s, 3H, OCH_3)	240 (17000)	345 (M^+–Br)
	3.70 (s, 3H, OCH_3)		330 (M^+–CH_3Br)
	6.34—7.25 (m, 12H, arom.)		
5	3.43 (s, 3H, OCH_3)	284 (15500)	382, 380 (M^+)
	3.58 (s, 3H, OCH_3)	240 (16400)	330 (M^+–CH_3Cl)
	6.42—7.23 (m, 12H, arom.)		
6	2.21 (s, 3H, OCH_3)	283 (11500)	410, 408 (M^+)
	3.47 (s, 3H, OCH_3)	235 (sh, 20000)	329 (M^+–Br)
	3.73 (s, 3H, OCH_3)		314 (M^+–CH_3 Br)
	6.40—7.30 (m, 12H, arom.)		
7	3.43 (s, 3H, OCH_3)	284 (10500)	396, 394 (M^+)
	3.73 (s, 3H, OCH_3)		315 (M^+–Br)
	6.40—7.25 (m, 13H, arom.)		300 (M^+–CH_3Br)

product other than **8**. Recrystallization (EtOH) gave white plates, mp 125—126 °C. NMR (CCl_4, δ): 3.58 (s, OCH_3), 3.68 (s, OCH_3), 6.58—7.62 (m, 12H, arom.). MS (m/e): 330 (M^+). Found: C, 80.13; H, 5.26%. Calcd for $C_{22}H_{18}O_3$: C, 79.98; H, 5.49%.

Reaction in AcOH: Vinyl bromide (**4**) (70 mg, 0.164 mmol) in AcOH (7 ml) with Na_2CO_3 (85 mg, 0.8 mmol) was refluxed for 27 h. The cooled solution was poured into water, extracted with ether, washed with saturated $NaHCO_3$ solution and water, dried over Na_2SO_4, and then the solvent was evaporated to give the precipitate. Recrystallization (EtOH) gave white needles, mp 124.5—125.5 °C, of **8**. The NMR spectrum of the crude product showed that **8** was probably the only product.

Reaction in 70% Aqueous DMF: Vinyl bromide (**4**) (120 mg, 0.283 mmol) in 70% aqueous DMF (20 ml) was kept in a sealed ampoule at 140 °C for 16 h. The NMR spectrum of the crude product showed the presence of **8** as the sole product.

Reaction in the Presence of Sodium Azide: Vinyl bromide (**4**) (70 mg, 0.165 mmol) in basic (NaOH, 0.4 mmol) 80% EtOH (20 ml) in the presence of sodium azide (650 mg, 10.0 mmol) was kept in a sealed ampould at 120 °C for 6 h. The NMR spectrum of the crude product showed the quantitative formation of **8**.

Reaction in the Presence of Sodium p-*Toluenethiolate*: Vinyl bromide (**4**) (210 mg, 0.49 mmol) and *p*-toluenethiol (87.1 mg, 0.7 mmol) in basic (NaOH, 0.7 mmol) 80% EtOH (7 ml) was sealed in an ampoule and kept at 120 °C for 4 h. After work-up of the solution, the NMR spectrum of the reaction mixture (in CCl_4) showed the presence of **8** (100%) and methyl *p*-tolyl sulfide (47%) (CH_3 at δ 2.02 and SCH_3 at 2.33) which was assigned by comparison with an authentic sample.[22] Since it was hoped that more of the methyl moiety would be trapped by the nucleophile *p*-toluenethiolate ions, the reaction of **4** (200 mg, 0.47 mmol) in basic (NaOH, 1.4 mmol) 80% EtOH (7 ml) in the presence of *p*-toluenthiol (1.4 mmol) was conducted under the same conditions. The NMR spectrum of the reaction mixture this time showed **8** (100%) and methyl *p*-tolyl sulfide (74%).

*Reaction of 2,2-Bis(*o-*methoxyphenyl)-1-(*p-*methoxyphenyl)-vinyl Chloride (5)*. Vinyl chloride (**5**) (60 mg, 0.16 mmol) in basic (NaOH, 0.5 mmol) 80% EtOH (20 ml) was sealed in an ampoule and kept at 160 °C for 25 h. After work-up of the reaction mixture, the NMR spectrum of the crude product showed the dominant formation of **8**.

*Reaction of 2,2-Bis(*o-*methoxyphenyl)-1-*p-*tolylvinyl Bromide (6)*. Vinyl bromide (**6**) (60 mg, 0.15 mmol) in 80% EtOH containing NaOH (0.5 mmol) was kept in a sealed ampoule at 160 °C for 43 h. Work-up of the reaction mixture gave the precipitate of 3-(*o*-methoxyphenyl)-2-*p*-tolylbenzofuran (**9**). The NMR spectrum (in CCl_4) of the crystallized product, mp 89—90 °C, which was identical with that of the crude product, had peaks at δ 2.29 (s, CH_3), 3.56 (s, OCH_3), 6.75—7.44 (m, 12H, arom.). UV: λ_{max} (80% EtOH); 306 nm (ε 26800), 240 (sh, 17200). MS (m/e): 314 (M^+). Found: C, 83.82; H, 5.85%. Calcd for $C_{22}H_{18}O_2$: C, 84.05; H, 5.77%.

*Reaction of 2,2-Bis(*o-*methoxyphenyl)-1-phenylvinyl Bromide (7)*. With protection from light, vinyl bromide (**7**) (0.31 g, 0.78 mmol) in AcOH (20 ml) containing silver acetate (0.84 g, 5 mmol) was refluxed for 21 h (100% reaction), followed by filtration, and the solvent was evaporated. Work-up of the reaction mixture gave an oil (0.23 g) which could not be induced to crystallize. An NMR spectrum (in CCl_4) of the crude product showed two different methoxyl proton peaks (singlet at δ 3.58 and 3.31) in addition to aromatic proton peaks (multiplet at δ 6.8—7.7) indicating the possibility of two different products, each one of which would have one methoxyl group. Integration of these methoxyl proton peaks showed two products to be present in the ratio of 91 : 9, respectively. Similarly, the reaction of **7** (63 mg, 0.16 mmol) in basic (NaOH, 0.5 mmol) 80% EtOH (20 ml) in a sealed ampoule at 160 °C for 204 h (95% reaction) and the reaction of **7** (55 mg, 0.136 mmol) in basic (NaOH, 7.0 mmol) 50% EtOH (14 ml) at 160 °C for 26 h (96% reaction) gave the two products in similar product ratios (93 : 7 for both). Twice attempted separation of the two products by thin-layer chromatography (TLC) on silica gel (benzene–hexane 1 : 2 or 1 : 3) gave only poor separations, as judged by the small changes in the relative NMR intensities of the two different methoxyl proton peaks. By treating the reaction mixture (0.103 g) with a hot saturated solution of picric acid in EtOH (3 ml) and allowing the solution to cool, a picrate was separated in orange-red needles (0.122 g), which were then recrystallized (EtOH), mp 108—109 °C. Found: C, 61.02; H, 3.62; N, 7.86%. Calcd for $C_{27}H_{19}O_9N_3$ (1 : 1 π-complex of picric acid and $C_{21}H_{16}O_2$): C, 61.25; H, 3.62; N, 7.94%. The picrate was split by chromatography on alumina and eluted with benzene to give a pale yellow oil. All attempted crystallizations failed. The NMR spectrum of this oil (in CCl_4) showed only one methoxyl singlet at δ 3.45 and an aromatic 13H multiplet at δ 6.9—7.7, indicating the isolated major product. MS (m/e): 330 (M^+). The UV spectrum in cyclohexane showed a characteristic absorption at 305 nm of 2-phenylbenzofuran

Table 2. Relationship between $\delta_A-\delta_B$ and (R,R′) in $RR'\overset{\oplus}{S}-OCH_AH_BR''$ and $RR'\overset{\oplus}{S}-N(R'')CH_AH_BR'''$

	R, R′		
	in $RR'\overset{\oplus}{S}-OCH_AH_B-Me$	in $RR'\overset{\oplus}{S}-OCH_AH_BCMe_3$	in $RR'\overset{\oplus}{S}-N(R'')CH_AH_BR'''$
$\delta_A-\delta_B=0$	(Ph, CH_2Ph) (Bu, Et) (*p*-MeC_6H_4,) (Ph,)		
$\delta_A-\delta_B\fallingdotseq0$	(Et, OMe) (Et, OCH_2CMe_3) (Et, $-O^{\ominus}$)	(Et, $-O^{\ominus}$) (Et, OEt) (Et, OMe)	
$\delta_A-\delta_B>0$	(*p*-MeC_6H_4, Me) (*p*-MeC_6H_4, $-O^{\ominus}$)	(Ph, Me) (*p*-MeC_6H_4, $-O^{\ominus}$)	(Ph, $-O^{\ominus}$) (Ph, OEt) (*p*-MeC_6H_4, OEt) (*p*-MeC_6H_4, $-O^{\ominus}$) (Me, $-O^{\ominus}$)

double bond character, the rotations around the N–$\overset{\oplus}{S}$ and O–$\overset{\oplus}{S}$ bonds are not restricted, since 2p-3d π overlaps in sulfur compounds are not much affected by S–N rotation.[13,14] Even under conditions of rapid rotation or in the absence of unequal populations of several conformers, methylene hydrogens α or β to a chiral sulfur atom can be non-equivalent.[12–15] Interpretation of the data shown in Tables 1 and 2 is not easy; accumulation of more data is necessary before one can reasonably explain these phenomena.

Experimental

PMR spectra were determined with a Hitachi Perkin-Elmer NMR Spectrometer R-20 (60 MHz) at 34 °C with CH_2Cl_2 (δ 5.30) as an internal standard.[16] The concentrations were about 10 wt %.

Neopentyl benzenesulfenate[17] was prepared by the reaction among benzenesulfenyl chloride (10.4 mmol), neopentyl alcohol (10.4 mmol), and pyridine (10.4 mmol) at −5 °C. Yield, 1.6 g (80%), bp, 80 °C/2 mmHg.

Alkyl triflates were prepared according to the methods described in the literature. CF_3SO_3Me, bp 100 °C (lit,[18] 99 °C). CF_3SO_3Et, bp 119 °C (lit,[19] 115 °C).

Sulfinates (or sulfinamides) were prepared either by the reaction between sulfinyl chlorides and alcohols (or amines) or by the condensation between sulfinic acids and alcohols (or amines) with *N,N′*-dicyclohexylcarbodiimide.[21] *N*-*p*-Toluenesulfinylpyrrolidine was prepared from pyrrolidine and *p*-toluenesulfinyl chloride in ether at 0°, and recrystallized from hexane; yield, 31%; mp 52—53 °C; NMR (CD_3NO_2) δ= 1.55—1.86 (m, 4, N–$CH_2C\underline{H}_2$–), 2.27 (s, 3, $C\underline{H}_3$–C_6H_4), 2.57—3.41 (m, 4, N–$C\underline{H}_2$), 7.10—7.53 (q, 4, –$C_6\underline{H}_4$–); Found: C, 62.77; H, 7.12; N, 6.36%. Calcd for $C_{11}H_{15}ONS$: C, 63.14; H, 7.23; N, 6.69%.

Ethoxysulfonium Triflates ***1a—c.*** They were prepared by mixing equimolar amounts of the corresponding sulfoxides and ethyl triflate in CD_3NO_2. Since they are oils which cannot be distilled, their elemental analyses were not carried out. *p*-$TolMe\overset{\oplus}{S}-OEt\ \overset{\ominus}{BF_4}$ was described in the literature,[6–8] but its PMR data were not shown. PMR: **1a**, δ=1.27 (t, 3, $C\underline{H}_3CH_2$–), 2.39 (s, 3, $C\underline{H}_3C_6H_4$–), 3.60 (s, 3, $C\underline{H}_3$–S), 4.16—4.48 (m, 2, CH_2), 7.40—8.10 (q, 4, –$C_6\underline{H}_4$–); **1b**, δ=1.22 (t, 3, $C\underline{H}_3CH_2$), 4.33 (q, 2, $CH_3C\underline{H}_2$), 5.05 (q, 2, S–CH_AH_B–Ph, $\Delta\delta_{AB}$=0.23 ppm, J_{AB}=12.8 Hz), 6.95—8.00 (m, 10, Ph); **1c**, δ=1.31 (t, 3, $C\underline{H}_3CH_2$–S), 1.39 (t, 3, $C\underline{H}_3CH_2$–O), 0.60—2.20 (m, 7, $C\underline{H}_3C\underline{H}_2C\underline{H}_2$–), 3.26—3.71 (m, 4, $C\underline{H}_2$–S–$C\underline{H}_2$), 4.36 (q, 3, CH_3–S), 3.92 (q, O–CH_AH_B–, J_{AB}=9.1Hz), 7.64—8.20 (m, 5, C_6H_5–).

Neopentyloxymethylphenylsulfonium Triflate ***1d.*** When an equimolar mixture of neopentyl benzenesulfenate and methyl triflate in nitromethane was allowed to stand for 10 min at 34 °C, its PMR spectrum showed that the sulfenate was converted to **1d**. After the solvent was evaporated, the residue was dissolved in a small amount of acetone, and an equimolar amount of $NaBPh_4$ was added. However, the corresponding anion-exchanged salt was not obtained, and only decomposition products were found.

When a CD_3NO_2 solution of **1d** was heated at 75 °C for 18 h, it completely decomposed. Its PMR spectrum showed absorptions at δ=0.85 (s, 9.0H, $(CH_3)_3C$–), 2.35 (s, 0.54H, $PhSC\underline{H}_3$), 2.44 (s, 0.64H, ?), 3.19 (s, 1.29H, ?), 3.63 (s, 1.94H, $Me_3CC\underline{H}_2\overset{\oplus}{O}H_2$), and 7.16—7.83 (m, Ar–H). When an equimolar amount of pentadeuteriopyridine was added, the absorptions of neopentyl alcohol was shifted to δ=0.75 ($(CH_3)_3C$–) and δ=3.12 (CH_2).

PMR of **1d** (CD_3NO_2), δ=0.80 (s, 9, $(CH_3)_3C$–), 3.57 (s, 3, CH_3–S), 4.92 (q, CH_AH_B–CMe_3), 7.64—8.20 (m, 5, Ph).

Alkoxyneopentyloxyethylsulfonium Triflates ***2a,b.*** They were prepared by the reaction of an equimolar mixture of neopentyl ethanesulfinate and ethyl or methyl triflate in CD_3NO_2 at 34 °C for 1 h. They were stable only in solution, and decomposed when the solvent was evaporated. PMR: **2a**, δ=0.92 (s, 9, $(CH_3)_3C$–), 1.41 (t, 3, $C\underline{H}_3CH_2S$–), 1.43 (t, 3, $C\underline{H}_3CH_2O$–), 3.66 (q, 2, $CH_3C\underline{H}_2S$–), 4.26 (q, 2, –OCH_AH_B–CMe_3, J_{AB}=8.8 Hz), 4.68 (q, 2, $OC\underline{H}_2CH_3$); **2b**, δ=0.90 (s, 9, $(CH_3)_3C$–), 1.37 (t, 3, $C\underline{H}_3CH_2S$–), 3.68 (q, 2, $CH_3C\underline{H}_2S$–), 4.29 (s, 3, CH_3O–), 4.29 (q, 2, OCH_AH_B, J=9.0 Hz); **2c**, δ=1.35 (t, 3, $C\underline{H}_3CH_2S$–), 1.42 (t, 3, $C\underline{H}_3CH_2O$–), 3.63 (q, 2, $CH_3C\underline{H}_2S$–), 4.25 (s, 3, CH_3O–), 4.66 (q, 2, $CH_3C\underline{H}_2O$–).

Alkoxyaminosulfonium Triflates ***4b—d.*** They were prepared by the reaction of an equimolar mixture of an arenesulfinamide and alkyl triflate in CD_3NO_2 at 34 °C for 1 h. Upon evaporation of the solvent, **4b** decomposed, whereas **4c** and **4d** could be isolated as oils. PMR(CD_3NO_2) of **4b**; δ= 1.49 (t, 3, $C\underline{H}_3CH_2O$–), 1.85—2.14 (m, 4, $-CH_2CH_2N$), 2.39

Spin Trapping of Benzoyloxycyclohexadienyl Radicals by 2,3,5,6-Tetramethylnitrosobenzene (Nitrosodurene) in the Decomposition of Dibenzoyl Peroxide in Benzene

Tadashi SUEHIRO, Mariko KAMIMORI, Hirochika SAKURAGI,*
Masayuki YOSHIDA,* and Katsumi TOKUMARU**

Faculty of Sciences, Gakushuin University, Mejiro, Toshima-ku, Tokyo 171
**Department of Chemistry, Faculty of Science, The University of Tokyo, Hongo, Bunkyo-ku, Tokyo 113*
***Department of Chemistry, The University of Tsukuba, Sakura-mura, Niihari-gun, Ibaraki 300-31*

(Received June 7, 1976)

The aroyloxycyclohexadienyl radicals (VIII), the key intermediates in the homolytic aromatic aroyloxylation, were detected and identified in the decomposition of dibenzoyl peroxide, bis(4-methylbenzoyl) peroxide, and bis(4-methoxybenzoyl) peroxide in benzene-d_6 as spin adducts of nitrosodurene.

Irradiation of dibenzoyl peroxide (BPO) in benzene causes a benzoyloxylation of the solvent benzene to give substantial yields of phenyl benzoate at room temperature, if molecular oxygen is present. Such a benzoyloxylation takes place also in the thermal decomposition of BPO in benzene, where the yield of phenyl benzoate increases with lowering of the reaction temperature.[1] The genesis of phenyl benzoate has been accounted for in terms of the reversible addition of benzoxyl radicals to benzene followed by the oxidation of the resulting benzoyloxycyclohexadienyl radicals (I) by molecular oxygen (Scheme 1).[1]

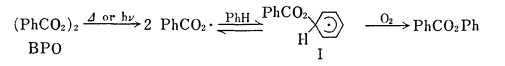

Scheme 1.

In the decomposition of bis(pentafluorobenzoyl) peroxide in the presence of benzene in hexachloro-1,3-butadiene CIDNP effects are detected in the proton NMR spectra of benzene and other products. The observed polarizations have been explained by assuming a singlet radical pair of a pentafluorobenzoyloxycyclohexadienyl radical and a pentafluorobenzoxyl radical.[2] Recently, the direct observation of the radical adduct of benzoxyl radicals to 1,3,5-tris(trimethylsiloxy)benzene was attained by ESR spectroscopy.[3] However, no definitive spectroscopic evidence indicating the formation of I has hitherto been reported in the decomposition of BPO in benzene. We showed previously that the decomposition of arylazotriphenylmethanes in the presence of 2,3,5,6-tetramethylnitrosobenzene (nitrosodurene) in benzene affords arylcyclohexadienyl 2,3,5,6-tetramethylphenyl nitroxides (arylcyclohexadienyl duryl nitroxides). Thus, success has been achieved in trapping arylcyclohexadienyl radicals, produced by the addition of aryl radicals to benzene, by nitrosodurene.[4] We therefore decided to employ this spin trapping technique for the detection of I.

Results and Discussion

Heating dibenzoyl peroxide (BPO) at 80 °C in benzene containing nitrosodurene under an atmosphere of argon gave an ESR spectrum consisting of three complex sets (a_N=9.5 gauss) ascribable to duryl phenyl nitroxides (VIa).[4,5] Apparently these radicals (VIa) are produced by the fast decarboxylation of benzoxyl radicals followed by trapping of the resulting phenyl radicals by nitrosodurene. When the decomposition was carried out at 40 °C in benzene, VIa could not be detected at all; instead an ESR signal (three triplets, a_N=9.7 and $a_{ortho\text{-}H}$=2.7 gauss) consistent with 4-benzoyloxyphenyl duryl nitroxide (III)[6] was observed. The structural assignment is mainly based on the value of the nitrogen hyperfine splitting constant (a_N) and the partially resolved splitting due to the two *ortho*-hydrogens. The possible assignment to 4-biphenylyl duryl nitroxide (V), which might be formed by the oxidation of a spin adduct of phenylcyclohexadienyl radicals (IV), can be eliminated, since no signals due to 4-biphenylyl duryl nitroxide (V) were detected in the decomposition of phenylazotriphenylmethane (PAT) in the presence of nitrosodurene at 40 °C in benzene; the phenyl radicals arising from PAT are trapped by nitrosodurene to yield VIa before they add to benzene. Further verification for the structural assignment of III was obtained in the trapping experiment by the photolysis of 4-iodophenyl benzoate (VII) in carbon tetrachloride (Scheme 2). The ESR spectrum obtained agrees well with that observed above.

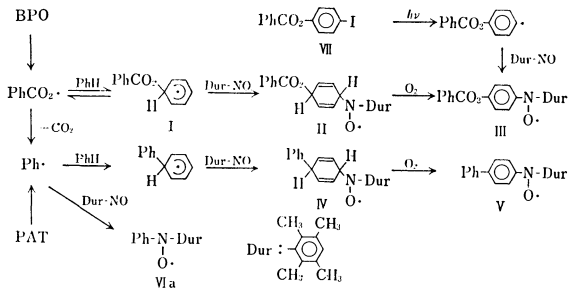

Scheme 2.

To gain more insight into the formation of III, BPO was decomposed in benzene-d_6 at 40 °C in the presence of nitrosodurene. The ESR spectrum showed three triplets (a_N=13.4 and $a_{\beta\text{-}D}$=1.5 gauss), which diminished in intensity on exposure to oxygen, while a new signal composed of a broad triplet (a_N=9.6 gauss) increased. The latter signal is attributed to the deuterated 4-benzoyloxyphenyl duryl nitroxide (Xa) by comparison of the a_N value with that of III. The magnitude of the nitrogen and β-hydrogen (deuterium) hyperfine splitting

CH_2, m), 3.20 (3H, OCH_3, s), 3.70 (1H, C-6 CH, dd, J=6.0, 10.0 Hz), 3.92 (1H, C-8 CH, br t, J=8.0 Hz), 6.30 (5H, aromatic-H, br s), 7.76—8.32 ppm (4H, aromatic-H, m). UV_{max} (CCl_4); 300 nm (ε: 2.8×10^3), 310 (2.6×10^3), 343 (4.5×10^2), UV_{max} (CH_3CN); 301 nm (ε: 2.6×10^3), 310 (2.4×10^3), 339 (4.5×10^2).

8-Hexyl-1-methoxy-3,4-benzobicyclo[4.2.0]oct-3-ene-2,5-dione (3e); colorless oil (yield, 40% after 90% of quinone was consumed on irradiation with the filter A.). Mass; m/e=300(M^+). IR (liq. film); 1690 cm^{-1} (C=O). ^{1}H-NMR (CCl_4); δ: 0.98 (3H, CH_3, br t, J=6.0 Hz), 1.00—1.84 (10H, aliphatic-H, m), 1.92—2.70 (3H, C-7 CH_2 and C-8 CH, m), 3.24 (3H, O-CH_3, s), 3.42 (1H, C-6 CH, dd, J=6.0, 10.0 Hz), 7.20—8.24 ppm (4H, aromatic-H, m). UV_{max} (CCl_4); 300 nm (ε: 1.4×10^3), 309 (1.3×10^3), 352 (1.3×10^2), UV_{max} (CH_3CN); 300 nm (ε: 1.5×10^3), 308 (1.4×10^3), 349 (1.7×10^2).

1-Ethoxy-8,8-diphenyl-3,4-benzobicyclo[4.2.0]oct-3-ene-2,5-dione (3f); white crystals (yield, 60%); mp 112.0—113.0 °C. Mass; m/e=382 (M^+). Found: C, 81.49; H, 5.80%. Calcd for $C_{26}H_{22}O_3$: C, 81.65; H, 5.80%. IR (KBr disk); 1680 cm^{-1} (C=O). ^{1}H-NMR (CCl_4); δ: 1.18 (3H, CH_3, t, J=8.0 Hz), 3.40 (2H, CH_2, q, J=8.0 Hz), 3.38 (3H, C-6 CH and C-7 CH_2, m), 6.72—7.90 ppm (14H, aromatic-H, m).

1-Isopropoxy-8-phenyl-3,4-benzobicyclo[4.2.0]oct-3-ene-2,5-dione (3g); white needles (yield, 41%); mp 91.0—92.0 °C. Mass; m/e=320 (M^+). Found: C, 79.07; H, 5.85%. Calcd for $C_{21}H_{20}O_3$: C, 78.75; H, 6.25%. IR (KBr disk); 2970 (CH), 1690, 1680 cm^{-1} (C=O). ^{1}H-NMR (CCl_4); δ: 0.68 (3H, CH_3, d, J=6.0 Hz), 0.90 (3H, CH_3, d, J=6.0 Hz), 2.14 (1H, C-7 CH, m), 2.83 (1H, C-7 CH, m), 3.60—4.00 (3H, O-CH, C-6 CH, and C-8 CH' s, m), 7.24 (5H, aromatic-H, br s), 7.60—8.24 ppm (4H, aromatic-H, m). UV_{max} ($CHCl_3$); 300 nm (ε: 2.3×10^3), 310 (1.8×10^5), 338 (3.3×10^2).

The Acetylation of the Photo-addition Compound, 4. The acetyl derivative **6** was prepared by standing the photo-addition compound, **4**, (115 mg) in acetic anhydride (5 ml) containing few drops of pyridine for 3 h at room temperature, and by then pouring the mixture into cold water (10 ml). After extraction with ether and subsequent purification using thin-layer chromatography on silica gel, 2-acetoxy-8-phenyl-3,4-benzo-1,2-epoxymethanobicyclo[4.2.0]oct-3-en-5-one, **6**, was obtained as white plates (110 mg; yield, 83%); mp 92.0—93.0 °C from petroleum ether. Mass; m/e=334 (M^+). IR (KBr disk); 1740, 1682 cm^{-1} (C=O). ^{1}H-NMR ($CDCl_3$); δ: 2.13 (3H, $OCOCH_3$, s), 2.60 (2H, C-7 CH_2, dd, J=6.0, 8.0 Hz), 3.56 (1H, C-6 CH, t, J=8.0 Hz), 3.84 (1H, C-8 CH, t, J=6.0 Hz), 4.52, 4.84 (2H, C-10 CH_2, AB-q, J=6.0 Hz), 7.30 (5H, aromatic-H, br s), 7.20—8.05 ppm (4H, aromatic-H, m).

The Acid-catalyzed Decomposition of the Photo-addition Compound, 4. The acid-catalyzed decomposition was completed by treating the photo-addition compound, **4** (200 mg) in chloroform (15 ml) with a few drops of concd hydrochloric acid or concd sulfuric acid at room temperature for 8 h. After the concentration of the reaction mixture and purification using thin-layer chromatography on silica gel, two isomers of 7-phenyl-3,4-benzobicyclo[4.2.0]oct-3-ene-2,5-dione, **7a** (61 mg; yield, 38%) and **7b** (35 mg; yield, 22%), were isolated as white crystals; **7a**; mp 112.0—115.0 °C. Mass; m/e=262 (M^+). IR (KBr disk); 1690 cm^{-1} (C=O). ^{1}H-NMR (CCl_4); δ: 2.70 (2H, C-8 CH_2, m), 3.40—3.70 (3H, C-1, C-6 and C-7 CH' s, m), 7.16 (5H, aromatic-H, br s), 7.92—8.10 ppm (4H, aromatic-H, m). **7b**; mp 147.0—148.0 °C. Mass; m/e=262 (M^+). IR (KBr disk); 1680 cm^{-1} (C=O). ^{1}H-NMR ($CDCl_3$); δ: 2.70—3.20 (2H, C-8 CH_2, m), 3.60—4.40 (3H, C-1, C-6, and C-7 CH's, m), 6.90—7.40 (5H, aromatic-H, m), 7.60—8.20 ppm (4H, aromatic-H, m).

The Photochemical Reaction of 1,4-Naphthoquinone with Styrene. A benzene solution (20 ml) of 1,4-naphthoquinone (158 mg) and styrene (210 mg) was submitted to the irradiation of a high-pressure Hg arc lamp. After the complete consumption of the quinone, **7a** (118 mg; yield, 45%) and **7b** (28 mg; yield, 11%) were isolated from the reaction mixture through purification by thin-layer chromatography on silica gel.

The Acetylation of 7a or 7b. 3,8-Diacetoxy-1-phenyl-1,2-dihydrocyclobuta[*b*]naphthalene, **8**, was prepared by refluxing a mixture of **7a** (or **7b**) (70 mg) and sodium acetate (200 mg) dissolved in acetic anhydride (15 ml) for 3 h. **8** was thus obtained in a 57% yield (53 mg) as white needles from benzene–hexane; mp 135.0 °C. Mass; m/e=346 (M^+). Found: C, 76.10; H, 5.38%. Calcd for $C_{22}H_{18}O_4$: C, 76.28; H, 5.25%. IR (KBr disk); 1750 cm^{-1} (C=O). ^{1}H-NMR (CCl_4); δ: 2.16 (3H, $COCH_3$, s), 2.42 (3H, $COCH_3$, s), 3.18 (1H, C-2 CH, dd, J=4.0 14.0 Hz), 3.82 (1H, C-2 CH, dd, J=8.0, 14.0 Hz), 4.78 (1H, C-1 CH, dd, J=4.0, 8.0 Hz), 7.24 (5H, aromatic-H, br s), 7.36—8.04 ppm (4H, aromatic-H,m).

The Bromination of the Photo-addition compound, 4. Bromine (100 mg) was added to a chloform solution (25 ml) of the photo-addition compound, **4** (300 mg), after which the mixture was allowed to stand for 15 h at room temperature. Two products, **9** and **10**, were isolated in 54% (189 mg) and 32% (122 mg) yields respectively after the purification of the reaction mixture using thin-layer chromatography on silica gel. 1-Bromo-7-phenyl-3,4-benzobicyclo[4.2.0]oct-3-ene-2,5-dione (**9**); white crystals from benzene–peroleum ether; mp 136.0—137.0 °C. Mass; m/e=342, 340 (M^+). IR (KBr disk); 1695 cm^{-1} (C=O). ^{1}H-NMR ($CDCl_3$); δ: 3.20—3.50 (2H, C-7 CH and C-8 CH, m), 3.78 (1H, C-8 CH, dd, J=8.0, 12.0 Hz), 4.74 (1H, C-6 CH, d, J=8.0 Hz), 7.10-7.50 (5H, aromatic-H,m), 7.70—8.40 ppm (4H, aromatic-H, m). 6-Bromo-2-hydroxy-8-phenyl-3,4-benzo-1,2-epoxymethanobicyclo[4.2.0]oct-3-en-5-one (**10**); white crystals. Mass; m/e=372, 370 (M^+). IR (KBr disk); 3400 (OH), 1670 cm^{-1} (C=O). ^{1}H-NMR ($CDCl_3$); δ: 2.94 (1H, C-7 CH, dd, J=10.0, 12.0 Hz), 3.10 (1H, OH, s), 3.26 (1H, C-7 CH, dd, J=8.0, 12.0 Hz), 3.92 (1H, C-8 CH, dd, J=8.0, 10.0 Hz), 4.64, 4.74 (2H, C-10 CH_2, AB-q, J=8.0 Hz), 7.30—8.00 ppm (9H, aromatic-H, m).

The Bromination of 6. By treating a chloroform solution (10 ml) of **6** (110 mg) with bromine (30 mg) for 15 h at room temperature, **9** (65 mg; yield, 50%) and **11** (49 mg; yield, 36 %) were obtained: 2-acetoxy-6-bromo-8-phenyl-3,4-benzo-1,2-epoxymethanobicyclo[4.2.0]oct-3-en-5-one (**11**); white needles from benzene–petroleum ether; mp 138.0—138.5 °C. Mass; m/e=414, 412 (M^+). IR (KBr disk); 1740, 1690 cm^{-1} (C=O). ^{1}H-NMR ($CDCl_3$); δ: 2.84 (3H, $COCH_3$, s), 2.80 (1H, C-7 CH, dd, J=8.0, 12.0 Hz), 3.42 (1H, C-7 CH, dd, J=8.0, 12.0 Hz), 3.92 (1H, C-8 CH, t, J=8.0 Hz), 4.68, 4.78 (2H, C-10 CH_2, AB-q, J=6.0 Hz), 7.26 (5H, aromatic-H, br s), 7.10—7.90 ppm (4H, aromatic-H, m). **11** was also isolated from the reaction mixture of the acetylation of **10** by acetic anhydride–pyridine.

The Bromination of 7b. **9** was also identified as one of the reaction products of **7b** (115 mg) with bromine (100 mg) in chloroform (10 ml) at room temperature for 20 h.

The Clemmensen Reduction of the Photo-addition Compound, 4. The photo-addition compound, **4** (500 mg), toluene (5 ml), amalgamated zinc (10 g), and concd hydrochloric acid (12 ml) were heated for 8 h. Three reaction products, **12**, **13**, and **14**, were isolated from the reaction mixture using thin-layer chromatography on silica gel in 17% (42 mg), 7% (20 mg), and 12% (37 mg) yields respectively; 8-methyl-1-phenyl-1,2-dihydrocyclobuta[*b*]naphthalene (**12**); colorless oil. Mass; m/e=244 (M^+). IR (liq. film); no OH or C=O. ^{1}H-NMR (CCl_4); δ: 2.56 (3H, CH_3, s), 2.70—3.20 (3H, C-1 CH and C-2 CH_2, m), 7.60 (5H, aromatic-H, br s), 7.10—8.00 ppm

(5H, aromatic-H, m). UV_{max} ($CHCl_3$); 243 nm (ε: 7.9×10^3), 276 (5.0×10^3), 307 (1.7×10^3), 322 (1.4×10^3). 4-Phenyl-3,4-dihydro-1H-oxeto[2′,3′: 3,4]naphtho[1,2-*b*]furan (**13**); white needles from benzene–petroleum ether; mp 137.0—139.0 °C. Mass; $m/e=274$ (M^+). Found: C, 83.06; H, 5.35 %. Calcd for $C_{19}H_{14}O_2$: C, 83.20; H, 5.15%. IR (KBr disk); no OH or C=O. ^{1}H-NMR ($CDCl_3$); δ: 3.14 (2H, C-3 CH_2, m), 4.82 (1H, C-4 CH, dd, $J=4.0$, 10.0 Hz), 5.44 (2H, C-1 CH_2, AB-q, $J=15.0$ Hz), 7.14—7.90 ppm (9H, aromatic-H, m). UV_{max} ($CHCl_3$); 242 nm (ε: 6.9×10^3), 266 (4.9×10^3), 274 (6.1×10^3), 280 (6.3×10^3), 291 (4.8×10^3), 307 (8.8×10^2), 313 (5.7×10^2), 322 (6.6×10^2). 2-(2-Hydroxy-2-phenylethyl)-4-methylnaphthalene-1,3-diol (**14**); colorless oil. Mass; $m/e=276$ (M^+-H_2O). IR (liq. film); 3850, 3400 cm^{-1} (OH). ^{1}H-NMR (CCl_4); δ: 2.56 (3H, CH_3, s), 3.18 (2H, CH, d, $J=6.0$ Hz), 4.82 (1H, CH, t, $J=6.0$ Hz), 7.10—8.00 ppm (9H, aromatic-H, m). UV_{max} ($CHCl_3$); 246 nm (ε: 7.2×10^3), 275 (4.4×10^3), 283 (3.8×10^3), 321 (1.2×10^3).

The Thermal Decomposition of ***12***. The thermal decomposition of **12** at 500 °C for 20 min in a sealed tube gave 1-methylnaphthalene, which was identified by gas-liquid-partition chromatography.

The Acetylation of ***14***. A monoacetylated product, **15**, was identified through the acetylation of **14** with sodium acetate–acetic anhydride: 4-Acetoxy-5-methyl-2-phenyl-2,3-dihydronaphthalene[1,2-b]furan (**15**); Mass; $m/e=328$ (M^+). IR (liq, film); 1730 cm^{-1} (C=O). ^{1}H-NMR (CCl_4); δ: 2.00 (3H, $COCH_3$, s), 2.56 (3H, CH_3, s), 3.18, 3.46 (2H, CH_2, d×AB-q, $J=6.0$, 12.0 Hz), 5.96 (1H, CH, t, $J=8.0$ Hz), 7.00—8.10 ppm (9H, aromatic-H, m).

The Thermal Decomposition of ***3a***. A 0.04 M-CCl_4 solution of **3a** was submitted to thermal decomposition at 75±1 °C; the rate was followed by means of ^{1}H-NMR. The half-life of **3a** was estimated to be about 92 min.

The Determination of the Quantum Efficiency. The light source was a high-pressure Hg arc lamp (300 W) with the filter, A. Irradiation carried out at a constant temperature (16±0.5 °C). The quanta of light absorbed by the reaction mixture was calibrated using an aqueous solution of potassium ferroxalate as a chemical actinometer;[22] it was estimated to be 2.07×10^{-5} mol/10.0 ml/min. The reaction mixture submitted to the measurement was a benzene solution of 2.00×10^{-2} mol/l of 2-methoxy-1,4-naphthoquinone and 4.00×10^{-2} mol/l of styrene. The quantum efficiency was calculated for the disappeaance of 2-methoxy-1,4-naphthoquinone and was estimated to be 0.18.

The author wishes to express his deep gratitude to Professor Kazuhiro Maruyama, Kyoto University, for his fruitful suggestions and invaluable encouragement. He also wishes to thank the Ministry of Education for the financial support for this research.

References

1) a) K. Maruyama and T. Otsuki, *Chem. Lett.*, **1974**, 129; b) T. Otsuki, *Bull. Chem. Soc. Jpn.*, **47**, 3089 (1974).
2) J. M. Bruce, *Quart. Revs.*, **21**, 405 (1967).
3) K. Maruyama, T. Otsuki, and Y. Naruta, *Chem. Lett.*, **1973**, 641; K. Maruyama, Y. Naruta, and T. Otsuki, *Bull. Chem. Soc. Jpn.*, **48**, 1553 (1975).
4) C. H. Krauch and S. Farid, *Tetrahedron Lett.*, **1966**, 4783.
5) K. Maruyama, T. Otsuki, A. Takuwa, and S. Kako, *Bull. Inst. Chem. Res., Kyoto Univ.*, **50**, 344 (1972).
6) J. A. Bartrop and B. Hesp, *J. Chem. Soc., C*, **1967**, 1625.
7) D. Bryce-Smith and G. A. Gilbert, *Tetrahedron Lett.*, **1964**, 3471.
8) S. P. Pappas and N. A. Portnoy, *Chem. Commun.*, **1970**, 1126, and the references cited therein.
9) K. Wallenfals and W. Mohler, *Ber.*, **76**, 924 (1943).
10) P. Zumman, *Coll. Czech. Chem. Commun.*, **27**, 2935 (1962).
11) F. A. L. Anett and D. P. Mullis, *Tetrahedron Lett.*, **1969**, 737.
12) J. E. Ellis and J. E. Jones, *J. Org. Chem.*, **40**, 485 (1975).
13) In the following discussion, the structures of the compounds derived from **5** are not illustrated because these structures should be excluded as trivial.
14) The stereochemistry of these isomers was concluded on the basis of an analysis of their ^{1}H-NMR spectra, as is illustrated in **7a** and **7b**. The possibility of the stereoisomers being centered at C-1 can be excluded completely because **4** (or **5**) could be derived from one of the stereoisomers at C-1 (**3d**).
15) D. J. Cram and A. C. Day, *J. Org. Chem.*, **31**, 1227 (1967).
16) N. J. Turro and D. S. Weiss, *J. Am. Chem. Soc.*, **90**, 2185 (1968).
17) A similar type of photo-rearrangement was also observed in another case when a cyclobutane-ring compound was isolated: that is, the photolysis of **3e** gave **2c**, and that of **3g** gave **2o**, both exclusively.
18) *Cf.* R. B. Woodward, F. Sondheimer, D. Taub, K. Hensler, and W. L. Lamore, *J. Am. Chem. Soc.*, **74**, 4223 (1952).
19) L. F. Fieser, *J. Am. Chem. Soc.*, **48**, 2922 (1926).
20) L. F. Fieser, *J. Am. Chem. Soc.*, **70**, 3165 (1948).
21) *Cf. Org. Synth.*, Coll. Vol. II, 606 (1966).
22) C. A. Parker, *Proc. R. Soc. London, Ser. A*, **220**, 104 (1952).
23) D. A. Hatchard and C. A. Parker, *Proc. R. Soc. London, Ser. A*, **235**, 518 (1956).

Table 2. The observed and calculated frequencies (cm^{-1}) of CH_3HgX

Assignments	Obsd (refs)	Calcd	Assignments	Obsd (refs)	Calcd
CH_3HgCH_3			E δ(C-Hg-As)	101 (17)	100.9
asym ν(Hg-C)	550 (4, 5)	550.0	CH_3HgSCN		
sym ν(Hg-C)	515 (4, 5)	515.0	ν(C-N)	2138 (15, 16)	2138.0
δ(C-Hg-C)	156 (4, 5)	156.0	ν(S-C)	792 (15, 16)	792.0
CH_3HgF			ν(Hg-C)	540 (15, 16)	540.0
ν(Hg-C)	561 (6)	561.0	δ(S-C-N)	*ca.* 480 (15, 16)	475.8
ν(Hg-F)	482 (6)	482.0	ν(Hg-S)	283 (15, 16)	283.0
δ(C-Hg-F)	170 (6)	170.0	δ(C-Hg-S)	150[a]	151.6
CH_3HgCl			CH_3HgSCH_3		
ν(Hg-C)	539 (7, 8, 9)	539.0	A′ ν(S-C)	698 (18, 19)	698.0
ν(Hg-Cl)	304 (7, 8, 9)	304.0	A′ ν(Hg-C)	533 (18, 19)	533.0
δ(C-Hg-Cl)	112 (7, 8, 9)	112.0	A′ ν(Hg-S)	329 (18, 19)	329.0
CH_3HgBr			A′ δ(Hg-S-C)	192 (18, 19)	192.0
ν(Hg-C)	538 (7, 8, 10, 11)	538.0	A′/A″ δ(C-Hg-S)	133 (18, 19)	126.0 (A″)
ν(Hg-Br)	202 (7, 8, 10, 11)	202.0			113.1 (A′)
δ(C-Hg-Br)	100 (7, 8, 10, 11)	100.0	$(CH_3Hg)_2S$		
CH_3HgI			B_2 ν(Hg-C)	530	528.0
ν(Hg-C)	526 (7, 8, 11—13)	526.0	A_1 ν(Hg-C)	525	527.0
ν(Hg-I)	173 (7, 8, 11—13)	173.0	B_2 ν(Hg-S)	344	344.0
δ(C-Hg-I)	97 (7, 8, 11—13)	97.0	A_1 ν(Hg-S)	300	300.0
CH_3HgCN			A_1/B_2 δ(C-Hg-S)	137	134.0 (B_2)
ν(C-N)	2180 (14)	2180.0			131.3 (A_1)
ν(Hg-CH_3)	565 (14)	565.0	A_1 δ(Hg-S-Hg)	80	77.0
ν(Hg-CN)	386 (14)	386.0	$(CH_3Hg)_3S^+$ ($\theta=105°$)		
δ(Hg-C-N)	306 (14)	303.1	E′ ν(Hg-C)	534	534.6
δ(C-Hg-CN)	75 (14)	73.3	A_1 ν(Hg-C)	529	529.4
$CH_3HgAs(CH_3)_3^+$			E′ ν(Hg-S)	329	327.4
E ν(As-C)	632 (17)	632.0	A_1 ν(Hg-S)	258	257.5
A_1 ν(As-C)	598 (17)	598.0	A_1/E' δ(C-Hg-S)	127	131.1 (E′)
A_1 ν(Hg-C)	537 (17)	537.0			130.1 (A_1)
A_1 ν(Hg-As)	253 (17)	253.0	A_1/E' δ(Hg-S-Hg)	86	126.5 (E′)
E δ(C-As-C)	219 (17)	219.0			73.7 (A_1)
A_1 δ(C-As-C)	167 (17)	167.0			

a) Assumed from the δ(C-Hg-S) values of the CH_3HgSCH_3, $(CH_3Hg)_2S$, and $(CH_3Hg)_3S^+$.

Table 3. Force constants (md/Å) of CH_3HgX

MeHgMe	K(Hg-C) 2.330		H(C-Hg-C) 0.0928	E(C···C) 0.010			
MeHgF	K(Hg-C) 2.55	K(Hg-F) 2.43	H(C-Hg-F) 0.123				
MeHgCl	K(Hg-C) 2.38_2	K(Hg-Cl) 1.67	H(C-Hg-Cl) 0.063				
MeHgBr	K(Hg-C) 2.37_7	K(Hg-Br) 1.41	H(C-Hg-Br) 0.056				
MeHgI	K(Hg-C) 2.27	K(Hg-I) 1.41	H(C-Hg-I) 0.053				
MeHgCN	K(Hg-C) 2.61	K(Hg-CN) 2.13	H(C-Hg-CN) 0.033	K(C-N) 17.47	H(Hg-C-N) 0.105		
$MeHgAsMe_3^+$	K(Hg-C) 2.37	K(Hg-As) 1.53	H(C-Hg-As) 0.084	K(As-C) 2.75	H(C-As-C) 0.140	F(Hg···C) 0.098	F(C···C) 0.034
MeHgSCN	K(Hg-C) 2.39	K(Hg-S) 1.50	H(C-Hg-S) 0.11	K(C-N) 15.38	K(S-C) 5.87	H(S-C-N) 0.29	
MeHgSMe	K(Hg-C) 2.33	K(Hg-S) 1.52	H(C-Hg-S) 0.078		K(S-C) 2.90	H(Hg-S-C) 0.183	
$(MeHg)_2S$	K(Hg-C) 2.38	K(Hg-S) 1.46	H(C-Hg-S) 0.118	H(Hg-S-Hg) 0.15	F(Hg···Hg) 0.0		
$(MeHg)_3S^+$ ($\theta=105°$)	K(Hg-C) 1.86	K(Hg-S) 0.79	H(C-Hg-S) 0.06	H(Hg-S-Hg) 0.06	F(Hg···Hg) 0.30	F(C···S) 0.48	

8.10 (m, 4H, aromatic-H), 11.83 (s, 1H, OH). Found: C, 73.04; H, 6.71; N, 4.54%. Calcd for $C_{19}H_{21}NO_3$: C, 73.29; H, 6.80, N, 4.54%. 1,2-Dihydroxy-4-naphthalenecarbonitrile monooctanoate [**5**: R=$CH_3(CH_2)_6$, R_1=R_3=H, R_2=CN]: white needles (21 mg, 6.2%), mp 91—92 °C. IR: ν_{OH} 3225; ν_{CH} 2970, 2945, 2870; ν_{CN} 2235; $\nu_{C=O}$ 1760 cm^{-1}. PMR (CCl_4), δ: 0.85 (t, 3H, CH_3), 1.15—1.89 (m, 10 H, $(CH_2)_5$), 2.68 (t, 2H, $COCH_2$), 6.80 (1H, OH), 7.40—8.21 (m, 5H, aromatic-H). Found: C, 73.00; H, 6.57; N, 4.44%. Calcd for $C_{19}H_{21}NO_3$: C, 73.29; H, 6.80; N, 4.50%.

(ix) Nonanal: 1,2-Dihydroxy-3-nonanoyl-4-naphthalenecarbonitrile [**4**: R=$CH_3(CH_2)_7$, R_1=CN, R_2=H]: orange plates (63 mg, 17.6%), mp 93—94 °C. IR: ν_{OH} 3300; ν_{CH} 2955, 2930, 2860; ν_{CN} 2225; $\nu_{C=O}$ 1638 cm^{-1}. PMR ($CDCl_3$), δ: 0.88 (t, 3H, CH_3), 1.20—1.95 (m, 12H, $(CH_2)_6$), 3.49(t, 2H, $COCH_2$), 6.78 (1H, OH), 7.50—8.30 (m, 4H, aromatic-H), 11.99 (s, 1H, OH). Found: C, 73.49; H, 6.87; N, 4.22%. Calcd for $C_{20}H_{23}NO_3$: C, 73.82; H, 7.12; N, 4.30%. 1,2-Dihydroxy-4-naphthalenecarbonitrile monononanoate [**5**: R=$CH_3(CH_2)_7$, R_1=R_3=H, R_2=CN]: white needles (11 mg, 3.1%), mp 91—92 °C. IR: ν_{OH} 3280; ν_{CH} 2970, 2940, 2865; ν_{CN} 2237; $\nu_{C=O}$ 1765 cm^{-1}. PMR(CCl_4), δ: 0.87 (t, 3H, CH_3), 1.20—1.83 (m, 12H, $(CH_2)_6$), 2.61 (t, 2H, $COCH_2$), 6.91 (1H, OH), 7.45—8.24 (m, 5H, aromatic-H). Found: C, 73.96; H, 7.00; N, 4.21%. Calcd for $C_{20}H_{23}NO_3$: C, 73.82; H, 7.12; N, 4.30%.

(x) Decanal: 1,2-Dihydroxy-3-decanoyl-4-naphthalenecarbonitrile [**4**: R=$CH_3(CH_2)_8$, R_1=CN, R_2=H]: orange plates (82 mg, 22%), mp 156—157 °C. IR: ν_{OH} 3300; ν_{CH} 2925, 2885; ν_{CN} 2215; $\nu_{C=O}$ 1638 cm^{-1}. PMR($CDCl_3$), δ: 0.86—1.86 (m, 17H, $CH_3(CH_2)_7$), 3.52(t, 2H, $COCH_2$), 6.75 (1H, OH), 7.53—8.33 (m, 4H, aromatic-H), 11.98 (s, 1H, OH). Found: C, 74.41; H, 7.26; N, 4.03%. Calcd for $C_{21}H_{25}NO_3$: C, 74.31; H, 7.42; N, 4.13%. 1,2-Dihydroxy-4-naphthalenecarbonitrile monodecanoate [**5**: R=$CH_3(CH_2)_8$, R_1=R_3=H, R_2=CN]: white needles (19 mg, 5.1%), mp 156—157 °C. IR: ν_{OH} 3235; ν_{CH} 2957, 2940, 2858; ν_{CN} 2243; $\nu_{C=O}$ 1760 cm^{-1}. PMR(CCl_4), δ: 0.80—1.96 (br. m, 17H, $CH_3(CH_2)_7$), 2.60 (t, 2H, $COCH_2$), 6.89 (1H, OH), 7.48—8.32 (m, 5H, aromatic-H). Found: C, 74.09; H, 7.50; N, 4.10%. Calcd for $C_{21}H_{25}NO_3$: C, 74.31; H, 7.42; N, 4.13%.

Photo-addition Products of 6-Bromo-1,2-naphthoquinone with Aliphatic Aldehydes. (i) Acetaldehyde: 3-Acetyl-6-bromo-1,2-naphthalenediol [**4**: R=CH_3, R_1=H, R_2=Br]: orange yellow needles (90 mg, 38%), mp 159.5—160.5 °C. IR: ν_{OH} 3440; $\nu_{C=O}$ 1650 cm^{-1}. PMR(CCl_4), δ: 2.78 (s, 3H, CH_3), 5.98 (s, 1H, OH), 7.48—8.05 (m, 4H, aromatic-H), 11.56 (s, 1H, OH). Found: C, 51.17; H, 3.31%. Calcd for $C_{12}H_9BrO_3$: C, 51.27; H, 3.23%. 6-Bromo-1,2-naphthalenediol monoacetate [**5**: R=CH_3, R_1=R_2=H, R_3=Br]: white needles (40 mg, 16.9%), mp 136—137 °C. IR: ν_{OH} 3310; $\nu_{C=O}$ 1742 cm^{-1}. PMR($CDCl_3$), δ: 2.43 (s, CH_3, 70%), 2.52 (s, CH_3, 30%), 7.12—8.18 (m, aromatic-H+OH). Found: C, 51.48; H, 3.17%. Calcd for $C_{12}H_9BrO_3$: C, 51.27; H, 3.23%.

(ii) Propionaldehyde: 3-Propionyl-6-bromo-1,2-naphthalenediol [**4**: R=CH_3CH_2, R_1=H, R_2=Br]: orange prisms (64 mg, 25.7%), mp 143—144.5 °C. IR: ν_{OH} 3375; $\nu_{C=O}$ 1640 cm^{-1}. PMR(CCl_4), δ: 1.30(t, 3H, CH_3), 3.14 (q, 2H, CH_2), 5.92 (s, 1H, OH), 7.37—7.92 (m, 4H, aromatic-H), 11.52 (s, 1H, OH). Found: C, 53.17; H, 3.61%. Calcd for $C_{13}H_{11}BrO_3$: C, 52.91; H, 3.76%. 6-Bromo-1,2-naphthalenediol monopropionate [**5**: R=CH_3CH_2, R_1=R_2=H, R_3=Br]; white crystals (60 mg, 24%), mp 140.5—142 °C. IR: ν_{OH} 3400; $\nu_{C=O}$ 1735 cm^{-1}. PMR($CDCl_3$), δ: 1.31 (t, CH_3, 70%), 1.38 (t, CH_3, 30%), 2.69 (q, CH_2, 70%), 2.78 (q, CH_2, 30%), 7.00—8.00 (m, aromatic-H+OH). Found: C, 52.81; H, 3.65%. Calcd for $C_{13}H_{11}BrO_3$: C, 52.91; H, 3.76%.

(iii) Butyraldehyde: 3-Butyryl-6-bromo-1,2-naphthalenediol [**4**: R=$CH_3(CH_2)_2$, R_1=H, R_2=Br]: orange prisms (67 mg, 25.8%), mp 126.5—128.5 °C. IR: ν_{OH} 3430; ν_{CH} 2960, 2940, 2880; $\nu_{C=O}$ 1655 cm^{-1}. PMR(CCl_4), δ: 1.08 (t, 3H, CH_3), 1.74 (sex, 2H, CH_2), 3.06 (t, 2H, $COCH_2$), 5.95 (s, 1H, OH), 7.38—7.98 (m, 4H, aromatic-H), 11.58 (s, 1H, OH). Found: C, 54.53; H, 4.09%. Calcd for $C_{14}H_{13}BrO_3$: C, 54.39; H, 4.24%. 6-Bromo-1,2-naphthalenediol monobutyrate [**5**: R=$CH_3(CH_2)_2$, R_1=R_2=H, R_3=Br]: white needles (75 mg, 28.8%), mp 131.0—132.5 °C. IR: ν_{OH} 3300; ν_{CH} 2960; $\nu_{C=O}$ 1720 cm^{-1}. PMR($CDCl_3$), δ: 1.08 (t, 3H, CH_3), 1.84 (sex, 2H, CH_2), 2.65 (t, 2H, $COCH_2$), 7.10—8.08 (m, 6H, aromatic-H+OH). Found: C, 54.26; H, 4.37%. Calcd for $C_{14}H_{13}BrO_3$: C, 54.39; H, 4.24%.

(iv) Isobutyraldehyde: 3-Isobutyryl-6-bromo-1,2-naphthalenediol [**4**: R=$(CH_3)_2CH$, R_1=H, R_2=Br]: orange plates (40 mg, 15.4%), mp 116.5—118.0 °C. IR: ν_{OH} 3450; ν_{CH} 2980, 2940; $\nu_{C=O}$ 1650 cm^{-1}. PMR(CCl_4), δ: 1.29 (d, 6H, $(CH_3)_2$), 3.67 (sep, 1H, OH), 5.90 (s, 1H, OH), 7.31—7.96 (m, 4H, aromatic-H), 11.58 (s, 1H, OH). Found: C, 54.72; H, 4.36%. Calcd for $C_{14}H_{13}BrO_3$: C, 54.39; H, 4.24%. 6-Bromo-1,2-naphthalenediol monoisobutyrate [**5**: R=$(CH_3)_2CH$, R_1=R_2=H, R_3=Br]: white prisms (105 mg, 40.4 %), mp 153.0—154.5 °C. IR: ν_{OH} 3440; ν_{CH} 2990, 2950, 2890; $\nu_{C=O}$ 1735 cm^{-1}. PMR($CDCl_3$), δ: 1.40 (d, 6H, $(CH_3)_2$), 2.91 (sep, 1H, CH), 7.02—8.01 (m, 6H, aromatic-H). Found: C, 54.39; H, 4.19%. Calcd for $C_{14}H_{13}BrO_3$: C, 54.39; H, 4.24%.

(v) Valeraldehyde: 3-Valeryl-6-bromo-1,2-naphthalenediol [**4**: R=$CH_3(CH_2)_3$, R_1=H, R_2=Br]: orange needles (49 mg, 18.1%), mp 101—102 °C. IR: ν_{OH} 3450; ν_{CH} 2950, 2880; $\nu_{C=O}$ 1650 cm^{-1}. PMR(CCl_4), δ: 0.98 (t, 3H, CH_3), 1.31—1.88 (m, 4H, $(CH_2)_2$), 3.03 (t, 2H, $COCH_2$), 5.93 (s, 1H, OH), 7.04—7.94 (m, 4H, aromatic-H), 11.65 (s, 1H, OH). Found: C, 55.58; H, 4.52%. Calcd for $C_{15}H_{15}BrO_3$: C, 55.57; H, 4.68%. 6-Bromo-1,2-naphthalenediol monovalerate [**5**: R=$CH_3(CH_2)_3$, R_1=R_2=H, R_3=Br]: white needles (73 mg, 26.9%), mp 121—122 °C. IR: ν_{OH} 3400; ν_{CH} 2960, 2945, 2880; $\nu_{C=O}$ 1722 cm^{-1}. PMR (CCl_4), δ: 0.97 (t, 3H, CH_3), 1.33—1.89 (m, 4H, $(CH_2)_2$), 2.60 (t, 2H, $COCH_2$), 6.10 (s, 1H, OH), 7.00—8.06 (m, 5H, aromatic-H). Found: C, 55.83; H, 4.71%. Calcd for $C_{15}H_{15}BrO_3$: C, 55.75; H, 4.68%.

(vi) Isovaleraldehyde: 3-Isovaleryl-6-bromo-1,2-naphthalenediol [**4**: R=$(CH_3)_2CHCH_2$, R_1=H, R_2=Br]: orange yellow needles (45 mg, 16.6%), mp 117—118 °C. IR: ν_{OH} 3460; ν_{CH} 2960; $\nu_{C=O}$ 1655 cm^{-1}. PMR(CCl_4), δ: 1.04 (d, 6H, $(CH_3)_2$), 2.31 (m, 1H, CH), 2.92 (d, 2H, $COCH_2$), 5.96 (s, 1H, OH), 7.42—7.97 (m, 4H, aromatic-H), 11.69 (s, 1H, OH). Found: C, 55.62; H, 4.61%. Calcd for $C_{15}H_{15}BrO_3$: C, 55.75; H, 4.68%. 6-Bromo-1,2-naphthalenediol monoisovalerate [**5**: R=$(CH_3)_2CHCH_2$, R_1=R_2=H, R_3=Br]: white crystals (75 mg, 27.7%), mp 150—151 °C. IR: ν_{OH} 3420; ν_{CH} 2960; $\nu_{C=O}$ 1720 cm^{-1}. PMR (CCl_4), δ: 1.06 (d, 6H, $(CH_3)_2$), 1.10(d, 6H, $(CH_3)_2$), 2.25(br. m, 2H, CH), 2.45 (t, 2H, $COCH_2$), 2.55 (t, 2H, $COCH_2$), 6.40 (br, 2H, OH), 6.93—8.03 (m, 10H, aromatic-H). Found: C, 55.65; H, 4.75%. Calcd for $C_{15}H_{15}BrO_3$: C, 55.75; H, 4.68.

(vii) Hexanal: 3-Hexanoyl-6-bromo-1,2-naphthalenediol [**4**: R=$CH_3(CH_2)_4$, R_1=H, R_2=Br]: orange plates (64 mg, 22.4%), mp 98—99 °C. IR: ν_{OH} 3450; ν_{CH} 2950, 2875; $\nu_{C=O}$ 1655 cm^{-1}. PMR($CDCl_3$), δ: 0.94 (t, 3H, CH_3), 1.27—1.92 (m, 6H, $(CH_2)_3$), 2.99 (t, 2H, $COCH_2$), 6.02 (s, 1H,

OH), 7.25—7.92 (m, 4H, aromatic-H), 11.65 (s, 1H, OH). Found: C, 56.89; H, 5.14%. Calcd for $C_{16}H_{17}BrO_3$: C, 56.99; H, 5.08%. 6-Bromo-1,2-naphthalenediol monohexanoate [**5**: $R=CH_3(CH_2)_4$, $R_1=R_2=H$, $R_3=Br$]: white crystals (95 mg, 33.6%), mp 106—108 °C. IR: ν_{OH} 3410; ν_{CH} 2970, 2948, 2875; $\nu_{C=O}$ 1725 cm^{-1}. PMR (CCl_4), δ: 0.86—1.90 (m, 11H, $CH_3(CH_2)_4$), 6.19 (br. s, 1H, OH), 7.05—8.05 (m, 5H, aromatic-H). Found: C, 56.71; H, 5.10%. Calcd for $C_{16}H_{17}BrO_3$: C, 56.99; H, 5.08%.

(viii) Heptanal: 3-Heptanoyl-6-bromo-1,2-naphthalenediol [**4**: $R=CH_3(CH_2)_5$, $R_1=H$, $R_2=Br$]: yellow crystals (59 mg, 20%), mp 72—73 °C. IR: ν_{OH} 3440, ν_{CH} 2945, 2875, $\nu_{C=O}$ 1655 cm^{-1}. PMR (CCl_4), δ: 0.91 (t, 3H, CH_3), 1.25—1.90 (m, 8H, $(CH_2)_4$), 3.06 (t, 2H, $COCH_2$), 5.94 (s, 1H, OH), 7.42—7.96 (m, 4H, aromatic-H), 11.67 (s, 1H, OH). Found: C, 58.31; H, 5.52%. Calcd for $C_{17}H_{19}BrO_3$: C, 58.13; H, 5.45%. 6-Bromo-1,2-naphthalenediol monoheptanoate [**5**: $R=CH_3(CH_2)_5$, $R_1=R_2=H$, $R_3=Br$]: white plates (74 mg, 25%), mp 107—108 °C. IR: ν_{OH} 3440; ν_{CH} 2970, 2970, 2945, 2870; $\nu_{C=O}$ 1722 cm^{-1}. PMR(CCl_4), δ: 0.93 (t, 3H, CH_3), 1.26—1.90 (br. m, 8H, $(CH_2)_4$), 2.57 (t, 2H, $COCH_2$), 6.13 (s, 1H, OH), 7.00—8.05 (m, 5H, aromatic-H). Found: C, 58.06; H, 5.50%. Calcd for $C_{17}H_{19}BrO_3$: C, 58.13; H, 5.45%.

(ix) Octanal: 3-Octanoyl-6-bromo-1,2-naphthalenediol [**4**: $R=CH_3(CH_2)_6$, $R_1=H$, $R_2=Br$]: orange plates (71 mg, 23.2%), mp 86—88 °C. IR: ν_{OH} 3440; ν_{CH} 2950, 2925, 2860; $\nu_{C=O}$ 1655 cm^{-1}. PMR(CCl_4), δ: 0.89 (t, 3H, CH_3), 1.20—1.87 (br. m, 10H, $(CH_2)_5$), 3.02 (t, 2H, $COCH_2$), 5.96 (s, 1H, OH), 7.40—7.97 (m, 4H, aromatic-H), 11.67 (s, 1H, OH). Found: C, 59.37; H, 5.63%. Calcd for $C_{18}H_{21}BrO_3$: C, 59.19; H, 5.63%. 6-Bromo-1,2-naphthalenediol monooctanoate [**5**: $R=CH_3(CH_2)_6$, $R_1=R_2=H$, $R_3=Br$]: white crystals (91 mg, 29.7%), mp 99—100 °C. IR: ν_{OH} 3410; ν_{CH} 2960, 2930, 2860; $\nu_{C=O}$ 1738 cm^{-1}. PMR (CCl_4), δ: 0.88 (t, 3H, CH_3), 0.91 (t, 3H, CH_3), 1.81—1.92 (br. m, 20 H, $(CH_2)_{10}$), 2.55 (t, 2H, $COCH_2$), 2.66 (t, 2H, $COCH_2$), 6.14 (2H, OH), 6.88—8.02 (m, 10H, aromatic-H). Found: C, 58.08; H, 5.72%. Calcd for $C_{18}H_{21}BrO_3$: C, 59.19; H, 5.79%.

(x) Nonanal: 3-Nonanoyl-6-bromo-1,2-naphthalenediol [**4**: $R=CH_3(CH_2)_7$, $R_1=H$, $R_2=Br$]: yellow crystals (66 mg, 20.8%), mp 77—78 °C. IR: ν_{OH} 3425; ν_{CH} 2930, 2860; $\nu_{C=O}$ 1655 cm^{-1}. PMR (CCl_4), δ: 0.89 (t, 3H, CH_3), 1.15—1.91 (br. m, 12 H, $(CH_2)_6$), 3.04 (t, 2H, $COCH_2$), 5.94 (s, 1H, OH), 7.41—7.96 (m, 4H, aromatic-H), 11.67 (s, 1H, OH). Found: C, 59.93; H, 6.10%. Calcd for $C_{19}H_{23}BrO_3$: C, 60.17; H, 6.11%. 6-Bromo-1,2-naphthalenediol monononanoate [**5**: $R=CH_3(CH_2)_7$, $R_1=R_2=H$, $R_3=Br$]: white crystals (98 mg, 30.3%), mp 97—98 °C. IR: ν_{OH} 3430; ν_{CH} 2940, 2860; $\nu_{C=O}$ 1740 cm^{-1}. PMR (CCl_4), δ: 0.85—1.92 (br. m, 30H, $CH_3(CH_2)_6$), 2.56 (t, 2H, $COCH_2$), 2.68 (t, 2H, $COCH_2$), 6.07 (1H, OH), 6.19 (1H, OH), 6.91—8.03 (m, 10 H, aromatic-H). Found: C, 60.24; H, 6.27%. Calcd for $C_{19}H_{23}BrO_3$: C, 60.17; H, 6.11%.

(xi) Decanal: 3-Decanoyl-6-bromo-1,2-naphthalenediol [**4**: $R=CH_3(CH_2)_8$, $R_1=H$, $R_2=Br$]: orange crystals (38 mg, 11.5%), mp 92—93 °C. IR: ν_{OH} 3420; ν_{CH} 2910, 2870; $\nu_{C=O}$ 1650 cm^{-1}. PMR(CCl_4), δ: 0.86 (t, 3H, CH_3), 1.16—1.88 (br. m, 14H, $(CH_2)_7$), 3.02 (t, 2H, $COCH_2$), 5.91 (s, 1H, OH), 7.41—7.94 (m, 4H, aromatic-H), 11.65 (s, 1H, OH). Found: C, 61.08; H, 6.33%. Calcd for $C_{20}H_{25}BrO_3$: C, 61.08; H, 6.41%. 6-Bromo-1,2-naphthalenediol monodecanoate [**5**: $R=CH_3(CH_2)_8$, $R_1=R_2=H$, $R_3=Br$]: white crystals (121 mg, 36.7%), mp 89.0—89.5 °C. IR: ν_{OH} 3425; ν_{CH} 2940, 2860; $\nu_{C=O}$ 1720 cm^{-1}. PMR (CCl_4), δ: 0.88 (t, 3H, CH_3), 1.20—1.87 (br. m. 14H, $(CH_2)_7$), 2.56 (t, 2H, $COCH_2$), 6.14 (1H, OH), 7.02—8.06 (m, 5H, aromatic-H). Found: C, 61.24; H, 6.50%. Calcd for $C_{20}H_{25}BrO_3$: C, 61.08; H, 6.41%.

Photo-addition Products of 6-Methyl-1,2-naphthoquinone with Aliphatic Aldehydes. (i) Acetaldehyde: 3-Acetyl-6-methyl-1,2-naphthalenediol [**4**: $R=CH_3$, $R_1=H$, $R_2=CH_3$]: orange plates (25 mg, 10%), mp 156—157 °C. IR: ν_{OH} 3330 (br); $\nu_{C=O}$ 1650 cm^{-1}. PMR(CCl_4), δ: 2.26 (s, 3H, CH_3), 2.69 (s, 3H, CH_3), 5.86 (s, 1H, OH), 7.24—8.04 (m, 4H, aromatic-H), 11.47 (s, 1H, OH). Found: C, 72.21; H, 5.63%. Calcd for $C_{13}H_{12}O_3$: C, 72.21; H, 5.59%. 6-Methyl-1,2-naphthalenediol monoacetate [**5**: $R=CH_3$, $R_1=R_2=H$, $R_3=CH_3$]: white plates (15 mg, 6%), mp 127—128 °C. IR: ν_{OH} 3360; $\nu_{C=O}$ 1720 cm^{-1}. PMR(CCl_4), δ: 2.29 (s, 3H, $COCH_3$), 2.39 (s, 3H, $COCH_3$), 2.47 (s, 6H, CH_3), 6.10 (2H, OH), 7.08—8.10 (m, 10H, aromatic-H). Found: C, 72.10; H, 5.48%. Calcd for $C_{13}H_{12}O_3$: C, 72.21; H, 5.59%.

(ii) Propionaldehyde: 3-Propionyl-6-methyl-1,2-naphthalenediol [**4**: $R=CH_3CH_2$, $R_1=H$, $R_2=CH_3$]; yellow plates (55 mg, 15.2%), mp 148—149 °C. IR: ν_{OH} 3448; $\nu_{C=O}$ 1647 cm^{-1}. PMR(CCl_4), δ: 1.27 (t, 3H, CH_3), 2.45 (s, 3H, CH_3), 3.14 (q, 2H, CH_2), 5.85 (s, 1H, OH), 7.16—7.95 (m, 4H, aromatic-H), 11.03 (s, 1H, OH). Found: C, 73.22; H, 5.59%. Calcd for $C_{14}H_{14}O_3$: C, 73.03; H, 6.13%. 6-Methyl-1,2-naphthalenediol monopropionate [**5**: $R=CH_3CH_2$, $R_1=R_2=H$, $R_3=CH_3$]: white crystals (50 mg, 13.9%), mp 114—116 °C. IR: ν_{OH} 3400 (br); $\nu_{C=O}$ 1722 cm^{-1}. PMR(CCl_4), δ: 1.33 (t, 3H, CH_3), 2.42 (s, 3H, CH_3), 2.72 (q, 2H, CH_2), 5.81 (1H, OH), 6.93—7.53 (m, 5H, aromatic-H). Found: C, 72.89; H, 6.05%. Calcd for $C_{14}H_{14}O_3$: C, 73.03; H, 6.13%.

(iii) Butyraldehyde: 3-Butyryl-6-methyl-1,2-naphthalenediol [**4**: $R=CH_3(CH_2)_2$, $R_1=H$, $R_2=CH_3$]: yellow orange needles (25 mg, 10.4%), mp 117—118 °C. IR: ν_{OH} 3490; ν_{CH} 2960, 2940, 2880; $\nu_{C=O}$ 1635 cm^{-1}. PMR (CCl_4), δ: 1.05 (t, 3H, CH_3), 1.80 (sex, 2H, CH_2), 2.43 (s, 3H, CH_3), 3.04 (t, 2H, $COCH_2$), 5.87 (s, 1H, OH), 7.18—7.96 (m, 4H, aromatic-H), 11.55 (s, 1H, OH). Found: C, 74.00; H, 6.68%. Calcd for $C_{15}H_{16}O_3$: C, 73.75; H, 6.60%. 6-Methyl-1,2-naphthalenediol monobutyrate [**5**: $R=CH_3(CH_2)_2$, $R_1=R_2=H$, $R_3=CH_3$]: white plates (28 mg, 11.5%), mp 99.0—99.5 °C. IR: ν_{OH} 3300(br); ν_{CH} 2980, 2945, 2890; $\nu_{C=O}$ 1725 cm^{-1}. PMR (CCl_4), δ: 1.03 (t, 3H, CH_3), 1.08 (t, 3H, CH_3), 1.65—1.96 (m, 4H, CH_2), 2.45 (s, 3H, CH_3), 2.54 (t, 2H, $COCH_2$), 2.66 (t, 2H, $COCH_2$), 6.00 (2H, OH), 6.91—8.07 (m, 10H, aromatic-H). Found: C, 73.71; H, 6.51%. Calcd for $C_{15}H_{16}O_3$: C, 73.75; H, 6.60%.

(iv) Isobutyraldehyde: 3-Isobutyryl-6-methyl-1,2-naphthalenediol [**4**: $R=(CH_3)_2CH$, $R_1=H$, $R_2=CH_3$]: yellow prisms (31 mg, 7.8%), mp 155—156 °C. IR: ν_{OH} 3450; ν_{CH} 2990, 2940; $\nu_{C=O}$ 1645 cm^{-1}. PMR(CCl_4), δ: 1.29 (d, 6H, $(CH_3)_2$), 2.42(s, 3H, CH_3), 3.75 (sep. 1H, OH), 5.90 (s, 1H, OH), 7.20—8.00 (m, 4H, aromatic-H), 11.65 (s, 1H, OH). Found: C, 73.63; H, 6.47%. Calcd for $C_{15}H_{16}O_3$: C, 73.75; H, 6.60%. 6-Methyl-1,2-naphthalenediol monoisobutyrate [**5**: $R=(CH_3)_2CH$, $R_1=R_2=H$, $R_3=CH_3$]: white needles (126 mg, 31.9%), mp 118—119 °C. IR: ν_{OH} 3325; ν_{CH} 2980, 2930, 2890; $\nu_{C=O}$ 1720 cm^{-1}. PMR(CCl_4), δ: 1.34 (d, 6H, $(CH_3)_2$), 2.46 (s, 3H, CH_3), 2.82 (sep, 1H, CH), 5.96 (1H, OH), 6.94—8.08 (m, 5H, aromatic-H). Found: C, 73.49; H, 6.65%. Calcd for $C_{15}H_{16}O_3$: C, 73.75; H, 6.60%.

(v) Valeraldehyde: 3-Valeryl-6-methyl-1,2-naphthalenediol [**4**: $R=CH_3(CH_2)_3$, $R_1=H$, $R_2=CH_3$]: yellowish orange needles (58 mg, 13.5%), mp 101—102 °C. IR: ν_{OH} 3410; ν_{CH} 2960, 2930, 2880; $\nu_{C=O}$ 1650 cm^{-1}. PMR(CCl_4), δ: 1.01 (t, 3H, CH_3), 1.30—1.90 (m, 4H, $(CH_2)_2$), 2.48 (s, 3H, CH_3), 3.10 (t, 2H, $COCH_2$), 5.88 (s, 1H, OH), 7.10—8.01 (m, 4H,

aromatic-H), 11.61 (s, 1H, OH). Found: C, 74.43; H, 7.08%. Calcd for $C_{16}H_{18}O_3$: C, 74.40; H, 7.02%. 6-Methyl-1,2-naphthalenediol monovalerate [**5**: R=$CH_3(CH_2)_3$, R_1=R_2=H, R_3=CH_3]: white needles (66 mg, 15.4%), mp 92—94 °C. IR: ν_{OH} 3390; ν_{CH} 2960, 2930, 2880; $\nu_{C=O}$ 1722 cm^{-1}. PMR(CCl_4), δ: 0.96 (t, 3H, CH_3), 1.30—1.86 (m, 4H, $(CH_2)_2$), 2.46 (s, 3H, CH_3), 2.55 (t, 2H, $COCH_2$), 5.98 (s, 1H, OH), 6.29—8.07 (m, 5H, aromatic-H). Found: C, 74.28; H, 6.95%. Calcd for $C_{16}H_{18}O_3$: C, 74.40; H, 7.02%.

(vi) Isovaleraldehyde: 3-Isovaleryl-6-methyl-1,2-naphthalenediol [**4**: R=$(CH_3)_2CHCH_2$, R_1=H, R_2=CH_3]: yellow needles (41 mg, 10%), mp 89—91 °C. IR: ν_{OH} 3400; ν_{CH} 2970, 2890; $\nu_{C=O}$ 1645 cm^{-1}. PMR(CCl_4), δ: 1.05 (d, 6H, $(CH_3)_2$), 2.05 (m, 1H, CH), 2.45 (s, 3H, CH_3), 2.94 (d, 2H, $COCH_2$), 5.87 (s, 1H, OH), 7.25—7.94 (4H, aromatic-H), 11.60 (s, 1H, OH). Found: C, 74.33; H, 6.89%. Calcd for $C_{16}H_{18}O_3$: C, 74.40; H, 7.02%. 6-Methyl-1,2-naphthalenediol monoisovalerate [**5**: R=$(CH_3)_2CHCH_2$, R_1=R_2=H, R_3=CH_3]: white needles (89 mg, 21%), mp 99—100 °C. IR: ν_{OH} 3410 (br); ν_{CH} 2980; $\nu_{C=O}$ 1735 cm^{-1}. PMR(CCl_4), δ: 1.06 (d, 6H, $(CH_3)_2$), 1.10 (d, 6H, $(CH_3)_2$), 2.26 (br. m, 2H, CH), 2.44 (d, 2H, $COCH_2$), 2.46 (s, 6H, CH_3), 2.56 (d, 2H, $COCH_2$), 5.74 (1H, OH), 5.94 (1H, OH), 6.92—8.08 (m, 10H, aromatic-H). Found: C, 74.21; H, 7.01%. Calcd for $C_{16}H_{18}O_3$: C, 74.40; H, 7.02%.

(vii) Hexanal: 3-Hexanoyl-6-methyl-1,2-naphthalenediol [**4**: R=$CH_3(CH_2)_4$, R_1=H, R_2=CH_3]: yellowish orange needles (81 mg, 17.4%), mp 88—89 °C. IR: ν_{OH} 3430; ν_{CH} 2960, 2940, 2880; $\nu_{C=O}$ 1643 cm^{-1}. PMR(CCl_4), δ: 0.80—1.90 (br. m, 9H, $CH_3(CH_2)_3$), 2.43 (s, 3H, CH_3), 3.04 (t, 2H, $COCH_2$), 5.85 (s, 1H, OH), 7.20—8.00 (4H, aromatic-H), 11.58 (s, 1H, OH). Found: C, 74.73; H, 7.52%. Calcd for $C_{17}H_{20}O_3$: C, 74.97; H, 7.40%. 6-Methyl-1,2-naphthalenediol monohexanoate [**5**: R=$CH_3(CH_2)_4$, R_1=R_2=H, R_3=CH_3]: white lieves (48 mg, 11%), mp 78—80 °C. IR: ν_{OH} 3390; ν_{CH} 2970, 2930, 2870; $\nu_{C=O}$ 1720 cm^{-1}. PMR (CCl_4), δ: 0.80—2.00 (br. m, 18H, $CH_3(CH_2)_3$), 2.48 (s, 6H, CH_3), 2.54 (t, 2H, $COCH_2$), 2.68 (t, 2H, $COCH_2$), 6.00 (2H, OH), 6.92—8.15 (m, 10H, aromatic-H). Found C, 75.11; H, 7.48%. Calcd for $C_{17}H_{20}O_3$: C, 74.97; H, 7.40%.

(viii) Heptanal: 3-Heptanoyl-6-methyl-1,2-naphthalenediol [**4**: R=$CH_3(CH_2)_5$, R_1=H, R_2=CH_3]: orange needles (62 mg, 14%), mp 76—77 °C. IR: ν_{OH} 3370; ν_{CH} 2960, 2930, 2860; $\nu_{C=O}$ 1640 cm^{-1}. PMR(CCl_4), δ: 0.90 (t, 3H, CH_3), 1.23—1.86 (br. m, 8H, $(CH_2)_4$), 2.42 (s, 3H, CH_3), 3.03 (t, 2H, $COCH_2$), 5.85 (s, 1H, OH), 7.18—7.95 (4H, aromatic-H), 11.54 (s, 1H, OH). Found: C, 75.54; H, 7.60%. Calcd for $C_{18}H_{22}O_3$: C, 75.50; H, 7.74%. 6-Methyl-1,2-naphthalenediol monoheptanoate [**5**: R=$CH_3(CH_2)_5$, R_1=R_2=H, R_3=CH_3]: white plates (41 mg, 9.2%), mp 76—77 °C. IR: ν_{OH} 3375 (br); ν_{CH} 2960, 2930, 2860; $\nu_{C=O}$ 1735, 1710 cm^{-1}. PMR(CCl_4), δ: 0.90 (t, 3H, CH_3), 1.25—1.88 (br. m, 8H, $(CH_2)_4$), 2.45 (s, 3H, CH_3), 2.56 (t, 2H, $COCH_2$), 5.95 (s, 1H, OH), 6.95—8.10 (m, 5H, aromatic-H). Found: C, 75.26; H, 7.81%. Calcd for $C_{18}H_{22}O_3$: C, 75.50; H, 7.74%.

(ix) Octanal: 3-Octanoyl-6-methyl-1,2-naphthalenediol [**4**: R=$CH_3(CH_2)_6$, R_1=H, R_2=CH_3]: orange plates (21 mg, 4.4%), mp 76—77 °C. IR: ν_{OH} 3440; ν_{CH} 2925, 2860; $\nu_{C=O}$ 1655 cm^{-1}. PMR(CCl_4), δ: 0.90 (t, 3H, CH_3), 1.25—1.88 (br. m, 10H, $(CH_2)_5$), 2.43 (s, 6H, CH_3), 3.05 (t, 2H, $COCH_2$), 5.84 (s, 1H, OH), 7.20—7.97 (4H, aromatic-H), 11.57 (s, 1H, OH). Found: C, 75.63; H, 7.92%. Calcd for $C_{19}H_{24}O_3$: C, 75.97; H, 8.05%. 6-Methyl-1,2-naphthalenediol monooctanoate [**5**: R=$CH_3(CH_2)_6$, R_1=R_2=H, R_3=CH_3]: white crystals (22 mg, 4.7%), mp 77—78 °C. IR: ν_{OH} 3425; ν_{CH} 2960, 2930, 2860; $\nu_{C=O}$ 1740 cm^{-1}. PMR(CCl_4), δ: 0.88—1.88 (br. m, 26H, $CH_3(CH_2)_5$), 2.43 (s, 6H, CH_3), 2.53 (t, 2H, $COCH_2$), 2.66 (t, 2H, $COCH_2$), 5.74 (1H, OH), 6.00 (1H, OH), 6.93—8.07 (m, 10H, aromatic-H). Found: C, 75.89; H, 7.86%. Calcd for $C_{19}H_{24}O_3$: C, 75.97; H, 8.05%.

(x) Nonanal: 3-Nonanoyl-6-methyl-1,2-naphthalenediol [**4**: R=$CH_3(CH_2)_7$, R_1=H, R_2=CH_3]: reddish orange plates (72 mg, 13.8%), mp 74—75 °C. IR: ν_{OH} 3470; ν_{CH} 2940, 2865; $\nu_{C=O}$ 1650 cm^{-1}. PMR(CCl_4), δ: 0.87 (t, 3H, CH_3), 1.18—1.88 (br. m, 12H, $(CH_2)_6$), 2.42 (s, 3H, CH_3), 3.00 (t, 2H, $COCH_2$), 5.86 (s, 1H, OH), 7.16—7.95 (4H, aromatic-H), 11.54 (s, 1H, OH). Found: C, 76.40; H, 8.39%. Calcd for $C_{20}H_{26}O_3$): C, 76.40; H, 8.33%. 6-Methyl-1,2-naphthalenediol mononononanoate [**5**: R=CH_3, R_1=R_2=H, R_3=CH_3]: white crystals (105 mg, 20.2%), mp 76—77 °C. IR: ν_{OH} 3440; ν_{CH} 2940, 2870; $\nu_{C=O}$ 1740 cm^{-1}. PMR(CCl_4), δ: 0.80—1.88 (br. m, 34H, $CH_3(CH_2)_7$), 2.43 (s, 6H, CH_3), 2.53 (t, 2H, $COCH_2$), 2.64 (t, 2H, $COCH_2$), 5.85 (1H, OH), 6.05 (1H, OH), 6.93—8.07 (m, 10H, aromatic-H). Found: C, 76.09; H, 8.39%. Calcd for $C_{20}H_{26}O_3$: C, 76.40; H, 8.33%.

(xi) Decanal: 3-Decanoyl-6-methyl-1,2-naphthalenediol [**4**: R=$CH_3(CH_2)_8$, R_1=H, R_2=CH_3]: orange plates (53 mg, 9.8%), mp 70—71 °C. IR: ν_{OH} 3450; ν_{CH} 2930, 2855; $\nu_{C=O}$ 1650 cm^{-1}. PMR(CCl_4), δ: 0.87 (t, 3H, CH_3), 1.18—1.90 (br. m, 14H, $(CH_2)_7$), 2.41 (s, 3H, CH_3), 3.02 (t, 2H, $COCH_2$), 5.85 (s, 1H, OH), 7.18—7.95 (4H, aromatic-H), 11.55 (s, 1H, OH). Found: C, 76.75; H, 8.43%. Calcd for $C_{21}H_{28}O_3$: C, 76.79; H, 8.59%. 6-Methyl-1,2-naphthalenediol monodecanoate [**5**: R=$CH_3(CH_2)_8$, R_1=R_2=H, R_3=CH_3]: white crystals (41 mg, 7.6%), mp 64—65 °C. IR: ν_{OH} 3420; ν_{CH} 2930, 2860; $\nu_{C=O}$ 1740, 1720 cm^{-1}. PMR(CCl_4), δ: 0.81—1.92 (br. m, 34 H, $CH_3(CH_2)_7$), 2.44 (s, 6H, CH_3), 2.55 (t, 2H, $COCH_2$), 2.67 (t, 2H, $COCH_2$), 5.82 (1H, OH), 6.03 (1H, OH), 6.93—8.07 (m,10H, aromatic-H). Found: C, 77.03, H, 8.49%. Calcd for $C_{21}H_{28}O_3$: C, 76.79; H, 8.59%.

Irradiation of 3-Chloro-1,2-naphthoquinone in the Presence of Acetaldehyde. *(a)* A benzene solution of quinone (200 mg, 1.04 mmol) and acetaldehyde (500 mg) was irradiated for 4 days. Paraldehyde was detected by PMR analysis of the reaction mixture. The solvent and paraldehyde were removed at 60 °C under reduced pressure, and the residue was worked up as usual.

(b) The quinone (300 mg) in acetaldehyde (15 g) was irradiated for 5 days; the metaldehyde which deposited (120 mg) was filtered off and the paraldehyde (13.5 g) was removed at 60 °C under reduced pressure, then the residue was chromatographed over silica gel.

Photo-addition Products of 3-Chloro-1,2-naphthoquinone with Aliphatic Aldehydes. *(i) Acetaldehyde*: 3-Chloro-1,2-naphthalenediol monoacetate [**5**: R=CH_3, R_1=Cl, R_2=R_3=H] white needles (95 mg, 38.7%), mp 149—150 °C. IR: ν_{OH} 3335 (br), $\nu_{C=O}$ 1757 cm^{-1}. PMR ($CDCl_3$), δ: 2.48 (s, 3H, CH_3), 7.33—8.24(m, 6H, aromatic-H+OH). Found: C, 60.85; H, 3.88%. Calcd for $C_{12}H_9ClO_3$: C, 60.90; H, 3.83%. 3-Chloro-4-acetyl-1,2-naphthoquinone: reddish orange needles (12 mg, 4.9%), mp 197—200 °C. IR: $\nu_{C=O}$ 1700, 1685 cm^{-1}. MS, *m/e*: 234 (M^+), 206 (M−CO), 199 (M−Cl), 178 (M−2CO), 171 (M−Cl−CO). PMR($CDCl_3$), δ: 2.30 (s, 3H, CH_3), 7.04—8.16 (m, 4H, aromatic-H). 3-Acetyl-1,2-naphthalenediol(2.1 mg, 1%) was identical (IR spectrum) with the photo-adduct of 1,2-naphthoquinone and acetaldehyde.

(ii) Propionaldehyde: 3-Chloro-1,2-naphthalenediol mono-

TABLE 1. YIELDS AND PHYSICAL DATA FOR THE PHOTOPRODUCTS FROM **1a** TO **1d**

	Yield %	Mp °C	UV in EtOH λ(nm)	UV in EtOH ε	IR (cm^{-1})	Mass (*m/e*)	NMR (δ in $CDCl_3$)	Anal. Found (Calcd) C%	H%	N%
2a	23—54	230[a]	264	13900	1716	182[b]	2.49 (s, 3H), 2.73 (s, 3H),	52.80	5.58	15.24
			307	6650	3430	150	3.94 (s, 3H), 12.93 (s, 1H)	(52.74)	(5.53)	(15.34)
2b	20	220.5	264	18800	1703	196[b]	1.40 (t, 3H), 2.48 (s, 3H),	55.09	6.25	14.55
		221.0	308	4500	3430	151	2.72 (s, 3H), 4.42 (q, 2H),	(55.10)	(6.17)	(14.28)
						123	12.93 (s, 1H)			
2c	36	180[a]	285	13800	1689	166[b]	2.45 (s, 3H), 2.58 (s, 3H),	57.60	6.09	16.56
					3430	151	2.69 (s, 3H), 12.80 (s, 1H)	(57.82)	(6.07)	(16.86)
2d	small amount		295			228[b]				
3a	27	152	266	14000	1722	298[b]	1.12 (t, 3H), 1.22 (d, 3H),	56.40	7.46	9.45
		154	322	5300	3270	225	2.17 (s, 3H), 2.40 (s, 3H),	(56.30)	(7.51)	(9.39)
						193	3.38 (q, 2H), 3.76 (s, 6H),			
						165	4.28 (q, 1H), 5.04 (bs, 1H)			
3c	33	liquid	234	5400	1698	220				
			288	8000	3380	205				
						193				
4a	20	152	267	14000	1733	296[b]	2.00 (m, 4H), 2.20 (s, 3H),	56.68	6.85	9.40
		153.5	331	3900	3340	226	2.40 (s, 3H), 3.77 (s, 6H),	(56.74)	(6.80)	(9.45)
						193	3.85 (m, 1H), 4.60 (t, 2H),			
						165	5.00 (bs, 1H)			
4c	35	liquid	234	9000	1730	220				
			289	13900	3375	177				
						164				

a) Decomposition. b) Molecular ion.

The results are shown in Fig. 1. Upon irradiation, the absorption (A) of **1a** at 289 nm rapidly decreased. At the same time, a new absorption (B) appeared at 330 and 505 nm and increased quickly. Then the color of the solution changed from colorless to red. If the irradiation was interrupted at the stage when the peak of (B) was at its maximum and the solution was then kept in the dark, the spectrum of the solution returned to **1a**. This indicates that the change of (A) to (B) is reversible. The first-order rate constant of the change of (A), measured from the decrease in the peak at 289 nm of **1a**, was $3.5\times10^{-3}\ s^{-1}$, while that of the regeneration of (A) from (B), measured from the decrease in the peak at 330 nm of (B), was $2.0\times10^{-4}\ s^{-1}$. Upon further irradiation, another new absorption (C) appeared at about 260 nm and increased with the decrease in (B). The formation of (C) was irreversible, so (C) did not return to (B) or (A) upon remaining in the dark.

In the case of **1a—d**, similar behavior was observed, and the same change occurred in tetrahydrofuran, diethyl ether, and 2-propanol. The peaks of the **1** absorption (A), (B), and (C) in 2-propanol are shown in Table 2. This spectrobehavior was similar to that of phenazine (which has a pyrazine ring in a molecule) upon irradiation.[7] To investigate the relationship between phenazine and pyrazine derivatives, three pyrazine derivatives, **1e**, **1f**, and **1g**, with structures similar to phenazine were synthesized, and the spectral change in them upon irradiation were studied. These results are also shown in Table 2. In the irradiation of

TABLE 2. THE VARIATION IN THE ABSORPTION SPECTRA OF PYRAZINE DERIVATIVES IN 2-PROPANOL

Pyrazine	**1** (A) (nm)	(B) (nm)		(C) (nm)
1a	289	330	505	260
b	288	320	502	256
c	298	384	—	292
d	290	384	—	237
e	317	372	502	290
f	317	366	520	282
g	290	290		290

2g (which does not have an α-carbonyl group), no spectral change similar to that of **1a—f** was shown. In the case of **1e**, the first-order rate constant of the change of (A) to (B), as measured from the decrease in the peak at 318 nm of **1e**, was $4.5\times10^{-2}\ s^{-1}$, while that of the regeneration of (A) from (B), as measured from the decrease in the peak at 374 nm of (B) was $6.7\times10^{-3}\ s^{-1}$.

Colored Compound. The solution of **1c** in diethyl ether gave a violet-colored compound, **5c**, upon irradiation; in the case of **1e** a red-brown-colored compound, **5e**, was precipitated. Both **5c** and **5e** were unstable and turned to **1c** and **1e** respectively after a few weeks in the solid state. They were difficult to dissolve and turned to **1c** and **1e** as soon as they are dissolved. Therefore, the UV spectra were measured in acetic acid under an argon atmosphere, they agreed with the (B) absorption of **1c** and **1e** (**5c**: 384 nm;

TABLE 1. ELECTRONIC SPECTRAL BANDS, MAGNETIC MOMENTS AND ELEMENTAL ANALYSIS OF NITRATED BINARY IMINE, DIAMINE, AND MIXED DIAMINE Cu(II) SCHIFF BASE COMPLEXES

No.	Complex	Analytical data %								λ_{max} in nm	$\mu_{eff.}$ in B.M.
		Calcd				Found					
		Cu	C	H	N	Cu	C	H	N		
1	Bis[1-(2-hydroxy-3,5-dinitrophenyl)ethylideneamine]Cu(II)	12.42	37.53	2.34	16.41	12.75	37.97	2.66	16.29	530	1.88
1a	Bis[1-(2-hydroxy-3,5-dinitrophenyl)ethylideneamine]Cu(II)	12.42	37.53	2.34	16.41	12.30	37.40	2.52	15.98	—	1.90
2	Bis[1-(2-hydroxy-5-nitro-*m*-tolyl)ethylideneamine]Cu(II)	14.13	48.05	4.00	12.45	13.70	47.80	4.42	11.99	530	1.82
2b	Bis[1-(2-hydroxy-5-nitro-*m*-tolyl)ethylideneamine]Cu(II)	14.13	—	—	12.45	14.08	—	—	12.00	—	1.86
3	Bis[1-(6-hydroxy-5-nitro-*m*-tolyl)ethylideneamine]Cu(II)	14.13	48.05	4.00	12.45	13.85	47.94	4.06	13.00	—	1.89
3c	Bis[1-(6-hydroxy-5-nitro-*m*-tolyl)ethylideneamine]Cu(II)	14.13	48.05	4.00	12.45	13.92	48.65	3.64	12.23	550	1.92
4	Bis[1-(2-hydroxy-3,5-dinitro-*p*-tolyl)ethylideneamine]Cu(II)	11.77	40.03	2.95	15.56	11.75	39.74	2.94	15.05	590	1.92
4d	Bis[1-(2-hydroxy-3,5-dinitro-*p*-tolyl)ethylideneamine]Cu(II)	11.77	—	—	15.56	11.50	—	—	15.15	—	1.90
5	*N,N'*-ethylene bis[1-(2-hydroxy-3,5-dinitrophenyl)ethylideneaminato]Cu(II)	11.82	40.18	2.60	15.62	12.19	40.68	2.67	16.12	540	1.84
5e	*N,N'*-ethylene bis[1-(2-hydroxy-3,5-dinitrophenyl)ethylideneaminato]Cu(II)	11.82	—	—	15.62	11.98	—	—	15.82	—	1.85
6	*N,N'*-propylene bis[1-(2-hydroxy-3,5-dinitrophenyl)ethylideneaminato]Cu(II)	11.52	41.33	2.90	15.23	11.69	40.97	2.68	15.40	550	1.80
6f	*N,N'*-propylene bis[1-(2-hydroxy-3,5-dinitrophenyl)ethylideneaminato]Cu(II)	11.52	—	—	15.23	11.42	—	—	15.15	—	1.78
7	*N,N'*-ethylene[3,5-dinitrosalicylideneaminato, 1-(2-hydroxy-3,5-dinitrophenyl)ethylideneaminato]Cu(II)	12.13	38.96	2.29	16.04	12.00	38.75	2.21	15.95	560	1.94
8	*N,N'*-propylene[3,5-dinitrosalicylideneaminato, 1-(2-hydroxy-3,5-dinitrophenyl)ethylideneaminato]Cu(II)	11.82	40.18	2.60	15.62	11.78	40.00	2.52	15.42	560	1.95
9	*N,N'*-ethylene[3,5-dinitrosalicylideneaminato, 1-(2-hydroxy-5-nitro-*m*-tolyl)ethylideneaminato]Cu(II)	12.90	—	—	14.21	12.75	—	—	14.02	560	1.86
10	*N,N'*-propylene[3,5-dinitrosalicylideneaminato, 1-(2-hydroxy-5-nitro-*m*-tolyl)ethylideneaminato]Cu(II)	12.54	—	—	13.82	12.42	—	—	13.50	560	1.91
11	*N,N'*-ethylene[3,5-dinitrosalicylideneaminato, 1-(2-hydroxy-3,5-dinitro-*p*-tolyl)ethylideneaminato]Cu(II)	11.82	—	—	15.62	11.65	—	—	15.25	550	1.84
12	*N,N'*-propylene[3,5-dinitrosalicylideneaminato, 1-(2-hydroxy-3,5-dinitro-*p*-tolyl)ethylideneaminato]Cu(II)	11.52	—	—	15.23	11.48	—	—	15.00	550	1.82
13	*N,N'*-ethylene[3,5-dinitrosalicylideneaminato, 1-(6-hydroxy-5-nitro-*m*-tolyl)ethylideneaminato]Cu(II)	12.90	43.85	3.04	14.21	12.62	43.55	3.00	14.00	550	1.87
14	*N,N'*-propylene[3,5-dinitrosalicylideneaminato, 1-(6-hydroxy-5-nitro-*m*-tolyl)ethylideneaminato]Cu(II)	12.54	45.01	3.35	13.82	12.35	44.98	3.23	13.52	550	1.89

a, b, c, and d prepared from nitrated ligand. e and f prepared from imine nitrated complex.

Table 1. Analytical data

	Name of compound	Metal % Calcd	Metal % Found	C, H % Calcd	C, H % Found	Nitrogen % Calcd	Nitrogen % Found	λ_{max} nm	ε	μ Effective in B.M.
1a″	(Salicylideneaminato)(2-hydroxy-1-naphthylmethyleneaminato)Ni(II)	16.83	16.28	C=61.94 H= 4.01	C=62.37 H= 4.40	8.02	7.56	550	303	Diamagnetic
2a′	{*N,N′*-Ethylene(salicylaldeneaminato-2-hydroxy-1-naphthylmethyleneaminato)}Ni(II)	15.66	16.10			7.47	7.30	530	418	Partially paramagnetic
3a′	{*N,N′*-Propylene(salicylaldeneaminato-2-hydroxy-1-naphthylmethyleneaminato)}Ni(II)	15.10	14.90			7.20	6.50	550	343	0.956 Partially paramagnetic
4a′	(*N*-Methylsalicylaldeneaminato)(*N*-methyl-2-hydroxy-1-naphthylmethyleneaminato)Ni(II)	15.58	15.44			7.43	6.60	560 590	213 213	Partially paramagnetic
5a′	(*N*-Ethylsalicylaldeneaminato)(*N*-ethyl-2-hydroxyl-1-naphthylmethyleneaminato)Ni(II)	14.50	14.91	C=65.23 H= 5.43	C=66.40 H= 5.46	6.91	6.48	520 570 596	318 275 275	Partially paramagnetic
6a″	(Salicylideneaminato)(2-hydroxy-1-naphthylmethyleneaminato)Cu(II)	17.97	17.78			7.91	7.29	530 550	123 123	1.83
7a′	{*N,N′*-Ethylene(salicylaldeneaminato-2-hydroxy-1-naphthylmethyleneaminato)}Cu(II)	16.74	16.36	C=63.23 H= 4.74	C=63.45 H= 4.28	7.37	6.90	560	410	1.83
8a′	{*N,N′*-Propylene(salicylaldeneaminato-2-hydroxy-1-naphthylmethyleneaminato)}Cu(II)	16.10	15.80			7.00	6.70	490 550	319 478	1.83
9a′	(*N*-Methylsalicylaldeneaminato)(*N*-methyl-2-hydroxy-1-naphthylmethyleneaminato)Cu(II)	17.65	17.52			7.33	6.33	530 570	252 213	1.86
10a′	(*N*-Ethylsalicylaldeneaminato)(*N*-ethyl-2-hydroxy-1-naphthylmethyleneaminato)Cu(II)	16.51	15.99			6.83	6.12	490	533	1.98
11a‴	{*N,N′*-Propylene(salicylaldeneaminato-2-hydroxy-1-naphthylmethyleneaminato)}Cu(II)	16.10	16.32			7.00	6.72	490	320	1.89

a′=Ammine exchange; a″=compound found from metal amine; a‴=en to pn exchange.

valent each of alcoholic solution of salicylaldehyde and 2-OH-1-naphthaldehyde. The mixture was refluxed (75 min) and stirred. The compound obtained was filtered, washed with water and finally with 50% alcohol. The compound was recrystallized from chloroform and analyzed.

Preparation of Methyl and Ethyl Amino Schiff's Base Complexes. Imine Schiff's base complex(I) was treated with methyl or ethylamine solution (0.5 M) and refluxed gently on a water-bath for 3—4 h. Green crystalline solids were obtained. They were washed with water and 50% alcohol, dried and recrystallized from chloroform and analyzed. Ethylamine compound could be obtained in about 3—4 h, whereas refluxing had to be carried out for about 6—7 h in the case of methyl amine reaction.

Preparation of Diamine Schiff's Base Complexes in Case of Cu(II) or Ni(II). {N,N-*Ethylene or Propylene(salicylideneaminato-2-hydroxy-1-naphthylmethyleneaminato}Cu(II) or Ni(II)*: The complexes were obtained by substitution reactions. The preformed mixed imine Schiff's base complexes of Cu(II) or Ni(II) (2 g) were refluxed (3 h) with en (2 ml) or pn (2 ml) in ethanol (25 ml). The reaction mixture was stirred thoroughly to obtain the compounds. It was filtered, washed, dried and recrystallized from chloroform and analyzed.

General Properties of Complexes. All the complexes were found to be crystalline, stable in atmosphere and insoluble in water. All the compounds are soluble in organic solvents.

In order to characterize and determine the structures of complexes the following studies were undertaken.

Analysis. Cu was estimated by complexometric titration against standard EDTA disodium salt solution, using Fast Sulphon Black F as an indicator. Ni was estimated gravimetrically as dimethylglyoximate. The results of metal, carbon, hydrogen, and nitrogen analyses are presented in the table.

TLC Anslysis. TLC analyses of all the complexes were carried out on a silica gel G(Sichen) using a mixture of chloroform–ether (6:4) as a solvent. The solvent was selected after several trials. A mixture of 1:1 bis(salicylaldeneaminato)M-(II) and bis(2-hydroxy-1-naphthylmethyleneaminato)Ni(II) complexes was prepared. On subjecting it to TLC analysis, the mixture was found to give two spots whereas the mixed ligand complex is pure and a single compound rather than the mixture of bis complexes of the two ligands.

Magnetic Measurements. Magnetic measurements were carried out at room temperature (28 °C) using Guoy balance.

Conductance. Conductivity measurements were carried out in chloroform using Toshniwal Conductivity Bridge Type C LO/O1A.

Spectrophotometric Measurements. The visible spectra of all the complexes were a studied in chloroform solution, on a DU2 Beckman Spectrophotometer at room temperature (30 °C) using 1 cm quartz cell in the range 300—1000 nm.

IR Measurements. IR spectra was recorded in Nujol in the range 4000—625 cm^{-1} on a Perkin-Elmer Model 427.

None of the complexes had adequate solubility in the solvents for NMR studies.

Results and Discussion

The molar conductance of all the complexes in chloroform show them to be non electrolytes.

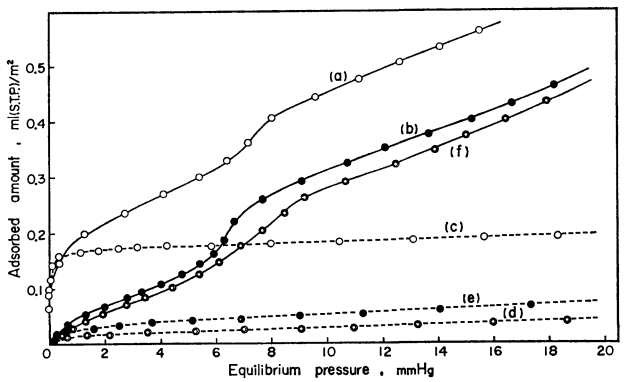

Fig. 1. Adsorption isotherms of H_2O and NH_3 at 25 °C on ZnO surfaces controlled in the amount of chemisorbed H_2O or NH_3. Solid line, H_2O adsorption; broken line, NH_3 adsorption. (a) and (c), on dehydroxylated surface; (b) and (e), on fully hydroxylated surface; (d) and (f), on ammoniated surface.

hydroxylated surfaces, respectively. A large difference is observed between the two curves, because of chemisorption of H_2O on the dehydroxylated surface of ZnO, a distinct discontinuity in the isotherm appearing in the range of relative pressure 0.2—0.3, similar to the case of the ZnO–S sample.[10,13,21-25] Appearance of the discontinuity has been elucidated in terms of the formation of closed hydrogen bonding between the surface hydroxyls on the well-developed $(10\bar{1}0)$ planes of the wurtzite structure.[22]

Curve c is the adsorption isotherm of NH_3 at 25 °C on the dehydroxylated surfaces of ZnO–K, curve d being the second adsorption isotherm of NH_3 on the same sample evacuated at 25 °C after the measurement of the first adsorption isotherm. The two curves are of the Langmuir type and seem to be parallel to each other. It seems that the difference of these two isotherms gives the amount of NH_3 chemisorbed on the surface, as in the case of H_2O adsorption. It should be noted that the amount of NH_3 physisorbed at 25 °C on the NH_3-chemisorbed surfaces, which is represented by the second adsorption isotherm, is much smaller than that of H_2O physisorbed at 25 °C, but the amount of chemisorbed NH_3 seems to be as much as that of chemisorbed H_2O. Curve e is the adsorption isotherm of NH_3 at 25 °C on the fully hydroxylated surfaces of ZnO–K. It is seen that the physisorption of NH_3 on the surface hydroxyls is also as small as that on the ammoniated surface (curve d).

The monolayer capacity calculated on these isotherms is given in Table 1, together with the data on ZnO–S. The V_m and V_p values are the monolayer capacity for the first and second adsorption isotherms, calculated by applying the B-point method to the H_2O adsorption isotherms and the Langmuir equation to the NH_3 adsorption isotherms. Since the difference between V_m and V_p gives the chemisorbed amount, we can obtain the chemisorbed amount V_c by subtracting V_p from V_m. As a small amount of chemisorbed H_2O equal to the H_2O content V_h remains on the 450 °C-treated surface, the total amount of chemisorbed H_2O is calculated by summing the values V_c and V_h. The results (Table 1) indicate that the number of NH_3 molecules chemisorbed on dehydroxylated surfaces of ZnO is almost equal to that of chemisorbed H_2O on the same surfaces. This suggests that a molecule of NH_3 is chemisorbed on the sites formed by dehydroxylation of the two neighboring hydroxyls.

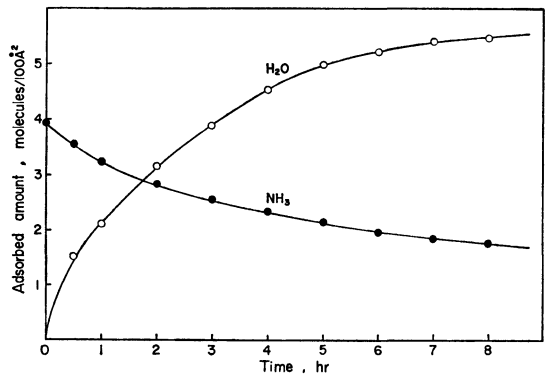

Fig. 2. Exchange reaction of chemisorbed NH_3 on ZnO with H_2O vapor.

Exchange Reaction of Chemisorbed NH_3 on ZnO with H_2O Vapor. Curve f (Fig. 1) is the adsorption isotherm of H_2O at 25 °C on the ammoniated surface of ZnO. The discontinuity in the isotherm reappears in a higher pressure region than in the case of the fully hydroxylated surface of ZnO. Infrared spectroscopic studies have shown qualitatively that NH_3 chemisorbed on ZnO is replaced by H_2O to form hydroxylated surface when exposed to H_2O vapor.[19] Figure 2 shows the change in the amount of chemisorbed H_2O and gaseous NH_3 with time, which was obtained when the ammoniated surface of ZnO was kept in H_2O vapor of the relative pressure 0.7. The equilibrated mixed gas was analyzed by the same procedure as described above. The results (Fig. 2) clearly show that the exchange reaction occurs between the chemisorbed NH_3 and H_2O vapor. The apparently queer phenomenon (curve f, Fig. 1) can thus be interpreted as follows: 1) on account of the exchange reaction the ammoniated surface of ZnO is converted in to the hydroxylated surface, which leads to the appearance of the discontinuity in the adsorption isotherm of H_2O; 2) the shift of the discontinuity to a higher pressure region results from the additional partial pressure of evolved NH_3.

Table 1. H_2O and NH_3 adsorbed on ZnO surface

Sample	Surface area (m^2/g)	H_2O adsorption: V_m (H_2O molecules/100 Å²)	V_p	V_c	V_h	V_c+V_h (OH/100Å²)	$\frac{V_p}{V_c+V_h}$ (H_2O/OH)	NH_3 adsorption: V_m (NH_3 molecules/100 Å²)	V_p	V_c	$\frac{V_p}{V_c}$	$\frac{V_c(NH_3)}{V_c(H_2O)}$
ZnO–K	8.40	11.03	7.50	3.53	0.50	8.06	0.93	5.30	1.35	3.95	0.34	1.05
ZnO–S	3.16	10.63	7.40	3.23	0.65	7.76	0.95	4.69	1.14	3.55	0.32	1.10

TABLE 1. GENERIC NAMES OF ROTATIONAL ISOMERS

Molecule[a)]	Generic name	Conformations
CH_3CH_2–CH_2X	T	t
XCH_2–CH_2X	G	g^+, g^-
XCH_2–CH_2Y		
CH_3Z–CH_2CH_3		
CH_3CH_2–Z–CH_2CH_3	TT	tt
XCH_2–CH_2–CH_2X	TG	tg^+, tg^-, g^+t, g^-t
	GG	g^+g^+, g^-g^-
	GG′	g^+g^-, g^-g^+
CH_3CH_2–CH_2–CH_2X	TT	tt
XCH_2–CH_2–CH_2Y	TG	tg^+, tg^-
CH_3W–CH_2–CH_2CH_3	GT	g^+t, g^-t
CH_3W–CH_2–CH_2X	GG	g^+g^+, g^-g^-
	GG′	g^+g^-, g^-g^+
XCH_2–CH_2–CH_2–CH_2X	TTT	ttt
CH_3Z–CH_2–CH_2–ZCH_3	TTG	ttg^+, ttg^-, g^+tt, g^-tt
	TGT	tg^+t, tg^-t
	TGG	tg^+g^+, tg^-g^-, g^+g^+t, g^-g^-t
	GTG	g^+tg^+, g^-tg^-
	TGG′	tg^+g^-, tg^-g^+, g^+g^-t, g^-g^+t
	GTG′	g^+tg^-, g^-tg^+
	GGG	$g^+g^+g^+$, $g^-g^-g^-$
	GGG′	$g^+g^+g^-$, $g^-g^-g^+$, $g^+g^-g^-$, $g^-g^+g^+$
	GG′G	$g^+g^-g^+$, $g^-g^+g^-$
CH_3CH_2–CH_2–CH_2–CH_2X	TTT	ttt
XCH_2–CH_2–CH_2–CH_2Y	TTG	ttg^+, ttg^-
CH_3CH_2–W–CH_2–CH_2CH_3	TGT	tg^+t, tg^-t
CH_3W–CH_2–CH_2–CH_2CH_3	GTT	g^+tt, g^-tt
CH_3O–CH_2–CH_2–SCH_3	TGG	tg^+g^+, tg^-g^-
	GTG	g^+tg^+, g^-tg^-
	GGT	g^+g^+t, g^-g^-t
	TGG′	tg^+g^-, tg^-g^+
	GTG′	g^+tg^-, g^-tg^+
	GG′T	g^+g^-t, g^-g^+t
	GGG	$g^+g^+g^+$, $g^-g^-g^-$
	GGG′	$g^+g^+g^-$, $g^-g^-g^+$
	GG′G	$g^+g^-g^+$, $g^-g^+g^-$
	GG′G′	$g^+g^-g^-$, $g^-g^+g^+$

a) X, Y=F, Cl, Br, or I; Z=CH_2, O, or S; W=O or S.

force constants of ethers. Structural parameters and symmetry coordinates used in the calculation and a final set of the force constants are reported in a separate paper.[6)]

The force constants of the ethers were determined in the following way. The force constants associated with a methyl or methylene group which is not bound directly to an oxygen atom were assumed to be the same as those for the paraffin molecules.[18)] The force constants associated with the ether group, including those of neighboring methyl and methylene groups, were refined in the least-squares adjustment with initial values transferred from the results by Shimanouchi *et al.*,[19)] Snyder and Zerbi,[7)] and Matsuura and Miyazawa.[20)] Some of the ether force constants, which were unestimable from the observed frequencies, were assumed to have the same values as those for the corresponding paraffin force constants.

Table 2 shows the procedure of the least-squares calculation. The calculation began with the simplest ethers in the extended form, and then the molecules to be treated were extended to the longer ethers and the non-extended forms. The various deuterated derivatives of ethyl methyl ether and diethyl ether were also included in the force constants refinement. A total of 83 force constants associated with the ether group were determined from 690 Raman and infrared frequencies of 46 forms of 19 molecular species.

Results

Figures 1—9 show the Raman and infrared spectra in the gaseous, liquid, glassy and crystalline states. The observed frequencies and the assignment based on the calculated potential-energy distributions are listed in Tables 3—5. The observed spectra were analyzed with reference to the results of the normal coordinate treatment.

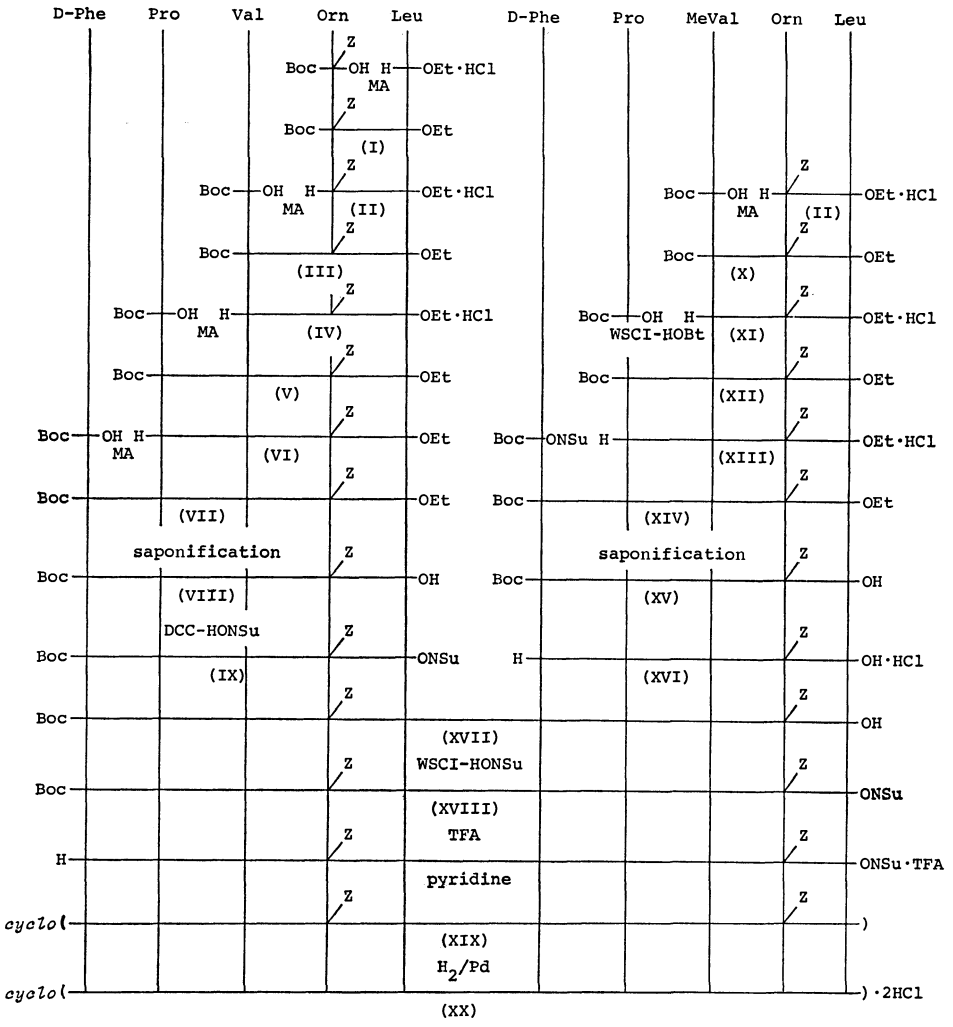

Scheme 1. Synthesis of [MeVal[1]]-GS.

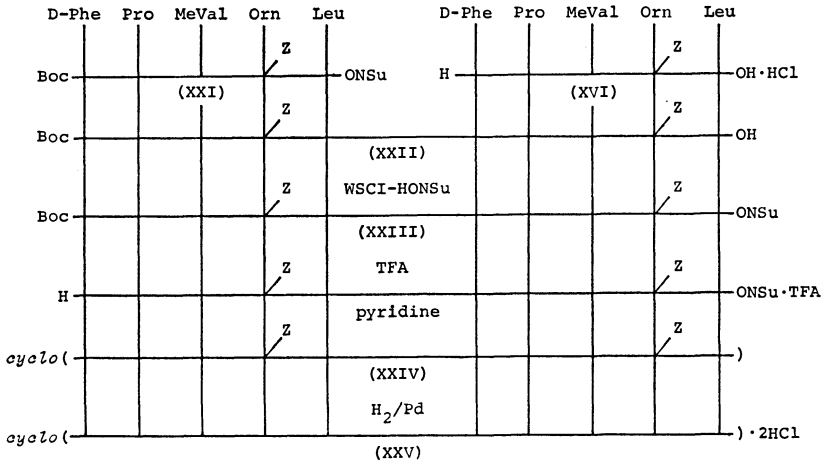

Scheme 2. Synthesis of [MeVal[1,1']]-GS.

tide–ONSu in a satisfactory yield of 66%.

For the syntheses of final [MeVal[1]]-GS and [MeVal[1,1']]-GS, each Z-substituted cyclodecapeptide (XIX and XXIV) was subjected to hydrogenolysis, and the desired analogs were obtained as crystalline dihydrochlorides (XX and XXV). Their homogeneity was confirmed by paper and thin-layer chromatography, paper electrophoresis and elemental analysis.

Antibacterial activity toward several microorganisms was examined, the results being given in Table 1. The two analogs were found to exhibit weak activity for Gram-positive microorganisms, whereas GS showed strong activity. The antibacterial potency of [MeVal[1]]-GS is slightly higher than that of the [MeVal[1,1']]-

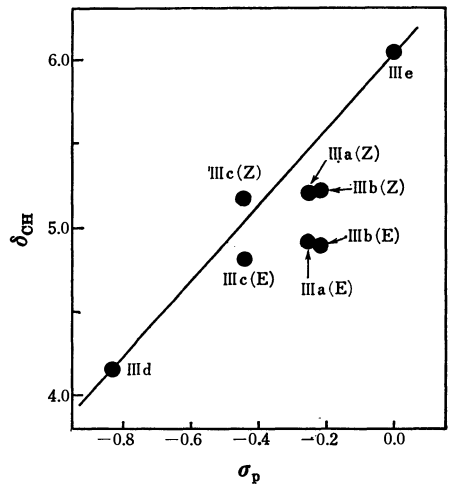

Fig. 1. Hammett's plot of δ_{CH} of ylides III.

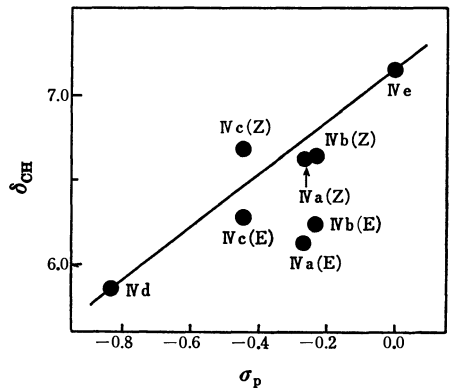

Fig. 2. Hammett's plot of δ_{CH} of oxosulfonium ions IV.

Another result is the decomposition of IVe. Compound IVe was stable in the crystalline state, but it decomposed entirely in a chloroform solution after 24 h at 34.5 °C to give vinyl sulfoxide(V) and methyl iodide in quantitative yields. Compound V(mp 68.5—70 °C) showed one *S*-methyl peak at δ 2.06, SOMe at 2.76, and an olefinic proton at 6.61 in the NMR spectrum. On UV irradiation V gave new peaks at 2.41 (SMe), 2.66 (SOMe), and 6.15 (olefinic proton). Fractional crystallization afforded VI with a mp of 138—140.5 °C, which again gave V on irradiation. The V: VI equilibrium ratio was 1 : 2. Using the values of Pascuel, Meier, and Simon[13] for the chemical shifts of the vinyl protons, the vinyl sulfoxides, V and VI, were confirmed to be the Z and *E* isomers respectively. Thus, we confirmed IIIe to be the *Z* isomer.

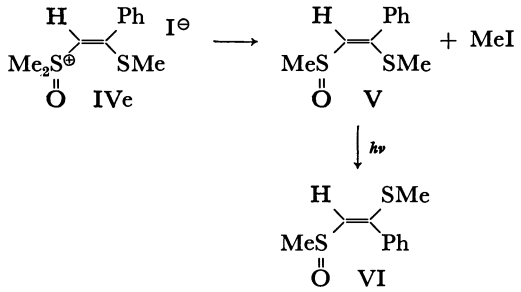

Compound IVd decomposed entirely at 40 °C for 3 days in chloroform to give a mixture of unidentifiable compounds (NMR and TLC). IVa, on the other hand, decomposed easily in $CDCl_3$ at 34.5 °C for 20 h to give a new carbonyl-stabilized ylide, I(R=SMe), and methyl iodide in quantitative yields. Although IVb,c also decomposed at 34.5 °C for 3 days to yield a mixture of I (R=SMe) and vinyl sulfoxides (NMR study), no effort was made to isolate them.

Reaction of III with Carbon Disulfide. A number of reactions of sulfur ylides with olefins and carbonyl compounds have been reported.[18] The reactions of IIIb with dimethyl fumarate or maleate failed, since the reagents were recovered after 48 h in THF at reflux. It has been reported that II(R=Ph)[2] reacts with carbon disulfide to give a 1,3-dithiane derivative in chloroform and a 1,2,4-trithiole derivative in ethanol.

The IIIb—e ylides reacted easily with carbon disulfide, even at room temperature, to give 1,2-dithiole-3-thione, VII, in moderate yields (Table 4). The products were confirmed to be VII, by comparison with known samples (VIId,e) and by analyses (VIIb,c) not 1,3-dithiole-2-thione. No crystalline compound was isolated from a reaction mixture of IIIa and carbon disulfide.

The reactivity of III decreased in this order; IIId> IIIb,c>IIIe. This is also the order of the pK_a values of

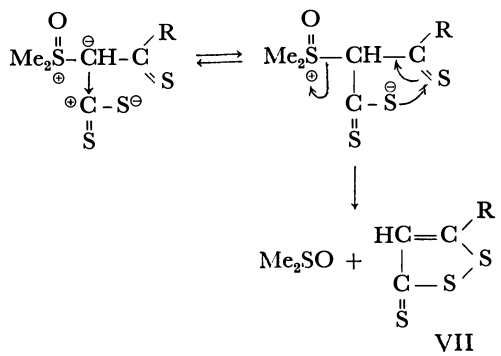

Table 4. Yields and physical properties of VII's

	VIIb	VIIc	VIId	VIIe
Yield (%)	27	18	55	48
Mp (°C)	82—82.5	59.5—60.5	199—201	124.5—126.5
IR (KBr) $\nu_{C=S}$ cm^{-1}	1180	1190	1190	1180
NMR Solvent	$CDCl_3$	CCl_4	$CDCl_3$	$CDCl_3$
δ CH	6.66	6.62	6.46	7.27
δ R	4.27q	4.72sept	3.22	7.5—7.8m
δ (J(Hz))	1.49t (7.1)	1.48d (6.5)		

a) Ref. 20. b) Ref. 21.

IR (KBr): 3450 (OH), 1710, 1670 cm^{-1} (C=O). PMR (CCl_4): δ; 0.92 (s, 3H), 1.16 (s, 3H), 1.48 (s, 3H), 1.51 (s, 3H), 2.30 (s, 3H), 4.62 (s, 1H; OH), 6.8—7.5 ppm (m, 8H). Found: C, 78.25; H, 7.45%. Calcd for $C_{22}H_{24}O_3$: C, 78.54; H, 7.19%. **8d**; white prisms; mp 137.5—138.0 °C. IR (KBr): 1730, 1705 cm^{-1} (C=O). PMR (CCl_4): δ; 1.18 (s, 3H), 1.41 (s, 3H), 1.53 (s, 3H), 1.56 (s, 3H), 2.40 (s, 3H), 5.53 (s, 1H), 7.0—7.8 ppm (m, 8H). Found: C, 78.59; H, 7.36%. Calcd for $C_{22}H_{24}O_3$: C, 78.54; H, 7.19%.

Photochemical Reaction of **1** *with* p-*Isopropylbenzaldehyde.* A solution of **1** (134 mg, 0.6 mmol) and *p*-isopropylbenzaldehyde (332 mg, 2.0 mmol) in benzene was irradiated by the use of the filter solution to give 3-hydroxy-3-*p*-isopropylbenzoyl-1,1,4,4-tetramethyl-2-tetralone, **7e** (149 mg, 66%), and 3-*p*-isopropylbenzoyloxy-1,1,4,4-tetramethyl-2-tetralone, **8e** (71 mg, 32%). **7e**; white needles; mp 126.0—127.0 °C. IR (KBr): 3420 (OH), 1720, 1675 cm^{-1} (C=O). PMR (CCl_4): δ; 0.91 (s, 3H), 1.15 (s, 3H), 1.16 (s. 3H), 1.22 (s, 3H), 1.43 (d, 6H), 2.8 (m, 1H), 4.56 (s, 1H; OH), 6.9—7.4 ppm (m, 8H). Found: C, 79.14; H, 7.82%. Calcd for $C_{24}H_{28}O_3$: C, 79.07; H, 7.76%. **8e**; white prisms; mp 117.0—118.0 °C. IR (KBr): 1735, 1710 cm^{-1} (C=O). PMR (CCl_4): δ; 1.20 (s, 3H), 1.25 (s, 3H), 1.32 (s, 3H), 1.44 (s, 3H), 1.48 (d. 6H), 2.92 (m, 1H), 5.60 (s, 1H), 7.0—7.9 ppm (m, 8H). Found: C, 79.03; H, 7.98%. Calcd for $C_{24}H_{28}O_3$: C, 79.07; H, 7.76%.

Photochemical Reaction of **1** *with Benzaldehyde.* A benzene solution of **1** (131 mg, 0.6 mmol) and benzaldehyde (397 mg, 3.7 mmol) was irradiated by the use of the filter solution. The products were 3-benzoyl-3-hydroxy-1,1,4,4-tetramethyl-2-tetralone, **7f** (79 mg, 38%), and 3-benzoyloxy-1,1,4,4-tetramethyl-2-tetralone, **8f** (27 mg, 13%). **7f**; white needles; mp 169.0—171.0 °C. IR (KBr): 3400 (OH), 1710, 1670 cm^{-1} (C=O). PMR (CCl_4): δ; 0.92 (s, 2H), 1.19 (s, 3H), 1.50 (s, 6H), 4.64 (s, 1H; OH), 6.9—7.7 ppm (m, 9H). Found: C, 78.02; H, 6.78%. Calcd for $C_{21}H_{23}O_3$: C, 78.23; H, 6.88%. **8f**; white prisms; mp 134.5—135.5 °C. IR (KBr): 1735, 1710 cm^{-1} (C=O). PMR (CCl_4): δ; 1.22 (s, 2H), 1.45 (s, 2H), 1.58 (s, 3H), 1.61 (s, 3H), 5.70 (s, 1H), 7.2—8.2 ppm (m, 9H). Found: C, 78.01; H, 6.72%. Calcd for $C_{21}H_{22}O_3$: C, 78.23; H, 6.88%.

Photochemical Reaction of **1** *with* p-*Chlorobenzaldehyde.* A benzene solution of **1** (126 mg, 0.6 mmol) and *p*-chlorobenzaldehyde (396 mg, 3.7 mmol) was irradiated by the use of the filter solution to give 3-*p*-chlorobenzoyl-3-hydroxy-1,1,4,4-tetramethyl-2-tetralone, **7g** (53 mg, 26%), and 3-*p*-chlorobenzoyloxy-1,1,4,4-tetramethyl-2-tetralone, **8g** (32 mg, 15%). **7g**; white needles; mp 153.0—153.5 °C. IR (KBr): 3430 (OH), 1710, 1670 cm^{-1} (C=O). PMR (CCl_4): δ; 0.92 (s, 3H), 1.18 (s, 3H), 1.48 (s, 6H). 4.56 (s, 1H; OH), 6.9—7.5 ppm (m, 8H). Found: C, 70.38; H, 5.94; Cl, 9.85%. Calcd for $C_{21}H_{21}O_3Cl$: C, 70.67; H, 5.94; Cl, 9.93%. **8g**; white prisms; mp 164.0—164.5 °C. IR (KBr): 1735, 1710 cm^{-1} (C=O). PMR (CCl_4): δ; 1.16 (s, 3H), 1.38 (s, 3H), 1.50 (s, 5H), 1.52 (s, 3H), 5.44 (s, 1H), 6.9—7.1 (m, 4H), 7.2—7.8 ppm (AB-q, 4H). Found: C, 70.87; H, 6.24; Cl, 9.74%. Calcd for $C_{21}H_{21}O_3Cl$: C, 70.67; H, 5.94; Cl, 9.93%.

Photochemical Reaction of **1** *with Isobutyraldehyde.* The photolysis of **1** (187 mg, 0.9 mmol) and isobutyraldehyde (193 mg, 2.7 mmol) in benzene by the use of the filter solution gave a mixture of 3-hydroxy-3-isobutyryl-1,1,4,4-tetramethyl-2-tetralone, **7h** (49 mg, 17%), 3-isobutyryloxy-1,1,4,4-tetramethyl-2-tetralone, **8h** (127 mg, 47%), 3-hydroxy-3-isopropyl-1,1,4,4-tetramethyl-2-tetralone, **12** (20 mg, 10%), and the reduced product, **3** (22 mg, 11%), accompanied by the evolution of a gas (carbon monoxide) (49—63%), which was identified by means of palladium chloride-test paper; the color changed from yellow to brown. The yield of carbon monoxide was measured volumetrically. **7h**; white needles; mp 84.5—85.5 °C. IR (KBr): 3420 (OH), 1690 cm^{-1} (C=O). PMR (CCl_4): δ; 0.88 (d, 3H), 0.96 (s, 3H), 1.00 (d, 3H), 1.38 (s, 6H), 1.50 (s, 3H), 3.20 (m, 1H), 4.82 (s, 1H; 0H), 7.2—7.3 ppm (m, 4H). Found: C, 74.95; H, 8.54%. Calcd for $C_{18}H_{24}O_3$: C, 74.97; H, 8.39%. **8h**; colorless oil. IR (liq. film): 1740, 1730 cm^{-1} (C=O). PMR (CCl_4): δ; 1.08 (s, 2H), 1.22—1.24 (dd, 6H), 1.40 (s, 3H), 1.49 (s, 3H), 1.54 (s, 3H), 2.66 (m, 1H), 5.40 (s, 1H), 7.1—7.4 ppm (m, 4H). Mass: *m/e*; 288 (M^+). Found: C, 75.25; H, 8.48%. Calcd for $C_{18}H_{24}O_3$: C, 74.97; H, 8.39%. **12**; white crystals; mp 36.0—37.0 °C. IR (KBr); 3470, 3420 (OH), 1695 cm^{-1} (C=O). PMR (CCl_4): δ; 0.56 (d, 3H), 0.89 (d, 3H), 0.98 (s, 3H), 1.48 (s, 3H), 1.53 (s, 3H), 1.56 (s, 3H), 2.00 (m, 1H), 3.84 (s, 1H; OH), 7.1 ppm (m, 4H). Mass: *m/e*; 260 (M^+). Found: C, 78.27; H, 9.38%. Calcd for $C_{17}H_{24}O_2$: C, 78.42; H, 9.29%.

References

1) See, for example, B. M. Monroe, and S. A. Weiner, *J. Am. Chem. Soc.*, **91**, 450 (1969).

2) Presented at the 31st Annual Meeting of the Chemical Society of Japan, Sendai (1974).

3) G. E. Geam, P. C. Paice, and C. C. R. Ramsay, *Aust. J. Chem.*, **20**, 1671 (1967).

4) M. B. Rubin and Z. Neuwirth-Weiss, *J. Am. Chem. Soc.*, **94**, 6048 (1972).

5) R. Kaptein, *J. Chem. Soc., Chem. Commun.*, **1971**, 732.

6) The *g*-value of the semidione radical is probably very close to that of the acetoin radical (*cf.* H. Zeldes and R. Livingston, *J. Chem. Phys.*, **47**, 1465 (1967)).

7) The *g*-value of the xanthenyl radical is probably close to that of the diphenylmethyl radical (*cf.* A. L. Lepley and G. L. Closs, "Chemically Induced Magnetic Polarization," John Wiley & Sons, New York (1973), p. 108.

8) The polarized signals observed in the region of methyl protons coincide with those of the product, **2**. So far there are no experimental results on the coupling sign of methyl protons of **5**, but, according to a recent review F. W. King, *Chem. Rev.*, **76**, 157 (1976), the sign of the long-range *hfc* may be positive. Thus, our experimental results may indicate the in-cage combination of **5** and **6**. The absorption polarized signal due to the methine proton on the xanthenyl moiety of the product, **2**, also supports this condideration.

9) H. A. Bruson, F. W. Grant, and E. Bobko, *J. Am. Chem. Soc.*, **80**, 3634 (1958).

10) J. M. Pink and R. Steward, *Can. J. Chem.*, **49**, 649 (1971).

11) G. E. Gream, J. C. Paice, and C. C. R. Ramsay, *Aust. J. Chem.*, **22**, 1229 (1969).

12) A. Schönberg, "Preparative Organic Photochemistry," 2nd ed., Springer-Verlag, Berlin (1968), p. 491.

13) A. A. Bother-By and C. Naar-Colin, *J. Am. Chem. Soc.*, **83**, 231 (1961).

14) R. W. Ferrenden and R. H. Schuler, *J. Chem. Phys.*, **39**, 2147 (1963).

15) See, for example, N. S. Issacs, "Reactive Intermediates in Organic Chemistry," John Wiley & Sons, New York (1974), p. 325.

16) K. Maruyama, T. Otsuki, H. Shindo, and T. Maruyama, T. Otsuki, A. Takuwa, and S. Arakawa, *Bull. Chem. Soc. Jpn.*, **46**, 2470 (1973).

17) A. W. Bergstrahler and M. O. Abdel-Rahman, *J. Am. Chem. Soc.*, **85**, 173 (1963).

TABLE 1. PROTON MAGNETIC RESONANCE DATA FOR 4-*t*-BUTYL-1-METHYL-1-SILACYCLOHEXYL DERIVATIVES ($X(CH_3)SiCH_2CH_2CH(t\text{-}Bu)CH_2CH_2$)

Compound		δ, ppm[a]		
No.	X	$SiCH_3$	$C(CH_3)_3$	Si–X
2a	H	0.12 (d) (J=3.5 Hz)	0.86 (s)	3.95—3.78 (m) (3.91)[d]
2b	H	0.07 (d) (J=3.5 Hz)	0.86 (s)	3.93—3.53 (m) (3.80)[d]
3a[b]	Cl	0.42 (s)	0.86 (s)	
3b[b]	Cl	0.38 (s)	0.87 (s)	
4a	$OCH(CH_3)_2$	0.10 (s)	0.86 (s)	1.10 (d), 3.96 (sep) (J=6.0 Hz)
4b	$OCH(CH_3)_2$	0.02 (s)	0.86 (s)	1.14 (d), 3.99 (sep) (J=6.0 Hz)
5a	OCH_3	0.10 (s)	0.86 (s)	3.36 (s)
5b	OCH_3	0.01 (s)	0.85 (s)	3.41 (s)
6a	$OC(CH_3)_3$	0.13 (s)	0.86 (s)	1.21 (s)
6b	$OC(CH_3)_3$	0.06 (s)	0.85 (s)	1.26 (s)
7a	C_6H_5	0.35 (s)	0.96 (s)	7.63—7.22 (m)
7b	C_6H_5	0.26 (s)	0.84 (s)	7.73—7.25 (m)
8a	*p*-Br–C_6H_4	0.27 (s)	0.89 (s)	7.37—7.41 (m)
8b	*p*-Br–C_6H_4	0.12 (s)	0.80 (s)	7.42—7.44 (m)
9a	*p*-Cl–C_6H_4	0.22 (s)	0.84 (s)	7.31—7.34 (m)
9b	*p*-Cl–C_6H_4	0.09 (s)	0.77 (s)	7.36—7.42 (m)
10a[c]	$Si(CH_3)_2H$	0.10 (s)	0.84 (s)	0.10 (d), 3.56 (sep) (J=4.5 Hz)
10b[c]	$Si(CH_3)_2H$	0.04 (s)	0.84 (s)	0.16 (d), 3.69 (sep) (J=4.5 Hz)
11a[b]	F	0.25 (d) (J=7.3 Hz)	0.88 (s)	
11b[b]	F	0.18 (d) (J=7.3 Hz)	0.88 (s)	

a) NMR spectra were taken as carbon tetrachloride solution with Varian Associates HA-100 and A-60D. b) Isomers were not separated, chemical shift being determined with a mixture. c) Preparation and determination of this material were described in the previous paper.[12] Details will be published later. d) Center of the chemical shift determined by decoupling.

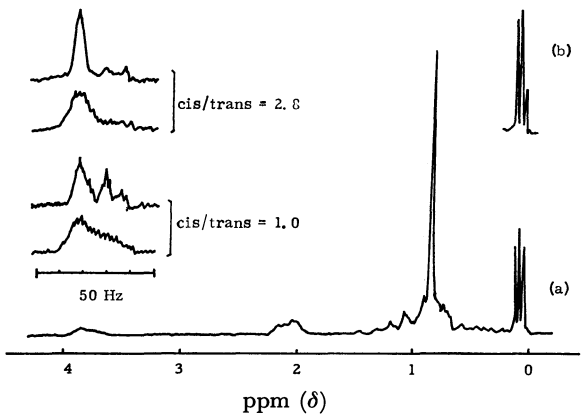

Fig. 1. (a) NMR spectra of **2** (1:1 *cis-trans* mixture) prepared from di-Grignard reagent from **1** and methyldichlorosilane and (b) methyl signals of **2** (2.8:1 *cis-trans* mixture) prepared by reduction of **3** with $LiAlH_4$. Left part of the spectra shows each SiH signals in addition to decoupling signals of **2** irradiated at Si–CH_3.

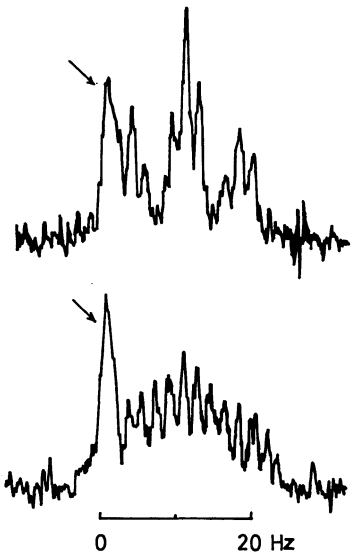

Fig. 2. SiH signal of **2b** (lower) and SiH signal irradiated at the $SiCH_3$ signal of **2b** (upper). The arrows indicate a signal due to unknown impurity.

assign the stereochemistry. The axial Si–Me (*e.g. cis* compounds) gives rise to a resonance at lower field (δ 0.12) than the equatorial SiMe (δ 0.07), whereas the axial hydrogen (δ 3.80) appears at higher field than the equatorial hydrogen (δ 3.91). A similar relationship has been observed for cyclohexane derivatives. Incidentally, West proposed the structure of silacyclohexane ring as a deformed chair form.[15]

Many observations show that the chemical shifts of protons in the functional groups attached to six-membered rings are related to their configuration and that these relations afford a reasonable basis for stereochemical assignments as shown in Table 2.[16] Compounds listed in Table 1 were assigned for their *cis* and *trans* structures on the basis of NMR spectra assuming that the compound with a methyl signal of NMR appearing at lower

Found: C, 91.79; H, 8.17%. Calcd for $C_{28}H_{30}$: 91.73; H, 8.27%. PMR ($CDCl_3$, δ) 1.44 (s, 3H, CH_3), 1.7—3.2 (m, 16H, CH_2), 2.39 (s, 3H, CH_3), 4.90 (s, 1H, ArH), 5.05 (s, 1H, ArH), 5.48 (s, 1H, ArH), 5.63 (d, J=1 Hz, 2H, ArH), 6.79 (s, 1H, ArH), 7.09 (d, J=1 Hz, 2H, ArH). MS m/e 366 (M^+).

The second eluate gave the monosulfur compd **32** (22 mg, 24%), colorless plates from ethanol, mp 187—188 °C.

Found: C, 84.63; H, 7.62; S, 8.17%. Calcd for $C_{28}H_{30}S$: C, 84.37; H, 7.59; S, 8.04%. NMR ($CDCl_3$, δ) 1.71 (s, 3H, CH_3), 2.2—3.6 (m, 16H, CH_2), 2.37 (s, 3H, CH_3), 4.92 (s, 1H, ArH), 5.11 (s, 1H, ArH), 5.49 (s, 1H, ArH), 5.60 (d, J=1 Hz, 2H, ArH), 6.87 (s, 1H, ArH), 7.10 (d, J=1 Hz, 2H, ArH). MS m/e 398 (M^+).

*18,27-Dithia[3.3]paracyclo(4,6)[2.2]metacyclophane (**34**).* A soln of 4,6-bis(bromomethyl)[2.2]metacyclophane **33**[6b] in 35 ml of benzene and a soln of 1,4-bis(mercaptomethyl)-benzene **19** (0.31 g, 1.8 mmol) and sodium hydroxide (0.15 g, 3.8 mmol) in a mixture of water (2 ml) and ethanol (33 ml) were added dropwise and simultaneously over a period of 4 h to boiling ethanol (100 ml) with stirring in a nitrogen atmosphere. The mixture was refluxed for additional 12 h and worked up in the usual way. Chromatography of the product over neutral alumina (30 g, Woelm act. II) using hexane-benzene (1 : 1) gave the desired dithiacyclophane **34** (0.31 g, 34%), colorless needles from benzene-alcohol (1 : 1), mp 238—239 °C.

Found: C, 77.80; H, 6.36; S, 15.78%. Calcd for $C_{26}H_{26}S_2$: C, 77.55; H, 6.52; S, 15.92%. PMR ($CDCl_3$, δ) 1.5—4.0 (m, 17H, CH_2 and one ArH), 4.54 (bs, 1H, ArH), 5.43 (s, 1H, ArH), 7.13 (bs, 4H, ArH), 7.21 (m, 3H, ArH). MS m/e 402 (M^+), 104.

[2.2]Metacyclo(4,6)[2.2]metaparacyclophane (m-m, m-p) *(**9**).* *a) By the Stevens Rearrangement-Raney Nickel Desulfurization.* A mixture of the above dithiacyclophane **34** (0.60 g, 1.5 mmol) and the Borch reagent[11] (1.00 g, 6.2 mmol) in 20 ml of dichloromethane was refluxed with stirring for 15 h. The resulting ppt was filtered and stirred with sodium hydride (0.12 g, 4.8 mmol), washed with dry ether, in dry dimethyl sulfoxide (10 ml) at 20 °C under a nitrogen atmosphere for 1.5 h. The mixture was poured into ice-water to quench the reaction. The resulting ppt was filtered, dried, and then refluxed with 7 ml of Raney nickel (W-II) in benzene (5 ml) and ethanol (50 ml) for 15 h. Raney nickel was filtered and washed with benzene. The filtrate and the washings were combined and concentrated, and then the residue was chromatographed on silica gel (40 g, Merck act. II) using hexane-benzene (9 : 1). The first eluate gave the desired cyclophane **9** (96 mg, 19%), colorless prisms from toluene, mp 209—210 °C.

Found: C, 92.08; H, 7.75%. Calcd for $C_{26}H_{26}$: C, 92.24; H, 7.76%. PMR ($CDCl_3$, δ) 1.5—3.5 (m, 16H, CH_2), 3.66 (s, 1H, ArH), 5.62 (s, 1H, ArH), 5.70 (bs, 1H, ArH), 6.48 (d, J=2 Hz, 2H, ArH), 7.3 (m, 3H, ArH), 7.46 (d, J=2 Hz, 2H, ArH). MS m/e 338 (M^+), 234, 104.

b) By Photodesulfurization. In the same manner as **8** b), irradiation of a soln of **34** (60 mg, 0.15 mmol) in triethyl phosphite (20 ml) for 15 h and purification by column chromatography gave the same compd **9** (19 mg, 35%).

*4,6-Bis(mercaptomethyl)[2.2]metacyclophane (**35**).* A mixture of 4,6-bis(bromomethyl)[2.2]metacyclophane **33** (2.36 g, 6 mmol) and thiourea (1.0 g, 13 mmol) was refluxed in 50 ml of ethanol for 3 h and concd to dryness. The thiouronium salt was hydrolyzed by refluxing with 85% potassium hydroxide (7.30 g) in 50 ml of water for 7.5 h and worked up as usual. The crude product was filtered through a short column of neutral alumina with hexane–benzene (1 : 1) to afford pure dithia compound **35** (1.53 g, 85%), colorless prisms from hexane–benzene, mp 92—93 °C.

Found: C, 71.97; H, 6.71; S, 21.11%. Calcd for $C_{18}H_{20}S_2$: C, 71.94; H, 6.72; S, 21.34%. PMR ($CDCl_3$, δ) 1.80 (t, J=7 Hz, 2H, SH), 3.0—3.5 (m, 8H, CH_2), 3.81 (d, J=7 Hz, 4H, SCH_2), 4.17 (s, 1H, ArH), 4.43 (bs, 1H, ArH), 7.0—7.5 (m, 4H, ArH). MS m/e 300 (M^+).

*21,24-Dimethyl-18,27-dithia[3.3]paracyclo(4,6)[2.2]metacyclophane (**36**).* A soln of 2,5-bis(chloromethyl)-*p*-xylene **10** (1.02 g, 5 mmol) in 40 ml of benzene and a soln of 4,6-bis(mercaptomethyl)[2.2]metacyclophane **35** (1.50 g, 5 mmol) in 40 ml of 80% ethanol were added dropwise and simultaneously over a period of 3.5 h to boiling ethanol (100 ml) under nitrogen and the refluxing was continued for 12 h. The mixture was worked up in the usual way. The crude product was purified by chromatography over alumina (Woelm act. II) with hexane–benzene (4 : 1) to give the pure dithiacyclophane **36** (1.62 g, 74%), colorless fine crystals from ethanol, mp 165—166 °C.

Found: C, 78.23; H, 7.17; S, 14.85%. Calcd for $C_{28}H_{30}S_2$: C, 78.23; H, 6.98; S, 14.90%. PMR ($CDCl_3$, δ) 2.22 (s, 3H, CH_3), 2.32 (s, 3H, CH_3), 2.9—4.0 (m, 16H, CH_2), 4.09 (bs, 1H, ArH), 4.34 (s, 1H, ArH), 5.46 (s, 1H, ArH), 6.9—7.5 (m, 5H, ArH). MS m/e 430 (M^+).

*12,15-Dimethyl[2.2]metacyclo(4,6)[2.2]metaparacyclophane (**37**).* The Stevens rearrangement-Raney nickel desulfurization method was carried out as in the synthesis of **8**. The following conditions were used; methylation of **36** (1.10 g, 2.6 mmol) with the Borch reagent (1.66 g, 10 mmol) in dichloromethane (20 ml) under reflux for 3.5 h, the Stevens rearrangement with potassium *t*-butoxide (3.0 g, 27 mmol) in dry tetrahydrofuran (25 ml) under reflux for 5 h, and desulfurization with Raney nickel (6 ml) in 60 ml of benzene–ethanol (1 : 5) under reflux for 15 h. After chromatography, the desired product **37** was obtained as an oil, which was solidified when treated with a small amount of pentane (141 mg, 15%), colorless fine crystals from toluene, mp 131—132 °C.

Found: C, 91.51; H, 8.06%. Calcd for $C_{28}H_{30}$: C, 91.73; H, 8.27%. PMR ($CDCl_3$, δ) 1.7—3.4 (m, 32H, CH_2), 1.49 (s, 3H, CH_3), 1.98 (s, 3H, CH_3), 2.44 (s, 3H, CH_3), 2.58 (s, 3H, CH_3), 3.71 (s, 2H, ArH), 4.20 (s, 1H, ArH), 5.07 (bs, 1H, ArH), 5.39 (s, 1H, ArH), 5.60 (s, 1H, ArH), 5.80 (bs, 1H, ArH), 6.21 (s, 1H, ArH), 6.87 (s, 1H, ArH), 6.9—7.3 (m, 7H, ArH). MS m/e 366 (M^+).

The present work was partially supported by a Grant-in-Aid for Scientific Research from the Ministry of Education, to which the authors' thanks are due.

References

1) Part XXXIV, T. Toyoda, A. Iwama, T. Otsubo, and S. Misumi, *Bull. Chem. Soc. Jpn.*, **49**, 3300 (1976).

2) D. J. Cram, R. C. Helgeson, D. Lock, and L. A. Singer, *J. Am. Chem. Soc.*, **88**, 1324 (1966); D. T. Hefelfinger and D. J. Cram, *ibid.*, **92**, 1073 (1970); *ibid.*, **93**, 4754, 4767 (1971).

3) F. Vögtle, *Chem. Ber.*, **102**, 3077 (1969); *Angew. Chem.*, **81**, 258 (1969).

4) S. Akabori, S. Hayashi, M. Nawa, and K. Shiomi, *Tetrahedron Lett.*, **1969**, 3727.

5) S. A. Sherrod and V. Boekelheide, *J. Am. Chem. Soc.*, **94**, 5513 (1972); S. A. Sherrod and R. L. da Costa, *Tetrahedron Lett.*, **1973**, 2083; S. A. Sherrod, R. L. da Costa, R. A. Barnes, and V. Boekelheide, *J. Am. Chem. Soc.*, **96**, 1565 (1974).

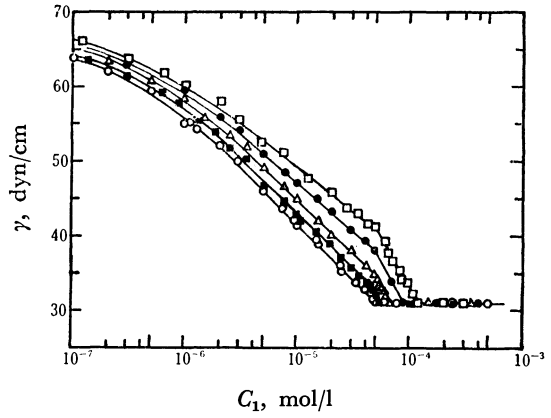

Fig. 1. Surface tension *vs.* concentration curves of $D(EO)_6$ solution at various concentrations of urea. ○: 0 M, ■: 0.04 M, △: 0.40 M, ●: 2.5 M, □: 4.0 M.

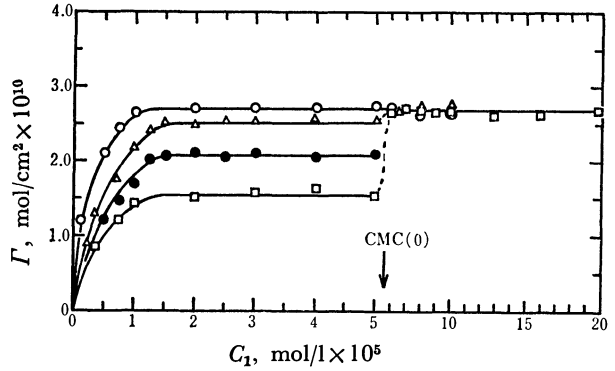

Fig. 2. Adsorption isotherms of $D(EO)_6$ at various concentrations of urea.
○: 0 M, △: 0.04 M, ●: 2.5 M, □: 4.0 M.

characterized by the following two parts above and below about 5.5×10^{-5} mol/l of $D(EO)_6$, which corresponds approximately to the CMC(0) of a $D(EO)_6$ solution without urea. Below the CMC(0) value, adsorption of $D(EO)_6$ obviously decreases with the increasing urea concentration present in the solution as is shown in a previous paper,[1] and reaches saturation. This suggests that urea may directly interact with the poly(oxyethylene) group of $D(EO)_6$ and probably forms some kind of urea–nonionic aggregations. If urea affects the solution by breaking the water structure, the isotherm should not give such a saturated adsorption as that shown in Fig. 2, but should only increase gradually depending on the change in the activity of $D(EO)_6$ in the urea solution. Above the CMC(0) value, the isotherms at varying urea concentrations coincide with the isotherm of the simple $D(EO)_6$ solution. These phenomena will be discussed in later section.

Adsorption of D(EO)$_6$. An attempt was made to apply the Gibbs adsorption isotherm to the calculation of the surface excess of nonionic in the urea–nonionic solution. The Gibbs isotherm is generatlly written as:[7]

$$-d\gamma = RT\sum \Gamma_i \, d\ln a_i \qquad (1)$$

where γ denotes the surface tension, Γ_i and a_i the surface excess and activity of the i-th components of the solution, respectively, and R and T the gas constant and absolute temperature, respectively. The interaction between urea and $D(EO)_6$ in the solution can be expressed implicitly as an activity coefficient (f_i) in Eq. 1. At constant urea concentration, Eq. 1 can be rewritten using the Gibbs-Duhem equation for bulk solutions,

$$-\left(\frac{\partial\gamma}{RT\partial\ln C_1}\right)_{2,3} = \Gamma_1 - \left\{\Gamma_1\frac{C_2}{C_1}-\Gamma_2\right\}\left(\frac{\partial\ln f_2}{\partial\ln C_1}\right)_{2,3} - \Gamma_1\frac{C_3}{C_1}\left(\frac{\partial\ln f_3}{\partial\ln C_1}\right)_{2,3} \qquad (2)$$

where C_i is the concentration of the i-th component in the solution, and the subscripts 1, 2 and 3 refer to $D(EO)_6$, urea and water, respectively. The last term on the right-hand side of Eq. 2 can reasonably be neglected, because the activity coefficient of water in the urea–nonionic solution should be constant at concentrations, C_1, less than 5.5×10^{-5} mol/l. If the cross-differentiation relation of Eq. 3 can be adopted for this system as a good approximation,[13]

$$\left(\frac{\partial\ln f_1}{\partial C_2}\right)_1 = \left(\frac{\partial\ln f_2}{\partial C_1}\right)_2 \qquad (3)$$

Eq. 2 is reduced to:

$$-\left(\frac{\partial\gamma}{RT\partial\ln C_1}\right)_2 = \Gamma_1\left\{1-\left(\frac{\partial\ln f_1}{\partial\ln C_2}\right)_1\right\} \qquad (4)$$

since $C_1/C_2 \ll 1$, *e.g.* $C_1 \leq 5.5\times10^{-5}$ and $C_2 \geq 4.0\times10^{-2}$ mol/l in this study. Tajima *et al.* have reported the following empirical relation from a study on the salting-in effect of urea upon the adsorption of $D(EO)_6$:[1]

$$\Gamma_D = -\frac{4.5\times10^{-11}}{\Delta}C_u^{0.15} \qquad (5)$$

where Γ_D is the surface excess of $D(EO)_6$, C_u ($=C_2$) the concentration of urea and $\Delta=(\partial\ln f_1/\partial\ln C_2)_1$. Substituting Eq. 5 into Eq. 4, we finally obtain

$$\Gamma_1 = -\left(\frac{\partial\gamma}{RT\partial\ln C_1}\right)_2 - 4.5\times10^{-11}C_2^{0.15} \qquad (6)$$

The Γ_1 value in Eq. 6 may be calculated from the data in Fig. 1 at constant concentration, C_2. The calculated and observed values for Γ_1 at various urea concentrations are shown in Table 1, where Γ_1 is compared at 4.0×10^{-5} mol/l for C_1 in the region of saturated adsorption. The values of Γ_1 calculated using Eq. 6 are in good agreement with the observed results. Therefore, it is seen that the adsorption of $D(EO)_6$ in the urea solution takes place according to the relation expressed by Eq. 6, which has a term which is a function of C_2.

Adsorption of Urea. Urea adsorption on the

TABLE 1. COMPARISON OF THE CALCULATED AND OBSERVED VALUES OF $D(EO)_6$ ADSORPTION AT VARIOUS UREA CONCENTRATIONS ($C_1=4.0\times10^{-5}$ mol/l)

C_2 mol/l	δ[a] mol/cm² ×10¹⁰	$-\left(\frac{\partial\gamma}{RT\partial\log C_1}\right)_2$ mol/cm² ×10¹⁰	Γ_1^{calcd} mol/cm² ×10¹⁰	Γ_1^{obsd} mol/cm² ×10¹⁰
0	0	2.72	2.72	2.73
0.040	0.277	2.60	2.32	2.41
0.40	0.392	2.48	2.09	2.09
4.0	0.554	2.09	1.54	1.57

a) See Eq. 10′.

Table 9. Results for the mercapto internal rotation

Barrier (cal/mol)[a]	Present work		Schmidt and Quade		Manocha *et al.*	
V_1	−207 (67)		−186		−123 (63)	
V_2	−386 (27)		−386		−392 (20)	
V_3	1305 (20)		1258		1355 (6)	
V_6	——		——		−37 (3)	
Kinetic coef. (cm^{-1})	CH_3CH_2SH	CH_3CH_2SD	CH_3CH_2SH	CH_3CH_2SD	CH_3CH_2SH[b]	CH_3CH_2SD[b]
$\mu_\alpha^{(0)}$	10.870	6.091	10.78	6.02	10.9735	6.0756
$\mu_\alpha^{(1)}$	−0.011	−0.046	——	——	−0.1617	−0.1601
$\mu_\alpha^{(2)}$	0.020	0.006	——	——	0.0362	0.0424
$\mu_\alpha^{(3)}$	——	——	——	——	−0.0017	−0.0034
$\mu_\alpha^{(4)}$	——	——	——	——	0.0002	0.0004
Energy dif. (cm^{-1})[c]						
$g0_+-g0_-$	0.05851 (−3) (p)	0.00234 (20) (p)	0.058 (−2) (q)	0.0023 (3) (q)	0.05851 (318) (p)[e]	0.00234 (40) (p)[e]
$t0-t1$	158.0 (−15) (r)	125.0 (−24) (r)	154.0 (0) (q)	——	158.0 (−25) (r)[e]	125.0 (0) (r)
$g0_+-g1_-$	193.0 (2) (r)	148.5 (−15) (r)	192.0 (50) (q)	147.0 (10) (q)	193.0 (−1) (r)[e]	148.5 (0) (r)
$g0_--g1_+$	191.8 (4) (r)				191.8 (0) (r)[e]	
$g1_+-g2_-$	——	135.1 (15) (r)	——	——	——	135.1 (0) (r)
$g1_--g2_+$	——	134.1 (19) (r)	——	——	——	134.1 (0) (r)
$t0-g0_\pm$	142.0 (−21) (q)[d]	138.0 (−90) (q)[d]	142.0 (40) (q)	138.0 (−40) (q)	——	——

a) Figures in parentheses indicate the uncertainties attached to the last significant figures. b) Quoted from the paper by Inagaki *et al.* (Ref. 11). Manocha *et al.* used these values for the CH_3CH_2SD species in their determination of the barrier values. c) $g0_+-g0_-$ indicates the energy difference between the 0_+ and 0_- levels for the *gauche* isomer. Figures in parentheses indicate the deviations of the observed values from the calculated and symbols in parentheses indicate the method used for obtaining the data quoted, that is, (p); the splitting analysis of the microwave spectra by the present authors, (q); the splitting analysis and the relative intensity measurements of the microwave spectra by Schmidt and Quade (Ref. 3); (r); the far-infrared spectra by Manocha *et al.* (Ref. 12). d) These data were not included in a least squares analysis since they were considered to have relatively large uncertainties. e) These data were not used by Manocha *et al.* in the determination of the V values. Deviations of the observed values from the calculated were not shown in their paper but we calculated them using their parameters.

Table 6. PMR spectral data for [Co(sal_2en)(Amino acid anion)] in methanol (δ, ppm)

Amino acid and No. of complex	Soon after dissolution		At equilibrium condition	
	H-C=N of sal_2en[a]	R of amino acid	H-C=N of sal_2en[a]	R of Amino acid
gly (1)	8.00(1) 8.30(1)	(c)	8.00(1) 8.30(1)	(c)
L-ala (2)	7.92(1) 8.26(1)	CH_3(a) 1.44(1.5), 1.56(1.5) CH_3(b) 1.26(1.5), 1.38(1.5)	7.92(1) 8.26(1)	CH_3(a) 1.44(1.2), 1.56(1.2) CH_3(b) 1.26(1.8), 1.38(1.8)
L-val (3)	8.00(1) 8.28(1)	CH_3(a) 0.97(1.5), 1.09(1.5), 0.92(1.5), 1.04(1.5) CH_3(b) 0.80(1.5), 1.02(1.5), 0.70(1.5), 0.82(1.5)	8.00(1) 8.28(1)	CH_3(a) 0.97(1.2), 1.09(1.2), 0.92(1.2), 1.04(1.2) CH_3(b) 0.80(1.8), 1.02(1.8), 0.70(1.8), 0.82(1.8)
L-leu (4)	8.00(1) 8.30(1)	CH_3, 0.95[b]	8.00(1) 8.30(1)	CH_3, 0.90[b]
L-isoleu (5)	8.02(1) 8.30(1)	CH_3, 0.95[b]	8.02(1) 8.30(1)	CH_3, 0.95[b]
L-met[c] (6)	8.03(1) 8.32(1)	CH_3(a) 2.10(1.5) CH_3(b) 2.02(1.5)	8.03(1) 8.32(1)	CH_3(a) 2.10(1.2) CH_3(b) 2.02(1.8)
L-thr (8)	7.90(1) 8.24(1)	CH_3(b) 1.10(3), 1.21(3)	7.90(1) 8.24(1)	CH_3(a) 1.19(0.6), 1.30(0.6) CH_3(b) 1.10(2.4), 1.21(2.4)
L-phe (10)	(b) 8.25(2)	(c)	(a) 7.97(0.4), 8.27(0.4) (b) 8.25(1.6)	(c)
L-tyr[c] (11)	(a) 7.97(*ca.* 0.2) (b) 8.26(*ca.* 1.8)	(c)	(a) 7.97(0.17) (b) 8.26(1.83)	(c)
L-trp (12)	(b) 8.11(2)	(c)	(a) 7.82(0.11) (b) 8.11(1.89)	(c)

( ) corresponds to the number of proton(s). (a), peak(s) corresponding to $(+)_{435}$-isomer. (b), peak(s) due to $(-)_{435}$-isomer. (c), not clear due to overlap with other peaks.
a) CH_2-CH_2 protons appear at 3.4—4.6 ppm as broad multiplet, phenyl protons appear between 6.5 and 7.5 ppm as multiplet. b) Center of broad multiplet. c) This complex shows $CHCl_3$ signal at 7.77 ppm.

14—16, and **20** (in the case of L-thr-complex **20**, as shown in Fig. 5 C′, the CH_3–C=N singal splits into three peaks soon after dissolution). These PMR spectral behaviors clearly indicate that the complexes **2—6**, **14—16**, and **20** exist each as an 1 : 1 mixture of the two isomers soon after dissolution, but they exist each as a mixture of the two isomers in which one isomer is over the other at equilibrium conditions. On the other hand, as shown in Figs. 5 B and B′, the L-met-complex **18** shows only one signal for the methyl group of the coordinated L-methionine anion soon after dissolution ,but the signal decreases its intensity and another methyl signal appears at a somewhat lower field at the equilibrium condition. Similar behaviors are seen for the complexes **8** and **17**. Therefore, it is concluded that these three complexes are isolated each as a pure isomer, but they exist each in a mixture of two isomers in solution. By comparison of the time dependences between the optical rotations at 435 nm of the complexes and their PMR spectra, the signals of the alkyl groups of amino acid anions at higher field are assigned to those for $(-)_{435}$-isomers and the lower field signals to $(+)_{435}$-isomers. Thus, the isomer's ratio, $(-)_{435}$-isomer/$(+)_{435}$-isomer, can easily be estimated from the PMR intensity ratio. The ratios for the complexes **2**, **3**, **6**, **8**, **14**, **15**, **18**, and **20** are listed in Table 8.

On the contrary, as shown in Figs. 5 D, D′ and E and E′, the complexes **10—12** and **22—24** in which the amino acid anions have phenyl group show the time dependences not only for the signals of the amino acid anions but for the signals of H–C=N or CH_3–C=N. This is due to the anisotropic effect of the phenyl group. Since the PMR spectral behaviors of these H–C=N and CH_3–C=N signals are similar to those of the alkyl signals of amino acid anions mentioned above, the compositions of $(-)_{435}$- and $(+)_{435}$-isomers both soon after dissolution and at equilibrium conditions are easily estimated; the isomer's ratios in the complexes **10—12** and **22—24** at the equilibrium conditions are listed in Table 8.

In the cases of the L-leu- and L-isoleu-complexes

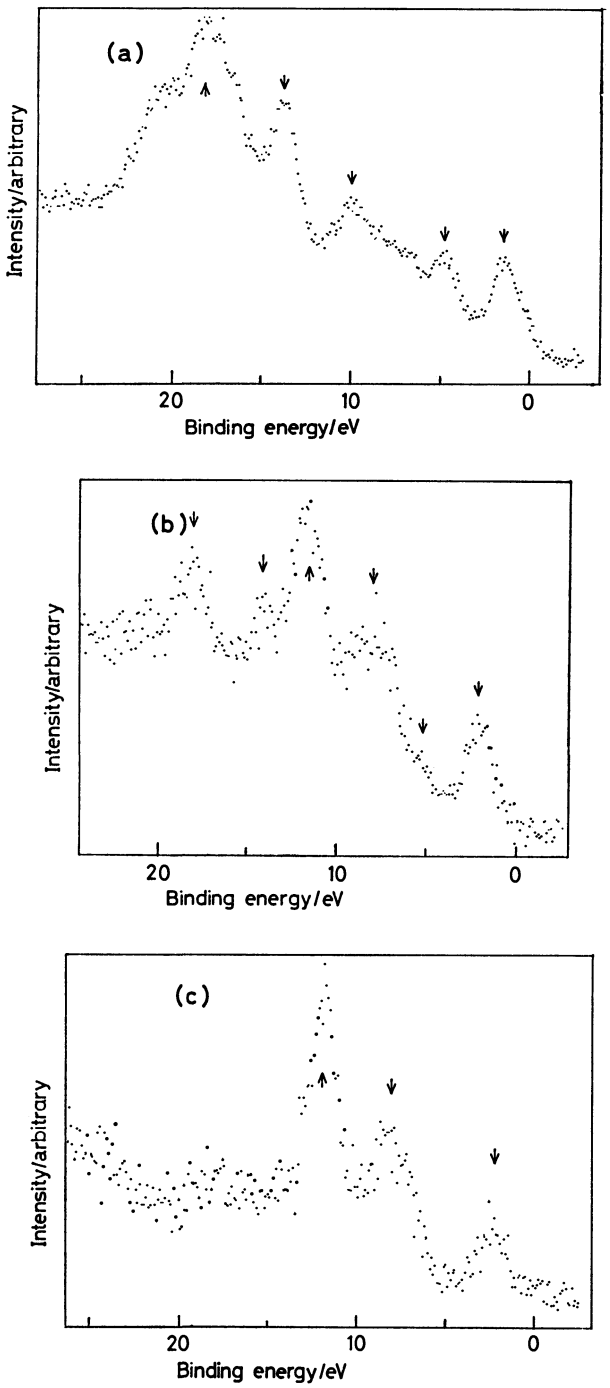

Fig. 1. The valence region of XPS spectra of a) Cr $(C_6H_6)_2$, b) $Cr(C_6H_6)(CO)_3$, and c) $Cr(CO)_6$.

The fact that the binding energies localized on both a central metal atom and ligands give the same shift shows that the magnitude of the matrix effects is constant over a molecule, and that the observed binding energies are little affected by Madelung and polarization energies which may depend upon the lattice points.

The fact must be also true in the case of core electrons, that is, we could obtain the binding energies of core electrons referred to vacuum level as given in Table 1.

The Estimation of the Charge Distribution from XPS Data. It has been shown that the binding energy, BE, of a carbon ls electron can be expressed as follows in terms

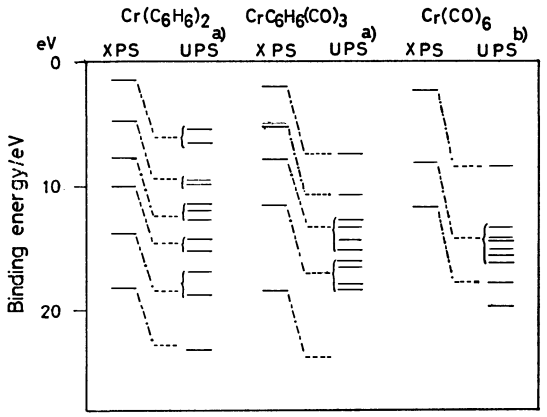

Fig. 2. The comparison of the energy level diagrams observed by XPS method and UPS method. Broken lines denote the corrected binding energies. a) : Ref. 4. b) : Ref. 5.

Table 1. Binding energies of core electrons refered to the vacuum level (eV)

Compound	C 1s	O 1s	Cr 3p
$Cr(CO)_6$	292.9	539.2	50.8
$Cr(C_6H_6)(CO)_3$	292.0	538.4	49.8
	290.1[a]		
$Cr(C_6H_6)_2$	289.7	—	47.9

a) the C 1s binding energy due to carbon atom in benzene.

of the charge density q_C on the carbon atom of the interest:[8]

$$BE = k_C q_C + V + E_R + l_C \quad (1)$$

where V denotes the electrostatic potential at the nuclear caused by surrounding atoms and E_R gives relaxation energy based on the sudden approximation. k_C and l_C are constant to be decided from experiments. Snyder[9] and Gelius[10] suggestes that E_R may also be expressed in terms of q_C. For the group of carefully selected compounds, such a linear relation can be found in Fig. 3 where calculated relaxation energies[11] were plotted against the charge density on the carbon atom obtained by CNDO/2 method. This is expected on the basis of the study of relaxation energies done by H. Siegbahn *et al.*[12] According to their notation, the following equation may be settled for a certain authorized group

$$k^T \cdot \Delta q_A(j) + \Delta V_A(j) + l^T - l = \text{const.}$$

where the constants of k and l for the transition state are denoted by k^T and l^T. In other words, it can be said that the flow of charge onto the ionized atom and potential energy change at the site of the ionized atom as a result of charge reorganization in the rest of the molecule are similar within a certain group.

When the following substitution reaction proceeds

the carge density on the carbon atom may increase by amounts of Δq. It is shown that the chemical shift in

Syntheses of D-Arabinofuranosyl and 2'-Deoxy-D-ribofuranosyl Pyrazolecarboxamides

Osamu MAKABE,* Jutaro YAJIMA, and Sumio UMEZAWA**

Department of Applied Chemistry, Faculty of Engineering, Keio University, Hiyoshi, Kohoku-ku, Yokohama, Kanagawa 223

(Received December 27, 1975)

Several D-arabino- and 2'-deoxy-D-ribonucleosides of carbamoylpyrazoles were synthesized by an acid-catalyzed fusion reaction of 1-*O*-acetyl derivatives of the corresponding sugars with pyrazole derivatives. Spectral evidences for their *N*-glycosylation sites and anomeric configurations were presented.

In a previous paper we have reported[1] the synthesis of a cytotoxic nucleoside, 1-(β-D-ribofuranosyl)pyrazole-3-carboxamide, which is closely related to the antiviral antibiotic of pyrazomycin[2] [3-(β-D-ribofuranosyl)-4-hydroxypyrazole-5-carboxamide]. Our continued interest in the nucleosides of pyrazolecarboxamide has prompted us to synthesize the corresponding nucleosides, *i.e.*, D-arabino- and 2'-deoxy-D-ribonucleosides of pyrazolecarboxamide and related nucleosides.

Since D-arabinosylation of heterocycles has often been successful in yielding antiviral and cytotoxic activities as exemplified[3] by 1-(β-D-arabinofuranosyl)-cytosine and 9-(β-D-arabinofuranosyl)adenine, we undertook a synthetic investigation of the arabinosylpyrazolenucleoside (**13β**). The β-nucleoside(1',2'-*cis*) was synthesized by use of 1-*O*-acetyl-2,3,5-tri-*O*-benzyl-D-arabinofuranose (**1**) in which the hydroxyl group at *C*-2 is blocked with benzyl group (a nonparticipating group). The 1-*O*-acetyl sugar **1** was prepared by acetylation of 2,3,5-tri-*O*-benzyl-D-arabinofuranose.[4] Fusion of **1** with ethyl pyrazole-3-carboxylate[5] (**2**) in the presence of bis(*p*-nitrophenyl) hydrogenphosphate[6] gave a mixture of ethyl 1-(2,3,5-tri-*O*-benzyl-α-D-arabinofuranosyl)pyrazole-3-carboxylate (**5α**) and its β-anomer (**5β**) in a ratio of *ca.* 3 : 5 together with a small amount of 5-ethoxycarbonyl isomer (**6α**). These products were separated by chromatography and then treated with methanolic ammonia to give 1-(2,3,5-tri-*O*-benzyl-α-D-arabinofuranosyl)pyrazole-3-carboxamide (**9α**), its β-anomer (**9β**), and the α-anomer of 5-carboxamide (**10α**), respectively. Catalytic hydrogenolysis then afforded 1-(α-D-arabinofuranosyl)pyrazole-3-carboxamide (**13α**), its β-anomer (**13β**), and 5-carboxamide (**14α**), respectively.

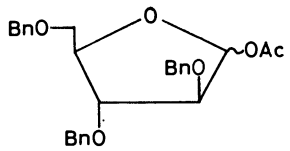

1
(Bn=$CH_2C_6H_5$)

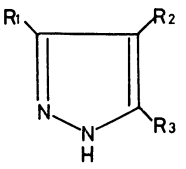

2, $R_1=CO_2Et$, $R_2=R_3=H$
3, $R_1=R_3=CO_2Et$, $R_2=H$
4, $R_1=R_3=CO_2Et$, $R_2=NO_2$

Chart 1

A similar fusion reaction of diethyl pyrazole-3,5-dicarboxylate[1] (**3**) with **1** afforded an anomeric mixture of (**7**), from which, by treatment with methanolic ammonia followed by chromatographic separation, 1-(2,3,5-tri-*O*-benzyl-α-D-arabinofuranosyl)pyrazole-3,5-dicarboxamide (**11α**) and its β-anomer (**11β**) were obtained in a ratio of 5 : 1. Catalytic hydrogenolysis of the major product **11α** gave 1-(α-D-arabinofuranosyl)-pyrazole-3,5-dicarboxamide (**15α**).

A fusion of diethyl 4-nitropyrazole-3,5-dicarboxylate[1] (**4**) with **1** followed by chromatographic separation afforded diethyl 1-(2,3,5-tri-*O*-benzyl-α-D-arabinofuranosyl)-4-nitropyrazole-3,5-dicarboxylate (**8α**) and its β-anomer (**8β**) in a ratio of 11 : 3. The major product (**8α**) was treated with methanolic ammonia to give the carboxamide (**12α**), which was converted by catalytic hydrogenation into 4-amino-1-(α-D-arabinofuranosyl)-pyrazole-3,5-dicarboxamide (**16α**).

The structures of these nucleosides were assigned on the basis of their PMR and UV spectra. Substitution by the anisotropic carbamoyl group at *C*-5 of the pyrazole portion results in the downfield shift of anomeric proton signal[1,10] and it is observed that the anomeric proton signals of **14α** (δ 6.89), **15α** (δ 6.90), and **16α** (δ 6.41) show downfield shifts as compared with those of **13α** (δ 5.82) and **13β** (δ 6.06). The *H*-5 signals of **13α** (δ 8.17) and **13β** (δ 8.04) were observed in lower field than the *H*-3 signal of **14α** (δ 7.75). The anomeric proton signals of 1',2'-*cis* nucleosides have been shown[7] to occur at lower field than those of the corressponding *trans* anomers. The anomeric proton signals of the nucleoside **13α** and **13β** occurred at δ 5.82 and 6.06, respectively. These data suggested α-configuration(1',2'-*trans*) for **13α** and β-configuration(1',2'-*cis*) for **13β**. Comparison of the PMR spectrum of **8α**(1',2'-*trans*) with that of **8β**(1',2'-*cis*) showed a downfield shift for the anomeric proton of **8β** as expected for a 1',2'-*cis* nucleoside. This suggested α-configuration(1',2'-*trans*) for **16α**. The anomeric configuration of **14α** was suggested as α by the coupling constant ($J_{1',2'}=2.8$ Hz) of its benzyl derivative (**10α**).

Syntheses of the 2'-deoxy-D-ribonucleosides were next performed by use of 1-*O*-acetyl-2-deoxy-3,5-di-*O*-(*p*-nitrobenzoyl)-D-*erythro*-pentofuranose (**17**) which was obtained from methyl 2-deoxy-3,5-di-*O*-(*p*-nitro-

* Present address: Research Laboratories, Meiji Seika Kaisha, Morooka-cho, Kohoku-ku, Yokohama, Kanagawa 222.

** Present address: Institute of Bio-organic Chemitry, Nakahara, Kawasaki-shi 211.

$C_{30}H_{31}O_5N_3$: C, 70.16; H, 6.08; N, 8.18%.

*1-(2,3,5-Tri-O-benzyl-α-D-arabinofuranosyl)pyrazole-5-carboxamide (**10α**).* By a procedure similar to that for **9α**, **6α** (150 mg, 0.28 mmol) gave **10α**, 118 mg (82%), as a colorless syrup; $[\alpha]_D^{25}$+25.0° (*c* 0.50, chloroform). PMR ($CDCl_3$): δ 7.73 (d, 1H, H-3), 7.40 (d, 15H, Ar), 6.95 (d, 1H, H-4), 6.60 (br d, 2H, $CONH_2$), 6.03 (d, 1H, $J_{1',2'}$=2.8 Hz, H-1'), 4.80 (t, 1H, H-2'), 4.60 (s, 6H, CH_2-Ar), 4.80 (m, 2H, H-3', H-4'), 3.71 (d, 2H, H-5',5''). Found: C, 69.94; H, 6.11; N, 8.13%. Calcd for $C_{30}H_{31}O_5N_3$: C, 70.16; H, 6.08; N, 8.18%.

*1-(2,3,5-Tri-O-benzyl-α-D-arabinofuranosyl)pyrazole-3,5-dicarboxamide (**11α**) and Its β-Anomer (**11β**).* A solution of **7** (330 mg, 0.537 mmol) in absolute methanol (30 ml) saturated with ammonia at 0 °C was kept at room temperature for 12 h. After removal of methoanol by evaporation, the resulting syrup was dissolved in acetone and chromatographed on a column of silica gel (15 g, 1×10 cm, packed with 6 : 1 chloroform–acetone) with the same solvent system. The effluent was fractionated into 3 mls.

Fraction Nos. 8—10 gave colorless crystals of **11β**, 46 mg (15.4%); mp 200—202 °C. $[\alpha]_D^{25}$−89.1° (*c* 1.0, dioxane). PMR (CD_3OD): δ 7.50 (m, 16H, Ar, H-4), 7.28 (d, 1H, $J_{1',2'}$=4.9 Hz, H-1'), 4.85—4.20 (m, 9H, CH_2-Ar, H-2', H-3', H-4'), 3.70 (d, 2H, H-5', 5''). Found: C, 66.95; H, 6.01; N, 9.80%. Calcd for $C_{31}H_{32}O_6N_4$: C, 66.89; H, 5.80; N, 10.07%.

Fraction Nos. 13—18 gave a colorless solid of **11α**, 221 mg (74%); $[\alpha]_D^{25}$+72.8° (*c* 1.0, dioxane). PMR (CD_3OD): δ 7.48 (d, 16H, Ar, H-4), 7.22 (d, 1H, $J_{1',2'}$=3.2 Hz, H-1'), 5.03 (dq, 1H, H-2'), 4.75—4.20 (m, 8H, CH_2-Ar, H-3', H-4'), 3.72 (d, 2H, H-5' H-5''). Found: C, 67.02; H, 5.93; N, 10.04%. Calcd for $C_{31}H_{32}O_6N_4$: C, 66.89; H, 5.80; N, 10.07%.

*1-(2,3,5-Tri-O-benzyl-α-D-arabinofuranosyl)-4-nitropyrazole-3,5-dicarboxamide (**12α**).* By a method similar to that described above, **8α** (440 mg 0.668 mmol) gave an oil, which was chromatographed on silica gel column (20 g, 1×15 cm, packed with 3 : 1 benzene–ethyl acetate). Evaporation of the portion containing the product gave a colorless syrup of **12α**, 354 mg (88%); $[\alpha]_D^{25}$+101.3° (*c* 1.0, methanol). PMR (CD_3OD): δ 7.40 (s, 15H, Ar), 6.29 (d, 1H, $J_{1',2'}$=3.2 Hz, H-1'), 5.10 (dt, 1H, H-2'), 4.75—4.00 (m, 8H, CH_2-Ar, H-3', H-4'), 3.69 (d, 2H, H-5',5''). Found: C, 62.06; H, 5.37; N, 11.68%. Calcd for $C_{31}H_{31}O_8N_5$: C, 61.89; H, 5.19; N, 11.64%.

*1-(2,3,5-Tri-O-benzyl-β-D-arabinofuranosyl)-4-nitropyrazole-3,5-dicarboxamide (**12β**).* By a procedure similar to that described above, **8β** (110 mg, 0.167 mmol) gave **12β**. Its recrystallization from methanol afforded its pure sample (79 mg, 78.5%); mp 188—200 °C. $[\alpha]_D^{25}$ −113° (*c* 0.83, dioxane). PMR (CD_3OD): δ 7.40 (s, 15H, Ar), 6.34 (d, 1H, $J_{1',2'}$=5.2 Hz, H-1'), 3.70 (d, 2H, H-5',5''). Found: C, 62.17; H, 5.39; N, 11.42%. Calcd for $C_{31}H_{31}O_8N_5$: C, 61.89; H, 5.19; N, 11.64%.

*1-(α-D-Arabinofuranosyl)pyrazole-3-carboxamide (**13α**).* A solution of **9α** (402 mg, 0.78 mmol) in methanol (40 ml) was hydrogenated in the presence of palladium black at 3.5 atm for 24 h. After removal of the catalyst, the methanol was evaporated and the residue was chromatographed on a silica gel column with 4 : 4: 2 : 3 1-butanol–ethanol–chloroform–17% aqueous ammonia. Evaporation of the portion containing the product gave a colorless glass of **13α** (129 mg, 68%); $[\alpha]_D^{25}$ +30.6° (*c* 0.41, water). PMR (DMSO-d_6): δ 8.17(d, 1H, H-5), 7.50 (br d, 2H, $CONH_2$), 6.84 (d, 1H, H-4), 5.92 (br s, 1H, OH), 5.82 (d, 1H, $J_{1',2'}$=4.7 Hz, H-1'), 5.60 (br s, 1H, OH), 4.85 (br d, 1H, OH), 4.65 (t, 1H, H-2'), 4.30—3.83 (m, H, H-3', H-4'), 3.70 (m, 2H, H-5',5''). UV: λ_{max}^{water} 231 (ε 12800), λ_{max}^{pH1} 198 (ε 13000), λ_{max}^{pH13} 219 nm (ε 11800). Found: C, 42.76; H, 5.51; N, 16.53%. Calcd for $C_9H_{13}O_5N_3$ 1/2H_2O: C, 42.82; H, 5.58; N, 16.65%.

*1-(β-D-Arabinofuranosyl)pyrazole-3-carboxamide (**13β**).* By a procedure similar to that described above, **9β** (560 mg, 1.09 mmol) gave 13β. Its recrystallization from ethanol and benzene afforded its pure sample (198 mg, 74.6%); mp 126—127.5 °C. $[\alpha]_D^{25}$ −22.4° (*c* 0.67, water). PMR (DMSO-d_6): δ 8.04 (d, 1H, H-5), 7.40 (br d, 2H, $CONH_2$), 6.80 (d, 1H, H-4), 6.06 (d, 1H, $J_{1',2'}$=5.2 Hz, H-1'), 5.50 (d, 2H, OH), 5.02 (t, 1H, OH), 4.25 (m, 2H, H-2', H-3'), 3.75 (m, 3H, H-4', H-5',5''). UV: λ_{max}^{water} 213 (ε 11500), λ_{max}^{pH1} 198 (ε 12000), λ_{max}^{pH13} 219 nm (ε 11000). Found: C, 44.16; H, 5.29; N, 17.13%. Calcd for $C_9H_{13}O_5N_3$: C, 44.44; H, 5.39; N, 17.28%.

*1-(α-D-Arabinofuranosyl)pyrazole-5-carboxamide (**14α**).* By a procedure similar to that described above followed by recrystallization from ethanol, **10α** (108 mg, 0.21 mmol) gave crystals of **14α**, 41.2 mg (78%); mp 189—191 °C. $[\alpha]_D^{25}$ +64.0° (*c* 0.88, water). PMR (DMSO-d_6): δ 7.85 (br d, 2H, $CONH_2$), 7.75 (d, 1H, H-3), 7.06 (d, 1H, H-4), 6.89 (d, 1H, $J_{1',2'}$=4.6 Hz, H-1'), 5.58 (q, 2H, OH), 4.80 (m, 2H, OH, H-2'), 4.00 (m, 2H, H-3', H-4'), 3.60 (m, 2H, H-5',5''). UV: λ_{max}^{water} 219 (ε 13700), λ_{max}^{pH1} 221 (ε 10800), 198 (ε 14000), λ_{max}^{pH13} 220 nm (ε 10100). Found: C, 44.42; H, 5.38; N, 17.07%. Calcd for $C_9H_{13}O_5N_3$: C, 44.44; H, 5.39; N, 17.28%.

*1-(α-D-Arabinofuranosyl)pyrazole-3,5-dicarboxamide (**15α**).* A solution of **11α** (210 mg, 0.377 mmol) in 21 ml methanol and dioxane (1 : 1) was hydrogenated with palladium black and hydrogen for 48 h to give a solid, which was recrystallized from methanol and benzene to give crystals of **15α** (63 mg, 58%); mp 237—239 °C. $[\alpha]_D^{25}$ +77.4° (*c* 0.5, water). PMR (DMSO-d_6): δ 7.65 (br d, 2H, $CONH_2$), 7.45 (s, 1H, H-4), 6.90 (d, 1H, $J_{1',2'}$=4.5 Hz, H-1',) 5.70 (d, 1H, OH), 6.40 (d, 1H, OH), 4.85 (m, 2H, OH, H-2'), 4.10 (m, 2H, H-3', H-4'), 3.65 (m, 2H, H-5',5''). UV: λ_{max}^{water} 205 (ε 12000), λ_{max}^{pH1} 207 (ε 10600), λ_{max}^{pH13} 219 nm (ε 8900). Found: C, 42.06; H, 5.00; N, 19.35%. Calcd for $C_{10}H_{14}O_6N_4$: C, 41.96; H, 4.93; N, 19.58%.

*4-Amino-1-(α-D-arabinofuranosyl)pyrazole-3,5-dicarboxamide (**16α**).* A solution of **12α** (300 mg, 0.499 mmol) in methanol (8 ml) was hydrogenated in the same way as described for **13α**. The resulting solid was recrystallized from methanol and benzene to give **16α**, 91.5 mg (61%); mp 208—209 °C. $[\alpha]_D^{25}$ +108.9° (*c* 0.8, water). PMR (DMSO-d_6): δ 7.48 (br s, 4H, $CONH_2$), 6.41 (d, 1H, $J_{1',2'}$= 4.0 Hz, H-1'), 5.65 (d, 1H, OH), 5.31 (br s, 3H, NH_2, OH), 4.85 (m, 2H, OH, H-2'), 3.97 (br d, 2H, H-3', H-4'), 3.60 (m, 2H, H-5',5''). UV: λ_{max}^{water} 204 nm (ε 11000), λ_{max}^{pH1} 207 (ε 98000), 304 (ε 2900), λ_{max}^{pH13} 219 (ε 18000), 302 nm (ε 6800). Found: C, 39.45; H, 4.99; N, 22.98%. Calcd for $C_{10}H_{15}O_6N_5$: C, 39.45; H, 5.02; N, 23.25%.

*1-O-Acetyl-2-deoxy-3,5-di-O-(p-nitrobenzoyl)-D-erythro-pentofuranose (**17**).* Methyl 2-deoxy-3,5-di-*O*-(*p*-nitorobenzoyl)-D-*erythro*-pentoside (4.5 g, 10.1 mmol) was dissolved in a mixture of glacial acetic acid (5 ml) and acetic anhydride (10 ml) under cooling at −15 °C, and concentrated sulfuric acid (0.3 ml) was added with stirring, after which the stirring was further continued for 30 min at −15 °C. The mixture was poured onto ice–water (300 ml) and extracted with chloroform (100 ml). The organic layer was washed successively with water (100 ml×2), saturated aqueous sodium hydrogencarbonate solution, and water, and dried over anhydrous sodium sulfate. Evaporation under reduced

Pressure Effect on the Isomerization Velocities of β-[Co(edda)(tn)]$^+$ and β-[Co(edda)(en)]$^+$ in Solution

Yoichi KITAMURA

Department of Chemistry, Faculty of Science, Ehime University, Matsuyama, Ehime 790

(Received July 26, 1975)

The rates of the isomerization of β-[Co(edda)(tn)]$^+$ and β-[Co(edda)(en)]$^+$ to the α-isomers in a 0.2 M Na_2CO_3–0.2 M $NaHCO_3$ buffer solution have been measured under pressures of 1, 1000, 2000, and 3000 kg cm^{-2}. The activation volumes have been found to be 14.7 and 20.0 ml mol^{-1} respectively. It may be concluded that these reactions proceed through the SN1 CB mechanism.

The investigation of the pressure effect on a reaction velocity gives the value of the activation volume through the $\Delta V^{\neq} = -RT(\mathrm{d}\ln k/\mathrm{d}P)$ relation and, therefore, some information about the reaction mechanism.[1] Such investigations were carried out for several reactions of complex ions in solution, and the reaction mechanisms were deduced on the basis of the activation volume ($\Delta V^{\neq}$) and the total volume change (ΔV).[2] For an isomerization reaction, since the ligands of the reactant and of the resultant are identical, the total volume change can be assumed to be very small; hence, $\Delta V^{\neq}$ must be directly related to the reaction pathway.

Kuroda found that β-[Co(edda)(tn)]$^+$ and β-[Co(edda)(en)]$^+$ isomerize to the α-isomers in basic solutions, and proposed the Co–N bond rupture as the activation step.[3,4] In this study, the pressure dependence of the reaction rate was involved, and so the mechanism proposed by Kuroda was re-examined from the standpoint of the pressure effect.

Experimental

Materials. The α- and β-ethylenediamine-*N*,*N*′-diacetato(trimethylenediamine)cobalt(III) perchlorate, α- and β-[Co(edda)(tn)]ClO_4 (β-isomer is the monohydrate), were synthesized by the method developed by Kuroda and were identified by the agreement of the absorption spectra with those obtained by him.[3] The β-ethylenediamine-*N*,*N*′-diacetato(ethylenediamine)cobalt(III) perchlorate, β-[Co(edda)(en)]ClO_4, was provided by Kuroda.[5] Commercial reagent-grade chemicals were used. The water was distilled after an ion exchange.

Measurements. On the initiation of a reaction, about 20 mg of the complex salt and 10 ml of a 0.2 M Na_2CO_3–0.2 M $NaHCO_3$ buffer solution (pH=9.47 at 60 °C) at the reaction temperature were mixed in a beaker, and then 4 ml of the mixed solution was immediately poured into a glass syringe. The excess of the solution was quenched by putting the beaker in cold water, and the initial concentration was calculated from the absorption intensity of this quenched solution. The top of the syringe was sealed with a Teflon tape and was then set into liquid paraffin in a special steel cylinder, which had been maintained at the reaction temperature. The cylinder was set between the two plates of a press and pressurized rapidly. After a definite time, the pressure was released and the solution was quenched immediately. The absorption spectrum was measured subsequently.

The temperature of the cylinder block was controlled by circulating water from a thermostat and measured by a copper-constantan thermocouple, inserted in a hole of the cylinder block. It was maintained at 60±0.2 °C for the reaction of β-[Co(edda)(tn)]$^+$ and at 65±0.2 °C for that of the β-[Co(edda)(en)]$^+$.[6] The thermometer and the thermocouple were calibrated within ±0.1 °C by a standard thermometer made by the T. L. M. G. Co., Germany. The pressure value of the press was measured by means of a Bourdon gauge and controlled within ±2 kg cm^{-2}. The gauge was calibrated by a free piston gauge, and the pressure value was reproducible within ±1 kg cm^{-2}. The pressure generated in the cylinder was estimated from the piston-area ratio (22.56).

Results

Figure 1 illustrates the spectra of the initial solution of β-[Co(edda)(tn)]$^+$ and that after a definite reaction time. The three isosbestic points lie within ±4 nm from the positions obtained by Kuroda.[3] The concentration of each isomer was calculated from the absorption intensity at 503 nm, using the absorption coefficients of 153.8 and 64.8 l mol^{-1}cm^{-1} for the β- and the α-isomer respectively. A similar spectral change was observed for the reaction of β-[Co(edda)(en)]$^+$; the three isosbestic points lay within ±5 nm from the positions obtained by Kuroda.[4] The concentration of each isomer was calculated from the absorption intensity at 494 nm, using the absorption coefficient of 150.7 and 56.4 l mol^{-1} cm^{-1} for the β- and the α-isomers respectively.

These reactions have been known to be opposing first-order reversible reactions with respect to the

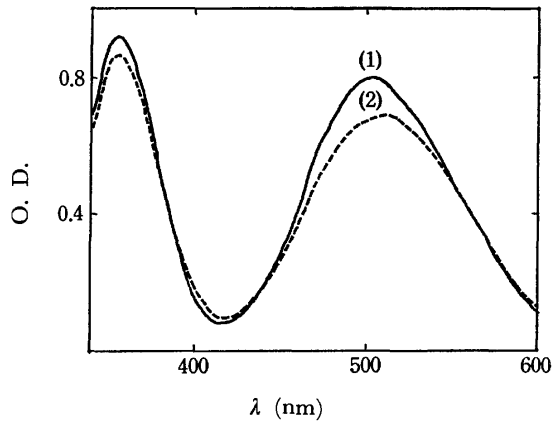

Fig. 1. Change of the absorption spectrum of β-[Co(edda)(tn)]$^+$ in 0.2 M Na_2CO_3–0.2 M $NaHCO_3$ solution.
1: Initial, 2: after reaction for 383 min at 58.6 °C and 3000 kg cm^{-2}.

complex ions at normal pressure.[3,4] This was ascertained to be also true under high pressures, and the rate constants were calculated from the following equations:

$$\beta\text{-[Co(edda)(tn or en)]}^{+} \rightleftharpoons \alpha\text{-[Co(edda)(tn or en)]}^{+}$$

$$k_1 = \frac{1}{(1+1/K)t} \ln \frac{m}{m-x}, \quad K = \frac{k_1}{k_{-1}}, \quad m = \frac{k_1 b - k_{-1} a}{k_1 + k_{-1}}$$

where

k_1, k_{-1}: rate constants of the forward and the backward reactions; K: the equilibrium constant; t: the reaction time at a high pressure; a, b: the concentrations of the α-isomer and of the β-isomer at the biginning of the pressurization, and x: the concentration isomerized during time t

Kuroda has reported, for the β-[Co(edda)(tn)]$^+$ solution, that, at equilibrium, 88.3—89.5% of the initial β-isomer isomerizes to the α-isomer, irrespective of the reaction temperature and the pH value of the solution.[3] For this complex ion in the 0.2 M Na_2CO_3–0.2 M $NaHCO_3$ solution, an 89% isomerization was found after 11 half-lives at 1000 kg cm^{-2} and 68.6 °C. K=7.93, which corresponds to an 88.8% (average value) isomerization, was used throughout the calculations at each pressure. For β-[Co(edda)(en)]$^+$ in the 0.2 M Na_2CO_3–0.2 M $NaHCO_3$ solution at 68.6 °C, a 95.3% isomerization was found after 9 half-lives at normal pressure and a 93.3% isomerization after 8 half-lives at 1000 kg cm^{-2}. The k_1 value is not very much influenced by the small variations in K value, and so K=20.3, which corresponds to a 95.3% isomerization, was used throughout the calculations for this complex. a and b were estimated from the initial concentration and a consideration of the progress of the reaction during the time from the mixing to the attainment of a high pressure. It took about 3 min. Similarly, for the estimation of x, the progress during the time from the release of the pressure to the quenching was taken into account. It took about 2 min.

The rate constants at each pressure are summarized in Table 1. The real reaction temperature in the syringe was slightly lower than the block temperature because of the heat loss through the cylinder bottom and the piston. For the estimation of the temperature difference, the rate constants at a normal pressure in Table 1 were compared with those obtained in a flask in an ordinary thermostat controlled at 60 °C for β-[Co(edda)(tn)]$^+$ (k_1=6.20×10^{-3} m^{-1}) and at 65 °C for β-[Co(edda)(en)]$^+$ (k_1=10.0×10^{-3} m^{-1}). Taking the activation energies into account, the temperature difference was estimated to be 1.4 °C. The rate constants were fitted to the formula: $\ln(k_{1p}/k_{10}) = cP + dP^2$, by the least-mean-square method, where k_{1p} and k_{10} represent the rate constants at a high pressure and at zero pressure respectively.[1] The relationships are shown in Fig. 2. The activation volumes at zero pressure were calculated from the $\Delta V^{\neq} = -RTc$ relation as 19.9 ml mol^{-1} for β-[Co(edda)(tn)]$^+$ and as 25.2 ml mol^{-1} for β-[Co(edda)(en)]$^+$.

Kuroda measured the rate constants at 65 °C at different OH^- ion concentrations. His results show that k_1 is linearly dependent on [OH^-] for β-[Co(edda)-(tn)]$^+$ and that k_1 is expressed as $k_1 = k'_1[OH^-] + k_0$, where k_0 is a parameter.[3] For this complex, k_1 was also measured in the 0.08 M Na_2CO_3–0.32 M $NaHCO_3$ solution (pH=8.90 at 60 °C) at 58.6 °C; it was found to be 2.06×10^{-3}, 1.10×10^{-3}, and 0.46×10^{-3} m^{-1} at 1, 1000, and 2000 kg cm^{-2} respectively. Assuming a linear relationship between k_1 and [OH^-], the k_0 value was obtained to be 1.01×10^{-3}, 0.64×10^{-3}, and 0.15×10^{-3} m^{-1} at 1, 1000, and 2000 kg cm^{-2} respectively. This pressure dependence of k_0 is approximately equal to that of k_1, at least in the lower pressure range ($\leq$1000 kg cm^{-2}); therefore, the pressure dependence of $k'_1[OH^-]$ may be taken as equal to that of k_1. For β-[Co(edda)(en)]$^+$, k_1 is approximately proportional to [OH^-] and may be expressed as $k_1 = k'_1[OH^-]$ for a relatively small range of [OH^-].[4]

The OH^- ion concentration in this buffer solution is given by: $[OH^-] = K_w[CO_3^{2-}]/K_2[HCO_3^-]$, where

Table 1. Rate constants for the isomerization of β-[Co(edda)(tn)]$^+$ and β-[Co(edda)(en)]$^+$ in 0.2 M Na_2CO_3–0.2 M $NaHCO_3$ solution[a]

	β-[Co(edda)(tn)]$^+$ at 58.6 °C			
P (kg cm^{-2})	1	1000	2000	3000
$k_1/10^{-3}$ m^{-1}	4.82(116)	2.54(366)	1.20(480)	0.62(383)
	5.06(99)	2.36(184)	1.46(362)	0.68(191)
	4.87(88)	2.19(126)	1.25(261)	
average	4.92	2.36	1.30	0.65
	β-[Co(edda)(en)]$^+$ at 63.6 °C			
P (kg cm^{-2})	1	1000	2000	3000
$k_1/10^{-3}$ m^{-1}	7.75(132)	3.49(242)	1.43(410)	0.84(410)
	7.54(60)	3.61(131)	1.42(264)	0.75(340)
			1.44(121)	
average	7.65	3.55	1.43	0.80

a) The figure in the parentheses denotes the pressure duration in min.

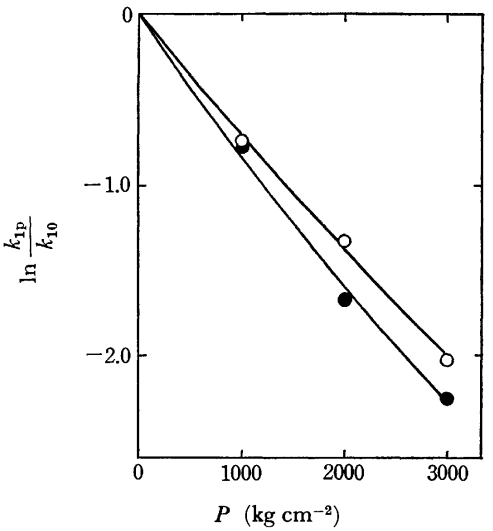

Fig. 2. The relation between $\ln(k_{1p}/k_{10})$ and P (kg cm^{-2}).
○: For β-[Co(edda)(tn)]$^+$, $c = -7.09\times10^{-4}$, $d = 1.26\times10^{-8}$.
●: For β-[Co(edda)(en)]$^+$, $c = -8{,}84\times10^{-4}$, $d = 4{,}11\times10^{-8}$.

K_w is the ionic product of water and where K_2 is the 2nd dissociation constant of carbonic acid.[7] When the buffer concentration is sufficiently high, as in this case, the pressure-induced change in pH does not significantly alter the $[CO_3^{2-}]/[HCO_3^-]$ ratio term.[8] Hence,

$$-RT\frac{d\ln k_1}{dP} = -RT\left[\frac{d\ln k_1'}{dP}+\frac{d\ln[OH^-]}{dP}\right]$$
$$= -RT\left[\frac{d\ln k_1'}{dP}+\frac{d\ln K_w}{dP}-\frac{d\ln K_2}{dP}\right]$$

The pressure dependence of K_w has been measured by Hamann, and that of K_2, by Distèche and Distèche.[9,10] From their measurements, the ΔV value for $H_2O=H^++OH^-$ was calculated to be -20.4 ml mol^{-1} at 25 °C, and that for $HCO_3^-=H^++CO_3^{2-}$, to be -25.6 ml mol^{-1} at 22 °C. Thus, $\Delta V^{\ddagger 1}=-RT\mathrm{d}\ln k_1'/dP$ can be calculated; 14.7 ml mol^{-1} and 20.0 ml mol^{-1} were obtained for β-[Co(edda)(tn)]$^+$ and β-[Co(edda)(en)]$^+$ respectively.

Discussion

Two reaction mechanisms are conceivable in view of the k_1 dependence on [OH$^-$]. One is the associative (SN2) mechanism, and the other is the dissociative (SN1 CB) mechanism. In the associative case, the rate-determining process is the association of the β-isomer with an OH$^-$ ion to form a seven-coordinated intermediate:

$$\beta\text{-[Co(edda)(tn or en)]}^+ + OH^- \rightarrow \beta\text{-[Co(edda)(tn or en)(OH)]}$$

An analogous case would be the substitution reaction of [Pt(dien)X]$^+$ by Y$^-$ (X$^-$=Cl$^-$, Br$^-$, I$^-$, N_3^-; Y$^-$=N_3^-, NO_2^-, I$^-$, SCN$^-$) through the five-coordinated neutral intermediate; activation volumes of -5——-12 ml mol^{-1} were obtained for these reactions.[11] Therefore, negative values of $\Delta V^{\ddagger\prime}$ may be expected in the associative case.

The activation volume would result partly from the intrinsic volume change accompanying the bond formation, and partly from the release of the solvated water molecules owing to the neutralization of the ionic charges of reactant ions, *i.e.*, the electrostrictive volume change. The electrostrictive part for the complex ion may be interpreted by means of Born's equation, which is considered to be valid for a large ion.[12] It amounts to 2 ml mol^{-1}, since the radius of the complex ion may be estimated as 3 Å from the Co–O and Co–N bond distances and the molecular extensions.[13,14] For the OH$^-$ ion, the crystal radius is 1.38 Å, and the absolute partial molal volume, $\overline{V}_{OH^-}$, may be estimated as 1.5 ml mol^{-1} at 60 °C, taking a reasonable average value of $\overline{V}_{H^+}$ (-6.2 ml mol^{-1}) from several reported values.[15] For a singly charged ion of this crystal radius in water, the disordered or the void space volume, $\overline{V}_{disord}$, and the electrostrictive volume, $\overline{V}_{elect}$, have been semiempirically estimated as 9 ± 3 ml mol^{-1} and 7 ± 3 ml mol^{-1} respectively.[15]

The activation process of the substitution reaction of [Pd(Et$_4$dien)X]$^+$ by Y$^-$ (X$^-$=Cl$^-$, Br$^-$, I$^-$; Y$^-$=Br$^-$, I$^-$, N_3^-) is considered to be the incorporation of a water molecule into the complex ion; activation volumes of -14——-10 ml mol^{-1} were obtained.[11] A water molecule has the same crystal radius as the OH$^-$ ion, and the arrangement of the solvent molecules around them must be similar. Therefore, the intrinsic change caused by OH$^-$-ion incorporation would be of a nature analogous to that of a H_2O incorporation, and it may be assumed that

$$\Delta V(H_2O \text{ incorporation})/\Delta V_{int}(OH^- \text{ incorporation}) = \overline{V}_{H_2O}/\overline{V}_{OH^-int}.$$

$\overline{V}_{H_2O}$ may be taken as 18.3 ml mol^{-1} at 60 °C from the water density.

In this situation, the upper limit of the activation volume in the associative case is obtained by assuming the highest value for $\overline{V}_{OH^-elect}$, or the highest value for $\overline{V}_{OH^-disord}$, to give the $\overline{V}_{OH^-}=1.5$ ml mol^{-1};

$\overline{V}_{OH^-int}=\overline{V}_{OH^-cryst}+\overline{V}_{OH^-disord}=6.6+12=18.6$ ml mol^{-1},

$\overline{V}_{OH^-elect}=\overline{V}_{OH^-int}-\overline{V}_{OH^-}=18.6-1.5=17.1$ ml mol^{-1}.

Then the upper limit may be given by $(-10\times18.6/18.3)+2+17.1=8.9$ ml mol^{-1}. This is still considerably smaller than the obtained values of $\Delta V^{\ddagger\prime}$, so the possibility of the associative mechanism can be excluded.

For the SN1 CB mechanism, by analogy with the base hydrolysis of [Co(NH$_3$)$_5$X]$^{2+}$ (X$^-$=Cl$^-$, Br$^-$,NO_3^-), the reaction series may be written as:

$$\beta\text{-[Co(edda)(H}_2\text{N-R-NH}_2\text{)]}^+ + OH^- \rightleftharpoons \beta\text{-[Co(edda)(HN-R-NH}_2\text{)]} + H_2O$$
$$\beta\text{-[Co(edda)(HN-R-NH}_2\text{)]} \rightarrow \alpha\text{-[Co(edda)(HN-R-NH}_2\text{)]}$$
$$\alpha\text{-[Co(edda)(HN-R-NH}_2\text{)]} + H_2O \rightleftharpoons \alpha\text{-[Co(edda)(H}_2\text{N-R-NH}_2\text{)]}^+ + OH^-,$$

where the 1st and 3rd steps are assumed to be rapid and where the 2nd is assumed to be the rate-determining process.[16] Hence, $k'_1=k''_1K_{pre}$, where k''_1 is the rate constant of the 2nd step and where K_{pre} is the equilibrium constant of the 1st step. Thus,

$$-RT\frac{d\ln k_1'}{dP} = -RT\left[\frac{d\ln k_1''}{dP}+\frac{d\ln K_{pre}}{dP}\right],$$
$$\text{or } \Delta V^{\ddagger\prime} = \Delta V^{\ddagger\prime\prime} + \Delta V_{pre}$$

The volume change accompanying the pre-equilibrium (ΔV_{pre}) may be estimated as $\Delta V_{pre}=\overline{V}_{H_2O}-\overline{V}_{OH^-}+\Delta V_{el}$, where ΔV_{el} is the partial molal volume difference between the conjugate base form and the acid form of the β-isomer. ΔV_{el} may be estimated as 2 ml mol^{-1} from Born's equation.[12] Hence, ΔV_{pre} amounts to 18.8 ml mol^{-1} at 60 °C. Then, $\Delta V^{\ddagger\prime\prime}$, which is attributed to the activation of the rate-determining process, is -4.1 mol ml^{-1} and 1.2 ml mol^{-1} for β-[Co(edda)(tn)]$^+$ and for β-[Co(edda)(en)]$^+$ respectively. These magnitudes of $\Delta V^{\ddagger\prime\prime}$ are comparable with that expected from a bond rupture and the resulting solvations, and the SN1 CB mechanism seems reasonable.[17–19]

The activation energy and activation entropy were measured for these reactions by Kuroda; the values of 36.0 kcal mol^{-1} and 29.7 e.u. for β-[Co(edda)(tn)]$^+$ and of 42.1 kcal mol^{-1} and 46.5 e.u. for β-[Co(edda)-(en)]$^+$ were obtained.[3] The large positive values of

the activation entropies are in accordance with the qualitative proportionality relation between the activation volume and the activation entropy.[20] The energy and entropy changes for the pre-equilibrium must be approximately equal for these two complexes, and the differences in the activation energy and in the activation entropy should be attributed to the activation of the rate-determining process.

Following the proposal by Kuroda that the activation of the rate-determining process is the Co–N bond rupture of *tn* or *en*,[3,4] the obtained magnitudes of $\Delta V^{\neq\prime\prime}$ may be interpreted as follows. For β-[Co(edda)-(tn)]$^+$, the long trimethylenediamine chain was rather loosely attached in the complex and could move rather freely in its initial state. Hence, the intrinsic volume change resulting from the bond rupture was rather small, and the negative contribution owing to the solvation to the unoccupied site of the intermediate ion and to the partly liberated polar R–NH_2 group was the dominant factor. In contrast, for β-[Co(edda)-(en)]$^+$, the ethylenediamine chain is rather firmly and compactly attached in the complex; hence, the Co–N bond rupture results in a rather large intrinsic volume change, which compensates for the solvation effects.

The author wishes to thank Professor Jiro Osugi of Kyoto University for the use of the high-pressure apparatus and Professor Kashiro Kuroda of Ehime University for kindly providing the sample and for his valuable suggestions throughout this work.

References

1) T. W. Swaddle, *Coord. Chem. Rev.*, **14**, 217 (1974).
2) D. R. Stranks, *Pure Appl. Chem.*, **38**, 303 (1974).
3) K. Kuroda, *Chem. Lett.*, **1974**, 17.
4) K. Kuroda and F. Mohri, *Chem. Lett.*, **1972**, 719.
5) K. Kuroda, *Chem. Lett.*, **1972**, 197.
6) The reaction temperature is slightly lower than the block temperature, as will be shown later.
7) H. Menzel, *Z. Phys. Chem.*, **100**, 276 (1922).
8) R. C. Neuman, Jr., W. Kauzmann and A. Zipp, *J. Phys. Chem.*, **77**, 2687 (1973).
9) S. D. Hamann, *J. Phys. Chem.*, **67**, 2233 (1963).
10) A. Distèche and S. Distèche, *J. Electrochem. Soc.*, **114**, 330 (1967).
11) D. A. Palmer and H. Kelm, "Proceedings of the 4th International Conference on High Pressure," Kyoto 1974, p. 657. The $\Delta V^{\neq}$ (2) values on Table 3 in the report should show a minus sign (private communication). Et_4dien means *N,N,N′N′*-tetraethyldiethylene-triamine.
12) $\overline{V}_{el}=(Nz^2e^2)(dD/dP)/(2rD^2)$, where r, D, z and e represents the ionic radius, dielectric constant of the solvent, Avogadro number, ionic valence and electric charge, respectively.
13) H. Kuroya, *Nippon Kagaku Zasshi*, **92**, 905 (1971).
14) A. Bonamartini Corradi, C. G. Palmieri, M. Nardelli, M. A. Pellinghelli and M. E. Vidori Tani, *J. Chem. Soc., Dalton*, **1973**, 655.
15) See for example, "Water and Aqueous Solutions, Structure, Thermodynamics and Transport Processes", ed. by R. A. Horn, Wiley-Interscience, a Division of John Wiley and Sons, Inc., New York (1972), pp 519—560.
16) See for example, F. Basolo and R. G. Pearson, "Mechanisms of Inorganic Reactions," 2nd ed., John Wiley and Sons, Inc., New York (1967), p. 183.
17) H. R. Hunt and H. Taube, *J. Am. Chem. Soc.*, **80**, 2642, (1958).
18) W. E. Jones, L. R. Carey, and T. W. Swaddle, *Can, J. Chem.*, **50**, 2739 (1972).
19) G. Guastalla and T. W. Swaddle, *Can. J. Chem.*, **51**, 821 (1973).
20) K. J. Laidler and D. T. Y. Chen, *Can. J. Chem.*, **37**, 599 (1959).

The Inner-Sphere Mechanism Interpreted by the Hydrogen Ion Effect on the Fe^{2+} Reduction Rate of Oxalato-, Malonato-, Glycolato-, and Chloro-Cobalt(III) Complexes in Aqueous Solution

Kousaburo OHASHI

Department of Chemistry, Ibaraki University, Mito 310

(Received September 1, 1975)

The hydrogen ion effect on the rate of the Fe^{2+} reduction of oxalato-, glycolato-, and chloro-cobalt(III) complexes was investigated kinetically. It was found that the rates of the Fe^{2+} reduction of cobalt(III) complexes such as *trans*(*N*)-Co(ox)(β-ala)$_2^-$, *trans*(*N*)-Co(ox)(gly)$_2^-$, *trans*(*N*)-Co(ox)(gly)(en), Co(ox)$_3^{3-}$, and *trans*-(O,Cl)-Co(Cl)(am)(dien)$^+$ (am=glycinate, α-alaninate or β-alaninate ions) increase with an increase in the hydrogen ion concentration. This result can be explained by accounting for the protonation of the oxygen atom of the carbonyl group of the nonbridging ligand. The inner-sphere mechanism can be deduced for the Fe^{2+} reductions of these complexes due to the hydrogen-ion effect. Moreover, a kinetic study of the Fe^{2+} reduction reaction of Co(Hmalo)$(NH_3)_5^{2+}$ and Co(malo)$(NH_3)_5^+$ was carried out. An inner-sphere mechanism for these reactions is proposed from an analysis of the kinetic data. Discussion of the structure of the precursor complex and of the rate determining step for the Fe^{2+} reduction reactions of cobalt(III) complexes are also made.

One of the major problems of the Fe^{2+} reduction reaction of cobalt(III) complexes is to determine whether electron-transfer reactions proceed through the inner- or outer-sphere mechanisms. It was demonstrated that the reactions of Co(Cl)$(H_2O)_5^{2+}$,[1] and Co(Cl)(Hedta)$^-$ [2] with Fe^{2+} proceed through an inner-sphere mechanism from the kinetic measurements of the formation and decay of the transient species of these reactions. Such a direct evidence of the inner-sphere mechanism for the Fe^{2+} reduction of cobalt (III) complexes has not been so often obtained due mainly to the experimental difficulty caused by the slow rate of formation of transient products of the Fe^{3+} and the possibility of subsequent substitution.

In previous kinetic studies concerning the effect of the nonbridging ligand on the Fe^{2+} reductions of oxalato-,[3] azido,[4] chloro-[5-7] and nitrilopolyaminocarboxylato[8]-cobalt(III) complexes, the present author was inclined to favor the inner-sphere mechanism.

One of the purposes of the present work is to indirectly determine the mechanism of the Fe^{2+} reductions of some oxalato-, malonato-, glycolato-, and chloro-cobalt(III) complexes due to the effect of the hydrogen ion on the electron-transfer rate. Another purpose is the investigation of the structure of the precursor complex for the Fe^{2+} reductions of some oxalato-, malonato-, and chloro-cobalt(III) complexes. The rate-determining step is also discussed.

Experimental

Preparation of Cobalt(III) Complexes. *trans*(*N*)-K[Co(ox)(gly)$_2$],[9,10] *trans*(*N*)-K[Co(ox)(β-ala)$_2$],[11] K$_3$[Co(ox)$_3$],[12] [Co(ox)$(NH_3)_4$](ClO_4),[13] [Co(Hmalo)$(NH_3)_5$]$(ClO_4)_2\cdot 2H_2O$,[14] [Co(glyco)$(en)_2$]Cl$\cdot H_2O$,[15] *trans*(O,Cl)-[Co(Cl)(gly)(dien)](ClO_4),[16] *trans*(O,Cl)-[Co(Cl)(α-ala)(dien)](ClO_4),[16] and *trans*(O,Cl)-[Co(Cl)(β-ala)(dien)](ClO_4),[16] used as oxidants were prepared by the methods described in the references cited. The purities and identities of the complexes were ascertained by microanalysis for carbon, hydrogen, and nitrogen and by comparing the absorption spectra with those reported in the references.

Materials. The preparation of the iron(II) stock solution and the determinations of the concentrations of the iron(II), hydrogen, and perchlorate ions in this solution were carried out by the methods similar to those described in the previous paper.[5] The other reagents were G. R. grade chemicals.

Measurements of the Reaction Rate. The rates for the aquation reactions of the cobalt(III) complexes in strong acid media are negligibly small as compared with those of the Fe^{2+} reduction reactions. The Fe^{2+} reduction rates of the cobalt(III) complexes, except for Co(ox)$_3^{3-}$, were determined by the usual spectrophotometric method. The kinetic runs for Co(ox)$_3^{3-}$ were carried out by a Yanagimoto EPS-1-type stopped flow spectrophotometer under pseudo-first order conditions, the concentration of iron(II) ion being notably in excess of that of the cobalt(III) complex. The decrease in absorption was observed at a wavelength in the vicinity of the first absorption maximum of the complexes.

The concentration of the perchlorate ion in the solution was controlled by the addition of a sodium perchlorate solution. The hydrogen ion concentrations were varied from 0.05 M to 1.3 M by the addition of perchloric acid.

Results and Discussion

Figure 1 shows the dependence of the second-order rate constant on the hydrogen ion concentration for the Fe^{2+} reduction of *trans*(*N*)-Co(ox)(gly)$_2^-$ when the

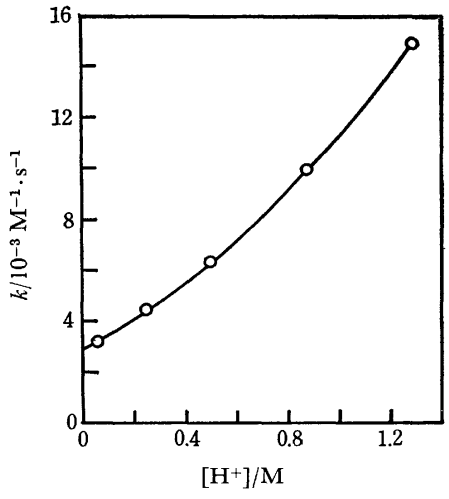

Fig. 1. The relation between the second-order rate constant of *trans*(*N*)-Co(ox)(gly)$_2^-$ and hydrogen ion concentration. $\Sigma[ClO_4^-]=1.30$ M, 25 °C, $NaClO_4$-$HClO_4$ medium.

ionic strength was maintained by the addition of sodium perchlorate. The second-order rate constant increases with the hydrogen-ion concentration. Similar results were obtained in the cases of *trans*-(*N*)-Co(ox)(β-ala)$_2^-$, Co(ox)$_3^{3-}$ (Table 1), *trans*(*N*)-Co(ox)(gly)(en) (Fig. 2),

Table 1. The effect of hydrogen ions on the Fe^{2+} reduction rate of $Co(ox)_3^{3-}$ and $Co(glyco)(en)_2^+$

Complex ion	[H$^+$] / M	Rate constant / m^{-1} s^{-1}
$Co(ox)_3^{3-}$ a)	0.10	1.3×10
	0.50	2.7×10
	1.00	4.1×10
$Co(glyco)(en)_2^+$ b)	0.10	5.3×10^{-6}
	0.50	5.2×10^{-6}
	1.00	5.3×10^{-6}

a) $NaClO_4$-$HClO_4$ medium, $\Sigma[ClO_4^-]=1.0$ M, 25 °C.
b) $NaClO_4$-$HClO_4$ medium, $\Sigma[ClO_4^-]=1.0$ M, 25 °C.

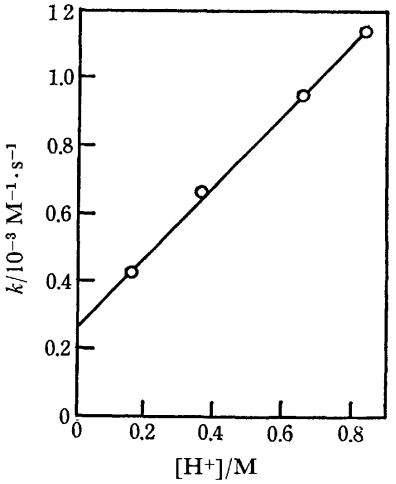

Fig. 2. The relation between the second-order rate constant of *trans*(*N*)-Co(ox)(gly)(en) and hydrogen ion concentration. $\Sigma[ClO_4^-]=2.5$ M, 39.8 °C, $NaClO_4$–$HClO_4$ medium.

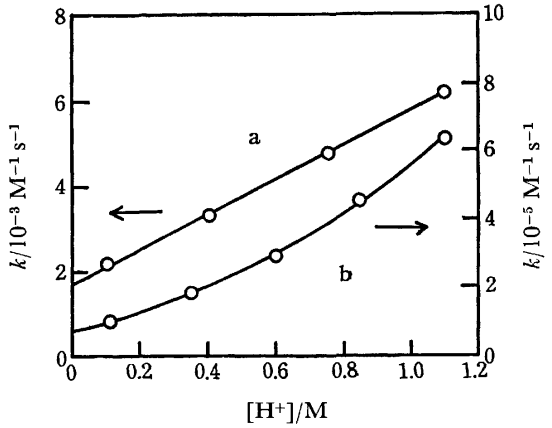

Fig. 3. The relation between the second-order rate constant of *trans* (O,Cl)–Co(Cl)(gly)(dien)$^+$ and *trans*-(O,Cl)–Co(Cl)(β-ala)(dien)$^+$ and hydrogen ion concentration.

trans(O,Cl)-Co(Cl)(gly)(dien)$^+$ (Fig. 3), *trans*(*N*)-Co(Cl)(β-ala)(dien)$^+$ (Fig. 3), and *trans*(O,Cl)-Co(Cl)-(α-ala)(dien)$^+$. In the cases of Co(ox)$(NH_3)_4^+$,[17] Co(ox)$(en)_2^+$, Co(glyco)$(en)_2^+$ (Table 1), and *cis*-Co(Cl)-(A)$(en)_2^{2+}$ (A=alkylamine),[6] however, no evidence of the hydrogen ion dependence was observed. The enhancement of the rate can be explained by the protonation of the carbonyl group of the carboxylate ion of the ligand which cannot be an electron mediator. Protonation would reduce the difficulty of stretching the ligand from the cobalt(III) center before the electron-transfer reaction takes place.

Independent evidence for the protonation of the carbonyl oxygen was obtained in the kinetic study of the acid-catalyzed oxygen exchange reaction between oxalato-cobalt(III) complexes with $H_2{}^{18}O$.[18] Further proof of the protonation of the nonbridging ligand was also indirectly obtained in the Fe^{2+} reduction of *trans*-Co$(N_3)_2(NH_3)_4^+$[19] and *trans*-Co$(N_3)_2(en)_2^+$.[4] For the Fe^{2+} reduction of *trans*-Co$(N_3)_2(NH_3)_4^+$, the kinetic study suggested the inner-sphere mechanism. Therefore, the acid-catalyzed reduction of *trans*(O,Cl)-Co(Cl)-(am)(dien)$^+$ may suggest that the reaction proceeds through the chloride-bridged activated state. As mentioned above, the reduction rates of Co(ox)$(NH_3)_4^+$, Co(ox)$(en)_2^+$, and Co(glyco)$(en)_2^+$ are independent of the hydrogen ion concentration. However, for *trans*-(*N*)-Co(ox)(gly)(en) in which one of the ethylenediamine molecules in the Co(ox)$(en)_2^+$ is replaced with a glycinate ion, an acid-catalyzed enhancement of the rate is observed (Fig. 2). For this complex, the inner-sphere mechanism may be proposed. The hydrogen ion may attack the oxygen atom of the carbonyl group of the glycinate ion of *trans*(*N*)-Co(ox)(gly)(en). The possible structure of the precursor complex for the Fe^{2+} reduction of Co(ox)$(NH_3)_4^+$ may be represented in Fig. 4. The rate of the Fe^{2+} reduction reaction which proceeds by the formation of the precursor complex shown in Fig. 4 should be much larger than that which proceeds by the formation of the iron(II) non-chelated precursor complex.

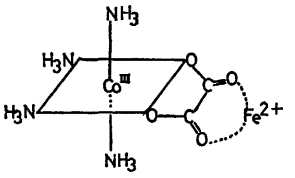

Fig. 4. The structure of the precursor complex for the Fe^{2+} reduction of Co(ox)$(NH_3)_4^+$.

The inner-sphere electron-transfer reaction between cobalt(III) complexes and Fe^{2+} should proceed *via* the following three steps:

$$RCo^{III}L + Fe^{II}(H_2O)_6 \rightleftharpoons RCo^{III}LFe^{II}(H_2O)_{6-n} + nH_2O \quad (1)$$

$$RCo^{III}LFe^{II}(H_2O)_{6-n} \rightleftharpoons RCo^{II}LFe^{III}(H_2O)_{6-n} \quad (2)$$

$$RCo^{II}LFe^{III}(H_2O)_{6-n} + mH_2O \rightleftharpoons RCo^{II}(H_2O)_m + LFe^{III}(H_2O)_{6-n} \text{ (or } RCo^{II}L + Fe^{III}(H_2O)_6) \quad (3)$$

where reactions (1), (2), and (3) indicate the formation of the precursor complex, electron-transfer, and the decomposition of the successor complex, respectively.

The reaction of *trans*-$Co(HCO_2)(en)_2^+$ [20] and *trans*-$Co(N_3)_2(en)_2^+$ [21] with V^{2+} is independent of the hydrogen ion concentration, whereas the reaction of *trans*-$Co(HCO_2)_2(en)_2^+$ with Cr^{2+} [22] involves an important term of first-order with respect to the hydrogen ion concentration. However, the V^{2+} and Cr^{2+} reductions of *cis*-$Co(HCO_2)_2(en)_2^+$ do not exhibit an acid-catalyzed effect. Such a different behavior of the hydrogen ion on the *trans*-$Co(HCO_2)_2(en)_2^+$ has been ascribed to the difference of the rate-determining steps.[22] For the Cr^{2+} reactions, the electron-transfer step is rate determining. This step requires a change in the inner-sphere and the electronic energy levels of the two metal centers. Protonation of the trans ligand on the oxidant appears to have the effect of facilitating such changes and lowering the energy of the acceptor orbital.[22] Therefore, the electron-transfer rate may be accelerated by the addition of a hydrogen ion. With V^{2+} as the reductant, the formation of the precursor complex appears to be rate-determining.[20,21]

The reactivity of the cobalt(III) complex with Fe^{2+}, in general, is strikingly affected by the ligand coordinated to the cobalt(III) center. In a strong acid medium, the successor complex, $Co^{II}LFe^{III}$ should much easily decompose because of the susceptibility of Co(II) and Fe(III) complexes to substitution and of the low stability of Co(II) complexes. The rates of the Fe^{2+} reduction of the oxalato- and chloro-cobalt(III) complexes are notably smaller than that of water exchange between $Fe(H_2O)_6^{2+}$ and $H_2{}^{18}O$.[23] Consequently, water molecule removal from the first-coordination sphere of $Fe(H_2O)_6^{2+}$ in forming a bridged activated state cannot be, in general, a rate-determining step. On the basis of the acid-catalyzed rate enhancement observed in the Fe^{2+} reductions of oxalato- and chlorocobalt(III) complexes, the present author is inclined to favor the electron-transfer step as the rate-determing one. With the rate-determing step being electron-transfer, reorganization of the first coordination sphere of the cobalt(III) complex would be needed before the electron-transfer reaction occurs. The previous investigation showed that the change in the reactivity of $Co(ox)(N_4)^+$ ($N_4=(NH_3)_4$, $(en)_2$, (trien), $(phen)_2$, $(bpy)_2$) with the iron(II) ion was mainly ascribed to the change in the enthalpy of activation.[3] This fact may mean that the rate-determining step is electron-transfer and that the reorganization of the first-coordination sphere of the Co(III) complex is a very important factor in the determination of the electron-transfer rate.

The acid dissociation constant for malonate ions (Hmalo), $Co(Hmalo)(NH_3)_5^{2+}$, which was determined in this work, is $K_a=6.3\times10^{-4}$ M at 25 °C and $I=1.0$. In the $[H^+]$ range from 0.02 M to 0.10 M, the predominant species is $Co(Hmalo)(NH_3)_5^{2+}$, and the concentration of $Co(malo)(NH_3)_5^+$ is very small. Assuming the large reactivity of $Co(malo)(NH_3)_5^+$, the results of the kinetic study on the Fe^{2+} reduction conform to the reaction path shown in reaction (4).

$$\begin{array}{ccc} Co(Hmalo)(NH_3)_5^{2+} & \overset{K_a}{\rightleftharpoons} & Co(malo)(NH_3)_5^+ + H^+ \\ {\scriptstyle Fe^{2+}}\downarrow{\scriptstyle k_{H^+}} & & {\scriptstyle Fe^{2+}}\downarrow{\scriptstyle k_0} \\ Co(II) + Fe(III) & & Co(II) + Fe(III) \end{array} \qquad (4)$$

Then, the observed rate constant k_{obsd} of the form $-d[Co(III)]/dt=k_{obsd}[Co(III)][Fe^{2+}]$ can be expressed as:

$$k_{obsd}=\frac{k_{H^+}[H^+]+k_0K_a}{[H^+]+K_a} \qquad (5)$$

where k_{H^+} and k_0 are the second-order rate constants for $Co(Hmalo)(NH_3)_5^{2+}$ and $Co(malo)(NH_3)_5^+$, respectively. Under the condition that $K_a \ll [H^+]$, k_{H^+} and k_0 can be obtained conveniently by plotting k_{obsd} *vs.* $1/[H^+]$ (Fig. 5). The rate constants obtained are listed along with those for $Co(Hox)(NH_3)_5^{2+}$ and $Co(ox)(NH_3)_5^+$ in Table 2. The reactivities of $Co(ox)(NH_3)_5^+$ and $Co(malo)(NH_3)_5^+$ are about 10^3 times larger than

Table 2. The second-order rate constant for the iron(II) reduction of $Co(L)(NH_3)_5^{n+}$ ($L=Hox^-$, ox^{2-} $Hmalo^-$, $malo^{2-}$) and the pK_a of $Co(Hox)(NH_3)_5^{2+}$ and $Co(Hmalo)(NH_3)_5^{2+}$

Complex ion	Rate constant $M^{-1}s^{-1}$	pK_a
$Co(Hox)(NH_3)_5^{2+}$	5×10^{-4} a)	2.06 a)
$Co(ox)(NH_3)_5^+$	4.3×10^{-1} a)	
$Co(Hmalo)(NH_3)_5^{2+}$	1.5×10^{-6} b)	3.2 b)
$Co(malo)(NH_3)_5^+$	1.3×10^{-3} b)	

a) From Ref. 24, $I=0.52$, 25 °C. b) Present work, $I=1.0$, 25 °C, in a $NaClO_4$-$HClO_4$ medium.

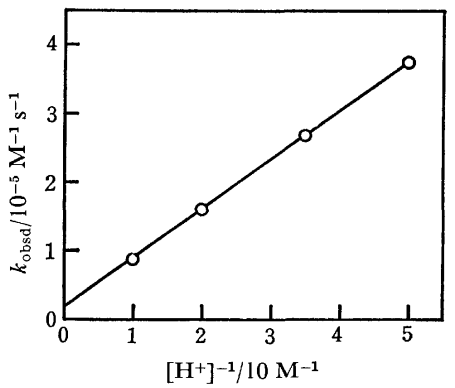

Fig. 5. The relation between the apparent second-order rate constant of $Co(Hmalo)(NH_5)_3^{2+}$ and hydrogen ion concentration. $\sum[ClO_4^-]=1.0$ M, 25 °C.

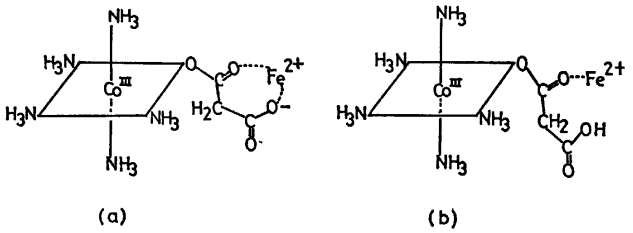

Fig. 6. The structure of the precursor complex for the Fe^{2+} reduction of $Co(Hmalo)(NH_3)_5^{2+}$ and $Co(malo)$-$(NH_3)_5^+$.

those of the corresponding protonated species (Table 2). The striking variation in the rate between the protonated species and the deprotonated species may be due mainly to the difference in the thermodynamic stability of the precursor complex, although an effect of the difference in charge on the cobalt(III) complex is not completely excluded. In the transition state for the Fe^{2+} reduction of $Co(malo)(NH_3)_5^+$, iron(II) is expected to chelate to a malonate ion(Fig. 6a). The reaction of $Co(Hmalo)(NH_3)_5^{2+}$ should proceed *via* the iron(II) non-chelated precursor complex (Fig. 6b). Moreover, the rate constants of $Co(Hox)(NH_3)_5^{2+}$ and $Co(ox)(NH_3)_5^+$ are larger by a factor of approximately 10^3 than that of the corresponding malonato-cobalt(III) complex. Possibly the difference in reactivity between the oxalato-cobalt(III) complex and the malonato-cobalt(III) complex may be related to the difference in the stabilities of the precursor complex and/or the efficiency of the bridging ligand as the electron mediator.

The author wishes to express his thanks to Professor K. Yamamoto for his helpful discussions.

References

1) T. J. Conochioli, G. Nancollas, and N. Sutin, *J. Am. Chem. Soc.*, **86**, 1453 (1964).
2) A. Haim and N. Sutin, *J. Am. Chem. Soc.*, **88**, 5343 (1966).
3) K. Ohashi, *Bull. Chem. Soc. Jpn.*, **45**, 3093 (1973).
4) K. Ohashi, K. Yamamoto, K. Yokouchi, and Y. Kurimura, *Nippon Kagaku Kaishi*, **1972**, 740.
5) Y. Kurimura, K. Ohashi, T. Ohtsuki, and K. Yamamoto, *Bull. Chem. Soc. Jpn.*, **44**, 1293 (1971).
6) K. Ohashi, *Bull. Chem. Soc. Jpn.*, **45**, 947 (1972).
7) K. Ohashi, K. Yamamoto, I. Hirako and Y. Kurimura, *Bull. Chem. Soc. Jpn.*, **45**, 1712 (1972).
8) K. Ohashi, *Bull. Chem. Soc. Jpn.*, **46**, 1880 (1973).
9) M. Matsuoka, J. Hidaka and Y. Shimura, *Bull. Chem. Soc. Jpn.*, **40**, 1868 (1967).
10) The gly, ala ox, glyco, malo, bpy, phen, dien, and trien abbreviations represent glycinate, alaninate, oxalate, glycolate, malonate ions, 2,2′-bipyridine, 1,10-phenanthroline, diethylenetriamine and triethylenetetraamine, respectively.
11) J. Hidaka and Y. Shimura, *Bull. Chem. Soc. Jpn.*, **40**, 2312 (1967).
12) S. P. L. Sorensen, *Z. Anorg. Chem.*, **11**, 2 (1896).
13) W. Schramm, *Z. Anorg Chem.*, **167**, 177 (1929).
14) D. K. Sebera and H. Taube, *J. Am. Chem. Soc.*, **83**, 1785 (1961).
15) M. D. Alexander and D. H. Busch, *Inorg. Chem.*, **5**. 1590 (1966).
16) K. Ohkawa, S, Yano, and J. Fujita, *Bull. Chem. Soc. Jpn.*, **41**, 2224 (1968).
17) C. Hwang, and A. Haim, *Inorg. Chem.*, **9**, 500 (1970).
18) J. A. Broomhead, *J. Chem. Soc.*, **1971**, 645.
19) A. Haim, *J. Am. Chem. Soc.*, **85**, 1016 (1963).
20) T. P. Przystas and A. Haim, *Inorg. Chem.*, **11**, 1016 (1972).
21) K. W. Hicks, D. L. Toppen, and R. G. Linck, *Inorg. Chem.*, **11**, 310 (1972).
22) J. A. Ward and A. Haim, *J. Am. Chem. Soc.*, **92**, 475 (1970).
23) T. E. Swift and R. E. Connick, *J. Chem. Phys.*, **37**, 302 (1962).
24) J. H. Espenson, *Inorg. Chem.*, **4**, 121 (1965).

Some Mixed-Ligand Iron(III) Complexes Produced by Reactions of Tris(acetylacetonato)iron(III) with Hydrogen Halides in Organic Solvents

Kenji TAKEDA*, Kiyoshi ISOBE, Yukio NAKAMURA, and Shinichi KAWAGUCHI

Department of Chemistry, Faculty of Science, Osaka City University, Sumiyoshi-ku, Osaka 558

(Received September 16, 1975)

Tris(acetylacetonato)iron(III) $Fe(acac)_3$ reacts with an equimolar and double molar amounts of a hydrogen halide in dichloromethane to afford the mixed-ligand iron(III) complexes, $FeX(acac)_2$ and $FeX_2(acac)H_2O$, respectively, where X is Cl or Br. They are all high-spin iron(III) complexes and exist as monomeric five-coordinate molecules in non-coordinating solvents, but behave as uni-univalent electrolytes in methanol. Further reactions of $FeX_2(acac)H_2O$ with an excess of hydrogen halides in dichloromethane followed by the addition of twice as many moles of 1,10-phenanthroline produced $[FeX_2(phen)_2]X$. The reactions of $FeX_2(acac)H_2O$ with excesses of pyridine and 2,2′-bipyridine in tetrahydrofuran gave the six-coordinate complexes $FeX_2(acac)(py)_2$ and $FeX_2(acac)(bipy)$, respectively.

In the present series of studies on the reactions of metal acetylacetonates with bromine and hydrogen bromide in organic solvents, different kinds of products have previously been isolated and characterized.[1] For instance, dibromo(acetylacetone)cobalt(II) $CoBr_2$-(acacH), a novel complex containing an acetylacetone molecule as the bidentate ligand, was produced by the reaction of $Co(acac)_3$ with bromine in dichloromethane. However, an attempt to isolate the intermediary cobalt(III) complex, assumed to be a precursor of the cobalt(II) complex, was unsuccessful.[2] On the other hand, $Mn(acac)_3$ is reduced by hydrogen halides in organic solvents, ultimately resulting in manganese(II) chloride, bromide, or $Mn(acac)_2$, and the intermediary Mn(III) products, $MnX(acac)_2$, where X is Cl, Br, or I, could be isolated from the equimolar reactions.[3]

Collman[4] demonstrated that halogen substitution at the central carbon atom of metal acetylacetonate can be successfully carried out under electrophilic substitution reaction conditions. Thus, $Fe(acac)_3$ was directly brominated with *N*-bromosuccinimide in chloroform[5] or with bromine in buffered acetic acid.[6] On the contrary, one acetylacetonate ring of the acid labile tris-chelate was displaced in the reaction with picric acid in benzene–ethanol, affording the cationic iron(III) complex, $[Fe(acac)_2(H_2O)_2]$picrate.[7] The present paper reports some mixed-ligand iron(III) complexes which were isolated and characterized as intermediary products in the reactions between $Fe(acac)_3$ and hydrogen halides in organic solvents.[8]

Experimental

Materials. Tris(acetylacetonato)iron(III) was prepared and recrystallized according to Ref. 9. Found: Fe, 15.85; C, 51.12; H, 6.12%. Hydrogen chloride was generated by the reaction of hydrochloric acid with sulfuric acid, dried over calcium chloride, and dissolved in dichloromethane (*ca.* 0.2 mol/l). Hydrogen bromide was produced by the reaction between tetralin and bromine, dried over calcium bromide, and dissolved in dichloromethane (*ca.* 0.2 mol/l). Dichloromethane and acetonitrile were distilled twice over phosphorus pentaoxide. Benzene was distilled over metallic sodium. Nitromethane and methanol were also distilled.

The Reactions of Tris(acetylacetonato)iron(III) with Hydrogen Halides. A solution of $Fe(acac)_3$ in dichloromethane was placed in a three-necked flask equipped with a buret, a glass tube containing calcium chloride, and another outlet tube. A solution (*ca.* 0.1 mol/l) of hydrogen chloride or bromide in dichloromethane was added dropwise from the buret to the above solution with magnetic stirring. The usual precautions were taken for preventing moisture during filtration of the reaction product.

Isolation of Chlorobis(acetylacetonato)iron(III): To a solution of $Fe(acac)_3$ in dichloromethane was added a solution of an equimolar amount of hydrogen chloride in dichloromethane from the buret. After the reaction, a dark red precipitate was separated out by the addition of petroleum ether. The precipitate was filtered, washed with petroleum ether and dried *in vacuo*. Found: Fe, 19.88; Cl, 12.40; C, 41.43; H, 4.88%. Calcd for $FeCl(acac)_2=C_{10}H_{14}O_4ClFe$: Fe, 19.29; Cl, 12.25; C, 41.15; H, 4.87%.

Isolation of Bromobis(acetylacetonato)iron(III): A dichloromethane solution of $Fe(acac)_3$ was allowed to react with an equimolar amount of hydrogen bromide in dichloromethane. The initially red-brown solution turned to dark red. The solution was concentrated to a quarter of its original volume, whereupon a red-brown precipitate separated out. The precipitate was filtered, washed with petroleum ether and dried *in vacuo*. Found: Fe, 17.08; Br, 24.37; C, 35.67; H, 4.23%. Calcd for $FeBr(acac)_2=C_{10}H_{14}O_4BrFe$: Fe, 16.72; Br, 23.93; C, 35.96; H, 4.23%.

Isolations of Dichloro(acetylacetonato)aquairon(III) and Dibromo-(acetylacetonato)aquairon(III): When a red-brown solution of $Fe(acac)_3$ in dichloromethane was forced to react with twice as many moles of hydrogen chloride or bromide in dichloromethane, its color turned to dark red. Petroleum ether was added slowly to the reaction mixture producing a dark red precipitate. This was filtered, washed with petroleum ether and dried *in vacuo*. Found for the chloro complex: Fe, 23.09; Cl, 28.86; C, 24.73; H, 3.77%. Calcd for $FeCl_2(acac)H_2O=C_5H_9O_3Cl_2Fe$: Fe, 22.90; Cl, 29.07; C, 24.62; H, 3.72%. Found for the bromo complex: Fe, 16.90; Br, 47.86; C, 18.19; H, 2.80%. Calcd for $FeBr_2$-$(acac)H_2O=C_5H_9O_3Br_2Fe$: Fe, 16.78; Br, 48.02; C, 18.05; H, 2.73%. The same compounds were also produced from the equimolar reactions between $FeX(acac)_2$ and HX (X=Cl or Br) in dichloromethane in a manner similar to that described above.

Further Reactions of $FeCl_2(acac)H_2O$ and $FeBr_2(acac)H_2O$ with Excess Hydrogen Chloride and Bromide. Isolation of FeX_3 as $[FeX_2(phen)_2]X$, where X is Cl or Br: To a suspension of $FeX_2(acac)H_2O$ (X=Cl or Br) in dichloromethane was added an excess of hydrogen chloride or bromide dissolved in the same solvent, whereupon a transparent solution was

* Present address: Toyama Chemical Co., Ltd., Shimookui, Toyama.

produced. Twice as many moles of 1,10-phenanthroline as that of the iron(III) complex used were dissolved in a minimum quantity of dichloromethane and added to the above clean solutions to separate out the precipitates, which were yellow-brown (chloride) and red-brown (bromide), respectively. The precipitates were recrystallized from ethanol and dried *in vacuo*. Found for chloride: C, 51.13; H, 3.08; N, 9.94%. Calcd for $[FeCl_2(phen)_2]Cl=C_{24}H_{16}N_4Cl_3Fe$: C, 51.60; H, 2.89; N, 10.03%. Found for bromide: C, 44.08; H, 3.04; N, 8.21%. Calcd for $[FeBr_2(phen)_2]Br=C_{24}H_{16}N_4Br_3Fe$: C, 43.94; 2.46; N, 8.54%.

Preparation of $FeX_2(acac)(py)_2$ and $FeX_2(acac)(bipy)$, where X is Cl or Br. To tetrahydrofuran solutions of $FeX_2(acac)H_2O$ (X=Cl or Br) was added an excess of pyridine or 2,2′-bipyridine in tetrahydrofuran. The solution was stirred magnetically for about 1 hour, whereupon a precipitate gradually separated out. Found for the dichlorobispyridine complex: Fe, 14.43; Cl, 18.45; C, 46.89; H, 4.52; N. 7.09%. Calcd for $FeCl_2(acac)(py)_2=C_{15}H_{17}O_2N_2Cl_2Fe$: Fe, 14.54; Cl, 18.46; C, 46.91; H, 4.46; N, 7.29%. Found for the dibromobispyridine complex: Fe, 11.29; Br, 33.51; C, 39.07; H, 3.79; N, 5.91%. Calcd for $FeBr_2(acac)(py)_2=C_{15}H_{17}O_2N_2Br_2Fe$: Fe, 11.81; Br, 33.79; C, 38.10; H, 3.62; N, 5.92%. Found for the dichloro(2,2′-bipyridine) complex: Fe, 14.44; Cl, 18.46; C, 47.09; H, 4.25; N, 7.39%. Calcd for $FeCl_2(acac)(bipy)=C_{15}H_{15}O_2N_2Cl_2Fe$: Fe, 14.62; Cl, 18.56; C, 47.16; H, 3.96; N, 7.33%. Found for the dibromo-(2,2′-bipyridine) complex: Fe, 12.09; Br, 34.06; C, 38.42; H, 3.28; N, 6.03%. Calcd for $FeBr_2(acac)(bipy)=C_{15}H_{15}O_2N_2Br_2Fe$: Fe, 11.86; Br, 33.93; C, 38.26; H, 3.21; N, 5.95%.

Analysis. Each compound was subjected to elemental analysis after drying *in vacuo* at room temperature. Iron was determined gravimetrically as iron(III) oxide, and chlorine and bromine as the silver salts. The concentrations of hydrogen chloride and bromide in dichloromethane were measured by the method reported previously.[1]

Measurements. The visible and ultraviolet absorption spectra were measured by means of a Hitachi EPS-3T autorecording spectrophotometer. The infrared spectra were taken in Nujol with JASCO IR-E (4000—700 cm^{-1}), Hitachi EPI-L (700—200 cm^{-1}) and FIS-3 (400—30 cm^{-1}) infrared spectrophotometers.

The magnetic susceptibility was measured at room temperature or at various temperatures down to 80 K by the Faraday method with an automatically recording magnetic balance MB-2 of the Shimadzu Seisakusho Co., Ltd. Mercury(II) tetraisothiocyanatocobaltate(II) (room temperature) and hexaammine chromium(III) chloride (lower temperature) were used as reference compounds.

The molecular weight was determined by vapor-pressure osmometry with an apparatus manufactured by the Knauer Co. of Germany. Benzene, nitromethane, acetonitrile and methanol were used as solvents, and benzil as a reference. The electric conductivity was measured in nitromethane or methanol by means of an MY-7 apparatus of the Yanagimoto Seisakusho, Ltd.

Results

Tris(acetylacetonato)iron(III) reacts in a stepwise manner with an equimolar amount or twice as many moles of hydrogen chloride or bromide to produce halogenobis(acetylacetonato)iron(III) or dihalogeno-(acetylacetonato)aquairon(III), respectively.

Halogenobis(acetylacetonato)iron(III) Complexes. Chloro- and bromo-bis(acetylacetonato)iron(III) complexes were isolated from the equimolar reaction mixtures of $Fe(acac)_3$ and HX, where X is Cl or Br, by the addition of petroleum ether or the evaporation of the solution, respectively, and the composition of $FeX(acac)_2$ was confirmed by elemental analysis. As shown in Table 1, the compounds have magnetic moments typical of high-spin d^5 systems.

The molecular weights determined in benzene are close to the calculated values, indicating that each of the chloro and bromo complexes exists essentially as a discrete molecule in the non-coordinating solvent. The molar conductances in nitromethane at room temperature also indicate that the complexes are essentially non-electrolytes in this solvent.

In methanol, the complexes dissociate almost completely and the observed molecular weights are near to half of the formula weight. The molar conductances (λ_M) in the same solvent reveal that the complexes behave practically as uni-univalent electrolytes, although the values are smaller in comparison with 9.10 Ω^{-1} cm^2mol^{-1} of tetraethylammonium iodide in methanol. It may be presumed that the complexes are solvolyzed in methanol, affording a six-coordinate iron(III) cation and a halide ion:

$$FeX(acac)_2 + 2CH_3OH \rightarrow Fe(acac)_2(CH_3OH)_2^+ + X^-$$

Although the assumed compounds $[Fe(acac)_2(CH_3OH)_2]X$ could not be isolated, similar cationic complexes $[Fe(acac)_2(H_2O)_2]$picrate and $[Fe(acac)_2(TOPO)_2]ClO_4$ (TOPO=trioctylphosphine oxide) have been prepared by Aly[7] and Aggett.[10] The former is weakly dissociated in dichloromethane and the Λ_M value (31.3 $\Omega^{-1}cm^2mol^{-1}$) in the solvent is appreciably smaller

Table 1. Molecular weight, conductance and magnetic moment data of $FeX(acac)_2$ and $FeX_2(acac)H_2O$ (X=Cl or Br)[a]

Complex	Molecular weight in C_6H_6	Molecular weight in CH_3NO_2	Molecular weight in CH_3OH	Calcd	Molar conductance/ $\Omega^{-1}cm^2mol^{-1}$ in CH_3NO_2	Molar conductance/ $\Omega^{-1}cm^2mol^{-1}$ in CH_3OH	Magnetic moment at 27°C/B.M.
$FeCl(acac)_2$	304		140	290	17.6	61.1	6.11
$FeBr(acac)_2$	324		181	334	20.9	70.8	5.94
$FeCl_2(acac)H_2O$		224	95	244	35.6	65.1	5.76
$FeBr_2(acac)H_2O$		338	139	333	28.6	77.0	5.88

a) The molecular weight was measured at (1.0—5.0)$\times 10^{-2}$ M, and the molar conductance at 1.0×10^{-2} M, both at room temperature.

than that observed for $FeX(acac)_2$ in methanol.

Puri and Mehrotra,[11] and Cox and his coworkers[12] prepared $FeCl(acac)_2$, either by refluxing the appropriate quantities of anhydrous iron(III) chloride and acetylacetone in benzene or by the reaction of stoichiometric amounts of anhydrous $FeCl_3$ and $Fe(acac)_3$ in chloroform. The complex has been shown [13] to possess a slightly distorted square-pyramidal structure, with the iron atom situated 0.51 Å above the basal plane.

Infrared Spectra: In a previous paper,[3] the present authors have discussed the infrared spectra of $FeX(acac)_2$ in comparison with those of $MnX(acac)_2$ in the 1600—700 cm^{-1} region, and therefore, only the far-infrared spectra are discussed here. There are one or two intense bands in the 400—250 cm^{-1} region as shown in Fig. 1. The band at 298 cm^{-1} in the parent complex, $Fe(acac)_3$, is isotopically assigned to the pure ν(Fe–O) vibration.[14] Thus, the peak around 310—300 cm^{-1} is readily attributed to the corresponding vibration in the two $FeX(acac)_2$ complexes.

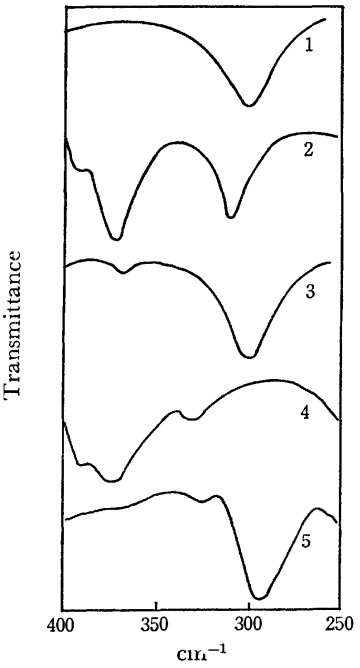

Fig. 1. Infrared spectra in the low-frequency region of $Fe(acac)_3$ (curve 1), $FeX(acac)_2$, where X=Cl (curve 2) or Br (curve 3), and $FeX_2(acac)H_2O$, where X=Cl (curve 4) or Br (curve 5).

The stretching band of the terminal Fe(III)–Cl bond of the five-coordinate iron(III) complexes is usually observed in the 300—400 cm^{-1} region and the exact position is affected by the coexisting ligands: 309 cm^{-1} for $FeCl(S_2CNEt_2)_2$[15], 355 and 375 cm^{-1} for $FeCl_3$-(1,2-dimethoxyethane)[16], 380 cm^{-1} for $FeCl_3$(1,4-dioxane)[17] and 378 cm^{-1} for four-coordinate iron(III) ion $FeCl_4^-$.[18] Thus, the strong band observed at 373 cm^{-1} for $FeCl(acac)_2$ can be reasonably assigned to the ν_t(Fe–Cl) vibration. For the same metal, the ratio ν(M–Br)/ν(M–Cl) is usually 0.77—0.74,[19] and hence the corresponding ν_t(Fe–Br) absorption in the FeBr-(acac)$_2$ complex appears to be incorporated in the ν(Fe–O) band at 300 cm^{-1}.

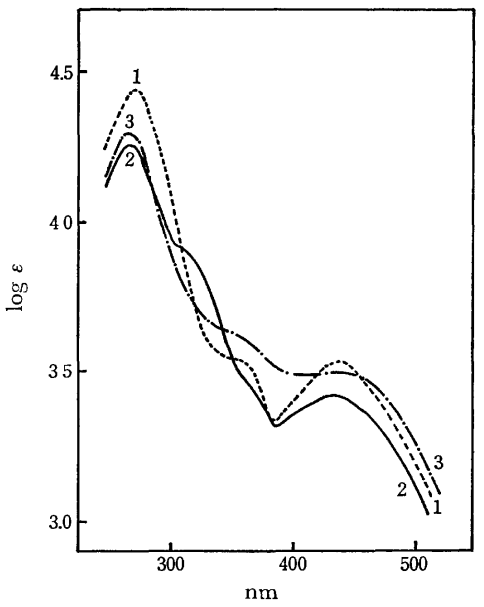

Fig. 2. Absorption spectra of $Fe(acac)_3$ (curve 1) and $FeX(acac)_2$ in CH_2Cl_2, where X=Cl (curve 2) or Br (curve 3).

Electronic Spectra: The electronic spectra of the present $FeX(acac)_2$ complexes in dichloromethane are shown in Fig. 2 together with the curve for the parent complex, $Fe(acac)_3$. The spectrum of $Fe(acac)_3$ has three absorption bands in the 200—600 nm region, and the most intense band at 270 nm is assigned to the intra-ligand π-π^* transition. The other two bands in this region are assigned to a metal-to-ligand($t_{2g}\rightarrow\pi^*$) charge transfer (CT) at 353 nm and a ligand-to-metal ($\pi\rightarrow e_g$) charge transfer (CT) at 436 nm.[20] On the other hand, $FeCl(acac)_2$ exhibits a shoulder on the longer wavelength side (*ca.* 310 nm) of the π-π^* transition band in addition to the original three bands. The new band can be feasibly assigned to a chlorine-to-metal CT transition. For the spectra of $[FeCl_2(bipy)_2][FeCl_4]$

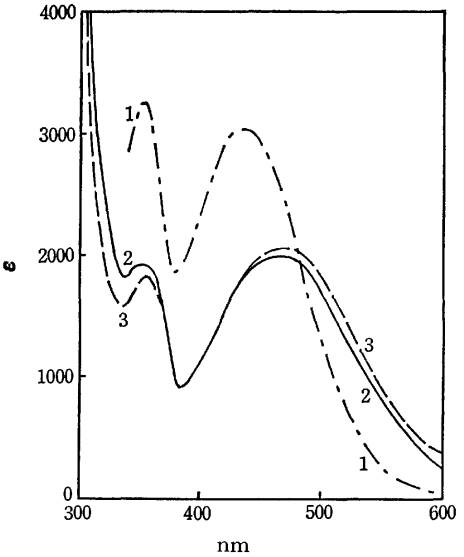

Fig. 3. Absorption spectra of $Fe(acac)_3$ (curve 1) and $FeX(acac)_2$ in methanol, where X=Cl (curve 2) or Br (curve 3).

in dichloromethane, a band at 365 nm is attributed to the same transition.[21] The corresponding bromine-to-metal CT band is not easy to assign in the spectrum of the bromo complex, $FeBr(acac)_2$, but an unusual increase in the absorption intensity is observed around 400 nm, as shown in Fig. 2. This may suggest that the band is obscured by the broad absorption at 435 nm.

The spectra of $FeCl(acac)_2$ and $FeBr(acac)_2$ in methanol are shown in Fig. 3. The measurements were made with 2×10^{-2} M solutions, of which the concentration was almost the same as those used in the molecular weight and molar conductance measurements, by the use of a cell with a 0.1 mm light path. The spectra of both the complexes show a pattern similar to that of the parent complex $Fe(acac)_3$ in methanol, and no absorption due to the halogen-to-metal CT transition was observed. This fact supports the assumed dissociation of a halide ion in methanol.

Dihalogeno(acetylacetonato)aquairon(III) Complexes. The complexes $FeX_2(acac)H_2O$ (X=Cl or Br) were produced by the reaction of $Fe(acac)_3$ with twice as many moles of HX or by the reaction of $FeX(acac)_2$ with an equimolar amount of HX in dichloromethane. The complexes are only slightly soluble in benzene, and hence the molecular weights were measured in nitromethane or in methanol. As shown in Table 1, the values determined in nitromethane are near to the formula weights, suggesting that each of the $FeX_2(acac)H_2O$ complexes also exists in the solvent essentially as a five-coordinate, monomeric complex. The Λ_M values obtained in the same solvent at room temperature also indicate that the complexes are practically non-electrolytes in this solvent, but the slightly large value for $FeCl_2(acac)H_2O$ may suggest some dissociation of a chloride ion.

In methanol, the molecular weights are one-half to one-third of the calculated values, while the Λ_M values imply that the complexes behave substantially as uni-univalent electrolytes in the same solvent. These results suggest that the $FeX_2(acac)H_2O$ complexes liberate only one of their two X^- ligands, and the resulting cations $FeX(acac)(H_2O)(CH_3OH)_2^+$ are partially solvolyzed to replace the aqua ligand with a solvent molecule:

$$FeX_2(acac)H_2O + 2CH_3OH \rightarrow FeX(acac)(H_2O)(CH_3OH)_2^+ + X^-$$

$$-CH_3OH \left\| \right. + CH_3OH$$

$$FeX(acac)(CH_3OH)_3^+ + H_2O$$

The electronic spectra of the complexes in methanol also support this assumption. As shown in Fig. 4, a band due to the halogen-to-metal CT transition reappears at 330 nm in the spectrum of $FeCl_2(acac)H_2O$ and at 410 nm in that of the dibromo analog. Thus, it can be concluded that one halide ligand is still coordinated to the metal in the complex cation produced by the dissociation in methanol.

The magnetic susceptibilities were measured over the temperature range from 300—80 K. As shown in Table 1, the room-temperature moments are close to or slightly less than the 5.92 B.M. predicted by the spin-only formula and these values are independent of temperatures down to 77 K. The plots of χ_A^{-1} against T (Fig. 5) gave straight lines in accordance with the Curie-Weiss law $\chi_A=c/(T+\theta)$. The θ values were obtained from an extrapolation of the straight line and found to be 4 and 8 K for the dichloro and dibromo complexes, respectively. These facts show that each of the $FeX_2(acac)H_2O$ complexes exists as a magnetically dilute molecule in the solid state and that the complexes have no antiferromagnetic interactions with each other.

The infrared spectra of the dihalogeno complexes $FeX_2(acac)H_2O$ in the 4000—700 cm^{-1} region resemble those of the mono-halogeno complexes, except for additional absorption bands due to the coordination of an aqua ligand. As shown in Fig. 1, the strong band at 375 or 294 cm^{-1} in each spectrum of the dihalogeno

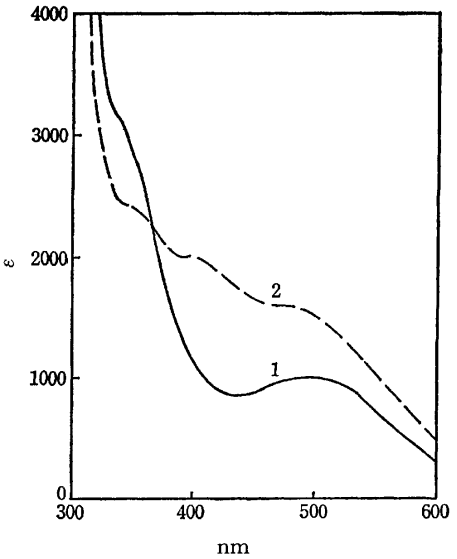

Fig. 4. Absorption spectra of $FeX_2(acac)H_2O$ in methanol, where X=Cl (curve 1) or Br (curve 2).

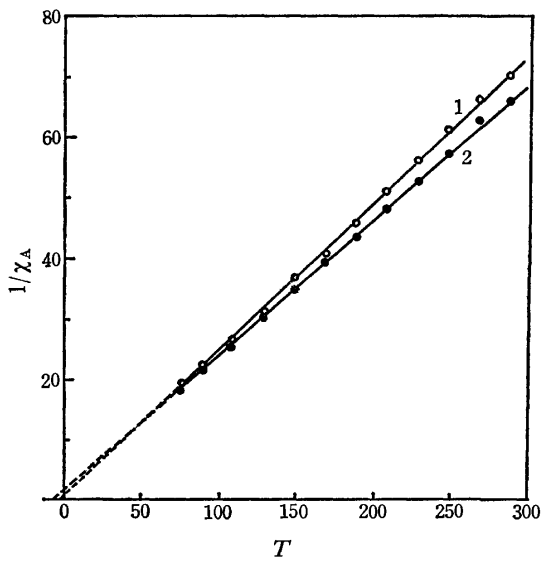

Fig. 5. Curie-Weiss plots for $FeCl_2(acac)H_2O$ (1) and $FeBr_2(acac)H_2O$ (2).

TABLE 2. MOLECULAR WEIGHT, CONDUCTANCE AND MAGNETIC MOMENT DATA OF $FeX_2(acac)(py)_2$ AND $FeX_2(acac)(bipy)$ (X=Cl or Br)[a]

Complex	Molecular weight				Molar conductance/ $\Omega^{-1}\,cm^2\,mol^{-1}$		Magnetic moment at 27 °C/B.M.
	in CH_3CN	in CH_3NO_2	in CH_3OH	Calcd	in CH_3NO_2	in CH_3OH	
$FeCl_2(acac)(py)_2$	330	178	130	384	28.7	105.6	5.96
$FeBr_2(acac)(py)_2$	385	259	158	473	38.9	150.6	5.82
$FeCl_2(acac)(bipy)$		193	136	382	7.1	66.6	5.85
$FeBr_2(acac)(bipy)$		272	156	471	22.1	84.8	5.77

a) The molecular weight was measured at $(1.0—5.0)\times10^{-2}$ M, and the molar conductance at 1.0×10^{-2} M, with both at room temperature.

complexes can be readily assigned to the stretching vibration of the terminal Fe(III)–X bond in comparison with the corresponding band of the monohalogeno complexes. In contrast to the Fe(III)–X stretching band, it is not easy to specify the band due to the Fe(III)–O(acac) stretching vibration because of its weak intensity. The weak band at 330 cm^{-1} for the dichloro complex and that at 326 cm^{-1} for the dibromo analog were tentatively assigned to the ν(Fe–O(acac)) vibration.

Puri and Mehrotra have also prepared $FeCl_2(acac)$ by the equimolar reaction of anhydrous iron(III) chloride and acetylacetone in benzene, but the compound does not contain an aqua ligand. Unfortunately, its properties and structure have not been reported.[11]

The Six-coordinate Mixed Ligand Fe(III) Complexes. Further reactions of the $FeX_2(acac)H_2O$ complexes with excess hydrogen halides followed by an addition of twice as many moles of phen as that of the complex used gave the precipitate composed of $FeX_3(phen)_2$. A compound of the same composition, $FeCl_3(phen)_2$ was prepared as an acetic acid adduct by Harris and Lockyer[22] and was formulated as a cationic iron(III) complex, $[FeCl_2(phen)_2]Cl\cdot2CH_3CO_2H$. Other similar compounds, $[FeCl_2(phen)_2]X\cdot nCH_3CO_2H$ (X=ClO_4, n=1; X=$FeCl_4$, n=0.5), containing the same cation were also prepared.

The five-coordinate complexes $FeX(acac)_2$ and $FeX_2(acac)H_2O$ have a vacant site to allow for the coordination of another monodentate base B. The former reacted with B to cause a disproportionation reaction, affording exclusively the dihalogeno complexes $FeX_2(acac)B_2$. Thus, the isolation of the six-coordinate complexes of the type $FeX(acac)_2B$ was not successful, whereas the neutral six-coordinate complexes $FeX_2(acac)(py)_2$ and $FeX_2(acac)(bipy)$ (X=Cl or Br) were isolated from the reaction of $FeX_2(acac)H_2O$ with excess pyridine or 2,2′-bipyridine, respectively, in tetrahydrofuran. Molecular weight, conductance and magnetic moment data of these mixed-ligand complexes are shown in Table 2. The magnetic moments at 27 °C lie in the range of 5.77—5.96 B.M., indicating that they are all high-spin Fe(III) complexes.

The molecular weights of the pyridine complexes in acetonitrile are slightly less than the formula weights, while they are close to half of the calculated values in nitromethane. The Λ_M values in nitromethane are not as large as expected for electrolytes. These results might indicate that the $FeX_2(acac)(py)_2$ complexes dissociate a pyridine molecule in this solvent. On the other hand, in methanol the molecular weights of both the pyridine complexes are about one-third of the formula weights, while the Λ_M values of the dichloro and dibromo complexes are comparable to or appreciably larger than that of a uni-univalent electrolyte, respectively. Hence, it may be presumed that both the complexes are solvolyzed in methanol in the following manner:

$$FeCl_2(acac)(py)_2 + 2CH_3OH \rightarrow FeCl(acac)(py)(CH_3OH)_2^+ + Cl^- + py$$

$$FeBr_2(acac)(py)_2 + 2CH_3OH \rightarrow Fe(acac)(py)_2(CH_3OH)_2^{2+} + 2Br^-$$

The affinity of iron(III) for the halide ions is in the order of F>Cl>Br>I. Such a trend might be reflected in the dissociation pattern of the second halide ion.

The electronic spectra of the $FeX_2(acac)(py)_2$ complexes in methanol are shown in Fig. 6. The absorption bands present at *ca.* 350 and *ca.* 450 nm are due to the metal-to-ligand(acac) and the ligand(acac)-to-metal CT transitions, respectively. As can be seen from the figure, in the spectrum of the dichloro complex a chlorine-to-metal CT band appears at *ca.* 330 nm as a

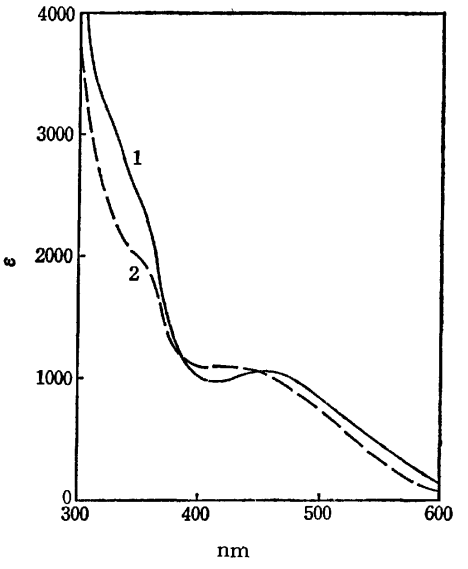

Fig. 6. Absorption spectra of $FeX_2(acac)(py)_2$ in methanol, where X=Cl (curve 1) and Br (curve 2).

discernible shoulder, while a corresponding bromine-to-metal CT band which is expected to appear around 410 nm is not observed for the bromo analog. This seems to reflect the dissociation patterns in methanol described above.

The behaviors of the 2,2′-bipyridine complexes $FeX_2(acac)(bipy)$ in nitromethane and methanol are very similar to those of the $FeCl_2(acac)(py)_2$ complex in the same solvents. Therefore, it can be concluded that they dissolve in nitromethane to dissociate a 2,2′-bipyridine molecule, but are solvolyzed in methanol to give a cation $FeX(acac)(CH_3OH)_3^+$ and a halide ion in addition to a 2,2′-bipyridine molecule:

$$FeX_2(acac)(bipy) + 3CH_3OH \rightarrow FeX(acac)(CH_3OH)_3^+ + X^- + bipy$$

As shown in Fig. 7, the electronic spectra of the $FeX_2(acac)(bipy)$ complexes in methanol show a band due to the halogen-to-metal CT transition at 340 nm for the dichloro complex and at 400 nm for the dibromo analog, respectively, in addition to the two CT metal-to-ligand(acac) and ligand(acac)-to-metal bands. Thus the spectral data are again in accord with the suggested dissociation pattern in methanol.

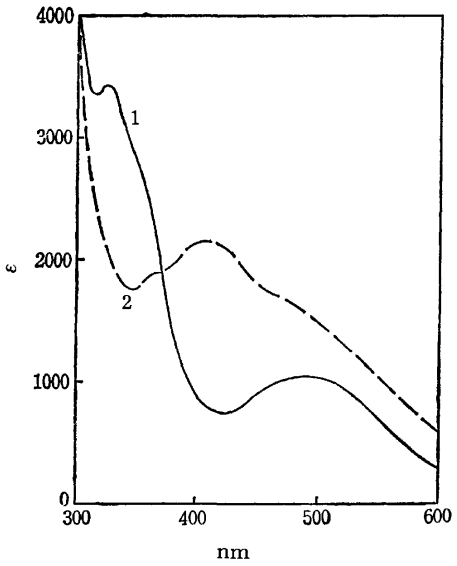

Fig. 7. Absorption spectra of $FeX_2(acac)(bipy)$ in methanol, where X=Cl (curve 1) and Br (curve 2).

Discussion

Despite the biological importance of iron-containing systems, there is a comparative lack of interest in the coordination chemistry of iron, especially in the case of tervalent iron. This can largely be attributed to the properties of the d^5 ion.[23] The present work extends the studies[1-3] of the reactions of metal acetylacetonates with bromine and hydrogen halides in organic solvents to include the iron(III) complex. In some metal acetylacetonates previously studied, the oxidation state of the metal was finally reduced in the reactions with these reagents, but in the present case no reduction to an iron(II) complex occurred throughout the reactions of Fe(acac)$_3$ with HX (X=Cl or Br) in dichloromethane. The detailed mechanism of these reactions could not be established in this investigation, but the reaction steps leading to the dihalogeno complex seem to proceed in the following sequence:

$$Fe(acac)_3 \xrightarrow{+HX} \left[(acac)_2Fe\begin{matrix}X\\ \diagdown\\ acacH\end{matrix}\right] \xrightarrow{-acacH} \begin{matrix}X\\ |\\ (acac)Fe(acac)\end{matrix}$$

Intermediate **1**

$$\begin{matrix}X\\ |\\ (acac)Fe(acac)\end{matrix} \xrightarrow{+HX} \left[\begin{matrix}X\\ |\\ (acac)Fe\\ \diagdown\\ acacH\end{matrix}\begin{matrix}\\ \\ \diagup\\ X\end{matrix}\right]$$

Intermediate **2**

$$\xrightarrow[+H_2O]{-acacH} FeX_2(acac)H_2O$$

Intermediates **1** and **2** have not been identified, but the latter has a composition similar to the chromium (III) complex $CrBr_2(acac)(acacH)$, which has previously been isolated from the reaction of Cr(acac)$_3$ with HBr in dichloromethane containing excess acetylacetone.[24] However, any attempts to isolate intermediate **2** in the present reactions were unsuccessful. This intermediate may be essentially labile, and change irreversibly to the insoluble complex, $FeX_2(acac)H_2O$, upon the addition of petroleum ether to the reaction mixture of Fe(acac)$_3$ and twice as many moles of hydrogen halides in dichloromethane.

In a preceding paper,[3] the present authors have reported that Mn(acac)$_3$ reacted with excess HX to liberate some Mn(II) products, but no reduction occurred in the present case. Such a difference in reactivity could be due to a difference in the reduction potentials of Mn(III) (E=1.51 V) and Fe(III) (E=0.77 V). It was assumed that FeX_3 was produced in the reaction mixture of $FeX_2(acac)H_2O$ with excess HX in dichloromethane:

$$FeX_2(acac)H_2O \xrightarrow[+(n-1)H_2O]{+HX} FeX_3\cdot nH_2O + acacH$$

The existence of FeX_3 in solution has not been confirmed directly, but $[FeX_2(phen)_2]X$ was precipitated from the solution upon the addition of 1,10-phenanthroline:

$$FeX_3\cdot nH_2O + 2phen \rightarrow [FeX_2(phen)_2]X + nH_2O$$

Although the base adducts $FeX_2(acac)B_2$ were readily obtained from $FeX_2(acac)H_2O$, $FeX(acac)_2$ was disproportionated by the reaction with the base B to deposit the dihalogeno complex $FeX_2(acac)B_2$ exclusively:

$$2FeX(acac)_2 + 2B \rightarrow FeX_2(acac)B_2 + Fe(acac)_3$$

Contrary to the Fe(III) complexes, it was noted previously[3] that $MnX(acac)_2B$ (B=dioxane, 4-methylpyridine or pyridine oxide) are stable enough to be isolated in reactions of $MnX(acac)_2$ with B, while $MnCl_2(acac)(O\text{-}py)_2$ is unstable at room temperature and was obtained only at −78 °C.

All the complexes prepared in this work, with the exception of $FeCl_2(acac)H_2O$ and $FeBr_2(acac)(bipy)$, have magnetic moments of 5.82—6.11 B.M. at 27 °C, which are close to the calculated spin-only value of

5.92 B.M. The room-temperature magnetic moments (5.76 and 5.77 B.M.) of the complexes $FeCl_2(acac)H_2O$ and $FeBr_2(acac)(bipy)$ are slightly less than 5.92 B.M. Apparently the former complex retains the possibility of polymeric structure in the solid state, which induces the magnetic interaction between neighboring iron atoms. In practice, however, it obeys the Curie-Weiss law between room temperature and 80 K, and the θ value of 4 K is not so large as to indicate an antiferromagnetic interaction.

Frazer, Qureshi and Taylor[25] studied the reactions of 8-quinolinol or its iron(III) complex with iron(III) halides in organic solvents, and prepared $FeX(oxin)_2$ and $FeX_2(oxin)$(oxin=8-quinolinolate ion and X=Cl or Br). These compounds were concluded to have a polymeric structure in the light of their insolubility and magnetic data. Only a small number of examples of high-spin iron(III) complexes which exist as five-coordinate monomers in solid state have been discovered up to now. They include adducts of $FeCl_3$ with 1,2-dimethoxyethane[16] and 1,4-dioxane,[17] *N*-substituted salicylideneamine complexes, $FeX(sal=NR)_2$ (X=Cl or Br),[26] *N*,*N*′-bis(salicylidene)ethylenediamine complexes, FeX(salen)monomer (X=Cl, Br, Ph or CH_2Ph)[27] and other Schiff-base iron(III) complexes[28] and some iron(III) porphyrins.[29] Both the present complexes, $FeX(acac)_2$ and $FeX_2(acac)$-H_2O, are new examples of this group.

The authors are grateful to Mr. J. Gohda for the elemental analysis. The financial aid of the Ministry of Education is also acknowledged.

References

1) K. Isobe, K. Noda, Y. Nakamura, and S. Kawaguchi, *Bull. Chem. Soc. Jpn.*, **46**, 1699 (1973), and references cited therein.
2) Y. Nakamura, M. Gotani, and S. Kawaguchi, *Bull. Chem. Soc. Jpn.*, **45**, 457 (1972).
3) K. Isobe and S. Kawaguchi, *Bull. Chem. Soc. Jpn.*, **48**, 250 (1975).
4) J. P. Collman, *Adv. Chem. Ser.*, **37**, 78 (1963); *Angew. Chem., Int. Edn.*, **4**, 132 (1965); "Transition Metal Chemistry," Vol. 2, (1966), p. 1.
5) R. W. Kluiber, *J. Am. Chem. Soc.*, **82**, 4839 (1960): J. P. Collman, R. A. Moss, H. Maltz, and C. C. Heindel, *ibid.*, **83**, 531 (1961).
6) P. R. Singh and R. Sahai, *Aust. J. Chem.*, **20**, 639 (1967).
7) M. M. Aly, *J. Inorg. Nucl. Chem.*, **35**, 537 (1973).
8) K. Isobe, K. Takeda, Y. Nakamura, and S. Kawaguchi, *Inorg. Nucl. Chem. Lett.*, **9**, 1283 (1973).
9) R. C. Charles and M. A. Pawlikowski, *J. Phys. Chem.*, **62**, 440 (1958).
10) J. Aggett, *J. Inorg. Nucl. Chem.*, **32**, 2767 (1970).
11) D. M. Puri and R. C. Mehrotra, *J. Less-Common Metals*, **5**, 2 (1963).
12) M. Cox, B. W. Fitzsimmons, A. W. Smith, L. F. Larkworthy, and K. A. Rogers, *J. Chem. Soc., A*, **1971**, 2158.
13) P. F. Lindley and A. W. Smith, *Chem. Commun.*, **1970**, 1355.
14) K. Nakamoto, C. Udovich, and J. Takemoto, *J. Am. Chem. Soc.*, **92**, 3973 (1970).
15) R. L. Martin and A. H. White, *Inorg. Chem.*, **6**, 712 (1967).
16) G. W. A. Fowles, D. A. Rice, and R. A. Walton, *J. Inorg. Nucl. Chem.*, **31**, 3119 (1969).
17) G. W. A. Fowles, D. A. Rice, and R. A. Walton, *J. Chem. Soc., A*, **1968**, 1842.
18) R. J. H. Clark and T. M. Dunn, *J. Chem. Soc.*, **1963**, 1198.
19) R. J. H. Clark and C. S. Williams, *Inorg. Chem.*, **4**, 350 (1965).
20) R. L. Lintvedt and L. K, Kernitsky, *Inorg. Chem.*, **9**, 491 (1970).
21) G. M. Bryant and J. E. Fergusson, *Aust. J. Chem.*, **24**, 275 (1971).
22) C. M. Harris and T. N. Lockyer, *Chem. Ind.*, **20**, 1231 (1958).
23) S. A. Cotton, *Coord. Chem. Rev.*, **8**, 185 (1972).
24) Y. Nakamura, K. Isobe, H. Morita, S. Yamazaki, and S. Kawaguchi, *Inorg. Chem.* **11**, 1573 (1972).
25) M. J. Frazer, A. H. Qureshi, and F. B. Taylor, *J. Chem. Soc., A*, **1971**, 1712; D. Cunningham, M. J. Frazer, A. H. Qureshi and F. B. Taylor, *J. Chem. Soc., Dalton*, **1972**, 1090.
27) A. van den Bergen, K. S. Murray, M. J. O'Connor, N. Rehak, and B. O. West, *Aust. J. Chem.*, **21**, 1505 (1968); A. van den Bergen, K. S. Murray, and B. O. West, *ibid.*, **21**, 1517 (1968): J. E. Davies and B. M. Gatehouse, *Chem. Commun.*, **1970**, 1166; J. A. Bertrand, J. L. Breece, and P. G. Eller, *Inorg. Chem.*, **13**, 125 (1974).
27) M. D. Hobday and T. D. Smith, *Coord. Chem. Rev.*, **9**, 311 (1973).
28) T. Tsumaki, S. Antoku, and M. Shito, *Bull. Chem. Soc. Jpn.*, **33**, 1096 (1960); B. W. Fitzsimmons, A. W. Smith, L. F. Larkworthy, and K. A. Rogers, *J. Chem. Soc., Dalton*, **1973**, 676.
29) E. B. Fleischer, *Acc. Chem. Res.*, **3**, 105 (1970).

Studies on Mixed Chelates. V. Mixed Nickel(II) Chelates with *N,N,N',N'*-Tetraethylethylenediamine and β-Diketones[1]

Yutaka FUKUDA, Reiko MORISHITA (née FUKUSHIMA), and Kozo SONE

Department of Chemistry, Faculty of Science, Ochanomizu University, Bunkyo-ku, Tokyo 112

(Received September 30, 1975)

Fourteen mixed nickel(II) chelates with the general formula, Ni teen(β-dik)X, were newly obtained. Here teen is *N,N,N',N'*-tetraethylethylenediamine, *i.e.*, a sterically hindered ligand with four bulky ethyl groups on the donor *N* atoms, β-dik is a β-diketonate ion, and X is an anion such as $B(C_6H_5)_4^-$, ClO_4^-, NO_3^- or β-dik. According to the coordination ability of the anion X, the structure of the mixed chelate changes from square planar to octahedral, remarkable solvent effects being observed on the absorption spectra of these chelates. The steric influence of the ligand "teen" was compared with that of the ligand "tmen", *i.e.*, its tetramethyl analog.

Many complexes of nickel(II) with ethylenediamine or its derivatives have been studied.[2-7] The structures of these complexes are sometimes square planar and sometimes octahedral. Although the principal factors which determine the structures are steric and electronic, the former seems to be predominant in a number of cases. Thus *N,N,N',N'*-tetramethylethylenediamine (tmen*) forms a dimeric chelate, $[Ni\ tmen(OH)]_2^{2+}$, instead of the bis-chelate $[Ni\ tmen_2]^{2+}$ in which a strong interligand repulsion occurs.[3] On the other hand, the combination of tmen and the ligand which has no bulky group around the donor atom can form stable mixed complexes, *i.e.*, [Ni tmen(AA)][1,8] or [Ni tmen X_2].[9]

In the present study, a ligand with more bulky groups on the donor *N* atoms, *N,N,N',N'*-tetraethylethylenediamine, which has been studied only little as a chelating agent, was chosen in order to obtain a series of new mixed chelates, Ni teen(β-dik)X, and the properties of the chelates were compared with those of the corresponding chelates of tmen.[1,8]

Experimental

Materials. Commercial "Extra Pure" products were used except for $Ni(ClO_4)_2 \cdot 6H_2O$ prepared from freshly prepared nickel carbonate and perchloric acid and purified by recrystallization.[10] Solvents for spectral measurements were of "Extra Pure" or "Spectro" grade. 1,2-Dichloroethane for electric conductivity measurements was redistilled and dehydrated.

Preparation of the Chelates. *[Ni teen dpm]$B(C_6H_5)_4$*, *[Ni teen aca]$B(C_6H_5)_4$* *and* *[Ni teen dbm]$B(C_6H_5)_4$*: Equimolar amounts of nickel nitrate and an appropriate β-diketone (10 mmol each) were dissolved in 30 ml of acetone. To this solution, 5 mmol of Na_2CO_3 and an excess of teen (slightly above 15 mmol) were added with stirring. After filtration, the resulting mixture was dried up with a rotary evaporator, and the solid obtained was dissolved in 1,2-dichloroethane and filtered in order to separate a white precipitate. When solid $NaB(C_6H_5)_4$ (15 mmol) was added to this solution, the color of the solution turned from green to red, a white powder being precipitated. This was found to be a mixture of $NaNO_3$ and $NaB(C_6H_5)_4$ from the IR spectra. After filtration, the solution was concentrated in a silica-gel desiccator. Brilliant red crystals were obtained from the solution (except in the case of [Ni teen aca]$B(C_6H_5)_4$) and recrystallized from the same solvent. It was difficult to crystallize the aca mixed chelate, but it could be obtained as a crystalline powder from the red solution by addition of ether in excess and cooling with stirring. The same procedure was repeated for purification.

[Ni teen dpm]ClO_4 *and* *[Ni teen bza]ClO_4*: Equimolar amounts of nickel perchlorate and an appropriate β-diketone (10 mmol each) were dissolved in 30 ml of acetone, and 5 mmol of Na_2CO_3 and 15 mmol of teen were added with stirring. After filtration, the solution was dried up with a rotary evaporator and the red solid product was dissolved in 1,2-dichloroethane and concentrated by blowing air stream. A red crystalline powder was finally obtained by addition of ether to the concentrated dichloroethane solution. In the case of dpm, [Ni teen dpm_2] was obtained from the filtrate as a by-product.

[Ni teen aca NO_3], *[Ni teen bza NO_3]* *and* *[Ni teen dbm NO_3]*: Equimolar amounts of nickel nitrate and an appropriate β-diketone(10 mmol each) were dissolved in 30 ml of acetone, and 5 mmol of Na_2CO_3 and an excess of teen (15 mmol) were added with stirring. The solution was concentrated by blowing air stream. The blue or green crystals obtained were recrystallized from 1,2-dichloroethane.

[Ni teen dpm_2], *[Ni teen aca_2]*, *[Ni teen bza_2]*, *[Ni teen dbm_2]*, *[Ni teen tfa_2]* *and* *[Ni teen hfa_2]*: Some of these chelates were obtained as by-products in the preparation of the mixed perchlorate chelates. In the case of tfa and hfa, however, only this type of chelate, [Ni teen $\beta\text{-dik}_2$], could be obtained as crystalline products. The general procedure of preparation of this type of chelate is as follows: 10 mmol of nickel sulfate or nitrate and 20 mmol of an appropriate β-diketone were dissolved in 50 ml of acetone, and 20 mmol of KOH suspended in 20 ml of methanol was added in order to neutralize the β-diketone. To the pale greenish blue solution in which $[Ni\ (\beta\text{-dik})_2(S)_2]$(where S=solvent molecule) was formed, an excess of teen(slightly more than 10 mmol) was added and then filtered. The solution was dried up with a rotary evaporator. After the crude blue or green solid obtained was dissolved in 1,2-dichloroethane, the filtrate was concentrated by blowing air stream until the crystals appeared. The crude product was recrystallized from 1,2-dichloroethane.

Physical Measurements. The electronic spectra of the chelate solutions in the range 340—1500 nm were recorded with a Hitachi EPS-3T spectrophotometer using 10 mm silica cells. The reflection spectra of solid samples in the range 400—750 nm were recorded with a Shimadzu Multi-convertible D-40R spectrophotometer with a reflection

* Other abbreviations used in this article are: teen=*N,N,N',N'*-tetraethylethylenediamine, dpm=dipivaloylmethanate, aca=acetylacetonate, bza=benzoylacetonate, dbm=dibenzoylmethanate, tfa=trifluoroacetylacetonate, hfa=hexafluoroacetylacetonate, diam=diamine, β-dik= a β-diketonate ion, and AA=a bidentate ligand such as β-dik.

Table 1. Analytical data and other properties of the chelates obtained

Chelate	Color	C%[a]	H%[a]	N%[a]	μ_{eff}(BM)	$\Lambda_M(\Omega^{-1}\,cm^2\,M^{-1})$[b]
[Ni teen dpm]$B(C_6H_5)_4$	Red	69.46(73.68)	8.10(8.67)	3.68(3.82)	Dia.	27.2
[Ni teen aca]$B(C_6H_5)_4$	Red	69.21(72.13)	7.47(7.93)	4.00(4.31)	(1.08)	27.2
[Ni teen dbm]$B(C_6H_5)_4$	Red	75.48(76.08)	6.95(7.18)	3.59(3.62)	Dia.	27.1
[Ni teen dpm]ClO_4	Red	51.36(49.09)	8.44(8.49)	5.54(5.45)	(0.28)	31.2
[Ni teen bza]ClO_4	Red	48.24(48.86)	7.03(6.77)	5.51(5.70)	Dia.	30.3
[Ni teen aca NO_3]	Blue	45.19(45.94)	8.09(7.97)	11.03(10.70)	3.10	0.7
[Ni teen bza NO_3]	Green	51.47(52.87)	7.08(7.32)	9.26(9.25)	3.11	0.5
[Ni teen dbm NO_3]	Green	57.95(58.16)	6.44(6.83)	8.11(8.14)	3.08	0.0
[Ni teen dpm_2]	Blue	63.85(64.10)	10.96(10.76)	4.66(4.67)	3.07	0.0
[Ni teen aca_2]	Blue	56.66(55.96)	9.23(8.92)	6.60(6.52)	3.07	0.0
[Ni teen bza_2]	Green	65.47(65.11)	7.80(7.65)	5.04(5.06)	3.07	0.0
[Ni teen dbm_2]	Green	70.73(70.91)	6.84(6.84)	4.11(4.14)	3.05	0.0
[Ni teen tfa_2]	Blue	44.50(44.71)	6.02(6.00)	5.21(5.21)	3.10	0.0
[Ni teen hfa_2]	Green	36.90(37.24)	3.88(4.06)	4.30(4.34)	3.18	0.0

a) Calculated values in parentheses. b) 1.0×10^{-3} M solution in 1,2-dichloroethane at 25 °C.

attachment and MgO disks for reference. Measurements were performed at room temperature, *ca.* 20 °C. The magnetic susceptibility was measured by the Faraday method with a Shimadzu Tortion Magnetometer MB-100 using $HgCo(NCS)_4$ and Mohr's salt as standard samples for calibration. The IR spectra of the solid chelates in the range 400—4000 cm^{-1} were recorded with a JASCO IR-G spectrophotometer by the Nujol-mull method. The electric conductivity measurements were carried out with a Yanagimoto Conductivity Outfit MY-7 using 1,2-dichloroethane as the solvent.

Results and Discussion

General Properties of the Chelates. The compositions of the chelates obtained as crystals or fine crystalline powders can be expressed with the general formula, Ni teen (β-dik) X, where X is an anion such as $B(C_6H_5)_4^-$, ClO_4^-, NO_3^- or β-dik. The results of chemical analyses and other properties are given in Table 1. As in the case of the tmen chelates,[1,8] these chelates can be classified into two types. Type 1 chelates with $B(C_6H_5)_4^-$ or ClO_4^- are diamagnetic and red,** while type 2 chelates with NO_3^- or one more β-diketone are paramagnetic (*ca.* 3 BM) and green or blue. These facts, together with the spectral features give the formula for each chelate (Table 1).

Table 1 also gives the electric conductivity data of the chelates in 1,2-dichloroethane solution. According to the criterion by Geary[11] who has pointed out that a 1 : 1 electrolyte in 1,2-dichloroethane shows a molar conductivity of *ca.* 23 $ohm^{-1}\,M^{-1}\,cm^2$, all type 1 chelates should be 1 : 1 electrolytes, while all the type 2 chelates are clearly non-charged complexes. This also supports the formulation of these chelates given in Table 1.

Electronic Spectra. Figures 1, 2, and 3 show the absorption spectra of the mixed chelates, Ni teen bza X, in various solvents and in solid state. The other mixed chelates also show similar spectra. Their spectral data are given in Table 2.

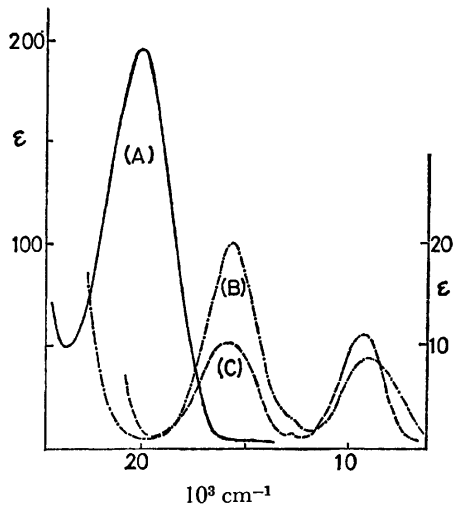

Fig. 1. Absorption spectra of the chelates of the bza series in 1,2-dichloroethane. (A), [Ni teen bza]ClO_4; (B), [Ni teen bza NO_3]; (C), [Ni teen bza_2]. The scale on the left refers to (A), and that on the right to (B) and (C).

The general features of these spectra are similar to those of the corresponding tmen chelates.[1,8] These data indicate that type 1 chelates in 1,2-dichloroethane (a very weakly coordinating solvent) and in solid state are all square planar,[12,13] while type 2 chelates in the same solvent have octahedral structures, in which not only a β-diketonate ion but also a nitrate ion seem to act as a bidentate ligand. They show that, in a strongly coordinating solvent like DMF, the square planar chelate cation [Ni teen β-dik]$^+$ in type 1 chelates are quantitatively converted into the octahedral solvated species [Ni teen β-dik S_2]$^+$ (S= solvent molecule); on the other hand, in a solvent with intermediate coordinating ability like acetone, the spectra indicate that these two species coexist in

** Weak paramagnetism, shown by two of them, might be due to impurities. In fact, type 1 chelates (especially the aca chelate; *cf.* Experimental) were difficult to purify, and even after repeated trials some of them could not be made as pure as most of the type 2 chelates.

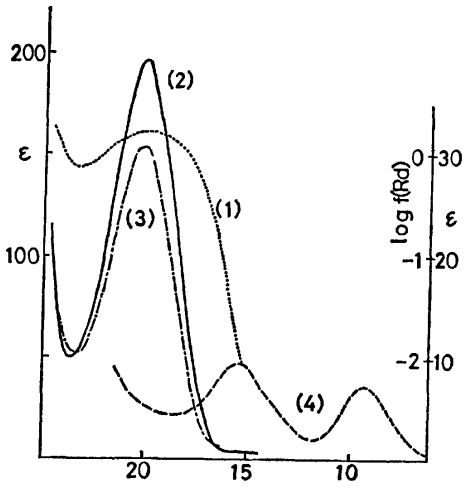

Fig. 2. Absorption spectra of the chelate, [Ni teen bza]ClO_4, in various organic solvents. (1), solid reflectance spectrum; (2), in 1,2-dichloroethane; (3), in acetone; (4), in DMF. The scale on the left refers to (2) and (3), and those on the right to (1) and (4).

equilibrium.***

$$[\text{Ni teen } \beta\text{-dik}]^+ + 2S \rightleftharpoons [\text{Ni teen } \beta\text{-dik } S_2]^+ \quad (1)$$

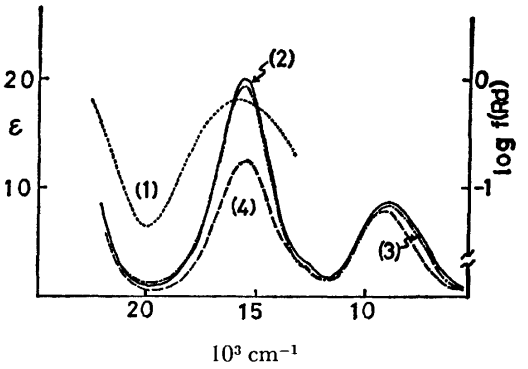

Fig. 3. Absorption spectra of the chelate, [Ni teen bza NO_3], in various organic solvents. Notations are the same as those in Fig. 2. The scale on the right refers to (1), and that on the left to the others.

As can be seen from Fig. 3 and Table 2, there is a small but noticeable difference between the spectrum of a nitrate chelate in 1,2-dichloroethane and that in DMF, and the outlook of the latter spectrum is similar to that of [Ni teen β-dik S_2]$^+$. These facts, together with the information from conductivity data and IR data, lead to the view that a nitrate chelate has the structure [Ni teen β-dik NO_3] both in solid state and in an inert solvent, while in a solvent with stronger

Table 2. Electronic spectra of the chelates in solid state and in various solvents (10^3 cm^{-1}, ε_{max} in parentheses)

Chelate	Solid	$C_2H_4Cl_2$	Acetone	DMF
[Ni teen dpm]$B(C_6H_5)_4$	20.12	20.12(137)	20.16(142)	15.5(6.08) 9.40(5.90)
[Ni teen aca]$B(C_6H_5)_4$	20.16	20.20(146)	20.20(120)	15.5(7.59) 9.29(7.01)
[Ni teen dbm]$B(C_6H_5)_4$	20.16	20.12(232)[a]	20.20(190)[a]	15.5(7.32) 9.26(6.37)
[Ni teen dpm]ClO_4	20.12	20.16(148)	20.12(154)	15.5(6.68) 9.35(6.85)
[Ni teen bza]ClO_4	19.92	20.12(195)[a]	20.12(154)	15.5(9.53) 9.30(7.32)
[Ni teen aca NO_3]	15.90	15.6(19.6) 9.01(8.84)	15.6(18.2) 9.03(9.51)	15.5(11.7) 9.22(7.55)
[Ni teen bza NO_3]	15.90	15.6(19.9) 9.01(8.84)	15.6(19.3) 9.03(8.33)	15.5(12.5) 9.17(7.95)
[Ni teen dbm NO_3]	15.65	15.6(20.9) 9.01(9.12)	15.6(20.9) 9.03(9.30)	15.5(14.1) 9.17(7.95)
[Ni teen dpm_2]	16.00	15.9(9.60) 9.30(10.0)	insoluble	insoluble
[Ni teen aca_2]	16.10	15.7(7.05) 9.17(9.90)	15.7(7.85) 9.23(10.1)	15.7(7.10) 9.20(9.60)
[Ni teen bza_2]	15.92	15.9(10.3) 9.30(11.1)	15.9(10.7) 9.30(11.3)	15.8(9.80) 9.30(10.4)
[Ni teen dbm_2]	16.31	16.0(14.2) 9.30(12.2)	insoluble	16.0(14.2) 9.30(9.86)
[Ni teen tfa_2]	15.90	15.7(9.65) 9.35(9.30)	15.8(9.50) 9.35(9.40)	15.7(10.6) 9.30(9.10)
[Ni teen hfa_2]	16.00	15.8(13.0) 9.51(8.60)	15.8(13.2) 9.50(8.05)	15.8(14.2) 9.43(9.02)

a) Apparent values which are probably somewhat higher than the true ones because of the partial overlap of this band with the strong ligand band (or CT band) in the UV.

*** The coexistence of these two species is more evident in the case of the tmen chelates (*cf.* Table 5), but a comparison of the data shows that the same situation takes place with the teen chelates.

coordinating power the following equilibrium is established:

$$[\text{Ni teen } \beta\text{-dik } NO_3] + 2S \rightleftharpoons [\text{Ni teen } \beta\text{-dik } S_2]^+ + NO_3^- . \quad (2)$$

Finally, the spectra of the bis-β-diketonate chelates show that they retain their octahedral structures in the solid state and also in any solvent. All the structural information correspond very closely to that obtained in the studies of the tmen chelates.[1,8]

Infrared Spectra. The IR spectra of all these chelates are naturally highly complicated. The discussion will be restricted to those of the perchlorate and nitrate anions. As to the perchlorate ion, the spectra show that it merely acts as a counter ion of the square planar cation [Ni teen β-dik]$^+$.[15] In the IR spectra of the nitrate chelates, it was not easy to assign the bands to a coordinated nitrate or the simple counter ion with sufficient accuracy.

Lever *et al.* pointed out the usefulness of the weak band at *ca.* 1750 cm^{-1} (a combination band of ν_1 and ν_4) as a criterion to distinguish whether a nitrate ion in a complex is a coordinating ligand or merely a counter ion.[14] From a large number of data, they concluded that, (1) when this band is not split, the nitrate ion is not bound in the complex, and acts only as a counter ion; (2) when it is split slightly (about 5 to 20 cm^{-1}), the ion acts as a monodentate ligand; and (3) when the splitting is much larger (about 30 to 50 cm^{-1}), the ion acts as a bidentate ligand.

According to this criterion, the nitrate ions in the mixed chelates [Ni teen β-dik NO_3] are apparently bidentate ligands. As an example, the IR data of a nitrate chelate, [Ni teen aca NO_3], are shown in Fig. 4, in which important bands are marked with arrows. They are at 1723 and 1774 cm^{-1}, respectively, and the splitting is 51 cm^{-1}. The corresponding bands of the other nitrate chelates [Ni teen bza NO_3] (B) and [Ni teen dbm NO_3] (C) are also shown.

In previous papers,[1,8] a number of mixed nitrate chelates [Ni tmen β-dik NO_3] were characterized and concluded to be octahedral and to contain a bidentate nitrate ion, by means of the d-d spectra, electric conductivities and IR spectra. Application of the criterion of Lever *et al.* to these tmen chelates confirmed that they contain the bidentate nitrate ion as expected, with a *ca.* 50 cm^{-1} splitting. The values are given in Table 3 together with those of the teen chelates. It seems that the formulation of the nitrate chelates of teen and tmen as [Ni diam β-dik NO_3] with a bidentate nitrate ion is well established.

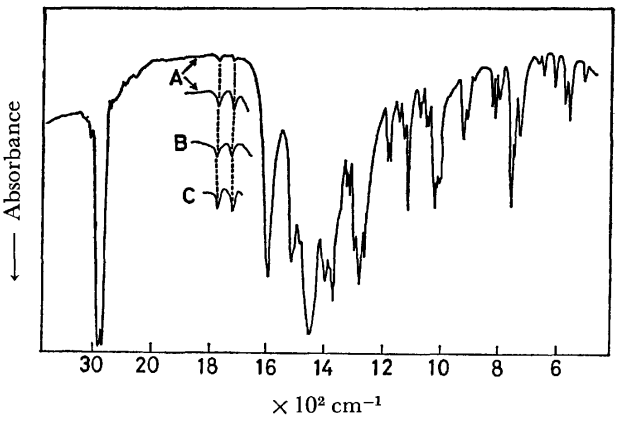

Fig. 4. IR spectra of the chelates; (A), [Ni teen aca NO_3]; (B), [Ni teen bza NO_3]; (c), [Ni teen dbm NO_3]. The data of the latter two are shown only in the range of 1700—1800 cm^{-1}.

Table 3. IR data of the nitrate chelates of tmen and teen

Only bands in the 1700—1800 cm^{-1} region useful as a criterion of the mode of coordination of the nitrate ion are given. Δ is the difference between the ν values of the two bands.

Chelate	ν(cm^{-1})		Δ(cm^{-1})
[Ni tmen aca NO_3]	1766	1718	48
[Ni tmen bza NO_3]	1767	1717	50
[Ni tmen dbm NO_3]	1767	1720	47
[Ni tmen tfa NO_3[	1769	1721	48
[Ni teen aca NO_3]	1774	1723	51
[Ni teen bza NO_3]	1773	1724	49
[Ni teen dbm NO_3]	1768	1720	48

Comparison of the Mixed Chelates of Teen with Those of Tmen. There are great similarities between the teen chelates obtained in this study and the tmen chelates studied before. The differences between the two groups of chelates will now be considered in some detail.

Ease of Formation and Isolation of the Chelate: Although various mixed chelates containing teen and β-diketonate ions have been obtained, they are not so numerous as those of tmen. The ease of preparation of the mixed chelates is shown in Table 4 for a comparison of teen and tmen. The circle shows that the corresponding chelate can be more or less easily obtained, the triangle that the chelate cannot be isolated as solid crystals, although there is definite spectral evidence that it actually exists in solution, and the cross that the chelate cannot be obtained and that there is no evidence of its formation even in solution. It can be seen that the formation of the teen chelates is, in general, more difficult than that of the tmen chelates.

Ligand Field Strength in the Chelates: Although the coordination ability of the ligand "teen" has not been studied thoroughly, it is easy to see that the steric hindrance caused by the ethyl groups in teen, which increases the interligand repulsion in its chelate, will be much more effective than that of the methyl groups in tmen.

In this connection, it is of interest to compare the apparent ligand field strength(1.f.s.) in the teen chelate with that in the tmen chelate. Spectral data of the square planar species, [Ni teen β-dik]$B(C_6H_5)_4$ in 1,2-dichloroethane are given in Table 2, and those of the corresponding chelates of tmen in Table 5. From a comparison of [Ni teen aca]$B(C_6H_5)_4$ and [Ni tmen aca]$B(C_6H_5)_4$, we see that the 1.f.s. in the former is slightly weaker than that in the latter. This probably reflects the increased steric hindrance of the ethyl

Table 4. Variations in the ease of formation and isolation of the mixed chelates, Ni diam β-dik X (A) is a mixed chelate containing teen as a diamine, (B) the corresponding tmen chelate. As to the remarks, ○ shows that the corresponding chelate could be obtained, △ the chelate could not be obtained but was found to exist in solution, × no chelate formation could be found in this study.

β-dik	X									
	$B(C_6H_5)_4$		ClO_4		$2H_2O \cdot ClO_4$		NO_3		β-dik	
	(A)	(B)	(A)	(B)	(A)	(B)	(A)	(B)	(A)	(B)
dpm	○	○	○	○	×	×	△	△	○	○
aca	○	○	△	○	×	○	○	○	○	○
bza	△	○	○	○	×	○	○	○	○	○
dbm	○	○	△	○	×	○	○	○	○	○
tfa	×	○	×	×	×	×	×	○	○	○
hfa	×	×	×	×	×	×	×	×	○	○

Table 5. Spectral data of the square planar mixed chelates with tmen in solid state and in various solvents (10^3 cm^{-1}, ε_{max} in parentheses)[1,8]

Chelate	Solid	$C_2H_4Cl_2$	Acetone	DMF
[Ni tmen dpm]$B(C_6H_5)_4$	20.33	20.49(153)	20.37(75.1) 9.47(6.5)	16.08(8.4) 9.70(9.5)
[Ni tmen aca]$B(C_6H_5)_4$	20.33	20.53(151)	20.49(31.5) 16.26(8.9) 9.43(8.3)	15.87(7.8) 9.60(9.5)
[Ni tmen dbm]$B(C_6H_5)_4$	20.66	20.49(263)	20.00(sh[a]) 16.03(9.7) 9.49(9.3)	16.08(9.4) 10.13(9.5)
[Ni tmen dpm]ClO_4	20.62	20.53(150)	20.37(56.5) 15.90(sh[a]) 9.45(4.6)	15.97(6.3) 9.74(7.6)
[Ni tmen bza]ClO_4	20.83	20.45(176)	20.33(16.4) 16.00(8.7) 9.43(8.9)	15.97(8.6) 9.58(9.8)

a) sh=shoulder

groups in the diamine, to which the decreased ease of formation of the teen chelates also seems to be related.

Relative Stability of the Square Planar Chelates: Another point of interest is that, in the case of a teen chelate of type 1, the equilibrium (1) established in a solvent of intermediate coordination ability is shifted remarkably to the left hand side, in comparison with that of the corresponding tmen chelate. This can be seen in acetone solutions, but a better comparison can be made with the use of a mixed solvent containing a large amount of an inert solvent and a little of a strongly coordinating solvent. Figure 5 shows the absorption spectra of [Ni teen dpm]$B(C_6H_5)_4$ and [Ni tmen dpm]$B(C_6H_5)_4$ in various mixtures of 1,2-dichloroethane and DMF. In both these cases, the intensity of the band at *ca.* 20000 cm^{-1} decreases with the increase of the DMF content in the solvent, but the decrease in the case of the tmen chelate is far more drastic, showing that the equilibrium in 1,2-dichloroethane,

$$[\text{Ni diam } \beta\text{-dik}]^+ + 2\text{DMF} \rightleftharpoons [\text{Ni diam } \beta\text{-dik } (\text{DMF})_2]^+$$

is shifted more strongly to the right hand side. Approximate calculations with these data and also with the spectral data in acetone solution (Tables 2 and 5), lead to the values in Table 6.†

We see that the apparent value of the equilibrium constant, K, of Eq. 1 in acetone increases *ca.* 20—40 times with the change of [Ni teen β-dik]$^+$ to their

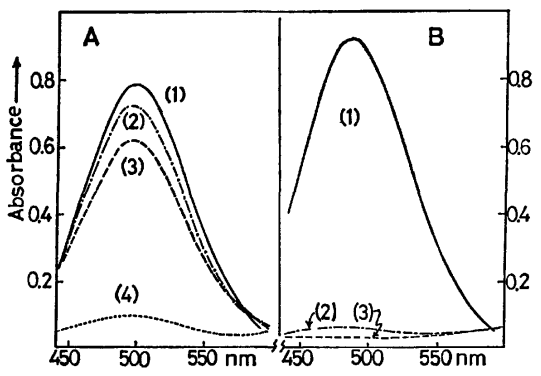

Fig. 5. Absorption spectra of the chelates, [Ni diam dpm]$B(C_6H_5)_4$, dissolved in various $C_2H_4Cl_2$-DMF mixtures. A and B show the case of the teen chelate (conc. 6.1×10^{-3} M) and that of the tmen chelate (conc. 5.9×10^{-3} M), respectively. The content of DMF in the solvent is: 0%; (2), 0.5%; (3), 1%; (4), 5%.

† In these calculations it was assumed that the true molar extinction coefficient of the band at *ca.* 20000 cm^{-1} of a square planar chelate is, in any solvent, practically equal to that in 1,2-dichloroethane.

TABLE 6. PERCENTAGE OF [Ni teen β-dik]$^+$, REMAINING UNSOLVATED IN THE EQUILIBRIUM MIXTURES PRODUCED BY DISSOLVING TYPE 1 CHELATES OF teen IN ACETONE AND IN 1,2-DICHLOROETHANE CONTAINING 1% DMF

The value for [Ni tmen dpm]$B(C_6H_5)_4$ in the mixed solvent ($C_2H_4Cl_2$ + 1% DMF), obtained from Fig. 5, is very low (<4%).

Chelate	Acetone[a)]	$C_2H_4Cl_2$ + 1%DMF
[Ni teen dpm]$B(C_6H_5)_4$	100(49)	82
[Ni teen dpm]ClO_4	100(38)	75
[Ni teen aca]$B(C_6H_5)_4$	82(21)	65
[Ni teen bza]ClO_4	78(9)	46
[Ni teen dbm]$B(C_6H_5)_4$	83(8)	29

a) The values for the corresponding tmen chelates are given in parentheses.

tmen analogs. It can also be seen that the K values among the teen chelates increase in the order dpm→aca→bza→dbm, which is just the same as that observed among the tmen chelates.[1)]

As regards this remarkable difference between the chelates of teen and those of tmen, it is natural to expect that the more bulky ethyl groups on teen hinder the coordination of the solvent molecules at the 5th and 6th coordinating sites of the square planar chelate cation more strongly than the smaller methyl groups on tmen. The fact that the chelates [Ni diam β-dik $(H_2O)_2$]ClO_4, which could be easily obtained with tmen and a number of β-dik, could not be obtained at all with teen (*cf.* Table 4) may also be due to the same kind of steric effect.

All the perceptible differences between the chelates of teen and those of tmen are thus ascribed to the difference in magnitude of the steric effect caused by the *N*-alkyl groups of their ligands. The observed differences are, however, rather small, and the formation of octahedral complexes is by no means made impossible with the use of teen in spite of the great increase in the bulkiness of these groups.

The authors wish to thank Prof. Hiroshi Kakisawa, Tokyo Kyoiku University, for permission to use the Hitachi EPS-3T Spectrophotometer in his laboratory, and also Dr. Ichiro Fujita and Mrs. Etsuko Fujita, Georgia Institute of Technology, for kindly supplying a sample of teen from Aldrich Chem. Co., Milwaukee. This work was financially supported by a grant-in-aid from the Ministry of Education.

References

1) Part IV of this series: Y. Fukuda and K. Sone, *J. Inorg. Nucl. Chem.*, **37**, 455 (1975).
2) D. A. Baldwin and G. J. Leigh, *J. Chem. Soc., A*, **1968**, 1431.
3) D. W. Meek and S. A. Ehrhardt, *Inorg. Chem.*, **4**, 584 (1965).
4) S. F. Pavkovic and D. W. Meek, *Inorg. Chem.*, **4**, 20 (1965).
5) D. M. L. Goodgame and L. M. Venanzi, *J. Chem. Soc.*, **1963**, 616.
6) D. M. L. Goodgame and L. M. Venanzi, *J. Chem. Soc.*, **1963**, 5909.
7) F. Basolo, Y. T. Chen, and R. K. Murmann, *J. Am. Chem. Soc.*, **76**, 956 (1954).
8) Y. Fukuda and K. Sone, *J. Inorg. Nucl. Chem.*, **34**, 2315 (1972).
9) L. Sacconi, I. Bertini, and F. Mani, *Inorg. Chem.*, **6**, 262 (1967).
10) H. Ito, *Nippon Kagaku Zasshi*, **77**, 1383 (1956).
11) W. J. Geary, *Coord. Chem. Rev.*, **7**, 81 (1971).
12) A. B. P. Lever, "Inorganic Electronic Spectroscopy," Elsevier, Amsterdam (1968).
13) L. Sacconi, "Transiton Metal Chemistry," ed. by R. L. Carline, Vol. 4, Marcel Dekker (1968), p. 199.
14) A. B. P. Lever, E. Mantovani, and B. S. Ramaswamy, *Can. J. Chem.*, **49**, 1957 (1971).
15) K. Nakamoto, "Infrared Spectra of Inorganic and Coordination Compounds," 2nd ed., Wiley-Interscience, New York (1970).

Diprotonated Bimetallic Complex between Copper(II) with 3,3′-Bis[*N*,*N*-bis(carboxymethyl)aminomethyl]-*o*-cresolsulfonphthalein*

Mutsuo YAMADA

Department of Chemistry, Faculty of Science, Hokkaido University, Sapporo 060

(Received November 25, 1975)

The solution chemistry for complexes of copper(II) with 3,3′-bis[*N*,*N*-bis(carboxymethyl)aminomethyl]-*o*-cresolsulfonphthalein(XO) is studied by spectrophotometric measurement. Copper(II) is found to form a diprotonated bimetallic complex with XO in weakly acidic medium. Stability constant and molar absorptivity of the complex are evaluated to be log $K_{Cu_2LH_2}=9.86\pm0.05$ and $\varepsilon_{574nm}=3.73\times10^4$ M^{-1} cm^{-1}, respectively, at 25.0 °C and $I=0.1$ M. Thermodynamic parameters are calculated to be $\Delta H=4.3$ kcal·mol^{-1} and $\Delta S=64$ eu at 25.0 °C and $I=0.1$ M.

Xylenol Orange forms mononuclear 1 : 1, 1 : 2 or binuclear 2 : 2 complexes with various metal ions in solution.[1] Nickel(II) and cobalt(II) have been found to form mononuclear monoprotonated 1 : 1 complexes[2] in the presence of an excess of the metal ions to the ligand at pH 3.5—4.4.

However, copper(II) does not form mononuclear 1 : 1 complex but bimetallic 2 : 1 complex in the presence of an excess of the metal ion to the ligand at pH 3.5—5.5. In the present paper the anomalous behavior in copper(II) complex of XO is discussed in terms of the degree of protonation, the stability constant and the thermodynamic parameters of the bimetallic 2 : 1 complex. The structure of the complex is estimated, whose structure would give an important suggestion to the reaction mechanisms of complexation between XO and metal ions.[3,4]

Experimental

Materials. *Reagents*: All the chemicals used were of analytical grade, unless otherwise specified. Water was deionized and distilled.

Xylenol Orange: The acid from of the "*pure*" specimen[5,6] was used. 1.0×10^{-3} M stock solution of XO was prepared by weight. The solution was very stable in a refrigerator.

Copper(II) Perchlorate: Copper(II) perchlorate was prepared from recrystallized copper(II) chloride by heating with a small excess of perchloric acid. Perchlorate was further recrystallized twice from water. The solution was standardized by EDTA titration using PAN as indicator.

Sodium Perchlorate: The purified salt[2] was heated at *ca.* 200 °C to prepare anhydrous salt. The concentration of the solution was determined by weight. The ionic strength of the solution was adjusted to 0.1 M with the sodium perchlorate.

Buffer Solutions: They were prepared from 1.0 M acetic acid and 1.0 M sodium acetate.

Measurements. The equilibria of complexation were measured with a Hitachi 139 spectrophotometer at 574 nm of the maximum absorption for copper(II) complex. Absorption spectra were recorded with a Hitachi recording spectrophotometer Model EPS-3T. A 1-cm glass or quartz cell was used.

The pH values of the solutions were measured with a Radiometer pH Meter 4d (Copenhagen) equipped with a glass electrode Type G 202B and a saturated calomel electrode Type K 401.

Temperature of the solution was maintained constant by circulating thermostated water from a Coolnics Model CTR-1B with a circulator CTE-1A.

Results

Absorption Spectra. Figure 1 shows the absorption spectra for the total concentrations of copper(II) and XO, $T_{Cu}=(0.40—1.20)\times10^{-4}$ M and $T_L=1.60\times10^{-5}$ M, at pH 4.308±0.005, at 25.0 °C and $I=0.1$ M.

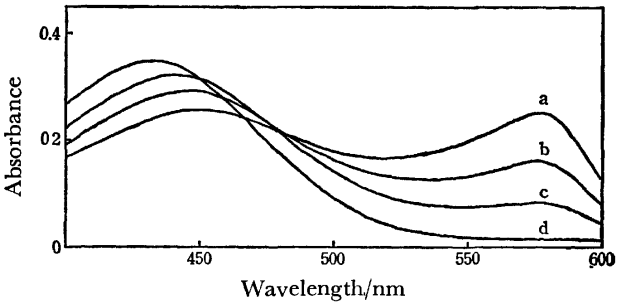

Fig. 1. Absorption spectra of copper(II) complex at various concentrations of copper(II).
T_{Cu}: a) 1.20×10^{-4} M, b) 2.00×10^{-5} M, c) 1.28×10^{-5} M, and d) 0 M. $T_L=1.60\times10^{-5}$ M. pH=4.308±0.005, $I=0.1$ M, 25.0 °C.

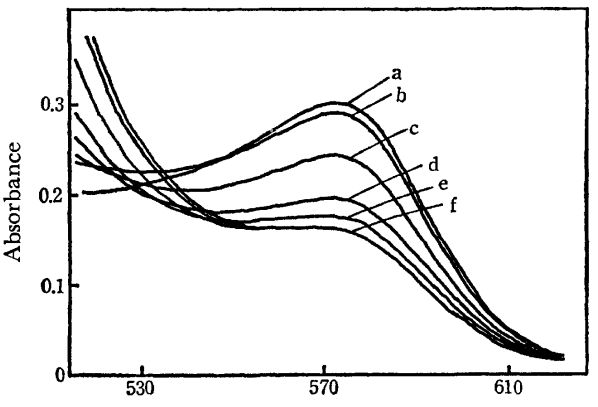

Fig. 2. Absorption spectra of copper(II) complex at various concentrations of XO.
T_L: a) 2.00×10^{-5} M, b) 3.00×10^{-5} M, c) 4.00×10^{-5} M, d) 6.00×10^{-5} M, e) 8.00×10^{-5} M, and f) 1.80×10^{-4} M. $T_{Cu}=4.00\times10^{-5}$ M. pH=4.284±0.024, $I=0.1$ M, 25.0 °C.

* Presented in part at the 25th Annual Meeting on Coordination Chemistry, Tokyo, October 8, 1975, Abstract, p. 161.

The absorption maximum of copper(II) complex is 574 nm, while those of nickel(II) and cobalt(II) are 584 nm.[2] Surprisingly, there is only a little increase in the absorbance at the absorption maximum with the increase of the copper(II) concentration compared with the case of nickel(II) and cobalt(II) complexes with XO.[2] Figure 2 indicates that a successive reaction occurs for $T_{Cu}=8.00\times10^{-5}$ M and $T_L=(0.20—1.80)\times10^{-4}$ M at pH 4.284±0.024 and at 25.0 °C and I=0.1 M.

The Composition of the Complex. The method of molar ratio at 574 nm at pH 4.308±0.005 indicates that the complex species contains 2 copper(II) and 1 XO and that another species of different composition exists as expected in Fig. 2. The curve exhibits an inflection at lower mole fractions of copper(II) (Fig. 3).

Degree of Protonation, Molar Absorptivity and Stability Constant of the Bimetallic Complex. Figure 4 shows pH-dependence of the absorbance of Cu_2XO at 574 nm for $T_{Cu}=2.00\times10^{-4}$ and $T_L=1.60\times10^{-5}$ M at pH 3.458—5.498 at 25.0 °C and I=0.1 M. Under these conditions the ligand and the complex exist predominantly in the form of LH_3^{3-} [7] and Cu_2XO, respectively. So the following equilibrium is postulated for the copper(II) complex. (Charges on the metal and the ligand ions are omitted.)

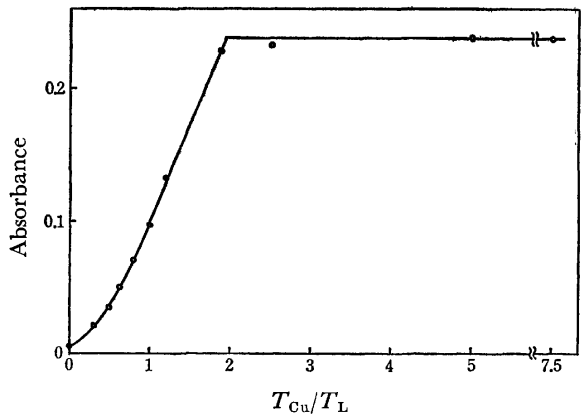

Fig. 3. Curve of molar ratio for copper(II) complex at 574 nm. pH=4.308±0.005, I=0.1 M, 25.0 °C.

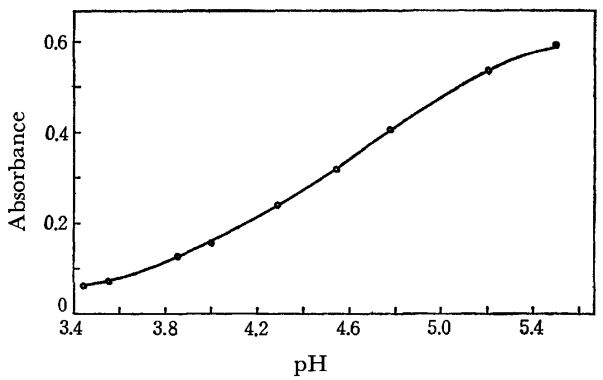

Fig. 4. pH-Dependence of the absorbance for copper(II) complex at 574 nm.
$T_{Cu}=2.00\times10^{-4}$ M and $T_L=1.60\times10^{-5}$ M. I=0.1 M, 25.0 °C.

$$2Cu + LH_3 \rightleftarrows Cu_2LH_i + (3-i)H \quad (1)$$

Applying the law of mass action, we obtain

$$K = [Cu_2LH_i][H]^{3-i}/[Cu]^2[LH_3] \quad (2)$$

and the absorbance of the solution is given by

$$A = \varepsilon_L[LH_3] + \varepsilon_1[Cu_2LH_i], \quad (3)$$

where ε_L and ε_1 are molar absorptivities of LH_3 and Cu_2LH_i, respectively. Analytical concentrations of copper(II) ion and XO are

$$T_{Cu} = [Cu] + 2[Cu_2LH_i] \quad (4)$$

$$T_L = [LH_3] + [Cu_2LH_i]. \quad (5)$$

Combining Eqs. 2—5, and rearranging one leads to

$$\frac{T_L}{A-\varepsilon_L T_L} = \frac{1}{\varepsilon_1-\varepsilon_L} + \frac{[H]^{3-i}}{(\varepsilon_1-\varepsilon_L)K\left\{T_{Cu}-\dfrac{2(A-\varepsilon_L T_L)}{\varepsilon_1-\varepsilon_L}\right\}^2} \quad (6)$$

Under the experimental conditions, Eq. 6 is approximated to Eq. 6′

$$\frac{T_L}{A-\varepsilon_L T_L} = \frac{1}{\varepsilon_1-\varepsilon_L} + \frac{[H]^{3-i}}{\varepsilon_1-\varepsilon_L K T_{Cu}^2} \quad (6')$$

The plot of $T_L/(A-\varepsilon_L T_L)$ against $[H]^{3-i}$ using the data obtained in Fig. 4 gives a straight line for i=2 for copper(II) complex (Fig. 5).

The complex is found to be the diprotonated bimetallic species Cu_2LH_2. The intercept gives 0.313×10^{-4} M cm. From this value and Eq. 6, the exact value 0.270×10^{-4} M^{-1} cm^{-1} is obtained by plotting $T_L/(A-\varepsilon_L T_L)$ against $[H]/\{T_{Cu}-2(A-\varepsilon_L T_L)/(\varepsilon_1-\varepsilon_L)\}^2$. ε_L is evaluated to be 300 M^{-1} cm^{-1} at 574 nm. The molar absorptivity at 574 nm is calculated to be $(3.70+0.03)\times10^4=3.73\times10^4$ M^{-1} cm^{-1} for Cu_2LH_2.

The stability constant of the complex Cu_2LH_2 is determined as follows,

$$2Cu + LH_2 \rightleftarrows Cu_2LH_2 \quad (7)$$

$$K = [Cu_2LH_2]/[Cu]^2[LH_2] \quad (8)$$

$$A = \varepsilon_L' C_L + \varepsilon_1[Cu_2LH_2], \quad (9)$$

where ε_L' and C_L are the apparent molar absorptivity and the total concentration of the free XO, respectively. Total concentrations of copper(II) and XO are

$$T_{Cu} = [Cu] + 2[Cu_2LH_2] \quad (10)$$

$$T_L = C_L + [Cu_2LH_2] \quad (11)$$

and

$$C_L = [LH_2] + [LH_3] + [LH_4]. \quad (12)$$

Combination of Eqs. 7 to 12 and a rearrangement lead to

$$K = \frac{(A-\varepsilon_L' T_L)\alpha}{(\varepsilon_1-\varepsilon_L')\left\{T_{Cu}-\dfrac{2(A-\varepsilon_L' T_L)}{\varepsilon_1-\varepsilon_L'}\right\}^2\left(T_L-\dfrac{A-\varepsilon_L' T_L}{\varepsilon_1-\varepsilon_L'}\right)} \quad (13)$$

and

$$\alpha = 1 + K_1[H] + K_1K_2[H]^2 \quad (14)$$

$$LH_2 + H \rightleftarrows LH_3; \quad K_1 = 10^{6.74}\ [7] \quad (15)$$

$$LH_3 + H \rightleftarrows LH_4; \quad K_2 = 10^{2.85}\ [7] \quad (16)$$

The result is summarized in Table 1. The stability

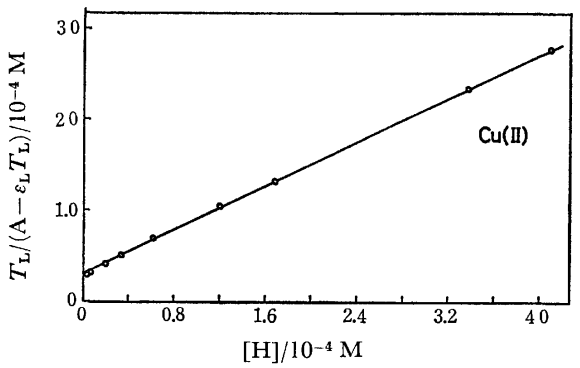

Fig. 5. Plot of $T_L/(A-\varepsilon_L T_L)$ for copper(II) complex against $[H]^{3-i}$ for $i=2$.

Table 1. Stability constant and molar absorptivity for Cu_2LH_2

pH	$-\log[H]$	$\log K$
3.458	3.377	9.91
3.552	3.471	9.89
3.854	3.773	9.86
4.000	3.919	9.83
4.288	4.207	9.81
4.548	4.467	9.81
4.778	4.697	9.84
5.204	5.123	9.91
5.498	5.417	9.85

av. $\log K=9.86\pm0.05$
$\varepsilon_{574\,nm}=3.73\times10^4\ M^{-1}\ cm^{-1}$

constant of the diprotonated bimetallic complex of copper(II) and XO is found to be $\log K=9.86\pm0.05$.

The thermodynamic parameters are spectrophotometrically determined for $T_{Cu}=8.00\times10^{-5}$ M and $T_L=1.60\times10^{-5}$ M and at 15.0, 20.0, 25.0 and 30.0 °C and I=0.1 M. Since the acid-association constants K_1's of XO at 15.0—30.0 °C are spectrophotometrically determined, the calculation of the stability constant $K_{Cu_2LH_2}$ is carried out at higher pH region where it is possible to neglect the concentration of LH^{2-1}. At the higher pH region, $\alpha=1+K_1[H]$.

$K_{Cu_2LH_2}$ is a little larger than 9.86. ΔH is determined to be 4.3 kcal·mol^{-1} by a graphical solution[8] of the following equation

$$\log K = (\Delta S-\Delta H/T)/2.303R$$

and

$$\Delta S_{298} = (\Delta H-\Delta G)/T$$
$$= (4.3+14.7)\times10^3/298$$
$$= 64\ \text{e.u.}$$

Discussion

Xylenol Orange forms mononuclear 1 : 1, 1 : 2 or binuclear 2 : 2 complexes with many metal ions but it is found that XO forms bimetallic 2 : 1 complex with copper(II) ion. Low stability constant of the 2 : 1 copper(II) complex implies the existence of a larger-membered chelate ring than five. Formation of the diprotonated complex species indicates that amine protons of XO do not dissociate but a phenolic proton dissociates on complexation. It is also supported by the fact that a bathochromic shift upon complexation between XO and metal ions is due to the dissociation of a phenolic proton.[9] Furthermore, the endothermicity of the complexation of copper(II) with XO ($\Delta H=4.3$ kcal·mol^{-1}) strongly supports that copper(II) atoms do not coordinate to the nitrogen atoms.[10]

As the amine proton does not dissociate in the experimental pH region, the copper(II) atom in the complex could not be in a plane of three oxygen atoms—a phenolic or a quinoidal and two carboxylic oxygen atoms, but would be a little above or below the plane. Therefore, the copper(II) atom could not take an octahedral or a square-planar structure but a more or less distorted tetrahedral structure.

The structure of Cu_2LH_2 with four nine-membered rings and two eight-membered rings is proposed (Fig. 6). The resonance stabilization due to the bimetallic structure of the complex may contribute to the stability of such structure.

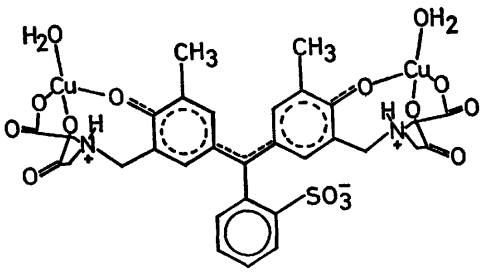

Fig. 6. Proposed structure of Cu_2LH_2 complex.

Despite of large-membered chelate rings, a large positive entropy 64 eu is obtained. It may be due to the reduction of the ordered arrangement of the inner-sphere water molecules around the reactant ions by the formation of the uncharged bimetallic species. The decrease in the coordination number of copper(II), presumably from six to four, also contributes to the positive entropy. The increase in entropy is sufficiently large to overcome the endothermicity of this complexation reaction.

The formation of large chelate rings is also kinetically supported:[4] The overall rate constant of the complex formation of copper(II) with XO is smaller approximately by 3 orders of magnitude than the value expected from the normal substitution reactions of aqua copper(II) ion. Therefore, the complexation reaction of copper(II) ion and XO is a sterically controlled substitution reaction.

The bimetallic diprotonated species Cu_2LH_2 shows reversible thermochromism at pH about 4. The aqueous solution containing $T_{Cu}=2.0\times10^{-4}$ M and $T_L=1.60\times10^{-5}$ M is orange at room temperature and changes reddish purple at about 70 °C and green at 77 K. The phenomena relate to the configurational change around the copper(II), which affects in turn the π-electron system of the coordinated XO. The thermochromism of Cu_2LH_2 would provide a support

for the proposed structure of bimetallic complex Cu_2LH_2. The further details are now in progress.

The author should like to thank to Professor M. Fujimoto for general discussion and reading this manuscript and to Professor T. Ito for the valuable discussion on the configuration of the complex Cu_2LH_2.

References

1) B. Buděšínský, "Chelate in Analytical Chemistry," Vol. 1, ed. by H. A. Flaschka and J. A. Barnard, Jr., Marcel Dekker, Inc., New York, N. Y. (1967), pp. 15—47.

2) M. Yamada and M. Fujimoto, *Bull. Chem. Soc. Jpn.*, to be published.

3) M. Yamada and M. Fujimoto, *Bull. Chem. Soc. Jpn.*, in preparation.

4) M. Yamada, *Bull. Chem. Soc. Jpn.*, in preparation.

5) M. Yamada and M. Fujimoto, *Bull. Cohem. Sc. Jpn.*, **44**, 294 (1971).

6) M. Yamada and M. Fujimoto, *Bull. Chem. Soc. Jpn.*, to be published (50636). "Preparative Thin-Layer Chromatography of Semi-Xylenol Orange and Xylenol Orange by Developing with Solvents Giving Discrete pH Change on the Plate."

7) M. Murakami, T. Yoshino, and S. Harasawa, *Talanta*, **14**, 1293 (1967).

8) F. J. C. Rossotti, "Modern Coordination Chemistry," ed. by J. Lewis and R. G. Wilkins, Interscience Publishers, Inc., New York, N. Y. (1960).

9) P. N. Kovalenko, K. H. Badgasarov, I. E. Shelenin, and M. A. Shemyakina, *Zh. Obshch. Khim.*, **38**, 2015 (1968).

10) J. J. Christensen, D. J. Eatouch, and R. M. Izatt, "Handbook of Metal Ligand Heats," Marcel Dekker, Inc., New York, N. Y. (1975).

Derivatographic Studies on Transition Metal Complexes. XVII.[1] Solid-phase Deaquation-anation of Some Optically Active Aqua-cobalt(III) Complexes[2]

Ryokichi TSUCHIYA, Masakatsu OMOTE, Akira UEHARA, and Eishin KYUNO

Department of Chemistry, Faculty of Science, Kanazawa University, Kanazawa 920

(Received December 17, 1975)

Stereochemical changes involved in the solid-phase deaquation-anation of the following optically active aqua-cobalt(III) complexes were investigated: $(+)_{546}$-*cis*-$[Co(H_2O)_2en_2]X_3\cdot 2H_2O$ (X=Cl or Br), $(+)_{589}$-*cis*-$[CoCl(H_2O)en_2]Cl_2\cdot H_2O$, $(-)_{589}$-*cis*-$[CoCl(H_2O)en_2]Br_2\cdot H_2O$, $(+)_{589}$-α-$[CoCl(H_2O)trien]Cl_2\cdot H_2O$ and $(+)_{589}$-α-$[CoCl(H_2O)trien]Br_2\cdot 2H_2O$, where en and trien denote ethylenediamine and triethylenetetramine, respectively. Thermal deaquation-anation processes for each complex were observed with a derivatograph, polarimeter, and UV and CD spectrophotometers. *cis*-$[Co(H_2O)_2en_2]Cl_3\cdot 2H_2O$ was converted into *cis*-$[CoCl(H_2O)en_2]Cl_2$ at first and then *cis*-$[CoCl_2en_2]Cl$; the stereochemical changes during the first step and the second step were found to be retention and racemization, respectively. In contrast, a predominant stereochemical change involved in the deaquation-anation of *cis*-$[Co(H_2O)_2en_2]Br_3\cdot 2H_2O$ was *cis*-to-*trans* isomerization. The deaquation-anation of *cis*-$[CoCl(H_2O)en_2]Cl_2\cdot H_2O$ and *cis*-$[CoCl(H_2O)en_2]Br_2\cdot H_2O$ was found to be accompanied by racemization and by greater parts of *cis*-to-*trans* isomerization, respectively. However, both α-$[CoCl(H_2O)trien]Cl_2\cdot H_2O$ and α-$[CoCl(H_2O)trien]Br_2\cdot 2H_2O$ undergo deaquation-anation with retention.

Werner found that *cis*- and *trans*-$[Co(H_2O)_2en_2]Cl_3$ evolve waters *in vacuo* or heating at 115 °C to yield the violet product *cis*-$[CoCl_2en_2]Cl$.[3] Chang and Wendlandt studied various *cis*- and *trans*-$[Co(H_2O)_2en_2]X_3$ complexes (X=Cl, Br or NO_3) from the standpoint of thermal deaquation-anation in the solid-phase. They suggested that the variation of the counter anions sometimes causes geometrical isomerization (*cis*↔*trans*) during the course of deaquation-anation.[4]

In addition to the isomerization, other stereochemical changes such as racemization should also be included during the course of deaquation-anation. However, no information has been obtained on such stereochemical changes, except for the report by Mathieu that (+)-*cis*-$[CoCl(H_2O)en_2]Cl_2$ racemizes when heated at 100 °C in the solid-phase.[5]

More detailed information would be obtained if optically active aqua-cobalt(III) complexes were employed for studying deaquation-anation.

We have undertaken to (1) derivatographically investigate the solid-phase deaquation-anation of three types of optically active aqua-cobalt(III) complexes: *cis*-$[Co(H_2O)_2en_2]X_3$, *cis*-$[CoCl(H_2O)en_2]X_2$ and α-$[CoCl(H_2O)trien]X_2$ (X=Cl or Br), and (2) obtain further information on the stereochemical changes during the course of deaquation-anation.

Experimental

Preparation of Complexes. $(+)_{546}$-*cis*-$[Co(H_2O)_2en_2]Cl_3\cdot 2H_2O$ (I) and $(+)_{546}$-*cis*-$[Co(H_2O)_2en_2]Br_3\cdot 2H_2O$(II) were prepared from optically active $[CoCO_3en_2]Cl$.[6]

Complex I, Found: C, 13.58; H, 6.86; N, 14.89%. Calcd for $[Co(H_2O)_2en_2]Cl_3\cdot 2H_2O$: C, 13.42; H, 6.71; N, 15.66%. $[\alpha]_{546}=300°$.

Complex II, Found: C, 10.27; H, 4.90; N, 11.42%. Calcd for $[Co(H_2O)_2en_2]Br_3\cdot 2H_2O$: C, 9.78; H, 4.94; N, 11.42%. $[\alpha]_{546}=200°$.

$(+)_{589}$-*cis*-$[CoCl(H_2O)en_2]Cl_2\cdot H_2O$ (III) and $(-)_{589}$-*cis*-$[CoCl(H_2O)en_2]Br_2\cdot H_2O$ (IV) were obtained through the resolution of racemic *cis*-$[CoCl(H_2O)en_2]Cl_2$ with ammonium (+)-3-bromocamphor-8-sulfonate ((+)-BCS).[7]

Complex III, Found: C, 15.10; H, 6.62; N, 17.43%. Calcd for $[CoCl(H_2O)en_2]Cl_2\cdot H_2O$: C, 14.94; H, 6.28; N, 17.43%. $[\alpha]_{589}=280°$.

Complex IV, Found: C, 11.87; H, 5.15; N, 13.32%. Calcd for $[CoCl(H_2O)en_2]Br_2\cdot H_2O$: C, 11.70; H, 4.88; N, 13.65%. $[\alpha]_{589}=-240°$.

$(+)_{589}$-α-$[CoCl(H_2O)trien]Cl_2\cdot H_2O$ (V) and $(+)_{589}$-α-$[CoCl(H_2O)trien]Br_2\cdot 2H_2O$ (VI) were prepared from α-$[CoCl_2trien]Cl$ and (+)-BCS.[8]

Complex V, Found: C, 20.68; H, 6.68; N, 15.95%. Calcd for $[CoCl(H_2O)trien]Cl_2\cdot H_2O$: C, 20.73; N, 16.12%. $[\alpha]_{589}=610°$.

Complex VI, Found: C, 16.08; H, 5.42; N, 12.68%. Calcd for $[CoCl(H_2O)trien]Br_2\cdot 2H_2O$: C, 15.78; H, 5.34; H, 5.34; N, 12.34%. $[\alpha]_{589}=590°$.

The other complexes, *cis*- and *trans*-$[CoCl_2en_2]Cl$,[9] $(+)_{589}$-*cis*-$[CoCl_2en_2]Cl\cdot H_2O$,[9] *cis*-$[CoBrClen_2]Br\cdot H_2O$,[10] *trans*-$[CoBrClen_2]NO_3$,[10] *cis*-$[CoBr_2en_2]Br\cdot H_2O$[11] and *trans*-$[CoBr_2en_2]NO_3$[11] were prepared in a manner similar to that described in literature, and they were used as the reference complexes.

Derivatographic Measurement. Measurements were carried out with a MOM Derivatograph Typ-OD-102 under constant flow of nitrogen at the heating rate of 1 °C/min. Five tenths grams of the samples was used in each run.

Spectral Measurement. Visible and UV, and CD spectra of the samples were recorded on a Hitachi Recording Spectrophotometer 322, and a JASCO Model DRD/UV-5 Spectrophotometer, respectively.

Polarimetric Measurement. Specific rotatory powers of the samples were measured with a JASCO Model DIP-SL Polarimeter.

Determination of the Ratios of cis- *to* trans-$[CoBr_2en_2]^+$ *and of* cis *to* trans-$[CoBrClen_2]^+$. The ratios of two isomers in the products after heating were determined spectrophotometrically in a manner similar to that reported previously.[12]

Results and Discussion

Diaquabis(ethylenediamine)cobalt(III) Complexes. $(+)_{546}$-cis-$[Co(H_2O)_2en_2]Cl_3\cdot 2H_2O$ *(I).*[13] Figure 1 shows the derivatogram of complex I, together with that of $(+)_{546}$-*cis*-$[Co(H_2O)_2en_2]Br_3\cdot 2H_2O$ (II). We see that the complex evolves three moles of water at first at 46—75 °C and then one mole of water at

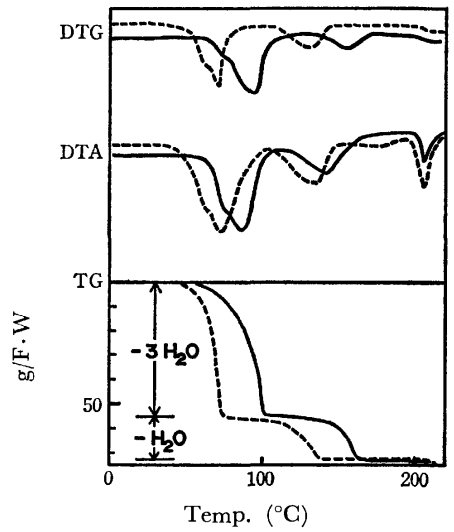

Fig. 1. Derivatograms of complexes I (----) and II (——).

112—138 °C. The initial red color of the complex turned red-violet at first and then violet in each dehydration step. The split DAT and DTG curves for the first water evolution step indicate that three moles of water are evolved in two steps.

Electronic spectra were measured in DMF solution to identify the red-violet and the violet products. Figure 2 shows the electronic spectra of complex I, the red-violet product, the violet product, and the reference complexes *cis*-$[CoCl(H_2O)en_2]Cl_2 \cdot H_2O$ and *cis*-$[CoCl_2en_2]Cl \cdot H_2O$. The numerical values for their absorption bands due to d-d transition are summarized in Table 1, together with those for the other series of complexes. Resemblance in the spectra between the red-violet product and *cis*-$[CoCl(H_2O)en_2]Cl_2 \cdot H_2O$ and between the violet product and *cis*-$[CoCl_2en_2]Cl \cdot H_2O$ proves that the original complex is converted successively into *cis*-$[CoCl(H_2O)en_2]Cl_2$ and then *cis*-$[CoCl_2en_2]Cl$.

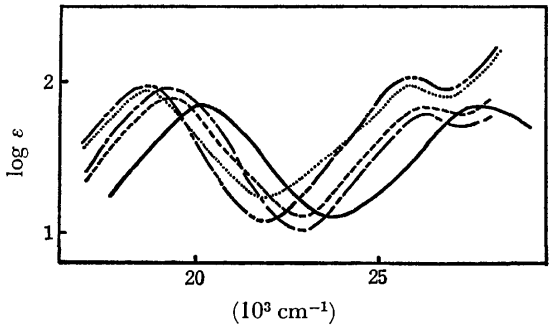

Fig. 2. Electronic spectra of complex I (——), the red-violet product (— — —), the violet product (……), and the reference complexes *cis*-$[CoCl(H_2O)en_2]Cl_2 \cdot H_2O$ (----) and *cis*-$[CoCl_2en_2]Cl \cdot H_2O$ (— — —).

CD spectra were measured to obtain information on the stereochemical changes of the complex during the course of deaquation-anation (Fig. 3). Figure 3(A) shows the CD spectra of complex I, the red-

Table 1. Absorption bands due to d-d transition (10^3 cm^{-1})

Complex	$\tilde{\nu}_I$		$\tilde{\nu}_{II}$
cis-$[Co(H_2O)_2en_2]X_3$ series[a]			
$(+)_{546}$-*cis*-$[Co(H_2O)_2en_2]Cl_2 \cdot 2H_2O$ (I)	20.20		28.10
Red-violet product	19.30		26.45
Violet product	18.66		25.57
cis-$[CoCl_2en_2]Cl \cdot H_2O$	18.64		25.52
$(+)_{546}$-*cis*-$[Co(H_2O)_2en_2]Br_3 \cdot 2H_2O$ (II)	20.20		28.10
First greenish violet product	15.27	18.18	*
Second greenish violet product	15.27	18.18	*
cis-$[CoBr_2en_2]Br \cdot H_2O$	18.10		*
trans-$[CoBr_2en_2]NO_3$	15.20	21.70(sh)[e]	*
cis-$[CoCl(H_2O)en_2]X_2$ series[a]			
$(+)_{589}$-*cis*-$[CoCl(H_2O)en_2]Cl_2 \cdot H_2O$ (III)	19.38		26.67
Violet product	18.66		25.57
$(-)_{589}$-*cis*-$[CoCl(H_2O)en_2]Br_2 \cdot H_2O$ (IV)	19.38		26.62
Greenish violet product	18.42	15.77	*
cis-$[CoBrClen_2]Br \cdot H_2O$	18.38		*
trans-$[CoBrClen_2]NO_3$	15.75		*
α-$[CoCl(H_2O)trien]X_2$ series[b]			
$(+)_{589}$-α-$[CoCl(H_2O)trien]Cl_2 \cdot H_2O$ (V)[c]	19.80		27.03
Violet product	18.48		26.30
α-$[CoCl_2$ trien$]Cl$[d]	18.52		26.32
$(+)_{589}$-α-$[CoCl(H_2O)trien]Br_2 \cdot 2H_2O$ (VI)	19.84		27.10
Violet product	18.28		*

* These bands could not be clearly detected because of the overlap with the subsequent CT bands due to Br^- ions. a) Spectra measured in DMF. b) Spectra measured in water. c) Data identical with those reported in Ref. 16. d) Data cited from Ref. 16. e) sh denotes shoulder.

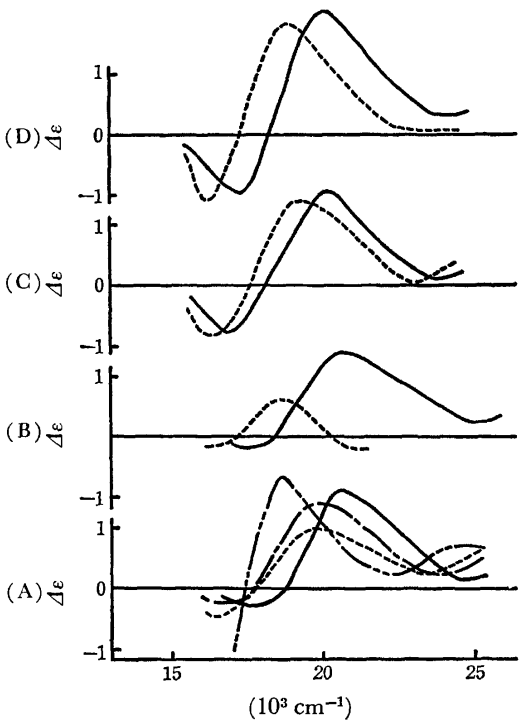

Fig. 3. CD spectra.
(A): complex I (——), the red-violet product (----), $(+)_{589}$-*cis*-$[CoCl(H_2O)en_2]Cl_2 \cdot H_2O$ (----) and $(+)_{589}$-*cis*-$[CoCl_2en_2]Cl \cdot H_2O$ (-----); (B): complex II (——) and the first greenish violet product (----); (C): complex V (——) and the violet product (----); (D): complex VI (——) and the violet product (----).

violet product and the reference complexes $(+)_{589}$-*cis*-$[CoCl(H_2O)en_2]Cl_2 \cdot H_2O$ and $(+)_{589}$-*cis*-$[CoCl_2en_2]Cl \cdot H_2O$. All the CD spectra show positive signs in similar patterns, indicating that the red-violet product still remains in an optically active form, the configuration during the process *cis*-$[Co(H_2O)_2en_2]Cl_3 \cdot 2H_2O \rightarrow$ *cis*-$[CoCl(H_2O)en_2]Cl$ being retained. The measurements of CD spectra and specific rotatory powers demonstrate that the violet product is completely optically inactive.

The stereochemical changes during the deaquation-anation of complex I are summarized in Table 2; the first step *cis*-$[Co(H_2O)_2en_2]Cl_3 \cdot 2H_2O \rightarrow$ *cis*-$[CoCl(H_2O)en_2]Cl_2$ involves retention and the second step *cis*-$[CoCl(H_2O)en_2]Cl_2 \rightarrow$ *cis*-$[CoCl_2en_2]Cl$, racemization.

$(+)_{546}$-cis-$[Co(H_2O)_2en_2]Br_3 \cdot 2H_2O$ (II). We see from the TG curve of the bromide (complex II, Fig. 1) that the mass losses of the complex take place in a pattern similar to that of the corresponding chloride (complex I) except that the former decomposes at somewhat higher temperatures than the latter. Complex II evolves three moles of water at 55—100 °C and then one mole of water at 130—162 °C. The complex changes to greenish violet from red, no further change being observed.

From the measurements of the electronic spectra of the greenish violet products obtained at the first and the second steps, it was found that both the products have two absorption bands at 15270 and 18180 cm^{-1}; these bands quite resemble the first bands of *trans*-$[CoBr_2en_2]NO_3$ (15200 cm^{-1}) and *cis*-$[CoBr_2en_2]Br \cdot H_2O$ (18100 cm^{-1}), respectively. Both the greenish violet products seem to consist of a mixture of *cis*- and *trans*-$[CoBr_2en_2]^+$.

The ratios of *cis*- to *trans*-isomers in the product were determined spectrophotometrically in a manner similar to that reported previously.[12] It was found that both the products contain 23% *cis*- and 77% *trans*-isomers. In the case of the bromide, the *cis*-to-*trans* isomerization is a predominant stereochemical change involved in the deaquation-anation.

Such a *cis*-to-*trans* isomerization inevitably causes a considerable reduction in optical activity. However, CD spectral measurements should afford another information on the stereochemical changes. Figure 3(B) shows the CD spectra of complex II and the first and the second greenish violet products (the spectrum of the second product coincides with the base line). A small but clear positive sign is seen in the CD spectrum of the first product, but none was detected in that of the second product. This suggests that optical activities still remain in the first product, but not in the second product.

We see that the stereochemical change during the process *cis*-$[Co(H_2O)_2en_2]Br_3 \cdot 2H_2O \rightarrow$ *cis*- and *trans*-$[CoBr_2en_2]Br \cdot H_2O$ involves most parts of *cis*-to-*trans* isomerization with small portions of retention and the remaining change in the process *cis*- and *trans*-$[CoBr_2en_2]Br \cdot H_2O \rightarrow$ *cis*- and *trans*-$[CoBr_2en_2]Br$ involves racemization (Table 2).

Chloroaquabis(ethylenediamine)cobalt(III) Complexes.
$(+)_{589}$-cis-$[CoCl(H_2O)en_2]Cl_2 \cdot H_2O$ (III).[13]
Figure 4 shows the derivatogram of complex III, together with that of $(-)_{589}$-*cis*-$[CoCl(H_2O)en_2]Br_2 \cdot H_2O$ (IV). Complexes III and IV evolve two moles of water in analogous fashion to each other at 70—130 °C and 45—126 °C, respectively.

The original red-violet chloride (complex III) turned violet at the end of the liberation of two moles of water. Electronic spectral measurements showed that the $\tilde{\nu}_I$ and $\tilde{\nu}_{II}$ of the violet product appear at 18660 and 25570 cm^{-1}, these values being almost the

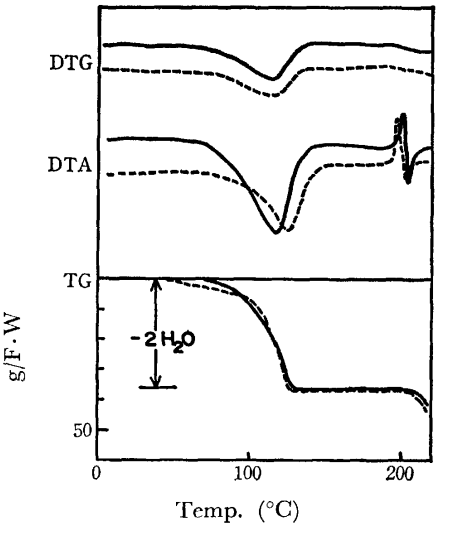

Fig. 4. Derivatograms of complexes III (——) and IV (----).

Table 2. Summary of the stereochemical changes involved in the deaquation-anation

Type of complex	X	Deaquation-anation process	Stereochemical change in the deaquation-anation
cis-$[Co(H_2O)_2en_2]X_3$ series	Cl	*cis*-$[Co(H_2O)_2en_2]Cl_3\cdot 2H_2O$ (I) (red) $\xrightarrow[46-75\,^\circ C]{-3\,H_2O}$ *cis*-$[CoCl(H_2O)en_2]Cl_2$ (red-violet) Step 1	Step 1: retention
		$\xrightarrow[112-138\,^\circ C]{-H_2O}$ *cis*-$[CoCl_2en_2]Cl$ (violet) Step 2	Step 2: racemization
	Br	*cis*-$[Co(H_2O)_2en_2]Br_3\cdot 2H_2O$ (II) (red) $\xrightarrow[55-100\,^\circ C]{-3\,H_2O}$ *cis*- and *trans*-$[CoBr_2en_2]Br\cdot H_2O$ (greenish violet) Step 1	Step 1: greater parts of *cis*-to-*trans* isomerization with small parts of retention
		$\xrightarrow[130-162\,^\circ C]{-H_2O}$ *cis*- and *trans*-$[CoBr_2en_2]Br$ (greenish violet) Step 2	Step 2: racemization
cis-$[CoCl(H_2O)en_2]X_2$ series	Cl	*cis*-$[CoCl(H_2O)en_2]Cl_2\cdot H_2O$ (III) (red-violet) $\xrightarrow[70-130\,^\circ C]{-2\,H_2O}$ *cis*-$[CoCl_2en_2]Cl$ (violet)	racemization
	Br	*cis*-$[CoCl(H_2O)en_2]Br_2\cdot H_2O$ (IV) (red-violet) $\xrightarrow[45-126\,^\circ C]{-2\,H_2O}$ *cis*- and *trans*-$[CoBrCl en_2]Br$ (greenish violet)	greater parts of *cis*-to-*trans* isomerization with small parts of racemization
α-$[CoCl(H_2O)trien]X_2$ series	Cl	α-$[CoCl(H_2O)trien]Cl_2\cdot H_2O$ (V) (red-violet) $\xrightarrow[38-105\,^\circ C]{-2\,H_2O}$ α-$[CoCl_2 trien]Cl$ (violet)	retention
	Br	α-$[CoCl(H_2O)trien]Br_2\cdot 2H_2O$ (VI) (red-violet) $\xrightarrow[50-85\,^\circ C]{-2\,H_2O}$ α-$[CoCl(H_2O)trien]Br_2$ (red-violet) Step 1	Step 1: evolution of lattice water alone
		$\xrightarrow[85-124\,^\circ C]{-H_2O}$ α-$[CoBrCl trien]Br$ (violet) Step 2	Step 2: retention

same as those (18640 and 25520 cm^{-1}) of *cis*-$[CoCl_2en_2]Cl\cdot H_2O$ (Table 1). From the CD spectra and specific rotatory powers, it was confirmed that the violet product is completely optically inactive.

It can be concluded in the case of complex III that the deaquation-anation proceeds with racemization, the result agreeing with that observed in the second step of the deaquation-anation of complex I.

$(-)_{589}$-cis-$[CoCl(H_2O)en_2]Br_2\cdot H_2O$ (IV). The bromide turned greenish violet from initial red-violet at the final stage of the evolution of two moles of water. As seen from Table 1, the electronic spectrum of the greenish violet product gives two peaks at 18.42 and 15.77 cm^{-1}, each of which satisfactorily agrees with the first bands of *cis*-$[CoBrCl en_2]Br\cdot H_2O$ (18380 cm^{-1}) and *trans*-$[CoBrCl en_2]NO_3$ (15750 cm^{-1}). This indicates that the greenish violet product is in the mixed form of *cis*- and *trans*-isomers. From the spectrophotometrical determination of the ratios of *cis*- to *trans*-isomers, it was found that the product contains 35% *cis*- and 65% *trans*-isomers.

If the configuration of the remaining *cis*-isomer were retained, the product should be, more or less, optically active. However, the measurements of CD spectra and specific rotatory powers revealed that the product is completely optically inactive. It seems that the stereochemical change during the deaquation-anation involves major parts of *cis*-to-*trans* isomerization with small portions of racemization.

Chloroaquatriethylenetetraminecobalt(III) Complexes.[13] Figure 5 shows the derivatograms of complexes V and VI. The chloride (complex V) loses two moles of water at 38—105 °C, turning violet from red-violet. The $\tilde{\nu}_I$ and $\tilde{\nu}_{II}$ for the violet product are respectively 18480 and 26300 cm^{-1}, which coincide with the values (18520 and 26320 cm^{-1}) for α-$[CoCl_2 trien]Cl$. Figure

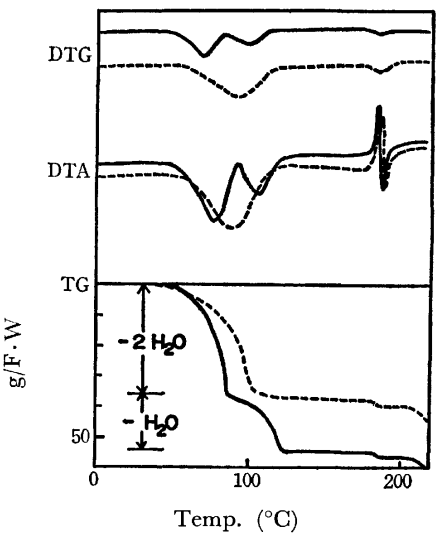

Fig. 5. Derivatograms of complexes V (----) and VI (——).

3(C) shows the CD spectra of the original chloride and the violet product. The CD spectrum of the violet product displays a positive sign similar to that of the original chloride. The measurement of the specific rotatory powers of the violet product indicates that the $[M]_D$ of the product is 2570° (Value of the reference complex α-[$CoCl_2$ trien]Cl: 2770° [8]). It can be concluded from these results that the stereochemical change during the deaquation-anation of complex V is retention.

On the other hand, the bromide (complex VI) evolves two moles of water at first at 50—85 °C and then one mole of water at 85—124 °C. The initial red-violet color of the complex remained unchanged at the first step, but changed to violet at the second step. The first step is probably simple evolution of lattice water and the second step may correspond to deaquation-anation. In the case of complex VI, the absence of the reference complexes such as α-[CoBrCltrien]$^+$ makes it impossible to identify the configuration of the violet product. However, the violet product may be regarded as optically active α-[CoBrCltrien]Br[14] for the following two reasons. Firstly, the spectrum pattern in the first band of the violet product was similar to that of α-[$CoCl_2$trien]Cl_2[8] (not shown) except that the $\tilde{\nu}_I$ of the violet product appears at slightly smaller wave number regions (18280 cm^{-1}) as compared with that (18520 cm^{-1}) of α-[$CoCl_2$trien]Cl. The slight shift may be due to the coordination of a Br^- ion as a consequence of the deaquation-anation. Secondly, the CD spectral changes observed during the deaquation-anation of complex VI are in the same tendency as that found in complex V (Fig. 3(C) and (D)). It might be concluded that the configuration is retained during the course of deaquation-anation.

LeMay and Bailar studied the solid-phase racemization of optically active *cis*-[Cr or $CoCl_2en_2$]Cl·H_2O.[15] They tentatively interpreted the racemization in terms of an aquation-anation mechanism, but obtained no conclusive experimental evidence. Their suggestion may, however, be supported by our present result in which the racemization takes place in the process *cis*-[$CoCl(H_2O)en_2$]Cl_2→*cis*-[$CoCl_2en_2$]Cl.

In the case of the bromides II and IV of the en complexes, the predominant stereochemical changes during the deaquation-anation are *cis*-to-*trans* isomerization, but the case is not the same for the corresponding trien complex.

As for the trien complexes V and VI, the configuration is retained irrespective of the kind of counter anions throughout the deaquation-anation. The trien complexes differ from the corresponding en complexes (the en complexes contain two chelate rings) as regards the inclusion of three fused chelate rings. Owing to the presence of the three fused chelate rings, the configuration of the trien complexes may be more tightly fixed than that of the en complexes.

References

1) Part XVI: R. Tsuchiya, K. Manzaki, S. Sekiya, A. Uehara, and E. Kyuno, *Bull. Chem. Soc. Jpn.*, **48**, 2805 (1975); Part XV: R. Tsuchiya, T. Ohoki, A. Uehara, and E. Kyuno, *Thermochim. Acta*, **12**, 413 (1975).

2) Presented at the 9th Symposium on the Society of Calorimetry and Thermal Analysis, Osaka, November, 1973.

3) A. Werner, *Chem. Ber.*, **40**, 263 (1907).

4) F. C. Chang and W. W. Wendlandt, *J. Inorg. Nucl. Chem.*, **32**, 3775 (1970); *Thermochim. Acta*, **1**, 495 (1970).

5) J. P. Mathieu, *Bull. Soc. Chim. Fr.*, **4**, 687 (1937).

6) F. P. Dwyer, A. M. Sargeson, and I. K. Reid, *J. Am. Chem. Soc.*, **85**, 1215 (1963).

7) Gmelins Handbuch der Anorganischen Chemie, **58B**, 168 (1930).

8) E. Kyuno, L. J. Boucher, and J. C. Bailar, Jr., *J. Am. Chem. Soc.*, **87**, 4458 (1965).

9) J. C. Bailar, Jr., *Inorg. Synth.*, **2**, 222 (1964).

10) J. W. Vaughn and R. D. Lindholm, *Inorg. Synth.*, **9**, 163 (1967).

11) Page 250 of Ref. 7.

12) R. Tsuchiya, Y. Natsume, A. Uehara, and E. Kyuno, *Thermochim. Acta*, **12**, 147 (1975).

13) (+)-$[Co(H_2O)_2en_2]^{3+}$, (+)-$[CoCl(H_2O)en_2]^{2+}$ and (+)-α-$[CoCl(H_2O)trien]^{2+}$ ions have been assigned a lamda, *Λ*, absolute configuration: L. J. Boucher, E. Kyuno, and J. C. Bailar, Jr., *J. Am. Chem. Soc.*, **86**, 3656 (1964).

14) E. Kyuno and J. C. Bailar, Jr., unpublished work.

15) H. E. LeMay and J. C. Bailar, Jr., *J. Am. Chem. Soc.*, **90**, 1729 (1968).

16) E. Kyuno and J. C. Bailar, Jr., *J. Am. Chem. Soc.*, **88**, 1120 (1966).

Copper(II) Chelates with Some Photographic Color Intermediates. Structure-Stability Relationships

Ahmad S. SHAWALI*, Ahmad E. EL-HILALY, and Mohammad S. EL-EZABY

Department of Chemistry, Faculty of Science, University of Kuwait, Kuwait

(Received November 10, 1975)

Acid dissociation constants, pK_1, of a series of benzoylacetanilides (Ia—i) have been determined potentiometrically in 50 vol% ethanol-water media at 30 °C. The stability constants, $\log \beta_1$, of their copper(II) chelates have also been determined. The effects of substituents on the anilide moiety of the ligand on the equilibria are discussed. The data were correlated by the equations: $pK_1 = 9.39 - 0.916\,\sigma$; $\log \beta_1 = 1.34\,pK_1 - 5.42$; and $\log \beta_1 = 7.20 - 1.44\,\sigma$. These results were taken to imply that the stabilization by dative metal-to-ligand π-bonding is not significant in copper(II)-benzoylacetanilide complexes.

Benzoylacetanilides (I) are useful intermediates in the color photographic process.[1] The chelating ability of these compounds to form stable metal chelates has recently elicited interest. Syntheses of iron(III),[2] copper(II),[3] oxo-vanadium(IV),[4] dioxo-molybdenum-(III),[5] dioxo-uranium(VI),[6] titanium(IV),[7] and chromium(III)[8] complexes, and reports concerning the estimation of titanium, vanadium, and mercury[4,7,9] are all that have appeared so far. In continuation of our studies on the relationship between structure and properties of I,[10,11] we have investigated the effects of substituents on the chelating tendency of a series of benzoylacetarylamides (Ia—i) towards copper(II). The acid dissociation constants and stability constants of these ligands and copper(II) cation were determined potentiometrically in 50 vol% ethanol–water solution at 30 °C ±0.1.

$C_6H_5COCH_2CONHC_6H_4R$

I

a, R=4-MeO	d, R=H	g, R=3-Cl
b, R=4-Me	e, R=3-MeO	h, R=3-Br
c, R=3-Me	f, R=4-Cl	i, R=4-EtOOC-

The object of the present work was, on one hand, to test the applicability of the Hammett equation to correlate the stability constants of copper(II)–benzoylacetanilide complexes, and on the other, to determine the extent of copper(II)-ligand π-bonding in such chelates.

Experimental

Benzoylacetanilides (Ia—i) were prepared by condensation of equimolecular amounts of ethyl benzoylacetate and the appropriate aniline as previously described.[12] The physical constants of the compounds prepared agreed with those in literature.[12,13] The stock solution of each anilide was prepared by dissolving the appropriate weight of the anilide in ethanol.

Absolute ethanol (BDH AnalaR reagent) was used. Carbonate-free sodium hydroxide solution was prepared in 50 vol% ethanol-water. A stock solution (0.1 M) copper nitrate was prepared in doubly distilled water and the copper (II) concentration was determined by standardization with EDTA using Eriochrome Black-T as indicator.[14] A solution of potassium nitrate (0.5 M) was also prepared in 50 vol% ethanol–water.

Titrations were performed using a Radiometer pH meter (type 63) equipped with a combined glass electrode type GK 2311C. The thermostated vessel of 50 ml capacity was tightly covered with a special electrode head through which passed the glass electrode, the nitrogen inlet tube and the delivery tube from the auto-burette. Auto-burette type Metrohm Herisau Multi-Dosimat E 415, accurate to ±0.01 ml was used.

In a typical titration, a 25 ml solution was prepared by mixing the appropriate volume of the ligand solution, 5 ml of potassium nitrate solution, and 0.25 ml of copper(II) solution, and the mixture was diluted to the mark. The concentration of copper(II) was always 1×10^{-3} M and those of ligand were 1×10^{-3} and 2×10^{-3} M. The solution was then transferred to the titration cell. A stream of nitrogen gas, traces of oxygen and carbon dioxide being removed by the method of Albert and Serjeant[15], was bubbled through. A complete titration consisted of successive addition of 0.05 ml or less of the titrant. One minute to two minutes after each addition, the pH meter reading was recorded. The titration was continued up to pH~7.00 in most cases. Visual precipitation occurred at pH~6.50. Each titration was repeated at least twice giving reproducibility of ±0.01 pH units along the titration. The pH readings were caliberated before, and checked after each titration using standard Radiometer buffers of pH's 4.01±0.01 and 7.00±0.01.

Calculated amounts of nitric acid and sodium hydroxide were used to check the pH in 50 vol% ethanol–water. A calibration curve was made and corrections for pH's were recorded.

Results and Discussion

The potentiometric titration curves for some of the ligands studied are illustrated in Fig. 1. No clear inflection was observed at all in the neutralization of these active methylene ligands. The acid dissociation constants of these reagents were calculated from the titration curves as follows. The pH meter readings (B) in 50 vol% ethanol–water solution are converted to hydrogen ion concentration $[H^+]$ by means of the widely used relation,[16] namely:

$$-\log [H^+] = B + \log U$$

where U is the correction factor. The value of $\log U$ in 50 vol% ethanol–water medium at 30 °C was determined and was found to be −0.35. The pK_1 value of the ligand HL was then calculated using the equation:

$$K_1 = \frac{(aT_L + [H^+] - [OH^-])[H^+]}{T_L(1-a) - [H^+] + [OH^-]}$$

* To whom all inquiries should be addressed.

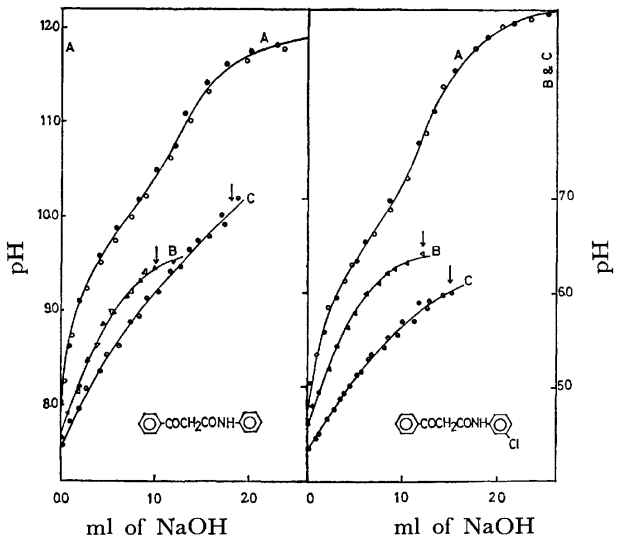

Fig. 1. Titration curves of some benzoylacetanilide-copper(II) systems in 50 vol% ethanol-water media at 30 °C, μ 0.1.
●○: ligand alone, $1.0\times10^{-}$ M
△▲: [HL]=[Cu^{2+}]=1.0×10^{-3} M
◓◒: [HL]=2.0×10^{-3}; [Cu^{2+}]=1.0×10^{-3} M.

Table 1.

Ligand	σ	$pK_1\pm s$[a)]	$\log\beta_1\pm s$	S_f[b)]
Ia	−0.27	9.68±0.03	7.56±0.03	+0.57
Ib	−0.17	9.60±0.05	7.41±0.05	+0.34
Ic	−0.07	9.45±0.04	7.22±0.05	0.00
Id	0.00	9.43±0.02	7.24±0.02	0.00
Ie	+0.05	9.40±0.03	7.10±0.06	−0.17
If	+0.23	9.20±0.03	6.89±0.04	−0.58
Ig	+0.37	9.11±0.02	6.73±0.06	−0.83
Ih	+0.39	9.10±0.02	6.80±0.05	−0.77
Ii	+0.45	8.98±0.04	6.64±0.05	−1.05

a) s=standard deviation. b) S_f=stabilization factor

where a is the ratio of the mole base added to mole of ligand. The results of the computations are given in Table 1.

The pK_1 values, so obtained, correspond to the overall dissociation constant of the two tautomers of benzoylacetanilide as given by the equation:

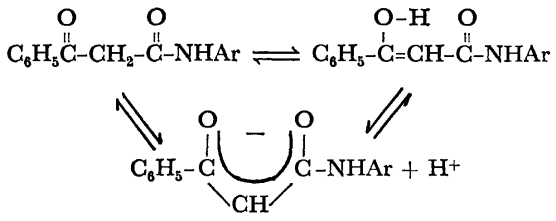

The data show that the magnitude of the pK_1 value of I depends on the nature of the substituent on the anilide ring. Electron withdrawing groups increase the acidity whereas electron-donating ones have an opposite effect. The relationship between the acidity constants, pK_1, and the Hammett substituent constant, σ, is shown in Fig. 2. It is obvious that the pK_1 values of the series studied are fairly correlated with σ constant. Using the least squares method, the values of the slope, ρ,

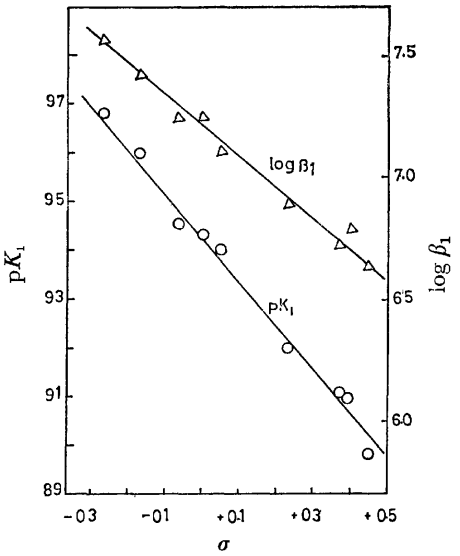

Fig. 2. Correlation of pK_1 and $\log\beta_1$ with Hammett substituent constant, σ.

and the intercept, pK_1, were found to be 0.916 and 9.39 respectively (correlation coefficient, r=0.989). The value of the reaction constant, ρ, so obtained, is somewhat higher than that (ρ=0.741) reported by Pelizzetti *et al.*[17] for related series of anilides. This difference is undoubtedly due to solvent effects.[18] The latter authors have evaluated the value of the reaction constant from measuring the dissociation constants spectrophotometrically at 25 °C in aqueous solutions containing less than 1% organic solvent.

The potentiometric titration curves for copper(II)–benzoylacetanilide systems (1 : 1; 1 : 2) are illustrated in Fig. 1. Similar curves were obtained for other systems investigated. The low solubility of the 1 : 2 Cu(II) chelates caused early precipitation during many of the titrations. Thus the stability constant, β_1, for the 1 : 1 complex species only was calculated and compared. This constant was calculated using the equation:

$$\beta_1 = \bar{n}/(1-\bar{n})L$$

where

$$L = ((1-a)T_L-[H^+])/([H^+]/K_1)$$

and

$$\bar{n} = T_L-(L([H^+]/K_1)+1))/T_M.$$

In these equations T_L and T_M correspond to the total ligand and metal ion concentrations used respectively, and $\bar{n}$ is the average number of ligand bound to the metal ion. The calculated values of $\log\beta_1$ are summarized in Table 1.

As the relation between Cu(II) and these ligands is regarded as a Lewis acid-base reaction, the $\log\beta_1$ value is plotted against the acid dissociation constant, pK_1, in Fig. 3. As shown, the $\log\beta_1$ values are linearly related to the pK_1 values. This implies that the stability of the chelates is mainly dependent upon the basicity, *i.e.*, the pK_1 value, of the ligand. A slope value of 1.34 of the straight line obtained (Fig. 3) was found as calculated by the least squares method. This result suggests that Cu(II) in the complexes studied does

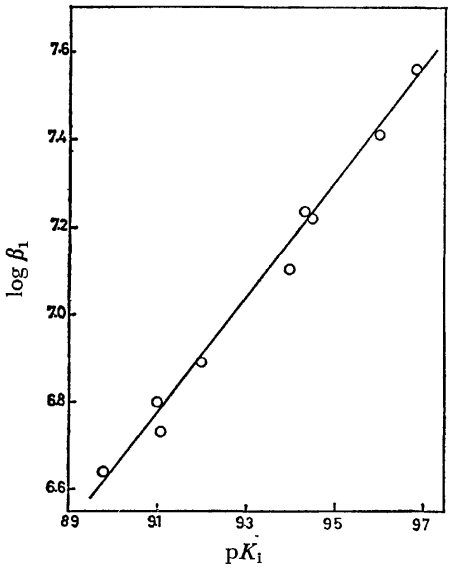

Fig. 3. Relation between acid dissociation constants of benzoylacetanilides, pK_1, and stability constants, log β_1, of their copper(II) chelates.

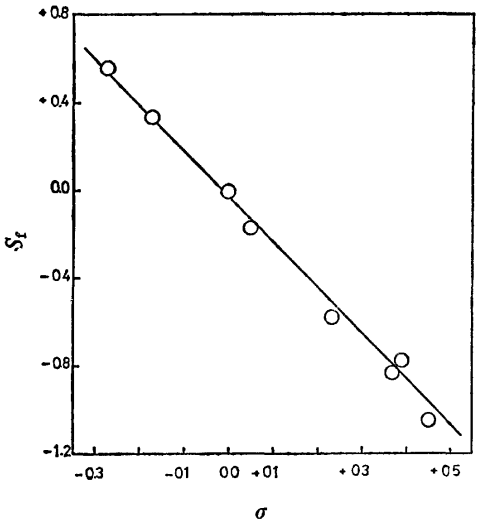

Fig. 4. Correlation of stabilization factor, S_f, with Hammett substituent constant, σ, for 1 : 1 complexes of copper(II) with benzoylacetanilides.

not function as π-electron donor, as it was suggested for copper(II) complexes with substituted benzoic acids.[19] If the 1 : 1 complexes of benzoylacetanilides with Cu(II) were stabilized by back-electron donation from the metal ion to the ligand, the slope of the plot of log β_1 *vs.* pK_1 should be less than unity.[20]

In order to confirm the foregoing conclusion, the stability constants, log β_1 (Table 1), were correlated with the Hammett substituent constant, σ. Figure 2 shows such a correlation. The equation of the straight line obtained is:

$$\log \beta_1 = 7.20 - 1.44\,\sigma.$$

The goodness of this correlation can be judged from the value of the correlation coefficient, r, of 0.955. This observed linear correlation indicates that the mode of chelation between Cu(II) and the ligand does not vary with the substituent; otherwise irregularities would have resulted. Again, the negative value of the reaction constant, *i.e.*, the slope of the plot, can only mean that the reaction studied is favored by electron donation to the metal. This explanation is further supported by plotting the so-called stabilization factor, S_f,[21] defined by the equation:

$$S_f = \log (\beta_1/K_1)_X - \log (\beta_1/K_1) = \rho\sigma$$

versus σ. As shown in Fig. 4, the plot is linear with a nagative slope; $S_f = -2.124\,\sigma$. This result is contrary to what has been reported for Cu(II) complexes of substituted benzoic acids, and for pyridine adducts of Cu(II) acetylacetonates.[21,22] Accordingly, it is not unreasonable to conclude that the explanation of the stabilization of Cu(II) complexes, based on the back donation of electrons from the metal to the ligand, does not seem likely in the Cu(II)–benzoylacetanilide chelates. This conclusion is also in agreement with the recently reported[3] spectral characteristics of the solid benzoylacetanilide complexes of copper(II).

References

1) C. E. K. Mees, "The Theory of the photographic process," MacMillan, New York (1969).
2) A. Syamal, *Can. J. Chem.*, **46**, 1693 (1969); K. P. Srivastava and A. D. Taneja, *Microchem. J.*, **17**, 540 (1972).
3) P. R. Johnson and D. A. Thornton, *J. Inorg. Nucl. Chem.*, **37**, 461 (1975) and the references cited therein.
4) A. K. Sarker and J. Das, *Anal. Lett.*, **1**, 323 (1968).
5) A. Syamal, *J. Indian Chem. Soc.*, **45**, 755 (1968).
6) A. Syamal, *J. Inorg. Nucl. Chem.*, **4**, 543 (1968); S. K. Mandel and J. Das, *J. Indian Chem. Soc.*, **50**, 426 (1973).
7) A. K. Sarker and J. Das, *Anal. Chem.*, **39**, 1608 (1967); A. Syamal, *J. Inorg. Nucl. Chem.*, **31**, 1850 (1969).
8) A. Syamal, *J. Prakt. Chem.*, **312**, 954 (1971); A. D. Taneja and K. P. Srivastava, *J. Inorg. Nucl. Chem.*, **34**, 3573 (1972).
9) N. Chaudhuri and J. Das, *J. Indian Chem. Soc.*, **50**, 446 (1973).
10) A. S. Shawali, M. M. Naoum, and S. A. Ibrahim, *Bull. Chem. Soc. Jpn.*, **45**, 2504 (1972).
11) A. S. Shawali and B. Akrawi, *Indian J. Chem.*, **12**, 1074 (1974).
12) C. J. Kibler and A. Weissberger, "Organic Synthesis," Coll. Vol. III, p. 108 (1955).
13) G. H. Brown, J. Figueras, R. J. Gledhill, C. J. Kibler, F. C. McCrossen, S. M. Parmerter, P. W. Vittum, and A. Weissberger, *J. Am. Chem. Soc.*, **79**, 2929 (1957).
14) G. Schwarzenbach and H. Flaschka, "Complexometric Titrations," 2nd ed, translated by H. M. N. H. Irving, Methuen & Co., N. Y. (1969).
15) A. Albert and E. P. Serjeant, "Ionization Constants of Weak Acids and Bases," John Wiley & Sons, N. Y. (1962), p. 20.
16) L. G. Van Uitert and C. G. Haas, *J. Am. Chem. Soc.*, **75**, 451 (1953).
17) E. Pelizzetti and C. Verdi, *J. Chem. Soc., Perkin II*, **1973**, 808.
18) J. E. Leffler and E. Grunwald, "Rates and Equilibria of Organic Reactions," John Wiley & Sons, N. Y. (1963).
19) W. May and M. Jones, *J. Inorg. Nucl. Chem.*, **24**, 511 (1962).
20) J. G. Jones and J. B. Poole, J. C. Tomkinson, and R. J. P. Williams, *J. Chem. Soc.*, **1958**, 2001.
21) J. J. R. Da Silva and J. G. Calado, *J. Inorg. Nucl. Chem.*, **28**, 125 (1966).
22) W. May and M. Jones, *J. Inorg. Nucl. Chem.*, **25**, 507 (1963).

Non-isothermal Studies of Adduct Molecules of Metallic Halides with Oxo Compounds in Solid State. II

N. Ray CHAUDHURI and S. MITRA

Inorganic Chemistry Laboratory, Indian Association for the Cultivation of Science, Calcutta 700032, India

(Received April 28, 1975)

Non-isothermal studies of several adduct molecules of metallic halides with oxo-compounds as the type $MX_2(THF)_y$ in solid state were carried out with a Derivatograph, where M is Mn(II), Co(II), Ni(II), Cu(II) or Cd(II), X is Cl^- or Br^-, THF is the abbreviated form of tetrahydrofuran and y is 0.25—2.00. These adduct molecules lost tetrahydrofuran in single or multiple steps upon heating. Thermally stable intermediate products were isolated and characterised by elemental analysis and IR spectral measurement. The activation energy for each step of decomposition of the adducts was evaluated from the analysis of TG, DTG, and DTA curves of the respective derivatograms. Enthalpy change was evaluated from DTA peak area and order of reaction was found to be unity for each step of decomposition. Thermal parameters for the above adducts were compared with those of the adducts of dioxane.

The works on the adduct molecules with tetrahydrofuran had been carried out by several workers.[1-13] They only prepared and characterised some adduct molecules of metallic halides with tetrahydrofuran. Rossmanith and Blaha[8,10] studied the thermal decomposition of the adducts of some rare earth bromides. On the other hand, Barnes and Duncan[12] carried out the thermal decomposition of tetrahydrofuran adducts of $CdCl_2$ and $CdBr_2$ with differential scanning calorimeter. They reported the value of enthalpy changes and decomposition temperatures of the adducts. But they did not evaluate the activation energy and order of reaction for the decomposition of the adducts.

In continuation of our previous work on dioxane,[14] the present paper deals with thermal decomposition of tetrahydrofuran adducts of some metallic halides to evaluate the activation energy for decomposition of the adducts from the results by the simultaneous TG, DTG and DTA measurements as well as the order of reaction (n) from TG curve, ΔH from DTA peak area and thermal stability from the first DTG peak temperature. This paper reveals a comparative picture on the thermal properties of the adducts which are similar in composition and also discusses the thermal properties of the adducts with tetrahydrofuran comparing with those of dioxane[14] studied by us.

Experimental

All the adducts were prepared by using the method described in the earlier work[14] and characterised by elemental analysis and IR spectral measurement. The tetrahydrofuran used was sufficiently purified according to the standard procedure.[15]

The following adducts of the metal halides were prepared

1. $MnCl_2 \cdot 0.50$ THF
2. $MnBr_2 \cdot 2.00$ THF
3. $CoCl_2 \cdot 0.50$ THF
4. $NiCl_2 \cdot 0.25$ THF
5. $NiBr_2 \cdot 0.75$ THF
6. $CuCl_2 \cdot 0.70$ THF
7. $CuBr_2 \cdot 1.00$ THF
8. $CdCl_2 \cdot 1.00$ THF
9. $CdBr_2 \cdot 1.00$ THF

where THF represents tetrahydrofuran.

A Paulik-Paulik-Erdey type MOM Derivatograph was used for thermal analysis. The particle size of the sample was 150—200 mesh. Heating rate was 1.5 °C/min. The volume of the sample in each run was nearly the same. Platinum crucible was used for these studies. All these experiments were conducted in static air.

Results

The adducts of $CuBr_2$, $CdCl_2$ and $CdBr_2$ have the similar composition to each other and lose one molecule of THF in a single step upon heating as indicated by their respective derivatograms in Fig. 1. While the composition of the adduct of $NiBr_2$ is not similar to that of the above adducts, it loses all molecules of THF in a single step as shown in Fig. 2. Derivatogram of $NiCl_2 \cdot 0.25$ THF in Fig. 3 shows a single step decomposition, whereas its DTA and DTG curves are indicative of double step decomposition. The adducts of $MnCl_2$ and $CoCl_2$ are similar in composition and they lose THF molecule in two steps passing through an intermediate as follows: $MCl_2 \cdot 0.50\ THF \rightarrow MCl_2 \cdot 0.25\ THF$ where M=Mn(II) or Co(II). From the comparison of the TG curve of these two adducts, the range giving a plateau in $MnCl_2 \cdot 0.25$ THF is slightly larger than that of $CoCl_2 \cdot 0.15$ THF. The adduct $CuCl_2 \cdot 0.70$ THF loses oxo-compound in three steps upon heating in the following way as seen in Fig. 2: $CuCl_2 \cdot 0.70\ THF \rightarrow CuCl_2 \cdot 0.50\ THF \rightarrow CuCl_2 \cdot 0.50\ THF/CuCl_2$. The TG curve of $CuCl_2 \cdot 0.70$ THF shows that decomposition of $CuCl_2 \cdot 0.50\ THF \rightarrow CuCl_2 \cdot 0.15$ THF is more rapid than the decomposition of $CuCl_2 \cdot 0.15\ THF \rightarrow CuCl_2$ though both the intermediate products *i.e.*, $CuCl_2 \cdot 0.50$ THF and $CuCl_2 \cdot 0.15$ THF are thermally unstable. The adduct $MnBr_2 \cdot 2.00$ THF loses tetrahydrofuran molecules in three steps as observed in Fig. 3 as follows: $MnBr_2 \cdot 2.00\ THF \rightarrow MnBr_2 \cdot 1.00\ THF \rightarrow MnBr_2 \cdot 0.88\ THF \rightarrow MnBr_2$. The intermediate $MnBr_2 \cdot 1.00$ THF is thermally stable, whereas $MnBr_2 \cdot 0.88$ THF is thermally unstable as observed in its thermogram. However, the existence of $MnBr_2 \cdot 0.88$ THF was verified by repeated analysis.

The decomposition of all the adducts gives endotherm in DTA. Temperature ranges of decomposition and DTG peak temperatures for the adducts are listed in the second and third columns in Table 1 respectively. Enthalpy change for each step of decomposition of the adducts was evaluated by the method of Sano[16] using copper sulfate pentahydrate as the standard and the values are also tabulated in the last column in Table 1. When the two DTA curves are too much overlapped with each other, the ΔH

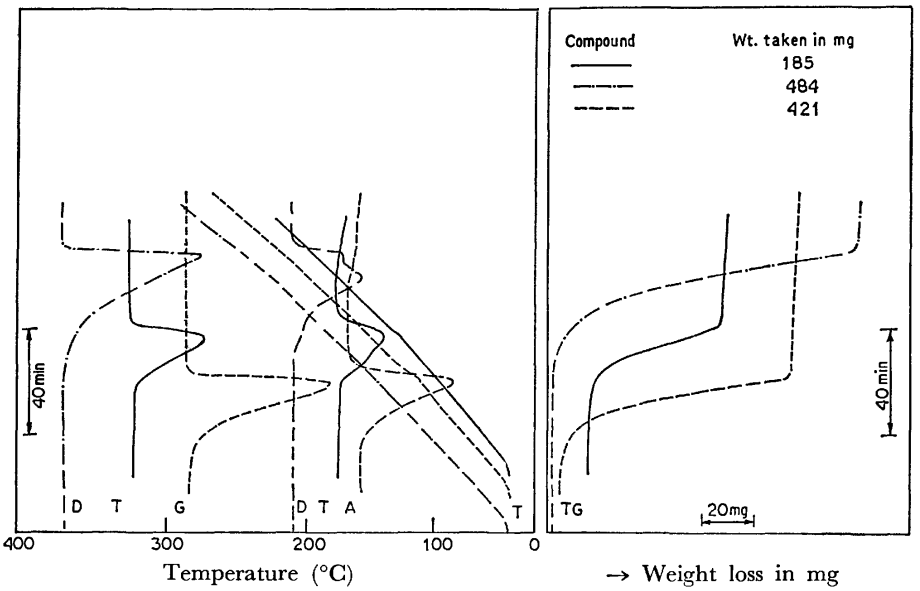

Fig. 1. The derivatograms for $CdCl_2 \cdot 1.00$ THF (——), $CuBr_2 \cdot 1.00$ THF (—·—) and $CdBr_2 \cdot 1.00$ THF (----).

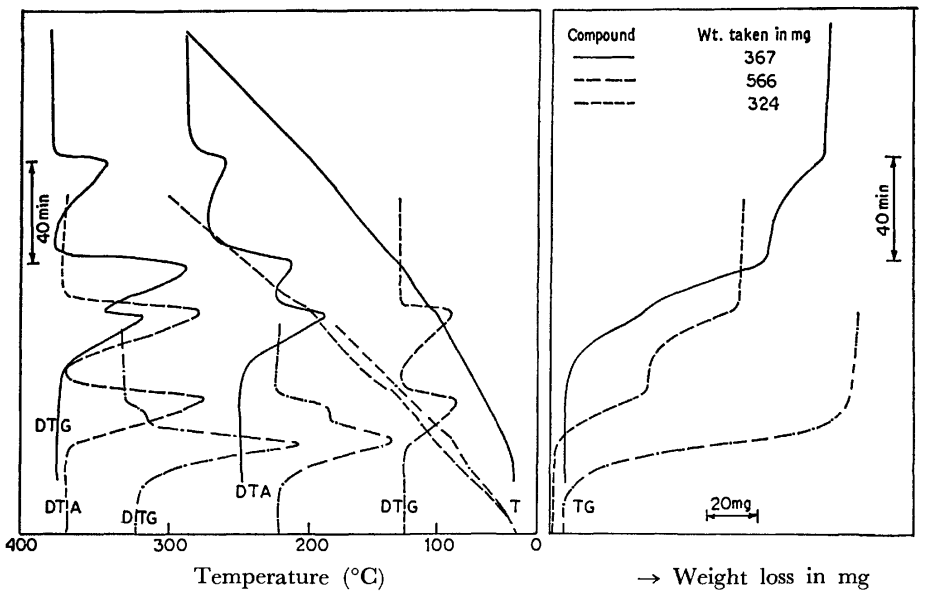

Fig. 2. The derivatograms for $CuCl_2 \cdot 0.70$ THF (——), $NiBr_2 \cdot 0.75$ THF (—·—) and $MnCl_2 \cdot 0.50$ THF (----).

values are evaluated from the overall area of the DTA peaks concerned.

The activation energy for each step of decomposition of the adduct molecules was evaluated from the analysis of the TG curves using Freeman and Carroll's[17] equation. The values are tabulated in the fourth column of Table 1 and the plots of

$$\Delta \log \frac{dw}{dt} \Big/ \Delta \log W_r \text{ vs. } [\Delta T^{-1} / \Delta \log W_r] \times 10^3$$

from TG curves are shown in Fig. 4.

The corresponding values were also evaluated from the analysis of the DTG curve using Dave and Chopra's[18] equation and from the analysis of DTA curve using Brochardt's[19] equation for the first order reaction. These values are tabulated in the fifth and sixth columns in Table 1 respectively. Arrhenius plots of $\log k$ *vs.* $T^{-1} \times 10^3$ from DTG and DTA curves are shown in Figs. 5 and 6 respectively.

IR spectra of the adducts were taken to ensure the presence of tetrahydrofuran molecule in the adduct.

Discussion

The adduct of $MnCl_2$ has been isolated as $MnCl_2 \cdot 1.50$ THF by some workers.[5,12] We have failed to isolate $MnCl_2 \cdot 1.50$ THF. The adduct of this salt with THF we isolated differs in composition from the corresponding adduct with dioxane (D) studied by us. The dioxane adduct of this salt lost oxo compounds in a single step upon heating, whereas $MnCl_2 \cdot 0.50$ THF loses tetrahydrofuran in double step passing

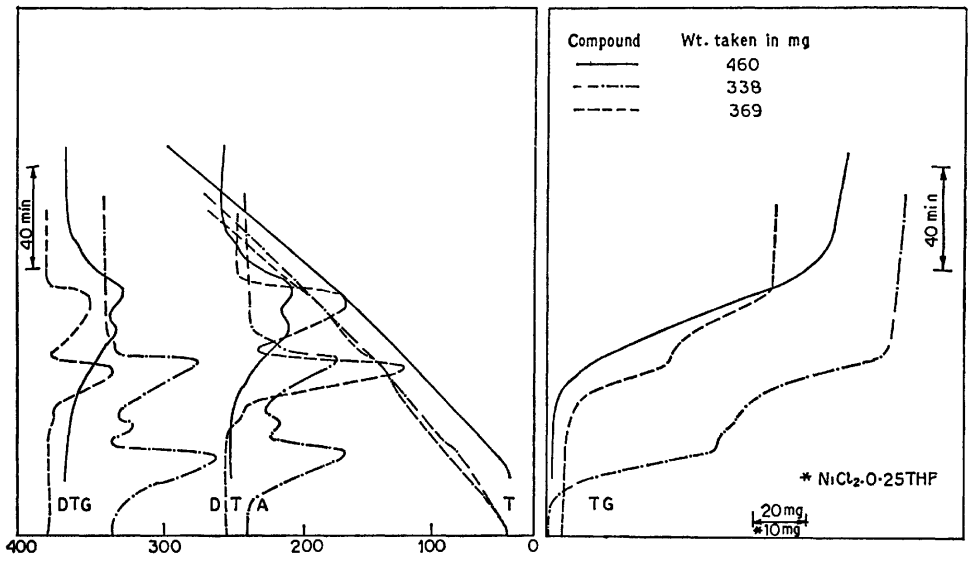

Fig. 3. The derivatograms for $NiCl_2 \cdot 0.25$ THF (——), $MnBr_2 \cdot 2.00$ THF (—·—) and $CoCl_2 \cdot 0.50$ THF (----).

Table 1. Thermal parameters for the decomposition of adduct molecules of some metallic halides with tetrahydrofuran

	Decomposition reactions	Temp. range °C	DTG peak temp. °C	Activation energy E_a kcal/mol of THF			Enthalpy change ΔH kcal/mol of THF
				TG	DTG	DTA	
Ia.	$MnCl_2 \cdot 0.50L \rightarrow MnCl_2 \cdot 0.25L$	88—135	125	41.4	39.0	41.4	61.5
b.	$MnCl_2 \cdot 0.25L \rightarrow MnCl_2$	157—205	195	72.2	71.5	71.5	58.6
IIa.	$MnBr_2 \cdot 2.00L \rightarrow MnBr_2 \cdot 1.00L$	41— 80	73	30.7	30.7	30.7	18.2
a'.	$MnBr_2 \cdot 1.00L \rightarrow MnBr_2 \cdot 0.88L$	95—108	100	b)	b)	b)	b)
b.	$MnBr_2 \cdot 0.88L \rightarrow MnBr_2$	108—148	140	55.2	55.2	55.2	22.5
IIIa.	$CoCl_2 \cdot 0.50L \rightarrow CoCl_2 \cdot 0.25L$	100—145	127	41.8	37.6	37.6	62.5
b.	$CoCl_2 \cdot 0.25L \rightarrow CoCl_2$	145—205	192	46.0	46.0	46.0	57.7
IV.	$NiCl_2 \cdot 0.25L \rightarrow NiCl_2$	78—234	145	30.7	b)	b)	45.0[a]
V.	$NiBr_2 \cdot 0.75L \rightarrow NiBr_2$	40—126	88	19.7	b)	b)	19.1
VIa.	$CuCl_2 \cdot 0.70L \rightarrow CuCl_2 \cdot 0.50L$	63— 98	94	38.9	b)	b)	38.8[a]
b.	$CuCl_2 \cdot 0.50L \rightarrow CuCl_2 \cdot 0.15L$	98—135	128	44.2	b)	b)	
c.	$CuCl_2 \cdot 0.15L \rightarrow CuCl_2$	135—200	197	36.0	36.0	36.0	24.1
VII.	$CuBr_2 \cdot 1.00L \rightarrow CuBr_2$	155—250	244	34.5	35.5	b)	14.7
VIII.	$CdCl_2 \cdot 1.00L \rightarrow CdCl_2$	80—135	125	31.2	32.9	29.6	12.7 (10.4 ± 0.2)[c]
IX.	$CdBr_2 \cdot 1.00L \rightarrow CdBr_2$	36—116	108	28.8	33.4	33.4	15.4 (15.1 ± 0.4)[c]

L: Represents tetrahydrofuran. a) Indicates overall enthalpy change. b) Evaluation of activation energy was not possible due to overlapping of the corresponding curves. c) Value in the parentheses evaluated by Barnes and Duncan.

through a thermally stable intermediate $MnCl_2 \cdot 0.25$ THF. The thermal stability of $MnCl_2 \cdot 1.00$ D is greater than that of $MnCl_2 \cdot 0.50$ THF but smaller than that of $MnCl_2 \cdot 0.25$ THF. The value of activation energy and enthalpy change for the decomposition of both the steps of this adduct are high in comparison with that of the adduct with dioxane.

The composition of the adducts $MnBr_2 \cdot 2.00$ THF is similar to the corresponding adduct with dioxane but their nature of decomposition differs from each other. Dioxane adduct of the salt lost oxo compound in two steps passing through a thermally stable intermediate $MnBr_2 \cdot 1.00$ D. Whereas, the corresponding tetrahydrofuran adduct loses oxo compound in three steps passing through a stable intermediate $MnBr_2 \cdot 1.00$ THF like dioxane and then through an unstable intermediate $MnBr_2 \cdot 0.88$ THF. The thermal stability of $MnBr_2 \cdot 2.00$ THF is low in comparison with that of the corresponding adduct with dioxane. The activation energy for the first step of decomposition of the adduct with tetrahydrofuran is also low in comparison with that of the dioxane but the value of enthalpy of this adduct is high in comparison with that of the adduct with dioxane. The thermal stability of the

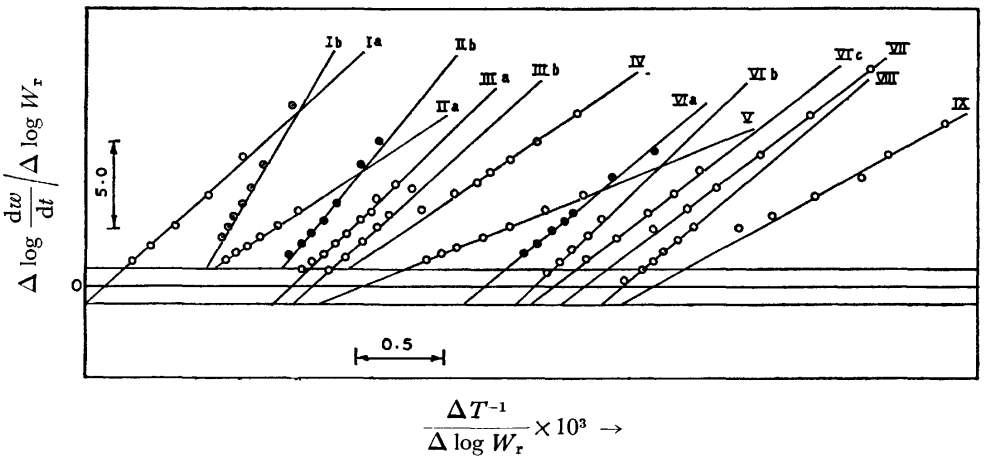

Fig. 4. Plots of $\Delta \log \frac{dw}{dt} / \Delta \log W_r$ *vs.* $\Delta T^{-1} / \Delta \log W_r \times 10^3$ from TG for the decomposition of $MnCl_2 \cdot 0.50\ THF \rightarrow MnCl_2 \cdot 0.25\ THF$ (Ia), $MnCl_2 \cdot 0.25\ THF \rightarrow MnCl_2$ (Ib), $MnBr_2 \cdot 2.00\ THF \rightarrow MnBr_2 \cdot 1.00\ THF$ (IIa), $MnBr_2 \cdot 0.88\ THF \rightarrow MnBr_2$ (IIb), $CoCl_2 \cdot 0.50\ THF \rightarrow CoCl_2 \cdot 0.25\ THF$ (IIIa), $CoCl_2 \cdot 0.25\ THF \rightarrow CoCl_2$ (IIIb), $NiCl_2 \cdot 0.25\ THF \rightarrow NiCl_2$ (IV), $NiBr_2 \cdot 0.75\ THF \rightarrow NiBr_2$ (V), $CuCl_2 \cdot 0.70\ THF \rightarrow CuCl_2 \cdot 0.50\ THF$ (VIa), $CuCl_2 \cdot 0.50\ THF \rightarrow CuCl_2 \cdot 0.15\ THF$ (VIb), $CuCl_2 \cdot 0.15\ THF \rightarrow CuCl_2$ (VIc), $CuBr_2 \cdot 1.00\ THF \rightarrow CuBr_2$ (VII), $CdCl_2 \cdot 1.00\ THF \rightarrow CdCl_2$ (VIII) and $CdBr_2 \cdot 1.00\ THF \rightarrow CdBr_2$ (IX).

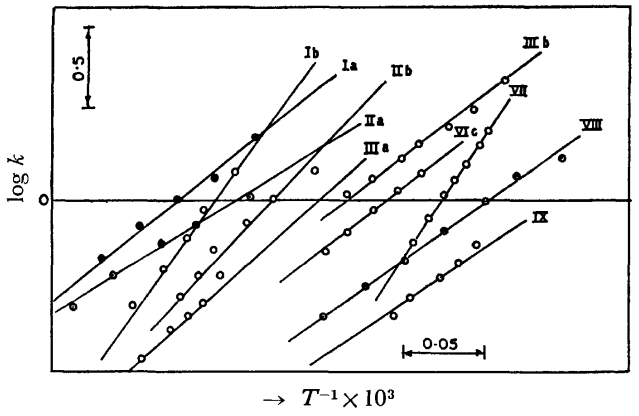

Fig. 5. Arrhenius plots of $\log k$ *vs.* $T^{-1} \times 10^3$, from DTG for the decomposition of $MnCl_2 \cdot 0.50\ THF \rightarrow MnCl_2 \cdot 0.25\ THF$ (Ia), $MnCl_2 \cdot 0.25\ THF \rightarrow MnCl_2$ (Ib), $MnBr_2 \cdot 2.00\ THF \rightarrow MnBr_2 \cdot 1.00\ THF$ (IIa), $MnBr_2 \cdot 0.88\ THF \rightarrow MnBr_2$ (IIb), $CoCl_2 \cdot 0.50\ THF \rightarrow CoCl_2 \cdot 0.25\ THF$ (IIIa), $CoCl_2 \cdot 0.25\ THF \rightarrow CoCl_2$ (IIIb), $CuCl_2 \cdot 0.15\ THF \rightarrow CuCl_2$ (VIc), $CuBr_2 \cdot 1.00\ THF \rightarrow CuBr_2$ (VII), $CdCl_2 \cdot 1.00\ THF \rightarrow CdCl_2$ (VIII) and $CdBr_2 \cdot 1.00\ THF \rightarrow CdBr_2$ (IX).

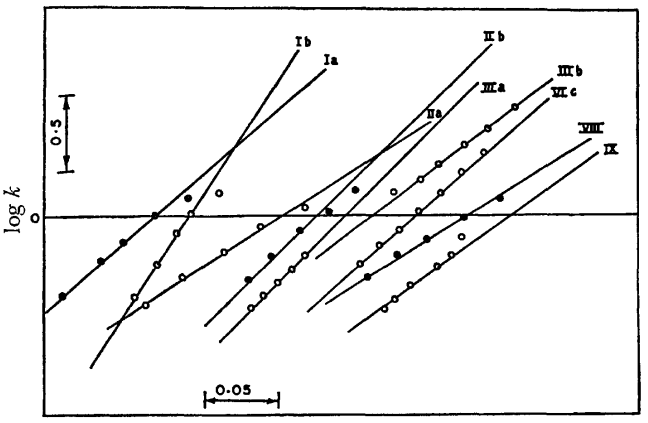

Fig. 6. Arrhenius plots of $\log k$ *vs.* $T^{-1} \times 10^3$, from DTA for the decomposition of $MnCl_2 \cdot 0.50\ THF \rightarrow MnCl_2 \cdot 0.25\ THF$ (Ia), $MnCl_2 \cdot 0.25\ THF \rightarrow MnCl_2$ (Ib), $MnBr_2 \cdot 2.00\ THF \rightarrow MnBr_2 \cdot 1.00\ THF$ (IIa), $MnBr_2 \cdot 0.88\ THF \rightarrow MnBr_2$ (IIb), $CoCl_2 \cdot 0.50\ THF \rightarrow CoCl_2 \cdot 0.25\ THF$ (IIIa), $CoCl_2 \cdot 0.25\ THF \rightarrow CoCl_2$ (IIIb), $CuCl_2 \cdot 0.15\ THF \rightarrow CuCl_2$ (VIc), $CdCl_2 \cdot 1.00\ THF \rightarrow CdCl_2$ (VIII) and $CdBr_2 \cdot 1.00\ THF \rightarrow CdBr_2$ (IX).

intermediate $MnBr_2 \cdot 1.00\ THF$ is also low in comparison with $MnBr_2 \cdot 1.00\ D$.

The adducts of $CoCl_2$ with tetrahydrofuran isolated by Kern[5] and also by Fowles *et al.*[13] were similar in composition *i.e.*, $CoCl_2 \cdot 1.50\ THF$. We isolated the adduct of the same salt with tetrahydrofuran as $CoCl_2 \cdot 0.50\ THF$ which is similar in composition to the adduct with dioxane isolated by us. The composition and the nature of decomposition of $CoCl_2 \cdot 0.50\ THF$ are similar to the adduct of $MnCl_2$ with this oxo compound. Both undergo decomposition through an intermediate $MCl_2 \cdot 0.25\ THF$, where M=Co or Mn. Although the adduct of the same salt with dioxane is similar in composition, it eliminated oxo compound in single step. The values of activation energy and enthalpy change for the decomposition of $CoCl_2 \cdot 0.50\ THF \rightarrow CoCl_2 \cdot 0.25\ THF$ are slightly low in comparison with that of the decomposition $MnCl_2 \cdot 0.50\ THF \rightarrow MnCl_2 \cdot 0.25\ THF$. The activation energy for the decomposition of $CoCl_2 \cdot 0.25\ THF \rightarrow CoCl_2$ is very low in comparison with that for the corresponding step of decomposition of adduct of $MnCl_2$ with THF, whereas the value of enthalpy change for the decomposition of $CoCl_2 \cdot 0.25\ THF$ is slightly higher than the corresponding adduct of $MnCl_2$ with dioxane. It is observed that the activation energy and enthalpy change for the decomposition of $CoCl_2 \cdot 0.50\ D \rightarrow CoCl_2$ is low in comparison with those for the decomposition of the corresponding adduct of $CoCl_2$ with THF though

$CoCl_2 \cdot 0.50$ D decomposes at a temperature higher than that of $CoCl_2 \cdot 0.50$ THF. This may be due to the fact that the adducts differ from each other in the nature of decomposition.

Kern[5] isolated the adduct of $NiCl_2$ as $NiCl_2 \cdot 2.00$ THF by starting from $NiCl_2 \cdot CH_3CN$ complex. Whereas we isolated the adduct as $NiCl_2 \cdot 0.25$ THF alone by starting from anhydrous nickel chloride. The composition of this adduct is similar to that of the intermediate product of the adducts of $MnCl_2$ and $CoCl_2$ with this oxo compound but differs from the adduct of the same salt with dioxane. The thermal stability and the values of activation energy and enthalpy change of decomposition of $NiCl_2 \cdot 0.25$ THF are lower than those of the decomposition of $MnCl_2 \cdot 0.25$ THF$\rightarrow MnCl_2$ and $CoCl_2 \cdot 0.25$ THF$\rightarrow CoCl_2$. Whereas the value of activation energy of decomposition of $NiCl_2 \cdot 1.50$ D$\rightarrow NiCl_2$ is close to the value obtained for the decomposition of $NiCl_2 \cdot 0.25$ THF though the value of enthalpy change for the decomposition of the latter is higher than that of the former.

We isolated the adduct of $NiBr_2$ with this present oxo-compound as $NiBr_2 \cdot 0.75$ THF, but the adduct of dioxane we isolated was simple in composition, though single step of decomposition is observed in both the adducts. This adduct molecule is thermally less stable than the adduct with dioxane. The value of activation energy of this adduct is also lower than that of the adduct with dioxane. Whereas, enthalpy change of $NiBr_2 \cdot 0.70$ THF is higher than that of the adduct with dioxane.

The adduct of $CuCl_2$ with THF was reported earlier by Kern[5] as $CuCl_2 \cdot 0.80$ THF. We isolated the adduct of $CuCl_2$ as $CuCl_2 \cdot 0.70$ THF. The dioxane adduct of $CuCl_2$ was reported earlier by us[14] as $CuCl_2 \cdot 0.75$ D which lost oxo compound in single step, whereas the adduct $CuCl_2 \cdot 0.70$ THF loses oxo compounds in three steps. The thermal stability of the adduct $CuCl_2 \cdot 0.70$ THF is lower than that of the adduct with dioxane we isolated. Whereas, the value of activation energy of this adduct is higher than that of the adduct with dioxane. The intermediate product $CuCl_2 \cdot 0.50$ THF shows similarity in composition with the adduct of $MnCl_2$ and $CoCl_2$ with this oxo compound. The thermally unstable $CuCl_2 \cdot 0.50$ THF decomposes through an intermediate $CuCl_2 \cdot 0.15$ THF which differs in composition from the intermediate product of the adduct of $MnCl_2$ and $CoCl_2$ with THF.

The composition of the adduct of $CuBr_2$ with THF is not similar to that of the adduct of the same salt with dioxane and $CuBr_2 \cdot 1.00$ D as an intermediate product of $CuBr_2 \cdot 2.00$ D corresponds to the adduct with this oxo compound isolated by us. The adduct $CuBr_2 \cdot 1.00$ THF decomposes at higher temperature than that of adduct with dioxane. The activation energy for the decomposition of this adduct is slightly lower than that of the adduct with dioxane but the corresponding enthalpy change is high in comparison with that of the dioxane adduct.

The adduct $CdCl_2 \cdot 1.00$ THF isolated by us is similar in composition to the adduct reported earlier.[12] The composition of dioxane adduct of $CdCl_2$ differs from the adduct of the same salt with tetrahydrofuran but both the adducts lose their oxo compounds in a single step upon heating. The thermal stability, activation energy and enthalpy change for decomposition of this tetrahydrofuran adduct is lower than those of the adduct with dioxane. Barnes and Duncan[12] investigated the thermal decomposition of $CdCl_2 \cdot 1.00$ THF with differential scanning calorimeter, where the heating rate was 8 °C/min. The initial decomposition temperature and peak temperature for this adduct reported by them were 105 and 147 °C respectively. Whereas we observe 80 and 125 °C as the initial decomposition temperature and peak temperature respectively, though the value of enthalpy change evaluated by us is very close to the value reported by them.

The tetrahydrofuran adduct of $CdBr_2$ reported earlier[12] is same in composition to the adduct isolated by us and also similar in composition to the corresponding adduct of dioxane.[14] Both the adducts lose their oxo compounds in a single step. This tetrahydrofuran adduct is thermally less stable than the corresponding dioxane adduct. Whereas, the values of activation energy and enthalpy change for the decomposition of adduct with tetrahydrofuran are very close to that of dioxane. Barnes and Duncan[12] also carried out the thermal decomposition of $CdBr_2 \cdot 1.00$ THF and reported 62 and 177 °C as initial and maximum decomposition temperatures respectively, whereas in our cases these temperatures are 36 and 108 °C respectively. But the value of enthalpy change evaluated by them is very close to the value reported by us.

Thermal stability of the adducts of the composition $MBr_2 \cdot 1.00$ THF where M=Mn(II), Cu(II) and Cd(II) owing to the difference of DTG peak temperature increases in the order Mn<Cd<Cu. The values of activation energy for the decomposition of the adducts of $CuBr_2$ and $CdBr_2$ are close. The values of enthalpy change for these two adducts are also same. Thermal stability of the adduct of $CdCl_2$ is higher than that of the corresponding bromide adduct. Whereas, the value of enthalpy change is higher in the case of bromide adduct than that of chloride, though the values of activation energy of both are close. The general comparative review shows that thermal stability of the adducts of dioxane is higher than the corresponding tetrahydrofuran adducts with a few exception in $CuBr_2 \cdot 1.00$ THF and the corresponding dioxane adduct.

The difference of the values of activation energy for the decomposition of adducts evaluated from TG, DTG and DTA curves is not too much. This shows that all the methods used for the evaluation of activation energy are standard. In general, the value of activation energy for the latter step of decomposition gives larger value than the former. This phenomenon is observed in the decomposition of adducts with tetrahydrofuran like the adducts with dioxane. However, there is exception in the value of activation energies for the first and second step of decompositions of $CuCl_2 \cdot 0.70$ THF like the values obtained for the second and third step of decomposition of $CoBr_2 \cdot 2.00$ D reported by us.

It is noticed that the value of enthalpy change for the decomposition of the adduct is related with the

composition of the adducts; it shows low value where the composition of the adduct is simple, *i.e.*, 12.7 kcal/mol for $CdCl_2 \cdot 1.00$ THF and high value where the composition of the adduct is not so simple, *i.e.*, 63.5 kcal/mol for $CoCl_2 \cdot 0.50$ THF. In general the latter decomposition gives larger ΔH value than the former one. But such tendencies are not observed in the decomposition of all the adducts.

References

1) P. M. Hamilton, R. McBeth, W. Bekebred, and H. H. Sisler, *J. Am. Chem. Soc.*, **75**, 2881 (1953).
2) R. F. Rolsten and H. H. Sisler, *ibid.*, **79**, 1068, 1819 (1957).
3) W. Herwing and H. H. Zeiss, *J. Org. Chem.*, **23**, 2404 (1958).
4) E. Kurras, *Naturwissenschaften*, **46**, 171 (1959).
5) R. J. Kern, *J. Inorg. Nucl. Chem.*, **24**, 1105 (1962).
6) R. J. H. Clark, J. Lewis, D. J. Machin, and R. S. Nyholm, *J. Chem. Soc.*, **1963**, 379.
7) B. E. Bridgland, G. W. A. Fowles, and R. A. Walton, *J. Inorg. Nucl. Chem.*, **27**, 383 (1965).
8) K. Rossmanith, *Monatsh. Chem.*, **97**, 1357 (1966).
9) G. W. A. Fowles, P. T. Greene, and T. E. Lester, *J. Inorg. Nucl. Chem.*, **29**, 2365 (1967).
10) K. Rossmanith and H. Blaha, *Monatsh. Chem.*, **98**, 1060 (1967).
11) G. W. A. Fowles, D. F. Lewis, and R. A. Walton, *J. Chem. Soc., A*, **1968**, 1468.
12) J. C. Barnes and C. S. Duncan, *J. Chem. Soc., A*, **1969**, 1746.
13) G. W. A. Fowles, D. A. Rice, and R. A. Walton, *J. Inorg. Nucl. Chem.*, **31**, 3119 (1969).
14) N. Ray Chaudhuri, S. Mitra, and G. K. Pathak, *Bull. Chem. Soc. Jpn.*, **48**, 2375 (1975).
15) L. F. Fieser and M. Fieser, "Reagents for Organic Synthesis," John Wiley and Sons, New York (1967), p. 1140.
16) K. Sano, *Sci. Rep. Tohoku Imp. Univ., 1st Ser.*, **24**, 719 (1936).
17) E. S. Freeman and B. Carroll, *J. Phys. Chem.*, **62**, 394 (1958).
18) N. G. Dave and S. K. Chopra, *Z. Phys. Chem.*, **48**, 257 (1966).
19) H. J. Brochardt and F. Daniels, *J. Am. Chem. Soc.*, **79**, 41 (1957).

The Participation of Solvents in the Reaction of Alkenes with Manganese(III) Acetate*

Masayoshi OKANO

Faculty of Integrated Arts and Sciences, Hiroshima University, Higashisendamachi, Hiroshima 730

(Received December 4, 1974)

1-Hexene and 2-methyl-2-pentene were heated with manganese(III) acetate at 100 °C in two mixed solvents of glacial acetic acid and acetic anhydride and of propionic acid and propionic anhydride in a nitrogen flow. γ-Acyloxy carboxylic acids, γ-lactones and saturated and unsaturated carboxylic acids were obtained, these oxidative products being considered to be adducts of acetic and propionic acids. Additional investigations were carried out on a mutual reaction of the oxidant and the solvents and on the thermal analysis of manganese(III) acetate. The reaction was explained by a solvent-participating free-radical mechanism.

The present author has reported on the formation of γ-butyrolactones and acetates in the reaction of *d*-limonene, *i.e.*, 1-methyl-4-isopropyl-1-cyclohexene, with manganese(III) acetate in acetic acid.[2] He has subsequently reported on the formation of saturated mono- and diacetates and certain kinds of allylic acetates in the heating of *d*-carvomenthene with a reagent in glacial acetic acid[3] and the formation of carboxymethyl adducts in the heating of *d*-limonene, *d*-carvomenthene, 1-methylcyclohexene, cyclohexene and 1-decene in glacial acetic acid containing catalytic amounts of potassium acetate.[4]

In addition, the formation of γ-lactones has been reported by Bush[5] in refluxing phenyl- and methyl-substituted ethylenes with manganese(III) acetate in a mixed solvent of acetic acid and acetic anhydride, and by Heiba[6] in refluxing certain alkenes, such as *trans*-β-methylstyrene, 1-octene, *trans*-4-octene, cyclooctene, styrene and *trans*-stilbene with manganese(III) acetate in glacial acetic acid containing potassium acetate. Allylic acetate has also been detected by Gilmore and Kasahara[7] in the reaction of cyclohexene, 1-methylcyclohexene, α- and β-methylstyrene. Heiba[6] has described that in these reactions, manganese(III) acetate reacts with olefins *via* a free-radical pathway leading to γ-butyrolactone. Whether or not the solvent participates in the reaction and the detailed mechanism of this reaction, however, have not yet been reported.

Results and Discussion

Characterization of Reaction Products. 1-Hexene and 2-methyl-2-pentene were separately heated with manganese(III) acetate dihydrate at 100 °C in two kinds of mixed solvents of acetic acid and acetic anhydride (solvent A) and of propionic acid and propionic anhydride (solvent P) in flowing nitrogen; the compounds listed in Table 1 were obtained as reaction products. The characterization of the products from the reaction of 1-hexene in solvent A depends upon the establishment of the chemical correlation for structually-known compounds as follows.

*γ-Lactone of 4-Hydroxyoctanoic Acid (**2**)*: The product with the lowest boiling point, $C_8H_{14}O_2$, from the reaction of 1-hexene in solvent A exhibited an IR absorption band characteristic of γ-lactone at 1775 cm^{-1}. Its reduction with lithium aluminum hydride furnished viscous 1,4-octanediol, which was converted into a methyl ester of a keto acid in a good yield by potassium permanganate oxidation followed by the treatment with diazomethane together with a small amount of the returned original γ-lactone. The keto ester was then subjected to Clemmensen reduction to give methyl octanoate. The structure of this compound is thus certain.

*3-Octenoic and 4-Octenoic Acids (**3**,**4**)*: An acidic substance isolated from the middle fraction of the reaction products, after being methylated, was separated into two unsaturated methyl esters by means of preparative gas chromatography, the quickly eluted one being identified as methyl 3-octenoate and the other as an unsaturated methyl ester containing a *trans*-disubstituted double bond, which gave methyl octanoate after catalytic hydrogenation. On the other hand, potassium permanganate oxidation of the mixed acidic substance furnished butyric and valeric acids. This evidence indicates the presence of 3-octenoic and 4-octenoic acids.

*4-Acetoxyoctanoic Acid (**1**)*: The product with the highest boiling point, $C_{10}H_{20}O_4$, was found to possess a carboxyl group (2670, 1710 cm^{-1}, 10.02 ppm) and an acetoxy group in its IR and NMR spectra. The compound was reduced *via* methylation with $LiAlH_4$ into 1,4-octanediol obtained in a similar treatment of **2**, and it was heated at 250 °C and converted into **2** and acetic acid in good yields together with a small amount of 3-octenoic and 4-octenoic acids.

The structures of the reaction products obtained in the other runs were determined based on spectral evidence and the structural analogy of the above-mentioned products.

Participation of the Solvent in the Reaction. Several kinds of products obtained from 1-hexene and 2-methyl-2-pentene in the manganese(III) acetate oxidation in two solvents are classified into acyloxy carboxylic acids, γ-lactones and unsaturated and saturated carboxylic acids; all the classes of these compounds were uniformly isolated in each run with the exception of acyloxy carboxylic acid which was not formed in the reaction of 2-methyl-2-pentene with solvent P. In these classes acyloxy carboxylic acids were a new class in the oxidation of alkenes with manganese(III) acetate. On the other hand, the reaction products from solvent A are considered as adducts of acetic acid, while those

* A part of the result has been preliminarily reported.[1]

Table 1. Products of the reaction of 1-hexene and 2-methyl-2-pentene with manganese(III) acetate

Solvent A (acetic acid and acetic anhydride)		Solvent P (propionic acid and propionic anhydride)	
	1-Hexene		
	Yield		Yield
(1) $CH_3(CH_2)_3CH(OAc)(CH_2)_2COOH$	61%	(6) $CH_3(CH_2)_3CH(OPr)CH_2CH(CH_3)COOH$	44%
(2) 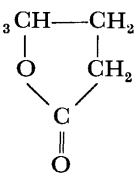	19%	(7) 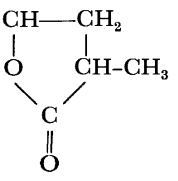	15%
(3) $CH_3(CH_2)_3CH{=}CHCH_2COOH$	5%	(8) unsaturated carboxylic acid	trace
(4) $CH_3(CH_2)_2CH{=}CH(CH_2)_2COOH$	8%		
(5) $CH_3(CH_2)_6COOH$	7%	(9) $CH_3(CH_2)_5CH(CH_3)COOH$	41%
	2-Methyl-2-pentene		
(10) 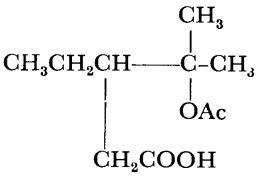	14%		
(11) 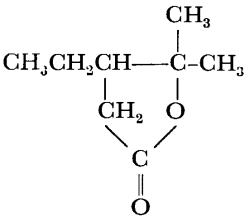	55%	(14) 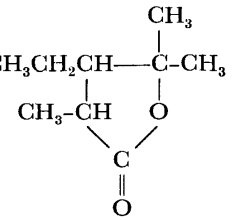	35%[a]
(12) 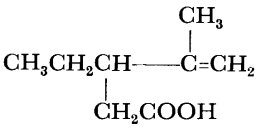	22%	(15) 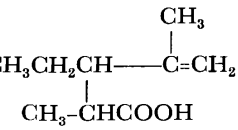	38%
(13) 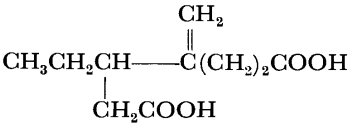	9%	(16) 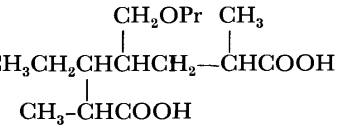	27%[b]

a) This compound was separated into two diastereoisomers in relative amounts of 13 to 1. b) This compound was separated into two diastereoisomers in relative amounts of 5 to 1.

from solvent P are recognized to be adducts of propionic acid.

Furthermore, when the reaction of 1-methylcyclohexene with manganese(III) acetate was carried out in acetic acid containing acetic acid-^{14}C, radioactive γ-lactone[8,9] and acetates[9] were obtained. This indicates that the solvent participates in the reaction of alkenes with manganese(III) acetate.

Thermal Decomposition of Manganese(III) Acetate Dihydrate. The thermal analysis of manganese(III) acetate dihydrate was performed to determine the weight loss and differential thermal analysis curves, shown in Fig. 1 for a standard of silicone dioxide. In the weight loss curves about 50 to 100 °C corresponds to the loss of the two hydrated waters of manganese acetate molecule and about 100 to 130 °C to the loss of one acetic acid residue from the molecule. When manganese(III) acetate dihydrate itself was also heated in a flask by gradually raising the temperature in flowing nitrogen gas, violent evolution of carbon dioxide was observed at about 110 °C. Both results indicate that at the reaction temperature used in the present investigation manganese(III) acetate dihydrate decomposes into manganese(II) acetate *via* two steps: the first step is the release of the two hydrated waters, which may be promoted by the acetic anhydride, and the second is the rupture of one acetic acid residue.

Thermal Reaction of Manganese(III) Acetate Dihydrate in the Solvent. Manganese(III) acetate dihydrate was heated at 100 °C in solvent A and P without the

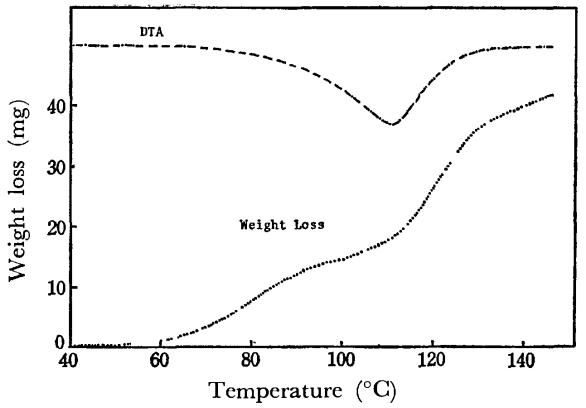

Fig. 1. Thermal analysis of $Mn(OAc)_3 \cdot 2H_2O$.*

reactant, an appreciable amount of succinic acid and a trace of acetoxyacetic acid being isolated in the heating with solvent A, and *dl*-2-propionyloxypropionic acid and 2,3-dimethylsuccinic acids which consisted of *dl*- and *meso*-isomers in a ratio of 3 : 1 being obtained in the heating with solvent P. Together with the fact that, in the above reaction of alkene in solvent P, only propionic acid adducts were isolated, this result demonstrates that $\cdot CH_2COOH$, $CH_3COO\cdot$, $\cdot\dot{C}HCOOH$

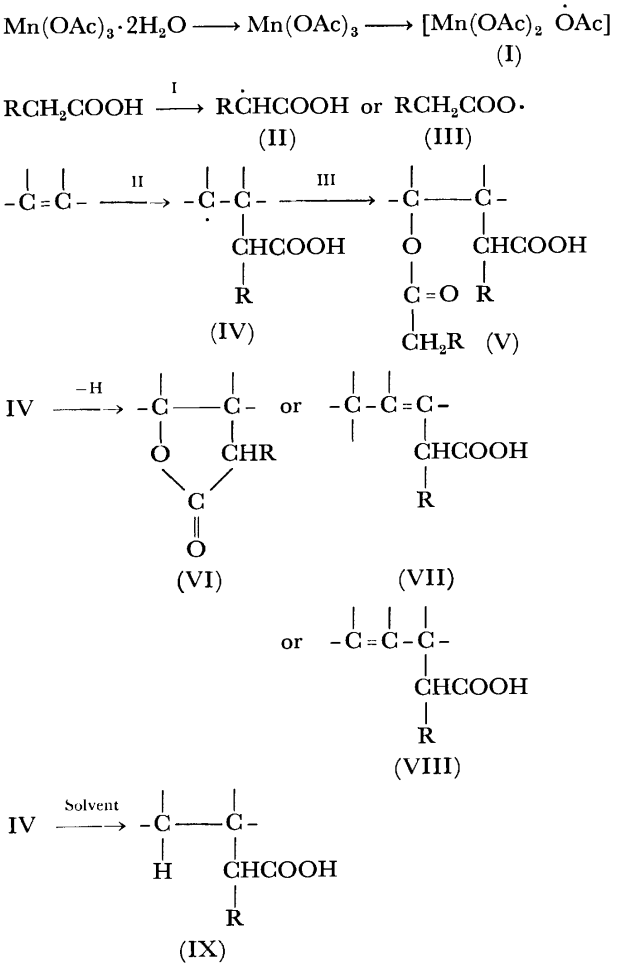

Sceme 1. Reaction mechanism.

* 104.8 mg of $Mn(OAc)_3 \cdot 2H_2O$ was used.

and $CH_3CH_2COO\cdot$ radicals were formed with the participation of the solvents in the manganese (III) acetate reaction.

Reaction Mechanism. On the basis of this evidence, the reaction of alkenes with manganese(III) acetate in the solvent may be explained by the reaction mechanism presented in Scheme 1.

For the first time, hydrated water of manganese(III) acetate is abstracted by acid anhydride. The anhydrous molecule of manganese(III) acetate thus produced is thermally decomposed releasing an acetoxy radical, which should be stabilized within the coordination sphere of the manganous ion. This radical does not react directly with the substrate, but with a surrounding molecule of the solvent to furnish an alkyl carboxymethyl(II) or an acyloxy(III) radical.

The addition of II to a double bond of alkene gives a radical intermediate (IV), which may be immediately stabilized by the following reactions: 1) the addition of an acyloxy radical(III) to give γ-acyloxy carboxylic acid (V), 2) the release of a hydrogen atom to give γ-lactone (VI) and unsaturated carboxylic acid (VII or VIII), and 3) the abstraction of a hydrogen atom from the solvent to give saturated carboxylic acid (IX).

Experimental

Analytical and preparative GLC were carried out on a Hitachi 023 gas chromatograph equipped with a thermocouple detector in connection with a stainless steel column (3 mm in diameter) which was packed with Celite 545 (40—60 mesh) impregnated with 20% PEG-20M or 25% DEGS. The NMR spectra were determined on a JEOL model JNM-MH-60 spectrometer in CCl_4, $CDCl_3$ or C_6D_6 with an internal reference of tetramethylsilane. The mass spectra were taken on a Hitachi RMS-4 instrument with a 70-eV ionization voltage and a 200 °C ionization chamber temperature. The molecular weight was determined on a Hitachi Perkin-Elmer 115 MW apparatus in benzene. Thermal analysis was carried out on a Shimadzu model DTB-2B DTA-TG apparatus.

Reagents. A Tokyo Kasei guaranteed reagent of 1-hexene and extra-pure reagent of 2-methyl-2-pentene were used. These materials each showed one peak in the GLC and the IR and NMR spectra were coincident with authentic samples.

Preparation of Manganese(III) Acetate Dihydrate. $Mn(OAc)_2 \cdot 4H_2O$ was oxidized with potassium permanganate according to a modification of the procedure of Heiba.[10] Crystallized $Mn(OAc)_3 \cdot 2H_2O$ filtering up from the reacted mixture was washed with ether, and preserved over sodium hydroxide *in vacuo* for a week. The purity was 99% according to iodometric titration.

Reaction of 1-Hexene and 2-Methyl-2-pentene with Manganese(III) Acetate. 1-Hexene and 2-methyl-2-pentene (8.4 g, 100 mmol of each) were added to a solution of manganese(III) acetate (53.6 g, 200 mmol) in a mixed solvent (400 ml) of acetic acid and acetic anhydride (v/v, 1 : 1, solvent A) or of propionic acid and propionic anhydride (v/v, 1 : 1, solvent P) drop by drop at 70 °C in flowing nitrogen, the mixture being stirred with a gradual increase of the reaction temperature up to 100 °C. When the brown color of the Mn(III) ions disappeared, the stirring was stopped, and the reaction mixture was cooled, diluted with water (*ca.* 300 ml)

and extracted with ether. Brown oily substances were obtained (from 1-hexene, 12 g in solvent A and 16 g in solvent P; from 2-methyl-2-pentene, 7 g in solvent A and 9 g in solvent P). The oily substances were then separated by a combination of fractionation and preparative gas chromatography into individual compounds whose characterizations were carried out as follows.

*Reaction of 1-Hexene in Solvent A. 4-Acetoxyoctanoic Acid (**1**)*: The highest boiling product was isolated as a colorless viscous substance which showed a blue-violet spot after the spraying of a vanillin-sulfuric acid reagent and a yellow spot with a solution of BCG indicator in TLC using silica gel and a mixed solvent of hexane and ethyl acetate (v/v 1 : 4) at R_f: 0.0—0.3 (tailing). ν_{max}^{neat} 2670 and 1710 (COOH), 1240 cm^{-1}(acetate); $\delta_{ppm}^{CCl_4}$ 0.91t(3H, J=5 Hz), 1.1—1.7 m(6H), 1.97s(4H), 1.8—2.1m(6H), 4.84t(1H, J=6 Hz), 10.02s(1H, exchangeable with D_2O)

It was treated with diazomethane to give a colorless liquid methyl ester. $C_{10}H_{20}O_4$(MS and elementaly analysis). *m/e* 173(7%, $M^+-C_2H_3O$), 142(4%, $M^+-C_3H_6O_2$), 117 (81%, $M^+-C_2H_3O-C_4H_7$), 85(42%, $M^+-C_3H_6O_2-C_4H_9$), 74 (17%, $C_3H_6O_2$), 55(35%, C_4H_7), 43(100%, C_2H_3O); ν_{max}^{neat} 1740(ester), 1240 cm^{-1}(acetate); $\delta_{ppm}^{CCl_4}$ 0.92t(3H, J=5 Hz), 1.1—1.6 m(6H), 1.96 m(6H), 1.7—2.5 m(4H), 3.60s(3H), 4.80t(1H, J=6 Hz). Found: C, 61.30; H, 9.11%; mol wt, 216±2. Calcd for $C_{10}H_{20}O_4$: C, 61.11; H, 9.26%; mol wt, 216.

In the reduction of the methyl ester (0.4 g) with $LiAlH_4$ (LAH, 0.4 g), 1,4-octanediol (0.3 g) was obtained. $C_8H_{18}O_2$ (MS). *m/e* 89(18%, $M^+-C_4H_9$), 87(12%, $M^+-C_3H_7O$), 71(100%, $M^+-C_4H_9-H_2O$), 69(40%, $M^+-C_3H_7O-H_2O$) 59(5%, C_3H_7O), 57(15%, C_4H_9); ν_{max}^{neat} 3330 cm^{-1} (OH); $\delta_{ppm}^{CCl_4}$ 0.91t(3H, J=5 Hz), 1.34bs(6H), 1.51bs(4H), 3.50bs(2H, exchangeable with D_2O).

In heating at 100 °C with solvent A, the compound showed no decomposition, but it (0.5 g) decomposed at 250 °C to give acetic acid (*ca.* 0.1 g) and the γ-lactone of 4-hydroxyoctanoic acid (*ca.* 0.30 g) described below. On the other hand, **1** was not obtained by refluxing **2** in solvent A.

*γ-Lactone of 4-Hydroxyoctanoic Acid (**2**)*: The compound was isolated as the oily product with lowest boiling point. The IR and NMR spectra were coincident with those of authentic samples. $C_8H_{14}O_2$(MS). *m/e* 142(2%, M^+), 85(100%, $M^+-C_4H_9$); ν_{max}^{neat} 1775 cm^{-1} (γ-lactone); $\delta_{ppm}^{CCl_4}$ 0.93t(3H, J=5 Hz), 1.1—1.8 m(6H), 1.8—2.6 m (4H), 4.31 m(1H).

In reduction with LAH (0.4 g), it (0.4 g) gave 1,4-octanediol (0.38 g), which was also obtained by LAH reduction of **1**. The oxidation of 1,4-octanediol (0.20 g) with potassium permanganate (0.5 g) followed by treatment with diazomethane gave, together with a minor amount of returned **2**, methyl 4-oxooctanoate as a main product. $C_9H_{16}O_3$(MS). *m/e* 141(8%, M^+-CH_3O), 130(13%, $M^+-C_3H_6$), 98 (24%, $M^+-C_3H_6-CH_4O$), 115(22%, $M^+-C_4H_9$), 87(19%, $M^+-C_4H_9-CO$), 59(65%, $M^+-C_7H_{13}O$), 57(100%, C_4H_9); ν_{max}^{neat} 1740(ester), 1720 cm^{-1} (ketone); $\delta_{ppm}^{CCl_4}$ 0.93t (3H, J=5 Hz), 2.3bs(2H), 2.51bs(2H), 3.59s(3H).

Methyl 4-oxooctanoate (0.10 g) was reduced to methyl octanoate in the Clemmensen reaction, which was indicated by admixing with the authentic sample in GLC and analysis of the MS, IR and NMR spectra.

*3-Octenoic Acid (**3**), 4-Octenoic Acid (**4**) and Octanoic Acid (**5**)*: The treatment of the middle fractions with diazomethane gave a mixture of three methyl esters which furnished common methyl octanoate by hydrogenation over a Raney nickel catalyst (W-2) in hexane in an autoclave. After three methyl esters were separated by preparative GLC, two were identified as methyl esters of **3** and **5** by gas chromatographic and spectrometric comparisons with authentic samples. The remaining methyl ester eluted in the middle position of the GLC exhibited and IR spectrum closely resembling that of methyl 3-octanoate, but the NMR spectrum was somewhat different. ν_{max}^{neat} 1740(ester), 970 cm^{-1} (*trans*); $\delta_{ppm}^{CCl_4}$ 0.87t(3H, J=6 Hz), 1.1—2.1m(4H), 2.24s(4H), 3.54s(3H), 5.33t(2H, J=3 Hz).

The potassium permanganate oxidation of the fraction (0.20 g) followed by a treatment with diazomethane gave methyl esters (*ca.* 0.15 g) of butyric acid, valeric acid and unchanged octanoic acid, which were identified by admixing the authentic samples and analysis by GLC.

*Reaction of 1-Hexene in Solvent P. 2-Methyl-4-propionyloxyoctanoic Acid (**6**)*: The product with the highest boiling in the reaction. $C_{12}H_{22}O_4$(MS). *m/e* 156(2%, $M^+-C_3H_6O_2$), 74(100%, $C_3H_6O_2$); ν_{max}^{neat} 2650 and 1705(COOH), 1735(ester), 1180 cm^{-1} (propionate); $\delta_{ppm}^{CCl_4}$ 0.87t(3H, J=5 Hz), 1.0—2.0(14H), 1.06t(J=7 Hz), 1.15d(J=7 Hz), 2.23q (2H, J=7 Hz), 4.86 m(1H), 11.18 s(1H).

In heating at 260 °C, the acid (0.5 g) decomposed into propionic acid and the lactone (**7**) described in the following section.

After methylation, the substance was separated into equivalent amounts of diastereoisomers by means of preparative GLC. The quickly eluted isomer: $C_{13}H_{24}O_4$ (MS). *m/e* 187(19%, $M^+-C_3H_5O$), 88(78%, $C_4H_8O_2$), 57(100%, C_3H_5O); ν_{max}^{neat} 1735(ester), 1190 cm^{-1} (propionate); $\delta_{ppm}^{CCl_4}$ 0.90t (3H, J=5 Hz), 1.10t(3H, J=7 Hz), 1.12d(3H, J=7 Hz), 2.19q (3H, J=7 Hz), 3.56s(3H), 4.72m(1H). Found: C, 64.04; H, 9.91%. Calcd for $C_{13}H_{24}O_4$: C, 63.88; H, 9.91%. The slowly eluted isomer: $C_{13}H_{24}O_4$(MS). *m/e* 187(16%, $M^+-C_3H_5O$), 88(100%, $C_4H_8O_2$), 57(100%, C_3H_5O); ν_{max}^{neat} 1735(ester), 1185 cm^{-1} (propionate); $\delta_{ppm}^{CCl_4}$ 0.90t(3H, J=5 Hz), 1.10t(3H, J=7 Hz), 1.12q(3H, J=7 Hz), 2.21q (3H, J=7 Hz), 3.54s(3H), 4.78s(1H).

*γ-Lactone of 4-Hydroxy-2-methyloctanoic Acid (**7**)*: The oily product with the lowest boiling in the reaction. $C_9H_{16}O_2$ (MS). *m/e* 156(1%, M^+), 99(100%, $M^+-C_4H_9$); ν_{max}^{neat} 1770 (γ-lactone); $\delta_{ppm}^{CCl_4}$ 0.92t (3H, J=5 Hz), 1.0—2.0 (11H), 1.20d(J=6 Hz), 2.45m(1H), 4.24m(1H); $\delta_{ppm}^{C_6D_6}$ 0.82t (3H, J=5 Hz), 0.95d(1.5 H, J=6 Hz), 1.00d(1.5 H, J=6Hz), 1.0—1.5 m(4H), 2.08m(2H), 3.80m(1H). These spectral data suggest the γ-lactone to be a mixture of two diastereoisomers.

*2-Methyloctanoic Acid (**9**)*: Colorless oil. $C_9H_{18}O_2$ (MS). *m/e* 158(1%, M^+), 74(100%, $C_3H_6O_2$); ν_{max}^{neat} 2650 and 1705 (COOH); $\delta_{ppm}^{CCl_4}$ 0.88t(3H, J=5 Hz), 1.0—1.6(13H), 1.15d (J=7 Hz), 1.28bs(10H), 2.30m(1H), 11.96s(1H); amide mp 80—81 °C (lit,[11] 80—81 °C).

*Reaction of 2-Methyl-2-pentene in Solvent A. 4-Acetoxy-3-ethyl-4-methylpentanoic Acid (**10**)*: Upon treatment with diazomethane, the acid was converted into a colorless liquid methyl ester. $C_{11}H_{20}O_4$ (MS and elementaly analysis). *m/e* 157(5%, $M^+-C_2H_4O_2$), 127(15%, $M^+-C_2H_4O_2-CH_3O$), 97(21%, $M^+-C_2H_4O_2-C_2H_3O_2$), 96(41%, $M^+-2C_2H_4O_2$), 59(38%, $C_2H_3O_2$), 55(91%, $M^+-2C_2H_4O_2-C_3H_5$), 43 (100%, $C_2H_3O_2$), 41(62%, C_3H_5); ν_{max}^{neat} 1735(ester), 1250 cm^{-1} (acetate); $\delta_{ppm}^{CDCl_3}$ 0.97t(3H, J=5 Hz), 1.0—2.1 (5H), 1.92s (3H), 1.40s (3H), 1.48s (3H), 3.66s (3H).

The methyl ester (0.1 g) was reduced with LAH (0.1 g) to give a diol which was identical with that obtained in the LAH reduction of **11**.

*γ-Lactone of 3-Ethyl-4-hydroxy-4-methylpentanoic Acid (**11**)*: Colorless oil. $C_8H_{14}O_2$ (MS). *m/e* 142(5%, M^+), 127(44%, M^+-CH_3), 69(40%, C_5H_9), 59(100%, C_3H_7O); ν_{max}^{neat} 1775 (γ-lactone), 1390 and 1375 cm^{-1}(*gem*-dimethyl); $\delta_{ppm}^{CCl_4}$ 0.96t(3H,

J=5 Hz), 1.20s(3H), 1.39s(3H), 2.25d(2H, J=7 Hz).

Upon reduction with LAH (1.0 g), the compound (0.1 g) gave 3-ethyl-4-methyl-1,4-pentanediol, mp 44—45 °C, (*ca.* 0.9 g). $C_8H_{18}O_2$(MS). *m/e* 131(2%, M^+-CH_3), 113(14%, $M^+-CH_3-H_2O$), 84(6%, $M^+-CH_3-H_2O-C_2H_5$), 57 (100%, C_3H_7O); ν_{max}^{neat} 3330(OH), 1150(*tert.* OH), 1050 (*prim.* OH), 1380 and 1355 cm^{-1} (*gem*-dimethyl); $\delta_{ppm}^{CCl_4}$ 0.98t (3H, J=6 Hz), 1.05s(3H), 1.20s(3H), 1.56m(3H), 3.52m (2H), 5.02bs(2H, exchangeable with D_2O).

The diol (0.2 g) was oxidized with potassium permanganate (0.5 g) and returned to the original γ-lactone. It (0.6 g) was also treated with a mixture (5 ml) of acetic anhydride and pyridine (1 : 3, v/v) to give 3-ethyl-4-hydroxy-4-methylpentyl acetate as a colorless oily substance (*ca.* 0.6g). $C_{10}H_{20}O_3$ (MS). *m/e* 113 (21%, $M^+-C_2H_4O_2-CH_3$), 110 (17%, $M^+-C_2H_4O_2-H_2O$), 59(92%, $C_2H_3O_2$), 43(100%, C_2H_3O); ν_{max}^{neat} 3450(OH), 1740(ester), 1250(acetate), 1150 cm^{-1} (*tert.* OH); $\delta_{ppm}^{CCl_4}$ 0.93t(3H, J=5 Hz), 1.03s(3H), 1.13s (3H), 1.80s(1H, exchangeable with D_2O), 1.93s(3H), 4.03t (2H, J=7 Hz). Dehydration of this acetate (0.5 g) with acetic anhydride (1 ml) at 250 °C gave 3-isopropenyl-1-pentyl acetate as a colorless liquid (*ca.* 0.4 g). $C_{10}H_{18}O_2$ (MS). *m/e* 110(35%, $M^+-C_2H_4O_2$), 69(37%, $M^+-C_2H_4O_2-C_3H_5$), 43(100%, C_2H_3O), 41(80%, C_3H_5); ν_{max}^{neat} 3070, 1640 and 890 (C=C), 1740(ester), 1245 cm^{-1} (acetate); $\delta_{ppm}^{CCl_4}$ 0.83t(3H, J=7 Hz), 1.60s(3H), 1.92s(3H), 3.90t(2H, J=7 Hz), 4.72m(2H).

Upon treatment with LAH (0.3 g), the above acetate (0.3 g) was reduced to 3-isopropenyl-1-pentanol (0.2 g). Colorless oil. $C_8H_{16}O$ (MS). *m/e* 128(3%, M^+), 113(2% M^+-CH_3), 110(3%, M^+-H_2O), 84(64%, $M^+-CH_3-C_2H_5$) 81(23%, $M^+-H_2O-C_2H_5$), 69(80%, $M^+-H_2O-C_3H_5$), 41(100%, C_3H_5); ν_{max}^{neat} 3340 and 1055 (*prim.* OH), 3080, 1640 and 890 cm^{-1} (C=C). The unsaturated primary alcohol (0.1 g) was hydrogenated over a Raney nickel catalyst in ethanol to give 3-isopropyl-1-pentanol which was identified by means of gas chromatographic and IR and NMR spectrometric comparisons with an authentic sample synthesized as the final description.

*3-Isopropenylpentanoic Acid (**12**)*: After methylation, the acid was isolated as a colorless liquid in a highly homologous state from the highest fraction of the reaction product together with a dimethyl ester of the following dibasic acid (**13**). $C_9H_{16}O_2$ (MS). *m/e* 156 (7%, M^+), 141(6%, M^+-CH_3), 125(9%, M^+-CH_3O), 124(13%, M^+-CH_4O), 97 (20%, $M^+-C_2H_3O_2$), 96(48%, $M^+-C_2H_4O_2$), 59(27%, $C_2H_3O_2$), 55(100%, $M^+-C_2H_4O_2-C_3H_5$), 41(59%, C_3H_5); ν_{max}^{neat} 3070, 1645 and 890 (C=C), 1740 cm^{-1} (ester); $\delta_{ppm}^{CCl_4}$ 0.82t (3H, J=6 Hz), 1.65s(3H), 2.40s(2H), 3.64s(3H), 4.74bs(2H).

Upon reduction with LAH (0.1 g), the methyl ester (0.1 g) gave 3-isopropenyl-1-pentanol as a colorless oil, which was also derived from **11**.

*3-Ethyl-4-methyleneheptanedioic Acid (**13**)*: The compound was isolated from the highest fraction after methylation. $C_{12}H_{20}O_4$(MS and elementaly analysis). *m/e* 196(9%, M^+-CH_3O), 168(9%, $M^+-C_2H_3O_2$), 166(5%, M^+-2CH_3O), 116(8%, $M^+-2C_2H_3O_2$), 59(100%, $C_2H_3O_2$); ν_{max}^{neat} 3075, 1640 and 890 (C=C), 1735 cm^{-1} (ester); $\delta_{ppm}^{CCl_4}$ 0.84t(3H, J=6 Hz), 1.0—1.9 m(3H), 2.41bs(6H), 3.64s(3H), 3.66s(3H), 4.81bs (2H). Found: C, 62.94; H, 9.16%. Calcd for $C_{12}H_{20}O_4$: C, 63.11; H, 8.84%. Reduction of the methyl ester (0.1 g) with LAH (0.1 g) gave 3-ethyl-4-methylene-1,7-heptanediol as a colorless oily substance. ν_{max}^{neat} 3330 and 1055 (*prim.* OH).

*Reaction of 2-Methyl-2-pentene in Solvent P. γ-Lactone of 2,4-Dimethyl-3-ethyl-4-hydroxypentanoic Acid (**14**)*: From the lowest boiling fraction of the reaction products two colorless liquids determined to be diastereoisomers were separated in the relative amounts of 13 : 1 by preparative GLC. Quickly eluted isomer: $C_9H_{16}O_2$ (MS). *m/e* 141 (25%, M^+-CH_3), 112(18%, M^+-CO_2), 97(12%, $M^+-CO_2-CH_3$), 55(100%); ν_{max}^{neat} 1770 (γ-lactone), 1390 and 1375 cm^{-1} (*gem*-dimethyl); $\delta_{ppm}^{CCl_4}$ 0.8—1.8(15H), 1.02t(3H, J=5 Hz), 1.20d(3H, J=7 Hz), 1.21s(3H), 1.41s(3H), 2.17m(1H); $\delta_{ppm}^{C_6D_6}$ 0.60t(3H, J=5 Hz), 0.81s(3H), 1.10s(3H), 1.05d(3H, J=6 Hz), 0.5—1.5 m(3H), 1.87m(1H). Slowly eluted isomer:$C_9H_{16}O_2$ (MS). *m/e* 141(25%, M^+-CH_3), 112(16%, M^+-CO_2), 97(12%, $M^+-CO_2-CH_3$), 55(100%); ν_{max}^{neat} 1765 (γ-lactone), 1390 and 1375(*gem*-dimethyl); $\delta_{ppm}^{CCl_4}$ 0.81—1.7 m(2H), 0.97t(3H, J=6 Hz), 1.20d(3H, J=7 Hz), 1.26s(3H), 1.39s(3H), 2.11m (1H), 2.57m(1H); $\delta_{ppm}^{C_6D_6}$ 0.55t(3H, J=6 Hz), 0.91s(3H), 1.02s(3H), 0.97d(3H, J=6 Hz), 1.58q(2H), 2.31q(1H, J=8 Hz).

*3-Ethyl-2,4-dimethyl-4-pentenoic Acid (**15**)*: Colorless oily substance. $C_9H_{16}O_2$ (MS). *m/e* 156 (9%, M^+), 83(75%, $M^+-C_3H_5O_2$), 55(100%); ν_{max}^{neat} 2650 and 1710(COOH), 1650 and 895 (C=C); $\delta_{ppm}^{CCl_4}$ 0.7—1.6 (11H), 0.77t(3H, J=6 Hz), 1.14d(3H, J=6 Hz), 1.53s(3H), 2.31m(2H), 4.78s (1H), 4.87s(1H), 11.3s(1H). Upon treatment with diazomethane, it gave a colorless oily methyl ester: ν_{max}^{neat} 3080, 1640 and 895 (C=C), 1735 cm^{-1} (ester); $\delta_{ppm}^{CCl_4}$ 0.75t(3H, J=6 Hz), 0.96d(3H, J=6 Hz), 1.0—1.4m(2H), 1.50s(3H), 2.10m (2H), 3.48s(3H), 4.61s(1H), 4.67s(1H).

*3-Ethyl-2,6-dimethyl-4-propionyloxymethyl-1,7-heptanedioic Acid (**16**)*: By preparative GLC of the fraction with the highest boiling point (0.5 g) of the reaction products, two colorless isomeric esters were separated in a ratio of 5 : 1 after treatment with diazomethane. Quickly eluted ester: $C_{17}H_{30}O_6$ (MS). *m/e* 154 (7%, $M^+-2C_4H_8O_2$), 139(13%, $M^+-2C_2H_3O_2-C_3H_5O_2$), 95(18%, $M^+-2C_4H_8O_2-C_2H_3O_2$), 88 (18%, $C_4H_8O_2$), 59 (8%, $C_2H_3O_2$), 57(100%, $C_3H_5O_2$); ν_{max}^{neat} 1735(ester), 1195 cm^{-1} (propionate); $\delta_{ppm}^{CCl_4}$ 1.05t(3H, J=6 Hz), 1.14d(6H, J=7 Hz), 1.68 m(7H), 2.20q(4H, J=7 Hz), 3.56s(6H), 4.80m(2H). Slowly eluted ester: $C_{17}H_{30}O_6$ (MS) *m/e* 154 (3%, $M^+-2C_4H_8O_2$), 139(11%, $M^+-2C_2H_3O_2$), 95(63%, $M^+-2C_4H_8O_2-C_2H_3O_2$), 88(48%, $C_4H_8O_2$), 59 (19%, $C_2H_3O_2$), 57(100%, $C_3H_5O_2$); ν_{max}^{neat} 1735(ester), 1195 cm^{-1} (propionate); $\delta_{ppm}^{CCl_4}$ 1.07t(3H, J=6 Hz), 1.14d(6H, J=7 Hz), 1.70m(7H), 2.18q(4H, J=7 Hz), 3.56s(6H), 5.02m (2H). Since sixteen isomers are possible for 3-ethyl-2,6-dimethyl-4-propionyloxymethyl-1,7-heptanedioic acid, these substances should still be mixed esters.

Reactions of $Mn(OAc)_3\cdot 2H_2O$ in Solvents A and P. $Mn(OAc)_3\cdot 2H_2O$ (26.8 g, 100 mmol) was heated with solvent A (200 ml) without a reactant for 6 h in a manner similar to the above reaction in flowing nitrogen. The reacted mixture was concentrated as a viscous liquid, which produced a small amount of white crystals when allowed to stand. The crystals, mp 184—186 °C, 1.3 g, showed no depression during a mixed mp determination with an authentic sample of succinic acid and the IR spectrum was coincident with that of an authentic sample. The liquior remaining after filtration of the crystals was methylated and then the reacted mixture was separated by preparative gas chromatography. Together with succinic acid, acetoxyacetic acid was isolated and it was identified based on gas chromatographic and spectrometric comparisons with an authentic sample prepared from hydroxyacetic acid. During heating, the nitrogen gas passing through the reaction flask passed into a saturated aqueous solution of calcium hydroxide (200 ml); although the solution became slightly cloudy, no precipitate was formed.

$Mn(OAc)_3\cdot 2H_2O$ (53.6 g, 200 mmol) was also heated with solvent P (400 ml). A similar treatment of the reacted mixture gave a mixture (1.7 g) of *meso-* (2 mmol, mp 196—

198 °C, lit,[11] 198 °C) and *dl*-2,3-dimethylsuccinic acid (6 mmol) and *dl*-2-propionyloxypropionic acid (2 mmol). They were separated by preparative GLC after methylation. *dl*-2-Propionyloxypropionic acid was identified by IR and NMR spectral comparisons with an authentic sample synthesized from *dl*-lactic acid. Similarly *dl*-2,3-dimethylsuccinic acid was identified by its MS, IR and NMR spectra. $C_8H_{14}O_4$ (MS). *m/e* 143 (28%, M^+-CH_3O), 115(30%, $M^+-C_2H_3O_2$), 59(100%, $C_2H_3O_2$); ν_{max}^{neat} 1740 cm^{-1} (ester); $\delta_{ppm}^{CCl_4}$ 1.11d(6H, J=6Hz), 2.71m(2H), 3.65s(6H).

Thermal Analysis of $Mn(OAc)_3 \cdot 2H_2O$. The thermal analysis of $Mn(OAc)_3 \cdot 2H_2O$(104.8 mg) was carried out with a Shimadzu DTA-TG apparatus with temperature programming of 2°C/min in flowing nitrogen, and the weight loss (mg) and differential thermal analysis were recorded using a standard of fused SiO_2 (Fig. 1). On the other hand, $Mn(OAc)_3 \cdot 2H_2O$ (26.8 g, 100 mmol) was gradually heated up to 130 °C in flowing nitrogen, and the emerging gas from a reaction flask was bubbled into a saturated solution (200 ml) of calcium hydroxide. When the temperature reached 110 °C, the formation of a white precipitate was observed.

Synthesis of 3-Isopropyl-1-pentanol. 2-Methyl-3-pentanol (9.0 g, 88 mmol) which was prepared from propionaldehyde and isopropylmagnesium bromide[12] was oxidized with Jones reagent at room temperature for 6 h to give 2-methyl-3-pentanone, bp 113—118 °C (lit,[11] 115—116 °C), as a colorless liquid (7.5 g, yield 85%). The Reformatsky reaction[13] of 2-methyl-3-pentanone (7.5 g, 75 mmol) thus obtained with methyl bromoacetate(12.2 g, 80 mmol) gave methyl 3-hydroxy-3-isopropylpentanoate (8.5 g, 48.8 mmol); ν_{max}^{neat} 3530(OH), 1730 and 1715 (ester), 1385 and 1370 cm^{-1} (isopropyl); $\delta_{ppm}^{CCl_4}$ 0.87t(3H, J=7 Hz), 1.50q(2H, J=6 Hz), 1.90 d(6H, J=7 Hz), 2.40bs(2H), 3.69s(3H), 3.15bs(1H, exchangeable with D_2O). The alcohol, after dehydration with acetic anhydride, was subjected to catalytic hydrogenation to give methyl 3-isopropylpentanoate as a colorless liquid (bp 163—164 °C, 2.4 g, yield 59%). $C_9H_{18}O_2$ (MS). *m/e* 127(11%, M^+-CH_3O), 84(17%, $M^+-C_3H_6O_2$), 74 (100%, $C_3H_6O_2$), 59(31%, $C_2H_3O_2$); ν_{max}^{neat} 1745 (ester), 1390 and 1370 cm^{-1} (isopropyl); $\delta_{ppm}^{CCl_4}$ 0.91t(3H, J=4 Hz), 0.86 t (3H, J=6 Hz), 0.89d(3H, J=6Hz), 2.15 m(2H), 3.59s(3H).

Reduction of this methyl 3-isopropylpentanoate (1.0 g) with LAH(1.0 g) gave 3-isopropyl-1-pentanol (*ca.* 0.9 g). $C_8H_{18}O$ (MS). *m/e* 112 (2%, M^+-H_2O), 84(23%, $M^+-H_2O-C_2H_4$), 44(100%, C_3H_8), 40(96%, C_3H_4); ν_{max}^{neat} 3340 and 1055 (*prim.* OH), 1385 and 1367 cm^{-1} (isopropyl); $\delta_{ppm}^{CCl_4}$ 0.84d(6H, J=6 Hz), 3.46t(2H, J=7 Hz), 3.18s(1H, exchangeable with D_2O).

Thanks are expressed to Professor Shūichi Hayashi of Hiroshima University, for his guidance and encouragement throughout this work and to Dr. Kōzō Akabori of the same institution for the measurements of the thermal analysis of manganese(III) acetate dihydrate.

References

1) M. Okano, *Chem. Lett.*, **1973**, 165.
2) M. Okano and T. Aratani, *Mem. Fac. Gen. Ed. Hiroshima Univ.*, III, **1**, 31 (1967).
3) M. Okano and T. Aratani, *J. Sci. Hiroshima Univ., Ser. A-II*, **33**, 71 (1969).
4) M. Okano, *Chem. Ind. (London)*, **1972**, 423.
5) J. B. Bush, Jr. and H. L. Finkbeiner, *J. Am. Chem. Soc.*, **90**, 5903 (1968).
6) E. I. Heiba, R. M. Dessau, and W. J. Koehl, Jr., *J. Am. Chem. Soc.*, **90**, 5905 (1968).
7) J. R. Gilmore and J. M. Mellor, *J. Chem. Soc., C*, **1971**, 2355; A. Kasahara, R. Saito, and T. Izumi, *Bull. Chem. Soc, Jpn.*, **46**, 2610 (1973).
8) M. Okano and T. Aratani, *Yuki Gosei Kagaku Kyokai Shi*, **30** (6), 568 (1972).
9) M. Okano, to be published in *J. Sci. Hiroshima Univ., Ser. A-II*, **40**, no. 1 (1976).
10) E. I. Heiba, R. M. Dessau, and W. J. Koehl, Jr., *J. Am. Chem. Soc.*, **91**, 138 (1968).
11) A. H. Cook, H. M. Bundury, and D. H. Hey, "Dictionary of Organic Compounds," Maruzen, Tokyo (1965).
12) C. J. Pouchert, "The Aldrich Library of Infrared Spectra," (1970).
13) R. L. Shriner, *Org. React.* **1**, 1–37 (1957).

The Hydrogen-Deuterium Exchange of 3,5-Dimethylisoxazoles

Choji KASHIMA, Yasuhiro YAMAMOTO, Yoshihiko TSUDA, and Yoshimori OMOTE
Department of Chemistry, University of Tsukuba, Sakura-mura, Niihari-gun, Ibaraki 300-31
(Received December 27, 1974)

By the hydrogen-deuterium exchange reaction in methanol-d_4, 3,5-dimethylisoxazole (**1**) was found to react regioselectively at the C-5 methyl group. This methyl group was, however, less reactive than the methyl groups of 2-picoline or quinaldine. This reaction was shown to be retarded by the electron-donating substituents, and to be accelerated by the electron-withdrawing substituents, at the C-4 position of **1**.

The isoxazole derivatives frequently show some pharmaceutical activities, and they are also employed as intermediates for the syntheses of peptides[1] and natural products.[2] Previously, we reported that 3,5-dimethylisoxazole (**1**) reacted with various kinds of electrophiles in the presence of bases to give 5-substituted 3-methylisoxazoles.[3-5] For example, 3-methyl-5-ethylisoxazole was obtained by the treatment of **1** with methyl iodide in the presence of sodium amide in liquid ammonia.[3] For the development of these reactions, it is necessary to investigate the application and the limitation of these reactions. However, no quantitative study has yet been reported.

The reaction of active methyl and methylene groups on the heteroaromatic compounds, such as 2-picoline[6] and quinaldine,[7] has been extensively investigated. White and Anderson[8] reported that the hydrogen on the methyl group of 5-methylisothiazole was exchanged with the activation energy of 5.61×10^4 J/mol in deuterium oxide. Also, Zatspina *et al.*[9] reported that the activation energies of the hydrogen exchange of 2-picoline and quinaldine are 1.03×10^5 and 8.70×10^4 J/mol respectively in deuterium oxide. In these papers, the rate-determining step of these reactions is supposed to be the formation of the corresponding carbanions by proton abstraction from active methyl and methylene groups.

The rate-determining step of the reaction of **1** with the electrophiles should be the formation of the carbanion of **1**. Therefore, the stability of an intermediate carbanion was calculated by means of the MINDO/2 method. Also, the present study will report the results of the sodium methoxide-d_3 catalyzed isotopic exchange of **1** in methanol-d_4 in order to compare the reactivity of **1** with those of the heteroaromatic compounds with a methyl group. Furthermore, the substituent effect of 4-substituted 3,5-dimethylisoxazoles is discussed in terms of the hydrogen-deuterium-exchange reaction rates.

Results and Discussion

Regioselectivity. Two methyl groups of 3,5-dimethylisoxazole (**1**) are expected to be activated by the isoxazole ring. When the proton abstraction from the active methyl group is considered to be the rate-determining step, the stability of the carbanion should reflect the reactivity of the corresponding methyl groups. The total energies of the (3-methyl-5-isoxazolyl)methyl carbanion (**2**) and the (5-methyl-3-isoxazolyl)methyl carbanion (**3**) were calculated by means of the MINDO/2 calculation method. The calculation showed that **2** is more stable than **3** by 3×10^3 J/mol. These results were roughly supported by the following data. The carbanions introduced from **1** were prepared by the treatment of **1** with butyllithium in ether. After equilibration for 3 h at room temperature, the resulting carbanions were quenched by deuterium oxide. The deuterated products were then analyzed by mass spectrometry; the results are summarized in Table 1. In this table, the relative intensity of *m/e* 98 showed that the monodeutero derivative was formed in a yield of 37%. The peak of *m/e* 82 was assigned to the **4** ion, while the peak of *m/e* 54 was assigned to the **5** ion.[10] In both ions, **4** and **5**, the C-5 methyl group was expelled from the molecule. When the mass spectrum of **1** was compared with that of the deuterated products, the isotopic peaks of **4** and **5**, *m/e* 83 and 55, were observed to have a difference in relative intensity.

Table 1. Mass Spectral data of **1** and the deuterated derivative

m/e	Relative intensity	
	1	Deuterated derivative
99	0.9	6.1
98	11.9	36.2
97	78.6	49.0
83	5.1	7.1
82	100.0	100.0
56	2.0	5.0
55	30.4	31.7
54	70.3	67.5

The hydrogen-deuterium exchange rates of very weak acids often parallel the acidities of this type of heteroaromatic compound.[11] This parallelism can be expected from the Brønsted catalysis law.[12] The relative reactivity of the methyl group of **1** was studied kinetically by means of a hydrogen-deuterium exchange reaction at 110.6 °C in the presence of sodium methoxide-d_3 in methanol-d_4 (16.5 mg/282 mg). Actually, the hydrogen-deuterium exchange was monitored by the decreases in the NMR peaks of **1** at δ 2.13 and 2.30 ppm, which were identified as C-3 methyl and C-5 methyl groups respectively. The pseudo-first-order rate constants of this reaction were found to be $k=3.3\times10^{-4}$ s^{-1} at the C-5 methyl group and $k=1.2\times10^{-6}$ s^{-1} at the C-3 methyl group. That is, the C-5 methyl group was activated 280 times as much as the C-3 methyl group.

Reactivity. The reaction rates of the hydrogen-deuterium exchange on the C-5 methyl group of **1**

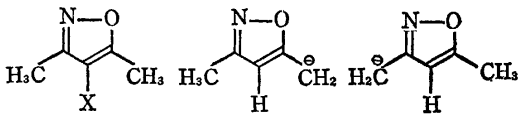

1 X=H **2** **3**
6 X=OCH_3
7 X=CH_3
8 X=Cl
9 X=I
10 X=$COOCH_3$
11 X=NO_2

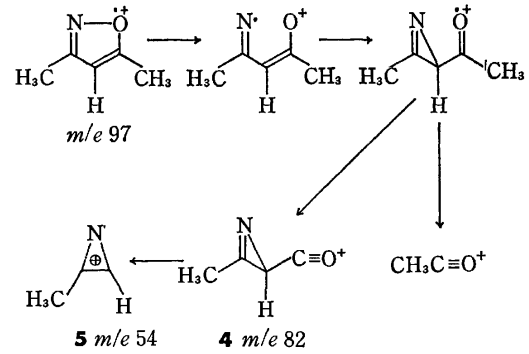

m/e 97

5 *m/e* 54 **4** *m/e* 82

were also measured at 80.1, 89.0, 100.0, and 121.2 °C in methanol-d_4. The activation parameters for the C-5 methyl group of **1** were calculated to be $E_{act}=(1.200\pm0.008)\times10^5$ J/mol and log $A=12.76$, while those for the methyl groups of 2-picoline and quinaldine were $E_{act}=1.03\times10^5$ J/mol; log $A=9.86$ and $E_{act}=8.70\times10^4$ J/mol; log $A=9.77$, respectively.[9] Apparently the C-5 methyl group of **1** is less reactive than those of 2-picoline and quinaldine.

Effect of Substituents. The hydrogen-deuterium exchange reaction rates for the C-5 methyl group of 4-substituted 3,5-dimethylisoxazoles were measured in order to clarify the effects of the substituents. The 4-methoxy- (**6**), 4-methyl- (**7**), 4-chloro- (**8**), 4-iodo- (**9**), 4-carbomethoxy- (**10**), and 4-nitro- 3,5-dimethylisoxazoles (**11**) were prepared and the exchange rates were measured in methanol-d_4 in the presence of sodium methoxide-d_3 at 34.2, 80.1, and/or 110.6 °C. The results are presented in Table 2. Unfortunately, the reaction of **10** was too fast for us to determine the exchange rate accurately at 34.2 °C. The NMR peak of the C-5 methyl group of **11** could not be observed even 1 min after the **11** and methoxide-d_3 were dissolved in methanol-d_4 at room temperature. Table 2 shows that the hydrogen-deuterium exchange was retarded by the electron-donating groups at the C-4 position of the isoxazole ring.

TABLE 2. HYDROGEN-DEUTERIUM EXCHANGE REACTION RATES OF 4-SUBSTITUTED 3,5-DIMETHYLISOXAZOLES

4-Substituents	Temp (°C)	Reaction rate (s^{-1})	
		C-3 CH_3	C-5 CH_3
OCH_3	110.6	6.4×10^{-7}	1.3×10^{-5}
CH_3	110.6	4.1×10^{-7}	7.8×10^{-5}
H	110.6	1.2×10^{-6}	3.3×10^{-4}
	80.1	—	9.5×10^{-6}
Cl	80.1	—	5.5×10^{-4}
I	110.6	7.7×10^{-5}	8.0×10^{-3}
	80.1	—	9.4×10^{-4}
$COOCH_3$	34.2	—	$>2\times10^{-3}$

Experimental

MINDO/2 Calculations. Using the coordinates shown in Table 3, the total energies of the **2** and **3** carbanions were calculated as −1252.483 and −1252.149 eV respectively by means of the MINDO/2 method.

TABLE 3. THE COORDINATES OF **2** AND **3**

Isoxazole ring			
Bond length		Bond angle	
O-N	1.39 Å	C-5-O-N	107°
N-C-3	1.33 Å	O-N-C-3	110°
C-3-C-4	1.42 Å	N-C-3-C-4	108°
C-4-C-5	1.37 Å	C-3-C-4-C-5	107°
C-5-O	1.39 Å	C-4-C-5-O	108°
C-3-C	1.50 Å	N-C-3-C	126°
C-4-H	1.08 Å	C-3-C-4-H	126.5°
C-5-C	1.50 Å	O-C-5-C	126°
Side chain methyl			
Bond length of C-H		1.08 Å	
Bond angle of H-C-H		109.5°	
Bond angle of C-C-H		109.5°	
Dihedral angle of C-4-C-C-H		0°	
Side chain methylene			
Bond length of C-H		1.08 Å	
Bond angle of H-C-H		120°	
Bond angle of C-C-H		120°	
Dihedral angle of C-4-C-C-H		0°	

Materials. *3,5-Dimethylisoxazole (**1**)* was prepared by the method of Lampe[13] from acetylacetone and hydroxylamine hydrochloride. Yield, 59%; bp 139—141 °C (lit, 140—142 °C[13]).

*3,5-Dimethyl-4-methoxyisoxazole (**6**).* According to the method of Katritzky,[14] **6** was prepared from diazomethane and 3,5-dimethyl-4-hydroxyisoxazole [NMR: δ^{CDCl_3} 2.17 (s, 3H), 2.27 (s, 3H), and 5.5 ppm (broad s, 1H)]; yield (from 4-acetoxy-2,4-pentanedione), 8%; bp 106—115 °C/2 mmHg. NMR: δ^{CD_3CD} 2.19 (s, 3H), 2.53 (s, 3H) and 3.78 ppm (s, 3H).

*3,4,5-Trimethylisoxazole (**7**).* According to the method of Sokolov,[15] **7** was prepared from 3-methyl-2,4-pentanedione, hydroxylamine hydrochloride, and anhydrous potassium carbonate. Yield, 26%; bp 98—99 °C/69 mmHg. NMR: δ^{CD_3OD} 1.89 (s, 3H), 2.16 (s, 3H), and 2.28 ppm (s, 3H).

*3,5-Dimethyl-4-chloroisoxazole (**8**).* According to the method of Sokolov,[15] **8** was prepared from 3-chloro-2,4-pentanedione and hydroxylamine hydrochloride. Yield, 63%; bp 82 °C/25 mmHg. NMR: δ^{CD_3OD} 2.22 (s, 3H), and 2.37 ppm (s, 3H).

*3,5-Dimethyl-4-iodoisoxazole (**9**).* According to the method of Kochetkov,[16] **9** was prepared from **1**, iodine, and a catalytic amount of nitric acid. Yield, 59%; mp 51—53.5 °C (lit, 51.5—53 °C[16]). NMR: δ^{CD_3OD} 2.21 (s, 3H), and 2.42 ppm (s, 3H).

*3,5-Dimethyl-4-carbomethoxyisoxazole (**10**).* According to the method of Stork,[17] **10** was prepared from nitroethane and methyl acetoacetate. Yield, 30%; bp 95—98 °C/3 mmHg. NMR: δ^{CD_3OD} 2.34 (s, 3H), 2.59 (s, 3H), and 3.83 ppm (s, 3H).

*3,5-Dimethyl-4-nitroisoxazole (**11**).* By the method of Morgan,[18] **1** was nitrated by nitric acid and concentrated sulfuric acid. Yield, 60%, mp 62—64 °C (lit, 63.5 °C[18]). NMR: δ^{CD_3OD} 2.50 (s, 3H), and 2.75 ppm (s, 3H).

Hydrogen-Deuterium Exchange Reaction Rate. Isoxazole (0.45 mmol) was treated with sodium methoxide-d_3 (16.5 mg) in methanol-d_4 (282 mg) in sealed tubes at the refluxing temperature of tetrachloroethylene (bp 121.2 °C), toluene (bp 110.6 °C), water (bp 100.0 °C), aqueous *p*-dioxane (bp 89.0 °C), or benzene (bp 80.1 °C), and at appropriate time intervals the NMR spectra were measured at 34.2 °C, using cyclohexane as the internal standard, by means of a JEOL H-100 NMR spectrometer. From the NMR data, the reaction rates were calculated; they are summarized in Table 2.

Mass Spectral Analysis of Deuterated Derivative. To a solution of **1** (1.01 g) in anhydrous ether, a 15% hexane solution of butyllithium (6 ml) was added at −70 °C. The mixture was then stirred for 3 h at room temperature under a nitrogen atmosphere. After the addition of deuterium oxide (1.97 g), the stirring was continued for another 0.5 h at room temperature. The reaction mixture was separated. The organic layer was washed with dilute hydrochloric acid, water, and aqueous sodium chloride, and dried over anhydrous sodium sulfate. After the solvent had been removed, the residue was distilled. Yield, 0.21 g; bp 135—142 °C. NMR: δ^{CDCl_3} 2.21 (s), 2.33 (s), and 5.78 ppm (s); the intensity ratio is 30 : 26 : 11.

The authors are indebted to Dr. Osamu Kikuchi, Department of Chemistry, University of Tsukuba, for doing the MINDO/2 calculations.

References

1) R. B. Woodward, R. A. Olofson, and Y. Kobayashi, *J. Org. Chem.*, **32**, 388 (1967).
2) G. Stork, S. Danishefsky, and M. Ohashi, *J. Am. Chem. Soc.*, **89**, 5459 (1967).
3) C. Kashima, S. Tobe, N. Sugiyama, and M. Yamamoto, *Bull. Chem. Soc. Jpn.*, **46**, 310 (1973).
4) C. Kashima and Y. Tsuda, *Bull. Chem. Soc. Jpn.*, **46**, 3533 (1973).
5) C. Kashima, N. Mukai, and Y. Tsuda, *Chem. Lett.*, **1973**, 539.
6) D. Taub, R. D. Hoffsommer, C. H. Kuo, and N. L. Wendler, *J. Org. Chem.*, **30**, 3229 (1965).
7) F. W. Bergson and A. Moffat, *J. Am. Chem. Soc.*, **59**, 1494 (1937).
8) J. A. White and R. C. Anderson, *J. Heterocycl. Chem.*, **6**, 199 (1969).
9) N. N. Zatsepina, I. F. Tupitsyn, and L. S. Efros, *Dokl. Akad. Nauk SSSR*, **154**, 148 (1964).
10) M. Ohashi, H. Kamachi, H. Kakisawa, A. Tatematsu, H. Yoshizumi, H. Kano, and H. Nakata, *Org. Mass. Spectrom.*, **2**, 195 (1969).
11) A. Streitwieser, Jr., J. I. Brauman, J. H. Hammons, and A. H. Pudjiaatmaaka, *J. Am. Chem. Soc.*, **87**, 384 (1965).
12) A. A. Frost and R. G. Pearson, "Kinetics and Mechanism," John Wiley & Sons, Inc., New York, N. Y. (1953), p. 209.
13) W. Lampe and L. Smalinska, *Roczniki. Chem.*, **28**, 163 (1954).
14) G. Bianchi, M. J. Cook, and A. R. Katritzky, *Tetrahedron*, **27**, 6133 (1971).
15) S. D. Sokolov, L. A. Kazitsyna, and L. K. Guseva, *Zh. Organ. Khim.*, **2**, 731 (1966).
16) N. K. Kochetkov, S. D. Sokolov, N. M. Vagurtova, and E. E. Nifant'ev, *Dokl. Akad, Nauk SSSR*, **133**, 598 (1960).
17) G. Stork and J. E. McMurry, *J. Am. Chem. Soc.*, **89**, 5461 (1967).
18) G. T. Morgan and H. Burgess, *J. Chem. Soc.*, **1921**, 697.

Studies of Tritylated Pentoses and Methyl Pentoses. I. The *O*-Tritylation of Methyl α-D-Fucopyranoside

Toshiki OTAKE and Toru SONOBE*

Nippon Electric Varian, Ltd., Yotsuya, Fuchu-shi Tokyo 183

**Tobishi Pharmaceutical Co., Ltd., Omori-Nishi, Ota-ku, Tokyo 143*

(Received March 17, 1975)

Two trityl derivatives of fucose, methyl 2-*O*- (II) and 3-*O*-trityl α-D-fucopyranoside (III), were obtained in good yields by the reaction of methyl α-D-fucopyranoside (I) and trityl chloride in pyridine. The ratio of II and III in the reaction mixture was about 3 : 2. The structures were mainly established by NMR with appropriate derivatives. The gas chromatography-mass spectrometry of the partial methyl ethers of I was also discussed.

O-Tritylation[1] usually proceeds much more rapidly on primary hydroxyl groups. It has been used to determine quantitatively the number of primary hydroxyl groups in a molecule, or to protect the group for further synthetic procedures. However, in some cases, equatorial secondary hydroxyl groups are also tritylated rapidly. Hocket and Hudson[2] reported that methyl α-L-fucopyranoside, which contains only secondary hydroxyl groups, reacted readily with trityl chloride to form a mono-*O*-trityl ether. However, they did not describe its structure.

This paper will deal with the *O*-tritylation of I and with the etherified positions of the trityl derivatives. The *O*-tritylation of various pentoses and methyl pentoses can give information about the reactivity of secondary hydroxyl groups in different environments and can be used to protect a certain hydroxyl group for further synthetic procedures. This paper will also deal with the mass spectra of the partially methylated methyl fucosides prepared from the trityl derivatives.

Results and Discussion

The reaction of I with trityl chloride in a 1 : 2 mole ratio readily formed substituted derivatives under the conditions described by Helferich.[1] The tritylated product gave two adjacent spots on a thin-layer chromatogram and two peaks on a high-speed liquid chromatogram, as is shown in Fig. 1. The compound corresponding to the first peak(II) was isolated as a pyridine complex and was then recrystallized as monoethyl alcoholate. The second peak(III) was separated by liquid chromatography, and crystallized as monohydrate. The analyses and PMR spectra of the appropriate derivatives of II and III indicated that they both consisted of mono-*O*-trityl ether of I.

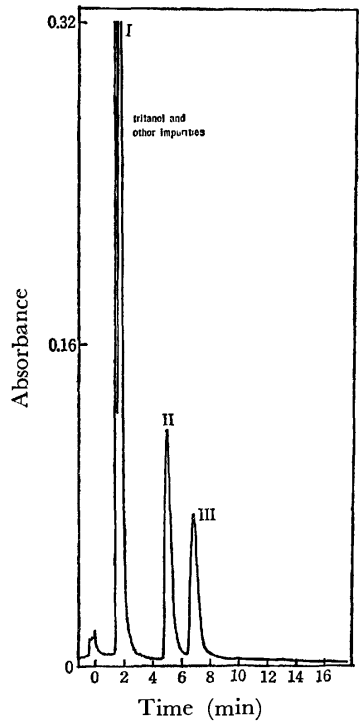

Fig. 1. Liquid chromatogram of the reaction mixture column: MicroPak si-10 2 mm×20 cm; solvent: 20% hexane/methylene chloride; flow rate: 50 ml/h; detector: UV (254 nm).

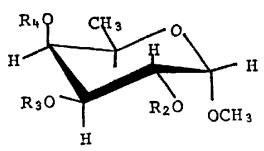

I	$R_2=R_3=R_4=H$	VIII	$R_3=Tr, R_2=Ac, R_4=H$
II	$R_2=Tr, R_3=R_4=H$	IX	$R_3=Tr, R_2=R_4=CH_3$
III	$R_3=Tr, R_2=R_4=H$	X	$R_3=H, R_2=R_4=CH_3$
IV	$R_2=Tr, R_3=R_4=Ac$	XI	$R_3=Ac, R_2=R_4=CH_3$
V	$R_2=Tr, R_3=R_4=CH_3$	XII	$R_4=H, R_2=R_3=CH_3$
VI	$R_2=H, R_3=R_4=CH_3$	XIII	$R_4=Ac, R_2=R_3=CH_3$
VII	$R_2=Ac, R_3=R_4=CH_3$		

All the methine-proton signals in a PMR spectrum of the peracetyl derivative of II (IV) were assigned with the aid of the decoupling technique shown in Fig. 2. The signals of H-3 and H-4 lay in the *O*-acetylmethine-proton area, while the H-2 resonated at a higher field than would be expected for an *O*-tritylmethine-proton. Most of the methine protons attached to alkoxylated or hydroxylated carbon resonate at δ4.0—2.5. However, trityl groups may sometimes cause anomalous chemical shifts of the adjacent protons by means of their strong anisotropic effect.[3,4] To confirm the structure, the PMR of a methyl di-*O*-methyl mono-*O*-acetylfucoside (VII) which had been derived from permethyl ether of II (V) was analyzed by the aid of the homodouble-resonance technique,[5]

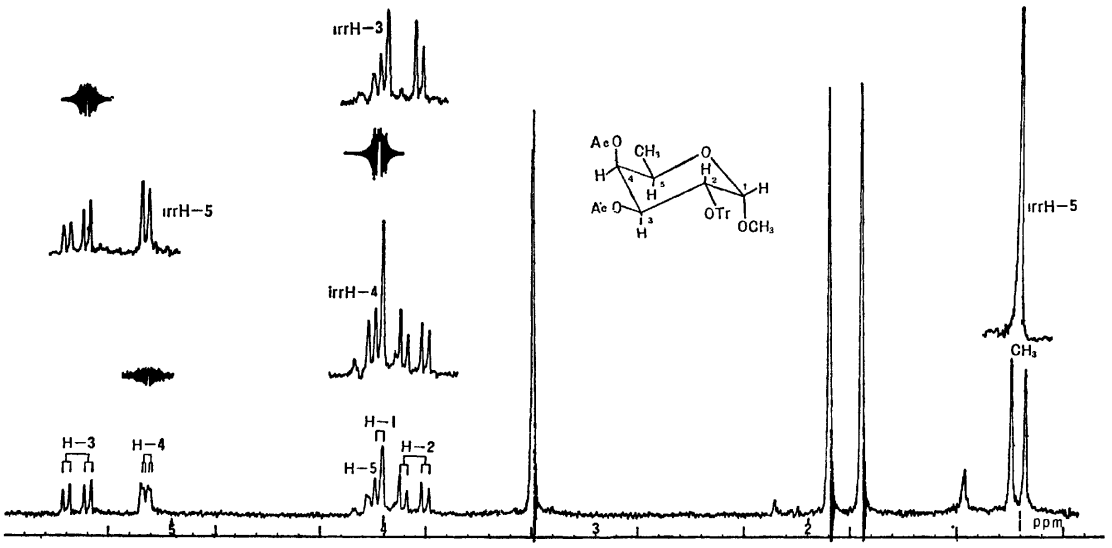

Fig. 2. Parts of the NMR spectrum at 100 MHz of IV.

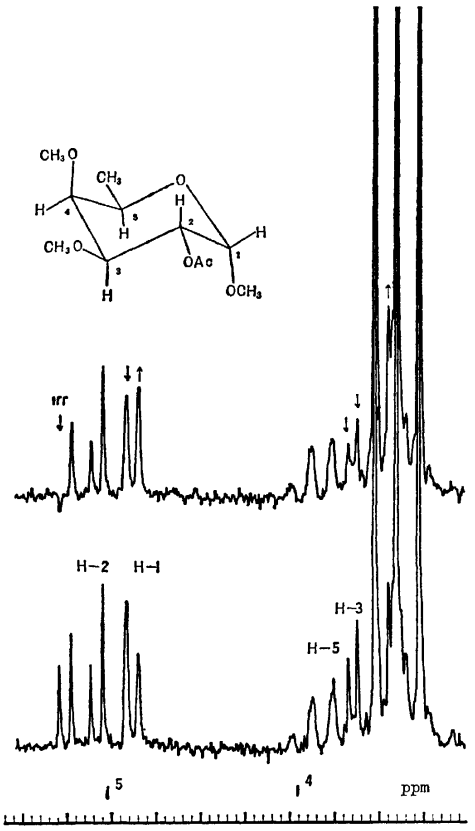

Fig. 3. A part of the NMR spectrum at 60 MHz (FT-mode) of VII. No. of scans: 10. Arrows show increasing or decreasing of signal intensities compared with those on the normal spectrum.

irradiating with a selective π-pulse at a resonance line of δ5.25, and observing the signal intensities using the Fourier transform mode, as is shown in Fig. 3. The spectrum showed that the H-2 was an *O*-acetylmethine proton, judging from the chemical shift. Accordingly, Compound II was confirmed to be 2-*O*-trityl α-D-fucopyranoside.

A PMR spectrum of the acetylation product of III (VIII) indicated that the hydroxyl group at C-2 alone was replaced by an acetyl group. Since protons of hydroxylmethine and alkoxylmethine resonate in a common area, however, the complete identification of VIII is difficult. In the PMR spectrum of di-*O*-methyl mono-*O*-acetylfucoside (XI) derived from the permethyl ether of III (IX) through its detritylation product (X), all the methine-proton signals were

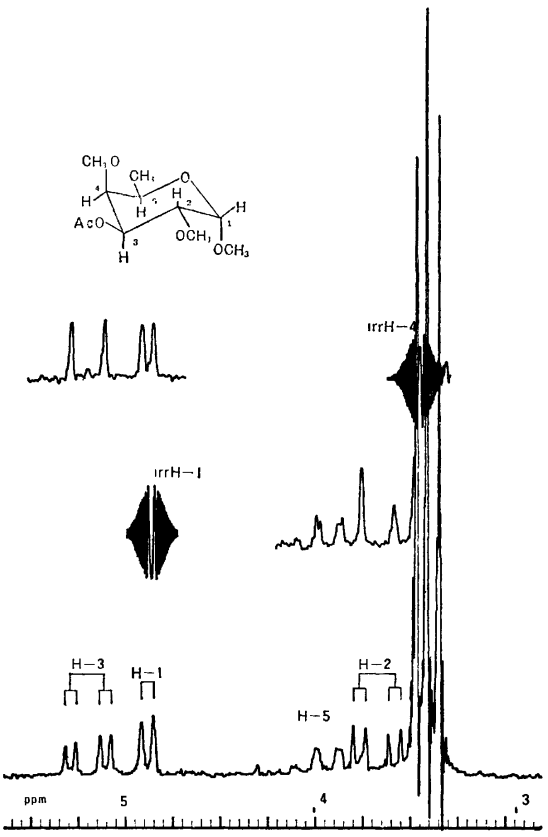

Fig. 4. A part of the NMR spectrum at 60 MHz of XI.

assigned with the aid of the decoupling technique, as is shown in Fig. 4. The H-3 was regarded as an acetylmethine proton from its chemical shift, and Compound III was identified as methyl 3-*O*-trityl α-D-fucopyranoside.

During these studies, the mass spectra of methyl di-*O*-methylfucoside (VI and X) were also analyzed. The mass spectra of methyl ethers of methyl glycosides have previously been studied in detail. For example, Kochetkov *et al.*[6-9] and Heyns *et al.*[10-11] have assigned the peaks on the mass spectra of permethylated methyl glycosides and calculated the contributions of isomeric ions to the total peak intensities. Later, Heyns *et al.*[12] analyzed the peaks of partially methylated methyl glucoside.

Some of the structures of ions and their contributions to the total peak intensities are presented below.

m/e	Structure[a]	Designation[9,12]	Contribution[b]
58 72	$[CH_3\text{-}CH{=}CH\text{-}OR(4)]^+$	K_1	100
74 88	$[R(2)O\text{-}CH{=}CH\text{-}OR(3)]^+$	H_1^2	78
75	$[CH_3(3)O{=}CH{=}OCH_3(1)]^+$	J_1^1	60
87 101	$R(4)O\text{-}CH{=}CH\text{-}CH{=}O^+R(2)$	F_1^2	62
87 101	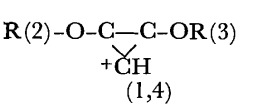	G_1^4	15
119	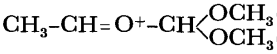	D_1	100
115 129	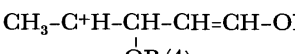	C_2	48
161	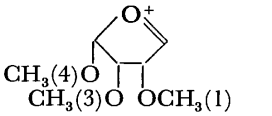	J_4	
	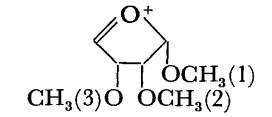	J_3	

a) R's are CH_3 or OH, and the numbers in parentheses agree with the attached positions of the OR-groups in the original ethers.

b) The contributions were calculated with methyl 2,3,4-tri-*O*-methyl β-D-fucoside.

c) The peaks at *m/e* 119 and 75 are mainly formed by the migration of the methoxyl (3). Therefore, their hydroxyl analogues are scarcely afforded at all.

The relative intensities of the characteristic peaks of VI, X, and those of methyl 2,3-di-*O*-methyl α-D-fucopyranoside (XII) are presented in Table 1, while the mass spectra of these compounds are in Fig. 5.

The mass spectra of these ethers are well elucidated by the structures of ions and their contributions to the total peak intensities. For example, the comparatively low intensities of the peaks at *m/e* 75, 88, and 119 in the spectrum of X indicate the absence of methoxyl (3). The major ions which contribute to these peak intensities all include this methoxyl group.

TABLE 1. THE RELATIVE INTENSITIES ON MASS SPECTRA OF PARTIALLY METHYLATED METHYL α-D-FUCOPYRANOSIDES

m/e	VI	X	XII	Permethyl α-D-fucose[14]
72	50	42	2	20
74	91	100	15	1
75	54	18	30	38
85	14	8	42	2
87	19	8	10	2
88	100	43	100	100
101	6	23	18	20
102	2	15	3	1.5
115	6	5	2	1
119	5.2	0.4	2.2	1.7
129	1.5	3.9	0	1.6
130	4.5	0.6	6.5	0
143	1.8	2.4	2.4	0
157	0.2	0.6	0.1	0.4
161	2.0	0.2	1.3	0
175	0.5	1.9	0.7	0
176	0	0	0	1.0
189	0	0	0	1.4

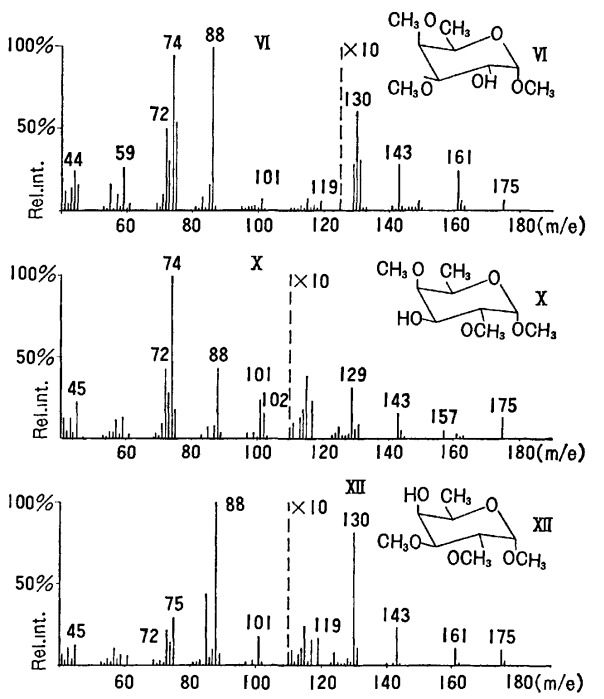

Fig. 5. Gas chromatography-mass spectra of VI, X and XII.

Similarly, the low intensity of the peak at *m/e* 101 in the spectrum of VI, and that of the peak at *m/e* 72 in the spectrum of XII, are elucidated by the absence of methoxyl (2) and methoxyl (4) respectively. The pathway of fragmentation should also be taken into consideration. The comparatively low intensity of the peak at *m/e* 101 in the spectrum of X may be explained by the lack of methoxyl (3). Because the F_1^2 ion is formed by the migration of methoxyl (3) from C-3 to C-1, in the case of permethylated methyl fucopyranoside, the absence of this group would reduce

the contribution of F_1[2] to the peak intensity.

The formation of *m/e* 161 (J_3,J_4) accompanies proton-transfers from OH (2) or OH (4) to the ring oxygens of VI or XII, indicating the presence of hydroxyl gorups at C-2 or C-4 in molecular ions.

There were other peaks, like *m/e* 157, 130, and 102, which were characteristic of each isomeric ether. The peak at *m/e* 157 appeared only in the spectrum of X and was considered as a dehydrated fragment of an ion of *m/e* 175:

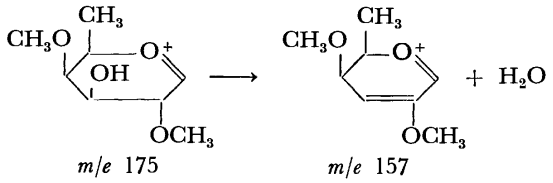

The peak at *m/e* 130 appeared in the spectra of VI and XII. The peak at *m/e* 102 appeared in the spectrum of X. The pathway of the fragmentation was assumed to be as follows:

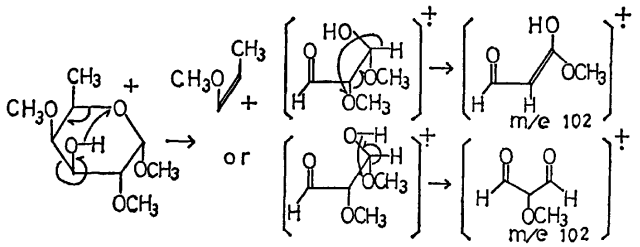

Experimental

General Methods. For high-performance liquid chromatography, a Varian Model 8520 Liquid Chromatograph, equipped with a Micro Pak Si-10 column, was used. The solvent for elution was 20% hexane/methylene chloride. Thin-layer chromatography was effected using Merck silica gel G as an adsorbent in a thickness of 0.25 mm, with a solvent system of acetone-benzene. Preparative column chromatography was carried out using silica gel, 60—80 mesh (Kanto Chemical Co.). The PMR spectra were recorded on a Varian HA-100D (100 MHz) apparatus and an NV-14 (60 MHz) spectrometer equipped with Adapts, a computor system (Varian Data Machins), using chloroform-*d* with tetramethylsilane as the internal lock, the signal positions being expressed in δ values. Gas chromatography-mass spectrometry was carried out using a Varian MAT 111 GC/MS system.

Tritylation of I. A mixture of 0.593 g of I ($[\alpha]_D^{25}$+ 189°) and 1.853 g of recrystallized trityl chloride was dissolved in 20 ml of dry pyridine, and was then allowed to stand for 120 h at room temperature. At the end of the reaction period, 1 ml of water was added to the solution. The solution was then concentrated *in vacuo* at 40 °C until it became hard syrup. A thin-layer chromatogram with a solvent system of 20% acetone/benzene showed spots corresponding to II and III, with R_f values of 0.69 and 0.63 respectively. On a high-performance liquid chromatogram, two peaks corresponding to II and III had retention times of 5°00′ and 6°48′ respectively, with a flow rate of 50 ml/h. The reaction concentrate was chromatographed on 15 g of silica gel. After the column had been washed with benzene (300 ml), trityl ethers were eluted with 4% acetone/benzene (300 ml). The evaporation of the last solvent left 1061 mg of a glass which consisted of II and III. The combined yield of the ethers was about 71%.

Methyl 2-O-Trityl α-D-Fucopyranoside (II). The derivative, II, was crystallized as a pyridine complex from the pyridine solution of the glass. Then it was recrystallized several times from the ethanol solution as monoethyl alcoholate, which melted at 68—70 °C and which had an $[\alpha]_D^{20}$ of +55.5 °(*c* 1, chloroform).

Found: C, 72.07; H, 7.00%. Calcd for $C_{26}H_{28}O_5 \cdot C_2H_5OH$: C, 72.08; H, 7.35%.

The monoethyl alcoholate was dried over phosphorous pentoxide at 60 °C for 24 h.

PMR data for unhydrous II (100 MHz): δ 1.15 (d, 3H, $J_{5,6}$ 6.5 Hz, CH_3), δ 3.25 (s, 3H, OCH_3).

Found: C, 73.96; H, 6.74%. Calcd for $C_{26}H_{28}O_5$: C, 74.26; H, 6.71%.

Methyl 3-O-Trityl α-D-Fucopyranoside (III). The mother liquid of the recrystallization of II from the pyridine solution was dried *in vacuo* and chromatographed on 10 g of silica gel. The column was washed with 2% acetone/benzene (200 ml) and with 2.5% acetone/benzene (200 ml). The eluent was divided into eight 50-ml fractions. Each of them was dried *in vacuo*, and each residue was chromatographed on a thin-layer plate. The combined solid from the fractions which consisted of III weighed 417 mg. The crude III was recrystallized as monohydrate from a 60% methanol solution. The crystalline III had an $[\alpha]_D^{20}$ of +81.4° (*c* 1, chloroform) and melted at 71—74 °C.

PMR data for III (60 MHz): δ 0.98 (d, 3H, $J_{5,6}$ 6.5 Hz, CH_3), δ2.03 (dd, 1H, $J_{4,5}$ 1.5 Hz, $J_{3,4}$ 2.8 Hz, H-4), δ3.27 (s, 3H, OCH_3), δ3.41 (qd, 1H, H-5), δ 4.66 (d, 1H, $J_{1,2}$ 3.2 Hz, H-1).

Found: C, 71.04; H, 6.62%. Calcd for $C_{26}H_{28}O_5 \cdot H_2O$: C, 71.23; H, 6.85%.

Acetylation of II and III. About 0.1 g of each sample was dissolved in 2 ml of dry pyridine and then acetylated with 0.2 ml of acetic anhydride and allowed to stand for 24 h. Each residue of the evaporation *in vacuo* was chromatographed on 10 g of silica gel. The peracetyl product of II (IV) was eluted with 1% acetone/benzene (200 ml) after the column had been washed with benzene (200 ml). The acetylation of III only gave a monoacetyl product (VIII). It was eluted with 2% acetone/benzene (200 ml) from the column. The yields were almost theoretical. The repeated crystallization of IV from 80% aqueous acetone gave needles; mp 172—174 °C, $[\alpha]_D^{20}$ +38.02° (*c* 1, chloroform).

Found: C, 71.00; H, 6.68%. Calcd for $C_{30}H_{32}O_7$: C, 71.41; H, 6.40%.

PMR data for IV (100 MHz): δ 1.01 (d, 3H, $J_{5,6}$ 6.5 Hz, CH_3), δ 1.75 (s, 3H, OAc), δ 1.90 (s, 3H, OAc), δ 3.30 (s, 3H, OCH_3), δ 3.80 (dd, 1H, $J_{1,2}$ 3.5 Hz, $J_{2,3}$ 10 Hz, H-2), δ 4.04 (qd, 1H, $J_{4,5}$ 1.5 Hz, H-5), δ 4.02 (d, 1H, H-1), δ 5.12 (dd, 1H, $J_{3,4}$ 3.5 Hz, H-4), δ 5.45 (dd, 1H, H-3).

PMR data for VIII (60 MHz): δ 1.00 (d, 3H, $J_{5,6}$ 6.5 Hz, CH_3), δ 2.02 (s, 3H, OAc), δ 2.25 (dd, 1H, $J_{4,5}$ 1.5 Hz, $J_{3,4}$ 3.5 Hz, H-4), δ 3.22 (s, 3H, OCH_3), δ 3.47 (qd, 1H, H-5), δ4.07 (dd, 1H, $J_{2,3}$ 10 Hz, $J_{3,4}$ 3.5 Hz, H-3), δ4.75 (d, 1H, $J_{1,2}$ 3.8 Hz, H-1), δ 5.31 (dd, 1H, H-2).

Methylation of II and III. Each of the trityl ethers (0.1 g) was methylated in dry *N,N′*-dimethylformamide (5 ml) with methyl iodide (0.4 ml) and 0.8 g of a 1 : 1 mixture of silver oxide and barium oxide for 24 h. After filtration, each filtrate was concentrated *in vacuo*, and the residue was resolved in an admixture of methyl ethyl ketone and benzene (1 : 1 v/v) (20 ml), after which the solution was filtered to remove any insoluble matter. Each residue of the evaporation was chromatographed on 10 g of silica gel. The per-

methylated products, V and IX, were eluted with 1% acetone/benzene (200 ml). The yields were about 60% in both cases. The preparation of V and IX showed spots of R_f-values of 0.67 and 0.45 respectively on a thin-layer chromatogram with 6% acetone/benzene. Both derivatives were crystallized from 80% ethanol solutions as prisms; mp for V: 124 °C and mp for IX: 131—133 °C. The $[\alpha]_D^{20}$ of V was +24.5 ° (*c* 1.6, chloroform), and the $[\alpha]_D^{20}$ of IX was +131.1° (*c* 1.5, chloroform).

PMR data for V (60 MHz): δ 1.09 (d, 3H, $J_{5,6}$ 6.5 Hz, CH_3), δ 2.96 (s, 3H, OCH_3), δ 3.17 (d, 1H, $J_{1,2}$ 3.4 Hz, H-1), δ 3.47 (s, 3H, OCH_3), δ 3.57 (s, 3H, OCH_3), δ 4.13 (dd, 1H, $J_{2,3}$ 10.0 Hz, H-2).

PMR data for IX (60 MHz-FT): δ 0.89 (d, 3H, $J_{5,6}$ 6.7 Hz, CH_3), δ 1.72 (s broad, 1H, H-4), δ 3.23 (s, 3H, OCH_3), δ 3.27 (s, 3H, OCH_3), δ^{ca} 3.33 (H-5), δ 3.63 (s, 3H, OCH_3), δ^{ca} 3.85 (dd, 1H, $J_{1,2}$ 3.3 Hz, $J_{2,3}$ 10.0 Hz, H-2), δ^{ca} 4.13 (dd, 1H, $J_{3,4}$ 2.2 Hz, H-3), δ 4.77 (d, 1H, H-1).

Found for V: C, 74.96; H, 7.25%. Calcd for $C_{28}H_{32}O_5$: C, 74.97; H, 7.19%.

Found for IX: C, 74.91; H, 7.20%. Calcd for $C_{28}H_{32}O_5$: C, 74.97; H, 7.19%.

Detritylation of V and IX. Each 50-mg portion of V and IX was dissolved with 80% acetic acid (0.5 ml) and heated at 90 °C in a sealed tube for 30 min. The solutions were then concentrated with toluene (3 ml) *in vacuo*. The residue of evaporation were chromatographed on 5 g of silica gel. The detritylation products, VI and X, were eluted with chloroform (100 ml). The subsequent evaporation of the eluting solvent left VI and X in almost theoretical yields. Retention index (I_R)[13] on GLC (He: 22 ml/min, column: 5′×1/8″, glass, column temperature: 140 °C) for VI: 2026 (5% NPGS/Chromosorb W) and 1526 (2% OV 17/Chromosorb W), for X: 2035 (5% NPGS) and 1584 (2% OV 17). Both ethers were crystallized from hexane solutions as needles; mp for VI: 82—85 °C, and mp for X: 74—78 °C, $[\alpha]_D^{20}$ for VI: +201.1 ° (*c* 0.9, chloroform) and $[\alpha]_D^{20}$ for X: +175.4° (*c* 1.2, chloroform).

Found for VI: C, 52.25; H, 8.57%. Calcd for $C_9H_{18}O_5$: C, 52.41; H, 8.80%.

Found for X: C, 52.23; H, 8.53%. Calcd for $C_9H_{18}O_5$: C, 52.41; H, 8.80%.

Methyl 2,3-Di-O-methyl α-D-Fucopyranoside (XII). Methyl 2-*O*-methyl α-D-fucopyranoside (0.5 g) was methylated in almost the same manner as is described above with methyl iodide (0.25 ml). After the removal of the catalyzer and the silver iodide, the residue of evaporation was chromatographed on 10 g of silica gel. The partially methylated products, X and XII, were eluted with 9% acetone/benzene (200 ml). The eluent was divided into five 40-ml fractions. Then it was re-chromatographed four times, while the fractions were gradually returned to the column with additional eluting solvent to get thirteen fractions. Each residue of evaporation was chromatographed on a thin-layer plate. The combined fractions, which contained only XII, were dried *in vacuo*. The residue weighed about 60 mg and had an $[\alpha]_D^{20}$ of +145.0 ° (*c* 1.0, chloroform). The structure of XII was confirmed by PMR as its acetylated derivative (XIII). I_R for XII: 2000 (5% NPGS) and 1584 (2% OV 17).

Found: C, 52.10; H, 8.60%. Calcd for $C_9H_{18}O_5$: C, 52.41; H, 8.80%.

Acetylation of VI, X and XII. The acetylation procedure used for these ethers was almost the same as that used for II and III. The acetylation products, VII, XI, and XIII, were purified by chromatography, after having been eluted with 1% acetone/benzene (200 ml) from silica gel column (10 g). The evaporation of the eluting solvent left the acetylation products in an almost theoretical yield as glass: $[\alpha]_D^{20}$ for VII; +156.4° (*c* 0.3, chloroform), for XI; +156.0° *c* 1.3, chloroform), and for XIII; +138.7° (*c* 0.6, chloroform). I_R for VII; 2095 (5% NPGS) and 1700 (2% OV 17), for XI; 2112 (5% NPGS) and 1770 (2% OV 17) and for XIII; 1981 (5% NPGS) and 1667 (2% OV 17).

PMR data for VII (60 MHz): δ 1.25 (d, 3H, $J_{5,6}$ 6.5 Hz, CH_3), δ 2.08 (s, 3H, OAc), δ 3.34 (s, 3H, OCH_3), δ 3.45 (s, 3H, OCH_3), δ 3.57 (s, 3H, OCH_3), δ 3.87 (qd, 1H, H-5), δ 4.85 (d, 1H, $J_{1,2}$ 3.7 Hz, H-1), δ 5.12 (dd, 1H, $J_{2,3}$ 10.0 Hz, H-2), for XI (60 MHz): δ 1.22 (d, 3H, $J_{5,6}$ 6.5 Hz, CH_3), δ 2.10 (s, 3H, OAc), δ 3.37 (s, 3H, OCH_3), δ 3.43 (s, 3H, OCH_3), δ 3.48 (s, 3H, OCH_3) δ^{ca} 3.48 (H-4), δ 3.70 (dd, 1H, $J_{1,2}$ 3.7 Hz, $J_{2,3}$ 10.3 Hz, H-2), δ 3.93 (qd, 1H, H-5), δ4.82 (d, 1H, H-1), δ 5.10 (dd, 1H, $J_{3,4}$ 3.2 Hz, H-3), and for XIII (100 MHz): δ 1.17 (d, 3H, $J_{5,6}$ 6.5 Hz, CH_3), δ2.20 (s, 3H, OAc), δ 3.44 (s, 3H, OCH_3), δ 3.46 (s, 3H, OCH_3), δ 3.55 (s, 3H, OCH_3), δ 4.03 (qd, 1H, H-5), δ 4.89 (d, 1H, $J_{1,2}$ 3.2 Hz, H-1), δ 5.36 (dd, 1H, $J_{4,5}$ 1.2 Hz, $J_{3,4}$ 3.0 Hz, H-4).

Relative peak intensities on MS for VII: *m/e* 72; 77, *m/e* 74; 82, *m/e* 75; 86, *m/e* 88; 100, *m/e* 97; 5.0, *m/e* 101; 18, *m/e* 116; 23, *m/e* 129; 14, *m/e* 157; 0.5, *m/e* 185; 4.0, *m/e* 204 ($M-CH_3CHO$); 0.8, *m/e* 217 ($M-CH_3O$); 0.3, for XI; *m/e* 72; 51, *m/e* 74; 100, *m/e* 75; 38, *m/e* 88; 36, *m/e* 97; 20, *m/e* 101; 30, *m/e* 116; 40, *m/e* 129; 24, *m/e* 157; 6.0, *m/e* 185, 1.2, *m/e* 204 ($M-CH_3CHO$); 0, *m/e* 217 ($M-CH_3O$); 1.0, and for XIII: *m/e* 72; 2.0, *m/e* 73; 18, *m/e* 74; 10, *m/e* 75; 44, *m/e* 85; 24, *m/e* 88; 100, *m/e* 97; 4.5, *m/e* 101; 8.5, *m/e* 116; 3.0, *m/e* 125; 5.4, *m/e* 129; 5.5, *m/e* 157; 0.8, *m/e* 185; 1.2, *m/e* 204 ($M-CH_3CHO$); 1.0, *m/e* 217 ($M-CH_3O$); 1.4.

The authors wish to thank Mr. Katsuhiko Kushida for determining the NMR spectra.

References

1) B. Helferich, "Advances in Carbohydrate Chemistry," 3rd ed., Academic Press, New York (1948), p. 106.
2) R. C. Hockett and C. S. Hudson, *J. Am. Chem. Soc.*, **56**, 1414 (1936).
3) T. Otake, *Bull. Chem. Soc. Jpn.*, **43**, 3199 (1970).
4) T. Otake, *Bull. Chem. Soc. Jpn.*, **45**, 2895 (1972).
5) K. Kushida, K. Aoki, and S. Sato, *J. Am. Chem. Soc.*, **97**, 443 (1975).
6) N. Kochtkov and O. Chizov, *Tetrahedron*, **21**, 55, (1965).
7) N. Kochetkov, N. Wulfson, O. Chizov, and B. Zolotarev, *Tetrahedron*, **19**, 2204 (1963).
8) N. Kochetkov and O. Chizov, *Biochem. Biophys. Acta*, **83**, 134 (1964).
9) N. Kochetkov, *Tetrahedron*, **21**, 2029 (1965).
10) K. Heyns and O. Muller, *Tetrahedron*, **21**, 55 (1965).
11) K. Heyns and H. Schorman, *Tetrahedron*, **21**, 507 (1965).
12) K. Heyns, K. Sperling, and H. Grutzmacher, *Carbohyd. Res.*, **9**, 79 (1969).
13) A. Wehrli and E. Kovats, *Helv. Chim. Acta*, **42**, 2709 (1959).
14) T. Otake and T. Sonobe, unpublished data.

A Convenient Synthesis of β-Acetyl-γ-substituted-γ-butyrolactones and γ-Acetyl-δ-substituted-δ-valerolactones

Toshio SATO, Junichi HANNA, Hideo NAKAMURA, and Teruaki MUKAIYAMA*

Laboratory of Organic Chemistry, Tokyo Institute of Technology, Ookayama, Meguro-ku, Tokyo 152

(Received April 16, 1975)

A convenient method for the preparation of β-acetyl-γ-substituted-γ-butyrolactones (III) and γ-acetyl-δ-substituted-δ-valerolactones (IV) is described. It was established that α-angelicalactone (I) and 3,4-dihydro-6-methyl-2*H*-pyran-2-one(II) react with various aldehydes in the presence of boron trifluoride etherate ($BF_3 \cdot OEt_2$) to afford the corresponding γ and δ-lactones, respectively, in good yields.

In the course of our continuing studies of useful synthetic reactions promoted by $TiCl_4$, it was found recently that trimethylsilyl enol ethers or isopropenyl acetate react with various aldehydes, ketones, or acetals to give the aldol type addition products in good yields.[1] For example, isopropenyl acetate reacts with aldehydes to afford β-acetoxy methylketones along with β-chloroketones and α,β-unsaturated ketones. The latter two products are formed by the subsequent displacement or elimination reaction

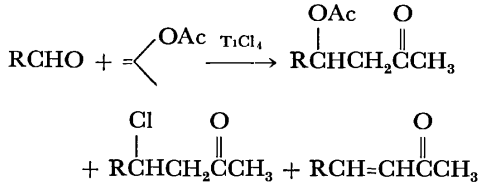

of the β-acetoxy methylketones initially formed.

In the present experiment, it was found that β-acetyl-γ-substituted-γ-butyrolactones (III)[2] and γ-acetyl-δ-substituted-δ-valerolactones (IV) are synthesized in good yields by the reactions of α-angelicalactone (I) or 3,4-dihydro-6-methyl-2*H*-pyran-2-one (II), chosen as cyclic enol esters in place of isopropenyl acetate in the above experiment, with various aldehydes activated by $BF_3 \cdot OEt_2$.

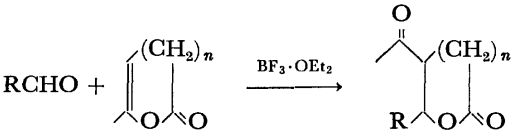

I, II I, III ($n=1$) III, IV

II, IV ($n=2$)

Rothe *et al.*[3] reported that β-acetyl-γ-butyrolactones are produced by treating levulinic acid and aldehydes with potassium carbonate; however, this is not suited to the preparative method since the reaction was carried out under rather severe conditions and the yields were very low.

Results and Discussion

In the present experiment, it was found that, when the mixture of α-angelicalactone (I) and 3-phenylpropanal in methylene chloride was stirred in the presence of $TiCl_4$ or $SnCl_4$ at room temperature over night, β-acetyl-γ-phenethyl-γ-butyrolactone (IIIa) was obtained in 54% or 44% yield, respectively, along with a considerable amount of levulinic acid produced by hydrolysis of α-angelicalactone. In the above experiment, the reaction was carried out in a heterogeneous system, since $TiCl_4$ or $SnCl_4$ formed solid complexes between the aldehydes, α-angelicalactone, and the products in methylene chloride. On the other hand, when $BF_3 \cdot OEt_2$ is used in place of $TiCl_4$ or $SnCl_4$ in the above experiment, the reaction was carried out in a homogeneous system and the corresponding lactone was obtained in 94% yield after 8 h at 0 °C. This result showed that $BF_3 \cdot OEt_2$ was more suitable for this reaction than $TiCl_4$ and $SnCl_4$. It was also found that the lactone was produced in 94 or 87% yield, respectively, when a half molar or a catalytic amount of $BF_3 \cdot OEt_2$ was used.

Table 1. The effect of solvent on the yield of the γ-butyrolactone (IIIa)

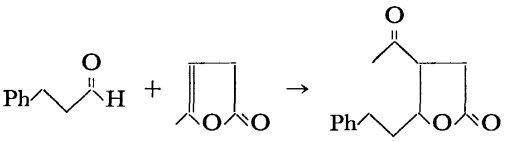

Solvent	Temp	Time (h)	Yield of IIIa (%)
CH_2Cl_2	0 °C	1	85
C_6H_5	r. t.	1	84
CCl_4	0 °C	6	71
Et_2O	0 °C	12	83
	r. t.	20	

Concerning the effect of solvents, it was shown that benzene and methylene chloride are more suitable solvents than diethyl ether and carbon tetrachloride with respect to yield and reaction velocity, as shown in Table 1.

In a similar manner, the reaction of α-angelicalactone with various aldehydes, such as benzaldehyde, cinnamaldehyde, chloroacetaldehyde, dichloroacetaldehyde, and formaldehyde, were carried out in the presence of an equimolar amount of $BF_3 \cdot OEt_2$ in methylene chloride, and the corresponding β-acetyl-γ-butyrolactones were obtained in good yields, as shown in Table 2.

Next, it was established that γ-acetyl-δ-phenethyl-δ-valerolactone (IVa) was obtained in 69% yield by treating 3,4-dihydro-6-methyl-2*H*-pyran-2-one (II) with 3-phenylpropanal in the presence of $BF_3 \cdot OEt_2$ in methylene chloride at 0 °C over night. The yield of the lactone was increased to 84% by employing two molar amounts of II against one molar amount

* Department of Chemistry, Faculty of Science, The University of Tokyo, Hongo, Buykyo-ku, Tokyo 113.

Table 2. Synthesis of β-acetyl-γ-butyrolactones (III) and γ-acetyl-δ-valerolactones (IV)

Compound	Reaction condition		Bp °C/Torr Mp °C	Analysis (%)			
				Calcd		Found	
	Temp (h)	Yield (%)		C	H	C	H
IIIa (R=$PhCH_2CH_2$)	0 °C(8)	94	157—158/0.03	72.39	6.24	72.36	7.11
IIIb (R=Ph)	r. t.(24)	62	165—170/0.35	70.57	5.92	70.59	6.02
IIIc (R=PhCH=CH)	0 °C(12)	79[a]	(91.5—92.0)[a]	73.02	6.13	72.81	6.16
			(53—63)[a]	73.02	6.13	73.22	6.23
IIId (R=$ClCH_2$)	0 °C(1)	90	122—123/0.09	47.60	5.13	47.62	5.12
IIIe (R=Cl_2CH)	0 °C(12)	60	116—117/0.062	39.85	3.79	40.01	3.83
IIIf (R=H)	0 °C(1)	93	120—121/4[b]	56.24	6.29	56.19	6.28
IVa (R=$PhCH_2CH_2$)	0 °C(14—15)	84	174—176/0.4	73.14	7.37	72.88	7.26
IVb (R=CH_3CH_2)	0 °C(14—15)	78	107—108/0.01	63.51	8.29	63.22	8.57
IVc (R=$ClCH_2$)	0 °C(14—15)	65	oil[c]	50.40	5.81	50.62	5.88
IVd (R=$PhCH_2$)	0 °C(14—15)	61	152—154/0.05	72.39	6.94	72.21	7.10
IVe (R=Ph)	0 °C(14—15)	75	(106—109)	71.54	6.47	71.78	6.57
IVf (R=H)	0 °C(0.33)	90	111—113/0.16	59.14	7.09	58.92	7.38

a) Two isomers (*trans* (higher melting point) : *cis*(lower melting point)=8 : 1) were isolated by silica gel chromatography (solvent: benzene–ethyl acetate). These were isomerized by $BF_3 \cdot OEt_2$ in methylene chloride and the ratio of *trans* and *cis* was 8 : 1 at equilibrium. b) Lit, 118—125/5.[3] c) Decomposed during the course of vacuum distillation.

of 3-phenylpropanal, based on the observation that II reacted with aldehydes more slowly than α-angelicalactone and that II was gradually decomposed by $BF_3 \cdot OEt_2$.

Similarly, various γ-acetyl-δ-valerolactones were obtained by the reaction of II with various aldehydes, such as propionaldehyde, chloroacetaldehyde, phenylacetaldehyde, benzaldehyde, and formaldehyde, as shown in Table 2.

This reaction may be explained by assuming an initial formation of aldehyde–$BF_3 \cdot OEt_2$ complex, which in turn reacts with α-angelicalactone (I) or 3,4-dihydro-6-methyl-2*H*-pyran-2-one (II) to give an addition product of V or VI. The intermediate

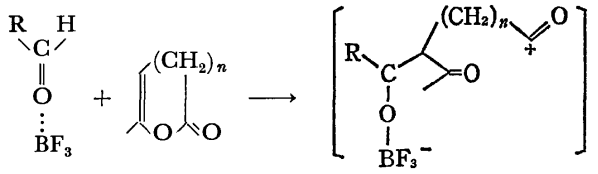

I, II V, VI

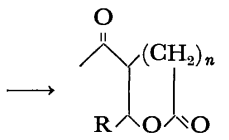

III, IV

I, III, V (n=1)
II, IV, VI (n=2)

adduct (V or VI) immediately cyclizes to form γ or δ-lactone (III or IV).

It is expected that the present reaction provides a simple and useful method for the syntheses of naturally occurring γ or δ-lactone derivatives. Actually, we recently reported the stereospecific synthesis of antibiotic botriodiplodin from β-acetyl-α-methyl-γ-butyrolactone produced by the reaction of α-methyl-α-angelicalactone with formaldehyde.[4]

Experimental

All boiling points and melting points were uncorrected. The IR spectra were recorded with a Hitachi Model EPI G3 spectrometer. The proton NMR spectra were obtained in carbon tetrachloride or deuterio chloroform solutions on a Varian T-60 spectrometer with TMS as an internal standard.

α-Angelicalactone (I) was prepared from levulinic acid. Bp 56—58 °C/12 Torr.[5] 3,4-Dihydro-6-methyl-2*H*-pyran-2-one (II) was prepared according to Shiroyan *et al.*[6] Bp 82—83 °C/23 Torr.

Reaction of α-Angelicalactone with 3-Phenylpropanal. $BF_3 \cdot OEt_2$ (0.142 g, 1 mmol) in 4 ml of methylene chloride was added slowly at 0 °C into a mixture of α-angelicalactone (0.098 g, 1 mmol) and 3-phenylpropanal (0.134 g, 1 mmol) in 6 ml of methylene chloride. The reaction mixture was stirred for 8 h at 0 °C. After being quenched with saturated NaCl solution, it was extracted with benzene. The extract was dried over anhydrous sodium sulfate. After removal of the solvent, 0.201 g (94%) of β-acetyl-γ-phenetyl-γ-butyrolactone (IIIa) was isolated by silica gel chromatography (solvent: benzene–ethyl acetate).

Similarly, IIIb—d were obtained under the reaction conditions shown in Table 2. The NMR and IR spectra of IIIa—f are shown in Table 3.

Reaction of α-Angelicalactone with Formaldehyde. Formaldehyde gas, prepared by thermal cracking of paraformaldehyde (0.604 g, 20 mmol) at 200 °C, was introduced into α-angelicalactone (0.982 g, 10 mmol) in 25 ml of methylene chloride at 0 °C. After stirring for 15 min, $BF_3 \cdot OEt_2$ (1.42 g, 10 mmol) in 5 ml of methylene chloride was added slowly into the reaction mixture at 0 °C and the reaction mixture was stirred for 1 h. After being quenched with saturated sodium hydrogen carbonate solution, it was extracted with methylene chloride. The extract was dried over anhydrous sodium sulfate, concentrated, and the residue was chromatographed on silica gel (solvent: benzene–ethyl acetate) to

mixture was stirred for 30 min at 0 °C, it was worked up as in the preparation of IIIf, to afford 0.255 g, (90%) of γ-acetyl-δ-valerolactone (IVf).

References

1) T. Mukaiyama, K. Narasaka, and K. Banno, *Chem. Lett.*, **1973**, 1011; T. Mukaiyama and M. Hayashi, *ibid.*, **1974**, 15; T. Mukaiyama, T. Izawa, and K. Saigo, *ibid.*, **1974**, 323. It was found recently that diketene reacts with acetals to afford δ-alkoxy-β-ketoesters. T. Izawa and T. Mukaiyama, *ibid.*, **1974**, 1189.

2) T. Mukaiyama, T. Hanna, T. Inoue, and T. Sato, *Chem. Lett.*, **1974**, 381.

3) J. Rothe and H. Zimmer, *J. Org. Chem.*, **24**, 586 (1959).

4) T. Mukaiyama, M. Wada, and J. Hanna, *Chem. Lett.*, **1974**, 1181.

5) Y. Iwakura and K. Hayashi, "Yukikagoubutsu Gouseiho," Vol. 11, ed. by The Society of Synthetic Organic Chemistry, Gihodo, Japan (1959), p. 3.

6) F. R. Shiroyan, L. V. Khazhakyan, A. K. Mkrtchyan, A. G. Terzyan, and G. T. Tatevosyan, *Arm. Khim. Zh.*, **20**, 649 (1967) [Chem. Abstr., **69**, 10387V (1968)].

Hydrolysis of Carbohydrates in the Presence of a Reversed Micelle. I. Hydrolysis of Sucrose in a Dioxane-Water Mixed Solvent

Kenichiro ARAI, Yoshitaka OGIWARA, and Kazuyoshi EBE

Faculty of Engineering, Gunma University, Kiryu, Gunma 376

(Received April 18, 1975)

Formation of a reversed micelle by dodecybenzenesulfonic acid (DBSH) in a dioxane-water mixed solvent was discussed in terms of the behavior of critical micelle concentration and NMR study. Hydrolysis of sucrose in the presence of the reversed micelle was then investigated. The pseudo-first-order rate constant of the reaction showed a tendency to increase with decreasing substrate concentration and increasing dioxane composition, and the maximum rate acceleration obtained in the present experiment was 21-fold on the basis of the reaction in aqueous solution. The rate acceleration may result from the solvent effect of dioxane relating to the structuredness of water and the substrate binding effect due to the formation of the reversed micelle.

The hydrolysis of carbohydrates in the presence of catalysts has been studied.[1-3] Numerous studies have been made on catalysis in the presence of a micelle[4] and also in the presence of a reveresed micelle.[5-9] In the present work the hydrolysis of sucrose as a model substance of carbohydrates in the presence of a reversed micelle was investigated. First the formation of the reversed micelle in the dioxane–water mixed solvent was examined, since carbohydrates are not sufficiently soluble in a polar solvents such as benzene and cyclohexane for the reaction rate to be followed accurately. If dodecylbenzenesulfonic acid (DBSH) can form a reversed micelle in the mixed solvent and the carbohydrates are bound into the micelle, it can be expected that the hydrolysis rates of sucrose are affected; the carbohydrates bound into the micelle are hydrolyzed in the presence of locally concentrated protons in the interior of the micelle.

There is little information on the reversed micelle in a mixed solvent, and its behavior was predicted to be very complicated.[10] The analyses were therefore carricd out with emphasis on the rate enhancement.

Experimental

Materials. Reagent grade sucrose, dioxane and hydrochloric acid (Wako Chemical Co., Tokyo) were used. Deionized and distilled water was used. Commercial sodium dodecybenzenesulfonate (Tokyo Chemical Co., Tokyo) was passed through a cation-exchange resin column in order to obtain free acidic surfactant.

Measurement of the Reaction Rate. DBSH was dissolved in a dioxane–water mixture and added to a sucrose aqueous solution, and the resulting mixture was kept at 40 °C. Aliquots of the mixture were taken out at intervals and the optical rotatory powers were measured by an automatic digital polarimeter (Nippon Bunko Co., Tokyo, DIP-180; accuracy ±0.002°). The logarithm of the difference between the optical rotatory powers, m_t at a reaction time t and m_∞ at infinite time (practically at ten times half life), was plotted against the reaction time, and the pseudo-first-order rate constant, k_1, was estimated from the slope (Fig. 1).

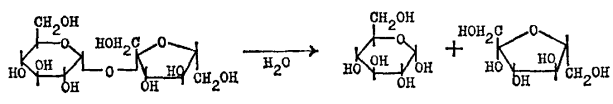

$[\alpha]_D^{20} = 66.45$ $[\alpha]_D^{20} = -19.7 + 0.36C$

C; concentration in g·dl^{-1}

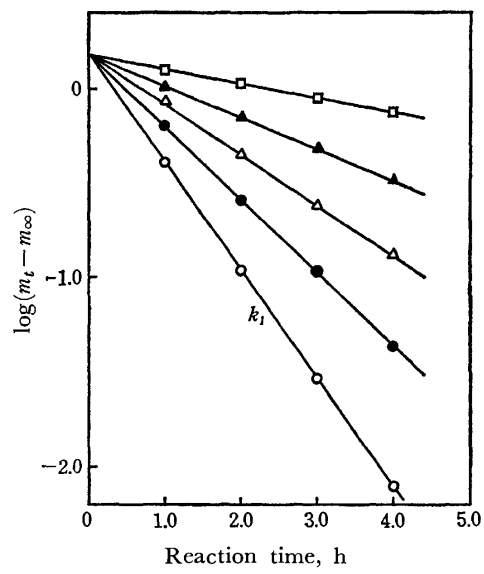

Fig. 1. Typical first-order plots of the changes in the optical rotatory power of sucrose at 40 °C.
m_t and m_∞ are the optical rotatory powers at a reaction time t and infinity. Dioxane composition, 70 vol%. DBSH concn, mM: ○; 100, ●; 80, △; 60, ▲; 40, □; 20.

A fairly good straight line was obtained for each plot. The changes in optical rotatory powers in water are as above.

Critical Micelle Concentration (CMC). Electric conductances of DBSH–dioxane–water mixed solutions were measured with an electric conductance titrator (Mitamura Riken Co., Tokyo) at various concentrations of DBSH, specific electric conductances being plotted against the concentration of DBSH. The maximum experimental error of specific conductance was ±0.001 S. The CMC was estimated from the break in the plots.

NMR Study. NMR spectra were obtained with an analytical NMR spectrometer (Nichiden-Varian Co., Varian A-60D, 60 MHz) at various concentrations of DBSH and hydrochloric acid, the chemical shifts of water-proton being measured. Sodium 3-trimethylsilylpropanesulfonate was used as a reference.

Results and Discussion

Formation of Reversed Micelle. First we examined whether reversed micelle could be formed by DBSH. Figure 2 shows the plots of the electric conductance of DBSH–dioxane–water mixtures against the con-

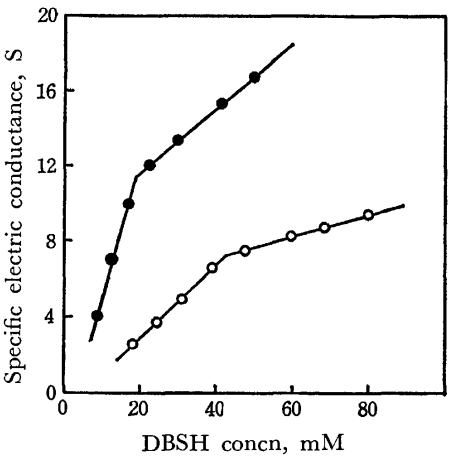

Fig. 2. The plots of the specific electric conductance of DBSH in dioxane-water mixtures against the concentration of DBSH at 40 °C.
Solvent: ○; dioxane 70 vol%, ●; dioxane-free.

centration of DBSH at compositions of dioxane 0 and 70 vol%. The concentration of surfactant corresponding to the break point of the straight lines obtained is considered to be CMC. The break point of the straight line can be clearly seen for the mixture with dioxane composition of 70 vol% as well as in the dioxane-free medium (Fig. 2), although it has been reported that the CMC of a reversed micelle is not clear.[11] This suggests the formation of a micelle even at higher dioxane composition.

Figure 3 shows the temperature dependence of the CMC estimated by the electric conductance method. It was found that the CMC is scarcely influenced by temperature. This behavior is in approximate agreement with the general characteristics of the micelle of ordinary alkylbenzenesulfonates.

Figure 4 shows the changes in CMC with the concentration of added sucrose. The CMC in the mixed solvent of dioxane 70 vol% decreases with addition of sucrose up to about 50 mM, and then levels off, but hardly changes in the dioxane-free solvent. The decrease in CMC with the addition of polar substrate was also found by Fendler *et al.*[6] in the reversed micelle system, and might indicate substrate binding into the micelle. The leveling off of the CMC with increasing sucrose concentration at higher dioxane compositions might be due to the fact that the amount of sucrose bound into the micelle does not increase any more with increasing concentration of sucrose under the conditions.

Figure 5 shows the relationship between the CMC and dioxane composition in the mixed solvents. DBSH was found to be insoluble in the range 20—50 vol% of dioxane. This suggests that the micelle formed at above 60 vol% of dioxane is the reversed micelle. The CMC is scarcely influenced by the dioxane composition in the lower range. In the higher range of dioxane composition, however, the CMC increases with increasing dioxane composition, and then shows a maximum at 80 vol% of dioxane. In the higher range of dioxane composition than those shown in Fig. 5, measurement of CMC was impossible because of the phase separation. The increase in CMC with increasing dioxane composition does not necessarily rule out the possibility of the reversed micelle formation, since the size of the micelle in the mixed solvent probably changes remarkably with changing solvent composition.[10]

The proton magnetic resonance shifts of water-proton in the presence of DBSH and hydrochloric acid in the dioxane–water mixed solvent at various concentrations were measured in order to investigate the reversed micelle formation. It has been established that the chemical shift of the proton magnetic resonance is concentration-dependent in the solutions of electrolytes which yield hydrogen-containing ions. The chemical exchange averages the chemical shifts in the proton resonance position over the different chemical species, and the averaged shifts observed are correlated with the dissociation of the solute.[12–15] Figure 6 shows the plots of averaged chemical shift *vs.* acid concentrations in the aqueous solution and in the dioxane–water mixed solvent with 70 vol% of dioxane. In the aqueous solution, the changes in the chemical shift with addition of acids were relatively small and

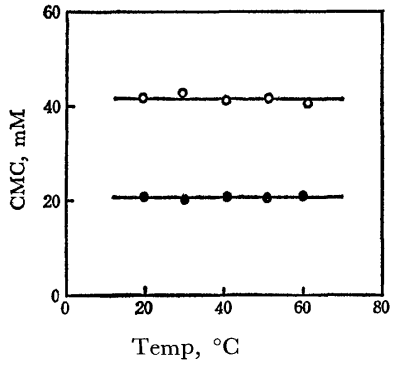

Fig. 3. Temperature dependence of CMC. Solvent: ○; dioxane 70 vol%, ●; dioxane-free.

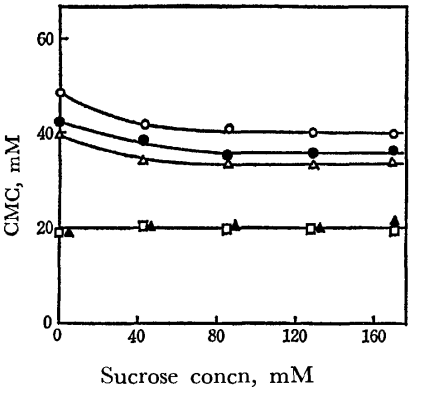

Fig. 4. Changes in CMC with addition of surcose at 40 °C. Dioxane compositions, vol%: ○; 80, ●; 70, △; 60, ▲; 10, □; 0.

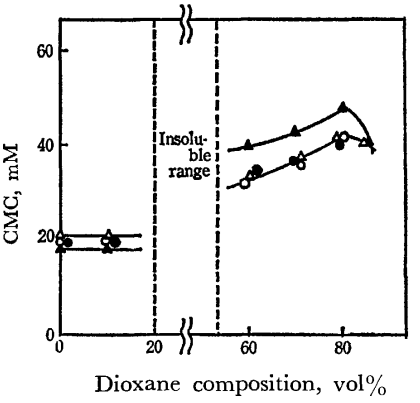

Fig. 5. Relationships between CMC and dioxane composition in the mixed solvents at 40 °C. Sucrose concn, mM: ○: 124.8, ●; 83.2, △; 41.6, ▲; 0.

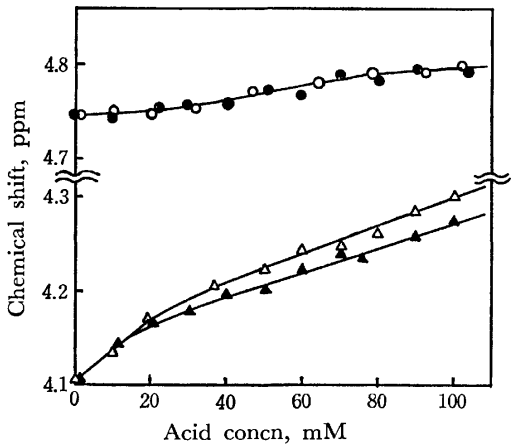

Fig. 6. The plots of averaged chemical shift of water-proton magnetic resonance *vs.* acid concentration. Acid: DBSH, ▲; dioxane 70 vol%, ●; dioxane free: hydrochloric acid, △; dioxane 70 vol%, ○; dioxane-free.

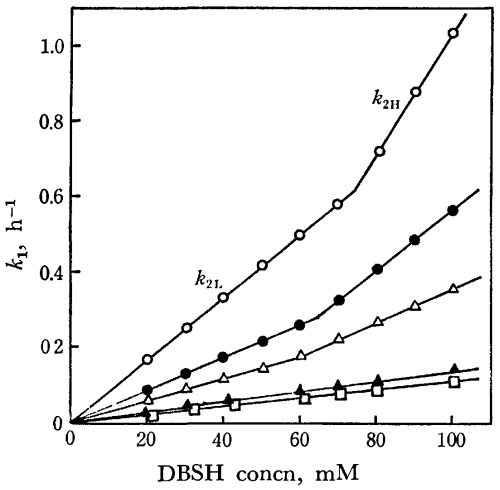

Fig. 7. Plots of the pseudo-first-order rate constant, k_1, *vs.* DBSH concentration at 40 °C. Sucrose concn, 83.2 mM. Dioxane composition, vol%. ○; 80, ●; 70, △; 60, ▲; 10, □; 0.

the difference in the chemical shifts of DBSH and hydrochloric acid appeared to be within the error limit. In the mixed solvent the chemical shift shifted to higher magnetic field with addition of dioxane, the changes in the chemical shift with addition of acids being greater than those in aqueous solution. The shifts may be related to the changes in structuredness of water. The changes in chemical shift were found to become smaller with addition of DBSH than with that of hydrochloric acid with an increase in acid concentration above 30 mM. The difference may result from the decrease in dissociation of DBSH due to "concentration" of sulfonic acid groups in the interior of the reversed micelle.

It seems that DBSH could form a reversed micelle in a dioxane–water mixed solvent with dioxane above 60 vol%, although the micelle might be less stable than the typical reversed micelle formed in neat apolar solvents.

Hydrolysis of Sucrose in the Presence of the Reversed Micelle. Hydrolysis of sucrose in dioxane–water mixed solvents in the presence of the reversed micelle mentioned above was investigated. Figure 7 shows the plots of the pseudo-first-order rate constant, k_1, estimated from the changes in the optical rotatory power of the reaction mixture (see Fig. 1) *vs.* the concentration of DBSH. Above 60 vol% of dioxane each plot gives two half lines, whereas below 10 vol% it gives only one straight line. In the hydrolysis of sucrose in the presence of hydrochloric acid, each similar plot of k_1 gives only one straight line independent of dioxane composition in the mixed solvent. Since k_1 was defined as the pseudo-first-order rate constant at a constant concentration of DBSH, the slope of the straight lines gives the apparent second-order rate constant, k_2, when the changes in the amount of water in the mixed solvent are not considered. Above 60 vol% of dioxane, k_2's in the lower and higher concentration ranges of DBSH are denoted by k_{2L} and k_{2H}, respectively. k_2 for the hydrolysis of sucrose in the presence of hydrochloric acid is denoted by k_{2HCl}. Although the concentration of DBSH corresponding to the break point on the straight line was slightly higher than the CMC estimated by the electric conductance method under the same conditions, the concentration may be considered as CMC, since CMC is known to be slightly affected by the measuring method and also the changes in concentration corresponding to the break point with change in concentration of DBSH and sucrose qualitatively agree with those of the CMC estimated by the electric conductance method (Table 1). Fendler *et al.*[7] also found a change in rate constant at a certain concentration by changing the concentration of surfactant. The hydrolysis of sucrose seems to be accelerated with formation of reversed micelle.

k_2's estimated at various concentrations of sucrose and dioxane are summarized in Table 2. It was found that k_2's increased with increasing dioxane composition in the mixed solvents for all of the k_{2H}, the k_{2L} and the k_{2HCl}. The increase may arise from the increase in activities of proton and water molecules due to the decrease in structuredness of water with addition of dioxane.[16] At the same composition of dioxane, k_{2L}'s were always smaller than k_{2HCl}. These differences may be due to the differences in the degree of dissociation. Above 60 vol% of dioxane and higher concentration range of DBSH, however, k_{2H}'s were greater than k_{2L}'s and even greater than k_{2HCl}. This rate enhancement might result from the substrate binding into the reversed micelle in which protons

Table 1. DBSH concentration corresponding to the break point of the straight lines obtained in the plots of k_1 *vs.* DBSH concentration, mM

Dioxane composition, vol%	Sucrose concn, mM		
	41.6	83.2	124.8
80	77	74	68
70	67	65	65
60	67	61	61

Table 2. Second-order rate constants, k_2's, in $M^{-1}h^{-1}$, for sucrose hydrolysis in the presence of DBSH or hydrochloric acid at 40 °C

Catalyst	Sucrose concn, mM		Dioxane composition, vol% 85	80	70	60	10	0
DBSH	41.6	k_{2L}	13.0	8.3	4.5	2.6	1.4	1.3
		k_{2H}	27.0	19.0	9.5	4.5		
		k_{2H}/k_{2L}	2.1	2.3	2.1	1.7	—	—
	83.2	k_{2L}	—	8.3	4.5	3.0	1.4	1.3
		k_{2H}	—	16.8	7.9	4.6		
		k_{2H}/k_{2L}	—	2.0	1.8	1.5	—	—
	124.8	k_{2L}	—	10.7	5.3	3.4	1.6	1.4
		k_{2H}	—	16.5	8.0	5.1		
		k_{2H}/k_{2L}	—	1.6	1.5	1.5	—	—
Hydrochloric acid	124.8	k_{2HCl}	—	14.0	6.5	3.5	1.6	1.5

were concentrated. The ratio k_{2H}/k_{2L} could be regarded as a measure of rate enhancement produced by the formation of reversed micelle. The ratios were found to increase with increasing dioxane composition. It is presumed that the stability of reversed micelle increases with lowering polarity of the mixed solvent or increasing dioxane composition, the effect leading to rate enhancement. The ratio k_{2H}/k_{2L} was also found to decrease with increasing sucrose concentration. The decrease could be explained as the result of averaging of reaction rates in and out of the reversed micelle, since the amount of sucrose bound into the micelle was presumed not to change, at least remarkably, with increasing total amount of sucrose, while the amount of sucrose existing out of the micelle increased, and the averaged reaction rate or the rate enhancement decreased with increasing total amount of sucrose. This explanation is supported by some investigations published so far. For example, Konno and Kitahara[17] reported that a small amount of water solubilized in reversed micelle is firmly bound into the micelle, but the binding become more loose, even less than that of free water, with the increase in amount of water solubilized. Kitahara[18] found that the change in the amount of water solubilized in the anionic surfactant reversed micelle scarcely influences the amount of micelle. The value of k_{2H}/k_{2L} corresponding to the sucrose concentration 41.6 mM and dioxane 85 vol% was found to deviate from the tendency mentioned above (Table 2). A similar deviation of the value of CMC estimated by the electric conductance method under the same conditions is shown in Fig. 5.

It may be concluded that DBSH forms a reversed micelle in dioxane–water mixture with above 60 vol% of dioxane and the micelle accelerates the hydrolysis of sucrose by binding the substrate inside. The maximum rate enhancement obtained in the present investigation was *ca.* 21-fold, and it was predicted to increase with decreasing sucrose concentration. The rate enhancement may result from the solvent effect of dioxane relating to the structuredness of water and the substrate binding effect due to the formation of reversed micelle.

We are very grateful to Professor Norio Ise, Kyoto University, Kyoto, for his helpful discussion.

References

1) K. Arai and N. Ise, *Makromol. Chem.*, **176**, 37 (1975).
2) K. Arai and Y. Ogiwara, *Makromol. Chem.*, **176**, 2491, 2501 (1975).
3) K. Arai, Y. Ogiwara, and N. Ise, *Makromol. Chem.*, **176**, 2871 (1975).
4) For example: J. Albrizzio, J. Archila, T. Rudulfo, and E. H. Cordes, *J. Org. Chem.*, **37**, 871 (1972); J. R. Cho and H. Morawetz, *J. Am. Chem. Soc.*, **94**, 345 (1972); J. H. Fendler and R. R. Liechti, *J. Chem. Soc. Chem., Commun.*, **1972**, 1041; S. Friberg and S. I. Ahmad, *J. Am. Chem. Soc.*, **94**, 5196 (1972).
5) S. Friberg and S. I. Ahmad, *J. Phys. Chem.*, **75**, 2001 (1971).
6) J. H. Fendler, E. J. Fendler, R. T. Medary, and V. A. Woods, *J. Am. Chem. Soc.*, **94**, 7288 (1972).
7) C. J. O'Connor, E. J. Fendler, and J. H. Fendler, *J. Am. Chem. Soc.*, **96**, 370 (1974).
8) C. J. O'Connor, E. J. Fendler, and J. H. Fendler, *J. Chem. Soc., Dalton*, **1974**, 625.
9) P. H. Elworthy and D. S. McIntosh, *Kollord Z. Z. Polym.*, **195**, 27 (1964).
10) S. R. Palit, *J. Colloid Sci.*, **4**, 523 (1949).
11) For example: G. Y. Markovits, O. Levy, and A. S. Kertes, *J. Colloid Interface Sci.*, **47**, 424 (1974).
12) H. S. Gutowsky and A. Saika, *J. Chem. Phys.*, **21**, 1688 (1953).
13) G. C. Hood, O. Reulich, and C. A. Reilly, *J. Chem. Phys.*, **22**, 2067 (1954).
14) R. Radeglia, *Z. Phys. Chem.*, **231**, 339 (1966).
15) L. Kotin and M. Nagasawa, *J. Am. Chem. Soc.*, **83**, 1026 (1961).
16) J. Tokura, "Yobaiwa," Kagaku Dojin, Kyoto (1973), p. 87.
17) K. Konno and A. Kitahara, *J. Colloid Interface Sci.*, **35**, 409 (1971).
18) A. Kitahara, *J. Phys. Chem.*, **69**, 2788 (1965).

Solvent Effects on Stereo and Regioselectivities of Ring-opening Reaction of Epoxide with Aluminum Chloride

Masashi INOUE, Toshio SUGITA,* Yoshiaki KISO, and Katsuhiko ICHIKAWA

Department of Hydrocarbon Chemistry, Faculty of Engineering, Kyoto University, Sakyo-ku, Kyoto 606

(Received May 31, 1975)

The ring-opening of 2,3-epoxybutane with aluminum chloride yielding 3-chloro-2-butanol was carried out in several different solvents. The reaction proceeds with 94% retention of configuration in a nitromethane solvent. The retentive ring-opening was observed to variable extents when nitro compounds, ethers, and aromatics were utilized as the solvents, but a complete inversion resulted in the other solvents. The regioselectivity was examined using 1,2-epoxypropane. The composition of the 1-chloro-2-propanol and 2-chloro-1-propanol thus produced was also strongly affected by the solvent. The latter was exclusively produced in nitromethane, though the former predominated in several other solvents. The structure of aluminum chloride in various solvents is discussed, and aluminum chloride–solvent 1 : 1 addition compounds in solution are concluded to be important for retentive and abnormal ring-opening.

Much has been written regarding the ring-opening reaction of epoxides. Nevertheless, the stereo and regioselectivities of the reaction are still somewhat confused subjects.[1] Ring-openings of epoxides with a nucleophile are generally accompanied with inversion of configuration at the point of attack, and can be explained by S_N2 mechanism. Reactions which proceed with retention of configuration have been reported in some cases of phenyl and acyl substituted epoxides. A double inversion mechanism with neighboring groups and a four-centered mechanism with an ion-pair have been proposed for these reactions.[2-5] Parker and Isaacs proposed that the reactions which proceed with racemization take place not by S_N1, but by concurrent S_N2 and S_Ni mechanisms.[1a]

When unsymmetrically substituted epoxides are involved, ring-opening can occur in either of two different directions:

$$\text{R-CH(O)CH}_2 \xrightarrow{\text{HA}} \text{R-CH(OH)-CH}_2\text{A} + \text{R-CH(A)-CH}_2\text{OH}$$

Normal product Abnormal product

In general, a reaction to cleave the bond between less substituted carbon and oxygen is termed "normal ring-opening," while the other direction is termed "abnormal." In the case of base-induced reactions of epoxides, normal ring-opening is predominant, but acid-catalyzed substitution reactions usually give considerable amounts of abnormal products.

Yielding chlorohydrins by the reaction of epoxides with aluminum chloride is well known not only as a side reaction of the Friedel-Crafts reaction, but also as a modification of catalyst in cationic polymerizations of epoxides. We reported in a previous paper that an alkyl-substituted epoxide, propylene oxide, afforded a chlorohydrin with a retained configuration in a reaction with aluminum chloride in a nitromethane solution.[6] In the present paper, we wish to report the solvent effect on the stereo and regioselectivities of the ring-opening reaction of epoxide with aluminum chloride.

* To whom all correspondence should be addressed.

Results and Discussion

Stereoselectivity. The ring-opening reaction of *cis*- and *trans*-2,3-epoxybutane (**1**) with aluminum chloride (**2**), yielding *erythro*- and *threo*-3-chloro-2-butanols (**3**), was examined in several different kinds of solvents. The stereochemical results are summarized in Table 1. It was also confirmed that the stereochemistry of the product was not affected in the course of hydrolysis of the produced aluminum alkoxide, since no ^{36}Cl was introduced into the product when the reaction mixture was hydrolyzed with aqueous $H^{36}Cl$.

$$\underset{\textbf{(1)}}{\text{CH}_3\text{-CH(O)CH-CH}_3} \xrightarrow[\text{ii) } H_3O^+]{\text{i) } AlCl_3\ (2)} \underset{\textbf{(3)}}{\text{CH}_3\text{-CH(OH)-CH(Cl)-CH}_3} \quad (1)$$

The solvents in which the reaction proceeds with retention of configuration are limited to aromatics, ethers, and nitro compounds. The product corresponding to the retention of configuration predominated only in the solvents of nitro compounds.

The ring-opening of **1** with **2** was carried out in carbon disulfide containing variable amounts of nitro-

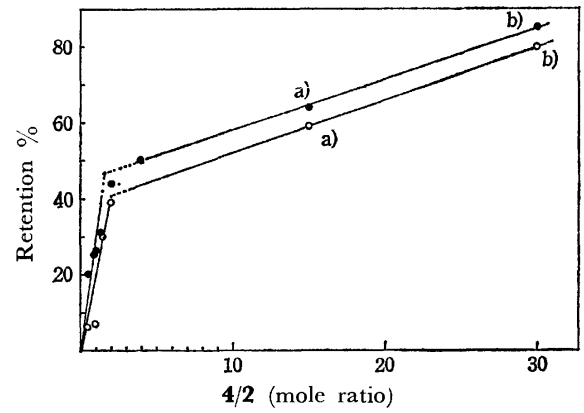

Fig. 1. Plot of $CH_3NO_2/AlCl_3$ *vs.* stereochemistry of ring-opening reaction of 2,3-epoxybutane: (●) *cis*-**1**, (○) *trans*-**1**.
Reactions were run in carbon disulfide (8 ml) at 0 °C. An equivalent amount (4 mmol) of **2** to **1** was used. a) Neat **4** (4 ml) was used as a solvent. b) Neat **4** (8 ml) was used as a solvent.

Table 1. Stereochemistry of ring-opening reaction of 2,3-epoxybutane with $AlCl_3$[a]

Solvent	1	Reaction temperature[b] °C	3 Yield %	Steric course Retention %
Carbon disulfide	*cis*	0	15.0	0
Chloroform	*cis*	0	42.3	0
Acetonitrile	*cis*	0	38.1	0
Acetone	*cis*	0	4.6	0
Ethanol	*trans*	0	76.1	0
Nitromethane (**4**)	*cis*	−10	24.1	94
Nitromethane	*cis*	0	12.7	85
Nitromethane	*cis*	18	13.2	36
Nitromethane	*cis*	27	10.6	25
Nitromethane	*trans*	−11	18.5	93
Nitromethane	*trans*	0	13.8	80
Nitromethane	*trans*	24	12.3	30
Nitromethane + Chloroform[c]	*trans*	0		65
1-Nitropropane	*trans*	0	24.1	59
2-Nitropropane	*trans*	0	30.3	49
Nitrobenzene	*trans*	0	14.4	48
Benzene	*trans*	7	5.9	trace
Toluene	*trans*	0	3.8	0.6
Mesitylene	*trans*	0	1.4	2.8—4.9
Ethyl ether	*trans*	0	16.5	52
Anisole	*trans*	0	4.2	2
Diphenyl ether	*trans*	28	8.3	0
DMSO	*trans*	0	4.6	0
DMF	*trans*	0	7.8	0
Sulfolane	*cis*	27	17.0	trace
Sulfolane + 1,2-Dichloroethane[d]	*cis*	0		0[g]
Dimethyl sulfone + 1,2-Dichloroethane[e]	*cis*	0		0
Pyridine-*N*-oxide + Chloroform[f]	*cis*	0		3
Triethylamine	*cis*	0	42.5	0

a) Reactions were run in 8 ml of the solvent unless specified otherwise on 4 mmol scale of **1** with 1.5 equiv. of **2** for 2 h. b) Cooling bath temperature. c) **1** (4.88 mmol), **2** (5.59 mmol), **4** (4 ml), $CHCl_3$ (4 ml). d) **1** (2.80 mmol), **2** (5.60 mmol), sulfolane (39.4 mmol), $(CH_2Cl)_2$ (4 ml). e) **1** (5.30 mmol), **2** (5.48 mmol), $(CH_3)_2SO_2$ (100 mmol), $(CH_2Cl)_2$ (20 ml). f) **1** (4.35 mmol), **2** (5.07 mmol), C_5H_5NO (17.0 mmol), $CHCl_3$ (10 ml). g) Nakajima reported that the ring-opening reaction of 1,2-epoxypropane with **2** proceeds with 12% retention of configuration in a mixed solvent of sulfolane and 1,2-dichloroethane.[7]

methane (**4**). In Fig. 1, the percentages of retention are plotted against the amounts of **4** added. Nearly linear correlations between the amounts of **4** added and the percentage of retention are observed in the regions of **4**/**2**<0.5 and **4**/**2**>4. From the intersection to these two straight lines, values of **4**/**2**=1.4 and 1.8 are obtained for *cis*- and *trans*-**1** respectively. This fact seems to indicate that the ring-opening is connected with the 1 : 1 addition compound of **2** and **4**, although the possibility of the participation of the 1 : 1.5 or 1 : 2 addition compound cannot be completely excluded. On the other hand, it has been reported that nitroalkanes and many aromatic nitro compounds react with **2** to form crystalline solids, generally with the formula of $AlCl_3 \cdot RNO_2$, but also, in a few cases, that of $AlCl_3 \cdot 2RNO_2$.[8a]

Table 2. Stereochemistry of ring-opening of 2,3-epoxybutane with $AlCl_3$ in the presence of nitrobenzene derivatives (p-X-C_6H_4-NO_2)[a]

X	Stereochemistry Retention %	Hammett $\sigma_p - \sigma_m$
H[b]	60	—
CH_3[b]	61	−0.109
Cl[b]	65	−0.146
OCH_3[b]	75	−0.383
CN[c]	0	+0.100
NH_2[c]	1.3	−0.49
OH[c]	2.4	−0.82

a) Reactions were carried out using *cis*-**1** in 1,2-dichloroethane containing nitrobenzene derivatives (1.0 M) at 0 °C, **2**/**1**=1.0−1.4, nitrobenzene derivatives/**2**=8.6−8.9. b) Reaction is homogeneous. c) Reaction is heterogeneous.

The substituent effects of p-substituted nitrobenzenes were investigated in order to account for the specificity of nitro compounds; the results are shown in Table 2. Within the nitro compounds which are soluble in 1,2-dichloroethane, a good correlation is obtained between the percentages of retention and the $\sigma_p - \sigma_m$ values of the substituents, which have been suggested as measures of the resonance effect of the given substituents. This fact indicates that the resonance between π-electrons of an aromatic ring and a nitro group is very significant in the retention process. On the other hand, the $\sigma_p - \sigma_m$ values should reflect the stabilities of the 1 : 1 addition compounds, of which structural information has been reported by Gagnaux.[9] Thus, the more stable 1 : 1 addition compounds, $AlCl_3 \cdot Sv$ (**5**, Sv=solvent), increases the retentive ring-opening reaction.

p-Cyano-, p-hydroxy- and p-amino-nitrobenzenes are insoluble in 1,2-dichloroethane, and the reaction systems are heterogeneous. A nonpolar solvent capable of undergoing a homogeneous reaction was searched for in vain. The reaction is accompanied with an almost complete steric inversion when these nitrobenzenes were added. In these cases, the group coordinating to aluminum may be not nitro, but cyano, hydroxyl or amino group, even if these compounds form complexes with **2**.

The proportions of the retention slightly increase in the order of: benzene<toluene<mesitylene, although the Friedel-Crafts reactions occur predominantly in these solvents. It is still less certain that **2** interacts with aromatic hydrocarbon, but these has been evidence of weak complex formation from solubility measurements.[8b] Roberts[10] reported that the susceptibility toward a **2**-induced rearrangement of n-propyl side chains decreased in the series of n-propylbenzene, n-propyltoluene, and n-propylxylene. He attributed

this to the postulate that the catalyst is progressively less active due to complex formation with aromatics with increasing Lewis basicities. In the present case, the percentage of retention is also proportional to the stability order of the aluminum chloride complexes to be formed.

The same conclusion can also be drawn from a series of aliphatic nitro compounds. It is well-known that the steric effects have an important influence on the stability of the 1 : 1 complexes of Lewis acids and bases.[11] Brown[12] reported that the stabilities of the 1 : 1 complexes of boron trifluoride and ethers decreased in the order of: $Me_2O \cdot BF_3 > Et_2O \cdot BF_3 > i\text{-}Pr_2O \cdot BF_3$. The stabilities of the complexes of **2** and nitro compounds are expected as: $MeNO_2 \cdot AlCl_3 > n\text{-}PrNO_2 \cdot AlCl_3 > i\text{-}PrNO_2 \cdot AlCl_3$. The sequence is actually consistent with the observed order of the percentages of retention.

In the earlier reports on the ring-opening reactions of epoxides which proceeded with retention of configuration, the mechanism was discussed in the following terms: 1) a double inversion with the participation of neighboring groups, and 2) a four-centered or an ion-pair mechanism. Although the mechanism 1 was proposed for the case of phenyl- and carbonyl-substituted epoxides,[2,3,5] it is improbable for an alkyl-substituted epoxide in the present case. The mechanism 2 was proposed by Wasserman and Aubrey[5] as a possible explanation of the results of the reaction of dypnone oxide with hydrogen chloride. Brewster[4] also supposed an ion-pair in a solvent cage to explain the *cis* ring-opening of *trans*-α-methylstilbene oxide with acetic acid. An analogous mechanism, shown in Scheme 1, seems to be applicable to the present case.

Solvates of different compositions are known for **2** containing from one to six donor molecules per molecule of **2**. Solvents of a weak coordinating affinity give 1 : 1 addition compounds, and those of better coordinating properties give 1 : 1, 1 : 1.5, and 1 : 2 compounds, while 1 : 4 and 1 : 6 compounds are limited only to some powerful coordinating solvents. A solvate of the $AlCl_3 \cdot Sv$ type was regarded as an acceptor solvate,[13] since it is capable of accepting further solvent or other donor molecules.

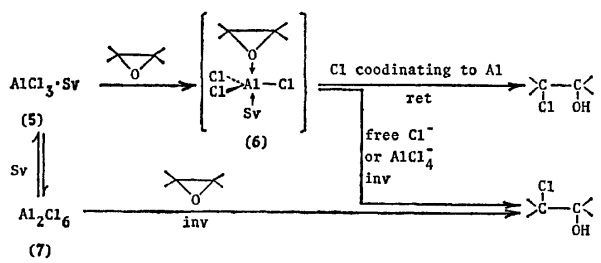

Scheme 1.

On the addition of epoxide, the solvated aluminum chloride (**5**) may accept lone-pair electrons of epoxide and is transformed into the complex **6**. The collapse of **6** gives chlorohydrin of a retained configuration whose chlorine comes from the coordinating site to aluminum. On the contrary, the inverted product can be derived by the attack of the free chloride ion in the solution on the solvated complex **6**. An analogous mechanism involving a common intermediate leading to both *cis* and *trans* oxymercurials was recently proposed by Bach and Richter.[14] Furthermore, in the present case, the solvated complex **5** may be equilibrated with the aluminum chloride dimer (**7**). **2** is well-known to exist as a dimer in carbon disulfide or in chloroform. Since a chlorohydrin with an inverted configuration is obtained in these solvents, the reaction of epoxide and **7** is considered to proceed with inversion. In the system involving a stable addition compounds, the equilibrium should lie towards the complex **5** rather than **7**; that is, the more stable addition compounds afford an increased amount of the chlorohydrin with a retained configuration.

If the ring-opening of epoxide with **2** is assumed to follow Scheme 1, free ion species and also **7** should not exist in the system which produces a chlorohydrin with a retained configuration. However, an inconsistency inheres in this condition. To satisfy the condition, the solvent must be moderately basic; free chloride ion may be formed by the cleavage of Al–Cl bonds if the solvent basicity is too strong.

Table 3. Stereochemistry of ring-opening of 2,3-epoxybutane with $AlCl_3$ in nitromethane. Effects of the additional lithium halide

Lewis acid (mole ratio)	Stereochemistry Retention %
2	85
2+LiCl (1 : 1)	6
2+HCl (1 : 1)	3
2+HCl (1 : 0.03)	72
2+LiBr (1 : 1)	2[a]
$AlBr_3$+LiCl (1 : 1)	1[a]
(LiCl)	No reaction
(LiBr)	No reaction

a) The product is 3-bromo-2-butanol containing trace of **3**.

In order to discuss the effect of a free ion, the ring-opening reaction of **1** was pursued in **4** by the addition of lithium salts as a source of free ions. The results are tabulated in Table 3. The reaction process alters from retention to inversion by the addition of an equivalent amount of lithium chloride. In the experiments using $Li^{36}Cl$, the produced **3** contained 22.6% of the activity. This result indicates that all the chlorines of lithium chloride and **2** are equivalent within the limits of experimental error. The addition of lithium chloride creates an equilibrium:

$$AlCl_3 \cdot Sv + LiX \overset{Sv}{\rightleftharpoons} LiSv_n^+ + AlCl_3X^- \qquad (2)$$

The anion, $AlCl_4^-$, formed in this equilibrium attacks epoxide, and the reaction proceeds with inversion of configuration.

A mechanism involving the back-side shielding by a solvent may be expected, but it is inadequate for the present system by the facts that a high retention of configuration is observed only in nitro compound

solvents, and that the reaction proceeds with complete inversion in acetonitrile, which exhibits a good back-side shielding effect in solvolysis.[15] The substitution reaction of epoxides under acidic conditions was claimed not to proceed by the *A*1 mechanism, but by the borderline *A*2 mechanism even in a system stabilizing the carbonium ion such as styrene oxide.[16] It was also reported that the rearrangement of oxirane to carbonyl compounds does not occur through a planar carbonium ion, but occurs in a more concerted manner.[17] The temperature effect on the stereoselectivity shown in Table 1 seems to constitute evidence for the arguments on the intermediacy of the fully developed carbonium ion. If the ring-opening in **4** proceeds by means of the carbonium ion–back-side shielding mechanism, the ratio of racemization would increase at higher temperatures. At 27 °C, the result is 25% retention and 75% inversion, which means 50% inversion and 50% racemization. As inversion and racemization at 18 °C are 28 and 72% respectively, an inversion process prevails at higher temperatures. The observed temperature effects cannot be explained by assuming the formation of a carbonium ion. These results suggest a larger activation entropy and enthalpy for the reaction accompanied with steric inversion than for the reaction with retention. Taking the cyclic transition state, the S_Ni reaction can be expected to have a smaller activation enthalpy and a larger negative value of activation entropy than the S_N2 reaction. The observed temperature effect is explainable by assuming the S_N2 mechanism for the ring-opening reaction with inversion and the S_Ni mechanism for the reaction with retention. However, the differences in the relative rates due to the reaction temperature are too large to be accounted for by only the competition of S_N2 and S_Ni reactions. These differences may also be due to an equilibrium between **5** and **7**, as is indicated in Scheme 1.

The ring-opening reaction proceeds with inversion of configuration in nonpolar solvents, such as carbon disulfide and chloroform, in which **2** is dimeric. In these solvents, however, it is difficult to assume a free ionic species which attacks the coordinated epoxide from the back-side. Therefore, it seems to be difficult to explain an inversion mechanism by a model for the transition state at a single metal atom center. A mechanism which involves two separate metal sites has been proposed by Price for the triethylaluminum–water catalyzed epoxide polymerization, which proceeds with inversion of configuration at the carbon atom undergoing ring-opening attack.[18] We propose, on these bases, a most plausible mechanism for the ring-opening of epoxide with **7** in a nonpolar solvent (Scheme 2), although we expected a mechanism including two molecules of **2** for the reaction in a previous paper.[6]

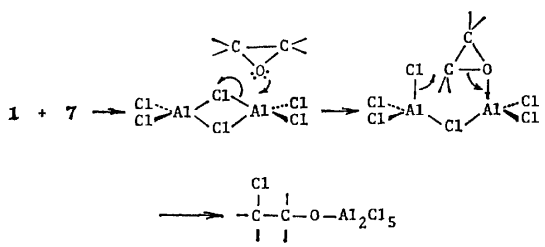

Scheme 2.

Many studies have been made concerning the structure of **2** in solutions; among them, the investigation by means of NMR appears to be most reliable. The solution structures of **2** can be classified into the following four groups on the basis of the experimental results obtained by NMR techniques:

Type 1. Solutions in which **2** is completely dissociated into ions.

Solutions of **2** in protic and aprotic polar solvents belong to this group. In dimethyl sulfoxide (DMSO)[19] and ethanol,[20] the Al–Cl bonds are completely dissociated into ions, and the aluminum cation is coordinated by six molecules of the solvents.

$$AlCl_3 + 6Sv \longrightarrow AlSv_6^{3+} + 3Cl^- \quad (3)$$

Type 2. Solutions in which disproportionation occurs.

The apparent solvation number of **2** in acetonitrile is 1.5,[21] and the Al–Cl bonds dissociate partially into ions.[20,22]

$$4AlCl_3 + 6Sv \longrightarrow AlSv_6^{3+} + 3AlCl_4^- \quad (4)$$

Type 3. Solutions in which **2** forms 1 : 1 addition compounds with the solvents.

$$AlCl_3 + Sv \longrightarrow AlCl_3 \cdot Sv \quad (5)$$

Although many compounds are reported to form 1 : 1 addition compounds in the crystalline state with **2**, the existence of the 1 : 1 compounds in solution has been confirmed in a few cases. Nitro compounds are considered to form the 1 : 1 adduct in solution.[23] Ether and benzene may also form 1 : 1 adducts in the equilibrium state.[20,24] The 1 : 1 adducts are acceptor solvates, as has been mentioned before.

Type 4. Solutions in which **2** exists as a dimer.

2 exists as a dimeric form (**7**) in nonpolar solvents, such as carbon disulfide and chloroform.[25] Ether and benzene are considered to contain **7** under equilibrium with the 1 : 1 adducts.[20,24]

The ring-opening of epoxide with **2** proceeds with retention of configuration only in the solvents of Type 3. In mixed solvents, the one with the stronger ability to coordinate to aluminum determines the nature of the solution; *e.g.*, the solution structures of the mixed solvents of Types 1 and 2, and of Types 2 and 3 are dominated by the solvent natures of Types 1 and 2 respectively. When an equivalent amount of **4** to **2** is added to an acetonitrile solvent, the structure of the solution is Type 2, and the epoxide is ring-opened with 100% inversion. This result is in good contrast with that of the reaction carried out in a carbon disulfide solution containing **4**.

Haraguchi reported the order of coordination affinity against aluminum as $H_2O > EtOH \gg I > Br > Cl > PhCN > CH_3CN$.[20,24] If lithium halide is added to the solutions of Types 2 and 3, aluminum in the solution will mostly be in the state of $AlCl_3X^-$, since the halogen has a stronger affinity than the solvent does. In these systems, the reaction proceeds with inversion.

Regioselectivity. The reaction was carried out in a way similar to that mentioned in the stereochemical section, using 1,2-epoxypropane (**8**) instead of **1**. The isomer distributions of the produced chloropropanols (**9**) are summarized in Table 4.

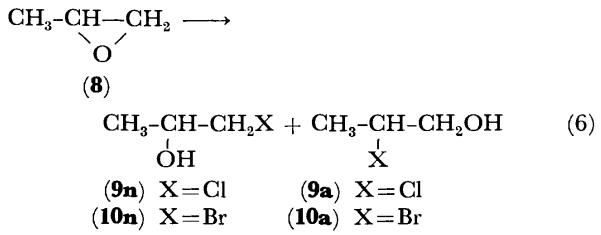

(**8**)

$$CH_3\text{-}CH(OH)\text{-}CH_2X \quad (\mathbf{9n})\ X=Cl \quad (\mathbf{10n})\ X=Br$$
$$+\ CH_3\text{-}CH(X)\text{-}CH_2OH \quad (\mathbf{9a})\ X=Cl \quad (\mathbf{10a})\ X=Br \qquad (6)$$

Table 4. Ring-opening reaction of 1,2-epoxypropane with $AlCl_3$ in various solvents[a]

Solvent	Yield **9** (%)	Product ratio (%)	
		9n	**9a**
CS_2	54.0	47	53
$ClCH_2CH_2Cl$	71.0	17	83[b]
Et_2O	26.3	57	43
CH_3NO_2	51.6	2	98
CH_3CN	97.5	87	13
EtOH	96.4	91	9
DMSO	18.7	81	19

a) Experimental conditions are **8** : **2** : solvent = 1 : 1 : 50. b) The proportion of **9a** depends upon the rate of addition of **8**, and it decreases until a minimum 18% when **8** is added rapidly.

In contrast with the fact that normal ring-opening is predominant in acetonitrile, ethanol, and DMSO, the proportion of the abnormal ring-opening product (**9a**) is increased in ether, carbon disulfide, and 1,2-dichloroethane. Furthermore, an extensive abnormal ring-opening as much as 98% is observed in nitromethane. A few reactions are known which proceed with more than 90% abnormal ring-opening. In these cases, nucleophiles preferably attack the hindered carbon atom.

Although several different mechanisms have been called into play to explain the divergent results of ring-opening reactions of epoxides, a consistent explanation can be given in terms of a "push-pull" mechanism.[26] Because of the strain in the three-membered ring of epoxide, the cleavage of the C–O bond will be important, especially in acid-catalyzed reactions, in which proton or Lewis acid coordinates to the epoxide oxygen. The coordination of these acids provides a strong pull in the displacement. As a result, steric factors are less influential than usual.

The ring-opening of aliphatic epoxide with **2** in **4** cannot be considered to involve a fully developed carbonium ion, but the 1 : 1 adduct of **2** and **4** is an acceptor solvate and can coordinate on the epoxide oxygen. Thus, favorable bond-breaking may occur between secondary carbon and oxygen giving the abnormal product (**9a**).

Such mode of reaction is often observed in the substitution reactions of heterocyclic compounds.[27] For example, the Friedel-Crafts reaction of **8** proceeds with inversion of configuration, accompanied with a complete abnormal ring-opening.[6] The ring cleavage of cyclic sulfate has been considered to proceed by S_N1 mechanism under acidic conditions, because the reaction of unsymmetrical cyclic sulfate from 1,3-butanediol with hydrochloric acid takes place on the secondary carbon.[28] However, the ring-opening of the cyclic sulfate of 2,4-pentanediol with hydrochloric acid proceeds with complete inversion of configuration, yielding 4-chloro-2-pentanol.[29]

As has been postulated in the foregoing stereochemical section, $AlCl_3 \cdot Sv$ (**5**) is the reacting species in **4** and ether solutions, and the chlorine atom of the products comes from the coordination sphere of aluminum. In DMSO, ethanol, and acetonitrile, on the contrary, chloride and $AlCl_4^-$ ions play an important role in the nucleophilic substitution of epoxide. The dissociated aluminum cation is completely solvated, fulfilling its coordination number, and it seems no longer to provide a strong pull by the coordination of the epoxide oxygen.

It has also been reported that the ring-opening reaction of **8** with hydrochloric acid proceeds concurrently by the two paths shown in Eqs. 7 and 8.[16] Analogous courses can be considered for the reaction of **8** with **2** in polar solvents (Eqs. 9 and 10):

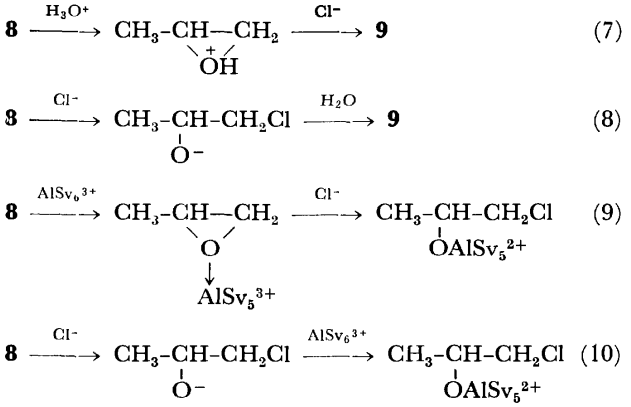

$$\mathbf{8} \xrightarrow{H_3O^+} CH_3\text{-}CH(\overset{+}{O}H)\text{-}CH_2 \xrightarrow{Cl^-} \mathbf{9} \qquad (7)$$

$$\mathbf{8} \xrightarrow{Cl^-} CH_3\text{-}CH(O^-)\text{-}CH_2Cl \xrightarrow{H_2O} \mathbf{9} \qquad (8)$$

$$\mathbf{8} \xrightarrow{AlSv_6^{3+}} CH_3\text{-}CH(O\rightarrow AlSv_5^{3+})\text{-}CH_2 \xrightarrow{Cl^-} CH_3\text{-}CH(OAlSv_5^{2+})\text{-}CH_2Cl \qquad (9)$$

$$\mathbf{8} \xrightarrow{Cl^-} CH_3\text{-}CH(O^-)\text{-}CH_2Cl \xrightarrow{AlSv_6^{3+}} CH_3\text{-}CH(OAlSv_5^{2+})\text{-}CH_2Cl \qquad (10)$$

The nucleophiles produced in DMSO and ethanol are free and solvated chloride ions respectively, but $AlCl_4^-$ ion is the nucleophile in acetonitrile.[19,20,22] Equation 9 may be considered as a usual acid-catalyzed reaction *via* an onium ion, and Eq. 10, as a reaction with a base. It is well known that the base-induced reaction of epoxide exclusively results in the normal ring-opening. As the normal product (**9n**) is favored in DMSO, ethanol, and acetonitrile, the respectable part of the ring-opening in these solvents is expected to proceed by means of Eq. 10.

The regioselectivity of the ring-opening reaction appears to depend upon the counterbalance of the pull by Lewis acids and the push by nucleophiles. The result that the normal product predominates in the polar solvents may reflect the weak pull by the $AlSv_6^{3+}$ cation and the strong push by the chloride and $AlCl_4^-$ ions. This is in good contrast with the results of the Friedel-Crafts reaction, in which a bulky and weak nucleophile, benzene, provides only a weak push, while **2** pulls very strongly; thus, the result is a complete abnormal ring-opening, as has been mentioned before.

Table 5. Ring-opening reaction of 1,2-epoxypropane in the presence of salts[a)]

Solvent	Addendum	Yield 9+10 (%)	Product ratio (%)			
			9n	9a	10n	10a
CH_3NO_2	none	48.3	4	96		
CH_3NO_2	LiCl	72.6	62	38		
CH_3NO_2	NaCl	53.3	58	42		
CH_3NO_2	KCl	58.4	73	27		
CH_3NO_2	LiBr	81.5	14	4	69	13
CH_3NO_2	KBr	65.4	15	4	73	8
Et_2O	none	34.8	57	43		
Et_2O	LiBr	37.8	4	1	89	6
Et_2O	NaBr	29.0	61	39	0	0
Et_2O	KBr	33.0	57	43	0	0

a) Experimental condition; **8** : **2** : addendum : solvent = 1 : 1 : 1 : 50.

Table 6. Solvent effect on the ring-opening of 1,2-epoxypropane in the presence of lithium bromide[a)]

Solvent	Yield 9+10 (%)	Product ratio (%)			
		9n	9a	10n	10a
CS_2	36.3	61	34	5	trace
$ClCH_2CH_2Cl$	37.9	44	40	9	3
Et_2O	34.8	21	3	70	6
CH_3NO_2	84.9	11	3	75	11
CH_3COCH_3	92.7	12	1	83	4
CH_3CN	96.1	8	1	86	5
DMF	22.1	63	7	29	1
DMSO	13.8	69	13	17	1
EtOH	80.4	69	8	21	2
EtOH	100	49	6	43	2

a) Experimental condition; **8** : **2** : LiBr : solvent = 1 : 1 : 1 : 20.

To confirm these considerations we examined the effect of added alkali metal halide on the regioselectivity of the ring-opening of **8** with **2**. Quite a different regioselectivity was observed when the salts are added to **4** and ether solvents.

The results shown in Table 5 can be summarized as follows: 1) the normal ring-opening becomes predominant when the salts are added, and bromides are more effective than chlorides; 2) the bromopropanols (**10**) predominate when bromides are added, except in the cases of sodium and potassium bromides in ether; 3) the difference of cation has little influence on the product compositions.

As is shown in Table 6, the product distribution in acetonitrile is similar to those obtained in **4** and ether; in these solvents $AlCl_3Br^-$ is a reacting species, but it distinctly differs from those in DMSO and ethanol, in which the added salts completely dissociate into ions. This fact indicates that the regioselectivity is related intimately to the anionic species. It has been reported that AlX_4^- has nucleophilicity to some extent, though it is a weaker nucleophile than halide ion.[30)]

If the equilibrium 2 is taken into account, lithium cation should be the acid providing the pull in Eq. (9) when the solvents of the second and third types are used. Although it has been reported that lithium salts have catalytic activities in the ring-opening and rearrangement reactions of epoxides,[31)] only a weak participation of lithium cation may be displayed by the electrostatic interaction in the present case, since not only lithium but potassium salt is effective and the reaction is not so much affected by the change of cations. As the pull provided by the lithium cation may be much weaker compared with that by **5**, the more normal ring-opening results when the lithium halides are added to **4**. When sodium and potassium bromides are added, the equilibrium 2 stays far to the left in ether, because these salts are insoluble in this solvent. Thus, these salts seem to have no influence on the regioselectivity in an ether solvent.

As affinity of bromide ion to aluminum is stronger than that of chloride,[24)] the formation of AlX_4^- species in the equilibrium is more satisfactory when lithium bromide instead of chloride is added. As a result, the more normal ring-opening product is obtained by the addition of lithium bromide.

The results shown in Table 6 can be explained appropriately by taking the before-mentioned types of the solution structure into account. The first class of solvent, consisting of polar solvents such as DMSO, DMF, and ethanol, can completely dissociate **2** and lithium salts into ions. In these solvents, metal cations are strongly coordinated by the solvent molecules. The distribution of the halohydrins produced depends upon the nucleophilicities of the halide ions. In aprotic polar solvents, halide ions are not solvated and their nucleophilicities depend upon their basicities, $Cl^- > Br^-$.[32)] On the contrary, halide ions are solvated in protic solvents, their nucleophilicities do not depend upon the basicities, and the order of nucleophilicities has been well established as $Br^- > Cl^-$.[33)] Accordingly, the predominant product is **9** in aprotic polar solvents, and the extended proportion of **10** results in protic solvents.

In the moderately basic solvents of the second type (acetonitrile, acetone, *etc.*), and in **4** and ether of the third type, a larger amount of **10** was yielded than was to be expected from the nucleophilicities of halide ions in aprotic solvents. The reaction without the addendum in **4** and ether proceeds *via* the complex **6**, where no ionic species are present. An $AlCl_3Br^-$ ion is formed according to Eq. 2 when the lithium bromide is added to solvents of the second and the third classes. It is most reliable that the ring-opening is caused by the attack of $AlCl_3Br^-$ instead of free chloride or bromide ions in these systems. However, insufficient evidence is available to us at this time to interpret the predominant formation of **10** with the use of $AlCl_3Br^-$. One of the most reasonable elucidations for this subject may be offered by Pearson's HSAB principle. Bromine is a softer base within four halogens in $AlCl_3Br^-$, and the carbon atom of epoxide is a soft acid. As a soft acid is favorable to react with a soft base, **10** should be the predominant product of the reaction with $AlCl_3Br^-$.

If the reaction conditions of LiBr/**8**$\geqq$1 are satisfied

Table 7. Effects of mole ratio of the reagents on the ring-opening reaction[a)]

Mole ratio			Product ratio (%)			
8	**2**	LiBr	**9n**	**9a**	**10n**	**10a**
1	1	1	7	1	85	7
1	1	0.5	37	9	50	4
1	1	2	2	trace	89	9
1	0.5	1	4	1	87	8
1	2	1	4	2	86	8
0.5	1	1	5	1	84	10
2	1	1	36	8	51	5

a) Solvent: Et_2O (100 mol eq.)

as is shown in Table 7, **10** is the principal product and no difference is observed in the product distributions. The exhaustive formation of **10** in the system of **8** : **2** : LiBr=1 : 2 : 1 may be indicative that the reaction rate of $AlCl_3Br^-$ and **8** is faster than that of **5** and **8**, for the same amount of **5** as $AlCl_3Br^-$ should exist in the system even if Eq. 2 is completely shifted to the right under these conditions.

In the nonpolar solvents which are classified as the fourth type (carbon disulfide, dichloroethane, *etc.*), the abnormal ring-opening product indicates a tendency to predominate over the normal product. The addition of lithium bromide shows little effects, as is shown in Tables 4 and 6. The composition of the normal ring-opening product, **9n**, was increased in the order of 17, 27 and 37% with an increase in the mole ratio of **8**/**2**=1.0, 2.0, and 3.0 in 1,2-dichloroethane. These results indicate that the alkoxyaluminum chloride, which is given by the reaction of **8** and **2**, reacts with additional **8** to give more **9n** than in the reaction of **2**. The proportion of normal ring-opening seems to increase in the order of **2**<$AlCl_2OR$<$AlCl(OR)_2$; these reacting species may be present as dimers in such solvents. As the Lewis acidities generally increase with an increase in the electronegativities of X in metal salts, MX_n, the Lewis acidities decrease in the order of **2**>$AlCl_2OR$>$AlCl(OR)_2$. Thus, the abnormal ring-opening should be favored in the cases of stronger Lewis acids. The product distribution was strongly affected by the rate of addition of **8** to **2**, and the proportion of **9n** was varied from 17 to 82% by rapid addition. As **2** is less soluble in these solvents, the reaction was initially heterogeneous, but **2** was completely dissolved when an equivalent amount of **8** had been carefully added. When **8** is added rapidly, the ring-opening reaction with $AlCl_2$-OR and $AlCl(OR)_2$ may not be neglected. The reactions in these nonpolar solvents are insufficiently reproducible. Since the dissolving rate of **2** should be significantly influenced by the nature of the crystal of **2** and with the mechanical stirring efficiency, the insufficiency of reproducibility appears to be due to these facts.

The results of the present paper are summarized in Table 8.

Experimental

Materials. *cis*-2,3-Epoxybutane (*cis*-**1**) and *trans*-2,3-epoxybutane (*trans*-**1**) were prepared by the method of Pasto and Cumbo.[34] VPC analysis (a 45 m polypropylene glycol Ucon oil LB-550X capillary column was employed) indicated the *trans*-**1** to be free of any *cis*-isomer, whereas *cis*-**1** was accompanied with 1.4% of the *trans*-isomer. Commercial 1,2-epoxypropane (**8**, special grade) was distilled before use. Commercial special grade aluminum chloride (**2**) was purified by sublimation three times under a reduced pressure before each use. Lithium chloride and bromide were dried over P_2O_5 at 140 °C in vacuum. All the solvents were dried by the most efficient ways appeared in the literature[35] and were distilled before use.

A Typical Procedure of Ring-opening Reaction. Into a solution of **2** (0.877 g, 6.58 mmol) in 4 ml of acetonitrile,[36] **1** (0.318 g, 4.69 mmol) in 4 ml of acetonitrile was slowly added under well-stirring in an ice bath. It took 2 h for the addition at a constant temperature, and stirring was continued for an additional 30 min. After the duration, the reaction mixture was poured into a mixture of 10 ml of concd HCl and 50 g of ice. The organic layer was separat-

Table 8. Solution structure of $AlCl_3$ and the ring-opening reaction of epoxides

Type	Solution structure[a)]	Solvation number	Typical solvent	Selectivity	
				Stereo	Regio
1	$AlSv_6^{3+}+3Cl^-$	6	DMSO, DMF	inv	nor
1′	$AlSv_6^{3+}+3ClSv_n^-$	6	EtOH	inv	nor
2	$AlSv_6^{3+}+3AlCl_4^-$	1.5	CH_3CN	inv	nor
3	$AlCl_3\cdot Sv$	1	CH_3NO_2	ret	abnor
4	Al_2Cl_6	—	CS_2, $CHCl_3$	inv	mixture

In the presence of lithium bromide		Selectivity		Product
Type	Solution structure[a)]	Stereo	Regio	
1	$AlSv_6^{3+}+LiSv_m^++3Cl^-+Br^-$	inv	nor	**9**>**10**
1′	$AlSv_6^{3+}+LiSv_m^++3ClSv_p^-+BrSv_q^-$	inv	nor	**9**≧**10**
2	$AlCl_3Br^-+LiSv_m^+$	inv	nor	**10**
3	$AlCl_3Br^-+LiSv_m^+$	inv	nor	**10**
4	Al_2Cl_6	inv	mixture	**9**

a) Those indicated in italics are the active species of each reaction.

ed and washed with 20 ml of water. The combined aqueous layer was saturated with NaCl and extracted twice with 30 ml and then with 20 ml of ether. The combined organic layer was dried over Na_2SO_4 after the addition of mesitylene as an internal standard. The solvent was evaporated off, and the residual product was submitted to VPC analysis. *erythro*-3-Chloro-2-butanol (**3**) was obtained in 38% yield based on **1**, and neither *threo*-**3** nor the unreacted **1** was detected. The product was identified by a comparison of the VPC retention time with those of the authentic samples.[37] The product was converted into *trans*-**1** with dil. NaOH.

When 1,2-epoxypropane (**8**) was treated with **2** in ether, 1-ethoxy-2-propanol (yield 8.1%) was obtained, accompanied with chloropropanols (**9**, yield 26.3%). The former was identified after the product mixture had been treated with dil. NaOH, converting **9** to **8**, by comparisons of the VPC retention time and the NMR spectrum with those of an authentic sample prepared from **8** and sodium ethoxide.

A Typical Reaction Procedure in the Presence of Lithium Bromide. In a cold nitromethane (30.5 g, 500 mmol), 1.4 g (10 mmol) of **2** was dissolved, then 0.87 g (10 mmol) of lithium bromide was added, the mixture turned to a brown homogeneous solution. To the well-stirred solution, 0.61 g (10.5 mmol) of **8** was added dropwise during a period of 20 min in an ice bath. After a duration of 40 min, the reaction mixture was worked up as mentioned above. The yields of **9** and **10** were 8.6 and 37.8% respectively by VPC analysis, the product ratio was 14.0 (**9n**), 4.5 (**9a**), 68.6 (**10n**), and 12.9% (**10a**).

It was confirmed that the products compositions did not change after they were treated again under the reaction conditions.

Vapor-phase Chromatographic (VPC) Analyses. The VPC analyses were carried out on Hitachi K-53 and Shimadzu 3AH gas chromatographs. The retention times of *threo*- and *erythro*-**3**, *threo*- and *erythro*-3-bromo-2-butanols, and mesitylene were 7.4, 8.9, 13.7, 15.7, and 10.4 min respectively on a 2 m column packed with 25% tricresyl phosphate and 1.5% H_3PO_3 on Chamelite CK at a column temperature of 100 °C. The retention times of **9n**, **9a**, **10n**, **10a**, and tetraline (an internal standard) were 3.2, 3.9, 4.8, 6.1, and 9.1 min respectively on a 3 m column of 10% PEG-20M on Celite 545 at 120 °C.

TABLE 9. RESULTS OF ^{36}Cl TRACER EXPERIMENTS OF RING-OPENING REACTION OF 2,3-EPOXYBUTANE WITH $AlCl_3$ IN NITROMETHANE SOLVENTS

Entry	Sample (mmol)	Automatic external standard ratio	dpm	dpm/mmol
1	Blank	0.8777	47.0	
2	**3** (0.292)[a]	0.8817	63.9	
3	$H^{36}Cl$ (1.94×10^{-3})	0.6604	2839.9	1473.7×10^3
4	**3** (0.0534)[b]	0.8965	43.1	807.1
5	$Li^{36}Cl$ (0.0292)	0.6959	14465.8	495404
6	**3** (0.183)[c]	0.8718	20481.3	111920

a) An authentic non-active sample. b) The product obtained by hydrolyzing the non-active reaction mixture with $H^{36}Cl$ specified in entry 3. **2**: 15.58 mmol, $H^{36}Cl$: 4.85 mmol, ^{36}Cl/total Cl: 9.40%. c) The product obtained by the reaction with **2** (15.25 mmol) and $Li^{36}Cl$ (entry 6; 15.29 mmol), ^{36}Cl/total Cl: 25.2%, ^{36}Cl taken into **3**/total Cl: 22.6% (111920/495404).

^{36}Cl Tracer Experiments. The radioactivity measurements were performed by means of a Packard Tri-Carb liquid scintillation spectrometer model 3380. VPC preparation was made on an Aerograph Auto-prep A-700 chromatograph. Radioactive lithium chloride was prepared from lithium carbonate and 1 N $H^{36}Cl$; it was dried at 140 °C in vacuum until the weight was constant.

The crude **3** obtained by the reaction was purified by means of preparative VPC (Carbowax-20 M 20%, 20 ft column) and then submitted to measurements of the radioactivity. A solution of PPO (4 g) and dimethyl-POPOP (0.1 g) diluted with toluene to 1.0 l was used as the scintillator. The radioactivities of $H^{36}Cl$ and $Li^{36}Cl$ were measured in homogeneous solutions prepared by the addition of small amounts of ethanol or ethanol and water. Quenching corrections were carried out with the use of an external standard channel ratio method. The results of the experiments are summarized in Table 9.

We wish to express our thanks to Professors S. Suga and T. Nakajima, Kanazawa University, for their many helpful discussions. We are especially indebted to Drs. M. Hamada and R. Kiritani, Radiation Center of Osaka Prefecture, where the radioactive tracer experiments were carried out. This work was supported in part by a Scientific Research Grant from the Ministry of Education, Japan (No, 911511).

References

1) For general reviews on the epoxides ring-opening, see a) R. E. Parker and N. S. Isaacs, *Chem. Rev.*, **59**, 737 (1959); b) E. L. Eliel, "Steric Effects in Organic Chemistry," ed. by M. S. Newman, John Wiley & Sons, New York, N. Y. (1956), p. 106; c) J. G. Buchanan and H. Z. Sable, "Selective Organic Transformations," Vol. 2, ed. by B. S. Thyagarajan, Wiley-Interscience, New York, N. Y. (1972), p. 1.

2) D. Y. Curtin, A. Bradley, and Y. G. Hendrickson, *J. Am. Chem. Soc.*, **78**, 4064 (1956).

3) H. O. House and G. D. Ryerson, *J. Am. Chem. Soc.*, **83**, 979 (1961); J. R. Doherty, D. D. Keane, K. G. Marathe, W. I. O'Sullivan, E. M. Philbin, R. M. Simons, and P. C. Teague, *Tetrahedron*, **26**, 2545 (1970).

4) J. H. Brewster, *J. Am. Chem. Soc.*, **78**, 4061 (1956).

5) H. Wasserman and N. Aubrey, *J. Am. Chem. Soc.*, **78**, 1726 (1956).

6) T. Nakajima, S. Suga, Sugita, and K. chikawa, *Tetrahedron*, **25**, 1807 (1969).

7) T. Nakajima, private communication.

8) N. N. Greenwood and K. Wade, "Friedel-Crafts and Related Reactions," Vol. 1, ed. by G. A. Olah, Interscience Publishers, New York, N. Y. (1963), a) p. 584, b) p. 581 and references cited therein.

9) P. Gagnaux and B. P. Susz, *Helv. Chim. Acta*, **44**, 1128, 1132 (1961).

10) R. M. Roberts, A. A. Kalaf, and J. E. Douglass, *J. Org. Chem.*, **29**, 1511 (1964).

11) H. C. Brown, *J. Chem. Soc.*, **1956**, 1248.

12) H. C. Brown and R. M. Adams, *J. Am. Chem. Soc.*, **64**, 2557 (1942); A. C. Rutenberg, A. A. Palko, and J. S. Drury, *ibid.*, **85**, 2702 (1963).

13) M. Baaz and V. Gutmann, p. 371 of Ref. 8.

14) R. D. Bach and R. F. Richter, *J. Am. Chem. Soc.*, **94**, 4747 (1972).

15) K. Okamoto, I. Nitta, M. Dohi, and H. Shingu, *Bull. Chem. Soc. Jpn.*, **44**, 3220 (1971).

16) J. K. Addy and R. E. Parker, *J. Chem. Soc.*, **1963**,

915; *ibid.*, **1965**, 644.
17) P. L. Barili, G. Berti, B. Macchia, F. Macchia, and L. Monti, *J. Chem. Soc., C*, **1970**, 1168; G. Berti, B. Macchia, F. Macchia, and L. Monti, *ibid.*, **1971**, 3371.
18) C. C. Price and R. Spector, *J. Am. Chem. Soc.*, **88**, 4171 (1966); also refer to J. P. Kennedy, N. V. Desai, and S. Sivaram, *ibid.*, **95**, 6386 (1973).
19) F. A. Cotton and R. Francis, *J. Am. Chem. Soc.*, **82**, 2986 (1960).
20) H. Haraguchi and S. Fujiwara, *J. Phys. Chem.*, **73**, 3467 (1969).
21) I. Y. Ahmed and C. D. Schmulbach, *Inorg. Chem.*, **11**, 228 (1972).
22) J. F. Hon, *Mol. Phys.*, **15**, 57 (1968); C. D. Schmulbach, *J. Inorg. Nucl. Chem.*, **26**, 745 (1964).
23) G. A. Olah and C.-H. Lin, *J. Am. Chem. Soc.*, **90**, 6468 (1968).
24) H. Haraguchi, *Kagaku no Ryoiki*, **24**, 802 (1970).
25) See, for example, N. V. Sidgwick, "The Chemical Elements and Their Compounds," Vol. 1, Oxford Univ. Press, London (1950), p. 424; C. A. Thomas, "Anhydrous Aluminum Chloride in Organic Chemistry," Reinhold Publishing, New York, N. Y. (1941), p. 19.
26) A. Feldstein and C. A. VanderWerf, *J. Am. Chem. Soc.*, **76**, 1626 (1954); R. Fuchs and C. A. VanderWerf, *ibid.*, **76**, 1631 (1954).
27) L. A. Paquett, "Principles of Modern Heterocyclic Chemistry," W. A. Benjamin, New York, N. Y. (1968), p. 26.
28) D. S. Breslow and H. Skalnik, "Multi-Sulfur and Sulfur and Oxygen Five- and Six-membered Heterocycles," Part 2, in "The Chemistry of Heterocyclic Compounds," ed. by A. Weissberger, Interscience Publishers, New York, N. Y. (1966), p. 653.
29) O. Itoh, Y. Yokoyama, and K. Ichikawa, unpublished data.
30) H. Perst, "Oxonium Ions in Organic Chemistry," Academic Press, London (1971), p. 17, 37.
31) E. Schwenk, K. Gulbins, M. Rath, G. Benzing, R. Maysenholder, and K. Hamann, *Makromol. Chem.*, **51**, 53 (1962); B. Rickborn and R. M. Gerkin, *J. Am. Chem. Soc.*, **93**, 1693 (1971).
32) R. F. Rodewald, K. Mahendran, J. L. Bear, and R. Fuchs, *J. Am. Chem. Soc.*, **90**, 6698 (1968); W. M. Weaver and J. D. Hutchison, *ibid.*, **86**, 261 (1964).
33) A. J. Parker, *Quart. Rev. (London)*, **16**, 163 (1962).
34) D. J. Pasto and C. C. Cumbo, *J. Org. Chem.*, **30**, 1271 (1965).
35) J. A. Riddick and W. B. Bunger, "Organic Solvents," 3rd ed., Wiley Interscience, New York, N. Y. (1970).
36) When DMSO is used as a solvent, one should carefully add **2** to DMSO under nitrogen atmosphere since an explosive reaction has occurred.
37) S. Winstein and H. J. Lucas, *J. Am. Chem. Soc.*, **61**, 1576 (1939); C. A. Stewart and C. A. VanderWerf, *ibid.*, **76**, 1259 (1954).

Preparation of Phorone

Yasuo NAKADA, Yasuo YURA, and Keisuke MURAYAMA
Central Research Laboratories, Sankyo Co., Ltd., Hiromachi, Shinagawa-ku, Tokyo 140

(Received June 5, 1975)

A new method for preparation of 2,6-dimethylhepta-2,5-dien-4-one (**4**; phorone) from isobutene and carbon tetrachloride is described. A redox addition of carbon tetrachloride to isobutene in the presence of ferric chloride, benzoin, and diethylamine hydrochloride yielded 3-methyl-1,1,1,3-tetrachlorobutane (**1**). 2,6-Dimethyl-2,4,4,6-tetrachloroheptane (**2**) was obtained by the addition of **1** to isobutene or the twofold addition of carbon tetrachloride to isobutene. Treating **2** with ethanolic potassium hydroxide gave 2,6-dimethylhepta-1,5-dien-3-yne (**3**). Hydration of **3** by treating with methanolic boron trifluoride in the presence of mercuric oxide and with aqueous sulfuric acid gave **4**.

Phorone has been chiefly prepared by dehydrative trimolecular condensation of acetone (method A) under various catalysts such as beryllium chloride[1], ferric oxide[2], and bromomagnesium alcoholate[3], but with less satisfactory results on yield and selectivity. Colonge and Dumont[4] reported another method (method B) treating β,β-dimethylacrylyl chloride with isobutene in the presence of stannic chloride to yield phorone selectively.

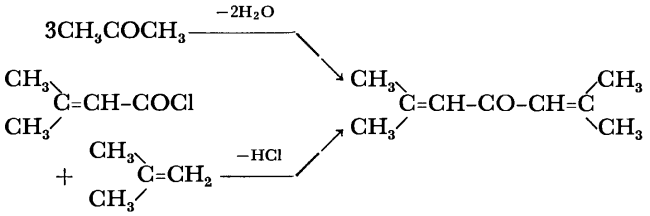

The redox addition of haloalkanes to olefins using copper or iron salts as catalysts have been known[5]. Recently, Moore[6] reported the twofold redox addition of carbon tetrachloride to olefins.

$$CCl_4 + 2CH_2{=}CHR \longrightarrow (RCHClCH_2)_2CCl_2$$

We now wish to report a new preparation method of phorone from isobutene and carbon tetrachloride *via* the twofold addition product as shown in Scheme I.

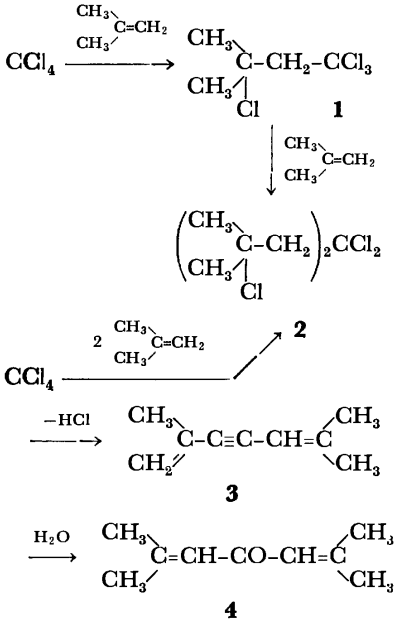

Scheme I.

The method has the following advantages over the methods described above in spite of having three steps. The yield and selectivity of each steps are better than those of the method A, and starting materials, isobutene and carbon tetrachloride are easily available by comparison with the method B.

According to the procedure of Asscher and Vofsi,[5] the redox addition of carbon tetrachloride to isobutene in the presence of ferric chloride, benzoin, and diethylamine hydrochloride afforded 3-methyl-1,1,1,3-tetrachlorobutane (**1**)[7] in a high yield. The compound **1** was treated with an additional mol of isobutene to yield 2,6-dimethyl-2,4,4,6-tetrachloroheptane (**2**) in 46% yield. Also, the compound **2** was directly obtained from 1 mol of carbon tetrachloride and 2 mol of isobutene under the same conditions in 47% yield. The mass spectrum of **2** showed peaks at *m/e* (relative intensity): 235 (1), 233 (8), 231 (20), and 229 (20, M−35) suggesting 1 : 2 adduct of carbon tetrachloride and isobutene. The NMR spectrum of **2** showed two singlet peaks at τ 8.15 (12H) and τ 6.96 (4H) corresponding to four equivalent methyl groups and two equivalent methylene groups respectively. Since 2,6-dimethyl-2,4,4,6-tetrachloroheptane (**2**) is a key compound for the preparation of phorone (**4**), we sought the optimum conditions for these redox addition. The results are summarized in Table 1. Thus an optimum result was obtained in Run No. 2. At a temperature above 60 °C the yield of **2** decreased and a dehydrochlorinated product of **2** (**5**; 2,6-dimethyl-4,4,6-trichlorohept-1-ene) and a large amount of distillation residue were formed.

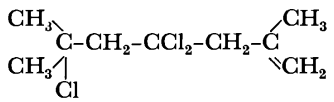

5

At a lower temperature the yield of **2** also decreased.

Dehydrochlorination of **2** with excess ethanolic potassium hydroxide gave 2,6-dimethylhepta-1,5-dien-3-yne (**3**) and 4-chloro-2,6-dimethyl-6-ethoxyhepta-2,4-diene (**6**) in 62 and 23% yields respectively by GLC analysis (silicone DC 550, 125 °C). The IR spectrum of **3** showed characteristic absorptions at 2200 (−C≡C−) and 895 cm^{-1} (>C=CH_2).

According to the procedure of Islam and Raphael,[8] **3** was hydrated by treating with methanolic boron trifluoride in the presence of mercuric oxide and with

Table 1. Preparation of 2,6-dimethyl-2,4,4,6-tetrachloroheptane (2)

Run number	Reactants: Haloalkane	Reactants: Mole ratio Haloalkane/Isobutene[a]	Reaction condition: Temperature (°C)	Reaction condition: Time (h)	Products (%): 2	Products (%): 1
1	CCl_4	1/2	70	23	16	9[b,c]
2	CCl_4	1/2	60	23	47	17[b]
3	CCl_4	1/2	60	16	40	26[b]
4	CCl_4	1/2	50	47	45	15[b]
5	CCl_4	1/2	50	23	31	12[b]
6	CCl_4	1/1	60	23	14	39[b]
7	CCl_4	2/1	80	6	0	80[d]
8	CCl_4	2/1	60	23	0	63[d]
9	**1**	1/1	60	20	46	—[b]

a) Isobutene; 0.30 mol, 2-propanol; 0.45 mol, ferric chloride hexahydrate; 0.0022 mol, benzoin; 0.0022 mol, and diethylamine hydrochloride; 0.0033 mol were used. b) Based on haloalkane. c) A dehydrochlorinated product (**5**; 3%) and a distillation residue(14.3 g) were obtained. d) Based on isobutene.

aqueous sulfuric acid to give 2,6-dimethylhepta-2,5-dien-4-one (**4**, phorone) and 2,6-dimethyl-6-methoxyhept-2-en-4-one (**7**) in 57 and 13% yields respectively by GLC analysis (silicone DC 550, 140 °C). The compound **4** was treated in the same manner as **3** to afford **7** in 62% yield. The structure of **4** was identified by comparing its IR, UV, and NMR spectra with those of an authentic sample.

The treatment of **6** with aqueous sulfuric acid in the presence of mercuric sulfate in water–dioxane (1 : 1) afforded **4** in 27% yield. When **6** was treated with aqueous sulfuric acid in the absence of the mercuric salt, **4** and 2,6-dimethylhept-5-en-3-yn-2-ol (**8**) were obtained in 17 and 72% yields respectively.

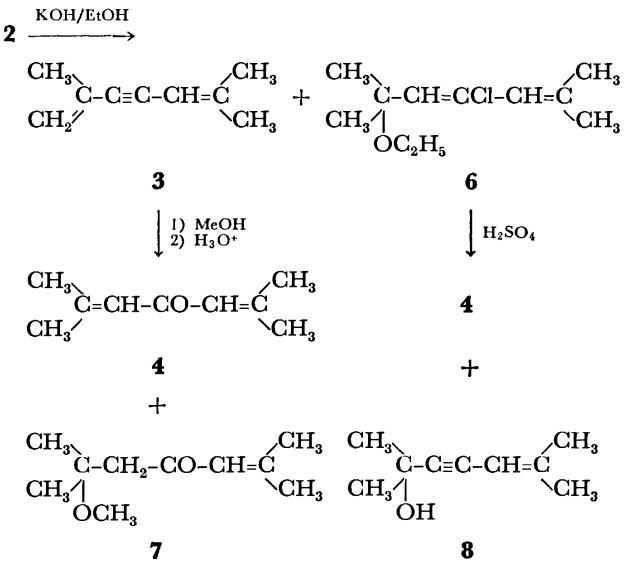

The mechanism of formation of **8** is not clear. An IR spectrum of **8** showed characteristic absorptions at 3400 (–OH) and 2220 cm^{-1} (–C≡C–). The structure of **8** was identified by comparing its IR, UV, and NMR spectra with those of an authentic sample which was synthesized independently by the route shown in Scheme II. Thus treating acetone with propargyl aluminium bromide[9] gave 2-methylpent-4-yn-2-ol (**9**). The compound **9** was brominated by phosphorus tribromide to afford 4-bromo-4-methylpent-1-yne (**10**), which was treated with excess lithium amide in liquid ammonia, followed by addition of acetone to give **8**.

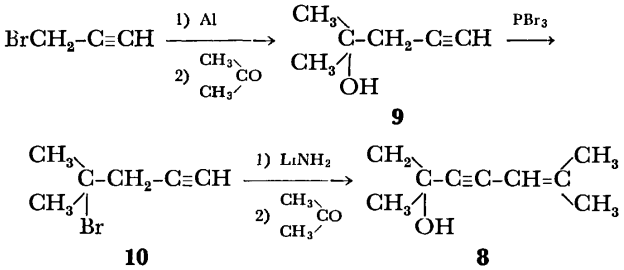

Scheme II.

Experimental

3-Methyl-1,1,1,3-tetrachlorobutane (1). According to the procedure of Asscher and Vofsi,[5] a mixture of carbon tetrachloride (92.4 g, 0.60 mol), liquid isobutene (28.5 ml, 0.30 mol), isopropanol (27.0 g, 0.45 mol), ferric chloride hexahydrate (0.60 g, 0.0022 mol), benzoin (0.45 g, 0.0022 mol), and diethylamine hydrochloride (0.36 g, 0.0033 mol) was heated at 80 °C for 6 h to afford 3-methyl-1,1,1,3-tetrachlorobutane (**1**) in 80% yield (Table 1, Run 7): bp 75—77 °C (18 Torr), lit,[7] bp 43—45 °C (3 Torr); IR, ν_{max} cm^{-1}: 710 (C–Cl): NMR (CCl_4): τ 8.13 (s, 6H) and 6.61 (s, 2H); MS, *m/e* (relative intensity): 179(1), 177(7), 175 (17), and 173 (20, M−35).

2,6-Dimethyl-2,4,4,6-tetrachloroheptane (2). A 1 : 1 mixture of **1** and isobutene (Run 9) or 1 : 2 mixture of carbon tetrachloride and isobutene was treated in the similar procedure to the above giving 2,6-dimethyl-2,4,4,6-tetrachloroheptane (**2**) in yields as shown in Table 1: bp 73—75 °C (0.28 Torr); IR, ν_{max} cm^{-1}: 690 (C–Cl); NMR (CCl_4): τ 8.15 (s, 12H) and 6.96 (s, 4H); MS, *m/e* (relative intensity): 235 (1), 233 (8), 231 (20), 229 (20, M−35), 197 (12), 195 (57), and 193 (78, M−71). The reaction was carried out at 70 °C to give 2,6-dimethyl-4,4,6-trichlorohept-1-ene (**5**), which was separated by preparative GLC (carbowax 20 M, 130 °C): IR, ν_{max} cm^{-1}: 1642 and 680; NMR (CCl_4): τ 8.18 (s, 6H), 8.04 (d, 3H; J=1.0 Hz), 7.14 (s, 2H), 6.93 (s, 2H), and 4.8—5.1 (m, 2H); MS, *m/e* (relative intensity): 234 (1), 232 (6), 230 (13), 228 (13, M^+), 197 (20), 195 (98), and 193 (147, M−35).

Dehydrochlorination of **2**. A solution of **2** (5.3 g, 0.020 mol) and potassium hydroxide (9.0 g, 0.16 mol) in ethanol (20 ml) was heated under reflux for 6 h and cooled. After addition of saturated aqueous sodium chloride, the reaction mixture was extracted with ethyl acetate. The extracts were dried over anhydrous magnesium sulfate and evaporated to give 2,6-dimethylhepta-1,5-dien-3-yne (**3**) and 4-chloro-2,6-dimethyl-6-ethoxyhepta-2,4-diene (**6**) in 62 and 23% yields respectively by GLC analysis (silicone DC 550, 125 °C).

Compound **3** and **6** were separated by preparative GLC and their spectral data were obtained as follows: compound **3**[10]; IR, ν_{max} cm^{-1}: 2200, 1610, and 895; UV, λ_{max}^{EtOH} mμ: 241, 252, and 265; NMR (CCl_4): τ 8.24 (d, 3H; J=1.0 Hz), 8.20 (d, 6H; J=1.0 Hz), 4.8—5.0 (m, 2H), and 4.7—4.8 (m, 1H); MS, *m/e* (relative intensity): 120 (14, M$^+$) and 105 (10, M−15) and compound **6**; IR, ν_{max} cm^{-1}: 1635 and 855; UV, λ_{max}^{EtOH} mμ: 234; NMR (CCl_4): τ 8.88 (t, 3H; J=6.8 Hz), 8.62 (s, 6H), 8.05—8.25 (m, 6H), 6.64 (q, 2H; J=6.8 Hz), and 4.3—4.5 (m, 2H); MS, *m/e* (relative intensity): 204 (10), 202 (24, M$^+$), 189 (15), 187 (39, M−15), 167 (44, M−35), 158 (65), and 156 (169, M−46).

Phorone (**4**). Products were separated by preparative GLC and their yields were determined by analytical GLC (silicone DC 550, 140 °C).

Hydration of **3**. A mixture of methanol (1.5 ml), mercuric oxide (0.10 g, 0.00046 mol), ethereal boron trifluoride (0.05 ml), and trichloroacetic acid (trace) was heated under reflux for 10 min and cooled. A solution of **3** (0.12 g, 0.001 mol) in methanol (1.5 ml) was added to the mixture in an ice water bath and stirred at room temperature for 20 min. After pouring into cooled 10% aqueous sulfuric acid (20 ml) the mixture was extracted with ether. The extracts were dried over anhydrous sodium carbonate and evaporated to yield phorone (**4**) and 2,6-dimethyl-6-methoxyhept-2-en-4-one (**7**) in 57 and 13% yields respectively. Also **7** was given in 62% yield by stirring phorone and methanol under the same catalyst for 2 h at room temperature. Following spectral data of **7** were obtained: IR, ν_{max} cm^{-1}: 1680, 1619, and 850; UV, λ_{max}^{EtOH} mμ: 240; NMR (CCl_4): τ 8.83 (s, 6H), 8.15 (d, 3H; J=1.0 Hz), 7.91 (d, 3H; J=1.0 Hz), 7.55 (s, 2H), 6.88 (s, 3H), and 3.9—4.1 (m, 1H); MS, *m/e* (relative intensity): 170 (10, M$^+$) and 138 (16, M−32).

Hydrolysis of **6**. A solution of **6** (0.13 g, 0.00064 mol) in dioxane (1 ml) was added to a solution of mercuric oxide (0.10 g, 0.00046 mol) in 20% aqueous sulfuric acid (1.2 ml) and stirred at room temperature for 3 h. After addition of water the mixture was extracted with ether. The extracts were dried over anhydrous sodium sulfate and evaporated to give phorone in 27% yield. In the absence of mercuric oxide in this system phorone and 2,6-dimethylhept-5-en-3-yn-2-ol (**8**) were obtained in 17 and 72% yields respectively. Following spectral data of **8**[10] were obtained; IR, ν_{max} cm^{-1}: 3400, 2220, and 1630; UV, λ_{max}^{EtOH} mμ: 232; NMR (CCl_4): τ 8.60 (s, 6H), 8.2—8.4 (m, 6H), 7.95 (s, 1H), and 4.7—4.9 (m, 1H); MS, *m/e* (relative intensity): 138 (18, M$^+$), 123 (111, M−15), and 121 (10, M−17).

2-Methylpent-4-yn-2-ol (**9**). According to the procedure of Eiter and Oediger[9], a mixture of propargyl aluminium bromide, prepared from aluminium strips (2.4 g, 0.089 atom), propargyl bromide (1.42 g, 0.12 mol), and mercuric chloride (two spoons), and acetone (7.5 g, 0.13 mol) in tetrahydrofuran (35 ml) was stirred at 0 °C for 1 h to obtain 2-methylpent-4-yn-2-ol (**9**) in 69% yield: bp 68—71 °C (115 Torr); IR, ν_{max} cm^{-1}: 3400, 3310, and 2140; UV, λ_{max}^{EtOH} mμ: 238; NMR[11] (CCl_4): τ 8.74 (s, 6H), 8.05 (t, 1H; J=2.4 Hz), 7.17 (d, 2H; J=2.4 Hz), and 7.44 (s, 1H); MS, *m/e* (relative intensity): 83 (25, M−15) and 81 (10, M−17).

4-Bromo-4-methylpent-1-yne (**10**). A solution of phosphorus tribromide (3.3 g, 0.012 mol) in ether (10 ml) was dropwise added to a solution of **9** (3.0 g, 0.030 mol) and pyridine (1.2 g, 0.015 mol) in ether (20 ml) below 0 °C and stirred for 30 min at 0 °C. After pouring into ice, the mixture was extracted with ether. The extracts were washed with 5% hydrochloric acid and 5% aqueous sodium carbonate and dried over anhydrous sodium carbonate. Evaporation of ether gave crude **10** in 28% yield, which was not purified further because of its unstability. The IR spectra showed characteristic peaks at 3300, 2210, and 650 cm^{-1}.

2,6-Dimethylhept-5-en-3-yn-2-ol (**8**). A solution of **10** (1.0 g, 0.0062 mol) in ether (20 ml) was dropwise added at −60 °C to a solution of lithium amide in liquid ammonia (100 ml) and stirred at −65 °C for 3 h. A solution of acetone (1.3 g, 0.020 mol) in ether (15 ml) was dropwise added to the mixture and stirred at −60 °C for 3 h. After addition of ammonium chloride the mixture was allowed to stand overnight to evaporate ammonia. After addition of water the mixture was extracted with ether. The extracts were washed with 5% hydrochloric acid, 5% aqueous sodium hydrogen carbonate, and saturated aqueous sodium chloride successively, and dried over anhydrous sodium sulfate. Evaporation, followed by distillation gave 0.36 g (42%) of **8**, bp 63—67 °C (6 Torr).

References

1) H. Bredereck, G. Lehmann, E. Fritzsche, and C. Schonfeld, *Angew. Chem.*, **52**, 445 (1939).
2) H. Midorikawa, *Rept. Sci. Research Inst.*, **24**, 405 (1948); *Chem. Abstr.*, **45**, 4202e (1951).
3) Y. Y. Tsmer, *Zhur. Prikład. Khim.*, **34**, 1628 (1961); *Chem. Abstr.*, **55**, 27029e (1961).
4) J. Colonge and P. Dumont, *Bull. Soc. Chim. Fr.*, **1947**, 38.
5) H. Asscher and D. Vofsi, *J. Chem. Soc.*, **1963**, 1887.
6) L. O. Moore, *J. Org. Chem.*, **37**, 2633 (1972).
7) Recently, T. Sato, M. Seno, and T. Asahara reported the same reaction. *Yuki Gosei Kagaku Kyokai Shi*, **32**, 184 (1974).
8) A. M. Islam and R. A. Raphael, *J. Chem. Soc.*, **1952**, 4086.
9) K. Eiter and H. Oediger, *Justus Liebigs Ann. Chem.*, **682**, 62 (1965).
10) S. O. Badanyan, M. G. Voskanyan, G. G. Kuhdoyan, and R. G. Agababyan, *Arm. Khim. Zh.*, **27**, 401 (1974); *Chem. Abstr.*, **81**, 90948q (1974).
11) A. Ghenciulescu and M. Hanack, *Tetrahedron Lett.*, **1970**, 2827.

Table 1. IR spectra of I, II, III, IV and V (in CCl_4)

Compound	Ester C=O ν (cm^{-1})	Ketone C=O ν (cm^{-1})	OH ν (cm^{-1})	OH Intensity (%) 0.1 M/l	0.01 M/l	0.001 M/l
I	1740	1703				
II	1740	1730				
III	1736		3620	23	62	72
	1720 (sh)		3480—3440	77	38	28
IV	1736		3620	28	71	89
	1720 (sh)		3500—3400	72	29	11
V	1744		3580	90	89	91
	1700		3460	10	11	9

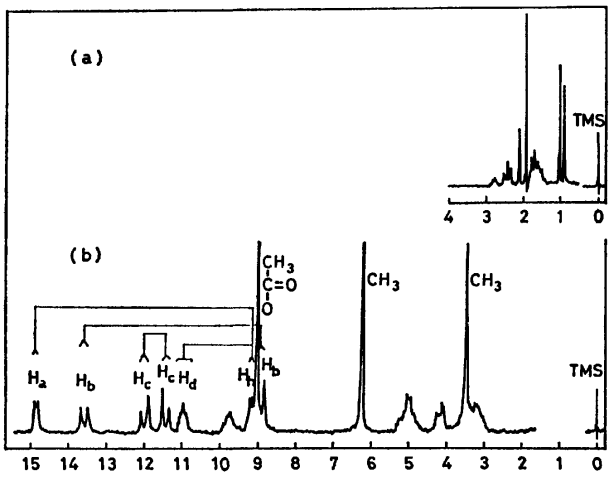

Fig. 1. The NMR spectra of I in CCl_4 (20 mg/0.4 ml) at 90 MHz (a) without $Eu(DMP)_3$ and (b) with 60 mg $Eu(DPM)_3$.

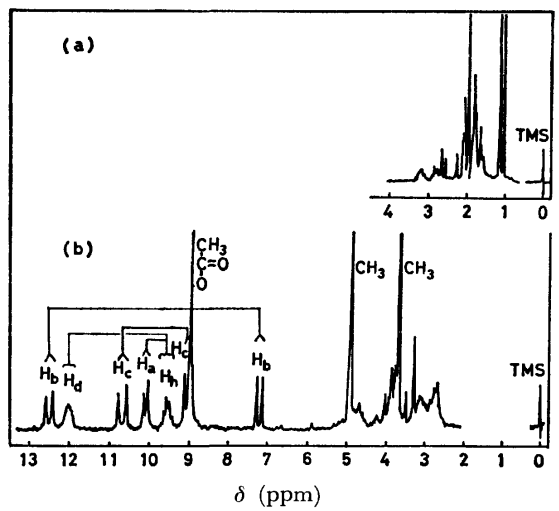

Fig. 2. The NMR spectra of II in CCl_4 (20 mg/0.4 ml) at 90 MHz (a) without $Eu(DPM)_3$ and (b) with 60 mg $Eu(DPM)_3$.

carrying out proton decoupling in this state. When the NMR spectra of I and II are measured by changing the amount of $Eu(DPM)_3$ added—that is, by adding 5, 10, 15, 20, 30, 40 or 60 mg of $Eu(DPM)_3$, the chemical

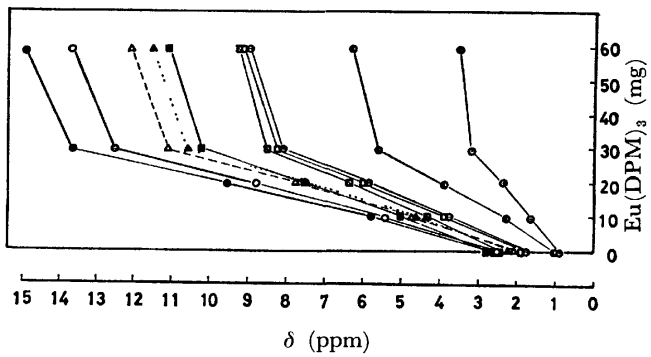

Fig. 3. Variation in chemical shift for each proton of I *vs.* the amount of added $Eu(DPM)_3$ in CCl_4 (20 mg/0.4 ml). ● H_a; ○ ⊖ H_b; △ ▲ H_c; ■ H_d; ⊠ H_h; □ CH_3COO; ⊙ ◐ CH_3.

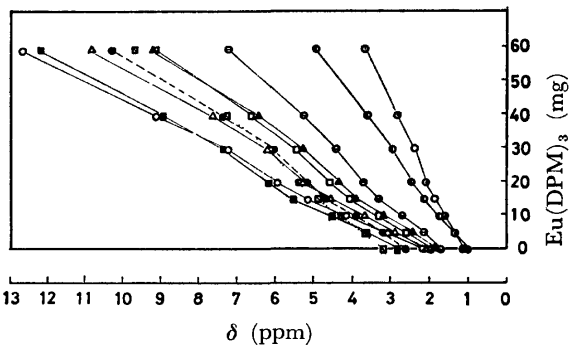

Fig. 4. Variation in chemical shift for each proton of II *vs.* the amount of added $Eu(DPM)_3$ in CCl_4 (20 mg/0.4 ml). ● H_a; ○ ⊖ H_b; △ ▲ H_c; ■ H_d; ⊠ H_h; □ CH_3COO; ⊙ ◐ CH_3.

shift of each proton varies with the amount of $Eu(DPM)_3$ added in the manner shown in Figs. 3 and 4. It is hence possible to determine by interpolation the chemical shift of each proton in the absence of $Eu(DPM)_3$. The values thus obtained are shown in Table 2. The coupling constants of protons are given in Table 3.

The difference in chemical shift for each proton before and after the addition of 60 mg of $Eu(DPM)_3$, designated as $\Delta\delta$, is shown in Table 2. In the case of the addition of 60 mg of $Eu(DPM)_3$, the values of $\Delta\delta$ suggest that $Eu(DPM)_3$ forms complexes with both ketone and ester groups. A comparison of the $\Delta\delta$

TABLE 2. THE CHEMICAL SHIFTS OF I AND II WITH 60 mg Eu(DPM)$_3$ AND WITHOUT Eu(DPM)$_3$ (in CCl_4)

Compd	Eu(DPM)$_3$ (mg)	H_a		H_b				H_c			
		δ	$\Delta\delta$	δ	$\Delta\delta$	δ	$\Delta\delta$	δ	$\Delta\delta$	δ	$\Delta\delta$
I	0	2.6	12.3	1.75	7.15	2.5	11.1	2.1	9.9	2.2	9.2
	60	14.9		8.9		13.6		12.0		11.4	
II	0	2.65	7.45	1.7	5.5	2.15	10.35	1.9	7.15	2.05	8.65
	60	10.1		7.2		12.5		9.05		10.7	

Compd	Eu(DPM)$_3$ (mg)	H_d		H_h		CH_3COO		CH_3		CH_3	
		δ	$\Delta\delta$	δ	$\Delta\delta$	δ	$\Delta\delta$	δ	$\Delta\delta$	δ	$\Delta\delta$
I	0	2.8	8.2	2.45	6.7	1.9	7.1	1.0	5.25	0.9	2.6
	60	11.0		9.15		9.0		6.25		3.5	
II	0	2.85	9.2	3.2	6.35	1.95	7.05	1.1	2.55	1.0	3.9
	60	12.05		9.55		9.0		3.65		4.9	

(I or II; 20 mg/0.4 ml CCl_4)

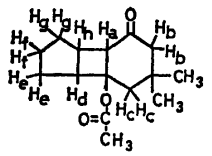

TABLE 3. COUPLING CONSTANTS

Compd	$J_{H_aH_h}$	$J_{H_bH_b}$	$J_{H_cH_c}$	$J_{H_dH_h}$
I	7 Hz	15	16	6
II	8 Hz	15	17	7

values reveals information on the configurations of I and II. As is shown in Table 2, the H_a of I has a considerably larger $\Delta\delta$ value than the H_a of II. It is likely that the proximity of H_a and –OAc in I, or a *cis* configuration as suggested by the IR data, results in a larger shift for H_a, while a *trans* configuration for H_a and –OAc in II is affected less by the shift reagent. On the other hand, the spatial relationship between H_a and the ketone carbonyl group seems not to differ from I to II. Now, the $\Delta\delta$ for the H_d of II is larger than that for the H_d of I, although the difference here is not so pronounced as in the $\Delta\delta$ for H_a. In considering the configuration of H_d and –OAc, it is likewise assumed that the shift appears larger in II because of the *cis* configuration for H_d and –OAc, while the shift is smaller in I on account of the *trans* configuration for H_d and –OAc. Moreover, H_h is little affected by the shift reagent, as it is located in the β-position relative to both carbonyl and ester groups; only a small difference in chemical shift is found between I and II.

In the NMR spectra measured in the absence of the shift reagent, I shows the chemical shift of H_h at a normal value of $\delta=2.5$, while II shows it in an unusually low magnetic field of $\delta=3.2$. The configuration for H_h and –OAc is *cis* in II; that is, H_h is nearer to the ester carbonyl group. The anisotropy[5] of this ester carbonyl group seems to account for the appearance of the chemical shift of H_h in the lower magnetic field. On the contrary, the lack of such a phenomenon in I suggests that H_h and the ester group in I are not *cis* to each other.

In summary, the above-mentioned results indicate that I assumes a *cis-anti-cis* configuration, while II assumes a *cis-anti-trans* configuration. The fusion of the five-membered and four-membered rings is *cis* in both I and II.

IR Spectra of III, IV, and V. The infrared spectra were measured on the III, IV, and V alcohols which had been obtained from I and II by reduction with $NaBH_4$ in order to determine whether or not there was an intramolecular hydrogen bond between the alcoholic OH and the carbonyl oxygen or ether oxygen of the ester group. The measurements were made in carbon tetrachloride at concentrations of 0.1, 0.01, and 0.001 mol/l. The absorptions due to OH stretching look alike in III and IV. As is shown in Table 1, the alcohol, III or IV, arising from the reduction of I produces an absorption peak due to free hydroxyl at 3620 cm^{-1} and a broad absorption peak due to the hydrogen-bonded hydroxyl group near 3500 cm^{-1}; the relative intensity of these peaks varies with the concentration. The absorption near 3500 cm^{-1} becomes exceptionally strong at high concentrations (0.1 mol/l), but it weakens as the concentration diminishes. This indicates that the absoption near 3500 cm^{-1} is due to an intermolecular hydrogen bond. On the other hand, the compound, V, which has been obtained by the reduction of II shows a strong and sharp absorption peak at 3580 cm^{-1} and a weak but sharp absorption peak at 3460 cm^{-1}, and the relative intensity of these two peaks is not affected at all by the concentration in the range from 0.1 to 0.001 mol/l. It is, therefore, likely that these two absorptions are due to intramolecular hydrogen bonding.

Corresponding to these OH absorptions, V shows an absorption of ester carbonyl at 1744 cm^{-1}, as is shown in Table 1. This peak is shifted towards the larger-wave-number side from 1740 cm^{-1}, where the ester carbonyl absorption of II appeared before reduction. It is known that hydrogen bonding between OH and ester carbonyl shifts the infrared absorption of the carbonyl towards the smaller-wave-number side, while hydrogen bonding between OH and ether oxygen of

the ester group shifts it towards the larger-wave-number side.[6] It is, therefore, assumed that the principal hydrogen bond of V (OH absorption at 3580 cm^{-1}) gives rise to a six-membered ring involving the OH and ether oxygen of the ester group. The carbonyl absorption of V has a shoulder at 1700 cm^{-1} which seems to be due to some contribution from a hydrogen bond between OH and ester carbonyl (the formation of an eight-membered ring); the weak but sharp OH absorption at 3460 cm^{-1} is likely to correspond to such a hydrogen bond.

Let us suppose that II assumes a *cis-anti-trans* configuration as has been mentioned above. The six-membered ring would then be in the chair form and hydride would attack a less hindered site in the $NaBH_4$ reduction to produce only an alcohol with a configuration such as V. The construction of a molecular model shows that the OH group is axial and comes very close to the ether oxygen of the -OAc group to facilitate formation of an intramolecular hydrogen bond. On the other hand, if one assumes a *cis-anti-cis* configuration for I, the six-membered ring would not be in the chair form, but rather, in the boat form or labile form, and hydride would attack the carbonyl group from both sides in the $NaBH_4$ reduction to yield two alcohols, III and IV. Molecular models of III and IV show that the OH group and the ester group are sufficiently separated to make the formation of an intramolecular hydrogen bond impossible.

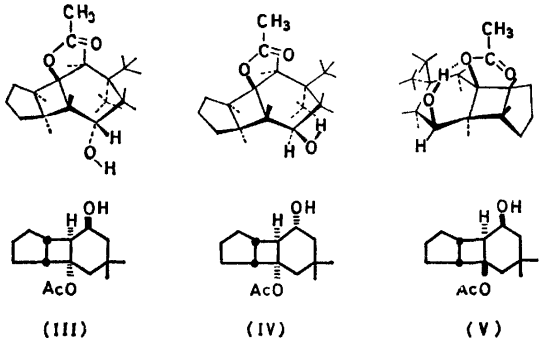

Scheme 2.

NMR Spectra of III, IV, and V. The NMR spectra of III, IV, and V, like those of I and II, do not show much differences in chemical shift, and the definite assignment of each proton is not possible. However, the proton linked to the carbon carrying the OH group can be distinguished because its signal appears in lower magnetic fields than the other protons. Table 4 shows the chemical shift and the half-width ($W_{1/2}$) of this signal. When three or more protons are present on neighboring carbon atoms, as in $-CH_2-CH(OH)-CH<$, the proton on the carbon atom carrying the OH group has a larger coupling constant and, hence, ordinarily a larger half-width of the signal in the axial conformation than in the equatorial conformation —in general, 16 Hz or more in the axial conformation and 12 Hz or less in the equatorial conformation.[7] If this is applied to III, IV, and V, the proton in question is equatorial in III and V and axial in IV, as is shown in Table 4. These results agree with those obtained from the IR data on V mentioned above and support the configuration of V.

Table 4. The NMR signals for 6-hydrogen of III, IV, and V

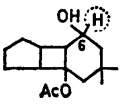

Compd	δ	$W_{1/2}$ (Hz)	Conformation of 6-hydrogen
III	3.77	9	equatorial
IV	4.05	18	axial
V	4.01	10	equatorial

Table 5. The rate constants of I and II→VI at 25 °C

Comp.	Initial concentration a=[NaOH] (mol/l)	k (s^{-1})
I	8.40×10^{-5}	8.87×10^{-5}
II	8.34×10^{-5}	2.25×10^{-4}

Rate of Formation of α,β-Unsaturated Ketone (VI) from I or II. I or II loses acetic acid in an alkaline solution to yield an α,β-unsaturated keton (VI). The rate of this reaction was determined in ethanol at 25 °C. An ethanol solution of sodium hydroxide was used as an alkali. The reaction is first-order, and a plot of $\log(a-x)$ against t gave a linear relationship wherein a is the initial concentration of I or II, x is the amount of VI formed, and t is the reaction time. The rate constant, k, obtained from the slope of this straight line is given in Table 5.

The rate constant, k, in this case varies with the concentration of alkali. Since the alkaline concentration is the same for I and II, equal to the initial concentration of I or II, the k for II is about 2.7 times as large as that for I. In general, the ionic elimination reaction proceeds more readily in a *trans* configuration than in a *cis* configuration; this also supports the idea that the ring fusion of the four-membered and six-membered rings is *trans* in II and *cis* in I.

Any of the above-mentioned results indicates that I has a *cis-anti-cis* configuration, while II has a *cis-anti-trans* configuration.

Mass Spectra of I, II, and VI. The mass spectra of I and II are shown in Figs. 5(a) and 5(b) respectively. Neither shows any molecular peak corresponding to m/e=250 indicating a cleavage of the cyclobutane ring. On the other hand, the elimination of acetic acid also takes place. In particular, II shows a mass spectral pattern similar to that of the α, β-unsaturated ketone (VI) shown in Fig. 5(c), signifying a ready occurrence of the elimination of acetic acid. I undergoes the elimination of acetic acid only slightly, about 1/20 as much as II; it primarily suffers a cleavage of the cyclobutane ring.

The principal fragment ions and estimated fragmentations are shown below. A metastable peak is observed at m/e=108.8; this indicates the formation of a fragment ion of m/e=141 from a fragment ion of

rate of the elimination reaction of acetic acid (I or II→VI) was followed spectrophotometrically at the absorption maximum of 250 nm.

The solutions of I (2.80×10^{-3} mol/l), II (2.78×10^{-3} mol/l), and sodium hydroxide (8.01×10^{-3} mol/l) in ethanol were each thermally equilibrated at 25 °C. To a 100-ml volumetric flask, 3 ml of a solution of I or II was added, after which the solution was diluted with ethanol (equilibrated at 25 °C) to a volume of nearly 89 ml. Then an equimolar portion of sodium hydroxide solution was added to the flask (1.05 ml for I and 1.04 ml for II), and finally the mixture was diluted to 100 ml with ethanol. The flask was placed in a thermostatic bath at 25 °C. Suitable aliquots of the sample solution were withdrawn at 10—30 min intervals, and immediately the absorbance was measured against an ethanol blank at 250 nm. The concentration of VI (x) was calculated from its extinction coefficient (ε, 9250). In these experiments, the initial concentration of I was 8.40×10^{-5} mol/l, and that of II was 8.34×10^{-5} mol/l. The results are shown in Table 5.

Referencese

1) P. de Mayo and H. Takeshita, *Can. J. Chem.*, **41**, 440 (1963); P. de Mayo, H. Takeshita, and A. B. M. A. Sattar, *Proc. Chem. Soc.*, **1962**, 119; P. de Mayo, *Pure Appl. Chem.*, **9**, 597 (1964); H. Hikino and P. de Mayo, *J. Am. Chem. Soc.*, **86**, 3582 (1964); P. de Mayo, *Acc. Chem. Res.*, **4**, 41 (1971).

2) J. K. M. Sanders and D. H. Williams, *J. Am. Chem. Soc.*, **93**, 641 (1971); S. G. Levine and R. E. Hicks, *Tetrahedron Lett.*, **1971**, 311; P. Kristiansen and T. Ledaal, *ibid.*, **1971**, 2817; L. H. Keith, *ibid.*, **1971**, 3.

3) T. S. Cantrell, W. S. Haller, and J. C. Williams, *J. Org. Chem.*, **34**, 509 (1969).

4) E. J. Corey, J. D. Bass, R. LeMahieu, and R. B. Mitra, *J. Am. Chem. Soc.*, **86**, 5570 (1964).

5) G. J. Karabatsos, G. C. Sonnichsen, N. Hsi, and D. J. Fenoglio, *J. Am. Chem. Soc.*, **89**, 5067 (1967).

6) R. Biggins, T. Cairns, G. Eglinton, E. Haslam, and R. D. Haworth, *J. Chem. Soc.*, **1963**, 1750.

7) Y. Kawazoe, Y. Sato, T. Okamoto, and K. Tsuda, *Chem. Pharm. Bull.*, **11**, 328 (1963); R. U. Lemieux, R. K. Kullnig, H. J. Bernstein, and W. G. Schneider, *J. Am. Chem. Soc.*, **80**, 6098 (1958).

Studies of Unusual Amino Acids and Their Peptides. VI. The Syntheses and the Optical Resolutions of β-Methylphenylalanine and Its Dipeptide Present in Bottromycin

Yoshiharu KATAOKA,* Yasuhiko SETO,** Masaaki YAMAMOTO,*** Takashi YAMADA, Shigeru KUWATA, and Hiroshi WATANABE

Laboratory of Chemistry, Faculty of Science, Kōnan University, Okamoto, Higashinada, Kobe 658

(Received July 25, 1975)

β-Methyl-phenylalanine was prepared by the condensation of α-methylbenzyl bromide with acetaminomalonate, followed by the hydrolysis and decarboxylation of the condensate. The decarboxylation occurred diastereoselectively to some extent. The *erythro* and the *threo* isomers could be separated by the fractional crystallization of their benzoyl derivatives, and differentiated by means of their NMR spectra. The optical resolution of the respective isomers was attained by treating the benzyloxycarbonyl derivatives with qunine or quinidine; thus, the four isomers could be obtained in a pure state. A dipeptide present in the C-terminal of bottromycin was synthesized by coupling N-protected *erythro*-L-β-methyl-phenylalanine with either L-β-(2-thiazolyl)-β-alanine ester or, more conveniently, with the DL-compound, and by separating thereafter.

Bottromycin, a peptidic antibiotic discovered in the fermentation broths of *Streptomyces bottropensis* by Waisvisz and his co-workers,[1] contains many unusual amino acids. Structural studies of this antibiotic were carried out by Waisvisz[1,2] and by Umezawa *et al.*;[3] the formula shown in Fig. 1 has been proposed by the latter.

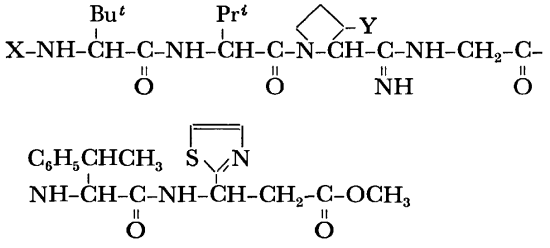

X=Pivaloyl or Δ^1-isocaproyl
Y=H or CH_3

Fig. 1. Structure of bottromycin.

In a previous paper[4] we have made clear the absolute configuration of β-(2-thiazolyl)-β-alanine, situated at the carboxyl terminal in this peptide oligomer, by resolving the synthesized racemate into antipodes and by then investigating their ORD curves.

This paper will treat β-methyl-phenylalanine, the amino acid just neighboring β-(2-thiazolyl)-β-alanine. Umezawa and his co-workers[3] attributed this amino acid to the L-series from the facts that its dithioethoxycarbonyl derivative shows a positive Cotton effect in methanol and that the amino acid is not decomposed by D-amino acid oxidase. Arold and his co-warkers[5] have shown that the amino acid present in bottromycin belongs to the *erythro*-L series by preparing *ethythro*-β-methyl-phenylalanine and by then resolving it into antipodes. We, too, prepared this amino acid by another route and succeeded in obtaining the four possible isomers by resolving both *erythro*- and *threo*-

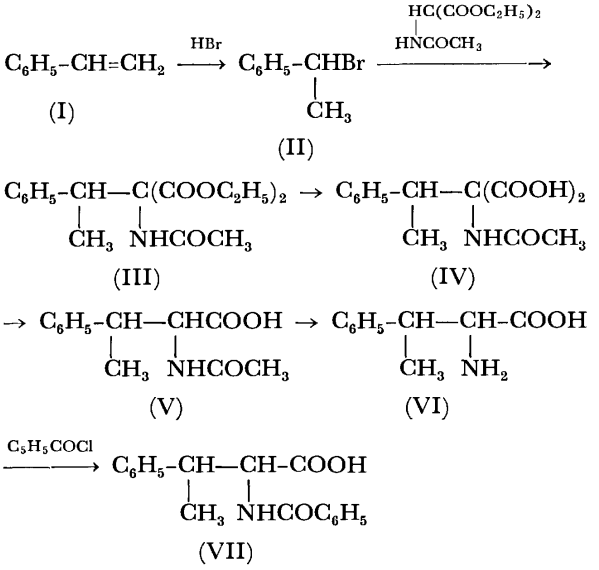

Scheme 1. Synthetic route of β-Methyl-phenylananine.

compounds into antipodes; the scheme is illustrated in Schemes 1 and 2. α-Methylbenzyl bromide, prepared by the addition of hydrogen bromide to styrene according to Walling,[6] was condensed with acetaminomalonate. The condensate, α-methylbenzylacetaminomalonate (III), was then hydrolyzed with aqueous sodium hydroxide and decarboxylated without isolation of the intermediate hydrolysate (IV). In order to separate the product mixture into *erythro*- and *threo*-compounds, it was first converted into the easily crystallizable benzoyl derivative, which was then separated, by crystallization from aqueous ethanol, into two : A high-melting substance (mp 188—190 °C)(VII-a) and a low-melting one (mp 130—132 °C) (VII-b).

It has been reported that *erythro* and *threo* isomers can easily be differentiated by means of a comparison of their NMR spectra; *i.e.*, in β-alkylsubstituted α-amino acids, the coupling constant ($J_{\alpha\beta}$) between C_α–H and C_β–H is larger in the *erythro* form than in the *threo* form.[7] In our case, the β-methyl-phenylalanines obtained from VII-a always gave larger values than those obtained from VII-b, as may be seen in Table 1. This suggests that the former belongs to an *erythro* type.

* Department of Chemistry, Tsukuba University, Ibaragi Prefecture.
** Protein Research Foundation, Minoh, Osaka.
*** Yamamoto Seiyakusho Co. Ltd., Nishimatsushimacho, Amagasaki.

Table 2. Salt formation of acyl-β-methyl-phenylalanine with alkaloid bases

Solvent	Quinine			Chinchonine			Brucine		
	Bz	Ac	Z	Bz	Ac	Z	Bz	Ac	Z
Acetone	±	−	+		−	−	−	−	−
Methanol	−			−					
Ethanol		−	+		−	−	−	−	−
1-Propanol	−	−	±	−	−	−		−	−
Ethyl acetate		−		±		−			
Benzene						−			
Chloroform			−			−		−	−

Bz=Benzoyl derivative; Ac=Acetyl derivative; Z=Benzyloxycarbonyl derivative. +, crystal; ±, trace; −, no precipitate.

with hydrogen bromide in acetic acid to remove the benzyloxycarbonyl group. We thus obtained a free amino acid of $[\alpha]_D$+28.4°. From the soluble quinine salt, its antipode of $[\alpha]_D$−30.6° was isolated. The latter is identical with the β-methyl-phenylalanine ($[\alpha]_D$−31°) obtained from bottromycin by Umezawa and his co-workers[3] as well as with the one belonging to the *erythro*-L form reported by Arold.[5] Another way to isolate the *erythro*-L isomer was to treat the benzyloxy-carbonyl compound with quinidine and to regenerate the free amino acid from the less soluble alkaloid salt. In this case, it was not the D-isomer but the L-isomer that made the less soluble salt, so it was more convenient to obtain the L-isomer present in bottromycin, though the yield was somewhat inferior to that of the preceding method. In a similar way, the *threo*-compound was also resolved into its antipodes. Thus, all four theoretically possible isomers were successfully prepared.

Now both the optically-active amino acids present in the carboxyl terminal of bottromycin, *i.e.*, L-β-(2-thiazolyl)-β-alanine and L-β-methyl-phenylalanine, could be prepared, so we tried to build up the dipeptide which constitutes the most important part of bottromycin.[8] *N*-Benzyloxycarbonyl-*erythro*-L-β-methyl-phenylalanine was coupled with L-β-(2-thiazolyl)-β-alanine methyl ester by the carbodiimide method; the desired protected dipeptide was thus obtained in a 70% yield. As the standard sample was prepared in this way, we attempted a more convenient method of synthesizing this dipeptide by coupling the optically-active β-methyl-phenylalanine with the racemic β-(2-thiazolyl)-β-alanine, and by then separating the product mixture into its respective diastereomers. After coupling the components by the carbodiimide method, the product was fractionally recrystallized from ethanol; we thus obtained a diastereomer with a mp of 159—161 °C, and one with a mp of 182—182.5 °C in *ca.* a yield 60% of the theoretical amount respectively. The ORD curve and IR spectrum of the former were completely identical with those of the standard sample described above. The other compound must be a diasteromer composed of L-β-methyl-phenylalanine and D-β-(2-thiazolyl)-β-alanine, because it has a different melting point and a different value of $[\alpha]_{300}$ from those of the L-L-compound, though the IR spectra of the two compounds in chloroform coincided completely. In order to ascertain the configuration of the β-(2-thiazolyl)-β-alanine contained in this dipeptide, it was hydrolyzed by refluxing with 6 M hydrochloric acid for a short time (1.5 h); the desired amino acid was then isolated by silica-gel dry-column chromatography. Its ORD curve apparently showed that it belongs to the D-series, though the values of α are very small because of its easily racemizable property under acid-hydrolytic conditions.[4] The phenomenon that the curve shifts to the positive side when 2 drops of 6 M hydrochloric acid or a concentrated sodium hydroxide solution (more remarkably) are added supports this conclusion.[9]

Experimental[10]

α-Methylbenzyl Bromide (II). This compound was prepared according to the method of Walling[6] by passing dry hydrogen bromide gas to freshly distilled styrene under ice-cooling; bp 79—80 °C/8 mmHg, n_D^{22} 1.564. lit,[11]: bp 78—82 °C/10 mmHg, n_D^{20} 1.5612.

Diethyl α-Methylbenzylacetaminomalonate (III). Diethyl acetaminomalonate (9.1 g) was dissolved in a sodium ethoxide solution in ethanol (sodium, 0.97 g; absolute ethanol, 50 ml); II (9.3 g) was then added, and the mixture was kept at 30 °C for 20 h. After the sodium bromide had then been filtered off and washed with hot ethanol, the combined ethanolic solution was concentrated *in vacuo*. The residual solid was recrystallized from 50% aqueous ethanol. The yield was 9.9 g (73%); mp 122—122.5 °C. Found: C, 63.31; H, 7.41; N, 4.40%. Calcd for $C_{17}H_{23}NO_5$: C, 63.54; H, 7.21; N, 4.36%.

N-*Acetyl*-DL-*β-methyl-phenylalanine (V).* III (6.43 g) was hydrolyzed by refluxing with a 10% sodium hydroxide solution (30 ml) for 30 min; then to this boiling solution 3 M hydrochloric acid (*ca.* 23 ml) was carefully added, drop by drop, until no more evolution of carbon dioxide was observed. The resulting mixture was allowed to stand in a refrigerator overnight, after which the separated acetylamino acid (V) was collected. The yield was 3.91 g (88%). The crude product was used for the next reaction without further purification, though it showed a broad melting point.

Diastereomeric Mixture of erythro- *and* threo-DL-*β-Methyl-phenylalanine Hydrochloride (VI).* V was refluxed with 6 M hydrochloric acid for 8 h, after which the solution was concentrated to dryness *in vacuo*. The residue was diluted with some water and concentrated again; the repetition of this operation gave a crude diastereomeric mixture (VI) in an almost quantitative yield. TLC and a paper chromatogram showed only one spot. For analysis it was recrystallized from water; mp 181—190 °C. Found: C, 55.56; H, 6.48; N, 6.68%. Calcd for $C_{10}H_{13}NO_2 \cdot HCl$; C, 55.69; H, 6.49; N, 6.49.%

N-*Benzoyl*-DL-*β-methyl-phenylalanine and Its Separation into* erythro- *and* threo-*Forms.* VI was benzoylated in a usual manner in a 93% yield. When the crude product was fractionally crystallized from aqueous ethanol, compounds melting at 188—190 °C (VII-a) and 130—132 °C (VII-b) were obtained.

Determination of the Structures of the erythro- *and the* threo-*Compounds (VII-a and VII-b) by Means of the NMR Data.* Both the *N*-benzoylated derivatives (VII-a and VII-b) were hydrolyzed with 6 M hydrochloric acid, and the resulting hydrochlorides were converted into free amino acids by treating them with an ion-exchange resin (Amberite IR 120). The

NMR data of both the amino acids are shown in Table 1. In order to estimate the *erthro/threo* ratio of the decarboxylation product (V), the crude sample of V was hydrolyzed to a free amino acid mixture and its NMR spectrum was measured. From the intensity of the peaks corresponding to the two α-H signals (100 MHz), the *erythro/threo* ratio was calculated as 1.7 : 1. The free amino acids derived from the acetaminomalonate in one step by treating it with 6 M hydrochloric acid also gave a similar *erythro/threo* ratio (1.5 : 1), as estimated from their NMR spectra.

N-Benzyloxycarbonyl erythro- *and* threo-DL-*β-Methyl-phenylalanine (IX-a and IX-b).* VII-a and VII-b were hydrolyzed with 6 M hydrochloric acid and benzyloxycarbonylated by the usual method (yields, >90%).

VIII-a derived from VII-a (mp 117—118 °C). Found: C, 68.95; H, 6.20; N, 4.48%. Calcd for $C_{18}H_{19}NO_4$: C, 69.00; H, 6.11; N, 4.47%.

VIII-b derived from VII-b (mp 132—134 °C). Found: C, 69.09; H, 6.16; N, 4.63%.

Separation of the N-*Benzyloxycarbonylated β-Methyl-phenylalanine into the* erythro- *and the* threo-*Derivatives.* The amino acid mixture obtained by the hydrolysis of V was benzyloxycarbonylated as usual. Part of the crude reaction product crystallized easily and could be isolated by filtration, though the rest remained oily (the ratio of the oil to the crystal was about 2 : 1). The crystalline compound was found to be identical with the *threo*-compound (VIII-b) derived from VII-b, and the residual oil was concluded to be composed of the *erythro*-derivative contaminated with some *threo*-compound, judging from the NMR spectrum of the free amino acid reproduced from it.

NMR data of VIII-a and VIII-b (60 MHz, DMSO-d_6):

VIII-a (*erythro*): δ 1.27 (3H, CH_3, d, J=7.2 Hz), 3.15 (1H, H_β, d-q, J=9.1 Hz and 7.1 Hz), 4.29 (1H, H_α, t, J=9.0 Hz), 4.99 (2H, benzyl-CH_2, s).

VIII-b (*threo*): δ 1.25 (3H, CH_3, d, J=7.5 Hz), 3.26 (1H, H_β, qi, J=7.0 Hz), 4.27 (1H, H_α, d-d, J=6.9 Hz and 9.0 Hz), 5.01 (2H, benzyl-CH_2, s), 7.66 (1H, NH, d, J=9.0 Hz).

Optical Resolutions of N-*Benzyloxycarbonyl*-erythro- *and* threo-DL-*β-Methyl-phenylalanine.* Equimolar amounts of VIII-a and quinine were dissolved in hot ethanol, and the solution was allowed to stand overnight. A white crystalline salt which separated as needles was collected. From the salt, the quinine was removed by treatment with 2 M hydrochloric acid in ether; thus *N*-benzyloxycarbonyl-*erythro*-D-*β*-methylphenylalanine was obtained. From the mother liquor, the *erythro*-L-derivative was obtained by a similar treatment. By the same proceddre, the *threo*-D-compound was obtained from VIII-b through easily crytallizable quinine salt, and the *threo*-L-compound, from the mother liquor. The results are summarized in Scheme 2.

Similarly, VIII-a was treated with quinidine, and from the less soluble salt (mp 171—171.5 °C (from chloroform–ethanol) $[\alpha]_D^{20}$ +122.1° (*c* 1, $CHCl_3$)), the L-compound ($[\alpha]_D^{20}$ +17.6° (*c* 1, C_2H_5OH)) was obtained in a 62% yield.

Four Isomers of Optically Active β-Methyl-phenylalanine. Four isomers of the optically-active benzyloxycarbonyl derivative of the amino acid obtained above were debenzyloxycarbonylated by hydrogen bromide in acetic acid and converted into free amino acids by treatment with an ion-exchange resin (Amberlite IR 120). Their optical properties are shown in Scheme 2.

Methyl β-(2-Thiazolyl)-β-alaninate Dihydrochloride. Thionyl chloride (1.31 g) was gradually stirred into methanol (30 ml) at about −10 °C, and to the resulting solution DL-*β*-(2-thiazolyl)-*β*-alanine[4] (1.72 g) was added. After stirring for 1 h at that temperature and for 6 h at room temperature, the reaction mixture was concentrated to dryness *in vacuo*, and after which anhydrous ether was added. The colorless crystals (1.72 g; 73%) precipitated were collected and recrystallized from methanol–ether. The yield was 1.16 g (48%); mp 153—155 °C. Found: C, 32.29; H, 4.79; N, 10.76%. Calcd for $C_7H_{10}N_2O_2S \cdot 2HCl$: C, 32.44; H. 4.67; N, 10.81%.

Similarly, the L-compound was prepared; mp 152—153 °C, $[\alpha]_{270}^{19}$ −8.8° (*c* 1, CH_3OH).

N-Benzyloxycarbonyl-erythro-L-*β*-*methyl-phenylalanyl*-L- *and* DL-*β*-(2-*thiazolyl*)-*β*-*alanine Methyl Ester and Its Resolution into Diastereomers.* Into a solution of *N*-benzyloxycarbonyl-*erythro*-L-*β*-methyl-phenylalanine (175 mg) in dichloromethane (4 ml), dicyclohexylcarbodiimide (115 mg) in the same solvent (2 ml) was stirred under ice-cooling. After 5 min, a solution of methyl L-*β*-(2-thiazolyl)-*β*-alanine dihydrochloride (145 mg) and *N*-methylmorpholine (113 mg) in dichloromethane (4 ml) was added, and the mixture was stirred overnight at room temperature. After treatment as usual, the crude dipeptide was obtained; 256 mg (95%); mp 152—155 °C. Recrystallization from aqueous ethanol gave a sample with a mp of 159.5—162 °C, $[\alpha]_{300}^{19}$ +89.3° (*c* 0.268, $CHCl_3$). Found: C, 62.34; H, 5.70; N, 8.62%. Calcd for $C_{25}H_{27}N_3O_5S$: C, 62.35; H, 5.65; N, 8.73%.

The coupling of the *erythro*-L-acid (1.38 g) and the DL-ester (1.08 g) was quite similarly carried out by using triethylamine in place of *N*-methylmorpholine. The crude dipeptide (1.89 g; 89%) was fractionally crystallized from 70% ethanol and could be separated into two components:

L-D-Compound, mp 182—182.5 °C, $[\alpha]_{300}^{27}$ +103.7° (*c* 0.27, $CHCl_3$). Found: C, 62.65; H, 5.69; N, 8.60%.

L-L-Compound, mp 159—161 °C, $[\alpha]_{300}^{19}$ +90.0° (c, 0.242, $CHCl_3$). Found: C, 62.33; H, 5.68; N, 8.56%.

References

1) J. M. Waisvisz, M. G. VAN DER Hoeven, J. VAN Peppen, and W. C. M. Zwennis, *J. Am. Chem. Soc.*, **79**, 4520 (1957).

2) J. M. Waisvisz, M. G. VAN DER Hoeven, and B. TE Nijenhuis, *J. Am. Chem. Soc.*, **79**, 4524 (1957).

3) S. Nakamura and H. Umezawa, *J. Antibiot.* **19**, 10 (1966); S. Nakamura, T. Yajima, Y. C. Lin, and H. Umezawa, *ibid.*, **20**, 1 (1967).

4) Y. Seto, K. Torii, K. Bori, K. Inabata, S. Kuwata, and H. Watanabe, *Bull. Chem. Soc. Jpn.*, **47**, 151 (1974).

5) H. Arold, M. Eule, and S. Reissmann. *Z. Chem.*, **9**, 447 (1969).

6) C. Walling, M. S. Kharasch, and F. R. Mayo, *J. Am. Chem. Soc.*, **61**, 2693 (1939).

7) J. Shōji, K. Tori, and H. Ōtsuka, *J. Org. Chem.*, **30**, 2772 (1965); K. Ōkubo and Y. Izumi, *Bull. Chem. Soc. Jpn.*, **43**, 1541 (1970); *cf.* S. Futagawa, T. Inui, and T. Shiba, *ibid.*, **46**, 3308 (1973).

8) S. Nakamura, S. Ōmura, T. Nishimura, N. Tanaka, and H. Umezawa, *J. Antibiot.*, **20A**, 162 (1967).

9) Y. Seto, T. Yamada, K. Niwa, S. Miwa, F. Tanaka, S. Kuwata, and H. Watanabe, *Chem. Lett.*, **1973**, 151.

10) All the melting points are uncorrected. The optical rotations were measured by means of a Yanagimoto Polarimeter OR-20. ORD-curves were recorded on a JASCO ORD/UV-5 spectropolarimeter. NMR spectra were recorded on JEOL PS-100 and Hitachi R-20A spectrometer, using DSS as the internal standard. Thin-layer chromatographies were performed on Merck silica gel G using 1-butanol–acetic acid–water (4 : 1 : 2 v/v, upper layer) as the developing solvent. Circular paper chromatographies were performed on Toyo Roshi No. 2.

11) Dictionary of Organic Compounds, Vol. 1, 4th ed., p. 443, Eyre & Spottiswoode, London (1965).

Reactions of Perfluoro-2-methyl-2-pentene and Octafluoroisobutylene with Arylamines

Nobuo Ishikawa and Akira Nagashima

Tokyo Institute of Technology, Department of Chemical Engineering, Ookayama, Meguro-ku, Tokyo 152

(Received August 4, 1975)

Treatment of perfluoro-2-methyl-2-pentene with four moles of arylamine provided 1-aryl-2,4-bis(arylimino)-3-(1-arylimino-2,2,3,3,3-pentafluoropropyl)azetidine, 3-(*N*,*N*′-diarylamidino)-4-arylamino-2-(pentafluoroethyl)-quinoline and 2,4-bis(arylamino)-3-(1-arylimino-2,2,3,3,3-pentafluoropropyl)quinoline, depending on the basicity of the arylamine and on the solvent used. Octafluoroisobutylene also yielded similar azetidine and quinoline derivatives.

As has been previously reported,[1] perfluoro-2-methyl-2-pentene (**1**) is much more reactive with *O*-nucleophiles than another isomer of hexafluoropropene dimer, perfluoro-4-methyl-2-pentene. Reactions of **1** with alcohols and phenol very easily produced addition and substitution products. Now we wish to report on reactions of **1** with primary arylamines, which proceeded with similar facility, but with much more complexity.

Results and Discussion

Reaction of Perfluoro-2-methyl-2-pentene with Arylamines. Haszeldine and his co-workers[2] very recently reported that two moles of arylamine react with **1** affording a quinoline derivative, **3**. They presumed that the reaction occurs with the formation of a ketenimine, **2**, followed by intramolecular cyclization. We had independently found this quinoline ring formation using about two moles of aniline, toluidines and chloroanilines in *N*,*N*-dimethylformamide.[3] The results of this quinoline formation are summarized in Table 1.

However, we further found that as much as four moles of arylamine react with **1** to give azetidine and quinoline derivatives, **5**—**7**, depending on the basicity of the arylamine and on the solvent used.

For example, when a large excess of aniline was allowed to react with **1** in the presence of triethylamine in diethyl ether, yellow crystals of 1-phenyl-2,4-bis(phenylimino)-3-(1-phenylimino-2,2,3,3,3-pentafluoropropyl)azetidine, **5** (Ar=Ph), was obtained in a fair yield (52%). The structure of this compound was established on the basis of the spectral data. In the IR spectrum, a strong, wide absorption band at 1660 cm^{-1} was observed, which should be due to the C=N groups adjacent to the azetidine ring. A sharp band at 1765 cm^{-1} was ascribed to a similar group apart from the ring. In the PMR, one singlet signal at τ 4.90 and several signals in the region of τ 1.7—4.6 were assigned to one >CH proton and fifteen aromatic protons, respectively. In the MS, the parent peak and the fragment peaks appeared appropriately (Experimental section). These spectral data, in contrast with those of the quinoline derivatives, strongly supported the azetidine structure.

Naturally, this compound was susceptible to reactions with acids and alkalies, *e.g.*, acetic and hydrochloric acids, and aqueous alkali hydroxide solutions, and these reactions produce several decomposition products.

Interestingly, when this azetidine compound was treated with ethanolic hydrochloric acid at room temperature, it isomerized into a quinoline derivative, **6** (Ar=Ph; X=H) in a 34% yield.

The structure of **6** was evident also from its spectral analysis. The IR spectrum revealed the presence of N–H groups by the two absorption bands at 3400 and 3350 cm^{-1}. In the mass spectrum, a peak at *m/e* 440 (M^+—NHPh) was observed, which confirmed the structure of **6**, but not that of another isomeric quinoline derivative, **7**.

When *p*-toluidine was used instead of aniline under the same conditions, the quinoline derivative **3** (Ar=*p*-MeC_6H_4; X=6-Me) was obtained as a main product (38%).

Table 1. Physical data of quinoline and azetidine derivatives

Compound No	Ar	X	Yield %	Mp °C	F-Anal % (Calcd)	IR (KBr) cm^{-1}	^{19}F NMR ($CHCl_3$) δ[a]	^{1}H NMR ($CDCl_3$) τ
3	Ph	H	53	99.5—100	37.8 (37.4)	3450 (N-H), 1100—1240 (C-F)	−24.3 (CF_3), +29.0, +0.3 (CF_2CF_3)	1.8—3.3 (Ar)
	o-MeC_6H_4	8-Me	77	99.5—100	34.9 (35.0)	3420 (N-H), 1050—1250 (C-F)	−23.8 (CF_3), +28.7, +0.6 (CF_2CF_3)	2.4—3.7 (Ar), 7.28, 7.58 (CH_3)
	p-MeC_6H_4	6-Me	63	94.5—95	34.7 (35.0)	3400 (N-H), 1100—1250 (C-F)	−24.1 (CF_3), +29.6, +0.4 (CF_2CF_3)	2.04—3.4 (Ar), 7.78 (CH_3)
	o-ClC_6H_4	8-Cl	17	124—125	31.1 (32.0)	3420 (N-H), 1100—1240 (C-F)	−23.4 (CF_3), +28.7, +1.0 (CF_2CF_3)	2.1—3.7 (Ar)
	m-ClC_6H_4	7-Cl	21	103—104	31.9 (32.0)	3450 (N-H), 1100—1240 (C-F)	−23.7 (CF_3), +29.8, +1.2 (CF_2CF_3)	1.8—3.5 (Ar)
	p-ClC_6H_4	6-Cl	37	120—121	32.0 (32.0)	3455 (N-H), 1100—1240 (C-F)	−23.2 (CF_3), +29.7, +1.2 (CF_2CF_3)	1.8—3.5 (Ar)
5	Ph	—	52	128—129.5	17.7 (17.8)	1765, 1660 (C=N), 1060—1260 (C-F)	+31.2, +2.3 (CF_2CF_3)	4.9 (>CH), 1.8—4.6 (Ar)
	p-ClC_6H_4	—	34	145—146	13.4 (14.2)	1780, 1680 (C=N), 1080—1280 (C-F)	+33.2, +1.8 (CF_2CF_3)	5.00 (>CH), 1.8—4.6 (Ar)
	p-FC_6H_4	—	34	129—130	28.8 (28.3)	1767, 1680 (C=N), 1100—1260 (C-F)	+33.0, +2.0 (CF_2CF_3)	4.83 (>CH), 1.8—4.5 (Ar)
6	Ph	H	5 (34)[b]	132—132.5	17.7 (17.8)	3400, 3350 (N=H), 1628 (C=N), 1100—1250 (C-F)	+30.7, +1.7 (CF_2CF_3)	1.9—3.6 (Ar, NH)
	m-ClC_6H_4	7-Cl	16	169.5—170	14.5 (14.2)	3415, 3375 (N-H), 1655 (C=N), 1050—1260 (C-F)	+30.2, +1.7 (CF_2CF_3)	1.9—3.7 (Ar, NH)
7	*m*-ClC_6H_4	7-Cl	18	129.5—130	14.0 (14.2)	3460, 3415 (N-H), 1640 (C=N), 1050—1270 (C-F)	+32.4, +1.7 (CF_2CF_3)	2.1—3.4 (Ar), 4.35 (NH)
9	*p*-MeC_6H_4	—	18	124.5—125	13.6 (13.5)	1775, 1675 (C=N), 1100—1300 (C-F)	−14.5 d (CF_3), J_{H-F}=6.2 Hz	5.05 q (>CH)
10	*p*-MeC_6H_4	6-Me	12	131—131.5	13.6 (13.5)	3405, 3500 (N-H), ~1300 (C-F)	−24.8 s	2.2—3.4 (Ar, NH), 3.67 (NH), 7.65, 7.72 (CH_3)

a) Given in δ ppm from ext. CF_3CO_2H. b) Yield obtained by isomerization of **3** (Ar=Ph).

When *p*-fluoro- and *p*-chloroaniline were used, the azetidine derivatives (**5**) were obtained as in the case of aniline (Table 1).

m-Chloroaniline, however, gave two quinoline derivatives, **6** and **7** (Ar=*m*-ClC_6H_4; X=Cl), in yields of 16 and 18%, respectively. In this case, these isomeric quinoline derivatives were separated from each other by means of a column chromatography. A fraction which was assumed to contain azetidine derivative was obtained, but no confirmation of compound **5** (Ar=*m*-ClC_6H_4) could be made.

Assignments for the two quinoline derivatives, **6** and **7**, were rather easy. In their IR spectra, both compounds showed absorption at about 1650 cm^{-1}, characteristic of a C=N group. However, the C=N absorption of **6** was situated in that of the amidino group, so it was much stronger than that of **7**. The mass spectra gave more unambiguous evidence. Besides the parent peak at M^+ 668, the amidinoquinoline **6** showed a strong peak at *m/e* 542 ($M^+-NHC_6H_4Cl$), whereas arylaminopentafluoropropylquinoline **7** gave a peak at *m/e* 549 ($M^+-C_2F_5$). The former peak of *m/e* 542 was absent in the spectrum of **7**, and *vice versa*.

The reaction mechanisms assumed for the formation of the azetidine and quinoline derivatives are shown in the scheme. Four moles of aniline nucleophilically attacked **1**, replacing fluorine atoms successively to give the ketenimine intermediate **4**. When the positive carbon atom of the ketenimine attacked the nitrogen atom of ArNH, the azetidine ring was formed to give **5**. On the other hand, when the positive carbon atom attacked the *ortho* position of the aromatic ring of arylimino group, either Ar* or Ar**, a quinoline ring was formed to give **6** or **7**.

In general, the amino group should be kinetically more readily attacked by the ketenimine group to give azetidine, **5**. The azetidine derivatives thus formed are thermodynamically less stable than the quinoline derivative, so that **5** will isomerize into **6** by means of an acid or a base. This was confirmed experimentally as mentioned above. Presumably, the electron donative methyl group of toluidine prompted the intramolecular attack of the ketenimine group of **2** on the toluidino ring, and further retarded the reaction of **2** with other toluidino molecules.

When *p*-halogenoanilines were used, the *ortho* position to the amino group, *i.e.*, the *meta* position to the halogen, should be electron deficient, which means they are rarely attacked by the ketenimine group. Thus no quinoline derivatives, neither **6** nor **7**, could be obtained from *p*-chloro or *p*-fluoroaniline.

On the other hand, the amino group of *m*-halogenoaniline is less basic than that of the *p*-isomer, so that it will retard the formation of the azetidine ring. Conversely, the *ortho* position to the amino group, *i.e.*, *para* position to the halogen, may be attacked more easily by the ketenimine group than that of *p*-halogenoaniline. Thus, only quinoline derivatives **6** and **7** from *m*-chloroaniline could be obtained, though in poor yields.

Reaction of Octafluoroisobutylene with Arylamine. As has been mentioned previously, perfluoro-2-methyl-2-pentene (**1**) reacts easily with primary aromatic amines

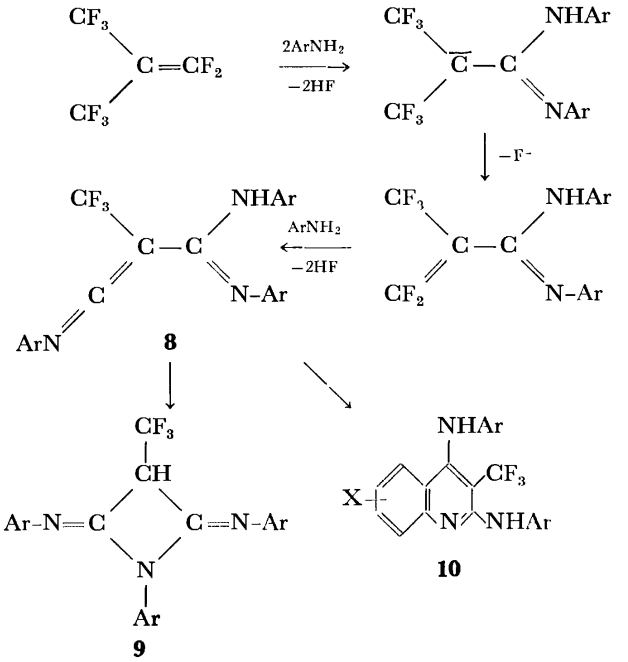

to give azetidine and quinoline derivatives. This high reactivity and the mode of the reaction should have resulted from the existence of a *gem*-bis(trifluoromethyl) methylene group, $=C(CF_3)_2$. This prompted us to examine the similar reaction with octafluoroisobutylene, the simplest olefin of this type. We carried out the reaction of octafluoroisobutylene with an excess of *p*-toluidine in diethyl ether in the presence of triethylamine, and in *N,N*-dimethylformamide.

In diethyl ether in the presence of triethylamine, three moles of *p*-toluidine reacted, giving the azetidine derivative **9** (Ar=*p*-MeC_6H_4) in a 18% yield.

In *N,N*-dimethylformamide, also three moles of toluidine reacted, and as expected, a quinoline derivative **10** (Ar=*p*-MeC_6H_4; X=6-Me) was obtained in a 12% yield. In each case, large quantities of by-products were formed. The by-products could not be identified, but they were assumed to be other imidoyl fluoride derivatives.[4]

The structures of these azetidine and quinoline derivatives were evident from the spectral data. In particular, in the ^{19}F and ^1H NMR spectra of **9**, there appeared a doublet due to C**F**$_3$ and a quartet due to C**H**. This means that a $CH(CF_3)$ group is present in the molecule, and this fact strongly supports the azetidine structure.

The reaction mechanism is understood in a similar way, as in the case of **1**. Arylamine should have attacked the terminal difluoromethylene groups successively, thereby forming an amidinoketenimine intermediate, **8**. When the positive carbon of the ketenimine attacked the nitrogen atom in the arylamino group, the azetidine derivative was formed. On the other hand, if the *ortho* position of the arylimino group was attacked, the quinoline derivative was produced.

Experimental

*2-Pentafluoroethyl-3-trifluoromethyl-4-anilinoquinoline (**3**(Ar=Ph; X=H)).* A solution of aniline (2.23 g, 0.022 mol)

in *N,N*-dimethylformamide (5 ml) was added into an ice-cooled mixture of perfluoro-2-methyl-2-pentene (**1**) (3.0 g, 0.01 mol) and *N,N*-dimethylformamide (15 ml) in a pressure vessel. After sealing, the mixture was heated with stirring at 70 °C for 2.5 h, and the reaction mixture was poured into water (100 ml). The resulting precipitate was separated by filtration to give a crude product (3.3 g, mp 84—89 °C). Recrystallization from hexane yielded a pure quinoline derivative **3** (2.2 g), mp 99—100 °C, in a 53% yield.

Found: C, 53.51; H, 2.48; N, 7.03; F, 37.8%. Calcd for $C_{18}H_{10}N_2F_8$: C, 53.20; H, 2.48; N, 6.90; F, 37.4%. MS: 406 (M^+), 337 (M^+-CF_3), 218 ($M^+-CF_3-C_2F_5$).

In the above procedure, toluidines and chloroanilines were used instead of aniline. The formed quinoline derivatives (**3**) are tabulated in Table 1.

*1-Phenyl-2,4-bis(phenylimino)-3-(1-phenylimino-2,2,3,3,3-pentafluoropropyl)azetidine (**5** (Ar=Ph)).* Into a solution of aniline (8.2 g, 0.088 mol) and triethylamine (14.2 g, 0.154 mol) in diethyl ether (30 ml), a solution of perfluoro-2-methyl-2-pentene (6.0 g, 0.02 mol) in diethyl ether (15 ml) was added dropwise, while keeping the temperature at 35—40 °C. After the addition, the mixture was stirred at room temperature for 1 h. The reaction mixture was washed with dilute hydrochloric acid to remove excess triethylamine, and with water, and then dried over magnesium sulfate. On removing the ether, yellow crystals were produced, which were collected to give the crude product (7.1 g, 67%), mp 102—118 °C. Recrystallization from hexane yielded pure **5** (Ar=Ph), mp 128—129.5 °C (5.5 g, 52%).

Found: C, 67.62; H, 3.87; N, 10.55; F, 17.7%. Calcd for $C_{30}H_{21}N_4F_5$: C, 67.66; H, 3.97; N, 10.52; F, 17.8%. MS: *m/e* 532 (M^+), 338 (M^+–Ph–N=C=N–Ph), 219 (PhN=C–CH=C=NPh), 194 (PhN=C=NPh).

p-Fluoro- and *p*-chloroanilines were used instead of aniline in the above reaction and similar azetidine derivatives were obtained (Table 1).

*2-Pentafluoroethyl-3-(N,N'-diphenylamidino)-4-anilinoquinoline (**6** (Ar=Ph; X=H)).* The azetidine compound **5** (Ar=Ph) (0.5 g) was dissolved in ethanol (15 ml), and a small amount of conc. hydrochloric acid (5 drops) was added. The mixture was stirred at room temperature for 3 h and poured into water (200 ml). The resulting oily material containing crystals was taken into diethyl ether, and the ethereal solution was washed with water, and dried over magnesium sulfate. The ether was removed and the residue (0.7 g) was crystallized from petroleum ether, giving **6** (Ar=Ph; X=H) (0.17 g, 34%), mp 132—132.5 °C.

Found: C, 67.71; H, 3.76; N, 10.59; F, 17.7%. Calcd for $C_{30}H_{21}N_4F_5$: C, 67.66; H, 3.97; N, 10.52; F, 17.8%.

*2-Pentafluoroethyl-3-[N,N'-bis(m-chlorophenyl)amidino]-4-(m-chloroanilino)-7-chloroquinoline (**6** (Ar=m-ClC_6H_4; X=7-Cl)) and 2,4-bis(m-chloroanilino)-3-(1-m-chlorophenylimino-2,2,3,3,3-pentafluoropropyl)-7-chloroquinoline (**7** (Ar=m-C_6H_4; X=7-Cl)).* Into a solution of *m*-chloroaniline (5.6 g) and triethylamine (7.1 g) in diethyl ether (15 ml), a solution of perfluoro-2-methyl-2-pentene (3.0 g) in diethyl ether (15 ml) was added dropwise at ~40 °C. After 1 h of stirring at room temperature, the reaction mixture was washed with dilute hydrochloric acid and water, then dried over magnesium sulfate. The ether was removed, leaving a semi-solid mass (7.0 g). This crude product was subjected to silica-gel column chromatography, using a mixture of benzene and hexane as the eluent. Of the two main yellow bands observed, the first band was eluted. Evaporation of the eluate provided crystals (1.21 g, 18%), which were recrystallized from hexane yielding pure **7** (Ar=*m*-ClC_6H_4, H=7-Cl), mp 129.5—130 °C.

Found: C, 54.09; H, 2.50; N, 9.08; F, 14.0%. Calcd for $C_{30}H_{17}N_4Cl_4F_5$: C, 53.76; H, 2.56; N, 8.36; F, 14.2%. MS: 668 (M^+), 549 ($M^+-C_2F_5$), 111 (ClC_6H_4).

Elution of the second main band, followed by evaporation of the solvent, provided more of the product (1.07 g, 16%). Recrystallization from hexane gave pure **6** (Ar=*m*-ClC_6H_4; X=7-Cl), mp 169.5—170 °C.

Found: C, 54.25; H, 2.58; N, 8.65; F, 14.5%. Calcd for $C_{30}H_{17}N_4Cl_4F_5$: C, 53.76; H, 2.56; N, 8.36; F, 14.2%. MS: *m/e* 668 (M^+), 542 ($M^+-NHC_6H_4Cl$), 126 (NHC_6H_4Cl).

*1-(p-Tolyl)-2,4-bis(p-tolylimino)-3-(trifluoromethyl)azetidine (**9** (Ar=p-MeC_6H_4)).* *p*-Toluidine (7.07 g, 0.066 mol), triethylamine (11.1 g, 0.11 mol) and diethyl ether (25 ml) were placed in a glass pressure tube equipped with a mechanical stirrer. This reaction vessel was cooled to *ca.* −50 °C into which liquefied octafluoroisobutylene (4.0 g, 0.02 mol) was introduced. The mixture was stirred for 1 h at −20 to −5 °C, for 30 min at 0 °C, then for 1 h at room temperature. After the unreacted octafluoroisobutylene was driven off by an aspirator, the reaction mixture was washed with dilute hydrochloric acid and water, and was dried over magnesium sulfate. Diethyl ether was evaporated and the remaining oily material (7.1 g) was recrystallized from petroleum ether. The azetidine derivative **9** (1.5 g, 18%), mp 122—123 °C, was thus obtained, and was recrystallized further to give the pure product, mp 124.5—125 °C.

Found: C, 71.74; H, 5.44; N, 10.27; F, 13.6%. Calcd for $C_{25}H_{22}N_3F_3$: C, 71.24; H, 5.26; N, 9.97; F, 13.5%. MS: *m/e* 421 (M^+), 352 (M^+-CF_3), 222 (Ar–N=C=N–Ar), 199 (M^+—Ar–N=C=N–Ar).

*6-Methyl-2,4-bis(p-toluidino)-3-(trifluoromethyl)quinoline (**10** (Ar=p-MeC_6H_4; X=6-Me)).* *p*-Toluidine (3.54 g, 0.033 mol), *N,N*-dimethylformamide (15 ml) and octafluoroisobutylene (2.0 g, 0.01 mol) were placed in a reaction vessel as described above. The mixture was stirred for 30 min at room temperature, then for 2.5 h at 65—70 °C. A considerable amount of unidentified yellow crystals (2.33 g, mp 205—211 °C) were produced. This solid was removed by filtration and the filtrate was poured into water. The solid material thus obtained (0.50 g, 12%) was recrystallized from hexane to give pure **10**, mp 131—131.5 °C.

Found: C, 71.28; H, 5.49; N, 10.15; F, 13.6%. Calcd for $C_{25}H_{22}N_3F_3$: C, 71.24; H, 5.26; N, 9.97; F, 13.5%. MS: *m/e* 421 (M^+), 380 ($M^+-2HF-H$), 91 ($C_6H_5CH_2^+$).

References

1) N. Ishikawa and A. Nagashima, *Bull. Chem. Soc. Jpn.*, **49**, 502 (1976).

2) W. T. Fowlers, R. N. Haszeldine, C. R. Owen, and A. Thomas, *J. Chem. Soc. Chem. Commun.*, **1974**, 134.

3) N. Ishikawa, A. Nagashima, and A. Sekiya, *Chem. Lett.*, **1974**, 1225.

4) Yu. V. Zeifman, D. P. Del'tsova, E. V. A. Avetisyan, N. P. Gambaryan, and I. L. Knunyants, *Izv. Akad. Nauk SSSR, Ser. Khim.*, **1973**, 1795.

Steroids. I. The bromination of 1α-Methyl and 1α-Phenyl-3-keto Steroids

T. Tomoyoshi TAKAHASHI and J. Yasuo SATOH*

Department of Chemistry, The Jikei University School of Medicine, Kokuryo, Chofu, Tokyo 182
**Department of Chemistry, St. Paul's (Rikkyo) University, Nishi-Ikebukuro, Tokyo 171*

(Received September 23, 1975)

1α-Phenyl-5α-cholestan-3-one was prepared from 5α-cholestan-1-en-3-one by treatment with the Grignard reagent in the presence of copper (I) chloride. In the mono- and dibromination of 1α-methyl-3-keto steroids, it was found that the position and configuration of bromine were the same as in the case of the 1-nonsubstituted 3-keto steroid. The A-ring conformations of these bromoketones were studied by means of NMR and ORD.

Synthetic and conformational studies of physiologically active 1-methyl-3-keto steroids have been made by several groups.[1] Kirk and Hartshorn[2a] stated that 3-keto-1-en-5α-steroids undergo the conjugate addition of methyl Grignard reagents to give 1β-methyl derivatives. This fact was explained by assuming that the β attack is sterically favored by the convexity of the β face of the molecule. However, other workers contend that this statement is wrong since 1α-methyl derivatives are formed. Recently, Pelc *et al.*[3] reported that the A ring of 1α-methyl-5α-androstan-3-one is in a chair conformation with the α-oriented C_1 methyl group. The α-attack of Grignard reagents is explained by the steric hindrance of the C_{10} methyl group.[4] From the fact that 1α-methyl-5β-cholestan-3-one (Va), which is derived from 1α-methyl-5α-cholestan-3-one (IIa), showed an unusual rotatory dispersion curve, Mori[5] suggested that the A ring of Va has a boat conformation. However, only very little information can be found on 1-alkyl-3-keto steroids concerning the synthesis of their derivatives and their reactivity.

In the present paper, we will describe the bromination of 1-methyl-3-keto steroids and will discuss the conformations of 1-methyl bromoketones.

Results and Discussion

The bromination of 5α- and 5β-cholestan-3-one occurred at the $C_{2\alpha}$ and $C_{4\beta}$ positions respectively.[6] The direction of bromination is dependent on that of enolization. The strong preference for a C_2-enolization in the 5α-series can be accounted for by both the 6β/19 interactions and the "hyperconjugation" of the C_1-methylene group.[2b] In the case of the 5β-series, the preference for C_4-enolization can be explained in terms of the relief of the nonbonded interactions between the 4α-hydrogen and the 7α- and 9α-hydrogens when a trigonal center is formed at C_4.[2b] Accordingly, 1-substituted 3-keto steroids are particularly interesting in the point of whether or not they show the same results as 1-unsubstituted 3-keto steroids on enolization and subsequent bromination.

Mori[5] reported that the bromination of IIa gave a C_4 brominated product, which was not purified. The bromination at the C_4-position was determined by the formation of 1α-methyl-cholest-4-en-3-one (IV) when the crude bromoketone was treated with LiCl/DMF. In our case, pure bromoketone (IIIa) was isolated; its configuration was determined by means of ORD and NMR (Tables 1 and 2).

The rotatory dispersion of this pure bromoketone

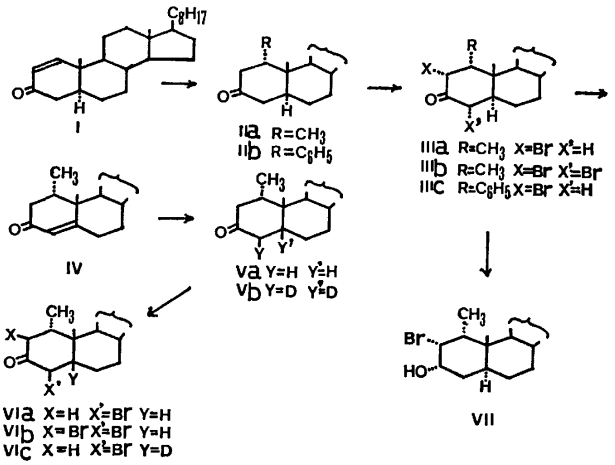

TABLE 1. ORD AND CD DATA OF 1-SUBSTITUTED 2- AND 4-BROMO-3-KETO STEROIDS

	$[\phi]_1$(nm)	$[\phi]_2$(nm)	a	$[\theta]$(nm)
IIa	2320(317)	−2132(273)	45	3416(296)
IIIa	1779(313)	−3319(272)	51	3531(298)
IIIb	402(310)			2112(288)
Va	848(314)	161(272)	7	848(290)
VIa	2532(313)	1204(268)	37	3029(292)
VIb	−369(367)	1285(300)	−17	−1143(337)
IIb	2897(311)	2014(285)	9	1667(297)
IIIc	3528(317)	925(277)	26	3976(294)

(IIIa) does not change the nature of the Cotton effect, and the wavelength shifts are negligible or tend toward shorter wavelength region, compared with the case of the parent ketone (IIa). The NMR spectrum showed peaks at 5.00 ppm (doublet, J=4.8 Hz) due to -CHBr-. Accordingly, the bromination product of (IIa) is concluded to be a 2α-bromo compound (IIIa) in a normal chair conformation. The dihedral angle, which was calculated using the Karplus equation from the coupling constant, also supported the results (Table 2). The dehydrobromination of IIIa with $CaCO_3$/DMF gave IV. This reaction was accompanied by a rearrangement of the bromine atom in the elimination reaction from C_2 to C_4 to give IV. If the 1,2-*trans* diaxial elimination of IIIa occurs, the A-ring requires a boat conformation in the process of elimination. In this reaction, the A-ring can not adopt a boat form by the nonbonded interaction of the 1α-methyl/11-methylene group. Therefore, the rearrangement of the substituent must have occurred.

Table 2. Chemical shifts, coupling constants, and dihedral angles of 2- and 4-bromo-3-keto steroids

Compound	CHBr (ppm)	J (Hz)	$\phi_{H_1\beta H_2}$ [c]	$\phi_{H_4H_5}$ [c]
5α-Cholestan-3-one derivative				
2α-Bromo-[a]	4.83(dd)	6.5	44°	
2α,4α-Dibromo-[a]	4.80(d)	12.7		161°
	4.45(dd)	6.2	45°	
IIIa	5.00(d)	4.8	52°	
IIIb	4.46(d)	12.0		156°
	5.11(d)	4.5	53°	
IIIc	5·14(d)	6.0	46°	
5β-Cholestan-3-one derivative				
4β-Bromo-[b]	4.98(d)	12.5		159°
2β,4β-Dibromo-[b]	4.82(dd)	14.6	180°	
	5.08(d)	11.4		153°
VIa	4.64(d)	10.5		149°
VIb	4.37(d)	13.5		166°
	4.55(d)	8.3	35°	

a) C. W. Shoppee, T. E. Bellas, R. E. Lack, and S. Sternhell, *J. Chem. Soc.*, **1965**, 2483. b) C. W. Shoppee, A. B. Devine, and R. E. Lack, *J. Chem. Soc.*, **1965**, 6458. c) R. J. Abraham and J. S. E. Holker, *J. Chem. Soc.*, **1963**, 806.

The reduction of IIIa with $NaBH_4$ gave a bromohydrine as the only product. The NMR spectrum of the bromohydrine showed peaks at 4.66 ppm (d,d, J= 3.0 and 4.8 Hz) attributable to –CHBr–. Moreover, the bromohydrine was identified as 1α-methyl-2α-bromo-5α-cholestan-3α-ol (VII) on the basis of the small coupling constants (*i.e.*, not diaxial vicinal coupling constants). Because of shielding for the reducing reagent by the 1α-methyl group, the reduction of the 3-keto group occurred only on the β-side. The bromination product of IIa was also determined to be a 2α-bromo compound (IIIa) from the above fact that IIIa had no diaxial vicinal coupling constants.

The 1α-phenyl derivative, with its bulky substituent at the C_1 position, is interesting in the point of the direction of bromination. Therefore, the introduction of a phenyl group at the C_1 position was tried for the 1,4-addition with PhMgI in a manner similar to that used with CH_3MgI. The NMR spectrum of this reaction product (IIb) showed peaks at 7.10 ppm (m, 5H) and 3.25 ppm (bd, J=6.0 Hz, 1H) due to the aromatic protons and –CHPh– respectively. From the relatively small coupling constant of the C_1 proton, its configuration was equatorial. Therefore, it appears that the phenyl group was also introduced at the $C_{1\alpha}$-position, in a manner similar to that in the case of the methyl group.

The NMR spectrum of the monobromination product of IIb had peaks at 3.58 ppm (d, J=6.0 Hz, $C_{1\beta}$–H) and 5.14 ppm (d, J=6.0 Hz, C_2–H). Its ORD curve did not change the nature of the Cotton effect, and the wavelength shifts were negligible compared with those of the parent ketone (IIb) (Table 1). From this spectral evidence, the bromination product was determined to be 1α-phenyl-2α-bromo-5α-cholestan-3-one (IIIc), with an equatorial bromine atom. From the coupling constants of IIIc, the dihedral angle of C_1H_e–C_2H_a was calculated using the Karplus equation. This calculation resulted in 46°(44° in 2α-bromo-5α-cholestan-3-one[7]) (Table 2); hence, the A-ring conformation of phenyl bromoketone (IIIc) seemed to be of approximately a normal chair form.

The above results do not show any differences in the 1α-substituent with respect to the direction of bromination and A-ring conformation.

The NMR spectrum of the dibromination product of IIa revealed peaks at 4.46 ppm (d, $J_{4\beta,5\alpha}$=12.0 Hz) and 5.11 ppm (d, $J_{1\beta,2\beta}$=4.5 Hz) due to vicinal diaxial coupling and equatorial-axial coupling respectively. Accordingly, the dibromination product was determined to be 1α-methyl-2α,4α-dibromo-5α-cholestan-3-one (IIIb). The dihedral angles ($\phi_{4\beta,5\alpha}$ and $\phi_{1\beta,2\beta}$) were calculated using the Karplus equation. It was found that the A-ring conformation of IIIb is a nearly normal chair form. These values are also listed in Table 2.

1α-Methyl-5β-cholestan-3-one (Va), which has been synthesized by following the procedure of Mori,[5] was brominated. The monobrominated product (VIa) of Va showed a peak at 4.64 ppm (d, J=10.5 Hz) attributed to –CHBr– in the NMR spectrum. It can not be determined from the above NMR data whether the bromine atom is attached to the C_2 or C_4 position. In order to determine the brominated position, IV was reduced with deuterium in cyclohexane. From the fact that the mass spectrum showed a peak at *m/e* 402 [M^+], this reduced product was found to be 1α-methyl-4β,5-dideuterio-5β-cholestan-3-one (Vb). The reaction of Vb with bromine in acetic acid gave a monobromoketone, melting at 136—139 °C. This product was determined to be 1α-methyl-4-bromo-5-deuterio-5β-cholestan-3-one (VIc) from the fact that the NMR spectrum showed a singlet at 4.64 ppm due to –CHBr–. From the above facts, it was found that the bromination of Va occurs at the C_4 position. The configuration of the C_4 bromine atom was determined to be equatorial (β-linkage) in the A-ring with the boat conformation from the fact that the rotatory dispersion of 1α-methyl-4β-bromo-5β-cholestan-3-one (VIa) does not change the nature of the Cotton effect; the wavelength shifts are negligible compared with those of the parent ketone, Va. If the A-ring takes a normal chair conformation, the ORD curve can be expected to show a negative Cotton effect. The dibromination of Va produced 2,4-dibromoketone (VIb); it showed a negative Cotton curve with a small amplitude (−17) and a red shift of 53 nm from that of the parent keton (Va). From these results, we may conclude that the two bromine atoms are attached to an axial-like bond. Because of the counteraction of the opposite contribution due to 2- and 4-bromine for the Cotton effect, it seems that the amplitude is small. From the coupling constants, $J_{1,2}$=8.3 Hz and $J_{4,5}$=13.5 Hz, of the dibromoketone, the dihedral angles were calculated using the Karplus equation; we obtained 35° and 166° respectively. These values differ from those for the angles of 2β,4β-dibromo-5β-cholestan-3-one (Table 2). From these data, it was concluded that the dibromoketone was 1α-methyl-2β,4β-dibromo-5β-cholestan-3-one

(VIb), with a twist boat conformation.

All of the facts observed in these experiments with respect to the direction and orientation proved to be the same as those in the case of 1-unsubstituted 3-keto steroids; thus, these seems to be no drastic 1α-substituent effect.

Experimental

All the melting points are uncorrected. The IR spectra were measured (KBr) with a Hitachi model 215 grating infrared spectrophotometer. The ORD spectra were obtained in dioxane with a JASCO model J-20 instrument. The NMR spectra were recorded in carbon tetrachloride, with tetramethylsilane as the internal standard, using a Hitachi-Perkin Elmer R-20A apparatus. The mass spectra were obtained with a Hitachi RMU-6M spectrometer at 20 eV.

1α-Phenyl-5α-cholestan-3-one (IIb). To Mg (0.9 g) in absolute ether (24 ml), under a nitrogen atomosphere was added dropwise iodobenzene (9.6 g) with stirring. After 30 min, absolute tetrahydrofuran (40 ml) was slowly added. The solvent was distilled until the boiling point was 62 °C; the mixture was then cooled to room temperature, and CuCl (0.2 g) and 5α-cholestan-1-en-3-one (2.0 g) in tetrahydrofuran (21 ml) were added. To facilitate stirring, tetrahydrofuran (40 ml) was added. After 30 min, the mixture was cooled to 0 °C, a saturated ammonium chloride solution was added, the mixture was extracted with ether, the aqueous solution was discarded, and the organic phase was washed successively with a sodium thiosulfate solution, the saturated ammonium chloride solution, and water. After a usual work-up, the resulting oil was distilled under reduced pressure at 180 °C to remove the non-keto substance. The residue was chromatographed on silica gel. Elution with benzene afforded 1α-phenyl-5α-cholestan-3-one (IIb) (1.2 g), which crystallized from ethanol as needles; mp 140—141 °C; IR cm^{-1}: ν_{max} 1707, 1600, and 703; NMR: 3.25 ppm (bd, J=6.0 Hz, 1H) and 7.10 ppm (m, 5H); Found: C, 85.60; H, 11.00, $C_{33}H_{50}O$ requires C, 85.65; H, 10.89%.

1α-Methyl-2α-bromo-5α-cholestan-3-one (IIIa). 1α-Methyl-5α-cholestan-3-one (2 g) in acetic acid (62 ml) was treated with bromine (0.811 g) in acetic acid (19 ml) containing a few drops of 48% hydrobromic acid at room temperature for 25 min. The reaction mixture was then treated in the usual manner. The crystallization of the resulting oil from ethanol gave IIIa (1.54 g); mp 177—180 °C; IR cm^{-1}: ν_{max} 1726 and 890; NMR: 5.00 ppm (d, J= 4.8 Hz, 1H); Found: C, 70.18; H, 9.80, $C_{28}H_{47}OBr$ requires C, 70.12; H, 9.88%.

1α-Methyl-2α, 4α-dibromo-5α-cholestan-3-one (IIIb). To a solution of IIa (0.300 g) in acetic acid (18 ml) and one drop of 48% hydrobromic acid was added bromine (0.231 g) in acetic acid (15 ml) with stirring for 30 min at room temperature. The reaction mixture was then taken up in ether, and the ether extracts were washed, dried, and evaporated. On the chromatography of the residue with silica gel, elution with benzene-petroleum ether (1 : 1) gave an oily product. The crystallization of the resulting oil from ethanol afforded needles (0.125 g) of IIIb; mp 145—148 °C, IR cm^{-1}: ν_{max} 1740 and 613; NMR: 4.46 ppm (d, J=12.0 Hz, 1H) and 5.11 ppm (d, J=4.5 Hz, 1H); Found: C, 59.92; H, 8.07%, $C_{28}H_{46}OBr_2$ requires C, 60.22; H, 8.30%.

1α-Phenyl-2α-bromo-5α-cholestan-3-one (IIIc). The bromination of IIb (0.5 g) was carried out using the technique for the synthesis of IIIa. After the usual work-up, the resulting oil was chromatographed on silica gel. Elution with benzene-petroleum ether (1 : 1) afforded IIIc (0.400 g), which crystallized from ethanol-methanol as needles; mp 74—76 °C, IR cm^{-1}: ν_{max} 1723 and 789; NMR: 3.58 ppm (d, J=6.0 Hz, 1H), 5.14 ppm (d, J=6.0 Hz, 1H), and 7.20 ppm (m, 5H); Found: C, 73.35; H, 9.30%, $C_{33}H_{49}OBr$ requires C, 73.17; H, 9.12%.

1α-Methyl-4β,5-dideuterio-5β-cholestan-5-one (Vb). The synthesis was carried out following the procedure of Shapiro and Djerassi.[8] A mixture of IV (0.168 g), palladium black (0.100 g), and cyclohexane (30 ml) was shaken in a deuterium atmosphere. The deuterium uptake was completed within 7 h. The catalyst was then removed by filtration, and the filtrate was evaporated. The residue was recrystallized from methanol to give Vb (0.079 g); mp 84—85 °C, IR cm^{-1}: ν_{max} 1718 (1718, CCl_4); MS: m/e 402 (M^+).

1α-Methyl-4β-bromo-5β-cholestan-3-one (VIa). The bromination of Va (0.100 g) was carried out using the technique used for the synthesis of IIIa. The crystallization of the resulting oil from ethanol gave VIa (0.094 g); mp 136—139 °C; IR cm^{-1}: ν_{max} 1718 (1730, CCl_4) and 572; NMR: 4.64 ppm (d, J=10.5 Hz, 1H), Found: C, 70.30; H, 9.62%, $C_{28}H_{47}OBr$ requires C, 70.12; H, 9.88%.

1α-Methyl-2β, 4β-dibromo-5β-cholestan-3-one (VIb). The dibromination of Va (0.300 g) was carried out using the technique used for the synthesis of IIIb. The crystallization of the resulting oil from ethanol gave VIb (0.180 g); mp 139—144 °C; IR cm^{-1}: ν_{max} 1733 (1720, CCl_4) and 624; NMR: 4.37 ppm (d, J=13.5 Hz, 1H) and 4.55 ppm (d, J=8.3 Hz, 1H), Found: C, 60.12; H, 8.00%, $C_{28}H_{46}OBr_2$ requires C, 60.22; H, 8.30%.

1α-Methyl-4β-bromo-5-deuterio-5β-cholestan-3-one (VIc). The bromination of Vb (0.060 g) was carried out using the technique used for the synthesis of IIIa. The crystallization of the resulting oil from ethanol gave VIc (0.045 g); mp 136—139 °C, IR cm^{-1}: ν_{max} 1718 (1730, CCl_4) and 572; NMR: 4.64 ppm (s, 1H); MS: m/e 480 and 482 (M^+).

1α-Methyl-2α-bromo-3α-hydroxy-5α-cholestane (VII). The synthesis used was virtually identical with the method of Fieser.[9] A solution of IIIa (0.400 g) and sodium borohydride (0.050 g) in methanol (60 ml) was stirred at room temperature for 30 min. After the usual work-up, the crystallization of the resulting oil from ethanol gave VII (0.315 g); mp 148—152 °C; IR cm^{-1}: ν_{max} 3499 and 1030; NMR: 3.96 ppm (m, 1H) and 4.66 ppm (dd, J= 3.0 and 4.8 Hz, 1H); Found: C, 70.01; H, 10.40%, $C_{28}H_{49}OBr$ requires C, 69.83; H, 10.26%.

The authors wish to thank Professors Jisaku Kuroda, Machiko Tozawa, and Tsunetaka Kushimoto of the Jikei University School of Medicine for their great support during this work.

References

1) a) A. Zaffaromi, *Acta Endocrinol., Suppl. 50*, **34**, 139 (1960). b) R. Wiechert and E. Kaspar, *Chem. Ber.*, **93**, 1710 (1960). c) D. Bertin and J. Perronnet, *Bull. Soc. Chem. Fr.*, **1964**, 2732. d) W. J. Wechter, *J. Org. Chem.*, **29**, 163 (1964). e) W. J. Wechter, G. Slomp, and F. A. Mackellar, *Tetrahedron*, **21**, 1625 (1965). f) B. Pelc, *Collect. Czech. Chem. Commun.*, **30**, 3468 (1965). g) B. Pelc and J. Hodkova, *ibid.*, **30**, 3575 (1965). h) B. Pelc and J. Hodkova, *ibid.*, **31**, 1064 (1966).

2) a) D. N. Kirk and M. P. Hartshorn, "Steroid Reaction Mechanisms," Elsevier, Amsterdam (1968), p. 196;

b) *ibid.*, p. 161.
3) B. Pelc and J. K. M. Sanders, *J. Chem. Soc., Perkin Trans. 1*, **1972**, 1219.
4) C. C. Bolt and F. J. Zeelen, *Recueil*, **92**, 1267 (1973).
5) H. Mori, *Chem. Pharm. Bull. (Tokyo)*, **10**, 386 (1962).
6) S. Coffey, "Rodd's Chemistry of Carbon Compounds," Elsevier, Amsterdam (1970), pp. 119, 124.
7) C. W. Shoppee, T. E. Bellas, R. E. Lack, and S. Sternhell, *J. Chem. Soc.*, **1965**, 2483.
8) R. H. Shapiro and C. Djerassi, *Tetrahedron*, **20**, 1987 (1964).
9) L. F. Fieser and R. Ettore, *J. Am. Chem. Soc.*, **75**, 1700 (1953).

The Effects of Phosphorus Ligands on the Stereoselectivity of the Nickel-catalyzed Dimerization of Norbornadiene

Susumu YOSHIKAWA,* Jitsuo KIJI,** and Junji FURUKAWA
Department of Synthetic Chemistry, Kyoto University, Kyoto 606
(Received September 25, 1975)

The effects of phosphorus ligands on the stereoselectivity of the nickel-catalyzed 2+2 cyclodimerization of norbornadiene have been studied. The electronic factor, $\nu_{CO}(A_1)$, of $Ni(CO)_3L$ (where L is the ligand) is correlated with the ratio of the *exo-trans-exo* (X-t-X) to the *exo-trans-endo* (X-t-N) isomers of the product, but no simple correlation is apparent between the steric parameter and the selectivity. A three-coordinated Ni(0) species is proposed as the intermediate. The values of $\Delta H^{\neq}_{X\text{-}t\text{-}X}-\Delta H^{\neq}_{X\text{-}t\text{-}N}$ and $\Delta S^{\neq}_{X\text{-}t\text{-}X}-\Delta S^{\neq}_{X\text{-}t\text{-}N}$ are large and negative.

Ligand effects in homogeneous catalytic reactions are generally divided into electronic and steric factors. Contrary to the electronic factor, the estimation of the steric factor is rather complicated, and little appears to be known about the steric effect on the selectivity of a reaction. Stereoselective organic syntheses have been attracted increasing interest in recent years. Our work in this series was initiated in order to clarify the factors which control the steric course of some homogeneous catalytic reactions. In the previous paper we described that the steric effect of trivalent phosphorus ligands dominates the steric course of the 4+2 cycloaddition of norbornadiene (NBD) with acrylonitrile (AN) catalyzed by bis(acrylonitrile)nickel $Ni(AN)_2$ (Eq. 1).[1]

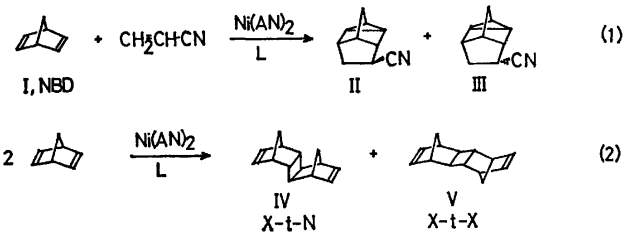

A steric parameter, the cone angle,[2] was correlated with the ratio of the stereo-isomers (II and III). It seems to us that the reaction of norbornadiene is simple enough for the evaluation of the effect of the added ligands, because both isomerization and retro-reaction can be minimized by temperature control under these conditions. The dimerization (Eq. 2) is catalyzed by various transition metal complexes.[3] In the nickel carbonyl-catalyzed dimerization,[4] ir-radiated $Ni(CO)_4$ with ultraviolet gives a different selectivity from that of the dark reaction.[5] If a ligand added to this system, instead of irradiating, alters the stereoselectivity, the effects of the ligand can be evaluated from the product distribution.

This paper will deal with the dominant role of the electronic effect in the 2+2 cyclodimerization of norbornadiene (Eq. 2).

Results

The present study employed bis(acrylonitrile)nickel $Ni(AN)_2$ combined with phosphorus ligands as the catalyst. Early in the reaction, $Ni(AN)_2$ was insoluble, but it was gradually dissolved by complexing with the phosphorus ligands. With a strong donor ligand, $Ni(AN)_2$ was rapidly dissolved and the system turned reddish-yellow. During the reaction, the acrylonitrile, which was coordinated to the nickel, reacted with norbornadiene to give II and III as the by-products. The radio of II and III was controlled by the cone angle of the phosphorus ligands used, as has been described in the previous paper.

The dimers, *exo-trans-endo* (IV, abbreviated as X-t-N) and *exo-trans-exo* (V, X-t-X), were the major products.[6] The ratio of IV to V is considered to reflect the stereoselectivity of the reaction under these conditions (65.8—130 °C), because neither isomerization nor retro-reaction occurred. In fact, the purified product, IV or V was heated with the catalyst. In this case, however, the isomer was recovered unchanged. Figure 1 shows the effects of the added triphenylphosphine on the yield and on the ratio of IV to V. An inspection of Fig. 1 reveals that the selectivity is independent of the amount of triphenylphosphine (P/Ni>2). This observation shows that the active species is specified not by the amount but by the kind of the phosphorus ligand added. This is consistent with the previous observation.[1] A correlation for the temperature indicated that the IV isomer was preferably formed as the temperature rises.

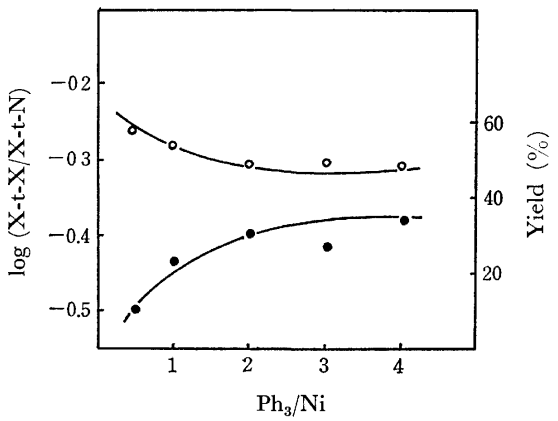

Fig. 1. Effects of added triphenylphosphine on the yield and the selectivity. ○, selectivity; ●, yield. Conditions: NBD, 8 mmol; $Ni(AN)_2$, 0.04 mmol; 100 °C for 5 h.

* Present address: Government Industrial Research Institute, Osaka, Midorigaoka, Ikeda, Osaka 563.
** To whom correspondence should be addressed.

As has been reported earlier,[1] the electronic and steric factors of the ligands were estimated by means of the $\nu_{CO}(A_1)$ of $Ni(CO)_3L$ and the cone angle, θ,

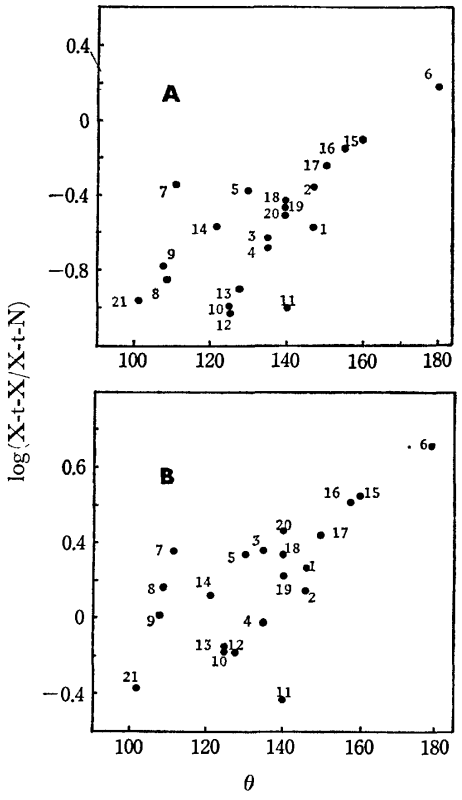

Fig. 2. Selectivity *vs.* cone angle. A, 110°; B, 7.15 °C. Ligands numbers refer to Experimental section.

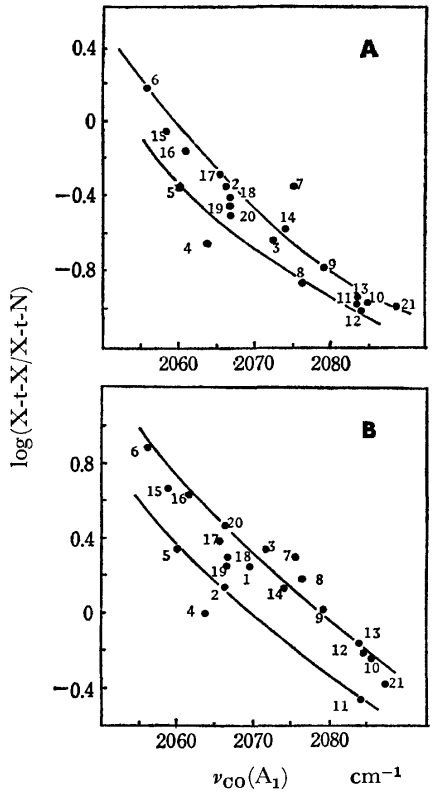

Fig. 3. Selectivity *vs.* ν_{CO}. A 110°; B, 71.5 °C.

respectively. The ratio of IV to V was correlated with ν_{CO} rather than with θ, as is shown in Figs. 2 and 3. No simple correlation is apparent between the cone angle and the selectivity. For example, ligands of different bulkiness, $(O\text{-}o\text{-}C_6H_4CH_3)_3P$ (**11**), $(O\text{-}m\text{-}C_6H_4CH_3)_3P$ (**12**), $(C_6H_5O)_3P$ (**10**), and $CH_3C(CH_2O)_3P$ (**21**), gave a similar ratio. This is in marked contrast to the 4+2 cycloaddition of norbornadiene with acrylonitrile, where a clear-cut correlation of the bulkiness of the ligands with the selectivity was found.

On the other hand, the importance of the electronic effect is indicated by the rather good correlation between $\nu_{CO}(A_1)$ and log V/IV. No appreciable difference in the effects was observed between phosphines and phosphites, except that the former gave higher yields than the latter.

The solvent effect was investigated by using PPh_3 as the auxiliary ligand at 92 and 110 °C. Solvents similar in their volume to norbornadiene were used. Figure 4 shows the relation between their molar polarizability and the selectivity. Acetonitrile behaved

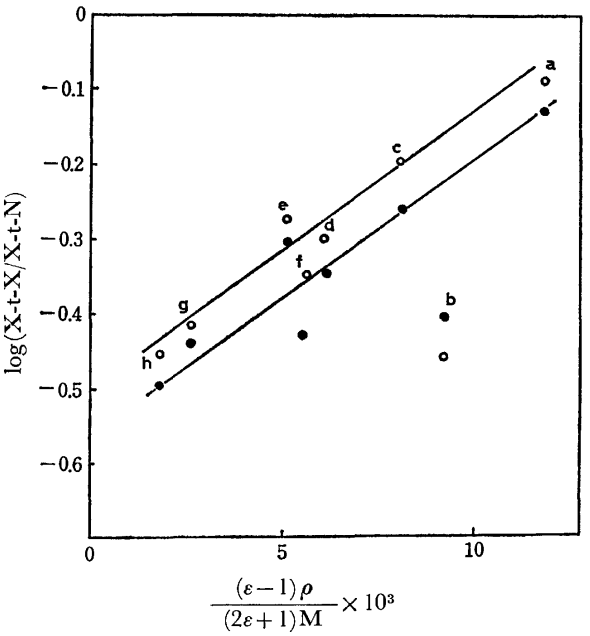

Fig. 4. Solvent effect. a, methanol; b, acetonitrile: c, ethanol; d, 2-propanol; e, tetrahydrofuran; f, pyridine; g, benzene; h, triethylamine. ●, 110 °C; ○, 92 °C. Conditions: NBD, 6 mmol; $Ni(AN)_2$, 0.04 mmol; PPh_3, 0.12 mmol; solvent, 1 ml; 3 h.

differently from the other solvents. This is attributable to the coordination of the CN group to the nickel. The increase in the polarity of the solvent preferred the formation of the X-t-X isomer. However, the solvent effect was smaller than that of the ligand.

It is noteworthy that the 4+2 cycloaddition of norbornadiene to acrylonitrile is strongly influenced by the cone angle of the ligands coordinated to the nickel, while the 2+2 cyclodimerization of norbornadiene is influenced by their electronic factor. This difference is attributable to the limited coordination number of the central metal. Due to a steric inter-

action of reactants in the coordination sphere, the reaction follows an unexpected course. The reaction of acetylenes with norbornadiene is an example.[7] Bulky diphenylacetylene undergoes 2+2 cycloaddition with norbornadiene on nickel, while dicarbomethoxyacetylene undergoes 4+2 cycloaddition. The failure of the 4+2 cycloaddition of diphenylacetylene may be ascribed to the steric interaction of the bulky phenyl group. In the reaction (Eq. 1) the tetrahedral configuration around the nickel was assumed. Zerovalent nickel (d^{10}) has the maximum coordination number 4, and the stabilization energy of its ligand field is highest. However, the steric interaction caused by adding the fourth bulky ligand may cost more energy than would be gained by completing the coordination number, 4. In fact, Seidel and Tolman[8] have reported that, in the homolog of NiL_4, coordinatively unsaturated NiL_3 is obtained with bulky $P(O\text{-}o\text{-}C_6H_4CH_3)_3$.

A supposed intermediate of the dimerization is shown in Fig. 5, where one molecule of norbornadiene is bidentately coordinated, and the other, unidentately, by assuming that the C–Ni bond is 2.1 Å. In this configuration the cone angle of the ligand coordinated to the fourth site must be smaller than 95°. None of the phosphorus ligands used in the present study can occupy the site, because they are too bulky to be coordinated to the nickel. Therefore, a three-coordinated Ni(0) species is here proposed as the intermediate.[9] This assumption is in striking contrast to that used for the reaction of norbornadiene with acrylonitrile.[1]

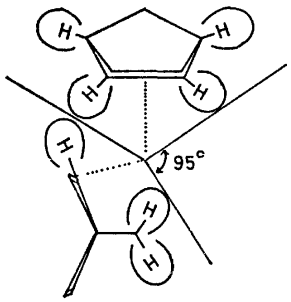

Fig. 5. Proposed coordination of bidentate and unidentate norbornadiene.

Plots of V/IV (the ratio of X-t-X to X-t-N formed) against $1/T$ were used to determine the values of $\Delta H^{\ddagger}_{X\text{-t-}X}-\Delta H^{\ddagger}_{X\text{-t-}N}$ ($\Delta\Delta H^{\ddagger}$) and $\Delta S^{\ddagger}_{X\text{-t-}X}-\Delta S^{\ddagger}_{X\text{-t-}N}$ ($\Delta\Delta S^{\ddagger}$), by assuming that the ratio of the products formed reflects that of the rate constants. The values of $\Delta\Delta H^{\ddagger}$ and $\Delta\Delta S^{\ddagger}$ are large and negative, in general (Fig. 6). The isokinetic temperature is derived as 79 °C.

The thermally "forbidden" dimerization of norbornadiene is here considered to proceed *via* a metal-carbon bonded intermediate.[10] In fact, an analogous iridocycle has been prepared and can be regarded as a stabilized intermediate.[11] The stercochemistry of the carbon–carbon bond formation on the iridium metal is not altered during the reductive elimination, which gives the 2+2 cycloaddition products. That is, no isomerization is involved in these steps. Before

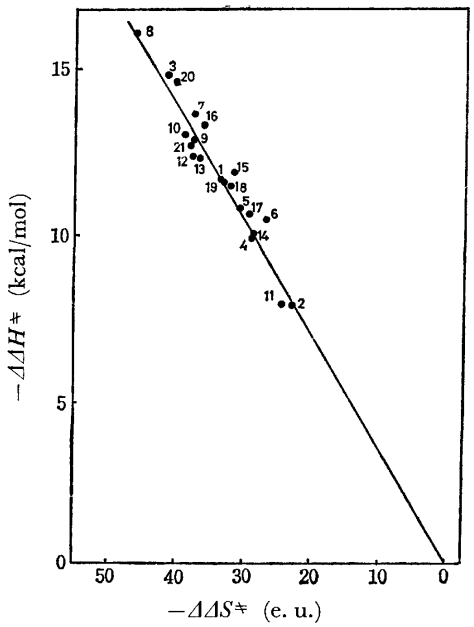

Fig. 6. Isokinetic relation. Ligands numbers refer to Experimental section.

the coupling of two double bonds, the coordination of both reactants to the central metal is required. In the nickel-catalyzed 2+2 cycloaddition of norbornadiene with a strained olefinic double bond, the transient bidentate (*endo*) coordination of norbornadiene is assumed, because this catalytic system gives exclusively an adduct having *endo* stereochemistry.[12] The mode of the coordination before the coupling is considerd to determine the stereochemistry of the products.

In general, due to its strain each double bond of norbornadiene can participate in the coordination;[9] thus, the *endo* coordination through chelation is inherent in the present reaction. Consequently, prior to the coupling of norbornadiene, the corresponding *exo-endo* (VII) and *exo-exo* (VIII) coordinations can be assumed with likelihood; they afford *exo-trans-endo* (IV) and *exo-trans-exo* (V) isomers respectively.

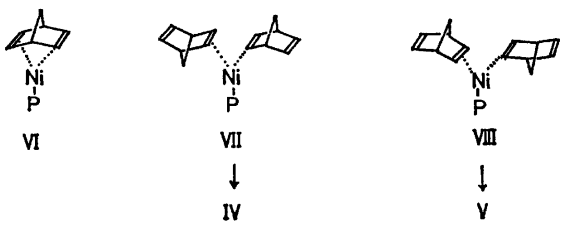

No sufficient explanation of the electronic effect of the phosphorus ligands on the reaction can be made on the basis of the present study. However, the following explanation is possible. The donor ligand increases the electron density of the nickel. The coordination of norbornadiene on the less-hindered *exo* side gives a greater overlap of the orbitals between the nickel and the double bond.[13] The terms of enthalpy dominates the formation of VIII. On the other hand, the formation of VII is favorable in terms of its smaller entropy loss on the basis of the assumption that both VII and VIII are derived from VI by substituting one and two

double bonds of the originally *endo*-coordinated norbornadiene with the incoming norbornadiene. A higher temperature also favors the formation of IV (Fig. 3). Therefore, the entropy term is considered to be dominant in the formation of VII. If the intermediates (VII and VIII) participate in the product-determining step, the selectivity is determined by the ease of their formation.

Experimental

Commercially available phosphorus compounds were used without further purification. All the reactions were carried out in glass tubes (8 mm in diameter) without stirring. The reaction conditions are indicated in the figures. The separation of the isomers was performed by gas chromatography on a Silicon DC 550 column (3 m) at 180 °C. They were identified by comparing the NMR spectra of the gas chromatographically collected samples with those of the reported ones.[4d] The yields were determined by gas chromatography, using tetralin as the internal standard. The total yields (X-t-X and X-t-N formed) of a typical reaction (NBD, 8 mmol) in the presence of $Ni(AN)_2$ (0.04 mmol) and the ligand (0.12 mmol) in benzene (1 ml) are as follows (% at 71.5 °C for 15 h, 110 °C for 3 h): $(C_6H_5)_3P$ (**1**), (65.2, 49.0); $(p\text{-}CH_3C_6H_4)_3P$ (**2**), (70.2, 59.2); $(C_6H_5)_3As$ (**3**), (46.4, 4.8); $(C_2H_5)_2(C_6H_5)P$ (**4**), (55.0, 3.7); $(n\text{-}C_4H_9)_3P$ (**5**), (43.9, 35.7); $(C_6H_{11})_3P$ (**6**), (36.6, 24.5); $(C_4H_9O)_3P$ (**7**), (47.1, 15.3); $(C_2H_5O)_3P$ (**8**), (27.4, 3.6); $(CH_3O)_3P$ (**9**), (20.8, 1.9); $(C_6H_5O)_3P$ (**10**), (32.2, 1.4); $(O\text{-}o\text{-}C_6H_4CH_3)_3P$ (**11**), (31.6, 0.9); $(O\text{-}m\text{-}C_6H_4CH_3)_3P$ (**12**), (27.6, 0.5); $(O\text{-}p\text{-}C_6H_4CH_3)_3P$ (**13**), (36.7, 0.9); $(C_2H_5O)_2(C_6H_5)P$ (**14**), (35.4, 6.9); $(o\text{-}C_6H_4CH_3)_3P$ (**15**), (42.3, 31.6); $(o\text{-}C_6H_4OCH_3)_2(C_6H_5)P$ (**16**), (59.8, 23.1); $(o\text{-}C_6H_4OCH_3)(C_6H_5)_2P$ (**17**), (55.0, 20.1); $(C_6H_5)_2PCH_2P(C_6H_5)_2$ (**18**), (47.6, 10.4); $(C_6H_5)_2PCH_2CH_2P(C_6H_5)_2$ (**19**), (36.2, 15.9); $(C_6H_5)_2P(CH_2)_3P(C_6H_5)_3$ (**20**), (41.6, 7.3); $CH_3C(CH_2O)_3P$ (**21**), (25.8, 3.6).

References

1) S. Yoshikawa, J. Kiji, and J. Furukawa, *Bull. Chem. Soc. Jpn.*, **48**, 3239 (1975).
2) C. A. Tolman, *J. Am. Chem. Soc.*, **92**, 2956 (1970).
3) G. N. Schrauzer, *Chem. Ber.*, **95**, 2764 (1962).
4a) R. Pettit, *J. Am. Chem. Soc.*, **81**, 1266 (1959). b) C. W. Bird, D. L. Colinese, R. C. Cookson, J. Hudec, and R. O. Williams, *Tetrahedron Lett.*, **1961**, 373 . c) D. M. Lemal and K. S. Shim, *ibid.*, 368 (1961). d) D. R. Arnord, D. J. Trecker, and E. B. Whipple, *J. Am. Chem. Soc.*, **87**, 2596 (1965).
5) G. E. Vock, P. W. Jennings, G. D. Smith, and C. N. Caughlan, *J. Org. Chem.*, **37**, 1460 (1972).
6) When phosphite was used as the ligand, *endo-trans-endo* isomer was formed in very low yield.
7) G. N. Schrauzer and T. Glockner, *Chem. Ber.*, **97**, 2451 (1964).
8) W. C. Seidel and C. A. Tolman, *Inorg. Chem.*, **9**, 2554 (1970).
9) C. A. Tolman, *J. Am. Chem. Soc.*, **96**, 2780 (1974).
10) S. Yoshikawa, K. Aoki, J. Kiji, and J. Furukawa, *Tetrahedron*, **30**, 405 (1974).
11) A. R. Fraser, P. H. Bird, S. A. Bezman, J. R. Shapley, R. White, and J. A. Osborn, *J. Am. Chem. Soc.*, **95**, 597 (1973).
12) R. Noyori, T. Ishigami, N. Hayashi, and T. Takaya, *J. Am. Chem. Soc.*, **95**, 1674 (1973).
13) Reaction of bicycloheptene with cyclododecatriene-nickel gives tris(bicycloheptene)nickel, which reacts with one molecule of phosphine or phosphite to give bis(olefin)-nickel. The nickel of this complex is assumed to occupy the *exo* position, P.W. Jolly and G. Wilke, "The Organic Chemistry of Nickel," Vol. 1, Academic Press, New York and London (1974), p. 257.

Bromination and Mercuration of Bis-dimethlglyoximato(1-octenyl)-pyridinecobalt(III), 1-Octenyl Cobaloxime

Masaru TADA, Minoru KUBOTA, and Hiraku SHINOZAKI

Department of Chemistry, School of Science and Engineering, Waseda Univerity, Shinjuku, Tokyo 160

(Received October 2, 1975)

cis-1-Octenyl(pyridine)cobaloxime (I) and *trans*-1-octenyl(pyridine)cobaloxime (II) were prepared by the reaction of cobaloxime anion with *cis*- and *trans*-1-halooctene, respectively. Bromination of I and II in polar solvents gave preferentially *trans*-1-bromooctene. Bromination of I in carbon disulfide also gave preferentially *trans*-1-bromooctene, but bromination of II gave more *cis*-1-bromooctene. Mercuration of I and II with mercuric acetate in DMF gave preferentially 1-octenylmercury(II) compound with retention of configuration, but the mercuration in acetic acid gave *ca.* 1 : 2 mixture of *cis* and *trans*-1-octenylmercury(II) compound. Two mechanisms are proposed for these electrophilic displacement reactions; one involves the addition of electrophile as a first step, followed by the elimination of cobaloxime moiety, and the other involves the addition of bromonium or mercury(II) ion, followed by the elimination of cobaloxime moiety.

In recent years much attention has been paid to the electrophilic displacement of alkyl metal-complexes,[1] especially bis-dimethylglyoximato(alkyl)pyridinecobalt-(III).[2-5] Kinetic studies[6,7] and the stereochemical consequences of these reactions suggest that the nature of these reactions is a concerted S_E2 reaction with inversion of the configuration at the reaction center. Little is known about the electrophilic displacement of alkenyl cobalt-complex. Johnson and Meeks[8] recorded in a preliminary report that the halogenation of bis-dimethylglyoximato(styryl)pyridinecobalt(III) in acetic acid proceeded with retention of configuration to give β-halostyrene.

In this paper we wish to report the steric course of the electrophilic displacement, bromination, and mercuration of bis-dimethylglyoximato(*cis*-1-octenyl)pyridinecobalt(III) (I) and bis-dimethylglyoximato(*trans*-1-octenyl)pyridinecobalt(III) (II), for which the conventional name octenyl(pyridine)cobaloxime is used hereafter, and to discuss the reaction mechanism.

Experimental

Preparation of cis *and* trans-*1-Octenyl(pyridine)cobaloxime (I and II).* To the stirred mixture of *cis*-1-bromooctene (382 mg, 2 mmol) and dimeric pyridinecobaloxime,[9] $(Co(dmgH)_2py)_2$ (368 mg, 0.5 mmol) in 20 ml of ethanol containing sodium hydroxide (0.01 mol/l) was added under nitrogen 1.3 g of zinc powder in portions over the period of 3 days. The reaction mixture was filtered and the filtrate was condensed under reduced pressure. The condensate was passed through a column of Florisil (10 g) with dichloromethane to remove impurities. Evaporation of the solvent from the eluate gave essentially pure *cis*-1-octenyl(pyridine)-cobaloxime (I) in 35% yield. Recrystallization of I from acetonitrile gave pure cobaloxime.

The same procedure starting with *trans*-1-chlorooctene gave *trans*-1-octenyl(pyridine)cobaloxime (II) in the yield of 33%. I, mp 149—151 °C. Found: C, 52.47; H, 7.31; N, 14.87%. Calcd for $C_{21}H_{34}N_5O_4Co$: C, 52.61; H, 7.15; N, 14.61%. IR (KBr): 2940, 2855, 1598, 1439, 1230, 1080, and 725 cm^{-1}. NMR($CDCl_3$):[10] 8.75 (d, J=6.5, 2H), 7.80 (t, J=6.5, 1H), 7.40 (t, J=6.5, 2H), 5.80 (d, J=7, 1H), 4.96 (q, J=7, 1H), 2.08 (s, 12H), 1.0—1.4 (m, 10H), and 0.88 ppm (δ) (t, J=6, 3H).

II, mp 171—173 °C. Found: C, 52.32; H, 7.35; N, 14.90%. Calcd for $C_{21}H_{34}N_5O_4Co$: C, 52.61, H, 7.15; N, 14.61%. IR(KBr): 2940, 2860, 1600, 1560, 1442, 1225, 1082, and 945 cm^{-1}. NMR($CDCl_3$): 8.74 (d, J=6.5, 2H), 7.81 (t, J=6.6, 1H), 7.40 (t, J=6.6, 2H), 5.71 (d, J=14, 1H), 5.08 (quintet, J=14 and 7, 1H), 2.08 (s, 12H), 1.0—1.4 (m, 10H), and 0.82 ppm (δ) (t, J=6.5, 3H).

Bromination of 1-Octenyl(pyridine)cobaloximes (I and II). The solution of I or II (120 mg, 0.25 mmol) in one of the solvents (10 ml) was treated with one equivalent of bromine or NBS dissolved in 10 ml of the same solvent, and the mixture was stirred for 30 min at ambient temperature. After evaporation of most of the solvent, the products were dissolved in hexane. When DMF was used as the solvent, the reaction mixture was added to water and extracted with hexane. Passing of the hexane solution through the column of alumina (Merck activity II-III, 500 mg) gave the eluate containing 1-bromooctene. This eluate was subjected to GLC analysis (N_2, 5% Carbowax 20 M on Chromosorb W, 90 °C) for the determination of the product composition. Evaporation of the solvent of the eluate gave 1-bromooctenes in the yields listed in the tables. Assignment of the bromides to *cis* and *trans*-1-bromooctene was made by the comparison of GLC, IR, and NMR spectra of the products with those of the authentic samples. The reaction in carbon disulfide at a controlled temperature was carried out using a cooling bath (−50 °C) or by boiling the reaction mixture (46 °C). The effect of bromide ion on the product composition was determined by using a mixture of DMF and water (9 : 1) containing a certain amount of tetraethylammonium bromide.

Mercuration of 1-Octenyl(pyridine)cobaloximes (I and II). The solution of I or II (120 mg, 0.25 mmol) in DMF or acetic acid (5 ml) was treated with 1.2 equivalents of mercuric acetate and the mixture was stirred for 30 min at ambient temperature. The mixture was further stirred for 10 min after addition of 4 ml of saturated aqueous solution of sodium chloride and extracted with dichloromethane after further addition of water (20 ml). The extract was washed with water and then condensed at reduced pressure to remove any residual DMF. The crude product thus obtained was passed through a column of Florisil (1.2×15 cm) using dichloromethane, and evaporation of the solvent gave 1-octenylmercury(II) chloride (IVa and IVb) in the yields listed in Table 3. The product composition was determined by the relative intensities of the NMR signals of olefinic hydrogen of this product mixture in $CDCl_3$. Recrystallization of the product from hexane gave pure *cis* and *trans*-1-octenylmercury(II) chloride (IVa and IVb). The structures of IVa and IVb were deduced by transforming these organomercury(II) compounds into *cis* and *trans*-1-bromooctene with bromine in pyridine.

IVa, low melting solid. IR(KBr): 3005, 1598, 1460,

965, 950, and 690 cm^{-1}. NMR($CDCl_3$): 6.74 (double t, J=10 and 7, 1H), 6.03 (d, J=10, 1H), 2.28 (m, 2H), 1.2—1.6 (8H), and 0.91 ppm (δ) (t, J=6.5, 3H). IVb, mp 103—104 °C.[11] IR(KBr): 3005, 1600, 1462, 969, 952, and 717 cm^{-1}. NMR($CDCl_3$): 5.81 (m, 2H), 2.20 (m, 2H), 1.1—1.6 (8H), and 0.90 ppm (δ) (t, J=6.5, 3H).

Results and Discussion

cis-1-Octenyl(pyridine)cobaloxime and *trans*-1-octenyl (pyridine)cobaloxime (I and II) were prepared by the action of the cobaloxime anion on *cis*-1-bromooctene and *trans*-1-chlorooctene, respectively (Eqs. 1 and 2). The cobaloxime anion was usually prepared *in situ* from dimethylglyoxime, pyridine, cobalt(II) chloride, and sodium tetrahydroborate in methanol, but the yield (*ca.* 15%) of 1-octenyl(pyridine)cobaloxime was moderate by this method. We prepared the cobaloxime anion conveniently by the reduction of dimeric pyridinecobaloxime $(Co(dmgH)_2py)_2$[9] with zinc powder in ethanol containing sodium hydroxide (0.01 mol/l). The yields of 1-octenyl(pyridine)cobaloximes were always over 30%, though we did not maximize the yields.

The stereochemistry of 1-octenyl(pyridine)cobaloximes (I and II) can be easily assigned by examination of the coupling constants of the olefinic hydrogens, J=7 Hz for I and 14 Hz for II. The stereochemistry of 1-octenyl(pyridine)cobaloxime is the same as that of the starting halooctenes; this is in sharp contrast to the inversion of the configuration at the reaction center when the displacement of alkyl halide is carried out

$$n\text{-}C_6H_{13}\!\!\diagdown\!\!=\!\!\diagup X + [Co(dmgH)_2py]_2 \xrightarrow[NaOH/EtOH]{Zn} \underset{(I)}{n\text{-}C_6H_{13}\!\!\diagdown\!\!=\!\!\diagup Co(dmgH)_2py} \quad (1)$$

$$n\text{-}C_6H_{13}\!\!\diagdown\!\!=\!\!\diagdown X + [Co(dmgH)_2py]_2 \xrightarrow[NaOH/EtOH]{Zn} \underset{(II)}{n\text{-}C_6H_{13}\!\!\diagdown\!\!=\!\!\diagdown Co(dmgH)_2py} \quad (2)$$

with cobaloxime anion.[1] These facts suggest that the formation of alkenyl cobaloxime results from the addition of cobaloxime anion to 1-haloalkene and the elimination of halide anion. This process usually proceeds with retention of configuration,[12,13] whereas the reaction of alkyl halide with cobaloxime anion takes S_N2 process with inversion of configuration.[14]

The reaction of bromine with *cis*- and *trans*-1-octenyl-(pyridine)cobaloxime (I and II) was carried out in polar solvents such as acetic acid, pyridine, DMF, and methanol; the bromine was consumed smoothly at ambient temperature (*ca.* 20 °C). The reaction gave only *cis* and *trans*-1-bromooctene (IIIa and IIIb); the results are shown in Table 1. The yields listed in the table were obtained from the isolated bromides; the yields analyzed by GLC gave much better figures. The relative ratio of the two isomeric bromides of the isolated products was essentially the same as the ratio of the crude products, and we did not maximize the isolated yields. The results summarized in Table 1 show that the bromination of *cis*-cobaloxime I in polar solvents proceeds almost completely with inversion of the configuration, whereas *trans*-cobaloxime II takes a different steric course, retention.

$$\left.\begin{array}{l} n\text{-}C_6H_{13}\!\!\diagdown\!\!=\!\!\diagup Co(dmgH)_2py \\ \quad (I) \\ n\text{-}C_6H_{13}\!\!\diagdown\!\!=\!\!\diagdown Co(dmgH)_2py \\ \quad (II) \end{array}\right\} \xrightarrow{Br_2} \left.\begin{array}{l} n\text{-}C_6H_{13}\!\!\diagdown\!\!=\!\!\diagup Br \\ \quad (IIIa) \\ + \\ n\text{-}C_6H_{13}\!\!\diagdown\!\!=\!\!\diagdown Br \\ \quad (IIIb) \end{array}\right. \quad (3)$$

The bromination of *cis* and *trans*-1-octenyl(pyridine)-cobaloxime (I and II) in carbon disulfide gave the results shown in Table 2. *cis*-Cobaloxime I gave preferentially *trans*-1-bromooctene (IIIb) with inversion, and *trans*-1-octenyl(pyridine)cobaloxime (II) gave more *cis*-1-bromooctene IIIa again with predominant inversion. The temperature effect on the product composition is opposite for I and II; a lowering of temperature induces more retention with I and more inversion with II. The stereoselectivity of the reaction in carbon disulfide is worse than in polar solvents, even at the lower temperatures. The low stereoselectivity in the bromination of 1-octenyl(pyridine)cobaloximes in carbon disulfide suggests the possibility of the intrusion of a radical mechanism. Bromination of the cobaloximes in the presence of 2,4,6-tri-*t*-butylphenol (2 equivalents), however, changed the isomeric ratio of the products by less than 5%. In the case of *trans*-cobaloxime II, addition of 2,4,6-tri-*t*-butylphenol gave products with more *cis*-bromide IIIa (64%) than its *trans*-isomer IIIb (36%). The preferential formation of thermo-

Table 1. Stereochemical compositions of 1-bromooctene

Starting material	Solvent	Yield[a] (%)	IIIa[b] (%)	IIIb[b] (%)
I	Methanol	67	2	98
	Pyridine	73	5	95
	Acetic acid	67	8	92
II	Methanol	68	10	90
	DMF	58	8	92

a) Isolated yield; some part of the products was lost on evaporation of the solvents. b) Calculated from the ratio of the peak area in GLC analysis.

Table 2. Dependence of the stereoselectivity of bromination in CS_2 on reaction temperature

Starting material	Reaction temperature	Yield[a] (%)	IIIa[b] (%)	IIIb[b] (%)
I	46 °C	80	11	89
	20 °C	72	13	87
	−50 °C	80	17	83
	20 °C[c]		14	86
II	46 °C	80	56	44
	20 °C	67	59	41
	−50 °C	65	72	28
	20 °C[c]		64	36

a) Isolated yield; some part of the products was lost on evaporation of the solvent. b) Calculated from the ratio of the peak area in GLC analysis. c) Carried out in the presence of 2 equivalents of 2,4,6-tri-*t*-butylphenol.

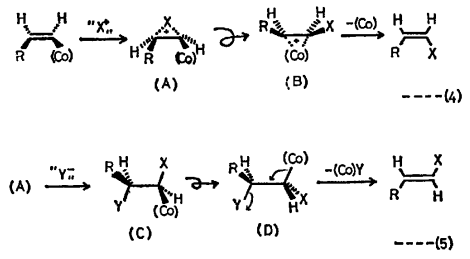

dynamically unstable *cis*-bromide IIIa from *trans*-cobaloxime II and the slight effect on the product composition from the radical inhibitor, 2,4,6-tri-*t*-butylphenol, exclude the possibility that the bromination of I and IIb is a radical process. The minor temperature effect on the product composition can be understood by considering a slight thermal isomerization of IIIa to IIIb under reaction conditions. Vinyl-type organocobaloxime is more stable than the corresponding alkyl cobaloxime; inparticular the former resists photodecomposition and photo-oxygenation under the conditions in which the latter decomposes with extreme easiness, giving alkyl radical as an intermediate. This feature is one of the reasons for eliminating a radical process for the bromination of cobaloxime I and II. A concerted S_E2 reaction also does not seem reasonable since the S_E2 reaction of alkyl cobaloxime has been settled to proceed with inversion of configuration due to the steric hindrance of the front side by dimethylglyoximato-ligand.[1] Bromination in the present study, nevertheless, proceeds with preferential retention under some conditions. These discussions imply a π-participated mechanism, as is generally believed to be responsible for the halogenation of vinyl-type organometallic compounds vinyl borane,[15] vinyl silicone,[16] and vinyl mercury(II) compound.[17] We prefer, therefore, the π-participated mechanisms depicted in Eq. 4 for the bromination with retention and in Eq. 5 for the bromination with inversion. There is large steric repulsion between the alkyl group and dimethylglyoximato-ligand in the intermediate (A) and also between alkyl and bromide in the intermediate (B). The bromination of *cis*-1-octenyl(pyridine)cobaloxime (I) *via* the route depicted in Eq. 4 must be disadvantageous for this reason. In the case of *trans*-1-octenyl(pyridine)-cobaloxime (II), the lack of severe steric repulsion in the intermediates of the types of (A) and (B) drives the reaction, as in Eq. 4, almost completely in non-polar solvents and appreciably in carbon disulfide. The reaction of *trans*-cobaloxime II in carbon disulfide, however, proceeds still preferentially with inversion, especially at the lower temperature. This means that the bridged carbonium ions (A) and (B) from *trans*-cobaloxime II are not sufficiently stabilized in polar solvents and an addition-elimination mechanism (Eq. 5) is still the favorable one. This concept is supported by the effect of temperature on the product composition—the lowering of temperature induces more inversion. In the latter mechanism (Eq. 5), we preclude the *cis*-elimination of halo-cobaloxime (CoY) from the intermediate (C) by the following reasons. Organo-(pyridine)cobaloxime has a central cobalt(III) ion whose coordination number is saturated by six ligand sites to take the nominal electronic structure of an inert gas. In support of this concept, notice that *trans*-2-hydroxycyclohexyl(pyridine)cobaloxime (IV) enters the elimination reaction with extreme easiness, giving cyclohexene, whereas its *cis* isomer V does not eliminate the cobaloxime residue easily.[1] These features are nicely illustrated by the halogen displacement of vinyl boronate (VI), in which *trans*-elimination takes place from the intermediate (E) in the presence of sodium methoxide (Eq. 6)[18] and *cis*-elimination takes place from the intermediate (F) in the presence of a weaker base (Eq. 7).[19] In these examples the intermediate (E) has the boron with saturated coordination number, whereas the intermediate (F) has the boron with unsaturated coordination number.

Next we examined the effect of the anion on the steric course of the reaction. Succinimide anion is considered to be a poor nucleophile, as exemplified in the oxybromination of olefin by *N*-bromosuccinimide in water or alcohol.[20] The use of *N*-bromosuccinimide as a bromonium ion source forces the reaction to take the route shown in Eq. 4, and the reaction proceeded more stereospecifically with retention of configuration, I : 72% retention and II : 71% retention in carbon disulfide. It is of special interest that the stereoselectivity was reversed, more retention, when *N*-bromosuccinimide was used. On the same ground, the existence of more bromide ions in the reaction system may induce more inversion as a result of the enhanced probability of giving the intermediate (C). Actually addition of tetraethylammonium bromide upon bromination of II with bromine in DMF caused more inversion—IIIa(*cis*)/IIIb(*trans*)=8/92, 14/86, and 29/71 when 0, 1.9, and 7.7 equivalents, respectively, of tetraethylammonium bromide was added.

The reaction of *cis*- and *trans*-1-octenyl(pyridine)-cobaloxime (I and II) with mercuric acetate followed by the treatment with sodium chloride was less stereospecific and gave *cis* and *trans*-1-octenylmercury(II) chloride (Eq. 8), as summarized in Table 3.

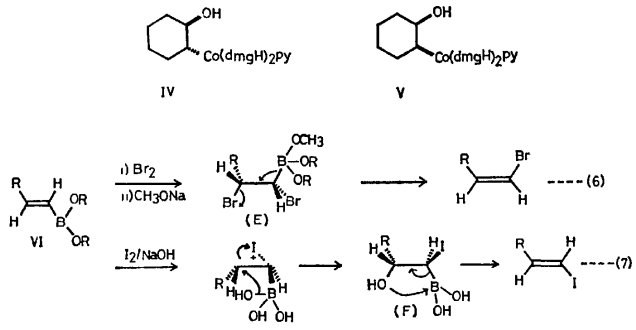

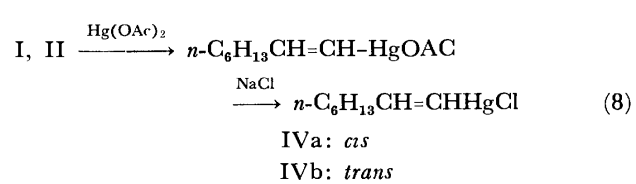

1-Octenylmercury(II) chloride thus formed was identified by transformation of these mercury-compounds

TABLE 3. ISOMERIC COMPOSITION OF 1-OCTENYLMERCURY(II) CHLORIDE FROM 1-OCTENYL(PYRIDINE)COBALOXIME

Starting material	Solvent	Yield[a] (%)	IVa[b] (%)	IVb[b] (%)
I	DMF	80	74	24
	Acetic acid	93	35	65
II	DMF	50	37	63
	Acetic acid	70	31	69

a) Isolated yield. b) Determined by the relative intensity of the NMR signals of olefinic hydrogen.

into *cis* and *trans*-1-bromooctene (IIIa and IIIb) by treatment with bromine in pyridine. In DMF, mercuration of I and II gave more products with retention. The low stereospecificity is not due to the isomerization of the starting *cis* and *trans*-cobaloxime (I and II), since mercuration of the cobaloxime with less than one equivalent of mercuric acetate recovered the starting cobaloxime in intact form. The reaction of *cis*-cobaloxime I in acetic acid, however, gave predominantly *trans*-1-octenylmercury(II) chloride (IVb). One of the possible courses is an addition-elimination mechanism due to the nucleophilic nature of acetic acid to give the intermediate of type (C) (Y=OAc) in Eq. 5, since the intermediate (A) and (B) are rather unstable due to the steric repulsion between alkyl and mercury (II) ion. A radical mechanism resulting from the initial electron transfer from the cobaloxime to mercury (II) ion (Eq. 9)[21] may be a mechanistic candidate, but the preferential formation of thermodynamically unstable *cis*-1-octenylmercury(II) chloride (IVa) from *cis* cobaloxime in DMF can be a justification for precluding the radical mechanism. Thus the mercuration of 1-octenyl(pyridine)cobaloxime (I and II) in polar solvents such as acetic acid and DMF can be considered to take both paths depicted in Eq. 4 and 5 competitively.

$$C_6H_{13}CH{=}CH{-}Co(dmgH)_2py + Hg^{2+} \longrightarrow [C_6H_{13}CH{=}CH{-}Co(dmgH)_2py]^+ + Hg^+ \xrightarrow{-Co(dmgH)_2py^+} C_6H_{13}CH{=}CH\cdot + Hg^+ \longrightarrow C_6H_{13}CH{=}CHHg^+ \quad (9)$$

In conclusion, the electrophilic substitution of 1-octenyl(pyridine)cobaloxime takes two competitive reaction paths—a stepwise mechanism involving bridged carbonium ions (Eq. 4) and a mechanism involving addition-elimination (Eq. 5). The relative importance of the two mechanisms depends on the stereochemistry of the starting 1-octenyl(pyridine)cobaloxime, the nature of the electrophilic reagent, and the solvent system of the reaction.

References

1) H. Shinozaki, H. Ogawa, and M. Tada, *Bull. Chem. Soc. Jpn.*, **49**, 775 (1976) and references cited therein.
2) M. Tada and H. Ogawa, *Tetrahedron Lett.*, (**1973**), 2639.
3) F. R. Jensen, V. Madan, and D. H. Buchanan, *J. Am. Chem. Soc.*, **93**, 5283 (1971).
4) S. N. Anderson, D. H. Ballard, J. Z. Chrzastowski, D. Dodd, and M. D. Johnson, *J. Chem. Soc., Chem. Commun.*, **1972**, 685.
5) H. L. Fritz, J. H. Espenson, D. A. Williams, and G. A. Molander, *J. Am. Chem. Soc.*, **96**, 2378 (1974).
6) G. N. Schrauzer, J. H. Weber, T. M. Beckham, and R. K. Ho, *Tetrahedron Lett.*, **1971**, 275.
7) V. E. Magnuson and J. H. Weber, *J. Organomet. Chem.*, **74**, 135 (1974).
8) M. D. Johnson and B. S. Meeks, *J. Chem. Soc., Chem. Commun.*, **1970**, 1027.
9) "Inorganic Syntheses," ed. by W. L. Jolly, McGraw Hill, N. Y., (1968) Vol. XI, p. 61.
10) The symbols d, t, q, and m denote doublet, triplet, quartet, and multiplet, respectively. A coupling constant is shown in Hz.
11) R. Pappa and P. W. Collins, *Tetrahedron Lett.*, **1972**, 2617.
12) C. Modena, *Acc. Chem. Res.*, **4**, 73 (1971).
13) W. D. Stohrer, *Tetrahedron Lett.*, **1975**, 207.
14) F. R. Jensen, V. Madan, and D. H. Buchanan, *J. Am. Chem. Soc.*, **92**, 1414 (1970).
15) D. S. Matteson and J. D. Leidtke, *J. Am. Chem. Soc.*, **87**, 1526 (1965).
16) R. B. Miller and T. Reichenbach, *Tetrahedron Lett.*, **1974**, 543.
17) C. P. Casey, G. M. Whitesides, and J. Kurth, *J. Org. Chem.*, **38**, 3406 (1973).
18) H. C. Brown, T. Hamaoka, and N. Ravindran, *J. Am. Chem. Soc.*, **95**, 6456 (1973).
19) H. C. Brown, T. Hamaoka, and N. Ravindran, *J. Am. Chem. Soc.*, **95**, 5786 (1973).
20) J. P. Pizey, "Synthetic Reagents," Vol. II, Ellis-Horwood, Chichester (1974) p. 27.
21) J. Halpern, M. S. Chan, J. Hanson, T. S. Roche, and J. A. Toich, *J. Am. Chem. Soc.*, **97**, 1606 (1975).

A Convenient Synthesis of Indolotropones and 6-Substituted 5-Azabenz[*b*]azulenes*

Kameji YAMANE and Kunihide FUJIMORI

Department of Chemistry, Faculty of Science, Shinshu University, Matsumoto 390

(Received October 6, 1975)

Several substituted indolo[2,3-*b*]tropones were prepared by the dehydrobromination of 7,7-dibromo-7,8,9,10-tetrahydrocyclohept[*b*]indole-6(5*H*)-ones (**2a—h**), which had been obtained by the bromination of 7,8,9,10-tetrahydrocyclohept[*b*]indol-6(5*H*)-ones (**1a—h**) with phenyltrimethylammonium tribromide (PTAB). 6,7,8,9-Tetrahydrocyclohept[*b*]indole-10(5*H*)-one (**5a**) and 6,7,8,9-tetrahydro-5-methylcyclohept[*b*]indol-10(5*H*)-one (**5b**) were obtained by the oxidation of hexahydrocyclohept[*b*]indole (**4a**) and the 5-methyl derivative (**4b**) with dichlorodicyanobenzoquinone (DDQ). Indolo[3,2-*b*]tropones (**6a** and **6b**) were derived from **5a** and **5b** respectively. The reactions of 6-chloro-5-azabenz[*b*]azulene (**8**) with nucleophilic reagents gave the corresponding substituted products (**9a—j**).

In a previous paper,[1] it has been reported that cyclohept[*b*]indol-6(5*H*)-ones (indolo[2,3-*b*]tropones) were obtained by using 2-hydrazinotropones as the starting material.

We will outline here a convenient method for the synthesis of cyclohept[*b*]indol-6(5*H*)-ones and cyclohept[*b*]indol-10(5*H*)-ones (indolo[3,2-*b*]tropones) by a modification of the synthetic method of G. Jones and his co-workers for heterocyclic tropones.[2] It will also be described for substitution reactions of 6-chloro-5-azabenz[*b*]azulene, obtained from **3a**, with several nucleophilic reagents.

Results and Discussion

Cyclohept[b]*indol-6(5*H*)-ones.* 7,8,9,10-Tetrahydrocyclohept[*b*]indol-6(5*H*)-one (**1a**) was brominated with phenyltrimethylammonium tribromide (PTAB) in dry tetrahydrofuran to give 7,7-dibromo-7,8,9,10-tetrahydrocyclohept[*b*]indol-6(5*H*)-one (**2a**). The dehydrobromination of the dibromo compound (**2a**) with lithium chloride in boiling *N*,*N*-dimethylformamide (DMF) gave yellow micro needles (mp 245—246 °C).

The IR spectrum was identical with that of the cyclohept[*b*]indol-6(5*H*)-one prepared by the dehydrogenation of 1,2,3,4-tetrahydrocyclohept[*b*]indol-6(5*H*)-one with chloranil or 2,3-dichloro-5,6-dicyanobenzoquinone (DDQ).[1]

Further, several substituted cyclohept[*b*]indol-6(5*H*)-ones (**3b—h**) were obtained from the corresponding 7,8,9,10-tetrahydrocyclohept[*b*]indol-6(5*H*)-ones (**1b—h**) in the same way. The results are shown in Tables 1, 2, and 3.

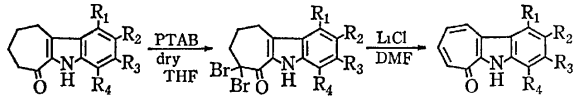

1 **2** **3**

a: $R_1=R_2=R_3=R_4=H$
b: $R_2=CH_3$, $R_1=R_3=R_4=H$
c: $R_4=CH_3$, $R_1=R_2=R_3=H$
d: $R_2=NO_2$, $R_1=R_3=R_4=H$
e: $R_4=NO_2$, $R_1=R_2=R_3=H$
f: $R_2=R_4=CH_3$, $R_1=R_3=H$
g: $R_3=R_4=CH_3$, $R_1=R_2=H$
h: $R_2=Cl$, $R_1=R_3=R_4=H$

* Presented at the 32nd Annual Meeting of the Chemical Society of Japan, Tokyo, April, 1975.

Cyclohept[b]*indol-10(5*H*)-ones.* 5,6,7,8,9,10-Hexahydrocyclohept[*b*]indole (**4a**) reacts rapidly with DDQ at room temperature in wet dioxane to give colorless micro prisms (mp 224—225 °C).

The analytical data revealed a composition with the formula of $C_{13}N_{13}ON$. The IR spectrum does not agree with that of **1a**.

The structure of this product was confirmed by a direct comparison with an authentic sample of 6,7,8,9-tetrahydrocyclohept[*b*]indol-10(5*H*)-one (**5a**) prepared[4] from the phenylhydrazone of 5-acetylvaleric acid.

Compound **5a** has also been prepared[4] by the hydrolysis of 5,6,7,8,9,10-hexahydro-10-*p*-tolylsulphonyliminocyclohept[*b*]indole or by the irradiation of acridine *N*-oxide, followed by hydrogenation.

6,7,8,9-Tetrahydro-5-methylcyclohept[*b*]indol-10-(5*H*)-one (**5b**) was also obtained by the reaction of hexahydro-5-methylcyclohept[*b*]indole (**4b**) with DDQ by a similar method. It was identical with the material obtained by the methylation of **5a** with dimethyl sulfate.

The bromination of **5a** and **5b** with PTAB afforded α,α-dibromo ketones **6a** and **6b**, which were then converted to cyclohept[*b*]indol-10(5*H*)-ones **7a**[4b] and **7b** respectively by dehydrobromination with lithium chloride.

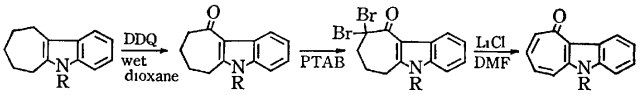

4 **5** **6** **7**

a R=H
b $R=CH_3$

Nucleophilic Substitution Reactions of 6-Chloro-5-azabenz[b]*azulene.* In the previous paper,[1] we have reported that 6-chloro-5-azabenz[*b*]azulene (8-chlorobenz[*b*]-1-azaazulene) (**8**) was obtained when cyclohept[*b*]indol-6(5*H*)-one (**3a**) was heated with phosphoryl chloride or thionyl chloride.

The treatment of Compound **8** with sodium methoxide, sodium hydrosulfide, dimethylamine, aniline, *etc.* in ethanol or dimethyl sulfoxide gave the corresponding substituted products (**9a—j**). The results are shown

TABLE 1. 7,7-DIBROMO-7,8,9,10-TETRAHYDROCYCLOHEPT[*b*]INDOL-6(5*H*)-ONES (**2**)

Compound	Mp (°C)	Yield (%)	Formula	Elemental analysis Found (Calcd) (%)				IR (KBr) (cm^{-1})	
				C	H	N	Br	NH	C=O
2a	154—155	91	$C_{13}H_{11}ONBr_2$	43.87 (43.73	3.15 3.11	3.98 3.92	44.14 44.76)	3363	1618
2b	180 (dec)	87	$C_{14}H_{13}ONBr_2$	45.24 (45.31	3.52 3.53	3.64 3.78	42.98 43.07)	3358	1623
2c	158—159	93	$C_{14}H_{13}ONBr_2$	44.99 (45.31	3.46 3.53	3.82 3.78	42.67 43.07)	3378	1625
2d	>250	78	$C_{13}H_{10}O_3N_2Br_2$	39.00 (38.83	2.81 2.51	7.00 6.97	40.00 39.75)	3385	1626
2e	173—174	87	$C_{13}H_{10}O_3N_2Br_2$	38.98 (38.83	2.64 2.51	7.20 6.97	39.99 39.75)	3463	1626
2f	182 (dec)	84	$C_{15}H_{15}ONBr_2$	46.77 (46.78	3.82 3.93	3.66 3.64	41.50 41.50)	3370	1615
2g	177—178	92	$C_{15}H_{15}ONBr_2$	47.00 (46.78	3.95 3.93	3.75 3.64	41.50 41.50)	3336	1630
2h	183 (dec)	79	$C_{13}H_{10}ONClBr_2$	39.15 (39.88	2.40 2.51	3.85 3.53	40.43 40.82)	3378	1625

TABLE 2. CYCLOHEPT[*b*]INDOL-6(5*H*)-ONES (**3**)

Compound	Mp (°C)	Yield (%)	Formula	Elemental analysis Found (Calcd) (%)			IR (KBr) (cm^{-1})	
				C	H	N	NH	C=O
3a[1]	245—246	82	$C_{13}H_9ON$				3195	1614
3b	242—244	100	$C_{14}H_{11}ON$	79.92 (80.36	5.26 5.30	6.70 6.70)	3183	1610
3c	135—136	92	$C_{14}H_{11}ON$	80.22 (80.36	5.32 5.30	6.77 6.70)	3190	1605
3d	>300	100	$C_{13}H_8O_3N_2$	64.60 (65.00	3.26 3.36	11.56 11.66)	3165	1616
3e	287—288	100	$C_{13}H_8O_3N_2$	65.17 (65.00	3.31 3.36	11.52 11.66)	3310	1611
3f	245—247	100	$C_{15}H_{13}ON$	80.85 (80.69	5.75 5.87	6.29 6.27)	3200	1615
3g	245—246	100	$C_{15}H_{13}ON$	80.62 (80.69	5.75 5.87	6.20 6.27)	3190	1610
3h	292—293	100	$C_{13}H_8ONCl$	67.58 (67.99	3.41 3.51	6.43 6.10)	3203	1608

TABLE 3. ULTRAVIOLET AND VISIBLE ABSORPTION MAXIMA OF CYCLOHEPT[*b*]INDOL-6(5*H*)-ONE (**3**)

Compound	λ_{max} nm (log ε) (in CH_3OH)
3b	278(4.34), 313(4.24), 326(4.23), 338(4.19), 392(3.68) (sh), 409(3.82)
3c	281(4.32), 309(4.13), 323(4.11), 337(4.02), 390(3.72) (sh), 407(3.83)
3d	255(4.34), 296(4.32), 305(4.27) (sh), 320(4.27), 376(4.01), 397(4.02)
3e	254(4.45), 338(4.09), 366(4.13), 386(4.15)
3f	282(4.35), 316(4.21), 326(4.22), 338(4.14), 396(3.81) (sh), 409(3.88)
3g	286(4.36), 310(4.30), 326(4.21) (sh), 337(4.11) (sh), 390(3.80) (sh), 408(3.90)
3h	275(4.32), 317(4.19) (sh), 324(4.22), 338(4.16), 384(3.72), 402(3.84)

TABLE 4. NUCLEOPHILIC SUBSTITUTION REACTION PRODUCTS (**9**) FROM 6-CHLORO-5-AZABENZ[*b*]AZULENE (**8**)

Compound	Mp (°C) Apearance (color, crystal form)	Yield (%)	Formula	Elemental analysis Found (Calcd) (%) C	H	N	IR (KBr) (cm^{-1})
9b	(Picrate) 203—204 (yellow micro needles)	26[a]	$C_{20}H_{14}O_8N_4$	54.64 (54.80	3.44 3.22	12.81 12.78)	
9c	(Picrate) 219—220 (yellow micro needles)	10[a]	$C_{21}H_{16}O_8N_4$	55.55 (55.75	3.60 3.57	12.30 12.39)	
9d	215 (dec) (orange micro needles)	85[a]	$C_{13}H_9NS$	73.47 (73.92	4.20 4.30	6.81 6.63)	3226, 1616, 1601, 1498, 1478, 1433
9e	96— 98 (a) (red prisms) (b)	70[a] 94[b]	$C_{15}H_{14}N_2$	81.37 (81.37	6.34 6.25	12.43 12.61)	1599, 1561, 1504
9f	112—114 (a) (red prisms) (b)	49[a] 85[b]	$C_{19}H_{14}N_2$	84.54 (84.41	5.14 5.22	10.35 10.37)	1611, 1586, 1526, 1474
9g	86— 87 (orange prisms)	59[a]	$C_{20}H_{16}N_2$	84.75 (84.47	5.70 5.67	9.93 9.85)	3413, 1614, 1599, 1539
9h	231—233 (yellow plates)	54[a]	$C_{19}H_{13}N_3O_2$	72.09 (72.37	4.18 4.15	12.89 13.33)	3391, 1616, 1591, 1541, 1519, 1499
9i	138—139 (red needles)	50[a]	$C_{17}H_{16}N_2O$	77.38 (77.25	6.09 6.10	10.76 10.60)	2957, 2857, 1601, 1567, 1498
9j	136—137 (red prisms)	43[a]	$C_{20}H_{17}N_3$	80.20 (80.24	5.89 5.73	13.86 14.04)	3394, 1521, 1496, 1481

a) General procedure (a). b) General procedure (b).

TABLE 5. ULTRAVIOLET AND VISIBLE ABSORPTION MAXIMA OF SUBSTITUTED 5-AZABENZ[*b*]AZULENES (**9**)

Compound	λ_{max} nm (log ε)
9d	234(4.30), 300(4.41), 403(3.94), 461(4.17) (in MeOH)
9e	236(4.20), 268(4.16), 301(4.45), 311(4.49), 363(4.13), 382(4.22), 400(3.95)(sh), 507(3.68) (in cyclohexane)
9f	277(4.22), 305(4.32), 372(4.18) (in MeOH)
9g	281(4.20), 304(4.36), 473(4.20) (in MeOH)
9h	277(4.31), 323(4.20), 421(4.31) (in MeOH)
9i	237(4.29), 279(4.27), 305(4.48), 315(4.50), 370(4.11), 389(4.22), 408(4.03), 513(3.55) (in cyclohexane)
9j	249(4.44), 303(4.25), 363(4.07) (in MeOH)

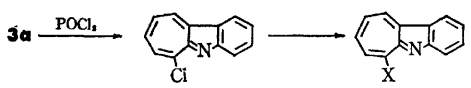

8 **9**

a: X=$NHNH_2$[1)]
b: X=OCH_3
c: X=OCH_2CH_3
d: X=SH
e: X=$N(CH_3)_2$
f: X=NHC_6H_5
g: X=$NHC_6H_4CH_3$
h: X=$NHC_6H_4NO_2$
i: X=N O
j: X=$NHNC_6H_5$ with CH_3

in Tables 4 and 5.

Compound **9d** can exist in two tautomeric forms, such as **A** and **B**:

A **B**

The IR spectrum contained a band at 3226 cm^{-1} due to NH, but no band due to SH between 2600—2550 cm^{-1}. On the UV and visible absorption spectra, the absorption maxima of the visible portion was shifted to shorter wavelengths than those of **8**, **9e**, and **9i**, which could take only the type-B tautomeric form. Therefore, it is assumed that Compound **9d** takes the type-A tautomeric form.

Also, we can consider a similar tautomerism on Compounds **9a**, **9f**, **9g**, **9h**, and **9j**. However, it is difficult to decide on the basis of only the UV and IR spectra toward which form the equilibria of these compounds tend.

Experimental**

All the melting points are uncorrected.

Bromination of 7,8,9,10-Tetrahydrocyclohept[b]*indole-6(5*H*)-ones (**1a—h**) with PTAB.* *7,7-Dibromo-7,8,9,10-tetra-*

** The authors are grateful to the Sankyo Co., Ltd., for doing some of the elemental analyses.

hydrocyclohept[b]*indol-6(5H)-one (2a)*: To a solution of **1a** (0.3 g) in dry tetrahydrofuran (15 ml), we added phenyltrimethylammonium tribromide (PTAB) (1.1 g) at room temperature. The mixture was stirred for 15 h. The precipitate was filtered and washed with tetrahydrofuran. The combined tetrahydrofuran solutions were evaporated, and the residue was recrystallized from methanol to give **2a** as yellow micro needles (0.49 g, 91%); mp 154—155 °C.

Dibromo compounds (**2b—h**) were also prepared from the corresponding cyclic ketones (**1b—h**) by a method similar to that described above. The results are given in Table 1.

Dehydrobromination of 7,7-Dibromo-7,8,9,10-tetrahydrocyclohept[b]*indol-6(5H)-ones (2a—h). Cyclohept*[b]*indol-6(5H)-one (3a)*: A mixture of **2a** (0.6 g) and lithium chloride (0.2 g) in DMF (20 ml) was refluxed under nitrogen for 3 h. The solvent was then removed under reduced pressure, after which the residue was diluted with water to give a precipitate. The separated material was collected and dried. Recrystallization from benzene gave **3a** as yellow micro needles, (0.27 g, 82%); mp 245—246 °C.

Cyclohept[*b*]indol-6(5*H*)-ones (**3b—h**) were also prepared from the dibromo compounds (**2b—h**) by a method similar to that described above. The results are given in Table 2.

6,7,8,9-Tetrahydrocyclohept[b]*indol-10(5H)-one (5a)*. Into a solution of 5,6,7,8,9,10-hexahydrocyclohept[*b*]indole (**4a**) (1.0 g) in dioxane (100 ml) and water (10 ml), we stirred DDQ (2.4 g) at 5 °C. After 10 min, the precipitate was filtered off, and the filtrate was evaporated. The residue was extracted with chloroform. The chloroform layer was washed with a dilute sodium hydrogencarbonate solution, dried over anhydrous sodium sulfate, and evaporated to leave a residue. It recrystallized from benzene–ethanol to give **5a** as colorless micro prisms (0.73 g, 68%); mp 224—225 °C.

9,9-Dibromo-6,7,8,9-tetrahydrocyclohept[b]*indol-10(5H)-one (6a)*. To a solution of **5a** (0.3 g) in dry tetrahydrofuran (30 ml) we added PTAB (1.1 g). The mixture was then treated by a method similar to that used for the preparation of **2a—h**. Yellow prisms (0.48 g, 89%); mp 182—184 °C (dec). IR(KBr): 3238, 2925, 1610, 1595, and 1445 cm^{-1}. Found: C, 43.92; H, 3.15; N, 3.79; Br, 44.68%. Calcd for $C_{13}H_{11}ONBr_2$: C, 43.73; H, 3.11, N, 3.92; Br, 44.76%.

Cyclohept[b]*indole-10(5H)-one (7a)*. A mixture of **6a** (0.3 g) and lithium chloride (0.11 g) in DMF (10 ml) was refluxed under nitrogen for 3 h. The reaction mixture was treated by a method similar to that used for the preparation of **3a—h**. Yellow micro prisms (0.27 g, *ca.* 100%); mp 285—286 °C.

6,7,8,9-Tetrahydro-5-methylcyclohept[b]*indol-10(5H)-one (5b)*. (*a*): To a solution of hexahydro-5-methylcyclohept[*b*]indole (**4b**) (1.0 g) in dioxane (50 ml) and water (5 ml), we added DDQ (2.28 g). The mixture was treated by a method similar to that used for the preparation of **5a**. Colorless scales (0.47 g, 44%), were recrystallized from cyclohexane; mp 136—137 °C.

(*b*): A mixture of **5a** (0.2 g) and dimethyl sulfate (0.24 g) in acetone (10 ml) and 1 M sodium hydroxide (3 ml) was heated at 90 °C for 30 min. The reaction mixture was then diluted with water and extracted with chloroform. The chloroform layer was dried over anhydrous sodium sulfate and evaporated to leave a oily residue. It was recrystallized from cyclohexane to give colorless scales (0.08 g, 38%); mp 135—136 °C.

The IR spectrum was identical with that of a sample prepared by Method (a), and the mixed melting point was not depressed.

9,9-Dibromo-6,7,8,9-tetrahydro-5-methylcyclohept[b]*indol-10(5H)-one (6b)*. To a solution of **5b** (0.3 g) in dry tetrahydrofuran (30 ml), we added PTAB (1.1 g). The mixture was then treated by a method similar to that used for the preparation of **2a—h**. Pale yellow prisms (0.41 g, 79%); mp 173 °C (dec). IR(KBr): 2962, 2939, 1624, 1511, 1471, 1406, and 1414 cm^{-1}. Found: C, 45.00; H, 3.47; N, 3.72; Br, 42.83%. Calcd for $C_{14}H_{11}ONBr_2$: C, 45.31; H, 3.53; N, 3.78; Br, 43.07%.

5-Methylcyclohept[b]*indol-10(5H)-one (7b)*. A mixture of **6b** (0.1 g) and lithium chloride (0.04 g) in DMF (5 ml) was refluxed under nitrogen for 3 h. The reaction mixture was then treated by a method similar to that used for the preparation of **3a—h**. Yellow micro needles (0.05 g, 89%); mp 169—170 °C. IR(KBr): 1628, 1556, and 1478 cm^{-1}. Found: C, 79.84; H, 5.28; N, 6.64%. Calcd for $C_{14}H_{11}ON$: C, 80.36, H, 5.30; N, 6.69%.

The Reaction of 6-Chloro-5-azabenz[b]*azulene with Nucleophilic Reagents. General Procedure*: (*a*); A solution of **8** (0.0005 mol) and a nucleophilic reagent (0.0007 mol) in ethanol (6 ml) was refluxed for 30 min on a water bath. The solvent was then removed. The resdiue was diluted with water, made slightly alkaline by adding aqueous sodium hydrogencarbonate, and extracted with benzene. The benzene layer was concentrated and passed through a silica gel column. The product obtained from the main effluent was recrystallized from cyclohexane, hexane, or cyclohexane–benzene.

(*b*); A mixture of **8** (0.0005 mol) and a nucleophilic reagent (0.0007 mol) in dimethyl sulfoxide (5 ml) was stirred for 15 min at room temperature. The reaction mixture was then diluted with water to separate the precipitate. The solid was collected, dried under reduced pressure, and recrystallized from cyclohexane. The results are given in Tables 4 and 5.

The authors wish to express their gratitude to Professor Gurnos Jones of the University of Keele for his kind discussion.

References

1) T. Nozoe, J-K Sin, K. Yamane, and K. Fujimori, *Bull. Chem. Soc. Jpn.*, **48**, 314 (1975).

2) G. Jones, R. K. Jones, and M. J. Robinson, *J. Chem. Soc., Perkin Trans. 1*, **1973**, 968.

3) 7,8,9,10-Tetrahydrocyclohept[*b*]indol-6(5*H*)-ones were obtained according to the procedure of M. Muhlstadt *et al.* M. Muhlstadt and W. Treibs, *Justis Liebigs Ann. Chem.*, **608** 38 (1957).

4) a) A. S. Baily and J. F. Seager, *J. Chem. Soc., Perkin Trans. 1*, **1974**, 763. b) M. Ishikawa, C. Kaneko, and S. Yamada, *Tetrahedron Lett.*, **1968**, 4519; C. Kaneko, S. Yamada, I. Yokoe, and M. Ishikawa, *ibid.*, **1967**, 1873.

The Reaction of Anhydrochloralurethanes with Ketene Acetals

Tetsuo AKIYAMA, Nobuaki URASATO, Takeshi IMAGAWA, and Mituyosi KAWANISI

Department of Industrial Chemistry, Faculty of Engineering, Kyoto University, Yoshida, Sakyo-ku, Kyoto 606

(Received October 6, 1975)

The reaction of anhydrochloralurethanes (I) with ketene acetals (II) has been found to give novel carbamate derivatives (III) in quantitative yield. The intermediacy of a cyclic intermediate, an oxazine derivative (IV), was confirmed by spectroscopic methods, although several attempts to isolate IV have been unsuccessful. The mechanism for formation of IV is discussed.

In 1968 Ulrich and coworkers[1] established the structure and the synthetic method of *N*-(2,2,2-trichloroethylidene)alkoxycarbonylamine (I), commonly called anhydrochloralurethane. They also reported that the C=N double bond of I was highly reactive and easily attacked by several nucleophiles, such as water, alcohols, and amines.[1]

In a previous report from this laboratory, we have demonstrated the potentiality of I as a dienophile in a Diels-Alder reaction.[2]

A literature survey reveals that investigations about the reactivity of I have mainly noted the C=N double bond.[1-3]

Since the CCl_3 group is equivalent to the CO_2H group, I might be valuable for constructing the α-amino acid skelton. However, the synthetic application of I is rather limited.[4]

As judged from the structure of I, we have been intrigued with the supposition that I, as a heterodiene (C=N–C=O),[5] might formally undergo a [4+2] Diels-Alder type reaction with inverse electron demand against an electron-abundant nucleophilic olefin to give an adduct.

In this report, we should like to present the results obtained in the reaction of I with ketene acetal (II) to give novel acyclic carbamates (III), and also convincing evidence for the intermediacy of cyclic oxazine derivatives (IV) which could arise from the above-mentioned reaction.

Results and Discussion

When I ($R=C_2H_5$) and excess II ($R'=C_2H_5$) in benzene were heated under reflux for 15 h, a single product was obtained in a quantitative yield. Elementary analysis as well as spectral investigations established the structure as IIIa. Although its parent peak was missing, the mass spectrum had a peak corresponding to M^+-CCl_3 fragment ion as the base peak originating from the fragmentation β at the nitrogen atom. The NMR spectrum showed a typical ABX pattern corresponding to $-CH_2CH(CCl_3)-$, accompanied by the signals of NH and two $-OCH_2CH_3$.

A plausible mechanism for the formation of III is shown in Scheme 1:

A Diels-Alder type reaction between I and II in a sense of inverse electron demand affords a dihydro-1,3-oxazine (IV),[6] hydrolysis (by atomospheric moisture or work-up) of which will give III.

Although the adduct (IV) was not obtained in a pure state, its existence was confirmed as follows. The crude product-mixture just after the reaction gave an additional peak in GLC along with that of III. Taking as an example the case of the reaction between Ia and IIa, in the mass spectrum [Fig. 1(a)], the parent peak

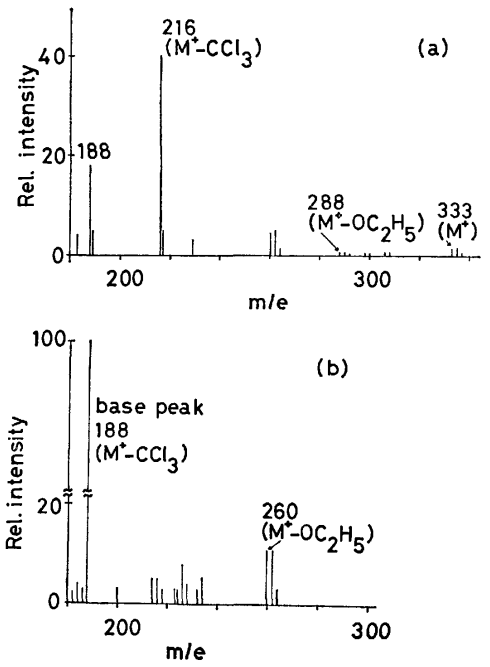

Fig. 1. Mass spectra of the reaction products between Ia and IIa.

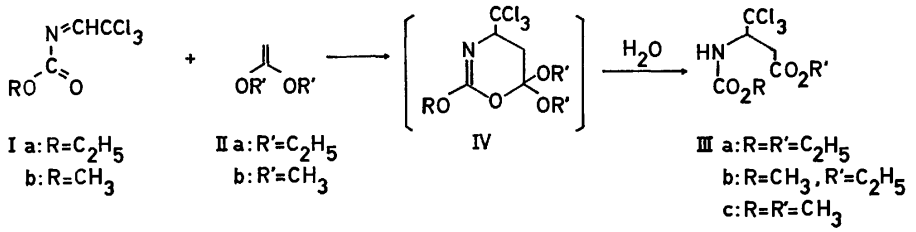

Scheme 1.

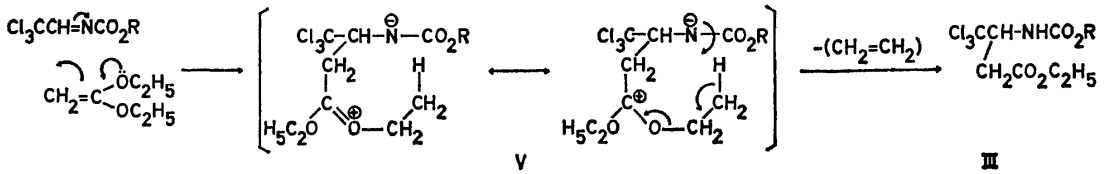

Scheme 2.

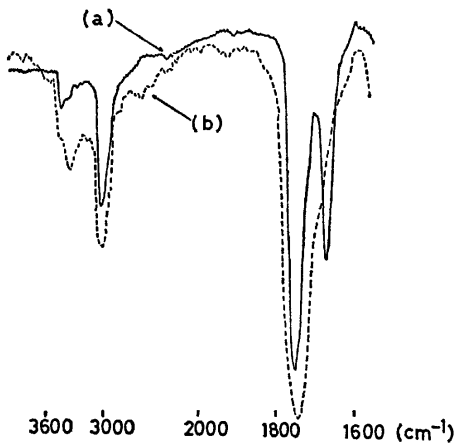

Fig. 2. IR spectra of the reaction products between Ia and IIa.
(a) For the crude products in the reaction of Ia and IIa. (b) For the analytically pure IIIa.

of IV (R=R'=C_2H_5), *m/e* 333, and the peak due to $M^+ - CCl_3$ of IV, *m/e* 216, which were absent in the spectrum of IIIa [Fig. 1(b)], were clearly observed. The IR spectrum in CCl_4 solution [Fig. 2(a)] had only a small NH absorption band, which grew gradually significant after several hours in air, when the absorption band at 1680 cm^{-1} due to the C=N bond became disappeared. The crude reaction mixture was gradually hydrolyzed by atmospheric moisture. The intentional treatment of the reaction mixture with dil hydrochloric acid rapidly afforded III. It should be noted that the addition reaction giving IV is highly regioselective as far as the product is concerned.

An alternative path giving III from I and II may be the one shown in Scheme 2, in which a zwitterionic intermediate (V) would expel the neutral ethylene molecule as the leaving group. This mechanism could also explain the regioselectivity of the reaction.

However, this scheme cannot be compatible with the spectral data mentioned above, and the fact that the reaction Ib with IIb gave a similar product IIIc cannot be adequately explained by this scheme (In this case a neutral molecule as a good leaving group cannot exist).

More recently, Arbuzov *et al.* reported[7] that the reaction between *N*-(2,2,2-trichloroethylidene)acetamide (VI) and 2,3-dimethylbutadiene (VII) gave an oxazine derivative (VIII) together with the normal Diels-Alder adduct (IX). The oxazine derivative (VIII) and its crystalline salt, on reaction with strong acids, were obtained in pure form (Scheme 3).

We expected similar oxazine derivatives to be isolable

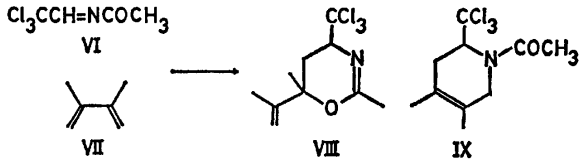

Scheme 3.

in the reaction between VI, instead of anhydrochloralurethane (I), with ketene acetal. However, also in this case the adduct (XI) was not stable toward any conventional methods of purification, and the hydrolyzed product X was again produced in quantitative yield (Scheme 4).

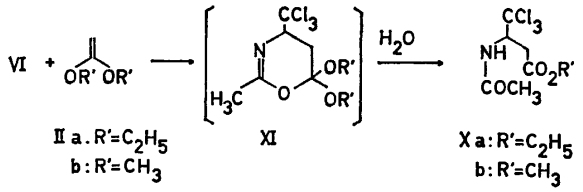

Scheme 4.

Based on these facts, we can safely conclude that the mechanism depicted in Scheme 1 is highly plausible.

In summary, a Diels-Alder type reaction with inverse electron demand between anhydrochloralurethane and ketene acetal takes place, giving novel carbamate derivatives. This reaction might emerge as a powerful synthetic route to α-amino acids. The investigation aiming at this point is currently under way in this laboratory.

Experimental

All the temperatures are uncorrected. The IR spectra were obtained on a Shimadzu IR-27 spectrometer. The mass spectra were taken by Hitachi RMS-4 Mass Spectrometer. The NMR spectra were obtained on a Varian EM-360 spectrometer, TMS being chosen as the internal standard.

Reaction of N-*(2,2,2-Trichloroethylidene)ethoxycarbonylamine (Ia) with Ketene Diethyl Acetal (IIa).* Refluxing a benzene (26 ml) solution of $CCl_3CH{=}NCO_2C_2H_5$ (Ia) (260 mg, 1.19 mmol) and ketene diethyl acetal (360 mg, 3.10 mmol) for 15 h gave a yellow oily mixture after evaporation of benzene and ketene diethyl acetal. After hydrolysis with dil hydrochloric acid, this mixture was distilled under vacuum to afford a quantitative yield (365 mg, 1.19 mmol) of IIIa, bp 100—104 °C/0.15 mmHg. IR (CCl_4): 3320, 1740 (broad) cm^{-1}. MS: *m/e* 260 (11%, $M^+-OC_2H_5$), 262 (11), 264 (3), 188 (100, M^+-CCl_3), 142 (33), 116 (41), 70 (36), 59 (81), 56 (37). NMR (CCl_4): δ 1.28 ppm (t, 6H, $-OCOCH_2-$

CH_3), 2.68 [dd, 1H, J=15.2, 3.6 Hz, $-CH_2CH(CCl_3)-$], 3.18 [dd, 1H, J=15.2, 9.0 Hz, $-CH_2CH(CCl_3)-$], 4.16 (q, 4H, $-OCOCH_2CH_3-$), 4.91 (m, 1H, $-CHCCl_3-$), 5.48 (d, 1H, J=10.0 Hz, NH). Found: C, 34.82; H, 4.74; N, 4.60%. Calcd for $C_9H_{14}Cl_3NO_4$: C, 35.26; H, 4.60; N, 4.57%.

Reaction of Ib with IIa. Refluxing a benzene (32 ml) solution of Ib (320 mg, 1.56 mmol) and an excess of IIa for 15 h gave an oily mixture. After being left at room temperature for several days, the reaction mixture turned into a white solid of IIIb (458 mg) quantitatively, mp 71.5—73.5 °C after recrystallization from hexane. IR (Nujol): 3300, 1750, 1710 cm^{-1}. MS: *m/e* 260 (3%, M^+-OCH_3), 262 (3), 264 (1), 246 (11, $M^+-OC_2H_5$), 248 (11), 250 (3), 174 (100, M^+-CCl_3), 132 (30), 128 (52). NMR (CCl_4): δ 1.27 ppm (t, 3H, $-OCH_2CH_3$), 2.69 (dd, 1H, $-CH_2CH(CCl_3)-$], 3.07 [dd, 1H, $-CH_2CH(CCl_3)-$], 3.71 (s, 3H, $-OCOCH_3$), 4.18 (q, 2H, $-OCOCH_2CH_3$), 4.92 (m, 1H, $-CHCCl_3-$), 5.50 (d, 1H, NH). Found: C, 32.74; H, 4.18; N, 4.80%. Calcd for $C_8H_{12}Cl_3NO_4$: C, 32.85; H. 4.13; N, 4.79%.

IIIc was similarly obtained from Ib and IIb (15 h; 100%), mp 96—99 °C (hexane). IR (Nujol): 3350, 1760, 1730 cm^{-1}. MS: *m/e* 246 (8%, M^+-OCH_3), 248 (7.5), 250 (2), 160 (100, M^+-CCl_3), 138 (80). NMR (CCl_4): δ 2.69 ppm [dd, 1H, $-CH_2CH(CCl_3)-$], 3.08 [dd, 1H, $-CH_2CH(CCl_3)-$], 3.70 (s, 6H, $-OCOCH_3$), 4.88 (m, 1H, $-CHCCl_3-$), 5.50 (d, 1H, NH). Found: C, 30.24; H, 3.64; N, 5.04%. Calcd for $C_7H_{10}Cl_3NO_4$: C, 30.19; H, 3.62; N, 5.03%.

Reaction of N-(2,2,2-Trichloroethylidene)acetamide (VI) with Ketene Acetals (II). In a manner similar to the above, Xa was obtained from VI and IIa (15 h at 80 °C, 100%), mp 61.5—63.0 °C (hexane). IR (Nujol): 3300, 1740, 1680 cm^{-1}. MS: *m/e* 230 (9%, $M^+-OC_2H_5$), 232 (9), (9), 234 (3), 158 (44, M^+-CCl_3), 116 (100). NMR (CCl_4+$CDCl_3$): δ 1.27 ppm (t, 3H, $-OCH_2CH_3$), 2.08 (s, 3H, $-COCH_3$), 2.72 [dd, 1H, $-CH_2CH(CCl_3)-$], 3.13 [dd, 1H, $-CH_2CH(CCl_3)-$], 4.17 (q, 2H, $-OCH_2CH_3$), 5.32 (m, 1H, $-CHCCl_3-$), 6.43 (d, 1H, NH). Found: C, 34.49; H, 4.44; N, 5.28%. Calcd for $C_8H_{12}Cl_3NO_3$: C, 34.75; H, 4.37; N, 5.06%.

Similarly, Xb was obtained from VI and IIb (15 h at 80 °C, 100%), mp 132.0—132.5 °C from hexane and benzene (1 : 1). IR (Nujol): 3300, 1760, 1680 cm^{-1}. MS: *m/e* 230 (4%, M^+-OCH_3), 232 (4), 234 (1), 144 (33, M^+-CCl_3), 102 (100). NMR (CCl_4+$CDCl_3$): δ 2.09 ppm (s, 3H, $-COCH_3$), 2.73 [dd, 1H, $-CH_2CH(CCl_3)-$], 3.10 [dd, 1H, $-CH_2CH(CCl_3)-$], 3.73 (s, 3H, $-OCOCH_3$), 5.27 (m, 1H, $-CHCCl_3-$), 6.27 (d, 1H, NH). Found: C, 32.13; H, 3.85; N, 5.36%. Calcd for $C_7H_{10}Cl_3NO_3$: C, 32.03; H, 3.84; N, 5.34%.

References

1) H. Ulrich, B. Tucker, and A. A. R. Sayigh, *J. Org. Chem.*, **33**, 2887 (1968).

2) T. Imagawa, K. Sisido, and M. Kawanisi, *Bull. Chem. Soc. Jpn.*, **46**, 2922 (1973).

3) M. S. Raasch, *J. Org. Chem.*, **40**, 161 (1975).

4) C. Kashima, Y. Aoki, and Y. Omote, The 32th Annual Meeting of the Chemical Society of Japan, Tokyo 1G34 (1975).

5) a) W. Seeliger and W. Diepers, *Justus Liebigs Ann. Chem.*, **697**, 171 (1966). b) R. R. Schmidt, *Angew. Chem. Int. Ed. Engl.*, **4**, 241 (1965); *ibid.*, **8**, 602 (1969).

6) It is not implied that the formation of IV from I and II should follow a concerted pathway. We feel it to be probable to allot a polar transition state for this reaction. However the precise mechanism is still undetermined.

7) Y. A. Arbuzov, E. I. Klimova, N. D. Autonova, and Y. V. Tomilov, *Zh. Org. Khim.*, **10**, 1164 (1974).

Aminocyclitols. 33. Synthesis of Diaminocyclopentanetriols[1]

Kinnichi TADANO, Yasufumi EMORI, Mitsukuni AYABE, and Tetsuo SUAMI

Department of Applied Chemistry, Faculty of Engineering, Keio University, Hiyoshi, Yokohama 223

(Received October 2, 1975)

Three hitherto unknown 2,5-diamino-1,3,4-cyclopentanetriols have been prepared. Their structures were established by chemical evidence.

We have been studying a synthesis of carbocyclic nucleoside analogs[2] and during the course of this study, we needed 2,5-diamino-1,3,4-cyclopentanetriols with analogous configurations as those of the pentose moiety of naturally occurring nucleoside antibiotics, such as puromycin[3] and 3'-amino-3'-deoxyadenosine.[4]

In the first attempt for this aim, 5-acetamido-1-*O*-benzoyl-1,2,3,4-cyclopentanetetrol (**2**) seemed to be an adequate starting material, which was obtained by mono-*O*-benzoylation of 2,3-*O*-cyclohexylidene-(1,4/2,3,5)-5-acetamido-1,2,3,4-cyclopentanetetrol (**1**),[5] followed by mild acid hydrolysis. Sodium metaperiodate oxidation of **2** afforded the corresponding dialdehyde (**3**) and then **3** was cyclized with nitromethane in the presence of sodium ethoxide. The product was catalytically hydrogenated and subsequently acetylated. The product was purified on a silica gel column to give penta-*N*,*O*-acetyl-2,5-diamino-1,3,4-cyclopentanetriol (**4**) as a main product in 11% yield. A few minor products were detectable on TLC, but they were not isolated in a crystalline state.

There are ten theoretically possible stereoisomers (A—J) in 2,5-diamino-1,3,4-cyclopentanetriols. In the present reaction, three new chiral centers are introduced in the product and therefore, seven stereoisomers are possible for **4**. Since the PMR spectrum of **4** indicated a lack of a molecular symmetry, five stereoisomers: E, F, G, H and J are possible. On the other hand, when 2-*O*-tosyl- (**5**)[8] or 2-*O*-mesyl-DL-(1,4/2,3,5)-5-acetamido-1,2,3,4-cyclopentanetetrol (**6**)[8] was heated with sodium azide in *N*,*N*-dimethylformamide (DMF), an azido derivative was obtained. The product was hydrogenated and subsequently acetylated to give the same compound **4**.

Considering from the reaction employed, the configurations on C-3, 4 and 5 are not changed. Therefore, three stereoisomers: F, G and H are possible for **4**. To distinguish these three, following reactions have been attempted.

Since a possibility of neighboring group participation on the azidolysis of **6** is avoided by methylating the hydroxyl groups on C-1 and 4, 1,4-di-*O*-methyl derivative of **6** (**10**) has been submitted to the azidolysis. The azide derivative thus obtained was hydrogenated and *N*-acetylated to give 2,5-diacetamido-1,4-di-*O*-methyl-1,3,4-cyclopentanetriol. The product was further *O*-methylated to give 2,5-diacetamido-1,3,4-tri-*O*-methyl-1,3,4-cyclopentanetriol (**8**), which was identified with the compound derived from **4** *via* **7**. This fact indicated that the displacement of the mesyloxy group by a highly nucleophilic azide ion occurred in a direct S_N2 mechanism with a Walden inversion of the configuration on C-2.[6,7] Therefore, the configuration of **4** was established to be H.

In the second attempt, two other stereoisomers of 2,5-diamino-1,3,4-cyclopentanetriols (**14** and **15**) were prepared by azidolysis of 2,3-di-*O*-mesyl-(1,4/2,3,5)-5-acetamido-1,2,3,4-cyclopentanetetrol[8] (**11**). Azidolysis of **11**, followed by acetylation afforded two diastereomers of 1,3,4-tri-*O*-acetyl-5-acetamido-2-azido-1,3,4-cyclopentanetriols (**12** and **13**) in 32 and 7% yield respectively. The corresponding penta-*N*,*O*-acetyl-2,5-diamino-1,3,4-cyclopentanetriols (**14** and **15**) were prepared from **12** and **13**.

The configurations of **14** and **15** were established to be those of I and F respectively by the following evidence. (1) Both diacetamido-cyclopentanetriols (**16** and **17**) which were prepared from **14** and **15** respectively,

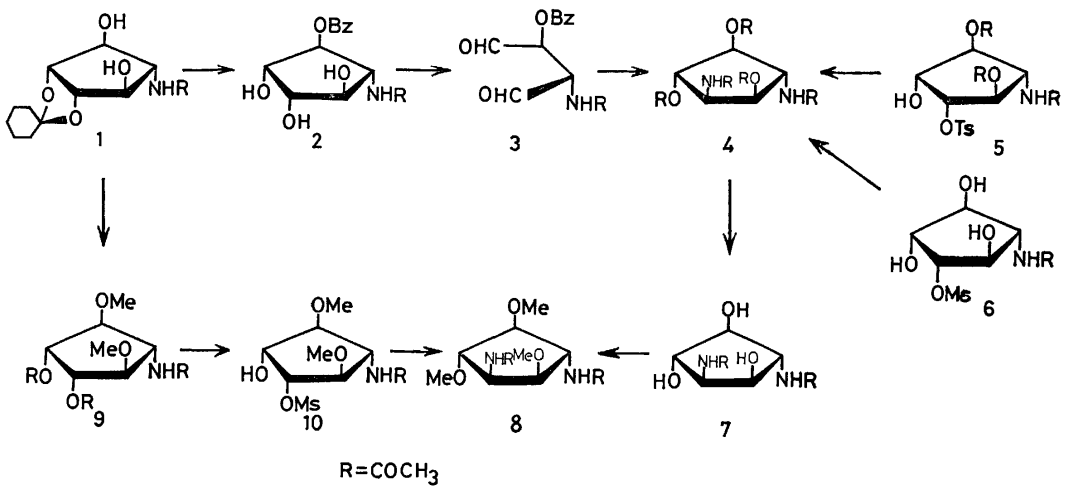

Scheme 1.

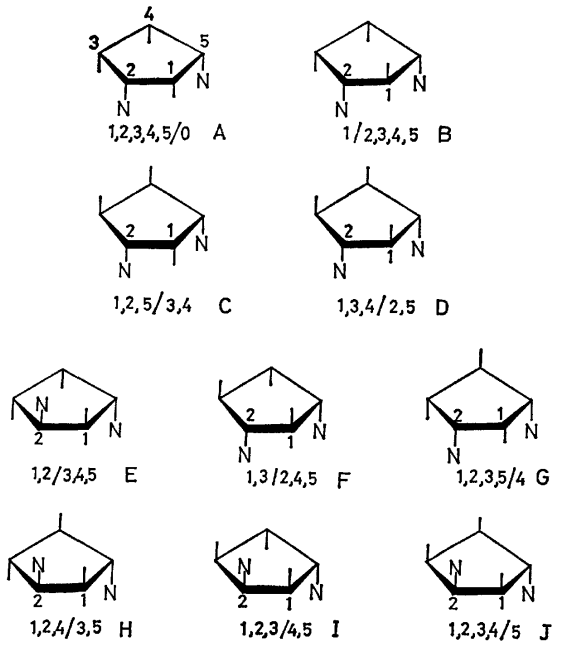

Scheme 2. 2,5-Diaminocyclopentanetriols.

consumed one molar equivalent of periodate respectively, and this fact indicated that they had two acetamido groups on C-2 and 5 (not on C-1 and 5). (2) Displacement of the mesyloxy group on C-3 of **11** proceeded *via* an intermediary epoxide with a participation of the hydroxyl group on C-4 and the epoxide was attacked by a hydroxide ion to give *trans*-3,4-diol.[8] Therefore, four stereoisomers: F, G, H and I are likely for **14** and **15**, but none of them is identical with **4** (H-configuration). Also a formation of a compound with G-configuration is hardly explained without a big contradiction of *cis*-opening of an intermediary epoxide between C-1 and C-2 by an azide ion. (3) When the azido-acetates (**12** and **13**) were catalytically hydrogenated, **12** gave a ninhydrin negative product and **13** gave a ninhydrin positive product. This fact suggested that the former had an acetyl group migration from O to N between a vicinal *cis*-located amino-acetate and I-configuration was given to **12**. Accordingly, F-configuration was given to **13**. (4) This was further confirmed by a formation of di-*N*,*O*-isopropylidene derivatives in the case of **16** and a formation of mono-*N*,*O*-isopropylidene derivative in the case of **17**.[10]

A direct S_N2 mechanism is proposed to the displace-

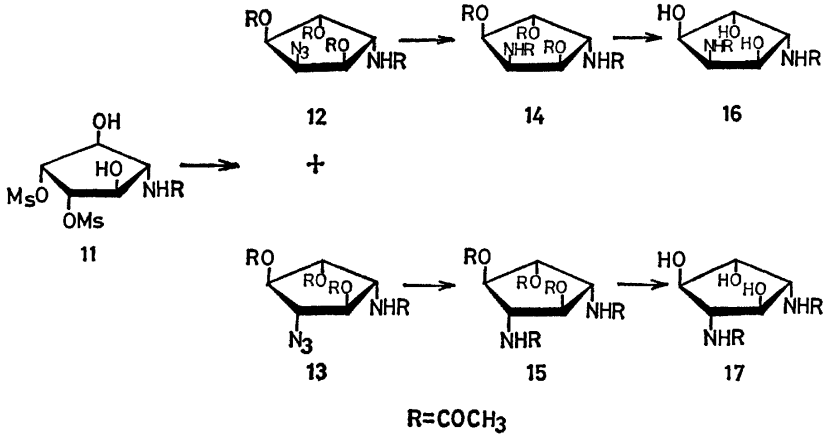

Scheme 3.

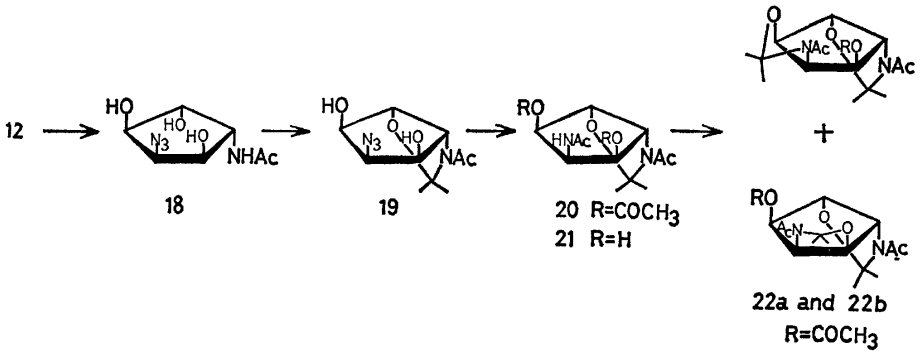

Scheme 4.

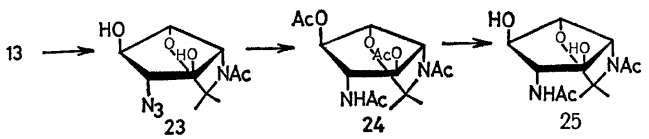

Scheme 5.

ment of the mesyloxy group on C-2 of **11** by an azide ion in a formation of **12**, and an anchimeric reaction mechanism is proposed in a formation of **13**.

Experimental

Mps were measured in capillary tubes and are uncorrected. Acetylation was carried out in the usual manner with acetic anhydride in pyridine. De-*O*-acetylation was performed in methanolic ammonia. Hydrogenation was carried out with Raney nickel in a hydrogen atmosphere (3.4 kg/cm^2) in Parr shaker apparatus. Silica gel (Wakogel C-200, Wako Pure Chemical Ind. Ltd.) was used for column chromatography and TLC was performed on a Wakogel B-10 plate in benzene–ethanol (5 : 1, v/v) solvent system. PMR spectrum was measured at 60 MHz on a Varian A-60D spectrometer in $CDCl_3$ with reference to tetramethylsilane as an internal standard and the peak positions are given in τ values. Elemental analyses were performed by Mr. Saburo Nakada, to whom our thanks are due.

*2,3-O-Cyclohexylidene-(1,4/2,3,5)-5-acetamido-1,2,3,4-cyclopentanetetrol (**1**).* The compound was prepared by the method described in the previous paper.[5]

*1-O-Benzoyl-*DL*-(1,4/2,3,5)-5-acetamido-1,2,3,4-cyclopentanetetrol (**2**).* Compound **1** (5.0 g) was dissolved in dry pyridine (50 ml), and benzoyl chloride (3.5 ml) was added to the solution drop by drop under ice cooling with mechanical agitation. After settled overnight at room temperature, the reaction solution was poured into ice cold water to give crystalline precipitates (7.97 g) which consisted of two components of R_f 0.7 and 0.5 on TLC. The precipitate was heated in 50% aqueous acetic acid for 2 h under reflux and then evaporated. The residue was dissolved in cold water (150 ml) and the solution was extracted with chloroform repeatedly. From the combined chloroform layers, 1,4-di-*O*-benzoyl derivative[9] was obtained in 31% yield.

The aqueous layer was evaporated and the residue was recrystallized from ethanol to give 1.84 g (34%) of **2**, mp 163—165 °C.

Found: C, 56.66; H, 5.88; N, 4.58%. Calcd for $C_{14}H_{17}NO_6$: C, 56.94; H, 5.80; N, 4.74%.

*Periodate Oxidation of **2**.* Sodium metaperiodate (675 mg) was dissolved in ice cold water (35 ml) and **2** (775 mg) was added to the solution under ice cooling with agitation. After 1 h another crop of sodium metaperiodate (576 mg) was added to the solution and the reaction solution was settled overnight in a refrigerator. Crystalline products which appeared in the solution were collected by filtration to give 546 mg (79%) of the dialdehyde (**3**), mp 138—142 °C. The product was used for the successive reaction without any purification.

*Nitromethane Cyclization of **3**.* Compound **3** (546 mg) was dissolved in methanol (10 ml) and nitromethane (0.7 ml) was added to the solution in the presence of 0.9 M methanolic sodium methoxide (7 ml) under ice cooling with agitation. After settled overnight in a refrigerator, the solution was adjusted to pH 5 with glacial acetic acid and then catalytically hydrogenated for 18 hr. After the catalyst was filtered off, the solution was evaporated and the residue was acetylated. The product was fractionated on a silica gel column. Fractions which showed a single spot at R_f 0.4 on TLC were combined and evaporated to give a crystalline residue (100 mg). Recrystallization from ether afforded 80 mg (11%) of 1,3,4-tri-*O*-acetyl-DL-(1,2,4/3,5)-2,5-diacetamido-1,3,4-cyclopentanetriol (**4**), mp 191—193 °C; PMR: τ 8.04 (s, 6, 2NAc), 7.95 (s, 3, OAc), 7.93 (s, 3, OAc), 7.90 (s, 3, OAc), 3.48 (d, 1, J=8 Hz, NH), 2.67 (d, 1, J=8 Hz, NH).

Found: C, 50.58; H, 6.13; N, 7.54%. Calcd for $C_{15}H_{22}N_2O_8$: C, 50.28; H, 6.19; N, 7.82%.

*Azidolysis of 1,4-Di-O-acetyl-2-O-tosyl-*DL*-(1,4/2,3,5)-5-acetamido-1,2,3,4-cyclopentanetetrol (**5**).* Compound **5**[8] (0.50 g) was heated with sodium azide (0.76 g) in DMF (10 ml) at 120 °C for 10 h with agitation. The reaction mixture was filtered and the filtrate was evaporated. The residue was extracted with warm ethyl acetate and the ethyl acetate solution was catalytically hydrogenated for 40 h. After the catalyst was removed by filtration, the filtrate was settled in a refrigerator to give 28 mg (9%) of crystalline product, mp 226—228 °C. The product was acetylated and then recrystallized from ether to give 30 mg (7%) of **4**, which was identified with an authentic sample.

The ethyl acetate mother liquor was evaporated and the residue was acetylated. The product was fractionated on a silica gel column to give 109 mg (26%) of 1,2,3,4-tetra-*O*-acetyl-DL-(1,2,4/3,5)-5-acetamido-1,2,3,4-cyclopentanetetrol, mp 110—111 °C, which was identified with an authentic sample.[8]

*Azidolysis of 2-O-Mesyl-*DL*-(1,4/2,3,5)-5-acetamido-1,2,3,4-cyclopentanetetraol (**6**).* Compound **6**[8] (0.65 g) was heated in DMF (20 ml) at 115 °C with sodium azide (1.57 g) for 10 h with agitation. The mixture was filtered and the filtrate was evaporated. The residue was acetylated overnight and the reaction solution was poured into ice cold water. The mixture was extracted with chloroform repeatedly and the combined chloroform layer was evaporated. The residue was hydrogenated in ethanol (12 ml) and the product was acetylated to give 0.59 g (68%) of **4**, 189—191 °C, which was identified with an authentic sample.

*DL-(1,2,4/3,5)-2,5-Diacetamido-1,3,4-cyclopentanetriol (**7**).* Compound **4** (188 mg) was de-*O*-acetylated and the product was recrystallized from ethanol to give 84 mg (69%) of **7** as hygroscopic crystals, mp 171—172 °C.

*1,3,4-Tri-O-methyl-*DL*-(1,2,4/3,5)-2,5-diacetamido-1,3,4-cyclopentanetriol (**8**).* Compound **7** (99 mg) was treated with methyl iodide (0.17 ml) in DMF (2 ml) in the presence of silver oxide (0.44 g) for 70 h with agitation. The reaction mixture was filtered and the filtrate was evaporated. The residue was extracted with warm ethanol and the alcoholic solution was evaporated. The residue was recrystallized from ethyl acetate–petroleum ether to give 40 mg (34%) of **8**, mp 193—194 °C; PMR: τ 8.00 (s, 3, NAc), 7.97 (s, 3, NAc), 6.60 (s, 3, OCH_3), 6.58 (s, 6, $2OCH_3$), 3.73 (d, 1, J=8 Hz, NH), 2.92 (d, 1, J=9 Hz, NH).

Found: C, 52.43; H, 7.83; N, 10.27%. Calcd for $C_{12}H_{22}N_2O_5$: C, 52.54; H, 8.09; N, 10.21%.

*2,3-Di-O-acetyl-1,4-di-O-methyl-(1,4/2,3,5)-5-acetamido-1,2,3,4-cyclopentanetetrol (**9**).* Compound **1** (2.81 g) was methylated analogously as described in the preparation of **8**. The product was hydrolyzed in 0.1 M hydrochloric acid for 2 h under reflux, and then the solution was evaporated. The residue was acetylated and the product was purified on a silica gel column. The product was recrystallized from benzene to give 1.72 g (55%) of **9**, mp 98—99 °C; PMR τ 7.99 (s, 3, NAc), 7.95 (s, 6, 2OAc), 6.62 (s, 6, $2OCH_3$), 3.74 (d, 1, J=9 Hz, NH).

Found: C, 51.76; H, 7.13; N, 4.51%. Calcd for $C_{13}H_{21}NO_7$: C, 51.48; H, 6.98; N, 4.62%.

*2-O-Mesyl-1,4-di-O-methyl-*DL*-(1,4/2,3,5)-5-acetamido-1,2,3,4-cyclopentanetetrol (**10**).* Compound **9** (2.63 g) was de-*O*-acetylated to give 2.36 g of syrup. The syrup was *O*-mesylated with mesyl chloride (1.5 ml) in pyridine (8 ml) overnight with agitation. After an excess of mesyl chloride was decomposed by adding cold water (4 ml), the reaction solution was evaporated. The residue was extracted with

chloroform, and the extract was purified on a silica gel column. Fractions which showed a single spot at R_f 0.37 on TLC were combined and evaporated to give crystals. Recrystallization from ethyl acetate afforded 1.37 g (53%) of **10**, mp 115—116 °C; PMR ($CDCl_3$–pyridine-d_5 3 : 1, v/v): τ 7.95 (s, 3, NAc), 6.82 (s, 3, OSO_2CH_3), 6.51 (s, 3, OCH_3), 6.47 (s, 3, OCH_3), 2.00 (d, 1, J=8 Hz, NH).

Found: C, 40.58; H, 6.32; N, 4.56; S, 10.67%. Calcd for $C_{10}H_{19}NO_7S$: C, 40.40; H, 6.44; N, 4.71; S, 10.78%.

Acetylation of **10** (30 mg) yielded 29 mg (85%) of the corresponding mono-*O*-acetyl derivative, mp 79—80 °C; PMR τ 7.98 (s, 3, NAc), 7.87 (s, 3, OAc), 6.95 (s, 3, OSO_2CH_3), 6.57 (s, 3, OCH_3), 6.53 (s, 3, OCH_3), 3.84 (d, 1, J= 9 Hz, NH).

Found: C, 42.71; H, 6.11; N, 4.01; S, 9.27%. Calcd for $C_{12}H_{21}NO_8S$: C, 42.47; H, 6.24; N, 4.13; S, 9.45%.

From the fractions (R_f 0.57), 0.29 g (9%) of 2,3-di-*O*-mesyl derivative, mp 132—133 °C, was obtained. PMR ($CDCl_3$–pyridine-d_5 1 : 1, v/v): τ 7.96 (s, 3, NAc), 6.80 (s, 6, $2OSO_2CH_3$), 6.48 (s, 6, $2OCH_3$), 2.15 (d, 1, J=12 Hz, NH).

Found: C, 35.21; H, 5.49; N, 3.65; S, 16.88%. Calcd for $C_{11}H_{21}NO_9S_2$: C, 35.19; H, 5.64; N, 3.73; S, 17.08%.

Azidolysis of ***10***. Compound **10** (1.00 g) was heated with sodium azide (2.2 g) in DMF (10 ml) at 95 °C for 42 h, and the product was treated analogously as described in the azidolysis of **6**. The product was purified on a silica gel column to give 123 mg (14%) of 1,4-di-*O*-methyl-DL-(1,2,4/3,5)-2,5-diacetamido-1,3,4-cyclopentanetriol, mp 179—180 °C.

Found: C, 50.69; H, 7.60; N, 10.60%. Calcd for $C_{11}H_{20}N_2O_5$: C, 50.76; H, 7.75; N, 10.76%. A 376 mg portion of the starting material **10** was recovered from the column.

The above mentioned diacetamido derivative (120 mg) was further *O*-methylated and then purified on a silica gel column to give 58 mg (46%) of **8**, 191—192 °C, which was identified with an authentic sample.

*Azidolysis of 2,3-Di-*O*-mesyl-(1,4/2,3,5)-5-acetamido-1,2,3,4-cyclopentanetetrol (**11**).* Compound **11**[8] (3.00 g) was heated with sodium azide (5.67 g) in DMF (25 ml) at 125 °C for 3 hr, and the product was acetylated. The acetylated product was recrystallized from ethyl acetate to give 692 mg (23%) of 1,3,4-tri-*O*-acetyl-DL-(1,2,3/4,5)-5-acetamido-2-azido-1,3,4-cyclopentanetriol (**12**), mp 163—164 °C; PMR τ 8.04 (s, 3, NAc), 7.92 (s, 3, OAc), 7.88 (s, 6, 2OAc), 3.71 (d, 1, J=8 Hz, NH).

Found: C, 45.49; H, 5.19; N, 16.55%. Calcd for $C_{13}H_{18}N_4O_7$: C, 45.61; H, 5.30; N, 16.37%. The mother liquor was evaporated and the residue was fractionated on a silica gel column to give 240 mg (8%) of **12** (Rf 0.3 on TLC) and 216 mg (7%) of 1,3,4-tri-*O*-acetyl-DL-(1,3/2,4,5)-5-acetamido-2-azido-1,3,4-cyclopentanetriol (**13**), mp 110—112 °C (recrystallized from ether); R_f 0.4 on TLC; PMR: τ 8.06 (s, 3, NAc), 7.90 (s, 9, 3OAc), 3.84 (d, 1, J=8 Hz, NH).

Found: C, 45.51; H, 5.23; N, 16.54%. Calcd for $C_{13}H_{18}N_4O_7$: C, 45.61; H, 5.30; N, 16.37%.

*1,3,4-Tri-*O*-acetyl-DL-(1,2,3/4,5)-2,5-diacetamido-1,3,4-cyclopentanetriol (**14**).* Compound **12** (921 mg) was catalytically hydrogenated in ethanol (15 ml) for 5 hr, and subsequently acetylated. The product was recrystallized from ethanol to give 651 mg (68%) of **14**, mp 205—206 °C; PMR (pyridine-d_5) τ 8.19 (s, 3, NAc), 8.06 (s, 3, NAc), 8.04 (s, 3, OAc), 8.01 (s, 3, OAc), 7.98 (s, 3, OAc), 1.93 (d, 1, J=9 Hz, NH), 0.61 (d, 1, J=9 Hz, NH).

Found: C, 50.48; H, 6.31; N, 7.65%. Calcd for $C_{15}H_{22}N_2O_8$: C, 50.28; H, 6.19; N, 7.82%.

*1,3,4-Tri-*O*-acetyl-DL-(1,3/2,4,5)-2,5-diacetamido-1,3,4-cyclopentanetriol (**15**)* Compound **13** (534 mg) was hydrogenated analogously as described in the preparation of **14** to give 232 mg (41%) of **15**, mp 206—207 °C; PMR (pyridine-d_5): τ 8.14 (s, 3, NAc), 8.07 (s, 3, NAc), 8.04 (s, 3, OAc), 7.95 (s, 3, OAc), 7.89 (s, 3, OAc), 1.26 (d, 1, J=8 Hz, NH), 0.85 (d, 1, J=8 Hz, NH).

Found: C, 50.17; H, 6.27; N, 7.58%. Calcd for $C_{15}H_{22}N_2O_8$: C, 50.28; H, 6.19; N, 7.82%.

*DL-(1,2,3/4,5)-2,5-Diacetamido-1,3,4-cyclopentanetriol (**16**).* Compound **14** (0.70 g) was de-*O*-acetylated and the product was recrystallized from ethanol to give 395 mg (87%) of **16**, mp 193—194 °C.

Found: C, 46.46; H, 7.05; N, 12.08%. Calcd for $C_9H_{16}N_2O_5$: C, 46.54; H, 6.96; N, 12.06%. Compound **16** consumed 0.9 molar equivalent of periodate in 0.05 M sodium metaperiodate solution for 2 h at room temperature.

*DL-(1,3/2,4,5)-2,5-Diacetamido-1,3,4-cyclopentanetriol (**17**).* Compound **15** (216 mg) was de-*O*-acetylated and the product was recrystallized from ethanol to give 93 mg (66%) of **17**, mp 180—181 °C.

Found: C, 46.86; H, 6.96; N, 11.73%. Calcd for $C_9H_{16}N_2O_5$: C, 46.54; H, 6.96; N, 12.06%. Compound **17** consumed 0.9 molar equivalent of periodate in the same conditions as described above.

*Structural Determinations of **12** and **13** by Acetyl Migration.* Compound **12** (33 mg) was hydrogenated in the presence of platinum oxide in ethanol (5 ml) overnight to give a practically ninhydrin negative product (28 mg). The product was de-*O*-acetylated and subsequently treated with Amberlite IR-120 (H^+) to give 19 mg (85%) of a ninhydrin negative product, mp 193—194 °C, which was identified as **16** by a comparison with an authentic sample.

Compound **13** (22 mg) was hydrogenated analogously as described above to give 15 mg (74%) of a ninhydrin positive product as a syrup.

*DL-(1,2,3/4,5)-5-Acetamido-2-azido-1,3,4-cyclopentanetriol (**18**).* Compound **12** (707 mg) was de-*O*-acetylated to give 340 mg (76%) of **18**, mp 168—169 °C.

Found: C, 38.77; H, 5.74; N, 25.60%. Calcd for $C_7H_{12}N_4O_4$: C, 38.89; H, 5.60; N, 25.92%.

*4,5-*N,O*-Isopropylidene-DL-(1,2,3/4,5)-5-acetamido-2-azido-1,3,4-cyclopentanetriol (**19**).* Compound **18** (280 mg) was treated with 2,2-dimethoxypropane (0.7 ml) in DMF (12 ml) at room temperature in the presence of *p*-toluenesulfonic acid (3 mg) for 46 h. After neutralized with Amberlite IRA-400 (OH^-), the reaction solution was evaporated and the residue was recrystallized from ethyl acetate to give 228 mg (69%) of **19**, mp 131—133 °C.

Found: C, 46.70; H, 6.23; N, 22.06%. Calcd for $C_{10}H_{16}N_4O_4$: C, 46.87; H, 6.29; N, 21.86%.

*1,3-Di-*O*-acetyl-4,5-*N,O*-isopropylidene-DL-(1,2,3/4,5)-2,5-diacetamido-1,3,4-cyclopentanetriol (**20**).* Compound **19** (396 mg) was hydrogenated in hydrogen atomosphere (3.4 kg/cm^2) in the presence of Raney nickel in ethanol (24 ml) overnight. The hydrogenation product was acetylated and the product was recrystallized from ethyl acetate to give 363 mg (66%) of **20**, mp 167—168 °C; PMR: τ 8.49 and 8.31 (each 3, CMe_2), 8.01 (s, 3, NAc), 7.93 (s, 3, NAc), 7.85 (s, 6, 2OAc), 4.21 (d, 1, J=9 Hz, NH).

Found: C, 53.76; H, 6.76; N, 7.94%. Calcd for $C_{16}H_{24}N_2O_7$: C, 53.93; H, 6.79; N, 7.86%.

*4,5-*N,O*-Isopropylidene-DL-(1,2,3/4,5)-2,5-diacetamido-1,3,4-cyclopentanetriol (**21**).* Compound **20** (323 mg) was de-*O*-acetylated and the product was recrystallized from ethyl acetate to give 229 mg (93%) of **21**, mp 163—164 °C.

Found: C, 52.65; H, 7.27; N, 10.29%. Calcd for $C_{12}H_{20}N_2O_5$: C, 52.93; H, 7.40; N, 10.29%.

O-*Acetyl-di*-N,O-*isopropylidene*-DL-*(1,2,3/4,5)-2,5-diacetamido-1,3,4-cyclopentanetriols (**22a** and **b**).* Compound **21** (149 mg) was treated with 2,2-dimethoxypropane (0.3 ml) in DMF (10 ml) in the presence of *p*-toluenesulfonic acid (3 mg) at room temperature for 21 h. After neutralized with Amberlite IRA-400 (OH^-), the reaction solution was evaporated to give 168 mg of a crystalline residue. The residue was fractionated on a silica gel column with benzene–ethanol as an eluate to give 119 mg of a main product and 30 mg of a minor product. The main product showed a single spot of R_f 0.5 and the minor one showed a single spot of R_f 0.4 on TLC in benzene–ethanol (5 : 1, v/v).

A 50 mg portion of the main product was acetylated to give 40 mg (70%) of **22a**, mp 197—198 °C (recryst. from ether); PMR: τ 8.50, 8.47, 8.38 and 8.32 (each 3, $2CMe_2$), 7.90 (s, 3, 2NAc), 7.85 (s, 3, OAc).

Found: C, 57.79; H, 7.33; N, 7.85%. Calcd for $C_{17}H_{26}N_2O_6$: C, 57.61; H, 7.40; N, 7.90%.

A 30 mg portion of the minor product was acetylated to give 20 mg (57%) of **22b**, mp 135—136 °C (recryst. from ether); PMR: τ 8.46, 8.43, 8.34 and 8.30 (each 3, $2CMe_2$), 8.00 (s, 6, 2NAc), 7.88 (s, 3, OAc).

Found: C, 57.39; H, 7.28; N, 7.72%. Calcd for $C_{17}H_{26}N_2O_6$: C, 57.61; H, 7.40; N, 7.90%.

4,5-N,O-*Isopropylidene*-DL-*(1,3/2,4,5)-5-acetamido-2-azido-1,3,4-cyclopentanetriol (**23**).* Compound **13** (293 mg) was de-*O*-acetylated to give 243 mg of colorless syrup. The syrup was treated with 2,2-dimethoxypropane (0.6 ml) in DMF (8 ml) in the presence of a catalytic amount of *p*-toluenesulfonic acid (3 mg) for 49 h at room temperature. After neutralized with Amberlite IRA-400 (OH^-), the solution was evaporated. The residue was recrystallized from ethyl acetate–petroleum ether to give 55 mg (25%) of **23**, mp 111—112 °C.

Found: C, 46.83; H, 6.33; N, 21.91%. Calcd for $C_{10}H_{16}N_4O_4$: C, 46.87; H, 6.29; N, 21.86%.

1,3-Di-O-*acetyl-4,5*-N,O-*isopropylidene*-DL-*(1,3/2,4,5)-2,5-diacetamido-1,3,4-cyclopentanetriol (**24**).* Compound **23** (36 mg) was acetylated and subsequently hydrogenated in the presence of Raney nickel in ethanol (2 ml) in hydrogen atmosphere (3.4 kg/cm²) for 5 h. The product was acetylated to give 27 mg (54%) of **24** as a syrup; PMR: τ 8.45 and 8.25 (each 3, CMe_2), 8.03 (s, 3, NAc), 7.88 (s, 9, NAc and 2OAc), 3.63 (d, 1, J=9 Hz, NH).

Found: C, 53.71; H, 6.70; N, 7.93%. Calcd for $C_{16}H_{24}N_2O_7$: C, 53.93; H, 6.79; N, 7.86%.

A 72 mg portion of **24** was de-*O*-acetylated give to 58 mg of 4,5-*N,O*-isopropylidene-DL-(1,3/2,4,5)-2,5-diacetamido-1,3,-4-cyclopentanetriol (**25**) as a syrup.

Compound **25** (58 mg) was treated with 2,2-dimethoxypropane as described in the preparation of **22a** and **b**, but only **24** was recovered in 88% yield (67 mg).

References

1) A part of this work was presented at the 7th International Symposium on Carbohydrate Chemistry, Bratislava, Czechoslovakia, August 5, 1974.

2) T. Suami, S. Nishiyama, K. Tadano, and F. W. Lichtenthaler, *Bull. Chem. Soc. Jpn.*, **46**, 2562 (1973).

3) J. N. Porter, R. I. Hewitt, C. W. Hesseltine, G. Kraupka, J. A. Lowery, W. S. Wallace, N. Bohonos, and J. H. Williams, *Antibiotics Chemotherapy*, **2**, 409 (1952).

4) C. A. Ammann and R. S. Safferman, *Antibiotics Chemotherapy*, **8**, 1 (1958).

5) T. Suami, Y. Sakota, K. Tadano, and S. Nishiyama, *Bull. Chem. Soc. Jpn.*, **44**, 2222 (1971).

6) B. R. Baker and A. H. Haines, *J. Org. Chem.*, **28**, 442 (1963).

7) T. Suami, F. W. Lichtenthaler, and S. Ogawa, *Bull. Chem. Soc. Jpn.*, **39**, 170 (1966).

8) T. Suami, K. Tadano, S. Nishiyama, and F. W. Lichtenthaler, *J. Org. Chem.*, **38**, 3691 (1973).

9) T. Suami, K. Tadano, and S. Horiuchi, *Bull. Chem. Soc. Jpn.*, **48**, 2895 (1975).

10) A. Hasegawa and M. Nakajima, *Carbohyd. Res.*, **29**, 239 (1973).

The Electrochemical Fluorination of Trifluoromethyl-substituted Benzenes

Michimasa YONEKURA,* Shunji NAGASE, Hajime BABA, Kazuo KODAIRA, and Takashi ABE

Government Industrial Research Institute, Nagoya, Hirate-machi, Kita-ku, Nagoya 462

(Received October 13, 1975)

The electrochemical fluorination of benzenes containing one or two trifluoromethyl groups has been carried out. They afforded perfluorocyclohexane derivatives with the trifluoromethyl group in good yields. Chlorobenzenes containing a trifluoromethyl group yielded chlorine-containing perfluorocyclohexane derivatives carrying the trifluoromethyl group. Trifluoromethylbenzonitriles gave perfluoro(dimethylcyclohexane)s, whereupon the nitrile group was converted into a trifluoromethyl group, thus releasing nitrogen trifluoride. The electrochemical fluorination of a trifluoromethylnaphthalene gave perfluoro(methyldecahydronaphthalene) only in a small yield.

Alicyclic fluorocarbons for practical use have received much attention, for example, in the electrical field,[1] because of their unique chemical inertness and physical properties. The preparation of these compounds by the electrochemical fluorination of aromatic hydrocarbons had been known to be unsatisfactory because of the conversion of the starting materials into tar in an electrolytic cell and the formation of polymeric substances on the surface of electrodes which impede the further smooth passage of the current. Sander and Blöch[2] obtained perfluoro compounds in good yields by the electrochemical fluorination of partially fluorinated cyclic alkanes.

In continuing our work on the electrochemical fluorination of aromatic compounds,[3] we have now found that the alicyclic fluorocarbons can be obtained in a reasonable yield by the fluorination of benzenes containing a trifluoromethyl group. However, in the case of the fluorination of trifluoromethyl-substituted naphthalene, the amount of the perfluorinated product was limited.

This report will further deal with the results of the electrochemical fluorination of (trifluoromethyl)benzenes carrying a nitrile group, which was found to be converted into a trifluoromethyl group by releasing nitrogen as nitrogen trifluoride during the fluorination. Thus, trifluoromethylbenzonitriles gave perfluoro-(dimethylcyclohexane)s. These perfluorocyclohexane derivatives have often been prepared by the exhaustive fluorination of cyclic hydrocarbons with high-valency metallic fluorides.[4]

Results and Discussion

The trifluoromethyl group attached to the benzene nucleus had a good effect in increasing the yields of polyfluorinated products in the electrochemical fluorination. For example, benzylidyne trifluoride afforded perfluoro(methylcyclohexane) (I) in a 47.6% yield, together with a small amount of perfluoro(1,2-dimethylcyclopentane) (II). The results are shown in Table 1. The fragmented fluorocarbons, such as carbon tetrafluoride and hexafluoroethane, were among the by-products. No unsaturated fluorocarbons were isolated. The electrochemical fluorination of benzylidyne trifluoride could be carried out even without using a conductivity additive, such as sodium fluoride (Run 2).

Benzenes containing two trifluoromethyl groups gave the expected products, perfluoro(dimethylcyclohexane)s (Runs 3 and 4). As has been shown in the electrochemical fluorination of chlorobenzenes,[3] the chlorine atom attached to the benzene ring was retained during the fluorination, giving chlorine-containing perfluorocyclohexane derivatives. Thus, trifluoromethyl-substituted chlorobenzenes yielded chlorotrifluoromethyldecafluorocyclohexanes (Runs 5, 6, and 7). However, I was obtained as the main product. This indicates that the carbon–carbon bond between the trifluoromethyl group and the benzene ring of the chlorotrifluoromethylbenzenes is much more stable to the electrochemical fluorination than the carbon–chlorine bond.

The fluorination of these aromatic compounds may proceed by the successive addition of fluorine radicals to the benzene nucleus to produce partially fluorinated cyclohexane derivatives; the replacement of the hydrogens by fluorines is expected to follow, yielding perfluoro compounds. The cleavage of the carbon–carbon bond may occur in this replacement stage by means of the energy liberated by the formation of the hydrogen-fluorine and carbon-fluorine bonds. II is probably produced by the rearrangement of the carbon skeleton of the partially fluorinated cyclohexanes. Rearrangements like this have often been observed in the electrochemical fluorination of such cyclic compounds, for example, perfluoro(methylcyclopentane) from benzene.[3] The isomerization of the cyclohexane ring to methylcyclopentane has also been known.[5]

The fact that the benzenes stabilized by the trifluoromethyl group give perfluorocyclohexane derivatives in good yields in the electrochemical fluorination may be explained as follows. First, these compounds do not generate such radicals as fluorocyclohexylmethyl or benzyl, which, among others, seem to be responsible for tar formation. For example, toluene, which has been known to yield only a very small amount of C_7 fluorocarbons, but a considerable amount of tarry materials, in the electrochemical fluorination,[2,6] can be expected to produce radicals of this type. Second, the introduction of trifluoromethyl group to the benzene nucleus could give higher solubilities in anhydrous hydrogen fluoride than those of the corresponding aromatic hydrocarbons[7] because of the increased polarity of the molecule.

The trifluoromethyl group attached to the naphtha-

* Present address: Asahi Denka Kogyo Co., Ltd., 7-1, Higashiogu, Arakawa-ku, Tokyo 116.

TABLE 1. FLUORINATION OF TRIFLUOROMETHYL-SUBSTITUTED BENZENES

Run No.	Starting material (mol)	Electricity passed (A·h)	Total amount of fluorocarbons obtained[b] (g)	Principal product	
				Yield[c,d] (%)	Amount[f] (g)
1	Benzylidyne trifluoride(0.197)	129	43.1	I[e] 47.6, II 6.1	37.2
2	Benzylidyne trifluoride(0.197)	123[a]	35.1	I 34.8, II 11.9	32.2
3	1,3-Bis(trifluoromethyl)-benzene(0.197)	148	25.2	I 1.7, III 23.9	20.0
4	1,4-Bis(trifluoromethyl)-benzene(0.200)	143	24.6	I 1.8, perfluoro(1,4-dimethylcyclohexane)[e] 23.5	20.1
5	1-Chloro-2-trifluoromethyl-benzene(0.202)	151	36.9	I 27.7, II 2.2, 1-chloro-2-trifluoromethyl-decafluorocyclohexane 14.5	31.8
6	1-Chloro-3-trifluoromethyl-benzene(0.204)	151	29.3	I 19.1, II 1.1, 1-chloro-3-trifluoromethyl-decafluorocyclohexane 10.1	22.0
7	1-Chloro-4-trifluoromethyl-benzene(0.203)	159	22.6	I 16.8, II 1.0, 1-chloro-4-trifluoromethyl-decafluorocyclohexane 9.4, perfluorocyclohexane 0.6	20.0
8	1-Trifluoromethylnaphthalene (0.102)	127	4.2	perfluoro(1-methyldeca-hydronaphthalene) 4.4	2.3
9	2-Trifluoromethylbenzonitrile (0.204)	150	10.8	I 1.1, perfluoro(1,2-dimethylcyclohexane)[e] 9.7	8.7
10	3-Trifluoromethylbenzonitrile (0.188)	150	27.8	I 5.3, III 20.5	18.9
11	3,5-Bis(trifloromethyl)benzonitrile (0.199)	150[a]	4.2	III 1.3, perfluoro(1,3,5-trimethylcyclohexane)[e] 2.6	3.4

a) Carried out without using the conductivity additive. b) Includes fragmented products such as CF_4 and C_2F_6. c) Yields were calculated as follows; (moles of respective product/moles of starting material) × 100. d) I=perfluoro(methylcyclohexane), II=perfluoro(1,2-dimethylcyclopentane), III=perfluoro(1,3-dimethylcyclohexane). e) IR spectra of these compounds agree with those listed in Ref. 13. f) Total amount of the principal products.

lene ring was not obviously effective. The electrochemical fluorination of 1-trifluoromethylnaphthalene afforded perfluoro(1-methyldecahydronaphthalene) only in a poor yield, 4.4% (Run 8). A considerable amount of tarry materials was found in the cell.

Trifluoromethylbenzonitriles are soluble in anhydrous hydrogen fluoride. In the fluorination, the carbon–nitrogen bond of the nitrile group was extensively cleaved, but the carbon–carbon bond between the benzene ring and the nitrile group remained intact; consequently, the nitrile group was converted into the trifluoromethyl group. The adsorption of the hetero-atom compounds at the active sites on the nickel anode may produce the proper conditions for the preferential attack of fluorine on the nitrogen atom.[8] Thus, perfluoro(dimethylcyclohexane)s (Runs 9 and 10) and perfluoro(1,3,5-trimethylcyclohexane) (Run 11) were obtained, but the yields of the products were depressed by the formation of a polymeric material. The presence of the nitrile group of the starting materials may assist the polymerization reaction.

Experimental

Materials and Apparatus. 1-Trifluoromethylnaphthalene,[9] 3-trifluoromethylbenzonitrile, and 4-trifluoromethylbenzonitrile[10] were prepared according to the methods described in the literature. The other reagents were commercial products and were used as received. The anhydrous hydrogen fluoride was more than 99.5% pure.

The electrolytic cell used was similar to that described previously.[11] Analytical gas chromatography was carried out with a Shimadzu GC-2C chromatograph using Col. A [1.5 m (3 mm diam.), silica gel (60—80 mesh), 80—100 °C], and Col. B [6 m (3 mm diam), 15% Silicone DC QF-1 on Chromosorp P-AW (60—80 mesh), 25—50 °C]. For the semi-preparative work, a Shimadzu GC-1C chromatograph [10 m (6 mm diam), 25% Silicone DC QF-1 on Chromosorp P-AW (60—80 mech)], was used. The IR spectra were recorded on a Hitachi EPI-S2 spectrometer, and the mass spectra, on a Hitachi RMU-7 instrument at 70 eV, as before.[3]

Fluorination of Trifluoromethyl-substituted Benzenes (Run 1). To electrically purified anhydrous hydrogen fluoride (1.28 l) in the cell, sodium fluoride (10 g) was added, and, then benzylidyne trifluoride (28.8 g, 0.197 mol) was introduced into the cell continuously over a period of 2 h by means of a micro-pump in the early period of the reaction. This process was accompanied by the continuous passage of an electric current with an anodic current density of 0.9—1.4 A/dm^2 (the effective surface areas of the anodes and cathodes were each 20 dm^2), a cell voltage of 5.5—5.8 V, and a cell temperature of 5—7 °C. During the reaction, helium (150 ml/min) was blown into the cell through a bubbler, made of poly(tetrafluoroethylene) fiber, fitted in the bottom of the cell.

The gases evolving from the cell were passed through a reflux condenser kept at −15 °C and then consecutively through an iron tube packed with sodium fluoride pellets, polyethylene- and glass-made gas washing bottles filled with an aqueous solution of potassium sulfite containing a small amount of potassium iodide, and finally a series of cold traps immersed in ice and in liquid nitrogen respectively.

The products formed were sufficiently volatile under these conditions so that the major portion of them moved with the stream of hydrogen and the carrier gas of helium from the cell into these traps. The total quantity of electricity passed through was 129 A·h over a period of 5 h. After the electrolysis was over, the blowing of helium was continued for 1.5 h to forward the portion of the products still remaining in the reaction system.

The products (43.1 g) collected in the cold traps were separated into two fractions by trap-to-trap distillation. Each fraction was further subjected to gas-chromatographic analysis (the compositions were calculated on the basis of the chromatographic peak areas, assuming, as usual, equal weight sensitivities for all components),[12] using Col. A for the lower-boiling portion (1.4 g) and Col. B for the higher-boiling portion (41.6 g). The following compounds were thus obtained: CF_4 (0.6 g), C_2F_6 (0.1 g), CHF_3 (0.1 g), CH_2F_2 (0.1 g), *n*-C_4F_{10} (trace), *n*-C_5F_{12} (trace), $CF_3\overline{CF(CF_2)_3}CFCF_3$ (4.2 g), $\overline{CF_2(CF_2)_4}CFCF_3$ (33.0 g), and others (4.9 g, an unidentified complex mixture). These compounds were identified on the basis of their known IR spectra[13] or by a spectral comparison with authentic samples, as before.[3] The authentic sample of perfluoro(1,2-dimethylcyclopentane) was prepared by the electrochemical fluorination of *cis*-1,2-dimethylcyclopentane. Bp 72 °C (lit,[14] bp 71.5—71.8 °C). (All the boiling points are uncorrected). MS: *m/e* 331 [M−F], 281 [M−CF_3], 243 [C_6F_9), 231 [C_5F_9], and 219 [C_4F_9].

The procedures for the other runs (Runs 2, 3, and 4) were essentially the same as those described above; the results obtained for the principal products are shown in Table 1. (Run 2 was carried out without using sodium fluoride).

Fluorination of Trifluoromethyl-substituted Chlorobenzenes (Run 5). 1-Chloro-2-trifluoromethylbenzene (36.5 g, 0.202 mol) was fluorinated, in the presence of sodium fluoride (10 g), with an anodic current density of 1.1—1.5 A/dm², a cell voltage of 5.1—6.0 V, and a cell temperature of 7—8 °C. A total quantity of electricity of 151 A. hr was supplied for a period of 6 hr. The flow rate of helium was 150 ml/min. After the electrolysis was over, the blowing of helium was continued for 1.5 hr.

The products (33.8 g) in the cold traps were separated into lower- (1.7 g) and higher-boiling portions (32.2 g) by trap-to-trap distillation, and each was subjected to gas-chromatographic (Col. A, and Col. B) and spectral analyses. In addition to these products, a small amount of a clear, heavy liquid was drained from the cell through the drain-cock by breaking the bubbler; this liquid was washed with water and with an alkaline solution, dried over anhydrous sodium sulfate, and subjected to gas chromatography (Col. B). This portion (3.1 g) was found to consist of mostly 1-chloro-2-trifluoromethyldecafluorocyclohexane,[15,16] which was also obtained in the cold traps. Bp 103 °C (lit,[15] bp 103 °C). MS: *m/e* 366 [M], 347 [M−F], 331 [M−Cl], 312 [C_7F_{12}], and 297 [C_6ClF_{10}]. The summarized results of the analyses for these three portions of the products are as follows: CF_4 (0.5 g), C_2F_6 (0.6 g), $CClF_3$ (0.5 g), $CF_3\overline{CF(CF_2)_3}CFCF_3$ (1.6 g), $\overline{CF_2(CF_2)_4}CFCF_3$ (19.6 g), $\overline{CFCl(CF_2)_4}CFCF_3$ (10.7 g) and others (3.5 g). For the other runs (Runs 6 and 7), the results obtained for the principal products are shown in Table 1. The 1-chloro-3-trifluoromethyldecafluorocyclohexane obtained in Run 6 had a bp of 103 °C (lit,[16] bp 102—103 °C). MS: *m/e* 366 [M], 347 [M−F], 331 [M−Cl], 312 [C_7F_{12}], and 297 [C_6ClF_{10}]. The 1-chloro-4-trifluoromethyldecafluorocyclohexane obtained in Run 7 had a bp of 103 °C (lit,[16] bp 102—103 °C). MS: *m/e* 366 [M], 347 [M−F], 331 [M−Cl], 312 [C_7F_{12}], and 297 [C_6ClF_{10}].

Fluorination of 1-Trifluoromethylnaphthalene. By following procedures similar to those used for Run 1, 1-trifluoromethylnaphthalene (20.0 g, 0.102 mol) was fluorinated in the presence of sodium fluoride (10 g), with an anodic current density of 1.2—1.4 A/dm², a cell voltage of 5.0—6.8 V, and a cell temperature of 10—11 °C. A total quantity of electricity of 127 A·h was supplied for a period of 5 hr. The flow rate of helium was 50 ml/min.

After the electrolysis was over, most of the anhydrous hydrogen fluoride was distilled off from the cell; the remaining vaporizable residue was driven out with the helium carrier gas from the cell, which had been heated to 70 °C, into a polyethylene bottle containing water. A small amount of fluorocarbons was condensed at the bottom of the bottle. It was separated from water, washed with an alkaline solution, and dried over anhydrous sodium sulfate. This product (2.3 g) was found to consist of mostly perfluoro(1-methyldecahydronaphthalene) (Col. B, 100 °C), bp 159 °C (lit,[17] bp 161 °C). MS: *m/e* 512 [M], 493 [M−F], 443 [M−CF_3], 424 [$C_{10}F_{16}$], and 405 [$C_{10}F_{15}$]. The formation of possible isomers such as perfluoro(perhydroindan)s[2] could not be confirmed under the present conditions. From the tarry residue in the bottom of the cell, 1-trifluoromethylnaphthalene (9.5 g) was recovered unchanged by acetone extraction. No other isolable product was found. The products (1.9 g) obtained in the cold traps consisted of the following compounds: CF_4 (1.1 g), C_2F_6 (0.1 g), CHF_3 (0.2 g), CH_2F_2 (0.2 g), and others (0.3 g).

Fluorination of Trifluoromethyl-substituted Benzonitriles (Run 9). An initial portion of 3-trifluoromethylbenzonitrile was added into the cell, drop by drop, through a sampling valve; electrolysis was then carried out in the presence of sodium fluoride (10 g) with an anodic current density of 1.1—1.6 A/dm², a cell voltage of 5.3—7.2 V, and a cell temperature of 5—7 °C. After a 50 A·h electrolysis, a second portion of 3-trifluoromethylbenzonitrile was added to the cell to bring the total of the two portions to 32.2 g (0.188 mol), after which the electrolysis was continued. A total quantity of electricity of 150 A·h was supplied for a total period of 5.5 h. The flow rate of helium was 150 ml/min. After the electrolysis was over, the blowing of helium was continued for 1.5 h.

The products (27.8 g) obtained in the cold traps were separated into lower- (6.1 g) and higher-boiling portions (21.6 g) by trap-to-trap distillation, and each was subjected to gas chromatography (Col. A and Col. B). The following compounds were obtained: CF_4 (1.9 g), NF_3 (2.4 g), C_2F_6 (0.3 g), CHF_3 (0.8 g), C_3F_8 (0.5 g), *n*-C_5F_{12} (trace), $\overline{CF_2(CF_2)_4}CFCF_3$ (3.5 g), $CF_3\overline{CFCF_2CF(CF_3)(CF_2)_2}CF_2$ (15.4 g), and others (2.9 g). Perfluoro(1,3-dimethylcyclohexane) had a bp of 101 °C (lit,[14] bp 101.7—101.9 °C). MS: *m/e* 381 [M−F], 331 [M−CF_3], 312 [C_7F_{12}], 293 [C_7F_{11}], and 281 [C_6F_{11}]. The results obtained for the principal products of this series of fluorinations (Runs 10 and 11) are shown in Table 1. (Run 11 was carried out without using sodium fluoride.)

The authors wish to thank the Daikin Industries Corporation for supplying the anhydrous hydrogen fluoride.

References

1) a) S. W. Green, *Chem. Ind.*, No. 3, 63 (1969); b) M. Hill, *ibid.*, No. 3, 118 (1975).

2) a) M. Sander and W. Blöchl, *Chem. Ing. Tech.*, **37**, 7 (1965); b) Ger. Pat. 1119262 (1961).
3) Y. Inoue, S. Nagase, K. Kodaira, H. Baba, and T. Abe, *Bull. Chem. Soc. Jpn.*, **46**, 2204 (1973).
4) For example, M. Stacey and J. C. Tatlow, "Advances in Fluorine Chemistry," Vol. 1, ed. by M. Stacey, J. C. Tatlow, and A. G. Sharpe, Butterworths Scientific Publications, London (1960), p. 166.
5) A. L. Glasebrook and W. G. Lovell, *J. Am. Chem. Soc.*, **61**, 1717 (1939).
6) J. H. Simons, U. S. Pat. 2519983 (1950).
7) J. H. Simons, "Fluorine Chemistry," Vol. 1, ed. by J. H. Simons, Academic Press, New York (1950). p. 239.
8) B. Chang, H. Yanase, K. Nakanishi, and N. Watanabe, *Electrochim. Acta*, **16**, 1179 (1971).
9) K. Hosokawa and K. Inukai, 23th Annual Meeting of the Chemical Society of Japan, Tokyo, 1970, April, Abstracts, IV, p. 2264.
10) Y. Maki and K. Inukai, *Kogyo Kagaku Zasshi*, **67**, 807 (1964).
11) S. Nagase, H. Baba, K. Tanaka, and T. Abe, *Kogyo Kagaku Zasshi*, **67**, 2062 (1964).
12) K. Okazaki, S. Nagase, H. Baba, and K. Kodaira, *J. Fluorine Chem.*, **4**, 387 (1974).
13) IR spectra of perfluorocyclohexane derivatives [perfluoro- (methyl-, 1,2-dimethyl-, 1,4-dimethyl-, and 1,3,5-trimethyl-cyclohexanes)] are listed in "Infrared Spectral Data," American Petroleum Institute, Research Project 44, Carnegie Institute of Technology, 1959, Serial number 996—1003.
14) W. B. Burford III, R. D. Fowler, J. M. Hamilton, Jr., H. C. Anderson, C. E. Weber, and R. G. Sweet, *Ind. Eng. Chem.*, **39**, 319 (1947).
15) R. N. Haszeldine and J. E. Osborne, *J. Chem. Soc.*, **1956**, 61.
16) W. B. Ligett, U.S. Pat. 2654789 (1953).
17) E. T. McBee and L. D. Bechtol, *Ind. Eng. Chem.*, **39**, 380 (1947).

Catalytic Reduction of Sulfoxide by Bromine–Hydrogen Bromide System

Tetsuo AIDA, Takeshi AKASAKA, Naomichi FURUKAWA, and Shigeru OAE

Department of Chemistry, The University of Tsukuba Sakura-mura, Niihari-gun, Ibaraki 300-31

(Received October 15, 1975)

A small amount of hydrogen halides or halogens was found to catalyze the decomposition of dimethyl sulfoxide (DMSO), affording dimethyl sulfide (DMS) and other oxidized products. Of the halides or halogens, either bromine or hydrogen bromide is the most effective. DMSO decomposes until it is completely consumed. This catalytic decomposition takes place with other sulfoxides such as diethyl or tetramethylene sulfoxide but sluggishly with alkyl aryl or diaryl sulfoxides. The reaction with bromine apparently proceeds *via* the initial α-bromination of DMSO to afford α-bromomethyl methyl sulfoxide which is oxidized by (Kornblum Reaction) to afford such products as formaldehyde, methanesulfonic acid, and hydrogen bromide. These consecutive reactions form a process of "Oxidation-Reduction Cycle" between bromine–hydrogen bromide and DMSO–DMS. The effects of salts and DMS on the rate of decomposition are discussed.

Recently, halide ions were found to catalyze the Stevens-type rearrangement of *S*-alkyl *S*-phenyl *N*-*p*-tosylsulfilimine in DMSO or *N*,*N*-dimethylformamide.[1] However, when DMSO was used as a solvent, an unexpected reduction of DMSO was observed besides the above rearrangement. The rate and amount of reduction vary with the halide ion. The catalyzed reduction of DMSO was attained most effectively with bromide ion, while the yield of dimethyl sulfide did not depend upon the amount of sulfilimide and bromide ion used. Reduction did not proceed in the absence of either the sulfilimine or bromide ion. These observations seem to indicate that the reduction is "triggered" by some species which is formed as a transient intermediate in the initial reaction of the sulfilimine and bromide ion (SB-System). A trapping experiment with a nucleophilic olefin confirmed that molecular bromine is formed during the course of reaction of the sulfilimine with bromide ion. Thus, the reduction is considered to be catalyzed by the molecular bromine formed during the course of reaction. This is supported by the fact that a drop of bromine or aqueous hydrobromic acid solution is enough to reduce DMSO to DMS completely upon heating. This catalytic reduction also takes place with other sulfoxides such as diethyl and tetramethylene sulfoxides. Although the reduction of sulfoxides with other acids has been reported,[2] this is the most facile and convenient catalytic reduction of sulfoxides.

This paper describes detailed observations on this new catalytic reduction of the sulfoxide triggered by the reaction of the sulfilimine with bromide ion and the implication of the reaction.

Results and Discussion

Reaction of N-p-*Tosylsulfilimines with Halide Ion in DMSO.* The reactions of *S*-methyl *S*-phenyl *N*-*p*-tosylsulfilimine with lithium halides were carried out in DMSO at 110 °C for 5 h. The products and yields obtained are summarized in Table 1.

In the case of bromide ion (SB-System) the reaction was apparently quite different from others (chloride ion or iodide ion), a large amount of dimethyl sulfide being obtained. The reaction with iodide ion gave a small amount of molecular iodine. In order to clarify the nature of this abnormal reaction with bromide ion, the yield of dimethyl sulfide was examined by changing the concentration of the bromide ion in DMSO. The results are given in Table 2.

Even though the total yield of dimethyl sulfide calculated from the amount of the SB-System markedly depends upon the initial concentration of the SB-System, the net yields of dimethyl sulfide calculated from the amount of DMSO used always remain at *ca.* 55%. During the course of reaction, about a half molar amount of DMSO used was reduced to the sulfide until DMSO was consumed. This suggests that the SB-System acts only as a "trigger" in the reduction of DMSO, and apparently a certain active species is generated from the SB-System during the course of reduction.

In order to understand the mechanism of the reaction with SB-System and the active species involved, the effect of structure of the sulfilimine on this reaction

TABLE 1. REACTION OF SULFILIMINE WITH HALIDE ION

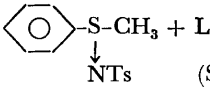

(Sulfilimine/LiX = 1/4; molar ratio)

X	Products and Yields (%)			
	$TsNHCH_3$	PhSSPh	CH_3SCH_3	Others
Cl	93	88	0	—
Br	43	43	1400	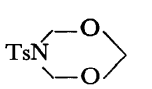 (34), $(CH_2O)_n$ (12)
I	71	62	30	I_2 (15)

TABLE 2. CONCENTRATION DEPENDENCY OF THE SB-SYSTEM

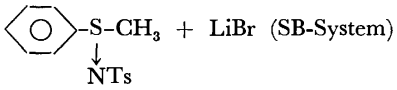

Molar ratio (SB-System/DMSO)		0.01	0.05	0.25
Yield of DMS (%)	a)	615	1166	2420
	b)	55	53	56

a) Calculated from the amount of the SB-System.
b) Conversion percentage for DMSO.

TABLE 3. EFFECT OF THE STRUCTURE OF THE SULFILIMINE

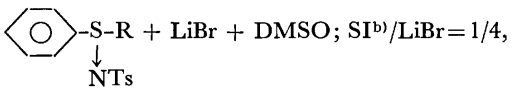

R	Me	Et	*i*-Pr	$PhCH_2$	Ph
k_{rel}[a]	1.0	0.5	4.0	200.0	0

a) Calculated from the yield of DMS obtained after a certain reaction time. b) Sulfilimine.

TABLE 4. EFFECT OF SUBSTITUENT

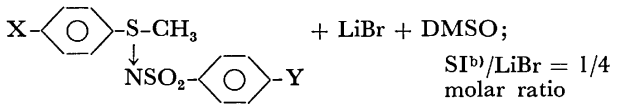

X	*p*-MeO	H	*p*-NO_2	H
Y	H	H	H	*m*-NO_2
k_{rel}[a]	0.1	1.1	18.0	5.0

a) Calculated from the yield of DMS obtained after a certain reaction time. b) Sulfilimine.

was investigated. The reactivity was determined by comparing the amount of dimethyl sulfide formed after a certain reaction time. The results are summarized in Tables 3 and 4.

The ability of the triggered system (sulfilimine–lithium bromide system) toward the reduction of DMSO appears to depend considerably on the structure of the sulfilimine (Table 3), the reduction proceeding favorably in the order $PhCH_2$>*i*-Pr>Me>Et>Ph. This trend of order does not seem to fit any single conceivable factor. In addition, β-elimination apparently takes place with the sulfilimines having β-hydrogen,[3] *i.e.*, Et- and *i*-Pr- derivatives, playing an important role in the catalytic reduction. The sulfenamides (1 or 2) which are formed in both reactions (rearrangement and β-elimination) seem to be the key compounds (Scheme 1).

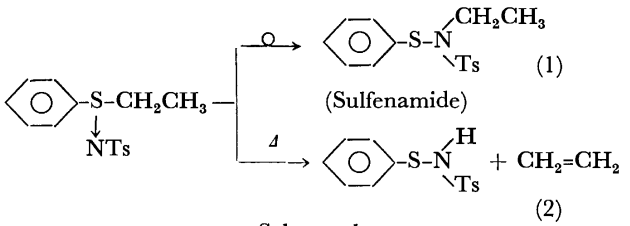

(Sulfenamide) (1) (2)

Scheme 1.

A study on the effect of substituent in the sulfilimine on this reaction reveals that the reduction is accelerated by the electron-withdrawing substituent. This trend is in line with the Stevens rearrangement reaction of the sulfilimine with halide ion.

In order to clarify the nature of the active species formed in the reaction of the SB-System and acting as a catalyst for the reduction of DMSO, the controlled experiments were carried out with various substances. The results are summarized in Table 5. All the compounds seem to have a similar triggering ability for the reduction of DMSO, and the common active species is considered to be either bromine or hydrogen bromide since both benzyl bromide and ethyl bromide generate bromine or hydrogen bromide in the reactions with DMSO, (Kornblum reaction[3] and reduction[2]), as shown in Scheme 2.

TABLE 5. CATALYTIC REDUCTION OF DMSO

DMSO + Catalytic System; 100 : 3 (molar ratio)

Catalytic System	SB-System	$PhCH_2Br$	EtBr	Br_2	HBr
DMS-% (*vs.* DMSO)	55	55	54	56	56

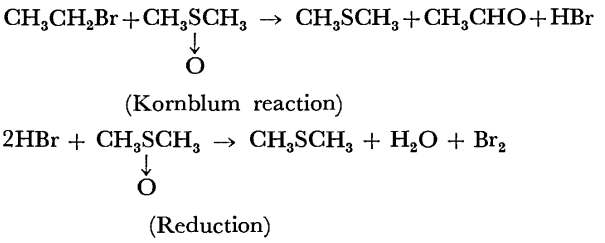

(Kornblum reaction)

(Reduction)

Scheme 2.

The effect of additional third components on the reduction of DMSO with the SB-System was examined. The results are given in Table 6. The active species is very likely to be molecular bromine, since the reduction was retarded remarkably when styrene was added in the reaction system, while a small amount of (1,2-dibromoethyl)benzene was detected by GLC. Although no bromo-derivative could be detected in the case of phenol, phenol is known to react readily with molecular bromine affording the corresponding *o*- or *p*-substituted derivative, thus trapping molecular bromine.

Thus, the generation of active species (bromine or hydrogen bromide) is suggested as shown in Scheme 3.

Product Analysis of the Catalytic Reduction of DMSO by Molecular Bromine. In order to simplify the catalytic system for the reduction of DMSO, molecular bromine was used as a catalyst and both the products and yields

TABLE 6. EFFECT OF ADDITION OF THIRD COMPONENT

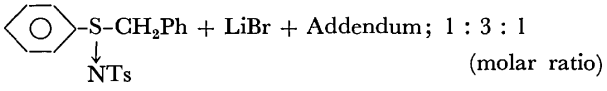

(molar ratio)

Addendum	None	Styrene[a]	Cyclo-hexene	Phenol	Hydro-quinon
DMS(%)[b]	1400	30	0	0	0

a) 1,2-Dibromoethylbenzene was detected by means of GlC. b) Conversion percentage for sulfilimine.

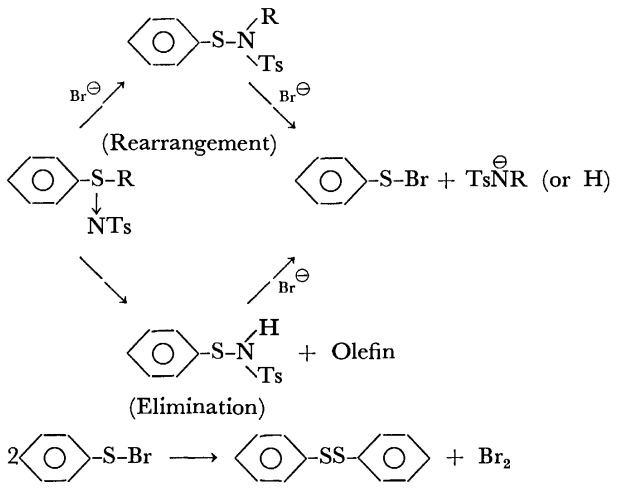

Scheme 3.

Table 7. Product distribution of the reduction of DMSO by bromine
(DMSO/Br_2=100/1; molar ratio)

Products	Yields (%)	
	%-Br_2[a]	%-DMSO[b]
CH_3SCH_3	1860	56
$(CH_3)_3S^+$ $CH_3SO_3^-$	400	12
CH_3SO_3H	232	7
$(CH_2O)_n$	600	18

a) Calculated from a molar amount of Br_2. b) Conversion percentage for DMSO.

were examined. The results are given in Table 7. The reduced product is dimethyl sulfide, while the oxidized products are both methanesulfonic acid derivatives and formaldehyde, the yields of which are nearly equal.

A similar product distribution was also observed in the reduction of DMSO by a catalytic amount of hydrogen bromide or benzyl bromide (Table 4). In order to confirm the applicability of this catalytic reduction, the same experiments were carried out with various sulfoxides. The results are summarized in Table 8. Apparently the reduction depends on the structure of the sulfoxide (R or R'). Diphenyl sulfoxide is non-reactive and was recovered quantitatively even under drastic reaction conditions. This suggests that the presence of acidic hydrogen is essential. The sequence of reactivities of these sulfoxides, Me>Et>$-(CH_2)_4-$>*n*-Bu, seems to suggest that both steric and inductive effects of alkyl substituent are important in the rate determining step of the reduction.

The yield of DMS in the reduction of DMSO by bromine was followed by means of GLC (Fig. 1.). The formation of DMS increases gradually at the initial stage of the reduction, and then the increase becomes remarkably when the reduction reaches near to completion. The formation of DMS was apparently accelerated by the initial addition of DMS. This suggests that there are at least two routes for the catalytic formation of DMS whose relative rates differ and DMS itself may accelerate the reduction. Since the reduction is not affected by radical initiating reagents such as 2,2'-azobisisobutyronitrile and oxygen atmosphere, it is undoubtedly an ionic reaction.

Table 8. Catalytic reduction of various sulfoxides R-S-R' by molecular bromine
(Sulfoxide/Br_2=100/1; molar ratio)

R	R'	Reaction conditions		Yield of sulfide	
		Temp (°C)	Time (h)	%-Br_2[a]	%-Sulfoxide[b]
Me	Me	100	5	1860	56
Et	Et	100	24	2310	69
n-Bu	*n*-Bu	100	240	1450	43[c]
$-(CH_2)_4-$		100	72	1810	54
Ph	Me	100	240	200	6[c]
Ph	Ph	100	100	0	0
				(recovered quant)	

a) Calculated from a molar amount of Br_2. b) Conversion percentage for sulfoxide. c) The starting materials were recovered in 36% and 82% for di-*n*-butyl and methyl phenyl sulfoxide, respectively.

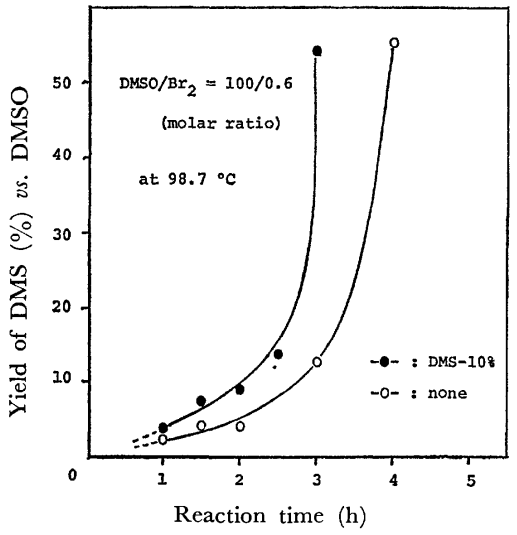

Fig. 1. The effect of DMS for the reduction of DMSO.

The effects of various salts on the reduction were also investigated (Fig. 2). Lithium chloride apparently accelerates, while both lithium bromide and lithium perchlorate retard the reduction.

These and other observations such as product analyses and the rate of formation of DMS, suggest that the reduction can be explained in terms of two main catalytic cycles (Scheme 4). The reaction is obviously initiated by the facile bromination of DMSO or DMS by bromine. The α-bromo-sulfoxide or sulfide reacts with DMSO (Kornblum reaction) affording the sulfide and oxidation products, accompanied by hydrogen bromide which is known to reduce the sulfoxide to the sulfide, forming bromine and water.[2]

If these catalytic cycles work competitively in this reaction while the cycle (2) proceeds faster than the cycle (1), an explanation can be given for the char-

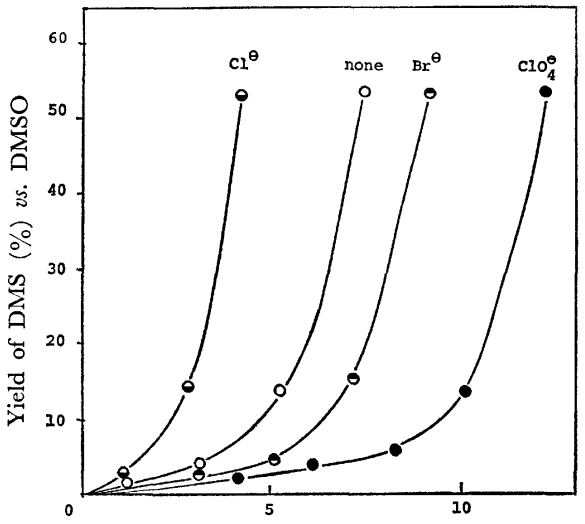

Fig. 2. Salt-effect of reduction of DMSO by bromine.
DMSO/Br_2/Salt=100/0.35/0.35 (molar ratio)
○=none, ◒=LiCl, ◓=LiBr, ●=$LiClO_4$

Catalytic Cycle-(1)

$DMSO + Br_2 = [CH_3SCH_2Br] + HBr$

$[CH_3SCH_2Br] + DMSO = [CH_3SCHO] + DMS + HBr$

$DMSO + 2HBr = DMS + Br_2 + H_2O$

$[CH_3SCHO] + H_2O = [CH_3SOH] + CH_2O$

$[CH_3SOH] + DMSO = DMS + CH_3SO_3H$

+)

$4DMSO = 3DMS + CH_2O + CH_3SO_3H$

Calcd Yield; 75% 25% 25%

Catalytic Cycle-(2)

$DMS + Br_2 = [CH_3SCH_2Br] + HBr$

$[CH_3SCH_2Br] + DMSO = [CH_3SCHO] + DMS + HBr$

$DMSO + 2HBr = DMS + Br_2 + H_2O$

$[CH_3SCHO] + H_2O = [CH_3SOH] + CH_2O$

$[CH_3SOH] + 2DMSO = 2DMS + CH_3SO_3H$

+)

$4DMSO = 3DMS + CH_2O + CH_3SO_3H$

Calcd Yield; 75% 25% 25%

Scheme 4.

acteristic phenomenon of the formation of DMS, namely the gradual increase of DMS at an early stage, followed by a remarkable increase during the reaction. At the initial stage of the reaction, cycle (1) would work predominantly since the amount of DMS in the reaction mixture is too small for cycle (2) to operate; however, the accumulation of DMS during the course of reduction would gradually change the main reaction from cycle (1) to cycle (2). Since cycle (2) proceeds faster than cycle (1), the formation of DMS would increase remarkably near the completion of the reaction.

The Kornblum reaction is probably the slowest one in cycle (1), while the rate-determining step of the reaction is the proton abstraction from the oxo-sulfonium salt (3) by the counter anion (Scheme 5), in view of the interesting salt effects. Since bromide ion acts as a common salt which prevents the formation of the oxo-sulfonium salt(3), and perchlorate ion is a

$CH_3SCH_2Br + DMSO = [CH_3SCH_2\text{-}O\text{-}\overset{\oplus}{S}(CH_3)_2]Br^{\ominus}$ (or $Cl^{\ominus}$, $ClO_4^{\ominus}$)

(3)

$[CH_3SCHO] + DMS + HBr \leftarrow CH_3S\text{-}CH\text{-}O\text{-}\overset{\oplus}{S}(CH_3)_2$ (3)

$+ Br^{\ominus}$ (or $Cl^{\ominus}$, $ClO_4^{\ominus}$)

Scheme 5.

$CH_3SCH_2\text{-}O\text{-}\overset{\oplus}{S}(CH_3)_2 + Br^{\ominus} \longrightarrow [CH_3SCH_2OSCH_3] + CH_3Br$

$CH_3SCH_3 + CH_3Br \longrightarrow [CH_3\overset{\oplus}{S}(CH_3)_2]Br^{\ominus}$

$\underset{HBr}{\overset{CH_3SO_3H}{\rightleftarrows}} [CH_3\overset{\oplus}{S}(CH_3)_2]CH_3SO_3^{\ominus}$

Scheme 6.

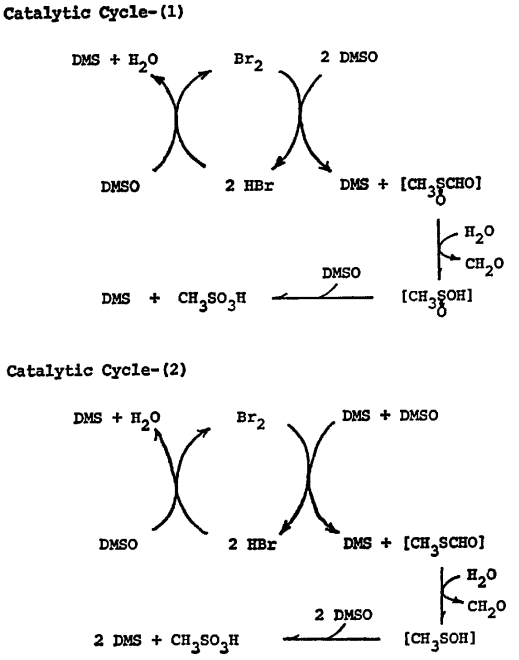

Fig. 3. Mechanism of catalytic reduction of DMSO by Br_2.

weaker base than bromide ion to abstract the proton of the oxo-sulfonium salt(3), the reduction would be retarded by perchlorate ion. Chloride ion is a stronger counter anion than bromide or perchlorate ion. Thus, the whole scheme of the catalytic reduction DMSO to DMS may be illustrated as shown in Fig. 3. The formation of trimethylsulfonium methanesulfonate ($(CH_3)_3S^+CH_3SO_3^-$) is shown in Scheme 6.

Experimental

Materials. N-p-*Tosylsulfilimine*: All the *N-p*-tosylsulfilimines were prepared from the corresponding sulfides and chloramine-T by the modified Mann-Pope reaction.[5] These sulfilimines were identified by comparison of their mp, IR, and NMR spectra with those reported.[5]

Lithium Halide and Perchlorate: Commercial anhydrous products were used without purification.

Sulfoxide: Commercial DMSO was dried over calcium hydride and distilled before use. Diethyl, tetramethylene, dibutyl, methyl phenyl and diphenyl sulfoxides were prepared by oxidation of the corresponding sulfides with bromine in acetic acid.[6]

Other Reagents: Commercial dimethyl sulfide, benzyl bromide, ethyl bromide and cyclohexene were used after distillation. Commercial styrene and phenol were distilled in order to remove the stabilizer. Commercial bromine and aqueous hydrobromic acid solution were used without purification.

Reaction of S-*Methyl* S-*Phenyl*-N-p-*Tosylsulfilimine with Halide Ion in DMSO.* A typical run is as follows; a mixture of *S*-methyl *S*-phenyl *N-p*-tosylsulfilimine (3 mmol) and lithium bromide (12 mmol) was dissolved in DMSO (5 g) containing 0.5 g of benzene as an internal standard for GLC. The solution was heated in a sealed tube at 110 °C for 12 h. The reaction mixture was then cooled to ice-water temperature. In order to determine the yield of dimethyl sulfide formed in the reaction, it was injected into the GLC-column and then poured into 30 ml of cold water. The products were extracted from the solution with chloroform and separated by column chromatography (silica gel; benzene); $TsNHCH_3$ 43%, CH_3SCH_3 1400%, $(CH_2O)_n$ 10% and 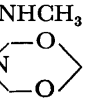 34%, respectively. The yields were calculated from the molar amount of the sulfilimine used. The structure of 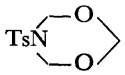 was determined by the following data; IR ν_{SO_2} 1340, 1160 cm^{-1} ν_{COC} 1160 cm^{-1}; NMR is shown in Fig. 4.

Found: C, 50.2; H, 5.35; N, 5.93%. Calcd for $C_{10}H_{13}NO_4S$: C, 49.4; H, 5.35; N, 5.77%.

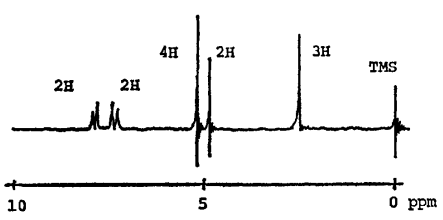

Fig. 4. NMR spectrum of Ts- 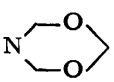 (in $CDCl_3$).

Reactions of Various N-p-*Tosylsulfilimines with Lithium Bromide in DMSO.* A mixture of the *N-p*-tosylsulfilimine (3 mmol) and lithium bromide (12 mmol) was dissolved in DMSO (5 g) containing benzene (0.5 g) as an internal standard for GLC. The solution was heated in a sealed tube at 110 °C. for 5 h, and then cooled to ice-water temperature. The isolation and determination of the products formed in the reaction were carried out as described above.

Catalytic Reduction of DMSO by Various Bromides. As a typical example, a solution of ethyl bromide (0.33 g; 3 mmol) and DMSO (8.0 g; 100 mmol) was placed into a sealed tube, and heated at 100 °C for 24 h. The yield of dimethyl sulfide was determined by GLC.

Product Analysis in the Reduction of DMSO by Bromine. The reaction was carried out by heating an ampouled mixture of bromine (1 mmol) and DMSO (8.0 g; 100 mmol) at 100 °C for 5 h. After the reaction, the reaction mixture was separated into two layers. From the upper layer dimethyl sulfide was detected by GLC as the sole product (56%). The under layer was poured into 100 ml of acetone, and then the crystalline precipitates were filtrated off and recrystallized from acetone–ethanol. The compound was identified as trimethylsulfonium methanesulfonate ($(CH_3)_3S^+CH_3SO_3^-$) by comparison of its IR and NMR spectra with those of an authentic sample prepared from trimethylsulfonium iodide ($(CH_3)_3S^+I^-$) and methanesulfonic acid. The yield of the sulfonium salt was 12%. Methanesulfonic acid was separated from the filtrate by means of the anion exchange resine (7%). Paraformaldehyde condensed in the cold part of the sealed tube (18%).

Catalytic Reductions of Various Sulfoxides by Bromine. A typical run is as follows; a mixture of bromine (0.1 mmol) and dibutyl sulfoxide (0.62 g; 10 mmol) was put into a sealed tube and heated at 100 °C for 10 days. The yield of the corresponding sulfide was determined by GLC.

Measurement of the Rate of Formation of Dimethyl Sulfide. A typical run is as follows; a mixture of bromine (0.35 mmol) and DMSO (8.0 g; 100 mmol) containing benzene (0.5 g) as an internal standard for GLC was divided into six portions which were put into separate ampoules. The ampoules were heated in a constant temperature oil bath (100 °C) at the same time, and then removed at set intervals. The yield of dimethyl sulfide was determined by GLC. The effect of the initial addition of dimethyl sulfide (5%) was observed by the same procedure as described above. Addition of various lithium salts to the reaction mixture was also carried out, the molar ratio of DMSO, bromine and lithium salt being 100 : 0.35 : 0.35.

References

1) N. Furukawa, T. Aida, and S. Oae, *Int. J. Sulfur Chem.*, **A2**, 181 (1972); S. Oae, T. Aida, and N. Furukawa, *J. Chem. Soc., Perkin Trans. 2*, **1974**, 1231.

2) I. A. Smythe, *J. Chem. Soc.*, **95**, 349 (1909); E. N. Karaulova and G. D. Galpern, *Zhur. Obsh. Khim.*, **29**, 3033 (1959); T. L. Flecher and H. L. Pan, *J. Org. Chem.*, **24**, 141 (1959).

3) N. Kornblum, W. J. Jones, and G. J. Anderson, *J. Am. Chem. Soc.*, **81**, 4113 (1959).

4) K. Tsujihara, N. Furukawa, K. Oae, and S. Oae, *Bull. Chem. Soc. Jpn.*, **42**, 2631 (1969).

5) S. Oae, Y. Ohnishi, S. Kozuka, and W. Tagaki, *Bull. Chem. Soc. Jpn.*, **39**, 364 (1966).

Synthetic Studies on Phosphorylating Reagent. V. A Convenient Synthesis of 2′,3′-Cyclic Coenzyme A

Yoshihiko TAGUCHI, Noriyuki NISHIMURA, Toshio KAKIMOTO, and Yoshitaka MUSHIKA

Research Laboratory of Applied Biochemistry, Tanabe Seiyaku Co., Ltd., 16-89, Kashima-3-chome, Yodogawa-ku, Osaka 532

(Received October 17, 1975)

A convenient method has been developed for the preparation of 2′,3′-cyclic Coenzyme A (**5**). It was readily prepared in a good yield from the reaction of adenosine-5′ 2-dimethylamino-4-nitrophenyl phosphate (**3**) with D-pantethine-4′,4″-diphosphate (**4**) in the presence of acetic acid in pyridine. Compound **3** and the diphosphate **4** were prepared in a good yield from the condensation of adenosine (**1**) with 2-dimethylamino-4-nitrophenyl phosphate (**2**) in the presence of dicyclohexylcarbodiimide (DCC) and the phosphorylation of D-pantethine with **2**, respectively.

Phosphate **5** was hydrolyzed with 0.1 M-hydrochloric acid and subsequently reduced with 2-mercaptoethanol to confirm its structure of **5**. One of the products, Coenzyme A (reduced form) (**6**) showed 102% activity with phosphotransacetylase.

It was reported in the previous papers[1–4] that the selective phosphorylation of the hydroxyl group of polyalcohols and amino alcohols including nucleosides, such as adenosine and cytidine *etc.*, was achieved by employing 2-dimethylamino-4-nitrophenyl phosphate (**2**), a new phosphorylating reagent having "an activatable protecting group" to afford the corresponding phosphate esters such as glycerol-1-phosphate, 2-aminoethyl phosphate, adenosine-5′-phosphate and adenosine-3′,5′-cyclic phosphate.

In the present paper, we will describe a convenient preparation of 2′,3′-cyclic Coenzyme A (**5**) using the phosphorylating reagent **2**. There are several papers[5–9] concerning the total synthesis of Coenzyme A (**6**). All methods comprised the synthesis of 2′,3′-cyclic Coenzyme A (**5**) as a precursor of Coenzyme A. However, these methods seem to be impractical because of the difficulties of isolation and purification. Phosphate **5** has not been isolated yet from the reaction mixture and the exact character of **5** has remained unknown. We have attempted the synthesis[10] of **5** using the new phosphorylating reagent **2**. The synthesis of **5** was carried out according to the route shown in Scheme 1.

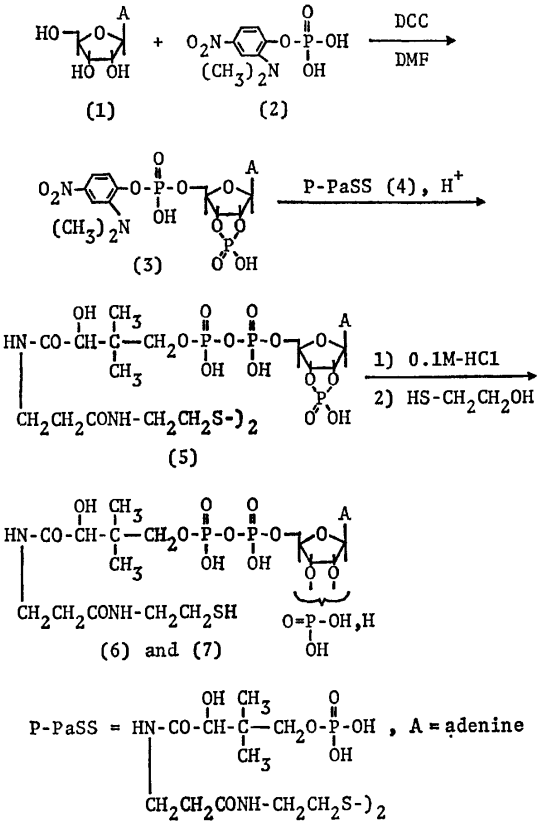

Scheme 1.

Adenosine-2′,3′-cyclic phosphate-5′ 2-dimethylamino-4-nitrophenyl phosphate (**3**), which acts as a phosphorylating reagent, was prepared by the condensation of the unprotected adenosine (**1**) and the reagent **2** with DCC. Formation of the phosphate **3** was observed in the reaction of **1** and **2** with DCC.[1] Phosphate **3** was obtained as a by-product, the yield being very low. The coupling reaction was reinvestigated in order to find optimum conditions. As a result, phosphate **3** was obtained in quantitative yield when 3 equiv. of the monotriethylammonium salt of **2**, 1 equiv. of adenosine (**1**) and 10 equiv. of DCC were used in the reaction carried out at room temperature in *N,N*-dimethylformamide (DMF). Isolation and purification of product **3** were easily achieved by column chromatography on DEAE-Sephadex according to the usual procedure. Phosphate **3** was obtained in 93% yield as its dilithium salt.

The other component of Coenzyme A (**6**), D-pantetheine-4′-phosphate or D-pantethine-4′,4″-diphosphate (**4**) was necessary for the preparation of **6**. We chose D-pantethine-4′,4″-diphosphate (**4**) as a starting material since the thiol group of D-pantetheine-4′-phosphate would be unfavorable for making the pyrophosphate linkage of **6**. Diphosphate **4** was prepared by Michelson.[6] His method consists of three steps, phosphorylation of D-pantetheine with dibenzyl phosphorochloridate, debenzylation of dibenzyl D-pantetheine-4′-phosphate and oxidation of the thiol group. The procedure seemed to be somewhat intricate. Consequently, a one step synthesis of diphosphate **4** was undertaken with the use of **2**. Thus, the desired diphosphate **4** was readily obtained in 62% yield as its barium salt when a mixture of 1 equiv. of D-pentethine and 2 equiv. of monotriethylammonium salt of **2**

in pyridine was heated under reflux in the presence of 3 equiv. of acetic acid. All the materials including D-pantethine should be thoroughly dried to obtain good results, since this reaction is especially sensitive to the presence of water. The complete drying of D-pantethine was very difficult.

The final step in the preparation of **5** was carried out as follows. The desired pyrophosphate **5** was obtained in 65% yield when 1 equiv. of the triethylammonium salt of **3** was reacted with 3 equiv. of the pyridinium salt of **4** at 50—60 °C for 5 days in pyridine without acid. On the other hand, the yield of **5** increased to 93% when 3 equiv. of glacial acetic acid was added. DMF used in place of pyridine gave the poorest results. The effects of the other acidic media on the yield of **5** are listed in Table 1. The separation of **5** was successfully achieved by eluting a column of DEAE-Sephadex with a linear gradient (0.005—0.30 M) of triethylammonium hydrogencarbonate after applying the reaction mixture to the column and washing with a sufficient amount of water. Analytically pure **5** was obtained as its trilithium salt, a white powder melting at 247—249 °C. The data concerning paper partition chromatography (PPC) and paper electrophoresis (PEP) of compound **5** and the related ones are summarized in Table 2. The structure of **5** was also comfirmed, biologically and chemically, by converting **5** into Coenzyme A (**6**) and *iso*-Coenzyme A (**7**) according to the method of Moffatt and Khorana.[5] Compound **5** (disulfide form) was treated with 0.1 M-hydrochloric acid at room temperature for 1 hr to cleave the cyclic phosphate ring and to reduce subsequently the disulfide linkage with 2-mercaptoethanol at pH 6.0. The products, **6** and **7**, which were isolated as their lithium salts, were chromatographically and electrophoretically identical to a commercially available sample of **6**. The enzymatic assay of the mixture of **6** and **7** by the phosphotransacetylase method[11] showed 102% activity on the basis of **6**.

Table 1. 2′,3′-Cyclic Coenzyme A

Solvent	Acid	Yield (%)
Pyridine	no acid	65
Pyridine	CH_3COOH	93
Pyridine	H_2SO_4	89
Pyridine	CF_3COOH	80
Pyridine	p-$CH_3C_6H_4SO_3H$	78
Pyridine	BF_3-$(C_2H_5)_2O$	65
DMF	BF_3-$(C_2H_5)_2O$	74
DMF	H_2SO_4	48

In conclusion, the key intermediate for the synthesis of Coenzyme A, adenosine-2′,3′-cyclic phosphate-5′ 2-dimethylamino-4-nitrophenyl phosphate (**3**), was easily prepared in one step by the DCC coupling reaction of adenosine (**1**) and the phosphorylating reagent (**2**) in a high yield. A simpler preparation of D-pantethine-4′,4″-diphosphate (**4**) was achieved by using **2**. It was clear that the mild reactivity of phosphate **3** was due to protonation on the nitrogen atom, and **3** reacted with **4** to afford the oxidized form of 2′,3′-cycle Coenzyme A in a good yield.

This method should be useful for the syntheses of other nucleotides having pyrophosphate linkages.

Experimental

Paper chromatography (PPC) was carried out by descending technique using Toyo Roshi No. 51A paper. Solvent systems used were: A, EtOH–0.5 M ammonium acetate buffer (pH 3.8) (5 : 2); B, EtOH–1 M ammonium acetate buffer (pH 7.5) (5 : 2); C, 1-butanol–acetic acid–water (5 : 2 : 3).

Paper electrophoresis (PEP) was performed at pH 7.5 (0.05 M triethylammonium hydrogencarbonate, 900 V/40 cm). The spots of adenosine derivatives on chromatograms were detected with UV lamp (2540 Å). The phsphorus-containing compounds were detected with the Hanes and Isherwood reagent.[12] Chromatographic and electrophoretic mobilities are given in Table 2.

Table 2. Paper chromatography and paper electrophoresis

Compound	R_f in solvent A	B	C	Electrophoretic mobility[a]
Adenosine-2′,3-cyclic phosphate-5′ 2-dimethylamino-4-nitrophenyl phosphate	0.60			0.83
2′,3′-Cyclic Coenzyme A (SS)	0.10	0.08	0.11	1.17
Coenzyme A (SS)	0.07	0.06	0.08	1.20
Coenzyme A (SH)	0.23	0.24	0.23	1.15
Pantethine-4′,4″-diphosphate			0.55	0.50

a) Mobility relative to adenosine-5′-phosphate.

Melting points were determined on a Yamato apparatus, MP-21. The NMR spectra were determined on a Hitachi Perkin-Elmer R-20A instrument (DSS as internal standard). IR spectra were determined on a Shimadzu IR-27G spectrophotometer.

*Adenosine-2′,3′-cyclic Phosphate-5′ 2-Dimethylamino-4-nitrophenyl Phosphate (**3**).* A DMF solution (20 ml) of adenosine (**1**) (0.27 g, 1 mmol), DCC (2.06 g, 10 mmol) and pyridinium 2-dimethylamino-4-nitrophenylphosphate (**2**), prepared from ammonium salt of **2** (0.84 g, 3 mmol) by the cation exchange method on Dowex 50W×8 resin (pyridinium form), was allowed to stand at room temperature for 2 days. After removal of the precipitate by filtration, the filtrate was applied to a column (1.8×60 cm) of DEAE-Sephadex (HCO_3^- form) and eluted with a linear gradient of 0.0005 M and 0.1 M of triethylammonium hydrogencarbonate solution (2 l each). The eluates were continuously followed by the UV-monitor (260 nm). The desired compound, adenosine-2′,3′-cyclic phosphate-5′ 2-dimethylamino-4-nitrophenyl phosphate (**3**), was eluted at roughly 0.07 M salt concentration. The combined fractions containing **3** were evaporated to dryness after complete removal of the volatile compounds by co-evaporation of two 10-ml portions of methanol. The residue was dissolved in methanol (5 ml) and a stoichiometric amount of lithium chloride was added. Acetone (20 ml) was added to the methanolic solution to give the crude dilithium salt

of **3** as a yellow precipitate. The recrystallization of the crude product from a mixture of ethanol and acetone gave 0.63 g (93%) of pentahydrate of dilithium salt of **3**. It was confirmed by PPC, PEP and NMR spectroscopy that phosphate **3** was identical to an authentic sample prepared previously.[1]

D-Pantethine-4′,4″-diphosphate (4). To a pyridine solution (30 ml) of D-pantethine (2.77 g, 5 mmol), which was well dried by co-evaporation with three 30-ml portions of pyridine, were added monotriethylammonium 2-dimethylamino-4-nitrophenyl phosphate (**2**) (3.62 g, 10 mmol), acetic acid (1.80 g, 30 mmol) and triethylamine (1.01 g, 10 mmol) and the solution was refluxed for 3 hr. After evaporating the reaction mixture, the residue was dissolved in water (50 ml) and subsequently applied to a column (1.3×75 cm) of Dowex 50W×8 resin (H^+ form). Th column was washed with water (3000 ml) and the aqueous washings were adjusted to pH 7.5 with barium hydroxide. After removal of the precipitate by filtration, the filtrate was evaporated to dryness at a temperature below 40 °C. The residue was treated with ethanol (100 ml) to give 3.05 g (62%) of dibarium D-pantethine-4′,4″-diphosphate (**4**) as white precipitate; NMR (D_2O, ppm): 0.81 (s, 6H, $CH_3\times2$), 0.97 (s, 6H, $CH_3\times2$), 2.50 (t, 4H, $CH_2\times2$), 2.85 (s, 4H, $CH_2\times2$), 3.40—3.63 (m, 12H, $CH_2\times6$), 4.09 (s, 2H, $CH\times2$). IR (Nujol, cm^{-1}): 3280 (OH), 1655, 1563, 1545 (CONH), 1240 (P=O), 1120, 1080 (P–O–C). These data were identical with those of an authentic sample prepared according to Michelson's method.[6]

2′,3′-Cyclic Coenzyme A (5). Typical Procedure: An aqueous solution of dibarium D-pantethine-4′,4″-diphosphate (1.48 g, 3 mmol) was passed through a column of Dowex 50W×8 resin (pyridinium form) and the column was washed with water. The combined eluate and washings were evaporated to dryness. The residue was well dried by co-evaporation with three 10-ml portions of pyridine. After adding the triethylammonium salt of adenosine-2′,3′-cyclic phosphate-5′ 2-dimethylamino-4-nitrophenyl phosphate (**3**) (0.72 g, 1 mmol) to the above residue, the mixture was again dried by co-evaporation with two 25-ml. portions of pyridine. To a solution of the residue in pyridine (25 ml) was added acetic acid (0.18 g, 3 mmol) and the solution was allowed to stand at 50—60 °C for 5 days. After evaporating the solvent, an aqueous solution (500 ml) of the residue was applied to a column (2.4×50 cm) of DEAE Sephadex (HCO_3^-) and the column was washed with water until the optical density of the washings became negligible. The column was then eluted with a linear gradient of 0.005 M and 0.3 M of triethylammonium hydrogencarbonate solution (4 l each) and four hundred 20-ml portions of the fractions were collected. The desired compound, 2′,3′-cyclic Coenzyme A (**5**), was eluted with *ca.* 0.13 M salt solution. The combined fractions, which contained the product **5**, were evaporated to dryness at a temperature below 40 °C. After adding a stoichiometric amount of lithium chloride to a solution of the residue in methanol, the solution was diluted with acetone (40 ml) to give the crude lithium salt of **5**. Repeated reprecipitation of the crude product **5** from methanol and acetone gave 0.77 g (93%) of the pure lithium salt of **5** as white powder; mp 247—249 °C (dec.); NMR (D_2O, ppm): 1.27 (s, 6H, $CH_3\times2$), 1.39 (s, 6H, $CH_3\times2$), 2.75—3.58 (m, 8H, $CH_2\times4$), 3.87—4.29 (m, 18H, $C_5'H_2\times2+C_4'H\times2+CH_2\times6$), 4.37—5.14 (m, 6H, $C_2'H\times2+C_3'H\times2+CH\times2$), 6.11 (d, 2H, $C_1'H\times2$), 8.17 (s, 2H, $C_2H\times2$), 8.52 (s, 2H, $C_8H\times2$). IR (Nujol, cm^{-1}): 3320 (OH), 1655, 1610, 1545 (CONH), 1240 (P=O), 1120, 1080 (P–O–C), 945 (P–O–P). Found: C, 30.07; H, 4.14; N, 11.60%. Calcd for $C_{42}H_{60}N_{14}O_{30}S_2P_6Li_6\cdot8H_2O$: C, 30.08; H, 4.57; N, 11.70%.

Hydrolysis of 2′,3′-Cyclic Coenzyme A (5) with 0.1 M-HCl. An aqueous solution (5 ml) of 2′,3′-cyclic Coenzyme A (disulfide form) (6510 OD units) was allowed to stant at room temperature for 1 hr after its pH had been adjusted to 1.0 with 0.1 M-HCl. The solution was then readjusted to pH 6.0 with ammonium hydroxide. To the neutral solution was added 2-mercaptoethanol (20 ml) and the solution was left overnight. After diluting with water (500 ml), the reaction mixture was applied to a column (3.5×30 cm) of DEAE Sephadex (Cl^- form) and the column was washed with water until the optical densities of the washings became negligible. The column was than eluted with a linear gradient of 2 l of 0.003 M-hydrochloric acid (mixing vessel) and 2 l of 0.003 M-hydrochloric acid containing of 12.72 g (0.3 mol) of lithium chloride (reservoir). Twenty-ml portions of fractions were collected and the elution curve is shown in Fig. 1.

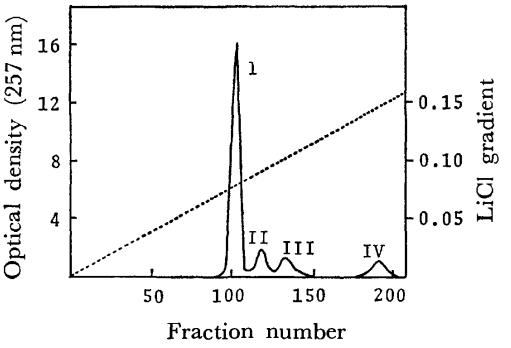

Fig. 1. Chromatography on a DEAE-Sephadex column. Products of the acidic hydrolysis and reduction with 2-mercaptoethanol of 2′,3′-cyclic Coenzyme A (disulfide form).
Peak I, Coenzyme A + *iso*-Coenzyme A; Peak II and III, unidentified; Peak IV, Coenzyme A + *iso*-Coenzyme A (disulfide form).

Peak I (3460 OD units, 49.4%) was a mixture of Coenzyme A and *iso*-Coenzyme A. Peak II (5.8 %) and Peak III (5.5%) could not be identified. Peak IV (320 OD units, 4.6%) was a mixture of oxidized Coenzyme A and *iso*-Coenzyme A. Assay of the mixture of Coenzyme A and *iso*-Coenzyme A, which was obtained from Peak I, by the phosphotransacetylase method[11] using purified commercially available Coenzyme A as the standard proved to be 102% activity on the basis of Coenzyme A, as the ratio of Coenzyme A and *iso*-Coenzyme A was presumed to be 1 : 1.[5]

We wish to express our thanks to Professor Yasumitsu Tamura, Drs. Takashi Takayanagi, Ichiro Chibata, Muneji Miyoshi, Naoto Yoneda, and Ichizo Inoue for their valuable discussions and suggestions.

References

1) Part IV: Y. Taguchi and Y. Mushika, *Bull. Chem. Soc. Jpn*, **48**, 1528 (1975).
2) Y. Taguchi and Y. Mushika, *Tetrahedron Lett.*, **1975**, 1913.
3) Y. Taguchi and Y. Mushika, *J. Org. Chem.*, **40**, 2310 (1975).
4) Y. Taguchi and Y. Mushika, *Chem. Pharm. Bull.* **23**, 1586 (1975).

5) J. G. Moffatt and H. G. Khorana, *J. Am. Chem. Soc.*, **83**, 663 (1961).
6) A. M. Michelson, *Biochim. Biophys. Acta*, **93**, 71 (1964).
7) W. Gruber and F. Lynen, *Ann.*, **659**, 139 (1962).
8) M. Shimizu, O. Nagase, S. Okada, Y. Hosokawa, H. Tagawa, Y. Abiko, and T. Suzuki, *Chem. Pharm. Bull.*, **15**, 655 (1967).
9) M. Hashimoto and T. Mukaiyama, *Chem. Lett.*, **1972**, 595.
10) The usual methods employ the hydrolysis of **5** with dilute hydrochloric acid to obtain Coenzyme A (**6**). However, this usually gives a mixture of Coenzyme A (**6**) and *iso*-Coenzyme A (**7**), which has no activity to the enzyme, the ratio of the two products being about 1 : 1.
11) G. D. Novelli, "Methods of Biochemical Analysis", Vol. 2. Interscience Publishers, New York (1955), pp. 201—207.
12) C. S. Hanes and F. A. Isherwood, *Nature*, **164**, 1107 (1949).

Effects of Alkali Metal Cation, Solvent, and Alkylating Agent on the Alkylation of Alkali Metal Enolates of Ethyl Acetoacetate

Yoshinori HARA and Minoru MATSUDA

Chemical Research Institute of Non-aqueous Solutions, Tohoku University, Katahira 2-Chome, Sendai 980

(Received October 20, 1975)

Alkylation of Li^+, Na^+, and K^+ enolates of ethyl acetoacetate by dimethyl sulfite in dimethyl sulfoxide, hexamethylphosphoric triamide, and *N,N*-dimethylformamide at 50 °C has been studied. The ratio of O/(C+C,C)-alkylation is considerably dependent on the size of the counter cation and the solvent. The tightness of the ion pair is responsible for determining the ratio. The structure of alkylating agents has also influence upon the alkylation ratio. Dimethyl sulfite gives a higher O/(C+C,C)-alkylation ratio than methyl halides which may be ascribed to the hard methyl sulfite anion as leaving group.

It seems to be of interest to determine the factors affecting the alkylation site of ambident anions such as alkali metal enolates of ethyl acetoacetate. Several studies of this area have revealed that the ratio of O/(C+C,C) in alkylation reactions is remarkably dependent on the structure of the alkylating agents, the size of the metal cations, the solvent, and the temperature.[1-6] In connection with our previous studies concerned with the syntheses of organic compounds having sulfite linkages,[7,8] our attention has been focused on the use of dimethyl sulfite in organic reactions in order to understand the chemical properties of the relatively less known alkyl sulfite as alkylating agent.[9] We will report here the alkylation reaction of the alkali metal enolates of ethyl acetoacetate by dimethyl sulfite and the results are discussed in terms of the effects of the size of alkali metal cations, the solvent, and the alkylating agent.

Results

Solvent Effects on the Isomer Ratio in Alkylation Reaction. Results obtained from alkylation of sodium enolate of ethyl acetoacetate by dimethyl sulfite in several solvents at 50 °C are listed in Table 1. The O/(C+C,C)-alkylation ratio increases in the order of diglyme< *N,N*-dimethylformamide (DMF)<dimethyl sulfoxide (DMSO)<hexamethylphosphoric triamide (HMPA)< liquid SO_2. Reaction in liquid SO_2 proceeds in a heterogeneous system. The yield of C,O-isomers is negligibly small.

Counter Cation Effects. Results obtained in DMSO at 50 °C are listed in Table 2. The O/(C+C,C)-alkylation ratio increases in the order of $Li^+<Na^+<K^+$

TABLE 1. ALKYLATION OF SODIUM ENOLATE OF ETHYL ACETOACETATE BY DIMETHYL SULFITE IN VARIOUS SOLVENTS[a]

Solvent	Reaction time (h)	Total yield (mol%)	Products (mol%)			Donicity number	Dielectric constant
			C-isomer	C,C-isomer	O-isomer		
HMPA	48	50	37	2	61	38.8	30
DMSO	44	50	53	1	46	29.8	~45
DMF	44	42	54	2	44	30.9	35
DMSO (70 vol. %) —*t*-BuOH	46	51	58	2	40		
Diglyme[b]	48	19	66	~0	34		
liquid SO_2[c]	48	18	13	<1	86		

a) [Enolate]=1.0 mol/l. b) [Enolate]=0.25 mol/l. c) Heterogeneous.

TABLE 2. METHYLATION OF THE ALKALI METAL ENOLATES OF ETHYL ACETOACETATE BY VARIOUS ALKYLATING AGENTS AT 50 °C[a]

Alkylating agent	Alkali metal	r_c^{+}[c] (Å)	Solvent	Reaction time (h)	Total yield (mol%)	Products (mol%)		
						C-isomer	C,C-isomer	O-isomer
$CH_3OS(O)OCH_3$	Li^+	0.60	DMSO	52	38	63	2	35
$CH_3OS(O)OCH_3$	Li^+		DMSO	120	46	66	2	32
$CH_3OS(O)OCH_3$	Na^+	0.96	DMSO	39	52	47	1	52
$CH_3OS(O)OCH_3$	K^+	1.33	DMSO	40	39	41	1	58
CH_3I	Na^+		DMSO	22	quant.	81	16	3
$CH_3OS(O_2)OCH_3$	Na^+		DMSO	22	77	55	7	38
CH_3OTs[b]	K^+		HMPA		96	7	4	89
CH_3Br[b]	K^+		HMPA		87	42	44	14
CH_3I[b]	K^+		HMPA		93	31	64	5

a) [Enolate]=0.5 mol/l. b) Data cited from Ref. 6, [enolate]=0.25 mol/l at 20 °C. c) Alkali metal cation radius.

depending on the size of the counter cation radius (r_c^+).

Leaving Group Effects. Results are listed in Table 2 together with the results reported for other methylating agents. Although it is difficult to compare rigorously among the data which have been obtained under the different reaction conditions,[6] the O/(C+C,C)-alkylation ratio increases roughly in the order $I^- < Br^- < CH_3OS(O_2)O^- < CH_3OS(O)O^- < TsO^-$ (as listed in Table 2 data of Br^- and TsO^- cited from Ref. 6 and these have been obtained in HMPA with potassium salts). Methyl iodide in DMSO yields the C,C-isomer in higher yield compared with dimethyl sulfite.

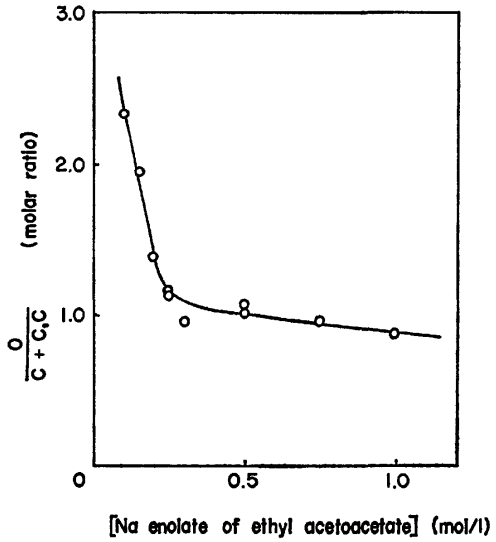

Fig. 1. Dilution effects on the O/(C+C,C)-alkylation ratio obtained with the sodium enolate of ethyl acetoacetate in DMSO at 50 °C.

Dilution Effects. As depicted in Fig. 1 the O/(C+C,C)-alkylation ratio tends to increase with increasing dilution, especially in a region of low enolate concentrations less than 0.3 mol/l pronounced dilution effects in DMSO was clearly appreciable.

Discussion

As shown in the preceding section the O/(C+C,C)-alkylation ratio of the alkali metal enolates of ethyl acetoacetate is affected by the size of the counter cation, solvent, leaving group, and dilution. The alkylation scheme is represented in Fig. 2 and according to this scheme an enhanced O/(C+C,C)-alkylation ratio of ambident anions is expected from the free ions. Kurts *et al.* measured the conductances of solutions containing alkali metal enolates and explained the enhanced ratios by the increased fraction of free ions.[4-6] Dilution effects observed in a region of the low enolate concentrations less than about 0.3 mol/l also reflect the formation of the free ions (see Fig. 1).

On the other hand, solvent effects (Table 1) and counter cation effects in DMSO (Fig. 3) observed in the higher enolate concentration region more than 0.3 mol/l can be explained by the relative amounts of the two species, the contact and solvent-separated ion pairs, which were found to depend on the counter cation and the nature of the solvent. The solvent-separated ion pairs play an important role in the O/(C+C,C)-alkylation ratio when the fraction of the dissociated species, the free ions, is small, which is the similar situation to that proposed by Winstein *et al.* to account for the observed salt effects in the solvolysis of certain arene sulfonates.[10]

The observed order of the solvent effects may be correlated to the solvating power to alkali metal ca-

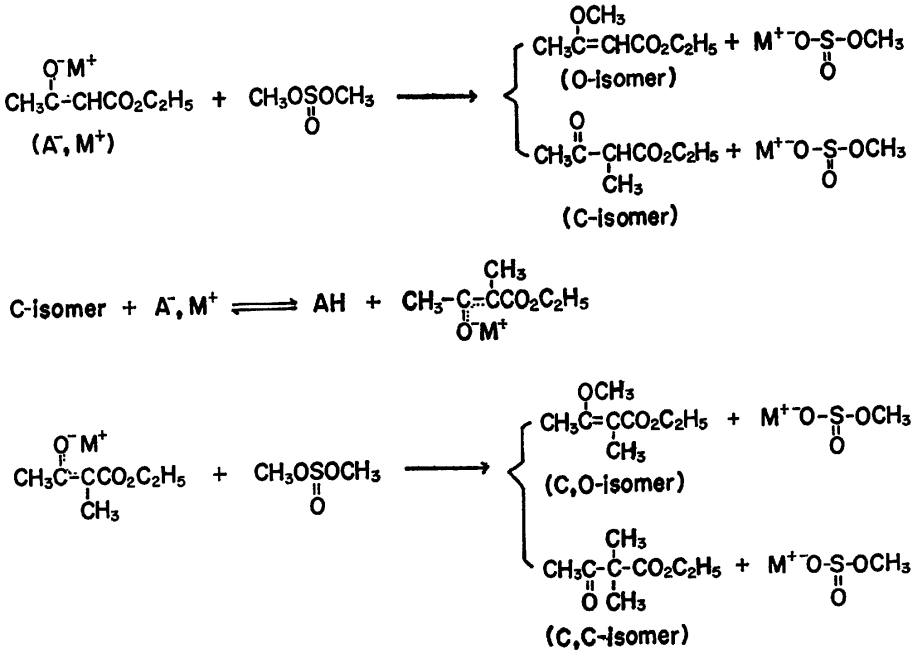

Fig. 2. Reaction scheme.

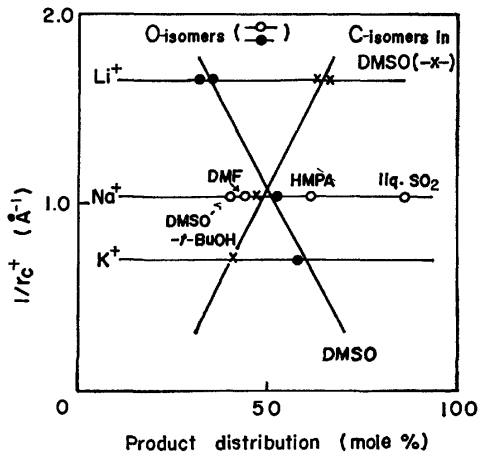

Fig. 3. Relationship between the inverse of the alkali metal cation radius ($1/r_c^+$) and the product distribution at 50 °C. ●, O-isomers in DMSO. ○, O-isomers in other solvents. ×, C-isomers in DMSO. Concentration of enolate was being kept constant at 0.5 mol/l.

tions. The solvating power does not depend on their dielectric constants, but on their ability to donate the negative charge to the cations.[11] The donor property is measured, for example, by solvent's "donicity"[12] and our O/(C+C,C)-alkylation ratio would be correlated with the donicity numbers rather than dielectric constants (see Table 1). DMSO and DMF are polarizable powerful bases like HMPA and the negative charge in their solvents is localized on a bare oxygen atom (nucleophilicity is centered on this oxygen[13]). The external solvation of HMPA, DMSO, or DMF to alkali metal cation tends to disperse the cationic charge and may contribute to weakening the coulombic interaction between the oxygen atom of the ambident anions and alkali metal cations. Thus in the DMSO, DMF, and HMPA, most of the fluorenyl salts (carbanions)[14] and thiolate salts (sulfur anions)[15] form solvent-separated ion pairs, even at room temperature. The polyethyleneglycol dimethyl ethers with the general formula, $CH_3O(CH_2CH_2O)_nCH_3$, referred to as glymes are effective alkali metal-solvating reagents[11] and have often been used to enhance the reactivity of organo-alkali metal compounds. Diglyme, $x=2$ in the general formula, can coordinate alkali metal cations using three coordinate sites. Our observed O/(C+C,C)-alkylation ratio in digylme is small than those in DMF, DMSO, and HMPA. Similar has been reported by Kornblum *et al.* that the O/C-alkylation ratio of sodium β-naphthoxide with benzyl bromide increased in the order tetrahydrofuran≃diglyme<DMF<DMSO[16] which is in accord with order observed in this study. Zook and Miller also found that the O/C-alkylation ratios of sodium enolate in DMSO are substantially larger than in diglyme and rates of enolate alkylation in DMSO are 10^3-fold greater than in glyme solvents.[17] These results may probably be due to the use of the sodium counter cation, and reactivity of diglyme is the most extensive for lithium salts.[18] The addition of *t*-butyl alcohol to DMSO lowered the O/(C+C,C)-alkylation ratio, since the protic solvent prevents the alkylating agent from approaching the oxygen atom of the ambident anion due to the formation of hydrogen bonding.

The size of the alkali metal cations strongly affects the fraction of tight ion pairs formed under otherwise identical conditions. Zaugg and Schaefer[18] found for the anions of phenols and enols that the fraction of the tight ion pairs decreases with increasing cation radius and that the absence of appreciable covalency interactions with alkali metals. The relationship between the inverse of the alkali metal cation radius ($1/r_c^+$) and the product distribution is depicted in Fig. 3. The larger the cation yields the higher the O-isomer; the fraction of O-isomer is proportional to the cation radius in DMSO. The oxygen atom of the alkali metal enolates of ethyl acetoacetate would be associated neither with solvent used nor with cations in these media except for liquid SO_2 (Reaction in liquid SO_2 is discussed below).

The structure of alkylating agents has also influence upon the alkylation. Although the results listed in Table 2 have been obtained under the different reaction conditions, the formation of enol ethers by methylating agents obviously depends on the nature of the leaving groups. In accordance with the hard soft acid base principle[20] the leaving group effects have been explained in terms of the symbiotic stabilization of the transition state; the more essential stabilization must be expected when both the leaving group and nucleophile are soft (or hard) Lewis bases.[21] Our results obtained by dimethyl sulfite, relatively high O/(C+C,C)-alkylation ratio, may be ascribed to that methyl sulfite anion as leaving group displays a fairly hard base, since the oxygen atom of enolate anions is a hard center.

The methylation in liquid SO_2 proceeds in a heterogeneous system which is rather assist to obtain the C-isomers. The observed O/(C+C,C)-alkylation ratio in liquid SO_2 is rather strangeness on the basis of the results obtained in aprotic and electron donating solvents, HMPA, DMSO, and DMF. Liquid SO_2 is also dipolar aprotic solvent, but behaves as an electron acceptor toward most of olefins and a large number of organic compounds having lone pair electrons.[22] Solvation of liquid SO_2 to alkali metal cations is not conceivable. Effects of liquid SO_2 is probably due to the stabilization for leaving groups, *i.e.*, methyl sulfite anion may be stabilized by the presence of electron accepting liquid SO_2.

Experimental

Solvents, HMPA, DMSO, DMF, diglyme, and liquid SO_2, were purified by usual methods. The alkali metal enolates of ethyl acetoacetate were prepared by addition of ethyl acetoacetate to the corresponding ethoxide salts, followed by the careful removal of ethanol and the dissolution of the remaining solid in solvent. Dimethyl sulfite was enclosed in the glass ampoule which was broken in a closed reaction vessel containing the alkali metal enolate of ethyl acetoacetate solution. Quantitative analysis of the four products was carried out by means of VPC.

References

1) R. Chong and P. S. Clezy, *Tetrahedron Lett.*, **1966**,

741.
2) W. J. Noble and J. E. Puerta, *Tetrahedron Lett.*, **1966**, 1087.
3) W. J. Noble and H. Morris, *J. Org. Chem.*, **34**, 1969 (1969).
4) A. L. Kurts, A. Macias, I. P. Beletskaya, and O. A. Reutov, *Tetrahedron*, **27**, 4759 (1971).
5) A. L. Kurts, P. I. Dem'yanov, A. Macias, I. P. Beletskaya, and O. A. Reutov, *Tetrahedron*, **27**, 4769 (1971).
6) A. L. Kurts, N. K. Genka, A. Macias, I. P. Beletskaya, and O. A. Reutov, *Tetrahedron*, **27**, 4777 (1971).
7) Y. Hara and M. Matsuda, *J. Org. Chem.*, **40**, 2786 (1975).
8) M. Matsuda, F. Akiyama, and Y. Hara, *Kobunshi Kagaku*, **32**, 660 (1975).
9) H. F. Van Woerden, *Chem. Rev.*, **63**, 557 (1963).
10) S. Winstein and G. C. Robinson, *J. Am. Chem. Soc.*, **80**, 169 (1958).
11) R. V. Slates and M. Szwarc, *J. Am. Chem. Soc.*, **89**, 6043 (1967).
12) V. Gutmann, "Coordination Chemistry in Non-aqueous Solutions," Springer-Verlag, Berlin (1968).
13) A. J. Parker, *Chem. Rev.*, **69**, 1 (1969).
14) T. E. Hogen-Esch and J. Smid, *J. Am. Chem. Soc.*, **89**, 669 (1965); *ibid.*, **88**, 307 (1966).
15) T. Miyashita, T. Aoki, and M. Matsuda, *Bull. Chem. Soc. Jpn.*, **49**, 231 (1976).
16) N. Kornblum, R. Seltzer, and P. Haberfield, *J. Am. Chem. Soc.*, **85**, 1148 (1963).
17) H. Zook and J. Miller, *J. Org. Chem.*, **36**, 1112 (1971).
18) L. L. Chan, K. H. Wong, and J. Smid, *J. Am. Chem. Soc.*, **92**, 1955 (1970).
19) H. E. Zaugg and A. D. Schaefer, *J. Am. Chem. Soc.*, **87**, 1857 (1965).
20) R. G. Pearson and J. Songstad, *J. Am. Chem. Soc.*, **89**, 1827 (1967).
21) R. G. Pearson and J. Songstad, *J. Org. Chem.*, **32**, **2899** (1967).
22) M. Matsuda, M. Iino, T. Hirayama, and T. Miyashita, *Macromolecules*, **5**, 240 (1972).

The Enzyme-like Reaction Catalyzed by Flavin-Reduced Keratin Systems

Fujio Takahashi, Tatsuo Ogasa, Morio Hirano, and Shuichi Suzuki

Research Laboratory of Resources Utilization, Tokyo Institute of Technology, Meguro-ku, Tokyo 152

(Received October 24, 1975)

The reduced keratin (RK), which was obtained by the reductive cleavage of human hair, was found to act as an apoenzyme and to furnish the reaction field for flavin adenine dinucleotide (FAD): the absorbance of the succinic acid–FAD–RK system in solution increased in the region of 200—250 nm with the lapse of time. From this system fumaric acid was isolated. FAD was found to form a complex with RK and the FAD–RK complex exhibited a catalytic activity for the dehydrogenation reaction of succinic acid to fumaric acid. FAD was reduced in this reaction and the reduced FAD was oxidized by oxygen. It was found that the process of the dehydrogenation reaction obeyed the Michaelis-Menten kinetics; the equilibrium constants of the complex formation between FAD and RK were determined by measuring the initial velocities of the dehydrogenation reaction. The binding site of FAD and RK in the complex was discussed.

It has been known that a coenzyme locates in the active center of an enzyme and exhibits a catalytic activity which can not be realized without an apoenzyme.[1,2] As a plausible speculation, we would assume that an apoenzyme might furnish a coenzyme with a reaction field, in which the coenzyme could exhibit the catalytic activity. If this assumption is true, we can expect that a catalytic reaction may occur in a solution containing the coenzyme combined with a compound which could produce the reaction field, like apoenzyme.

Keratin is known to be one of the albuminoids and contains 10—15% cystine residues, which can be reduced to form thiol groups.[3] The physico-chemical properties of RK obtained by the reductive cleavage of human hair have already been reported.[4] It was expected in the viewpoint of practical use that RK might be utilized as a catalyst. Alcohol dehydrogenase and succinate dehydrogenase are known to be thiol enzymes.[3] The former contains nicotinamide adenine dinucleotide (NAD) and the latter FAD as the coenzyme, respectively. Supposing a thiol group can stimulate NAD and FAD to exhibit the catalytic activity, RK may furnish the reaction field for NAD and FAD.

Aiming at the preparation of an artificial enzyme and the practical use of keratin in our study, preliminary experiments were made for an ethanol–NAD–RK system and a succinic acid–FAD–RK system. No reaction was found to occur in the former case. On the other hand it was found that the dehydrogenation of succinic acid to fumaric acid occurred in the latter case as follows:

$$\mathrm{FAD} + \mathrm{RK} \rightleftharpoons \mathrm{FAD{\cdot}RK} \tag{1}$$

$$\mathrm{FAD{\cdot}RK} + \text{Succinic acid} \underset{k_{-1}}{\overset{k_1}{\rightleftharpoons}} \mathrm{FAD{\cdot}RK{\cdot}Succinic\ acid\ complex} \xrightarrow{k_2} \mathrm{FADH_2RK} + \text{Fumaric acid} \tag{2}$$

$$\mathrm{FADH_2RK} + 1/2\mathrm{O_2} \longrightarrow \mathrm{FAD{\cdot}RK} + \mathrm{H_2O} \tag{3}$$

The dehydrogenation of succinic acid catalyzed by a FAD and FAD-protein system has not been known so far. Takemoto *et al.* have reported the redox reaction of isoalloxazine residues which are introduced in the vinyl polymer, but they did not discuss the reaction field in the polymer.[5]

This paper will present the results of spectrophotometric studies for the verification of Eqs. 1—3 and the isolation of the reaction product.

Calculation

The association constant, K, in Eq. 1 is expressed as

$$K = \frac{[\mathrm{FAD{\cdot}RK}]}{[\mathrm{FAD}][\mathrm{RK}]} \tag{4}$$

where [FAD], [RK], and [FAD·RK] are the concentrations of free FAD, free RK, and the FAD–RK complex. The value of K can be determined by Eq. 10, which is obtained by the following derivation. If the reaction in Eq. 2 obeys the Michaelis-Menten kinetics and makes the rate-determining step, then the initial velocity, v_0, of the succinate dehydrogenation could be expressed as:

$$v_0 = k_2[\mathrm{FAD{\cdot}RK{\cdot}S}] \tag{5}$$

where [FAD·RK·S] is the concentration of the three component complex of FAD, RK, succinic acid.

When the condition of the reactions of Eqs. 2 and 3 reach the steady state, the following equation is given:

$$\frac{\mathrm{d}[\mathrm{FAD{\cdot}RK{\cdot}S}]}{\mathrm{d}t} = k_1[\mathrm{FAD{\cdot}RK}][\mathrm{S}] - (k_{-1}+k_2)[\mathrm{FAD{\cdot}RK{\cdot}S}] = 0 \tag{6}$$

The Michaelis constant, K_m, is expressed as:

$$K_\mathrm{m} = \frac{k_{-1}+k_2}{k_1} \tag{7}$$

Therefore from Eqs. 6 and 7 we obtain,

$$K_\mathrm{m} = \frac{[\mathrm{FAD{\cdot}RK}][\mathrm{S}]}{[\mathrm{FAD{\cdot}RK{\cdot}S}]} \tag{8}$$

where [S] is the concentration of succinic acid. Let F, R, and S be the concentration of total FAD, total RK, and total succinic acid. And let R and S be greater then F, and S be constant; then

$$\left.\begin{aligned} \mathrm{F} &= [\mathrm{FAD}] + [\mathrm{FAD{\cdot}RK}] + [\mathrm{FAD{\cdot}RK{\cdot}S}] \\ &\ll \mathrm{R} \fallingdotseq [\mathrm{RK}] \\ \mathrm{F} &\ll \mathrm{S} \fallingdotseq [\mathrm{S}] \end{aligned}\right\} \tag{9}$$

From Eqs. 4, 5, 8, and 9, the following equation is obtained:

$$\frac{1}{v_0} = \left(\frac{K_\mathrm{m}}{k_2\mathrm{FSK}}\right)\left(\frac{1}{\mathrm{R}}\right) + \frac{1}{k_2\mathrm{F}}\left(1+\frac{K_\mathrm{m}}{\mathrm{S}}\right) \tag{10}$$

From Eq. 10, a plot of $1/v_0$ *vs.* 1/R yields a straight line, from which the value of K can be determined.

Experimental

Materials. The RK was prepared in the same way as was described in the previous paper.[4] The molecular weight of RK was 4500 (by viscometry). Thiol group: 0.21 mg-eq/g and S content: 2.7%. All the other chemicals were of reagent grade or the best commercially available.

The Measurements of Initial Velocities. Stock solutions of 2.5×10^{-5} M FAD, 2.5×10^{-4} M RK, and various concentrations of succinic acid in 1/30 M phosphate buffer were prepared. The requisite amounts of FAD and RK stock solutions were poured into 10-ml volumetric flasks and enough 1/30 M phosphate buffer were added to reach the 10-ml mark. The sample solution was prepared by pipetting 4 ml of FAD-RK solution out of the volumetric flask and adding it into 1 ml of succinic acid solution. The reference solution contains the same concentration of FAD and RK as the sample solution, except that succinic acid is omitted. The initial velocities were determined from the slopes of absorbance-time curves which were obtained by measuring the absorbance change at 225 nm ($\varepsilon=5.7\times10^3$) and 240 nm ($\varepsilon=2.1\times10^3$) for fumaric acid with the lapse of time. Measurements of absorption spectra were made with a Shimadzu spectrophotometer UV-200 at controlled temperatures.

Results and Discussion

Absorbance-Time Relation for the Flavin–RK–Succinic Acid Systems. Various flavins and/or RK were dissolved into 1/30 M phosphate buffer (pH 7.5) and then succinic acid was added. With these solutions differential absorption spectra were measured. The absorbance of each solution was found to increase in the region of 200—250 nm and the absorption maximum at 206 nm appeared in the case of the FAD-solution (inserted figure in Fig. 1). The results for the absorbance (at 225 nm) *vs.* time relation are shown in Fig. 1. The initial velocity was calculated from the slope of each line at zero time in Fig. 1. No reaction occurred without flavin. The initial velocities in the solution containing riboflavin (RF), flavin mononucleotide (FMN), and FAD were obtained to be 4×10^{-8}, 2×10^{-8}, and 5×10^{-7} M/min, respectively.

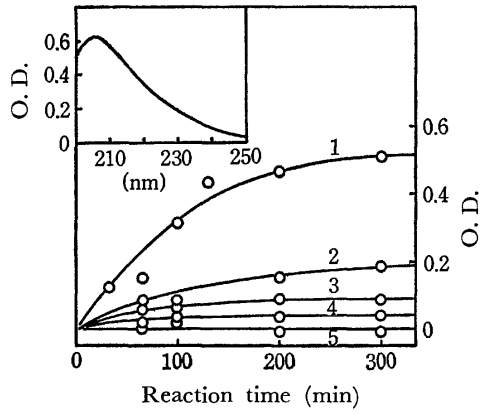

Fig. 1. The absorbance change during reaction. 1/30 M Phosphate buffer (pH 7.5), 35 °C. FAD, FMN, RF: 1.0×10^{-5} M, RK: 1.3×10^{-4} M, Succinic acid (S): 1.0×10^{-4} M. 1: S-FAD-RK, 2: S-RF-RK, 3: S-FMN-RK, 4: S-FAD, 5. S-RK.

ly. It could be thought that the adenine moiety of FAD might combine with RK to form a complex. A little activity (2×10^{-8} M/min) was observed in the case of FAD-succinic acid solution without RK. From this fact, it could be speculated that RK might furnish FAD with the reaction field, as was expected. Paper chromatogram (1-butanol : formic acid : water=10 : 2 : 15)[6] of the succinic acid–FAD–RK system showed one spot (R_f=0.73), assigned to be succinic acid, before reaction. Another spot (R_f=0.84), assigned to be fumaric acid, appeared with the lapse of time. Maleic acid (R_f=0.46) was not found. From the results of absorption spectra and paper chromatography it was suggested that succinic acid was dehydrogenated to form fumaric acid in this reaction.

The absorbance (at 450 nm) of the succinic acid–FAD–RK system, through which nitrogen gas was passed, was found to decrease with the lapse of time and increase again by the aeration. It can be thought that FAD may be reduced to form reduced FAD ($FADH_2$) during the reaction and $FADH_2$ may be reoxidized by oxygen. These results suggested that Eq. 2 might be the rate-determining step in the reaction of Eqs. 2 and 3.

Isolation of Fumaric Acid. Fumaric acid was isolated from the solution of the succinic acid–FAD–RK system as follows: Into distilled water, 5 mmol (590 mg) succinic acid, 1 mmol FAD, and 1.3 mmol RK were dissolved, and sodium hydroxide solution was added to adjust to pH 7.0. Finally, the total volume of the mixture was set to 1000 ml by adding distilled water. The solution was allowed to stand at 25 °C with occasional aeration. The reaction was broken off after 4 days because of the coagulation of RK. The conversion of succinic acid to fumaric acid was estimated to be nearly 20% by the determination of absorption spectra. The solution of the succinic acid–FAD–RK system was concentrated by evaporation and adjusted to pH below 1 by adding hydrochloric acid. Precipitation occurred. Precipitates were separated by centrifugation and then suspended in methanol. The methanol solution separated from insoluble matter was evaporated. The extraction with ethyl ether was carried out and ether was removed from the extract. A white crystal from the residual matter was obtained by recrystallization from water. Yield: 23 mg. The yield can be raised if the separation processes are repeated. The elemental analysis: Found: C, 41.0; H, 3.8%. Calcd for fumaric acid ($C_4H_4O_4$), C, 41.4; H, 3.5%. NMR: 6.84 ppm, singlet in CD_3OD (succinic acid: 2.57, maleic acid; 6.40 ppm).

It was found that a higher yield of fumaric acid could not be obtained because of the activity change of the FAD–RK system during the reaction or the preservation in solution. A stock solution of 1/30 M phosphate buffer (pH 7.5) containing 1.1×10^{-5} M FAD and 1.4×10^{-4} M RK was prepared and divided into two parts. One was bubbled by air, and nitrogen gas was passed through the other. Both were preserved at 25 °C. After the requisite time each was mixed with 1/30 M phosphate buffer (pH 7.5) containing succinic acid and the mixture was aerated. After

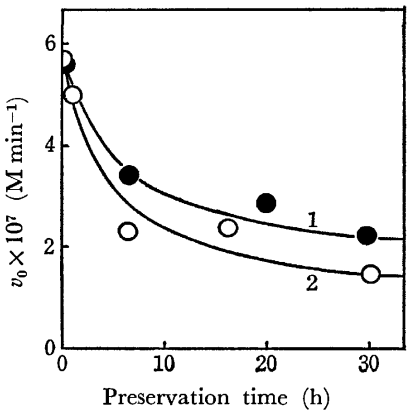

Fig. 2. Activity changes of FAD-RK systems during preservation. 1: Nitrogen gas passed. 2: Aerated.

that the initial velocity of the reaction was calculated by measuring the absorbance change at 225 nm. The mixture contained 1.0×10^{-5} M FAD, 1.3×10^{-4} M RK, and 1.0×10^{-4} M succinic acid. The activities were found to decrease during the preservation, as showin in Fig. 2. The activity change in the solution containing oxygen was larger. Oxidation of RK by oxygen might be the cause of the activity change.

pH Profile. The initial velocities at different pH were determined at 35 °C to obtain the optimum pH for the dehydrogenation of succinic acid. The sample solutions were composed of 1.0×10^{-5} M FAD, 1.0×10^{-4} M RK, and 2.0×10^{-4} M succinic acid in 1/30 M phosphate buffer (pH 6.6—8.4). The optimum pH was found to be in the region of pH 7.5—7.7 (Fig. 3).

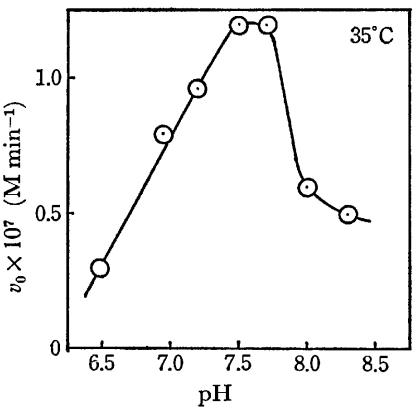

Fig. 3. pH profile.

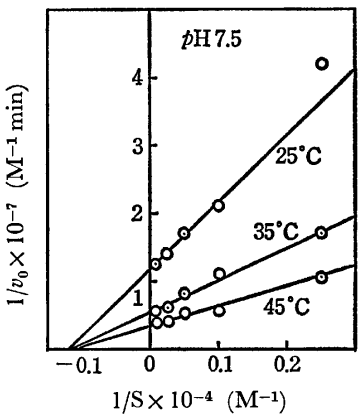

Fig. 4. Lineweaver-Burk plots.

Michaelis-Menten Kinetics. The final concentrations of FAD, RK, and succinic acid in 1/30 M phosphate buffer (pH 7.5) were 1.0×10^{-5}, 1.0×10^{-4}, and 0—10×10^{-4} M, respectively. The initial velocities were measured at different temperatures. The Lineweaver-Burk plots fell on straight lines (Fig. 4), which means that the reaction obeys Michaelis-Menten kinetics. From the straight lines the values of K_m and V_{max} were calculated. The results are summarized in Table 1. The reaction velocity at 60 °C decreased lower than that at 45 °C.

Table 1 Maximum velocities, michaelis constants, and equilibrium constants

	25 °C	35 °C	45 °C
V_{max} (M min^{-1})	8.7×10^{-8}	2.0×10^{-7}	3.3×10^{-7}
K_m (M)	8.7×10^{-5}	9.4×10^{-5}	1.0×10^{-4}
K (M^{-1})	3.8×10^{3}	3.7×10^{3}	3.5×10^{3}

The K_m values of the succinic acid–FAD–RK complex are about half as big as that of the succinate dehydrogenase.[7]

Equilibrium Constant of FAD–RK Complex. The final concentrations of FAD, succinic acid, and RK in 1/30 M phosphate buffer (pH 7.5) were 1.0×10^{-5}, 2.0×10^{-4}, and 0—2.0×10^{-4} M, respectively. Plots of $1/v_0$ *vs.* 1/R gave straight lines, as shown in Fig. 5, from which the assumptions for the derivation of Eq. 10 seemed to be verified. The values of K were calculated (Table 1) by using Eq. 10 with the K_m values and slopes and intercepts obtained from the straight lines. In the solution containing 1.0×10^{-5} M FAD, 1.0×10^{-4} M RK, and 1.0×10^{-3} M succinic acid, 80% (25 °C), 79% (35 °C), and 77% (45 °C) of FAD forms the succinic acid–FAD–RK complex, whose concentration can be calculated from K_m and K values. In turn, the values of k_2 can be obtained to be 1.1×10^{-2} (25 °C), 2.6×10^{-2} (35 °C), and 4.4×10^{-2} (45 °C) min^{-1} from Eq. 5 with the values of V_{max}. These values are 10^5 time smaller than that of succinate dehydrogenase.[7] The activation energy was determined to be 13 kcal/mol from an Arrhenius plot, using the values of k_2 (Fig. 6). The values of enthalpy change and entropy change of the formation

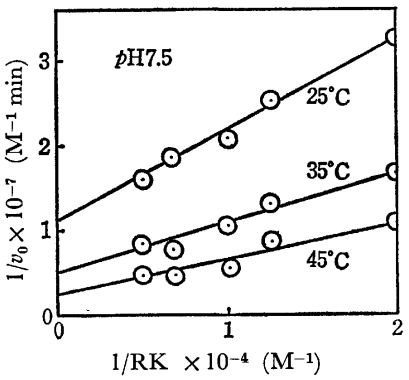

Fig. 5. Plots of $1/v_0$ *vs.* 1/RK.

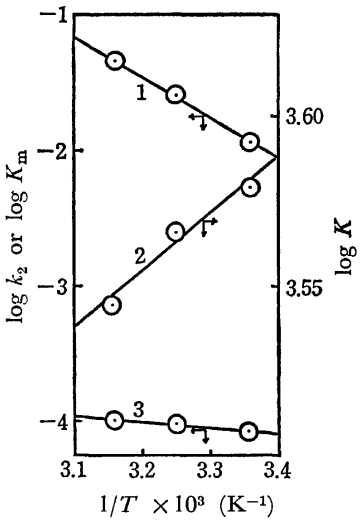

Fig. 6. van't Hoff's plots and Arrhenius plot.
1: log k_2-1/T plot, 2: log K-1/T plot, 3: log K_m-1/T plot.

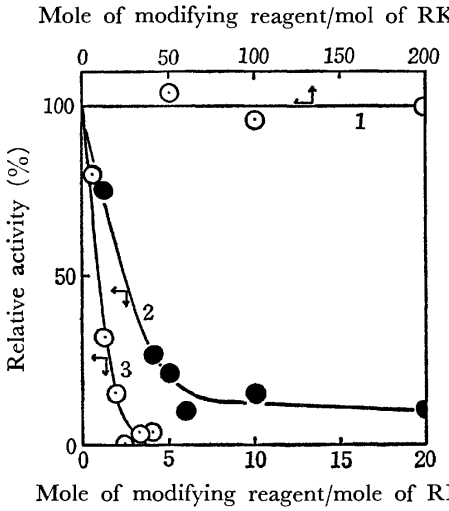

Fig. 7. Effect of the modifying reagents to the catalytic activity of FAD-RK complex.
1: *N*-Acetylimidazole, 2: Glyoxal, 3: *p*-Chloromercuribenzoate.

Table 2. The thermodynamic parameters

	ΔH kcal/mol	ΔS e. u.
FAD-RK complex formation	−0.8	+14
Succinic acid-FAD-RK complex formation	−1.3	+15

of the FAD–RK complex and the succinic acid–FAD–RK complex calculated by the van't Hoff's plots (Fig. 6) are summarized in Table 2.

It is known that the overall entropy changes for the formation of an ES complex in many enzymatic reactions give positive values caused by the elimination process of water molecules. It is plausible that a similar process may occur in the formation of the FAD-RK complex and the succinic acid–FAD–RK complex.

The Amino Acid Residues' Part in Catalytic Activity. Various chemical modification reagents were added to the RK solution in order to modify the specific functional groups in RK, and the amino acid residues which play a part in the catalytic activity were assigned from the changes of the reaction velocity caused by the modification of the amino acid residues.

p-Chloromercuribenzoic acid, *N*-acetylimidazole, and glyoxal were used for the chemical modification reagents of cysteine, tyrosine, and arginine residues, respectively.[8–10] The results are summarized in Fig. 7.

The modification of thiol groups made the FAD–RK system inactive. It is very possible that the thiol group participates in the catalysis. However a question still remains: A bulky group of *p*-mercuribenzoate may hinder sterically the complex formation for the dehydrogenation. The initial velocity in the FAD solution containing RK modified by glyoxal is comparable to that in the FMN–RK system. It seems that the adenine moiety of FAD may not interact with modified RK. The arginine residue in RK may made a binding site for the adenine moiety of FAD. Tyrosine residues may not play any part in the catalytic activity.

As a conclusion we suggest that the FAD–RK complex can be formed by the interaction between an arginine residue of RK and an adenine moiety and pyrophosphate linkage of FAD, and that the catalytic activity can be exhibited by the interaction between an isoalloxazine moiety of FAD and a thiol group of RK.

The FAD–RK complex cannot be a model of succinate dehydrogenase, because succinate dehydrogenase is an iron-sulfur flavoprotein and the product of reduced flavin and oxygen is hydrogen peroxide, not water. However, it is significant that the FAD–RK complex exhibits the catalytic activity of an artificial enzyme.

References

1) M. L. Bender, "Mechanism of Homogenous Catalysis from Protons to Proteins," Wiley-Interscience, New York (1971), p. 539.
2) E. T. Kaiser and F. J. Kézdy, "Progress in Bioorganic Chemistry," Wiley-Interscience, Vol. 1, New York (1971), p. 106.
3) M. Friedman, "The Chemistry and Biochemistry of the Sulfhydryl Group in Amino Acids, Peptides, and Proteins," Pergamon, Braunschweig (1973), pp. 205, 362.
4) F. Takahashi, T. Ogasa, and S. Tanaka, *Nipopn Kagaku Kaishi*, **1975**, 738.
5) K. Kondo, T. Fujita, and K. Takemoto, *Makromol. Chem.*, **174**, 7 (1973).
6) G. Zweig and J. Sherma, editors, "Handbook of Chromatography," Vol. 1, CRC Press, Cleveland (1972), p. 299.
7) C. L. Tober, P. Nicholls, and J. D. Brodie, *Arch. Biochem. Biophys.*, **138**, 506 (1970).
8) P. D. Boyer, *J. Am. Chem. Soc.*, **76**, 4331 (1954).
9) K. Shibata, "The Experiments of Biochemistry C-1 (in Japanese)," University of Tokyo Press, (1969), pp. 40, 94, 103.
10) R. T. Simpson, J. F. Riordan, and B. L. Vallee, *Biochemistry*, **2**, 616 (1963).

Backbone Rearrangements of 3α,4α-Epoxyshionane into Bacchar-12-en-3α-ol and D : B-Friedo-bacchar-5(10)-en-3α-ol[1]

Shûzô YAMADA, Sachiko YAMADA, Kazuo TACHIBANA, Yoshihiko MORIYAMA, Yoshiaki TANAHASHI, Takahiko TSUYUKI, and Takeyoshi TAKAHASHI

Department of Chemistry, Faculty of Science, The University of Tokyo, Bunkyo-ku, Tokyo 113

(Received November 26, 1975)

Upon treatment with boron trifluoride etherate, 3α,4α-epoxyshionane (**7**) rearranged into bacchar-12-en-3α-ol (**9**) and D : B-friedo-bacchar-5(10)-en-3α-ol (**10**), and their structures have been determined. Revision of the structure for the latter product from previously reported D : C-friedo-bacchar-8-en-3α-ol (**20**) to **10** was described.

A structure of baccharis oxide,[2] obtained from dried roots of *Baccharis halimifolia* L., has been proposed as **1b**[2,3] and then revised to **1a** by X-ray study.[4] Dihydrobaccharis oxide was shown to rearrange into bacchar-12-en-3β-ol (**2**) by treatment with boron trifluoride etherate.[2]

Being interested in close biogenetic relationship between baccharis oxide (**1a**) and shionone (**3**)[5,6] and in their acid-catalyzed backbone rearrangements, we examined a backbone rearrangement reaction of 3α,4α-epoxyshionane (**7**) catalyzed by boron trifluoride etherate.

Shion-3-ene (**6**),[7] prepared from shionone (**3**) *via* shionan-3-one (**4**) and shionan-3β-ol (**5**), was subjected to epoxidation with *m*-chloroperbenzoic acid in benzene at room temperature. The reaction mixture was separated by silica gel chromatography to give two epoxides in a ratio of *ca.* 7 : 3. Assignment of the epoxide group was easily accomplished by PMR measurement using Eu(fod)$_3$-d_{27} as a shift reagent.

The signals due to all methyl groups of the minor epoxide suffered downfield shifts (Fig. 1), while in the case of the major epoxide the signals due to four methyl groups suffered downfield shifts and the signals due to other four methyl groups caused upfield shifts (Fig. 2). Assuming that the shift reagent is associated with the epoxide oxygen atom as shown in Figs. 1 and 2, the fact that the signals due to the four methyl groups caused upfield shifts would be explicable only in the case of 3α,4α-epoxyshionane (**7**) and these four methyl groups could be assigned to 13α-, 20β-, and the side chain two methyl groups which would be placed outside of a cone area suffered an upfield shift (Fig. 2). The epoxide ring of the major epoxide (**7**) was thus shown to be in an α-configuration. The 3β,4β-epoxide structure (**8**) follows for the minor isomer.

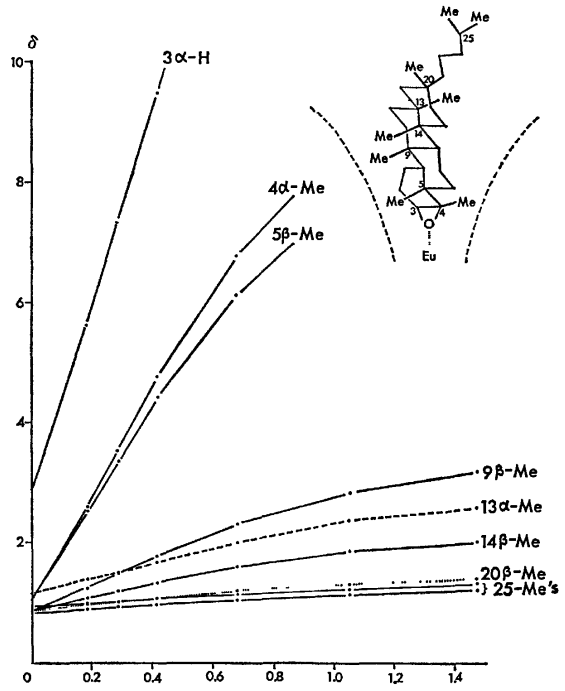

Fig. 1. Induced paramagnetic shifts for the 3β,4β-epoxide (**8**). [Eu(fod)$_3$-d_{27} was added to a 4% (w/v) solution of **8** in $CDCl_3$].

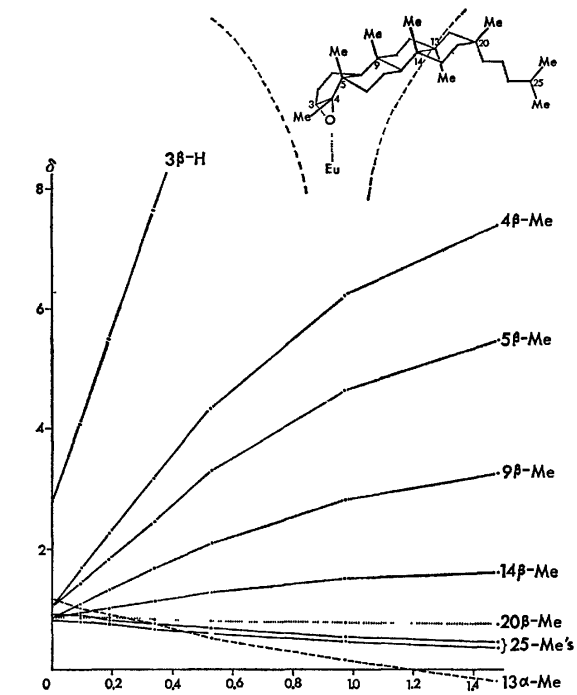

Fig. 2. Induced paramagnetic shifts for the 3α,4α-epoxide (**7**). [Eu(fod)$_3$-d_{27} was added to a 4% (w/v) solution of **7** in $CDCl_3$].

3α,4α-Epoxyshionane (**7**) in dry benzene was treated with boron trifluoride etherate at room temperature. Examination by thin layer chromatography (TLC) showed that the starting material was consumed within 10 min and that a complex mixture was formed. The resulting mixture was separated by column chro-

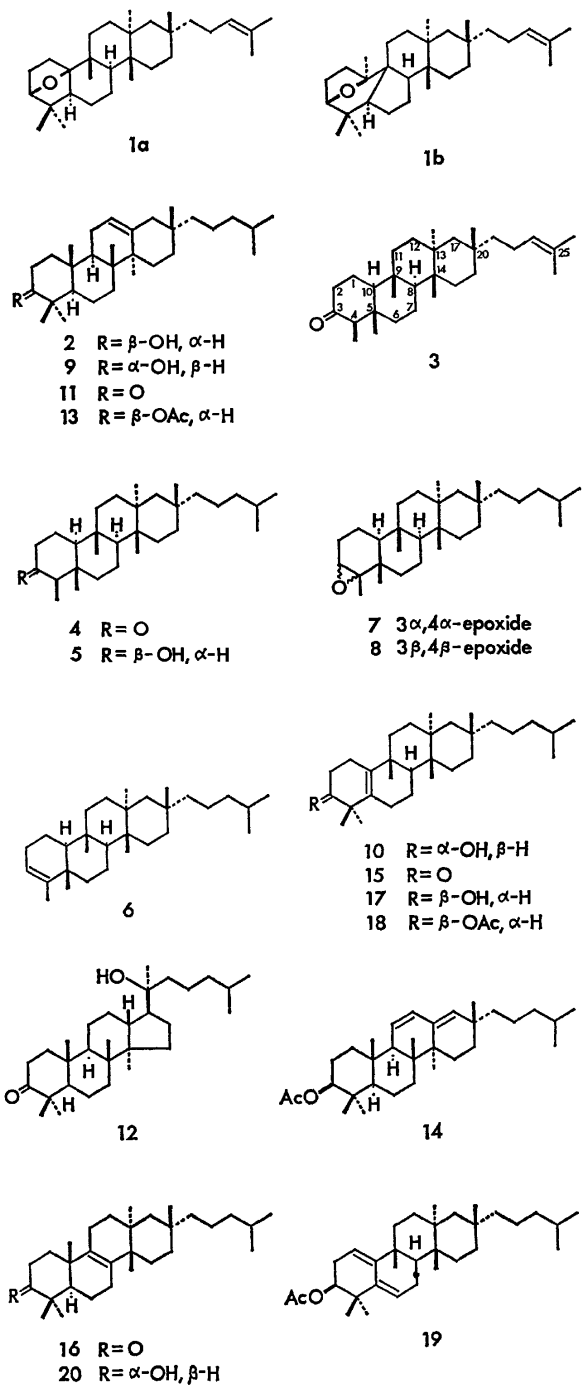

matography to give a mixture, which was later shown to be a mixture of bacchar-12-en-3α-ol (**9**) and D : B-friedo-bacchar-5(10)-en-3α-ol (**10**).

The mixture (**9** and **10**) without further separation was then subjected to the Collins oxidation to give after column chromatographic separation two unsaturated ketones (**11** and **15**).

A more polar ketone, crystallized from methanol, showed mp 111—112 °C (previously reported 102—102.5 °C[1]); IR (Nujol) 1710 and 815 cm^{-1}, and was shown to be bacchar-12-en-3-one (**11**) by the following evidence and derivation. The enone (**11**) showed PMR signals at δ 2.43 (2H, m) and 5.27 (1H, t-like, J=*ca.* 2 Hz). The former signal due to α-methylene protons to the carbonyl group is similar to those of triterpenes bearing 3-oxo-4,4,10-trimethyl moiety such as β-amyrone and lupenone. The latter signal is due to an olefinic proton. The CD data of **11** ($[\theta]_{290}$+2600, $[\theta]_{325}$−90 in methanol) was almost the same as those of dipterocarpol (**12**).[8] The A/B/C ring junctures were therefore suggested to be the same as those of **12**.

Reduction of bacchar-12-en-3-one (**11**) with sodium borohydride gave an alcohol. On column chromatographic separation followed by crystallization from methanol, there obtained pure bacchar-12-en-3β-ol [**2**; mp 143.5—144 °C (lit,[2] 147—148 °C); M^+ at *m/e* 428 (lit,[2] 428.403); $[\alpha]_D$ +55° (lit,[2] +39°)]. The PMR signals due to an axial proton at C-3 bearing an equatorial hydroxyl group were observed at δ 3.23 as double doublets (J=5 and 8 Hz) and an olefinic proton at C-12 resonated at δ 5.11 as a multiplet. On acetylation with acetic anhydride and pyridine, bacchar-12-en-3β-ol (**2**) afforded an acetate (**13**; mp 177—178 °C. lit,[2] 181—182 °C).

The acetate (**13**) was treated with selenium dioxide in acetic acid at 85 °C for 4 h to give bacchara-11,13-(17)-dien-3β-yl acetate[6] [(**14**; UV λ_{max}^{EtOH} 250 nm (ε 12500), 241 (19400), and 234 (17000); M^+ at *m/e* 468]. The PMR, UV, and mass spectral data were completely identical with those of the authentic sample[2] which was kindly donated from Dr. T. Bruun.

A less polar ketone (**15**) was previously reported as D : C-friedo-bacchar-8-en-3-one (**16**) on the basis of the following evidence. The ketone showed no signals due to olefinic proton and the molecular formula was shown to be $C_{30}H_{50}O$ by the elemental analysis and the mass spectrometry. These findings suggested that the ketone must contain a tetrasubstituted double bond and could be formulated as either D : C-friedo-bacchar-8-en-3-one (**16**) or D : B-friedo-bacchar-5(10)-en-3-one (**15**). The previously reported melting point, 174.5—177.5 °C[1] was not coincident with that of D : B-friedo-bacchar-5(10)-en-3-one (mp 78—80 °C[9]), which was prepared from shionan-3-one (**4**). These facts led to the conclusion that the ketone was not D : B-friedo-bacchar-5(10)-en-3-one (**15**), but was, instead, D : C-friedo-bacchar-8-en-3-one (**16**).

However, on reinvestigation of the less polar ketone, it was found that the melting point was 84—84.5 °C and the previously reported melting point (174.5—177.5 °C) was that of the decomposition product. The misinterpretation seemed to be mainly due to a fragility of the ketone. Thus, it is shown that the previous assignment (**16**) must be withdrawn and the ketone should be represented by D : B-friedo-bacchar-5(10)-en-3-one (**15**). The conclusion was supported by a direct comparison (mp, mixed mp (84—84.5 °C), TLC, IR and PMR spectra) with D : B-friedo-bacchar-5(10)-en-3-one (**15**; 84—84.5 °C), prepared from shionan-3-one (**4**) *via* D : B-friedo-bacchara-1,5(10)-dien-3-one.[10]

The ketone (**15**) was reduced with sodium borohydride to give D : B-friedo-bacchar-5(10)-en-3β-ol (**17**), mp 140.5—141 °C (lit, mp 135—136 °C[1]; 140.5—141 °C[9]; 141.5—142 °C[10]). The PMR signals due to 3α-(axial) proton were observed at δ 3.42 as double doublets (J=5 and 10 Hz).

The alcohol (**17**) was converted by a usual procedure into an acetate (**18**), mp 147—148 °C. Oxidation of the acetate (**18**) with selenium dioxide in acetic acid under reflux gave D : B-friedo-bacchara-1(10),5-dien-3β-yl acetate (**19**), mp 123—123.5 °C, which showed characteristic ultraviolet absorption bands due to heteroannular transoid dienone at 248 (sh. ε 12100), 238 (20900), and 231 nm (19400).[11]

The formation of the alcohols (**9** and **10**) from the α-epoxide (**7**) by boron trifluoride etherate-catalyzed rearrangement was thus shown. The structure of D : C-friedo-bacchar-8-en-3α-ol (**20**)[1] previously given for the latter product (**10**) should be revised to **10**.

Experimental

IR and UV spectra were measured on a Hitachi EPI-G2 and EPS-2 spectrometers, respectively. Mass spectra were taken on a Hitachi RMU-6-Tokugata mass spectrometer operating at 70 eV with a direct inlet system. PMR spectra were measured using a JEOL JNM PS-100 (100 MHz), a Hitachi R-20 (60 MHz) or a Hitachi R-24 (60 MHz) spectrometer. Chemical shifts were expressed in ppm downfield from TMS as an internal standard (δ value) and coupling constants in Hz. ORD and CD measurements were carried out on a JASCO ORD/UV-5 spectrometer. Measurements of optical rotation were carried out using a JASCO polarimeter DIP-SL. Thin layer chromatography (TLC) was carried out on Kieselgel G or PF_{254} (E. Merck) in 0.25 mm thickness. Wakogel C-200 (Wako Pure Chemical Ind.) was used for column chromatography. All melting points were determined on a hot block and reported uncorrected.

*3α,4α-Epoxyshionane (**7**).* A solution of *m*-chloroperbenzoic acid (516 mg) in benzene (12 ml) was added to shion-3-ene[7] (**6**; 1.00 g) in benzene (10 ml) at room temperature. The reaction mixture was allowed to stand for 1.5 h, and washed with a saturated sodium hydrogencarbonate solution and then with brine. After usual work-up, a residue (1.04 g), which gave two spots on TLC, was subjected to silica gel chromatographic separation quickly. 3α,4α-Epoxyshionane (**7**; 0.70 g) was eluted with benzene and crystallized from acetone to give colorless needles, mp 147—148 °C; PMR (100 MHz, $CDCl_3$) δ 0.86 (s; 3×*t*-CH_3), 0.87 (d, J=5.5 Hz; 2×*s*-CH_3), 1.04 (s; 2×*t*-CH_3), 1.17 (s; *t*-CH_3), and 2.83 (t, J=3 Hz; $C_{(3)}$–H); mass spectrum *m/e* 428 (M^+); Found: C, 84.12; H, 12.37%. Calcd for $C_{30}H_{52}O$: C, 84.04; H, 12.21%.

Further elution with the same eluent afforded 3β,4β-epoxyshionane (**8**; 0.28 g) mp 154—155 °C; PMR (100 MHz, $CDCl_3$) δ 0.86 (s: 3×*t*-CH_3), 0.88 (d, J=5 Hz; 2×*s*-CH_3), 1.05, 1.06, 1.16 (each s; *t*-CH_3), and 2.89 (t, J=*ca.* 1 Hz; $C_{(3)}$–H); mass spectrum *m/e* 428 (M^+); Found: C, 84.00; H, 12.14%. Calcd for $C_{30}H_{52}O$: C, 84.04; H, 12.21%.

The PMR spectral data using Eu(fod)$_3$-d_{27} as a shift reagent were given in Figs. 1 and 2.

*Reaction of 3α,4α-Epoxyshionane (**7**) with Boron Trifluoride Etherate.* To a solution of 3α,4α-epoxyshionane (**7**; 1.00 g) in benzene (40 ml, dried over sodium), freshly distilled boron trifluoride etherate (1.0 ml) was added with swirling. The reaction was monitored by TLC examination. After 10 min, the starting material completely disappeared and two new major spots were observed on TLC. The reaction was stopped by addition of a saturated sodium hydrogencarbonate solution, and the organic layer was washed with brine, dried over sodium sulfate, and evaporated to give a colorless oil (1.13 g).

The resulting oil was dissolved in benzene, passed through a column of silica gel (200 g), and eluted with the following solvents (each fraction 100 ml): frs 1—15, benzene; frs 16—19, benzene–ether (97 : 3). From fractions 6—9, a mixture of alcohols (**9** and **10**; 598 mg) was obtained.

*Collins Oxidation of the Alcohol Mixture (**9** and **10**).* The alcohol mixture (**9** and **10**; 596 mg), without further separation, was dissolved in dichloromethane (11 ml) and added to the Collins reagent (prepared from chromium trioxide (0.844 g), dry pyridine (1.4 ml), and dichloromethane (10 ml, dried over Zeolite)). After the solution was kept at room temperature for 2 h, the reaction mixture was passed through a short column of silica gel and eluted with ether. The eluates were combined and evaporated to yield a yellow oil (437 mg), which was dissolved in benzene, passed through a dry column of silica gel (300 g), and eluted with benzene (each fraction 100 ml). Fractions 5—8 gave D : B-friedo-bacchar-5(10)-en-3-one (**15**; 289 mg), fraction 9 gave a mixture (45 mg) of **15** and **11**, and fractions 10—16 gave bacchar-12-en-3-one (**11**; 69 mg).

D : B-Friedo-bacchar-5(10)-en-3-one (**15**) was crystallized from methanol to give colorless fine needles, mp 84—84.5 °C; IR (Nujol) 1715 cm^{-1}; PMR: no signal due to olefinic proton; mass spectrum *m/e* 426 (M^+); $[\alpha]_D$ −103° (*c* 0.10, methanol); ORD *a*=−66 (*c* 0.10, methanol); Found; C, 84.51; H, 11.51%. Calcd for $C_{30}H_{50}O$: C, 84.44; H, 11.81%.

Bacchar-12-en-3-one (**11**) was crystallized from methanol and gave mp 111—112 °C; IR (neat) 1710 and 815 cm^{-1}; PMR (100 MHz, $CDCl_3$) δ 2.43 (m; 2×$C_{(2)}$–H) and 5.27 (t-like, J=2 Hz; $C_{(12)}$–H); ORD *a*=+33 (*c* 0.10, methanol); CD $[\theta]_{290}$+2600, $[\theta]_{325}$−90 (*c* 0.10, methanol); Found: C, 84.57; H, 11.97%. Calcd for $C_{30}H_{50}O$: C, 84.44; H, 11.81%.

*Reduction of Bacchar-12-en-3-one (**11**) with Sodium Borohydride.* To a solution of bacchar-12-en-3-one (**11**; 47 mg) in methanol (10 ml), sodium borohydride (52 mg) was added and the reaction mixture was allowed to stand overnight at room temperature. After addition of dilute hydrochloric acid and removal of the solvent under reduced pressure, the reaction products were extracted with ether three times. On usual work-up, a residue (45 mg) was obtained, which was subjected to separation by silica gel (25 g) dry column chromatography. Elution with benzene (270 ml) afforded an oily product (4 mg) and successive elution with the same solvent (410 ml) gave bacchar-12-en-3β-ol (**2**; 36 mg), mp 143.5—144 °C (crystallized from methanol); IR (neat) 3400, 1045, and 820 cm^{-1}; PMR (100 MHz, $CDCl_3$) δ 3.23 (dd, J=5 and 6 Hz; $C_{(3)}$–H) and 5.11 (m; $C_{(12)}$–H); $[\alpha]_D$+55° (*c* 0.49, methanol); mass spectrum *m/e* 428 (M^+). (lit,[2] mp 147—148 °C; $[\alpha]_D$+39° (*c* 1.82); mass spectrum *m/e* 428.403).

*Acetylation of Bacchar-12-en-3β-ol (**2**).* A solution of bacchar-12-en-3β-ol (**2**; 17 mg) in pyridine (0.3 ml) was treated with acetic anhydride (0.2 ml) and was allowed to stand overnight at room temperature. Methanol was added and the reaction mixture was poured into water and extracted with ether twice. On usual work-up, a pale yellow crystal (18 mg) was obtained, which was recrystallized from methanol to give bacchar-12-en-3β-yl acetate (**13**; 8 mg) as colorless crystals, mp 177—178 °C; IR (neat) 1735, 1280, 1030, and 815 cm^{-1} (lit,[2] mp 181—182 °C; $[\alpha]_D$+21° (*c* 1.58); mass spectrum *m/e* 470.411).

*Bacchara-11,13(17)-dien-3β-yl Acetate (**14**).*[6] A mixture of bacchar-12-en-3β-yl acetate (**13**; 14 mg) in acetic acid (1 ml) and selenium dioxide (15 mg) in 96% aqueous

acetic acid solution (0.2 ml) was heated at 85 °C for 4 h. Extraction with ether and usual work-up gave a yellow solid (14 mg), which was subjected to separation by silica gel chromatography to afford bacchara-11,13(17)-dien-3β-yl acetate (**14**; 6.5 mg) as a pale red solid; IR (Nujol) 1735, 1280, 1245, and 875 cm^{-1}; UV λ_{max}^{EtOH} 250 nm (ε 12500), 241 (19400), and 234 (17000); PMR (100 MHz, $CDCl_3$) δ 2.03 (s; $-OCOCH_3$), 4.53 (dd, J=7 and 9 Hz; $C_{(3)}$–H), 5.23 (br. s; $C_{(17)}$–H), 5.55 (dd, $J_{11,12}$=10 Hz, $J_{9,12}$=1 Hz; $C_{(12)}$–H), and 5.92 (dd, $J_{11,12}$=10 Hz, $J_{9,11}$=3 Hz; $C_{(11)}$–H); mass spectrum *m/e* 468 (M^+) [lit,[2] mp 152—153 °C; PMR (60 MHz, $CDCl_3$) δ 5.16 (br. s; $C_{(17)}$–H), 5.40 (dd, $J_{11,12}$=10.5 Hz, $J_{9,12}$=1 Hz; $C_{(12)}$–H), and 5.82 (dd, $J_{11,12}$=10.5 Hz, $J_{9,11}$=3 Hz; $C_{(11)}$–H); mass spectrum *m/e* 468.397 (M^+)].

The PMR, UV, and mass spectra of Bruun's authentic sample were measured under the same conditions as mentioned above. These spectral data were shown to be completely superimposable with ours.

*Reduction of D : B-Friedo-bacchar-5(10)-en-3-one (**15**) with Sodium Borohydride.* D : B-Friedo-bacchar-5(10)-en-3-one (**15**; 246 mg) in methanol (50 ml) was treated with sodium borohydride (200 mg) as the same procedure as described for bacchar-12-en-3-one (**11**) to afford a residue (239 mg), which gave two spots on TLC (a more polar spot was predominant). This was dissolved in benzene and passed through a dry column of silica gel (100 g). A minor component was eluted first with 600 ml of benzene, and successive elution with the same solvent (750 ml) afforded D : B-friedo-bacchar-5(10)-en-3β-ol (**17**; 176 mg), which was crystallized from methanol to give fine needles, mp 140.5—141 °C; IR (Nujol) 3350, 1175, 1120, 1070, 1040, 1030, and 980 cm^{-1}; PMR (100 MHz, $CDCl_3$) δ 3.42 (dd, J=10 and 5 Hz; $C_{(3)}$–H); Found: C, 83.90; H, 12.53%. Calcd for $C_{30}H_{52}O$: C, 84.04; H, 12.21%.

*Acetylation of D : B-Friedo-bacchar-5(10)-en-3β-ol (**17**).* Acetic anhydride (2 ml) was added to a solution of D : B-friedo-bacchar-5(10)-en-3β-ol (**17**: 123 mg) in pyridine (3 ml), and the solution was kept at room temperature for 2 h and then at 70 °C for 2 h. After addition of methanol to decompose excess of the reagent, the solution was poured into water and extracted with ether twice. Usual treatment gave a residue (162 mg), which was crystallized from methanol to give D : B-friedo-bacchar-5(10)-en-3β-yl acetate (**18**), mp 147—148 °C; IR (Nujol) 1725, 1250, 1025, and 970 cm^{-1}; PMR (100 MHz, $CDCl_3$) δ 2.03 (s; $-OCOCH_3$) and 4.64 (dd, J=10 and 5 Hz; $C_{(3)}$–H).

*D : B-Friedo-bacchara-1(10),5-dien-3β-yl Acetate (**19**).* A mixture of D : B-friedo-bacchar-5(10)-en-3β-yl acetate (**18**; 90 mg) in acetic acid (10 ml) and selenium dioxide (158 mg) in water (2 ml) was heated under reflux (bath temperature 100—130 °C) for 4.5 h. After addition of a cold aqueous potassium hydroxide solution, the mixture was extracted with ether twice, washed with a potassium hydroxide solution and then with brine. The ethereal layer was dried over sodium sulfate and evaporated. On standing for 2 days, the residue crystallized. The product was subjected to separation by silica gel (20 g) dry column chromatography using benzene as an eluent (each fraction 30 ml). Fractions 1 and 2, showing two spots on TLC, were combined and further separated by preparative TLC (2 plates (20×20 cm), SiO_2 0.5 mm in thickness; detection: I_2) to give D : B-friedo-bacchara-1(10),5-dien-3β-yl acetate (**19**; 43 mg), mp 123—123.5 °C; UV λ_{max}^{EtOH} 248 nm (sh. ε 12100), 238 (20900), and 231 (19400); PMR (100 MHz, $CDCl_3$) δ 2.04 (s; $-OCOCH_3$), 4.72 (dd, J=6 and 10 Hz; $C_{(3)}$–H), 5.28, and 5.68 (each m; $C_{(1)}$–H and $C_{(6)}$–H); mass spectrum *m/e* 468 (M^+).

The authors wish to thank Dr. T. Bruun for the generous gifts of the authentic bacchara-11,13(17)-dien-3β-yl acetate and of the IR and PMR spectra of bacchar-12-en-3β-ol and its acetate.

References

1) A preliminary report: S. Yamada, S. Yamada, Y. Moriyama, Y. Tanahashi, and T. Takahashi, *Tetrahedron Lett.*, **1972** 5043.

2) T. Anthonsen, T. Bruun, E. Hemmer, D. Holme, A. Lamvik, E. Sunde, and N. A. Sørensen, *Acta Chem. Scand.*, **24**, 2479 (1970).

3) E. Suokas and T. Hase, *Acta Chem. Scand.*, **25**, 2359 (1971).

4) F. Mo, T. Anthonsen, and T. Bruun, *Acta Chem. Sand.*, **26**, 1287 (1972).

5) Y. Moriyama, Y. Tanahashi, T. Takahashi, and G. Ourisson, *Bull. Soc. Chim. Fr.*, **1968**, 2890; T. Tsuyuki, T. Hoshino, M. Ito, and T. Takahashi, *ibid.*, **1968**, 2895. And references cited therein.

6) A nomenclature following biogenetic standpoint is applied in the present paper.

7) Y. Tanahashi, T. Takahashi, F. Patil, and G. Ourisson, *Bull. Soc. Chim. Fr.*, **1964**, 584.

8) P. Witz, H. Herrmann, J. -M. Lehn, and G. Ourisson, *Bull. Soc. Chim. Fr.*, **1963**, 1101.

9) Y. Tanahashi, Y. Moriyama, T. Takahashi, F. Patil, J. -F. Biellmann, and G. Ourisson, *Bull. Soc. Chim. Fr.*, **1966**, 1670.

10) K. Tachibana, S. Yamada, S. Yamada, T. Tsuyuki, and T. Takahashi, *Bull. Chem. Soc. Jpn.*, **48**, 3425 (1975).

11) The discrepancy, stated in the footnote 11 in the previous paper,[1] was found to be due to the impurity of the 3β-acetoxy-1(10),5-diene[1] which had been prepared from the less polar ketone by the same procedures now reinvestigated in the present paper.

Compounds Related to Acridine. XIII.[1] Reactions of 9-Vinyl- and 9-Ethynylacridine with *C,N*-Diarylnitrones

Otohiko Tsuge* and Akiyoshi Torii**

Research Institute of Industrial Science, Kyushu University, Hakozaki, Higashi-ku, Fukuoka 812

***Department of Industrial Chemistry, Kurume Technical College, Kurume 830*

(Received December 19, 1975)

The reaction of 9-vinylacridine (**1**) with *C,N*-diarylnitrones (**3**) in xylene under reflux afforded 5-(9-acridinyl)-2,3-diarylisoxazolidines (**4**) and/or 9-acridinyl styryl ketones (**5**). On heating isoxazolidines **4** were readily converted into the styryl ketones **5** with the elimination of anilines: this is a new type of thermal decomposition of isoxazolidine ring. However, thermal decomposition of 3-(9-acridinyl)-2,5-diarylisoxazolidines (**9**) which were prepared from *N*-(9-acridinylmethylene)aniline *N*-oxide (**7**) and styrene (**8**), did not observed. On the other hand, the reaction of 9-ethynylacridine (**2**) with nitrones **3** in ethanol under the influence of hydrochloric acid proceeded smoothly to give the reversed 4-(9-acridinyl)-4-isoxazolines (**11**), which on heating were converted into the corresponding 4-oxazolines **12.**

It is known that the reactions of *C*-aryl-*N*-alkyl(or aryl)nitrones with mono-substituted alkenes proceed regioselectively to give only the 5-substituted isoxazolidines.[2-6] However, Huisgen, *et al.*[7,8] observed diminished regioselectivity in the cycloaddition reaction of *C*-phenyl-*N*-methylnitrone with methyl propiolate. Recently, it has been reported that *C*-phenyl-*N*-methylnitrone added to electron-deficient monosubstituted dipolarophiles such as nitroethylene and cyanoacetylene to yield only the reversed 4-substituted cycloadducts.[9]

Thus, it seemed of interest to investigate the reactions of 9-vinyl- (**1**) and 9-ethynylacridine (**2**) with nitrones, because the 9-acridinyl group is rather bulky and electron-withdrawing. In this paper we wish to report the reactions of **1** and **2** with *C,N*-diarylnitrones which revealed some unusual phenomena.

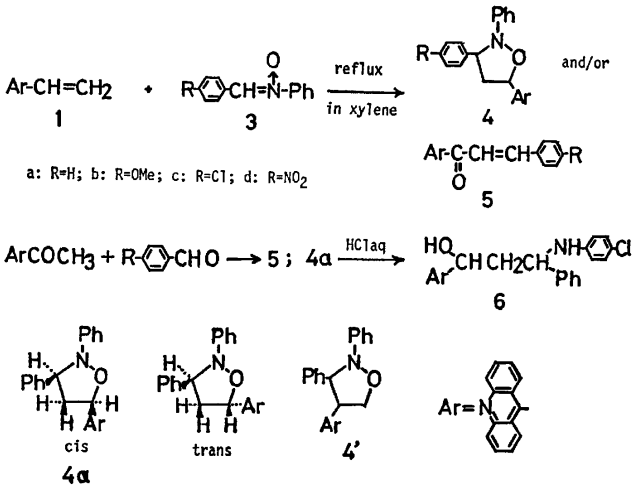

Scheme 1.

Results and Discussion

The reaction of 9-vinylacridine (**1**) with *C,N*-diphenylnitrone (**3a**) in boiling benzene did not take place. When a solution of equimolar quantities of **1** and **3a** in xylene was refluxed for 1.5 h, an 1 : 1 adduct **4a**, mp 188—189 °C, and 9-acridinyl styryl ketone (**5a**)[1] were obtained in 11 and 1% yields respectively, together with tarry materials.

On the basis of the chemical conversion and spectral data, **4a** was assigned to be 5-(9-acridinyl)-2,3-diphenylisoxazolidine (normal cycloadduct). Hydrolysis of **4a** with 20% aqueous hydrochloric acid at room temperature for 1.5 h afforded 1-(9-acridinyl)-3-(*p*-chloroanilino)-3-phenyl-1-propanol (**6**), mp 216—217 °C, in 60% yield. However, the configuration of **6** could not be determined, because the measurement of NMR spectrum of **6** was unsuccessful owing to its insolubility in solvents. Previously,[10] we have reported that hydrolysis of *cis*-2,3,5-triphenylisoxazolidine gave 1,3-diphenyl-3-(*p*-chloroanilino)-1-propanol. Thus, the reversed 4-(9-acridinyl) isomer **4'** can be excluded form the possibility for the structure of **4a**.

An inspection of Dreiding models indicates that there is a significant steric interaction between the acridinyl and *N*-phenyl groups in *trans*-isoxazolidine, but not in *cis*-isoxazolidine. Therefore, *cis*-configuration seems to be favorable to **4a**.

Under similar conditions, **1** reacted with *C*-*p*-anisyl-*N*-phenylnitrone (**3b**) to afford a normal cycloadduct **4b**, mp 202—203 °C, in 11% yield. However, the reaction of **1** with *C*-*p*-chlorophenyl- (**3c**) and *C*-*p*-nitrophenyl-*N*-phenylnitrone (**3d**) did not give the cycloadducts, but only acridinyl styryl ketones **5c**, mp 241—242 °C, and **5d**, mp 284 °C, were obtained in 27 and 13% yields respectively. The structures of **5c** and **5d** were confirmed by comparison with the authentic samples prepared from 9-acetylacridine and the corresponding benzaldehydes.

When heated in boiling xylene, isoxazolidines **4a** and **4b** were quantitatively converted into the corresponding acridinyl styryl ketones **5a** and **5b**, mp 200—201 °C. Thus, the formation of styryl ketones **5** in the reaction of **1** with **3** may be explained as arising from the corresponding isoxazolidines **4**. Little attention has been paid to the thermal decomposition of isoxazolidines. To our knowledge, the only one example has been reported on thermal isomerization of a bicyclic isoxazolidine.[11]

The transformation of isoxazolidines **4** into α,β-unsaturated ketones **5** is noteworthy as a new type of thermal decomposition of isoxazolidine ring. Although the exact pathway for the formation of **5** from **4** is not clear, we tentatively proposed the potential one as

* To whom all correspondence should be addressed.

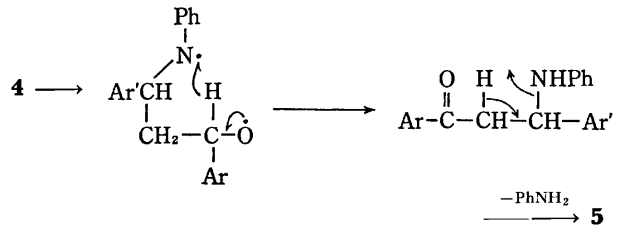

Ar=9-acridinyl: Ar'=*p*-substituted phenyl

depicted below. The cleavage of N–O bond of **4**, followed by the hydrogen shift gives 1-(9-acridinyl)-3-anilino-3-(*p*-substituted phenyl)propanone. Subsequent elimination of aniline from the propanone yields the final acridinyl styryl ketone **5**.

In this context, it appeared of interest to know whether a positional isomer of **4** is thermally decomposed or not. The reaction of *N*-(9-acridinylmethylene)-aniline *N*-oxide (**7**) with styrene (**8a**) in xylene under reflux afforded the expected 3-(9-acridinyl)-2,5-diphenylisoxazolidine (**9a**), mp 202—203 °C, in 37% yield. The structure of **9a** was confirmed by the spectral data as well as by the result of hydrolysis.

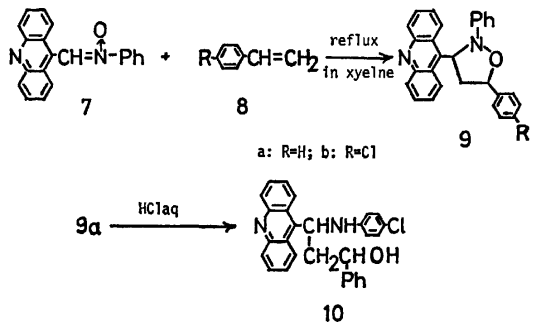

Scheme 2.

Hydrolysis of **9a** with 20% aqueous hydrochloric acid gave 3-(9-acridinyl)-3-(*p*-chloroanilino)-1-phenyl-1-propanol (**10**), mp 112—113 °C, in 68% yield. Similarly, *p*-chlorostyrene (**8b**) reacted with nitrone **7** to give 3-(9-acridinyl)-5-(*p*-chlorophenyl)-2-phenylisoxazolidine (**9b**), mp 205—206 °C, in 41% yield. Even when heated in boiling xylene for a long while, isoxazolidines **9a** and **9b** were recovered quantitatively.

On the other hand, the reaction of 9-ethynylacridine (**2**) with nitrones **3** in xylene under reflux yielded only tarry materials. However, we found that **2** reacted with *C*,*N*-diphenylnitrone (**3a**) in ethanol under the influence of hydrochloric acid at room temperature to afford a 1 : 1 cycloadduct **11a**, mp 115—115 °C (dec); whose yield depended on the amounts of hydrochloric acid used as shown in Table 1.

Table 1. Reaction of **2** with **3a**[a]

HCl, ml	**11a**, Yield (%)	HCl, ml	**11a**, Yield (%)
0.01	37	0.1	33
0.02	59	0.3	30
0.05	45	0.5	21

a) A mixture of **2** (1.0 g), **3a** (1.0 g), and the specified amount of hydrochloric acid (d^{27} 1.1748) in ethanol 20 ml) was stirred at room temperature for 10 min.

On the basis of the spectral data and chemical conversion, the structure of **11a** was deduced to be a reversed cycloadduct, 4-(9-acridinyl)-2,3-diphenyl-4-isoxazoline. The NMR spectrum (CS_2) of **11a** exhibited two doublets (each 1H, J=2 Hz) at δ 5.83 (3-H) and 6.83 ppm (5-H), besides aromatic protons (18H). As will be described below, **11a** was readily converted into the corresponding 4-oxazoline. These observations agreed with the assigned structure **11a**, but not with a normal cycloadduct, 5-(9-acridinyl) isomer **11'** (Scheme 3).

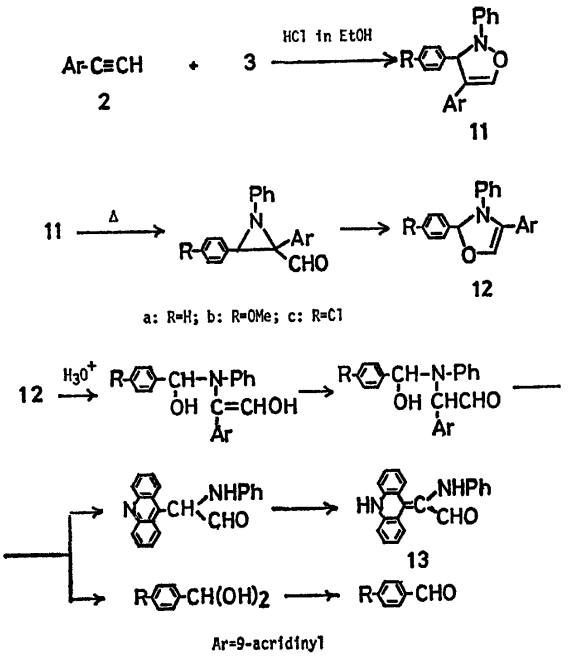

Scheme 3.

Similarly, the reaction of **2** with nitrones, **3b** and **3c** afforded the corresponding 4-(9-acridinyl)-4-isoxazoline compounds **11b**, mp 119 °C (dec), and **11c**, mp 85—86 °C (dec), in fairly good yields.

Previously, we have found that hydrochloric acid is an extremely effective catalyst for the reactions of 9-alkyl-,[12–14] 9-vinyl-,[15] and 9-ethynylacridine[16] with nitrosobenzenes. Although the reaction of **1** with *C*,*N*-diarylnitrones in the presence of hydrochloric acid afforded only tarry materials, hydrochloric acid was also very effective for the reaction of **2** with **3**. Catalytic behaviour of hydrochloric acid in the above reactions is not clear at the present stage.

Baldwin, *et al.*[17] demonstrated the existence of the facil thermal valence rearrangement of 4-isoxazolines to 2-acylaziridines, and subsequently to 4-oxazolines. Although attempts to isolate an acylaziridine intermediate were unsuccessful, heating of 4-isoxazoline **11a** in boiling benzene afforded 4-(9-acridinyl)-2,3-diphenyl-4-oxazoline (**12a**), mp 142—143 °C (dec), in 70% yield. Under similar conditions, 4-isoxazolines **11b** and **11c** were converted into the corresponding 4-oxazolines **12b**, mp 168 °C (dec), and **12c**, mp 114—115 °C (dec), in 85 and 50% yields respectively.

The structures of 4-oxazolines **12** were deduced on the basis of the spectral data and chemical conversion. Hydrolysis of **12a** with 20% aqueous hydrochloric acid at room temperature afforded violet prisms **13** ($C_{21}H_{16}N_2O$), mp 192—193 °C, in a good yield, and from the reaction mixture benzaldehyde was identified as its 2,4-dinitrophenylhydrazone. Similarly, **12b** and **12c** yielded **13** and *p*-methoxy- or *p*-chlorobenzaldehyde.

The IR spectrum of **13** displayed the absorption bands at 3360, 3280 (NH) and 1620 cm^{-1} (conjugated C=O), and a strong absorption band appeared at 523 nm in the UV spectrum. The NMR spectrum (DMSO-d_6) exhibited signals at δ 6.7—8.3 (14H, N**H** and aromatic protons), 9.1 (1H, s, C**H**O) and 11.95 ppm (1H, s, N**H**). The above observations indicated that **13** was (9,10-dihydro-9-acridinylidene)anilinoacetaldehyde.

The pathway for the formation of **13** from **12** is shown in Scheme 3. Previously,[18] we have reported that 9-methyleneacridine compounds were easily transformed into 9,10-dihydro-9-acridinylidene compounds. Thus, hydrolysis of **12** gives 9-acridinylanilinoacetaldehyde with the elimination of benzaldehyde, and then isomerization yields the stable 9,10-dihydro-9-acridinylidene compound **13**. The formation of **13** from **12** strongly supported the assigned structure **12**.

Although hydrolysis of 4-isoxazoline **11a** under similar conditions afforded **13** and benzaldehyde, this result may be understood in terms of an initial isomerization of **11a** to **12a**, followed by hydrolysis of **12a**.

Experimental

All the melting points are uncorrected. The NMR spectra were determined with a Hitachi R-20 Model spectrometer, with TMS as the internal standard. The IR spectra were measured as KBr disks, and the mass spectra were obtained on a Hitachi RMS-4 mass spectrometer with a direct inlet and an ionization energy of 70 eV.

*Reaction of 9-Vinylacridine (**1**) with* C,N-*Diphenylnitrone (**3a**).* A solution of **1**[19] (1.0 g) and **3a** (1.0 g) in xylene (10 ml) was refluxed under a stream of nitrogen for 1.5 h. Then, the reaction mixture was evaporated *in vacuo*, and the residue was chromatogaphed on alumina using benzene as the eluent, giving 0.32 g (11%) of 5-(9-acridinyl)-2,3-diphenylisoxazolidine (**4a**), mp 188—189 °C, as pale yellow needles, and 20 mg (1%) of 9-acridinyl styryl ketone (**5a**), mp 258 °C (lit,[1] mp 258 °C), as pale yellow prisms. The NMR spectrum ($CDCl_3$) of **4a**: δ ppm 2.93 (1H, ddd, 4-**H** (*cis*), J=9, 12, and 13 Hz), 3.3 (1H, ddd, 4-**H** (*trans*), J=7, 9, and 13 Hz), 5.15 (1H, t, 3-**H**, J=9 Hz), 6.55 (1H, dd, 5-**H**, J=7 and 12 Hz), 7.0—8.7 (18H, m, aromatic protons). Mass spectrum: *m/e* 402 (M^+). Found: C, 84.81; H, 5.61; N, 6.01%. Calcd for $C_{28}H_{22}N_2O \cdot C_6H_6$: C, 84.97; H, 5.87; N, 5.83%.

Similarly, the reaction of **1** with C-*p*-anisyl-N-phenylnitrone (**3b**) afforded 5-(9-acridinyl)-3-(*p*-anisyl)-2-phenylisoxazolidine (**4b**), mp 202—203 °C, as pale yellow prisms in 11% yield. NMR spectrum ($CDCl_3$): δ ppm 2.9, 3.3 (each 1H, m, 4-**H**), 3.85 (3H, s, OC**H**$_3$), 4.92 (1H, dd, 3-**H**, J=6 and 9 Hz), 6.8—8.8 (18H, m, >C**H** and aromatic protons). Mass spectrum: *m/e* 416 (M^+). Found: C, 83.64; H, 5.80; N, 6.93%. Calcd for $C_{29}H_{24}N_2O$: C, 83.47; H, 5.94; N, 7.15%.

On the other hand, the reaction of **1** with *C-p*-chlorophenyl-(**3c**) or *C-p*-nitrophenyl-*N*-phenylnitrone (**3d**) for 0.5 h under similar conditions afforded only the corresponding styryl ketone **5c** or **5d** in 27 or 13% yield respectively. The styryl ketones **5c** and **5d** were identical with the authentic samples prepared from the reaction of 9-acetylacridine with *p*-chloro- and *p*-nitrobenzaldehyde in the presence of sodium hydroxide in ethanol.

9-Acridinyl *p*-chlorostyryl ketone (**5c**): mp 241—241 °C, yellow prisms. IR spectrum: 1680 cm^{-1} (C=O). Mass spectrum: *m/e* 345, 343 (M^+). Found: C, 77.17; H, 4.04; N, 4.17%. Calcd for $C_{22}H_{14}NOCl$: C, 76.86; H, 4.08; N, 4.08%.

9-Acridinyl *p*-nitrostyryl ketone (**5d**): mp 284 °C, yellow prisms. IR spectrum: 1680 cm^{-1} (C=O). Mass spectrum: *m/e* 354 (M^+). Found: C, 74.80; H, 3.80; N, 7.91%. Calcd for $C_{22}H_{14}N_2O_3$: C, 74.56; H, 3.98; N, 7.91%.

*Thermal Decomposition of Isoxazolidine **4b**.* A solution of **4b** (0.1 g) in xylene (10 ml) was refluxed under a stream of nitrogen for 2 h. Then, the mixture was evaporated *in vacuo* to leave yellow crystals, which on recrystallization from benzene gave 80 mg (*ca.* 100%) of 9-acridinyl *p*-methoxystyryl ketone (**5b**), mp 200—201 °C, as pale yellow prisms. This compound was identical with the authentic sample prepared from 9-acetylacridine and *p*-anisaldehyde. Found: C, 82.55; H, 5.02; N, 3.94%. Calcd for $C_{23}H_{17}NO_2$: C, 82.39; H, 5.05; N, 4.13%.

Similarly, thermal decomposition of isoxazolidine **4a** afforded **5a** quantitatively.

*Hydrolysis of Isoxazolidine **4a**.* A suspension of **4a** (50 mg) in 20% aqueous hydrochloric acid (2 ml) was stirred at room temperature for 1.5 h. Then, the mixture was neutralized with aqueous ammonia to give yellow prisms, which on recrystallization from benzene afforded 30 mg (60%) of 1-(9-acridinyl)-3-(*p*-chloroanilino)-3-phenyl-1-propanol (**6**), mp 216—217 °C, as yellow prisms. IR spectrum: 3200—3400 (OH and NH), 830 cm^{-1}. Mass spectrum: *m/e* 440, 438 (M^+), 422, 420 (M^+-H_2O), 311 ($M^+-H_2NC_6H_4Cl$), 222 (acridinyl–CH–CH_2), 218, 216 (Ph$\overset{+}{C}$HNH–C_6H_4Cl), 208 (9-acridinyl–$\overset{+}{C}$HOH), 205, 193, 178. Found: C, 76.30; H, 5.42; N, 6.06%. Calcd for $C_{28}H_{23}N_2OCl$: C, 76.27; H, 5.67; N, 6.35%.

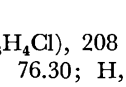

Reaction of N-*(9-Acridinylmethylene)aniline* N-*oxide (**7**) with Styrene (**8a**).* A solution of nitrone **7**[12] (0.2 g) and **8a** (0.1 g) in xylene (3 ml) was refluxed under a stream of nitrogen for 1.5 h. Then, the mixture was evaporated *in vacuo* to leave yellow crystals, which on recrystallization from benzene afforded 50 mg (37%) of 3-(9-acridinyl)-2,5-diphenylisoxazolidine (**9a**), mp 202—203 °C, as pale yellow prisms. NMR spectrum ($CDCl_3$): δ ppm 2.9—3.5 (2H, m, >C**H**), 5.45 (1H, dd, >C**H**, J=6 and 12 Hz), 6.3 (1H, dd, >C**H**, J=10 and 12 Hz), 6.9—8.5 (18H, m, aromatic protons). Mass spectrum: *m/e* 402 (M^+). Found: C, 83.26; H, 5.33; N, 6.67%. Calcd for $C_{28}H_{22}N_2O$: C, 83.55; H, 5.51; N, 6.92%.

Similarly, the reaction of **7** with *p*-chlorostyrene (**8b**) afforded a 41% yield of 3-(9-acridinyl)-5-(*p*-chlorophenyl)-2-phenylisoxazolidine (**9b**), mp 205—206 °C, as pale yellow needles. NMR spectrum ($CDCl_3$): δ ppm 2.6—3.4 (2H, m, >C**H**), 5.4 (1H, dd, >C**H**, J=5 and 13 Hz), 6.1—6.4 (1H, m, >C**H**), 6.7—8.5 (17H, m, aromatic protons). Mass spectrum: *m/e* 438, 436 (M^+). Found: C, 76.89; H, 4.61; N, 6.65%. Calcd for $C_{28}H_{21}N_2OCl$: C, 76.97; H, 4.81; N, 6.14%.

*Hydrolysis of Isoxazolidine **9a**.* A suspension of **9a** (0.25 g) in 20% aqueous hydrochloric acid (10 ml) was

stirred at 90 °C for 1 h. The mixture was neutralized with aqueous ammonia to give yellow crystals, which on recrystallization from a mixture of benzene and petroleum ether (bp 60—85 °C) afforded 0.17 g (68%) of 3-(9-acridinyl)-3-(*p*-chloroanilino)-1-phenyl-1-propanol (**10**), mp 112—113 °C, as yellow prisms. IR spectrum: 3200—3400 (OH and NH), 830 cm^{-1}. Mass spectrum: *m/e* 440, 438 (M^+), 422, 420 (M^+-H_2O), 319, 317 ($M^+-PhCH(OH)CH_2$), 206, 204, 193, 178. Found: C, 78.80; H, 5.58; N, 5.58%. Calcd for $C_{28}H_{23}N_2OCl\cdot C_6H_6$: C, 78.99; H, 5.61; N, 5.42%.

*Reaction of 9-Ethynylacridine (**2**) with* C,N-*Diphenylnitrone (**3a**).* A solution of **2**[16] (1.0 g) and **3a** (1.0 g) in ethanol (20 ml) containing concd hydrochloric acid (0.02 ml) was stirred at room temperature for 10 min. Filtration gave yellow crystals, which were washed with ethanol (20 ml×3) to leave 4-(9-acridinyl)-2,3-diphenyl-4-isoxazoline (**11a**), mp 115—116 °C (dec), as pale yellow prisms. Isoxazoline **11a** was subjected to microanalysis without further purification. NMR spectrum (CS_2): δ ppm 5.83 (1H, d, >C**H**, J= 2 Hz), 6.83 (1H, d, >C**H**, J=2 Hz), 7.0—8.1 (18H, m, aromatic protons). Mass spectrum: *m/e* 400 (M^+). Found: C, 83.77; H, 5.24; N, 6.71%. Calcd for $C_{28}H_{20}N_2O$: C, 83.97; H, 5.03; N, 7.00%.

The results of other reactions under varying amounts of hydrochloric acid are shown in Table 1.

Similarly, the reaction of **2** with *C-p*-anisyl- (**3b**) and *C-p*-chlorophenyl-*N*-phenylnitrone (**3c**) gave the corresponding 4-isoxazolines **11b**, mp 119 °C (dec), **11c**, mp 85—86 °C (dec), in 73 and 41% yields respectively.

4-(9-Acridinyl)-3-(*p*-anisyl)-2-phenyl-4-isoxazoline (**11b**). NMR spectrum (CS_2): δ ppm 3.51 (3H, s, OCH_3), 5.8 (1H, d, >C**H**, J=2 Hz), 6.8 (1H, d, =C**H**, J=2 Hz), 6.4—8.1 (17H, m, aromatic protons). Mass spectrum: *m/e* (M^+). Found: C, 81.09; H, 5.09; N, 6.30%. Calcd for $C_{29}H_{22}N_2O$: C, 80.90; H, 5.15; N, 6.51%.

4-(9-Acridinyl)-3-(*p*-chlorophenyl)-2-phenyl-4-isoxazoline (**11c**). NMR spectrum (CS_2): δ ppm 5.82 (1H, d, >C**H**, J=2 Hz), 6.84 (1H, d, =C**H**, J=2 Hz), 6.6—8.1 (17H, m, aromatic protons). Mass spectrum: *m/e* 436, 434 (M^+). Found: C, 77.16; H, 4.37; N, 6.34%. Calcd for $C_{28}H_{19}N_2OCl$: C, 77.16; H, 4.16; N, 6.05%.

*Thermal Isomerization of 4-Isoxazoline **11a**.* A solution of **11a** (0.2 g) in benzene (5 ml) was refluxed for 5 min. Then, the mixture was evaporated *in vacuo* to leave orange crystals, which on recrystallization from petroleum ether (bp 60—85 °C) afforded 0.14 g (70%) of 4-(9-acridinyl)-2,3-diphenyl-4-oxazoline (**12a**), mp 142—143 °C (dec), as orange prisms. NMR spectrum (CS_2): δ ppm 6.6—8.1 (18H, m, aromatic protons), 8.6, 8.73 (each 1H, d, J= 2 Hz). Mass spectrum: *m/e* 400 (M^+), 371 (M^+-CHO), 323 (M^+-Ph), 294 ($M^+-PhCHO$), 281 (9-acridinyl-$C\equiv\overset{+}{N}$-Ph, base peak). Found: C, 84.26; H, 4.93; N, 6.83%. Calcd for $C_{28}H_{20}N_2O$: C, 83.97; H, 5.03; N, 7.00%.

Similarly, other 4-isoxazolines **11b** and **11c** were easily isomerized into the corresponding 4-oxazolines. 4-(9-Acridinyl)-2-(*p*-anisyl)-3-phenyl-4-oxazoline (**12b**), mp 168 °C (dec), as orange prisms (from petroleum ether). Yield, 85%. NMR spectrum (CS_2): δ ppm 3.81 (3H, s, OCH_3), 6.6—8.2 (17H, m, aromatic protons), 8.64, 8.75 (each 1H, d, J=2 Hz). Mass spectrum: *m/e* 430 (M^+), 401 (M^+-CHO), 323 ($M^+-MeOC_6H_4$), 294 ($M^+-MeOC_6H_4CHO$), 281 (base peak). Found: C, 80.90; H, 4.99; N, 6.36%. Calcd for $C_{29}H_{20}N_2O_2$: C, 80.90; H, 5.15; N, 6.51%.

4-(9-Acridinyl)-2-(*p*-chlorophenyl)-3-phenyl-4-oxazoline (**12c**), mp 114—115 °C (dec), as orange prisms (from benzene). Yield, 50%. NMR spectrum (CS_2): δ ppm 6.6—8.2 (17H, m, aromatic protons), 8.55, 8.68 (each 1H, d, J= 2 Hz). Mass spectrum: *m/e* 436, 434 (M^+), 407, 405 (M^+-CHO), 323 ($M^+-ClC_6H_4$), 294 ($M^+-ClC_6H_4CHO$), 281 (base peak). Found: C, 78.25; H, 4.81; N, 5.75%. Calcd for $C_{28}H_{19}N_2OCl\cdot 1/2C_6H_6$: C, 78.48; H, 4.62; N, 5.91%.

*Hydrolysis of 4-Oxazoline **12b**.* A solution of **12b** (0.3 g) in ethanol (5 ml) was stirred with 20% hydrochloric acid (5 ml) at room temperature for 2 h, and then the mixture was neutralized with aqueous ammonia. Filtration gave violet crystals, which on recrystallization from chloroform afforded 0.21 g (96.7%) of (9,10-dihydro-9-acridinylidene)-anilinoacetaldehyde (**13**), mp 192—193 °C, as violet prisms. UV spectrum (EtOH): λ_{max} nm (log ε) 252 (4.9), 362 (3.8), 380 (3.9), 399 (3.8), 523 (3.1). Found: C, 80.50; H, 5.04; N, 8.98%. Calcd for $C_{21}H_{16}N_2O$: C, 80.75; H, 5.16; N, 8.97%.

From the filtrate *p*-anisaldehyde was identified as its 2,4-dinitrophenylhydrazone.

Similarly, hydrolysis of 4-oxazolines **12a** and **12c** gave **13** and the corresponding benzaldehydes.

References

1) Part XII of this series: A. Torii and O. Tsuge, *Heterocycles*, **3**, 557 (1975).
2) R. Huisgen, R. Grashey, H. Hauck, and H. Seidl, *Chem. Ber.*, **101**, 2043 (1968).
3) R. Huisgen, R. Grashey, H. Hauck, and H. Seidl, *Chem. Ber.*, **101**, 2548 (1968).
4) R. Huisgen, R. Grashey, H. Seidl, and H. Hauck, *Chem. Ber.*, **101**, 2559 (1968).
5) R. Huisgen, H. Hauck, R. Grashey, and H. Seidl, *Chem. Ber.*, **101**, 2568 (1968).
6) R. Huisgen, H. Seidl, and I. Brüning, *Chem Ber.*, 1102 (1969).
7) H. Seidl, R. Huisgen, and R. Knorr, *Chem Ber.*, **102**, 904 (1969).
8) R. Huisgen, H. Seidl, and J. Wulff, *Chem. Ber.*, **102**, 915 (1969).
9) J. Sims and K. N. Houk, *J. Am. Chem. Soc.*, **95**, 5798 (1973).
10) O. Tsuge, M. Tashiro, and Y. Nishihara, *Nippon Kagaku Zasshi*, **92**, 72 (1971).
11) G. R. Delpierre and M. Lamchen, *J. Chem. Soc.*, **1963** 4693.
12) O. Tsuge, M. Nishinohara, and M. Tashiro, *Bull. Chem. Soc. Jpn.*, **36**, 1477 (1963).
13) O. Tsuge, M. Nishinohara, and K. Sadano, *Bull. Chem. Soc. Jpn.*, **38**, 2037 (1965).
14) A. Torii, H. Higashiuchi, and O. Tsuge, *Heterocycles*, **2**, 615 (1974).
15) O. Tsuge and A. Torii, *Bull. Chem. Soc. Jpn.*, **45**, 3187 (1972).
16) O. Tsuge and A. Torii, *Bull, Chem. Soc. Jpn.*, **43**, 2920 (1970).
17) J. E. Baldwin, R. G. Pudussery, A. K. Qureshi, and B. Sklarz, *J. Am. Chem. Soc.*, **90**, 5325 (1968).
18) O. Tsuge and A. Torii, *Bull. Chem. Soc. Jpn.*, **46**, 283 (1973).
19) O. Tsuge, A. Torii, and T. Tomita, *Nippon Kagaku Zasshi*, **90**, 1263 (1969).

Oxidation of 4-Alkyl-1-hydroxyimino-2,4,6-tri-*t*-butyl-2,5-cyclohexadienes: Formation of 4-Alkyl-2,6-di-*t*-butylnitrobenzenes *via* Iminoxyl Radical

Yoshio INAGAKI, Renji OKAZAKI, and Naoki INAMOTO

Department of Chemistry, Faculty of Science, The University of Tokyo, Hongo, Tokyo 113

(Received December 19, 1975)

Reactions of 4-alkyl-1-hydroxyimino-2,4,6-tri-*t*-butyl-2,5-cyclohexadienes (**1**) with silver(I) oxide afforded 4-alkyl-2,6-di-*t*-butylnitrobenzenes (**2**) mainly, which were found to be formed *via* an iminoxyl radical on the base of the ESR spectra and by-products, 4-alkyl-1-*t*-butoxyimino-2,4,6-tri-*t*-butyl-2,5-cyclohexadienes (**3**). This reaction is a novel oxidative decomposition of iminoxyl radical and provides a practical preparative method for the nitrobenzenes (**2**). Oxidation of **1** with other reagents (nickel peroxide and *m*-chloroperbenzoic acid) and oxidation of 6-alkyl-1-hydroxyimino-2,4,6-tri-*t*-butyl-2,4-cyclohexadienes (**5**) have also been described.

Although many iminoxyl radicals have been studied by means of ESR, there have been only two examples of iminoxyl radicals which were so stable as to be isolated.[1,2] We attempted to prepare and isolate another type of stable iminoxyl radicals by hydrogen abstraction from highly sterically hindered oximes, 4-alkyl-1-hydroxyimino-2,4,6-tri-*t*-butyl-2,5-cyclohexadienes (**1**) which were prepared from 2,4,6-tri-*t*-butylnitroso-[3a] and -nitrobenzenes.[3b] Intermediary iminoxyl radical was observed by ESR, but could not be isolated because of further reaction. We describe here the novel oxidative decomposition of the iminoxyl radical found during this attempt and the usefulness of this reaction as a preparative method for 4-alkyl-2,6-di-*t*-butylnitrobenzenes (**2**).[4]

Oxidation with Silver(I) Oxide or Nickel Peroxide. The reaction of the oxime (**1**) with excess silver(I) oxide or nickel peroxide[5] in benzene at room temperature gave 4-alkyl-2,6-di-*t*-butylnitrobenzene (**2**) mainly, along with 4-alkyl-1-*t*-butoxyimino-2,4,6-tri-*t*-butyl-2,5-cyclohexadienes (**3**) and 2,4,6-tri-*t*-butylnitrobenzene (**4**) as minor products. The yields of the products and reaction conditions are summarized in Table. The products were isolated by means of thin layer chromatography (TLC) and characterized by their spectral and analytical data except for **2d** where the pure specimen free from **4** has not been obtained owing to the similar R_f value of **2d** and **4**, and the yield was determined by means of high speed liquid chromatography with a UV detector assuming that both **2d** and **4** have the same molar extinction coefficient at 254 nm.

There has been no practical method for the synthesis of 1-substituted 4-alkyl-2,6-di-*t*-butylbenzenes except for phenols and their derivatives:[6] the preparation of nitrobenzenes (**2**) by nitration of the corresponding hydrocarbons is very difficult owing to the bulky *t*-butyl groups, and for example, Mhyre *et al.* reported that nitration of 3,5-di-*t*-butyltoluene affords the corresponding 2- and 4-nitro derivatives in 98.5 and 1.5% yields respectively.[7] Therefore, the present reaction provides a convenient method for the synthesis of **2**. Furthermore, in view of a key role of a nitro group in synthetic chemistry, this reaction might also give an access to other various derivatives.

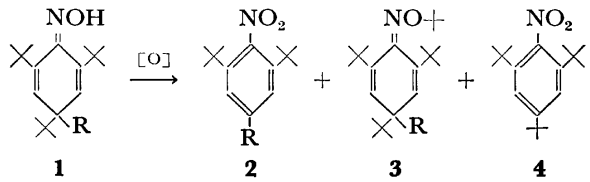

1 **2** **3** **4**

a: R=Et; **b**: R=*i*-Pr; **c**: R=PhCH$_2$; **d**: R=1-Ad

Similar oxidation of 1-hydroxyimino-6-methyl-2,4,6-tri-*t*-butyl-2,4-cyclohexadiene (**5**) with silver(I) oxide afforded 2,4-di-*t*-butyl-6-methylnitrobenzene (**6**), the corresponding nitrosobenzene (**7**), and 1-*t*-butoxyimino-2,4,6-tri-*t*-butyl-6-methyl-2,4-cyclohexadiene (**8**) (see Table).

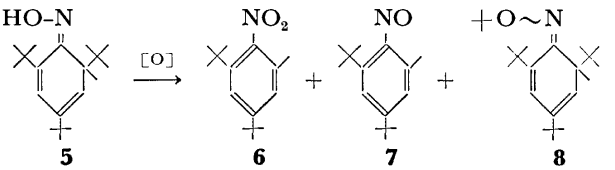

5 **6** **7** **8**

TABLE. YIELDS OF THE PRODUCTS

No.	Oxime	R	Oxidizing agent	Reaction time (h)	**2** (%)	Other product (%)
1	**1a**	Et	Ag_2O	24.5	56	**3a**(17)
2	**1b**	*i*-Pr	Ag_2O	24	96	
3[a]	**1b**	*i*-Pr	Ag_2O	24.5	56	**3b**(13)
4	**1b**	*i*-Pr	Ni-PO	22.3	37	
5	**1c**	$PhCH_2$	Ag_2O	24.5	55	**3c**(9), **4**(10)
6	**1c**	$PhCH_2$	MCPBA[b]	24	37	
7	**1d**	1-Ad[c]	Ag_2O	21	48	**4** (26)
8	**1d**	1-Ad[c]	MCPBA[b]	22.5	10	**4** (28)
9	**5**		Ag_2O	0.5		**6**(14), **7**(14), **8**(16)

a) Reaction in a degassed system. b) *m*-Chloroperbenzoic acid. c) 1-Adamantyl group.

ESR Study of the Reaction. During the reactions of **1** with a defficient amount of nickel peroxide (Ni-PO), lead(IV) dioxide (PbO_2), or silver(I) oxide (Ag_2O), a strong ESR signal (Type A; a_N=32 G, a_H=4 G, g=2.006) was recorded irrespective of the 4-substituent (Fig. 1). This signal was identical with that observed in the reaction of **1** with photo-excited benzophenone,[8] which has been reported to be an excellent reagent for the formation of an iminoxyl radical from an oxime.[9] Therefore, Type A signal is assignable to the corresponding iminoxyl radical (**9**). The signal was so stable that the intensity was not reduced even after a day at room temperature under air. The line shape varied reversibly with temperature (Fig. 2), and this may be ascribed to a conformational change. The line shape was also changed by the solvent (Fig. 2).

When an excess amount of Ni-PO, PbO_2, or Ag_2O, was used, Type A signal was recorded at first, but the signal rapidly decreased in its intensity and changed into a signal due to another iminoxyl radical (Type B; a_N=32 G, g=2.006) (Fig. 3), whose structure remains unknown.

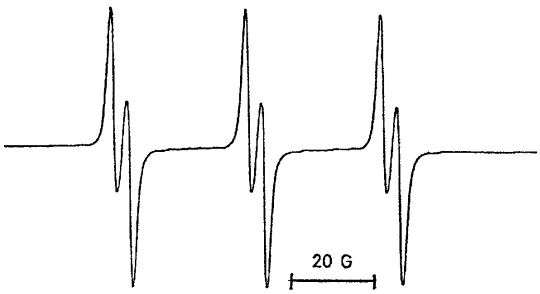

Fig. 1. Type A signal obtained by the reaction of **1b** with Ni-PO in benzene at room temperature.

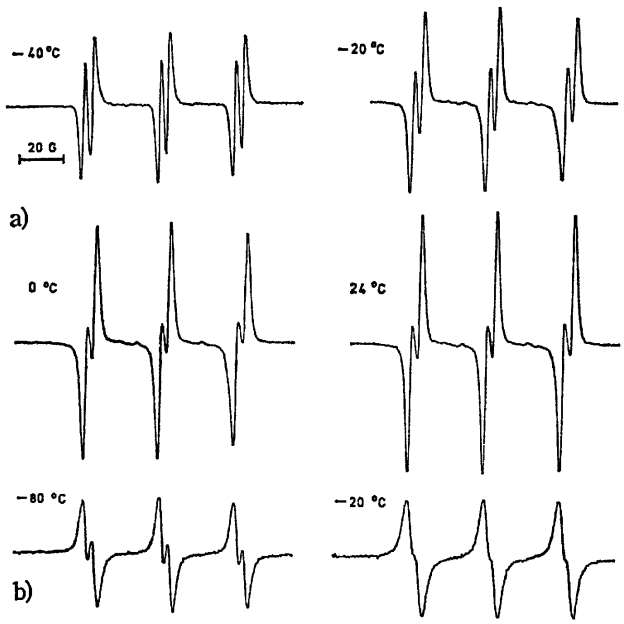

Fig. 2. Temperature and solvent dependence of the line shape of Type A signal: a) **1b**+photoexcited benzophenone in CH_2Cl_2, b) **1b**+photoexcited benzophenone in hexane.

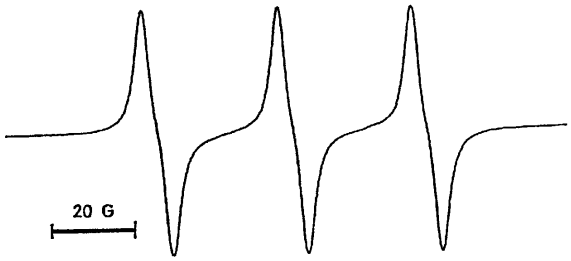

Fig. 3. Type B signal obtained by the reaction of **1c** with an excess amount of Ni-PO in hexane at room temperature.

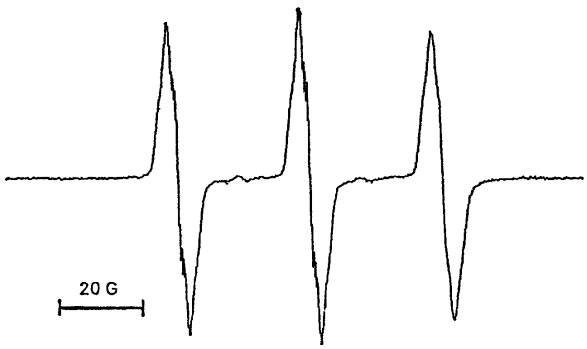

Fig. 4. Type C signal obtained by the reaction of **5** with photoexcited benzophenone in CH_2Cl_2 at −84 °C.

On the other hand, Type C signal (a_N=32 G, g=2.006) (Fig. 4) was observed during the oxidation of oxime (**5**) with photo-excited benzophenone and this may be assigned to the iminoxyl radical (**10**). Reaction of oxime (**5**) with excess Ni-PO, PbO_2, or Ag_2O gave a signal similar to Type B signal (a_N=32 G, g=2.006).

The iminoxyl radical (**9**) showed a splitting due to one of the protons on the 3- or 5-position; such a long range coupling is characteristic of iminoxyl radicals[10] and often observed in σ-radicals.[11] It is interesting that the iminoxyl radical (**10**) did not show any such splitting due to the ring proton.

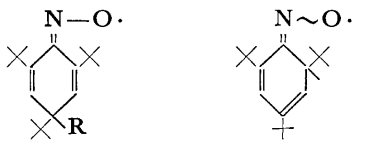

9 **10**

Reaction Mechanism. The nitrobenzenes (**2**) are considered to be formed *via* the initially produced iminoxyl radicals (**9**) in the following manner.

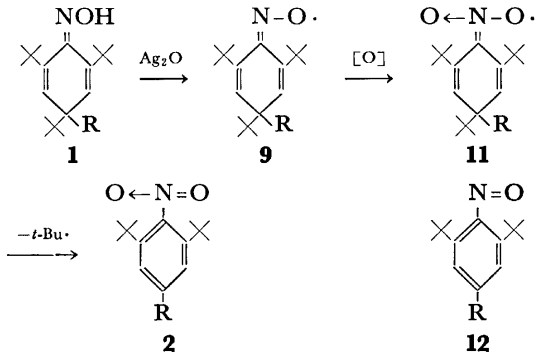

This pathway is supported by the observation of a strong ESR signal due to **9**, which was destroyed by excess oxidizing agents, and the formation of the oxime ether (**3**) by the combination between **9** and *t*-butyl radical.

An alternative route *via* 4-alkyl-2,6-di-*t*-butylnitrosobenzene (**12**), which might be formed by the elimination of a *t*-butyl radical from **9** can be ruled out, because 2,4,6-tri-*t*-butylnitrosobenzene was never oxidized into **4** by Ni-PO or Ag_2O at room temperature even after a day.

We consider a similar mechanism can also be applied to the oxidation of **5**. In this case, however, elimination of *t*-butyl radical from the initially formed iminoxyl radical (**10**) also took place as suggested by the formation of a considerable amount of 2,4-di-*t*-butyl-6-methylnitrosobenzene (**7**).

The source of the oxygen which is responsible for the oxidation of **1** into **2** remains obscure: although involvement of stubbornly adsorbed oxygen may be possible, the oxygen seems to stem from the silver(I) oxide, because **9** is fairly stable even under air as suggested by before-mentioned ESR spectroscopy, also because the formation of **2** was still observed even in the degassed solvent and with degassed silver(I) oxide. The reaction of **1b** in a degassed system (No. 3 in Table) afforded also **3b** besides **2b** in contrast to the reaction under air. This formation of **3b** is probably ascribed to the prolonged life times of **9b** and the eliminated *t*-butyl radicals in the absence of oxygen. Therefore, it seems preferable to carry out the reaction in the presence of atmospheric oxygen in order to obtain **2** in a high yield.

This reaction is a novel type of fragmentation of iminoxyl radicals and the first example of the formation of nitro compound in silver(I) oxide oxidation of oximes. This unusual reaction is ascribable to the following two reasons: first, the bulky *t*-butyl groups on **9** make a barrier against intermolecular coupling which is a main decomposition pathway in usual iminoxyl radicals; secondly, an inclination of the cyclohexadienone oxime system to aromatize by an elimination of the bulky *t*-butyl group favours the reaction energetically.

In the cases of **1a** and **1b**, the selective elimination of the *t*-butyl group took place, while in the cases of **1c** and **1d**, a considerable amount of **4** which represents the elimination of benzyl or 1-adamantyl group, respectively, was obtained. These facts imply that the elimination of 1-adamantyl radical which is less stable than *t*-butyl radical[12] competed with that of *t*-butyl radical, and that the elimination of *t*-butyl radical was favorable over that of benzyl radical although the latter is more stable than the former. Therefore, it is concluded that the more bulky group is selectively eliminated, although elimination of a small group can competitively occur if it is more stable as a free radical than a bulky group.

Oxidation with m-*Chloroperbenzoic Acid.* The reaction of **1** with *m*-chloroperbenzoic acid is interesting, because it is expected that the reaction is initiated by heterolytic oxidation of the nitrogen of the oxime, suggesting elimination of *t*-butyl group as a cation. Thus there must be some differences in the reaction products compared with the silver(I) oxide oxidation. The reaction afforded similar products to those obtained in the silver(I) oxide oxidation (Table), but the product ratio **2d**/**4** was inversed. Although the yields of the nitro compounds were relatively low, this inversion seems to imply the mechanistic difference between the two reactions.

Experimental

All melting points were not corrected. The IR and UV spectra were recorded with Hitachi EPI-G2 and EPS-3 spectrophotometers respectively. The NMR spectra were measured with a Hitachi R-24 (60 MHz) spectrometer using tetramethylsilane as an internal standard. The mass spectra were recorded with a Hitachi RMU-6L mass spectrometer. The ESR spectra were recorded with a JEOL JES-ME spectrometer and *g* values were determined on the basis of Mn^{2+} marker. Solvents were not degassed unless otherwise noted.

Materials. 4-Alkyl-1-hydroxyimino-2,4,6-tri-*t*-butyl-2,5-cyclohexadienes (**1**),[3] 1-hydroxyimino-2,4,6-tri-*t*-butyl-6-methyl-2,4-cyclohexadiene (**5**),[3] 2,4,6-tri-*t*-butylnitrosobenzene,[13] 2,4-di-*t*-butyl-6-methylnitrosobenzene (**7**),[13] 2,4,6-tri-*t*-butylnitrobenzene (**4**),[14] and 2,4-di-*t*-butyl-6-methylnitrobenzene (**6**)[14] were prepared by the reported methods.

*Oxidation of 1-Hydroxyimino-2,4,6-tri-t-butyl-4-ethyl-2,5-cyclohexadiene (**1a**) with Silver(I) Oxide.* To a suspension of a few hundred miligrams of silver(I) oxide in 2 ml of benzene was added a benzene solution (2 ml) of 40.4 mg (0.132 mmol) of **1a**. After the mixture was stirred for 24.5 h at room temperature, the insoluble part was filtered off. After removal of the solvent from the filtrate, the residue was treated with TLC (silica gel, hexane–benzene (4 : 1)), and each fraction was eluted with ether. The first fraction (R_f=0.83) gave 8.0 mg (17%) of 1-*t*-butoxyimino-2,4,6-tri-*t*-butyl-4-ethyl-2,5-cyclohexadiene (**3a**) as a tarry material, which was purified by TLC (silica gel, hexane) followed by molecular distillation. IR (neat): 965 cm^{-1} (NO); NMR (CCl_4): δ 0.65 (t, J=7 Hz, 3H), 0.82 (s, 9H), 1.22 (s, 9H), 1.28 (s, 9H), 1.32 (s, 9H), 1.65 (q, J=7 Hz, 2H), and 5.75 (ABq, $\Delta\delta$=0.13, J=2 Hz, 2H); λ_{max} (hexane): 258 nm (ε 5940); MS: *m/e* 304 (M−57, 32%) and 57 (100%).

The second fraction (R_f=0.67) gave 19.3 mg (56%) of **2a** which was recrystallized four times from aqueous methanol, mp 100.5—101.5 °C; IR (KBr): 1525 and 1375 cm^{-1} (NO_2); NMR (CCl_4): δ 1.31 (t, J=7 Hz, 3H), 1.42 (s, 18H), 2.70 (q, J=7 Hz, 2H), and 7.23 (s, 2H); λ_{max} (hexane): 247 (ε 960) and 348.5 nm (180); MS: *m/e* 263 (M^+, 19%) and 248 (100).

Found: C, 72.84; H, 9.43; N, 5.51%. Calcd for $C_{16}H_{25}NO_2$: C, 73.00; H, 9.51; N, 5.32%.

Another reaction under similar conditions afforded 64% of **2a**.

*Oxidation of 1-Hydroxyimino-2,4,6-tri-t-butyl-4-isopropyl-2,5-cyclohexadiene (**1b**) with Silver(I) Oxide.* Reaction of 50.0 mg (0.156 mmol) of **1b** and a large excess of silver(I) oxide in 4.5 ml of benzene for 24 h followed by treatment with TLC (silica gel, hexane–benzene (4 : 1)), afforded 41.6 mg (96%) of 2,6-di-*t*-butyl-4-isopropylnitrobenzene (**2b**) as white crystals (R_f=0.78—0.61), which were recrystallized twice from aqueous methanol, mp 101—103 °C; IR (KBr): 1525 and 1370 cm^{-1} (NO_2); NMR (CCl_4): δ 1.25 (d, J=7 Hz, 6H), 1.35 (s, 18H), 2.88 (sep, J=7 Hz, 1H),

and 7.21 (s, 2H); λ_{max} (hexane): 246 sh (ε 1740) and 340 nm (350); MS: *m/e* 277 (M^+, 17%) and 262 (100). Crude material showed a peak at *m/e* 291 (trace) which indicates the contamination of trace of 2,4,6-tri-*t*-butylnitrobenzene (**4**).

Found: C, 73.68; H, 9.68; N, 4.98%. Calcd for $C_{17}H_{27}NO_2$: C, 73.65; H, 9.75; N, 5.05%.

*Reaction of **1b** with Silver(I) Oxide in Degassed System.* A few hundred miligrams of silver(I) oxide in 3.5 ml of dry benzene was degassed four times, and a solution of 44.3 mg (0.139 mmol) of **1b** in 0.5 ml of dry benzene was added under argon atmosphere. After the mixture was stirred for 24.5 h at room temperature, the insoluble part was filtered off. The filtrate was evaporated *in vacuo* and treated with TLC (silica gel, hexane–benzene (4 : 1)). A fraction with R_f of 0.78 gave 6.8 mg (13%) of 1-*t*-butoxyimino-2,4,6-tri-*t*-butyl-4-isopropyl-2,5-cyclohexadiene (**3b**) as colorless oil, IR (neat): 975 cm^{-1} (NO); NMR (CCl_4): δ 0.90 (s, 9H), 1.22 (s, 9H), 1.29 (s, 9H), 1.32 (s, 9H), 5.89 (ABq, $\Delta\delta$=0.15, J=2 Hz, 2H), and the signals due to the isopropyl group were obscure; λ_{max} (hexane): 259 nm (ε 7590); MS: *m/e* 318 (M−57, 23%) and 57 (100),

Found: C, 80.00; H, 12.36; N, 3.69%. Calcd for $C_{25}H_{45}NO$: C, 79.93; H, 12.08; N, 3.92%.

A fraction with R_f of 0.5 gave 21.6 mg (56%) of **2b**, which was identified by the IR and NMR spectra.

*Reaction of **1b** with Nickel Peroxide.* Reaction of **2b** (60.7 mg, 0.190 mmol) with a large excess of nickel peroxide in 5 ml of benzene for 22.3 h at room temperature followed by treatment with TLC (silica gel, hexane–benzene (4 : 1)) gave 18.6 mg (37%) of **2b**.

*Reaction of 1-Hydroxyimino-4-benzyl-2,4,6-tri-t-butyl-2,5-cyclohexadiene (**1c**) with Silver(I) Oxide.* Reaction of **1c** (46.2 mg, 0.126 mmol) and a large excess of silver(I) oxide in 4 ml of benzene for 24.5 h at room temperature followed by TLC (silica gel, hexane–benzene (4 : 1)) afforded the following compounds. The first fraction (R_f=0.89) gave 5.0 mg (9%) of 1-*t*-butoxyimino-4-benzyl-2,4,6-tri-*t*-butyl-2,5-cyclohexadiene (**3c**) as white crystals, which were recrystallized from aqueous methanol, mp 107—109 °C; IR (KBr): 750 cm^{-1} (NO); NMR (CCl_4): δ 0.91 (s, 9H), 0.98 (s, 9H), 1.19 (s, 9H), 1.27 (s, 9H), 2.93 (s, 2H), 5.89 (s, 2H), and 7.12 (s, 5H); λ_{max} (hexane): 259 nm (ε 9540); MS: *m/e* 366 (M−57, 21%) and 57 (100).

Found: C, 82.34; H, 11.09; N, 3.34%. Calcd for $C_{29}H_{45}NO$: C, 82.21; H, 10.71; N, 3.30%.

A fraction with R_f of 0.72 gave 3.9 mg (10%) of **4**. A fraction with R_f of 0.56 afforded 22.7 mg (55%) of 4-benzyl-2,6-di-*t*-butylnitrobenzene (**2c**) as white crystals, mp 110—112 °C (from aqueous methanol); IR (KBr): 1525 and 1375 cm^{-1} (NO_2); NMR (CCl_4): δ 1.32 (s, 18H), 3.95 (s, 2H), and 7.1—7.3 (m, 7H); λ_{max} (hexane): 249 (ε 1380), 254.5 (1380), 259 (1330), 262 sh (1250), 265 sh (1140), 269.5 (1202), and 345 nm (200); MS: *m/e* 325 (M^+, 29%) and 310 (100).

Found: C, 77.40; H, 8.58; N, 4.41%. Calcd for $C_{21}H_{27}NO_2$: C, 77.50; H, 8.37; N, 4.31%.

Another reaction under similar condition afforded **2c** (68) and **3c** (16%).

*Reaction of 1-Hydroxyimino-4-(1-adamantyl)-2,4,6-tri-t-butyl-2,5-cyclohexadiene (**1d**) with Silver(I) Oxide.* Reaction of **1d** (21.9 mg, 0.053 mmol) with a large excess of silver(I) oxide in benzene (2 ml) for 21 h at room temperature followed by treatment with TLC (silica gel, hexane–benzene (4 : 1)) gave 13.5 mg of white crystalline material, which was a mixture of **4** and 4-(1-adamantyl)-2,6-di-*t*-butylnitrobenzene (**2d**). The molar ratio was determined to be 1 : 2.3 (**4**; 26%, **2d**; 48%) by means of high speed liquid chromatography (styrene–divinylbenzene copolymer, methanol–aqueous ammonia (1%)) with a UV detector assuming that both **4** and **2d** have the same molar extinction coefficient at 254 nm. The spectral data of the mixture were as follows, IR (KBr): 1525 and 1380 cm^{-1} (NO_2); NMR (CCl_4): δ 1.37 (s, 18H), 1.78 (m, 15H), 7.32 (s, 2H), and signals due to **4**; MS: *m/e* 369 (M^+ of **2d**, 13%), 354 (53), 291 (M^+ of **4**, 8), 276 (55), 135 (Ad^+, 32), and 57 (100).

*Reaction of 1-Hydroxyimino-4-benzyl-2,4,6-tri-t-butyl-2,5-cyclohexadiene (**1c**) with m-Chloroperbenzoic Acid.* A dichloromethane solution (4 ml) of **1c** (50.0 mg, 0.14 mmol) and 98.1 mg (0.74 mmol) of *m*-chloroperbenzoic acid was stirred for 24 h at room temperature. Subsequently, the reaction mixture was shaken with an aqueous sodium hydrogen carbonate and extracted with dichloromethane. The extract was washed with water and dried over anhydrous magnesium sulfate. After removal of the solvent, the residue was treated with TLC (silica gel, hexane–benzene (4 : 1)). A fraction with R_f of 0.63—0.51 gave 14.8 mg (37%) of consumed **1c** of **2c**. From a fraction with R_f of 0.26—0.17, 5.8 mg (11.6%) of **1c** was recovered.

*Reaction of 1-Hydroxyimino-4-(1-adamantyl)-2,4,6-tri-t-butyl-2,5-cyclohexadiene (**1d**) with m-Chloroperbenzoic Acid.* A dichloromethane solution (4 ml) of *m*-chloroperbenzoic acid (132 mg, 0.765 mmol) and **1d** (48.2 mg, 0.117 mmol) was stirred for 22.5 h at room temperature. Usual work-up afforded 13.5 mg of white crystals, which were a mixture of **4** and **2d** according to the NMR and IR spectra, and the yields were calculated to be 28 and 10% respectively.

*Reaction of 1-Hydroxyimino-2,4,6-tri-t-butyl-6-methyl-2,4-cyclohexadiene (**5**) with Silver(I) Oxide.* A mixture of **5** (134.4 mg, 0.46 mmol) and a large excess of silver(I) oxide in 8 ml of benzene was stirred for 35 min at room temperature. The mixture was worked up as usual and treated with TLC (silica gel, hexane–benzene (4 : 1)). A fraction with R_f of 0.86–0.72 afforded 26.1 mg (16%) of 1-*t*-butoxyimino-2,4,6-tri-*t*-butyl-6-methyl-2,4-cyclohexadiene (**8**) as white crystals, mp 76—79 °C (from aqueous methanol); IR (KBr): 970 cm^{-1} (NO); NMR (CCl_4): δ 0.86 (s, 9H), 1.09 (s, 9H), 1.31 (s, 18H), 1.55 (s, 3H), 5.20 (d, J=2 Hz, 1H), and 6.13 (d, J=2 Hz, 1H); λ_{max} (hexane): 314 nm (ε 6400); MS: *m/e* 290 (M^+−*t*-Bu, trace), 204 (75%), 57 (94), and 41 (100). Fraction (R_f=0.50—0.56) and a fraction (R_f=0.39—0.47) afforded 14.8 mg (14%) of 2,4-di-*t*-butyl-6-methylnitrosobenzene (**7**) and 15.9 mg (14%) of 2,4-di-*t*-butyl-6-methylnitrobenzene (**6**) respectively, which were identified by comparing the spectral data with those of the authentic samples.

ESR Measurements. An oxime and an oxidizing agent were mixed in a solvent and transferred into a sample tube directly or in a pyrex capillary just before a measurement. A procedure for a reaction between an oxime and photo-excited benzophenone was as follows: a mixed solution of an oxime and a carbonyl compound whose concentration was controlled to be *ca.* 0.1 mol/l for the oxime and *ca.* 0.05 mol/l for benzophenone, was placed in a pyrex capillary, which was transferred into a sample tube and irradiated with a high pressure mercury lamp in a cavity of ESR spectrometer.

References

1) G. D. Mendenhall and K. U. Ingold, *J. Am. Chem. Soc.*, **95**, 2963 (1973).

2) J. H. Wiering, H. Wynberg, and J. Strating, *Tetrahedron*, **30**, 3053 (1974); D. Lindsay, E. C. Horswill, D. W.

Davidson, and K. U. Ingold, *Can. J. Chem.*, **52**, 3554 (1974); K. U. Ingold and S. Brownstein, *J. Am. Chem. Soc.*, **97**, 1817 (1975).

3) a) Y. Inagaki, R. Okazaki, and N. Inamoto, *Bull. Chem. Soc. Jpn.*, **48**, 612 (1975); b) *ibid.*, **48**, 3727 (1975).

4) Preliminary report: R. Okazaki, Y. Inagaki, and N. Inamoto, *Chem. Lett.*, **1974**, 1543.

5) R. Konaka, *Yuki Gosei Kagaku Kyokai Shi*, **30**, 479 (1972).

6) R. Okazaki, *Yuki Gosei Kagaku Kyokai Shi*, **32**, 704 (1974).

7) P. C. Mhyre, M. Beug, and L. L. James, *J. Am. Chem. Soc.*, **90**, 2105 (1968).

8) The signal once obtained remained unchanged even after irradiation was stopped.

9) T. -S. Lin, S. H. Mastin, and N. Ohkaku, *J. Am. Chem. Soc.*, **95**, 6845 (1973).

10) R. O. C. Norman and B. C. Gilbert, *J. Phys. Chem.*, **71**, 14 (1967); B. C. Gilbert and R. O. C. Norman, *J. Chem. Soc., B*, **1966**, 86.

11) G. Cauquis, M. Genis, H. Lemaire, A. Rassat, and J. P. Ravet, *J. Chem. Phys.*, **47**, 4642 (1967); P. J. Krusic and T. A. Rettig, *J. Am. Chem. Soc.*, **92**, 722 (1970).

12) C. Ruchardt, *Angew. Chem. Int. Ed. Engl.*, **9**, 830 (1970).

13) R. Okazaki, T. Hosogai, E. Iwadare, M. Hashimoto, and N. Inamoto, *Bull. Chem. Soc. Jpn.*, **42**, 3611 (1969).

14) J. Burgers, M. A. Hoefnagel, P. E. Verkade, H. Visser, and B. M. Wepster, *Rec. Trav. Chim. Pays-Bas*, **77**, 491 (1958).

NOTES

BULLETIN OF THE CHEMICAL SOCIETY OF JAPAN, VOL. 49(4), 1147—1148 (1976)

Vapor-Phase Photolysis of *cis*-Cyclononene

Yoshihisa INOUE,* Setsuo TAKAMUKU, and Hiroshi SAKURAI
The Institute of Scientific and Industrial Research, Osaka University, Suita, Osaka 565
(Received September 12, 1975)

Synopsis. Direct and sensitized photolyses of *cis*-cyclononene (**1c**) vapor were investigated. The direct irradiation of **1c** gave 1,8-nonadiene(**2**) and vinylcycloheptane *via* the thermally-activated ground state produced by rapid internal conversion from the excited singlet state initially generated. On the other hand, the sensitized photolysis of **1c** gave **2** and five bicyclononanes, which are interpreted in terms of intramolecular hydrogen transfer reactions.

We have investigated the direct and sensitized photolyses of alkenes.[1] On direct irradiation in the vapor phase, the excited singlet alkene generated was reported to suffer rapid internal conversion to thermally-activated ground state molecule.[1e,2] On the other hand, the vibrationally-excited triplet alkene produced in vapor-phase photosensitization has been demonstrated to undergo intramolecular hydrogen transfer reactions[1a,d,f] along with the well-known *cis-trans* isomerization and allylic bond cleavage.[3] As for the photochemistry of cycloalkenes, little is known of the photochemical behavior of medium-ring alkenes, although considerable study has been made of the sensitized photolysis of common-ring alkenes.[4] We wish now to report the results of the direct and sensitized photolyses of cyclononene vapor.

Experimental

All the experiments were carried out at room temperature and under static conditions. The apparatus and basic procedures employed were the same as described previously.[1d,e] The light source of the direct photolysis at 1849 Å was a 30 W low-pressure mercury lamp fitted with a Suprasil envelope. In the sensitized photolyses, radiation from the lamp was filtered by a Toshiba UV-25 filter. The products were analyzed by GLC on a 6 m column of 15% polyethylene glycol-6000 and a 3 m column of 15% tritolyl phosphate. All the products had retention times on GLC identical to those of the authentic specimens or, in the case of *cis*- and *trans*-bicyclo-[5.2.0]nonanes, to those reported in the literature.[5] Attempts for the separation on GLC of *trans*-cyclononene from the *cis*-form were unsuccessful.

Preparation of cis-*Cyclononene (**1c**).* Cyclononanone, prepared from dimethyl azerate according to procedures similar to those described in "Organic Syntheses,"[6,7] was reduced with $LiAlH_4$ to cyclononanol. The alcohol was heated with phosphoric acid to yield *cis*-cyclononene(**1c**), which was purified to 99.5% by preparative GLC.

Preparative Photolysis. The mercury photosensitization of *cis*-cyclononene(**1c**) with 10% nitric oxide was carried out at the pressure of 1.5 Torr for 12 h using the 30 W mercury lamp and a preparative irradiation apparatus which was made up of a 5 l Pyrex vessel, two quartz cells for irradiation, and a thermosiphone for circulation of the gas. Isolation of the products, **2**, **5c** and **6c**, was performed by preparative GLC. The NMR and mass spectra of the products separated above made the identification certain.

*Independent Syntheses of the Authentic Specimens. 1,8-Nonadiene(**2**)* was synthesized by pyrolysis of nonamethylene glycol diacetate at 500 °C according to the method of Marvel and Stile.[8]

*Vinylcycloheptane(**3**)* was synthesized by pyrolysis of **1c** at 800 °C.[9]

cis-*Bicyclo[4.3.0]nonane(**4c**)* was prepared by hydrogenation of indene on Raney nickel W-2 at 180°C for 3 h at the hydrogen pressure of 200 atm in an autoclave.

trans-*Bicyclo[4.3.0]nonane(**4t**)* was prepared by acetone-sensitized photoepimerization of **4c**.[10]

cis-*Bicyclo[6.1.0]nonane(**6c**)* was synthesized by a Simmons-Smith reaction of cyclooctene with diiodomethane in the presence of zinc-copper(II) chloride mixture, according to the procedure described by Rawson and Harrison.[11]

Results and Discussion

The products resulting from the direct and sensitized photolyses of *cis*-cyclononene(**1c**) vapor are shown in Table 1.

On direct photolysis of **1c** at 1849 Å, 1,8-nonadiene (**2**) and vinylcycloheptane(**3**) were obtained as the major products. The formation of **2** and **3** was also observed in the pyrolysis of **1c** at 520—720 °C.[9] The electronically-excited singlet state of simple alkenes has been shown in other systems to undergo rapid internal conversion.[1e,2] Thus, it may be inferred that the electronically-excited singlet of **1c** generated by the direct irradiation suffers rapid internal conversion to a thermally-activated ground state, which gives the products similar to those from the pyrolysis of **1c**. The absence of the bicyclic products, **4**, **5**, and **6**, indicates the low efficiency of the S→T intersystem crossing process, since the photoisomerization to the bicyclic products is characteristic of the triplet species, as shown below in the photosensitization of **1c**.

In sensitized photolysis, mercury and benzene vapor were used as the sensitizers. The products of the photosensitization of **1c** were 1,8-nonadiene(**2**), *cis*- and *trans*-bicyclo[4.3.0]nonanes (**4c** and **4t**), *cis*- and *trans*-bicyclo[5.2.0]nonanes(**5c** and **5t**), and *cis*-bicyclo-[6.1.0]nonane(**6c**), as shown in Table 1. The marked difference in the product distribution between the mercury and benzene sensitizations is attributable to the different triplet energies of the sensitizers; the triplet energies of mercury and benzene are 113 and 84 kcal/mol, respectively. Since the benzene sensitization of **1c** in the liquid phase did not afford any of these products, it is considered that the intermediate

TABLE 1. PHOTOLYSES OF *cis*-CYCLONONENE (**1c**)

Photolysis mode	Pressure, Torr	Exposure time, min	Product, μmol						
			2	**3**	**4t**	**4c+5t**	**5c**	**6c**	H_2
Direct[a]	1.0	3.0	0.29	0.13	c)	c)	c)	c)	d)
Mercury-sensitization	1.0	2.0	0.07	c)	0.11	0.12	0.54	1.18	0.04
Benzene-sensitization[b]	1.0	30	0.05	c)	0.23	0.08	0.02	0.02	c)

a) A small amount (0.04μmol) of unidentified C_9H_{16} product was also obtained. b) One Torr of benzene vapor was added as the sensitizer. c) Not detected (<0.01μmol). d) Not determined.

involved in the vapor-phase photosensitization is a vibrationally-excited triplet of **1c** and that the vibrational activation in the triplet state enhances the photorearrangement. Similarly to the mechanism shown in the norcarane formation in the mercury photosensitization of cycloheptene,[1b] the formation of **6c** is interpreted in terms of a 1,2-shift of allylic hydrogen followed by ring closure of the resulting 1,3-biradical (Scheme). The intramolecular hydrogen abstractions by the excited C=C double bond *via* two possible six-membered transition states give cyclic 1,4- and 1,6-biradicals, and the subsequent β-cleavage or recombination of the resulting biradicals leads to the products **2**, **5**, and **4**.

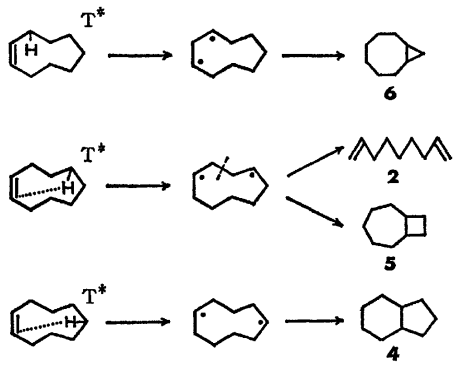

Scheme.

It is thus confirmed in this system that the 1,2-shift of allylic hydrogen and the intramolecular hydrogen abstractions *via* six-membered transition states are the main course of the photo-sensitization of simple alkenes in the vapor phase.

References

1) a) S. Takamuku, K. Moritsugu, and H. Sakurai, *Bull. Chem. Soc. Jpn.*, **44**, 2562 (1971); b) Y. Inoue, M. Kadohira, S. Takamuku, and H. Sakurai, *Tetrahedron Lett.*, **1974**, 459 ; c) Y. Inoue, S. Takamuku, and H. Sakurai, *J. Chem. Soc. Chem. Commun.*, **1975**, 577; d) Y. Inoue, K. Moritsugu, S. Takamuku, and H. Sakurai, *J. Chem. Soc. Perkin Trans. 2*, in press (5/1299); e) Y. Inoue, S. Takamuku, and H. Sakurai, *Bull. Chem. Soc. Jpn.*, **48**, 3101 (1975); f) Y. Inoue, S. Takamuku, and H. Sakurai, *J. Chem. Soc., Chem. Commun.*, **1975**, 896.

2) R. B. Cundall, F. J. Flecher, and D. G. Milne, *Trans. Faraday Soc.*, **60**, 1146 (1964); J. P. Chesick, *J. Chem. Phys.*, **45**, 3934 (1966).

3) J. G. Calvert and J. N. Pitts, Jr., "Photochemistry," Wiley, New York (1966), chapter 2.

4) W. A. Gibbons, W. F. Allen, and H. E. Gunning, *Can. J. Chem.*, **40**, 568 (1962); G. R. De Maré, O. P. Strausz, and H. E. Gunning, *ibid.*, **43**, 1329 (1965); G. R. De Maré, *Bull. Soc. Chim. Belges*, **81**, 459 (1972).

5) C. D. Gutche and J. W. Baum, *J. Am. Chem. Soc.*, **90**, 5862 (1968).

6) N. L. Allinger, "Organic Syntheses," Col. Vol. IV, p. 840.

7) A. C. Cope, J. W. Barthel, and R. D. Smith, "Organic Syntheses," Col. Vol. IV, p. 218.

8) C. S. Marvel and J. K. Stille, *J. Am. Chem. Soc.*, **80**, 1740 (1958).

9) J. K. Crandall and R. J. Watkins, *J. Org. Chem.*, **36**, 913 (1971).

10) R. G. Salomon and J. K. Kochi, *Tetrahedron Lett.*, **1973**, 4387.

11) R. J. Rawson and I. T. Harrison, *J. Org. Chem.*, **35**, 2057 (1970).

BULLETIN OF THE CHEMICAL SOCIETY OF JAPAN, VOL. 49(4), 1149—1150 (1976)

Comments on the Energy Calibration in X-Ray Photoelectron Spectroscopy

Shuichi KINOSHITA, Toshiaki OHTA, and Haruo KURODA

Department of Chemistry, Faculty of Science, University of Tokyo, Hongo, Tokyo 113

(Received November 14, 1975)

Synopsis. The change of the contact potential difference between the sample and spectrometer was examined on the adsorbed carbon/Au system by observing the low kinetic energy limit of the X-ray photoelectron spectrum. Discussions are given on the use of the contamination carbon for energy calibration.

In X-ray photoelectron spectroscopy (XPS) of solid materials, the observed kinetic energies of photoelectron peaks are affected not only by the contact potential difference between the sample and spectrometer, but also by the charge-up of sample caused by X-ray irradiation. The latter, called "charging effect", is known to be particularly significant in the case of insulating samples. There are two methods most widely used to calibrate the energies of photoelectron peaks; the one is to use the C 1s peak of "contamination carbon" as the reference, and the other to use the Au $4f_{7/2}$ peak of a very thin gold film deposited on the sample surface.

It has been pointed out by Ascarelli and Missoni[1] that the contact potential difference between the spectrometer and sample under the condition of the measurement of XPS spectrum can be directly known by observing the low kinetic-energy limit of the photoelectron spectrum. This low energy limit can be observed if an appropriate potential difference is externally applied between the sample and spectrometer. When a voltage $V_{ext.}$ is externally applied on the sample against the spectrometer, the following relation is expected,

$$E_k^0 = (\Phi - \Phi_{sp}) - eV_{ext.} \quad (1)$$

where E_k^0 is the observed kinetic energy of the low-energy limit of the photoelectron spectrum, and Φ and Φ_{sp} are the work functions of the sample and spectrometer, respectively. This method provides another way to calibrate the energies of photoelectron peaks.[2]

In the present study, we have examined if the above three calibration methods do provide results consistent with each other. We carried out experiments with McPherson ESCA 36 electron spectrometer employing Al$K\alpha_{1,2}$ (1486.6 eV). We prepared a gold film by evaporating gold onto an aluminum plate within the sample chamber of the spectrometer, and observed the changes in the Au $4f_{7/2}$ peak of the film and the C 1s peak of "contamination carbon".[3] At the same time, we observed the low kinetic energy limit of photoelectron spectrum by applying −50 volt on the sample against the spectrometer. The low kinetic energy limit appeared as a sharp edge, of which position was able to be determined with an accuracy of ±0.03 eV. Throughout the experiment the vacuum of the sample chamber was kept at about 10^{-8} Torr by means of the combined action of a turbomolecular pump and a cryopump.

As shown in Fig. 1, the intensity of C 1s peak of contamination carbon gradually increased with time, which being accompanied by a decrease of the intensity of Au $4f_{7/2}$ peak. These changes ceased after about two hours, and thereafter, the intensities of both peaks remained constant. On the other hand, no trace of C 1s peak was observed during the measurement. Accordingly, the saturation of the growth of C 1s peak is likely to correspond to the complete coverage of the sample surface with adsorbed hydrocarbon. Thus we took the ratio of the C 1s intensity observed at a given time to the intensity at the saturated state as a measure of surface coverage.

From the low kinetic energy limit of photoelectron spectrum, we estimated the contact potential difference $\Delta\Phi$ according to Eq. 1. The change of $\Delta\Phi$ from the initial value is plotted in Fig. 2 against the surface coverage by adsorbed carbon. We note that the

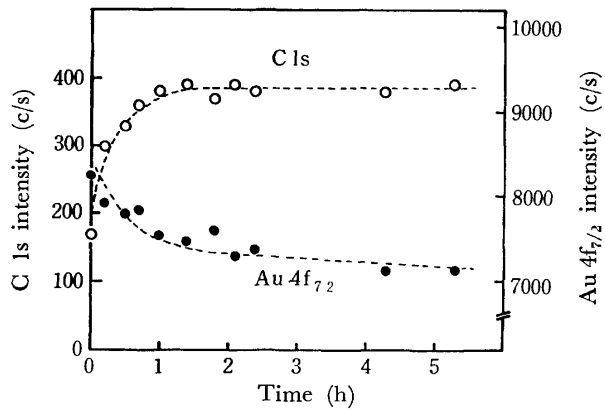

Fig. 1. The variations of the intensities of C 1s and Au $4f_{7/2}$ peaks with time.

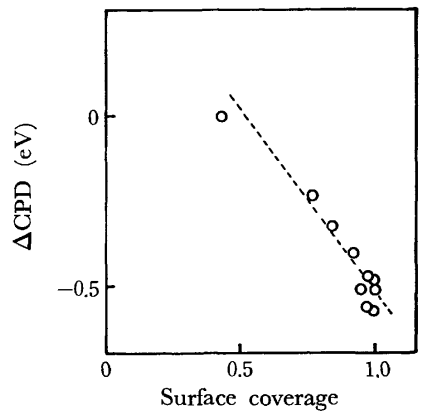

Fig. 2. The relation between the contact-potential-difference change (ΔCPD) and the amount of adsorbed carbon.

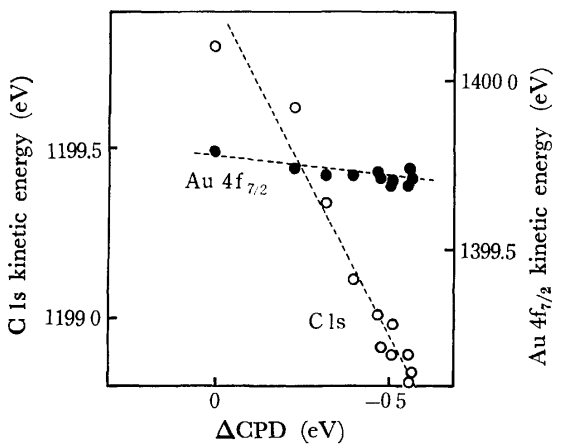

Fig. 3. The dependences of the energies of Au $4f_{7/2}$ and C 1s peaks on the contact-potential-difference.

contact potential difference decreases on increasing the surface coverage. This is consistent with the reported effect of hydrocarbon adsorption on the surface potentials of metals.[4]

In Fig. 3, we have plotted the observed kinetic energies of the C 1s and Au $4f_{7/2}$ peaks against the change of the contact potential difference (CPD). We found that the C 1s peak was shifted to lower kinetic energy linearly depending on the decrease of contact potential difference, whereas the $Au4f_{7/2}$ peak remained almost at the same position.

The above result seems quite reasonable since the Fermi level of the gold film must be little affected by the adsorption of hydrocarbons on its surface while the carbon atoms of the adsorbed layer are under the strong influence of the electrical double layer formed on the surface by the adsorption.

Several conclusion may be derived from the present result. First, the energy of the C 1s peak of "contamination carbon" adsorbed on metal surface can vary depending on the amount of adsorption, consequently its use as the reference of energy calibration seems to be dubious in some cases, especially for metallic samples. Second, the contact potential difference determined from the low kinetic energy limit of photoelectron spectrum, sensitively reflects only the very surface properties, and not necessarily useful to calibrate the energies of the photoelectron peaks associated with the bulk material. One could expect that it might be useful at least for the calibration of the energies of the peaks associated with the adsorbed layer. In this respect, however, it should be noted that, although the observed energy of the C 1s peak of adsorbed carbon was found to be linearly dependent on the change of contact potential difference, its shift was about two times of the value expected from the latter change. This indicates the difficulty in employing the average contact potential difference determined from the low energy limit of photoelectron spectrum even for the purpose of energy calibration of the photoelectron peaks of adsorbed layer. Finally, we wish to point out the possibility that the photoelectron peaks of the bulk material can be distinguished from those of the surface by examining their dependence on the change of contact potential difference as demonstrated by the results shown in the present paper.

References

1) P. Ascarelli and G. Missoni, *Discuss. Faraday Soc.*, **54**, 298 (1972).

2) S. Evans, *Chem. Phys. Lett.*, **23**, 134 (1973).

3) We do not know its exact origin. One of the possible origins could be the oil seal of the turbomolecular pump.

4) R. V. Culver and F. C. Tompkins, *Adv. Catal.*, **11**, 67 (1959).

BULLETIN OF THE CHEMICAL SOCIETY OF JAPAN, VOL. 49(4), 1151—1152 (1976)

Primary Photochemical Process of Sulfur in Solution

Chiho NISHIJIMA,* Nobuaki KANAMARU,** and Katsumi KIMURA

Physical Chemistry Laboratory, Institute of Applied Electricity, Hokkaido University, Sapporo 060

(Received December 27, 1975)

Synopsis. A photochemical intermediate possibly attributed to linear S_8 has been found with a flash-photolysis technique and a rigid-glass technique. The decay behavior of transient in ethanol at room temperature between 10 and 100 ms may be interpreted in terms of the dimerization and polymerization of the linear S_8.

Since a very early work by Lallemand,[1] several groups[2] have studied the phenomenon of photopolymerization of sulfur in solution. Previously, the photoproduct has been explained in terms of allotropes and called "photosulfur". However, no studies on its reaction mechanism and intermediate species have been published so far. In the present work we considered it interesting to study the primary process of the formation of photosulfur in solution by means of a flash photolysis technique as well as a low-temperature UV-irradiation technique.

Experimental

Sulfur (Wako Chemical 99.999%) was recrystallized from carbon disulfide. Low temperature photolysis experiments of sulfur were carried out in EPA glass (2 : 2 : 5) by UV light in the region 250—350 nm using a high-pressure mercury lamp combined with a filter system which consists of an aqueous $NiSO_4$ solution and a Toshiba UV-D25 glass filter. In the low-temperature experiments, absorption spectrum measurements were carried out with a Cary Model 15 spectrophotometer, a quartz cell of 1-cm path length being used. Flash photolysis experiments were carried out with degassed solutions of sulfur in ethanol at room temperature using a flash photolysis apparatus described previously[3] and using a quartz cell of 15 cm long.

Results and Discussion

Sulfur in EPA glass at 77 K shows absorption peaks at 262 and 278 nm ($\varepsilon \approx 6 \times 10^3$ l/mol cm), as shown by Curve 1 in Fig. 1. When an EPA glass containing sulfur (4×10^{-4} M) at 77 K was irradiated by the 250—350 nm light for about 2—3 min, the absorption spectrum shown by Curve 2 was obtained, indicating a new absorption band peaking at 420 nm with an optical density of 0.15 which disappears by warming.[7] Meyer *et al.*[4-6] have recently published the visible absorption bands of S_2, S_3, and S_4 photolytically produced from S_2Cl_2, S_3Cl_2, and S_4Cl_2, respectively, in rigid matrices. The photo-induced 420 nm band in Fig. 1 more or less differs from those of S_2, S_3, and S_4. As far as each S_8 molecule is trapped in EPA glass at 77 K, it may be difficult to consider that a further

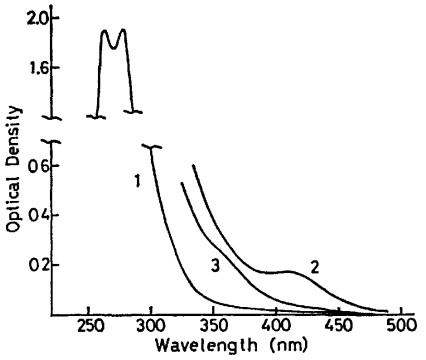

Fig. 1. Electronic absorption spectra before and after the Hg-lamp irradiation of sulfur in EPA glass at 77 K, shown by Curves 1 and 2, respectively. Curve 3 is the spectrum obtained when the irradiated glass was warmed up to room temperature.

dissociation forming $S+S_7$, S_2+S_6, S_3+S_5, or $2S_4$ takes place in the 77-K matrix. Therefore, the photo-induced spectrum (Curve 2, Fig. 1) may be assigned to the linear S_8 biradical formed by ring opening.

$$S_8 \xrightarrow{h\nu} \cdot S_8 \cdot \text{ (linear)} \qquad (1)$$

The flash UV-irradiation of a degassed ethanol solution of sulfur (1×10^{-5} M) at room temperature gave rise to the transient spectra shown in Fig. 2 in which the upper spectra (Curves 1—3) were obtained within about 30 μs after flash, while the lower spectrum was obtained at 10 ms that resembles the low-temperature spectrum (Curve 2, Fig. 1). However, transient spectra taken within about 30 μs are somewhat complicated, suggesting several short-lived transients. Under non-degassed conditions, no transients were detected (possibly because of quenching by oxygen).

The second- and first-order plots of the absorbances of the transients against the time (t) at various wave-

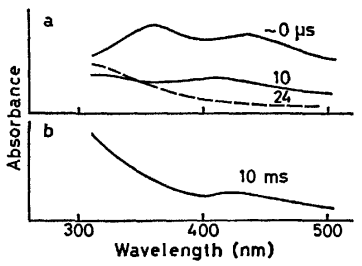

Fig. 2. Transient absorption spectra obtained by the flash photolysis of degassed ethanol solutions of sulfur at room temperature. a) The spectra obtained with a photographic method within about 30 μs after flash. b) The spectrum obtained photoelectrically at 10 ms. The concentrations of sulfur are (a) 1×10^{-5} M and (b) 2×10^{-5} M.

* Present address: Kagawa Nutrition College, 251 Chiyoda, Sakado-machi, Saitama

** Present address: The Institute of Physical and Chemical Research, Wako-shi, Saitama.

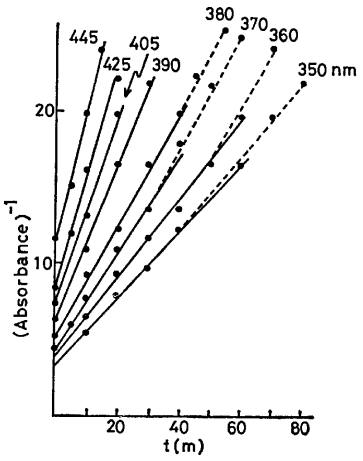

Fig. 3. Second-order decay plots of the transient absorbances obtained at various wavelengths at room temperature under degassed conditions. (An ethanol solution of 2×10^{-5} M sulfur was used.)

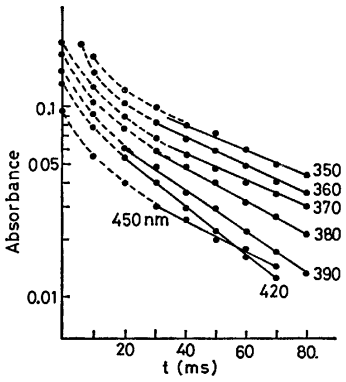

Fig. 4. First-order decay plots of the transient absorbances obtained at various wavelengths at room temperature under degassed conditions. (An ethanol solution of 2×10^{-5} M sulfur was used.)

lengths are shown in Figs. 3 and 4, respectively, suggesting that the 350—450 nm absorption may be ascribed to a single species in the time scale 10—100 ms with a minor contribution from other species. The rate of second-order decay obtained from the plots of the 350—380 nm and 440—450 nm absorptions in Fig. 3 is $C_0k_2=75\pm10$ s^{-1}, where C_0 is the initial concentration of the transient species. (There is some anomaly in the region 390—430 nm) Similarly, we obtained the rate of first-order decay $k_1=16$ s^{-1}, using the plots of the 350—380 nm and 440—450 nm absorptions in Fig. 4.

From the present experimental results, it may be suggested that the intense flash irradiation of sulfur in ethanol solution gives rise to the linear S_8 as well as its some decomposed species (such as S and S_7) which decay much faster than the linear S_8. The observed second- and first-order decays in the range 10—100 msec may be interpreted in terms of the dimerization and polymerization of the linear S_8,

$$2S_8 \longrightarrow S_{16} \quad (2)$$

$$S_8 + S_{8n} \longrightarrow S_{8(n+1)} \quad (3)$$

where $n\geq2$. Such mechanisms seem to be consistent with the formation of photosulfur which has been understood as a polymeric substance of sulfur for a long time.[2)]

The main conclusion obtained here is that the decay of transient species around 10—40 ms may be interpreted mainly in terms of the dimerization of the linear S_8 biradical, whereas the decay observed after about 40 ms may be explained mainly with the polymerization of the linear S_8.

References

1) M. A. Lallemand, *Compt. Rend.*, **70**, 182 (1870).
2) For instance, see B, Meyer, *Chem. Rev.*, **64**, 429 (1964).
3) N. Kanamaru and K. Kimura, *Mol. Photochem.*, **5**, 427 (1973).
4) B. Meyer, T. V. Oommen, and D. Jensen, *J. Phys. Chem.*, **75**, 912 (1971).
5) B. Meyer, T. Stroyer-Hansen, D. Jensen, and T. V. Oommen, *J. Am. Chem. Soc.*, **93**, 1034 (1971).
6) B. Meyer, T. Stroyer-Hansen, and T. V. Oommen, *J. Mol. Spectrosc.*, **42**, 335 (1972).
7) It should also be mentioned that a further UV-irradiation at 77 K for a much longer time, *e.g.*, about 30 min, gives rise to another spectrum (with absorption maxima at about 370 and 420 nm) which disappears at higher temperature. The 370-nm band may be possibly due to some photo-decomposed species such as S and S_7.

BULLETIN OF THE CHEMICAL SOCIETY OF JAPAN, VOL. 49(4), 1153—1154 (1976)

The Crystal Structures of Sterigmatocystin and *O*-Methylsterigmatocystin, Metabolites of the Genus *Aspergillus*

Keiichi FUKUYAMA, Kensaku HAMADA, Tomitake TSUKIHARA, Yukiteru KATSUBE, Takashi HAMASAKI,* and Yuichi HATSUDA*

Faculty of Engineering, Tottori University, Koyama, Tottori 680

(Received December 27, 1975)

Synopsis. The crystal and molecular structures of sterigmatocystin and *O*-methylsterigmatocystin have been studied by the X-ray diffraction method. Both compounds crystallized in the space group $P2_1$ with $Z=2$. The cell dimensions are $a=16.068$, $b=4.293$, $c=11.243$ Å, and $\beta=113.23°$ for sterigmatocystin, and $a=8.835$, $b=16.769$, $c=5.403$ Å, and $\beta=109.21°$ for *O*-methylsterigmatocystin.

Sterigmatocystin (I) was isolated as a metabolite of *Aspergillus versicolor* (Vuillemin) Tiraboschi.[1] The structure and absolute configuration have been determined by chemical and X-ray methods.[2,3] *O*-Methylsterigmatocystin (II) was isolated by Burkhardt *et al.* from *Aspergillus flavus* Link ex Fries, and was synthesized by the methylation of sterigmatocystin.[4] In the series of studies of the structures of the metabolites of the genus *Aspergillus*,[5] X-ray structure analyses of the title compounds have been undertaken.

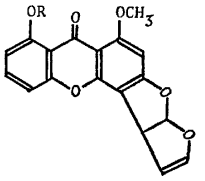

(I) R:H
(II) R:CH_3

Sterigmatocystin crystallized from aqueous acetone solution in the form of pale yellow needles elongated along the b axis. *O*-Methylsterigmatocystin crystallized from acetone solution in the form of colorless prisms elongated along the c axis. The crystal data for each compound are listed in Table 1. The intensities of each compound were measured up to $\sin\theta/\lambda=0.53$ on a Toshiba four-circle diffractometer with Ni-filtered Cu $K\alpha$ radiation. The approximate size of specimen used in the intensity measurement was $0.10\times0.35\times0.12$ mm for sterigmatocystin and $0.11\times0.14\times0.31$ mm for *O*-methylsterigmatocystin. The stationary-crystal stationary-counter method was used, with a counting time of 30 s. The background for each reflection was taken from plots of background as a function of 2θ. The intensities were corrected only for Lorentz and polarization factors.

TABLE 1. CRYSTAL DATA

	Sterigmatocystin	*O*-Methylsterigmatocystin
Molecular formula	$C_{18}H_{12}O_6$	$C_{19}H_{14}O_6$
Molecular weight	324.3	338.3
Crystal system	Monoclinic	Monoclinic
Space group	$P2_1$	$P2_1$
a	16.068(5) Å	8.835(4) Å
b	4.293(2)	16.769(6)
c	11.243(3)	5.403(3)
β	113.23(8)°	109.21(8)°
Z	2	2
D_x	1.51 g/cm³	1.49 g/cm³
D_o	1.50	1.50
μ(for Cu$K\alpha$)	9.7 cm^{-1}	9.6 cm^{-1}

* Faculty of Agriculture, Tottori University, Koyama, Tottori 680.

Sterigmatocystin. The structure was solved by interpretation of Patterson function followed by successive Fourier syntheses. The structure was refined to $R=0.08$ by a block-diagonal least-squares method with anisotropic temperature factors for non-hydrogen atoms. The positions of all the hydrogen atoms were determined from difference synthesis. Including positional parameters and isotropic temperature factors of hydrogen atoms, the refinement reduced the R value to 0.074 for 1018 independent reflections ($R=0.060$ for non-zero reflections). The weighting scheme adopted in the final calculations was; $w=0.3$ for $F_o=0$, $w=1.0$ for $0<F_o\leqq20$, and $w=1.0/(1.0+0.75(F_o-20))$ for $20<F_o$. The final atomic parameters are given in Tables 2(a) and 3(a).

O-Methylsterigmatocystin. The structure was solved by application of the convolution molecule method[6] followed by Fourier syntheses. The refinement was carried out in the same way as that of sterigmatocystin. The final R value is 0.060 for 973 independent reflections ($R=0.055$ for non-zero reflections). The weighting scheme adopted in the final calculations was; $w=0.2$ for $F_o=0$, $w=1.0$ for $0<F_o\leqq15$, and $w=1.0/(1.0+0.83(F_o-15))$ for $15<F_o$. The final atomic parameters are given in Tables 2(b) and 3(b). The atomic scattering factors were taken from the International Tables for X-ray Crystallography.[7]

The bond lengths and angles with their estimated standard deviations are shown in Fig. 1. The difference Fourier synthesis indicates that sterigmatocystin molecule has a intramolecular hydrogen bond, O(3)–H(O3)···O(2). The methoxy groups of both compounds are nearly coplanar with xanthone skeleton; the torsion angle of C(1)–C(2)–O(1)–C(18) in sterigmatocystin is −8.0°, and the angles of C(1)–C(2)–O(1)–C(18) and C(7)–C(6)–O(3)–C(19) in *O*-methylsterigmatocystin are 0.3° and 1.2° respectively. The dihedral angle between the xanthone skeleton and the terminal five-membered ring in sterigmatocystin is 64.9°, and that in *O*-methylsterigmatocystin is 61.0°.

The crystal structure for each compound is shown in Fig. 2. The molecules of sterigmatocystin are stacked with the interplanar distance of xanthone skeleton of 3.4 Å along the b axis to form a column. In *O*-

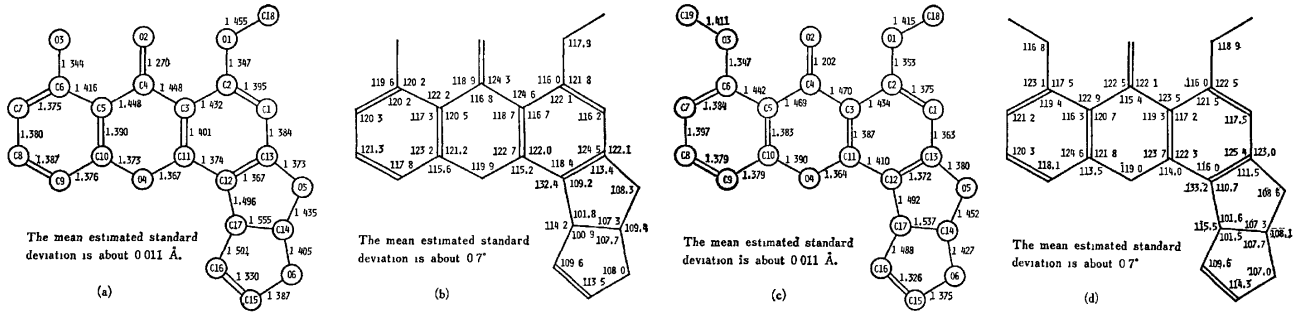

Fig. 1. Bond lengths and angles. (a) and (b) are those in sterigmatocystin, and (c) and (d) are in *O*-methylsterigmatocysten.

Table 2. Final atomic parameters and e.s.d.'s ($\times 10^4$) for non-hydrogen atoms

The anisotropic temperature factors are of the form; $\exp(-\beta_{11}h^2-\beta_{22}k^2-\beta_{33}l^2-\beta_{12}hk-\beta_{13}hl-\beta_{23}kl)$.

(a) Sterigmatocystin

	x	y	z	β_{11}	β_{22}	β_{33}	β_{12}	β_{13}	β_{23}
C(1)	4396(4)	886(18)	2598(5)	46(3)	613(47)	95(6)	13(23)	40(7)	-33(34)
C(2)	3989(4)	1957(18)	1326(6)	50(3)	598(47)	103(6)	-10(22)	61(8)	-32(33)
C(3)	3084(4)	1102(17)	491(5)	40(3)	545(43)	86(6)	9(21)	35(7)	-77(31)
C(4)	2628(4)	2126(19)	-837(5)	43(3)	675(49)	103(6)	50(22)	45(7)	-48(32)
C(5)	1725(4)	925(18)	-1549(5)	43(3)	534(43)	88(6)	54(21)	30(7)	-65(31)
C(6)	1218(4)	1698(19)	-2863(6)	54(3)	740(56)	101(7)	76(26)	48(8)	-46(37)
C(7)	353(5)	571(20)	-3492(6)	71(4)	565(48)	105(7)	79(27)	18(9)	-66(34)
C(8)	-22(4)	-1361(20)	-2855(6)	56(4)	630(52)	112(7)	20(26)	-3(8)	14(38)
C(9)	447(4)	-2132(20)	-1563(6)	46(3)	750(60)	130(7)	-36(26)	24(8)	-37(40)
C(10)	1312(4)	-987(18)	-946(5)	47(3)	610(49)	100(6)	29(24)	34(7)	-94(35)
C(11)	2626(4)	-908(18)	1008(5)	46(3)	603(47)	87(6)	4(23)	43(7)	-2(33)
C(12)	3012(4)	-1966(17)	2262(5)	51(3)	495(43)	90(6)	20(21)	49(7)	-9(30)
C(13)	3880(4)	-1090(19)	3006(5)	50(3)	746(53)	75(6)	70(26)	33(7)	4(34)
C(14)	3494(4)	-4153(20)	4359(6)	68(4)	666(52)	95(6)	8(21)	47(8)	59(36)
C(15)	2376(5)	-1723(23)	4739(7)	82(5)	855(65)	160(9)	14(33)	131(11)	15(47)
C(16)	1992(5)	-2297(20)	3475(6)	72(4)	596(51)	128(8)	31(27)	93(9)	109(38)
C(17)	2656(4)	-3933(18)	3054(6)	55(3)	633(49)	91(6)	-8(25)	41(7)	21(34)
C(18)	5375(4)	4522(21)	1572(7)	46(3)	882(66)	142(8)	-36(27)	41(9)	120(43)
O(1)	4421(2)	3889(13)	816(4)	47(2)	712(35)	114(5)	-27(17)	49(5)	16(24)
O(2)	2970(3)	3976(14)	-1403(4)	53(2)	834(40)	114(5)	-37(18)	49(5)	76(26)
O(3)	1579(3)	3532(14)	-3503(4)	64(2)	839(39)	103(4)	51(19)	47(5)	80(26)
O(4)	1754(2)	-1859(12)	325(3)	44(2)	690(34)	90(4)	-32(15)	19(4)	39(22)
O(5)	4192(3)	-2252(12)	4243(4)	58(2)	646(34)	92(4)	-47(17)	22(5)	32(23)
O(6)	3244(3)	-2930(16)	5330(4)	87(3)	1078(48)	99(5)	-1(22)	78(6)	-55(28)

(b) O-Methylsterigmatocystin

	x	y	z	β_{11}	β_{22}	β_{33}	β_{12}	β_{13}	β_{23}
C(1)	2662(9)	-1503(5)	-634(15)	154(12)	44(3)	484(34)	38(11)	313(34)	-9(18)
C(2)	1427(8)	-1781(5)	152(14)	142(12)	35(3)	479(33)	6(11)	210(32)	3(18)
C(3)	772(8)	-1310(4)	1768(14)	115(10)	31(3)	408(31)	-11(9)	180(29)	-4(15)
C(4)	-597(9)	-1564(5)	2555(16)	180(13)	36(3)	525(36)	-22(11)	314(37)	-34(18)
C(5)	-1105(8)	-994(5)	4190(14)	128(11)	40(3)	414(32)	-8(10)	206(30)	16(16)
C(6)	-2416(9)	-1147(5)	5158(14)	137(12)	43(3)	433(33)	3(10)	240(32)	21(17)
C(7)	-2799(9)	-585(5)	6735(14)	143(12)	58(4)	414(32)	34(12)	222(33)	39(20)
C(8)	-1977(9)	139(5)	7324(15)	158(12)	39(3)	492(37)	18(11)	282(35)	-12(19)
C(9)	-739(9)	303(5)	6378(15)	144(11)	45(3)	419(34)	-9(11)	230(33)	-18(19)
C(10)	-344(8)	-266(5)	4853(13)	136(12)	43(3)	350(28)	19(10)	198(31)	9(17)
C(11)	1453(8)	-566(4)	2544(13)	122(11)	33(3)	376(28)	15(9)	181(29)	19(15)
C(12)	2741(8)	-277(5)	1805(13)	116(11)	45(3)	359(28)	9(10)	169(29)	1(17)
C(13)	3256(8)	-764(5)	205(14)	134(12)	39(3)	418(32)	14(10)	229(32)	11(17)
C(14)	4918(9)	329(5)	966(15)	145(12)	43(3)	469(36)	20(11)	234(34)	41(19)
C(15)	3460(10)	1405(6)	-894(17)	191(14)	51(4)	501(38)	12(13)	314(39)	-10(20)
C(16)	2832(9)	1196(5)	926(17)	145(13)	37(3)	633(41)	-39(11)	287(37)	-65(19)
C(17)	3680(9)	481(5)	2352(15)	138(11)	43(3)	445(34)	-29(10)	271(33)	-39(17)
C(18)	1381(13)	-3012(6)	-2081(21)	262(19)	43(4)	822(58)	2(14)	502(56)	-74(25)
C(19)	-4395(10)	-2012(6)	5628(18)	174(14)	57(4)	672(44)	-32(13)	401(43)	49(24)
O(1)	776(7)	-2513(3)	-511(12)	222(11)	40(2)	719(33)	-30(9)	432(32)	-94(15)
O(2)	-1223(9)	-2204(4)	1957(17)	348(16)	58(3)	1272(54)	-114(12)	1017(51)	-235(22)
O(3)	-3177(6)	-1852(3)	4541(11)	165(9)	46(2)	680(29)	-23(8)	383(27)	-14(15)
O(4)	936(6)	-48(3)	4040(10)	160(8)	37(2)	472(23)	-20(7)	337(22)	-38(11)
O(5)	4521(6)	-429(3)	-388(11)	170(9)	47(3)	599(26)	-31(8)	413(26)	-60(14)
O(6)	4729(6)	940(4)	-953(10)	189(9)	46(2)	550(27)	7(8)	367(27)	29(14)

Table 3. Final positional parameters ($\times 10^3$) and isotropic temperature factors ($\times$Å^{-2}) for hydrogen atoms

	(a) Sterigmatocystin				(b) O-Methylsterigmatocystin			
	x	y	z	B	x	y	z	B
H(C1)	506(4)	128(19)	314(5)	4.0(16)	323(8)	-188(5)	-151(14)	2.6(16)
H(O3)	217(4)	345(21)	-313(6)	4.8(17)	-378(9)	-69(5)	733(15)	3.5(18)
H(C7)	1(4)	128(19)	-445(5)	4.3(17)	-215(8)	59(4)	852(15)	2.4(16)
H(C8)	-68(4)	-241(21)	-333(6)	4.2(16)	-11(8)	86(5)	696(14)	2.3(16)
H(C9)	10(4)	-350(20)	-131(6)	4.4(17)	624(9)	23(5)	717(15)	3.0(17)
H(C14)	380(4)	-613(19)	464(6)	3.8(16)	312(9)	189(5)	-221(14)	2.4(16)
H(C15)	210(4)	-81(21)	533(6)	4.6(18)	186(9)	143(5)	119(16)	3.7(19)
H(C16)	139(4)	-145(22)	282(6)	5.6(19)	425(8)	55(5)	442(14)	2.3(17)
H(C17)	242(4)	-626(19)	265(5)	3.5(15)	251(11)	-308(6)	-173(19)	6.1(25)
H(C18)	571(4)	278(22)	179(6)	5.4(18)	95(12)	-280(7)	-399(21)	6.7(26)
H(C18)	552(4)	516(24)	260(6)	6.0(19)	77(10)	-357(5)	-223(16)	4.5(21)
H(C18)	555(4)	607(22)	120(6)	5.4(19)	H(C19)	-493(12)	-252(5)	496(19)	4.1(20)
					H(C19)	-382(10)	-203(6)	766(16)	4.1(20)
					H(C19)	-525(9)	-151(5)	504(16)	2.5(16)

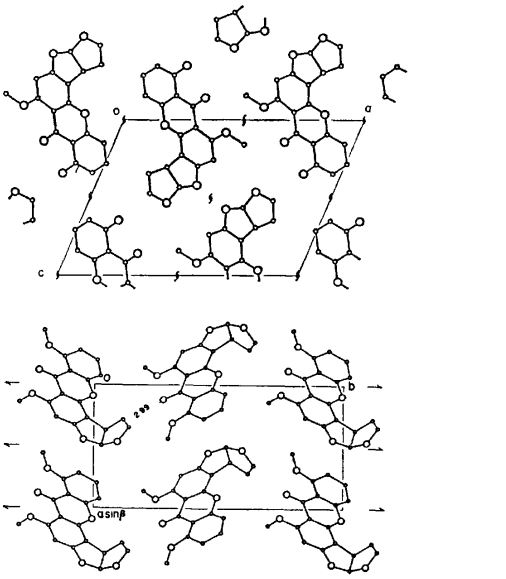

Fig. 2. Projections of the crystal structures of (a) sterigmatocystin and (b) *O*-methylsterigmatocystin.

methylsterigmatocystin the interplanar distance of the xanthone skeletons related by unit translation along the c axis is 3.5Å. The xanthone planes related by screw axis make an angle of 76° in sterigmatocystin, while the angle is 48° in *O*-methylsterigmatocystin. The closest intermolecular contact in the crystal of *O*-methylsterigmatocystin is observed between the terminal of the dihydrofuranofuran moiety and carbonyl oxygen atom. The distances between the C(15) and O(2) atoms and between the H(C15) and O(2) atoms are 2.99 Å and 2.3Å respectively. No intermolecular hydrogen bond is observed in both crystals.

The authors wish to thank Mr. Isao Tanaka and Professor Tamaichi Ashida of Nagoya University for computer programs. They are also indebted to Mr. Fumiyoshi Nishimura for the assistance in this work.

References

1) Y. Hatsuda and S. Kuyama, *Nippon Nogei Kagaku Kaishi*, **28**(12), 989 (1954).
2) E. Bullock, J. C. Roberts, and J. G. Underwood, *J. Chem. Soc.*, **1962**, 4179.
3) J. S. E. Holker and L. J. Mulheirn, *J. Chem. Soc., Chem. Commun.*, **1968**, 1576; K. Fukuyama, T. Tsukihara, Y. Katsube, N. Tanaka, T. Hamasaki, and Y. Hatsuda, *Bull. Chem. Soc., Jpn.*, **48**, 1980 (1975).
4) H. J. Burkhardt and J. Forgacs, *Tetrahedron*, **24**, 717, (1968).
5) K. Fukuyama, H. Kawai, T. Tsukihara, K. Tsukihara, Y. Katsube, T. Hamasaki, Y. Hatsuda, and H. Kuwano, *Bull. Chem. Soc. Jpn.*, **48**, 2949 (1975).
6) "Crystallographic Computing," ed. by F. R. Ahmed, Munksgaard, Copenhagen (1970).
7) "International Tables for X-Ray Crystallography," Vol. III, Kynoch Press, Birmingham (1962), p. 202.

BULLETIN OF THE CHEMICAL SOCIETY OF JAPAN, VOL. 49(4), 1155—1156 (1976)

The Infrared Frequency Shift and Half Width of the Hydrogen-Bonded Band in Some Phenol–Nitrile Systems

Inam JAWED

Department of Physical Chemistry, Peshawar University, Peshawar, Pakistan

(Received March 18, 1975)

Synopsis. The relationship between the infrared frequency shift and half width of the hydrogen bonded band for a number of phenol–nitrile systems has been studied. A linear relationship, $(\Delta\nu_{1/2})_{\text{bonded}}=0.31\,\Delta\nu+21.7\ \text{cm}^{-1}$, has been obtained. It seems that in such plots the intercept is about the magnitude of the half width of the free or unbonded ν(XH) band; *i.e.*, at zero value of the frequency shift, the half width of the bonded band equals that of the free band.

Huggins and Pimental[1] were first to report a linear relationship between half width and frequency shift of the hydrogen bonded ν(XH) vibrational band and further noted that the same plot was applicable to a wide variety of intermolecular hydrogen bonded systems. Their equation was:

$$(\Delta\nu_{1/2})_b = 0.72\,\Delta\nu + 2.5\ \text{cm}^{-1}$$

Since then, many workers have found similar relationships for different hydrogen bonded systems.[2-6] Recently, Lopes and Thompson[7] reported the following correlation for some phenol–nitrile systems:

$$(\Delta\nu_{1/2})_b = 0.58\,\Delta\nu + 2.0\ \text{cm}^{-1}$$

The present study was undertaken to investigate this relationship further for a number of phenol–nitrile systems. However, this investigation differs from the previous one[7] in that here the dependence of the spectroscopic parameters on the concentration of proton acceptors has also been taken into account. This concentration dependence is now more or less established.[8-10]

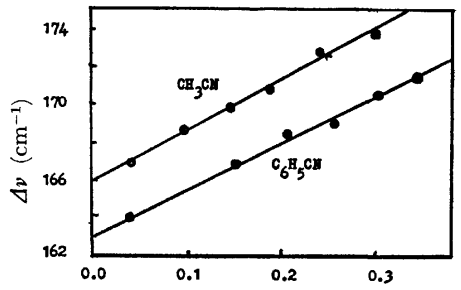

Fig. 1. Frequency shift *vs.* nitrile concentration.
Proton donor: *p*-chlorophenol.

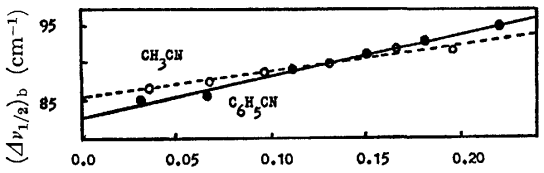

Fig. 2. Half width of the bonded band *vs.* nitrile concentration.
Proton donor: *p*-nitrophenol.

Experimental

The spectra were recorded on a Perkin-Elmer model 125 infrared grating spectrophotometer using an expanded scale(1 cm=5 wave nos.). Tetrachloroethylene was used as the solvent which was dried and fractionally distilled. Quartz cells, 20 mm long, were used. All measurements were made at 25 °C.

The concentration of proton donors is found to have no effect on the spectroscopic parameters whereas that of acceptor has a marked effect. Hence the values of half width and frequency shift are those obtained by extrapolation to infinite dilution of the proton acceptors as shown in Figs. 1 and 2. The concentrations of the proton donors and acceptors used were as follows:

p-Methoxyphenol, phenol and *p*-chlorophenol	5.0×10^{-5} M.
p-Cyanophenol and *p*-nitrophenol	2.5×10^{-5} M.
Trichloroacetonitrile	0.2 M to 1.5 M.
Benzonitrile and acetonitrile	0.03 M to 0.35 M.
t-Butyl cyanide	0.015 to 0.2 M.

Results and Discussion

Tables 1 and 2 give the values of frequency shift and half width respectively of the bonded bands for the systems investigated. Using this data, the following straight-line correlation was obtained by the method of least squares (Fig. 3):

$$(\Delta\nu_{1/2})_b = 0.31\,\Delta\nu + 21.7\ \text{cm}^{-1}$$

The slope and intercept of this straight line are widely different from those obtained by Lopes and Thompson.[7]

TABLE 1. INFRARED FREQUENCY SHIFTS (at 25 °C)

Phenol	Frequency shifts (cm^{-1}) for nitriles			
	Cl_3CCN	C_6H_5CN	CH_3CN	$(CH_3)_3CCN$
p-Methoxyphenol	60.5	142.0	145.0	155.0
Phenol	63.5	148.0	152.5	162.5
p-Chlorophenol	71.0	163.0	166.0	179.0
p-Cyanophenol	91.0	194.0	197.5	215.5
p-Nitrophenol	95.5	207.0	209.5	226.0

TABLE 2. HALF WIDTH OF THE BONDED BANDS (at 25 °C)

Phenol	Half width of the bonded band (cm^{-1})			
	Cl_3CCN	C_6H_5CN	CH_3CN	$(CH_3)_3CCN$
p-Methoxyphenol	37.0	64.0	68.5	75.0
Phenol	40.0	70.5	75.5	74.0
p-Chlorophenol	39.5	75.0	80.0	78.0
p-Cyanophenol	49.0	80.0	82.5	84.5
p-Nitrophenol	55.0	83.5	85.5	86.5

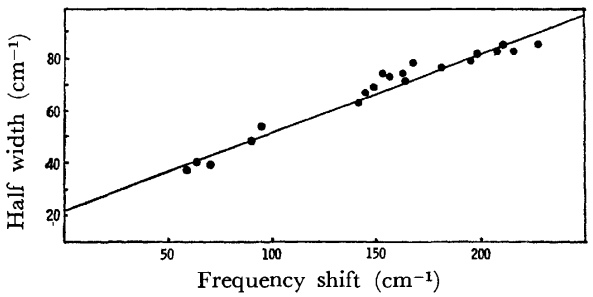

Fig. 3. Plot of frequency shift against half width of the hydrogen bonded band for phenol-nitrile systems.

However, there is an interesting point about our relationship. We note that the intercept of the $(\Delta\nu_{1/2})_b$-axis is just about the average of the half widths of the free ν(OH) bands of the phenols under study. This finding is quite reasonable if we consider both the frequency shift and half width of the bonded band to be related to the strength of the hydrogen bond. Then smaller frequency shift and half width would mean weaker hydrogen bond and hence a stronger X–H link. In the case of no hydrogen bonding at all, the X–H bond should return to its original strength, *i.e.*, it should show the frequency and half width of the free ν(XH) band. Present results should be more reliable since the values of frequency shift and half width used here are those obtained by extrapolation to infinite dilution of the proton acceptors. This concentration dependence of the spectroscopic parameters has been frequently overlooked in previous works.

The author is grateful to Professor Sir Harold Thompson, Physical Chemistry Laboratory, Oxford, for help with this work and to the Government of Pakistan for a fellowship.

References

1) C. M. Huggins and G. C. Pimental, *J. Phys. Chem.*, **60**, 1615 (1956).
2) E. D. Becker, *Spectrochim. Acta*, **17A**, 436 (1961).
3) G. Aksnes and T. Gramstad, *Acta Chim. Scand.*, **14**, 1485 (1960).
4) T. Gramstad, *Acta Chem. Scand.*, **15**, 1337 (1960).
5) M. L. Josien and P. Pineau, "Advances in Molecular Spectroscopy," Vol. 2, ed. by A. Mangini, (1962), p. 924. (Proc. Int. Conf. on Molecular Spectroscopy, 4th Bologne, 1959).
6) S. C. White and H. W. Thompson, *Proc. Roy. Soc., Ser. A*, **291**, 460 (1966).
7) M. C. S. Lopes and H. W. Thompson, *Spectrochim. Acta*, **24A**, 1367 (1968).
8) H. Tsubomura, *J. Chem. Phys.*, **23**, 2130 (1955).
9) S. S. Mitra, *J. Chem. Phys.*, **36**, 3286 (1962).
10) A. Allerhand and P. v. R. Schleyer, *J. Am. Chem. Soc.*, **85**, 371 (1963).

BULLETIN OF THE CHEMICAL SOCIETY OF JAPAN, VOL. 49(4), 1157—1158 (1976)

Syntheses of 3,4-Dimethylpyrrole

Kunihiro ICHIMURA, Susumu ICHIKAWA,* and Kazuo IMAMURA*

Research Institute for Polymers and Textiles, Sawatari 4, Kanagawa-ku, Yokohama 221

(Received August 25, 1975)

Synopsis. Treatment of *N*-sulfinyl compound with 2,3-dimethylbutadiene gives a cycloadduct which affords 3,4-dimethylpyrrole in satisfactory yields by heating in a strongly alkaline methanolic solution.

From an interest in synthesizing porpyrins, we have attempted to prepare a large amount of 3,4-dimethylpyrrole (I). Although various pyrrole syntheses have been worked out,[1] 3,4-disubstituted pyrroles have been available only *via* several steps. The Knorr synthesis affords in *ca.* 50% yield ethyl 2,3,4-trimethylpyrrole-5-carboxylate which we converted into I in 20–40% yield based on Fischer's procedure.[2] The unsatisfactory results prompted us to find a new synthetic route to I.

Alkaline hydrolysis of 2-aryl-3,6-dihydro-4,5-dimethyl-1,2-thiazine 1-oxide gives 1-aryl-3,4-dimethylpyrrole in high yields[3] whereas various 2-substituted 3,6-dihydrothiazine 1-oxide exclusively yield γ,δ-unsaturated amine by acidic, neutral or even alkaline hydrolysis.[4] We have carefully investigated the alkaline hydrolysis of some derivatives of dihydrothiazine 1-oxide (III), the 2-position of which is substituted by ester groups.

The *N*-sulfinylamides (IIa R=CO_2Et,[5] IIb R=CO_2Ph, IIc R=$PO(OEt)_2$[6]) were obtained in excellent yields by the action of thionyl chloride and dry pyridine upon the corresponding carbamate or phosphoramidate. In order to attain a good yield, thionyl chloride and pyridine should be added dropwise to a benzene solution of carbamate or phosphoramidate at the same rate. A poor yield was attained when thionyl chloride was added to a solution of urethane and pyridine.[5b] The *N*-sulfinyl compounds were not purified on account of the high sensitivity toward heat and moisture, as characterized by means of IR spectra. IIb crystallized on cooling. The IR spectrum exhibits bands at 1260 and 1100 cm^{-1} characteristic of the N=S→O group [4a] and at 1750 cm^{-1} due to the carbonyl group. After pyridine hydrochloride had been removed under protection from moisture, 2,3-dimethylbutadiene was added to the solution of crude *N*-sulfinylamide followed by refluxing to give the cycloadduct (III). 2-Ethoxycarbonyl (IIIa)[5a] and diethoxyphosphonyl (IIIc) derivatives have a high boiling point and were not purified because of reduction in yield caused by distillation. They were characterized by IR spectra. 2-Phenoxycarbonyl derivative (IIIb) was purified by recrystallization from cyclohexane to give 79.5% yield of hydroscopic crystals, mp 84—86 °C, which decompose with the evolution of sulfur dioxide on being left to stand at room temperature.

When cycloadducts (III) were heated in strongly alkaline methanol, 3,4-dimethylpyrrole was formed (Table 1) although Levchenko and coworkers described the exclusive formation of γ,δ-unsaturated amine by the action of 2.5 mol sodium hydroxide on IIIa in ethanol.[5a] The pyrrole was isolated by steam-distillation. A dark resinous substance remained. Evolution of hydrogen sulfide and sulfur dioxide was observed on acidification of the aqueous residue. The strength of alkali played a key role for the formation of the pyrrole; when the cycloadduct were heated in aqueous alkali, the yield of the pyrrole was always smaller than in methanol (run 5, Table 1).

Table 1. Syntheses of 3,4-dimethylpyrrole

Exp. run	R in III	Alkali[a]	Mol of alkali	Solv.	Yield (%)[b]
1	CO_2Et	NaOMe	4	MeOH	5—10
2	CO_2Et	KOH	8	MeOH	34—48
3	CO_2Et	NaOMe	7	MeOH	62
4	CO_2Ph	NaOH	5	MeOH	40
5	CO_2Ph	NaOH	5	H_2O	trace[c]
6	CO_2Ph	NaOMe	7	MeOH	59
7	$PO(OEt)_2$	KOH	8	EtOH-H_2O	22
8	$PO(OEt)_2$	NaOMe	6	MeOH	27

a) Alkali hydroxide; 20—30 w/w% in methanol or water. Sodium methoxide: *ca.* 10 w/w% in methanol. b) Based on the crude cycloadduct (III) except runs 4—6 where the purified cycloadduct was used. c) Ehrlich's test was positive.

Similarly, 3-methylpyrrole was obtained in 13% overall yield when isoprene was used instead of dimethylbutadiene. The poor yield of the pyrrole in this case should results from less sufficient cycloaddition.

Attempts to isolate 2-unsubstituted 3,6-dihydrothiazine 1-oxide (III; R=H) by the reaction of IIb with such weaker bases as ammonia and aniline were unsuccessful.

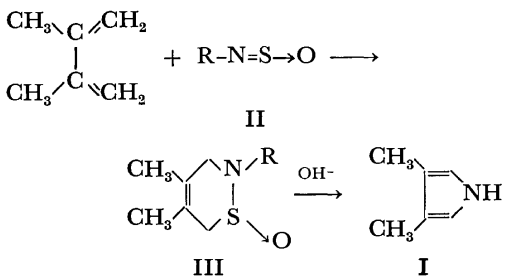

II III I

IIa and IIIa; R=CO_2Et, IIb and IIIb; R=CO_2Ph, IIc and IIIc; R=$PO(OEt)_2$.

Experimental

Materials. Benzene was dried over sodium wire, and pyridine over potassium hydroxide. Thionyl chloride

* Department of Chemistry, Faculty of Technology, Kanagawa University, Kanagawa, Yokohama.

was distilled just before use.

3,4-Dimethylpyrrole (Starting From Ethyl Carbomate). In a 1 l round-bottomed flask, equipped with a mechanical stirrer, a reflux condenser attached with a calcium chloride tube, and two 100 ml dropping funnels, were placed 27.1 g ethyl carbamate and 150 ml dry benzene. Pyridine and thionyl chloride were added dropwise at the same rate with efficient stirring and cooling with cold water. After the mixture was further stirred for one hour at room temperature, 25.0 g 2,3-dimethylbutadiene was added in one portion. The mixture was heated under mild refluxing and stirring and then allowed to stand overnight. After voluminous pyridine hydrochloride was filtered and washed with benzene, the filtrates were evaporated under reduced pressure to afford an oily residue of crude 2-ethoxycarbonyl-3,6-dihydro-4,5-dimethyl-1,2-thiazine 1-oxide, ν_{max} (neat); 1725, 1317, 1250, 1100 cm^{-1}. To the residue was added 135 g potassium hydroxide dissolved in 300 ml methanol, and the dark colored mixture was refluxed 2 h. The solvent was distilled under ordinary pressure, and the reaction mixture was steam-distilled to give an oily substance which was extracted repeatedly with ether. The extracts were dried over anhydrous potassium carbonate, and the solvent was removed. Vacuum distillation of the oily residue gave 13.77 g 3,4-dimethylpyrrole of bp_{25} 67—70 °C (lit, bp_{14} 65.5–66 °C).[7] The yield was 47.7% based on ethyl carbamate.

2-Phenoxycarbonyl-3,6-dihydro-4,5-dimethyl-1,2-thiazine 1-Oxide. After 30.0 g phenyl carbamate was treated with 35.1 ml pyridine and 15.1 ml thionyl chloride in 250 ml benzene in the same manner as above, pyridine hydrochloride was filtered off and washed with dry benzene. To the combined benzene solutions was added 19.8 g 2,3-dimethylbutadiene, and the mixture was refluxed for 1 h after being left standing overnight. The solvent was removed by vacuum distillation to afford crystalline residue which was recrystallized from cyclohexane. The 1,2-thiazine 1-oxide weighed 46.1 g (79.6% based on phenyl carbamate) and melted at 84—86 °C. ν_{max}(KBr); 1745, 1342, 1211, 1080 cm^{-1}. Found: C, 58.84; H, 6.14; N, 5.26%. Calcd for $C_{13}H_{15}NO_3S$: C, 58.84; H, 5.69; N, 5.28%. The crystals decomposed gradually with evolution of sulfur dioxide. Treatment of this compound with alkali yielded 3,4-dimethylpyrrole as shown in Table 1.

Phenyl *N*-sulfinylcarbamate was isolated when the benzene solution was removed *in vacuo* under protection from moisture, after the reaction of phenyl carbamate with thionyl chloride in the presence of pyridine. The new *N*-sulfinyl derivative crystallized on cooling in a refrigerator, showing characteristic IR bands at 1260 and 1100 cm^{-1} due to N=S→O groups.[4a]

3-Methylpyrrole. In the same way as mentioned above, crude ethyl *N*-sulfinylcarbamate, obtained by the reaction of 30.0 g ethyl carbamate with 40.0 g thionyl chloride and 26.5 g pyridine, was treated with 28.0 g isoprene. The mixture was refluxed for 3 h. After pyridine hydrochloride had been removed by filtration, the salt was washed with benzene. The benzene was distilled *in vacuo* to afford an oily residue which was heated with 130 g potassium hydroxide in 300 ml methanol for 3 h. The solvent was distilled off, and the residue was steam-distilled. The distillate was extracted with ether, and the solvent was distilled off after the ether had been dried with potassium carbonate. Distillation of the residue gave 6.60 g crude 3-methylpyrrole which was purified by redistillation: 3.93 g (13% based on ethyl carbamate), bp 140—145 °C (lit,[2a] bp 142—143 °C).

References

1) a) A. H. Corwin, "*Heterocyclic Compounds*," Vol. I, ed. by R. C. Elderfield, John Wiley & Sons, Inc., New York, N. Y. (1959), p. 227; b) E. Baltazzi and L. I. Krismen, *Chem. Rev.*, **62**, 511 (1962).

2) a) H. Fischer and B. Walach, *Liebigs Ann. Chem.*, **450**, 109 (1926); b) H. Booth, A. W. Johnson, F. Johnson, and R. A. Langdale, *J. Chem. Soc.*, **1963**, 650; c) R. L. N. Harris, A. W. Johnson, and I. T. Kay, *J. Chem. Soc., C*, **1966**, 22.

3) J. Rocek, *Chem. Listy*, **47**, 1781 (1953); *Chem. Abstr.*, **49**, 1055b (1955).

4) a) G. Kresze, A. Maschke, R. Albrecht, K. Bederke, H. P. Patzschke, H. Smalla, and A. Trede, *Angew. Chem.*, **74**, 135 (1962); b) G. Kresze, "1,4-Cycloaddition," ed. by J. Hamer, A. Academic Press, New York and London (1967), p. 453.

5) a) E. S. Levchenko, Ya. G. Bal'on, and A. V. Kirsanov, *Zh. Org. Khim.*, **30**, 1883 (1967); *Chem. Abstr.*, **68**, 29658 k (1968). b) J. Hancock and A. R. Markert, *Tetrahedron Lett.*, **1966**, 6157; c) H. -H. Hoerhold, *Angew. Chem.*, **79**, 312 (1967).

6) J. Wieczorkowski, *Chem. Ind., (London)*, **1963**, 825.

7) H. Plieninger, H. Bauer, W. Buehler, J. Kurze, and U. Lerch, *Liebigs Ann. Chem.*, **680**, 69 (1964).

BULLETIN OF THE CHEMICAL SOCIETY OF JAPAN, VOL. 49(4), 1159—1160 (1976)

A Synthesis of Methyl 2-Dimethylphosphoenolpyruvate by Dephosphorylation

Kugako WATANABE, Michiko (KATO) ISHIMATSU, and Koa TASAKA

Division of National Science, International Christian University, Osawa, Mitaka-Shi, Tokyo 181

(Received September 25, 1975)

Synopsis. Methyl 2-dimethylphosphoenolpyruvate was obtained by base-catalyzed dephosphorylation of methyl 2,3-bis(dimethylphospho)glycerate.

Phosphoenolpyruvate(PEP) has a very large free energy of hydrolysis among the so called "energy-rich" phosphates in biological systems.[1] In glycolysis, it is considered that 3-phosphoglycerate is transformed into 2-phosphoglycerate by phosphoglycerate mutase with the help of 2,3-diphosphoglycerate, and the PEP is formed by dehydration of 2-phosphoglycerate[2]. Organic syntheses of PEP have been performed by various methods.[3]

In the present work, a synthesis of methyl 2-dimethylphosphoenolpyruvate by dephosphorylation was investigated. The term "dephosphorylation" is used here for the reaction in which a phosphoric acid or ester is eliminated from a mono-, di- or tri-ester of phosphoric acid to form an alkene;

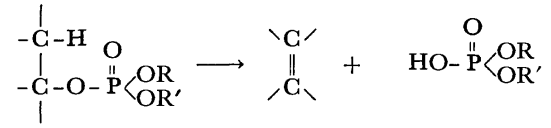

Dephosphorylation of bis-phosphate should lead to the formation of enolphosphate.

No decomposition took place when 1,2-bis(dimethylphospho)propanediol was subjected to pyrolysis at 250 °C. Methyl 2,3-bis(dimethylphospho)glycerate was prepared by the phosphorylation of methyl glycerate, decomposition taking place at 250 °C. The reaction mixture turned dark brown. It was difficult to isolate the products. On the other hand, when the reaction was carried out in the presence of triethylamine, the dephosphorylation occurred at a much lower temperature. The amine acts not only as a catalyst but it is consumed by forming a salt. Pyridine could be also used as a base, but was found less effective.

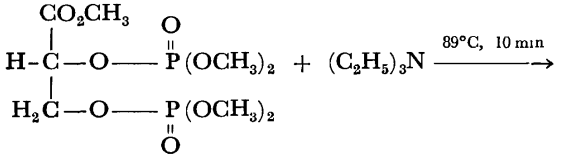

(1)

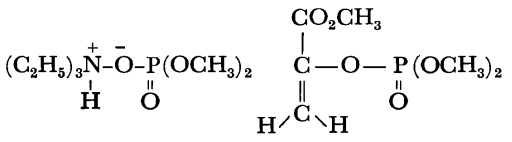

(2)

When a mixture of diphosphoglycerate(**1**) and two mole equivalent of triethylamine was kept in a oil-bath of 89 °C for 10 min and the ammonium salt was removed, the methyl ester of phosphoenolpyruvate was obtained in 50% yield by use of a short-path distillation apparatus *in vacuo*. The distillate showed identical H^1-NMR and IR spectra with those of phosphoenolpyruvate methyl ester (**2**) prepared by the Perkow reaction from methyl β-bromopyruvate and trimethyl phosphite.[4] 2,3-Diphosphoglycerate is known to be extremely stable toward hydrolysis among the biologically important phosphoric esters[5]. However, the lability of its esters toward elimination is not known. We are investigating the dephosphorylation of 2,3-diphosphoglycerate and its other esters under various conditions.

Experimental

The IR spectra were taken with a JASCO IRA-2 spectrophotometer, and NMR spectra with a Hitachi-Perkin Elmer R-20 spectrometer. The chemical shifts in NMR measurement were recorded in δ values relative to tetramethylsilane (TMS) as an internal standard.

*Preparation of Methyl 2,3-Bis(dimethylphospho)glycerate(**1**)* Glyceric acid was converted into methyl ester by the usual way,[6] and the methyl glycerate was phosphorylated with dimethylphosphorochloridate in the following way. To an ethereal solution of methyl glycerate(1.2 g, 0.01 mol) and pyridine(1.6 ml, 0.02 mol) was added dimethylphosphorochloridate(3.0 g, 0.02 mol) dropwise under cooling and stirring. The mixture was left to stand overnight at room temperature and the pyridinium salt was removed by decantation and extraction with water from chloroform solution. After removal of the solvent, methyl 2,3-bis(dimethylphospho)-glycerate(**1**) (1.5 g, 45%, bp 80 °C/0.1 mmHg) was obtained by distillation. NMR δ ppm (in $CDCl_3$); 2.92(12H, doublet, $POCH_3$, J=11.3 Hz), 3.00(2H, multiplet, CH_2), 3.17(3H, singlet, $COCH_3$), 3.90(1H, multiplet, CH). IR νcm^{-1} (in $CHCl_3$); 1270(s) νP=O, 1185(m), νC–O–P, 1035(s) νC–O–P.

*Dephosphorylation of Methyl 2,3-Bis(dimethylphospho)glycerate (**1**).* A mixture of methyl 2,3-bis(dimethylphospho)-glycerate (0.42 g, 12 mmol) and triethylamine (0.20 g, 24 mmol) was kept in an oil-bath of 89 °C for 10 min and extracted with CCl_4 at room temperature. The extract was concentrated under reduced pressure and distilled *in vacuo*. Methyl 2-dimethylphosphoenolpyruvate(**2**), 0.13 g (50.0%, bp 60—64 °C/0.02 mmHg), was obtained as a colorless liquid. NMR δ ppm(in CCl_4); 3.79(3H, singlet, CO_2CH_3), 3.80(6H, doublet, P–OCH_3, J=11.3 Hz), 5.56 and 5.86 (2H, two triplets, $=CH_2$). IR ν cm^{-1} (in CCl_4); 3020(w) νH–C=, 1750(vs) νC=O, 1650(s) νC=C, 1290(vs) νP=O, 1160(vs) νC–O–(C), 1050(vs) νP–O–(C). The IR and NMR spectra of the compound were identical with those of **2** prepared by the Perkow reaction.

*Preparation of Methyl 2-Dimethylphosphoenolpyruvate(**2**) by Perkow Reaction.* Compound **2** was synthesized from α-bromopyruvate (0.83 g., 5 mmol) and trimethyl phosphite (0.57 g, 5 mmol) in benzene according to the procedure of Cramer and Garther[4]. The product was distilled at 65—67 °C/0.03 mmHg, and **2** was obtained in 68.5% yield.

References

1) A. L. Lehninger, "Bioenergetics," W. A. Benjamin, Inc., (1965), p. 59.
2) E. W. Sutherland, T. Posternak ,and C. F. Cori, *J. Biol. Chem.*, **181**, 153 (1949).
3) S. P. Colowick and N. t. Kaplan, Ed., "Methods in Enzymology," Vol. III, Academic Press, N. Y., 1957, p. 223.
4) F. Cramer and K. G. Garther, *Chem. Ber.*, **91**, 704 (1958).
5) S. P. Colowick and N. O. Kaplan, Ed., "Methods in Enzymology," Vol. III, Academic Press, N. Y. (1957), p. 221.
6) J. Cheymol and P. Chabrier, *C. R. Acad. Sci.*, **247**, 1014 (1958).

BULLETIN OF THE CHEMICAL SOCIETY OF JAPAN, VOL. 49(4), 1161—1162 (1976)

NMR Spectroscopic Studies on the Tautomerism in Schiff Bases of Tenuazonic Acid Analogs

Tatsuaki YAMAGUCHI, Kimitoshi SAITO, Toshio TSUJIMOTO,* and Hidetaka YUKI*

Laboratory of Organic Chemistry, Chiba Institute of Technology, Narashino, Chiba 275

**Faculty of Pharmaceutical Sciences, Osaka University, Yamadakami, Suita, Osaka 565*

(Received October 13, 1975)

Synopsis. A NMR spectroscopic study of ^{15}N-enriched Schiff bases of such tenuazonic acid analogs as 3-acetyltetramic acid, 3-acetyltetronic acid, and 3-acetylthiotetronic acid showed the predominance of ketamine forms in their tautomeric equilibria in $CDCl_3$. The ratios of "external tautomers" between two different ketamine forms, as calculated from the ^{15}N–H signal intensities, were compared favorably with the ratios obtained from the ring methylene signals.

In connection with the study[1] of the antitumor activities of Schiff bases of tenuazonic acid analogs,[2] their tautomeric structures were examined by means of NMR spectroscopy. These Schiff bases[3] may exist in a solution in any form of "external tautomers" (B_N, $B_O \rightleftharpoons C_N$, C_O), besides "internal tautomers" ($B_N \rightleftharpoons B_O$, $C_N \rightleftharpoons C_O$), as Forsén and coworkers have suggested for unsymmetrical β,β'-triketones.[4] They have also estimated the ratios of the "external tautomers" of unsymmetrical cyclic β,β'-triketones from the intensities of the split NMR signals of the ring methylene.

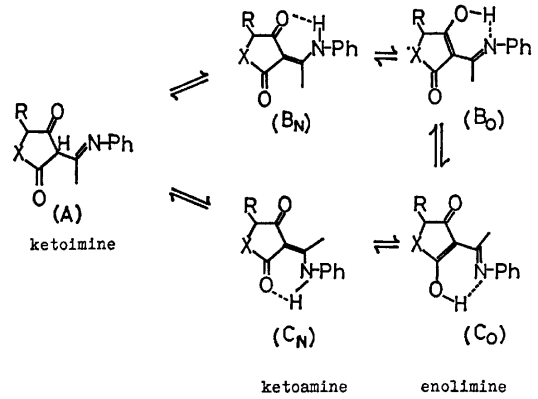

Chart 1.

Results and Discussion

The presence of "external tautomers" in the Schiff bases of these tenuazoinc acid analogs was detected from the splitting of the ring methylene (5-position) signals (3.70—4.53 ppm) in their NMR spectra. The counterpart in the higher field of the split methylene signals can be assigned to the tautomeric pair of B_N and B_O, and the lower one, to the pair of C_N and C_O, since the anisotropic effect[5] of the neighboring carbonyl group (4-position) can be expected to be more pronounced in the forms of C_N and C_O than in B_N and B_O, in which the carbonyl groups are hydrogen-bonded (B_N) or enolized (B_O). The ratios of the "external tautomers", B_N+B_O to C_N+C_O, for these Schiff bases were calculated from intensities of the corresponding signals (Table 1).

The observed NMR spectra of these Schiff bases showed a broad doublet arising from the active hydrogen in the region of 11.66—13.67 ppm (Table 2). In order to elucidate the exact assignment of these signals to the tautomeric structures, the Schiff bases of tenuazonic acid analogs were synthesized using commercially available aniline-^{15}N, since sharp signals can be expected for protons bonded to the ^{15}N-nucleus ($I=1/2$), and the ^{15}N–H spin coupling constant of *ca.* 90 Hz makes possible a ready detection of any "internal" tautomerization between N–H and O–H.[6]

The spectrum of the ^{15}N-substituted Schiff base (IA) from 3-acetyltetramic acid contained two pair of sharp doublets at nearly the same position relative to the corresponding ^{14}N-compound (Fig. 1). The observed ^{15}N–H spin coupling constant was 90.0 Hz for each doublet at 34 °C in $CDCl_3$. Upon raising the sample temperature to +60 °C or lowering it to −70 °C, no changes were observed in the chemical shifts, signal intensities, or coupling constants of this compound. Therefore, it can be concluded that IA primarily exists in the ketoamine forms, B_N and C_N. The intensity ratio of the higher-field doublet to the lower one showed a good coincidence with the ratio of "external tautomers" calculated from the intensities of the ring methylene signals (Table 1). Accordingly, the higher-field doublet can be ascribed

Table 1. Ratios of "external tautomers" calculated from the intensity ratios of ring methylene signals and ^{15}NH signals

No.	Compounds X	Compounds R	B_N+B_O/C_N+C_O (from CH_2)	B_N/C_N (from ^{15}NH)
IA	NH	H	1.13	1.17
IB	NH	$CH_2C_6H_5$	1.39	1.41
II	O	H	0.37	0.36
III	S	H	0.34	0.32

Table 2. Chemical shifts of active hydrogens

No.	δ^{14}_{NH} (ppm)		δ^{15}_{NH} (ppm) B_N form	(J^{15}_{N-H}) (Hz) C_N form
IA	12.09	12.44	12.17 (90.0)	12.52 (90.0)
IB	12.08	12.40	12.11 (90.0)	12.48 (90.0)
II	11.66	12.44	11.61 (90.0)	12.57 (91.8)
III	12.89	13.67	12.86 (90.9)	13.66 (86.4)

to the B_N form, and the lower one to the C_N form.

The observed spectra of the other compounds showed patterns similar to that of IA and indicated the same conclusion in the assignment of the signals. However, the observed ^{15}N–H coupling constant (86.4 Hz) of the C_N form in the Schiff base (III) of 3-acetylthiotetronic acid is found to be markedly smaller than the values for the others. This suggests that *ca.* 5% of the C_O form is present at 34 °C in the $CDCl_3$ solution of this compound. The presence of the C_O form in III is also supported by the results for the ^{13}C-NMR spectrum of III, which showed an additional small signal of enolic carbon at 193.88 ppm (from TMS) besides two signals at 195.18 and 198.81 ppm arising from free carbonyl carbon and hydrogen-bonded carbonyl carbon respectively. The exceptional feature of III could be explained by the geometry of the molecule. Simple molecular orbital calculation are in progress to obtain further insights in this field.

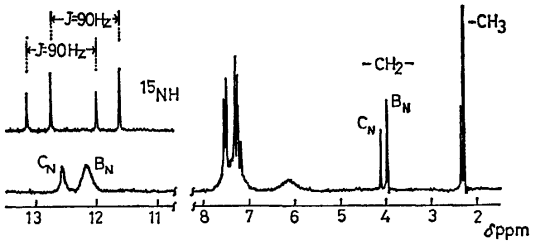

Fig. 1. NMR spectrum of 3-(1'-anilinoethylidene)-pyrrolidine-2,4-dione (IA) in $CDCl_3$ at 90 MHz.

Experimental

Materials. The IA,[7] IB,[7] II,[8] and III[9] were prepared according to the procedures described in the literature cited. Aniline-^{15}N (95% isotopic purity) was obtained from Prochem BOC, Ltd.

Measurements. The NMR spectra were measured with a Hitachi Perkin-Elmer R-22 spectrometer at 90 MHz at 34 °C, using TMS as the internal standard. Solutions were made so as to contain 1.5×10^{-4} mol of compounds in 0.4 ml of $CDCl_3$.

The ^{13}C-NMR spectra measured on a JNM-FX60 spectrometer equipped with a PFT-100 Fourier transform accessory at 25.1 MHz, using TMS as the internal reference and a 10-mm-diameter NMR tube. The spectra were obtained by 5000-times accumlations measured on a broad-band proton decoupler. The solution contained 200 mg of the sample in 2 ml of $CDCl_3$.

The authors are grateful to Mr. Muneki Ohuchi of the Japan Electron Optics Laboratory for the ^{13}C-NMR measurement.

References

1) (a) H. Yuki, E. Kitanaka, A. Yamao, and Y. Hashimoto, *GANN*, **62**, 199 (1971). (b) H. Yuki, K. Kariya, and Y. Hashimoto, *Chem. Pharm. Bull.*, **15**, 727 (1967). (c) H. Yuki, Y. Kaizu, S. Yoshida, and K. Takiura, *ibid.*, **19**, 1664 (1971).

2) Common names were consciously introduced for these compounds in order to express the mixed systems of complicated tautomers.

3) Although the ketoimine form (A) is another possible tautomer, there is no evidence for its presence in any of these Schiff bases.

4) (a) S. Forsén and M. Nilsson, "The Chemistry of the Carbonyl Group," Vol. 2, J. Zabicky, ed., John Wiley & Sons, London (1970), p. 157. (b) S. Forsén, F. Merényi, and M. Nilsson, *Acta Chem. Scand.*, **21**, 620 (1967).

5) Z. Bankowsa and I. Zadrozna, *Rocz. Chem. Ann. Soc.*, **45**, 183 (1971).

6) a) G. O. Dudek and E. P. Dudek, *J. Am. Chem. Soc.*, **86**, 4283 (1964). (b) G. O. Dudek and G. P. Volpp, *J. Org. Chem.*, **30**, 50 (1965). (c) G. O. Dudek and E. P. Dudek, *J. Am. Chem. Soc.*, **88**, 2407 (1966). (d) G. O. Dudek and E. P. Dudek., *J. Chem. Soc., B*, **1971**, 1356. (e) B. Sunners, L. H. Pitte, and W. G. Schneider, *Can. J. Chem.*, **38**, 681 (1960).

7) R. N. Lacey, *J. Chem. Soc.*, **1954**, 832.

8) R. N. Lacey, *J. Chem. Soc.*, **1954**, 850.

9) D. M. O'Mant, *J. Chem. Soc., C*, **1968**, 1501.

BULLETIN OF THE CHEMICAL SOCIETY OF JAPAN, VOL. 49(4), 1163—1164 (1976)

Pyridoxal Model Compounds. II. The Diels-Alder Reaction of 9-Substituted 2-Methoxyanthracenes

Masaaki IWATA and Sakae EMOTO

The Institute of Physical and Chemical Research, Wako-shi, Saitama 351

(Received November 10, 1975)

Synopsis. The Diels-Alder reactions of several 2-methoxyanthracenes with tetracyanoethylene (TCNE), dimethyl acetylenedicarboxylate (DMAD), and maleic anhydride (MA) were examined. TCNE gave charge-transfer complexes, but not an addition product in every case. MA gave one-to-one adducts with anthracenes, while DMAD afforded no adduct.

Following the regioselective formylation of 2-methoxyanthracenes,[1] the Diels-Alder reactions of maleic anhydride (MA), tetracyanoethylene (TCNE), and dimethyl acetylenedicarboxylate (DMAD) with 9-substituted 2-methoxyanthracenes were examined in an attempt to synthesize a possible precursor of asymmetric inversion catalysts. The anthracene derivatives used are shown in Fig. 1.

The qualitative results obtained are shown in Table 1. These results clearly show that only MA was effective

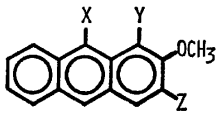

1 X=CH_3, Y=Z=H
2 X=4-isopropyl-*o*-tolyl, Y=Z=H
3 X=4-isopropyl-*o*-tolyl, Y=CHO, Z=H
4 X=3-tolyl, Y=Z=H
5 X=4-isopropyl-*o*-tolyl, Y=H, Z=CHO
6 X=phenyl, Y=Z=H
7 X=2,6-xylyl, Y=Z=H
8 X=2-methoxyphenyl, Y=Z=H

Table 1. The qualitative results of the Diels-Alder reaction of dienophiles with 9-substituted 2-methoxyanthracenes

Compounds	TCNE[a]	DMAD[b]	MA[c]	(Yield %)
1	NR[e]	—	—	
2	C[d]	NR	A[f]	(14)
3	C	NR	A	(42)[g]
4	NR	NR	A	(20)[h]
5	—	NR	A	(40)[h]
6	—	—	A	(87)
7	—	—	A	(80)[h]
8	—	—	A	(75)

a) In THF at ambient temperature. b) With or without solvent such as xylene or ethanol at temperature lower than 100 °C. c) See Experimental. d) C stands for complex formation. e) NR represents that no reaction occured. f) A stands for the formation of one-to-one adduct. g) Yield after hydrolysis followed by esterification of the adduct. h) Apparent yield on TLC.

in the Diels-Alder addition to 9-substituted 2-methoxyanthracenes; this is consistent with the fact that, in early reports concerning the Diels-Alder addition to 9-arylanthracenes, MA was frequently used as a dienophile.[2] Contrary to our expectation, however, TCNE resulted in only the formation of the corresponding charge-transfer complex, and DMAD gave no addition product. The lack of reactivity in these dienophiles may be explained by the steric interaction in the transition state between the aryl group at C_9 and the bulky functional group of the dienophiles.[3]

In relation to our interest in the construction of asymmetric inversion catalysts, the confirmation of the structure of adducts between MA and **3** was important. Thus, the reaction mixture was treated with aqueous 5% trimethylamine and then with diazomethane to convert the products to esters. Mainly, four products were detected on a thin-layer chromatogram; their R_f values were 0.5, 0.35, 0.25, and 0.18. The R_f=0.35 and 0.18 compounds were separated by elution chromatography with silica gel and shown to be one-to-one adducts of **3** with dimethyl maleate; the structures were unequivocally assigned to **9** and **10** respectively on the basis of their NMR spectra and lanthanide-induced NMR spectra. A comparison of the NMR spectra of **9** with that of **10** showed that two methoxycarbonyl groups, at C_{11} and C_{12}, were parallelly disposed to the nearer direction to the formyl-substituted benzeno-ring in **9** and to the more remote direction in **10**, because the two ester methyl groups in **10** showed the same chemical shifts at 3.58 ppm.

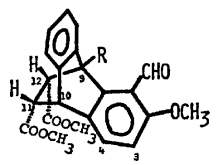

9

R=4-isopropyl-*o*-tolyl

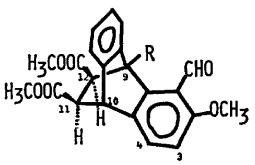

10

R=4-isopropyl-*o*-tolyl

The ratio of the yield of **9** to that of **10** was 47 : 53; it was probably caused by the dipole interaction of the groups between the formyl group at C_1 of **3** and maleic anhydride.

Experimental

The IR spectra were obtained using a Shimadzu IR-27 apparatus. The ^{1}H-NMR spectra were recorded on a Varian HA-100D apparatus, with tetramethylsilane as the internal standard. The chemical shifts and the coupling constant were represented in δ and Hz units respectively. The UV spectra were measured by means of a Hitachi 124

spectrophotometer. Merck Art. 7734 and Wakogel B-5 FM were used for the preparative separation of the products on a silica gel column by elution chromatography and for thin-layer chromatography (TLC) respectively. The melting points are uncorrected.

Materials. All the dienophiles used, TCNE, DMAD, and MA, are commercially available. Compounds **1** through **8** were prepared by the previously reported method.[1b]

Reaction of Anthracenes with MA. In general, MA equivalent in weight to the anthracene derivative used was treated in a suitable amount of *m*-dichlorobenzene at 125—165 °C, and the reaction was monitored by TLC.

9-(4-Isopropyl-*o*-tolyl)-2-methoxyanthracene (**2**) gave a one-to-one adduct in a 14% yield after a reaction for 6 days; mp 210—211 °C. Found: C, 79.15; H, 6.04%. Calcd for $C_{29}H_{26}O_4$: C, 79.43; H, 5.98%.

A mixture of 9-(4-isopropyl-*o*-tolyl)-2-methoxy-1-anthracenecarbaldehyde (**3**) (1.5 g) and 1.5 g of MA in 10 ml of *m*-dichlorobenzene was heated without stirring at 135—145 °C for 40 h. In order to obtain the products as esters, the reaction was then treated with 20 ml of aqueous 5% trimethylamine at room temperature for 2 h, followed by treatment with an ether solution of diazomethane after a usual work-up. Mainly four products were detected on TLC (benzene–ethyl acetate=9 : 1 v/v); their R_f values were 0.5, 0.35, 0.25, and 0.18. On the basis of the color reaction of the products when sprayed with a $FeCl_3$(2 g)–concd HCl (5 ml)–H_2O(95 ml) solution,[4] the products, R_f=0.35 and 0.18, were the compounds bridged between the C_9 and C_{10} of the anthracene ring.

The compound showing R_f=0.35 was obtained in a 19.6% yield and found to be a racemic mixture of dimethyl (9R,10R,11R,12R)-1-formyl-9-(4-isopropyl-*o*-tolyl)-2-methoxy-9,10-dihydro-9,10-ethano-11,12-anthracenedicarboxylate (**9**) and its enantiomer on the basis of the following properties: colorless fine needles from ethanol, mp 189—190 °C. Found: C, 75.04; H, 6.19%. Calcd for $C_{32}H_{32}O_6$: C, 74.98; H, 6.29%. IR (KBr disk): 1740 (–$COOCH_3$), 1705(–CHO), and 1215(=C–O–C) cm^{-1}. UV(ethanol): λ_{max} (log ε) 212 (4.60), 272(3.49), 280(3.53), and 290(3.53)nm. NMR(CCl_4): 1.32(6H, d, J=7.0, –CH($\underline{CH_3}$)$_2$), 1.65(3H, s, Ar–$\underline{CH_3}$), 2.94(1H, quin, J=7.0, –$\underline{CH}$(CH_3)$_2$), 3.66(3H, s, –OCH_3), 3.33 (3H, s, C_{11}– or C_{12}–COO$\underline{CH_3}$), 3.48(3H, s, C_{12}– or C_{11}–COO$\underline{CH_3}$), 3.08 (1H, quar, J=1.75 and 10.75, C_{11}–$\underline{H}$), 3.94 (1H, d, J=10.75, C_{12}–$\underline{H}$), 4.61(1H, d, J=1.75, C_{10}–$\underline{H}$), 6.66 (1H, d, J=8.5, C_3–$\underline{H}$), 7.23(1H, d, J=8.5, C_4–$\underline{H}$), and 9.06 (1H, s, –CHO). MS: (M^+)*m/e* 512.

The compound showing R_f=0.18 was obtained in a 22.5% yield and found to be a racemic mixture of dimethyl (9*R*,10R,11S,12S)-1-formyl-9-(4-isopropyl-*o*-tolyl)-2-methoxy-9,10-dihydro-9,10-ethano-11,12-anthracenedicarboxylate (**10**) and its enantiomer on the basis of the following data: colorless crystals from ethanol, mp 195—196 °C. Found: C, 75.08; H, 6.00%. Calcd for $C_{32}H_{32}O_6$: C, 74.98; H, 6.29%. IR (KBr disk): 1760(–$COOCH_3$), 1690(–CHO), and 1260 (=C–O–C) cm^{-1}. UV(ethanol): 212(4.60), 261(3.79), 270 (sh)(3.68), 281(sh)(3.51), and 318(3.56) nm. NMR($CDCl_3$–CCl_4 1 : 1 v/v): 1.31(6H, d, J=7.0, –CH($\underline{CH_3}$)$_2$), 3.75(3H, s, –OCH_3), 3.58(6H, s, C_{11}– and C_{12}–COO$\underline{CH_3}$), 3.17(1H, quar, J=1.75 and 11.0, C_{11}–$\underline{H}$), 3.80(1H, d, J=11.0, C_{12}–$\underline{H}$), 4.69(1H, d, J=1.75, C_{10}–$\underline{H}$), 6.86(1H, d, J=8.25, C_3–$\underline{H}$), 7.47(1H, d, J=8.25, C_4–$\underline{H}$), and 9.30(1H, s, –CHO). MS: (M^+) *m/e* 512.

9-Phenyl-2-methoxyanthracene (**6**) gave a one-to-one adduct in a 87% yield after a reaction for 14.5 h; colorless crystals, mp 224—226 °C. Found: C, 78.25; H, 4.66%. Calcd for $C_{25}H_{18}O_4$: C, 78.52; H, 4.74%.

9-(*m*-Tolyl)-2-methoxyanthracene (**4**), 9-(4-isopropyl-*o*-tolyl)-2-methoxy-3-anthracenecarbaldehyde (**5**), 9-(2,6-xylyl)-2-methoxyanthracene (**7**), and 9-(2-methoxyphenyl)-2-methoxyanthracene (**8**) were found to react with MA to give yields of 20% (after 18 h) for **4**, 40% (6 days) for **5**, (2 days) for **7**, and 75% (14 h) for **8** on the basis of the TLC spots.

The author wishes to thank Mr. Jun Uzawa and Mrs. Tamiko Chijimatsu for their NMR spectral measurements, and the staff of the Organic Microanalysis Lab. in this Institute for their elemental analyses. This study was supported in part by a Grant for Life Science from this Institute.

References

1) (a) M. Iwata and S. Emoto, *Chem. Lett.*, **1973**, 477; (b) M. Iwata and S. Emoto, This Bulletin, **47**, 1687 (1974).

2) (a) C, Dufraise and L. Velluz, *Bull. Soc. Cheim. Fr.*, **5**, 1073 (1938); (b) E. de B. Barneet, N. F. Goodway, A. G. Higgins, and C. A. Lawrence, *J. Chem. Soc.*, **1934**, 1224; (c) W. E. Bachmann and M. C. Kloetzel, *J. Am. Chem. Soc.*, **60**, 481 (1938).

3) The noncoplanarity between the anthracene ring and the 9-aryl substituent is shown by several workers; (a) von H. Hartmann and H. Grunert, *Z. Naturforsch.*, **5a**, 168 (1950); (b) H. Preuss, *Tetrahedron*, **19**, 51 (1963); (c) E. Heilbronner, P. A. Straub, O. Chalvet, and R. Daudel, *C. R. Acad. Sci.*, **261**, 5330 (1965); (d) E. D. Bergmann, M. Rabinovitz, M. J. Aroney, R. J. W. Le Fevre, L. Radom, and G. L. D. Ritchie, *J. Chem. Soc., B* ,**1968**, 1551.

4) The compounds, R_f=0.5 and 0.25, were detected as brown spots and, on the other hand, the compounds, R_f=0.35 and 0.18, as green spots.

BULLETIN OF THE CHEMICAL SOCIETY OF JAPAN, VOL. 49(4), 1165—1166 (1976)

The Structure and Reactivity of $[Zn(OMe)_2 \cdot (EtZnOMe)_6]$

Michihiro ISHIMORI, Tokio HAGIWARA, Teiji TSURUTA, Yasushi KAI*, Noritake YASUOKA*, and Nobutami KASAI*

Department of Synthetic Chemistry, Faculty of Engineering, University of Tokyo, Bunkyo-ku, Tokyo 113

**Department of Applied Chemistry, Faculty of Engineering, Osaka University, Yamadakami, Suita, Osaka 565*

(Received December 8, 1975)

Synopsis. The molecular structure of $[Zn(OMe)_2 \cdot (EtZnOMe)_6]$, an enantiomorphic catalyst for the polymerisation of methyloxirane, has been determined.

It has been reported that zinc dialkoxide exhibits an excellent stereoselective behaviour as a catalyst for the polymerisation of methyloxirane. In the systematic studies of organozinc compounds as polymerisation catalysts, a complex, $[Zn(OMe)_2 \cdot (EtZnOMe)_6]$ has been isolated in colourless crystalline form.[1] All the stereochemical results so far obtained led to the conclusion that polymerisation of methyloxirane with a catalyst involving zinc dialkoxide proceeds by an enantiomorphic catalyst site control mechanism,[2] similar to the polymerisation of α-olefin to an isotactic polymer with Ziegler-Natta catalyst.[3] The structure of such catalyst sites, however, has not been studied in detail. Thus, elucidation of the structure of zinc dialkoxide complex, $[Zn(OMe)_2 \cdot (EtZnOMe)_6]$, is of particular interest.

The complex was prepared by addition of 16 mmol of methanol to 14 mmol of diethylzinc in 10 ml of heptane under an argon atmosphere (a typical example). The complex has been formulated as $[Zn(OMe)_2 \cdot (EtZnOMe)_6]$, based on the cryoscopic measurement in benzene as well as analyses by EDTA titration for Zn^{2+}, by VPC for CH_3OH and by ethane evolution after hydrolysis. The 100 MHz NMR spectra of the complex in benzene were recorded at 5 to 10 w/v %. The chemical shifts (δ) of CH_2 at 0.54 (relative intensity, 2), CH_3 at 1.46 (3) and CH_3O at 3.51 (4) were observed at room temperature (23 °C). In contrast, the resonance of CH_3O group was split into a doublet having the intensity ratio of 1 : 3 at 80 °C; 0.53 (2) for CH_2, 1.43 (3) for CH_3 and 3.56 (1) and 3.58 (3) for CH_3O. Coupling constants, $J_{CH_2-CH_3}$, were 8.0 Hz in both cases. There was no sign of dissociation for this complex by an equilibrium involving $ZnEt_2$, $(EtZnOMe)_4$, $[Zn(OMe)_2 \cdot (EtZnOMe)_6]$, *etc.* (*cf.* $Me_6Zn_7(OMe)_8$[4]).

In accord with the line split of methoxy groups, the complex showed catalytic activity for methyloxirane at 80 °C, whereas no catalytic activity was observed at room temperature; methyloxirane/complex=2.1(mol/mol), methyloxirane/benzene(solvent)$=5.8\times10^{-2}$(v/v), 3 days : methyloxirane converted=97% at 80 °C and 0% at 30 °C, CH_3O group reacted per mol of the complex=0.58 mol at 80 °C and 0 mol at 30 °C. Under the conditions of methyloxirane/complex=150 (mol/mol) at 80 °C for 4 days, high molecular weight poly(methyloxirane) was obtained in 56% yield.

The molecular structure of $[Zn(OMe)_2 \cdot (EtZnOMe)_6]$ was determined by maens of X-ray diffraction. In spite of very careful sealing in glass-capillary tubes in argon, most of the crystals decomposed after a few days, only one crystal being found useful to some extent for the X-ray analysis.

Crystal Data: $C_{20}H_{54}O_8Zn_7$, M 880.24, monoclinic, $P2_1/c$, $a=11.276(3)$, $b=15.741(3)$, $c=10.715(2)$ Å, $\beta=106.68(2)°$, $U=1821.9(7)$ Å^3, $1.59/D_m/1.63$ g·cm^{-3}. (floatation in cyclohexyl iodide and *n*-butyl iodide), $Z=2$, $D_c=1.604$ g·cm^{-3}.

The determination of unit-cell dimensions and collection of intensity data were carried out on a Rigaku automated, single crystal diffractometer using Nickel-filtered Cu$K\alpha$ radiation. A total of 1884 integrated intensities was measured by θ-2θ scan technique up to $(\sin\theta)/\lambda=0.50$, of which only 942 reflexions were above the background because of rapid decrease of diffraction intensity in high angle region. The structure was solved by the heavy-atom method and refined by the block-diagonal least squares procedure. Applying isotropic temperature factors for non-hydrogen atoms except zinc the R index converged to 0.142 for observed reflexions. The temperature factors were relatively large especially for the terminal methyl carbon atoms of ethyl groups.

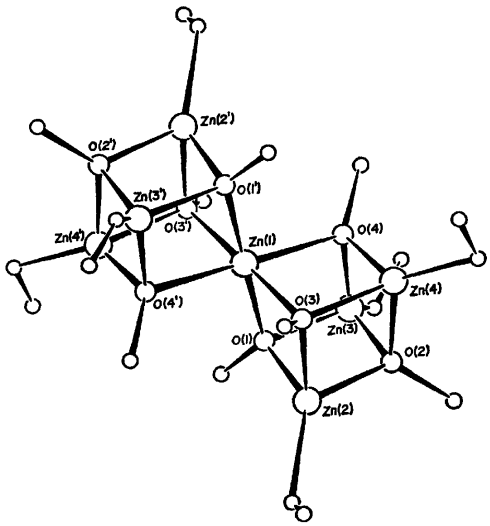

The molecular structure is shown in the Figure. The centrosymmetric complex consists of two enantiomorphic distorted cubes which share a corner, the center of symmetry. Each distorted cube is similar to that of $(MeZnOMe)_4$; the zinc atoms occupy the corners of a tetrahedron and oxygen atoms the corners of an interpenetrating but smaller tetrahedron. The average bond distances and bond angles are : Zn–O 2.06, O–C 1.48, Zn–C 2.07 Å, O–Zn–O 82.5°, and Zn–O–Zn 97.0°. The largest distortions are observed

in the geometry of the central zinc atom, Zn(1), Zn(1)–O(4) (2.18(3) Å) and Zn(1)–O(3) (2.12(3) Å) being longer and O–Zn(1)–O angles (average 80.2°) smaller than the average values of other zinc atoms.

The X-ray results suggest the cleavage of two zinc(1)–oxygen bonds involving Zn(1)–O(4) and/or Zn(1)–O(4') at elevated temperatures. This reasonably explains the results of NMR and reactivity of [Zn-$(OMe)_2$·$(EtZnOMe)_6$]. Namely, the zinc dialkoxide part has vacant seats for coordination of methyloxirane under the influence of chiral circumstance at 80 °C, by a process of dissociation of two methoxy groups.

References

1) M. Ishimori, T. Tomoshige, and T. Tsuruta, *Makromol. Chem.*, **120**, 161 (1968).
2) T. Tsuruta, *J. Polym. Sci., D*, 6, 179 (1972).
3) M. Goodman, in "Topics in Stereochemistry." N. L. Allinger and E. L. Eliel, Eds., Vol. 2, Interscience, New York (1967) p. 173; G. Allegra, *Makromol. Chem.* ,**145**, 235 (1971).
4) G. Allen, J. M. Bruce, D. W. Farren, and F. G. Hutchinson, *J. Chem. Soc., B*, **1966**, 799.
5) H. M. M. Shearer and C. B. Spencer, *J. Chem. Soc., Chem. Commun.*, **1966**, 194.

BULLETIN OF THE CHEMICAL SOCIETY OF JAPAN, VOL. 49(4), 1167—1168 (1976)

An Improved Synthesis of Dibenzoxanthene

Koki OTA and Taketoshi KITO

Department of Chemistry, Kyushu Institute of Technology, Tobata-ku, Kitakyushu-shi 804

(Received October 2, 1975)

Synopsis 14*H*-Dibenzo[*a*,*j*]xanthene was easily synthesized by heating alkali (K or Na) 2-naphthyloxide under CO and CO_2 pressure.

14*H*-Dibenzo[*a*,*j*]xanthene (DBX) and its derivatives have been synthesized by several methods. A mixture of DBX, dibenz[*a*,*j*]acridine, *N*-formyl-2-naphthylamine, 1-methyl-2-naphthol, and bis(2-hydroxy-1-naphthyl)methane (HNM) was formed by heating a mixture of 2-naphthol and formamide.[1] In this reaction, however, DBX was always not the main product, in addition, it was hard to separate from the other products. 3,11-Dimethyl-14*H*-dibenzo[*a*,*j*]-xanthene was obtained in a good yield from the reaction of 2-naphthol and formaldehyde, followed by internal cyclization using phosphoryl chloride.[2,3] Now, we wish to report a one-step synthesis of DBX in a higher state of purity.

Results and Discussion

DBX was obtained by heating alkali (K or Na) 2-naphthyloxide in a nonpolar solvent under an atmosphere of CO and CO_2. Such solvents as *N*,*N*-dimethylformamide and dioxane, in which alkali 2-naphthyloxide dissolves, prevent the reaction. The yield of DBX increases slightly in a reaction of more than 2 h, but the temperature affects the yield considerably. The presence of both CO and CO_2 is essential for the present reaction, and the pressure of CO appreciably affects the yield of DBX. The CO_2 may act as a neutralization agent of alkali salt, in which case the alkali metal would be consumed as alkali carbonate. Thus, the yield of 35% was attained in the reaction at 250 °C for 2 h under a pressure of CO (50 kg/cm^2) and CO_2 (8 kg/cm^2).

Pure DBX was formed as needles when the reaction was carried out in the presence of an alcohol, such as 1-butanol, 1-pentanol, 1-octanol, and 6-methyl-1-heptanol, although the yield of DBX fell slightly upon the alkylation of 2-naphthol by alcohol.[4] For example, the maximum yield of 26.0% was obtained from a reaction at 240 °C for 8 h under pressure of CO (56 kg/cm^2) and CO_2 (10 kg/cm^2) in the presence of octanol; the molar ratio of $C_8H_{17}OH$/2-$C_{10}H_7OK$ was 3.5.

Sodium 2-naphthyloxide gave DBX in a poorer yield than the potassium salt.

The thermal stability of DBX was also examined. A mixture of DBX, 1-butanol-*d*, potassium carbonate, and cyclohexane was heated under CO and CO_2 pressure at 240 °C for 1 h; 93.6% of the DBX was recovered and in it no deuterium was found. As a result, it was concluded that DBX is a thermally stable product; in other words, the two methylene hydrogens were thermally inactive under these conditions. On the other hand, at least four deuteriums were found in DBX when a mixture of potassium 2-naphthyloxide, 1-butanol-*d*, and cyclohexane was heated under CO and CO_2 pressure at 240 °C for 2.5 h (this was examined by means of a high-resolution mass spectrometer). Moreover, it was confirmed by NMR analyses that the two methylene protons of this DBX were almost entirely replaced by deuteriums. This fact suggests that the aromatic nucleus is also activated in the transition state and that the two hydrogen atoms in the methylene group of DBX come from both the aromatic nucleus and alcohol.

Experimental

The NMR spectra were obtained on a Japan Electron Optics Laboratory spectrometer (JNM, C-60 HL), with TMS used as the internal standard. The mass spectra were obtained on a Hitachi mass spectrometer (RMU-6L), using an electron-accelerating voltage of 70 eV. The IR spectrum was measured with a Japan Spectroscopic spectrometer (IRA-2).

DBX. One example will be described in detail. In a 300 ml autoclave, with an electromagnetic stirrer, we placed potassium 2-naphthyloxide (4.01 g), and cyclohexane (40 ml). After the air had been replaced by N_2, CO (50 kg/cm^2) and CO_2 (7 kg/cm^2) were introduced into the autoclave. The autoclave was then heated at 250 °C for 2 h. After cooling, aq. 2% NaOH was added to the reaction mixture, and the insoluble product (crude DBX) was filtered on a glass filter. The crude DBX was washed with small amounts of MeOH and then excess water, and the DBX was dissolved with trichloroethylene. The DBX was then obtained as a residue by the evaporation of the trichloroethylene. Yield, 1.09 g (35%, based on potassium 2-naphthyloxide). The melting point, MS, NMR, and IR of this product were consistent with those of authentic DBX.

Analyses of DBX. (i) Elementary analysis, Found: C, 88.91%; H, 4.96%. Calcd for $C_{21}H_{14}O$: C, 89.33%; H, 5.00%. (ii) MS: M^+=282 ($C_{21}H_{14}O$), 65%. (iii) NMR (δ value in CS_2 at 24 °C): 4.50, s(2H): 7.1—8.1, m(12H). (iv) IR(cm^{-1}): no absorptions in the range of 1800—1600; 1585, m; 1390, m; 1230, s; 950, m~w; 800, m; 760, m~w; 740, m. (v) Mp. 194 °C (from CS_2) determined by DTA.

Thermal Stability of DBX. A mixture of DBX (1.00 g), 1-butanol-*d* (0.58 g), potassium carbonate (0.57 g), and cyclohexane (35 ml) was heated under pressure of CO (34 kg/cm^2) and CO_2 (8 kg/cm^2) at 240 °C for 1 h (the pressure at 240 °C was 82 kg/cm^2). The recovery of the DBX was 93.6%.

*Reaction in the Presence of 1-Butanol-*d. A mixture of potassium 2-naphthyloxide (2.05 g), 1-butanol-*d* (5.20 g), and cyclohexane (40 ml) was heated under pressure of CO (65 kg/cm^2) and CO_2 (10 kg/cm^2) at 240 °C for 2.5 hr. The yield of DBX was 0.35 g. The results of the high resolution mass spectra of the DBX were as follows; *m*/*e*=282 (62%), 283 (71%), 284 (77%), 285 (45%), and 286 (19%). In

the NMR spectrum of this DBX, the ratio of aromatic protons/methylene protons was 0.042. The calculated ratio is 0.167.

Authentic DBX. HNM was prepared according to the directions;[2] DBX was thus obtained, with reference to the synthesis of 3,11-dimethyl-14*H*-dibenzo[*a*,*j*]xanthene,[3] by treating phosphoryl chloride on HNM.

References

1) N. Saito, C. Tanaka, and M. Okubo, *Pharm. Soc. Jpn.*, **76**, 359 (1956).
2) R. Robinson and F. Weygand, *J. Chem. Soc.*, **1941**, 386.
3) R. Royer, *Ann. Chim.*, XII, **1**, 395 (1946).
4) T. Kito and K. Ota, *Chem. Lett.*, **1975**, 1019.

BULLETIN OF THE CHEMICAL SOCIETY OF JAPAN, VOL. 49(4), 1169—1170 (1976)

Branched-chain Sugars. VI. Reaction of Methylene Dimagnesium Bromide with Uloses[1]

Juji YOSHIMURA, Ken-ichi SATO, Hiroo WAKAI, and Masuo FUNABASHI

Laboratory of Chemistry for Natural Products, Faculty of Science, Tokyo Institute of Technology, Meguro-ku, Tokyo, 152

(Received December 5, 1975)

Synopsis Application of methylene dimagnesium bromide, instead of the Wittig reagent, to several uloses gave the corresponding methylene derivatives in nearly equal yields, when the hydroxyl groups vicinal to the carbonyl function are protected with alkaline-stable groups.

The Wittig reaction with uloses is widely used for synthesis of the corresponding substituted and unsubstituted methylene derivatives, which are useful intermediates for preparation of branched-chain sugars as well as for elongation of carbon-chain of monosaccharides.[2]

Bertini *et al.*[3] reported that methylene dimagnesium bromide prepared from dibromomethane and magnesium amalgam in ether–benzene (1 : 1), instead of magnesium turnings in ether only, easily reacts with aldehydes and ketones to afford the corresponding methylene derivatives in good yields. If this method is applicable to uloses, it might be rather easier than the Wittig reaction to handle a large amount of compounds. The present paper describes the results obtained by the reaction of methylene dimagnessium bromide with uloses in comparison with the Wittig reaction.

Results and Discussion

Examination of the conditions for preparation of methylene dimagnesium bromide disclosed that the addition of catalytic amount of iodine and mercuric chloride, instead of magnesium amalgam, easily activates magnesium turnings. (Method A). Moreover, preparation and concurrent reaction of methylene dimagnesium bromide with uloses, by the final addition of dibromomethane to a suspension of an ulose and activated magnesium turnings in tetrahydrofuran gave the best results both in the yield and in handling. (Method B). Such a concurrent preparation-reaction system may prevent the formation of unreactive species of methylene dimagnesium bromide[4], even though tetrahydrofuran was used as a solvent.[3]

As uloses, 1,2 : 5,6-di-*O*-isopropylidene-α-D-*ribo*-hexofuranos-3-ulose (**1**)[5], 1,2-*O*-isopropylidene-3-*O*-methyl-6-*O*-trityl- (**2**)[6] and -6-*O*-benzyl-α-D-*xylo*-hexofuranos-5-ulose[6] (**3**), and methyl 2-*O*-benzoyl-4,6-*O*-benzylidene-α-D-*ribo*-hexopyranos-3-ulose[7] (**4**) were used. The yields of methylene derivatives are summarized in Table 1, together with that of the Wittig reaction reported in literatures. The structure of products were confirmed by elemental and spectrometric analyses and also by the melting point of admixture. In the case of **4**, only an intractable sirup was obtained both in the Grignard and Wittig reactions. These results indicate that methylene dimagnesium bromide is almost as useful as the corresponding Wittig reagent for preparation of methylene derivatives of uloses.

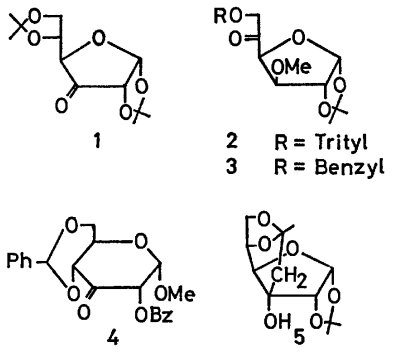

TABLE 1. COMPARISON OF YIELDS OF THE METHYLENE DERIVATIVES (**1**, **2** AND **3**)

Uloses	Yields (%)	
	Wittig reaction	Grignard reaction
1	55[9b], 60[1,9a]	60[a], 72[b]
2	50[6] c)	70[a]
3	85[6]	50[a], 60[b]

a) Method A, b) Method B, c) The yield was 80% in the case of the corresponding 3-*O*-benzyl derivative.[1]

Although the lack of reproducibility remained unexplained, a peculiar compound (**5**) was obtained in 86% yield, in the case of **1** in the method A without ether.

NMR spectrum of **5** showed the appearance of a quartet of isolated methylene group and a very broad signal of a hydroxyl proton, and the disappearance of one methyl signal of isopropylidene group.

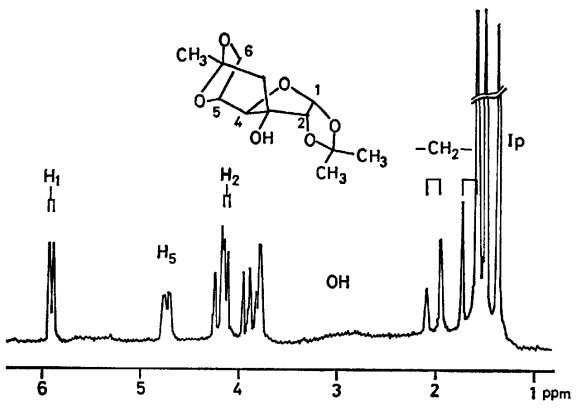

Fig. 1. NMR spectrum of **5**.

From this fact, in addition to the disappearance of the absorption of carbonyl group in IR spectrum, and elemental analysis, the structure **5** was tentatively determined to be 1,2-*O*-isopropylidene-3-*C*-(2'-oxopropyl)-α-D-allofuranose-(2'-*C*, 5-*O*, 6-*O*)-ketal. Examination of the structure with Dreiding model indicates no steric hindrance in this fused-ring system, and a similar structure is known in 1,2-*O*-isopropylidene-[3-*C*, 5-*O*, 6-*O*-(methylmethylidyne)]-α-D-allofuranose.[8]

Experimental

Optical rotations were measured in a 0.5 dm tube with a Carl Zeiss LEP-Al polarimeter. IR spectra were measured with a Hitachi Model EPI-G2 spectrometer. NMR spectra were taken with JEOL 4H-100 spectrometer in deuteriochloroform containing TMS as an internal refernce. Chemical shifts and coupling constants were recorded in δ and Hz units, and IR in cm^{-1}.

Reaction of Uloses with Methylene Dimagnesium Bromide. *Method A.* A suspension of magnesium turning (1.46 g, 60 m atom), catalytic amount of iodine and mercuric chloride in benzene (40 ml) and ether (40 ml) was refluxed for the activation of magnesium, and then the addition of dibromomethane (4.35 g, 25 mmol) to the above suspension with stirring, under cooling if necessary, to form methylene dimagnesium bromide. A solution of uloses (5 mmol) in benzene was added dropwise into the Grignard solution with stirring at room temperature, and the mixture was poured into saturated ammonium chloride after stirring for 1 h. The resulting solution was filtered, and the filtrate was concentrated into a half volume, extracted with chloroform. Concentration of the extracts gave the corresponding methylene derivatives, which were purified by the methods reported in the literatures and identified with authentic specimens.

Method B. To a suspension of magnesium activated as mentioned in method A in tetrahydrofuran, was added, in turn, a solution of uloses in THF and dibromomethane with stirring, under cooling if necessary. The reaction mixture was treated in the same way as above.

1,2-O-Isopropylidene-3-C-(2'-oxopropyl)-α-D-allofuranose-(2'-C, 5-O,6-O)-ketal (5). As an example, methylene dimagnesium bromide (the same scale as method A) was prepared in benzene only. 1,2 : 5,6-Di-*O*-isopropylidene-α-D-*ribo*-hexofuranos-3-ulose was then added to the Grignard solution. The work-up of the reaction mixture gave crude crystals which were recrystallized from benzene to give needles having mp 139—140° and $[\alpha]_D^{23}$ −2.8° (*c* 1.1, $CHCl_3$). IR: 3500 (OH), NMR: 5.91 (H_1; d, $J_{1,2}$=3.75), 4.74 (H_5; q), 4.13 (H_2; d), 4.3—3.7 (H_3, H_4, H_6, H_6'; m), 2.02 and 1.66 (CH_2; q, J_{gem}=17.5), 1.60, 1.50 and 1.38 ($3\times CH_3$).

Found: C, 55.66; H, 7.14%. Calcd for $C_{12}H_{18}O_6$: C, 55.80; H, 7.03%.

References

1) M. Funabashi, H. Sato, and J. Yoshimura, Part V, *Bull. Chem. Soc. Jpn.*, **49**, 788 (1976).

2) Yu. Z. Zhdanov, Yu. E. Alexeev, and V. G. Alexeeva, "Adv. Carbohyd. Chem.", Vol. 27, ed. by R. S. Tipson and D. Horton, Academic Press, New York and London (1972), p. 227.

3) F. Bertini, P. Grasselli, and G. Zubiani, *Tetrahedron*, **26**, 1281 (1970).

4) D. A. Fidler, J. R. Jones, S. L. Clark, and H. Stange, *J. Am. Chem. Soc.*, **77**, 6634 (1955).

5) P. J. Beynon, P. M. Collins, and W. G. Overend, *Proc. Chem. Soc.*, **1964** 342: K. Onodera, S. Hirano, and K. Kashimura, *J. Am. Chem. Soc.*, **87**, 4651 (1965).

6) J. Yoshimura, T. Iida, H. Wakai, and M. Funabashi, *Bull. Chem. Soc. Jpn.*, **46**, 3207 (1973).

7) F. A. Carey and K. O. Hodgson, *Carbohyd. Res.*, **12**, 463 (1970).

8) D. C. Baker, D. K. Brown, D. Horton, and R. G. Nickol, *Carbohyd. Res.*, **32**, 299 (1974).

9) (a) W. A. Szarek, J. S. Jewell, I. Szarek, J. K. N. Jones, *Can. J. Chem.*, **47**, 4473 (1969); (b), A. Rosenthal and M. Sprinzl, *Can. J. Chem.*, **47** 3941 (1969).

BULLETIN OF THE CHEMICAL SOCIETY OF JAPAN, VOL. 49(4), 1171—1172 (1976)

The Inclusion Effects of Cyclodextrins on the Photolysis of *p*-Benzoquinone in Aqueous Solution

Kazutoshi YAMADA, Shigeo KOHMOTO, and Hirotada IIDA

Department of Synthetic Chemistry, Faculty of Engineering, Chiba University, Yayoi-cho, Chiba 280

(Received December 20, 1975)

Synopsis. The additive effects of cyclodextrins on the photolysis of *p*-benzoquinone in water were investigated spectrophotometrically. By applying Michaelis-Menten keinetics, the dissociation constant of the inclusion complex was determined. The quantum yield for the formation of hydroquinone from the complex increased, while that of 2-hydroxy-1,4-benzoquinone decreased.

The cyclodextrin inclusion effects are known as a good enzymatic action model and many reports on their catalytic activities have been published.[1] Cyclodextrins associate with a variety of organic substances in aqueous solution. This complexation leads to their catalytic selectivity. In the previous papers, we reported the photochemical reaction control by cyclodextrins.[2] In this note, we wish to report the effects of cyclodextrins on the photolysis of *p*-benzoquinone in aqueous solution and to show that the addition of water to *p*-benzoquinone must be inhibited.

Recently several investigations of the photolysis of quinones in an aqueous solution have been reported. In the photolysis of *p*-benzoquinone (**1**) in aqueous solution, hydroquinone (**4**) has been isolated as the sole stable product in addition to the transient formation of 1,2,4-benzenetriol (**2**) and 2-hydroxy-1,4-benzoquinone (**3**)[3]. Kurein and Robins[4] suggested in their spectrophotometric study that the primary photochemical process of this photolysis was the conversion of **1** into **2**. According to their report, **3** and **4** are formed by dark reaction between **1** and **2**, and the result is the approximately equal quantity of **3** and **4**. Kano and Matsuo[5] tried this photolysis of **1** in the presence of the surfactants. The quantum yield for the disappearance of **1** was accelerated by the addition of the anionic surfactant, but was suppressed by the cationic one. Shirai and Tanaka[6] suggested an electrophilic attack of the excited **1** on water.

α-Cyclodextrin (α-CDX) and β-cyclodextrin (β-CDX) were used in this work. CDX was dissolved in an aqueous solution of **1**. CDX has little absorption above 230 nm and no spectral change was observed within experimental errors after the addition of CDX. After irradiation with 254 nm light, the reacted solution was quickly converted to acidic (because **3** is not stable in the neutral pH range), and the curve resolution was carried out to determine the yield conversions of **3** and **4**. In the absence of CDX, oxidation of the reacted solution by $Ce(SO_4)_2$, the same method used by Robins, showed that products were about equal quantity of **3** and **4**, and also the curve resolution showed the same value. Scheme 1 shows the processes of the CDX catalyzed photolysis of **1**. Here, we assumed that **1** and CDX would make a 1 : 1 complex. In this scheme, K_d represents the dissociation

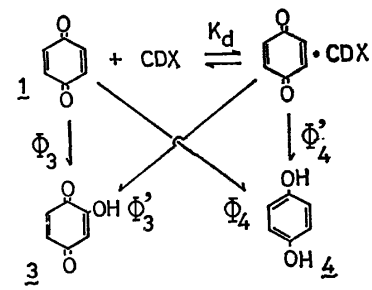

Scheme 1. The mechanism of CDX catalyzed photolysis of **1**.

constant of the inclusion complex, Φ_3 and Φ_4, the quantum yield for the formation of **3** and **4** from **1**, respectively, and Φ'_3 and Φ'_4, the quantum yield for the formation of **3** and **4** from the inclusion complex, respectively. The modified form of Michaelis-Menten's equation[7] was applied to this system. The equation was modified by using the quantum yield instead of the first order rate constant[8]. This equation was used separately for the formation of **3** and **4**. The following equations were used in our calculations.

$$(1-\Phi_{obs}/\Phi_3)^{-1} = (1-\Phi_3'/\Phi_3)^{-1} + K_d(1-\Phi_3'/\Phi_3)^{-1}[CDX]^{-1} \quad (1)$$

$$(\Phi_{obs}/\Phi_4-1)^{-1} = (\Phi_4'/\Phi_4-1)^{-1} + K_d(\Phi_4'/\Phi_4-1)^{-1}[CDX]^{-1} \quad (2)$$

In these equations, Φ_{obs} represents the observed quantum yields for the formation of **3** and **4** when CDX was added. Figure 1 shows the plots of the modified form of Michalis-Menten's equation in the case where α-CDX was added. The plots obtained from Eqs. 1 and 2 were strictly linear and these two lines were coincident. This means that the quantum yield for the formation of **3** from the inclusion complex decreases,

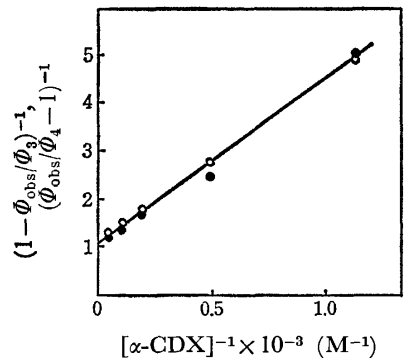

Fig. 1. The plots of Michaelis-Menten's equation.
—○—: Plots for **3** calculated from Eq. 1.
—●—: Plots for **4** calculated from Eq. 2.

Table 1. Values of the quantum yield ratios and the dissociation constants obtained from the modified form of Michaelis-Menten's equation

	α-CDX	β-CDX
Φ_3'/Φ_3	0.2±0.1	0.1±0.1
Φ_4'/Φ_4	1.9±0.2	2.1±0.4
$K_d \times 10^3$ (M)	2.1±0.1[a)] / 1.9±0.2[b)]	2.0±0.1[a)] / 2.3±0.6[b)]

a) Obtained from Eq. 1. b) Obtained from Eq. 2.

but on the other hand that of **4** increases. This was also true when β-CDX was added and the same linear relationship was obtained. Obtained values of Φ and K_d by Eqs. 1 and 2 are showed in Table 1. In Table 1 Φ'_3/Φ_3 is nearly zero while Φ'_4/Φ_4 is nearly two and K_d obtained from Eqs. 1 and 2 quite agree with each other, in both complexes.

Next, we examined the additive effects of α-methyl D(+)-glucoside (α-MG) and poly(vinyl alcohol) (PVA, $n=500$). α-MG has only one glucopyranose unit which is contained in CDX. PVA has a helix structure and was reported to make an inclusion complex with iodine[9]. Both α-MG and PVA showed the same tendency as CDX. But this tendency is very weak for α-MG. From the above results, we conclude that CDX makes the 1 : 1 inclusion complex with **1** in aqueous solution and conformationally inhibits the addition of water to **1**, and probably the excited **1** will abstract hydrogen from CDX.

Experimental

The light source used in this work is USHIO ULO-6DQ 6 watt low pressure mercury lamp. For the counting of the photons irradiated, potassium ferrioxalate actinometry was used. Irradiations were carried out in the spectrophotometric cell (width 1 cm) according to the method proposed by Parker[10]. The light intensity at 254 nm measured in our irradiation system is $(3.54+0.57)\times 10^{17}$ quanta/s·l. three ml of arerobic solution of **1** was pipeted in the spectrophotometric cell (4.4×10^{-5} M), and after the irradiation for constant time 1 ml of 2M-H_2SO_4 solution was added to the reacted solution, and UV spectrum was measured. The curve resolution was carried out at 246 nm and 256 nm to determine the yield conversions of **3** (λ_{max} 256 nm, ε 13700, ε at 246 nm is 11100) and **4** (λ_{max} 289 nm, ε at 246 nm is 180, and ε at 256 nm is 190). To ensure this curve resolution, parrallel experiment, oxidation of the reacted solution by $Ce(SO_4)_2$ was carried out. **2** is converted into **3**, and **4** is converted into **1** quantitatively by $Ce(SO_4)_2$. This oxidation gave nearly same values of conversion which obtained by the curve resolution. CDX did not disturb this oxidation. After the complete photolysis (40 min irradiation), both the curve resolution and oxidation of the reacted solution suggested that the products were about equal quantity of **3** and **4**. The quantum yield for dissaperance of **1** is 0.44± 0.09, and for appearance of **3** and **4** is *ca.* 0.22 without CDX.

References

1) D. W. Griffiths and M. L. Bender, *Adv. Catal.*, **23**, 209 (1973).
2) K. Yamada, J. Morimoto, and H. Iida, *J. Fac. Eng. Chiba Univ.*, **24**, 71 (1973); *ibid.*, **26**, 85 (1975).
3) S. Hashimoto, K. Kano, and H. Okamoto, *Bull. Chem. Soc. Jpn.*, **45**, 966 (1972).
4) K. C. Kurien and P. A. Robins, *J. Chem. Soc., B*, **1970**, 855.
5) K. Kano and T. Matsuo, *Chem. Lett.*, **1973**, 1127.
6) M. Shirai, T. Awatsuji, and M. Tanaka, *Bull. Chem. Soc. Jpn.*, **48**, 1329 (1975).
7) H. Lineweaver, and D. Burk, *J. Am. Chem. Soc.*, **56**, 658 (1934).
8) The modified form of Michaelis-Mentens equation.

$$S + C \underset{K_d}{\rightleftharpoons} S\cdot C \xrightarrow[k_2]{} \text{Products}$$

$k_1 \downarrow$

Products

S, substrate C, CDX

The modified form of Michaelis-Mentens' equation was showed by the following form. See Refs. 1 and 7.

$$(k_{obs}-k_1)^{-1} = (k_2-k_1)^{-1} + K_d(k_2-k_1)^{-1}\,C^{-1} \quad (3)$$

k_1, the uncatalyzed first order rate constants
k_2, the catalyzed first order rate constants

We can show the quantum yield by the next equation. Here, we assume that the products effect little on the absorption of photons by substrate at the irradiating wavelength.

$$\Phi = \frac{C_0\cdot V\cdot \Delta x\cdot N_A}{\int_t^{t+\Delta t} N_{pabs}\cdot V\cdot(1-x)\,dt} \quad (4)$$

C_0, the initial concentration of the substrate
V, the volume of the solution
x, the conversion of the substrate at the reaction time "t"
$x+\Delta x$, the conversion of the substrate at the reaction time "$t+\Delta t$"
N_A, Avogadro number
N_{pabs}, the number of photons absorbed at the initial concentration

Next, we assume that this photochemical reaction proceeds according to the first order rate law, following equation will be applied.

$$\ln\frac{1}{1-x} = kt \quad (5)$$

k, the first order rate constant

From Eqs. 4 and 5 we get the very simple relation between the quantum yield and the first order rate constant.

$$\Phi = \frac{C_0\cdot N_A\cdot k}{N_{pabs}} \quad (6)$$

From Eqs. 3 and 6, we obtain the Eqs. 1 and 2.

9) M. M. Zwick, *J. Appl. Polym. Sci.*, **9**, 2392 (1965).
10) C. G. Hatchard and C. A. Parker, *Proc. Roy. Soc., A*, **235**, 518 (1956).

BULLETIN OF THE CHEMICAL SOCIETY OF JAPAN, VOL. 49(4), 1173—1174 (1976)

Phosphinidenes and Related Intermediates. V.[1] Reactions of Phosphinylidenes with *cis*- and *trans*-Stilbene Oxides

Shigenobu NAKAYAMA, Masaaki YOSHIFUJI, Renji OKAZAKI, and Naoki INAMOTO
Department of Chemistry, Faculty of Science, The University of Tokyo, Hongo, Tokyo 113

(Received January 16, 1976)

Synopsis. Reactions of phenyl- and cyclohexylphosphinylidenes with *trans*-stilbene oxide gave *trans*-stilbene and 4-hydroxybutyl 2-hydroxy-1,2-diphenylethyl phosphonate derivatives. In the case of cyclohexylphosphinylidene, 2-cyclohexyl-3,4-diphenyl-1,2-oxaphosphetane 2-oxide was also formed. Reactions with *cis*-stilbene oxide gave *cis*- and *trans*-stilbenes.

In the previous paper,[1] we reported that phosphinothioylidenes reacted with *cis*- and *trans*-stilbene oxides to give 1,3,2-oxathiaphospholane derivatives stereospecifically in most cases and *cis*- and/or *trans*-stilbenes. On the other hand, the reaction of phosphinylidenes gave different products except the formation of stilbenes.

Phenylphosphonic dichloride (**1a**) was allowed to react with magnesium in the presence of *trans*-stilbene oxide in tetrahydrofuran (THF) under nitrogen. *trans*-Stilbene (**2**), *meso*-1,2-diphenylethane-1,2-diol (**3**), and 4-hydroxybutyl 2-hydroxy-1,2-diphenylethyl phenylphosphonate (**4a**) were obtained in 10, 36, and 12% yields, respectively. A similar reaction using cyclohexylphosphonic dichloride (**1b**) gave 2,3,4-hydroxybutyl 2-hydroxy-1,2-diphenylethyl cyclohexylphosphonate (**4b**), and 2-cyclohexyl-3,4-diphenyl-1,2-oxaphosphetan 2-oxide (**5b**) in 11, 9, 12, and 8% yields, respectively.

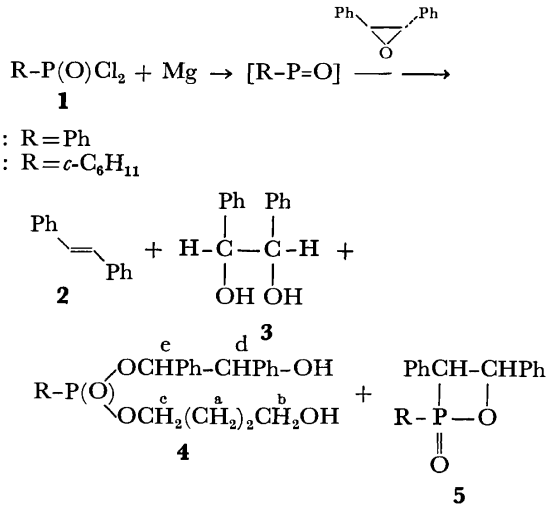

The structures of **4** and **5** were determined by the elemental analyses and spectral data.

In the NMR spectrum of **4a**, the presence of the multiplet at δ 3.5—4.0 ppm would rule out another possible structure **4a'**.

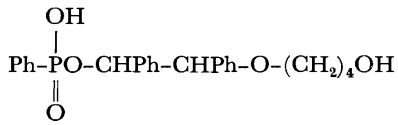

4a'

Comparison of the NMR spectrum of **4b** with that of **4a** suggests that **4b** is a mixture of isomers concerning with two methine parts (see Experimental). The IR spectrum of **5b** showed a strong broad band at 3150 cm^{-1} which is probably assignable to water of crystallization.

The fact that the reaction of *trans*-stilbene oxide with magnesium-magnesium(II) chloride did not give **3**[1] suggests a participation of phosphinylidene in the formation of **3**.

Reaction of phenylphosphinylidene with *cis*-stilbene oxide gave *cis*- and *trans*-stilbenes, *dl*-1,2-diphenylethane-1,2-diol (**6**), and *threo*-2-chloro-1,2-diphenylethanol (**7**), but the corresponding product of **4** could not be isolated in a pure state. A similar reaction of cyclohexylphosphinylidene gave *cis*- and *trans*-stilbenes and **7**.

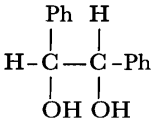

6

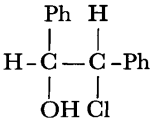

7

Experimental

All reactions were carried out under nitrogen.

Reaction of ***1a*** *with Magnesium and* trans-*Stilbene Oxide.* A solution of **1a**[2] (3.90 g, 20 mmol) in THF (5 ml) was added dropwise to a stirred mixture of magnesium (0.53 g, 21.8 mmol) and *trans*-stilbene oxide[3] (2.00 g, 10.3 mmol) in THF (40 ml) at room temperature, and the mixture was stirred until exothermic reaction had ceased (*ca.* 1 h). Unchanged magnesium (10 mg) was filtered off and the solvent was evaporated *in vacuo* from the filtrate. The residue was extracted with $CHCl_3$. The extract was washed with aq. NH_4Cl and dried over $MgSO_4$. After evaporation, the residue was chromatographed on a silica gel dry column to give 0.13 g (0.7 mmol) of unchanged oxide, 0.18 g (1 mmol) of *trans*-stilbene (**2**), 0.74 g (3.5 mmol) of **3**, mp 136—138 °C (from CCl_4) (lit,[4] 137 °C), and 0.47 g (1.1 mmol) of **4a**. The yields of **2**, **3**, and **4a** were 10, 36, and 12%, respectively, based on *trans*-stilbene oxide consumed.

4a: mp 116—119 °C (from CCl_4); IR (KBr): 3345 (OH), 1218 (P=O), 1138 (P-Ph), 1000, and 988 cm^{-1} (P-O-C); NMR ($CDCl_3$): δ 1.4—1.8(m, 4H, $2CH_2$), 2.95(s, 2H, 2 OH), 3.2—3.5(m, 2H, $C\underline{H}_2OH$), 3.5—4.0(m, 2H, $POCH_2$), 4.95 (d, J_{HCCH} 5 Hz, 1H, $C\underline{H}PhOH$), 5.8(dd, J_{HCCH} 5, J_{POCH} 9 Hz, 1H, $POC\underline{H}Ph$), and 6.9—7.9(m,15H, 3Ph); MS: *m/e* 338 ($PhP(OH)_2OCHPhCHPh^+$ or $PhP(OH)OCHPhCHPhOH^+$, 19%), 230 ($PhP(O)OCHPh^+$, 24), 178($PhC{\equiv}CPh^+$, 86), 167($PhP(O)OC_2H_3^+$, 72), 159 ($PhPO_3H_3^+$, 34), 141 ($PhPO_2H^+$, 61), 124 ($PhPO^+$, 31), and 77 (Ph^+, 100).

Found: C, 65.86; H, 6.46; P. 6.52%. Calcd for $C_{24}H_{27}O_5P \cdot 3/5H_2O$: C, 65.93; H, 6.50; P, 7.08%.

Reaction of ***1b*** *with Magnesium and* trans-*Stilbene Oxide.* A solution of **1b**[5] (4.02 g, 20 mmol) in THF (5 ml) was added

dropwise to a stirred mixture of magnesium (0.53 g, 21.8 mmol) and *trans*-stilbene oxide (2.00 g, 10.3 mmol) in THF (40 ml) at room temperature, and the mixture was stirred overnight. After a usual treatment, dry column chromatography on silica gel gave unchanged oxide (0.52 g, 2.7 mmol), **2**(0.14 g, 0.8 mmol), **3**(0.14 g, 0.7 mmol), **4b**(0.40 g, 0.9 mmol), and **5b**(0.20 g, 0.6 mmol) in 11, 9, 12, and 8% yields, respectively, based on *trans*-stilbene oxide consumed.

4b: mp 113.5—116.5 °C (from hexane); IR (KBr): 3390 (OH), 1228, 1200 (P=O), 995, and 985 cm^{-1} (P–O–C); NMR ($CDCl_3$): δ 0.8—2.0(m, 15H, *c*-C_6H_{11} and $2CH_2$), 2.8(bs, 2H, 2 OH), 3.25—4.0(m, 4H, $2CH_2O$), 4.93 (d+d, $J_{H^dH^e}$ 6 and 4 Hz, 1H, H^d), 5.56(dd+t, $J_{H^dH^e}$ 6 and 4 Hz, J_{POCH^e} 14 and 4 Hz, 1H, H^e), and 6.9—7.6 (m, 10H, 2Ph); MS: *m/e* 344 (*c*-$C_6H_{11}P(OH)_2OCHPhCHPh^+$ or *c*-C_6H_{11}-$P(OH)OCHPhCHPhOH^+$, 10%), 178($PhC{\equiv}CPh^+$, 63), 163(*c*-$C_6H_{11}PO_3H^+$, 16), 91($C_7H_7^+$, 70), and 55($C_4H_7^+$, 100).

Found: C, 64.00; H, 7.44; P, 7.13%. Calcd for $C_{24}H_{33}$-$O_5P\cdot H_2O$: C, 63.99; H, 7.83; P, 6.88%.

5b: mp 172—173 °C (from aq. EtOH); IR (KBr): 3150(br) (H_2O), 1213 (P=O), 1180, 1168, 1159, 1140, and 1090 cm^{-1} (P–O–C); NMR ($CDCl_3$): δ 0.8—2.4 (m, 11H, *c*-C_6H_{11}), 4.5—4.8 (m, 2H, 2CH), and 7.1—7.6 (m, 10H, 2Ph); MS: *m/e* 196 ($CHPhCHPhO^+$, 3%) and 167 ($PhC_2H_3O_2P^+$, 100).

Found: C, 72.35; H, 7.63; P, 8.86%. Calcd for $C_{20}H_{23}$-$O_2P\cdot 2/5H_2O$: C, 72.01; H, 7.19; P, 9.29%.

Reaction of ***1a*** *with Magnesium and* cis-*Stilbene Oxide.* Dichloride **1a** (6.01 g, 30.8 mmol) in THF (5 ml) was added dropwise to a mixture of *cis*-stilbene oxide[6] (3.00 g, 15.3 mmol) and magnesium (0.81 g, 33.3 mmol) in THF (45 ml) with stirring at room temperature over 1 h and the mixture was refluxed for 3 h. After a similar treatment, the residue was chromatographed on a silica gel dry column to afford unchanged oxide (0.21 g, 1.1 mmol), *cis*-(0.24 g, 1.3 mmol, 4.4%), and *trans*-stilbenes (1.9 g, 1.1 mmol, 3.7%), and **6** (0.10 g, 0.5 mmol, 1.7%), mp 121.5—122.5 °C (from CCl_4) (lit,[4] 120 °C). An oily fraction analogous to **4** (0.7 g) was obtained, but could not be purified. In addition, **7** (0.6 g, mp 43—45 °C (from hexane) (lit,[7] 47 °C) was obtained. The yields were calculated based on *cis*-stilbene oxide consumed.

Reaction of ***1b*** *with Magnesium and* cis-*Stilbene Oxide.* The reaction was carried out in the same scale as that of **1a**, and *cis*-(0.68 g, 3.7 mmol, 11%) and *trans*-stilbenes (1.22 g, 6.8 mmol, 22%), and **7** (0.15 g, 1.1 mmol, 3.7%) were obtained.

This work was supported by a grant-in-aid from the Ministry of Education.

References

1) For Part IV see: S. Nakayama, M. Yoshifuji, R. Okazaki, and N. Inamoto, *Bull. Chem. Soc. Jpn.*, **48**, 3733 (1975).

2) A. D. F. Toy, *J. Am. Chem. Soc.*, **70**, 186 (1948).

3) D. J. Reif and H. O. House, *Org. Synth.*, Coll. Vol. 4, 860 (1963).

4) J. H. Stocker and D. H. Kern, *J. Org. Chem.*, **33**, 291 (1968).

5) R. Graf, *Chem. Ber.*, **85**, 9 (1952).

6) D. Y. Curtin and D. B. Kellom, *J. Am. Chem. Soc.*, **75**, 6011 (1953).

7) D. Reulos and S. Le Tellier, *C. R. Acad. Sci.*, **217**, 698 (1943); *Chem. Abstr.*, **39**, 926[4] (1945).

BULLETIN OF THE CHEMICAL SOCIETY OF JAPAN, VOL. 49(4), 1175—1176 (1976)

Metal Phosphinylides and Phosphinothioylides. VI.[1] Some Observations in Reactions of Diphenylphosphinic Chloride with Tetrahydrofuran in the Presence of Metal Chlorides

Koshiro GODA and Naoki INAMOTO

Department of Chemistry, Faculty of Science, The University of Tokyo, Hongo, Tokyo 113

(Received January 16, 1976)

Synopsis. ^{31}P-NMR data showed a formation of a stable 1 : 1 complex between diphenylphosphinic chloride (**1**) and aluminum chloride. The effect of common chloride ion on the reaction of **1** with tetrahydrofuran in the presence of zinc or cuprous chloride supported a cationic mechanism in the former case, and no free radical but homolytic mechanism in the latter.

We reported in a previous paper[2] that diphenylphosphinic chloride (**1**) reacted with tetrahydrofuran (THF) in the presence of cuprous, cupric, zinc, aluminum or ferric chloride to give *O*-4-chlorobutyl diphenylphosphinate (**2**) in all cases, and it was suggested that **2** was formed through no free radical but homolytic mechanism in the case of cuprous chloride. This note describes on further observation in the above reactions.

Though zinc, aluminum, and ferric chlorides are typical Lewis acids, the latter two chlorides give **2** in a moderate yield.[2]

^{31}P-NMR data showed that **1** formed a stable 1 : 1 complex (**3**) with aluminum chloride (see Table 1) as reported in analogous systems,[3] but that, in the case of zinc chloride, ^{31}P chemical shift of **1** did not change within the experimental error. Therefore, it is considered that the reactivity of **1** becomes very low in the presence of aluminum chloride, because of the formation of the stable complex (**3**). Thus, zinc chloride becomes more effective as a catalyst than aluminum chloride.

$$\underset{\underset{\mathbf{1}}{\|}}{\underset{O}{Ph_2P\text{-}Cl}} + AlCl_3 \longrightarrow \underset{\underset{\mathbf{3}}{\|}}{\underset{O\rightarrow AlCl_3}{Ph_2P\text{-}Cl}}$$

Table 1. Changes in ^{31}P chemical shift of **1** in the presence of aluminum chloride in nitrobenzene

$AlCl_3$/**1** (mol/mol)	0	0.28	0.56	0.62	0.83	1.05	1.38	2.06
$-\delta^{31}$P (ppm)	42.8	44.1	46.5	49.6	55.9	60.6	60.5	60.6

Similarly, ^{31}P-NMR data also showed that **1** did not form a complex with cuprous chloride in acetonitrile.

These tendency were also similar in the case of diphenylphosphinothioic chloride.

In order to make clear a difference in mechanisms in the presence of zinc or cuprous chloride, effects of addition of lithium chloride on the yields of **2** were scrutinized. The results are shown in Table 2.

$$\underset{\mathbf{1}}{Ph_2P(O)Cl} + THF \xrightarrow[\text{or CuCl}]{ZnCl_2} \underset{\mathbf{2}}{Ph_2P(O)O(CH_2)_4Cl}$$

Table 2. Effect of addition of lithium chloride on yields of **2** (at 120 °C for 6 h)

a) In the case of zinc chloride

[LiCl]/**1** (mol/mol)	[LiCl]/[$ZnCl_2$]	Yield of **2** (%)
0	0	36
2.4×10^{-2}	1.3	62
9.2×10^{-2}	5.2	61
16×10^{-2}	10.1	58
34×10^{-2}	18.6	55

b) In the case of cuprous chloride

[LiCl]/**1** (mol/mol)	[LiCl]/[CuCl]	Yield of **2** (%)
0	0	38
1.9×10^{-2}	1.1	7
8.1×10^{-2}	4.6	9
17×10^{-2}	9.0	12
31×10^{-2}	17.0	12
98×10^{-2}	∞[a]	13

a) In the absence of cuprous chloride.

The effect of the common chloride ion showed an extreme contrast in both cases as shown in Table 2, suggesting a different mechanism in each case. Increase in yield of **2** in the case of zinc chloride is in agreement with the following ionic mechanism.

$$Ph_2P(O)Cl + ZnCl_2 \rightarrow Ph_2\overset{\delta+}{P}(O)\cdots\overset{\delta-}{Z}nCl_3 \xrightarrow{THF} \left[\overset{+}{O}\text{-}P(O)Ph_2 + ZnCl_3^- \text{ (or } Cl^-)\right] \rightarrow \mathbf{2} + ZnCl_2$$

Furthermore, in the case of cuprous chloride, ten times molar amounts (based on cuprous chloride) of cupric acetate w re added in place of lithium chloride under the same condition, but 4-acetoxybutyl diphenylphosphinate could not be detected. The product was only **2** (45%). This result ruled out a cationic mechanism.

The **1**-CuCl system did not result in isomerization of *cis*-stilbene in acetonitrile at 120 °C for 24 h, indicating the absence of free $Ph_2\dot{P}O$ radical. Therefore, a mechanism containing an inner-sphere electron transfer as shown in the following scheme might be more reasonable.

$$\underset{\underset{O}{\|}}{Ph_2P\text{-}Cl} + CuCl \rightleftarrows \underset{\underset{O}{\|}}{Ph_2\dot{P}\text{-}Cu^{II}Cl_2} \xrightarrow{THF} \left[\underset{\underset{O}{\|}}{Ph_2\bar{P}\text{-}\overset{+}{O}}\right] CuCl_2 \rightarrow \mathbf{2} + CuCl$$

The remarkable decrease in the yield of **2** in the presence of chloride ion is understandable, assuming that chloride ion coordinates with cuprous chloride and the electron transfer becomes difficult. A similar effect of lithium chloride has been reported in a carbon tetrachloride–cuprous chloride–olefin system.[4]

The yield of **2** is expected to decrease by addition of acetonitrile which can coordinate to cuprous chloride. In fact, addition of 3.5 times amounts of acetonitrile decreased the yield of **2** from 38% to 29%.

Moreover, the yield of **2** was better in the presence of cupric chloride than in the presence of cuprous chloride.[2] In order to make this point clear, cupric chloride was heated in THF at 120 °C for 24 h, and 12% of cuprous chloride was formed. Thus, the previous result is explained by the formation of more reactive cuprous chloride *in situ*.

Experimental

The ^{31}P-NMR spectra were measured with a Hitachi R-20 B-R-204-PB spectrometer using 85% phosphoric acid as an external standard. All reactions were carried out under nitrogen in a sealed tube.

*Reaction of Diphenylphosphinic Chloride (**1**) with THF in the Presence of Metal Chloride.* *1) Zinc Chloride*: A mixture of **1**[5] (6.2—6.8 mmol) and zinc chloride (0.11—0.12 mmol) in 8 ml of THF was heated in the presence of an appropriate amount of lithium chloride for 6 h at 120 °C. The reaction mixture was treated with methanol, concentrated, and determined by gas chromatography (column: H 523 on Diasolid at 210 °C) with methyl diphenylphosphinodithioate as an internal reference.

2) *Cuprous Chloride*: A mixture of **1** (5.6—5.8 mmol) and cuprous chloride (0.10—0.11 mmol/mmol of Cu atom) in 9 ml of THF was heated in the presence of an appropriate amount of lithium chloride for 6 h at 120 °C. The reaction mixture was treated similarly.

We are grateful to Dr. M. Yoshifuji and Dr. T. Kawashima of our laboratory for ^{31}P-NMR measurements. This work was supported by a grant-in-aid from the Ministry of Education.

References

1) For Part V see: K. Goda, R. Okazaki, K. Akiba, and N. Inamoto, *Tetrahedron Lett.*, **1976**, 181.
2) K. Goda, M. Yoshifuji, R. Okazaki, and N. Inamoto, *Bull. Chem. Soc. Jpn.*, **48**, 2484 (1975).
3) M. E. Peach and T. C. Waddington, *J. Chem. Soc.*, **1962**, 3450; M. Becke-Goehring and A. Slawisch, *Z. Anorg. Allg. Chem.*, **346**, 295 (1966).
4) Y. Mori and J. Tsuji, *Synth. Commun.*, **2**, 51 (1972).
5) W. A. Higgins, P. W. Vogel, and W. G. Craig, *J. Am. Chem. Soc.*, **77**, 1864 (1955).

BULLETIN OF THE CHEMICAL SOCIETY OF JAPAN, VOL. 49(4), 1177 (1976)

Olefination of Aldehydes by Methylenedicalcium Diiodide

Nariyoshi KAWABATA,* Michiharu NAKA, Takao KOMAZAWA, and Shinzo YAMASHITA

Department of Chemistry, Faculty of Polytechnic Science, Kyoto Institute of Technology, Matsugasaki, Sakyo-ku, Kyoto 606

(Received December 15, 1975)

Synopsis. Reaction of diiodomethane with calcium in tetrahydrofuran gave methylenedicalcium diiodide in 17% yield. Reaction of the calcium compound with aldehydes was shown to give the corresponding olefins in estimated yields of 53—94%.

Only a few works are available in the literature on the reaction of organocalcium compounds. We have demonstrated that methylcalcium iodide is a useful organometallic reagent in several organic reactions.[1,2] This paper describes the reaction of methylenedicalcium diiodide with carbonyl compounds. *gem*-Dimetallic compounds of lithium,[3] magnesium,[4] and zinc[5] are known to olefinate carbonyl compounds, but no information is available in the literature on the reaction of methylenedicalcium dihalides with carbonyl compounds.

Reaction of diiodomethane with calcium in tetrahydrofuran at −30 °C gave methylenedicalcium diiodide in 17% yield. Gas chromatographic analysis showed that diiodomethane was not remained in the reaction mixture. The yield was determined based on the amount of methane evolved by the addition of methanol. The geminal dimetallic nature of the organocalcium compound was confirmed by carboxylation, which gave malonic acid in 12% yield based on diiodomethane (71% based on methylenedicalcium diiodide).

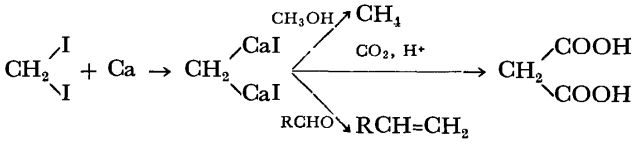

Reaction of diiodomethane with calcium in the presence of aldehydes at room temperature in tetrahydrofuran was found to give the corresponding olefins in 9–16% yields based on diiodomethane as is shown in Table 1. Since the yield of methylenedicalcium diiodide was 17% based on diiodomethane, the yields of olefins based on the organocalcium compound was estimated to be 53—94%. The reaction of bromoiodomethane with calcium in the presence of *p*-tolualdehyde gave *p*-methylstyrene though in a lower yield, but dibromomethane and dichloromethane did not react with calcium under the conditions. The reaction of diiodomethane with calcium in the presence of ketones did not give the corresponding olefins.

Experimental

Diiodomethane and aldehydes were purified by distillation. Bromoiodomethane was prepared by a conventional method.[6] Tetrahydrofuran and nitrogen were purified, and metallic calcium was rasped as described in our previous papers.[7,8] Methylenedicalcium diiodide was prepared from 0.26 g (6.50 mmol) of calcium and 0.74 g (2.76 mmol) of diiodomethane in 5.0 ml of tetrahydrofuran at −30 °C according to our previous procedure[8] with minor modifications. Carboxylation of methylenedicalcium diiodide was carried out at −70 °C according to our previous procedure[2] with minor modifications. Olefination of aldehydes was carried out by the addition of dihalomethane to a mixture of metallic calcium and aldehyde in tetrahydrofuran at room temperature under a nitrogen atmosphere. The reaction mixture was allowed to remain at room temperature for an additional 1 h, and worked up in the usual manner. Yields were determined by gas chromatographic analyses of the reaction mixture.

References

1) N. Kawabata, H. Nakamura, and S. Yamashita, *J. Org. Chem.*, **38**, 3403 (1973).
2) N. Kawabata, H. Yoshimura, and S. Yamashita, *Bull. Chem. Soc. Jpn.*, **47**, 2822 (1974).
3) R. West and E. G. Rochow, *J. Org. Chem.*, **18**, 1739 (1953).
4) F. Bertini, P. Grasselli, G. Zubiani, and G. Cainelli, *Tetrahedron*, **26**, 1281 (1970) and references cited therein.
5) S. Miyano, M. Hida, and H. Hashimoto, *J. Organometal. Chem.*, **12**, 263 (1968) and references cited therein.
6) S. Miyano and H. Hashimoto, *Bull. Chem. Soc. Jpn.*, **44**, 2864 (1971).
7) N. Kawabata, A. Matsumura, and S. Yamashita, *J. Org. Chem.*, **38**, 4268 (1973).
8) N. Kawabata, A. Matsumura, and S. Yamashita, *Tetrahedron*, **29**, 1069 (1973).

TABLE 1. OLEFINATION OF ALDEHYDES BY METHYLENEDICALCIUM DIHALIDE[a]

Calcium (mmol)	Dihalomethane	(mmol)	Aldehyde	(mmol)	Olefin (Yield, %)[b]
3.24	CH_2I_2	0.74	C_6H_5CHO	0.57	11
8.16	CH_2I_2	4.08	*p*-$CH_3C_6H_4CHO$	4.08	16
7.41	CH_2BrI	4.63	*p*-$CH_3C_6H_4CHO$	3.47	5
6.09	CH_2I_2	3.33	*trans*-CH_3CH=$CHCHO$	3.23	9
9.88	CH_2I_2	2.37	$CH_3(CH_2)_3CHO$	2.06	10

a) Reactions were carried out at room temperature in 5.0 ml of tetrahydrofuran under a nitrogen atmosphere.
b) Based on dihalomethane.

* To whom correspondence should be addressed.

Electronic Structure of Porphyrins. I. SCF-MO-CI Calculation Based on π-Electron Approximation

Kotaro TOMONO and Kichisuke NISHIMOTO

Department of Chemistry, Osaka City University, Sumiyoshi-ku, Osaka 558

(Received June 6, 1975)

The electronic structure and electronic spectra of metal free and metal porphyrins have been investigated by the MO method. In order to elucidate the effect of electron correlation on the electronic transitions, a new approximation for electron repulsion integral has been examined. For metal free porphyrin, the effect of hydrogen bondings on the electronic transitions has also been investigated. In metal porphyrin, the present calculation showed that almost two units of charges are transferred from the ligand porphyrin to the central metal ion through σ-type co-ordination bond. A satisfactory agreement between the calculated results and the experimental data was obtained when a new expression for electron repulsion integral, in which the effect of electron correlation is considered, was used. It was found that the Soret band of metal free porphyrin consists of almost degenerated B_x and B_y species.

Metal porphyrins are very important molecules in the field of biochemistry and biology. From this reason, a number of studies of the physico-chemical properties of these molecules have been carried out.[1] It is well known that hemoglobin, myoglobin, and cytochrome contain iron porphyrins. Vitamin B_{12} and chlorophyll also contain porphyrins. The porphyrin parts play most important roles in the chemical behavior of these molecules. Howver, their electronic spectra have not been clarified. Kobayashi,[2] Weiss *et al.*[3] and others[4-6] have calculated two strong allowed transitions for metal free porphyrin in the region of 400 nm. However, the observed spectra show only one strong absorption band in this region, so-called the Soret band. The excited energy levels of the molecule should be important, for understanding its photo-chemical behavior. One of the main purposes of this paper is to elucidate the nature of the Soret band, so that we have carried out SCF-MO-CI calculations. The effect of electron correlation on the electronic transitions is an interesting theoretical subject. So that, we used two kinds of approximations for electron repulsion integrals, one of them is older one[7] and another[8] is newly derived from a quantum field theory.

Calculation

SCF-MO-CI calculation based on π-electron approximation was carried out. Parameters were evaluated as following manner.

(*A*) *The Framework and Core Charges.* Webb and Fleischer[9] studied the crystal structure of metal free porphyrin by X-ray analysis. They treated the two hydrogen atoms attached to the nitrogens as four half-atoms. The two hydrogen can be considered to be statistically disordered or involved in the rapid interconversion of N–H tautomers. From the infrared spectroscopy,[10] it has been confirmed that inner hydrogens form hydrogen bonds with neighboring non-bonded nitrogens (Fig. 1). In order to elucidate the effect of hydrogen bond on the electronic structure of the porphyrin, we carried out MO calculations in which the core charges of nitrogens are assumed to change with the hydrogen bond formation. For the sake of simplicity, we assumed the D_{4h} symmetry for the porphyrin molecular frame-work. The bond distances and the bond angles were taken to be the same as those for the metal porphyrins. However, this causes no serious effect on the calculated results of electronic structure, since we used the variable β approximation.[11] Fleischer,[12] and Fleischer *et al.*[13] measured molecular dimensions of various metal porphyrins by X-ray analysis. The average interatomic distances associated with C–N, β–β, α–β, α–meso, and metal–N bonds are 1.38 Å, 1.35 Å, 1.44 Å, 1.40 Å, and 2.00 Å, respectively. In this paper we assumed the following interatomic distances: C–C 1.40 Å, C–N 1.38 Å, N:N (opposite to each other) 4.00 Å. When the value of CNC angle is assumed to be 108°, the other bond angles can be evaluated as shown in Fig. 2, because of the D_{4h} symmetry.

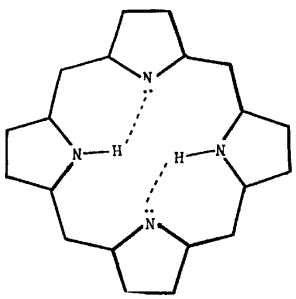

Fig. 1. Hydrogen bonds in metal free porphin.

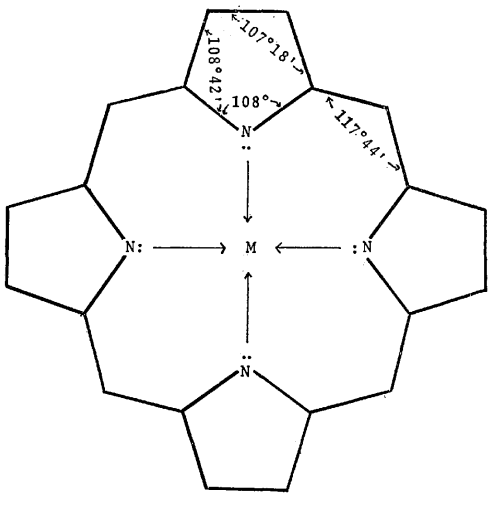

Fig. 2. Assumed porphin frame-work.

The number of π electrons is assumed to be 26 which is the same as that of free porphyrin. In the metal porphyrin, the lone pair electrons of a nitrogen should be largely transferred to the central metal ion by the formation of σ-type co-ordination bond. The net charge of central divalent metal ion is, therefore, expected to be considerably decreased. We have assumed the following various core charges for a nitrogen, +1.0, +1.3 and +1.5, which correspond to the net charges of the central metal ion, +2.0, +0.8, and 0.0, respectively.

(B) One-center Core Integral. When we neglect the penetration integrals, the core integral $\alpha_{\mu\mu}$ can be written as

$$\alpha_{\mu\mu} = \int \phi_\mu(1) H_{\text{core}}(1) \phi_\mu(1) d\tau = -I_\mu - \sum_{\nu \neq \mu} Q_\nu \gamma_{\mu\nu} \quad (1)$$

where ϕ_μ: 2pπ AO of atom μ

I_μ: valence state ionization potential of atom μ

Q_ν: core charge of atom ν

$\gamma_{\mu\nu}$: two-center electron repulsion integral.

I_μ can be represented by the following quadratic equation of core charge Q:[14]

$$I_\mu(Q) = (1/2)\{I(2) - 2I(1) + EA\}Q^2 - (1/2)\{I(2) - 4I(1) + 3EA\}Q + EA \quad (2)$$

where $I(2)$: second ionization potential

$I(1)$: first ionization potential

EA: electron affinity.

(C) Two-center Core Integral. The two-center core integral $\beta_{\mu\nu}$ associated with μ–ν bond,

$$\beta_{\mu\nu} = \int \phi_\mu(1) H_{\text{core}}(1) \phi_\nu(1) d\tau$$

has been evaluated by the variable β approximation.[11]

They are expressed as,

$$\beta_{\mu\nu}(\text{C–C}) = -0.51 P_{\mu\nu} + \beta^0(\text{C–C}) \text{ eV}$$
$$\beta_{\mu\nu}(\text{C–N}) = -0.53 P_{\mu\nu} + \beta^0(\text{C–N}) \text{ eV} \quad (3)$$

where $P_{\mu\nu}$ is the bond order associated with μ–ν bond. For non-neighbors, the $\beta_{\mu\nu}$'s are neglected. The values of β^0's are estimated to reproduce the lowest transition energy of the molecule.

(D) One-center Electron Repulsion Integral. This integral can be evaluated by the Pariser-Parr approximation:

$$\gamma_{\mu\mu} = \int \phi_\mu^2(1)(e^2/r_{12}) \phi_\mu^2(2) d\tau = I_\mu - EA_\mu \quad (4)$$

where EA_μ represents the electron affinity associated with ϕ_μ. When we consider a core charge dependence on the valence state energy, $\gamma_{\mu\mu}$ will be given by the following linear equation of core change Q.[14]

$$\gamma_{\mu\mu}(Q) = \{\gamma_{\mu\mu}(2) - \gamma_{\mu\mu}(1)\}Q + 2\gamma_{\mu\mu}(1) - \gamma_{\mu\mu}(2) \quad (5)$$

where

$$\gamma_{\mu\mu}(2) = I_\mu(2) - I_\mu(1)$$
$$\gamma_{\mu\mu}(1) = I_\mu(1) - EA_\mu$$

The values of parameters are summarized in Table 1.

(E) Two-center Electron Repulsion Integral. Two-center repulsion integral,

$$\gamma_{\mu\nu} = \int \phi_\mu^2(1)(e^2/r_{12}) \phi_\nu^2(2) d\tau$$

are calculated by two kinds of approximation, NM[7] and KHN[8]. In NM approximation, $\gamma_{\mu\nu}$ is given by

Table 1. The values of parameters

Atom	Q	I (eV)	EA (eV)	$\gamma_{\mu\mu}$ (eV)
C	+1.0	11.16	0.03	11.13
N	+1.0	14.12	1.78	12.34
N	+1.1	15.37	2.52	12.85
N	+1.2	16.62	3.26	13.36
N	+1.5	20.38	5.49	14.89
N	+1.8	24.17	7.75	16.42
N	+1.9	25.43	8.50	16.93
N	+2.0	26.70	9.26	17.44

$$\gamma_{\mu\nu} = e^2/(R + a)$$

where R is the interatomic distance between μ and ν atoms. Recently, we[8] have derived the following expression for $\gamma_{\mu\nu}$ from Brueckner equation,[15] by assuming ZDO and point charge interaction.

$$\gamma_{\mu\nu} = e^2/(R + (\Delta E_B/\Delta E)A_B) = e^2/(R + kA_B) \quad (6)$$

where A_B: parameter for benzene

ΔE_B: average transition energy of benzene

ΔE: average transition energy of the molecule

k: correlation parameter $(\Delta E_B/\Delta E)$.

NM expression can be obtained, when we put $k=1$. For the porphyrin molecule, $\Delta E_B/\Delta E$ is estimated to be 2.0 from the Soret band. In order to examine the effect of k on the electronic transition energies, the value is varied from 1 to 2.5.

Results and Discussion

Electronic Spectra. In order to elucidate the effect of σ-donation from the ligand porphyrin to the central metal ion, SCF-MO-CI calculations based on various models for the σ-framework have been carried out. First of all, we used NM approximation for two-center repulsion integrals and various β^0's. Models and the values of β^0 are shown in Table 2. In the calculation of metal porphyrin, we neglected the dπ-pπ interaction. The calculated results are summarized in Tables 3 and 4, together with the experimental data. It was found that better results are obtained by Model

Table 2. Various models for free and metal porphins

(A) Free porphin

Model	Core charge of: pyrrole type nitrogen	Core charge of: pyridine type nitrogen	β^0 (C–C) (eV)	β^0 (C–N) (eV)
I	2.0	1.0	−1.80	−1.86
II	2.0	1.0	−2.04	−2.24
III	1.9	1.1	−2.04	−2.24
IV	1.8	1.2	−2.04	−2.24

(B) Metal porphin

Model	Core charge of nitrogen	β^0 (C–C)	β^0 (C–N)
V	1.3	−1.80	−1.86
VI	1.5	−1.80	−1.86
VII	1.0	−2.04	−2.24
VIII	1.3	−2.04	−2.24
IX	1.5	−2.04	−2.24

Table 3. Calculated transition energies (in eV) and oscillator strengths for free porphin (NM approximation)

Model		Q_x	Q_y	B_x	B_y
I	ΔE	1.69	2.01	3.00	3.40
	f	(0.008)	(0.028)	(0.461)	(2.30)
II	ΔE	1.91	2.21	3.27	3.61
	f	(0.018)	(0.057)	(0.666)	(2.60)
Expt[a)]	ΔE	2.01	2.39	3.13	
	$\varepsilon\times10^3$	(0.86)	(2.64)	(2.60)	

a) Ref. 17.

Table 4. Calculated transition energies (in eV) and oscillator strengths for metal porphin (NM approximation)

Model		Q	B	N
V	ΔE	1.80	3.20	3.86
	f	(0.014)	(2.34)	(2.41)
VI	ΔE	1.87	3.41	3.98
	f	(0.018)	(5.30)	(1.19)
VII	ΔE	1.78	3.23	4.05
	f	(0.092)	(3.45)	(1.84)
VIII	ΔE	2.02	3.48	4.32
	f	(0.048)	(5.01)	(1.09)
IX	ΔE	2.09	3.62	4.29
	f	(0.045)	(5.81)	(1.03)
Expt[a)] (Cu-porphin)	ΔE	2.23	3.13	
	f	(0—0.1)	(1.1—1.6)	

a) Ref. 18.

II for free porphyrin and Model IX for metal porphyrin. These results suggest that the appropriate values of β^0's are β^0 (C–C) $=-2.04$ eV and β^0 (C–N) $=-2.24$ eV, respectively. The values fit benzene and its derivatives. According to our previous work,[11] the best value of β^0 is usually reduced with an increase in the size of the cata-condensed hydrocarbon system. Since porphyrin is a much larger conjugated system than benzene, the present estimation seems to be unusual. However, there are some exceptions. For an example, in polyenes, it is not necessary to decrease the value of β^0 with increase in the length of conjugated system.[16] An improvement was obtained in the present study as compared with the previous investigation.[3] However, the calculated interval between Q and B bands is still too large.

In order to examine the effect of electron correlation on the electronic transitions, we have carried out SCF-MO-CI calculation based on KHN approximation. In the calculation, correlation parameter k in Eq. 6 is used as an adjusting parameter. We have varied the value of k from 1.0 to 2.5. The calculated results are given in Tables 5 and 6. The interval between Q and B bands decreases considerably with the increase in the value of k. A satisfactory agreement between the experimental and calculated results is obtained for $k=2.0$. In KHN approximation, the value of k is given by the ratio of the transition energy associated with p-band of benzene to that of a given molecule. In porphyrin, the value is to be 2.0, which agrees with the above mentioned best value. It is of interest to

Table 5. Calculated transition energies (in eV) and oscillator strengths of metal free porphin (KHN approximation)

Model			Q_x	Q_y	B_x	B_y
II	$k=1.5$ 22 CI[a)]	ΔE	1.87	2.28	3.07	3.26
		f	(0.049)	(0.040)	(0.879)	(2.45)
II	$k=2.0$ 22 CI	ΔE	1.84	2.32	2.93	3.03
		f	(0.087)	(0.025)	(1.05)	(2.34)
II	$k=2.0$ 4 CI	ΔE	1.89	2.33	3.05	3.10
		f	(0.098)	(0.024)	(2.68)	(2.83)
II	$k=2.5$ 22 CI	ΔE	1.81	2.35	2.83	2.87
		f	(0.126)	(0.012)	(1.18)	(2.27)
III	$k=2.0$ 22 CI	ΔE	1.90	2.30	2.99	3.06
		f	(0.073)	(0.022)	(1.53)	(2.54)
IV	$k=2.0$ 22 CI	ΔE	1.97	2.26	3.03	3.07
		f	(0.061)	(0.022)	(1.99)	(2.70)

a) Number of singly excited configurations included in the CI calculation

Table 6. Calculated transition energies (in eV) and oscillator strengths for metal porphin (KHN approximation)

Model			Q	B	N
IX	$k=1.5$ 20 CI	ΔE	2.12	3.30	4.06
		f	(0.056)	(5.69)	(0.585)
IX	$k=2.0$ 25 CI	ΔE	2.13	3.08	3.88
		f	(0.069)	(5.29)	(0.596)
IX	$k=2.0$ 4 CI	ΔE	2.15	3.10	
		f	(0.064)	(5.84)	
IX	$k=2.5$ 25 CI	ΔE	2.12	2.92	3.79
		f	(0.093)	(5.12)	(0.506)

note that the results are not affected by the number of excited configurations taken into the calculation of configuration interaction. Namely, a satisfactory result is also obtained by a so-called four orbital model. This fact suggests us that KHN approximation takes fairly well the effect of electron correlation into account. In the case of free porphyrin, Rimington *et al.*[17] pointed out that the B_y band should lie very close to the strongest B_x band. Their suggestion seems to be of significance in porphyrin chemistry. This has been justified by the present study. Recently, Hatano[19] showed from MCD experiment that the Soret band consists of very closed B_x and B_y species. The calculated oscillator strengths of free porphyrin based on KHN approximation are considerably influenced by σ-framework. The second band (Q_y) seems to be too weak theoretically. However, there is a possibility of acquiring an intensity from the neighboring very intense Soret band, similar to the case of benzene's p-band.

It has been suggested by infrared spectroscopy[10] that there are hydrogen bonds between inner hydrogens and pyridine type nitrogens in free porphyrin. The wave function of a hydrogen bonded system can be, to a first approximation, expressed by the linear combinations of a non-dative and a proton transferred dative structure. Thus, in a simple treatment, the effect of hydrogen bond formation on the electronic structure of porphyrin can be considered by the variation of

Table 7. Calculated orbital energies (in eV) of highest occupied (HOMO) and lowest unoccupied (LUMO) orbitals (NM approximation)

Model	I	II	V	VI	VII	VIII	IX
HOMO	−8.06	−8.10	−5.38	−7.99	−1.36	−5.40	−8.03
LUMO	−3.72	−3.65	−1.05	−3.57	2.75	−0.96	−3.49

core charges of nitrogens. Models III and IV were used for this purpose (Table 2). The calculated results are given in Table 5. It is expected that when the degree of proton transfer from N–H bond to pyridine type nitrogen increases, the interval between Q_x and Q_y and also that of B_x and B_y decrease.

Orbital Energy. According to Koopmans' theory,[20] the ionization potential and the electron affinity of a molecule can be calculated by the orbital energies associated with the highest occupied and the lowest unoccupied molecular orbitals. The calculated results are given in Table 7. As seen from this Table, Model IX for metal porphyrin gives almost the same ionization potential and electron affinity with those of free porphyrin. The experimental values of the half-wave potentials of metal porphyrins for oxidation[21] and reduction[22] are very close to those of free porphyrin.[21] This experimental result can be explained fairly well by means of Model IX. This provides another evidence that the Model IX in which the core charge of nitrogen is assumed to be 1.5 should be most appropriate for metal porphyrin. The model suggests that the net charge of the central metal ion varies from +2.0 to 0 by the formation of σ-type co-ordination bond.

The calculated MO energies of free porphyrin and the metal porphyrin are summarized in Tables 8 and 9, respectively. When k increases, the orbital spacings become narrow. The reason for this is as follows. Larger k corresponds to an increase in the effect of electron correlation. As a result, the two-center electron repulsion integral is reduced, so that the magnitude of off-diagonal Hartree-Fock element becomes small.

Table 8. Orbital energies (in eV) of free porphin calculated by model II

Symmetry	k=1.0	k=1.5	k=2.0
$5A_{1u}$	1.807	1.231	0.850
$4A_{1u}$	0.720	0.234	−0.092
$5B_{2g}$	0.544	0.073	−0.238
$5B_{3g}$	0.332	−0.155	−0.493
$6B_{1u}$	−0.116	−0.554	−0.861
$3A_{1u}$	−1.986	−2.380	−2.645
$4B_{2g}$	−3.550($4B_{3g}$)	−3.808	−3.927
$4B_{3g}$	−3.651($4B_{2g}$)	−3.848	−4.047
$5B_{1u}$	−8.101	−7.904	−7.752
$2A_{1u}$	−8.734	−8.515	−8.347
$3B_{2g}$	−9.991	−9.514	−9.193
$4B_{1u}$	−10.037	−9.566	−9.251
$3B_{3g}$	−10.783	−10.388	−10.097
$2B_{2g}$	−11.155($3B_{1u}$)	−10.757	−10.409
$3B_{1u}$	−11.230($2B_{2g}$)	−10.777	−10.494
$2B_{3g}$	−11.271	−10.906	−10.660
$1A_{1u}$	−12.375	−11.828	−11.457
$2B_{1u}$	−13.902	−13.365	−12.999
$1B_{2g}$	−14.188	−13.604	−13.210
$1B_{3g}$	−15.536	−15.030	−14.702
$1B_{1u}$	−15.598	−15.078	−14.742

Table 9. Orbital energies (in eV) of metal porphin calculated by model IX

Symmetry	k=1.0	k=1.5	k=2.0
$4A_{2u}$	2.024	1.451	1.061
$6E_g$	1.936	1.379	1.001
$3B_{1u}$	1.864	1.321	0.954
$2A_{1u}$	0.924	0.423	0.084
$5E_g$	0.662	0.166	−0.176
$3B_{2u}$	0.141	−0.326	−0.657
$2B_{1u}$	−1.891	−2.257	−2.513
$4E_g$	−3.492	−3.707	−3.865
$3A_{2u}$	−8.033	−7.839	−7.698
$1A_{1u}$	−8.585	−8.357	−8.194
$3E_g$	−10.485($2B_{2u}$)	−10.044	−9.737
$2B_{2u}$	−10.488($3E_g$)	−10.046	−9.742
$2A_{2u}$	−10.516	−10.074	−9.768
$2E_g$	−10.914	−10.488	−10.195
$1B_{1u}$	−12.164	−11.630	−11.272
$1B_{2u}$	−14.161	−13.627	−13.268
$1E_g$	−14.700	−14.120	−13.734
$1A_{2u}$	−15.049	−14.446	−14.046

Electron Density and Bond Order. The effect of correlation parameter k on the electron distribution in the ground state of free porphyrin is shown in Fig. 3. When k increases, the electron density of α-carbon decreases slightly and that of nitrogen increases, for the pyrrole type ring. Reverse changes are found in another ring which has no N–H bond. Referring to the bond orders associated with aromatic hydrocarbons, we might say that mobile π-electrons move along bonds,

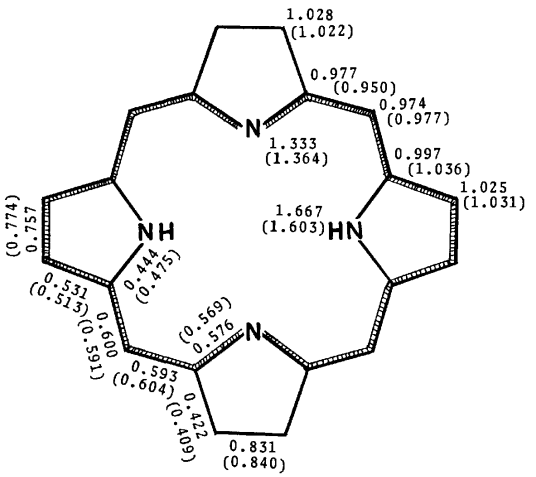

Fig. 3. Charge densities and bond orders of free porphin in the ground state, calculated by k=2.0. The results calculated by k=1.0 are shown in the parentheses.

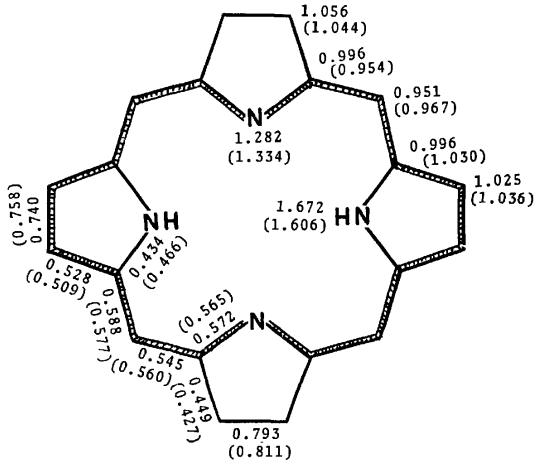

Fig. 4. Charge densities and bond orders of free porphin in the lowest excited singlet state, calculated by $k=2.0$. The results calculated by $k=1.0$ are shown in the parentheses.

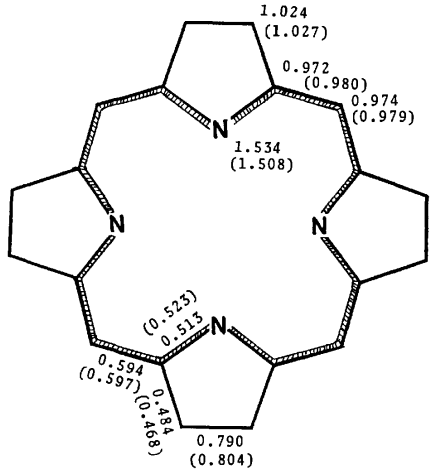

Fig. 5. Charge densities and bond orders of metal porphin in the ground state, calculated by $k=2.0$. The results calculated by $k=1.0$ are shown in the parentheses.

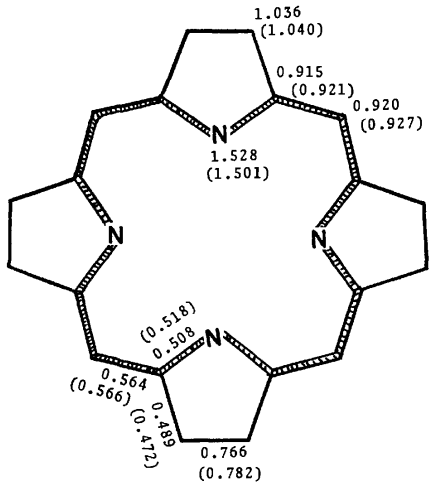

Fig. 6. Charge densities and bond orders of metal porphin in the lowest excited singlet state, calculated by $k=2.0$. The results calculated by $k=1.0$ are shown in the parentheses.

where bond orders are in the range 0.5—0.75. Thus, the path of mobile electrons in metal free porphyrin can be described by a shaded line in Fig. 3. The electron correlation might cause a slight increase in the mobility of π-electrons. The molecular diagram of free porphyrin in the lowest excited singlet state calculated by Model II is shown in Fig. 4. The effect of excitation causes a very small decrease in the electron densities of meso carbon and pyridine type nitrogen. The effect of k value on the electron distribution in metal porphyrin calculated by Model IX is shown in Fig. 5. It is seen from this figure that the mobility of π-electron along the outer ring increases slightly with increase in the value of k. The shaded framework includes 17.75 π-electrons; namely Huckel's $4n+2$ rule is approximately satisfied.

The 0–0 transitions of the Soret bands of both free and metal porphyrins are extremely intense. This fact suggests that the change of molecular framework by an excitation is very small. The molecular diagram of metal porphyrin in the lowest excited singlet state is shown in Fig. 6. The present calculation predicts that the changes of bond orders by an electronic transition are very small.

References

1) For example, a) "Porphyrins and Related Compounds," ed. by T. W. Doodwin, Academic Press, New York (1968); b) J. E. Falk, "Porphyrins and Metalloporphyrins," Elsevier Publish. Co., New York (1964).
2) H. Kobayashi, *J. Chem. Phys.*, **30**, 1362 (1959).
3) C. Weiss, H. Kobayashi, and M. Gouterman, *J. Mol. Spectrosc.*, **16**, 415 (1965).
4) A. J. Mchugh and M. Gouterman, *Theoret. Chim. Acta.*, **24**, 346 (1972).
5) M. Sundbom, *Acta Chem. Scand.*, **22**, 1317 (1968).
6) B. Roos and M. Sundbom, *J. Mol. Spectry.*, **36**, 8 (1970).
7) K. Nishimoto and N. Mataga, *Z. Phys. Chem.*, **12**, 335 (1957).
8) K. Kitaura, J. Hata, and K. Nishimoto, "Abstract of the Bunshikozo Sogo Toronkai," held at Nagoya, 1973, p. 63.
9) L. E. Webb and E. B. Fleischer, *J. Chem. Phys.*, **43**, 3100 (1965).
10) J. E. Falk and J. B. Willis, *Australian J. Sci. Res.*, **4A**, 579 (1951); S. F. Mason, *J. Chem. Soc.*, **1958**, 976; G. M. Badger, R. L. N. Harris, R. A. Jones, and J. M. Sasse, *ibid.*, **1962**, 4329.
11) K. Nishimoto and L. S. Forster, *Theor. Chim. Acta*, **3**, 407 (1965).
12) E. B. Fleischer, *J. Am. Chem. Soc.*, **85**, 146 (1963).
13) E. B. Fleischer, C. K. Millerand, and L. E. Webb, *J. Am. Chem. Soc.*, **86**, 2342 (1964).
14) K. Nishimoto, K. Nakatsukasa, R. Fujishiro, and S. Kato, *Theor. Chim. Acta*, **14**, 80 (1969).
15) K. A. Brueckner, *Phys. Rev.*, **96**, 508 (1954).
16) L. S. Forster, *Theor. Chim. Acta*, **5**, 81 (1966).
17) C. Rimington, S. F. Mason, and O. Kennard, *Spectrochim. Acta*, **12**, 65 (1958).
18) G. D. Dorough, J. R. Miller, and F. M. Huennekens, *J. Am. Chem. Soc.*, **73**, 4315 (1951).
19) M. Hatano
20) H. Koopmans, "Kernmomente Akademische Verlagsgesellschaft," m.b.H., Leipzig, Sec 26—5 (1940).
21) A. Wolberg and J. Manassen, *J. Am. Chem. Soc.*, **92**, 2982 (1970).
22) R. Felton, Ph. D. Thesis, Harvard University (1964).

X-Ray Photoelectron Spectra of Aryl-nickel Complexes

Manabu SENŌ, Shinji TSUCHIYA, Masanobu HIDAI,* and Yasuzo UCHIDA*

Institute of Industrial Science, The University of Tokyo, 7-22, Roppongi, Minato-ku, Tokyo 106

**Department of Industrial Chemistry, Faculty of Engineering, The University of Tokyo, 7-3, Hongo, Bunkyo-ku, Tokyo 113*

(Received July 3, 1975)

The nature of bondings in aryl–nickel complexes has been clarified by means of X-ray photoelectron spectroscopy (XPS). Pi bonding between nickel and aryl ligand seem to be of little importance. Ni–Cl bondings are of partially ionic character. A correlation between stereochemical structure and satellites has been discussed. It is suggested that the aryl-nickel complexes examined have diamagnetic square-planar structures. Measurements of solid-state susceptibilities support this view.

The stability of the aryl-nickel complexes is extremely high in contrast to the instability of transition metal-alkyl complexes. The increasing stability is probably ascribed to either or both of the following two factors; the substitution of β hydrogen atoms to the metal atom, and the stabilization by π acceptor ligands. Pi bonding between the transition metal and the aryl-ligand has been discussed in various aspects since the work by Chatt and Shaw.[1] It could be said that the stability of the complex is related with the energy difference (ΔE) between the highest occupied d orbital and the lowest unoccupied orbital. Since π bonding between the metal d orbital and the aryl-ligand reduces the energy of the d orbital and increases ΔE, the stability of the complex increases. Experimental evidence for this interaction is still ambiguous.

Recent studies on coordination complexes by X-ray photoelectron spectroscopy (XPS) revealed its usefulness, and we have applied this method to examination of a series of aryl-organometallic complexes.[2] Through measurements of the binding energies, we obtained some information on the nature of metal-ligand bondings. We also found the satellites associated with the 2p photoelectron lines of the nickel compounds. These satellites seem to originate from the shake-up process related to the paramagnetism.[2,3] A detailed discussion is given on the stereochemical structure on which the magnetic state depends.

Results and Discussion

The Nature of Nickel-Ligand Bondings. The observed values of Ni 2p, Cl 2p, and P 2s binding energies are summarized in Table 1. The structures of aryl-nickel complexes are shown in I.

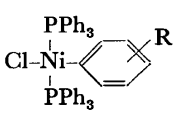

I

Ni 2p binding energies of aryl-nickel compounds are lower than those of $NiCl_2$ (**1**) and $Ni(PPh_3)_2Cl_2$ (**2**). It could be pointed out from these results that the positive charge less than that of (**1**) or (**2**) is assigned to Ni atom in aryl-nickel complexes, and the coordinated aryl group donates considerably more electron density to nickel atom than the chlorine ligand. Hence, the nickel-aryl π bonding or back-donation seems to be of little importance in the aryl-nickel complexes. If metal-aryl π bonding does exist, it would be the most important in square-planar *ortho*-substituted aryl-nickel complexes where the ligands locate to form a conformation ensuring a maximum $p\pi$-$d\pi$ overlap by steric constraints. However, for even *ortho*-substituted aryl-nickel complexes $Ni(PPh_3)_2Cl$- 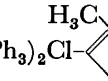 (**9**) and $Ni(PPh_3)_2Cl$- 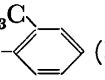 (**10**), a high binding energy could not be observed. Similar results have been obtained by Fahey and Baldwin.[4]

TABLE 1. Ni $2p_{3/2}$, Cl 2p, AND P 2s BINDING ENERGIES ON NICKEL COMPLEXES

		Ni $2p_{3/2}$	Cl 2p	P 2s
1	$NiCl_2$	857.3	199.5	—
2	$Ni(PPh_3)_2Cl_2$	856.2	198.4	189.0
3	$Ni[P(n\text{-}C_4H_9)_3]_2Cl_2$	854.3	198.3	189.5
4	$Ni(PPh_3)_2Cl$-	854.6	198.4	188.4
5	$Ni(PPh_3)_2Cl$- -Cl	855.0	200.4 198.5	189.3
6	$Ni(PPh_3)_2Cl$- -OMe	854.4	198.9	189.5
7	$Ni(PPh_3)_2Cl$- -CH_3	854.4	198.3	188.9
8	$Ni(PPh_3)_2Cl$-	855.3	199.0	189.5
9	$Ni(PPh_3)_2Cl$-	854.8	198.5	189.4
10	$Ni(PPh_3)_2Cl$-	854.7	198.8	188.7
11	$Ni(PPh_3)_2Cl$-	854.1	199.0	188.9

P 2s binding energies of nickel complexes remain constant for all the series of compounds. A small or no change is expected in P 2s binding energies on coordination of phosphine to a metal atom. From a comparison of Ni 2p binding energy of $NiCl_2$ (857.3 eV) with that of $Ni(PPh_3)_2Cl_2$ (856.2 eV), it is suggested that a net electron transfer from phosphines to a nickel atom might occur.

Cl 2p binding energies of some compounds containing

Table 2. Cl 2p binding energies of related compounds

	Cl 2p
$NiCl_2$	199.5
NH_4Cl	196.9[a]
Cl_3CCONH_2	200.2
$Cl_2CHCONH_2$	199.1
$ClCH_2CONH_2$	198.6
2,3-Dichloro-1,4-naphthoquinone	200.3
Chloranil	200.1
$Ni(PPh_3)_2Cl$-	198.3—199.0
$Ni(PPh_3)_2Cl$-	198.5, 200.4

a) J. Escard, G. Mavel, J.E. Guerchais, and R. Kergoat, *Inorg. Chem.*, **13**, 695 (1974).

chlorine are summarized in Table 2. Cl 2p binding energies vary considerably in the series of related compounds. We see that Cl 2p binding energy takes a maximum value in chlorine combining to aryl group and a minimum in NH_4Cl (Tables 1 and 2). Cl 2p binding energies in aryl-nickel complexes (198.3—199.0 eV) are lower than that of $NiCl_2$ (199.5 eV), but higher than that of NH_4Cl (196.9 eV). This shows that, although Cl 2p binding energies are highly affected through a Madelung contribution in these ionic structures, the electron density on Cl in aryl-nickel complexes increases by coordination of PPh_3 or aryl group and nickel-chlorine bond has partially ionic character. On the other hand, it is revealed from measurements of a series of chloroacetamides that, when the chlorine combines to the atom with higher electron density, the electron density on chlorine should increase and the Cl 2p binding energies in aryl-nickel complexes have about the same value of Cl 2p binding energy in α-chloroacetamide. This suggests that the chlorine in aryl-nickel complexes withdraws the electron on nickel atom to which the electron is supplied from the ligand.

As for complex Cl- 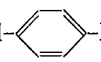 -$Ni(PPh_3)_2Cl$ (**5**), the Cl peak corresponding to binding energy of 198.5 eV is assigned to Cl coordinated directly to central Ni atom and the peak of binding energy of 200.4 eV to Cl bonded to aryl group. The large difference in energy shows that the two bonds differ largely from each other in nature. Cl 2p binding energies do not change among chlorine atoms bonded to aryl group in the compounds such as chloranil, 2,3-dichloro-1,4-naphthoquinone, and Cl- -$Ni(PPh_3)_2Cl$. The results indicate that the electron withdrawing from Ni to the aryl substituent in the complex (5) is not probable and, therefore, back-donation is of minor importance.

Stereochemical Structure and Satellites. We have observed photoelectron satellites accompanied by the Ni 2p line. Generally, the satellites associated with the 2p photoelectron lines of Ni compounds are interpreted to be due to promotion of a nickel 3d electron into an unoccupied level, this being called a shake-up phenomenon.[3] Matienzo *et al.* reported the selection rule ($\Delta L_v=0$, $\Delta S_v=0$) for the monopole shake-up transitions and discussed the correlation between

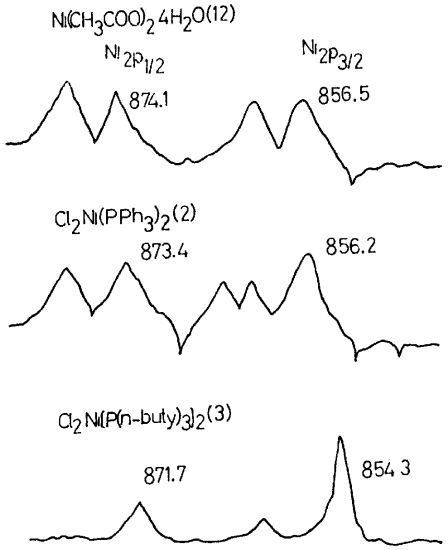

Fig. 1. Ni 2p XPS spectra of octahedral (**12**), tetrahedral (**2**), and square-planar (**3**) compounds of nickel.

paramagnetism and shake-up satellites. They suggested that, for the same ligand under different stereochemical geometries, the 2p binding energies of the nickel ion increase in the order, planar<tetrahedral<octahedral.[5] However, experimental evidence is insufficient for confirming the suggestion. For the sake of clarification, we have measured Ni 2p binding energies of $Ni(AcO)_2 4H_2O$ (**12**) (octahedral), $Ni(PPh_3)_2Cl_2$ (**2**) (tetrahedral), and $Ni[P(n\text{-}C_4H_9)_3]_2Cl_2$ (**3**) (square-planar). The results are shown in Fig. 1. It was found for paramagnetic nickel compounds **2** and **12** that parent lines are broad and large shake-up satellites appear, whereas for diamagnetic nickel compound(**3**) narrow parent lines and a small satellite only for $3p_{3/2}$ peak appear. The result for paramagnetic nickel compounds is consistent with that of previous studies, but not for diamagnetic compounds; no satellites were observed in the XPS spectra of diamagnetic nickel compounds reported previously.[2,5] Thus, the cause of the appearance of the small satellite for **3** is uncertain in the present state. A possibility is as follows; A paramagnetic substance is partially formed in the surface region of complex **3** on X-ray irradiation. Two satellites for Ni $2p_{3/2}$ of complex **2** would be assigned

Table 3. Ni 2p binding energies of nickel complexes

Compound	Ni $2p_{3/2}$	Sat.	Ni $2p_{1/2}$	Sat.
1	857.3	862.6	874.5	878.8
2	856.2	862.1, 865.3	873.4	879.8
3	854.3	861.8	871.7	—
4	854.6	861.3	871.8	880.7
5	855.0	861.8	871.8	880.3
6	854.4	861.8	871.0	881.8
7	854.4	861.3	871.7	881.1
8	855.3	861.8	871.7	880.3
9	854.8	862.3	872.0	—
10	854.7	862.8	872.2	—
11	854.1	861.6	871.6	—

to two type transitions, probably 3d→4s and 3d→ligand transitions. The possibility of development of a satellite due to the 3d→ligand transition is discussed by Frost *et al.*[3] Figure 1 also indicates that a definite correlation exists between the binding energy and stereochemistry of complexes. Hence, it is confirmed that information on the stereochemistry can be obtained through the measurements of the binding energy and satellites.

Table 4. Molar magnetic susceptibilities of nickel complexes

	Compound	Molar magnetic susceptibilities (emu/mol)
2	$Ni(PPh_3)_2Cl_2$	$+4.86\times10^{-3}$
4	$Ni(PPh_3)_2Cl$–	-2.70×10^{-4}
6	$Ni(PPh_3)_2Cl$– –OMe	-1.16×10^{-4}
11	$Ni(PPh_3)_2Cl$– 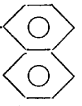	-2.97×10^{-4}

The main peak (Ni 2p) and satellites in the aryl-nickel complexes are summarized in Table 3. For all the aryl-nickel complexes, small satellites are observed on core level of nickel. In the case of aryl-nickel complexes **4**, **5**, **6**, **7** and **8**, there is a satellite for each parent peak, while in the case of aryl-nickel complexes **9**, **10** and **11**, there is a satellite only for $2p_{3/2}$. We have no good explanation for these satellites, but it is to be noted that the satellites observed in the complexes **9**, **10** and **11** are as sharp and weak as those in the diamagnetic complex **3** as shown in Fig 2. It is not clear whether the weak satellites associated with Ni $2p_{1/2}$ peak in the complexes **4**—**8** are of intrinsic origin or are due to the partial decomposition by X-ray irradiation. However, these satellites are very weak and the parent lines are narrow and sharp as compared with those observed for typical paramagnetic complexes like **12** and **2**. The binding energies of the Ni 2p peaks in these complexes are lower than those observed for complexes **12** and **2**. The difference between complexes

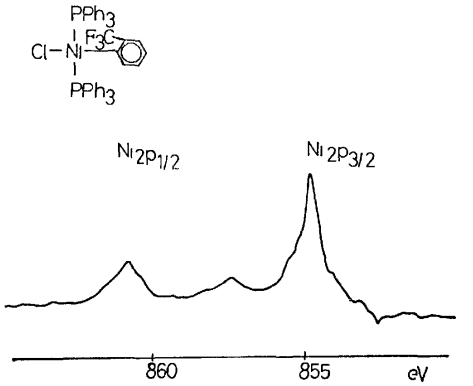

Fig. 2. Ni 2p XPS spectra of aryl-nickel complex (**10**).

4—**8** and complexes **9**—**11** is considered to be due to the stabilization of the latter complexes by the *ortho*-substitution of ligand.[1] It could be deduced from these considerations that all the aryl-nickel complexes examined have the diamagnetic square-planar nickel.

For the sake of confirmation, we have measured solid-state magnetic susceptibilities. The result shows that the aryl-nickel complexes are diamagnetic (Table 4). The conclusion from XPS measurements is thus supported.

Experimental

Aryl-nickel complexes were prepared as described in a previous report.[6]

Photoelectron spectra were taken with a JASCO ESCA-1 electron spectrometer. The Mg*K*α X-ray line (1253.6 eV) was used as a photoelectron excitation source. The samples were used as fine powder dusted onto aluminum foil or Scotch tape which was mounted on a copper sample holder. The recorded binding energies were recorded in triplicate, accuracy being within ±0.25 eV in most cases. All raw binding energies were corrected to C ls value of 284 eV. The procedure appeared very reasonable in the case where the compound contained many carbons. The binding energy of $NiCl_2$ were calibrated by using ls line of the impurity carbon. An attempt was made to refer the spectra to the Au($4f_{7/2}$) photoelectron line. The photoelectron line of Au($4f_{7/2}$) deposited *in vacuo* onto the samples were defined as 83 eV. The results from the two methods agreed with each other.

Solid-state magnetic susceptibilities were measured with a Faraday balance at room temperature.**

References

1) J. Chatt and B. L. Shaw, *J. Chem. Soc.*, **1959**, 705.

2) J. Escard, G. Mavel, J. E. Guerchais, and R. Kergoat, *Inorg. Chem.*, **13**, 695 (1974); S. O. Grim, L. J. Matienzo, and W. E. Swartz, Jr. *ibid.*, **13**, 447 (1974); L. O. Pont, A. R. Siedle, M. S. Lazarus, and W. L. Jolly, *ibid.*, **13**, 483 (1974); C. A. Tolman, W. M. Riggs, W. J. Linn, C. M. King, and R. C. Wendt, *ibid.*, **12**, 2770 (1973).

3) D. C. Frost, A. Ishitani, and C. A. McDowell, *Mol. Phys.*, **24**, 861 (1972); K. S. Kim, *J. Electron Spectrosc. Relat. Phenom.*, **3**, 217 (1974); W. L. Jolly, in D. A. Shirley (editor), "Electron Spectroscopy," North-Holland, Publ. Co., Amsterdam (1972); T. Novakov, *Phys. Rev. B*, **3**, 2693 (1971); T. Novakov and P. Prins, *Solid State Commun.*, **9**, 1975 (1972); A. Rosencwaig, G. K. Wertheim, and H. J. Guggenheim, *Phys. Rev. Lett.*, **27**, 479 (1971).

4) D. R. Fahey and B. A. Baldwin, *J. Organometal. Chem.*, **70**, C11, (1974).

5) L. Yin, I. Adler, T. Tsang, L. T. Matienzo, and S. O. Grim, *Chem. Phys. Lett.*, **24**, 81 (1974); L. J. Matienzo, L. Yin, S. O. Grim, and W. E. Swartz, Jr. *Inorg. Chem.*, **12**, 2762 (1973).

6) M. Hidai, T. Kashiwagi, T. Ikeuchi, and Y. Uchida, *J. Organometal. Chem.*, **30**, 279 (1971).

** Measurements were carried out at the University of Tokyo, Department of Chemistry, Faculty of Science. The authors' thanks are due to Mr. T. Sugano for the measurements and also to Prof. H. Kuroda for helpful discussion.

Studies of Spontaneous Emulsification. II. The Effect of Nonionic Surfactants

Keizo OGINO and Motoki OTA

Faculty of Science and Technology, Science University of Tokyo, Noda, Chiba 278

(Received August 26, 1975)

At the oil/water interface, spontaneous emulsification occurs when oil containing certain oil-soluble substances such as cholesterol is allowed to stand in contact with aqueous nonionic surfactant solutions. In this study, the interfacial tension between oil and water phases was measured in the presence of various oil-soluble substances, such as cholesterol, 1-dodecanol, and *cis*-9-octadecene-1-ol, added as ingredients in oil and various nonionic and anionic surfactants added in water, this study ascertained their effects on the emulsification.

When oil and water phases are brought quietly into contact, spontaneous emulsification sometimes occurs on one or both sides of the interface without any external mechanical work. The spontaneous emulsification is considered to be a result of one or more of the following three reasons[1,2]: i) The instability of the interface due to a non-uniform diffusion of the components of the phases across the interface, which causes a kicking of the interface violent enough to break off droplets of the adjacent bulk phases. ii) An accompanying diffusion of oil and an additive into the water, which results in a dilution of the additive with the water, leaving oil droplets stranded and thus forming the emulsion. iii) The temporary appearance of a negative interfacial tension, which causes an enlargement of the interfacial area.

Schulman and Cockbain[3] have shown that, when a complex is formed between an oil-soluble substance and a water-soluble surfactant at the oil/water interface, spontaneous emulsification occurs, and that the molecular interaction at the interface is sensitively influenced by the stereochemical configuration and the kinds of the polar groups of the two interacting molecules. Davies and Haydon[4] have reported that hexadecanol in toluene and sodium decyl sulfate in water are spontaneously brought into emulsion in the presence of surfactant or alcohol at concentrations higher than certain levels. In this system, interfacial tension was measured at low concentrations of solutes, this tension was proved to be negative when extrapolated to the higher concentration range of the solutes. From this result, they have estimated that a negative interfacial tension is the cause of the spontaneous emulsification. In such a system, emulsification does not occur spontaneously below a certain concentration of the solutes. To clarify the cause of this emulsification, therefore, the detailed measurement of interfacial tension with various concentrations of solutes is essential.

The present investigation was undertaken to reveal the mechanism of the spontaneous emulsification by measuring the interfacial tension in a system including oil-soluble substances and nonionic surfactants at various concentrations; also, the molecular interaction at the Nujol/water interface was studied in relation to the kinds of additives and to the tendency of spontaneous emulsification.

Experimental

Materials. *Surfactants*: The anionic surfactant, sodium dodecyl sulfate (SDS), and various nonionic surfactants were obtained from the Nikko Chemical Co. The characteristic properties of the nonionic surfactants are shown in Table 1. The surface tension *vs.* concentration curves of these nonionic surfactants are shown in Fig. 1.

Oil-soluble Substances: Cholesterol, 1-dodecanol, and *cis*-9-octadecene-1-ol (oleyl alcohol) of an extra pure grade (Tokyo

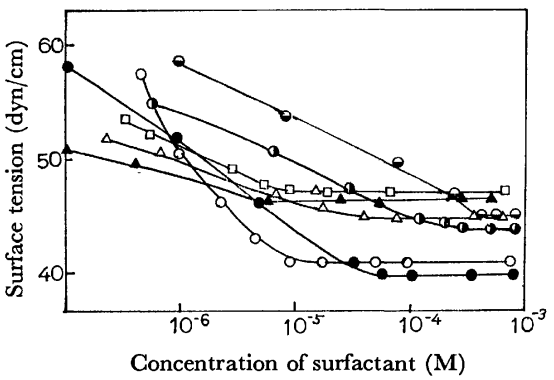

Fig. 1. Surface tension of aqueous solution of surfactants. ○ PCA-20; △ PCA-30; □ PCA-40; ● POA-20 ▲ POA-50; ◑ PS-40; ◒ POPA-30.

TABLE 1. CHARACTERISTIC PROPERTIES OF USED NONIONIC SURFACTANTS

Chemical composition	Abbr.	Number of ethylene oxide unit	HLB	CMC (mol/l)
Polyoxyethylene stearate	PS-40	40	17.4	2.45×10^{-4}
Polyoxyethylene hexadecyl ether	PCA-20	20	13.9	8.90×10^{-6}
Polyoxyethylene hexadecyl ether	PCA-30	30	16.0	3.21×10^{-5}
Polyoxyethylene hexadecyl ether	PCA-40	40	16.9	9.99×10^{-6}
Polyoxyethylene *cis*-9-octadecene-1-ol ether	POA-20	20	13.4	4.36×10^{-5}
Polyoxyethylene *cis*-9-octadecene-1-ol ether	POA-50	50	18.0	2.03×10^{-5}
Polyxyethylene *p*-hexadecylphenyl ether	POPA-30	30	16.9	3.28×10^{-4}

Kasei Co.) were adopted.

Water and Oil: Deionized and distilled water and liquid paraffin (commercial grade "Nujol") were used.

Apparatus. The interfacial tension and its time-course were measured by a Wilhelmy-type surface-tension meter (Shimadzu Surface Tensiometer ST-1).

Procedure. The oil-soluble substances and surfactants were dissolved in oil and water respectively, and the interfacial tension was measured at various concentrations of the solutes in each of the systems at 25 °C. These measurements were started 6 min (in the case of the anionic surfactants) 12 min (in the case of the nonionic surfactants) after the beginning of contact between the two phases, because the equilibria at these interfaces were reached after 5 min and 10 min respectively.

Results and Discussion

The Effects of Oil-soluble Substances. Figure 2 shows the effects of the oil-soluble substances on the interfacial tension in the Nujol/PCA-20 solution. In the figure, the dotted line shows the interfacial tension at which spontaneous emulsification occurs, while the arrow indicates the limit concentration of the component corresponding to the beginning of the emulsification, where the phases show a milky turbidity.

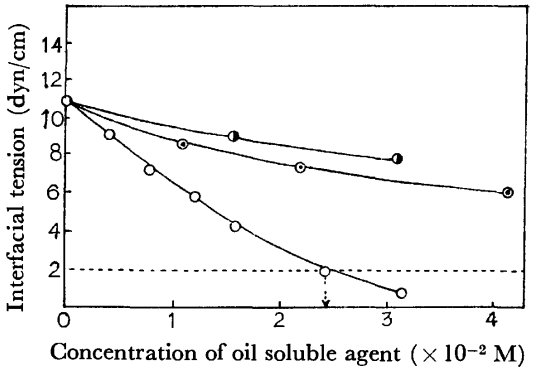

Fig. 2. Effect of oil soluble agents on the interfacial tension at Nujol/PCA-20 soln. interface.
Water phase; 2.7×10^{-3} M. PCA-20 soln.
○ Cholesterol; ◑ 1-dodecanol; ⊙ *cis*-9-octadecene-1-ol.

As shown in Fig. 2, it is clear that the interfacial tension is greatly lowered by the addition of oil-soluble substances; the degree of lowering is in the following order; cholesterol>*cis*-9-octadecene-1-ol>1-dodecanol. It is also clear that the most strongly effecting substance is cholesterol, suggesting that the interaction between cholesterol and a nonionic surfactant should be the strongest in these systems. In the system of cholesterol, spontaneous emulsification takes place at the level of 2.5×10^{-2} M; therefore, the interfacial tension is estimated to be about 2 dyn/cm. Unlike systems including SDS,[5] *cis*-9-octadecene-1-ol has more effects than 1-dodecanol in the systems including nonionic surfactants.

The Effects of Surfactants. The Influence of the Structures of Surfactants: In systems in which cholesterol is included in the oil phase, surfactant molecules with various bond structures and nearly the same HLB were examined for their effects on the interfacial tension

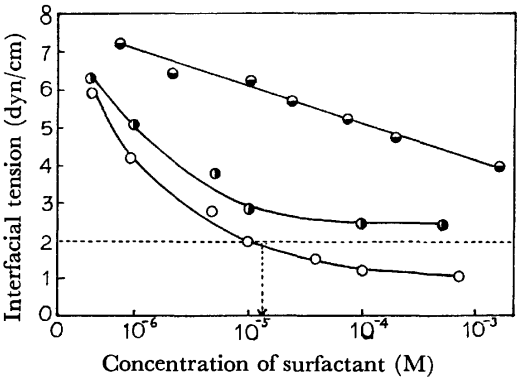

Fig. 3. Effect of surfactants on the interfacial tension at Nujol containing cholesterol/water interface.
Oil phase; 3 M/100 cholesterol soln.
○ PCA-40; ◑ PS-40; ◒ POPA-30.

(Fig. 3). As is shown in Fig. 3, the interfacial tension between water containing the surfactants and Nujol including cholesterol is effected in this order; ether type>ester type>phenyl ether type. In these systems, spontaneous emulsification was observed for the ether-type at an interfacial tension of about 2 dyn/cm.

The Influence of the Hydrophobic Group in Surfactants: Since ether-type nonionic surfactants are most effective in causing spontaneous emulsification, the influence of the hydrophobic group in the surfactants on the interfacial tension between Nujol containing cholesterol

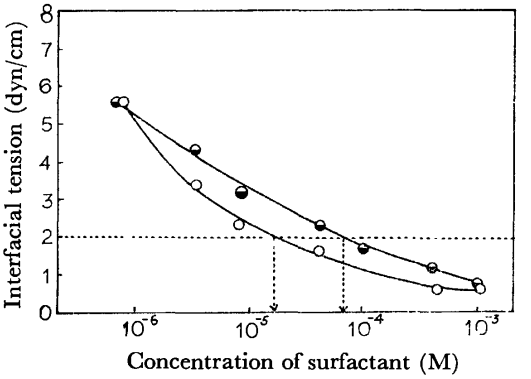

Fig. 4. Effect of surfactants on the interfacial tension at Nujol containing cholesterol/water interface.
Oil phase; 3M/100 cholesterol.
○ PCA-20; ◒ POA-20.

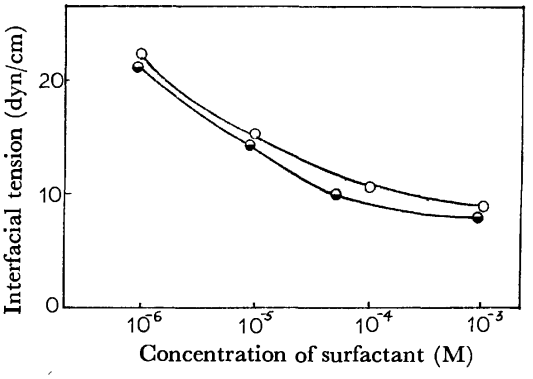

Fig. 5. Effect of surfactants on the interfacial tension at Nujol/water interface.
○ PCA-20; ◒ POA-20.

and water was studied; the results are plotted in Fig. 4. The surfactants consited of 20 units of ethylene oxide and had nearly equal HLB values. Figure 5 shows the equal intensity of the influence on the interfacial tension of the system in which the oil phase contains no oil-soluble substances. As can be seen in Fig. 5, cis-9-octadecene-1-ol ether-type nonionic surfactants lower the interfacial tension more intensively than do hexadecyl ether-type ones, in agreement with the results of Wrigley *et al.*[6] However, when the oil phase contains cholesterol, hexadecyl ether-type surfactants lower, the interfacial tension more than do *cis*-9-octadecene-1-ol ether-type ones, as is shown in Fig. 4. Therefore, it may be presumed that hexadecyl ether-type nonionic surfactants interact with cholesterol more strongly than do *cis*-9-octadecene-1-ol ether-type ones.

The Influence of Hydrophilic Chain Length in Surfactants, The relation between the hydrophilic chain length in surfactants and the effect on the interfacial tension at a Nujol-containing cholesterol/water interface was studied; the results are in Figs. 6 and 7. The hydrophobic group was the same in all kinds of surfactants. The interfacial tension was reduced to a larger extent by the surfactants with longer hydrophilic chains in the lower concentration range, but the degree of reduction is reversed in the higher concentration range of the surfactants, and in the case of *cis*-9-octadecene-1-ol ether-type nonionics, spontaneous emulsification was not observed with the surfactant containing 50 units of ethylene oxide groups. Therefore, it may be presumed that the interaction between the surfactants and cholesterol decreases with an increase in the hydrophilic chain length above 20 units of ethylene oxide groups.

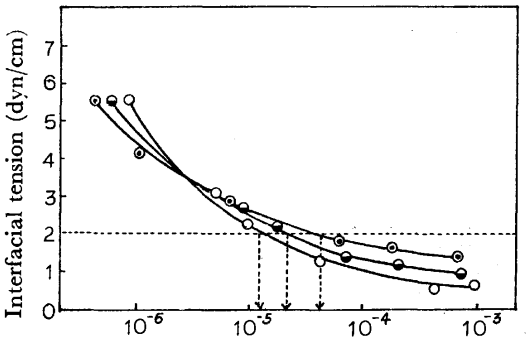

Fig. 6. Effect of surfactants on the interfacial tension at Nujol containing cholesterol/water interface.
Oil phase; 3M/100 cholesterol soln.
○ PCA-20; ◒ PCA-30; ⊙ PCA-40.

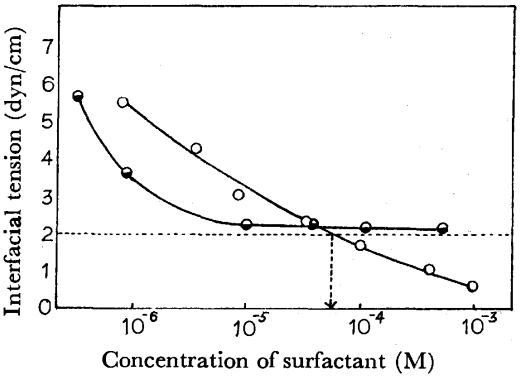

Fig. 7. Effect of surfactants on the interfacial tension at Nujol containing cholesterol/water interface.
Oil phase; 3M/100 cholesterol soln.
○ POA-20; ◒ POA-50.

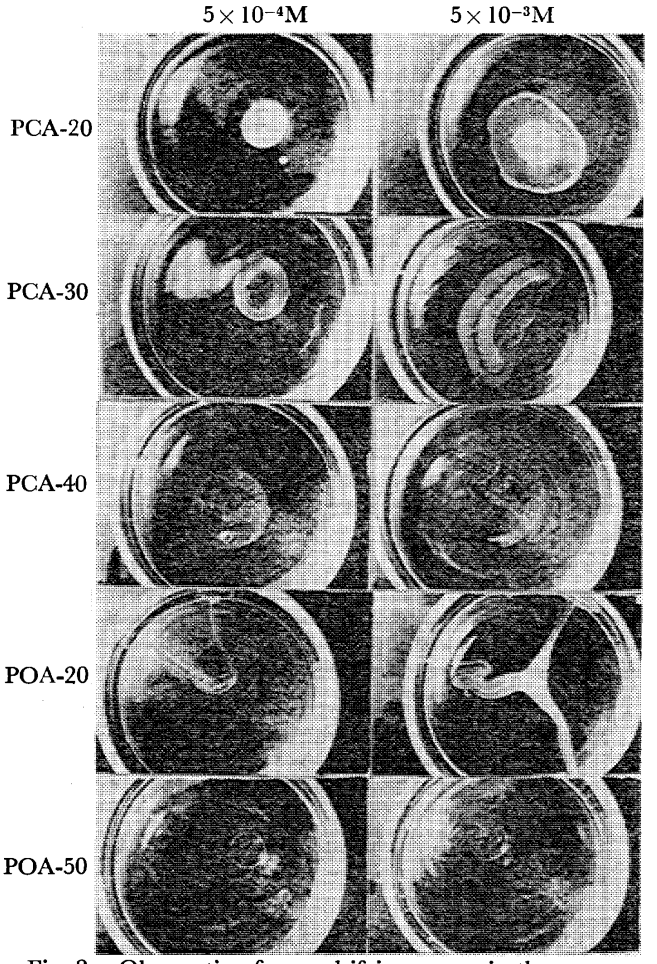

Fig. 8. Observation for emulsifying power in the system of Nujol with 3×10^{-2}M cholesterol/surfactant aqueous soln.

Figure 8 shows the appearance of spontaneous emulsification on the addition of a drop of oil containing 3×10^{-2} M cholesterol to aqueous solutions containing ether-type surfactants at 5×10^{-4} M and 5×10^{-3} M concentrations. The photograph shows the greater deformation of an oil drop and the higher turbidity, *i.e.*, the easier spontaneous emulsification. The emulsifying power of a surfactant decreases with an increase in the ethylene oxide chain length; that is, the interaction of nonionic surfactants with cholesterol decreases with the increase in the effect of hydrophilic groups in the surfactant. This agrees with the results shown in Figs. 6 and 7.

Further, the above results and the results for anionic surfactant systems, such as the cholesterol-sodium-dodecyl sulfate system, in which spontaneous emulsification occurs in the oil phase by means of the formation of a complex drawn up into the oil phase,[5] lead us to presume that a shorter length of the polyoxyethylene chain exhibits a greater likelihood of forming a complex

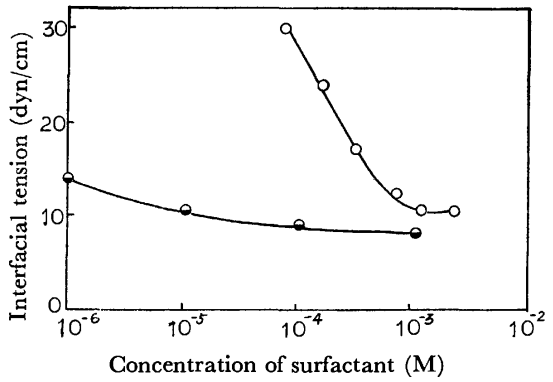

Fig. 9. Effect of surfactants on the interfacial tension at Nujol/water interface.
○ SDS; ◒ PCA-20.

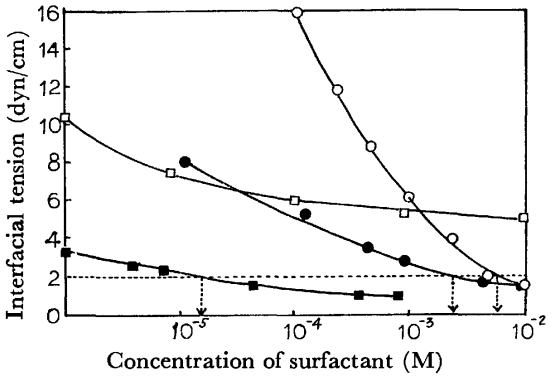

Fig. 10. Comparison between anionic and nonionic surfactants on the interfacial tension at Nujol containing cholesterol/water interface.
Oil phase: M/100 cholesterol–water phase; ○ SDS, □ PCA-20.
Oil phase: 3M/100 cholesterol–water phase; ● SDS, ■ PCA-20.

and causing spontaneous emulsification.

Comparison between Anionic and Nonionic Surfactants, Figures 9 and 10 show the effects of anionic and nonionic surfactants comparatively. When an oil phase contains no substances, the interfacial tension in the SDS system is 30 dyn/cm at the concentration of 5×10^{-4} M, as is shown in Fig. 9. That is, the interfacial tension of the PCA-20 system is lower than that of the SDS system at lower concentrations. On the other hand, as is shown in Fig. 10, when an oil phase contains 1×10^{-2} M cholesterol, the interfacial tension of the SDS system is lowered to a greater extent than that of the PCA-20 system above the surfactant concentration of 1.5×10^{-3} M, and spontaneous emulsification occurs above the concentration of 4.6×10^{-3} M. Therefore, it may be presumed that SDS interacts with cholesterol stronger than PCA-20.

Nevertheless, when an oil phase contains 3×10^{-2} M cholesterol, three times the above concentration, the interfacial tension *vs.* concentration curve shifts down turned and emulsification occurs at the level of 1.8×10^{-5} M in the case of PCA-20, while in the system of SDS emulsification occurs at 2.2×10^{-3} M. The case of SDS is not very different. That is, in the SDS system spontaneous emulsification occurs at a level about 100 times that in the PCA-20 system.

In a previous work[5] we found, with anionic surfactants containing different polar groups, that the oil-soluble cholesterol interacted in the following order: sodium dodecyl sulfate>sodium dodecanoate>sodium dodecylbenzene sulfonate.

From the above results, the molecular interaction between oil-soluble cholesterol and water-soluble surfactants may be thought to vary with the concentration of cholesterol in the oil phase, and its interaction with nonionic surfactants may be thought to be larger than that with anionic ones above a certain concentration of cholesterol in the oil phase.

Summary

In a Nujol/water system the oil phase of which contains both oil-soluble additives and water and the water phase contains oil and a surfactant, spontaneous emulsification scarcely occurs at all, while in systems composed of an oil phase containing a substance and of a water phase containing a surfactant, spontaneous emulsification is apt to take place, whereupon molecular interaction is presumed to occur to form a complex at the oil/water interface. This interaction is sensitive to the stereochemical configuration and polar groups of anionic surfactants molecules in the case of anionic surfactants and sensitive to bond structures, hydrophobic groups, and the polyoxyethylene chain length of nonionic surfactants.

Comparing anionic surfactants with nonionic ones, the former cause emulsification at lower concentrations than the latter in the presence of polar substances at low concentrations in the oil phase, but in the higher concentration range of the polar substances, on the contrary, nonionic surfactants interact with polar substances more strongly than do anionic ones, and spontaneous emulsification occurs at lower concentrations.

References

1) J. T. Davies and E. K. Rideal "Interfacial Phenomena," Academic Press, New York and London (1961), p. 360.
2) J. T. Davies and D. A. Haydon, *Proc. 2nd Internat. Congr. Surface Activity* **1**, 417, Butterworths, London (1957).
3) J. H. Schulman and E. G. Cockbain, *Trans. Faraday Soc.*, **36**, 651 (1940).
4) J. T. Davies and D. A. Haydon, *Proc. 2nd Internat. Congr. Surface Activity* **1**, 417—425 (1957).
5) K. Ogino and M. Ota, *Yukagaku*, **23**, 28 (1974).
6) A.N. Wrigley, F.D. Smith, and A.J. Stirton, *J. Am. Oil Chem. Soc.*, **34**, 39 (1957).

An X-Ray Study of Non-stoichiometric $Pr_{0.6}Gd_{0.4}O_{1.5+\delta}$

Kazuhiro ENDO*, Shigeru YAMAUCHI*, Kazuo FUEKI**, and Takashi MUKAIBO*

*Department of Industrial Chemistry, Faculty of Engineering, The University of Tokyo, Hongo, Bunkyo-ku, Tokyo 113

**Department of Synthetic Chemistry, Faculty of Engineering, The Uniuerity of Tokyo, Hongo, Bunkyo-ku, Tokyo 113

(Received August 27, 1975)

Non-stoichiometric $Pr_{0.6}Gd_{0.4}O_{1.5+\delta}$ (δ=0.000, 0.075, 0.120, and 0.157), with a bixbyite structure, was investigated by X-ray diffraction. The intensities of the superlattice lines were found to decrease with an increase in δ. The structure analysis has revealed that metal ions gradually move to the ideal positions of the fluorite structure with an increase in δ and that excess oxygen ions preferentially occupy the Z-sites.

The bixbyite structure common in rare-earth sesquioxides is closely related to the fluorite structure. For example, the X-ray powder pattern of the bixbyite structure can be interpreted as the superposition of the superlattice lines on the pattern of the fluorite structure. The unit cell of the bixbyite structure[1] (space group Ia3) is composed of eight unit cells with the fluorite structure, in which one-fourth of the oxygen-ion sites are vacant. These vacant sites, named Z-sites by Anderson,[2] can be regarded as interstitial positions for the bixbyite structure. Oxygen ions, O(1), occupy the general positions (48e) of Ia3. One-fourth of the metal ions, M(1), occupy the (8b) special positions, with the remaining three-fourths, M(2), occupy the (24d) special positions. As is shown in Fig. 1, the coordination polyhedron around M(2) is a cube consisting of six oxygen ions and two Z-sites. The Z-sites occupy the face diagonal corners, and the position of the M(2) ion is displaced from the centre of this cube.

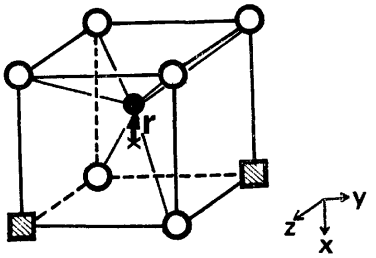

Fig. 1. Schematic drawing of the coordination polyhedron surrounding M (2) ion.
○: oxygen ion, ▨: Z-site, ●: M(2) ion, ×: the centre of the cube, $\boldsymbol{r}$: the displacement vector.

Rare-earth sesquioxides, such as $CeO_{1.5+\delta}$, $PrO_{1.5+\delta}$, and $TbO_{1.5+\delta}$, change their non-stoichiometry, δ, with the change in the oxygen partial pressure and the temperature. On the basis of the ordered intermediate phases of Pr_nO_{2n-2} (n=7, 9, 10, 11, 12), Hyde and his co-investigators[3] suggested that the excess oxygen ions in the non-stoichiometric σ-phase of $PrO_{1.5+\delta}$ occupy the Z-sites. Bratton[4] measured the density and lattice constants of yttria doped with zirconia and concluded that the predominant point defects are not cation vacancies but interstitial anions. Subbarao and his co-workers[5] obtained a similar result on yttria doped with thoria and inferred that such interstitial positions were Z-sites.

The present authors have carried out an X-ray diffraction study of non-stoichiometric $Pr_{0.6}Gd_{0.4}O_{1.5+\delta}$ and have found that the intensities of the superlattice lines decrease with the increase in δ. The purpose of the present study is to elucidate the relationship between the intensities of the superlattice lines and the non-stoichiometry of $Pr_{0.6}Gd_{0.4}O_{1.5+\delta}$, which has a wide non-stoichiometric range.

Experimental

Praseodymium oxide and gadolinium oxide supplied by the Shin-etsu Chemical Co. were used as the starting materials. The purity of the oxides was 99.99%. Each oxide was dissolved in G. R. -grade nitric acid, and the two solutions were mixed in such a ratio that a composition of Pr: Gd= 3: 2 was obtained. Then an excess amount of a G. R. -grade oxalic acid solution was added, and the resulting oxalate precipitate was separated by filtration, oven-dried, and decomposed into oxide in air at 900 °C. Then the oxide sample was ground in an agate mortar, cold-pressed at 7 ton/cm^2, and sintered at 1550 °C for 20 h to homogenize the solid solution. The samples thus treated were placed in a quartz basket, suspended from a beam of a Cahn RG electrobalance,[6] and equilibrated with gas mixtures of argon and oxygen at 900 °C so that δ-values of 0.000, 0.075, 0.120, and 0.157 could be obtained. Then the samples were quenched to room temperature as soon as possible. The X-ray diffraction study was carried out using Rigaku Rotaflex PV 100 with Ni-filtered Cu$K\alpha$ radiation. The intensity calculation was done by means of a HITAC-8700/8800 computer. The atomic scattering factors were taken from the International Table for X-ray Crystallography.[7] The program used for the computation was the full matrix least-squares program for X-ray powder diffraction.[8] In the least-squares calculations, the quantity of $\sum(I_o-I_c)^2$ was minimized. The reliability factor, R, was defined as $\sum|I_o-I_c|/\sum I_o$. Twenty-nine reflection lines observed in each sample were used in the calculation.

Results and Discussion

Table 1 shows the relative intensities of typical superlattice lines of $Pr_{0.6}Gd_{0.4}O_{1.5+\delta}$ as a function of the non-stoichiometry, δ. The strongest line, (222), is

Table 1. Observed intensities of superlattice lines as a function of non-stoichiometry of $Pr_{0.6}Gd_{0.4}O_{1.5+\delta}$

hkl	$(Ihkl)\times 10^2/I(222)$			
	δ=0.000	δ=0.075	δ=0.120	δ=0.157
112	8.5	7.2	4.7	1.7
114	5.0	4.3	2.4	1.4
233	4.2	3.6	2.6	1.3
143	7.2	6.1	3.5	2.2
253	4.7	4.0	2.6	1.3
154	4.6	3.9	2.6	1.3
163	6.8	5.9	3.9	2.0

Table 2. Atomic and lattice parameters with their standard deviations[a)]

δ	O(1)				Z-sites		M(2)	R	a_0
	A_1	x	y	z	A_z	x	u		
0.000	1.27	0.392	0.133	0.405	0.23	0.447	−0.0307	0.046	11.006 Å
	(0.08)	(0.008)	(0.010)	(0.006)	(0.08)	(0.012)	(0.0017)		(0.006)
0.075	1.67	0.392	0.161	0.364	−0.09	0.157	−0.0275	0.047	10.957
	(0.10)	(0.010)	(0.007)	(0.008)	(0.10)	(0.049)	(0.0019)		(0.007)
0.120	1.32	0.384	0.145	0.384	0.30	0.219	−0.0233	0.027	10.927
	(0.06)	(0.008)	(0.007)	(0.007)	(0.06)	(0.011)	(0.0015)		(0.006)
0.157	1.39	0.387	0.147	0.373	0.27	0.054	−0.0166	0.037	10.897
	(0.08)	(0.009)	(0.011)	(0.009)	(0.08)	(0.009)	(0.0017)		(0.005)

a) M(1) atoms are at (1/4 1/4 1/4) and its equivalents, and M(2) at (u 0 1/4) and the equivalents. O(1) atoms are at (x y z) and the equivalents, and Z-sites are (x x x) and the equivalents.

taken as the standard for the calculation of the relative intensities. As may be seen in the table, the intensities of the superlattice lines decrease with increase in δ. In the structure analysis, it was assumed that gadolinium and praseodymium ions are randomly distributed between M(1) and M(2) cation sites and that the atomic scattering factors for the ions equal those for neutral atoms. Two distribution parameters, A_1 and A_z, were introduced for the analysis. A_1 and A_z are the average numbers of oxygen ions on O(1) sites and on Z-sites respectively per metal ion. The numbers of total oxygen ions (*i.e.*, A_1+A_z), O(1) sites, and Z-sites per metal ion are $1.5+\delta$, 1.5, and 0.5 respectively. The intensities were calculated by the least-squares method by changing the A_1, A_z, and positional parameters. In a preliminary calculation, minimum R-value was obtained for the over-all temperature factor, B, of 1 Å^2. Therefore, the least-squares calculations were carried out on the assumption of $B=1$ Å^2. The smallest values of the reliability factor, R, were obtained when the distribution and positional parameters had the values given in Table 2. The standard deviations and lattice parameters are also given in the same table. The R-values ranging from 2.7 to 4.7% are satisfactorily small from the point of view of X-ray powder diffraction analysis. The atomic parameters of the oxygen ions have much larger standard deviations than those for the M(2) ions.

In order to examine the dependence of the observed u-values (the positional parameters of the M(2) ions) upon the atomic parameters of the oxygen ions, a calculation was made on the assumption that excess oxygen ions occupy the ideal positions of the Z-sites. The results are shown in Table 3, where the standard deviations are also given in parentheses. The values of u and R are similar to those in Table 2. This means that the u-values estimated by the least-squares method are reliable and are nearly independent of the atomic parameters of the oxygen ions.

Table 3. Atomic parameters obtained on the assumption that excess oxygen ions occupy the ideal position of the Z-sites

δ	O(1)			M(2)	R
	x	y	z	u	
0.000	0.400	0.128	0.413	−0.0296	0.057
	(0.006)	(0.007)	(0.005)	(0.0017)	
0.075	0.389	0.164	0.367	−0.0273	0.045
	(0.010)	(0.005)	(0.008)	(0.0017)	
0.120	0.404	0.133	0.405	−0.0232	0.031
	(0.004)	(0.005)	(0.004)	(0.0013)	
0.157	0.399	0.153	0.364	−0.0167	0.044
	(0.013)	(0.007)	(0.011)	(0.0019)	

As has been mentioned above, the Pr and Gd ions are assumed to be randomly distributed between M(1) and M(2) sites. In order to verify the validity of this assumption in the present discussion, the intensities of the superlattice lines were calculated in such extreme cases that M (1) sites were occupied by only Pr or Gd ions. The intensities were found to agree with those shown in Table 1, within the range of experimental error. This result indicates that the intensities of the superlattice lines are nearly independent of the distribution of Pr and Gd ions. This is probably caused by the small difference in scattering factors between the two kinds of cations.

The relationship between u and δ is plotted in Fig. 2. The u-value expresses the degree of displacement of M(2) ions from the centre of the coordination polyhedron. The displacement vector, $\boldsymbol{r}$, in Fig. 1 has a component of $(-u, 0, 0)$. Clearly, the displacement

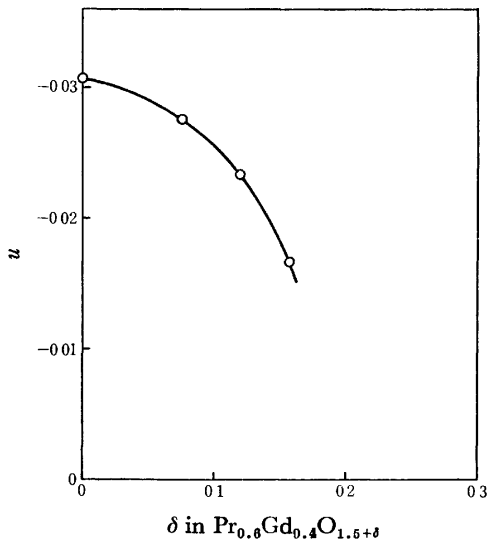

Fig. 2. Dependence of u on δ.

of the M(2) ions from the ideal positions in the fluorite structure decreases as δ increases. The negative value of u indicates that the M(2) ions shift from the ideal positions in the fluorite to the opposite direction against the plane including Z-sites. Such a tendency is generally observed in α-Mn_2O_3[9,10], In_2O_3[11], and rare-earth sesquioxides,[9-12] such as Y_2O_3, Dy_2O_3, and Tm_2O_3. Mertens and Zemann[13] have calculated the Madelung constant of yttria as a function of u and found that the Madelung energy increases with the increase in u and reaches a maximum at the observed u-value. Probably the displacement of yttrium ions is caused by the anisotropic arrangement of the oxygen ions surrounding the yttrium ions. Accordingly, the u-value can be regarded as a measure of the Coulombic anisotropy around the M(2) ions. Excess oxygen ions occupying the Z-sites would decrease the anisotropy; consequently, the M(2) ions would return to the ideal positions in the fluorite structure when the non-stoichiometry becomes large.

At δ=0.157, more than 30% of the Z-sites are occupied by excess oxygen ions, while the u-value is about 50% of that at δ=0.000. This means that a considerable degree of anisotropy still remains even at δ=0.157. From the above discussion, it may be concluded that excess oxygen ions preferentially occpy the Z-sites.

The authors wish to express their gratitude to professor Goro Yamaguchi, the University of Tokyo, for his valuable discussions and also for allowing them to use his computer program.

References

1) L. Pauling and M. D. Shappell, *Z. Krist.*, **75**, 128 (1930).
2) J. S. Anderson, "Modern Aspects of Solid State Chemistry," ed. by C. N. R. Rao, Plenum Press, New York-London (1970), p. 78.
3) B.G. Hyde, D. J. M. Bevan, and L. Eyring, *Phil. Trans. Roy. Soc.*, (London), **259A**, 583 (1966).
4) R. J. Bratton, *J. Am. Ceram. Soc.*, **52**, 213 (1969).
5) E. C. Subbarao, P. H. Sutter, and J. Hrizo, *J. Am. Ceram. Soc.*, **48**, 443 (1965).
6) S. Kurihara, K. Fueki, T. Mukaibo, and Y. Wada, *Bull. Chem. Soc. Jpn.*, **43**, 2761 (1970).
7) "International Table for X-Ray Crystallography," Vol. III, Kynoch Press, Birmingham (1968), p. 211.
8) G. Yamaguchi and H. Miyabe, *Ceramics*, **9**, 176 (1974).
9) A. Fert, *Bull. Soc. Fr. Mineral. Cristallogr.*, **85**, 267 (1962).
10) W. Hase, *Phys. Stat. Sol.*, **3**, K446 (1963).
11) M. Betzl, W. Hase, K. Kleinstuck, and J. Tobisch, *Z. Krist.*, **118**, 473 (1963).
12) M. G. Paton and E. N. Maslen, *Acta Crystallogr.*, **19**, 307 (1965).
13) Helga-Elizabeth v. Mertens and J. Zemann, *Acta Crystallogr.*, **21**, 467 (1966).

ENDOR Studies of the Hindered Internal Rotation of Alkyl Groups in the 1,4-Dialkyl Naphthalene Radical Anions

Fujito NEMOTO

Department of Chemistry, Faculty of Science, Ehime University, Bunkyo-cho, Matsuyama 790

(Received September 16, 1975)

The ENDOR spectra were measured for the anion radicals of 1,4-dimethylnaphthalene, 1,4-diethylnaphthalene, and 1,4-dipropylnaphthalene. The β-proton splittings of the alkyl groups were 3.30, 2.85, and 2.44 G at -80 °C for 1,4-dimethyl-, 1,4-diethyl-, and 1,4-dipropylnaphthalene respectively, and the positive temperature dependence of the β-proton splitting was demonstrated. Based on the Heller-McConnell relationship, $a^{\beta}_{1,4}=(B_0+B_2\cos^2\theta)\rho^{\pi}_{1,4}$ the β-proton splittings and their temperature dependence were interpreted in terms of a modified model of the restricted internal rotation of ethyl and propyl groups over two kinds of potential barriers. The rotational potential barriers thus estimated were 3.0 and 0.7 kcal/mol for the 1,4-diethylnaphthalene anion and 6.0 and 1.2 kcal/mol for the 1,4-dipropylnaphthalene anion. In the ENDOR spectra of potassium 1,4-diethylnaphthalene observed in THF solutions, two ENDOR lines attributed to the non-equivalent alkyl β-protons were observed at -110 °C, these lines collapsed to a single line when the temperature was raised to -70 °C. This phenomenon can be understood on the assumption that the steric effect of the solvated cation alters the rotational potential curve from a symmetric to an asymmetric one.

Based on the ESR observation, the evidence of an internal restricted rotation on the alkyl groups has now been widely established, and the temperature dependence of the alkyl β-proton splitting has been well understood in terms of the $\cos^2\theta$ rule, as has been discussed by Stone and Maki.[1] In particular, for the *para*-substituted alkylbenzene and 9-alkylanthracene, the hindered internal rotation of the ethyl group was investigated in detail. According to the ESR studies of the 4,4'-diethylbiphenyl anion radical,[2] the ethyl group may undergo a restricted rotation in the twofold-potential well, which has a barrier height of 1 kcal/mol. On the other hand, the ethyl group in 9-ethylxanthyl[3] is thought to be strongly restrained, and the ethyl β-proton is almost fixed at the most stable conformation ($\theta_0=\pi/3$).

In this context, studies of the hindered internal rotation of the alkyl groups in 1,4-dialkylnaphthalene become very intersting, because the motion of the alkyl group in 1,4-dialkylnaphthalene is thought to be restricted by two different steric repulsions, due to the neighboring α-CH and β-CH groups of the naphthalene moiety. The former steric repulsion is similar to that restricting the motion of the alkyl group in 9-alkylxanthyl, while the other is analogous to the case in 4,4'-dialkylbiphenyl.

From the investigation of the hindered internal rotation of the alkyl group in the 1,4-dialkylnaphthalene, one can expect to obtain a revised view of the rotational potentials of the alkyl groups in the alkylated aromatic radicals previously reported. Nevertheless, the ESR spectra of 1,4-dialkylnaphthalene anion radicals have never been reported, except for the case of the 1,4-dimethylnaphthalene anion.[4]

The ESR spectra observed for the 1,4-diethyl- and 1,4-dipropylnaphthalene anion radicals revealed a poor resolution because of the superposition of the hyperfine components due to the ring 2- and ring 6-proton hyperfine couplings. Furthermore, the extra alkyl γ-proton splittings bring additional complexities to the ESR hyperfine structures. In order to determine the hyperfine coupling constants, it seemed desirable to apply the ENDOR technique.[5,6]

Experimental

The 1,4-dimethylnaphthalene was synthesized from *p*-xylene by the method previously reported by Barnet *et al.*[8] The other 1,4-dialkylnaphthalenes were prepared by the Friedel-Crafts reaction of the appropriate acylhalide and α-alkylnaphthalene, and by subsequent reduction.[9,10] The materials were purified by means of preparative fractional gas chromatography. The materials thus obtained were all recrystallized from ethanol at *ca.* -20——-30 °C.

The anion radicals were prepared by reduction with lithium, sodium, or potassium metal in several different solvents, such as tetrahydrofuran (THF), 1,2-dimethoxyethan (DME), and *N*,*N*-dimethylformamide (DMF).

The ESR and ENDOR spectra were recorded in the temperature ranges from $+20$ °C to -120 °C, and from -60 °C to -120 °C, respectively. The ESR and ENDOR spectrometers employed here and their operating conditions have been described in previous papers.[11,12]

Results and Discussion

ESR Spectra. The ESR spectra of the 1,4-dimethylnaphthalene anion, the reference compound of the 1,4-dialkyl derivatives, have already been reported by Gerson *et al.*[4] The spectra of the 1,4-diethylnaphthalene anion observed in DME, DMF, and THF solutions are shown in Fig. 1. The analysis of the spectra of DME and DMF solutions was hindered by the complicated overlapping of the hyperfine structures due to the alkyl γ-proton splitting (70 mG), which was detected in the temperature range between -20 °C and -50 °C. On the other hand, the ESR spectrum of the THF solution could be roughly analyzed; the results are listed in Table 1. However, the temperature dependence of the hyperfine coupling constants was not precisely determined due to line broadening. For the 1,4-dipropylnaphthalene anion, only a poorly resolved spectrum was observed everywhere, as is shown in Fig. 2; the hyperfine coupling constants could not be determined.

ENDOR Observation. The ENDOR spectra of the 1,4-dimethyl-, 1,4-diethyl-, and 1,4-dipropylnaphtha-

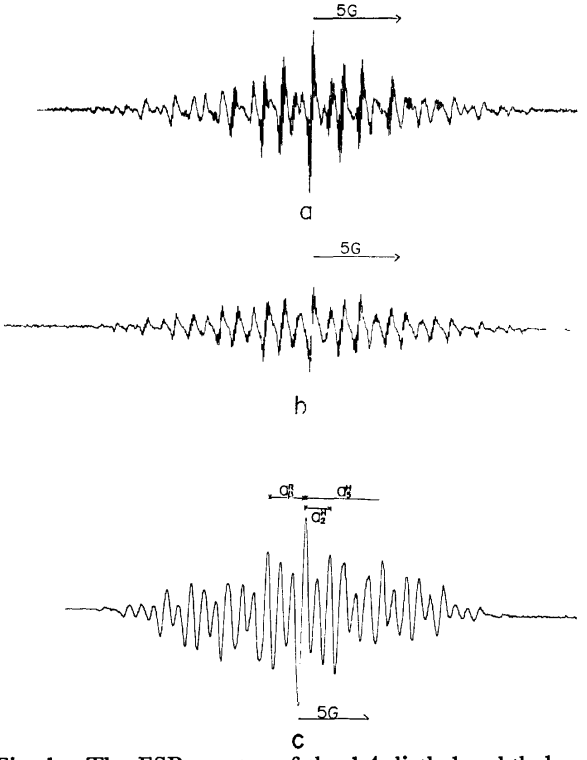

Fig. 1. The ESR spectra of the 1,4-diethylnaphthalene anion by reduction with potassium. a) DME solution at −40 °C, b) DMF solution at −40 °C, c) THF solution at +10 °C.

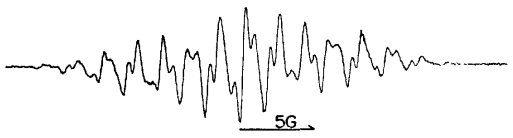

Fig. 2. The ESR spectrum of the 1,4-dipropylnaphthalene anion by reduction with potassium observed with the THF solution at +20 °C.

lene anion radicals observed in DME are shown in Fig. 3.

The spectra can be easily analyzed with reference to the ESR spectra of 1,4-dimethylnaphthalene anions. For example, 1,4-diethylnaphthalene reveals absorptions at 14.0, 16.2, 16.4, 17.9, and 21.4 MHz, which are assigned to the splitting due to the alkyl γ-, the 2,3-ring, the 6,7-ring, the alkyl β-, and the 5,8-ring protons respectively.

Of particular interest is the fact that γ-protons of the propyl group give rise to two different hyperfine coupling constants (0.17 G and 0.05 G), although the ethyl γ-protons reveal only one hyperfine coupling constant. The results are summarized in Table 1. The experimental results indicate that the coupling constants due to ring protons remain almost unchanged on the substitution of alkyl groups.

When the 1,4-dialkylnaphthalene anion radicals were prepared in THF by reduction with potassium, the alkyl β-protons exhibited anomalous hyperfine interactions. The methyl β-proton splitting of 1,4-dimethylnaphthalene showed the minimum value (3.11 G); furthermore, the methylene protons of the ethyl group

Fig. 3. The ENDOR spectra of the 1,4-dialkylnaphthalene anions by reduction with potassium observed with the DME solution at −80 °C. a) 1,4-dimethylnaphthalene, b) 1,4-diethylnaphthalene, c) 1,4-dipropylnaphthalene.

exhibited non-equivalent splittings at 17.4 and 17.9 MHz below −110 °C. When the temperature was gradually elevated, the two lines of alkyl β-protons were merged into a single line (17.6 MHz), as is shown in Fig. 4. The propyl β-protons also exhibited two different signals (at 17.3 and 18.3 MHz) at −110 °C, as is

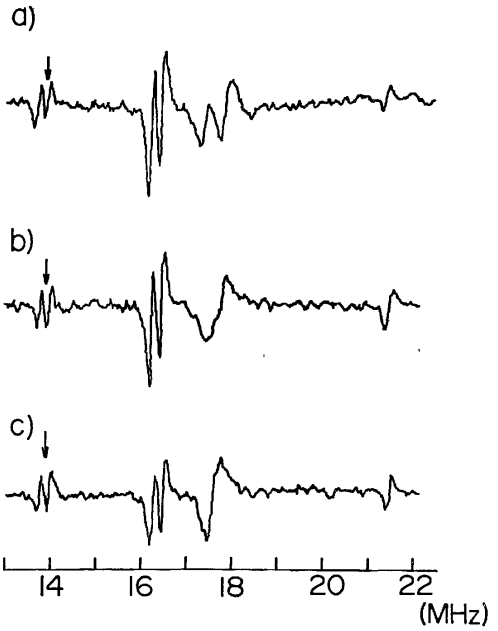

Fig. 4. The ENDOR spectra of the 1,4-diethylnaphthalene anion by reduction with potassium observed with the THF solution. a) −110 °C b) −90 °C, c) −70 °C.

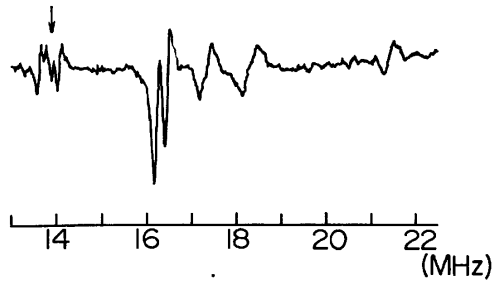

Fig. 5. The ENDOR spectrum of the 1,4-dipropylnaphthalene anion by reduction with the THF solution at −110 °C.

shown in Fig. 5, but the β-proton splittings could not be detected clearly above −110 °C.

Measurements of the β-proton splittings were extensively performed in other systems, such as DME–Na, DME–Li, THF–Na, THF–Li, and DMF–K, but the alkyl β-protons exhibited the equivalent splitting everywhere.

Table 1. Proton hyperfine coupling constants of 1,4-dialkylnaphthalene radical anions (G)

		Temp °C	a_2^H	a_6^H	a_5^H	$a_{1,4}^\beta$	$a_{1,4}^\gamma$
Methyl	K-DME[b]	−70	1.66	1.83	5.45	3.30	
	K-DME[b]		1.63	1.79	5.17	3.26	Lit. 13)
	K-DME[a]	−70	1.67	1.83	5.29	3.29	
	Li-DME[a]	−90	1.68	1.85	5.21	3.29	
	K-THF[a]	−100	1.70	1.86	5.32	3.14	
	Na-THF[a]	−100	1.65	1.82	5.32	3.41	
	Li-THF[a]	−100	1.68	1.85	5.25	3.40	
Ethyl	K-DME[a]	−80	1.68	1.86	5.27	2.87	0.09
	Li-DME[a]	−80	1.68	1.86	5.21	2.86	0.09
	K-THF[b]	−75	1.76	1.76	5.56	2.80	
	K-THF[a]	−110	1.69	1.84	5.34	(2.52, 2.89)	0.08
	K-THF[a]	−70	1.70	1.87	5.34	2.63	0.08
	Na-THF[a]	−110	1.69	1.83	x	2.80	0.08
	Li-THF[a]	−110	1.67	1.82	5.28	2.77	0.08
Propyl	K-DME[a]	−80	1.69	1.86	5.25	2.45	(0.06, 0.16)
	Li-DME[a]	−80	1.70	1.86	5.21	2.46	(0.05, 0.15)
	K-THF[a]	−100	1.71	1.88	5.29	(2.49, 3.16)	(0.06, 0.16)
	Na-THF[a]	−100	1.67	1.85	x	2.38	(0.06, 0.16)
	Li-THF[a]	−100	1.72	1.86	5.21	2.42	(0.05, 0.18)

a) ENDOR, b) ESR
(x); The observation of signal was failed to.

Temperature Dependence of the Alkyl β-Proton Splittings. The ENDOR spectra in solution can be observed in only a limited temperature range because of the complicated relaxation mechanism which determines the ENDOR intensity.[17] The temperature dependences of the alkyl β-proton splittings of the 1,4-dialkylnaphthalene anions, therefore, have been examined in different solvents with various alkali metal cations.

As is shown in Fig. 6, the ethyl β- and the propyl β-proton hyperfine coupling constants show a positive temperature dependence. The slope of the temperature dependence for the propyl β-proton splitting is slightly larger than that for the ethyl β-proton splitting.

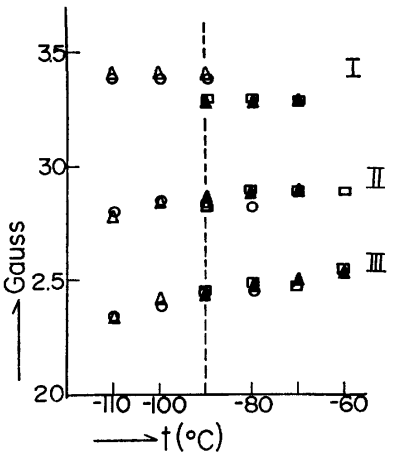

Fig. 6. Temperature dependence of the β-proton splittings observed with the 1,4-dialkylnaphthalene anions. I) 1,4-dimethylnaphthalene, II) 1,4-diethylnaphthalene, III) 1,4-dipropylnaphthalene.
□; K-DME, ▲; Li-DME, ○; Na-THF, △; Li-THF.

The reduction in the alkyl β-proton splitting from the methyl proton splitting has been successfully explained in terms of the hindered internal rotation of the alkyl group.[1,2,3,6]

To calculate the β-proton splitting as a function of the temperature, the following equations were used:[2,3,6,7]

$$Q(\theta) = B_0 + B_2 \cos^2\theta \tag{1}$$

$$a_{1,4}^\beta = \langle Q(\theta)\rangle \rho_{1,4}^\pi = B\rho_{1,4}^\pi \langle \cos^2\theta\rangle,\ \theta = \alpha + \theta_0 \tag{2}$$

$$\langle \cos^2\theta\rangle = \frac{\sum_{i=0}^{\infty}\langle \Phi_i(\alpha)|\cos^2(\alpha+\theta_0)|\Phi_i(\alpha)\rangle e^{-E_i/kT}}{\sum_{i=0}^{\infty} e^{-E_i/kT}} \tag{3}$$

Where B_0 and B_2 are the empirical parameters, $\rho_{1,4}^\pi$ is the spin density on the ring carbon atom adjacent to the alkyl group, and θ is the dihedral angle between the aliphatic C–H bond and the symmetry axis of the 2 p_z orbital on the aromatic carbon atom.[1,2] In Eq. 2, the contribution from B_0 was neglected and the value of $B\rho_{1,4}^\pi$ was estimated to be 2×3.35 G from the methyl proton splitting of the 1,4-dimethylnaphthalene anions by assuming the free rotation of the methyl group.[13] In Eq. 3, the wave function, $\Phi_i(\alpha)$, and the eigenvalue, E_i, were obtained by solving this equation:

$$-\left(\frac{\hbar^2}{2I}\right)\left(\frac{d^2\Phi_i}{d\alpha^2}\right) + [V(\alpha) - E_i]\Phi_i = 0 \tag{4}$$

where the moment of inertia, I, of the molecule fragment, Φ-R, was calculated to be 0.55×10^{-38} g·cm² for 1,4-diethylnaphthalene and 2.65×10^{-38} g·cm² for 1,4-dipropylnaphthalene, assuming that a preferred rotation of the residual group occurs about the C_1–C_4 axis of the molecule of 1,4-dialkylnaphthalenes.

In order to determine the rotational potentials, $V(\alpha)$, in Eq. 4, we assumed that the potential barrier arises from

an intermolecular interaction between the alkyl group and the aromatic ring. The external barrier sources, such as a solvation of anions, were neglected, because the dependence of the β-proton splittings on the solvents and counter cations is very small, as is shown in Fig. 6.

For 1,4-diethyl- and 1,4-dipropylnaphthalene, there are two distinct steric repulsions. The major steric repulsions are those between the γ-methyl and the γ-ethyl groups, respectivery, and the 5-CH or 8-CH group of the naphthalene moiety. The other is between the γ-alkyl group and the 2-CH or 4-CH group of the naphthalene moiety. Thus, the appropriate potential function of the ethyl and propyl groups has two maxima with different heights, as is illustrated in Fig. 7. The equilibrium conformation corresponds to the (B) state given in Fig. 7. The calculation of the Lennard-Jones repulsion energy between the non-bonded ethyl and the neighboring aromatic protons supported this result. According to the above consideration, the rotational potential can be approximated as:

$$V(\alpha) = \sum_{i=0}^{3} a_i \cos i\alpha$$

$$a_0 = \frac{1}{4}(V_a + V_c), \quad a_1 = \frac{3}{8}(V_a - V_c),$$

$$a_2 = \frac{1}{4}(V_a + V_c), \quad a_3 = \frac{1}{8}(V_a - V_c) \qquad (5)$$

where V_a and V_c are the potential energies corresponding to the (A) state and the (C) state respectively, as is given in Fig. 7.

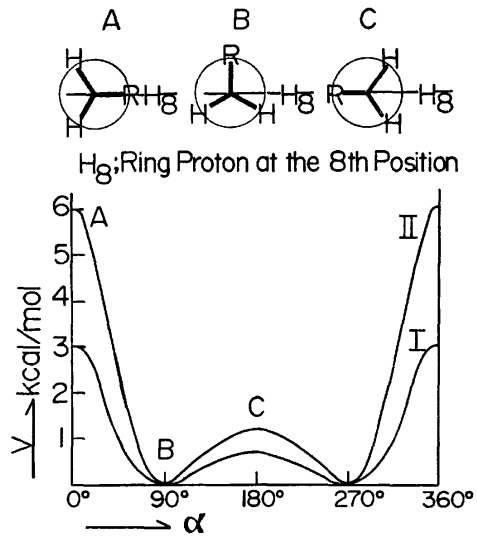

Fig. 7. Possible equilibrium conformations of the 1,4-dialkylnaphthalene anion and the rotational potential curve of the alkyl groups as a function of α. I) 1,4-diethylnaphthalene, II) 1,4-dipropylnaphthalene.

At the (A) conformation, the dihedral angle, θ_0, of the β-proton in Eq. 2 is equal to $\pi/6$. The matrix, $|\langle i|H|j\rangle|$, was diagonalized by expanding the function into a Fourier series:

$$\Phi_i(\alpha) = \sum_{j=0}^{\infty}(C_{ij}\sin j\alpha + D_{ij}\cos j\alpha) \qquad (6)$$

The $\langle\cos^2\theta\rangle$ values calculated for 1,4-diethyl- and 1,4-dipropylnaphthalene in the temperature range

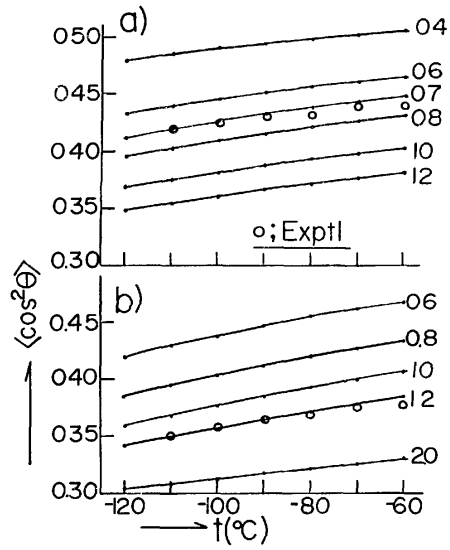

Fig. 8. Theoretical temperature dependence of $\langle\cos^2\theta\rangle$ for rotating alkyl groups. Numerical calculations were carried out by taking the potential barrier, V_c, as a variable parameter, where the barrier height, V_a, was fixed to 3 and 6 kcal/mol for 1,4-diethyl- and 1,4-dipropylnaphthalene, respectively. a) 1,4-diethylnaphthalene, b) 1,4-dipropylnaphthalene.

from -120 °C to -60 °C for various values of V_a and V_c are shown in Fig. 8.

The best agreement between the calculated and experimental temperature dependence of $\langle\cos^2\theta\rangle$ was obtained with V_a=3.0, V_c=0.7, and V_a=6.0, V_c=1.2 kcal/mol for 1,4-diethyl- and 1,4-dipropylnaphthalene respectively.

Based on the theoretical calculation and the experimental result, it can be said that, at room temperature, the ethyl group in the 1,4-diethylnaphthalene rotates in the rotational potential in Fig. 7. On the other hand, the motion of the propyl group is thought to be a torsional oscillation around the equilibrium conformation (B) rather than a restricted rotation.

Non-equivalent Alkyl β-Proton Splittings. In the ENDOR spectra for the 1,4-diethylnaphthalene-THF-K system, two signals attributed to the non-equivalent splittings of the β-methylene protons were recorded at -110 °C. They collapsed into a single line as the temperature was raised to -70 °C (see Fig. 4.). Previous ESR and ENDOR studies[14,15] of non-equivalent alkyl β-proton splittings have established a tightly locking model of an alkyl group. The Heller-McConnell relationship gives nearly $2\pi/3$ for the sum of the two dihedral angles of the non-equivalent β-protons.[16] On the contrary, for the 1,4-diethyl- and 1,4-dipropylnaphthalene anions, the sum of the dihedral angles does not coincide with $2\pi/3$, but is much smaller. It would appear that the splitting of the methylene lines for the 1,4-diethylnaphthalene anion arises neither from rotational isomers nor from the tightly locked ethyl group.

In order to explain the anomalous non-equivalene splitting detected for the two β-methylene ENDOR lines at -110 °C, it is postulated that the steric repulsion between the solvated cation and the rotating alkyl

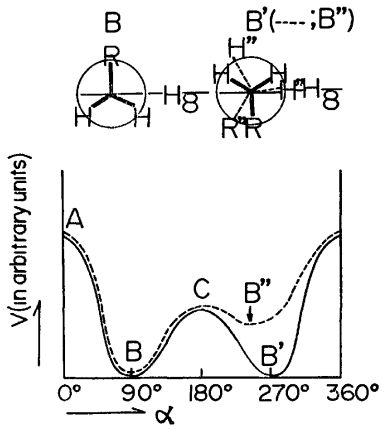

Fig. 9. Schematic diagram of the change in the potential curve due to the steric effect of the solvated-cation. (B"); Probable equilibrium conformation.

groups alters the rotational potential curve from a symmetric to an asymmetric one, where the motion of the alkyl groups take the fast rotational limit. In consequence, the averaged $\cos^2\theta$ in Eq. 3 for each alkyl β-proton may have a different value.

Based on the conductivity and ESR measurements,[18-20] it is well established that the naphthalene anions form solvent-separated ion pairs in THF solutions at low temperatures (<-70 °C) and that a potassium ion, which becomes fully coordinated with THF molecules, is located on the plane of the aromatic ring. The separation between the two opposite charges has been estimated to be 6.5—7 Å for the naphthalene anion,[21] and it has been considered to be insensitive to the aromatic moiety, as has been discussed by Chang *et al.*[19] The radius of the THF-coordinated potassium ion, which is larger than those of lithium and sodium, may be more than 4 Å[21] In 1,4-diethylnaphthalene, the ethyl substitution increases the averaged halfthickness of the aromatic moiety by about 4 Å. At the equilibrium configuration, B', shown in Fig. 9, the γ-methyl group, which is perpendicular to the aromatic plane, gives rise to a strong steric repulsion between the alkyl group and solvated cation. If the steric repulsion due to the solvated cation is negligible, the populations at the (B) and (B') states will be equal in a symmetric rotational potential. The steric effect of the solvated cation, however, destabilizes the (B') state more than the (B) state and, at the same time, the (B') state is converted into a new equilibrium conformation (B"), as is shown in Fig. 9. The rotational potential, therefore, is altered from a symmetric to an asymmetric one, and the averaged $\cos^2\theta$ for each alkyl β-proton in an asymmetric potential may take a different value. The nonequivalent alkyl β-proton splittings observed for the 1,4-dipropylnaphthalene anion may be understood on the basis of the same assumption.

At -75 °C, two signals attributed to the β-methylene protons collapsed into a single line. This means that the thermal activation energy accelerated the motion of the alkyl group; thus, the averaged thickness of the anion were increased. The distance between the paired ions becomes greater, and the asymmetry potential again approaches the original symmetric one.

The numerical calculations were carried out on the FACOM 230-75 at the Data Processing Center, Kyoto University.

The author wishes to thank Professor Kazuhiko Ishizu and Dr. Kazuo Mukai for their helpfull advice and discussion.

References

1) E. W. Stone and A. H. Maki, *J. Chem. Phys.*, **32**, 1535 (1960).
2) F. Nemoto and K. Ishizu, *J. Phys. Chem.*, **79**, 1730(1975).
3) N. D. Sevilla and G. Vincow, *J. Phys. Chem.*, **72**, 3647 (1968).
4) F. Gerson, B. Weidman, and E. Heilboronner, *Helv. Chim. Acta*, **47**, 1951 (1964).
5) For example, see J. S. Hyde, R. Breslow, and C. De Boer, *J. Am. Chem. Soc.*, **84**, 4763 (1966), and K. Ishizu, F. Nemoto, K. Yamamoto, and M. Nakazaki, *Bull. Chem. Soc. Jpn.*, **48**, 2168 (1975).
6) F. Nemoto, F. Shimoda, and K. Ishizu, *Bull. Chem. Soc. Jpn.*, **48**, 2627 (1975).
7) N. L. Bauld, J.D. McDermed, C.E. Hudson, Y.S. Rim, J. Zoeller, Jr., R.D Gordon, and J.S. Hyde, *J. Am. Chem. Soc.*, **91**, 6666 (1969).
8) E. B. Barnett and F. G. Sanders, *J. Chem. Soc., Part 1*, **1933**, 434.
9) L. M. Long and H. R. Henze, *J. Am. Chem. Soc.*, **63** 1939 (1941).
10) H. Minion, *J. Am. Chem. Soc.*, **68**, 2487 (1946).
11) K. Ishizu, *Bull. Chem. Soc. Jpn.*, **36**, 938 (1963).
12) T. Yamamoto, K. Sato, and T. Miyamae, *Jpn. J. Appl. Phys.*, **11**, 1508 (1972).
13) The averaged value is used and the curves shown in Fig. 8 are accurate within 3% for $3.3 \leqq a_{1,4}^{Me} \leqq 3.4$ G.
14) K. Ishizu, F. Nemoto, H. Hasegawa, K. Yamamoto, and M. Nakazaki, *Bull. Chem. Soc. Jpn.*, **46**, 140 (1973).
15) K. Ishizu, F. Nemoto, K. Mukai, M. Kohno, and H. Hasegawa, *Bull. Chem. Soc. Jpn.*, **48**, 1635 (1975).
16) C. Heller and H. M. McConnell, *J. Chem. Phys.*, **32**, 1535 (1960).
17) J. H. Freed, *J. Chem. Phys.*, **43**, 2313 (1965).
18) D. Nicholls, C. Sutphen, and M. Szwarc, *J. Phys. Chem.*, **72**, 1021 (1968).
19) P. Chang, R. V. States, and M. Szawarc, *J. Phys. Chem.*, **70**, 3180 (1966).
20) N. Hirota, *J. Phys. Chem.*, **71**, 127 (1967), and N. M. Atherton and S. I. Weissman, *J. Am. Chem. Soc.*, **83**, 1330(1961).
21) R. C. Roberts and M. Szwarc, *J. Am. Chem. Soc.*, **87**, 5542 (1965), and C. Carvajal, K. J. Tolle, J. Smid, and M. Szwarc, *ibid.*, **87**, 5548 (1965).

The Tribosorption of Hydrogen to Silicon Carbide

Koji Ichioka, Tomoyasu Ito,* Toshiaki Shirakawa, Keio Toi, and Taneki Tokuda
Department of Chemistry, Faculty of Science, Tokyo Metropolitan University, Setagaya-ku, Tokyo 158
(Received September 26, 1975)

The tribosorption of hydrogen into granular silicon carbide was studied under shaking in the pressure range of 0.04—1 Torr at room temperature. The sorption was observed when the frequencies of the vibration were 10.0 and 13.3 Hz, but was not observed when they were 0 and 6.7 Hz. The rate of tribosorption evaluated from the change in the pressure of gas had its maximum value when the sample was shaken for 20—40 h. It was found that this tribosorption could be attributed to an absorption to the solid and could be treated as a diffusion process. The time dependence of the diffusion coefficient showed a behavior similar to that of the lattice defect. It is suggested that the chemical properties of hydrogen and the activation of the solid play important roles in the tribosorption process.

Chemical reactions generally take place by the absorption of heat, radiation, *etc.* On the other hand, reactions have been known to be similarly induced by mechanical treatments of a solid, *e.g.*, by friction, compression, or impact.[1,2] That is to say, such mechanical workings gradually produce various disturbances in the crystal lattice, such as bond rupture, irregular atomic displacement, strain, and lattice defect, and chemical reactions or phase transitions proceed in and on the solid. In the last one and a half decades Heinicke and his co-workers[3-5] have made an extensive study of tribochemical reactions, especially in the presence of gases, through phenomenological observations of the reaction and measurements of lattice disorders induced in the solid, and so on. In addition, the relations between the so-called tribosorption and the tribochemical reactions have been discussed by them.

In tribochemistry many parameters participate in a reaction, so that it is necessary to select the most simple reaction system in order to obtain reproducible experimental results and to clarify the reaction mechanism. In this sense, a homomolecular isotopic exchange reaction is considered to be one of the most probable. Therefore, a study of a hydrogen–deuterium gas system, $H_2+D_2=2HD$, was made under the mechanical treatment of granular silicon carbide,[6] and an increase in the reaction rate with the shaking time was found. For a further discussion of the experimental results, and investigation of tribosorption is necessary.

Recently Heinicke *et al.*[7] investigated the tribosorption of the system consisting of powdered silicon carbide and hydrogen. They dealt mainly with the primary and secondary changes in the structure produced in the silicon carbide powder during mechanical working in the presence of hydrogen; they found a close correlation between the disturbances in the lattice and the amount of tribosorption. However, an analysis of the sorption process itself has been scarcely done.

In the present paper, the tribosorption of hydrogen into granular silicon carbide was carried out with the intention of analysing the sorption process kinetically, and some discussion is given of the mechanism of the tribosorption.

Experimental

The silicon carbide (Showa Denko K. K.) employed was black, *ca.* 1.2 mm in granular size, 98.5% pure; it was α-SiC in the hexagonal crystal system. One to twenty grams of SiC, which had been evacuated at 850 °C for a period of more than 10 h, was shaken in a 100 ml quartz vessel by a Irie Model TS-3 shaker in 0.04—1 Torr H_2 at room temperature; its amplitude was 10 mm, and the vibrational frequencies were 6.7, 10.0, and 13.3 Hz. The sorption rate was measured through the continuous measurement of the pressure change of H_2 in the system (total volume: 1.3 l) by a Pirani gauge. The existence of the reaction products was checked by means of a Hitachi Model RM-50 mass spectrometer.

In order to observe the changes of the SiC granules with the shaking, their surface area was measured by the BET adsorption method using krypton at the boiling point of liquid nitrogen, and the changes in their surface state were photographed with the aid of a JEOL Model JSM-15 scanning electron microscope.

Results and Discussion

Tribosorption Rate. When the granular SiC was left at room temperature in H_2 without shaking, no sorption was observed. On the other hand, when the mechanical treatment was used, the pressure of H_2 decreased, and tribosorption was observed. This sorption rate showed a steep increase in the initial stage of the shaking time; it reached its maximum value near 20 to 40 h, after which there was a monotonous decrease (Fig. 1). In a usual sorption which takes place ther-

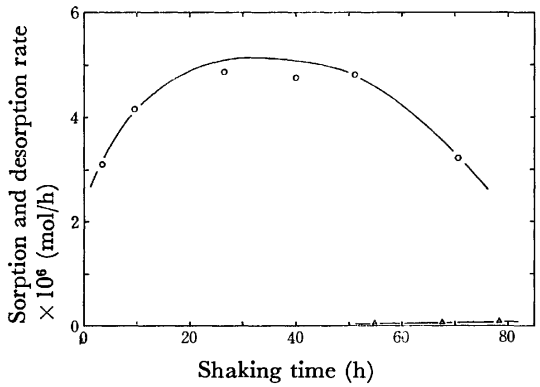

Fig. 1. The shaking time dependence of the sorption rate at 0.04—1 Torr and the desorption rate: Vibrational frequency $f=13.3$ Hz; weight of SiC $W=10$ g. ○, sorption rate; △, desorption rate.

* To whom correspondence should be addressed.

mally, no such maximum of the sorption rate is observed generally. Consequently, the appearance of this maximum may be considered to be one of the most important features of the tribosorption.

Prior to the investigation of the tribosorption mechanism, the contributions of the inner wall of the quartz vessel and the quartz powder which might be produced by abrasion to the observed tribosorption were examined. First, in order to see the effect of the inner wall of the vessel, the effect of the amount of SiC on the sorption rate was investigated. The sorption rate was found to be proportional to the amount of SiC (Fig. 2).

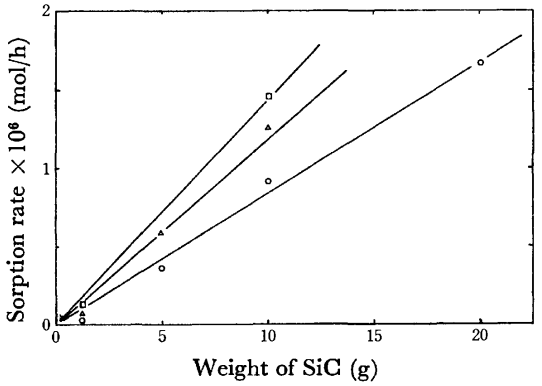

Fig. 2. The effect of SiC amount on the sorption rate: $f=10$ Hz; hydrogen pressure $P=0.04$—1 Torr. Shaking time: ○, 3 h; △, 10 h; □, 30 h.

Then, tribosorption was carried out by adding the quartz glass powder to SiC. The sorption in this case showed no increase but, rather, a little decrease compared with that in the case free from additives (Fig. 3). From the results of these experiments, it can be seen that the sorption occurred exclusively on SiC.

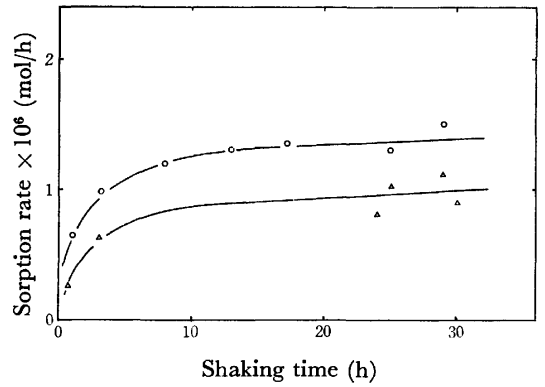

Fig. 3. The effect of quartz glass powder on the sorption rate: $f=10$ Hz; $P=0.04$—1 Torr. ○, SiC 10 g; △, SiC 10 g+glass powder 10 mg.

Next, it is necessary to distinguish whether the sorption is due to adsorption or absorption. For this purpose, the sorption rate was measured in two regions of H_2 pressure, namely, 0.02—0.2 and 5—15 Torr. In spite of the pressure difference of a factor of about 100, the ratio of the two sorption rates was merely about 2:1. This result indicates that the pressure dependence of the sorption rate is effectively nil; hence, the surface of SiC is always saturated with hydrogen. Heinicke *et al.*[4] also showed that the adsorption was very fast and immediately attained equilibrium when CO_2 was tribosorbed into metals. If the observed sorption was due chiefly to adsorption, the shaking time dependence of the sorption amount should, therefore, correspond to that of the surface area of SiC. The measurement of the surface area resulted in an initial rapid increase and a subsequent slower one, while the sorption amount had an induction time at the same initial stage (Fig. 4). Consequently, there is no simple correspondence between the two.

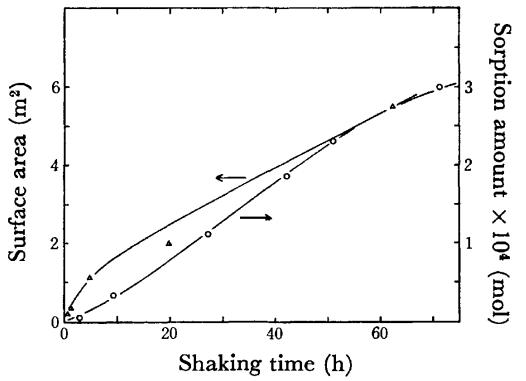

Fig. 4. The variations of the sorption amount and the surface area of SiC with shaking time: $f=13.3$ Hz; $P=0.04$—1 Torr; $W=10$ g. ○, sorption amount; △, surface area of SiC.

If this sorption is mainly absorption, the rate of resorption on SiC which, after the sorption experiment for a long period, has been evacuated under shaking to make the concentration near the surface vanishingly small, can be expected to be at its maximum at the beginning, to decrease slowly, and finally to attain the value extrapolated from the first run. Our measurement of the re-sorption after the 160 h tribosorption gave the result just anticipated, and the sorption rate attained the extrapolated value after 20 h (Fig. 5). In addition, Henning[8] showed that SiC absorbed about 10 times of the monolayerly adsorbed amount of H_2; Heinicke *et al.*[4] also reported that absorption occurred in many tribochemical processes. On the basis of these

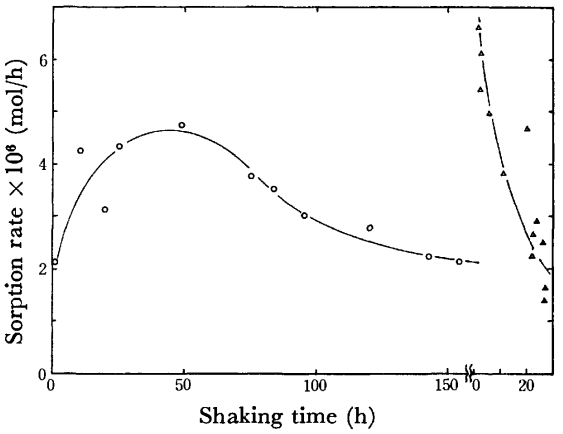

Fig. 5. The resorption rate of triboevacuated SiC after long time sorption: $f=10$ Hz; $P=5$—15 Torr; $W=20$ g. ○, sorption rate; △, resorption rate.

facts, it can be seen that the observed tribosorption results mainly from the absorption phenomenon.

Analysis of the Tribosorption Curves. Considering that the adsorption rate on the SiC surface was very rapid and that the re-sorption rate attained the extrapolated original value after a considerably long time, about 20 h, as is shown in Fig. 5, the tribosorption attributed to an absorption may be treated as a diffusion process. However, the diffusion coefficient obtained from the sorption rate may include the effects of the quartz glass powder and the tribo-desorption. As has previously been mentioned, the quartz glass powder caused a slight decrease in the sorption rate (Fig. 3). However, the amount of powder produced, which was estimated from the weight change in the vessel in each sorption experiment, was considerably less than the quantity added in the run shown in Fig. 3. Therefore, the effect of the quartz powder can be virtually neglected. If it is clearly seen that the already absorbed hydrogen and the tribochemical reaction products are desorbed from the SiC surface during the tribosorption, the sorption rate evaluated from the pressure change in the gas phase does not give a true value. However, SiC which had just been subjected to a tribosorption experiment exhibited a very small tribo-desorption rate (Fig. 1), and the results of a mass-spectrometric analysis of the gas which remained in the vessel after the sorption experiment under conditions favorable for the formation of the reaction products indicated the presence of only small amounts of methane and ethane, with a large amount of hydrogen. In addition, all the gas in the system was evacuated and H_2 was refreshed within 15 h in the sorption experiments. Therefore, the tribo-desorption may be thought to influence the sorption rate scarcely at all.

Absorption rate decreases monotonously in a usual simple diffusion system. However, a maximum in the rate can be expected in the case of a varying surface concentration or in the case of a varying diffusion coefficient with the time.[9] The former is inapplicable to the present case because of the rapid adsorption rate and because of the quick attainment to the saturated surface concentration. The following discussion will be concerned with the latter case.

In the tribosorption, the structures and properties of the solid will change during the shaking. Thus, the diffusion coefficient changes with the time. A more quantitative analysis is performed through the application of Fick's diffusion equation to the observed sorption rate by regarding the SiC granule as a sphere. Two assumptions are adopted here; one is that the radius of the granule does not vary during the shaking, and the other is that H_2 is absorbed mainly by the granular SiC and not by the powdery SiC produced during the shaking. Actually, neither the variation in the granular size nor the presence of large broken pieces was much observed after the tribosorption. Furthermore, granular SiC (10 g) was shaken with powdery SiC (0.44 g), but the sorption rate was scarcely influenced at all. Consequently, the above two assumptions seem reasonable. Then, in case of radial diffusion in a sphere of radius a, the equation takes this form:[10]

$$\frac{\partial U}{\partial t} = D\frac{\partial^2 U}{\partial r^2}, \tag{1}$$

where t is the diffusion time; D, the diffusion coefficient; r, the distance from the center of the sphere, and $U=Cr$, where C is the surface concentration. When the diffusion coefficient depends on t, T is defined as follows:

$$\mathrm{d}T = D\mathrm{d}t. \tag{2}$$

Under the following conditions:

$$\begin{aligned} U &= 0 \quad & r &= 0 \quad & t &> 0, \\ U &= aC \quad & r &= a \quad & t &> 0, \\ U &= 0 \quad & 0 &< r < a \quad & t &= 0, \end{aligned} \tag{3}$$

the solution of Eq. (1) is given by:

$$\frac{M_t}{M_\infty} = 1 - \frac{6}{\pi^2}\sum_{n=1}^{\infty}\frac{1}{n^2}\exp\left(-n^2\pi^2 T/a^2\right), \tag{4}$$

where M_t and M_∞ are the sorption amounts at the times of t and infinity respectively.

Here let us deal with the case shown in Fig. 1. It is assumed that each unit cell of SiC can finally absorb one hydrogen atom (M_∞=30 mmol as H_2) and that, from the granular size, a^2 is equal to 3.6×10^{-7} m^2. When M_t observed at t is substituted into Eq. (4), the time dependence of the diffusion coefficient is obtained by Eqs. (2) and (4) (Fig. 6). In the above treatment,

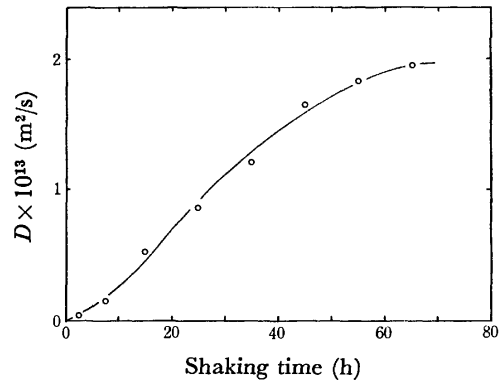

Fig. 6. The shaking time dependence of the diffusion coefficient calculated from Eqs. (2) and (4).

if the surface area effective for diffusion increases with the time, the apparent value of D should vary. The surface area observed by the BET method increased by a factor of about 10 during 60 h (Fig. 4). On the other hand, as has previously been described, the sorption rate in the case of adding powdery SiC was approximately equal to that without the powder. Accordingly, we may consider that the enlargement of the surface area observed is mainly attributable to the production of powdery SiC and powdery quartz glass, and that this increase scarcely contributes to the enlargement of the surface area effective for diffusion. It can, therefore, be understood that the time dependence of D results exclusively from that of the activity of the solid for diffusion. In fact, a scanning electron microscope showed that, at least on the surface, roughness grew during the tribosorption (Fig. 7).

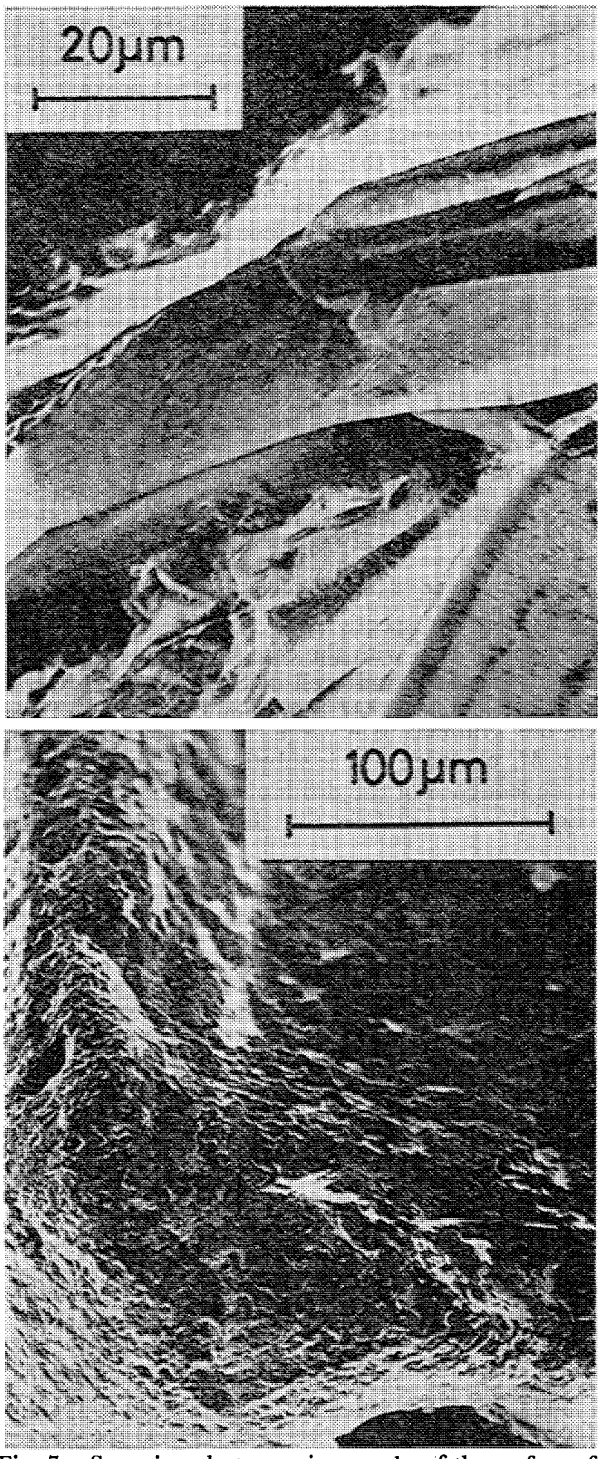

Fig. 7. Scanning electron micrographs of the surface of SiC: (a), before shaking; (b), after shaking.

Heinicke *et al.*[7] carried out the experiments of X-ray diffraction and ESR, together with the tribosorption of H_2 on SiC powders, and measured quantitatively the changes in the disturbances of the solid, such as the size of the primary grain, the disorder of the lattice, and the concentration of the free radical, *etc.* of SiC. In thier experiments all these disturbances exhibited similar time dependence, and their patterns were analogous to that of D obtained in our experiment. In particular, the disorder of the lattice is regarded as an activity which indicates the ease of hydrogen diffusion in the solid. From this point of view, too, it may be reasonable that the diffusion coefficient exhibited the variation shown in Fig. 6.

The powder system used by Heinicke *et al.*[7] had no maximum in its tribosorption rate, but only a monotonous decrease. In this regard, our experimental results differ from theirs. This probably comes from the difference in experimental condition; the granular system in the shaker and the powder system in the ball mill. In terms of the amounts of hydrogen absorbed at the same shaking time, the value obtained by Heinicke *et al.* was greater than ours by a factor of about 100. There may also be a maximum in the sorption rate at the very initial stage in their powder system.

Mechanism of the Diffusion. Then the sorption experiments of inert gases were carried out in a similar manner to ascertain whether the sorption process of SiC–H_2 system is a physical or chemical one. Helium, with a smaller molecular radius than hydrogen, and krypton, with a larger, were used, and neither of them was tribosorbed at all. Therefore, it may be seen that the sorption process of hydrogen proceeds not as a merely physical one but as a process with chemical interaction between SiC and hydrogen. Further, when deuterium was subjected to the sorption experiment, the isotope effect was not found. This information suggests that the activation step of diffusion needs an extremely high energy. Thus, as the mechanism of the tribodiffusion of hydrogen in SiC, it may be assumed that H_2 is dissociated into atomic hydrogen at high-energy points, *e.g.*, the lattice distortion and the so-called magma plasma which are produced by the collision of solids, and that the atomic hydrogen diffuses into the distorted lattice with chemical bonding processes.

As has previously been mentioned, the sorption rate was independent of the H_2 pressure and proportional to the SiC weight (Fig. 2). The surface area effective for the diffusion and activity of SiC are usually functions of the time. Therefore, D may be expressed as follows:

$$D = kP^0WA(t)S(t), \qquad (5)$$

where k is the constant; P, the gaseous pressure; W, the weight of SiC; A, the activity of the solid for diffusion, and S, the effective specific surface area. In addition, considering the vibrational frequency, no sorption was observed at 6.7 Hz, and the sorption rate at 10 Hz was one-third of the sorption rate at 13.3 Hz. The variation in the vibrational frequency seems to influence in a complicated manner the diffusion coefficient through A, S, and the activation of hydrogen.

There may be much problems in the application of Fick's equation to such a complex process as tribosorption. In the present case, all the factors due to rough approximation must be included in the activity, A, of Eq. (5). However, A and the distortion of the solid showed similar patterns in their time dependences. Hence, this treatment is correct, at least qualitatively.

In conclusion, the tribosorption of H_2 into SiC can be interpreted as a diffusion process which is essentially chemical in its nature. The diffusion coefficient in this case varies during the shaking; its variation may be caused by the activity change in the solid under mechanical treatment in the presence of H_2.

The authors wish to thank Assistant Professor Y. Tanabe of this university for his valuable suggestions. They are also grateful to Mr. Y. Shimizu for his assistance in the electron-microscopic observations.

References

1) "Symposium of Mechanochemistry," *Kogyo Kagaku Zasshi*, **71**, 1301 (1968).
2) T. Kubo, "Outline of Mechanochemistry," Tokyo Kagaku Dozin Co., Ltd., Tokyo (1971).
3) G. Heinicke, *Schmiertechnik*, **13**, 81 (1966).
4) G. Heinicke and E. Schober, *Z. Chem.*, **11**, 219 (1971).
5) G. Heinicke and K. Sigrist, *Chem. Tech. (Leipzig)*, **26**, 70 (1974).
6) T. Shirakawa, K. Shimizu, K. Toi, and T. Ito, *Chem. Lett.*, **1975**, 1097.
7) G. Heinicke, H. -P. Hennig, and U. Steinike, *Krist. Tech.*, **8**, 379 (1973).
8) H. -P. Hennig, Dissertation (Humboldt University, 1970), cited in reference 7).
9) J. Crank, "The Mathematics of Diffusion," Oxford University Press, London (1956), pp. 87, 147.
10) J. Crank, "The Mathematics of Diffusion," Oxford University Press, London (1956), p. 84.

Study of Cholesteryl Formate and Cholesteryl Octanoate by Means of Thermal Analytic Microscopy with a Thermoelement

Kazuko SASAKI KUNIHISA and Seiichi HAGIWARA*

National Chemical Laboratory for Industry, Honmachi, Shibuya-ku, Tokyo 151

**Tokyo Riko Company, Kitamachi, Hoya-shi, Tokyo 188*

(Received June 6, 1975)

A simple apparatus using a thermoelement was constructed for thermal analytic microscopy and the phase transitions of cholesteryl formate and cholesteryl octanoate were studied. The isotropic–cholesteric transition of cholesteryl formate and the cholesteric–smectic transition of cholesteryl octanoate were observed microscopically but not thermally. Upon slow cooling cholesteryl octanoate gives large spherulites with a cholesteric focal conic texture. The spherulites are optically negative. They give rise to the vortices which turn to smectic reeled yarns in specimens with appropriate thickness. The solar spectrum which appears at the cholesteric-smectic transition of cholesteryl octanoate was observed repeatedly, namely, blue, yellow, red, blue, *etc.* A melt recrystallized sample of cholesteryl formate forms a block similar to a sphere in the thermal cell. Both solid phases of cholesteryl formate and octanoate grow radially in the microscopic cell plates.

One of the authors (K.S.K.) developed thermal analytic microscopy, simultaneous observation by polarizing microscopy and by DTA.[1] This was applied to cholesteryl myristate using an improved apparatus with a modified sample holder.[2] The present work was carried out in order to systematically study (1) the aliphatic esters of cholesterol and (2) the operation of the apparatus using a thermoelement in place of the thermocouple for DTA. The temperature sensitivity of the thermoelement is 180 μV/°C based on the contact potential difference between copper and the thermoelement,[3] three or four times EMF of thermocouple. Cholesteryl formate (Ch. F.) and cholesteryl octanoate (Ch.O.) were studied. The interior of a hot stage for a microscope was reconstructed.

Apparatus

Only the reconstructed part will be described. Three thermoelements protrude like arms from the copper block wall as shown in Fig. 1. This protrusion is necessary to make the thermoelement sensitive to the temperature gradient between the specimen and the heat wall. The center arm has a copper ring at the terminal to hold a microscopic sample which is sandwiched between two quartz plates (1 mm thick). The sample thickness usually is 10—15 μ. Both side arms have their copper cell holders attached to DTA cells which are also made of copper (inside volume, 130 μl). The leads to the amplifier extend from the bases of the holders for the purpose of detecting the potential proportional to the temperature difference between the sample and the reference substance (Al_2O_3).

The copper block is surrounded by a manganin heater and has no cover. It is assumed that the temperature distribution near the specimen is approximately homogeneous due to nearly equivalent conduction of heat through the thermoelements. The temperature of the sample was measured by setting a copper–constantan thermocouple (0.1 mm ϕ) at the center ring for microscopy. The thermocouple for temperature monitoring, also copper–constantan (0.3 mm ϕ), is placed between the block wall and the manganin wire. The central part of the bottom of the block is made of glass for the sake of light transmission. The light source is an ordinary tungsten lamp of 30 W. The surroundings of the hot stage are covered with moltprene and teflon sheets.

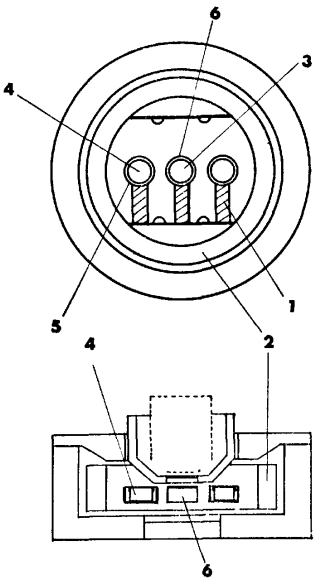

Fig. 1. Hot stage devised for thermal analytic microscopy.
1: Thermoelement, 2: copper block, 3: quartz cell, 4: copper DTA cell, 5: copper cell holder, 6: copper ring.

Sample

Commercial Ch. F. and Ch. O. were successively recrystallized from 1-pentanol[4] and ethanol, washed with acetone and dried at 60 °C for one day, as in the case of cholesteryl myristate (Ch.M.).[2]

Performance of the Apparatus

Stearic acid recrystallized from benzene was used to calibrate the heats of transition. The heats of transition were determined by taking three copies for the respective peaks and weighing the copied peak areas.

Table 1. Transition values for cholesteryl myristate

		Cryst.-Sm.		Sm.-Ch.		Ch.-Iso.	
		T °C	Q cal/g	T °C	Q cal/g	T °C	Q cal/g
Heating	This work	70.6	18.2	78.4	0.5	83.5	0.3
	Barrall II *et al.*[5]	73.6	18.7	79.7	0.41	85.6	0.41
	Davis *et al.*[6]	70.5	18.6	77.8	0.56	83.2	0.41
Cooling	This work	52—67	16.3	78.5	0.6	83.5	0.5
	Barrall II *et al.*[5]	36.7	16.8	70.0	0.56	76.5	0.44

This was done for the purpose of averaging the fluctuations (about 2%) of the density of the paper and of the mode of trimming the peak area.

Table 1 gives the transition values for Ch.M., which was further purified from the compound previously studied.[2] Thermal data are available for Ch.M.[9] since it is a typical sample giving rise to both liquid crystalline states, cholesteric and smectic, which are enantiotropic. The result of Davis *et al.*[6] is the most recent. The work of Barrall II *et al.*[5] refers to the cooling data besides heating ones. Our values of the heat of transition do not exceed the reference ones in accuracy mainly due to the fluctuations in the copy paper density. However, the transition temperatures show a better agreement between heating and cooling than the reference ones regarding every transition. The precision of the transition temperatures on heating is ± 1 °C, which is independent of the scanning rate (0.25, 0.5, 1, 2, and 4 °C/min).

Results and Discussion

The transition points of both esters on heating (mp) were reproducible and independent of the heating rate (0.25, 0.5, 1, 2, and 4 °C/min), but not those on cooling. The transition temperatures on cooling change with cooling rate and sample. Both Ch.F. and Ch.O. sometimes crystallize leaping over the mesophases, as pointed out by Friedel.[10] Discrepancy was found between the temperature determined by the DTA peak and that determined by the microscopic change. Table 2 gives the results of Ch. F. The mesophase transition was not detectable by DTA curves,** while the cholesteric texture appears microscopically a few degrees above the solidification temperature. In most cases, solidification temperature determined by DTA was higher than that by microscopy.

Table 2. Transition temperatures of cholesteryl formate, depending on DTA or microscopic samples and the cooling rates

Cooling rate	Transition temperatures (°C)		
	DTA	Microscopy	
°C/min	Crystn. point	Ch. focal conic	Crystn.
0.25	61.2	58.5	56.4
1	60.3	58.0	55.0
4[a]	57.6	57.7	52.4

a) The practical rate was 1.2 °C/min around 60 °C, due to no water circulation.

In order to clarify the discrepancies, the temperatures of thermal and microscopic samples were measured simultaneously by setting another thermocouple on the DTA cell holder of sample side. The temperature difference between the microscopic sample and the DTA sample diminishes with the decrease in the scanning rate. Both temperatures coincided within ± 1 °C below 100 °C. It seems that the difference in shape of the two sample cells causes the discrepancy rather than the inhomogeneity of the temperature distribution in the block, even taking into account the instability of the

Table 3. Transition values for cholesteryl formate and cholesteryl octanoate

		Heating		Cooling			
		Cryst.-Iso.		Cryst.-Ch.		Ch.-Iso.	
		T °C	Q cal/g	T °C	Q cal/g	T °C	Q cal/g
Ch.F.	This work	96.0	12.4	55.0	9.4	(58.0)	(0.1)
	Berrall II *et al.*[5]	97.3	12.8	50	8.6	97.1	0.2
	Davis *et al.*[6]	96.6	12.6	—	—	57.1[a]	0.08[a]
	Gray[7]	97.5	—	—	—	60.5	—
Ch.O.	This work	108	13.9	81	11.1	87	0.2
	Barrall II *et al.*[8]	112.7	17.5—18.9	81.7	14.2—13.5	92.7	0.45—0.38
	Gray[7]	110	—	69.5	—	96.5	—

a) *cf.* Ref. 6.

** The mesophase transition of Ch. F. in DTA appeared only once. The heat evolution was estimated to be 0.1 cal/g (shown in parentheses in Table 3).

mesophase of Ch.F. Translational or rotational motions start easily in the DTA sample in liquid state in the free space inside the cylindrical cell, solidifying directly without taking the mesophase. On the other hand, a microscopic sample in the thin space between the quartz plates is not free since it receives adhesive forces at the boundaries, being forced to take the course to the mesophase.

Multiplicate runs on a microscopic sample give rise to some depression of the transition temperature of Ch.F. It seems that the space in the plates becomes thinner due to flowing out of the sample by repetition of melting. The sample can hardly undergo transformation against the boundary forces. This is supported by the fact that a thick sample of Ch.F. for microscopy shows no cholesteric texture, solidifying at 59.6 °C under 1 °C/min cooling. No quantitative relations between the mesophase appearance and the sample thickness were studied.

The transition temperatures become lower with the increase of the cooling rate also in DTA samples as shown in Table 2. This indicates that the transformation can not follow the cooling rate above a certain rate. The lowest cooling rate 0.25 °C/min gave the highest crystallization temperature 61.2 °C.

Disagreement of the transition temperatures determined by DTA with those by microscopy also occurred in the case of Ch.O. However, the isotropic–cholesteric transition was observed by DTA and microscopy. The cholesteric–smectic transition was observed by microscopy but not by DTA. The transition temperatures of Ch.O. on cooling (Table 3) are the most probable values, their fluctuations being ± 5 °C. The reported values of both substances also markedly differ (Table 3).[5-9] The results of Ch.F. and Ch.O. may be due to the unstable properties of the mesophases as well as to the apparatus conditions. Davis *et al.*[6] concluded from their DSC studies that the lowest molecular weight saturated aliphatic ester of cholesterol to show mesophase behavior is the propionate.

Microscopy. Optical studies on aliphatic esters of cholesterol were carried out by Fridel[10] and others.[7] The studies dealt with the characteristic color reflections of the cholesteric phases and the results were restricted to liquid crystalline states. Our results might give some new information on the morphological mechanism of the transformation. The observations for the solid states may be useful to elucidate their liquid crystalline states.

Cholesteryl Formate. Ch.F. shows a mesophase similar to the cholesteric focal conic texture of Ch.M. a few degrees above the solidification temperature. When the cholesteric texture appears slowly, the phase front makes spherulitic balls and then takes them in the texture (Photo. 1). The view field is faintly light (turns faintly orange by taking off analyser) until the texture appears. Indigo blue appears near the boundary of the texture in a specimen of proper thickness. Photograph taken with a color sensitive plate gives an ordered cholesteric phase somewhat like woolen texture (Photo. 2).

The solidification speed is considerably great as compared with that of the cholesteric phase growth. The solid phase develops radially like a film which seems to retain the liquid property. The cholesteric texture is once destroyed and transformed into isotropic (dark in view) before solidification. In a properly thick specimen, the flow caused by the texture destruction appears in dark vermilion and dark green under crossed polars. The two color directions appear to make a right angle.

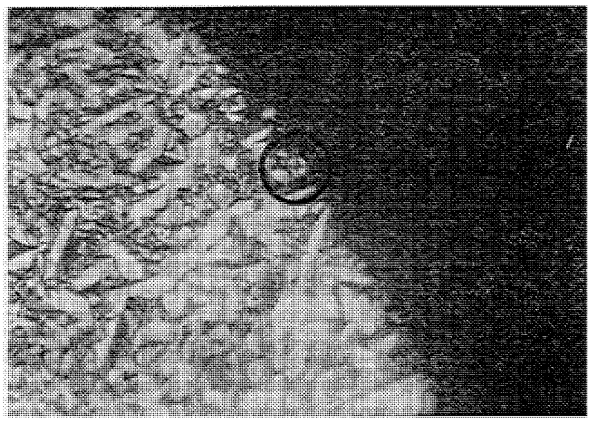

Photo. 1. Cholesteric texture appearance of cholesteryl formate. 0.25 °C/min cooling at 58.5 °C, The circle in the photograph indicates the spherulitic ball.

Radial cleavages occur after solidification. Photograph 3 shows the center of a radially grown solid phase which indicates a spherulitic growth. A sample recrystallized after melting in the DTA cell forms a block similar to a sphere and to an illustration, drawn by G. W. Gray, for an explanation of a smectic phase.[11]

Cholesteryl Octanoate. In this work, the homeotropic texture gave colors from blue to yellow. The most retainable color was sapgreen. Both the brilliance and hue are dependent on the thickness of sample. The color increases in luminosity and approaches the longer wavelength with the thickness, similar to the case of Ch.M.

Ch.O. lies in the series of aliphatic esters of cholesterol whether the smectic phase appears or not. The focal conic texture is sometimes similar to the cholesteric focal conic of Ch.M. and at others to the smectic focal conic of Ch.M. With a very thin specimen ($<10\,\mu$) the cholesteric focal conic texture disappears and turns isotropic, a smectic texture like the smectic strings of Ch.M. appearing at the transformation into solid phase. The strings turn many small spherulites before a solidification wave front appears discontinuously.

Photographs 4—9 show the course of spherulitic growth of the cholesteric focal conic texture from occurrence to destruction by invasion of the solidification wave front. It is evident by means of a color sensitive plate that the large spherulite is also optically negative.***

The spherulite causes a rapid rotation around the center somewhat like a spinning wheel or a vortex just

*** The colors, yellow and blue, of the quadrants of the spherulite interchange their positions by photography.

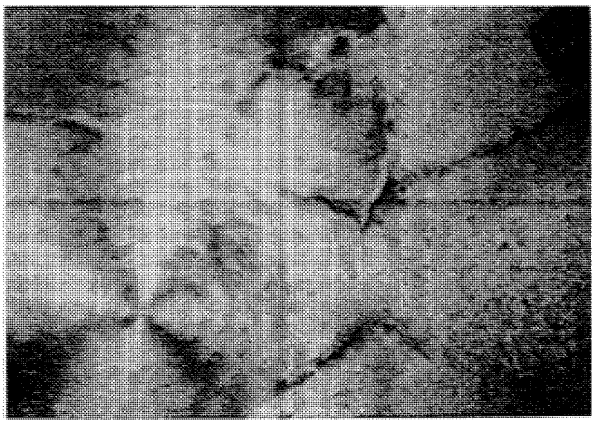

Photo. 10. Generation of the spherulites in the cholesteric phase.

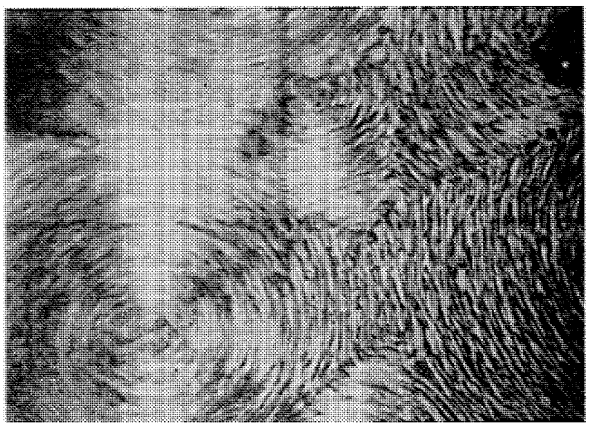

Photo. 11. Vortices around the spherulitic centers, just before the solidification.

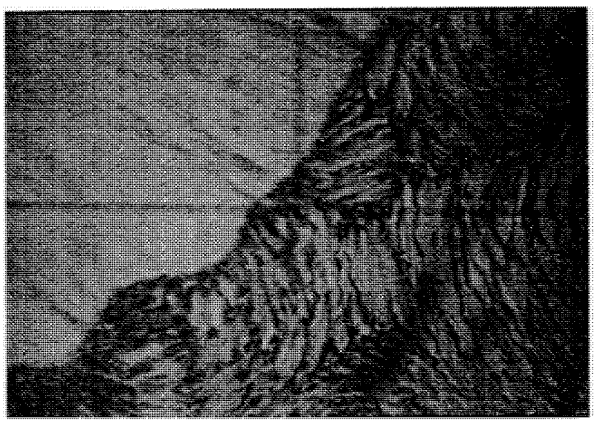

Photo. 12. The solid wave front and the smectic phase as the finish of the vortices.

Photos. 10—12. Vortices caused by the spherulites in cholesteryl octanoate.
All the photographs show observation under crossed nicols. (×100)
A color sensitive plate was used for Photos. 2, 3, 5, 7, 8, and 9.

before solidification (Photos. 10—12). The vortex is accompanied by iridescent colors, blue, yellow, red, blue and so on. The colors do not end at red but blue appears successively. It seems that the visible spectrum does not reflect the characteristic wavelength at a certain temperature but repeats from short wavelength to long one at the transformation. The color intensity decreases with the lowering of the rotational speed. We cannot observe the repetition of the solar spectrum completely. In many cases, blue does not appear a second time. The vortex turns a state similar to big reels of yarn, which suggest a smectic texture when the speed is lowered. The yarns are suddenly invaded by the solid phase. The domains formed by the growths of the cholesteric spherulites hold their regions when the smectic phase appears. The boundaries are clarified by the formation of the smectic yarns (Photo. 12).

The solid phase of Ch.O. also grows radially but the center of the growth is entirely independent of the center of the mesophase spherulite. Photograph 13 shows a dendritic growth of the solid phase with a free surface. A radially grown solid sample is gradually transformed into regular ordered state similar to Photo. 13.

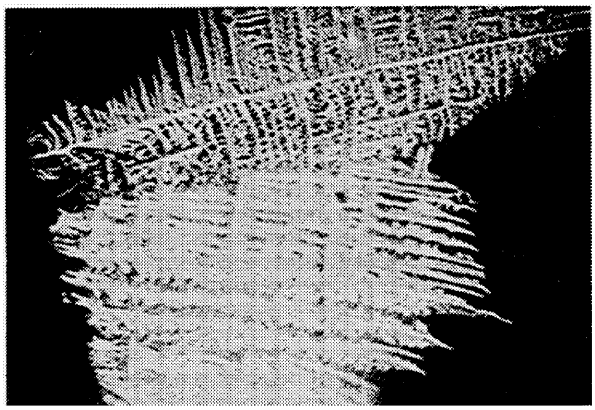

Photo. 13. Dendritic crystal growth of cholesteryl octanoate with the free surface.

The above results can be classified as follows.

Spherulitic Growths at the Phase Transitions. We observed spherulitic growths in both mesophases of Ch.F. and Ch.O. "Focal conic texture" as called by Friedel might be interpreted as the resultant texture of the spherulitic growth. According to Friedel's study, a cholesteric phase is optically negative while the smectic phase is optically positive. The cholesteric spherulites of both Ch.F. and Ch.O. are also optically negative. It is not clear whether the smectic spherulites of Ch.O. are optically positive because they appear only for an instant. Ch.M. makes small but very stable smectic spherulites which show themselves to be optically positive. It seems to be of significance that the optical sense of the spherulites coincides with that of the mesophase.

We also observed the radial growths, that is the spherulitic growths of the solid phases in the large scales. The texture has an almost spherical symmetry even in the large scale (Photo. 3). Many kinds of spherulites seem to have been studied in the field of polymer. Fischer[12] and Kobayashi[13] found that a spherulite in polymer is constructed by the layers which have essentially the same structure as the single crystals deposited from the solutions. Studies of spherulites in polymer field may be useful for elucidating the spherulitic

growths of the liquid crystals.

Color Appearance and Phase Transition. Coloration appears twice, in Ch.O., before the appearance of the cholesteric focal conic texture and the smectic phase. The former color covers the range from blue to yellow and the latter from blue to red repeatedly.

Ch.F. which is colorless, still scatters iridescent colors just before solidification, when it is rapidly quenched.

Vortices Caused by the Cholesteric Spherulites. The vortices seem to be of interest. It is not clear whether they are a characteristic of Ch.O. or not. The formation of the smectic reeled yarns was observed with a sample of proper thickness. The aggregation force of the strings may be strong enough for them to reel themselves up in a large quantity, but not in a small amount, due to hindrance by quartz boundaries.

DTA Peaks and Their Textures. Ch.F. shows the mesophase thermally only once but displays the cholesteric texture microscopically. Since the smectic phase of Ch.O. appears microscopically for an instant just before solidification it can not be detected thermally.

Both isotropic–cholesteric transition points of Ch.F. and Ch.O. are a few degrees above their solidification temperatures.

We wish to express out sincere gratitude to Dr. S. Tanaka and Dr. M. Goto of the National Chemical Laboratory for Industry for their help and encouragement.

References

1) K. S. Kunihisa, *Bull. Chem. Soc. Jpn.*, **46**, 2862 (1973).
2) K. S. Kunihisa and T. Shinoda, *Bull. Chem. Soc. Jpn.*, **48**, 3506 (1975).
3) S. Hagiwara, *Powder and Industry* (in Japanese), **5**, 1 (1973).
4) G. J. Davis and R. S. Porter, *Mol. Cryst. Liq. Cryst.*, **6**, 377 (1970).
5) E. M. Barrall II, R. S. Porter, and J. F. Johnson, *J. Phys. Chem.*, **71**, 1224 (1967).
6) G. J. Davis, R. S. Porter, and E. M. Barrall II, *Mol. Cryst. Liq. Cryst.*, **10**, 1 (1970).
7) G. W. Gray, *J. Chem. Soc.*, **1956**, 3733.
8) E. M. Barrall II, J. F. Johnson, and R. S. Porter, *Thermal Analysis*, **1**, 555 (1969).
9) G. J. Davis, R. S. Porter, and E. M. Barrall II, *Mol. Cryst. Liq. Cryst.*, **11**, 319 (1970).
10) G. Friedel, *Ann. Phys.*, (Paris), (9) **18**, 273 (1922).
11) G. W. Gray, "Molecular Structure and the Properties of Liquid Crystals," (1962).
12) F. W. Fischer, *Kolloid Z.*, **159**, 108 (1958).
13) K. Kobayashi, Intern. Conference of Electron Microscopy, Berlin (1958).

Magnetic Properties of $[(H_2O)_2M\{(OH)_2Coen_2\}_2](X)_2\cdot nH_2O$ (M=Ni or Co, X=SO_4 or S_2O_6 and n=5 or 7)

Hanako KOBAYASHI, Kazuo OHKI, Ikuji TSUJIKAWA, Keiji OSAKI,* and Norikiyo URYÛ*

Faculty of Science, Kyoto University, Sakyo-ku, Kyoto 606

**Faculty of Engineering, Kyushu University, Hakozaki, Fukuoka 812*

(Received October 8, 1975)

The magnetic properties of $[(H_2O)_2Ni\{(OH)_2Coen_2\}_2](SO_4)_2\cdot 7H_2O$, $[(H_2O)_2Co\{(OH)_2Coen_2\}_2](SO_4)_2\cdot 5H_2O$, $[(H_2O)_2Co\{(OH)_2Coen_2\}_2](SO_4)_2\cdot 7H_2O$, and $[(H_2O)_2Co\{(OH)_2Coen_2\}_2](S_2O_6)_2\cdot 5H_2O$ were investigated on powder samples. The paramagnetism of these compounds was considered to be that of the central Ni^{2+} or Co^{2+} ion. From the fits of the experimental data with the calculated magnetic susceptibilities and the simulations of the ESR derivative curves, the ligand field parameters and g-values were determined. The ligand field around the Co^{2+} ion in $[(H_2O)_2Co\{(OH)_2Coen_2\}_2](SO_4)_2\cdot 5H_2O$ was concluded to be tetragonal and in the other samples the ligand fields at the central divalent ions were found to be rhombic.

Werner[1] obtained a series of tri-nuclear $[(H_2O)_2Co\{(OH)_2Coen_2\}_2]$ salts from the partly oxidized mixtures of cobalt(II) salts and ethylendiamine. Cambi[2] later observed the magnetic susceptibility of the sulfate at room temperature. The main structure of the complex ion is considered to be a Co^{2+} ion linked to two Co^{3+} ions on wings through double OH bridges. Two other ligand sites for the central Co^{2+} ion are occupied by two H_2O molecules and four other ligand sites of each Co^{3+} ion by two ethylendiamines, as shown in Fig. 1. The magnetic properties of such complex compounds with mixed valencies are of interest because the magnetic properties of the mixed valency compounds[3,4] are not well known, except for the double exchange interaction in mixed compounds of $LaMnO_3$ and $BaMnO_3$.[3] In the course of this investigation, a new method of synthesis of this kind of complex compound was discovered by Mori *et al.*[5] in which $[(H_2O)_2M\{(OH)_2Coen_2\}_2]X_2\cdot nH_2O$, where M=$Ni^{2+}$, Co^{2+}, Mg^{2+}, Zn^{2+} or Cd^{2+}, X=SO_4^{2-}, $S_2O_3^{2-}$ or $S_2O_6^{2-}$ and n=5 or 7, were synthesized. Samples synthesized by the new method were offered by Mori *et al.* for the present investigation.

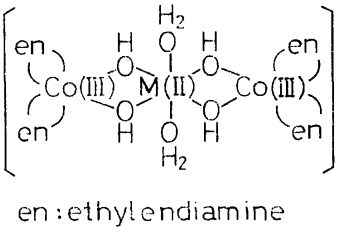

Fig. 1. The schema of $[(H_2O)_2M\{(OH)_2Coen_2\}_2]^{4+}$ complex ion.

In the present paper, the magnetic properties of $[(H_2O)_2Ni\{(OH)_2Coen_2\}_2](SO_4)_2\cdot 7H_2O$, $[(H_2O)_2Co\{(OH)_2Coen_2\}_2](SO_4)_2\cdot 5H_2O$, $[(H_2O)_2Co\{(OH)_2Coen_2\}_2](SO_4)_2\cdot 7H_2O$ and $[(H_2O)_2Co\{(OH)_2Coen_2\}_2](S_2O_6)_2\cdot 5H_2O$ are examined. Mori *et al.*[5] observed the reflection spectra of these salts on powder. The d-d bands of the magnetic central Ni^{2+} or Co^{2+} ions were not discernible because of the much smaller absorptivity in comparison with those of the d-d bands of the trivalent cobalt chromophores. It was, therefore, impossible to determine the orbital energy levels by optical measurements.

Experimental

Preparation of Samples. $[(H_2O)_2M(II)\{(OH)_2Coen_2\}_2](SO_4)_2\cdot nH_2O$ with M=Mg, Co, Ni(n=7) and Zn, Cd (n=5) were prepared according to the method of Mori *et al.*[5] The new procedure gave only this product with seven molecules of water of crystallization for the salt of M=Co, so that $[(H_2O)_2Co\{(OH)_2Coen_2\}_2](SO_4)_2\cdot 5H_2O$ was prepared according to the original method of Werner *et al.* with a slight modification. One hundred and forty-five grams of cobalt(II)sulfate heptahydrate were dissolved in 180 ml of water, and 300 ml of a 10% ethylenediamine aqueous solution was added to it. After about four hours, a green precipitate, with a pink precipitate, was filtered off. From the filtrate a massive amount of pink silky crystals soon began to precipitate. The silky precipitate was filtered through a glass filter and washed with water. Then the precipitate was placed between unglazed plates (Ton platten).

The results of the chemical analysis are as follows. For $[(H_2O)_2M(II)\{(OH)_2Coen_2\}_2](SO_4)_2\cdot 7H_2O$, Found: M=Mg(II), 3.07; Co(III), 14.13%. Calcd for: Mg(II), 3.02; Co(III), 14.13%. Found: M=Co(II), 7.01; Co(III), 13.65%. Calcd for: Co(II), 7.02; Co(III), 14.04%. Found: M=Ni(II), 6.69; Co(III), 13.38%. Calcd for: Ni(II), 7.00; Co(III), 13.38%. Found: M=Zn(II), 7.79; Co(III), 13.49%. Calcd for: Zn(II), 8.07; Co(III), 14.55%. Found: M=Cd(II), 13.25; Co(III), 13.82%. Calcd for: Cd(II), 13.12; Co(III), 13.75%. For $[(H_2O)_2Co\{(OH)_2Coen_2\}_2](SO_4)_2\cdot 5H_2O$, Found: H, 6.21; C, 11.17; Co, 21.33; N, 13.37%. Calcd for: H, 6.28; C, 11.98; Co, 22.02; N, 13.95%, and for $[(H_2O)_2Co\{(OH)_2Coen_2\}_2](S_2O_6)_2\cdot 5H_2O$, Found: H, 4.96; Co, 23.06; N, 12.31%. Calcd for: H, 5.41; Co, 22.96; N, 12.03%.

The hepta hydrate of $[(H_2O)_2Co\{(OH)_2Coen_2\}_2](SO_4)_2$ prepared from the penta hydrate by the Werner method did not give good analytical values.

Magnetic Susceptibilities. Magnetic susceptibilities at liquid helium and liquid hydrogen temperatures were measured with a Hartshorn alternating current bridge. A Faraday magnetic balance with a field strength of *ca.* 9000 Oe was also employed for magnetic susceptibilities between 4.2 K and room temperature. The magnetic susceptibility of anhydrous hexaamminechromium(III) chloride powder was used as a "thermometer" which was calibrated at each run to an atmospheric liquid helium temperature with corrections for the Hg-barometer and gravitational constant following procedure of Linder.[6] The accuracy for all the measure-

Table 1. Diamagnetic part of the magnetic susceptibility per mole (cgs emu)

Compound	Estimated from expt	Calcd by Pascal's rule
$[(H_2O)_2Zn\{(OH)_2Coen_2\}_2](SO_4)_2\cdot 5H_2O$	−0.00041	−0.00036
$[(H_2O)_2Co\{(OH)_2Coen_2\}_2](SO_4)_2\cdot 5H_2O$	−0.00042	−0.00037
$[(H_2O)_2Mg\{(OH)_2Coen_2\}_2](SO_4)_2\cdot 7H_2O$	−0.00031	−0.00038
$[(H_2O)_2Ni\{(OH)_2Coen_2\}_2](SO_4)_2\cdot 7H_2O$	−0.00032	−0.00040
$[(H_2O)_2Co\{(OH)_2Coen_2\}_2](SO_4)_2\cdot 7H_2O$	−0.00033	−0.00040

ments was not less than 5% in the case of the AC bridge method and 10% in the case of the Faraday method.

Taking into account the isomorphism[5] of the sulfates with the same number of water molecules of crystallization, the corrections for the diamagnetic part of the susceptibilities were performed as follows: for the estimation of the diamagnetic part of the susceptibility of $[(H_2O)_2Co\{(OH)_2Coen_2\}_2](SO_4)_2\cdot 5H_2O$, e.g., the diamagnetic susceptibility of a free Zn^{2+} ion in the literature[7] was subtracted from the observed susceptibility at room temperature for $[(H_2O)_2Zn\{(OH)_2Coen_2\}_2](SO_4)_2\cdot 5H_2O$, then the diamagnetic susceptibility of a free Co^{2+} ion was added. A similar correction for the heptahydrate salts was made using the observed susceptibility of $[(H_2O)_2Mg\{(OH)_2Coen_2\}_2](SO_4)_2\cdot 7H_2O$. Table 1 shows these corrections together with the diamagnetic susceptibilities calculated from Pascal's rule.

Electron Spin Resonance. The electron spin resonance of a powder sample was measured using a Japan Electron Optics Laboratory Co., Ltd., JES-3 ESR spectrometer at liquid helium temperatures. X-Band spectra were observed with an 80 Hz modulation of 15 V. The external magnetic field was swept to about 23 kOe. Sixty minutes/3000 Oe scans were usually made.

Results and Discussion

Molar magnetic susceptibilities of $[(H_2O)_2Ni\{(OH)_2Coen_2\}_2](SO_4)_2\cdot 7H_2O$ are shown as a function of temperature in Fig. 2 and Table 2. The compound was paramagnetic down to 1.3 K, *i.e.*, magnetic interactions between magnetic ions in this complex compound are negligibly small compared to the thermal energy except at very low temperatures. The effective Bohr magneton number of 3.17 in the higher temperature region shown in Fig. 3 indicates that the paramagnetism is due to a Ni^{2+} ion, and that the two Co^{3+} ions may be in low spin states of the complex ion. The Ni^{2+} ion is surrounded by six oxygen atoms, of which four oxygen atoms are part of –OH– bridges and two oxygen atoms are part of co-ordinated water molecules, provided we accept the idea of Werner. No preliminary calculations of the temperature dependence of the susceptibility, ignoring the rhombic terms, show any agreement with the observed susceptibility, and therefore, a rhombic symmetry of the ligand field formed by six co-ordinated oxygen atoms was assumed for the components of the magnetic susceptibility. A temperature-independent paramagnetic susceptibility, that is, a high-frequency term, was graphically obtained from extrapolation of the plots of the observed molar mag-

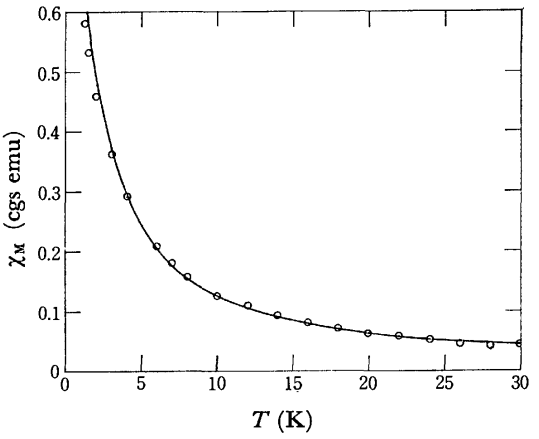

Fig. 2. The molar magnetic susceptibilities of $[(H_2O)_2Ni\{(OH)_2Coen_2\}_2](SO_4)_2\cdot 7H_2O$ (cgs emu) as a function of temperatures (K). ○: Experimental values corrected for the diamagnetic susceptibility and the temperature independent paramagnetic susceptibility. —: Calculated values with parameters, $D=-3.0$ cm^{-1}, $E=-1.0$ cm^{-1}, $g=2.25$ and $\theta=0$.

Table 2. Molar magnetic susceptibilities of $[(H_2O)_2Ni\{(OH)_2Coen_2\}_2](SO_4)_2\cdot 7H_2O$ (cgs emu)

Temp K	χ_M expt	χ_M calcd	Temp K	χ_M expt	χ_M calcd
1.20		(0.5800)	30.0	0.0391	(0.0418)
1.25	0.5799		70.0	0.01885	(0.0179)
2.00	0.4589	(0.4696)	77.0	0.01672	(0.0163)
4.00	0.2909	(0.2850)	100.0	0.01262	(0.0125)
6.00	0.2084	(0.1990)	140.0	0.00922	(0.00898)
10.0	0.1294	(0.1237)	180.0	0.00732	(0.00699)
14.0	0.0949	(0.0888)	220.0	0.00579	(0.005719)
16.0	0.0819	(0.0779)	260.0	0.00456	(0.004839)
18.0	0.0719	(0.0695)	290.0	0.00430	(0.004339)
20.0	0.0629	(0.0626)	293.7	0.00429	

The experimental χ_M values are corrected for the diamagnetic susceptibility and the temperature-independent paramagnetic susceptibility.

The χ_M values calculated from Eq. 2, with $D=-3.0$ cm^{-1}, $E=-1.0$ cm^{-1}, $g=2.25$, and $\theta=-0.1$ K, are shown in parentheses.

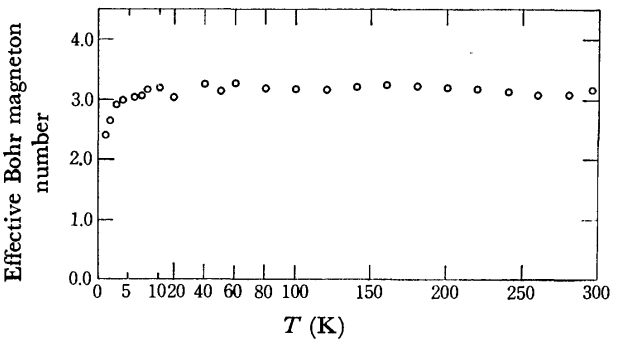

Fig. 3. The effective Bohr magneton numbers of $[(H_2O)_2Ni\{(OH)_2Coen_2\}_2](SO_4)_2\cdot 7H_2O$ *versus* temperatures.

netic susceptibilities *versus* reciprocal temperatures for $1/T \to 0$. The temperature-independent paramagnetic susceptibility per mole was 0.0001 cgs emu., from which the energy difference between the ground orbital state and the first-excited orbital state was estimated to be about 10^4 cm^{-1}.[8] A nickel ion in the nickel Tutton salts is also co-ordinated by six oxygen atoms. In this case, the F state of the nickel ion is split into two triplet and one singlet substates by the cubic ligand field, and the energy splitting between the lowest singlet and the lower triplet is estimated to be about 8000 cm^{-1}. Though it is not known how the lower triplet is further split by the non-cubic ligand field, the temperature-independent paramagnetic susceptibility mentioned above is considered to show a cubic-field splitting similar to that of the nickel Tutton salt. The magnetic susceptibility was calculated, therefore, following the spin Hamiltonian

$$H = DS_z^2 + E(S_x^2 - S_y^2) + g\beta HS, \qquad (1)$$

where D and E are axial and rhombic ligand field parameters, respectively, β is the Bohr magneton and H the applied magnetic field. In order to obtain a molar magnetic susceptibility corrected for the diamagnetic susceptibility and the temperature-independent paramagnetic susceptibility, a fit with a calculated magnetic susceptibility was made assuming fairly small magnetic interactions. The formula[9] used for the calculation, in which the magnetic interaction is considered to be corrected for temperature, is:

$$\chi_{\text{powder}} = \frac{1}{3}(\chi_x + \chi_y + \chi_z), \qquad (2)$$

where

$$\chi_x = \frac{2Ng^2\beta^2}{\frac{D+E}{2}} \frac{\sinh \frac{D+E}{2k(T-\theta)}}{\exp\left(\frac{-3E-D}{2k(T-\theta)}\right) + 2\cosh \frac{D+E}{2k(T-\theta)}},$$

$$\chi_y = \frac{2Ng^2\beta^2}{\frac{D-E}{2}} \frac{\sinh \frac{D-E}{2k(T-\theta)}}{\exp\left(\frac{-3E-D}{2k(T-\theta)}\right) + 2\cosh \frac{D-E}{2k(T-\theta)}},$$

and

$$\chi_z = \frac{2Ng^2\beta^2}{E} \frac{\sinh \frac{E}{k(T-\theta)}}{\exp\left(\frac{D}{k(T-\theta)}\right) + 2\cosh \frac{E}{k(T-\theta)}}.$$

Assuming isotropic g values, a fairly good fit was obtained for $D = -2.9 \sim -3.0$ cm^{-1}, $E = -1.0$ cm^{-1}, $g = 2.25$ and $\theta = -0.1$ K, as is seen in Fig. 2 and Table 2. In conformity with the above values of D and E, the X-band ESR of this sample at 4.2 K gave no signal up to 23 kOe of the applied magnetic field.

The effective Bohr magneton number was 3.17 in the temperature region above 8 K and at lower temperatures it decreased showing the effect of the rhombic ligand field and antiferromagnetic interactions among magnetic complex ions.

The molar magnetic susceptibilities of $[(H_2O)_2Co\{(OH)_2Coen_2\}_2](SO_4)_2 \cdot 5H_2O$, corrected for diamagnetic susceptibility, are shown in Figs. 4a and 4b and Table 3. The compound is paramagnetic down to 1.3 K, *i.e.*, the magnetic interactions among the magnetic ions are very weak, but the temperature dependence of the susceptibility is not simply that of the Curie-

TABLE 3. MOLAR MAGNETIC SUSCEPTIBILITIES (cgs emu)

Temp K	$[(H_2O)_2Co\{(OH)_2Coen_2\}_2](SO_4)_2 \cdot 5H_2O$ χ_M		$[(H_2O)_2Co\{(OH)_2Coen_2\}_2](SO_4)_2 \cdot 7H_2O$ χ_M		$[(H_2O)_2Co\{(OH)_2Coen_2\}_2](S_2O_6)_2 \cdot 5H_2O$ χ_M	
	expt	calcd	expt	calcd	expt	calcd
1.0		(1.8972)		(1.8782)		(2.0084)
1.4	0.960		1.062		0.395	
1.5	0.896	(1.2675)	0.890	(1.2255)	0.403	(1.3420)
2.0	0.712	(0.95269)	0.790	(0.94350)	0.4045	(1.0089)
4.0	0.403	(0.48045)	0.451	(0.47616)	0.3205	(0.50914)
6.0	0.283	(0.32303)	0.305	(0.32039)	0.262	(0.34256)
8.0	0.216	(0.24433)	0.265	(0.24250)	0.215	(0.25927)
10.0	0.170	(0.19710)	0.197	(0.19576)	0.181	(0.20929)
12.0	0.144	(0.16562)	0.1685	(0.16461)	0.156	(0.17598)
14.0	0.136	(0.14313)	0.146	(0.14235)	0.136	(0.15218)
16.0	0.110	(0.12626)	0.1252	(0.12566)	0.115	(0.13433)
18.0	0.0988	(0.11315)	0.112	(0.11268)	0.103	(0.12045)
20.0	0.090	(0.10205)	0.1036	(0.10230)	0.0948	(0.10935)
40.0	0.052	(0.055427)	0.0591	(0.055561)	0.0593	(0.059371)
60.0	0.037	(0.039674)	0.0421	(0.039951)	0.0443	(0.042681)
80.0	0.034	(0.031743)	0.0330	(0.032036)	0.0347	(0.034222)
100.0	0.0292	(0.026879)	0.02768	(0.027119)	0.0283	(0.028971)
140.0	0.0225	(0.020962)	0.02102	(0.021051)	0.02124	(0.022493)
180.0	0.0186	(0.017257)	0.01728	(0.017253)	0.01700	(0.018440)
220.0	0.0152	(0.014607)	0.01275	(0.014580)	0.01382	(0.015587)
260.0	0.0126	(0.012592)	0.01120	(0.012582)	0.01180	(0.013448)
290.0	0.0112	(0.011371)	0.01110	(0.011384)	0.01140	(0.012163)

The experimental χ_M values are corrected only for the diamagnetic susceptibility.

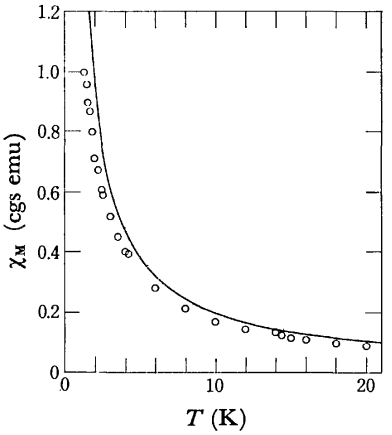

Fig. 4a. The molar magentic susceptibilities of $[(H_2O)_2Co\{(OH)_2Coen_2\}_2](SO_4)_2\cdot 5H_2O$ (cgs emu) *versus* temperatures lower than 20 K. ○: Experimental values which were corrected for the diamagnetic susceptibility. —: Calculated values with parameters, $g_{//}=5.915$, $g_{\perp}=3.566$, $\alpha=1.450$ and $\alpha'=1.950$.

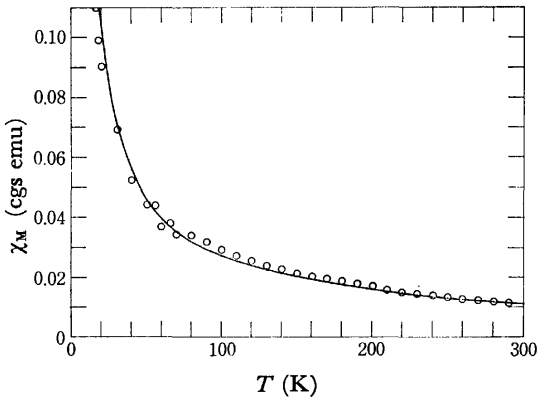

Fig. 4b. The molar magnetic susceptibilities of $[(H_2O)_2Co\{(OH)_2Coen_2\}_2](SO_4)_2\cdot 5H_2O$ (cgs emu) *versus* temperatures between 20 K and room temperature. ○: Experimental values which were corrected for the diamagnetic susceptibility. —: Calculated values with the same parameters as those in Fig. 4a.

Weiss law. In the case of a Co^{2+} ion co-ordinated by oxygen atoms in the form of an octahedron, it is known that the Co^{2+} ion has an effective spin of 1/2 at very low temperatures, where the spins are populated only in the lowest energy level. The Weiss constant of from −0.4 to −0.6 K, which was determined at liquid helium temperatures, was considered to be mainly due to the magnetic interaction. The high-frequency term was graphically obtained from data between 150 K and room temperature, that is, the extrapolation of the molar magnetic susceptibility as a function of the reciprocal temperature for $1/T\rightarrow 0$ was about 0.0007 cgs emu per mole. A similar extrapolation of the molar magnetic susceptibilities for $1/T\rightarrow 0$ from data between 14 and 20 K did not result in the same value, but it appears that the high-frequency term is not temperature independent suggesting that there are some excited levels of low excitation energy. The high-frequency term cannot be uniquely determined in these cases. On the other hand, the effective Bohr magneton number was also temperature dependent as

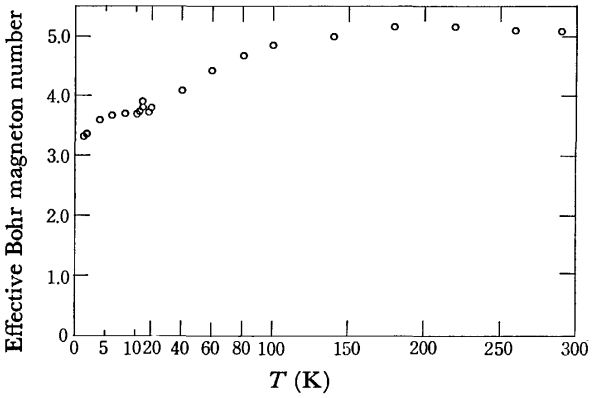

Fig. 5. The effective Bohr magneton numbers of $[(H_2O)_2Co\{(OH)_2Coen_2\}_2](SO_4)_2\cdot 5H_2O$ *versus* temperatures.

shown in Fig. 5. The value was about 5.1 at room temperature and gradually decreased to about 3.3 at 1.4 K. This decrease is more than that due to the antiferromagnetic interactions, indicating that the ground orbital level splits due to the ligand field of low symmetry.

The ESR derivative curve of this sample in powder form at 4.2 K is shown in Fig. 6. The signal intensity was weaker than that for $Co(NH_4)_2(SO_4)_2\cdot 6H_2O$ powder at 4.2 K, as shown in Fig. 7, but shapes of these two signals are quite similar. In $Co(NH_4)_2(SO_4)_2\cdot 6H_2O$, each Co^{2+} ion is surrounded by six oxygen atoms of coordinated water molecules with tetragonal symmetry and its g-values have been measured for single crystals by Bleaney and Ingram[10] to be $g_{\perp}=3.06\pm 0.06$ and $g_{//}=6.45\pm 0.13$. Simulations of the

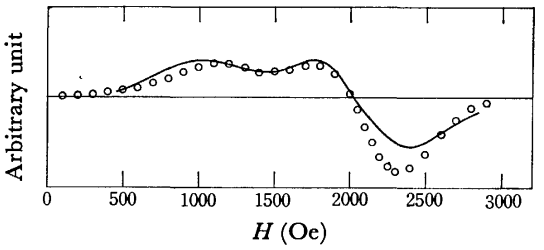

Fig. 6. ESR derivative curve of $[(H_2O)_2Co\{(OH)_2Coen_2\}_2](SO_4)_2\cdot 5H_2O$ on powder at 4.2 K. —: Experimental curve. ○: Simulation with parameters of $g_1=2.900$, $g_2=2.901$, $g_3=5.80$, $I=7/2$, $A_1=21.0$ Oe, $A_2=22.0$ Oe, $A_3=260.0$ Oe and line width=350 Oe.

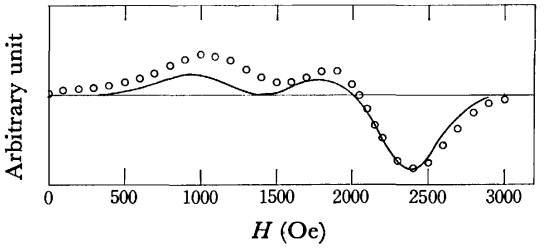

Fig. 7. ESR derivative curve of $Co(NH_4)_2(SO_4)_2\cdot 6H_2O$ on powder at 4.2 K. —: Experimental curve. ○: Simulation with parameters of $g_1=3.000$, $g_2=3.002$, $g_3=6.60$, $I=7/2$, $A_1=21.0$ Oe, $A_2=22.0$ Oe, $A_3=260.0$ Oe and line width=350 Oe.

ESR spectrum of $Co(NH_4)_2(SO_4)_2\cdot 6H_2O$ powder with g-value, hyperfine constant and line width parameters according to the Kneübuhl method[11] were attempted to see if simulation is applicable to this sort of compound. Computations were performed with a FACOM 230—75 computer at Kyoto University using a program of Kuwada.[12] The best fit simulation for $Co(NH_4)_2(SO_4)_2\cdot 6H_2O$ was obtained with the parameters: g-values, $g_1=3.000$, $g_2=3.002$, and $g_3=6.60$, hyperfine constants, $A_1=21.0$, $A_2=22.0$, and $A_3=260.0$ Oe and a line width of 350 Oe. The results are plotted in Fig. 7. The fair agreement between these g-values and those for single-crystal ESR proves that simulation can be used to estimate g-values. The hyperfine constants used are equal to those determined by Bleaney and Ingram[10] in single-crystal experiments. These constants were also used in simulations of $[(H_2O)_2Co\{(OH)_2Coen_2\}_2](SO_4)_2\cdot 5H_2O$, $[(H_2O)_2Co\{(OH)_2Coen_2\}_2](SO_4)_2\cdot 7H_2O$ and $[(H_2O)_2Co\{(OH)_2Coen_2\}_2](S_2O_6)_2\cdot 5H_2O$. The line shapes of cobalt ammonium Tutton salt and $[(H_2O)_2Co\{(OH)_2Coen_2\}_2](SO_4)_2\cdot 5H_2O$ are quite similar, and the best fit for the latter was obtained with $g_1=2.900$, $g_2=2.901$ and $g_3=5.80$ and line width of 350 Oe, as is shown in Fig. 6. Thus, the symmetry of a Co^{2+} ion in $[(H_2O)_2Co\{(OH)_2Coen_2\}_2](SO_4)_2\cdot 5H_2O$ was concluded to be tetragonal as for the cobalt ammonium Tutton salt, though a difference of 0.001 between the values of g_1 and g_2 was necessary for a satisfactory fit. In Fig. 8, an example of simulations of ESR derivative curves is shown. All the curves were calculated for the same g_1 and g_3 values, that is, $g_1=3.060000$ and $g_3=6.450000$, but with the g_2 value varying from 3.060000 to 5.060000. It is worthwhile to note that when the anisotropy of the g values are almost tetragonal, the shapes of the ESR derivative curves are very sensitive to the anisotropy between the g_1 and g_2 values.

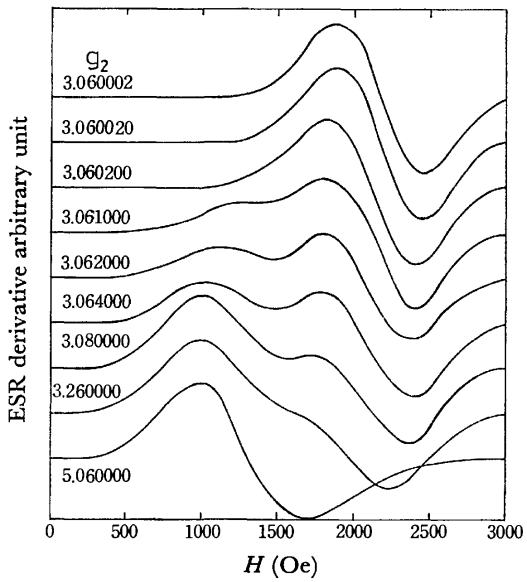

Fig. 8. Simulations of ESR derivative curves, where $g_1=3.060000$ and $g_3=6.450000$ are kept through all the cruves, but g_2 is varied from 3.060000 to 5.060000, which are written in the graph. The hyper-fine interaction is not considered.

The magnetic susceptibilities of Co^{2+} ions in the Tutton salts have been calculated by several authors[13] on the basis of the theory of Abragam and Pryce.[14] Calculations of the magnetic susceptibilities of $[(H_2O)_2Co\{(OH)_2Coen_2\}_2](SO_4)_2\cdot 5H_2O$ were attempted assuming tetragonal symmetry and considering spin-orbit interaction in order to obtain a fit with the experimental values. The calculation was performed using the equations proposed by Bose *et al.*,[13] but with orbital levels up to the third level taken into consideration. Some good fits were obtained though the g-values were not completely equal to those from the ESR simulation. The best fit to the results are given in Table 3 in parentheses and are shown in Figs. 4a and 4b. The parameters of the best fit are $g_{//}=5.915$ and $g_{\perp}=3.566$ and $\alpha=1.450$ and $\alpha'=1.950$, where $-\alpha$ and $-\alpha'$ are the effective axial and perpendicular Landé factors,[14] respectively, in the spin-orbit coupling terms expressed by the fictitious orbital angular momentum. The energy

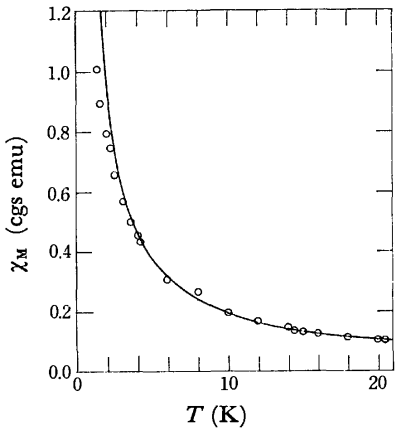

Fig. 9a. The molar magnetic susceptibilities of $[(H_2O)_2Co\{(OH)_2Coen_2\}_2](SO_4)_2\cdot 7H_2O$ (cgs emu) as a function of temperatures (K) lower than 20 K. ○: Experimental values which were corrected for the diamagnetic susceptibility. —: Calculated values with parameters, $B_4^0=-2.00\ cm^{-1}$, $B_2^2=75.0\ cm^{-1}$, $B_2^0=40.0\ cm^{-1}$, $\alpha_x=1.62$, $\alpha_y=1.52$, $\alpha_z=1.35$, $g_x=4.126$, $g_y=5.961$ and $g_z=2.690$.

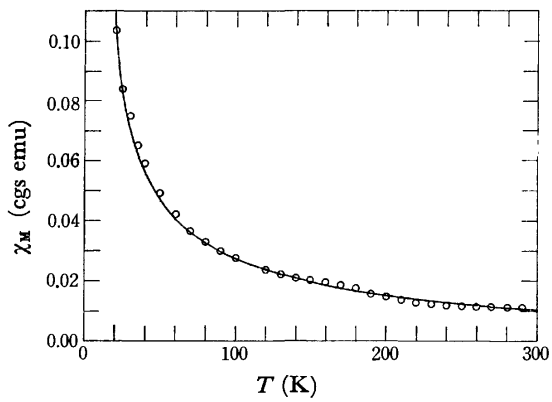

Fig. 9b. The molar magnetic susceptibilities of $[(H_2O)_2Co\{(OH)_2Coen_2\}_2](SO_4)_2\cdot 7H_2O$ (cgs emu) as a function of temperatures between 20 K and room temperature. ○: Experimental values which were corrected for the diamagnetic susceptibility. —: Calculated values with the same parameters as those in Fig. 9a.

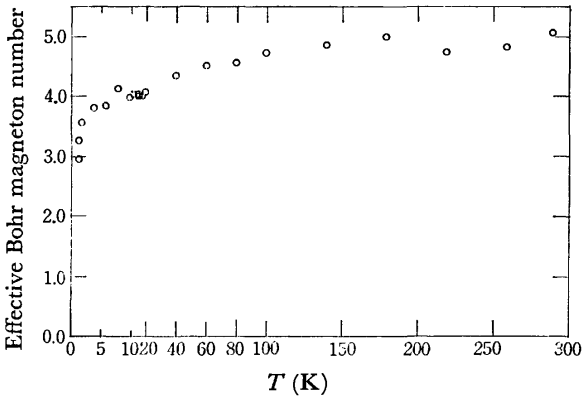

Fig. 10. The effective Bohr magneton numbers of $[(H_2O)_2Co\{(OH)_2Coen_2\}_2](SO_4)_2 \cdot 7H_2O$ *versus* temperatures.

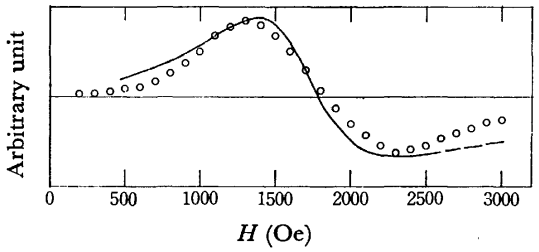

Fig. 11. ESR derivative curve of $[(H_2O)_2Co\{(OH)_2Coen_2\}_2](SO_4)_2 \cdot 7H_2O$ on powder at 1.3 K. —: Experimental curve. ○: Simulation with parameters of $g_1=2.00$, $g_2=3.00$, $g_3=4.50$, $I=7/2$, $A_1=21.0$ Oe, $A_2=22.0$ Oe, $A_3=260.0$ Oe, and line width=400 Oe.

difference between the ground level and the first-excited level is about 280 k, which is comparable to that of the Tutton salt.[13] If we follow the idea of the hexa coordination proposed by Werner,[1] it is reasonable to assume tetragonal symmetry.

The molar magnetic susceptibility of $[(H_2O)_2Co\{(OH)_2Coen_2\}_2](SO_4)_2 \cdot 7H_2O$ was close to that of $[(H_2O)_2Co\{(OH)_2Coen_2\}_2](SO_4)_2 \cdot 5H_2O$, as is seen in Figs. 9a and 9b and 10, and Table 3, but the ESR of the former is much more difficult to observe than that of the latter. The derivative curves of ESR were quite different, as is shown in Figs. 6 and 11. Because of the very broad line width, which seems to be more than 400 Oe, simulations would include numerous ambiguities. A calculated ESR derivative curve with g-values of 2.00, 3.00, and 4.50 and a line width of 400 Oe is shown in Fig. 11, this curve being one of the best fits though the g-values are unexpectedly small. This anisotropy of the g-values of a Co^{2+} ion in $[(H_2O)_2Co\{(OH)_2Coen_2\}_2](SO_4)_2 \cdot 7H_2O$ suggests that the ligandation of water molecules is different from that of penta hydrate. The Weiss constant of −0.6 to −0.7 K, which was obtained in the lowest temperature region, of the hepta hydrate is a little larger in absolute value than that of the penta hydrate. However, the hepta hydrate is, on the whole, considered to be more dilute for magnetic ions than the penta hydrate, suggesting some changes of the superexchange interaction paths. It was thought that the symmetry of the ligand field in the hepta hydrate is lower than that of the

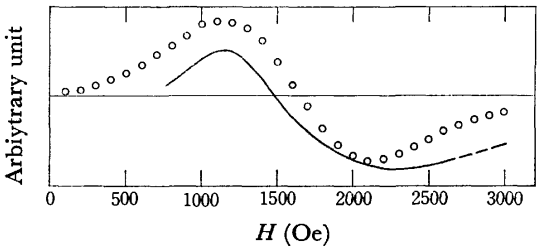

Fig. 12. ESR derivative curve of $[(H_2O)_2Co\{(OH)_2Coen_2\}_2](S_2O_6)_2 \cdot 5H_2O$ on powder at 4.2 K. —: Experimental curve. ○: Simulation with parameters of $g_1=2.30$, $g_2=5.20$, $g_3=5.80$, $I=7/2$, $A_1=21.0$ Oe, $A_2=22.0$ Oe $A_3=260.0$ Oe, and line width=600 Oe.

tetragonal from the symmetry of the g-values. On the other hand, the ESR derivative curve of $[(H_2O)_2Co\{(OH)_2Coen_2\}_2](S_2O_6)_2 \cdot 5H_2O$ was different from both the sulfate penta hydrate and the sulfate hepta hydrate, as is shown in Fig. 12. The simulation of this dithionate penta hydrate gave g-values of $g_1=2.30$, $g_2=5.20$, and $g_3=5.80$ with a width of 600 Oe. This anisotropy of the g-values is of the type $g_1<g_2\approx g_3$. A dithionate ion is larger in size than a sulfate ion, so it was supposed that $[(H_2O)_2Co\{(OH)_2Coen_2\}_2](S_2O_6)_2 \cdot 5H_2O$ would be magnetically more dilute than $[(H_2O)_2Co\{(OH)_2Coen_2\}_2](SO_4)_2 \cdot 5H_2O$. However, the observed magnetic susceptibility resulted in a negative Weiss constant having an absolute value larger than that of the penta hydrate and with a maximum near 2 K. The magnetic interactions may be operating *via* anions and some water molecules, and the dithionate ion does not result in a weaker linkage among the complex ions than does the sulfate ion in this case.

An attempt was made to calculate the magnetic susceptibilities of the dithionate penta hydrate and the sulfate hepta hydrate under the assumption of a rhombic ligand field symmetry. The method of calculation using the operator equivalents,[15] for which octahedral ligandation of oxygen atoms was assumed, is described in the appendix. The parameters for the best fit were as follows: for the dithionate penta hydrate, $\Delta r=8800$ cm^{-1}, $B_4^0=2.00$ cm^{-1}, $B_2^2=30.00$ cm^{-1}, $B_2^0=100.0$ cm^{-1}, $\alpha_x=1.81$, $\alpha_y=1.74$, $\alpha_z=0.90$, $g_x=5.044$, $g_y=5.768$ and $g_z=2.286$ and for the sulfate hepta hydrate, $\Delta r=8800$ cm^{-1}, $B_4^0=-2.00$ cm^{-1}, $B_2^2=75.00$ cm^{-1}, $B_2^0=40.0$ cm^{-1}, $\alpha_x=1.62$, $\alpha_y=1.52$, $\alpha_z=1.35$, $g_x=4.126$, $g_y=5.961$, and $g_z=2.690$. The calculated magnetic susceptibilities of the best fits are shown in Table 3 in parentheses and Figs. 9a and 9b, and 13a and 13b. As mentioned above, the dithionate penta hydrate showed that it has antiferromagnetic interactions, and therefore, in the lowest temperature region, the observed susceptibilities deviate from the calculated susceptibilities, for which magnetic interactions between magnetic ions are not taken into consideration. The discrepancy between the g-values from the ESR simulation and those from the magnetic susceptibility calculation is small in the case of $[(H_2O)_2Co\{(OH)_2Coen_2\}_2](S_2O_6)_2 \cdot 5H_2O$, however, the case of the sulfate hepta hydrate cannot be explained. If it is recalled that $[(H_2O)_2Ni\{(OH)_2Coen_2\}_2](SO_4)_2 \cdot 7H_2O$ has a rhombic ligand field for Ni^{2+} ion, a fairly good fit of the calculated magnetic

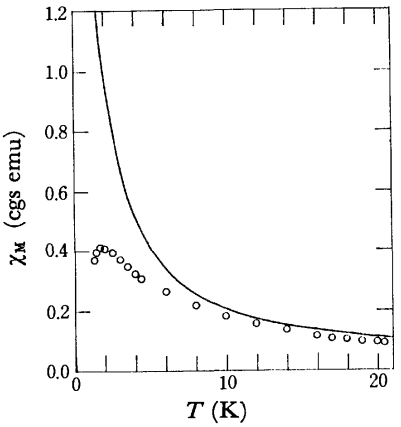

Fig. 13a. The molar magnetic susceptibilities of $[(H_2O)_2Co\{(OH)_2Coen_2\}_2](S_2O_6)_2\cdot 5H_2O$ (cgs emu) as a function of temperatures (K) lower than 20 K. ○: Experimental values which were corrected for the diamagnetic susceptibility. —: Calculated values with parameters of $B_4^0=2.00\ cm^{-1}$, $B_4^2=30.00\ cm^{-1}$, $B_2^0=100.0\ cm^{-1}$, $\alpha_x=1.81$, $\alpha_y=1.74$, $\alpha_z=0.90$, $g_x=5.044$, $g_y=5.768$, and $g_z=2.286$.

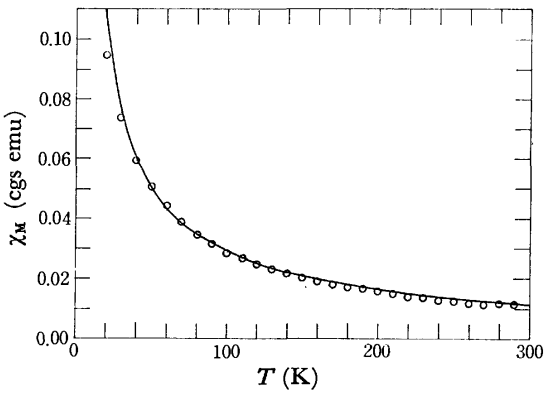

Fig. 13b. The molar magnetic susceptibilities of $[(H_2O)_2Co\{(OH)_2Coen_2\}_2](S_2O_6)_2\cdot 5H_2O$ (cgs emu) as a function of temperatures (K) between 20 K and room temperature. ○: Experimental values which were corrected for the diamagnetic susceptibility. —: Calculated values with the same parameters to those in Fig. 13a.

susceptibility for $[(H_2O)_2Co\{(OH)_2Coen_2\}_2](SO_4)_2\cdot 7H_2O$ under the assumption of rhombic anisotropy appears reasonable.

In conclusion, the magnetic properties of the $[(H_2O)_2M\{(OH)_2Coen_2\}_2]^{4+}$ ion, where M=Ni^{2+} or Co^{2+}, can be explained by those of the central divalent ion, that is, roughly speaking, the Co^{3+} ions in the wings are diamagnetic. In the solid state, the magnetic properties of the $[(H_2O)_2M\{(OH)_2Coen_2\}_2]^{4+}$ ion are not independent of the anion and crystalline water molecules, that is, the ligand field of sulfate penta hydrate was concluded to be tetragonal while those of sulfate hepta hydrate and dithionate penta hydrate were found to be rhombic, and the superexchange interactions were also to some extent dependent on the anions and crystalline water molecules.

This work was completed with the cooperation of Professor Masayasu Mori, Dr. Takashi Shibahara and Mr. Moriyoshi Hatta of Osaka City University, to whom the authors wish to express their deep gratitude for having provided the new compounds used in these experiments.

The authors wish to thank Professor Keiji Kuwada of Osaka University and Professor Shunichi Ohnishi of Kyoto University for valuable discussions on ESR simulation.

Appendix

Orbital energy levels, g-values of the lowest orbital level and molar magnetic susceptibilities for a ^4F state ion with a rhombic ligand field were calculated using the method of operator equivalents.[15] The operator equivalent method is based on the fact that, within a multiplet, the matrix elements of the potential function of the ion are proportional to the matrix elements of the appropriate polynomials of the orbital angular momentum operator.

The ligand field potential V that has been considered is

$$\begin{aligned} V &= V_K + V_{T2} + V_{T4} + V_{R2} \\ &= 20A_4(x^4+y^4+z^4-\frac{3}{5}r^4) + A_2^0(3z^2-r^2) \\ &\quad + A_4^0(35z^4-30z^2r^2+3r^4) + A_2^2(x^2-y^2), \end{aligned} \tag{3}$$

where V_K is the cubic potential function, V_{T2} and V_{T4} are the second- and fourth-order tetragonal potential functions, respectively, and V_{R2} is the second-order rhombic potential function. A_4, A_2^0, A_4^0, and A_2^2 are the coefficients of these potential functions, V_K, V_{T2}, V_{T4}, and V_{R2}, respectively. V_K is assumed to be much larger than V_{T2}, V_{T4}, and V_{R2}, so that the contributions from the latter terms can be treated as a perturbation. The matrix[16] of the cubic potential V_K for the orbital states $|M_L\rangle$ ($M_L=\pm 3, \pm 2, \pm 1, 0$) is

$$60B_4 \times \begin{pmatrix} 3 & 0 & 0 & 0 & \sqrt{15} & 0 & 0 \\ 0 & -7 & 0 & 0 & 0 & 5 & 0 \\ 0 & 0 & 1 & 0 & 0 & 0 & \sqrt{15} \\ 0 & 0 & 0 & 6 & 0 & 0 & 0 \\ \sqrt{15} & 0 & 0 & 0 & 1 & 0 & 0 \\ 0 & 5 & 0 & 0 & 0 & -7 & 0 \\ 0 & 0 & \sqrt{15} & 0 & 0 & 0 & 3 \end{pmatrix}, \tag{4}$$

where $B_4=-2A_4\langle r^4\rangle/315$. The eigenstates of this secular matrix are the singlet Γ_2 and the triplets Γ_5 and Γ_4, for which the wave functions are

$$\varphi_1 = \sqrt{\frac{3}{8}}|-1\rangle+\sqrt{\frac{5}{8}}|+3\rangle = |\Gamma_4, 1\rangle,$$

$$\varphi_2 = -|0\rangle = |\Gamma_4, 0\rangle,$$

$$\varphi_3 = \sqrt{\frac{5}{8}}|-3\rangle+\sqrt{\frac{3}{8}}|+1\rangle = |\Gamma_4, -1\rangle,$$

$$\phi_1 = \sqrt{\frac{5}{8}}|-1\rangle-\sqrt{\frac{3}{8}}|3\rangle = |\Gamma_5, 1\rangle,$$

$$\phi_2 = \frac{1}{\sqrt{2}}(|2\rangle+|-2\rangle) = |\Gamma_5, 0\rangle,$$

$$\phi_3 = \sqrt{\frac{5}{8}}|1\rangle-\sqrt{\frac{3}{8}}|-3\rangle = |\Gamma_5, -1\rangle,$$

and

$$\chi = \frac{1}{\sqrt{2}}(|2\rangle-|-2\rangle) = |\Gamma_2, 0\rangle.$$

$$\begin{pmatrix} 6B_2^0+135B_4^0 & 0 & 6B_2^2 & -3\sqrt{15}(B_2^0+5B_4^0) & 0 & \sqrt{15}B_2^2 \\ 0 & -12B_2^0+360B_4^0 & 0 & 0 & 2\sqrt{15}B_2^2 & 0 \\ 6B_2^2 & 0 & 6B_2^0+135B_4^0 & \sqrt{15}B_2^2 & 0 & -3\sqrt{15}(B_2^0+5B_4^0) \\ -3\sqrt{15}(B_2^0+5B_4^0) & 0 & \sqrt{15}B_2^2 & 105B_4^0+\Delta_\Gamma & 0 & 0 \\ 0 & 2\sqrt{15}B_2^2 & 0 & 0 & -420B_4^0+\Delta_\Gamma & 0 \\ \sqrt{15}B_2^2 & 0 & -3\sqrt{15}(B_2^0+5B_4^0) & 0 & 0 & 105B_4^0+\Delta_\Gamma \end{pmatrix}, \quad (5)$$

Following the process introduced by Abragam and Pryce[14] for the case of ligand fields of low symmetry, we take into account the orbitals Γ_4 and Γ_5, but neglect the contribution from the Γ_2 orbital.

The matrix elements of V_{T2}, V_{T4}, and V_{R2} based on $\{\varphi_i\}$ and $\{\varphi_i\}$ $(i=1, 2, 3)$ are, if we set $B_2^0=-2A_2^0\langle r^2\rangle/105$, $B_2^2=-2A_2^2\langle r^2\rangle/105$, and $B_4^0=-2A_4^0\langle r^4\rangle/315$,
where Δ_Γ is the separation between the Γ_4 and Γ_5 levels and is equal to $480|B_4|$. The orbital levels obtained by the diagonalization of (5) are shown in Fig. 14.

The components of the orbital angular momentum L based on $\{\varphi_i\}$ and $\{\varphi_i\}$ $(i=1, 2, 3)$ are represented as follows,

$$L_x=\frac{1}{2}\begin{pmatrix} 0 & \frac{-3}{2}\sqrt{2} & 0 & 0 & \sqrt{\frac{15}{2}} & 0 \\ \frac{-3}{2}\sqrt{2} & 0 & \frac{-3}{2}\sqrt{2} & -\sqrt{\frac{15}{2}} & 0 & -\sqrt{\frac{15}{2}} \\ 0 & \frac{-3}{2}\sqrt{2} & 0 & 0 & \sqrt{\frac{15}{2}} & 0 \\ 0 & -\sqrt{\frac{15}{2}} & 0 & 0 & \frac{\sqrt{2}}{2} & 0 \\ \sqrt{\frac{15}{2}} & 0 & \sqrt{\frac{15}{2}} & \frac{\sqrt{2}}{2} & 0 & \frac{\sqrt{2}}{2} \\ 0 & -\sqrt{\frac{15}{2}} & 0 & 0 & \frac{\sqrt{2}}{2} & 0 \end{pmatrix},$$

$$L_y=\frac{-i}{2}\begin{pmatrix} 0 & \frac{-3}{2}\sqrt{2} & 0 & 0 & -\sqrt{\frac{15}{2}} & 0 \\ \frac{3}{2}\sqrt{2} & 0 & \frac{-3}{2}\sqrt{2} & \sqrt{\frac{15}{2}} & 0 & -\sqrt{\frac{15}{2}} \\ 0 & \frac{3}{2}\sqrt{2} & 0 & 0 & \sqrt{\frac{15}{2}} & 0 \\ 0 & -\sqrt{\frac{15}{2}} & 0 & 0 & \frac{-\sqrt{2}}{2} & 0 \\ \sqrt{\frac{15}{2}} & 0 & -\sqrt{\frac{15}{2}} & \frac{\sqrt{2}}{2} & 0 & \frac{-\sqrt{2}}{2} \\ 0 & \sqrt{\frac{15}{2}} & 0 & 0 & \frac{\sqrt{2}}{2} & 0 \end{pmatrix},$$

and

$$L_z=\begin{pmatrix} \frac{-3}{2} & 0 & 0 & \frac{\sqrt{15}}{2} & 0 & 0 \\ 0 & 0 & 0 & 0 & 0 & 0 \\ 0 & 0 & \frac{3}{2} & 0 & 0 & \frac{-\sqrt{15}}{2} \\ \frac{\sqrt{15}}{2} & 0 & 0 & \frac{-1}{2} & 0 & 0 \\ 0 & 0 & 0 & 0 & 0 & 0 \\ 0 & 0 & \frac{-\sqrt{15}}{2} & 0 & 0 & \frac{1}{2} \end{pmatrix}. \quad (6)$$

The lowest three orbital states ξ_1, ξ_2, and ξ_3 in matrix (5) are given by

$$\xi_1=\mu_1\varphi_1+\mu_1'\varphi_3+\nu_1\phi_1+\nu_1'\phi_3,\ \xi_2=\mu_2\varphi_2+\nu_2\phi_2,$$
$$\text{and } \xi_3=\mu_3\varphi_1+\mu_3'\varphi_3+\nu_3\phi_1+\nu_3'\phi_3. \quad (7)$$

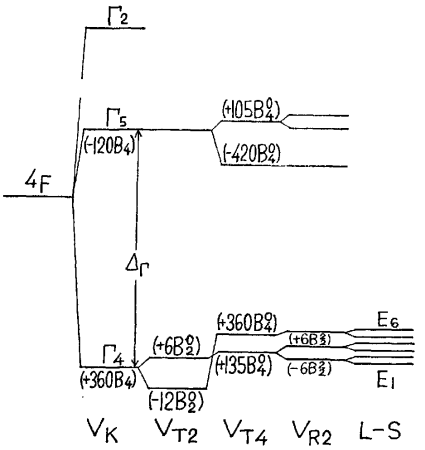

Fig. 14. Orbital energy level splittings of a ^4F state in a field of rhombic symmetry.

The components of the angular momentum based on $\{\xi_i\}$ $(i=1, 2, 3)$ are

$$L_x=\frac{1}{2}\begin{pmatrix} 0 & \rho_x & 0 \\ \rho_x & 0 & \rho_x' \\ 0 & \rho_x' & 0 \end{pmatrix},$$

$$L_y=\frac{-i}{2}\begin{pmatrix} 0 & \rho_y' & 0 \\ -\rho_y' & 0 & \rho_y \\ 0 & -\rho_y & 0 \end{pmatrix},$$

and

$$L_z=\begin{pmatrix} \rho_z' & 0 & \rho_z \\ 0 & 0 & 0 \\ \rho_z & 0 & \rho_z'' \end{pmatrix}, \quad (8)$$

where ρ_v, ρ_v', and ρ_v'' $(v=x, y, z)$ are, using (7),

$$\rho_x=\frac{-3\sqrt{2}}{2}\mu_2(\mu_1+\mu_1')+\sqrt{\frac{15}{2}}\{\nu_2(\mu_1+\mu_1')-\mu_2(\nu_1+\nu_1')\}+\frac{\sqrt{2}}{2}\nu_2(\nu_1+\nu_1'),$$

$$\rho_x'=\frac{-3\sqrt{2}}{2}\mu_2(\mu_3+\mu_3')+\sqrt{\frac{15}{2}}\{\nu_2(\mu_3+\mu_3')-\mu_2(\nu_3+\nu_3')\}+\frac{\sqrt{2}}{2}\nu_2(\nu_3+\nu_3'),$$

$$\rho_y=\frac{3\sqrt{2}}{2}\mu_2(\mu_3-\mu_3')+\sqrt{\frac{15}{2}}\{\nu_2(\mu_3-\mu_3')+\mu_2(\nu_3-\nu_3')\}+\frac{\sqrt{2}}{2}\nu_2(\nu_3-\nu_3'),$$

$$\rho_y'=\frac{3\sqrt{2}}{2}\mu_2(-\mu_1+\mu_1')+\sqrt{\frac{15}{2}}\{\nu_2(-\mu_1+\mu_1')+\mu_2(-\nu_1+\nu_1')\}+\frac{\sqrt{2}}{2}\nu_2(-\nu_1+\nu_1'),$$

$$\rho_z = \frac{-3}{2}(\mu_1\mu_3-\mu_1'\mu_3')+\sqrt{\frac{15}{2}}(\mu_1\nu_3+\nu_1\mu_3-\mu_1'\nu_3'-\nu_1'\mu_3') -\frac{1}{2}(\nu_1\nu_3-\nu_1'\nu_3'),$$

$$\rho_z' = \frac{-3}{2}(\mu_1^2-\mu_1'^2)+\sqrt{15}(\mu_1\nu_1-\mu_1'\nu_1')-\frac{1}{2}(\nu_1^2-\nu_1'^2),$$

and $$\rho_z'' = \frac{-3}{2}(\mu_3^2-\mu_3'^2)+\sqrt{15}(\mu_3\nu_3-\mu_3'\nu_3')-\frac{1}{2}(\nu_3^2-\nu_3'^2).$$

The solution of the secular equation shows that $\mu_1'=\mu_1, \nu_1'=\nu_1$, $\mu_3'=-\mu_3$, and $\nu_3'=-\nu_3$ in the case of orthorhombic ligand fields, and therefore,

$$\begin{aligned}\xi_1 &= \mu_1(\varphi_1+\varphi_3)+\nu_1(\phi_1+\phi_3),\\ \xi_2 &= \mu_2\varphi_2+\nu_2\phi_2,\\ \text{and}\quad \xi_3 &= \mu_3(\varphi_1-\varphi_3)+\nu_3(\phi_1-\phi_3).\end{aligned} \tag{9}$$

If we define the α_v ($v=x, y, z$) as follows

$$\alpha_x = \frac{-\rho_x}{2} = \frac{3\sqrt{2}}{2}\mu_1\mu_2-\sqrt{\frac{15}{2}}\{\mu_1\nu_2-\mu_2\nu_1\}-\frac{\sqrt{2}}{2}\nu_1\nu_2,$$

$$\alpha_y = \frac{\rho_y}{2} = \frac{3\sqrt{2}}{2}\mu_2\mu_3+\sqrt{\frac{15}{2}}\{\nu_2\mu_3+\nu_3\mu_2\}+\frac{\sqrt{2}}{2}\nu_2\nu_3,$$

and $$\alpha_z = -\rho_z = 3\mu_1\mu_3-\sqrt{15}(\mu_1\nu_3+\nu_1\mu_3)+\nu_1\nu_3, \tag{10}$$

and it is known that

$$\rho_x' = \rho_y' = \rho_z' = \rho_z'' = 0,$$

then the components of the angular momentum can be written as follows,

$$L_x = -\alpha_x\begin{bmatrix}0&1&0\\1&0&0\\0&0&0\end{bmatrix} = -\alpha_x l_x',$$

$$L_y = -\alpha_y\begin{bmatrix}0&0&0\\0&0&i\\0&-i&0\end{bmatrix} = -\alpha_y l_y',$$

and $$L_z = -\alpha_z\begin{bmatrix}0&0&1\\0&0&0\\1&0&0\end{bmatrix} = -\alpha_z l_z', \tag{11}$$

where $l_x'^2+l_y'^2+l_z'^2 = l(l+1) = 2,\ (l=1).$

The α_x, α_y, and α_z indicate the contributions from the Γ_5 orbital level. When there is no contribution from the Γ_5 level, that is, when the lowest triplet Γ_4 state consists of only the wave functions $\{\varphi_1\}$, α_x, α_y, and α_z are

$$\alpha_x = \alpha_y = \alpha_z = 1.5.$$

The potential function (3) is replaced by the equivalent angular momentum operators[15] as follows,

$$\begin{aligned}\hat{V} &= \hat{V}_K+\hat{V}_{T2}+\hat{V}_{T4}+\hat{V}_{R2}\\ &= B_4(O_4^0+5O_4^4)+B_2^0O_2^0+B_4^0O_4^0+B_2^2O_2^2,\end{aligned} \tag{12}$$

where $B_4 = \langle L\|\beta\|L\rangle A_4\langle r^4\rangle$,
$B_2^0 = \langle L\|\alpha\|L\rangle A_2^0\langle r^2\rangle$,
$B_4^0 = \langle L\|\beta\|L\rangle A_4^0\langle r^4\rangle$,
and $B_2^2 = \langle L\|\alpha\|L\rangle A_2^2\langle r^2\rangle$.

$\langle L\|\alpha\|L\rangle$ and $\langle L\|\beta\|L\rangle$ are the proportional coefficients,[16] $-2/105$ and $-2/315$, respectively, and $\langle r_j\rangle$ is the average of r_j over the radial part of the wave function. O_3^0, O_2^2, O_4^0, and O_4^4 can be written using the orbital angular momentum operator L, thus

$$\begin{aligned}O_2^0 &= 3L_z^2-L(L+1),\\ O_2^2 &= \frac{1}{2}(L_+^2+L_-^2),\\ O_4^0 &= 35L_z^4-30L(L+1)L_z^2+25L_z^2\\ &\quad -6L(L+1)+3L^2(L+1)^2,\\ \text{and}\quad O_4^4 &= \frac{1}{2}(L_+^4+L_-^4).\end{aligned} \tag{13}$$

Using the α_x, α_y, and α_z mentioned above and $l=1$, the V_{T2}, V_{T4}, and V_{R2} (in Eq. 12) can be written as follows,

$$\begin{aligned}\hat{V}_{T2} &= \frac{1}{4}B_2^0Q_2^0,\\ \hat{V}_{T4} &= B_4^0Q_4^0,\\ \hat{V}_{R2} &= \frac{1}{4}B_2^2Q_2^2,\end{aligned} \tag{14}$$

where $Q_2^0 = (8\alpha_z^2+2p)l_z^2-4p-q(l_+^2+l_-^2)$,
$Q_4^0 = u_1l_z^2+u_2(l_+^2+l_-^2)+u_3$,
$Q_2^2 = p(l_+^2+l_-^2)-2ql_z^2+4q$,
$p = \alpha_x^2+\alpha_y^2$,
$q = \alpha_x^2-\alpha_y^2$,
$u_1 = 8\alpha_z^4-12p\alpha_z^2+19\alpha_z^2+3p-\frac{9}{4}p^2+\frac{3}{4}q^2$,
$u_2 = \frac{3}{2}q\left(\frac{p}{2}-4\alpha_z^2-1\right)$,
and $u_3 = 3p(p-2)$.

The first-order perturbation Hamiltonian containing the spin-orbit interaction is

$$\begin{aligned}\mathcal{H} &= \frac{1}{4}B_2^0Q_2^0+B_4^0Q_4^0+\frac{1}{4}B_2^2Q_2^2\\ &\quad -\lambda(\alpha_xl_xS_x+\alpha_yl_yS_y+\alpha_zl_zS_z).\end{aligned} \tag{15}$$

When the rhombic symmetry is taken into account, $m(=l_z+S_z)$ is not a good quantum number. The secular matrix of Eq. 15 represented in the basis set of $|l_z, S_z\rangle$ is

$$\begin{array}{cccccc}|-1,\tfrac{3}{2}\rangle & |-1,\tfrac{-1}{2}\rangle & |1,\tfrac{3}{2}\rangle & |1,\tfrac{-1}{2}\rangle & |0,\tfrac{1}{2}\rangle & |0,\tfrac{-3}{2}\rangle\\ |1,\tfrac{-3}{2}\rangle & |1,\tfrac{1}{2}\rangle & |-1,\tfrac{-3}{2}\rangle & |-1,\tfrac{1}{2}\rangle & |0,\tfrac{-1}{2}\rangle & |0,\tfrac{3}{2}\rangle\end{array}$$

$$\begin{pmatrix}
T_f+R_f+\frac{3}{2}\alpha_z\lambda & 0 & \frac{1}{2}(pB_2^2-qB_2^0)+2u_2B_4^0 & 0 & \frac{-\sqrt{6}}{4}r\lambda & 0\\
0 & T_f+R_f-\frac{1}{2}\alpha_z\lambda & 0 & \frac{1}{2}(pB_2^2-qB_2^0)+2u_2B_4^0 & \frac{-\sqrt{2}}{2}s\lambda & \frac{-\sqrt{6}}{4}r\lambda\\
\frac{1}{2}(pB_2^2-qB_2^0)+2u_2B_4^0 & 0 & T_f+R_f-\frac{3}{2}\alpha_z\lambda & 0 & \frac{-\sqrt{6}}{4}s\lambda & 0\\
0 & \frac{1}{2}(pB_2^2-qB_2^0)+2u_2B_4^0 & 0 & T_f+R_f+\frac{1}{2}\alpha_z\lambda & \frac{-\sqrt{2}}{2}r\lambda & \frac{-\sqrt{6}}{4}s\lambda\\
\frac{-\sqrt{6}}{4}r\lambda & \frac{-\sqrt{2}}{2}s\lambda & \frac{-\sqrt{6}}{4}s\lambda & \frac{-\sqrt{2}}{2}r\lambda & 0 & 0\\
0 & \frac{-\sqrt{6}}{4}r\lambda & 0 & \frac{-\sqrt{6}}{4}s\lambda & 0 & 0
\end{pmatrix}, \tag{16}$$

where
$$T_f = \left(2\alpha_z^2 + \frac{1}{2}p\right)B_2^0 + u_1 B_4^0,$$
$$R_f = -\frac{1}{2}qB_2^2,$$
$$r = \alpha_x + \alpha_y,$$
and
$$s = \alpha_x - \alpha_y.$$

The six Kramers doublets, which are deduced from the lowest orbital triplet, are obtained through the diagonalization of (16). The energy levels of the six Kramers doublets are expressed as E_i ($i=1, 2, ..., 6$) and their wave functions as $\Phi_{\pm i}$ ($i=1, 2, ..., 6$). Then

$$\Phi_{+i} = \sum_{j=1}^{6} C_{ij}\zeta_j,$$
and
$$\Phi_{-i} = \sum_{j=1}^{6} C_{ij}\zeta_j^*, \qquad (17)$$

where $\{\zeta_j\}$ is the base of the secular matrix (16) and its coefficient of linear combination, C_{ij}, can be determined from the solution of the secular equation. The g factors of the lowest Kramers doublet are given as follows:

$$\begin{aligned}
g_x &= 2\langle\Phi_{+1}|-\alpha_x l_x + 2S_x|\Phi_{-1}\rangle \\
&= -2\sqrt{2}\,\alpha_x(C_{11}C_{16}+C_{12}C_{15}+C_{13}C_{16}+C_{14}C_{15}) \\
&\quad +4\sqrt{3}\,(C_{11}C_{14}+C_{12}C_{13}+C_{15}C_{16})+8C_{12}C_{14}+4C_{15}^2, \\
g_y &= 2\langle\Phi_{+1}|-\alpha_y l_y + 2S_y|\Phi_{-1}\rangle \\
&= -2\sqrt{2}\,\alpha_y(-C_{11}C_{16}-C_{12}C_{15}+C_{13}C_{16}+C_{14}C_{15}) \\
&\quad +4\sqrt{3}\,(C_{11}C_{14}+C_{12}C_{13}-C_{15}C_{16})-8C_{12}C_{14}+4C_{15}^2, \\
g_z &= 2\langle\Phi_{+1}|-\alpha_z l_z + 2S_z|\Phi_{+1}\rangle \\
&= 2[(C_{11}^2+C_{12}^2-C_{13}^2-C_{14}^2)\alpha_z+3(C_{11}^2+C_{13}^2-C_{16}^2) \\
&\quad -C_{12}^2-C_{14}^2+C_{15}^2]. \qquad (18)
\end{aligned}$$

The magnetic susceptibility per mole is given by

$$\chi_v = \frac{N\beta^2}{Z}\left(\frac{G^v}{kT}+2G'^v\right), \quad (v=x, y, z)$$

where
$$G^v = \sum_{i=1}^{6} G_i^v \exp\frac{-(E_i-E_1)}{kT},$$
$$G_i^v = \sum_{\pm}|\langle\Phi_{\pm i}|-\alpha_v l_v+2S_v|\Phi_{\pm i}\rangle|^2,$$
$$G'^v = \sum_{i=1}^{6} G'^v_i \exp\frac{-(E_i-E_1)}{kT},$$
$$G'^v_i = \sum_{j(\neq i)}^{6} G'^v_{ij},$$
$$G'^v_{ij} = \sum_{\pm}\frac{|\langle\Phi_{\pm i}|-\alpha_v l_v+2S_v|\Phi_{\pm j}\rangle|^2}{E_j-E_i},$$
and
$$Z = 2\sum_{i=1}^{6}\exp\frac{-(E_i-E_1)}{kT}.$$

The G_i^v and G'^v_{ij} are

$$\begin{aligned}
G_i^x &= 2[-\sqrt{2}\,\alpha_x(C_{i1}C_{i6}+C_{i2}C_{i5}+C_{i3}C_{i6}+C_{i4}C_{i5}) \\
&\quad +2\sqrt{3}\,(C_{i1}C_{i4}+C_{i2}C_{i3}+C_{i5}C_{i6})+4C_{i2}C_{i4}+2C_{i5}^2]^2, \\
G_i^y &= 2[\sqrt{2}\,\alpha_y(C_{i1}C_{i6}+C_{i2}C_{i5}-C_{i3}C_{i6}-C_{i4}C_{i5}) \\
&\quad +2\sqrt{3}\,(C_{i1}C_{i4}+C_{i2}C_{i3}-C_{i5}C_{i6})-4C_{i2}C_{i4}+2C_{i5}^2]^2, \\
G_i^z &= 2[\alpha_z(C_{i1}^2+C_{i2}^2-C_{i3}^2-C_{i4}^2)+3(C_{i1}^2+C_{i3}^2-C_{i6}^2) \\
&\quad -C_{i1}^2-C_{i4}^2+C_{i5}^2]^2,
\end{aligned}$$

$$\begin{aligned}
G'^x_{ij} &= \frac{2}{E_j-E_i}[\sqrt{3}\,(C_{i1}C_{j4}+C_{i4}C_{j1}+C_{i2}C_{j3}+C_{i3}C_{j2} \\
&\quad +C_{i5}C_{j6}+C_{i6}C_{j5})-\frac{\sqrt{2}}{2}\alpha_x(C_{i1}C_{j6}+C_{i6}C_{j1}+C_{i2}C_{j5} \\
&\quad +C_{i5}C_{j2}+C_{i3}C_{j6}+C_{i6}C_{j3}+C_{i4}C_{j5}+C_{i5}C_{j4}) \\
&\quad +2(C_{i2}C_{j4}+C_{i4}C_{j2}+C_{i5}C_{j5})]^2,
\end{aligned}$$

$$\begin{aligned}
G'^y_{ij} &= \frac{2}{E_j-E_i}[\sqrt{3}\,(C_{i1}C_{j4}+C_{i4}C_{j1}+C_{i2}C_{j3}+C_{i3}C_{j2} \\
&\quad -C_{i5}C_{j6}-C_{i6}C_{j5})+\frac{\sqrt{2}}{2}\alpha_y(C_{i1}C_{j6}+C_{i6}C_{j1}+C_{i2}C_{j5} \\
&\quad +C_{i5}C_{j2}-C_{i3}C_{j6}-C_{i6}C_{j3}-C_{i4}C_{j5}-C_{i5}C_{j4}) \\
&\quad -2(C_{i2}C_{j4}+C_{i4}C_{j2}-C_{i5}C_{j5})]^2,
\end{aligned}$$

$$\begin{aligned}
G'^z_{ij} &= \frac{2}{E_j-E_i}[\alpha_z(C_{i1}C_{j1}+C_{i2}C_{j2}-C_{i3}C_{j3}-C_{i4}C_{j1}) \\
&\quad +3(C_{i1}C_{j1}+C_{i3}C_{j3}-C_{i6}C_{j6})-C_{i2}C_{j2}-C_{i4}C_{j4} \\
&\quad +C_{i5}C_{j5}]^2.
\end{aligned}$$

We must estimate the error in the operator equivalent method used in the above calculation. The method is valid for the lowest multiplet ^4F. The effect of mixing with the upper state of a different multiplet, *e.g.*, the Γ'_4 state arising from ^4P, can be estimated from the matrix element of $\hat{V}_{T2}+\hat{V}_{T4}+\hat{V}_{R2}$ between the lowest and the excited multiplets. Roughly, the contribution of the mixing with the upper mul-

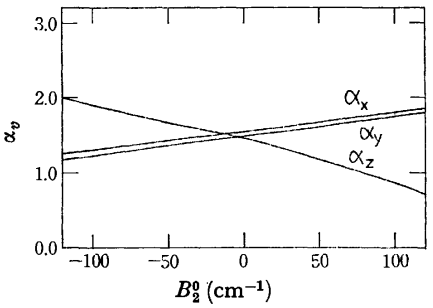

Fig. 15. α_v as a function of B_2^0. The graph is calculated for $\Delta\Gamma=8800$ cm^{-1}, $B_4^0=2.00$ cm^{-1}, and $B_2^2=30.0$ cm^{-1}.

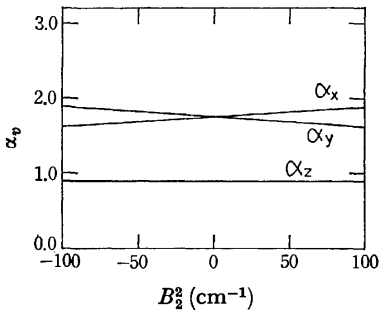

Fig. 16. α_v as a function of B_2^2, where $\Delta\Gamma=8800$ cm^{-1}, $B_2^0=100$ cm^{-1} and $B_4^0=2.00$ cm^{-1} were used.

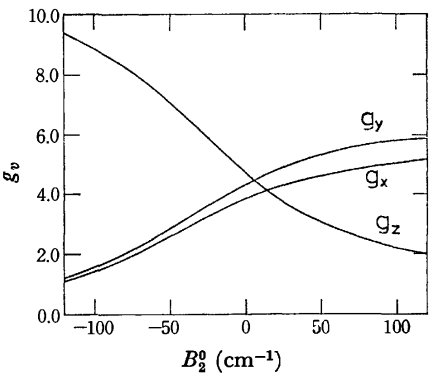

Fig. 17. g_v as a function of B_2^0 where $\Delta\Gamma=8800$ cm^{-1}, $B_4^0=2.00$ cm^{-1}, and $B_2^2=30.0$ cm^{-1} were used.

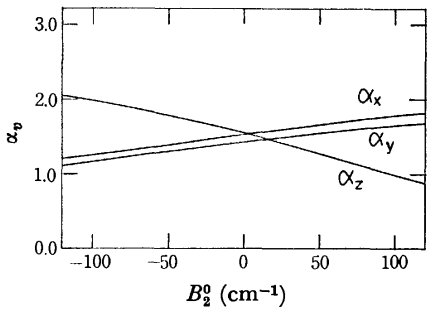

Fig. 18. α_v as a function of B_2^0, where $\Delta_\Gamma=8800$ cm^{-1}, $B_4^0=-2.00$ cm^{-1}, and $B_4^0=75.0$ cm^{-1} were used.

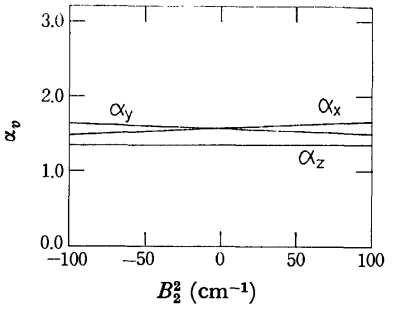

Fig. 19. α_v as a function of B_2^2, where $\Delta_\Gamma=8800$ cm^{-1}, $B_2^0=40.0$ cm^{-1}, and $B_4^0=-2.00$ cm^{-1} were used.

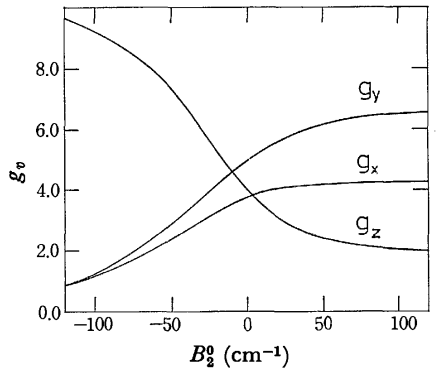

Fig. 20. g_v as a function of B_2^0, where $\Delta_\Gamma=8800$ cm^{-1}, $B_4^0=-2.00$ cm^{-1} and $B_2^2=75.0$ cm^{-1} were used.

tiplet to $\Delta\alpha$, the difference between α_v and 1.5, will be of the order of the ratio of the matrix element $\langle L=3|\hat{V}_{T2}+\hat{V}_{T4}+\hat{V}_{R2}|L\neq 3\rangle$ to the energy difference between the multiplets. Within the lowest multiplet, the more the Γ_5 level is separated from the Γ_4 level, the less the deviation of α_v from 1.5. The case of $\alpha_v=1.5$ has been analyzed by Uryû *et al.*[17] who dealt with $CoCl_2\cdot 6H_2O$. The same g-values as those of the Co Tutton salt[9] are found with the following parameters: $\alpha_x=\alpha_y=\alpha_v=1.5$, $B_4^0=2.00$ cm^{-1}, $B_2^0=-70.0$ cm^{-1}, and $B_2^2=0.00$ cm^{-1}.

In Figs. 15 and 16, α_v, $(v=x, y, z)$, is plotted as a function of B_2^0 and B_2^2, respectively. In Fig. 17, g_v, $(v=x, y, z)$, is shown as a function of B_2^0. In Figs. 15—17, the functions are calculated using the parameters, $\Delta_\Gamma=8800$ cm^{-1}, $B_4^0=2.00$ cm^{-1} and $B_2^0=100$ cm^{-1} or $B_2^2=30.0$ cm^{-1}, that is, those which showed the best fit for $[(H_2O)_2Co\{(OH)_2Coen_2\}_2](S_2O_6)_2\cdot 5H_2O$. In Figs. 18—20, similar calculations are shown using the parameters, $\Delta_\Gamma=8800$ cm^{-1}, $B_4^0=-2.00$ cm^{-1}, and $B_2^0=40.0$ cm^{-1} or $B_2^2=75.0$ cm^{-1}, that is, those which showed the best fit for $[(H_2O)_2Co\{(OH)_2Coen_2\}_2](SO_4)_2\cdot 7H_2O$.

Numerical computations in the appendix and those of the magnetic susceptibilities were performed with a FACOM 230—45 computer at the Computer Center of Kyushu University.

References

1) A. Werner, *Berichte*, **40**, 4426 (1907).
2) L. Cambi, *Atti. accad. nazl. Lincei, Rend., classe sci. fis., mat. e nat.*, **18**, 581 (1955) and C. A. **50**, 5347d (1956).
3) G. H. Jonker and J. H. Van Santen, *Physica*, **16**, 337, 599 (1950); J. B. Goodenough, *Phys. Rev.*, **100**, 564 (1955); P. W. Anderson and H. Hasegawa, *ibid.*, **100**, 675 (1955).
4) D. C. Jicha and D. H. Busch, *Inorg. Chem.*, **1**, 872, 878 (1962); D. H. Busch and D. C. Jicha, *ibid.*, **1**, 884 (1962); P. S. Poskozim, R. Shute, R. Taylor, and J. Wysocki, *J. Inorg. Nucl. Chem.*, **55**, 687 (1973).
5) M. Mori, M. Hatta, and T. Shibahara, *Proc. XV I. C. C. C.*, **I**, 272 (1973); M. Hatta, T. Shibahara, and M. Mori, to be published.
6) C. T. Linder, Research Report, R-94433-2-A (Westinghouse Research Laboratories).
7) A. V. Jagnnadham, *Proc. Rajasthan Acad. Sci.*, **1**, 6 (1950); C. A., **45**, 9948 (1951).
8) J. H. E. Griffiths and J. Owen, *Proc. R. Soc. London, Ser. A*, **213**, 459 (1952).
9) T. Haseda and M. Date, *J. Phys. Soc. Jpn.*, **13**, 175 (1958).
10) B. Bleaney and D. J. E. Ingram, *Proc. R. Soc. London, Ser. A*, **208**, 143 (1951).
11) F. K. Kneubühl, *J. Chem. Phys.*, **33**, 1074 (1960).
12) K. Kuwada, "Saikin no Bunsekikagaku," Vol. 20, Kagaku Dojin, Kyoto, p. 123.
13) K. Kambe, *Prog. Theor. Phys.*, **7**, 15 (1952); N. Uryû, *J. Phys. Soc. Jpn.*, **11**, 770 (1956); A. Bose, A. S. Chakravarty, and R. Chatterjee, *Proc. R. Soc. London, Ser. A*, **261**, 431 (1961),
14) A. Abragam and M. H. L. Pryce, *Proc. R. Soc. London, Ser. A*, **206**, 173 (1951).
15) K. W. H. Stevens, *Proc. Phys. Soc. London*, **A65**, 209 (1952).
16) H. Kamimura, S. Sugano, and Y. Tanabe, "Ligand Field Theory and Its Applications," 2nd ed., Syokabo, Tokyo (1970); A. Abragam and B. Bleaney, "Electron Paramagnetic Resonance of Transition Ions," Clarendon Press, Oxford (1970); K. Osaki and N. Uryû, *Technology Reports of the Kyushu Univ.*, **47**, 575 (1974).
17) N. Uryû, J. Skalyo, Jr., and S. A. Friedberg, *Phys. Rev.*, **144**, 689 (1966).

An Investigation of the Triplet State Dynamics of *p*-Chloroaniline by Microwave Induced Changes in the Phosphorescence Intensity and by Triplet ← Singlet Absorption

Nobuyuki NISHI and Minoru KINOSHITA

The Institute for Solid State Physics, The University of Tokyo, Roppongi, Minato-ku, Tokyo 106

(Received October 18, 1975)

The phosphorescent triplet state T_1 of *p*-chloroaniline (PCA) in a *p*-xylene host, in a neat crystal (n-trap), and in a PCA crystal doped with *p*-dichlorobenzene (x-trap) has been studied with the aid of phosphorescence spectra, optically detected zero-field magnetic resonance, and $T_1 \leftarrow S_0$ absorption spectra at temperatures below 4.2 K. The dynamic properties, particularly the radiative properties, of the individual spin states of T_1 are discussed in detail using the emission spectra for each spin state obtained with microwave techniques. For the x-trap system, the emissions from the T_y and T_z sublevels are found to be coincident in contrast to the other two systems. From this observation, it is suggested that the characters of the T_y and T_z states of normal PCA are mixed together in the x-trap.

The populating rates for the individual spin states were examined for the PCA crystal systems as a function of the excitation energy, when the excitation was induced by light having wavelengths in the $T_1 \leftarrow S_0$ absorption region. The relative populating rates thus obtained are dependent on the excitation energy. Therefore, it is concluded that the spin alignment produced by direct optical pumping from the ground state to the triplet manifold of the crystal is conserved during the vibrational relaxation and energy transfer processes. By using this unique wavelength dependence of the populating rates, the nature of the n- and x-traps is discussed and the vibrational structure of the $T_1 \leftarrow S_0$ spectrum is analyzed.

Detailed information on the static and dynamic properties of the phosphorescent triplet state of aromatic molecules has been successfully obtained in the past few years by using microwave techniques in combination with the conventional optical methods. In a previous paper,[1] it was shown that the emissions from the individual spin states in the lowest triplet state of *p*-chloroaniline (PCA) in *p*-xylene can be well separated at 1.3 K by applying the technique of microwave induced delayed phosphorescence (MIDP). This MIDP spectroscopy has proved to be useful in determining the mechanism of the $T_1 \rightarrow S_0$ radiative processes and in analyzing the vibrational structure of the phosphorescence. This work has been extended to two more PCA systems: a neat crystal and a PCA crystal doped with a small amount of *p*-dichlorobenzene. In these crystals, the phosphorescence is found to arise from the trap PCA molecules. It will be shown in this paper that the sublevel emissions of these traps are quite different from one system to another, although the phosphorescence spectra look much the same. From this observation the nature of the emitting centers will be deduced.

The $T_1 \leftarrow S_0$ absorption spectrum of a PCA crystal has also been observed and an attempt was made to analyze its vibrational structure using populating rates obtained by microwave techniques. Under the condition that spin-lattice relaxation is well suppressed, the spin directions produced by direct optical pumping into the triplet manifold are expected to be conserved during the vibrational relaxation, energy transfer, and phosphorescence decay processes. Therefore, the relative populating rates, if determined when the excitation is made by light of wavelengths corresponding to those of each vibronic band of the $T_1 \leftarrow S_0$ spectrum, are considered to be selective, and therefore, to be useful in the vibrational analysis of the spectrum.

Experimental

p-Chloroaniline, *p*-dichlorobenzene, and *p*-xylene were purchased from Tokyo Kasei Co. The former two materials were zone-refined (about 60 passes) and the purified portions were further sublimed in a vacuum. *p*-Xylene was purified by multiple distillation.

The light sources for the emission measurements were an Ork CH-612 1-kW mercury arc lamp and an Ushio UXL-1000D-O 1-kW DC xenon lamp. The exciting light was passed through a Corning 7-54 glass filter and a saturated $NiSO_4$ aqueous solution filter, and chopped with an Uniblitz L12 type electromagnetic shutter. The exciting light for photo-excitation experiments or the emission light from the sample was isolated by a Spex 1700-III 3/4-m spectrometer. The observing time was controlled by using an Uniblitz 26 type shutter in front of an EMI 6256-SA photomultiplier. The signal was fed into a low-pass filter and measured through a signal averager system (Nomura Electric Co. NP-800 or Ortec Model 4620/4623) or a PAR Model 128 lock-in amplifier. Hewlett-Packard Model 8620A and Weinschel Model 221 sweep oscillators were used as the microwave source with an appropriate microwave filter. The MIDP spectra were measured in a manner similar to that described in detail in a previous paper.[1] The repetition rate for the excitation and observation cycles was controlled to be 0.1—1 Hz by an Ortec 4653/4654 pulse generator system.

The light source for the absorption measurements was an Ushio UXL-500 500 W DC xenon lamp. The light transmitted through a 6 mm thick crystal was observed in the second order diffraction of the 3/4-m spectrometer.

The populating rate ratios for the triplet sublevels for each excitation energy were obtained by the fast passage PMDR method, first used by Winscom and Maki,[2] or a modified MIDP method. In the analysis of the signals, the values of the total decay and the relative radiative decay rate constants obtained by the ordinary MIDP techniques[3,4] were used.

Factor Group States

The crystal structure of PCA has been studied by

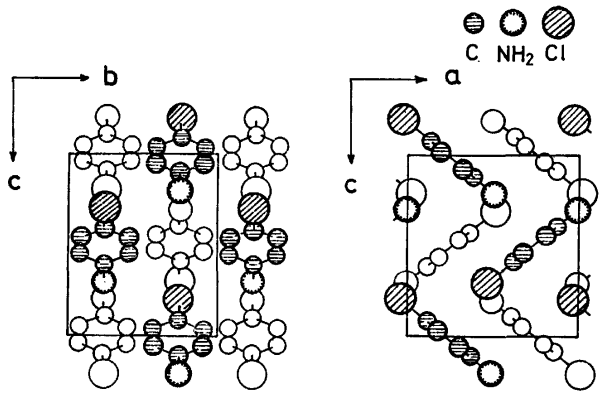

Fig. 1. The crystal structure of *p*-chloroaniline projected along the a and b axes.

Palm and was found to belong to the orthorhombic space group P_{nma} (D_{2h}^{16}),[5] as is shown in Fig. 1. The unit cell contains four PCA molecules. The long molecular axis (z: N–Cl direction) makes a larger projection on the a axis than on the c axis, and the medium in-plane axis (y: perpendicular to the long axis) is exactly parallel to the b axis. The molecular plane makes an angle of 39°40′ with the ab plane and the angle between the planes of two molecules is 79°20′. The coincidence of the molecular y axis with the crystal b axis offers many advantages in studying the optical properties of a PCA crystal.

TABLE 1. THE TOTAL SYMMETRIES OF THE THREE SPIN STATES IN THE FOUR ELECTRONIC FACTOR GROUP STATES

	T_a	T_b	T_c
^3A_g	B_{1g}	B_{2g}	B_{3g}
$^3B_{1u}$	A_u	$B_{3u}(c)$	$B_{2u}(b)$
$^3B_{2g}$	B_{3g}	A_g	B_{1g}
$^3B_{3u}$	$B_{2u}(b)$	$B_{1u}(a)$	A_u

The excited triplet A_1 (π,π^*) state of the free PCA molecule splits into the four factor group states of B_{1u}, B_{3u}, A_g and B_{2g} in the crystal. The three spin substates of the exciton level are designated by T_a, T_b and T_c, and their total symmetries are summarized in Table 1 with the polarization characteristics of the transition between the ground state and each substate. The crystal vectors a, b and c are designated as B_{1u}, B_{2u} and B_{3u}, respectively. Four of the twelve substates in Table 1 have the possibility of carrying dipole activity. If we assume that the one-center spin-orbit interaction between the (π,π^*) and (σ,π^*) states is predominant in acquiring the dipole activity, only two substates remain as strongly active substates: the $T_b(B_{3u})$ substate in the B_{1u} factor group state and the $T_b(B_{1u})$ substate in the B_{3u} factor group state. The transition involving the former state is polarized parallel to the c axis and the one involving the latter parallel to the a axis. By following the theoretical treatment of Hochstrasser and using the crystal geometry, the intensity ratio of the (0,0) transition of $^3B_{1u}\leftarrow{}^1A_g$ to that of $^3B_{3u}\leftarrow{}^1A_g$ is estimated to be about 1.5. In the high-resolution $T_1\leftarrow S_0$ absorption spectrum of a PCA crystal, the (0,0) band is found to split into two lines, the lower-energy component being 3–4 times stronger than the higher-energy one. Although this observed intensity ratio is larger than the ratio calculated on the basis of the crystal structure, we can safely conclude that the lowest dipole-allowed component has the strongest intensity and is assigned to the $^3B_{1u}$ state.

It has been found by Marchetti[6] that the ordering of the crystal zero-field levels of this state is $T_b>T_a>T_c$ and the top sublevel has the strongest dipole activity. This ordering in the crystal system leads to the following ordering of the molecular zero-field levels: $T_y>T_z>T_x$. These facts eliminate the possibility of the $^3B_2(\pi,\pi^*)$ state as the phosphorescent state of the free PCA molecule. The assignments of the $^3A_1(\pi,\pi^*)$ state to T_1 of isolated PCA and the $^3B_{1u}$ state to the lowest exciton state coincide well with the results presented below.

Results and Discussion

Phosphorescence Spectra, Zero-field Splittings and Kinetic Constants. The phosphorescence spectra of PCA were observed in three different systems: (1) in PCA molecules doped in a *p*-xylene crystal in which the PCA molecules are considered to be not too distorted by the host lattice, (2) in a neat PCA crystal the phosphorescence of which arises mainly from a trap 283 cm^{-1} below the $T_1\leftarrow S_0$ absorption origin, and (3) in a PCA crystal which has been doped with a small amount of *p*-dichlorobenzene. The phosphorescence origin of this latter crystal is lower by 67 cm^{-1} than the absorption origin of the crystal. The trap thus induced by *p*-dichlorobenzene is hereafter referred to in this text as an x-trap, because the appearnce of this trap resembles that of the so-called x-trap produced by doping quinoxaline in a naphthalene crystal[7]. The trap of the neat crystal is referred to as an n-trap for convenience. The phosphorescence spectra of these n- and x-traps are similar in shape to the spectrum reported previously for the PCA-doped xylene system[1].

The MIDP signals were observed at 4.559, 2.495 and 2.064 GHz for PCA isolated in *p*-xylene. The first two signals were strong but the latter was very weak. For the other systems, very strong PMDR and MIDP signals were observed. The x-trap phosphorescence produced signals at 4.539, 2.308 and 2.23 GHz and the n-trap at 4.063, 2.533 and 1.53 GHz.

The kinetic constants were obtained from an analysis of the MIDP signals by means of the method described by Schmidt *et al.*[3,4] with some modifications. The total decay rate constants of the sublevel emissions and

TABLE 2. ZERO-FIELD SPLITTINGS AND DECAY RATE CONSTANTS OF *p*-CHLOROANILINE

	PCA in *p*-xylene	n-trap	x-trap
D cm^{-1}	0.1176	0.1099	0.1128
E cm^{-1}	0.0344	0.0255	0.0385
k_y s^{-1}	9.5	42	16
k_z s^{-1}	6.8	20	12
k_x s^{-1}	0.1	1.1	0.5

the zero-field splitting constants in each system are summarized in Table 2. The zero-field microwave transitions were assigned according to the results stated in the previous section and the spin-orbit selection rule.

The D and E values are both positive for every system. Decreases in the D and E values of the n-trap system are noticeable. The latter value is reduced to about 66% of that observed in the x-trap system. While the total decay rate constant k_y for the n-trap is about four times larger than that for PCA in xylene, k_x increases by about 10 times in the n-trap. As will be seen, this increase in k_x for the PCA-crystal systems is attributed to the external heavy-atom effect. On the other hand, the changes in k_y and k_z in the n-trap may be correlated to the decrease in the E value.

Spin-Lattice Relaxation Rates. It has been shown that the spin-lattice relaxation rates in the phosphorescent triplet state in a zero magnetic field can be obtained from steady-state microwave induced phosphorescence experiments, if one knows the three total decay rates obtained in isolation.[8] Following the treatment of Antheunis,[8] one can derive the following equation for the spin-lattice relaxation rates, W_{xy} and W_{xz}* between the T_x and T_y sublevels and the T_x and T_z sublevels, respectively, as:

$$(k_x/k_y+1)W_{xy} + W_{xz} = \left(\frac{h_{x-y}(0;\ \mathrm{ISOL.})}{h_{x-y}(0;\ T;\ \mathrm{y=z})} - 1\right)k_x$$

where h_{x-y} (0;ISOL.) is the height of the microwave induced change in the steady-state phosphorescence intensity on sweeping through the T_x—T_y resonance in isolation and h_{x-y} (0;T; y=z) is the height under continuous microwave contact between T_y and T_z at temperature T. If $k_y \gg k_x'$ the left-hand side of the equation becomes the sum of the spin-lattice relaxation rates, *i.e.*, $W_{xy}+W_{xz}$.

In the n-trap system of the PCA crystal, $k_x/k_y=0.026$ and the approximation of $1+k_x/k_y \cong 1$ can be applied to within the error of the k_x value. The sum of the relaxation rates for the n-trap triplet state is plotted against the temperature in Fig. 2, which indicates that the isolation condition is well fulfilled below 1.8 K.

Vibrational Analysis of the $T_1 \rightarrow S_0$ Spectrum. The phosphorescence spectrum of each system was decomposed into the three sublevel emission spectra using MIDP techniques. The MIDP spectra for the three systems at 1.3 K are shown in Figs. 3–5.

For the PCA-doped xylene system, the vibrational

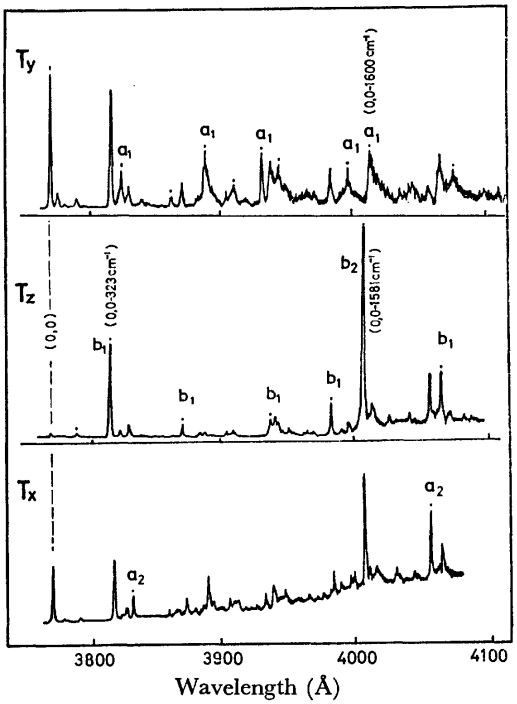

Fig. 3. The MIDP spectra of *p*-chloroaniline in *p*-xylene at 1.3 K. The spectrum denoted by T_u is the emission from the T_u sublevel (u=x, y, and z).

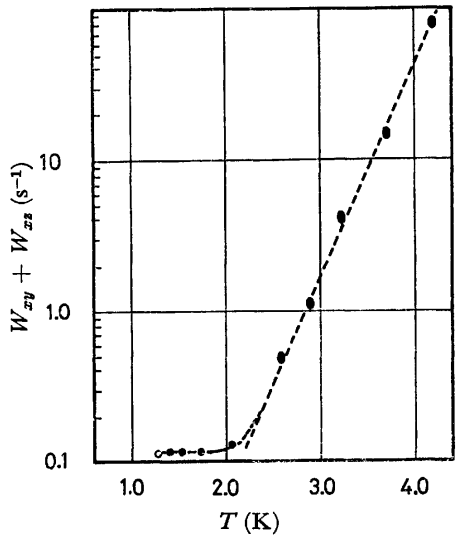

Fig. 2. The sum of the spin-lattice relaxation rates, $W_{xy}+W_{xz}$, as a function of temperature.

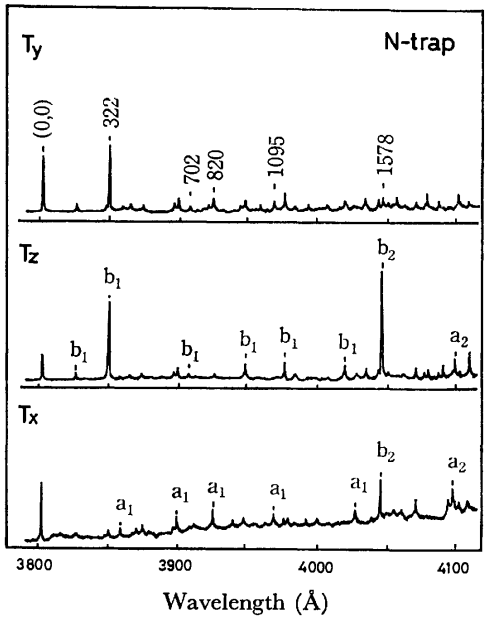

Fig. 4. The MIDP spectra of the *p*-chloroaniline neat crystal at 1.3 K.

* The approximation, $W_{xy}=W_{yx}$ and $W_{xz}=W_{zx}$, are used.

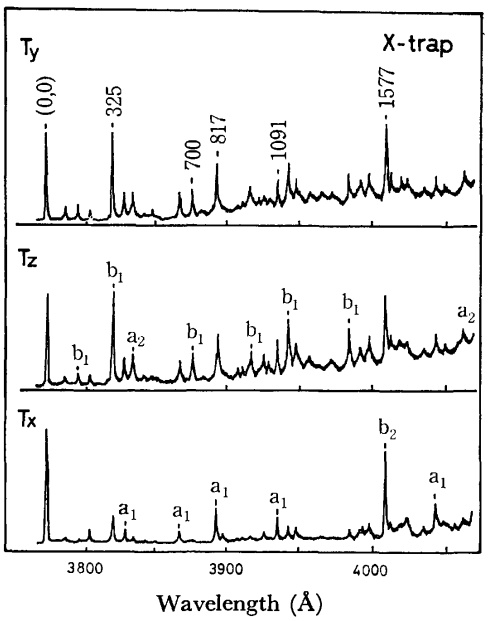

Fig. 5. The MIDP spectra (at 1.3 K) of the x-trap induced by doping *p*-dichlorobenzene into the *p*-chloroaniline crystal.

Table 3. Vibrational analysis of the phosphorescence spectrum of *p*-chloroaniline in *p*-xylene at 1.5 K[a)]

ν (cm^{-1})	$\Delta\nu$ (cm^{-1})	Relative intensity	Assignment
26513		s	(0, 0)
26470	43	w	lattice
26372	141	w	b_1
26189	323	s	b_1 (C–Cl bend. o.p.)
26129	384	m	a_1 (C–C bend. i.p.)
26097	416	m	a_2
25864	649	w	a_1 (2×323)
25811	702	m	b_1 (323+384)
25694	818	m	a_1 (C–C str.)
25583	930	vw	b_1
25415	1098	m	a_1
25376	1137	w	b_1 (323+818)
25338	1175	w	a_1 (C–H bend.)
25091	1421	m	b_1 (323+1098)
25016	1497	w	a_1 (C=C str.)
24932	1581	m	b_2 (C=C str.)
24913	1600	w	a_1 (C=C str.)
24609	1904	vw	a_2 (323+1581)
24592	1921	w	a_1 (818+1098)
24549	1964	w	b_2 (384+1581)

a) Relative intensity: s > m > w > vw, bend: bending mode, str: stretching mode, o.p.: out-of-plane, i.p.: in-plane.

analysis indicated in Table 3 has been reported previously.[1)] First, the band at 0—323 cm^{-1} was assigned to the out-of-plane b_1 vibration and that at 0—1581 cm^{-1} to the in-plane vibration of b_2 symmetry. Then the other bands were analyzed using the following characteristics of the MIDP spectra of Fig. 3:

1) The bands involving totally symmetric vibrations are active in the emission from the T_y spin state.

2) The bands involving the vibrations of b_1 symmetry are active in the emissions from T_y, T_z and T_x.

3) The bands involving the vibrations of b_2 symmetry are active in the emissions from T_z and T_x.

The mechanisms whereby each sublevel of the isolated PCA molecule acquires its dipole activity are summarized in Table 4 along with the observed intensities of the individual vibronic species in the sublevel spectra.

For the other two systems, the analysis was also performed in a similar manner. For the n-trap, the characteristics of the MIDP spectra are almost identical to those described for isolated PCA with the exception of the fact that the b_1 vibrations are less active than the a_1 vibrations in the T_x spectrum. The same statement holds for the T_x spectrum of the x-trap. However, the T_y and T_z spectra of the x-trap are quite different from those of the n-trap. They are considered to be a mixture of the T_y and T_z spectra of the n-trap. Using these features and the results in Table 3, a vibrational analysis of the phosphorescences of the n- and x-traps was completed as shown in Tables 5 and 6.

Radiative Properties of the Triplet Sublevels. The relative radiative decay rates for the main vibronic bands were examined by the method of Schmidt *et al.*[4)] and the results obtained for the (0,0), (0,0—320 cm^{-1}) and (0,0—1580 cm^{-1}) bands are tabulated in Table 7. Since the height of each vibronic band in the sublevel spectra of Figs. 3—5 is nearly proportional to the radiative decay rate k_u^r for that band (u=x, y and z), the relative values of k_u^r for the other bands may be estimated from Figs. 3—5 and Table 7.

Although the phosphorescence spectra are not shown here, the T_y spectrum of each system is almost identical to the phosphorescence spectrum of the respective system except for the intensity of the (0,0—1580 cm^{-1}) band. The intensity of this band in the phosphorescence spectra of the isolated PCA and of the n-trap results from the T_z emission, as can be seen from Table

Table 4. Main perturbing mechanisms for the $^3A_1 \rightarrow {}^1A_1$ radiative transition for *p*-chloroaniline in *p*-xylene

Triplet sublevel	Vibrational symmetry	Observed intensity	Intermediate state	Perturbing state
$^3A_1(T_y)$	a_1	very strong	first order	$^1B_1(\sigma, \pi^*)$
	b_1	very strong	$^{3,1}B_1(\sigma, \pi^*)$	$^1A_1(\pi, \pi^*)$
$^3A_1(T_z)$	b_2	very strong	$^3B_2(\pi, \pi^*)$, $^1A_2(\sigma, \pi^*)$	$^1B_1(\sigma, \pi^*)$
	b_1	strong	$^3B_1(\sigma, \pi^*)$, $^1A_2(\sigma, \pi^*)$	$^1B_2(\pi, \pi^*)$
	a_2	medium	$^{3,1}A_2(\sigma, \pi^*)$	$^1A_1(\pi, \pi^*)$
$^3A_1(T_y)$	a_2	weak	$^3A_2(\sigma, \pi^*)$, $^1B_2(\pi, \pi^*)$	$^1B_1(\sigma, \pi^*)$
	b_2	weak	$^3B_2(\pi, \pi^*)$, $^1B_2(\pi, \pi^*)$	$^1A_1(\pi, \pi^*)$

Table 5. Vibrational analysis of the phosphorescence spectrum of *p*-chloroaniline n-trap at 1.3 K[a)]

ν (cm^{-1})	$\Delta\nu$ (cm^{-1})	Relative intensity	Assignment
26295		s	(0, 0)
26140	155	w	b_1
25992	303	vw	a_1 (2×155)
25973	322	s	b_1 (C–Cl bend. o.p.)
25920	375	w	a_1 (C–C bend. i.p.)
25874	421	w	a_2
25822	473	w	a_1 (155+322)
25673	622	vw	b_1 (2×155+322)
25652	643	m	a_1 (2×322)
25593	702	vw	b_1 (322+375)
25497	798	w	
25475	820	m	a_1 (C–C str.)
25350	945	w	b_1
25333	962	m	b_1 (3×322)
25200	1095	w	a_1
25173	1122	vw	b_2 (C–H bend.)
25153	1142	m	b_1 (322+820)
25116	1179	w	a_1 (C–H bend.)
24882	1413	m	
24792	1503	m	a_1 (C=C str.)
24717	1578	s	b_2 (C=C str.)
24694	1601	mw	a_1 (C=C str.)
24624	1671	w	
24565	1720	w	
24399	1896	m	a_2 (322+1578)
24337	1958	m	b_2 (375+1578)

a) Relative intensity: s > m > mw > w > vw, bend.: bending mode, str.: stretching mode, o.p.: out-of-palne, i.p.: in-plane.

Table 6. Vibrational analysis of the phosphorescence spectrum of *p*-chloroaniline x-trap at 1.3 K[a)]

ν (cm^{-1})	$\Delta\nu$ (cm^{-1})	Relative intensity	Assignment
26511		s	(0, 0)
26460	51	vw	
26422	89	w	
26360	151	w	b_1
26186	325	s	b_1 (C–Cl bend. o.p.)
26132	379	m	a_1 (C–C bend. i.p.)
26104	407	vw	
26092	419	m	a_2
26033	478	vw	a_1 (151+325)
25867	644	m	a_1 (2×325)
25811	700	m	b_1 (325+379)
25694	817	ms	a_1 (C–C str.)
25578	933	w	b_1
25541	970	m	b_1 (3×325)
25463	1048	vw	b_1
25420	1091	m	a_1
25370	1141	ms	b_1 (325+817)
25338	1173	m	a_1 (C–H bend.)
25095	1416	m	
25056	1455	mw	
25009	1506	m	a_1 (C=C str.)
24934	1577	s	b_2 (C=C str.)
24913	1598	m	a_1 (C=C str.)
24841	1670	m	
24779	1732	w	
24605	1906	m	a_2 (325+1577)
24555	1956	m	b_2 (375+1577)

a) Relative intensity: s > ms > m > mw > w > vw, bend.: bending mode, str.: stretching mode, o.p.: out-of-plane, i.p.: in-plane.

7 and Figs. 3 and 4. For the x-trap system, on the other hand, the spectra of the T_y and T_z emissions resemble each other as is seen in Fig. 5 and the emissions contribute nearly equally to the phosphorescence, as is shown in Table 7. For the T_x spectra, the non-totally symmetric vibrations appear relatively strongly in the isolated PCA system, while the totally symmetric vibrations are dominant in the n- and x-trap systems.

For the isolated PCA system, the characteristic appearance of the (0,0−323 cm^{-1}) b_1 band in each sublevel spectrum can be understood in terms of the internal heavy-atom effect which enhances the spin-orbit coupling between the $^{3,1}A_1$ (π,π^*) and $^{1,3}B_1$ (σ,π^*) states. The b_2 band at 0−1581 cm^{-1} which has a notable intensity in the T_z spectrum was assigned to the ν_{8b} type C=C stretching vibration. The ν_{8b} vibration was also observed in the phosphorescence spectra of benzene[9)] and toluene[10)]. The notable appearance of this vibration has been discussed in relation to the pseudo-Jahn-Teller interaction between the phosphorescent $^3(\pi,\pi^*)$ state and nearby $^3(\pi,\pi^*)$ state. The fact that this in-plane non-totally symmetric vibration bands has a considerable intensity in the phosphorescence spectrum indicates that the second order spin-orbit vibronic process plays a role comparable to the first order process producing the (0,0) band intensity. However, the oscillator strength of the $^1B_1$ (σ,π^*)←$^1A_1$ transition is considered to be smaller by a factor of 10^{-2}–10^{-4} than that of the $^1B_2$ (π,π^*)←$^1A_1$ transition. It is therefore concluded that a strong vibronic interaction exists between the $^3A_1$ (π,π^*) and $^3B_2$ (π,π^*) states *via* the ν_{8b} type vibration, which leads to the pseudo-Jahn-Teller distortion.

The sublevel spectra for the x-trap have structures quite different from those for isolated PCA. The T_y

Table 7. Relative values of radiative decay rate constants of *p*-chloroaniline

System	PCA in *p*-xylene			n-trap			x-trap		
Symmefry $\Delta\nu$	a_1 (0, 0)	b_1 323 cm^{-1}	b_2 1581 cm^{-1}	a_1 (0, 0)	b_1 322 cm^{-1}	b_2 1578 cm^{-1}	a_1 (0, 0)	b_1 325 cm^{-1}	b_2 1577 cm^{-1}
k_y^r	1.0	1.0	1.0	1.0	1.0	1.0	1.0	1.0	1.0
k_z^r	0.007	0.22	9.0	0.12	0.26	0.83	1.0	0.9	0.8
k_x^r	0.001	0.001	0.07	0.02_6	0.006	0.05	0.09	0.02	0.06_6

The maximum experimental error is estimated to be 25%.

and T_z spectra resemble each other except for the small intensity difference in the individual vibronic bands. These are considered to be a mixture of the T_y and T_z characters of isolated PCA. Each spectrum contains the strong (0,0), (0,0−325 cm^{-1}) and (0,0−1577 cm^{-1}) bands which belong to the a_1, b_1 and b_2 symmetries, respectively. On the other hand, the T_y and T_z spectra of the n-trap system seem to show a feature similar to those of isolated PCA. The (0,0) band in the T_z spectrum is weaker than the (0,0−322 cm^{-1}) band, but the relative intensity of the (0,0−1578 cm^{-1}) band is extremely strong compared with that in the T_y spectrum. This anomalous behavior of the two types of traps in the PCA crystals is considered to originate from a distortion of the electronic structure induced by impurity molecules (*p*-dichlorobenzene for the x-trap) or by defects in the crystal.

The lifetime of the T_x sublevel emission of isolated PCA in *p*-xylene is about 10 s or about 100 times longer than that of the T_y emission. Although the presence of the out-of-plane vibrations is well understood by the mechanisms given in Table 4, the strong appearance of the ν_{8b} type vibration and the (0,0) band in the T_x spectrum cannot be explained by the selection rule for the C_{2v} symmetry, because the spin-orbit coupling between the $^3A_1$ (π,π^*) and $^1B_2$ (π,π^*) states is small. The emission from the weakly radiative T_x sublevel seems to be sensitively affected by the crystal field.

The T_x spectra of the n- and x-traps contain strong (0,0) and (0,0−1577 cm^{-1}) bands and have similar stuctures except for the quasi-continuum background intensity. The intensities of the totally symmetric vibration bands apparently exceed those of the out-of-plane vibronic bands. This phenomenon can be attributed to the external heavy-atom effect due to the chlorine atoms of the nearby PCA molecules.

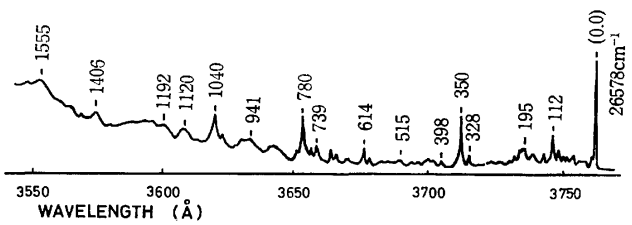

Fig. 6. The $T_1 \leftarrow S_0$ absorption spectrum of the *p*-chloroaniline crystal.

Direct Pumping of Each Triplet Vibronic Level, Energy-Transfer and Nature of the Traps. The $T_1 \leftarrow S_0$ absorption spectrum of a PCA crystal is shown in Fig. 6. The spectrum exhibits a relatively strong (0,0) band at 26578 cm^{-1} and resembles that of a symmetry allowed transition. On the shorter wavelength side of 3650 Å, it becomes much broader. The excitation spectrum was also observed with a high-pressure mercury arc lamp and nearly the same band widths as those in the absorption spectrum were obtained. Under the same conditions as those for the observation of the excitation spectrum, the dependence of the relative populating rates for the three sublevels on the excitation energy was examined by means of the MIDP and fast passage PMDR techniques. Typical fast passage

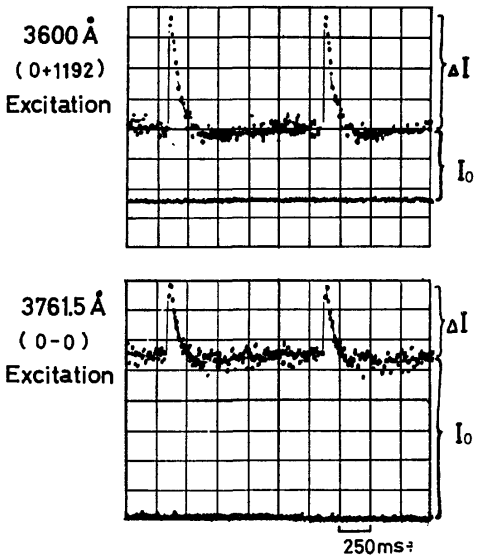

Fig. 7. Typical examples of the fast passage PMDR signals obtained by observing the total phosphorescence of the x-trap when the sample was excited at the (0,0) band (bottom) and at the (0,0+1192 cm^{-1}) band (top) of the $T_1 \leftarrow S_0$ spectrum.

PMDR signals for the two different excitation energies are shown in Fig. 7. The quantity, $\Delta I/I_0$, in Fig. 7 is a measure of the population difference between the sublevels connected by the resonant microwave pulse. After some manipulation, it yields the relative populating rate.

The transition probability for excitation to each sublevel in the triplet manifold is expected to change with the electronic and geometrical stucture of the excited vibronic state. In other words, the populating rate obtained by pumping one of the vibronic levels in the lowest triplet state of the crystal and by monitoring the trap emission is expected to reflect the transition probability for excitation to one of the individual spin states in that vibronic level, if spin alignment is conserved during the processes of vibrational relaxation, energy transfer and phosphorescence decay.

The vibrational relaxation to the lowest exciton level is believed to be fast enough to preserve the selective pumping probabilities. For the triplet-triplet energy transfer process, El-Sayed *et al.* have shown that the spin directions are conserved in the case of the x-trap emission of a naphthalene crystal doped with quinoxaline.[11,12] These authors have concluded that the triplet-triplet energy transfer takes place by the electron exchange mechanism and the probability of transfer between one spin direction in the molecular framework of a donor and the three spin directions in the molecular framework of an acceptor is proportional to the squares of the projection of the spin direction of the donor onto the spin directions of the acceptor.

The dependence of the relative populating rates on the excitation energy for both the n- and x-traps are shown in Fig. 8. As can be seen from the figure, the populating rate ratios change dynamically from one vibronic band to another. Figure 8 shows the following important facts:

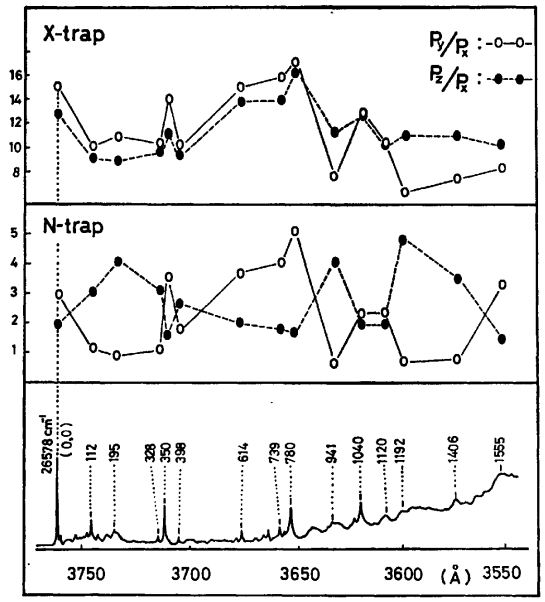

Fig. 8. The populating rate ratios obtained at 1.3 K by pumping each of the vibronic levels in the triplet manifold of the neat crystal (middle) and the *p*-chloroaniline crystal doped with *p*-dichlorobenzene (top) are plotted against the excitation energy. At the bottom, the $T_1 \leftarrow S_0$ absorption spectrum is shown for convenience.

1) The ratios P_u/P_x (u=y and z) change in a similar way with the excitation energy in the x-trap system, while they change in a different manner in the n-trap system.

2) The P_u/P_x ratios for (0,0) band excitation are in good agreement with the (0,0) band k_u^r/k_x^r ratios for the x-trap, while for the n-trap they are much smaller than the k_u^r/k_x^r ratios.

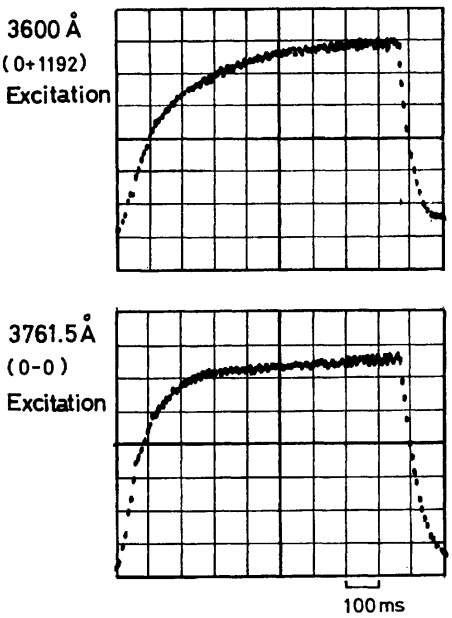

Fig. 9. The phosphorescence rise curves for the x-trap obtained by exciting at the (0,0) band (bottom) and at the (0,0+1192 cm^{-1}) band (top) of the $T_1 \leftarrow S_0$ absorption. After the excitation for about 860 ms, the exciting light was removed to observe the initial part of the decay.

In order to check the growing process of the sublevel population, the phosphorescence rise curves for the respective exciting energies were examined under the same conditions as those for the observation of the excitation spectrum. Typical examples are shown in Fig. 9, where the initial part of the phosphorescence decay is also recorded after the observation of the growth curve for about 860 ms. The two curves in Fig. 9 apparently indicate that the growing rate of the longer lifetime component is considerably faster than the decay rate and that the optical pumping of the crystal spin state from which the relaxation occurs mainly to the T_x sublevel is fairly enhanced on the excitation in the (0,0+1192 cm^{-1}) band compared with that in the (0,0) band.

The marked changes in the rise curves and the populating rates for trap molecule systems suggest that the spin-lattice relaxation in the exciton spin states scarcely affects the deactivation processes to the sublevels of the emitting trap molecules. The fact that the x- and n-traps in the PCA crystals have different populating rate ratios for the same exciting energy is considered to give support to the conclusion obtained by El-Sayed *et al.*[11,12]

In the x-trap system, the characters of the T_y and T_z sublevels are different from those in isolated PCA. The sublevel spectra and the ratios of the radiative decay rates of the x-trap can be explained by the mixing of the T_y and T_z states of isolated PCA. If *p*-dichlorobenzene molecules are substituted into the PCA crystal, one of the two chlorine atoms of the *p*-dichlorobenzene is found at a position otherwise occupied by an amino group, and is expected to interact with the two neighboring chlorine atoms of the nearby PCA molecules, because these three chlorine atoms are located closely together on a plane nearly paralled to the bc plane of the crytal, as is shown in Fig. 10. Therefore, repulsive forces act between the chlorine atoms, and the chlorine

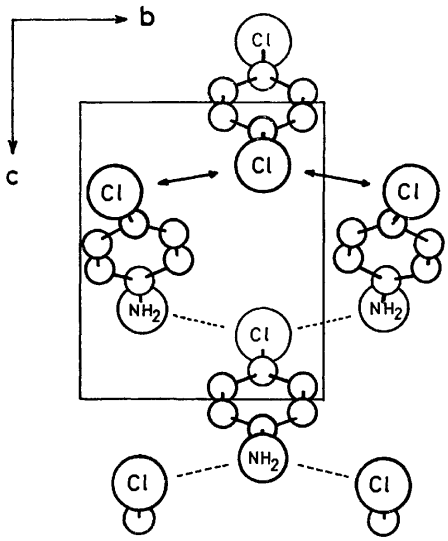

Fig. 10. Illustration of a possible structure of the x-trap induced in the *p*-chloroaniline crystal by doping *p*-dichlorobenzene. The solid arrow indicates the repulsive force and the dotted line shows attractive force.

atoms of these PCA molecules approach the neighboring amino groups. The y axes of the PCA molecules are thus expected to be distorted so as to be bent from the crystal b axis, which otherwise coincides with the y axis. Electronic distortion of these molecules is also expected to occur mainly in the molecular yz plane. This model seems to explain well the observed results for the x-trap system, where the z spin axis is considered to change its direction from the molecular long (N–Cl) axis toward the crystal b axis.

By using the conclusion of El-Sayed *et al.*, the spin directions or, equivalently, the populating rates for the trap sublevels under (0,0) band excitation are explained by the squares of the direction cosines between the crystal spin axes and those in the trap molecules. The (0,0) band pumping is expected to excite the crystal selectively to the T_b spin state, and also to a small extent to the T_a and T_c states by means of the external heavy-atom effect. Spin-orbit coupling which gives the transition intensity for the (0,0) band excitation of the $T_a \leftarrow S_0$ and $T_c \leftarrow S_0$ transitions comes from three-center integrals and is weaker than the external heavy-atom perturbation in the PCA crystal as mentioned above. However, the transition probability to the T_a or T_c spin state is not considered to exceed 10% of that to the T_b state, because the k_y^r/k_x^r values in the n- and x-trap systems are large enough for the (0,0) band emission. Since excitation at the (0,0) origin of the $^3B_{1u}$ or $^3B_{3u}$ factor group state results mostly in the population of the T_b spin state, the observed ratio of $P_y/P_z \cong 1.2$ is then expected to represent the ratio $\cos^2\theta_{by}/\cos^2\theta_{bz}$, where $\cos\theta_{by}$ and $\cos\theta_{bz}$ are the projections of the crystal b axis onto the y- and z-spin axes of the x-trap molecule, respectively. By assuming that the angle between the y- and z-spin axes is 90° and the yz plane includes the b axis, θ_{by} and θ_{bz} are estimated to be about 42° and 48°, respectively. Spin axis rotation of 45° has been recently reported for the case of tetramethylpyrazine in durene.[13]

The populating rate ratios P_u/P_x are small in the n-trap or, equivalently, the populating rate P_x is relatively large. This cannot be explained by the external heavy-atom effect alone, as mentioned previously. The large P_x is considered to be caused by the trapping process from the crystal T_b state to the trap T_x state. Considering the experimental errors in the populating rate ratios obtained, one may roughly estimate the range of the angles of the n-trap molecule to be $35° \lesssim \theta_{by} \lesssim 45°$, $53° \lesssim \theta_{bz} \lesssim 63°$ and $60° \lesssim \theta_{bx} \lesssim 70°$. We already know that the radiative decay rate ratios for the n-trap molecules are not so different from those of the isolated PCA molecules in *p*-xylene. Therefore, we can conclude that the deviation in orientation of the n-trap molecules does not affect its electronic structure as much as in the case of the x-trap, where the intermolecular interaction between the trap PCA and the neighboring *p*-dichlorobenzene is considered to play an important role in determining its electronic structure. Probably, the n-trap is not induced by a chemical impurity, but is produced by a crystal defect characteristic of the PCA crystal, because the n-trap is produced quite generally and no strong emissions from other traps can be found in the same spectral region.

Vibrational Analysis of the $T_1 \leftarrow S_0$ Spectrum. The variations of the P_u/P_x ratios with the excitation energy reflect the characteristics of the vibronic levels in the triplet manifold, and are thus utilized for the vibrational analysis of the $T_1 \leftarrow S_0$ absorption spectrum of the PCA crystal. Although the vibronic selection rule for the $T_1 \leftarrow S_0$ transition of the crystal depends on the representations of the factor group states, it is expected that the selection rule is correlated with the vibronic characteristics of the emission spectrum.

From the feature described for the n-trap system in the section on the vibrational analysis of the phosphorescence spectrum and the results shown in Fig. 8, it can be said that the transitions involving totally symmetric vibrations give a relatively large P_y/P_x ratio and a small P_z/P_x ratio, while the transitions involving the vibrations of b_2 symmetry give a relatively small P_y/P_x ratio and a large P_z/P_x ratio for the populating processes in the n-trap. On the other hand, it seems rather difficult to predict the P_u/P_x ratios for transitions involving the out-of-plane a_2 and b_1 vibrations.

The out-of-plane vibrations are expected to have low frequencies in the T_1 state. The bands at $0+112$, $0+195$, $0+328$ and $0+398\ cm^{-1}$ show small P_y/P_x ratios and large P_z/P_x ratios, and all of these low-frequency vibrations appear to have little possibility of belonging to the b_2 in-plane mode. If we attach considerable importance to the facts that they have relatively large P_u/P_x values and low-vibrational frequencies, these bands could be assigned to transitions to the out-of-plane vibronic levels.

The transitions corresponding to the band at $0+350\ cm^{-1}$ is active in the processes to T_y and T_x and this vibration can possibly be assigned to the a_1 or b_1 vibration in the crystal system. By assuming a mirror-image relation of the spectral features for emission and absorption, this strong band might be assigned to the transition to the b_1 vibrational level. The corresponding emission band appears at $0-323\ cm^{-1}$ in the PCA-doped xylene system. However, it should be noted that this ν_{10} type out-of-plane mode in *p*-dichlorobenzene shows no frequency change in the triplet and ground states and the frequencies of other vibrations also change very little[14]. If the band at $0+350\ cm^{-1}$ is due to the ν_{10} type vibration, which involves an out-of-plane C–Cl bending, the increment in frequency becomes about 8% upon transfer to the excited state. This seems to be too large. The line at $0+350\ cm^{-1}$ is more reasonably assigned as being due to a totally symmetric C–Cl bending vibration that is at $379\ cm^{-1}$ in the ground state in the *p*-xylene solution, since the populating rate ratios for excitation to this level are close to those obtained for the (0,0) band excitation, and the strong totally symmetric vibration band has been observed at $0+356\ cm^{-1}$ in the $^1B_2\ (\pi,\pi^*) \leftarrow {}^1A_1$ spectrum by Marchetti.[15]

In the wavelength region shorter than 3650 Å, the spectrum becomes broader and the bands, which can be assigned to b_2 vibrations, appear. The intensities of these b_2 bands, however, are not too strong. Burland, Castro and Robinson have studied the $^3B_{1u} \leftarrow {}^1A_{1g}$ absorption spectrum of benzene using the phosphores-

cence photo-excitation method.[16] They concluded that the ν_8 type vibration, the direction of which is related to the direction of the molecular distortion, is shifted by the pseudo-Jahn-Teller interaction from 1600 cm^{-1} in the ground state to 250 cm^{-1} in the excited triplet state.[16] In PCA, this normal mode splits into the ν_{8a} (a_1) and ν_{8b} (b_2) vibrations. The frequencies of these normal modes in the ground state are 1600 and 1581 cm^{-1}, respectively, in the *p*-xylene solution.[1] The absorption band at $0+1555$ cm^{-1} is reasonably assigned as being due to the a_1 fundamental corresponding to the ν_{8a} type vibration. The frequency change is about -3%, but larger than those found in *p*-dichloro- and *p*-dibromo-benzenes, where the frequency changes are $+0.3$ and $+0.2\%$, respectively.[14]

This ν_{8a} assignment leads to the conclusion that the force constants for the C=C stretching vibration in the excited state is much the same as in the ground state and does not produce such a low frequency for the antisymmetric ν_{8b} type vibration as in the case of benzene. The geometrical change caused by the pseudo-Jahn-Teller interaction is not expected to be large. This conclusion seems to be consistent with the fact that the (0,0) band in the T_z sublevel spectrum of PCA in *p*-xylene is extremely weak. The most probable band due to the ν_{8b} type mode is the one at $0+1406$ cm^{-1}.

The final results of the analysis of the main bands observed in the absorption spectrum of the PCA crystal are summarized in Table 8, where the frequencies of each state are compared. The frequency changes in the observed normal modes in the ground state, in the first excited singlet and triplet states are relatively small and the structural difference of the molecule between the first excited singlet and triplet states is also regarded as being very small.

Table 8. Vibrational analysis of the $T_1 \leftarrow S_0$ absorption spectrum of *p*-chloroaniline crystal and comparison of the vibrational frequencies (in units of cm^{-1})

	T_1	S_0[a]	S_1[b]	T_1 of DCB[c]
(0, 0)				
112	b_1 or a_2	145	144(ac)	97
195	b_1 or a_2	223		192
328	b_1	318		299(b_{2g})
350	a_1(C–Cl bend.)	379	356(abc)	330(a_g)
398	a_2	(416)[d]	408(ac)	406(a_u)
614	a_1(C–Cl str.)	637	631(ac)	
739	(a_1)	—	696(ac)	668(a_g)
780	a_1(C–C str.)	826	797(abc)	
941	b_2(C–H bend.)	1118		
1040	a_1(C–H bend.)	1090	1059(abc)	1051(a_g)
1120	(a_1)	1171	1132(ac)	1081(a_g)
1192	b_2(C–H bend.)	1380	1208(b)	
1406	b_2(C=C str.)	1596	1400(b)	
1555	a_1(C=C str.)	1602		1578(a_g)

a) V. B. Singh, R. N. Singh, and I. S. Singh, *Spectrochim. Acta*, **22**, 927 (1966). b) Ref. 15. c) DCB= *p*-dichlorobenzene, Ref. 14. d) This value is from the phosphorescence spectrum in the *p*-xylene solution.

References

1) E. Kanezaki, N. Nishi, M. Kinoshita, and K. Niimori, *Chem. Phys. Lett.*, **29**, 529 (1974).
2) C. J. Winscom and A. H. Maki, *Chem. Phys. Lett.*, **12**, 264 (1971).
3) J. Schmidt, W. S. Veeman, and J. H. van der Waals, *Chem. Phys. Lett.*, **4**, 341 (1969).
4) J. Schmidt, D. A. Antheunis, and J. H. van der Waals, *Mol. Phys.*, **22**, 1 (1971).
5) J. H. Palm, *Acta Crystallogr*, **21**, 473 (1966).
6) A. P. Marchetti, *J. Chem. Phys.*, **57**, 5475 (1972).
7) H. Port and H. C. Wolf, *Z. Naturforsch.*, **23a**, 315 (1968).
8) D. A. Antheunis, Thesis, University of Leiden, The Netherlands (1974).
9) E. R. Bernstein, S. D. Colson, D. S. Tinti, and G. W. Robinson, *J. Chem. Phys.*, **48**, 4632 (1968).
10) D. M. Haaland and G. C. Nieman, *J. Chem. Phys.*, **59**, 4423 (1973).
11) M. A. El-Sayed, D. S. Tinti, and E. M. Yee, *J. Chem. Phys.*, **51**, 5721 (1969).
12) M. A. El-Sayed, *J. Chem. Phys.*, **54**, 680 (1971).
13) D. A. Antheunis, B. J. Botter, J. Schmidt, and J. H. van der Waals, *Mol. Phys.*, **29**, 49 (1975).
14) G. Castro and R. M. Hochstrasser, *J. Chem. Phys.*, **46**, 3617 (1967).
15) A. P. Marchetti, *J. Chem. Phys.*, **56**, 5101 (1972).
16) D. M. Burland, G. Castro, and G. W. Robinson, *J. Chem. Phys.*, **52**, 4100 (1970).

Degradation Spectra and the *G*-values for Ionization and Excitation of the Mixtures of Noble Gases

Kiyoshi OKAZAKI, Eizo OKU, and Shin SATO

Department of Applied Physics, Tokyo Institute of Technology, Ookayama, Meguro-ku, Tokyo 152

(Received October 31, 1975)

Degradation spectra of electrons and the *W*-values in the mixtures of He–Ne, He–Ar, Ne–Ar, and Ne–Kr irradiated by 100 keV electrons have been calculated by using the binary-encounter theory and the theory of the degradation spectrum. On the basis of these calculations, the Jesse effect, the negative Jesse effect, and the non-metastable Penning effect have been reconsidered. It was shown that at least a part of the negative Jesse effect and the non-metastable Penning effect are explicable as due to the degradation spectra of electrons.

The yield of electrons in a binary mixture of noble gases irradiated by charged particles has been measured by several investigators. In some cases, a drastic change in the yield with the change of mixing ratio has been found. In 1952 Jesse and Sadauskis found that the yield of electrons, G_e, in helium is increased remarkably by the addition of a very small amount (~0.01%) of argon (the Jesse effect).[1] They attributed this increase to the well-known metastable Penning ionization. Hurst and his co-workers also found that the yield of electrons in argon is increased after the addition of foreign gases.[2] In order to explain this increase, they considered not only the metastable Penning ionization but also the resonance state Penning ionization which occurs through photon imprisonment. Kubota measured the yield of electrons in a helium–neon mixture, in which the metastable Penning ionization cannot energetically occur; however, he obtained a positive deviation as if the Penning ionization were occurring.[3] He attributed this deviation to the non-metastable Penning ionization. Klots observed an extraordinary behavior of the yield of electrons in the mixtures of Ne–Ar, Ne–Kr, and He–CH_4.[4] For example, when krypton is added to neon, the yield of electrons rapidly increases to a high value symptomatic of the Jesse effect, but then plummets to a minimum before finally climbing up again to the value characteristic of pure krypton (the negative Jesse effect). He interpreted this phenomenon in terms of the Hornbeck-Molnar process and some process competing with it. In this manner, the variation of the yield of electrons with the change of components in binary mixtures has been interpreted in terms of the metastable, resonance state, and non-metastable Penning ionizations and also of the Hornbeck-Molnar process. There is definite evidence for the metastable Penning ionization,[5,6] but no explicit evidence exists for the non-metastable Penning ionization and for the quenching of the Hornbeck-Molnar process.

Previously, we estimated the *G*-values for ionizations and excitations of pure noble gases irradiated by 100 keV electrons by a combination of the binary encounter collision theory and the theory of degradation spectrum.[7–11] The calculated *G*-values of electrons in pure noble gases are in fair accordance with the experimental values obtained by considering the double collision and the inner shell excitation. In that paper, we predicted that the yields for ionizations and excitations in the mixture greatly depend on the components, because the degradation spectra of electrons are quite dependent upon the type of noble gas.

In this paper, we apply the calculating method to estimate the *G*-values for ionizations in the mixtures of noble gases irradiated by 100 keV electrons and investigate the effect of the degradation spectra on the change of the yields of ionizations and excitations. We choose the mixtures of He–Ne, He–Ar, Ne–Ar, and Ne–Kr, because in these mixtures drastic changes of the *G*-values of electrons have been reported.

Method of Calculation

We consider a mixture of A and B gases. The basic procedure for the calculation on the mixture is analogous to that of a pure gas. The equations of the differential cross section, $\sigma_E(T)$, and of the cross section for ionization and excitation, $Q_s(T)$, are the same as those shown in the previous papers.[7,8] The cross sections for the double collisions and the inner shell excitations are also the same as those shown previously.[8]

Stopping Power. First we calculate the stopping power of the pure A gas, $S_A(T)$, and that of the pure B gas, $S_B(T)$, by use of the equation described previously.[7] Then, the stopping power of A–B mixture, $S_m(T)$, may be described as the combination of $S_A(T)$ and $S_B(T)$:

$$S_m(T) = \frac{p_A}{p_A+p_B}S_A(T) + \frac{p_B}{p_A+p_B}S_B(T) \qquad \text{(I)}$$

for $T \geq E_{t,A}$. Here, $E_{t,A}$ is the energy of the lowest excited triplet state of the A gas and $E_{t,A} > E_{t,B}$ is assumed. $E_{t,B}$ is the energy of the lowest excited triplet state of the B gas. p_A and p_B are the partial pressures of each component. Equation (I) holds only in the energy range where both A- and B-components can contribute to the energy loss of the incident electron.

When the energy of the incident electrons is lower than $E_{t,A}$, the A-component cannot contribute to the energy loss and only the B-component participates in the energy loss of the electrons. That is, when $E_{t,B} \leq T < E_{t,A}$, the first term of the right-hand side of Eq. (I) disappears; when $T < E_{t,B}$, both terms disappear.

Degradation Spectrum. On the assumption of a continuous slowing down, the degradation spectrum of the incident electron in the mixture may be expressed in a manner similar to that described previously:[7]

$$y_1(T) = 1/S_m(T) \qquad \text{(II)}$$

The degradation spectrum of the secondary electrons

consists of two terms, which correspond respectively to the ionizations of the A- and B-components.

$$y_2(T) = \frac{p_A}{p_A+p_B}\frac{N}{S_m(T)}\sum_i n_{i,A}\int_T^{(T_0-I_{i,A})/2}\int_{2T_2+I_{i,A}}^{T_0} \times y_1(T_1)\sigma_A(T_1, T_2)\mathrm{d}T_1\mathrm{d}T_2 + \frac{p_B}{p_A+p_B}\frac{N}{S_m(T)}\sum_i n_{i,B}\int_T^{(T_0-I_{i,B})/2}\int_{2T_2+I_{i,B}}^{T_0} \times y_1(T_1)\sigma_B(T_1, T_2)\mathrm{d}T_1\mathrm{d}T_2 \quad \text{(III)}$$

Here, N is the number of atoms in a unit volume, n_i is the number of electrons in the i-th shell, T_0 is the energy of the incident electrons, I_i is the binding energy of the electron in the i-th shell, and $\sigma(T_1, T_2)$ is the differential cross section for the production of a secondary electron with the energy of T_2 in a collision between the atomic electron in the i-th shell and the incident electron with the energy of T_1. The suffixes A and B correspond to A- and B-components. Similar equations may be constructed for the electrons ejected in the later steps.

The total degradation spectrum, $y(T)$, is the sum of the above spectra:

$$y(T) = \sum_k y_k(T) \quad \text{(IV)}$$

The $y(T)$ thus obtained contains the electrons produced in the ionization of the B-component in the collision with the electrons ejected from the A-component and *vice versa*.

Once $y(T)$ is obtained, the yields of ionizations and excitations can be calculated by using the following equation:

$$N_s = \int_{T_s}^{T_0} Ty(T)Q_s(T)\mathrm{d}\ln T \quad \text{(V)}$$

$$G_s = 100N_s/T_0 \quad \text{(VI)}$$

Here, N_s is the number of species produced in the s-process, T_s is the threshold energy for the s-process and G_s is the G-value of s-process.

The constants used for the calculation are the same as those reported in the previous paper.[7,8]

Results

He–Ne Mixture. Figure 1 shows the component dependence of $y(T)$ in the helium–neon mixture under a constant total pressure (1 atm). The $y(T)$ in pure helium is completely separated from those calculated for the mixtures in the whole energy range.

In order to investigate the effect of the change of $y(T)$ on the yield of ionization, the $Ty(T)\,Q_s(T)$'s for the ionization of helium and for that of neon are plotted as a function of ln T in Figs. 2A and 2B, respectively. The $Ty(T)\,Q_s(T)$ for helium in the 1:1 mixture is about 0.13 times that in pure helium, while that for neon is about 0.91 times that in pure neon; *i.e.*, the changes in the ionization yield do not compensate with each other.

Figures 3A and 3B show the G-values for the ionizations and excitations of helium and neon as a function of the parameter Z. This parameter was used by Kubota and equals the ratio of $p_{Ne}/(p_{Ne}+0.316\,p_{He})$.[3] p_{Ne} and p_{He} are the partial pressures of neon and helium, and 0.316 is the ratio of the stopping powers of the two gases. As Fig. 3A shows, the decreasing curve of the G-value for the ionization of helium is concave, while the increasing curve for neon is convex, and the total G-values of ionization do not lie on a straight line. In this figure, the energy exchange between Ne and He is not taken into account.

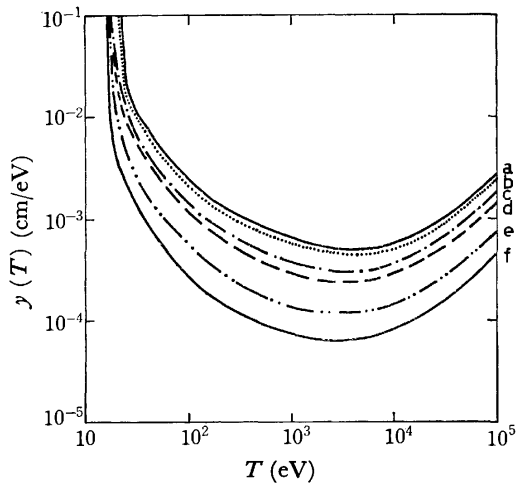

Fig. 1. The component dependence of $y(T)$ in the He–Ne mixture as a function of ln T.
a, $p_{Ne}/(p_{He}+p_{Ne})=0$; b, 0.038; c, 0.096; d, 0.162; e, 0.473; f, 1.0.

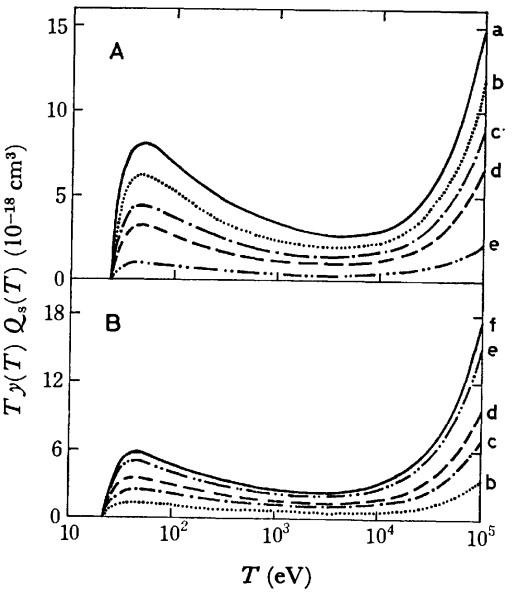

Fig. 2. The component dependence of $Ty(T)\,Q_s(T)$ in the He–Ne mixture as a function of ln T.
A, ionization of He; B, ionization of Ne from the 2p shell.
a, $p_{Ne}/(p_{He}+p_{Ne})=0$; b, 0.038; c, 0.096; d, 0.162; e, 0.473; f, 1.0.

He–Ar Mixture. Figure 4 shows $y(T)$'s for the helium–argon mixtures. The curves are similar to those for the helium–neon mixtures shown in Fig. 1. Figures 5A and 5B show the component dependence of the $Ty(T)\,Q_s(T)$'s for the ionization of helium and for that of argon from the 3p shell. The $Ty(T)\,Q_s(T)$ for helium decreases smoothly with a decrease in the partial pressure of helium, while the $Ty(T)\,Q_s(T)$ for argon behaves strangely in the electron energy range below

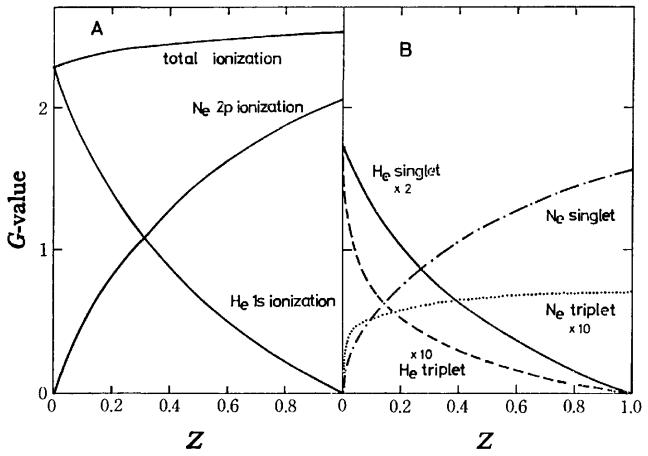

Fig. 3. The G-values for the ionizations and excitations of He and Ne in the He–Ne mixture as a function of Z.
A, Ionization; B, excitation.

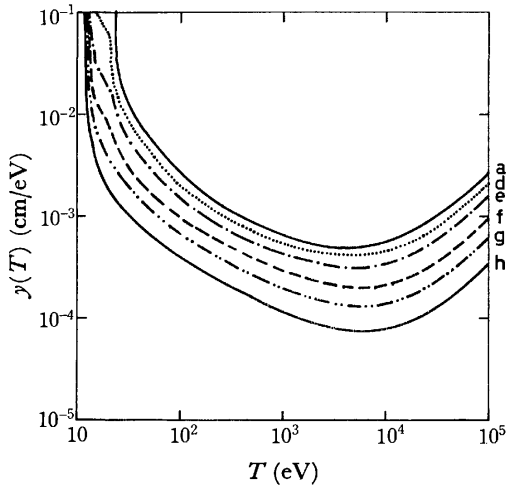

Fig. 4. The component dependence of $y(T)$ in the He–Ar mixture as a function of ln T.
a, $p_{Ar}/(p_{He}+p_{Ar})=0$; d, 0.040; e, 0.112; f, 0.274; g, 0.5; h, 1.0.

20 eV. This part of $T\,y(T)\,Q_s(T)$ does not decrease with a decrease in the partial pressure of argon. The reason is obviously that, since the lowest triplet state of helium is 19.8 eV, the electrons whose kinetic energies are lower than 19.8 eV cannot lose their energies in the collision with helium, but lose their energies only in the collision with argon.

Figures 6A and 6B show the G-values for ionizations and excitations of each component as a function of the parameter Z. This parameter equals $2.79\,p_{Ar}/(2.79\,p_{Ar}+p_{He})$. Here, 2.79 is the ratio of the stopping powers of two gases in the treatment of Klots.[4] It is characteristic in Fig. 6B that the G-value for the triplet excitation of Ar in the mixture with helium is larger than that in pure argon. In this mixture, we must also consider the Penning ionization, which will be discussed later.

Ne–Ar Mixture. Figure 7 shows the component dependence of $y(T)$ in the neon–argon mixture. It is noticeable that the curves for $y(T)$ intersect at two points, where the energies of electrons are 56 and 10^4 eV.

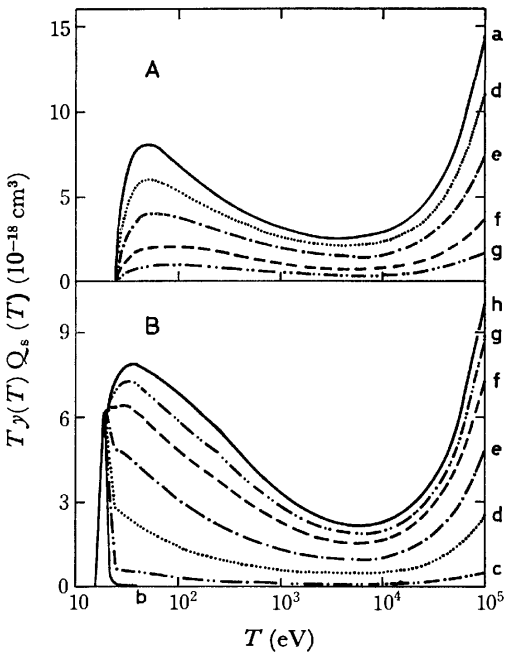

Fig. 5. The component dependence of $T\,y(T)\,Q_s(T)$ in the He–Ar mixture as a function of ln T.
A, Ionization of He; B, ionization of Ar from the 3p shell.
a, $p_{Ar}/(p_{He}+p_{Ar})=0$; b, 0.001; c, 0.007; d, 0.040; e, 0.112; f, 0.274; g, 0.5; h, 1.0.

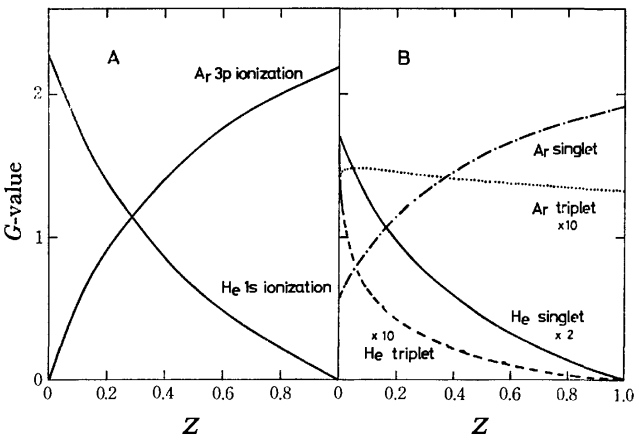

Fig. 6. The G-values for the ionizations and excitations of He and Ar in the He–Ar mixture as a function of Z.
A, Ionization; B, excitation.

Such crossings were not obtained in the mixtures of helium–neon and helium–argon.

Figure 8 shows the component dependence of the $T\,y(T)\,Q_s(T)$ for the ionization of argon from the 3p shell. There is a non-decreasing part at about 20 eV with the decrease in the partial pressure of argon. This is similar to the $T\,y(T)\,Q_s(T)$ for the ionization of argon in the He–Ar mixture.

Figures 9A and 9B show the G-values for the ionizations and excitations of each component. Here the parameter $Z=p_{Ar}/(p_{Ar}+0.75\,p_{Ne})$ is used as the abscissa, according to the treatment of Klots.[4] It is noticeable in Fig. 9A that the tendency of the change of the G-values for the ionizations in the Ne–Ar mixture is oppo-

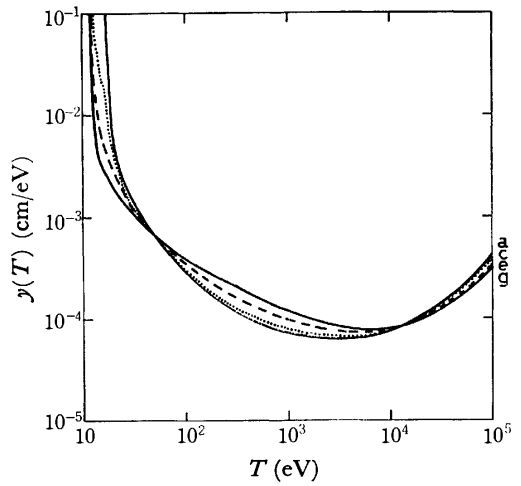

Fig. 7. The component dependence of $y(T)$ in the Ne–Ar mixture as a function of ln T.
a, $p_{Ar}/(p_{Ne}+p_{Ar})=0$; c, 0.165; e, 0.543; g, 1.0.

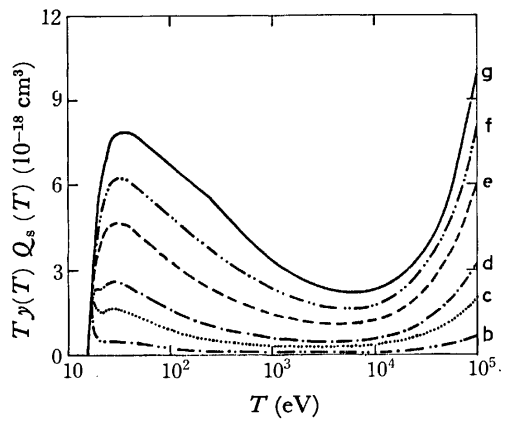

Fig. 8. The component dependence of $T\,y(T)\,Q_s(T)$ for the ionization of Ar from the 3p shell in the Ne–Ar mixture as a function of ln T.
b, $p_{Ar}/(p_{Ne}+p_{Ar})=0.05$; C, 0.165; d, 0.274; e, 0.543; f, 0.760; g, 1.0.

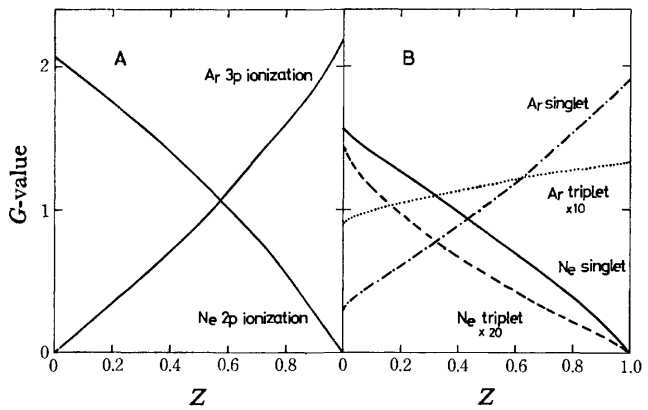

Fig. 9. The G-values for the ionizations and excitations of Ne and Ar in the Ne–Ar mixture as a function of Z.
A, Ionization; B, excitation.

Fig. 10. The component dependence of $y(T)$ in the Ne–Kr mixture as a function of ln T.
a, $p_{Kr}/(p_{Ne}+p_{Kr})=0$; c, 0.234; d, 0.5; f, 1.0.

Fig. 11. The component dependence of $T\,y(T)\,Q_s(T)$ for the ionization of Kr from the 4p shell in the Ne–Kr mixture as a function of ln T.
b, $p_{Kr}/(p_{Ne}+p_{Kr})=0.019$; c, 0.234; d, 0.5; e, 0.75; f, 1.0.

Fig. 12. The G-values for the ionizations and excitations of Ne and Kr in the Ne–Kr mixture as a function of Z.
A, Ionization; B, excitation.

site to that in the He–Ar mixture: *i.e.*, the curve of the G-value for the ionization of neon, whose ionization potential is higher than that of argon, is convex, while the curve for the ionization of argon is concave. The situation of the excitations in the Ne–Ar mixture is also quite different from that in the He–Ne and He–Ar mix-

tures. For example, the change of the G-values for singlet excitation of neon shows an S-shaped curve.

Ne–Kr Mixture. The $y(T)$'s and $Ty(T)\ Q_s(T)$'s for the Ne–Kr mixture are similar to those for the Ne–Ar mixture. These are shown in Figs. 10 and 11. Figures 12A and 12B show the G-values for the ionizations and excitations of each component. The abscissa is the parameter Z, which is equal to $p_{Kr}/(p_{Kr}+0.465\ p_{Ne})$ according to the treatment of Klots.[4] The general tendency of each curve is similar to that for the Ne–Ar mixture.

Discussion

He–Ne Mixture. Since the lowest excited states of helium are located at 19.8 (^{3}S) and 21.2 eV (^{1}P) and the ionization potential of neon is known to be 21.56 eV, the so-called Penning ionization cannot energetically occur in this mixture. Consequently, Haeberli *et al.* expected that the W-values in this mixture should satisfy this equation:[12]

$$1/W_m = (1/W_A - 1/W_B)Z + 1/W_B \qquad (1)$$

Here, $Z=[p_A+(S_B/S_A)\ p_B]^{-1}\ p_A$. A and B stand for He and Ne in the present case, and S_A and S_B for the stopping powers of the two gases. However, Kubota observed that the experimental results do not satisfy Eq. 1: *i.e.*, the total G-value of ionization deviates positively from the straight line expected from Eq. 1.[3] He explained this positive deviation as due to the non-metastable Penning ionization. According to the present calculation, however, a similar positive deviation can be obtained as the result of the change of $y(T)$. This is shown in Fig. 3.

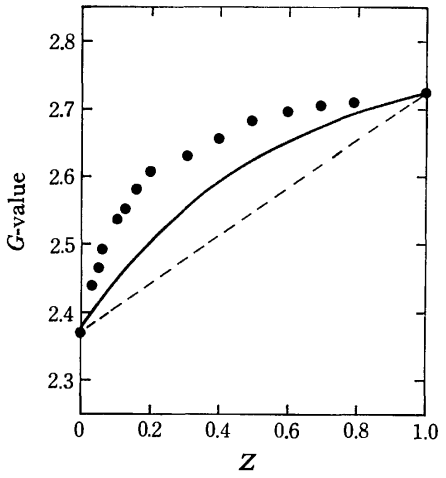

Fig. 13. The total G-value of electrons in the He–Ne mixture as a function of Z.
—, Calculated; ●, Kubota's experimental.

In order to check the deviation quantitatively, Kubota's experimental results are reproduced in Fig. 13 together with the calculated curve. The absolute G-values for ionizations in pure states calculated and experimentally obtained do not coincide with each other. Therefore, the following correction has been made for the calculated G-values:

$$G_{ion}' = G(A^+)f_A + G(B^+)f_B \qquad (2)$$

Here, $G(A^+)$ and $G(B^+)$ are the calculated G-values of A^+ ion and B^+ ion in a mixture and f_A and f_B are the ratios of the experimentally obtained G-values to the calculated G-values in the pure states of A and B.

As Fig. 13 shows, about a half of positive deviation can be explained as the result of the change of $y(T)$. It may be obvious from this figure that the non-metastable Penning ionization is not a unique explanation for the deviation from the straight line expected from Eq. 1.

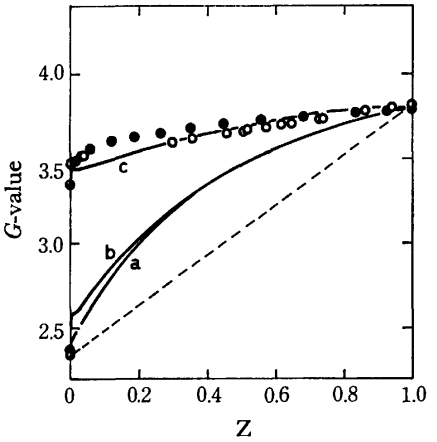

Fig. 14. The total G-value of electrons in the He–Ar mixture as a function of Z.
—, Calculated; ●, Kubota's experimental; ○, Klots' experimental.

He–Ar Mixture. There are two sets of experimental data for this mixture: one is that of Klots,[4] the other of Kubota.[3] They are reproduced in Fig. 14, together with the calculated curve. The curve a was obtained in a manner similar to that used in the case of the He–Ne mixture. In this mixture, we have to consider the Penning ionization, because the ionization potential of argon (15.7 eV) is much lower than the energy of the lowest triplet state of helium (19.8 eV).

If the metastable Penning ionization is taken into account:

$$He(^3S)^* + Ar \longrightarrow He + Ar^+ + e^- \qquad (3)$$

the calculated G-values increase to the curve b. The curve c was drawn by taking into account the so-called resonance state-Penning ionization.

$$He(^1P)^{**} + Ar \longrightarrow He + Ar^+ + e^- \qquad (4)$$

The radiative lifetime of the $He(^1P)^{**}$ is very short; however, the photon imprisonment will prolong its apparent lifetime.[13] The agreement between experimental plots and the calculated curve is very good.

Ne–Ar Mixture. In the case of this mixture, Klots did not show the experimental data in his paper, but did report the parameters obtained by his interpretation.[4] Using his parameters, the curve for the ionization has been reproduced in Fig. 15. The curves a,b, and c have been drawn by using the calculated values in a manner similar to that in curves a,b, and c in Fig. 14. The calculated curve does not agree at all with the curve obtained experimentally. However, there is another

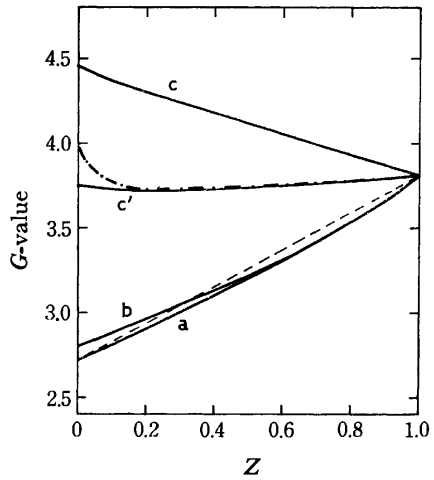

Fig. 15. The total G-value of electrons in the Ne–Ar mixture as a function of Z.
—, Calculated; —·—, Klots' experimental.

problem we have to consider here: *i.e.*, the ratio between the calculated G-value and the experimentally obtained G-value for the excitation is not necessarily equal to the ratio for the ionization, f_A or f_B. If the ratio between the calculated G-value and the experimental one for the singlet excitation of the A gas, Ne in the present case, is assumed to be 0.58, then the curve c′ in Fig. 15 can be obtained. In spite of this modification, the agreement between experiment and calculation could not be attained, especially in the range of small partial pressure of Ne. This disagreement might reflect some invalidity in the present explanation; however, a detailed inspection of the following mixture suggests that our explanation is one of the possibilities.

Ne–Kr Mixture. Klots' experimental data is reproduced in Fig. 16. The curves a, b, and c were drawn in a manner similar to that used in the case of the Ne–Ar mixture. Although the curve c does not agree at all with the experimental data, a small bump observed at a very small concentration of Kr is reproduced in the curve c. In the interpretation by Klots, this bump comes from the incomplete quenching of the excited state of Ne by Kr atoms. However, the small bump in the curve c is the result of a calculation in which the incomplete quenching was not taken into account.

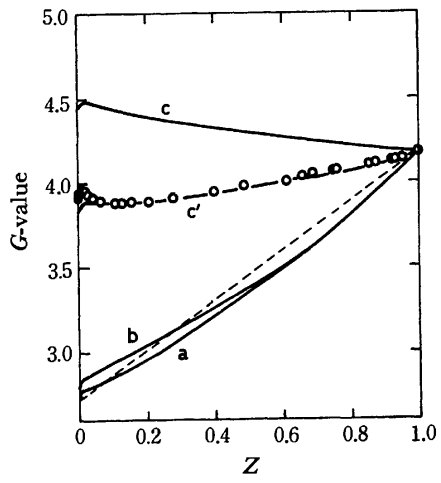

Fig. 16. The total G-value of electrons in the Ne–Kr mixture as a function of Z.
—, Calculated; ○, Klots' experimental.

As was done in the case of the Ne–Ar mixture, if the ratio between the experimentally obtained G-value and the calculated one for the singlet excitation of Ne is assumed to be 0.63, the curve c′ can be obtained. The experimental plots lie close to the curve c′.

Conclusion

In order to explain the change of the W-values in binary rare gas mixtures with the change of the mixing ratio, unestablished processes such as the non-metastable Penning ionization and the quenching of the Hornbeck-Molnar process have so far been proposed. As has been shown above, we can explain some of the change of the W-values which accompanies the change of the mixing ratio in terms of the change of the degradation spectra. Consequently, it may be conclude that, when we discuss the W-value of a binary mixture, we have to consider the degradation spectrum in detail.

References

1) W. P. Jesse and J. Sadauskis, *Phys. Rev.*, **88**, 417 (1952).
2) T. E. Bortner and G. S. Hurst, *Phys. Rev.*, **93**, 1236 (1954). C. E. Melton, G. S. Hurst, and T. E. Bortner, *ibid.*, **96**, 643 (1954). H. J. Moe, T. E. Bortner, and G. S. Hurst, *J. Phys. Chem.*, **61**, 422 (1957). G. S. Hurst, T. E. Bortner, and R. E. Glick, *J. Chem. Phys.*, **42**, 713 (1965). J. E. Parks, G. S. Hurst, T. E. Stewart, and H. L. Weidner, *ibid.*, **57**, 5467 (1972).
3) S. Kubota, *J. Phys. Soc. Jpn.*, **29**, 1017 (1970).
4) C. E. Klots, *J. Chem. Phys.*, **46**, 3468 (1967).
5) M. L. Coleman, R. Hammond, and J. W. Dubrin, *Chem. Phys. Lett.*, **19**, 271 (1973).
6) G. Lantschner and A. Niehaus, *Chem. Phys. Lett.*, **23**, 223 (1973).
7) S. Sato, K. Okazaki, and S. Ohno, *Bull. Chem. Soc. Jpn.*, **47**, 2174 (1974).
8) K. Okazaki, S. Sato, and S. Ohno, *Bull. Chem. Soc. Jpn.*, **48**, 1411 (1975).
9) S. Ohno, H. Nagayama, K. Okazaki, and S. Sato, *Bull. Chem. Soc. Jpn.*, **48**, 2153 (1975).
10) K. Okazaki, S. Sato, and S. Ohno, *Bull. Chem. Soc. Jpn.*, **49**, 174 (1976).
11) K. Okazaki and S. Sato, *Bull. Chem. Soc. Jpn.*, **48**, 3523 (1975).
12) W. Haeberli, P. Huber, and E. Baldinger, *Helv. Phys. Acta*, **26**, 145 (1953).
13) A. C. G. Mitchell and M. W. Zemansky, "Resonance Radiation and Excited Atoms," Cambridge University Press, London (1934).

An Analytical Study of pre-Inca Pigments, Dyes, and Fibers

K. Maresuke KASHIWAGI

Department of Textiles and Clothing, Kyoritsu Women's University, Hitotsubashi, Chiyoda-ku, Tokyo 101

(Received November 12, 1975)

The total analysis of 800-year-old Peruvian pigments with regard to the inorganic elements was carried out; some typical pigments, like mercury sulfide and iron oxide, are shown. Some characteristic pre-Inca (6—7 th century Tiahaunaco and 13—14 th century Chancay) dyes including cochineal, indigo, and probably logwood were identified from old fabrics by means of absorption spectroscopy and also chromatographic analysis. Two kinds of fiber constituting those fabrics were also investigated, and a few chemical analyses, including that of the amino-acid composition of protein fiber and that of the extent of the degradation of old cellulose fiber, were made.

Aside from the marvellous weaving technology of the pre-Inca period, which was developed at a very early date (2000 B.C.) and which remains in use today, the colors developed by those people present very interesting scientific problems today. Our present knowledge of those ancient dyestuffs is limited because the Incas did not leave any written documents and because those Indios who are their descendants have not yet been completely assimulated into Western culture.

Two kinds of dyed fabrics and five kinds of pigments were obtained by the courtesy of Mr. Yoshitaro Amano of the Museo Amano, Lima, Peru. One kind of fabrics was identified at the museum as from Chancay in the 13—14 th century, and the other, as from Tiahaunaco in the 6—7 th century. The pigments, all in powdered state, were found at Lauri, 87 km north of Lima, some time ago and were identified as of pre-Inca times (about 800 years ago).

Experimental

In addition to our previous methods–namely, paper chromatography[1,2] and the modern knowledge of organic chemistry,[3,4] all of which were successfully applied to the identification of certain dyestuffs in the old textiles, the present author adopted mass spectroscopy and high-frequency plasma spectroscopy of old inorganic pigments and absorption spectroscopy with regard to the extracted dyes.

Analysis of Pigments. About 10^{-2} g of each substance was dissolved by heating in a mixture of 0.5 ml of sulfuric acid and 2 ml of nitric acid, the mixture was then diluted to make a 20 ml solution. A Hitachi high-frequency plasma torch instrument, Model 300, was used to measure the characteristic spectra of each element at temperatures higher than 6000 °C. The mass spectroscopic measurements were carried out by the use of a Hitachi Mass Spectrometer, RNU6MG.

Analysis of Dyes. Dye extraction from the fabrics was made mostly according to Saltzman's method[5] using sulfuric acid, which destroyed the substrate fiber. However, we sometimes used our previous method for extraction employing ethanol and a small amount of hydrochloric acid.[2] Paper chromatography experiments were carried out at 30 °C with a developing solvent composed of butanol–acetic acid–water (4–1–1 by volume) except for the blue dyes of the indigo type. The developing solvent for the blue dye was composed of the supernatant solution from a mixture methyl acetate–2-propanol–25% aq. NaOH (45–35–20). The absorption spectra of those extracted dyes were measured by means of a Shimadzu Spectrophotometer, MPS-50L.

Analysis of Fibers. The fabrics were composed of Peruvian cotton and animal fiber of a Llama or Alpaca type, both of which could easily be recognized under a microscope.[6] The two kinds of fiber were further examined under a scanning electron microscope, Shimadzu EMX-SM. To estimate the extent of deterioration of the cellulose fiber, a small amount of white cellulose was removed from one of the Chancay fabrics and nitrated to measure the degree of polymerization by way of viscometry.[7] The amino acid composition of the protein fiber was determined by the use of the JLC-5AH analyzer at the Kanagawa Industrial Research Institute.

Results and Discussion

The analytical results for those pigments are shown in Table 1, together with some additional data from mass-spectroscopic measurements. According to Table 1, showing information which is here disclosed for the first time, we may suppose that the pre-Inca people did have a good knowledge of iron, contrary to a common belief that they did not know how to use iron.

Among the possible red dyes used in those days, cochineal was very widely known in this area.[8,9] Other possible dyes were kermes, lac-dye, and a mixture of those with cochineal.[9] Those dyes are known to contain compounds structurally related to one another, all being derivatives of anthraquinone, as is shown in Fig. 1.[10,11] Beside those, a shell fish dye called purpula could supply red color depending on the kind of mordant used.[9]

The dyes extracted from the red parts of the Chancay and Tiahaunaco fabrics gave a single red spot at values between 0.51 and 0.54 of R_f on a paper chromatogram, while cochineal itself showed a single red spot at 0.54. The absorption spectra of those red dyes in dilute sul-

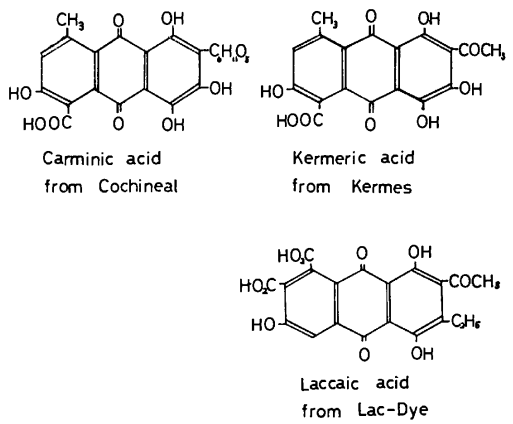

Fig. 1. Some anthraquinone dyes.

TABLE 1. ANALYSIS OF PIGMENTS USED 800 YEARS AGO IN CHANCAY AREA

Specimen	Color	Elements found (principal constituent and other minor ingradients)	Main constituent
1	red	Hg≫Sr, Na, Zn, Fe, Mg, Cu, Ni, Cr, Ca, Al, K	HgS
2	brown red	Fe≫Na, Zn, Mn, Mg, Cu, Ca, Al, K, Sr, Pb	Fe_2O_3
3	green	Cu≫P, Zn, Fe, B, Si, Mn, Mg, Ni, Cr, Ti, Mo, Ca, Al, K, Sr, Na	$CuCO_3Cu(OH)_2$ Marachite
4	dark yellow	mainly organic, metals found are Cu, Zn, Fe, Mg, Ca, Al, K, Na	lake with absorp. max. at 230 and 270 nm in acidic media
5	yellow	Fe≫Zn, Mg, Cu, Ca, Al, K, Sr, Na	$Fe_2O_3 \cdot H_2O$ or FeOOH

Other evidences found by Mass Spectra are:

1. Isotope conposition of Hg are the following.

Atomic wt.	Ratio%
198	10
199	16
200	23
201	13
202	30
203	0
204	7

4. Important constituent is organic.

furic acid were quite similar to that of cochineal, as is shown in Fig. 2. Moreover, the pH shifts of the absorption maxima of the dyes were quite identical to that of conhineal; they all exhibited maxima at 490 nm in acidic, 520—530 nm in neutral, and 550—560 nm in alkaline media.

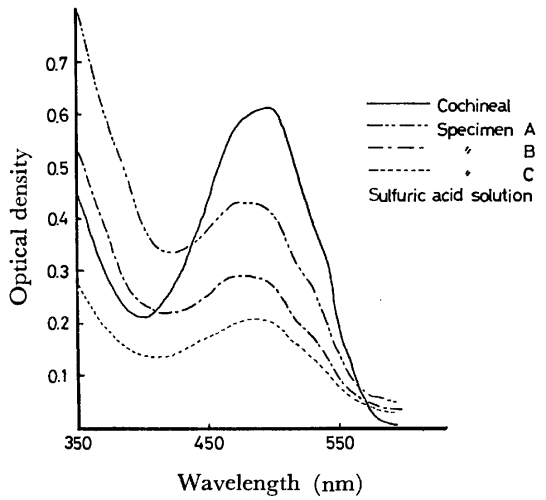

Fig. 2. Absorption spectra of the pre-Inca dyes and cochineal.

The blue dyes were extracted from the blue part of the old fabrics with sulfuric acid and chloroform. The extracts showed one blue spot at values from 0.68 to 0.72 of R_f in a paper chromatograph, while synthetic indigo showed one at 0.69.

The absorption spectra of those solution containing the blue dye extracted from fabrics and that of synthetic indigo are compared in Fig. 3. There seems to be little doubt that the blue dyes from the old fabrics were indigo; therefore, we can conclude that those blue colors must have been from a certain indigo-producing plant.

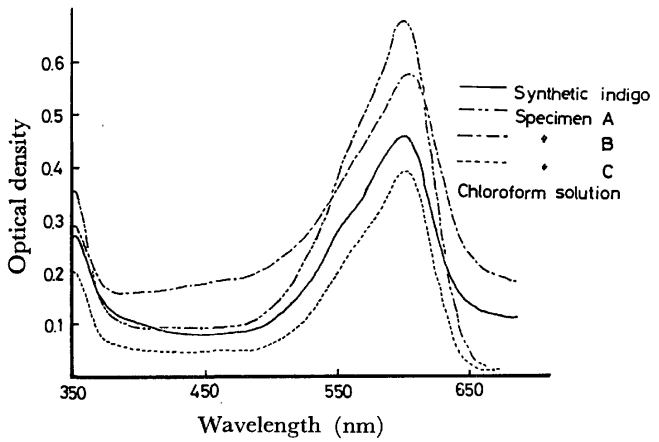

Fig. 3. Absorption spectra of the pre-Inca blue dyes and synthetic indigo.

Beside this indigo spot, another red spot with an R_f value of 0.84 appeared on the paper chromatogram. We tried to assign this red dye to some flavonoid compound by means of absorption spectra[12] and also by a few spot tests,[13] but we have not succeeded thus for. The pre-Inca people might, as in some other parts of the world, have attempted to produce a purple color from red and blue (mostly indigo),[9,14] as well as the famous purpula.

Black and golden yellow colors were often found in those fabrics. The dye extracted from the black parts of the fabrics exhibited two spots paper-chromatographically, one at 0.54 and the other at 0.34 of R_f, both of a dark yellow color. Moreover, the extracted golden yellow dye showed exactly the same spots as the black. This is taken to show that both colors originate from the same material, probably only the difference being the kind of mordant used. We further found that those two spots agreed with those from logwood extracts (R_f: 0.35 and 0.53). Logwood is well known to contain haematoxylin, which, on exposure to air, becomes

oxidized to haematein.

In addition, a series of dyeing experiments were undertaken, in them, among other items of interest, only logwood (Haematoxylon capechianum L.) exhibited both black as a result of the mordanting of $CuSO_4$ with a small amount of Fe and golden yellow color as a result of the use of acetic acid on silk cloth. We have not yet been successful in obtaining dependable absorption spectra and there is even a possibility that this dye polymerizes,[15] but it appears that both the black and golden yellow colors in those fabrics are probably from logwood.

Many pre-Inca fabrics were composed of cotton and animal protein fiber, one as warp and the other as weft, but sometimes the fabrics were interwoven in a more complicated manner. Those two kinds of fibers from one of the Chancay fabrics are shown in Fig. 4.

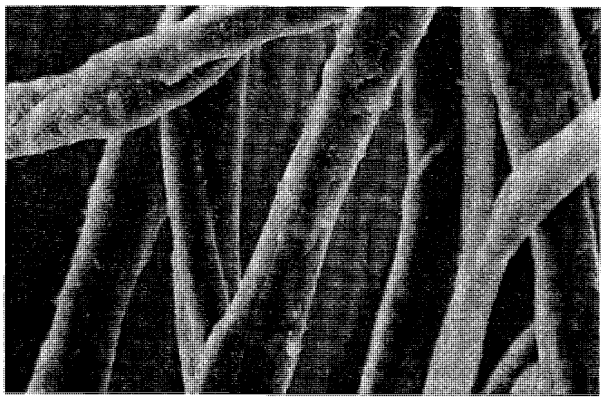

Cotten fiber.

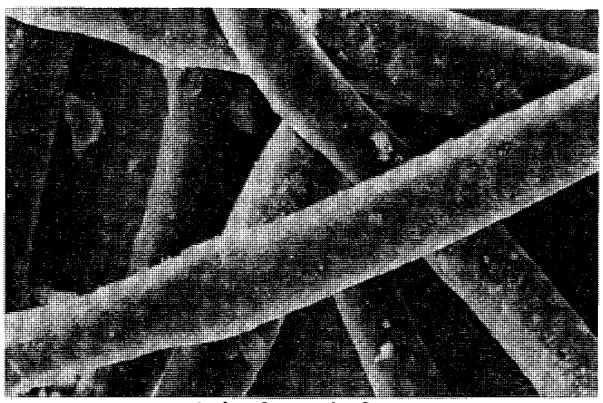

Animal protein fiber.

Fig. 4. Two kinds of old Peruvian textile fibers.

Many soil particles were often found everywhere along the fiber surfaces, and surface scratches were found under close examination. This evidence probably indicates that the fabrics had deteriorated over the long period of aging. To investigate the deterioration more quantitatively, both the degree of polymerization of cellulose (*DP*) and the total amino acid composition of the protein fiber were determined. The average *DP* for the old cellulose fiber thus calculated was 585, which was obviously lower than for natural cotton fiber. The following relation may approximately hold for cellulose deterioration under limited conditions.[16]

$1/DP - 1/DP_0 = kt$, where *DP* is the degree of polymerization at a certain time, DP_0 is the initial *DP* of cellulose, k is a constant, and t is the number of years elapsed. If k is assumed to be 1.86×10^{-6} and if DP_0 be 3500,[16] then we get $t=766$ years which corresponds to the early 13 th century. Table 2 shows the amino acid composition of pre-Inca protein fiber from fabrics which are known to be of the Llama type.

TABLE 2. AMINO ACID COMPOSITION OF PROTEIN FIBER (mol/10^5 g)

Amino acid	pre-Inca fiber	Llama	Camel	Merino wool
Lys.	14.7	19.3	20.9	20.6
His.	2.4	4.0	3.8	5.9
Arg.	50.6	55.8	56.0	52.0
Asp.	43.0	50.1	45.8	52.4
Thr.	43.1	47.2	47.5	53.6
Ser.	60.1	80.0	77.7	99.6
Glu.	120.0	109.0	114.0	94.7
Gly.	48.7	59.0	56.8	73.6
Ala.	38.2	40.4	39.8	44.7
Cys.	10.9	43.6	44.3	40.1
Val.	35.5	35.9	35.4	43.0
Met.	4.0	3.7	4.7	3.6
iso Leu.	19.9	20.8	20.0	21.5
Leu.	51.6	56.9	55.9	62.0
Tyr.	14.2	20.9	19.0	31.3
Phe.	15.1	24.1	16.4	23.9
Pro.	86.0	80.0	83.0	56.4

For comparison, the amino acid analyses of three other fresh protein fibers—llama, camel, and merino wool—was carried out; the results are shown in Table 2. From Table 2 it appears that the pre-Inca protein fiber was more similar to that of camel rather than that of llama, except for the difference in cystine content (10.9/44.3). Whether this and other minor differences in amino acid content are attributable to selective degradation due to long aging, or, to the pre-Incan people's use of other kinds of animal fiber, like vicuna or alpaca, is not clear at this stage.

The author wishes to thank especially Mr. Yoshitaro Amano of the Museo Amano, Lima, Peru for his courtesy and Prof. T. Yamanobe for his encouragement. He also appreciates the cooperation of Hitachi Ltd. and other organizations, including the Shimadzu Seisakusho Ltd. and the Kanagawa Industrial Research Institute. The expences were jointly taken care of by Kyoritsu Women's University and the Foundation Foreign Service for Private Universities, Japan.

References

1) M. Kashiwagi, *J. Home Economics (Jpn.)*, **22**, 253 (1971).
2) M. Kashiwagi and N. Kondo, *J. Home Economics (Jpn.)*, **22**, 258 (1971).
3) K. M. Kashiwagi, *Textile Res. J.*, **43**, 404 (1973).
4) M. Kashiwagi and N. Kondo, *J. Home Economics (Jpn.)*, **25**, 610 (1974).
5) M. Saltzman, A.M. Keay, and J. Christenesen, *Dyestuff*, **44**, 241 (1963).
6) Identification of Textile Materials by Textile Institute, Manchester (1965), pp. 11—54.
7) W. J. Alexander and R. L. Mitchell, *Anal. Chem.*, **12**

1497 (1949).
8) J. M. Diehl, "Textile Conservation," ed. by J. E. Leene, Butterworth, London (1972), p. 25.
9) R. J. Forbes, "Studies in Ancient Technology," IV, E. J. Brill, Leiden (1964), pp. 102—127.
10) S. Hattori and M. Shimokoriyama, "Plant and Animal Pigments," Asakura, Tokyo (1973), p. 121.
11) B. S. Joshi, "Recent Progress in the Chemistry of Natural and Synthetic Coloring Matters," ed. by T. S. Gore, B. S. Joshi, S. V. Sunthankar, and B. D. Tilak, Academic Press, New York (1962), pp. 127—136.
12) L. Jurd, "The Chemistry of Flavonoid Compounds," ed. by T. A. Geissman, Macmillan, New York (1962), pp. 107—131.
13) E. Haslam, "Chemistry of Vegetable Tannins," Academic Press, New York (1966), p. 20, 37.
14) T. Yoshioka, "Studies in Natural Dyes," Mitsumura Suikodo, Kyoto (1974), pp. 160—175.
15) R. H. Thomson, "Recent Progress in the Chemistry of Natural and Synthetic Coloring Matters," Academic Press, New York (1962), pp. 99—113.
16) M. Nagano, Private communication.

The Conformations of Oligosaccharides. III. The Crystal and Molecular Structure of Melibiose Monohydrate*

Ken HIROTSU and Taiichi HIGUCHI

Department of Chemistry, Faculty of Science, Osaka City University, Sugimoto-cho, Sumiyoshi-ku, Osaka 558

(Received November 12, 1975)

The crystal structure of α-melibiose monohydrate ($C_{12}H_{22}O_{11}\cdot H_2O$) was determined by direct methods using two-dimensional cosine invariants. The space group is $P2_12_12_1$, with $Z=4$ and unit cell dimensions of $a=15.814$ (5), $b=10.924$ (5), $c=8.903$ (4) Å. The structure was refined to $R=0.044$ for 1439 reflections measured with Mo$K\alpha$ radiation. Difference synthesis indicated the partial (15%) random substitution of α-melibiose molecules by the β-anomer. The molecular conformation of α-melibiose is almost the same as that previously found in the melibiose moiety of raffinose, although some of the bond lengths and angles are significantly different. The molecules are linked by complex hydrogen-bond systems which consist of six-link finite chains and five-membered closed loops.

The crystal structure of α-melibiose monohydrate has been determined as a part of a series of reports on the X-ray diffraction of carbohydrates.[1,2] α-Melibiose (*O*-α-D-galactopyranosyl-(1→6)-α-D-glucopyranoside) is the principal disaccharide of the melibiose group. It contains a galactose and a glucose moiety as shown in (I). The first purpose of this investigation was to compare the conformation of the melibiose unit in different intermolecular environments, *i.e.*, in this molecule and in the melibiose moiety of raffinose (Berman 1970).[3] The second purpose was to compare the bond lengths and bond angles common to melibiose and raffinose. The hydrogen bond scheme in the crystal is also of interest.

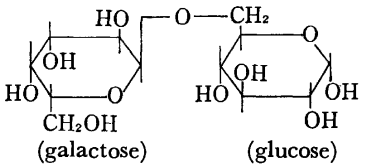

(I)

Experimental

Crystal Data. $C_{12}H_{22}O_{11}\cdot H_2O$, mol wt=360.3, orthorhombic, $a=15.814$ (5), $b=10.924$ (5), $c=8.903$ (4) Å, $U=1538.0$ Å^3. $D_m=1.54$ g·cm^{-3} (by flotation), $Z=4$, $D_c=1.556$ g·cm^{-3}. Mo$K\alpha$ radiation, $\lambda=0.7107$ Å, μ (Mo$K\alpha$) $=1.32$ cm^{-1}. Space group $P2_12_12_1$ (D_2^4, No. 19).

The crystal was grown by slow evaporation from a saturated aqueous solution of commercially available α-melibiose monohydrate. Unit cell parameters were determined using a standard Philips PW1100 X-ray diffractometer computer program, which investigates rows in the reciprocal lattice through the origin and scans the four highest weighted reflections and their anti-reflections (weighted by intensity and sin θ). The centers of gravity of these eight profiles are then used in a least-squares refinement of the spacing for that row.

Intensity Measurement. A crystal with the dimensions $0.22\times0.30\times0.18$ mm was used to measure the cell parameters and intensities with a Philips PW 1100 four-circle automatic diffractometer. The $\omega/2\theta$ scan method was employed (scan speed 0.03° s^{-1}, scan width $1°+0.3°\times\tan\theta$). The background was measured for 15 s on either side of the peak. Data were collected to a maximum θ of 27.5° with graphite-monochromated Mo$K\alpha$ radiation ($\lambda=0.7107$ Å). Of the 2062 independently measured reflections, 1439 were considered to be observed with $I>2.5\,\sigma(I)$, where $\sigma(I)=[(0.04I)^2+S+TAU^2\times B]^{1/2}$ S=scan count, B=total background count, and TAU=ratio of scan time to total background time. The intensities were corrected for Lorentz and polarization factors but not for absorption.

Structure Determination and Refinement. The structure was determined by a phasing procedure, based on the two-dimensional structure invariants $\cos(\phi_1+\phi_2+\phi_3)$ whose values were calculated with the following modified triple product formula[4] at an E threshold level of 1.85:

$$\cos(\phi_1+\phi_2+\phi_3) \simeq \frac{K\Psi}{|E_1E_2E_3|} + \frac{R_3}{|E_1E_2E_3|} \qquad (1)$$

where

$$\Psi = \langle(|E_{\vec{k}}|^{1/2}-\overline{|E|^{1/2}})(|E_{\vec{h}_1+\vec{k}}|^{1/2}-\overline{|E|^{1/2}})\times (|E_{-\vec{h}_1+\vec{k}}|^{1/2}-\overline{|E|^{1/2}})\,\big|\,|E_{\vec{k}}|>t\rangle_{\vec{k}},$$

$$\overline{|E|^{1/2}} = \langle|E_{\vec{k}}|^{1/2}\rangle_{\vec{k}},$$

$$\phi_i = \phi_{\vec{h}_i},\ |E_i| = |E_{\vec{h}_i}|,\quad i=1,2,3$$

$$R_3 = \frac{\sigma_3}{4\sigma_2^{3/2}}\left[\frac{3}{2}(|E_1E_2|^2+|E_2E_3|^2+|E_3E_1|^2) + |E_1|^2+|E_2|^2+|E_3|^2-\frac{7}{2}\right],$$

$h_1+h_2+h_3=0$, and the parameter K is the sliding scale factor. The phasing process was similar to that described by Duax, Weeks and Hauptman (1972).[5] The positions of 24 non-hydrogen atoms were easily located from the E-map and further confirmed by a least-squares refinement. Six cycles of isotropic block-diagonal least-squares refinement followed by two cycles of anisotropic refinement resulted in an R $(=\sum||F_o|-|F_c||/\sum|F_o|)$ value of 0.082. A difference map revealed hydrogen atoms attached to all carbon atoms and some of the hydroxyl hydrogen atoms. The electron density (1.22 e·Å^{-3}) of the peak at the position for the hydrogen atom attached to C(1) was about three times that of the other peaks (0.31—0.52 e·Å^{-3}). The second difference map after three cycles of anisotropic refinements, in which hydrogen atoms were included with an isotropic temperature factor, revealed the remaining hydrogen atoms. This map additionally showed a residual electron density of 0.95 e·Å^{-3} near the position assigned to H(Cl), which probably indicates the presence of a small amount of the β-anomer. The β-oxygen atom was located at about 1.38 Å from C(1). A similar example was found in the structure of α-lactose monohydrate (Fries, Rao and Sundaralingam, 1971).[6] Refinement of the carbon, oxygen and hydrogen parameters and of the occupancy factors for αO(1) and βO(1) was completed

* The papers in *Chem. Lett.*, **1973**, 83 and *Bull. Chem. Soc. Jpn.*, **47**, 1872 (1974) are designated as parts I and II, respectively, of this series.

TABLE 1. FRACTIONAL ATOMIC COORDINATES AND THERMAL PARAMETERS IN MELIBIOSE MONOHYDRATE
The anisotropic temperature factor is of the form of $\exp[-(\beta_{11}h^2+\beta_{22}k^2+\beta_{33}l^2+\beta_{12}hk+\beta_{13}hl+\beta_{23}kl)]$. Numbers in parentheses refer to standard deviations of the last place.

	$x\times10^4$	$y\times10^4$	$z\times10^4$	$\beta_{11}\times10^4$	$\beta_{22}\times10^4$	$\beta_{33}\times10^4$	$\beta_{12}\times10^4$	$\beta_{13}\times10^4$	$\beta_{23}\times10^4$
C(1)	2398(2)	384(4)	6648(4)	23(1)	83(4)	89(5)	1(4)	4(5)	13(8)
C(2)	2672(2)	−935(4)	6784(4)	24(1)	80(4)	56(4)	−18(4)	15(4)	−2(7)
C(3)	3567(2)	−1082(3)	7376(4)	32(2)	57(3)	55(4)	13(4)	6(4)	−9(7)
C(4)	4186(2)	−230(3)	6600(4)	24(1)	68(3)	58(4)	9(4)	7(4)	−36(7)
C(5)	3829(2)	1068(3)	6589(4)	22(1)	66(3)	59(4)	5(4)	6(4)	−24(7)
C(6)	4380(2)	2009(3)	5860(4)	28(1)	56(3)	88(5)	−9(4)	−11(5)	8(7)
C(1′)	5135(2)	2547(3)	3694(4)	27(1)	35(3)	105(5)	4(4)	7(5)	−2(7)
C(2′)	5058(2)	2492(3)	1983(4)	24(1)	74(3)	94(5)	−20(4)	6(5)	46(7)
C(3′)	5351(2)	1247(3)	1417(4)	37(2)	72(4)	90(5)	−41(4)	2(5)	4(8)
C(4′)	6245(2)	980(3)	2011(4)	38(2)	47(3)	109(5)	9(4)	29(5)	−15(8)
C(5′)	6255(2)	1103(3)	3716(4)	29(1)	44(3)	117(5)	−1(4)	16(5)	31(7)
C(6′)	7130(2)	954(4)	4390(5)	33(2)	78(4)	143(7)	11(5)	2(6)	50(9)
O(1)	2243(2)	828(3)	8069(3)	39(1)	72(3)	80(4)	30(4)	32(4)	−3(6)
O(2)	2089(2)	−1624(2)	7667(3)	33(1)	85(3)	87(3)	−34(3)	26(3)	−15(5)
O(3)	3845(2)	−2307(2)	7222(3)	38(1)	58(2)	113(4)	13(3)	14(4)	6(5)
O(4)	5000(2)	−253(2)	7308(3)	24(1)	83(3)	131(4)	12(3)	−27(4)	−47(6)
O(5)	3022(1)	1065(2)	5848(3)	22(1)	65(2)	77(3)	2(3)	−1(3)	20(5)
O(6)	4550(1)	1730(2)	4324(3)	24(1)	57(2)	71(3)	−21(3)	6(3)	0(5)
O(2′)	4235(2)	2812(3)	1525(3)	27(1)	128(4)	128(4)	0(3)	−15(4)	109(7)
O(3′)	5319(2)	1176(3)	−171(3)	52(1)	131(4)	79(4)	−65(4)	3(4)	−33(6)
O(4′)	6806(2)	1837(3)	1326(3)	30(1)	90(3)	115(4)	−4(3)	23(4)	6(6)
O(5′)	5972(1)	2311(2)	4153(3)	23(1)	59(2)	92(3)	−7(3)	1(3)	4(5)
O(6′)	7096(2)	939(3)	5998(3)	49(1)	123(4)	134(5)	36(4)	−37(5)	18(7)
W	6408(2)	−1477(3)	6203(3)	42(1)	97(3)	111(4)	−4(3)	−20(4)	0(6)
βO(1)	1618(11)	463(16)	6136(19)	3.51(4)[a]					

	$x\times10^3$	$y\times10^3$	$z\times10^3$	B		$x\times10^3$	$y\times10^3$	$z\times10^3$	B
H(C1)	186	53	604	2.4	H(C6′)	749	172	414	3.9
H(C2)	266	−129	583	1.6	H′(C6′)	738	9	401	2.4
H(C3)	358	−87	838	1.4	H(O1)	209	144	799	5.1
H(C4)	426	−49	559	1.4	H(O2)	208	−139	842	2.7
H(C5)	376	123	758	1.6	H(O3)	359	−268	770	4.4
H(C6)	487	206	646	3.8	H(O4)	498	7	−188	5.2
H′(C6)	411	277	590	2.2	H(O2′)	387	239	180	4.9
H(C1′)	501	340	402	1.8	H(O3′)	566	160	−53	5.2
H(C2′)	548	309	158	2.0	H(O4′)	728	157	133	5.6
H(C3′)	494	65	180	3.2	H(O6′)	685	6	610	8.2
H(C4′)	642	14	175	2.5	H(W)	617	−165	539	6.6
H(C5′)	590	48	414	1.8	H′(W)	593	−103	663	6.8

a) Isotropic temperature parameter. The occupancy parameters of O(1) and βO(1) are 0.848 and 0.152, respectively.

by the full matrix least-squares program. The total of the occupancy parameters was constrained to unity through the refinement. The function minimized was $\sum w(|F_o|-k\times|F_c|)^2$, where $w=1/\sigma(F)^2$. The final cycle gave an R value of 0.044 for all reflections. The occupancy parameter of αO(1) was 0.848 and that of βO(1) was 0.152. The atomic scattering factors used were those of the International Tables for X-ray Crystallography[7] and for the hydrogen atoms, those of Stewart, Davidson, and Simpson (1965).[8] The final positional and thermal parameters are given in Table 1; corresponding structure factors are listed in Table 2.**

** Table 2 has been submitted to, and is kept by the office of the Chemical Society of Japan, 5, 1-Chome, Kanda-Surugadai, Chiyoda-ku, Tokyo 101. (Document No. 7614).

Discussion

The molecular conformation of melibiose monohydrate is shown in Fig. 1, where the atomic numbering of the galactose moiety is primed.

Bond Lengths and Angles. The bond lengths and angles involving carbon and oxygen atoms are shown in Fig. 2, excluding those involving the βO (1) atom. The standard deviations are 0.004—0.005 Å for C–C and C–O bonds and 0.3° for the valence bond angles. E.s.d's for the C–H and O–H distances are 0.03—0.04 Å. The C(1)–βO(1) length is 1.32 Å. The C(2)–C(1)–βO(1) and O(5)–C(1)–βO(1) angles are 110.0° and 116.2°, respectively. The C(5)–C(6) bond length of the (1→6) linkage is 1.496 Å, which is rather short for a

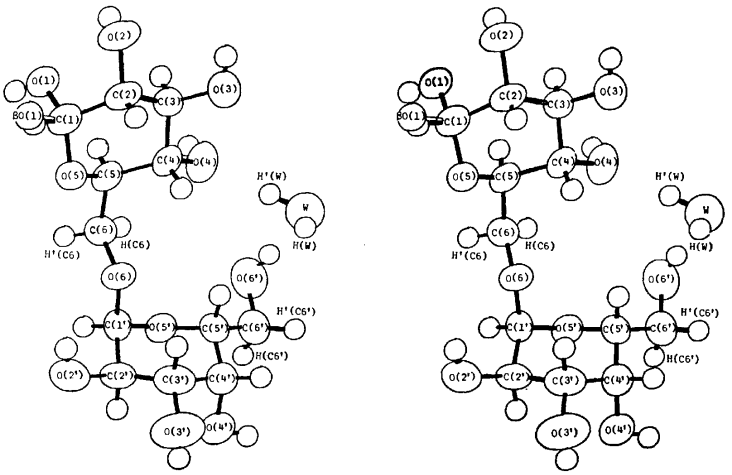

Fig. 1. Molecular conformation and atomic numbering in melibiose monohydrate. The 74% probability thermal ellipsoids are shown for the carbon and oxygen atoms.

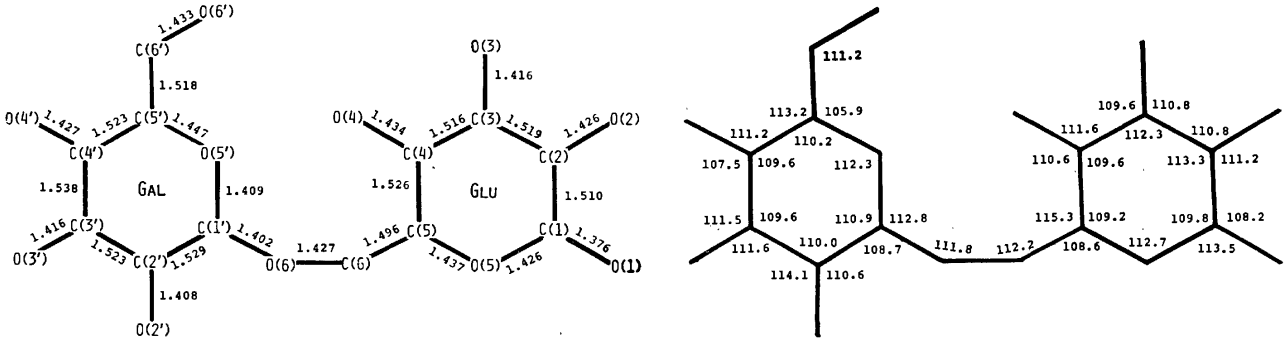

Fig. 2. Bond lengths (l/Å) and bond angles (ϕ/°).

TABLE 3. COMPARISON OF C–O BOND LENGTHS FOR HEMI-ACETAL GROUPS IN DI- AND TRISACCHARIDES

Compound	Pyranose ring	Configuration of C(1)–O(1) bond	C(5) — O(5) — C(1)	O(5) — C(1)	C(1)—O(1)	—R	References
α-Melibiose	Glu[a]	axial	1.437Å	1.426Å	1.376Å	H	this work
	Gal[b]	axial	1.447	1.402	1.402	$C_6H_{11}O_5$	
β-Lactose	Gal	equatorial	1.440	1.413	1.402	$C_6H_{11}O_5$	2
	Glu	equatorial	1.436	1.431	1.388	H	
α-Lactose	Gal	equatorial	1.448	1.427	1.389	$C_6H_{11}O_5$	6
	Glu	axial	1.425	1.443	1.387	H	
β-Cellobiose	Glu	equatorial	1.436	1.425	1.397	$C_6H_{11}O_5$	10
	Glu	equatorial	1.437	1.435	1.381	H	
Methyl β-cellobioside	Glu	equatorial	1.430	1.432	1.390	$C_6H_{11}O_5$	11
	Glu	equatorial	1.432	1.434	1.379	CH_3	
Trehalose	Glu	axial	1.433	1.421	1.415	$C_6H_{11}O_5$	14
	Glu	axial	1.431	1.404	1.422	$C_6H_{11}O_5$	
Methyl β-mal Topyranoside	Glu	axial	1.440	1.408	1.416	$C_7H_{13}O_5$	15
	Glu	equatorial	1.430	1.427	1.375	$C_6H_{11}O_5$	
Sucrose (X-ray)	Glu	axial	1.443	1.413	1.428	$C_6H_{11}O_5$	16, 17
Sucrose (Neutron)			1.439	1.411	1.422		
Isomaltulose	Glu	axial	1.430	1.427	1.397	$C_6H_{11}O_5$	18
Melezitose	Glu	axial	1.435	1.405	1.424	$C_{12}H_{21}O_{10}$	1
	Glu	axial	1.436	1.419	1.415	$C_{12}H_{21}O_{10}$	
Planteose	Glu	axial	1.430	1.416	1.415	$C_{12}H_{21}O_{10}$	9
	Gal	axial	1.444	1.418	1.414	$C_{12}H_{21}O_{10}$	
Raffinose	Glu	axial	1.433	1.419	1.402	$C_6H_{11}O_5$	3
	Gal	axial	1.436	1.422	1.428	$C_{12}H_{21}O_{10}$	
1-Kestose	Glu	axial	1.441	1.410	1.417	$C_{12}H_{21}O_{10}$	19

a) Glu=glucopyranose ring. b) Gal=galactopyranose ring.

TABLE 4. IMPORTANT TORSION ANGLES IN THE GLUCOSE AND GALACTOSE MOIETIES

	Glucose moiety		Galactose moiety	
Intracyclic torsion angles	C(1)–C(2)	50.4°	C(1′)–C(2′)	57.3°
	C(2)–C(3)	−46.3	C(2′)–C(3′)	−53.8
	C(3)–C(4)	49.1	C(3′)–C(4′)	54.3
	C(4)–C(5)	−57.7	C(4′)–C(5′)	−57.1
	C(5)–O(5)	65.6	C(5′)–O(5′)	61.6
	O(5)–C(1)	−61.0	O(5′)–C(1′)	−61.3
Extracyclic torsion angles	O(1)–C(1)–C(2)–O(2)	51.6°	O(6)–C(1′)–C(2′)–O(2′)	59.7°
	O(2)–C(2)–C(3)–O(3)	64.9	O(2′)–C(2′)–C(3′)–O(3′)	57.3
	O(3)–C(3)–C(4)–O(4)	−64.5	O(3′)–C(3′)–C(4′)–O(4′)	57.4
	O(4)–C(4)–C(5)–C(6)	56.3	O(4′)–C(4′)–C(5′)–C(6′)	−56.8
			O(5′)–C(5′)–C(6′)–O(6′)	65.6
			C(4′)–C(5′)–C(6′)–O(6′)	−173.5

C–C single bond. In planteose[9] also, the C(5)–C(6) bond of the (1→6) linkage is 1.494 Å. However, the corresponding bond in raffinose[3] is not markedly short (1.520 Å). A slight shortening of the exocyclic C(5)–C(6) bond has been observed in many carbohydrate structures.[2,6,10–12]

The C(1)–O(1) and C(1′)–O(6) bond lengths of melibiose are rather short. This shortening effect in the anomeric positions has been generally observed in oligosaccharides[13] and investigated theoretically.[14,15] The C–O bonds in both pyranoside rings show the same type of systematic disproportion. The C(1′)–O(5′) and C(5′)–O(5′) bond lengths in the galactose moiety are 1.409 and 1.447 Å, respectively, the latter bond being longer than the former by about 9σ. The same trend is observed in glucose moiety. The ring C–O and anomeric C–O bond lengths for the hemi-acetal group in di- and trisaccharides which contain glucose or galactose moiety are listed in Table 3. When R (the substituent at O(1)) is H or CH_3, the C(1)–O(1) lengths are markedly short. Systematic disproportion is not observed in ring C–O distances. When R is a pyranosyl group and O(1) is in an equatorial position, the mean distance of the C(1)–O(1) bonds is 1.391 Å. When O(1) is in an axial position, the corresponding mean distance is 1.416 Å, which is slightly longer than that of the axial C(1)–O(1) bond. The systematic disproportion, C(5)–O(5)>O(5)–C(1), is distinctly observed in both α- and β-pyranosides, excluding methyl β-cellobioside and isomultulose. The mean distances of C(5)–O(5) and O(5)–C(1) are 1.438 and 1.415 Å, respectively. There is a correlation between C(1)–O(1) and the ring C–O lengths of di- and trisaccharides given in Table 3. The difference between the C(5)–O(5) and O(5)–C(1) bond lengths becomes small with a shortening of the C(1)–O(1) bond. The difference becomes large with a lengthening of the C(1)–O(1) bond to the normal C–O single bond length.

The valence angles shown in Fig. 2 are not remarkable. The C(5)–C(6)–O(6) angle is 112.2°, which is larger by 4.2° than the corresponding angle in raffinose. The C(1′)–O(6)–C(6) angle is 111.8°

Molecular Conformation. The conformational angles in the pyranose rings are listed in Table 4. The torsion angles of the galactose moiety range from 53.8° to 61.6° with an average value of 57.6°. Those of the glucose moiety range more widely from 46.3° to 65.6° with an average value of 55.0°. The corresponding angles in the melibiose moiety of raffinose range from 52.7° to 59.5° and from 53.8° to 62.2° for the glucose and galactose moieties, respectively. The torsion angles around the ring C–O bonds are the largest, while those around C(2)–C(3), C(3)–C(4), C(2′)–C(3′), and C(3′)–C(4′), which are at the positions opposite to the ring C–O bonds, are the smallest. In the glucose moiety of melibiose, this trend is distinct. The difference between the torsion angles C(1)–C(2)–C(3)–C(4) and C(2)–C(3)–C(4)–C(5) is −95.4°, while the difference between the torsion angles C(4)–C(5)–O(5)–C(1) and C(5)–O(5)–C(1)–C(2) is 126.6°. This indicates smaller puckering in the region of C(3) and larger puckering in the region of O(5). Also, in the exocyclic torsion angles, those of the glucose moiety range more widely than those of the galactose moiety.

The conformation of the C(5′)–C(6′) bond of the galactose moiety is *plus synclinal*, while that of the corresponding bond of raffinose is *antiperiplanar*. From intramolecular interactions, these two conformations seem to be equally preferable, while *minus synclinal* conformation should be unfavorable because this conformation would have short O(6′)···O(4′) intramolecular contact.

TABLE 5. A COMPARISON OF THE TORSION ANGLES OF THE (1→6) LINKAGE IN MELIBIOSE AND RAFFINOSE

	Melibiose	Raffinose
O(5)–C(5)–C(6)–O(6)	−63.3°	−64.8°
C(4)–C(5)–C(6)–O(6)	59.6	58.4
C(5)–C(6)–O(6)–C(1′)	−173.9	−169.5
C(6)–O(6)–C(1′)–C(2′)	−160.5	−167.6
C(6)–O(6)–C(1′)–O(5′)	76.1	71.9

The conformation around the (1→6) linkage is of interest in that it determines the overall molecular form, and gives basic data which can be used to construct a model of macromolecular polysaccharides with a (1→6) linkage. The torsion angles around the (1→6) linkage in melibiose and raffinose are listed in Table 5. The conformations around the bridge bond of these two compounds are almost the same. The C(1′)–O(6) conformation is *plus synclinal*, the C(6)–O(6) conforma-

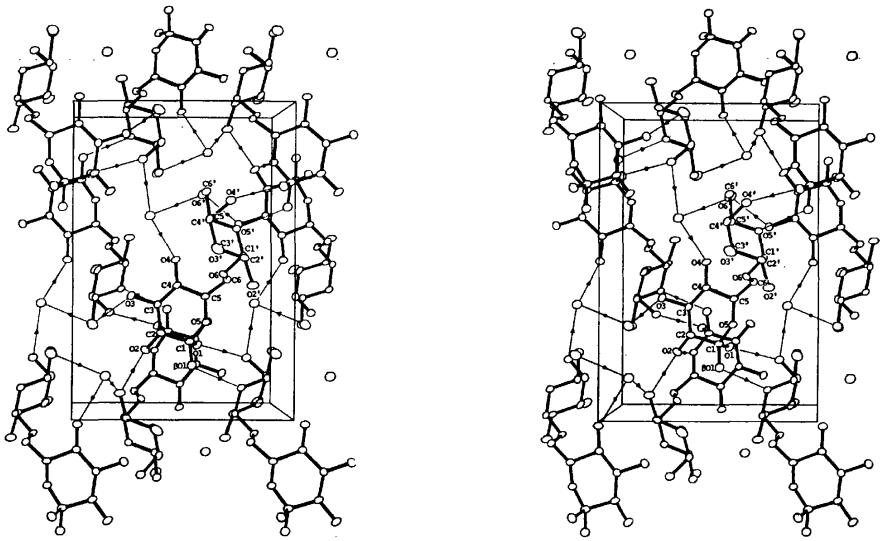

Fig. 3. Stereogram of melibiose monohydrate viewed down the c axis showing the packing and the hydrogen bonding scheme including that of the disordered oxygen atom βO(1).

TABLE 6. HYDROGEN BONDING

i	j	k	l	j-l	j-k	i-j-l	j-k-l	Symmetry code of l
C(1)	O(1)	H(O1)	O(4′)	2.697 Å	0.71 Å	124.2°	156°	(h)
C(2)	O(2)	H(O2)	O(5)	2.902	0.72	117.8	167	(d)
C(3)	O(3)	H(O3)	O(6′)	2.898	0.72	114.4	172	(l)
C(4)	O(4)	H(O4)	O(3′)	2.780	0.82	120.5	161	(b)
C(2′)	O(2′)	H(O2′)	O(2)	2.666	0.78	119.6	169	(f)
C(3′)	O(3′)	H(O3′)	O(3)	2.797	0.79	127.1	154	(i)
C(4′)	O(4′)	H(O4′)	W	2.854	0.81	122.7	162	(e)
C(6′)	O(6′)	H(O6′)	W	2.861	1.04	95.1	178	(a)
	W	H(W)	O(2′)	2.745	0.84		172	(k)
	W	H′(W)	O(4)	2.777	0.97		176	(a)
C(1)	βO(1)		O(5′)	2.683		118.4		(h)

Symmetry code

The letters refer to the symmetry operations to be applied to the coordinates listed in Table 1.

(a)	x,	y,	z	(g)	$-1/2+x$, $1/2-y$, $-z$
(b)	x,	y,	$1+z$	(h)	$-1/2+x$, $1/2-y$, $1-z$
(c)	x,	y,	$-1+z$	(i)	$1-x$, $1/2+y$, $1/2-z$
(d)	$1/2-x$,	$-y$,	$1/2+z$	(j)	$1-x$, $1/2+y$, $3/2-z$
(e)	$3/2-x$,	$-y$,	$-1/2+z$	(k)	$1-x$, $-1/2+y$, $1/2-z$
(f)	$1/2-x$,	$-y$,	$-1/2+z$	(l)	$1-x$, $-1/2+y$, $3/2-z$

tion is *antiperiplanar*, and the C(5)–C(6) conformation is *minus synclinal*. C(5), C(6), O(6), and C(1′) in melibiose are coplanar to within 0.04 Å. The same conformation of the (1→6) linkage is maintained in these two compounds in different intermolecular environments.

Hydrogen Bonding. The arrangement of the molecules in the structure is shown in Fig. 3. The molecules are linked by the complex system of hydrogen bonds given in Table 6. There are two major hydrogen bond sequences. One comprises a six-link finite chain:

O (1) (c) → O (4′) (g) → W (i) → O (2′) (a) → O (2) (f) → O (5) (a)

where → indicates the donor direction and the small letters refer to the symmetry codes given in Table 6. The other system consists of a five-membered closed loop:

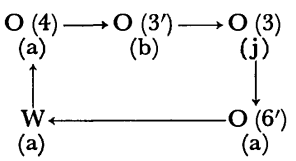

As shown in Table 6, the separation between βO(1) and O(5′) (2.683 Å) corresponds to the hydrogen bond distances. When the α-anomer in the crystalline melibiose is replaced by a β-anomer, the hydrogen bond, O(1)···O(4′), is missing, but there appears to be one compensating hydrogen bond between βO(1) and O(5′). Thus, the β-anomer can easily be accomodated in the crystal.

Each hydroxyl group except O(1)–H participates in two hydrogen bonds, in one as a donor and in the other as an acceptor. O(1)–H serves only as a donor. A

water molecule serves as a donor for two hydrogen bonds and an acceptor for two others. The ring oxygen O(5) takes part in hydrogen bonds as an acceptor. About 15% of the O(5′) atoms should be hydrogen bond acceptors. The glycosidic linkage oxygen atom is not involved in hydrogen bonds, just as in all crystal structures of di- and trisaccharides. There are no intramolecular hydrogen bonds.

Computer Programs

All calculations were performed on a FACOM 270/30 computer at the Computer Center of Osaka City University using the following programs: RSSFR-3,[20] HBLS-IV,[20] RSFLS-4,[20] MTPF (calculation of cosine invariants),[21] PHASE III (tangent refinement),[22] BOND (molecular dimensions),[23] and TECS (stereoscopic drawing of crystal and molecular structures).[24]

References

1) K. Hirotsu and A. Shimada, *Chem. Lett.*, **1973**, 82.
2) K. Hirotsu and A. Shimada, *Bull. Chem. Soc. Jpn.*, **47**, 1872 (1974).
3) H. M. Berman, *Acta Crystallogr.*, **B26**, 290 (1970).
4) H. A. Hauptman, "Crystal Structure Determination," Plenum Press, New York-London (1972), p. 287.
5) W. L. Duax, C. M. Weeks, and H. Hauptman, *Acta Crystallogr.*, **B28**, 1857 (1972).
6) D. C. Fries, S. T. Rao, and M. Sundaralingam, *Acta Crystallogr.*, **B27**, 994 (1971).
7) "International Tables for X-ray Crystallography," Vol. IV, Kynoch Press, Birmingham (1974).
8) R. F. Stewart, E. R. Davidson, and W. T. Simpson, *J. Chem. Phys.*, **42**, 3175 (1965).
9) D. C. Rohrer, *Acta Crystallogr.*, **B28**, 425 (1972).
10) S. S. C. Chu and G. A. Jeffrey, *Acta Crystallogr.*, **B24**, 830 (1968).
11) J. T. Ham and D. G. Williams, *Acta Crystallogr.*, **B26**, 1373 (1970).
12) G. M. Brown and H. A. Levy, *Science*, **147**, 1038 (1965).
13) H. M. Berman, S. S. C. Chu, and G. A. Jeffrey, *Science*, **157**, 1576 (1967).
14) G. A. Jeffrey, J. A. Pople, and L. Radom. *Carbohyd. Res.*, **25**, 117 (1972).
15) G. A. Jeffrey, J. A. Pople, and L. Radom, *Carbohyd. Res.*, **38**, 81 (1974).
16) G. M. Brown and H. A. Levy, *Acta Crystallogr.*, **B29**, 790 (1973).
17) J. C. Hanson, L. C. Sieker, and L. H. Jensen, *Acta Crystallogr.*, **B29**, 797 (1973).
18) W. Breissig and P. Luger, *Acta Crystallogr.*, **B29**, 514 (1973).
19) G. A. Jeffrey and Y. J. Park, *Acta Crystallogr.*, **B28**, 257 (1972).
20) "The Universal Crystallographic Computing System (I)," ed. by T. Sakurai, The Crystallographic Society of Japan (1967).
21) K. Hirotsu, unpublished work.
22) K. Hirotsu, unpublished work.
23) H. Yoshioka, unpublished work.
24) F. Takusagawa, unpublished work.

Formation Constants of Dibenzo-18-crown-6 Complexes with Alkali Metal Ions in DMSO, DMF, and PC at 25 °C

Niro MATSUURA, Kisaburo UMEMOTO, Yasuyuki TAKEDA, and Atsuko SASAKI

Department of Pure and Applied Sciences, College of General Education, The University of Tokyo, Komaba, Meguro-ku, Tokyo 153

(Received November 12, 1975)

The formation constants (K_f) for the 1:1 complexes of dibenzo-18-crown-6 (DBC) with alkali metal ions in DMSO (dimethyl sulfoxide), DMF (*N,N*-dimethyl formamide), and PC (propylene carbonate) have been determined conductometrically. The formation constant sequences of the alkali metal ions with DBC in DMSO, DMF, and PC are $K^+ > Rb^+ > Cs^+ \cong Na^+ \gg Li^+$, $K^+ > Rb^+ > Cs^+ > Na^+ > Li^+$, and $K^+ \gg Na^+ > Rb^+ > Cs^+ > Li^+$ respectively. The K_f value series about the same alkali metal ion among these nonaqueous solvents are given in the order of DMSO<DMF<PC. These results show that the selectivity of DBC toward the alkali metal ions is dependent on the ionic diameter and the ring-hole size of DBC, and that the donor number of the organic solvent as a component factor is important in determining the process of the formation of the DBC complexes constant.

In a number of recent papers Pedersen[1] has described many macrocyclic polyethers synthesized by him; these compounds form complexes with various salts. The complexing of alkali cations by neutral molecules is an uncommon and only recently observed phenomenon. The formation of the complexes between cyclic polyethers and alkali metal salts has been determined by several methods, for example, by a calorimetric titration technique by Izatt *et al.*,[2] by potential and conductance measurements by McLaughlin *et al.*,[3] by spectroscopic methods by Wong *et al.*,[4] by UV spectra and solvent extraction by Pedersen,[1b] and by potentiometry with cation-selective electrodes by Frensdorff.[5] They have reported the formation constants for complexing of these polyethers with several cations, and suggested that the specificity of the complexation is due to the surrounding solvent for the free cation and the required fit between the ionic radius and the hole size of the cyclic polyether ring. The present study was undertaken in order to quantify the strength of complexing in a solution as a function of the ionic radius, the hole size of the cyclic polyether ring, and the physical properties of the solvent. In this paper the formation constants for 1:1 complexes of dibenzo-18-crown-6 (DBC) with alkali metal ions (Li^+, Na^+, K^+, Rb^+, Cs^+) in DMSO (dimethyl sulfoxide), DMF (*N,N*-dimethyl formamide) and PC (propylene carbonate) have been determined conductometrically.

Experimental

Conductance Cell. The conductance cell was similar to those reported previously.[6]

Apparatus and Procedure. The measurements were carried out by means of a Yokogawa-Hewlette-Packard Universal Bridge. Cell solutions were thermostated to 25± 0.02 °C in a double water bath. The solution in the cell was stirred by means of a magnetic stirrer so that we might quickly obtain a temperature equilibrium. The cell temperature change was readily detected by the shift of resistance readings exceeding 0.01%. For the first run, DBC and alkali metal perchlorate were dissolved in the solvent in order to make the concentration of DBC equal that of alkali metal perchlorate. After a constant value of resistance had been attained, a 30-ml portion of the solution was siphoned out and equal volume of the solvent was added to the cell. This procedure was continued. The concentration range was from 7.6×10^{-4} to 3.1×10^{-3} M. For the second run, DBC of about 7.5×10^{-3} M was added to the solvent in the cell and the resistance of the solution was measured. Then a step-by-step increase in the alkali metal perchlorate concentration was effected by a quick transfer from the weighing bottle to the conductance cell. The concentration range was from 1.0×10^{-4} to 1.5×10^{-2} M. The Λ *vs.* $\sqrt{C}$ curve for this series is given by (3) in Figs. 1—5.

Materials. The method of the purification of solvents and electrolytes was as has previously been described.[7] Dibenzo-18-crown-6 was obtained from the Aldrich Chemical Company, Inc. DBC was dissolved in chloroform and filtered.

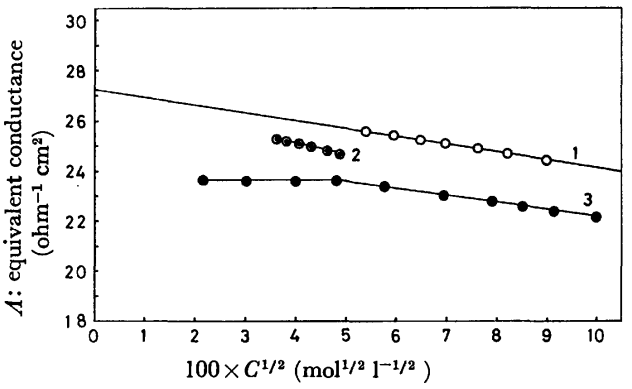

Fig. 1. Λ *vs.* $\sqrt{C}$ curves for $LiClO_4$ and its complex with DBC in PC at 25 °C.

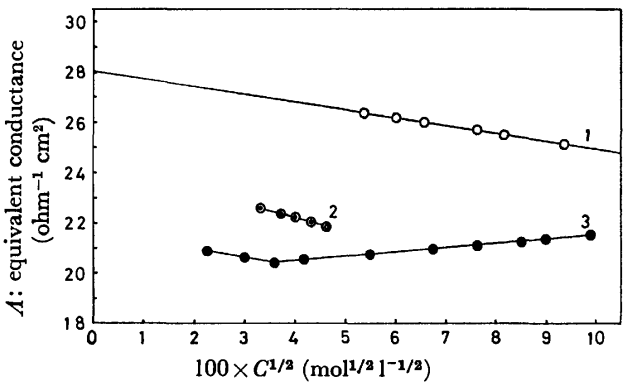

Fig. 2. Λ *vs.* $\sqrt{C}$ curves for $NaClO_4$ and its complex with DBC in PC at 25 °C.

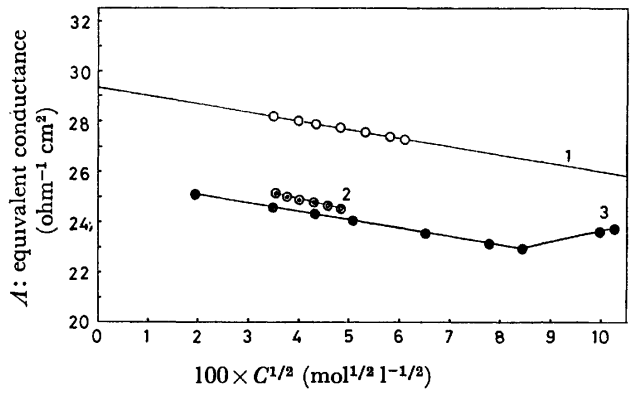

Fig. 3. Λ *vs.* $\sqrt{C}$ curves for $KClO_4$ and its complex with DBC in PC at 25 °C.

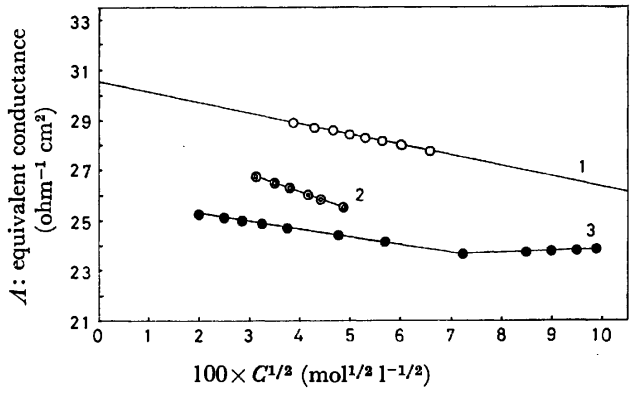

Fig. 4. Λ *vs.* $\sqrt{C}$ curves for $RbClO_4$ and its complex with DBC in PC at 25 °C.

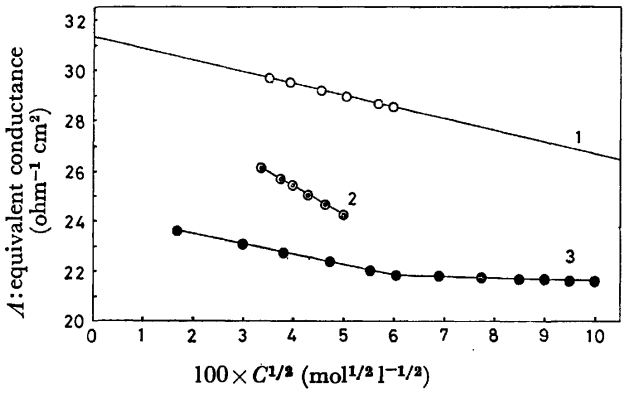

Fig. 5. Λ *vs.* $\sqrt{C}$ curves for $CsClO_4$ and its complex with DBC in PC at 25 °C.

1: Λ *vs.* $\sqrt{C}$ curve for alkali metal perchlorate in PC at 25 °C —phoreogram-1.

2: Λ *vs.* $\sqrt{C}$ curve for the same concentration of alkali metal perchlorate as that of DBC in PC at 25 °C —phoreogram-2.

3: Λ *vs.* $\sqrt{C}$ curve for the stepwise increase of the alkali metal perchlorate concentration against the constant DBC concentration in PC at 25 °C — phoreogram-3.

Then it was recrystallized from benzene five times and, before use, dried at 50 °C in a vacuum oven.

Results

The Λ *vs.* $\sqrt{C}$ curves for alkali metal perchlorates and their complexes with DBC in PC at 25 °C are given in Figs. 1—5. Figures 1,2,3,4, and 5 correspond to the cases of lithium, sodium, potassium, rubidium, and cesium perchlorate respectively. The experimental curves in DMSO and DMF are similar and hence have been omitted. The phoreogram-3 consists of either one linear line or two different ones. The former is found only in the case of $NaClO_4$ in DMSO, and the slope of the Λ *vs.* $\sqrt{C}$ curve is negative. The latter has three types. In the case of the first type, the slope changes from positive to negative with an increase in the concentration, as can be seen in Fig. 1. This type can also be seen in the case of the $NaClO_4$ in DMF. In the case of the second type, the slope changes from negative to positive, as can be seen in Figs. 2—4. In the case of the last type, both slopes are negative, the absolute values of these two slopes are different from each other, and the absolute value of the slope changes from large to small with an increase in the concentration, as can be seen in Fig. 5. This type can also be seen in the cases of $LiClO_4$, $KClO_4$, $RbClO_4$, and $CsClO_4$ in DMSO and DMF. Accordingly, the phoreogram-3 obtained can be classified into the four types. In every case, however, the phoreogram-2 always lies between the phoreogram-1 and the phoreogram-3. That is, the phoreogram-1 is at the top, the phoreogram-2 is in the middle, and the phoreogram-3 is at the bottom. It may be noted from Figs. 1—5 that the distance from the phoreogram-2 to the phoreogram-1 differs from that from the phoreogram-2 to the phoreogram-3 in the concentration range of the phoreogram-2. These tendencies in DMSO and DMF are similar. It seems that the 1:1 complex of DBC with the alkali metal ion is larger than the alkali metal ion itself. Therefore, it can be supposed that the former is more mobile than the latter in these solutions. Judging from the above, it is assumed that, in the case of the phoreogram-3, most of the alkali metal ions form complexes with DBC and that these complexes are of the 1:1 type when the concentration of DBC exceeds that of alkali metal ions. As the phoreogram-2 lies between the phoreogram-1 and the phoreogram-3, it is considered that the uncomplexed cation and the complexed cation attain to a chemical equilibrium in the case of the phoreogram-2. The equilibrium equation is given by;

$$\underset{C(1-\alpha)}{M^+} + \underset{C(1-\alpha)}{DBC} \overset{K_f}{\rightleftharpoons} \underset{C\alpha}{M(DBC)^+} \qquad (1)$$

where C is the initial molar concentration of the alkali metal ion and DBC, while α is the fraction of the cation in the 1:1 complex. Accordingly, the complex formation constant, K_f, is given by;

$$K_f = \frac{[M(DBC)^+]}{[M^+][DBC]} = \frac{\alpha}{C(1-\alpha)^2} \qquad (2)$$

where $[M^+]$, $[M(DBC)^+]$, and [DBC] are the molarities of the uncomplexed cation, the complexed cation, and uncomplexed DBC respectively. The observed specific conductance, κ_{ob}, is given by;

$$\kappa_{ob} = \kappa_{M^+} + \kappa_{M(DBC)^+} + \kappa_{ClO_4^-} \qquad (3)$$

where κ_{M^+}, $\kappa_{M(DBC)^+}$, and $\kappa_{ClO_4^-}$ are the specific conductances of the uncomplexed cation, the complexed cation, and the perchlorate ion respectively. The ionic equivalent conductances are given by;

$$\lambda_{M^+} = \frac{\kappa_{M^+}}{[M^+]} = \frac{\kappa_{M^+}}{C(1-\alpha)} \quad (4)$$

$$\lambda_{M(DBC)^+} = \frac{\kappa_{M(DBC)^+}}{[M(DBC)^+]} = \frac{\kappa_{M(DBC)^+}}{C\alpha} \quad (5)$$

$$\lambda_{ClO_4^-} = \frac{\kappa_{ClO_4^-}}{[ClO_4^-]} = \frac{\kappa_{ClO_4^-}}{C} \quad (6)$$

where λ_{M^+}, $\lambda_{M(DBC)^+}$, and $\lambda_{ClO_4^-}$ are the ionic equivalent conductances of the uncomplexed cation, the complexed cation, and the perchlorate ion respectively. As a consequence of Eqs. 4, 5, and 6, Eq. 3 would be transformed into;

$$\Lambda_{ob} = \frac{\kappa_{ob}}{C} = (1-\alpha)\Lambda_{MClO_4} + \alpha\Lambda_{M(DBC)ClO_4} \quad (7)$$

where Λ_{ob} is the observed equivalent conductance and where Λ_{MClO_4} and $\Lambda_{M(DBC)ClO_4}$ are the equivalent conductances of alkali metal perchlorate and alkali metal DBC perchlorate respectively. If the α value is obtained, the value of K_f at each concentration can be calculated. The procedure for obtaining the α value is as follows. First, the α value is estimated arbitrarily. Using this α value, the concentrations of alkali metal perchlorate and alkali metal DBC perchlorate are found to be $C(1-\alpha)$M and $C\alpha$M respectively. As the values of Λ_{MClO_4} and $\Lambda_{M(DBC)ClO_4}$ at these concentrations can be obtained from the phoreogram-1 and the phoreogram-3 respectively, the right side of Eq. 7 can be calculated. As the value of the left side of Eq. 7 is the observed one, these calculations are continued until the value of the right side of Eq. 7 becomes equal to that of the left side of Eq. 7. When the value of α is finally obtained, K_f can be calculated from Eq. 2. As a result, the formation constants of the 1:1 complexes of DBC with alkali metal ions for each concentration are as shown in Table 1. It may be noted from Figs. 1—5 and Table 1 that the closer the phoreogram-2 approaches the phoreogram-3, and the more the phoreogram-2 departs from the phoreogram-1, the larger the value of the K_f of each concentration becomes. These phenomena in DMSO and DMF are similar. The formation constant sequences of the alkali metal ions with DBC in PC at 25 °C are $K^+ \gg Na^+ > Rb^+ > Cs^+ > Li^+$. In the cases of DMSO and DMF, however, they are $K^+ > Rb^+ > Cs^+ \cong Na^+ \gg Li^+$ and $K^+ > Rb^+ > Cs^+ > Na^+ > Li^+$ respectively.

Table 1. Formation constants for the 1:1 complexes for alkals cations with DBC

10^3C	DMSO $10^{-3}K_f$				
	Li^+	Na^+	K^+	Rb^+	Cs^+
1.44	nil	1.99	2.44	2.28	2.01
1.52	nil	2.03	2.47	2.32	2.03
1.60	nil	2.04	2.68	2.34	2.04
1.68	nil	2.05	2.74	2.39	2.07
1.76	nil	2.03	2.61	2.34	2.07

10^3C	DMF $10^{-3}K_f$				
	Li^+	Na^+	K^+	Rb^+	Cs^+
1.44	0.99	2.11	3.43	3.20	2.99
1.52	0.98	2.26	3.59	3.30	3.03
1.60	1.15	2.19	3.54	3.49	3.09
1.68	1.12	2.39	3.66	3.57	3.16
1.76	1.21	2.31	3.72	3.55	3.20

10^3C	PC $10^{-3}K_f$				
	Li^+	Na^+	K^+	Rb^+	Cs^+
1.44	1.86	7.60	131	5.86	3.43
1.52	1.68	7.20	125	5.55	3.49
1.60	1.81	7.50	119	5.74	3.32
1.68	1.96	7.14	113	5.96	3.66
1.76	2.00	7.50	110	5.22	3.77

Discussion

The K_f value series about the same alkali metal ion among these nonaqueous solvents are given in the order of DMSO<DMF<PC from Table 1. The formation constant sequences of the complex in PC differ from those in DMSO and DMF. Of all the alkali metal ions, the K_f value of K^+ is the largest, and that of Li^+ is the smallest, in each solvent. These results show that the ability of the alkali metal ion to form complexes with DBC in these solvents is dependent on the ionic diameter, as can be seen in Table 2, and that the solvent used is important in determining the formation constant in these systems. This can be considered to reflect the competition between complex formation and solvation. This is supported by the K_f values in Table 1, which show, that for alkali metal cations of approximately the same ionic diameters, *i.e.*, K^+ (2.66 Å), the K_f value of K^+ is the largest. Pedersen[1] has observed that the complexing power can be expected to be weak when the hole of the polyether is too small or too large for the cation, because the salt-polyether complexes are formed by ion-dipole interaction between the cation and the negatively charged oxygen atoms symmetrically arranged in the polyether ring. In addition, the poor selectivity for Li^+ is probably due to its small size (ionic diameter, 1.20 Å) as compared to the size of the hole of DBC (hole size, 2.6—3.2 Å). The solvation is very important in determining cation selectivity, and in this respect it will be more difficult to strip the solvent molecules from Li^+ than from all the other alkali metal ions. Of course, this will depend very greatly on the nature of the solvent. The potential series on the

Table 2. Ionic diameters and hole size (Å)[a]

Cation	Ionic diameter	Polyether	Hole size
Li^+	1.36		
Na^+	1.94	All 18-crown-6	2.6—3.2
K^+	2.66		
Rb^+	2.94		
Cs^+	3.34		

a) H. K. Frensdorff, *J. Am. Chem. Soc.*, **93**, 600 (1971).

normalized potential scale were given in the order of DMSO<DMF<PC, indicating that the metal ion-solvent interaction increases with an increase in the electron-donor property of the solvent.[8] The K_f value sequences were given in the order of DMSO (ε=46.7[9])<DMF (ε=36.7[9])<PC (ε=64.4[9]). Accordingly, it seems that the donor number of the solvent is a very influential factor in the alkali metal ion-DBC complexing. Pedersen[1b] has reported that the selectivity of polyethers with respect to the complexation of alkali metal ions increases as the dielectric constant of the organic solvent is lowered. However, it seems that the donor number is a main factor in determining the selectivity of DBC for the alkali metal ion in the organic solvent.

References

1) (a) C. J. Pedersen, *J. Am. Chem Soc.*, **89**, 7017 (1967); (b) C. J. Pedersen, *Fed. Proc., Fed. Am. Soc. Exp. Biol.*, **27**, 1305 (1968); (c) C. J. Pedersen, *J. Am. Chem. Soc.*, **92**, 386 (1970); (d) C. J. Pedersen, *ibid.*, **92**, 391 (1970).

2) R. M. Izatt, J. H. Rytting, D. P. Nelson, B. L. Haymore, and J. J. Christensen, *Science*, **164**, 443 (1969).

3) S. G. A. McLaughlin, G. Szabo, G. Eisenman, and S. Ciani, Abstracts, 14th Annual Meeting of the Biophysical Society, Baltimore, Md., Feb. 25—27, 1970, p. 96a.

4) K. H. Wong, G. Konizer, and J. Smid, *J. Am. Chem. Soc.*, **92**, 666 (1970).

5) H. K. Frensdorff, *J. Am. Chem. Soc.*, **93**, 600 (1971).

6) N. Matsuura, K. Umemoto, and Y. Takeda, *Bull. Chem. Soc. Jpn.*, **48**, 2253 (1975).

7) N. Matsuura, K. Umemoto, and Z. Takeuchi, *Bull. Chem. Soc. Jpn.*, **47**, 813 (1974).

8) N. Matsuura and K. Umemoto, *Bull. Chem. Soc. Jpn.*, **47**, 1324 (1974).

9) (a) J. A. Riddick and W. B. Bunger, "Techniques of Chemistry," Vol. 2 (Organic Solvents), 3rd ed., Wiley-Interscience, New York (1972); (b) G. J. Janz and R. P. T. Tomkins, "Nonaqueous Electrolytes Handbook," Vol. 1, New York (1972).

Pulse Radiolysis of $HgBr_2$ in Aqueous Solutions

Shin-ichi FUJITA, Hideo HORII, Toshiaki MORI, and Setsuo TANIGUCHI
Radiation Center of Osaka Prefecture Shinke-cho, Sakai, Osaka 593

(Received November 20, 1975)

Pulse radiolysis of aqueous $HgBr_2$ solutions was investigated in the range from visible to 260 nm. $HgBr_2$ is reduced by e_{aq}^-, H, CO_2^-, and some alcohol radicals except *t*-butyl alcohol radical to yield a transient species, HgBr, having an absorption spectrum with a maximum at 350 nm ($\varepsilon^{350}=(4.3\pm0.2)\times10^3$ M^{-1} cm^{-1}). $k(e_{aq}^-+HgBr_2)$ was determined by the pseud-first order decay of e_{aq}^- observed at 500 nm as $(4.0\pm0.3)\times10^{10}$ M^{-1} s^{-1}. The reactivities of the other reducing species toward $HgBr_2$ were estimated to be in the order $e_{aq}^->CO_2^-\gtrsim$ĖtOH≈*i*-ṖrOH>MeOH by comparing the absorption yields of HgBr in equimolar $HgBr_2$ solutions containing the parent substances of the respective species. HgBr was found to decay following a second order rate law ($2k=(1.0\pm0.1)\times10^{10}$ M^{-1} s^{-1}), producing Hg_2Br_2. $HgBr_2$ reacts also with the OH radical to give a transient species which shows a similar spectrum to that of Br_2^-. It is considered that the transient may be $HgBr_3$ instead of Br_2^-.

Pulse radiolysis of aqueous solutions of various mercuric salts has recently been investigated in order to find unstable mercurous species[1,2] and to clarify their behavior before they fall into the stable state.[3,4] It was found that the mercurous species behave in different ways depending on the pair anions attached. The results obtained for aqueous of mercuric bromide are described in the present report.

Experimental

Details of pulse radiolysis measurements have been described previously.[2,3] The dose per pulse was controlled by changing the pulse duration ($\lesssim1$ μs) and the thickness of aluminum plate situated between the reaction cell and the outlet of the beam. With a thickness of 1—3 mm the delivered doses to the cell depended linearly on the coulomb values monitored by the system.[2] The light source used was a 500 W xenon lamp. All the solutions were prepared with guaranteed reagents and triply distilled water.

Results and Discussion

The spectra were obtained in a deaerated aqueous solution of 500 μM $HgBr_2$ containing 10 mM *t*-BuOH on irradiation with about 1 μs electron pulses (Fig. 1). The immediate absorption after the pulse has a peak at 350 nm. It decays rapidly following a second order rate law. Concurrently with the decay of the transient a residual intense absorption appears at shorter wavelengths within about 100 μs. Most of these absorptions were reduced by saturation of N_2O.

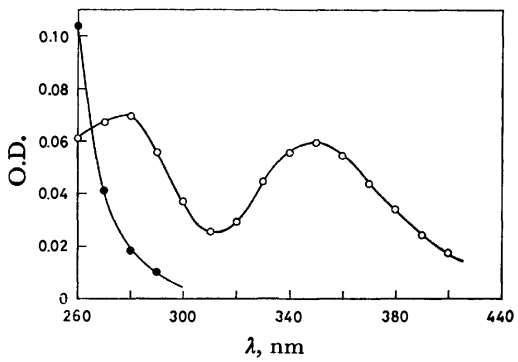

Fig. 1. Absorption spectra obtained in an deaerated aqueous solution of 500 μM $HgBr_2$ and 10 mM *t*-BuOH, immediately (○) and 100 μs (●) after the pulse; average dose, 2500 rad.

Irradiation of water with electron pulses produces the e_{aq}^-, H and OH radicals as reactive species. The OH radical is, however, scavenged by *t*-BuOH.[5] Since N_2O is known to react rapidly with the e_{aq}^-,[6] it is expected that the initial absorption is due to Hg(I) resulting from reduction of $HgBr_2$ by e_{aq}^-, the residual one being due to its dimer, $Hg_2(I)$.

$$e_{aq}^- + HgBr_2 \longrightarrow Hg(I) \quad (1)$$

$$Hg(I) + Hg(I) \longrightarrow Hg_2(I) \quad (2)$$

By observing the life time of e_{aq}^- at 500 nm in the range 10—30 μM $HgBr_2$, the rate constant, $k(e_{aq}^-+HgBr_2)$, was determined to be $(4.0\pm0.3)\times10^{10}$ M^{-1} s^{-1}.

Entirely similar spectra were found in a deaerated 500 μM $HgBr_2$ solution with 10 mM *t*-BuOH at pH 2 where e_{aq}^- was converted into the H radical by the reaction with H^+.[7] It is accepted, therefore, that the H radical also reduces $HgBr_2$ rapidly.

$$H + HgBr_2 \longrightarrow Hg(I) \quad (3)$$

In the presence of other OH scavengers, such as formate ion, methanol, ethanol, and 2-propanol, additional growth curves appeared. Consequently the total absorption yields at 350 nm increased up to nearly twice as much as that in Fig. 1 in the case of formate ion as a scavenger. The resultant absorption spectra in these systems were also similar to those shown in Fig. 1. These results were not influenced essentially by saturation of N_2O in solutions.

Thus, it seems that the OH radical contributes to the reduction of $HgBr_2$ through its reaction products with scavengers.

$$OH + HCO_2^- \longrightarrow CO_2^- + H_2O \quad (4)$$

$$CO_2^- + HgBr_2 \longrightarrow Hg(I) + CO_2 \quad (5)$$

$$OH + ROH \longrightarrow \dot{R}OH + H_2O \quad (6)$$

$$\dot{R}OH + HgBr_2 \longrightarrow Hg(I) + \text{aldehyde or ketone} \quad (7)$$

where Reactions 4 and 6 are known to be very fast.[8,9] $k(CO_2^-+HgBr_2)$ was found to be 9×10^9 M^{-1} s^{-1} from the formation curve of the Hg(I) absorption at 350 nm. This value should, however, be accepted as an upper limit because, owing to its fast decay, Hg(I) could not attain the full equivalent for the CO_2^- yield. Thus,

Table 1. Transient absorption yields in deaerated aqueous solutions of 0.87 mM $HgBr_2$ containing various OH-scavengers at a dose of 2700 rad

Scavengers	O. D.$_{max}$	O. D.$_{relative}$ [a)]
HCO_2Na	0.103	1.0
i-PrOH	0.092	0.89
EtOH	0.090	0.87
MeOH	0.065	0.63

a) Normalized to the value for HCO_2Na.

as to similar reactivities of some alcohol radicals, the order among each other was determined on the basis of the observed Hg(I) yield. Table 1 gives the maximum optical densities of the absorptions obtained in solutions of 0.87 mM $HgBr_2$ containing 10 mM respective alcohols or the formate ion at a dose of 2700 rad. Each maximum optical density should depend on the formation rate constant, k_5 or k_7, since the Hg(I) absorption decays rapidly at almost a uniform rate under these conditions. The values relative to the one for the formate ion are listed in the third column of Table 1. The results and the kinetic data show that the reactivities toward $HgBr_2$ are in the order $e_{aq}^- > CO_2^- > \dot{E}tOH \approx i\text{-}\dot{P}rOH > \dot{M}eOH$.

In a *t*-BuOH contained solution of 0.87 mM $HgBr_2$, a linearity of the absorption quantities *vs.* dose per pulse was obtained up to *ca.* 3000 rad. From the slope of the line the absorption coefficient of Hg(I) was calculated to be $\varepsilon^{350}=(4.3\pm0.2)\times10^3\ M^{-1}\ cm^{-1}$ on the basis of $G(Hg\ (I))=G_H+G_{e_{aq}^-}=3.3$.

The results of the tests of a second order rate law for the decay of the transient at 350 nm at different doses in $HgBr_2$ solutions containing various OH-scavengers are given in Fig. 2. All the plots are linear, their slopes ($=2k_2/\varepsilon l$), giving the same value of $(1.6\pm0.1)\times10^6\ s^{-1}$ for all the scavengers except *t*-BuOH. Thus, $2k_2=(1.0\pm0.1)\times10^{10}\ M^{-1}\ s^{-1}$ ($l=1.5$ cm). The rate constant was not affected by ionic strength of the solutions. The transient might be assigned to HgBr with no charge.

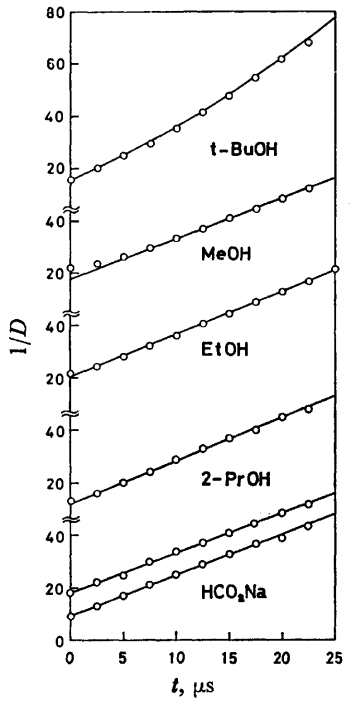

Fig. 2. Test of second order kinetics for the decay of Hg(I) at 350 nm in the presence of various OH-scavengers: $[HgBr_2]=500\ \mu M$, [scavenger]$=10$ mM; dose, ranging between 1300—2700 rad. In the case of HCO_2Na the dose giving the lower result is as nearly twice as that giving the higher one.

The corresponding plots for solutions containing *t*-BuOH deviate slightly from the straight line (Fig. 2), indicating that *t*-butyl alcohol radical interacts with HgBr. In reference to the results for HgCN,[4] it is expected that the other alcohol radicals also react with HgBr. In the present system, however, the deviation from linearity in the decay kinetics may be negligible, because the attainable radical concentration is kept low owing to Reaction 7.

The residual absorbing species at shorter wavelengths may be ascribed to be Hg_2Br_2 in view of the similarity with the $HgCl_2$ system (Fig. 1).[1] It may be supported by the fact that the slow increase of the absorption at 260 nm occurs simultaneously with the second order decay of HgBr (Fig. 3).

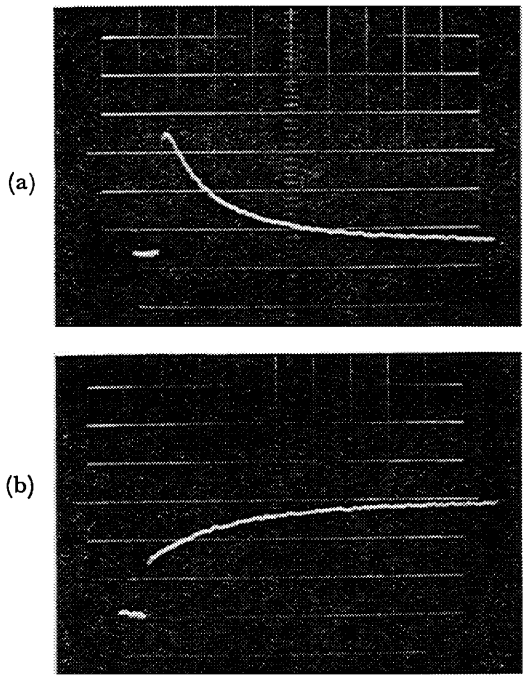

Fig. 3. Oscillographic traces obtained in a deaerated aqueous solution of 500 μM $HgBr_2$ and 10 mM *i*-PrOH: (a) 350 nm, (b) 260 nm; average dose, 2100 rad; ordinates, 4.5%/div., abscissa, 10 μs/div.

Figure 4 shows the absorption spectra obtained in a N_2O-saturated solution of $HgBr_2$. Two kinds of species are recognized: one absorbing at shorter wavelengths appears just after the pulse and disappears rapidly, while the other with an absorption maximum at 355 nm builds up slowly and decays according to a second order kinetics. The formation rate of the latter becomes greater with increasing $HgBr_2$ concentration. No residual absorption was found in this system.

In N_2O-saturated aqueous solutions the OH radical should work mainly as reactive species to solutes with

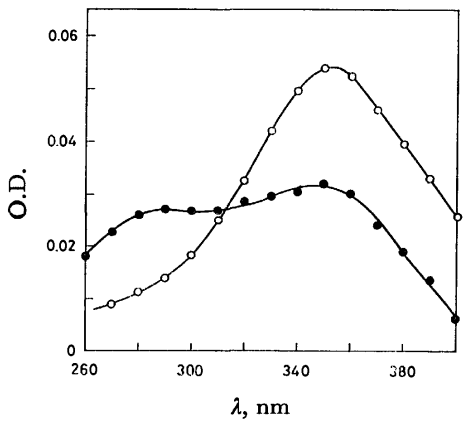

Fig. 4. Absorption spectra obtained in a N_2O-saturated aqueous solution of 500 μM $HgBr_2$, immediately (●) and 7 μs (○) after the pulse; average dose, 1600 rad.

$G(OH)=G_{e_{aq}^-}+G_{OH}=5.5$.[10] Most of the former absorption, however, may be due to HgCl reduced by the H radical and some part of the e_{aq}^- in view of the results obtained in deaerated solutions. Though the absorption quantity at 280 nm seemed somewhat larger (initially about twice as much) than that in the solution containing *t*-BuOH as an OH scavenger, no evidence was obtained suggesting a species other than HgCl. The latter absorption would be interpreted by the occurrence of the oxidation of Br^-, since no evidence that mercury(II) ions in some other complexes are further oxidized by the OH radical.[2-4]

Radiolysis of aqueous solutions of KBr gives rise to transient Br_2^- ions having an absorption spectrum with a maximum at 360 nm ($\varepsilon^{360}=8200$ M^{-1} cm^{-1}),[12] which is similar to the one at 7 μs after the pulse (Fig. 4).

$$Br^- + OH \longrightarrow Br + OH^- \quad (8)$$

$$Br + Br^- \longrightarrow Br_2^- \quad (9)$$

Contribution of the free Br^- to Br_2^- formation, however, should be ruled out, because $HgBr_2$ is little dissociable and little hydrolyzed in aqueous solutions.[13] Thus, the following processes might take place.

$$HgBr_2 + OH \longrightarrow HgBrOH + Br \quad (10)$$

$$Br + HgBr_2 \xrightarrow{H_2O} HgBrOH + Br_2^- + H^+ \quad (11)$$

If these processes actually occur, Br_2^- should recombine to produce the stable Br_3^- having an intense absorption with a peak at 267 nm ($\varepsilon\approx40000$ M^{-1} cm^{-1})[14]

$$2Br_2^- \longrightarrow Br_3^- + Br^- \quad (12)$$

It was found, however, that even in the case of a N_2O–KBr system such an intense absorption was observed only in the acidic solutions (pH 2). No residual absorption was observed in N_2O-saturated $HgBr_2$ solutions at the same pH. The results suggest that the 355 nm-transient species is not Br_2^- (Fig. 4). This may be supported by some characteristic differences between the transient and Br_2^-:

(i) ε^{360} of the transient obtained in N_2O-saturated $HgBr_2$ solutions (100—500 μM) is *ca.* 75% of that of Br_2^- appearing in a N_2O-saturated 1 mM KBr solution. Both values were compared with each other at very low doses (30—150 rad), to avoid the effect of decay (Fig. 5).

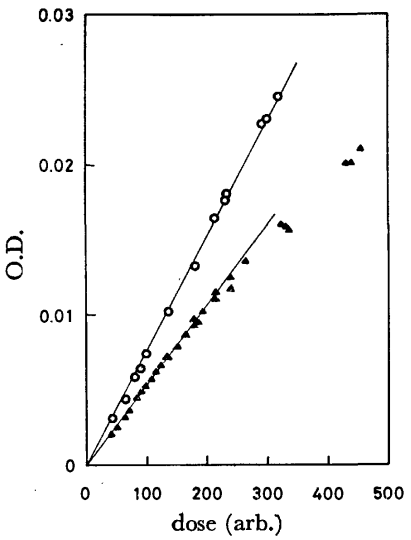

Fig. 5. Comparison between the 355 nm-absorption yields from Br_2^- in a N_2O-saturated KBr solution and the transient in a N_2O-saturated $HgBr_2$ solution: ○: N_2O+1 mM KBr, ▲: N_2O+500 μM $HgBr_2$. The dose unit is roughly in agreement with "rad", though not calibrated.

(ii) $2k/\varepsilon^{360}$ of the transient calculated from the slope of the plots of $1/D$ *vs.* t is about twice as much as that of Br_2^- (6.0 and 3.4×10^5 $cm\ s^{-1}$, respectively, where the latter value is consistent with the reported one[15]).

Čerček pointed out the existence of the Br_3^{2-} ion in aqueous solutions of highly concentrated KBr.[16] It can be assumed that the transient can be a complex molecule such as $HgBr_3$ in view of the charge equivalency.

$$Br + HgBr_2 \longrightarrow HgBr_3 \quad (13)$$

If the assumption is correct, Hg(II) seems to increase the stability of Br_3^{2-} structure since there exist few free Cl^- ions in the solution. Since the transient gives rise to no Br_3^- absorption after the second order decay, the bimolecular reaction of $HgBr_3$ would produce Br_2, though the determination of Br_2 was not carried out.

$$2HgBr_3 \longrightarrow 2HgBr_2 + Br_2 \quad (14)$$

The second order rate constant of the transient formation was determined to be 9×10^8 M^{-1} s^{-1} from the analysis of the formation curve in N_2O-saturated solutions of 100—200 μM $HgBr_2$.

References

1) N. B. Nazhat and K. -D. Asmus, *J. Phys. Chem.*, **77**, 614 (1973).
2) S. Fujita, H. Horii, and S. Taniguchi, *J. Phys. Chem.*, **77**, 2868 (1973).
3) S. Fujita, H. Horii, T. Mori, and S. Taniguchi, *J. Phys. Chem.*, **79**, 960 (1975).
4) S. Fujita, H. Horii, T. Mori, and S. Taniguchi, *Bull. Chem. Soc. Jpn.*, **48**, 3067 (1975).
5) M. Anbar and P. Neta, *Int. J. Appl. Radiat. Isot.*, **18**, 493 (1967).

6) J. H. Bexendale *et al.*, *Nature (London)*, **201**, 468 (1964).
7) L. M. Dorfman and I. A. Taub, *J. Am. Chem. Soc.*, **85**, 2370 (1963); S. Gordon, E. J. Hart, M. S. Matheson, J. Rabani, and J. K. Thomas, *ibid.*, **85**, 1375 (1963).
8) E. J. Hart, J. K. Thomas, and S. Gordon, *Rad. Res. Suppl.* **4**, 74 (1964).
9) G. E. Adams, J. W. Boag, J. Currant, and B. D. Michael, "Pulse Radiolysis," ed. by M. Ebert, J. P. Keene, A. J. Swallow, and J. H. Baxendale, Academic Press, London, (1965), p. 131.
10) G represents the number of species per 100 eV absorbed energy. Primary reactive species are produced with $G(e_{aq}^-)=2.7$, $G(OH)=2.8$, and $G(H)=0.6$, respectively.[11]
11) M. S. Matheson and L. M. Dorfman, "Pulsed Radiolysis," The M. I. T. Press, Cambridge, Mass. (1969).
12) H. C. Sutton, G. E. Adams, J. W. Boag, and B. D. Michael, "Pulse Radiolysis," ed. by M. Ebert, J. P. Keene, A. J. Swallow, and J. H. Baxendale, Academic Press, London (1965), p 61.
13) B. J. Aylet, "Comprehensive Inorganic Chemistry," Vol. 3, ed. by J. C. Bailar, H. J. Emeléus, R. Nyholm, and A. F. Trotman-Dickenson, Pergamon Press, Oxford (1973), p. 296.
14) A. Rafi and H. C. Sutton, *Trans. Faraday Soc.*, **61**, 877 (1965).
15) M. S. Matheson, W. A. Mulac, J. L. Weeks, and J. Rabani, *J. Phys. Chem.*, **70**, 2092 (1966).
16) B. Čerček, *Int. J. Radiat. Phys. Chem.*, **4**, 25 (1972).

Hydrates of Organic Compounds. II. The Effect of Alkyl Groups on the Formation of Quaternary Ammonium Fluoride Hydrates

Haruo NAKAYAMA and Kazuichi WATANABE

Department of Chemistry, Faculty of Engineering, Yokohama National University, Ooka-machi, Minami-ku, Yokohama 233

(Received December 25, 1975)

The solid–liquid phase diagrams for the binary mixtures of water with various quaternary ammonium fluorides, $(n\text{-}C_4H_9)_3RNF$ (R=H, CH_3, C_2H_5, $n\text{-}C_3H_7$, $i\text{-}C_3H_7$, $n\text{-}C_4H_9$, $i\text{-}C_4H_9$, $n\text{-}C_5H_{11}$, $i\text{-}C_5H_{11}$, $n\text{-}C_6H_{13}$, $n\text{-}C_7H_{15}$, and $C_6H_5CH_2$), have been determined in order to see the effect of alkyl groups on the formation of clathrate hydrates. It has been found that, among these compounds, not only $(n\text{-}C_4H_9)_4NF$, which has been known as a clathrate hydrate-forming salt, but also several other compounds with R=C_2H_5, $n\text{-}C_3H_7$, $i\text{-}C_3H_7$, $i\text{-}C_4H_9$, $n\text{-}C_5H_{11}$, and $i\text{-}C_5H_{11}$ can form hydrate type. These hydrates are believed to be of the clathrate hydrates since they have almost the same hydration numbers as that of $(n\text{-}C_4H_9)_4NF$ hydrate. From the melting points of these hydrates, it has been concluded that the most suitable alkyl chain length of quaternary ammonium salts for their clathrate-hydrate formation is C_4-chain (butyl or isopentyl). In the cases of R=CH_3 and $C_6H_5CH_2$, hydrates having lower melting points and smaller hydration numbers than those of the above group of hydrates have been detected. No hydrates have been observed for the salts with R=H, $n\text{-}C_6H_{13}$ and $n\text{-}C_7H_{15}$.

In 1940 the formation of a variety of crystalline hydrates of tetra butyl and tetra isopentyl quaternary ammonium salts was reported by Kraus and his coworkers.[1] Later McMullan and Jeffrey[2-4] carried out a detailed X-ray structural analysis of the hydrates formed by a large number of these salts and have found that they were the clathrate type, similar to the gas hydrates.[5] In these hydrates, the central N^+ atom lies at a common vertex of four large polyhedra formed by the association of water molecules through hydrogen bondings, and each of the four alkyl chains extends into one of the polyhedral cages. Up to the present it has been known that these hydrates have various characteristic features: 1) an unusually high proportion of water of crystallization; 2) high melting points as compared with ordinary gas hydrates; 3) the capability of forming hydrates with various kinds of anions. However, so far as we know, no systematic investigation of these properties, particularly of their thermodynamic properties, such as heats of fusion of the hydrates and vapor pressure of water molecules which form polyhedral cages, has been extensively done. There is no doubt that such information would be very helpful for the studies of aqueous solutions of these compounds, particularly in connection with the structural modification of water molecules in the vicinity of hydrophobic solutes.[6]

First of all, we are here concerned mainly with the effect of alkyl chain length and/or shape on the stability of the clathrate hydrates of quaternary ammonium salts. It has been reported that quaternary ammonium salts having either a butyl or an isopentyl group can make fairly stable crystalline hydrates. On the other hand an attempt to make the hydrates of tetra propyl ammonium salts was unsuccessful.[7] We have examined as well the solid–liquid phase diagram of the system $(n\text{-}C_3H_7)_4NF$+water and concluded that $(n\text{-}C_3H_7)_4NF$ certainly does not form a clathrate hydrate; the phase diagram of this system is shown in Fig. 1. These facts indicate that the stability of the clathrate hydrate of a quaternary ammonium salt depends significantly on the type of its alkyl group.

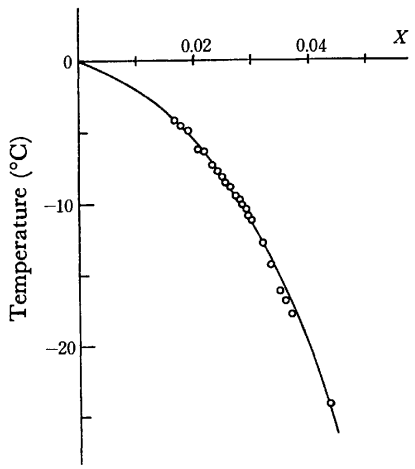

Fig. 1. The solid–liquid phase diagram for the $(n\text{-}C_3H_7)_4NF$+water system; X is the mole fraction of $(n\text{-}C_3H_7)_4NF$.

In order to make this point clearer and, at the same time, to determine what conditions are required for this type of hydrate to be formed (with respect to the length and/or shape of alkyl groups of quaternary ammonium cations), we have examined the formation of hydrates of quaternary ammonium fluorides in which one of the four butyl chains of tetra butylammonium fluoride is substituted for by various kinds of alkyl chains R, *i.e.*, $(n\text{-}C_4H_9)_3RNF$.

Experimental

Alkyltributylammonium iodides (or bromides), $(n\text{-}C_4H_9)_3RNI$ (or Br), were prepared by the quaterization of tributylamine with the appropriate alkyl iodide (or bromide): HI; CH_3I; C_2H_5I; $n\text{-}C_3H_7I$; $i\text{-}C_3H_7I$; $n\text{-}C_4H_9I$; $i\text{-}C_4H_9I$; $n\text{-}C_5H_{11}I$; $i\text{-}C_5H_{11}I$; $n\text{-}C_6H_{13}Br$; $n\text{-}C_7H_{15}Br$; $C_6H_5CH_2Br$. The obtained solid products were recrystallized from ethyl acetate+acetone mixtures and confirmed by the NMR spectra. The aqueous solutions of their fluorides were prepared by the triple decomposition of a mixture of BaF_2, Ag_2SO_4, and the corresponding iodide (or bromide) by using

stoichiometric amounts of the latter two components and an excess of the former.[8] The mixture of the silver salts was removed by filtration.

Each solution (about 5 ml) of a known concentration was sealed in a glass ampoule and was cooled until the solid phase appeared. After being annealed at low temperature for several hours, each ampoule was warmed very slowly in a constant temperature bath with vigorous shaking. By measuring the temperatures, for each ampoule, at which the solid phase disappeared completely, the solid-liquid phase diagram was determined. The differential scanning calorimeter[6] was also employed when the determination of the dissolution temperature was somewhat ambiguous. The water content of each solution was determined by the Karl Fischer titration method.

Results and Discussion

The solid-liquid phase diagrams for the systems water+$(n\text{-}C_4H_9)_3RNF$ with R=H—$n\text{-}C_4H_9$ are shown in Fig. 2, those for the systems water+$(n\text{-}C_4H_9)_3RNF$ with R=$n\text{-}C_5H_{11}$—$n\text{-}C_7H_{15}$, and $C_6H_5CH_2$ are shown in Fig. 3, and those for the systems water+$(n\text{-}C_4H_9)_3$-RNF, with R a branched alkyl group ranging from isopropyl to isopentyl, are shown in Fig. 4. For comparison, the curve for the system water+$(n\text{-}C_4H_9)_4NF$ is also included in Figs. 3 and 4.

As is obvious from these figures, among this series of compounds, the salt $(n\text{-}C_4H_9)_4NF$ forms a hydrate which has the highest melting point, *i.e.*, the most stable hydrate. The melting point and hydration number of this hydrate have been determined to be 28.3 °C and 28.0 (34.1 wt %) respectively. These values are somewhat different from those reported by McMullan and Jeffrey, who reported 24.9±0.1 °C[8] for the melting point and for hydration number 34.0[8] by chemical analysis and 32.8[4] by crystallographic analysis. It is

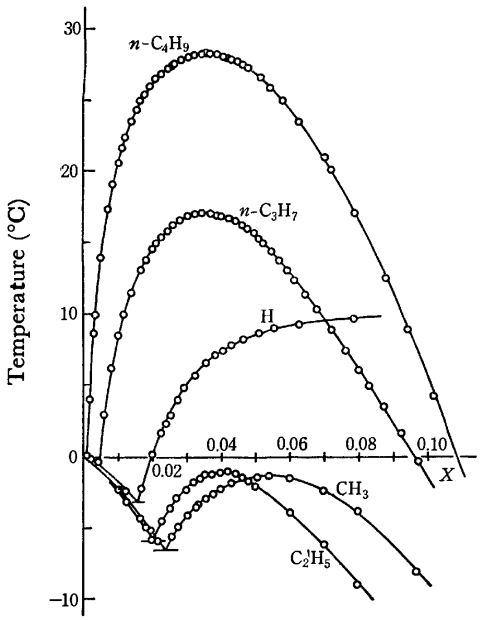

Fig. 2. The solid-liquid phase diagrams for the $(n\text{-}C_4N_9)_3RNF$+water systems; R=H, CH_3, C_2H_5, $n\text{-}C_3H_7$, and $n\text{-}C_4H_9$. X is the mole fraction of the salts.

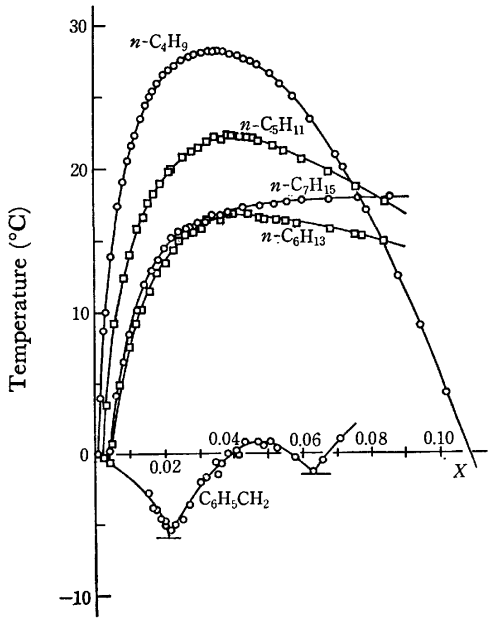

Fig. 3. The solid-liquid phase diagrams for the $(n\text{-}C_4H_9)_3RNF$+water systems; R=$n\text{-}C_4H_9$, $n\text{-}C_5H_{11}$, $n\text{-}C_6H_{13}$, $n\text{-}C_7H_{15}$ and $C_6H_5CH_2$. X is the mole fraction of the salts.

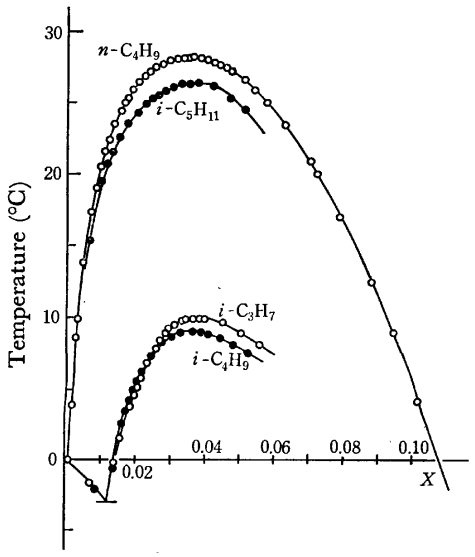

Fig. 4. The solid-liquid phase diagrams for the $(n\text{-}C_4H_9)_3RNF$+water systems; R=$i\text{-}C_3H_7$, $i\text{-}C_4H_9$, $i\text{-}C_5H_{11}$, and $n\text{-}C_4H_9$. X is the mole fraction of the salts.

conceivable that these discrepancies can be attributed to the fact that our values are for the hydrate which is in equilibrium with an aqueous solution of the same composition as that of the hydrate itself. It has been noticed that the composition of the hydrate which is separated from its solution phase and is exposed to the atmosphere varies considerably with time and as a result of this its apparent melting point decreases. Such a property and some other thermodynamic properties of the $(n\text{-}C_4H_9)_4NF$ hydrate are now in under investigation and the results will be published in the near future.

TABLE 1. MELTING POINTS AND HYDRATION NUMBERS OF THE HYDRATES OF TRIBUTYL MONOALKYL AMMONIUM FLUORIDES, $(n\text{-}C_4H_9)_3RNF$

R	Melting point (°C)	Hydration number
CH_3	−1.5	17.5[a)]
C_2H_5	−1.1	26.0
$n\text{-}C_3H_7$	17.1	27.1
$i\text{-}C_3H_7$	10.0	27.6
$n\text{-}C_4H_9$	28.3(24.9[6)])	28.0(32.8[4)]; 34.0[6)])
$i\text{-}C_4H_9$	9.1	28.0
$n\text{-}C_5H_{11}$	22.1	25.4
$i\text{-}C_5H_{11}$	26.4	27.8(32.8[7)])
$C_6H_5CH_2$	1.0	21.5[a)]

a) See text.

Figures 2—4 indicate that $(n\text{-}C_4H_9)_3(C_2H_5)NF$, $(n\text{-}C_4H_9)_3(n\text{-}C_3H_7)NF$, $(n\text{-}C_4H_9)_3(i\text{-}C_3H_7)NF$, $(n\text{-}C_4H_9)_3(i\text{-}C_4H_9)NF$, $(n\text{-}C_4H_9)_3(n\text{-}C_5H_{11})NF$, and $(n\text{-}C_4H_9)_3(i\text{-}C_5H_{11})NF$ can also make hydrates. The melting points and hydration numbers of these hydrates are summarized in Table 1, together with the values reported before. These hydrates are considered to be of the clathrate type since they have hydration numbers similar to that of the $(n\text{-}C_4H_9)_4NF$ hydrate. This indicates the fact that a formation of a clathrate hydrate of quaternary ammonium salts is not limited only to salts containing either butyl or isopentyl chains, though the melting point is very much affected by a change in length and/or shape of the alkyl chain. The formation of the clathrate hydrate of $(n\text{-}C_4H_9)_3(i\text{-}C_5H_{11})NF$ has been known.[7)] However, as in the case of $(n\text{-}C_4H_9)_4NF$ hydrate, there is some difference in hydration number between our value (27.8) and the reported one (32.8 ± 1).[7)] This discrepancy may also be explained, at least partly, by the same reason as given above in connection with the $(n\text{-}C_4H_9)_4NF$ hydrate.

From Table 1, it can be seen that, for the salts whose R is either a propyl or butyl chain, the hydrate of salt having a normal alkyl chain has a higher melting point than that having a branched alkyl chain; on the contrary, in the hydrates of the salts containing a pentyl group, the isopentyl chain can stabilize the hydrate more effectively than the pentyl chain. These results undoubtedly indicate that the most suitable length of an alkyl chain of quaternary ammonium salt for the formation of a clathrate hydrate is C_4-chain (butyl or isopentyl chain).

The solid-liquid equilibrium curves for the systems of water+$(n\text{-}C_4H_9)_3(CH_3)NF$ and water+$(n\text{-}C_4H_9)_3(C_6H_5CH_2)NF$ (Figs. 2 and 3) suggest a formation of hydrates. However, these hydrates do not seem to belong to the same group as the $(n\text{-}C_4H_9)_4NF$ hydrate since the hydration numbers (Table 1) are rather low as compared with that of the $(n\text{-}C_4H_9)_4NF$ hydrate. For the systems $(n\text{-}C_4H_9)_3HNF$+water, $(n\text{-}C_4H_9)_3(n\text{-}C_6H_{13})NF$+water, and $(n\text{-}C_4H_9)_3(n\text{-}C_7H_{15})NF$+water, the formation of hydrates was not recognized. Although the solid-liquid phase equilibrium curve exhibits a slight maximum in the system of $(n\text{-}C_4H_9)_3(n\text{-}C_6H_{13})NF$+water (Fig. 3), it is dubious whether this is due to the formation of a hydrate, since in the solutions whose concentrations are higher than $X=0.04$ (X is the mole fraction of the salt) the appearance of droplets of an oily substance has been observed. This oily substance was identified as tributylamine by means of its NMR spectrum. The same phenomena was also noted in the $(n\text{-}C_4H_9)_3(n\text{-}C_7H_{15})NF$+water system.

In conclusion, it has been found that there is some permitted limit for the length and/or shape of alkyl groups of quaternary ammonium salts if their clathrate hydrates are to be formed. That is, though it seems clear that the most suitable alkyl-chain length for their clathrate-hydrate formation is C_4-chain (butyl or isopentyl chain), other alkyl groups such as propyl, isopropyl, pentyl, and even ethyl, have some ability to make clathrate hydrates.

References

1) D. L. Fowler, W. V. Loebenstein, D. B. Pall, and C. A. Kraus, *J. Am. Chem. Soc.*, **62**, 1140 (1940).
2) D. Feil and G. A. Jeffrey, *J. Chem. Phys.*, **35**, 1863 (1961).
3) M. Bonamico, R. K. McMullan, and G. A. Jeffrey, *J. Chem. Phys.*, **37**, 2219 (1962).
4) R. K. McMullan, M. Bonamico, and G. A. Jeffrey, *J. Chem. Phys.*, **39**, 3295 (1963).
5) M. von Stackelberg, *Z. Elektrochem.*, **58**, 24 (1954).
6) H. Nakayama and M. Tahara, *Bull. Chem. Soc. Jpn.*, **46**, 2965 (1973).
7) G. Beurskens, G. A. Jeffrey, and R. K. McMullan, *J. Chem. Phys.*, **39**, 3311 (1963).
8) R. K. McMullan and G. A. Jeffrey, *J. Chem. Phys.*, **31**, 1231 (1959).

Physico-Chemical Properties of Aqueous Solutions of $C_{n-1}H_{2n-1}OCH_2COONa$

Masakatsu HATO,* Kōzō SHINODA, and Tōru MIYAGAWA

Department of Chemistry, Faculty of Engineering, Yokohama National University, Ooka, Minami-ku, Yokohama 233

(Received December 26, 1975)

Properties of aqueous solutions of surfactants, $C_{n-1}H_{2n-1}OCH_2COONa$ ($n-1=12$—18), which may be non-toxic, non-allergic and bio-degradable, have been studied. The Krafft points in aqueous solutions of these surfactants are close (+8.5——1.5 °C) to those of the corresponding fatty acid soaps R_nCOONa. The critical micelle concentrations are also close to those of corresponding fatty acid soaps in spite of the introduction of an oxygen atom in the hydrocarbon chain. A study of the effect of water hardness on the solubility revealed that this type of surfactant is, unlike soap, soluble in town water (hardness 4°) in the presence of equal weight of tripolyphosphate.

The majority of ionic surfactants used nowadays are sodium alkyl or alkylaryl sulfonates or sulfates. Great consumption of such substances is undesirable from the viewpoint of environmental preservation and biological recycling. It is expected that compounds composed solely of carbon, hydrogen and oxygen atoms and whose structures resemble fatty acids or their analogues may be easily bio-degradable, non-toxic and non-allergic. However, fatty acid soaps are insoluble in hard water and scum forms in washing process. Thus, surfactants whose ionic groups are carboxyl and are more soluble in hard water could be of some advantage. The present investigation was undertaken to prepare such compounds and study their physico-chemical properties in aqueous solutions.

Experimental

Materials. $R_{n-1}OCH_2COONa$($R_{n-1}=C_{n-1}H_{2n-1}$; $n-1=12$—18) were synthesized from respective alcohols, $C_{n-1}H_{2n-1}OH$, and sodium chloroacetate. These acids were purified by vacuum distillation and then neutralized. Their melting points and boiling points and purity determined by gas chromatography are summarized in Table 1.

TABLE 1.

Molecular formula	Mp °C	Bp °C	Purity
$R_{12}OCH_2COOH$	46.0	147(0.06 mmHg)	99.8
$R_{14}OCH_2COOH$	56.2	150(0.025 mmHg)	99.4
$R_{16}OCH_2COOH$	64.3	176(0.025 mmHg)	99.8
$R_{18}OCH_2COOH$	70.8	208.5(0.023 mmHg)	99.2

Procedure. The critical micelle concentration (CMC) was determined by electrical conductivity measurements. The Krafft point was determined from the change in solubility with temperature.[1] It was also confirmed from the color change of pinacyanol chloride since the solubility and the cmc agree at the Krafft point.

Results and Discussion

Critical Micelle Concentration (CMC). The CMC values determined from electrical conductivity *vs.* concentration curves are summarized in Table 2.

TABLE 2.

Molecular formula	CMC mmol/l	Krafft point (°C)
$R_{12}OCH_2COONa$	7.5(55.0 °C)	42
$R_{14}OCH_2COONa$	2.2(64.9 °C)	49
$R_{16}OCH_2COONa$	0.73(75.1 °C)	56
$R_{18}OCH_2COONa$	0.40(75.5 °C)	62

The CMC values of the corresponding fatty acid soaps, R_nCOONa, are close to those of $R_{n-1}OCH_2COONa$. Insertion of oxygen atom in the hydrocarbon chain has little effect on the CMC. Klevens empirically found that the logarithms of the CMC values and the fatal lengths of surfactant molecules from the terminal carbon atom to the atom carrying the charge change linearly.[2] The relation fortuitously holds in several ordinary ionic surfactants. It is evident, however, that the relation will not hold in the case of $C_nH_{2n+1}O(CH_2CH_2O)_mSO_3Me$,[3-5] since the CMC is determined by the free energy change of respective groups at micellization.[6] The ether oxgen atom in R_nOCH_2COONa might increase the hydrophilic property of this surfactant on one hand, but the water and gegenions distributed around polar groups might depress the electrical repulsion on the

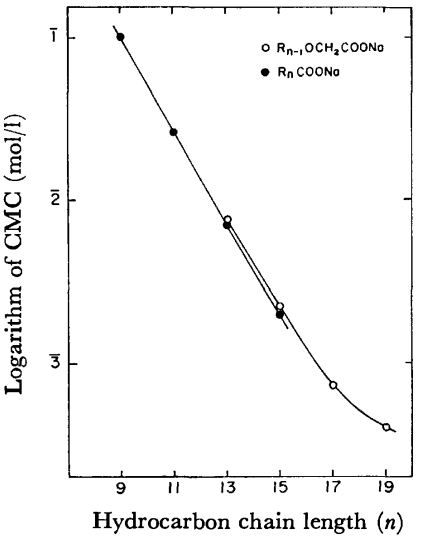

Fig. 1. The CMC values of $R_{n-1}OCH_2COONa$ and R_nCOONa as a function of hydrocarbon chain length of respective surfactants. The CMC values have been determined slightly above respective Krafft points.

* Address: Research Institute for Polymers and Textiles, Sawatari, Kanagawa-ku, Yokohama 221.

other hand. A comparison of the CMC values of these surfactants with those of fatty acid soaps as a function of hydrocarbon chain length is shown in Fig. 1.[2] Since the change in CMC value with temperature is relatively small over 20—70 °C,[7,8] the CMC values slightly above the Krafft points were plotted.

The logarithms of the CMC values decrease linearly up to 15 carbon atoms, but the slope *vs.* hydrocarbon chain length gradually decreases above 17 carbon atoms. The CMC values as a function of hydrocarbon chain length are expressed as follows:

$$\ln \mathrm{CMC} = -\frac{1}{1+K_g}\frac{m\omega}{kT} - K_0 \qquad (1)$$

where ω is the free energy increase transferring one methylene group from the interior of micelle to aqueous environment, K_g a constant obtained from the change of CMC with the concentration of gegenions, m the number of carbon atoms in hydrocarbon chain and K_0 the experimental constant.[9]

Krafft Point. The Krafft point was determined from the change of solubility of $R_{n-1}OCH_2COONa$ with temperature and the CMC value (Fig. 2).

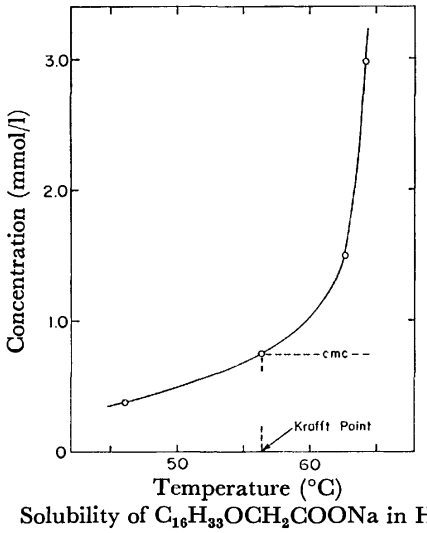

Fig. 2. The change of solubility of $C_{16}H_{33}OCH_2COONa$ in water with temperature and the Krafft point.

The results are summarized in Table 2. The Krafft point is a temperature at which hydrated solid surfactant melts.[1] Thus the Krafft points and melting points of corresponding acids are closely related. The relation is plotted in Fig. 3.

Krafft points of fatty acid soaps are about 20 °C lower than those of the corresponding fatty acids, whereas the Krafft point of $R_{n-1}OCH_2COONa$ is not so low compared with the melting points of $R_{n-1}OCH_2COOH$. The melting points of $R_{n-1}OCH_2COOH$ are merely 3—8 °C lower than those of $R_{n-1}CH_2COOH$. It is evident that the insertion of oxygen atom in the hydrocarbon chain neither depresses the Krafft points nor increases the CMC values. However, the Krafft point of $R_{12}(OCH_2CH_2)OCH_2COONa$ is below 0 °C.

The Change of Krafft Point of $R_{n-1}OCH_2COONa$ as a Function of Water Hardness. Ordinary soaps are salted out by the addition of a very small amount of

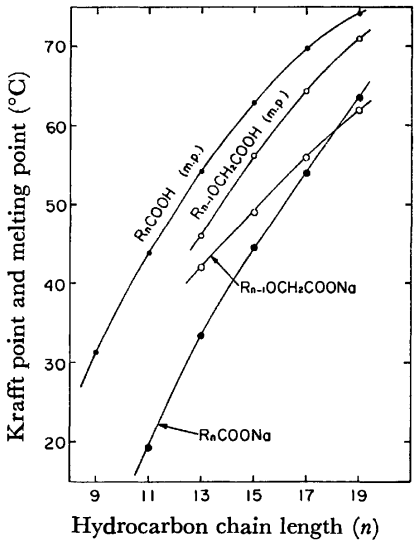

Fig. 3. The comparison among Krafft points of $R_{n-1}OCH_2COONa$ and R_nCOONa and melting points of corresponding acids.

multi-valent cations. In the case of $R_{n-1}OCH_2COONa$, however, the Krafft point is gradually enhanced with added calcium chloride, particularly in the presence of the chelating agent, tripolyphosphate. The results are plotted in Fig. 4 as a function of the water hardness.

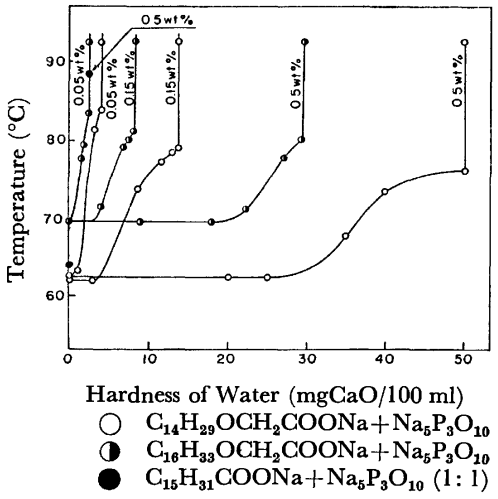

Fig. 4. The change of Krafft point as a function of the concentration of calcium chloride (water hardness).

The solubility gradually decreases with time, because the tripolyphosphate slowly becoming degraded. Since the solutions contained the same weight of tripolyphosphate and surfactants, concentrated solutions were less sensitive to the calcium ions added. Surfactants are usually used at about 0.05 wt % and contain roughly the same weight of tripolyphosphate. It is clear from Fig. 4 that 0.05 wt % solutions of $R_{14}OCH_2COONa$ and $R_{16}OCH_2COONa$ are durable up to about 4° and 2.5°, respectively. Whereas 0.05 wt % $R_{15}COONa$ in the presence of equal weight of tripolyphosphate was salted out at the hardness of 0.3°.

The authors express their sincere thanks to Dr. K. Nagase of Kao-Soap Co. for the synthesis and purification of $R_{n-1}OCH_2COOH$, and to Mr. M. Tahara for the experiments on added salts.

References

1) K. Shinoda, T. Nakagawa, B. Tamamushi, and T. Isemura, "Colloidal Surfactants," Academic Press Inc., New York (1963), p. 7.
2) H. B. Klevens, *J. Am. Oil Chem. Soc.*, **30**, 74 (1953).
3) F. Tokiwa and K. Ohki, *J. Phys. Chem.*, **71**, 1343 (1967).
4) F. Tokiwa, *J. Phys. Chem.*, **72**, 1214 (1968).
5) M. Hato and K. Shinoda, *J. Phys. Chem.*, **77**, 378 (1973).
6) Ref. 1, p. 41.
7) B. D. Flockhart, *J. Colloid Sci.*, **16**, 484 (1961).
8) K. Shinoda, 6th International Congress on Surface Active Substances, Zürich, 1972, Band II, 2, 891, Carl Hanser Verlag, München 1973.
9) Ref. 1, p. 42.

The Microwave Spectra of Sulfur Tetrafluoride in the Excited Vibrational States. The Vibrational Assignment for ν_4 and ν_9

Hiroshi INOUE, Akio NARUSE, and Eizi HIROTA

Department of Chemistry, Faculty of Science, Kyushu University, Higashi-ku, Fukuoka 812

(Received January 16, 1976)

The vibrational satellites of SF_4 have been observed for the two lowest bending modes, ν_4 and ν_9. The relative intensities which were observed are consistent with the vibrational assignment of Frey *et al.* but are incompatible with Levin's assignment. Consideration of the Coriolis interaction between the two modes lead to the same conclusion. The centrifugal distortion constants are evaluated and are compared with the observed.

In 1970 Christie and Sawodny[1] revised the previous assignments for the vibrational modes of sulfur tetrafluoride, by observing the Raman spectra in the gaseous state. Shortly after Frey *et al.*[2] proposed an assignment in which they reversed the two antisymmetric stretching bands, ν_6 and ν_8, based upon comparison with the vibrational spectra of the related molecules. Christie *et al.*[3] recently arrived at the same conclusion by evaluating the force constants. On the other hand Levin[4] observed two bands at 245 cm^{-1} and 206 cm^{-1} in the Raman spectrum of solid SF_4, which he ascribed to the two lowest bending modes, ν_4 and ν_9. Berney[5] has, however, shown that the band at 206 cm^{-1} is due to randomly-oriented oligomers. Christie *et al.*[3] also critisized the assignment of Levin by comparing the calculated mean amplitudes with the observed.

The rotational spectra in the excited states may provide us with information on the vibrational assignment, particularly in cases where two modes in near resonance are coupled by the Coriolis interaction[6]. If the ν_4 and ν_9 vibrations are nearly degenerate in the gas phase as argued by Levin, the rotational spectra in the two excited states would exhibit the effects of the Coriolis resonance, provided that the coupling constant is large enough. In the present work we observed the rotational spectra of SF_4 in the excited states of the ν_4 and ν_9 modes and obtained results which are consistent with the vibtational assignment of Frey *et al.*

Experimental

A sample of sulfur tetrafluoride was obtained by a method described in Inorganic Syntheses.[7] It is known that SF_4 reacts easily with water to form SOF_2. Our sample contains about 5—10% of SOF_2. Fortunately the microwave spectra of SOF_2 have recently been investigated in detail,[8] and thus we could identify easily the lines of SOF_2 in our observed spectra. Sulfur tetrafluoride decomposes quite rapidly in a glass vessel, and hence we stored the sample in a stainless steel holder equipped with a needle valve. Sulfur tetrafluoride was found quite stable in a Stark cell; we did not observe any appreciable decrease in intensity for two hours. We observed the microwave spectra of SF_4 at room temperature using a microwave spectrometer with a 120 kHz square-wave oscillator as a Stark modulator.

Rotational Spectra

The intensities of the ν_4 satellites relative to those of the ground state are the same for all types of the transitions, whereas those of the ν_9 satellites are dependent upon the parity of the K_{+1} number because of the two pairs of the equivalent fluorine nuclei. Table 1 lists the relative intensities which are calculated at $T=300$ K for the two vibrational assignments. It is to be noted that Levin assigned the bands at 228 cm^{-1} and at 233 cm^{-1} to ν_4 and ν_9 (or ν_9 and ν_4) in the gas phase, respectively.

TABLE 1. RELATIVE INTENSITIES OF THE ν_4 AND ν_9 SATELLITES OF SF_4 AT 300 K[a]

Vibration	Transition	Frey *et al.*	Levin
ν_4 (A_1)	ee—oe, oo—eo	0.320	0.320
ν_9 (B_2)	ee—oe	0.103	0.187
	oo—eo	0.285	0.520

a) Relative to the ground-state transition.

Because several low-J R-branch transitions of $J=2\leftarrow 1$ and $J=3\leftarrow 2$ show characteristic Stark patterns, we first concentrated to search the vibrational satellites around the corresponding ground-state transitions, which were reported by Tolles and Gwinn[9]. Aside from the Stark patterns we also utilized the following relation among the three R-branch frequencies:

$$4\nu(3_{22}\leftarrow 2_{12}) = 3[\nu(2_{21}\leftarrow 1_{11}) + \nu(2_{11}\leftarrow 1_{01})].$$

Since the centrifugal distortion effects are very small for SF_4 as shown below, this relation holds accurately. In Fig. 1 we plotted $\nu(2_{11}\leftarrow 1_{01})/2$, $\nu(3_{22}\leftarrow 2_{12})/3$, and $\nu(2_{21}\leftarrow 1_{11})/2$ in equidistance. We adjusted the abscissa slightly so that the three ground-state lines are in line.

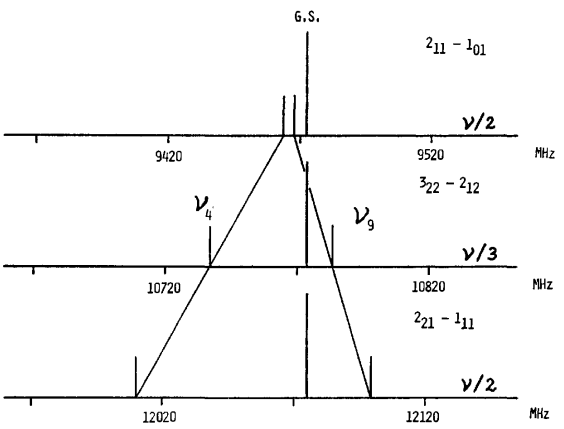

Fig. 1. Plot of the three R-branch frequencies, $\nu(2_{11}\leftarrow 1_{01})/2$, $\nu(3_{22}\leftarrow 2_{12})/3$, and $\nu(2_{21}\leftarrow 1_{11})/2$.

TABLE 2. OBSERVED FREQUENCIES OF SF_4 IN THE ν_4 AND ν_9 STATES (MHz)

Transition	ν_4		ν_9	
	Obsd	Δ[a]	Obsd	Δ[a]
$2_{11}-1_{01}$	18 929.188	0.082	18 935.565	0.076
$2_{20}-1_{10}$	23 331.027	−0.053	23 518.939	−0.053
$2_{21}-1_{11}$	24 020.927	0.049	24 199.162	−0.023
$2_{20}-2_{12}$	10 476.062	−0.012		
$3_{12}-2_{02}$	27 617.464	−0.060	27 568.640	−0.004
$3_{21}-2_{11}$	30 474.066	0.014	30 620.687	0.053
$3_{22}-2_{12}$	32 212.423	−0.015	32 350.800	−0.049
$3_{30}-3_{22}$	15 070.894	−0.011	15 429.284	−0.040
$3_{31}-3_{21}$	14 136.150	−0.039	14 562.058	0.071
$3_{21}-3_{13}$			12 701.624	−0.008
$4_{31}-4_{23}$	15 695.438	−0.033	16 002.389	0.081
$4_{32}-4_{22}$	13 065.330	0.019		
$4_{40}-4_{32}$	20 636.163	0.072		
$5_{32}-5_{24}$	17 057.299	−0.054		
$5_{33}-5_{23}$	11 443.225	−0.071		
$5_{42}-5_{32}$	19 938.522	0.002		
$5_{50}-5_{42}$	26 489.208	−0.065		
$5_{41}-5_{33}$			21 178.940	−0.086
$6_{06}-5_{14}$	27 574.120	0.107		
$6_{25}-5_{33}$	26 652.792	−0.102		
$6_{34}-6_{24}$	9 409.653	−0.056		
$6_{43}-6_{33}$	18 901.345	0.013		
$6_{52}-6_{42}$	26 223.992	−0.032		
$6_{51}-6_{43}$			27 060.470	0.015
$7_{52}-7_{44}$	26 232.490	0.096	26 929.460	0.010
$8_{35}-8_{27}$	28 913.758	0.193		
$8_{53}-8_{45}$	26 203.110	0.063		
$9_{45}-9_{37}$	26 075.965	−0.096		
$9_{54}-9_{46}$	26 460.532	0.105		
$9_{64}-9_{54}$	31 527.507	0.052		
$10_{46}-10_{38}$	30 489.551	−0.109		
$10_{55}-10_{47}$	27 302.000	0.028	27 713.130	−0.002
$10_{64}-10_{56}$	31 613.132	−0.283		
$11_{56}-11_{48}$	29 126.547	−0.077		
$11_{65}-11_{57}$	31 539.739	0.037		
$11_{66}-11_{56}$	29 480.457	0.068		
$12_{66}-12_{58}$	31 822.525	0.078		
$13_{67}-13_{59}$	32 788.690	0.038		
$15_{79}-15_{69}$	31 377.473	0.031		
$16_{7,10}-16_{6,10}$	27 945.594	−0.078		
$19_{8,12}-19_{7,12}$	31 166.284	0.019		

a) Obsd − Calcd The calculated frequencies are obtained using the constants listed in Table 3.

TABLE 3. ROTATIONAL CONSTANTS AND CENTRIFUGAL DISTORTION CONSTANTS OF SF_4 IN THE ν_4 AND ν_9 STATES (MHz)[a]

Constants	ν_4	ν_9
A	6641.7081 (84)	6707.7928 (71)
B	4095.8118 (89)	4075.9354 (94)
C	3213.7530 (90)	3217.9307 (93)
τ_{aaaa}	−0.01052 (76)	−0.0225 (19)
τ_{bbbb}	−0.00464 (63)	−0.0138 (19)
τ_{cccc}	−0.00136 (66)	0.0044 (43)
T_1[b]	−0.0085 (11)	−0.0178 (33)
T_2[b]	−0.00024 (84)	−0.0111 (27)

a) Values in parentheses denote the standard deviations and apply to the last significant digits. b) $T_1=\tau_{aabb}'+[(A-B)/(A-C)]\tau_{ccaa}'$ and $T_2=\tau_{bbcc}'+[(B-C)/(A-C)]\cdot\tau_{ccaa}'$.

Two sets of the vibrational satellites indicated in Fig. 1 obviously satisfy the above equation. Table 2 summarizes the observed frequencies of the two sets of the spectra. The rotational constants listed in Table 3 were determined by a least-squares analysis, where the centrifugal distortion effects were taken into account to the first order. The τ constants are not well determined as shown in Table 3.

Vibrational Assignment

The relative intensities of the two sets of the observed spectra are in good agreement with those given in Table 1 for the vibrational assignment of Frey *et al.* Further evidence which supports this conclusion is obtained by analyzing the Coriolis interaction.

The two modes under consideration couple with each other by the Coriolis interaction associated with the a-axis. Levin[4] gave the force constants of valence-force type, which reproduce the vibrational frequencies corresponding to the two assignments. These force constants result in the Coriolis coupling constants $\zeta_{4,9}^{(a)}$ which are listed in Table 4.

TABLE 4. CORIOLIS COUPLING CONSTANT AND VIBRATIONAL CHANGES OF THE A CONSTANTS OF SF_4 IN THE ν_4 AND ν_9 STATES

Constants	Frey *et al.*	Levin
$\zeta_{4,9}^{(a)}$	0.670	0.778
$\Delta A_\pm$ ν_4 (MHz)	−22.2	−723
$\Delta A_\pm$ ν_9 (MHz)	+22.2	+723

Obsd $A_4-A_0=-46.029$ MHz, $A_9-A_0=20.056$ MHz

In the second-order approximation the Coriolis interaction contributes $\Delta A_\pm=\pm D^2/\Delta E$ to the A rotational constant where

$$D = A[(\nu_4/\nu_9)^{1/2}+(\nu_9/\nu_4)^{1/2}]\zeta_{4,9}^{(a)},$$
$$\Delta E = \nu_4 - \nu_9,$$

and the + and − signs apply to ν_4 and ν_9, respectively.[10] Table 4 shows $\Delta A_\pm$ calculated for the two

TABLE 5. ROTATIONAL CONSTANTS AND CENTRIFUGAL DISTORTION CONSTANTS OF SF_4 IN THE GROUND STATE (MHz)[a]

Constants	Obsd	
	This work	Tolles, Gwinn (Ref. 9)
A	6687.737 (11)	6687.71
B	4086.689 (12)	4086.68
C	3219.949 (12)	3219.95

Constants	Obsd	Calcd	
	This work	Frey *et al.*	Levin
τ_{aaaa}	−0.0152 (11)	−0.0160	−0.0167
τ_{bbbb}	−0.0078 (11)	−0.0057	−0.0059
τ_{cccc}	−0.0049 (10)	−0.0034	−0.0032
T_1[b]	−0.0147 (20)	−0.0153	−0.0138
T_2[b]	−0.0052 (16)	−0.0027	−0.0031

a) Values in parentheses denote the standard deviations and apply to the last digits. b) See Footnote b) of Table 3.

assignments. The observed A_4 and A_9 constants differ from the ground-state A constant by −46.029 MHz and +20.056 MHz, respectively. The $\Delta A_{\pm}$ values for Levin's assignment are obviously too large in magnitude.

Centrifugal Distortion Constants

We remeasured some of the ground-state transitions reported by Tolles and Gwinn, and analyzed them with a few added lines by a least-squares analysis. Table 5 lists the rotational constants and the centrifugal distortion constants thus derived. The rotational constants which were obtained are in very good agreement with those of Tolles and Gwinn. The observed τ constants are compared with those calculated using the force fields mentioned previously. Both assignments give the τ constants which are in fair agreement with the observed.

Discussion and Conclusion

The vibrational satellites of SF_4 in higher excited states would be possible to observe, but it would be very hard to assign the ν_6 and ν_8 satellites, because there are too many lower states including the overtone and combination states of the lower-frequency modes. No information was thus obtained for the two antisymmetric stretching vibrations, but the present work eliminates definitely Levin's assignment for the ν_4 and ν_9 modes.

The computation in the present work was carried out at the Computation Center of Kyushu University.

References

1) K. O. Christie and W. Sawodny, *J. Chem. Phys.*, **52**, 6320 (1970).
2) R. A. Frey, R. L. Redington, and A. L. K. Aljibury, *J. Chem. Phys.*, **54**, 344 (1971).
3) K. O. Christie, W. Sawodney, and P. Pulay, *J. Mol. Struct.* **21**, 158 (1974).
4) I. W. Levin, *J. Chem. Phys.*, **55**, 5393 (1971).
5) C. V. Berney, *J. Mol. Struct.*, **12**, 87 (1972).
6) See, for example, E. Hirota, *J. Mol. Spectrosc.*, **7**, 242 (1961).
7) F. S. Fawcett and C. W. Tullock, *Inorg. Synth.*, Vol. VII, ed. by J. Kleinberg, McGraw-Hill Book Co., New York (1963), p. 119.
8) R. C. Ferguson, *J. Am. Chem. Soc.*, **76**, 850 (1954); N. J. D. Lucas and J. G. Smith, *J. Mol. Spectrosc.*, **43**, 327 (1972); A. Dubrulle and J. L. Destombes, *J. Mol. Struct.*, **14**, 461 (1972); D. F. Rimmer, J. G. Smith, and D. H. Whiffen, *J. Mol. Spectrosc.*, **45**, 114 (1973); I. Yamaguchi, O. Ohashi, H. Takahashi, T. Sakaizumi, and M. Onda, *Bull. Chem. Soc. Jpn.*, **46**, 1560 (1973).
9) W. M. Tolles and W. D. Gwinn, *J. Chem. Phys.*, **36**, 1119 (1962).
10) E. Hirota and M. Sahara, *J. Mol. Spectrosc.*, **56**, 21 (1975).

The Crystal Structure and the Absolute Configuration of (−)-Argemonine Methiodide

Tsuguhiro KANEDA, Noriyoshi SAKABE, and Jiro TANAKA
Department of Chemistry, Faculty of Science, Nagoya University, Chikusa, Nagoya 464
(Received January 30, 1976)

The crystal structure of (−)-argemonine methiodide has been investigated by the X-ray method. The crystal system is orthorhombic, and the space group is $P2_12_12_1$. The cell dimensions are $a=13.443$, $b=20.838$, and $c=8.485$ Å. The structure parameters were refined by the block-diagonal least-squares method, and the final R-value was 0.055. The absolute configuration was determined by the Mo$K\alpha$ anomalous scattering to be 1S5S, which is consistent with the CD result.

Argemonine is an alkaloid from *Argemone hispida G* and *Argemone munita*, and its structure was determined by Martell, Soine, and Kier[1] to be identical with (−)-*N*-methylpavine, which was synthesized by Battersby and Binks.[2] The absolute configurations of (−)-argemonine and its related alkaloids have been established by Barker and Battersby[3] by the chemical correlation method. Mason and his coworkers[4,5] have investigated the CD spectra of these molecules and further investigations on the conformation and the absolute configuration by the X-ray method will be of much interest.

In this paper we present a precise structure analysis of (−)-argemonine methiodide and its absolute configuration by the X-ray method.

Experimental

Argemonine methiodide was kindly gifted from Prof. T. O. Soine of Minnesota Univ., and it was recrystallized from water for the X-ray examination. The space group was determined from oscillation and Weissenberg photographs. The density was measured by the flotation method in a mixed solution of cyclohexane and carbon tetrachloride. The cell dimensions were determined by the least-squares method, using 12 reflections which had been carefully measured on a Hilger-Watts four circle diffractometer with Ni-filtered Cu$K\alpha$ radiation ($\lambda=1.5418$ Å). The crystal data are shown in Table 1.

Table 1. Crystal data

M.F.: $C_{22}H_{28}NO_4I\cdot 2H_2O$
M.W.: 533.41
Crystal system: orthorhombic
Space group: $P2_12_12_1$
$a=13.443(2)$, $b=20.838(2)$, $c=8.485(2)$ Å;
$V=2376.9$ Å^3, $Z=4$,
$D_m=1.486$, $D_c=1.491$ g·cm^{-3}
$\mu=15.81$ cm^{-1} (for Mo$K\alpha$ radiation).

Intensity data were measured on the diffractometer in ω-2θ scanning mode using Zr-filtered Mo$K\alpha$ radiation ($\lambda=0.7107$ Å) with the crystal whose size was $0.5\times0.7\times0.8$ mm. Non-zero data of 2766 independent reflections within $\theta\leq26°$ were collected and no correction were made for absorption or extinction.

Structure analysis

The crystal structure was determined by the heavy atom method. Iodine atom was found from a Patterson map and a Fourier synthesis using the coordinate of the iodine atom revealed all the other non-hydrogen atoms including two water molecules of crystallization. A diagonal-least-squares method was applied to the refinement of structure parameters by using all non-zero data and the R-value was reduced to 0.098. Successively a block-diagonal least-squares method was applied to further refinement with anisotropic thermal factors for all atoms and the R-value was converged to 0.055. No other significant peaks were found in the final Fourier and difference Fourier maps. All atomic scattering factors were taken from the International Tables for X-ray Crystallography.[6] The computation was carried out with the program of HBLS-IV coded by Prof. Ashida

Table 2. Atomic coordinates and their standard deviations

	x	y	z
I	0.13050(6)	0.22007(4)	0.98752(9)
O(1)	0.4788(6)	0.4495(4)	0.7229(9)
O(2)	0.5317(6)	0.4585(3)	0.4340(9)
O(3)	0.6618(5)	0.0708(4)	0.2969(9)
O(4)	0.7034(8)	0.0714(4)	0.5914(9)
C(1)	0.3223(8)	0.2369(5)	0.6432(12)
C(2)	0.3749(7)	0.2966(4)	0.5722(10)
C(3)	0.4013(7)	0.3026(5)	0.4139(11)
C(4)	0.3721(9)	0.2519(4)	0.2928(11)
C(5)	0.3490(7)	0.1882(5)	0.3761(12)
C(6)	0.4420(6)	0.1589(4)	0.4458(11)
C(7)	0.4684(7)	0.1589(5)	0.6060(12)
C(8)	0.4003(8)	0.1941(5)	0.7266(12)
N(9)	0.2736(5)	0.1999(3)	0.5105(11)
C(10)	0.4020(8)	0.3457(4)	0.6829(12)
C(11)	0.4507(7)	0.3976(5)	0.6293(12)
C(12)	0.4786(7)	0.4036(4)	0.4684(12)
C(13)	0.4547(7)	0.3571(4)	0.3631(12)
C(14)	0.5084(7)	0.1286(4)	0.3360(12)
C(15)	0.5943(7)	0.1009(4)	0.3913(12)
C(16)	0.6171(7)	0.1015(4)	0.5531(11)
C(17)	0.5554(7)	0.1312(4)	0.6582(12)
C(18)	0.1841(7)	0.2392(5)	0.4519(14)
C(19)	0.2334(8)	0.1345(5)	0.5665(15)
C(20)	0.4621(10)	0.4427(6)	0.8886(12)
C(21)	0.5556(9)	0.4684(6)	0.2693(13)
C(22)	0.6520(9)	0.0778(6)	0.1308(13)
C(23)	0.7258(9)	0.0684(6)	0.7602(14)
OW(1)	0.6677(9)	0.5134(5)	0.6943(12)
OW(2)	0.7493(8)	0.5707(6)	0.4245(14)

TABLE 3. ANISOTROPIC THERMAL FACTORS ($\times 10^4$) AND THEIR STANDARD DEVIATIONS

The anisotropic thermal factors are of the form of $\exp\{-(h^2B_{11}+k^2B_{22}+l^2B_{33}+hkB_{12}+hlB_{13}+klB_{23})\}$

	B_{11}	B_{22}	B_{33}	B_{12}	B_{13}	B_{23}
I	59(0)	28(0)	122(1)	−3(1)	11(1)	0(1)
O(1)	70(6)	21(2)	107(11)	−10(6)	−12(14)	−21(8)
O(2)	64(5)	18(2)	112(11)	−19(5)	−3(13)	7(7)
O(3)	61(5)	27(2)	115(11)	27(6)	19(13)	−17(9)
O(4)	42(4)	26(2)	124(11)	17(5)	−10(12)	6(9)
C(1)	43(6)	16(2)	105(14)	−5(6)	3(16)	9(9)
C(2)	34(5)	14(2)	105(12)	8(6)	0(15)	−2(8)
C(3)	38(5)	17(2)	97(13)	4(6)	−15(14)	−5(9)
C(4)	54(6)	16(2)	101(13)	−2(7)	−51(20)	−9(9)
C(5)	32(5)	17(2)	113(14)	0(6)	3(14)	9(10)
C(6)	32(5)	13(2)	95(13)	0(5)	1(13)	−12(9)
C(7)	36(5)	16(2)	96(14)	−6(6)	7(15)	7(10)
C(8)	51(6)	20(2)	92(14)	14(7)	42(16)	3(10)
N(9)	30(4)	17(2)	122(12)	−4(4)	24(15)	−10(10)
C(10)	50(6)	13(2)	101(14)	10(6)	21(15)	−11(9)
C(11)	41(5)	18(2)	100(14)	0(6)	−27(15)	−13(10)
C(12)	38(5)	14(2)	120(16)	−3(5)	−15(16)	19(10)
C(13)	40(5)	16(2)	99(14)	2(6)	−14(15)	2(10)
C(14)	39(5)	13(2)	119(15)	2(6)	17(16)	−13(10)
C(15)	41(5)	14(2)	114(15)	−1(6)	20(15)	−4(10)
C(16)	37(5)	15(2)	124(14)	1(6)	−3(15)	14(9)
C(17)	39(5)	15(2)	101(14)	0(6)	−4(15)	10(9)
C(18)	37(5)	27(3)	149(19)	15(7)	−7(17)	1(12)
C(19)	48(6)	20(3)	184(21)	−4(7)	35(20)	18(12)
C(20)	89(9)	24(3)	75(14)	10(9)	−12(20)	−18(11)
C(21)	64(7)	22(3)	107(15)	−5(8)	17(19)	29(11)
C(22)	65(8)	32(3)	103(15)	9(9)	49(19)	−6(13)
C(23)	50(7)	33(4)	117(16)	17(9)	−21(19)	5(14)
OW(1)	91(8)	45(4)	183(17)	−46(9)	−18(20)	−12(14)
OW(2)	116(10)	50(4)	245(22)	−62(11)	43(26)	−13(16)

and those written by ourselves on a FACOM 230-60 computer at Nagoya University Computation Center.

The atomic coordinates and the anisotropic thermal parameters with their standard deviations are listed in Tables 2 and 3, respectively. The observed and calculated structure factors are listed in Table 4.[7]

Results and discussion

Argemonine is a rigid molecule which has a bicyclo-[3.3.1]nona-diene skeleton. Figure 1 shows the conformation and atomic labels, and thermal ellipsoids drawn by the program ORTEP coded by Dr. Johnson. The bond lengths and angles are shown in Tables 5 and 6, respectively. The average bond distance of dimethoxybenzene ring A {C(2), C(3), C(10), C(11), C(12), and C(13)} and that of dimethoxybenzene ring B {C(6) C(7), C(14), C(15), C(16), and C(17)} are 1.39 Å and

TABLE 5. BOND LENGTHS AND THEIR STANDARD DEVIATIONS

C(6)–C(7)	1.40(1) Å	C(2)–C(3)	1.39(1) Å
C(6)–C(14)	1.44(1)	C(2)–C(10)	1.44(1)
C(7)–C(17)	1.38(1)	C(3)–C(13)	1.41(1)
C(14)–C(15)	1.37(1)	C(10)–C(11)	1.34(1)
C(15)–C(16)	1.41(1)	C(11)–C(12)	1.42(1)
C(16)–C(17)	1.37(1)	C(12)–C(13)	1.36(1)
C(1)–C(2)	1.55(1)	C(5)–C(6)	1.51(1)
C(1)–C(8)	1.55(1)	C(4)–C(5)	1.54(1)
C(3)–C(4)	1.53(1)	C(7)–C(8)	1.56(1)
C(1)–N(9)	1.51(1)	C(5)–N(9)	1.55(1)
C(18)–N(9)	1.54(1)	C(19)–N(9)	1.54(1)
C(11)–O(1)	1.39(1)	C(15)–O(3)	1.36(1)
C(12)–O(2)	1.38(1)	C(16)–O(4)	1.36(1)
C(20)–O(1)	1.43(1)	C(22)–O(3)	1.42(1)
C(21)–O(2)	1.45(1)	C(23)–O(4)	1.46(1)

TABLE 6. BOND ANGLES AND THEIR STANDARD DEVIATIONS

C(2)–C(3)–C(13)	119.7(9)°	C(6)–C(7)–C(17)	121.7(9)°
C(2)–C(10)–C(11)	118.4(9)	C(6)–C(14)–C(15)	119.0(9)
C(3)–C(2)–C(10)	120.1(8)	C(7)–C(6)–C(14)	118.1(8)
C(3)–C(13)–C(12)	119.6(9)	C(7)–C(17)–C(16)	119.7(9)
C(10)–C(11)–C(12)	121.6(9)	C(14)–C(15)–C(16)	120.9(9)
C(11)–C(12)–C(13)	120.5(9)	C(15)–C(16)–C(17)	120.6(9)
C(1)–C(2)–C(10)	115.6(8)	C(5)–C(6)–C(14)	116.0(8)
C(4)–C(3)–C(13)	118.9(8)	C(8)–C(7)–C(17)	119.0(9)
C(5)–C(6)–C(7)	126.0(8)	C(1)–C(2)–C(3)	124.1(8)
C(6)–C(7)–C(8)	119.2(8)	C(2)–C(3)–C(4)	121.4(9)
C(2)–C(1)–C(8)	109.3(8)	C(4)–C(5)–C(6)	111.2(8)
C(3)–C(4)–C(5)	109.9(8)	C(1)–C(8)–C(7)	111.7(8)
C(2)–C(1)–N(9)	108.5(8)	C(6)–C(5)–N(9)	108.5(8)
C(8)–C(1)–N(9)	109.9(8)	C(4)–C(5)–N(9)	109.6(8)
C(10)–C(11)–O(1)	124.3(9)	C(14)–C(15)–O(3)	123.5(9)
C(12)–C(11)–O(1)	114.0(8)	C(16)–C(15)–O(3)	115.6(8)
C(11)–C(12)–O(2)	114.4(8)	C(15)–C(16)–O(4)	114.6(8)
C(13)–C(12)–O(2)	125.1(9)	C(17)–C(16)–O(4)	124.9(9)
C(11)–O(1)–C(20)	116.1(9)	C(15)–O(3)–C(22)	118.2(8)
C(12)–O(2)–C(21)	116.0(8)	C(16)–O(4)–C(23)	115.4(9)
C(1)–N(9)–C(18)	107.9(7)	C(5)–N(9)–C(19)	108.5(7)
C(1)–N(9)–C(19)	111.9(8)	C(5)–N(9)–C(18)	111.0(8)
C(1)–N(9)–C(5)	110.2(7)		
C(18)–N(9)–C(19)	107.2(7)		

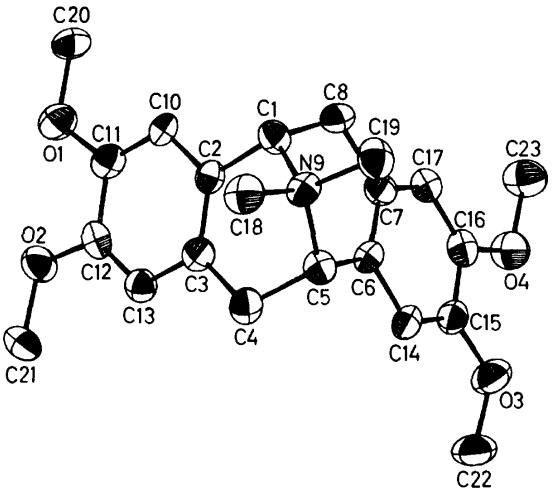

Fig. 1. The conformation and atomic labels. The atoms are represented as thermal ellipsoids of a size such that the center of the vibrating atoms have a 50% probability of being found within them.

1.40 Å, respectively. The distances of four methoxyl groups are normal. The C–C single bond distances at the part of the bicyclo ring are also normal with the average value of 1.54 Å.

The bond angles of two benzene rings are in the range of 120±2°. The external angles around C(2), C(3), C(6), and C(7) are 115.6—119.0°, while the internal angles of bicyclo site are 119.2—126.0°. These trends are noticed in triptycene derivatives which have a bicyclo[2.2.2]octatriene skeleton.[8]

Intermolecular distances within 3.6 Å are listed in Table 7, and the closest contact of 3.29 Å occurs between O(3) and C(23) (3/2−x, −y, −1/2+z). Projection

Table 7. Intermolecular distances less than 3.6 Å[a]

O(2) ····· C(19^{i})	3.33 Å
O(2) ····· C(22^{ii})	3.55
O(3) ····· C(23^{iii})	3.29
O(4) ····· C(20^{iv})	3.49
OW(1) ····· C(19^{iv})	3.50
C(12) ····· C(19^{i})	3.53
C(13) ····· C(23^{v})	3.60
C(14) ····· C(21^{iv})	3.56
C(16) ····· C(18^{i})	3.44
C(16) ····· C(20^{iv})	3.51
C(17) ····· C(18^{i})	3.34
C(19) ····· C(21^{v})	3.50
C(20) ····· C(21^{vi})	3.50
C(22) ····· C(23^{vii})	3.30

Symmetry code superscript	Symmetry operator		
i	1/2+x	1/2−y	1−z
ii	1−x	1/2+y	1/2−z
iii	3/2−x	−y	−1/2+z
iv	1−x	−1/2+y	3/2−z
v	−1/2+x	1/2−y	1−z
vi	x	y	1+z
vii	x	y	−1+z

a) The Roman numerals represent the symmetry operators relevant to the atoms listed second.

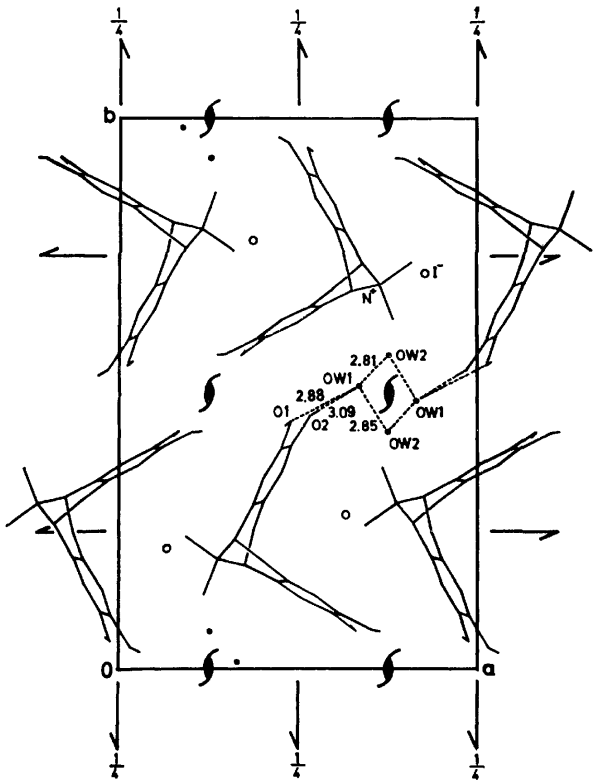

Fig. 2. Projection along the c axis.

along the c axis is shown in Fig. 2. There is a hydrogen bond network including four hydrogen bonds around the screw axis.

The planarity of the benzene rings, A and B, is remarkably good. The least-squares planes of the two rings are given by the following equations.

(1) Ring A

$$0.8652X - 0.4652Y + 0.1869Z - 2.3957 = 0$$

(2) Ring B

$$0.4855X + 0.8650Y - 0.1267Z - 5.2726 = 0$$

Deviations of atoms from these planes are listed in Table 8. C(1) and C(4) deviate 0.08 and −0.05 Å from the A plane, respectively, and C(8) deviates 0.06 Å from

Table 8. Deviations from the least-squares plane

(1) Dimethoxybenzene-ring plane (A)			
C(2)	0.00 Å	C(1)*	0.08 Å
C(3)	−0.01	C(4)*	−0.05
C(10)	0.01	C(20)*	0.10
C(11)	−0.01	C(21)*	−0.05
C(12)	0.00	O(1)*	−0.04
C(13)	0.01	O(2)*	0.03
		N(9)*	−0.34
(2) Dimethoxybenzene-ring plane (B)			
C(6)	0.00 Å	C(5)*	−0.01 Å
C(7)	0.00	C(8)*	0.06
C(14)	0.00	C(22)*	0.24
C(15)	0.00	C(23)*	−0.12
C(16)	−0.01	O(3)*	0.00
C(17)	0.01	O(4)*	−0.03
		N(9)*	−0.43

* Atoms not included in the least-squares calculation.

TABLE 9. DETERMINATION OF ABSOLUTE CONFIGURATION

h	k	l	$100\times\{I(hkl)-I(\bar{h}\bar{k}\bar{l})\}/I(hkl)$ Obsd	Calcd
1	6	6	13.2	9.4
1	6	7	−12.0	−13.2
1	15	2	−11.6	−12.4
2	5	7	4.3	9.8
2	7	7	−8.6	−10.2
3	5	6	−7.1	−11.9
3	7	2	15.4	12.8
3	10	5	6.1	11.2
4	2	1	−10.7	−10.7
4	2	6	−5.8	−11.0
4	6	3	11.3	14.6
5	2	7	−8.3	−10.2
5	3	1	−14.3	−14.9
5	3	8	8.2	10.0
6	4	2	−5.1	−10.3
7	2	3	−5.7	−10.3
7	2	5	15.6	13.0
7	4	3	8.4	9.4
8	3	4	−5.2	−10.1
8	4	1	6.1	10.4
9	5	1	13.3	9.2
11	9	2	−10.8	−9.7

the B plane. The methoxyl carbons, C(22) and C(23), which are attached to oxygen atoms not taking part in hydrogen bonding, deviate 0.24 and −0.12 Å from the B plane, respectively, while C(20) and C(21) do not deviate from the A plane so much. The dihedral angle between A and B planes is 90.4°.

The absolute configuration was determined by the Bijvoet method using the anomalous scattering of Mo$K\alpha$ radiation by the iodine atom. The $\Delta f'$ and $\Delta f''$ values were taken from the International Tables for X-ray Crystallography.[6] The observed intensity differences and calculated ones between 22 Bijvoet pairs are listed in Table 9. The signs of observed values are in good agreement with those calculated based on the positional paramenters of Table 2 in the right-handed coordinate system. The absolute configuration thus determined is 1S5S as is illustrated in Fig. 1. This result is in perfect agreement with those by the chemical correlation method of Barker and Battersby,[3] and by the CD spectral analysis of Mason *et al.*[4,5] The structural data will be still useful for the theoretical calculation of the CD spectra.

The authors are gratefull to Professor T.O.Soine for his kind gift of the crystals.

References

1) M. J. Martell, T. O. Soine, and L. B. Kier, *J. Am. Chem. Soc.*, **85**, 1022 (1963).
2) A. R. Battersby and R. Binks, *J. Chem. Soc.*, **1955**, 2888.
3) A. C. Barker and A. R. Battersby, *J. Chem. Soc., C*, **1967**, 1317.
4) S. F. Mason, K. Schofield, R. J. Wells, J. S. Whitehurst, and G. W. Vane, *Tetrahedron Lett.*, **1967**, 137.
5) S. F. Mason, G. W. Vane, and J. S. Whitehurst, *Tetrahedron*, **23**, 4087 (1967).
6) "International Tables for X-ray Crystallography," Vol. III, Kynoch Press, Birmingham (1968), p. 201.
7) Table 4 has been submitted to, and is kept by the office of the Chemical Society of Japan, 1-5, Kanda-Surugadai, Chiyoda-ku, Tokyo (Document No. 7615).
8) T. Kaneda, N. Sakabe, and J. Tanaka, *Bull. Chem. Soc. Jpn.*, **47**, 1858 (1974).

Theoretical Calculations of the Raman Intensities by the Vibronic Method. II. The In-plane Vibrations of Ethylene

Hiroyuki SHINODA

Department of Applied Chemistry, Faculty of Science and Engineering, Waseda University, Nishi-Ohkubo, Shinjuku-ku, Tokyo 160

(Received January 20, 1976)

The values of the transition moment of Raman scattering have been calculated according to the formula derived from the vibronic method. The calculations have been performed for the in-plane vibrational modes of ethylene determined by three different sets of force constants. The electronic wave functions were calculated by the CNDO/2-CI method. From the relative Raman intensities of three A_{1g}-vibrations of ethylene in the respective cases, it was found that the Raman intensities are sensitive to the vibrational modes. Also, the Raman intensities of ethylene were calculated by the polarizability method in order to compare the results with those obtained from the vibronic method. From the results of these calculations, the conclusions of the previous work have been confirmed.

In a previous paper,[1] which will hereafter be called Part I, the Raman intensities of the symmetric stretching vibrations of several small molecules and of the normal vibrations of methane were calculated by means of the semi-empirical molecular orbital method.[2] In Part I, the Raman intensities were calculated by two methods: the polarizability method and the vibronic method. In the polarizability method, the values of the Raman tensor were obtained by fitting the calculated polarizabilities to a cubic function with respect to the normal coordinate and by taking the first derivative at the equilibrium molecular position. In the vibronic method, the expression of the Raman tensor was derived from the Kramers-Heisenberg dispersion formula by applying the Herzberg-Teller expansion. The results calculated by the two methods were compared with each other, and it was concluded that the vibronic method is more suitable for the theoretical calculation of the Raman intensity than is the other one.

The polarizability derivatives for small polyatomic molecules have been calculated by several investigators[3] by means of the semi-empirical molecular orbital technique. In all of those calculations, the vibrations of diatomic molecules or the symmetric stretching vibrations of some polyatomic molecules have been treated by means of the polarizability method. Moreover, Bleckmann[4] recently calculated the Raman intensities of the normal vibrations of cyclopropenon by the polarizability method. In his work, the polarizabilities were evaluated by means of the finite perturbation technique using the CNDO/2 method.[2] However, his results contradicted the observed ones because the calculated Raman intensities of some non-totally symmetric vibrations were stronger than those of the totally symmetric ones. He attributed the contradiction to the insufficiency of the method of calculation: when the z-axis has its direction perpendicular to the molecular plane, the zz-component of the Raman tensor for the in-plane vibrations of the planar molecules was always zero. Also, the result from the polarizability method in Part I was contradictory to the observed one; the calculated Raman intensity of the ν_2 vibration of methane was stronger than that of the ν_1 vibration, which is observed as the strongest Raman line. From these results (Ref. 4 and Part I), it may be considered that the polarizability method within the framework of the CNDO method leads to unsatisfactory results for the theoretical evaluation of Raman intensities.

In the present work, the Raman intensities of the in-plane vibrations of ethylene have been calculated by the vibronic method. It acquires additional interest from the fact that different kinds of sets of force constants of ethylene have been presented by various investigators.[5-7] Therefore, three sets of force constants have been used in this calculation, and the influence of the different sets on the calculated values of the Raman intensity has been discussed. In order to confirm the conclusion in Part I, furthermore, the calculation has been repeated by the polarizability method.

Methods of Calculation

The total intensity of a Raman line after averaging all the molecular orientations is given as follows:

$$I_{mn} = \frac{2^3\pi}{3^2c^4} I_0 \omega^4 \sum_{\rho,\sigma} |(\alpha_{\rho\sigma})_{mn}|^2, \tag{1}$$

where c is the velocity of light; I_0, the intensity of the incident light; ω, the frequency of the scattered light; m, the initial state; n, the final state, and $(\alpha_{\rho\sigma})_{mn}$, the $\rho\sigma$-th component of the polarizability tensor for the $m \rightarrow n$ transition. The sum goes over $\rho=x,y,z$ and $\sigma=x,y,z$, which refer to the molecular fixed coordinate system. The final expression of $(\alpha_{\rho\sigma})_{mn}$ has been given as follows:[1,8]

$$(\alpha_{\rho\sigma})_{mn} = A + B + C, \tag{2}$$

$$A = -\sum_a \sum_{r \neq g} \left[\frac{\langle g^\circ|R_\sigma|r^\circ\rangle\langle r^\circ|h_a|r^\circ\rangle\langle r^\circ|R_\rho|g^\circ\rangle}{(\varepsilon_r^\circ - \varepsilon_g^\circ - E_0)^2} + \frac{\langle g^\circ|R_\sigma|r^\circ\rangle\langle r^\circ|h_a|r^\circ\rangle\langle r^\circ|R_\rho|g^\circ\rangle}{(\varepsilon_r^\circ - \varepsilon_g^\circ + E_0)^2} \right] \langle \psi_m^g | Q_a | \psi_n^g \rangle, \tag{3}$$

$$B = -\sum_a \sum_r \sum_{s \neq r} \left[\frac{\langle g^\circ|R_\sigma|r^\circ\rangle\langle r^\circ|h_a|s^\circ\rangle\langle s^\circ|R_\rho|g^\circ\rangle}{(\varepsilon_r^\circ - \varepsilon_g^\circ - E_0)(\varepsilon_s^\circ - \varepsilon_g^\circ - E_0)} + \frac{\langle g^\circ|R_\rho|s^\circ\rangle\langle s^\circ|h_a|r^\circ\rangle\langle r^\circ|R_\sigma|g^\circ\rangle}{(\varepsilon_r^\circ - \varepsilon_g^\circ + E_0)(\varepsilon_s^\circ - \varepsilon_g^\circ + E_0)} \right] \langle \psi_m^g | Q_a | \psi_n^g \rangle, \tag{4}$$

and

$$C = -\sum_a \sum_{r \neq g} \sum_{s \neq g} \left[\frac{\langle g^\circ|h_a|s^\circ\rangle\langle s^\circ|R_\sigma|r^\circ\rangle\langle r^\circ|R_\rho|g^\circ\rangle}{(\varepsilon_r^\circ - \varepsilon_g^\circ - E_0)(\varepsilon_s^\circ - \varepsilon_g^\circ)} + \frac{\langle g^\circ|h_a|s^\circ\rangle\langle s^\circ|R_\rho|r^\circ\rangle\langle r^\circ|R_\sigma|g^\circ\rangle}{(\varepsilon_r^\circ - \varepsilon_g^\circ + E_0)(\varepsilon_s^\circ - \varepsilon_g^\circ)} \right.$$

$$+\frac{\langle g^\circ|R_\sigma|r^\circ\rangle\langle r^\circ|R_\rho|s^\circ\rangle\langle s^\circ|h_a|g^\circ\rangle}{(\varepsilon_r^\circ-\varepsilon_g^\circ-E_0)(\varepsilon_s^\circ-\varepsilon_g^\circ)}$$
$$+\frac{\langle g^\circ|R_\rho|r^\circ\rangle\langle r^\circ|R_\sigma|s^\circ\rangle\langle s^\circ|h_a|g^\circ\rangle}{(\varepsilon_r^\circ-\varepsilon_g^\circ+E_0)(\varepsilon_s^\circ-\varepsilon_g^\circ)}\Big]\langle\psi_m^g|Q_a|\psi_n^g\rangle, \quad (5)$$

where the superscript o denotes the equilibrium nuclear position in the electronic ground state; $|g^\circ\rangle$ is the electronic ground state, and $|r^\circ\rangle$ and $|s^\circ\rangle$ are the electronic excited states; ε_g°, ε_r°, and ε_s° are the energies of $|g^\circ\rangle$, $|r^\circ\rangle$, and $|s^\circ\rangle$ respectively; E_0 is the energy of the incident light; $|\psi_m^g\rangle$ and $|\psi_n^g\rangle$ are the wave functions of the m-th and n-th vibrational states respectively in the electronic ground state; Q_a is the normal coordinate of the a vibrational mode; R_ρ and R_σ are the operators of the ρ- and σ-components respectively of the electronic dipole operator, and $h_a=(\partial H/\partial Q_a)$, the first-order vibronic coupling operator introduced initially by Herzberg and Teller.[9] The Raman tensor for the a normal vibration, $(\alpha_{\rho\sigma}^a)'$, can be defined by the following equation:

$$(\alpha_{\rho\sigma})_{mn}=\sum_a(\alpha_{\rho\sigma}^a)'\langle\psi_m^g|Q_a|\psi_n^g\rangle \quad (6)$$

The wave functions of the electronic states and the molecular integrals appearing in the above expressions were calculated by the methods described in Part I.

The different sets of the force constants of ethylene used in the calculation will now be described. The first set, which will be called Set 0 for convenience, consists of the modified Urey-Bradley force constants offered by Scherer and Overend.[6] This set is a modification of the simplified Urey-Bradley force field obtained by adding the *trans*-interaction, so called by them; it may be the most reliable set because the transferability of their set of force constants was successful in discussing the experimental results of several bromoethylenes. The second and third sets of the force constants used in this work were Proposed by Crawford *et al.*;[7] these sets will be called Set I and II below. There are differences in their force constants with respect to the symmetry coordinates of the A_{1g} symmetry species. In the calculation with Set 0, the equilibrium configuration of ethylene followed the data in Ref. 6, while in the calculations with Sets I and II it followed the data in Ref. 7.

Results and Discussion

In the calculations, the wavelength of the incident light was fixed at 5145 Å, the wavelength of an Ar^+ laser line. Five Raman-active in-plane vibrations, which include three vibrations of A_{1g} symmetry species and two of B_{1g}, will be discussed. The other vibrations will be omitted from the discussion because the values of their calculated Raman intensities were practically equal to zero. The vibrational modes obtained by the usual **GF** method with Sets 0, I, and II of the force constants are shown in Figs. 1—3 respectively.

In this work, the differential cross section, $(d\sigma/d\Omega)_{//}$, instead of the total cross section has been calculated because there are the experimental results of $(d\sigma/d\Omega)_{//}$ which can be used in the discussion. $(d\sigma/d\Omega)_{//}$ is expressed as follows:

$$(d\sigma/d\Omega)_{//}=\frac{\omega^4}{c^4}\langle\psi_m^g|Q_a|\psi_n^g\rangle^2\left\{(\bar{\alpha}_a')^2+\frac{4}{45}(\gamma_a')^2\right\}, \quad (7)$$

where $\bar{\alpha}_a'$ and γ_a' are the mean part and the anisotropy part of the Raman tensor of the a normal vibration. The values of the $(d\sigma/d\Omega)_{//}$ caluculated by the vibronic method with Sets 0, I, and II are shown in Table 1; the experimental results are also included. The calculated values of the $(d\sigma/d\Omega)_{//}$ for the A_{1g}-vibrations are larger than the experimental ones. The cause of the overestimations in the calculated results will be discussed later on the basis of the results shown in Table 3. The rela-

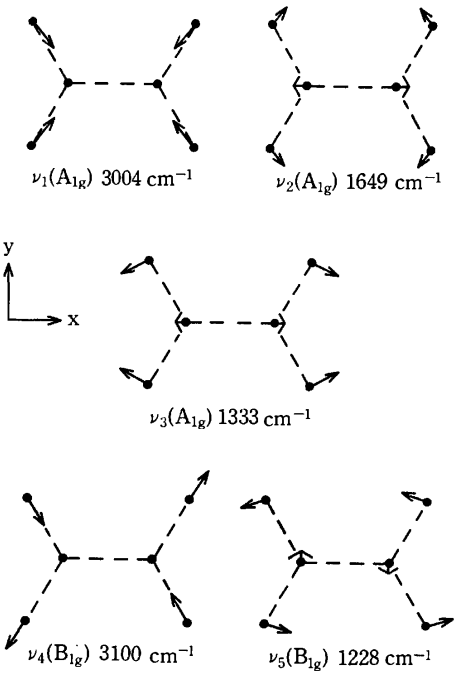

Fig. 1. Vibrational modes of ethylene obtained from the **GF** calculation with the force constants of Set 0.

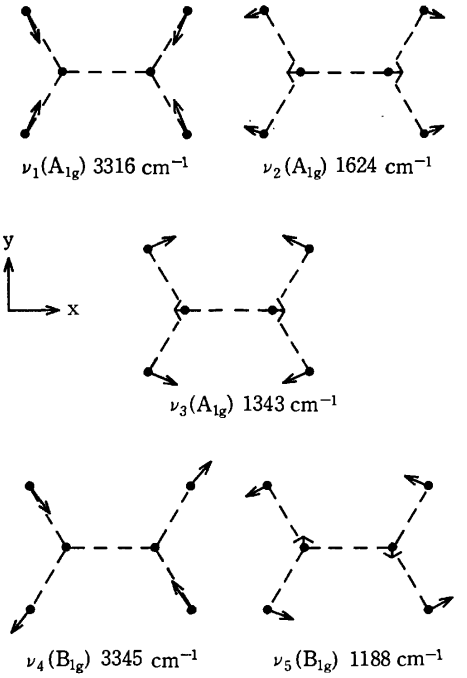

Fig. 2. Vibrational modes of ethylene obtained from the **GF** calculation with the force constants of Set I.

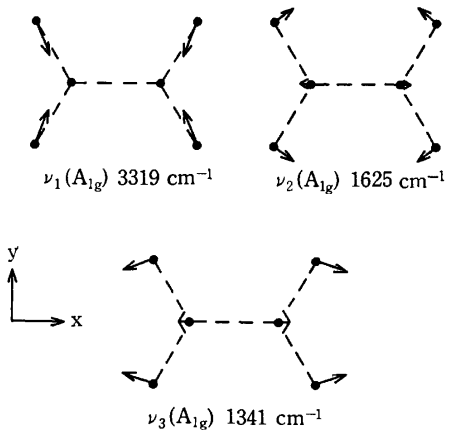

Fig. 3. Vibrational modes of ethylene obtained from the **GF** calculation with the force constants of Set II; ν_4 and ν_5 are the same as those in Fig. 2.

Table 1. The Raman intensity of ethylene calculated by the vibronic method

	$(d\sigma/d\Omega)_{//}\times 10^{30}$[cm^2]					
	Calcd			Obsd		
	Set 0	Set I	Set II	Ref. 10	Ref. 11	Ref. 12
$\nu_1(A_{1g})$	110.1	91.4	91.7	15[a]		vs
$\nu_2(A_{1g})$	58.9	126.9	39.1	5.6[a]	10.6[a,b] 0.74[b,c]	vs
$\nu_3(A_{1g})$	69.4	20.2	114.6	9.0[a]		vs
$\nu_4(B_{1g})$	0.0009	0.0003[d]				s
$\nu_5(B_{1g})$	0.0607	0.0698[d]				w

a) The wavelength of the incident light is 3371 Å.
b) The values correspond to $(d\sigma/d\Omega)$ which expresses as $(\omega^4/c^4)\langle\psi_m^g|Q_a|\psi_n^g\rangle^2\{(\bar{\alpha}_a')^2+(7/45)(\gamma_a')^2\}$.
c) The wavelength of the incident light is 5145 Å.
d) The values are common for Set I and Set II.

tive Raman intensities among the A_{1g}-vibrations calculated with one set of force constants are different from those with another set. The results calculated with Set 0 appear to be in good agreement with the ones observed by Shimizu *et al.*[10] The results from Sets I and II differ from the experimental ones in the order of the intensities. If the suitabilities of Set I and Set II are compared with each other after the manner of the discussion by Crawford *et al.*, it appears, from the calculated Raman intensities, that Set II is appropriate to the force constants of ethylene, although Crawford *et al.* pointed out that Set I is more correct than Set II in view of the constancy of the C=C frequency of olefins. The reason for the situation in the present work is found partly in the similarity of the vibrational modes decided from Sets 0 and II (see Figs. 1 and 3).

In an effort to discuss the importance of the *trans*-interaction introduced to Set 0 of the force constants, $(d\sigma/d\Omega)_{//}$ value swere calculated while neglecting the *trans*-interaction term. The calculated values of the ν_1, ν_2, and ν_3 vibrations are 0.111×10^{-27}, 0.661×10^{-28}, and 0.593×10^{-28} cm^2 respectively. The relative intensities among them are less in agreement with the observed ones than with the results obtained with the original set including the *trans*-interaction term. The results show that the introduction of the *trans*-interaction to the set of force constants is very meaningful.

In the measurement of the Raman intensities, by Blumenfeld *et al.*,[12] for the ν_4 and ν_5 vibrations with B_{1g} symmetry species, the former was observed with a strong intensity and the latter, with a very weak one, although the assignment of the latter was somewhat uncertain. However, both the calculated intensities for these Raman lines are very weak and the intensity of the ν_4 vibration is weaker than that of the ν_5 vibration. A similar situation for the non-totally symmetric vibrations was obtained in the treatment for methane in Part I. The calculated Raman intensity of the ν_2 vibration is very weak, less than those of the ν_3 and ν_4 vibrations; this contradicts the observed result. It will be shown in a future paper that the 2p-orbitals of the hydrogen atom play an important role in the theoretical calculation of the Raman intensities for these non-totally symmetric vibrations.

The calculated values of the depolarization ratios,

Table 2. The depolarization ratio, ρ_n, of ethylene calculated by the vibronic method

	Set 0	Set I	Set II
$\nu_1(A_{1g})$	0.236	0.239	0.239
$\nu_2(A_{1g})$	0.223	0.230	0.224
$\nu_3(A_{1g})$	0.225	0.197	0.228
$\nu_4(B_{1g})$	0.857	0.857[a]	
$\nu_5(B_{1g})$	0.857	0.857[a]	

a) The values are common for Set I and Set II.

Table 3. Raman tensors of ethylene calculated by the vibronic method with set 0, $(\alpha_{\rho\sigma}^a)'\times10^4$[cm^{2}g$^{-1/2}$]

	Term A[a]	Term B[a]	Term C[a]	Total[b]
$\nu_1(A_{1g})$				
$(\alpha_{xx})'$	−18.77	0.0105	0.0644	−18.70
$(\alpha_{yy})'$	−6.568	0.2335	0.1698	−6.165
$(\alpha_{zz})'$	−2.893	0.0	0.0	−2.893
$(\alpha_{xy})'=(\alpha_{yx})'$	0.0	0.0	0.0	0.0
$\nu_2(A_{1g})$				
$(\alpha_{xx})'$	−8.465	−0.1099	0.0610	−8.514
$(\alpha_{yy})'$	−2.814	−0.2899	0.0707	−3.033
$(\alpha_{zz})'$	−1.373	0.0	0.0	−1.373
$(\alpha_{xy})'=(\alpha_{yx})'$	0.0	0.0	0.0	0.0
$\nu_3(A_{1g})$				
$(\alpha_{xx})'$	−8.004	−0.0888	0.0552	−8.038
$(\alpha_{yy})'$	−2.684	−0.2169	0.0717	−2.829
$(\alpha_{zz})'$	−1.287	0.0	0.0	−1.287
$(\alpha_{xy})'=(\alpha_{yx})'$	0.0	0.0	0.0	0.0
$\nu_4(B_{1g})$				
$(\alpha_{xx})'$	0.0	0.0	0.0	0.0
$(\alpha_{yy})'$	0.0	0.0	0.0	0.0
$(\alpha_{zz})'$	0.0	0.0	0.0	0.0
$(\alpha_{xy})'=(\alpha_{yx})'$	0.0	0.0413	−0.0993	−0.0580
$\nu_5(B_{1g})$				
$(\alpha_{xx})'$	0.0	0.0	0.0	0.0
$(\alpha_{yy})'$	0.0	0.0	0.0	0.0
$(\alpha_{zz})'$	0.0	0.0	0.0	0.0
$(\alpha_{xy})'=(\alpha_{yx})'$	0.0	0.0536	−0.2952	−0.2416

a) See text. b) Sum of the terms *A*, *B*, and *C*.

ρ_n, are shown in Table 2. The values calculated with the different sets of force constants are similar to each other. The calculated values for the A_{1g}-vibrations are all about 0.23, with the one exception of 0.197, while those for the B_{1g}-vibrations are 0.857, this value being expected in view of the group theory.

The values of the elements of the Raman tensors calculated with the force constants of Set 0 are shown in Table 3. From these values, the effective terms in the theoretical calculation of the Raman intensities can be discussed. For the A_{1g}-vibrations, the term A gives the main contribution to the intensities; no off-diagonal elements of the Raman tensor contribute to the intensities. Moreover, the mean part of the Raman tensor is more effective on the intensities of the A_{1g}-vibrations than is the anisotropy part, judging from the results on ρ_n shown in Table 2. Therefore, it can be said that the intensity of the A_{1g}-vibrations arises mainly from the mean part referring to the term A, $\bar{\alpha}_a'(A)$, which is written as follows

$$\bar{\alpha}_a'(A) = \frac{1}{3}\sum_{\sigma}\sum_{r\neq g}\left[\frac{\langle g^\circ|R_\sigma|r^\circ\rangle\langle r^\circ|h_a|r^\circ\rangle\langle r^\circ|R_\sigma|g^\circ\rangle}{(\varepsilon_r^\circ-\varepsilon_g^\circ-E_0)^2} + \frac{\langle g^\circ|R_\sigma|r^\circ\rangle\langle r^\circ|h_a|r^\circ\rangle\langle r^\circ|R_\sigma|g^\circ\rangle}{(\varepsilon_r^\circ-\varepsilon_g^\circ+E_0)^2}\right]$$
$$= \frac{1}{3}\sum_{r\neq g}\left[\frac{1}{(\varepsilon_r^\circ-\varepsilon_g^\circ-E_0)^2}+\frac{1}{(\varepsilon_r^\circ-\varepsilon_g^\circ+E_0)^2}\right] \times \frac{\langle r^\circ|h_a|r^\circ\rangle}{(\varepsilon_r^\circ-\varepsilon_g^\circ)} f_{rg},$$

where f_{rg} is the oscillator strength of the electronic transition from the ground state to the r-th excited state. The value of f_{rg} calculated by the semi-empirical molecular orbital calculation is usually 2—3 times larger than the observed one.[13] This fact partly explains the overestimation of the $(d\sigma/d\Omega)_{//}$ of the A_{1g}-vibrations. In the calculated results for the non-totally symmetric vibrations, the contribution of the term C to the intensities is larger than that of the term B. This result is opposite to the usual conception that the contribution of the term C is small in comparison with that of the term B, because the energy separations between the electronic excited states appearing in the denominators of the term B are smaller than those between the electronic ground state and the excited states in the denominators of the term C. In the derivation of the terms B and C used in this work, there is only one approximation—the vibronic energy, E_{ri} in Eqs. 3 and 4 in Part I, is regarded as constant over the vibrational states. Therefore, if we want to determine the effective terms which contribute to the intensities of the non-totally symmetric vibrations, a theoretical calculation without the approximation described just above must be done.

The Raman intensities and the depolarization ratios of ethylene were calculated by the polarizability method with the force constants of Set 0 in order to compare these results with those obtained from the vibronic method. The polarizability method leads to undesirable results, as will be mentioned below (see Table 4). The intensity of the ν_4 vibration, the non-totally symmetric one, is stronger than that of the ν_2 vibration, the totally symmetric one. In the depolarization ratio, the value for the ν_3 vibration is larger than that generally found for the totally symmetric vibrations.

TABLE 4. RAMAN INTENSITIES, DEPOLARIZATION RATIOS, AND RAMAN TENSORS OF ETHYLENE CALCULATED BY THE POLARIZABILITY METHOD WITH SET 0

	$(d\sigma/d\Omega)_{//}\times10^{30}$ [cm^2]	ρ_n	$(\alpha_{\rho\sigma})'\times10^4$[cm^2 g$^{-1/2}$]			
			$(\alpha_{xx})'$	$(\alpha_{yy})'$	$(\alpha_{zz})'$	$(\alpha_{xy})'=(\alpha_{yx})'$
$\nu_1(A_{1g})$	2.80	0.236	1.728	2.662	0.034	0.0
$\nu_2(A_{1g})$	0.345	0.194	0.049	0.573	0.381	0.0
$\nu_3(A_{1g})$	2.92	0.747	2.150	−0.917	0.007	0.0
$\nu_4(B_{1g})$	1.61	0.857	0.0	0.0	0.0	2.454
$\nu_5(B_{1g})$	0.0005	0.857	0.0	0.0	0.0	0.021

Conclusions

From the results in Tables 1—4, the following conclusions can be drawn;

(a) The conclusions in Part I are almost all confirmed in the present work.

(b) The Raman intensity calculated by the vibronic method is sensitive to the set of force constants used in the calculation.

(c) The *trans*-interaction in the modified Urey-Bradley force field introduced by Scherer and Overend plays an important role not only in the frequencies, but also in the Raman intensities.

The author is grateful to Professor Tomoo Miyazaki for giving him the opportunity of publishing this work. He is also indebted to Professor Hiroaki Takahashi for his helpful advice.

References

1) H. Shinoda, *Bull. Chem. Soc. Jpn.*, **48**, 1777 (1975).
2) J. A. Pople, D. P. Santry, and G. A. Segal, *J. Chem. Phys.*, **43**, S129 (1965); J. A. Pople and G. A. Segal, *ibid.*, **43**, S136 (1965); J. A. Pople and G. A. Segal, *ibid.*, **44**, 3289 (1966).
3) N. S. Hush and M. L. Williams, *Theor. Chim. Acta (Berl.)*, **26**, 141 (1972); H. Yamada, *Kwansei Gakuin Univ. Ann. Studies*, **21**, 95 (1972); H. Shinoda and T. Miyazaki, *Chem. Lett.*, **1973**, 563.
4) P. Bleckmann, *Z. Naturforsch.*, **29a**, 1485 (1974).
5) T. Shimanouchi, *J. Chem. Phys.*, **26**, 594 (1957); W. H. Fletcher and W. T. Thompson, *J. Mol. Spectrosc.*, **25**, 240 (1968); J. M. Comerford, W. H. Snyder, and H. S. Kimmel, *Spectrosc. Lett.*, **4**, 9 (1971).
6) J. R. Scherer and J. Overend, *J. Chem. Phys.*, **33**, 1681 (1960).
7) B. L. Crawford, Jr., J. E. Lancaster, and R. G. Inskeep, *J. Chem. Phys.*, **21**, 678 (1953).
8) J. Tang and A. C. Albrecht, "Raman Spectroscopy," Vol. 2, ed. by H. A. Szymanski, Plenum Press, New York-London (1970), pp. 33—68.
9) G. Herzberg and E. Teller, *Z. Phys. Chem. (Leipzig)* **B21**, 410 (1933).
10) H. Shimizu, T. Kobayashi, and H. Inaba, *Oyo Buturi*, **42**, 889 (1973).
11) Y. Udagawa, N. Mikami, K. Kaya, and M. Ito, *J. Raman Spectrosc.*, **1**, 341 (1973).
12) S. M. Blumenfeld, S. P. Reddy, and H. L. Welsh, *Can. J. Phys.*, **48**, 513 (1970).
13) R. S. Mulliken, *J. Chem. Phys.*, **7**, 20 (1939); W. Moffitt, *ibid.*, **22**, 320 (1954).

The Crystal and Molecular Structure of Silver(I) *N,N*-Diethyldithiocarbamate

Hiroko YAMAGUCHI, Azuma KIDO, Tetsuo UECHI,* and Kazuo YASUKOUCHI

Department of Industrial Chemistry, Faculty of Engineering, Kumamoto University, Kurokami, Kumamoto 860

**General Education Department of Kyushu University, Fukuoka 810*

(Received June 16, 1975)

The crystal structure of silver(I) *N,N*-diethyldithiocarbamate was determined by the X-ray diffraction method. The crystals are monoclinic, with the space group $P2_1/c$, and with two hexameric molecules in a unit cell with dimensions of $a=10.90\pm0.02$, $b=24.72\pm0.01$, $c=11.51\pm0.02$ Å, and $\beta=125.8\pm0.1°$. The structure was solved by a heavy-atom method and was refined by block-diagonal least-squares methods to a final *R*-value of 0.029 for 2108 observed reflections. The structure consists of hexameric molecules, $[AgS_2CN(C_2H_5)_2]_6$. The hexameric structure was essentially consistent with Hesse's preliminary result (1960). The terminal silver atom in one molecule is bridged by a sulfur atom to that in the adjacent hexamer, forming a chain structure along the a axis. All the silver atoms are connected to five atoms (either 1Ag and 4S or 2Ag and 3S). The dithiocarbamate ligands are classified into three types: bidentate, intra-, and inter-molecule tetradentate.

The use of silver(I) *N,N*-diethyldithiocarbamate (Ag-EtDC) in the microdetermination of arsenic has been widely accepted in the last ten years,[1] and the mechanism of color development has been investigated in some detail.[2] The crystal and molecular structure of this interesting reagent was studied by Hesse. He reported that the molar ratio of metal and ligand contents was 1:1,[3] and that the six silver atoms of a hexameric molecule formed a doubly bent chain in the crystal,[4] although the detailed structure was left undetermined. Hitherto, the crystal structures of many other metal-EtDC complexes have also been studied; among them, the structure of Ag-PrDC[5] (silver dipropyldithiocarbamate) was reported by Hesse in detail.

Our precise determination of the crystal and molecular structure of Ag-EtDC was carried out in an attempt to reveal the relations between the arrangement of the silver atoms and the terminal alkyl group, and between the solubility and the molecular structure.

Experimental

Ag-EtDC (Dotite Arsemate of Dojindo Labs.) was recrystallized from pyridine. The crystals were light-yellow transparent prisms. The lattice parameters were determined using 15 reflections measured by a Syntex automated diffractometer ($P\bar{1}$) using Mo$K\alpha$ radiation monochromated with a graphite crystal (taken as 0.71069 Å). The density was measured by flotation in a mixed solution of methyl iodide and ethyl alcohol.

TABLE 1. THE CRYSTAL DATA

Silver (I) *N,N*-Diethyldithiocarbamate
Formula: $Ag_6[S_2CN(C_2H_5)_2]_6$
Crystal Class: Monoclinic prismatic
Space Group: $P2_1/c$
Cell Parameters:
$a=10.90\pm0.02$ Å
$b=24.72\pm0.01$ Å
$c=11.51\pm0.02$ Å
$\beta=125.8\pm0.1°$
Volume of Unit Cell: $V=2514.4\pm5.7$ Å^3
Density: $D_m=2.048$ g cm^{-3}
$D_x=2.082$ g cm^{-3}
Number of Formula per Unit Cell: $Z=2$
μ for Mo$K\alpha$: $\mu=31.3$ cm^{-1}

The crystal data are summarized in Table 1. A single crystal was ground by Bond's method[6] to make it a sphere with a diameter of 0.348 mm ($\mu r=0.545$ for Mo$K\alpha$ radiation); this sphere was then used for the intensity measurement. The intensity data were collected by the θ–2θ scan technique with a variable scan rate from 4.0 to 24.0°/min on a Syntex ($P\bar{1}$) four-circle diffractometer, using Mo$K\alpha$ radiation monochromated by a graphite crystal. The intensities were corrected for the Lorentz, polarization, and absorption effects. A total of 2108 observed reflections whose intensity was larger than three times their standard deviations was obtained within a range of $2\theta<40°$.

Structure Analysis

The positions of three unique silver atoms were deduced from a three-dimensional Patterson synthesis. The remaining non-hydrogen atoms were located by successive Fourier syntheses. Six cycles of block-diagonal least-squares refinement led an *R* value (defined as $\sum||F_o|-|F_c||/\sum|F_o|$) of 0.095 for the observed reflections. Subsequently, six further cycles of least-squares refinements with anisotropic thermal factors reduced the *R* value to 0.047. At this point, a difference Fourier synthesis was computed; all hydrogen atoms could be allocated with peak heights varying from 0.2 to 0.3 eÅ^{-3}. Introducing the hydrogen atoms with isotropic temperature factors brought the *R* value down to 0.032. Refinement was terminated when the shifts of the parameters for the non-hydrogen atoms were less than one-tenth of their estimated standard deviations. The final *R* value was 0.029. A final difference Fourier synthesis showed no significant features of the undulations, with ranged from −0.2 to 0.1 eÅ^{-3}. The atomic scattering factors for Ag^+, S, N, C, and H were taken from the International Tables for X-ray Crystallography.[7] The anomalous dispersion correction was not taken into account. In the least-squares procedure, the quantity minimized was $\sum w(k|F_o|-|F_c|)^2$, where *k* was a scale factor and $w=1$ for all the observed reflections. The final atomic coordinates and thermal parameters are given in Tables 2 and 3, along with their estimated standard deviations. The

TABLE 2. FINAL ATOMIC COORDINATES AND THERMAL PARAMETERS WITH THEIR STANDARD DEVIATIONS
(Numbers in parentheses here and elsewhere in this paper are the estimated standard deviations in the least significant digits.)

atom	x/a	y/b	z/c	β_{11}	β_{22}	β_{33}	β_{12}	β_{13}	β_{23}
Ag(1)	0.2828(1)	0.0278(0)	0.3660(1)	126(1)	14(0)	137(1)	6(1)	188(2)	3(1)
Ag(2)	0.1421(1)	0.1065(0)	0.1442(1)	160(1)	20(0)	88(1)	24(1)	126(2)	−6(1)
Ag(3)	0.1100(1)	0.0110(0)	−0.0288(1)	110(1)	18(0)	103(1)	19(1)	139(2)	15(1)
S(1A)	0.1220(3)	0.0878(1)	0.3964(3)	130(4)	11(0)	125(4)	3(2)	193(7)	0(2)
S(1B)	0.2209(3)	0.1844(1)	0.3126(3)	156(4)	12(0)	93(3)	−6(2)	173(7)	−3(2)
S(2A)	0.4825(2)	0.0071(1)	0.3320(2)	70(3)	13(0)	68(3)	−2(2)	85(5)	5(2)
S(2B)	0.3165(3)	0.0826(1)	0.0757(3)	82(3)	18(1)	83(3)	10(2)	90(6)	24(2)
S(3A)	0.1420(3)	−0.0874(1)	0.0214(2)	116(4)	14(1)	75(3)	7(2)	131(6)	3(2)
S(3B)	0.1006(2)	−0.0609(1)	0.2534(2)	72(3)	11(0)	61(3)	1(2)	83(5)	−1(2)
N(1)	0.1496(9)	0.1876(3)	0.4957(8)	151(13)	13(2)	104(11)	21(7)	184(21)	0(7)
N(2)	0.6071(7)	0.0623(3)	0.2264(7)	85(11)	15(2)	78(10)	3(7)	105(18)	8(6)
N(3)	0.3225(8)	−0.1210(3)	0.2898(7)	87(11)	9(1)	80(10)	11(6)	49(18)	−5(6)
C(11)	0.1645(9)	0.1571(3)	0.4098(8)	53(12)	13(2)	52(11)	2(7)	35(19)	−2(7)
C(12)	0.0970(12)	0.1664(4)	0.5819(11)	198(20)	20(2)	151(17)	12(11)	262(36)	6(10)
C(13)	0.2233(14)	0.1579(5)	0.7353(13)	230(23)	25(3)	159(18)	−4(13)	260(36)	5(12)
C(14)	0.1767(12)	0.2464(4)	0.5039(11)	212(20)	9(2)	128(15)	33(10)	183(31)	−5(9)
C(15)	0.0309(17)	0.2744(5)	0.3923(16)	321(32)	17(3)	286(28)	22(15)	334(52)	−12(14)
C(21)	0.4815(9)	0.0516(3)	0.2156(8)	69(12)	12(2)	57(11)	−13(7)	71(20)	−11(7)
C(22)	0.6108(11)	0.0965(4)	0.1233(10)	126(16)	27(3)	111(14)	6(11)	176(27)	30(10)
C(23)	0.6406(18)	0.1554(5)	0.1665(16)	402(35)	20(3)	261(26)	−31(16)	478(54)	22(14)
C(24)	0.7560(10)	0.0388(4)	0.3401(10)	78(14)	22(2)	111(14)	−2(9)	111(24)	5(9)
C(25)	0.7857(14)	−0.0105(5)	0.2860(13)	233(23)	27(3)	195(21)	57(14)	305(39)	23(13)
C(31)	0.2012(9)	−0.0920(3)	0.1999(9)	76(13)	8(2)	68(11)	−18(7)	52(20)	−6(7)
C(32)	0.4211(11)	−0.1432(4)	0.2541(11)	133(16)	15(2)	175(17)	26(9)	212(29)	8(10)
C(33)	0.3875(17)	−0.1993(5)	0.2012(16)	324(30)	19(3)	329(29)	−23(15)	503(53)	−60(14)
C(34)	0.3775(11)	−0.1289(4)	0.4427(10)	141(17)	14(2)	87(13)	45(9)	68(25)	9(8)
C(35)	0.3160(17)	−0.1789(5)	0.4647(13)	357(32)	28(3)	152(19)	−32(16)	33(43)	4(13)

β_{ij} as given here are defined by: $T=\exp(-10^{-4}(h^2\beta_{11}+k^2\beta_{22}+l^2\beta_{33}+hk\beta_{12}+hl\beta_{13}+kl\beta_{23}))$

TABLE 3. COORDINATES AND ISOTROPIC TEMPERATURE FACTORS FOR HYDROGEN ATOMS

Atom	x/a	y/b	z/c	B(Å^2)	Atom	x/a	y/b	z/c	B(Å^2)
H(11)	0.057(10)	0.129(4)	0.544(10)	2.69	H(26)	0.752(10)	0.027(4)	0.419(9)	2.63
H(12)	0.005(10)	0.184(4)	0.559(10)	2.89	H(27)	0.838(10)	0.068(5)	0.373(10)	3.05
H(13)	0.294(12)	0.133(4)	0.730(11)	4.85	H(28)	0.873(11)	−0.020(5)	0.352(11)	4.21
H(14)	0.160(9)	0.141(3)	0.768(8)	0.99	H(29)	0.720(11)	−0.033(5)	0.238(10)	4.07
H(15)	0.300(11)	0.186(4)	0.776(11)	4.46	H(210)	0.819(11)	0.000(5)	0.218(11)	5.13
H(16)	0.275(10)	0.255(4)	0.521(9)	2.33	H(31)	0.444(11)	−0.119(5)	0.233(10)	4.17
H(17)	0.197(11)	0.258(4)	0.594(11)	3.95	H(32)	0.447(13)	−0.158(6)	0.306(12)	7.26
H(18)	0.038(11)	0.300(4)	0.393(10)	4.09	H(33)	0.337(13)	−0.226(6)	0.205(12)	6.45
H(19)	−0.049(12)	0.263(4)	0.413(11)	5.46	H(34)	0.463(12)	−0.207(4)	0.173(11)	5.21
H(110)	−0.024(15)	0.259(5)	0.273(15)	8.98	H(35)	0.275(12)	−0.197(4)	0.108(11)	4.67
H(21)	0.518(12)	0.094(4)	0.038(11)	4.60	H(36)	0.341(8)	−0.102(3)	0.465(8)	0.87
H(22)	0.672(10)	0.081(4)	0.109(10)	3.23	H(37)	0.447(14)	−0.172(5)	0.479(13)	9.42
H(23)	0.562(13)	0.166(5)	0.177(12)	6.11	H(38)	0.380(12)	−0.182(5)	0.587(12)	5.64
H(24)	0.754(15)	0.143(5)	0.248(14)	9.46	H(39)	0.215(11)	−0.165(4)	0.419(10)	3.80
H(25)	0.659(11)	0.168(4)	0.104(11)	4.79	H(310)	0.347(12)	−0.201(4)	0.433(11)	5.25

calculated and observed structure factors are listed in Table 4.**

Results and Discussion

The Crystal Structure. The crystal structure of Ag-EtDC (except hydrogen atoms), projected along the c axis, is shown in Fig. 1. The crystal is composed of hexameric molecules, $[AgS_2CN(C_2H_5)_2]_6$. Each molecule has a center of symmetry. The molecular structure was essentially consistent with Hesse's preliminary result.[4] As is shown in Table 6, the distance between Ag(1) and S(2A″) in the neighboring molecule is 2.994 Å. The distance is longer than any other inner-hexameric bond, but it is nearly the same as that, 2.965 Å, of Hg–S in the β form of Hg-$(EtDC)_2$.[8] Since

** Table 4 is deposited as Document No. 7616 at the Office of the Editor of the Bulletin of the Chemical Society of Japan.

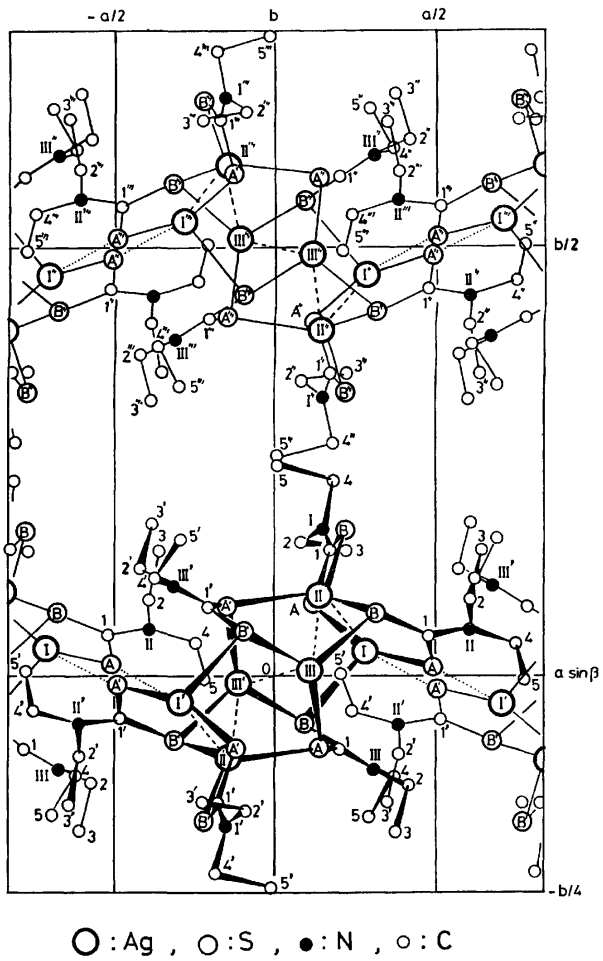

Fig. 1. The crystal structure of Ag-EtDC projected along the c axis.

the sum of the ionic radii of Ag and S (3.10 Å) is larger than the distance of Ag(1)–S(2A″) (2.994 Å), it is concluded that the terminal silver atom is bridged by a sulfur atom to the silver atom of the adjacent hexameric molecule and that the hexameric molecules form a chain polymer along the a axis. In the crystal, these chains sparsely contact with each other by van der Waals interaction. The inter-molecular distances are listed in Table 5; the limit of 0.3 Å is greater than the sum of the relevant van der Waals radii cited by Pauling.[9]

The Molecular Structure. A schematic drawing of the hexameric molecule of Ag-EtDC, which is a part of the chain polymer, is shown in Fig. 2. The hexamer contains three types of diethyldithiocarbamate ligands-1, 2, and 3. The atomic arrangement of the three types of ligands is shown in Fig. 3. The bond distances and angles are listed in Tables 6 and 7.

In the case of hexamers of univalent metal carbamates,[5,12,13] the geometrical arrangement of the metal atoms is usually octahedral, as is shown in Table 8. However, in the Ag-EtDC hexamer, the metal atoms do not form an octahedron, but instead form a doubly bent chain, as may be seen in Fig. 2. The silver-silver distances, Ag(1)–Ag(2), Ag(2)–Ag(3), and Ag(3)–Ag(3′) (2.841, 2.974, and 2.890 Å respectively), are similar to that of the metallic Ag–Ag bond (2.889 Å at

Table 5. Van der Waals contacts between molecules (Å)

Ag(1)···Ag(1′)	4.091(1)	S(1A)···H(26′)	3.31(9)
Ag(1)···C(24′)	4.000(13)	S(1A)···H(27)	2.99(13)
Ag(1)···C(34′)	3.906(10)	S(1A)···H(28′)	3.31(13)
Ag(2)···C(14″)	4.083(11)	S(1B)···H(37′)	2.96(11)
Ag(2)···C(15″)	3.798(15)	S(1B)···H(17″)	2.78(13)
Ag(3)···C(25′)	3.742(19)	S(2A)···H(36′)	3.07(7)
		S(3A)···H(22′)	3.15(14)
S(2A)···S(2A′)	3.674(4)	S(3B)···H(210)	3.24(13)
S(1A)···C(24)	3.845(12)	S(3B)···H(26′)	3.22(10)
S(1A)···C(25′)	3.703(15)	C(13)···H(29′)	3.12(10)
S(1B)···C(14″)	3.711(14)	C(13)···H(34′)	3.18(13)
S(1B)···C(34′)	3.814(10)	C(23)···H(38′)	3.04(16)
S(2A)···C(34′)	3.671(10)	C(25)···H(13′)	3.13(11)
S(3B)···C(25)	3.872(18)	C(32)···H(13′)	3.02(15)
		C(33)···H(38″)	3.20(12)
C(13)···C(25′)	3.648(18)	C(35)···H(110‴)	3.12(12)
C(15)···C(35‴)	3.784(16)	H(11)···H(27)	2.52(15)
C(21)···C(34′)	3.795(14)	H(13)···H(29′)	2.52(11)
		H(13)···H(31′)	2.66(19)
Ag(1)···H(26′)	3.02 (12)	H(15)···H(34′)	2.35(19)
Ag(2)···H(17″)	3.52 (10)	H(19)···H(33‴)	2.61(18)
Ag(2)···H(18″)	3.34 (11)	H(19)···H(35‴)	2.54(20)
Ag(3)···H(210′)	2.73 (15)	H(23)···H(38′)	2.43(20)

unprimed; (x, y, z), single-primed; $(a-x, -y, -z)$, double-primed; $(x, b/2-y, c/2+z)$, triple-primed; $(-x, b/2+y, c/2-z)$

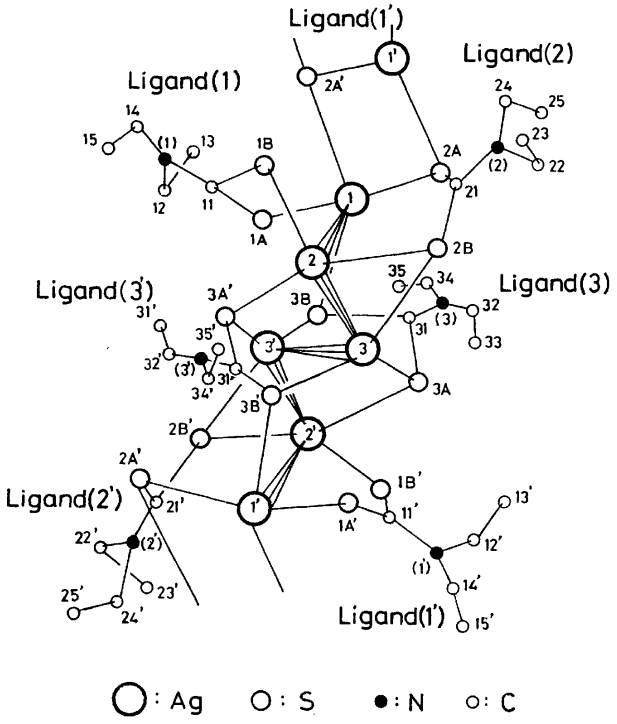

Fig. 2. Schematic drawing of Ag-EtDC hexamer.

20 °C);[14] they are slightly shorter than those of octahedrons, such as Ag-PrDC[5] and Ag-PrMC (silver dipropylmonothiocarbamate).[13] The Ag(1)···Ag(3), Ag(1)···Ag(3′), Ag(2)···Ag(3′), and Ag(1)···Ag(2′) distances

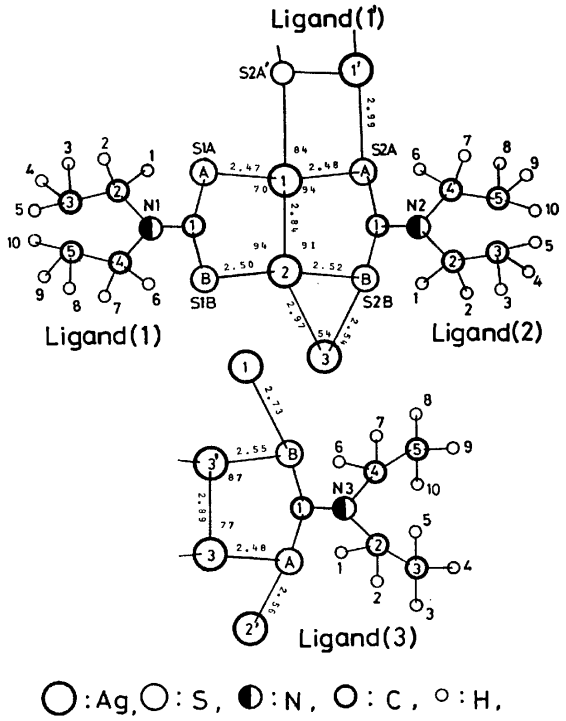

Fig. 3. Main bond distances (Å) and angles (°) of ligand 1, 2, and 3 in Ag-EtDC hexamer.

(3.786, 3.855, 3.673, and 5.928 Å respectively) are considerably longer than those of the octahedral conformation (3.20—3.28 Å). It seems that the unusual arrangement of the metal atoms causes the formation of a chain polymer and also a complicated coordination of the six ligands to the metal atoms, as will be discussed later. The thermal ellipsoids of atoms projected along the b axis are shown in Fig. 4. The atoms in the outer part of the molecule vibrate more than those of the inner part. The thermal vibrations of the terminal methyl carbons are the largest, as was expected.

The Coordination. All diethyldithiocarbamate

TABLE 6. BOND DISTANCES WITH THEIR e.s.d.'s (Å)

Ag(1)–Ag(2)	2.841(1)	Ag(2)–S(1B)	2.500(3)
Ag(2)–Ag(3)	2.974(1)	Ag(2)–S(2B)	2.519(4)
Ag(3)–Ag(3′)	2.890(2)	Ag(2)–S(3A′)	2.557(2)
Ag(1)–S(1A)	2.471(3)	Ag(3)–S(2B)	2.544(3)
Ag(1)–S(2A)	2.481(3)	Ag(3)–S(3A)	2.478(3)
Ag(1)–S(3B)	2.725(2)	Ag(3)–S(3B′)	2.554(2)
Ag(1)–S(2A″)	2.994(2)		

	Ligand 1	Ligand 2	Ligand 3
S(A)–C(1)	1.734(9)	1.727(10)	1.760(10)
S(B)–C(1)	1.710(2)	1.738(7)	1.721(12)
N( )–C(1)	1.340(14)	1.328(14)	1.315(9)
N( )–C(2)	1.501(19)	1.471(16)	1.465(18)
N( )–C(4)	1.476(12)	1.482(10)	1.503(14)
C(2)–C(3)	1.487(14)	1.521(17)	1.473(16)
C(4)–C(5)	1.504(16)	1.488(19)	1.497(20)

single-primed ($-x$, $-y$, $-z$); double-primed ($a-x$, $-y$, $-z$)

TABLE 7. BOND ANGLES WITH THEIR e.s.d.'s (degrees)

Ag(1)–Ag(2)–Ag(3)	81.23(3)	Ag(2)–Ag(1)–S(1A)	70.24(7)
Ag(2)–Ag(3)–Ag(3′)	77.57(4)	Ag(2)–Ag(1)–S(2A)	93.52(7)
		Ag(2)–Ag(1)–S(3B)	105.34(5)
Ag(2)–S(2B)–Ag(3)	71.94(9)	Ag(1)–Ag(2)–S(1B)	94.08(6)
Ag(2′)–S(3A)–Ag(3)	93.69(7)	Ag(1)–Ag(2)–S(2B)	90.62(6)
Ag(1)–S(3B)–Ag(3′)	93.76(8)	Ag(1)–Ag(2)–S(3A′)	108.90(7)
Ag(1)–S(2A)–Ag(1″)	96.25(5)	Ag(3)–Ag(2)–S(1B)	169.31(8)
		Ag(3)–Ag(2)–S(2B)	54.42(6)
S(1A)–Ag(1)–S(2A)	155.03(9)	Ag(3)–Ag(2)–S(3A′)	74.78(7)
S(1A)–Ag(1)–S(3B)	99.80(9)	Ag(2)–Ag(3)–S(2B)	53.64(8)
S(2A)–Ag(1)–S(3B)	102.83(9)	Ag(2)–Ag(3)–S(3A)	132.70(8)
S(1B)–Ag(2)–S(2B)	116.39(10)	Ag(2)–Ag(3)–S(3B′)	88.73(6)
S(1B)–Ag(2)–S(3A′)	115.90(10)	Ag(3′)–Ag(3)–S(2B)	130.30(9)
S(2B)–Ag(2)–S(3A′)	122.00(9)	Ag(3′)–Ag(3)–S(3A)	77.49(8)
S(2B)–Ag(3)–S(3A)	127.42(7)	Ag(3′)–Ag(3)–S(3B′)	87.03(7)
S(2B)–Ag(3)–S(3B′)	99.49(8)		
S(3A)–Ag(3)–S(3B′)	129.09(7)	Ag(2)–S(1B)–C(11)	95.74(30)
S(2A)–Ag(1)–S(2A″)	83.74(5)	Ag(2)–S(2B)–C(21)	112.00(42)
		Ag(2)–S(3A′)–C(31′)	108.35(34)
Ag(1)–S(1A)–C(11)	114.97(41)	Ag(3)–S(2B)–C(21)	106.31(31)
Ag(1)–S(2A)–C(21)	112.53(35)	Ag(3)–S(3A)–C(31)	103.96(29)
Ag(1)–S(3B)–C(31)	95.13(29)	Ag(3)–S(3B′)–C(31′)	103.72(28)

	Ligand 1	Ligand 2	Ligand 3		Ligand 1	Ligand 2	Ligand 3
S(A)–C(1)–S(B)	121.34(63)	122.16(63)	120.88(42)	C(1)–N( )–C(4)	120.92(95)	122.77(86)	121.33(98)
S(A)–C(1)–N( )	119.35(84)	121.04(54)	117.79(88)	C(2)–N( )–C(4)	116.08(99)	113.73(89)	115.13(71)
S(B)–C(1)–N( )	119.30(69)	116.76(71)	121.31(81)	N( )–C(2)–C(3)	112.80(109)	112.68(116)	115.02(122)
C(1)–N( )–C(2)	122.91(81)	123.43(66)	123.28(91)	N( )–C(4)–C(5)	109.02(82)	110.23(75)	113.21(78)

single-primed ($-x$, $-y$, $-z$); double-primed ($a-x$, $-y$, $-z$)

TABLE 8. BOND DISTANCES IN SOME COINAGE METALS DITHIOCARBAMATES AND MONOTHIOCARBAMATES

Compound	Metal arrangement	Bond distances (Å)					Ref.
		Metal–Metal	Metal–S	S–C	C–N	N–C(Et)	
$[Ag\text{-}EtDC]_6$	doubly bent chain	2.84—2.97	2.471—2.994	1.71—1.76	1.32—1.34	1.47—1.50	this work
$[Au\text{-}PrDC]_2$	pair	2.76	2.28	1.70	1.32	1.50	10
$[Cu\text{-}EtDC]_4$	tetrahedron	2.66—2.76	2.25—2.29	1.71	1.41	1.48	11
$[Cu\text{-}PrMC]_6$	octahedron	2.70—3.06	2.20—2.25	1.78	1.37	1.50	12
$[Ag\text{-}PrMC]_6$	octahedron	2.94—3.28	2.44—2.49				13
$[Ag\text{-}PrDC]_6$	octahedron	2.90—3.20	2.48—2.58	1.71	1.38	1.50	5

A comparison of bond distances in various Metal-EtDC complexes

Metal-EtDC	Metal–S	S–C	C–N	N–C(Et)	Ref.
$Ni\text{-}(EtDC)_2$	2.195—2.207	1.707	1.330	1.485	15
$[Cu(II)\text{-}(EtDC)_2]_2$	2.297—2.339	1.717	1.330	1.470	16
$[Zn\text{-}(EtDC)_2]_2$	2.331—2.815	1.727	1.325	1.473	17
$Co\text{-}(EtDC)_3$	2.258—2.260	1.704	1.319	1.496	18
$Na\text{-}EtDC\cdot 3H_2O$	—	1.726	1.344	1.417	19
$\alpha\ Hg_2\text{-}(EtDC)_4$	2.418—2.698	1.728	1.33	1.495	8
β Hg-$(EtDC)_2$	2.398—2.965	1.737	1.29	1.485	8
$[Ag\text{-}EtDC]_6$	2.471—2.994	1.732	1.328	1.483	this work

ligands are bidentate to the bivalent metals[8,15–17] and are bidentate[10] or tridentate[5,11–13] to the univalent metals. All six ligands in the hexamer, Cu(I)-PrMC,[12] Ag-PrDC,[5] and Ag-PrMC,[13] are tridentate. On the other hand, in the case of Ag-EtDC, there are three types of ligands in the hexameric molecules (i) Both sulfur atoms [S(1A), S(1B)] of the ligand-1 are monodentate (coordination number of the ligand-1, $p_1=2$). (ii) In the ligand-2, one [S(2A)] is mono- and the other [S(2B)] is bidentate. In addition, the sulfur atom [S(2A)] of the ligand-2 coordinates to another silver atom [Ag(1')] of the adjacent hexameric molecule ($p_2=3+1$). (iii) The two sulfur atoms [S(3A), S(3B)] of the ligand-3 are bidentate ($p_3=4$), as is shown in Figs. 2 and 3. Consequently, each silver atom in a hexamer has five combined atoms (one silver and four sulfur atoms, or two silver and three sulfur atoms). It seems that the greater coordination number tends to give the shorter distance of C–N, and the longer distance of C–S, as is shown in Table 6. It may be considered that these three types of coordinations have influence on the different electron transfer from the nitrogen through carbon to the sulfur atoms.

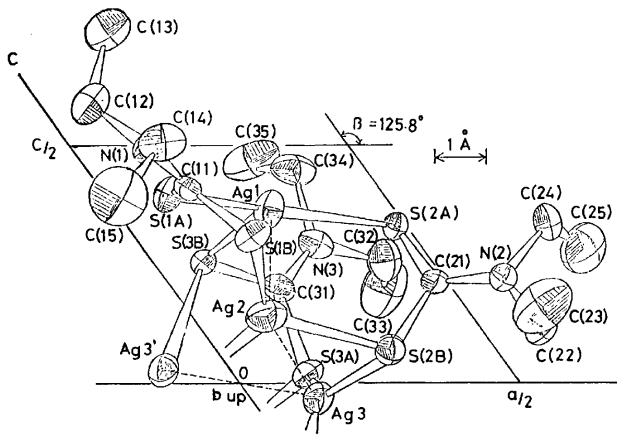

Fig. 4. Atomic arrangements of Ag-EtDC in an asymmetric unit (b axis projection).

The Ligand Structure. A comparison of the bond distances in various univalent metal-EtDC complexes is shown[8,15–19] in Table 8. The bond distances of S–C and C–N obtained in the present work are nearly the same as those of the other compounds. The bond distance of Ag–S in Ag-EtDC is, however, slightly longer than in the other Ag-complexes. This may be attributable to the doubly bent chain of the silver atom and to the formation of the chain polymer in the Ag-EtDC crystal. The distances between carbon and nitrogen show a double-bond character. All the ligands of the hexamer are planar except for the terminal alkyl groups, as is shown in Fig. 1. The terminal methyl groups of the ligands-1 and 2 take a *trans*-configuration, whereas those of the ligand-3 take a *cis*-configuration. This is the first example of an alkyldithiocarbamate complex in which the ligand molecules have both *trans*- and *cis*-type methyl groups. It may be caused by complicated packing among the hexameric molecules.

The C–H bond distances are around 0.96 Å, varying from 0.61 to 1.23 Å.

It seems that the solubility of a crystal depends on the polymerity of the molecule in the crystal. Whereas Ag-PrDC is a simple hexamer, in the case of Ag-EtDC the hexameric molecules form a chain polymer along the a axis. This agrees with the fact that Ag-PrDC is readily soluble, while Ag-EtDC is hardly soluble, in an organic solvent.

We wish to express our hearty thanks to Professor I. Ueda, Professor K. Ueno, and Assistant Prof. S. Kawano, Kyushu University, for their kind valuable advice throughout this work. Thanks are also due to Prof. T. Kato, Yamaguchi University, for his advice on the computation process. We wish also to thank to Prof. T. Kawasaki and his co-workers at the Faculty of Pharmacy of Kyushu University for making available the Syntex automated diffractometer.

References

1) V. Stara and J. Stary, *Talanta*, **17**, 341 (1970).
2) H. Bode and K. Hachmann, *Z. Anal. Chem.*, **241**, 18 (1968).
3) R. Hesse, *Acta Crystallogr.*, **13**, 1025 (1960).
4) "Advances in the Chemistry of the Coordination Compounds," ed. by S. Kirschner, New York (1961), p. 314.
5) R. Hesse and L. Nilson, *Acta Chem. Scand.*, **23**, 825 (1969).
6) W. L. Bond, *Rev. Sci. Instrum.*, **22**, 344 (1951).
7) "International Tables for X-Ray Crystallography," Vol. III. Kynoch Press, Birmingham (1962), p. 202.
8) H. Iwasaki, *Acta Crystallogr.*, **B29**, 2115 (1973).
9) L. Paulling, "The Nature of the Chemical Bond," Cornell Univ. Press, Ithaca (1960), p. 260.
10) R. Hesse and P. Jennische, *Acta Chem. Scand.*, **26**, 3855 (1972).
11) R. Hesse, *Arkiv. Kemi.*, **20**, 481 (1963).
12) R. Hesse and U. Aava, *Acta Chem. Scand.*, **24**, 1355 (1970).
13) P. Jennische and R. Hesse, *Acta Chem. Scand.*, **25**, 423 (1971).
14) "International Tables for X-Ray Crystallography," Vol. III. Kynoch Press, Birmingham (1962), p. 278.
15) M. Bonamico, G. Dessy, C. Mariani, A. Vaciago, and L. Zambonelli, *Acta Crystallogr.*, **19**, 619 (1965).
16) M. Bonamico, G. Dessy, A. Mugnoli, A. Vaciago, and L. Zambonelli, *Acta Crystallogr.*, **19**, 886 (1965).
17) M. Bonamico, G. Mazzone, A. Vaciago, and L. Zambonelli, *Acta Crystallogr.*, **19**, 898 (1965).
18) S. Merlino, *Acta Crystallogr.*, **B24**, 1441 (1968).
19) M. Colapietro, A. Domenicano, and A. Vaciago, *Chem. Commun.*, **1968**, 572 (1968).

On the Solvent-Induced Changes of Electronic Structures of Intramolecular Exciplexes

Shinzaburo MASAKI, Tadashi OKADA, Noboru MATAGA,*
Yoshiteru SAKATA,** and Soichi MISUMI**

The Department of Chemistry, Faculty of Engineering Science, Osaka University, Toyonaka, Osaka 560
***The Institute of Scientific and Industrial Research, Osaka University, Suita, Osaka 565*

(Received September 16, 1975)

Effects of solvent polarity upon the electron donor-acceptor interactions in the excited state of p-$(CH_3)_2N\,C_6H_4$-$(CH_2)_n$-(9-anthryl) (n=0, 1, 2, 3) and p-$(CH_3)_2NC_6H_4$-$(CH_2)_n$-(1-pyrenyl) (n=1, 2, 3) have been investigated by means of fluorescence spectral measurements and theoretical calculations based on some simplified models. The solvent-induced electronic structural changes during the excited state lifetime have been demonstrated for some of the above intramolecular exciplexes.

The nature of the CT (charge transfer) interaction in the excited electronic state is a subject under the most lively investigation at present. For example, it is well-known that many aromatic molecules in solution form exciplexes in the singlet excited state.[1] Detailed studies on the structures and dynamic behaviors of exciplex systems are now being made, mainly by means of time-resolved fluorescence measurements as well as transient absorption spectral measurements by the laser photolysis method. On the other hand, similar studies have been made on the excited state of CT complexes (which are stable in the ground state), such as the TCNB(1,2,4,5-tetracyanobenzene)-aromatic hydrocarbon complexes.[2-6] Owing to these investigations, the nature of the CT interactions in the excited electronic state has been elucidated to a considerable extent and the results of these investigations appear to be important from the viewpoint of the photochemical reaction mechanisms in solution.

Upon increasing the solvent polarity, both the fluorescence quantum yield and the decay time of some typical heteroexcimers, such as pyrene-DMA (*N,N*-dimethylaniline) and anthracene-DEA (*N,N*-diethylaniline), decrease, and the fluorescence yield decreases more rapidly with increasing solvent polarity than does the corresponding fluorescence lifetime.[7,8] There are two alternative interpretations of these observations.

(a) Solvent-induced Change of Electronic and Geometrical Structure of the Exciplex.[7] The exciplex state may be considered as a resonance hybrid of the electron transfer configuration (A^-D^+) mixed with the locally excited configuration (A*D) or (AD*). The solvation of the exciplex by the polar solvents will oppose the electronic delocalization between A and D since the solvation energy increases with increasing charge separation in the exciplex, *i.e.*, with its increasing dipole moment. This is true whether the solvation can be approximated by the interaction of a solute dipole with the surrounding dielectric continuum[9] or it is described by the 1 : n electrostatic complex formation with the polar solvent molecules.[10,11] Furthermore, the strong solvation may induce the change of geometrical structure of the exciplex leading to the decrease of the electronic delocalization interaction between A and D. Thus, the exciplex electronic structure may become more polar with increasing polarity of the solvent and this change of the electronic structure would lead to the decrease of the radiative transition probability. The radiationless transition probability, however, increases with solvent polarity because the energy gap between the relevant electronic levels becomes smaller in a more polar solvent and, furthermore, because of the ionic dissociation of the complex in a more or less polar solvent.

(b) Competition between the Ionic Dissociation and the Fluorescent Exciplex Formation in the Encounter Complex.[8]

$$A^* + D \rightarrow A^* \cdots D \begin{cases} \xrightarrow{k_c} (A^-D^+)^* \xrightarrow{k_f} \\ \xrightarrow{k_{ip}} (A_s^- \cdots D_s^+) \end{cases} \xrightarrow{k_d} A_s^- + D_s^+$$

where $(A^-D^+)^*$ is the fluorescent exciplex and ($A_s^- \cdots D_s^+$) represents a solvated ion-pair which is non-fluorescent. Almost complete charge transfer between D and A in the exciplex is assumed here, while partial charge transfer is postulated in the case of (a). It is assumed that k_{ip} and k_i are increased in polar solvents while k_c is almost independent of the solvent polarity and, moreover, the electronic structure of the complex may be independent of the solvent polarity.

According to the recent laser photolysis studies,[12] the solvent-induced electronic structural change does not seem to be very important for the interpretation of the effect of solvent polarity upon the fluorescence yield and decay time of such strongly polar exciplexes as pyrene-DMA and anthracene-DEA systems. However, the phenomenon of the solvent-induced electronic structural change may exist in principle and seems to be of some importance in general for the interpretation of electronic structures of molecular complexes in solution, since they have more flexible structures than the ordinary molecules. The observation by Schneider and Lippert[13] that the fluorescence spectra of 9,9'-bianthryl depends considerably on the solvent polarity, showing a red shift as the polarity is increased, seems to be a special case of a competition between the delocalization tendency and the solvation as described in (a). Namely, in the case of 9,9'-bianthryl, which consists of two weakly interacting identical moieties, there arise energy minima corresponding to solvated polar (unsymmetrical) states which are more stable than the nonpolar symmetrical ones at sufficiently high solvent polarities.[14]

* To whom all correspondence should be addressed.

Recently, we have examined the solvent effect upon the $S_n \leftarrow S_1$ spectra of this compound by using the mode-locked ruby laser.[15] Although the $S_n \leftarrow S_1$ spectra in hexane are not the same as those of anthracene, they are somewhat similar to each other. The spectra observed in acetone are quite different from those in hexane and rather similar to those of anthracene ions.[15] This is a direct demonstration of the solvent-induced electronic structural change. This result of a remarkable solvent effect on the $S_n \leftarrow S_1$ spectra is similar to the case of the solvent effect upon the $S_n \leftarrow S_1$ spectra of 9-(4-dimethylaminophenyl)anthracene which we have observed previously.[16]

Now, in order to elucidate the electronic structures and the mechanisms of the dynamical behaviors of exciplex systems, we have been making detailed studies of the following intramolecular exciplex systems: *p*-$(CH_3)_2N$ C_6H_4-$(CH_2)_n$-(9-anthryl) (n=0, 1, 2, 3, abbreviated as A_0, A_1, A_2, A_3, respectively) and *p*-$(CH_3)_2N$ C_6H_4-$(CH_2)_n$-(1-pyrenyl) (n=1, 2, 3, abbreviated as P_1, P_2, P_3, respectively). The solvent shifts of the fluorescence bands of these intramolecular exciplexes have been measured and analyzed by a theoretical method which is an extension of the previous ones,[17,18] and the solvent-induced electronic structural change has been demonstrated.

In the following the results of these investigations will be described from the viewpoint of the solvent-induced electronic structural change of the composite molecular systems and of the geometrical restrictions on the exciplex formation.

Experimental

Synthesis of the compounds, A_0, A_1, A_2, A_3, P_1, P_2, and P_3, will be reported in a separate paper.[19]

The following solvents were used for the measurements. (The numbers in parentheses are those attached to the observed points in the figures.) Hexane (3), methylcyclohexane (4), cyclohexane (5), dibutyl ether (9), diethyl ether (13), chloroform (14), isobutyl acetate (17), ethyl acetate (18), methyl acetate (19), tetrahydrofuran (20), dichloromethane (21), pyridine (23), isopentyl alcohol (25), 1-butanol (26), 1-propanol (28), acetone (29), and acetonitrile (31), were spectrograde reagents and used without purification. Isopentane (1), pentane (2), decalin (6), tetralin (7), diisopentyl ether (8), dipropyl ether (10), acetal (11), diisopropyl ether (12), 1-hexanol (24), isobutyl alcohol (27), and ethanol (30), were purified by the standard method.[20] Butylacetate (15), ethyl butyrate (16), 1,1,2,2-tetrachloroethane (22), were G. R. grade reagents and used without purification.

Fluorescence spectra were measured by an Aminco-Bowman or a Hitachi MPF-2A spectro-photofluorometer. Solutions were deaerated by means of the freeze-pump-thaw cycles or flushed with nitrogen. For the measurements at low temperatures, a cuvette was immersed in ethanol in a quartz Dewar vessel and the temperature of ethanol was controlled by dropping liquid nitrogen. For the measurements at higher temperatures than room temperature, the cuvette was immersed in hot water in the quartz Dewar.

Results and Discussion

Solvent Effects upon Fluorescence Spectra. Absorption spectra of A_1, A_2, A_3, P_1, P_2, and P_3 do not show any indication of the ground state interaction. However, the absorption spectra of A_0 are a little broadened compared with those of anthracene, indicating a weak ground state interaction between the two moieties. The longest wavelength absorption band of A_0 may be a superposition of the anthracene band slightly modified by the substitution and a very weak CT band.[16,21] Although the absorption spectra of these systems show little dependence on the solvent polarity, the latter affects considerably their fluorescence spectra. For instance, the fluorescence spectra of A_2 and P_1 show remarkable solvent dependence, as indicated in Fig. 1. Quite similar results have been obtained for A_1.

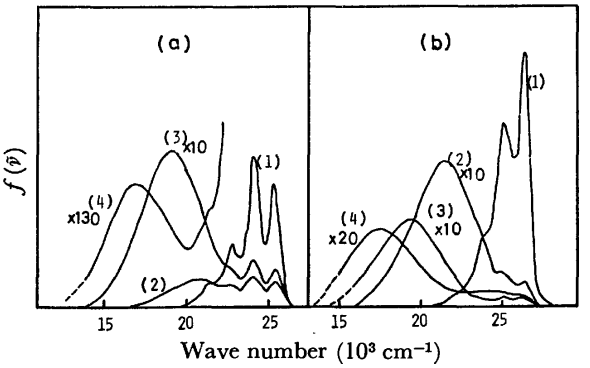

Fig. 1. Fluorescence quantum spectra of A_2 (a) and P_1 (b) in various solvents.
Solvents: 1. hexane, 2. diethyl ether, 3. isobutyl acetate, 4. isobutyl alcohol.

The fluorescence spectra of A_1, A_2, and P_1 in nonpolar solvent can be ascribed to the anthracene or pyrene part (LE (local excited state) fluorescence). In polar solvents, they show the exciplex fluorescence band in addition to the LE fluorescence band. The exciplex band shows a remarkable red shift with increase of the solvent polarity, while the wave number of the LE band does not depend on the solvent polarity. Thus, A_1, A_2 and P_1 show dual fluorescence spectra in polar solvents, but not in nonpolar solvents.

The fluorescence spectra of P_2 and P_3 in various solvents are indicated in Fig. 2. The results for A_3

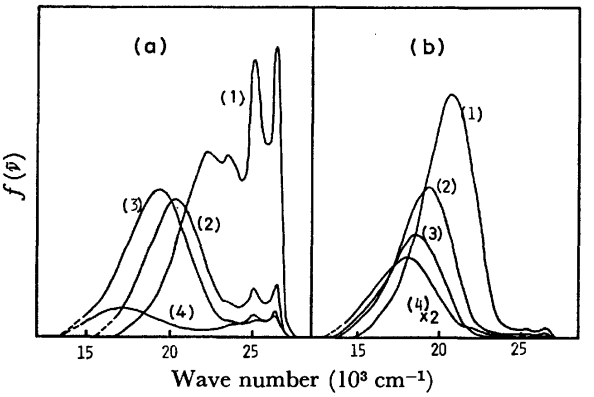

Fig. 2. Fluorescence quantum spectra of P_2 (a) and P_3 (b) in various solvents.
Solvents: 1. hexane, 2. diethyl ether, 3. butyl acetate, 4. isobutyl alcohol.

are rather similar to those in Fig. 2. In the case of these systems, both the exciplex fluorescence and the LE fluorescence bands can be observed even in nonpolar solvents, although the exciplex fluorescence yield of P_3 in a nonpolar solvent is much larger than that of P_2.

The above results for P_2 and A_2 suggest that the geometrical structure of P_2 is more favorable for the exciplex formation than that of A_2, since the electron affinity of pyrene is almost equal to or a little smaller than that of anthracene.

In contrast to the fluorescence spectra of $A_n(n=1,2,3)$ and $P_n(n=1,2,3)$, A_0 exhibits a single fluorescence band and shows a continuous red shift with increase of the solvent polarity.[16]

We have plotted the energy of the fluorescence ($h\nu_f$) of these compounds against the polarity parameter $f(\varepsilon,n)=(2(\varepsilon-1/2\varepsilon+1)-(n^2-1/2n^2+1))$, where ε and n are the dielectric constant and the refractive index of the solvent, respectively. Of course, the solute-solvent interaction may be a more or less specific molecular interaction, so that the points in the figures are rather scattered around the average values.

The plot for A_0 cannot be represented by one straight line; it is curved or represented by a superposition of several lines of different slopes.[16] This result indicates the solvent-induced change of excited electronic structure. The change of the electronic structure in the case of A_0 can be concluded also from the solvent dependence of the fluorescence yield and lifetime as well as the solvent effect on the $S_n \leftarrow S_1$ absorption spectra.[16,21]

In the case of A_1, A_2, and P_1, the CT fluorescence appears at the values of the polarity parameter $f(\varepsilon,n)\approx 0.3$—$0.4$, where its red shift with the solvent polarity is especially large. Compared with the case of sandwich type exciplexes, the stabilization of the CT state due to the Coulomb force between the pair may be smaller in these cases owing to the larger separation between

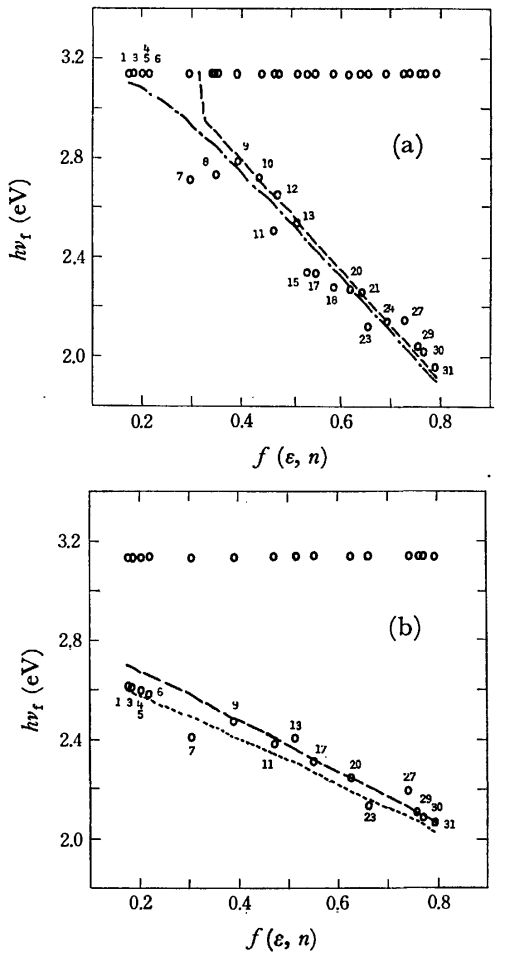

Fig. 3. Comparison between the observed and the calculated $h\nu_f$ values of A_1 (a) and A_3 (b).
o: observed value.
Calculated curves.
a. ———: $\alpha=0.05$ eV, — — —: $\alpha=0.3$ eV.
b. ———: $\alpha=0.0$ eV, ·····: $\alpha=0.3$ eV.

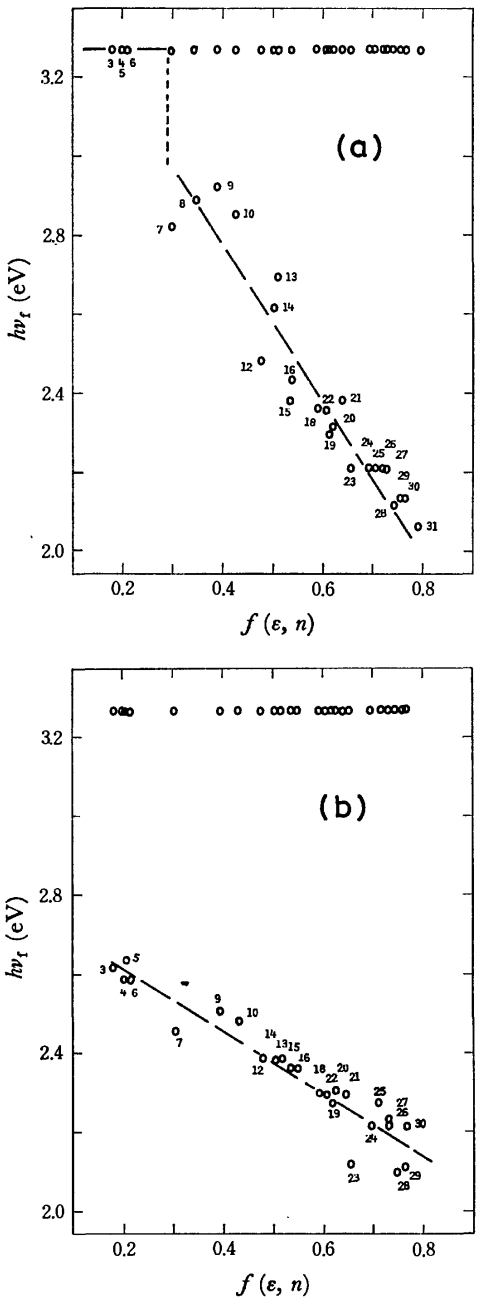

Fig. 4. Observed $h\nu_f$ *vs.* $f(\varepsilon, n)$ relations for P_1 (a) and P_3 (b).

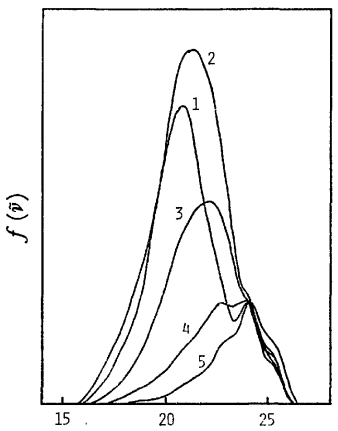

Fig. 6. Temperature effect on the fluorescence of A_1 in *n*-butylether. The spectra are normalized at the peak of anthracence LE fluorescence (24.2×10^3 cm^{-1}). Temperature (°C): (1) −61.5, (2) −25.3, (3) −3.5, (4) 26.5, (5) 78.5.

the exciplex fluorescence band appears, becomes stronger, and shifts to red. At sufficiently low temperatures, the LE band is again a little strengthened in addition to the further red shift of the exciplex band. At high temperatures, the CT state will not be stabilized sufficiently for the exciplex band to appear because of the weak solvation. There seems to be a competition between the LE fluorescence and the change of the excited electronic structure due to solvation. At sufficiently low temperatures, the solvation process as well as the accompanying structural changes may become slow because of the high viscosity, leading to a strengthening of the LE band.

The plot of the energy of the exciplex fluorescence against the solvent polarity parameter $f(\varepsilon, n)$ in the case of P_3 and A_3 can be represented approximately by an almost straight line. Therefore, only small solvent-induced electronic structural changes seem to arise in the case of these exciplexes and their electronic structures may be considerably polar even in a nonpolar solvent, since their CT states are presumably lower than the LE state even in nonpolar solvents due to the strong Coulomb interaction between the two moieties. The situation in the case of P_2 seems to be analogous. However, the plot of $h\nu_f$ against $f(\varepsilon, n)$ appears a little curved, indicating a small change of the electronic and, presumably, geometrical structures of the exciplex fluorescent state induced by the interaction with polar solvent molecules.

Remarks on the Mechanism of Charge Transfer Process in the Intramolecular Exciplex Systems. At any rate, the CT fluorescence state should be formed from the LE state owing to the solvation as well as the change of the geometrical structure, as indicated in Eq. 3.

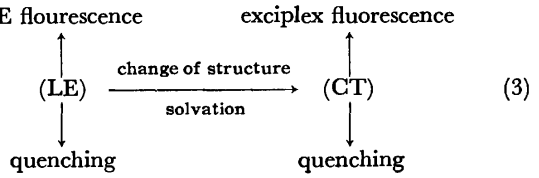

(3)

For example, the fluctuation of the relative orientations of two aromatic rings into the configuration most suitable for the charge transfer will occur frequently in the case of A_1 and P_1. The charge transfer from the *N,N*-dimethylaniline group to an anthracene or pyrene nucleus might be induced by this orientational fluctuation as well as those of polar solvent molecules, and the generated CT state may be stabilized by the orientational relaxation of solvents, *i.e.*, by the solvation process.

The change of structure seems to be especially important for A_2 and P_2 as well as A_3 and P_3 to form the exciplex fluorescent state. In the case of A_2 and P_2, their structures in the ground and the excited FC state are presumably *trans* or *gauche* form with respect to the CH_2–CH_2 single bond. They will change partly to *cis* form where the charge transfer occurs, and will be solvated in the polar solvent, resulting in the exciplex fluorescence. As was pointed out already, the Coulomb interaction energy between the donor cation and acceptor anion in the *cis* form of P_2 seems to be larger than that of A_2, since the exciplex fluorescence of P_2 can be observed even in nonpolar solvents. The situation in the case of A_3 and P_3 seems to be analogous: namely, their ground state structure may be an extended form and the sandwich structure seems to be formed during the excited state lifetime.

Analysis of the Observed Results on the Basis of Some Theoretical Models. Now, we will try to explain the above experimental results on the basis of some theoretical models. We assume the wave function of Eq. 4 for the intramolecular exciplex systems.

$$\Psi = C_1\Psi(A^-D^+) + C_2\Psi(A^*D) + C_3\Psi(AD) \qquad (4)$$

where the 1st term represents the lowest CT configuration, the 2nd is the locally excited (^1L_a) configuration, and the last term is the ground configuration. The Hamiltonian of the system may be given by:

$$\mathcal{H} = \mathcal{H}_0 + \mathcal{H}' \qquad (5)$$

where $\mathcal{H}_0$ is the Hamiltonian of the exciplex in the absence of the solvent and $\mathcal{H}'$ represents the electrostatic interaction with the solvent molecules. Since the solute-solvent interaction is essentially "molecular" interaction between a solute molecule and the surrounding solvent molecules, the above treatment in terms of a dielectric continuum model may be only a rough approximation. Presumably, a more appropriate treatment is to regard the interaction of the solute with the nearest neighbor solvent molecules as a $1:n$ electrostatic complex formation and to approximate the interactions with solvent molecules further apart using the dielectric continuum model. This is a rather old problem in the theoretical treatment of the molecular interactions in liquid solutions, but even at present a rather difficult problem.

If we regard the solute-solvent interaction as an electrostatic molecular complex formation, we must calculate the interaction energy for an individual case by using the wave function of Eq. 4 in which it is necessary to assume some specified form of $\mathcal{H}'$ for several interacting molecules. However, such a calculation is rather difficult in practice. In view of the fact

that the solvent-induced changes of fluorescence spectra of A_1, A_2 and P_1 can be well interpreted by assuming the interaction of an excited solute dipole with the surrounding solvent molecules to be approximated by the dielectric continuum, we approximate here $\mathcal{H}'$ by a simple continuum model using the Onsager's reaction field. On the basis of this simplified model, we try to give an interpretation of the general features of the solvent effects on the exciplex fluorescence.

We put

$$\mathcal{H}' = -\vec{\mu}_{op}\vec{F} = -\vec{\mu}_{op}\vec{\mu}f_\varepsilon \tag{6}$$

where $\vec{\mu}_{op}$ is the dipole operator, $\vec{F}$ is the Onsager's reaction field, and $\vec{\mu}$ is given by:

$$\begin{aligned}\vec{\mu} &= \langle\Psi|\vec{\mu}_{op}|\Psi\rangle \simeq C_1^2\langle\Psi(A^-D^+)|\vec{\mu}_{op}|\Psi(A^-D^+)\rangle \\ &= C_1^2\vec{\mu}_0\end{aligned} \tag{7}$$

We denote the matrix elements of the Hamiltonian as follows:

$$\begin{aligned}\langle\Psi(A^-D^+)|\mathcal{H}|\Psi(A^-D^+)\rangle &= \langle\Psi(A^-D^+)|\mathcal{H}_0|\Psi(A^-D^+)\rangle \\ &\quad + \langle\Psi(A^-D^+)|\mathcal{H}'|\Psi(A^-D^+)\rangle \\ &= E_c - \langle\Psi(A^-D^+)|\vec{\mu}_{op}\vec{F}|\Psi(A^-D^+)\rangle \\ &= E_c - C_1^2\vec{\mu}_0^2 f_\varepsilon\end{aligned} \tag{8}$$

$$\left.\begin{aligned}&\langle\Psi(A^-D^+)|\mathcal{H}|\Psi(A^*D)\rangle \simeq \langle\Psi(A^-D^+)|\mathcal{H}_0|\Psi(A^*D)\rangle = \alpha \quad (a)\\ &\langle\Psi(A^-D^+)|\mathcal{H}|\Psi(AD)\rangle \simeq \langle\Psi(A^-D^+)|\mathcal{H}_0|\Psi(AD)\rangle = \beta \quad (b)\\ &\langle\Psi(A^*D)|\mathcal{H}|\Psi(A^*D)\rangle \simeq \langle\Psi(A^*D)|\mathcal{H}_0|\Psi(A^*D)\rangle = E_e \quad (c)\\ &\langle\Psi(AD)|\mathcal{H}|\Psi(AD)\rangle \simeq \langle\Psi(AD)|\mathcal{H}_0|\Psi(AD)\rangle = E_g \quad (d)\end{aligned}\right\} \tag{9}$$

In terms of these matrix elements, the secular equations may be written as:

$$\begin{aligned}&C_1(E_c - C_1^2\mu_0^2 f_\varepsilon - E) + C_2\alpha + C_3\beta = 0\\ &C_1\alpha + C_2(E_e - E) = 0\\ &C_1\beta + C_3(E_g - E) = 0\end{aligned} \tag{10}$$

Thus, the wave function Ψ depends upon the solute-solvent interaction $\mathcal{H}'$, while $\mathcal{H}'$ depends on the charge distribution determined by Ψ. Therefore, one must solve the nonlinear Eq. 10. However, in the present case, the solution can be obtained by solving Eq. 11, instead of doing an iterative calculation.

$$\left\{E_c - E - \frac{\alpha^2}{E_e - E} + \frac{\beta^2}{E}\right\}\left\{1 + \frac{\alpha^2}{(E_e - E)^2} + \frac{\beta^2}{E^2}\right\} = \mu_0^2 f_\varepsilon \tag{11}$$

In order to obtain the energies relevant to the frequency of the exciplex emission, one must add to the energy obtained from Eq. 11 the polarization energy of the solvent, $E_{pol} = (1/2)\vec{\mu}\vec{F}$. We denote the lowest and the 2nd lowest eigenvalues obtained from Eq. 11 as E_0 and E_1, respectively. Then, the energies of the excited equilibrium state (E_e^{eq}) and the FC ground state (E_g^{FC}) may be given by Eq. 12 and Eq. 13, respectively.

$$E_e^{eq} = E_1 + \frac{1}{2}\vec{\mu}_e^{eq}\vec{F}_e^{eq} = E_1 + \frac{1}{2}\mu_e^{eq'} f_\varepsilon = E_1 + \frac{1}{2}C_1^4\mu_0^2 f_\varepsilon \tag{12}$$

$$\begin{aligned}E_g^{FC} &= E_0 - \vec{\mu}_g^{FC}\vec{\mu}_e^{eq}(f_\varepsilon - f_n -) \mu_g^{FC'} f_n + \frac{1}{2}\mu_e^{eq'}(f_\varepsilon - f_n) + \frac{1}{2}\mu_g^{FC'} f_n \\ &= E_0 - C_1'^2 C_1^2 \mu_0^2 (f_\varepsilon - f_n) + \frac{1}{2}C_1^4\mu_0^2(f_\varepsilon - f_n) \\ &\quad - \frac{1}{2}C_1'^4\mu_0^2 f_n\end{aligned} \tag{13}$$

where μ_g^{FC} is the dipole moment of the FC ground state and C_1 and C_1' represent respectively the coefficients of $\Psi(A^-D^+)$ in the lowest excited and the ground state wave functions obtained by solving Eq. 10 and Eq. 11. Thus, the energy of the exciplex fluorescence may be given by

$$h\nu_f = E_1 - E_0 + \frac{1}{2}(C_1^4 + C_1'^4)\mu_0^2 f_n + C_1^2 C_1'^2 \mu_0^2 (f_\varepsilon - f_n) \tag{14}$$

The solvent shift of the fluorescence of A_1, for example, can be well reproduced by means of the following parameters, as indicated in Fig. 3: $E_c = 3.70$ eV, $E_e = 3.14$ eV, $|\vec{\mu}_0| = 28.0$ D, $\alpha = 0.05$ eV, and $\beta = 0$. Since α is very small and $\beta = 0$, this case can be regarded as a solvation induced reversal of two energy levels, which is the same conclusion as already obtained by the simplified procedure. We have obtained a similar calculated result for P_1. Although we have not made any detailed calculation for A_2, the circumstances in A_2 seems to be rather similar to those in A_1.

In the case of A_0, however, we cannot neglect β, but we must use fairly large values for both α and β in order to reproduce the observed result. We have confirmed that the result of calculation using the following values of parameters: $E_c = 3.1$ eV, $|\vec{\mu}_0| = 20.1$ D, $\alpha = 0.4$ eV, and $\beta = 0.3$ eV or $\beta = 0.4$ eV, is rather close to the experimental result. The calculated value of C_1^2 shows a gradual increase with the increase of the solvent polarity, in contrast to the case of A_1 where C_1^2 shows a sudden increase at $f(\varepsilon, n) \approx 0.33$. However, recent results[21] of detailed studies upon the solvent dependence of the fluorescence yield and lifetime of A_0 indicate a rather drastic change of electronic structure when the solvent is changed from diethyl ether ($f(\varepsilon, n) = 0.512$) to isobutylacetate ($f(\varepsilon, n) = 0.548$). In order to explain this drastic structural change, we need a more sophisticated theoretical treatment. Therefore, roughly speaking, the plot of $h\nu_f$ *vs.* $f(\varepsilon, n)$ for A_0 might be represented approximately by the superposition of two lines of different slopes. Nevertheless, the solvent-induced electronic structural change of excited A_0 is different from those in the case of A_1, A_2 and P_1, in the fact that A_0 shows a single fluorescence band. The single fluorescence band of A_0 seems to be ascribed to a stronger electronic interaction between two moieties than in the case of A_1, A_2 and P_1, which is consistent with the larger values of parameters α and β.

In the case of A_3 and P_3, the solvation induced electronic structural change is not large and the electronic structure of the exciplex seems to be considerably polar even in a nonpolar solvent. Actually, in order to reproduce the observed result, it was found for A_3 that $E_c = 2.90$ eV, which is lower than the LE state, leading to the strongly polar structure of the exciplex,

and $\alpha \approx 0$—0.3 eV and β can be neglected. The calculated result is compared with the experimental values in Fig. 3. The change of C_1^2 with solvent polarity was rather small. We have not made such a calculation for P_3, but the results may be very similar to the present one. Although we have not made any calculation in the case of P_2, a similar calculation with smaller values of the energy gap ($E_e - E_c$) than those for the case of $n=3$, might explain the observed results.

Concluding Remarks

We have demonstrated that the electronic structure of some molecular composite systems are liable to change remarkably by the interaction with polar solvent molecules in the excited electronic state. Although the strongly polar intermolecular exciplex systems undergo ionic dissociation, the present intramolecular exciplex systems cannot dissociate. Instead, some of them show the solvent-induced electronic structural change, and they show a quite large red shift of exciplex fluorescence in the strongly polar solvents, in which the fluorescence of the intermolecular exciplex cannot be observed because of the ionic dissociation. Thus, restricting the geometrical structure of the exciplex system by connecting two moieties with the methylene chain, we have found some new phenomena which cannot be observed in the case of the strongly polar intermolecular exciplexes. Furthermore, the present results indicate clearly that the plane parallel sandwich structure is not necessary for the fluorescent exciplex in polar solvents.

For the more detailed elucidations of the behaviors of these intramolecular exciplexes, measurements of fluorescence quantum yields, rise and decay times, and $S_n \leftarrow S_1$ spectra are necessary. We have made such studies and the results will be reported in a separate paper.

References

1) See for example, (a) N. Mataga and T. Kubota, "Molecular Interactions and Electronic Spectra," Marcel-Dekker Inc., New York, N. Y. (1970); (b) M. Ottolenghi, *Acc. Chem. Res.*, **6**, 153 (1973).

2) N. Mataga and Y. Murata, *J. Am. Chem. Soc.*, **91**, 3144 (1969); T. Kobayashi, K. Yoshihara, and S. Nagakura, *Bull. Chem. Soc. Jpn.*, **44**, 2603 (1971); Y. Torihashi, Y. Furutani, K. Yagii, N. Mataga, and A. Sawaoka, *ibid.*, **44**, 2985 (1971).

3) K. Egawa, N. Nakashima, N. Mataga, and C. Yamanaka, *Chem. Phys. Lett.*, **8**, 108 (1971); *Bull. Chem. Soc. Jpn.*, **44**, 3287 (1971).

4) R. Potashnik and M. Ottolenghi, *Chem. Phys. Lett.*, **6**, 525 (1970); H. Masuhara and N. Mataga, *ibid.*, **6**, 608 (1970); H. Masuhara and N. Mataga, *Z. Phys. Chem. N. F.*, **80**, 113 (1972); H. Masuhara, N. Tsujino, and N. Mataga, *Bull. Chem. Soc. Jpn.*, **46**, 1088 (1973); N. Tsujino, H. Masuhara, and N. Mataga, *Chem. Phys. Lett.*, **21**, 301 (1973); H. Masuhara and N. Mataga, *ibid.*, **22**, 305 (1973).

5) H. Masuhara, M. Shimada, and N. Mataga, *Bull. Chem. Soc. Jpn.*, **43**, 3316 (1970); H. Masuhara, M. Simada, N. Tsujino, and N. Mataga, *ibid.*, **44**, 3310 (1971); M. Shimada, H. Masuhara, and N. Mataga, *Chem. Phys. Lett.*, **15**, 364 (1972); M. Shimada, H. Masuhara, and N. Mataga, *Bull. Chem. Soc. Jpn.*, **46**, 1903 (1973).

6) H. Masuhara, N. Tsujino, and N. Mataga, *Chem. Phys. Lett.*, **12**, 481 (1972); N. Tsujino, H. Masuhara, and N. Mataga, *ibid.*, **15**, 357 (1972).

7) N. Mataga, T. Okada, and N. Yamamoto, *Bull. Chem. Soc. Jpn.*, **39**, 2562 (1966); *Chem. Phys. Lett.*, **1**, 119 (1967).

8) H. Knibbe, K. Röllig, F. P. Schäfer, and A. Weller, *J. Chem. Phys.*, **47**, 1184 (1967).

9) E. Lippert, *Z. Naturforsch.* **10a**, 541 (1955); N. Mataga, Y. Kaifu, and M. Koizumi, *Bull. Chem. Soc. Jpn.*, **28**, 690 (1955).

10) E. A. Chandross and H. T. Thomas, *Chem. Phys., Lett.*, **9**, 397 (1971).

11) N. Mataga, Y. Torihashi, and K. Ezumi, *Theor. Chim. Acta (Berl)*, **2**, 158 (1964): N. Nakashima and N. Mataga, *Bull. Chem. Soc. Jpn.*, **46**, 3016 (1973).

12) Y. Taniguchi, Y. Nishina, and N. Mataga, *Bull. Chem. Soc. Jpn.*, **45**, 764 (1972): Y. Taniguchi and N. Mataga, *Chem. Phys. Lett.*, **13**, 596 (1972).

13) F. Schneider and E. Lippert, *Ber. Bunsenges. Phys. Chem.*, **72**, 1155 (1968).

14) F. Schneider and E. Lippert, *Ber. Bunsenges. Phys. Chem.*, **74**, 624 (1970); H. Beens and A. Weller, *Chem. Phys. Lett.*, **3**, 666 (1969).

15) N. Nakashima, M. Murakawa, and N. Mataga, *Bull. Chem. Soc. Jpn.*, to be published. Picosencond Flash Spectroscopy of Solvent-Induced Intramolecular Electron Transfer in the Excited 9,9′-Bianthryl.

16) T. Okada, T. Fujita, M. Kubota, S. Masaki, N. Mataga, R. Ide, Y. Sakata, and S. Misumi, *Chem. Phys. Lett.*, **14**, 563 (1972).

17) H. Beens, Thesis, Free University of Amsterdam, Amsterdam, 1970.

18) S. Yomosa, *J. Phys. Soc. Jpn.*, **35**, 1738 (1973).

19) R. Ide, M. Tsutsui, Y. Sakata, and S. Misumi, *Bull. Chem. Soc. Jpn.*, to be published. Synthesis of Intramolecular Exciplexes Containing Condensed Aromatic Hydrocarbon and *N,N*-Dimethylaniline Moieties.

20) A. Weissberger, Ed., "Technique of Organic Chemistry," Vol. III, Interscience, New York (1955).

21) T. Okada, T. Fujita, and N. Mataga, *Z. Phys. Chem. N. F.*, to be published. Intramolecular Charge Transfer Interactions and Dynamic Behaviors of Excited *p*-(9′-Anthryl)-*N,N*-dimethylaniline.

Studies of the Ruthenium(III) Complexes. XII[1] Kinetic Studies of the Deammonation-anation Reactions of Halogenopentaammineruthenium(III) Complexes in the Solid State

Akira Ohyoshi, Susumu Kohata, Masanobu Nishimori, Yoshiaki Shimura, and Noriko Iwasaki

Department of Industrial Chemistry, Faculty of Engineering, Kumamoto University, Kumamoto 860

(Received June 9, 1975)

The kinetics of the thermal substitution reaction of chloro- and bromopentaammineruthenium(III) complexes has been studied in the solid state. The reaction rates and kinetic parameters were determined for these reactions: $[RuX(NH_3)_5]Y_2(s) \rightarrow [RuXY(NH_3)_4]Y(s) + NH_3(g)$, and (X=Cl, Br: Y=Cl, Br, I, NO_3). The values of the rate constant (s^{-1}), the activation energy (kcal mol^{-1}), and the activation entropy (cal mol^{-1} K^{-1}) were 1.70×10^{-5} (at 222 °C), 41.8, and 0.7 for $[RuCl(NH_3)_5]Cl_2$; 1.02×10^{-4} (at 226 °C), 30.2, and −19.6 for $[RuCl(NH_3)_5]Br_2$; 1.35×10^{-4} (at 208 °C), 25.3, and −26.6 for $[RuCl(NH_3)_5]I_2$; 8.47×10^{-3} (at 162 °C), 29.7, and −11.5 for $[RuCl(NH_3)_5](NO_3)_2$; 1.26×10^{-4} (at 219 °C), 21.8, and −35.1 for $[RuBr(NH_3)_5]Cl_2$, and 1.17×10^{-3} (at 162 °C), 14.7, and −40.0 for $[RuBr(NH_3)_5](NO_3)_2$ respectively. The S_N1-like mechanism is favorable for the deammonation-anation reaction of all the chloropentaamine series except for the iodide, while the S_N2-like mechanism is more probable for the corresponding reaction of the bromopentaammine series. The reaction mechanism is predominantly controlled by the coordinating ability of the inner-sphere halide ion and secondarily by that of the outer-sphere anion.

The thermal decomposition of a series of halogenopentaammine halides[2,3] and nitrates[4] of cobalt(III) has been studied. The results suggest that the thermal dissociation reaction involves the following steps:

$$[CoX(NH_3)_5](NO_3)_2(s) \longrightarrow [CoX(NO_3)(NH_3)_4]NO_3(s) + NH_3(g)$$

$$[CoX(NO_3)(NH_3)_4]NO_3(s) \longrightarrow [CoX(NO_3)_2(NH_3)_3](s) + NH_3(g)$$

$$[CoX(NO_3)_2(NH_3)_3](s) \longrightarrow Co_3O_4(s) + \text{decomposition products.}$$

A recent kinetic study[5] of the thermal decomposition reaction of the series of ammine complexes of chromium(III) has reported that the thermal substitution reaction of the chloropentaamminechromium(III) chloride proceeded through the intermediate of *trans*-$[CrCl_2(NH_3)_4]Cl$.

Our own previous papers[6,7] exhibited that the thermal reactions of halogenopentaammine- *cis*-dihalogenotetraammine- and hexaammineruthenium(III) complexes were initiated by the replacement of coordinated ammonia by the outer-sphere halide ion, and the reaction mechanisms of the hexaammine- and *cis*-dihalogenotetraammineruthenium(III) complexes were proposed. In this paper, the kinetic studies of the thermal anations of $[RuX(NH_3)_5]Y_2$ (X=Cl, Br; Y=Cl, Br, I, NO_3) will be demonstrated. The influence of both inner-sphere and outer-sphere ions on the reaction mechanism will be discussed in comparison with those of the hexaammine and tetraammine series of ruthenium(III) complexes.

Experimental

Preparation of Complexes. The complexes, $[RuX(NH_3)_5]X_2$ (X=Cl, Br), were prepared by the method described in the literature.[8] $[RuCl(NH_3)_5]Y_2$ (Y=Br, I, NO_3) and $[RuBr(NH_3)_5]Y_2$ (Y=Cl, I, NO_3) were precipitated from a cold solution of ammonium halide and nitric acid.

The complexes were confirmed by elemental analysis and by visible and UV spectral measurements. $[RuCl(NH_3)_5]Cl_2$. Found: ν_{max}, 30.5×10^3 cm^{-1}; ε, 1.89×10^3 cm^{-1} M^{-1}. Ref. Value[8]: ν_{max}, $30.5\times10^3 cm^{-1}$; ε, 1.93×10^3 cm^{-1} M^{-1}. $[RuCl(NH_3)_5]Br_2$. Found: H, 4.05; N, 18.85%. Calcd: H, 3.96; N, 18.36%. $[RuCl(NH_3)_5]I_2$. Found: H, 3.15; N, 14.57%. Calcd: H, 3.18; N, 15.38%. $[RuCl(NH_3)_5](NO_3)_2$. Found: H, 4.67; N, 28.24%. Calcd: H, 4.37; N, 28.36%. $[RuBr(NH_3)_5]Br_2$. Found: ν_{max}, 25.1×10^3 cm^{-1}; ε, 1.93×10^3 cm^{-1} M^{-1}. Ref. Value[8]: ν_{max}, 25.1×10^3 cm^{-1}; ε, 1.92×10^3 cm^{-1} M^{-1}. $[RuBr(NH_3)_5]Cl_2$. Found: H, 4.15; N, 21.21%. Calcd: H, 4.49; N, 20.78%. $[RuBr(NH_3)_5]I_2$ Found: H, 3.03; N, 13.89%. Calcd: H, 2.91; N, 13.47%. $[RuBr(NH_3)_5](NO_3)_2\cdot1/2H_2O$. Found: H, 4.05; N, 25.39%. Calcd: H, 3.88; N, 25.13%.

Differential Thermal Analysis, Thermogravimetry and Isothermal Kinetic Measurement. The differential thermal analysis (DTA) and the thermogravimetry (TG) of the complexes were carried out using a Shimadzu DTG 20-type micro-differential thermobalance. All the experiments were made in a constant helium stream at a heating rate of 5 °C/min., using about a 10 mg sample in each run. In the isothermal kinetic measurement, the temperature was rapidly elevated so as to depress the decomposition of the sample before measurement and was then kept constant within ±0.5 °C. The kinetic plots were made based on mass-loss measurements at several temperatures.

A Shimadzu UV-200 recording spectrophotometer and a JASCO Model DS-403G Grating Infrared spectrophotometer were used for the measurement of the absorption spectra of the initial compounds and the reaction products.

Results and Discussion

DTA and TG Studies. The DTA and TG curves of the chloropentaammineruthenium(III) bromide and iodide, and the bromopentaammineruthenium(III) chloride and iodide are given together in Fig. 1, while those of the nitrates are given in Fig. 2.

The DTA curves are characterized by endothermic peaks for the chloropentaammine series at 327 °C (bromide) and 291 °C (iodide). Shoulders were found, however, corresponding to the mass-loss of one or two

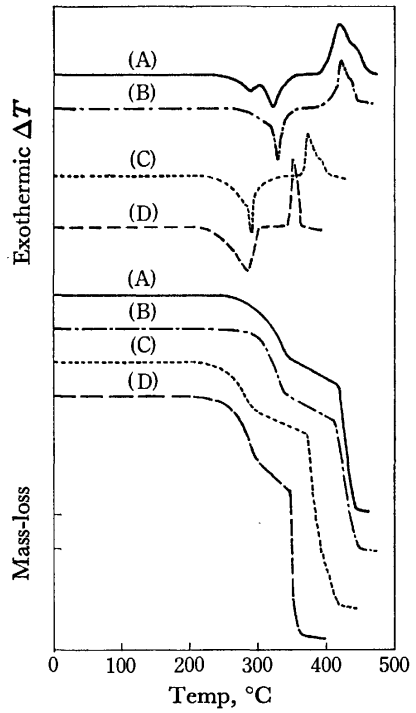

Fig. 1. DTA and TG curves of the halogenopentaammineruthenium(III) halides.
$[RuCl(NH_3)_5]Y_2$; bromide (B), iodide (C).
$[RuBr(NH_3)_5]Y_2$; chloride (A), iodide (D).

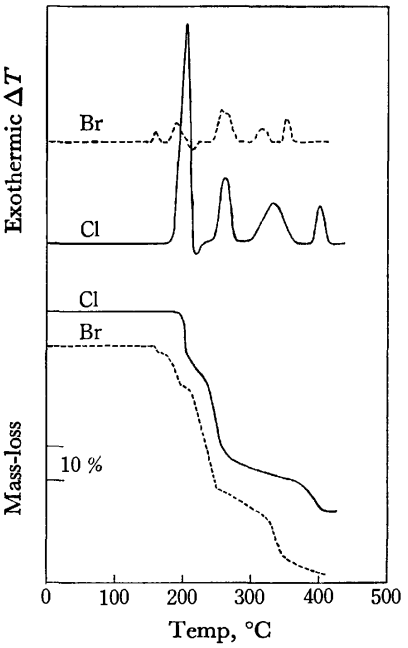

Fig. 2. DTA and TG curves of the halogenopentaammineruthenium(III) nitrate.
$[RuX(NH_3)_5](NO_3)_2$; (X=Cl, Br).

moles of ammonia at 310 °C and 285 °C respectively. For the bromopentaammine chloride, a small endothermic peak at 288 °C was clearly found, besides a large broad endothermic peak at 320 °C, and a broad endothermic peak was found at 284 °C for the bromopentaammine iodide. On the other hand, the DTA curves of the nitrates for both series are characterized by several exothermic peaks, different from those of the halides. For the bromopentaammine nitrate, the first exothermic peak at 158 °C was found, by the elemental analysis and the mass-loss measurement, to be corresponding to the liberation of $1/2 \cdot H_2O$. This may be attributable to the physico-chemical rearrangements of the crystalline lattice or the coordination structure after the coordinated water liberation. However, a detailed interpretation must await further investigations.

The initial temperature of mass-loss for the deammonation is as follows: $[RuBr(NH_3)_5](NO_3)_2$ (176 °C), $[RuCl(NH_3)_5](NO_3)_2$ (190 °C), $[RuCl(NH_3)_5]I_2$ (215 °C), $[RuBr(NH_3)_5]I_2$ (239 °C), $[RuCl(NH_3)_5]Br_2$ (243 °C), $[RuBr(NH_3)_5]Br_2$ (244 °C), $[RuCl(NH_3)_5]Cl_2$ (246 °C), $[RuBr(NH_3)_5]Cl_2$ (247 °C).

The main decomposition reaction, probably taking place during the first endo- or exothermic reaction, might be accompanied by the continuous evolution of such gases as ammonia, free halogen, or ammonium halide, as reported in a previous paper[6] on the halogenopentaammine halides. On the other hand, for the nitrates, only the ammonia gas was identified in the initial period of the thermal decomposition; the analyses of such gases as NO, N_2O, N_2 and H_2O which were identified in the thermal decomposition of halogenopentaamminecobalt(III) nitrate[4] have not yet been successful.

As a result, there were not so many differences among the thermal decomposition reactions of the halogenopentaammine series of complexes, except for those of the nitrates. However, the nitrates and the iodides all seem to be thermally unstable.

Stoichiometry and Kinetic Study. It has already been reported[6] that the thermal decomposition reactions of chloropentaammine chloride (at 246—396 °C) and bromopentaammine bromide (at 244—398 °C) can be expressed by Eq. 1:

$$[RuX(NH_3)_5]X_2 \longrightarrow [RuX_3(NH_3)_3] + 2NH_3 \quad (X=Cl, Br) \qquad (1)$$

In the present isothermal experiment it was found that the reaction actually proceeded *via* successive steps which were composed of unimolecular deammonations, because the isothermal decomposition products of the initial complex were each composed of one mole of ammonia and dihalogenotetraammine halides or nitrate. All the solid reaction products were identified by elemental analysis or absorption spectrophotometry; the results are listed in Tables 1 and 2. The results for the elemental analysis of a reaction product are not necessarily in agreement with the calculated value for chemical formulas corresponding to the liberation of one molar ammonia, except for the chlorobromotetraammine bromide. This might be attributed to the instability of the reaction product at the decomposition temperature or to the low reproducibility in this sort of thermal decomposition reaction. Unfortunately, the configurations of tetraammine complexes can not be clearly determined from the absorption spectra, especially for the mixed halide-ligand complexes. In the IR spectra of $[RuCl(NH_3)_5](NO_3)_2$ and its reaction

Table 1. Analysis of the reaction product of chloropentaammineruthenium(III)

Initial complex	Chloride	Bromide	Iodide	Nitrate
Sample color	dark green	dark yellow	black	brown
Chemical formula assigned	$[RuCl_2(NH_3)_4]Cl$	$[RuClBr(NH_3)_4]Br$	$[RuClI(NH_3)_4]I$	$[RuCl(NO_3)(NH_3)_4]$ (NO_3)
Elemental analysis (H%, N%) found	(4.82, 21.10)	(3.31, 15.50)	(2.18, 11.28)	(3.89, 27.14)
Elemental analysis (H%, N%) calcd	(4.40, 20.38)	(3.32, 15.38)	(2.64, 12.22)	(3.68, 25.57)
Electronic spectrum (ν_{max}, 10^3cm^{-1}, ε; 10^3M^{-1} cm^{-1})	(30.6, 1.70) (35.7, 2.19)	(30.6, 0.93) (25.6, 1.10)	(30.6, 0.65) (18.3, 1.24)	(30.6, 1.60)
Initial spectrum	(30.5, 1.89) (30.5, 1.93)[a]	(30.6, 1.56)	(30.6, 1.92)	(30.6, 1.89)

a) Published value from Ref. 8.

Table 2. Analysis of the reaction product of bromopentaammineruthenium(III)

Initial complex	Chloride	Bromide	Iodide	Nitrate
Sample color	brown	brown	black	yellow
Chemical formula assigned	$[RuClBr(NH_3)_4]Cl$	$[RuBr_2(NH_3)_4]Br$	$[RuBrI(NH_3)_4]I$	$[RuBr(NO_3)(NH_3)_4](NO_3)$
Elemental analysis (H%, N%) found	(4.13, 17.23)	(3.61, 14.46)	(2.67, 11.80)	(3.38, 23.57)
Elemental analysis (H%, N%) calcd.	(3.78, 17.51)	(2.96, 13.70)	(2.41, 11.14)	(3.25, 22.53)
Electronic spectrum (ν_{max}, 10^3cm^{-1}, ε; 10^3M^{-1} cm^{-1})	(25.1, 1.14) (30.5, 1.41)	(25.2, 1.12) (30.3, 1.83)	(18.3, 2.10) (25.6, 1.06)	(25.2, ——)
Initial spectrum	(25.2, 1.72)	(2.51, 1.95) (2.51, 1.92)[a]	(25.2, 2.20)	(25.2, 1.40)

a) Published value from Ref. 8.

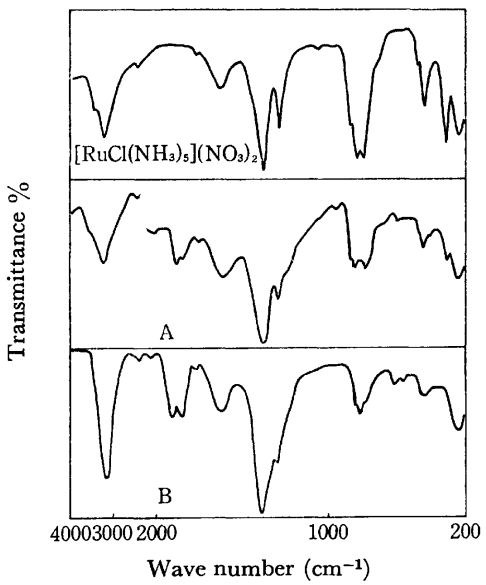

Fig. 3. IR spectra of initial complex and thermal decomposition products.
Chemical formura assigned
A: $[RuCl(NO_3)(NH_3)_4](NO_3)$
B: $[RuBr(NO_3)(NH_3)_4](NO_3)$

products, shown in Fig. 3, new absorption bands were found at 1850—1900 cm^{-1} and 570—600 cm^{-1}; the former was assigned to the ν(NO) of the coordinated NO_3^- and the latter, to the ν(Ru–NO_3) or ν(Ru–ONO_2).[9,10]

Thus, the thermal decomposition reaction can be expressed by Eqs. 2 and 3:

$$[RuCl(NH_3)_5]X_2 \longrightarrow [RuClX(NH_3)_4]X + NH_3 \quad (X=Br, I, NO_3) \quad (2)$$

$$[RuBr(NH_3)_5]X_2 \longrightarrow [RuBrX(NH_3)_4]X + NH_3 \quad (X=Cl, I, NO_3) \quad (3)$$

In the isothermal kinetic measurements, the ranges of temperature applied were decided with reference to the results of DTA and TG studies. Plots of $\ln\{a/(a-x)\}$ *vs.* the reaction time for Reactions 2 and 3 obtained from the isothermal measurements are illustrated in Figs. 4 and 5, where a is the initial mass of the sample, and $a-x$ the mass at the reaction time t. The plots give a straight line with a good reproducibility in each measurement. A similar relationship was obtained for the other complexes. As a result the thermal decomposition can be regarded as a first-order reaction with respect to the reactant. The Arrhenius plots for the reactions are given in Fig. 6, while the rate constants obtained from the slope of the straight line are listed in

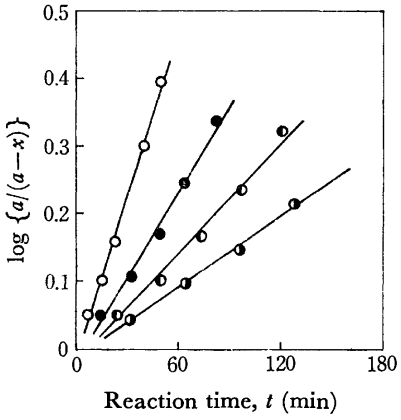

Fig. 4. Plots of a first-order rate equation for the deammonation-anation reaction of $[RuCl(NH_3)_5]Br_2$.
○ 243 °C, ● 237 °C, ◐ 226 °C, ◑ 219 °C

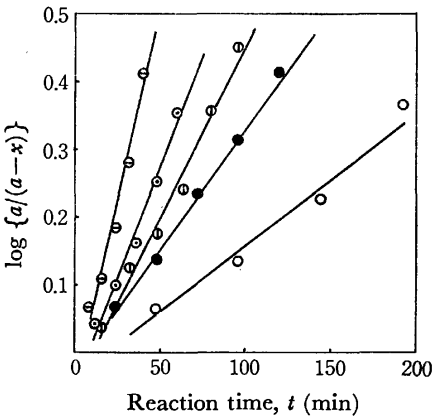

Fig. 5. Plots of a first-order rate equation for the deammonation-anation reaction of $[RuCl(NH_3)_5](NO_3)_2$. ⊖ 168 °C, ⊙ 166 °C, ⓘ 162 °C, ● 154 °C, ○ 151 °C

Table 3. Kinetic parameters for the deammonation-anation reaction of Ru(III) and Cr(III) compounds

Compound	$k\times10^5$ s^{-1} (177 °C)	E_a (kcal/mol)	ΔS^* (e.u.)	log A
$[Ru(NH_3)_6]Br_3$	5.05	23.3	−29.3	7.0
$[Ru(NH_3)_6]I_3$	27.1	20.7	−31.6	6.5
$[RuCl(NH_3)_5]Cl_2$	0.02	41.8	0.7	13.6
$[RuCl(NH_3)_5]Br_2$	0.36	30.2	−19.6	9.2
$[RuCl(NH_3)_5]I_2$	1.96	25.3	−26.8	7.6
$[RuCl(NH_3)_5](NO_3)_2$	29.2	29.7	−11.5	13.1
$[RuBr(NH_3)_5]Cl_2$	1.44	21.8	−35.1	5.8
$[RuBr(NH_3)_5]Br_2$	0.42	26.1	−34.3	7.5
$[RuBr(NH_3)_5]I_2$	10.34	15.6	−44.9	3.6
$[RuBr(NH_3)_5](NO_3)_2$	314	14.7	−40.0	4.6
cis-$[RuCl_2(NH_3)_4]Cl$	6.75	33.1	−6.9	11.9
cis-$[RuBr_2(NH_3)_4]Br$	10.0	31.3	−10.1	11.2
$[Cr(NH_3)_6]Cl_3$	4.0(174)	30	−12	} a)
$[CrCl(NH_3)_5]Cl_2$	2.8(198)	39	1.4	
cis-$[CrCl_2(NH_3)_4]Cl$	16 (142)	31	−2.3	

a) From Ref. 5.

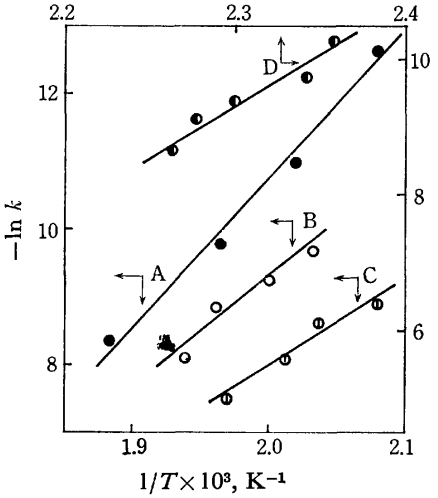

Fig. 6. Arrhenius plots of the substitution reaction for chloropentaammineruthenium(III). $[RuCl(NH_3)_5]Y_2$; chloride (A), bromide (B), iodide (C), nitrate (D).

Table 3, together with the kinetic parameters.

It can be seen that, in general, the rate constants for the deammonation reactions of the chloropentaammine series are smaller than those of the bromopentaammine series. In both cases, the influence of the outer-sphere anion species on the reaction rate is to enhance it in the following order; $Cl<Br<I<NO_3$.

By a comparison with the other ammine complexes, it was found that the rate constants decrease in the order of tetraammine>hexaammine>pentaammine, as has also been seen for the chromium(III) chloride complexes (Table 3). However, the activation energies do not necessarily decrease with the increase in rate constants. Moreover, the values of the activation entropy are smaller in this order: tetraammine>pentaammine≈hexaammine. These facts suggest that the reaction mechanisms for the deammonation and the anation of the outer-sphere anion are different from each other among the reactions of the three series of ammine complexes. It may be considered that the coordinated halide ligand is also one of the determinants on the reaction mechanism.

Reaction Mechanism of the Deammonation-anation. In a previous paper,[7] we discussed how the mechanism seems to belong to the S_N2 category for the substitution reaction of the hexaammine series of complexes, while the S_N1 mechanism is favorable for that of the tetraammine series, considering the values of the kinetic parameters and the contribution of the π-bonding nature between the metal and the ligand.

The reaction rates of the chloropentaammine series of complexes are smaller than those of the corresponding bromopentaammine series, and the former reveal large values of the activation energy. Yet the values of the activation entropy of the former (0——20 cal·mol^{-1}·K^{-1}) are larger than those of the latter (−34——45 cal·mol^{-1}·K^{-1}). Therefore, for the substitution reaction of the chloropentaammine series of complexes, the S_N1-like mechanism may be favorable.

The activation energies of deammonation-anation reactions should be rather close to each other, but there are some differences among the values of the activation energies for the reactions of complexes with different outer-sphere anions. This suggests that the substitution reaction mechanism is affected by the nucleophilic characters of the coordinated ligand and the outer-sphere anion. That is to say, in the chloropentaammineruthenium(III) iodide and nitrate, the deammonation-anation reaction may proceed *via* the S_N1-like (partially the S_N2-like) mechanism. On the other hand, considering the small values of the activation energy (15—26 kcal·mol^{-1}) and the large negative values of the activation entropy (−34——45 cal·mol^{-1}·K^{-1}), the mechanism for the reaction of the bromopentaammine series seems to belong to the S_N2 category.

Reviewing the thermal substitution reactions of the hexaammine-, pentaammine-, and tetraammineruthenium(III) complexes, the rate constants increase in the following order of the outer-sphere anion: $Cl<Br<I<NO_3$. That the nitrates gave the largest value of the rate constants may be attributable to the nucleophilic character, as has also been in the kinetic study[11] of the

deaquation-anation reaction of the aquapentaammine-ruthenium(III) series. The iodides also gave larger values of the rate constants than those for the other halide ions. This might be attributed to the back-donation of π-electrons from the 4d-orbital electron of the ruthenium(III) ion to the vacant d orbitals of the iodide ion, for the outer-sphere anion might be fixed by the lattice energy.

The reaction mechanisms thus determined can be classified by the order of the frequency factor as is shown in Table 3. The order of the frequency factor, A, is $10^3\,s^{-1}$—$10^7\,s^{-1}$ for the S_N2 mechanism, while that for the S_N1 mechanism ranges from $10^9\,s^{-1}$ to $10^{13}\,s^{-1}$. A reasonable discussion of this classification can now be undertaken.

The authors wish to thank the Ministry of Education for the financial support (No. 847009) granted to this research.

References

1) Part XI of this series; A. Ohyoshi, H. Sakamoto, H. Makino, and K. Hamada, *Bull. Chem. Soc. Jpn.*, **48**, 3179 (1975).
2) N. Tanaka and M. Nanjo, *Bull. Chem. Soc. Jpn.*, **37**, 1330 (1964).
3) W. W. Wendlandt and J. P. Smith, *J. Inorg. Nucl. Chem.*, **25**, 843 (1963).
4) W. W. Wendlandt and J. P. Smith, *J. Inorg. Nucl. Chem.*, **26**, 445 (1964).
5) N. Tanaka and K. Nagase, *Bull. Chem. Soc. Jpn.*, **40**, 546 (1967).
6) A. Ohyoshi, S. Hiraki, and H. Kawasaki, *Bull. Chem. Soc. Jpn.*, **47**, 841 (1974).
7) A. Ohyoshi, S. Hiraki, T. Odate, S. Kohata, and J. Oda, *Bull. Chem. Soc. Jpn.*, **48**, 230 (1975).
8) H. Hartman and C. Bushbeck, *Z. Phys. Chem.*, **11**, 120 (1957).
9) E. Miki, *Bull. Chem. Soc. Jpn.*, **41**, 1835 (1968).
10) E. E. Mercer, W. A. McAllister, and J. R. Durig, *Inorg. Chem.*, **5**, 1881 (1966).
11) A. Ohyoshi, S. Hiraki, T. Odate, S. Kohata, and J. Oda, *Bull. Chem. Soc. Jpn.*, **48**, 262 (1975).

Effects of Additives on Solid State Reaction. III. Effects of Halide Additives on the Formation of $MgFe_2O_4$

Shiro SHIMADA, Ryusaburo FURUICHI, and Tadao ISHII

Department of Applied Chemistry, Faculty of Engineering, Hokkaido University, Sapporo 060

(Received July 3, 1975)

The promoting effects of halide additives on the formation of $MgFe_2O_4$ have been studied on the basis of both kinetic and thermoanalytical data. A mixture of MgO and α-Fe_2O_3 powder containing 10 mol % additive (LiF, NaF, MgF_2, BaF_2, NaCl, or KCl) and that without additive were isothermally heated in a vacuum ($P_{O_2}=10^0$—10^1 mmHg) in the temperature range 666—1018 °C. High temperature X-ray analysis on MgO–Fe_2O_3 and MgO–Fe_2O_3–additive systems was carried out at a heating rate of 3 °C/min *in vacuo*, ($P_{O_2}=10^{-1}$ mmHg). In the case of fluoride, it seems that the reactions between the fluoride and the reactants, α-Fe_2O_3 or MgO, promote $MgFe_2O_4$ formation in the initial stage and that compounds produced by the initial reaction accelerate diffusion in the later stage. The same promoting mechanism seems to be applicable to the case of chloride additives. The interaction between solids of NaCl and α-Fe_2O_3 occurring just before the melting of NaCl seems to initiate $MgFe_2O_4$ formation.

Solid state reactions are affected by various factors such as impurity or additive,[1,2] preparation history of the reacting material[3] and atmosphere.[4-6] The mechanism for the promoting effects of fluoride and chloride additives on $MgAl_2O_4$ formation has been systematically discussed from kinetic and thermoanalytical viewpoints.[7-9] In the case of fluoride additives,[8,9] the formation of $MgAl_2O_4$ was initiated by the reaction between fluoride and reactants of α-Al_2O_3 and MgO, the cations of fluoride playing an important role in accelerating the reaction in the later stage. In the case of chloride,[7,8] the $MgAl_2O_4$ formation was accelerated *via* the dissolution process of MgO particle in molten chloride.

We have investigated the promoting effects of the halides of alkali and alkaline earth on $MgFe_2O_4$ formation on the basis of both kinetic and thermoanalytical results.

Experimental

Sample. α-Fe_2O_3 samples were prepared by calcining commercial ferric oxide (Kanto Chemical Co., 99% pure) at 1100 °C in the air. The particle size of α-Fe_2O_3 was microscopically determined to be in the range 0.5—2 μ with an average size of 1 μ. MgO particles (av. 0.1 μ) were prepared by a similar way to that described in the previous paper.[8] Powders of MgO, α-Fe_2O_3 and additive were thoroughly mixed in the molar ratio 1 : 1 : 0.1. The additives used were LiF, NaF, MgF_2, BaF_2, NaCl, or KCl (Kanto, Wako or Morita Companies), which were stored in a desiccator with silica gel before experiments. The mixtures were pressed into pellets at 150 kg/cm^2.

DTA and High Temperature X-Ray Diffraction Experiments. DTA experiments on MgO–Fe_2O_3 and MgO–Fe_2O_3–additive systems were carried out in a vacuum ($P_{O_2}=10^{-1}$ mmHg) at a heating rate of 10 °C/min. The temperature was measured with a Pt–Pt13Rh thermocouple. α-Al_2O_3 was used as a standard material. The high temperature X-ray diffraction experiments were carried out *in vacuo* ($P_{O_2}=10^{-1}$ mmHg) at a heating rate of 3 °C/min.

Isothermal Kinetic Experiments. The pellet was kept on a Pt boat placed in a fused-silica tube connected to a vacuum system ($P_{O_2}=10^0$—10^1 mmHg) and then heated isothermally in the Pt-furnace at 666—1018 °C. The temperature was measured with a Pt–Pt13Rh thermocouple. After heating, the pellet was quenched at room temperature by withdrawal of the tube from the hot zone of the furnace. Fractional conversion of $MgFe_2O_4$ was determined by measuring the amount of MgO or α-Fe_2O_3 remaining after the reaction. The MgO unreacted was extracted by dissolving the pellet in 10% NH_4Cl solution. The Mg^{2+} ion concentration of the solution was then determined by titration with a standard solution of EDTA. This procedure was applied to the products obtained in the experiments of both MgO–Fe_2O_3 and MgO–Fe_2O_3–additive (LiF or NaF) systems. The amount of α-Fe_2O_3 unreacted was determined by quantitative X-ray analysis by use of NaCl as an external standard. The method was applied to the products in MgO–Fe_2O_3–additive (MgF_2 or BaF_2) system.

Analyis of Fe^{2+}. The amount of Fe^{2+} ion in the samples, obtained after isothermal experiments or the high temperature X-ray diffraction experiments, was colorimetrically determined.[10] The solution for colorimetry was prepared by dissolving the sample in concd H_2SO_4. 2M NH_4F and 1% *o*-phenanthroline were used as masking agent for Fe^{3+} and color-producing agent for Fe^{2+}.

Results

Figures 1 and 2 show the rates of $MgFe_2O_4$ formation in MgO–Fe_2O_3 and MgO–Fe_2O_3–alkali fluoride systems, and MgO–Fe_2O_3–alkaline earth fluoride system, respectively. The rate of reaction between solid reactant particles is generally governed by either chemical reaction at phase-boundary or diffusion process.[11] The rate equations for the diffusion-controlled reaction have been given by Jander,[12] Serin-Ellickson,[13] Ginstling-Brounshtein,[14] and Carter.[15] It was found that the reaction rate of MgO–Fe_2O_3 system is best represented by Jander's equation:

$$[1-(1-\alpha)^{1/3}]^2 = kt \qquad (1)$$

where α=fractional conversion, k=rate constant, t=reaction time. A part of the data plotted according to Eq. (1) is shown in Fig. 3. We see that the data of all systems fit Jander's equation up to about $\alpha=70\%$. The straight lines obtained for NaF, MgF_2 and BaF_2 additives intersect at $t=0$ the ordinate with values corresponding to $\alpha=20$—30%. On the other hand, the lines for non-additive and LiF additive fall on the origin. The activation energies are given in Table 1,

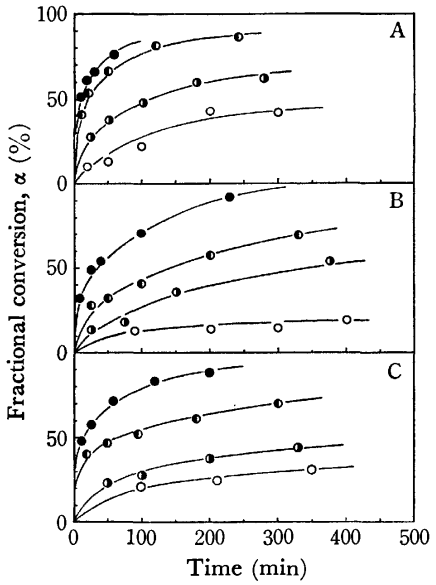

Fig. 1. Formation rate of $MgFe_2O_4$ for $MgO–Fe_2O_3$ and $MgO–Fe_2O_3$–alkali fluoride systems.
A: $MgO–Fe_2O_3$ system
○: 853 °C, ◑: 915 °C, ◐: 972 °C, ●: 1018 °C
B: $MgO–Fe_2O_3$–LiF system
○: 666 °C, ◑: 715 °C, ◐: 760 °C, ●: 814 °C
C: $MgO–Fe_2O_3$–NaF system
○: 754 °C, ◑: 798 °C, ◐: 850 °C, ●: 901 °C

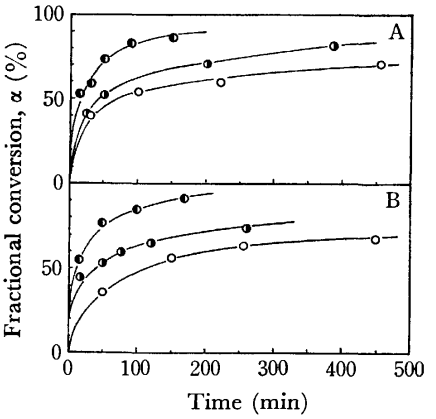

Fig. 2. Formation rate of $MgFe_2O_4$ for $MgO–Fe_2O_3$–alkaline earth fluoride system.
A: $MgO–Fe_2O_3–MgF_2$ system
○: 847 °C, ◑: 895 °C, ◐: 940 °C
B: $MgO–Fe_2O_3–BaF_2$ system
○: 847 °C, ◑: 895 °C, ◐: 940 °C

for which the rate constants k were calculated from the results shown in Figs. 1 and 2 by means of Eq. (1). The samples obtained by the isothermal experiments of all systems showed no trace of Fe^{2+}.

Figure 4 shows DTA curves of $MgO–Fe_2O_3$–LiF (curve A) and $MgO–Fe_2O_3$–NaF (curve B) systems. Curve A has two endothermic peaks at 670 °C and 730 °C. The peak at 730 °C is considered to be due to the formation of the liquid phase, since an exothermic peak was obtained at *ca.* 730 °C by cooling the sample (curve A) from 930 °C as indicated by arrows. The liquid phase seems to result from melting of LiF.

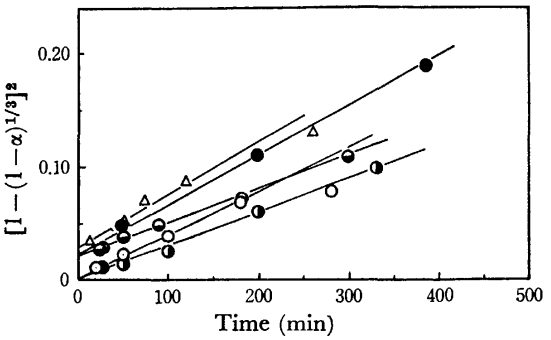

Fig. 3. Plots of $[1-(1-\alpha)^{1/3}]^2$ *vs.* t according to the Jander's equation.
○: non-additive (915 °C), ◑: LiF (760 °C), ◒: NaF (850 °C) ●: MgF_2 (895 °C), △: BaF_2 (895 °C)

TABLE 1. VALUES OF ACTIVATION ENERGY

Additive	E^* (kcal/mol)
Non-additive	70± 4
LiF	57± 4
NaF	59± 4
MgF_2	65±10
BaF_2	60± 5

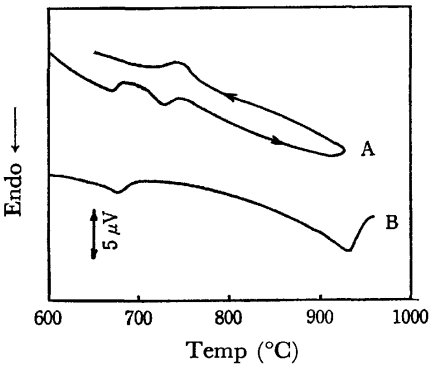

Fig. 4. DTA curves of reaction in $MgO–Fe_2O_3$–LiF (curve A) and $MgO–Fe_2O_3$–NaF (curve B) systems. Heating rate: 10 °C/min, sample weight: 400 mg, 1:1:0.1 mixture of MgO, Fe_2O_3, and LiF or NaF in molar ratio.

Similarly, curve B has two endothermic peaks at 670 °C and 930 °C. The peak at 930 °C probably corresponds to melting of NaF. DTA curves of the systems with non-additive, MgF_2 and BaF_2 additives showed no thermal change in the range 20—1000 °C except for the endothermic peak near 670 °C, which showed a reversible one. This peak corresponds to the Curie point of α-Fe_2O_3.[16,17]

Figures 5A–D and 6A–D show the results of high temperature X-ray diffraction analysis for the systems $MgO–Fe_2O_3$, $MgO–Fe_2O_3$–NaCl, $MgO–Fe_2O_3$–KCl, Fe_2O_3–NaCl, $MgO–Fe_2O_3$–LiF, $MgO–Fe_2O_3$–NaF, $MgO–Fe_2O_3–MgF_2$, and $MgO–Fe_2O_3–BaF_2$. We see that the amounts of α-Fe_2O_3 and MgO decrease at *ca.* 700 °C and then $MgFe_2O_4$ begins to appear at 820 °C (Fig. 5-A). Addition of NaCl (Fig. 5-B) lowers the initiation temperature of $MgFe_2O_4$ formation by more than 60 °C, as compared with that of the $MgO–Fe_2O_3$ system. This initiation temperature, 760 °C, is lower

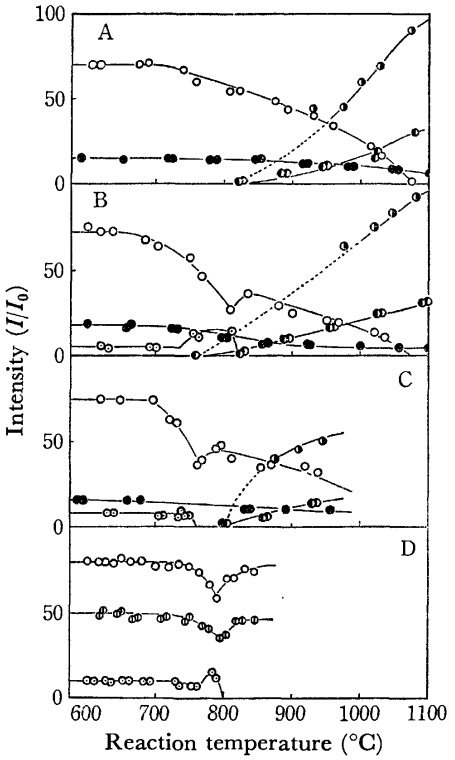

Fig. 5. High temperature X-ray diffraction patterns of the reaction in the systems for $MgO–Fe_2O_3$ (A), $MgO–Fe_2O_3$–NaCl (B), $MgO–Fe_2O_3$–KCl (C), and Fe_2O_3–NaCl (D).
Molar mixing ratio: 1: 1: 0.1 in MgO: Fe_2O_3: chloride and 1: 0.2 in Fe_2O_3: NaCl, heating rate: 3 °C/min.
○: α-Fe_2O_3 (104), ●: MgO (200), ◑ and ◐: Mg-Fe_2O_4 (311) and (200), respectively, B-⊙: NaCl (200), C-⊙: KCl (200), D-ⓘ, -○ and -⊙: α-Fe_2O_3 (104), α-Fe_2O_3 (110) and NaCl (200), respectively.

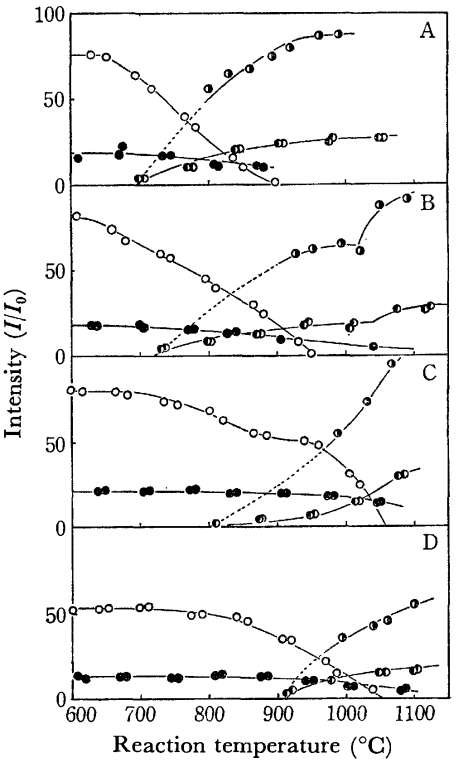

Fig. 6. High temperature X-ray diffraction patterns of the reaction in systems for $MgO–Fe_2O_3$–LiF (A), $MgO–Fe_2O_3$–NaF (B), $MgO–Fe_2O_3–MgF_2$ (C) and $MgO–Fe_2O_3–BaF_2$ (D).
Molar mixing ratio: 1: 1: 0.1, heating rate: 3 °C/min
○: α-Fe_2O_3 (104), ●: MgO (200), ◑ and ◐: Mg-Fe_2O_4 (311) and (200), respectively

than the melting point of NaCl (mp 808 °C). In the case of KCl (Fig. 5-C), $MgFe_2O_4$ begins to form at *ca.* 800 °C after melting of KCl (mp 776 °C). The discontinuous changes in the X-ray intensities of α-Fe_2O_3 and NaCl for $MgO–Fe_2O_3$–NaCl system (Fig. 5-B), and of α-Fe_2O_3 for $MgO–Fe_2O_3$–KCl system (Fig. 5-C) are observed just before the melting of chloride additives. Such phenomena are also observed in the binary system of $NaCl–Fe_2O_3$ (Fig. 5-D). Addition of LiF (Fig. 6-A) lowers the initiation temperature of $MgFe_2O_4$ formation to 700 °C. This temperature is close to that of the liquid phase formation (730 °C) in $MgO–Fe_2O_3$–LiF system (Fig. 4). In the case of NaF (Fig. 6-B), the initiation temperature is also lowered, the intensity of $MgFe_2O_4$ increasing abruptly at 1020 °C.

Table 2. The initiation temperature of $MgFe_2O_4$ formation

Additive	Init. temp (°C)
Non-additive	820
LiF	700
NaF	725
MgF_2	800
BaF_2	900
NaCl	760
KCl	800

In the case of MgF_2 (Fig. 6-C), $MgFe_2O_4$ begins to form at 800 °C. On the other hand, the initiation temperature of the system with BaF_2 (Fig. 6-D) is somewhat higher in comparison with that of other systems. The initiation temperatures of the $MgFe_2O_4$ formation in all the systems are summarized in Table 2. It is seen that α-Fe_2O_3 in $MgO–Fe_2O_3$ system disappears at temperatures higher than 1075 °C, but MgO still exists at these temperatures (Fig. 5-A). Similar phenomena are also observed at 1075 °C, 950 °C, 1060 °C, or 1050 °C in $MgO–Fe_2O_3$–NaCl, –NaF, $–MgF_2$, or $–BaF_2$, respectively. The samples obtained after the high temperature X-ray diffraction experiments (Figs. 5-A, -B and 6-A, -B, -C, -D) showed traces of Fe^{2+}.

Discussion

It was found[9] that the lower the melting point of the fluoride additives, the lower the initial temperature of $MgAl_2O_4$ formation, and that AlF_3 formed by the reaction between fluorides and α-Al_2O_3 initiates the formation of $MgAl_2O_4$. For the $MgO–Fe_2O_3$–fluoride systems, a linear correlation of the melting point of the fluoride with the initiation temperature of $MgFe_2O_4$ formation (Table 1) was also observed (Fig. 7). Deviation of the point for BaF_2 from a straight line may be due to the poor crystallinity of $MgFe_2O_4$ formed, since although the initial temperature of $MgFe_2O_4$ formation is at *ca.* 900 °C (Fig. 6-D), the fractional conversion

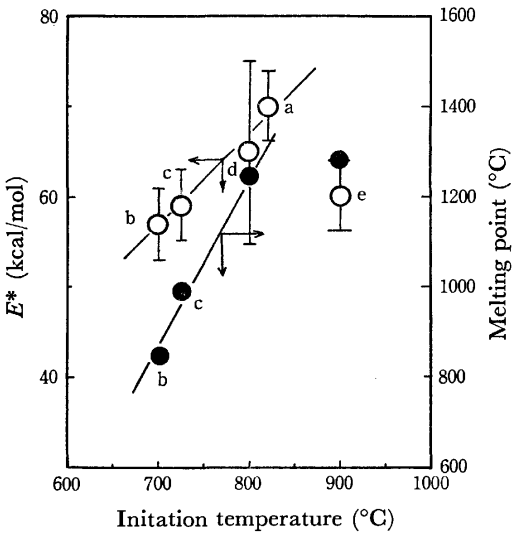

Fig. 7. Plots of the melting points of halide and the E^* values *vs.* the initiation temperature of $MgFe_2O_4$ formation.
a: non-additive, b: LiF, c: NaF, d: MgF_2, e: BaF_2

determined from the amount of unreacted α-Fe_2O_3 after the isothermal experiments goes up to $\alpha=36\%$ at 847 °C for 50 min in MgO–Fe_2O_3–BaF_2 system. The correlation in Fig. 7 suggests that the fluoride of lower melting point easily reacts with reactants α-Fe_2O_3 or MgO and that the reaction promotes the $MgFe_2O_4$ formation in the initial stage, as described for MgO–Al_2O_3–fluoride system. The reaction of fluoride with reactants may result in the formation of compounds such as magnesium or iron fluoride. The formation of such compounds results in the lowering of the melting point of LiF (mp 845 °C) or NaF (mp 992 °C) by more than 100 °C or 60 °C, respectively (Fig. 4). On the other hand, the melting point of the binary systems such as MgO–LiF or –NaF and Fe_2O_3–LiF or –NaF nearly agreed with that of pure LiF or NaF. However, X-ray analysis for the products obtained in the DTA experiments did not indicate the formation of compounds such as magnesium or iron fluoride, or Li–, Na–, or Ba–ferrite. This might be due to too small amounts of the compounds for detection by X-ray analysis.

Reijnen[18] studied the solid state reaction in the MgO–Fe_2O_3 system, and proposed two possible mechanisms of counter diffusion of cations for the formation of $MgFe_2O_4$ at a given oxygen pressure and temperature, *i.e.* Mg^{2+} and Fe^{3+}, or Mg^{2+} and Fe^{3+} or Fe^{2+} diffuse through the spinel layer. The Fe^{2+} diffusion is accompanied by the diffusion of one cation vacancy and by the transport of oxygen in the gas phase. Carter[19] assumed the mechanism of the counter diffusion of Mg^{2+} and Fe^{3+}. Lindner[20,21] reported that the activation energy for the self-diffusion of Mg^{2+} in MgO single crystal is 79 kcal/mol and that of Fe^{3+} in $ZnFe_2O_4$ polycrystal is 82 kcal/mol. These can be regarded as values for the volume or grain boundary diffusion. It was found from the results given in Fig. 3 and Table 1 that the formation rate of $MgFe_2O_4$ in MgO–Fe_2O_3 system is controlled by the diffusion with the activation energy of 70 ± 4 kcal/mol, which is comparable to the above values. Since no Fe^{2+} was found in the samples obtained by the isothermal experiments, it seems that $MgFe_2O_4$ formation in MgO–Fe_2O_3 system proceeds by the counter diffusion of Mg^{2+} and Fe^{3+} and that the volume or grain-boundary diffusion is operative in the formation of $MgFe_2O_4$. The presence of fluorides lowers the value of the activation energy E^* by 5—13 kcal/mol (Table 1), which might indicate that the fluorides accelerate the diffusion along grain boundary or within bulk. There is a possibility that the dissolution or incorporation of compounds formed by the reaction of fluoride with α-Fe_2O_3 into the $MgFe_2O_4$ layer facilitates the diffusion of Mg^{2+} or Fe^{3+}. It can be considered in the case of LiF or NaF additive that the liquid phase formation at *ca.* 700 °C or 800 °C accelerates further diffusion by acting as a vehicle of transporting MgO or α-Fe_2O_3. It is observed that the lower the E^* value, the lower the initiation temperature of $MgFe_2O_4$ formation (Fig. 7).

The accelerating mechanism of $MgFe_2O_4$ formation by the presence of chloride was explained as follows: MgO particles dissolve in molten chloride to spread uniformly over the outer surface of α-Al_2O_3 particles and then MgO particles transport into the inner part of α-Al_2O_3 particles consisting of crystallites. In the MgO–Fe_2O_3–NaCl system, discontinuous changes in X-ray diffraction intensities of α-Fe_2O_3 and NaCl were observed before melting of NaCl, the initial for mation of $MgFe_2O_4$ beginning simultaneously (Fig. 5-B). The discontinuous changes of X-ray intensities seem responsible for the initial formation of $MgFe_2O_4$, although no explanation can be given at present. In the case of KCl, $MgFe_2O_4$ was formed after melting of KCl, although a discontinuous change of α-Fe_2O_3 intensity was also observed (Fig. 5-C). There may be a difference in the action of solids NaCl and KCl on the $MgFe_2O_4$ formation. It is considered that after chloride melts, the formation of $MgFe_2O_4$ is promoted by the dissolution process of MgO particles in molten chloride.

It was found in the high temperature X-ray experiments that α-Fe_2O_3 disappears at temperatures where MgO still exists (Figs. 5 and 6) and that a trace of Fe^{2+} is present in the samples after the experiments. This suggests that a part of Fe^{3+} is reduced at high temperatures to ferrous ions by the dissolution of α-Fe_2O_3 in $MgFe_2O_4$ phase at relatively high vacuum ($Po_2=10^{-1}$ mmHg) in comparison with that in the isothermal experiments ($Po_2=10^0$—10^1 mmHg), and that the $MgFe_2O_4$ formation proceeds by the counter diffusion mechanism of Mg^{2+} and Fe^{3+} accompanied by partial participation of Fe^{2+} in the diffusion, as proposed by Reijnen.[18]

References

1) B. Delmon, "Reactivity of Solids," ed. by J. S. Anderson, London (1972), p. 567.
2) J. Deren, J. Haber, A. Podyorecka, and W. Tur, *Z. Anorg. Allg. Chem.*, **402**, 221 (1973).
3) R. Furuichi, T. Ishii, and K. Kobayashi, *J. Thermal Anal.*, **6**, 305 (1974).
4) G. Henrich, *Z. Electrochem.*, **58**, 183 (1954).
5) H. Schmalzried, *Ber. Dtsh. Keram. Ges.*, **42**, 11 (1969).

6) K. J. Mackenzie, *Trans. Brit. Ceram. Soc.*, **63**, 103 (1969).
7) S. Shimada and T. Ishii, *Nippon Kagaku Kaishi*, **1972**, 1234.
8) S. Shimada, R. Furuichi, and T. Ishii, *Bull. Chem. Soc. Jpn.*, **47**, 2026 (1974).
9) S. Shimada, R. Furuichi, and T. Ishii, *Bull. Chem. Soc. Jpn.*, **47**, 2031 (1974).
10) H. Tamura, K. Goto, T. Yotsuyanagi, and M. Nagayama, *Talanta*, **21**, 314 (1974).
11) K. J. Laidler, "Chemical Kinetics," McGraw-Hill, New York (1964), p. 316.
12) W. Jander, *Z. Anorg. Allg. Chem.*, **163**, 1 (1927).
13) B. Serin and R. J. Ellickson, *J. Chem. Phys.*, **9**, 742 (1941).
14) A. M. Ginstling and B. J. Brounshtein, *J. Appl. Chem.*, **23**, 1327 (1950).
15) R. E. Carter, *J. Chem. Phys.*, **34**, 2010 (1961).
16) M. Iwata, *Oyobuturi*, **34**, 812 (1965).
17) S. L. Blum, A. E. Paladino, and L. G. Tubin, *Ceram. Bull.*, **36**, 175 (1957).
18) P. Reijnen, "Reactivity of Solids," ed. by G. M. Schwab, Amsterdam (1965), p. 562.
19) R. E. Carter, *J. Am. Ceram. Soc.*, **44**, 116 (1961).
20) R. Lindner and G. D. Parfitt, *J. Chem. Phys.*, **26**, 182 (1957).
21) R. Lindner, *Z. Electrochem.*, **59**, 967 (1955).

Indium(III) Complexes of DL-Penicillamine in Aqueous Solution. Evidence for the Formation of Protonated and Hydrolyzed Complexes

Nakao KOJIMA, Yukio SUGIURA, and Hisashi TANAKA

Department of Pharmaceutical Radiochemistry, Faculty of Pharmaceutical Sciences, Kyoto University, Yoshida, Sakyo-ku, Kyoto 606

(Received September 8, 1975)

The penicillamine–In(III) system has been investigated with potentiometric titration over a wide range of metal concentration at 21°C and I=0.1 (KNO_3). In dilute concentration of metal (0.00025—0.0005 M) and ligand (free base), single species (InL and InL_2) are predominantly formed. In higher concentration of metal (0.0025—0.005 M) and ligand (with an equimolar HCl), the protonated and hydrolyzed complexes (InLH, InL(LH), and InL(OH)) are also formed together with the simple species. The formation constants calculated with non-linear least-squares program were found to be: log β_{110}=15.330, log β_{120}=29.789, log β_{11-1}=18.858, log β_{12-1}=33.391, and log β_{111}=11.25 for InL, InL_2, InLH, InL(LH), and InL(OH) species, respectively. The formation constants and ultraviolet spectra indicate that the proton in the protonated complex is attached to the amino-group of penicillamine.

^{113m}In[1] and ^{111}In[2] as well as ^{99m}Tc are a few of the radioisotopes recommended for the scanning of various organs or tissues among those introduced in the field of nuclear medicine. Recently, the use of some complexing agents with these radioisotopes has made a wide variety of scanning possible. However, knowledge of the complex formation of these metals is still insufficient for the development of new effective scanning agents. Some thiols, of which penicillamine is the most popular, have been used as the complexing agents with ^{99m}Tc. The complex formation together with hydrolysis reaction have been studied in connection with the preparation of the effective scanning agents which localize to some organs or tissues.[3] We planned a series of studies on the complex formation of In(III) with some complexing agents in an aqueous solution and also the reaction of In(III) with proteins for the better understanding on the mechanism of the localization of In(III) complexes *in vivo*. As the first step of this study, we adopted penicillamine as a complexing agent.

Although Habeeb and Tuck[4] have extensively investigated coordination compounds of In(III), most of which are prepared in organic solvent, studies on complex formation of In(III) in an aqueous solution are relatively few. Sarin and Munshi[5-7] reported that the order of the stability constants of β-substituted propionic acid–In(III) complexes decreases in the order SH>OH>NH_2 in various substituted groups. Their estimates for the stability constants are made on the assumption that three simple species, InL, InL_2 and InL_3 are present. On the other hand, Perrin and Sayce[8] detected the protonated penicillamine complexes with Zn(II) which has the isoelectronic configuration for d^{10}-In(III).

We have investigated the complex formation of In(III) with penicillamine with the use of potentiometric titration and absorption spectra. The presence of the protonated and hydrolyzed species is discussed.

Experimental

Materials. Indium metal (99.99%, Wako Pure Chemical Industries, Ltd.) was used. An accurately weighed amount of metal was dissolved in a small amount of hydrochloric acid by heating and diluted to 1 liter with deionized water after cooling. Solution of In(III) was freshly prepared and standardized with 8-quinolinol method.[9] Hydrochloric acid added to prevent hydrolysis of In(III) was standardized potentiometrically.

DL-Penicillamine (Sigma Chemical Company) was dried under vacuum over phosphoric oxide at room temperature. Stock solutions were stored under nitrogen, and checked by pH titration.

Carbonate-free potassium hydroxide solutions (1M and 0.1M) were prepared by an ion-exchange method,[10] and standardized by a conventional method. All other reagents used of commercial reagent grade.

Potentiometric Titrations. The potentiometric titrations were performed with a Radiometer titrator, Type TTT-2 equipped with a Radiometer G202B glass electrode and a K401 saturated calomel electrode. The pH readings with standard buffer solutions (0.05M potassium hydrogen phtalate, pH 4.00, and 0.05M sodium tetraborate, pH 9.22) were constant within 0.01 pH unit for periods exceeding 1 day. Titration was carried out with standard carbonate-free potassium hydroxide solutions with a specially designed, water-jacketed titration vessel at 21.00±0.05°C in an air-conditioned room (21±1°C), the solution being stirred continuously with a stirrer under pure nitrogen gas supply. In(III) (0—0.005 M), penicillamine (0.001—0.01 M) and potassium nitrate (0.1M) were placed in the vessel, and the total volume was adjusted to 20 ml by adding deionized water. All potentiometric measurements were repeated at least twice in order to obtain satisfactory reproducibility required for the computer-based analysis.

Absorption Spectra. Optical spectra were determined in an aqueous solution with a Shimadzu recording spectrophotometer, Model Double 40-R. Sample solutions consisted of penicillamine (0.00016M), or the ligand and In(III) (0.00008 M), and a very small amount of 1M potassium hydroxide and 1M hydrochloric acid was added for the adjustment of pH. The visible and ultraviolet spectra of the penicillamine solutions containing Fe(III), Cu(II), Pb(II), Hg(II), Cd(II), or Zn(II) were also measured.

Calculations

The proton dissociation constant(Ka_1) of the carboxyl-group in penicillamine was obtained by the usual method

from the potentiometric titration data for the sample solution containing 0.05 M penicillamine and an equimolar HCl. The remaining two ionization constants Ka_2 and Ka_3 for the amino- and thiol-groups are defined by the following equation which can be deduced from the total ligand concentration($[L]_T$) and electroneutrality.

$$[H^+]([L]_T-\gamma)Ka_2 + (2[L]_T-\gamma)Ka_2Ka_3 = \gamma[H^+]^2 \quad (1)$$

In this equation, γ is defined as

$$\gamma = [H^+] + [K^+] - [OH^-]$$

where $[K^+]$ is the concentration of base added. The Ka_2 and Ka_3 values were defined simultaneously by the linear least-squares method for Eq. (1) under the condition of $[L]_T=0.0015$ M. These three constants were further refined by the non-linear Fortran IV computer program on a FACOM 230-75 Computer, the Kyoto University Computer Center. The values of $pKw=14.130$[11] at 21°C and $[H^+]=10^{-pH}$ were used in the calculations.

The titration curve of 1:2 In(III) to penicillamine (free base) indicates the formation of the complex InL_2. Formation constants (K_1 and K_2) are defined as follows.

$$K_1 = [InL^+]/[In^{3+}][L^{2-}] \quad (2)$$

$$K_2 = [InL_2^-]/[InL^+][L^{2-}] \quad (3)$$

The constants were calculated by the least-squares method of the Irving and Rossotti equation.[12,13]

$$\bar{n}(\bar{n}-1)[L^{2-}] = (2-\bar{n})[L^{2-}]K_1K_2(\bar{n}-1) - K_1 \quad (4)$$

The theoretical $\bar{n}$ values are evaluated by the constants obtained. From the constants, theoretical titres (x ml) are also expressed as follows.

$$Ax^3 + Bx^2 + Cx + D = 0 \quad (5)$$

where

$$A = a(K_1K_2Qa^2+K_1PQa+P^2Q)$$

$$B = 3K_1K_2a^2b+K_1PQa(Va+2b)-0.5K_1[L]_TP^2Va + P^2Q(2Va+b)-[L]_TP^3V$$

$$C = 3K_1K_2a^2b+K_1PQb(2Va+b)-0.5K_1[L]_TP^2V(Va+b) + P^2QV(Va+2b)-2[L]_TP^3V^2$$

$$D = K_1K_2Qb^3+K_1PQVb^2-0.5K_1[L]_TP^2V^2b+P^2QV^2b - [L]_TP^3V^3$$

$$a = [OH^-] - [H^+] - [K^+]$$

$$b = V(2[L]_T+[Cl^-]+[OH^-]-[H^+])$$

$$P = 3(H^+)^3/Ka_1Ka_2Ka_3+2(H^+)^2/Ka_2Ka_3+(H^+)/Ka_3$$

$$Q = (H^+)^3/Ka_1Ka_2Ka_3+(H^+)^2/Ka_2Ka_3+(H^+)/Ka_3+1$$

V = initial volume

$[L]_T$ = total ligand concentration

$[Cl^-]$ = concentration of inorganic acid (if any)

Equation (5) was solved by the use of subroutine CALDND, Scientific Subroutine Library, the Kyoto University Computer Center.

No simple procedures exist for obtaining the stability constants of metal complexes from $[L^{2-}]$ and $\bar{n}$ values, if polynuclear, protonated or hydroxo complexes are formed. In such cases, various computer programs based on the non-linear least-squares method have been used.[14-17] At each point of the titration, equilibrium takes place among the various species expressed by the general formula $M_lL_mH_{-n}$ (M=metal, L=ligand), where n is positive for a hydrolyzed species and negative for a protonated species. The concentration of the species $M_lL_mH_{-n}$ at each point is given by

$$[M_lL_mH_{-n}] = \beta_{lmn}[M]^l[L]^m(H^+)^{-n} \quad (6)$$

where β_{lmn} is the formation constant of the species under consideration.

For each point, the followoing mass-balance equations should hold.

$$[M]_T = [M] + \sum l\beta_{lmn}[M]^l[L]^m(H^+)^{-n} \quad (7)$$

$$[L]_T = [L] + \sum m\beta_{lmn}[M]^l[L]^m(H^+)^{-n} \quad (8)$$

$$[H]_T = [H^+] + \sum(-n)\beta_{lmn}[M]^l[L]^m(H^+)^{-n} \quad (9)$$

where $[M]_T$, $[L]_T$ and $[H]_T$, are the analytical concentrations of the metal, ligand, and acid, respectively. The unknown parameters in these equations are [M] and [L] for each point and the stability constants β_{lmn}. The values of (H^+) are obtained from the potentiometric measurement. In the present case, [M] and [L] are obtained by considering a set of plausible values for the stability constants and by calculating the starting values of [M] and [L] from Eqs. (7) and (8) for each point, using the Newton-Raphson iteration. Computed [M] and [L] for the first point are used as initial estimates for the second point, and so on. Using the obtained [M] and [L], the concentration of $M_lL_mH_{-n}$ is calculated from Eq. (6), and $[H]_T$ from (9) for each data point. Theoretical titre of base is obtained from $[H]_T$. If the agreement between the experimental and calculated titres is not satisfactory, the values of the constants β_{lmn} are varied in turn so as to minimize the error-square sum in titre. The standard deviations of the parameters are the square-roots of the diagonal elements of the variance-covariance matrix of the parameters.

This program was also used for the calculation of pKa and hydrolysis constants of the metal ion.

Results and Discussion

Practical Association Constants. Table 1 shows the result of the calculation for "practical' association constants defined by the following equations.

$$\beta_{01-1} = [LH^-]/(H^+)[L^{2-}]$$

$$\beta_{01-2} = [LH_2]/(H^+)^2[L^{2-}]$$

$$\beta_{01-3} = [LH_3^+]/(H^+)^3[L^{2-}]$$

The constants were refined with non-linear program. The calculated $\log\beta_{01-1}$ and $\log\beta_{01-2}$ are in good agreement with that ($\log\beta_{01-1}=10.679$ and $\log\beta_{01-2}=18.714$) reported by Perrin and Sayce.[8] The value ($pKa_1=$

Table 1. Ionization constants of DL-penicillamine at 21°C and $I=0.1$ (KNO_3)[a]

LH	$\log\beta_{01-1}=10.669\pm0.004$
LH_2	$\log\beta_{01-2}=18.774\pm0.006$
LH_3	$\log\beta_{01-3}=20.839\pm0.005$[b]

a) Uncertainty intervals associated with all the values are the standard deviations. b) Obtained from 0.05 M solutions, others from 0.0015 M solutions.

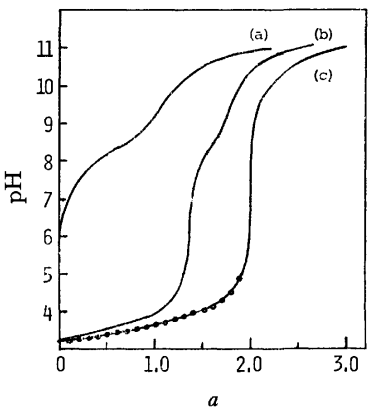

Fig. 1. Titration curves of the penicillamine (free base)–In(III) complexes: (a) ligand alone; (b) L: In=3: 1; (c) L: In=2: 1. Total ligand concentrations are 0.0015, 0.0015, and 0.001 M, respectively. Each point on the curve (c) was calculated by the use of the formation constants. a=moles of KOH added per mole of protonated ligand with regard to the thiol- and amino-groups.

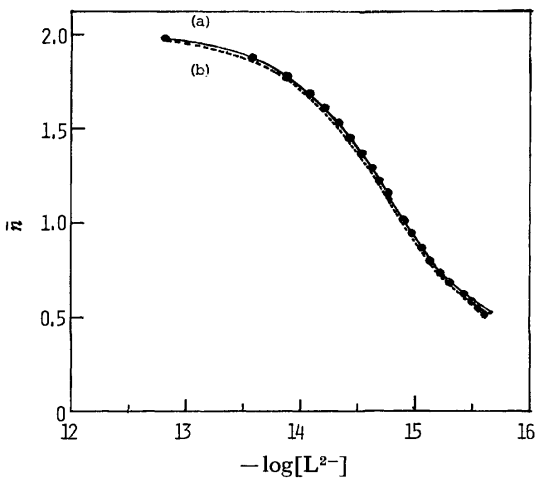

Fig. 2. Formation curves of the penicillamine (free base)–In(III) complexes: (a) L: In=2: 1, (b) L: In=3: 1. Total ligand concentrations are 0.001 and 0.0015 M respectively. Each point represents the calculated value as for curve (a).

2.065) obtained from $\log\beta_{01-3}$ and $\log\beta_{01-2}$ differs slightly from that (pKa_1=2.44) reported by Kuchinskas and Rosen.[18] The difference is due to the low concentration (0.0033 M) of the latter case.

Simple InL and InL_2 System. Figure 1 shows the titration curves of 2: 1 and 3: 1 penicillamine (free base) to In(III) (0.0005 M). The sharp inflections of pH were observed at a=1.33 and 2 in the 3: 1 and 2: 1 systems, respectively. The two formation curves could be superimposed (Fig. 2). It was impossible even under the condition of 3: 1 (ligand to metal) to obtain $\bar{n}$ values greater than 2. The findings indicate that in our experimental conditions the mononuclear species, InL and InL_2, are present predominantly. In the titration curve of the 3: 1 system, therefore, the inflections at a=1.33 and 1.67 are associated with the formation of the complex InL_2 and the dissociation of the thiol-group of the excess ligand, respectively.

The constants ($\log K_1$=15.44 and $\log K_1K_2$=29.85) were obtained from Eq. (4) using $\bar{n}$ and $[L^{2-}]$ values at each point. With use of these constants, theoretical $\bar{n}$ values were also calculated by Eq. (4). Validity of these constants was confirmed by the coincidence with the experimental and calculated formation curves (Fig. 2, (a)). From the K_1 and K_1K_2 values, the titration curve (Fig. 1, (c)) was recalculated by the use of Eq. (5) and compared with that obtained experimentally.

These constants determined by the Irving Rossotti method were further refined by the non-linear computer program. The final values ($\log\beta_{110}$=15.425±0.010 and $\log\beta_{210}$=29.844±0.006) fitted the data to within a standard deviation in titre of 0.0015 ml, as compared with the value (0.0021 ml) obtained in fitting the simple pKa titration data. From these constants, a distribution diagram of various complexes was calculated for various pH (Fig. 3).

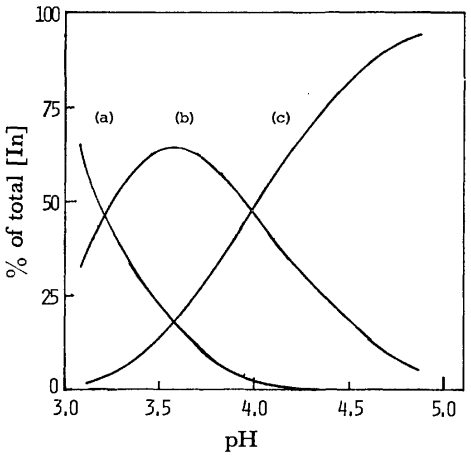

Fig. 3. Distribution diagram for the penicillamine (free base) (0.001M)–In(III)(0.0005M) system: (a) In^{3+}; (b) InL; (c) InL_2.

Penicillamine as a terdentate ligand has been predicted to form metal complexes with various coordination types. In dilute penicillamine(free base)–In(III) systems, however, the simple species InL and InL_2 only were formed. The constant ($\log\beta_{110}$=15.425) for the species InL is much larger than those for the corresponding penicillamine 1: 1 complex of Zn(II) (9.589), Ni(II) (10.749),[8] Cd(II) (10.92) and Pb(II) (12.88),[19] respectively. It is of interest that the formation constant is comparable to that (16.4) of the Hg(II) complex.[19]

InL, InL_2, InLH, InL(LH), and InL(OH) Systems. Titration was extensively carried out in the systems of various metal concentrations and metal-ligand ratios. An equimolar HCl was added to the penicillamine solution in order to protonate the carboxyl-group in the ligand. The total metal concentrations were 0.00025, 0.0005, 0.0025, and 0.005 M, and the total ligand concentrations were 0.001, 0.001, 0.01, and 0.01 M, respectively. Plots of $\bar{n}$ against $\log[L^{2-}]$ are shown in Fig. 4. Failure of superposition in the formation curve indicates that besides InL and InL_2, other complex species are formed with an increase in metal concentra-

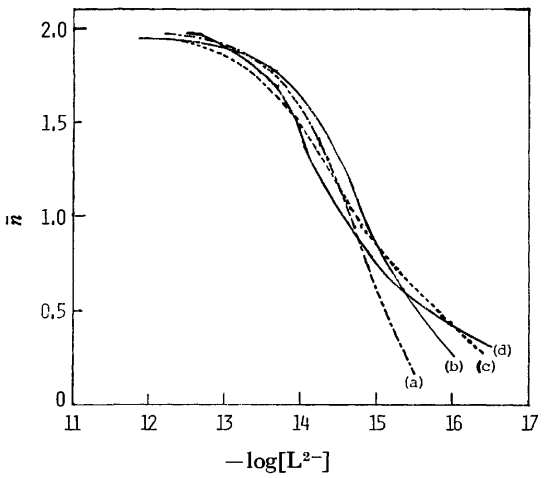

Fig. 4. Formation curves of the penicillamine (HCl)–In(III) complexes: (a) L: In=4: 1; (b) L: In=2: 1; (c) L: In=4: 1; (d) L: In=2: 1. Total ligand concentrations are 0.001, 0.001, 0.01, and 0.01M, respectively.

tion. However, the curves do not converge towards Biedermann and Sillén's "mononuclear wall."[20] Accordingly, the systems could contain no "core plus links" series of complexes.[21] Formation of mononuclear protonated and/or hydroxo species was assumed.

In order to characterize the hydrolyzed In(III) species which give the hydroxo complexes to associate with ligand, a brief inspection on the hydrolysis equilibrium of In(III) ion was carried out. Potentiometric titration of 0.0005 M In(III) solution containing 0.00026 M HCl at 21°C and I=0.1(KNO_3), afforded $\log \beta_{101} = -3.634 \pm 0.037$ after refinement by the non-linear program.

$$In^{3+} \rightleftarrows In(OH)^{2+} + H^+$$

$$[In(OH)^{2+}] = [InH^{2+}_{-1}] = \beta_{101}[In^{3+}](H^+)^{-1}$$

(β_{101} is not precisely the formation constant for the complex In(OH), but is related to it through $Kw = (H^+)(OH^-)$ since $\beta'[In^{3+}](OH^-) = \beta'[In^{3+}](H^+)^{-1}Kw$, *i.e.*, $\beta_{101} = \beta' \times Kw$, where β' is the true formation constant for the complex In(OH).) Besides a large amount of In(OH), a small amount of $In(OH)_2$ was also formed. Biedermann[22] reported $\log \beta_{202} = -5.21$ and $\log \beta_{304} = -9.90$ for 0.05 M In(III) perchlorate at 25° in 3 M $NaClO_4$. However, no such complexes were detected in our dilute system which is close to the "metal ion wall." The species In(OH) and $In(OH)_2$ were used as the hydrolyzed In(III) species which participate in the hydroxo complex formation with penicillamine.

On the other hand, the protonated mononuclear species to be considered are InL, InL_2, InLH, InL(LH), and $In(LH)_2$. The best fit to the experimental results was sought by the use of a computer program, with automatic refinement of estimated stability constants. The initial value of unknown constant for the complex InLH was estimated as below. Each equilibrium constant for the next three reaction were defined as follows.

$$In^{3+} + L^{2-} + H^+ \rightleftarrows InLH^{2+}; \quad \beta_{11-1}$$

$$In^{3+} + LH^- \rightleftarrows InLH^{2+}; \quad K^{In}_{InLH}$$

$$L^{2-} + H^+ \rightleftarrows LH^-; \quad K^{H}_{LH}$$

where β_{11-1} was given by

$$\beta_{11-1} = [InLH^{2+}]/[In^{3+}][L^{2-}](H^+)$$
$$= [InLH^{2+}]K^{H}_{LH}/[In^{3+}][LH^-]$$
$$= K^{In}_{InLH}K^{H}_{LH}$$

According to Sarin and Munshi,[5] the constant ($\log K_1$) for the In(III)–β-aminopropionic acid complex ($\widehat{NO}$ coordination type) was 2.72, which is much smaller than that of the In(III)–penicillamine complex. This suggests that the thiol-group coordinates to the metal in the protonated complex(InLH). The assignment of pKa value (10.67) to the dissociation of the protonated amino-group is supported by absorption spectral measurements. The constants ($\log K_1$) for the In(III) complexes of *N*-acetyl-*L*-cysteine ($\widehat{SO}$ coordination type) and 2-aminoethanethiol ($\widehat{SN}$ type) are 10.24 and 13.96, respectively. If the proton in InLH attaches to the carboxyl- or amino-group, $\log \beta_{11-1}$ values are obtained as follows.

$$\log \beta_{11-1} = 13.96 + 2.07 = 16.03$$

$$\log \beta_{11-1} = 10.24 + 10.67 = 20.91$$

The two values were refined by the program in the system of 0.005 M In(III) and 0.01 M penicillamine (HCl), together with the constants for the complexes

Table 2. Values (logarithmic units) of the formation constants in the successive trials for the In(III) (0.005 M)–penicillamine(HCl) (0.01 M) system[a]

Trial	Complex species						Std. dev. in titre (ml)
	InL	InL_2	InLH	InL(LH)	$In(LH)_2$	InL(OH)	
1	15.803 (0.016)	29.610 (0.038)					0.0168
2	15.778 (0.008)	29.860 (0.011)	18.662 (0.014)				0.0022
3	15.728 (0.008)	29.761 (0.012)	18.718 (0.012)			11.752 (0.045)	0.0015
4	15.688 (0.016)	29.865 (0.007)	18.754 (0.015)	33.000 (0.065)			0.0015
5		29.885 (0.010)	18.796 (0.020)	33.604 (0.017)	36.61 (1.03)		0.0018
6	15.696 (0.014)	29.804 (0.017)	18.747 (0.014)	32.79 (0.14)		11.47 (0.13)	0.0014

a) Standard deviations in parentheses.

InL and InL_2. In each case, the final value of $\log \beta_{11-1}$ converged to 18.662, *viz.*, the intermediate between two initial estimates (Table 2, trial 2). Introduction of this complex (InLH) gave a remarkable improvement as compared with trial 1. For trial 1 inclusion of the hydroxo complex (InL(OH)) caused no improvement, but for trial 2 it gave a better fit to the experimental data (trial 3). However, the inclusion of $InL(OH)_2$ did not significantly improve the fit. Trials 4—6 gave acceptable fits of a series of a trial and error approach. Trial 5 indicates that the complex $In(LH)_2$ is negligible. Trials 3 and 4 gave the equal standard deviations in titre. In trial 6, the standard deviation in titre is slightly improved, neverthless the standard deviations of the constants of InL(LH) and InL(OH) are larger. This result may be due to the fact that a small amount of the two species are formed in similar pH regions. It is difficult to make a selection from trials 3, 4, and 6 by pH titration. Figure 5 shows the distribution diagram of the complexes obtained from trial 6.

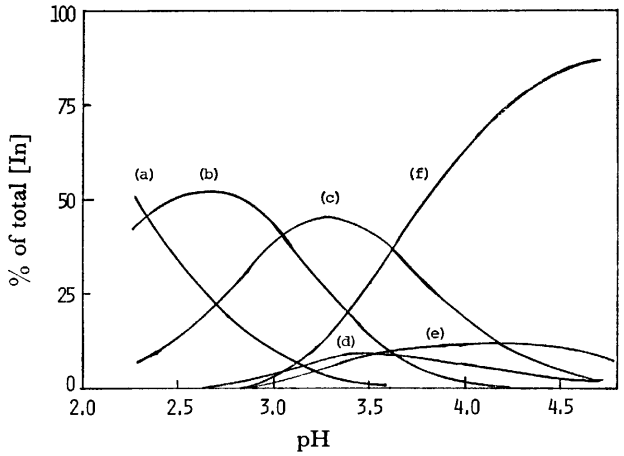

Fig. 5. Distribution diagram for the penicillamine(HCl) (0.01M)–In(III)(0.005M) system, as for Table 2, trial 6: (a) In^{3+}; (b) InLH; (c) InL; (d) InL(LH); (e) InL(OH); (f) InL_2.

The sulfur-bridged polymers are formed in aqueous solutions containing ligands of the types RS^- and the first transition metals.[8,23,24] However, introduction of various polynuclear or olated species caused no improvement in the results. Probably, the methyl groups in penicillamine prevent the formation of sulfur-bridging species.

The same investigation on the other three formation curves suggests that the presence of InL(LH) and InL(OH) becomes negligible with the decrease in concentration of the metal. A comparison with Figs. 3 and 5 also suggests that the species (InLH) becomes negligible, unless the system is acidified by addition of HCl in the lower metal concentration.

A final refinement of all these constants over the whole range of the experimental data (4 experiments, 166 data points) yielded the constants listed in Table 3. The calculated and experimental titres coincided within a standard deviation of 0.0087 ml. Although this value seems to be somewhat large, it is acceptable when the appreciable change in concentration of the complex

Table 3. Stability constants of In(III) complexes with DL-penicillamine at 21°C and I=0.1 (KNO_3)[a]

InL	$\log \beta_{110} = 15.330 \pm 0.058$
InL_2	$\log \beta_{120} = 29.789 \pm 0.038$
InLH	$\log \beta_{11-1} = 18.858 \pm 0.043$
InL(LH)	$\log \beta_{12-1} = 33.391 \pm 0.079$
InL(OH)	$\log \beta_{111} = 11.25 \pm 0.11$

a) Uncertainty intervals associated with all the values are the standard deviations.

species present in the various systems is taken into account.

Calculation of the constant for the protonated complex InLH yielded the intermediate value between the two initial estimates for the species of the $\widehat{SO}$ or $\widehat{SN}$ type. Figure 5 shows, however, that the two protonated species InLH and InL(LH) exhibit maxima at pH 2.7 and 3.3, respectively, where the carboxyl-group in penicillamine is fully ionized. Therefore, these protons are assumed to attach on the amino-group in the ligand. When the value of pKa_3=10.669 is assigned to the ionization constant of the amino-group, the constant K^{In}_{InLH} in the reaction ($In^{3+}+LH^- \rightleftarrows InLH^{2+}$) is calculated by the following equations using the refined constant $\log \beta_{11-1}$=18.858.

$$K^{In}_{InLH} = \beta_{11-1}/Ka = 10^{18.858}/10^{10.669}$$

$$\log K^{In}_{InLH} = 8.189$$

The value is smaller than that ($\log \beta_{110}$=10.242) of *N*-acetyl-L-cysteine complex with In(III). Presumably, the difference is attributed to the electrostatic effect, that is, the reaction species with In^{3+} is LH^- in penicillamine but L^{2-} in *N*-acetyl-L-cysteine. In the solutions containing 0.0015 M ligands, the 1 : 1 (ligand to metal) complexes reach their maxima at pH 3.5 and 5.0 in *N*-acetyl-L-cysteine and 2-aminoethanethiol, respectively. This indicates that the coordination of the amino-group occurs at a relatively high pH.

Ultraviolet Absorption Spectra. The absorption of penicillamine in the 228—236 nm region is based on the form of RS^- ion. The absorbances increased rapidly in the pH range 7.5—8.5, and slightly in 10.5—11.5. Hence, we can assign the ionization constant pKa_2=

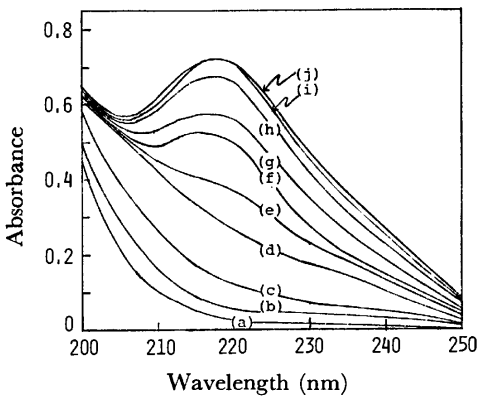

Fig. 6. Absorption spectra of the penicillamine (0.00016 M)–In(III)(0.00008M) system at various pH's: (a) pH 2.04; (b) pH 2.54; (c) pH 3.06; (d) pH 3.78; (e) pH 3.97; (f) pH 4.19; (g) pH 4.40; (h) pH 4.90; (i) pH 6.52; (j) pH 8.64.

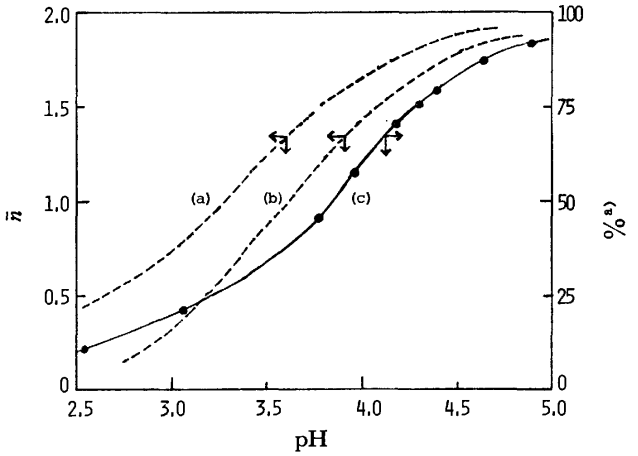

Fig. 7. Absorbance (solid line) and $\bar{n}$ values (dashed lines) of the 2: 1 (penicillamine to In(III)) solutions: Total metal concentrations are 0.005M (a), 0.0005M (b), and 0.00008M (c), respectively.
a) Absorbance at maximum is taken to be 100%.

8.105 to the thiol-group approximately, although the acid strength of the amino- and thiol-groups cannot be easily defined. According to Benesch and Benesch[25] the red shift with increasing pH is related to the change in the ratio of the forms of S^-RNH_2 and $S^-RNH_3^+$. Penicillamine gives a larger shift than cysteine, their thiol- and amino-groups microscopic constants pK_S and pK_N being 8.45 and 8.58, respectively.[26]

The absorption spectrum of the In(III) complex with penicillamine exhibits maximum at 217.5 nm ($\varepsilon = 4\times10^3$), which differs a great deal from that of penicillamine only. On the other hand, In(III) ion(d^{10}) shows no absorption. The absorption spectra of the solution containing 0.00008 M In(III) and 0.00016 M penicillamine are shown in Fig. 6. The absorption curvature at 215 nm appears at pH≈4, reaches its maximum at pH≈6 and is accompanied by a red shift of 2.5 nm, when pH increases. Figure 7 shows plots of the absorbance against pH. In this case, the absorbance at maximum is regarded as 100%. In the lower pH range (having no curvature), the absorbances at 215 nm are plotted. Figure 7 also contains plots of $\bar{n}$ against pH obtained from the pH titration data in the 0.01 M and 0.001 M penicillamine solutions containing 0.005 M and 0.0005 M In(III), respectively. Curves are parallel with a spacing, $\Delta\log[In]_T$, proportional to ΔpH. However, the relation does not hold below pH 3.5, the absorption and formation curves intersecting each other.

The In(III) complex with $\widehat{SO}$ type ligand has λ_{max} at ≈200 nm, and exhibits the tail in the range of ≈215 nm. The absorption spectra in the pH range 2—3.5 are similar to those of the corresponding $\widehat{SO}$ type complex (Fig. 6). These findings also support the formation of the protonated complex InLH ($\widehat{SO}$ type), which has λ_{max} at <200 nm and ε differing from that of the $\widehat{SNO}$ type complex InL. The absorption of InLH appears as a tail at 215 nm, and is considered to be superimposed upon that of InL. Crossing between the absorption and formation curves occurs below pH 3.5, where the species InL is absent.

The shift from 215 to 217.5 nm seems to be caused by the reaction $InL(LH)\rightarrow InL_2$, which leads to the change in the ratio of the forms of $S^-RNH_3^+$ and S^-RNH_2. Under the condition of $[In]_T=0.00008$ M, however, no formation of the species InL(LH) was confirmed from the pH titration data. The shift is, therefore, due to the reaction $InL\rightarrow InL_2$.

Precipitation of the meta hydroxide appears at pH 3.1 in 0.05 M metal ion solution, because of high hydrolyzability of In(III). The In(III) complexes with the usual amino-acids are unstable, whereas the In(III) complexes containing the thiol-group are very stable. The high stability might be attributed to the $d\pi$ back-donation of d^{10} electrons to the empty d orbitals of sulfur. This π-bonding character is reflected in the ultraviolet absorption. The charge transfer bands (λ_{max}) of the various metal-sulfide complexes[27] are correlated to the absorption maxima of the correspond-

Table 4. Charge transfer bands (λ_{max}) of sulfides- and penicillamine-metals complexes

Metal	Sulfide[a] (nm)	Penicillamine (nm)
Fe(III)	>500	570
Cu(II)	>375	520
Pb(II)		268
Hg(II)	300	260
Cd(II)	~250	217
Zn(II)	<200	217
In(III)		217.5

a) Ref. 27.

ing penicillamine–metal complexes (Table 4). The absorption at 217.5 nm of the penicillamine–In(III) complex is assigned to the charge transfer band. The band of Zn(II) complex, having an isoelectronic configuration for In(III), is at <200 nm for the sulfides, and at 217 nm for penicillamine. This is related closely to the fact that the corresponding band of In(III) is at <200 nm for β-mercaptopropionic acid, at ≈217 nm for penicillamine and 2-aminoethanethlol. Thus it seems that the absorptions at ≈217 nm in the penicillamine–In(III) and –Zn(II) result from M–S and M–N coordinations.

The authors thank Dr. H. Aiba, Kyoto University, for his helpful discussions, and the staff of the Kyoto University Computer Center for use of the FACOM 230-75 Computer.

References

1) H. H. Kramer and H. S. Stern, *J. Nucl. Med.*, **7**, 365 (1966).
2) D. A. Goodwin, R. A. Finston, L. G. Colombetti, J. E. Beaver, and H. Hupf, *J. Nucl. Med.*, **10**, 337 (1969).
3) M. Tubis, G. T. Krishnamurthy, J. S. Endow, and W. H. Blahd, *J. Nucl. Med.*, **13**, 652 (1972).
4) For example, J. J. Habeeb, and D. G. Tuck, *Can. J. Chem.*, **52**, 3950 (1974).
5) R. Sarin and K. N. Munshi, *Aust. J. Chem.*, **25**, 929 (1972).
6) R. Sarin and K. N. Munshi, *J. Inorg. Nucl. Chem.*, **34**, 581 (1972).

7) R. Sarin and K. N. Munshi, *J. Inorg. Nucl. Chem.*, **35**, 201 (1973).
8) D. D. Perrin and I. G. Sayce, *J. Chem. Soc., A*, **1968**, 53.
9) Lószló Erdey, "Gravimetric Analysis," Part II. Pergamon Press, New York, N. Y. (1965).
10) A. Albert and E. P. Serjeant, "Ionization Constants of Acids and Bases," Chap. 2, Mathuen, London (1962).
11) H. S. Harned and B. B. Owen, "The Physical Chemistry of Electrolytic Solutions," 3rd ed., Reinhold Publishing Corp., New York, N. Y. (1958).
12) H. Irving and F. J. C. Rossotti, *J. Chem. Soc.*, **1953**, 3397.
13) A. Albert and E. P. Serjeant, "Ionization Constants of Acids and Bases," Chap. 9, Mathuen, London (1962).
14) L. G. Sillén, *Acta Chem. Scand.*, **16**, 159 (1962).
15) R. S. Tobias and M. Yasuda, *Inorg. Chem.*, **2**, 1307 (1963).
16) I. G. Sayce, *Talanta*, **15**, 1397 (1968).
17) A. Sabatini, A. Vacca, and P. Gans, *Talanta*, **21**, 53 (1974).
18) E. J. Kuchinskas and Y. Rosén, *Arch. Biochem. Biophys.*, **97**, 370 (1962).
19) Y. Sugiura, A. Yokoyama, and H. Tanaka, *Chem. Pharm. Bull.*, **18**, 693 (1970).
20) G. Biedermann and L. G. Sillén, *Acta Chem. Scand.*, **10**, 1011 (1956).
21) L. G. Sillén, *Acta Chem. Scand.*, **8**, 299 (1954).
22) G. Biedermann, *Ark. Kemi.*, **9**, 277 (1956).
23) D. L. Leussing, *J. Am. Chem. Soc.*, **81**, 4208 (1959).
24) D. D. Perrin and I. G. Sayce, *J. Chem. Soc., A*, **1967**, 82.
25) R. E. Benesch and R. Benesch, *J. Am. Chem. Soc.*, **77**, 5877 (1955).
26) G. E. Clement and T. P. Hartz, *J. Chem. Educ.*, **48**, 395 (1971).
27) B. L. Valee and W. E. C. Wacker, "The Proteins," Vol. V, Academic Press, Inc., New York, N. Y. (1970).

The Structure of Ion-pairs of Λ- and Δ-$[Co(en)_3]^{3+}$ Ions with L-Tartrate and Related Anions as Deduced from Circular Dichroism Spectra*

Miho FUJITA** and Hideo YAMATERA

Department of Chemistry, Faculty of Science, Nagoya University, Chikusa, Nagoya 464

(Received October 20, 1975)

The circular dichroism (CD) spectra of optical antipodes of $[Co(en)_3]^{3+}$ and $[Co(pn)_3]^{3+}$ were measured in the presence of L-tartrate, L-tartranilate or related dicarboxylate ions. L-Tartrate(2−) ions gave a large and stereoselective effect on the CD spectra; the CD change was greater for the Λ-complex than for the Δ-complex. Hydrogen-L-tartrate(1−) and L-tartranilate(1−) ions also caused stereoselective CD changes. On the other hand, succinates-(2−) and L-malate(2−) ions gave small and non-stereoselective CD changes, and undissociated tartaric acid gave no CD change. From a comparison of the results, it was concluded that two hydroxyl and one carboxylate groups of the L-tartrate ion form hydrogen bonds with three N–H groups of the tris(diamine)cobalt(III) ion of the *lel* form.

In a previous papar,[1] we reported the stereoselective hydrogen-deuterium exchange rate of optically active $[Co(en)_3]^{3+}$ ions in D_2O solutions containing L-tartrate ions; the rate was faster for the Δ-isomer of the complex than for the Λ-isomer. The stereoselectivity of L-tartrate ions for optically active $[Co(en)_3]^{3+}$ ions has also been observed in optical rotatory dispersion, circular dichroism, UV absorption spectra,[2-4] and electrophoresis;[5] values have been obtained for the association constants of L-tartrate ions with Λ- and Δ-$[Co(en)_3]^{3+}$.[2,6]

However, neither the orgin of the stereoselective interaction nor the structure of the ion-pair seems to have been established. Ogino[2] suggested that two carboxylate groups of a L-tartrate ion participate in hydrogen-bonding with a $[Co(en)_3]^{3+}$ ion, and that the right-handed screw of $^-COO-C-C-COO^-$ in the gauche structure with two hydroxyl groups at *trans* position to each other is particularly important for the stereoselectivity. In contrast to this suggestion, our preliminary experiments on the hydrogen-deuterium exchange showed that hydroxyl groups may take a role as important as that of carboxylate groups.

Therefore, the present study was undertaken to investigate the role of each group of the L-tartrate ion in the stereoselective ion-paring with $[Co(en)_3]^{3+}$ or $[Co(pn)_3]^{3+}$ by a comparison of the effect of added dicarboxylate ions on the CD spectra.

Experimental

$[Co(en)_3]Br_3 \cdot H_2O$ was prepared by the usual method and resolved into the optical isomers by using silver L-tartrate and D-tartrate. The $[\alpha]_D$ values of the Λ- and Δ-$[Co(en)_3]$-$Br_3 \cdot H_2O$ were +124° and −123°, respectively. Λ (+) $[Co\{(+)pn\}_3]Br_3$ and $\Delta(-)[Co\{(-)pn\}_3]Br_3$ were prepared according to the literature.[7] Their $[\alpha]_D$ values were +221° and −223°, respectively. L-Tartranilic acid was prepared in the same way as described by Montzka *et al.*[8] Found: C, 52.9; H, 4.89; N, 6.04%. Calcd for $C_4H_{11}NO_5$: C, 53.3; H, 4.92; N, 6.22%. The acids were neutralized with an equivalent amount of sodium hydroxide if necessary. Series of sample solutions, 0.01 M in either Λ- or Δ-$[Co(en)_3]$-Br_3 and 0—0.1M in one of the dicarboxylates, were prepared by mixing solutions of the components. Sample solutions were made in pairs; two solutions of a pair were equivalent to each other except that each contained one antipode of the complex. Series of sample solutions of the optically active $[Co(pn)_3]Br_3$ were also prepared in the same way with sodium L-tartrate and with sodium succinate.

Circular dichroism spectra of these solutions were measured in the region of the first absorption band (600 nm—350 nm) with a JASCO ORD/UV5 spectrophotometer by using a 1 cm quartz cell at 25±1 °C.

Results

A typical result is shown in Fig. 1. Λ-$[Co(en)_3]^{3+}$ shows a CD spectrum with two peaks in the region of the first absorption band (corresponding to the $T_{1g} \leftarrow A_{1g}$ transition in an octahedral ligand field). The positive peak at the larger wavelength has been assigned to the E component and the negative peak at the smaller wavelength to the A_2 component.[9] In the presence of L-tartrate(2−) ion, the CD spectrum was modified in such a way that the intensity of the E component decreased and that of the A_2 component increased, as

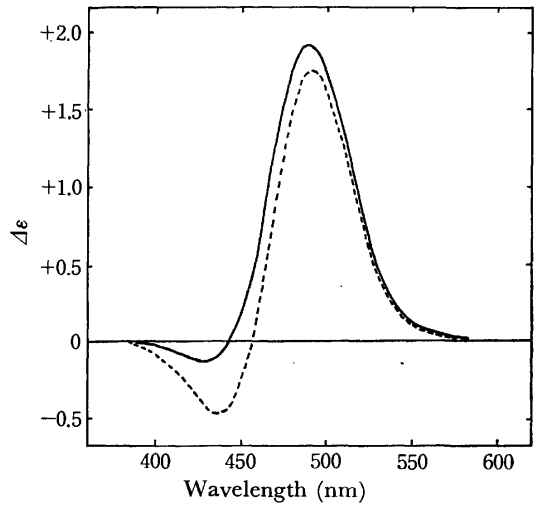

Fig. 1. CD spectra of 0.01 M Λ-$[Co(en)_3]Br_3 \cdot H_2O$ in the absence (—) and in the presence (---) of 0.15 M Na_2(L-tartrate) in the region of the first absorption band.

* The major part of the present study was presented at the 25th Annual Meeting of the Chemical Society of Japan, Tokyo, 1972.

** Present address: Department of Chemistry, Nagoya City University, Mizuho, Nagoya 467.

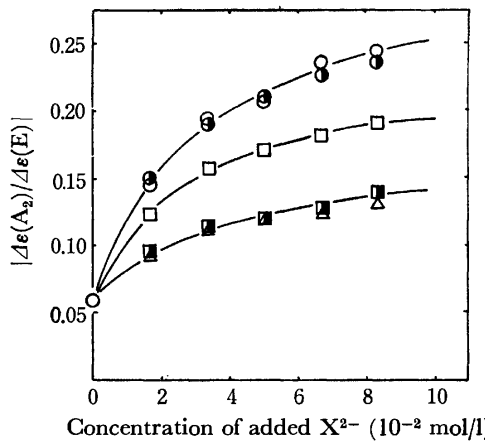

Fig. 2. Effects of the concentration of added dicarboxylate ions (X^{2-}) on the $|\Delta\varepsilon(A_2)/\Delta\varepsilon(E)|$ values of Λ- and Δ-$[Co(en)_3]^{3+}$ (0.01 M). ○: Λ-complex, X=L-tartrate, □: Δ-complex, X=L-tartrate. ◑: Λ- and Δ-complex, X=*meso*-tartrate. ◧: Λ- and Δ-complex, X=L-malate. △: Λ- and Δ-complex, X=succinate.

TABLE 1. VALUES OF $|\Delta\varepsilon(A_2)/\Delta\varepsilon(E)|$ IN THE ABSENCE AND PRESENCE OF CARBOXYLATE AND OTHER ANIONS (The concentrations are 0.01 M in the complexes and 0.084 M in the added anions.)

Anion	Λ-$[Co(en)_3]^{3+}$	Δ-$[Co(en)_3]^{3+}$
None	0.06	0.06
Bromide	0.06±0.01	0.06±0.01
Fumarate(2−)	0.09	0.09
Succinate(2−)	0.14	0.14
meso-Tartrate(2−)	0.23	0.23
L-Tartrate(2−)	0.24	0.19
H(L-Tartrate)(1−)	0.19	0.15
H_2(L-Tartrate)	0.06_7	0.07_0
L-Malate(2−)	0.14_8	0.14_8
L-Tartranilate(1−)	0.16	0.12
	Λ-$[Co\{(+)pn\}_3]^{3+}$	Δ-$[Co\{(-)pn\}_3]^{3+}$
None	0.30	0.30
Succinate(2−)	0.41	0.41
L-Tartrate(2−)	0.62	0.50

shown by the dotted line in Fig. 1. The same tendency was observed with all the carboxylates to some extent.

For ready comparison, the ratios of the CD intensity at the A_2 peak to that at the E peak (denoted by $|\Delta\varepsilon(A_2)/\Delta\varepsilon(E)|$) were plotted against the concentration of L-tartrate (Fig. 2). The effect of added L-tartrate was greater for the Λ-complex than for the Δ-complex. L-Tartaric acid, H_2 (L-tartrate), gave no change within the error of measurements and naturally showed no stereoselectivity. Nor did sodium bromide give appreciable effects.

Table 1 summarizes the $|\Delta\varepsilon(A_2)/\Delta\varepsilon(E)|$ values measured for several kinds of dicarboxylate ions which have carbon skeletons similar to a L-tartrate ion. Optically active L-malate(2−) gave only a small CD change, similar to that due to succinate(2−), and showed no stereoselectivity. On the other hand, *meso*-tartrate(2−) gave an effect almost identical to that of L-tartrate, but without any stereoselectivity. The L-tartranilate(1−) ion, in which a carboxylate group of the L-tartrate(2−) ion is replaced by an acid-anilide group, showed a distinct stereoselectivity. As is seen from Table 1, however, the magnitude of CD change due to L-tartranilate was smaller than that due to L-tartrate at the same carboxylate concentration. This can be ascribed to the difference in the charge between the L-tartranilate(1−) and L-tartrate(2−) ions. If the difference in the ionic charge is taken into account, L-tartranilate seems to be comparable to L-tartrate in the stereoselectivity for the optically active $[Co(en)_3]^{3+}$ ions. A similar result was observed with the monohydrogen-L-tartrate(1−) ion, H(L-tartrate)$^-$.

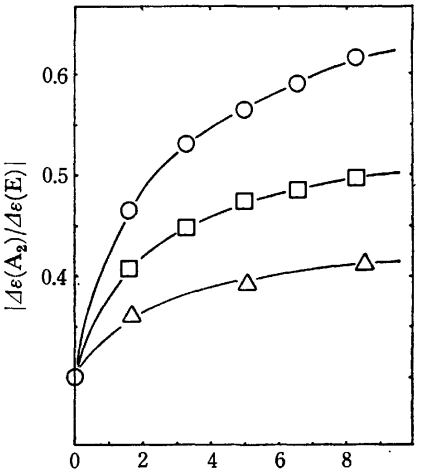

Fig. 3. Effects of the concentration of added L-tartrate and succinate ions on $|\Delta\varepsilon(A_2)/\Delta\varepsilon(E)|$ values of Λ-$[Co\{(+)pn\}_3]^{3+}$ and Δ-$[Co\{(-)pn\}_3]^{3+}$ (0.01 M). ○: Λ-complex, L-tartrate. □: Δ-complexes, L-tartrate. △: Λ- and Δ-complex, succinate.

Measurements on the optically active $[Co(pn)_3]^{3+}$, Λ-$[Co\{(+)pn\}_3]^{3+}$ and Δ-$[Co\{(-)pn\}_3]^{3+}$, resulted in nearly the same pattern of CD changes as those of Λ-$[Co(en)_3]^{3+}$ and Δ-$[Co(en)_3]^{3+}$, respectively. Figure 3 shows the relationship between the $|\Delta\varepsilon(A_2)/\Delta\varepsilon(E)|$ value and the concentration of L-tartrate (and of succinate, as a reference). The $|\Delta\varepsilon(A_2)/\Delta\varepsilon(E)|$ values at the same concentration of different carboxylates are compared in Table 1. A comparison of Fig. 3 with Fig. 2 shows that the stereoselectivity of L-tartrate for the optically active $[Co(pn)_3]^{3+}$ ion corresponds to that for the optically active $[Co(en)_3]^{3+}$ ion.

Discussion

The Λ-$[Co\{(+)pn\}_3]^{3+}$ ion is known to have the *lel* conformation and one of two N–H bonds at each end of the propylenediamine lies nearly parallel to the C_3 (or quasi-C_3) axis of the complex. Thus a set of three N–H hydrogens at each end of the complex can be conveniently used for hydrogen bonding with anions approaching the complex ion along the C_3 axis. This is also the case with the *lel* form of $[Co(en)_3]^{3+}$, which predominates over the *ob* form in aqueous solutions.

Thus the formation of an ion-pair between tris(diamine)-cobalt(III) and phosphate ions with a set of three N–H··· O hydrogen bonds was proposed by Mason and Norman in order to explain the marked changes in the CD spectrum of the complex observed in the presence of phosphate ions.[10]

A tartrate ion has two carboxylate and two hydroxyl groups which can be used for hydrogen bonding with the N–H groups of the complex ion. In analogy with Mason's model, it is very probable that three of these four groups participate in the hydrogen bonding. The two possibilities for the formation of three hydrogen bonds, with two carboxylate and one hydroxyl groups or with two hydroxyl and one carboxylate groups, will be discussed in connection with the experimental results.

From the fact that sodium bromide and tartaric acid (the fully protonated tartrate) caused only slight CD changes, the free carboxylate group seems to play an important role in causing CD changes. The fumarate-(2−) ion, of which only one of the two carboxylate groups can be used for hydrogen bonding with a tris(diamine)-cobalt(III) ion, caused only a small CD change, whereas the succinate ion capable of forming hydrogen bonds through two carboxylate groups caused greater CD changes. The L-malate ion which has two carboxylate and one hydroxyl groups caused a CD change similar to that caused by the succinate ion. These experimental results might be taken as an indication that carboxylate groups play a principal role in the CD changes of the tris(diamine)cobalt(III) ions. However, this is not likely to be the case, since further greater CD changes were caused by the hydrogen-L-tartrate(1−) ion which has only one free carboxylate group. The greatest CD changes were observed when the L-tartrate-(2−) ion was added to solutions containing tris(diamine)-cobalt(III) ions, especially of the *A*-form. Considering that introduction of the second hydroxyl group into the malate(2−) ion gives the tartrate(2−) ion, the second hydroxyl group seems to play an important role in the ion association and thus in the great CD changes.

Thus we propose a model of the ion-pair in which two hydroxyl and one carboxylate groups form hydrogen bonds with three N–H groups of tris(diamine)cobalt(III) ion of the *lel* form. This model of the ion-pair can also give a satisfactory explanation of the stereoselective CD changes, as can be seen from Fig. 4, which shows a schematic representation of the structures of tartrate and related ions. The clockwise arrangement of the COO^-, OH, and OH groups are characteristic of the isomers causing greater CD changes for the *A*-complexes. Thus the hydrogen-L-tartrate and L-tartranilate ions, which have the same configuration as that of L-tartrate as far as one carboxylate and two hydroxyl groups are concerned, caused stereoselective CD changes, which are large considering the lower ionic charge. The *meso*-tartrate ion has two asymmetric carbons of the *R* and *S* chiralities, and differs from the L-tartrate in that

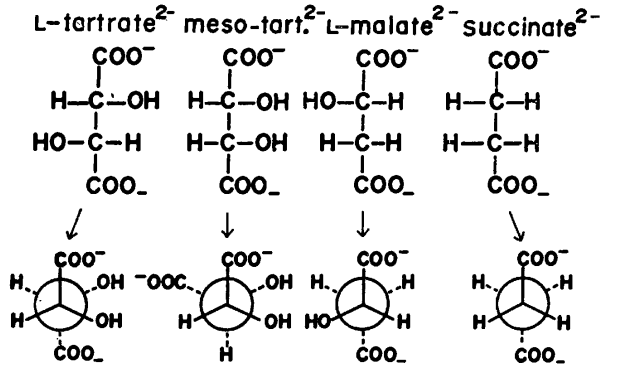

Fig. 4. Schematical representation of the structures of tartrate and related ions.

the carboxylate and hydrogen attached to the *S* carbon are interchanged. This appears to explain why meso-tartrate causes great CD changes in the CD spectra of both isomers of the complex.

During the preparation of this manuscript, an X-ray analysis was carried out on a crystal of *A*(+)$[Co(en)_3]$-Br(L-tartrate)·$5H_2O$ by Kushi *et al.*[11] Their result seems to confirm our model for the ion-pair described above. In addition, we recently prepared two types of optically active Sephadex cation exchangers with L-tartrate groups, and applied them to a direct column-chromatographic resolution of $[Co(en)_3]^{3+}$.[12] The exchanger with tartrate groups of the ester type showed higher efficiency than that with tartrate groups of the ether type. This is also a support for our model.

The authors wish to thank Dr. Yuzo Yoshikawa of Nagoya University for his helpful suggestions.

References

1) H. Yamatera and M. Fujita, *Bull. Chem. Soc. Jpn.*, **42**, 3043 (1969).
2) K. Ogino and U. Saito, *Bull. Chem. Soc. Jpn.*, **40**, 826 (1967).
3) K. Ogino, *Bull. Chem. Soc. Jpn.*, **42**, 447 (1969).
4) B. Norden, *Acta Chem. Scand.*, **26**, 111 (1972).
5) H. Yoneda and T. Miura, *Bull. Chem. Soc. Jpn.*, **43**, 574 (1970); **45**, 2126 (1972).
6) M. Fujita and H. Yamatera, Presented at the 21st Symposium on Coordination Chemistry of the Chemical Society of Japan, Nagoya, 1971.
7) F. P. Dwyer, F. L. Garvan, and A. Shulman, *J. Am. Chem. Soc.*, **81**, 290 (1959).
8) T. A. Montzka, T. L. Pindell, and J. D. Matiskella, *J. Org. Chem.*, **33**, 3993 (1968).
9) A. J. McCaffery and S. F. Mason, *Mol. Phys.*, **6**, 359 (1963).
10) S. F. Mason and B. J. Norman, *J. Chem. Soc., A*, **1966**, 307.
11) Y. Kushi, M. Kuramoto, and H. Yoneda, *Chem. Lett.*, **1976**, 135.
12) M. Fujita, Y. Yoshikawa, and H. Yamatera, *Chem. Lett.*, **1974**, 1515; **1975**, 473.

The Complexing of the Thallium(I) Ion with Other Solvents in Acetonitrile. Investigation Using a Cation-sensitive Glass Electrode

Toshio NAKAMURA

Chemistry Department, Faculty of Science, Shinshu University, Asahi, Matsumoto 390

(Received October 27, 1975)

The complexing of the thallium(I) ion with other common solvents has been studied in acetonitrile by using a univalent cation-sensitive glass electrode. A method similar to that developed to study the complexing of sodium[1] and lithium ions[2] was employed. Mono-, di-, and tri-solvated species were formed with DMF, SDMF, DMA, pyridine, formamide, and DMSO. Tetra-solvated species were also formed with *N*-methylformamide and HMPA. The complex formation constants for the mono-solvated thallium(I) ion were 4.1 with DMF, 5.6 with SDMF, 6.9 with DMA, 11 with pyridine and formamide, 12 with *N*-methylformamide, 15 with DMSO, and 1.0×10^2 with HMPA. Prior to these experiments, the cation-sensitive glass electrode was confirmed to respond to the thallium-(I)-ion activity in different solvents by comparing its behavior with that of a thallium-amalgam electrode. When water was the complexing solvent the potential of the glass electrode was not stable, and therefore, a thallium-amalgam electrode was used instead of a glass electrode to obtain the hydration constants of the thallium(I) ion in acetonitrile. Mono- and di-solvated species were formed with water and the hydration constant for the mono-solvated species was 1.1. The amalgam electrode and the glass electrode were used to obtain the constants with DMSO.

In previous papers,[1,2] the author and collaborators have reported a potentiometric method to obtain the formation constants of complexing for the sodium and lithium ions with other common solvent molecules in acetonitrile (AN). A univalent cation-sensitive glass electrode was used as an indicator. In the present experiment, a similar method was used to determine the formation constants of the complexing of the thallium(I) ion with other solvents in AN. Emf measurements of Cell I were carried out.

$$\underset{\text{glass electrode}}{\text{Ag}|0.005\text{M } AgNO_3(\text{AN})\|\underset{(A)}{0.1\text{M } Et_4NClO_4(\text{AN})}\|\underset{(B)}{5\times10^{-4}\text{M } TlClO_4+0.01\text{M } Et_4NClO_4(\text{AN}+\text{D})}|}$$

Cell I

A solution of 0.1 M of tetraethylammonium perchlorate (Et_4NClO_4) in AN was in compartment B in place of the 0.1 M of tetraethylammonium picrate(Et_4NPi) used in previous work,[1,2] in order to avoid the interaction between thallium(I) and picrate ions. The dissociation constant pK^d of thallium(I) picrate in AN at 25 °C has been determined using a conductometric method to be 2.6.[3] The validity of this substitution of the bridge electrolyte in compartment B has been discussed.[4,5] To obtain the complex formation constants the following relations were used:

$$\beta_x = \frac{(M^+_{xD})}{(M_s^+)[D]^x} \tag{1}$$

$$R_1 = \left\{\frac{(M_s^+)_{AN}}{(M_s^+)_{AN-D}} - 1\right\}/[D] = \sum_{i=1}\beta_i[D]^{i-1} \tag{2}$$

$$R_j = (R_{j-1}-\beta_{j-1})/[D] = \sum_{j=2}\beta_j[D]^{j-2} \tag{3}$$

$$\frac{(M_s^+)_{AN}}{(M_s^+)_{AN-D}} = 10^{(E_{AN}-E_{AN-D})/59} \tag{4}$$

All symbols have the same meaning as those in a previous report.[2] Assumptions similar to those in previous papers[1,2] were made: (i) solvent D in the AN–D mixtures is monomeric, (ii) the activity of AN does not change upon the addition of D and is equal to unity, (iii) the salt-effect activity coefficient of the thallium(I) ion, as calculated using the Debye-Hückel equation, is equal for both pure AN and AN–D mixtures, (iv) the amount of D consumed by the solvation of the ions of an indifferent electrolyte is negligible, and (v) the liquid-junction potential between the solutions in the salt bridge B and compartment C in Cell I does not change upon the addition of D. All of these assumptions appear to be satisfied approximately under the experimental conditions of these experiments when $[\text{AN}]\gg[\text{D}]$.

Using this method, formation constants β_x for such D as methanol, *N*,*N*-dimethylformamide (DMF), *N*,*N*-dimethylthioformamide (SDMF), *N*,*N*-dimethylacetamide (DMA), pyridine, formamide, *N*-methylformamide, dimethyl sulfoxide (DMSO), hexamethylphosphoric triamide (HMPA) were obtained, and the constants β_x for water were obtained with the thallium-amalgam electrode instead of the glass electrode, as will be described later.

Prior to the determination of the formation constants, the glass electrode was confirmed to respond well to the activity of the thallium(I) ions with a Nernstian slope in such diverse solvents as AN, methanol, DMF, and DMSO. This is shown in Fig. 1, where the relation between the potentials of the glass electrode and the thallium-amalgam electrode is plotted. When water was the solvent, the plot deviated from a straight line, as shown in Fig. 1, and more time was needed to attain a steady potential than in the cases of the other solvents.

Apparatus and Reagents

Apparatus. Most of the apparatus and experimental techniques for the determination of the formation constants β_x are the same as those in previous reports.[1,2] The arrangement of Cell I is that shown in Fig. 1 of Ref. 1, except that

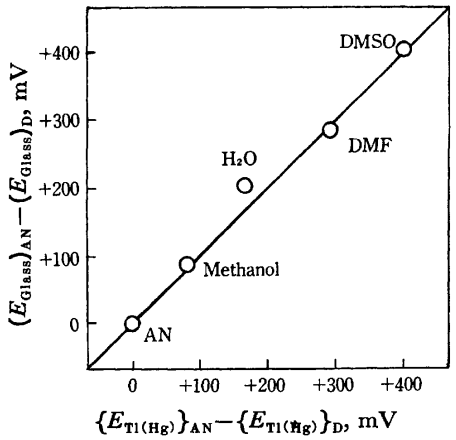

Fig. 1. Relation between potentials of monovalent cation-sensitive glass electrode and those of the thallium-amalgam electrode in various solvents both referred to the values in AN.

5×10^{-4} M of $TlClO_4$ was used in place of 10^{-3} M of $NaClO_4$ or 10^{-3} M of $LiClO_4$ in compartment C and 0.1 M of Et_4N-ClO_4 was used in place of 0.1 M of Et_4NPi in the compartment B. The thallium-amalgam electrode was used to obtain the hydration constants for thallium(I) ions in AN (*cf.* Cell II).

Reagents. Thallium(I) perchlorate was prepared by neutralizing perchloric acid with an aqueous thallium(I) hydroxide solution prepared by passing a thallium(I) formate solution through a column of Amberlite IRA 411 ion-exchange resin in OH-form[3] and was dried at 70 °C in a high vacuum. The SDMF was prepared from DMF and phosphorus pentasulfide, according to the method of Willstatter and Wirth.[6] The other solvents and reagents used in this experiment were prepared by the same methods as those described in previous reports.[1,2]

Results

Response of the Glass Electrode to the Activity of Thallium(I) Ions in Different Solvents. The glass electrode used in this study had a slope of 58 mV on a logarithm scale of the thallium(I)-ion concentration between 2×10^{-3} and 1.6×10^{-5} M in AN–0.01 M Et_4NClO_4. If corrected for a change in the salt-effect activity coefficient, the response to pa_{Tl^+} is very near the Nernstian slope of 59 mV. The glass electrode also responds well to differences in the activity of thallium(I) ions in several different solvents except water as indicated above and Ref. 4.

Complexing of Thallium(I) Ions with Other Solvents in AN. From the emf measurements using Cell I, the values of

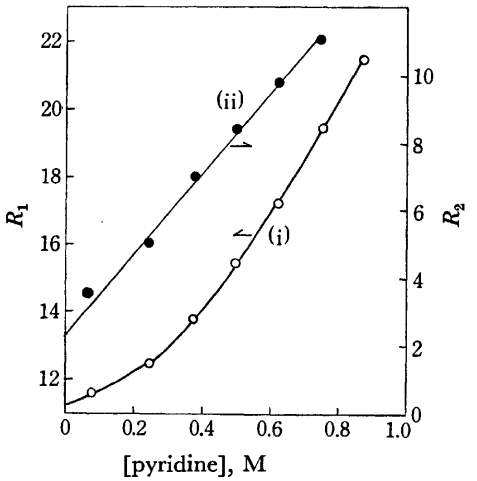

Fig. 2. R_1–[pyridine] (Curve i) and R_2–[pyridine] (Curve ii) relations.

Table 1. Complex formation constants of thallium(I) ions with other solvents in AN

Solvent	Upper mol added (M)	β_1	β_2	β_3	β_4
PC	0.4	(<0.3)			
Methanol	1.0	$0._9$			
		(4.5) [1.1]	($6._7$) [0.4]		
H_2O	0.8	1.1*	$0._2$*		
		[1.8]	[1.8]		
DMF	0.9	4.1	$3._1$	$3._4$	
		(16) [2.5]	(1.1×10^2) [$2._1$]	($6._7\times10$) [$1._2$]	
SDMF	0.5	5.6	12	$3._8\times10$	
DMA	0.5	6.9	$4._6$	$1._5\times10$	
		(62) [5.3]	(8.7×10^2) [11]	($1._9\times10^3$) [$6._4$]	
Pyridine	0.9	11	$2._0$	$1._2\times10$	
		(5.2) [0.7]	($2._7$) [0.5]		
Formamide	0.8	11	$8._1$	$2._0\times10$	
		(20)	(90)		
N-Methylformamide	0.5	12	15	$1._9\times10$	$2._0\times10^2$
		(25)	(2.5×10^2)		
DMSO	0.5	15	54	$1._2\times10^2$	
		15*	45*	$1._2\times10^2$*	
		(49) [6.0]	(9.7×10^2) [11]	($3._2\times10^3$) [$1._4\times10$]	
HMPA	0.06	1.0×10^2	$2._1\times10^3$	$2._2\times10^4$	$7._3\times10^5$
		(2.1×10^3) [29]	(3.1×10^5) [$3._2\times10^2$]	[$1._3\times10^3$]	

Each value of β is the average of two measurements. Values in parentheses ( ) and brackets [ ] are those for lithium[2] and sodium ions,[1] respectively. Asterisks indicate the values obtained with the thallium-amalgam electrode. (at 25±0.1 °C)

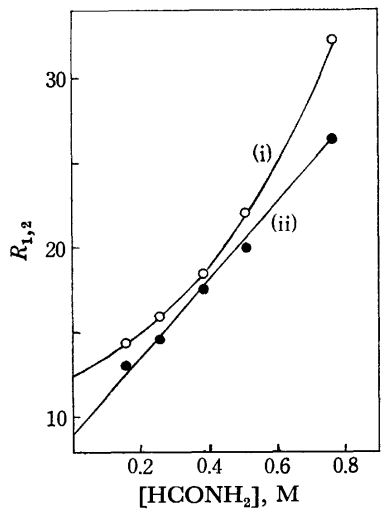

Fig. 3. R_1–[HOCNH$_2$] (Curve i) and R_2–[HOCNH$_2$] (Curve ii) relations.

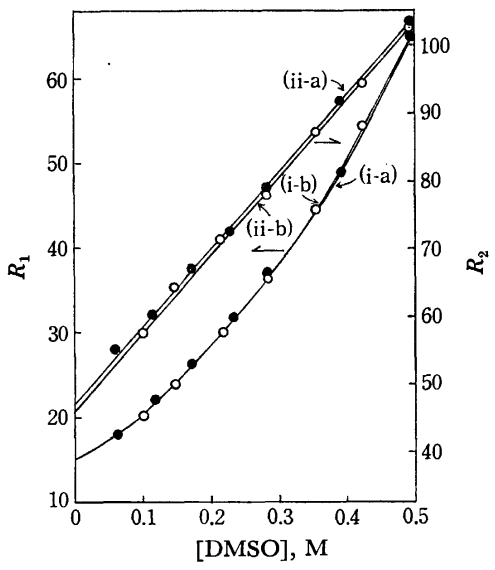

Fig. 4. R_1–[DMSO] (Curve i-a, i*-b) and R_2–[DMSO) (Curve ii-a, ii*-b) relations. * results obtained with the amalgam electrode.

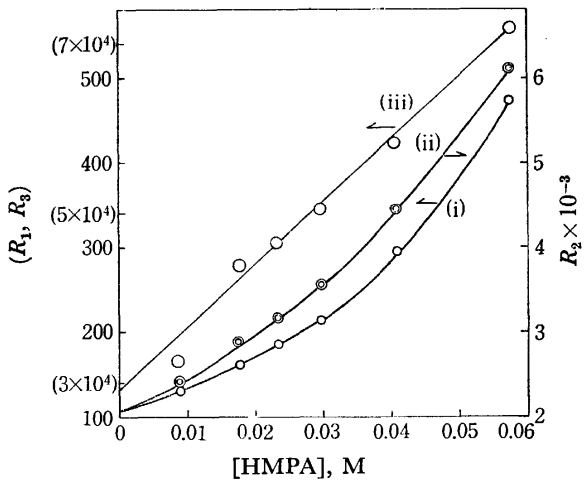

Fig. 5. R_1–[HMPA] (Curve i), R_2–[HMPA] (Curve ii), and R_3–[HMPA] (Curve iii) relations.

the formation constant β_X were calculated using Eqs. 2—4. The results are summerized in Table 1. The maximum concentrations of D added to the AN solution are also shown in Table 1. Figures 2—5 show several examples of the R_1–[D], R_2–[D], and R_3–[D] relations for the determination of the formation constants. When water was added as the complexing solvent D to the compartment C of the Cell I, the rate of potential change was very slow and the steady potential attained was not reproducible. Hydration constants were thus obtained using the thallium-amalgam electrode (Cell II) instead of the glass electrode (Cell I).

Ag|0.005M $AgNO_3$(AN)‖0.1M Et_3NClO_4(AN)‖
(A) (B)

5×10^{-4}M $TlClO_4$ + 0.01M Et_4NClO_4(AN+D)|
(C)

thallium-amalgam electrode

Cell II

The thallium content in the amalgam (5.4×10^{-2} M) was determined by the same titration method as that of Ref. 4. The amalgam electrode was sufficiently stable during the period of the emf measurements, so long as the solution in compartment C in Cell II was deaerated. Prior to the determination of the hydration constants of thallium(I) ions with DMSO in AN was also studied with the thallium-amalgam electrode and the formation constants obtained with the two different electrodes agreed fairly well (*cf.* Table 1). Figures 4 and 6 show some examples of the R_1–[DMSO], R_2–[DMSO], and R_1–[H_2O] relations obtained with the amalgam electrode.

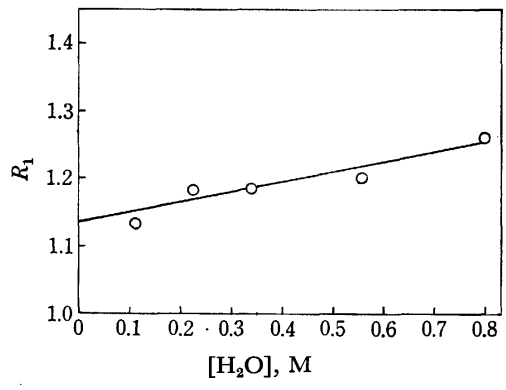

Fig. 6. R_1–[H_2O] relation.

Discussion

From Fig. 1, it appears reasonable to consider that the glass electrode can respond to the activity of thallium(I) ions in solvents of different species or compositions.

It was indicated in previous reports[1,2] that pyridine, which has a strong basic character but a low dielectric constant, solvates to sodium and lithium ions only to a small extent. The β_1 increased in the case of sodium ions in order: pyridine<methanol<H_2O<DMF<DMA<DMSO, and in the case of lithium ions: methanol<pyridine<DMF<DMSO<DMA. On the other hand, in the case of thallium(I) ions, β_1 increased in order: methanol<H_2O<DMF<DMA<pyridine<

DMSO. The strong complexing of pyridine with thallium(I) ions seems to be acceptable considering the strong basic character of pyridine. In the complexing of thallium(I) ions in AN with other solvents formation constants up to β_4 were obtained in the cases of *N*-methylformamide and HMPA. On the other hand, in the cases of lithium ions in AN with these solvents only β_1 and β_2 were obtained. The results may be explained by the fact that the radius (r_c) of the thallium(I) ion is considerably greater than that of the lithium ion. SDMF must solvate to thallium(I) ions more strongly than DMF on the basis of considerations of hard and soft acids and bases. This trend appears in the values in Table 1. In general, the degree of complexing β_x of thallium(I) ions with these solvents in AN was intermediate between those of lithium and sodium ions.

Table 2. Effect of the concentration of an indifferent electrolyte on the complex formation constants of thallium(I) ions with DMSO in AN

Concn of Et_4ClO_4(M)	β_1	β_2	β_3
0	1.5×10	4.4×10	$1._3\times10^2$
	1.5×10	4.8×10	$1._1\times10^2$
0.01	1.5×10	4.8×10	$1._1\times10^2$
	1.5×10	6.0×10	$1._4\times10$
0.1	1.2×10	3.9×10	$6._4\times10$
	1.3×10	3.7×10	$6._2\times10$

From the results of Table 2, the effect of the concentration of the indifferent electrolyte on complex formation constants of thallium(I) ions with DMSO in AN may be recognized, that is, the values of β_3 for 0.1 M of Et_4NClO_4 are about one-half of those in 0 and 0.01 M of Et_4NClO_4. In the presence of 0.1 M Et_4NClO_4, ion association between thallium(I) and perchlorate ions may occur. The association constant of thallium(I) perchlorate in AN is 32,[7] compared with the constants for sodium and lithium perchlorates of *ca.* 11[8] and *ca.* 4[9] respectively. The addition of DMSO to the AN solution may cause the dissociation of the ion-associated thallium(I) perchlorate and decrease the potential change, and then the apparent value of β_x may become small. Dissociation, of course, may occur as the DMSO content in AN increases. But a complete discussion cannot be made concerning the results in Table 2, because the reliability of these constants (β_x) obtained using the present method appears to be within $\pm10\%$ for β_1 for the dipolar aprotic solvents and might be somewhat less for β_1 for the other solvents and for β_2–β_4.

Many studies have been made concerning solvation phenomena of the sodium ion as noted previously.[1] Recently, Kuntz and Cheng have published the results of experiments on the solvation of some protic solvents with ions in non-aqueous systems using IR measurements,[10] in which the solvation constants (β_1) of lithium ions with methanol and sodium ions with water in AN were described to be 3.4 and 1.3, respectively. These values agree fairly well with those shown in Table 1.

The author wishes to express his sincere thanks to Prof. Kosuke Izutsu of the Chemistry Department of Shinshu University for his suggestions and discussions and to Mr. Yuji Goi for his earnest support. This work was supported in part by a Grant-in-Aid for Scientific Research from the Ministry of Education.

References

1) K. Izutsu, T. Nomura, T. Nakamura, H. Kazama, and S. Nakajima, *Bull. Chem. Soc. Jpn.*, **47**, 1657 (1974).
2) T. Nakamura, *Bull. Chem. Soc. Jpn.*, **48**, 1447 (1975).
3) I. M. Kolthoff and M. K. Chantooni, Jr., *J. Phys. Chem.*, **76**, 2024 (1972).
4) T. Nakamura, *Bull. Chem. Soc. Jpn.*, **48**, 2967 (1975).
5) K. Izutsu and T. Nakamura, unpublished results.
6) R. Willstatter and T. Wirth, *Ber.*, **42**, 1908 (1909); J. W. Diggle and D. Bogsányi, *J. Phys. Chem.*, **78**, 1018 (1974).
7) H. L. Yeager and B. Krátochvil, *J. Phys. Chem.*, **74**, 963 (1970).
8) R. L. Key, B. J. Hales, and G. P. Cunningham, *J. Phys. Chem.*, **71**, 3925 (1967).
9) F. Accascina, *Ric. Sci. Rend.*, **7**, 556 (1966).
10) I. D. Kuntz, Jr. and C. J. Cheng, *J. Am. Chem. Soc.*, **97**, 4852 (1975).

The Crystal Structure and Magnetic Property of the Alkoxo-Oxygen Bridged Tetranuclear Copper(II) Complex, $Cu_4\{(n\text{-}C_3H_7)_2N(CH_2)_2O\}_4Cl_4$

Naohide MATSUMOTO, Ikuhiko UEDA,* Yuzo NISHIDA, and Sigeo KIDA

Department of Chemistry, Faculty of Science, Kyushu University, Hakozaki, Higashi-ku, Fukuoka 812

**Department of General Education, Kyushu University, Ropponmatsu, Fukuoka 810*

(Received December 27, 1975)

The crystal structure of the alkoxo-oxygen bridged tetranuclear copper(II) complex, $Cu_4\{(n\text{-}C_3H_7)_2N(CH_2)_2O\}_4Cl_4$, has been determined from the three-dimensional X-ray diffraction method. The crystals are orthorhombic with the space group Pbcn. The cell dimensions are $a=15.965$ (4), $b=14.941$ (1), $c=19.305$ (2) Å. The structure has been determined from the heavy atom method and refined by the block-diagonal least-squares method to give $R=7.52\%$. The complex is of a cubane type structure formed by four copper and four alkoxide oxygen atoms. Each copper atom has a distorted square pyramidal environment. The correlation between the magnetic property and the structure was discussed on some homologous compounds of cubane structure.

Hein and his coworkers[1] prepared a series of copper(II) complexes of *N,N*-dialkylaminoethanol with the general formula $Cu(R_2NCH_2CH_2O)X$ (R=CH_3, C_2H_5, n-C_4H_9 *etc.* and X=Cl, Br) whose basic structure was assumed to be a binuclear unit as shown in Fig. 1.

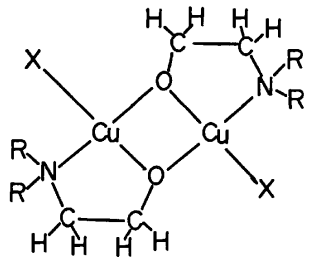

Fig. 1. An assumed basic structure of $[Cu(R_2(CH_2)_2O)X]$, where R=alkyl group and X=Cl, Br, NCS.

Uhlig and Staiger[2] measured magnetic moments and optical spectra, and found that their magnetic moments at room temperature distribute in a wide range (from 1.9 BM to practically zero). Recently Kida and his coworkers[3-5] prepared a number of copper(II) complexes of various aminoalcohols with the general formulas $[Cu(R_2N(CH_2)_nO)X]$ (hereafter abbreviated as Cu(R-n)X, where R=CH_3, C_2H_5, n-C_3H_7, n-C_4H_9 and X=Cl, Br, NCS) and $[Cu(R_2N(CH_2)_nNH(CH_2)_mO)]Y$ (hereafter abbreviated as [Cu(R-n-m)]Y, where n and m=2 or 3, and Y denotes a mono-negative ion), and proposed a new criterion for the classification of the extended series of alkoxo-bridged copper(II) complexes on the basis of temperature dependence of the magnetic susceptibilities,[5] *i.e.*, (A) those whose χ_A-T curves can be fitted by the Bleaney-Bowers equation[6], (B) those whose χ_A-T curves obey the Curie-Weiss law with positive Weiss constant, (C-1) those whose χ_A-T curves obey Curie-Weiss law with negative Weiss constant, and (C-2) whose χ_A-T curves can not be fitted by the Bleaney-Bowers equation, though showing subnormal magnetic moments at room temperature. They also showed that there is a close relationship between the presence of the near-ultraviolet absorption band and the intramolecular spin-exchange interaction.

In order to elucidate the above properties on the molecular structural basis, single-crystal X-ray analyses are desirable for a series of key compounds. The structures of some alkoxo-bridged copper(II) complexes were already determined.[7-12] In this study, crystal structure of chloro *N,N*-dipropyl-2-aminoethanolato copper(II), Cu(pr-2)Cl, which belongs to the above-mentioned C-1 group, was determined by the three-dimensional X-ray diffraction techniques. It was found that the compound is of a cubane type structure formed by four copper and four alkoxide oxygen atoms. This result and the already reported data of the three related compounds[7-9,12] make a series of cubane structures with stepwise differing magnetic properties. Thus, the present result has made it possible to discuss the correlation between magnetic property and molecular structure.

Experimental

The complex was prepared according to Hein.[1] Single-crystals were obtained by slow evaporation of absolute ethanol solution at room temperature. They are green rhombic prisms elonagated along the c-axis. Unit cell dimensions were determined by the least-squares method from fifteen reflections measured on a Syntex P$\bar{1}$ diffractometer. The crystal data are listed in Table 1. A suitable crystal for the intensity measurement was ground to a sphere of radius $r=0.151$ mm. Since the crystal is liable to decompose in the air, it was coated with clear varnish. Three-dimensional intensity data were collected by the 2θ-θ scan technique on a Syntex P$\bar{1}$ four-circle diffractometer using Mo$K\alpha$ radiation monochromated by a graphite plate. Three reflections were monitored after every measurement of 47 reflections, and the monitored data showed a satisfactory stability. Of 3929

TABLE 1. CRYSTAL DATA OF Cu(pr-2)Cl

$Cu_2Cl_2O_2N_2C_{16}H_{36}$	F.W.=486.4
Orthorhombic	
$a=15.965$ (4) Å	
$b=14.941$ (1)	
$c=19.305$ (2)	
$V=4596.8$ Å^3	
$D_m=1.399$ g·cm^{-3} (by floatation)	
$D_x=1.405$ g·cm^{-3} (for $Z=8$)	
μ(Mo$K\alpha$, $\lambda=0.71069$Å)=21.24 cm^{-1}	
Space group=Pbcn	
systematic absences;	
$h\ k\ 0$ for $h+k=$odd	
$h\ 0\ l$ for $l=$odd	
$0\ k\ l$ for $k=$odd	

TABLE 2. FRACTIONAL ATOMIC COORDINATES AND FINAL ANISOTROPIC TEMPERATURE FACTORS ($\times 10^4$) WITH THEIR STANDARD DEVIATIONS IN PARENTHESES

The temperature factor is of the form; $\exp[-(B_{11}h^2+B_{22}k^2+B_{33}l^2+B_{12}hk+B_{13}hl+B_{23}kl)]$.

	x/a	y/b	z/c	B_{11}	B_{22}	B_{33}	B_{12}	B_{13}	B_{23}
CuOA	4496 (2)	6792 (1)	3227 (1)	72 (1)	56 (1)	21 (0)	40 (2)	−6 (2)	−12 (1)
CuOB	4118 (2)	5276 (1)	2108 (1)	54 (1)	62 (1)	31 (0)	−26 (2)	13 (2)	−31 (2)
CLOA	4929 (5)	6942 (4)	4313 (2)	105 (5)	86 (4)	22 (1)	40 (8)	−9 (5)	−20 (4)
CLOB	2828 (4)	5070 (4)	2531 (3)	59 (3)	80 (4)	51 (2)	−47 (6)	21 (5)	−33 (6)
OXBA	4209 (9)	6695 (8)	2241 (6)	52 (7)	47 (7)	24 (4)	10 (12)	3 (9)	−10 (9)
OXBB	5296 (8)	5357 (8)	1854 (6)	52 (7)	41 (6)	24 (4)	3 (11)	6 (9)	−22 (9)
NITA	3553 (13)	7693 (14)	3305 (10)	65 (12)	86 (14)	43 (7)	42 (22)	−10 (16)	−34 (18)
NITB	4043 (13)	4380 (12)	1318 (8)	72 (12)	62 (10)	26 (5)	−6 (19)	25 (14)	−29 (13)
CAR1	3556 (15)	7274 (15)	2040 (12)	56 (13)	55 (12)	40 (8)	35 (21)	−22 (18)	0 (18)
CAR2	3050 (17)	7499 (15)	2700 (13)	93 (18)	86 (18)	43 (10)	−50 (25)	63 (22)	−72 (23)
CAA1	3724 (18)	8533 (16)	3697 (16)	75 (17)	52 (13)	78 (14)	26 (26)	36 (26)	−48 (24)
CAA2	4555 (26)	9017 (23)	3491 (19)	148 (31)	96 (23)	76 (16)	−64 (45)	70 (38)	−8 (32)
CAA3	4954 (31)	9519 (22)	4222 (22)	186 (36)	90 (21)	107 (21)	−35 (50)	70 (48)	−69 (37)
CAB1	2845 (19)	7263 (27)	3745 (29)	47 (16)	156 (33)	214 (38)	−66 (39)	63 (43)	−254 (62)
CAB2	2072 (29)	7470 (44)	3729 (26)	127 (34)	322 (69)	111 (24)	−159 (84)	−32 (38)	−29 (71)
CAB3	1595 (26)	6916 (32)	4314 (31)	86 (25)	163 (38)	184 (37)	−66 (53)	56 (53)	−18 (65)
CBR1	4782 (18)	4555 (18)	880 (13)	91 (19)	96 (18)	42 (9)	−88 (30)	81 (22)	−96 (22)
CBR2	5570 (17)	4763 (15)	1317 (12)	82 (16)	58 (13)	37 (8)	37 (25)	15 (20)	−46 (18)
CBA1	4060 (20)	3471 (14)	1659 (13)	116 (21)	38 (11)	46 (9)	13 (26)	24 (25)	−34 (17)
CBA2	3968 (27)	2634 (20)	1155 (20)	161 (33)	61 (17)	91 (19)	30 (40)	20 (42)	−34 (31)
CBA3	4130 (22)	1803 (19)	1654 (22)	99 (22)	63 (16)	117 (22)	−8 (33)	35 (39)	40 (33)
CBB1	3232 (21)	4470 (23)	894 (17)	89 (20)	124 (25)	60 (13)	−67 (38)	−63 (28)	10 (30)
CBB2	3029 (21)	5392 (22)	663 (16)	95 (21)	117 (24)	52 (12)	14 (38)	−37 (27)	−5 (29)
CBB3	2296 (28)	5495 (34)	192 (21)	132 (33)	223 (47)	81 (18)	−19 (64)	−132 (42)	54 (50)

independent reflections collected in $2\theta \leqq 48°$, 1557 ones greater than 2.33σ (F) were used in the analysis. They were corrected for Lorentz and polarization effects, but corrections for absorption were not applied ($\mu r = 0.32$).

Solution and Refinement

There are eight formula units (a formula unit = $Cu_2Cl_2O_2N_2C_{16}H_{36}$) in a unit cell. The structure has been determined by the heavy atom method. The positions of copper atoms were obtained from the three-dimensional Patterson syntheses. Those of chlorine atoms were obtained from the minimum function based on the copper atoms. A three-dimensional electron-density map was then calculated with all observed reflections phased by the copper and chloride atoms, thus obtaining the positions of oxygen and nitrogen atoms. By successive Fourier syntheses and the block-diagonal least-squares method the positions of all the nonhydrogen atoms were determined except some carbon atoms of the propyl group, whose most probable positions were determined by the D-Fourier syntheses. Six-cycles of the block-diagonal least-squares refinement was applied to the positional and isotropic thermal parameters of the non-hydrogen atoms. Further five-cycles refinement was carried out, introducing anisotropic temperature factors, and R decreased to 7.52%. Maximum shifts of the positional and thermal parameters in the final cycle did not exceed half of their standard deviations. The scattering factors for all the atoms were taken from the International Tables for X-ray Crystallography.[13] In the least-squares procedures, weight w was taken equal to one for $|F_o| \geqq 5.0$ and zero for $|F_o| < 5.0$. The F_o–F_c table is kept at the office of this Bulletin, as Document No. 7617. The final positional and thermal parameters with the standard deviations are shown in Table 2.

Description of the Structure

The projection along the b-axis and the numbering system are shown in Fig. 2. The unit cell contains four molecules, each of which has a so-called "cubane" structure formed by four copper and four alkoxide

TABLE 3. INTERATOMIC DISTANCES WITH THEIR STANDARD DEVIATIONS

Coordination sphere			Chelate ring (B)		
CuOA	CuOA′	3.237 (5)	OXBB	CBR2	1.43 (2)
CuOB	CuOB′	3.219 (5)	CBR2	CBR1	1.54 (3)
CuOA	CuOB	3.190 (5)	NITB	CBR1	1.47 (3)
CuOA	CuOB′	3.238 (5)			
CuOA	OXBA	1.963 (11)	Propyl group (A)		
CuOA	OXBA′	2.260 (14)	NITA	CAA1	1.49 (3)
CuOB	OXBB	1.947 (13)	CAA1	CAA2	1.56 (4)
CuOB	OXBB′	2.212 (12)	CAA2	CAA3	1.71 (6)
CuOA	OXBB′	2.175 (12)	NITA	CAB1	1.55 (4)
CuOB	OXBA	2.140 (12)	CAB1	CAB2	1.27 (8)
CuOA	NITA	2.025 (20)	CAB2	CAB3	1.60 (9)
CuOB	NITB	2.032 (16)			
CuOA	CLOA	2.220 (4)	Propyl group (B)		
CuOB	CLOB	2.236 (6)	NITB	CBA1	1.50 (2)
			CBA1	CBA2	1.59 (6)
Chelate ring (A)			CBA2	CBA3	1.59 (6)
OXBA	CAR1	1.40 (2)	NITB	CBB1	1.53 (3)
CAR1	CAR2	1.54 (3)	CBB1	CBB2	1.48 (4)
NITA	CAR2	1.45 (3)	CBB2	CBB3	1.49 (6)

oxygen atoms. Each molecule contacts with Van der Waals forces, the shortest intermolecular Cu–Cu distance being 8.12 Å. The molecule has a twofold axis which passes through the center of the top and the bottom faces of the cubane structure. The symmetry group of the molecule may be approximated by S_4 point group. Each copper atom of the molecule has a distorted tetragonal pyramidal environment. The bond lengths and angles with their standard deviations are given in Tables 3 and 4.

Some least-squares planes are given in Table 5 together with the distances of the individual atoms from

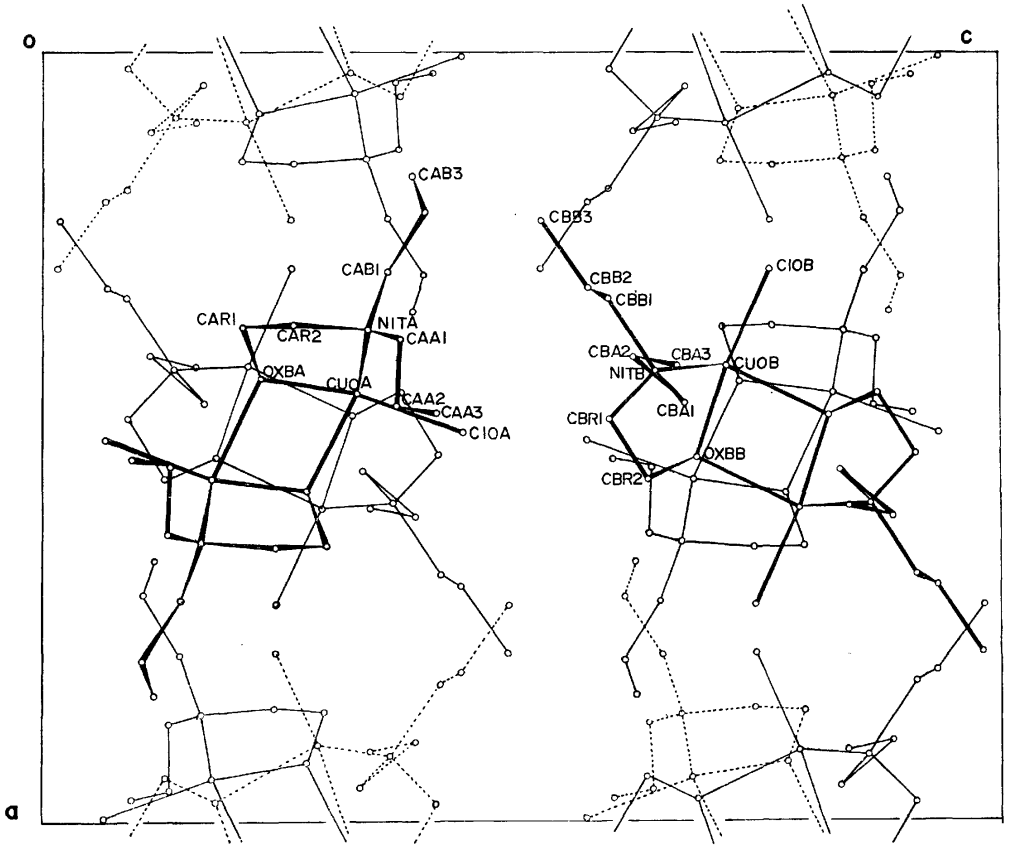

Fig. 2. Projection of the crystal structure along the b-axis

TABLE 4. BOND ANGLES AND ESTIMATED STANDARD DEVIATIONS

CuOA	OXBA	CuOA′	99.8 (5)	CuOA′	OXBB	CBR2	120 (1)
CuOB	OXBB	CuOB′	100.1 (5)				
CuOA	OXBA	CuOB	101.8 (5)	CuOA	NITA	CAT2	103 (1)
CuOA	OXBB′	CuOB	93.1 (4)	NITA	CAR2	CAR1	114 (1)
CuOA	OXBA′	CuOB′	94.4 (5)	CAR2	CAR1	OXBA	107 (1)
CuOA	OXBB′	CuOB′	103.0 (5)				
OXBA	CuOA	OXBA′	79.6 (5)	CuOB	NITB	CBR1	105 (1)
OXBA	CuOA	NITA	87.0 (6)	NITB	CBR1	CBR2	111 (1)
NITA	CuOA	CLOA	95.3 (5)	CBR1	CBR2	OXBB	105 (1)
CLOA	CuOA	OXBA′	95.7 (3)				
OXBA	CuOA	OXBB′	83.8 (4)	CuOA	NITA	CAA1	117 (1)
OXBA′	CuOA	OXBB′	76.6 (4)	NITA	CAA1	CAA2	114 (2)
OXBB	CuOB	OXBB′	79.4 (4)	CAA1	CAA2	CAA3	108 (3)
OXBB	CuOB	NITB	84.8 (6)	CuOA	NITA	CAB1	107 (1)
NITB	CuOB	CLOB	97.3 (6)	NITA	CAB1	CAB2	126 (5)
CLOB	CuOB	OXBB′	93.7 (3)	CAB1	CAB2	CAB3	108 (5)
OXBB	CuOB	OXBA	84.4 (5)				
OXBB′	CuOB	OXBA	78.9 (4)	CuOB	NITB	CBA1	105 (1)
CuOA	OXBA	CAR1	113 (1)	NITB	CBA1	CBA2	115 (2)
CuOA′	OXBA	CAR1	121 (1)	CBA1	CBA2	CBA3	103 (3)
CuOB	OXBA	CAR1	121 (1)	CuOB	NITB	CBB1	113 (1)
CuOB	OXBB	CBR2	116 (1)	NITB	CBB1	CBB2	115 (2)
CuOB′	OXBB	CBR2	119 (1)	CBB1	CBB2	CBB3	116 (3)

Table 5. Best least-squares planes defined by atomic positions

1)	Plane defined by CuOA, CuOA', OXBA, OXBA'			
	Distances of atoms from this plane (Å)			
	CuOA	0.07	ClOA	0.29
	CuOA'	0.07	NITA	1.41
	OXBA	−0.07	CAR1	0.79
	OXBA'	−0.07	CAR2	1.12
2)	Plane defined by CuOB, CuOB', OXBB, OXBB'			
	Distances of atoms from this plane (Å)			
	CuOB	−0.06	ClOB	−0.36
	CuOB'	−0.06	NITB	−1.39
	OXBB	0.06	CBR2	−0.81
	OXBB'	0.06	CBR1	−1.13

these planes. The carbon atoms of the chelate ring, and nitrogen and chlorine atoms are situated far from the plane, probably due to a steric repulsion.

Discussion

The cubane type structure similar to the present complex has been known in the related complexes, Cu(et-2)Cl[7,8] and Cu(bu-2)Cl.[9] The copper complex with a tridentate ligand, Cu(eia), where eia is a Schiff base formed by the condensation of aminoethanol and acetylacetone has also been known to be of a cubane structure.[12] A remarkable trend is found in those compounds that in-plane Cu–O bonds involving chelate ring are of normal Cu–O bond lengths, while the other in-plane Cu–O bonds (labeled with (d) in Fig. 3) are considerably elongated.[7–9,12] It is also to be noted that in all the above complexes the bridging alkoxide group is involved in a five-membered chelate ring. No cubane type tetranuclear complex, which has a six-membered chelate ring involving bridging alkoxide, has yet been known.

Some bond distances and angles of the series of cubane type structure are listed in Table 6 in the order of

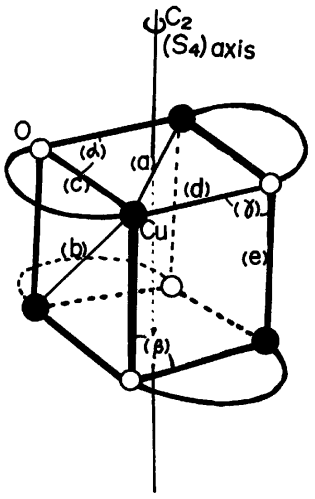

Fig. 3. The cubane type structure formed by the copper and oxygen atoms.
The bond distances and angles, which may be closely related to the magnetic property, are defined in the figure.

Table 6. Bond lengths and angles of cubane structure

	Cu(et-2)Cl[7,8]	Cu-(eia)[12]	Cu(pr-2)Cl	Cu(bu-2)Cl[9]
μ_{eff} (BM) (k)	1.66	1.83	1.85	1.95
	−102	+10	−27	+32
group	C-1	B	C-1	B
Cu–Cu (a)	2.935	3.006	3.228	3.383
(b)	3.435	3.259	3.214	3.169
Cu–O (c)	1.945	1.98	1.955	1.942
(d)	1.986	2.00	2.236	2.410
(e)	2.471	2.32	2.157	2.069
Cu–O–Cu (α)	96.6	97.8	100.4	101.3
(β)	102.1	98.2	102.4	105.7
(γ)	99.5	97.6	93.8	90.5

The notations of bonds are defined in Fig. 3.

increasing μ_{eff} values. As seen in Table 6, bond distances and angles are closely related to magnetic moments for the three homologous compounds.* In this series, Cu(et-2)Cl and Cu(bu-2)Cl take both extreme values in either structural and magnetic data. In the former, the in-plane Cu–O (d and c) bonds are much stronger than the out-of-plane Cu–O (e) bonds and the molecule may be regarded to be formed from two basic binuclear units of Fig. 1. On the other hand, in the latter the out-of-plane Cu–O (e) bonds are much shortened and Cu–O (d) bonds are elongated. Thus the axis of the squar pyramid of copper ion is changed from the Cu–O (e) (in the case of Cu(et-2)Cl) to the Cu–O (d) (in the case of Cu(bu-2)Cl) axis. The presently analysed complex, Cu(pr-2)Cl, lies between the both extremes in either structural and magnetic values. However, it should be remarked that the structural trend of Cu(pr-2)Cl is definitely similar to that of Cu(bu-2)Cl rather than that of Cu(et-2)Cl, *i.e.*, in Cu(pr-2)Cl and Cu(bu-2)Cl Cu–Cu (a)>(b) and Cu–O (d)>(e)>(c), though magnetically Cu(pr-2)Cl belongs to the same group C-1[5] as Cu(et-2)Cl, since they both give negative Weiss constant, while Cu(bu-2)-Cl gives positive Weiss constant as shown in Table 6. This implies that in this series of compounds the change of sign in Weiss constant accompanies no discontinueous change of structure.

The calculations were performed on the FACOM 230-75 computer of the Computer Center of Kyushu University, using the UNICS program system.[14]

We are grateful to Professor T. Komori of Kyushu University for the kind advices and allowing us to use the Syntex PĪ automatic diffractometer. Thanks are also due to Mr. T. Uechi of this university for valuable advices and discussion.

References

1) F. Hein and W. Beerstechen, *Z. Anorg. Allg. Chem.*, **282**, 93 (1955).

* For Cu(eia) the μ_{eff} value slightly deviates from the value expected from the interpolation of the data of the three homologous compounds, probably due to the change of the chemical environment of copper atom.

2) E. Uhlig and K. Staiger, *Z. Anorg. Allg. Chem.*, **346**, 21 (1966).
3) Y. Ishimura, Y. Nonaka, Y. Nishida, and S. Kida, *Bull. Chem. Soc. Jpn.*, **46**, 3728 (1973).
4) Y. Nishida, F. Numata, and S. Kida, *Inorg. Chim. Acta*, **11**, 189 (1974).
5) Y. Nishida and S. Kida, *J. Inorg. Nucl. Chem.*, **38**, 451 (1976).
6) B. Bleaney and K. D. Bowers, *Proc. Roy. Soc., Ser. A*, **214**, 451 (1952).
7) E. D. Estes and D. J. Hodgson, *Inorg. Chem.*, **14**, 334 (1975).
8) W. Haase, *Chem. Ber.*, **106**, 3132 (1973).
9) R. Mergehenn and W. Haase, R. Allmann, *Acta Crystallogr.*, **B31**, 1847 (1975).
10) R. Mergehenn and W. Haase, *Z. Naturforsch., Teil B*, **30**, 155 (1975).
11) A. C. Villa, L. Coghi, A. G. Manfredotti, and C. Guastini, *Cryst. Struct. Commun.*, **1974**, 543.
12) J. A. Bertrand and J. A. Kelley, *Inorg. Chim. Acta*, **4**, 203 (1970).
13) "International Tables for X-ray Crystallography," Vol. III, Kynock Press, Birmingham (1962).
14) "The Universal Crystallographic Computation Progrgram System." Crystallographic Society of Japan (1967).

Complexation between Copper(II) Ion and Large Excess Histidine in Aqueous Solution

Hiroji AIBA,* Yoshihiro KURODA, and Hisashi TANAKA
Faculty of Pharmaceutical Sciences, Kyoto University, Sakyo-ku, Kyoto, 606
(Received January 12, 1976)

The complexation between copper(II) ion and large excess histidine has been studied by visible absorption, proton and C-13 NMR spectral methods, in comparison with histamine–copper(II) system. The predominant species were considered to be ML_2H^+ and $ML_2H_2^{2+}$ at $a=0$ and ML_2 at $a=1$ and 2, respectively from the spectral data in visible region, where a represents moles of base added per mole of diprotonated ligand. In ML_2H^+, one histidine is bound histamine-like with a carboxylate coordinated in apical position and the other glycine-like with a protonated imidazolium group, and in $ML_2H_2^{2+}$, both histidine molecules are bound glycine-like. Two histidine molecules are both tridentate with apical carboxylates in ML_2. In histamine–copper(II) system, the coordination of the third histamine molecule in the apical position was suggested at $a=1$ and 2. The proton and the C-13 NMR spectra were reasonably interpreted in view of the above situation. A difference in the line-broadening of PMR signals was observed between histidine–copper(II) and histamine–copper(II) systems. This is mainly due to the difference in the exchange rates of the coordinated ligands of two systems.

On account of the importance of interaction between imidazole group and copper(II) ion in biological systems, copper(II)–histidine complexes in aqueous solution have been studied by many workers. Most of the experiments were performed at stoichiometric conditions such as ligand to copper(II) ion ratio of 2: 1 or 1: 1. Sigel and McCormick investigated the interaction at ligand to metal ion ratio of 2×10^3 by means of proton NMR spectroscopy.[1] By comparing the line-broadening of imidazole proton signals of neutral histidine with that of its derivatives, they concluded that the predominant species is 2: 1 complex where one histidine is bound histamine-like and the other glycine-like. On the other hand, based on a kinetic consideration Sundberg and Martin have suggested that histidine may interact with copper(II) ion in only a monodentate mode at extraordinarily large ratios of ligand to metal ion.[2] The purpose of the present study is to obtain detailed information about the mode of complexation in the presence of large excess histidine by means of NMR and visible spectral methods.

Experimental

Materials. L-Histidine monohydrochloride monohydrate, histamine dihydrochloride, and $CuCl_2\cdot2H_2O$ were obtained from Nakarai Chemicals, Ltd., Kyoto. The deuterated compounds, D_2O, NaOD, and TSP (sodium 3-trimethylsilyltetradeuteriopropionate) were obtained from E. Merck AG, Darmstadt.

Visible Absorption Spectra. A Shimadzu Double 40-R spectrophotometer was used to obtain the visible absorption spectra. The measurements were carried out on the solutions containing a ligand (4×10^{-1} M) and copper(II) ion (2×10^{-3} M) or a ligand (2×10^{-2} M) and copper(II) ion (10^{-2} M) at room temperature. The spectra were obtained at various pH values corresponding to each a value, in which a represents moles of base added per mole of diprotonated ligand.

NMR Spectra. The proton NMR spectra were measured on a Varian A-60 NMR spectrometer. The spectra were obtained on the D_2O solutions of a ligand (0.25 M) in the absence and the presence of 1/500- or 1/2000-fold copper(II) ion at each a value. TSP was used as an internal reference The temperature variation was made with a Varian temperature variable accessory unit (V-6040) calibrated by ethylene glycol. The C-13 NMR spectra were measured on a Nippon Electric Varian NV-21 NMR spectrometer. The spectra were obtained on D_2O solutions of histidine (0.4 M) in the absence and the presence of 1/4000-fold copper(II) ion at each a value. Dioxane was used as an internal reference.

* Present address: Faculty of Medicine, Kyoto University, Sakyo-ku, Kyoto 606.

Results and Discussion

Visible Absorption Spectra. The spectral characteristics at each a value of the 200: 1 ligand–copper(II) system are shown in Table 1 together with those of 2: 1 complexes at $a=2$.

TABLE 1. VISIBLE ABSORPTION CHARACTERISTICS OF 200: 1 AND 2: 1 LIGAND–COPPER(II) SYSTEMS

	a value[a]	λ_{max}(nm)	ε_{max}(cm^{-1} M^{-1})
Histidine–Cu(II) 200: 1	0 (3.66)	623	60
	1 (7.81)	640	86
	2 (11.70)	635	94
Histamine–Cu(II) 200: 1	0 (3.03)	800	20
	1 (8.09)	610	96
	2 (11.68)	610	105
Histidine–Cu(II) 2: 1	2 (7.60)	640	86
Histidine–Cu(II)–1-methylhistidine 1: 1: 1	2 (7.52)	615	60
1-Methylhistidine–Cu(II) 2: 1	2 (7.50)	628	57
Histamine–Cu(II) 2: 1	2 (7.85)	600	85

a) The value of a represents moles of KOH added per diprotonated ligand. The values in parentheses are pH values.

In the 200: 1 histidine–copper(II) system at $a=0$, an absorption maximum was observed at 623 nm, which is an intermediate between that in 1: 1: 1 histidinate–Cu(II)–1-methylhistidinate complex and that in 2: 1 1-methylhistidinate–Cu(II) complex. This finding sug-

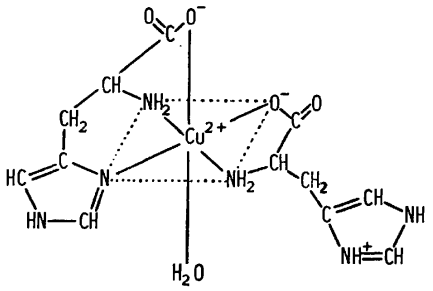

I, ML_2H^+

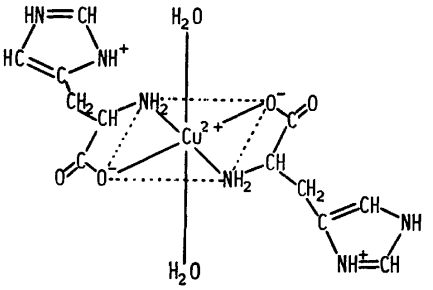

II, $ML_2H_2^{2+}$

gests the presence of the complex ML_2H^+(I), where one histidine is bound histamine-like with a coordinated apical carboxylate and the other glycine-like with a protonated imidazolium group and the complex $ML_2H_2^{2+}$(II), where both histidine molecules are bound glycine-like. Such complexes are known to be present in a weak acid pH region in the stoichiometric histidine–copper(II) systems, too.[2-4] On the other hand, the very weak ligand field (λ_{max}=800 nm) observed at a=0 in the 200: 1 histamine–copper(II) system means little complex formation between histamine and copper(II) ion. This remarkable difference in the degree of the complexation at a=0 between two systems suggests that the carboxylate group plays an important role in the complexation in the histidine–copper(II) system.

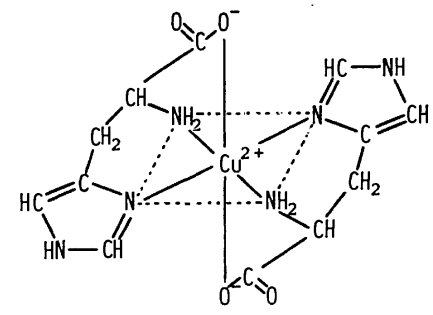

III, ML_2

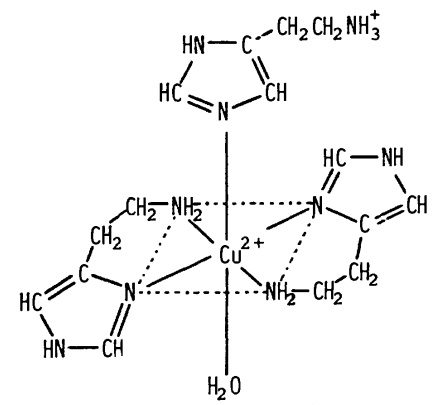

IV, ML_2LH^{3+}

The spectral characteristic, λ_{max}=640 nm (ε=86), at a=1 in the 200: 1 histidine–copper(II) system agrees completely with that of the 2: 1 histidinate–copper(II) complex ML_2. This means the formation of ML_2 as an exclusively predominant species in the 200: 1 histidine–copper(II) system. The structure of the 2: 1 complex ML_2, which is shown by III, has been discussed in detail.[5] The spectrum at a=1 in the 200: 1 histamine–copper(II) system exhibits an absorption maximum at 610 nm (ε=96), which is longer than that of 2: 1 normal histamine–copper(II) complex. This result suggests the coordination of the third histamine molecule in the apical position as shown by IV (ML_2LH^{3+}).

A little blue shift of the absorption maximum at a=2 in 200: 1 histidine–copper(II) system shows the partial deprotonation from the pyrrole nitrogen of the coordinated histidine molecules.[5] In comparison of the absorption spectrum of the 200: 1 histamine–copper(II) system at a=2 with that at a=1 the λ_{max} was the same whereas the absorptivity was higher. This observation may be interpreted by the strengthening of the apical coordination due to the deprotonation of the ammonium group and the partial deprotonation from the pyrrole nitrogen.

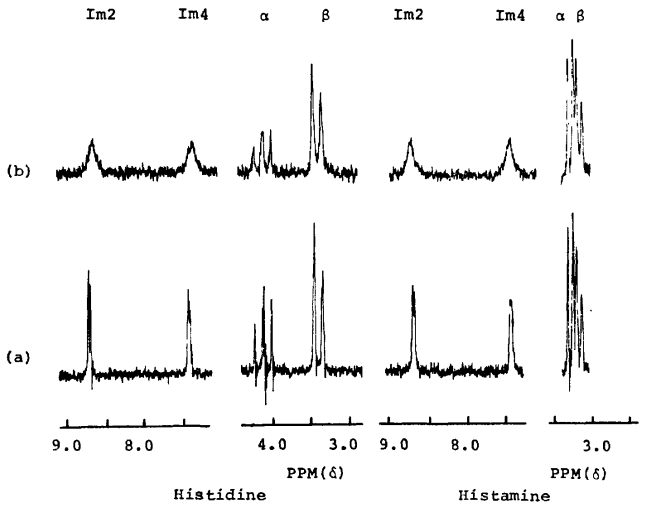

Fig. 1. PMR spectra of histidine and histamine at a=0 in the absence and the presence of 1/500-fold copper(II) ion: concentration of ligand=0.25 M; (a) ligand alone, (b) ligand+1/500 $CuCl_2$.

Proton Magnetic Resonance Spectra. The proton magnetic resonance spectra of histidine and histamine at a=0 in the absence and the presence of 1/500-fold copper(II) ion are shown in Fig. 1. In the 2000: 1 ligand–copper(II) systems, no evident broadening of the signals is observed. The signal of α-methine proton is broadened together with the signals of imidazole-2 and -4 protons in the 500: 1 histidine–copper(II) system, suggesting the involvement of the amino and the imidazole groups in the complex formation. This observation corresponds fully to the mode of complexation estimated by the visible spectral properties. The signals of the imidazole protons are broadened in the 500: 1 histamine–copper(II) system in the same manner

as in the 500: 1 histidine–copper(II) system. It is noteworthy that the broadening of imidazole signals is observed in the same degree in both systems in spite of the remarkable difference in the degrees of complex formation. This observation may be based on the different exchange rates in both systems.

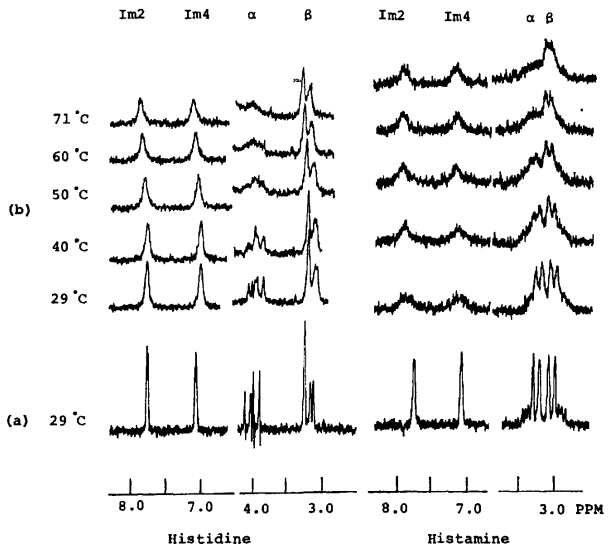

Fig. 2. PMR spectra of histidine and histamine at $a=1$ in the absence and the presence of 1/2000-fold copper (II) ion: concentration of ligand=0.25 M;
(a) ligand alone, (b) ligand+1/2000 $CuCl_2$.

Figure 2 shows the PMR spectra with temperature variation at $a=1$ in the histidine–copper(II) and the histamine–copper(II) systems. The broadening of the PMR signals is evident in both systems, giving remarkably different degrees of the broadening on the imidazole proton signals. This difference was observed on the solutions of histidine and histamine at pD 8.1 by Sigel and McCormick.[1] We measured the PMR spectra at constant a value, where the dissociation steps of both ligands are equal. In our experiment, a more remarkable difference in the broadening was observed. The previous workers concluded that such a difference is based on the different degrees of the participation of the imidazole group in complex formation, assuming that the exchange rates of the coordinated ligand are the same in both systems.[1] However, the validity of such assumption is difficult to justify. In the histidine–copper(II) system the line width of all the signals increases with increasing temperature. On the other hand, in the histamine–copper(II) system the line width of the imidazole proton signals decreases slightly with increasing temperature. This result suggests that the exchange rates of the coordinated ligands are different between two systems. In the presence of copper(II) ion, the line width at half height of signal $1/T_2$ is given by the following equation, if only one paramagnetic environment is present in solution.[6,7]

$$1/T_2 = 1/T_{2L} + P_M/P_L(1/(T_{2M}+\tau_M)) \quad (1)$$

Here, T_{2L} is the transverse relaxation time for the uncoordinated ligand, T_{2M} is that for the coordinated ligand, P_M/P_L is the ratio of the concentration of the coordinated ligand to that of the uncoordinated ligand, and τ_M is the life-time for chemical exchange of the coordinated ligand. Equation 1 is applicable to the histidine–copper(II) and the histamine–copper(II) systems to calculate the values of $1/(T_{2M}+\tau_M)$, because the presence of the main complex species, ML_2 for the histidine–copper(II) and ML_2LH^{3+} for the histamine–copper(II) systems are shown by the visible absorption spectra. We calculated the values of $1/(T_{2M}+\tau_M)$ using the line-broadening data on the imidazole-2 and -4 protons. In the histidine–copper(II) system, $1/(T_{2M}+\tau_M)$ is nearly equal to $1/\tau_M$, since the line width increases with increasing temperature and in this case τ_M is much larger than T_{2M}. The exchange rate $1/\tau_M$ is calculated to be about $3—5\times10^3\ s^{-1}$. On the other hand in the histamine–copper(II) system, $1/(T_{2M}+\tau_M)$ is calculated to be about $2—3\times10^4\ s^{-1}$. Since the line width of the imidazole proton signals in the histamine–copper(II) system decreases with increasing temperature, T_{2M} should be larger than τ_M.[6] Therefore, the exchange rate $1/\tau_M$ is much larger than $2—3\times10^4\ s^{-1}$. These results suggest that the difference in the line broadening in both systems is mainly due to different exchange rates. The relatively slower exchange rate histidine–copper(II) complex can be accounted for its coordination structure, that is, the copper(II) complex, where two histidine molecules are tridentate with apical carboxylates, is not easily accessible for an incoming ligand molecule.

In the PMR spectra at $a=2$, the signals are more broadened than those at $a=1$, especially in the histidine–copper(II) system, and the line width decreases slightly with increasing temperature. This may be explained on the basis of faster exchange rate caused by the deprotonation of the ammonium group.

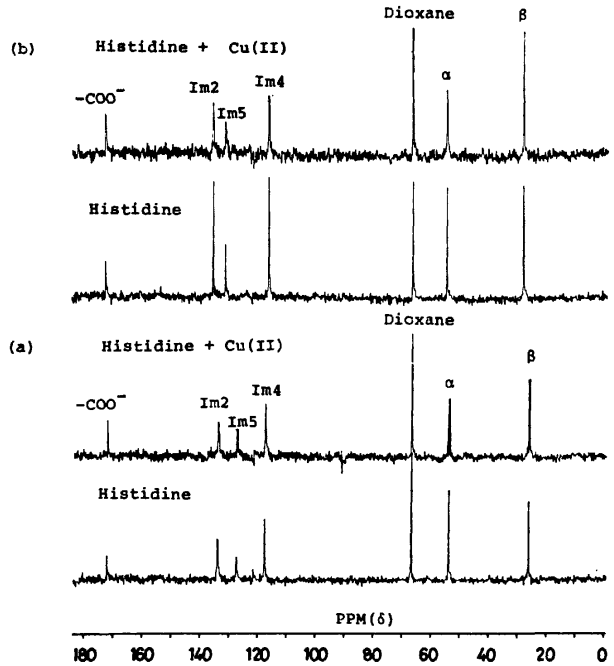

Fig. 3. C-13 NMR spectra of histidine in the absence and the presence of 1/4000-fold copper (II) ion: concentration of histidine=0.4 M;
(a) spectra at $a=0$, (b) spectra at $a=1$.

TABLE 2. THE RELATIVE SIGNAL HEIGHTS OF C-13 NMR SPECTRA OF HISTIDINE IN THE PRESENCE AND IN THE ABSENCE OF COPPER(II) ION

	$a=0$		$a=1$	
	Chemical shift (ppm)	Ratio	Chemical shift (ppm)	Ratio
Dioxane	67.40	1.00	67.40	1.00
β	26.69	1.00	28.90	1.00
α	54.44	0.66	55.54	0.53
Im4	118.51	0.89	117.62	0.44
Im5	128.24	1.16	132.67	0.56
Im2	134.75	0.85	136.87	0.40
$-COO^-$	173.02	1.53	174.35	0.95

C-13 Magnetic Resonance Spectra. Figure 3 shows C-13 NMR spectra of histidine in the absence and the presence of 1/4000-fold copper(II) ion at $a=0$ and 1 together with the assignments by Freedman *et al.*[8] The effect of copper(II) ion on the C-13 NMR signals is observed at each a value. To estimate the effect quantitatively, the relative signal heights in the presence and in the absence of copper(II) ion were compared. Table 2 shows the ratios of these heights, in which the smaller value means the larger effect of copper(II) ion, except for the carboxyl and the imidazole-5 carbons. The values for these signals are larger than 1.00 at $a=0$. This is probably due to their relatively long spin lattice relaxation times resulting from the lack of bound hydrogen atoms which can act as dipolar relaxers. By the addition of paramagnetic substance such as copper(II) ion, spin lattice relaxation time decreases and unsaturated signals may be recorded. At $a=0$ the value with the signal of α-methine carbon is smaller than those of the imidazole-2 and -4 carbons. On the other hand, the values with these three signals are roughly equal each other at $a=1$. These results give another support for the presence of ML_2H^+ and $ML_2H_2^{2+}$ at $a=0$ and ML_2 at $a=1$.

It the NMR line broadening experiments, histidine was suggested to interact with copper(II) ion in only a monodentate mode.[2] However, the present data show that histidine molecules bind to copper(II) ion in the tridentate or bidentate modes at extraordinarily large ratios of ligand to metal ion in a similar manner as at the stoichiometric conditions. The difference in the complexation between such two conditions has been found in the histamine–copper(II) system. The more remarkable difference has been observed in glycine-like ligands, which possess one amino and one carboxyl groups.[9]

NMR spectroscopic technique has been utilized to obtain structural information about copper(II) complexes. However, in NMR experiments attention should be called to the presence of large excess ligand. The mode of complexation at extraordinarily large ratios of ligand to metal ion may not be the same as those at stoichiometric ratios.[2] In addition, recently, Martin *et al.* have pointed out some criteria or disadvantage in the NMR line broadening method.[2,10] The use of visible spectral method together with NMR method will compensate such disadvantage and will give further detailed information about the mode of complexation of copper(II) ion in the presence of large excess ligand.

The authors wish to express their thanks to Miss M. Sugiura of Kobe Women's College of Pharmacy for the measurement of C-13 NMR spectra.

References

1) H. Sigel and D. B. McCormick, *J. Am. Chem. Soc.*, **93**, 2041 (1971).
2) R. J. Sundberg and R. B. Martin, *Chem. Rev.*, **74**, 471 (1974).
3) T. P. A. Kruck and B. Sarkar, *Can. J. Chem.*, **51**, 3550 (1973).
4) T. P. A. Kruck and B. Sarkar, *Can. J. Chem.*, **51**, 3563 (1973).
5) H. Aiba, A. Yokoyama, and H. Tanaka, *Bull. Chem. Soc. Jpn.*, **47**, 1003 (1974).
6) T. J. Swift and R. E. Connick, *J. Chem. Phys.*, **37**, 307 (1962).
7) R. G. Pearson and M. M. Anderson, *Angew. Chem.*, **77**, 361 (1965).
8) M. H. Freedman, J. S. Cohen, and I. M. Chaiken, *Biochem. Biophys. Res. Commun.*, **42**, 1148 (1971).
9) H. Aiba, Y. Kuroda, and H. Tanaka, unpublished data.
10) W. G. Espersen, W. C. Hutton, S. T. Chow, and R. B. Martin, *J. Am. Chem. Soc.*, **96**, 8111 (1974).

Liquid Phase Disproportionation of Propylene over MoO_3-Al_2O_3 Catalyst in the Presence of Solvents

Eisuke OGATA, Toshiaki SODESAWA, and Yoshio KAMIYA

Department of Reaction Chemistry, Faculty of Engineering, University of Tokyo, Hongo, Bunkyo-ku, Tokyo 113

(Received February 26, 1975)

Liquid phase disproportionation of propylene using hydrocarbon solvents over MoO_3–Al_2O_3 (atomic ratio: Mo/Al=1/25) catalyst was investigated at 80 °C at a pressure of 50 kg/cm². The catalytic activity in heptane solution was preserved for a long time, because the small amount of polyolefins produced by polymerization reactions was entirely dissolved in the heptane and carried away from the catalyst surface. Selectivity for ethylene and butenes increased slightly in the heptane solvent. Benzene was not a suitable solvent because of poor solubility of the polymers and the formation of alkylbenzenes. A small amount of dissolved hydrogen also was found to be somewhat effective in lengthening the catalyst life. The polymers were found to be composed of larger amounts of ethylene than propylene and to have two molecular weight distribution maxima.

Disproportionation of olefins has been studied by numerous investigators in heterogeneous gas and homogeneous liquid phases. From an industrial point of view, it is important that the catalytic activity be preserved for a long time. In gas-phase disproportionation over MoO_3–Al_2O_3 catalyst, the catalytic activity decreases rapidly with reaction time on stream.[1,2] The catalyst life and selectivity have been improved by the addition of third materials to the catalysts, but this is not yet fully successful.[1–5] Previously,[6] the present authors have shown that the activity of MoO_3–Al_2O_3 in liquid-phase propylene disproportionation is preserved much longer than in the gas phase, and decreases very slowly after a long time at low temperatures. It was assumed that the main effect of deactivation of the catalyst was due to the covering of the active site with the polymers produced. If this is true, a longer life of the catalyst can be expected using a solvent which dissolves the polymers and maintains a clean active site for disproportionation.

In this paper, the catalytic activity, selectivity, and catalyst life in propylene disproportionation over MoO_3–Al_2O_3 catalyst in the presence of solvents were investigated. In addition, the formation of polymers was studied by measuring the molecular weight and constituents of the polymers produced.

Experimental

The disproportionation reaction was carried out in an ordinary up-flow system of a fixed-bed catalyst in the liquid phase at a total reaction pressure of 50 kg/cm². About 0.025 to 1.000 g of the catalyst and twice that amount of γ-alumina were used as a catalyst bed and packed in the middle of a tube reactor with an 8 mm inside diameter and a 400 mm length. The upper and lower spaces of the catalyst bed were filled with γ-alumina. Propylene and the solvent were introduced into the catalyst bed from two cylindrical pumps after mixing in the lower part of the catalyst bed. The reaction products were analyzed by gas chromatography as reported in a previous paper.[7]

The preparation method and composition of the MoO_3–Al_2O_3 (atomic ratio: Mo/Al=1/25) catalyst, pretreatment of the catalyst for activation, and propylene used were the same as indicated in a previous paper.[6] Heptane and benzene were of purities above 99.7% and added after drying with a 13X molecular sieve and the removal of the small amount of air in the solution by the bubbling of helium, nitrogen or hydrogen gases.

The polyolefins produced by a side reaction of the disproportionation were analyzed by the following method in order to determine their molecular weights. Polymers soluble in heptane and benzene were dried at 95 °C at 1 mmHg for 1 h. Polymers adhering to the catalyst surface were extracted by tetrahydrofuran using a Soxhlet extractor at 65 °C for 15 h, and the extracts were dried at 95 °C under 1 mmHg for 1 h. The number average molecular weight $\overline{M}_n$ for the polymers was measured in a tetrahydrofuran solution using a Mechrolab Inc. vapor pressure osmometer (Model 301A). The molecular weight distributions of the polymers were measured in a tetrahydrofuran soluble at 20 °C and 40 °C using a Toyo Soda Manufacturing Co., Ltd. high-speed liquid chromatograph of the gel-permeation type (Model HLC-801A). The column used was 4 feet in length and packed with a TSK GEL MIX. of the polystyrene type prepared by the Toyo Soda Co. Samples for liquid chromatography were prepared as about 1 wt% polymer solutions in tetrahydrofuran. Six kinds of paraffinic hydrocarbons (C_{12}–C_{32}) and eight kinds of mono-disperse polystyrene standards (with molecular weights of 2100—2000000) prepared by the Pressure Chemical Co. were used as standard molecular weight samples. The estimate of the molecular weight distribution was corrected for the mono-disperse polystyrene standard by multiplying by a factor of 0.6 and for paraffinic hydrocarbon by multiplying by a factor of 1.2. Infrared spectra of the polymers were measured using the KBr pellet method, as well as the film method using a Hitachi Co., Ltd. Model IRA-2.

Results and Discussion

Effects of Reaction Temperature. The results of propylene disproportionation over MoO_3–Al_2O_3 catalyst in the liquid phase are shown in Table 1 and Fig. 1. In a run at 0 °C, the propylene conversion was very low in the initial period and gradually increased with reaction time. The conversion showed a broad maximum after 100 to 200 h and was still at about 80% of the maximum even after 460 h. The reaction time when the conversion fell to one-half its maximum value ($\tau_{1/2}$) was more than 1000 h.

On the other hand, the activity of the MoO_3–Al_2O_3 catalyst at 80 °C increased rapidly and showed maximum conversion for as short as 25 h (Run No. 2). Thereafter, the catalytic activity decreased rapidly with in a $\tau_{1/2}$ of about 25 h.

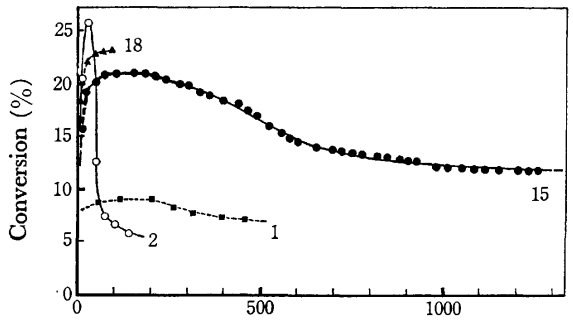

Fig. 1. Effects of reaction temperature and solvent on preservation of activity of MoO_3–Al_2O_3 catalyst in liquid phase disproportionation of propylene under 50 kg/cm².
Numbers correspond to the Run No. in Table 1.

Effect of Hydrogen. The effect of hydrogen in the liquid phase disproportionation of propylene was studied because it is known that hydrogen gas in the reaction system increases the catalytic activity and prolonges the catalyst life in the gas-phase disproportionation of propylene and 1-butene over a Co–Mo/Al_2O_3 catalyst.[8] As shown in Fig. 2, it was found that the catalyst retained its activity slightly longer in the presence of 0.1—3.5 mol% of dissolved hydrogen (Run No. 3—7). The hydrogen effect was much less marked than in the gas-phase reaction.[8] The product distribution shows that most dissolved hydrogen in the feed was consumed by the hydrogenation of propylene to propane, and the optimum amount of hydrogen in the reaction system was estimated to be about 0.1—0.3 mol% for ethylene and butenes production and for the prolongation of the catalyst life.

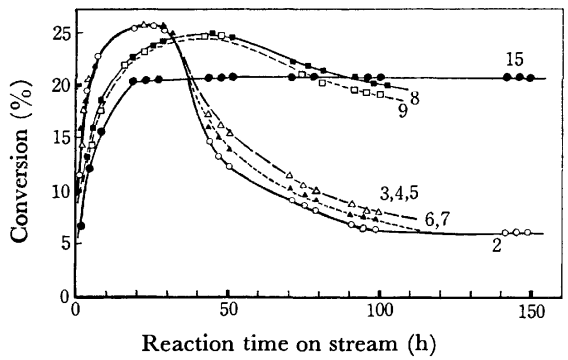

Fig. 2. Solvent and hydrogen effects on preservation of activity of MoO_3–Al_2O_3 catalyst in liquid phase disproportionation of propylene at 80 °C under 50 kg/cm².
Numbers correspond to the Run No. in Table 1.

Effect of Heptane Solvent. The effect of solvents was investigated at 80 °C where remarkable deactivation was observed. Since the catalyst activated in nitrogen was more active than that activated in air as reported previously,[6] oxygen must be poisonous to the active site of olefin disproportionation.[2] The decrease in activity of disproportionation in the heptane solvent purged by helium (Run No. 8) or nitrogen (Run No. 9)

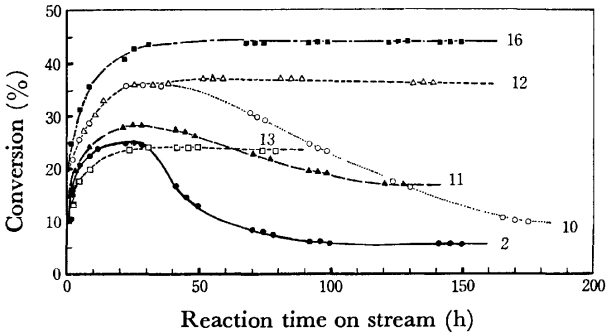

Fig. 3. Solvent effects on preservation of activity of MoO_3–Al_2O_3 catalyst in liquid phase disproportionation of propylene at 80 °C under 50 kg/cm².
Numbers correspond to the Run No. in Table 1.

was less extensive than that in the absence of the solvent (Run No. 2) as shown in Fig. 2. Heptane containing about 0.3 mol% hydrogen was more effective for prolonging the catalytic activity. As shown in Fig. 3, $\tau_{1/2}$ was increased by a factor of about three by using a half-liquid volume of heptane to feed (Run No. 10) as compared with neat propylene. The duration of catalytic activity and the pressure drop in the reactor were improved by increasing the heptane/propylene ratio (Run No. 12—16).

According to the catalytic activity duration test at a heptane/propylene volume ratio of two and a large liquid hourly space velocity of 120 (Run No. 15), the propylene conversion after 1250 h decreased to 58% of the maximum, and $\tau_{1/2}$ was estimated by extrapolation to be about 2000 h. As shown in Table 1, propylene conversion is mostly dependent on the space velocity of the propylene and is affected only slightly by the total space velocity. These results indicate that the adsorption of propylene on the active site is hardly affected by the use of heptane as the solvent.

The selectivity to ethylene and butenes always increases with reaction time on stream. The selectivity was 95—97% within the initial period of 20 h, and it increased to about 99% after 50 h. When heptane was used as the solvent, the selectivity of disproportionation was improved about 0.3% as compared with the case of neat propylene. As shown in Table 2, comparatively more polymers were produced doing the initial period and most oligomers and polymers produced were carried away from the catalyst surface by the heptane solution, because the amount of polymers (Polymer C) extracted from the catalyst bed was much less than that (Polymer B) soluble in heptane (Run No. 14). On the average, 0.028 wt% of solid products (Polymer E) based on the converted propylene was recovered by concentrating to one-fiftieth of the heptane solution obtained from Run No. 15. Further evacuation of the heptane solution gave viscous hydrocarbons (Polymer D, 0.32 wt% on the average). Small amounts of white solid polymers were observed in the space down stream of the reaction system after a reaction time of 1250 h.

These results show that various kinds of polymers, that is, very soluble, slightly soluble, and insoluble polymers, in heptane were produced by the accompanied

TABLE 1. EFFECTS OF REACTION TEMPERATURE, HYDROGEN, AND SOLVENT ON THE PRESERVATION OF ACTIVITY OF THE MoO_3–Al_2O_3 CATALYST IN THE LIQUID-PHASE DISPROPORTIONATION OF PROPYLENE AT 50 kg/cm²

Run No.	Temp (°C)	Solvent	Purging gas[a]	Solv./C_3H_6 (vol/vol)	LHSV(h^{-1})			Max. conv. (%)	$\tau_{1/2}$[b]
					C_3H_6	Solv.	Total		
1	0	none	none	0.0	3	0	3	9.3	~1000
2	80	none	none	0.0	30	0	30	25	~25
3	80	none	H_2 (0.1)	0.0	30	0	30	25	~35
4	80	none	H_2 (0.2)	0.0	30	0	30	25	~35
5	80	none	H_2 (0.5)	0.0	30	0	30	25	~35
6	80	none	H_2 (3.0)	0.0	30	0	30	25	~30
7	80	none	H_2 (3.5)	0.0	30	0	30	25	~30
8	80	*n*-C_7H_{16}	He (0.3)	2.0	30	60	90	24	—
9	80	*n*-C_7H_{16}	N_2 (0.3)	2.0	30	60	90	24	—
10	80	*n*-C_7H_{16}	H_2 (0.3)	0.5	20	10	30	35	~90
11	80	*n*-C_7H_{16}	H_2 (0.3)	0.8	25	20	45	29	—
12	80	*n*-C_7H_{16}	H_2 (0.3)	2.0	20	40	60	37	—
13	80	*n*-C_7H_{16}	H_2 (0.3)	2.0	30	60	90	24	—
14	80	*n*-C_7H_{16}	H_2 (0.3)	2.0	30	60	90	—	—
15	80	*n*-C_7H_{16}	H_2 (0.3)	2.0	40	80	120	21	~2000
16	80	*n*-C_7H_{16}	H_2 (0.3)	4.0	10	40	50	44	—
17	80	C_6H_6	H_2 (0.3)	2.0	30	60	90	—	—
18	80	C_6H_6	H_2 (0.3)	2.0	30	60	90	23	—

a) The gas used to remove oxygen from the solvent. The numbers in parentheses are the contents (in mol %) of the gas in propylene (Run No. 3—7) or in the solvent (Run No. 8—18).
b) The reaction time when the conversion falls to one-half of its maximum value.

TABLE 2. PRODUCT DISTRIBUTIONS IN LIQUID-PHASE PROPYLENE DISPROPORTIONATION AT 80 °C, 50 kg/cm², A VOLUME RATIO OF SOLVENTS/PROPYLENE OF 2, AND AN LHSV OF 90

Solvent	Heptane[a]		Benzene[a]			
Run No.	14	15	17			18
Reaction time (h)	0—10	0—1250	0—1	9—10	0—10	0—100
Total propylene conversion (%)	23.45	16.05	—	—	20.64	23.81
Disproportionation (%)	23.00 (98.07)	16.00 (99.65)	14.3	16.2	15.00 (72.66)	23.00 (97.5)
Alkylation (%)	— (—)	— (—)	8.3	4.0	5.00 (24.22)	0.81 (3.5)
Soluble polymers in solv. (%)	0.41 (1.76)[b]	0.05 (0.35)[d]	—	—	0.39 (1.90)[e]	— (—)
Insoluble polymers on cat. (%)	0.04 (0.17)[c]	— (—)	—	—	0.25 (1.22)[f]	— (—)
Components of diisopropylbenzene produced (mol %) *o*-	—	—	25.2	12.8	20.0	—
m-	—	—	33.6	31.8	32.6	—
p-	—	—	41.3	55.4	47.4	—
Components of isopropylbutylbenzene produced (mol %) *o*-	—	—	—	—	13.2	—
m-	—	—	—	—	29.5	—
p-	—	—	—	—	57.3	—

a) The numbers in parentheses are the selectivity of converted propylene. b) Polymer B. c) Polymer C. d) Polymer D+Polymer E. e) Polymer F. f) Polymer G.

polymerization.

Effect of Benzene Solvent. When benzene was used as the solvent (Run No. 17 and 18), the conversion during the initial period was nearly equal to that for the heptane solution. However, after a comparatively short time on stream, the introduction of propylene and benzene mixtures became difficult due to the increased flow resistance, caused by the produced polymers adhering on the down stream side of the reaction system. As shown in Table 2, about 24% of the converted propylene was comsumed in the alkylation of benzene within the first 10 h (Run No. 17), but the alkylation decreased rapidly to 3.5% after 100 h (Run No. 18). The composition of alkylbenzenes decreased in the following order: cumene, butylbenzenes, diisopropylbenzenes, styrene and isopropylbutylbenzenes. From the results in Table 2, it is clear that large amounts of polymers (Polymer G) insoluble in benzene were produced, and the solubility of the polymers in benzene is lower than in heptane. Therefore, benzene was not a suitable solvent for the propylene disproportionation.

Molecular Weight Determination of Polymers Produced. When the reaction was carried out without any solvent at an LHSV below two (80 °C), large amounts of oligomers and polymers (Polymer A) were produced in the reaction system and propylene could no longer be introduced after 10 hr.

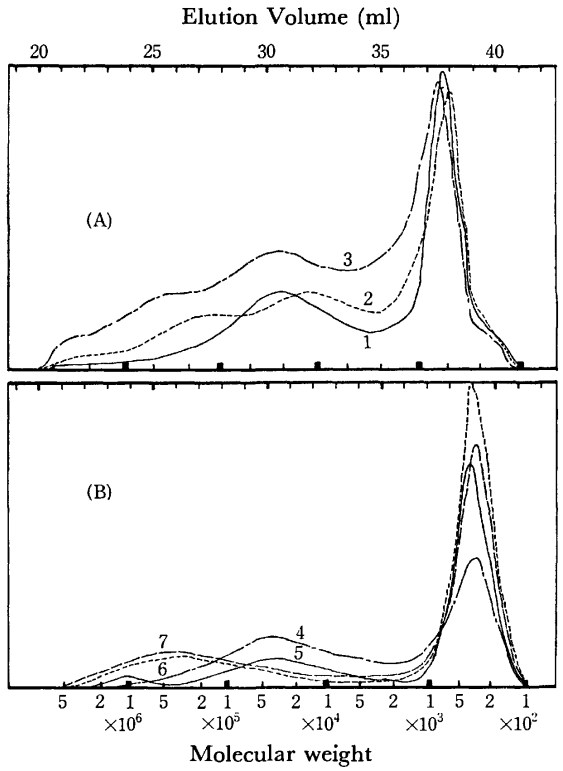

Fig. 4. Molecular weight distribution of polymers produced in liquid phase disproportionation of propylene at 80 °C under 50 kg/cm².
Condition of high speed liquid chromatograph (Toyo Soda, HLC-801A);
Column; TSK GEL MIX. (G3000H-G7000H), 4 ft., Solvent; tetrahydrofuran, Flow rate; 1.4 ml/min, Temperature; 20 °C (Fig. 4, A) and 40 °C (Fig. 4, B), Sample: 1 wt% solution in tetrahydrofuran, Detector; refractive index.
1: Polymer A, 2: Polymer D, 3: Polymer E, 4: Polymer B, 5: Polymer C, 6: Polymer F[a]; 7: Polymer G.
a): Polymers soluble in benzene obtained from Run No. 17.

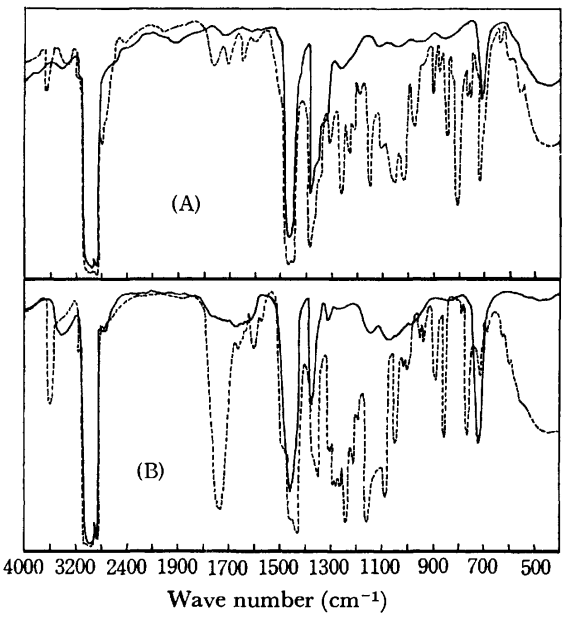

Fig. 5. Infrared spectra of polymers produced in the disproportionation of propylene over MoO_3–Al_2O_3 catalyst in the presence of heptane and benzene.
[A]: ·····; Polymer B, film method on NaCl,
——; Polymer E, film method on KBr,
[B]: ·····; Fraction of Polymer G soluble in heptane, film method on NaCl,
——; Fraction of Polymer G slightly soluble in heptane, film method.

TABLE 3. NUMBER AVERAGE MOLECULAR WEIGHTS AND COMPONENTS OF POLYMERS PRODUCED IN PROPYLENE DISPROPORTIONATION AT 80 °C AND 50 kg/cm²

Polymers	States	$\overline{M}_n$[a]	Propylene content[b] (%)
Polymer A	Gummy materials	900	34
Polymer B	Viscous liquid	—	45
Polymer D	Viscous liquid	1300	23
Polymer E	Solid	1800	40
Polymer G[c]	Solid	—	20

a) Number average molecular weights determined using a vapor pressure osmometer. b) Propylene contents of polymers determined by infrared spectroscopic analysis on the assumption that the polymers were produced only by the polymerization of ethylene and propylene. c) Fraction of Polymer G slightly soluble in heptane.

Although the number average molecular weight $\overline{M}_n$ of all polymers determined was between 900 and 1800 (Table 3), very small amounts of lower molecular weight materials were observed in both gas and liquid chromatographic analyses of the products.

The molecular weight distribution of these polymers is shown in Fig. 4. Each polymer has two maxima at molecular weights of 300 to 500 and 20000 to 200000. Each sample includes a small amount of higher polymers with molecular weights of several millions. Polymers produced in the benzene solvent contained larger amounts of high molecular-weight fractions and of sligptly soluble polymers than the polymers produced in the heptane solvent. About 1 wt% of Polymers A, E, and G homogeneously dissolved in tetrahydrofuran at temperatures above 60 °C, while at 20 °C some of them precipitated. Therefore, still higher fractions than observed in Fig. 4 may be included in the original polymer solution.

Component of Polymers by Infrared Spectroscopic Analysis, Infrared spectra of the polymers produced in the propylene disproportionation are shown in Fig. 5. The absorption bands at 1380 and 1460 cm^{-1} are assigned respectively to the methyl symmetrical C–H bending vibration and the methylene C–H scissoring vibration. On the assumption that the polymers are produced only by the polymerization of ethylene and propylene, the propylene contents of the polymers were measured using the method of Corish[9] with the results shown in Table 3. The propylene contents varied with the polymer samples, but they were always less than that for ethylene. Methyl groups in polymers should also be produced to some extent by the polymerization of ethylene as the terminal and branched methyl groups. Therefore, the real propylene contents in each polymer may be lower than those measured by the method of

Corish.[9] Since the absorption band at 722 cm^{-1} was stronger than those at 733, 752, and 815 cm^{-1}, it is clear that the n-values in $\{CH_2\}_n$ are higher than four according to the reports of Bucci.[10] Hashimoto *et al.* reported that the polymerization rate of ethylene over MoO_3–Al_2O_3 catalyst reduced at 400 °C at a hydrogen pressure of 150 mmHg was larger by a factor of seven to ten than that for propylene.[11] In a previous paper[6] it was shown that the polymerization rate decreases in the following order: ethylene, propylene, and butenes. The tendencies of the polymerization and oligomerization rates of the various olefins over MoO_3–Al_2O_3 catalysts activated in nitrogen must be similar to those over reduced catalysts. As shown in Fig. 5 (A and B), polymers produced in the initial period have some absorption bands in the regions of 1700—1750 and 3400—3700 cm^{-1}, which may be related to oxygen compounds. These results imply that the oxygen compounds are produced by the oxidation of olefins with oxygen of the catalyst, reducing the catalyst at more highly active stated.

The authors wish to express their thanks to Dr. Etsuo Niki of the Faculty of Engineering, University of Tokyo for useful discussions.

References

1) S. Furukawa, Y. Kamiya, and N. Ohta, *Kogyo Kagaku Zasshi*, **74**, 2471 (1971).
2) R. Nakamura and E. Echigoya, *Nippon Kagaku Kaishi*, **1972**, 500; *ibid.*, **1972**, 2276; *ibid.*, **1973**, 244; *Chem. Lett.*, **1972**, 273.
3) R. L. Banks and G. G. Bailey, *Ind. Eng. Chem. Prod. Res. Develop.*, **3**, 170 (1964).
4) T. P. Kobylinski and H. Swift, *J. Catal.*, **26**, 416 (1972).
5) C. P. C. Bradshow, E. J. Bawman, and L. Turner, *J. Catal.*, **7**, 269 (1967).
6) E. Ogata and Y. Kamiya, *Ind. Eng. Chem. Prod. Res. Develop.*, **13**, 170 (1974).
7) E. Ogata, Y. Kamiya, and N. Ohta, *J. Catal.*, **29**, 296 (1973).
8) H. J. Alkema and R. V. Helden, Brit. 1117968 (1968).
9) P. J. Corish and M. E. Tunnicliffe, *J. Polym. Sci. Part C*, **7**, 187 (1964).
10) G. Bucci and J. Simonazzi, *J. Polym. Sci., Part C*, **7**, 203 (1964).
11) K. Hashimoto, S. Watanabe, and K. Tarama, *Nippon Kagaku Kaishi*, **1974**, 409.

Lanthanide Induced Shifts of the PMR Spectra of Polyaza-aromatic Compounds

Yoshinobu NAGAWA, Makoto ONO, Minoru HIROTA,* Yoshiki HAMADA,+ and Isao TAKEUCHI+

Department of Applied Chemistry, Faculty of Engineering, Yokohama National University, Minami-ku, Yokohama 233

+Faculty of Pharmacy, Meijo University, Yagoto-Urayama, Tempaku-cho, Nagoya 468

(Received June 3, 1975, in revised form November 25, 1975)

The LIS's were determined with the equimolar mixtures of two monoaza-aromatic compounds, and the relative coordinating ability of each ligand was estimated from these LIS's. The coordinating ability index is defined as the ratio of the complexed species of the monoaza-aromatics to that of pyridine, and is proved to be transferable to the nitrogen atom of similar steric circumstances. Thus, $Eu(fod)_3$ induced shifts of the protons in several unsymmetrical naphthyridines and related heterocycles were estimated by the sum of the induced shifts of the corresponding monofunctional equivalents weighted by the relative abundances of the complexed species which were obtained from the coordinating ability measurements. The method is applicable to other bifunctional compounds of rigid conformation.

Since the first success reported by Hinckley,[1] lanthanide shift reagents have been applied to many stereochemical problems, and their uses are known as a routine technique of resolving the overlapping NMR signals. However, their application is limited within the monofunctional compounds in most cases, and relatively few examples have previously been reported concerning the lanthanide-induced shifts (LIS) of bi- and poly-functional compounds.[2] In the field of the chemistry of nitrogen heterocycles, their uses were focused on relatively simple compounds, such as pyridine, quinoline, and related compounds. An extensive work on six-membered nitrogen heterocycles including diazanaphthalenes has also been reported by Armarego and coworkers.[3] However, the discussion on the preferred site of complexation is qualitative and rather inconclusive.

In order to use shift reagents on polyfunctional compounds, it is necessary to decide the preferred site of complexation. Further, it is desirable to know quantitatively the relative abundances of the complexed molecules on two or more competing sites. In general, the coordinating ability of the ligand is affected by the electronic and steric factors.[4] In the case of shift reagent-substrate complexes, it is demonstrated that the coordinating ability is mainly governed by the steric factors which control the approach of the bulky Eu(III) complexes.

In this investigation, the LIS's were determined on the equimolar mixture of the two monofunctional compounds carrying similar functional groups in different steric circumstances. This offers an approach to determine the coordinating abilities of various substrates to the shift reagent by intermolecular competition.[5] Then, the LIS's of bifunctional compounds were estimated by the weighted summation of the induced shift of every equivalent monofunctional compound $[S_i^{(m)}]$. To accomplish this, the induced shifts of each monofunctional compound carrying a functional group of almost same circumstances as in the bifunctional one were measured first. Then, their induced shifts were again determined with an equimolar mixture of the two equivalent monofunctional compounds. The ratios of the induced shifts in the mixed solution to the one component LIS's give the relative abundances of the complexed monofunctional equivalents. The ratios thus obtained are nearly indifferent irrespective of the nature of protons in the molecule, and may be usable as a measure for the relative coordinating ability of the two substrates. The sequence of the relative coordinating ability indices will be a more reliable criterion for the steric effect than the LIS itself, since the steric factor of the McConnel-Robertson equation,[6] $(3\cos^2\theta-1)/r^3$, will also affect the LIS values

The coordinating ratios can be assumed to reproduce the complexation in two sites of the bifunctional compound. Then, the induced shifts (S_i) of each proton (i) in a bifunctional compound is calculated by summing up the each induced shift of the monofunctional model compound $(S_i^{(m)})$ weighted by the normalized relative abundance $(P^{(m)})$ obtained by the competitive complexation among the monofunctional model compounds.

$$S_i = \sum_{(m)} S_i^{(m)} \cdot P^{(m)} \qquad (1)$$

The above equation is derived by assuming that the electronic and other through bond effects between the two functional groups are negligible, and applies to the bifunctional compounds in which the two functional groups are located moderately apart from each other. Diaza-aromatic compounds carrying nitrogen atoms in different rings are suitable examples, and the LIS's of these heterocycles can be estimated properly from those of monoaza-aromatic compounds of similar structural feature.

Experimental

Materials used in this investigation were synthesized according to the methods previously reported,[7] or obtained by purification of commercially available materials. Proton NMR spectra were measured with chloroform-*d* solutions employing a JNM C-60H spectrometer operating at 60 MHz. The concentrations of the solutions were adjusted approximately at 0.3 $mol \cdot l^{-1}$ with respect to substrates, and $Eu(fod)_3$ was employed as the shift reagent throughout this work except the cases otherwise remarked. The induced shift was measured by adding the shift reagent in small portions to the solution containing an excess of the substrate. To eliminate the

* To whom correspondences should be addressed.

effect of imperfect complexation (equilibrium constants), the concentration of substrates were carefully adjusted to be constant throughout this investigation.

Results and Discussion

The LIS's of Monoaza-Aromatic Compounds and Evaluation of the $P^{(m)}$ *Values.* The lanthanide-induced shift was estimated, as usual, from the slope of the $\Delta\delta$ *vs.* [Eu(fod)$_3$]/[Substrate] plot, where $\Delta\delta$ refers to the chemical shift change induced by the shift reagent. The slope from the least squares fit of the plot was used as the LIS value (denoted by S in Tables and equations). The LIS's of various six-membered monoaza-aromatic compounds are given in Table 1. As expected, both the LIS's and the coordinating abilities (in Tables 2 and 5) decrease with increasing streic hindrance around the nitrogen atoms. This tendency is illustrated by the fact that the LIS decreases in the order of pyridine>2-methylpyridine>2,6-dimethylpyridine in the series of pyridine homologs. A remarkable difference is observed between the LIS's of 3- and 5-protons of 2-methylpyridine (**2**). Though the influence of the contact shift is not negligible for this compound, its contribution is concluded to be not predominant in the case of proton spectra.[8] Thus, the magnitudes of the LIS's can be interpreted that the bulkier methyl group expels the coordinated Eu(fod)$_3$ molecule to the opposite side of the C_4–N axis and changes the contribution of the steric factor on the 3- and 5-protons. This effect will be discussed quantitatively in the succeeding part of this paper. Similar deviations in coordination sites are also observed with 6-chloro-2-methylquinoline (**5**) and 6-chloro-8-methylquinoline (**6**). In the case of the 6-chloro-2-methyl derivative (**5**), the LIS of 7-proton is considerably larger than that in the 6-chloro-8-methyl derivative (**6**). This must also be the consequence of the different location of Eu(III) ion relative to the nitrogen ligand.

In order to determine the coordinating ability by intermolecular competition method, the LIS's of each substrate in the solution of the equimolar mixture of the two substrates were measured in a similar manner. Then the coordination ratio for every proton was calculated by comparison of the apparent LIS value ($S_i^{ap(m)}$) with that of each component ($S_i^{o(m)}$). By averaging the coordination ratios $P_i^{(m)}$ of all protons in the molecule m, the coordination ratio of the molecule ($P^{(m)}$) is calculated.[9] The coordination ratios of several aza-aromatic compounds to Eu(fod)$_3$ are given in Table 2. In the cases of shift reagents, the coordinating ability is mainly governed by the steric factor. Thus, the ability estimated from the coordination ratios of quinoline is nearly identical with those of 2-methylpyridine (**2**) and 6-chloroquinoline (**4**) with which the steric circumstances of the donor nitrogen atoms are similar to quinoline. Analogously, the coordinating abilities of 2,6-dimethylpyridine (**3**) and 6-chloro-8-methylquinoline (**6**) are almost identical with those of 6-chloro-2-methylquinoline (**5**) and 1-azaphenanthrene (**7**), respectively. 2-Methylpyridine might possess a little larger coordinating ability than 6-chloroquinoline, because the free rotation of the methyl group in the former can operate to lessen the steric hindrance in contrast to the rigid 8-H in quinoline. The same discussion is also applicable to the series of 2,6-dimethylpyridine (**3**), 6-chloro-2-methylquinoline (**5**), and acridine (**8**). The order of coordinating ability is: 2,6-dimethylpyridine>6-chloro-2-methylquinoline>acridine. However, the differences in coordinating abilities among these compounds are smaller than those among the compounds of dissimilar steric circumstances. In short, the competitive complexation experiments given in Table 2 reveal the fact that the steric circumstances are the dominating factor to the coordinating abilities of these heterocycles.

A shift to higher field is observed with the 2-H of 1,8-naphthyridine (**10**) by addition of Eu(fod)$_3$. 1,8-

Table 1. The LIS's of several monoaza-aromatic compounds

Compound	2-CH_3	8-CH_3	2-H	3-H	4-H	5-H	6-H	7-H	8-H	9-H	10-H
Pyridine (**1**)	—	—	35.37	11.11	11.00	11.11	35.37	—	—	—	—
	—	—	(1.00)	(0.31)	(0.31)	(0.31)	(1.00)	—	—	—	—
2-Methylpyridine (**2**)	23.37	—	—	8.56	5.34	4.60	13.89	—	—	—	—
	(1.00)	—	—	(0.37)	(0.23)	(0.20)	(0.59)	—	—	—	—
2,6-Dimethylpyridine	7.29	—	—	2.48	2.09	2.48	—	—	—	—	—
(**3**)	(1.00)	—	—	(0.34)	(0.29)	(0.34)	—	—	—	—	—
6-Chloroquinoline (**4**)	—	—	26.64	8.80	10.33	7.34	—	5.57	33.63	—	—
	—	—	(0.79)	(0.26)	(0.31)	(0.22)	—	(0.17)	(1.00)		
6-Chloro-2-methyl-	5.06	—	—	1.75	1.29	0.84	—	0.57	5.92	—	—
quinoline (**5**)	(0.85)	—	—	(0.30)	(0.22)	(0.14)	—	(0.10)	(1.00)	—	—
6-Chloro-8-methyl-	—	4.13	4.04	0.44	0.59	0.18	—	1.29	—	—	—
quinoline (**6**)	—	(1.00)	(0.98)	(0.11)	(0.14)	(0.04)	—	(0.31)	—	—	—
1-Azaphenanthrene	—	—	2.72	0.43	0.55	<0.5	<0.5	<0.5	<0.5	<0.5	3.92
(**7**)	—	—	(0.69)	(0.11)	(0.14)	(<0.13)	(<0.13)	(<0.13)	(<0.13)	(<0.13)	(1.00)
Acridine (**8**)	—	—	1.0	1.0	8.05	8.05	<1.0	<1.0	<1.0	1.71	—
	—	—	(0.12)	(0.12)	(1.00)	(1.00)	(<0.12)	(<0.12)	(<0.12)	(0.21)	—
2,8-Dimethylquinoline	1.79	1.98	—	0.81	0.75	<0.5	<0.5	<0.5	—	—	—
(**9**)	(0.90)	(1.00)	—	(0.41)	(0.38)	(<0.25)	(<0.25)	(<0.25)	—	—	—
1,8-Naphthyridine	—	—	−1.04	3.63	5.17	5.17	3.63	−1.04	—	—	—
	—	—	(−0.20)	(0.70)	(1.00)	(1.00)	(0.70)	(−0.20)	—	—	—

The LIS's defined by $S^{\circ}=\Delta\delta/([Eu(fod)_3]/[Substrate])$ are given in this table. Relative LIS values with respect to the largest are given in parentheses.

TABLE 2. RESULTS ON THE COMPETITIVE COORDINATION EXPERIMENTS BETWEEN TWO SUBSTRATES

Run No.	Predominantly Complexed Substrate		Less Predominantly Complexed Substrate	
	Compound 1	P_1 (%)	Compound 2	P_2 (%)
1	1,8-Naphthyridine	92	Pyridine	8
2	Isoquinoline	56	Pyridine	44
3	Pyridine	87	2-Me-Pyridine	13
4	Pyridine	88	2,6-Me_2-Pyridine	12
5	Pyridine	87	6-Cl-Quinoline	13
6	Pyridine	91	6-Cl-2-Me-Quinoline	9
7	Pyridine	93	6-Cl-8-Me-Quinoline	7
8	Pyridine	88	Acridine	12
9	Pyridine	93	1-Azaphenanthrene	7
10	Pyridine	97	2,8-Me_2-Quinoline	3
11	2-Me-Pyridine	58	6-Cl-Quinoline	42
12	2-Me-Pyridine	78	2,6-Me_2-Pyridine	22
13	Quinoline	52	6-Cl-Quinoline	48
14	6-Cl-Quinoline	77	2,6-Me_2-Pyridine	23
15	6-Cl-Quinoline	72	6-Cl-2-Me-Quinoline	28
16	6-Cl-Quinoline	74	6-Cl-8-Me-Quinoline	26
17	6-Cl-Quinoline	71	Acridine	29
18	2,6-Me_2-Pyridine	68	6-Cl-2-Me-Quinoline	32
19	2,6-Me_2-Pyridine	73	6-Cl-8-Me-Quinoline	27
20	2,6-Me_2-Pyridine	65	Acridine	35
21	6-Cl-2-Me-Quinoline	63	6-Cl-8-Me-Quinoline	37
22	6-Cl-2-Me-Quinoline	51	Acridine	49
23	6-Cl-2-Me-Quinoline	62	1-Azaphenanthrene	38
24	Acridine	64	6-Cl-8-Me-Quinoline	36
25	Acridine	61	1-Azaphenanthrene	39
26	1-Azaphenanthrene	54	6-Cl-8-Me-Quinoline	46
27	6-Cl-8-Me-Quinoline	53	2,8-Me_2-Quinoline	47

* P_1 and P_2 are the coordinating ratios in percent, which are estimated by employing the following equation: $P_i = S_i^{ap}/S_i^{\circ}$

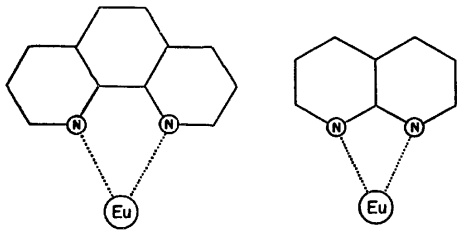

Fig. 1. Eu^{3+}–1,10-phenanthroline and 1,8-naphthyridine complexes. These bases behave as bidentate ligands in the complex formation.

naphthyridine (**10**) is a bidentate ligand, forming a chelate compound with $Eu(fod)_3$ (as shown in Fig. 1), and this may be the reason for its anomalous LIS. Thus, the system gains additional stabilization energy, and its coordinating power is strengthened remarkably. The above discussion applies to the peculiar stability of the 1,10-phenanthroline- and 2,2′-bipyridine-$Eu(fod)_3$ complexes.

The $P^{(m)}$ values are convenient to compare the coordinating abilities of the two nitrogen donors, but inconvenient for the comparison among several nitrogen donors of different steric circumstances. Thus, the coordinating ability index (C) is defined as the ratio of $P^{(m)}$ to the $P^{(m)}$ of pyridine. The most probable values of coordinating ability indices were calculated from the $P^{(m)}$'s listed in Table 2 by least squares optimization technique, and are given in Table 5.

The intermolecular competition offers a more reliable method to determine the abundances of the complexed species, since the LIS's depend not only on the population of the complexed species but also on the steric factor (in Eq. 3). The LIS's of some protons are shown in Table 3. These protons occupy nearly equivalent positions relative to the nitrogen atoms. By comparing these LIS's with the coordinating ability

TABLE 3. THE LIS'S OF SOME PROTONS OCCUPYING NEARLY EQUIVALENT POSITIONS RELATIVE TO THE NITROGEN ATOMS

Compound	**1**	**2**	**3**	**4**	**5**	**6**	**7**	**8**	**9**	**10**
LIS	35.37	13.89	7.29	26.64	5.06	4.04	8.05	2.72	1.79	−1.04[a]
Position	2-H	6-H	2-CH_3	2-H	2-CH_3	2-H	4-H	2-H	2-CH_3	2-H

a) Shift to the higher field.

indices in Table 5, it is shown that the LIS's are not always proportional to the coordinating abilities. The coordinating ability indices are rather insensitive to the electronic effect. Thus, the coordinating ability indices for quinoline and its 6-chloro-derivative are 0.153 and 0.145, respectively. However, a small but definite effect is observed when a substituent is attached directly to the hetero-aromatic ring. The coordinating ability indices for pyridine, 4-chloropyridine, and 4-methylpyridine are 1.00, 0.79, and 1.22, respectively, and, as expected, the electron donating ability of the substituent favors the complex formation. In conclusion the relative values of the coordinating ability indices are transferable to the nitrogen ligand of similar local steric circumstances.

Estimation of the LIS's of Polyaza-aromatic Compounds. As the coordinating abilities of the nitrogen atoms in the heterocycles are dependent mainly upon their steric circumstances, the LIS's of polyaza-aromatic compounds can be estimated from the coordinating abilities of monoaza-aromatic compounds of which nitrogen atoms occupy similar steric circumstances. The method is quite successful in estimating the LIS's of polyaza-aromatic compounds without polyaza-rings. Thus, the induced shifts of the ring protons of 1,6- and 1,7-naphthyridines were estimated from those of quinoline and isoquinoline. $Eu(fod)_3$ was employed as the shift reagent throughout this work, and the induced shift was measured by adding the shift reagent in small portions. To avoid the effect of the di-coordinated species $C_8H_6N_2 \cdot 2Eu(fod)_3$, the induced shift was estimated from the chemical shift displacement ($\Delta\delta$) in the range of lower [$Eu(fod)_3$]/[substrate] ratios. From the experiment of the competitive complexation with the equimolar quinoline–isoquinoline mixture in chloroform-*d*, the mean coordinating abilities for quinoline ($P^{(1)}$) and isoquinoline ($P^{(2)}$) have already been estimated to be 0.14 and 0.86, respectively. Then, the induced shifts for the protons in the naphthyridines were estimated by Equation 1 as shown in Table 4.

The estimated relative induced shifts agree almost quantitatively with the observed values except the case of 8-H in 1,7-naphthyridine. The lower estimated value of S_8 in 1,7-naphthyridine can be improved considerably by assuming the equal $S_i^{(2)}$ values for 6-H and 8-H of 1,7-naphthyridine (which correspond to those of 3-H and 1-H in isoquinoline, respectively). This assumption is exactly true if pyridine is employed as a model monofunctional compound.

Similar estimations again result proper relative values for the LIS's of 2-methyl- and 4-methyl-1,5-naphthyridines (as shown in Table 4). The magnitudes of the induced shifts can also be estimated in fair agreement by this method. However, the relative values fit more closely with the observed ones.

Table 4. The observed and the estimated LIS's of some naphthyridines

Naphthyridine		Reference monoaza-aromatics and the ratios					
(1) 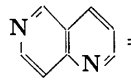		= 0.86 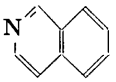 + 0.14 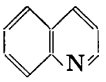					
Position		2	3	4	5	7	8
S_i	obsd	8.46	5.63	8.23	29.20	37.74	16.28
	calcd	6.45	4.58	7.76	25.55	31.06	13.30
$S_i/(S_i)_{max}$	obsd	0.22	0.15	0.22	0.77	1.00	0.43
	calcd	0.21	0.15	0.25	0.82	1.00	0.42
(2) 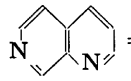		= 0.86 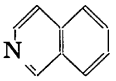 + 0.14 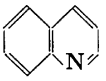					
Position		2	3	4	5	6	8
S_i	obsd	6.25	4.31	7.39	9.29	29.27	32.62
	calcd	6.49	4.58	7.76	9.96	31.06	28.89
$S_i/(S_i)_{max}$	obsd	0.19	0.13	0.23	0.28	0.90	1.00
	calcd	0.22	0.16	0.27	0.34	1.08	1.00
(3) 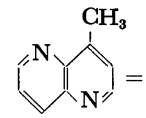		= 0.74 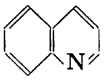 + 0.26 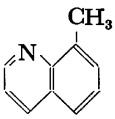					
Position		2	3	6	7	8	CH_3
S_i	obsd	42.02	15.06	11.95	10.28	58.71	15.68
	calcd	19.84	6.85	5.49	4.23	25.04	—
$S_i/(S_i)_{max}$	obsd	0.72	0.26	0.20	0.18	1.00	0.27
	calcd	0.79	0.27	0.22	0.17	1.00	—
(4) 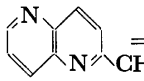		= 0.72 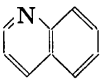 + 0.28 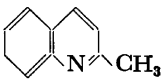					
position		3	4	6	7	8	CH_3
S_i	obsd	6.41	33.66	25.43	9.44	12.18	5.41
	calcd	4.50	24.57	19.37	6.50	9.10	—
$S_i/(S_i)_{max}$	obsd	0.19	1.00	0.76	0.28	0.36	0.16
	calcd	0.18	1.00	0.79	0.26	0.37	—

Estimation of the Locations of Eu(III) in the Shift Reagent-Substrate Complexes and Calculation of the $S_i^{(m)}$'s for the Protons Void in the Model Monofunctional Compounds. In order to correlate the coordinating ability with the location of Eu(III) ion and to use in estimating some LIS's of polyfunctional compounds, the most probable location of the complexed Eu(III) ion was determined by evaluating the agreement factors[10] defined by the folowing equation.

Table 5. The Eu–N distances (d_{Eu-N}), distortion angles (φ), and coordinating ability indices (C) of some aza-aromatic compounds

Compound	1	2	3	4	5	6	7	8	9	10
d_{Eu-N}, Å	3.3	—	4.0	—	4.2	5.1	4.2	5.3	—	—
	(3.9)	4.7		(4.8)	(5.7)	(4.6)				
φ°	0	—	0	—	4	10	18	0	—	—
	(0)	(5)		(16)	(9)	(23)				
C	[1.00]	0.177	0.097	0.158	0.084	0.058	0.070	0.096	0.040	11.5

a) The distances and angles in paretheses refer to those of $Pr(fod)_3$–substrate complexes.

$$R = \left(\frac{[(S_{obsd})_i - (S_{calcd})_i]^2}{(S_{obsd})_i^2} \right)^{1/2} \quad (2)$$

The calculations were carried out with a HITAC 8250 digital computer by assuming the following: a) The lanthanide-substrate interaction is entirely, or at least predominantly, of pseudocontact nature usually evaluated by the McConnell-Robertson equation,

$$S = K(3\cos^2\theta - 1)/r^3 \quad (3)$$

where θ is the N–Ln–H internuclear angle and r is the Ln–H distance. b) The coordination site is located on the plane of the heteroaromatic ring. The Eu–N distances thus obtained are given, together with the relative coordinating ability indices, in Table 5. Some of the results are illustrated also in Fig. 2. The calculated locations of Eu(III) ions are in accordance with the degree of the steric hinrdance qualitatively estimated from the coordinating abilities. The results illustrate that there exists an approximately linear relation between the coordinating ability indices and the Eu–N distances. If the substrate molecule carries some groups, such as methyl, which cause the steric hindrance to the coordination, the coordination site of $Eu(fod)_3$ may shift, and both the Eu–N distance and the orientation of the Eu–N axis deviate from those of pyridine. The methyl and the benzo groups of 8-methylquinoline and 1-azaphenanthrene, respectively, hinder the access of the shift reagent more remarkably than those of 2-methylquinoline and acridine. Angular distortion of the Eu–N axes in the Eu complexes of the former may play an important role to increase the steric hindrance. The steric circumstances of the electron

TABLE 6. THE OBSERVED AND THE ESTIMATED LIS'S OF SOME DIAZAPHENANTHRENES

Diazaphenanthrene		Reference monoaza-aromatics and the ratio[a]							
(5)		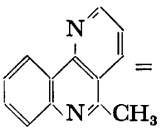 = 0.38 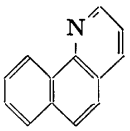 + 0.62 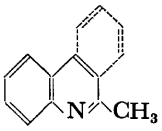							
Position		2	3	4	7	8	9	10	CH_3
S_i	obsd	1.52	0.59	1.06	4.71	<0.5	<0.5	2.37	3.46
	calcd	1.52	0.65	1.15	3.75	0.54	0.61	2.01	—
$S_i/(S_i)_{max}$	obsd	0.32	0.13	0.23	1.00	<0.1	<0.1	0.50	0.73
	calcd	0.40	0.17	0.30	1.00	0.14	0.16	0.53	—
(6)		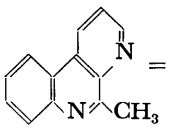 = 0.63 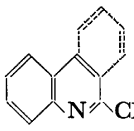 + 0.37 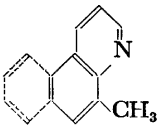							
Position		1	2	3	7	8	9	10	CH_3
S_i	obsd	0.80	0.54	1.55	4.62	<0.5	<0.5	0.74	4.17
	calcd	0.84	0.58	1.94	3.90	0.49	0.59	0.82	—
$S_i/(S_i)_{max}$	obsd	0.17	0.12	0.34	1.00	<0.1	<0.1	0.16	0.90
	calcd	0.22	0.15	0.50	1.00	0.13	0.15	0.21	—
(7)		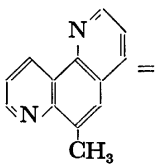 = 0.54 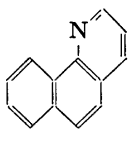 + 0.46 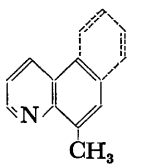							
Position		2	3	4	5	8	9	10	CH_3
S_i	obsd	2.09	0.61	0.77	1.26	4.07	0.55	3.39	4.35
	calcd	1.64	0.42	0.52	0.86	2.13	0.47	2.39	—
$S_i/(S_i)_{max}$	obsd	0.62	0.18	0.23	0.37	1.20	0.16	1.00	1.28
	calcd	0.69	0.18	0.22	0.36	0.89	0.20	1.00	—
(8)		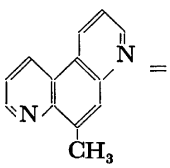 = 0.74 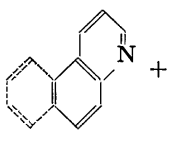 + 0.26 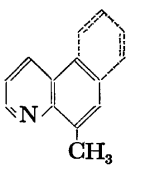							
Position		1	2	3	5	8	9	10	CH_3
S_i	obsd	9.78	8.60	24.94	28.71	3.86	3.30	6.97	3.08
	calcd	7.82	6.61	19.80	25.22	2.35	1.78	3.28	—
$S_i/(S_i)_{max}$	obsd	0.34	0.30	0.87	1.00	0.13	0.11	0.24	0.11
	calcd	0.31	0.26	0.79	1.00	0.09	0.07	0.13	—

a) The reference monoaza-aromatic compound is lacking in the aromatic ring illustrated by the broken line, and the $S_i^{(m)}$ values were estimated by the method described in the text.

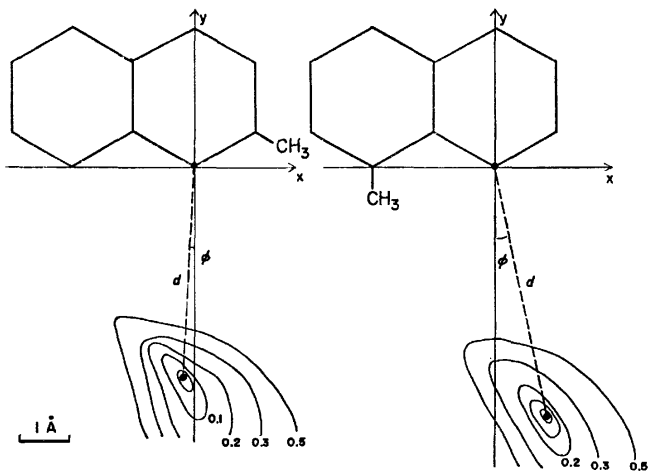

Fig. 2. The most probable location of europium (III) ion in the shift reagent–substrate complex estimated by the evaluation of the R values.

donating nitrogen atom affect remarkably the coordination with the shift reagent.

On estimating the induced shifts (S_i's) of the protons in bifunctional compounds by Eq. 1, the induced shifts of the monofunctional reference compounds ($S_i^{(m)}$'s) are required. When the reference monofunctional compounds have the same skeletal structure with that of the bifunctional compound, the $S_i^{(m)}$ values can be obtained experimentally, as exemplified by the cases (1) to (4) in Table 4. However, such reference monofunctional compounds are not always available easily when the bifunctional compound has a more complex structure. Even in such cases, the induced shifts $S_i^{(m)}$ of the protons on the rings distant from the functional group can be estimated from the d_{Eu-N} and ϕ values by employing the McConnell-Robertson equation. For example, the induced shifts of the protons in 5-methyl-1,6-diazaphenanthrene is estimated from the $S_i^{(m)}$'s of 2-methylquinoline and 1-azaphenanthrene (as shown in Table 6). Since 2-methylquinoline is void of the aromatic ring illustrated by the broken lines in Table 6, the $S_i^{(m)}$'s for the protons at 2, 3, and 4 positions due to the complexation on the 6-nitrogen atom are estimated by calculating relative LIS's of these protons by Eq. 3. As the induced shifts $S_i^{(m)}$'s of the distant protons are small, the approximation is permissible in spite of the considerable inaccuracy accompanying to this method of evaluation. The results are shown in Table 6, together with those of 5-methyl-4,6-diaza-, 6-methyl-1,7-diaza-, and 6-methyl-4,7-diaza-phenanthrenes. Here again the estimated LIS's are rather smaller than the observed ones, however, the agreement between the relative values is excellent in most cases. And the method is proved to be applicable to the prediction of the LIS's of the heteroaromatic compounds of this class.

The authors are grateful to Prof. Hiroshi Kakiuchi, Yokohama National University, for his valuable advice and encouragement throughout this work. They also express their hearty thanks to Mrs. Shigeko Yoshida for her technical assistance on of the measurements NMR spectra.

References

1) C. C. Hinckley, *J. Am. Chem. Soc.*, **91**, 5160 (1969).

2) a) A. Ius, G. Vecchio, and G. Carrea, *Tetrahedron Lett.*, **1972**, 1543. b) C. C. Hinckley, M. R. Klotz, and F. Patil, *J. Am. Chem. Soc.*, **93**, 2417 (1971). c) J. K. M. Sanders, S. W. Hanson, and D. H. Williams, *J. Am. Chem. Soc.*, **94**, 5325 (1972).

3) a) G. Beech and R. J. Morgan, *Tetrahedron Lett.*, **1974**, 973. b) W. L. F. Armarego, T. J. Batterham, and J. R. Kershaw, *Org. Magn. Resonance*, **3**, 575 (1971). c) P. V. Demarco, B. J. Cerimere, R. W. Crane, and A. L. Thakkar, *Tetrahedron Lett.*, **1972**, 3539.

4) a) L. Ernst and A. Mannschreck, *Tetrahedron Lett.*, **1971**, 3023. b) C. Beaute, Z. W. Wolkowski, and N. Thoai, *Tetrahedron Lett.*, **1971**, 817.

5) H. Hart and G. M. Love, *Tetrahedron Lett.*, **1971**, 625.

6) *H. M. McConnell and R. E. Robertson, J. Chem. Phys.*, **29**, 1361 (1958).

7) These quinolines were synthesized by a slight modification of the method described in the following paper. Y. Hamada, I. Takeuchi, and M. Hirota, *Chem. Pharm. Bull.* (Tokyo), **19**, 1751 (1971).

8) D. R. Eaton, *J. Am. Chem. Soc.*, **87**, 3097 (1965).

9) The procedure is formulated as follows;

$$P_i^{(m)} = \frac{(S_i^{ap})_i^{(m)}}{(S^o)_i^{(m)}} \qquad P^{(m)} = \sum_{i=1}^{n} P_i^{(m)}/n,$$

where n is the number of protons over which $P_i^{(m)}$'s are averaged.

10) a) M. R. Willcott III, R. E. Lenkinski, and R. E. Davis, *J. Am. Chem. Soc.*, **94**, 1742 (1972). b) I. M. Armitage, L. D. Hall, A. G. Marshall, and L. G. Werbelow, *J. Am. Chem. Soc.*, **95**, 1473 (1973). c) T. Heigl and G. K. Mucklow, *Tetrahedron Lett.*, **1972**, 649.

The Oxidation Activity and Acid-base Properties of Mixed Oxide Catalysts Containing Titania. I. The TiO_2-MoO_3 and TiO_2-V_2O_5 Systems

Mamoru Ai

Research Laboratory of Resources Utilization, Tokyo Institute of Technology, Ookayama, Meguro-ku, Tokyo 152

(Received July 1, 1975)

The amounts of both the acidic and basic sites of two series of catalysts, TiO_2–MoO_3 and TiO_2–V_2O_5, with different compositions were measured by studying the adsorption of the basic and acidic molecules in the gas phase, using both the static and pulse methods. The acidity of TiO_2–MoO_3 catalysts is very high at Mo=40—60 atom%, though those of the TiO_2-rich (Mo<30 atom%) and MoO_3-rich (Mo>80 atom%) catalysts are fairly low. The acidity of the TiO_2–V_2O_5 increases steadily with the V_2O_5 content. The basicity of the catalysts is remarkably enhanced by the introduction of a small amount of MoO_3 or V_2O_5. It can be said that the catalysts are basic at Mo <20 atom% or V<10 atom%, while the MoO_3-rich or V_2O_5-rich catalysts are acidic. The vapor-phase oxidation of 1-butene, butadiene,and acetic acid, the dehydration and dehydrogenation of isopropyl alcohol (IRA), and the isomerization of 1-butene were carried out in the presence of an excess of air, and the relationship between the catalytic behavior and the acid-base properties was investigated. It was concluded that the activities and selectivities can be relatively well explained by the acid-base properties between the catalyst and the reactant.

Single TiO_2 is impractical as a catalyst because of its low activity. However, mixed-oxide systems combining TiO_2 with such oxides as V_2O_5, MoO_3, P_2O_5, K_2SO_4, SiO_2, and ZnO are known to be effective for certain reactions.[1–5] These combinations seem to induce an unexpectedly great change in the catalytic behavior. Above all, the characteristic features of the selectivity become completely different as different sorts of oxides are introduced into TiO_2. However, the function of these second components has not yet been firmly established.

According to our recent studies,[6] it has been found that TiO_2, much like UO_3, SnO_2, and Fe_2O_3, is a metal oxide included in Group B, intermediate between such acidic metal-oxides as V_2O_5, MoO_3, and WO_3 (Group A) and such basic metal-oxides with a high oxidation powder as NiO, Co_2O_3, MnO_2, CuO, and Cr_2O_3 (Group C), and that its acid-base properties are significantly modified by the introduction of a small quantity of acidic or basic elements, such as P_2O_5, MoO_3, and K_2O.

It seemed, therefore, that it would be very interesting to find how the incorporation of certain oxides intoTiO_2 modifies the acid-base properties of the catalyst and how this modification in turn induces a change in the catalytic behavior.

The present paper will deal with the first part of an investigation concerning the oxidation activity of the TiO_2-based catalyst systems. We attempted to ascertain how the incorporation of various amounts of MoO_3 and V_2O_5 into TiO_2 modified the acid-base properties as well as the oxidation activity and selectivity, and examined to see whether or not the catalytic behavior can be explained by the acid-base properties of the catalyst system, as in the cases of the V_2O_5–MoO_3,[7] V_2O_5–P_2O_5,[8] MoO_3–P_2O_5,[9] MoO_3–Bi_2O_3–P_2O_5,[10–12] MoO_3–P_2O_5–X_nO_m[13] SnO_2–V_2O_5,[14,15] and SnO_2–MoO_3[14,16] systems.

Experimental

Catalysts. Two series of TiO_2-based binary catalysts, TiO_2–MoO_3 and TiO_2–V_2O_5, with different compositions were prepared as follows. The required quantity of $TiCl_4$ was dissolved in water containing ice. To this solution, dilute aqueous ammonia was added to precipitate the hydroxide. After filtering and washing, the paste-like hydroxide was added to an aqueous solution of $(NH_4)_6Mo_7O_{24}\cdot 4H_2O$ or NH_4VO_3–oxalic acid, and 10—20 mesh pumice was mixed with the solution; then the mixture was evaporated with vigorous stirring. The amount of pumice was 500 ml (about 150 g) per g atom of titanium and molybdenum or titanium and vanadium. The catalyst was calcined under flowing air at 500 °C for about 4—5 h.

Acidity and Basicity Measurements. Since the TiO_2–MoO_3 and TiO_2–V_2O_5 catalysts are colored and small in surface area, the determination of the acidity and basicity by an ordinary titration method seems to be difficult; therefore, the adsorption amounts of the basic and acidic molecules in the gas phase were measured, much as in a previous work.[12]

(a) Static Method: NH_3 and CO_2 were chosen as the basic and acidic adsorbates respectively. The adsorption measurements were carried out using an ordinary BET apparatus modified to measure small areas. About a 20-g portion of the catalyst was put in an adsorption vessel (about 25 ml) and heat-treated in an electric furnace at 500 °C for 2 h under a stream of dried air. Immediately after the vessel had then been taken out of the furnace, it was quickly connected to the adsorption apparatus and pumped out. A known amount of NH_3 or CO_2 was introduced into the adsorption system, after which it was allowed to stand for 20 min before the pressure changes were read. Subsequently, the catalyst was pumped out for 30 min at the same temperature. Similar adsorption procedures were then repeated, and the amount of readsorption was measured. The amount of NH_3 or CO_2 irreversibly adsorbed at the pressure of 300 mm Hg was obtained as the difference between the amount of readsorption and that of the first adsorption; this was adopted as a measure of the acidity or basicity of the catalysts.

(b) Gas-chromatographic Pulse Technique: The apparatus used was a conventional gas chromatograph equipped with a U-tube of stainless steel (4 mm in internal diameter and 40 cm in length). The catalyst (1.0 g) was packed in the U-tube and heat-treated in a stream of air at 500 °C for 1 h. Immediately after the U-tube had then been taken out from the furnace, it was quickly connected to the gas chromatographic column, unless otherwise indicated, and placed in another

furnace kept at 130 °C or 160 °C. Then the carrier gas (He: 50 ml NTP/min) was introduced into the system.

In the case of the basicity measurements acetic acid was chosen as the acidic adsorbate, much as in previous works.[12,15,16] A sequence of the pulses of an heptane solution of 1.0 M acetic acid was injected into the U-tube (130 °C) at intervals of about 2 min. The volume of the pulses was 3—10 μl, adjusted to be about one-tenth of the total adsorption amount obtained by preliminary measurements. The adsorbate uptake was obtained from the gas chromatographic analysis at both the inlet and the exit of the U-tube. The peak of acetic acid at the exit is not observed upon the initial injections; as the number of pulse increases, the catalyst is saturated with the acetic acid, and so the peak appears. Thus, the amount adsorbed can be evaluated. Subsequently, the carrier gas was allowed to pass through for 30 min at the same temperature. Then the same procedures were repeated, and the readsorbed amount was obtained. The amount irreversibly adsorbed was obtained as the difference between the amount of readsorption and that of the first adsorption; it was adopted as a measure of the basicity.

In the case of the acidity measurements, butene pulses consisting of 2 ml of a mixture of air and 1-butene (0.7 mol%) and pyridine pulses consisting of 2—5 μl of an hexane solution of 0.25 M pyridine were fed into the U-tube (160 °C) alternately and separately; the amount of pyridine required to inhibit the isomerization of 1-butene completely was adopted as a measure of the acidity.

Catalytic-activity Measurements. The vapor-phase oxidation of 1-butene, 1,3-butadiene, and acetic acid, the isomerization of 1-butene, and the dehydration and dehydrogenation of isopropyl alcohol (IPA) were carried out in an ordinary continuous-flow-type reaction system. The concentrations of butene, butadiene, acetic acid, and IPA were about 0.67, 0.67, 1.5, and 1.65 mol% respectively in air, unless otherwise indicated. The total flow rate (at 25 °C) was kept constant at 1.5 l/min, and the amount of the catalyst used was 1.0—25 g. The reactor and the experimental and analytical procedures were the same as those employed in previous works.[6-16]

Results

Surface Areas. The surface areas of the TiO_2–MoO_3 and TiO_2–V_2O_5 catalysts were checked by the BET method using nitrogen at −195 °C. The results are shown in Table 1. The surface area increases sharply upon the addition of even 2 atom% of MoO_3 to TiO_2, but with a further increase in the MoO_3 content it gradually decreases.

Table 1. Surface area of the TiO_2–MoO_3 and TiO_2–V_2O_5 catalysts used

Composition Mo/(Ti+Mo)	Surface area (m^2/g)	Composition V/(Ti+V)	Surface area (m^2/g)
0	2.0	0	2.0
0.02	45.2	0.02	4.3
0.05	38.8	0.05	5.7
0.10	38.5	0.10	8.0
0.20	39.2	0.20	4.2
0.33	27.4	0.33	4.0
0.50	13.3	0.50	4.1
0.70	14.9	0.70	4.0
0.80	10.0	0.90	4.8
0.90	8.5	1.0	2.8
0.95	7.5		
1.0	2.6		

Acidity. Since even single TiO_2 has a fair amount of acidic sites,[4,17,18] probably of a very weak acid strength compared with the MoO_3-rich or V_2O_5-rich catalysts, NH_3 was adsorbed even on the pure TiO_2 and on the TiO_2-rich catalysts to almost the same extent as on the MoO_3-rich or V_2O_5-rich catalysts at room temperature. However, at a higher temperature (more than 350 °C), the decomposition of NH_3 was enhanced and adsorption measurement became impossible.

In the case of adsorption measurements by the pulse method, the TiO_2-rich catalysts adsorbed pyridine at 130 °C to the same extent as the MoO_3-rich or V_2O_5-rich catalysts. This means that the pure TiO_2 has a fair amount of certain acidic sites and that this method is not proper.

Therefore, as a measure of the acidity, the amount of pyridine required to poison the isomerization of butene completely was adopted.[15,16,19] However, the defect of this method is that the isomerization must be catalyzed mainly by acidic sites; when the isomerization is catalyzed by other factors, *i.e.*, when the catalyst is basic rather than acidic, this method cannot be used. To remove this defect, prior to the adsorption measurements the heat-treated catalysts were placed under a stream of a mixed gas of air and 1-butene (0.67 mol%) at 250 °C for 30 min; this was done because of the experimental evidence that, under the circumstances of the oxidation of butene, the isomerization of butene is uniquely dependent on the acidic sites of the catalyst (as will be described below).

The acidity per unit of the surface area of the TiO_2–MoO_3 and TiO_2–V_2O_5 catalysts, as determined both by the amount of NH_3 irreversibly adsorbed at 200 °C and 250 °C and by that of pyridine required to poison completely the isomerization activity for 1-butene at 160 °C, is plotted as a function of the MoO_3 or V_2O_5 content in Figs. 1 and 2.

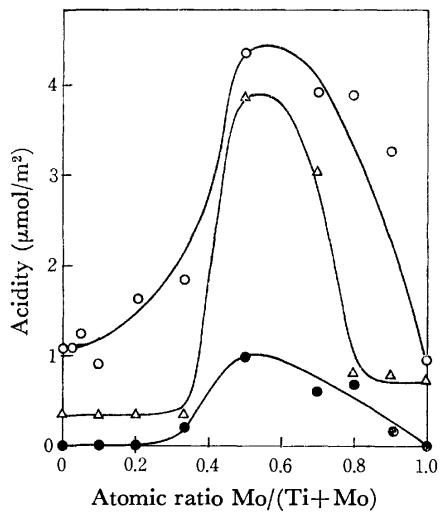

Fig. 1. Acidity of TiO_2–MoO_3 as a function of the MoO_3 content. Irreversible adsorption of NH_3 (static method) at 200 °C: ○, at 250 °C: △, pyridine required to poison the isomerization activity for 1-butene at 160 °C (pulse method): ●.

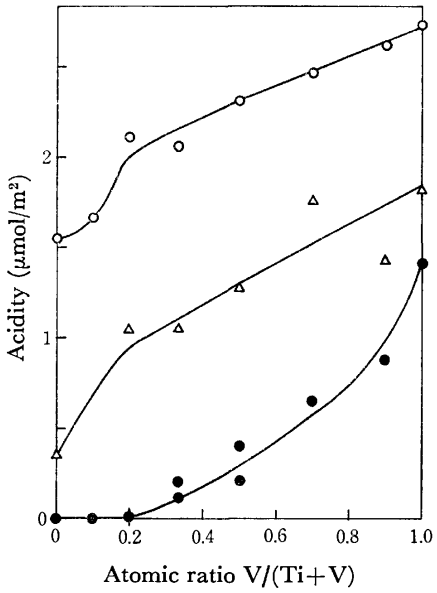

Fig. 2. Acidity of TiO_2–V_2O_5 as a function of the V_2O_5 content. Irreversible adsorption of NH_3 (static method) at 200 °C: ○, at 250 °C: △, pyridine required to poison the isomerization activity for 1-burene at 160 °C (pulse method): ●.

Parallels were found between the amounts of NH_3 obtained by means of the static method and those of pyridine obtained by means of the pulse method; these parallels may indicate the validity of these results, though the value of NH_3 was much higher than that of pyridine. It is believed that, even at 250 °C, NH_3 is still adsorbed on the acidic sites of a weak acid strength, which cannot serve to catalyze the isomerization.

The results show that the acidity is fairly low in the low range of the MoO_3 content (Mo<30 atom%), but that it increases rapidly with the MoO_3 content, shows a maximum at about Mo=40—60 atom%, and then decreases again to a very low value of pure MoO_3. It is also found that, in the case of the TiO_2–V_2O_5 catalysts, the acidity increases steadily with the V_2O_5 content.

Basicity. The basicity per unit of surface area of the TiO_2–MoO_3 and TiO_2–V_2O_5 catalysts, as determined by the irreversible adsorption of acidic molecules in the gas phase, is shown in Figs. 3 and 4 as a function of the MoO_3 and V_2O_5 content. Parallels were found between the amounts of CO_2 obtained by means of the static method and those of acetic acid obtained by means of the pulse method. The difference may be attributed to the difference in acid strength between CO_2 and acetic acid, and the acetic acid may be adsorbed on the basic sites of a lower base strength than CO_2.

It is evident at least that, with an increase in the MoO_3 and V_2O_5 content, the basicity sharply increases at first, passes through a maximum at about Mo=5 atom% or V=5 atom%, and then decreases of the very low value of the pure MoO_3 or V_2O_5 catalyst.

Dehydration and Dehydrogenation Activities for IPA. Because of the difficulty implicit in the titration method, we used, in our previous studies,[6–11,13,14] the catalytic activity for the dehydration of IPA to propylene as a measure of the acidity of the catalyst, and the (dehydrogenation rate)/(dehydration rate) ratio in the reaction of IPA as a measure of the basicity, assuming that the dehydration is catalyzed at acidic sites and that the dehydrogenation is catalyzed at both acidic and basic sites. It is, therefore, very interesting and important to confirm whether or not these measures of acidity and basicity obtained from the catalytic activities for IPA really represent their true values.

A gaseous mixture of IPA and air was passed through a bed of the catalyst held at a temperature of 165—185 °C. The amount of the catalyst was changed in the 3—30 g range. Apart from propylene and acetone, only di-isopropyl ether was found in the product, but the

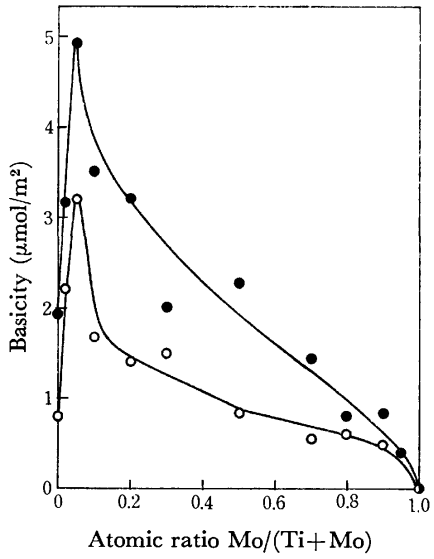

Fig. 3. Basicity of TiO_2–MoO_3 as a function of the MoO_3 content. Irreversible adsorption of CO_2 at 20 °C (static method): ○, acetic acid at 130 °C (pulse method): ●.

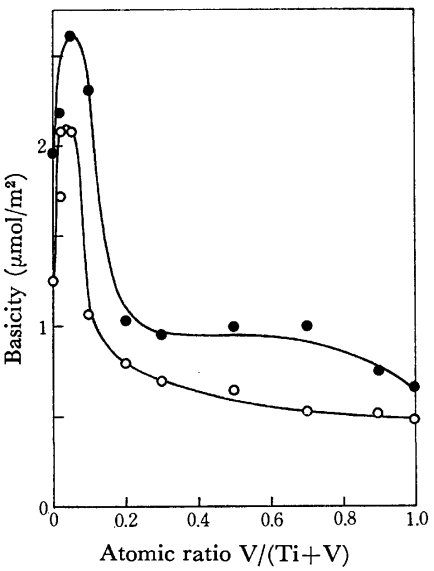

Fig. 4. Basicity of TiO_2–V_2O_5 as a function of the V_2O_5 content. Irreversible adsorption of CO_2 at 20 °C (static method): ○, irreversible adsorption of acetic acid at 130 °C (pulse method): ●.

amount of this ether was very small compared with the amount of the other two compounds. The initial rates of the dehydration and dehydrogenation at 175 °C, r_p and r_a (mol/h m²-cat), were measured; they are plotted, together with the r_p/r_a ratio, in Figs. 5 and 6.

At Mo<20 atom% or V<20 atom%, the dehydrogenation takes place rather than the dehydration, but at Mo>40 atom% or V>60 atom% the dehydration is predominant. As the content of MoO_3 or V_2O_5 increases, the values of r_p and r_a/r_p vary in the same direction as the acidity and basicity (Figs. 1—4).

Isomerization Activity for Butene. The isomerization of butene is sometimes accompanied by its oxidation. The relationship between the catalytic activity for the isomerization and the acid-base properties was investigated. The reaction was carried out at 0.67 mol% of 1-butene in air and at 225 °C by changing the catalyst amount in the 1—20 g range. As a measure of the isomerization activity, we adopted, for convenience, the ratio of (*cis*-2-C_4H_8+*trans*-2-C_4H_8)/(1-C_4H_8+*cis*-2-C_4H_8+*trans*-2-C_4H_8) corresponding to 1 m² of the catalyst, *I*.

The results are plotted as a function of the catalyst composition in Figs. 7 and 8. It is found that the isomerization activity changes in a manner similar to the acidity shown in Figs. 1 and 2.

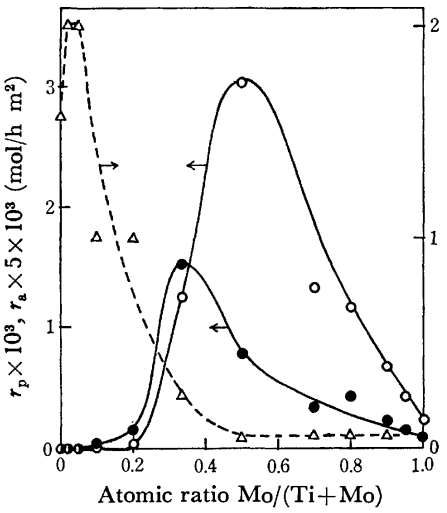

Fig. 5. The dehydration and dehydrogenation activities for IPA, r_p and r_a, and the r_a/r_p ratio as a function of the MoO_3 content.
Catalyst=TiO_2–MoO_3, T=175 °C, IRA=1.65 mol% in air, Dehydration: ○, Dehydrogenation: ●. r_a/r_p: △.

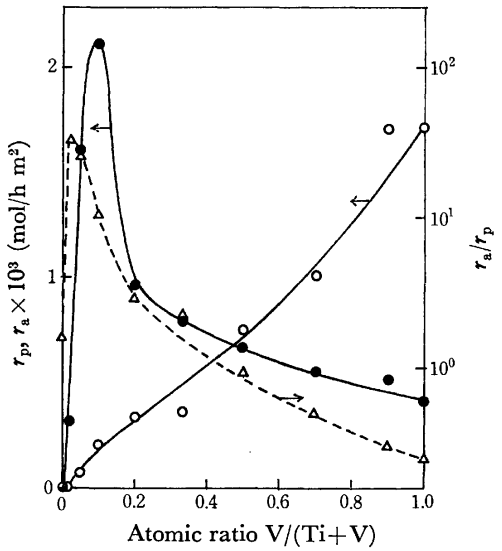

Fig. 6. The dehydration and dehydrogenation activities for IPA, r_p and r_a, and the r_a/r_p ratio as a function of the V_2O_5 content.
Catalyst=TiO_2–V_2O_5, T=175 °C, IPA=1.65 mol% in air, Dehydration; ○, Dehydrogenation: ●, r_a/r_p: △.

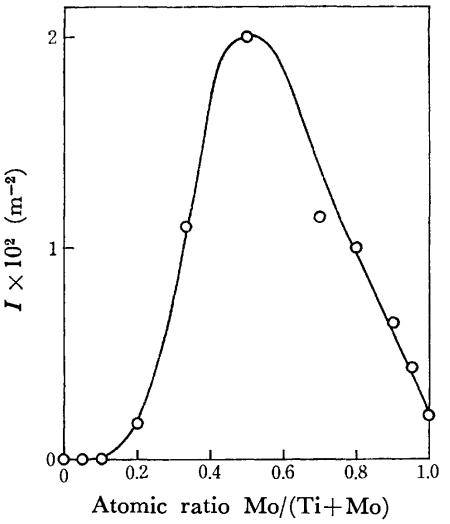

Fig. 7. The isomerization activity for 1-butene as a function of the MoO_3 content. Flow rate=1.5 l/min, 1-C_4H_8=0.67 mol% in air, T=225 °C, I=ratio of (*cis*-2-C_4H_8+*trans*-2-C_4H_8)/(1-C_4H_8+*cis*-2-C_4H_8+*trans*-C_4H_8) corresponding to 1 m² of the catalyst.

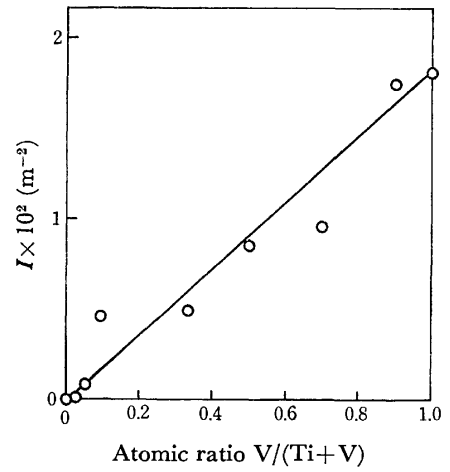

Fig. 8. The isomerization activity for 1-butene as a function of the V_2O_5 content. Total flow rate=1.5 l/min, 1-C_4H_8=0.67 mol% in air, T=225 °C,

Oxidation Activity for Butadiene. First, in order to examine the oxidation activity for basic reactants, butadiene was oxidized in an excess of air. The initial rate of the overall consumption of butadiene, at 320 °C

in the case of the TiO_2–MoO_3 catalysts and at 290 °C in the case of the TiO_2–V_2O_5, r_B (mol/h m^2-cat), was adopted, for convenience in the experimental procedures, as a measure of the oxidation activity. It is plotted as a function of the catalyst composition in Figs. 9 and 10.

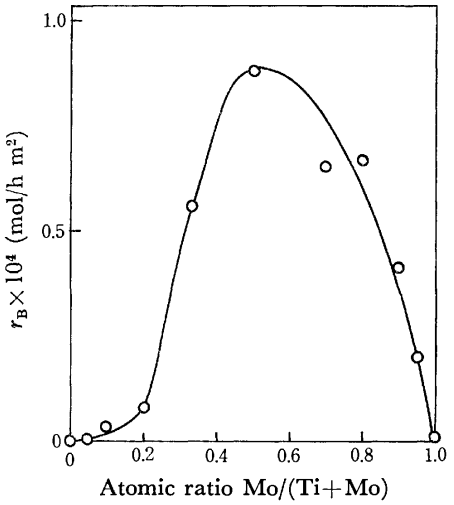

Fig. 9. The oxidation activity for butadiene as a function of the MoO_3 content. Catalyst=TiO_2–MoO_3, Butadiene=0.67 mol% in air, T=320 °C,

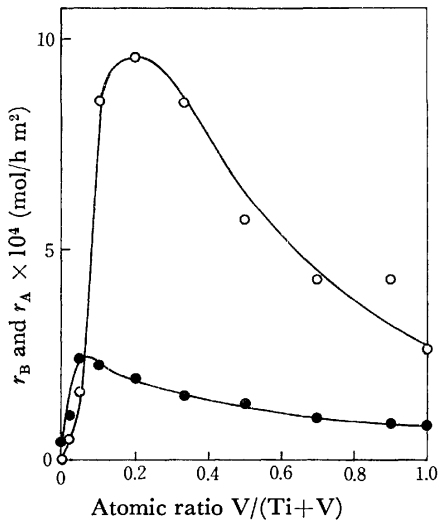

Fig. 10. The oxidation activities for butadiene and acetic acid as a function of the V_2O_5 content. Catalyst=TiO_2–V_2O_5,
○: butadiene, C_4H_6=0.67 mol% in air, T=290 °C,
●: acetic acid, $C_2H_4O_2$=1.5 mol% in air, T=290 °C.

The oxidation activity of TiO_2–MoO_3 catalysts increases with the MoO_3 content and attains a maximum at about Mo=50 atom%. The trend of the r_B curve is in agreement with that of the acidity shown in Fig. 1. On the other hand, in the case of TiO_2–V_2O_5 catalysts, the r_B increases sharply with the addition of even a small amount of V_2O_5 and attains a maximum at V=20 atom%. The trend of the r_B curve is quite different from that of the acidity shown in Fig. 2.

Oxidation Activity for Acetic Acid. Next, the oxidation activity for acidic compounds was examined in the case of TiO_2–V_2O_5 catalsts. Acetic acid was chosen as the acidic reactant, and the initial rate of the oxidation to CO_2 at 290 °C in the presence of an excess of air, r_A (mol/h m^2-cat), was taken as the oxidation activity. The results are shown in Fig. 10. The r_A increases with an increase in the V_2O_5 content and passes through a maximum at about V=10 atom%.

Selectivity in the Oxidation of Olefin. The starting materials in selective oxidations are mostly such basic compounds as olefinic and aromatic hydrocarbons. The reactions, therefore, can be divided into two types in terms of the acid-base characteristics of the products:[6,10–12,14–16]

Type 1: Basic reactant ⟶ acidic product
Type 2: Basic reactant ⟶ basic product

As a model reaction of Type 1, the oxidation of butadiene to maleic anhydride in the presence of an excess of air (0.67 mol% C_4H_8) was chosen. The

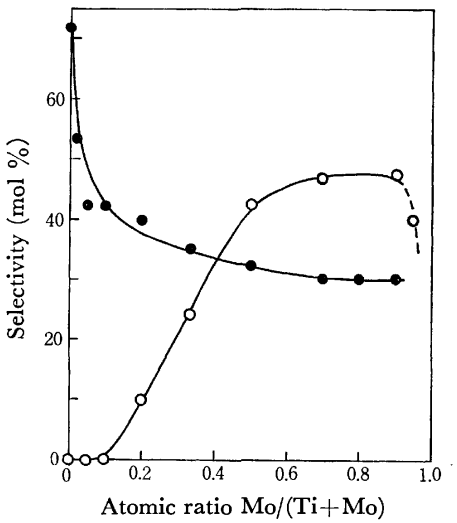

Fig. 11. Selectivity *versus* the MoO_3 content.
○: selectivity of butadiene to maleic anhydride,
●: selectivity of 1-butene to butadiene.

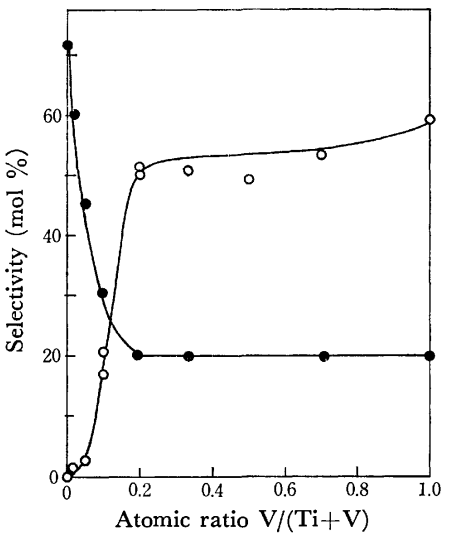

Fig. 12. Selectivity *versus* the V_2O_5 content.
○: selectivity of butadiene to maleic anhydride,
●: selectivity of 1-butene to butadiene.

selectivity at a conversion of about 40—50% was measured for every catalyst; it is plotted as a function of the catalyst composition in Figs. 11 and 12.

On the other hand, as a model of the Type 2 reactions, the oxidation of 1-butene to butadiene at a low oxygen concentration (O_2=0.34—1.3 mol% and C_4H_8=0.67 mol%) was chosen. The selectivity at a conversion of about 30—40% was measured; it is also plotted in Figs. 11 and 12.

A high selectivity to maleic anhydride is obtained over the acidic catalysts (Mo>50 atom% and V>20 atom%), while the selectivity to butadiene decreases steadily with the MoO_3 and V_2O_5 content.

Discussion

These experiments first show that the incorporation of MoO_3 and V_2O_5 induces a change in the surface area; this change directly contributes to the catalytic activity.

Next, the incorporation of MoO_3 and V_2O_5 modifies, to a significant extent, the acid-base properties of the catalyst systems. In a MoO_3-poor (Mo<20 atom%) or V_2O_5-poor (V<10 atom%) composition, the catalysts are basic; the catalysts containing more than 40 atom% Mo or 20 atom% V are acidic. It should be noted that, although MoO_3 and V_2O_5 are typical acidic elements, the incorporation of a minor amount of MoO_3 (Mo=2—10 atom%) or V_2O_5 (V=2—10 atom%) into TiO_2 remarkably enhances the basicity, much as in the cases where MoO_3 and V_2O_5 were combined with SnO_2 and Fe_2O_3.[14–16,20] This phenomenon resembles the fact that the incorporation of a minor amount of Bi_2O_3, which is a basic element, into MoO_3–P_2O_5 enhances the acidity.[10–12] The acidity per unit of the surface area of the TiO_2–MoO_3 system attains a sharp maximum at about 50 atom% Mo, much as in the case of the SnO_2–MoO_3 system. However, the acidity of the TiO_2–MoO_3 system at Mo=50 atom% is considerably lower than that of the SnO_2–MoO_3 at Mo=50 atom%.[14,16,20] The incorporation of V_2O_5 to TiO_2 never enhance the acidity per unit of the surface area more than V_2O_5 itself, unlike the case of the TiO_2–MoO_3 and MoO_3–V_2O_5 systems.[7]

A comparison of the catalytic activities for IPA with the acidity-basicity data reveals that the activity for the dehydration to propylene, r_p, respresents the acidity of the catalyst, and that the value of the r_a/r_p ratio is also valid enough as a rough index of the basicity, much as in the cases of the MoO_3–Bi_2O_3–P_2O_5,[12] SnO_2–V_2O_5,[15] and SnO_2–MoO_3 systems.[16] Therefore, this indirect method of acidity-basicity measurement, based on the catalytic activity, may be recommended especially in the cases of catalysts whose surface area are too small for the amount of adsorption to be measured.

The isomerization activity for butene is correlated only with the acidity, not with the basicity, and the product ratio of *cis*-/*trans*-2-butene is 1—2. These pieces of evidence prove that, under the circumstances of the oxidation, the isomerization is catalyzed only by the acidic sites.[4,17,18] The same results have been observed in all the catalyst systems examined by us, such as V_2O_5–MoO_3, V_2O_5–P_2O_5, MoO_3–P_2O_5, MoO_3–Bi_2O_3–P_2O_5, MoO_3–P_2O_5–X_nO_m, SnO_2–V_2O_5, and SnO_2–MoO_3.[6–16] This means that the basic sites which can also catalyze the isomerization in the absence of oxygen in a closed or a pulse-reaction system are poisoned by CO_2, H_2O, or other acidic oxidation-products under the circumstances o the oxidation.

The similarity of the r_B curve in Fig. 9 to the acidity curves in Fig. 1 suggests that, in the case of TiO_2–MoO_3 catalysts, the acidic sites play an important role in the oxidation of olefin, probably in the activation of the olefin, much as in the cases of the V_2O_5–MoO_3, V_2O_5–P_2O_5, MoO_3–P_2O_5, MoO_3–Bi_2O_3–P_2O_5, MoO_3–P_2O_5–X_nO_m, and SnO_2–MoO_3[7–14,16] systems.

On the other hand, in the case of the TiO_2–V_2O_5 system, the shapes of the r_B curves (Fig. 10) are completely different from those of the acidity curves in Fig. 2. This implies that acidic sites are not the sole factor deciding the oxidation activity for butadiene. To explain these results, we envisage that, when the catalyst is highly acidic and scarcely basic, as in the cases of the V_2O_5–MoO_3,[7] V_2O_5–P_2O_5,[8] and MoO_3–P_2O_5 systems,[9] the oxidation activity for such a basic reactant as olefin is controlled only by the activation of olefin, which is performed at the acidic sites of the catalyst. However, as the acidic property of the metal-oxide catalst decreases and as the basic property increases, the contribution of the acidic sites to the oxidation activity decreases, while that of the activation of oxygen, which is connected, presumably, with the number of basic sites, *i.e.*, O^{2-} sites, on the surface of the catalyst as well as with oxygen-mobility of the sites increases.[12,20] Practically, in the case of oxidation over such scarcely acidic catalysts as the Ni, Co, Cr, Mn, and Cu metal oxides, the oxidation activity must be controlled entirely by the activity of surface oxygen—that is, by the oxidizing power of surface oxygen.[6,21]

Therefore, it may be speculated that, in the case of the TiO_2–V_2O_5 system, both the acidic and basic sites participate in the oxidation to a certain extent; when the V_2O_5 content is low and the catalyst is rather basic, the oxidation is affected to a considerable extent by the activity of the surface oxygen, while, as the V_2O_5 content increases, the contribution of the acidic sites increases, and when the V_2O_5 content is high and the catalyst becomes highly acidic, the contribution of the acidic sites becomes predominant. The fact that the oxidation activity of the TiO_2–MoO_3 system is much lower than that of the TiO_2–V_2O_5 system, though the former has a much higher acidity than the latter, may also support the theory of the participation of the factor relating to the activation of surface oxygen.

The characteristics of the r_A curve in Fig. 10 are similar to those of the r_a curves in Fig. 6. This may suggest that basic sites play a fairly important role in the oxidation, probably in the activation of the acidic compound.[6,12,20]

It is evident at least that, when the V_2O_5 content is low (V<5 atom%) where the TiO_2–V_2O_5 catalyst is basic, the catalyst is less active for the oxidation of a base reactant such as butadiene than for the oxidation

of an acidic reactant such as acetic acid, while when the catalyst is rich in V_2O_5 content and highly acidic, the catalyst is more active for butadiene than for an acidic compound.

With regard to the selectivity, the characters of the maleic anhydride curves in Figs. 11 and 12 support our opinion[6-16] that one requirement for an effective catalyst in this type of reaction (acid-formation reaction) is the acidic property; this may be concluded for two reasons: (1) the acidic catalyst is active in the oxidation of the reactant, and (2) it is inactive in the degradation of the acidic compound produced. On the other hand, the character of the curve of the butadiene formation may reveal that TiO_2 itself has both the acidic and basic properties proper to the selectivity of this type of reaction (base-formation reaction) and that the increase in the acidic character as a result of the MoO_3 or the V_2O_5 addition leads to a decrease in the selectivity. It should be noted that, in the cases of SnO_2 and Fe_2O_3, which are less acidic and more basic than TiO_2,[14,16,20] the selectivity increases with the addition of a small amount of such acidic elements as MoO_3 and V_2O_5. It seems probable that the presence of the acidic character is desirable in enhancing the activity for the reactant; however, when the acidic character is too high, butadiene is oxidized more rapidly than butene,[10-12] because butadiene is more basic that butene (the ionization potential of butadiene 8.75—9.18 eV, is lower than that of butene, 9.3—9.8 eV). These results also support our opinion[6-16] that one requirement for an effective catalyst in a base-formation reaction is a moderate character both in an acid and a base.

It can be concluded that the oxidation activity and selectivity of the TiO_2–MoO_3 and TiO_2–V_2O_5 catalysts can be relatively well interpreted in connection with their acid-base properties, which are strongly changed by the catalyst composition.

References

1) D. J. Hucknall, "Selective Oxidation of Hydrocarbons," Academic Press, London/New York (1974).
2) T. Ohara, *Yuki Gosei Kagaku Kyokai Shi*, **29**, 51 (1971).
3) K. Tarama, "Hannobetsu Jitsuyo Shokubai (List of Practical Catalysts)," Kagakukogyosha, Tokyo (1970).
4) M. Itoh, H. Hattori, and K. Tanabe, *J. Catal.*, **35**, 225 (1974).
5) K. Tanabe, C. Ishiya, I. Ichikawa, and H. Hattori, *Bull. Chem. Soc. Jpn.*, **45**, 47 (1972).
6) M. Ai and S. Suzuki, *Shokubai*, **15**, 159p (1973).
7) M. Ai and S. Suzuki, *Nippon Kagaku Kaishi*, **1973**, 260.
8) M. Ai and S. Suzuki, *Bull. Chem. Soc. Jpn.*, **47**, 3074 (1974).
9) M. Ai and S. Suzuki, *J. Catal.*, **30**, 362 (1973).
10) M. Ai and S. Suzuki, *J. Catal.*, **26**, 202 (1972).
11) M. Ai and S. Suzuki, *Bull. Jpn. Petrol. Inst.*, **16**, 118 (1974).
12) M. Ai and T. Ikawa, Preprint of 35th Shokubai (Catalyst) Meeting (Sendai), p. 88 (1974): *J. Catal.*, **40**, 203 (1975).
13) M. Ai and S. Suzuki, *Bull. Jpn. Petrol. Inst.*, **15**, 18 (1973).
14) M. Ai, Preprint of 7th Sanka-hanno (Oxidation reaction) Meeting (Nagoya), p. 98 (1973).
15) M. Ai, *J. Catal.*, **40**, 318 (1975).
16) M. Ai, *J. Catal.*, **40**, 327 (1975).
17) K. Tanabe, "Solid Acids and Bases," Kodansha, Tokyo and Academic Press, London/New York (1970).
18) K. Morishige, H. Hattori, and K. Tanabe, *Shokubai*, **17**, 29p (1975).
19) Y. Murakami, F. Nozaki, and J. Turkevich, *Shokubai* **5**, 262 (1963).
20) M. Ai and T. Ikawa, *Shokubai*, **17**, 10p (1975).
21) W. M. H. Sachtler and N. H. de Boer, *Proc. Intern. Congr. Catal.* 3rd, (Amsterdam, 1964), **I**, 252 (1965).

Identification of Stereoisomers of Methyl Hexopyranosides by Mass Spectrometry of Their Trifluoroacetates

Susumu ANDO,* Toshio ARIGA,** and Tamio YAMAKAWA

Department of Biochemistry, Faculty of Medicine, University of Tokyo, Hongo, Bunkyo-ku, Tokyo 113

(Received September 20, 1975)

The mass spectra of the trifluoroacetates of methyl hexopyranosides and their partially deuterated derivatives were measured. The trifluoroacetyl derivatives were found to be very useful for identification of some stereoisomeric hexoses. The mass spectra were characterized by abundant peaks in the high mass range, the presence of a recognizable molecular ion, and sensitive spectral differences due to different stereoisomers. Glucose, galactose and mannose were distinguished from each other by comparing the intensities of the fragment ions due to the loss of trifluoroacetyl groups or cleavage of the pyranose ring. Alfa and β-anomers were distinguished by differences in the abundance of fragment ions produced by the loss of glycosidic methoxyl groups.

Monosaccharides have been examined by measuring the mass spectra of their methyl,[1,2] acetyl,[3] trimethylsilyl (TMS)[4-6] and isopropylidene derivatives.[7,8] However, use of the mass spectra of these derivatives has the disadvantages of the absence of a molecular ion and small differences in the specral patterns of different stereoisomers (*e.g.* epimers or anomers). Chizhov *et al.*[9] reported that the trifluoroacetyl (TFA) derivatives of alditols give sufficiently intense molecular ions to allow direct determination of their molecular weights. TFA derivatives were previously used in gas chromatographic analysis of methyl glycosides because of their high volatility.[10,11] The present paper reports studies on the mass spectra of the TFA derivatives of methyl hexopyranosides. The major fragmentation processes are proposed on the basis o results of deuterium-labeling experiments.

Experimental

Methyl α-D-glucopyranoside (Ia) and methyl β-D-glucopyranoside (Ib) were obtained from Sigma Chemical Co. Methyl α-, and β-D-galactopyranosides (IIa and IIb) were prepared by refluxing D-galactose with 1% methanolic HCl and were separated by Dowex (1×4) column chromatography as described by Matsushima and Miyazaki.[12] Methyl α-, and β-D-mannopyranosides (IIIa and IIIb) were obtained in a similar way. Deuteriomethyl α-, and β-D-galactopyranosides (VIa and VIb) were also prepared with the use of methanol-d_4 instead of methanol.

Methyl α-, and β-D-Glucopyranoside-2-d and Deuteriomethyl α-, and β-D-Glucopyranoside-2-d (IVa, IVb, Va, and Vb). Deuteration of the C_2 position was carried out as described by Lemieux and Stevens.[13] 2-*O*-benzyl-D-glucose[14] (750 mg) was dissolved in 3 ml of deuterium oxide (d, 99.5%) and lyophilized. The treatment was repeated three times. The lyophilized material was then dissolved in 3 ml of 1.7 M NaOD, and left to stand for 10 days at room temperature. The solution was neutralized with acetic acid-d_1 and extracted five times with 10 ml volumes of ethyl acetate. The extracts were combined and evaporated to dryness. The residue was recrystallized from ethyl acetate to yield 670 mg of 2-*O*-benzyl-D-glucose-2-*d*; mp, 176—178 °C; NMR(D_2O) ppm, 5.26(1-H_{eq}, singlet), 4.70 (1-H_{ax}, singlet), 7.4 (phenyl protons). 2-*O*-benzyl-D-glucose-2-*d* (600 mg) was dissolved in 20 ml of 95% ethyl alcohol and subjected to hydrogenolysis for 24 h under atmospheric pressure with 5% Pd on charcoal. The reaction mixture was filtered and evaporated to yield 540 mg of D-glucose-2-*d*; syrupy; NMR (D_2O) ppm, 5.24 (1-H_{eq}, singlet), 4.94 (1-H_{ax}, singlet). No detectable phenyl proton. Methyl α-, and β-glucopyranoside-2-*d* (IVa and IVb) and deuteriomethyl α-, and β-glucopyranoside-2-*d* (Va and Vb) were derived from D-glucose-2-*d* using acidic methanol and deuteriomethanol, respectively. Each anomer was purified by Dowex 1 column chromatography as described above.

Methyl α-, and β-D-glucopyranoside-6-d_2 (VIIa and VIIb). To a solution of methyl D-glucuronic acid methyl ester (100 mg) in 2 ml of water was added dropwise a solution of $NaBD_4$ (50 mg) in 3 ml of cold water. The mixture was left to stand for 6 h at room temperature, treated with Dowex 50 (H^+ form) and IR-45 (OH^-), and evaporated to dryness. VIIa and VIIb were separated on a column of Dowex 1.

Trifluoroacetylation of Sugars. The dried material (3 mg) was allowed to react with a mixture of 0.1 ml of ethyl acetate and 0.2 ml of trifluoroacetic anhydride at 100 °C for 8 min.[10] The reaction mixture was then evaporated under a stream of nitrogen at 40 °C and the residual trifluoroacetic acid was removed as an azeotropic mixture with carbon tetrachloride.

Mass spectra were measured on a Hitachi model RMS-4 mass spectrometer, temperature of the ion source being 200°C, ionizing potential 70 eV and accelerating voltage 3 kV. Samples were vaporized in a 1 l glass reservoir at 140 °C. Mass spectra were recorded on a photographic chart. Peak intensities were expressed in percentage of that of total ions above *m/e* 100 (% Σ_{100}).

Results and Discussion

The physical properties of the methyl hexopyranosides used are listed in Table 1. The deuterium contents in the deuterated sugars were determined from the isotope peaks. The deuterium content at position C_2 of IVa was 95.8% and that at C_6 of VIIa 97.1%. The deuterium content in the methoxyl group of VIa was 98.2%.

The major fragment ions of the TFA derivatives of methyl glucosides, galactosides and mannosides are listed in Table 2. The TFA derivatives of hexopyranosides all showed a molecular ion (*m/e* 578), whereas the acetyl,[3] methyl[1,2] and TMS derivatives[4-6] of monosaccharides gave $(M-CH_3CO)^+$, $(M-CH_3O)^+$ and $(M-CH_3)^+$, respectively, as the highest ions.

* Present address: Department of Biochemistry, Tokyo Metropolitan Institute of Gerontology, 35—2 Sakae-cho, Itabashi-ku, Tokyo 173.

** Present address: Sankyo Ltd., Central Research Laboratory, 1-2-58 Hiromachi, Shinagawa-ku, Tokyo 140.

Table 1. Physical properties of methyl hexopyranosides

Compound	mp, °C	$[\alpha]_D^{17}$ in H_2O
Ia	167—8	+158.2
Ib	107—8	− 28.6
IIa	112—3	+193.5
IIb	175—8	0
IIIa	191—2	+ 84.6
IIIb	66—9	− 64.0
IVa	167—9	+160.9
IVb	105—7	− 30.9
Va	165—7	+152.7
Vb	106—7	− 29.2
VIa	108—111	+193.9
VIb	174—7	+ 0.8
VIIa	166—8	+156.2
VIIb	103—6	—

Table 2. Relative intensities ($\%\sum_{100}$) of major fragment ions of methyl *O*-TFA hexopyranosides. *m/e* 177 was base peak in all the compounds tested.

Fragment ions *m/e*		Ia	Ib	IIa	IIb	IIIa	IIIb
M^+	578[a)]	0.05	0.11	0.06	0.14	0.04	0.08
g	547[b)]	0.04	0.02	0.07	0.04	0.08	0.02
a	465	1.54	1.49	1.42	1.48	1.78	1.00
d	405	4.30	4.17	3.20	4.37	4.94	3.66
	404	2.02	1.75	0.89	1.18	2.11	1.57
b	351	0.75	1.07	1.70	1.36	1.27	0.65
h	319[b)]	2.06	1.05	1.70	0.96	2.20	0.92
e	291[c)]	2.50	2.50	1.85	1.88	2.94	2.64
j	265[c)]	2.92	2.64	0.99	1.75	3.03	2.90
k	252[c)]	1.35	1.39	0.55	0.92	1.54	1.46
c	237[c)]	1.99	2.35	0.99	2.16	3.48	2.82
	221	1.30	1.26	0.58	0.82	1.58	1.31
i	205[b)]	0.41	0.21	0.28	0.16	0.41	0.21
	196	1.47	1.36	0.63	1.33	1.13	1.63
l	193	2.44	2.64	1.22	2.39	2.73	2.54
m	183	1.97	1.77	0.98	1.73	2.72	2.09
f	177	13.21	11.87	8.33	14.60	12.90	12.49
n	170	4.92	2.73	1.80	1.88	7.55	4.10
p	157	6.30	3.72	2.73	3.37	8.62	5.23
o	153	2.30	2.50	1.43	2.80	2.32	2.69
	149	5.93	5.68	4.42	8.93	6.00	6.64
	129	3.62	2.80	2.01	3.28	4.17	3.39
	109	2.25	1.75	1.60	2.62	2.19	2.32

a) Peak intensity of β-anomer is greater than that of the corresponding α-anomer. b) Peak intensity of α-anomer is greater than that of the corresponding β-anomer. c) Intensities decrease in the order of mannoside, glucoside and galactoside.

A typical mass spectral pattern of the TFA derivative of methyl α-D-glucopyranoside is shown in Fig. 1-b, with that of the corresponding TMS derivative (Fig. 1-a) for comparison. Relatively abundand peaks were observed in the high mass range (above *m/e* 177) of the spectra of the TFA derivatives, whereas the mass spectra of the methyl,[1,2] acetyl[3] or TMS derivatives were characterized by peaks of extremely low intensity

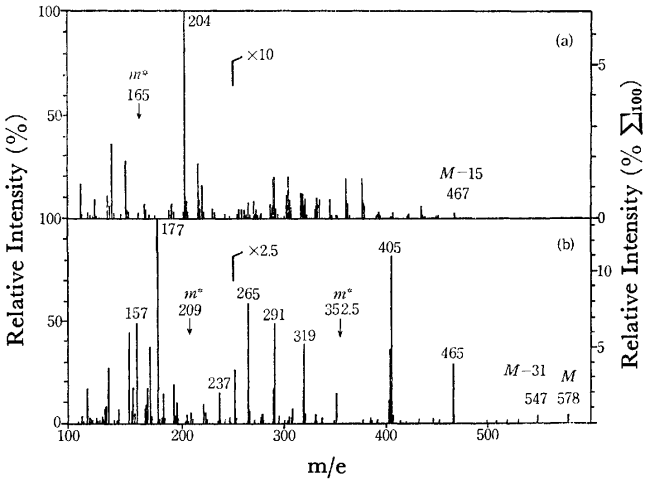

Fig. 1. Mass spectra of (a) TMS- and (b) TFA-derivatives of methyl α-D-glucopyranoside.

in the high mass range. TFA groups may effectively stabilize the molecular and fragment ions in the high mass range.

Fragmentation Process. Three modes of fragmentation are presented. The fragmentation mode in series **A** (Scheme 1) was produced by sequential elimination of

Scheme 1. Fragmentation due to elimination of TFA groups and ring scission at C_1–C_2 and C_5–O (series **A**).
Relative intensities are shown in parentheses.

Molecular ion	−TFA → **a**	−TFA → **b**	−TFA → **c**[c)]
Ia	465 (1.54)	351 (0.75)	237 (1.99)
IVa	466 (1.33)	351 (0.36)	237 (1.22)
		352 (0.51)	238 (1.08)
VIa	468 (1.61)	354 (1.24)	240 (1.73)
VIIa	467 (1.14)	353 (0.78)	238 (0.40)
			239 (2.62)
	↓ −60		
	d	−TFA → **e**	−TFA → **f**
Ia	405 (4.30)	291 (2.50)	177 (13.21)
IVa	406 (4.58)	292 (2.53)	178 (12.61)
VIa	405 (4.39)	291 (3.11)	177 (13.89)
VIIa	406 (2.32)	292 (0.93)	178 (7.07)
	407 (4.58)	293 (2.49)	179 (4.57)

c) Intensities decrease in the order of mannoside, glucoside and galactoside.

TFA groups. A similar sequential elimination of TFA groups was reported in the mass spectra of TFA alditols.[9] In the course of the fragmentation, ring scissions occurred at C_1–C_2 and C_5–O bonds to produce the fragment ions *m/e* 405(**d**) or 404. The fragment ion **d** further released TFA groups to yield the ions **e** and **f**. These degradation processes were confirmed by the presence of the following metastable ions: *m/e* 352.5 (*m/e* 465→405), *m/e* 209.0 (*m/e* 405→291) and *m/e* 107.5 (*m/e* 291→177). All the deuterium atoms of IVa

Table 3. Fragment ions derived from methyl α-glucopyranoside and its deuterated compounds by ring scissions (series **C**)

Compound	Fragment ion, *m/e* (%Σ_{100})						
	j	**k**	**l**	**m**	**n**	**p**	**o**
Ia	265 (2.92)	252 (1.35)	193 (2.44)	183 (1.97)	170 (4.92)	157 (6.30)	153 (2.30)
IVa	265 (0.70)	252 (0.13)	193 (0.34)	183 (0.80)	170 (0.55)	157 (6.47)	153 (1.51)
	266 (2.07)	253 (1.23)	194 (2.15)	184 (1.47)	171 (5.32)		154 (1.14)
Va	265 (0.39)	252 (0.15)	193 (0.38)	183 (0.52)	170 (0.95)	160 (6.04)	153 (1.63)
	266 (1.90)	253 (1.18)	194 (2.14)	186 (0.72)	171 (0.50)		154 (1.14)
				187 (1.42)	173 (0.37)		
					174 (5.54)		
VIIa	265 (3.04)	252 (1.65)	193 (0.72)	183 (2.50)	170 (4.26)	157 (6.31)	153 (1.20)
			194 (0.55)		171 (1.78)		154 (1.20)
			195 (1.79)				155 (2.20)

and VIIa remained in fragment **a**, and 2-**d** (IVa) and 6-d_2 (VIIa) were still retained in **d** and **b**, respectively. The fragmentation, **c**→**f**, seems unlikely, because of the difference in the deuterium contents of the two fragments. The deuterium content at the C_2 position of fragment ion **c** was reduced to 47%, but not the deuterium content of fragment ion **f**. During the fragmentation from M^+ to **c**, elimination of TFA groups caused only a little loss of the hydrogens at the C_6 position. After the ring scissions at C_1–C_2 and C_5–O bonds, sequential elimination of TFA groups was not accompanied by removal of the hydrogen at the C_2 position. Scarcely any fragment ions due to loss of F-, CF_3-, or CF_3CO- radicals were detected.

The second fragmentation mode in series **B** was characterized by elimination of the methoxyl group from the parent molecule or the fragments **b** or **c** without ring opening (Scheme 2).

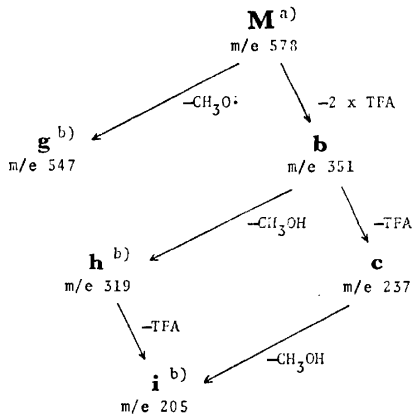

Scheme 2. Fragmentation due to elimination of methoxyl groups (Series B).
a) Peak intensity of β-anomer is greater than the corresponding α-anomer. b) Intensity of α-anomer, greater than the corresponding β-anomer.

The third mode of fragmentation in series **C** included several kinds of ring scissions. Simultaneous cleavage of C_1–C_2 and C_5–O linkages produced fragment ion *m/e* 405 from the tris-TFA fragment (**a**, *m/e* 465) (Scheme 1). The path was confirmed by the loss of deuteriomethoxyl groups from the corresponding fragment ion **a** of VIa and VIb. Other ring scissions produced some characteristic ions, *m/e* 265, 252, 193, 183, 170, 157 and 153, from the fragments **a**, **b** and **c** (Table 3).

Differentiation of Anomers. The relative intensities of the molecular ions of β-anomer were more than twice those of α-anomers (Table 2). Similar phenomena have been observed with the methyl ethers of methyl hexosides.[1,2] However, the difference in abundance of the high mass fragments of the methyl derivatives was not so large. The TFA derivatives of gluco-, galacto- and mannopyranosides gave reproducible results when they were introduced into a mass spectrometer through a heated reservoir or a gas chromatograph. The two anomers of the TFA derivatives were also distinguished by the difference in abundance of the fragment ions produced by the loss of glycosidic methoxyl groups (series **B**, Scheme 2, Table 2). The relative intensities of the fragment ions, **g**, **h** and **i**, derived from the α-anomers were about twice as large as those of the corresponding fragments from β-anomers. The difference in abundance of these ions may be caused by steric effects of the configuration of methoxyl groups.

Differentiation of Epimers. Differences in the spectra of some epimers have been reported.[2,3,7] Kochetkov and Chizhov[2] studied methylated hexosides and reported that the abundance of the fragment *m/e* 149 from galactose and that of the fragment *m/e* 145 from mannose were relatively large. DeJongh and Biemann[7] found differences in the spectra of the isopropylidene derivatives of glucose, galactose and mannose. However, no significant difference was observed between the spectra of acetylated hexoses.[3]

The TFA derivatives of glucose, galactose and mannose could be distinguished from each other by the abundance of various fragments (Table 2). In particular, differences in the abundance of the fragment ions, **c**, **e**, **j** and **k**, could be used to differentiate these monosaccharides. The two former ions are produced in the fragmentation process of series **A**, and the two latter in the process of series **C**.

References

1) N. K. Kochetkov, N. S. Wulfson, O. S. Chizhov, and B. M. Zolotarev, *Tetrahedron*, **19**, 2209 (1963); *ibid.*, **21**, 2029 (1965).

2) N. K. Kochetkov and O. S. Chizhov, *Biochim. Biophys. Acta*, **83**, 132 (1964).

3) K. Biemann, D. C. DeJongh, and H. K. Schnoes, *J. Am. Chem. Soc.*, **85**, 1763 (1963).
4) D. C. DeJongh, T. Radford, J. D. Hribar, S. Hanessian, M. Bieber, G. Dawson, and C. C. Sweeley, *J. Am. Chem. Soc.*, **91**, 1728 (1969).
5) O. S. Chizhov, N. V. Molodtsov, and N. K. Kochetkov, *Carbohydrate Res.*, **4**, 273 (1967).
6) J. Vink, J. H. W. BruinsSlot, J. J. de Ridder, J. P. Kamerling, and J. F. G. Vliegenthart, *J. Am. Chem. Soc.*, **94**, 2542 (1972).
7) D. C. DeJongh and K. Biemann, *J. Am. Chem. Soc.*, **86**, 67 (1964).
8) K. Biemann, H. K. Schnoes, and J. A. McClosky, *Chem. Ind. (London)*, **1963**, 448.
9) O. S. Chizhov, B. A. Dmitriev, B. M. Zolotarev, A. Ya. Chernyak, and N. K. Kochetkov, *Org. Mass Spectrometry*, **2**, 947 (1969).
10) S. Ando and T. Yamakawa, *J. Biochem.*, **70**, 335 (1971).
11) S. Ando, T. Ariga, and T. Yamakawa, *J. Biochem.*, **73**. 663 (1973).
12) Y. Matsushima and T. Miyazaki, *J. Biochem.*, **55**, 464 (1964).
13) R. U. Lemieux and J. D. Stevens, *Can. J. Chem.*, **44**, 249 (1966).
14) A. Klemer, G. Drolshagen, and H. Lukonesky, *Chem. Ber.*, **96**, 634 (1963).

Cyanamide Derivatives. Part 99.* Electrolytic Oxidation of Cyanamide

Koji KUBO,** Tsutomu NONAKA, and Keijiro ODO

Department of Electrochemistry, Tokyo Institute of Technology, Ookayama, Meguro-ku, Tokyo 152

(Received September 25, 1975)

Cyanamide was electrochemically oxidized with a platinum anode in aqueous potassium hydroxide. Electrolysis was carried out at 1.30 V *vs.* SCE of anode potential. Oxidation products consist of several unknown 1,2,3,5-tetrazine compounds and known linear cyano compounds.

A number of studies have been performed on the catalytic and electrolytic reduction of cyanamide, but only one paper dealing with the oxidation of cyanamide was published by Calcagni and Lazzari.[1] They electrolyzed cyanamide in aqueous sulfuric acid but gave no details except for the formation of nitric and nitrous acids.

Cyanamide is considerably stable in strongly alkaline and acidic solutions because it is an amphoteric compound, while it is easily converted into dicyandiamide by dimerization and into urea by hydration in weakly alkaline and acidic solutions, respectively. Potassium hydroxide was used as an electrolyte in this work. The advantage of a strongly alkaline electrolyte is not only that cyanamide can be stabilized but also that its anionic form ($NC-NH^-$ or $NC-N^{2-}$) favorable to migration to an anode surface can be formed.

Results and Discussion

Cyanamide was electrolyzed with a platinum anode in 2 M potassium hydroxide. Several products were isolated from the anolyte neutralized with hydrochloric acid or carbon dioxide.

Of the products, dicyanoimine(I), cyanourea(II), and dicyandiamide(III) are known compounds and were identified with authentic samples, while the structures of VII and VIII could not been confirmed. Cyanic acid in the form of potassium salt was also confirmed IR-spectroscopically without being isolated. On the other hand, 4-amino-6-cyanamino-1,2,3,5-tetrazine (IV), 4-amino-6-cyanoguanidino-1,2,3,5-tetrazine(V), and 4-ureido-6-cyanoguanidino-1,2,3,5-tetrazine(VI) are new compounds with a rare 1,2,3,5-tetrazine ring.[2] Their structures were confirmed as follows.

The potassium salts of these compounds exhibited the absorption for C≡N and cyclic –N=N–N– groups at 2160—2190 and 1200—1300 cm^{-1},[3] respectively.

IV was converted into V by addition of cyanamide in aqueous potassium carbonate.

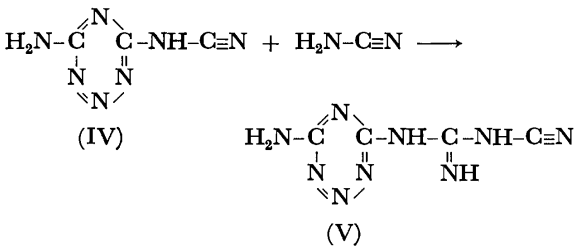

(IV) (V)

Amidinobiuret and nitrogen were formed in 73 and 80% yields, respectively, when IV was warmed at 40 °C in dilute sulfuric or hydrochloric acid. Neither carbon dioxide nor ammonia was detected. IV also decomposed slowly,

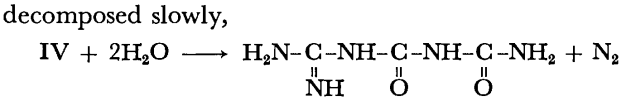

accompanied by evolution of nitrogen in aqueous potassium hydroxide at room temperature, and finally giving ammeline in a 45% yield after being left to stand for 24 h. The decomposition seems to involve cyanoamidinourea or cyanocarbamoylguanidine as an intermediate.[4]

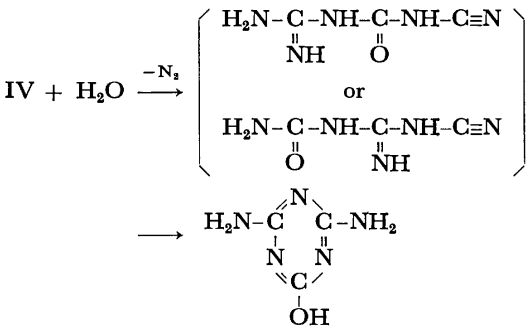

In order to obtain the free acid of IV, hydrogen chloride gas was introduced into a dry acetone solution of potassium salt of IV. The resulting precipitate was not the desired free acid but the hydrochloride of a base which gave 2,4-diamino-6-chloro-1,3,5-triazine by treatment with water. The basic intermediate exhibited no absorption for –C≡N group. It is presumed to be 4-amino-6-(iminochloromethyl)amino-1,2,3,5-tetrazine on the basis of its elemental analysis.

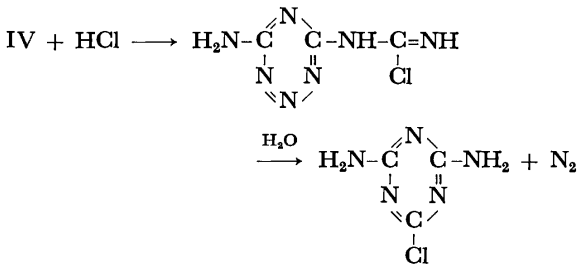

V decomposed to melamine (yield, 88%), ammonia (91%), carbon dioxide (63%) and nitrogen (82%), when heated in dilute minearal acid.

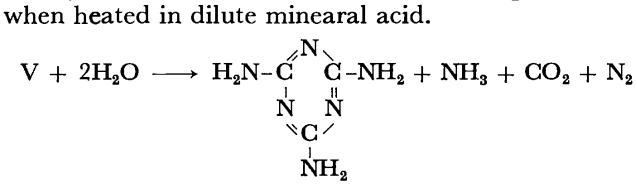

* Part 98: *J. Syn. Org. Chem. Jpn.*, **34**, 417 (1976).

** Present address: Bridgestone Tire Co., Ltd., 2800-1, Ogawahigashi-machi, Kodaira, Tokyo 178

TABLE 1. PROPERTIES OF PRODUCTS

Compounds (Formula)	IR spectrum cm^{-1}	UV spectrum λ_{max} (log ε) nm in CH_3OH	in H_2O	in 2×10^{-3} M KOH	D.p. °C	Appearance
IV($C_3H_2N_7K$)	3360, 3130, 2190 1645, 1550, 1451 1270, 1196, 1018	320 (4.34)			171	Pale yellow fine needles
V($C_4H_4N_9K$)	3350, 3160, 2180 1675, 1630, 1525 1230, 986		335 (4.43)	334 (4.43) 205 (3.77)	225	Yellow needles
V($C_4H_5N_9$)	3300, 3150, 2210 1660, 1588, 1414 1245, 1012, 930	333 (4.24) 306 (4.22)		336 (4.27) 226 (4.00)	130[a]	Yellow powder
VI($C_5H_4N_{10}OK_2$)	3350, 3150, 2160 1610, 1510, 1272 1190, 1080, 982		340 (4.52)	340 (4.53) 214 (4.00)	217	Yellow granules
VII($C_3H_2N_7O_2K$)	3450, 3330, 2180 1650. 1314, 1281 1155, 995		301 (4.34)		131	Yellow needles
VIII(?)	3400, 3170, 2160 1700, 1596, 1355 1230, 1089, 948		299 (—)		162	White powder

a) Explosive.

TABLE 2. RESULTS OF ELECTROLYSIS OF CYANAMIDE

Neutralizing reagent of anolyte	Yield of products g (%) I[b]	II	III	IV[c]	V[c]	VI[d]	VII	VIII	N_2[e]	Recovered cyanamide[f] g (%)
HCl	0.72 (8)	+	—	0.84 (19)	0.04 (1)	—	+	+	5	0.18 (1)
CO_2	0.70 (8)	+	+	0.20 (5)	1.11 (26)	0.35 (7)	—	+	5	0.45 (2)

a) 0.101 F of electricity was passed through an anolyte containing 4.20 g (0.10 mol) of cyanamide.
b) Monoammonium salt. c) Monopotassium salt. d) Dipotassium salt. e) ml under 1 atm at 0 °C.
f) Disilver salt.

VI also decomposed to melamine (yield, 80%), ammonia, carbon dioxide and nitrogen under similar conditions.

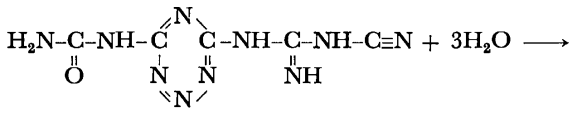

(VI)

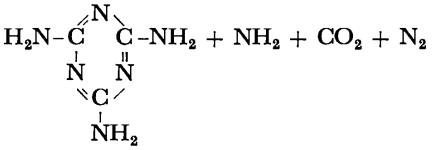

No detailed mechanism could be established for hydrolytic decompositions of IV, V and VI. However, the above results might bring some reliable information for determination of the structures of these compounds. At least the formation of amidinobiuret and 2,4-diamino-6-chloro-1,3,5-triazine suggests the existence of the skeletons of N–C–N–C–N–C≡N and N–C–N–C–N–C≡N, respectively. The evolution of nitrogen in the course of decomposition also suggests that a –N=N– bond is involved in IV. The most probable structure of IV is thus represented as shown above. It is further supported by the fact that the decomposition of V derived from IV is reasonable from a stoichiometric aspect.

Only V could be successfully converted into the corresponding free acid. Although the free acid gave no molecular peak even in a high resolution mass spectrum measured carefully because of its thermolability, the spectrum indicated a N_3^+ fragment at *m/e* 42.0109 (pattern coefficient, 26%; calcd *m/e* 42.0125). This is an evidence for the existence of the –N=N–N– group. The highest *m/e* value of peak in the spectrum was 151.0601 (pattern coefficient, 15%) corresponding to a $C_4H_5N_7^+$ fragment (calcd *m/e* 151.0606) formed by elimination of N_2 from a molecule ($C_4H_5N_9$). The properties and the amounts of the products are listed in Tables 1 and 2, respectively.

The distribution of products derived from an anolyte neutralized with hydrochloric acid differs from that derived from the one neutralized with carbon dioxide. This suggests that an unstable intermediate may be left active in an anolyte even after electrolysis.

Experimental

Electrolytic Cell and Procedure. An H-type cell divided with a sintered glass diaphragm was used. Both anode and cathode were platinum plates (3×4 cm). 75 ml of 2 M potassium hydroxide was used as anolyte and catholyte. 4.20 g (0.10 mol) of cyanamide was added to the anolyte and electricity was supplied. The anode potential and the temperature of anolyte were maintained at 1.30 V *vs.* SCE (an initial anodic current density, 20 amp/dm²) and below 10 °C,

respectively, during electrolysis. When the anodic current density lowered to 2 amp/dm^2 after 3.5 h, electricity was turned off. The amount of passed electricity was 1.01 F/mol.

Separation of Products. After electrolysis, the anolyte was neutralized to pH 8—9 with carbon dioxide and then evaporated to dryness under reduced pressure at below 20 °C.[5] The residue was extracted with 150 ml of acetone. When the insoluble solid in acetone was treated with 50 ml of water, the crude monopotassium salt of V, which was purified by recrystallization from water, was left as a yellow solid. Found: C, 22.11; H, 2.18; N, 58.70%. Calcd for $C_4H_4N_9K$: C, 22.11; H, 1.86; N, 58.63%. The aqueous solution was neutralized to pH 6.5 with hydrochloric acid and 400 ml of ethanol was added. The resulting precipitate (potassium hydrogen carbonate) was filtered off and the filtrate was evaporated to dryness. When the residue was treated with 10 ml of water, dipotassium salt of VI, which was recrystallized from a small amount of water, was left as a yellow solid. Found: C, 20.29; H, 1.28; N, 47.63%. Calcd for $C_5H_4N_{10}OK_2$: C, 20.13; H, 1.35; N, 46.95%. 50 ml of ethanol was added to the aqueous solution and the resulting precipitate (potassium carbonate) was filtered off. After aqueous ammonia was added to the filtrate, it was evaporated to dryness. When the residue was extracted with 10 ml of acetone, monoammonium salt of II was left as a white solid. The ammonium salt was dissolved in dilute hydrochloric acid and the solution was evaporated to dryness. The residue was treated with ethanol in order to remove ammonium chloride. When the ethanolic solution was again evaporated to dryness, the free acid of II, which was recrystallized from ethanol, was left as a white solid. When the acetone solution was evaporated to dryness, ammonium salt of I, recrystallized from a mixture of acetone and ether, was left as white needles.

On the other hand, when the acetone solution prepared at the first stage was concentrated to one-third of its original volume, a small amount of VIII, which was recrystallized from acetone, crystallized out of the solution as white powder. Found: C, 16.62; H, 1.22; N, 49.24%. The structure of VIII could not be determined. The acetone solution was evapoated to dryness and the residue was extracted with ether. The ether extract was again evaporated to dryness and the residue was dissolved in dilute ammonia. When an aqueous solution of silver nitrate was added to the ammoniacal solution, disilver salt of recovered cyanamide precipitated as yellow powder. When the insoluble solid in ether was extracted with 10 ml of cold water, III, which was recrystallized from hot water, was left as a white solid. The aqueous solution was evaporated to dryness and the residue was again dissolved in 100 ml of acetone. When 20 ml of ether was added to the acetone solution, monopotassium salt of IV crystallized out of the solution as pale yellow needles. IV was purified by recrystallization from acetone containing a small amount of ether. Found: C, 20.23; H, 1.06; N, 55.94%. Calcd for $C_3H_2N_7K$: C, 20.56; H, 1.15; N, 55.97%.

In the case where an original anolyte was neutralized to pH 6.4—6.8 with dilute hydrochloric acid, the products were separated by a similar method to the above.

Decomposition of IV in Acidic Solution. 0.35 g (2 mmol) of potassium salt of IV, a small glass ampoule containing 2 ml of concentrated hydrochloric acid, and 50 ml of water were placed in a flask connected with a gas burette. The flask was heated at 40 °C and then the ampoule was broken with a magnet hammer. 36 ml (yield, 80%) of nitrogen generated for 30 min. The reaction mixture was evaporated to dryness and then was dissolved in dilute ammonia. When a saturated solution of ammonium picrate was added to the ammoniacal solution, 0.35 g (yield, 65%) of potassium picrate crystallized out of the solution. When the mother liquor was acidified with acetic acid, 0.55 g (yield, 73%) of amidinobiuret picrate crystallized out of the solution.

Decomposition of IV in Alkaline Solution. 0.35 g (2 m mol) of potassium salt of IV and 20 ml of 2M potassium hydroxide were placed in a flask similar to that described above. 20 ml (yield, 45%) of nitrogen generated for 24 h. 0.11 g (yield, 45%) of ammeline crystallized out of the solution, when the reaction mixture was neutralized with acetic acid.

Decomposition of IV with Hydrogen Chloride in Acetone. Dry hydrogen chloride gas was introduced into 50 ml of an acetone solution containing 0.075 g (0.43 mmol) of potassium salt of IV at 0 °C. After the resulting potassium chloride had been filtered off, the reaction mixture was evaporated to dryness. 0.067 g (yield, 75%) of white residue, which could not be purified, was presumed to be 4-amino-6-(iminochloromethyl)amino-1,2,3,5-tetrazine monohydrochloride. Found: C, 17.87; H, 2.11; N, 46.95; Cl, 32.44%. Calcd for $C_3H_5N_7Cl_2$: C, 17.16; H, 2.40; N, 46.68; Cl, 33.76%. This residue was converted into 2,4-diamino-6-chloro-1,3,5-triazine by treatment with water.

Decomposition of V in Acidic Solution. 0.49 g (2.2 mmol) of V was dissolved in 30 ml of cold 0.5M hydrochloric acid. The reaction mixture was heated at 75 °C for 1 h. The gas evolved consisted of 41 ml (yield, 82%) of nitrogen and 32 ml (yield, 63%) of carbon dioxide. When the reaction mixture was cooled in an ice bath, 0.32 g (yield, 88%) of melamine hydrochloride precipitated. The amount of ammonium chloride in the mother liquor was estimated to be 2.04 mmol (yield, 91%) by the hypobromite method.

Decomposition of VI in Acidic Solution. 0.24 g (0.8 mmol) of dipotassium salt of VI was decomposed by a similar procedure to that in the case of V. 0.10 g (yield, 80%) of melamine hydrochloride and 0.60 mmol (yield, 75%) of ammonia were obtained from the reaction mixture. The gaseous product consisted of nitrogen and carbon dioxide, but their volumes were not measured.

Free Acid of V. 0.27 g (yield, 58%) of the free acid of V precipitated as yellow powder, when 2 ml of 2M hydrochloric acid was added to 5 ml of cold aqueous solution containing 0.57 g (2.6 mmol) of potassium salt of V. The free acid was purified by recrystallization from water. Found: C, 26.63; H, 2.75; N, 69.12%. Calcd for $C_4H_5N_9$: C, 26.82; H, 2.81; N, 70.37%.

References

1) G. Calcagni and G. Lazzari, *Ann. Chim. Applicata*, **26**, 43 (1936); *CA*, **30**, 6651 (1936).

2) V. P. Wystrach, "Heterocyclic Compounds," Vol. 8, ed. by R. C. Elderfield, John Wiley and Sons, Inc., New York, N. Y. (1967), p. 106.

3) F. R. Benson "Heterocyclic Compounds," Vol. 8, ed. by R. C. Elderfield, John Wiley and Sons, Inc., New York, N. Y. (1967), p. 4.

4) Yu. I. Mushkin and A. I. Finkel'stein, *Zh. Org. Khim.* **3**, 507 (1967).

5) Evaporation of the solution was carried out under such conditions in order to avoid the decomposition of the compounds.

Vinyl Polymerization. 341.[1] A Proposal of a Mechanism for Radical Polymerization of Vinyl Monomers with Sodium Polymethallylsulfonate

Minoru IMOTO, Yoshiaki NAKAMURA, and Tatsuro OUCHI

Department of Applied Chemistry, Faculty of Engineering, Kansai University, Suita-shi, Osaka 564

(Received October 1, 1975)

In aqueous solution, sodium polymethallylsulfonate (PMAS-Na) can initiate a radical polymerization of vinyl monomer which has positively charged vinyl group. In the polymerization of MMA, Michaelis-Menten equation was applicable. From the results obtained, a bimolecular initiation mechanism, involving hydrogen atom transfer, was concluded to be reasonable. The relationships between pH of the aqueous layer and conversion and between polymerization temperature and conversion were of downward bell type. By Stewart model, it was found that PMAS-Na has a very rigid conformation. This structure can be compared with a rigid tertiary structure of enzyme, and the reaction appearances of enzyme and PMAS-Na can be considered to resemble very much each other.

Recently we reported[2] that an aqueous solution of sodium polymethallylsulfonate (PMAS-Na) could polymerize some vinyl monomers in the absence of any usual initiator. In the present paper, we would like to propose a probable mechanism for the generation of an initiating radical species by the reaction of sulfonate group with vinyl monomer, *i.e.* a generation by the interaction of two molecules of vinyl monomer through the Flory's mechanism.[3]

Experimental

Materials. PMAS-Na was prepared by the polymerization of sodium methallylsulfonate with ammonium peroxodisulfate in water, as described in the former report[2]: [η] 0.08 dl/g (30 °C, in water). Peroxide group and metallic ion in PMAS-Na were hardly detected by KI-method and atomic absorption spectrometry technique, respectively.

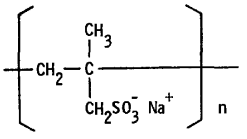

PMAS-Na

Styrene (St), methyl methacrylate (MMA) and acrylonitrile (AN) were of commercial and purified by usual method. *p*-Nitrostyrene (*p*-NO_2-St)[4] and *p*-methoxystyrene (*p*-CH_3O-St)[5] were synthesized according to the literatures. Water was ion-exchanged.

Procedure. Vinyl monomer and an aqueous solution of PMAS-Na were placed in a tube and seald under vacuum after thawing with nitrogen. The tube was heated at 85 °C for 1 h under shaking. The content was poured into a large amount of methanol to precipitate the polymer. The collected polymer was washed throughly with water and the polymer of vinyl monomer was separated. After drying, the polymer was weighed.

Results and Discussion

Proof of Radical Mechanism. In a mixture of 3 ml of MMA and an aqueous solution of 0.05 g of PMAS-Na in 5 ml of water, diphenylpicrylhydrazyl, hydroquinone or benzoquinone was added in an amount of 0.1 g, as radical scavenger. Another polymerization without radical scavenger was carried out in air. In all cases, formation of poly-MMA was not observed. Thus, it was concluded that the polymerization proceeded through a radical mechanism.

Efficiency of Grafting. In the polymerization of MMA, the efficiency of grafting was measured by extracting the polymer obtained with benzene. The results showed that the grafting reaction did not take place.

Selectivity of Vinyl Monomer. A solution of 0.05 g of PMAS-Na in 5 ml of water and 3 ml of vinyl monomer were reacted as described in a former section. Five kinds of monomer were used. The conversions observed were drawn in Fig. 1. Here, "e" is the Alfey-Price's polymerization factor.[6] The conversion was found to be linearly proportional to the "+*e*"-value of the monomer. The "*e*"-value of −0.3 is considered to be the point at which a vinyl monomer behaves as a non-polarized molecule.

From the results, it was confirmed that only the vinyl monomer having plus-charged vinyl group could be polymerized by PMAS-Na. This conclusion agrees well with the consideration in which the plus-charged vinyl group is adsorbed on the minus-charged sulfonate group.

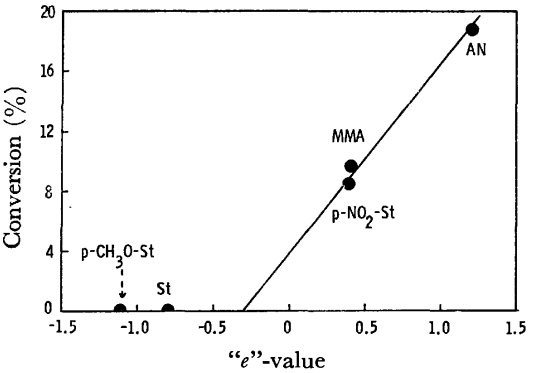

Fig. 1. Conversions of vinyl monomers *vs.* their "*e*"-values.

Relationship between Amounts of PMAS-Na and Polymer Yield. Using various amounts of MMA, the polymerization was carried out at 85 °C for 1 h to obtain the results shown in Fig. 2. The yield of polymer increased with the added amount of MMA and reached

a constant yield at a certain point of the amount of MMA. Beyond the point, the yield became to be independent of the amount of MMA. This relationship between the polymer yield and the feeded amount of MMA resembles well to the relationship between the rate of reaction and the amount of substrate in enzymatic reaction.

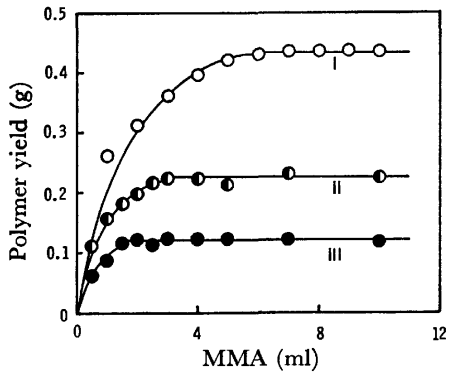

Fig. 2. Polymer yield *vs.* feeded amount of MMA.
H_2O: ○ 10 ml, ◐ 5 ml, ● 2.5 ml.
[PMAS-Na]=0.01 g per 1 ml of water. 85°C, 1 h.

Application of Michaelis-Menten Equation to the Polymerization of MMA. The results obtained in Fig. 2 were found to fit in Michaelis-Menten Equation (1);

$$E + S \underset{k_2}{\overset{k_1}{\rightleftharpoons}} ES \xrightarrow{k_3} E + P \qquad (1)$$

where E is PMAS-ion, S is MMA, ES is a adsorbed complex of MMA on PMAS-ion and P is a radical initiator. From Eq. 1, Lineweaver-Burk's Equation (2) is obtained.

$$\frac{1}{R_p} = \frac{K_a}{k_3[E]} \times \frac{1}{[S]} + \frac{1}{k_3[E]}$$
$$K_a = (k_2+k_3)/k_1 \qquad (2)$$

Here, as "P", we adopted poly-MMA instead of radical initiator. Accordingly, R_p in Eq. 2 is the rate of polymerization. By application of Eq. 2, the reciprocals of R_p were coordinated with those of the feeded amounts of MMA, as shown in Fig. 3. Straight lines were obtained. From the intercepts of the ordinate at the zero point and from the inclinations of the lines, $k_3[E]$ and Michaelis-Constant, K_a, were calculated as shown in Table 1.

As can be seen, K_a was obtained as a constant value of 1.06 ± 0.09, and $k_3[E]$ was almost proportional to [E]. Thus it was confirmed that Michaelis-Menten Equation fits in the present polymerization.

Table 1. Values of K_a and k_3 [E]
(PMAS-Na 0.01 g/ml H_2O; 85 °C, 1 h)

Case	H_2O (ml)	K_a (g)	$k_3[E]$ g/h
III	2.5	1.15	0.222
II	5	0.98	0.285
I	10	1.05	0.500

Effect of pH of the Aqueous Phase on the Rate of Polymerization of MMA. The effect of pH of the aqueous phase on the conversion of MMA was observed as shown in Fig. 4. It was very interesting that this radical polymerization showed the most rapid rate at the pH near to 6. It is considered that at such pH the PMAS-ion can exist in a bare state as sulfate anion apart from Na^+ cation. At acidic area, sulfate anion of PMAS-Na becomes to unionized sulfonic acid and to be difficult to adsorb a positively charged vinyl group. On the other hand, in alkaline area, hydroxide ion surrounds a positive part of vinyl monomer to put it apart from sulfate ion.

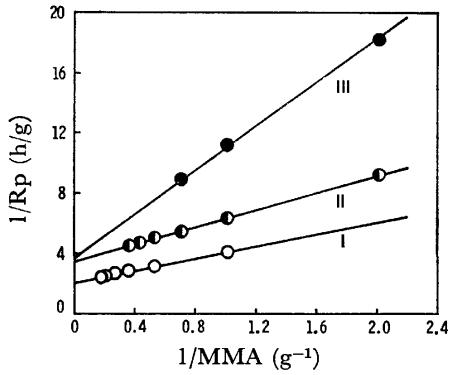

Fig. 3. Application of Eq. 2 to the results obtained in Fig. 2.

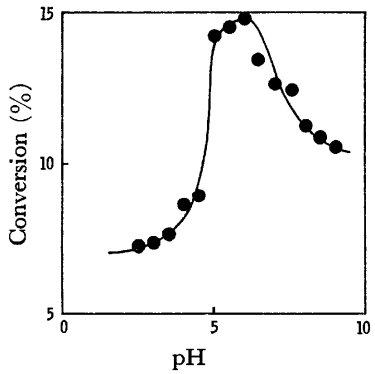

Fig. 4. Conversion of MMA *vs.* pH of the aqueous layer of the reaction system.
(MMA 3 ml, PMAS-Na 0.05 g, buffered water 5 ml; 85 °C, 1 hr. Buffer solutions were prepared by the following systems; pH 2.5—6.0, M/10 citric acid-M/5 Na_2HPO_4; pH 6.5—7.5, M/10 HCl-M/20 $Na_2B_4O_7$; pH 7.5—9.5, M/15 Na_2HPO_4-M/15 KH_2PO_4)

Effect of Reaction Temperature on the Rate of Reaction. The polymerization of MMA initiated with an aqueous solution of PMAS-Na was carried out at the temperature between 55 and 120 °C. The result can be seen in Fig. 5. The maximum conversion was obtained at 90 °C. Over this temperature, the degree of adsorption of MMA by $PMAS^{n-}$ is concluded to decrease.

From three points of A, B and C in Fig. 5, an overall activation energy, E, was calculated to be 12.8 kcal/mole, as shown in Fig. 6. Granting that $(2E_p-E_t)$ is 9.0 kcal/mol,[7] the activation energy of initiation, E_i, was calculated to be 16.6 kcal/mol from the equation, $2E=E_i+2E_p-E_t$. Here E_p and E_t are activation energies of propagation and termination reactions, respectively.

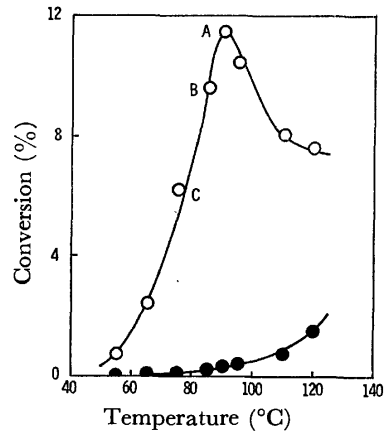

Fig. 5. Conversion of MMA *vs.* polymerization temperature. (MMA 3 ml, H_2O 5 ml, PMAS-Na 0.0 g (●) or 0.05 g (○); 1 h)

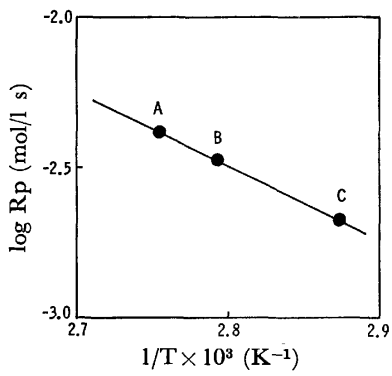

Fig. 6. Arrhenius plot of three points of A, B, and C in the former figure.

Mechanism of the Initiation Reaction. Figure 1 indicates that a mechanism which accomodates the results is one in which the plus-charged methylene of vinyl monomer is adsorbed to the SO_3^- group of PMAS^{n-} and goes into reaction. The formula of polarized vinyl monomer having "$+e$"-value on CH_2 group is expressed as the formula (3).

$$\overset{\delta+}{C}H_2{=}CH{-}R^{\delta-} \qquad (3)$$

On the other hand, $-SO_3^-$ groups of PMAS^{n-} repel each other and situate separately as far as they can. Thus, it is a reasonable consideration that the macromolecule of PMAS^{n-} has a structure near to syndiotactic configuration. A probable Stewart's model of PMAS^{n-} is shown in Fig. 7. In this model, only three units were taken. However, the structure of PMAS^{n-} was found to be very rigid. In Fig. 7, furthermore, two adsorbed molecule of acrylonitrile were also shown. From the model it was concluded that the two vinyl monomers could exist within a van der Waals distance.

The rigid structure of PMAS^{n-} is considered to correspond to a rigid tertiary structure of enzyme by which an enzyme can afford a specificitic reactivity to substrate.

As usually known, in enzymatic reaction, a relationship between rate of reaction and reaction temperature or pH of the reaction system is of downward bell type. Michaelis-Menten Equation was verified to be applicable. Thus, the observations obtained in the present paper agreed very well with enzymatic reaction figures.

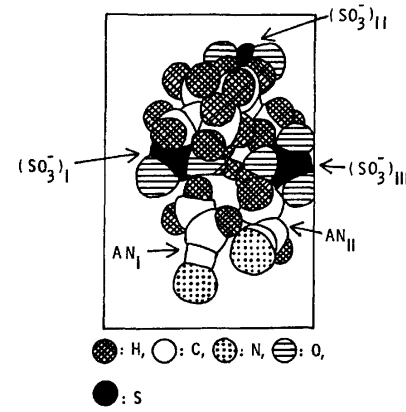

Fig. 7. Stewart's model of 3 units in PMAS^{n-}.

From the results obtained above, the mechanism of the initiation reaction was concluded to be as shown in the following Scheme 1.

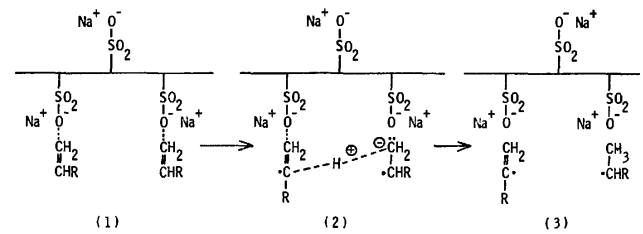

Scheme 1. Initiation mechanism of vinyl monomer by PMAS-Na.

By complexing of $-SO_3^-$ anion with positively charged $CH_2=$ group of the monomer, a following partial electron transfer may proceed.

$$-\overline{O}^{-}\cdots\overset{\delta+}{C}H_2{=}CH{-}R \qquad (4)$$

Thus, electron density around the carbon atom of $=CH-$ increases and becomes easier to donate its electron. In other words, a charge-transfer complex (CT-complex) becomes easier to be formed.

$$(1) \longrightarrow CH_2{=}\overset{+}{C}H\cdots\overset{-}{C}H_2{-}\dot{C}H \longrightarrow (2) \qquad (5)$$
$$\qquad\qquad\quad R \qquad\quad R$$
$$\text{CT-complex}$$

This initiating mechanism corresponds well to the Flory's mechanism which was proposed as Eq. (6) in 1937.[3]

$$2CH_2{=}CH \xrightarrow[\text{of H· atom}]{\text{Transfer}} CH_3{-}\dot{C}H + CH_2{=}\dot{C}\cdot \qquad (6)$$
$$\quad R \qquad\qquad\qquad\quad R \qquad\quad R$$

This mechanism was denied from the standpoint of the reaction energy. However, recently the Flory's mechanism involving hydrogen transfer was taken up as an initiation mechanism of the radical polymerization which proceeds through a charge-transfer (CT) complex. For example, one of the present authors (M. Imoto)[8]

assumed the following initiation mechanism as shown in Eq. (7):

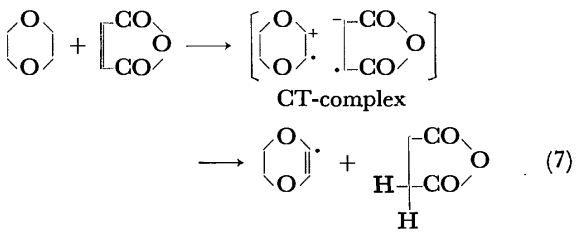

(7)

Otsu and Sato succeeded to prove this H· transfer mechanism using the spin-trapping method.[9] Accordingly, the mechanism proposed as shown in Scheme 1 may be recognizable to be reasonable.

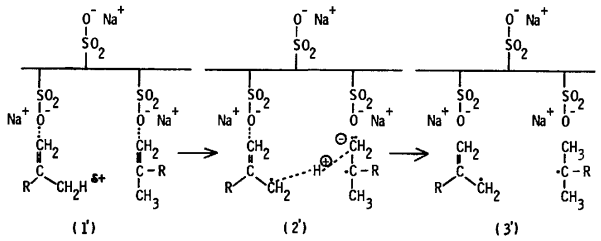

Scheme 2. Initiation of the polymerization of MMA. ($R\text{-}COOCH_3$)

In the case of MMA having no hydrogen atom at the vinyl carbon atom attached directly to the substituent, the transfering hydrogen atom is considered to be one in the α-CH_3 group. The mechanism is concluded to be as in Scheme 2. One of the generated radicals is an allyl radical which may make easier the hydrogen transfer.

The authors wish to express their hearty thanks to Dr. T. Takada of Toho Beslon Co. for his affording of methallyl sulfonate.

References

1) Part 340: T. Kimura, T. Nakaya, M. Imoto, *Makromol. Chem.*, **176**, 1945 (1975).
2) M. Imoto, T. Ouchi, Y. Nakamura, and H. Ogushi, *J. Polym. Sci., Polym. Lett. Ed.*, **13**, 131 (1975).
3) P. J. Flory, *J. Am. Chem. Soc.*, **59**, 241 (1937).
4) R. A. Gregg and C. Walling, *J. Am. Chem. Soc.*, **69**, 2141 (1947).
5) R. Quelet, *Bull. Soc. Chem. Fr.*, **7**, 196 (1940).
6) G. E. Ham, "Copolymerization," Interscience Publisher, New York, (1964).
7) K. S. Bagdasariyan, "Theory of Radical Polymerization," (Moscow, 1966), p. 116.
8) M. Imoto, *Kobunshi*, **15**, 789 (1966).
9) T. Otsu and T. Sato, unpublished.

The Reaction between Hydrocarbon and Hydrogen Chloride in Silent Electrical Discharge. I. The Reaction of Ethylene with Hydrogen Chloride

Kazuaki KAWAMOTO, Keiko TAMURA, and Setsuko HIKASA

Institute of Commodities, Faculty of Economics, Kagawa University, Takamatsu, Kagawa 760

(Received October 1, 1975)

Silent discharge was found to induce the reaction of ethylene and hydrogen chloride and to give mainly addition and telomerization products. Discharge on a mixture of ethylene and hydrogen chloride in an ozonizer under atmospheric pressure gave chloroethane, 1-chlorobutane, and 1,4-dichlorobutane as the main products. Besides these compounds, chloroethylene, 2-chlorobutane, 1,3-dichlorobutane, 2,3-dichlorobutane, 1,2-dichlorobutane, 1-chlorohexane, 1,2-dichloroethane, and gaseous products were also formed. The maximum yield of the liquid products was obtained when ethylene and hydrogen chloride were mixed in the ratio of approximately 1 : 1. The formation of telomers was favored by a low ratio of the hydrogen chloride to the ethylene concentration, and by a low temperature in the discharge reaction. On the other hand, gaseous products increased with the rise in the discharge temperature and with an increase in the ratio of ethylene to hydrogen chloride. Judging from the product distribution, the reaction may be explained in terms of radical reactions involving vinyl, ethyl, and chlorine radicals. Among the reactions between ethylene and HX, such as hydrogen cyanide, hydrogen sulfide, and hydrogen chloride, the highest conversion was obtained by using the hydrogen chloride as the reactant.

In recent years, the oxidation of hydrocarbons in silent electrical discharge has been studied by Sugino *et al.*[1]

In particular, the reactions of ethylene with ammonia or oxygen in silent electrical discharge have been reported by them and by Tsutsumi *et al.*[2]

In previous papers,[3] the reactions of a hydrocarbon (ethylene, propylene, and cyclohexane) with hydrogen cyanide, and of a hydrocarbon (ethylene and propylene) with hydrogen sulfide in a silent discharge were reported. When a mixture of ethylene and hydrogen cyanide was discharged in an ozonizer, acrylonitrile could be prepared in one step. Besides this compound, the formation of telomers was observed. Moreover, when a mixture of ethylene and hydrogen sulfide was discharged in an ozonizer, the formation of such telomers as ethanethiol and 1-butanethiol was also observed.

The reaction of ethylene with hydrogen halide has been reported by many investigators. The photochemical addition of hydrogen bromide to olefins has been investigated by Vaughan *et al.*[4] Hanford *et al.*[5] reported the formation of mixtures of straight chain primary alkyl chlorides, ranging from chloroethane to greases and waxes, by the reaction between ethylene and hydrogen chloride in the presence of catalysts and water at a high temperature under a high pressure. It was recognized by Raley *et al.*[6] that the vapor-phase addition of hydrogen chloride to ethylene, as initiated by ultraviolet light or peroxide, yielded chloroethane and small amounts of hydrogen and ethane.

Moreover, it was found by Ford *et al.*[7] that when the reaction of ethylene with hydrogen chloride was carried out in the presence of free-radical initiators and water under ethylene pressures of 100—1000 atm, telomerization took place. The radiation-induced addition of hydrogen chloride to ethylene produced 1-chlorobutane and chloroethane, and this reaction was supposed to be a vapor-phase radical chain reaction.[8] No detailed study of the interaction of ethylene and hydrogen chloride in the silent discharge has yet been reported.

The present study was undertaken to find out whether or not the direct formation of such chloro compounds as chloroethylene, chloroethane, and 1-chlorobutane results from the reaction of ethylene with hydrogen chloride in a silent electrical discharge. Moreover, the differences among the reactions of ethylene with hydrogen cyanide, with hydrogen sulfide, and with hydrogen chloride were discussed. In this research, the silent discharge was carried out in a Siemens ozonizer for 8 h, using a voltage of 15 kV.

Experimental

Materials. The ethylene was purchased from the Nihon Sekiyu Co., Ltd. (Kawasaki), the hydrogen chloride, chloroethylene, and chlorine from the Seitetsu Chemicals Co. (Osaka), and chloroethane from the Tokyo Kasei Co. (Tokyo). These materials were used without further purification. No impurity was found in these reagents by gas chromatographic analysis. (Columns of activated charcoal, Silica gel, and Silicone GE SF-96 were used.)

Apparatus. In this experiment, the apparatus illustrated in Fig. 1 was used. (1) Helium, hydrogen chloride, and ethylene coming from each bomb were passed over calcium chloride (A). (2) The molar ratios of ethylene, hydrogen chloride, chloroethane, chloroethylene, and chlorine were

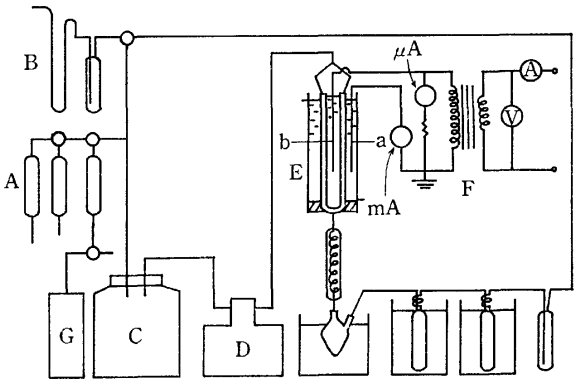

Fig. 1. Apparatus.

roughly determined by means of a manometer (B), and the quantitative analysis of the mixed gas in this experiment was performed by gas chromatography. (A column of Silicone GE SF-96 was used.) (3) The reservoir (C) was filled with a mixture of ethylene, hydrogen chloride, and helium. (4) The mixed gas was circulated by means of a pump (D) at the rate of 2 l/min. (5) The outside (a) of the discharge tube (E) was filled with water, and the inner tube (b) with a 3% copper sulfate solution. (6) The discharge tube (E) used was a Pyrex tube 25 cm in effective length, 3 cm in outside diameter, and with a space gap of 0.25 cm. (7) The electrical energy was supplied by a 15-kV transformer (F).

Procedure. Air in the system was completely replaced by helium, by repeated evacuation and introduction of helium. The volume of the reaction system was 20.7 l. As a diluent, one-third volume (about 6.9 l) of helium was put into the reaction system, then a mixture of ethylene and hydrogen chloride (chloroethane, chloroethylene, and chlorine) at the molar ratios shown in Tables 1, 3, and 5 was put into it. The mixed gas was made homogeneous by using a pump (D) for 30 min and was then passed through the discharge tube at a regular velocity of 2 l/min for the period of the reaction. A current of 60 cycles was passed through a voltage regulator and the voltage was stepped up by a transformer to give the required value. The products coming out of the discharge tube were condensed by passing them through a condenser, then they were collected by being passed through two traps cooled at −50 °C or −70 °C by acetone–Dry Ice. The liquid products were analyzed by the method described below, while the non-condensable gases were analyzed by gas chromatography at intervals of 30 min. The pressure in the system during the period of the reaction was measured at intervals of 30 min.

Identification and Analysis of the Reaction Products. The liquid products obtained by these reactions were identified by comparing their retention times on the gas chromatogram with those of authentic samples. (Columns of tricresyl phosphate, Silicone GE SF-96, Silicone DC 550). In addition, the reaction products were fractionally distilled, and the constituents of the fraction were identified by examining the infrared spectrum. The gaseous products obtained by these reactions were also analyzed by gas chromatography. (Columns of activated charcoal, tricresyl phosphate, silica gel, and Silicone GE SF-96). The gaseous products could not be determined quantitatively. The quantitative analysis of the liquid products in this experiment was performed by gas chromatography.

Results and Discussion

The results obtained by running ethylene with hydrogen chloride in an ozonizer under the conditions described in Tables 1 and 3 are summarized in Tables 2 and 4, respectively. Further, the results obtained by the reactions of chloro compounds with and without ethylene under the conditions listed in Table 5 are summarized in Table 6. The yields of each compound shown in these tables are an average of three experiments under constant operating conditions. The fluctuation in the yields of the compounds obtained in repeated experiments was less than 1 per cent. The gaseous products given by the reaction of ethylene and hydrogen chloride consisted of hydrogen, chlorine, methane, ethane, acetylene, propane, propylene, butane, 1-butene, and 1,3-butadiene.

Influence of the Molar Ratio of Ethylene to Hydrogen Chloride. As can be seen in Table 2, the yield of the reaction products depends upon the molar ratio of ethylene to hydrogen chloride; when the mixed components of the reactant were approximately in the ratio of 1 : 1, the maximum yield of the liquid reaction products was obtained. However, the product distribution depended upon the molar ratio of the reactants as follows: (1) In the case of the range of discharge temperatures from 5 to 50 °C, when ethylene and hydrogen chloride were mixed in the ratio of approximately 1 : 1, the proportion of chloroethane in the liquid products was at its maximum. (2) On the other hand, 1-chlorobutane decreased with the increase in the ratio of hydrogen chloride to ethylene. Thus, it may be said that the yield of telomer with $n=2$ is favored by a low ratio of the hydrogen chloride to the ethylene concentration. (3) The yields of dichloro and trichloro compounds of butane increased with the increase in the ratio of the hydrogen chloride to the ethylene. (4) A small amount of dichloro compounds of ethane were obtained, and their yields increased slightly with an increase in the ratio of the hydrogen chloride to the ethylene. (5) When the discharge reaction was performed at a higher ratio of the hydrogen chloride to the ethylene, a solid black deposit was formed on the wall of discharge tube, and the yield of the solid product thus obtained increased with a rise in the discharge temperature. Chloroethane, 1-chlorobutane, and 1-

Table 1. Influences of the molar ratio of ethylene to hydrogen chloride and of the discharge temperature on the yield of reaction products (Experimental conditions)

Experiment No.	1	2	3	4	5	6	7	8	9	10	11	12
Materials used (l)												
Ethylene	5.45	7.66	9.67	5.11	7.56	9.81	4.70	7.39	9.70	3.95	7.67	10.01
Hydrogen chloride	8.26	6.08	4.17	8.64	6.05	3.93	8.93	6.49	4.06	9.72	6.00	3.81
Molar ratio (C_2H_4/HCl)	0.65	1.26	2.26	0.59	1.26	2.44	0.53	1.14	2.39	0.42	1.26	2.65
Temp. of discharge tube (°C)												
Inside	5—27	5—26	5—25	25—45	25—45	25—46	50—76	50—76	50—76	75—94	75—95	75—98
Outside	5	5	5	25	25	25	50	50	50	75	75	75
Discharge time (h)	8	8	8	8	8	8	8	8	8	8	8	8
Second voltage (kV)	15	15	15	15	15	15	15	15	15	15	15	15
Second current (mA)	2.5	2.5	2.4	2.7	2.7	2.6	2.9	3.0	3.1	3.1	3.2	3.1

TABLE 2. INFLUENCES OF THE MOLAR RATIO OF ETHYLENE TO HYDROGEN CHLORIDE AND OF THE DISCHARGE TEMPERATURE ON THE YIELD OF REACTION PRODUCTS (Experimental results)

Experiment No.	1	2	3	4	5	6	7	8	9	10	11	12
Liquid product collected (g)	10.27	12.09	9.59	10.39	13.52	11.76	9.86	12.53	11.82	9.71	11.04	11.55
Conversion efficiency[a] (%)	50.7	62.0	50.8	50.8	70.0	64.0	48.3	63.3	63.0	46.7	57.0	61.7
Composition of liquid reaction products[b] (%)												
Chloroethylene	T	1.0	1.4	T	1.3	2.0	T	0.9	1.5	T	0.7	1.4
Chloroethane	28.7	50.6	46.2	29.0	58.2	53.5	28.6	61.1	54.7	30.5	55.5	57.6
1-Chlorobutane	8.6	16.6	23.2	8.3	12.9	17.5	8.0	11.8	16.7	7.5	11.7	15.4
2-Chlorobutane	4.6	2.9	2.1	5.2	2.9	2.0	4.8	3.2	2.0	4.8	3.5	1.7
1,4-Dichlorobutane	22.1	16.3	15.2	18.0	13.0	11.2	14.5	11.2	9.7	12.2	10.7	8.2
1,3-Dichlorobutane	7.6	3.4	1.4	8.2	3.4	1.4	8.5	3.5	1.5	8.7	5.1	1.6
2,3-Dichlorobutane	6.1	1.4	0.2	6.9	1.5	0.8	8.7	1.6	1.0	9.2	1.9	1.2
1,2-Dichlorobutane	5.5	0.2	T	6.2	0.2	T	8.6	0.4	T	9.1	0.9	T
1-Chlorohexane	2.4	0.4	T	2.0	0.4	T	1.9	0.4	T	1.7	0.4	T
1,1-Dichloroethane	2.4	0.5	0.4	2.0	0.4	0.3	2.3	0.4	0.4	1.9	0.4	0.3
1,2-Dichloroethane	4.8	1.9	1.3	4.0	1.3	1.1	4.0	1.2	0.8	3.7	1.2	0.6
1,2,4-Trichlorobutane	3.5	0.2	0	5.1	0.4	0	6.7	0.5	0	6.9	0.8	0
1-Chloropropane	0.6	1.2	2.1	0.7	1.1	2.2	0.6	1.0	2.3	0.6	1.2	2.0
2-Chloropropane	0.5	0.6	0.9	0.6	0.8	1.0	0.5	0.8	1.0	0.5	1.0	1.0
1,2-Dichloropropane	0.9	0.2	T	0.9	0.2	T	1.0	0.2	T	1.0	0.3	T
1,3-Dichloropropane	1.7	0.2	T	1.4	0.2	T	1.3	0.2	T	1.3	0.2	T
1-Butene	T	0.4	2.0	T	0.4	2.4	T	0.5	2.8	T	0.9	3.0
Butane	T	0.5	2.1	T	0.5	2.5	T	0.7	2.9	T	1.0	3.1
1,3-Butadiene	T	0.3	1.5	T	0.3	2.1	T	0.4	2.7	T	0.7	2.9
Unidentified products	T	1.2	T	1.5	0.6	T	T	T	T	0.4	1.9	T

T: Trace. a) The conversion efficiency was given by (grams of liquid product/grams of materials (ethylene+hydrogen chloride) used) × 100. b) The yields of each compound produced were given by (grams of each compound/grams of total reaction product) × 100.

TABLE 3. INFLUENCE OF THE DISCHARGE TIME ON THE YIELD OF REACTION PRODUCTS (Experimental conditions)

Experiment No.	13	14	15	16[a]	17[a]
Materials used (l)					
Ethylene	4.60	4.88	4.90	6.30	5.73
Hydrogen chloride	9.07	8.90	8.79	7.37	8.03
Molar ratio (C_2H_4/HCl)	0.53	0.55	0.56	0.85	0.72
Discharge time (h)	4	2	1	8	4
Temp. of discharge tube (°C)					
Inside	25—48	25—47	25—47	25—45	25—47
Outside	25	25	25	25	25
Second voltage (KV)	15	15	15	15	15
Second current (mA)	2.8	2.5	2.4	2.8	2.5

a) Experiment Nos. 16 and 17 show the results when the products coming out of the discharge tube were collected by being passed through two traps cooled at −70 °C by acetone–Dry Ice.

chlorohexane seem to be formed by the telomerization between ethylene and hydrogen chloride. The formation of 1-chlorooctane (1 : 4 telomer) and one-to-five or more products could not be observed by gas chromatographic analysis.

Influence of the Discharge Temperature. The discharge reactions were performed at 5, 25, 50, and 75 °C, as shown in Table 1. As may be seen from the results of these experiments shown in Table 2, the conversion efficiency [grams of liquid product/grams of materials (ethylene+hydrogen chloride) used × 100] depends upon the temperature at which the discharge is carried out; when the molar ratio of the reactants was about 1 : 1, the maximum yield of the liquid products was obtained at 25 °C, the proportions of 1-chlorobutane and 1,4-dichlorobutane in the liquid product decreased with increasing temperature, and the gaseous products increased with the rise in the discharge temperature and the increase in the ethylene concentration. It may be said that the telomer formation with $n=2$ is favored by a low temperature.

Influence of the Discharge Time. The discharge reaction was carried out with various reaction times (1, 2, 4, and 8 h), as is shown in Table 3; the results are summarized in Table 4. The total pressure in the reaction system was measured at intervals of 30 min. The results shown in Fig. 2 and Table 4 show that lowering the total pressure increases the amount of the

Table 4. Influence of the discharge time on the yield of reaction products (Experimental results)

Experiment No.	13	14	15	16	17
Liquid product collected (g)	9.90	5.30	2.34	10.77	10.74
Conversion efficiency (%)	48.2	25.7	11.4	54.2	53.1
Composition of liquid reaction products (%)					
Chloroethylene	0.5	0.9	1.0	0.2	1.4
Chloroethane	66.7	70.9	72.7	61.5	73.0
1-Chlorobutane	5.1	4.6	4.2	7.1	4.5
2-Chlorobutane	1.9	1.2	0.7	2.0	1.4
1,4-Dichlorobutane	13.9	13.4	12.9	12.8	10.9
1,3-Dichlorobutane	3.0	2.5	1.5	4.4	2.1
2,3-Dichlorobutane	1.3	0.6	0.4	2.4	0.6
1,2-Dichlorobutane	1.0	0.3	T	2.3	0.1
1-Chlorohexane	0.3	0.2	0.2	0.8	0.1
1,1-Dichloroethane	0.7	0.4	0.3	1.4	0.4
1,2-Dichloroethane	2.2	1.8	1.7	2.6	1.7
1,2,4-Trichlorobutane	0.9	0	0	T	0
1-Chloropropane	0.4	0.2	0.2	0.5	0.3
2-Chloropropane	0.4	T	T	0.1	T
1,2-Dichloropropane	0.4	0.1	T	0.2	0.2
1,3-Dichloropropane	0.6	0.1	0.1	0.8	0.3
1-Butene	0.1	0.2	0.2	T	0.3
Butane	0.1	0.2	0.2	T	0.4
1,3-Butadiene	0.1	0.2	0.2	T	0.3
Unidentified products	0.4	2.2	3.5	0.9	2.0

Table 5. The reactions of ethylene with chloro compounds in silent electrical discharge (Experimental conditions)

Experiment No.	18[a)]	19[a)]	20[b)]	21[b]	22
Materials used (l)					
Ethylene	—	4.14	—	4.42	6.66
Chloroethane	5.29	4.73	—	—	—
Chloroethylene	—	—	4.61	4.74	—
Hydrogen chloride	8.48	4.66	9.21	4.69	—
Chlorine	—	—	—	—	7.16
Temp. of discharge tube (°C)					
Inside	25—41	25—40	25—45	25—45	25—40
Outside	25	25	25	25	25
Discharge time (h)	8	8	8	8	3
Second voltage (kV)	15	15	15	15	15
Second current (mA)	2.1	2.3	2.2	2.2	2.8

a) Experiment Nos. 18 and 19 show the results when the products were collected by two traps cooled at 10 °C. b) The products were collected by being passed through two traps cooled at −10 °C by acetone–Dry Ice.

liquid product. The yield of the reaction products and the velocity of the reduced pressure in the reaction system increased rapidly until 4 h of reaction time, while beyond this, they increased only gradually. Chloroethane in the reaction products decreased with the progress of the discharge time. As may be seen from Experiment No. 4 of Table 2 and Experiment No. 16 of Table 4, when the reaction product coming out of the discharge tube was cooled at −70 °C by acetone–Dry Ice, the conversion efficiency and the yield of chloroethane increased. When the reaction product coming out of the discharge tube was cooled at −50 °C, the yields of telomer with $n=2$ and dichloro compounds of butane increased. These results suggest that the noncondensable chloroethane is concerned in the secondary process.

The Reaction of Ethylene with Chloro Compounds

The mixture of ethylene and several chloro compounds, such as chloroethane, chloroethylene, hydrogen chloride, and chlorine was discharged in an ozonizer under the reaction conditions shown in Table 5; the results are summarized in Table 6. In the reaction of ethylene and chlorine, the main product was 1,2-dichloroethane. This suggests that the addition reaction occurs predominantly on account of the high reactivity of chlorine. As can be seen from Experiment Nos. 18 and 19 in Tables 5 and 6, when the mixtures of chloroethane and hydrogen chloride or of both compounds and ethylene

TABLE 6. THE REACTIONS OF ETHYLENE WITH CHLORO COMPOUNDS IN SILENT ELECTRICAL DISCHARGE (Experimental results)

Experiment No.	18	19	20	21	22
Liquid product collected (g)	7.73	4.40	20.69	8.89	24.70
Composition of liquid reaction products (%)					
Chloroethylene	T	0.2	1.7	8.2	T
Chloroethane	11.9	23.3	1.6	5.1	1.0
1-Chlorobutane	1.0	9.3	0.4	9.3	0.4
2-Chlorobutane	0.7	3.1	0.2	2.9	0.2
1,4-Dichlorobutane	17.8	27.2	1.9	11.8	0.6
1,3-Dichlorobutane	20.7	19.3	3.3	13.6	0
2,3-Dichlorobutane	15.2	5.7	3.1	7.1	0
1,2-Dichlorobutane	14.1	3.8	3.1	2.1	0
1-Chlorohexane	T	1.3	T	1.5	0
1,1-Dichloroethane	0.9	0.6	0.9	1.4	0.4
1,2-Dichloroethane	1.7	1.5	8.4	5.9	92.8
1,2,4-Trichlorobutane	11.5	1.2	53.2	24.2	0
1-Chloropropane	0.1	0.7	0	0.6	0
2-Chloropropane	0.3	0.1	0	0.1	0
1,2-Dichloropropane	1.2	0.4	T	0.4	0
1,3-Dichloropropane	1.6	1.1	T	0.9	0
1-Butene	T	0.1	0.1	T	T
Butane	T	0.1	T	T	T
1,3-Butadiene	T	0.1	T	T	T
Unidentified products	1.3	1.9	22.1	4.9	4.6

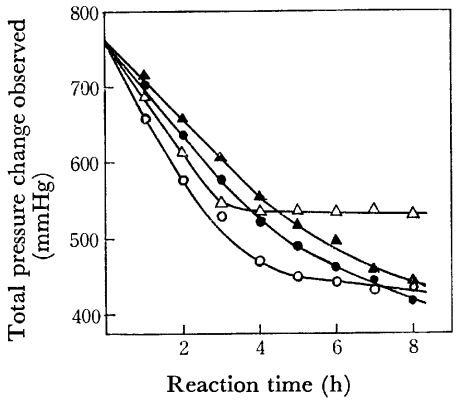

Fig. 2. Relation between total pressure in reaction system and time of reaction.
Experiment No., ▲: No. 2, △: No. 4, ●: No. 5, ○: No. 11.

were discharged, they were mainly transformed into the dichloro compounds of butane. Similar experiments (Nos. 20 and 21) with chloroethylene showed formation of considerable amounts of the trichloro compound (1,2,4-trichlorobutane) and the dichloro compounds of butane. When a mixture of ethylene and hydrogen chloride was discharged in an ozonizer a small amount of chloroethylene in the liquid products was obtained. This suggests that the chloroethylene may be formed by the primary process, but will be rapidly involved in the secondary process owing to its great activity.

The Mechanism of the Formation of the Main Products Obtained by the Reaction of Ethylene and Hydrogen Chloride. The molecules excited by the silent discharge are considered to change into radicals or atoms, and into small amounts of ionized molecules as has been reported by many workers.[9] Accordingly, the reaction of ethylene with hydrogen chloride in a silent electrical discharge is guessed to be a vapor-phase radical reaction. Egloff *et al.*[10] reported that a vinyl radical was formed from ethylene in the electrical discharge, and that it was produced by breaking a carbon-hydrogen bond. Tsutsumi[11] reported that the vinyl radical was produced by two molecular processes,[12] as is shown below. Franklin *et al.*[13] reported the formation of activated monochloroethyl radicals in the photochlorination of ethylene. Golden and Ausloos[14] reported that the vacuum-ultraviolet photolysis of ethylene led essentially to three types of processes, as is indicated below.[15]

The mechanism of the formation of chloroethane, 1-chlorobutane, and 1-chlorohexane by the reaction of ethylene with hydrogen chloride may be represented as follows: The first step is the activation of the ethylene molecule and the hydrogen chloride molecule by electron impact, while the second step consists of both (1) the reaction of the excited ethylene molecule with a normal ethylene molecule to give the vinyl radical and the ethyl radical,[12] and (2) the decomposition of the activated molecules to give the vinyl radical, the chlorine radical, and the hydrogen atom. Chloroethane may be formed by four paths: (1) the combination of the ethyl radical and the chlorine radical; (2) the reaction of the chlorine radical with ethylene, and the reaction between hydrogen chloride and the monochloroethyl radical so formed; (3) the addition of hydrogen atom to the monochloroethyl radical produced by (2); and (4) the formation of chloroethylene by the combination of the vinyl radical and chlorine radical, and then the addition of hydrogen atoms to the chloroethylene thus obtained. The formation of acetylene, 1,3-butadiene, and 1-butene may show the existence of the vinyl radical. And the formation of ethane, butane, and 1-butene may indicate the production of the ethyl

radical. Since chloroethylene as described above has high activity in the presence of hydrogen chloride and ethylene under a silent discharge, it is changed into the dichloro compounds and the trichloro compound (1,2,4-trichlorobutane) of butane. The formation of 1-chlorobutane and 1-chlorohexane may be represented as follows:

$$CH_2{=}CH_2 + \cdot Cl \longrightarrow \dot{C}H_2CH_2Cl$$
$$\dot{C}H_2CH_2Cl + CH_2{=}CH_2 \longrightarrow \dot{C}H_2(CH_2)_3Cl$$
$$\dot{C}H_2(CH_2)_3Cl + HCl \longrightarrow CH_3(CH_2)_3Cl + \cdot Cl$$
$$\dot{C}H_2(CH_2)_3Cl + CH_2{=}CH_2 \longrightarrow \dot{C}H_2(CH_2)_5Cl$$
$$\dot{C}H_2(CH_2)_5Cl + HCl \longrightarrow CH_3(CH_2)_5Cl + \cdot Cl$$

The mechanism mentioned above is the telomerization reaction in which hydrogen chloride acts as the telogen. The addition reaction of the $\cdot CH_2(CH_2)_5Cl$ radical to ethylene in these reaction mechanisms need not be considered, since no products beyond 1-chlorooctane (1:4 telomer) were obtained. Compared with the yield of 1-chlorobutane (1:2 telomer), the yield of 1-chlorohexane (1:3 telomer) decreased remarkably. Therefore, it is considered that the unpaired electron of the end CH_2 and the Cl atom in the $CH_2(CH_2)_3Cl$ radical form a pseudo cyclic arrangement.* On the other hand, the formation of 1,4-dichlorobutane may proceed by two paths: (1) the reaction between $\cdot CH_2(CH_2)_3Cl$ radical and hydrogen chloride or chlorine radical, (2) the coupling reaction between two $\cdot CH_2CH_2Cl$ radicals. Other dichloro compounds of butane may be formed by various secondary processes. The formation of 2-chlorobutane was also observed. 2-Chlorobutane may be formed by two paths: (1) the isomerization of 1-chlorobutane, and (2) the reaction between hydrogen chloride or ethylene and chloroethylene, the addition of CH_3–$\dot{C}HCl$ radical thus obtained to ethylene, and then the reaction of the CH_3CHCl–CH_2–$\dot{C}H_2$ radical and hydrogen chloride.

The Reactions between HX, such as Hydrogen Cyanide, Hydrogen Sulfide, and Hydrogen Chloride, and Ethylene. The reactions of ethylene with hydrogen cyanide or hydrogen sulfide in the silent electrical discharge were carried out.[3] The results obtained are summarized in Table 7. In the case of the reaction between ethylene and hydrogen cyanide, the main product was acrylonitrile. Besides this compound, ethyl cyanide, butyl cyanide, and *s*-butyl cyanide *etc.* were obtained. No compound combined with two CN groups was obtained. In the case of the reaction between ethylene and hydrogen sulfide, the main product was ethanethiol. However, the product (1,2-ethanedithiol) combined with two SH groups was formed. As may be seen from Tables 2 and 7, when hydrogen chloride, hydrogen sulfide, and hydrogen cyanide as reactants (HX) were used, the yields of the liquid products decrease in the following order: HCl>H_2S>HCN. When the hydrogen chloride was used, the yield of liquid product was especially remarkable.

Table 7. The reactions between ethylene and hydrogen sulfide or hydrogen cyanide in silent electrical discharge

Experiment No.	23[a]	24[b]
Materials used (l)		
Ethylene	19.6	27.6
Hydrogen sulfide	29.4	—
Hydrogen cyanide	—	44.8
Molar ratio (C_2H_4/HX)[c]	0.7	0.6
Second voltage (kV)	12	15
Second current (mA)	2.1	2.1
Discharge time (h)	6	9
Discharge temp. (°C)		
Inside	19—49	10—26
Outside	19—41	10
Liquid product collected (g)	7.00	6.47
Composition of liquid reaction products (%)		
$CH_2{=}CHX$	0	45.9
CH_3CH_2X	61.6	12.9
$CH_3CH_2CH_2CH_2X$	3.5	17.1
$CH_3CH_2CHXCH_3$	0.1	10.2
$CH_3(CH_2)_4CH_2X$	T	T
XCH_2CH_2X	24.2	0

a) The discharge tube used was a Pyrex tube of the Siemens type with a space gap of 2.5 mm and an effective length of 45 cm. b) This experiment was performed by using the flow system. c) X: SH or CN radicals.

References

1) K. Sugino and E. Inoue, *Bull. Chem. Soc. Jpn.*, **24**, 93 (1951); K. Sugino and E. Inoue, *Nippon Kagaku Zasshi*, **75**, 10, 617 (1954); E. Inoue, *J. Electrochem. Soc. Jpn.*, **22**, 668 (1954); E. Inoue, *ibid.*, **23**, 18, 76, 403, 452, 574, 648 (1955); E. Inoue and K. Sugino, *ibid.*, **24**, 33 (1956); T. Matsuda, K. Oto, and K. Sugino, *Nippon Kagaku Zasshi*, **79**, 325 (1958); K. Sugino, E. Inoue, K. Shirai, T. Koseki, and T. Gomi, *ibid.*, **86**, 114 (1965).

2) S. Yamamoto, N. Sonoda, and S. Tsutsumi, Preprints for the 17th Annual Meeting of the Chemical Society of Japan, (April, 1964), p. 24; N, Sonoda, S. Yamamoto, K. Okumura, S. Noda, and S. Tsutsumi, "Oxidation of Organic Compounds," Vol. II, Advances in Chemistry Series 76, American Chemical Society, Washington (1968), pp. 352—362.

3) K. Kawamoto, N. Sonoda, and S. Tsutsumi, *Bull. Chem. Soc. Jpn.*, **41**, 1376 (1968); K. Kawamoto, *ibid.*, **41**, 2161 (1968); K. Kawamoto and Y. Nishimura, *ibid.*, **42**, 1105 (1969); Y. Nishimura and K. Kawamoto, *ibid.*, **45**, 274 (1972).

4) W. E. Vaughan, F. F. Rust, and T. W. Evans, *J. Org. Chem.*, **7**, 477 (1942).

5) W. E. Hanford and J. Harmon, U. S. 2418832 (1947); U. S. 2440801 (1948).

6) J. H. Raley, F. F. Rust, and W. E. Vaughan, *J. Am. Chem. Soc.*, **70**, 2767 (1948).

7) T. A. Ford, W. E. Hanford, J. H. Harmon, and R. D. Lipscomb, *J. Am. Chem. Soc.*, **74**, 4323 (1952).

* Beer and Besprozvannyi[16] found, from their data on the telomerization of ethylene in carbon tetrachloride and chloroform, that compounds ($ClCH_2(CH_2)_3CCl_3$ and $CH_3(CH_2)_3CCl_3$) with $n=2$ were formed over a wide range of ethylene concentration. They suggested that the predominance of telomers with $n=2$ resulted from the stabilization of the trichloroamyl radical by a "pseudo cyclic" configuration between the unpaired electron of the end CH_2 and the electrophilic CCl_3 groups.

8) A. Terakawa, J. Nakanishi, and T. Hirayama, *Bull. Chem. Soc. Jpn.*, **39**, 892 (1966).
9) H. Wiener and M. Burton, *J. Am. Chem. Soc.*, **75**, 5815 (1953); J. C. Devins and M. Burton, *ibid.*, **76**, 2618 (1954); E. Inoue, *J. Electrochem. Soc. Jpn.*, **23**, 76 (1955).
10) C. L. Thomas, G. Egloff, and J. C. Morell, *Chem. Rev.*, **28**, 1 (1941).
11) S. Tsutsumi, *Kagaku Kogyo*, **16**, 623 (1965).
12) $CH_2=CH_2+e^* \rightarrow CH_2=CH_2^*+e$
$CH_2=CH_2^*+CH_2=CH_2 \rightarrow CH_2=\dot{C}H+CH_3\dot{C}H_2$
13) J. A. Franklin, P. Goldfinger, and G. Huybrechts, *Ber. Bunsenges. Phys. Chem.*, **1968**, 72 (2), 173.
14) R. Golden Jr. and P. Ausloos, *J. Chem. Phys.*, **47**, 1799 (1967).
15) $C_2H_4^* \rightarrow C_2H_2+H_2$, $C_2H_4^* \rightarrow C_2H_3+H$, $C_2H_4^* \rightarrow C_2H_2+2H$
16) A. A. Beer and M. A. Besprozvannyi, *Khim. Nauka i Prom.*, **4**, 547 (1959).

Chemistry of 1,3-Glycol Derivatives. I. The Reactions of 2,4-Pentanediol Derivatives

Osamu ITOH, Yasunori ICHIKAWA, Hiroaki KATANO, and Katsuhiko ICHIKAWA

Department of Hydrocarbon Chemistry, Faculty of Engineering, Kyoto University, Yoshida, Kyoto 606

(Received October 16, 1975)

Cyclic orthoacetates of *meso*- and *dl*-2,4-pentanediol (*cis*- and *trans*-2-ethoxy-2,4,6-trimethyl-1,3-dioxane, **1**) were prepared and characterized by NMR. The stereochemical courses of the reactions of **1** with water, hydrogen chloride, trityl chloride, and acetic acid were investigated. The reactions with water gave 4-acetoxy-2-pentanol (**4**) with complete retention of configuration, while those with the other reagents gave 4-acetoxy-2-chloropentane (**3**) and 2,4-diacetoxypentane with complete inversion. Acetolyses of **3** and the tosylate of **4** gave 2,4-diacetoxypentane predominantly with retention in the absence of water. Hydrolysis of the tosylate gave **4** with almost complete inversion. These results can be explained by the mechanism that the reactions proceed mainly through acetoxonium cation intermediate involving six-membered ring. The fluoroborate salt of this acetoxonium cation was prepared and characterized by NMR.

As a case of neighboring group participation, acetoxy participation has been studied extensively by Winstein and his co-workers.[1] Participation of acetoxy group attached to the carbon α to the cationic carbon forms acetoxonium cation of five-membered ring (AcO-5 cation). Participation of the same group at the β-position should from acetoxonium cation of six-membered ring (AcO-6 cation).

AcO-5 cation

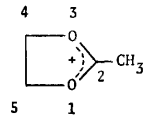

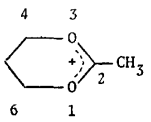

AcO-6 cation

So far, most part of the studies has been concerned with the former type of participation, and only few papers by Kovács and his co-workers[2] discussed the latter type, although the idea was reviewed by Schneider without presenting experimental data.[3]

This paper describes the preparation of *cis*- and *trans*-2-ethoxy-2,4,6-trimethyl-1,3-dioxane (*cis*- and *trans*-**1**) from *meso*- and *dl*-2,4-pentanediol (*meso*- and *dl*-**2**) and ethyl orthoacetate, and the formation of AcO-6 cation from **1**. The stereochemistry of the reactions of **1** with water, hydrogen chloride and trityl chloride is also reported together with the results of the acetolyses of 4-acetoxy-2-chloropentane (**3**) and the tosylate of 4-acetoxy-2-pentanol (**4**) which proceeded mainly through AcO-6 cation.

Preparation and Characterization of cis- *and* trans-*1*. From the reduction product of acetylacetone with sodium borohydride, *meso*- and *dl*-**2** were separated by the method of Pritchard and his co-workers.[4] The diols were converted to cyclic sulfite by the reaction with thionyl chloride and then subjected to fractional distillation. Hydrolysis of the lower boiling fraction gave pure *meso*-**2** and that of higher boiling fraction gave *dl*-isomer of 98% purity.

The method for the preparation of five-membered cyclic orthoester by Newman and his co-workers[5] was applied successfully to the present case of six-membered cyclic system. The reactions of *meso*- and *dl*-**2** with ethyl orthoacetate in benzene containing catalytic amounts of monochloroacetic acid gave *cis*-**1** and *trans*-**1** in more than 80% yields, respectively. Both *cis*-**1** and *trans*-**1** were very sensitive to atmospheric moisture and could not be stored for more than two days unless special precautions were made. However, both of them could be analyzed by gas chromatography, although slight extents of decomposition were observed.

NMR data of *cis*-**1** and *trans*-**1** are shown in Table 1.

TABLE 1. NMR DATA OF **1** IN DEUTERIOCHLOROFORM

	cis-**1**			*trans*-**1**		
	δ			δ		
C_2–CH_3	1.47	s	3H	1.45	s	3H
C_4–CH_3	1.16	d	6H	1.19(e)	d	3H
C_6–CH_3				1.34(a)	d	3H
C_5H_2	1.55	m	2H	1.54	m	2H
C_4H	4.17	m	2H	4.26(a)	m	1H
C_6H				4.06(e)	m	1H
OCH_2CH_3	1.22	t	3H	1.20	t	3H
OCH_2CH_3	3.52	q	2H	3.55	q	2H

Eliel and his co-workers reported extensive studies on the conformational analyses of 1,3-dioxane system. When methyl group is attached to C_2 of 1,3-dioxane system, the equatorial position is preferred to the axial by 3.6—4.1 kcal/mol, because of the strong crowding between the axial methyl at C_2 and hydrogens or methyl groups at C_4 and C_6. On the other hand, alkoxy group at C_2 prefers the axial position (by 0.35 kcal/mol in the case of 2-alkoxy-1,3-dioxane) by a substantial anomeric effect.[6] Applying these conclusion, the configurations and conformations of *cis*- and *trans*-**1** are depicted in Fig. 1. The NMR data can be explained reasonably.

The protons of two methyl groups attached to C_4 and C_6 of *cis*-**1** give only one doublet at $\delta=1.16$ because the two methyl groups are equivalent, while those of *trans*-**1** give two doublets at $\delta=1.19$ and 1.34. Two methyl groups of *cis*-**1** must be equatorial, since the signals should be observed at much lower fields, if they were axial. Protons at C_4 and C_6 of *cis*-**1** give only one multiplet at 4.17 because they are equivalent, while those of *trans*-**1** give two multiplets at 4.06 and 4.26. In general, the diaxial repulsion in dioxane system is larger than that in cyclohexane system because of the shorter length of C–O bond than that of C–C. It appears, therefore, to be unnecessary to consider the possibility that all of the two methyl and ethoxy groups

are axial, since the steric effects will prevent the formation of such a highly strained compound. Since Eliel suggested that 2,2-*trans*-4,6-tetramethyl-1,3-dioxane takes skew boat conformation predominantly, the same conformation must be considered in the case of *trans*-**1**. To discriminate the chair and skew boat conformations, it is necessary to determine the coupling constants between C_4–H and C_5–H and C_5–H and C_6–H exactly. From the spectrum obtained, however, it is difficult to estimate these coupling constants. Whether the chair form or the skew boat form is preferred cannot be discussed at present. NMR data can be explained reasonably in terms of both conformations. In the case of *cis*-**1**, skew boat conformation appears to be unlikely because of the strong 1,3-repulsions.

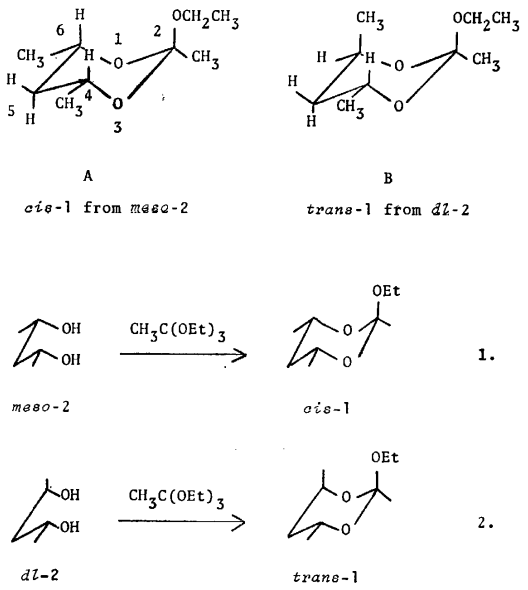

Fig. 1. Conformations and configurations of *cis*-**1** and *trans*-**1** and the stereochemistry of the formation of *cis*-**1** and *trans*-**1**.

Stereochemistry of the Reaction of **1** *with Water, Hydrogen Chloride, and Trityl Chloride.* Although a number of cyclic orthoester has been prepared by Newman and his co-workers, it appears that the stereochemistry of the nucleophilic substitution has been studied only for those with trityl chloride and trimethylsilyl chloride in methylene chloride by the same authors which proceeded with inversion. They explained the results by assuming the ionization of the substrates to AcO-5 cations and the subsequent attack of the nucleophile on the cations.[5] We have examined the stereochemical courses of the reactions of **1** with several kinds of reagent.

Treatments of *cis*- and *trans*-**1** with water–ethanol mixture (20: 80 by volume) at room temperature gave *erythro*- and *threo*-4-acetoxy-2-pentanol (**4**) in almost quantitative yields, respectively. The results show that the reactions proceeded with complete retention. On the other hand, the reactions of the same *cis*- and *trans*-**1** with trityl chloride (under reflux) or hydrogen chloride (at 0 °C) in methylene chloride gave *threo*- and *erythro*-4-acetoxy-2-chloropentane (**3**) also in almost quantitative yields, respectively. It is clear that the reactions proceeded with complete inversion. The sharp contrast of the stereochemical courses mentioned above makes it clear that the mechanism of the reactions with water–ethanol mixture is different from those with trityl chloride or hydrogen chloride in methylene chloride.

Since the stereochemistry of the latter reactions is the same as that of the case of five-membered cyclic orthoester by Newman, it appears that the mechanism is also the same.

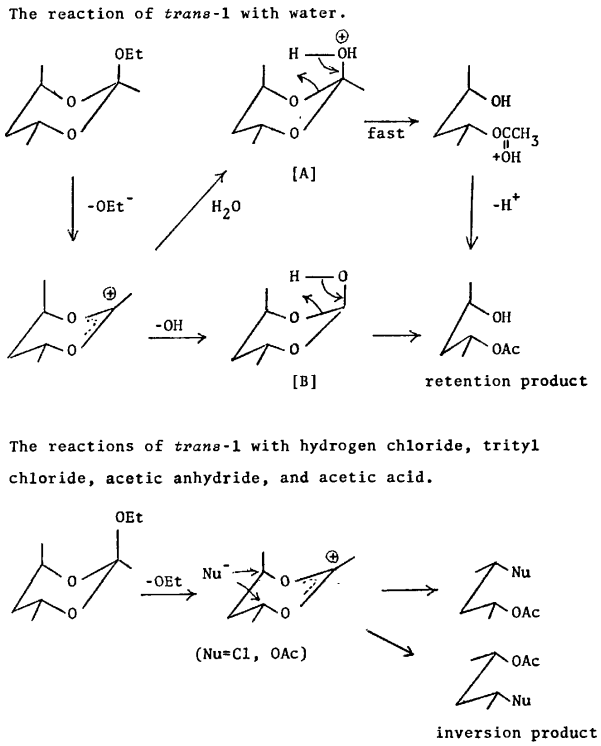

Fig. 2. Mechanisms of the reactions of *trans*-**1** (*cis*-isomer follows the same mechanism).

The most probable mechanism to explain the retentive course of the reaction with water–ethanol mixture is depicted in Fig. 2. If the product **4** is obtained by the reaction of water or hydroxide ion with the AcO-6 cation from **1** as in the cases of hydrogen chloride and trityl chloride, the stereochemistry should be inversion. The mechanism proposed to explain the results of retention assumes the ionization of **1** to form AcO-6 cation, the subsequent reaction with water or hydroxide ion to yield oxonium ion type intermediate (A) or its deprotonated type (B), and the collapse of A or B to form the final product **4** by bond reconstruction involving proton transfer. Since the stereochemistry of the reaction with the same water–ethanol (20: 80 by volume) mixture containing 2 M NaOH was also complete retention, it appears that both reaction routes through A and B are operative.

The steric courses of the reactions of **1** with several other reagents were examined qualitatively by analyzing the reaction mixtures at room temperature directly by gas-chromatography. Acetic anhydride which was completely free from water gave 2,4-diacetoxypentane

results reasonably. Here again, however, the acetolysis without participation as a minor reaction appears to be operative, since the products with inversion were obtained as the minor products. In moist acetic acid–acetic anhydride mixture, the primary main product of the reaction of *threo*-**3** was *erythro*-**4** with inversion showing that the reaction of water with AcO-6 cation is very fast as already mentioned. After a sufficient reaction time, the main product became *meso*-**6** by the acetylation of **4** under the condition. Undoubtedly, the acetylation does not change the configuration of the substrate since the bond breaking of C–OH is not involved in this reaction step. It is concluded, therefore, that the AcO-6 cation formation which was assumed in the reactions of steroid[7] and (2-acetoxycyclohexyl)-methyl cation system[2] is also important in the solvolysis of acyclic 1-acetoxy-3-ol system and that the presence of water changes the steric course of the reaction.

Structural assignments of 2, 3, 4, 5, and 6. The structural assignments of *erythro* and *threo* or *meso* and *dl* of the substrates and products can be made by converting them to **2** or **6** whose physical constants (mp) are known. By NMR, however, the discriminations are possible also. Methylene signal of *dl*-**6** is a doublet (J=8 Hz) of doublet (J=6 Hz), while that of *meso*-isomer is a doublet (J=14 Hz) of triplet (J=6 Hz). This difference is due to the fact that the *dl*-isomer is more symmetrical than *meso* about the the central carbon C_3. According to this principle, the assignments of the other compounds have been made. In the case of **4**, methylene signal of *threo*-isomer was a triplet (J=9 Hz) of doublet (J=3 Hz) at δ 1.61, while the signals of the *erythro* were two pairs of multiplet at δ 1.57 and 1.85. The relationship between the symmetry of the structure and the shape of the signal can be applied to the case of methine proton too. The methine signals of **5** at C_2 and C_4 should be different, since the substituents are different, although they are very similar. In the case of *erythro*-isomer, the two methine protons gave a sextet at δ 4.96 and a broad multiplet at δ 4.92 and those of *threo* gave a triplet-like signal at δ 1.79. NMR data are summarized in Table 3.

Preparation of Fluoroborate salt of 2,4,6-Trimethyl-1,3-dioxane-2-ylium Cation. Many kinds of 1,3-dioxolan-2-ylium cation (AcO-5 cation type) salt have been prepared by various methods.[8] On AcO-6 type cation salt, however, only few papers are found in the literature.[9] We have prepared the fluoroborate salt of the present AcO-6 cation.

Dropwise addition of boron trifluoride–ether complex to ether solution of **1** at room temperature resulted in the formation of oily drops which became colorless crystals after standing for several days in refrigerator. The crystals were so hygroscopic that elemental analysis and IR and mp measurements by usual methods were difficult. The raw crystals, just after filtration, were dissolved into dry nitrobenzene and subjected to NMR measurement. In Fig. 4, the spectra of the salt and

Table 3. NMR data of **2**, **3**, **4**, **5**, and **6**, δ in ppm

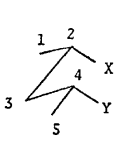

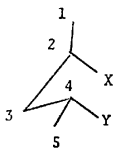

			C^1H_3	C^5H_3	C^2H	C^4H	C^3H_2CO	CH_3CO
2	X=OH Y=OH	*meso*	1.18 d		3.99 broad m		1.55 m	
		dl	1.21 d		4.13 sextet		1.58 t	
3	X=Cl Y=OAc	*erythro*	1.53 d	1.25 d	4.03 m	5.07 m	1.80 (1H) m 2.13 (1H) m	2.02 s
		threo	1.51 d	1.24 d	4.03 m	5.08 m	1.86 m	2.01 s
4	X=OH Y=OAc	*erythro*	1.21 d	1.26 d	3.88 sextet	5.05 sextet	1.57 (1H) d of t 1.85 (1H) d of t	2.04 s
		threo	1.19 d	1.27 d	3.75 m	5.15 m	1.61 t of d	2.08 s
5	X=OTs Y=OAc	*erythro*[a]	1.17 d	1.31 d	4.69 m	4.92 m	b)	2.05 s
		threo[c]	1.19 d	1.35 d	4.83 broad sextet		1.79 broad t-like	1.98 s
6	X=OAc Y=OAc	*meso*	1.24 d		4.98 sextet		b)	2.04 s
		dl	1.22 d		4.91 sextet		1.75 d of d	2.02 s

a) CH_3 bonded to phenyl, 2.50. b) Because of the overlapping with the peak of acetyl protons, the signals could not be determined. c) CH_3 bonded to phenyl, 2.47.

precursor **1** are shown. In the former, the signals due to ethoxy group disappeared and all signals shifted to lower fields as compared to the corresponding signals of **1**. The shifts are especially remarkable in those of C_2-methyl protons and C_4 and C_6 methine protons. In the case of the cation from *trans*-**1**, methyl protons attached to C_4 and C_6 gave only one doublet at δ 1.87 and two methine protons of the same C_4 and C_6 gave also only one multiplet at δ 5.67. It appears that the rapid flattering of the six-membered ring resulted in such observations. In the case of the cation from *cis*-**1** the flattering is considered to be difficult because the diaxial form should be much less stable than the di-equatorial form by the strong steric crowding.

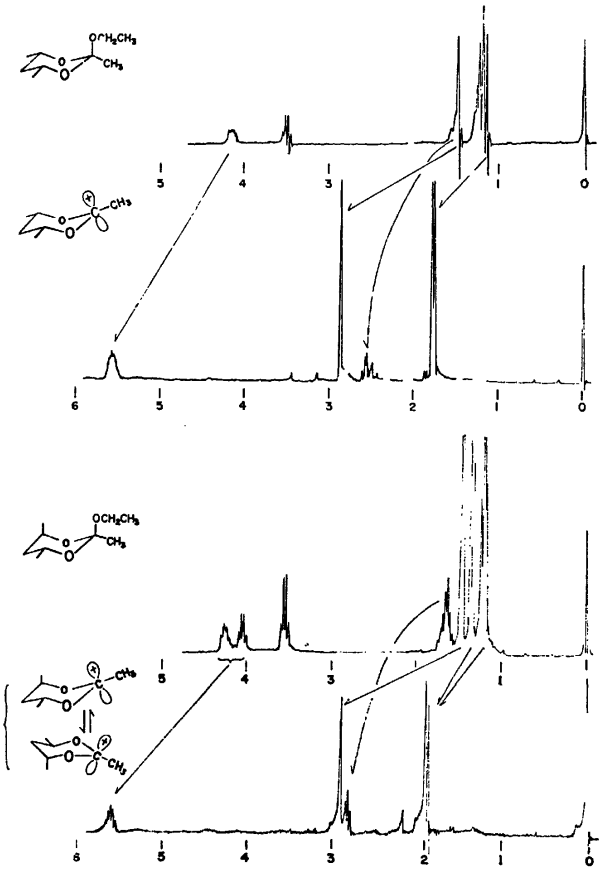

Fig. 4. NMR spectra of *cis*- and *trans*-**1** and fluroborate salts of the corresponding cations.

TABLE 4. NMR DATA OF FLUOROBORATES OF *cis*- AND *trans*-2,4,6-TRIMETHYL-1,3-DIOXANE-2-YLIUM CATIONS

	Cation from *cis*-**1**			Cation from *trans*-**1**		
	δ ppm			δ ppm		
C_2–CH_3	2.97	s	3H	2.93	s	3H
C_4–CH_3, C_6–CH_3	1.83	d	6H	1.87	d	6H
C_5H_2	2.58	m	2H	2.84	m	2H
C_4H, C_6H	5.78	m	2H	5.67	m	2H

Experimental

Preparation of dl-*and* meso-**2**. According to the method reported by Pritchard *et al.*, 2,4-pentanediol, which was obtained by sodium borohydride reduction of acetylacetone, was converted to cyclic sulfite by equivalent amount of thionyl chloride. Fractional distillation gave *cis*-(bp 57.8 °C/6 Torr) and *trans*-sulfite fraction (bp 65.4 °C/6 Torr). Analyses by gas-chromatography (EGSS-X 1m column) showed that the purities were 96 and more than 98%, respectively. Hydrolyses of the both fractions gave *meso*-**2** (bp 85—87 °C/7 Torr) and *dl*-**2** (99—100 °C/11 Torr, mp 47.5—49 °C), respectively.

Preparation of cis- *and* trans-*1*. Into a benzene (50 ml) solution containing 11.4 g of *meso*-**2** and catalytic amount (ca. 100 mg) of monochloroacetic acid, 25 g of freshly distilled ethyl orthoacetate were added under stirring. After refluxing for 3 h, benzene and ethanol formed were removed. Distillation under vacuum gave *cis*-**1** (bp 81—83 °C/40 Torr, 15.1 g). IR (liquid film): 1255 (s, ν_{as} C–O–C), 1195 (m), 1150 (m), 1120 (m), 1100 (sh), 1060 (s, ν_s C–O–C) cm^{-1}.

By the same method, *trans*-**1** was obtained from *dl*-**2** in 87% yield (bp 82.5 °C/40 Torr). IR (liquid film): 1245 (s, ν_{as} C–O–C), 1180 (m), 1150 (m), 1140 (sh), 1115, and 1055 (s, ν_s C–O–C) cm^{-1}.

Reaction of 1 with Water. Into 80 ml of 80% ethanol, 27.9 g of *cis*-**1** were added under stirring at room temperature After 1 h, ethanol was distilled off from the reaction mixture. Ether extract of the residue was washed with aqueous saturated sodium chloride solution, dried with sodium sulfate and then distilled to give *erythro*-**4** (bp 107—109 °C/22 Torr) in 94% yield (22.2 g). Analysis by glc. with EGSS-X column showed that the purity was more than 98%. IR in CCl_4: ν_{OH}, 3620 (sh), 3480 (br); ν_{CO}, 1740 (br), 1720 (sh); 1150, 1110 (br), 1035, 1020, 955 cm^{-1}.

From 17.3 g of *trans*-**1**, 13.0 g (90% yield) of *threo*-**4** of more than 96% purity were obtained by the same procedure. IR in CCl_4: ν_{OH}, 3630 (w), 3520 (br); ν_{CO}, 1740 (sh), 1720; 1280 (sh), 1260, 1250, 1150, 1020, 1010, 970, and 940 cm^{-1}.

The half esters of *erythro*- and *threo*-**4** were converted to *meso*- and *dl*-**6** by acetylation with acetyl chloride in pyridine, respectively. The physical constants and IR and NMR spectra were identical with those of the authentic samples which were prepared from *meso*- and *dl*-**2** by the reported method.[10]

Reaction of 1 with Hydrogen Chloride. Into a methylene chloride (50 ml) solution of *cis*-**1** (3.5 g), dry hydrogen chloride (0.04 mmol, 2 equivalents) was added at 0 °C. After 30 min, the reaction mixture was washed with water, dried with sodium sulfate and subjected to distillation. *threo*-**3** was obtained (2.3 g, 70% yield, bp 82—84 °C/22 Torr). Analysis by GLC showed that no detectable amount of by-product was formed. By the same experimental method, the reaction of *trans*-**1** gave *erythro*-**3** in 68% yield (83.5—86.5 °C/25 Torr).

Reaction of 1 with Trityl Chloride. A mixture containing 3.48 g of *cis*-**1**, 5.58 g of trityl chloride and 50 ml of methylene chloride was kept at 42 °C for 3.5 h. Distillation of the reaction mixture gave 2.75 g of *threo*-**3** (83% yield). By the same experimental procedure, *erythro*-**3** (2.70 g) was obtained from *trans*-**1**. Both products were shown to contain no other products by GLC. The IR and NMR spectra were identical with those of the products obtained by acetylation of *erythro*- and *threo*-**4**, respectively.

Preparation of 3. Thionyl chloride (3.8 g) was added to an ether (15 ml) solution of *threo*-**4** (2.48 g). The mixture was heated under reflux for 2 h, washed with saturated aqueous solution of sodium hydrogencarbonate, extracted with ether, dried, and distilled. The product was *threo*-**3**, bp 82—84 °C/22 Torr, 1.83 g (65 % yield).

Similarly, *erythro*-**3**, bp 82—83 °C/22 Torr, was obtained from *erythro*-**2** in 78% yield.

Preparation of 5. Into pyridine (50 ml) solution of

Table 5. Analytical data

		Calcd for			Observed		
		C	H	Cl, S	C	H	Cl, S
cis-**1**	$C_9H_{18}O_3$	62.04	10.41		61.85	10.33	
trans-**1**					62.06	10.65	
meso-**2**	$C_5H_{10}O_2$	57.66	11.61		57.85	11.58	
dl-**2**					57.69	11.64	
erythro-**3**	$C_7H_{13}O_2Cl$	51.07	7.96	21.54	51.34	8.03	21.57
threo-**3**					51.29	7.85	21.51
erythro-**4**	$C_7H_{14}O_3$	57.51	9.65		57.57	9.81	
threo-**4**					57.81	9.72	
erythro-**5**	$C_{14}H_{20}O_5S$	55.98	6.71	10.67	55.95	6.82	10.56
threo-**5**					56.02	6.89	10.66

erythro-**4** (2.96 g), *p*-toluenesulfonyl chloride (6.1 g) was added dropwise under cooling with ice bath. The mixture was kept in refrigerator (−15—−18 °C) for two days, poured into ice-water, extracted with ether and dried with K_2CO_3–Na_2SO_4. When ether was removed, oily product was obtained. This product was dissolved into 200 ml of petroleum ether, heated to about 40 °C and filtered to remove impurities. After standing in refrigerator for 24 h, crystals formed were collected and recrystallized from the same solvent, mp 32—34 °C (5.15 g, 86% yield). The structure of *erythro*-**5** was confirmed by NMR spectrum. From *threo*-**4**, *threo*-**5**, mp 60—61 °C, was obtained in 82% yield similarly.

Solvolysis Reactions. The reactions were carried out in ampoules. The experimental procedure was analogous to that of the reaction of **1** with water.

Preparation of 2,4,6,-trimethyl-1,3-dioxane-2-ylium fluoroborate. Into 15 ml of dry ether, 5.55 g of *cis*-**1** was dissolved. Boron trifluoride–ether complex (5.2 g) was added slowly. The mixture was kept in refrigerator for two days. Removing ether, 6.48 g of the salt were obtained and characterized by NMR. The same procedure gave the salt of *trans*-isomer.

NMR spectra were recorded on a Varian Associates HR-220 at 220 MHz at room temperature. Gas-chromatograph analyses were carried out with YANACO GC-550 TPH. IR spectra were recorded on HITACHI EPI-G2.

This work was partially supported by a Grant-in-Aid for Scientific Research from the Ministry of Education, Japan (No. 911503).

References

1) See, for example, S. Winstein, E. Grunwald, R. E. Buckles, and C. Hanson, *J. Am. Chem. Soc.*, **70**, 812 and 716 (1948).

2) Ö. Kovács, G. Schneider, L. K. Láng, and J. Apjok, *Tetrahedron*, **23**, 4181 (1967). Ö. Kovács, G. Schneider, and L. K. Láng, *Proc. Chem. Soc., London*, **1963**, 374. L. J. Dolby and M. J. Schwarz, *J. Org. Chem.*, **30**, 3581 (1965).

3) G. Schneider, *Tetrahedron Lett.*, **1966**, 5921.

4) J. G. Pritchard and R. L. Vollmer, *J. Org. Chem.*, **28**, 1545 (1963).

5) M. S. Newman and C. H. Chen, *J. Am. Chem. Soc.*, **95**, 278 (1973).

6) E. L. Eliel, *Acc. Chem. Res.*, **3**, 1 (1970).

7) M. J. Cooper, M. P. Hartshorn, and D. N. Kirk, *J. Chem. Soc., C*, **1966**, 576. E. J. Tarlton, M. Fieser, and L. F. Fieser, *J. Am. Chem. Soc.*, **75**, 4423 (1953). A. D. Cross, E. E. Denot, R. Acevedo, R. Urquiza, and A. Bowere, *J. Org. Chem.*, **29**, 2195 (1964).

8) See, for example, C. U. Pittman, Jr., S. P. McManus, and J. W. Larsen, *Chem. Rev.*, **72**, 357 (1972).

9) H. Paulsen and H. Behre, *Chem. Ber.*, **104**, 1264, 1281, and 1299 (1971).

10) M. Shirai and S. Nagai, *Nippon Kagaku Zasshi*, **81**, 144, (1960).

^{13}C NMR Spectra of Some Methyl Cyclohexanecarboxylates

Yasuhisa SENDA, Jun-ichi ISHIYAMA, and Shin IMAIZUMI

Department of Applied Science, Faculty of Engineering, Tohoku University, Aoba, Sendai 980

(Received October 23, 1975)

^{13}C NMR spectra of a series of stereoisomeric-substituted methyl cyclohexanecarboxylates have been obtained. The resonances for ring carbons of the isomers, in which both the methoxycarbonyl and the other groups have equatorial orientations, usually appear at a field lower than those of the isomers in which one of the two substituents has an axial orientation. No appreciable difference in shift due to the configurational change is observed in the resonances for the substituents. Observed chemical shifts are compared with predicted values.

In ^{13}C NMR spectra it is generally found that various substituents exert shielding effects which are additive for families of compounds. As a result, the positions of ^{13}C signals for closely related materials may often be predicted with good precision in a wide variety of systems.[1] It has been reported that the ^{13}C chemical shifts predicted from those of conformational isomers of cyclohexanol and substituent parameters already reported are in good agreement with those observed in previous studies on series of stereoisomeric substituted 1-methylcyclohexanols[2] and menthols.[3] This paper is a report on a study of the ^{13}C NMR spectra of some substituted stereoisomeric methyl cyclohexanecarboxylates. The ^{13}C chemical shifts observed are compared with those predicted.

Results and Discussion

Natural-abundance 25.15-MHz ^{13}CFT NMR spectra were obtained using the ^{1}H noise decoupling technique. The signals were assigned by comparing signal shifts due to differences of structure between closely related compounds and by the use of the ^{1}H off-resonance decoupling technique.[1] The chemical shifts δ obtained are listed in Table 1.

Ring Carbons. The resonances for ring carbons of isomers, in which the methoxycarbonyl and other groups have an equatorial orientation, usually appear at a field lower than those of isomers, in which one of the two substituents has an axial orientation, except for the C-3 and C-4 resonances in methyl 4-*t*-butylcyclohexanecarboxylate (Table 2).

From the observed ^{13}C chemical shifts of *t*-butylcyclohexane and of stereoisomeric methyl 4-*t*-butylcyclohexanecarboxylates, substituent parameters for a methoxycarbonyl group on ring carbons were estimated. These are tabulated in Table 2.

Parent cyclohexanecarboxylate exists in a conformational mixture, the population of which is estimated as being approximately 89.5% of the equatorial conformer and 10.5% of the axial conformer, since the conformational free energy of a methoxycarbonyl group on a cyclohexane ring is 1.25 kcal/mol.[4] As a cnsequence, the carbon chemical shifts predicted are obtained from those of each set of conformers according to a previously outlined procedure.[2] These values are in good agreement with those observed. Conformational free energies of a methyl and a hydroxyl group on a cyclohexane ring are 1.7 and 0.7 kcal/mol, respectively. The conformational distribution of *cis* 2- and 4- or

TABLE 1. OBSERBED AND PREDICTED ^{13}C CHEMICAL SHIFTS OF METHYL CYCLOHEXANECARBOXYLATES[a,b]

Methyl cyclohexanecarboxylate			C-1	C-2	C-3	C-4	C-5	C-6	OMe	C=O	Me
Parent		Obsd[c]	43.19	29.18	25.60	25.96	25.60	29.18	51.32	176.31	
			43.1	*29.0*	*25.4*	*25.8*	*25.4*	*29.0*	*51.2*	*176.3*	
		Pred[d]	43.6	29.5	26.0	26.5	26.0	29.5	51.3	176.3	
		Diff[e]	−0.4	−0.3	−0.4	−0.5	−0.4	−0.3	0	0	
2-Methyl-	*cis*	Obsd	45.98	31.85	31.60	24.51	22.08	24.51	51.02	175.27	15.65
		Pred	48.8	32.8	32.2	25.1	24.2	26.9	51.3	175.7	21.0
		Diff	−2.8	−0.9	−0.6	−0.6	−2.1	−2.4	−0.3	−0.4	−5.3
	trans	Obsd	51.44	34.52	34.52	26.02	25.60	30.03	51.14	176.37	20.68
		Pred	53.0	35.3	35.2	26.5	26.0	29.7	51.3	176.4	22.8
		Diff	−1.6	−0.8	−0.7	−0.5	−0.4	0.3	−0.2	0	−2.1
3-Methyl-	*cis*	Obsd	43.56	32.27	37.67	34.64	25.72	28.81	51.32	176.18	22.69
		Pred	44.1	38.6	31.9	35.4	26.3	29.4	51.3	176.4	22.8
		Diff	−0.5	−0.9	0.4	−0.8	−0.6	−0.6	0	−0.2	−0.1
	trans	Obsd	31.19	35.73	27.96	33.91	22.08	28.45	51.32	175.88	21.29
		Pred	39.3	36.4	28.3	34.5	22.7	28.5	51.3	176.4	21.0
		Diff	−0.1	−0.7	−0.3	−0.6	−0.6	0	0	−0.5	0.3
4-Methyl-	*cis*	Obsd	40.43	26.33	31.54	30.82	31.54	26.33	51.26	176.43	21.11
		Pred	40.8	26.9	32.2	30.6	32.2	26.9	51.3	176.4	21.0
		Diff	−0.5	−0.6	−0.7	0.2	−0.7	−0.6	0	0	0.1
	trans	Obsd	43.19	29.24	34.46	32.21	34.46	29.24	51.32	176.43	22.56
		Pred	43.8	29.7	35.2	32.1	35.2	29.7	51.3	176.4	22.8
		Diff	−0.6	−0.5	−0.7	0.1	−0.7	−0.5	0	0	−0.2

Table 1 Continued

Methyl cyclohexanecarboxylate			C-1	C-2	C-3	C-4	C-5	C-6	OMe	C=O	Me
2-Hydroxy-	*cis*	Obsd	47.01	66.85	32.15	20.20	24.87	23.66	51.63	175.81	
		Pred	49.3	68.9	32.0	21.0	24.9	23.7	51.3	176.1	
		Diff	−2.3	−2.0	0.2	−0.8	0	0	0.3	−0.3	
	trans	Obsd	51.69	70.86	34.15	24.51	25.05	28.45	51.69	175.82	
		Pred	52.3	73.2	34.5	24.4	25.0	27.5	51.3	176.4	
		Diff	−0.6	−2.3	−0.3	0.2	0.1	1.0	0.4	0.6	
3-Hydroxy-	*cis*	Obsd	41.98	37.91	69.40	34.82	23.47	28.21	51.63	176.61	
		Pred	41.9	37.9	69.8	34.7	24.1	28.4	51.3	176.1	
		Diff	0.1	0	−0.4	0.1	−0.6	−0.2	0.3	0.5	
	trans	Obsd	37.67	35.49	65.64	32.70	19.89	28.15	51.63	175.76	
		Pred	37.3	35.7	65.1	33.1	20.0	28.6	51.3	176.4	
		Diff	0.4	−0.2	0.5	−0.4	−0.1	−0.4	0.3	−0.6	
4-Hydroxy-	*cis*	Obsd	41.31	23.84	32.03	66.43	32.03	23.84	51.57	176.00	
		Pred	42.2	23.7	32.0	66.2	32.0	23.7	51.3	176.1	
		Diff	−0.9	0.1	0	0.2	0	0.1	0.3	−0.1	
	trans	Obsd	42.28	27.36	34.40	69.40	34.40	27.36	51.57	176.24	
		Pred	42.8	27.5	34.5	70.0	34.5	27.5	51.3	176.4	
		Diff	−0.5	−0.1	−0.1	−0.6	−0.1	−0.1	0.3	−0.2	
2-Methoxycarbonyl-	*cis*	Obsd	42.71	42.71	26.39	23.90	23.90	26.39	51.57	174.12	
		Pred	43.3	43.3	26.5	24.3	24.3	26.5	51.3	175.9	
		Diff	−0.6	−0.6	−0.1	−0.4	−0.4	0.1	0.3	−1.8	
	trans	Obsd	44.89	44.89	29.06	25.36	25.36	29.06	51.63	175.27	
		Pred	46.3	46.3	28.6	25.4	25.4	28.6	51.3	176.4	
		Diff	−1.4	−1.4	0.5	0	0	0.5	0.3	−1.1	
3-Methoxycarbonyl-	*cis*	Obsd	42.53	31.18	42.53	28.45	24.93	28.45	51.50	175.33	
		Pred	43.0	31.9	43.0	28.7	25.2	28.7	51.3	176.4	
		Diff	−0.5	−0.7	−0.5	−0.2	−0.3	−0.2	0.2	−1.1	
	trans	Obsd	39.07	29.56	39.07	27.96	22.10	27.96	51.50	175.33	
		Pred	39.4	30.4	39.4	28.2	22.5	28.2	51.3	175.9	
		Diff	−0.3	−0.8	−0.3	−0.2	−0.4	−0.2	0.2	−0.6	
4-Methoxycarbonyl-	*cis*	Obsd	40.71	26.14	26.14	40.71	26.14	26.14	51.44	175.15	
		Pred	41.1	26.5	26.5	41.1	26.5	26.5	51.3	175.9	
		Diff	−0.4	−0.4	−0.4	−0.4	−0.4	−0.4	0.1	−0.6	
	trans	Obsd	42.46	28.15	28.15	42.46	28.15	28.15	51.50	175.76	
		Pred	43.1	28.6	28.6	43.1	28.6	28.6	51.3	175.4	
		Diff	−0.6	−0.4	−0.4	−0.6	−0.4	−0.4	0.2	0.4	
1,3-Cyclohexanecarbolactone		Obsd	39.07	(37.67)	77.90	(28.75)	18.50	(26.57)		178.91	

a) The values in parentheses have not been assigned to specific carbons. b) The values in italics are taken from M. Gordon, S. H. Grover, and J. B. Stothers, *Can. J. Chem.*, **51**, 2092 (1973). c) Observed (δ) d) Predicted (δ) e) Difference (ppm); the observed chemical shift minus the predicted value.

TABLE 2.

^{13}C chemical shift (δ) of		C-1	C-2	C-3	C-4	OMe	C=O	Me	$\underline{C}Me_3$
t-Butylcyclohexane[a]		26.87	27.42	27.78	48.53			27.60	32.58
		27.2	*27.8*	*28.2*	*48.9*			*27.7*	*32.7*[b]
Methyl 4-*t*-butylcyclohexanecarboxylate	*cis*	39.01	28.15	23.96	48.11	51.26	175.40	27.54	32.51
		38.9	*28.0*	*23.8*	*47.9*	*51.2*	*175.4*	*27.4*	*32.4*[c]
	trans	43.50	29.66	23.96	47.56	51.26	176.37	27.54	32.39
		43.4	*29.5*	*26.6*	*47.3*	*51.2*	*176.4*	*27.4*	*32.3*[c]
Substituent parameter (ppm) of									
COOMe	Axial	12.1	0.7	−3.8	−0.4				
	Equatorial	16.6	2.2	−1.1	−1.0				

a) The numbering system follows the methyl *t*-butylcyclohexanecarboxylate. b) These values are taken from J. D. Roberts, F. J. Weigert, J. I. Kroschwitz, and H. J. Reich, *J. Am. Chem. Soc.*, **92**, 1338 (1970). c) These values are taken from M. Gordon, S. H. Grover, and J. B. Stothers, *Can. J. Chem.*, **51**, 2092 (1973).

trans 3-methylcyclohexanecarboxylates, therefore, are estimated to be approximately 67% of the equatorial methyl conformers and 33% of their axial methyl counterparts, and those of *cis* 2- and 4- or *trans* 3-hydroxycyclohexanecarboxylates are estimated to be approximately 28% of the equatorial hydroxyl conformers and 72% of their axial hydroxyl counterparts. Taking into account the substituent parameters of the methyl group reported by Grant and Dalling[5] and those of the hydroxyl group which are estimated from the chemical shifts for *t*-butylcyclohexane and stereoisomeric 4-*t*-butylcyclohexanols,[2] the chemical shifts predicted are obtained in a way similar to those of the parent cyclohexanecarboxylate. *cis* 1,2- and 1,4- or *trans* 1,3-Cyclohexanedicarboxylates undergo rapid interconversion between equivalent conformers, while alternatives exist exclusively in more stable conformations. These chemical shifts are also tabulated in Table 1. Most of them are in good agreement with those observed, deviations being within $\pm$0.9 ppm.*

Appreciable deviations between predicted and observed values appear in 2-substituted cyclohexanecarboxylates, especially for C-1 and C-2 resonances. The δ values observed are smaller than those predicted. Grant and Dalling[5] also found that the upfield shift caused by some of the gross effects appeared for the C-1 and C-2 resonances in 1,2-dimethylcyclohexanes. These shifts may be due to the bond deformation of these carbons by the gauche interaction between two vicinal substituents.

Substituents. The resonances for the carbonyl carbons of the ester groups in *cis* and *trans* 4-*t*-butylcyclohexanecarboxylates appear at δ 175.40 and 176.37, respectively. No shift difference is observed for the carbon of the ester methyl group in a set of stereoisomers. These results show that the orientational difference of the methoxycarbonyl group has a slight effect on the chemical shifts of their own carbons. Practically, very small shift differences occur in each pair of isomers. The ^{13}C NMR spectra of stereoisomeric 1-*t*-butyl-4-methylcyclohexanes show that the chemical shift for an axial methyl group in a cyclohexane ring is δ 17.53 and that that for an equatorial group is δ 22.53.[3] Using these δ values, the chemical shifts predicted for the methyl groups of methylcyclohexanecarboxylates are estimated (Table 1). In the case of 2-methylcyclohexanecarboxylate, there are appreciable shift differences between the observed and predicted values, while the chemical shifts for 3- and 4-methylcyclohexanecarboxylate are in good agreement with the predicted values, deviations being within $\pm$0.3 ppm. Such deviations for 2-methyl isomers suggest that the gauche interaction between these two vicinal substituents plays a major role in shifts to higher field.

The ^{13}C NMR spectrum of the lactone of 3-hydroxycyclohexanecarboxylic acid (1,3-cyclohexanecarbolactone) was obtained. The cyclohexane ring of this compound is considered to be more puckered than that of ordinary cyclohexanes produced by lactone formation. Since C-5 is the γ-position of both axial alkoxycarbonyl and acyloxy groups, a significant upfield shift is expected. The resonance at δ 18.50 corresponds to this carbon. The resonances at δ 37.67 and 28.75 cannot be assigned to specific carbons.

^{1}H NMR spectra of cyclohexanecarboxylates were also examined. ^{1}H signals for the methyl groups on the cyclohexane ring appear at about δ 0.83—0.90 and those for the methoxycarbonyl groups at about δ 3.60—3.67. Only a very small shift difference was observed in a set of stereoisomeric cyclohexanecarboxylates.

Since ^{13}C chemical shifts are affected by stereochemical differences, the predicted chemical shifts derived from the A values and the substituent parameters are helpful to a certain extent in assigning the resonance signals to specific carbons.

Table 3. ^{1}H chemical shifts for methyl groups of methyl cyclohexanecarboxylates[a,b]

Methyl cyclohexanecarboxylate	COOMe		Me	
	cis	*trans*	*cis*	*trans*
Parent	3.65		—	—
4-*t*-Butyl-	3.64	3.60	0.83	0.85
2-Methyl-	3.60	3.63	0.89	0.86
			(7.6)	(6.0)
3-Methyl-	3.64	3.61	0.89	0.90
			(6.8)	(6.4)
4-Methyl-	3.64	3.61	0.89	0.88
			(5.6)	(5.6)
2-Hydroxy-	3.65	3.67	—	—
3-Hydroxy-	3.64	3.62	—	—
4-Hydroxy-	3.64	3.64	—	—
2-Methoxycarbonyl-	3.63	3.62	—	—
3-Methoxycarbonyl-	3.64	3.64	—	—
4-Methoxycarbonyl-	3.63	3.63	—	—

a) All chemical shifts are expressed in δ (ppm downfield from internal Me_4Si). b) The values in parentheses are coupling constants, J(Hz).

* Positive values represents shifts toward lower field.

Experimental

NMR Spectra. The ^{13}CFT-NMR spectra were obtained at 25.15 MHz on a JEOL JNM-MH-100 instrument equipped with a JNM-MFT-100 Fourier transform accessory. The instrument was controlled with a JEC-6 spectrum computer. Samples were dissolved in $CDCl_3$, the deuterium signal of which provided a field frequency lock; the concentrations were 30% (w/v). Measurement conditions were as follows: pulse width, 27.5 μs (*ca.* 45°); repetition time, 4 s; spectral width, 6.25 kHz; data points, 8192; acquisition time, 0.655 s. Noise modulated proton decoupling was carried out at a nominal power of 20 W. All chemical shifts are expressed in δ (ppm downfield from internal Me_4Si). Each observed chemical shift is estimated to be accurate to within δ $\pm$0.05.

Materials. All the materials employed in this work are known compounds. *o*-Toluic acid was hydrogenated over PtO_2 in AcOH to give 2-methylcyclohexanecarboxylic acid. The composition of the resulting mixture was 92% of the *cis* and 8% of the *trans* acids. A part of this was refluxed with KOH in ethylene glycol giving mixture of 78% of the *trans* and 22% of the *cis* isomers. The PtO_2 hydrogenation of *p*-toluic acid gave a mixture of 95% *cis* and 5% *trans* 4-methylcyclohexanecarboxylic acids, the isomerization of which gave a mixture of 84% of the *trans* and 16% of the *cis* isomers. The

PtO_2 hydrogenation of *m*-toluic acid gave 83% of *cis* and 17% of *trans* 3-methylcyclohexanecarboxylic acids. Methyl hydroxycyclohexanecarboxylates were prepared by the method of Kilpatrick and Morse.[6] *cis* and *trans* Cyclohexane-1,2-dicarboxylic acids and *cis* cyclohexane-1,4-dicarboxylic acid were obtained commercially. Isomerization of *cis* cyclohexane-1,4-dicarboxylic acid with KOH, followed by recrystallization from H_2O gave pure *trans* isomer. Cyclohexane-1,3-dicarboxylates were prepared from isophthalic acid by the method of Smith and Byrne.[7] The Raney Ni hydrogenation of methyl *p*-*t*-butylbenzoate at high hydrogen pressure and high temperature gave a mixture of 60% *cis* and 40% *trans* methyl 4-*t*-butylcyclohexanecarboxylates. All carboxylic acids were converted to methyl esters by treatment with diazomethane in the usual manner. Each mixture of methyl 2-, 3- or 4-methylcyclohexanecarboxylates, or methyl 4-*t*-butylcyclohexanecarboxylates was subjected to preparative gas chromatography to give a pure *cis* or *trans* isomer.

References

1) (a) G. C. Levy and G. L. Nelson, "Carbon-13 Nuclear Magnetic Resonance for Organic Chemists," Wiley Interscience, New York, (1972); (b) J. B. Stothers, "Carbon-13 NMR Spectroscopy," Academic Press, New York (1972).

2) Y. Senda, J. Ishiyama, and S. Imaizumi, *Tetrahedron*, **31**, 1601 (1975).

3) Y. Senda and S. Imaizumi, *Tetrahedron*, **31**, 2905 (1975).

4) J. A. Hirsch, "Topics in Stereochemistry," Vol. 1, ed. by N. L. Allinger and E. L. Eliel, Wiley Interscience, New York (1967), p. 199.

5) D. K. Dalling and D. M. Grant, *J. Am. Chem. Soc.*, **89**, 6612 (1967).

6) M. Kilpatrick and J. G. Morse, *J. Am. Chem. Soc.*, **75**, 1846 (1953).

7) H. A. Smith and F. P. Byrne, *J. Am. Chem. Soc.*, **72**, 4406 (1950).

Trifluoroacetylation at the 3 Position of 1-(2-Aminophenyl)-2,5-dimethylpyrrole in Trifluoroacetic Acid. Possible Remote Control of an Amino Group in Electrophilic Substitution

Kimie IMURO and Terukiyo HANAFUSA

Chemistry Department, Faculty of Science, Hiroshima University, Higashi-senda-cho, Hiroshima 730

(Received October 23, 1975)

Spontaneous trifluoroacetylation at the β position of the pyrrole ring in 1-(2-aminophenyl)-2,5-dimethylpyrrole (**1**) was observed in trifluoroacetic acid. The half-life of the reaction was about 3.5 h at 25 °C. This unexpected result might be explained in terms of the 1,5-participation of the amino group in the electrophilic substitution reaction.

The pyrrole ring is known as one of the most sensitive aromatics in electrophilic substitutions. Even trifluoroacetic anhydride, which dose not acylate benzene derivatives without a catalyst, reacted quite readily with a pyrrole to afford a trifluoroacetyl derivative.[1] The partial rate factor for the α position of pyrrole has been estimated up to 10^{18} compared with a single position of benzene.[2] We now wish to report the trifluoroacetylation of 1-(2-aminophenyl)-2,5-dimethylpyrrole (**1**) in trifluoroacetic acid (TFA).

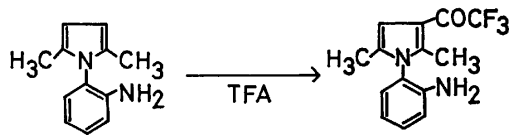

(1) (2)

Results and Discussion

It was incidentally observed during the NMR measurement that the spectrum of **1** in TFA gradually changed from its initial pattern to another spectrum. When the solution was kept at 25 °C for 48 h, a substance (mp 84—86 °C) was isolated by quenching the solution with a base. Judging from the spectral data given in Table 1, the substance thus obtained was easily identified as the 3-trifluoroacetyl derivative (**2**) of **1**. Since the NMR spectrum of **2** in TFA was almost identical with the final spectrum of **1**, the substance (**2**) was shown to be the major product under the conditions.

Despite the presumption that the *N*-trifluoroacetylation of an amino group in **1** is more feasible than *C*-acylation at the β position of the pyrrole ring, the trifluoroacetylamino derivative could not be detected. Also, there was no such significant alteration in the NMR spectrum of the other substituted derivatives, including the 2-hydroxy (**5**), 2-iodo (**7**) and 4-amino substituents (**8**), in a solution of TFA, even at higher temperatures. In these cases, the materials were recovered without any substantial change after quenching. Thus, trifluoroacetylation at the β position of **1** may be regarded as a unique example among these pyrrole derivatives.

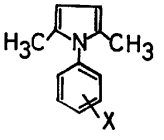

	X
1	2'-NH_2
3	2'-$NHCOCF_3$
4	H
5	2'-OH
6	2'-CH_3
7	2'-I
8	4'-NH_2
9	4'-Cl

The following explanation might be proposed for this phenomenon. Powerful mineral acids, such as nitric or sulfuric acids, function by themselves as electrophilic reagents toward aromatics. Since TFA is almost as acidic as nitric acid, it may be anticipated that TFA would autocatalytically produce a trifluoroacetyl cation which could in turn bring about electrophilic substitution with highly reactive aromatic compounds. Also, the electrophilic substitution of five-membered hetero-aromatics generally proceeds to the transition state very close to the intermediate cation, *i.e.*, the σ complex.[3] Thus, extraordinary stabilization would have to work in the reaction intermediate of the present example.

An amino group generally plays an important role in the neighbouring-group participation of various reactions in which cationic species are the intermediates. Especially, 1,5-participation by this group has been eminent in solvolytic displacement.[4] Since 1-(4-aminophenyl)-2,5-dimethylpyrrole and other derivatives did not give the trifluoroacetyl compound under the same conditions, 1,5-participation by the 2-amino group would operate in the rate-determining formation of the cationic intermediate, as is shown below.

Another possible interpretation is the rearrangement of the 2-trifluoroacetylamino derivative (**3**) into **2**. The

TABLE 1. SPECTRAL DATA FOR 1-(2-AMINOPHENYL)-2,5-DIMETHYL-3-(TRIFLUOROACETYL)PYRROLE (**2**)

Mass	282 (M^+)
IR	3390, 3490, 1660, 1620
PMR	7.40—6.63, 4H, m; 6.50—6.30, 1H, m; 3.69—3.36, 2H, bs; 2.33, 3H, s; 1.96, 3H, s
FMR	5.20, d, J=2 Hz[a)]

a) Chemical shift is reported in ppm downfield from trifluoroacetic acid as an external standard. Coupling of the fluorine atom with a proton at position-4 in the pyrrole ring was confirmed by double resonance technique.

1H, d, $J=7$; 7.7—7.3, 4H, m; 5.96, 2H, s; 1.96, 6H, s. The NMR spectrum of **3** dissolved in TFA did not change substantially when it was kept at 25 °C for 48 h. The sample could be recovered from the solution after quenching, although deep coloring and some decomposition were observed.

(2) The starting material (500 mg), identified by a comparison of its spectral data with those of an authentic sample.

(3) 1-(2-Trifluoroacetylaminophenyl)-2,5-dimethyl-3-tri-, fluoroacetylpyrrole; mp 100—103 °C (26 mg) IR: 3500 3400, 1740, 1680; NMR: 8.13, 1H, d, $J=7$; 7.7—7.1, 4H, m; 6.56, 1H, m; 2.30, 3H, s; 1.96, 3H, s. Found: C, 50.81; H, 3.16; N, 7.41%. Calcd for $C_{16}H_{12}N_2O_2F_6$: C, 50.81; H, 3.17; N, 7.45%.

(4) **2** (134 mg); the identity of this compound with the sample obtained from **1** in TFA was established by a comparison of their spectral data and by a mixed-melting-point determination.

The authors are grateful to Miss Yukiko Hayashi for her skillfulness in doing part of experiments and to Mr. Yoshio Takai, The Institute for Scientific and Industrial Research, Osaka University, for his measurement of ^{19}F NMR spectrum.

References

1) S. Clementi, F. Genel, and G. Marino, *Chem. Commun.*, **1967**, 498.
2) P. Linda and G. Marino, *Chem. Commun.*, **1967**, 499.
3) G. P. Bean, *Chem. Commun.*, **1971**, 421 and references cited therein.
4) B. Capon, *Quart. Rev.*, **20**, 301 (1966).
5) R. Alan, *Aust. J. Chem.*, **19**, 289 (1966).
6) C. Paal and C. W. Th. Schneider, *Chem. Ber.*, **19**, 558 (1886).
7) W. S. Bishop, *J. Am. Chem. Soc.*, **67**, 2261 (1945).

The Base-Catalyzed Condensation Reaction of *o*-Nitroisobutyrophenone in Liquid Ammonia

Kimiko YAMAGUCHI

Department of Chemistry, Faculty of Science, Osaka City University, Sumiyoshi-ku Osaka 558

(Received October 29, 1975)

The base-catalyzed condensation reaction of *o*-nitroisobutyrophenone (III) with sodium acetylide in liquid ammonia gave 1-ethynyl-2-methyl-1-(*o*-nitrophenyl)-1-propanol (**G**) as the main product and *o,o'*-azoxybenzamide (**C**), 2-carbamoyl-2'-carboxyazoxybenzene (**C'**), 2,2-dimethyl-3-indolinone (**D**), 1-hydroxy-2,2-dimethyl-3-indolinone (**E**), and 1-hydroxy-2,2-dimethyl-1,2-dihydro-4-quinazolone (**F**) as minor products. On the other hand, with sodium amide the ketone (III) gave Compounds **C** and **C'** as the main products and Compounds **D**, **E**, and **F** as the minor products. These products were formed by the α-proton abstraction.

The base-catalyzed condensation of *o*-nitrophenones in liquid ammonia gave rise to abnormal reactions.[1]

The treatment of *o*-nitroacetophenone (I) with sodium acetylide in liquid ammonia mainly gave Compound (**A**): 1,3-dihydroxy-3-methyl-2-(*o*-nitrophenacylidene)-indoline.[2,3] In the case of *o*-nitropropiophenone (II), 2-(1-carbamoylethyl)-1-(*o*-hydroxyphenyl)-2-methyl-3-indolinone (**B**) was obtained as the main product.[4]

In this experiment, *o*-nitroisobutyrophenone (III) was subjected to a similar reaction. The structures of these products and the mechanisms of their formations will be discussed.

Results

o-Nitroisobutyrophenone (III) was synthesized by the following two methods, analogous to these used in preparation of *o*-nitropropiophenone: 1) the hydrolytic decarboxylation of methyl *o*-nitrobenzoyldimethylacetate,[5,6] and 2) the treatment of 2-diazopropane[7] with *o*-nitrobenzaldehyde.

The treatment of III with an equimolar amount of sodium acetylide in liquid ammonia at −70 °C gave **G** as the main product and **C**, **C'**, **D**, **E**, and **F** as the minor products. On the other hand, the reaction with sodium amide gave **C** and **C'** as the main products and **D**, **E** and **F** as the minor products (Chart 1).

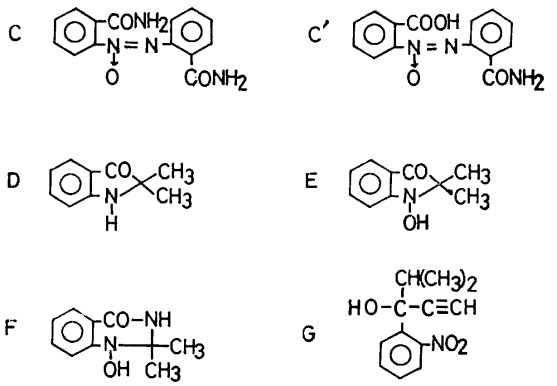

Chart 1.

Compound **C** was identified with *o,o'*-azoxybenzamide.[8] Compound **C'** was identical with the 2-carbamoyl-2'-carboxyazoxybenzene prepared by the alkaline reduction of *o*-nitrobenzamide with glucose or arsenious acid.[9]

The IR spectrum of **D** showed absorption bands of the NH group at 3380 cm^{-1} and of the C=O group at 1675 cm^{-1}. The UV spectrum of **D** revealed the absorption maxima at 237 (ε 4.33), 257 (3.78) and 398 nm (3.60) due to the 3-indolinone nucleus. Further, the NMR spectrum showed the signals for the methyl protons at δ 1.30 (s, 6H) and the imino proton at 5.15 (broad, 1H). These data were identical with those of 2,2-dimethyl-3-indolinone.[10]

The IR spectrum of **E** showed absorption bands of the OH group at 3310 cm^{-1} and of the C=O group at 1685 cm^{-1}. The UV spectrum revealed the absorption maxima at 240 (ε 4.37), 259 (3.81), and 381 nm (3.45) due to the 3-indolinone nucleus. **E** was methylated with diazomethane to give a methyl ether. The IR spectrum of the latter compound showed absorption bands due to the OCH_3 group at 2800 and 1150 cm^{-1} instead of those of the OH group at 3310 cm^{-1} of **E**. From these results, **E** was assumed to be 1-hydroxy-2,2-dimethyl-3-indolinone.

The IR spectrum of **F** showed absorption bands of the NH group at 3200 cm^{-1} and of the C=O group at 1655 cm^{-1}. The UV spectrum of **F** revealed the absorption maxima characteristic of the quinazoline nucleus at 228 (ε 4.42) and 328 nm (3.41). From the above results, **F** was assumed to be 1-hydroxy-2,2-dimethyl-1,2-dihydro-4-quinazolone, which was synthesized by the condensation of *o*-hydroxylaminobenzamide with acetone in acetic acid.

The IR spectrum of **G** showed the absorption bands of the C≡CH group at 3300 and 2101 cm^{-1}, of the NO_2 group at 1535, 1375, and 850 cm^{-1}, and of the OH group at 3550 cm^{-1}. The NMR spectrum of **G** showed the signals for the proton of alkyne at δ 2.77 (s, 1H), for the methyl protons at 1.05 (d, 3H), and 1.10 (d, 3H), for the methine proton at 2.75 (m, 1H), and for the hydroxyl proton at 3.00 (s, 1H). From the results, **G** was assumed to be 1-ethynyl-2-methyl-1-(*o*-nitrophenyl)-1-propanol.

Consequently, the reaction of III with sodium acetylide gave the normal condensation product without the participation of the nitro group.

G was oxidized to confirm its structure. The ozonolysis of **G** gave an acid, 2-hydroxy-3-methyl-2-(*o*-nitrophenyl)butyric acid, and a neutral fraction having the absorption band of the CHO group at 1700 cm^{-1}. The latter compound was immediately oxidized with silver oxide or aqueous hydrogen peroxide to the same

acid which was obtained from the acid fraction. These acid fractions were further oxidized with lead tetraacetate to yield III. Further, the oxidation of **G** with potassium permanganate gave the acid described above.

Discussion

It has been pointed out that the base-catalyzed condensations of *o*-nitrobenzoyl derivatives undergo cyclization to isatogenes.[1]

The reaction of *o*-nitroisobutyrophenone (III) with sodium acetylide gave Compound **G** as the main product and Compounds **C**, **C'**, **D**, **E**, and **F** as minor products (Scheme 1).[1]

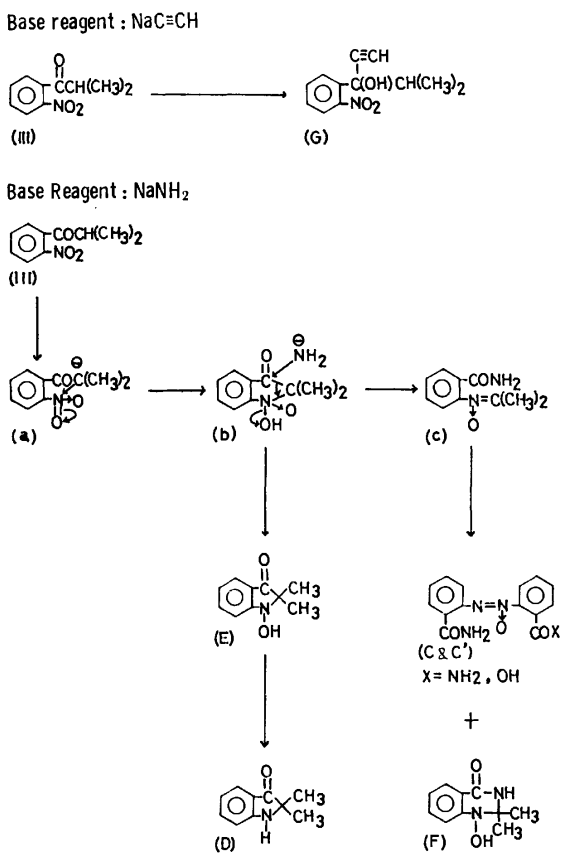

Scheme 1.

Various reasons for the results described above may be considered.[11,12] First, the increase in the number of alkyl groups on the α carbon of the carbonyl group decreases the acidity of the α-proton. Consequently, *o*-nitroisobutyrophenone (III) will react with the acetylide anion through nucleophilic addition at the carbonyl group rather than through the α-proton abstraction.

Second, in the *o*-nitrophenones, the increase in the steric hindrance between the alkyl and nitro groups competes with the repulsion by dipole-dipole interaction between the carbonyl and nitro groups.

In acetophenone or propiophenone, with small alkyl groups, the nitro group may be located in the neighborhood of the alkyl group undergoing the abstraction of the α-proton, but in the case of *o*-nitroisobutyrophenone, with a larger alkyl group, the situation is reversed.

On the other hand, with sodium amide the ketone (III) gave Compounds **C** and **C'** as the main products and Compounds **D**, **E** and **F** as the minor products.

These products are formed by the α-proton abstraction. The conjugate base of *o*-nitroisobutyrophenone causes an intramolecular reaction with the nitro group containing the electrophilic center to form an intermediate (b) of the 3-indolinone type, which is subsequently reduced to form the products, **D** and **E**.

In the next step, the addition of the amide anion to the carbonyl group of the intermediate (b) cleaved the heterocyclic ring to form a nitrone (c). The nitrone was derived to Compound **F**, an unknown product of the weak acidity, by the addition of the amide group to the C=N double bond of the nitrone.[13,14]

On the other hand, Compounds **C** and **C'** were assumed to be formed by the oxidation-reduction reaction of *o*-hydroxylaminobenzamide, which was formed by the cleavage of the intermediate (c).

Experimental

The IR spectra were measured with JASCO IR-E and Hitachi EPI-2 spectrophotometers, using neat or Nujol mull; the UV spectra, with a Hitachi EPS-2 spectrophotometer, using 95% EtOH as the solvent, and the NMR spectra, with JEOLCO C-60, using $CDCl_3$ as the solvent.

Preparation of o-Nitroisobutyrophenone (III). Methylation Method: A solution of 42 g (0.18 mol) of methyl *o*-nitrobenzacetate in 60 ml of absolute methanol was added in one portion to a sodium methoxide solution prepared from 4.1 g of sodium metal, followed by the drop-by-drop addition of an absolute methanol solution of methyl iodide (0.36 mol); then the mixture was refluxed at 65 °C for 30 min. The reaction mixture was cooled with ice–water, and then another molar equivalent of sodium methoxide was added in one portion. The mixture was subsequently treated with methyl iodide and refluxed at 65 °C for 3 h. The insoluble material was filtered off, and the filtrate was evaporated to give a residue, which was taken up with ether and washed thoroughly with 10% aqueous sodium hydroxide. This product was refluxed with a mixture of 13.5 ml of acetic acid, 7.5 ml of concd hydrochloric acid, and 7ml of water for 75 min. After being made alkaline with 20% aqueous sodium hydroxide, the reaction product was extracted with ether; the subsequent evaporation of the ethereal layer gave a crude product, which was distilled under reduced pressure; bp 115—130 °C/4 Torr. It was recrystallized from petroleum benzine; mp 46—47 °C; yield, 65—81%.

2-Diazopropane Method[7]: A solution of 25.7 g (0.17 mol) of *o*-nitrobenzaldehyde in an arbitrary volume of dry ether was added to 0.17 mol of 2-diazopropane (prepared from acetone-hydrazone) at −20 °C. The reaction mixture was stirred for 2 h at the same temperature and then warmed to room temperature. The insoluble material was removed by filtration. The filtrate was washed with a saturated sodium hydrogen sulfite solution to remove the unchanged aldehyde. The evaporation of the ether layer gave colorless crystals (mp 46—48 °C) from petroleum benzine; yield, 65—72%. IR (cm^{-1}): 1705 (C=O); 1530, 1350, and 860 (NO_2). Found: C, 62.52; H, 5.88; N, 7.23%. Calcd for $C_{10}H_{11}NO_3$: C, 62.16; H, 5.74; N, 7.25%.

The Condensation of o-Nitroisobutyrophenone (III) with Sodium Acetylide. A mixture of 0.23 g (0.01 g-atom) of sodium and 100—150 ml of liquid ammonia was saturated with dry acetylene. The mixture was cooled at −70 °C, and then a solution of 1.93 g (0.01 mol) of *o*-nitroisobutyrophenone in 10 ml of dry ether was added in one portion. After the mixture had stood at −60 °C for one hour, during which it turned from grey to yellow, ammonium chloride (1.0 g) was added; then the liquid ammonia was evaporated while 50 ml of dry ether was added. Next, 50 ml of water was added, the reaction mixture was filtered to remove an insoluble material (a), and the ethereal layer (b) was separated from the aqueous layer (c). The insoluble material (a) was recrystallized from water or dilute alcohol to give Compound **C** in a 0.2-g yield; mp 245—246 °C (lit,[8] mp 242 °C). Found: C, 59.10; H, 4.41; N, 19.52%. Calcd for $C_{14}H_{12}N_4O_3$: C, 59.15; H, 4.26; N, 19.71%. The aqueous layer (c) was acidified with 6M-HCl and continuously extracted with ether. The extract was evaporated and recrystallized from methanol to give Compound **C'** (mp 209—211 °C) in a 50-mg yield. Found: C, 59.04; H, 3.90; N, 14.79%. Calcd for $C_{14}H_{11}N_3O_4$: C, 58.94; H, 3.89; N, 14.79%. The ethereal layer (b) was successively extracted with aqueous sodium hydrogen carbonate and aqueous sodium hydroxide to leave a neutral fraction as the organic layer (d), which was purified by column chromatography on silica gel with chloroform to give **G** in 1.04 g (60.1%). Found: C, 65.31; H, 6.03; N, 6.39%. Calcd for $C_{12}H_{13}NO_3$: C, 65.74; H, 5.98; N, 6.39%.

The Condensation of o-Nitroisobutyrophenone (III) with Sodium Amide. Sodium amide was prepared from 0.23 g (0.01 g-atom) of sodium and 100—150 ml of liquid ammonia, using ferric nitrate($9H_2O$) as a catalyst. The mixture was cooled at −70 °C, and then a solution of 1.93 g (10 mmol) of *o*-nitroisobutyrophenone in 10 ml of dry ether was added in one portion. After standing at −60 °C for one hour, ammonium chloride (1.0 g) was added, and then the liquid ammonia was evaporated while 50 ml of dry ether was added. The post-treatment was then carried out as has been described above. The insoluble material (a) gave 1.7 g (23%) of **C** (mp 254—256 °C), and the aqueous layer (c) gave 0.9 g (12%) of **C'** (mp 209—211 °C). The ethereal layer (b), after have been washed an alkaline solution, gave 0.5—0.9 g (10—19%) of **D** (mp 86—87 °C) from petroleum ether. Found: C, 74.29; H, 6.90; N, 8.69%. Calcd for $C_{10}H_{11}NO$: C, 74.51; H, 6.88; N, 8.69%. The acid fraction obtained by the extraction with aqueous sodium hydroxide, after purification by column chromatography on silica gel with chloroform, gave 0.4 g (9.5%) of **F** (mp 196—197 °C (chloroform or ether)) and 0.1 g (2.3%) of **E** (mp 102—103 °C (petroleum benzine)). **E**, Found: C, 67.45; H, 6.32; N, 7.89%. Calcd for $C_{10}H_{11}NO_2$: C, 67.78; H, 6.29; N, 7.91%. **F**, Found: C, 62.10; H, 6.13%. Calcd for $C_{10}H_{12}N_2O_2$: C, 62.48; H, 6.29%. This compound was identified with the synthetic specimen (see below) by IR spectroscopy.

Preparation of F. A solution of 20 ml of acetone and 20 ml of acetic acid was added to 1.5 g (0.02 mol) of *o*-hydroxylaminobenzamide during refluxing at 85—86 °C for about 13 h. The black solution was evaporated under reduced pressure to leave a tar substance, which was then chromatographed on silica gel with chloroform. The first fraction was recrystallized from ether to give pearl grey and twinkle crystals; mp 197—200 °C; yield, 725 mg. IR (cm^{-1}): 3160 (OH), 1655, 1600 (CONH), and 1380 (CH_2). Found: C, 62.18; H, 6.36; N, 14.32%. Calcd for $C_{10}H_{12}N_2O_2$: C, 62.48; H, 6.29; N, 14.58%.

Ozonolysis of G. Ozone gas was passed into a solution of 2.8 g (13 mmol) of **G** in acetic acid at 5—6 °C for 30 min. The reaction mixture was then diluted with water and heated in a water bath. The solvent was removed under reduced pressure, and the residue was separated into acid and neutral fractions by the usual method. The oil from the acid part solidified in due time and was recrystallized from ether and petroleum benzine to give white crystals; mp 143—145 °C (1.0 g, 40.7%). The oil from the neutral part was oxidized with silver oxide or hydrogen peroxide in an alkaline solution to form the same product as the acid part. The IR spectrum of the acid part (cm^{-1}): 3550 (OH), 2900, 2500, 930 (COOH), 1720 (C=O), 1540, 1375, 825 (NO_2), and 770 (*o*-subst. benzene). Found: C, 55.70; H, 5.61 N, 5.83%. Calcd for $C_{11}H_{13}NO_5$: C, 55.23; H, 5.48; N, 5.86%.

Oxidation of G with $KMnO_4$. Formation of the Acid Fraction: Into an acetone (10 ml) solution of 32 mg (0.15 mmol) of **G** we added a small amount of $KMnO_4$; the purple color disappeared at once. The addition of $KMnO_4$ was continued at room temperature until the purple color remained ($KMnO_4$: 47 mg in total). The filtered reaction mixture was evaporated to remove the acetone, acidified with 2 M-HCl, and extracted with ether; the extract was then evaporated to give the acid compound.

Oxidation of Acid Compound with Lead Tetraacetate. Formation of III: A mixture of 100 mg (0.44 mmol) of an acid compound and 203 mg of $Pb(OAc)_4$ in 20 ml of dry benzene was stirred at reflux for 8 h. The reaction mixture was then cooled, and the $Pb(OAc)_2$ was filtered off and washed with ether. The combined filtrates were washed with a sodium hydrogen carbonate solution, dried with sodium sulfate, and evaporated to give 407 mg of III (mp 41—42 °C).

References

1) J. D. London and G. Tennant, *Quart. Rev.*, **18**, 389 (1964).
2) T. Sakan, K. Kusuda, and T. Miwa, *Bull. Chem. Soc. Jpn.*, **37**, 1678 (1964).
3) T. Sakan, K. Kusuda, and T. Miwa, *Bull. Chem. Soc. Jpn.*, **38**, 18 (1965).
4) T. Sakan, S. Hayashi, and T. Miwa, *Bull. Chem. Soc. Jpn.*, **45**, 1485 (1972).
5) B. R. Baker, R. E. Schaub, and J. H. Williams, *J. Org. Chem.*, **17**, 116 (1952).
6) C. Schöf, G. Koepke, B. Kowald, F. Schülde, and D. Wunderlich, *Chem. Ber.*, **89**, 2884 (1956).
7) a) S. D. Andrews, A. C. Day, P. Raymond, and M. C. Whiting, *Org. Synth.*, **50**, 27 (1970). b) "Preparation and Reactions of Diazopropane": Dr. M. Frank-Newmann. Unpublished work, Private communication from Prof. J. Streith.
8) E. Bamberger and F. Elgre, *Ann.*, **371**, 65 (1910).
9) K. Yamaguchi, Unpublished work.
10) R. J. Sundberg and T. Yamazaki, *J. Org. Chem.*, **32**, 290 (1967).
11) A. T. Nielsen and W. J. Houlihan, *Org. React.*, Vol. 16 (1968), p. 1.
12) J. H. Boyer, "The Cemistry of the Nitro and Nitroso Groups": part 1 & 2, ed. by Henry Feuer, Interscience Publishers, New York, N. Y. (1969), p. 269.
13) P. A. S. Smith, "Molecular Rearrangements: part 1", ed. by P. de Mayo, Interscience Publishers, New York, N. Y. (1963), p. 507.
14) E. Buncel, "Mechanisms of Molecular Migrations," Vol. 1, ed. by B. S. Thyagaranjan, Interscience Publishers, New York, N. Y. (1968), p. 61.

Aldol Condensation of Aldehydes with Ketones Promoted by the Copper(II) Ion. Orientation to the Chemical Model for Metalloaldolases

Masaaki IWATA and Sakae EMOTO

The Institute of Physical and Chemical Research, Wako-shi, Saitama 351

(Received November 7, 1975)

The aldol condensation reactions of aromatic aldehydes such as **1** through **4** and **7** through **13**, and aliphatic aldehydes such as **5** and **6**, with a number of ketones promoted by the copper(II) ion were examined. The reactions were specifically promoted by the copper(II) ion, while such metal ions as zinc, cobalt(II), manganese(II), and magnesium were quite inactive as catalysts. All the aldehydes but **7** and **8** reacted with all the aliphatic ketones except ethyl acetoacetate, acetonitrile, and nitromethane to varying degrees in the Claisen-Schmidt type of reaction. Acetylacetone gave a condensation product of the Knoevenagel type. In the reaction of aldehydes with 2-butanone, aldehydes regiospecifically attacked the methylene group at C_3 of 2-butanone. Amines inhibited the reaction, while the coexistence effect of zinc or cobalt(II) was observed. It was shown that there existed a substrate selectivity depending greatly on the kinds of ketones in the reaction promoted by the copper(II) ion. As a consequence, possible intermediates in the reaction were proposed and the relationship of the aldol condensation reaction promoted by the copper(II) ion with the metalloaldolases was discussed, particularly in the light of the role of the metal ions in both catalytic mechanisms.

The aldol-condensation reaction is generally catalyzed by strong bases, such as alkali-metal hydroxide or alkoxide, or strong acids, such as hydrochloric or sulfuric acid.[1] However, no instances of an aldol condensation catalyzed by a transition-metal ion have been reported. This must be because there is no requirement of new catalysts superior to such bases or acids for general organic synthesis. In relation to enzymatic reactions, however, Rutter reported an important phylogenetic analysis in 1964 where he showed that there were two types of aldolases with distinct catalytic elements and molecular characteristics.[2] One type of aldolase (according to Rutter, Class I aldolases) catalyzes the aldol condensation of D-glyceraldehyde 3-phosphate with dihydroxyacetone phosphate to form fructose 1,6-diphosphate *via* a Schiff-base intermediate; the other type of aldolase (Class II aldolases) needs divalent metal ions to promote the same condensation reaction, the intermediate of which is evidently different from that of Class I aldolases. Later works by Rutter and his co-workers,[3-5] and by other groups[6] have given evidence of the presence of these two types of aldolases, and the catalytic mechanisms have been discussed. However, it has remained chemically unsolved whether or not the aldol-condensation reaction is really catalyzed by the transition-metal ion. On the other hand, we incidently found the novel aldol-condensation reaction promoted by the copper(II) ion of 2,6-dimethoxybenzaldehyde with acetone in the course of our studies concerning the demethylation of methoxy-substituted aromatic aldehydes,[7] and we briefly reported that the copper(II) ion specifically promoted the aldol condensation of acetone with several aromatic aldehydes to give benzylideneacetones.[8] In order to ascertain the scope and limitations of the aldol condensation promoted by the copper(II) ion and in order to approach a chemical elucidation of the role of metal ion in the catalytic mechanism of metalloaldolases, the method was further applied to the condensation of aliphatic and aromatic ketones with aliphatic and aromatic aldehydes. In this paper, the results obtained will be reported in detail and the relationship of the aldol-condensation reaction promoted by the copper(II) ion with enzymatic reactions will be discussed.

Results and Discussion

Reaction Systems. As aldehydes, benzaldehyde (**1**), *o*-anisaldehyde (**2**), *p*-anisaldehyde (**3**), 2,6-dimethoxybenzaldehyde (**4**), propanal (**5**), pentanal (**6**), salicylaldehyde (**7**), *p*-chlorobenzaldehyde (**8**), furfural (**9**), 2-thiophenecarbaldehyde (**10**), 2-pyridinecarbaldehyde (**11**), 3-pyridinecarbaldehyde (**12**), and 4-pyridinecarbaldehyde (**13**) were arbitrarily chosen. Acetone, 2-butanone, 2-pentanone, cyclopentanone, cyclohexanone, acetophenone, acetylacetone, and ethyl acetoacetate were used as ketones. Also, solvents with an active methylene group, such as acetonitrile and nitromethane, were examined as ketone analogues. In a typical experiment, we employed, unless otherwise stated, the procedure described in a previous report[8] where 8—10 mmol of a (hydrated) metal ion, such as zinc, cobalt(II), manganese(II), magnesium, or copper(II), all of which were selected in relation to the prothetic metal ions for the Class II aldolases,[3] and 5 mmol of an aldehyde were stirred in 20—30 ml (an excess amount) of the solvent ketone at room temperature. Also, on the basis of analogy with the enhancement effect of nucleophilic attack upon the addition of the zinc ion,[9] an amount of zinc chloride equimolar to that of the copper(II) ions was added to the reaction system.

Condensation of Aldehydes with Acetone. The results obtained in the presence of the copper(II) ion alone and in the coexistence of copper(II) and zinc ions are summarized in Table 1; the table shows that the yield of the condensation product after a comparable or shorter reaction time was strikingly increased by the addition of the zinc ion and that the **7** and **8** aldehydes gave no condensation product, presumably because of the occupation of the catalytic site of the metal ion by the electron-rich substituent or because of the decreasing electrophilicity of the aldehyde group as a result of the inductive and resonance effects of the

Table 1. The condensation of aromatic aldehydes with acetone in the presence of cupric ion alone and in the coexistence of cupric and zinc ions

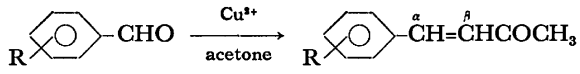

Aldehyde	R	Configuration of double bond of the product[a]	Yield (%) of benzylideneacetones[c] Cu^{2+} catal.	Reac. time, h	Cu^{2+}–Zn^{2+} catal.	Reac. time, h
1	H	E[10]	2	51	26	50
2	2-OCH_3	E[11]	trace	64	12	44
3	4-OCH_3	E[12]	4	84	20	65
4	2,6-di-OCH_3	E[13]	34	43	73	40
7	2-OH	—	—[b]	68	—[b]	67
8	4-Cl	—	—[b]	52	—[b]	52

a) The configuration of the double bond was determined by the coupling constants of NMR spectra. b) No reaction occurred and the starting material was recovered. c) Yield after the column chromatographic separation.

substituents. It was also of interest, from the synthetical point of view, that the copper(II) ion-promoted reaction of **4** in the coexistence of the zinc ion gave 2,6-dimethoxybenzylideneacetone in a considerably high yields. Furthermore, the yield of 2-methoxybenzylideneacetone in the coexistence of copper(II) and zinc ions was dramatically ameliorated when acetone was purified (Fig. 1). The aliphatic aldehydes, **5** and **6**, appeared to give no condensation product with acetone.

Condensation of Aldehydes with 2-Butanone. The reactions of 2-butanone with the aldehydes **1** through **6** and **9** through **13** in the presence of the copper(II) ion alone and in the coexistence of the copper(II) and zinc ions were examined. The results obtained are listed in Tables 2 and 3. It is of particular interest to note that all aldehydes attack the methylene group at C_3 of 2-butanone, but not the methyl group at C_1. The regiospecificity suggests that the copper(II) ion functions as a proton-like catalyst because it has been generally known that the mineral-acid-catalyzed aldol condensation of aldehydes with 2-butanone preferentially occurs at C_3, while the strong base-catalyzed aldol condensation preferentially occurs at C_1.[1] Also, it was demonstrated

Table 2. The condensation of aromatic aldehydes with 2-butanone in the presence of cupric ion alone and in the coexistence of cupric and zinc ions

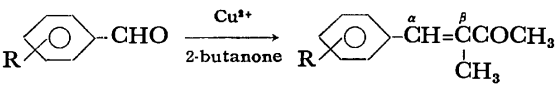

Aldehyde	R	Yield (%) of 3-benzylidene-2-butanones[a] Cu^{2+} catal.	Reac. time, h	Cu^{2+}–Zn^{2+} catal.	Reac. time, h	Ref.[b]
1	H	91	41	88	41	14)
2	2-OCH_3	48	28	63	44	15)
3	4-OCH_3	40	44	63	44	16)
4	2,6-di-OCH_3	45	20	23	20	

a) Yield after the column chromatographic separation. b) The condensation product obtained was identified in comparison with the reference cited.

Table 3. The condensation of aldehydes with 2-butanone in the presence of cupric ion alone and in the coexistence of cupric and zinc ions

Aldehyde	Product	Yield (%) Cu^{2+} catal.	Reac. time, h	Cu^{2+}–Zn^{2+} catal.	Reac. time, h
5	dehyd[a]	3[c]	48	2[c]	24
6	dehyd	—	—	27[c]	19
9	dehyd	15[d]	22	15[d]	22
10	dehyd	33[e]	24	77[e]	24
11	add[b]	70[d]	24	70[d]	24
12	add	40[d]	20	0	20
13	add	80[d]	22	30[d]	22

a) The condensation reaction gave dehydrated product, $RCH{=}C(CH_3)COOCH_3$, where R was the group in the aldehyde RCHO. b) The condensation reaction afforded addition product, $RCH(OH)CH(CH_3)COCH_3$, where R was the group in the aldehyde RCHO. c) Yield after the column chromatographic separation. d) On the basis of TLC spot. e) On the basis of gas chromatographic analysis (see Experimental part).

that the additional effect of the zinc ion was not so remarkable as has been shown in the case of acetone. It was of interest that the pyridinecarbaldehydes **11** through **13** gave only aldol-addition products to 2-butanone, but not dehydrated products, as was shown in all the other aldehydes, and that the aliphatic aldehydes **5** and **6** gave also the condensation products, unlike the case of acetone, but in a lower yield. The fact that the condensation of pyridinecarbaldehydes with 2-butanone gave the addition product led us to predict that the reaction of benzaldehydes with 2-butanone in the presence of pyridine would also afford the non-dehydrated product. However, no addition product was obtained; pyridine acted only as an inhibitor of the reaction.

Condensation of Miscelaneous Ketones and their Analogues with Aldehydes. The reactants and the results obtained are briefly shown in Table 4; no condensation product of aryl methyl ketone, β-keto ester, or alkyl (carbon number$>$3) methyl ketone was obtained in the presence of a copper(II) or copper(II)–zinc catalyst.

Table 4. The condensation of miscelaneous ketones with aldehydes in the presence of cupric ion or in the coexistence of cupric and zinc ions

Aldehyde	Ketone	Catalyst[a]	Reac. time, h	Yield (%)[b]
3	Acetophenone	A	139	N
3	Acetophenone	B	139	N
1	2-Pentanone	A	24	N
2	2-Pentanone	A	24	N
3	2-Pentanone	A	24	N
4	2-Pentanone	A	24	N
2	Acetylacetone	A	29	47
2	Acetylacetone	B	23	14
2	Ethyl acetoacetate	A	7 days	N
3	Acetonitrile	A	47	N
3	Acetonitrile	B	47	N
2	Nitromethane	A	23	N
2	Nitromethane	B	23	N

a) A; $CuCl_2 \cdot 2H_2O$ and B; $CuCl_2 \cdot 2H_2O$–$ZnCl_2$. b) yield after the column chromatographic separation and N represents non-reaction.

In addition, solvents with an active methylene group, such as acetonitrile and nitromethane, gave no condensation product with aldehydes in spite of the formation of certain copper complexes. On the other hand, of interest was the formation of 3-(2-methoxybenzylidene)-2,4-pentanedione (**14**) by the reaction of **2** with acetylacetone, while the reaction was not induced when bis(acetylacetonato)copper(II), which had previously been prepared by the reaction of copper(II) chloride dihydrate with twice the equimolar amount of acetylacetone, was treated with **2** in benzene. This seemed to indicate that it might be crucially important in the aldol condensation promoted by the copper(II) ion that the copper(II) ion was bound to the carbonyl moiety weakly, not tightly. Furthermore, it should be noted that, from the synthetical point of view, the formation of **14** was the first example of the Knoevenagel-type aldol condensation under weak acidic conditions; the reaction has usually been run in the presence of primary or secondary amines, ammonia, pyridine, or piperidine.[17]

Catalytic Activity of the Metal Ion. It is of particular interest to learn, in relation to the enzymatic reaction, whether the aldol condensation promoted by the copper(II) ion is specific for the copper(II) ion or equally applicable to other metal ions. In order to elucidate the specificity, zinc, magnesium, cobalt(II), and manganese(II) were examined under conditions similar to those of the copper(II) ion series. However, none of these metal ions which were prothetic to the Class II aldolases promoted the Claisen-Schmidt aldol condensation; that is, the aldol condensation promoted by the metal ion was specific for the copper(II) ion. The reaction was, however, affected by the addition of zinc or cobalt(II) in some aldehydes (see Experimental). As regards the effect of the counter anion of the copper(II) ion, copper(II) acetate was also effective in the condensation of **3** with acetone; the yield of the product was, however, considerably decreased in comparison with that catalyzed by copper(II) chloride.

Effect of Molar Ratio of Zn^{2+}/Cu^{2+} on the Condensation Reaction. The observations that the reaction yield of the aldol condensation promoted by the copper(II) ion depended greatly on the kinds of ketones and that it was greatly or slightly affected in the coexistence of the zinc ion led us to examine the possibility of the substrate selectivity of the aldol condensation. Thus, the effect of the molar ratio of Zn^{2+}/Cu^{2+} on the yields of the condensation reaction of *o*-anisaldehyde (**2**) as a representative aldehyde with acetone, 2-butanone, 2-pentanone, cyclopentanone, and cyclohexanone respectively was investigated. The results obtained are illustrated by plotting the molar ratio of Zn^{2+}/Cu^{2+} *vs.* the yield of the condensation product in Fig. 1. In the experiments, purified acetone was used, and a series of the reactions for each ketone was set up to keep consistency with respect to the reaction time and temperature in order to normalize the data. Also, the reaction yield was estimated by analyzing the gas chromatogram on the basis of the theoretical equation derived from several assumptions (see Experimental). The molar ratio of $Cu^{2+}/\mathbf{2}$ was at most 2, and that of $Zn^{2+}/\mathbf{2}$, at most 2. Figure 1 shows the following characteristic features; there is certainly a substrate selectivity in the condensation reaction in the presence of the copper(II) ion alone, since acetone and 2-pentanone hardly reacted with **2**, while cyclopentanone and cyclohexanone quantitatively gave the condensation product. In any cases, the condensation reaction was not induced without the copper(II) ion, and the zinc ion coexisting in the system affected the yield positively or negatively. Additionally, there was the optimum molar ratio of Zn^{2+}/Cu^{2+} to give the product in the best yield. The range showing the optimum ratio is limited in the case of 2-butanone, whereas it is very wide for acetone.

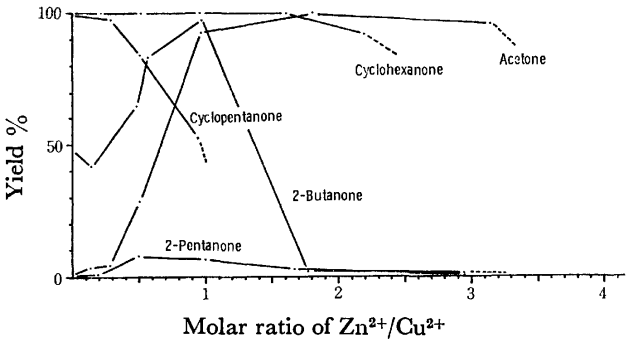

Fig. 1. The effect of the molar ratio of Zn^{2+}/Cu^{2+} on the condensation yield of various ketones with *o*-anisaldehyde (**2**).

Scope and Limitation of the Aldol Condensation Promoted by the Copper(II) Ion. In view of the stoichiometry of the reaction, 0.05 mol of **2** was treated with a mixture of 0.05 mol of 2-butanone, 0.01 mol of copper(II) chloride dihydrate, and 0.01 mol of zinc chloride in 30 ml of ethanol for 122 h. However, no benzylideneacetone derivative was obtained, and almost all of the starting materials were recovered. On the other hand, the reaction in which **3** and imidazole were added to the previously prepared acetone-copper(II) complex in the excess amount of acetone also gave no condensation

product. In addition, when the aceton–ceopper(II) complex which had previously been prepared was added to the mixture of **2** and 2-butanone, 3-(2-methoxybenzylidene)-2-butanone was produced after 28 h but no 2-methoxybenzylideneacetone was produced. Furthermore, it was of interest that methyl salicylate was formed in a 19% yield when **2** and the 2-butanone–copper(II) complex, previously prepared, were stirred in benzene for 48 h.

These observations, together with the afore-mentioned results, permit us to draw some conclusions with regard to the scope and limitations of the aldol condensation promoted by the copper(II) ion. That is, (a) the reaction will not stoichiometrically proceed with respect to ketone and thus should be conducted in a ketone solvent, which means that only liquid ketone can be used as a reactant for aldehyde. (b) A stable ketone–copper(II) complex such as bis(acetylacetonato)copper-(II) is unsuitable for the condensation with an aldehyde, while such an unstable ketone–copper(II) complex as acetone–copper(II), 2-butanone–copper(II), or an intermediarity formed copper(II) complex in a mixture of acetylacetone, aldehyde, and copper(II) ions will be effective for the condensation. This seems to be the case where enzymes catalyze the reactions in biological systems. (c) Ketone analogues with active hydrogen(s), such as acetonitrile, nitromethane, and the β-keto esters, are inactive in relation to the copper(II) ion. In the latter particularly, the hydrolysis of the ester rather than the condensation is promoted by copper(II) ion. (d) Aryl alkyl ketones will be unsuitable, while aliphatic ketones can be used. As regards aldehydes, hydroxyl, halogeno, and nitro substituents will inhibit the condensation, while the methoxy group and hetero atoms in the aromatic ring will allow the reaction.

Role of the Metal Ion in the Catalytic Mechanism of Metalloaldolases. The most remarkable feature of the aldol condensation promoted by the copper(II) ion is that the mixed condensation of aldehyde with ketone exclusively predominates over the self condensation of ketone, even if large excess amounts of ketone are present. This can be explained by the assumption that the ligation power of aldehydes to the copper(II) ion slightly predominates over that of ketones; thus, in the equilibrium, the copper(II) ion, present in twice the equimolar amount of aldehyde, coordinates both aldehyde and ketone. In fact, this assumption seems to be reasonable because the color of the intermediarily formed copper(II) complex in the reaction medium depends on the kinds of aldehydes and ketones used. In addition, such an intermediate will explain the inactivity of such metal ions as zinc, cobalt(II), magnesium, and manganese(II) in the consideration of coordination chemistry.[18]

Thus, we can deduce the processes of the aldol condensation promoted by the copper(II) ion from the initial formation of the mixed copper(II) complex of aldehyde and ketone, as is shown in Scheme 1. That is, in the initially formed copper(II) complex (**15**)-copper assists the enolization of ketone to give the intermediate (**16**), which then nucleophilically attacks the aldehyde moiety activated by the copper(II) ion to afford **17**. Subsequently, **17** releases the metal ion to prepare the addition product (**18**), which is then dehydrated to give **19** in almost all the aldehydes but the pyridinecarbaldehydes. In this reaction scheme, the dual role of the copper(II) ion, the enolization of ketone and the activation of aldehyde, is emphasized. If the mechanism has reality, it resembles the one proposed for the Class II aldolases with respect to the role of the metal ion.

As regards the mechanism of the action of the Class I aldolases, direct chemical evidence has been provided by many workers.[6a,19,20] Alternatively, as for the role of the metal ion in the catlytic mechanism of the Class II aldolases which require a divalent metal ion and are not inhibited in the presence of sodium borohydride, Rutter and his co-workers have proposed some intermediates, which can be illustrated as **20**, **21**, and **22** in Scheme 2.[3-6] Now, the similarity of the dual role of the copper(II) ion in the aldol condensation promoted by the copper(II) ion to that of the metal ion in the Class II aldolases is apparent, and the mixed complex is likely to exist in both the chemical and enzymatic processes.

We are, however, confronted with a large gap regarding indispensable metal ions for the aldol condensation between the chemical model and the natural metalloaldolases, in which Zn^{2+}, Co^{2+}, Ni^{2+}, Mn^{2+}, and Fe^{2+} restore the enzymatic activity to varying degrees. while Cu^{2+}, Hg^{2+}, Cd^{2+}, Mg^{2+}, and Fe^{3+} fail to restore activity to any measurable extent.[3] Although a hasty

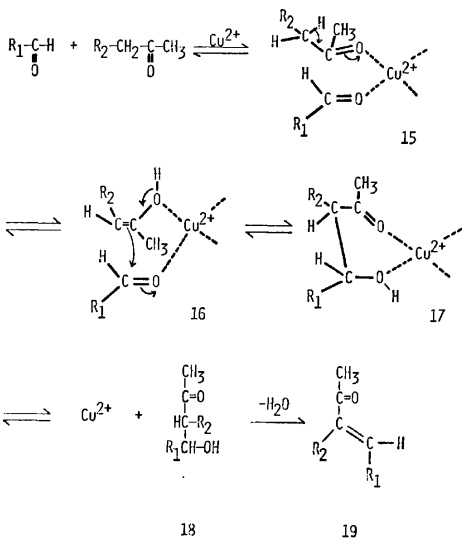

R_1=Aryl or Alkyl R_2=Alkyl

Scheme 1.

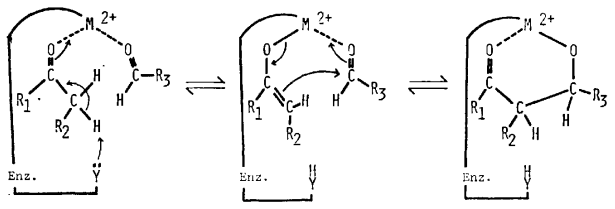

Scheme 2.

judgment may lead to an erroneous conclusion, we now consider that the gap is caused by the protein effects in enzyme such as proximity, orientation, strain, and microenvironmental factors; that is, the topochemical configuration of the catalytic site of a metal ion in the absence of an enzyme will be changed by these effects in the presence of enzyme. It is important to note that the coordination number and, thus, the stereochemical outcome are determined largely by the size and charge of the metal ion and ligand.[18] The investigation of the problem with which we are here concerned will bring about further fruitful results.

Experimental

The IR spectra were obtained using a Shimadzu IR-27 apparatus. The ^{1}H-NMR spectra were recorded on a Varian HA-100D apparatus, with tetramethylsilane as the internal standard. The chemical shift and the coupling constant were represented by δ and Hz units respectively. The mass spectra and exact mass measurements were obtained using a Japan Electron Optics Lab. Model JMS-OlSG instrument. Merck Art. 7734 (E. Merck, Darmstadt) was used for the preparative separation of the products on a silica gel column by elution chromatography, and Wakogel B-5 FM (Wako Pure Chem. Ind.), for the thin-layer chromatography (TLC). The measurements of the gas chromatography were performed by a Shimadzu GC-4A gas chromatograph with a flame ionization detector, using a 1.8 m×3 mm glass tube column packed with 5% Silicone GE-30 on Shimalite W 60—80 mesh and using helium gas as the carrier. The melting points are uncorrected. The elemental analyses were performed by the staff of the Organic Microanalysis Lab. in our Institute.

Materials. All the ketones and aldehydes, **1** through **13**, are commercially available.. Purified acetone was obtained by drying over Drierite after treatment with potassium permanganate, followed by distillation.[21] Copper(II) chloride dihydrate, zinc chloride, magnesium chloride hexahydrate, manganese(II) chloride tetrahydrate, cobalt(II) chloride, and copper(II) acetate monohydrate were used as metal chloride; all of them were commercially available.

Reaction Systems. The general procedure was described above. In the examination of the coexistence of copper(II) and zinc ions, an amount of zinc chloride equimolar to that of copper(II) chloride dihydrate was used unless otherwise stated. Although benzaldehydes are easily oxidized to the corresponding benzoic acid, the reaction system prevented the oxidation to a small extent, as has been shown by the comparative studies of the reaction of 2-butanone with benzaldehyde in the absence and in the presence of nitrogen gas. The final point of the reaction was decided by monitoring the TLC spots. After the completion of the reaction, the mixture was hydrolyzed by the addition of water and filtered through celite to remove the emulsive metal hydroxides. The filtrate was then extracted with ethyl acetate. The organic layer was dried over anhydrous sodium or magnesium sulfate, and the solvents were evaporated under reduced pressure. The residue was chromatographed on a silica gel column to give the products. In the case of the estimation of the yield by the aid of gas chromatography, the extract with ethyl acetate was used.

Analysis of Gas Chromatogram. In the case of the column chromatographic separation of the product, "yield" represents the real theoretical percentage of the product to the starting aldehyde. On the other hand, in the case of the estimation of the product yield by the use of gas chromatography, "yield" is evaluated on the basis of the following assumptions: (a) on the gas chromatogram, the product of the height of a band and the width of the band at half of its height nearly equals the relative area, which is directly proportional to the gram-molecular weight of the compound, and (b) the side products except for the condensation product are negligible (all the aldehyde consumed is converted to the condensation product). This second assumption (b) has a practical significance in this condensation reaction. According to these assumptions, the product yield ($Y_{\%}$) based on the gas chromatogram can generally be calculated by means of the following equation: $Y_{\%}=100\,r/(1+r)$, where r is the molar ratio of the condensation product to the aldehyde remaining on the gas chromatogram. Therefore, we can obtain the product yield by the estimation of r, which is calculated by the area ratio of the aldehyde to the product.

Under the conditions of the gas chromatograph (injection temp, 222 °C; detector oven temp, 230 °C; column temp, 89—189 °C (10 °C per min)) and a pressure of helium gas of 1.2—1.39 kg/cm^2, the retention times of *o*-anisaldehyde (**2**) and the condensation products were as follows: **2** was 5; 2-methoxybenzylideneacetone, 10; 3-(2-methoxybenzylidene)-2-butanone, 10; 3-(2-methoxybenzylidene)-2-pentanone, 12.7; 2-(2-methoxybenzylidene)cyclopentanone, 14; 2-(2-methoxybenzylidene)cyclohexanone, 9; 3-(2-methoxybenzylidene)-2,-4-pentanedione, 10.5; and 3-(2-furylmethylidene)-2-butanone, 20 min. Under an injection temp of 260 °C, a detector oven temp. of 220 °C, a column temp of 100—200 °C (10 °C per min), and a pressure of helium gas of 1.0—1.4 kg/cm^2, the retention time of 3-(2-thienylmethylidene)-2-butanone was 7, and that of thiophenecarbaldehyde, 1.8 min.

Additional Effect of Anhydrous $CoCl_2$ on the Aldol Condensation Promoted by the Copper(II) Ion. Various amounts of anhydrous $CoCl_2$ were added to the usual reaction system, and the mixture was stirred at the ambient temperature for 38 h. After a usual work-up, the yields of the product, 3-(2-methoxybenzylidene)-2-butanone, were determined on the basis of the analysis of the gas chromatogram. When 10, 5, 2.5, and 1.25 mmol of anhydrous $CoCl_2$ coexisted, the yields of the product were 59, 63, 69, and 70% respectively.

Condensation Product. Benzylideneacetone;[10] NMR (CCl_4); 2.32 (3H, s, $-CO\underline{CH_3}$), 6.65 (1H, d, $J=16.5$, C_β–H), and 7.45 (1H, d, $J=16.5$, C_α–H).

2-Methoxybenzylideneacetone[11] [mp 44—46 °C (lit, 50 °C)]; NMR (CCl_4); 2.34 (3H, s, $-COCH_3$), 3.90 (3H, s, $-OCH_3$), 6.66 (1H, d, $J=17.0$, C_β–H), and 7.80 (1H, d, $J=17.0$, C_α–H).

4-Methoxybenzylideneacetone[12] [mp 70—72 °C (lit, 73 °C)]; NMR (CCl_4); 2.26 (3H, s, $-CO\underline{CH_3}$), 3.82 (3H, s, $-OCH_3$), 6.50 (1H, d, $J=16.0$, C_β–H), and 7.37 (1H, d, $J=16.0$, C_α–H).

2,6-Dimethoxybenzylideneacetone[13] [mp 89—91 °C (lit, 88—90 °C)]; NMR (CCl_4); 2.26 (3H, s, $-CO\underline{CH_3}$), 3.88 (6H, s, $-O\underline{CH_3}$), 6.97 (1H, d, $J=16.6$, C_β–H), and 7.77 (1H, d, $J=16.6$, C_α–H).

3-Benzylidene-2-butanone;[14] NMR (CCl_4); 2.01 (3H, s, $C=C-\underline{CH_3}$), 2.40 (3H, s, $-CO\underline{CH_3}$), and 7.35 (1H, s, C_α–H).

3-(2-Methoxybenzylidene)-2-butanone[15]; NMR (CCl_4); 1.95 (3H, s, $C=C-\underline{CH_3}$), 2.42 (3H, s, $-CO\underline{CH_3}$), 3.87 (3H, s, $-O\underline{CH_3}$), and 7.63 (1H, s, C_α–H).

3-(4-Methoxybenzylidene)-2-butanone[16]; NMR (CCl_4); 2.02 (3H, s, $C-C-CH_3$), 2.37 (3H, s, $-COCH_3$), 3.82 (3H, s, $-OCH_3$), and 7.36 (1H, s, C_α–H).

3-(2,6-Dimethoxybenzylidene)-2-butanone; pale yellow crystals, mp 78—80 °C. Found: C, 70.59; H, 7.18%. Calcd for $C_{13}H_{16}O_3$: C, 70.89; H, 7.32%. NMR (CCl_4); 1.61 (3H,

s, C=C–$\underline{CH_3}$), 2.40 (3H, s, –CO$\underline{CH_3}$), 3.80 (6H, s, –O$\underline{CH_3}$), and 7.23 (1H, s, C_α–H).

3-(2-Thienylmethylidene)-2-butanone; a pale yellow liquid. Found: C, 65.17; H, 6.08; S, 19.10%. Calcd for $C_9H_{10}OS$: C, 65.03; H, 6.06; S, 19.29%. NMR (CCl_4); 2.10 (3H, d, J=0.7, C_β–CH_3), 2.36 (3H, s, –CO$\underline{CH_3}$), 7.09 (1H, d–d, J=3.75 and 5.0, ring C_4–H), 7.25 (1H, broad d, J=3.75, ring C_5–H), 7.46 (1H, broad d, J=5.0, ring C_2–H), and 7.58 (1H, d, J=0.7, C_α–H).

3-(2-Methoxybenzylidene)-2,4-pentanedione; light yellow crystals, mp 96—98 °C. Found: C, 71.51; H, 6.47%. Calcd for $C_{13}H_{14}O_3$: C, 71.54; H, 6.47%. IR (neat); 1705 and 1685 cm^{-1}. NMR (CCl_4); 2.15 and 2.35 (3H each, s, two –CO$\underline{CH_3}$), 3.85 (3H, s, –O$\underline{CH_3}$), and 7.71 (1H, s, C_α–H).

3-Methyl-3-octen-2-one; a pale yellow liquid. Found: C, 76.94; H, 11.14%. Calcd for $C_9H_{16}O$ (140.22): C, 77.09; H, 11.50%. MS; *m/e* 140 (parent). Exact mass measurement; Calcd, 140.120; Found, 140.123. NMR (CCl_4); 0.98 (3H, m, –CH_3), 1.43 (4H, m, –CH_2CH_2–), 1.72 (3H, s, C_3–CH_3), 2.00 (2H, m, –CH_2–), 2.22 (3H, s, –CO$\underline{CH_3}$), and 6.51 (1H, broad t, J=7.5, –$\underline{CH}$=C).

4-Hydroxy-3-methyl-4-(2-pyridyl)-2-butanone; colorless crystals, mp 72—74 °C (sublimation). MS; *m/e* 179 (parent). exact mass measurement; Calcd for $C_{10}H_{13}O_2N$, 179.094; Found, 179.099. NMR (CCl_4); 0.93 and 1.05 (3H each, d, J=7.0, C_3–CH_3) (ratio, 8: 5) and 2.11 and 2.18 (3H each, s, –CO$\underline{CH_3}$) (ratio, 5: 8). These results gave evidence of the presence of rotamers between C_α and C_β of the side chain.

4-Hydroxy-3-methyl-4-(3-pyridyl)-2-butanone; a pale yellow liquid. MS; *m/e* 179 (parent). Exact mass measurement; Calcd for $C_{10}H_{13}O_2N$, 179.094; Found, 179.092. NMR ($CDCl_3$); 0.92 and 1.08 (3H each, d, J=7.0, C_3–CH_3) (ratio, 96: 117), and 2.18 and 2.24 (3H each, s, –CO$\underline{CH_3}$) (ratio, 75: 78). These results gave evidence of the presence of rotamers between C_α and C_β of the side chain.

4-Hydroxy-3-methyl-4-(4-pyridyl)-2-butanone; a pale yellow viscous liquid. Found: C, 66.92; H, 7.34; N, 7.78%. Calcd for $C_{10}H_{13}O_2N$ (179.21): C, 67.02; H, 7.31; N, 7.82%. MS; *m/e* 179 (parent). Exact mass measurement; Calcd, 179.094; Found, 179.097. NMR ($CDCl_3$); 2.21 and 2.22 (3H each, s, –CO$\underline{CH_3}$) (ratio, 1: 1). Those results gave evidence of the presence of rotamers between C_α and C_β of the side chain.

Methyl salicylate; yield, 19%, exact mass measurement, Calcd for $C_8H_8O_3$, 152.047; Found, 152.049. IR (neat); 3530 (OH) and 1740 (C=O) cm^{-1}. NMR (CCl_4); 3.82 (3H, s, –O$\underline{CH_3}$).

The author wishes to thank Mr. Jun Uzawa and Mrs. Tamiko Chijimatsu for their NMR spectral measurements, Mr. Yasuaki Ezumi and Miss Kyoko Sugita for their measurements of the mass spectra, and the staff of the Organic Microanalysis Lab. of this Institute for their elemental analyses. This study was supported in part by a Grant for Life Science from this Institute.

References

1) A. T. Nielsen and W. J. Houlihan, *Org. React.*, Vol. 16 (1968).
2) (a) W. J. Rutter, *Federation Proc.*, **23**, 1248 (1964); (b) O. Warburg and W. Christian, *Biochem. Z.*, **314**, 149 (1943).
3) R. D. Kobes, R. T. Simpson, B. L. Valee, and W. J. Rutter, *Biochem.*, **8**, 585 (1969).
4) C. E. Harris, R. D. Kobes, D. C. Teller, and W. J. Rutter, *Biochem.*, **8**, 2442 (1969).
5) A. S. Mildvan, R. D. Kobes, and W. J. Rutter, *Biochem.*, **10**, 1191 (1971).
6) (a) E. J. Heron and R. M. Caprioli, *Biochem.*, **13**, 4371 (1974); (b) N. B. Schwarz, D. Abram, and D. S. Feigold, *ibid.*, **13**, 1726 (1974).
7) M. Iwata and S. Emoto, *Bull. Chem. Soc. Jpn.*, **47**, 2907 (1974).
8) M. Iwata and S. Emoto, *Chem. Lett.*, **1974**, 959.
9) K. Maeoka, K. Narasaka, and T. Mukaiyama, *Bull. Chem. Soc. Jpn.*, **46**, 3478 (1973).
10) L. Claisen and A. C. Ponder, *Ann.*, **223**, 137 (1884).
11) I. M. Heilbron and J. S. Buck, *J. Chem. Soc.*, **119**, 1500 (1921).
12) A. Einhorn and J. P. Gradfield, *Ann.*, **243**, 362 (1888).
13) M. Miyano, S. Muraki, T. Kusunoki, T. Morita, and M. Matsui, *Nippon Nogeikagaku Kaishi*, **34**, 683 (1960).
14) (a) G. Heller, H. Lauth, and A. Buchwaldt, *Ber.*, **55**, 483 (1922); (b) M. E. Kronenberg and E. Havinga, *Rec. Trav. Chim. Pays-Bas*, **84**, 17 (1965).
15) E. H. Woodruff and T. W. Conger, *J. Am. Chem. Soc.*, **60**, 465 (1938).
16) K. Iwamoto, *Bull. Chem. Soc. Jpn.*, **2**, 51 (1927).
17) For example, (a) M. Sekiya, T. Morimoto, and K. Suzuki, *Chem. Pharm. Bull.*, **21**, 1213 (1973); (b) P. Delest and R. Palland, *Compt. Rend.*, **246**, 1703 (1958); (c) E. Knoevenagel, *Ber.*, **36**, 2136 (1903); (d) D. F. Martin and W. C. Fernellius, *J. Am. Chem. Soc.*, **81**, 1509 (1959); (e) E. Hase and G. Stjernvall, *Suom. Kemistil. B*, **21**, 42 (1948); *Chem. Abstr.*, **42**, 8176c.
18) See, for example; "Inorganic Biochemistry," Vol. 1, ed. by G. L. Eichhorn, Elsevier, Amsterdam (1973).
19) (a) E. Grazi, T. Cheng, and B. L. Horecker, *Biochem. Biophys. Res. Commun.*, **7**, 250 (1962); (b) E. Grazi, P. T. Rowley, T. Cheng, O. Tchola, and B. L. Horecker, *ibid.*, **9**, 38 (1962).
20) P. Model, L. Ponticorvo, and D. Rittenberg, *Biochem.*, **7**, 1339 (1968).
21) A. Bramley, *J. Chem. Soc.*, **1916**, 496.

Transbutylation of Aromatic Hydrocarbons with Di-*t*-butylanisole[1)]

Keizo SHIMADA

Central Research Institute, Teijin Limited, 4-3-2, Asahigaoka, Hino, Tokyo 191

(Received November 18, 1975)

The trans-*t*-butylation of aromatic hydrocarbons with di-*t*-butylanisole in the presence of aluminum chloride was studied. It was found that the *t*-butyl group substituted at the *ortho* position to the methoxy group transfered easily to the hydrocarbons, but the *t*-butyl group of the *para* position did not transfer to the hydrocarbons. The transbutylation products did not suffer further isomerization when the catalyst aluminum chloride was less than 1/2 mol of the di-*t*-butylanisole used. Competitive trans-*t*-butylation was carried out and k_T/k_B, k_{m-X}/k_B, k_{O-X}/k_B, and k_{EB}/k_B were found to be 24, 2.2, 136, and 19, respectively.

Trans-*t*-butylation of aromatic hydrocarbons with *t*-butylbenzenes has been reported mainly in connection with the separation of *p*-xylene from a xylene mixture*.[2)] on the basis that *p*-xylene could not be *t*-butylated because of the steric hindrance of the *ortho* position to the methyl group.[3)]

However, no report is available concerning the use of a *t*-butylation reagent having substituents other than alkyl groups on the aromatic ring.

In this paper, the trans-*t*-butylation of aromatic hydrocarbons with 2,4-di-*t*-butylanisole is described.

Experimental

Materials. *Hydrocarbons*: Guaranteed pure reagents of benzene, toluene, ethyl- and isopropylbenzene were purified through distillation. The resulting purities were higher than 99.9%, as confirmed by gas chromatographic analysis. Guaranteed pure reagents of *m*-xylene were *t*-butylated with di-*t*-butyltoluene[2)] in the presence of $AlCl_3$ and the butyl-*m*-xylene separated by distillation was debutylated using toluene. The xylene fraction free of *p*-xylene thus obtained was purified by distillation. The resulting purity was greater than 99.5%. *o*-Xylene was purified in the same way. *t*-Butylbenzene was synthesized from benzene and *t*-butyl chloride.

Anisole: A guaranteed pure reagent of anisole was distilled after washing with a 10% sodium hydroxide aqueous solution and water, with a resulting purity greater than 99.5% (analyzed by gas chromatography).

t-Butyl chloride was synthesized from guaranteed pure reagents of *t*-butyl alcohol and hydrochloric acid (38%), washed well with water and distilled twice.

p-t-*Butylanisole*: To a solution of $AlCl_3$ (90 g) in anisole (756 g), maintained at 10 °C, *t*-butyl chloride (650 g) was added for 3 h. Afterward, the reaction mixture was stirred for 6 h, ice-water was added to the mixture and the catalyst was decomposed. The organic layer was washed with water and an alkaline aqueous solution, dried and distilled. The fraction boiling at 218—222 °C was collected. Yield 560 g. Further purification through redistillation was carried out (bp 220—221 °C, purity greater than 99.5%).

2,4-Di-t-butylanisole: To a solution of $AlCl_3$ (50 g) in anisole (540 g), 1100 g of *t*-butyl chloride was added and stirred for 6 h at 10 °C. After decomposition of the catalyst by the addition of ice-water, the organic layer was washed with water and an alkaline aqueous solution and dried. 2,4-Di-*t*-butylanisole was crystallized by cooling. It was recrystallized three times from methanol (mp 36 °C (lit, 36—37 °C),[4)] yield 350 g). An additional 110 g of pure 2,4-di-*t*-butylanisole was obtained from a parent solution (393 g) through distillation and recrystallization from methanol.

Reactions. To a mixture of 0.1 mol each of benzene or alkylbenzenes and di-*t*-butylanisole, the desired amount of $AlCl_3$ was added with stirring. In the case of competitive reactions, a desired amount of $AlCl_3$ was added to a mixture of 0.5 mol of each of the aromatic hydrocarbons and 0.1 mol of di-*t*-butylanisole with stirring. The competitive reaction of benzene and *o*-xylene was carried out using 0.5 mol of benzene and 0.1 mol of *o*-xylene. Samples were taken at appropriate times, poured into ice-water, washed and dried over calcium chloride. The samples were analyzed by gas chromatography using Apiezone L (10%) on a Diasolid S column (2 m) at 180 °C.

Results and Discussion

Butylation of Toluene: The results are shown in Table 1 and 2.

Friedel-Crafts *t*-butylation of toluene has been investigated by many authors. Allen and Yats[5)] have

Table 1. Butylation of toluene with di-*t*-butylanisole at 20 °C $AlCl_3$ 0.02 mol

Time	mol % of anisole deriv.		mol % of toluene deriv.	
	p-*t*-Butylanisole	di-*t*-Butylanisole	*t*-Butyltoluene	*p*-Isomer content in *t*-butyltoluene
5 min	42.9	57.1	43.0	92.3
30 min	53.6	46.4	53.5	93.1
1 hr	57.5	42.5	57.5	92.8
3 hr	66.4	33.6	66.5	94.5
10 hr	73.2	26.8	73.2	94.5
24 hr	82.1	18.9	82.0	94.6
100 hr	91.4	8.5	91.3	94.6

Table 2. Butylation of toluene with di-*t*-butylanisole $AlCl_3$ 0.01 mol

Time	25 °C		50 °C	
	Conversion (%)	*p*-Isomer content in *t*-butyltoluene (%)	Conversion (%)	*p*-Isomer content in *t*-butyltoluene (%)
5 min	19.3	94.4	37.3	89.9
15 min	30.6	94.3	49.0	90.8
30 min	35.6	94.3	58.0	91.2
1 h	40.2	94.6	66.8	91.7
2 h	46.6	94.8	73.2	92.1
6 h	56.5	95.7	82.5	92.4
24 h	68.3	95.8	90.0	92.8

* For references to previous research, see Ref. 2.

concluded, on the basis of the results of Schlatter.[6] that the initial isomer distribution of *t*-butyltoluene consisted of 7% *m*- and 93% *p*-isomers. Steric hindrance prevents the formation of the *o*-isomer. Usually, in the alkylation and especially transalkylation reaction conditions, subsequent or concurrent isomerization of the reaction mixture takes place and the higher *m*-isomer contents are observed.

However, in the present case, the *t*-butyltoluene produced by transbutylation from di-*t*-butylanisole maintains a high *p*-isomer content throughout the reaction, and there is no sign of secondary reactions, such as isomerization and disproportionation. A slight increase in the *p*-isomer content toward the end of the reaction may be due to further *t*-butylation of *m*-*t*-butyltoluene, forming 3,5-di-*t*-butyltoluene. A low reaction temperature and a low catalyst concentration favor the high *p*-isomer content.

TABLE 3. BUTYLATION OF BENZENE WITH DI-*t*-BUTYLANISOLE AT 20 °C $AlCl_3$ 0.02 mol

Time	Reaction products mol %				
	Benzene	*t*-Butylbenzene			*p*-Isomer % in Dibutylbenzene
		mono-	*m*-di-	*p*-di	
5 min	96.1	2.0	0.2	1.7	90
20 min	92.8	2.7	0.4	4.1	91
40 min	90.6	2.8	0.6	6.0	91
1.5 h	87.4	2.8	0.7	9.1	93
3 h	83.3	4.1	0.9	11.7	93
24 h	73.5	3.0	1.5	22.0	94
120 h	59.4	3.0	2.4	35.2	94

Butylation of Benzene: The results were shown in Table 3. The content of di-*t*-butylbenzenes increased with time, whereas the *t*-butylbenzene content remained almost constant. These results were realized on the assumption that the *t*-butylbenzene initially formed is more reactive than benzene and that the transbutylation of benzene by di-*t*-butylbenzene did not occur.

TABLE 4. BUTYLATION OF ALKYLBENZENE WITH DI-*t*-BUTYLANISOLE AT 25 °C $AlCl_3$ 0.01 mol

Time	Ethylbenzene		Isopropylbenzene		*t*-Butylbenzene	
	Conversion (%)	*p*-isomer (%)	Conversion (%)	*p*-isomer (%)	Conversion (%)	*p*-isomer (%)
5 min	18.8	94.0	19.8	92.0	15.9	93.0
10 min	25.7	94.0	26.0	93.0	21.1	92.5
30 min	35.4	94.6	36.3	93.0	30.2	93.0
1 h	41.2	94.6	41.6	93.3	34.9	93.5
2 h	47.0	94.5	47.8	93.5	40.7	93.5
6 h	55.7	94.8	56.3	93.6	50.4	93.4
24 h	67.0	94.9	67.8	93.3	62.8	93.5

Butylation of Ethyl-, Isopropyl-, and t-*Butylbenzenes*: The results are shown in Table 4. In the course of the reaction, there was no sign of either disproportionation of ethyl- or isopropylbenzene, or isomerization of butylated products.

TABLE 5. REACTION OF TOLUENE WITH *p*-*t*-BUTYLANISOLE AT 25 °C $AlCl_3$ 0.01 mol

Time	Butyltoluene yield (mol %)	Composition of anisole deriv. (mol %)		
		Anisole	*p*-*t*-Bu-	2,4-(t-Bu)$_2$-
20 min	0	2	97.5	1.3
30 min	0	1.9	96.1	2.0
2 h	0	1	95.6	2.2
45 h	6.4	10.9	84.6	4.5

Reaction of Toluene with p-t-*Butylanisole*: The results were shown in Table 5. *t*-Butylation of toluene by *p*-*t*-butylanisole did not occur. Instead, disproportionation of *p*-*t*-butylanisole was observed. Formation of *t*-butyltoluene after 45 h was considered to be the result of trans-*t*-butylation by 2,4-di-*t*-butylanisole.

Thus the *t*-butyl group of the *para* position to the methoxy group did not participate in this transbutylation.

Furthermore, confirmation that the *t*-butyl group of the *ortho* position transfers to the hydrocarbons was obtained by the result that 4-methyl-2-*t*-butylanisole reacts with toluene to form *t*-butyltoluene and 4-methylanisole. This result will be reported elsewhere.

Therefore, the trans-*t*-butylation of aromatic hydrocarbons with 2,4-di-*t*-butylanisole is shown by the following reaction.

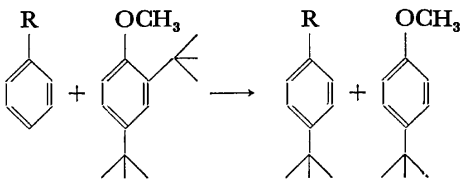

*Competitive Trans-*t-*butylation*: The results of the competitive *t*-butylations of benzene and toluene are shown in Table 6. When the amount of $AlCl_3$ catalyst was less than 1/2 mol to di-*t*-butylanisole, the competitive reaction proceeded normally. However, when an equimolar amount of a catalyst for di-*t*-butylanisole was used, secondary reactions took place and the apparent k_T/k_B value decreased.

Olah *et al.*[7] have investigated the Friedel-Crafts *t*-butylation of benzene and methylbenzenes with *t*-butyl bromide and with isobutylene. They pointed

TABLE 6. COMPETITIVE *t*-BUTYLATION OF BENZENE AND TOLUENE

Cat. mol ratio	0.1		0.5		1.0	
Time	k_T/k_B	*p*-Isomer in *t*-Butoluene	k_T/k_B	*p*-Isomer in *t*-Butoluene	k_T/k_B	*p*-Isomer in *t*-Butoluene
2 min	24.2		21.1	94.7	15.0	90.3
10 min	23.9	94.3	21.0	93.3	11.3	87.8
30 min	23.1	94.3	22.1	93.5	9.6	85.8
1 h	24.0	94.4	21.6	93.2	8.3	84.2
2 h	23.7	94.5	21.8	93.2	7.0	80.5
24 h	23.9	94.7			2.8	51.7
48 h	23.7	94.7				
	24.0±0.7		21.6±0.5			

Table 7. Competitive *t*-butylation of benzene and C_8 aromatics

Aromatic	k_{Ar}/k_B		
	This work	Olah[7]	
	Di-*t*-butylanisole	*t*-BuBr	Isobutylene
Benzene	1.00	1.00	1.00
Toluene	24.0	16.6	15.2
o-Xylene	136	44.3	47.8
m-Xylene	2.2	2.54	3.82
Ethylbenzene	22		

out that secondary isomerization occurred in the *t*-butylation conditions reported by Brown,[8] and found that k_T/k_B of the *t*-butylation was 14—16 for non-isomerized conditions. A higher k_T/k_B value (24) was observed in the trans-*t*-butylation with di-*t*-butylanisole.

The competitive *t*-butylation of toluene and C_8 aromatics was also carried out. The data obtained are summarized and compared with the results of Olah in Table 7.

From the data it is seen that the trans-*t*-butylation with di-*t*-butylanisole is the most selective *t*-butylation.

The author would like to acknowledge the continuing guidance and encouragement of Dr. Saburo Akiyoshi, now Professor Emeritus of Kyushu University. The author is also indebted to Dr. Shoichi Sakajiri, Director of the Central Research Institute, Teijin Limited, for publication permission.

References

1) The Alkylation and Transalkylation Reaction of Aromatic Hydrocarbons VI. Presented at the 20th Annual Meeting of The Chemical Society of Japan, April 1967.

2) K. Shimada and S. Nagahama, *Sekiyu Gakkai Shi*, **18**, 34 (1975).

3) A. Nakatsuchi, *Kogyo Kagaku Zasshi*, **32**, 1084 (1929).

4) M. S. Carpenter, W. M. Easter, and R. F. Wood, *J. Org. Chem.* **16**, 586 (1951).

5) R. H. Allen and L. D. Yats, *J. Am. Chem. Soc.*, **83**, 2799 (1961).

6) M. J. Schlatter and R. D. Clark, *J. Am. Chem. Soc.*, **75**, 261 (1953).

7) G. A. Olah, S. H. Flood, and M. E. Moffatt, *J. Am. Chem. Soc.*, **86**, 1060 (1964).

8) H. C. Brown and C. R. Smoot, *J. Am. Chem. Soc.*, **78**, 6255 (1956).

The Reductive *N*-Methylation of Amines with Tetracarbonylhydridoferrate-Formaldehyde

Yoshihisa WATANABE, Sang Chul SHIM, Take-aki MITSUDO, Masakazu YAMASHITA, and Yoshinobu TAKEGAMI

Department of Hydrocarbon Chemistry, Faculty of Engineering, Kyoto University, Sakyo-ku, Kyoto 606

(Received November 19, 1975)

Alcoholic tetracarbonylhydridoferrate combined with formaldehyde is an excellent reagent for reductive *N*-methylation of amines. The effects of reaction conditions such as temperature, atmosphere, and molar ratio (ferrate/formaldehyde/amine) on the reaction have been examined. The optimum condition for *N,N*-dimethylation of aniline is at 60 °C, under carbon monoxide, and at 1.0/2.2/1.0 for the molar ratio.

Recently, tetracarbonylhydridoferrate prepared from pentacarbonyliron and alkali metal hydroxide[1] has been shown to be a convenient, selective reagent for carbonylation and/or reduction of a variety of organic functional groups such as a nitro group,[2] an acetylenic bond,[2] olefinic bonds[3] of conjugated diene, enamine, and α,β-unsaturated carbonyl compound, alkyl halides,[4] and olefin oxides.[5] More recently, several works have demonstrated that the ferrate is effective for reductive alkylation of amines[6] and ketones[7] with carbonyl compounds. Several methods for the synthesis of *N*-alkylamines from amines and carbonyl compounds have been reported.[8] These methods generally give satisfactory results, but have limited applicabilities. For example, the Clarke-Eschweiler reaction, a simple method for *N*-methylation of amines using formaldehyde/formic acid, can be applied successfully only to aliphatic amines.

The present investigation deals with the reductive *N*-mono- and *N,N*-dimethylation of amines using the tetracarbonylhydridoferrate–formaldehyde system with a view to determine the factors affecting the reaction in some detail. A preliminary report of this work was published elswhere.[6b,c]

Experimental

Potassium tetracarbonylhydridoferrate was prepared according to the method described in a previous paper:[4a] 3.7—11 mmol of the ferrate was used in each run. Pentacarbonyliron, amines, and the other compounds employed were all commercial products.

Reaction Procedure. To the alcoholic ferrate, determined amounts of amines and aqueous formaldehyde were added at 50—78 °C under carbon monoxide or argon. After a certain reaction time, the reaction mixture was submitted to analysis.

Analytical Procedure. *N,N*-Dimethyl derivatives of aniline, toluidines, anisidines, benzylamine, and 2-aminoethanol were analyzed by GLPC using internal standards: a column (0.3 cm ϕ, 3 m) packed with 10% Versamid on Neopak 60—80 mesh. Other reaction products were isolated and identified by means of IR and NMR spectra, which were recorded on a 215 Hitachi grating spectrophotometer and a JEOL model 3H 60 NMR spectrometer, respectively. Products were isolated as follows: the reaction mixture was acidified with hydrochloric acid and solvents were evaporated to dryness. A residue was extracted with ether in the presence of sodium carbonate. The extract gave *N*-methylated amines after evaporating the solvent, and the amines were purified by vacuum distillation: *N*-methyl-2-aminopyridine, bp 57—58 °C/2 mmHg, yield 65%, NMR($CDCl_3$) τ 2.0 (m, 1H, α-H), 2.6 (m, 1H, γ-H), 3.5 (m, 2H, β-H), 5.0 (m, 1H, N–H), and 7.0 (m, 3H, N–CH_3); *N,N*-dimethyl-*o*-anisidine, bp 48—49 °C/2—3 mmHg, 82%, NMR($CDCl_3$) τ 3.25 (s, 4H, aromatic), 6.25 (s, 3H, O–CH_3), and 7.3 (s, 6H, $N(CH_3)_2$).

Results and Discussion

N-Methylation of Aniline. Aniline was converted into *N*-methyl- and *N,N*-dimethylaniline with tetracarbonylhydridoferrate–formaldehyde under different con-

TABLE 1. *N*-METHYLATION OF ANILINE WITH $KHFe(CO)_4$–HCHO

Exp. No.	Reaction Conditions			CO Absorbed[b]	Product (%)[e]	
	Ratio[a]	Temp (°C)	Time (h)		*N*-Methylaniline	*N,N*-Dimethylaniline
1	1.0/2.2/1.0	60	9	1.8	~0	~100
2[c]	1.0/2.2/1.0	60	0.5	—	52	10
			9	—	48	32
3[d]	1.0/2.2/1.0	60	9	~0	30	70
4	1.0/2.2/1.0	50	9	1.6	7	93
5	1.0/2.2/1.0	70	9	0.6	19	78
6	1.0/2.2/1.0	Reflux	9	~0	30	70
7	1.0/4.0/4.0	60	3.5	1.4	210	38
8	1.0/4.4/2.0	60	4	1.1	98	50
9	1.0/6.6/3.0	60	3	1.8	116	50
			18	1.8	115	82

a) Molar ratio; ferrate/formaldehyde/aniline. b) Mol/mol–$KHFe(CO)_4$. c) Under argon atmosphere. d) Water, 10 mol/mol–$KHFe(CO)_4$, was added. e) Determined by GLPC. Based on the amount of the ferrate used.

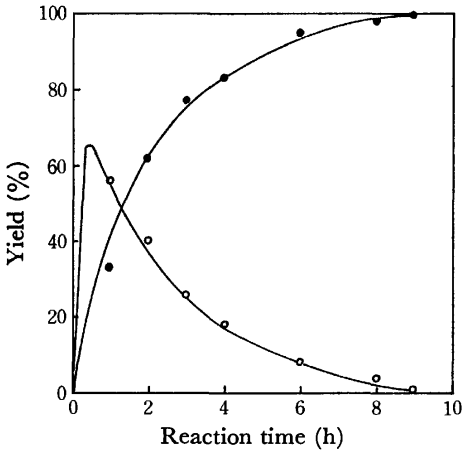

Fig. 1. *N*-Methylation of aniline with $KHFe(CO)_4$–HCHO. At 60 °C under carbon monoxide. Molar ratio, ferrate/formaldehyde/aniline, 1.0/2.2/1.0.
○: *N*-Methylaniline. ●: *N,N*-Dimethylaniline.

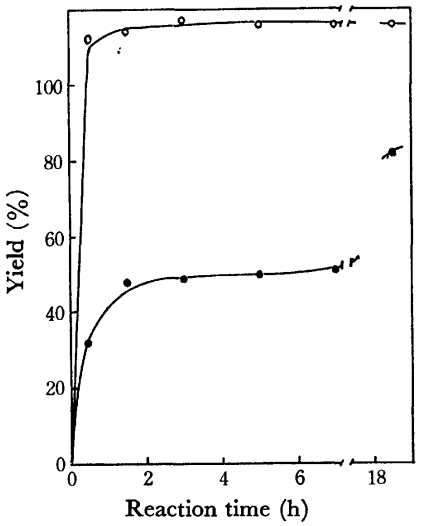

Fig. 2. *N*-Methylation of aniline with $KHFe(CO)_4$–HCHO. At 60 °C under carbon monoxide. Molar ratio, ferrate/formaldehyde/aniline, 1.0/6.6/3.0.
○: *N*-Methylaniline. ●: *N,N*-Dimethylaniline.

ditions. The formation of *N*-methylated anilines was highly affected by such reaction variables as reaction temperature, atmosphere, molar ratio (the ferrate/formaldehyde/aniline), and the addition of water. The results are shown in Table 1 and Figs. 1 and 2.

As Fig. 1 shows, *N*-methylaniline is dominant at first and then *N,N*-dimethylaniline dominates when aniline is methylated at 60 °C under carbon monoxide at 1.0/2.2/1.0 of the molar ratio. This fact shows that aniline is almost quantitatively converted into *N,N*-dimethylaniline *via* *N*-methylaniline under this condition. The reaction proceeds smoothly with an absorption of carbon monoxide; the gas absorbed amounts to 1.8 mol/mol-ferrate.

The reaction condition optimum for preparation of *N,N*-dimethylaniline is that of Exp. No. 1: at 60 °C under carbon monoxide in moist ethanol when the molar ratio is fixed at 1.0/2.2/1.0. Lower or higher temperatures, argon atmosphere, and addition of excess water are less favorable for the dimethylation and give *N*-methylaniline in considerable yields. (See Exps. 1—6). Higher temperatures (70 °C and reflux in ethanol) have an inhibitory effect on the dimethylation and carbon monoxide absorption is significantly retarded. By addition of excess water, the gas absorption is also retarded. Under argon, the reaction stops at the first stage to give *N*-methylaniline. These results show that the reducing power of the ferrate increases with an absorption of carbon monoxide.

N-Methylaniline predominates as the reaction product at 1.0/40/4.0 of the molar ratio (Exp. 7). The reaction appears to be completed in 2—3 h and the yields of *N*-methyl- and *N,N*-dimethylaniline are 210 and 38%, respectively. Accordingly the selectivity for mono- and dimethylation can be readily controlled by the ferrate/aldehyde/aniline ratio, and one mole of the ferrate has the power to methylate about 2.8 N–H bonds at maximum. Therefore, one mole of the ferrate corresponds to about 1.4 mol of aniline for dimethylation. The machanism of the reaction is not clear, but the reduction seems to proceed *via* Schiff bases and immonium salts and to include the reduction of carbon-nitrogen bonds.

$$-NH_2 + HCHO \longrightarrow$$
$$[-NH-CH_2OH \longrightarrow -N{=}CH_2] \xrightarrow{KHFe(CO)_4} -NHCH_3$$

Table 2. *N*-Methylation of primary amines with $KHFe(CO)_4$–HCHO[a]

Exp. No.	Primary amine	Reaction time (h)	CO absorbed[b]	Product (%)[c]	
				N-Methyl-amine	*N,N*-Dimethyl-amine
1	Aniline	9	1.8	~0	~100
10	*o*-Toluidine	16	2.0	~0	~100
11	*p*-Toluidine	6	2.0	~0	~100
12	*o*-Anisidine	36	1.6	~0	~100 (82)[d]
13	*p*-Anisidine	7	1.5	~0	~100
14	*o*-Chloroaniline	72	0.4	56	33
15	2-Aminopyridine	48	0.7	65[d]	—
16	Benzylamine	12	2.0	~0	~100
17	2-Aminoethanol	8	0.6	—	34

a) At 60°C under carbon monoxide. Molar ratio: $KHFe(CO)_4$/HCHO/Amine=1.0/2.2/1.0. b) Mol/mol-$KHFe(CO)_4$. c) Determined by GLPC. Based on the amount of the ferrate used. d) Isolated yield.

TABLE 3. *N*-METHYLATION OF SECONDARY AMINES WITH $KHFe(CO)_4$–HCHO[a]

Exp. No.	Amine	Reaction time (h)	CO absorbed[b]	Product (%)[c]	
18	*N*-Methylaniline	6	1.8	*N,N*-Dimethylaniline	~200
19	*N*-Ethylaniline	6	2.0	*N,N*-Ethylmethylaniline	195
20	*N*-Methylbenzylamine	3	1.4	*N,N*-Dimethylbenzylamine	~200
21	Piperidine	6	1.0	*N*-Methylpiperidine	~200
22	Morpholine	6	1.0	*N*-Methylmorpholine	~200
23	2-(Methylamino)ethanol	8	1.5	2-(Dimethylamino)ethanol	~200

a) At 60°C under carbon monoxide. Molar ratio: $KHFe(CO)_4$/HCHO/Amine=1.0/3.0/2.0. b) Mol/mol-$KHFe(CO)_4$. c) Determined by GLPC. Based on the amount of the ferrate used.

$$-NHCH_3 + HCHO \longrightarrow [-\underset{\underset{CH_3}{|}}{N}-CH_2OH \longrightarrow -\overset{+}{\underset{\underset{CH_3}{|}}{N}}=CH_2] \xrightarrow{KHFe(CO)_4} -N(CH_3)_2$$

Such a consideration may be supported by the fact that Schiff bases and immonium salts are reduced by the ferrate.[3d,6b] As a result, *N*-methylation of the N–H bond means reduction of the $-N=CH_2$ bond with the ferrate, and one mole of the ferrate with the power to methylate 2.8 N–H bonds corresponds to about 5.6 hydrogens as a reducing reagent in the reductive methylation of amines. At 1.0/6.6/3.0 of the molar ratio, in the presence of excess aniline, *N*-methylaniline is predominant as the product. (Fig. 2). For the reduction of conjugated diene and enamine, the most effective reaction variables are the atmosphere and the amount of water present.[3a,d] Under carbon monoxide in the presence of some water, the reaction proceeded most smoothly, and one mole of the ferrate corresponds to five hydrogens in the reduction of olefinic bonds.

N-*Methylation of Primary Amines.* Several primary amines were dimethylated under the conditions optimum for the dimethylation of aniline. The results are listed in Table 2. *o*-Methyl, methoxy, and chloro groups highly inhibit the dimethylation. For example, the dimethylation of *o*-anisidine required 36 h for completion, but that of *p*-anisidine only 7 h. Such effects of the substituents may be due to a steric hindrance, which would be the largest for the chloro group, followed by the methoxy and then the methyl group. *o*-Chloroaniline gave *N*-methyl-*o*-chloroaniline in 56% yield even after 3 days. 2-Aminopyridine gave only the *N*-monomethylated product. Benzylamine and 2-aminoethanol were dimethylated.

N-*Methylation of Secondary Amines.* As shown in Table 3, secondary amines were readily and almost quantitatively methylated to the corresponding tertiary amines by this method. The reaction completes in 3—8 h at 60 °C under carbon monoxide at 1.0/3.0/2.0 of the molar ratio.

References

1) P. Krumholz and H. M. A. Stettiner, *J. Am. Chem. Soc.*, **71**, 3035 (1949).

2) See, for example: H. W. Sternberg, R. Markby, and I. Wender, *J. Am. Chem. Soc.*, **79**, 6116 (1957); Y. Watanabe, T. Mitsudo, M. Yamashita, and Y. Takegami, *Bull. Chem. Soc. Jpn.*, **48**, 1476 (1975).

3) a) Y. Takegami, Y. Watanabe, I. Kanaya, T. Mitsudo, T. Okajima, Y. Morishita, and H. Masada, *Bull. Chem. Soc. Jpn.*, **41**, 2990 (1968); b) H. Masada, M. Mizuno, S. Suga, Y. Watanabe, and Y. Takegami, *ibid.*, **43**, 3824 (1970); c) R. Noyori, I. Umeda, and T. Ishigami, *J. Org. Chem.*, **37**, 1542 (1972); d) T. Mitsudo, Y. Watanabe, M. Yamashita, and Y. Takegami, *Chem. Lett.*, **1974**, 1385; e) T. Mitsudo, Y. Watanabe, M. Tanaka, S. Atsuta, K. Yamamoto, and Y. Takegami, *Bull. Chem. Soc. Jpn.*, **48**, 1506 (1975); f) M. Yamashita, Y. Watanabe, T. Mitsudo, and Y. Takegami., *Tetrahedron Lett.*, **1975**, 1867.

4) a) Y. Takegami, Y. Watanabe, H. Masada, and I. Kanaya, *Bull. Chem. Soc. Jpn.*, **40**, 1456 (1967); b) Y. Takegami, Y. Watanabe, T. Mitsudo, and T. Okajima, *ibid.*, **42**, 1992 (1969); c) H. Alper, *Tetrahedron Lett.*, **1975**, 2257.

5) Y. Takegami, Y. Watanabe, T. Mitsudo, and H. Masada, *Bull. Chem. Soc. Jpn.*, **42**, 202 (1969), and references cited therein.

6) a) T. Mitsudo, Y. Watanabe, M. Tanaka, K. Yamamoto, and Y. Takegami, *Bull. Chem. Soc. Jpn.*, **44**, 392 (1971); b) Y. Watanabe, M. Yamashita, T. Mitsudo, M. Tanaka, and Y. Takegami, *Tetrahedron Lett.*, **1974**, 1879; c) Y. Watanabe, T. Mitsudo, M. Yamashita, S. C. Shim, and Y. Takegami, *Chem. Lett.*, **1974**, 1265; d) G. P. Boldrini, M. Panunzio, and A. Umani-Ronchi, *Synthesis*, **1974**, 733; e) Y. Watanabe, S. C. Shim, T. Mitsudo, M. Yamashita, and Y. Takegami, *Chem. Lett.*, **1975**, 699, 995.

7) G. Cainelli, M. Panunzio, and A. Umani-Ronchi, *Tetrahedron Lett.*, **1973**, 2491; *J. Chem. Soc. Perkin Trans I*, **1975**, 1273; G. P. Boldrini, M. Panunzio, and A. Umani-Ronchi, *J. Chem. Soc., Chem. Commun.*, **1974**, 359.

8) W. S. Emerson, *Org. React.*, **4**, 174 (1948); M. L. Moor, *ibid.*, **5**, 301 (1949).

Thermal *Cis*-to-*Trans* Isomerization of Substituted Azobenzenes II.[1] Substituent and Solvent Effects

Norio NISHIMURA, Toshinobu SUEYOSHI, Hideyuki YAMANAKA, Etsuko IMAI, Shunzo YAMAMOTO, and Shigeo HASEGAWA

Department of Chemistry, Faculty of Science, Okayama University, Tsushima, Okayama 700

(Received November 25, 1975)

The thermal *cis*-to-*trans* isomerization rate of various azobenzenes was followed by means of spectrophotometric and flash photolysis techniques. For *para*-donor/*para'*-acceptor-substituted azobenzenes such as 4-nitro-4'-dimethylaminoazobenzene, the rate was distinctly accelerated, the activation energy decreasing with the increase in the polarity of solvents. Introduction of substituents in *para* positions with respect to azo group increased the rate irrespective of substituent. The effect is additive and a Hammett-type equation holds. For 4-dimethylamino- and 4-nitroazobenzenes, while the 2-methyl group accelerated the rate, the 2'-methyl group did not. The results suggest that the isomerization proceeds *via* inversion mechanism and the rate is controlled mainly by the resonance stabilization in the coplanar transition state. The inversion center for asymmetric azobenzenes is discussed.

The mechanism of *cis-trans* isomerization of azobenzenes and azomethines has attracted much attention from interest in its photochemistry. For their thermal *cis*-to-*trans* isomerization, two mechanisms have been proposed. One involves a rotation (torsion or twist) around the N=N double bond and includes a π-bond rupture. The other involves an inversion (in-plane lateral shift) through a linear state, the π-bond remaining intact.

The inversion mechanism has been assumed to hold for imines and azo compounds. However, recent accumulation of data of the isomerization has given rise to controversy on the mechanism.[2-9] Some authors explained their results in terms of different mechanisms,[6,7] and others suggested the possibility of a continuum of mechanisms between two limiting cases.[3] In addition to the study of activation parameters and solvent effects, a study of substituent effects on the rate of isomerization seemed to be the nearest way to solve the problem.

Recently, the present authors[1] presented a brief report on the *cis*-to-*trans* thermal isomerization of substituted 4-dimethylaminoazobenzenes as summarized below: (1) 2-Methyl group considerably accelerates the rate, while 2'-methyl group has virtually no effect on the rate. (2) All *para* substituents accelerate the rate, irrespective of the nature of the substituents. The effect is of an additive nature and an extended Hammett equation approximately holds:

$$\log k/k_0 = \sum\sigma_{c-t} \qquad (1)$$

where k and k_0 refer to the rate constants of *o*- and/or *p*-substituted and unsubstituted 4-dimethylaminoazobenzenes, respectively, and $\sum$ is the sum of the substituent constants for the substituents present in both benzene nuclei. (3) The logarithmic isomerization rate constants are roughly proportional to the molar extinction coefficients of the *trans*-isomers. The findings seemed to give us an useful suggestion regarding the rate-controlling factors for the isomerization.

This paper deals with the isomerization of various azobenzene derivatives for a better understanding of the isomerization mechanism and rate-controlling factors.

Experimental

Materials. The usual azobenzene derivatives were prepared by the procedures described previously.[10,11] For 2,6-dimethyl-4-dimethylaminoazobenzene derivatives, *N,N*-dimethyl-*m*-xylidine was prepared *via* 2,4,6-trimethylpyridinium perchlorate by the method of Diels and Alder.[12] It was then coupled with diazonium salts to give the final substances. Ryan's method[13] was used for the coupling. The final products were purified by dissolving them in benzene, passing through an alumina column, and then crystallizing them from benzene. *p*-Nitroazobenzene was prepared by condensing *p*-nitronitrosobenzene with aniline, the former being obtained by oxidation of *p*-nitroaniline with Caro's acid. Other *p*-nitroazobenzene derivatives were prepared by similar procedures. Melting point, NMR and UV spectra were utilized for identification. Elemental analysis was made for the new compounds. Their names, melting points and values in literature (in parentheses) are as follows: 4-Dimethylaminoazobenzene, 118—119 °C (119—120 °C); 4-Methyl-4'-dimethylaminoazobenzene, 169—170 °C (169.5—170 °C); 4-Chloro-4'-dimethylaminoazobenzene, 158—159 °C (158—158.5 °C); 3-Nitro-4'-dimethylaminoazobenzene, 157.5—158 °C (157—158 °C); 2-Methyl-4'-dimethylaminoazobenzene, 73—74 °C (73.5—74 °C); 2-Methyl-4-dimethylaminoazobenzene, 67—67.5 °C (68—68.5 °C); 2,4-Dimethyl-4'-dimethylaminoazobenzene, 136—137 °C (137 °C); 2-Methyl-4-chloro-4'-dimethylaminoazobenzene, 114—115 °C (117 °C); 2,4'-Dimethyl-4-dimethylaminoazobenzene, 125—126 °C (121 °C); 2-Methyl-4'-chloro-4-dimethylaminoazobenzene, 98—99 °C (96 °C); 2,2'-Dimethyl-5'-nitro-4-dimethylaminoazobenzene, 148—149 °C (148—148.5 °C); 2,2'-Dimethyl-4-dimethylaminoazobenzene, 77—78 °C (79—80 °C); 2,2',4'-Trimethyl-4-dimethylaminoazobenzene, 118—119 °C (120—121 °C); 2,2'-Dimethyl-4'-chloro-4-dimethylaminoazobenzene, 114.5—115 °C (115—116 °C); 4-Diethylaminoazobenzene, 96—97 °C (98 °C); 4-Methoxyazobenzene, 55—56 °C (55.5 °C); 4,4'-Bis(dimethylamino)azobenzene, sublimes at *ca.* 235 °C. Found: C, 71.73; H, 7.29; N, 20.58%. Calcd for $C_{16}H_{20}N_4$: C, 71.61; H, 7.51; N, 20.88%; 4,4'-Bis(diethylamino)azobenzene, 176—177 °C (171 °C); 4,4'-Dimethoxyazobenzene, 163.5—164.5 °C (164 °C); 4,4'-Dichloroazobenzene, 185 °C(183—184 °C); 4,4'-Dimethylazobenzene, 144 °C (144 °C); 4,4'-Dinitroazobenzene, 215 °C (216 °C); 4-Pyrrolidinoazobenzene, 166—167 °C (166—167 °C); 4-Aminoazobenzene, 125.5 °C (125—126 °C); 4-Amino-4'-methylazobenzene, 147—148 °C. Found: C, 74.20; H, 6.48;

TABLE 1. RATE CONSTANTS AND ACTIVATION PARAMETERS FOR THE *cis*-TO-*trans* THERMAL ISOMERIZATION OF AZOBENZENES[a]

No.	Substance	λ_{max}[b] (nm)	ε_{max}[b]	$10^2 k$, min^{-1} 25°C	30°C	35°C	40°C	45°C	50°C	55°C	60°C	65°C	70°C	75°C	E_a (kcal/mol)	ΔS^* (300K) (gibbs/mol)
1	4-Dimethylamino-azobenzene	390	31200	0.204	0.355	0.670	1.10								21.1	−10.7
2	4′-Methyl-DAAB[c]	400	31800	0.319	0.562	0.990	1.57								20.1	−12.5
3	4′-Chloro-DAAB	410	34100	0.386	0.713	1.14	1.97								20.0	−12.5
4	3′-Nitro-DAAB	420	31600	0.291	0.517	0.838	1.47								18.8	−17.4
5	2′-Methyl-DAAB	394	29900			0.594	0.935	1.59							19.2	−16.5
6	2-Methyl-DAAB	405	30200			1.87	3.32	5.10							20.1	−11.0
7	2′,4′-Dimethyl-DAAB	393	31000			0.99		2.90	4.93						21.0	−9.75
8	2′-Methyl-4′-chloro-DAAB	413	32600			1.16	1.75	3.74	5.90						21.5	−7.46
9	2,4′-Dimethyl-DAAB	405	30500		1.54	2.60	4.69	7.95	11.6						19.7	−12.0
10	2-Methyl-4′-chloro-DAAB	415	32800			3.98	6.03	11.3							19.7	−11.0
11	2,2′-Dimethyl-5′-nitro-DAAB	425	29800	0.755	1.18	2.33	4.02								20.4	−9.75
12	2,2′-Dimethyl-DAAB	400	28800	0.567	1.02	1.73	2.91								20.6	−9.75
13	2,2′,4′-Trimethyl-DAAB	399	29900	1.01	1.59	2.88	4.38								18.3	−16.9
14	2,2′-Dimethyl-4′-chloro-DAAB	411	31000			5.17										
15	4-Diethylamino-azobenzene	407	32300			0.993										
16	4-Methoxy-AB[d]	342	21350			0.194										
17	4,4′-Bis(dimethyl-amino)-AB	410	37000	1.61	2.81	4.69	7.49	11.1							19.2	−12.0
18	4,4′-Bis(diethyl-amino)-AB	431	39300	3.40	5.44	9.25	14.5								18.3	−13.9
19	4,4′-Dimethoxy-AB	353	26300			0.314										
20	4,4′-Dichloro-AB	331	26400			0.161										
21	4,4′-Dimethyl-AB	330	27000			0.173										
22	4,4′-Dinitro-AB	336	24600			2.40										
23	4-Pyrrolidino-AB	407	33000			0.865										
24	4-Amino-AB	363	29000			0.842										
25	4-Amino-4′-methyl-AB	363	28300			1.04										
26	4-Methyl-4′-pyrrolidino-AB	407	32800			1.15										
27	4-Chloro-4′-pyrrolidino-AB	417	35000			1.84										
28	4-Nitro-AB	330	25600			0.737										
29	2′-Methyl-4-nitro-AB	341	24100			0.491										
30	2-Methyl-4-nitro-AB	336	24600			1.16										
31	2,2′-Dimethyl-4-nitro-AB	345	21100			1.14										
32	2,2′,6′-Trimethyl-DAAB	377	26000						0.180	0.359	0.590	0.944	1.75		24.7	−4.71
33	2′,6′-Dimethyl-DAAB	389	23100								0.276	0.491	0.848	1.69	27.5	2.15
34	2,6-Dimethyl-DAAB	391	20000					0.480	0.914	1.40	2.84				24.5	−2.42
35	2,4′,6-Trimethyl-DAAB	395	24700				0.312	0.534	0.769	1.57	3.14				24.2	−2.88
36	2,2′,6-Trimethyl-DAAB	395	24800				0.850	1.34	2.03	3.44	5.30				19.2	−16.8

a) Substances **1**—**24**, **26**—**31** in cyclohexane, **25** in benzene and **32**—**36** in toluene. b) Wavelength and molar extinction coefficient at the maximum of the conjugation band in cyclohexane. c) DAAB: 4-Dimethylaminoazobenzene. d) AB: Azobenzene.

N, 19.45%. Calcd for $C_{13}H_{13}N_3$: C, 73.90; H, 6.20; N, 19.89%; 4-Methyl-4′-pyrrolidinoazobenzene, 187—188 °C (187—188 °C); 4-Chloro-4′-pyrrolidinoazobenzene, 197—198 °C (197—198 °C); 2,2′,6′-Trimethyl-4-dimethylaminoazobenzene, oil. Found: C, 76.33; H, 8.43; N, 15.28%. Calcd for $C_{17}H_{21}N_3$: C, 76.37; H, 7.92; N, 15.72%; 2,6-Dimethyl-4′-dimethylaminoazobenzene, 103.5—104.5 °C. Found: C, 75.87; H, 8.07; N, 16.81%. Calcd for $C_{16}H_{19}N_3$: C, 75.85; H, 7.56; N, 16.59%; 2,6-Dimethyl-4-dimethylaminoazobenzene, 91—92 °C. Found: C, 75.80; H, 8.03; N, 16.29%; 2,4′,6-Trimethyl-4-dimethylaminoazobenzene, 133—133.5 °C. Found: C, 76.24; H, 7.87; N, 15.99%. Calcd for $C_{17}H_{21}N_3$: C, 76.37; H, 7.92; N, 15.72%; 2,2′,6-Trimethyl-4-dimethylaminoazobenzene, 87.5—88 °C. Found: C, 76.24; H, 7.90; N, 15.59%; 4-Nitro-4′-dimethylaminoazobenzene, 228 °C (229—230 °C); 4-Nitro-4′-diethylaminoazobenzene, 151 °C (151 °C); 4-Nitro-3′-methyl-4′-dimethylaminoazobenzene, 121—122 °C (121—122 °C);4-Nitroazobenzene, 135—135.2 °C (135 °C); 2′-Methyl-4-nitroazobenzene, 81.5—82 °C. Found: C, 64.73; H, 4.58; N, 17.27%. Calcd for $C_{13}H_{11}N_3O_2$: C, 64.72; H, 4.60; N, 17.42%; 2-Methyl-4-nitroazobenzene, 98.5—99 °C (98—99 °C); 2,2′-Dimethyl-4-nitroazobenzene, 81.5—82 °C. Found: C, 66.26; H, 5.07; N, 16.20%. Calcd for $C_{14}H_{13}N_3O_2$: C, 65.87; H, 5.13; N, 16.46%.

Solvents. Benzene, toluene and acetone were purified, dried and distilled in the usual way. Cyclohexane was washed with a mixture of concentrated nitric acid and sulfuric acid. After repeated washing with distilled water, it was distilled over sodium wire. *N,N*-Dimethylformamide, dimethyl sulfoxide and pyridine of the reagent grade were used without further purification.

Measurements. An appropriate amount of the sample was dissolved in a solvent containing 0.2% piperidine* and allowed to stand overnight in the dark. The solution was transferred to a cylindrical cell (3 cm diam, 10 cm length) fitted with a glass window (3 mm thickness) at each end and equipped with a water jacket. Thermostated water was circulated. The solution was irradiated with a high pressure mercury lamp (Toshiba 400P) for 2 min. After irradiation, the absorbance at the peak of the conjugation band of *trans*-isomers was measured at appropriate time intervals with a Hitachi spectrophotometer Model 139. The rate constants were checked by duplicate runs, accuracy being within ±1%.

For rapid isomerization, flash technique was applied. A glass sample cell (1.5 cm diam, 10 cm length) was put into a flash box and a xenon flash lamp was fired at 100J (2 μF, 10 KV). After the flash, steady monitoring light beam from a tungsten projective lamp was passed through the cell perpendicular to the direction of the flash. After being passed through a Shimadzu prism monochromator, the transmitted light was received by a photomultiplier (Hamamatsu R 106) and transient signals were recorded on a dry-plate with the aid of an Iwasaki oscilloscope and a polaroid camera.

* Influence of adventitious catalytic action: When a solution of *trans*-isomers was irradiated by UV light in a quartz cell the solution was irreversibly photo-bleached. The rate of thermal isomerization was found to depend strongly on the time of irradiation. The factors affecting the rate have been studied by some authors.[14-16] When a small quantity of piperidine was added to the azobenzene solution and all light of $\lambda<310$ nm was cut by a glass filter, most azobenzenes restored the color almost completely after being kept in the dark. Reproducible data were obtained under the above conditions. However, some abnormal behavior was observed for azobenzene, 4-chloroazobenzene, 2,2′-dichloroazobenzene, and 2,2′-dibromoazobenzene. Since these substances did not reversibly return to the *trans*-form after visible light irradiation, they should have been partly decomposed. Therefore, the data for these substances were omitted.

Results

The thermal *cis*-to-*trans* isomerization of various kinds of azobenzene derivatives was carried out at various temperatures. The rate constants, estimated from excellent first-order plots, are listed in Tables 1—3 together with the activation parameters. Some of the rate constants (Tables 1 and 2) can be compared with those in literature (Table 4). The values of Schulte-Frohlinde[16] and Le Fèbre and Northcott[18] were estimated by interpolating the Arrhenius plot. It is to be noted that Schulte-Frohlinde, and Talaty and Fargo[17] used pure *cis*-isomers, while others used *trans*-isomers as the starting materials. In spite of the fact that the data were obtained under different conditions, the agreement is fair except for 4,4′-dinitro- and 4-nitroazobenzenes.

Table 2. Thermal isomerization rate constants for *para*-donor/*para*′-acceptor-substituted azobenzenes at 25 °C in various solvents

Solvent	k, min^{-1}		
	37[a]	38[b]	39[c]
Cyclohexane	2.4	3.6	1.8
Benzene	2.4	3.0	1.8
Pyridine	180	420	12
Acetone	150	240	8.4
DMF	3000	5100	120
DMSO	7200	11400	600

a) 4-Nitro-4′-dimethylaminoazobenzene, $\varepsilon_{max}=33500$, $\lambda_{max}=445$ nm. b) 4-Nitro-4′-diethylaminoazobenzene, $\varepsilon_{max}=37200$, $\lambda_{max}=458$ nm. c) 4-Nitro-3′-methyl-4′-dimethylaminoazobenzene, $\varepsilon_{max}=22700$, $\lambda_{max}=410$ nm.

Discussion

Linear Free Energy Relationship. A general linear enthalpy-entropy relationship has been discussed in relation to the simple interaction mechanism.[19-25] ΔS^* tends to increase with increase in E_a, although there exists a considerable scatter (Fig. 1). Leffler[23] has shown that such a case is a result of more than two interactions whose vectors move independently on the E_a *vs.* ΔS^* plane. It is difficult to interpret the scatter, but a tentative explanation is as follows: The rate is mainly governed by the electronic effect of substituents, small perturbations due to solvation and steric effects being involved. The Arrhenius parameters fall in a reasonable range as compared with those reported.[16,18,22]

According to Schulte-Frohlinde,[16] the observation of preexponential factors as large as 10^{11-12} precludes the intervention of a triplet exited state involving a rupture of the N=N π-bond. The barrier to rotation around the N=N double bond was calculated to be 55—84 kcal/mol,[26-28] whereas the activation energy for the *cis*-to-

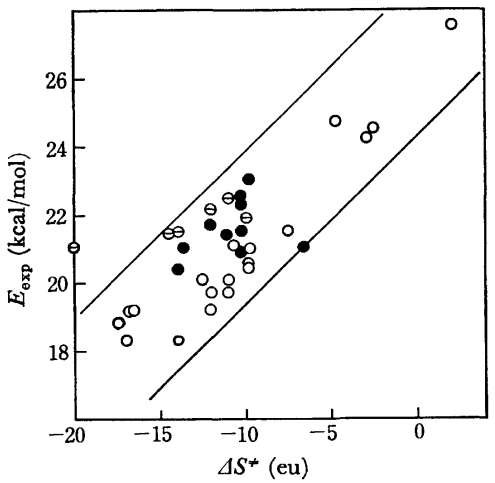

Fig. 1. Activation energy *vs.* entropy for the thermal *cis*-to-*trans* isomerization of azobenzenes.
○: This work; ●: Schulte-Frohlinde;[16] ◐: Brown and Granneman.[22]

trans thermal isomerization of azobenzene *via* inversion was calculated to be 32.9 kcal/mol by Ljunggren and Wettermark[28] by means of the CNDO/2 method, and improved to be 23.0 kcal/mol by Brown and Grannemann.[22]

On the other hand, Bineboym *et al.*[29] and Talaty and Fargo[17] suggested from the value of experimental activation energy that E_a of *ca.* 20 kcal/mol is too low to be compatible with the singlet transition state, because the corresponding isomerization of stilbenes considered to involve the rotation mechanism is followed by E_a of 34—37 kcal/mol in the liquid phase. They suggested therefore a transition state in which one or both azo-nitrogen atoms undergo a change in hybridization from sp^2- to sp-state. Thus it is likely that the lower activation energies support the inversion mechanism (Table 1).

However, recent evidence[30–32] has shown that there are some olefins and guanidinium salts which have activation energies of *ca.* 20 kcal/mol or even less, where only torsion is allowed. This has caused again much discussion on the mechanism of the *cis*-to-*trans* thermal isomerization of azomethines.[2–9] It was pointed out[4,7] that the lower activation energies cannot necessarily be regarded as a criteria of the inversion mechanism.

Solvent Effects. Although there are trials to relate the kinetic data to the properties of solvents such as dipole moment and dielectric constant, solvent effects in this field are generally ambiguous, and the rate varies only by a factor of a few times for most azobenzenes from solvent to solvent.[17,18] Wildes *et al.*,[9] however, observed a large solvent effect on the rate and activation energy for the thermal isomerization of *para*-donor/*para'*-acceptor-substituted azobenzenes. The isomerization rate of 4-diethylamino-4'-nitroazobenzene is about 10^5 times faster in *N*-methylformamide than in hexane. This seemed to contradict the former observation that the rate is not much affected by solvent.

Table 3. Activation parameters for the isomerization of **37** in various solvents

Solvent	E_a (kcal/mol)	ΔS^*(300K) (gibbs/mol)
Benzene	14	−14
Acetone	11	−20
DMF	10	−21
DMSO	9	−24

For the sake of confirmation, we followed the rate by means of the flash photolysis method, the results being given in Table 2. For 4-nitro-4'-dimethylaminoazobenzene, the activation parameters in various solvents are given in Table 3. The results are virtually in line with those of Wildes *et al.*[9] They suggested the rotation mechanism since the double bond character of the N=N bond and consequently the barrier to rotation would decrease with substituent.

Our view is as follows: Using a simple structure model, one can show that azobenzenes in no way take a coplanar

Table 4. Comparison of rate constants at 35°C

Azobenzene	$10^2 k$, min^{-1}				
	S-F[a]	T-F[b]	F-N[c]	W-P-I-W[d]	This work[e]
4-Dimethylamino-	0.98				0.670
4-Methoxy-	0.138	0.103	0.166		0.194
4,4'-Dimethoxy-	0.339				0.314
4-Chloro-	0.078	0.0556	0.067		
4-Nitro-	0.912	0.933	0.00021		0.74
Unsubstituted		0.0358	0.0416		
3-Nitro-	0.0371	0.0316			
4,4'-Dichloro-	0.324				0.161
4-Methyl-		0.0559	0.126		
4,4'-Dinitro-	0.252				2.40[f]
4,4'-Dimethyl-	0.098				0.173
4-Nitro-4'-dimethylamino-				120	240 (25 °C)
4-Nitro-4'-diethylamino-				180	360 (25 °C)

a) Shulte-Frohlinde;[16] in benzene; *k* at 35°C calcd by the Arrhenius equation. b) Talaty and Fargo;[17] in benzene. c) Le Fèvre and Northcott;[18] in benzene; *k* at 35°C calcd by the Arrhenius equation. d) Wildes, Pacifici, Irick and Whitten;[9] in benzene; temperature not specified. e) In cyclohexane containing 0.2% piperidine. f) In benzene containing 0.2% piperidine.

structure during rotation. On the other hand, if the inversion mechanism is accepted, a coplanar configuration is possible in the transition state (see **B–F** below). The dipole moment of this configurational structure may be as large as that for the *trans*-isomers (for example $\mu=$ 7.63D for **37**[10]). A considerable lowering in the free energy of activation and hence the increase in the rate for these species can be attributed to the large interaction with polar solvents. From a large decrease in the molar extinction coefficient (Table 2), the introduction of a methyl group in the *ortho* position with respect to the dimethylamino group would cause a considerable decrease in the dipole moment. This might be responsible for a much smaller solvent effect for **39** as compared with that for **37**. It should be noted that similarly substituted stilbenes, for which inversion is impossible, do not undergo facile thermal and photochemical isomerization in polar solvents.[33]

Table 5. Estimated substituent constants according to equation (1)

Substituent	σ_{c-t} [a]			
	This work	Talaty	S-F	Le Fèvre
2-CH_3	0.46*			
2'-CH_3	−0.01*			
4 (or 4')-Cl	0.33*	0.20	0.34	0.28
4 (or 4')-CH_3	0.19*	0.20		0.45
3 (or 3')-NO_2	0.11*	−0.05	0.02	
4-$N(CH_3)_2$	1.27		1.44	
4-$N(C_2H_5)_2$	1.44			
4-OCH_3	0.73	0.46		0.67
4-Pyrrolidino	1.38			
4-NH_2	1.37			
4-I			0.21	
4-NO_2		1.42	1.41	
4-$COCH_3$		0.52		
4-C_2H_5		0.19		
4-$CH(CH_3)_2$		0.35		
4-$C(CH_3)_3$		0.25		

*) DAAB is chosen as standard and σ-values are estimated from the possible combinations of the *k*-values of **1**—**14**. For σ-values with no asterisk, Talaty's *k*-value for azobenzene is chosen as a standard. a) *k*-values at 35 °C are used.

Substituent Effects. *para*-Substitutions invariably accelerate the isomerization rate, regardless of the nature of the substituents (Tables 1 and 2). This was first pointed out by Talaty and Fargo.[17] It was pointed out that this acceleration is of the additive nature and Eq. 1 is approximately valid for 4-dimethylaminoazobenzene derivatives.[1] From the data in Tables 1 and 2, the substituent constant, σ_{c-t} for various kinds of substituents has been estimated (Table 5). The first five σ_{c-t} values with an asterisk are obtained from the data of **1**—**14** in Table 1. Using these values, log k/k_0 are again plotted against σ_{c-t} according to Eq. 1 (Fig. 2). The correlation coefficient is calculated to be 0.987.

Using σ_{c-t}-values listed in the second column in Table 5, the same plots were made for substances **17**—**31** and **37**—**38** (Fig. 3) Although the correlation

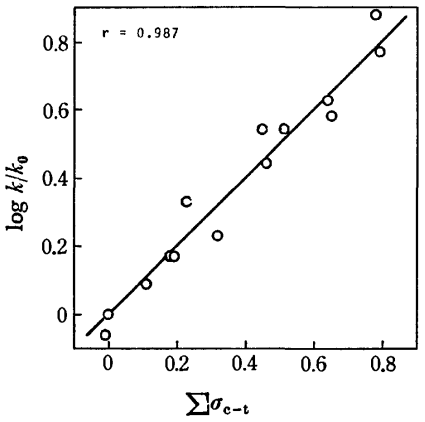

Fig. 2. Log k/k_0 *vs.* $\sum\sigma_{c-t}$ according to Eq. 1.

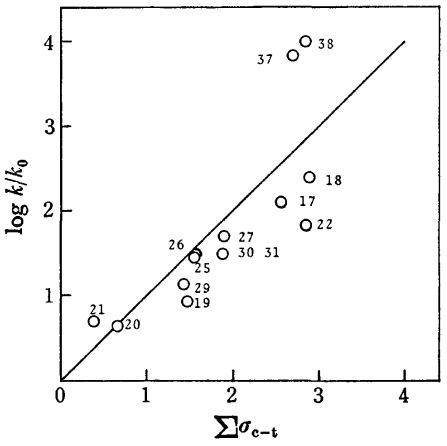

Fig. 3. Log k/k_0 against $\sum\sigma_{c-t}$ plot according to Eq. 1. Key is shown in Tables 1 and 2.

in this case is not so good as in Fig. 2, some interesting features may be noted. For 4-amino and 4-pyrrolidino derivatives, the deviation from the theoretical line is comparatively small. This means that the nature of these groups is virtually the same as that of dimethylamino group. For symmetrically substituted azobenzenes, the rate is usually not so accelerated as expected by the additivity rule. For *para*-donor/*para'*-acceptor-substituted azobenzenes, the rate is much more

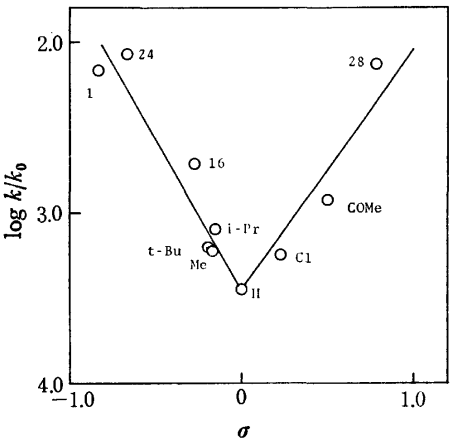

Fig. 4. The Hammett relationship. Key is shown in Table 1.

accelerated than expected from the rule. Hence the additivity rule, though it is useful to presume the effect of substituent on the rate of isomerization, has limited applicability.

In this connection, it may be worthwhile examining the Hammett relationship. The rate constants expressed in logarithmic scale, were plotted against σ for 4-monosubstituted azobenzenes. The plots are V-shaped with the minimum near σ equal to zero (Fig. 4).

Similar examples were reported recently by Hall *et al.*[6] and Herkstroeter[7] who found that the plots are all V-shaped for the isomerization of *N*-hexafluoroisopropylideneanilines, benzoylacetanilides, and pyrazolone azomethines. They explained the results in terms of the resonance stabilization in the transition state: If Z and Z′ in **A** are electron-accepting group, the rotation mechanism is

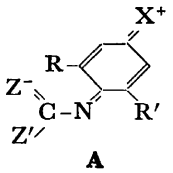

A

facilitated as the electron-donating strength of X increases as depicted, whereas growing electron-accepting capacity of X facilitates the isomerization by inversion, thus accounting for the V-plots. It is noted, however, that such a single bond character should substantiate only in the transition state through coplanar resonance structures. Such a coplanar structure is impossible through pure rotation. It does not seem plausible to assume such a drastic change in mechanism in going from electron-donating groups to electron-accepting groups. Further, the introduction of bulky substituent(s) to *ortho* position(s) with respect to azomethine nitrogen invariably accelerates the rate.[2,7,34-36] This cannot reasonably be explained in terms of the rotation mechanism, because the steric hindrance of R and R′ in **A** should destabilize the transition state a great deal. For the inversion mechanism, on the contrary, the steric effect may be less severe in the transition state than in the ground state for azomethines as has been explained successfully by Kessler *et al.* and others.[34-36]

The facilitated rate by *para*-substituents in azobenzenes, irrespective of their nature, may be explained in terms of a similar mesomeric effect, as depicted by resonance structures in the transition state **B**–**F**. If σ_{c-t} (or absolute Hammett σ) is regarded as a crude measure of the contribution of the resonance stabilization in the transition state, the deviation from the additivity rule may indicate that the contribution of the above resonance structures is not always additive (Fig. 3). As an example, an extra stabilization effect may arise from the resonance contribution depicted by $\mathbf{F}_3$, thus accounting for the upward deviation.

Steric Effects and Inversion Center. Complication arises for asymmetrical azobenzenes in which there are two distinct centers capable of inversion. In this case the empirical rate constant can be given by

$$k = k_1 + k_2 = A_1 e^{-E_1/RT} + A_2 e^{-E_2/RT} \qquad (2)$$

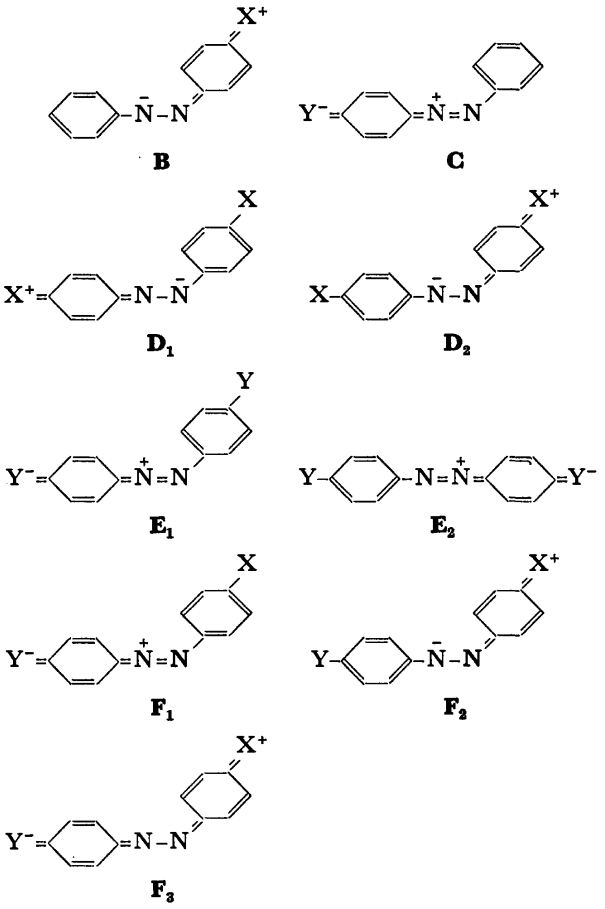

B **C** $\mathbf{D}_1$ $\mathbf{D}_2$ $\mathbf{E}_1$ $\mathbf{E}_2$ $\mathbf{F}_1$ $\mathbf{F}_2$ $\mathbf{F}_3$

where the suffixes 1 and 2 denote the two rate processes.[22] The rate constants in Tables 1, 2 and 4 correspond to k in Eq. 2.

It is of interest to distinguish the two centers. According to Brown and Granneman,[22] the difference in the activation energies for the two distinct inversion routes is calculated to be 1—2 kcal/mol by the CNDO/2 method. They predicted that the amount of curvature in the Arrhenius plots would be quite small. In the present study, the Arrhenius plots failed to distinguish the two routes. The CNDO/2 calculations predict that the isomerization is aided by the electron-withdrawal by the ring adjacent to the rehybridizing nitrogen. We also have a similar idea summarized as follows: Due to the steric hindrance the ground *cis*-state may have a folded conformation as depicted by **G**.

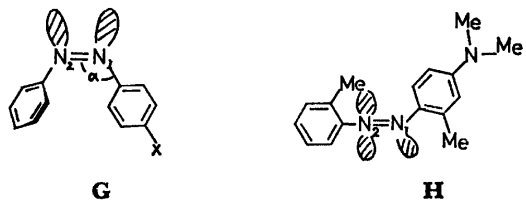

G **H**

If X is an electron-accepting group, the repulsive force among paired electrons on N_1 atom will be lowered, resulting in the increase in the s-character in the C–N_1 bond and the increase in the bond angle α. This should cause the inversion on N_1 atom more easily than on N_2. With X, as an electron donor, the reverse effect is expected.

A large difference in the effect of 2- and 2'-methyl groups on the rate for 4-dimethylaminoazobenzenes seems to indicate that the main inversion center is N_2 as will be understood by the conformation **H**. If the above view is valid, it is expected that the 2'-methyl group should facilitate the rate, but not the 2-methyl in the case of 4-nitroazobenzenes. As seen in Table 1 (**28**—**31**), the 2-methyl group accelerates the rate, but the 2'-methyl group retards it, contrary to expectation.

As an alternative, one may postulate that if X is a strong electron donor or electron acceptor, the approximately planar X- -N_1=N_2- moiety can take a "stiff" conformation through conjugation in the ground *cis*-isomer. If this is the case, the inversion center should be N_2. The distinctly different *ortho* effects between 2- and 2'-methyl groups on the isomerization rate could be interpreted tentatively by this assumption.

A study was made using 2,6- and 2',6'-dimethylated 4-dimethylaminoazobenzene derivatives. The steric effects may become so severe for these substances that at least one of the benzene rings may be considerably twisted with respect to the C–N=N–C plane in the transition state as in the ground *trans*-isomer,* and this may be responsible for the considerable decrease in rate. The most favorable conformation will be determined by the compromise between the energy stabilization through conjugation and the steric hindrance. Thus, although it is by no means decisive, favorable conformations in the transition state of 2,6- and 2',6'-dimethyl-4-dimethylaminoazobenzenes will be given by **I** and **J**, respectively.

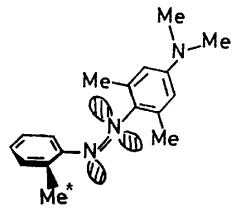

I

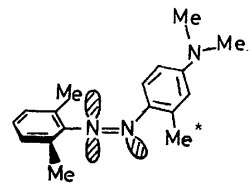

J

These conformations may be responsible for the acceleration effect due to the methyl group with an asterisk.

* A considerable decrease in the molar extinction coefficient of the conjugation band for **32**—**36** may be ascribed to the twist. For detail *cf.* Ref. 10.

References

1) T. Sueyoshi, N. Nishimura, S. Yamamoto, and S. Hasegawa, *Chem. Lett.*, **1974**, 1131.
2) H. Kessler and D. Leibfritz, *Tetrahedron*, **25**, 5127 (1969).
3) N. P. Marullo and E. H. Wagener, *Tetrahedron Lett.*, **1969**, 2555.
4) N. P. Marullo and E. H. Wagener, *J. Am. Chem. Soc.*, **88**, 5034 (1966).
5) D. Leibfritz and H. Kessler, *Chem. Commun., D*, **1970**, 655.
6) G. E. Hall, W. J. Middleton, and J. D. Roberts, *J. Am. Chem. Soc.*, **93**, 4778 (1971).
7) W. G. Herkstroeter, *J. Am. Chem. Soc.*, **95**, 8686 (1973).
8) J. M. Lehn, *Fortschr. Chem. Forsch.*, **15**, 311 (1970).
9) P. D. Wildes, J. G. Pacifici, Gether Irik, Jr, and D. G. Whitten, *J. Am. Chem. Soc.*, **93**, 2004 (1971).
10) S. Yamamoto, N. Nishimura, and S. Hasegawa, *Bull. Chem. Soc. Jpn.* **44**, 2018 (1971); *ibid.*, **46**, 194 (1973).
11) S. Yamamoto, *Bull. Chem. Soc. Jpn.*, **46**, 3139 (1973).
12) O. Diels and K. Alder, *Chem. Ber.* **60**, 716 (1927).
13) A. J. Ryan, *Tetrahedron*, **20**, 1547 (1964).
14) T. Kameo, T. Hirashima, O. Manabe, and H.Hiyama, *Kogyo Kagaku Zasshi*, **72**, 1327 (1969).
15) G. Wettermark, M. E. Langmuir, and D. G. Anderson, *J. Am. Chem. Soc.*, **87**, 476 (1965).
16) D. Schulte-Frohlinde, *Justus Liebigs Ann. Chem.*, **612**, 138 (1958).
17) E. R. Talaty and J. C. Fargo, *Chem. Commun.*, **1967**, 65.
18) R. J. W. Le Fèvre and J. Northcott, *J. Chem. Soc.*, **1953**, 867.
19) J. E. Leffler and E. Grunwald, "Rates and Equilibria of Organic Reactions," John Wiley and Sons, Inc., New York (1963).
20) J. E. Lefler, *J. Org. Chem.*, **20**, 1202 (1955).
21) S. Hasegawa, N. Nishimura, and K. Miura, *Bull. Chem. Soc. Jpn.*, **33**, 1323 (1960).
22) E. V. Brown and G. R. Granneman, *J. Am. Chem. Soc.* **97**, 621 (1975).
23) J. E. Leffler, *J. Org. Chem.*, **31**, 533 (1966).
24) R. C. Peterson, J. H. Markgraf, and S. D. Ross, *J. Am. Chem. Soc.*, **83**, 3819 (1961).
25) R. C. Peterson, *J. Org. Chem.*, **29**, 3133 (1964).
26) G. T. Armstrong and S. Marantz, *J. Chem. Phys.*, **38**, 169 (1962).
27) D. R. Kearns, *J. Phys. Chem.*, **19**, 1062 (1965).
28) S. Ljunggren and G. Wettermark, *Acta. Chem. Scand.*, **25**, 1599 (1971).
29) J. Binenboym, A. Burcat, A. Lifshitz, and S. Shamir, *J. Am. Chem. Soc.*, **88**, 5039 (1966).
30) A. S. Kende, P. T. Izzo, and W. Fulmer, *Tetrahedron Lett.*, **1966**, 3697.
31) G. Isakson, J. Sandstrom, and J. Wennerbeck, *Tetrahedron Lett.*, **1967**, 2233.
32) Y. Shvo, E. C. Taylor, and J. Batulin, *Tetrahedron Lett.*, **1967**, 3259.
33) D. Schule-Frohlinde, H. Blume, and H. Guster, *J. Phys. Chem.*, **66**, 2486 (1962).
34) H. Kessler, P. F. Bley, and D. Leibfritz, *Tetrahedron*, **27** 1687 (1971).
35) H. Kessler, *Angew, Chem.*, **82**, 237 (1970).
36) D. Wurmb-Gerlich, F. Vogtle, A. Mannschreck, and H. A. Staab, *Liebigs Ann. Chem.*, **708**, 36 (1967).

Synthesis of Pseudo-β-DL-galactopyranose and Pseudo-α-DL-altropyranose

Tetsuo SUAMI,* Seiichiro OGAWA, Takashi ISHIBASHI, and Isamu KASAHARA

Department of Applied Chemistry, Faculty of Engineering, Keio University, Hiyoshi, Yokohama 223

(Received December 20, 1975)

Pseudo-β-DL-galactopyranose and pseudo-α-DL-altropyranose pentaacetates (**10** and **11**) were obtained in a seven step reaction starting from DL-1,2-*O*-cyclohexylidene-5-deoxy-*chiro*-inositol (**2**).

The term "pseudo-sugar" was first given by McCasland and his coworkers[1] to a monosaccharide analog in which a ring oxygen is replaced by a methylene group. In connection with studies on aminocyclitols[2] and inositol derivatives,[3] we have attempted to synthesize validamine (**1**) which is a component of antibiotic validamycin.[4] Validamine has the structure (1*S*)-(1,2,4/3,5)-1-amino-5-hydroxymethyl-2,3,4-cyclohexanetriol[4] which is designated as pseudo-α-D-glucopyranosylamine.[5] It seems that a pseudo-hexopyranose with a proper configuration is the most promising intermediate for a synthesis of **1**.

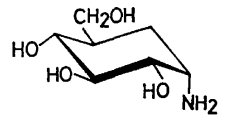

1

In the present study, DL-1,2-*O*-cyclohexylidene-5-deoxy-*chiro*-inositol (**2**) prepared from *myo*-inositol in four steps[6] was used as the starting material. Compound **2** was treated with 2,2-dimethoxypropane in the presence of a catalytic amount of *p*-toluenesulfonic acid to give DL-1,2-*O*-cyclohexylidene-5-deoxy-3,4-*O*-isopropylidene-*chiro*-inositol (**3**). Oxidation of **3** in dimethyl sulfoxide–acetic anhydride afforded DL-5,6-*O*-cyclohexylidene-2-deoxy-3,4-*O*-isopropylidene-*chiro*-inosose-1 (**4**) in 74% yield. Compound **4** was treated with diazomethane to give DL-1,1′-anhydro-5,6-*O*-cyclohexylidene-2-deoxy-1-*C*-hydroxymethyl-3,4-*O*-isopropylidene-*chiro*-inositol (**5**) and DL-1,1′-anhydro-2,3-*O*-cyclohexylidene-6-deoxy-1-*C*-hydroxymethyl-4,5-*O*-isopropylidene-*myo*-inositol (**6**) in 82 and 9% yields, respectively.

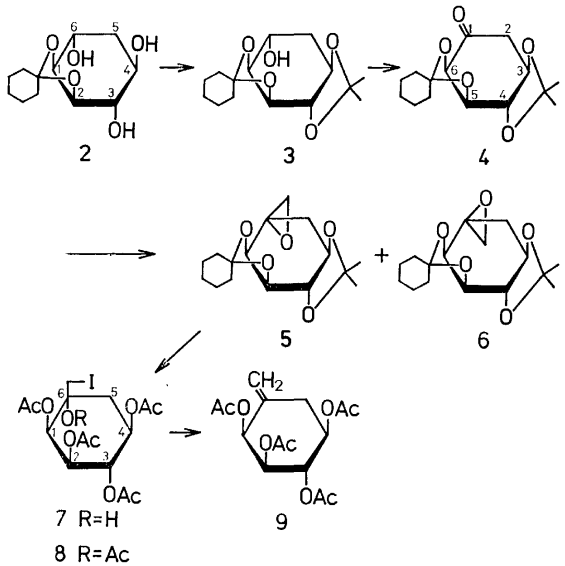

Compound **5** reacted with hydriodic acid under reaction conditions analogous to those employed by Angyal and his coworkers[7] for the preparation of methylenecyclohexanepentols, to give DL-1,2,3,4,6-penta-*O*-acetyl-5-deoxy-6-*C*-iodomethyl-*chiro*-inositol (**8**). Compound **8** was converted into DL-1,2,3,4-tetra-*O*-acetyl-5,6-dideoxy-6-methylene-*chiro*-inositol (**9**) by refluxing in glacial acetic acid in the presence of zinc powder.

Hydroboration[8] of **9**, followed by oxidation with alkaline hydrogen peroxide and subsequent acetylation afforded pseudo-β-DL-galactopyranose pentaacetate (**10**), pseudo-α-DL-altropyranose pentaacetate (**11**) and DL-1,2,3,4-tetra-*O*-acetyl-(1,3,4/2,5)-5-methyl-1,2,3,4-cyclohexanetetrol (**12**) in 13, 17 and 13% yields, respectively. Besides these compounds, DL-1,2,3,4,5-penta-*O*-acetyl-(1,3,4/2,5)-5-*C*-methyl-1,2,3,4,5-cyclohexanepentol (**13**) was obtained in 6.5% yield, which was identified with an authentic sample prepared by another route (**5**→**14**→**13**). This compound was an epimer of **16** prepared from **6** by an analogous reaction route (**6**→**15**→**16**).

In the above reaction from **9** to **10** and **11**, only two types of pseudo-hexopyranose pentaacetates, *viz.* β-DL-galacto and α-DL-altro type compound, can be obtained. Their PMR spectra were measured to distinguish the two compounds.

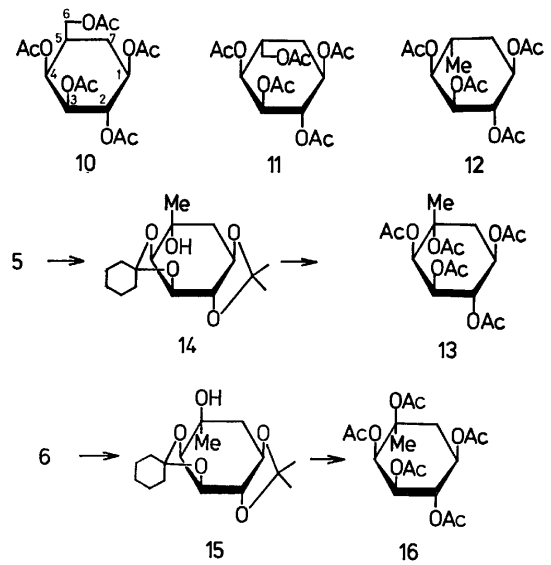

* To whom correspondence should be addressed.

The PMR spectrum of **10** revealed a singlet at δ 2.14 for an axial acetoxy group and three singlets at δ 2.05 (6H), 2.03 (3H) and 1.99 (3H) for three equatorial acetoxy groups[9] and one side chain acetoxy group.

The side chain methylene protons revealed an eight line signal pattern, each proton showing a pair of doublets at δ 4.03 and 3.86 with a geminal coupling of 11 Hz and vicinal couplings of 6 and 8.5 Hz. The ring methylene protons showed multiplets between δ 1.54—2.27 overlapped with a multiplet of the methine proton (H-5).

The ring proton (H-4) revealed its signal at δ 5.50 as a triplet with $J_{3,4}=J_{4,5}=3$ Hz. This was demonstrated on irradiating the H-5 proton (δ 2.3), the triplet collapsing to a doublet ($J_{3,4}=3$ Hz). The small coupling constant indicated the nonexistence of an axial-axial arrangement between H-4 and H-5. The proton H-3 revealed a pair of doublets at δ 4.90 with $J_{3,4}=3$ Hz and $J_{2,3}=10$ Hz, indicating the existence of two vicinal axial protons: H-2 and H-3. The proton H-2 showed a triplet at δ 5.40 with $J_{1,2}=J_{2,3}=10$ Hz. The proton H-1 showed an eight signal pattern centered at δ 4.94 with $J_{1,2}=10$ Hz, $J_{1,7a}=11.5$ Hz and $J_{1,7e}=5$ Hz. The PMR spectral assignment was consistent with the β-DL-galactopyranose pentaacetate, a side-chain equatorial favoring conformation. These spectral assignments are consistent with those of pseudo-α-DL-galactopyranose pentaacetate[1] except for the axial acetoxy group on C-1 in the case of the α-epimer.

The PMR spectrum of **11** revealed five sharp signals for the five acetoxy groups at δ 2.05, 2.06, 2.08, 2.10 and 2.12. These signals could not be attributed to an axial or an equatorial acetoxy methyl proton, owing to a deviation from their typical values.[9] This indicates that there is a rapid ring inversion between two chair conformations. This has also been deduced from the fact that methyl α-altropyranoside exists in two chair conformations: Cl and 1C.[10]

The PMR spectrum of **12** showed a similar signal pattern for the acetoxy methyl protons, suggesting an analogous ring inversion as was observed in the case of **11**. Thus the above described structure was proposed for **12**.

Experimental*

Melting points were determined in a capillary tube in a liquid bath and are uncorrected. PMR spectra were obtained on Varian A-60D (60 MHz) and Varian XL-100 (100 MHz) spectrometers in deuteriochloroform with reference to tetramethylsilane as an internal standard, peak positions being given in δ-values. Values given for coupling constants are of first order. Solutions were evaporated under diminished pressure at 40—50 °C. TLC was performed on silica gel plates (Wakogel B-10, Wako Pure Chemical Industries Ltd.).

DL-*1,2-O-Cyclohexylidene-5-deoxy-3,4-O-isopropylidene*-chiro-*inositol (3).* DL-1,2-*O*-Cyclohexylidene-5-deoxy-*chiro*-inositol[6] (**2**, 3.70 g) was treated with 2,2-dimethoxypropane (37 ml) in *N,N*-dimethylformamide (80 ml) at 85—95 °C for 40 min in the presence of *p*-toluenesulfonic acid (0.1 g). Sodium hydrogencarbonate (0.21 g) was added to the solution and the mixture was evaporated. The residue was extracted with warm ethyl acetate and the solution was evaporated. The residue was recrystallized from hexane to give 3.25 g (76%) of **3**, mp 82—83 °C; PMR: δ 1.42 (s, 6, $2CH_3$), 1.48—1.75 (m, 10, C_6H_{10}), 1.87—2.18 (m, 2, CH_2), 2.60 (s, 1, OH). Found: C, 63.18; H, 8.49%. Calcd for $C_{13}H_{24}O_5$: C, 63.36; H, 8.51%.

DL-*5,6-O-Cyclohexylidene-2-deoxy-3,4-O-isopropylidene*-chiro-*inosose-1 (4).* To a solution of **3** (5.0 g) in dimethyl sulfoxide (100 ml) was added acetic anhydride (15 ml). The reaction mixture was stirred in a refrigerator for 24 h and poured into ice cold sodium hydrogencarbonate solution. The crystalline precipitates were collected and recrystallized from ethanol to give 3.67 g (74%) of **4**, mp 138—139.5 °C; PMR; δ 1.48 (s, 6, $2CH_3$), 1.54—1.80 (m, 10, C_6H_{10}), 2.45 (q, 1, $J_{2a,3}=10.5$ Hz, $J_{gem}=18.0$ Hz, H-2a), 2.99 (q, 1, $J_{2e,3}=7.0$ Hz, H-2e), 3.55 (q, 1, $J_{3,4}=10.5$ Hz, $J_{4,5}=6.5$ Hz, H-4), 4.13 (m, 1, H-3), 4.50 (d, 1, $J_{5,6}=8.0$ Hz, H-6), 4.65 (q, 1, H-5). Found: C, 63.78; H, 7.69%. Calcd for $C_{15}H_{22}O_5$: 63.81; H, 7.85%.

DL-*1,1'-Anhydro-5,6-O-cyclohexylidene-2-deoxy-1-C-hydroxymethyl-3,4-O-isopropylidene*-chiro-*inositol (5) and* DL-*1,1'-anhydro-2,3-O-cyclohexylidene-6-deoxy-1-C-hydroxymethyl-4,5-O-isopropylidene*-myo-*inositol (6).* To an ethereal solution of diazomethane prepared from 50.0 g of nitrosomethylurea was added a solution of **4** (5.0 g) in chloroform (50 ml) under ice-cooling. The reaction solution was settled in a refrigerator for 17 h and evaporated. The crystals were filtered and washed with ethanol to give 484 mg (9%) of **6**, mp 196—197 °C; PMR: δ 1.46 (s, 6, $2CH_3$), 1.52—1.75 (m, 10, C_6H_{10}), 1.70—2.14 (m, 2, H-6a and 6e), 2.40 and 3.12 (dd,2, $J_{gem}=6.5$ Hz, CH_2), 3.66 (m, 1, H-5), 4.08 (q, 1, $J_{3,4}=8.0$ Hz. $J_{4,5}=9.5$ Hz, H-4), 4.30 (d, 1, $J_{2,3}=6.5$ Hz, H-2), 4.41 (q, 1, H-3).

Found: C, 65.10; H, 8.38%. Calcd for $C_{16}H_{24}O_5$: C, 64.84; H, 8.16%.

The filtrate and the ethanol washing were combined and evaporated to give 4.29 g (82%) of crude **5** as a syrup. PMR: δ 1.45 (s, 6, $2CH_3$), 1.51—1.82 (m, 10, C_6H_{10}), 2.08—2.41 (m, 2, H-2a and 2e), 2.81 and 2.95 (dd, 2, $J_{gem}=4.5$ Hz, CH_2), 3.56 (q, 1, $J_{3,4}=9.5$ Hz, $J_{4,5}=8.0$ Hz, H-4), 3.63 (d, 1, $J_{5,6}=6.0$ Hz, H-6), 3.74 (m, 1, H-3), 4.35 (1, 1, H-5).

DL-*1,2,3,4,6-Tetra-O-acetyl-5-deoxy-6-C-iodomethyl*-chiro-*inositol (7).* A 3.5-g portion of crude **5** was added to a saturated solution (25 ml) of sodium iodide containing 2.5 ml of concentrated hydriodic acid, and the mixture was agitated for 48 h. An insoluble matter was removed by filtration, and the filtrate was evaporated to dryness. The residue was acetylated in acetic anhydride (50 ml) with one drop of concentrated sulfric acid for 5 h. The solution was poured into ice-cold water (500 ml) to give 2.62 g (47%) of **7**, mp 209—211 °C; PMR: δ 1.98 (s, 3, OAc), 2.03 (s, 6, 2OAc), 2.15 (s, 3, OAc). Found: C, 38.46; H, 4.32; I, 26.84%. Calcd for $C_{15}H_{21}O_9I$: C, 38.15; H, 4.48; I, 26.87%.

The mother liquor was extracted repeatedly with chloroform and the chloroform solution was evaporated to give a mixture of **7** and **8** (1.96 g).

DL-*1,2,3,4,6-Penta-O-acetyl-5-deoxy-6-C-iodomethyl*-chiro-*inositol (8).* Compound **7** (2.62 g) was acetylated in acetic anhydride with a drop of concentrated sulfuric acid at 40 °C for 1 h, and the mixture was poured into ice cold water (400 ml) to give 2.37 g (83%) of **8**, mp 94—95 °C; PMR: δ 1.98 (s, 3, OAc), 2.03 (s, 6, 2OAc), 2.17 (s, 3, OAc), 2.21 (s, 3, OAc), 2.24—3.12 (m, 2, H-5a and 5e), 3.61 and 3.92 (dd, 2, $J_{gem}=11.5$ Hz, CH_2). Found: C, 39.91; H, 4.69; I, 24.52%. Calcd for $C_{17}H_{23}O_{10}I$: C, 39.90; H, 4.51; I, 24.68%.

Compound **8** (1.30 g) was obtained from a mixture of **7** and **8** (1.96 g) by the same procedure.

* Elemental analyses were performed by Mr. Saburo Nakada to whom our thanks are due.

DL-*1, 2, 3, 4-Tetra-*O*-acetyl-5, 6-dideoxy-6-methylene*-chiro-*inositol (9)*. A 3.0-g portion of **8** was heated in glacial acetic acid (40 ml) with zinc powder (25 g) under reflux for 1 h. The mixture was filtered and the filtrate was evaporated to give 1.2 g of crude **9**. The insoluble matter obtained by filtration was extracted twice with warm ethyl acetate and the ethyl acetate solution was evaporated to give another crop of **9**. Recrystallization from ethanol–hexane gave 1.44 g (75%) of **9**, mp 93—94 °C; PMR: δ 1.99 (s, 3, OAc), 2.01 (s, 3, OAc), 2.02 (s, 3, OAc), 2.10 (s, 3, OAc), 2.43—2.70 (m, 2, H-5a and 5e), 4.82 (m, 1, $J_{3,4}$=10 Hz, $J_{4,5a}$=10.5 Hz, $J_{4,5e}$=7.0 Hz, H-4), 4.86 (q, 1, $J_{1,2}$=3.5 Hz, $J_{2,3}$=10 Hz, H-2), 5.19 and 5.29 (dd, 2, J_{gem}=1.0 Hz, CH_2), 5.35 (t, 1, H-3), 5.65 (d, 1, H-1). Found: C, 54.91; H, 6.14%. Calcd for $C_{15}H_{20}O_8$: C, 54.88; H, 6.14%.

*Pseudo-β-*DL*-galactopyranose Pentaacetate (10) and Pseudo-α-*DL*-altropyranose Pentaacetate (11)*. Sodium tetrahydroborate (0.24 g) was added to a solution of **9** (0.60 g) in tetrahydrofuran (15 ml). A solution of freshly distilled boron trifluoride etherate (2.4 ml) in tetrahydrofuran (4.8 ml) was slowly added to the mixture. After the mixture was agitated for 4 h at 25 °C, 50% aqueous tetrahydrofuran (5.0 ml) was added. Then 3M sodium hydroxide (6 ml) and 30% hydrogenperoxide (3.0 ml) were added to the mixture. The mixture was agitated for 1 h at 35 °C and evaporated to dryness. The residue was acetylated in acetic anhydride (20 ml) with a drop of concentrated sulfuric acid overnight and the reaction solution was poured into ice cold water. The aqueous solution was extracted repeatedly with chloroform and the combined chloroform solution was evaporated. The residue was fractionated on a silica gel (Wakogel C-300, 40 g) column in 2-butanone–toluene (1:7, v/v). Fractions which showed a single spot at R_f 0.50 on TLC in 2-butanone–toluene (1:4, v/v) were combined and evaporated to give 93 mg (13%) of **10**, mp 123—124 °C; PMR: δ 1.99 (s, 3, OAc), 2.03 (s, 3, OAc), 2.05 (s, 6, 2OAc), 2.14 (s, 3, OAc), 3.86 (q, 1, $J_{5,6}$=6.0 Hz, J_{gem}=11.0 Hz, H-6), 4.03 (q, 1, $J_{5,6'}$=8.5 Hz, J_{gem}=11.0 Hz, H-6'), 4.90 (q, 1, $J_{2,3}$=10.0 Hz, $J_{3,4}$=3.0 Hz, H-3), 4.94 (qd, 1, $J_{1,7a}$=11.5 Hz, $J_{1,7e}$=5.0 Hz, $J_{1,2}$=10.0 Hz, H-1), 5.40 (t, 1, H-2), 5.50 (t, 1, $J_{4,5}$=3.0 Hz, H-4). Found: C, 52.52; H, 6.24%. Calcd for $C_{17}H_{24}O_{10}$: C, 52.58; H, 6.23%.

Fractions showing a single spot at R_f 0.47 on TLC in the same solvent were combined and evaporated to give 119 mg (17%) of **11**, mp 115—116 °C; PMR: δ 2.05 (s, 3, OAc), 2.06 (s, 3, OAc), 2.08 (s, 3, OAc), 2.10 (s, 3, OAc), 2.12 (s, 3, OAc), 2.38 (m, 1, H-5), 4.16 (d, 2, $J_{5,6}$=6.0 Hz, H-6 and 6'). Found: C, 52.87; H, 6.29%. Calcd for $C_{17}H_{24}O_{10}$: C, 52.58; H, 6.23%.

DL-2,3,4,5-Tetra-*O*-acetyl-(2,3,5/1,4)-1-methyl-2,3,4,5-cyclohexanetetrol (**12**, 77 mg, 13%), mp 111—112 °C, was obtained from fractions showing a single spot at R_f 0.60 on TLC. PMR: δ 0.96 (d, 3, J=6.0 Hz, CH_3), 1.45 (m, 2, CH_2), 1.97 (s, 3, OAc), 1.99 (s, 3, OAc), 2.00 (s, 3, OAc), 2.02 (s, 3, OAc). Found: C, 54.37; H, 6.73%. Calcd for $C_{15}H_{22}O_8$: C, 54.54; H, 6.71%.

From fractions showing a single spot at R_f 0.55 on TLC, DL-1,2,3,4,5-penta-*O*-acetyl-2-deoxy-1-*C*-methyl-*chiro*-inositol (**13**) was obtained as a syrup (46 mg, 6.5%), which was identified with an authentic sample prepared by the following reactions.

DL-*5, 6-*O*-Cyclohexylidene-2-deoxy-3, 4-*O*-isopropylidene-1-*C*-methyl*-chiro-*inositol (14)*. To a solution of compound **5** (516 mg) in tetrahydrofuran (14 ml) was added lithium aluminum hydride (0.3 g). The mixture was heated under reflux for 1.5 h and then cold water (3 ml) was added to the iced reaction mixture. The mixture was filtered and the filtrate was evaporated. The residue was recrystallized from hexane to give 228 mg (44%) of **14**, mp 113—114 °C. PMR: δ 1.40 (s, 6, $2CH_3$), 1.44 (s, 3, CH_3 at C-1), 1.50—1.75 (m, 10, C_6H_{10}), 2.00 (s, 1, OH), 3.43 (q, 1, $J_{3,4}$=10.5 Hz, $J_{4,5}$=9.0 Hz, H-4), 3.81 (td, 1, $J_{2a,3}$=$J_{3,4}$=10.5 Hz, $J_{4,5}$=9.0 Hz, H-3), 3.90 (d, 1, $J_{5,6}$=5.0 Hz, H-6), 4.31 (q, 1, H-5). Found: C, 64.12; H, 8.56%. Calcd for $C_{16}H_{26}O_5$: C, 64.40; H, 8.78%.

DL-*1, 3, 4, 5, 6-Penta-*O*-acetyl-2-deoxy-1-*C*-methyl*-chiro-*inositol (13)*. Compound **14** (120 mg) was heated in 80% aqueous acetic acid (10 ml) under reflux for 19 h. The solution was evaporated and the residue was acetylated with acetic anhydride and pyridine at 80—90 °C for 20 h. The acetate was purified on a silica gel column in 2-butanone–toluene (1:8 v/v). Fractions showing a single spot at R_f 0.38 on TLC in 2-butanone–toluene (1:6, v/v) were combined and evaporated to give 87 mg (56%) of **13** as a colorless syrup. PMR: δ 1.50 (s, 3, CH_3 at C-1), 1.96 (s, 3, OAc), 2.00 (s, 6, 2OAc), 2.11 (s, 3, OAc), 2.15 (s, 3, OAc), 2.22—2.91 (m, 2, CH_2 at C-2), 4.79—5.56 (m, 4, ring protons). Found: C, 52.86; H, 6.27%. Calcd for $C_{17}H_{24}O_{10}$: C, 52.58; H, 6.23%.

DL-*2, 3-*O*-Cyclohexylidene-6-deoxy-4, 5-*O*-isopropylidene-1-*C*-methyl*-myo-*inositol (15)*. Compound **6** (600 mg) was treated with lithium aluminum hydride (0.37 g) in tetrahydrofuran (25 ml) as in the preparation of **14**, to give 567 mg (94%) of **15** as an amorphous solid, mp 86—88 °C. PMR: δ 1.30 (s, 3, CH_3 at C-1), 1.41 (s, 6, $2CH_3$), 1.51—1.80 (m, 10, C_6H_{10}). Found: C, 64.72; H, 8.67%. Calcd for $C_{16}H_{26}O_5$: C, 64.40; H, 8.78%.

DL-*1, 2, 3, 4, 5-Penta-*O*-acetyl-6-deoxy-1-*C*-methyl*-myo-*inositol (16)*. Compound **15** (560 mg) was heated in 80% aqueous acetic acid (20 ml) under reflux for 20 h. The solution was evaporated and the residue was acetylated. The acetate was purified on a silica gel column in 2-butanone–toluene (1:8, v/v). Fractions showing a single spot at R_f 0.32 on TLC in 2-butanone–toluene (1:6, v/v) were combined and evaporated to give 407 mg (56%) of **16** as a syrup. PMR: δ 1.69 (s, 3, CH_3 at C-1), 1.94 (s, 3, OAc), 1.99 (s, 6, 2OAc), 2.03 (s, 3, OAc), 2.15 (s, 3, OAc), 2.25—2.56 (m, 2, CH_2 at C-6), 4.76—5.55 (m, 4, ring protons). Found: C, 52.82; H, 6.35%. Calcd for $C_{17}H_{24}O_{10}$: C, 52.58; H, 6.23%.

References

1) G. E. McCasland, S. Furuta, and L. J. Durham, *J. Org. Chem.*, **31**, 1516 (1966); ditto, *ibid.*, **33**, 2835, 2841 (1968).
2) T. Suami, K. Tadano, and S. Horiuchi, *Bull. Chem. Soc. Jpn.*, **48**, 2895 (1975).
3) T. Suami, S. Ogawa, and Y. Funaki, *Bull. Chem. Soc. Jpn.*, **48**, 1545 (1975).
4) Y. Kameda, S. Horii, and T. Yamano, *J. Antibiot.*, **28**, 298 (1975) and references cited therein.
5) Of the racemic diastereomers the enantiomer has been depicted, and the assignment of positional number in a pseudohexopyranose is used as for **10** and **11** in connection with the positional number of a true hexopyranose.
6) T. Suami, S. Ogawa, T. Ueda, and H. Uchino, *Bull. Chem. Soc. Jpn.*, **45**, 3226 (1972).
7) S. J. Angyal, J. E. Klavins, and A. Mills, *Aust. J. Chem.*, **27**, 1075 (1974).
8) A. Rosenthal and M. Sprinzl, *Carbohyd. Res.*, **16**, 337 (1971).
9) F. W. Lichtenthaler, *Chem. Ber.*, **96**, 2047 (1963).
10) E. L. Eliel, N. L. Allinger, S. J. Angyal, and G. A. Morrison, "Conformational Analysis," John Wiley & Sons, Inc., New York (1965), p. 370.

1*H*-2,3-Benzoxazin-1-ones. II. Action of Amines, Phenylhydrazine, Aluminium Chloride, and Grignard Reagents on 4-Aryl-1*H*-2,3-benzoxazin-1-ones

A. F. M. FAHMY, and Mrs. Nawal F. ALY
Faculty of Sciences, Ain Shams University, Cairo, Egypt
(Received September 30, 1974)

4-Aryl-1*H*-2,3-benzoxazin-1-one on reaction with amines by fusion gave *o*-aroyl benzamides. With benzylamine in benzene they gave (2-benzylcarbamoyl)-benzophenone oximes, and with phenylhydrazine they gave 1,3-diaryl-1,2-dihydrophthalazin-4-ones. However, with anhydrous $AlCl_3$ (12 mol) in reactive hydrocarbon substrates, they gave the corresponding *o*-aroylbenzophenone anils. With Grignard reagents they gave the corresponding *o*-aroyl-triaryl-methanols, which upon cyclization gave 1,1,4-triaryl-1(*H*)-2,3-benzoxazines.

Reaction of 1H-2,3-Benzoxazin-1-ones with Amines. We have found a new reaction of 1*H*-2,3-benzoxazin-1-one with amines.

4-Aryl-1*H*-2,3-benzoxazin-1-ones (Ia and b) react with benzylamine, and aniline by fusion to give *N*-substituted *o*-aroyl benzamides (IIa—d).

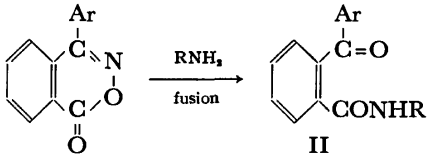

I II

	Ar	R
a: C_6H_5	a: C_6H_5	C_6H_5-CH_2
b: $C_6H_4CH_3$(-*p*)	b: $C_6H_4CH_3$(-*p*)	C_6H_5·CH_2
c: C_6H_4Cl(-*p*)	c: C_6H_5	C_6H_5
	d: $C_6H_4CH_3$(-*p*)	C_6H_5

It was found that IIIa—c were formed from the reaction of Ia—c with benzylamine in benzene.

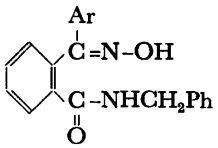

III

a: Ar=C_6H_5, b: Ar=$C_6H_4CH_3$(-*p*), c: C_6H_4Cl(-*p*).

Reaction of 1H-2,3-benzoxazin-1-ones with Phenylhydrazine. 4-Aryl-1*H*-2,3-benzoxazin-1-ones (Ia—c) react with phenylhydrazine to give the corresponding 1,3-diaryl-1,2-dihydrophthalazin-4-ones (IVa—c).

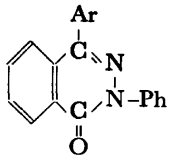

IV

a: Ar=C_6H_5, b: Ar=$C_6H_4CH_3$(-*p*),
c: Ar=C_6H_4Cl(-*p*)

The structure of IVa—c was confirmed:

(i) *Via* the reaction of the corresponding *o*-aroylbenzoic acids (Va—c) with phenylhydrazine.[2,3]

(ii) *From IR spectra*: IVa—c showed $\nu_{C=O}$ in the region 1700—1690 cm^{-1}.

The reaction possibly takes place according to the following mechanism (Scheme 1).

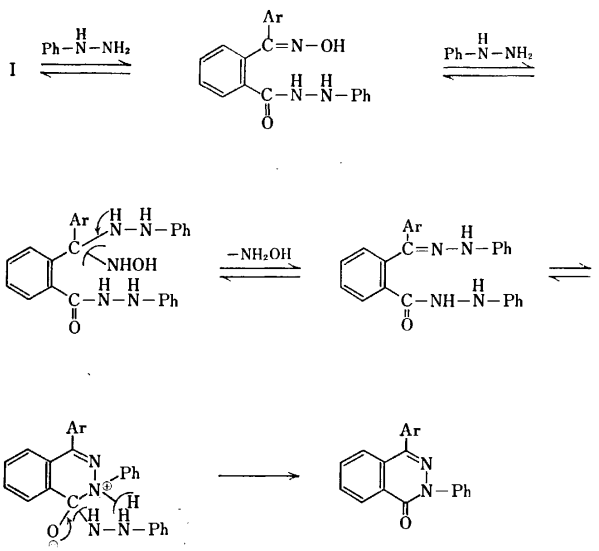

Scheme 1. The above mechanism was proved from the fact that benzophenone oxime reacts with hydrazines to give benzophenone hydrazones.[4]

Action of Anhydrous $AlCl_3$ in Reactive Aromatic Hydrocarbon Substrates. 4-Phenyl-1(*H*)-2,3-benzoxazin-1-one (Ia) reacts with hot benzene, toluene, and anisole in the presence of 12 mol anhydrous $AlCl_3$ to give 2-benzoyl-; 2-(*p*-toluoyl)-4'-methyl; and 2-(*p*-anisoyl)-4'-methoxybenzophenone anils (VIa—c), respectively. Under the same conditions 4-(*p*-tolyl)-, and 4-(*p*-chlorophenyl)-1*H*-2,3-benzoxazin-1-ones (Ib, and c) gave the corresponding 2-aroylbenzophenone *p*-methyl anils (VId—f) and 2-aroylbenzophenone *p*-chloro anils (VIg—i) respectively.

The structure of VIa—i was confirmed from IR spectra which revealed the presence of $\nu_{C=O}$ in the region 1720—1700 cm^{-1}. The reaction possibly takes place according to the following mechanism (Scheme 2).

Route A in the above scheme is the most probable one for the following reasons: (i) 3-Phenyliminophthalide (VII) is found to undergo Friedel-Crafts reaction with benzene to give *o*-benzoylbenzanilide (VIII)[5] (ii) formation of *N*-arylphthalimides, when chlorobenzene was used as a substrate,[1] indicates that the carbonium ion (IX) is formed as an intermediate.

o-Aroylbenzanilide (VIII) was found to be an intermediate in the above mechanism from the following:

(i) It was formed from reaction of I with benzene,

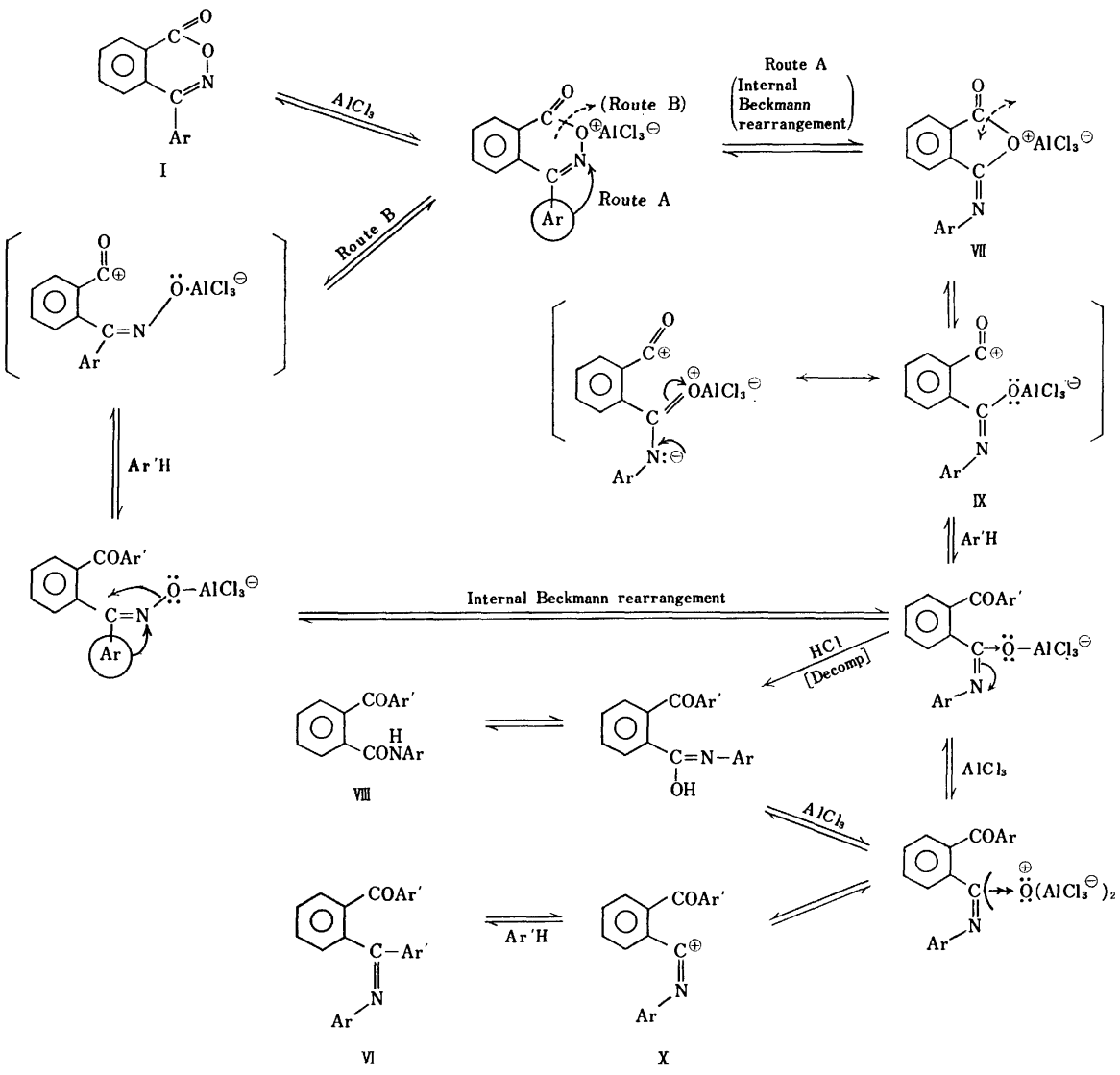

Scheme 2.

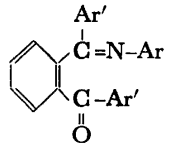

VI

Ar	Ar'
a: C_6H_5	C_6H_5
b: C_6H_5	$C_6H_4CH_3$(-*p*)
c: C_6H_5	$C_6H_4OCH_3$(-*p*)
d: $C_6H_4CH_3$(-*p*)	C_6H_5
e: $C_6H_4CH_3$(-*p*)	$C_6H_4CH_3$(-*p*)
f: $C_6H_4CH_3$(-*p*)	$C_6H_4OCH_3$(-*p*)
g: C_6H_4Cl(-*p*)	C_6H_5
h: C_6H_4Cl(-*p*)	$C_6H_4CH_3$(-*p*)
i: C_6H_4Cl(-*p*)	$C_6H_4OCH_3$(-*p*)

and toluene in presence of 6 mol $AlCl_3$.[1]

(ii) When VIIIa, and b were treated with benzene and toluene in 12 mol $AlCl_3$, they gave the corresponding *o*-aroylbenzophenone anils (VIa, and b) *via* carbonium ion X.

Action of Grignard Reagents. We have reinvestigated[6a,b] the problem of reaction of Grignard reagents with 4-aryl-1*H*-2,3-benzoxazin-1-ones (I).

Phenylmagnesium bromide reacts with 4-(*p*-tolyl)-, and 4(*p*-chlorophenyl)-1*H*-2,3-benzoxazin-1-ones (Ib and c) to give oximes of 2'-(*p*-toluoyl)-, and 2-(*p*-chlorobenzoyl)-triphenyl methanols (XIa and b), respectively.

Similarly, *o*-anisylmagnesium bromide reacts with

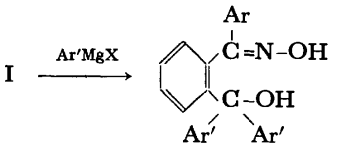

XI

Ar	Ar'
a: $C_6H_4CH_3$(-*p*)	C_6H_5
b: C_6H_4Cl(-*p*)	C_6H_5
c: C_6H_5	$C_6H_4CH_3O$(-*o*)
d: $C_6H_4CH_3$(-*p*)	$C_5H_4CH_3O$(-*o*)
e: C_6H_4Cl(-*p*)	$C_6H_4CH_3O$(-*o*)

Ia—c to give the corresponding oximes of *o*-aroyl-triarylmethanols (XIc—e).

The structure of XI was confirmed as follows: (i) *IR spectra* showed two ν_{OH} (bonded) in the regions 3520—3180 cm^{-1} and 3280—3050 cm^{-1} for oximes and *tert*-alcoholic groups. (ii) cyclization with (HCl/acetic) and/or (HCl/ethanol) to give 1,1,4-triaryl-1*H*-2,3-benzoxazines (XIIa—e).[6b]

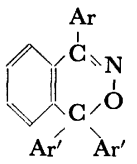

XII

	Ar	Ar′
a:	$C_6H_4CH_3$(-*p*)	C_6H_5
b:	C_6H_4Cl(-*p*)	C_6H_5
c:	C_6H_5	$C_6H_4CH_3O$(-*o*)
d:	$C_6H_4CH_3$(-*p*)	$C_6H_4CH_3O$(-*o*)
e:	C_6H_4Cl(-*p*)	$C_6H_4CH_3O$(-*o*)

Experimental

All mp's are not corrected, IR spectra were measured on a Unicam SP 1200 spectrophotometer by means of KBr wafer technique.

Action of Amines on 4-Aryl-1H-2,3-benzoxazin-1-ones (I a, b). Formation of IIa—d: A mixture of Ia, b (0.1 mol), and amine (0.6 mol) was heated at 150 °C on a sand bath for 12 hr. The excess amine was removed with concd-hydrochloric acid, and the solid product obtained was crystallized from methanol (Table 1).

Action of Benzylamine on Ia—c in Benzene. Formation of IIIa—c: To a solution of Ia—c (0.1 mol) in benzene (20 ml) was added benzylamine (0.3 mol). The reaction mixture was heated under reflux for about 12 hr, and then cooled. The solid product was filtered off, and crystallized from benzene (Table 2).

Action of Phenylhydrazine on Ia—c. Formation of IVa—c: A solution of Ia—c (0.1 mol) in glacial acetic acid (20 ml) was treated with phenylhydrazine (0.3 mol). The reaction mixture was heated under reflux for 2 hr and then cooled. The solid product was filtered off and crystallized from acetic acid (Table 3).

Action of Anhydrous $AlCl_3$ in Reactive Aromatic Hydrocarbon Substrates on Ia—c. Formation of VIa—i: Anhydrous aluminium chloride (12 mol) was added under stirring to a solution of Ia—c (0.1 mol) in dry aromatic substrates (20 ml). The reaction mixture was heated under reflux for 6 hr, and the complex formed was decomposed with ice-cold dilute hydrochloric acid. The solvent was steam distilled, and the residual solid was filtered off and crystallized from ethanol (Table 4).

Action of Anhydrous $AlCl_3$ (VIIIa, and b). Formation of VIa, and b: Anhydrous aluminium chloride (12 mol) was added under stirring to a solution of VIIIa and b (0.1 mol) in dry aromatic substrates (20 ml). The reaction mixture was

Table 1. Action of amines on Ia—c

Compd.	Mp °C	Yield %	Formula (M. Wt.)	Analysis %	Found	Required
IIa	178	68	$C_{21}H_{17}NO$ (315)	C	79.60	80.0
				H	5.50	5.4
				N	4.2	4.4
IIb	150	78	$C_{22}H_{19}NO_2$ (329)	C	80.70	80.24
				H	5.75	5.78
				N	4.30	4.25
IIc	191	80	$C_{20}H_{15}NO_2$ (301)	C	79.50	79.73
				H	4.90	4.98
				N	5.10	4.65
IId	213—215	78	$C_{21}H_{17}NO_2$ (315)	C	80.00	79.4
				H	5.4	5.2
				N	4.4	4.6

Table 2. Action of benzylamine on Ia—c in benzene

Compd.	Mp °C	Yield %	Formula (M. Wt.)	Analysis %	Found	Required
IIIa	172—173	80	$C_{21}H_{18}N_2O_2$ (330)	C	76.50	76.36
				H	5.70	5.45
IIIb	148	75	$C_{22}H_{20}N_2O_2$ (344)	C	76.6	76.7
				H	6.0	5.8
IIIc	178 (decomp)	70	$C_{21}H_{17}N_2O_2Cl$ (364.5)	C	69.5	69.1
				H	4.8	4.6
				Cl	9.9	9.7

Table 3. Action of phenylhydrazine on Ia—c

Compound	Mp °C	Yield %	Reference
IVa	168	80	2
IVb	140	79	3
IVc	169	82	3

Table 4. Action of anhydrous $AlCl_3$ on Ia—c

Compd.	Mp °C	Yield %	Formula (M. Wt.)	Analysis %	Found	Required
VIa	188	63	$C_{26}H_{19}NO$ (361)	C	86.7	86.4
				H	4.8	5.3
				N	3.8	3.9
VIb	194	68	$C_{28}H_{23}NO$ (389)	C	87.0	86.4
				H	6.1	5.8
				N	3.7	3.6
VIc	191	70	$C_{28}H_{23}NO_3$ (421)	C	79.8	79.8
				H	5.7	5.4
				N	3.5	3.3
VId	205—206	60	$C_{27}H_{21}NO$ (375)	C	86.1	86.4
				H	5.5	5.6
				N	3.8	3.7
VIe	282—284	63	$C_{29}H_{25}NO$ (403)	C	85.9	86.3
				H	5.9	6.2
				N	3.1	3.4
VIf	184	58	$C_{29}H_{25}NO_3$ (435)	C	79.7	80.0
				H	5.2	5.7
				N	3.0	3.2
VIg	220	60	$C_{26}H_{18}ClNO$ (395.5)	C	78.2	78.8
				H	4.6	4.6
				N	3.3	3.5
				Cl	9.4	8.97
VIh	230	65	$C_{28}H_{22}ClNO$ (423.5)	C	79.2	79.3
				H	5.2	5.2
				N	3.2	3.3
				Cl	8.2	8.4
VIi	160	58	$C_{28}H_{22}ClNO_3$ (455.5)	C	73.9	73.7
				H	4.8	4.9
				N	3.1	3.0
				Cl	7.8	7.5

heated under reflux for 6 hr, and the complex formed was decomposed with ice-cold dilute hydrochloric acid. The solvent was steam distilled, and the residual solid was filtered off and crystallized from ethanol, yield 70%. It was proved to be VIa and VIb prepared *via* the reaction of Ia and Ib with anhydrous $AlCl_3$ by mp and mixed mp.

Action of Grignard Reagents on Ia—c. Formation of XIa—c: A solution of the Grignard reagents (0.6 mol) in dry ether was added to a solution of Ia—c (0.1 mol) in dry ether (30 ml). The reaction mixture was heated under reflux for 6 hr, then left to stand overnight. The reaction mixture was decomposed with ice-cold concentrated solution of ammonium chloride. The ethereal layer was separated, dried over anhydrous sodium sulfate, and the solvent was distilled off. The solid product was filtered off and crystallized from benzene (Table 5).

Table 5. Action of Grignard reagent on Ia—c

Compd.	Mp °C	Yield %	Formula (M. Wt.)	Analysis %		
					Found	Required
XIa	170	58	$C_{27}H_{23}NO_2$ (393)	C	81.7	82.4
				H	6.2	5.8
XIb	172—174	68	$C_{26}H_{20}NO_2Cl$ (413.5)	C	75.2	75.5
				H	5.5	4.8
				Cl	8.6	8.56
XIc	218	64	$C_{28}H_{25}NO_4$ (439)	C	77.3	76.5
				H	5.9	5.7
XId	206—207	60	$C_{29}H_{27}NO_4$ (453)	C	77.0	76.8
				H	5.7	5.9
XIe	198—200	64	$C_{28}H_{24}NO_4Cl$ (473.5)	C	70.6	70.94
				H	4.8	5.07
				Cl	7.4	7.4

Cyclization of XIa—e with HCl/acetic. Formation of XIIa—c: A solution of XIa—e (0.1 mol) in a mixture of 10 ml acetic, 2 ml HCl was heated on a boiling water-bath for about 12 hr, cooled and then poured on ice-cold water. The solid obtained was filtered off, and crystallized from ethanol (Table 6).

Table 6. Cyclization of Ia—e

Compd.	Mp °C	Yield %	Formula (M. Wt.)	Analysis %		
					Found	Required
XIIa	209—211	40	$C_{27}H_{21}NO$ (375)	C	86.1	86.4
				H	5.3	5.3
XIIb	215—218	40	$C_{26}H_{18}NOCl$ (395.5)	C	78.6	78.8
				H	4.2	4.5
				Cl	8.5	8.9
XIIc	168—170	42	$C_{28}H_{23}NO_3$ (421)	C	79.9	79.8
				H	5.6	5.5
XIId	185—186	52	$C_{29}H_{25}NO_3$ (435)	C	79.9	80.0
				H	5.6	5.7
XIIe	208—209	60	$C_{28}H_{22}NO_3Cl$ (455.5)	C	73.9	73.76
				H	4.8	4.8
				Cl	8.0	7.8

The authors are indebted to Professor F. G. Baddar, Chem. Department., Kuwait University, Kuwait, for his kind help during the course of this work.

References

1) F. G. Baddar, A. F. M. Fahmy, Nawal F. Aly, *J. Chem. Soc., Perkin Trans. I*, **1973**, 2448.
2) W. Roser, *Ber.*, **18**, 805 (1885).
3) N. P. Buu-Hol, N. Hoan, and N. D. Xuong, *Rec. Trav. Chim. Pays-Bas*, **69**, 1092 (1950).
4) F. Just, *Ber.*, **19**, 1206 (1886).
5) D. Muller, *Ber.*, **45**, 294 (1912).
6) (a) A. Mustafa, W. Asker, M. Kamel, A. F. A. Shalaby, and A. E. Hassan, *J. Am. Chem. Soc.*, **77**, 1612 (1955). (b) A. Mustafa, A. H. Harhash, *ibid.* **82**, 2735 (1960).

NOTES

BULLETIN OF THE CHEMICAL SOCIETY OF JAPAN, VOL. 49 (5), 1395—1396 (1976)

Nuclear Magnetic Resonance Studies of Bicyclic Thiophene Derivatives. IV. Further Examples of Through-space H-F Coupling

Toshiyuki HIROHASHI, Shigeho INABA, and Hisao YAMAMOTO

Institute for Biological Science, Sumitomo Chemical Co., Takatsukasa, Takarazuka, Hyogo 665

(Received September 10, 1975)

Synopsis. Bicyclic thiophene derivatives, 3-methyl-4-(*o*-fluorophenyl)-2,3-dihydrothieno[2,3-*d*]-pyrimidin-2-ones (I) and *N*,5-dimethyl-4-(*o*-fluorophenyl)-5*H*-thieno[2,3-*c*]-pyrrole-6-carboxamides (II), have been prepared. Two sorts of ^{1}H, ^{19}F spin coupling over six bonds attributable to a through-space mechanism have been observed in the ^{1}H NMR spectra of these compounds.

In previous papers,[1-2] we reported that long-range spin couplings over six or seven bonds are observed in various bicyclic thiophene derivatives; the coupling was considered to arise from a through-space mechanism. In the course of our synthetic studies of biologically active thiophenes, we have also found in the ^{1}H NMR spectra of other kinds of bicyclic thiophene derivatives, I and II, the presence of two long-range couplings, $^6J_{HF}$, between *N*-methyl protons and fluorine as well as between the H_β of the thiophene ring and the fluorine; these are also considered to be through-space couplings. Myhre *et al.* have already reported through-space couplings between fluorine and two different protons in a molecule of 2,4,6-tri-*t*-butylfluorobenzene.[4] In this paper, we will present our observations of the $^6J_{HF}$ in these new compounds. As is shown in Table 1,

TABLE 1. J_{HF} IN COMPOUNDS I AND II

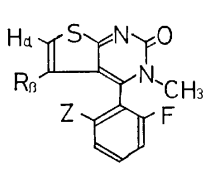

I

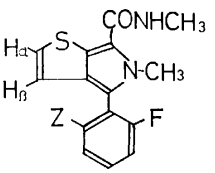

II

Compound	Z	R	$J_{H_\beta,F}$	$J(NCH_3,F)$
Ia[a]	H	H_β	0.6 d[b]	1.2 d
Ib[a]	F	H_β	1.0 t[c]	0.8 t
Ic	H	CH_3	—	0.5 d
IIa[a]	H	—	0.8 d	1.8 d
IIb[d]	F	—	1.0 t	1.3 t

a) J_{H_α,H_β}=6.3 Hz, b) doublet, c) triplet, d) J_{H_α,H_β}=5.3 Hz.

both *N*-methyl and H_β exhibit doublet signals in *o*-fluorophenyl-I and -II (Ia and IIa) and a triplet in 2,6-difluorophenyl-I and -II (Ib and IIb). These facts suggest the presence of a long-range coupling over six bonds between the *N*-methyl protons and fluorine as well as between the H_β of the thiophene ring and the fluorine. When the J_{HF} value of the *o*-fluorophenyl compound is compared with that of the corresponding 2,6-difluorophenyl compound, the $J(H_\beta, F)$ value is smaller for the former (Ia, 0.6 Hz; IIa, 0.8 Hz) than for the latter (Ib, 1.0 Hz; IIb, 1.0 Hz). On the contrary, the $J(CH_3, F)$ value is greater for the former (Ia, 1.2 Hz; IIa, 1.8 Hz) than for the latter (Ib, 0.8 Hz; IIb, 1.3 Hz). Since the torsional angle between the thiophene and the benzene-ring planes should be greater for the 2,6-difluorophenyl compound than for the *o*-fluorophenyl compound,[1] these facts reasonably suggest that, of the two possible conformers (A and B),

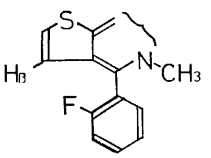

A

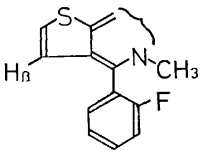

B

the B conformer in which the fluorine atom is more proximate to the *N*-methyl group, is much predominant in the *o*-fluorophenyl compounds, I and II. When H_β is replaced by a methyl group, the $J(CH_3, F)$ value is decreased from 1.2 Hz (Ia) to 0.5 Hz (Ic). This phenomenon can easily be understood because the torsional angle between the thiophene and the benzene planes should be greater for Ic than for Ia as a result of the steric hindrance between the methyl group of the thiophene and the benzene rings in Ic. This greater torsional angle should lead to an increase in the internuclear distance between the *N*-methyl protons and fluorine.

Experimental

Measurements. The ^{1}H NMR spectra were recorded on a Hitachi R-20-B spectrometer at 60 MHz, using $CDCl_3$ solutions (about 10%w/v) containing TMS as an internal reference at a probe temperature of 35 °C. The chemical shifts are expressed in δ (ppm) with a precision of $\pm$0.01. The coupling constants were measured by several sweepings at an expanded width (60 or 120 Hz) with an accuracy of $\pm$0.1 Hz. The IR spectra were recorded as Nujol mulls on a Hitachi EPI-G-3 spectrophotometer (wave number, cm^{-1}). The UV spectra (wavelength) were determined in 95% ethanol with a Hitachi-323 spectrophotometer. The melting points were measured on a Thomas-Hoover melting-point apparatus and are uncorrected.

Materials. The preparation of the following compounds has already been reported: 4-(*o*-fluorophenyl)-3-methyl-2,3-dihydrothieno[2,3-*d*]pyrimidin-2-one(Ia)[5] and

3,5-dimethyl-4-(*o*-fluorophenyl)-2,3-dihydrothieno[2,3-*d*]pyrimidin-2-one (Ic).[2] The other compounds were prepared by the following methods.

4-(2,6-Difluorophenyl)-3-methyl-2,3-dihydrothieno[2,3-d]pyrimidin-2-one (Ib). 2-Amino-3-(2,6-difluorobenzoyl)thiophene[1] and methyl isocyanate in benzene were heated under reflux to afford 4-(2,6-difluorophenyl)-4-hydroxy-3-methyl-1,2,3,4-tetrahydrothieno[2,3-*d*]-pyrimidin-2-one (yield, 36.9%; mp 212—217 °C), which was then heated at 240 °C to afford Ib. Yield, 11.0%; mp 188—190 °C (from ethanol–ether). IR: 3060, 1665, and 1620. NMR: 3.54 (3H, t, N–CH_3), 6.42 (1H, d–d, H_β) and 6.97 (1H, d, H_α). UV: 220.5 (19100), 251.5 (24300), 292 (2700) and 374 (5200). Found: C, 56.09; H, 3.09; N, 10.12%. Calcd for $C_{13}H_8N_2OSF_2$: C, 56.11; H, 2.90; N, 10.07%. The same procedure was applied to the synthesis of 3-methyl-4-phenyl-2,3-dihydroquinazolin-2-one by Metlesics *et al.*[6]

Compounds IIa and IIb. These compounds were prepared from 5-(*o*-fluorophenyl or 2,6-difluorophenyl)-1-methyl-1,3-dihydro-2*H*-thieno[2,3-*e*]-1,4-diazepin-2-one[1,5] with sodium hydride and methyl iodide. The same procedure was applied to the synthesis of 5-chloro-*N*, 2-dimethyl-3-phenyl-1-isoindolecarboxamide by Fryer *et al.*[7]

N,*5-Dimethyl-4-(o-fluorophenyl)-5H-thieno[2,3-c]pyrrole-6-carboxamide (IIa).* Yield, 31.1%; mp 131—132 °C (from ether). IR: 3300 and 1625. NMR: 3.04 (3H, d, J=4.9, $NHC\underline{H}_3$), 4.01 (3H, d, N^5–CH_3), 5.07 (1H, broad s, NH), 6.88 (1H, d–d, H_β) and 7.00 (1H, d, H_α). UV: 224 (14700), 251 (15800) and 324 (18900). Found: C, 62.60; H, 4.56; N, 9.92%. Calcd for $C_{15}H_{13}N_2OSF$: C, 62.49; H, 4.54; N, 9.71%.

4-(2,6-Difluorophenyl)-N,5-dimethyl-5H-thieno[2,3-c]pyrrole-6-carboxamide (IIb). Yield, 36.4%; mp 165—166 °C (from ethanol). IR: 3300 and 1627. NMR: 3.04 (3H, d, J=4.8, $NHC\underline{H}_3$), 4.00 (3H, t, N^5–CH_3), 5.67 (1H, broad s, NH), 6.83 (1H, d–t, H_β) and 7.03 (1H, d, H_α). UV: 221 (16200), 250.5 (15700) and 321 (18900). Found: C, 58.77; H, 4.05; N, 9.18%. Calcd for $C_{15}H_{12}N_2SOF_2$: C, 58.81; H, 3.95; N, 9.14%.

The authors wish to thank Professor Masamichi Tsuboi, The University of Tokyo, and Dr. Makoto Sunagawa of this Institute for their valuable suggestions. and Mr. Hiromi Sato for his cooperation in the synthetic experiments.

References

1) Part II: T. Hirohashi, S. Inaba, and H. Yamamoto, *Bull. Chem. Soc. Jpn.*, **48**, 974 (1975).
2) Part III: T. Hirohashi, S. Inaba, and H. Yamamoto, *Bull. Chem. Soc. Jpn.*, **48**, 3373 (1975).
3) See Part II and the references therein.
4) P. C. Myhre, J. W. Edmonds, and J. D. Kruger, *J. Am. Chem. Soc.*, **88**, 2459 (1966).
5) Part I: T. Hirohashi, S. Inaba, and H. Yamamoto, *Bull. Chem. Soc. Jpn.*, **48**, 147 (1975).
6) W. Metlesics, G. Silverman, V. Toome, and L. H. Sternbach, *J. Org. Chem.*, **31**, 1007 (1966).
7) R. I. Fryer, J. V. Earley, and L. H. Sternbach, *J. Org. Chem.*, **34**, 649 (1969).

BULLETIN OF THE CHEMICAL SOCIETY OF JAPAN, VOL. 49 (5), 1397—1398 (1976)

A MINDO/2′-MO Study of the Inversion Barriers of Some Molecules Involving First-Row Atoms

Katsutoshi OHKUBO, Yutaka AZUMA, and Masahide OKADA

Department of Synthetic Chemistry, Faculty of Engineering, Kumamoto University, Kurokami 860

(Received July 28, 1975)

Synopsis. The inversion barriers of CH_3^-, NH_3, CH_3NH_2, $(CH_3)_2NH$, $(CH_3)_3N$, NH_2OH, NH_2CHO, and OH_3^+ were investigated by means of the MINDO/2′ method. Although the calculated bond lengths are in satisfactory agreement with the experimental values, the calculated bond angles are too large and resulted in relatively low inversion barriers in comparison with the observed values.

In general, pyramid-like molecules involving an unshared pair on its central atom instead of a fourth substituent indicate the intramolecular motions which lead to inversion.

Inversion barriers are intimately related to the configurations (especially, bond angles) of molecules,[1] for instance, the smaller angles of phosphine, arsine, *etc.*, as compared with those of ammonia, make inversion more difficult.[2]

Recently, Allen and Arents[3] have argued that carefully parametrized semiempirical adaptations of the SCF-MO method can be useful for investigating inversion barriers. Stevenson and Burkey[4] have compared the effectiveness of several different versions of the CNDO and INDO methods in predicting the inversion barriers of AR(R′) (R″), where A=C, N, O, Si, P, and S, and they demonstrated a predominant utility of the INDO method. However, all previous semiempirical calculations of the inversion barriers[5] were performed without optimization of the molecular geometries for the compounds investigated.[6]

On the other hand, a few *ab initio* calculations have also been performed on the inversion barriers of small molecules such as NH_3; Rauk *et al.*[7] have obtained an inversion barrier of 5.08 kcal/mol (exptl.=5.8 kcal/mol[8]) for NH_3 using an *ab initio* method with a large gaussian basis set, while Sambe and Felton[9] have reported a negative barrier of −62.77 kcal/mol for the same molecule using an LCAO-X_α method without the nitrogen d-orbitals.

The present authors report, here, on an extensive study of the inversion barriers of CH_3^-, NH_3, CH_3NH_2, $(CH_3)_2NH$, $(CH_3)_3N$, NH_2OH, NH_2CHO, and OH_3^+, which were investigated by means of the MINDO/2′ method.[10]

Method of Calculation

The MINDO/2′ method used for the present study is a modified version of MINDO/2[11] which has already been found to suffer from serious defects, including: (a) an overestimation of the dipole moments, (b) an underestimation of the strain energies of small rings, and (c) an incomplete treatment of heteroatoms.[12] The integrations and parametrizations involved in the present method will not be repeated here, because they have been described in detail in Ref 10.

The optimizations were performed on the geometrical parameters for the ground-state and transition-state molecules in which the geometries of the substituents (R, R′, and R″) were fixed by the use of the standard bond lengths and angles[13] in order to simplify the computation.

Results and Discussion

Let us first examine the optimized geometries of the compounds investigated in their ground and transition states. As can be seen from Table 1, the calculated bond lengths except that of the N–O bond in NH_2OH are in satisfactory agreement with the observed values and the differences between the ground-state and transition-state configurations are not too great. The bond length for the N–O bond in NH_2OH, which is too short, is mainly attributable to an underestimation (caused by the neglect of two-center integrals involving one-center overlap) of the lone pair-lone pair interactions in the present method.[14] This trend was also found for the bond lengths of O–O (in H_2O_2) and N–N (in N_2H_4) calculated by the MINDO/2′ method,[14] which were also too short. The calculated bond angles are too large in comparison to the observed values except for

Table 1. Estimated molecular geometries, ionization potentials, and dipole moments obtained using the MINDO/2′ method

Compound	Molecular geometry		I_p/eV	μ/Debye
	Ground-state	Transition-state	Calcd (Obsd)	Calcd (Obsd)
CH_3^-	CH, 1.12; CHC, 95.05	CH, 1.05; CHC, 120.0	1.30	6.05
NH_3	NH, 0.979 (1.012[a]); HNH, 104.62 (106.7[a])	NH, 0.956; HNH, 120.0	10.483 (10.154[f])	2.117 (1.468[b])
CH_3NH_2	NH, 0.975 (1.014[b]); NC, 1.43 (1.47[b]); HNH, 109.02 (105.8[b]); HNC, 123.49 (112.2[b])	NH, 0.963; NC, 1.43; HNH, 115.5; HNC, 123.23	9.336 (9.56[g])	0.595 (1.29[b])
$(CH_3)_2NH$	NH, 0.989; NC, 1.44 (1.46[c]); HNC, 116.93; CNC, 126.22 (108.11[c])	NH, 0.986; NC, 1.44; HNC, 117.69; CNC, 123.86	8.975 (9.01[g])	0.263 (1.03[b])
$(CH_3)_3N$	NC, 1.45 (1.47[d]); CNC, 119.99 (108.7[d])	NC, 1.45; CNC, 120.0	8.748 (8.66[g])	0.182 (0.612[d])
NH_2OH	NH, 1.02 (1.01[b]); NO, 1.27 (1.46[b]); HNH, 94.15 (107[b]); HNO, 112.05 (105[b])	NH, 0.978; NO, 1.26; HNH, 121.04; HNO, 118.57	9.602	2.665 (2.45[b])
H_1 H_2 N–C=O	NH, 0.981 (1.002[e]); NC, 1.36 (1.38[e]); H_1NH_2, 106.04 (118.98[e]); H_1NC, 127.9 (117.2[e]); H_2NC, 126.1 (120.5[e])	NH, 0.980; NC, 1.36; H_1NH_2, 106.60; H_1NC, 128.11; H_2NC, 125.89	10.001 (10.83[h])	4.880 (3.79[i])
OH_3^+	OH, 0.965 (0.96[b]); HOH, 119.99 (117[b])	OH, 0.964; HOH, 120.0	22.778	4.810

The bond lengths are in Å and the bond angles are in degrees.
a) W. S. Bennett and E. K. Plyler, *Can. J. Phys.*, **35**, 1235 (1957). b) Ref. 13. c) Ref. 17. d) Ref. 18. e) C. C. Costain and J. M. Dowling, *J. Chem. Phys.*, **32**, 158 (1960). f) W. Watanabe and J. R. Mottl, *J. Chem. Phys.*, **26**, 1773 (1957). g) A. Stereitwieser, Jr., *J. Am. Chem. Soc.*, **82**, 4123 (1960). h) Monograph Ser. Res. Instit. Appl. Elect. Hokkaido Univ., No. 4 (1954—7). i) A. L. McClellan, "Table of Experimental Dipole Moments," W. H. Freeman, San Francisco, Calif. (1963). j) S. Tsunekawa, *J. Phys. Soc.*, **33**, 167 (1972).

Table 2. Inversion barriers for some molecules involving first-row central atoms

Compound	CNDO/2[a]	INDO[b]	MINDO/2′	Obsd
CH_3^-	16.2	11.7	17.58	(5.2[c])
NH_3	11.8	4.9	3.14	5.9[d]
CH_3NH_2	12.9	4.7	1.38	4.8[e]
$(CH_3)_2NH$	13.6	4.4	0.12	4.4[f]
$(CH_3)_3N$	15.0	5.1	0.00	8.2[d]
NH_2OH			9.04	(13.3[g])
				(12.9[h])
NH_2CHO			0.092	1.0[i]
OH_3^+	1.3	0.0	0.0	1.71[j]

Values are in kcal/mol.

a) From Ref. 4, the ground-state configurations were assumed to be tetrahedral except CH_3^- (optimized angle=107°), NH_3 (optimized angle=107°), and OH_3^+ (optimized angle=115°). b) From Ref. 4, the ground-state configurations were assumed to be tetrahedral except CH_3^- (optimized angle=106°), NH_3 (optimized angle=110°), and OH_3^+ (optimized angle=120°). c) *ab initio* result. P. Millie and G. Berthier, *Int. J. Quantum Chem., Symp.*, **2**, 67 (1968). d) R. E. Weston, Jr., *J. Am. Chem. Soc.*, **76**, 2645 (1954). e) M. Tsuboi, A. Y. Hirakawa, and K. Tamagake, *J. Mol. Spectrosc.*, **22**, 272 (1967). f) J. E. Wollrab and V. W. Laurie, *J. Chem. Phys.*, **48**, 5058 (1968). g) MINDO/1 result. M. J. S. Dewar and M. Shanshal, *J. Chem. Soc., A*, **1971**, 25. h) Value for $C_6H_5CH_2N(OCH_3)_2$: D. J. Griffith and J. D. Roberts, *J. Am. Chem. Soc.*, **87**, 4089 (1965). i) J. Issoire and C. V. Long, *Bull. Soc. Chim. Fr.*, **1964**, 2004. j) G. W. Koeppl, D. S. Safatys, G. S. Krishnamurthy, and S. I. Miller, *J. Am. Chem. Soc.*, **89**, 3396 (1967).

those of NH_3. This may be a result of the fact that the MINDO/2′ method, as well as the original version called MINDO/2, is still unsatisfactory for the parametrization (α and B) of heteroatoms, such as nitrogen, and overestimates nonbonded hydrogen-hydrogen repulsions in such molecules as $(CH_3)_2NH$ and $(CH_3)_3N$.[15]

It should be stressed here that the present MINDO/2′ calculations for the compounds (with fixed geometries of the substituents) listed in Table 1 result in almost the same bond lengths and angles as the calculations with no geometrical assumptions (with all bond lengths and angles variable), for example, an MINDO/2′ calculation of $(CH_3)_3N$ with no geometrical assumptions gave N–C=1.44 Å, C–H=1.082 Å, $\angle$CNC=119.99°, and $\angle$NCH=114.91°. Therefore, there are no serious defects in the geometrical assumptions for the substituents (R, R′, and R″) in terms of the calculated bond lengths and angles.

In connection with the unsatisfactory results for the optimization of the bond angles, dipole moments (μ) are calculated incorrectly with marked deviations from the experimentally determined values, although the calculated ionization potentials (I_p)[19] are in good overall agreement with the observations (see Table 1).

Now, we turn our attention to the inversion barriers of the compounds investigated. In Table 2, the calculated inversion barriers were listed together with those evaluated by the CNDO/2 or INDO method. As Table 2 indicates, the CNDO/2 method results in remarkably high inversion barriers in comparison with the INDO or MINDO/2′ method, probably because it not only excludes the one-center atomic exchange integrals but suffers markedly from the parametrization.[20] With regard to the results of the present MINDO/2′ calculations, the inversion barriers were predicted to be relatively low in comparison with the experimental values. This is due to inadequate optimization (*viz.*, overestimation) of the bond angles for the ground-state configuration of the molecule.

References

1) For instance, see F. W. Koeppl, D. S. Sagatys, G. S. Krishnamurthy, and S. I. Miller, *J. Am. Chem. Soc.*, **89**, 3396 (1967).

2) W. J. le Noble, "Highlights of Organic Chemistry," Marcel Dekker, New York (1974), pp. 149, 178.

3) L. C. Allen and J. Arents, *J. Chem. Phys.*, **57**, 181, (1972).

4) P. E. Stevenson and D. L. Burkey, *J. Am. Chem. Soc.* **96**, 3061 (1974).

5) See Ref. 4 and M. J. S. Dewar and M. Shashal, *J. Chem. Soc., A*, **1971**, 25.

6) The optimization of the bond angles of symmetrical molecules expressed by AR_3 (A: central atom; R: substituent) can be seen in some cases (see Ref. 4).

7) A. Rauk, L. C. Allen, and E. Clementi, *J. Chem. Phys.*, **52**, 4133 (1970).

8) J. D. Swalen and J. D. Ibers, *J. Chem. Phys.*, **36**, 1914 (1962).

9) H. Sambe and R. H. Felton, *J. Chem. Phys.*, **61**, 3862 (1974).

10) N. Bodor, M. J. S. Dewar, and D. H. Lo, *J. Am. Chem. Soc.*, **94**, 5296 (1972): The parametrization for the C–C, C–H, and H–H bonds were taken from Ref. 12.

11) M. J. S. Dewar and E. Haselbach, *J. Am. Chem. Soc.*, **92**, 590 (1970).

12) N. Bodor, M. J. S. Dewar, and D. H. Lo, *J. Am. Chem. Soc.*, **94**, 5303 (1972).

13) The standard bond lengths and angles were obtained from Ref. 4 and from L. E. Sutton, Editor, "Tables of Interatomic Distances, "The Chemical Society, London, Special Publication No. 11 (1958) and No. 18 (1965).

14) N. Bodor, M. J. S. Dewar, A. Harget, and E. Haselbach, *J. Am. Chem. Soc.*, **92**, 3854 (1970).

15) These problems are not overcome even in a modified version called MINDO/3[16] as is apparent from the calculated bond angles of C–N–C (129.4°) in $(CH_3)_2NH$ (obsd=108.11°[17]) and of C–N–C (119.8°) in $(CH_3)_3N$ (obsd=108.7°[18]), which are too large.

16) R. C. Bingham, M. J. S. Dewar, and D. H. Lo, *J. Am. Chem. Soc.*, **97**, 1285, 1294, 1302, 1307 (1975); M. J. S. Dewar, D. H. Lo, and C. A. Ramsden, *ibid.*, **97**, 1311 (1975).

17) S. H. Bauer, *J. Am. Chem. Soc.*, **60**, 524 (1938); P. W. Allen and L. E. Sutton, *Acta Cryst allogr.*, **3**, 46 (1950).

18) D. R. Lide, Jr. and D. E. Mann, *J. Chem. Phys.*, **28**, 572 (1958).

19) They were taken from the energy of the highest-occupied MO as positive numbers according to T. Koopmans, *Physica*, **1**, 104 (1933).

20) For the inversion barriers calculated by the CNDO method with different parameters, refer to A. Rauk, J. D. Andose, W. G. Frick, R. Tang, and K. Mislow, *J. Am. Chem. Chem. Soc.*, **93**, 6507 (1971).

BULLETIN OF THE CHEMICAL SOCIETY OF JAPAN, VOL. 49 (5), 1399—1400 (1976)

Polarographic Studies on Bipyridine Complexes. IV. The Polarography of the Dicyanobis(2,2′-bipyridine)iron(II) Complex

Tetsuo SAJI and Shigeru AOYAGUI*

Faculty of Engineering, Tokyo Institute of Technology, Ohokayama, Meguro-ku, Tokyo 152

(Received October 2, 1975)

Synopsis. Each electron added to the oxidant in the first two reduction waves of a polarogram for dicyanobis(2,2′-bipyridine)iron(II) is concluded to occupy a π^*-orbital localized on a bipyridine molecule, on the basis of the number of the reversible waves and the half-wave potential shift caused by the methyl substitution of ligand bipyridines.

In Parts I—III of this series,[1-3] the molecular orbital occupied by the electron added or removed in the course of oxidation-reduction reactions of tris(bipyridine) complexes of transition metals was discussed on the basis of the polarographic half-wave potentials. In this paper, the same discussion will be extended to dicyanobis(2,2′-bipyridine)iron (II).

Experimental

4,4′-Dimethyl-2,2′-bipyridine (4-dmbipy) and 5,5′-dimethyl-2,2′-bipyridine (5-dmbipy) were prepared according to the method of Sasse and Whittle.[4] Dicyanobis(2,2′-bipyridine)iron(II) and its dimethyl derivatives were prepared by the method of Shilt.[5] *N,N*-Dimethylformamide (DMF) was used as a solvent. The supporting electrolyte was 0.1 M tetrabutylammonium perchlorate (TBAP). The electrolysis cell[3] and the following experimental procedures have been described in previous papers: the preparation of TBAP and solutions,[6] the purification of DMF,[6] and the measurements of polarograms and cyclic voltammograms.[1] The measurements were carried out at room temperature. All the potentials were referred to a saturated calomel electrode (SCE).

Results and Discussion

Figure 1 shows a cathodic polarogram for $Fe(bipy)_2(CN)_2$ (bipy=2,2′-bipyridine). It exhibits three waves with half-wave potentials of −1.59, −1.90, and −2.6 V. The wave height at −2.6 V is higher than the others. The first two waves were concluded to be reversible one-electron wave on the basis of the cyclic voltammogram in Fig. 2, taken with an initial cathodic scan. They can be assigned to the following redox systems respectively: $Fe(bipy)_2(CN)_2/Fe(bipy)_2(CN)_2^-$ and $Fe(bipy)_2(CN)_2^-/Fe(bipy)_2(CN)_2^{2-}$.

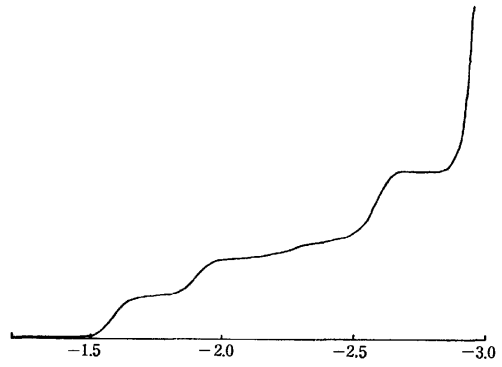

E/V *vs.* SCE

Fig. 1. Cathodic polarogram for 1 mM $Fe(bipy)_2(CN)_2$ in DMF containing 0.1 M TBAP.

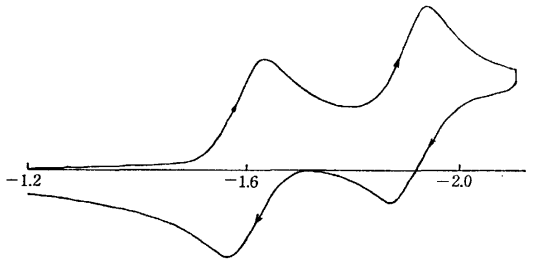

E/V *vs.* SCE

Fig. 2. Cyclic voltammogram with initial cathodic scan for 1 mM $Fe(bipy)_2(CN)_2$ in DMF containing 0.1 M TBAP. Scan rate: 0.1 V s^{-1}.

TABLE 1. THE REVERSIBLE HALF-WAVE POTENTIALS FOR $FeL_2(CN)_2$ (L=bipy, 4-dmbipy, 5-dmbipy), $E^{red}_{1/2,C}$, IN DMF CONTAINING 0.1 M TBAP

Complex	$E^{red}_{1/2,C}$/V *vs.* SCE	
	1st wave	2nd wave
$Fe(bipy)_2(CN)_2$	−1.59	−1.90
$Fe(4\text{-}dmbipy)_2(CN)_2$	−1.69	−1.98
$Fe(5\text{-}dmbipy)_2(CN)_2$	−1.73	−2.05

Similar polarograms and cyclic voltammograms were also obtained for the methyl-substituted complexes. The half-wave potentials of the redox systems, $FeL_2(CN)_2/FeL_2(CN)_2^-$ and $FeL_2(CN)_2^-/FeL_2(CN)_2^{2-}$ (L=bipy, 4-dmbipy, 5-dmbipy), became more negative in this order: bipy<4-dmbipy<5-dmbipy (Table 1). It should be noted that an empirical rule has been obtained concerning the order of the reversible half-wave potentials of tris(bipyridine) complexes of transition metals:[1] When an electron is added to a ligand π^*-orbital by the electrochemical reduction of a complex, the reduction half-wave potential, $E^{red}_{1/2,C}$, is shifted, on the methyl-substitution of ligand bipyridines, to a more negative potential in this order: bipy<4-dmbipy<5-dmbipy. The relation between the reduction half-wave potentials of free ligand molecules, $E^{red}_{1/2,L}$, and the $E^{red}_{1/2,C}$ for $FeL_2(CN)_2/FeL_2(CN)_2^-$ satisfies Eq. 3 in Part I,[1] as shown in Fig. 3. Consequently, it may be concluded that the electrons added to $FeL_2(CN)_2$ in the first two reduction steps occupy ligand π^*-orbitals.

It has been noted that there exsists a correlation be-

* To whom correspondence should be addressed.

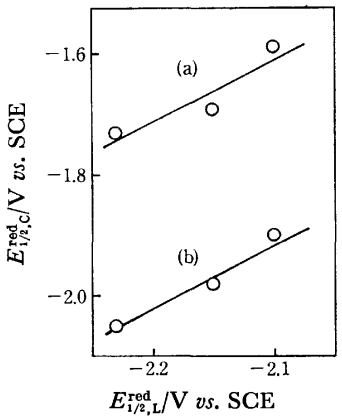

Fig. 3. Plot of half-wave potentials for (a) $FeL_2(CN)_2$/$FeL_2(CN)_2^-$ and (b) $FeL_2(CN)_2^-$/$FeL_2(CN)_2^{2-}$, $E^{red}_{1/2,C}$, *vs.* those for L/L^-, $E^{red}_{1/2,L}$, in DMF containing 0.1 M TBAP. L=bipy, 4-dmbipy, 5-dmbipy. The $E^{red}_{1/2,L}$ data can be found in Ref. 1.

tween the number of reversible reduction waves of a complex and the number of its ligands of a π-character:[1,7] The polarogram of this kind of complex is characterized by nearly neighboring one-electron waves, the number of which is identical with that of the ligands. This correlation can be found in the polarograms for bis(2,2′,2″-terpyridine)iron(II),[1,8,9] tris(4,7-diphenyl-1, 10-phenanthroline)iron(II),[7,10] tris(2,2′-bipyridine)iron(II),[1,8,11] tris(2,2′-bipyridine) ruthenium(II),[1,9] and tris(2,2′-bipyridine)osmium-(II).[1] It is evident that this rule holds also for Fe-$(bipy)_2(CN)_2$. This fact suggests that the lowest π^*-orbitals are nearly doubly degenerate. Thus, in the two reversible reduction waves for $Fe(bipy)_2(CN)_2$, each added electron should occupy one of the nearly degenerate orbitals successively.

References

1) T. Saji and S. Aoyagui, *J. Electroanal. Chem.*, **58**, 401 (1975).
2) T. Saji and S. Aoyagui, *J. Electroanal. Chem.*, **60**, 1 (1975).
3) T. Saji and S. Aoyagui, *J. Electroanal. Chem.*, **63**, 405 (1975).
4) W. H. F. Sasse and C. P. Whittle, *J. Chem. Soc.*, **1961**, 1347.
5) A. A. Shilt, *J. Am. Chem. Soc.*, **82**, 3000 (1960).
6) T. Saji, T. Yamada, and S. Aoyagui, *J. Electroanal. Chem.*, **61**, 147 (1975).
7) T. Saji, T. Fukai, and S. Aoyagui, *J. Electroanal. Chem.*, **66**, 81 (1975).
8) S. Musumeci, E. Rizzarelli, S. Sammartano, and R. P. Bonomo, *J. Inorg. Nucl. Chem.*, **36**, 853 (1974).
9) N. E. Tokel-Takvoryan, R. E. Hemingway, and A. J. Bard, *J. Am. Chem. Soc.*, **95**, 6582 (1973).
10) S. Musumeci, E. Rizzarelli, I. Fragala, S. Sammartano, and R. P. Bonomo, *Inorg. Chim. Acta*, **7**, 660 (1973).
11) N. Tanaka and Y. Sato, *Electrochim. Acta*, **13**, 335 (1968).

BULLETIN OF THE CHEMICAL SOCIETY OF JAPAN, VOL. 49 (5), 1401—1402 (1976)

Studies of the $\pi \rightarrow \pi^*$ Absorption Bands of 1,2-Naphthoquinone

Akira KUBOYAMA and Hiroshi ARANO

National Chemical Laboratory for Industry, Shibuya-ku, Tokyo 151

(Received October 30, 1975)

Synopsis. The $\pi \rightarrow \pi^*$ S–S absorption spectra up to the vacuum UV region of 1,2-naphthoquinone in solutions were obtained. Based on MO calculations, the observed five $\pi \rightarrow \pi^*$ bands of 1,2-naphthoquinone are assigned, and the alkyl-group substitution effects on the excitation energy of the longest-wavelength $\pi \rightarrow \pi^*$ band are discussed.

Previously, the present authors have theoretically and experimentally studied the $\pi \rightarrow \pi^*$ absorption bands of *p*-quinones[1] and 9,10-phenanthrenequinone[2] up to the vacuum UV region. In this note, the $\pi \rightarrow \pi^*$ absorption spectrum of 1,2-naphthoquinone (1,2-NQ), which has been studied by few workers, is reported.

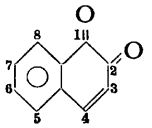

The absorption spectra were obtained in the same manner as in that described in previous reports.[1,2] The solvents, heptane and 1,1,1,3,3,3-hexafluoro-2-propanol (HFP) were the same as those used in previous works.[1,2] The 1,2-NQ was prepared according to the Fieser method[3] (mp 146 °C with decomp.).

TABLE 1. WAVELENGTHS AND MOLAR ABSORPTION COEFFICIENTS (IN PARENTHESES) OF THE ABSORPTION MAXIMA

Heptane	HFP	Band name
382 (nm)	425 (2180)	I
338 326	354 (3370)	II
251 245	255 (27500) 249 (27500)	III
195	196 (24300)	IV
	~170 (~22500)	V

In the P-P-P method calculations, the electronic integral values used were the same as those used in previous calculations,[1,2] except for the core resonance integral values for the carbon-carbon bonds. The latter were taken to be −1.5, −2.7, and −2.3 eV for the conventional single and double bonds, and the benzene-ring bonds, respectively. These values are close to those obtained by the Pariser-Parr method,[4] except for that of the double bond which is smaller than the latter by *ca.* 0.2 eV. In the CI calculation, all the singly-excited configurations were included. The molecular structure of 1,2-NQ was assumed to be planar. The lengths of the C–O bonds, the C(1)–C(2) bond, conventional C–C single and double bonds, and the benzene-ring bonds of 1,2-NQ were assumed to be 1.215, 1.49, 1.465, 1.35, and 1.40 Å, respectively.[1,2] All the valence angles in 1,2-NQ were assumed to be 120°.

TABLE 2. CALCULATED EXCITATION ENERGIES AND OSCILLATOR STRENGTHS OF THE SINGLET π, π^* EXCITED STATES AND THE CORRESPONDING $\pi \rightarrow \pi^*$ BANDS IN THE HEPTANE SOLUTION

	Calculated			Observed	
No.	Angle (°)	E (eV)	f	Band name	E (eV)
1	106	4.320	0.077	I	3.3
2	124	4.486	0.091	II	3.7
3	67	5.286	0.587	III	5.0
6	99	5.953	0.425	IV	6.4
7	23	6.189	0.585		
13	151	7.215	0.417	V	7.3[a]
14	168	7.412	0.344		

a) This value is that of the HFP solution.

The n$\rightarrow\pi^*$ absorption band of 1,2-NQ is near 520 nm.[5] In Fig. 1, five $\pi \rightarrow \pi^*$ bands can be observed for the HFP solution. These $\pi \rightarrow \pi^*$ bands are denoted as Bands I-V, as is shown in Table 1. As is seen in Fig. 1, the intensity ratio of Band I to Band II in the HFP solution is very different from that in the heptane

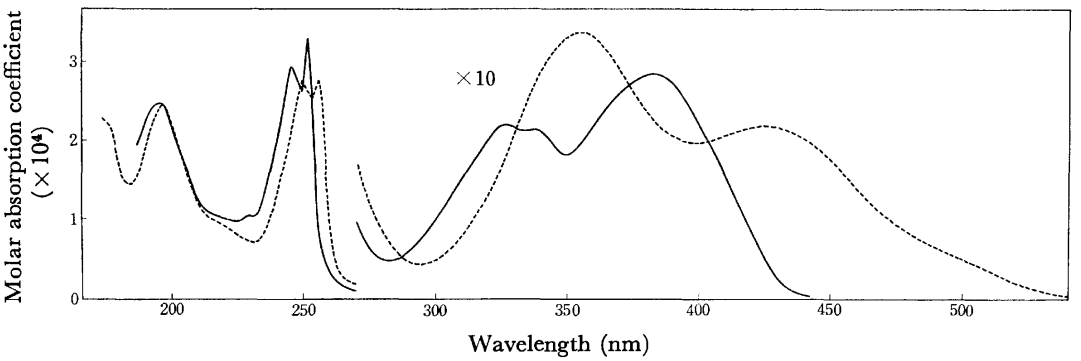

Fig. 1. Absorption spectra of 1,2-naphthoquinone in various solvents.
——: Heptane, ------: 1,1,1,3,3,3-hexafluoro-2-propanol.
In the heptane solution the scale of the ordinate is arbitrary.

solution and Bands I and II in the HFP solution show large red-shifts compared with those in the heptane solution. These facts may be due to the strong hydrogen-bond formation between 1,2-NQ and HFP.

In Table 2, the first column denotes an order based on the magnitude of the calculated excitation energies and the second column denotes the clockwise rotation angles of the directions of the transition moments with respect to the C(6)–C(7) bond axis. In this table, the data on the more highly-excited states with small *f*-values have been omitted. As may be seen in Table 2, the assignments of Bands I, II, and III based on the calculated results are reasonable, but those of Bands IV and V are not clear.

Table 3. The changes in the calculated excitation energy of the lowest π, π^* excited state of 1,2-NQ with alkyl-group substitutions at various positions

Position	ΔE (eV)[a]	Position	ΔE (eV)[a]
3	−0.067	6	+0.023
4	−0.018	7	−0.040
5	−0.043	8	−0.014

a) ΔE denotes the energy difference where the excitation energy of 1,2-NQ is subtracted from the corresponding energy for the substituted 1,2-NQ.

The changes in the calculated excitation energy of the lowest π,π^* excited states (state no. 1) with the alkyl-group substitutions are shown in Table 3. These calculations were carried out in the same manner as in previous works.[1,2] It is known that the methyl-group substitution at the 3-position of 1,2-NQ results in a relatively large red-shift of Band I.[6] In Table 3, the large energy decrease in the 3-position is consistent with this fact. In Table 3, the large energy increase in the 6-position is notable. Based on this result, a blue-shift of Band I of 6-alkyl-1,2-NQ compared with that of 1,2-NQ is expected. Since in 1,2-NQ the 6-position is the *para* position of the benzene nucleus with respect to the carbonyl group, this result is similar to that obtained for 9,10-phenanthrenequinone as reported in a previous paper.[2]

References

1) A. Kuboyama, S. Matsuzaki, M. Takagi, and H. Arano, *Bull. Chem. Soc. Jpn.*, **47**, 1604 (1974).

2) A. Kuboyama, F. Kobayashi, and S. Morokuma, *Bull. Chem. Soc. Jpn.*, **48**, 2145 (1975).

3) L. F. Fieser, "Experiments in Organic Chemistry," D. C. Heath and Co., Boston (1941), p. 230.

4) R. G. Parr, "Quantum Theory of Molecular Electronic Structure," W. A. Benjamin, New York (1964), p. 503; R. Parriser and R. G. Parr, *J. Chem. Phys.*, **21**, 767 (1953).

5) S. Nagakura and A. Kuboyama, *J. Am. Chem. Soc.*, **76**, 1003 (1954); *Nippon Kagaku Zasshi*, **74**, 97 (1953); A. Kuboyama, *Bull. Chem. Soc. Jpn.*, **33**, 1027 (1960).

6) A. Ebnöther, Th. M. Meijer, and H. Schmid, *Helv. Chim. Acta*, **35**, 910 (1952).

BULLETIN OF THE CHEMICAL SOCIETY OF JAPAN, VOL. 49 (5), 1403—1404 (1976)

An Observation of Compensation Effects between Enthalpy and Entropy Changes in the Interaction of Nickel-2,2′-bipyridine Complexes with Olefins

Akio YAMAMOTO and Takakazu YAMAMOTO

Research Laboratory of Resources Utilization, Tokyo Institute of Technology, O-okayama, Meguro, Tokyo 152

(Received November 13, 1975)

Synopsis. Compensation effects in the thermodynamic parameters $\Delta H°$ and $\Delta S°$ in the coordination of olefins with Ni(bpy) and NiR_2(bpy) (bpy=2,2′-bipyridine) and in the kinetic parameters $\Delta H^{\ddagger}$ and $\Delta S^{\ddagger}$ in reactions of NiR_2(bpy) with olefins have been observed; factors governing these compensation effects are discussed.

Coordination of an olefin to a transition metal having a σ-metal-carbon bond with a resultant activation of the metal-carbon bond constitutes a key step in various transition-metal promoted reactions of olefins. Despite the tremendous increase in the number of isolated olefin-metal complexes,[1] thermodynamic and kinetic data concerning the interaction of olefins with transition-metal complexes are quite meager and this situation seems to hinder the further understanding of the nature of the olefin-metal interaction. Dialkyl(2,2′-bipyridine)nickel(II), NiR_2(bpy) **1** (bpy=2,2′-bipyridine, R=CH_3, C_2H_5, C_3H_7, *i*-C_4H_9), and olefin-coordinated zerovalent nickel complexes, Ni(olefin)$_n$(bpy) **2** (n=1 or 2), have proved to be quite amenable to a quantitative investigation of the olefin-metal interaction.[2,3] Previous studies have established that the interaction of **1** with an olefin proceeds through the following reaction steps:

$$\underset{\mathbf{1}}{NiR_2(bpy)} + \text{olefin} \overset{K_1}{\rightleftharpoons} \underset{\mathbf{2}}{NiR_2(bpy)(olefin)} \qquad (1)$$

$$\underset{\mathbf{2}}{NiR_2(bpy)(olefin)} \xrightarrow{k} \underset{\mathbf{3}}{Ni(bpy)(olefin)} + 2R \qquad (2)$$

$2R=C_2H_6$, C_4H_{10} for R=CH_3, C_2H_5
$2R=C_3H_6+C_3H_8$, $C_4H_8+C_4H_{10}$ for R=C_3H_7, C_4H_9

Furthermore, the stability constants of the zerovalent olefin-nickel complexes in the following equilibria have been evaluated:

$$\text{Ni(bpy)(solvent)} + \text{olefin} \overset{K_2}{\rightleftharpoons} \underset{\mathbf{3}}{\text{Ni(bpy)(olefin)}} + \text{solvent} \qquad (3)$$

Examination of the enthalpy change ($\Delta H°$) and entropy change ($\Delta S°$) in equilibria (1) and (3) and of Eyring's enthalpy of activation ($\Delta H^{\ddagger}$) and entropy of activation ($\Delta S^{\ddagger}$) in the splitting of Ni–C bonds in **1** has revealed the presence of clear compensation effects between $\Delta H°$ and $\Delta S°$, as well as between $\Delta H^{\ddagger}$ and $\Delta S^{\ddagger}$. Here, results are reported in order to provide the basis for further discussions on transition metal-olefin interactions.

Compensation Effects between ΔH° and ΔS° in the Coordination of Olefins with Ni(bpy) and NiR_2(bpy). Figure 1 clearly demonstrates the presence of compensation effects in equilibria (1) and (3). Plots of $\Delta H°$ and $\Delta S°$ values for reaction (3) give a straight line over a very wide range (line A in Fig. 1), except for maleic anhydride, the only α,β-disubstituted olefin among the olefins examined. The plot of $\Delta H°$ and $\Delta S°$ values for Eq. 1 also gives a straight line with a steeper slope (line B in Fig. 1).[4] For the sake of numerical comparison, the following expression is used

$$\Delta S° = C_1 \Delta H° + C_2, \qquad (4)$$

where C_1 and C_2 are constants derived from the slopes and intercepts of straight lines A and B in Fig. 1. These values are tabulated in Table 1.

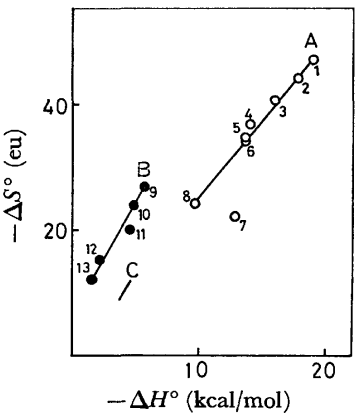

Fig. 1. The plots of $\Delta S°$ against $\Delta H°$ in the equilibria (1) and (3). Ni(bpy), line A: (1) acrylaldehyde, (2) acrylamide, (3) acrylonitrile, (4) methacrylonitrile, (5) methyl acrylate, (6) methyl vinyl ketone, (7) maleic anhydride, (8) methyl methacrylate. For NiR_2(bpy), line B: (9) R=C_2H_5, acrylaldehyde, (10) R=*n*-C_3H_7, acrylonitrile, (11) R=C_2H_5, acrylonitrile, (12) R=CH_3, acrylonitrile, (13) R=*i*-C_4H_9, acrylonitrile. The straight line C was taken from Fueno's paper.[5]

Table 1. The compensation effect between $\Delta H°$ and $\Delta S°$ in the coordination of olefins with metals

Metal	Olefin	$C_1 \times 10^3$ (eu/(cal/mol))	C_1T (at T=300)	C_2 (eu)
Ni(bpy)	β-Unsubstituted vinyl compound	2.1	0.6	+1
NiR_2(bpy)	β-Unsubstituted vinyl compound	3.3	1.0	+6
Ag^+	β-Unsubstituted vinyl ether[a]	3.0	0.9	−2

a) The values for the argentation of β-unsubstituted vinyl ethers were taken from Ref. 5.

Fueno and coworkers have previously observed a similar compensation effect in the argentation of vinyl ethers and alkenes over a narrower range as shown by line C in Fig. 1.[5] The C_1 and C_2 values are also included in Table 1. It is noteworthy to observe the presence of a compensation effect over such a wide range in the coordination of olefins bearing a variety of electron-withdrawing substituents with the nickel complexes, as well as in the argentation of olefins bearing electron-releasing substituents. Although it may be fortuitous, it is intriguing to observe that the extension of line A in Fig. 1 passes through line C. The presence of a compensation effect over this wide range implies that the interaction between the nickel complex and the variety of olefins is dominated by a single factor, namely, the complexation of the olefins with nickel through an olefinic double bond. The side-on coordination of methyl acrylate through the double bond to nickel in the solid Ni(bpy)(methyl acrylate)$_2$ has been recently established.[6] The lesser gradient in line A with a C_1T value of 0.6 at 300 K with respect to line B implies the greater contribution of the enthalpy effect on the stability of the π-olefin complexes **3**. This is in line with the anti-parallel relationship observed between log K_2 and the energy level of the π^*-orbital of the olefins,[2] a fact indicating the importance of back-donation from nickel to the olefin, which determines the stability of **3**.

In Eq. 1, on the other hand, the value of C_1T at room temperature is very close to unity, indicating the complete cancellation of the enthalpy change by the entropy change. In this case, the contribution of entropy is considered to be more important for the stabilization of the π-complexes **2** than in reaction (3) and the freedom of internal rotation of the nickel-bonded alkyl groups may exert a significant effect on the stability of **2** as reflected by the considerably smaller values of ΔS° and ΔH° observed in the complexation of acrylonitrile with the bulky isobutylnickel complex than those obtained for the propylnickel complex.

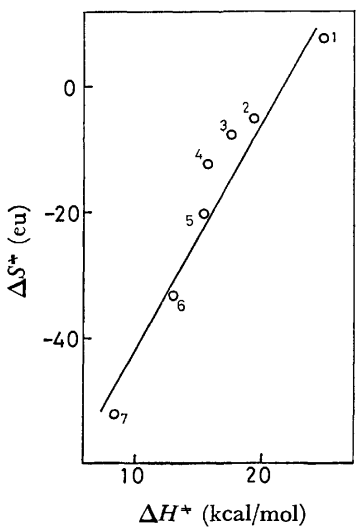

Fig. 2. Relationship between ΔH^* and ΔS^* in the reaction of Ni$(C_2H_5)_2$(bpy) with olefins. (1) methacrylonitrile, (2) acrylamide, (3) methyl vinyl ketone, (4) acrylaldehyde, (5) methyl acrylate, (6) styrene, (7) methyl methacrylate.

These results suggest that a seemingly small variation in the stability constant of a π-complex may not reflect a reater intrinsic change of interaction between an olefin and a transition-metal complex because of the presence of the compensation effect.

Compensation Effect between the Enthalpy of Activation and Entropy of Activation for the Splitting of Nickel–alkyl Bonds Induced by Olefin Coordination. Figure 2 shows that there is a fairly good correlation between ΔH^* and ΔS^* for reactions (1) and (2), which were taken from a previous paper.[2] The slope of the line in Fig. 2 is about 1/300 deg^{-1} which corresponds to a value of 1.0 for $T\Delta S^*/\Delta H^*$ at room temperature, indicating an almost complete cancellation of the entropy and enthalpy effects. The breaking of the Ni–C bond by the interaction with an olefin is a second-order reaction, whose rate constant can be expressed by K_1k in reactions (1) and (2). Since it is observed that $T\Delta S^\circ \fallingdotseq \Delta H^\circ$ in Eq. 1, the present compensation effect for the reaction allows us to deduce that there is a similar compensation effect for the splitting of Ni–alkyl bonds in the olefin coordinated diethyl (2,2′-bipyridine)nickel complex **2** given by reaction (2), namely, the acquired activation enthalpy is almost completely cancelled at room temperature by an increase in the entropy in the activated complex to be thermolyzed. A similar compensation effect in the thermolysis of alkylcopper complexes having tertiary phosphine ligands[7] has been observed.

References

1) For example, M. Herberhold, "Metal π-Complexes," Elsevier Publishing Co., Amsterdam, London, New York (1972) and references cited therein.

2) (a) T. Yamamoto, A. Yamamoto, and S. Ikeda, *J. Am. Chem. Soc.*, **93**, 3350 (1971); (b) *ibid.*, **93**, 3360 (1971).

3) T. Yamamoto, Y. Nakamura, and A. Yamamoto, *Bull. Chem. Soc. Jpn.*, **49**, 191 (1976).

4) The data for line B in Fig. 1 are taken from previously published data obtained by a visual method for the coordination of acrylaldehyde and acrylonitrile with a series of NiR$_2$-(bpy).[2] Later, somewhat more accurate data for the ethylnickel complex were obtained by an NMR method.[3] The values of ΔH° and ΔS° obtained by the NMR method also fall along the same straight line B although they have values that are somewhat more negative than those obtained by the visual method.

5) T. Fueno, O. Kajimoto, T. Okuyama, and J. Furukawa, *Bull. Chem. Soc. Jpn.*, **41**, 785 (1968).

6) P. Binger and C. Kruger, private communication.

7) A. Miyashita, Ph. D. Thesis, Tokyo Institute of Technology (1975).

BULLETIN OF THE CHEMICAL SOCIETY OF JAPAN, VOL. 49 (5), 1405—1406 (1976)

The Oxygen Gas Permselectivity of Dried Cellulose Acetate Membranes

Yoshio TANIGUCHI and Shinkichi HORIGOME

Central Research Laboratory, Hitachi Ltd., Kokubunji, Tokyo 185

(Received November 28, 1975)

Synopsis. The oxygen gas permselectivity of annealed cellulose di- and triacetate membranes were investigated. We have suggested that the permeation ratios of oxygen to nitrogen gases of these membranes attain 7—8 by annealing in air at 180 °C.

In recent years, cellulose diacetae membranes have came to play an important role in the reverse osmosis process. Therefore, there have been many investigations concerning the permselectivities for salts in aqueous solutions. However, the gas permselectivities of the cellulose acetate membranes have not been widely investigated. The cellulose diacetate membranes have, though, been found to show 2—3 times as much permeability to oxygen as to nitrogen.[1] Most polymer membranes thus far reported have oxygen permeation ratios to nitrogen ranging from 2 to 6.[2,3]

In this paper, we wish to report that the cellulose di- and triacetate membranes have a higher permeation ratio of oxygen gas than the reported values of this polymer, we have established this by investigating the conditions for the membrane preparation.

The cellulose di- and triacetate used in this study were Eastman's type E398-3 and Daicel's type LT-70 respectively. Two kinds of cellulose diacetate membranes, skinned and dense membrane, were prepared by the same procedure as in a previous paper.[4] Here, "skinned membrane" refers to the membrane consisting of a dense layer or skin, which is only 0.1 to 1.0 μm thick and which is responsible for the separation, on top of a highly porous structure which comprises about 99% of the overall thickness of the membrane. The skinned and dense membranes were both about 120 μm thick.

The cellulose triacetate dense membranes were prepared by a procedure essentially the same as that used for the cellulose diacetate dense membranes. In this case, the casting solvent consisted of 90 wt % dichloromethane and 10 wt % ethanol. The dense membranes were 10—30 μm thick. However, we could not make the skinned membrane of cellulose triacetate because we lack the knowledge of the most combination of solvents.

The skinned membranes were annealed in a water bath for 30 min at 80—90 °C and then freeze-dried in order to maintain the skinned structure of the membranes. The dense membranes were annealed in the air at 180 °C for 2 h.

The instrument for gas permeation measurment was driven by the pressure difference between the atmospheric and the diminished pressure; the gas permeation rates were calculated from the pressure change in the low-pressure region. Pure gases were used as the permeative gases.

The results of the gas permeation of the skinned membranes at 23 °C are shown in Fig. 1. In Fig. 1 the apparent gas permeation rates are used because the dense layer of the skinned membrane was not clear enough to be measured. Figure 1 shows some scatter, but this scatter seems to be result of the fluctuation in freeze-drying conditions. It is apparent from these results that the permeation ratio of oxygen to nitrogen increases with a decrease in the oxygen gas permeation rate, and with an increase in the annealing temperature; finally, it may reach the permeation ratio of the annealed dense membrane to be discussed below. It is also indicated that the non-annealed membranes deviate from this relationship, but the reason for this remains unknown.

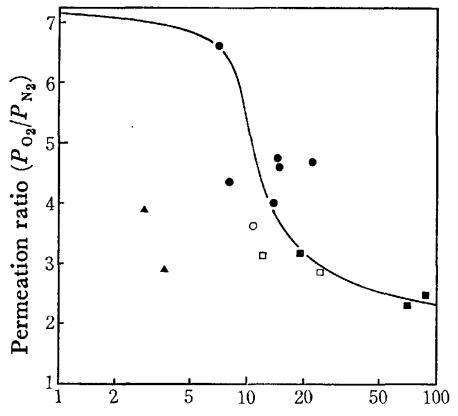

Fig. 1. Gas permeation property of skinned cellulose diacetate membranes.
▲: Non-annealed, ●: annealed at 90 °C, ○: annealed at 85 °C, □: annealed at 80 °C, ■: Gantzel's data.[1]

TABLE 1. GAS PERMEABILITY COEFFICIENTS OF DENSE CELLULOSE DIACETATE MEMBRANES

Annealing condition	Membrane thickness	P_{O_2} (cm²/s cmHg)	P_{O_2}/P_{N_2}
Non-annealed	30 μ	0.72×10^{-10}	3.2
4 h at 180 °C	30	0.93	7.3
Gantzel's data	—	0.78	2.8

TABLE 2. GAS PERMEABILITY COEFFICIENTS OF DENSE CELLULOSE TRIACETATE MEMBRANES

Annealing condition	Membrane thickness	P_{O_2} (cm²/s cmHg)	P_{O_2}/P_{N_2}
Non-annealed (1)	19 μ	1.6×10^{-10}	5.3
Non-annealed (2)	13	1.6	6.2
4 h at 180 °C (1)	18	1.9	7.8
4 h at 180 °C (3)	30	1.5	7.2

The results of the gas permeation of the dense membranes at 23 °C are shown in Tables 1 and 2. It can be noticed from these tables that upon the annealing of the dense membranes the oxygen gas permeation rates are

not affected, while the permeation ratios increase, and that the permeation ratios of cellulose di- and triacetate membranes attain 7.3 and 7.8 respectively. It is noteworthy that the oxygen gas permeation rate of the cellulose triacetate membrane is about twice that of the cellulose diacetate membrane.

It is well known that the gas permselectivity of polymer membranes is determined by the gas solubilities and the gas-diffusion coefficients of the membranes. We measured the oxygen and nitrogen gas solubilities of these membranes, but could not recognize any difference in the solubilities between the non-annealed and annealed membranes.[5] Consequently, we assume that the annealing process mainly influences the diffusion of the gases, and that the pore radii[6] in the cellulose di- and triacetate membranes might be made smaller by the annealing process. This annealing process would have greater effect on the diffusion of nitrogen gas, whose molecular size is larger than that of oxygen gas; therefore, the oxygen permeation ratio would increase.

As has been mentioned above, the cellulose triacetate membrane has a high permeability and permselectivity. Consequently, if one succeeded in making the skinned membrane of cellulose triacetate, it may be expected to be an excellent membrane for separating oxygen gas from nitrogen gas.

References

1) P. K. Gantzel and U. Merten, *Ind. Eng. Chem. Process Des. Develop.*, **9**, 331 (1970).
2) Y. Taniguchi and S. Horigome, *Polymer J.*, **7**, 519 (1975).
3) T. Nakagawa, *Japan Plastics*, **24** (12), 9 (1973).
4) Y. Taniguchi and S. Horigome, *J. Appl. Polymer Sci.*, **19**, 2743 (1975).
5) S. Horigome and Y. Taniguchi, to be published.
6) Y. Taniguchi and S. Horigome, *Desalination*, **16**, 395 (1975).

BULLETIN OF THE CHEMICAL SOCIETY OF JAPAN, VOL. 49 (5), 1407—1408 (1976)

Magnetic Susceptibility of Perylene-Iodine Complex

Minoru KINOSHITA,* Hisao KANDA,** and Hideo AKAMATU***

Department of Chemistry, Faculty of Science, The University of Tokyo, Hongo, Bunkyo-ku, Tokyo 113

(Received December 5, 1975)

Synopsis. The magnetic susceptibility of a highly conductive 2:3 charge-transfer complex of perylene with iodine has been examined as a function of temperature. The paramagnetic susceptibility, which was found to be nearly independent of temperature, is considered to be due only to the perylene cation radical.

Recently, much interest has centered on the tetracyanoquinodimethane (TCNQ) anion radical salts with high electrical conductivity such as quinolinium-$(TCNQ)_2$, *N*-methylphenazinium-TCNQ and tetrathiofulvalenium-TCNQ. In these complexes, the form of the acceptor has been well established by various electronic, as well as by X-ray crystallographic, analysis. The charge-transfer complexes formed between aromatic compounds and halogens fall into another class of highly-conductive substances.[1-3] The form of halogens in these complexes, however, is not well established

Some time ago, Singer and Kommandeur showed that the spin density of the 2:3 perylene-iodine complex changes exponentially with temperature with an activation energy of 0.019 eV,† which is the same as that for electrical conduction.[4] They measured the ESR absorption intensity in order to obtain the spin density. If the iodine molecule in the complex takes the form of I_2^-, as is commonly supposed in analogy to the TCNQ anion radical salts, it contributes to the paramagnetism.

However, the paramagnetism of I_2^- in the complex can not be detected in the ESR experiments for the following two reasons: (i) the ESR absorption of I_2^- appears over a wide magnetic-field range[5,6] because of the large nuclear spin ($I=5/2$) and the large magnetic moment of the iodine atom, while the absorption of the complex shows a linewidth of several gauss†† at 100—300 K,[4] and (ii) the *g*-values of I_2^- in alkali iodides (V_k center) have been reported to be $g_{//}=1.86$—1.89 and $g_\perp=2.27$—2.30,[6] whereas the average *g*-value of the complex is 2.0033 and the anisotropy is very small.[4] The observed ESR absorption is therefore considered to be due only to the perylene cation radical, even though the acceptor has a paramagnetic form.

It is therefore worthwhile to examine the static magnetic susceptibility of the complex and to compare the results with those obtained by the ESR method. Therefore, the static susceptibility of the 2:3 perylene-iodine complex was measured in the temperature range of 77—296 K. In this note, the data are presented on the basis of the molecular unit of $(C_{20}H_{12})\cdot(I_2)_{1.5}$.

TABLE 1. MOLAR MAGNETIC SUSCEPTIBILITIES OF PERYLENE, IODINE AND THEIR COMPLEX AT ROOM TEMPERATURE

	$-\chi_M/10^{-6}$ emu·mol^{-1}		
	This work	Literature	Ref.
Perylene ($C_{20}H_{12}$)	160	167	7
		159	2
		166—174	8
Iodine (I_2)	80.0	91.4	9
	77.8	89—92.4	8
Complex [$(C_{20}H_{12})\cdot(I_2)_{1.5}$]	217.8	210[a]	7
		217[b]	2

a) Mole ratio=1:1.34; b) Mole ratio=1:1.63.

The magnetic susceptibilities obtained for perylene, iodine and the complex at 290 K are given in Table 1. Although the values for iodine are a little different from those found in the literature, the present value of -80×10^{-6} emu/mol††† is used in the following. From these results, the diamagnetic contribution is estimated to be -280×10^{-6} emu/mol for $(C_{20}H_{12})\cdot(I_2)_{1.5}$. The discrepancy between the observed and calculated susceptibilities for the complex can then be reasonably ascribed to the paramagnetism resulting from the complex formation; *i.e.*, $\chi_p=62\times10^{-6}$ emu/mol at 290 K.

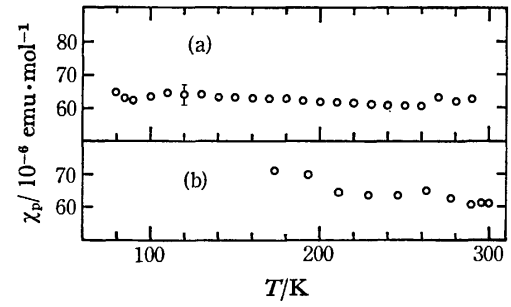

Fig. 1. Molar paramagnetic susceptibility of the perylene-iodine (2:3) complex as a function of temperature.
(a) The results by static susceptibility measurement. The error bar indicated on the point at 120 K applies to all the points.
(b) The susceptibility reproduced from the spin density data in Fig. 5 of Ref. 4.

By assuming that the diamagnetic part is independent of the temperature, the paramagnetic susceptibility at

* To whom inquiries may be addressed. Present address: The Institute for Solid State Physics, The University of Tokyo, Roppongi, Minato-ku, Tokyo 106.

** Present address: National Institute for Researches in Inorganic Materials, Sakura-mura, Niihari-gun, Ibaragi 300-31.

*** Present address: Institute for Molecular Science, Myodaiji, Okazaki, Aichi 444.

† 1 eV≃1.6021×10^{-19} J.

†† 1 G=10^{-4} T.

††† Molar magnetic susceptibility is expressed in m^3·mol^{-1} in the International System of Units; the values in emu·mol^{-1} should be multiplied by $4\pi\times10^{-6}$ to convert to SI units.

various temperatures is obtained as shown in Fig. 1, where the susceptibility calculated from the spin density data of Singer and Kommandeur is also shown for comparison.[4] If one considers the difficulty in the ESR intensity measurements, one may conclude that the results obtained by both methods are in complete agreement with each other.

The close agreement between the results by the resonance and static methods thus excludes the possibility that the iodine in the complex is in a paramagnetic form, such as I_2^-. The acceptor should be in diamagnetic form in the complex; it may be I_2, I_3^- or other higher polyiodides, although which cannot be said with certainty. In this connection, it may be noted that Matsunaga has suggested the existence of complex salts of phenothiazine, such as $(\text{phenothiazine})_2^+ \cdot (Br_2I)^-$,[10] and $(\text{phenothiazine})_2^+ \cdot (I_5^-)$[11] from the changes observed in the IR and electronic spectra and in the electrical resistivity when the iodine or phenothiazine was added to the phenothiazine bromide or phenothiazine-iodine complex.

The paramagnetic susceptibility of the complex was found to be independent of temperature. Similar results have been obtained for other systems such as highly conductive TCNQ complexes,[12] although no conclusive explanation has been given. One of the possible explanations is that the paramagnetism is due to the conduction electrons, as proposed by Singer and Kommandeur. In this case, there may be two possible ways to analyze the results. One is the way in which the phenomenon is regarded as Pauli paramagnetism; in which case, the susceptibility is expressed as

$$\chi_p = 2\mu_B^2 \cdot N(\varepsilon_F)$$

where μ_B is the Bohr magneton and $N(\varepsilon_F)$ is the density of states for one spin direction. By neglecting the diamagnetic contribution of the conduction electrons, the density of states for the complex is estimated to be about 1 $eV^{-1} \cdot molecule^{-1}$. This value can be compared with 7.5 $eV^{-1} \cdot molecule^{-1}$ for the quinolinium-$(TCNQ)_2$ complex.[12] The other is the way which has been adopted by Singer and Kommandeur.[4] They plotted $\ln(\chi_p \cdot T)$ against $1/T$ and obtained a straight line. However, in our case where the temperature range is much wider, as Fig. 1 shows, the plot does not give a straight line.

The experimental procedure was as follows. Synthesized perylene was recrystallized successively from benzene and glacial acetic acid, and finally sublimed in a vacuum. The iodine used was obtained by sublimation from a mixture of iodine, potassium iodide and calcium oxide in 10: 1: 2 weight ratios. Four samples of the complex were prepared by two different manners[2,3] and examined by the Faraday method using an apparatus described elesewhere.[13] The freshly-prepared polycrystalline complex was placed in a spherical (5 mm o.d.) thin-walled Pyrex glass container through a small capillary arm, and the container was sealed at the capillary portion with a small flame while the spherical part was immersed in a liquid nitrogen bath. After the measurement, the complex was taken out of the container and analyzed by the titration method.[2] The analysis showed that the complex examined was in a 1: 1.5 molar ratio to within the experimental error. Although only the typical results have been described here, the results obtained for other samples were essentially identical to within the range of experimental error.

References

1) H. Akamatu, H. Inokuchi, and Y. Matsunaga, *Nature*, **173**, 168 (1954); *Bull. Chem. Soc. Jpn.*, **29**, 213 (1956).
2) T. Uchida and H. Akamatu, *Bull. Chem. Soc. Jpn.*, **34**, 1015 (1961).
3) J. Kommandeur and F. R. Hall, *J. Chem. Phys.*, **34**, 129 (1961).
4) L. S. Singer and J. Kommandeur, *J. Chem. Phys.*, **34**, 133 (1961).
5) T. Shida, Y. Takahashi, H. Hatano, and M. Imamura, *Chem. Phys. Lett.*, **33**, 491 (1975).
6) E. Boesman and D. Schoemaker, *J. Chem. Phys.*, **37**, 671 (1962); T. Sidler, J. -P. Pellaux, A. Nouailhat, and M. A. Aegerter, *Solid State Commun.*, **13**, 479 (1973); J. -J. Pilloud and C. Jaccard, *ibid.*, **17**, 907 (1975).
7) Y. Matsunaga, *Bull. Chem. Soc. Jpn.*, **28**, 475 (1955).
8) "Landolt-Börnstein," Zahlenwerte und Funktionen, 6 Aufl. II Band, 10 Teil, Springer-Verlag (1967).
9) "International Critical Tables," Vol. VI, p. 355, McGraw-Hill (1929).
10) Y. Matsunaga and K. Shono, *Bull. Chem. Soc. Jpn.*, **43**, 2007 (1970); Y. Matsunaga and Y. Suzuki, *ibid.*, **46**, 719 (1973).
11) Y. Matsunaga, private communication.
12) R. G. Kepler, P. E. Bierstedt, and R. E. Merrifield, *Phys. Rev. Lett.*, **5**, 503 (1960); W. J. Siemons, P. E. Bierstedt and R. G. Kepler, *J. Chem. Phys.*, **39**, 3523 (1963); R. G. Kepler, *ibid.*, **39**, 3528 (1963).
13) Y. Sato, M. Kinoshita, M. Sano, and H. Akamatu, *Bull. Chem. Soc. Jpn.*, **40**, 2539 (1967).

BULLETIN OF THE CHEMICAL SOCIETY OF JAPAN, VOL. 49 (5), 1409—1410 (1976)

Chelation Effect of Alizarin Dyes on the Semiconductor-Aqueous Solution Systems

Michio MATSUMURA, Yoichi NOMURA, and Hiroshi TSUBOMURA

Department of Chemistry, Faculty of Engineering Science, Osaka University, Toyonaka, Osaka 560

(Received December 8, 1975)

Synopsis. The dye-sensitized photocurrents produced by some semiconductor (titanium dioxide single crystal or zinc oxide sinter) in electrolyte solutions containing alizarin dyes were studied. The photocurrent was concluded to be caused by the sensitization of the alizarin dyes chelated to the semiconductor electrodes.

When an *n*-type semiconductor is anodically polarized, a current is induced by light whose photon energy is greater than the band gap of the semiconductor.[1] In cases where the electrolyte solutions contain cyanine dyes or xanthene dyes, photocurrents arise by light absorbed by the dyes.[2] In many cases, such a dye-sensitized anodic photocurrent is believed to be caused by the electron transfer from the excited dye adsorbed on the electrode surface into the electrode.[3–7] However, the effect of light on the dye in the bulk of the solution to produce an electrochemically active species might also be present.[7] These two mechanisms cannot be distinguished experimentally, if one uses a dye-electrolyte solution, as has been done by most previous authors.

This paper presents some results on the sensitized photocurrent by alizarin dyes chelated to the semiconductor electrodes. Very recently, similar work was reported by Danzmann and Hauffe, mainly on azo dyes and zinc oxide single crystal.[8]

Experimental

Titanium dioxide single crystal disks with the (001) face and zinc oxide sintered disks, both *n*-type semiconductors, were used. The structure of the electrodes was mostly the same as described previously.[6,9] The surface of the TiO_2 disk was scratched by rough silicon carbide abrasive to make the surface area large. The potential of the semiconductor electrodes *vs.* the reference electrode (SCE) was controlled by a Hokutodenko HA-101 potentiostat and the current was measured with the aid of a Yokogawa Hewlett Packard LS-2D electrometer. A 500 W xenon lamp (Ushio electric Inc.) was used as a light source, the light being monochromatized by using a Japan Jarrell-Ash, 0.25 m, Ebert type monochromator. The solutions contained 0.2 mol/l Na_2SO_4 as the supporting electrolyte. Oxygen was removed by bubbling with high purity nitrogen gas before measurements. Alizarin, Alizarin S, and quinalizarin were used as the photosensitizer. They belong to the mordant dyes and are known to make lakes with metal oxides. A Simadzu SL-50L spectrometer was used for the measurements of absorption spectra.

Results and Discussion

When TiO_2 powder was added into an aqueous solution of alizarin at the pH of 4.3, the powder colored reddish purple. Figures 1 a) and b) show the absorption spectrum of an aqueous solution of alizarin and

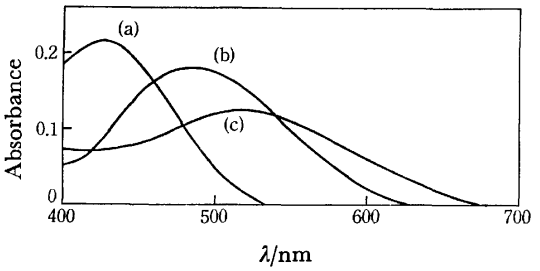

Fig. 1. Absorption spectra of alizarin and the colored powder; (a) a 5.2×10^{-6} mol/l aqueous solution of alizarin, pH=4.3, measured with a 10 cm cell, (b) colored TiO_2 powder in a KBr disk, the absorbance of TiO_2 powder being subtracted, (c) colored ZnO powder in a KBr disk, the absorbance of ZnO powder being subtracted.

that of a potassium bromide disk containing the colored powder, respectively. The absorption spectrum of an ethanol solution of titanium tetrachloride and alizarin nearly coincided with that of the colored TiO_2 powder. It is therefore concluded that the coloration is caused by a chelate compound formed between alizarin and titanium ion at the surface of the TiO_2 powder. The absorption spectrum of the chelate compound on a TiO_2 single crystal was measured through the single crystal, which was similar to that formed on the powder.

When ZnO powder was added into an aqueous alizarin solution, the powder colored purple whose absorption spectrum is shown by Fig. 1 c). This coloration is also considered to be due to the chelate formation at the ZnO surface.

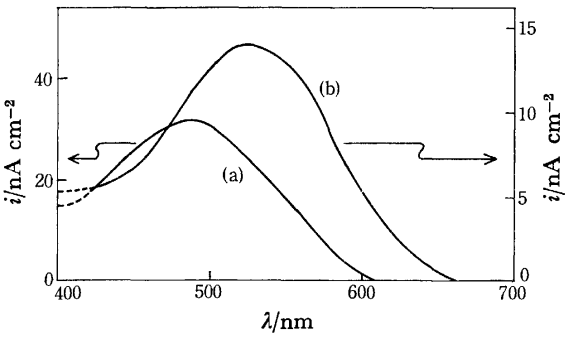

Fig. 2. Photocurrent action spectra in the solution of 5.2×10^{-6} mol/l alizarin at the anodic bias of 0.5 V. The photocurrents are corrected so that they correspond to the values for a uniform light intensity at all wavelengths. (a) For the TiO_2 electrode, with the illumination intensity $I=1.4\times10^{14}$ photons/cm² s. In these conditions the dark current i_d was 10 nA/cm². (b) For the ZnO electrode, $I=4.6\times10^{13}$ photons/cm² s. $i_d=4$ nA/cm².

Figure 2 shows the action spectra of the photocurrents for the TiO_2 and ZnO electrodes in the alizarin–electrolyte solution. They were obtained with a weak illumination intensity, so that the photocurrents did not change during the measurements and the wavelengths were scanned at the high speed of 250 nm/min. The intensity of the photocurrent was also confirmed to be proportional to the illumination intensity at several wavelengths. The action spectra nearly agree with the absorption spectra of the solutions. Consequently, the photocurrents are concluded to be caused by the sensitization due to the chelate compounds formed on the surface of the electrodes and not by the photochemical reactions of the dye in the solution. When each of the electrodes was dipped in a 5.2×10^{-6} mol/l alizarin solution for a while, washed with water, dipped into an electrolyte solution free from dye, and the photocurrents were measured, their action spectra agreed with those shown in Fig. 2. In this case, the intensities of the photocurrents were nearly the same as those observed in the alizarin–electrolyte solution systems. This indicates that the chelate compounds formed on the electrode surfaces are insoluble. The intensities of the photocurrent decayed gradually with illumination, the decay being the faster, the higher the illumination intensity. In the case of the TiO_2 electrode the decayed photocurrents recovered to the initial values, when the electrode was kept in the dark solution for a day. This seems to show that electrons are supplied by some means from the solution to the chelate compound.

Photocurrent measurements were also made for Alizarin S and quinalizarin which form chelate similar to that of alizarin. The action spectra for Alizarin S were confirmed to agree with the absorption spectra of the chelate compounds on the TiO_2 and ZnO powders. For the case of quinalizarin, the photocurrents also seem to be due to the chelate compounds, for their action spectra do not agree with the absorption spectrum of the dye in solution.

Concerning the photo-active species, two structures are considered; one is the alizarin dye directly coordinated to the metal ion which is still in the lattice of the oxide, and the other is the complete chelate compound physically adsorbed on the oxide surface. At present, we cannot decide which of the two models is the correct one. Trial to obtain a stoichiometric chelate compound in a pure state failed.

The present results show that the photo-electrochemical measurements provide a highly sensitive means to obtain the electronic spectra of very small quantities of materials on the solid–liquid interface.

The authors wish to express their gratitude to Wireless Research Laboratory, Matsushita Electric Industrial Co. Ltd. for the kind donation of zinc oxide sinter disks. The present work was partially supported by a Grant-in-Aid for Scientific Reserch from the Ministry of Education (No. 911504).

References

1) F. Lohmann, *Ber. Bunsenges. Phys. Chem.*, **70**, 87 (1966). H. Gerisher, *J. Electrochem. Soc.*, **113**, 1174 (1966).

2) H. Gerisher and H. Tributsch, *Ber. Bunsenges. Phys. Chem.*, **72**, 437 (1968). H. Tributsch and H. Gerisher, *ibid.*, **73**, 251 (1969). K. Hauffe, H. Pusch, and J. Range, *Z. Phys. Chem.*, **64**, 122 (1969). R. Memming and H. Tributsch, *J. Phys. Chem.*, **75**, 562 (1971). A Fujishima, T. Watanabe, O. Tatsuoki, and K. Honda, *Chem. Lett.*, **1975**, 13.

3) A. Fujishima, E. Hayashitani, and K. Honda, *Seisan-kenkyu*, **23**, 31 (1971).

4) B. Pettinger, H. -R. Schöppel, and H. Gerisher, *Ber. Bunsenges. Phys. Chem.*, **77**, 960 (1973).

5) W. P. Gomes and F. Cardon, *Ber. Bunsenges. Phys. Chem.*, **75**, 914 (1971).

6) M. Matsumura, K. Yamamoto, and H. Tsubomura, *Nippon Kagaku Kaishi*, **1976**, 399.

7) R. Memming, *Photochem. Photobiol.*, **16**, 325 (1972).

8) H. J, Danzmann and K. Hauffe, *Ber. Bunsenges. Phys. Chem.*, **79**, 438 (1975).

9) T. Ohnishi, Y. Nakato, and H. Tsubomura, *Ber. Bunsenges. Phys. Chem.*, **79**, 523 (1975).

BULLETIN OF THE CHEMICAL SOCIETY OF JAPAN, VOL. 49 (5), 1411—1412 (1976)

Charge-transfer Interaction in Supercooled Melts of Some Derivatives of *N*-Picrylaniline

Yoshio MATSUNAGA

Department of Chemistry, Faculty of Science, Hokkaido University, Sapporo 060

(Received December 12, 1975)

Synopsis. Supercooled melts of *N*-picrylaniline and its derivatives, the molecules of which consist of electron-donating and -accepting moieties, are colored more deeply than the crystals. Many of them exhibit glass transitions.

Some derivatives of *N*-picrylaniline have been known to be obtained in differently colored forms. For example, Grison has prepared *N*-picryl-*p*-iodoaniline in yellow, orange, and red forms, and determined the crystal and molecular structures.[1] The arrangement of the molecules is quite different in these polymorphic forms, but the structure of the molecule itself remains almost the same. In addition, he has noted that the melt is readily supercooled. Such a sample is red-colored and can be kept at room temperature without crystallization over a period of months. As we have reported for the dimorphic forms of *o*- and *p*-anisyl-*p*-benzoquinones,[2] the difference in color may be explained by the difference in the intermolecular charge-transfer (CT) interaction between the electron-donating moiety of a molecule and the accepting moiety of the neighboring molecule. Both the intensity and the location of the CT absorption are expected to be modified, to some extent, by the mode of molecular packing. As the readiness of supercooling might be correlated with an enhanced CT interaction, the spectral measurement and thermal analysis of supercooled melts have been attempted for a number of the derivatives.

The *N*-picrylanilines were prepared by the condensation reaction between picryl chloride and anilines in boiling ethanol.[3] The latter carried one of the following substituents: methyl, methoxy, ethoxy, chloro, bromo, and iodo. The compounds were melted in small aluminum pans, and then they were quickly cooled by being placed on a cold metal block. For the spectral measurements, the supercooled melts were ground with sodium chloride in concentrations of the order of one weight percent. The spectra were measured by means of a Beckman DK 2A spectroreflectometer as the difference in reflectance between the mixture and pure sodium chloride, and were plotted using the Kubelka-Munk function, $f(R)=(1-R)^2/2R$, where R is the reflectance.[4] The calorimetric curves were recorded on a Rigaku Denki differential scanning calorimeter, Model 8001 SL/C, at a heating rate of 5 °C/min. The glass transitions were measured with samples stored for several days at room temperature.

The color of all the compounds examined here becomes deeper upon melting. The melts are easily supercooled without color change. The most remarkable changes were observed with the derivatives carrying methyl. methoxy, and ethoxy groups. For example, *N*-picryl-*m*-anisidine is yellow in the crystalline state and is reddish orange in the molten and supercooled states. As is shown in Fig. 1, this change is ascribed to the appearance of an additional absorption on the longer wavelength side of the main absorption, having a maximum at about 400 nm. The former may be assigned to the intermolecular CT absorption, and the latter to the intramolecular CT absorption involving the transfer of an electron from the electron-donating moiety to the accepting moiety. The molecular packing in the crystalline state seems to be unfavorable to the intermolecular CT interaction, but a contact between the two moieties may be allowed by the disorder introduced by melting. If the interaction operating in the melt is strong, the disorder is to be conserved below the melting point. The color change observed with *N*-picryl-*o*-anisidine is similar to the afore-mentioned: namely, reddish orange in the crystalline state and deep red in the supercooled state. In this case, the spectral change suggests that the main absorption in the former state arises from the intermolecular CT interaction (see Fig. 1). The maximum of the intramolecular CT absorption may be located at 400 nm.

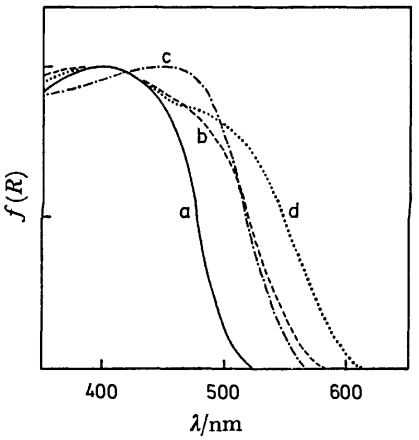

Fig. 1. Spectra of *N*-picryl-*m*-anisidine in the crystalline state (a) and in the glassy state (b) and those of *N*-picryl-*o*-anisidine in the crystalline state (c) and in the glassy state (d). The maximum is arbitrarily taken as 1.00 in each spectrum.

Another feature of interest is the appearance of a glass transition. For instance, the supercooled melt of *N*-picryl-*p*-iodoaniline described by Grison was found to show a small endothermic peak around 60 °C, a large exothermic one around 110 °C, and a large endothermic one near 190 °C. As the location of the last is close to the melting point of the red form, the large exothermic peak must be due to the crystallization of the supercooled melt. The above-mentioned temperature is consistent with Grison's observation that the crystallization into the orange form is rapid in the range from 100 to 120 °C. This form has been reported

Table 1. Glass transition temperatures and crystallization temperatures of supercooled melts of *N*-picrylanilines
(heating rate: 5 °C/min)

Substituent	Glass transition (°C)	Crystallization (°C)
None	—	70
o-Methyl	—	80
m-Methyl	40	—
p-Methyl	—	80
o-Methoxy	40	a)
m-Methoxy	45	—
p-Methoxy	—	75
o-Ethoxy	—	—
m-Ethoxy	30	90
p-Ethoxy	—	75
o-Chloro	—	85
m-Chloro	45	—
p-Chloro	50	90
m-Bromo	50	a)
p-Bromo	55	85
m-Iodo	55	—
p-Iodo	60	110

a) Partial crystallization occurred, but the peak was too broad to be located.

to be transformed into the red form around 145 °C, but this transition was not detected on our calorimetric curves. One may consider the small endothermic peak around 60 °C as an indication of a glass transition. Such peaks, with areas of 0.3—0.8 kcal/mol at the present heating rate, could be observed with many derivatives, as summarized in Table 1. All the *m*- and *p*-halo derivatives exhibit the transitions. The temperatures in the *p*-derivatives are consistently higher than those in the corresponding *m*-derivatives. In each group, the transition temperature becomes progressively higher with increasing the atomic weight of the halogen. On the other hand, the *m*-ethoxy derivative shows a peak located 15°C lower than the *m*-methoxy derivative; therefore, the transition in the *o*-ethoxy derivative might be below room temperature. It is particularly interesting to note that no crystallization can be observed in derivatives carrying the substituent on the *o*- or *m*-position upon heating to their melting points, suggesting the presence of strong molecular entanglement assisted by an intermolecular CT interaction.

References

1) E. Grison, *Acta Crystallogr.*, **2**, 410 (1949).
2) J. Aihara, G. Kushibiki, and Y. Matsunaga, *Bull. Chem. Soc. Jpn.*, **46**, 3584 (1973).
3) B. Linke, *Ber.*, **56**, 848 (1923).
4) W. W. Wendlandt and H. G. Hecht, "Reflectance Spectroscopy," Interscience Publishers, New York (1966), p. 62.

BULLETIN OF THE CHEMICAL SOCIETY OF JAPAN, VOL. 49 (5), 1413—1414 (1976)

Ultrasonic Absorption Mechanism in an Aqueous Solution of Isopropyl Alcohol

Sadakatsu NISHIKAWA, Mitsuo MASHIMA, and Tatsuya YASUNAGA*

Department of Chemistry, Faculty of Science and Engineering, Saga University, Honjo-machi, Saga 840
**Department of Chemistry, Faculty of Science, Hiroshima University, Higashisenda-machi, Hiroshima 730*

(Received December 26, 1975)

Synopsis. Ultrasonic absorption measurements in an aqueous solution of isopropyl alcohol were made in the frequency range from 5 to 220 MHz and in the concentration range from 3 to 10 M. The excess absorption which is characteristic of a single relaxation process was observed. The mechanism of the excess absorption was interpreted in terms of a reaction expressed by AB⇌A+B, where A and B are monomeric molecules of alcohol and water respectively. The rate constants for forward and backward reactions were determined from the concentration dependences of the relaxation frequencies. The results obtained were compared with those of aqueous solutions of other alcohols which had already been published.

The structural properties of aqueous solutions of various alcohols have been studied in relation to biological reaction mechanisms. The ultrasonic studies have been also applied to the investigations of the dynamical properties of aqueous solutions of alcohols.[1-3] The present authors have previously reported the results of the ultrasonic absorption measurements in aqueous solutions of propyl, *t*-butyl, and allyl alcohols, and they have interpreted the excess absorptions from the point of view of reaction kinetics.[4,5] In this paper, we will report the results of the ultrasonic absorption measurements in an aqueous solution of isopropyl alcohol; the results will be compared with those of other alcohols.

Experimental

The isopropyl alcohol was a reagent-grade commercial product and was distilled once. No impurity was observed by gas-chromatography. The water used in the experiments was doubly distilled. The sample solutions were made at the desired concentrations by weight. The concentration range of the experiments was from 3.00 to 10.01 M. The apparatus for the ultrasonic absorption and velocity measurements have been previously described in detail.[4,6] The frequency range of the ultrasonic absorption measurements was from 5 to 220 MHz, while the sound velocity was measured at 1.92 MHz by a sing-around technique. All the measurements were made at 25 °C.

Results and Discussion

Figure 1 shows the representative ultrasonic absorption spectra in an aqueous solution of isopropyl alcohol. All the spectra in the solution can be described by the following expression of a single relaxation in the frequency range measured.

$$\alpha/f^2 = A/[1+(f/f_r)^2] + B \qquad (1)$$

where α is the absorption coefficient; f, the frequency; f_r, the relaxation frequency, and A and B, constants. The relaxation parameters were determined by the usual procedure.[5] In Table 1, the obtained values of ultrasonic parameters are listed together with the sound velocities and densities.

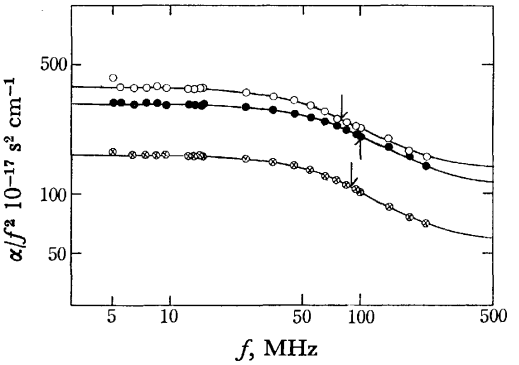

Fig. 1. Ultrasonic absorption spectra in an aqueous solution of isopropyl alcohol at 25 °C.
⊗; 4.00M, ○; 5.50M ●; 7.00M

Table 1. Relaxation parameters, sound velocities and densities in aqueous solution of isopropyl alcohol

C_a (M)	ρ (g ml^{-1})	c (m s^{-1})	f_r (MHz)	A (10^{-17} s^2 cm^{-1})	B
3.00	0.9718	1597	100	25.7	38.8
4.00	0.9620	1595	90	144	73.7
4.50	0.9570	1578	92	279	92.1
5.00	0.9500	1558	85	275	170
5.50	0.9428	1532	80	318	177
6.00	0.9324	1501	85	299	168
6.50	0.9310	1481	95	274	170
7.00	0.9146	1465	100	260	145
8.00	0.8995	1409	110	197	137
10.01	0.8551	1315	145	59.9	119

The sound absorption in aqueous solutions of propyl and *t*-butyl alcohols features a characteristic double relaxation; the mechanisms were interpreted in terms of the solute-solvent interaction and the molecular aggregation of alcohol by hydrophobic interaction. While, the excess absorption in an aqueous solution of allyl alcohol was expressed by a single relaxation process, and the mechanism was attributed to the solute-solvent interaction, as in a previous study.[5] Therefore, the cause of the ultrasonic absorption in an aqueous solution of isopropyl alcohol may be expected to be associated with the solute-solvent interaction, because the region of the relaxation frequency is roughly the same as that of allyl alcohol. The model for the relaxation process is as follows;

$$AB \underset{k_{21}}{\overset{k_{12}}{\rightleftharpoons}} A + B \qquad (2)$$

where A and B are the molecules of alcohol and water respectively, and k_{ij}, the rate constant. The relations for the relaxation frequency and the maximum excess absorption per wavelength are;

$$2\pi f_r = 1/\tau = k_{21}(C_2+C_3) + k_{12} \quad (3)$$

$$\mu_{max} = Af_r c/2 = \pi\rho c^2/[VRT(1/C_1+1/C_2+1/C_3-1/C_T)] \times (\Delta V-\alpha_p^\infty \Delta H/\rho C_p^\infty)^2 \quad (4)$$

All the symbols in these equations are defined as in the previous paper.[5] Equation 3 can be rewritten as:

$$2\pi f_r = 1/\tau = k_{21}\sqrt{(C_a-\beta C_w+K_{12})^2+4\beta C_w K_{12}} \quad (5)$$

where K_{12} is the equilibrium constant and C_a and C_w are the analytical concentrations of alcohol and water respectively. The parameter, β, is the mole fraction of the water monomer. The introduction of β into the interpretation of the excess absorption means that only the monomer of the water molecule can participate in the reaction expressed by Eq. 2. The values of k_{21}, β and K_{12} were determined so as to obtain a best fit of the data to Eq. 5. Here, the fact that the relaxation frequencies went through a minimum at the concentration of C_a=5.50 M was also used to estimate the parameters. The kinetic parameters obtained are listed in Table 2, along with those of aqueous solutions

Table 2. The reaction parameters and the stability of water structure in aqueous solutions of alcohols

Solute	k_{12} (s^{-1})	k_{21} ($M^{-1}s^{-1}$)	k_{23} a) ($M^{-2}s^{-1}$)	k_{32} a) (s^{-1})	β
t-Butyl alcohol	1.2×10^8	7.2×10^7	5.5×10^5	4.9×10^7	0.12
Propyl alcohol	1.6×10^8	6.2×10^7	2.2×10^5	6.9×10^7	0.15
Isopropyl alcohol b)	1.4×10^8	8.8×10^7	—	—	0.17
Allyl alcohol	1.5×10^8	6.3×10^7	—	—	0.19

a) The rate constants, k_{23} and k_{32}, are for the aggregation reaction by hydrophobic interaction. b) This work.

of other alcohols. The concentration dependence of the relaxation frequency calculated with these values and Eq. 5 is shown in Fig. 2 by a solid line; the circles indicate the experimental values. In order to confirm the excess absorption mechanism, it is appropriate to inspect the concentration dependence of the maximum excess absorption per wavelength, μ_{max}. From Eq. 4, μ_{max} may be expected to be approximately proportional to $\rho c^2(1/C_1+1/C_2+1/C_3-1/C_T)^{-1}$. In Fig. 3, the concentration dependence of the maximum excess absorption per wavelength is shown, together with that of the calculated values of $\rho c_2(1/C_1+1/C_2+1/C_3-1/C_T)^{-1}$. As may be seen in this figure, the tendency of the concentration dependence of the maximum excess absorption per wavelength is similar to that of the calculated curve (solid line). This confirms that the excess absorption mechanism in an aqueous solution of isopropyl alcohol may be attributed to the perturbation of the equilibrium expressed by Eq. 2.

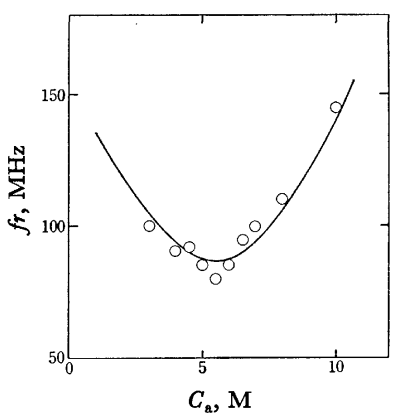

Fig. 2. Concentration dependence of the relaxation frequency in an aqueous solution of isopropyl alcohol.

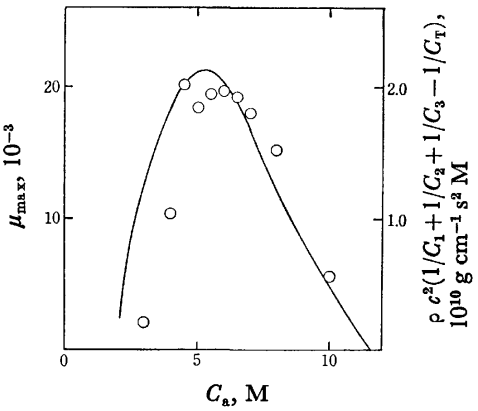

Fig. 3. The variations of μ_{max} and $\rho c^2(1/C_1+1/C_2+1/C_3-1/C_T)^{-1}$ with the concentration of isopropyl alcohol.

The dependencies of the forward and backward rate constants for the AB⇌A+B reaction on the solute molecules (see Table 2) are not remarkable. This may indicate that the complex formed by alcohol and water is due to a hydrogen bonding. However, the β parameter, which indicates the stability of the water structure, varies considerably depending on the solute molecules. When the strength of the hydrophobic interaction increases,[7] the β parameter decreases. In aqueous solutions of propyl and *t*-butyl alcohols, another excess absorption in the lower frequency range was observed; this mechanism was associated with the aggregation reaction of alcohol by hydrophobic interaction.[5] The strength of the hydrophobic interaction of isopropyl and allyl alcohols, however, is not so strong enough that these alcohols do not aggregate in aqueous solutions by hydrophobic interaction, and only a single relaxational absorption is observed in the frequency range measured

This work was in part supported by the Sakkokai Foundation.

References

1) M. J. Blandamer and D. Waddington, *Advn. Mole. Relaxation Processes*, **2**, 1 (1970).
2) K. Oda, R. Hayakawa, and Y. Wada, *Jpn. J. Appl. Phys.*, **14**, 1113 (1975).
3) K. Takagi and K. Negishi, *Jpn. J. Appl. Phys.*, **14**, 953 (1975).
4) S. Nishikawa, M. Mashima, and T. Yasunaga, *Bull. Chem. Soc. Jpn.*, **48**, 661 (1975).
5) S. Nishikawa, M. Mashima, M. Maekawa, and T. Yasunaga, *Bull. Chem. Soc. Jpn.*, **48**, 2353 (1975).
6) N. Tatsumoto, *J. Chem. Phys.*, **47**, 4561 (1967).
7) K. Shirahama and T. Kashiwabara, *J. Colloid Interface Sci.*, **36**, 65 (1971).

BULLETIN OF THE CHEMICAL SOCIETY OF JAPAN, VOL. 49 (5), 1415—1416 (1976)

The Photoconductivity of Poly(*N*-vinylcarbazole). VII.[1] The Effect of the Singlet and Triplet Quenchers on the Photoconductivity

Ken-ichi OKAMOTO, Norikazu ODA, Akira ITAYA, and Shigekazu KUSABAYASHI

Department of Chemical Engineering, Faculty of Engineering, Yamaguchi University, Ube 755

(Received January 20, 1976)

Synopsis. The singlet quenchers significantly reduce the photocurrents of poly(*N*-vinylcarbazole) and of brominated poly(*N*-vinylcarbazole), but the triplet quenchers do not do so at all regardless of the high efficiency of the polymer-to-quencher triplet energy transfer. This result excludes the possibility of the photocarrier generation from the triplet excited state in these polymers.

The photocarrier generation process in poly(*N*-vinylcarbazole) (PVCz) films, in the case of the singlet π-π^* excitation, has been widely investigated in the last few years.[2-4] It is considered that photocarriers in PVCz films are generated from the singlet excited states *via* either the intrinsic charge transfer exciton state in the case of the higher π-π^* excitation or the extrinsic exciplex state in the case of the lower π-π^* excitation. The exciplex state is considered to be formed efficiently, even if some electron-accepting impurities have very low concentrations, because of the high efficiency of the singlet exciton migration.[5]

On the other hand, the triplet excitation energy also migrates very efficiently in this polymer.[6-8] Furthermore, the triplet excitation energy of PVCz is fairly high (E_T=3.02 eV; *cf.* the singlet excitation energy, E_S= 3.55 eV) as compared with that of other aromatic vinyl polymers, such as poly(1-vinylnaphthalene) (E_T=2.5 eV, E_S=3.8 eV[9]). Therefore, the photocarrier generation from the triplet excited state in the case of the singlet π-π^* excitation may be possible in PVCz, as has been suggested by Yokoyama *et al.*[7] In order to decide on this possibility, we examined the effect of the triplet and singlet quenchers on the photoconductivity of PVCz and brominated poly(*N*-vinylcarbazole) (BPVCz).

Experimental

PVCz was prepared by free-radical polymerization and brominated by using *N*-bromosuccinimide. The BPVCz thus obtained had one bromine atom per 1.1 carbazolyl groups.[10] The copolymer of *N*-vinylcarbazole (VCz) with 1-vinylnaphthalene (VN) was also prepared by free-radical polymerization. These polymers were purified by repeated reprecipitations. Naphthalene and fluorene were used as the triplet quenchers of the carbazolyl chromophore, while anthracene and perylene were used as singlet and triplet quenchers. The scintillation-grade reagents were used after being purified by repeated recrystallizations, vacuum sublimation, and zone melting. The electrical measurements were made by the DC method in a vacuum of 10^{-5} Torr, as has been described previously.[11]

Results and Discussion

BPVCz has photoconductive properties similar to those of PVCz.[11] The magnitude of the photocurrent in BPVCz is twice as large as that in PVCz in the case of the hole current and is a most the same in the case of the electron current.

In both PVCz and BPVCz, the triplet quencher mixed or copolymerized does not affect the photoconductive properties at all. Anthracene and perylene acting as both singlet and triplet quenchers significantly reduce the photocurrent in magnitude, but do not affect the other photoconductive properties, such as the

TABLE 1. COMPARISON OF MAGNITUDES OF THE PHOTOCURRENT

Material			Number of samples	Magnitudes of the photocurrent[a]			
				Hole current/10^{-10} A cm^{-2}		Electron current/10^{-11} A cm^{-2}	
Polymer	Dopant	mol %		350 nm	330 nm	350 nm	330 nm
PVCz	None	0	7	(4.0±0.2)	(3.7±0.3)	(4.3±0.4)	(3.0±0.2)
	Fluorene	1.5	3	1.1±0.1	1.1±0.1	—	—
	Naphthalene	1.5	3	1.1±0.1	1.2±0.3	1.1±0.3	0.93±0.23
	Naphthalene	5.0	3	0.81±0.08	0.99±0.19	—	—
	Copolymerized	VN[b]	2	1.4±0.1	1.5±0.1	1.5±0.3	1.4±0.2
	Anthracene	3.0	2	0.18±0.07	0.23±0.09	0.09±0.01	0.14±0.01
	Perylene	2.0	3	0.20±0.06	0.22±0.09	0.13±0.05	0.25±0.08
VCz–VN (5 mol %) copolymer		0	2	(5.5±0.2)	(5.6±0.1)	(6.3±0.9)	(4.1±0.4)
	Anthracene	3.0	2	0.29±0.01	0.36±0.01	0.29±0.06	0.40±0.07
BPVCz	None	0	3	(7.2±0.2)	(7.0±0.2)	(3.2±0.2)	(2.6±0.1)
	Naphthalene	5.0	3	0.95±0.06	1.1±0.2	0.77±0.21	0.81±0.06
	Anthracene	3.0	2	0.16±0.03	0.19±0.02	0.37±0.03	0.54±0.06

a) The relative photocurrent values in the doped films taking the photocurrent values in the corresponding undoped films as unity. The values in parentheses are the photocurrent values in the undoped films measured under the condition of 35000 V/cm, 1×10^{13} photons/cm^2 s, 20 °C, and 1×10^{-5} Torr. b) VCz–VN (5 mol % in feed) copolymer.

voltage and the temperature dependences of the photocurrent. Table 1 shows a comparison of the magnitude of the photocurrent among the films undoped and doped with triplet or singlet quenchers. From this table, it is clear that, at the quencher concentrations of 1.5—5 mol%, the singlet quenchers reduce the photocurrent by a factor of about 5, while the triplet quenchers do not do so at all.

In both polymers, the triplet quenchers trap the freely-migrating triplet excitons rather than the trapped ones, resulting in both a significant decrease in the host phosphorescence and the appearance of the sensitized guest phosphorescence.[8] The host phosphorescence is completely replaced by the guest one at guest concentrations above 1 mol%.[8] It is, therefore, clear that the concentration of the freely-migrating triplet exciton in the films doped heavily (more than 1 mol%) with the triplet quenchers is remarkably reduced as compared with that in the undoped films. The situation is the same as for the case of the singlet quencher. Therefore, the present effect of the singlet and triplet quenchers on the photoconductivity excludes the possibility of photocarrier generation from the triplet state in these polymers under ordinary experimental conditions.

It is noted that the photocarrier generation from the singlet excited state is predominant even in BPVCz, which has a low efficiency of the singlet exciton migration because of the very short lifetime of the singlet exciton due to the enhanced intersystem crossing.[12] A similar example has been reported of the photoconductivity in tetracene crystals, where the low efficiency of the singlet exciton migation is attributed to the enhanced singlet fission into two triplet excitons.[13] In tetracene crystals, the photocarrier generation from the triplet excited state is possible only in the presence of a strong electron acceptor like *p*-chloranil.

Under the present experimental conditions, the two photon processes are negligible because of the weak light intensity. In the case of the lower singlet π-π^* excitation, the extrinsic photocarrier generation process with the participation of some electron-accepting impurities must be considered, whether the singlet channel or the triplet one is chosen. From the simple energetic calculation, this process is considered to be endothermic in the case of a weak electron acceptor such as some photoxidation products of carbazolyl chromophores, the most conceivable acceptors. In such an endothermic process, the energy difference between the singlet excitation energy and the triplet one (0.5 eV) seems to be determined in the choice between the singlet channel and the triplet one, although it is much smaller than those of other aromatic vinyl polymers. This is the reason for the lack of the photocarrier generation process from the triplet excited state in these polymers.

References

1) Part VI of this series; K. Okamoto, A. Itaya, and S. Kusabayashi, *Polym. J.*, **7**, 622 (1975).
2) G. Pfister and D. J. Williams, *J. Chem. Phys.*, **61**, 2416 (1974), and references therein.
3) M. Yokoyama, Y. Endo, and H. Mikawa, *Chem. Phys. Lett.*, **34**, 597 (1975).
4) K. Okamoto, N. Oda, A. Itaya, and S. Kusabayashi, *Chem. Phys. Lett.*, **35**, 483 (1975).
5) K. Okamoto, A. Yano, S. Kusabayashi, and H. Mikawa, *Bull. Chem. Soc. Jpn.*, **47**, 749 (1974).
6) W. Klöpffer and D. Fisher, *J. Polym. Sci. C*, **40**, 43 (1972).
7) M. Yokoyama, T. Tamamura, T. Nakano, and H. Mikawa, *J. Chem. Phys.*, in press.
8) A. Itaya, K. Okamoto, and S. Kusabayashi, *Bull. Chem. Soc. Jpn.*, in press.
9) R. B. Fox, T. R. Price, R. F. Cozzens, and J. R. McDonald, *J. Chem. Phys.*, **57**, 534 (1972).
10) Y. Murakami, K. Morimoto, A. Inami (Matsushita Electric Industrial Co., Ltd.), Japan Pat. 6929860 (1969).
11) K. Okamoto, S. Kusabayashi, and H. Mikawa, *Bull. Chem. Soc. Jpn.*, **46**, 2613 (1973).
12) A. Itaya, K. Okamoto, and S. Kusabayashi, 23rd Symposium on Macromolecules, (Tokyo) G11E09, October, 1974. To be published elsewhere.
13) E. L. Frankevich, *Disc. Faraday Soc.*, **51**, 37 (1972).

BULLETIN OF THE CHEMICAL SOCIETY OF JAPAN, VOL. 49 (5), 1417—1418 (1976)

Rate of Protonation of TCNQ Anion Radical in Water

Akihiko YAMAGISHI

Department of Chemistry, Faculty of Science, Hokkaido University, Sapporo 060

(Received January 27, 1976)

Synopsis. The protonation of TCNQ anion radical has been studied with an oxygen-free stopped-flow apparatus. The protonation rate is proportional to the square of $TCNQ^-$ concentration, being independent of the proton concentration. It is suggested that there exists an intramolecular step in which the electronic structure of $TCNQ^-$ changes into another one ready to accept a proton.

In the previous work, the protonation of 7,7,8,8-tetracyanoquinodimethane (TCNQ) anion radical was investigated in methanol, ethanol and acetonitrile.[1] On the basis of kinetic results, it was confirmed that the first attack of H^+ on $TCNQ^-$ was reversible according to $TCNQ^- + H^+ \rightleftharpoons TCNQH^\cdot$.

This paper reports the protonation of $TCNQ^-$ in water. It was intended to examine the effect of a dimer species on the reaction rate, since $TCNQ^-$ is known to dimerize in water.[2] The rate was determined using an oxygen-free stopped-flow apparatus in order to avoid the decomposition of $TCNQ^-$ under air.

Experimental

Li^+TCNQ^- was prepared by reducing TCNQ with LiI in acetonitrile. $HClO_4$ of reagent grade was used as proton source. The concentration of proton was equated to the proton activity at the investigated ionic strength (10^{-4}—10^{-2} M).

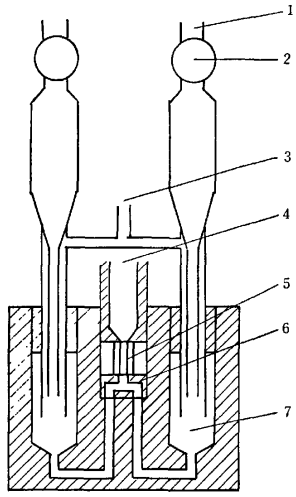

Fig. 1. A mixing part free from oxygen contamination; (1) to a vaccum line, (2) a gleaseless valve, (3) to a He tank, (4) to a rotary pump, (5) a quartz cell, (6) a mixer and (7) the reservoir of a sample solution.

The rate was measured with a Union Giken rapid scan stopped-flow spectrophotometer RA 1300. A mixing part free from oxygen contamination was newly constructed (Fig. 1).[3] The whole part was made of Teflon and Pyrex glass sealed by O-rings. About 10^{-3} mmHg vacuum was attainable under pumping. The sample solutions were directly drived by He gas pressure (*ca.* 0.5 kg/cm^2) without pistons. Thus the decomposition due to oxygen arose mainly from He gas impurity (nominal purity 99.9%). The samples were prepared in a vacuum line. The rate was followed by the absorbance change at 743 nm (a peak of $TCNQ^-$ monomer).

Results and Discussion

All measurements were performed under the condition that the initial concentration of $TCNQ^-$ was less than 10^{-5} M. At this concentration range, the contribution of a dimer to the total amount of $TCNQ^-$ is less than 5%. Thus the protonation rate is given by the decrease of a monomer species per unit time, $-d[TCNQ^-]/dt$, with a good approximation. The reactivity of a dimer may reflect on the observed rate through the rapid equilibrium below.[4]

$$2TCNQ^- \rightleftharpoons (TCNQ^-)_2 \qquad (1)$$

At the constant proton concentration, which is in large excess compared with $[TCNQ^-]$, the rate is expressed as below (Fig. 2).

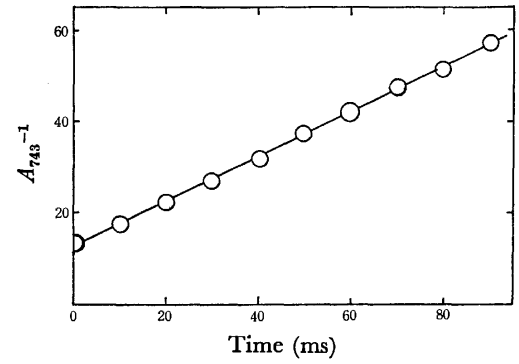

Fig. 2. Second-order plot of the disappearance of $TCNQ^-$; $[TCNQ^-]_0$ 3.9×10^{-6} M, and $[HClO_4]$ 3.98×10^{-3} M at 25±2 °C. The vertical scale is the reciprocal of the absorbance at 743 nm and the horizontal scale 20 ms/div.

$$-d[TCNQ^-]/dt = k[TCNQ^-]^2. \qquad (2)$$

k is found to be independent of the proton concentration for $[HClO_4]=(2.34\text{—}13.0)\times10^{-3}$ M. $k=(8.9\pm1.0)\times10^6$ $M^{-1}s^{-1}$ at 25±2 °C. From the temperature dependence of k between 14.5—35.0 °C, the apparent activation enthalpy is determined to be $\Delta H^*=10.1\pm0.3$ kcal mole^{-1}.

The second-order dependence of the rate on $[TCNQ^-]$ (Eq. 2) may seem to suggest the mechanism that the protonation takes place only by way of a dimer form, $(TCNQ^-)_2$. This possibility is, however, discarded on the following ground. If the dimer is an active species for protonation, k is expressed by

$$k = k_0 K_D$$

in which k_0 and K_D are the protonation rate of a dimer

and the equilibrium constant of reaction (1), respectively. Since k is independent of the proton concentration, k_0 may be the rate constant of some intramolecular step at which a dimer is activated. Taking $K_D = 2.5\times10^3\ M^{-1}$,[2] k_0 is obtained to be $3.6\times10^3\ s^{-1}$. Expressing k_0 as $\nu \exp(-\Delta H_0^*/RT)$, and equating $\Delta H_0^* = \Delta H^* - \Delta H_D$, in which ΔH_D is the enthalpy change of reaction (1), -10.4 kcal mol^{-1},[2] ΔH_0^* is obtained to be 20.5 kcal mol^{-1}. Substituting this value for the above expression of k_0, the frequentry factor, ν, is determined to be $3\times10^{18}\ s^{-1}$. ν exceeds the electronic vibration. It is very improbable to assume the presence of an activating mode with such a high frequency.

Therefore it is concluded that the second-order dependence of k on [TCNQ$^-$] arises from the same mechanism as observed previously in methanol, ethanol and acetonitrile. That is, the disproportionation takes place between protonated TCNQ$^-$, or HTCNQ$\cdot$, and TCNQ$^-$.

$$TCNQ^- + H^+ \rightleftharpoons HTCNQ\cdot \quad (3)$$

$$HTCNQ\cdot + TCNQ^- \longrightarrow HTCNQ^- + TCNQ \quad (4)$$

$$HTCNQ^- + H^+ \longrightarrow H_2TCNQ \quad (5)$$

The fact that k is independent of [H$^+$] suggests the presence of the intramolecular step in which TCNQ$^-$ is activated into a more basic species.

$$TCNQ^- \rightleftharpoons TCNQ^{-}* \quad (6)$$

Assuming the stationary conditions for both TCNQ^{-}* and HTCNQ$\cdot$, k is expressed by

$$k = \frac{k_6k_3k_4[H^+]}{(k_{-6}+k_3[H^+])k_{-3}}$$

Under the condition that $k_{-6} \ll k_3[H^+]$, k is reduced to

$$k = k_6k_4/k_{-3}$$

which is independent of the proton concentration as observed in Eq. 2.

One of the possibilities for the nature of the intramolecular step (6) is that TCNQ$^-$ transforms electronically into another species which accepts more readily a proton. For example, one of the carbon atoms in TCNQ$^-$ may become carbon anion, C$^-$, by destructing partially the solvation structures by water molecules.

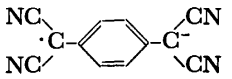

The author thanks Prof. Masatoshi Fujimoto for his encouragement.

References

1) A. Yamagishi and M. Sakamoto, *Bull. Chem. Soc. Jpn.*, **47**, 2152 (1974).

2) R. H. Boyd and W. D. Phillips, *J. Chem. Phys.*, **43**, 2927 (1965).

3) The author expresses thanks to Mr. Toshihiko Nagamura of Union Giken Co. Ltd. for constructing the mixing part.

4) A. Yamagishi, Y. Iida, and M. Fujimoto, *Bull. Chem. Soc. Jpn.*, **45**, 3482 (1972).

BULLETIN OF THE CHEMICAL SOCIETY OF JAPAN, VOL. 49 (5), 1419—1420 (1976)

The Crystal Structure of Bis[1-(2-thiazolylazo)-2-naphtholato]-iron(II)-Chloroform(2/3)

Masayasu KURAHASHI and Akira KAWASE*

National Research Institute for Metals, Nakameguro, Meguro-ku, Tokyo 153

(Received October 7, 1975)

Synopsis. The crystals of bis[1-(2-thiazolylazo)-2-naphtholato]iron(II)-chloroform (2/3) are triclinic, with unit-cell dimensions of: $a=12.509(7)$, $b=11.911(6)$, $c=10.460(4)$ Å, $\alpha=86.97(3)$, $\beta=97.24(4)$, and $\gamma=103.48(7)°$, $Z=2$ for $[Fe^{II}(C_{13}H_8N_3OS)_2]\cdot 1.5CHCl_3$, space group $P\bar{1}$. The complex is diamagnetic, and the iron atom is surrounded octahedrally by two terdentate ligands in the *mer* configuration.

The analytical use of heterocyclic azo dyestuffs, such as 1-(2-pyridylazo)-2-naphthol (Hpan) and 1-(2-thiazolylazo)-2-naphthol (Htan), has been the subject of a considerable number of papers; however, few crystallographic studies have been reported. We, therefore, have begun a systematic study of the structures of the metal chelates of these analytically important dyestuffs. It was thought that the determination of the crystal structures would be of great help in the design of new analytical reagents. The tan-complexes rather than the pan-complexes were selected because the coordination property of the thiazole ring appeared to be more interesting than that of pyridine. Thus far, the structures of Pd(II)-, Ni(II)-, Cu(II)-, and Co(III)-tan chelates have been determined.[1-4]

This note will deal with the structure of the Fe(II)-tan chelate, bis[1-(2-thiazolylazo)-2-naphtholato]iron(II) (abbr. as $[Fe^{II}(tan)_2]$). A preliminary work based on the photographic data has been published.[5]

Experimental

The single crystals of $[Fe^{II}(tan)_2]\cdot 1.5CHCl_3$ were obtained by recrystallization from a chloroform solution of $[Fe^{II}(tan)_2]$ by the slow evaporation of the solvent. The crystal data are: triclinic, $a=12.509(7)$, $b=11.911(6)$, $c=10.460(4)$ Å, $\alpha=86.97(3)$, $\beta=97.24(4)$, and $\gamma=103.48(7)°$, $V=1503.0$ Å^3, $D_m=1.63$, $D_x=1.64$ g·cm^{-3}, $Z=2$ for $[Fe^{II}(tan)_2]\cdot 1.5CHCl_3$, $\mu=95.7$ cm^{-1} (for Cu$K\alpha$), space group $P\bar{1}$. The specimen crystal had the dimensions of *ca.* $0.15\times0.3\times0.35$ mm. Both the determination of the cell constants and the collection of the intensity data were carried out on a Rigaku automated four-circle diffractometer using Cu$K\alpha$ radiation monochromatized with a graphite plate. The ω–2θ scan technique was employed at a scan rate of 4°/min in ω. Weak reflections with $|F|$ values less than $3\sigma(|F|)$ were omitted from the data, and a total of 1864 non-zero reflections ($\pm h, \pm k, l\geq 0$) were recorded in the range of $0°<2\theta<120°$. The intensities were corrected for the Lorentz and polarization factors, but not for absorption.

Structure Determination and Refinement

The centrosymmetric space group was indicated by the intensity statistics and has been used throughout. The structure was solved by the heavy-atom method. The analysis of a three-dimensional Patterson map gave the coordinates of Fe, S, and S′. The positions of the remaining non-hydrogen atoms were obtained from the successive Fourier and difference syntheses. After several cycles of least-squares refinement with isotropic temperature factors, anisotropic thermal parameters were introduced for Fe, S, S′, Cl(1), Cl(2), and Cl(3). At the final stage of the refinement, the calculated hydrogen positions and the isotropic temperature factor of 5.0 Å^2 were included in the structure factor calculations, but were not refined; the R value reached

TABLE 1. AVERAGE BOND DISTANCES AND ANGLES

Bond distances (Å)			Bond angles (°)			
Fe	–O	1.97(1)	O	–Fe	–N(1)	84(1)
Fe	–N(1)	1.88(2)	N(1)	–Fe	–N(3)	80(1)
Fe	–N(3)	1.95(2)	C(11)	–S	–C(12)	90(1)
S	–C(11)	1.71(2)	Fe	–O	–C(2)	110(1)
S	–C(12)	1.72(2)	Fe	–N(1)	–N(2)	121(1)
O	–C(2)	1.31(2)	Fe	–N(1)	–C(1)	115(1)
N(1)	–N(2)	1.31(2)	N(2)	–N(1)	–C(1)	123(2)
N(1)	–C(1)	1.40(2)	N(1)	–N(2)	–C(11)	107(2)
N(2)	–C(11)	1.39(3)	Fe	–N(3)	–C(11)	111(2)
N(3)	–C(11)	1.32(2)	Fe	–N(3)	–C(13)	139(2)
N(3)	–C(13)	1.41(3)	C(11)	–N(3)	–C(13)	111(2)
C(1)	–C(2)	1.39(3)	N(1)	–C(1)	–C(2)	110(2)
C(1)	–C(10)	1.44(3)	N(1)	–C(1)	–C(10)	127(2)
C(2)	–C(3)	1.45(3)	C(2)	–C(1)	–C(10)	122(2)
C(3)	–C(4)	1.37(3)	O	–C(2)	–C(1)	122(2)
C(4)	–C(5)	1.39(3)	O	–C(2)	–C(3)	118(2)
C(5)	–C(6)	1.44(3)	C(1)	–C(2)	–C(3)	120(2)
C(5)	–C(10)	1.44(3)	C(2)	–C(3)	–C(4)	117(2)
C(6)	–C(7)	1.35(4)	C(3)	–C(4)	–C(5)	124(2)
C(7)	–C(8)	1.41(4)	C(4)	–C(5)	–C(6)	121(2)
C(8)	–C(9)	1.40(3)	C(4)	–C(5)	–C(10)	121(2)
C(9)	–C(10)	1.41(3)	C(6)	–C(5)	–C(10)	117(2)
C(12)	–C(13)	1.33(3)	C(5)	–C(6)	–C(7)	122(2)
CH	–Cl(1)	1.71(6)	C(6)	–C(7)	–C(8)	121(2)
CH	–Cl(2)	1.83(6)	C(7)	–C(8)	–C(9)	120(2)
CH	–Cl(3)	1.81(6)	C(8)	–C(9)	–C(10)	121(2)
			C(1)	–C(10)	–C(5)	115(2)
			C(1)	–C(10)	–C(9)	125(2)
			C(5)	–C(10)	–C(9)	120(2)
			S	–C(11)	–N(2)	124(2)
			S	–C(11)	–N(3)	115(2)
			N(2)	–C(11)	–N(3)	122(2)
			S	–C(12)	–C(13)	113(2)
			N(3)	–C(13)	–C(12)	113(2)
			Cl(1)	–CH	–Cl(2)	106(3)
			Cl(1)	–CH	–Cl(3)	110(3)
			Cl(2)	–CH	–Cl(3)	104(3)

* Present address: National Chemical Laboratory for Industry, 5–5, 1-Chome, Honmachi, Shibuya-ku, Tokyo 151.

0.124 for 1864 observed reflections. A unit weight was given to each reflection. The atomic scattering factors were taken from International Tables for X-ray Crystallography.[6] The final atomic parameters and the list of structure factors are kept as Document No. 7618 at the Chemical Society of Japan.

Description of the Structure and Discussion

The perspective view of the molecules and the numbering of atoms are given in Fig. 1, while the electron density map is shown in Fig. 2. The iron atom is six-coordinated, surrounded octahedrally by two terdentate ligands in the *mer* configuration. The ligand, 1-(2-thiazolylazo)-2-naphtholato (tan) group coordinates to the iron atom through the phenolic oxygen, the azo nitrogen adjacent to the naphthol ring and the thiazole nitrogen atoms giving two five-membered chelate rings. This mode of attachment of the tan to the metal is common in all the tan-complexes studied.[1-5] The metal environment of the $[Fe^{II}(tan)_2]$ complex is just the same as those of $[Ni^{II}(tan)_2]$ and $[Co^{III}(tan)_2]^+$, but differs from those of $[Pd^{II}Cl(tan)]$ and $[Cu^{II}(tan)(H_2O)_2]^+$.

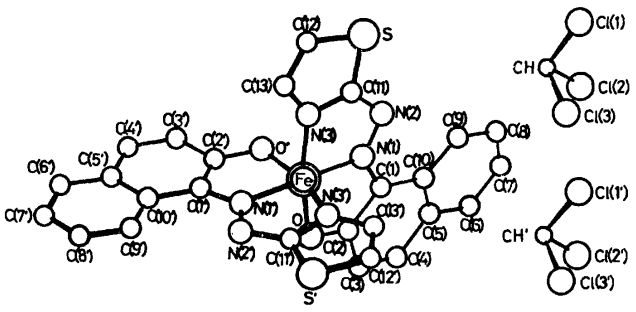

Fig. 1. Perspective view of the molecules and the numbering of atoms.

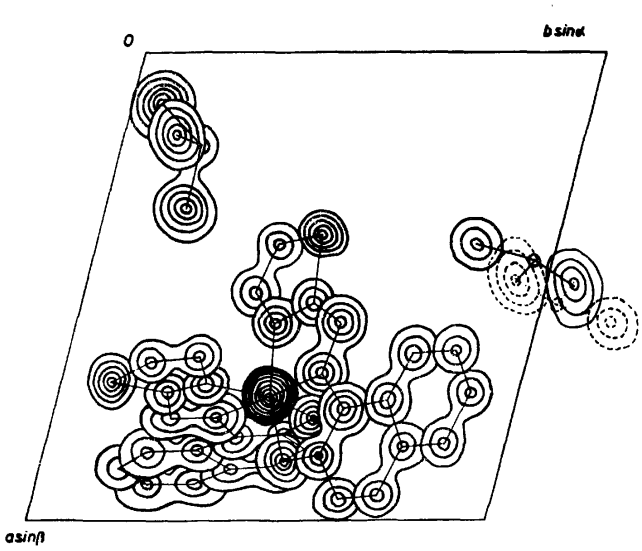

Fig. 2. Composite electron density map viewed down the c-axis. Contours are drawn at intervals of 2 e·Å^{-3} except for iron atom, the lowest contour being 2 e·Å^{-3}.

The average bond distances and angles, together with their e.s.d.'s, are given in Table 1. The bond angles around the metal, O–Fe–N(1) and N(1)–Fe–N(3), are compressed from the normal valence angles. This is attributable to the geometry of the tan ligand; a similar situation was observed for the other metal-tan complexes. The mean plane through Fe and the unprimed tan and that through Fe and the primed tan are roughly planar, and they are nearly perpendicular to each other.

It has been reported that the stability constants of metal chelates of tan and its analogues diminish in this order;[7]

$$Fe(II) > Ni(II) > Co(II) > Zn(II)$$

This order is the same as the stability series of Irving and Williams,[8] with the exception of Fe(II). This anomaly can be interpreted in terms of the orbital stabilization. Measurement of the magnetic moments confirmed that the iron atom utilizes d^2sp^3 orbitals, while the other three utilize sp^3d^2 orbitals.

The arrangment of the $[Fe^{II}(tan)_2]$ chelates is very similar to that observed in the crystals of $[Ni^{II}(tan)_2]$. However, the present crystal contains chloroform molecules (as a crystal solvent). One chloroform (CH, Cl (1), Cl (2), and Cl(3)) is in a general position, while the other chloroform (CH', Cl(1'), Cl(2'), and Cl(3'): half weight) is disordered and takes two possible orientations randomly and with equal probability about a center of symmetry at (1/2, 0, 0).

Calculations were carried out on the HITAC 5020F computer at the Computer Center of the National Aerospace Laboratory and on the NEAC 3100 computer at this Institute, using some UNICS programs.

The authors wish to express their deep thanks to Dr. Eiichi Asada and Mrs. Midori Goto of the National Chemical Laboratory for Industry, who kindly allowed them to use the X-ray diffractometer.

References

1) M. Kurahashi, *Bull. Chem. Soc. Jpn.*, **47**, 2045 (1974).
2) M. Kurahashi, *Bull. Chem. Soc. Jpn.*, **47**, 2067 (1974).
3) M. Kurahashi and A. Kawase, *Bull. Chem. Soc. Jpn.*, **49**, 127 (1976).
4) M. Kurahashi, *Chem. Lett.*, **1974**, 1271.
5) M. Kurahashi, A. Kawase, K. Hirotsu, M. Fukuyo, and A. Shimada, *Bull. Chem. Soc. Jpn.*, **45**, 1940 (1972).
6) "International Tables for X-ray Crystallography," Vol. III, Kynoch Press, Birmingham, England (1962).
7) A. Kawase, *Bunseki Kagaku*, **13**, 553 (1964).
8) H. Irving and R. J. P. Williams, *J. Chem. Soc.*, **1953**, 3192.

BULLETIN OF THE CHEMICAL SOCIETY OF JAPAN, VOL. 49 (5), 1421—1422 (1976)

Effect of Hydroxylation on the Thermal Reactivities of Fluorapatite and Chlorapatite[1)]

Hideki MONMA and Takafumi KANAZAWA

Department of Industrial Chemistry, Faculty of Technology, Tokyo Metropolitan University, Fukazawa, Setagaya-ku, Tokyo 158

(Received October 23, 1975)

Synopsis. Thermal self-decomposition of hydroxyapatite was notably suppressed by partial fluorination or chlorination. The volatility of halogen from fluorapatite and chlorapatite was reduced by the incorporation of hydroxide ions in the apatites. The reactivities of fluor-hydroxyapatite and chlor-hydroxyapatite with silica increased with increasing hydroxide content, which resulted in an increase in the halogen volatility.

In a preceding report by the authors,[2)] it was stated that in the presence of silica and water vapor, fluorapatite (FAp) and chlorapatite (CAp) could be dehalogenated by the substitution of hydroxide ions for halogen ions and by the subsequent destructive reaction of partially hydroxylated FAp or CAp with silica. The aim of the present study is to examine the effects of decreasing the ratios of F/OH and Cl/OH on the thermal and chemical stabilities of FAp-hydroxyapatite (HAp) solid solutions [$Ca_{10}(PO_4)_6F_{2(1-x)}(OH)_{2x}$, F_xAp] and CAp–HAp solid solutions [$Ca_{10}(PO_4)_6Cl_{2(1-x)}$-$(OH)_{2x}$, C_xAp]. The subscript x is the degree of substitution of OH^- for F^- or Cl^- and its value varies from 0 (for FAp or CAp) to 1 (for HAp).

Experimental

FAp (3.76% F), CAp (6.79% Cl) and HAp were prepared by the same methods as those described in a preceding paper.[2)] F_xAp was prepared by heating a mixture of $Ca_2P_2O_7$, CaF_2, and $CaCO_3$ having a molar ratio of 3: $(1-x)$: 8 at 1200 °C for 3 h in an atmosphere of water vapor (90—240 mmHg), followed by washing with a 10% NH_4Cl aqueous solution to remove the excess CaO. The formation of FAp–HAp solid solutions is judged from the fact that the thermal self-decomposition degree of F_xAp was not in proportion to the OH content (refer to Fig. 1). C_xAp was prepared by heating pure CAp in an atmosphere of water vapor (17—360 mmHg) for various retention times.[2)] The precise values of x for these solid solutions were determined by chemical analysis. The silica used was siliceous sand (α-quartz) for optical glass making. All the samples prepared were ground to a 200 inch-mesh before use. Heating runs were performed in flowing nitrogen gas (150 ml/min) containing a trace water vapor (0.6 mmHg). A heating time of 3 h and a mixing molar ratio of silica/apatite of 3 were adopted as adequate reaction conditions.[2)] The conversion fraction of F_xAp into tricalcium phosphate was determined by quantitative X-ray analysis the procedure for which is given in detail elsewhere.[2)] Fluorine and chlorine were analyzed by thorium nitrate and potassium thiocyanate titrations, respectively.

Results and Discussion

Fluor-hydroxyapatite. Figure 1 shows the conversion fractions for F_xAp. Scarcely any self-decomposition of F_xAp at 1300 °C was observed in the range of x of 0—0.8. However, F_xAp for values of x above 0.9 decomposed considerably. In other words, the thermal stability of HAp ($x=1$) was remarkably decreased by partially substituting F^- for OH^-. The decomposition of F_xAp by silica increased monotonically with x. The fluorine volatilities of F_xAp without silica during heating at 1000—1300 °C for 3 h were 8% for FAp ($x=0$) and less than 4% over the range of x from 0.1—1.0. The volatility was accelerated by the addition of silica. Figure 2 shows the fluorine volatilities from silica-added F_xAp. The volatility curves have trends similar to the

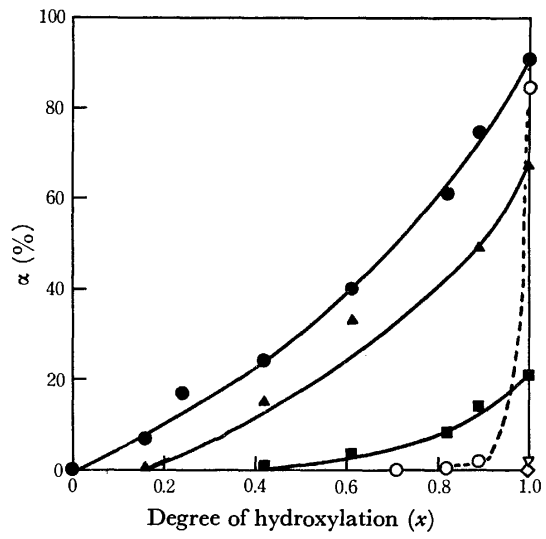

Fig. 1. Effects of hydroxylation and silica addition on conversion (α) of fluor-hydroxyapatite.
Sample: --- F_xAp, —F_xAp–silica mixture.
Temperature (°C): ○● 1300, ▽ 1250, ◇ 1200, ▲ 1100, ■ 1000.

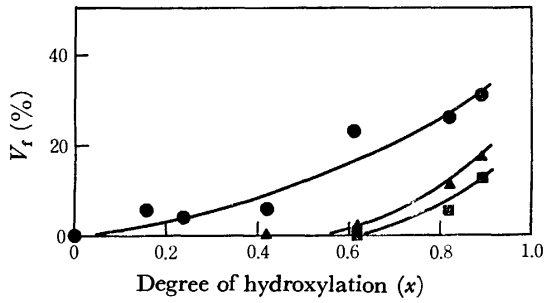

Fig. 2. Effects of hydroxylation and silica addition on fluorine volatility (V_f).
Sample: F_xAp–silica mixture. Temperature (°C): ● 1300, ▲ 1100, ■ 1000. V_f: [(Volatility for silica-added F_xAp)−(Volatility for F_xAp without silica)].

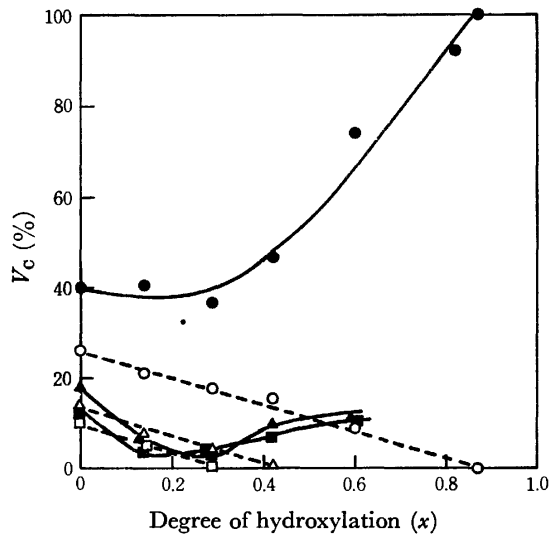

Fig. 3. Effects of hydroxylation and silica addition on chlorine volatility (V_C).
Sample: --- C_xAp, —C_xAp–silica mixture.
Temperature (°C): ○● 1300, △▲ 1100, □■ 1000.

decomposition curves in Fig. 1. This similarity supports the idea that the volatilization was mostly due to the destructive reaction of F_xAp with silica. However, the volatilities, which should be practially consistent with the decomposition fractions, were less than these fractions. This relationship suggests that a fluorine compound such as SiF_4 produced simultaneously during the destructive reaction may recombine with unreacted F_xAp.

Chlor-hydroxyapatite. The values of x for unreacted apatites after the heating of C_xAp with and without silica were determined by using a calibration curve of the lattice constant *vs.* x. The results are summarized as follows. The x values after heating became higher than those of the starting apatite under heating conditions permitting the stability of the apatite structure. This change of x was due possibly to the replacement of Cl^- with OH^- or O^{2-} of which a small amount was contained in the atmosphere as water vapor.[2] Under condition permitting the apatites structure to be unstable, the value of x of unreacted apatite agreed with those before heating. The chlorine volatilities from C_xAp and silica-added C_xAp are shown in Fig. 3. C_xAp without silica was structurally stable over the range of x from 0—0.9. This fact means that Cl ions incorporated into HAp also have a stabilizing effect on the apatite structure similar to that of F ions. The chlorine volatilities of C_xAp decreased linearly with x, while the volatilities of the C_xAp–silica mixture decreased in the range from 0—0.3 in which the apatite structure was stable and increased thereafter along with the decomposition of the apatite by silica. In conclusion, the volatility behavior of C_xAp in the presence of silica could be interpreted by both a suppression effect due to the incorporation of OH and an accelerating effect due to the decomposition reaction.

References

1) This paper was presented at the 32nd Annual Meeting of Spring of the Chemical Society of Japan, Tokyo, April, 1975.

2) H. Monma and T. Kanazawa, *Bull. Chem. Soc. Jpn.*, **48**, 1816 (1975).

BULLETIN OF THE CHEMICAL SOCIETY OF JAPAN, VOL. 49 (5), 1423—1424 (1976)

The Preparation and the Magnetic Property of Bis(*N*-*o*-nitrophenylsalicylideneaminato)copper(II)

Tadashi Tokii, Norimitsu Ohno, and Yoneichiro Muto

Department of Chemistry, Faculty of Science and Engineering, Saga University, Saga 840

(Received October 27, 1975)

Synopsis. A synthesis of bis(*N*-*o*-nitrophenylsalicylideneaminato)copper(II) is reported. The magnetic properties of the complex and the corresponding *p*-nitro complex are discussed in terms of the steric effect of the nitro group.

In the preparation of bis(*N*-nitrophenylsalicylideneaminato)copper(II) complexes, it is much more difficult to prepare complexes with a nitro group at the *o*-position of the phenyl ring than complexes with the substituent at the *m*- or *p*-position. Thus, the synthesis of bis(*N*-*o*-nitrophenylsalicylideneaminato)copper(II), Cu(sal·*N*-*o*-NO_2·Ph)$_2$, can not be accomplished by any of the following reactions which are used for the preparation of various bis(*N*-R-salicylideneaminato)copper(II) complexes (Fig. 1. I):[1] (1) Cu(sal)$_2$+2 R·NH_2; (2) 2 H·sal·N–R+Cu(Ac)$_2$·H_2O; (3) 2 H·sal+2 R·NH_2+Cu(Ac)$_2$·H_2O (where H·sal=salicylaldehyde, R=alkyl or aryl, H·sal·N–R=*N*-R-salicylideneamine and Ac=CH_3COO).

Verter and Frost[2] successfully prepared the *o*-NO_2 complex by the method of Charles[3]—that is, by the reaction of H·sal, *o*-nitroaniline, and Cu(Ac)$_2$·H_2O in the presence of sodium acetate. We have also succeeded in isolating this complex and the analogous complexes (R=*o*-NO_2-*p*-CH_3·Ph and *o*-NO_2-*p*-CH_3O·Ph) by methods different from that of Charles. Cryomagnetic measurements of the *o*-NO_2 complex and the corresponding *p*-NO_2 complex have been carried out; the results will be discussed in terms of the shielding effect of *o*-substituents.

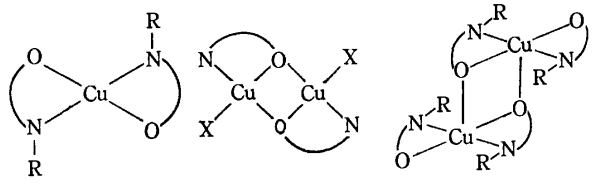

I II III

Fig. 1. Schematic representations of structures of I: Cu(sal·N–R)$_2$, II: [Cu(sal·N–R)X]$_2$, and III: [Cu(sal·N–R)$_2$]$_2$.

Preparation

A typical synthetic method was as follows: a mixture of Cu(sal)$_2$, Cu(Cl_2CHCOO)$_2$·$4H_2O$, and *o*-nitroaniline in a 1:1:2 mole ratio in ethanol was heated on a water bath under reflux for 1 h. The products were then recrystallized from *N*,*N*-dimethylformamide. They were all brown. The results of elemental analyses are given in Table 1, together with the calculated magnetic moments based on the observed magnetic susceptibilities at room temperature.

The synthesis of Cu(sal·*N*-*o*-NO_2·Ph)$_2$ was also achieved either by a similar procedure using Cu(Ac)$_2$·H_2O or Cu(ClO_4)$_2$·$6H_2O$ instead of Cu(Cl_2CHCOO)$_2$·$4H_2O$ or by the action of water on binuclear complexes of the II type shown in Fig. 1, [Cu(sal·*N*-*o*-NO_2·Ph)X]$_2$, which were prepared by the reaction of Cu(sal)$_2$, *o*-nitroaniline, and CuX_2(where X=Cl[4] or NO_3[5]).

Magnetic Property

The magnetic susceptibilities of Cu(sal·*N*-*p*-NO_2·Ph)$_2$ and Cu(sal·*N*-*o*-NO_2·Ph)$_2$ were measured in the temperature range of 80—300 K by the Gouy method; the results are shown in Fig. 2.

The cryomagnetic data for the *p*-NO_2 complex obeyed the Curie-Weiss law with a positive Weiss constant ($\theta \approx +2$ K), which was evaluated by extrapolating the $(\chi_m - N_\alpha)^{-1}$ *vs.* T curve; this indicated the existence of ferromagnetic interaction in this compound (where χ_m is the magnetic susceptibility per gram-ion of copper (II); N_α, the temperature independent paramagnetism per gram-ion of copper(II), and T, the absolute temperature). The ferromagnetic interaction was also reflected in the X-band ESR spectrum as measured on a powdered sample; *i.e.*, the spectrum showed a weak signal at *ca.* 1500 G due to the $\Delta M_s=2$ transition characteristic of magnetically coupled copper(II) ions,[6] and the intensity increased with a lowering of the temperature, suggesting that the ferromagnetic interaction leads to a triplet ground state. These magnetic properties are quite similar to those of such binuclear complexes as [Cu(sal·N–CH_3)$_2$]$_2$(*γ*-form),[7] [Cu(sal·N–CH_2CH_2–N·sal)]$_2$,[7,8] [Cu(dmg)$_2$]$_2$,[9] and [Cu(pyo)$_2$-

Table 1. Analytical data and magnetic moments

Complex	Analysis, % Found C	H	N	Cu	Calcd C	H	N	Cu	μ_{eff}[a] (°C) B. M.
Cu(sal·N-*o*-NO_2·Ph)$_2$	56.93	3.46	10.19	11.44	57.20	3.32	10.26	11.64	1.81 (21)
Cu(sal·N-*o*-NO_2-*p*-CH_3·Ph)$_2$	58.48	3.89	9.76	11.17	58.59	3.86	9.76	11.07	1.81 (24)
Cu(sal·N-*o*-NO_2-*p*-CH_3O·Ph)$_2$	55.24	3.75	9.00	10.59	55.49	3.66	9.24	10.48	1.81 (24)

a) Calculated from the expression $\mu_{eff}=2.83\sqrt{(\chi_m - N\alpha)\cdot T}$ assuming $N\alpha=60\times10^{-6}$ emu.

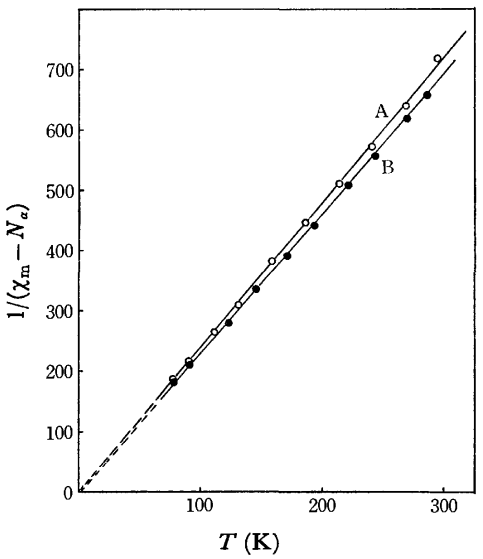

Fig. 2. Variation of reciprocal magnetic susceptibilities with temperature.
A: Cu(sal·N-*o*-NO_2·Ph)$_2$ B: Cu(sal·N-*p*-NO_2·Ph)$_2$
Pascal's constants were used for correction of diamagnetism (-255×10^{-6} emu/mol) and $N\alpha$ was assumed to be 60×10^{-6} emu.

$(NO_3)_2]_2$,[10] in which the coordination around the copper ion is square-based pyramidal, with the fifth position (out-of-plane) occupied by oxygen from an adjacent planar moiety (where dmg=dimethylglyoximato and pyo=pyridine *N*-oxide). The ferromagnetic spin interaction between copper ions in these complexes was interpreted in terms of a σ-type superexchange mechanism *via* the out-of-pane bonds.[7-10] Thus, the *p*-NO_2 complex very probably has a binuclear structure of the III type shown in Fig. 1, $[Cu(sal\cdot N\text{–}R)_2]_2$, in which the monomeric Cu(sal·N–R)$_2$ units are bridged by the Cu–O out-of-plane bonds.

On the other hand, for the *o*-NO_2 complex, magnetic behavior obeying the Curie law was observed within the range of experimental error. In the powder ESR spectrum, a strong signal at *ca.* 3100 G due to copper(II) ions with $S=1/2$ was observed, and, in contrast to the *p*-NO_2 complex, no absorption was detected near 1500 G over the temperature range of 80—300 K. On the basis of the magnetic data and the previous observation that the *o*-substituents in Cu(sal·N–Ph–Y)$_2$ complexes have a great tendency to shield the fifth coordination site of the copper ions,[4] it seems likely that, in the *o*-NO_2 complex, the shielding effect hinders the formation of a dimer of the III type; consequently, no magnetic interaction occurs between neighboring copper ions (where ph-Y=monosubstituted phenyl).

References

1) S. Yamada, *Coord. Chem. Rev.*, **1**, 415 (1966).
2) H. S. Verter and A. E. Frost, *J. Am. Chem. Soc.*, **82**, 85 (1960).
3) R. G. Charles, *J. Org. Chem.*, **72**, 677 (1957).
4) M. Kato, Y. Muto, H. B. Jonassen, K. Imai, K. Katsuki, and S. Ikegami, *Bull. Chem. Soc. Jpn.*, **42**, 2555 (1969).
5) M. Kato, Y. Muto, H. B. Jonassen, K. Imai, M. Kondo, K. Katsuki, and S. Ikegami, *Bull. Chem. Soc. Jpn.*, **42**, 3039 (1969).
6) B. Bleaney and K. D. Bowers, *Proc. Roy. Soc., Ser. A*, **214**, 451 (1952).
7) W. E. Hatfield, *Inorg. Chem.*, **11**, 216 (1972).
8) G. O. Carlisle and W. E. Hatfield, *Inorg. Nucl. Chem. Lett.*, **6**, 633 (1970).
9) J. F. Villa and W. E. Hatfield, *J. Chem. Phys.*, **55**, 4758 (1971).
10) W. E. Hatfield, J. A. Barnes, D. Y. Jeter, R. Whyman, and E. R. Jones, Jr., *J. Am. Chem. Soc.*, **92**, 4982 (1970).

BULLETIN OF THE CHEMICAL SOCIETY OF JAPAN, VOL. 49 (5), 1425—1426 (1976)

The Synthesis of Single Crystals of $HgX_2 \cdot 2HgS$ (X=Halogen)

Kunio TAKEI and Hitoshi HAGIWARA

Department of Industrial Chemistry, Faculty of Engineering, Miyazaki University, Miyazaki 880

(Received November 5, 1975)

Synopsis. Single crystals of $HgI_2 \cdot 2HgS$ ($3 \times 1.2 \times 0.2$ mm^3), $HgBr_2 \cdot 2HgS$ and $HgCl_2 \cdot 2HgS$ were prepared by means of a high-temperature vapor-phase reaction. X-Ray experiments showed that the crystal of $HgI_2 \cdot 2HgS$, the unit cell of which has dimensions of $a=9.36$ Å, $b=9.69$ Å, and $c=18.5$ Å, belongs to the rhombic system.

When powders of $HgI_2 \cdot 2HgS$ (yellow) and its related compounds are exposed to sunlight, they turn black in a few seconds; also, an absorption band is formed in all the visible regions. This process can be reversed, *i.e.*, bleaching occurs slowly in the dark after a few days or instantly when heated at 90 °C. The crystalline powders[1] of these compounds were easily prepared by the action of H_2S on the methanol solution of HgX_2. When a mixture of powdered HgX_2 and HgS (black) in a mole ratio of 1.1: 2 was heated at 170 °C for 1—2 h in an electric furnace, the same compounds as those of the hydrogen sulfide method were produced. In 1955, one of the present authors[2] synthesized a comparatively large single crystal by means of a vapor-phase reaction. About 30 g of a mixture of powdered HgI_2 and HgS (black) in a 1.1: 2 mole ratio were put into a glass tube (1 cm wide and 80 cm long) and placed in an electric furnace. After keeping the bottom of the tube at 520 °C for 30 min, the test tube was taken out and kept in the dark. Yellow crystals were observed inside the tube 40 cm from the bottom. These crystals were $HgI_2 \cdot 2HgS$, with rather small dimensions ($0.6 \times 0.7 \times 0.04$ mm^3). The purpose of the present investigation is to obtain a single crystal of $HgX_2 \cdot 2HgS$ as large as possible by using a more elaborate apparatus.

Vapor-phase Reaction between HgI_2, Hg, and S. A T-type glass tube (2 cm in inner diameter, 80 cm in length), whose two terminals were stopped with rubber stoppers, was put into a furnace consisting of two porcelain tubes (3 cm in inner diameter, 50 cm in length) and of 750 watts nicrom wires, as is shown in Fig. 1. The third terminal of the glass tube was connected to a water-stream pump in order to evacuate the inner air of the tube until the pressure became 748 mmHg. Asbestos was stuffed into the crevice between the furnace and the glass tube. The temperatures of the left and right parts of the furnace were kept at 280 °C and 500 °C respectively for 2 h by controlling the applied voltage at 50 V and 75 V with silidacs. Moreover, the temperatures at various positions of the two furnaces were measured by means of chromel–alumel thermocouples. The temperature of the B position (indicated in Fig. 1, 4—1 cm from the third terminal) was about 205—185 °C.

Next, a glass boat with 9 g of powdered HgI_2 was quickly placed into the left side of the glass tube, and another glass boat with 3 g of powdered black HgS was quickly put into the right side. The two terminals of the tube were closed again with rubber stoppers. HgI_2 molecules react in the vapor-phase with the Hg or S molecules produced by a decomposition of the HgS. These molecules also drive out oxygen in the tube. The reaction is as follows:

$$m\mathrm{HgI_2(g)} + n\mathrm{Hg(g)} + n\mathrm{S(g)} \longrightarrow \mathrm{HgI_2 \cdot 2HgS(s)} + (n-2)\mathrm{Hg(s)} + (n-2)\mathrm{S(s)} + (m-1)\mathrm{HgI_2(s)}$$

During the reaction, the temperature of the B part was higher than 180 °C. This shows that no crystals of $HgI_2 \cdot 2HgS$ were grown on the B position, because $HgI_2 \cdot 2HgS$ decomposes at 180 °C into HgI_2, Hg, and S. After the reaction had continued for 2 h, the applied voltage was slowly decreased and then cut off. It was observed that red and yellow crystals were deposited at the A and B cool parts respectively, and that gray powders were found at the C cool part, as is illustrated in Fig. 1. It is clear that the red crystals are HgI_2 and the gray ones are Hg and S. The yellow crystals ($3 \times 1.2 \times 0.2$ mm^3) show a phototropic character. The results of atomic light absorption analysis revealed the Hg content of this crystal to be 65.0% (calcd for $HgI_2 \cdot 2HgS$ 65.4%). These facts show that the crystals were $HgI_2 \cdot 2HgS$, which deposited upon cooling. In order to find the temperature which the crystal commences to deposit, the temperatures of the system while cooling were plotted against the time by using a big T-type glass tube (4 cm × 130 cm), two big furnaces, and 12 g of materials. When the temperatures of the left- and right-hand sides of the furnace were kept at 300 °C and 500 °C for 2 h and were then lowered at the rates of 5 °C and 7 °C per 10 min respectively, yellow crystals ($4 \times 2 \times 0.4$ mm^3) were found at a position corresponding to the C place in Fig. 1. In this case, the temperature of this position, which initially was 205 °C, was decreased at the rate of 2.5 °C per 10 min and then maintained between 175 °C and 150 °C for about 2 h.

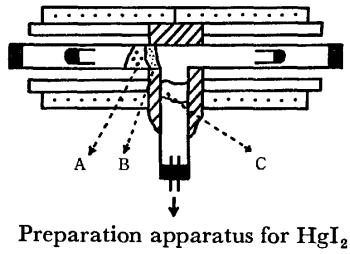

Fig. 1. Preparation apparatus for $HgI_2 \cdot 2HgS$.

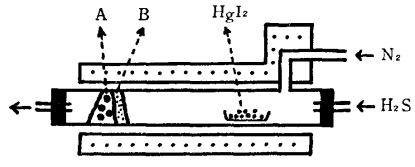

Fig. 2. Preparation apparatus for $HgI_2 \cdot 2HgS$.

It is certain that the crystals commenced to deposit in this temperature range.

High-temperature Reaction between HgI_2 and H_2S. Frerichs[3] prepared single crystals of CdS, CdSe, and CdTe by high-temperature reactions between Cd vapor and H_2S, H_2Se, or H_2Te. Crystals of $HgI_2 \cdot 2HgS$ could also be prepared by a similar method. As is shown in Fig. 2, a glass tube (2 cm in inner diameter, 2 m in length) was put into a horizontal electric furnace. At a point 20 cm from the entrance of the furnace, a glass boat with 5 g of HgI_2 powder was placed; a mixture of H_2S and N_2 was then introduced into the tube at a flow rate of 200 cm^3 per min. The temperature of the position near the glass boat was elevated up to 330 °C over a 1 h period and then kept at this condition for 2 h. After the electric source was cut off, it was observed that red and yellow crystals adhered to the A and B positions respectively, as is shown in Fig. 2. In the course of the reaction, the temperature of the B position was about 150 °C. The phototropy was observed from the yellow crystals deposited at the B place. These crystals are clearly $HgI_2 \cdot 2HgS$. By changing the experimental conditions, such a reaction was tried many times. It was found that $HgI_2 \cdot 2HgS$ crystals ($1.2 \times 0.5 \times 0.1$ mm^3) could also be obtained by this method.

Preparation of Single Crystals of $HgBr_2 \cdot 2HgS$ and $HgCl_2 \cdot 2HgS$. A glass tube (2 cm in inner diameter, 1 m in length) whose bottom had been sealed was placed in a vertical electric furnace. By putting into the bottom 5 g of a mixture of powdered $HgBr_2$ and HgS (black) in a mole ratio of 1 : 2 and by elevating temperature of the furnace, the temperature near the bottom was kept at 450 °C. A vapor-phase reaction was continued under their conditions for 30 h, as is shown in Fig. 3. The air in the tube was then evacuated by using a stream water pump. After the electric source had been cut off, yellow crystals ($1 \times 1 \times 0.5$ mm^3) were found inside the tube 25—29 cm from the bottom. It was easily confirmed by the curve between the temperature and the distance from the bottom that the temperature of this place was 160—200 °C. These crystals are clearly $HgBr_2 \cdot 2HgS$, because they showed phototropic behavior. When using a mixture of powdered $HgCl_2$ and HgS (black), white crystals ($1 \times 1 \times 0.5$ mm^3) were deposited 20 cm from the bottom. The temperature of this point was about 290 °C. These crystals correspond to $HgCl_2 \cdot 2HgS$. Their composition was confirmed by the atomic light absorption analysis; Hg content for $HgBr_2 \cdot 2HgS$: calcd 72.9%, obsd 72.5%; for $HgCl_2 \cdot 2HgS$: calcd 81.7%, obsd 81.3%.

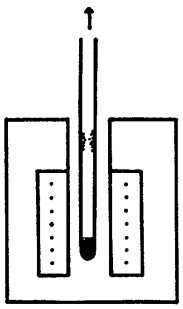

Fig. 3. Preparation apparatus for $HgBr_2 \cdot 2HgS$ or $HgCl_2 \cdot 2HgS$.

An investigation of the Laue photograph on a single crystal of $HgI_2 \cdot 2HgS$ showed that the Laue pattern is distributed with a 2-fold axis and that the symmetry planes of the spots are diagonal to each other. Observation of the single crystal by using a polarized microscope confirmed that this crystal has two light axes. The X-ray rotating-crystal method indicated the lattice constants of this crystal to be $a=9.36$ Å, $b=9.69$ Å, and $c=18.5$ Å. These facts established this crystal belongs to the rhombic system.

The X-ray experiments were carried out at the College of General Education, Kyushu University. The authors wish to express their hearty thanks to Professor Ikuhiko Ueda of Kyushu University for his continuous guidance and advice.

References

1) K. Takei, *Bull. Chem. Soc. Jpn.*, **28**, 408 (1955).
2) K. Takei, *Bull. Chem. Soc. Jpn.*, **28**, 406 (1955).
3) R. Frerichs and R. H. Bube, "Photoconductivity of Solids," John Wiley and Sons, New York (1960), p. 99.

BULLETIN OF THE CHEMICAL SOCIETY OF JAPAN, VOL. 49 (5), 1427—1428 (1976)

Aromaticity of Monocyclic Ions

Jun-ichi AIHARA

Department of Chemistry, Faculty of Science, Hokkaido University, Sapporo 060

(Received February 17, 1975)

Synopsis. The infinitely-large annulenes with additional formal charges were employed as reference structures to evaluate the reference energies of monocyclic ions. On this basis, the Hückel (4r+2) rule of aromaticity was verified within the framework of the HMO theory. The results obtained agree well with the available experimental evidence.

The aromatic criterion of Hess and Schaad[1] has been very successful for interpreting the aromatic character of cyclic conjugated systems within the framework of the Hückel molecular orbital (HMO) theory.[2,3] The resonance energy of a compound is given by the difference between the total π-energy of the compound and the π-energy of a hypothetically non-aromatic reference structure with the same molecular geometry. In previous papers,[4,5] the author has reported that the π-energy of the reference structure could sometimes be estimated from infinitely-large species of the same type.

However, no one has attempted an analogous approach to the ionic species, although some cyclic ions, such as cyclopropenyl and cycloheptatrienyl ions, are known to be aromatic.[6-8] It is the purpose of this paper to show that the HMO theory can be used to analyze the aromaticity of some carbocyclic ions, provided the author's reformulation of the aromatic criterion is employed. The HMO theory in its simplest form is used. All energies are given in units of β.

Theoretical

The total HMO π-energy of a monocyclic ion with a general formula of $C_nH_n^m$ is calculated by summing the π-energies of all its occupied levels. In the chemical formula, n and m respectively signify the numbers of carbon atoms and formal charges, the sign of m being indicative of the type of charge. The total HMO π-energy of $C_nH_n^m$, $E_{\mathrm{HMO}}(n,m)$, is then expressed in the analytical form:[9]

$$E_{\mathrm{HMO}}(n,m) = 2\sum_k g_k \cos\frac{2\pi k}{n}, \tag{1}$$

where g_k is the number of electrons which are present in the kth orbital.

On the other hand, an infinitely-large annulene should be neither aromatic nor antiaromatic, even though it bears formal charges. It should be similar to a charged linear polyene. For this reason, the infinitely-large charged annulene was used as the non-aromatic basis for the evaluation of the aromatic stabilization of the $C_nH_n^m$ series. In this case, the ratio of the number of additional charges to the number of carbon atoms, R, in the infinitely-large system must be adjusted to that of the ion under consideration, *i.e.*, m/n. For example, the reference structure of a cycloheptatrienyl cation is to be derived from the infinitely-large annulene from which a seventh part of the occupied π-electrons are removed.

If n is sufficiently large, Eq. 1 can be rewritten as:

$$\begin{aligned} E_{\mathrm{HMO}}(n,m) &\approx 4n\sum_k \frac{1}{n}\cos\frac{2\pi k}{n} \\ &\approx 4n\int_{\mathrm{occ.}} \cos 2\pi x\,dx \\ &= 4n\left\{\int_0^{1/4(1-m/n)} \cos 2\pi x\,dx + \int_{1/4(3+m/n)}^{1.0} \cos 2\pi x\,dx\right\} \\ &= \frac{4n}{\pi}\cos\left(\frac{m\pi}{2n}\right), \end{aligned} \tag{2}$$

where the integration is made over all occupied energy levels of $C_nH_n^m$. The regions of integration are indicated by arrows in Fig. 1. When n approaches infinity, the integrated value becomes solely dependent upon the ratio m/n and is denoted as $I(m/n)$.

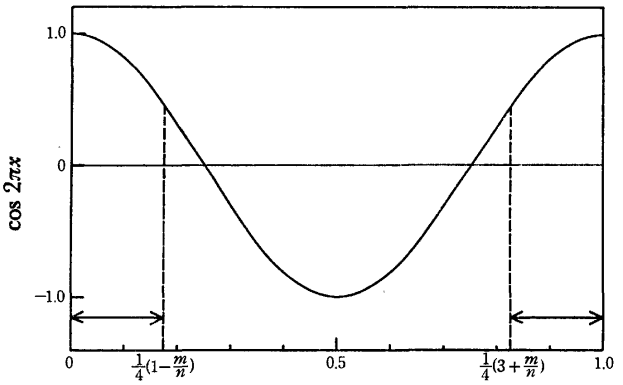

Fig. 1. The regions of integrations in Eq. 2.

Accordingly, the π-energy per π-bond, $E_{\mathrm{U}}(m/n)$, for an infinitely-large annulene with $R=m/n$ is derived from Eq. 2 as follows:

$$\begin{aligned} E_{\mathrm{U}}\left(\frac{m}{n}\right) &= \lim_{d\to\infty}\frac{E_{\mathrm{HMO}}(nd, md)}{nd} \\ &= 4I\left(\frac{m}{n}\right) = \frac{4}{\pi}\cos\left(\frac{m\pi}{2n}\right). \end{aligned} \tag{3}$$

The limiting π-energy per π-bond is exact. From this expression, the infinitely-large annulene can be regarded as a kind of alternant hydrocarbon, *i.e.*,

$$E_{\mathrm{U}}\left(\frac{m}{n}\right) = E_{\mathrm{U}}\left(-\frac{m}{n}\right). \tag{4}$$

Consequently, the π-energy, $E_{\mathrm{A}}(n,m)$, of the reference energy for $C_nH_n^m$ is defined as:

$$E_{\mathrm{A}}(n,m) = nE_{\mathrm{U}}\left(\frac{m}{n}\right) = \frac{4n}{\pi}\cos\left(\frac{m\pi}{2n}\right). \tag{5}$$

Such a derivation of the reference energy for a carbocyclic ion appears to be the best way imaginable at present, since the additive principle of localized π-bond

Table 1. Resonance energies of monocyclic ions in units of $|\beta|$

Species	E_{HMO}	E_A	E_{res}	Character
Two-Electron System ($n-m=2$)				
$C_3H_3^+$	4.0000	3.3080	0.6920	Aromatic
$C_4H_4^{2+}$	4.0000	3.6013	0.3987	Aromatic
Four-Electron Systems ($n-m=4$)				
$C_3H_3^-$	2.0000	3.3080	−1.3080	Antiaromatic
C_4H_4	4.0000	5.0930	−1.0930	Antiaromatic
$C_5H_5^+$	5.2361	6.0546	−0.8185	Antiaromatic
$C_6H_6^{2+}$	6.0000	6.6159	−0.6159	Antiaromatic
Six-Electron Systems ($n-m=6$)				
$C_4H_4^{2-}$	4.0000	3.6013	0.3987	Aromatic
$C_5H_5^-$	6.4721	6.0546	0.4175	Aromatic
C_6H_6	8.0000	7.6394	0.3606	Aromatic
$C_7H_7^+$	8.9879	8.6892	0.2987	Aromatic
$C_8H_8^{2+}$	9.6569	9.4106	0.2463	Aromatic
Eight-Electron Systems ($n-m=8$)				
$C_6H_6^{2-}$	6.0000	6.6159	−0.6159	Antiaromatic
$C_7H_7^-$	8.0978	8.6892	−0.5914	Antiaromatic
C_8H_8	9.6569	10.1859	−0.5291	Antiaromatic
$C_9H_9^+$	10.8229	11.2851	−0.4621	Antiaromatic
$C_{10}H_{10}^{2+}$	11.7082	12.1092	−0.4010	Antiaromatic
Ten-Electron Systems ($n-m=10$)				
$C_8H_8^{2-}$	9.6569	9.4106	0.2463	Aromatic
$C_9H_9^-$	11.5175	11.2851	0.2325	Aromatic
$C_{10}H_{10}$	12.9443	12.7324	0.2119	Aromatic
$C_{11}H_{11}^+$	14.0533	13.8631	0.1903	Aromatic
$C_{12}H_{12}^{2+}$	14.9282	14.7583	0.1699	Aromatic

energies is not applicable due to the lack of definite classical resonance structures. The resonance energy, E_{res}, for $C_nH_n^m$ is then given by the expression:

$$E_{res}(n, m) = E_{HMO}(n, m) - E_A(n, m). \quad (6)$$

The results obtained are presented in Table 1.

Results and Discussion

It is evident from Table 1 that the number of π-electrons is a significant factor which determines the aromaticity. All species with $(4r+2)$ π-electrons are predicted to be aromatic, because they have positive resonance energies, where r is an integer. Conversely, all species with $4r$ π-electrons are predicted to be antiaromatic with negative resonance energies. Note that this result is the best verification of the Hückel $(4r+2)$ rule of aromaticity within the Hückel theory.[10] These results are, of course, in qualitative agreement with the available experimental evidence.[6-8] In general, aromaticity or antiaromaticity decreases as the ring size increases.

Several years ago, Dewar and Venier defined a cyclic ion as being aromatic, if it has a greater π-energy than a corresponding open-chain system.[11] Their SCF-MO calculations appeared to be consistent with the predictions of the Hückel rule.[10] Subsequent free-electron molecular-orbital (FEMO) calculations, carried out by Hobey,[12] were also based on the same reference structures as were adopted by Dewar and Venier. However, one of the difficulties in using open-chain systems as reference structures appears to be that the molecular geometries and numbers of π-bonds are not preserved in them. To make the matter worse, the FEMO model cannot reproduce even the additivity of π-bond energies[1-5,11,13] for non-aromatic systems. However, the presently considered reference energies of monocyclic ions are free from these difficulties; the contributions from all π-bonds are counted in the present procedure. The HMO π-bond energies are sure to be additive in non-aromatic species.[1-5] For a general discussion, see Ref. 5.

Although our simple model neglects some significant effects arising from bond alternation and, more importantly, from interelectronic repulsion, the good agreement with experiment strongly suggests that the resonance energies obtained are good indices of aromaticity, at least, for the monocyclic ions investigated. It is expected that the gross features of the predicted aromatic character are not changed by these effects. On the contrary, it can be noted that the concept of aromaticity for ions thus introduced does not violate the simplicity and elegance of the HMO theory. Finally, it should be emphasized that the same approach can easily be extended to many other conjugated systems, as cited in Ref. 5.

We are grateful to the Hokkaido University Computing Center for the use of their FACOM 230-60, on which all calculations were performed.

References

1) B. A. Hess, Jr. and L. J. Schaad, *J. Am. Chem. Soc.*, **93**, 305 (1971).
2) B. A. Hess, Jr. and L. J. Schaad, *J. Am. Chem. Soc.*, **93**, 2413 (1971).
3) B. A. Hess, Jr. and L. J. Schaad, *J. Org. Chem.*, **36**, 3418 (1971).
4) J. Aihara, *Bull. Chem. Soc. Jpn.*, **48**, 517 (1975).
5) J. Aihara, *Bull. Chem. Soc. Jpn.*, **48**, 1501 (1975).
6) G. M. Badger, "Aromatic Character and Aromaticity," Cambridge University Press, London (1969).
7) F. Sondheimer, *Acc. Chem. Res.*, **5**, 81 (1972).
8) P. J. Garratt and M. V. Sargent, "Nonbenzenoid Aromatics," Vol. II, ed. by J. P. Snyder, Academic Press, New York, N. Y. (1971), Ch. 4.
9) C. A. Coulson and A. Streitwieser, Jr., "Dictionary of π-Electron Calculations," Pergamon, Oxford (1965).
10) E. Hückel, *Z. Phys.*, **70**, 204 (1931); **76**, 628 (1932).
11) M. J. S. Dewar, "The Molecular Orbital Theory of Organic Chemistry," McGraw-Hill, New York, N. Y. (1969), Ch. 5.
12) W. D. Hobey, *J. Org. Chem.*, **37**, 1137 (1972).
13) J. Aihara, *Bull. Chem. Soc. Jpn.*, **47**, 3169 (1974).

BULLETIN OF THE CHEMICAL SOCIETY OF JAPAN, VOL. 49 (5), 1429—1430 (1976)

On the Number of Aromatic Sextets in a Benzenoid Hydrocarbon[1)]

Jun-ichi AIHARA

Department of Chemistry, Faculty of Science, Hokkaido University, Sapporo 060

(Received May 15, 1975)

Synopsis. For a benzenoid hydrocarbon with a single sextet formula, the number of aromatic sextets in it is very close to the number of sextet-type resonance interactions per Kekulé structure.

An aromatic sextet is a benzene ring which can be isolated from a benzenoid hydrocarbon on condition that, if there is some residual π-system, at least, one Kekulé structure can be written for it.[2,3)] One or more aromatic sextets may be further isolated from the residual π-system. Clar has long stressed the importance of writing the structural formula of a benzenoid hydrocarbon with a maximum of aromatic sextets.[2,3)] These aromatic sextets, isolated from each other, have been considered as the only origin of aromatic stabilization. The structural formula thus defined is termed a sextet formula. Recently, Herndon showed,[4,5)] with the aid of a simple resonance theory, that the Dewar-type resonance energy[6–8)] of a benzenoid hydrocarbon is primarily associated with sextet-type resonance interactions, *i.e.*, resonance interactions related by a permutation of three double bonds within individual six-membered rings (sextets) of the structure.

In this article, I would like to point out that Clar's way of enumerating the sextets which give rise to aromaticity in the hydrocarbon is essentially the same as Herndon's, except for polyacenes and their derivatives. A somewhat complicated situation for the polyacenes with plural sextet formulas has already been examined in a separate paper.[9)] The present discussion will, hence, be limited to the benzenoid hydrocarbons for which only one sextet formula can be written.

Let N_C be the number of aromatic sextets in Clar's sextet formula of a benzenoid hydrocarbon,[2,3)] and let N_H be the number of sextet-type resonance interactions, divided by the number of possible Kekulé structures. According to Herndon,[4,5)] the sextet-type resonance interactions are enumerated by the excision of each six-membered ring of the structure in turn, with a summation of the number of possible Kekulé structures for the residual π-systems. The present problem is thus reduced to a comparison of the two quantities, N_C and N_H. For this purpose, N_H-values are calculated for almost all the relevant hydrocarbons imaginable.

Those adopted first are 52 benzenoid hydrocarbons from benzene (C_6H_6) to tetrabenzoheptacene ($C_{42}H_{22}$), which are all cited in Ref. 2. For example, 157 Kekulé structures can be written for dipyreno-(1′.3′: 10.2); (1″.3″: 5.7)-pyrene (I). The number of sextet-type resonance interactions assigned to each six-membered ring is entered in the ring concerned. The aromatic sextets specified in the sextet formula are therein marked with circles. Note that the number of the resonance interactions of this type is comparatively large at these aromatic sextets. This aspect of the aromatic sextets

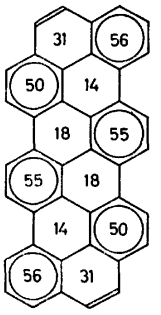

(I)

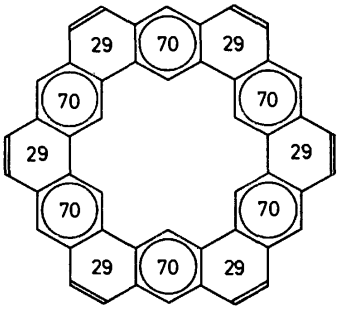

(II)

is common to all the hydrocarbons studied. The N_H-value is then calculated to be 5.707 for I, while the sextet formula is composed of six aromatic sextets and two fixed double bonds. Note, again, that the N_C-value of this compound agrees with the N_H-value within an accuracy of 5.1 percent of the latter value. The N_C-to-N_H value is 1.051. The analogous ratios for common hydrocarbons are as follows: phenanthrene, 1.000; pyrene, 1.000; dibenz[*a*,*h*]anthracene, 1.000; dibenz[*a*,*j*]anthracene, 1.000; triphenylene, 1.039; picene, 0.975; benzo[*d*]pyrene, 1.031; benzo[*ghi*]perylene, 1.000; peropyrene, 0.964; violanthrene, 0.988; ovalene, 1.000.

As may be suggested from these figures, the N_C-to-N_H ratios for the 52 benzenoid hydrocarbons were found to be densely distributed around 1.000. Interestingly, the number of aromatic sextets in the sextet formula nicely approximates the number of sextet-type resonance interactions per Kekulé structure, namely,

$$0.937 < N_C/N_H < 1.075. \quad (1)$$

It is noteworthy that, despite a variety of molecular geometries, the ratio for any compound with a single sextet formula is close to unity. It is possible to include in this relation two other hydrocarbons, coronene and circobiphenyl, which are classified as superaromatic species.[3)] Clar's sextet formulas for these two compounds can be written in two ways, although they are far from polyacene derivatives. Among the hydrocarbons investigated, coronene has the minimum ratio

of 0.9375, while hexa-*peri*-benzocoronene has the maximum ratio of 1.0749.

It goes without saying that the same features of the aromatic sextets are encountered in other kinds of benzenoid hydrocarbons which have not been referred to by Clar. In 1970, [12]coronaphene (II) was first prepared by Jenny *et al.*[10] 200 Kekulé structures can be written for this compound. The N_C-to-N_H ratio for II is calculated to be 1.010 with the use of $N_C=6$ and $N_H=5.940$. The numerical difference between the two ways of enumerating the sextets is only one percent of either value.

In conclusion, we can safely say that, as long as a maximum number of aromatic sextets are fixed in a benzenoid hydrocarbon, Clar's simple aromatic sextet theory[2,3] can predict the number of sextet-type resonance interactions in it; hence, it gives a rough estimate of the Dewar-type resonance energy.[7,8] Remember that the Dewar-type resonance energy, which has been the best aromaticity index available, is roughly proportional to N_H.[4,5] In this sense, Clar's concept of an aromatic sextet is evidently a simplified version of Herndon's theory of aromaticity.[4,5]

This resemblance between them reminds us of the correlation between Pauling's and Coulson's definitions of the bond order.[11] When only a single Kekulé structure is possible for a conjugated hydrocarbon, the double bonds in it indicate the correct locations where Coulson's bond order reaches its maximum values. In the same manner, we might say that, when a benzenoid hydrocarbon has a single sextet formula, the aromatic sextets in it specify the locations where the resonance energy is densely distributed.

References

1) Presented at the Symposium on Molecular Structures, Tokyo, Japan, October 1974.
2) E. Clar, "Polycyclic Hydrocarbons," Vols. I and II, Academic Press, New York, N. Y. (1964).
3) E. Clar, "The Aromatic Sextet," Wiley, London (1972).
4) W. C. Herndon, *J. Am. Chem. Soc.*, **95**, 2404 (1973).
5) W. C. Herndon and M. L. Ellzey, Jr., *J. Am. Chem. Soc.*, **96**, 6631 (1974).
6) M. J. S. Dewar and G. J. Gleicher, *J. Am. Chem. Soc.*, **87**, 685 (1965).
7) M. J. S. Dewar and C. de Llano, *J. Am. Chem. Soc.*, **91**, 789 (1969).
8) M. J. S. Dewar, "The Molecular Orbital Theory of Organic Chemistry," McGraw-Hill, New York, N. Y. (1969), Chapter 5.
9) J. Aihara, *Bull. Chem. Soc. Jpn.*, **48**, 3637 (1975).
10) W. Jenny, P. Baumgartner, and R. Paioni, in "Proceedings of the International Symposium on the Nonbenzenoid Aromatic Compounds," Sendai, Japan (1970), pp. 183—186.
11) W. B. Smith, "Molecular Orbital Methods in Organic Chemistry: HMO and PMO," Marcel Dekker, New York, N. Y. (1974), Chapter 3.

BULLETIN OF THE CHEMICAL SOCIETY OF JAPAN, VOL. 49 (5), 1431—1432 (1976)

Radical Anions Derived from 4-Picrylimino-2,6-disubstituted-2,5-cyclohexadiene-1-one

Eiichiro MANDA and Takehiko SHIMURA

National Chemical Laboratory for Industry Honmachi, Shibuya-ku, Tokyo 151

(Received July 10, 1975)

Synopsis. 4-Picrylimino-2,6-di-*t*-butyl (or bromo)-2,5-cyclohexadiene-1-ones were synthesized and radical anions were derived from them by one electron reduction with potassium metal. ESR measurement showed that an odd electron exists mainly on the quinone-imine moiety of the radical anion molecule.

A number of studies have been made on radical anions derived from quinones.[1] However, only one report[2] has appeared on radical anions derived from anils which are arylimino derivatives of *p*-benzoquinone. The title compounds are a new class of anils and are expected to give easily stable radical anions by one electron reduction since they have 2,6-disubstituted-*p*-benzoquinone and picryl moieties with known structures in the chemistry of stable radicals. In the present paper, we wish to report on the synthesis of the title compounds and some properties of radical anions derived from them.

Results and Discussion

Cyclohexadienones (II) were synthesized by ferricyanide oxidation of 4-*N*-picrylamino-2,6-disubstituted-phenols (I) prepared by the condensation of picryl chloride and 4-amino-2,6-disubstituted-phenol. The yield of each compound was moderate. One electron reduction of cyclohexadienone (II) (*ca.* 0.7 mg) in tetrahydrofuran (*ca.* 3 ml) with excess potassium metal was carried out *in vacuo* by using an apparatus shown in Fig. 2. The color of the reaction mixture turned immediately from yellow to violet (in case of *t*-butyl derivative), or to blue-violet (in case of bromo derivative). ESR measurement showed the presence of radical anions (III). Radical anions (III) were observed to change into some other species when they were in contact with excess potassium metal for some time, their color turning to brown in 20 min for the *t*-butyl derivative and in 3 min for the bromo derivative. Both radical anions (III) were found to be very stable in tetrahydrofuran when they were moved from excess potassium metal, remaining unchanged for a few days at room temperature *in vacuo*, though very unstable in air. ESR measurement for the decay of each radical anion (III) showed that radical anion (IIIa) was more stable than radical anion (IIIb). A solution of each radical anion (III) was therefore transferred to a cell

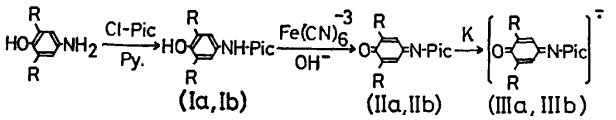

Fig. 1. Reaction path.
Pic; 2,4,6-trinitrophenyl, a; R=*t*-butyl, b; R=Br

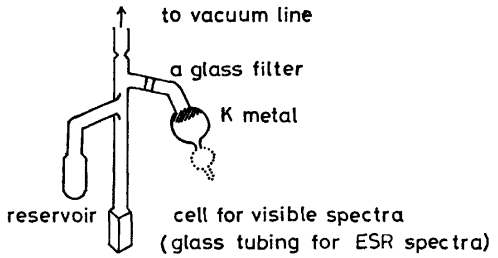

Fig. 2. An apparatus for reduction and spectral measurement.

from excess potassium metal before the color changed, and diluted to a suitable concentration for the spectral measurement with tetrahydrofuran condensed in a reservoir by chilling with liquid nitrogen. The absorption maxima in the electronic spectra of radical anions (III) is located at a greater wavelength (IIIa: 575 nm, IIIb: 583 nm) than the corresponding cyclohexadienones (IIa: 309 nm, IIb: 320 nm). These bathochromic shifts might be caused by the excitation of an odd electron in each radical anion molecule (III), as reported for many hydrocarbon radical anions.[3] The ESR spectrum of radical anion (IIIa) (Fig. 3) consists of a triplet (with hyperfine splitting of 4.38 G of an equal intensity) which might be due to an imino-nitrogen atom. The ESR spectrum of radical anion (IIIb) consists of a triplet (with hyperfine splitting of 6.25 G of an equal intensity) of a triplet (with hyperfine splitting of 1.88 G of intensity ratio=1:2:1) which might be due to an imino-nitrogen atom and two equivalent quinone-protons. The results suggest that unpaired electron distribution at an imino-nitrogen atom is maximal. The absence of the hyperfine splittings due to nitrogen atoms of picryl group suggests that an odd electron exists mainly on the quinone-imine moiety of the radical anion molecule (III). This may be explained by the fact that twisting of a picryl group disturbs the whole π-electron system of radical anion

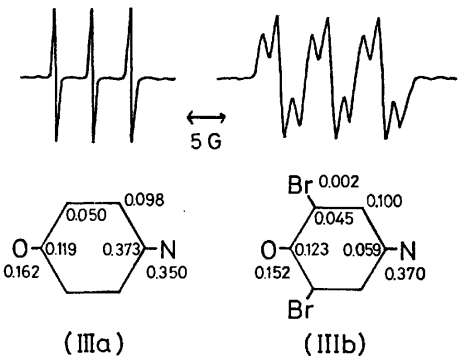

Fig. 3. ESR spectra and HMO spin density of radical anion (III).

(III),[4] and an odd electron exists on quinone-imine moiety which is considered to have greater electron affinity than a picryl group, since the electron affinity of 1,3,5-trinitrobenzene is 0.7 eV and that of 2,6-dibromo-*p*-benzoquinone is 1.2 eV.[5] The HMO unpaired electron distribution of each radical anion (III) was calculated by using parameters cited in the literature[6] for the π-electron system shown in Fig. 3, and the results are also shown in Fig. 3.

Experimental

4-N-Picrylamino-2,6-di-t-butyl (or bromo)-phenol (I). A saturated ethanol solution of 4-amino-2,6-di-*t*-butyl (or bromo)-phenol[7] (0.011 mol) containing pyridine (0.01 mol) was poured into a saturated ethanol solution of picryl chloride (0.01 mol). The reaction was continued for 3 h under refluxing in a stream of nitrogen. The solvent was distilled off as much as possible. The precipitates was filtered off, washed with cold hexane and water successively, and dried *in vacuo*. Recrystallization of each crude product from alcohol gave crystals of phenol (I). Phenol (Ia, R=*t*-butyl): red needles (1.4 g, 28%) from 1-propanol, mp 187—189 °C, Found: C, 55.76; H, 5.38; N, 12.96%; mol wt (MS) *m/e* 432 (M^+). Calcd for $C_{20}H_{24}O_7N_4$: C, 55.55; H, 5.59; N, 12.96%; mol wt 432.4. IR (KBr): 3640 (OH), 3350 (NH), 3070, 2960 (CH), 1625 (NH), 1590 (phenyl), 1530, 1340 (NO_2), 840 (CH) cm^{-1}; Phenol (Ib, R=Br): orange needles (3.0 g. 63%) from ethanol, mp 245—247 °C, Found: C, 30.32; H, 1.31; N, 12.02; Br, 33.41%; mol wt (MS) *m/e* 476 (M^+). Calcd for $C_{12}H_6O_7N_4Br_2$: C, 30.15; H, 1.27; N, 11.72; Br, 33.43%; mol wt 476.2, IR(KBr): 3400 (OH), 3300 (NH), 3070 (CH), 1615 (NH), 1590 (phenyl), 1525, 1355 (NO_2), 845 (CH) cm^{-1}.

4-Picrylimino-2,5-di-t-butyl (or bromo)-cyclohexadiene-1-one (II). The phenol (I) (0.001 mol) in benzene was oxidized with potassium ferricyanide (1.23 g, 0.004 mol) and potassium hydroxide (0.23 g, 0.0041 mol) in water (15 ml) by shaking the reaction mixture for 3 h at room temperature. The reaction mixture was then poured onto a large amount of water, and the organic layer was washed with water and dried over anhydrous sodium sulfate. A yellow powder was obtained after distilling off benzene from the organic layer, and each crude product was recrystallized from alcohol. Cyclohexadienone (IIa, R=*t*-butyl): yellow plates (0.37 g, 86%) from ethanol, mp 177—179 °C, Found: C, 54.29; H, 4.85; N, 13.53%; mol wt. (MS) *m/e* 430 (M^+). Calcd for $C_{20}H_{22}O_7N_4$: C, 55.81; H, 5.15, N, 13.02%; mol wt 430.4. IR (KBr) 3070, 2960 (CH), 1660 (C=N), 1640 (C=O), 1615 (C=C), 1550, 1345 (NO_2), 820 (CH) cm^{-1}. Cyclohexadienone (IIb, R=Br): yellow-brown plates (0.20 g, 42%) from ethanol, mp 220—221 °C. Found: C, 30.46; H, 0.92; N, 10.82; Br, 33.51%. Mol wt (MS) *m/e* 474 (M^+). Calcd for $C_{12}H_4O_7N_4Br_2$: C, 30.28; H, 0.85; N, 11.77; Br, 33.57%. Mol wt 474.2. IR (KBr); 3070 (CH), 1670 (C=O), 1615 (C=N), 1605 (C=C), 1535, 1350(NO_2), 825 (CH) cm^{-1}.

All the melting points were uncorrected. The infrared spectra were measured with a Shimadzu IR-27G grating spectrophotometer, the visible spectra with a Hitachi EPS-2U recording spectrophotometer and the ESR spectra with a Hitachi 771 electron spin resonance spectrometer.

The authors are indebted to Mr. Wasada for the mass spectra and Mr. Nishikawa for the HMO calculation.

References

1) B. W. Brandon and E. A. C. Rucken, *J. Chem. Soc.*, **1961**, 4273, G. Vincow, *J. Chem. Phys.*, **38**, 917 (1963), Y. Iida, *Bull. Chem. Soc. Jpn.*, **47**, 99 (1974), and literatures cited.

2) B. I. Shapiro and V. M. Kazakova, *Zh. Strukt. Khim.*, **1968**, 306.

3) D. E. Paul, D. Lipkin, and S. I. Weissman, *J. Am. Chem. Soc.*, **8**, 2002 (1956).

4) D. I. Williams, *J. Am. Chem. Soc.*, **88**, 5665 (1966).

5) G. Breigleb, *Angew. Chem.*, **76**, 326 (1964).

6) A. Streitwieser, Jr., "Molecular Orbital Theory," John Wiley & Sons, New York and London (1961), p. 135.

7) E. Manda, *Bull. Chem. Soc. Jpn.*, **47**, 2727 (1974), for *t*-butyl derivative and W. W. Hartman, J. B. Dickey, and J. G. Stampeli, *Org. Synth.*, Coll. Vol., **2** 175 (1948), for bromo derivative.

BULLETIN OF THE CHEMICAL SOCIETY OF JAPAN, VOL. 49 (5), 1433—1434 (1976)

The Reaction of the Butenyl Grignard Reagent with Trimethylchlorosilane

Hideki SAKURAI, Yoshihiko KUDO, and Heiichi MIYOSHI*

Department of Chemistry, Faculty of Science, Tohoku University, Aramaki Aza Aoba, Sendai 980
**Department of Synthetic Chemistry, Faculty of Engineering, Kyoto University, Sakyo-ku, Kyoto 606*

(Received September 5, 1975)

Synopsis. The reaction of trimethylchlorosilane with the butenyl Grignard reagent prepared from either 3-chloro-1-butene or 1-chloro-2-butene yielded *trans*-2-butenyltrimethylsilane, *cis*-2-butenyltrimethylsilane and 1-methyl-2-propenyltrimethylsilane, approximately in the ratio of 30/20/50. Structures of these isomeric butenylsilanes were elucidated by NMR and IR spectra.

During the course of a study on thermolysis of cyclopropylsilanes[1] and allyltrimethylsilane,[2] it became desirable to prepare *trans*- and *cis*-2-butenyltrimethylsilanes. Butenyltrimethylsilanes may be prepared by hydrosilylation of butadiene,[3] but these compounds can also be prepared by direct introduction of a butenyl group into silicon through an organometallic reagent. Accordingly, we prepared three allylic isomers of butenylsilanes by the reaction of trimethylchlorosilane with butenylmagnesium chloride. When the most of the work had been completed, we received reports of Seyferth and coworkers[4,5] who prepared the compounds in question with butenyllithium in the course of a study on the solution properties of the lithium reagent. Recently, they have published the detail of the experiment.[6] Slutsky and Kwart also reported the preparation of butenylsilanes recently.[7] In spite of these circumstances, we would like to publish our results briefly, since results with the Grignard reagent are somewhat different from those with the Grignard reagent in product distribution and we have elucidated the structures of butenyltrimethylsilane unequivocally by analyzing the complex NMR spectra.

Addition of trimethylchlorosilane at room temperature to the Grignard reagent, which was prepared from either 3-chloro-1-butene (I) or 1-chloro-2-butene (II), resulted in the formation of a mixture of *trans*- and *cis*-2-butenyltrimethylsilanes (III and IV) and 1-methyl-2-propenyltrimethylsilane (V) in 60—90% total yield.

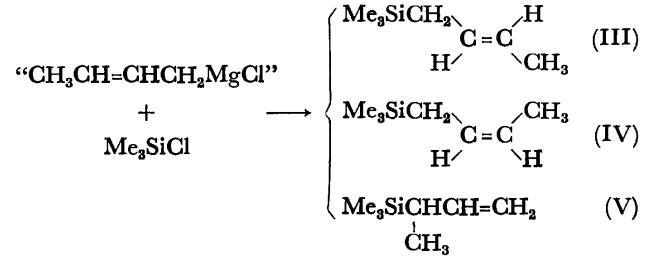

Product distribution was little affected by the structure of the starting chloride, by changing the solvent from ether to THF, and by the order of addition. Thus, relative yields of III/IV/V were, in %: (a) addition of trimethylchlorosilane to the Grignard reagent from I in ether, 27.7/20.4/51.9; (b) addition of trimethylchlorosilane to the Grignard reagent from II in ether, 30.1/21.5/48.4; (c) *in situ* reaction of trimethylchlorosilane, I and magnesium in THF, 26.7/19.8/53.4.

The reaction of the butenyllithium reagent, which was prepared from either *cis*- or *trans*-2-butenyltrimethyltin by *trans*-metallation, with trimethylchlorosilane gave an approximately 3/2 mixture of III/IV.[6] It was noted that V was not among the products in the reaction of the lithium reagent. This is the most significant difference between two reagents in the reaction with trimethylchlorosilane, although the same *trans*/*cis* ratio of approximately 3/2 is sustained in two experiments.

It is well established that the unsymmetric butenylmagnesium bromide consists mainly of the 2-butenyl isomer in mobile equilibrium with the very minor 1-methyl-2-propenyl isomer.[8] Therefore, the present finding confirms the rapid equilibration between two isomeric structures of the Grignard reagent.

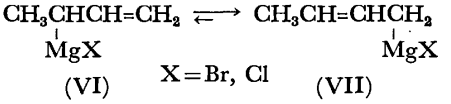

A path for the dominant formation of V, which must occur only in the reaction of the Grignard reagent, may be provided by the S_E2' type reaction of VII,[9] since the direct displacement reaction of VI (S_E2 reaction) with trimethylchlorosilane is unlikely because of both steric reason and unfavorable equilibrium concentration. The reaction of a secondary Grignard reagent with trimethylchlorosilane usually resulted in the reduction of the chlorosilane.[10]

The NMR spectra of III and IV are very complicated and have not been analyzed completely yet. We have

TABLE 1. NMR DATA OF $C_4H_7Si(CH_3)_3$ IN CCl_4

Compound	Chemical Shifts (δ) and Coupling Constants (Hz)
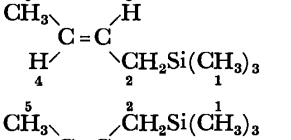	−0.03 (s, H_1), 1.46 (m, H_2), 5.23 (m, H_3 and H_4), 1.63 (m, H_5); $J_{H_3-H_4}=15.5$[a]
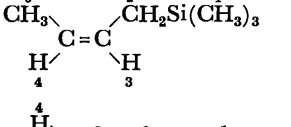	−0.01 (s, H_1), 1.45 (m, H_2), 5.28 (m, H_3 and H_4), 1.52 (m, H_5); $J_{H_3-H_4}=12.0$[a]
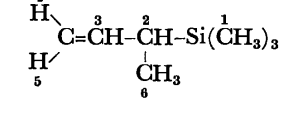	0.04 (s, H_1), 1.56 (m, H_2), 5.77 (d, d, d, H_3), 4.83 (m, H_4 and H_5), 1.04 (d, H_6); $J_{H_4-H_5}=1.5$[b], $J_{H_3-H_4}=11.0$, $J_{H_3-H_5}=16.5$, $J_{H_3-H_6}=6.0$, $J_{H_5-H_6}=7.5$

a) The coupling constants were obtained by irradiation at both H_2 and H_5. b) The coupling constant was obtained by irradiation at H_2.

Table 2. IR data of $C_4H_7Si(CH_3)_3$ (cm^{-1})

Mode of Vibration	Compound (III)	(IV)	(V)
$=CH_2$ stretching			3080 (m)
=CH– stretching	3020 (m)	3020 (m)	
C=C stretching	1660 (w)	1645 (m)	1625 (m)
CH in-plane deformation		1400 (m)	1415 (m)
CH out-of-plane deformation	965 (s)		900 (s)

determined all chemical shifts and coupling constants. by using triple resonance technique on pure samples The results are listed in Table 1. The data of IR spectra are listed in Table 2.

Experimental

NMR spectra were obtained at 100 MHz using a Varian HA-100 spectrometer. IR spectra were measured with a Nippon Bunko DS-402G Grating Infrared Spectrophotometer. 2-Chloro-1-butene and 1-chloro-2-butene were prepared from 1,3-butadiene and hydrogen chloride according to the literature.[11]

The Grignard reactions were carried out by the standard procedure. A typical example is shown below.

A solution of 1-chloro-2-butene (9.05 g, 0.1 mol) dissolved in ether (14 ml) was added to magnesium (3.16 g, 0.13 g-atom) in ether (14 ml) very slowly with stirring. After 6 h, a solution of trimethylchlorosilane (10.8 g, 0.1 mol) in ether (14 ml) was added to the mixture. After an exothermic reaction had ceased, the mixture was heated at reflux for 1 h and hydrolyzed with water. The dried organic layer was distilled using a short Vigreux column to give 9.5 g (74%) of a mixture of butenylsilanes, bp 110—118 °C.

The mixture was analyzed by GLC with a phenylacetonitrile–$AgNO_3$ column. Relative retention times were critically influenced by the silver content, and finally a column packed with *ca.* 30% by weight of an approximately 1 : 1 complex of $PhCH_2CN$–$AgNO_3$ on Celite 545 was used at 45 °C with 0.9 atom helium. Under these conditions the retention times were 2.0 min for III, 6.6 min for IV and 10.5 min for V. A portion of the mixture was also separated by GLC and identified by spectroscopic studies.

Mass spectra (25 eV) *m/e* (rel. intensity), (III): 128 (10.6), 113(5.5), 85(6.9), 73(100), 59(10.1), 55(11.1); (IV): 128(9.3), 113(4.8), 85(6.2), 73(100), 59(9.7), 55(14.5); (V): 128 (5.9), 113(4.3), 85(6.3), 73(100), 59(8.7), 55(6.7).

We wish to thank Dr. Y. Nakadaira for NMR measurements. We also thank Toshiba Silicone Co., Ltd., for gifts of chlorosilanes.

References

1) H. Sakurai, A. Hosomi, and M. Kumada, *Tetrahedron Lett.*, **1969**, 2469.
2) H. Sakurai, A. Hosomi, and M. Kumada, *Chem. Commun.*, **1970**, 767.
3) (a) V. F. Mironov and N. G. Maksimova, *Izv. Akad. Nauk SSSR, Otd Khim. Nauk*, **1962**, 1303; *Chem. Abstr.*, **58**, 5713 (1963); (b) M. S. Wrighton and M. A. Schroeder, *J. Am. Chem. Soc.*, **96**, 6236 (1974).
4) D. Seyferth and T. F. Jula, *J. Organomet. Chem.*, **8**, 13 (1967).
5) D. Seyferth, R. F. Jula, H. Dertouzos, and M. Pereyre, *J. Organomet. Chem.*, **11**, 63 (1968).
6) D. Seyferth and T. F. Jula, *J. Organomet. Chem.*, **66**, 195 (1974).
7) J. Slutsky and H. Kwart, *J. Am. Chem. Soc.*, **95**, 8678 (1973).
8) J. F. Nordlander, W. G. Young, and J. D. Roberts, *J. Am. Chem. Soc.*, **83**, 494 (1961).
9) H. Felkin and C. Frajerman, *Tetrahedron Lett.*, **1933**, 1045.
10) N. W. Cusca and F. S. Kipping, *J. Chem. Soc.*, **1933**, 1040.
11) A. L. Henne, H. Chanan, and A. Turk, *J. Am. Chem. Soc.*, **63**, 3473 (1941).

BULLETIN OF THE CHEMICAL SOCIETY OF JAPAN, VOL. 49 (5), 1435—1436 (1976)

Reduction and Oxidation Potentials of Metal-free and Cobalt Tetra(*p*-substituted phenyl)porphyrins

Meguru TEZUKA, Yasukazu OHKATSU, and Tetsuo OSA*

Department of Industrial Chemistry, Faculty of Engineering, The University of Tokyo, Hongo, Bunkyo-ku, Tokyo 113

(Received September 26, 1975)

Synopsis. Both reduction and oxidation potentials of metal-free and cobalt tetra(*p*-substituted phenyl)porphyrins were determined by means of cyclic voltammetry. They are correlated with Hammett σ values of the substituents when the electron transfer occurs at the porphin ring, but not in the electron transfer step in which the cobalt atom participates.

Great interest has been shown in the electrochemistry of porphyrins and metalloporphyrins from the standpoint that their redox properties play a significant role in biological systems.[1-4] Felton and Linschitz studied the polarographic reduction of various metallotetraphenylporphyrins (MTPP) in order to see if they were reduced step-wise through a one-electron transfer to yield the porphyrin anion radicals followed by the formation of the dianions; in the case of cobalt tetraphenylporphyrin (CoTPP), however, the central metal was reduced in the first electron transfer step.[5] On the other hand, Wolberg and Manassen investigated the oxidation of transition metal complexes of tetraphenylporphyrins and phthalocyanines and concluded that in the cases of Fe, Co, and Ni tetraphenylporphyrins, the central metal was oxidized first, whereas oxidation of the ligand was observed for Cu and Zn porphyrins, subsequent oxidation occurring at the ligand in all cases.[6] From these results, Manassen discussed the catalytic behavior of MTPP in a few pure chemical reactions, such as oxidative dehydrogenation and symmetry-forbidden rearrangement.[7]

Although a number of studies have been made on porphyrins and metalloporphyrins, little has been done to make a systematic examination of the substituent effect on their redox properties. We have determined both reduction and oxidation potentials of metal-free and cobalt (*p*-substituted phenyl)porphyrins by the cyclic voltammetric method. The effects of substituents on the redox properties and on the catalytic activity in the autoxidation of acetaldehyde are discussed.

Experimental

Materials. Metal-free tetraphenylporphyrin (H_2TPP) and its *p*-substituted derivatives, *viz.*, tetra(*p*-methylphenyl)-porphyrin[H_2(*p*-CH_3)TPP], tetra(*p*-methoxyphenyl)porphyrin [H_2(*p*-OCH_3)TPP] and tetra(*p*-chlorophenyl)porphyrin-[H_2(*p*-Cl)TPP] as well as the cobalt complexes of these porphyrins were synthesized and purified according to conventional methods. *N,N*-Dimethylformamide (DMF) was dried over "Drierite" for several days and distilled twice under reduced pressure of nitrogen. Tetraethylammonium perchlorate (TEAP) was synthesized and purified according to conventional methods.

Cyclic Voltammetry. Cyclic voltammograms of the saturated solutions of porphyrins in DMF were recorded with a platinum plate of 0.40 cm^2 at 25 °C. TEAP was used as a supporting electrolyte. The concentration of porphyrins was less than 2 mM in most cases. The potential was referred to saturated calomel electrode (SCE).

TABLE 1. CYCLIC VOLTAMMETRY OF METAL-FREE AND COBALT TETRA(*p*-SUBSTITUTED PHENYL)PORPHYRINS

Porphyrin	Peak potential (V)			
	Oxidation		Reduction	
H_2TPP		+1.13	−1.04	−1.42
H_2(*p*-CH_3)TPP		+1.08	−1.06	−1.48
H_2(*p*-OCH_3)TPP		+1.02	−1.08	−1.50
H_2(*p*-Cl)TPP		+1.18	−0.98	−1.36
CoTPP	+0.58	+1.20	−0.80	−1.90
Co(*p*-CH_3)TPP	+0.57	+1.16	−0.80	−1.88
Co(*p*-OCH_3)TPP	+0.62	+1.10	−0.80	−1.90
Co(*p*-Cl)TPP	+0.75	+1.26	−0.76	−1.79

Measurements were made on a platinum electrode in 0.1 M TEAP–DMF solution at 25 °C. The concentration of porphyrins was less than 2 mM in most cases. Potential sweep rate: 0.10 V/s. (V *vs.* SCE).

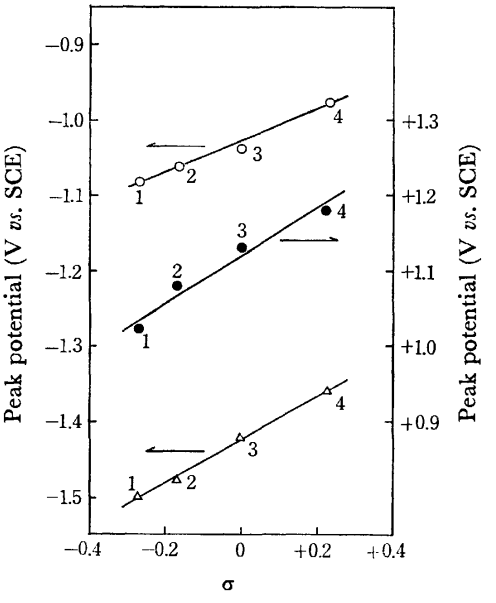

Fig. 1. Relation of peak potentials for the first (○), the second (△) reduction and oxidation (●) of metal-free tetra(p-substituted phenyl)porphyrins in DMF to Hammett substituent constants: 1, H_2(*p*-OCH_3)-TPP. 2, H_2(*p*-CH_3)TPP. 3, H_2TPP. 4, H_2(*p*-Cl)-TPP.

* Present address: Pharmaceutical Institute, Tohoku University, Aramaki, Sendai 980.

Results and Discussion

The cyclic voltammetric results are given in Table 1.

Metal-free porphyrins were reduced step-wise through a reversible one-electron transfer step to give porphyrin anion radicals followed by the formation of the dianions.[5] The irreversible waves, ascribed to the formation of porphyrin cation radicals, were also observed in the oxidation. These peak potentials of reduction and oxidation are correlated with Hammett σ values (Fig. 1). Each correlation is expressed as follows.

First reduction:

$$E_p = 0.205\sigma - 1.030\text{V} \quad (1)$$

Second reduction:

$$E_p = 0.295\sigma - 1.426\text{V} \quad (2)$$

Oxidation:

$$E_p = 0.317\sigma + 1.118\text{V} \quad (3)$$

The equations show that the electron-donating group increases the electron density on the porphin ring through the phenyl group, and consequently these peak potentials shift toward a negative direction while the reverse is seen for the electron-withdrawing group.

The reduction of cobalt porphyrins also proceeded reversibly through two one-electron steps. The first step has been accepted to be the addition of electron to cobalt, Co(II)→Co(I), and the second step also seems to involve the change in the valency of cobalt.[5,8] The oxidation consists of the two consecutive steps, the first and second steps being attributed to the oxidation of cobalt and porphin ring, respectively.[6] Contrary to the case of metal-free porphyrins, a good correlation with Hammett σ values was obtained in the second oxidation step (Fig. 2):

$$E_p = 0.296\sigma + 1.198\text{V} \quad (4)$$

whereas no distinct correlation was found in the first oxidation and reduction steps.

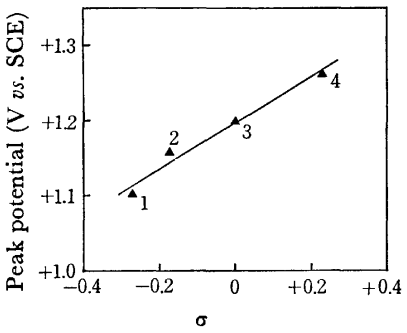

Fig. 2. Relation of peak potentials for the second oxidation of cobalt tetra(*p*-substituted phenyl)porphyrins to Hammett substituent constants: 1, Co(*p*-OCH_3)-TPP. 2, Co(*p*-CH_3)TPP. 3, CoTPP. 4, Co(*p*-Cl)-TPP.

It is thus concluded that the peak potentials are correlated well with Hammett σ values when the electron transfer occurs at the porphin ring as in the case of metal-free porphyrins or the second oxidation of cobalt porphyrins. This can be understood in terms of the resonance interaction between the substituents on phenyl groups and the porphin ring.[9] No correlation is substantially obtained when the electron transfer occurs at the cobalt atom. This indicates that the redox properties of central metal do not directly reflect those of the porphin ring.

CoTPP activates an oxygen molecule to the superoxide state through the electron donation from the central metal. The activated oxygen abstracts the hydrogen of acetaldehyde to initiate autoxidation. It was found that Co(*p*-CH_3)TPP possesses a remarkably high catalytic activity, almost ten times as much as those of the other cobalt porphyrins. The extraordinary activity of Co(*p*-CH_3)TPP cannot be explained in terms of the oxidation potentials of porphyrins. This is ascribed to the fact that the potentials indicate only the ease of the activation process of oxygen molecule. It seems that the substituent effect on the reactivity of an oxygen molecule which has been in activated condition should also be taken into account for clarifying the effect in autoxidation of acetaldehyde.

We would like to express our thanks to Prof. Taiseki Kunugi for his valuable advice and discussion.

References

1) J. H. Fuhrhop and D. Mauzerall, *J. Am. Chem. Soc.*, **91**, 4174 (1969).

D) J. Fajer, D. C. Borg, A. Forman, D. Dolphin, and R. H. Felton, *J. Am. Chem. Soc.*, **92**, 3451 (1970).

3) N. E. Tokel, V. Katonić, K. Farmery, L. B. Anderson, and B. H. Busch, *J. Am. Chem. Soc.*, **92**, 400 (1970).

4) K. M. Kadish, G. Larson, D. Lexa, and M. Momenteau, *J. Am. Chem. Soc.*, **97**, 282 (1975).

5) R. H. Felton and H. Linschitz, *J. Am. Chem. Soc.*, **88**, 1113 (1966).

6) A. Wolberg and J. Manassen, *J. Am. Chem. Soc.*, **92**, 2982 (1970).

7) J. Manassen, *Catal. Rev.*, **8**, 223 (1974).

8) L. D. Rollmann and R. T. Iwamoto, *J. Am. Chem. Soc.*, **90**, 1455 (1968).

9) P. Zuman, "Substituent Effects in Organic Polarography," Plenum Press, New York (1967).

BULLETIN OF THE CHEMICAL SOCIETY OF JAPAN, VOL. 49 (5), 1437—1438 (1976)

The Chlorination of 1,3- and 1,5-Cyclooctadienes with Various Chlorinating Agents

Sakae UEMURA, Akira ONOE, Hajime OKAZAKI, Masaya OKANO, and Katsuhiko ICHIKAWA*

Institute for Chemical Research, Kyoto University, Uji, Kyoto 611

**Department of Hydrocarbon Chemistry, Faculty of Engineering, Kyoto University, Yoshida, Kyoto 606*

(Received October 13, 1975)

Synopsis. The chlorination of 1,3-cyclooctadiene with various chlorinating agents gave an isomeric mixture of *trans*-3,4-, *cis*-3,4-, *trans*-3,8-, and *cis*-3,8-dichlorocyclooctene. From 1,5-cyclooctadiene an isomeric mixture of *trans*- and *cis*-5,6-dichlorocyclooctene was obtained. The isomer distribution depended a great deal on chlorinating agents in both cases.

Recently Lasne and Thuillier[1] have reported the chlorination of 1,3-cyclooctadiene (1,3-COD) with (dichloroiodo)benzene or copper(II) chloride which gave both 1,2- and 1,4-addition products. Since it has previously been reported[2] that 1,3-COD was chlorinated with copper(II) chloride to give only two isomeric 1,2-addition products, we reexamined the reaction products in the previous paper[2] and also carried out the chlorination of both 1,3- and 1,5-COD with many other chlorinating agents with which norbornene[3] and norbornadiene[4] were treated.

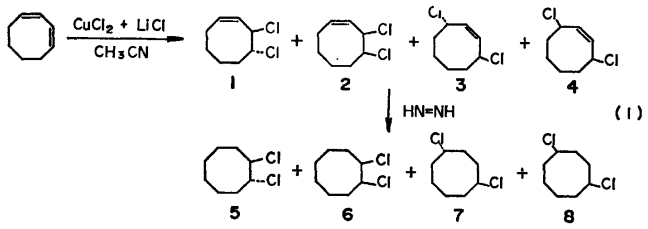

Scheme 1.

The product mixtures obtained from the reaction of 1,3-COD with $CuCl_2$[2] were hydrogenated with diimide in methanol[5] to the mixture of four isomeric dichlorocyclooctanes (**5**—**8** in Scheme 1). Each isomer was identified by comparison of retention time in GLC and the spectroscopic data with those of each authentic sample by the reported method.[6-8] From this result four isomers were revealed to be *trans*-3,4-(**1**), *cis*-3,4-(**2**), *trans*-3,8-(**3**), and *cis*-3,8-dichlorocyclooctene (**4**), respectively. Since we confirmed in separate experiments that no isomerization occurred during hydrogenation, the isomer ratio in **1**—**4** is considered to be the same as that in **5**—**8**. This isomer ratio was reproducible in each run and was not affected so much by prolonging the reaction time. The ratio of 1,2- to 1,4-addition was 53—51 : 47—49, being nearly the same as the reported value.[1] In order to compare with the reported data[1] chlorination with $PhICl_2$ was carried out under several conditions. It was revealed that the proportion of 1,4-addition was quite high (69—81%) in our case under any conditions, compared with the reported value[1] of 30%. Typical results are shown in Table 1. The chlorination was also carried out with several other chlorinating agents in which $PbCl_4$, $SeCl_4$, and Cl_2 gave **1**—**4** (Table 1). Tetrachlorocyclooctane was not formed under any conditions shown in

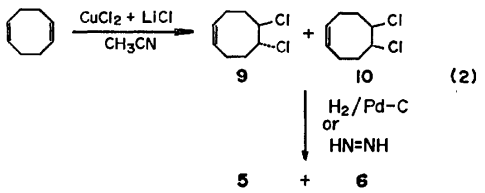

Scheme 2.

TABLE 1. CHLORINATION OF 1,3-CYCLOOCTADIENE

1,3-COD (mmol)	Chlorinating agents (mmol)	Solvent (ml)	React. Temp (°C)	React. Time (h)	Products Isomer distribution[a] 1	2	3	4	Yield (%)[b]
50	$CuCl_2$ 100+LiCl 100	CH_3CN 100	82	4	22	31	2	45	44
50	$CuCl_2$ 100+LiCl 100	CH_3CN 100	82	22	21	30	2	47	70
10	$PhICl_2$ 5	$CHCl_3$ 25[c]	25	1	17	4	62	17	42
10	$PhICl_2$ 5	$CHCl_3$ 25	25	1	27	4	54	15	41
10	$PhICl_2$ 5	$CHCl_3$ 25[c]	61	1	20	3	58	19	66
10	$PhICl_2$ 5	$CHCl_3$ 25	61	1	16	3	67	14	66
50	$PbCl_4$ 10	CH_2Cl_2 50	−40	2	31	4	21	44	82
10	$SeCl_4$ 3	CCl_4 50[c]	76	5	49	12	33	6	79
10	$SbCl_5$ 4	CCl_4 50[c]	5	0.1	19	35	0	46	33
50	Cl_2 50	CH_2Cl_2 100	−50	0.1	44	4	22	30	9
50	Cl_2 50	CH_2Cl_2 100	−50	0.5	45	3	24	28	44

a) Determined by GLC after diimide reduction of concentrated organic extract. b) Based on chlorinating agents charged as determined by GLC. c) Under N_2.

* Correspondence should be addressed to S. U.

Table 2. Chlorination of 1,5-cyclooctadiene

1,5-COD (mmol)	Chlorinating agents (mmol)	Solvent (ml)	React. Temp (°C)	React. Time (h)	Products Isomer distribution[a] 9	10	Yield (%)[b]
50	$CuCl_2$ 100+LiCl 100	CH_3CN 100	82	4	61	39	26
50	$CuCl_2$ 100+LiCl 100	CH_3CN 100	82	22	62	38	65
6	$PhICl_2$ 5	$CHCl_3$ 25[c]	25	1	23	77	53
6	$PhICl_2$ 5	$CHCl_3$ 25[c]	61	1	27	73	65
6	$PhICl_2$ 5	CCl_4 25[c]	76	1	20	80	47
50	$PbCl_4$ 10	CH_2Cl_2 50	−40	2	84	16	49[d]
11	$SeCl_4$ 3	CCl_4 50[c]	76	5	82	18	34[d]
21	$MoCl_5$ 4	CCl_4 100	27	3	8	92	48
50	Cl_2 50	CH_2Cl_2 50	−50	0.1	93	7	6
50	Cl_2 50	CH_2Cl_2 50	−50	0.5	93	7	18

a) Determined by GLC before reduction. b) Based on chlorinating agents charged as determined by GLC.
c) Under N_2. d) No improvement of the yield by prolonging the reaction time to 10 h.

Table 1, while variable amounts of high-boiling resinous products were always produced. In the case of $SbCl_5$ the yield of **1**—**4** was decreased by prolonging the reaction time or raising the temperature, producing the resinous products. In the case of Cl_2 it was necessary to carry out the reaction at low temperature. Otherwise very many unidentified products were formed as reported previously.[2] The reaction with $TlCl_3 \cdot 4H_2O$, VCl_4, and $MoCl_5$ at room or refluxing temperature gave only a trace amount of **1**—**4** together with lots of polymerized products.

The product mixtures obtained from chlorination of 1,5-COD with $CuCl_2$[2] were hydrogenated catalytically or with diimide to afford an isomeric mixture of **5** and **6** (Scheme 2), the ratio between two isomers being the same as that in the starting unsaturated compounds. The result showed that the products were *trans*-(**9**) and *cis*-5,6-dichlorocyclooctane (**10**). This means that both isomers have been assigned erroneously and reversely in the previous report.[2] Typical results were shown in Table 2 together with those of chlorination with some other metal chlorides and chlorine gas. The reactions were slow as compared to those of 1,3-COD and did not give tetrachlorocyclooctane in any cases. Although the chlorination of 1,5-COD with $SbCl_5$ gave an isomeric mixture of 2,8-dichlorobicyclo[3,2,1]octanes as the products,[9] such compounds were not formed by the use of chlorinating agents shown in Table 2. The characteristic *cis*-chlorination with $MoCl_5$ which has been observed with various olefins[10] was also found in this case.

Experimental

Experimental procedures were almost the same as those reported.[2-4] The IR and NMR spectra were recorded with a Hitachi EPI-S2 and a Varian A-60 or T-60 apparatus respectively. Gas chromatographies were carried out on Shimadzu 4BMPF apparatus using SE-30(3%)-Chromosorb-W (3 m) and EGSS-X(15%)-Chromosorb-W (3 m) columns (N_2 as carrier gas; ethyl benzoate as internal standard).

Anthentic Samples for GLC. **5** was prepared by the addition of chlorine to *cis*-cyclooctene.[6] A mixture of **5** and **6** (**5**:**6**=75:25) was prepared by the reaction of $PhICl_2$ with *cis*-cyclooctene.[7] A mixture of **7** and **8** (**7**:**8**=20:80) was prepared by the reaction of *cis*-cyclooctene with $PbCl_4$.[8]

Diimide Reduction of a Mixture of **1**—**4**. To a methanol (50 ml) solution of a mixture of **1**—**4** (0.6 g, 3.3 mmol, bp 62—69 °C/3 Torr) and hydrazine hydrate (80%, 10 g) was added 30% H_2O_2 (10 g) drop by drop at room temperature and then the mixture was heated to reflux for 1 h. The reaction mixtures were worked up by the following successive treatments; dilution with water, extraction with benzene, and then evaporation of benzene. The residue was analyzed by GLC on EGSS-X (3 m) column at 150 °C: **5** (21.7%), **6** (31.3%), **7** (2.2%), and **8** (44.8%); total yield, 3.1 mmol, 92%.

Similary a mixture of **9** and **10** was reduced to a mixture of **5** and **6** in a 95% yield as determined by GLC [EGSS-X or SE-30 (3 m) column at 150 °C].

References

1) M. -C. Lasne and A. Thuillier, *Bull. Soc. Chim. Fr.*, **1974**, 1142.
2) S. Uemura, A. Tabata, Y. Kimura, and K. Ichikawa, *Bull. Chem. Soc. Jpn.*, **44**, 1973 (1971).
3) S. Uemura, A. Onoe, and M. Okano, *Bull. Chem. Soc. Jpn.*, **48**, 3702 (1975).
4) A. Onoe, S. Uemura, and M. Okano, *Bull. Chem. Soc. Jpn.*, **49**, 345 (1976).
5) C. E. Miller, *J. Chem. Educ.*, **42**, 254 (1965).
6) N. L. Allinger and L. A. Tushaus, *Tetrahedron*, **23**, 2057 (1967).
7) M. -C. Lasne and A. Thuillier, *Bull. Soc. Chim. Fr.*, **1972**, 4594.
8) P. W. Henniger, L. J. Dukker, and E. Havinga, *Rec. Trav. Chim. Pays-Bas*, **85**, 1177 (1966).
9) S. Uemura, A. Onoe, and M. Okano, *J. Chem. Soc. Chem. Commun.*, **1975**, 210.
10) S. Uemura, A. Onoe, and M. Okano, *Bull. Chem. Soc. Jpn.*, **47**, 3121 (1974).
11) H. J. Lucas and E. R. Kennedy, "Organic Syntheses," Coll. Vol. III (1955), p. 482.

BULLETIN OF THE CHEMICAL SOCIETY OF JAPAN, VOL. 49 (5), 1439—1440 (1976)

Synthesis, Thermolysis and Photolysis of Trimethylammonium-*N*-diphenylphosphinylimine

Eiichi KAMEYAMA, Seiichi INOKUMA, and Tsunehiko KUWAMURA
Faculty of Engineering, Gunma University, Kiryu, Gunma 376

(Received October 14, 1975)

Synopsis. Ammonim-*N*-phosphinylimine was prepared from the corresponding hydrazinium salt. The ylid gave phosphinylnitrenes on thermolysis, predominantly in the singlet state. On photolysis, the ylid also gave a singlet product.

A number of aminimides have been studied extensively and reviewed.[1] Higher homologues of trialkylammonium-*N*-alkanoylimine and sulfonylimine have also been reported,[2,3] however, a similar type of nitrogen ylid with a phosphinyl group has received far less attention.

It is well known that the thermal decomposition of the aminimides gives corresponding isocyanates. In a previous paper,[3] the present authors have indicated that the photolysis of trialkylammonium-*N*-alkanoylimine was hindered by the introduction of a hydroxyl group into the 2-position of the alkyl chain attached to the positive nitrogen atom in the aminimide. Robson and Speakman[4] have found that trimethylammonium-*N*-dodecanoylimine afforded only an amide upon photolysis, and that a similar sulfonylimine underwent no photolysis, but instead thermally decomposed producing both singlet and triplet nitrenes.

This paper deals with the synthesis of a nitrogen ylid trimethylammonium-*N*-diphenylphosphinylimine (I), and the generation of phosphinylnitrene by the thermolysis and photolysis of I.

The nitrogen ylid I was synthesized from 1,1,1-trimethyl-2-diphenylphosphinylhydrazinium iodide (II), which was prepared from 1,1-dimethyl-2-diphenylphosphinylhydrazine (III) and methyl iodide.

The IR absorption frequencies assigned to the phosphinyl group of I are lower than those of II and III. A similar shift is known for a carbonyl group in aminimides and attributed to a delocalization of the negative charge on the imine nitrogen.[1] The shift was also found for a sulfonyl group in ammonium-*N*-sulfonylimines.[2] The base peak of the mass spectrum of I, due to the elimination of a methyl group, is a characteristic pattern for aliphatic amines. Three main peaks in the low mass region suggest that I decomposes to form phosphinylnitrene and trimethylamine. The differential thermal and thermogravimetric analysis data show that I has one mole of water of crystallization and decomposes producing trimethylamine at a temperature higher than its mp by about 60 °C. This decomposition temperature is higher than those for ammonium-*N*-acylimine and sulfonylimine.[2]

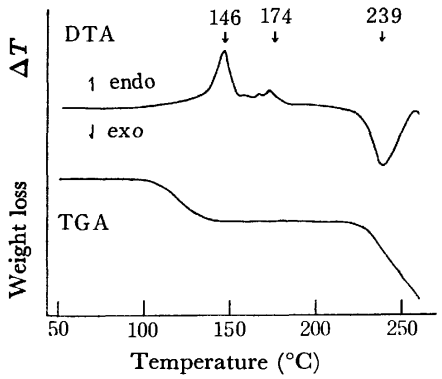

Fig. 1. DTA and TGA curves for $(CH_3)_3N^+N^-PO(Ph)_2$. α-Alumina standard; heating, 2.5 °C/min in air.

The aqueous solution of I was neutral, had a low electric conductivity and was titratable with an HCl aqueous solution at room temperature. When this acidic aqueous solution was boiled for a couple of minutes, I decomposed to give trimethylhydrazinium salt and diphenylphosphinic acid quantitatively.

Thermally, I was decomposed in DMSO and gave diphenylphosphinamide (IV) and *N*-diphenylphosphinyldimethylsulfoximine (V) with some unknown prod-

Table 1. Thermolysis of $(CH_3)_3N^+N^-$–X (5 h)

X	Solvent	Temp (°C)	Recovery (%)	Sulfoximine (mol %)	Amide (mol %)	Others (mol %)	Unknown (wt %)
$POPh_2$	DMSO	180	—	29	—	—	—
$POPh_2$	DMSO	150	50	19	11	—	2
$POPh_2$	DMSO	120	100	—	—	—	—
$POPh_2$	$C_{12}H_{25}OH$	180	13	—	22	29[a]	17
$POPh_2$	$C_{12}H_{25}OH$	150	46	—	13	18[a]	4
$POPh_2$	$C_{12}H_{25}OH$	120	100	—	—	—	—
COPh	DMSO	170	17	—	—	49[b]	—
COPh	DMSO	140	100	—	—	—	—
COR[c]	DMSO	170	—	—	—	21[b]	—
SO_2R[d]	DMSO	170	—	65	41	—	—

a) $(C_6H_5)_2POOC_{12}H_{25}$, b) *N,N'*-dialkylurea, c) R: $C_{11}H_{23}$, Ref. 4, d) R: $C_{12}H_{25}$, Ref. 4.

ucts. In 1-dodecanol, I gave IV and dodecyl diphenylphosphinate (VI). These results are shown in Table 1.

It can be assumed that diphenylphosphinylnitrene, produced in the singlet state, immediately reacts with DMSO to form V, on the other hand, in the presence of a poor singlet trap, the nitrene produces the triplet product IV by way of an intersystem crossing. The molar ratio of the singlet to triplet products was somewhat larger than that for the sulfonylimine. Moreover, I gave only V at 180 °C in DMSO. An almost identical proportion of I was decomposed in both DMSO and 1-dodecanol at a temperature lower than the mp of I.

Table 2. Photolysis of $(CH_3)_3N^+N^-$–X

X	Solvent	Time (h)	Recovery (%)	Sulfoximine (mol %)	Amide (mol %)	Unknown (wt %)
$POPh_2$	DMSO	12	22	29	51	13
$POPh_2$	amine[a)]	12	46	—	37	—
COPh	DMSO	14	100	—	—	—
COPh	DMSO	57	56	—	35	8
COPh	amine[a)]	14	100	—	—	—
$COC_{11}H_{23}$	amine[b)]	33	67	—	6	9

a) $(CH_3)_2NCH_2CH_2OH$. b) $(CH_3)_2NCH_2CH_2OH$+cyclohexane.

As in the case of thermolysis, the photolysis of I resulted in the smooth production of the singlet nitrene as shown in Table 2. In the presence of 2-(dimethylamino)ethanol, I transferred no additional products of the nitrene to the amine.

Experimental

All the melting points are uncorrected. The IR spectra were obtained using a Hitachi EPI-G3 infrared spectrometer. The NMR spectra were recorded on a Varian A-60D spectrometer in $CDCl_3$ at 60 MHz, using tetramethylsilane as an internal standard. The mass spectra were measured using a Nihon Denki JMS07 mass spectrometer operating at 25 eV. Differential thermal and thermogravimetric analyses were carried out using a Rigaku Denki Thermoflex DG-CIH.

Preparation of Trimethylammonium-N-diphenylphosphinylimine (I). Diphenylphosphinic chloride, prepared from chlorodiphenylphosphine in the usual way,[5)] was added to a benzene solution of two moles of 1,1-dimethylhydrazine at room temperature. The precipitated white crystal was washed thoroughly with water, and gave 1,1-dimethyl-2-diphenylphosphinylhydrazine (III) in a 40% yield, mp 178.2—178.5 °C (167—168 °C)[6)]; IR 1110, 1123, 1190, 1205 cm^{-1}. In ethanol, III was refluxed with an excess of methyl iodide to give 1,1,1-trimethyl-2-diphenylphosphinylhydrazinium iodide (II) in a 90% yield; IR 1103, 1122, 1200 cm^{-1}. At room tempera- ture II was treated with a 10% NaOH aq. solution. From the alkaline solution, I was extracted with chloroform in a 69% yield, mp 178.3—178.5 °C (from acetone); IR 1027, 1048, 1110, 1150 cm^{-1}; NMR δ 3.0—3.1 (s, *ca.* 2H, H_2O), 3.31 (s, 9H, CH_3), 7.2—8.2 (m, 10H, phenyl); mass spectrum (peaks more than 30% of the base peak) *m/e* (%) 58 (78), 59(59), 216 (33), 259 (100), 273 (50), 274 (47, M^+). The DTA and TGA curves are shown in Fig. 1. Found C, 61.36; H, 7.15; N, 9.42; P, 9.9%. Calcd for $C_{15}H_{19}N_2OP \cdot H_2O$: C, 61.63; H, 7.24; N, 9.58; P, 10.6%.

Thermolysis. In a stream of nitrogen, an approximately 7% solution of I in DMSO was heated. After 5 h, the solvent was distilled off at reduced pressure. Two products, diphenylphosphinamide (IV) and *N*-diphenylphosphinyldimethylsulfoximine (V) were isolated from the reaction mixture by recrystallization and/or by column chromatography. In addition, two or three unknown products were detected by TLC in the residue. In the same way as described above, I was decomposed in 1-dodecanol, and gave IV and dodecyl diphenylphosphinate (VI). These products, IV and VI, were confirmed by direct comparisons with authentic samples. On the basis of elemental analysis, IR and NMR spectra, V (mp 168.0—168.5 °C (from acetone)) was identified. Trimethylammonium-*N*-benzoylimine was also decomposed in DMSO and gave *N,N'*-diphenylurea.

Photolysis. Solutions of I and other aminimides (about 1 g) in 250 ml of DMSO or 2-(dimethylamino)ethanol were irradiated using a 10W low-pressure mercury arc lamp at room temperature. The products were isolated and identified in the same way as described for thermolysis.

References

1) W. J. McKillip, E. A. Sedor, B. M. Culbertson, and S. Wawzonek, *Chem. Rev.*, **73**, 255 (1973); H. J. Timpe, *Z. Chem.*, **12**, 250 (1972).

2) E. Kameyama, Y. Minegishi, and T. Kuwamura, *Nippon Kagaku Zasshi*, **71**, 1671 (1968); *ibid.*, **73**, 1018 (1970); *Yukagaku*, **18**, 897 (1969); E. Kameyama, S. Inokuma, A. Akagawa, and T. Kuwamura, *ibid.*, **22**, 434 (1973).

3) E. Kameyama, S. Inokuma, A, Akagawa, and T. Kuwamura, *Nippon Kagaku Kaishi*, **1974**, 1789.

4) P. Robson and P. R. H. Speakman, *J. Chem. Soc., B*, **1968**, 464.

5) L. R. Ocone, C. W. Schaumann, and B. P. Block, *Inorg. Synth.*, **8**, 71 (1966).

6) H. H. Sisler and R. P. Nielsen, *Inorg. Synth.*, **8**, 76 (1966). Prepared by air oxidation of (2,2-dimethylhydrazino)diphenylphosphine.

BULLETIN OF THE CHEMICAL SOCIETY OF JAPAN, VOL. 49 (5), 1441—1442 (1976)

Catalytic Oxidation of Mercaptans by Iodine-Hydrogen Iodide System in Dimethyl Sulfoxide

Tetsuo AIDA, Takeshi AKASAKA, Naomichi FURUKAWA, and Shigeru OAE

Department of Chemistry, The University of Tsukuba, Sakura-mura, Niihari-gun, Ibaraki 300-31

(Received October 15, 1975)

Synopsis. Mercaptans were oxidized readily by a catalytic amount of iodine or hydrogen iodide (*i.e.*, aq. HI-solution) in the presence of dimethyl sulfoxide to afford the corresponding disulfides nearly quantitatively.

As reported previously,[1] the reduction of sulfoxides, especially dialkyl sulfoxides (*e.g.*, dimethyl sulfoxide) was found to take place catalytically by either bromine or hydrogen bromide. The mechanism for this reaction was proposed to proceed *via* an initial bromination of the sulfoxide affording the corresponding α-bromo sulfoxide which then reacts with another sulfoxide regenerating the corresponding sulfide and hydrogen bromide (Kornblum Reaction).[2] Meanwhile, hydrogen bromide is well known to reduce the sulfoxide to the corresponding sulfide.[3] Thus, the whole process may form a kind of the Oxidation-Reduction Cycle by the bromine–hydrogen bromide system in the sulfoxide.

Therefore, if the above reaction system is treated with a third component which reacts with either bromine or hydrogen bromide, a new synthetic application of this system will be resulted.

Meanwhile, it is known that the oxidation of mercaptans proceeds in dimethyl sulfoxide (DMSO) solution, but the reaction requires high temperature and a prolonged reaction time.[4] While, iodine (I_2) is a mild and convenient oxidizing reagent for the preparation of disulfides from the corresponding mercaptans,[5] and the reaction is considered to proceed through the following reaction path.

$$RSH + I_2 \longrightarrow RSI + HI$$

$$RSI + RSH \longrightarrow RSSR + HI$$

Thus, if iodine is regenerated from hydrogen iodide (HI), this oxidation may be carried out by the use of a small amount of iodine or hydrogen iodide under a mild condition. Actually, when the oxidation of mercaptan was carried out in DMSO with a catalytic amount of iodine (or hydrogen iodide), the oxidation proceeded nearly quantitatively at room temperature affording the corresponding disulfide. Therefore, our present method is to be a simple and convenient preparation of disulfides.

The oxidation of mercaptan by iodine or hydrogen iodide was carried out under various reaction conditions. The results obtained are summarized in Table 1.

Inspection of the data in Table 1 shows that the oxidation of mercaptan by iodine or hydrogen iodide took place only in the presence of DMSO (Runs 6 and 7), and gave a nearly equal amount of dimethyl sulfide (DMS) to that of the corresponding disulfide. These observations suggest clearly that the oxidation of mercaptan and the reduction of DMSO occur simultaneously. Namely, iodine undoubtedly initiates the oxidation of mercaptan affording disulfide and hydrogen iodide which is readily oxidized by DMSO to iodine. Therefore, iodine acts only as a catalyst for the present reaction.

In order to generalize this catalytic oxidation of mercaptan by iodine, various mercaptans were reacted in sealed tubes at room temperature. The results

TABLE 2. CATALYTIC PREPARATION OF DISULFIDE FROM MERCAPTAN BY IODINE

RSH+I_2(1/100 mol %-RSH)+DMSO (excess)[a] in Benzene at Room Temperature for 5 h.

R	Products and yields[b] (%)	
	RSSR	DMS
Et	97	93
n-Pr	94	95
i-Pr	92	96
n-Bu	97	95
t-Bu	43	38
Ph	98	94
p-Tol	95	92
p-ClC_6H_4	97	93

a) Six times excess to that of mercaptan used.
b) Although iodine was detected, the yield was not determined.

TABLE 1. OXIDATION OF BUTYL MERCAPTAN BY IODINE OR HYDROGEN IODIDE IN BENZENE

Run	I_2 or HI[a] (mol %-SH)	DMSO	Reaction condition		Products (%)		
			Temp (°C)	Time (h)	(*n*-BuS)$_2$	DMS	Other
1	I_2 (50)	—	r.t.	0.1	96	—	I_2[c]
2	I_2 (50)	excess[b]	r.t.	0.1	93	98	I_2[c]
3	HI (100)	—	r.t.	0.1	—	—	—
4	HI (100)	excess[b]	r.t.	0.1	97	95	I_2[c]
5	I_2 (1)	—	40	3.0	—	—	I_2[c]
6	I_2 (1)	excess[b]	40	3.0	97	98	I_2[c]
7	HI (2)	excess[b]	40	3.0	95	94	I_2[c]

a) Aqueous HI-solution (*ca.* 40%) was used. b) Six times excess to that of mercaptan used. c) Iodine was detected, but the yield was not determined.

obtained are listed in Table 2.

These results shown in Table 2 reveal clearly that this reaction is a facile method to prepare disulfide from the corresponding mercaptan, while the plausible reaction scheme may be depicted as shown in Scheme 1.

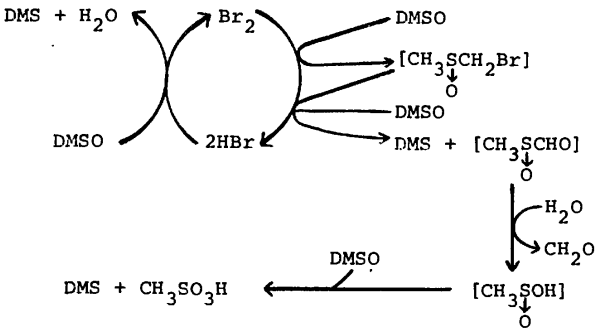

* DMS : Dimethyl Sulfide

Scheme 1.

Experimental

Materials. *Mercaptan*: Alkyl mercaptans and thiophenol were commercial products. *p*-Tolyl and *p*-chlorophenyl mercaptans were prepared from the corresponding sulfonyl chloride and zinc in sulfuric acid by a known method.[6]

Dimethyl sulfoxide: The commercial product was purified by usual method (dried over calcium hydride and then distilled).

Iodine and Hydrogen iodide: The commercial products (HI: *ca.* 40% aqueous solution) were used without further purification.

General Apparatus. GLPC analysis was performed with a Hitachi Gas Chromatography with a thermal conductivity detector, equipped with a 2 m×3 mmϕ stainless steel column packed with Silicon GE SE-30 on 60—80 mesh Chromosorb W (AW). Preparative column chromatography was performed with silica gel (Wakogel C-200) using benzene-hexane as an eluent.

Product Analysis. The yield of the disulfides was determined only by GLPC measurement, and the yield after the isolation slightly decreased. Dialkyl disulfides were separated by GLPC and preparative column chromatography and diaryl disulfides were separated by preparative column chromatography, and identified by comparing their mp and spectroscopic analyses with those of the authentic samples.

Oxidation of Mercaptan by Iodine. A typical run was as follows: Butyl mercaptan (0.2 g; 2.2 mmol), iodine (0.006 g; 0.02 mmol) and DMSO (1.0 g; 12.8 mmol) were dissolved in 5 ml of benzene. The mixture was placed in a sealed tube, and was allowed to stand at room temperature for 3 h. Then, the sealed tube was broken and 5 μl of the reaction mixture was directly injected into a column of GLPC to determine the amount of dimethyl sulfide. The yield was 95%. To the rest of the reaction mixture, 10 ml of aq. NaOH (1/10 M) solution was added, and after shaking the mixture vigorously, the benzene layer was separated. From the benzene layer, dibutyl disulfide was isolated by GLPC and preparative column chromatography. The yield was 97%. Meanwhile, the colorless reaction mixture turned to red at the completion of the reaction, and the red color faded away upon treatment with sodium hydrogen sulfite. This suggests that iodine was present in the reaction mixture.

All the other reactions were carried out as described above.

References

1) T. Aida, N. Fukukawa, and S. Oae, *Tetrahedron Lett.*, **1973**, 3853.

2) N. Kornblum, W. J. Jones, and G. J. Anderson, *J. Am. Chem. Soc.*, **81**, 4113 (1959).

3) J. A. Smythe, *J. Chem. Soc.*, **95**, 349 (1909); E. N. Karaulova and G. D. Galpern, *Zhur. Obsh. Khim.*, **29**, 3033 (1959); T. L. Flecher and H. -L. Pan, *J. Org. Chem.*, **24**, 141 (1959).

4) C. N. Yiannios and J. V. Karabinos, *J. Org. Chem.*, **28**, 3246 (1963); T. J. Wallace and H. A. Weiss, *Chem. Ind.*, **1966**, 1558.

5) L. D. Small, J. H. Bailey, and C. J. Cavallito, *J. Am. Chem. Soc.*, **69**, 1711 (1947).

6) R. Adams and C. S. Marvel, *Org. Synth.*, Coll. Vol. 1, 504 (1941).

BULLETIN OF THE CHEMICAL SOCIETY OF JAPAN, VOL. 49 (5), 1443—1444 (1976)

A Proton Magnetic Resonance Study of the Amide Configurations of 2-Acylaminopyrimidines

Michio KONDO

Central Research Laboratories, Sankyo Co., Ltd., Hiromachi, Shinagawa-ku, Tokyo 140

(Received October 16, 1975)

Synopsis. It has been found, from the ^1H NMR spectra at various temperatures, that 2-formylaminopyrimidine (**2**) exists in a *cis* configuration in chloroform and dimethyl sulfoxide, whereas 2-acetylaminopyrimidine (**3**) exists in a rapid rotational equilibrium between *cis* and *trans* configurations in $CDCl_3$, but almost exclusively in a *trans* configuration in DMSO at room temperature.

It is well known that *N*-monosubstituted amides undergo *cis-trans* rotational isomerism and that the equilibrium is a function of many factors. In the cases of acetylamino and higher acylamino derivatives, the isomers are almost all *trans*.[1] In polypeptides and proteins, it is also found that the peptide bonds are predominantly *trans*, except for a few peptide bonds in some cyclic oligopeptides.[2] For a few acetanilides with bulky *ortho* substituents, however, it has been reported that the *cis* isomers were appreciable.[3] On the other hand, formylamino derivatives usually exist as both *cis* and *trans* forms.[1b,4]

It seemed that it would be interesting, therefore, to find formylamino derivatives in a *cis* configuration exclusively or to find acetylamino derivatives without substituents in a *cis* configuration appreciably. This paper will be concerned with 2-acylaminopyrimidines as such compounds.

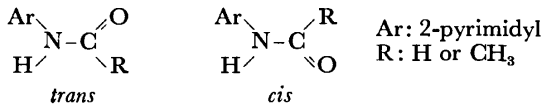

Experimental

2-Formylaminopyrimidine (2). Acetic anhydride (10 ml) was added to a solution of 2-aminopyrimidine (**1**) (5 g) in formic acid (20 ml). The reaction mixture became warm and foamed gently, and it was then allowed to stand overnight. Repeated recrystallizations of the precipitates from water gave pure **2**.

2-Acetylaminopyrimidine (**3**) was prepared from **1** and acetic anhydride.

The ^1H NMR spectra were recorded on a Varian A-60D spectrometer at various temperatures, using TMS as the internal standard. The concentration was 1% (w/v) unless otherwise noted. All the spectra were of the first order. The concentration dependence of the chemical shifts was examined for **3** in $CDCl_3$ and was found to be negligible for all protons but the amide proton.

Results and Discussion

The fact that H-4 and H-6 have the same chemical shift suggests a free flip-rotation around the C_{ring}–N_{amide} bond in **2** and **3** on the NMR time scale.

The chemical shift of the formyl proton is in good agreement with that reported for 2-formylamino-4-methylpyridine (**5**) in a *cis* form,[5] but it is fields lower than that of formanilide.[3a] This downfield shift can be attributed to a deshielding effect of an electric field due to the lone-pair electrons on the ring nitrogen atoms nearby.

The J_{CHONH} value was found to be about 10 Hz. A comparison of this value with two coupling constants for **5** (11 Hz for the *cis* and 2 Hz for the *trans* isomer)[5] leads to the conclusion that **2** in $CDCl_3$ and DMSO has a *cis* configuration almost exclusively. The two component peaks of the formyl proton signal in a DMSO solution coalesce at about 155 °C at almost the center of the doublet. This also seems to suggest a negligible contribution of **2** to the *trans* configuration, if any at all, because it has previously been reported that the formyl proton of **5** in the *trans* form resonated at a field higher by 0.92 ppm than did that in the *cis*.[5] Electrostatic repulsion between the lone-pair electrons on the ring nitrogen atoms and those on the carbonyl oxygen atom must play a key role, for **2** has a *cis* form, whereas 5 is subject to a *cis-trans* isomerism with a moderate equilibrium constant at room temperature.

The chemical shift of the acetyl protons of **3** in $CDCl_3$ is δ 2.53, lower by as much as about 0.4 ppm than that of acetanilide.[6] This fact strongly suggests that **3** has a configuration different from that of the latter compound, which has been proved to have a *trans* configuration. When the solvents were changed from $CDCl_3$ to DMSO, the acetyl signal was shifted upfield (−0.3 ppm); this shift was much larger than that observed for **4** upon the same solvent change. This large upfield shift could be explained in terms of a significant shift of the *cis-trans* equilibrium in **3** toward a *trans* preference, because the acetyl signal for the *trans* form can be expected to be at higher fields. It has been reported that the addition of DMSO to a $CDCl_3$ solution of formanilide shifted the equilibrium of the rotational isomers toward the intensification of the *trans* signal.[7]

Lowering the temperature of a $CDCl_3$ solution of **3** below 0 °C caused an appreciable broadening in the acetyl signal, and at −52 °C the acetyl signal split into a broad but clearly separated doublet (δ 2.33 and 2.73) with almost equal intensities. Of course, the amide proton gave two distinct signals, at δ 11.35 and 10.25. The ring proton signal also showed due complexity. The addition of a drop of DMSO to this solution caused an intensification of the upper-field signals for both the acetyl and amide protons at the expense of the lower-field ones. The acetyl proton signal of a solution of **3** in the $CDCl_3$–DMSO (3: 2) mixed solvent was observed at δ 2.23, almost equal to the value in DMSO. Lowering the temperature of the solution caused no splitting, but only a broadening, of the acetyl proton signal,

Table 1. Proton magnetic resonance spectral parameters of 2-amino- (**1**), 2-formylamino- (**2**), 2-acetylaminopyrimidine (**3**), and 2-acetylamino-4-methylpyridine (**4**)

Compd	Solvent	Chemical shift (δ)							Coupling constant (Hz)	
		H-3	H-4	H-5	H-6	NH	CHO	CH_3CO	$J_{4,5}$	J_{NHCHO}
1	$CDCl_3$	—	8.31	6.62	8.31	5.20	—	—	4.8	—
	DMSO-d_6	—	8.23	6.56	8.23	6.52	—	—	4.8	—
	C_6D_6	—	7.98	5.98	7.98	4.90	—	—	4.7	—
2	$CDCl_3$[a]	—	8.56	7.07	8.56	9.1	9.52	—	4.8	10
	DMSO-d_6	—	8.55	7.13	8.55	10.7	9.34	—	4.7	9.8
	C_6D_6[b]	—	—	—	—	—	—	—	—	—
3	$CDCl_3$	—	8.59	7.02	8.59	9.1	—	2.53	5.0	—
	DMSO-d_6	—	8.64	7.15	8.64	10.5	—	2.19	4.8	—
	C_6D_6	—	8.22	6.08	8.22	10.2	—	2.47	4.8	—
4	$CDCl_3$	8.07	2.37[c]	6.89	8.16	8.47	—	2.19		—
	DMSO-d_6	7.96	2.30[c]	6.93	8.18	10.3	—	2.08		—
	C_6D_6	8.45	1.89[c]	6.44	8.05	8.33	—	1.54		—

a) A saturated solution. b) Almost insoluble. c) CH_3.

probably as a result of a reduced mobility of solute molecules at an increased viscosity of the solvent. These observations are indicative of an almost complete preponderance of the *trans* form for **3** in DMSO.

The replacement of a formyl proton by a methyl group would cause significant change in the van der Waals interactions with the pyrimidine ring, but not in the electronic structure, as may be seen by the very close similarity in their UV spectra. In the case of **2**, the *trans* form is unfavorable from the viewpoints of both the van der Waals interaction and the electrostatic repulsion between the lone-pair electrons on the ring nitrogen and the carbonyl oxygen atoms, as compared with the *cis* form. As for **3**, however, the *cis* form is preferable to the *trans* form from the point of view of the electrostatic repulsion; on the contrary, though, the *trans* form is preferable from the point of view of the van der Waals' interaction. Therefore, the *trans* form is not so unfavorable in **3** as in **2**, resulting in an appreciable contribution of the *trans* form for **3** even in $CDCl_3$.

Consistent with the description given above, two absorption bands in the IR spectrum of **3** in a dilute $CDCl_3$ solution assignable to NH stretching vibrations were observed at 3425 and 3395 cm^{-1}. As for **2**, on the other hand, a single NH band was observed at 3390 cm^{-1}. Needless to say, there were other broad bands due to the amide protons involved in intermolecular associations.

The benzene-induced upfield shift is large for the acetyl protons of **4** (+0.65 ppm), whereas it is small for **3** (+0.06 ppm). As for the amide protons, on the contrary, the benzene-induced shift is very small for **4** (+0.14 ppm), but very large for **3** (−1.1 ppm). These observations are also indicative of different situations in the acetylamino groups of these two compounds, taking the specific interactions[8] between benzene molecules and these amide groups into account.

References

1) a) L. A. LaPlanche and M. T. Rogers, *J. Am. Chem. Soc.*, **85**, 3728 (1963); **86**, 337 (1964). b) R. F. C. Brown, L. Radom, S. Sternhell, and I. D. Rae, *Can. J. Chem.*, **46**, 2577 (1968). c) B. D. Andrews, I. D. Rae, and B. E. Reichert, *Tetrahedron Lett.*, **1969**, 1859.

2) a) G. N. Ramachandran and V. Sasiekharan, "Conformation of Polypeptides and Proteins," in "Advances in Protein Chemistry," Vol. 23, Academic Press, New York (1968). b) S. C. Jain and H. M. Sobell, *J. Mol. Biol.*, **68**, 1 (1972).

3) a) H. Kessler and A. Rieker, *Z. Naturforsch.*, **22b**, 456 (1967). b) H. Kessler and A. Rieker, *Justus Liebigs Ann. Chem.*, **708**, 57 (1967).

4) a) A. J. R. Bourn, D. G. Gillies, and E. W. Randall, *Tetrahedron*, **20**, 1811 (1964); **22**, 1825 (1966). b) I. D. Rae, *Can. J. Chem.*, **44**, 1334 (1966). I. Suzuki, M. Tsuboi, T. Shimanouchi, and S. Mizushima, *Spectrochim. Acta*, **16**, 471 (1960).

5) N. Enomoto and M. Kondo, *Bull. Chem. Spc. Jpn.*, **45**, 2665 (1972).

6) R. E. Carter, *Acta Chem. Scand.*, **21**, 75 (1967).

7) a) T. Nishiyama and F. Yamada, *Nippon Kagaku Zasshi*, **89**, 979 (1968). b) J. Niwa, *Bull. Chem. Soc. Jpn.*, **42**, 1726 (1969).

8) a) J. V. Hatton and R. E. Richards, *Mol. Phys.*, **3**, 253 (1960). b) N. Nakagawa, K. Nikki, Y. Takeuchi, and I. Kumagai, *Chem. Lett.*, **1972**, 1239. c) K. Nikki, N. Nakagawa, and Y. Takeuchi, *Bull. Chem. Soc. Jpn.*, **48**, 2902 (1975).

BULLETIN OF THE CHEMICAL SOCIETY OF JAPAN, VOL. 49 (5), 1445—1446 (1976)

The Photoreduction of *o*-Methoxycarbonylbenzophenone

Yuji TSUJIMOTO, Yasuo SHIGEMITSU, Takuji MIYAMOTO, and Yoshinobu ODAIRA

Department of Petroleum Chemistry, Faculty of Engineering, Osaka University, Suita-shi, Osaka 565

(Received October 27, 1975)

Synopsis. The photoreduction of *o*-methoxycarbonylbenzophenone (I) in a hydrogen-donating solvent, such as isopropyl alcohol and toluene, was shown to give diphthalidyl (II) or/and a coupling product (IV).

Recently we have studied the photoreactions of several aromatic compounds with the same carbonyl groups, such as tetramethyl pyromellitate[1] and *o*-dibenzoylbenzene.[2] In such a system, an interesting interaction between two carbonyls has been pointed out.[1-3] As an extension of these studies, we now wish to report the photoreduction of benzophenones substituted with an ester at the *ortho* position.

The irradiation of *o*-methoxycarbonylbenzophenone (I) in isopropyl alcohol through a Pyrex filter afforded diphthalidyl (II) in a good yield, together with an appreciable amount of methanol. However, no pinacol (III) was found at all.

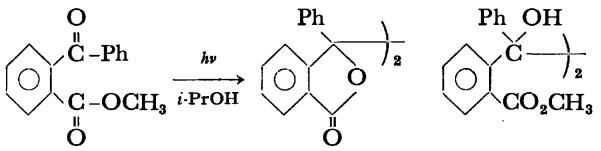

(I) (II) (III)

Moreover, the photoreaction of I with toluene gave benzyl-phthalide (IV), along with II and bibenzyl, whereas with a non-hydrogen-donating solvent such as acetonitrile, I was recovered almost quantitatively and the formation of II was negligible.

A ketyl radical (V), formed by the hydrogen abstraction of the n-π^* excited triplet of I from a solvent, such as isopropyl alcohol or toluene, may give (III) or/and (VI). III and VI subsequently undergo the lactonization, accompanied by the elimination of methanol, to give II and IV respectively.

In order to obtain information about the photoexcited state of I, the phosphorescence spectrum of I was measured and photocycloaddition to norbornene was examined.

In the phosphorescence spectrum, the entire shape of I resembles that of benzophenone, though fine structures do not appear clearly. In addition, the photocycloaddition of I to norbornene gave oxetane (VII) as a major product. These observations strongly suggest that I has the lowest n-π^* triplet level of benzoyl carbonyl.

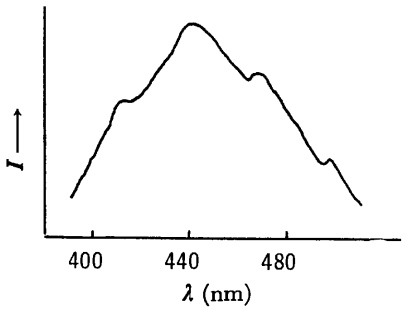

Fig. 1. Phosphorescence spectrum of I in MeOH–EtOH (1:3) at 77 K.

The following scheme may rationalize the above results:

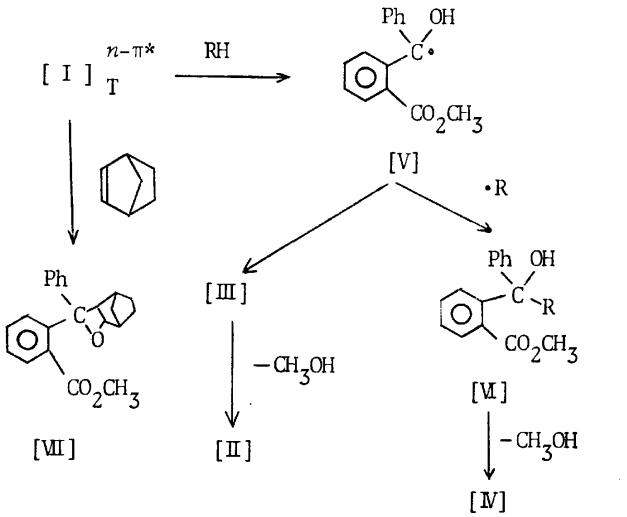

Furthermore, the photoreduction of 2,5-dimethoxycarbonylbenzophenone (VIII) (bichromophoric system)[4] was examined. The irradiation of VIII in toluene afforded diphthalidyl (IX) and benzyl-phthalide (X).

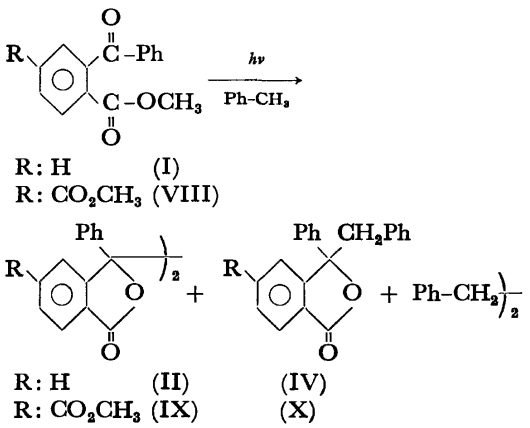

Experimental

Materials. *o*-Methoxycarbonylbenzophenone (I) (mp 48—50 °C, lit,[5] 51—51.6 °C) was prepared by the esterification of *o*-benzoylbenzoic acid (84%). 2,5-Dimethoxycarbonylbenzophenone ((VIII), mp 96—98 °C, lit,[6] 100—101 °C) was prepared by the following procedure: the Friedel-Crafts reaction[7] of *p*-xylene with benzoyl chloride gave 2,5-dimethylbenzophenone (91%), while the subsequent oxida-

tion of 2,5-dimethylbenzophenone with potassium permanganate gave benzophenone-2,5-dicarboxylic acid (16%). Finally the esterification of the diacid afforded VIII (99%).

Irradiation Procedure. All the irradiations were carried out with a 500-W high-pressure mercury lamp through a Pyrex filter at room temperature. The solutions were flushed for 15 min with nitrogen prior to irradiation.

Photoreduction of I. In isopropyl alcohol: a solution of I (1.5 g, 6.25 mmol) in isopropyl alcohol (45 ml) was irradiated for 7 h. Then, the precipitated crystals were filtered off; subsequent recrystallization from ethyl acetate gave 3,3′-diphenyl-diphthalidyl (II) (990 mg, 76%); mp 252—254 °C, lit,[8] 269—270 °C. From the volatile parts, methanol was detected by GLC (20% PEG 20M on Celite 545). In toluene: a solution of I (1.5 g, 6.25 mmol) in toluene (63 ml) was irradiated for 11 h. After the solvent had been removed *in vacuo*, the residue was chromatographed using a silica gel column. The insoluble parts [(II), (400 mg, 28%)] of the residue in benzene were removed before chromatography. The eluent of benzene with petroleum ether (60%) gave 3-phenyl-3-benzyl-phthalide (IV) (950 mg, 54%), mp 100—100.7 °C, lit,[9] 103—105 °C.

Photocycloaddition of I to Norbornene. A solution of I (2.0 g, 8.3 mmol) and 2-norbornene (4.1 g, 43.6 mmol) in benzene (40 ml) was irradiated for 10 h. The subsequent evaporation of the solvent gave a residue (3.1 g), which was then chromatographed on silica gel. The eluent of benzene with petroleum ether (20%) gave VII[10] (688 mg, 39%); mp 148—151 °C; IR (KBr) 1720, 970 cm^{-1}; NMR ($CDCl_3$) δ, 0.4—2.2 (m, 8H), 2.7 (d, 1H, J=6.0 Hz), 3.6 (s, 3H), 5.9 (d, 1H, J=6.0 Hz), 7.0—7.4 (m, 9H). Found: C, 78.96; H, 6.66%. Calcd for $C_{22}H_{22}O_3$: C, 79.01; H, 6.63%.

Photoreduction of VIII in Toluene. A solution of VIII (800 mg, 2.68 mmol) in toluene (32 ml) was irradiated for 7 h. After the evaporation of the solvent, small amounts of benzene were added. The insoluble parts were removed, and then the soluble parts were chromatographed on silica gel. The recrystallization of insoluble parts from benzene gave 3,3′-diphenyl-5,5′-dimethoxycarbonyl-diphthalidyl (IX) (118 mg, 16%); mp 280—284 °C; IR (KBr) 1785, 1740 cm^{-1}. Found: C, 71.85; H, 4.07%. Calcd for $C_{32}H_{22}O_3$: C, 71.90; H, 4.15%. The eluent of benzene containing petroleum ether (30%) gave 3-phenyl-3-benzyl-5-methoxycarbonyl-phthalide (X) (276 mg, 29%); mp 154—155 °C; IR (KBr) 1775, 1725 cm^{-1}; NMR (CCl_4) δ, 3.5, 3.7 (AB quartet, 2H, J=14 Hz), 3.9 (s, 3H), 6.8—8.2 (m, 13H). Found: C, 77.38; H, 4.95%. Calcd for $C_{23}H_{18}O_4$: C, 77.08; H, 5.06%.

References and Footnotes

1) K. Fukui, K. Senda, Y. Shigemitsu, and Y. Odaira, *J. Org. Chem.*, **37**, 3176 (1972).
2) Y. Shigemitsu, S. Yamamoto, T. Miyamoto, and Y. Odaira, *Tetrahedron Lett.*, **1975**, 2819.
3) W. C. Agosta, *J. Am. Chem. Soc.*, **89**, 3505 (1967).
4) VIII is expected to have two excited sites, the one is benzophenone moiety, the other dimethylterephthalate moiety.[11]
5) M. S. Newman, H. G. Koivila, and A. B. Garrett, *J. Am. Chem. Soc.*, **67**, 704 (1945).
6) "Beilstein Handbuch der Organischen Chemie," Band 10, Haupt (1927), p. 881.
7) K. Elbs and E. Larsen, *Chem. Ber.*, **17**, 2847 (1884).
8) M. V. Bhatt, K M. Kamath, and M. Ravindranathan, *J. Chem. Soc., C*, **1971**, 3344.
9) C. R. Hauser, *J. Org. Chem.*, **23**, 861 (1958).
10) NMR datum shows that VII is an exo isomer.
11) See Ref. 1.

BULLETIN OF THE CHEMICAL SOCIETY OF JAPAN, VOL. 49 (5), 1447—1448 (1976)

Bis(acetylacetonato)metal(II)-Catalyzed Addition of Acceptor Molecules to Acetylacetone[1]

Kaku UEHARA, Yoshiyuki OHASHI, and Makoto TANAKA

Department of Applied Chemistry, College of Engineering, University of Osaka Prefecture, Sakai-shi, Osaka 591

(Received November 6, 1975)

Synopsis. Bis(acetylacetonato)metal(II) ($M(acac)_2$) showed an effective catalytic activity for the addition of various acceptor molecules to acetylacetone to give 3-substituted 2,4-pentanediones.

Collman[2] found that $M(acac)_n$ undergoes electrophilic substitutions at the 3-position on the chelate ring in a similar manner to that of aromatic compounds and proposed that $M(acac)_n$ has some quasi-aromatic characters. However, the aromaticity of $M(acac)_n$ based on the electrophilic substitution is open to question.[3] In a previous communication,[4] we reported that $M(acac)_2$ undergoes an aldol addition of chloral to the 3-position on the chelate ring to give an adduct A and polychloral in the presence and absence of acetylacetone, respectively.

The present paper will show that $M(acac)_2$ undergoes not only the aldol addition but also another electrophilic reaction with a few acceptor molecules such as phenyl isocyanate and trichloroacetonitrile at the 3-position to give adduct B and C in the presence of acetylacetone. It is interesting to note that A can exist only in the keto form and that C is at first isolated as a crystalline keto-form but is easily transformed into an enolic form even in the solid state at room temperature within 24 h.

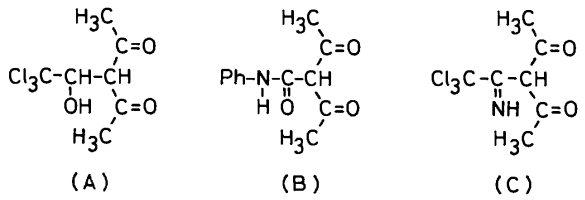

(A) (B) (C)

In the presence of piperidine instead of $M(acac)_2$ as a catalyst, chloral and trichloroacetonitile also reacted with acetylacetone to give the same reaction products (A and C), but not phenyl isocyanate since it reacted with piperidine to form urea. Carbon disulfide did not react with acetylacetone in the presence of $M(acac)_2$, but in the presence of piperidine it reacted to attack the 3-carbon of acetylacetone and the product was isolated as the piperidinium salt of dithiocarboxylic acid.[5] Acetonitrile was non-reactive to acetylacetone in the presence of either catalyst.

Bloodworth *et al.*[6] studied systematically the reactions of metal alkoxide with various acceptor molecules such as chloral, phenyl isocyanate, and carbon disulfide. They confirmed that these acceptor molecules were inserted into the oxygen-metal (O–M) bond of metal alkoxide (formation of O-adduct). However, we found that, for the $M(acac)_2$-catalyzed reaction of acetylacetone, the acceptor molecules which are highly polarized or have high polarizability react to attack the 3-position of acetylacetone and form C-adduct. This is not in line with the view that $M(acac)_n$ has the character of metal alcoholate. Hitherto, the initiation mechanisms of the polymerization of chloral and formaldehyde[7] and of the alternative copolymerization of maleic anhydride with epichlorohydrin[8] induced by $M(acac)_n$ have been explained in terms of the insertion of these monomers into the O–M bond of $M(acac)_n$ but without definite evidence.

Differing from the electrophilic substitution as reported by Collman,[2] these acceptors undergo only the electrophilic addition on the 3-carbon of $M(acac)_2$ without subsequent elimination of the proton. The present reaction, therefore, seem to be a novel type of reaction of $M(acac)_n$ as follows:

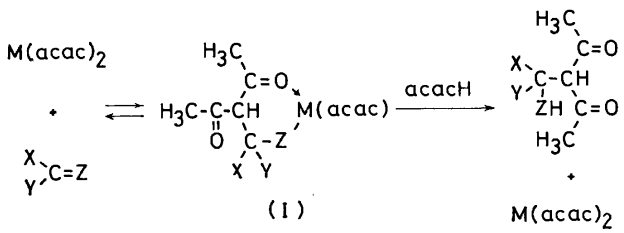

Attemps to isolate the adduct I from reaction mixtures were unsuccessful, presumably because the complex is unstable and readily decomposed to the acceptor molecule and $M(acac)_2$. However, there are several spectral evidences to support the existence of I in equilibrium with chloral and $M(acac)_2$. The tetrahydrofuran solutions of $Co(acac)_2$ and $Cu(acac)_2$ rapidly turned from pink to blue and from blue to green, respectively with the addition of chloral. The infrared spectrum ($CHCl_3$) shows the presence of $\nu_{C=O}$ (saturated ketone) at 1700 cm^{-1}, which is not detectable in chloral or $M(acac)_2$ (M=Co, Cu), independently.

Experimental

Materials. Chloral was prepared through the dehydration of commercial chloral hydrate by concentrated sulfuric acid and distilled under nitrogen prior to use. Phenyl isocyanate of G. R. grade was used without further purification. Commercial trichloroacetonitrile and carbon disulfide were distilled before use. Commercial acetylacetone was purified by distillation. $M(acac)_n$ and piperidine of G. R. grade were used without further purification.

Spectral Measurements. The IR spectra were measured with a Model 215 Hitachi grating infrared spectrophotometer. The NMR spectra were taken with a Hitachi Model R-20 spectrometer. Tetramethylsilan was used as an internal standard, and carbon tetrachloride as the solvent. The UV spectra were measured with a Shimadzu UV-200 spectrophotometer. The elemental analyses were carried out with a Yanagimoto Model MT-2 CHN analyzer.

Reaction of Chloral with Acetylacetone. To a mixture of 5.79 g (57.8 mmol) of acetylacetone and 8.48 g (57.5 mmol) of chloral was added 0.339 mmol of $M(acac)_2$(M=Mg(II), Co(II), Ni(II), Zn(II), Cu(II)). An exothermic reaction took place. The solution was cooled to 0 °C until the product was precipitated. The reaction mixture was poured into 20 ml of ligroin to give white crystals of 3-(1-hydroxy-2,2,2-trichloroethyl)-2,4-pentanedione (A). The yield was 91% ($Mg(acac)_2$) to 85% ($Cu(acac)_2$). Mp 83 °C (from benzene–ligroin). Found: C, 34.09; H, 3.62%. Calcd for $C_7H_9O_3Cl_3$: C, 33.97; H, 3.67%. IR spectrum (KBr disk); 3420 (s), 3300 (s), 1690 (vs, C=O), 1410 (m), 1360 (s), 1320 (m), 1275 (m), 1180 (s), 1150 (s), 1090 (s), 940 (m), 830 (w), 805 cm^{-1} (s). UV spectrum ($CHCl_3$); λ_{max} 290 nm, ε_{max} 140. NMR spectrum (CCl_4); 7.67 (6H, s, $COCH_3$), 5.35 (3H, m, OH, $Cl_3CCH(OH)$, and $CH(COCH_3)_2$). Spectral evidence for the aldol condensate is compatible with the structure A and shows that A exists only in keto form. A is reverted to chloral and acetylacetone in the presence of $M(acac)_2$ and other metal salts. The aldol reaction is also catalyzed by piperidine and gives the same product A in an 85% yield. $Co(acac)_3$ and $Cr(acac)_3$ are ineffective as catalyst.

Reaction of Phenyl Isocyanate with Acetylacetone. Phenyl isocyanate (2.12 ml, 19.5 mmol) was added to a mixture of $M(acac)_2$ (0.194 mmol, M=Mg(II), Co(II)) and acetylacetone (2 ml, 19.5 mmol) in dichloromethane (5 ml). An exothermic reaction took place. Ten ml of ligroin was added to the reaction mixture which was cooled to −78 °C, precipitating 3-phenylcarbamoyl-2,4-pentanedione (B) in a 76% yield (3.24 g). Mp 118—119 °C (lit,[9] 118—119 °C). IR spectrum (KBr disk); 3270 (NH) and 1640 cm^{-1} (C=O). The reaction mixture should not be allowed to stand for a long time in contact with air. In the presence of $M(acac)_2$, B is subject to hydrolysis to give acetic acid and acetoacetanilide as final products. In the presence of piperidine, phenyl isocyanate does not react with acetylacetone because it reacts with piperidine to form urea.

Reaction of Trichloroacetonitrile with Acetylacetone. Trichloroacetonitrile (3.96 g, 27.4 mmol) was added to a mixture of $Co(acac)_2$(0.0705 g, 0.274 mmol) and acetylacetone (2.74 g, 27.4 mmol). An exothermic reaction took place. Ten ml of ligroin was added to the reaction mixture which was cooled in an ice bath, precipitating 3-(1-imino-2,2,2-trichloroethyl)-2,4-pentanedione (C) in an 80% yield (5.37 g). C was precipitated as a keto-form crystal which was purified by the recrystallization from benzene–ligroin. It was easily transformed into the enol form even in the solid state, the color changing from white to pale yellow within 24 h on being left to stand at room temperature; mp of enol-form 58 °C (from benzene–ligroin). Found: C, 34.51; H, 3.07; N, 5.21%. Calcd for $C_7H_8O_2NCl_3$: C, 34.35; H, 3.27; N, 5.73%. IR spectrum of enol-form (KBr disk); 3340 (s, NH), 3080 (m), 1670 (s, C=N), 1595 (s, enol), 1450 (m), 1420 (m), 1360 (s), 1260 (s), 1220 (s), 1100 (m), 1030 (w), 1015 (w), 980 (m), 955 (m), 830 (s), 790 cm^{-1} (s). IR spectrum of keto-form (KBr disk); 3240 (s, NH), 1725 (s, C=O), 1700 (s, C=O), 1645 cm^{-1} (m, C=N). The reaction of trichloroacetonitrile with acetylacetone was also catalyzed by piperidine and gave C in a 1.0% yield.

References

1) Part XXI in the series "Catalytic Behavior of Metal Chelate Compounds," Part XX, K. Uehara, F. Kitamura, and M. Tanaka, *Bull. Chem. Soc. Jpn.*, **49**, 493 (1976).

2) J. P. Collman, *Angew. Chem.*, **77**, 154 (1965).

3) M. Kuhr and H. Musso, *Angew. Chem.*, **81**, 150 (1969).

4) K. Uehara, Y. Ohashi, and M. Tanaka, *Chem. Lett.*, **1974**, 827.

5) L. Dalgaad, H. Kolind-Andersen, and S. -O. Lawesson, *Tetrahedron*, **29**, 2077 (1973).

6) A. J. Bloodworth, A. G. Davies, and S. C. Vasishtha, *J. Chem. Soc., C*, **1967**, 1309.

7) T. Otsu, Y. Nishikawa, and S. Watanuma, *Makromol. Chem.*, **115**, 278 (1968). T. Otsu, S. Watanuma, and Y. Nishikawa, *Kogyo Kagaku Zasshi*, **72**, 1857 (1969). T. Ishii and T. Suzuki, *ibid.*, **72**, 2644 (1969).

8) A. Akimoto, *J. Polym. Sci. Polymer Chem. Ed.*, **11**, 2247 (1973).

9) A. G. Davies and R. J. Puddephatt, *J. Chem. Soc., C*, **1968**, 1479.

BULLETIN OF THE CHEMICAL SOCIETY OF JAPAN, VOL. 49 (5), 1449—1450 (1976)

Enzyme-like Reaction Catalyzed by Flavin-Reduced Keratin Systems. II. Binding Site in FAD-Reduced Keratin Complex[1)]

Fujio TAKAHASHI, Tatsuo OGASA, and M. B. RAHMAN*

Research Laboratory of Resources Utilization, Tokyo Institute of Technology, Meguro-ku, Tokyo 152

**Department of Chemistry, University of Rajshahi, Rajshahi, Bangladesh*

Synopsis. In order to confirm the binding site in the FAD-reduced keratin (RK) complex, polarographic and fluorometric studies were carried out and the FAD–RK complex was isolated. An adenine moiety of FAD was found to form a 1 : 1 complex with RK.

It has been reported in a previous paper that complex formation between FAD and reduced keratin (RK) occurs and that the complex catalyzes the dehydrogenation of succinic acid to fumaric acid.[1)] The binding site of FAD and RK in the complex was discussed and an arginine residue of RK and an adenine moiety and a pyrophosphate linkage of FAD were suggested as probable paths of ionic bond formation. This paper presents the results obtained by polarographic and fluorometric studies and by the isolation of the FAD–RK complex which throw light on the binding site in the FAD–RK complex.

Experimental

The RK used was prepared by the reductive cleavage of human hair with 2-mercaptoethanol and urea in a sodium hydroxide solution in accordance with the usual method.[2)] Molecular weight; 2800 (by viscometry), S-content; 2.7% as thiol groups; 0.36 mgeq/g (PCMB method[3)]) (1.0 thiol group/molecule of RK). The other chemicals used were the same as described in a previous paper.[1)]

Measurements of absorption and fluorescence spectra were made with a Shimadzu spectrophotometer UV-200 and a JASCO fluorescence spectrophotometer FP-4, respectively. The polarograms were determined with a dropping mercury electrode.

Results and Discussion

Polarography. From the dissimilar behavior between FAD and FMN with RK, it was expected that FAD and RK in solution would give different polarograms from FMN and RK in solution.

The sample solutions contained 2.5 mM of FAD or FMN and the requisite amount of RK in a 0.1 M phosphate buffer (pH 5.6 and 7.0). The results are shown in Figs. 1 and 2. The half-wave potentials of FAD without RK in solution at pH 5.6 and 7.0 were observed at −0.38 and −0.44 V *vs.* SCE at 25 °C. The same values were obtained when FMN containing solutions were measured. The wave height of the half-wave potential decreased when RK was introduced in the FAD or FMN solution. Another half-wave potential was found at −0.69 V *vs.* SCE on the polarograms of the FAD–RK system at pH 5.6 The wave height at the second half-wave potential increased with increasing RK concentration. The total of the two wave heights

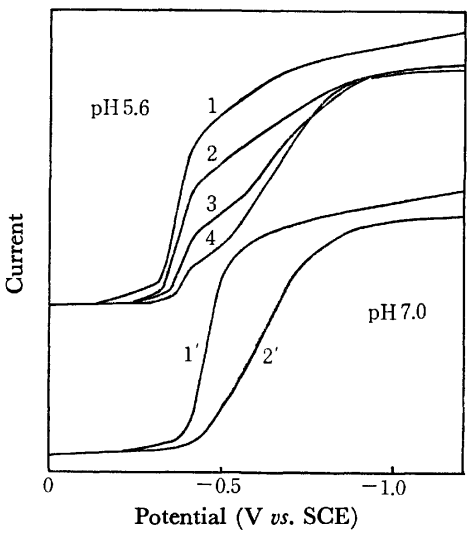

Fig. 1. FAD–RK polarography.
FAD 2.5 mmol/l
RK 1,1′: 0, 2: 0.07, 3: 0.14, 4,2′: 0.71 mmol/l

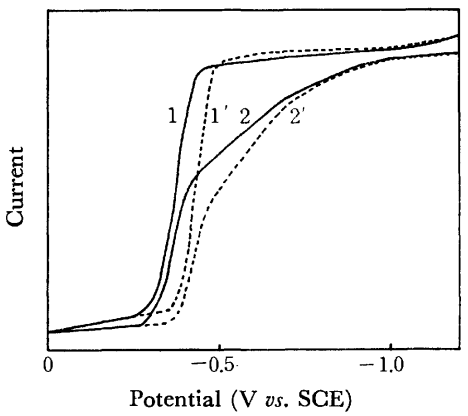

Fig. 2. FMN–RK polarography.
— pH 5.6, ---- pH 7.0
FMN 2.5 mmol/l
RK 1,1′: 0, 2,2′: 0.71 mmol/l

at the first and second half-wave potentials was found to remain constant.

It is known that sulfur- or nitrogen-containing compounds are readily absorbed on the surface of dropping mercury.[4)] Therefore, RK can very possibly be absorbed by mercury. The absorbed RK may interact with free FAD on the mercury surface and the reduction of FAD may be hindered so that the wave height at the first half-wave potential is decreased. Less influence on the wave height was observed for a solution containing FMN, for which complex formation with RK

was weaker than that for FAD. The second half-wave potential was assigned to the reduction of the FAD bound to RK. It is probably not possible that the reduction of free FAD is facilitated by the desorption of RK from the mercury surface at more negative potentials, because the second half-wave potential appeared at the same point, although the RK concentration had increased.

In the presence of an excess of RK, only the 1 : 1 complex is formed with RK. Then the equilibrium constant can be determined from the wave heights of the first and second half-wave potentials. The equilibrium constant was calculated to be about 2800 M^{-1} at pH 5.6 from Table 1.

Table 1. Equilibrium constant of the FAD-RK complex

FAD (mM)	RK (mM)	Wave height $(E_{1/2})_1$	Wave height $(E_{1/2})_2$	Equilibrium constant (M^{-1})
0.5	1.8	0.6	2.4	2.9×10^3
1.0	1.8	1.3	4.8	2.6×10^3
1.5	1.8	1.9	6.9	3.0×10^3

pH 5.6, 25 °C

Fluorescence Spectra. It was confirmed from the fluorescence spectra that the behavior of the interaction of FAD with RK was different from that of FMN with RK. The fluorescence intensity of FAD with RK (pH 7.0) at 522 nm (excited by 468 nm light) was found to be 7% higher than that of FAD without RK (Fig. 3). The fluorescence intensity of FMN was about 4 times stronger than that of FAD. It is known that the adenine moiety of FAD quenches the fluorescence caused by the intramolecular interaction.[5] It can be explained that quenching by RK may result in a decrease in the fluorescence intensity in the FMN-RK solution. In the FAD–RK case it is speculated that the interaction between the adenine moiety and isoalloxazine moiety may weaken when the adenine moiety bonds to RK, *i.e.*, the reduced influence of the adenine moiety on the isoalloxazine moiety decreases the quenching.

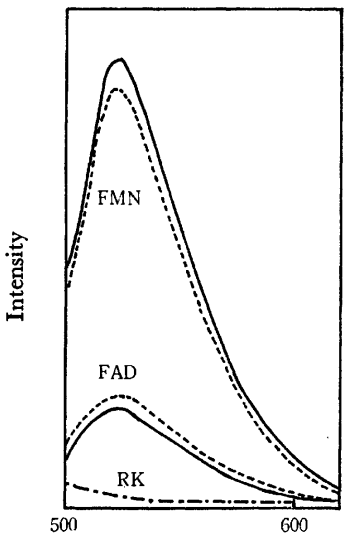

Fig. 3. Emission spectra of flavin-RK systems.
—— Flavin only, ------ Flavin-RK
Flavin 6 μmol/l, RK 3 μmol/l
λ_{EX}=468 nm, pH 7.0

Isolation of the FAD-RK Complex. Attempting further confirmation of complex formation in solution, the FAD–RK complex was isolated. Dissolving 0.071 mmol of RK and 0.11—0.42 mmol of FAD or FMN into distilled water and adding 1 M hydrochloric acid to adjust to pH 4, precipitation occurred. The precipitates were separated by centrifugation, washed by distilled water and dried. The determination of RK and flavin in the complex was carried out by analysis of the sulfur content and measurement of the absorption at 450 nm. It is seen from the results in Table 2 that a 1 : 1 complex was obtained from the FAD-RK solution. The FMN content in the precipitates obtained from the FMN-RK solution was found to be variable. These results confirm that the adenine moiety of FAD is a bonding site for RK.

Table 2. Analysis of flavin-RK complexes

	Flavin (mmol)	Flavin RK	Yield (%)	RK (mmol/g)	Flavin (mmol/g)
FAD	0.11	1.5	49	0.26	0.22
	0.42	5.9	50	0.30	0.26
FMN	0.11	1.5	37	0.33	0.09
	0.42	5.9	39	0.32	0.19

The authors express their sincere thanks to Professor Shuichi Suzuki of Tokyo Institute of Technology for his encouragement.

References

1) F. Takahashi, T. Ogasa, M. Hirano, and S. Suzuki: *Bull. Chem. Soc. Jpn.*, **49**, 1130 (1976).
2) M. Friedman, "The chemistry and biochemistry of the sulfhydryl group in amino acids, peptides and proteins," Pergamon Press, Braunschweig (1973), p. 205.
3) P. D. Boyer, *J. Am. Chem. Soc.*, **76**, 4331 (1954).
4) P. Zuman, "Organic polarography analysis," Pergamon Press, Oxford (1964), p. 99.
5) a) H. B. Burch, "Methods in enzymology," Vol III, Academic Press, New York (1957), p. 960. b) J. C. M. Tsibnis, D. B. McCornick, and L. D. Wright, *Biochemistry*, **4**, 504 (1965).

BULLETIN OF THE CHEMICAL SOCIETY OF JAPAN, VOL. 49 (5), 1451—1452 (1976)

Aromatic Nucleophilic Substitution. VI.[1] ^{1}H Nuclear Magnetic Resonance Evidence for the Rearrangement of 1,3- to 1,1-Anionic σ Complex in the Reactions of 1-Dialkylamino-2,4-dinitronaphthalenes with Potassium Alkoxides

Shizen SEKIGUCHI, Shigeru FUJISAWA, and Yumiko ANDO

Synthetic Chemistry Department, Gunma University, Tenjincho, Kiryu, Gunma 376

(Received December 12, 1975)

Synopsis. By use of NMR spectroscopy the rearrangement of 1,3- to 1,1-anionic σ complex (Meisenheimer complex) in the reactions of 1-dialkylamino-2,4-dinitronaphthalenes (dimethylamino-, diethylamino-, and *N*-methyl-*N*-butylamino, piperidyl) with potassium alkoxides in DMSO has been studied. The alkoxides used are potassium methoxide, ethoxide, isopropoxide, and *t*-butoxide. In the reactions of 1-dialkylamino-2,4-dinitronaphthalenes with the alkoxides the rearrangement could be spectrometrically analyzed. However, in the reaction of 1-dimethylamino-2,4-dinitro naphthalene with potassium *t*-butoxide the rearrangement was too fast to be clearly analyzed.

Regarding the 1,3-anionic σ complex (hereinafter referred to as 1,3-adduct) in the reaction of 1-methoxy-2,4-dinitronaphthalene with sodium methoxide, Millot and Terrier[2] reported the existence of the 1,3-adduct by use of visible spectra [λ_{max} 505, 550—600 (sh) nm], but showed no NMR evidence for it although NMR measurement would be a more conclusive means for confirming adducts. Fendler *et al.*, however, found no NMR evidence for the 1,3-adduct in the same reaction.[3] Although we carried out the reaction of 1-dialkylamino-2,4-dinitronaphthalenes with sodium methoxide in DMSO, no 1,3-adducts could be found.[4] Crampton and Gold reported that *N*,*N*-dimethylamino-2,4,6-trinitrobenzene with sodium methoxide gave the 1,3-adduct only[5] in MeOH, while Fyfe *et al.* found the rearrangement of the 1,3- to 1,1-adduct in the reaction of 3,5-dinitrocyanobenzene with sodium methoxide in DMSO.

Following our preliminary work[6] we now report that in the reactions of 1-dialkylamino-2,4-dinitronaphthaleneswith potassium alkoxides in DMSO the rearrangement could be followed by use of NMR spectroscopy as follows:

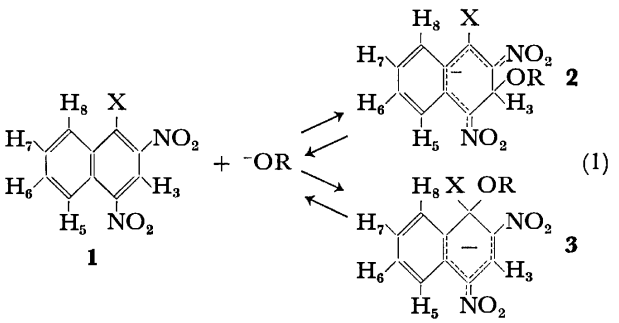

(1)

Replacing of sodium alkoxides by potassium ones is found to make possible measurement of NMR spectra on 1,3-adducts, which may be ascribed to the larger nucleophilicity of alkoxide ion in potassium alkoxides than in sodium ones. This greater nucleophilicity is considered to be caused by the increasing solvation of the cation (K^+) with alcohols.[7]

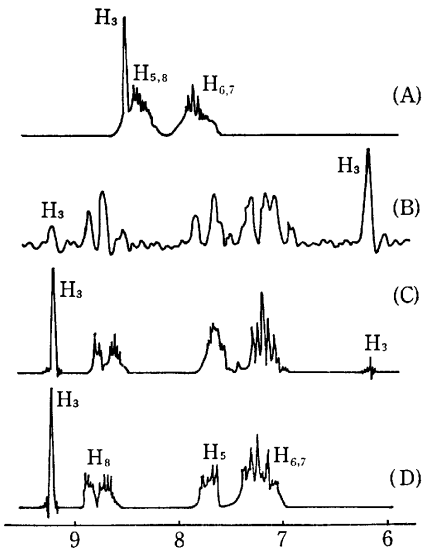

Fig. 1. NMR spectra relevant to the reaction of 1-piperidino-2,4-dinitronaphthalene (**1**, X=piperidino, 1.43×10^{-4} mol) with methanolic potassium methoxide (1.43×10^{-4} mol) in DMSO -d_6 (0.5 ml): A **1** before addition of potassium methoxide; B immediately after addition of potassium methoxide (500 Hz/50 s); C and D 2.5 min and 4 h after addition of potassium methoxide.

Immediately after addition of methanolic potassium methoxide (1.43×10^{-4} mol) to a DMSO solution (0.5 ml) of 1-piperidino-2,4-dinitronaphthalene (**1**, X=piperidino, 1.43×10^{-4} mol) at room temperature, the red solution gave the spectrum of Fig. 1B;[5,6,8] the poor resolution was due to the fast sweep time (500 Hz/150 s). The sharp singlet, attributable to H_3 of **2** (X=piperidino, R=CH_3), appeared at δ 6.21 with the resonance peak at δ 9.27, attributable to H_3 of **3** (X=piperidino, R=CH_3).[5,8] In 4 h after addition of potassium methoxide the 1,3-adduct (**2**) entirely rearranged to the 1,1-adduct (**3**). In addition, comparison of Fig. 1B with 1D shows that H_5, H_6, H_7, and H_8 resonance peaks of the 1,3- and 1,1-adducts do not substantially differ in position from each other. Similar results were obtained in other reactions of 1-dialkyl-

Table 1. H_3 Chemical shift (δ, ppm)[a]

Substrate[b]	$KOCH_3$		KOC_2H_5		$KOCH(CH_3)_2$		$KOC(CH_3)_3$	
	1,3-	1,1-	1,3-	1,1-	1,3-	1,1-	1,3-	1,1-
$CH_3\backslash N/CH_3$	6.33	9.31	6.39	9.27	6.52	9.31	—[c]	9.27
$C_2H_5\backslash N/C_2H_5$	6.37	9.27	6.26	9.23	6.51	9.27	6.58	9.27
$CH_3\backslash N/C_4H_9$	6.35	9.30	6.23	9.28	6.55	9.28	6.64	9.30
	6.21	9.27	6.25	9.20	6.35	9.24	6.28	9.23

a) In dimethyl sulfoxide with TMS as an internal standard. b) Only the substituents at C_1 of 2,4-dinitronaphthalene are indicated. c) Not clearly observed, perhaps owing to fast rearrangement.

amino-2,4-dinitronaphthalenes with potassium alkoxides studied. The fact that Fendler *et al.* could not find the existence of a 1,3-adduct is considered to be due to the fast rearrangement which is caused by the higher thermodynamic stability of **3** (X, OR; OCH_3) than **2** (X, OR; OCH_3).[3]

In the present case, therefore, both low reactivity of the 1-position of **2** and larger steric crowding at the 1-position of **3**, due to dialkylamino groups, would make the difference in stability between **2** and **3** smaller, and accordingly the rearrangement becomes so slow that the 1,3-adducts can be detected by use of NMR spectroscopy. Only the chemical shifts of H_3 of the adducts are summarized in Table 1.

In the reaction of 1-dimethylamino-2,4-dinitronaphthalene with potassium *t*-butoxide the low thermodynamic stability of **3** caused by addition of a bulky *t*-butoxide ion should make the difference in free energy between **2** and **3** larger, and accordingly make the rearrangement so fast that **2** can not clearly be observed.

Experimental

NMR spectra were recorded on a Varian A-60D spectrometer. 1-Dialkylamino-2,4-dinitronaphthalenes are prepared according to the method described in previous paper.[4]

We are grateful to the Ministry of Education and the Asahi Glass Foundation for the Contribution to Industrial Technology for financial support of this work.

References

1) Part V, S. Sekiguchi and K. Okada, *J. Org. Chem.*, **40**, 2782 (1975).
2) F. Millot and F. Terrier, *Bull. Soc. Chim. Fr.*, **1969**, 2692.
3) J. H. Fendler, E. J. Fendler, W. E. Byrne, and C. E. Griffin, *J. Org. Chem.*, **33**, 977 (1968).
4) S. Sekiguchi, K. Shinozaki, T. Hirose, K. Matsui, and K. Sekine, *Bull. Chem. Soc. Jpn.*, **47**, 2264 (1974).
5) M. R. Crampton and V. Gold, *J. Chem. Soc., B*, **1966**, 893.
6) S. Sekiguchi, K. Shinozaki, T. Hirose, K. Matsui, and T. Itagaki, *Tetrahedron Lett.*, **1974**, 1745.
7) A. J. Parker, *Quart. Rev.*, **16**, 163 (1962).
8) M. J. Strauss, *Chem. Rev.*, **70**, 667 (1970).

BULLETIN OF THE CHEMICAL SOCIETY OF JAPAN, VOL. 49 (5), 1453—1454 (1976)

A New Synthesis of the Pungent Principles of Ginger — Zingerone, Gingerol and Shogaol —

Kazuo BANNO[1] and Teruaki MUKAIYAMA

Department of Chemistry, Faculty of Science, The University of Tokyo, Hongo, Bunkyo-ku, Tokyo 113

(Received December 22, 1975)

Synopsis. The pungent principles of ginger —zingerone, gingerol and shogaol— are synthesized starting with vanillin in good yields by utilizing the Lewis acid-promoted cross aldol reaction in each key step.

In recent publications we reported a potential synthetic method[2] for the preparation of various cross aldols by the $TiCl_4$-promoted reactions of silyl enol ethers with carbonyl compounds. In the present paper, a successful application of the above mentioned method to the syntheses of the pungent principles of ginger[3] —zingerone, gingerol and shogaol— is described. Of these compounds, zingerone and shogaol were synthesized by Nomura *et al.*[3] according to the conventional base catalyzed aldol reaction, however, there is no report concerning the synthesis of gingerol.

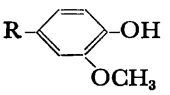

Zingerone R = $CH_2CH_2COCH_3$

Gingerol R = $CH_2CH_2COCH_2CH(CH_2)_4CH_3$ (OH)

Shogaol R = $CH_2CH_2COCH{=}CH(CH_2)_4CH_3$

Zingerone: When vanillin was treated with 2-trimethylsiloxy-1-propene (**2**) in the presence of $TiCl_4$, 2-methoxy-4-(3-oxo-1-butenyl)phenol(**3**) was obtained only in 7% yield and 90% of vanillin was recovered. Then, the reaction of **2** with vanillin was investigated in detail using various Lewis acids, and it was found that **3** was obtained in the optimum yield when $BF_3 \cdot OEt_2$ was employed (see the Table 1).

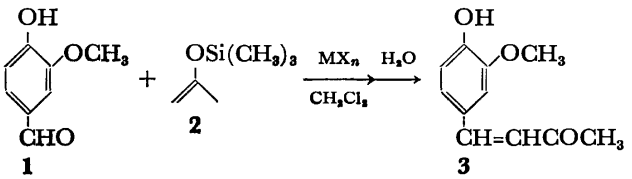

1 + **2** → (MX_n, H_2O, CH_2Cl_2) → **3**

TABLE 1. REACTION OF THE SILYL ENOL ETHER **2** WITH VANILLIN IN THE PRESENCE OF LEWIS ACID

Lewis acid	Temp (°C)	Time (h)	Yield of **3** (%)
$TiCl_4$	0	2	7
$SnCl_4$	0	2	4
$AlCl_3$	0	2	5
$BF_3 \cdot OEt_2$	0	2	68
	r.t.	3	89

The catalytic hydrogenation of **3** over Raney nickel afforded 2-methoxy-4-(3-oxobutyl)phenol (**4**) (zingerone: colorless needles, mp 36—37 °C) and 2-methoxy-4-(3-hydroxybutyl)phenol(**5**) in 75% and 16% yields, respectively.

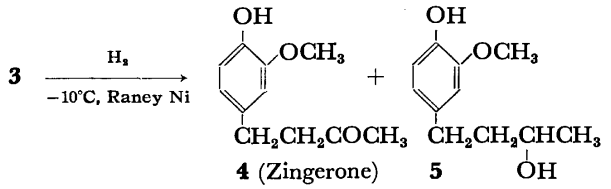

3 → (H_2, −10°C, Raney Ni) → **4** (Zingerone) + **5**

Gingerol and Shogaol: The silylation of **4** was carried out by a modification of House's method.[4] The treatment of a tetrahydrofuran solution of **4** with lithiodiisopropylamine, followed by addition of chlorotrimethylsilane, resulted in the formation of 2-methoxy-4-(3-trimethylsiloxy-3-butenyl)phenoxytrimethylsilane (**6**) in 69% yield. The reaction of **6** with hexanal in the presence of $TiCl_4$ gave *dl*-4-(5-hydroxy-3-oxodecyl)-2-methoxyphenol (**7**) (gingerol)[5] in 92% yield. 2-Methoxy-4-(3-oxo-4-decenyl)phenol (**8**) (shogaol) was obtained in 95% yield by the dehydration of **7** with TsOH–benzene. The structure of **8** was confirmed by comparison with the authentic sample (IR and NMR spectra).

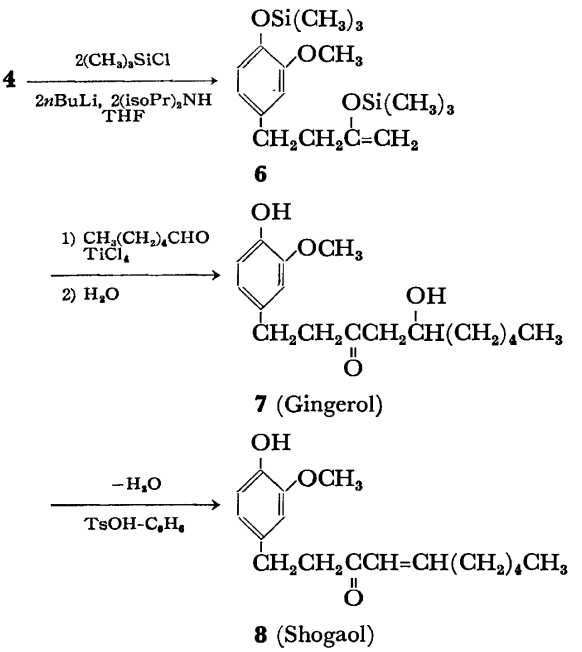

4 → ($2(CH_3)_3SiCl$, $2nBuLi$, $2(isoPr)_2NH$, THF) → **6**

6 → (1) $CH_3(CH_2)_4CHO$, $TiCl_4$; (2) H_2O) → **7** (Gingerol)

7 → ($-H_2O$, $TsOH\text{-}C_6H_6$) → **8** (Shogaol)

Experimental

Preparation of Zingerone (**4**). A dichloromethane (10 ml) solution of 1.30 g (10 mmol) of **2** was added dropwise into a mixture of 0.76 g (5 mmol) of **1** and 0.705 g (5 mmol) of $BF_3 \cdot OEt_2$ in dichloromethane (40 ml) under an argon atmosphere at room temperature, and the reaction mixture was stirred for 3 h. After hydrolysis with water (50 ml) at the temperature, the resulting organic layer was extracted with ether (100 ml), and the extract was washed with saturated NaCl solution (80 ml × 3) and dried over anhydrous Na_2SO_4.

The ethereal solution was condensed and then petroleum ether (30 ml) was added into the residue. The yellow precipitate was filtered and recrystallized from ligroin to yield 0.768 g (80%) of **3**. After evaporation of the filtrate, the residue was purified by preparative TLC (silica gel) using dichloromethane as a developer to give 0.086 g (9%) of **3** (total yield 89%) [IR (KBr disk): 3400, 1640, 1620 cm^{-1}; NMR ($CDCl_3$): δ 2.39 (s, 3H), 3.93 (s, 3H), 6.12 (b, 1H), 6.60 (d, J=16 Hz, 1H), 6.9—7.1 (m, 3H), 7.53 (d, J=16 Hz, 1H)]. A methanol (50 ml) solution of 3.92 g (20 mmol) of **3** was treated with hydrogen for 2 h at −10 °C in the presence of 0.3 g of Raney nickel (commercially produced Raney nickel was thoroughly washed with methanol). About 480 ml of hydrogen was absorbed. After filtration, the filtrate was evaporated, and the residual oil was purified by column chromatography (silica gel) using dichloromethane as a developer to give 2.91 g (75%) of **4** (zingerone)[IR(KBr disk): 3420, 1715 cm^{-1}; NMR (CCl_4): δ 2.04 (s, 3H), 2.69 (quasi s, 4H), 5.90 (b, 1H), 6.4—6.8 (m, 3H)] and 0.630 g (16%) of **5** [IR (neat): 3390 cm^{-1}; NMR (CCl_4): δ 1.21 (d, J=6 Hz, 3H), 1.3—4.0 (m, 5H), 3.81 (s, 3H), 6.18 (b, 1H), 6.9—7.1 (m, 3H)].

Trimethylsilylation of Zingerone (**6**). A hexane solution of 110 mmol of *n*-BuLi was added in 200 ml of THF. The resulting solution was treated with 11 g (110 mmol) of diisopropylamine at −10 °C. To this solution, 9.7 g (50 mmol) of **4** was added dropwise over a 20 min period with stirring at −10 °C. After stirring for an additional 30 min at the temperature, 1.19 g (110 mmol) of chlorotrimethylsilane was added into the mixture. The resulting mixture was stirred for 30 min, diluted with 300 ml of ether, and washed rapidly with two 200 ml portions of cold aq. 10% $KHSO_4$ and cold aq. $NaHCO_3$. The resulting organic layer was dried and concentrated Fractional distillation of the residue with a spinning Teflon-band column gave fraction 1; bp 172—173 °C/5.5 Torr, consisting of the pure **6** (11.6 g, 69%) [IR (neat): 1620 cm^{-1}; NMR (CCl_4): δ 0.18 (s, 9H), 0.20 (s, 9H), 2.0—3.0 (m, 4H), 3.76 (s, 3H), 3.97 (s, 2H), 6.63 (s, 3H)] and fraction 2; bp 173—179 °C/5.5 Torr, containing **6** and unknown compounds (4.5 g).

Preparation of Gingerol (**7**). To a dichloromethane (40 ml) solution of hexanal (0.347 g, 3.3 mmol) and $TiCl_4$ (0.567 g, 3 mmol) was added a dichloromethane (10 ml) solution of **6** (1.017 g, 3 mmol) at −78 °C, and the reaction mixture was stirred for 1 h at the temperature. After usual work-up, the resulting mixture was chromatographed on silica gel. Elution with dichloromethane afforded 0.828 g (92%) of **7** (gingerol) [IR (neat): 3450, 1710 cm^{-1}; NMR (CCl_4): δ 0.86 (t, J=5 Hz, 3H), 1.0—1.8 (m, 8H), 2.44 (d, J=5.5 Hz, 2H), 2.67 (s, 4H), 3.73 (s, 3H), 3.8—4.0 (m, 1H), 6.3—7.0 (m, 3H)].

Preparation of Shogaol (**8**). A solution of **7** (0.60 g, 2 mmol) in dry benzene (50 ml) was refluxed with *p*-toluenesulfonic acid (0.2 g). The resulting crude product was chromatographed on silica gel. Elution with benzene gave 0.534 g (75%) of **8** (shogaol) [IR (neat): 3430, 1665, 1630 cm^{-1}; NMR (CCl_4): δ 0.88 (t, J=5 Hz, 3H), 1.0—2.3 (m, 8H), 2.76 (s, 4H), 3.78 (s, 3H), 5.71 (d, J=18 Hz, 1H), 6.0—6.8 (m, 4H)].

References

1) Present address; The First Institute, Tokushima Faculty, Otsuka Pharmaceutical Company, Ltd., 463-10 Kagasuno, Kawauchi-cho Tokushima-Shi 771-01.

2) a) T. Mukaiyama, K. Narasaka, and K. Banno, *Chem. Lett.*, **1973**, 1011. b) T. Mukaiyama, K. Banno, and K. Narasaka, *J. Am. Chem. Soc.*, **96**, 7503 (1974). c) K. Banno and T. Mukaiyama, *Chem. Lett.*, **1975**, 741.

3) The pungent principles of ginger consist of zingerone, gingerol, and shogaol, which were isolated and assinged by Lapworth *et al.* and by Nomura *et al*: H. Nomura, *J. Chem. Soc.*, **111**, 769 (1917); A. Lapworth, L. K. Peason, and F. A. Royle, *ibid.*, **111**, 777 (1917); H. Nomura and S. Hotta, *Sci. Rep. Tohoku Imp. Univ.*, **7**, 67, 79 (1918); *ibid.*, **14**, 119, 131, 144 (1925); H. Nomura and S. Tsurumi, *ibid.*, **16**, 589 (1927); *ibid.*, **17**, 973 (1928).

4) H. O. House, L. J. Czuba, M. Gall, and H. D. Olmstead, *J. Org. Chem.*, **34**, 2324 (1969).

5) This product was led to the diacetate on treatment with acetic anhydride in pyridine and was confirmed by NMR and mass spectra [NMR (CCl_4): δ 0.89 (t, J=5 Hz, 3H), 1.0—1.8 (m, 8H), 1.91 (s, 3H, $COCH_3$), 2.25 (s, 3H, $COCH_3$), 2.50 (d, J=5 Hz, 2H), 2.71 (t, J=3 Hz, 4H), 3.74 (s, 3H), 5.10 (m, 1H), 6.5—6.9 (m, 3H); mass: *m/e* 378 (M^+)].

BULLETIN OF THE CHEMICAL SOCIETY OF JAPAN, VOL. 49 (5), 1455—1456 (1976)

Oxosulfonium Salts. IV. Preparation and Reactions of Methylphenyloxosulfonium Methylide[1]

Katsumi RYOKE, Hiroshi MINATO, and Michio KOBAYASHI
Department of Chemistry, Tokyo Metropolitan University, Fukazawa, Setagaya, Tokyo 158

(Received December 22, 1975)

Synopsis. Methylphenyloxosulfonium methylide was synthesized, and its reactions with several substrates possessing C=C and C=O bonds were investigated.

Sulfur ylides have proved to be very versatile and useful synthetic intermediates.[2,3] However, the majority of the ylides investigated so far are tri-coordinated ylides, and dimethyloxosulfonium methylide[4] (**1**) and (dialkylamino)methyloxosulfonium methylide[5] (**2**) are the only examples of tetracoordinated sulfur ylides reported in the literature.

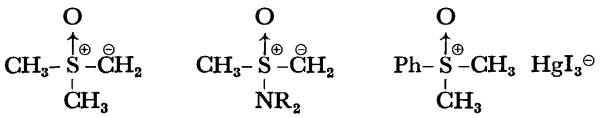

1 **2** **3**

Since oxosulfonium ylides are expected to show reactivities differing from those of sulfonium ylides and are of interest especially for application to asymmetric syntheses, we have investigated the synthesis of new oxosulfonium ylides.

The reason why oxosulfonium ylides other than **1** have not been investigated is that the syntheses of oxosulfonium salts are very difficult. Alkylation of sulfoxides always results in *O*-alkylation with very little *S*-alkylation,[6] although as an exceptional case the *methylation* of *dimethyl* sulfoxide produces trimethyloxosulfonium ion in a good yield.[4] We have overcome this difficulty by using mercury(II) iodide as the catalyst, and obtained dimethylphenyloxosulfonium salt **3** from methyl phenyl sulfoxide and methyl iodide in a 49% yield.[6]

3 was converted into perchlorate **4** by use of silver perchlorate, and **4** was converted into methylphenyloxosulfonium methylide **5** by use of butyllithium or dimsylsodium.

When **4** was treated with NaH in DMSO-d_6, the NMR spectrum of the methylide obtained showed multiplets at δ 8.2—7.5 ppm (5H; C_6H_5) and δ 2.5 (5H; $-CH_3$, and $-\bar{C}H_2$). This indicates that exchange of protons of $-CH_3$ and $-CH_2^-$ is rapid within the NMR time scale.

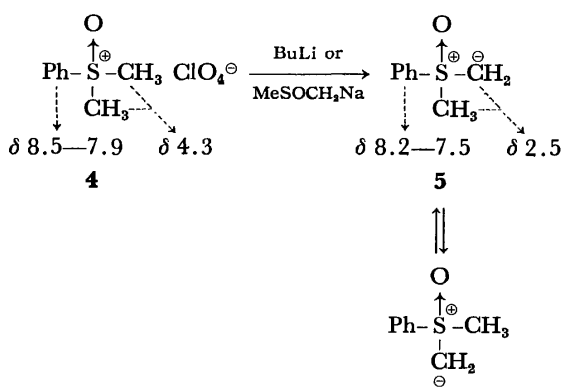

The aromatic hydrogens of **5** absorb in magnetic fields higher than those in **4**. This is reasonable since **5** has a negative charge next to the sulfonium sulfur atom.

The reactions between **5** and several substrates were investigated, and the results are summarized in the Table.

Other substrates examined were CO_2, $PhCH_2Br$, Me_3SiCl, PhNCO and $PhN_2^+BF_4^-$, but it was not

TABLE 1. PRODUCTS OF THE REACTIONS BETWEEN **5** AND SEVERAL SUBSTRATES

Substrate	mol/mol **5**	Products (mol % yield)[a]
Ph_2CO	1.02	$Ph_2C(O)CH_2$ (73%)
		PhSMe (63%)
PhCHO	1.02	PhCH(O)CH_2 (41%)
		PhSMe (32%)
	1.07	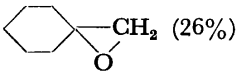 (26%)
		PhSMe (39%)
trans-Stilbene	1.09	*trans*-Stilbene (88%)
PhCH=CHCPh ‖ O	1.00	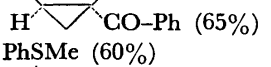 (65%)
		PhSMe (60%)
Dimethyl maleate	1.00	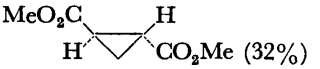 (32%)
		PhSMe (44%)
		Dimethyl fumarate (4%)
$Me_3O^+BF_4^-$	1.35	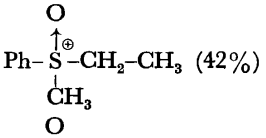 (42%)
PhCOCl	0.51	(70%)[b]

a) Based on the mol of **5** used. b) Based on half the mol of **5** used.

possible to isolate characterizable products.

As shown in the Table, the reaction between **5** and benzoyl chloride produced a stable oxosulfonium phenacylide. This can be explained by assuming the deprotonation of methylphenacylphenyloxosulfonium ion with **5**.

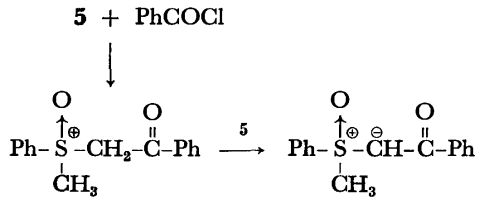

In the reaction with methyl maleate, the product of addition was not methyl cyclopropane-*cis*-dicarboxylate, but methyl cyclopropane-*trans*-dicarboxylate. One should note that methyl fumarate was produced in a 4% yield. These facts suggest that after **5** was added to methyl maleate the C=C bond in the adduct rotated, and the products were formed from the more stable conformation.

In the reaction with benzylideneacetophenone, **5** transfers the methylene to its C=C bond, whereas sulfonium ylide $PhMe\overset{+}{S}-\overset{-}{C}H_2$ transfers the methylene to the C=O bond.[7]

If optically-active $ArAr'\overset{+}{S}(\rightarrow O)\overset{-}{C}H_2$ could be synthesized, their reactions with various substrates would be of great interest.

Experimental

Conversion of 3 to 4. A saturated solution of $AgClO_4$ (25 g, 120.5 mmol) in acetone was added drop by drop to a stirred solution of **3** (25.5 g, 34.6 mmol) in acetone (400 ml), and the HgI_2 and AgI formed were filtered off. After the filtrate was evaporated in a vacuum, the residue was washed with ether and recrystallized three times from ethanol; the yield of **4**, 4.4 g (50%).

Conversion of 4 to 5. The following two methods were used. a) After **4** (0.8 g, 3.14 mmol) was dissolved in THF (30 ml; dried by refluxing with $LiAlH_4$ overnight) under a nitrogen atmosphere, the solution was cooled to −60 °C, and a hexane solution of butyllithium (1.6 M, 2.2 ml; 3.45 mmol) was added. The mixture was stirred for 1 h at −60 °C.

b) A slightly excess NaH (0.1 M mineral oil dispersion) was washed several times with petroleum ether in a three-necked flask under nitrogen, and then some DMSO (dried over CaH_2 for 3 h) was added. The mixture was heated to and kept at 70 °C until evolution of hydrogen ceased (about 1 h). After it was cooled to room temperature, a DMSO solution of **4** was slowly added.

References

1) Organic Sulfur Compounds. Part 51.

2) C. R. Johnson, "Ylide Chemistry," Academic Press, New York, N. Y., (1966).

3) B. M. Trost and L. S. Melvin, Jr., "Sulfur Ylides," Academic Press, New York, N. Y. (1975).

4) E. J. Corey and M. Chaykovsky, *J. Am. Chem. Soc.*, **84**, 867 (1962); *ibid.*, **84**, 3782 (1962); *ibid.*, **86**, 1640 (1964); *ibid.*, **87**, 1353 (1965).

5) C. R. Johnson, E. R. Janiga, and M. Haake, *J. Am. Chem. Soc.*, **90**, 3090 (1968); C. R. Johnson, M. Haake, and C. W. Schroeck, *ibid.*, **92**, 6544 (1970); C. R. Johnson and C. W. Schroeck, *ibid.*, **93**, 5305 (1971); C. R. Johnson and P. E. Rogers, *J. Org. Chem.*, **38**, 1798 (1973).

6) M. Kobayashi, K. Kamiyama, H. Minato, Y. Oishi, Y. Takada, and Y. Hattori, *Bull. Chem. Soc. Jpn.*, **45**, 3703 (1972); K. Kamiyama, H. Minato, and M. Kobayashi, *ibid.*, **46**, 2255 (1973).

7) E. J. Corey and M. Chaykovsky, *Tetrahedron Lett.*, **1963**, 169; C. R. Johnson, C. W. Schroeck, and J. R. Shanklin, *J. Am. Chem. Soc.*, **95**, 7424 (1973).

Shock Tube Studies of the Rate Constant for Chemical Excitation of Hydroxyl Radicals

Tohru KOIKE and Kihei MORINAGA

Department of Chemistry, National Defense Academy, Hashirimizu, Yokosuka 239

(Received August 7, 1975)

The $OH(^2\Sigma^{+2}\text{-}^2\Pi)$ chemiluminescence in the partial equilibrium region of the H_2—O_2 reaction in mixtures with $H_2/O_2/Ar=2/2/96$, $P_1=5$, 10, 20 Torr was studied in 1250—2000 K incident shock waves. The comparison between the temperature dependence of the $OH(^2\Sigma^+)$ emission and that of the computer simulation of the H_2—O_2 reaction yields the activation energy of the chemical excitation process, assuming the same bi-radical process as former investigators used. The evaluated $OH(^2\Sigma^+)$ profile, based on a simulation in which the chemical excitation, radiative, and non-radiative processes are accounted for, depends on the pre-exponential factor of the chemical excitation process. The correlations between the temperature dependence of the evaluated $OH(^2\Sigma^+)$ profile and that of the emission profile in the partial equilibrium region gave the pre-exponential factor of the chemical excitation process. Thus, we could estimate the rate constant for $O+H+Ar=OH(^2\Sigma^+)+Ar$ to be $1.0\times10^9\times\exp(-11000\ \text{cal}/RT)$.

The reactions of hydrogen and/or hydrocarbons with oxygen are accompanied by the emission of $OH(^2\Sigma^+\text{—}^2\Pi)$ transitions. The origin of $OH(^2\Sigma^+)$, hereafter OH*, could be attributed to both thermal and chemical excitations.

Kinetic studies of the OH* emission have been performed in $H_2/O_2/N_2$ flame,[1] in shock heated H_2/air mixtures,[2] H_2/O_2/Ar mixtures,[3] H_2/O_2/CO/Ar mixtures,[4] and in a flow system of O and H associations.[5]

Gardiner *et al.*[3] made a detailed comparison between the growth constant of the OH* emission and that of the ground state OH concentration measured by the Bi-lamp absorption technique; they concluded that the chemical excitation process or pre-association process of OH* is $O+H+M=OH^*+M$. Schott *et al.*[4] reached the same conclusion through the comparison between the OH* growth constant and the O growth constant, which were observed *via* OH* emission and CO+O emission using their end-on technique in shock tube experiments.

Strong evidence for the above conclusion was given by Schiff *et al.*,[5] who made it clear that the intensity of the OH* emission which accompanies O+H association in a microwave discharge flow system is proportional to the concentration product of ground state O and H.

Further studies of the OH chemiluminescence in a shock heated hydrogen/oxygen reaction were performed in the present work to evaluate the rate constant of the chemical excitation process of hydroxyl radicals in gas phase, accepting the above mechanism and adpoting a computer simulation technique for the estimation of the over-all reaction scheme.

Experimental

Shock Tube. Incident shock waves were actuated in the shock tube shown in Fig. 1, where the driver section A is made of a mild steel pipe of inner diameter 8.9 cm and length 120 cm, and the test section B is an extruded rectangular brass tubing of inner cross section 3.2×7.2 cm, thickness 0.4 cm, and length 400 cm, with three quartz windows of 10 mm thickness located 300 cm downstream from the diaphragm section. The windows and a triggering thermal gauge whose location is 5 cm upstream from the windows were carefully flat mounted at the bottoms onto the test section, avoiding any aerodynamic disturbance in the tube. The triggering gauge is a vacuum deposited thin tin film and the other five thermal gauges positioned downstream from the windows at 10 cm intervals are of thin platinum deposited by the baking of brush-painted Hanovia solution. The diaphragm section D was devised to employ the two diaphragm method but natural bursts of a single diaphragm were adopted throughout the present experiments. The diaphragms were press scored aluminium plates of 0.2 mm thickness. The test section could be evacuated to less than 1 micron by an oil diffusion pump with a liquid nitrogen trap and showed a leak rate of less than 2 micron/30 min.

Optical System and Electronic Devices. The emission from the reacting gas was monitored by a S-13 response photomultiplier (Hamamatsu-TV R292) with a filter which consisted of 3 mm of Corning 9863 glass and 6 mm of 50 g/100 g solution of $NiSO_4\cdot6H_2O$. This filter combination

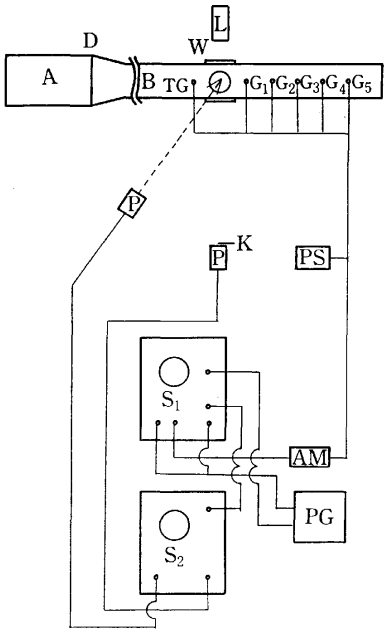

Fig. 1. Block Diagram of Apparatus.
A: Driver section, B: Test section, D: Diaphragm section, TG: Trigger gauge, G_1—G_5: Thermal gauges, W: Observation windows, L: Laser, K: Knife-edge, P: Photomultipliers, PS: Power supply, AM: Amplifier, PG: Pulse generator (Time mark, Triangle wave), $S_1\cdot S_2$: Oscilloscopes.

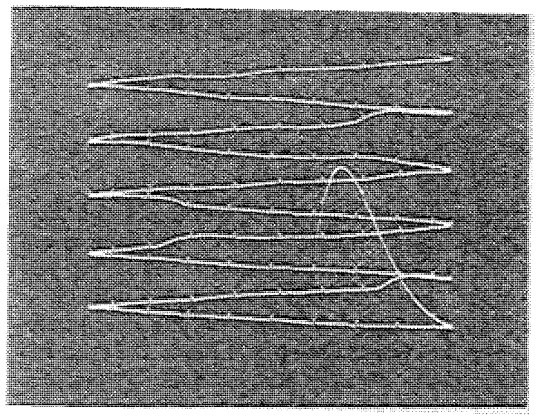

Fig. 2a. Signals of trigger gauge TG and thermal gauges G_1—G_5 are displayed on Raster sweep with 5-μs time marks.
$U_1 = 1350$ m/s, $T_2 = 1840$ K.

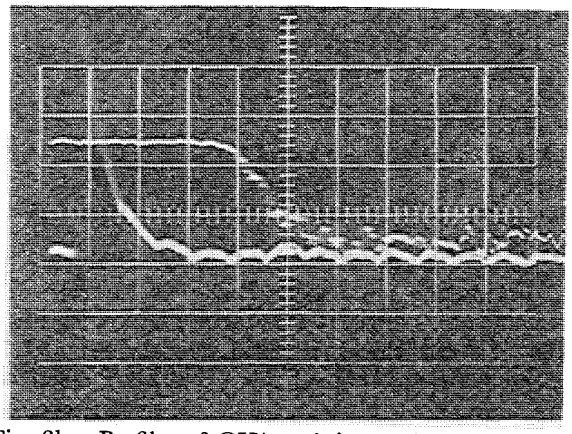

Fig. 2b. Profiles of OH* emission and laser schlieren.
Upper trace: OH* emission, gain = 1 mV/div.
Lower trace: Laser schlieren, gain = 10 mV/div.
Sweep rate = 10 μs/div.

had about 50% transmission at 306.7 nm, and its high- and low-cutoffs were 360.0 nm and 240.0 nm, respectively. Between the photomultiplier and the shock tube window two 2 mm slits were installed at a 20 cm separation. The emission from the reacting gas was observed through the slits in the direction in accordance with the minor latus of the rectangular cross section of the shock tube. A laser schlieren technique was adopted to detect any abnormality of the shock waves and any data with an abnormal laser schlieren image was discarded. The signals from the thermal resistance gauges were displayed on a Raster sweep oscilloscope along with 5 micro-second time marks from a quartz oscillator. An oscillogram of the Raster sweep is shown in Fig. 2a.

Gas Mixtures. The gases were taken from commercial cylinders whose purities, as assayed by the manufacturer, were not less than 99.9%, and were used without further purifications. Gas mixtures of the desired compositions were prepared manometrically and left to stand for at least 24 h before use. Blank tests of the emission were performed in the same manner as in the actual runs with Ar gas and H_2/Ar gas, and no appreciable emission was observed in either case.

The Computer Program. The computer program used in the present work was provided through the courtesy of W. C. Gardiner, Jr.,* and C. B. Wakefield and was modified to match the NEAC 2200 system. It was devised to calculate any of the incident or reflected shock waves with ideal, laminar, or turbulent flows. The thermodynamic data from the JANAF thermochemical tables[6] are included in it in the form of virial equations. Given the reaction mechanism to be a group of elementary reactions with forward rate constants, the program integrates the assembly of first order linear differential equations of the forward and reverse reactions *via* an implicit Adams method or Gear method, and gives the concentration profile of any desired species in relation to the time elapsed after the shock arrivals.

Results and Discussion

In studying the chemical excitation of OH*, Gaydon,[7] Schiff,[5] Gardiner,[3] and Schott[4] were not entirely consistent in their treatments of the third body M, though they were in accord for the bi-radical reaction of O and H. Gaydon *et al.*[7] presumed that a direct bi-radical reaction formed OH* in an unstable $^2\Sigma^-$ state and was followed by a radiationless transition to the stable $^2\Sigma^+$ state in order to explain the features obtained by flame spectroscopy. They posited three body collisions of O, H, and M to form OH* as the main process of OH* formation in a flame, through a consideration of the heat of formations. Schiff *et al.*[5] regarded the chemical excitation of OH* as a bi-radical reaction without a third body in their O and H association process in a low pressure flow system. Gardiner *et al.*[3] and Schott *et al.*[4] proposed a bi-radical reaction with or without a third body M to represent the OH* formation in their shock tube reaction of H_2 and O_2.

In the present study, we treated the chemical excitation process with a third body M to obtain a tentative pre-exponential factor and activation energy of the rate constant for formation of OH*. Thus, the reaction which includes OH* may be written as follows:

$$O + H + M = OH^* + M \quad (a)$$

$$OH^* + M' = OH + M' \quad (b)$$

$$OH^* = OH + h\nu \quad (c)$$

The fate of the OH* formed in reaction (a) is to follow either the non-radiative quenching process (b) in which a third body M′ is considered, or the radiative process (c) whose emission in the partial equilibrium region is now under consideration.

The reverse process (b) could be explained as a thermal excitation of OH. The activation energy of the thermal excitation process was assumed to be 93.4 kcal/mol, whereas the chemical excitation process to form OH* was characterized by a much smaller activation energy.[3] In the temperature region lower than 2000 K,[3] the contribution of the thermal excitation process to form OH* seemed to be less dominant than the chemical excitation process. The features of thermally excited OH* will be shown later in Fig. 6, along with the concentration profiles; here both chemical and thermal processes are taken into ac-

* The University of Texas at Austin, Austin, Texas, 78712 U. S. A.

count. The reverse reaction (c) is a self-absorption process whose extinction coefficient is very small.[8]

The steady state assumption of [OH*] leads to the equation:

$$[OH^*] = k_a[O][H][M]/(k_{-a}[M]+k_b[M']+k_c) \quad (1)$$

where the reverse processes (b) and (c) are disregarded by comparison with reaction (a). The reverse reaction (a) is a endothermic reaction of about 12 kcal/mol, whereas the reaction (b) is a exothermic reaction of 93.4 kcal/mol. The term $k_{-a}[M]$ is assumed to be very small compared with the term $k_b[M']$.

Bennett and Dalby[9] obtained the radiation life time of OH* and the collision cross-section between OH* and H_2O. Accepting their collision cross-section of 70 Å^2, the rate constant of reaction (b) could be evaluated by collision theory as:

$$k_b = 8.22\times10^{13}\times T^{0.5} \quad (cm^3\ mol^{-1}\ s^{-1}) \quad (B\,1)$$

and the value of k_c from the radiation life time is:

$$k_c = 9.9\times10^5 \quad (s^{-1}) \quad (C\,1)$$

In the partial equilibrium region, the concentration of H_2O computed under a sample condition of P_1=10 Torr and T_2=1500 K with $H_2/O_2/Ar$=2/2/96 is 2.5×10^{-8} mol/cm^3; then the value of $k_b[M']$ is 8.0×10^7 (s^{-1}). Thus, the value of k_c is 1/80 of the value of $k_b[M']$. If the other collision partners of OH* are taken into account along with H_2O, the value of k_c is far less than that of $k_b[M']$ and the term k_c in the denominator of Eq. 1 could reasonably be neglected. Therefore, the emission intensity I in the partial equilibrium region is given by:

$$I = Ck_c[OH^*] = Ck_ck_a[O][H][M]/k_b[M'] \quad (2)$$

where C is a correlation factor for the detector.

A sample oscillogram of an OH* emission profile is shown in Fig. 2b, along with a laser schlieren trace. In the partial equilibrium region, the OH* emission exhibits a flat plateau for the present mixtures of $H_2/O_2/Ar$=2/2/96. In Fig. 3, the OH* emission intensity I obtained from the oscillogram plateau height at various starting pressures is plotted against the concentration product of O and H of the computer simulations for each of the starting pressures. The validity of Eq. 2 and also that of reaction (a) are accordingly established by the linear relations shown in Fig. 3.

As noted previously, the computer program for the simulation requires a reaction mechanism with the forward rate constants, and the reverse rate constants incorporated into the calculation are determined from the equilibrium constants based on the JANAF thermochemical tables. The aggregation of elementary reactions and the rates used in the present work are shown in Table 1.

It is obvious that C and k_c in Eq. 2 are independent of temperature, and the activation energy of reaction (b) could be very small, as it is the rate constant for the reaction of highly activated OH*. The temperature dependence of the value of [O][H] can be evaluated from Fig. 4, where the concentration products of O and H of the computer simulations are plotted against $1/T$. The slope of the linear relations or pseudo-

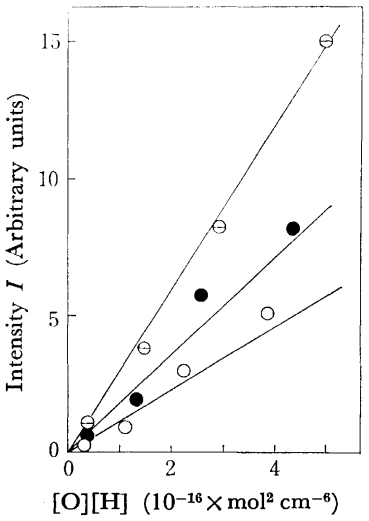

Fig. 3. The relation between emission intensity I and concentration product of [O] and [H] for different temperatures ($T\pm30$ K).
⊖: 1920 K, ●: 1550 K, ○: 1330 K.

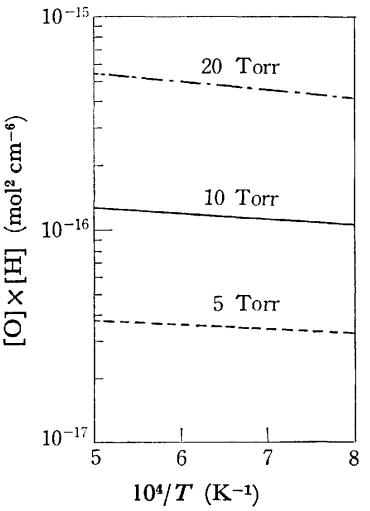

Fig. 4. The relation between concentration product ([O][H]) and $1/T$ for different starting pressures.

activation energy of the product, [O][H], is not so dominant. The above results yield the pseudo-activation energy of the product, [O][H], as 2500±700 cal/mol, where the limit of ±700 cal/mol represents the calculation's sensitivity to the variations (10-folds to 1/10-folds) of each of the rate constants in Table 1, except for the constant for the chain branching reaction of $H+O_2=OH+O$. For the latter rate constant, nearly equal values of the limit were obtained by 2-folds to 1/2-folds of the variations. The temperature dependence of the value of [M]/[M'] will be much less than that of the concentration product of O and H. Thus, it is concluded from Eq. 2 that the temperature dependence of I is the consequence of the temperature dependences of k_a and the [O][H] product in the temperature region where the thermal excitation is less dominant.[3] In Fig. 5, the emission intensity I in the partial equilibrium region was plotted against $1/T$. The apparent activation energy of the slopes

Table 1. Elementary reactions and kinetic parameters
$k=AT^n \exp(-E/RT)$ (cal, mol, cm, s units)

Reaction		A	n	E	Reference
$H_2+M=2H+M$	M=Ar, O_2	2.23×10^{12}	0.5	92600	11)
	M=H_2	5.58×10^{12}	0.5	92600	12)
	M=H	4.46×10^{13}	0.5	92600	12)
	M=H_2O	1.34×10^{13}	0.5	92600	13)
$O_2+M=2O+M$	M=Ar, H_2	1.85×10^{11}	0.5	95700	14)
	M=O	5.55×10^{12}	0.5	95700	14)
	M=O_2	1.85×10^{12}	0.5	95700	14)
$H_2+O_2=2OH$		2.0×10^{11}		20000	8)
$H+O_2=OH+O$		1.22×10^{17}	−0.91	16600	15)
$O+H_2=OH+H$		1.6×10^{14}		13500	16)
$OH+H_2=H_2O+H$		5.2×10^{13}		6500	16)
$H+O_2+M=HO_2+M$	M≠H_2O	2.0×10^{15}		−870	17)
	M=H_2O	5.0×10^{16}		−870	17)
$H+OH+M=H_2O+M$	M≠H_2O	7.5×10^{23}	−2.6		18)
	M=H_2O	1.5×10^{25}	−2.6		18)
$HO_2+H=2OH$		6.0×10^{13}			19)
$HO_2+O=OH+O_2$		1.0×10^{13}			19)
$OH+OH=H_2O+O$		5.5×10^{13}		7000	16)
$H_2+HO_2=H_2O+OH$		2.0×10^{11}		24000	20)

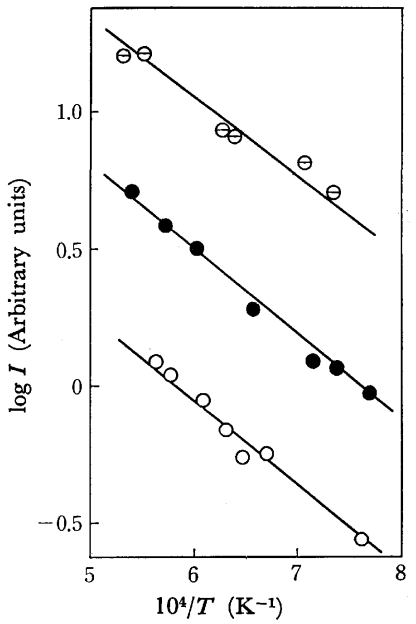

Fig. 5. The relation between log I and $1/T$ for different starting pressures.
⊖: 20 Torr, ●: 10 Torr, ○: 5 Torr.

in Fig. 5, which depends on the activation energy of k_a and the pseudo-activation energy of the [O][H] product, was obtained from the figure to be 13500 cal/mol. Thus the activation energy of k_a could be estimated from the above values as the difference, 13500—2500 cal/mol, and k_a could be expressed as:

$$k_a = A\exp(-11000\ \text{cal}/RT) \qquad \text{(A1)}$$

where A represents the pre-exponential factor of k_a. It is subjected to the following speculations.

The reaction mechanism shown in Table 1, used in the computation of the [O][H] product, does not include reactions which involve OH* because the concentration of OH* is much less than that of ordinary radicals.

To simulate the profile of OH* in the reaction, we added reactions (a), (b), and (c) to the above mechanism with the forward rate constants expressed in (A1), (B1), and (C1). Along with the rate constant expressed in (B1), we added the following rate constant (B2), evaluated by collision theory in which the collision partner is taken to be O_2 with the collision cross section of 7 Å^2, after Carrington.[10]

$$k_b = 1.84\times10^{12}\times T^{0.5}\ (\text{cm}^3\,\text{mol}^{-1}\,\text{s}^{-1}) \qquad \text{(B2)}$$

As the third body M of Eq. (a), Ar was employed in the course of the reaction simulations. For OH* and $h\nu$, the thermochemical properties were calculated by the equations based on the Mayer and Mayer representations in the JANAF thermochemical tables.[6] The mass of OH* and $h\nu$ were assumed to be OH*=OH and $h\nu=E/c^2$, where E corresponds to the 306.7 nm emission and c is the light velocity. The latter mass was provisionary assigned to carry out the computer program.

In Fig. 6, the calculated OH* concentration in the partial equilibrium region is shown *vs.* $1/T$, with parameters of the pre-exponential factor A of the expression (A1). It is obvious that the slopes of the curves depend on the parametric values of A. Calculations testing the sensitivity to reasonable variations in other rate constants showed that the pre-exponential factor has almost the total effect on the slopes of log[OH*] *vs.* $1/T$ in a definite temperature region. As the emission intensity I is proportional to the OH* concentration in the partial equilibrium region, the slope of log I *vs.* $1/T$ should accord with that of log[OH*] *vs.* $1/T$. The observed slope in Fig. 5 was fitted to the curve in Fig. 6, as is shown by thick line

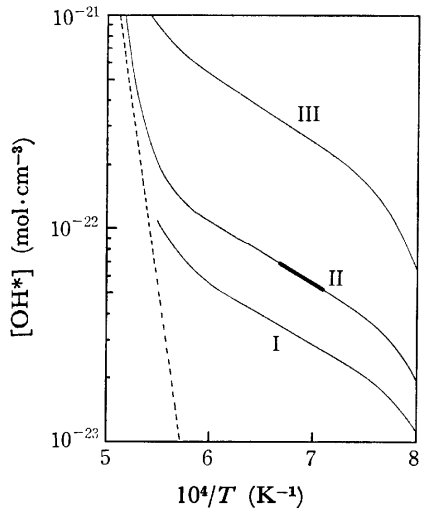

Fig. 6. The relation between calculated [OH*] and $1/T$. Broken line; The reactions (b) and (c) are taken into account. Solid line; The reactions (a), (b), and (c) are taken into account with the different A values of Eq. (A1).
I: $A=5.0\times10^8$, II: $A=1.0\times10^9$, III: $A=5.0\times10^9$.

in the latter figure. The best fit in the temperature range of 1400—1500 K was obtained when the parameter A was chosen to be 1.0×10^9 (cm^6 mol^{-2} s^{-1}).

Thus, we tentatively obtained the pre-exponential factor of reaction (a) assuming Ar as the collision partner M of the reaction. The rate constant k_a is expressed as:

$$k_a = 1.0\times10^9 \exp(-11000\ \text{cal}/RT) \quad (\text{cm}^6\ \text{mol}^{-2}\ \text{s}^{-1})$$

In the above expression of k_a, the activation energy is subjected to the error limit of the above discussion. Further investigations such as detection of the absolute emission intensity I are required to obtain a more rigorous pre-exponential factor A of the constant k_a.

The authors are grateful to Professor W. C. Gardiner, Jr. and Dr. C. B. Wakefield for providing us with the computer program "NIP", which was very helpful for the present studies.

References

1) W. E. Kaskan, *J. Chem. Phys.*, **31**, 944 (1959).
2) F. E. Belles and M. R. Lauver, *J. Chem. Phys.*, **40**, 415 (1964).
3) W. C. Gardiner, Jr., K. Morinaga, D. L. Ripley, and T. Takeyama, *Phys. Fluids Supplement*, **I**, 120 (1969).
4) D. Gutman, R. W. Lutz, N. F. Jacobs, E. A. Hardwidge, and G. L. Schott, *J. Chem. Phys.*, **48**, 5689 (1968).
5) S. Ticktin, G. Spindler, and H. I. Schiff, *Discuss. Faraday Soc.*, **44**, 218 (1967).
6) "JANAF Thermochemical Tables," Dow Chemical Company (1965).
7) A. G. Gaydon and H. G. Wolfhard, *Proc. R. Soc. Ser. A*, **208**, 63 (1951).
8) D. L. Ripley, Ph. D. thesis, University of Texas (1967).
9) R. G. Bennett and F. W. Dalby, *J. Chem. Phys.*, **40**, 1414 (1964).
10) T. Carrington, *J. Chem. Phys.*, **30**, 1087 (1959).
11) A. L. Myerson and W. S. Watt, *J. Chem. Phys.*, **49**, 425 (1968).
12) T. A. Jacobs, R. R. Giedt, and N. Cohen, *J. Chem. Phys.*, **47**, 54 (1967).
13) R. W. Getzinger and L. S. Blair, *Combust. Flame*, **13**, 271 (1969); A. Gay and N. H. Pratt, "Shock Tube Research: Proceedings of the 8th Shock Tube Symposium," Chapmann and Hall (1971), No. 39.
14) W. S. Watt and A. L. Myerson, *J. Chem., Phys.*, **51**, 1638 (1969).
15) G. L. Schott, *Combust. Flame*, **21**, 357 (1973).
16) W. C. Gardiner, Jr., W. G. Mallard, M. Mcfarland, K. Morinaga, J. H. Owen, W. T. Rawlins, T. Takeyama, and B. F. Walker, "14th Symp. Combust.," The Combustion Institute (1973), p. 61.
17) D. Gutman, E. A. Hardwidge, F. A. Dougherty, and R. W. Lutz, *J. Chem. Phys.*, **47**, 4400 (1967).
18) J. B. Homer and I. R. Hurle, *Proc. R. Soc. Ser. A*, **314**, 585 (1970).
19) W. G. Browne, D. R. White, and G. R. Smookler, "12th Symp. Combust.," The Combustion Institute (1969), p. 557.
20) V. V. Voevodsky, "7th Symp. Combust.," (1959), p. 34.

Kinetic Parameters of Thermal Dehydration and Decomposition of Zeise's Salt Hydrates

Manabu SENŌ, Kazutoshi IWAMOTO, and Teruzo ASAHARA

Institute of Industrial Science, University of Tokyo, Roppongi, Minato-ku, Tokyo 106

(Received November 17, 1975)

The kinetic parameters of the dehydration of Zeise's salt hydrates, $K[PtCl_3(olefin)]\cdot H_2O$, (olefin; $CH_2=CH_2$, $CH_3CH=CH_2$, $C_2H_5CH=CH_2$, n-$C_3H_7CH=CH_2$ and n-$C_4H_9CH=CH_2$) and the thermal decomposition of Zeise's dimers were determined by using DTA and TG. By comparing the kinetic parameters with the data of IR and the enthalpy change of dehydration, it was shown that the important factor in determining the kinetic behavior of the dehydration is an extent of deformation of lattice at the transition state. Similarly, it was suggested that the bulkiness of ligand olefin is an important factor in governing the kinetics of the thermal decomposition reactions.

In a previous paper,[1] it was shown from the investigation of the dehydration reaction of Zeise's salt that the dehydrated Zeise's salt contains some amount of the dimer. The content of the dimer was determined and the thermochemical properties of thermal decomposition reactions were examined. In the present paper, the kinetic parameters of the dehydration process of Zeise's salt and the thermal decomposition process of Zeise's dimer were determined from the data of differential thermal analysis (DTA) and thermogravimetry (TG). The activation energy and the activation entropy of dehydration process of Zeise's salts decrease remarkably as the ligand olefin becomes smaller. On the other hand, the decreasing order of the activation energy of the thermal decomposition process of Zeise's dimers is as follows;

$$[PtCl_2(n\text{-}C_4H_9CH=CH_2)]_2 > [PtCl_2(n\text{-}C_3H_7CH=CH_2)]_2 > [PtCl_2(C_2H_5CH=CH_2)]_2 \approx [PtCl_2(CH_2=CH_2)] > [PtCl_2(CH_3CH=CH_2)]_2$$

Experimental

Syntheses of Zeise's Salts $K[PtCl_3(olefin)]$. Zeise's salt hydrates $K[PtCl_3(olefin)]\cdot H_2O$ were prepared from K_2PtCl_4 and olefins according to the method described by MacNevin *et al.*[2] The products were recrystallized twice from 3% aqueous HCl solutions and dehydrated by storing in a $CaCl_2$ desiccator in 2—3 weeks. The purities were checked by elementary analyses.

Syntheses of Zeise's Dimers $[PtCl_2(olefin)]_2$. Dimers of Zeise's salts $[PtCl_2(olefin)]_2$ were prepared from Zeise's salts according to the method described by Moeller.[3] The products were confirmed by elementary analyses.

Measurements of Decomposition Processes. A thermal analyzer DT-20B (Shimadzu) and a thermo flex (Rigaku Denki) were used for characterization of thermal decomposition processes. Most of the measurements were carried out at the increasing rate of temperature of 1.25 °C/min under N_2 flow. The data of DTA, from which the kinetic parameters of the dehydration process were determined, were measured at the increasing rates of temperature of 5 °C/min, 10 °C/min, 20 °C/min and 40 °C/min, respectively.

Results and Discussion

Zeise's salt has one mole of crystalline water. The absorption peaks of the infrared spectra ascribed to the crystalline water in the complexes with various olefins are shown in Table 1. Asymmetric and symmetric stretching vibrations of the O–H band shift to a lower frequency side and the bending vibration shifts to a higher frequency side compared with those of a free water molecule, but these shifts are not so large as those in liquid water as being seen in Table 1. This means that the water molecule in Zeise's salt interacts with chlorine atoms to form partially hydrogen bonds. As a ligand olefin becomes large, the asymmetric stretching vibration shifts somewhat to a higher frequency. The other vibrations do not change so clearly as asymmetric stretching vibration.

TABLE 1. IR SPECTRA OF CRYSTALLINE WATER OF ZEISE'S SALT HYDRATE, $K[PtCl_3(olefin)]\cdot H_2O$

Complexes	Asym. stretch. vib.(cm^{-1})	Sym. strech. vib.(cm^{-1})	Bending vib.(cm^{-1})
$K[PtCl_3(C_2H_4)]\cdot H_2O$	3540	3480	1614
$K[PtCl_3(C_3H_6)]\cdot H_2O$	3540	3480	1618
$K[PtCl_3(\Delta'\text{-}C_4H_8)]\cdot H_2O$	3550	3500	1620
$K[PtCl_3(\Delta'\text{-}C_5H_{10})]\cdot H_2O$	3555	3500	1618
$K[PtCl_3(\Delta'\text{-}C_6H_{12})]\cdot H_2O$	3565	3500	1618
Free H_2O	3755.8	3654.5	1595.0[9]
Liquid H_2O	3430	3210	1650[9]

These observations are consistent with the results of X-ray analysis.[4,5] According to Black *et al.*,[5] $K[PtCl_3(CH_2=CH_2)]\cdot H_2O$ forms a monoclinic crystal, a= 10.750 Å b=8.405 Å, c=4.836 Å, β=97.73°. There are a chain of alternate potassium ions and triangles of chlorine atoms and a chain of hydrogen bonds ···Cl⁻···H–O–H··· parallel to the c axis and these two chains are cross-linked by the coordinate bonds within the complex ions and by the ionic interactions in chains of –O–K⁺– which are parallel to the b axis.

The dehydration reaction of Zeise's salt hydrates was analyzed by using DTA. Zeise's salt hydrates lose one mole of crystalline water by heating at about 60—80 °C. The activation energy and the order of dehydration reaction were estimated by using the method of Kissinger.[6] The following equations serve as a basis of analysis of DTA curve.

$$\ln\frac{\phi}{T_m^2} = \ln A - \frac{E_a}{RT_m} \quad (1)$$

$$n = 1.26S^{1/2} \quad (2)$$

$$S = \frac{(d^2x/dt^2)_1}{(d^2x/dt^2)_2} \quad (3)$$

Table 2. Activation energies and reaction orders of dehydration of Zeise's salt hydrate, $K[PtCl_3(olefin)]\cdot H_2O$

Complexes	Temp (°C)	n	E_a (kcal·mol^{-1})	ln A	$\Delta S^{\neq}$ (cal·K^{-1})	ΔH (kcal·mol^{-1})
$K[PtCl_3(C_2H_4)]\cdot H_2O$	67	0.72	46.7	70.0	80.7	15.5±0.5
$K[PtCl_3(C_3H_6)]\cdot H_2O$	76	0.90	30.8	44.8	30.6	15.3±0.5
$K[PtCl_3(\Delta'\text{-}C_4H_8)]\cdot H_2O$	73	1.11	26.8	38.4	17.9	16.0±1.0
$K[PtCl_3(\Delta'\text{-}C_5H_{10})]\cdot H_2O$	59	0.89	19.4	28.9	−1.0	13.3±1.0
$K[PtCl_3(\Delta'\text{-}C_6H_{12})]\cdot H_2O$	65	0.82	15.3	22.4	−13.9	14.0±1.0

ΔH is the enthalpy change in dehydration of Zeise's salt hydrate.[1]

In these equations, ϕ is the constant rate of temperature rise, T_m is the temperature giving a maximum rate of dehydration, n is the order of dehydration reaction, E_a is the activation energy, A is the frequency factor, R is the gas constant and S is called as a shape index. The values of T_m were determined at the rates of temperature rise ϕ of 5, 10, 20 and 40 °C/min and therefrom the kinetic parameters were obtained. The results of analyses are shown in Table 2. The activation energy of dehydration of the complexes decreases as the ligand olefin becomes larger. The values of $\Delta S^{\neq}$ are positive and larger for a smaller ligand olefin. The values of activation energy and activation entropy change greatly when the ligand olefin changes. On the other hand, the enthalpy change of dehydration does not change so remarkably as the activation energy and entropy. These results suggest that the bond energy of water in lattice is not an important factor which governs the transition state of dehydration reaction, but the energy required for deformation of lattice structure would be an important factor. During the process of dehydration, the lattice structure would be deformed markedly and the transition state would have a loose deformed structure, which ensures a large activation energy and a positive activation entropy.

For the complex with smaller ligand olefin such as ethylene, the transition state would be so far from the initial state and the deformation at the transition state becomes small as the ligand olefin is larger. This consideration accounts for the result in Table 2.

As being described in the preceding paper,[1] Zeise's salt hydrate loses crystalline water and at the same time rearranges partially into a dimer $[PtCl_2(olefin)]_2$. The above results for activation parameters of dehydration are for the overall reactions at the dehydration temperatures.

When the Zeise's salt is continued to heat after dehydration, it decomposes in two steps. The first step is the thermal decomposition of the dimer formed during the dehydration, as being revealed by the preceding paper.[1] The reaction order and the activation energy of the first step were calculated by using the Freeman-Carroll method.[7] The DTA curves of thermal decomposition of the dimers are too broad and obscure to calculate activation parameters by using the method of Kissinger and, since the decrease in weight is slow and large, the method of Freeman-Carroll is convenient. On the contrary, the dehydration process of Zeise's salt is too fast to measure exactly the weight loss, and the method of Kissinger is more convenient.

It was supposed[1] that the first step reaction proceeds as shown by Eq. 4,

$$[PtCl_2(olefin)]_2 \rightarrow Pt + PtCl_2 + Cl_2 + 2olefin \quad (4)$$

Then, the rate of decomposition reaction is tentatively assumed to be expressed by Eq. 5,

$$-\frac{dX}{dt} = kX^{\alpha} \quad (5)$$

where X is the amount of the reactant $[PtCl_2(olefin)]_2$ in the specimen, k is the rate constant and α is the reaction order with respect to the reactant. Now, the total amount of chemical species in this reaction system varies in progress of decomposition reaction and, therefore, we put

$$X=\frac{n}{N} \quad (6)$$

where n is the amount of the reactant and N is the total amount in molar unit in the reaction mixture at time t. Then,

$$\frac{-(E_a/R)\Delta(1/T)}{\Delta(\ln N-\ln n)} = \alpha + \frac{\Delta \ln(n\cdot dN/dt - N\cdot dn/dt) - 2\Delta \ln N}{\Delta(\ln N-\ln n)} \quad (7)$$

We could obtain the values of α and E_a from the plot $[\Delta\ln(n\cdot dN/dt - N\cdot dn/dt) - 2\Delta\ln N]/\Delta(\ln N-\ln n)$ against $\Delta(1/T)/\Delta(\ln N-\ln n)$ obtained by the thermogravimetric measurement. The results are shown in

Table 3. Activation energies, reaction orders and enthalpy changes of thermal decomposition of Zeise's dimers

Complexes	E_a (kcal mol^{-1})	α	ΔH[8] (kcal mol^{-1})
$[PtCl_2(C_2H_4)]_2$	36	3	15.5±0.5[a]
$[PtCl_2(C_3H_6)]_2$	30	−0.6	18.1±0.5*
$[PtCl_2(\Delta'\text{-}C_4H_8)]_2$	36	0	12.7±0.5[a]
$[PtCl_2(\Delta'\text{-}C_5H_{10})]_2$	42	2	7.4±1.0[b]
$[PtCl_2(\Delta'\text{-}C_6H_{12})]_2$	46	1	6.8±1.0[b]

a) Total enthalpy change in the two-step thermal decomposition. b) Enthalpy change in the second step of the thermal decomposition.

Table 3. These values would contain rather large errors and the reliability of α is estimated to be about ± 1, and that of activation energy to be about ± 2 kcal mol^{-1}. Except for the ethylene complex, the activation energy increases as the ligand olefin is larger.

There is no relation between the bond strength of π-bond and the activation energy. If the cleavage of π-bond is a rate determining step, the bond strength of π-bond would be closely related to the activation energy. The values of enthalpy change of Eq. 8 are different slightly among the complexes with various olefins.[8]

$$PtCl_4^{2-} + \text{olefin} \rightarrow [PtCl_3(\text{olefin})]^- + Cl^- \quad (8)$$

While, there is a fairly large difference between different olefin complexes in the activation energy of thermal decomposition. These results suggest that the bulkiness of ligand olefin would be an important factor in governing kinetics of thermal decomposition of Pt-olefin complexes.

References

1) M. Senō, K. Iwamoto, and T. Asahara, unpublished paper.
2) A. Giddings, W. MacNevin, and A. Foris, *Chem. Ind., London*, **1958**, 557.
3) "Inorganic Syntheses," ed. by T. Moeller, Vol. 5, MacGraw-Hill, New York (1957), p. 210.
4) J. A. Wunderlich and D. P. Mellor, *Acta Crystallogr.*, **7**, 130 (1954); **8**, 57 (1955).
5) M. Black, R. H. B. Maris, and P. G. Owston, *Acta Crystallogr.*, B**25**, 1753 (1969).
6) H. E. Kissinger, *Anal. Chem.*, **29**, 1702 (1957).
7) E. S. Freeman and B. Carroll, *J. Phys. Chem.*, **62**, 394 (1958).
8) M. Senō, K. Iwamoto, and T. Asahara, *Bull. Chem. Soc. Jpn.*, **47**, 2189 (1974).
9) G. Herzberg, "Infrared and Raman Spectra of Polyatomic Molecules," D. Van Nostrand Company, Inc., New York (1945).

Conductivity, Emf, and Spectrophotometric Study on the Participation of Na^+ and Cl^- into Acridine Orange-Poly(α,L-Glutamic Acid) Complex

Fumiyuki WATANABE

Department of Chemistry, Faculty of Science, Hokkaido University, Sapporo 060

(Received November 26, 1975)

Conductivity, emf and spectroscopic investigations were made for the dimerization process of Acridine Orange (AO) and for the complex formation of AO with poly(α,L-glutamic acid) (PLG) in water. The increase of the dimer species of AO by adding the neutral salt was quantitatively explained, taking the ionic strength into account. From the emf measurements, the inclusions of Cl^- into PLG–AO complex were concluded to be negligible, whereas Na^+ was included into this complex to a fairly appreciable extent. The association of Na^+ with carboxylate groups in the PLG–AO complex was described on the basis of the ordinary law of mass actions. The association constant K_1 was unaffected by the presence of AO even in the helical region of PLG. These results strongly support Schwarz's theory on cooperative binding.

Many authors have studied the interactions between Acridine Orange (AO) and a number of polyelectrolytes from various standpoints.[1-7] These investigations have shown that the addition of electrolytes affects the properties of the poly(α,L-glutamic acid) (PLG)–AO complex such as absorption spectra, circular dichroism, helix-coil transition, and so on.

To interpret the effects of Cl^- on the PLG–AO complex, two different assumptions were adopted. Sato *et al.* assumed that (i) Cl^- associates with AO dimer in the following manner:[5,8]

$$2AO^+ + Cl^- \rightleftharpoons (AO)_2Cl^+ \quad (1)$$

and then (ii) this $(AO)_2Cl^+$ is bound to the ionized carboxyl groups ($-COO^-$) of PLG. On the other hand, Schwarz *et al.* have assumed that AO dimer does not involve Cl^-.[3,4,9,10]

$$AO^+ + AO^+ \rightleftharpoons (AO)_2^{++} \quad (2)$$

Lamm and Neville, however, have found that it is impossible to distinguish the two mechanisms above by spectral means alone.[11]

To interpret the kinetic results for the reaction between AO and PLG, Schwarz offered the cooperative binding theory in which the binding of Na^+ to $-COO^-$ plays an important part in determining the rates.[2,3] He assumed that (i) AO^+ binds to $-COO^-$ cooperatively, while Na^+ binds to $-COO^-$ non-cooperatively and (ii) and Na^+ bind to $-COO^-$ competitively one another.

Now the following questions arise:

(a) What kind of a participation of Cl^- occurs when AO self-associates to dimer species?

(b) How many Cl^- and/or Na^+ ions are included into PLG–AO complex?

(c) Are Schwarz's assumptions above described correct?

No complete study, however, has been made on the equilibrium among many ionic species in the present system. In order to answer the questions above, the present paper reports the results obtained by conductivity, emf and spectrophotometric methods.

Experimental

Materials. Sodium salt of PLG (Na·PLG) purchased from Protein Research Foundation was used without further purification. The molecular weight of the sample (66000 in the acid form) was deduced from the intrinsic viscosity (1.42 dl/g) in 0.2 M NaCl at pH 7.3, using the calibration determined by Wada.[12] The concentration of the glutamyl residue was calculated using a value of 169 for the mean residue weight of monosodium glutamate monohydrate.

Acridine orange hydrochloride (AO·HCl), purchased from Wako Fine Chemical was recrystallized five times from water-methanol mixture. The apparent molar absorption coefficient at 492 nm was $5.0\times10^4\ M^{-1}\ cm^{-1}$ under the following condition; $[AO]=1.0\times10^{-5}$ M, pH=6.0 and 293 K. The elemental analysis showed that the AO·HCl purified in this way contained 3% NaCl as a contaminant. For the measurement of the activity of Cl^-, the total amount of Cl^- added was corrected by this excess Cl^-. The conductivity of AO-HCl solution was corrected in the following way:

$$k(\text{corrected}) = k(\text{observed}) - k(\text{excess NaCl})$$

where k(corrected) and k(observed) denote a corrected specific conductance and an observed specific conductance, respectively. k(excess NaCl) was the specific conductance of the solution containing the same amount of NaCl only as in the sample solution. For the spectroscopic measurements, this excess Cl^- was neglected, considering that an added NaCl was in large excess at least by a factor of 100.

Acridine orange zinc chloride $AO\cdot HZnCl_3$ (Merck) was three times recrystallized from ethanol. Other materials were reagent grade. Water was deionized and distilled once.

Instruments. The absorption spectra were obtained by a Hitachi EPS-3T recording spectrophotometer. The emf was measured with a Radiometer "PHM-4d." The electrochemical cells used for the measurements of Cl^- and Na^+ activities are

$$HgCl_2(s)/Hg \;|\; \text{satd KCl} \;\|\; \begin{matrix}AO\cdot HCl\\ \text{or}\\ AO\cdot HCl + Na\cdot PLG\end{matrix} \;\|\; Ag/AgCl \quad (3)$$

and

$$HgCl_2(s)/Hg \;|\; \text{satd KCl} \;\|\; \begin{matrix}Na\cdot PLG + AO\cdot HCl\\ \text{or}\\ Na\cdot PLG\end{matrix} \;|\; \begin{matrix}Na^+ \text{ selective}\\ \text{glass electrode}\end{matrix} \quad (4)$$

respectively. A Na^+ selective glass electrode No. 1512-05T was offered by the Horiba Co., Ltd. A silver-silver-chloride electrode was prepared by slowly depositing crystalline silver electrolytically onto a platinum wire sealed into a pyrex glass tube. The silver chloride was formed by electro-deposition in a 0.1 M aqueous solution of hydrochloride

with the silvered platinum as the anode.[14] Horiba No. 2010A was used as a saturated calomel electrode. The reproducibility of the emf measurements was within ±1 mV.

Conductivity was measured with a universal bridge BV-Z-3B (Yokogawa Electric Work Ltd.) at a frequency of 1 kHz, using an ordinary conductivity cell whose cell constant was 0.45. The pH values of the solutions were measured with a Horiba M-7 pH meter.

Preparations and Measurements. All the measurements were performed at 298±0.5 K. The pH values in the Na·PLG–AO·HCl solutions were adjusted at pH=4.53 (±0.03) and pH=7.51 (±0.03). 5 mM sodiu macetate-acetic acid buffer and 5 mM phosphate buffer were used for the measurements of Cl^- activity. For the measurements of Na^+ activity, 5 mM tetraethylammonium $(Et)_4N^+$ acetate-acetic acid buffer and 5 mM $(Et)_4N^+$-phosphate-phosphoric acid buffer were used. Considering that tetrapropylammonium ion is known to bind only slightly to polyanion,[15] the effect of $(Et)_4N^+$ on the association of Na^+ with $-COO^-$ was neglected. The activity of Na^+ was determined by comparing the measured emf values at each pH with those for NaCl solutions adjusted to pH=4.53 or pH=7.51 by the corresponding buffer.[13]

The specific conductivity of water used was $2\times10^{-6}\ \Omega^{-1}\ cm^{-1}$. The equivalent conductivity was obtained by the usual procedures[16] and was reproducible to about ±(5—10) $\Omega^{-1}\ mol^{-1}\ cm^2$ on repeated measurements.

The dimerization constant K_d of AO was obtained by the same procedure as Schwarz and Balthasar.[3]

Results and Discussion

I) The Role of Cl^- on the Dimerization Process of AO.

A) Conductance Measurements of AO–HCl: It is well known that the increase of the concentration of the aqueous AO causes the spectral change due to the increase of the aggregates containing more than two AO molecules.[5,11,17] In Fig. 1 the equivalent conductivity Λ is plotted against the square root of the concentration of the aqueous AO·HCl. Λ increases as [AOHCl] increases at first and then reaches the maximum value. If AO·HCl behaves as a univalent electrolyte, Λ would show a linear depence on [AO–HCl] as shown in Fig. 1 with a dashed line (A) in arbitrary unit. If the association between AO aggregates and Cl^- occurs, Λ of AO–HCl would fall down more rapidly than the case of (A). The increase of Λ at the concentration region from 2×10^{-4} M to 8×10^{-4} M, therefore, may be explained by the formation of the AO aggregates which scarcely contain Cl^- ions. An extrapolation of this curve to [AO·HCl]=0 gives a rough value to 85; Λ_0(AO·HCl)=85. Substracting the limiting equivalent conductance of Cl^-, $\Lambda_0(Cl^-)=76$,[16] from this value, we have the coarse limiting equivalent value of AO^+, $\Lambda_0(AO^+)=7$. Adopting this value, $\Lambda_0(AO^+)=7$, to the Stokes equation,[18] an apparent diameter of AO^+ is calculated to be $r=10$ Å.

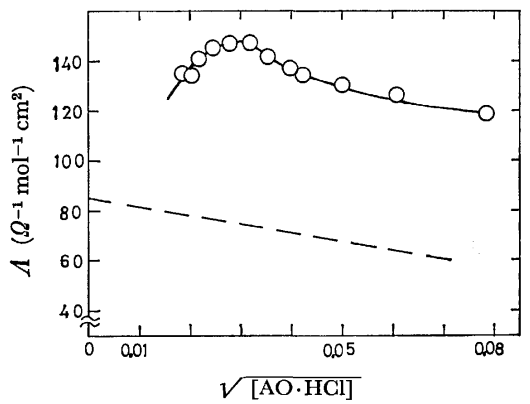

Fig. 1. The equivalent conductivity Λ of the aqueous AO·HCl plotted against square root of the concentration; ---- represents the equivalent conductivity in arbitrary unit, assuming that AO·HCl behaves as "strong electrolyte."

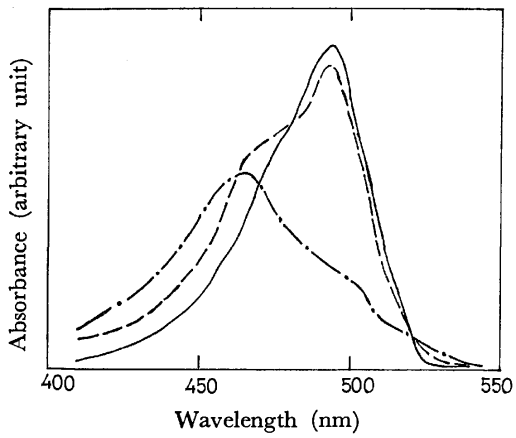

Fig. 2. Solvent dependence of AO-HCl spectrum: at 298 K.
—— in water/methanol 30/70 wt% mixture at [AO·HCl]=3×10^{-4} M. ---- in water at [AO·HCl]=1×10^{-5} M. —·— in water at [AO·HCl]=5×10^{-4} M. Coordinate is represented in arbitrary unit.

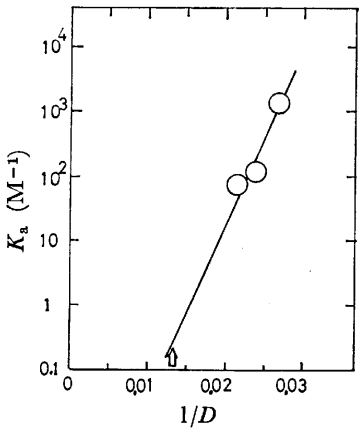

Fig. 3. The logarithm of the association constant K_a between AO^+ and Cl^- as a function of the reciprocal of the dielectric constant D. The notation ↑ indicates the point at $D=78.5$, which corresponds to that of water.

The conductivity measurements of AO–HCl were performed in water–methanol mixture at H_2O/CH_3OH =30/70, 20/80 and 10/90 (in wt.%). As shown in Fig. 2, the spectra of AO in these solvents clearly indicate that AO is present as monomer species.[17] Therefore the association constants, K_a, in the following equilibrium were obtained by the Shedlovsky's method.[19,20]

$$AO^+ + Cl \rightleftharpoons AOCl;\ K_a \qquad (5)$$

As shown in Fig. 3, the logarithm of K_a linearly decreases with the decrease of the reciprocal of the dielectric constant ($1/D$). From this linearity, it is reasonable to presume that even in water K_a should be dominated by a function of D in a way predicted by Bjerrum's theory.[16] Extrapolating the linear plot of log K_a *vs.* $1/D$ to the point $D=78.5$ which corresponds to the dielectric constant in water at 298 K, we obtained a rough value of K_a in water; $K_a=0.2\ M^{-1}$. It is concluded, therefore, that the association between AO^+ and Cl^- can be thoroughly neglected in the investigated AO–HCl concentration range.

B) Emf Measurements of Cl^- in the AO–$HZnCl_3$ System: In previous paper there have been reported the results of emf measurements of Cl^- activity in the aqueous AO–HCl solutions.[21] Figure 4 shows emf values plotted against the logarithm of the total amount of Cl^- added as AO·$HZnCl_3$, log[Cl]. The emf values for the AO–$HZnCl_3$ solution are in excellent agreement with those for the AO–HCl solution, that is, the emf values linearly decrease with log[Cl] at all concentrations from 1×10^{-5} to 5×10^{-3} M.

These results exclude the possibility that Cl^- might participate into the dimerization equilibrium of AO. This conclusion coincides with that in the results in section (*A*).

C) Effects of Ionic Strength on the AO Dimerization Equilibrium: The results in (*A*) and (*B*) exclude the possibility of the mechanism (1). Then the mechanism (2) should describe the dimerization process of AO correctly. The effect of the electrolyte on the dimerization equilibrium, therefore, would be interpreted in terms of the ionic strength.

Over the low concentration region, $(1-5)\times10^{-5}$ M, of AO at 298 K in water, there is an isosbestic point corresponding effectively to a monomer–dimer equilibrium.[11,22] The dimerization constant K_d is given by Eq. 6.

$$K_d = \frac{[(AO)_2{}^{2+}]}{[AO^+]^2} \qquad (6)$$

where $[AO^+]$ and $[(AO)_2{}^{2+}]$ denote the equilibrium concentrations of AO mono-cation and AO dimer, respectively. After Scatchard,[23] it is assumed that the activity coefficient, f_z, of a z-valent ion at an ionic strength I is given by the expression

$$-\log f_z = AZ^2\frac{\sqrt{I}}{1+1.5\sqrt{I}} \qquad (7)$$

where A is a constant. For aqueous solutions at 298 K, $A=0.5$. Assuming Eqs. 6 and 7, the Brønsted-Bjerrum equation becomes as follows:[24,25]

$$-\log K_d = \log K_t + 1.02\frac{\sqrt{I}}{1+1.5\sqrt{I}} \qquad (8)$$

where K_t is a tentative thermodynamic dimerization constant at $I=0$. In Fig. 5 the dimerization constant K_d was plotted against $\sqrt{I}/(1+1.5\sqrt{I})$. Ionic strength was varied from 7×10^{-3} to 0.2 M by NaCl, $NaNO_3$ and KCl. From the intercept of the straight line K_t was obtained to be $1\times10^4\ M^{-1}$. This value well coincides with Schwarz's value.[22] Thus the promotion

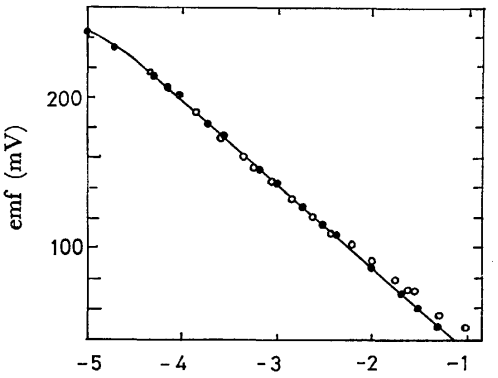

Fig. 4. Reversible emf values plotted against the logarithm of the total amount of Cl^- added as: ● NaCl (in water), ○ $AOHZnCl_3$ (in water) at 298 K.

of the dimerization of AO by an addition of electrolyte is explained quantitatively, considering the increase of the ionic strength.

II) Inclusion of Cl^- into PLG–AO Complex. From the results obtained in (*I*) and also the large negative charges of PLG, the inclusions of Cl^- into PLG–AO complex would be concluded to be improbable. This is confirmed by emf measurements as described below.

The emf measurements of Cl^- activity were performed in the following systems:

(a) Na·PLG + NaCl at pH = 4.53,

(b) Na·PLG + AO·HCl at pH = 4.53,

where the concentration of glutamyl residue was kept constant, varying the concentration of AO·HCl, and finally,

(c) Na·PLG + AO·HCl at pH = 4.53,

where the glutamyl residue to dye ratio (R/D) was kept constant at R/D=10. The results were exhibited in Fig. 6. The emf values for both the Na·PLG+AO·HCl systems (b) and (c) coincide with those for the Na·PLG+NaCl system. The results exactly show that there is no essential difference in the Cl^- activity among the systems (a), (b) and (c). An effect of PLG on the emf of Ag/AgCl electrode was discussed in ref. 21. It is reasonable to conclude that no signifi-

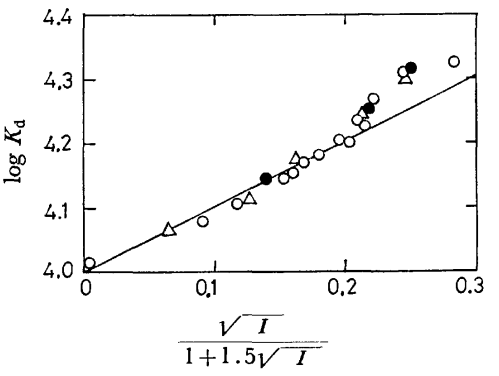

Fig. 5. The logarithm of the dimerization constant K_d of AO plotted as a function of the ionic strength I. ○ NaCl △ KCl ● $NaNO_3$.

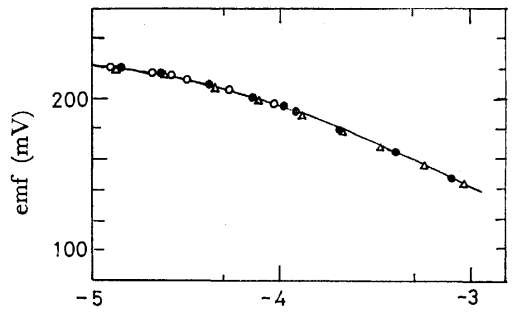

Fig. 6. Reversible emf of the cell (3) in the text as a function of the logarithm of the total chloride concentration added as AO-HCl or NaCl.
(a) ● Na·PLG+NaCl at pH=4.53, and at 298 K. (b) ○ Na·PLG+AO·HCl at pH=4.53; [Na·PLG] is constant at 4×10^{-3} M, and at 298 K. (c) △ Na·PLG+AO·HCl at pH=4.53; R/D=10 at 298 K in water.

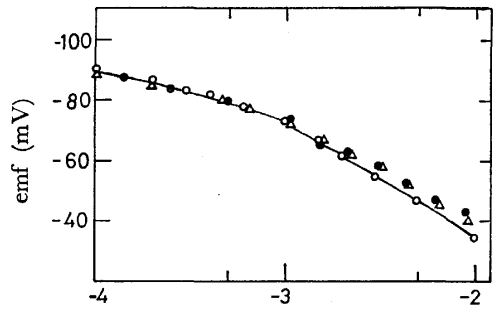

Fig. 7. Reversible emf of the cell (4) in the text as a fuuction of the logarithm of the total Na^+ concentration at pH=4.53 and 298 K in water.
(a) ○ NaCl+buffer, (b) ● Na·PLG+buffer, (c) △ Na·PLG+AO·HCl+buffer.

cant inclusion of Cl^- takes place into PLG–AO complex.

III) Effects of Na^+ on the PLG–AO Complex. As stated previously, Schwarz and Balthasar explained the interaction between AO and PLG in the random coil conformation in terms of the cooperative binding theory.[3] The assumptions made in this theory have been verified to be valid.[26] In order to interpret the interaction between AO and PLG in helical conformation, it would be worthwhile to examine the validity of the assumptions even in the helical region.

Figure 7 exhibits the emf values of the following systems at pH=4.53:

(a) NaCl in water,

(b) Na·PLG in water,

(c) Na·PLG + AO·HCl in water at R/D = 10.

At pH=4.53 PLG is present in the helix conformation with carboxyl groups partially ionized. The concentration of the ionized carboxyl groups, [-COO^-], was calculated from the degree of PLG ionization, α, defined by

TABLE 1. ASSOCIATION CONSTANT K_1 BETWEEN Na^+ AND -COO^- [28]

	In the random coil region (pH=7.51)	In the helix region (pH=4.53)
In the presence of AO	90±20 M^{-1} a)	48±20 M^{-1}
In the absence of AO	87±20 M^{-1} a)	50±20 M^{-1}

a) Cited from Ref. 26.

$$\alpha = \frac{[\text{-COO}^-]}{[\text{-COOH}]+[\text{-COO}^-]} \tag{9}$$

where [-COOH] denotes the concentration of the protonated carboxyl groups in PLG. The value of α was assumed to be α=0.35 at pH=4.53 according to Jacobson's data.[27] The association constant K_1 between Na^+ and -COO^- in the helical Na–PLG was obtained according to Eq. 10,

$$K_1 = \frac{[\text{-COONa}]}{[\text{-COO}^-][\text{Na}]} \tag{10}$$

where [Na] indicates the free Na^+ concentration obtained from the emf measurement. [-COO^-] and [-COONa] are free carboxylate ions and ion-paired carboxylate ions, respectively. They were calculated by Eq. 11,

$$\begin{aligned}[\text{-COO}^-] &= [\text{-COO}^-]_t - [\text{-COONa}] \\ [\text{-COONa}] &= [\text{Na}]_t - [\text{Na}]\end{aligned} \tag{11}$$

where $[\ ]_t$ indicates the total concentration of each ion. K_1 was obtained to be 50±25 M^{-1} in the range of $[Na]_t$ from 1×10^{-4} M to 1×10^{-3} M.[28] This value well agreed with Nitta and Sugai's data;[29] 20—30% of $[Na]_t$ are present as the ion-pair at [Na·PLG]=0.011 M. In the presence of AO, K_1 was calculated to be 48±20 M^{-1}, assuming that the three carboxyl groups are bound to the three nitrogen atoms in one AO molecule.[6,7]

The agreement between the two K_1 values reveals that the association between Na^+ and -COO^- can be described with the single association constant K_1 irrespective of the presence of AO. This conclusion has been found to hold also in the random coil region (at pH=7.51) as represented in Table 1.

These results show that the assumption in Schwarz's cooperative binding theory as stated in the introduction section is valid; namely Na^+ binds with -COO^- to a certain extent non-cooperatively even in the helical region. It has been also known that the reaction between AO and PLG in the helix conformation displays a non-exponential relaxation curve.[4]

Considering these findings, it is expected that this reaction may be described by the theory which is similar to Schwarz's cooperative binding theory and in which the association between Na^+ and -COO^- is taken into account.

The author would like to express hearty thanks to Horiba Co., Ltd. for kindly offering a Na^+ ion selective glass electrode. Thanks are also due to Professor Masatoshi Fujimoto for his encouragement and to Dr. Akihiko Yamagishi for his fruitful discussions.

References

1) V. Vitaglino and L. Costantino, *J. Phys. Chem.*, **74**, 1971 (1970).
2) G. Schwarz, *Eur. J. Biochem.*, **12**, 442 (1970).
3) G. Schwarz and W. Balthasar, *Eur. J. Biochem.*, **12**, 461 (1970).
4) G. C. Hammes and C. D. Hubbard, *J. Phys. Chem.*, **70**, 1615 (1966).
5) Y. Sato, M. Hatano, and M. Yoneyama, *Bull. Chem. Soc. Jpn.*, **46**, 1980 (1973).
6) R. E. Ballard, A. J. McCaffery, and S. F. Mason, *Biopolymers*, **4**, 97 (1966).
7) Y. Sato and M. Hatano, *Bull. Chem. Soc. Jpn.*, **46**, 3339 (1973).
8) G. R. Haugen and E. R. Hardwick, *J. Phys. Chem.*, **67**, 725 (1963).
9) D. J. Blears and S. S. Danyluk, *J. Am. Chem. Soc.*, **89**, 21 (1967).
10) R. E. Ballard and C. H. Park, *J. Chem. Soc., A*, **1970**, 1340.
11) M. E. Lamm and D. M. Neville. Jr., *J. Phys. Chem.*, **69**, 3872 (1965).
12) A. Wada, *J. Mol. Phys.*, **3**, 409 (1960).
13) J. C. T. Kwak, *J. Phys. Chem.*, **77**, 2790 (1973).
14) D. J. G. Ives and G. J. Janz, "Reference Electrodes," Academic Press, New York, N. Y. (1961).
15) H. P. Gregor and M. Frederick, *J. Polym, Sci.*, **23**, 451 (1957).
16) R. A. Robinson and R. H. Stokes, "Electrolyte Solutions," Butterworth Scientific Pub. London (1965).
17) V. Zanker, a) *Z. Phys. Chem.* **199**, 225 (1952), b) *ibid.*, **200**, 250 (1952).
18) E. A. Guggenheim and J. E. Prue, "Physicochemical Calculations," North-Holland Publishing Company.
19) T. Shedolovsky, *J. Franklin, Inst.*, **225**, 739 (1938).
20) T. Shedolovsky and R. L. Kay, *J. Phys. Chem.*, **60**, 151 (1956).
21) F. Watanabe, *J. Phys. Chem.*, **80**, 339 (1976).
22) B. H. Robinson, A. Löffier and G. Schwarz, *J. Chem. Soc. Faraday I*, **69**, 56 (1973).
23) G. Scatchard, *Chem. Rev.*, **19**, 309 (1936).
24) A. A. Frost and R. G. Pearson, "Kinetics and Mechanisms," John Wiley & Sons. Inc. (1961).
25) E. S. Amis, "Solvent Effects on Reaction Rates and Mechanisms," Academic Press, New York (1966).
26) F. Watanabe and A. Yamagishi, *Biopolymers*, in press.
27) A. L. Jacobson, *Biopolymers*, **2**, 237 (1964).
28) The association constant K_1 between Na^+ and $-COO^-$ varied considerably with the variation of α; for example, $K_1=78\pm35$ for $\alpha=0.30$, $K_1=50\pm20$ for $\alpha=0.35$, $K_1=36\pm15$ for $\alpha=0.40$ and $K_1=28\pm15$ for $\alpha=0.45$. At the present stage, therefore, we do not discuss whether K_1 in the helical region agrees with that in the random coil region or not.
29) K. Nitta and S. Sugai, *Ann. Rep. Res. Group Biophys. Jpn.*, **5**, 83 (1965).

Studies of the Effect of Ethanol and Sodium Chloride on the Micellization of Sodium Dodecyl Sulfate by Gel Filtration

Hitoshi SUZUKI

Department of Chemistry, Faculty of Science, Tokyo Metropolitan University, Setagaya, Tokyo 158

(Received November 26, 1975)

The effects of the addition of ethanol and sodium chloride to aqueous solutions of sodium dodecyl sulfate (SDS) were studied by the gel-filtration method. With an increase in the concentration of ethanol, the CMC decreased and then increased after passing a minimum, while the micellar weight increased and then decreased, showing a corresponding maximum. Above about 40 vol% ethanol, no micelle formation was observed. The micellar weight and aggregation number in the presence of ethanol were measured in the SDS concentration range of a constant elution rate of micelles. A decrease in the CMC and an increase in the micellar weight of SDS were observed with an increase in the concentration of NaCl from 0 to 10 mmol/l. The gel-filtration study enabled us to make a direct experimental confirmation of the effects of ethanol and NaCl on the micelle formation of SDS.

A number of studies have been made on the effects of additives on the CMC and micellar size of SDS.[1] However, relatively few have been reported concerning the effect of mixed solvents. According to Ward,[2] the CMC of aqueous SDS decreased with the addition of ethanol up to 10 vol% and then increased, while above 40 vol% no micellization occurred. Herrmann and Benjamin[3] and Becher[4] found a decrease in the micellar weight in water with an increase in the ethanol concentration for nonionic detergents. As for the effect of ethanol on the micellar size of SDS, only a few reports are available.[4]

Contrary to the effect of alcohol, the addition of NaCl to an aqueous SDS solution is known to decrease the CMC and to increase the micellar size.[1,5] In the present report, the effects of ethanol and NaCl on the micellar size and on the CMC of SDS in the aqueous solution have been studied by the gel-filtration method, which gives us direct experimental information.

Experimental

Materials. Sodium dodecyl sulfate prepared from 1-dodecanol and chlorosulfuric acid was purified by the extraction of the 1-dodecanol with diethyl ether and by subsequent recrystallization from ethanol.[6] Distilled water was degassed by boiling prior to use. Poly(vinyl alcohol)s (PVA), products of the Nippon Gosei Kogyo Co., Itd., and Blue Dextran 2000 obtained from pharmacia, Uppsala, Sweden, were used as the standard substances of the molecular weight. The purest grade ethanol was used after dehydration and distillation. The sodium chloride was purified by recrystallization from an aqueous solution by the addition of ethanol.

Apparatus and Procedure. The apparatus used for gel-filtration was essentially the same as that reported in the preceding papers.[6,7] The gels used were Sephadex G-50 and CPG-10 of Electro-Nucleonics, Inc. The gels were equilibrated with the mixed solvent of a known ethanol-water composition to be studied, and 30 ml of a SDS solution of the same ethanol-water composition was charged on top of the gel column. The elution was performed by using a mixed solvent of the same composition. An elution curve was obtained by recording the electrical conductance of the efluent as a function of the elution volume. The elution curve for a solution with a concentration larger than CMC

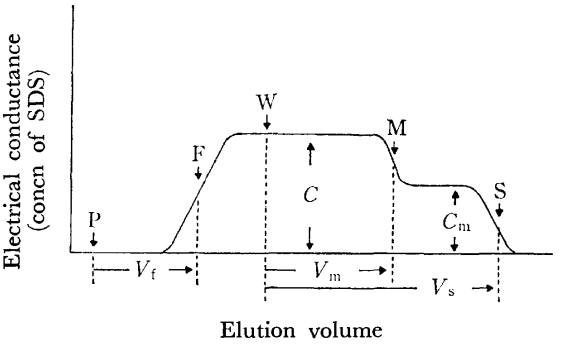

Fig. 1. Elution curve for SDS in ethanol-water solvent system.

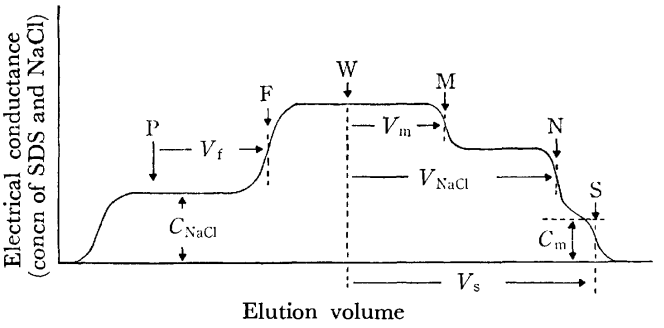

Fig. 2. Elution curve for SDS in aqueous sodium chloride solution, P, F, W, M, S, being the same as in Fig. 1. N; tail of NaCl.

is shown schematically in Fig. 1. In this figure, the ordinate is the conductance proportional to the concentration of SDS, while the abscissa is the volume eluted. P and W are the points of the sample and the water charges respectively, and F, M, and S, the front of the solution and the tails of micelles and single ions respectively. From this curve, the elution volumes of the SDS solution front, V_f; micelles, V_m, and single ions, V_s, were obtained; they are shown in Fig. 1. The lower plateau of Fig. 1 corresponds to the CMC of SDS (C_m), and the higher one, to the total concentration of SDS (C).

For the study of the effect of NaCl upon the CMC and the micellar size of SDS in aqueous solutions, Sephadex G-50 was used. The gel was equilibrated with an aqueous NaCl solution, and an aqueous solution of NaCl of the same

concentration, but containing SDS in addition, was charged on top of the gel column. The elution was performed by using an aqueous NaCl solution of the same concentration. The elution curve thus obtained is shown schematically in Fig. 2. The notations of P, W, M, S, and F are the same as in Fig. 1, while N is the tail of the NaCl solution. From the front and the three tails of the curve, the elution volumes of SDS front, V_f; the micelles, V_m; the single ions, V_s, and NaCl, V_{NaCl}, were obtained; they are shown in Fig. 2. The concentration of NaCl, C_{NaCl}, and the CMC of SDS, C_m, are estimated from the heights of the plateaus of the curve by using a conversion factor previously determined. The measurements were conducted at 30 °C throughout the experiments.

Results and Discussion

Effect of Ethanol and NaCl on CMC. The conductivity corresponding to the height of each plateau of the elution curve of SDS in the ethanol–water mixture shown in Fig. 1 is plotted against the total concentration of SDS in Fig. 3 for, for instance, the 10 vol% ethanol–water system. Three straight lines passing through a point which corresponds to the CMC of SDS in the mixture were obtained for both Sephadex and CPG-10 gel. The CMC's of the SDS obtained for ethanol–water mixtures are plotted as a function of the ethanol concentration at 30 °C in Fig. 4. Agreement is, as a whole, seen for both Sephadex and CPG gel. Since CPG-10 gel is more stable in a concentrated SDS solution than is Sephadex gel, plotting for a higher concentration has been possible for the former gel. Figure 4 shows that a small amount of ethanol in water lowers, while a larger amount raises, the CMC of SDS. The minimum at about 10 vol% of ethanol was in agreement with that reported by Ward.[2] The CMC above 20 vol% of ethanol was difficult to measure, since the step of the tail, M, corresponding to the micelles becomes obscure.

The elution volumes of front (V_f), micelles (V_m), and single ions (V_s) are plotted against ethanol concentrations up to 100 vol% at a constant SDS concentration (15 mmol/l) in Fig. 5. As may be seen, V_f increases above a 20 vol% ethanol concentration. From 30 up to 100 vol% ethanol, V_f becomes equal to V_s, the tail, M, disappears, and the elution curve observed is a simple one similar to that of the SDS solution below CMC. This means that in the solutions from 30 up to 100 vol% ethanol, the CMC is larger than 15 mmol/l. Presumably, at the SDS concentration a little above 30 mmol/l, as judged from the sharp rise of the curve of Fig. 4, CMC increases so rapidly that the micelle formation is practically prevented and the solute species is mainly of a single molecular type corresponding to V_s. A similar condition may prevail up to a 100% ethanol concentration, as may be seen from the coincidence of V_s and V_m in this region. Thus, the so-called micelles of the inverse type[8] could not be confirmed to form in an ethanol-rich solution or in a pure ethanol solution, at least experimentally by the gel filtration. The present results are rather in accord with those of Ward,[2] who reported a similar decrease in CMC upon the

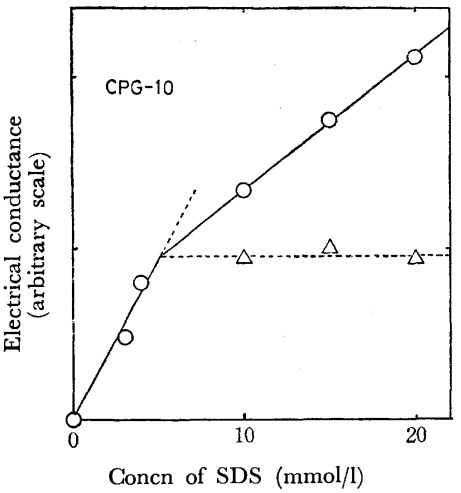

Fig. 3. Conductance of SDS solution obtained by gel-filtration using CPG-10 in the presence of 10 vol% ethanol. ○, conductance of the solution; △, conductance of tail part of solution.

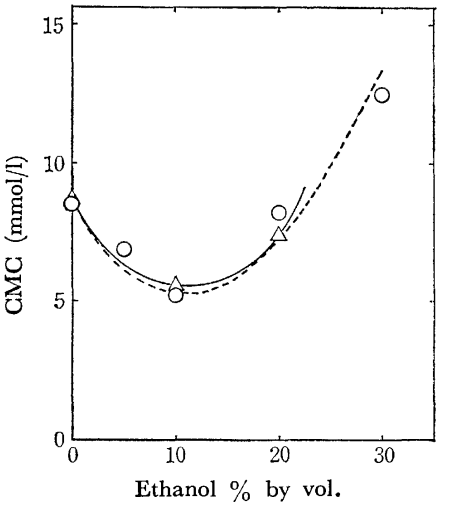

Fig. 4. Critical micelle concentration for SDS in aqueous ethanol. △, ——, Sephadex G-50 fine; ○, ----, CPG-10.

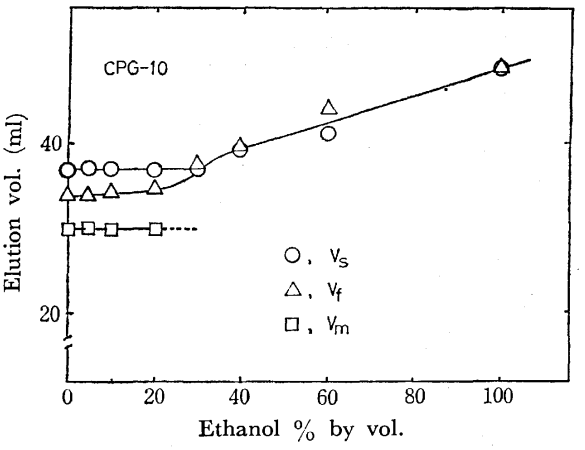

Fig. 5. Elution volume change in aqueous 15 mmol/l SDS solutions as a function of ethanol concentration.

Table 1.

NaCl	CMC
0 mmol/l	8.6 mmol/l
5 mmol/l	6.6 mmol/l
10 mmol/l	5.5 mmol/l
10 mmol/l	5.29 mmol/l[a)]

a) D. Sigter and K. J. Mysels, *J. Phys. Chem.*, **59**, 45 (1955).

ethanol addition and apparently no micellization in a mixed solvent with an ethanol concentration above 40 wt%.

As for the effect of ethanol addition upon CMC, a similar minimum in the concentration *vs.* partial molal volume of ethanol has been reported;[9)] this may suggest water-ethanol interaction affecting the micelle formation and CMC. However, it may be better explained by the fact that the solubilization of ethanol at low ethanol concentrations causes the decrease in the CMC, while the decrease in the amphipathy of the surfactant for a mixed solvent causes an increase in the CMC at high concentrations.

As for the effect of NaCl on CMC, the value of C_m in Fig. 2 is measured as a function of the NaCl concentration, which is shown in Table 1. As may be seen, C_m decreases with an increase in the concentration of NaCl and is in agreement with Stigter's data[13)] for the 10 mmol/l NaCl solution, which is also listed in the table. Further, the applicability of Eq. 8 derived in the previous paper:[6)]

$$\frac{R_m-R_s}{R_s}\cdot\frac{R_f}{R_m-R_f}=\frac{C}{C_m\cdot\alpha}-\frac{1-\alpha}{\alpha} \qquad (8)$$

was tested by plotting the left-hand side of Eq. 8 against the concentration of SDS (C). Here, R_f ($=V_s/V_f$), R_s($=V_s/V_s=1$), and R_m($=V_s/V_m$) ate the relative elution rates of the front, the single ions, and the micelles of SDS respectively; C, the total concentration of SDS; C_m, CMC, and α, the parameter of the rate of micelle decomposition.[6)] The results are shown in Fig. 6. As may be seen, the plots for 0, 5, and 10 mmol/l NaCl show straight lines passing through the point of origin, which confirms Eq. 8 to hold. The decomposition of micelles at the front is found to be instantaneous[6)] ($\alpha=1$) regardless of the NaCl concentration. The points of the intersections of these lines and the horizontal straight line of the ordinate, being unity, determine the C_m values, which are read for 0, 5, and 10 mmol/l NaCl solutions to be 8.6, 6.6, and 5.5 mmol/l respectively. These values are in agreement with the CMC estimated independently from the height of the plateaus of the elution curves, listed in Table 1. The effect of NaCl is also in accord with the general view of the effect of added salt on CMC.[1,10)]

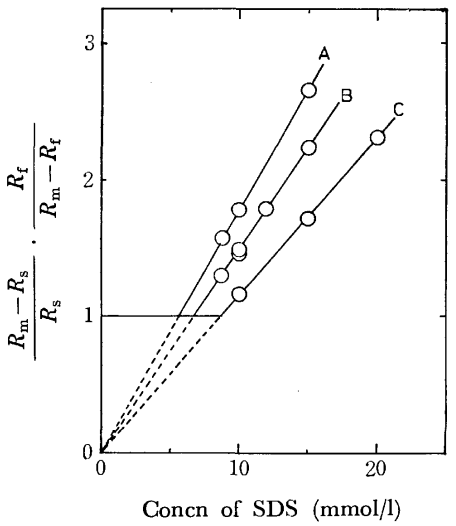

Fig. 6. Relationship between R_f and concentration of SDS in the presence of NaCl using CPG-10 gel. A, NaCl 10 mmol/l; B, NaCl 5 mmol/l; C, NaCl 0 mmol/l.

Effect of Ethanol and NaCl on Micellar Size. Since Sephadex gel suffers from a considerable shrinkage upon the addition of a concentrated ethanol solution, it is not suitable for micellar-size determination. Therefore, CPG-10 gel free from such an influence was mainly used in the gel-filtration, especially for the systems with high ethanol concentrations. Figure 7 shows the plots of R_m *vs.* the SDS concentration for each ethanol concentration. In the solutions with concentrations ranging from 0 to 20 vol% ethanol, it is seen that R_m, a measure of the micellar size, is constant independent of the SDS concentration from about 15 to 50 mmol/l SDS for each ethanol concentration, while the size decreases with an increase in the ethanol concentration. Up to 15 mmol/l SDS, R_m slightly increases with the increase of SDS for the system without ethanol.

The measurement of the micellar weight of SDS in an ethanol–water mixture is more complicated than that of SDS in an aqueous solution,[7)] although the basic principles are similar. For the micellar-weight determination of SDS in an aqueous solution, the calibration curve of the elution volume *vs.* the molecular weight of the unhydrated SDS micelle necessary for the calculation (SDS-W in Fig. 8) was obtained from the relation of the elution volume to the molecular

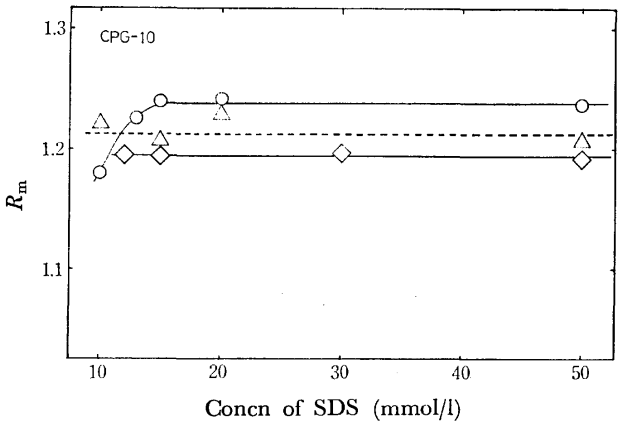

Fig. 7. R_m change of aqueous SDS solution as a function of ethanol concentration. ○, 0 vol% ethanol; △, 10 vol% ethanol; ◇, 20 vol% ethanol.

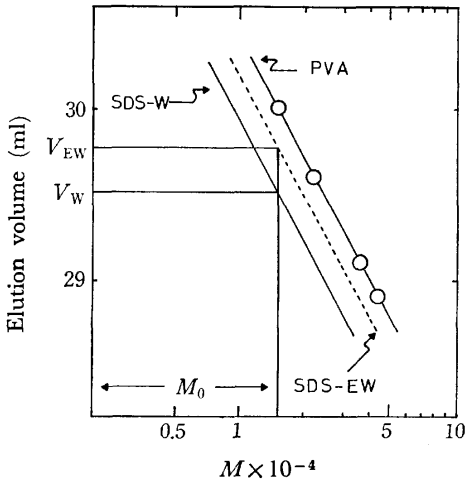

Fig. 8. CPG-10 system calibration curve showing the molecular weights of poly(vinyl alcohol)s relative to V_e as a linear log function.

weight of hydrated poly(vinyl alcohol) (PVA in Fig. 8). Thereby the difference between the amount of the hydration of poly(vinyl alcohol) and that of SDS was taken into account.[7]

To obtain a similar calibration curve for the micelles in an ethanol–water mixture, we measure the elution volume of the micelles both in water (V_W) and in the ethanol–water mixture (V_{EW}) and find the micellar weight (M_O) corresponding to V_W using the SDS-W relation shown in Fig. 8. Then the straight line passing through the point (M_O, V_{EW}) and parallel to the SDS-W line shown as the broken line (SDS-EW) in the figure may be drawn; it is used as the calibration curve for the determination of the micellar weight of SDS in an ethanol–water mixture. Actually, SDS micelles cannot be used for the measurement of V_W and V_{EW} since they undergo a change in size due to the change in solvent composition, while in the above calculation a micellar weight independent of the solvent composition is assumed.

To avoid this trouble, sodium poly(vinyl sulfate) of nearly the same elution volume as that of SDS micelles was used instead of SDS micelles, assuming that the chemical composition and the amount of hydration are like each other. From the measured elution volume of V_m in the ethanol–water mixture, we calculated the micellar weight and, the aggregation

Table 2.

Additives		Aggregation number of micelle		Amount of hydration of SDS (g/g)
		Standard M. W.	Laurent-Killander	
Ethanol	0 vol%	88	80	0.6
	10 vol%	102	—	0.1
	20 vol%	30	—	0.1
NaCl	5 mmol/l	93	91	0.6
	10 mmol/l	104	91	0.6

Concn of SDS, 15 mmol/l

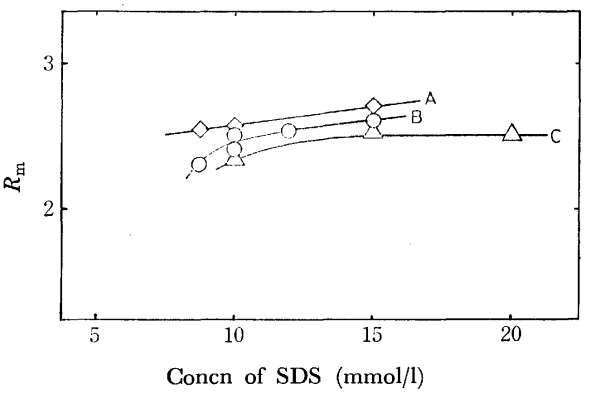

Fig. 9. Dependence of R_m on SDS concentration for different NaCl concentration. A, NaCl 10 mmol/l; B, NaCl 5 mmol/l; C, NaCl 0 mmol/l.

numbers of the SDS micelles. The results are listed in Table 2, together with the amount of hydration of SDS calculated. As may be seen, the aggregation number increases and then decreases with ethanol concentration after showing a maximum. The maximum corresponds to the minimum of CMC mentioned already. It may also be compared with the results of Becher[4] and Herrmann and Benjamin,[3] who showed a decrease in the micellar weight with an increase in the ethanol concentration for nonionic detergents. The amount of hydration is seen to decrease simply with an increase in the concentration of ethanol due to its dehydrating action.

The elution rate of micelles, R_m, in the presence of NaCl is further plotted against the total concentration of SDS (C) in Fig. 9. As may be seen, R_m increased with an increase in the concentration of NaCl.

For the determination of the micellar weight of SDS in an aqueous NaCl solution, a similar method was adopted, but replacing ethanol with NaCl. The elution volume *vs.* the molecular weight of unhydrated SDS micelles in an aqueous NaCl solution was obtained as in the case of Fig. 8. The results thus obtained are listed in Table 2.

The micellar radii of SDS were also calculated according to the Laurent-Killander equation, much as in an earlier report,[7] for both ethanol-water and aqueous NaCl systems; from the results, the aggregation numbers were calculated by taking account of the amount of hydration for the micelles of each system. The results are listed in Table 2. The aggregation numbers of micelles in the aqueous NaCl solution are, on the whole, in agreement with those given in the literature.[13,14] The micellar size was found to increase with an increase in the salt concentration, in agreement with the view that the reduction in the electrical repulsions of the head group of SDS facilitates micellization.[15] The difference in the aggregation numbers of an SDS micelle in water as estimated by the standard molecular weight method and by the Laurent-Killander equation may come from the difference in the methods of estimation, as has been seen in the literature.[13,14]

The author wishes to express his deep gratitude to

Professor Tsunetaka Sasaki of our University for his kind direction and valuable criticism throughout the work.

References

1) K. Shinoda, T. Nakagawa, B. Tamamushi, and T. Isemura, "Colloidal Surfactants," Academic Press, New York (1973).
2) A. F. H. Ward, *Proc. Roy. Soc., A*, **176**, 421 (1940).
3) K. W. Herrmann and L. Benjamin, *J. Colloid Interface Sci.* **23**, 478 (1967).
4) P. Becher, *J. Colloid Sci.*, **20**, 728 (1965).
5) M. I. Corrin and W. D. Harkins, *J. Phys. Colloid Chem.*, **69**, 683 (1947).
6) H. Suzuki and T. Sasaki, *Bull. Chem. Soc. Jpn.*, **44**, 2630 (1971).
7) H. Suzuki, *Bull. Chem. Soc. Jpn.*, **49**, 375 (1976).
8) H. Uehara and R. Matuura, Presented at the 20th Discussion Meeting of Colloid and Interface Science of Japan, Sapporo, Japan (1967).
9) F. Franks, "Physico-chemical Processes in Mixed Aqueous Solvents," Heineman (1967).
10) M. E. Hobbs, *J. Phys. Colloid Chem.*, **55**, 675 (1951).
11) T. C. Laurent and J. Killander, *J. Chromatogr.*, **14**, 319 (1964).
12) K. Shigehara, *Bull. Chem. Soc. Jpn.*, **39**, 2643 (1966).
13) D. Stigter and K. J. Mysels, *J. Phys. Chem.*, **59**, 45 (1955).
14) H. V. Tartar, *J. Colloid Sci.*, **14**, 115 (1959).
15) M. J. Vold and R. D. Vold, "Colloid Chemistry," Reinhold Publishing Corporation (1964).

Transition Dipole Interaction and Intermolecular Potential of Carbon Disulfide and Sulfur Dioxide Crystals

Yoshihiro KURODA and Katsunosuke MACHIDA

Faculty of Pharmaceutical Sciences, Kyoto University, Sakyo-ku, Kyoto 606

(Received December 11, 1975)

The optical active normal frequencies and the heats of sublimation of carbon disulfide and sulfur dioxide crystals have been calculated. The interaction between the transition dipoles associated with the infrared active intermolecular modes has been taken into account by introducing coupling terms between the equivalent coordinates of neighboring molecules. The coupling force constants estimated from the infrared absorption intensities explain the observed trend of the factor group splittings of the ν_3 mode of carbon disulfide and the ν_1 and ν_3 modes of sulfur dioxide. The splitting of the ν_2 mode of carbon disulfide has been reproduced by taking account of the long range Coulomb interaction between the atomic charges.

Appreciable factor group splittings in infrared and Raman spectra of crystals often arise from the interaction between the transition dipoles associated with the vibrations of neighboring molecules or ions.[1,2] The most straightforward way of incorporating this interaction in the potential function of crystal lattices is to introduce appropriate coupling constants between the equivalent coordinates of adjacent molecules in a unit cell. As shown by Decius,[3] such a coupling constant can be evaluated from the derivative of the molecular dipole moment with respect to the internal or the normal coordinate concerned.

For the crystals of alkaline earth carbonates, the dipole moment derivatives estimated from the factor group splittings agree with those obtained from the infrared reflection spectra.[4] On the other hand, the intermolecular coupling constants for the crystals of hydrogen chloride[5] and methyl chloride[6] have not fully been explained by the dipole moment derivatives obtained from infrared band intensities. Further studies are thus required to establish the theoretical basis of the coupling constants introduced empirically.

In this work, we have aimed at evaluating the intermolecular potential functions of carbon disulfide and sulfur dioxide crystals, and at clarifying how far the effect of the coupling terms are manifested in the observed vibrational spectra. In order to check the validity of the adopted potential parameters, the values of the potential functions for the equilibrium structure have also been calculated and compared with the heat of sublimation.

Method of Calculation

The frequencies of the optical active inter- and intramolecular normal modes were calculated according to the method of Harada and Shimanouchi.[7] The quadratic intramolecular force constants are those of the general valence type fitted to the observed fundamental frequencies in the gaseous state.[8] They are given in Table 1. The atomic coordinates were taken from the X-ray studies by Baenziger and Duax for carbon disulfide[9] and by Post *et al.* for sulfur dioxide.[10]

In order to distinguish the role of various types of intermolecular interactions, calculations were made for three kinds of intermolecular potentials. In calculation I, we took into account only the short range interactions due to the exchange repulsion and the van der Waals attraction, using the potential in the exp-6 form

$$V_{\mathrm{I}} = \sum_{i,j} [-Ar_{ij}^{-6} + B \exp(-Cr_{ij})], \tag{1}$$

where r_{ij} is the distance between the atoms i and j. Table 2 shows the values of the parameters A, B and C for the C···C, S···S and O···O interactions adopted in the present work.[11,12] The parameters for the asymmetrical C···S and S···O interactions were estimated from those for the two corresponding symmetrical interactions by taking the geometric means for A and B and the arithmetic means for C.[13] The summation limit for this short-range interaction was taken to be 6 Å.

Calculation II was carried out for the potential including the coupling terms due to the transition dipole interaction in the form

$$V_{\mathrm{II}} = V_{\mathrm{I}} + \sum_{a,b} \sum_{i} K_i^{ab} S_i^a S_i^b, \tag{2}$$

where S_i^a and S_i^b denote the i-th internal symmetry coordinate of the molecules a and b, respectively, and K_i^{ab} is the coupling force constant related to these coordinates. The summation limit was taken to cover only the nearest-neighbor interaction. The coupling constant was calculated, according to Decius,[3] by

$$K_i^{ab} = |\partial\mu/\partial S_i|^2[(\boldsymbol{e}_a \times \boldsymbol{R})\cdot(\boldsymbol{e}_b \times \boldsymbol{R}) - 2(\boldsymbol{e}_a \cdot \boldsymbol{R})(\boldsymbol{e}_b \cdot \boldsymbol{R})]/|\boldsymbol{R}|^5, \tag{3}$$

where $\boldsymbol{e}_a$ and $\boldsymbol{e}_b$ are the unit vectors along the transition dipoles formed in the molecules a and b, respectively, and $\boldsymbol{R}$ is the vector joining these dipoles. The transition dipoles were assumed to be at the central atoms (C for carbon disulfide and S for sulfur dioxide) for all the infrared active modes. The dipole moment derivatives for the normal coordinates, $\partial\mu/\partial Q_i$, were taken from the works on the infrared absorption intensities,[14,15] and were transformed into those for the internal symmetry coordinates, $\partial\mu/\partial S_j$, by assuming a simplified relation

$$\partial\mu/\partial S_j = (\partial\mu/\partial Q_i)/L_{ji}, \tag{4}$$

where L_{ji} is the $\boldsymbol{L}$ matrix element connecting Q_i with S_j. The relation is exact for the ν_2 and ν_3 modes of carbon disulfide and the ν_3 mode of sulfur dioxide, but not for the ν_1 and ν_2 modes of sulfur dioxide. The exact transformation in terms of the $\boldsymbol{L}^{-1}$ matrix elements[16] cannot be applied to these two modes since

TABLE 1. INTRAMOLECULAR FORCE CONSTANTS (in mdyn·Å^{-1})[a]

	CS_2	SO_2
k_1	7.5	9.97
k_{12}	0.6	0.0
k_δ/l^2	0.234	0.81

a) Notations in Ref. 8 are used.

TABLE 2. PARAMETERS FOR THE NON-BONDED ATOM-ATOM INTERACTION

Atomic pair	Å (kcal·Å/mol)	$B\times10^{-3}$ (kcal/mol)	C (Å^{-1})	Ref.
C···C	535	74.46	3.60	11
S···S	1430	220.8	3.62	12
O···O[a]	200	186.4	4.55	12

a) In calculation III′ for SO_2, the values of A and B were multiplied by 4.

the relative signs of $\partial\mu/\partial Q_1$ and $\partial\mu/\partial Q_2$ are not known. The symmetric stretching and the angle deformation modes of sulfur dioxide do not appreciably couple with each other, and the errors due to the approximation (4) are not serious for a crude estimation of splittings. The numerical values of the coupling constants and the related quantities are summarized in Table 3.

In calculation III, we adopted the potential including the terms due to the Coulomb interaction between the atomic charges as given by

$$V_{III} = V_{II} + \sum_{i,j} e_i e_j / r_{ij}, \qquad (5)$$

where e_i and e_j denote the charges carried by the atoms i and j, respectively. The atomic charges for carbon disulfide and sulfur dioxide were so estimated as to reproduce the observed values of the electric quadrapole moment[17] and the dipole moment,[18] respectively; $e_C=-2e_S=0.58$ for the former and $e_S=-2e_O=0.46$ for the latter in the electronic charge unit.

The summation limit for the Coulomb terms in Eq. 5 was determined in two steps. When the atomic pairs to be included in the sum are selected directly by comparing the individual interatomic distances with a given threshold, the net charge under the summation sign does not generally vanish and a smooth convergence of the sum is not expected. Accordingly, we selected first appropriate molecular pairs by referring to the distances between the central atoms, and then picked up all the intermolecular atomic pairs involved in each of these molecular pairs. For the critical distance to be used for the selection of the molecular pairs, several values between 20 and 50 Å were tested, and the distance of 40 Å was found to be large enough to secure a convergent sum.

In order to confirm the consistency between the adopted model potential and the observed heats of sublimation, the values of the potential functions V_I and V_{III} were calculated for the equilibrium structure. They were then corrected for the crystal zero-point energies by using the average Debye temperature.[19] The value of V_{II} is the same as that of V_I at the equilibrium where the transition dipole terms do not contribute to the energies. The numerical calculation was carried out on a FACOM 230-75 computer at the Data Processing Center, Kyoto University.

Results and Discussion

Carbon Disulfide. According to X-ray analysis, the crystal of carbon disulfide belongs to the space group $D_{2h}{}^{18}$-C_{mca}, two molecules being contained in the Bravais unit cell.[9] The calculated and the observed values of the vibrational frequencies and the heat of sublimation are given in Table 4. Based on the

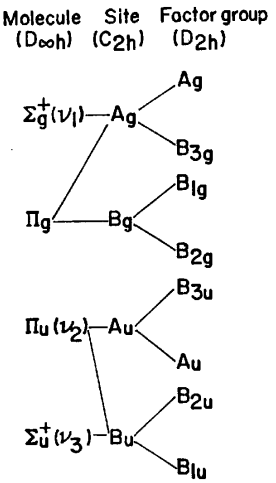

Fig. 1. Correlation diagram for vibrations of CS_2 crystal.

TABLE 3. DIPOLE MOMENT DERIVATIVES, L MATRIX ELEMENTS AND INTERMOLECULAR COUPLING CONSTANTS

	Mode(ν_i)	Internal symmetry coordinate (S_j)[a]	$\lvert\partial\mu/\partial Q_i\rvert$[b]	$\lvert L_{ji}\rvert$[c]	$\lvert\partial\mu/\partial S_j\rvert$[d]	K_j^{ab}[e]
CS_2	ν_2	$S_3=\Delta\phi$(in bc-plane)	20.12	0.4040	0.6418	0.0002[f]
	ν_3	$S_2=(\Delta r_1-\Delta r_2)/\sqrt{2}$	287.2	0.4446	8.3221	0.0318
SO_2	ν_1	$S_1=(\Delta r_1+\Delta r_2)/\sqrt{2}$	60.5	0.2794	2.7899	−0.0050
	ν_2	$S_2=\Delta\phi$	63.6	0.3037	2.6982	−0.0047
	ν_3	$S_3=(\Delta r_1-\Delta r_2)/\sqrt{2}$	165.9	0.3299	6.4791	0.0393

a) Δr_1 and Δr_2 are the two stretching coordinates and $\Delta\phi$ is the angle deformation coordinate. b) In esu·g$^{-1/2}$. c) In amu$^{-1/2}$ for ν_1 and ν_3, and in amu$^{-1/2}$·Å^{-1}·rad for ν_2 d) In debye·Å^{-1} for ν_1 and ν_3, and in debye·rad^{-1} for ν_2. e) In mdyn·Å^{-1} for ν_1 and ν_3, and in mdyn·Å·rad^{-2} for ν_2. f) For $S=\Delta\phi$(out of bc-plane), K_4^{ab} was calculated to be 0.0003 mdyn·Å·rad^{-2}.

TABLE 4. VIBRATIONAL FREQUENCIES (in cm^{-1}) AND HEAT OF SUBLIMATION (in kcal/mol) OF CARBON DISULFIDE CRYSTAL

		Obsd	Calcd		
			I	II	III
Internal modes					
ν_1	A_g	654[a]	656.3	656.6	655.8
	B_{2g}		656.4	656.4	656.6
ν_2	A_u		402.4	402.1	391.0
	B_{1u}	388.7[b]	400.8	400.5	394.8
	B_{2u}	400.1[b]	400.1	400.4	406.5
	B_{3u}	393.4[b]	402.2	402.6	399.9
ν_3	B_{1u}	1495[a]	1521.7	1507.6	1507.8
	B_{2u}	1528[a]	1521.5	1535.5	1538.8
External modes					
	A_g	73[a]	53	53	55
	B_{1g}		43	44	38
	B_{2g}		53	50	48
	B_{3g}	83[a]	54	53	62
	A_u		24	21	27
	B_{1u}	66[c]	56	56	59
	B_{2u}	66[c]	56	55	50
Heat of sublimation		9.02[d]	4.64	4.64	5.98

a) Ref. 20. b) Ref. 15. c) Ref. 21. d) Ref. 19.

correlation diagram (Fig. 1), the factor group splitting is expected for all the fundamentals, ν_1, ν_2 and ν_3. For the originally degenerate mode ν_2, the site group splitting is also expected. In the observed spectra,[15,20] ν_1 shows no splitting, while ν_2 and ν_3 split into as many components as expected theoretically. No empirical assignment of each component to proper symmetry species has been made because of the difficulty in measuring the low-temperature spectra of oriented crystals. The splittings could not be reproduced by calculation I which includes only the short range non-bonded atom-atom interaction terms (Table 4). Calculation I failed also in predicting the rotatory lattice frequencies[20] and the heat of sublimation,[19] but gave a fairly reasonable result for the translatory lattice modes.[21]

In calculation II, the intermolecular coupling constants K_2^{ab}, K_3^{ab} and K_4^{ab} were introduced between each molecule and its nearest neighbors lying on a common layer parallel to the bc plane. Since the ν_3 band in the infrared spectrum is very strong, splitting in the range 30—50 cm^{-1} observed for this band has been attributed to the interaction between the transition dipoles associated with the ν_3 mode.[15,20] In agreement with this interpretation, calculation II reproduced the observed splitting of the ν_3 mode satisfactorily. On the other hand, the ν_2 band in the infrared spectrum is very weak and the interaction between the transition dipoles is hardly expected to cause the observed splitting of the ν_2 mode.[15] Actually, the coupling constants K_3^{ab} and K_4^{ab} estimated from the infrared band intensity was found to give only one-tenth as large a splitting as the observed. For the lattice frequencies, calculations I and II gave almost

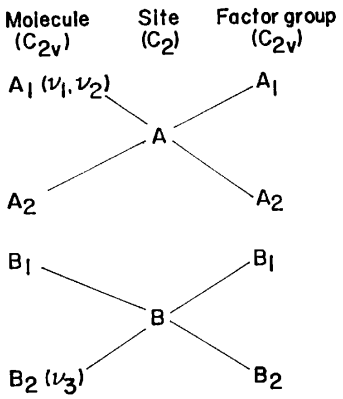

Fig. 2. Correlation diagram for vibrations of SO_2 crystal.

the same results, since the dipole-dipole coupling terms affect only the intramolecular modes in which the internal coordinates appearing in those terms vibrate appreciably.

As shown in Table 4, all the observed factor group and site group splittings were reproduced very well by calculation III. The long range Coulomb interaction exerts little effect on ν_3, for which the splitting has been explained to be due to the transition dipole interaction, but gives rise to the splitting of ν_2 into three components appearing at intervals of about 5 cm^{-1} just as in the observed spectrum. Addition of the Coulomb terms to the intermolecular potential does not much affect the lattice frequencies, but improves the heat of sublimation appreciably.

Sulfur Dioxide. A number of split bands have been observed in the infrared and Raman spectra of sulfur dioxide crystal, and have been interpreted in terms of the factor group splittings, the summation bands and the bands of the isotopic species $^{34}SO_2$.[22-24] According to the correlation diagram (Fig. 2), the factor group splitting of ν_3 is expected in both the infrared and Raman spectra while that of ν_1 and ν_2 only in the Raman spectrum. The calculated and the observed values of the vibrational frequencies and the heat of sublimation are listed in Table 5.

As in the case of carbon disulfide, none of ν_1, ν_2 and ν_3 is calculated to split appreciably when only the short range forces are taken into account (calculation I), whereas the observed splittings are 4 cm^{-1} for ν_1 and 18 cm^{-1} for ν_2.[24] The splitting of ν_3 is estimated to be between 10 and 30 cm^{-1} from the Raman spectrum at 77 K in which three peaks assignable to ν_3 appear in the region around 1300 cm^{-1}.[24] If the splittings of ν_1 and ν_2 are assumed to arise from the interaction between the transition dipoles, the high- and low-frequency components for each mode are attributed to the A_2 and the A_1 species, respectively, by using Eq. 3 with properly chosen vectors $\boldsymbol{e}_a$, $\boldsymbol{e}_b$ and $\boldsymbol{R}$. The result agrees with the assignment by Anderson and Savoie[24] based on a comparison of the infrared and Raman frequencies.

In calculation II, three coupling constants K_1^{ab}, K_2^{ab} and K_3^{ab} were introduced, each molecule being assumed to interact with the neighboring four molecules lying on a common layer parallel to the ac plane.

TABLE 5. VIBRATIONAL FREQUENCIES (in cm^{-1}) AND HEAT OF SUBLIMATION (in kcal/mol) OF SULFUR DIOXIDE CRYSTAL

		Obsd	Calcd			
			I	II	III	III′
Internal modes						
ν_1	A_1	1144[a]	1169.0	1167.7	1167.3	1169.6
	A_2	1148[a]	1169.7	1171.0	1170.6	1174.4
ν_2	A_1	524[a]	522.0	519.1	517.9	524.0
	A_2	542[a]	520.7	523.5	522.8	529.3
ν_3	B_1	1312[a]	1358.8	1348.1	1348.0	1350.2
	B_2	1324[a]	1358.2	1368.8	1369.6	1371.0
External modes						
	A_1	74[a]	42	42	34	60
	A_2		64	74	73	112
		67[a]	37	37	49	72
	B_1	160[b]	106	106	99	148
		101[b]	56	56	58	97
		67[b]	22	22	43	59
	B_2	141[b]	100	100	99	144
		101[b]	60	60	69	107
		67[b]	45	45	40	59
Heat of sublimation						
		8.91[c]	3.44	3.44	4.39	8.98

a) Ref. 24. b) Ref. 25. c) Ref. 19.

As shown in Table 5, the calculated splittings for ν_1 and ν_3 agree well with the observed ones, but not so for ν_2. In contrast to the case of carbon disulfide, addition of the Coulomb terms to the intermolecular potential of sulfur dioxide was found to give little effect on the magnitude of the factor group splittings, the discrepancy for ν_2 being left unreduced in calculation III. In order to obtain a satisfactory fit between the calculated and the observed splittings, it seems necessary to use more elaborate model potentials, for example by introducing polarizable charges.

The lattice frequencies and the heat of sublimation obtained in calculations I through III are far less than the observed values.[19,24,25] After several trials, the difficulty was overcome, without appreciable changes in the factor group splittings, by using about four times as large values of the parameters A and B for the O···O contact as those in calculations I, III and II (calculation III′, Table 5). Probably, the enhanced potential parameters do not faithfully represent the true feature of the non-bonded O···O interaction, but involve implicitly effects of some unknown interactions not considered herewith in this work.

References

1) D. A. Dows, in "Physics and Chemistry of the Organic Solid State," ed by D. Fox, M. M. Labes and A. Weissberger, Interscience, New York (1963).
2) A. S. Davydov, "Theory of Molecular Excitions," English Translation by M. Kasha and M. Oppenheimer, Jr., McGraw-Hill, New York (1962).
3) J. C. Decius, *J. Chem. Phys.*, **23**, 1290 (1955).
4) C. Hass and D. F. Hornig, *J. Chem. Phys.*, **26**, 707 (1957).
5) D. F. Hornig and G. L. Hiebert, *J. Chem. Phys.*, **27**, 752 (1957).
6) D. A. Dows, *J. Chem. Phys.*, **32**, 1342 (1960).
7) I. Harada and T. Shimanouchi, *J. Chem. Phys.*, **41**, 2651 (1964).
8) G. Herzberg, "Infrared and Raman spectra of Polyatomic Molecules," Van Nostrand, Princeton (1945).
9) N. C. Baenziger and W. L. Duax, *J. Chem. Phys.*, **48**, 2974 (1968).
10) B. Post, R. S. Schwartz, and I. Fankuchen, *Acta Crystallogr.*, **5**, 372 (1952).
11) D. E. Williams, *J. Chem. Phys.*, **45**, 3770 (1966).
12) E. Giglio, L. Mazzarella, and A. M. Liquori, *Lett. Nuovo Cimento Sic. Ital. Fis.*, **1**, 135 (1969).
13) E. A. Mason and W. E. Rice, *J. Chem. Phys.*, **22**, 522 (1954).
14) G. D. T. Tejwani, K. Fox, and R. J. Corice, Jr., *Chem. Phys. Lett.*, **18**, 365 (1973).
15) H. Yamada and W. B. Person, *J. Chem. Phys.*, **40**, 309 (1964).
16) E. B. Wilson, Jr., J. C. Decius, and P. C. Cross, "Molecular Vibrations," McGraw-Hill, New York (1955).
17) H. P. Huang and T. H. Spurling, *Aust. J. Chem.*, **23**, 377 (1970).
18) R. D. Nelson, Jr., D. R. Lide, Jr., and A. A. Maryott, in "Handbook of Chemistry and Physics," 50th ed., ed by R. C. Weast, The Chemical Rubber Co., Cleveland (1969—70), p. E-72.
19) W. Auer and K. Schäfer, in "Landolt-Börnstein Zahlenwerte und Funktionen," 6th ed., Vol. 2, Part 4, ed by K. Schäfer and E. Lax, Springer, Berlin (1961).
20) M. Ito, *J. Chem. Phys.*, **42**, 815 (1965).
21) G. W. Chantry, H. A. Gebbie, B. Lassier, and G. Wyllie, *Nature*, **214**, 163 (1967).
22) R. N. Wiener and E. R. Nixon, *J. Chem. Phys.*, **25**, 175 (1956).
23) P. A. Giguere and M. Falk, *Can. J. Chem.*, **34**, 1833 (1956).
24) A. Anderson and R. Savoie, *Can. J. Chem.*, **43**, 2271 (1965).
25) A. Anderson and S. H. Walmsley, *Mol. Phys.*, **10**, 391 (1965—66).

Coulomb Interactions and Optically-active Vibrations of Calcite-type Carbonates[1)]

Akio YAMAMOTO

Department of Chemistry, Faculty of Science, Hiroshima University, Higashisenda-machi, Hiroshima 730

(Received December 22, 1975)

Polarizable-ion model calculations are made for optically-active vibrations of five carbonates with calcite structures: calcite, magnesite, dolomite, rhodochrosite, and smithsonite. The fit to the experimental TO-LO splittings of the internal modes is found to be greatly improved by the introduction of ionic polarizabilities. It is also ascertained that the electronic polarizabilities of constituent atoms must be regarded as anisotropic in order to interpret the optical anisotropy. The resulting force constants for non-bonded oxygen-oxygen interactions can give the correct orders of magnitude for the Lennard-Jones potential constants.

This paper is complementary to a preceding paper,[2)] denoted as Paper I hereafter, on the lattice dynamics of sodium nitrate. There we described a method of polarizable-ion (PI) model calculations[3)] for partially ionic crystals, together with an illustrative example. The object of the present paper is to report the results of a systematic application of the PI model to several important carbonates with a calcite structure, *viz.*, $CaCO_3$, $MgCO_3$, $CaMg(CO_3)_2$, $MnCO_3$, and $ZnCO_3$, and also to test the adequacy of the force field in Paper I.

The structure and symmetry properties of calcite-type crystals have been described on several occasions,[4)] the structure being rhombohedral with 10 atoms in the primitive cell. As is shown in Fig. 1, the space groups of dolomite and the others[5,6)] are $R\bar{3}$ and $R\bar{3}c$ respectively. Our lattice dynamical interest in carbonate crystals is a result especially of the fact that their chemical bonds are fairly intermediate between those of ionic and covalent crystals: both the splittings of the transverse optic (TO) and longitudinal optic (LO) branches and the internal vibrations of quite high frequencies bear little resemblance to typical ionic and/or covalent crystals.

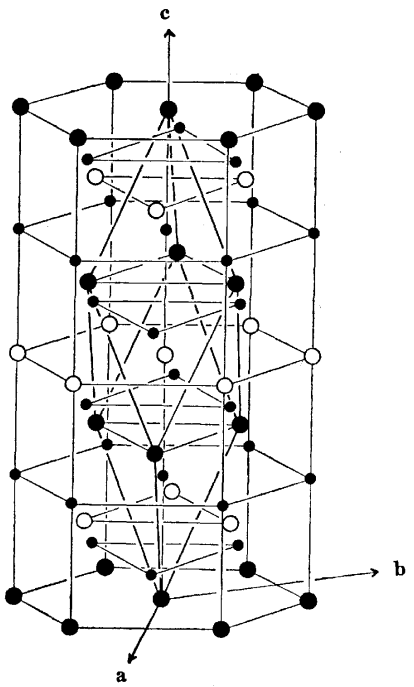

Fig. 1. Crystal structure of calcite-type carbonates. ○, ●: Metal, •: Carbonate.

In the vibration treatments, the estimation of the non-Coulomb contribution of carbonate groups to the potential energy is feassible by the use of a modified Urey-Bradley force field. On the other hand, the contribution due to the partially ionic nature of the bindings is characterized by using the method of lattice dynamics developed for simple crystals.[3)] One of the simplest models to take the Coulomb interactions explicitly may be the rigid-ion (RI) model[3,7)] with short-range forces. The present author and his coworkers have analyzed the optically-active vibrations of carbonate crystals[8,9)] on the basis of the RI model. It is concluded that the calculated TO-LO separations of the intermolecular vibration modes are fairly comparable with the experimental results, but that those of the intramolecular modes do not agree with the observed separations. Then we introduce a model where the effects of the electronic polarizabilities[3,10,11)] can be appropriately taken into account. The shell model[10)] may be one of the most elaborate models for such a purpose; it has been successfully used in the analysis of phonon dispersion relations and of specific heats of simple crystals. As for the shell model, however, we sometimes find it difficult to determine the unmanageable number of Coulomb parameters uniquely. Thus, the PI model of Born and Huang[3)] has been employed; this model is used with a certain extension in an attempt to incorporate the anisotropy of the electronic polarizability. The effects of the distortion of electronic distributions on the crystal vibrations can be rigorously estimated by the model; however, higher-order multipole effects are implicitly neglected, for we believe them to be much less important. In order to evaluate the Coulomb components of the dynamical matrix,[3)] we take the constituent atoms to be point ions of unknown charges and electronic polarizabilities; then those which can best explain the observed Coulomb interactions are determined to be the effective ionic charges and electronic polarizabilities.

Method of Calculation

The method has been described in detail in Paper I; here we shall merely quote the results relevant to the present work. From the Born and Huang theory,[3)] a dynamical matrix is constructed from four con-

stituents:

$$\mathbf{D} = \bar{\mathbf{M}}(\mathbf{F}^{N}+\mathbf{F}^{C}+\mathbf{F}^{I}+\mathbf{F}^{M})\bar{\mathbf{M}},$$

where $\bar{\mathbf{M}}_{\alpha\beta kk'}=\delta_{\alpha\beta}\delta_{kk'}m_k^{-1/2}$, where α and $\beta=x$, y or z, and where m_k and δ are the mass of the k-th kind of atom and the usual Kronecker delta symbol respectively. The first term arises from short-range non-Coulomb interactions; both the central force interactions of non-bonded atom pairs within 3.5 Å and the non-central force interactions of carbonate groups are taken into consideration. A complete description of them has been given elsewhere,[8,9] denoted by Papers II, and the notations of these papers are used here. The second and third terms are due to rigid-ion and induced-dipole interactions respectively. In the long-wavelength limit, the terms are thus far independent of the direction of the wave propagation. The last term is the macroscopic field part and is dependent on the direction.

Now, to proceed with the actual calculations we require the numerical values of the ionic charges and electronic polarizabilities of the constituent atoms. Unlike simple crystals, the situation is complicated here by the fact that the distribution of the ionic charges is not known in advance. Two disposable parameters, x and Z, have been introduced in order to represent the distribution under electrically neutral conditions: $Z_{Metal}=Z$, $Z_c=xZ$, and $Z_o=-(1+x)Z/3$. Furthermore, the ratio of Z_{Ca} to Z_{Mg} for dolomite was taken to be that of the Szigeti charges,[12] since the results do not depend on the ratio.[9] The electronic polarizability can be easily incorporated in tensor form by generalizing the Born and Huang expressions.[3] In order to reduce the number of disposable parameters, it is assumed that the off-diagonal elements of the polarizability tensors are negligibly small. It is then shown from the crystal symmetry that only two of the diagonal elements are independent, *i.e.*, $\alpha_{11}(k)=\alpha_{22}(k)$ $(=\alpha_\perp(k))\neq\alpha_{33}(k)(=\alpha_\parallel(k))$. The electronic polarizabilities of the constituent atoms were recalculated in order to take the anisotropy into account by using this expression:

$$\boldsymbol{\varepsilon}_\infty = \mathbf{I} + 4\pi v^{-1}\boldsymbol{\rho},$$

where $\boldsymbol{\varepsilon}_\infty$ is the macroscopic dielectric susceptibility tensor at a frequency higher than where the lattice vibration will contribute. $I_{\alpha\beta}=\delta_{\alpha\beta}$, v is the unit cell volume, and

$$\rho_{\alpha\beta} = \sum_{kk'}\{(\mathbf{I}'-\mathbf{AQ})^{-1}\mathbf{A}\}_{\alpha\beta kk'}.$$

In this expression, $I'_{\alpha\beta kk'}=\delta_{\alpha\beta kk'}$, $A_{\alpha\beta kk'}=\alpha_{\alpha\beta}(k)\delta_{kk'}$, $\boldsymbol{\alpha}(k)$ is the polarizability tensor of the k-th kind of atom, and $\mathbf{Q}$ denotes the Coulomb coefficient matrix. In practice, it has been found that the electronic polarizabilities of the metal atoms are fairly small as compared with those of carbonate groups[13] and that the frequencies given by the model are insensitive to the polarizabilities.[2] The polarizabilities were thus regarded as isotropic and set equal to the values determined by the other methods[13–16] in the final calculations.

The numerical work was performed using a TOSBAC 3400 TOPS 14 electronic computer at the Computing Center of Hiroshima University.

Results and Discussion

Electronic Polarizability. A considerable number of values have been reported for ionic and molecular polarizabilities.[13–16] Almost all of them have, however, been determined for isotropic crystals with simple structures; therefore, they cannot always apply to the present materials. As has been mentioned above, they were used only for less important metal atoms. The resulting electronic polarizabilities of oxygen and carbon atoms are shown in Fig. 2 for calcite, where all of the sets of values on the $\{\alpha_\perp(O), \alpha_\perp(C)\}$ and $\{\alpha_\parallel(O), \alpha_\parallel(C)\}$ curves were able to account for the high-frequency dielectric constants corresponding to the two refractive indices,[17,18] $n_\perp$ and $n_\parallel$ respectively. The determination of the electronic polarizabilities must, therefore, be based on a fit of the calculated to the observed vibrational frequencies.

In the present investigation, the off-diagonal elements of the polarizability tensor were neglected as a first approximation. The validity of the simplifying assumption is unclear at present, although it does predict the correct orders of magnitude for the Coulomb frequency splittings. It seems likely that the influence of the elements, if any, would be appreciable in the case of atoms with a lower site symmetry, such as oxygen atoms in the calcite lattices. Therefore, further work is required to clarify the significance of the off-diagonal elements.

Optically-active Vibrations. From the present calculations, certain frequency splittings in the intramolecular vibrations, *e.g.*, TO-LO and E_g-E_u splittings,[19–22] were found to be appreciably sensitive to the details of the electronic polarizabilities of oxygen and carbon atoms as well as to the charge distribution within the carbonate groups. The present calculations strongly suggest that the E_g-E_u splittings of the

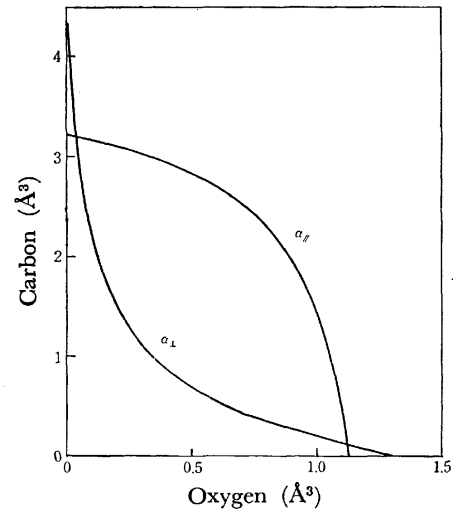

Fig. 2. Electronic polarizabilities of oxygen and carbon atoms for calcite. All of the sets of values on the curves are able to account for the observed high-frequency dielectric constants.
$\alpha_\perp$: Perpendicular component.
$\alpha_\parallel$: Parallel component.

Table 1. Observed and calculated vibrational frequencies (cm^{-1}) of calcite and magnesite

Sym.	Calcite									Magnesite								
	Observed[a]			PI Model			RI Model[b]			Observed[c]			PI Model			RI Model[b]		
	TO	LO	$\Delta\nu$	TO	LO	$\Delta\nu$	TO	LO	$\Delta\nu$	TO	LO	$\Delta\nu$	TO	LO	$\Delta\nu$	TO	LO	$\Delta\nu$
A_{1g}	1086			1086			1086			1096			1096			1095		
A_{2g}				883			884						853			906		
	309			282			254						394			349		
	172			177			192						322			315		
A_{1u}				1088			1088						1104			1101		
				257			255						376			345		
A_{2u}	872	890	18	876	887	11	874	885	11	876	911	35	882	905	23	881	899	18
	303	387	84	313	385	72	321	375	54	362	459	97	323	496	173	363	458	95
	92	136	44	100	101	~1	93	133	40	230	281	51	233	265	32	236	268	32
E_g	1434			1438			1424			1460			1459			1451		
	712			708			714			735			736			745		
	284			284			262			332			331			332		
	156			156			165			212			210			213		
E_u	1407	1549	142	1407	1551	144	1424	1429	5	1436	1599	163	1439	1605	167	1451	1459	8
	712	715	3	695	735	41	712	713	~1	747	783	36	745	813	68	743	745	2
	297	381	84	305	345	40	296	357	61	356	475	119	372	464	91	353	464	111
	223	239	16	218	242	24	226	234	8	301	315	14	284	329	45	310	314	4
	102	123	21	106	117	11	101	123	22	221	241	20	222	228	6	226	239	13

TO; Transverse optic mode. LO; Longitudinal optic mode. $\Delta\nu$; TO-LO separation.
a) Refs. 23, 25, and 29. b) Ref. 8. c) Refs. 25 and 41.

Table 2. Effective charge (electron unit) and electronic polarizability ($Å^3$)

	Magnesite	Dolomite	Calcite		Rhodochrosite	Smithsonite
x	0.25	0.30	0.35	x	0.27	0.30
Z_{Mg}	1.30	1.25		Z_{Mn}	1.19	
Z_{Ca}		1.08	1.11	Z_{Zn}		1.08
Z_C	0.32	0.35	0.39	Z_C	0.32	0.32
Z_O	−0.54	−0.50	−0.50	Z_O	−0.51	−0.47
α(Mg)	0.09	0.09		α(Mn)	0.92	
α(Ca)		1.10	1.10	α(Zn)		0.67
$\alpha_\perp$(C)	1.09	1.03	1.10	$\alpha_\perp$(C)	1.10	1.10
$\alpha_{//}$(C)	1.32	1.25	1.18	$\alpha_{//}$(C)	1.28	1.29
$\alpha_\perp$(O)	0.30	0.30	0.30	$\alpha_\perp$(O)	0.30	0.30
$\alpha_{//}$(O)	1.06	1.06	1.05	$\alpha_{//}$(O)	1.05	1.05
$\varepsilon_\perp^\infty$	2.95	2.82	2.75	$\varepsilon_\perp^\infty$	3.31	3.42
$\varepsilon_{//}^\infty$	2.30	2.25	2.21	$\varepsilon_{//}^\infty$	2.54	2.63

x, charge distribution parameter; //, parallel component; $\perp$, perpendicular component.

CO stretching and OCO angle deformation modes depend very sensitively on the polarizability, $\alpha_\perp$(O) or $\alpha_\perp$(C). If the values about 0.3 $Å^3$ are assigned to the $\alpha_\perp$(O) polarizability, a satisfactorily good agreement can be obtained with the experimental results; therefore, the value was set as 0.3 $Å^3$. On the other hand, it was found that the charge distribution affects the TO-LO separations of the CO stretching modes quite a bit. The distribution parameter was adjusted to explain the experimental separations. For the A_{2u} or A_u modes, the effects of the polarizabilities can be examined only for the TO-LO splitting of the out-of-plane angle deformation modes; the polarizability dependence of the splitting is, however, not so remarkable as that of the E_u modes. It was shown, from a careful analysis of the calculated results, that a polarizability set with $\alpha_{//}(O) \approx 1.05$ $Å^3$ yields a good agreement with the observed splitting. Any choice of isotropic polarizabilities, *i.e.*, $\alpha_\perp(O) = \alpha_{//}(O) = 0.3$ $Å^3$ or 1.05 $Å^3$, was found either to overestimate or to underestimate the experimental results seriously.

Calcite: A large number of experimental studies of the vibrational spectra of calcite have been carried out by means of IR absorption[23,24] or reflection[25-27] and of Raman scattering;[23,24,28] furthermore, the dispersion relations have been in part determined by neutron inelastic scattering.[29] The observed and calculated frequencies are given in Table 1, together with the results of the RI model calculations for comparison. It is shown that the E -E_u splitting of the CO stretching

Table 3. Observed and calculated vibrational frequencies (cm^{-1}) of dolomite

Sym.	Observed[a]			PI Model			RI Model[b]		
	TO	LO	$\Delta\nu$	TO	LO	$\Delta\nu$	TO	LO	$\Delta\nu$
A_g	1099			1099			1096		
	—			894			900		
	335			339			309		
	—			226			240		
A_u	—	—	—	1099	1100	~1	1098	1098	~0
	879	901	22	879	902	23	883	898	15
	361	429	68	362	446	84	374	436	62
	314	325	11	298	318	20	308	309	~1
	146	193	47	159	159	~0	149	190	41
E_g	1444			1459			1443		
	724			723			729		
	301			308			296		
	178			177			181		
E_u	1435	1580	145	1428	1577	150	1443	1449	6
	728	741	13	713	753	40	729	731	2
	345	439	94	337	412	75	348	418	70
	255	271	16	261	285	24	267	277	10
	150	173	23	155	164	9	152	176	24

The notation is the same as in Table 1. a) Refs. 25 and 43. b) Ref. 9.

modes is fairly comparable with the experimental separation, whereas the splitting of the OCO deformation modes seems to be somewhat overestimated. Recently, Onomichi *et al.*[30] have reported more accurate and reliable spectroscopic data for calcite: 1439 cm^{-1} and 720 cm^{-1} for the E_g modes, and 1411 cm^{-1} and 712 cm^{-1} for the E_u modes. Therefore, the present calculations do not always predict a tendency of the Coulomb shift opposite to that of the experimental data. The optimized set of the Coulomb parameters is listed in Table 2.

The vibrational analysis has been performed by many investigators;[22,29-35] however, only a few attempts have been made so far to examine the effects of the Coulomb interactions. Onomichi[36] performed the RI model analysis of the optically-active vibrations; the reproducibility of the observed frequencies seems not to be very good on account of the rough estimate of the disposable parameters. Plihal and Schaack[37,38] have analyzed the intermolecular vibrations based on a shell model; they explained the experimental results fairly well. They regarded the carbonate group as one large ion in order to reduce the shell-model parameters to manageable proportions, and the calcium atom was assumed to be unpolarizable. Of considerable interest is the recent work by Cowley and Pant;[29] the observed frequencies of the optically-inactive A_{2g} modes are in fair accord with the present results (see Table 1). They have determined the shell-model parameters with reference to the dispersion curves for several intermolecular modes. The resulting charge of calcium is read as 2.3 in electron units; this is the largest of the published charges (*viz.*, 1.5,[12] 1.53,[37] and the 1.11 determined presently). There appears to be considerable variation in the charge not only with the calculation models but also with the types of vibration referred to. It should be noted that the present charge can account for both the high- and low-frequency vibrations simultaneously, whereas the published charges were estimated with reference to the low-frequency vibrations only.

The charge distribution within the carbonate ion has been determined from energetic studies of the static lattices. Ladd[39] has recently assigned the following charges: $Z_C=0.31$ and $Z_O=-0.77$ in electron units, where (Z_C+3Z_O) is normalized to the formal ionic charge. The charge distribution seems to be far closer to the present dynamical distribution than that determined previously.[40]

Magnesite and Dolomite: The IR and Raman spectra have been reported by several workers,[25,41-44] but the theoretical analysis of the vibrations has been little attempted in terms of any force models.[8,9,35,37,45] The observed and calculated frequencies of magnesite and dolomite are compared in Tables 1 and 3 respectively. As has been ascertained for calcite, the theoretical frequency splittings of the intramolecular modes are in better agreement with the observed Coulomb splittings than those based on the RI model. The best-fit Coulomb parameters are listed in Table 2. On account of the lowering of the crystal symmetry, the disposable parameters for dolomite number about twice as many as those needed for calcite or magnesite. Accordingly, the initial values of these parameters for fitting-procedures were estimated with reference to both the optimized values on the basis of the RI model[8,9] and those of the PI model for calcite and magnesite. It is obvious, from a close inspection of the effective charges of calcite and magnesite, that a larger dipole moment is induced at each atom site in magnesite

Table 4. Observed and calculated vibrational frequencies (cm^{-1}) of rhodochrosite and smithsonite

Sym.	Rhodochrosite									Smithsonite								
	Observed[a]			PI Model			RI Model			Observed[a]			PI Model			RI Model		
	TO	LO	$\Delta\nu$	TO	LO	$\Delta\nu$	TO	LO	$\Delta\nu$	TO	LO	$\Delta\nu$	TO	LO	$\Delta\nu$	TO	LO	$\Delta\nu$
A_{1g}	1089			1089			1089			1096			1096			1095		
A_{2g}				869			887						878			903		
				339			291						359			304		
				231			255						246			280		
A_{1u}				1092			1093						1099			1100		
				238			230						217			219		
A_{2u}	865	—	—	868	891	23	866	887	21	878	—	—	878	898	20	879	903	24
	285	384	99	271	392	121	293	363	70	287	383	96	285	394	109	294	362	66
	176	—	—	176	181	5	174	211	37	198	—	—	198	198	~0	193	237	44
E_g	1420			1430			1409			1412			1430			1405		
	722			735			725			733			744			742		
	290			291			288			306			305			300		
	183			183			186			184			184			192		
E_u	1397	1556	159	1392	1550	158	1409	1419	10	1398	1559	161	1393	1551	157	1405	1417	12
	725	725	~0	710	782	72	724	726	2	743	743	~0	728	778	50	739	742	3
	285	368	83	306	356	50	278	362	84	287	368	81	306	342	36	275	361	86
	202	—	—	202	242	40	211	227	16	198	—	—	194	230	36	208	231	23
	160	—	—	157	159	2	171	180	9	130	—	—	130	135	5	176	180	4

The notation is the same as in Table 1. a) Refs. 46 and 48.

than in calcite; these features are well reflected in the observed TO-LO separations. The intermediate nature of dolomite between calcite and magnesite is appreciably brought out in the effective charges and short-range force constants; they are either calcite-like or magnesite-like.

Rhodochrosite and Smithsonite: There have been little vibrational data available for these crystals, and the crystal vibrations have not been analyzed in terms of any force models except in the work by Grandolfo[35] based on a short-range force model. The available data[28,46-48] are, however, barely sufficient to perform the detailed analysis. The observed IR reflectivities[48] were modified by employing the anisotropic refractive indices in the dielectric dispersion formulas: $n_\perp=1.818$ and $n_\parallel=1.595$ for rhodochrosite and $n_\perp=1.849$ and $n_\parallel=1.621$ for smithsonite.[17]

The optically-active vibrations of these crystals were analyzed on the basis of both the RI and PI models. The observed and calculated frequencies and the best-fit values of the Coulomb parameters are given in Tables 4 and 2 respectively. Because of the lack of reliable spectroscopic data for these crystals, the present results must be considered to be tentative. Although the physical significance of the values of the adjustable parameters is not clear, a general similarity in the values is found between these crystals and the other crystals investigated here.

Short-range Force Constants. The initial values of the force constants, f_1—f_6, were estimated with reference to those determined by the RI model,[8,9] and then they were refined by a least-squares method. The optimized values are listed in Table 5, where $F'=-0.1F$. The modified Urey-Bradley force field was ascertained to be satisfactory for the intramolecular vibrations of carbonate groups, although the physical meanings of the correction terms of relatively large values remain obscure. It is also found that some force constants between close atom pairs, such as intramolecular constants, are more affected by the ionic polarizabilities than those between distant pairs; an explanation of this can be found in the widely recognized concept that the interactions through the electronic polarizability are more short-range than the electrostatic interactions.

A rough estimation of the Lennard-Jones potential constants for non-bonded oxygen-oxygen interactions was possible from the resulting 17 force constants. The force constants are shown in Fig. 3. If the atoms are assumed to interact with central forces, the Lennard-Jones potential constants, A and B, of the form:[3,49]

$$U(r) = A\,r^{-9} - B\,r^{-6},$$

can be determined by the use of this relation:

$$f(r_0) = [\mathrm{d}^2U/\mathrm{d}r^2]_{r=r_0},$$

where $f(r_0)$ is the force constant at the interatomic distance of r_0. The optimized values for the potential constants were thus calculated to be $A=60\times10^{-82}$ erg·cm^9 and $B=350\times10^{-60}$ erg·cm^6. As Fig. 3 illustrates, the curve I of the carbonates seems to be intermediate between the curves II and III drawn from the self-consistent potential constants of oxides[49] and those of neon with the similar electron configuration to the O^{2-} ion[3] respectively. Figure 3 also indicates that Curve I is similar in the dependence on the interatomic distance to Curve II rather than to Curve III.

Comparison of PI Model with RI Model. The essential correctness of introducing the electronic polarizability is shown by the great improvement in the fit to the experimental Coulomb splittings of the

TABLE 5. SHORT-RANGE FORCE CONSTANTS (mdyn/Å)

FC[a]	Pair	Magnesite		Dolomite		Calcite		Pair	Rhodochrosite		Smithsonite	
		Dist.[e]	FC	Dist.[e]	FC	Dist.[e]	FC		Dist.[e]	FC	Dist.[e]	FC
K	C O	1.286	6.141	1.283	6.224	1.294	6.200	C O	1.286	5.761	1.286	5.832
H	O C O		0.908		0.962		0.952	O C O		0.964		0.962
F	O O	2.227	2.386	2.222	2.536	2.241	2.522	O O	2.227	2.554	2.227	2.556
α[b]	CO_3		0.392		0.367		0.325	CO_3		0.358		0.348
p[c]			−1.471		−1.544		−1.427			−1.422		−1.414
n[d]			0.950		1.298		1.220			1.069		1.208
f_1	Mg C	2.953	0.154	3.043	0.069			Mn C	3.051	0.148		
f_1'	Ca C			3.153	0.012	3.213	0.026	Zn C			2.964	0.103
f_2	Mg O	2.102	0.834	2.095	0.806			Mn O	2.916	0.765		
f_2'	Ca O			2.390	0.739	2.353	0.671	Zn O			2.111	0.800
f_3	C O	3.019	0.030	3.133	0.010			C O	3.152	0.011		
f_3'	C O			3.343	−0.005	3.406	0.001	C O			3.026	0.000
f_4	O O	2.849	0.111	3.009	0.080			O O	2.958	0.051		
f_4'	O O			3.086	0.070	3.189	0.064	O O			2.852	0.084
f_5	O O	2.924	0.255	2.916	0.174			O O	3.058	0.110		
f_5'	O O			3.304	0.005	3.249	−0.003	O O			2.943	0.149
f_6	O O	3.019	0.049	3.008	0.068			O O	3.152	0.012		
f_6'	O O			3.454	−0.010	3.406	−0.014	O O			3.026	0.003

a) The notation is the same as in Refs. 8 and 9. b) Out-of-plane angle deformation coordinate. c) Adjacent bond interaction. d) Adjacent angle interaction. Units of n in mdyn·Å. e) Interatomic distance in Å.

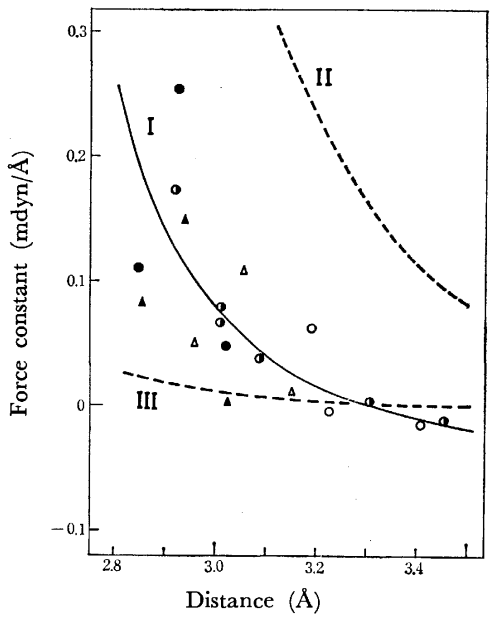

Fig. 3. Force constants for non-bonded oxygen-oxygen interactions. Curves II and III are drawn from the $O^{2-}\cdots O^{2-}$ potential of oxide crystals and Ne··· Ne potential, respectively. See text.
○: Calcite, ●: Magnesite, ◑: Dolomite,
△: Rhodochrosite, ▲: Smithsonite.

intramolecular modes. These splittings have been poorly accounted for on the basis of the RI model. With OCO angle deformation modes, the relatively weak absorption intensity makes it difficult to attain accurate and reliable determinations of the TO-LO separations. Consequently, the experimental separations seem to vary considerably with the five carbonates; nearly identical values are assigned to them in the case of CO stretching modes. We cannot, therefore, believe that all the variations arise from the specificity of each modification, although the Coulomb interactions of the angle deformation modes are seemingly reproduced less satisfactorily with the present model. Further experimentation is necessary to examine fully this apparent contradiction to the present results. The observed intermolecular mode frequencies are seen to be satisfactorily explained by both models: certain low-frequency modes are not very well fitted by the PI model, although this lack of fit is probably not significant.

As for the optically-active vibrations, the results of the present and of previous works[2] seem to indicate that the weak Coulomb interactions between moderately separated atoms can be fairly well accounted for by the RI model, and that, however, any strong interactions due to the distortion of electronic distributions can hardly be interpreted at all without the use of a model which takes rigorously ionic polarizations. Moreover, there are a large number of crystalline solids where we are obliged to be content with the oversimplified RI approximation because of the complexity inherent in elaborate models. Under these circumstances, we consider that the present work represents one step in the direction of obtaining a quantitative understanding of the Coulomb interactions in ionic crystals with intricate structures.

The author wishes to express his thanks to Professor Hiromu Murata for his continual encouragement during this work, and to Associate Professor Yuji Shiro for his valuable advice and discussion. Thanks are also due to Messrs. Masaru Ohsaku and Tamaki Utida and Miss Michiko Miura for their kind and helpful discussion and suggestions.

References

1) Coulomb Interactions and Optically-active Vibrations of Ionic Crystals. II. A part of this work was presented at the Symposium on Molecular Structure, Osaka, November (1975).
2) A. Yamamoto, T. Utida, H. Murata, and Y. Shiro, *J. Phys. Chem. Solids*, in press.
3) M. Born and K. Huang, "Dynamical Theory of Crystal Lattices," Oxford Univ. Press, London (1954).
4) See, for example, S. Bhagavantam and T. Venkatarayudu, "Theory of Groups and Its Application to Physical Problems," Andhra Univ. Press, Waltair (1951).
5) D. L. Graf, *Am. Mineral.*, **46**, 1283 (1961).
6) D. L. Graf, *Am. Mineral.*, **54**, 325 (1969).
7) E. W. Kellermann, *Phil. Trans. R. Soc.*, **238**, 513 (1940).
8) A. Yamamoto, Y. Shiro, and H. Murata, *Bull. Chem. Soc. Jpn.*, **48**, 1102 (1975).
9) A. Yamamoto, T. Utida, H. Murata, and Y. Shiro, *Spectrochim. Acta*, **31A**, 1265 (1975).
10) R. A. Cowley, *Proc. R. Soc. London*, **268A**, 109 (1962).
11) J. R. Hardy, *Phil. Mag.*, **7**, 315 (1962).
12) B. Szigeti, *Trans. Faraday Soc.*, **45**, 155 (1949).
13) J. Tessman, A. Kahn, and W. Shockley, *Phys. Rev.*, **92**, 890 (1953).
14) L. Pauling, *Proc. R. Soc. London*, **114A**, 191 (1927).
15) J. Pirenne and E. Kartheuser, *Physica*, **30**, 2005 (1962).
16) E. Uzan and V. Chandrasekharan, *J. Phys. Paris*, **33**, 771 (1972).
17) K. H. Hellwege and A. M. Hellwege, Ed., "Landolt-Börnstein Zahlenwerte und Funktionen," Vol. 8, 6-th ed., Springer, Berlin (1962).
18) P. Humbert and F. Plicque, *C. R. Acad. Sci. Paris*, **275B**, 391 (1972).
19) J. C. Decius, *J. Chem. Phys.*, **49**, 1387 (1968).
20) R. Frech and J. C. Decius, *J. Chem. Phys.*, **51**, 1536, 5315 (1969).
21) R. Frech and J. C. Decius, *J. Chem. Phys.*, **54**, 2374 (1971).
22) R. E. Carlson and J. C. Decius, *J. Chem. Phys.*, **58**, 4919 (1973).
23) A. K. Ramdas, *Proc. Indian Acad. Sci.*, **37A**, 441 (1953).
24) M. Tsuboi, Preprint of the International Symposium on Molecular Structure and Spectroscopy, Tokyo (1962).
25) K. H. Hellwege, W. Lesch, M. Plihal, and G. Schaack, *Z. Phys.*, **232**, 61 (1970).
26) P. J. Ring, *Infrared Phys.*, **12**, 237 (1972).
27) M. Ishigame, T. Sato, and T. Sakurai, *Phys. Rev.*, **3B**, 4388 (1971).
28) W. P. Griffith, *J. Chem. Soc. A*, **1970**, 132.
29) E. R. Cowley and A. K. Pant, *Phys. Rev.*, **8B**, 4795 (1973).
30) M. Onomichi, K. Kudo, and T. Arai, *J. Phys. Soc. Jpn.*, **31**, 1837 (1971).
31) L. Giulotto and A. Loinger, *Nuovo Cimento*, **8**, 475 (1951).
32) K. Venkateswarlu and K. Ramaswamy, *Indian J. Pure Appl. Phys.*, **2**, 209 (1964).
33) Y. Shiro, *J. Sci. Hiroshima Univ., Ser. A-II*, **32**, 77 (1968).
34) A. Yamamoto, Y. Shiro, and H. Murata, *Bull. Chem. Soc. Jpn.*, **47**, 265 (1974).
35) M. C. Grandolfo, *Diss. Abst. Int.*, **35B**, 2089 (1974).
36) M. Onomichi, *Sci. Light (Tokyo)*, **22**, 47 (1973).
37) M. Plihal and G. Schaack, *Phys. Stat. Sol.*, **42**, 485 (1970).
38) M. Plihal, *Phys. Stat. Sol.*, **56B**, 495 (1973).
39) M. F. C. Ladd, *J. Inorg. Nucl. Chem.*, **37**, 1529 (1975).
40) H. D. P. Jenkins and T. C. Waddington, *J. Chem. Phys.*, **56**, 5323 (1972).
41) D. Krishnamurti, *Proc. Indian Acad. Sci.*, **43A**, 210 (1956).
42) J. Morandat, V. Lorenzelli, and J. Lecomte, *J. Phys. Paris*, **28**, 156 (1967).
43) L. Couture, *C. R. Acad. Sci. Paris*, **221**, 235 (1945).
44) L. Couture, *Ann. Phys.*, **2**, 5 (1947).
45) K. D. Oh, H. Morikawa, S. Iwai, and H. Aoki, *Am. Mineral.*, **58**, 1029 (1973).
46) M. Donoghue, P. H. Hepburn, and S. D. Ross, *Spectrochim. Acta*, **27A**, 1065 (1971).
47) J. P. Pinan-Lucarre and N. T. Tai, *Bull. Soc. Fr. Mineral. Cristallogr.*, **95**, 15 (1972).
48) R. Vierne and R. Brunel, *Bull. Soc. Fr. Mineral. Cristallogr.*, **96**, 55 (1973).
49) R. H. Fowler, "Statistical Mechanics," Cambridge Univ. Press, London (1936).

X-Ray Photoelectron Spectroscopy of the Molecules Containing the C≡N Group

Takashi FUJIKAWA, Toshiaki OHTA, and Haruo KURODA

Department of Chemistry, Faculty of Science, University of Tokyo, Hongo, Tokyo 113

(Received December 24, 1975)

The gas-phase X-ray photoelectron spectra (with Mg$K\alpha$ radiation) were observed on acetonitrile, propionitrile, acrylonitrile and fumaronitrile. The ionization potentials were determined for all valence-electron levels of the above molecules by using the data derived from the observed valence-electron bands of X-ray photoelectron spectra and the reported data of ultraviolet photoelectron spectroscopy. It is shown that there is a linear relation between the observed ionization potential (IP) and the CNDO/2 orbital energy (ε): $IP=0.61(-\varepsilon)+3.2$ [eV], for σ-orbitals; $IP=0.38(-\varepsilon)+6.0$ [eV], for π-orbitals. The observed binding energies of the C 1s levels were analyzed by means of the electrostatic potential model and the charge densities calculated by CNDO/2 method. Discussion is given also on the shake-up satellite of core-electron peak.

The valence-electron levels of the molecules containing the C≡N group have been investigated by several authors by means of ultraviolet photoelectron spectroscopy (UPS), using He I resonance line as the stimulating radiation.[1-5] However, the informations which have been obtained by these UPS studies, are concerned mainly with the π-electron and lone-pair levels, and little has been known about σ-electron levels, in particular, those of higher ionization potentials.

For investigating valence-electron levels of a molecule, X-ray photoelectron spectroscopy (XPS) provides informations which are complementary to those obtainable by UPS; First, it is possible to investigate with XPS the deep-lying valence-electron levels which can not be studied by UPS, and, second, the prominent bands observable in the valence-electron region of a XPS spectrum are mostly associated with σ-orbitals, whereas, in UPS, π-orbitals usually give strong photoelectron bands.[6]

In the present paper, we report the gas-phase X-ray photoelectron spectra of the molecules containing the C≡N group. The valence-electron bands of the observed spectra will be analysed with the aids of the reported UPS data and the molecular orbital calculations by CNDO/2 method. Discussion will be also given on the core-electron peaks.

Experimental

The gas-phase X-ray photoelectron spectra of acetonitrile CH_3CN, propionitrile CH_3CH_2CN, acrylonitrile CH_2=CH-(CN) and fumaronitrile $^{NC}\diagdown CH{=}CH\diagdown^{CN}$ were measured with a McPherson ESCA 36 electron spectrometer, by employing Mg$K\alpha$ radiation (1253.6 eV). The purified sample of each compound was out-gassed by the freezing-and-pumping technique in a glass tube connected to the gas-handling system of the spectrometer, and then its vapor was introduced through the gas-handling system into the ionization cell installed in the sample compartment of the spectrometer.[7]

The binding energies of photoelectron peaks, referred to the vacuum level, were calibrated by using the N 1s peak (409.9 eV) of the nitrogen gas, mixed with the sample vapor, as the reference. The C 1s peak of the sample, induced by the weak Al$K\alpha$ radiation which came out as the secondary X-ray from the Al window of the X-ray source, was also used as a subsidiary reference for the calibrations of binding energies of valence-electron bands.

Results and Discussion

Valence-electron Bands. The valence-electron bands of the XPS spectrum of propionitrile is shown in Fig. 1, which exhibits five prominent peaks located at ~13, 17.5, 22.1, 25.2 and 29.7 eV, respectively. Since the propionitrile molecule has twenty two valence electrons, there must be eleven valence-electron levels. The UPS spectrum of propionitrile was studied by Lake and Thompson,[2] who observed seven photoelectron bands, and determined the vertical ionization potentials of the corresponding levels as 12.11, 12.91, 13.64, 13.86, 15.07, 16.59 and 17.46 eV, respectively. Lake and Thompson attributed the 12.11 eV band to the ionizations of the two π-orbitals localized on the C≡N group, and the 12.91 eV band to that of the lone-pair of the N atom, but gave no assignment on other photoelectron bands. Anyway, by the above UPS study, we already know the ionization potentials of eight levels among the eleven valence-electron levels, so that there remain only three levels on which the ionization potential must be determined. As we compare the XPS spectrum with the above UPS data, we note that there are three peaks (at 22.1, 25.5 and 29.7 eV) in the higher-energy region that can not be studied by UPS. Thus, we can safely conclude that these three peaks must be corresponding to the remaining three levels. By this way, we are able to know the ionization potentials of all valence-electron levels.

The relative intensities of valence-electron bands observed by XPS are known to have a relatively simple

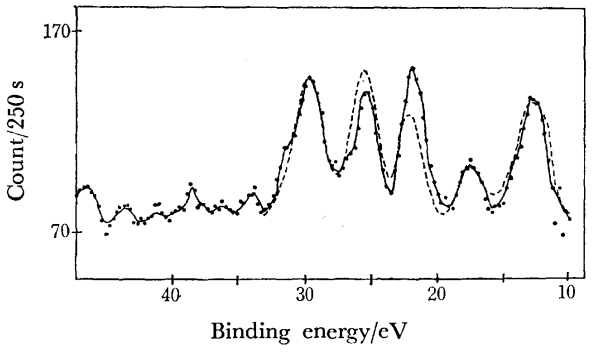

Fig. 1. Valence-electron bands of the XPS spectrum of propionitrile. The final results of simulation (see text) is shown with a broken line.

relation with the wave functions of the ionizing molecular orbitals. According to Gelius *et al.*, this can be approximately expressed as follows;[8]

$$I_j \propto \left(2+\frac{1}{2}\beta\right)\sum_{A\lambda} P_j(A\lambda)\,\sigma_{A\lambda}/\sigma_{C2s} \qquad (1)$$

where $P_j(A\lambda)$ is the atomic population on atom A from the atomic orbital $A\lambda$ in the ionizing molecular orbital j, $\sigma_{A\lambda}$ and σ_{C2s} are the photoionization cross sections of the atomic orbitals, $A\lambda$ and $C2_s$, for X-ray, and β is the asymmetric factor which can be taken as $\beta=2$ for σ-orbitals and -1 for π-orbitals. The relative photoionization cross section has been empirically determined by Gelius and others for various atomic orbitals.[8] The cross section of 2p orbital is reported to be almost one tenth of that of 2s orbital in the cases of the second row elements. Partly because of the small cross sections of 2p orbitals, and partly because of the asymmetric factor, π-orbitals usually have very small photoionization cross sections for X-ray as compared with σ-orbitals, whereas the photoelectron bands associated with π-orbitals strongly appear in the case of UPS. This situation gives us a way to distinguish the photoelectron bands due to π-orbitals from those due to σ- and n-orbitlas by comparing between the UPS and XPS spectra.

We calculated the molecular orbitals of propionitrile by CNDO/2 method, and estimated the relative intensities of XPS bands by using Eq. 1.[9] The results of the above calculations are given in Table 1. According to the calculated intensities, we should expect six prominent peaks in the XPS spectrum of propionitrile. We can safely assign the 22.1, 25.5 and 29.7 eV peaks of the observed spectrum to the 3σ, 2σ and 1σ orbitals, respectively. The 17.5 eV peak is likely to be mainly due to the ionization of the 4σ orbital. Then, we should consider that the band due to the 6σ orbital and the one due to the 7σ (lone pair) orbital are overlapping on each other to be a broad, strong peak at about 13 eV.

Since no peak is observed at 15 eV by XPS, we will attribute the 15.07 eV band observed by UPS, to the ionization of a π-orbital (1π). It is likely that in the XPS spectrum, the band corresponding to the 15.69 eV band of the UPS spectrum, is overlapping on the low-energy tail of the 17.5 eV peak. There remains some ambiguity as regards the assignments of the 13.64 and 13.86 eV bands observed by UPS. We will tentatively assign here the 13.64 eV band to the 2π orbital and the 13.86 eV band to the 6σ orbital. The ionization potential of each molecular orbital thus deduced is given in Table 1.

Using the ionization potentials mentioned above and the calculated relative intensities, we carried out a simulation of the valence electron bands of the XPS spectrum. We assumed here a Gaussian shape for each photoelectron peak, and adjusted peak width so that the best agreement was obtainable with the observed spectrum. The final result of simulation is shown in Fig. 1 with a broken line. We were able to obtain an excellent agreement between the calculated and observed spectra.

The valence-electron bands of the XPS spectrum of acetonitrile is shown in Fig. 2, which shows four peaks at 13.1, 17.3, 25.0 and 29.7 eV, respectively.[6] The situation is much more simple in this case than in the case of propionitrile. Lake and Thompson[2] observed four photoelectron bands (at 12.11, 13.14, 15.5

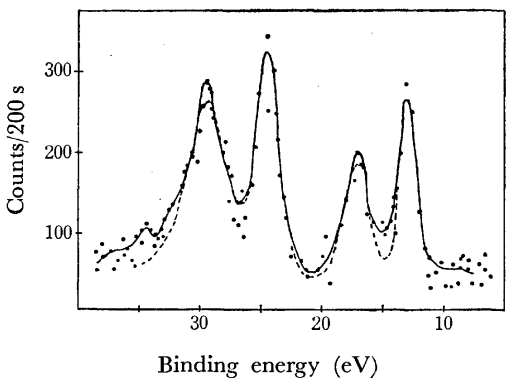

Fig. 2. Valence-electron bands of the XPS spectrum of acetonitrile. The broken line is the result of simulation.

Table 1. Molecular orbitals of propionitrile

	CNDO/2		Orbital[5] energy (*ab initio*) [eV]	*IP* (obs.)[eV]		
	Orbital energy[eV]	Relative intensity		UPS[2]	XPS	Peak width[eV]
4π (C≡N)	−15.43	0.07	−12.92	12.11		
3π (C≡N)	−15.76	0.11	−12.92			
7σ	−16.22	0.31	−14.86	12.91	~13	
2π	−18.57	0.07	−15.08	13.64		
6σ	−18.74	0.67	−15.38	13.86		
5σ	−21.71	0.16	−16.24	16.59		
1π (pseudo π)	−25.38	0.06	−18.36	15.07		
4σ	−25.41	0.39			17.5	
3σ	−31.60	1.00[a]			22.1	(2.5)
2σ	−38.51	1.91			25.5	(1.8)
1σ	−43.23	1.78			29.7	(2.2)

a) Assumed as the reference.

Table 2. Molecular orbitals of acetonitrile

	CNDO/2		*IP* (obsd) (eV)		
	Orbital energy[eV]	Relative intensity	UPS[2]	XPS	Peak width[eV]
2π (e) π(C≡N)	−15.98	0.11	12.11	—	
4σ (a_1) n(N atom)	−17.25	0.42	13.14	13.14	(1.6)
3σ (a_1) σ	−22.90	0.55	∼17	17.3	(2.4)
1π (e) mainly pseudo-π(CH_3)	−23.25	0.09	15.5	—	
2σ (a_1) σ	−36.51	1.00[a]	25.0	25.0	(2.2)
1σ (a_1) σ(mostly s-character)	−40.92	1.36		29.7	(3.6)

a) Assumed as the reference.

Table 3. Molecular orbitals of acrylonitrile

	CNDO/2		*IP* (obsd) [eV]		
	Orbital energy[eV]	Relative intensity	UPS[2]	XPS	Peak width[eV]
3π (out of plane)	−14.35	0.05	10.91	—	
7σ	−15.85	0.09	13.56		
2π (in plane, C≡N)	−16.35	0.08	12.36	∼13.3	
6σ (lone pair)	−18.87	0.35	13.04		
1π (out of plane)	−21.34	0.05	14.43	—	
5σ	−21.42	0.19	16.17	∼17.5	
4σ	−27.43	0.13	17.62		
3σ	−29.73	0.53		21.3	(2.0)
2σ	−38.96	0.95		25.3	(3.1)
1σ	−42.76	1.00[a]		29.7	(3.2)

a) Assumed as the reference.

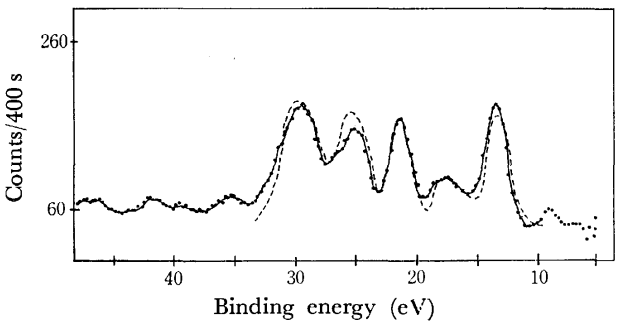

Fig. 3. Valence-electron bands of the XPS spectrum of acrylonitrile. The broken line is the result of simulation.

and about 17 eV) by UPS. By combining the above UPS data with our XPS ones, we can directly derive the ionization potentials of the six valence-electron levels of acetonitrile as 12.11, 13.14, 15.5, 17.3, 25.0 and 29.7 eV. At the same time, we can conclude that the 12.11 and 15.5 eV levels are of π-type since the bands associated with these levels do not appear in the XPS spectrum.

The orbital energies and relative intensities obtained by the CNDO/2 calculations are listed in Table 2. We will assign the 12.11 eV band observed by UPS to the ionization of the doubly-degenerated π-electron level, localized on the C≡N group, as reported by Lake and Thompson, and the 13.4 eV band to that of the lone pair. Then, other photoelectron bands can be assigned as shown in Table 2, assuming the sequence of levels as predicted by the CNDO/2 calculation.

The result of the simulation of the valence-electron bands of the XPS spectrum is shown in Fig. 2 with a broken line. Here, again, we obtained an excellent agreement between the calculated and observed spectra.

In the case of acrylonitrile, the ionization potentials are already known on seven levels among the total ten valence-electron levels through the UPS study by Lake and Thompson,[2] the reported values of the vertical ionization potentials being 10.91, 12.36, 13.04, 13.56, 14.43, 16.17 and 17.62 eV, respectively. By means of XPS, we can observe three prominent peaks at 21.3, 25.3 and 29.7 eV, in the region above 18 eV (see Fig. 3). Combining the above data, we were able to know the ionization potentials of all valence-electron levels.

The results of CNDO/2 calculations on acrylonitrile are shown in Table 3. According to Lake and Thompson, the 10.91 eV of the UPS spectrum is due to the π(C=C) orbital, and the 12.36 eV band to the π(C≡N) orbital. They assigned the 13.04 eV band to the ionization of the lone pair of the N atom. Thus we will attribute the 10.91, 12.36 and 13.04 eV bands to the 3π, 2π and 6σ orbitals, respectively. The calculation predicts a considerably high intensity for the 6σ band in the XPS spectrum. This is consistent with the observation which shows a prominent peak at about 13.3 eV. It is not possible to obtain a definite conclusion concerning the assignment of the 13.56 and

Table 4. Molecular orbitals of fumaronitrile

	CNDO/2		*IP* (obsd) [eV]		
	Orbital energy[eV]	Relative intensity	UPS[3]	XPS	Peak width[eV]
$5\pi(2a_u)$(out of plane)	−13.80	0.08	11.15	—	
$4\pi(6a_g)$(in plane)	−15.81	0.07	12.78	—	
$9\sigma(5a_g)$(partially, lone pair)	−16.21	0.32	(13.44)	—	
$3\pi(5b_u)$(in plane, C≡N)	−17.68	0.11	13.10	—	
$8\sigma(4b_u)$(lone pair)	−18.38	0.70	13.44	13.4	
$2\pi(1b_g)$(out of plane, C≡N)	−19.54	0.09	13.67	—	
$7\sigma(4a_g)$	−20.34	0.70	15.62	15.6	
$1\pi(1a_u)$(out of plane)	−23.01	0.08	14.41	—	
$6\sigma(3a_g)$	−24.07	0.43	18.2	18.0	(1.4)
$5\sigma(3b_u)$	−28.79	0.27	19.7	~20	(1.4)
$4\sigma(2b_u)$	−32.10	1.00		22.2	(1.4)
$3\sigma(2a_g)$	−39.05	1.58		25.6	(1.4)
$2\sigma(1b_u)$	−40.94	1.79		28.5	(2.5)
$1\sigma(1a_g)$	−44.47	1.64		30.2	(2.5)

a) Assumed as the reference.

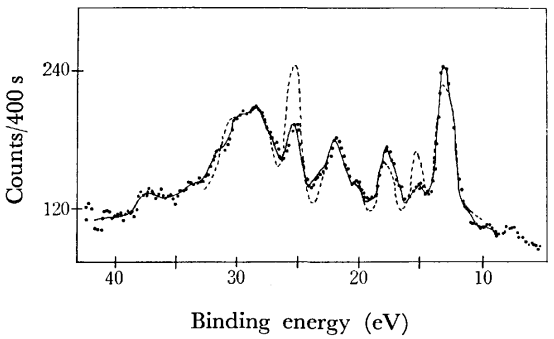

Fig. 4. Valence-electron bands of the XPS spectrum of fumaronitrile. The broken line is the result of simulation.

14.43 eV bands of the UPS spectrum. One of them must correspond to the 7σ orbital and the other to the 1π orbital. We tentatively assigned the 13.56 eV band to the 7σ orbital and the 14.43 band to the 1π orbital, since this assignment gave a better result in the simulation of the valence-electron bands of the XPS spectrum as compared with the alternative assignment. Seemingly, the weak band at about 17.5 eV in the XPS spectrum is due to the superposition of the two bands due to the 5σ and 4σ orbitals, which were separately observed by UPS at 16.17 and 17.62 eV.

We carried out the simulation of the XPS spectrum using the ionization potentials discussed above and the calculated intensities, and were able to obtain a good agreement between the calculated and observed spectra, as shown in Fig. 3.

As shown in Fig. 4, eight peaks were observed in the valence-electron region of the XPS spectrum of fumaronitrile, their maxima being located at 13.4, 15.6, 18.0, ~20, 22.2, 25.6, 28.5 and 30.2 eV, respectively. The UPS spectrum of fumaronitrile was studied by Bock and Stafast,[3] who observed nine photoelectron bands at 11.15, 12.78, 13.10, 13.44, 13.67, 14.41, 15.62, 18.2 and 19.7 eV, respectively, and carried out the assignments of these UPS bands on the bases of the analysis of vibrational structure and the molecular orbital calculation by extended Hückel method. By comparing the above UPS data with our XPS ones, we can conclude that the 11.15, 12.78, 13.10, 13.67 and 14.41 eV bands observed by UPS are due to the ionization of the π-orbitals because they are missing in the XPS spectrum.

The results of our CNDO/2 calculations are given in Table 4. The first strong peak at 13.4 eV in the XPS spectrum must correspond to the 13.44 eV photoelectron band observed by UPS, which was assigned to the ionization of the lone-pair. In effect, the 8σ orbital which has a character of the lone-pair orbital, is predicted to have a large photoionization cross section for X-ray. In the XPS spectrum, we can not find a peak corresponding to the ionization of the 9σ orbital. Seemingly, it is overlapping on the 13.4 eV peak. Assuming the sequence of other σ-orbitals as predicted by the CNDO/2 calculation, we will attribute the 30.2, 28.5, 25.6 and 22.2 eV peaks to the 1σ, 2σ, 3σ and 4σ orbitals, respectively. Since the 5σ orbital is predicted to have a relatively small intensity, we will attribute the weak peak at about 20 eV to the ionization of the above orbital. Then, the 18.0 and 15.6 eV peaks are attributable to the 6σ and 7σ orbitals. For the UPS bands associated with the π-orbitals, we will adopt the assignments given by Bock and Stafast since their results are consistent with our CNDO/2 calculation as regards the sequence of the orbitals. The ionization potential thus derived for each orbital is shown in Table 4.

The results of the simulation of the valence bands of the XPS spectrum is shown in Fig. 4 with a broken line, which is in a good agreement with the observed spectrum, except that the 15.6 and 25.6 eV peaks are predicted a little too strongly.

The results shown in Tables 1—4, clearly indicate that the observed ionization potentials are considerably

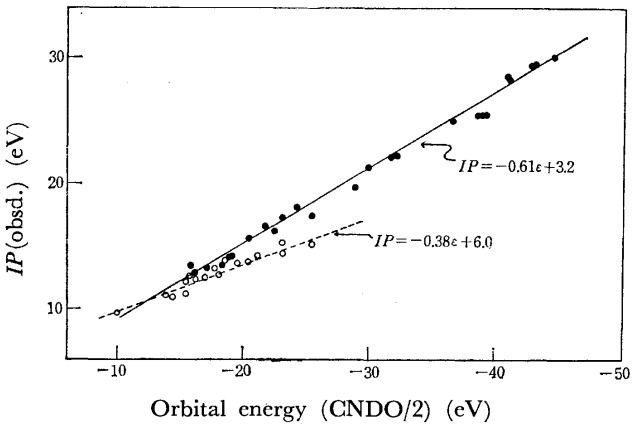

Fig. 5. Relation between ionization potential and CNDO/2 orbital energy: Filled circles are the data concerned with σ-orbitals, and open circles are those concerned with π-orbitals.

different from the values which are expected from the calculated orbital energies according to the Koopmans' theorem; the discrepancy between them is larger for deeper orbitals. In several UPS studies, it was mentioned that a reasonable value of ionization potential is obtainable when 4 eV is subtracted from the value given by Koopmans' theorem from the CNDO/2 orbital energy. However, the present data demonstrate that the above method is not satisfactory, in particular, for deeper orbitals.

In Fig. 5,[10] observed ionization potentials are plotted against CNDO/2 orbital energies. In this figure, the data concerned with π-orbitals are shown as open circles and those concerned with σ- and n-orbitals are shown as filled circles. Interestingly, the latters fall on a straight line and formers on another straight line. The relationship between the ionization potential (IP) and CNDO/2 orbital energy (ε) can be described as follows; for σ-orbitals,

$$IP = 0.61(-\varepsilon) + 3.2 \text{ [eV]} \quad (2)$$

and, for π-orbitals,

$$IP = 0.38(-\varepsilon) + 6.0 \text{ [eV]} \quad (3)$$

Probably, the above difference between the relation for σ-orbitals and that for π-orbitals is reflecting the problems concerned with the semiempirical parametrization in CNDO/2 method. It is also possible that the above difference is partly due to the difference in relaxation energy between σ- and π-orbitals. It should be noted that, because of the above relations between IP and ε, the locations of π-electron levels relative σ-electron levels are often incorrectly predicted by CNDO/2 method. This should be kept in mind when the results of CNDO/2 calculations are used for the assignment of photoelectron bands. The empirical relations, Eqs. 2 and 3, could be used to obtain the correct locations of valence electron levels, at least, in the cases of the molecules similar to those studied here.[11]

Core-electron Spectra. In all of the molecules studied here, one can generally expect that the charge density on the carbon atom of the C≡N group must be significantly different from those of other carbon

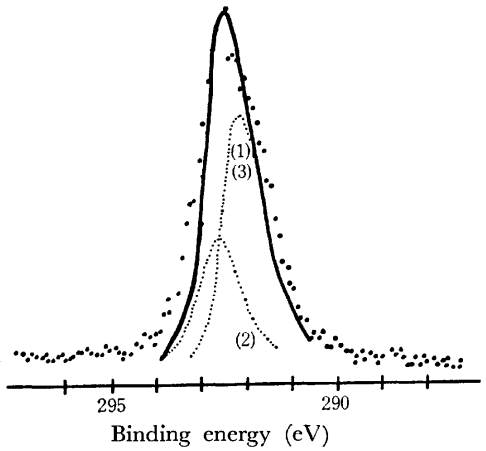

Fig. 6(a). C 1s peak of propionitrile. The observed data are shown by points. The solid line indicates the calculated peak shape which is obtained by superposing peaks due to different C 1s levels, illustrated with dotted lines. Their splitting being assumed as predicted from the CNDO/2 charge densities (see text). The peak number (i) is due to i-th C 1s (i= 1,2,3) (see Table 5).

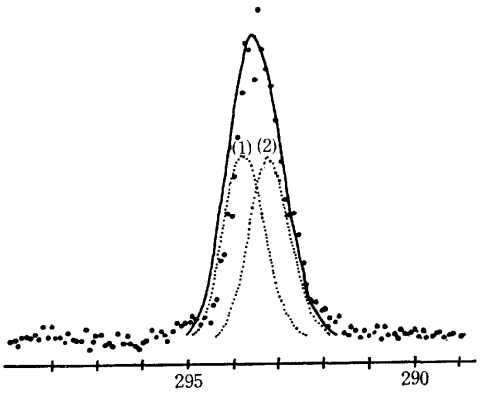

Fig. 6(b). C 1s peak of fumaronitrile. The observed data are shown by points. The solid line indicates the calculated peak shape which is a superposition of the two C 1s peaks shown with dotted lines. The peak number (1) is due to C(1) and (2) to C(2) (see Table 5).

atoms, and this difference of the charge densities will arise a relatively large splitting between the C 1s peak due to the former carbon atom and those due to the latter ones. However, the observed C 1s spectrum of each compound showed a single peak without a shoulder, although it is a little broad and asymmetric as illustrated by the spectra of propionitrile and fumaronitrile, shown in Fig. 6. This fact implies that the splitting of C1s levels must be smaller than 0.6 eV in all molecules studied here.

The net charge on each carbon atom, calculated by CNDO/2 method, is given in Table 5, where we can see that the carbon atom of the C≡N group has a charge of about $+0.09\,e$ whereas the net charges on other carbon atoms are $-0.02\,e \sim +0.02\,e$. According to the electrostatic potential model, the binding energy (E_i) of a core-electron level of the i-th atom can be

TABLE 5.

		q_i	ΔE [eV]	$\langle\Delta E\rangle$ [eV]	E_{obsd} [eV]	E_0 [eV]
$\overset{(2)}{C}H_3\overset{(1)}{C}N$	C_1	+0.090	0.71	0.55	293.1	292.5
	C_2	−0.023	0.38			
$\overset{(3)}{C}H_3\overset{(2)}{C}H_2\overset{(1)}{C}N$	C_1	+0.085	0.54			
	C_2	+0.017	1.07	0.72	292.4	291.7
	C_3	+0.002	0.54			
$\overset{(3)}{C}H_3\text{-}\overset{(2)}{C}H(\overset{(1)}{C}N)$	C_1	+0.092	0.47			
	C_2	+0.010	0.70	0.51	292.5	292.0
	C_3	−0.022	0.35			
$CH(CN)\text{=}\overset{(2)}{C}H(\overset{(1)}{C}N)$	C_1	+0.089	1.35	1.35	293.5	292.4
	C_2	+0.021	0.81			

related to the charge densities on the atoms in the molecule by the following equation,

$$E_i = E_0 + kq_i + \sum_{i \neq j} (q_j/R_{ij}) \quad (4)$$

where E_0 and k are the constants depending on the kind of atom, q_i and q_j are the charge densities on the i-th and j-th atoms, respectively, and R_{ij} is the interatomic distance.[13] In a previous paper, we showed that the binding energies of the C 1s levels of monosubstituted benzenes can be expressed as follows;[14]

$$E_i = 290.2 + 22.67\, q_i + 14.39 \sum_{i \neq j} (q_j/R_{ij}) \text{ [eV]} \quad (R_{ij}; \text{ in Å}) \quad (5)$$

thus E_0=290.2 eV and k=22.67 eV/unit charge. We can assume the same k value for the C 1s levels of the present molecules, but the value of E_0 could be different in the present cases since it depends, to some extent, on the relaxation energy.

We calculated the relative chemical shift of each C 1s level in a molecule by the following equation,

$$\Delta E_i = E_i - E_0 = 22.67 q_i + 14.39 \sum_{j \neq i} (q_j/R_{ij}) \quad (6)$$

The results are given in Table 5. In all molecules studied here, the difference between the relative chemical shifts of the C 1s levels is predicted to be less than 0.6 eV. This implies that the splitting of the C 1s levels is less than 0.6 eV in agreement with the results of observation. In effect, when we simulated the C 1s peak shape, by using the calculated relative chemical shifts, a good agreement was obtained in all cases between the observed and predicted peak shape as shown in Fig. 6.

If we consider that the binding energy of the observed C 1s peak gives the average of the binding energies of the C 1s levels in the molecule, we can derive the following relation.

$$E_0 = E_{obsd} - \langle\Delta E\rangle \quad (7)$$

where $\langle\Delta E\rangle$ is the average of the relative chemical shifts calculated by Eq. 6. Using the observed C 1s binding energy and the calculated $\langle\Delta E\rangle$, we estimated E_0 for each compound. The results are given in the last column of Table 5. Note that the E_0 values thus obtained are about 292 eV in all cases. The above values are about 2 eV larger than the E_0 value which we have previously obtained for the monosubstituted benzenes. As we have already mentioned, E_0 is dependent partly on the relaxation energy which should, in principle, vary depending on the electronic structure of each molecule. One might reasonably assume that the contribution of relaxation energy is nearly the same for the molecules of the same type as in the case of monosubstituted benzenes. However, it can be appreciably different for the type of molecules studied here from that for benzene derivatives. Seemingly, the difference between the E_0 value obtained in the present study and that previously obtained for benzene derivatives, demonstrates the importance of the contribution of the relaxation energy.

TABLE 6. N1s BINDING ENERGY AND CNDO/2 CHARGE OF THE N ATOM OF C≡N GROUP

	N1s binding energy [eV]	CNDO/2 charge
CH_3CN	405.6	−0.160
CH_3CH_2CN	405.3	−0.162
$CH_2\text{=}CH(CN)$	405.3	−0.152
$\overset{CN}{\underset{NC}{CH\text{=}CH}}$	405.9	−0.140
C_6H_5CN	405.0	−0.166
(N_2	409.9	0.000)

For the four molecules studied here, one can not expect a splitting of N 1s level. In effect, N 1s spectrum appeared as a single sharp peak. The observed binding energies are given in Table 6. As compared with the N 1s binding energy of the nitrogen molecule (409.9 eV), the observed N 1s binding energy is smaller by more than 4 eV in the cases of acetonitrile, propionitrile and acrylonitrile, and by 3 eV in the case of fumaronitrile. This fact indicates that the nitrogen atoms of the C≡N group is negatively charged by considerable amount. This is consistent with the results of CNDO/2 calculation.

Core-electron peaks of XPS spectra are often accompanied by satellites associated with the shake-up or shake-off transitions. In the present study, a prominent satellite was able to be observed only in the case of the N 1s peak of fumaronitrile. In this case, a satellite band is at 4.5 eV from the main N 1s peak as shown in Fig. 7.

According to the theory based on the sudden approximation, the relative probability of a shake-up process which yields the final state Ψ_k where a secondary

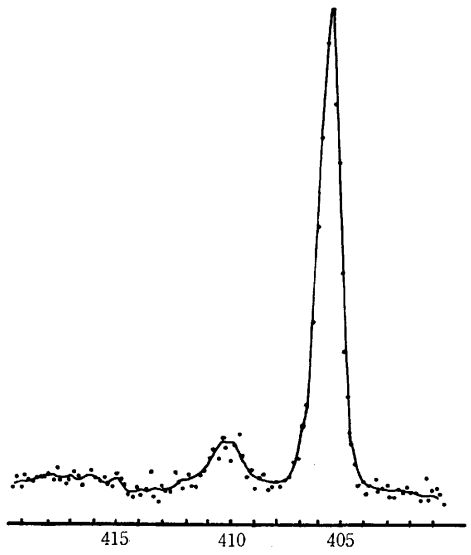

Fig. 7. N 1s spectrum of fumaronitrile: Note that there is a satellite peak at 4.5 eV from the primary peak.

excitation of a valence electron has occurred simultaneously with the photoionization of a core-electron level, can be given as follows;

$$P_k = |\langle \Phi_0 | \Psi_k \rangle|^2$$

where Φ_0 is the wave function of the core-hole ion, in which the valence-electron orbitals are taken the same as in the neutral molecule. By using the molecular orbitals obtained by CNDO/2 method,[15] we estimated the relative probabilities of various shake-up processes. In agreement with the observation, the above calculations predict the presence of a strong shake-up satellite only for the N 1s peak of fumaronitrile. In this case, the shake-up process associated with the lowest π-π^* transition was predicted to have probability of 10.8% relative to the total photoionization cross section of the N 1s level. No shake-up process is predicted to have a relative probability of more than 5% for the photoionizations of the C 1s levels of the same molecule. In the cases of the orther three molecules, all shake-up processes were predicted to have a relative probability of less than 5% for the ionizations of the C 1s levels as well as for those of the N 1s levels.

References

1) C. Baker and D. W. Turner, *Proc. R. Soc. London, Ser. A*, **308**, 19 (1968).
2) R. F. Lake and H. Thompson, *Proc. R. Soc., London Ser. A*, **317**, 187, (1970).
3) H. Bock and H. Stafast, *Chem. Ber.*, **105**, 1158 (1972).
4) I. Ikemoto, K. Samizo, T. Fujikawa, K. Ishii, T. Ohta, and H. Kuroda, *Chem. Lett.*, **1974**, 785.
5) P. Baybutt, M. F. Guest, and I. H. Hillier, *Mol. Phys.*, **25**, 1025 (1973).
6) T. Fujikawa, T. Ohta, and H. Kuroda, *Chem. Phys. Lett.*, **28**, 433 (1974).
7) The pressure of the sample vapor, read just after the needle valve of the gas-handling system was about 0.2 Torr. The actual vapor pressure in the ionization chamber is likely to be one order less than the above value.
8) For example, refer the following paper; U. Gelius and K. Siegbahn, *Faraday Discuss. Chem. Soc.*, **54**, 257 (1972).
9) We used Gelius' values for the relative cross sections of atomic orbitals.
10) The results obtained in our previous work on the UPS spectra of tetracyanoethylene and tetracyano-*p*-quinodimethane,[4] are also included in this figure.
11) On fluoromethanes, the following relation was given by Shirley *et al.*[12] between the observed ionization potential and the CNDO/2 orbital

$$IP = 0.8(-\varepsilon)$$

12) M. S. Banna, B. E. Mills, D. W. Davis, and D. A. Shirley, *J. Chem. Phys.*, **61**, 4780 (1974).
13) K. Siegbahn, C. Nordling, G. Johansson, J. Hedman, P. F. Heden, K. Hamrin, U. Gelius, T. Bergmank, L. O. Werme, R. Manne, and Y. Baer, "ESCA applied to Free Molecules," North-Holland, Amsterdam (1969).
14) T. Ohta, T. Fujikawa, and H. Kuroda, *Bull. Chem. Soc. Jpn.*, **48**, 2017 (1975).
15) The equivalent-core approximation was used to calculate the molecular orbitals of the core-hole ions. The method of calculation was described in our previous paper.[14]

The Structure of the Cyclodextrin Complex. II. The Crystal Structure of α-Cyclodextrin-Methyl Orange (2 : 1) Complex

Kazuaki HARATA

Research Institute for Polymers and Textiles, Sawatari-4, Kanagawa-ku, Yokohama 221

(Received December 25, 1975)

α-Cyclodextrin(α-CDx) forms 2 : 1 complexes with Methyl Orange sodium salt (MONa) and Methyl Orange potassium salt (MOK). The structures were investigated by the X-ray method. The crystals of both complexes belongs to the orthorhombic space group $P2_12_12$ with $Z=2$; the cell dimensions are $a=22.099(6)$, $b=16.359(3)$, and $c=8.296(1)$ Å for the MONa complex, and $a=22.120(4)$, $b=16.419(4)$, and $c=8.292(1)$ Å for the MOK complex. Weak streaks were observed between the layer lines in the oscillation photographs around the c* axis. The structures were determined by using 1566 reflections for the MONa complex and 2544 reflections for the MOK complex, and were refined by the least-squares method to the final R-values of 0.11 and 0.10 respectively. α-CDx is a doughnut-shaped molecule with a large cavity. The crystals have channel structures built up by the stacking of α-CDx rings along the c axes. The Methyl Orange anions are located in the channel with a statistical disorder of four different arrangements. The azo group and the benzene ring are included in the cavity of α-CDx, but the dimethylamino and sulfonato groups protrude from the cavity and are in contact with the adjacent α-CDx rings. The azo group is located at the "neck" of the cavity. The sulfonato group is hydrogen-bonded to the primary hydroxyl groups of α-CDx. No significant structural difference was observed between the MONa complex and the MOK complex.

Cyclodextrins, which are cyclic oligosaccharides consisting of α-1,4-linked D-glucose residues, have a cavity in the center of the molecule and form inclusion complexes with a number of organic compounds. Lautsch and his co-workers have used cyclodextrin-dye complexes as an enzyme model.[1] Cramer *et al.*[2] have measured the rate constants and equilibrium constants for the association of α-cyclodextrin (α-CDx) with a series of azo dyes, and suggested that the dyes are enclosed in the cyclodextrin ring. They have also indicated that α-CDx and Methyl Orange can form complexes with higher stoichiometric ratio than a 1 : 1 ratio.

The crystal structures of several α-CDx complexes have been determined by X-ray analysis,[3-8] and it has been shown that the "guest" molecule is included in the cavity of α-CDx. α-CDx forms a 2 : 1 complex with Methyl Orange. The cell dimensions and the space group of Methyl Orange complex have been determined by McMullan *et al.*[9] and it has been suggested that the structure is of a channel type. The reported space group is $P2_12_12_1$, but we have found that the α-CDx-Methyl Orange complex crystallizes in the space group of $P2_12_12$, the same as that of the α-CDx-potassium acetate complex.[3] A Methyl Orange anion is longer than the depth of the cavity of α-CDx. Therefore, it is of interest to know in what manner Methyl Orange forms the complex with α-CDx. The present X-ray analysis was undertaken in order to find the geometry of the complex and the interaction between α-CDx and Methyl Orange. Both salts, sodium (MONa) and potassium (MOK), were studied in order to investigate the effect of cations in the complex structure.

Experimental

Crystals of α-CDx-Methyl Orange complexes, which were obtained by cooling a hot aqueous solution containing α-CDx and Methyl Orange with a 2 : 1 molar ratio, are orange prisms elongated along the c axis. The density was measured by the flotation method in a mixture of chloroform and hexane. On oscillation photographs around the c* axis, weak streaks were found between the layer lines, as is shown in Fig. 1. The intensity data were measured on a Rigaku AFC four-circle diffractometer with a 2θ-ω scanning mode. The crystal was enclosed in a quartz capillary with a small amount of solvent, since the crystal breaks up in air. For the MONa complex, 3108 independent reflections were obtained with a graphite monochromatized Mo$K\alpha$ radiation up to 50° in 2θ, by using a specimen with dimensions of $0.3\times0.5\times0.5$ mm, but 1542 reflections with $|F_o|<3\sigma(F)$ were considered to be unobserved. For the MOK complex, four sets of independent reflections were obtained with Cu$K\alpha$ radiation up to 120° in 2θ, by using two specimens with dimensions of $0.2\times0.4\times0.4$ mm and $0.3\times0.3\times0.4$ mm. By averaging the intensities of equivalent reflections, 2544 reflections with $|F_o|>3\sigma(F)$ were used for the structure determination. The usual LP corrections were applied, but no correction was made for absorption and extinction. The crystal data are shown in Table 1.

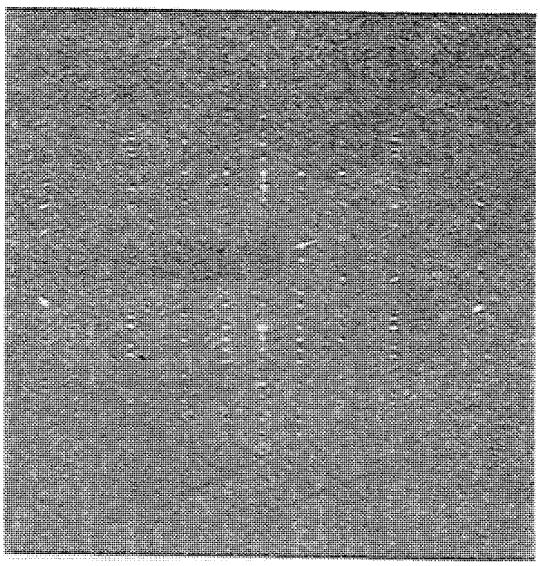

Fig. 1. An oscillation photograph around the c* axis.

TABLE 1. CRYSTAL DATA

		α-Cyclodextrin-Methyl Orange sodium salt complex $C_{36}H_{60}O_{30}\cdot 0.5C_{14}H_{14}O_3N_3SNa\cdot 9.75H_2O$	α-Cyclodextrin-Methyl Orange potassium salt complex $C_{36}H_{60}O_{30}\cdot 0.5C_{14}H_{14}O_3N_3SK\cdot 9.75H_2O$
Molecular weight		1312.2	1320.2
Cell dimensions	a	22.099(6) Å	22.120(4) Å
	b	16.359(3)	16.419(4)
	c	8.296(1)	8.292(1)
Cell volume	V	2998.9Å^3	3011.7Å^3
Space group		$P2_12_12$	$P2_12_12$
	Z	2	2
Density	D_0	1.45 g·cm^{-3}	1.48 g·cm^{-3}
	D_c	1.45	1.46

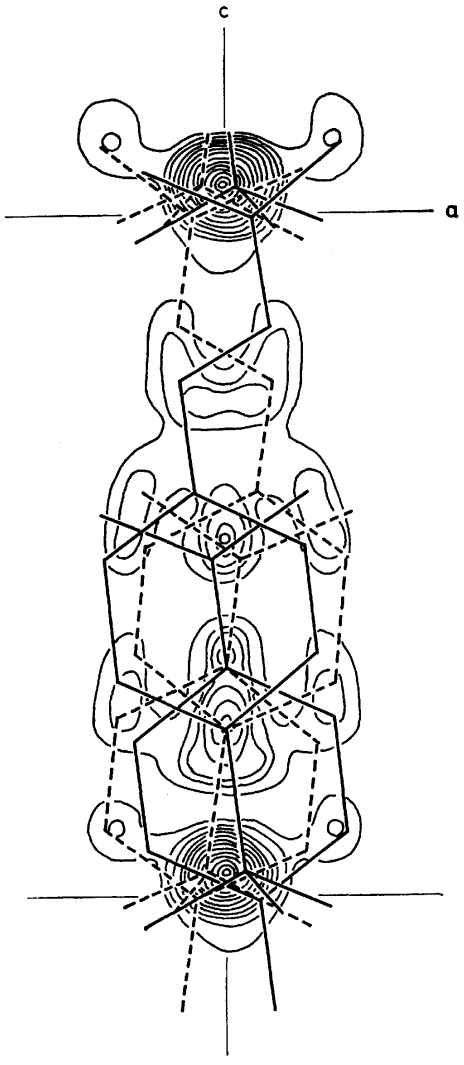

Fig. 2. The $Y=0$ section of a three-dimensional electron density map calculated by using the phases on the basis of α-cyclodextrin, showing Methyl Orange anion. The contours are at an arbitrary interval. The solid line represents a Methyl Orange anion and its shifted one overlapped in the same cell, and the broken line shows the anions related by the two-fold symmetry.

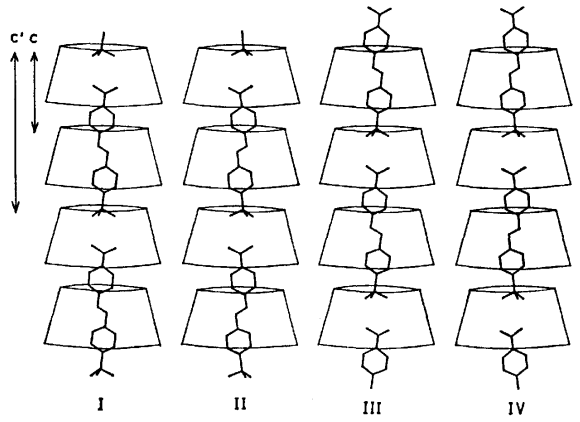

Fig. 3. Schematic drawings of the four arrangements of the Methyl Orange anion in the channel.

Determination and Refinement of the Structure

The cell dimensions of the crystals are similar to those of the α-CDx-potassium acetate complex[3] with the same space group. The potassium acetate complex gives $a=21.89$, $b=16.54$, and $c=8.30$ Å, and the space group is $P2_12_12$. Therefore, we considered that the framework of the crystal structure is the same as that of the potassium acetate complex. The positions and orientations of glucose residues were refined by the rigid-body least-squares method, starting from the same set of coordinates with the potassium acetate complex. Then, the parameters of each atom in α-CDx were refined by the block-diagonal least-squares method. At this stage, a Fourier map was calculated (Fig. 2). It showed that the Methyl Orange anion is located on the two-fold axis. The strongest peak was assigned to the sulfur atom of the sulfonato group; the arrangement of the anion was then considered to be as is shown in Fig. 2. The Methyl Orange anion is asymmetric, and in order to satisfy the two-fold symmetry required by the space group, the transposed structure must be considered. Since the length of the anion is nearly twice the c lattice unit, the shifted arrangement of anions along the c axis must be equally populated to accommodate a long molecule in a short cell. Therefore, the structure of the crystal must be

TABLE 2. FINAL ATOMIC COORDINATES AND THERMAL FACTORS ($\times 10^4$)
The anisotropic thermal factors are of the form:
$\exp[-(B_{11}h^2+B_{22}k^2+B_{33}l^2+B_{12}hk+B_{23}kl+B_{31}lh)]$.
OC indicates the occupancy factor.

α-Cyclodextrin-Methyl Orange Sodium Salt

	OC	x	y	z	B_{11}	B_{22}	B_{33}	B_{12}	B_{23}	B_{31}
C(1,G1)	1.00	1536(8)	2422(12)	3532(23)	22(5)	55(10)	140(32)	6(12)	19(36)	14(23)
C(2,G1)	1.00	1263(7)	2842(10)	4925(22)	16(4)	34(8)	144(28)	-10(10)	2(29)	-6(20)
C(3,G1)	1.00	613(7)	2603(10)	5132(19)	21(4)	32(8)	71(22)	5(9)	9(24)	-1(17)
C(4,G1)	1.00	252(7)	2775(10)	3596(18)	21(4)	36(8)	86(23)	-14(11)	11(27)	6(19)
C(5,G1)	1.00	559(9)	2346(12)	2178(23)	25(5)	48(10)	141(31)	3(13)	15(32)	-16(23)
C(6,G1)	1.00	267(9)	2635(14)	560(22)	24(5)	86(13)	145(32)	-6(15)	-33(39)	-5(23)
O(2,G1)	1.00	1587(5)	2651(8)	6354(14)	23(3)	56(7)	115(18)	-9(8)	-14(22)	-58(14)
O(3,G1)	1.00	324(6)	3033(8)	6470(15)	26(3)	56(6)	134(20)	4(9)	-35(23)	-10(16)
O(4,G1)	1.00	-336(5)	2428(7)	3793(13)	20(3)	37(5)	105(17)	4(7)	25(19)	1(14)
O(5,G1)	1.00	1184(5)	2627(8)	2092(13)	21(3)	51(6)	106(18)	-6(8)	52(20)	-1(14)
O(6,G1)	0.65	517(10)	2237(14)	-615(20)	41(7)	76(13)	67(26)	33(17)	4(33)	-3(23)
O(6',G1)	0.35	286(22)	3304(27)	113(54)	58(17)	73(24)	266(92)	-16(34)	223(89)	-153(72)
C(1,G2)	1.00	2488(9)	-549(11)	3461(22)	31(6)	41(9)	115(29)	10(12)	-8(30)	3(25)
C(2,G2)	1.00	2642(8)	-17(12)	4881(20)	21(5)	47(9)	111(25)	-1(12)	52(34)	-17(21)
C(3,G2)	1.00	2142(8)	663(10)	5117(20)	21(5)	30(8)	88(24)	-4(10)	-9(26)	2(19)
C(4,G2)	1.00	2059(8)	1137(10)	3594(20)	25(5)	34(8)	93(25)	1(10)	25(28)	-1(21)
C(5,G2)	1.00	1993(9)	574(11)	2102(19)	27(5)	40(9)	77(23)	20(12)	12(26)	-3(21)
C(6,G2)	1.00	2094(10)	1040(14)	509(22)	39(7)	72(13)	100(30)	11(16)	14(34)	-31(24)
O(2,G2)	1.00	2645(6)	-517(7)	6316(16)	37(5)	46(6)	146(21)	9(9)	16(23)	-72(19)
O(3,G2)	1.00	2326(5)	1227(7)	6326(14)	25(3)	39(6)	98(17)	-7(7)	18(20)	-12(15)
O(4,G2)	1.00	1545(5)	1578(6)	3791(13)	22(3)	31(5)	86(16)	3(7)	15(18)	-6(13)
O(5,G2)	1.00	2443(5)	-42(8)	2054(13)	22(3)	44(6)	125(18)	6(8)	16(21)	35(14)
O(6,G2)	0.65	1957(15)	583(14)	-723(26)	91(13)	56(12)	127(38)	31(21)	-4(38)	28(41)
O(6',G2)	0.35	2597(24)	1297(28)	107(58)	65(18)	81(26)	203(82)	-56(36)	183(87)	61(68)
C(1,G3)	1.00	834(8)	-2935(11)	3544(26)	21(5)	35(9)	192(36)	13(11)	-5(34)	-1(25)
C(2,G3)	1.00	1251(8)	-2890(12)	5019(27)	15(5)	58(10)	217(37)	7(12)	77(39)	0(23)
C(3,G3)	1.00	1477(7)	-2011(11)	5173(19)	11(4)	49(9)	101(25)	-12(10)	-46(29)	25(17)
C(4,G3)	1.00	1789(7)	-1738(10)	3553(20)	16(4)	38(8)	121(26)	-7(10)	55(29)	14(20)
C(5,G3)	1.00	1359(8)	-1833(11)	2167(19)	24(5)	47(9)	67(23)	-21(12)	-32(27)	33(18)
C(6,G3)	1.00	1713(10)	-1648(14)	550(22)	31(6)	75(13)	121(30)	-16(15)	29(35)	-33(24)
O(2,G3)	1.00	929(6)	-3158(9)	6289(19)	24(4)	68(8)	26(30)	1(9)	117(31)	5(20)
O(3,G3)	1.00	1936(6)	-1983(8)	6406(14)	29(4)	56(7)	104(18)	-2(9)	17(22)	-32(16)
O(4,G3)	1.00	1890(5)	-865(7)	3802(13)	14(3)	42(5)	87(16)	-6(7)	13(18)	12(13)
O(5,G3)	1.00	1169(5)	-2698(8)	2118(13)	19(3)	55(7)	118(19)	0(8)	-25(21)	20(14)
O(6,G3)	0.55	1320(14)	-1767(19)	-576(33)	53(11)	88(18)	169(53)	-56(24)	44(55)	84(40)
O(6',G3)	0.45	2112(16)	-2132(22)	-33(52)	48(12)	75(21)	375(88)	38(27)	169(82)	182(59)
Na	0.25	1758(19)	4793(40)	629(97)	14(11)	153(43)	1332(275)	-10(37)	-125(209)	201(98)
O(W1)	1.00	3315(7)	8409(10)	671(17)	45(5)	86(9)	146(24)	34(12)	-31(27)	25(19)
O(W2)	1.00	3820(11)	1227(13)	701(21)	117(11)	116(13)	186(31)	-90(21)	60(37)	-59(33)
O(W3)	1.00	4291(14)	9747(15)	3418(31)	141(15)	125(17)	504(58)	-33(27)	99(65)	105(55)
O(W4)	1.00	663(15)	4921(17)	2936(36)	158(16)	111(15)	793(85)	-76(30)	-60(84)	-190(66)
O(W5)	0.75	1582(13)	4936(17)	967(37)	64(10)	86(14)	645(83)	35(21)	46(80)	22(60)
O(W6)	0.25	0(-)	5000(-)	149(83)	90(29)	176(52)	448(157)	126(70)	0(-)	0(-)

Hydrogen Atoms

	OC	x	y	z	B
H(1,G1)	1.00	2013	2574	3336	4.9
H(2,G1)	1.00	1318	3499	4705	3.4
H(3,G1)	1.00	588	1951	5473	2.6
H(4,G1)	1.00	193	3429	3329	3.7
H(5,G1)	1.00	539	1669	2402	4.2
H(61,G1)	0.65	337	3285	396	5.1
H(62,G1)	0.65	-229	2488	555	5.1
H(61',G1)	0.35	407	2250	-446	5.1
H(62',G1)	0.35	-218	2435	501	5.1
H(1,G2)	1.00	2774	-1093	3233	4.2
H(2,G2)	1.00	3108	234	4707	4.0
H(3,G2)	1.00	1723	359	5505	2.7
H(4,G2)	1.00	2438	1604	3414	3.5
H(5,G2)	1.00	1549	227	2212	4.3
H(61,G2)	0.65	2550	1239	404	4.7
H(62,G2)	0.65	1772	1589	491	4.7
H(61',G2)	0.35	1854	753	-502	4.7
H(62',G2)	0.35	1768	1584	484	4.7
H(1,G3)	1.00	615	-3550	3319	4.9
H(2,G3)	1.00	1662	-3260	5164	4.7
H(3,G3)	1.00	1088	-1616	5477	2.8
H(4,G3)	1.00	2214	-2073	3252	2.9
H(5,G3)	1.00	953	-1431	2377	3.3
H(61,G3)	0.55	2074	-2100	397	4.8
H(62,G3)	0.55	1873	-1008	524	4.8
H(61',G3)	0.45	1895	-1019	554	4.8
H(62',G3)	0.45	1403	-1497	-430	4.8

Methyl Orange (OC=0.25)

	x	y	z	B
C(1,M)	23	-210	-2510	4.6
C(2,M)	595	-215	-3207	4.6
C(3,M)	657	-158	-4868	4.6
C(4,M)	146	-95	-5842	4.6
C(5,M)	-426	-90	-5145	4.6
C(6,M)	-488	-147	-3484	4.6
N(1,M)	208	-36	-7562	4.6
N(2,M)	-231	-100	1682	5.4
C(7,M)	-174	-114	-14	5.4
C(8,M)	-687	-128	-985	5.4
C(6,M)	-629	-142	-2651	5.4
C(10,M)	-59	-142	-3356	5.4
C(11,M)	455	-128	-2385	5.4
C(12,M)	397	-114	-719	5.4
N(3,M)	-1	-156	-4992	5.4
C(13,M)	-534	-170	-5962	5.4
C(14,M)	590	-156	-5719	5.4
S(1,M)	-82	-66	-475	4.3
O(1,M)	-237	740	114	4.3
O(2,M)	-506	-629	263	4.3
O(3,M)	511	-258	163	4.3

represented as a superposition of the four structures, I, II, III, and IV of Fig. 3, whose occupancies are 0.25 each.

The successive Fourier maps revealed the locations of the water molecules and cations. The cations are also statistically disordered with the population of 0.25, since there is only one Methyl Orange molecule in the unit cell in spite of four equivalent positions. On the electron density map, the sodium ion was not distinguished from water because of its low population. The location of the sodium cation was considered to be the same as that of the potassium cation, since no significant structural difference was observed between the MONa complex and the MOK complex. On

TABLE 2 (Continued)

α-Cyclodextrin-Methyl Orange Potassium Salt

	OC	x	y	z	B_{11}	B_{22}	B_{33}	B_{12}	B_{23}	B_{31}
C(1,G1)	1.00	1549(5)	2429(6)	3555(13)	24(3)	31(4)	100(16)	-13(6)	19(16)	17(12)
C(2,G1)	1.00	1259(5)	2844(7)	5025(16)	15(2)	41(5)	180(21)	-17(6)	22(20)	-10(13)
C(3,G1)	1.00	599(5)	2592(7)	5204(14)	18(3)	45(5)	114(18)	-9(6)	9(18)	-36(12)
C(4,G1)	1.00	258(4)	2772(6)	3665(12)	19(2)	29(4)	92(15)	-2(6)	-2(16)	5(11)
C(5,G1)	1.00	560(5)	2353(8)	2266(14)	17(2)	53(6)	124(19)	-2(7)	50(19)	-2(12)
C(6,G1)	1.00	274(5)	2618(10)	579(14)	18(3)	106(10)	125(20)	3(10)	3(27)	19(13)
O(2,G1)	1.00	1613(3)	2640(5)	6406(10)	18(2)	55(4)	157(14)	-3(5)	-38(15)	-35(9)
O(3,G1)	1.00	324(3)	3030(5)	6520(9)	21(2)	57(4)	97(12)	5(5)	-36(13)	9(9)
O(4,G1)	1.00	-336(3)	2423(4)	3849(8)	14(1)	35(3)	110(11)	-9(4)	14(11)	-8(8)
O(5,G1)	1.00	1193(3)	2631(5)	2163(9)	16(2)	53(4)	114(12)	-3(5)	69(13)	1(8)
O(6,G1)	0.65	530(6)	2192(12)	-618(15)	31(4)	124(12)	86(20)	1(12)	-4(28)	-6(15)
O(6',G1)	0.35	259(13)	3354(18)	184(32)	43(9)	90(17)	188(49)	-6(21)	230(53)	-93(36)
C(1,G2)	1.00	2466(5)	-538(7)	3483(16)	14(2)	35(5)	187(22)	5(6)	20(19)	-4(14)
C(2,G2)	1.00	2632(5)	5(8)	4940(14)	17(3)	46(5)	141(17)	-11(7)	2(22)	7(13)
C(3,G2)	1.00	2177(5)	661(7)	5165(13)	16(2)	37(5)	104(17)	-4(6)	12(16)	19(11)
C(4,G2)	1.00	2079(4)	1130(7)	3600(14)	14(2)	45(5)	125(18)	4(6)	7(19)	-11(12)
C(5,G2)	1.00	1990(6)	572(7)	2127(13)	30(3)	34(5)	82(16)	8(7)	-2(16)	3(13)
C(6,G2)	1.00	2061(7)	1052(8)	568(16)	38(4)	48(6)	158(24)	9(7)	23(22)	-10(17)
O(2,G2)	1.00	2668(3)	-517(5)	6339(10)	21(2)	56(4)	141(14)	10(5)	25(14)	-60(10)
O(3,G2)	1.00	2348(3)	1214(5)	6404(10)	24(2)	50(4)	110(12)	-3(5)	-19(13)	-25(9)
O(4,G2)	1.00	1534(3)	1585(4)	3827(10)	17(2)	38(3)	131(13)	-5(4)	24(12)	-3(8)
O(5,G2)	1.00	2443(3)	-57(5)	2089(8)	20(2)	40(3)	116(11)	2(4)	20(13)	34(8)
O(6,G2)	0.70	2007(9)	568(8)	693(16)	79(7)	48(7)	128(22)	16(12)	5(21)	-3(22)
O(6',G2)	0.30	2566(21)	1318(21)	15(66)	68(15)	52(17)	469(113)	-58(28)	144(83)	17(77)
C(1,G3)	1.00	844(5)	-2932(7)	3576(17)	14(2)	36(5)	206(24)	-6(6)	1(21)	9(14)
C(2,G3)	1.00	1266(5)	-2872(7)	5042(16)	18(3)	37(5)	180(22)	-1(6)	26(20)	-3(14)
C(3,G3)	1.00	1498(5)	-2008(7)	5199(13)	17(3)	47(5)	99(18)	-4(6)	11(18)	-1(11)
C(4,G3)	1.00	1791(5)	-1711(7)	3610(13)	17(2)	40(5)	109(17)	3(6)	29(17)	13(12)
C(5,G3)	1.00	1351(5)	-1841(8)	2189(14)	21(3)	50(6)	95(17)	-9(7)	-13(18)	2(12)
C(6,G3)	1.00	1677(6)	-1665(10)	538(14)	29(4)	85(9)	101(20)	-16(10)	16(23)	40(14)
O(2,G3)	1.00	945(4)	-3161(6)	6411(11)	23(2)	68(5)	176(16)	-10(5)	86(17)	-7(11)
O(3,G3)	1.00	1936(3)	-1979(5)	6432(9)	19(2)	61(4)	113(13)	0(5)	34(14)	-7(9)
O(4,G3)	1.00	1894(3)	-867(4)	3831(9)	13(1)	37(3)	105(11)	2(4)	-2(11)	8(8)
O(5,G3)	1.00	1159(3)	-2675(5)	2152(10)	18(2)	51(4)	149(14)	-9(5)	-43(14)	35(9)
O(6,G3)	0.55	1307(7)	-1776(14)	-642(19)	28(4)	140(16)	116(28)	-53(15)	59(38)	-13(19)
O(6',G3)	0.45	2067(11)	-2101(12)	74(30)	51(8)	47(10)	263(46)	-4(14)	-50(40)	142(35)
K	0.25	1747(9)	4846(8)	754(15)	30(3)	56(6)	193(22)	-13(8)	45(21)	-15(15)
O(W1)	1.00	3300(5)	8358(8)	612(12)	52(4)	101(7)	187(19)	67(9)	51(21)	60(15)
O(W2)	1.00	3786(9)	1225(9)	599(17)	116(8)	119(10)	270(30)	-105(16)	-4(30)	-60(28)
O(W3)	1.00	4293(11)	9785(14)	3383(33)	124(10)	160(16)	1040(91)	7(22)	245(79)	222(60)
O(W4)	1.00	669(11)	4927(11)	2998(27)	148(11)	89(9)	808(66)	11(20)	-43(60)	16(52)
O(W5)	0.75	1633(12)	4884(18)	902(31)	102(11)	173(19)	590(68)	11(27)	92(83)	-32(55)
O(W6)	0.25	0(-)	5000(-)	-137(94)	109(28)	297(71)	909(237)	219(80)	0(-)	0(-)

Hydrogen Atoms

	OC	x	y	z	B
H(1,G1)	1.00	2019	2589	3309	3.8
H(2,G1)	1.00	1267	3532	4937	3.9
H(3,G1)	1.00	555	1941	5508	3.1
H(4,G1)	1.00	260	3441	3398	3.3
H(5,G1)	1.00	523	1671	2522	4.0
H(61,G1)	0.65	357	3280	417	5.1
H(62,G1)	0.65	-223	2504	584	5.1
H(61',G1)	0.35	642	2293	-413	5.1
H(62',G1)	0.35	-195	2387	467	5.1
H(1,G2)	1.00	2797	-1056	3437	3.8
H(2,G2)	1.00	3076	297	4781	4.0
H(3,G2)	1.00	1765	361	5601	3.2
H(4,G2)	1.00	2421	1200	4570	3.2
H(5,G2)	1.00	1538	271	2231	3.9
H(61,G2)	0.70	2533	1300	476	5.1
H(62,G2)	0.70	1738	1565	474	5.1
H(61',G2)	0.30	1851	755	-468	5.1
H(62',G2)	0.30	1773	1605	537	5.1
H(1,G3)	1.00	658	-3563	3557	4.0
H(2,G3)	1.00	1664	-3296	4872	4.5
H(3,G3)	1.00	1128	-1604	5601	3.5
H(4,G3)	1.00	2235	-1992	3359	3.4
H(5,G3)	1.00	930	-1493	2422	3.8
H(61,G3)	0.55	2074	-2051	403	5.2
H(62,G3)	0.55	1835	-1002	540	5.2
H(61',G3)	0.45	1881	-1025	596	5.2
H(62',G3)	0.45	1360	-1584	-429	5.2

Methyl Orange (OC=0.25)

	x	y	z	B
C(1,M)	-6	-234	-254	6.7
C(2,M)	573	-180	-3194	6.7
C(3,M)	648	-116	-4851	6.7
C(4,M)	143	-105	-5860	6.7
C(5,M)	-436	-158	-5203	6.7
C(6,M)	-511	-223	-3546	6.7
N(1,M)	217	-38	-7576	6.7
N(2,M)	-234	-30	1728	7.4
C(7,M)	-172	-57	33	7.4
C(8,M)	-683	-123	-944	7.4
C(9,M)	-621	-149	-2609	7.4
C(10,M)	-48	-111	-3306	7.4
C(11,M)	463	-45	-2328	7.4
C(12,M)	401	-19	-663	7.4
N(3,M)	14	-137	-4940	7.4
C(13,M)	-517	-212	-5916	7.4
C(14,M)	608	-89	-5659	7.4
S(1,M)	-88	-69	-406	6.0
O(1,M)	-223	725	274	6.0
O(2,M)	-513	-638	313	6.0
O(3,M)	508	-293	161	6.0

the difference-Fourier map, the residual electron density was observed near the position of the cation. We considered it to be a water molecule (O(W5)) which occupies the position with the occupancy of 0.75 when the cation is absent. The O(6) atoms in α-CDx were found to be disordered. The occupancies were estimated from the electron density map, but they were not refined.

At this stage, the positions, orientations, and thermal parameters of the SO_3^-, C_6H_4–N, and N–C_6H_4–N-$(CH_3)_2$ groups in Methyl Orange were refined by the rigid-body least-squares method. The bond distances and angles were those from Hanson.[10] In the successive block-diagonal least-squares refinement, the positional and thermal parameters of the Methyl Orange anion were fixed, since the absurd bond lengths of 1.2—1.7 Å were found in benzene rings when the atomic parameters of Methyl Orange anion were allowed to move. Hydrogen atoms can not be found on the difference-Fourier map, but the positions of the

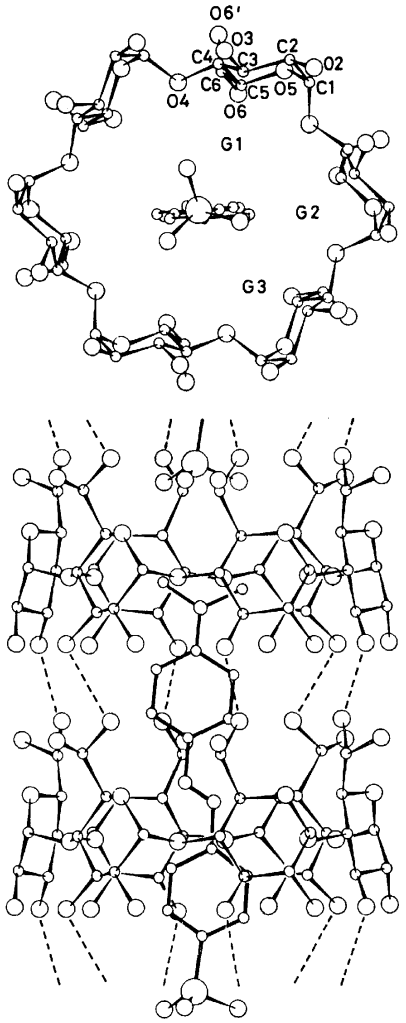

Fig. 4. The structure and numbering scheme of the complex. Dashed lines indicate O(3)···O(6) contacts.

hydrogen atoms attached to the carbon atoms in α-CDx were calculated and included in the structure factor calculation with isotropic thermal factors equal to those of the carbon atoms to which the hydrogen atoms are bonded. The final R-values were 0.11 for the MONa complex and 0.10 for the MOK complex. The quantity minimized was $\Sigma w(|F_o|-|F_c|)^2$ with $w=1.0$ for all the reflections used. The atomic scattering factors were taken from "International Tables for X-Ray Crystallography."[11] The atomic parameters are listed in Table 2, while the observed and calculated structure factors are given in Table 3.*

Description and Discussion of the Structure

The structure of the complex is shown in Fig. 4. Each glucose residue has the Cl chair conformation which is commonly found in α-CDx complexes. The α-CDx molecule is nearly hexagonal and has a two-fold symmetry axis. The α-CDx rings are stacked along the c axis with six hydrogen bonds which connect the O(3) with the O(6) of the adjacent α-CDx molecule, forming channels where Methyl Orange anions are located. The bond distances, angles, and conformation angles are listed in Table 4, the geometrical data for the α-CDx ring are given in Table 6, and the intermolecular distances less than 3.0 Å are shown in Table 7.

Bond Distances and Angles. No significant difference in bond distances and angles is observed between the MONa complex and the MOK complex. The C(1)–O(4*)–C(4*) angles of 117—121° are commonly observed values in α-CDx complexes. Similar values have been also observed in 1,4-linked disaccharides.[12–14]

In both MONa and MOK complexes, abnormally short distances are observed in the disordered C(6)–O(6) bonds. The effects of the thermal motion on the C(6)–O(6) and C(6)–O(6′) bonds were estimated according to Busing and Levy,[15] as is shown in Table 5. The shortening of C–O bonds may be ascribed to the riding motion, since the framework of the α-CDx ring is rigid. The corrected distances, however, are still too short, indicating that the correction for the riding motion is not strictly applicable in this case. The O(6) and O(6′) atoms are bonded to the C(6) atom, whose thermal motion is relatively large. The lower and upper limits for the corrected distances indicate that the effect of thermal motion is remarkably large. The normal C–O distance is found near the midst of the two limits or rather near the upper limit. Kim and Rosenstein[16] have found a similar phenomenon on the disordered C–O bond in α-L-sorbose; the C–O distances are 1.312 and 1.244 Å, and the C–C–O angles are 114.7 and 116.0°. They explained the shortening of the C–O bonds as being due to (1) the statistical overlap of the electron density of oxygen atoms with the hydrogen atoms attached to the carbon atom in the two disordered positions, and (2) a correlation of thermal displacements between C(6) and O(6), O(6)′ which has an effect similar to that of the anti-parallel thermal motion.

Conformation of α-Cyclodextrin. The glucose residues are in the Cl chair conformation and are α-1,4-linked. The disordered primary hydroxyl groups take two orientations: the C(6)–O(6) and C(6)-O(6′) bonds show *gauche-trans* and *gauche-gauche* conformations respectively. A similar disorder has been observed in the 1-propanol complex[7] and the *p*-iodoaniline complex.[8]

The macro-cyclic conformation of α-CDx is described by the conformation angles involving C(1)–O(4*)–C(4*) linkages: C(2)–C(1)–O(4*)–C(4*), O(5)–C(1)–O(4*)–C(4*)–C(1)–O(4*)–C(4*)–C(3*), and C(1)–O(4*)–C(4*)–C(5*). These angles in the Methyl Orange complexes are similar to those in the *p*-iodoaniline complex,[8] but a significant difference is observed in the water complex.[5] The two glucose residues in the water complex are inclined towards the inside of the cavity, thus reducing the empty volume and forming a hydrogen bond with water in it.

The α-CDx ring is distorted from the regular hexago-

* Table 3 is kept at the office of the Chemical Society of Japan. (Document No. 7619)

TABLE 4. BOND DISTANCES(l/Å), ANGLES(ϕ/°), AND CONFORMATION ANGLES(ϕ/°)
An asterisk(*) indicates the atom in the adjacent glucose residue.

α-Cyclodextrin-Methyl Orange Sodium Salt Complex

	G1	G2	G3	AVERAGE
C(1)-C(2)	1.475(26)	1.504(26)	1.534(27)	1.504
C(1)-O(5)	1.465(22)	1.435(22)	1.448(22)	1.449
C(1)-O(4*)	1.397(22)	1.447(22)	1.395(22)	1.413
C(2)-C(3)	1.499(24)	1.581(24)	1.528(26)	1.536
C(2)-O(2)	1.420(21)	1.445(22)	1.345(25)	1.403
C(3)-C(4)	1.529(23)	1.493(24)	1.575(23)	1.532
C(3)-O(3)	1.462(20)	1.422(20)	1.440(20)	1.441
C(4)-C(5)	1.529(25)	1.550(24)	1.499(24)	1.526
C(4)-O(4)	1.427(19)	1.355(20)	1.460(20)	1.414
C(5)-C(6)	1.563(28)	1.542(27)	1.582(27)	1.562
C(5)-O(5)	1.455(22)	1.417(21)	1.477(21)	1.450
C(6)-O(6)	1.297(29)	1.302(34)	1.290(36)	1.296
C(6)-O(6')	1.156(50)	1.233(54)	1.280(44)	1.223

	G1	G2	G3	AVERAGE
C(2)-C(1)-O(5)	108.3(1.5)	108.6(1.5)	109.4(1.5)	108.8
C(2)-C(1)-O(4*)	110.3(1.5)	105.2(1.4)	109.1(1.5)	108.2
O(5)-C(1)-O(4*)	111.0(1.4)	107.6(1.4)	111.3(1.4)	110.0
C(1)-C(2)-C(3)	111.1(1.5)	110.2(1.4)	108.0(1.5)	109.8
C(1)-C(2)-O(2)	110.2(1.4)	108.6(1.4)	106.9(1.6)	108.6
C(3)-C(2)-O(2)	109.3(1.4)	107.4(1.4)	114.4(1.6)	110.4
C(2)-C(3)-C(4)	110.9(1.3)	110.3(1.4)	109.8(1.4)	110.3
C(2)-C(3)-O(3)	112.3(1.3)	110.1(1.3)	108.7(1.4)	110.4
C(4)-C(3)-O(3)	108.5(1.3)	107.2(1.3)	106.8(1.3)	107.5
C(3)-C(4)-C(5)	109.0(1.4)	112.3(1.4)	110.4(1.3)	110.6
C(3)-C(4)-O(4)	107.8(1.3)	106.2(1.3)	102.9(1.2)	105.6
C(5)-C(4)-O(4)	108.1(1.3)	109.5(1.3)	107.8(1.3)	108.5
C(4)-C(5)-C(6)	109.8(1.5)	112.2(1.5)	108.5(1.4)	110.2
C(4)-C(5)-O(5)	108.3(1.4)	112.3(1.4)	107.5(1.3)	109.4
C(6)-C(5)-O(5)	104.8(1.5)	103.0(1.4)	107.5(1.4)	105.1
C(5)-C(6)-O(6)	108.5(1.8)	110.8(2.0)	104.6(2.0)	108.0
C(5)-C(6)-O(6')	123.1(2.9)	122.1(2.9)	122.9(2.4)	122.7
C(1)-O(5)-C(5)	113.1(1.3)	115.9(1.3)	112.4(1.3)	113.8
C(1)-O(4*)-C(4*)	121.3(1.3)	117.5(1.2)	117.7(1.3)	118.8

	G1	G2	G3	AVERAGE
C(1)-C(2)-C(3)-C(4)	-56.4	-54.6	-55.3	-55.4
C(2)-C(3)-C(4)-C(5)	54.8	47.8	56.6	53.1
C(3)-C(4)-C(5)-O(5)	-56.4	-47.7	-57.7	-53.9
C(4)-C(5)-O(5)-C(1)	62.1	54.8	63.8	60.2
C(5)-O(5)-C(1)-C(2)	-62.6	-61.0	-65.2	-62.9
O(5)-C(1)-C(2)-C(3)	57.9	58.6	59.6	58.7
O(4*)-C(1)-C(2)-O(2)	57.6	61.0	61.2	59.9
O(2)-C(2)-C(3)-O(3)	60.3	69.2	69.3	66.3
O(3)-C(3)-C(4)-O(4)	-64.4	-72.7	-71.0	-69.4
O(4)-C(4)-C(5)-C(6)	72.9	79.1	74.6	75.5
O(5)-C(5)-C(6)-O(6)	66.7	67.6	62.0	65.4
O(5)-C(5)-C(6)-O(6')	-52.9	-51.3	-44.7	-49.6
C(4)-C(5)-C(6)-O(6)	-177.2	-171.4	178.0	-176.9
C(4)-C(5)-C(6)-O(6')	63.2	69.8	71.3	68.1
C(2)-C(1)-O(4*)-C(4*)	-129.2	-134.6	-127.1	-130.3
O(5)-C(1)-O(4*)-C(4*)	110.8	110.7	112.1	111.2
C(1)-O(4*)-C(4*)-C(3*)	127.5	130.8	126.6	128.3
C(1)-O(4*)-C(4*)-C(5*)	-111.0	-112.6	-115.8	-113.1

nal symmetry. In the hexagon composed of O(4) atoms, the diagonal O(4,G3)···O(4,G3)* distance is longer by 0.8 Å than the O(4,G1)···O(4,G1)* distance (Table 6). In the 1-propanol complex, the diagonal O(4)···O(4) distances are 8.35—8.57 Å, indicating a nearly regular hexagon. In Methyl Orange complexes, the planarity of the six O(4) atoms is remarkably good; the deviation from the plane are less than 0.006 Å in the MONa complex and 0.012 Å in the MOK complex. In the other α-CDx complexes, the planarity is also rather good. The maximum deviations are 0.136 Å in the water complex, 0.144 Å in the 1-propanol complex, and 0.132 Å in the *p*-iodoaniline complex.

The α-CDx ring is tapered to the O(6) side. The diagonal distances of the cavity are smaller on the O(6) side than on the O(2), O(3) side (Table 6). Although the diagonal O(6)···O(6)* distances are shorter than the C(5)···C(5)* distances, the C(5)–H groups are oriented to the inside of the cavity and the diagonal H···H* distances are smaller than O(6)···O(6)* distances. This neck in the cavity is important in the geometry of the complex. The "guest" molecule may be included in the cavity to fit the slender part of the molecule to the "neck", as in the complexes with iodine and *p*-iodoaniline.

Geometry of Inclusion. The α-CDx molecules are stacked along the c axis to form endless channels with a head-to-tail arrangement, and the "guest" Methyl Orange anions are arranged in the channel. The azo group and one benzene ring are included

TABLE 4. (Continued)

α-Cyclodextrin-Methyl Orange Potassium Salt Complex

	G1	G2	G3	AVERAGE
C(1)-C(2)	1.538(16)	1.544(16)	1.538(16)	1.540
C(1)-O(5)	1.437(13)	1.399(13)	1.435(14)	1.424
C(1)-O(4*)	1.400(13)	1.406(13)	1.418(13)	1.408
C(2)-C(3)	1.522(16)	1.482(16)	1.508(16)	1.504
C(2)-O(2)	1.427(14)	1.442(14)	1.422(15)	1.430
C(3)-C(4)	1.512(15)	1.523(15)	1.545(15)	1.527
C(3)-O(3)	1.441(14)	1.419(13)	1.410(13)	1.423
C(4)-C(5)	1.506(15)	1.540(16)	1.545(16)	1.530
C(4)-O(4)	1.441(12)	1.426(13)	1.413(13)	1.427
C(5)-C(6)	1.597(18)	1.521(18)	1.574(18)	1.564
C(5)-O(5)	1.473(14)	1.436(13)	1.428(14)	1.446
C(6)-O(6)	1.340(21)	1.317(21)	1.287(23)	1.315
C(6)-O(6')	1.244(31)	1.287(48)	1.184(26)	1.238

	G1	G2	G3	AVERAGE
C(2)-C(1)-O(5)	107.8(0.8)	109.5(0.9)	109.7(0.9)	109.0
C(2)-C(1)-O(4*)	107.4(0.9)	105.8(0.9)	108.5(0.9)	107.2
O(5)-C(1)-O(4*)	110.0(0.8)	110.6(0.9)	110.1(0.9)	110.2
C(1)-C(2)-C(3)	110.9(0.9)	110.8(0.9)	109.5(0.9)	110.4
C(1)-C(2)-O(2)	107.6(0.9)	107.7(0.9)	107.9(0.9)	107.7
C(3)-C(2)-O(2)	112.5(0.9)	111.5(0.9)	114.4(0.9)	112.8
C(2)-C(3)-C(4)	110.0(0.9)	110.8(0.9)	111.3(0.9)	110.7
C(2)-C(3)-O(3)	110.0(0.9)	111.9(0.9)	109.0(0.9)	110.3
C(4)-C(3)-O(3)	109.3(0.9)	109.6(0.9)	108.7(0.9)	109.2
C(3)-C(4)-C(5)	109.9(0.9)	113.4(0.9)	110.1(0.9)	111.1
C(3)-C(4)-O(4)	106.7(0.8)	105.8(0.8)	105.4(0.8)	106.0
C(5)-C(4)-O(4)	107.7(0.8)	107.8(0.9)	109.5(0.8)	108.3
C(4)-C(5)-C(6)	112.0(0.9)	110.9(1.0)	110.6(0.9)	111.2
C(4)-C(5)-O(5)	108.9(0.9)	110.7(0.9)	109.6(0.9)	109.7
C(6)-C(5)-O(5)	103.9(0.9)	106.3(0.9)	106.9(0.9)	105.7
C(5)-C(6)-O(6)	109.8(1.2)	110.8(1.2)	110.3(1.3)	110.3
C(5)-C(6)-O(6')	120.4(1.6)	124.5(2.3)	120.4(1.6)	121.8
C(1)-O(5)-C(5)	113.8(0.8)	114.3(0.8)	113.9(0.8)	114.0
C(1)-O(4*)-C(4*)	118.0(0.8)	118.2(0.8)	118.0(0.8)	118.1

	G1	G2	G3	AVERAGE
C(1)-C(2)-C(3)-C(4)	-55.8	-52.0	-53.8	-53.9
C(2)-C(3)-C(4)-C(5)	56.4	47.0	52.6	52.0
C(3)-C(4)-C(5)-O(5)	-57.9	-47.2	-54.0	-53.0
C(4)-C(5)-O(5)-C(1)	62.5	56.5	61.0	60.0
C(5)-O(5)-C(1)-C(2)	-60.6	-62.2	-62.7	-61.8
O(5)-C(1)-C(2)-C(3)	56.4	59.4	57.2	57.7
O(4*)-C(1)-C(2)-O(2)	61.2	62.6	62.0	61.9
O(2)-C(2)-C(3)-O(3)	63.6	65.6	65.3	64.8
O(3)-C(3)-C(4)-O(4)	-66.6	-71.0	-69.5	-69.0
O(4)-C(4)-C(5)-C(6)	72.1	78.3	72.9	74.3
O(5)-C(5)-C(6)-O(6)	66.6	57.3	60.5	61.5
O(5)-C(5)-C(6)-O(6')	-60.6	-47.9	-51.3	-53.3
C(4)-C(5)-C(6)-O(6)	-176.1	177.7	179.8	-179.5
C(4)-C(5)-C(6)-O(6')	56.6	72.5	67.9	65.7
C(2)-C(1)-O(4*)-C(4*)	-130.5	-132.6	-127.9	-130.3
O(5)-C(1)-O(4*)-C(4*)	112.5	109.2	112.0	111.2
C(1)-O(4*)-C(4*)-C(3*)	126.2	130.2	127.3	127.9
C(1)-O(4*)-C(4*)-C(5*)	-112.3	-111.4	-115.0	-112.9

in the cavity; the azo group is located at the "neck" of the cavity. The dimethylamino and sulfonato groups protrude from the O(6) side and the O(2), O(3) side of the cavity respectively, and they are included in the cavities of the adjacent α-CDx molecules. The sulfonato group is located on the O(6) side of the cavity. In the potassium acetate complex, the acetate anion is located on the plane perpendicular to the c axis at a position similar to that of the sulfonato group. It is important that the ionized groups occupy the same position in both complexes, although the dimensions and shapes of the "guest" molecules are quite different. The sulfonato group may be hydrogen-bonded to the primary hydroxyl groups; the distances between oxygen atoms are 2.72, 2.89, 3.02, 3.11, 3.31, and 3.56 Å in the MONa complex, and 2.66, 3.01, 3.05, 3.08, 3.41, and 3.76 Å in the MOK complex. In the potassium acetate complex, the acetate anion is also hydrogen-bonded to four of the primary hydroxyl groups.

The Methyl Orange anion is almost planar except for the sulfonato group. The distortion of the hexagonal α-CDx ring may be ascribed to the inclusion of the bulky and planar "guest" molecule. A similar distortion has been observed in the *p*-iodoaniline complex.[8] The location of the benzene ring is nearly the same in the Methyl Orange complexes and in the *p*-iodoaniline complex. In both complexes, the longest diagonal O(4)···O(4)* distance is found to be nearly parallel to the benzene plane.

Crystal Structure. The framework of the crystal consists of stacked α-CDx molecules along the c axis.

TABLE 5. CORRECTED BOND DISTANCES, UPPER AND LOWER BOUNDS FOR THE C(6)-O(6) AND C(6)-O(6′) BONDS(l/Å)

	Uncorrected	Corrected for riding motion	Lower bound	Upper bound
(1) MONa complex				
C(6,G1)-O(6,G1)	1.297	1.302	1.297	1.549
C(6,G1)-O(6′,G1)	1.156	1.186	1.159	1.428
C(6,G2)-O(6,G2)	1.302	1.341	1.306	1.632
C(6,G2)-O(6′,G2)	1.233	1.259	1.236	1.503
C(6,G3)-O(6,G3)	1.290	1.294	1.290	1.572
C(6,G3)-O(6′,G3)	1.280	1.287	1.280	1.507
(2) MOK complex				
C(6,G1)-O(6,G1)	1.340	1.359	1.342	1.604
C(6,G1)-O(6′,G1)	1.244	1.261	1.245	1.438
C(6,G2)-O(6,G2)	1.317	1.356	1.322	1.613
C(6,G2)-O(6′,G2)	1.287	1.340	1.297	1.577
C(6,G3)-O(6,G3)	1.287	1.325	1.291	1.601
C(6,G3)-O(6′,G3)	1.184	1.193	1.185	1.439

TABLE 6. GEOMETRICAL DATA FOR THE HEXAGON DESCRIBED BY THE O(4) ATOMS

An asterisk(*) indicates the atom in the opposite glucose residue.

(1) Diagonal distances in the α-CDx ring (l/Å)

i) MONa complex

O(4,G1)-O(4,G1)*	8.08	O(6,G1)-O(6,G1)*	7.86
O(4,G2)-O(4,G2)*	8.56	O(6,G2)-O(6,G2)*	8.86
O(4,G3)-O(4,G3)*	8.82	O(6,G3)-O(6,G3)*	8.21
C(3,G1)-C(3,G1)*	8.94	C(5,G1)-C(5,G1)*	8.06
C(3,G2)-C(3,G2)*	9.71	C(5,G2)-C(5,G2)*	9.01
C(3,G3)-C(3,G3)*	9.27	C(5,G3)-C(5,G3)*	8.49

ii) MOK complex

O(4,G1)-O(4,G1)*	8.06	O(6,G1)-O(6,G1)*	7.55
O(4,G2)-O(4,G2)*	8.54	O(6,G2)-O(6,G2)*	9.06
O(4,G3)-O(4,G3)*	8.84	O(6,G3)-O(6,G3)*	8.20
C(3,G1)-C(3,G1)*	8.88	C(5,G1)-C(5,G1)*	8.08
C(3,G2)-C(3,G2)*	9.86	C(5,G2)-C(5,G2)*	8.99
C(3,G3)-C(3,G3)*	9.33	C(5,G3)-C(5,G3)*	8.48

(2) Least-squares planes through six O(4) atoms and deviations of atoms (l/Å)

i) MONa complex

$0.000X+0.000Y+1.000Z=3.148$

O(4,G1)	−0.002	O(4,G2)	−0.004	O(4,G3)	0.006
O(4,G1)*	−0.002	O(4,G2)*	−0.004	O(4,G3)*	0.006

ii) MOK complex

$0.000X+0.000Y+1.000Z=3.180$

O(4,G1)	0.012	O(4,G2)	−0.008	O(4,G3)	−0.004
O(4,G1)*	0.012	O(4,G2)*	−0.008	O(4,G3)*	−0.004

The weak streaks observed in the oscillation photographs indicate that there is a repetition unit of c' which is twice as long as the c length. The Methyl Orange anion is nearly twice as long as the c length, so the repetition unit in one channel may be c' as is shown in Fig. 3. A structure analysis by taking the unit cell length of c' is possible, but we did not attempt it because

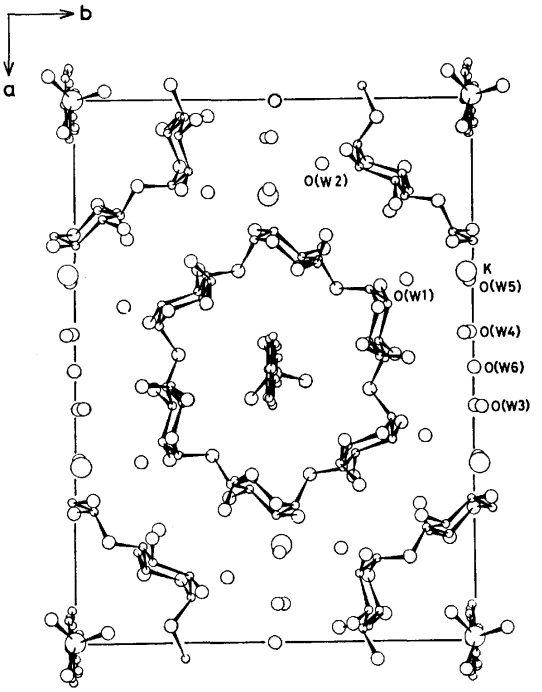

Fig. 5. The projection of the crystal structure of the α-cyclodextrin-Methyl Orange potassium salt complex along the c axis.

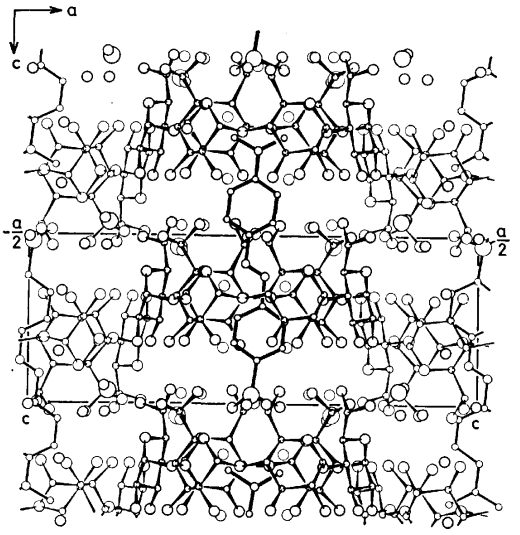

Fig. 6 The projection of the crystal structure of the α-cyclodextrin-Methyl Orange potassium salt complex along the b axis.

the reflections of $(l+1/2)$-th layers were so weak that no intensity measurement was tractable. The weak streaks can be explained if we assume some regularity that appears on the arrangements of the Methyl Orange anion, as is shown in Fig. 3. The disordered arrangements of "guest" molecules are plausible, since the inside of the channel has no contact with other channels. Therefore, the dimensions and shape of the "guest" molecule may be flexible in the channel-type structure, but the location of the ionized group may be very important because of the electrostatic interaction

Predictions of Molecular Geometries and Electronic Spectra of Complex Unsaturated Molecules from MC-LCAO-MO Method. II. 1,3-Butadiene and Cyclobutadiene

Mitsunobu NAKAYAMA, Moriyuki NISHIHIRA, and Yasumasa J. I'HAYA*

Department of Chemistry, Tokyo Kyoiku University, Otsuka, Tokyo 112

**Department of Materials Science, The University of Electro-Communications, Chofu-shi, Tokyo 182*

(Received December 26, 1975)

A multi-configuration (MC)-LCAO-MO method is applied to 1,3-butadiene and cyclobutadiene, predicting their molecular geometries and electronic spectra. The molecular ground state geometry, electronic spectrum and stabilization energy of the *trans*- to the *cis*-isomer of 1,3-butadiene are predicted to be in good accord with experiments and with those derived from the ordinary semi-empirical SCF-CI method. The results obtained for cyclobutadiene indicate that (a) the Jahn-Teller distortion occurs to favor a rectangular (D_{2h}) form, the stabilization energy being 0.3—0.9 eV depending on approximations, and (b) even in a square (D_{4h}) form a singlet (ground) state is more stable than a triplet state by *ca.* 0.3 eV. It is also shown that the lowest excited singlet and triplet states ($^3A_{2g}$ and $^1B_{1g}$) in the square form are not subjected to the Jahn-Teller effect. A discussion is given on a possible error in a CI treatment arising when degenerate molecular orbitals are expressed by real coefficients of atomic orbitals.

In previous papers,[1-4] a semi-empirical multi-configuration (MC)-LCAO-MO method in which a π-electron approximation is used was proposed in order to predict molecular geometries of ground and excited electronic states of unsaturated hydrocarbons, in particular those having open-shell MO's. The method was found to be useful, when applied to the benzene and triphenylene ions, for the examination of a static Jahn-Teller effect. One of the fruitful results obtained up to the present is that the method can be applied with the same degree of accuracy as the ordinary semi-empirical SCF-CI method to any unsaturated hydrocarbons independently of whether their electronic configurations are made up of closed shells or open shells and whether their MO's are degenerate or non-degenerate. This fact allows one to make use of the method securely for predictions of electronic structures of π-electron systems whose geometrical conformations are unknown.

The purpose of the present paper is twofold. One is to answer whether our MC-LCAO-MO method can be reliably used for predictions of molecular geometries and electronic structures of unsaturated open-chain molecules, thereby we have chosen 1,3-butadiene as a prototype of linear polyenes. As in the preceding paper[4] (called Part I of this series), we will compare the results obtained by our method with those of the usual SCF-CI calculation. We also discuss which isomer, *cis* or *trans*, is more stable.

The other is to complete our study of many years in a Jahn-Teller effect in unsaturated molecules by making use of the present method. We reported previously[5] a study of the effect in cyclobutadiene, which however was somewhat unsatisfactory in the selection of configuration functions taken for CI calculation and in the use of a bond order-bond length relationship that was found later to be not consistent with the whole scheme of the present MC-LCAO-MO method. Noting that there occur complicated CI mixings between different symmetry species of configuration functions when degenerate MO's are expressed by *real* coefficients of atomic orbitals, we carefully analyse the electronic structure of cyclobutadiene. We predict molecular geometry and spin multiplicity of the ground state, molecular geometries of some excited states, stabilization energies due to the Jahn-Teller effect and transition energies and oscillator strengths of square and rectangular cyclobutadiene.

Method of Calculation

In this section we will only give a brief outline of the method, the detail of which has been stated previously.

In order to construct a secular equation from which MO's are determined, we use throughout the calculation the formula

$$\alpha_p = -I_p - \sum_{q \neq p} (q : pp) \tag{1}$$

for the diagonal elements and the formulas

$$\beta_{pq} = \beta_0 \exp[-(r_{pq}-b)/a] \quad \text{(Approximation (1))} \tag{2a}$$

and

$$\beta_{pq} = -\frac{1}{2} K S_{pq}(I_p+I_q) \quad \text{(Approximation (2))} \tag{2b}$$

for the off-diagonal elements. Here I_p is an appropriate valence-state ionization potential of carbon p, (q : pp) the penetration integral, r_{pq} the carbon-carbon distance and S_{pq} is the overlap integral. The constants β_0, a, b, K, and I_p are set equal to the values -2.38 eV, 0.3938 Å, 1.397 Å, 0.86291, and 11.290 eV, respectively. Non-neighbor β_{pq}'s are also included.

The MO's thus obtained for a previously guessed molecular geometry are employed to calculate the matrix elements of the total Hamiltonian operator for CI mixing, in which the matrix elements of the one-electron Hamiltonian operator between MO's ϕ_i and ϕ_j are calculated to be

$$\varepsilon_{ij} = \delta_{ij}U_{ij} - \sum_p \sum_{q \neq p} C_{pi}C_{pj}(pp|qq) \tag{3}$$

where U_{ii} and C_{pi} are the eigenvalues and atomic orbital coefficients, respectively, of MO's ϕ_i. The two-center electronic repulsion integrals (pp|qq) are evaluated by the formula[6]

$$Z^{-1}(pp|qq) = 0.1227 - 0.005093\rho + 0.000070\rho^2 \tag{4}$$

(in a. u.) with $\rho = Zr_{pq}/a_0$. Here the effective nuclear

charge for carbon 2pπ AO's, $Z=3.250$, is assumed to be constant throughout the calculation and a_0 is the Bohr radius.

The π-bond orders P_{pq} obtained after each step of CI computation are used to revise the bond lengths in the next step of calculation through the relationship

$$r_{pq} = 1.523 - 0.193P_{pq} \quad (5)$$

and this process is repeated until a self-consistent solution is obtained with respect to bond lengths.

Electronic Structures of *trans*- and *cis*-1,3-Butadiene

To begin with, the MC-LCAO-MO method is applied to the calculation of the electronic structures of *trans*- and *cis*-1,3-butadiene; all the C–C–C bond angles are assumed to be 123° for both *trans*- and *cis*-butadiene. For comparison, the usual semi-empirical SCF-CI calculation is also carried out with the same atomic integrals, values of constants and species of configuration functions as in the MC-LCAO-MO method. The C–C bond lengths and C–C–C bond angles used in the SCF-CI calculation are taken from the experimental values obtained for the *trans*-isomer[7] (see the last column of Table 2), and assumed to be the same for the *cis*-form. The penetration integrals due to the hydrogen atoms are included for only nearest-neighbors, being given a constant value 0.627 eV.[6]

As shown in Table 1, the species of configuration functions employed in the CI calculation are classified according to the irreducible representations of the C_{2h} (*trans*) and C_{2v} (*cis*) symmetries. ϕ_i^k, ϕ_{ij}^{kl}, *etc.* are singly-, doubly-excited configuration functions, *etc.* (ϕ_i^k, for example, is constructed by promoting an electron in the occupied MO ϕ_i of the ground configuration ϕ_0 to the unoccupied MO ϕ_k) and are spin-eigenfunctions for the singlet and triplet states belonging to the corresponding symmetries. The explicit formulas of these singly- and doubly-excited configuration functions have been given previously[8]; triply- and quadruply-excited configuration functions are easily constructed in a similar way.

Table 1. Symmetry classification of configuration functions for *trans*- and *cis*-1,3-butadiene

C_{2h} (*trans*)	C_{2v} (*cis*)	Species of configuration function
^1A_g	$^1A_1$	ϕ_0, ϕ_2^4, ϕ_1^3, ϕ_{22}^{33}, ϕ_{22}^{44}, ϕ_{11}^{33}, ϕ_{11}^{44}, $\phi_{12}^{34}(1)$, $\phi_{12}^{34}(2)$, ϕ_{112}^{334}, ϕ_{122}^{344}, ϕ_{1122}^{3344}.
^3A_g	$^3A_1$	ϕ_2^4, ϕ_1^3, $\phi_{12}^{34}(I)$, $\phi_{12}^{34}(II)$, $\phi_{12}^{34}(III)$, ϕ_{112}^{334}, ϕ_{122}^{344}.
$^{1,3}B_u$	$^{1,3}B_2$	ϕ_2^3, ϕ_1^4, ϕ_{22}^{34}, ϕ_{11}^{34}, ϕ_{12}^{33}, ϕ_{12}^{44}, ϕ_{122}^{334}, ϕ_{112}^{344}.

Table 2. Bond lengths of 1,3-butadiene (Å)

Bond	Approximation (1)[a]		Approximation (2)[a]		Exptl.[7] (122.86°)[b]
	trans-	*cis*-	*trans*-	*cis*-	
1—2, 3—4	1.3454	1.3453	1.3484	1.3479	1.3439
2—3	1.4716	1.4713	1.4648	1.4659	1.4672

a) The columns under Approximation (1) and Approximation (2) are the results calculated with Eqs. 2a and 2b in the text, respectively. b) Observed C–C–C bond angle.[7]

In Table 2 are shown the bond lengths finally obtained for the ground states of *trans*- and *cis*-1,3-butadiene together with the corresponding observed values. It is found that the calculated values are in good accord with experiments.

The total energies for the two isomers of 1,3-butadiene are evaluated as

$$E_t = E + V. \quad (6)$$

Here the total electronic energy E is assessed through the formula

$$E = E_\pi + E_\sigma + E_c \quad (7)$$

where E_π and E_σ are, respectively, the π-electron and σ-electron energies to be obtained by the MC-LCAO-MO and/or the SCF-CI methods (the explicit forumla of E_σ depending upon bond lengths is given in Ref. 1; the value of E_σ determined by a fixed molecular geometry is to be just added in a SCF-CI calculation) and E_c is the sum of the effective internuclear interaction between π-electronless carbon cores and assumed to be

$$E_c = \sum_{p<q}\sum (pp|qq). \quad (8)$$

The term V is the sum of the energies due to the internuclear interactions between the non-neighbor carbon and hydrogen atoms (V_{CH}) and between the hydrogen atoms (V_{HH}), each being estimated according to Bartell's formulas[9] (in eV):

$$\left.\begin{aligned} V_{CH} &= 5.419[358\exp(-r/0.490) - 1]r^{-6} \\ V_{HH} &= 285.9\exp(-r/0.245) - 2.135r^{-6}. \end{aligned}\right\} \quad (9)$$

The C–H bond length is taken to be 1.094 Å.[7]

Table 3 gives the energy differences between *trans*- and *cis*-1,3-butadiene in their ground states calculated by the MC-LCAO-MO and the SCF-CI methods. The two methods predict the same result that the *trans*- is energetically more stable than the *cis*-species, though the difference in E appears to be negligibly small and the main term comes from the energy difference in V. The stabilization energies 0.11 eV calculated with Approximation (1) and 0.14 eV with Approximation (2) well compare with the value 0.12 eV obtained by a non-empirical SCF πMO method with a correction for nuclear repulsion[10] and with the value 0.22 eV obtained by an *ab initio* SCF-CI method.[11] The corresponding observed value is 0.10 eV, which was obtained a long time ago.[12]

Table 4 shows the calculated transition energies and oscillator strengths of the singlet and triplet transitions in 1,3-butadiene, together with the observed values. The MO's and the molecular geometries used are those obtained in the ground state calculation and the species of configuration functions listed in Table 1 are employed for the CI calculation. The first excited ^1A_g($^1A_1$ for *cis*) state comes out to be very close to the ^1B_u($^1B_2$ for *cis*) state which is to be expected as the lowest excited state and this is due to a strong interaction of the singly-excited configurations with the doubly-excited configurations, in the main with the configura-

TABLE 3. ENERGY DIFFERENCES BETWEEN *trans*- AND *cis*-1,3-BUTADIENE IN THEIR GROUND STATES (eV)

Method	Approximation (1)			Approximation (2)		
	ΔE_t [a]	ΔE	ΔV	ΔE_t [a]	ΔE	ΔV
MC-LCAO-MO	−0.1082	0.0103	−0.1185	−0.1377	−0.0180	−0.1197
SCF-CI	−0.1179	0.0071	−0.1250	−0.1444	−0.0194	−0.1250

a) $\Delta E_t = E_t(trans\text{-}) - E_t(cis\text{-})$, $E_t = E + V$.

TABLE 4. TRANSITION ENERGIES (eV) AND OSCILLATOR STRENGTHS FOR 1,3-BUTADIENE

State	Approximation (1)				Approximation (2)				Exptl.
	MC-LCAO-MO		SCF-CI		MC-LCAO-MO		SCF-CI		
	Energy	f	Energy	f	Energy	f	Energy	f	
trans									
^1A_g	0.000	ref.	0.000	ref.	0.000	ref.	0.000		
	5.960		5.972		5.399		5.466		
	7.524		7.545		7.316		7.347		(7.2) [a]
	9.542		9.566		9.273		9.325		
^1B_u	6.073	0.732	6.076	0.733	5.775	0.718	5.809	0.717	5.92[13]
	9.390	0.151	9.430	0.152	9.285	0.130	9.320	0.132	
	10.660	0.001	10.686	0.001	10.140	0.010	10.206	0.010	
^3A_g	4.368		4.395		4.156		4.188		4.91[13]
	7.791		7.809		7.630		7.671		
	11.909		11.958		11.565		11.628		
^3B_u	3.162		3.166		2.795		2.844		3.22[13]
	7.118		7.153		6.737		6.799		
	10.031		10.072		9.836		9.877		
cis									
$^1A_1$	0.000	ref.	0.000	ref.	0.000	ref.	0.000	ref.	
	5.965	0.005	5.976	0.006	5.390	0.012	5.446	0.012	
	7.799	0.531	7.820	0.533	7.515	0.439	7.545	0.441	(7.2) [a]
	9.101	0.017	9.115	0.017	8.778	0.073	8.820	0.073	
$^1B_2$	5.699	0.324	5.697	0.324	5.333	0.315	5.358	0.313	
	9.294	0.001	9.331	0.001	9.230	0.003	9.263	0.003	
	10.624	0.000	10.647	0.000	10.027	0.000	10.082	0.000	
$^3A_1$	4.380		4.406		4.149		4.177		
	7.705		7.720		7.554		7.589		
	11.915		11.961		11.546		11.603		
$^3B_2$	3.146		3.149		2.744		2.782		
	7.134		7.167		6.738		6.794		
	9.812		9.846		9.593		9.626		

a) This assignment appears to be incorrect.[13–15]

tion φ_{22}^{33}. A similar situation was found in an *ab initio* calculation.[11] As is well known, such lowering of the ^1A_g state is not obtained in the CI calculation in which only the singly-excited configurations are taken into account. Recent experimental[13] and more elaborate *ab initio*[14,15] studies of the electronic spectrum of *trans*-1,3-butadiene indicate that the transition in the 7.2 eV region should be assigned to a ^1B_u state of Rydberg character. We are not qualified for giving comments on this matter, since Rydberg-type transitions cannot be predicted by a minimal basis calculation such as the present treatment. The rest of the results shown in Table 4 appears to be in good agreement with experiments.

Electronic Structure of Cyclobutadiene

So far we have demonstrated that the present method is credible to reproduce the bond lengths and the electronic spectrum of 1,3-butadiene together with the stabilization energy of the *trans*-form against *cis*-, at least with the same accuracy as the usual SCF-CI method using a fixed molecular geometry. With this and accumulated confidence obtained in a series of papers hitherto, we challenge cyclobutadiene.

As for cyclobutadiene, if it exists as a stable entity, there are two problems of theoretical and experimental

interest: molecular geometry and spin multiplicity of the ground state. Up to date, various theoretical studies on cyclobutadiene have been carried out with CI[16-18] and without CI[19]; all of these results indicate that the molecule has a singlet ground state of a rectangular (the D_{2h} symmetry) form.[17-19] Recently, several authors[20,21] have reported studies of the photochemical synthesis and the infrared spectrum of cyclobutadiene and inferred its geometrical structure to be a square (the D_{4h} symmetry) form in its ground state. Cyclobutadiene, if it assumes to take a geometry of the D_{4h} symmetry, is considered theoretically to be subjected to the Jahn-Teller effect† in the ground and some excited states, because it has a pair of degenerate π-MO's partly occupied in the ground configuration.

In the following CI calculation for cyclobutadiene, we take account of all species of configuration functions which can be constructed by accommodating four π-electrons on four π-MO's, as in the case of 1,3-butadiene. The resulting configuration functions are classified into 20 singlets, 15 triplets and 1 quintuplet, the quintuplet state being not treated in the present study.

The four π-MO's are written, under the zero-differential overlap assumption, for cyclobutadiene of the D_{4h} geometry as in the following:

$$\left.\begin{array}{ll} a_{2u} & \phi_1 = \frac{1}{2}(\chi_1+\chi_2+\chi_3+\chi_4) \\ e_g & \left\{\begin{array}{l} \phi_2 = a(\chi_1-\chi_3) - b(\chi_2-\chi_4) \\ \phi_3 = c(\chi_1-\chi_3) + d(\chi_2-\chi_4) \end{array}\right. \\ b_{2u} & \phi_4 = \frac{1}{2}(\chi_1-\chi_2+\chi_3-\chi_4) \end{array}\right\} \quad (10)$$

where the orbital symmetries are determined by making use of the coordinate system shown in Fig. 1 and the MO's ϕ_2 and ϕ_3 are a pair of degenerate MO's. In the symmetry classification of configuration functions according to which each unit CI calculation is carried out, it should be noted that the irreducible representations to which some functions belong in the D_{4h} point group are varied depending upon whether the degenerate MO's are expressed by complex or real coefficients of atomic orbitals. This situation can be explained by taking up, for example, the singlet configuration functions having a g representation of the D_{4h} point group. If the degenerate MO's are expressed through the *complex* coefficients determined by the symmetry, that is, if the coefficients in Eq. 10 are set as $a=c=1/2$ and $b=d=-i/2$ (i: imaginary), then the species of configuration functions are classified as in Table 5. (Here we assume the ground configuration ψ_0 as $(\phi_1^2\phi_2^2)$, and as for the full symmetry classification of the other singlet and triplet configuration species,

† A word "second-order" or "pseudo" Jahn-Teller effect is sometimes used for the stabilization due to the second-order terms of an expanded Hamiltonian operator for the electronic motion in the field of nuclei. The ground state ($^1B_{1g}$) of cyclobutadiene is actually the case. On the other hand, the excited states ^1E_u and ^3E_u of cyclobutadiene receive the "first-order" Jahn-Teller effect. We hereafter use only the word "Jahn-Teller effect" for both ground and excited states of cyclobutadiene.

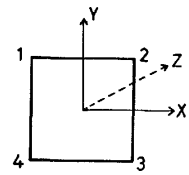

Fig. 1. Coordinate system of cyclobutadiene.

Table 5. Symmetry classification of g-singlet configuration functions: case of complex MO's

B_{2g}: $\psi_0-\psi_{22}^{33}$, $\psi_{12}^{34}(1)$, $\psi_{11}^{44}-\psi_{1122}^{3344}$;
B_{1g}: $\psi_0+\psi_{22}^{33}$, $\psi_{12}^{34}(2)$, $\psi_{11}^{44}+\psi_{1122}^{3344}$;
A_{1g}: ψ_2^2, $\psi_1^4+\psi_{122}^{334}$, ψ_{22}^{44}, ψ_{11}^{33}, ψ_{112}^{344}; A_{2g}: $\psi_1^4-\psi_{122}^{334}$.

Table 6. Symmetry classification of g-singlet configuration functions: case of real MO's

B_{2g}: $\psi_0-\psi_{22}^{33}$, $\psi_{12}^{34}(1)$, $\psi_{11}^{44}-\psi_{1122}^{3344}$;
B_{1g}: ψ_2^3, $\psi_1^4+\psi_{122}^{334}$, ψ_{112}^{344};
A_{1g}: $\psi_0+\psi_{22}^{33}$, $\psi_{12}^{34}(2)$, ψ_{22}^{44}, ψ_{11}^{33}, $\psi_{11}^{44}+\psi_{1122}^{3344}$;
A_{2g}: $\psi_1^4-\psi_{122}^{334}$.

see Refs. 5 and 16). On the other hand, if the MO's are *real* and all the coefficients a, b, c, and d are set equal to 1/2, then the symmetry species are determined as in Table 6. It should be noted that the species of the A_{1g} and B_{1g} configuration functions shown in Table 5 are different from the corresponding ones listed in Table 6. Furthermore, when the coefficients in the real MO's are set as $a=d$ and $b=c$ but $a\neq b$, the configuration species of the A_{1g} and B_{1g} symmetries shown in Table 6 mix partly with those of A_{2g} and B_{2g}, respectively, and the CI mixings to be allowed become more complicated.

In the previous study on cyclobutadiene,[5] we have carried out each unit CI computation by making use of the symmetry species of configurations classified as in Table 5, despite of the fact that the degenerate MO's used are real. This probably led to an unsatisfactory result not only in the symmetry assignment of the electronic states but also in the magnitudes of the transition energies. In the present study, therefore, we have chosen all the 12 configuration functions having a g representation for a unit CI calculation, from which the eigenvalues and eigenfunctions of the singlet A_{1g}, A_{2g}, B_{1g}, and B_{2g} states are obtained. As for the other states, 7 and 8 configuration functions are taken for the triplet g state and the singlet and triplet u states, respectively.

Table 7 shows the bond lengths obtained for the square and rectangular forms together with the corresponding π-bond orders. It is found that the lowest $^3A_{2g}$ and $^1B_{1g}$ states in the square form are not subjected to the Jahn-Teller distortion; that is, self-consistent solutions do not converge to a rectangular form but to the square form. A similar situation has been seen in the lowest excited states of the benzene anion and cation.[1,2] This is caused by the fact that the configuration ψ_2^3 shown in Table 6 is the main term in the CI mixing and gives a bond-order distribution which favors a square geometry.

TABLE 7. CALCULATED BOND LENGTHS (Å) AND π-BOND ORDERS IN CYCLOBUTADIENE

State	D_{4h}-geometry				State	D_{2h}-geometry[a]			
	Approx. (1)		Approx. (2)			Approx. (1)		Approx. (2)	
	Bond length	Bond order	Bond length	Bond order		Bond length	Bond order	Bond length	Bond order
$^1B_{2g}$	1.432	0.472	1.432	0.473	^1A_g	1.519	0.019	1.515	0.041
$^3A_{2g}$	1.431	0.478	1.430	0.479		1.341	0.941	1.346	0.915
$^1A_{1g}$	1.434	0.459	1.435	0.457	$^1B_{2u}$	1.523	0.000	1.523	0.000
$^1B_{1g}$	1.427	0.499	1.427	0.499		1.430	0.484	1.430	0.480
^1E_u	1.477	0.240	1.477	0.238	$^3B_{2u}$	1.523	0.000	1.523	0.000
^3E_u	1.479	0.229	1.478	0.234		1.433	0.468	1.432	0.474

a) The upper and lower figures in these column are the values for the 1—2 and 2—3 bonds, respectively.

TABLE 8. ENERGY LEVELS OF THE LOWER ELECTRONIC STATES OF CYCLOBUTADIENE IN D_{4h}-GEOMETRY (eV)

State	Approximation (1)			Approximation (2)		
	ΔE[a]	ΔE_π	ΔE_σ	ΔE[a]	ΔE_π	ΔE_σ
$^1B_{2g}$	0.000	0.000	0.000	0.000	0.000	0.000
$^3A_{2g}$	0.272	0.247	0.025	0.306	0.250	0.056
$^1A_{1g}$	1.291	1.339	−0.048	1.195	1.336	−0.141
$^1B_{1g}$	1.616	1.502	0.114	1.766	1.535	0.231

a) Energy difference referred to the $^1B_{2g}$ state, $E=E_\pi+E_\sigma$.

In Table 8 are shown the energy levels obtained for the lower electronic states of cyclobutadiene in the D_{4h} geometry given in Table 7. The energy differences due to the term E_c in Eq. 7 were omitted, since they were found to be negligibly small. Table 8 shows that the $^1B_{2g}$ state is more stable than the $^3A_{2g}$ state by *ca.* 0.3 eV, that is, the ground state of cyclobutadiene is likely to be the singlet state in the D_{4h} geometry rather than a triplet state. This result is consistent with what obtained by Buenker and Peyerimhoff,[17] except that in their prediction the $^3A_{2g}$ state has a slightly rectangular equilibrium form, but conflicts with that of Dewar *et al.*;[19] the latter authors have predicted the triplet to be more stable than the singlet in a square form.

The instability due to the Jahn-Teller effect is calculated for the ground ($^1B_{2g}$) state and the lowest excited states (^1E_u and ^3E_u) in the D_{4h} geometry. The entries in Table 9 are the energy differences, $\Delta E=\Delta E_\pi+\Delta E_\sigma$, between the corresponding species of the D_{2h} and D_{4h} geometries. The table shows that cyclobutadiene is no doubt subjected to the Jahn-Teller distortion in the ground and some excited states and the singlet ground state of the rectangular form is energetically most favorable. The latter conclusion agrees with those of all the other theoretical studies in the past,[17-19] but is not in accord with the recent experimental inferences[20,21] which indicate that the molecule should prefer a square rather than a rectangular form, probably in its ground state.

The previous study on cyclobutadiene,[5] in which the CI treatment was considered to be incomplete as mentioned above, misassigned the singlet A_{1g} and B_{1g} states of D_{4h}-cyclobutadiene and predicted the lowest $^1B_{1g}$ state to be slightly lower than the lowest $^1A_{1g}$ state. However, the conclusion on the Jahn-Teller effect in cyclobutadiene obtained in the previous study is essentially consistent with that mentioned above, though the previously obtained stabilization energy for the ground state is less than the present value by 0.2 eV.

Lastly, we show the calculated results for transition energies and oscillator strengths of the D_{4h} and D_{2h} species of cyclobutadiene. The MO's and the molecular geometries used are those obtained for the singlet ground states of both species. Table 10 lists a part of the results obtained from the full CI calculation. There can be seen a fairly definite difference between the energies of the lower excited states calculated under Approximations (1) and (2) in the D_{2h} geometry. This difference is mainly caused by the fact that Approximation (1) leads the ground state of cyclobutadiene to receive a more remarkable Jahn-Teller distortion in its molecular geometry and energy than Approximation (2) (*cf.* Tables 7 and 9).

The results listed in Table 10 are partly in agreement with those obtained by Allinger and Tai;[18] in particular, the singlet spectrum of the square form resembles each other. Though we have no experimental datum to compare with our prediction, we feel confident that

TABLE 9. STABILIZATION ENERGIES DUE TO THE JAHN-TELLER EFFECT IN CYCLOBUTADIENE (eV)

Reference state	Approximation (1)			Approximation (2)		
	ΔE[a]	ΔE_π	ΔE_σ	ΔE[a]	ΔE_π	ΔE_σ
$^1A_g-{}^1B_{2g}$	−0.921	−2.095	1.174	−0.300	−1.248	0.948
$^1B_{2u}-{}^1E_u$	−0.283	−0.537	0.254	−0.156	−0.410	0.254
$^3B_{2u}-{}^3E_u$	−0.319	−0.560	0.241	−0.170	−0.424	0.254

a) $\Delta E=E(D_{2h})-E(D_{4h})$, $E=E_\pi+E_\sigma$.

TABLE 10. CALCULATED TRANSITION ENERGIES (eV) AND OSCILLATOR STRENGTHS FOR CYCLOBUTADIENE

	D_{4h}-geometry					D_{2h}-geometry			
	Approx. (1)		Approx. (2)			Approx. (1)		Approx. (2)	
State	Energy	f	Energy	f	State	Energy	f	Energy	f
Singlet					Singlet				
B_{2g}	0.000	ref.	0.000	ref.	A_g	0.000	ref.	0.000	ref.
A_{1g}	1.204		1.175		B_{1g}	3.299		2.667	
B_{1g}	1.821		1.804		A_g	4.124		2.879	
E_u	5.698	0.052	5.394	0.072	B_{2u}	6.363	0.142	5.667	0.159
A_{1g}	7.515		7.208		B_{3u}	8.241	0.003	6.933	0.008
E_u	8.089	0.315	8.682	0.309	B_{2u}	8.597	0.670	8.833	0.597
A_{2g}	9.971		10.266		A_g	9.281		8.182	
B_{1g}	11.131		11.426		B_{1g}	10.219		10.378	
					B_{3u}	10.755	0.011	10.319	0.023
Triplet					Triplet				
A_{2g}	0.317		0.313		B_{1g}	1.787		1.173	
E_u	3.236		3.028		B_{2u}	3.863		3.289	
E_u	6.448		6.926		B_{3u}	5.827		4.592	
A_{2g}	8.888		9.178		B_{2u}	7.180		7.291	
B_{1g}	9.971		10.266		B_{3u}	8.923		8.360	
A_{1g}	9.971		10.266		B_{1g}	9.223		9.352	
B_{2g}	9.971		10.266		A_g	11.529		11.044	

the electronic spectra calculated for the square and rectangular forms of cyclobutadiene are about right from the viewpoint that the same method has been successful in reproducing the observed data for 1,3-butadiene and other unsaturated hydrocarbons.

Conclusion

The results obtained so far are summarized as in the following:

(a) The MC-LCAO-MO method can be applied, with about the same degree of accuracy as the usual semi-empirical SCF-CI method with fixed molecular geometry, to predictions of molecular geometries and electronic spectra of linear polyenes as well as cyclic polyenes, independently of whether configurations are made up of closed-shells or open-shells and whether MO's are degenerate or non-degenerate.

(b) The *trans*-1,3-butadiene is predicted to be stable than the *cis*- by 0.11—0.14 eV.

(c) The ground $^1B_{2g}$ state of square cyclobutadiene lies below the $^3A_{2g}$ state by 0.3 eV.

(d) The lowest $^3A_{2g}$ and $^1B_{1g}$ states in the square form are not subjected to the Jahn-Teller distortion.

(e) The Jahn-Teller distortion occurs to favor rectangular cyclobutadiene which has a singlet ground state, bond length expansion and contraction being 0.09 Å for the ground state and 0.04 Å for the lowest excited degenerate singlet and triplet states.

(f) The stabilization energy due to the Jahn-Teller effect for the ground state of cyclobutadiene is predicted to be 0.6 eV on the average, depending upon the approximation for the two-center core resonance integral.

An additional remark is as follows: When one uses degenerate MO's expressed by *real* coefficients of atomic orbitals, all the g (or u) state functions having the same multiplicity are recommended to be taken together in each unit CI calculation.

References

1) M. Nakayama and Y. J. I'Haya, *Int. J. Quantum Chem.*, **4**, 21 (1970).
2) M. Nakayama and Y. J. I'Haya, *Int. J. Quantum Chem.*, **4**, 43 (1970).
3) Y. J. I'Haya, M. Nakayama, and T. Iwabuchi, *Int. J. Quantum Chem.*, **S5**, 227 (1971).
4) M. Nakayama, K. Sazi, and Y. J. I'Haya, *Theor. Chim. Acta*, **38**, 327 (1975).
5) M. Nakayama and Y. J. I'Haya, *Rept. Univ. Electro-Commun.*, **23**, 31 (1967).
6) Y. J. I'Haya, "Advanced Quantum Chemistry," Vol. 1, ed. by P. O. Löwdin, Academic Press, New York, N. Y. (1964), p. 203.
7) W. Haugen and M. Traetteberg, *Acta Chem. Scand.*, **20**, 1726 (1966).
8) M. Nakayama and Y. J. I'Haya, *Rept. Univ. Electro-Commun.*, **30**, 73 (1971).
9) L. S. Bartell, *J. Chem. Phys.*, **32**, 827 (1960).
10) R. G. Parr and R. S. Mulliken, *J. Chem. Phys.*, **18**, 1339 (1950).
11) R. J. Buenker and J. L. Whitten, *J. Chem. Phys.*, **49**, 5381 (1968).
12) J. G. Aston, G. Szasz, H. W. Woolley, and F. G. Brickwedde, *J. Chem. Phys.*, **14**, 67 (1946).
13) O. A. Mosher, W. M. Flicker and A. Kuppermann, *J. Chem. Phys.*, **59**, 6502 (1973).
14) S. Shih, R. J. Buenker and S. D. Peyerimhoff, *Chem. Phys. Lett.*, **16**, 244 (1972).
15) R. P. Hosteny, T. H. Dunning Jr., R. R. Gilman, and A. Pipano, *J. Chem. Phys.*, **62**, 4764 (1975).
16) D. P. Craig, *Proc. R. Soc. London, Ser. A*, **202**, 498 (1950).
17) R. J. Buenker and S. D. Peyerimhoff, *J. Chem. Phys.*, **48**, 354 (1968).
18) N. L. Allinger and J. C. Tai, *Theor. Chim. Acta*, **12**, 29 (1968).
19) M. J. S. Dewar, M. C. Kohn, and N. Trinajstic, *J. Am. Chem. Soc.*, **93**, 3437 (1971).
20) O. L. Chapman, C. L. McIntosh, and J. Pacansky, *J. Am. Chem. Soc.*, **95**, 614 (1973).
21) A. Krantz, C. Y. Lin, and M. D. Newton, *J. Am. Chem. Soc.*, **95**, 2744 (1973).

Hybridization in Some Three-Membered Ring Organic Molecules

Hiroshi FUJIMOTO, Tsutomu MINATO, Satoshi INAGAKI, and Kenichi FUKUI

Faculty of Engineering, Kyoto University, Sakyo-ku, Kyoto 606

(Received December 26, 1975)

The molecular structures of some simple three-membered ring compounds, cyclopropane, cyclopropanone, ethylene oxide and ethylenimine, were studied by means of the orbital interaction between the fragments of a molecule. The relation between the carbon-carbon distance and the bending angle of the carbon-hydrogen bonds in ethylenic part of the three-membered rings is attributed primarily to the greater extent of mixing of the unoccupied π-like MO of ethylenic fragment into the occupied MO's of rings. The increase in the bending angle as going from ethylene oxide to cyclopropane is interpreted in terms of the interaction of an occupied σ-like orbital with the unoccupied π-like orbital of ethylenic fragment through the overlap with the orbital(s) of the residual part of rings. INDO MO and localized orbital calculations support the orbital interaction scheme. The same conclusion is derived also from the electrostatic theory of molecular geometries.

The differences in the structures of some three-membered ring molecules containing sulfur can be rationalized from the viewpoint of orbital interaction between the fragments, generated by a partitioning of the rings.[1] Thus, the long carbon-carbon bond in ethylene episulfone (1.590 Å)[2] in comparison with that in ethylene episulfide (1.492 Å)[3] was ascribed to the stronger interaction between ethylenic fragment and SO_2 than that between ethylenic fragment and sulfur orbitals. Although such an analysis is crude, it provides us with a theoretical insight into molecular geometry and suggests that, in some cases, the structure of molecules can be predicted simply by investigating the mode of orbital interaction between fragments.[4] In addition, the concept of orbital interaction primarily introduced in the theory of intermolecular interactions could be further extended to various chemical problems concerning the structure of molecules.[5]

We have developed a method for discussing the differences in the hybridized states of carbon atom in some simple three-membered ring molecules. The structures of cyclopropane, cyclopropanone, ethylene oxide and ethylenimine are given in Table 1.[6] The angle α, determined by the methylene plane and the carbon-carbon bond axis, increases with an increase in the carbon-carbon bond distance. The general tendency of the change in the bond distances with the change in hybridized states was studied by Bent, based on experimental observations.[7] The relation between the angle α and the bond distance of three-membered rings may be of interest for an MO theoretical study, since we frequently encounter similar problems in organic and inorganic chemistry.

Table 1. MOLECULAR STRUCTURES

	C–C Distance	Bending angle α
Cyclopropane	1.51 Å	30°
Cyclopropanone	1.575Å	29°7′
Ethylene oxide	1.472Å	20°36′
Ethylenimine	1.48 Å	20°36′[a]

a) Assumed.

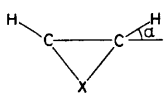

Orbital Interaction

Let us consider the orbital interaction in three-membered ring molecules CH_2CH_2X (X=>CH_2, >C=O, >NH, >O). We proceed in our usual way first by dividing the ring into two parts, the deformed ethylenic part and X.[1] The rehybridization can appropriately be represented by the "sigma-pi" interaction between the σ-like part and π-like part of the ethylenic fragment.[8,9] A stronger interaction indicates a greater rehybridization. The mode of orbital interaction chiefly responsible for the differences in the structure of the rings is illustrated in Fig. 1.[10] We have three significant MO's, ψ_1, ψ_2 and ψ_3, each consisting of the occupied σ and the unoccupied π^* MO's of the ethylenic fragment and an orbital λ of X. All of them are antisymmetric with respect to the plane, bisecting the ring. Figure 2 shows schematically the ways of mixing these three basis MO's to yield the

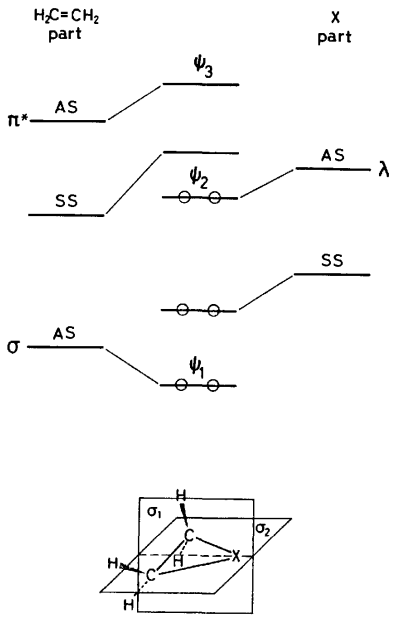

Fig. 1. A schematic illustration of orbital interaction between the fragments of three-membered rings.

Table 2. σ-π^* Mixing in ψ_1 and ψ_2 (ψ_2')

		Coefficient of σ	Coefficient of π^*	Product of coefficients	Orbital energy(λ)
Cyclopropane	ψ_1	0.9462	0.0977	0.0924	2.05 eV
	ψ_2	−0.2986	0.6295	−0.1880	
Cyclopropanone	ψ_1	0.8954	0.1336	0.1196	4.58 eV
	ψ_2'	−0.1318	0.6093	−0.0803	
	ψ_2	−0.4042	0.3261	−0.1318	
Ethylene oxide	ψ_1	0.9531	0.0982	0.0936	0.10 eV
	ψ_2	−0.2927	0.5336	−0.1571	
Ethylenimine	ψ_1	0.9560	0.0900	0.0860	1.73 eV
	ψ_2	−0.2779	0.5801	−0.1612	
			Orbital energy of π^*		3.95 eV

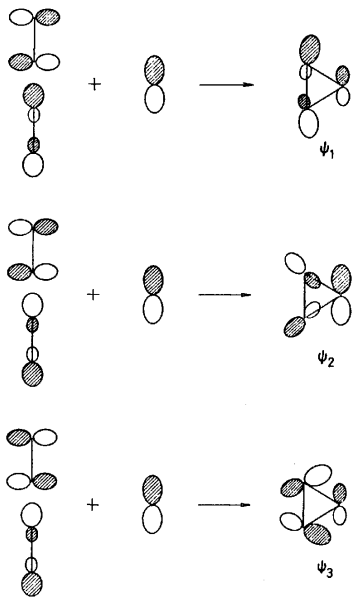

Fig. 2. The modes of orbital mixing.

MO's ψ_1, ψ_2 and ψ_3 of the composite system. The signs of the MO's σ and π^* were chosen in such a way as for both of them to have positive overlap integrals with the ortital λ. We then have no phase dislocation in ψ_1, one in ψ_2, and two in ψ_3.

Table 2 gives the products of the mixing coefficients of σ and π^* in ψ_1 and ψ_2 (and ψ_2' for cyclopropanone). The MO's were calculated by the INDO MO method,[11] and the expansion of the composite MO's in terms of the MO's of the fragments was carried out in the same way as in our previous works.[12] The remaining composite MO ψ_3 is unoccupied and has nothing to do with the electronic structure of the rings.[13] The calculation was carried out on an assumed geometry of cyclopropane, cyclopropanone and ethylenimine, holding the same framework of the ethylenic fragment as that in ethylene oxide. Greater extents of mixing of σ and π^* are observed in cyclopropane and cyclopropanone than in ethylene oxide and ethylenimine. It is noteworthy that the differences in the magnitude of the σ-π^* interaction are mainly attributed to ψ_2. This can readily be understood from the relative energy levels of σ, π^* and λ (Table 2) by application of simple MO perturbation theories.[14]

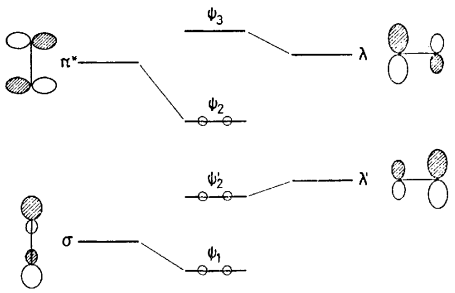

Fig. 3. The orbital interaction in cyclopropanone.

As the level λ comes closer to π^* in energy ($\varepsilon_\lambda < \varepsilon_{\pi^*}$), the contribution of π^* to ψ_2 becomes greater. If the MO λ happens to be higher than the π^* MO, the latter will be the dominant term in ψ_2. As a consequence, a greater extent of occupation of π^* results in the longer carbon-carbon bond and, at the same time, in a greater "sigma-pi" interaction. In the case of cyclopropanone, the high lying MO λ due to the anti-bonding property of the C=O bond would favor a greater contribution of π^* to ψ_2 and ψ_2' giving rise to the extraordinarily long carbon–carbon distance (Fig. 3). The σ-π^* mixing, however, is compatible with that in cyclopropane. Thus, the increase in α along with the stretching of the carbon-carbon bond can be generalized on the concept of the orbital interaction between the fragments.

Localized Orbitals

In order to work out the above reasoning quantitatively, we calculated the electron density of cyclopropane and ethylene oxide. Figure 4 shows the density distribution of valence electrons on the molecular plane. For the sake of comparison cyclopropane was subjected to such a deformation that the ethylenic fragment has the same nuclear framework as that of ethylene oxide. The points with the maximum electron densities in the carbon-hydrogen and the carbon-carbon bond regions are plotted. In cyclopropane, the locus of the maximum density extends from the carbon atom with somewhat larger α than that in ethylene oxide. In order to visualize this clearly, we transformed the MO's of cyclopropane and ethylene oxide into the localized orbitals, according to the

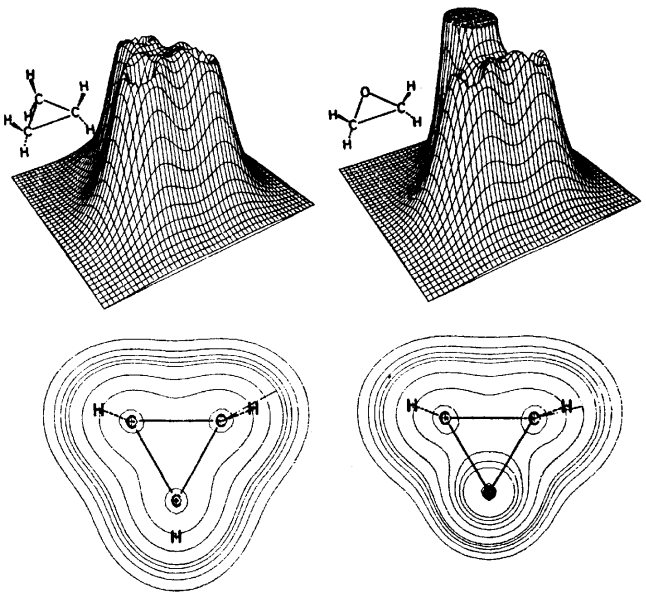

Fig. 4. The electron density distribution in cyclopropane and ethylene oxide.

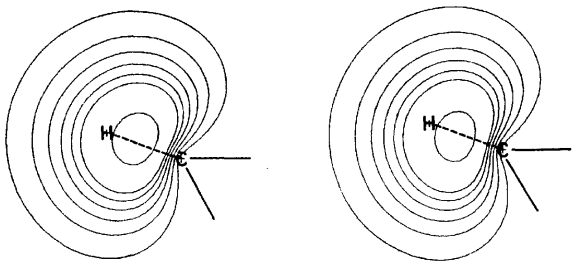

Cyclopropane Ethylene oxide

Fig. 5. The carbon-hydrogen bond orbitals in cyclopropane and ethylene oxide.

criterion postulated by Edmiston and Ruedenberg.[15] Figure 5 shows the cross sections of the localized MO's for a carbon-hydrogen bond on the ring plane. It is clear that the carbon-hydrogen orbital of cyclopropane tends to point to the "normal direction", opposing the geometrical constraint imposed upon the ethylenic fragment. To attain maximum bonding, the hydrogen resides in a position of a larger α than that assigned originally.

The localized orbital of cyclopropane is calculated to be

$$\phi_{C-H}(C_3H_6) = 0.390C_s + 0.298C_x + 0.476C_y - 0.148C_z + 0.709H_s - 0.011\lambda + \cdots\cdots$$

and the one for ethylene oxide is given by

$$\phi_{C-H}(C_2H_4O) = 0.412C_s + 0.299C_x + 0.474C_y - 0.083C_z + 0.711H_s - 0.007\lambda + \cdots\cdots$$

where C_s, C_x, C_y and C_z indicate the carbon 2s, $2p_x$, $2p_y$, and $2p_z$ atomic orbitals, respectively, and H_s denotes the hydrogen 1s atomic orbital. We see that the bond orbital of cyclopropane has a greater p_z component than that of ethylene oxide. By expanding the orbitals in terms of the MO's of the fragment, we obtain

$$\phi_{C-H}(C_3H_6) = 0.343\sigma + 0.089\pi^* + \cdots\cdots$$

and

$$\phi_{C-H}(C_2H_4O) = 0.356\sigma + 0.050\pi^* + \cdots\cdots$$

The σ-π^* mixing is more favorable in cyclopropane than in ethylene oxide, as was expected qualitatively from the consideration of the orbital interaction between the fragments.

In the above calculation, cyclopropane was compressed to have an unrealistic ethylenic fragment. In spite of such an artificial choice of atomic coordinates, the results of the calculation appear to be reasonable. Our intuitive interpretation of the differences in the ring structures based on a rather crude orbital interaction scheme seems to be supported by detailed numerical calculations.

Electrostatic Interaction

In addition to the orbital overlap interaction, the electrostatic effect should be taken into account. With an increase in the electronegativity of X, the charge shift from the carbon atoms to X is strengthened. Accordingly, the electrostatic interaction between the hydrogen atoms and X will be larger as X becomes more electronegative. However, such an electrostatic term in a classical sense, arising from the Coulombic interaction of the net charges, would not be so important in this case, since hydrogens have small net charges in general. Much more important is the binding force exerted on nuclei, originating from the overlap density.[16] Here, the electrostatic theory of molecular configurations proposed by Nakatsuji[17] might be useful. As the ethylenic fragment is distorted from planar structure, the exchange force developed by the carbon-hydrogen bonds and the carbon-carbon bond will pull carbon atoms back to the plane defined by the four hydrogen atoms. Thus, the ethylenic fragment is likely to remain in a planar or less distorted structure, opposing the "sigma-pi" interaction.

Chemical interaction between two systems generally causes electron redistributions, accompanied by the formation of new bonds between reaction sites and the weakening of old bonds of reactants to be broken in the course of reaction. The origin of the electron redistribution was analyzed in detail based on the concept of configuration interaction in chemical reactions.[18] In this case, the π like bonding between the carbon atoms of the ethylenic fragment is loosened and new bonds are formed between the fragments. The electron shift from the carbon-carbon bond region to the carbon-X bond regions takes place not through the mutual charge-transfer interaction between the fragments but through the crossing of the AS and SS type MO's.[19] The overlap density accumulated in the bond region between a carbon and X would attract the carbon toward X. The attracting force gets stronger as the overlap density becomes greater. The difference in the magnitude of the overlap density is determined mainly by the orbital overlap interaction between the π^* MO of the ethylenic fragment and λ of X. Thus, the overlap density is predominantly governed by the product of the mixing coefficients of

π^* and λ in ψ_2. The mixing in of π^* into ψ_2 gets poorer as the energy level of λ becomes lower (Table 2). The greater the electronegativity of X, the lower the energy level λ. The greater electronegativity of X indicates the smaller overlap density in the carbon-X bond region and less distorted ethylenic fragment.

Conclusion

The coupling of a partitioning analysis and an MO expansion procedure seems to be powerful in accurately reproducing MO quantity in a chemically acceptable manner, since we can obtain the exact expressions of the MO's of the composite system in terms of the MO's of the fragments. This kind of approach to the physical and chemical properties of molecular systems would be promising in discussing small but significant differences in similar systems. A simplified interpretation in regard to the difference in hybridization of three-membered rings given here seems to be independent of the approximation employed for the MO calculation.

The present semiquantitative calculation and qualitative concept for interaction revealed that the shorter carbon-carbon distance and smaller bending angle α in simple three-membered ring systems could be ascribed to the greater electronegativity of the central atom or group X. The concept developed here may be applicable to other cases in which changes in valence angles with the change in substituent is noticeable.[20] The assumption of the same bending angle α in ethylenimine as that in ethylene oxide deserves reinvestigation.

The MO computation was carried out at the Data Processing Center, Kyoto University with financial support from the Ministry of Education.

References

1) R. Hoffmann, H. Fujimoto, J. R. Swenson, and C. -C. Wan, *J. Am. Chem. Soc.*, **95**, 7644 (1973).

2) Y. Nakano, S. Saito, and Y. Morino, *Bull. Chem. Soc. Jpn.*, **43**, 368 (1970).

3) G. L. Cunningham Jr., A. W. Boyd, R. J. Meyers, and W. D. Gwinn, *J. Chem. Phys.*, **19**, 676 (1951).

4) A similar partitioning analysis of a molecule was made in discussing the stereochemical paths in intramolecular rearrangements; see, for example, K. Fukui and H. Fujimoto in "Mechanisms of Molecular Migrations," B. S. Thyagarajan, Ed., Interscience, Vol. 2, New York (1969), pp. 117—190.

5) See, for example, R. Hoffmann, C. C. Levin, and R. A. Moss, *J. Am. Chem. Soc.*, **95**, 269 (1973); N. D. Epiotis, *ibid.*, **95**, 3087 (1973); D. Cremer, J. S. Binkley J. A. Pople, and W. J. Hehre, *ibid.*, **96**, 6900 (1974).

6) Cyclopropane: S, Meiboom and L. C. Snyder, *J. Am. Chem. Soc.*, **89**, 1038 (1967). Cyclopropanone: J. M. Pochan, J. E. Baldwin, and W. H. Flygare, *ibid.*, **91**, 1896 (1969). Ethylene oxide: M. Igarashi, *Bull. Chem. Soc. Jpn.*, **26**, 330 (1953). Ethylenimine: T. E. Turner, V. C. Fiora, W. M. Kendrick, and B. L. Hicks, *J. Chem. Phys.*, **21**, 564 (1953). The angle α was assumed.

7) H. A. Bent, *Chem. Rev.*, **62**, 275 (1962).

8) K. Fukui and H. Fujimoto, *Bull. Chem. Soc. Jpn.*, **39**, 2116 (1966).

9) Sigma-pi separability (P. G. Lycos and R. G. Parr, *J. Chem. Phys.*, **24**, 1166 (1956); **25**, 1301 (1956).) does not hold in a strict sense, since the ethylenic fragment of the three-membered rings has the C_{2v} symmetry but not the D_{2h} symmetry. However, when the deviation from the planarity is small, the MO's of the fragment can approximately be classified into π-like MO's and σ-like MO's, each corresponding to the π and σ MO's of planar ethylene.

10) Considerable contribution of the MO's with other symmetry properties to the determination of the structure of the rings can be found. This is the case in the three-membered rings where d orbitals are available for X. The mixing of σ and π^* would be of importance even in these systems.

11) J. A. Pople and D. L. Beveridge, "Approximate Molecular Orbital Theory," McGraw-Hill, New York (1970).

12) a) H. Fujimoto, S. Kato, S. Yamabe, and K. Fukui, *J. Chem. Phys.*, **60**, 572 (1974). b) S. Kato, H. Fujimoto, S. Yamabe, and K. Fukui, *J. Am. Chem. Soc.*, **96**, 2024 (1974).

13) This is true only in the single-configuration approximation.

14) For a recent application of an MO perturbation theory to chemical problems, *cf.*, *e.g.*, L. Libit and R. Hoffmann, *J. Am. Chem. Soc.*, **96**, 1370 (1974).

15) C. Edmiston and K. Ruedenberg, *Rev. Mod. Phys.*, **35**, 457 (1963).

16) By the term "overlap density," we mean the two-center terms in the interference density. *Cf.*, *e.g.*, W. Kutzelnigg, *Angew. Chem., Int. Ed., Engl.*, **12**, 546 (1973); R. Ruedenberg, *Rev. Mod. Phys.*, **34**, 326 (1962).

17) H. Nakatsuji, *J. Am. Chem. Soc.*, **95**, 345, 354 (1973).

18) a); H. Fujimoto, S. Yamabe, and K. Fukui, *Bull. Chem. Soc. Jpn.*, **44**, 2936 (1971). b); K. Fukui, S. Kato, and H. Fujimoto, *J. Am. Chem. Soc.*, **97**, 1 (1975).

19) The symmetry classification is the same as that in Ref. 1.

20) P. Kollman, *J. Am. Chem. Soc.*, **96**, 4363 (1974).

Infrared Dichroism and Molecular Orientation of Ethyl 2-Hydroxyimino-3-oxo-3-phenylpropionate in Thin Films on Pd Metal Surfaces

Masatoshi Ōsawa, Aritada Hatta, Kaoru Harada*, and Wataru Suëtaka

Laboratory of Interface Science of Metals, Faculty of Engineering, Tohoku University, Aramaki, Aoba, Sendai 980

**Department of Chemistry, University of Tsukuba, Sakura-mura, Niihari, Ibaraki 300-31*

(Received January 5, 1976)

The infrared absorption spectra of ethyl 2-hydroxyimino-3-oxo-3-phenylpropionate, in differently oriented films, formed on Pd metal plates, were measured by using the high-sensitivity reflection method. The thin crystal film **A** was formed when the solvent was evaporated from the thin liquid film remaining on Pd. On the other hand, the film **B** resulted from the crystallization of the amorphous solid film which was initially formed on Pd when the liquid film was thick. From the infrared dichroism in the reflection spectra, the molecular orientations in thin films were obtained as follows. In the film **A**, the ketone C=O and C=N bonds are probably at a pseudo *s-cis* and are aligned in such a way that the C–C bond connecting the ketone carbonyl group with the C=N group are nearly parallel to the Pd surface. The NO bond is aligned parallel to the metal surface. The ester group is oriented nearly vertical to the metal surface, the C=O bond lying tilted to the surface. In the film **B**, the ester C=O and NO bonds are aligned nearly perpendicular to the Pd surface, while the ketone C=O bond is not so. The C···C axis of the ester is rather parallel to the surface. The orientation in the thin film **A** agrees well with the hypothetical chelation model.

The reflection infrared spectroscopy using the beam polarized parallel to the plane of incidence at high incident angles[1] (the high-sensitivity reflection method) is a very powerful tool of investigating various surface phenomena. The best known example is the absorption of gaseous molecules on metal surfaces.[2] In this method, the enhanced oscillating electric field normal to the metal mirror surface serves not only to detect the species adsorbed on the metal surface but also to obtain informations about the orientation of the adsorbed species.[3] This reflection method is also used successfully for the study of thin films of organic crystals formed on metal surfaces.[4] When an organic crystal is grown on a metal surface, the interaction with the metal surface may result in polymorphism or preferred orientation.[5] The preferred orientation and in particular the anomalous crystal structure are generally stable when the film is very thin. Since the crystal grows at the molecule strongly adsorbed on the substrate surface, which acts as the nucleous, the orientation of molecules in thin film crystal may be governed by that of the adsorbed molecule.[6,7] The orientation of adsorbed molecule may, therefore, be deduced from the infrared dichroism of thin crystal film.

On the other hand, the asymmetric synthesis of amino acids by hydrogenolytic asymmetric transamination using Pd hydroxide catalyst has been extensively investigated by one of the authors (Harada) and his co-workers.[8] They found that optically active α-amino acids could be synthesized from the Schiff base of α-keto acids or their esters with optically active α-alkylbenzylamines by catalytic hydrogenation and subsequent hydrogenolysis. In order to explain the reaction mechanism, Harada *et al.*[8] proposed the "chelate hypothesis" that the intermediate five membered cyclic complex[9] with a metal atom of the catalyst could be formed and then adsorbed on the catalyst surface. The intermediate complex assumed in elucidating the hydrogenation of ethyl 2-hydroxyimino-3-oxo-3-phenylpropionate is shown in Fig. 1.[10] Although there has been no direct evidence of the existence of such the chelate ring complex, it is perhaps reasonable to assume that an intermediate on the heterogeneous catalyst plays an important role in the determination of conformation of the resulting product. In this connection, it is interesting to observe the infrared dichroism arisen from the molecular orientation in the thin crystals of the Schiff base compounds formed on a palladium metal surface, because the molecular orientation of the intermediate may be deduced from the orientation of ethyl 2-hydroxyimino-3-oxo-3-phenylpropionate in thin films formed on the Pd surfaces, which can be determined by the high-sensitivity reflection technique.

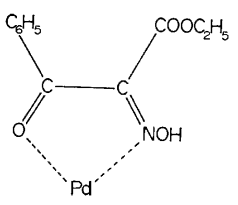

Fig. 1. Intermediate complex model.[10]

Experimental

The infrared spectra were taken by means of a JASCO IR-G grating spectrophotometer with an assembly of JASCO model PR-41 for double beam reflection. The sample of ethyl 2-hydroxyimino-3-oxo-3-phenylpropionate was prepared according to the method given in literature.[11] Pd plates (99.9% in purity) were used as substrate. To obtain high reflectivity, the Pd plate was polished with silicon carbide and chromium oxide to its maximum flatness. After treating with 20% NaOH aqueous solution at 80 °C, the Pd plate was subjected to ultrasonic cleaning for *ca.* 30 min in distilled water to remove remaining alkali and air dried. The Pd plate was then immersed into a 0.5% ethanol solution of the Schiff base. After standing for 24 h or more at 5 °C, the Pd plate was taken out of the solution, and was dried in air. Thin films of the compound were formed on the plates upon evaporation of solvent. Unstable amorphous or stable crystal films were obtained depending upon the quantity of the solution remaining on the Pd surfaces, as will be described below.

Results and Discussion

Assignments of vibrational bands. Since no infrared spectrum of ethyl 2-hydroxyimino-3-oxo-3-phenylpropionate, $C_6H_5COC(NOH)COOC_2H_5$ (abbreviated as EHOP) has appeared in literature, the infrared absorption bands of this compound must be assigned before the orientation of its molecule will be discussed. The assignment of the infrared bands of EHOP was made principally on the basis of comparison with the spectra of closely related compounds, $C_6H_5COC(NOH)COOCH_2C_6H_5$ (BHOP) and $CH_3COC(NOH)COOCH_2C_6H_5$ (BHOB), and their O-deuterated species.

Figure 2 shows the absorption spectrum of EHOP, obtained in KBr pellet in the range between 4000 and 600 cm^{-1}. The moderately strong band with maximum at 3310 cm^{-1}, which shifted on deuteration to 2445 cm^{-1}, can be assigned to the OH stretching vibration. A sharp band due to the free OH group was observed at 3555 and 3530 cm^{-1} in dilute CCl_4 and CS_2 solutions, respectively, and no band could be observed around 3310 cm^{-1}. The 3310 cm^{-1} band observed in the solid state is, therefore, certainly attributable to the intermolecular hydrogen bonded OH group. The strong bands at 1735 and 1675 cm^{-1} are assigned to the carbonyl stretching of ester and ketone, respectively.[12] Similar bands are observed in the solid state spectra of BHOP (1728 and 1682 cm^{-1}) and BHOB (1740 sh, 1732, and 1690 cm^{-1}).

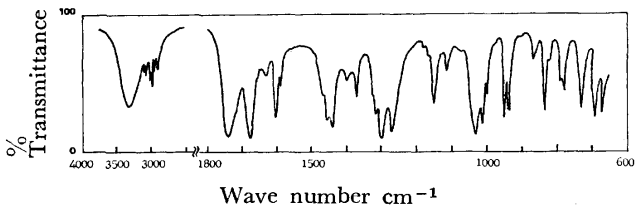

Fig. 2. Infrared absorption spectrum of $C_6H_5COC(NOH)COOC_2H_5$(KBr).

In most oximes, the C=N stretching band[13] appears at 1618—1660 cm^{-1}. This band corresponds to the weak one observed at 1627 cm^{-1} in this molecule. The weakness and low frequency of the C=N stretching band are probably due to the conjugations between the adjacent C=O groups.[14] The 1438 cm^{-1} band, which shifted to 1094 cm^{-1} on deuteration, is assigned to the OH in-plane deformation vibration.

In the region between 1300 and 1000 cm^{-1}, two intense bands are expected to appear,[12] *viz.*, the vibrations of ester C–O–C antisymmetric stretching and phenyl-carbonyl C–C stretching vibrations. EHOP does really give two strong bands, at 1298 (vs) and 1272 cm^{-1} (s), as is shown in Fig. 2. The 1298 cm^{-1} band disappeared on conversion of the ester group into COO^- group, while the 1272 cm^{-1} band remained unchanged. Therefore, the former band can be ascribed to the ester C–O–C antisymmetric stretching vibration and the latter to the phenyl–carbonyl C–C stretching vibration. This assignment is supported by the fact that BHOP also gives bands at similar frequencies, *i.e.*, at 1288 (vs) and 1273 (s), but BHOB shows only one band at 1240 cm^{-1} (s) around 1300 cm^{-1}.

Table 1. Observed frequencies and assignments of EHOP

Frequency (cm^{-1})	Assignment
3310 m	bonded OH str. (2445)
1735 s	ester C=O str.
1675 vs	ketone C=O str.
1627 vw	C=N str.
1597 m	phenyl ring
1583 w	phenyl ring
1452 sh	phenyl ring
1448 m	CH_3 asym. def.
1438 m	OH in-plane def. (1094)
1370 w	CH_3 sym. def.
1322 sh	CH_2 def.
1313 m	CH_2 def.
1298 vs	ester C-O-C anti-sym. str.
1272 s	phenyl-carbonyl C-C str.
947 m	OH out-of-plane def. (635)
935 m	NO str. (930)
693 m	phenyl C-H out-of-plane def.

Values in parentheses correspond to the peaks of O-deuterated compound.

Oximes give bands, in a range of 1000—900 cm^{-1} due to the NO stretching and OH out-of-plane deformation vibrations.[15] Because the band at 947 cm^{-1} decreased in intensity on partial deuteration and at the same time a new band appeared at 635 cm^{-1}, the 947 cm^{-1} band can be assigned to the OH out-of-plane deformation. The band at 935 cm^{-1} which shifted slightly toward lower frequency on deuteration may be attributed to the NO stretching, because the vibration is expected to be somewhat coupled with the OH in-plane deformation vibration. The assignments thus obtained are collected in Table 1.

Molecular Conformation. When EHOP was dissolved in CCl_4, the ester carbonyl band split into a doublet at 1752 and 1726 cm^{-1}. The doublet was also observed with BHOP at 1752 and 1725 cm^{-1} (see Fig. 3). Since the molecules are essentially free in the above mentioned dilute solutions, the observed bands at 1752 and 1726 cm^{-1} can be assigned to the nonbonded carbonyl group of ester.

It is well known that, in α,β-unsaturated carbonyl compounds, the carbonyl stretching band often splits in dilute solution into two bands corresponding to two rotational isomers. An example is seen in benzalacetone in CCl_4 solution.[16] Cromwell *et al.* ascribed to the band appearing at a high frequency to the *s-cis* form and the low frequency one to the *s-trans* form. By analogy, we assigned the 1752 and 1726 cm^{-1} bands mentioned above to the *s-cis* and *s-trans*, respectively (see Fig. 4). In the case of BHOB, solid state spectrum showed a doublet at 1740 (sh) and 1732 cm^{-1}, both ascribed to the carbonyl stretching of ester, while no doublet was observed in CCl_4 dilute solution but the ester carbonyl stretching band appeared at 1754 cm^{-1}. From its position, the 1754 cm^{-1} band is to be attributed

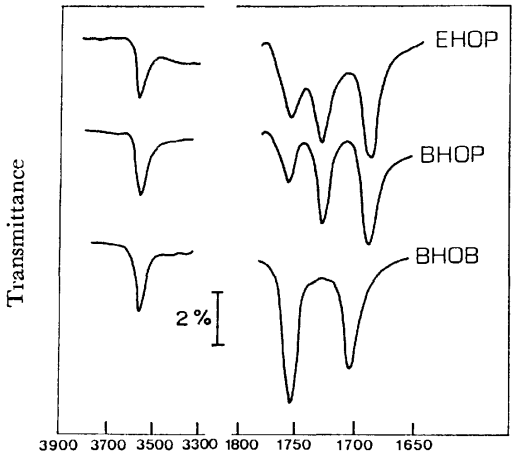

Fig. 3. Infrared spectra of ethyl 2-hydroxyimino-3-oxo-3-phenylpropionate (EHOP) and related compounds in 1×10^{-3} molal solutions in CCl_4 (0.5 mm layer): EHOP = $C_6H_5COC(NOH)COOC_2H_5$; BHOP = $C_6H_5COC(NOH)COOCH_2C_6H_5$; BHOB = $CH_3COC(NOH)COOCH_2C_6H_5$.

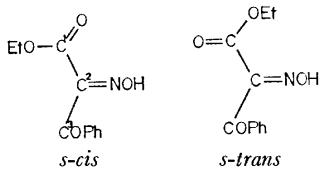

Fig. 4. Rotational isomers around the C^1–C^2 bond.

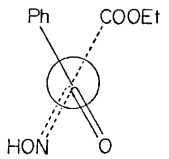

Fig. 5. Molecular conformation of EHOP, as viewed along the C^2–C^3 bond.

to the *s-cis* conformer. By structural analogy, the 1752 cm^{-1} (*s-cis*) band observed in the solution spectrum of EHOP probably corresponds to the 1735 cm^{-1} band observed in the solid phase, suggesting that the ester C=O (*s-cis*) group participates in the OH···O=C bond in the solid.

The rotational isomerism around the C^2–C^3 single bond is also possible in EHOP. However, the spectrum showed no doublet band of the ketone carbonyl stretching: the ketone C=O stretching band was observed at 1685 cm^{-1} in CCl_4 solution, slightly shifted toward higher wave numbers than the corresponding band in the solid phase.[16] This fact indicates that EHOP molecule exists in only one form around the C^2–C^3 bond. Taking into account the steric hindrance and electrostatic effects in this molecule, the most probable conformation of this molecule can be obtained as drawn in Fig. 5. In this figure the carbonyl bond adjacent to the phenyl group is assumed to be coplanar with the phenyl ring because of the predicted strong conjugation between them. The C=N bond and the ketone C=O bond are located at the non-planer *s-cis*

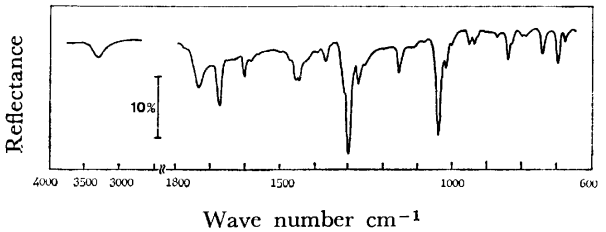

Fig. 6. High-sensitivity reflection spectrum of the thin film **A**.

for the reason that the fixation of these groups at the *s-trans* position would result in the sever repulsion a between lone-pair electrons of oxygen atom of the ketone carbonyl and those of ethoxy group. This conformation can be strongly supported by the infrared dichroisms of oriented EHOP films, as will be described below. The rotation of the ethyl group around the ester C–O bond will be mentioned later.

Reflection Spectra and Orientations. The evaporation of solvent from the thin liquid film remaining on Pd resulted in a continuous thin crystal film **A**. On the other hand, when the liquid film was thick, an amorphous solid film was formed which was unstable and crystallized into islands. The resulting film is called as **B**.

The high-sensitivity reflection spectrum of the film **A** is shown in Fig. 6. The absorption bands of the film appear at almost the same frequencies as in the transmission spectrum of the bulk crystals. However, differences in relative intensities are noticed between the thin film and the bulk crystals. Because the spectrum gave no new band in Fig. 6 and the possibility of decomposition during the treatment can be ruled out. As mentioned above, the spectrum obtained by means of the high-sensitivity reflection method is regarded as a polarized spectrum, because it results from the interaction of molecular vibration with oscillating electric field polarized normal to the plane of reflection or the Pd mirror surface. Therefore, the observed changes in band intensity is obviously ascribed to the molecular orientation in crystals.[3,4,17] Since the relative intensities of the observed bands depends on the orientation of the vibrational transition moments, the molecular orientation can be determined, based on the relative intensities and the vibrational assignments as mentioned above.

When the molecular and crystal structure of this compound is known, the orientation of all the groups of the molecule may be determined. Unfortunately, however, X-ray diffraction data is not available and the orientation will be discussed based on the molecular conformation assumed above. Because the electric vector of infrared radiation in the vicinity of Pd surface is practically normal to that surface, absorption bands must have the maximum intensity, when the vibrating electric vector is perpendicular to the palladium surface. The most noteworthy feature in Fig. 6, is the enhanced intensity of the band due to the ester C–O–C antisymmetric stretching and weakness of the ester C=O stretching. These facts can be used in determining the probable conformation of the ester group from

the two possible forms:

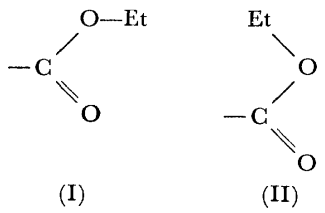

(I) (II)

The directions of the transition moments of the C=O stretching and the C–O–C antisymmetric stretching are approximately normal with each other in the conformation (I) and is parallel in the conformation (II). The relative intensities of the two bands mentioned above lead to the deduction that the conformation (I) is likely; this conformation agrees well with that known for normal acetate esters.[18] The high dichroic ratio obtained for the ester C=O stretching and the C–O–C antisymmetric stretching bands further shows that the ester group lies in a plane as a whole and that its plane is normal to the metal surface. The enhanced intensity of the ν_{as} (C–O–C) band indicates that the C–C axis of the ester probably lies perpendicular to the metal surface, whereas the C=O bond is nearly parallel to the surface. The carbonyl stretching band of ketone appears as a moderately intense band, indicating that this bond probably lies obliquely oriented to the metal surface. The fact that the band at 1275 cm^{-1}, due to the phenyl–carbonyl C–C stretching is much decreased in intensity, indicates that the C–C bond is largely tilted from the direction normal to the palladium substrate. No information is available from C=N stretching band as it is too weak in the thin film as well as in the bulk state spectrum to provide any useful information.

Other noticeable features in the spectrum of Fig. 6 are much decreased intensities of the bands at 947 and 935 cm^{-1}, arising from the OH out-of-plane deformation and NO stretching vibrations, respectively. The former gives information about the hydrogen bond as well as the OH alignment with respect to the substrate and will be noted later, while the latter indicates that the NO bond is oriented nearly parallel to the substrate surface. Based on the discussion mentioned above, the most probable molecular orientation in thin EHOP film on the Pd substrate can be obtained as shown in Fig. 7.

Figure 8 shows the high-sensitivity reflection spectrum of the thin crystal film **B**. Since the spectrum obtained

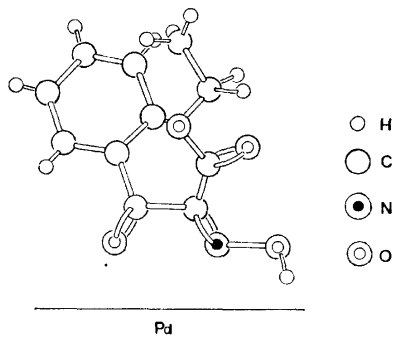

Fig. 7. Molecular orientation in the thin crystal **A**.

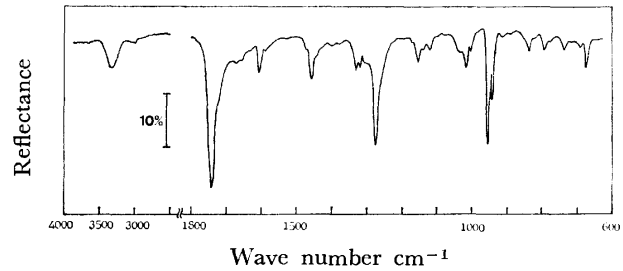

Fig. 8. High-sensitivity reflection spectrum of the thin film **B**.

just after evaporation of solvent ethanol was extremely weak and broad, this film may be regarded as amorphous. Although the relative intensity of the bands roughly agreed with that of the film **A**, the film was unstable and the crystallization soon occurred. After the crystallization, the absorption bands were much enhanced in intensity but the relative intensities of the bands differed remarkably from that in bulk spectrum of Fig. 2. The spectrum of the film **B** obtained by superposing the high-sensitivity reflection spectrum on the transmission one agrees well with the bulk spectrum, as will be described below. This fact clearly shows that the film was composed almost exclusively of EHOP and the change in relative intensity arose from the molecular orientation.

Most remarkable in Fig. 8 is the enhanced intensity of the band due to the ester C=O stretching and the extreme weakness of the ketone C=O stretching band. These facts indicate that the ester C=O bond is probably oriented perpendicular to the Pd surface, while the ketone C=O bond is not so.

The transmission measurement was carried out on film **B** formed on the sufficiently thin film of Pd deposited in a vacuum on a KBr window. The transmittance of the substrate plate used was about 30% throughout the examined frequency range. An ethyl alcohol solution of EHOP was put on the substrate surface. After evaporation of the solvent, the molecules soon crystallized in the same fashion mentioned above. To compensate the transmission loss of the substrate, a substrate prepared in the same procedure was placed in the reference beam. The signals were expanded by a factor of 5 on the recorder. The transmission spectrum obtained is shown in Fig. 9. Remarkable differences in band intensity can be seen when this spectrum is compared with that obtained by reflection method.

The spectrum obtained by superposing the reflection spectrum of the thin film on the transmission one is in good agreement with the spectrum of bulk sample

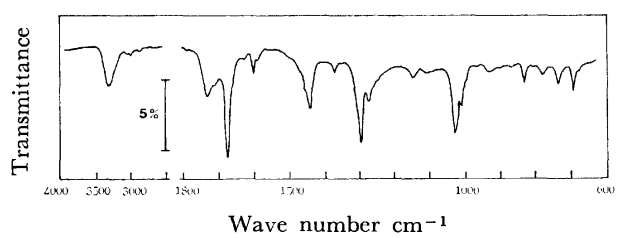

Fig. 9. Transmission spectrum of the thin film **B**.

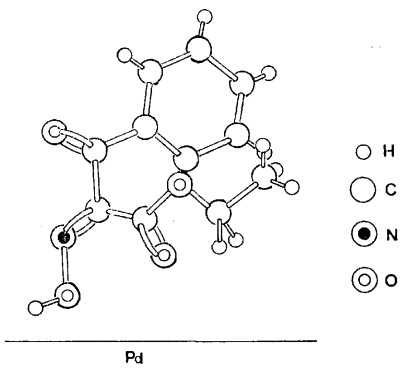

Fig. 10. Molecular orientation in the thin crystal **B**.

(Fig. 2), except slight shifts in band position caused by the difference in the measuring method. As can be seen in Fig. 9, the ketone carbonyl stretching and the ester C–O–C antisymmetric stretching bands are strongest in intensity, whereas the ester carbonyl stretching, the phenyl–carbonyl C–C stretching, and the NO stretching bands are weak. Because the electric field of incident radiation is parallel to the substrate surface and is orthogonal to that in the reflection method, the bands having enhanced intensity in the reflection spectrum must be weak in intensity in the transmission one, if the molecules are oriented. This is the case for the spectrum in Fig. 8 and that in Fig. 9, and the molecular orientation, mentioned above, is confirmed. The intensity of the OH out-of-plane deformation band is extremely weak in the spectrum of Fig. 9, indicating that the transition moment of the OH out-of-plane deformation vibration lies normal to the substrate surface. The transition moment of the OH in-plane deformation is in the plane of the OH···O unit and so stronger in intensity than the OH out-of-plane deformation in the transmission spectrum. These facts indicate that the OH···O plane in crystal **B** is lying nearly parallel to the Pd surface. Because the phenyl–carbonyl C–C stretching is observed as a moderately strong band in Fig. 8, the molecular orientation in the film **B** can be deduced as shown in Fig. 10. In accord with this orientation, NO stretching appears as an enhanced band as can be seen in Fig. 8.

In discussing the mechanism of the catalytic asymmetric hydrogenation, the direct determination of the orientation of species strongly adsorbed on the catalytic surface is quite desirable. However, the signal from such the species in a trace is too weak to provide any available information. It should be mentioned here that, according to recent experiments,[7] the orientation of molecules in a thin film is strongly governed by the orientation of the species which are adsorbed strongly on the substrate surface and which subsequently acts as the nuclei for crystal overgrowth. The molecular orientation thus taken place is generally maintained as far as the film is very thin. The orientations of the EHOP molecule in the thin film **A** may, therefore, correspond to that of species strongly adsorbed on the palladium surface. It must be mentioned that the molecular orientation in the extremely thin film **A** is essentially the same as the model proposed by Harada *et al.*[9] (see Fig. 1). Since the strain caused by crystallization may result in the change of orientation, and the molecular orientation in the film **B**, probably, does not correspond to that of the species strongly adsorbed on palladium.

References

1) W. Suëtaka, *Sci. Rept. Tohoku Univ., Ser. A*, **18**, Suppl., 129 (1966); R. G. Greenler, *J. Chem. Phys.*, **44**, 310 (1966).
2) M. L. Kottke, R. G. Greenler, and H. G. Tompkins, *Surface Sci.*, **32**, 231 (1972).
3) M. Ito and W. Suëtaka, *J. Phys. Chem.*, **79**, 1190 (1975).
4) W. Suëtaka, *Bunko Kenkyu*, **16**, 219 (1968); *Bull. Chem. Soc. Jpn.*, **40**, 2077 (1967).
5) K. Sëzuki, A. Hatta, and W. Suëtaka, *Chem. Lett.*, **1973**, 189; A. Hatta and W. Suëtake, *Bull. Chem. Soc. Jpn.*, **48**, 2428 (1975); A. Hatta, Y. Moriya, and W. Suëtaka, *ibid.*, **48**, 3441 (1975).
6) T. Takenaka, S. Tadokoro, and N. Uyeda, *Bull. Inst. Chem. Res., Kyoto Univ.*, **48**, 249 (1970).
7) K. Tanabe and N. Uyeda, *Bull. Inst. Chem. Res., Kyoto Univ.*, **52**, 616 (1974); M. Ashida, A. Hamada, and T. Watanabe, *Bull. Chem. Soc. Jpn.*, **45**, 2312 (1972); N. Uyeda, Y. Murata, T. Kobayashi, and E. Suito, *J. Cryst. Growth*, **26**, 267 (1974).
8) K. Harada and K. Matsumoto, *J. Org. Chem.*, **32**, 1794 (1967); *ibid.*, **33**, 4467 (1968); K. Harada, *Nature*, **212**, 1571 (1966); *J. Org. Chem.*, **32**, 1799 (1967); K. Harada and T. Yoshida, *Bull. Chem. Soc. Jpn.*, **43**, 921 (1970).
9) Y. Chang and W. H. Hartung, *J. Am. Chem. Soc.*, **75**, 89 (1953).
10) K. Harada and T. Yoshida, *J. Org. Chem.*, **37**, 4366 (1972).
11) W. H. Hartung, T. T. Dittrich, and Y. Chang, *J. Am. Chem. Soc.*, **75**, 238 (1953).
12) L. J. Bellamy, "The Infrared Spectra of Complex Molecules," 3rd ed., Chapman and Hall, London (1975).
13) A. Palm and H. Werbin, *Can. J. Chem.*, **31**, 1001 (1953).
14) D. Hadži, *J. Chem. Soc.*, **1956**, 2725.
15) N. B. Colthup, L. H. Daly, and S. E. Wiberley, "Introduction to Infrared and Raman Spectroscopy," Academic Press, New York (1964).
16) R. D. Campbell and N. H. Cromwell, *J. Am. Chem. Soc.*, **79**, 3456 (1957).
17) S. F. Francis and A. H. Ellison, *J. Opt. Soc. Am.*, **49**, 131 (1959).
18) M. Ōki and H. Nakanishi, *Bull. Chem. Soc. Jpn.*, **44**, 3144 (1971).

Interactions of Calcium Ions with Carbohydrates: Crystal Structure of Calcium D-Glucarate Tetrahydrate

Tooru TAGA and Kenji OSAKI
Faculty of Pharmaceutical Sciences, Kyoto University, Sakyo-ku, Kyoto 606

(Received January 12, 1976)

The crystal structure of calcium D-glucarate tetrahydrate has been determined from three dimensional X-ray data, and refined by the least squares method including an anisotropic temperature factor. The crystals are orthorhombic, space group $P2_12_12_1$ with $a=16.09$, $b=11.36$ and $c=6.68$Å. The calcium ion is bound to two glucarate molecules and three water molecules. The eight oxygen atoms form the calcium coordination shell of a distorted square-antiprism geometry. The carboxyl group including C(1) of D-glucarate has an eclipsed conformation relative to C(2) and O(2), and is coordinated with one calcium ion through the carboxyl oxygen O(1) and the α-hydroxyl oxygen O(2), and with the other calcium ion through the carboxyl oxygen O′(1) and the hydroxyl oxygens O(3) and O(4). The other carboxyl group including C(6) has an unusual staggered conformation relative to C(5) and O(5), and is not coordinated with calcium ions. However the oxygen atoms of the latter carboxyl group are attached by hydrogen bonds to a number of hydroxyl groups and water molecules, all of which are coordinated with calcium ions.

Studies on the binding of calcium ions to carboxylic sugars are important in relation to various biological systems which depend on the presence of calcium ions.[1-4] As part of a program of investigation of the structural characteristics of calcium binding, in this paper we describe the crystal structure of calcium D-glucarate tetrahydrate, $CaC_6H_8O_8\cdot 4H_2O$. D-Glucaric acid or D-saccharic acid, which is a dicarboxylic sugar acid derived from the oxidation of D-glyconic acid, is known to have a high affinity for calcium ions in alkaline solutions, and was expected to have structural characteristics typical of chelating agents.[5] In investigating the structure of calcium D-glucarate tetrahydrate we are interested therefore in interaction between calcium ions and the carboxyl groups and in particular the relationship between each carboxyl–calcium interaction and structural features which result from the conformation of the molecule as a whole.

Experimental

The crystals of strip shape were grown by slow evaporation from a dilute hydrochloride solution at room temperature. A preliminary examination showed that the crystals are orthorhombic, space group $P2_12_12_1$ as indicated by the systematic absences of $h00$, $0k0$ and $00l$ for h, k and l odd. $Z=4$, $D_x=1.74$ g/cm³, $D_m=1.77$ g/cm³ at 20 °C. The cell dimensions are $a=16.09(9)$, $b=11.36(7)$ and $c=6.68(5)$ Å. The reflection data were collected by visual estimations of the intensities from equi-inclination Weissenberg photographs obtained by rotating the crystal ($0.1\times0.15\times0.15$ mm) about the a- and c-axes, using Cu$K\alpha$ radiation. The reflection data were converted to structure amplitudes without absorption correction and the structure was solved by the direct method using the program MULTAN.[6] Three cycles of the full matrix least squares refinement using 913 reflections gave an R-value of 0.12. A further seven cycles of the block diagonal least squares refinement which included anisotropic thermal parameters reduced the R-value to 0.093. The weighting scheme used was $W^{-1}=(1+|F_o|+0.013|F_o|^2)$.[7] Scattering factors for all atoms were obtained from the International Table for X-ray Crystallography IV.[8] The positions of the hydrogen atoms were determined from the difference Fourier maps and included in the final cycle of the structure factor calculation.

Results and Discussion

The configuration and atomic numbering of the D-glucarate molecule are given in Fig. 1. The final heavy-atom parameters and their estimated standard deviations are listed in Table 1. Observed and calculated structure factors are listed in Table 2.[9] The bond distances and angles calculated from these parameters are given in Table 3. The C–C bond distances range from 1.52 to 1.58 Å with a mean value of 1.54 Å. The C–OH bond distances range from 1.42 to 1.47 Å with a mean value of 1.44 Å. The mean value for the C–C–C bond angle is 110.5° and the mean value for the C–C–OH bond angle is 110.1°. Each carboxyl group is symmetrical within the limits of experimental error. The four C–O bond distances range from 1.24 to 1.28 Å and the C–C–O angles range from 116° to 118°. The C–C–O bond angles are 126° and 128°. The carbon chain of D-glucarate has a bend conformation although the section C(2)–C(6) approximates to an extended planar zigzag. The C(1) atom is in a + synclinal position relative to C(4). (see Table 4) This conformation is unfavorable because of the repul-

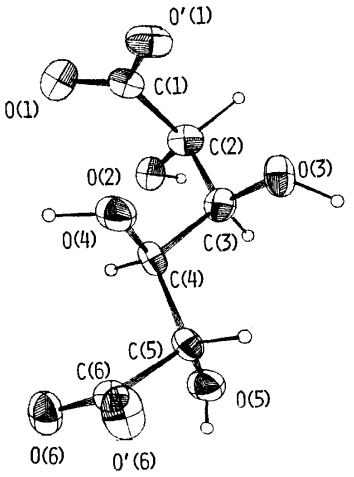

Fig. 1. The configuration and atomic numbering of the D-glucarate molecule.

TABLE 1. HEAVY-ATOM PARAMETERS AND THEIR ESTIMATED STANDARD DEVIATIONS
The values have been multiplied by 10^4. Temperature factors are in the form $T^{-1}=\exp(\beta_{11}h^2+\beta_{22}k^2+\beta_{33}l^2+2\beta_{12}hk+2\beta_{13}hl+2\beta_{23}kl)$.

	x	y	z	β_{11}	β_{22}	β_{33}	β_{12}	β_{13}	β_{23}
Ca	3100(1)	2259(2)	8596(4)	26(1)	39(1)	108(7)	−2(1)	−3(2)	−3(3)
C(1)	2714(6)	2528(9)	3565(21)	20(3)	48(9)	80(35)	5(4)	3(10)	31(14)
C(2)	3273(6)	3605(11)	3251(23)	24(4)	53(9)	127(43)	−2(5)	4(11)	30(16)
C(3)	4003(7)	3615(9)	4742(24)	27(4)	22(7)	191(45)	−6(4)	4(12)	17(14)
C(4)	4520(7)	2498(9)	4664(22)	24(3)	37(8)	105(44)	7(4)	11(10)	−16(13)
C(5)	5366(7)	2675(10)	5638(21)	21(3)	39(7)	105(33)	4(4)	12(9)	0(14)
C(6)	5760(7)	1405(10)	5884(24)	19(3)	50(9)	164(47)	1(5)	−2(10)	−10(15)
O(1)	2598(6)	1869(8)	2041(16)	40(4)	52(7)	120(27)	−9(4)	−13(9)	30(11)
O′(1)	2415(5)	2377(9)	5251(15)	19(2)	92(9)	82(27)	3(5)	15(7)	20(12)
O(2)	3557(5)	3652(7)	1161(15)	34(3)	41(6)	122(26)	−2(4)	−3(9)	16(11)
O(3)	3765(5)	3822(7)	6778(14)	36(3)	43(6)	78(26)	−3(4)	17(8)	−6(10)
O(4)	4076(5)	1622(7)	5749(16)	23(3)	39(6)	224(34)	3(3)	10(7)	14(11)
O(5)	5869(5)	3413(7)	4347(18)	23(3)	45(6)	251(36)	1(4)	5(8)	11(11)
O(6)	5945(6)	889(7)	4316(16)	38(4)	37(6)	181(32)	12(4)	−14(9)	−5(11)
O′(6)	5813(6)	1024(8)	7681(17)	46(4)	59(8)	133(31)	12(5)	−13(10)	2(12)
O(W1)	2467(8)	355(9)	8395(24)	54(5)	69(9)	361(49)	−4(6)	24(16)	−16(17)
O(W2)	4247(6)	1034(9)	9981(20)	37(4)	89(9)	205(35)	13(5)	6(10)	17(16)
O(W3)	1795(6)	3235(12)	8942(19)	37(4)	128(12)	195(38)	32(6)	−10(10)	−6(18)
O(W4)	5738(9)	4276(11)	335(27)	80(8)	83(11)	373(54)	9(8)	−15(18)	2(21)

sion between the parallel C(1)–C(2) and C(4)–O(4) bonds. (Jeffrey and Kim[10] have pointed out that parallel C–*n*-O [or C–*n*-C] and C–(*n*+2)-O [or C–(*n*+2)-C] bonds give rise to conformational instability in the carbohydrate chain.) The unfavorable C(1)–O(4) proximity in the +synclinal conformation is relaxed by a rotation of O(4) about the C(3)–C(4) bond. As a result of this rotation, O(3) and O(4) approach each other quite closely (2.64 Å). The carboxyl group at each end of the chain has a different conformation. The carboxyl group including C(1) is co-planar with the C(1)C(2)O(2) plane. The carboxyl oxygen O(1) is in an eclipsed position relative to C(2) and O(2), and is close to O(2) (2.61 Å). While the plane of the carboxyl group including C(6) is approximately perpendicular to the C(4)C(5)O(5) plane. The carboxyl oxygen O(6) is in a staggered position relative to C(4) and O(5) with the C(4)–C(5)–C(6)–O(6) torsional angle=67°. The latter staggered conformation is favorable with respect to the nonbonding interactions between the carboxyl oxygens and the atoms attached to C(5). However the former eclipsed conformation appears to be a feature of a number of carboxylic compounds. The stability of such an eclipsed form has been investigated by several workers without reaching any definite conclusion.[11–13]

The crystal packing and the coordination of calcium ions with glucarates and water molecules are shown in Figs. 2, 3, and 4. The calcium ion lies between three water molecules and two glucarate molecules which are related by translation along the c-axis, and is surrounded by eight oxygen atoms in a distorted square-antiprism arrangement. The Ca–O distances vary from 2.39 to 2.50 Å with a mean value of 2.46 Å. One glucarate molecule is coordinated with a calcium ion

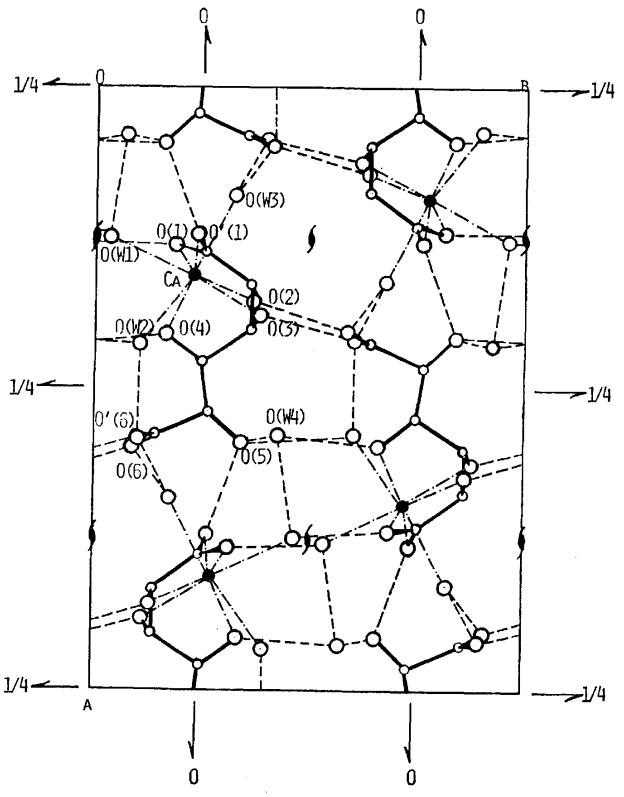

Fig. 2. The projection of the structure along the c-axis. The broken lines are hydrogen bonds.

through an O(1) carboxyl oxygen and an O(2) α-hydroxyl oxygen. The second glucarate is coordinated through the O′(1) carboxyl oxygen and the O(3) and O(4) hydroxyl oxygens arranged in a triangular form. The O–O distances in this formation are 2.64 Å for O(3)–O(4), 2.83 Å for O′(1)–O(3) and 2.91 Å for O′(1)–

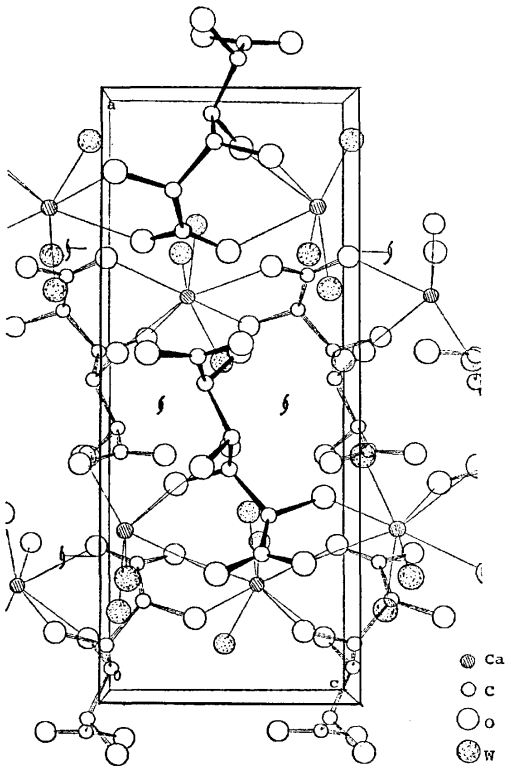

Fig. 3. A perspective view of the structure along the b-axis.

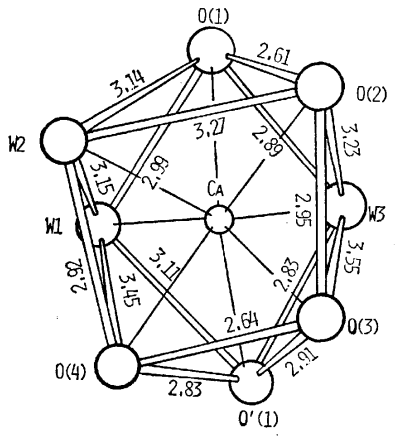

Fig. 4. The calcium coordination shell.

O(4). It has been demonstrated that in aqueous solutions the affinity of calcium ions for carboxylic acids is increased by the presence of an α-oxygen and this affinity is further enhanced by the presence of additional hydroxyl groups in the molecule.[14,15] In all the crystal structures of calcium salts of other carboxylic compounds determined to date,[16-23] the carboxyl oxygen and the α-oxygen are both coordinated with the calcium ion. Therefore the carboxylic oxygen and the α-hydroxyl oxygen in an eclipsed conformation as in O(1) and O(2) are generally coordinated with the calcium ion through the formation of a stable five membered ring O–C–C–O–Ca. The triangular structure of O'(1), O(3) and O(4) is a previously unobserved type of oxygen arrangement which excludes the α-oxygen atom. (In the structures determined for Ca D-xylo-5-hexalosonate $2H_2O$,[21] CaBr lactobionate $4H_2O$[22] and Ca arabonate $5H_2O$,[23] the α-hydroxyl oxygen is included in the 'oxygen triangle' coordinated with the calcium ion.) The nonbonding distance between O(3) and O(4) is shorter than that between O'(1) and O(3) and between O'(1) and O(4), and a stable five membered chelate ring including a calcium ion is formed through the O(3)–C(3)–C(4)–O(4) linkage.

Table 3. Intramolecular bond distances (Å) and angles (°) with their estimated standard deviations

Bond distance		Bond angle	
C(1)-C(2)	1.534(16)	C(1)-C(2)-C(3)	111.4(1.1)
C(2)-C(3)	1.540(19)	C(2)-C(3)-C(4)	112.9(1.1)
C(3)-C(4)	1.519(15)	C(3)-C(4)-C(5)	111.4(1.0)
C(4)-C(5)	1.522(17)	C(4)-C(5)-C(6)	106.3(0.9)
C(5)-C(6)	1.584(16)	C(2)-C(1)-O(1)	116.4(1.2)
C(1)-O(1)	1.277(17)	C(2)-C(1)-O'(1)	117.6(1.1)
C(1)-O'(1)	1.236(17)	C(5)-C(6)-O(6)	116.2(1.2)
C(6)-O(6)	1.237(18)	C(5)-C(6)-O'(6)	115.6(1.2)
C(6)-O'(6)	1.279(19)	C(1)-C(2)-O(2)	110.0(1.0)
C(2)-O(2)	1.469(18)	C(3)-C(2)-O(2)	112.1(1.0)
C(3)-O(3)	1.431(19)	C(2)-C(3)-O(3)	114.3(1.0)
C(4)-O(4)	1.424(15)	C(4)-C(3)-O(3)	108.5(1.1)
C(5)-O(5)	1.449(16)	C(3)-C(4)-O(4)	106.9(1.0)
Ca-O(1)	2.478(11)	C(5)-C(4)-O(4)	108.9(1.1)
Ca-O'(1)	2.495(10)	C(4)-C(5)-O(5)	108.8(1.1)
Ca-O(2)	2.445(10)	C(6)-C(5)-O(5)	111.4(0.9)
Ca-O(3)	2.402(9)	O(1)-C(1)-O'(1)	126.0(1.0)
Ca-O(4)	2.569(10)	O(6)-C(6)-O'(6)	128.1(1.1)
Ca-O(W1)	2.395(11)		
Ca-O(W2)	2.490(11)		
Ca-O(W3)	2.386(11)		

Another interesting feature of the structure of calcium D-glucarate is that calcium ions are not directly bound to the C(6) carboxyl group. The O(6) carboxyl oxygen in a staggered position is far from the O(5) hydroxyl oxygen. The O(5)–O(6) distance of 2.87 Å is sufficiently great to prevent the formation of a stable chelate ring with a calcium ion. Generally in the carboxyl oxygen in the staggered conformation the electron lone pairs are unshielded by intramolecular atoms, thus the carboxyl oxygens are more capable of forming intermolecular hydrogen bonds than in the case of carboxyl oxygens in the eclipsed form. In fact, the oxygen atoms of the C(1) carboxyl group form only two hydrogen bonds, whereas the oxygen atoms of the C(6) carboxyl group form five hydrogen bonds with the water molecules and the hydroxyl groups of the adjacent molecules. The hydrogen bonding scheme and their distances are given in Fig. 2 and Table 5, respectively. All of the hydroxyl groups and water molecules attached by hydrogen bonds to the C(6) carboxyl group are coordinated with calcium ions. Conversely, the C(6) carboxyl groups link the adjacent calcium centered oxygen polyhedrons.

From the data described here, it is apparent that the calcium-hydroxyl interaction is important in

Table 4. Torsional angles (°) about C-C bonds in D-glucarate molecule

O(1)-C(1)-C(2)-C(3)	−124.2	O′(1)-C(1)-C(2)-C(3)	56.1
O(1)-C(1)-C(2)-O(2)	0.8	O′(1)-C(1)-C(2)-O(2)	−179.0
C(1)-C(2)-C(3)-C(4)	55.7	O(2)-C(2)-C(3)-C(4)	−68.0
C(1)-C(2)-C(3)-O(3)	−68.9	O(2)-C(2)-C(3)-O(3)	167.4
C(2)-C(3)-C(4)-C(5)	162.4	O(3)-C(3)-C(4)-C(5)	−69.9
C(2)-C(3)-C(4)-O(4)	−78.7	O(3)-C(3)-C(4)-O(4)	49.0
C(3)-C(4)-C(5)-C(6)	168.0	O(4)-C(4)-C(5)-C(6)	50.3
C(3)-C(4)-C(5)-O(5)	−71.9	O(4)-C(4)-C(5)-O(5)	170.4
C(4)-C(5)-C(6)-O(6)	67.3	O(5)-C(5)-C(6)-O(6)	−51.1
C(4)-C(5)-C(6)-O′(6)	−109.9	O(5)-C(5)-C(6)-O′(6)	131.7

Table 5. Lengths (Å) of hydrogen bonds with their estimated standard deviations

O(1)···O(W1)	h	2.685(14)
O′(1)···O(5)	b	2.657(11)
O(6)···O(2)	e	2.683(11)
O(6)···O(W3)	c	2.755(16)
O′(6)···O(3)	f	2.617(12)
O′(6)···O(W2)	a	2.950(15)
O′(6)···O(W3)	d	2.879(16)
O(W4)···O(4)	g	2.777(16)
O(W4)···O(5)	a	2.860(21)
O(W4)···O(W1)	c	2.937(20)

Symmetry codes

a :	x,	y,	z
b :	$-1/2+x$,	$1/2-y$,	$1-z$
c :	$1/2+x$,	$1/2-y$,	$1-z$
d :	$1/2+x$,	$1/2-y$,	$2-z$
e :	$1-x$,	$-1/2+y$,	$1/2-z$
f :	$1-x$,	$-1/2+y$,	$3/2-z$
g :	$1-x$,	$1/2+y$,	$1/2-z$
h :	$1/2-x$,	$-y$,	$-1/2+z$

relation to the binding of calcium ions to carboxylic sugars. The intramolecular proximity of the hydroxyl groups and carboxyl oxygens is particularly relevant to the formation of a stable calcium chelate structure possibly accompanied by a conformational change of the ligand molecule to a more favorable arrangement of oxygen atoms. These structural characteristics readily account for the high stability of calcium D-glucarate crystals.

The authors wish to thank Dr. Robert Freeman for his kindness in the correction of this manuscript. All the computations were performed by using a new Kyoto X-Ray Program System, which is including the UNICS programs, on the FACOM 230-60 in the Data Processing Center, Kyoto University.

References

1) A. L. Lehninger, *Proc. Nat. Acad. Sci., U. S. A.*, **60**, 1069 (1968).
2) W. E. Pricer and G. Ashwell, *J. Biol. Chem.*, **246**, 4825 (1971).
3) E. R. Morris, D. A. Rees, and D. Thom, *J. Chem. Soc., Chem. Commun.*, **1973**, 245.
4) A. H. Hughes, I. C. Hancock, and J. Bacciley, *Biochem. J.*, **132**, 83 (1973).
5) C. L. Mehltretter, B. H. Alexander, and C. E. Rist, *Ind. Eng. Chem.*, **45**, 2782 (1953).
6) G. Germain, P. Main, and M. M. Woolfson, *Acta Crystallogr.*, **A27**, 368 (1971).
7) D. W. J. Cruickshank, "Computing Methods and the Phase Problem in X-Ray Crystal Analysis," Pergamon Press, New York (1961), p 45.
8) "International Tables for X-Ray Crystallography (IV)," Kynoch Press, Birmingam (1974), p 71.
9) Table 2 is kept in the office of the Chemical Society of Japan, 1-5 Kanda-Surugadai, Chiyoda-ku, Tokyo 113, (Document No. 7620).
10) G. A. Jeffrey and H. S. Kim, *Carbohyd. Res.*, **14**, 207 (1970).
11) J. A. Kanters, J. Kroon, A. F. Peerdeman, and J. C. Schoone, *Tetrahedron*, **23**, 4027 (1967).
12) G. A. Jeffrey and G. S. Parry, *Nature*, **169**, 1105 (1952).
13) R. Norrestam, P. E. Werner, and M. V. Glehn, *Acta Chem. Scand.*, **22**, 1395 (1968).
14) R. K. Cannan and A. Kibrick, *J. Biol. Chem.*, **124**, **437** (1938).
15) C. W. Davies, *J. Chem. Soc.*, **1938**, 277.
16) G. K. Ambady, *Acta Crystallogr.*, **B24**, 1548 (1968).
17) V. A. Uchtman and R. P. Oertel, *J. Am. Chem. Soc.*, **95**, 1802 (1973).
18) B. Sheldrick, *Acta Crystallogr.*, **B30**, 2056 (1974).
19) J. P. Glusker, J. A. Minkin, and C. A. Casciato, *Acta Crystallogr.* **B27**, 1284 (1971).
20) S. E. B. Gould, R. O. Gould, D. A. Rees, and W. E. Scott, *J. Chem. Soc., Perkin Trans. II*, **1975**, 237.
21) A. A. Balchin and C. H. Carlisle, *Acta Crystallogr.*, **19**, 103 (1965).
22) W. J. Cook and C. E. Bugg, *Acta Crystallogr.*, **B29**, 215 (1973).
23) S. Furberg and S. Helland, *Acta Chem. Scand.*, **16**, 2373 (1962).

Aromatic Nucleophilic Substitution. VII.[1] Electronic Structure of 1,1-Disubstituted 2,4-Dinitronaphthalene Meisenheimer Complexes

Shizen SEKIGUCHI,* Kinzo TSUTSUMI, Haruo SHIZUKA, Kohji MATSUI, and Takeshi ITAGAKI

Department of Synthetic Chemistry, Gunma University, Tenjincho, Kiryu, Gunma 376

(Received January 26, 1976)

The electronic structures of 1,1-disubstituted 2,4-dinitronaphthalene Meisenheimer complexes were studied by UV-visible and infrared spectrometry and compared with the results calculated by a semiempirical SCF-MO-CI method. The electronic transitions in the complexes were assigned to those of π-π^*. Calculated transition energies and intensities agree well with the observed values. The infrared spectra of the complex indicated that the complex is not a charge transfer complex or a radical anion, but an anionic σ complex.

Many Meisenheimer complexes such as I (hereinafter referred to as anionic σ complex) have been prepared by nucleophilic attack on polynitro aromatic compounds. These reactions have been extensively studied and the results are reviewed in detail.[2] Simple MO treatments of aromatic nucleophilic substitution have been attempted by several workers.[3] Abe[3g] has explained with the Hückel MO method the result that in the longer wavelength region one and two absorption bands are observed for di- and trinitrocyclohexadienate

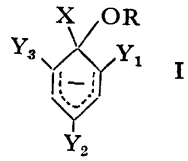

I

X=H, OR, halogen

(I, X=OCH_3, R=CH_3, Y_1=Y_2=NO_2, and Y_3=H; X=OCH_3, Y_1=Y_2=Y_3=NO_2), although the characters of the electronic transitions were not explained. Furthermore, Caveng *et al.*[3d] have reported with the aid of the HMO treatment that π-electrons in I (X=OCH_3, R=CH_3, Y_1=Y_2=Y_3=NO_2) are attracted by the three nitro groups such that the ring becomes positively charged. Criticizing the work of Abe and Caveng *et al.*, Hosoya *et al.*[3f] have indicated that nitro compounds are something beyond the limit of the HMO treatment, and they have performed the Pariser-Parr-Pople type SCF-MO-CI calculation for 1,3,5-trinitrocyclohexadienate (I, Y_1=Y_2=Y_3=NO_2, neglecting the effect of X and OR groups), indicating that the lower electronic transitions in this complex are assigned as due to charge transfer from the pentadienyl group to the nitro group. However, no SCF-MO-CI calculation has been performed for naphthalene anionic σ complexes. This paper will report the electronic transitions in 1,1-disubstituted 2,4-dinitronaphthalene anionic σ complexes with the aid of a semiempirical SCF-MO-CI calculation.

Method of Calculation

The π electronic structures of 1,1-disubstituted 2,4-dinitronaphthalene Meisenheimer complexes were studied by the variable β, γ procedure of semiempirical SCF-MO method combining with singly excited CI calculation. The parameters were taken as proposed by Nishimoto and Forster.[4] One-center repulsion integrals $\gamma_{\mu\mu}$ were estimated from the corresponding valence state ionization potentials (I_μ) and electron affinities (A_μ) by the Pariser-Parr approximation,[5] I_μ and A_μ being determined from spectroscopic data using the promotion energies of Hinze and Jaffé.[6] Two-center electron repulsion integrals $\gamma_{\mu\nu}$ were estimated by use of the Mataga-Nishimoto approximation.[7] Two-center core resonance integrals $\beta_{\mu\nu}$ were evaluated by the Nishimoto-Forster approximation.[4]

The geometry of the complex (II) was assumed as follows:

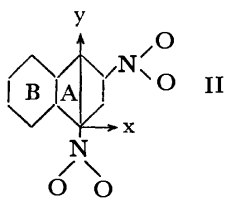

II

The C–C bond lengths and all bond angles were assumed to be 1.39 Å and 120°, respectively. The C–N and N–O bond lengths were assumed to be 1.486 and 1.210 Å, respectively. The computation was carried out with a HITAC 8800 located at the Computer Center of the University of Tokyo

Experimental

Materials. 1-Ethoxy-(III) and 1-methoxy-2,4-dinitronaphthalene (IV) were prepared by the action of $NaOC_2H_5$ on an ethanolic solution of 1-chloro-2,4-dinitronaphthalene (CDNN), mp 91—92 °C (lit, 93 °C[8] and 90—91 °C[9]) and 97—98 °C (lit. 97 °C[10] and 97.5—98 °C[11]). 1-Piperidino-(V) or 1-dimethylamino-2,4-dinitronaphthalene (VI) were prepared by the action of the corresponding amine on CDNN in DMSO according to the method of Orvik and Bunnett.[8] Recrystallization from 95% ethanol gave an analytical sample: V, yield 80%, mp 136—137 °C (Found: C, 60.05; H, 5.21; N, 14.23. Calcd for $C_{15}H_{15}N_3O_4$: C, 59.79; H, 5.02; N, 13.95%) and VI, yield 45%, mp 88—89 °C (Found: C, 55.39; H, 4,40; N, 16.30. Calcd for $C_{12}H_{11}N_3O_4$: C, 55.17; H, 4.24; N, 16.09%).

IR Spectra of the Reactions System of VI with $NaOCH_3$ in DMSO. 0.035 ml of methanolic $NaOCH_3$ (4.18 M) was added to a DMSO solution (0.15 ml) of VI (1.48×10^{-4} mol), in which the molar ratio VI to $NaOCH_3$ was one, and the spectra of the mixture were taken.

Results and Discussion

Absorption Spectra of the Reaction of 1-Ethoxy-2,4-dinitronaphthalene(III) with Piperidine and the Reaction of

Table 1. Calculated and observed transition energies, transition moments and oscillator strength of Meisenheimer complex (II)

	Transition energy (eV)			Transition moment		Oscillator strength		
	E_{calcd}	E_{obsd}				f_{calcd}	f_{obsd}	
		IIA	IIB	X	Y		IIA	IIB
S_1	2.815	2.372	2.376	1.282	1.322	0.835	0.30	0.33
S_2	3.729	3.388	3.308	−0.638	0.936	0.419	0.16	0.20
S_3	3.878	—	—	0.220	0.289	0.028	—	—
S_4	4.908	—	—	−0.175	−0.502	0.121	—	—

1-Methoxy-2,4-dinitronaphthalene(IV) with Dimethylamine in DMSO. Addition of excess piperidine to a DMSO solution of III at room temperature (III 2.60×10^{-5} M, piperidine 1.01 M) yielded a red solution, indicating the formation of an anionic σ complex as follows:[8,12,13]

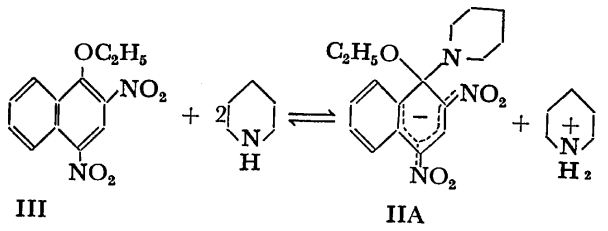

(1)

The complex IIA was catalyzed with piperidinium ion to form the replaced product V as shown in Eq. 2.[8] The absorption spectrum measured immediately

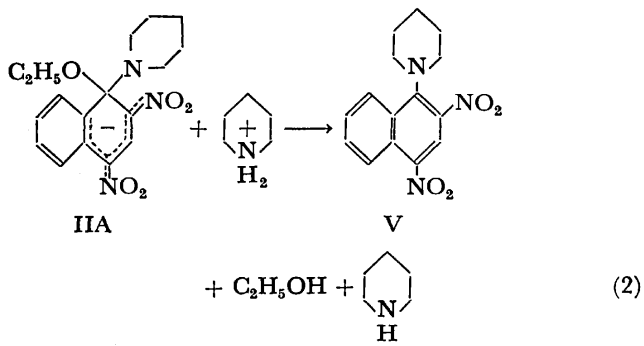

(2)

after mixing is shown in Fig. 1, in which the positions and intensities are typical of 1,1-disubstituted 2,4-dinitronaphalene anionic σ complexes.[13–15] In the case of the reaction of IV with dimethyl amine, a similar spectrum to that in Fig. 1 was obtained. The absorption spectra of IIA and IIB (1-methoxy-1-dimethylamino-2,4-dinitronaphthalene anionic σ complex) comprise two allowed transitions, Band I (ε 2.4×10^4 at 522 nm) and Band II (ε 1.7×10^4 at 357 nm) for IIA, and Band I (ε 2.7×10^4 at 519 nm) and Band II (ε 1.6×10^4 at 364 nm) for IIB, respectively.

The calculated and observed transition energies, transition moments, and oscillator strengths of the anionic σ complex are listed in Table 1. The calculated transition energies are smaller than those of the observed values, because the complex in the excited state, S_1 or S_2, is more stabilized in DMSO, a comparatively polar solvent, than that in the ground state, S_0, as can be seen from the result that the dipole moment in the excited state is about twice larger than that in the ground state.

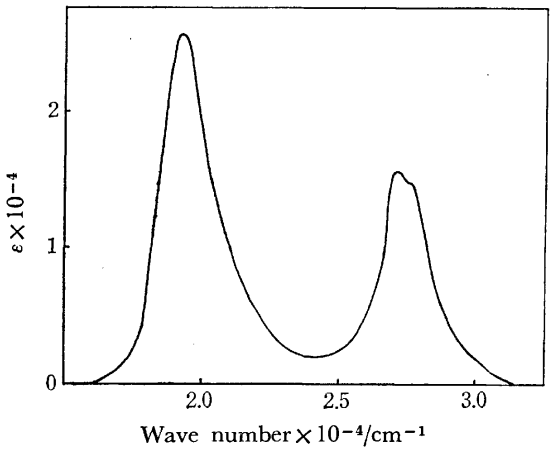

Fig. 1. Absorption spectrum relevant to the reaction of 2,4-dinitro-1-naphthylmethyl ether(IV, 3.30×10^{-5} M) with piperidine(2.00×10^{-1} M).

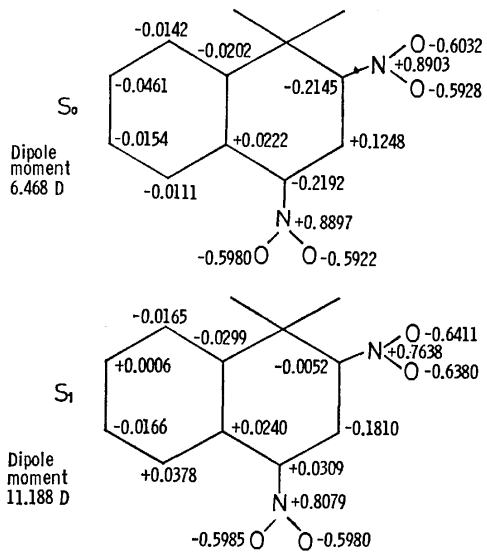

Fig. 2. π formal charge of the complex in the S_0 and S_1 states.

The π formal charges of the complex in the S_0 and S_1 states are shown in Fig. 2. In the S_0 state, the negative charge donated by a nucleophile to the π system is distributed on the two nitro groups to a large extent (*ca.* 60%). In the S_1 state, *ca.* 90% of

one negative charge is distributed on the two nitro groups, where the charge distribution on the nitro group attached to C_1 is larger in comparison with that on the nitro group attached to C_3 and *ca.* 10% of it distributed on the B ring. These facts indicate that Band I corresponds to that of an intramolecular CT. From the analysis of charge distribution in the complex, one can understand how the two nitro groups are responsible for electron acceptors resulting in the stability of II.

Naturally, the fact that the absorption spectra of IIA and IIB agree well with the result of SCF-MO-CI calculation of II based on the assumption of an 18 π-electron closed system indicates that IIA and IIB are not anion radicals but anionic σ complexes. Similar results have been obtained on 1,1-disubstituted tri- and dinitrocyclohexadienates by Hosoya *et al.*[3f]

IR spectra of the Reaction of N,N-*Dimethyl-2,4-dinitro-1-naphthylamine (VI) with Methanolic NaOCH$_3$ in DMSO.* We have recently found that VI reacts with NaOCH$_3$ in DMSO at room temperature to produce the same anionic σ complex as IIB,[9b] which is stable enough for a long time to be observed by IR measurement, different from IIB obtained in the similar way to Eqs. 1 and 2, as follows:[14]

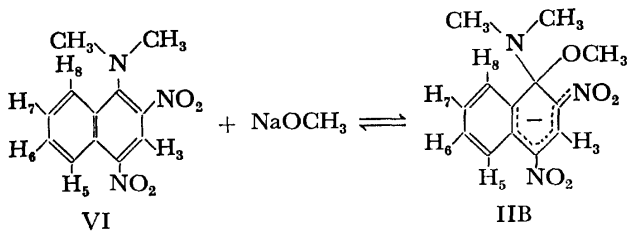

(3)

The IR spectra of the reaction system in Eq. 3 are shown in Fig. 3. Ohsawa[15] has stated that the strong and broad band characteristic of the ketal-like structure $>C\langle^{OR}_{NH_2}$ in Meisenheimer complexes appears at 1020—1040 cm^{-1}. The band appeared at 1040 cm^{-1}, therefore, is clearly attributable to the structure of $>C\langle^{OR}_{N\langle}$ bond, which indicates that the hybrid orbital of C_1 changes from sp^2 to sp^3 in conversion of V to IIB. Furthermore, in conversion of V to IIB, H_3 and H_8 resonance signals are shifted downfield, and H_5, H_6, and H_7 ones upfield, the shifts of which are characteristic of an anionic σ complex.[14] All these results show that IIB is an anionic σ complex.

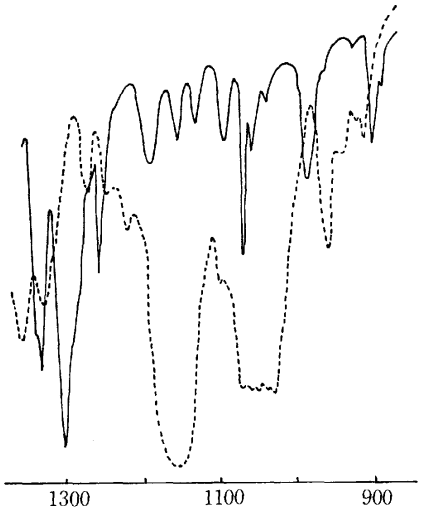

Fig. 3. Infrared spectra relevant to the reaction of *N,N*-dimethyl-2,4-dinitronaphthylamine(VI) with methanolic NaOCH$_3$ in DMSO.
——: VI, ----: IIB.

This work was supported in part by a Grant-in-aid of Industrial Scientific Research from the Asahi Glass Co., Ltd., and in part by a Grant from the Ministry of Education, to which the authors' thanks are due.

References

1) Part VI, S. Sekiguchi, Y. Ando, K. Matsui, and T. Hirose, submitted for publication in *Bull. Chem. Soc. Jpn.*

2) (a) F. Pietra, *Quart. Rev.*, **23**, 504 (1969); (b) T. J. de Boer and I. P. Dirkx, "The Chemistry of the Nitro and Nitroso Groups," Part I, H. Feuyer, Ed., Interscience, New York, N. Y. (1969), p.487; (c) J. Miller, "Aromatic Nucleophilic Substitution," Elsevier, New York, N. Y. (1968): (d) S. D. Ross, *Progr. Phys. Org. Chem.*, **1**, 31 (1963); (e) M. R. Crampton, *Adv. Phys. Org. Chem.*, **7**, 211 (1969); (f) R. Foster and C. A. Fyfe, *Rev. Pure Appl. Chem.*, **16**, 61 (1966); (g) E. Buncel, A. R. Norris, and K. E. Russell, *Quart. Rev.*, **22**, 123 (1968); (h) P. Buck, *Angew. Chem. Int. Edn.*, **8**, 120 (1969); (i) M. J. Strauss, *Chem. Rev.*, **70**, 667 (1970).

3) (a) R. Destro, C. Gramaccioli, and M. Simmonetta, *Acta Crystallogr.*, **23**, 1369 (1968); (b) S. Carra, M. Raimondi, and M. Simmonetta, *Tetrahedron*, **22**, 2673 (1966); (c) P. Beltrame, P. L. Beltrame, and M. Simmonetta, *ibid.*, **24**, 3043 (1968); (d) P. Caveng, P. B. Fisher, E. Heilbronner, A. L. Miller, and H. Zollinger, *Helv. Chim. Acta*, **50**, 848 (1967); (e) R. Destro, *Redn. Inst. Lombardo Sci. Lett.*, **101**, 725 (1967) (*Chem. Abstr.*, **69**, 46186t (1968)); (f) H. Hosoya, S. Hosoya, and S. Nagakura, *Theor. Chim. Acta*, **12**, 117 (1968); (g) T. Abe, *Bull. Chem. Soc. Jpn.*, **37**, 508 (1964); *ibid.*, **39**, 627 (1966); (h) J. Murto, *Suomen Kemi.*, **38**, 246 (1965); S. Nagakura, *Tetrahedron*, **19**, 361 (1963).

4) K. Nishimoto and L. S. Forster, *Theor. Chim. Acta*, **3**, 407 (1965); *ibid.*, **4**, 155 (1966).

5) R. Pariser and R. G. Parr, *J. Chem. Phys.*, **21**, 446, **767** (1953).

6) J. Hinze and H. H. Jaffé, *J. Am. Chem. Soc.*, **84**, 540 (1962).

7) N. Mataga and K. Nishimoto, *Z. Phys. Chem.*, **13**, 140 (1957).

8) P. H. Hiermann, *J. Prakt. Chem.*, **44**, 243 (1891).

9) J. A. Orvik and J. F. Bunnett, *J. Am. Chem. Soc.*, **92**, 2417 (1970).

10) F. Ullmann and W. Bruck, *Chem. Ber.*, **41**, 3932 (1908).

11) W. E. Byrne, E. J. Fendler, J. H. Fendler, and C. E. Criffin, *J. Org. Chem.*, **32**, 2506 (1967).

12) (a) S. Sekiguchi and T. Shiojima, *Bull. Chem. Soc. Jpn*, **46**, 693 (1973); (b) S. Sekiguchi, T. Itagaki, T. Hirose, K. Matsui, and K. Sekine, *Tetrahedron*, **29**, 3527 (1973).

13) C. F. Bernasconi, R. H. de Rossi, and C. L. Gehringer, *J. Org. Chem.*, **38**, 2838 (1973).

14) S. Sekiguchi, K. Shinozaki, T. Hirose, K. Matsui, and K. Sekine, *Bull. Chem. Soc. Jpn.*, **47**, 2264 (1974).

15) S. Ohsawa, *Nippon Kagaku Kaishi*, **8**, 1486 (1973).

Electronic Population Analysis Based on the Electron Pair Concept

Takashi OKADA and Takayuki FUENO

Department of Chemistry, Faculty of Engineering Science, Osaka University, Toyonaka, Osaka 560

(Received January 29, 1976)

The electronic population in molecular systems is analyzed on the basis of the spin coupling matrix. A proposal is made to define the pair-coupling population which is directly related to the electron pair concept. The theory is applied to the examinations of various types of wave functions used for three-centered two-, three-, and four-electron systems. The results permit clear comparisons of the characteristics of the various wave functions examined.

Recent progress in computer technology has made it possible to determine molecular electronic wave functions in fairly good accuracy. However, such wave functions are generally too intricate in form to permit naive interpretation by chemical intuition. Thus, a systematic procedure for obtaining a maximum insight into any type of wave function is necessitated. The first- and second-order reduced density matrices (hereafter referred to as 1- and 2-matrices, respectively) are the most appropriate starting point in this respect, because they contain enough information to specify the electronic structures in question. In particular, population analysis applied to the density matrices affords an interpretation of electronic structure in chemical language. Thus far, spinless 1- and 2-matrices have been successfully analyzed in several articles.[1–5]

In this paper, we analyze the spin coupling matrices, Q^0 and Q^2, and therefrom define the pair-coupling populations between AO's. The spin coupling matrices are directly related to the electron pair concept as studied in a previous paper.[6] Accordingly, the analysis of pair-coupling populations is expected to shed light on the classical Lewis-Langmuir theory as well as the valence bond interpretation. The specific examples which we will here investigate are the π-electron systems of C_3H_5, NO_2, HCO_2, and O_3 with 2 to 4 π-electrons. Population analysis has been carried out for various types of wave functions calculated by Linnett and coworkers.[7–10] The pair-coupling populations, together with the conventional populations so far employed, have been examined for each wave function. The results are compared, and the characteristics of molecules discussed.

I. Population Analysis

The 1- and 2-matrices in the Löwdin normalization[11] for an N-electron wave function $\Psi(x_1,x_2,\cdots x_N)$ are given by

$$\rho^{(1)}(x_1\,;\,x_1') = N\int \Psi(x_1,x_2,\cdots x_N) \times \Psi^*(x_1',x_2,\cdots x_N)\mathrm{d}x_2\cdots\mathrm{d}x_N \quad (1)$$

$$\rho^{(2)}(x_1,x_2\,;\,x_1',x_2') = \binom{N}{2}\int \Psi(x_1,x_2,x_3,\cdots x_N) \times \Psi^*(x_1',x_2',x_3,\cdots x_N)\mathrm{d}x_3\cdots\mathrm{d}x_N \quad (2)$$

The population analysis is to be made on spin-free density functions, so that we will make use of the following types of density matrices with space variables alone:

$$P_1(r_1\,;\,r_1') = \int_{s_1=s_1'} \rho^{(1)}(x_1\,;\,x_1')\mathrm{d}s_1 \quad (3)$$

$$Q_S(r_1\,;\,r_1') = 2\int_{s_1=s_1'} S_z(s_1)\,\rho_{st}^{(1)}(x_1\,;\,x_1')\mathrm{d}s_1 \quad (4)$$

$$P_2(r_1,r_2\,;\,r_1',r_2') = \int_{s_1=s_1',\,s_2=s_2'} \rho^{(2)}(x_1,x_2\,;\,x_1',x_2')\mathrm{d}s_1\mathrm{d}s_2 \quad (5)$$

$$Q^0(r_1,r_2\,;\,r_1',r_2') = \int_{s_1=s_1',\,s_2=s_2'} (-4/3)\boldsymbol{S}(s_1)\cdot\boldsymbol{S}(s_2) \times \rho^{(2)}(x_1,x_2\,;\,x_1',x_2')\mathrm{d}s_1\mathrm{d}s_2 \quad (6)$$

$$Q^2(r_1,r_2\,;\,r_1',r_2') = \frac{4(S+1)}{3(2S-1)}\int_{s_1=s_1',\,s_2=s_2'} [3S_z(s_1)\cdot S_z(s_2) - \boldsymbol{S}(s_1)\cdot\boldsymbol{S}(s_2)]\rho_{st}^{(2)}(x_1,x_2\,;\,x_1',x_2')\mathrm{d}s_1\mathrm{d}s_2 \quad (7)$$

where r_i and s_i are the space and spin variables, respectively, and where the subscript st denotes that a standard state with $\langle S_z\rangle = S$ is assumed.

The density functions defined as the diagonal elements of the spinless matrices (3) to (7) possess clear physical meanings. Thus, $P_1(r_1)$ and $P_2(r_1,r_2)$ stand for the charge and pair-electron densities. $Q_S(r_1)$ represents the spin density distribution. $Q^0(r_1,r_2)$ and $Q^2(r_1,r_2)$ are the spin-coupling functions,[6] which respectively denote the distributions of singlet- and triplet-type electron pairs.

In performing the population analysis, we assume that these density functions can be expanded by an atomic orbital basis set $(a,b,c,\cdots)$. The charge density function $P_1(r_1)$ is then expressed as follows:

$$P_1(r_1) = \sum_{a,b}\gamma_1(a\,|\,b)\,a(r_1)\,b^*(r_1) \quad (8)$$

The expansion coefficients $\gamma_1(a\,|\,b)$ lead to Mulliken's *gross* and *net populations*,[2] q_a and q_{aa}, for atomic orbital a as well as the *overlap population*[2] q_{ab} between atomic orbitals a and b:

$$q_a = \sum_b \gamma_1(a\,|\,b)\,s_{ab} \quad (9a)$$

$$q_{aa} = \gamma_1(a\,|\,a) \quad (9b)$$

$$q_{ab} = 2\gamma_1(a\,|\,b)\,s_{ab} \quad (9c)$$

where s_{ab} is the overlap integral between a and b. Populations of a total of N electrons are subject to the following constraints:

$$\sum_a q_a = N \quad (10a)$$

$$\sum_a q_{aa} + \sum\sum_{a>b} q_{ab} = N \quad (10b)$$

A similar partitioning procedure may be used for the other density functions. First, from the spin density function expressed in the form

$$Q_S(r_1) = \sum_{a,b} \delta_s(a|b)a(r_1)b^*(r_1), \tag{11}$$

we define the *spin population*:

$$q_a{}^s = \sum_b \delta_s(a|b)s_{ab} \tag{12}$$

Clearly, $q_a{}^s$ should satisfy the relationship:

$$\sum_a q_a{}^s = 2S. \tag{13}$$

Second, the two-particle density functions are expanded as follows:

$$P_2(r_1,r_2) = \sum_{a,b,c,d} \gamma_2(ab|cd)a(r_1)b(r_2)c^*(r_1)d^*(r_2) \tag{14}$$

$$Q^0(r_1,r_2) = \sum_{a,b,c,d} \delta^0(ab|cd)a(r_1)b(r_2)c^*(r_1)d^*(r_2) \tag{15}$$

$$Q^2(r_1,r_2) = \sum_{a,b,c,d} \delta^2(ab|cd)a(r_1)b(r_2)c^*(r_1)d^*(r_2) \tag{16}$$

from which we define the *pair populations*[12]

$$P_{aa} = \sum_{c,d} \gamma_2(aa|cd)s_{ac}s_{ad} \tag{17a}$$

$$P_{ab} = 2\sum_{c,d} \gamma_2(ab|cd)s_{ac}s_{bd} \tag{17b}$$

and the *pair-coupling populations*.

$$Q^0_{aa} = \sum_{c,d} \delta^0(aa|cd)s_{ac}s_{ad} \tag{18a}$$

$$Q^0_{ab} = 2\sum_{c,d} \delta^0(ab|cd)s_{ac}s_{bd} \tag{18b}$$

$$Q^2_{ab} = 2\sum_{c,d} \delta^2(ab|cd)s_{ac}s_{bd} \tag{19}$$

Obviously,

$$P_{aa} = Q^0_{aa}, \tag{20}$$

$$Q^2_{aa} = 0, \tag{21}$$

because the two electrons in the same AO have to be singlet coupled with each other.

The total sums of the above-defined two-particle populations are also bound. The pertinent relationships are as follows:

$$\sum_a P_{aa} + \sum_{a>b}\sum P_{ab} = N(N-1)/2 \tag{22}$$

$$\sum_a Q^0_{aa} + \sum_{a>b}\sum Q^0_{ab} = N/2 - 2S(S+1)/3 \tag{23}$$

$$\sum_{a>b}\sum Q^2_{ab} = 2S(S+1)/3 \tag{24}$$

It should be noted that a somewhat different method of population analysis has been proposed by Davidson[4] and Roby.[5] According to their proposal, the electronic population on each AO is defined as

$$n^0_{aa} = \sum_{b,c} s_{ab}\gamma_1(b|c)s_{ca} \tag{25}$$

The quantity n^0_{aa}/N is interpreted as expressing the probability that an electron belongs to orbital a. In this formalism, however, an electron in orbital a may be found simultaneously in orbital b, if a and b are not orthogonal to each other. Extension of this last method to two-particle density functions is easy. For example, the pair-coupling population is expressible in the form:

$$P^0_{ab} = 2\sum_{c,d,e,f} s_{ac}s_{bd}\delta^0(cd|ef)s_{ea}s_{fb} \tag{26}$$

The quantity is what we called the *generalized Penney-Dirac bond order* in a previous paper.[6] In this paper, however, we will not consider such populations as shown in Eqs. 25 and 26. For these populations, simple relations such as Eqs. 10a, 13 and 22—24 and as those that would be discussed in the next section do not hold.

II. Characteristics of the Populations

In a singlet state, the Q^0 function yields the charge density function by integrating over the second electron.[6]

$$P_1(r_1) = 2\int Q^0(r_1,r_2)\mathrm{d}r_2 \tag{27}$$

By expanding both sides of the above equation with respect to AO's and comparing the corresponding terms, we obtain the following relationship:

$$S = 0 : q_a = 2Q^0_{aa} + \sum_{b\neq a} Q^0_{ab} \tag{28a}$$

Thus, the gross population of each AO may be regarded as being composed of twice the ionic pair-coupling population on that AO and the sum of the covalent pair-coupling populations relevant to the same AO. This relationship is similar to that obtained on an orthogonalized AO basis set.[6] Analogous relations exist in the states with higher spin multiplicities.

$$S = \frac{1}{2}: \quad q_a = 2Q^0_{aa} + \sum_{b\neq a} Q^0_{ab} + q^s_a \tag{28b}$$

$$S \geqq 1: \quad q_a = 2Q^0_{aa} + \sum_{b\neq a} (Q^0_{ab} + Q^2_{ab}) \tag{28c}$$

The pair populations can likewise be related with the gross population.[12] The corresponding equations take the following forms:

$$P_1(r_1) = \frac{2}{N-1}\int P_2(r_1,r_2)\mathrm{d}r_2 \tag{29}$$

$$q_a = \frac{1}{N-1}(2P_{aa} + \sum_{b\neq a} P_{ab}) \tag{30}$$

For single-determinantal wave functions, 2-matrix can be expressed in terms of the products of 1-matrix. Hence, the pair and pair-coupling populations are expressed by

$$\begin{aligned}
Q^0_{aa} &= P_{aa} = \{(q_a)^2 - (q^s_a)^2\}/4 \\
Q^0_{ab} &= \{3(\boldsymbol{\gamma}_1\boldsymbol{s})_{ab}(\boldsymbol{\gamma}_1\boldsymbol{s})_{ba} - (\boldsymbol{\delta}_s\boldsymbol{s})_{ab}(\boldsymbol{\delta}_s\boldsymbol{s})_{ba} - 2q^s_a q^s_b\}/6 \\
Q^2_{ab} &= \{2(S+1)/3(2S-1)\}\{q^s_a q^s_b - (\boldsymbol{\delta}_s\boldsymbol{s})_{ab}(\boldsymbol{\delta}_s\boldsymbol{s})_{ba}\} \\
P_{ab} &= \{2q_a q_b - (\boldsymbol{\gamma}_1\boldsymbol{s})_{ab}(\boldsymbol{\gamma}_1\boldsymbol{s})_{ba} - (\boldsymbol{\delta}_s\boldsymbol{s})_{ab}(\boldsymbol{\delta}_s\boldsymbol{s})_{ba}\}/2
\end{aligned} \tag{31}$$

where $\boldsymbol{s}$ is the ordinary overlap matrix between AO's and where $\boldsymbol{\gamma}_1$ and $\boldsymbol{\delta}_s$ are the matrices composed of the expansion coefficients which appear in Eqs. 8 and 11, respectively.

The various populations investigated so far can be converted to atomic quantities by summing up the appropriate orbital populations. The resulting atomic and interatomic populations are invariant for the hybridization of AO's when the atomic orbitals on each atom are, as is usually the case, mutually orthogonal.

III. Applications to Three-center Systems

To illustrate the use of the population analysis above proposed, we apply it to various types of wave functions. The wave functions to be examined are those for the three-center systems calculated by Linnett and coworkers.[7-10] These have been chosen merely for the simplicity of arguments. The applications will clarify essential differences encountered on going from simple two-center cases to many-center problems. The sample systems here treated are the π-electron part of the allyl,[7] NO_2,[8] and HCO_2[9] radicals ($N=3$) as well as their cations ($N=2$) and anions ($N=4$). Ozone[10] ($N=4$) and its cation ($N=3$) and dication ($N=2$) will also be examined.

(A) Two-electron Systems. The three atomic orbitals involved are denoted as a, b, and c. The following basic functions constitute a complete set for the $^1A_1$ representation of the a–b–c system:

$$\begin{aligned}\Phi_1^{(2)} &= (a,b) + (b,a) + (b,c) + (c,b)\\ \Phi_2^{(2)} &= (a,c) + (c,a)\\ \Phi_3^{(2)} &= (a,a) + (c,c)\\ \Phi_4^{(2)} &= (b,b)\end{aligned} \tag{32}$$

Here, (a,b), for example, denotes a Slater determinant of the form:

$$(a,b) = \frac{1}{\sqrt{2}}\begin{vmatrix} a(1)\alpha(1) & b(1)\beta(1) \\ a(2)\alpha(2) & b(2)\beta(2)\end{vmatrix} \tag{33}$$

In all the Slater determinants the order of the spin function is $\alpha\beta$.

The wave function optimized over all these functions will be referred to as the configuration-interaction (CI) function $\Psi_{CI}^{(2)}$. In addition, the following approximate functions, each involving a smaller number of variational parameters, are considered.

1. Simple molecular orbital (MO) function:

$$\Psi_{MO}^{(2)} = (a+kb+c, a+kb+c) \tag{34}$$

2. Alternant molecular orbital (AMO) function[13]:

$$\begin{aligned}\Psi_{AMO}^{(2)} &= (a+k_1b+c, a+k_2b+c)\\ &\quad + (a+k_2b+c, a+k_1b+c)\end{aligned} \tag{35}$$

3. Valence bond (VB) functions:
Heitler-London type (HL)

$$\Psi_{HL}^{(2)} = (a,b) + (b,a) + (b,c) + (c,b) \tag{36}$$

Coulson-Fischer type (CF)

$$\begin{aligned}\Psi_{CF}^{(2)} &= (a+kb, b+ka) + (b+ka, a+kb)\\ &\quad + (c+kb, b+kc) + (b+kc, c+kb)\end{aligned} \tag{37}$$

Bond orbital type (BO)

$$\Psi_{BO}^{(2)} = (a+kb, a+kb) + (c+kb, c+kb) \tag{38}$$

4. Nonpaired spatial orbital (NP) functions:
Symmetrical form (NPA)

$$\Psi_{NPA}^{(2)} = (a+kb, kb+c) + (kb+c, a+kb) \tag{39}$$

Unsymmetrical form (NPB)

$$\begin{aligned}\Psi_{NPB}^{(2)} &= (a+kb, b+kc) + (b+kc, a+kb)\\ &\quad + (ka+b, kb+c) + (kb+c, ka+b)\end{aligned} \tag{40}$$

In Eqs. 34 to 40, k's are the variational parameters and the functions are not normalized.

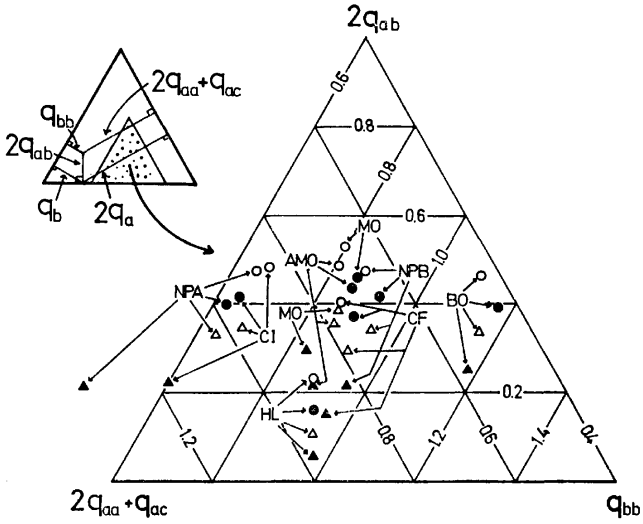

Fig. 1. The net and overlap populations for two-electron systems.
○: $C_3H_5^+$, △: NO_2^+, ●: HCO_2^+, ▲: O_3^{2+}
The length of the perpendicular from each point onto a base line shows the value of the population indicated at the opposite vertex.

The results of population analysis are shown in Figs. 1 and 2. The density distributions have been partitioned according to Eqs. 10b and 23. In two-electron systems, the function $P_2(r_1,r_2)$ is identical with $Q^0(r_1,r_2)$, so that there is no difference between the pair and pair-coupling populations. The numerical value for the population indicated at one vertex is equal to the length of the perpendicular onto the opposing base line (see Fig. 1). The sum of the lengths of three perpendiculars is invariant at any point. Thus, the gross populations q_a and q_b can be read simply as the lengths of the two perpendiculars drawn from the point at which the q_{ab} perpendicular intersects with the horizontal base line.

Let us first compare the results of the CI calculations for the four species: $C_3H_5^+$, NO_2^+, HCO_2^+ and O_3^{2+}. The polarity of molecules is reflected in the gross population q_a, which decreases in the order: $O_3^{2+} > HCO_2^+ \sim NO_2^+ > C_3H_5^+$. The overlap population q_{ab}, which corresponds to the strength of the bond a–b, decreases in the order: $C_3H_5^+ > HCO_2^+ > NO_2^+ > O_3^{2+}$. The pair-coupling populations shown in Fig. 2 are shifted regularly for $C_3H_5^+$, NO_2^+, and HCO_2^+; the populations, Q_{ab}^0 and Q_{ac}^0, decrease and increase, respectively, in that order. O_3^{2+} has a characteristic feature that Q_{bb}^0 is very small.

The shortcomings of the approximate functions compared with the CI treatment can readily be seen from Figs. 1 and 2. The molecular orbital method generally gives too large weights to the ionic terms Q_{aa}^0 and Q_{bb}^0. Moreover, q_b is overestimated. In the AMO method, the value of Q_{bb}^0 is improved, but the weight of the covalent term Q_{ab}^0 is unduly increased. In this latter sense, the AMO method cannot be regarded as an improvement over the MO method.

The valence bond functions (HL, CF, and BO) impart no weight to Q_{ac}^0. The variational parameters

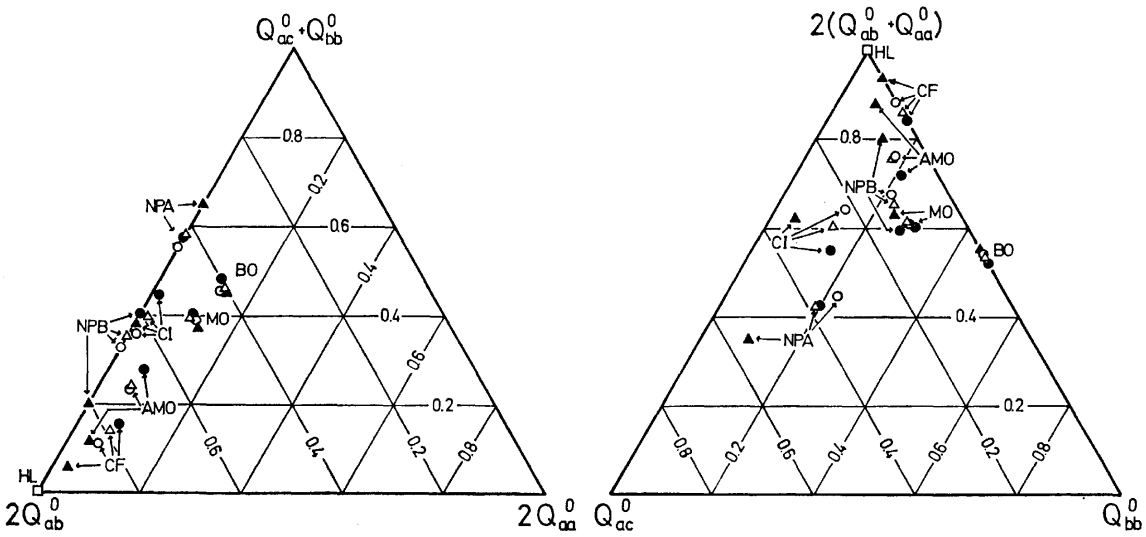

(i) (ii)

Fig. 2. The pair-coupling populations for two-electron systems.
○: $C_3H_5^+$, △: NO_2^+, ●: HCO_2^+, ▲: O_3^{2+}

introduced in the CF and BO functions serve to improve the value of q_{ab} as compared with the HL function, but this is so only at sacrifice of the polarity to be predicted.

The methods of nonpaired spatial orbitals provide relatively good values for the ionic terms Q^0_{aa} and Q^0_{bb}, reflecting the success of Linnett's idea to incorporate the Coulomb type correlation. Another advantage of $\Psi_{\mathrm{NPA}}{}^{(2)}$ is, as can be seen from Fig. 1, the results that the charge distributions calculated by this method are close to those obtained by the CI treatment.

(B) Three-electron Systems. We shall adopt the convention that each Slater determinant has the spin function $\alpha\beta\alpha$. The basic functions are represented by:

$$\begin{aligned}\Phi_1{}^{(3)} &= 2(a,b,c) + (a,c,b) + (b,a,c)\\ \Phi_2{}^{(3)} &= (a,a,c) + (a,c,c)\\ \Phi_3{}^{(3)} &= (a,b,b) + (b,b,c)\\ \Phi_4{}^{(3)} &= (a,a,b) + (b,c,c)\end{aligned} \tag{41}$$

The expressions for the approximate functions are as follows:

1. Simple molecular orbital (MO) function:

$$\Psi_{\mathrm{MO}}{}^{(3)} = (a+kb+c,\ a+kb+c,\ a-c) \tag{42}$$

2. Alternant molecular orbital (AMO) function:

$$\Psi_{\mathrm{AMO}}{}^{(3)} = \boldsymbol{O}(a+k_1b+c,\ a+k_2b+c,\ a-c) \tag{43}$$

3. Valence bond functions:

Heitler-London type (HL)

$$\Psi_{\mathrm{HL}}{}^{(3)} = \{(a,b,c)+(a,c,b)\} + \{(a,b,c)+(b,a,c)\} \tag{44}$$

Coulson-Fischer type (CF)

$$\begin{aligned}\Psi_{\mathrm{CF}}{}^{(3)} = {} & (a+kb,\ ka+b,\ c) + (ka+b,\ a+kb,\ c)\\ & - (kb+c,\ b+kc,\ a) - (b+kc,\ kb+c,\ a)\end{aligned} \tag{45}$$

Bond orbital type (BO)

$$\Psi_{\mathrm{BO}}{}^{(3)} = (a+kb,\ a+kb,\ c) + (a,\ kb+c,\ kb+c) \tag{46}$$

4. Nonpaired spatial orbital functions:

A type (NPA)

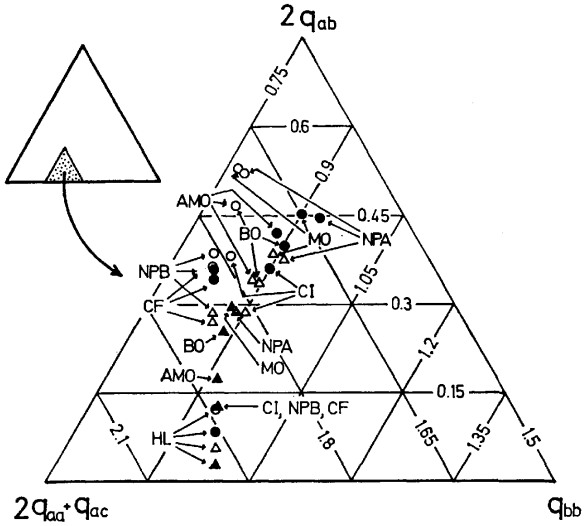

Fig. 3. The net and overlap populations for three-electron systems.
○:C_3H_5, △: NO_2, ●: HCO_2, ▲: O_3^+

$$\Psi_{\mathrm{NPA}}{}^{(3)} = \boldsymbol{O}(ka+b,\ b+kc,\ c) \tag{47}$$

B type (NPB)

$$\Psi_{\mathrm{NPB}}{}^{(3)} = \boldsymbol{O}(a+kb,\ b+kc,\ c) \tag{48}$$

where $\boldsymbol{O}$ is the projection operator to the $^2A_2$ state.

Figures 3 to 5 show the various populations obtained from the functions, $P_1(r_1)$, $Q^0(r_1,r_2)$, and $P_2(r_1,r_2)$, respectively. The pair populations P_{aa} and P_{bb} always take the same values as those of pair-coupling populations. Also, the relation, $Q^0_{ac}=(-1/2)Q^0_{ab}$, holds in these systems, so that we have shown only the sum of these pair-coupling populations in Fig. 4.

The results of the CI treatment characterize the O_3^+ ion as having extremely small overlap and ionic pair-coupling populations, thus indicating that the HL picture would be adequate for this species. For the other three radicals, the value of Q^0_{bb} becomes larger

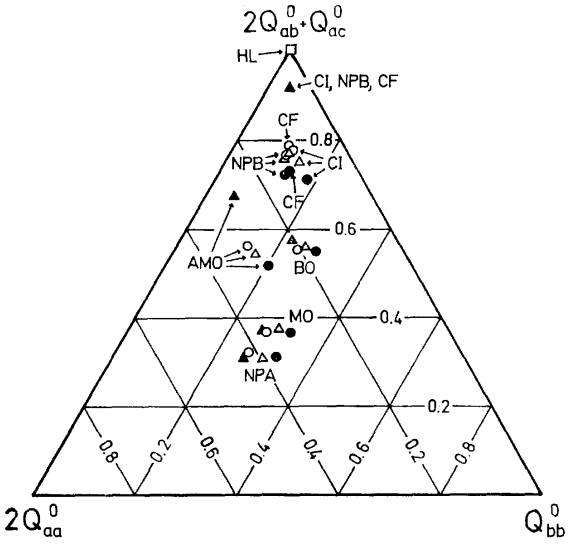

Fig. 4. The pair-coupling populations for three-electron systems.
○: C_3H_5, △: NO_2, ●: HCO_2, ▲: O_3^+
There exists a relation, $Q^0_{ac}=-\frac{1}{2}Q^0_{ab}$, so that these populations are not shown separately.

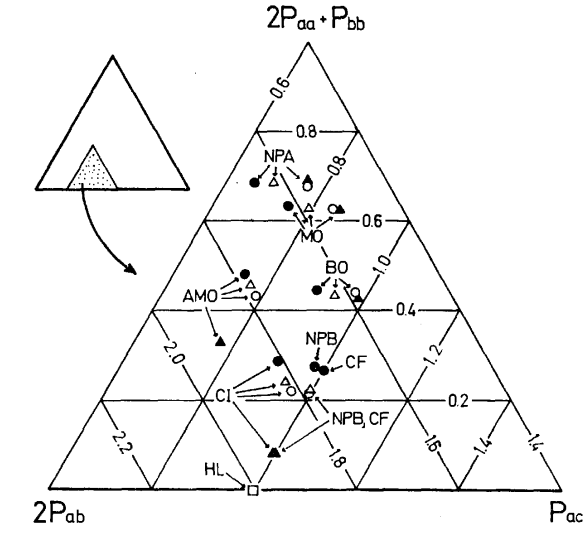

Fig. 5. The pair populations for three-electron systems.
○: C_3H_5, △: NO_2, ●: HCO_2, ▲: O_3^+
The pair populations P_{aa} and P_{bb} are identical respectively with the pair-coupling populations Q^0_{aa} and Q^0_{bb} shown in Fig. 4.

in the order, $C_3H_5<NO_2<HCO_2$, while the covalent pair-coupling population decreases simultaneously in the same order.

In the light of the above CI results, we examine the outcomings from the various approximate wave functions. Both $\Psi_{CF}^{(3)}$ and $\Psi_{NPB}^{(3)}$, providing the results close to each other, give good values for q_{ab}, $2Q^0_{ab}+Q^0_{ac}$, and $2Q^0_{aa}+Q^0_{bb}$. The shortcomings of these functions are that the ratios (Q^0_{aa}/Q^0_{bb}) and (P_{ab}/P_{ac}) are unreasonable and hence that the polarity of each species is not well reflected in the gross populations.

By contrast, all the other functions except $\Psi_{HL}^{(3)}$ give reasonable results for the above ratios. Thus, it

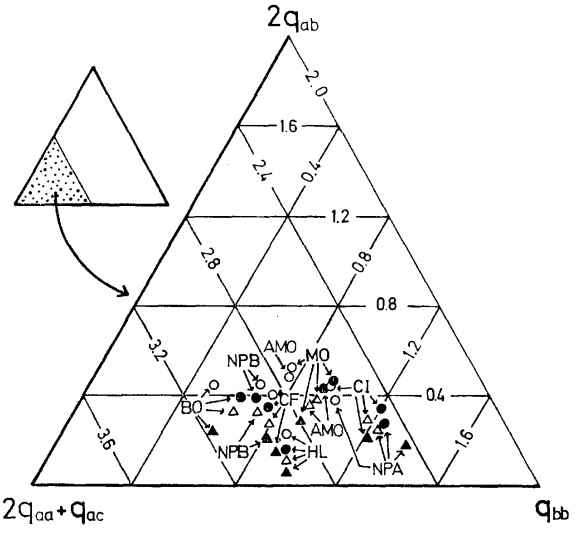

Fig. 6. The net and overlap populations for four-electron systems.
○: $C_3H_5^-$, △: NO_2^-, ●: HCO_2^-, ▲: O_3

may be suggested that a good wave function would result, if one combines the improvements from $\Psi_{HL}^{(3)}$ with the functions $\Psi_{CF}^{(3)}$ as well as $\Psi_{BO}^{(3)}$. For all kinds of populations, the AMO method gives much better results than does the MO treatment.

(C) Four-electron Systems. The order of the spin functions in all the Slater determinants is given as $\alpha\beta\alpha\beta$.

The basic functions pertinent to four-electron systems are

$$\begin{aligned}\Phi_1^{(4)} &= (a,a,b,c)+(a,a,c,b)+(c,c,b,a)+(c,c,a,b)\\ \Phi_2^{(4)} &= (a,b,b,c)+(c,b,b,a)\\ \Phi_3^{(4)} &= (a,a,c,c)\\ \Phi_4^{(4)} &= (a,a,b,b)+(c,c,b,b)\end{aligned} \tag{49}$$

The approximate wave functions to be considered are as follows:

1. Simple molecular orbital (MO) function:
$$\Psi_{MO}^{(4)} = (a+kb+c,\ a+kb+c,\ a-c,\ a-c) \tag{50}$$
2. Alternant molecular orbital (AMO) function:
$$\Psi_{AMO}^{(4)} = (a+k_1b+c,\ a+k_2b+c,\ a-c,\ a-c) + (a+k_2b+c,\ a+k_1b+c,\ a-c,\ a-c) \tag{51}$$
3. Valence bond functions:
Heitler-London type (HL)
$$\Psi_{HL}^{(4)} = (a,a,b,c)+(a,a,c,b)+(c,c,b,a)+(c,c,a,b) \tag{52}$$
Coulson-Fischer type (CF)
$$\Psi_{CF}^{(4)} = (a+kb,\ ka+b,\ c,c)+(ka+b,\ a+kb,\ c,\ c) + (c+kb,\ kc+b,\ a,\ a)+(kc+b,\ c+kb,\ a,\ a) \tag{53}$$
Bond orbital type (BO)
$$\Psi_{BO}^{(4)} = (a+kb,\ a+kb,\ c,\ c)+(c+kb,\ c+kb,\ a,\ a) \tag{54}$$
4. Nonpaired spatial orbital functions:
Symmetrical form (NPA)
$$\Psi_{NPA}^{(4)} = O(a,\ a+kb,\ kb+c,\ c) \tag{55}$$
Unsymmetrical form (NPB)
$$\Psi_{NPB}^{(4)} = O(a,\ a+kb,\ b+kc,\ c) \tag{56}$$

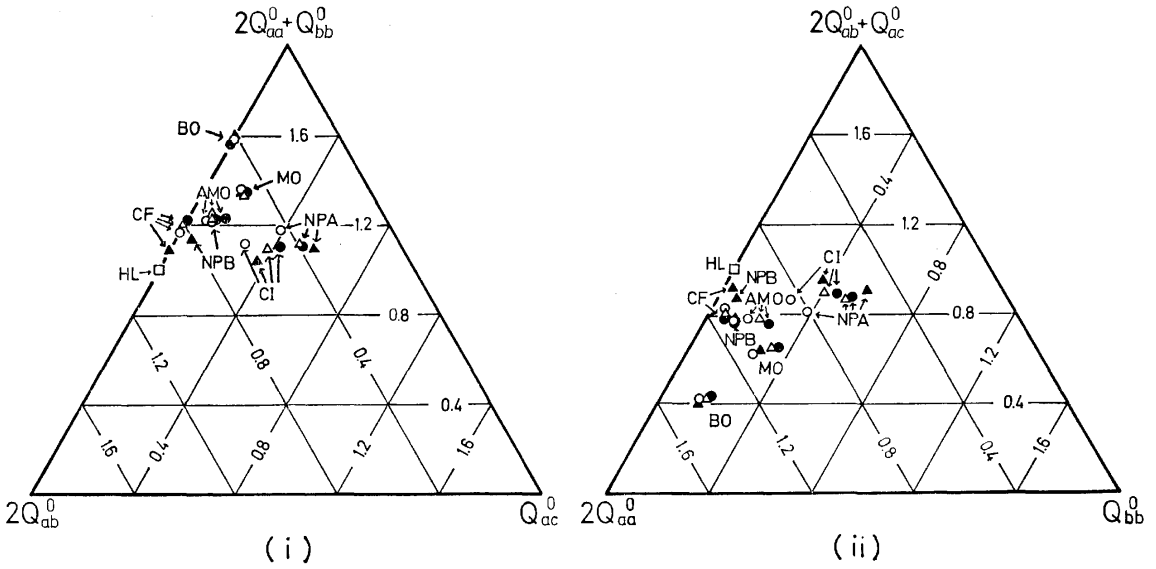

Fig. 7. The pair-coupling populations for four-electron systems.
○: $C_3H_5^-$, △: NO_2^-, ●: HCO_2^-, ▲: O_3

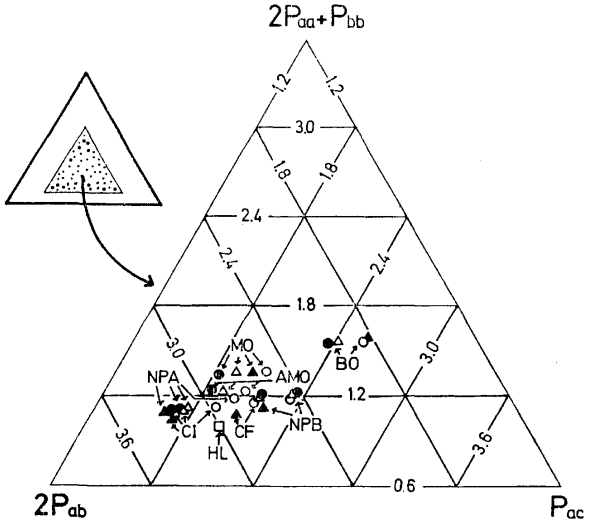

Fig. 8. The pair populations for four-electron systems.
○: $C_3H_5^-$, △: NO_2^-, ●: HCO_2^-, ▲: O_3
The pair populations for P_{aa} and P_{bb} are identical respectively with Q^0_{aa} and Q^0_{bb} in Fig. 7(ii).

Figures 6 to 8 show the results of population analysis for $C_3H_5^-$, NO_2^-, HCO_2^-, and O_3. It can be said from Fig. 6 that $C_3H_5^-$ concentrates its charge on the terminal atoms, while O_3 tends to have small values of q_{ab}. In Figs. 7 and 8, plots for the three ions $C_3H_5^-$, NO_2^-, and HCO_2^-, show a simple pattern that the three ratios, (Q^0_{ab}/Q^0_{ac}), (Q^0_{aa}/Q^0_{bb}), and (P_{ac}/P_{ab}), decrease in that order. The O_3 molecule shows a general trend that it takes relatively small values for the ionic pair-coupling populations, Q^0_{aa} and Q^0_{bb}.

Compared with other species, the value of Q^0_{ac} for O_3 is not particularly large. Therefore, it will be inadequate to attribute the well-known biradical character of ozone to the weight of the long-bond canonical structure, so far as Linnett's wave functions are concerned.

The function $\Psi_{NPA}{}^{(4)}$ appears to be the best of the approximate wave functions here examined, even though it fails to reproduce the CI results for ozone. The populations calculated from $\Psi_{CF}{}^{(4)}$ and $\Psi_{NPB}{}^{(4)}$ are nearly equal to each other. These latter wave functions can well give small ionic populations for ozone but do not improve other populations obtained by the HL treatment. The AMO treatment gives larger values for Q^0_{ab} than does the MO method, thus reducing the ionic pair-coupling populations. However, the improvements are still unsatisfactory.

IV. Concluding Remarks

We have shown in this study that the method of electronic population analysis can be extended to the analysis of the spin coupling matrices, by defining the pair-coupling populations. Interpretations of the electronic structure of molecules by the pair-coupling populations are similar to those by the resonance hybrid picture in the valence bond theory. The present method thus permits ready understandings of the characteristics of bonds by chemical intuition and yet is free from the arbitrariness in selecting the canonical structures.

It has frequently been found in the applications to three-center systems that an approximate wave function does not necessarily bring about improvements in populations, even when it improves energy. Of course, Linnett's wave functions are approximate ones even in the CI treatment. Nevertheless, the results for each species treated by use of various wave functions correctly demonstrate the characteristics of the molecular electronic structures to be represented by these wave functions. It should be emphasized that basic properties of the pair-electron density function $P_2(r_1,r_2)$ could best be understood when it is

looked at, as in this work, in the light of the distribution of pair-coupling populations in molecules.

References

1) R. McWeeny, *Rev. Mod. Phys.*, **32**, 335 (1960).
2) R. S. Mulliken, *J. Chem. Phys.*, **23**, 1833, 1841, 2338 (1955).
3) K. Ruedenberg, *Rev. Mod. Phys.*, **34**, 326 (1962).
4) E. R. Davidson, *J. Chem. Phys.*, **46**, 3320 (1967).
5) K. R. Roby, *Mol. Phys.*, **27**, 81 (1974); *Theoret. Chim. Acta*, **33**, 105 (1974).
6) T. Okada and T. Fueno, *Bull. Chem. Soc. Jpn.*, **48**, 2025 (1975).
7) D. M. Hirst and J. W. Linnett, *J. Chem. Soc.*, **1962**, 1035; **1962**, 3844; **1963**, 1068.
8) D. M. Hirst and J. W. Linnett, *J. Chem. Phys.*, **43**, S74 (1965).
9) W. H. Kirchhoff, J. Farren, and J. W. Linnett, *J. Chem. Phys.*, **42**, 1410 (1965).
10) R. D. Gould and J. W. Linnett, *Trans. Faraday Soc.*, **59**, 1001 (1963).
11) P. -O. Löwdin, *Phys. Rev.*, **97**, 1474 (1955).
12) The formulation is similar to the one described in Ref. 3.
13) For the results of alternant molecular orbital method, we refer to the book: R. Pauncz, "Alternant Molecular Orbital Method," W. B. Saunders Co., Philadelphia (1967).

The Crystal and Molecular Structure of (Acetylacetonato)(carboxymethyl)-(triphenylphosphine)palladium(II)

Yukio ZENITANI, Kaoru INOUE, Yasushi KAI, Noritake YASUOKA, and Nobutami KASAI

Department of Applied Chemistry, Faculty of Engineering, Osaka University, Yamadakami, Suita, Osaka 565

(Received February 7, 1976)

The molecular structure of (acetylacetonato)(carboxymethyl)(triphenylphosphine)palladium(II) [(acac)-(PPh_3)$PdCH_2COOH$] has been determined by means of X-ray diffraction. The crystal belongs to the triclinic system, space group $P\bar{1}$, with two formula units in a cell with dimensions of $a=10.433(2)$, $b=12.746(2)$, $c=10.224(2)$ Å, $\alpha=106.62(1)$, $\beta=112.41(2)$, and $\gamma=75.13(2)°$. $R=0.032$ for 4972 non-zero reflections. The palladium atom, σ-bonded to the methylene group of the acetic acid moiety (Pd-C=2.063(4) Å), has a square-planar geometry. The molecule forms a dimer with the adjacent molecule related by a center of symmetry through an inter-molecular hydrogen bonding between acetic acid moieties, O-H···O=2.621(4) Å.

Recently, in a series of studies of palladium complexes (Scheme 1), palladium(II) C,O-chelates of acetic acid have been prepared by the reaction of ketene and triphenylphosphine with bis(acetylacetonato)palladium(I) by Kawaguchi and his co-workers of Osaka City University.[1] In relation to this, the preparation of the following linkage isomers;

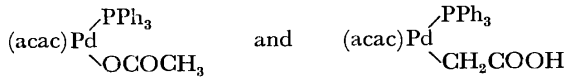

(VI) and (VII)

has also been reported.[3] The molecular structure of II, IV, and Vb have been determined and reported.[2,4] This paper will describe the molecular structure of VII. Interest in the Pd–C σ-bond also promoted this study.

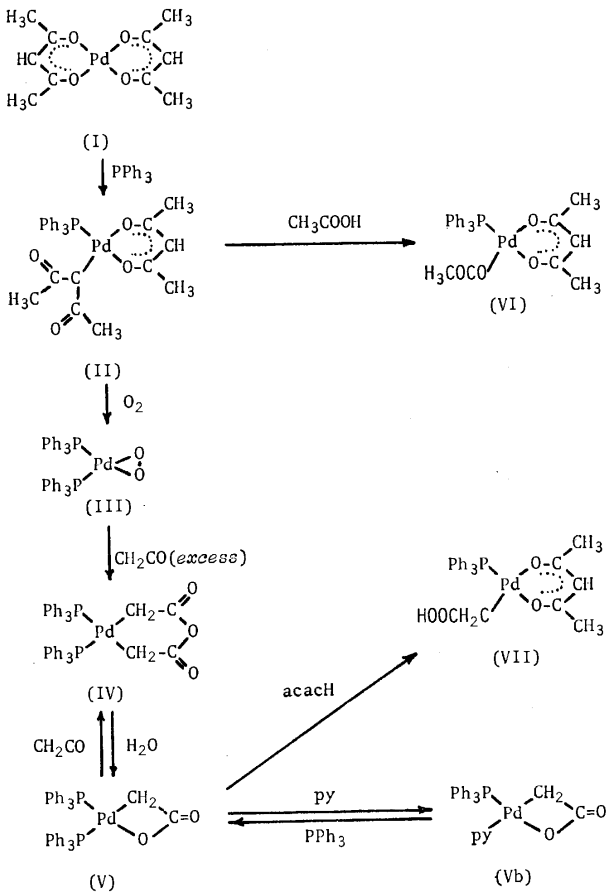

Scheme 1.

Experimental

Pale yellow, polyhedral crystals of [(acac)(PPh_3)$PdCH_2$-COOH] were kindly supplied by Professor Kawaguchi and his co-workers of Osaka City University. Preliminary photographic data showed that the crystals belong to the triclinic system. Accurate unit-cell dimensions were determined by a least-squares fit of the 2θ values of 24 high-order reflections as measured on a Rigaku automated, four-circle, single-crystal diffractometer.

Crystal Data: $C_{25}H_{25}O_4PPd$, $F.W.=527.4$, triclinic, space group $P\bar{1}$, $a=10.433(2)$, $b=12.746(2)$, $c=10.224(2)$ Å, $\alpha=106.62(1)$, $\beta=112.41(2)$, $\gamma=75.13(2)°$, $U=1187.6(3)$ Å^3, $D_m=1.48$ g·cm^{-3} (by flotation in carbon tetrachloride/hexane), $Z=2$, $D_x=1.47$ g·cm^{-3}, $\mu=8.57$ cm^{-1} (Mo$K\alpha_1$, $\lambda=0.70926$ Å).

A crystal with approximate dimensions of $0.23\times0.35\times0.23$ mm was used. Data were collected at 20 °C on a Rigaku diffractometer, using graphite-monochromatized Mo$K\alpha$ radiation. All data within a 2θ sphere of 54° ($\sin\theta/\lambda=0.64$) were measured using the θ-2θ scan technique. The integrated intensity was determined by scanning over the peak at a rate of 4°/min and by subtracting the background obtained by averaging the two values measured for 5 s at both ends of a scan; the scan width of each reflection was: $\Delta\theta=1.0°+0.35°\tan\theta_c$, where θ_c is the calculated Bragg angle for λ(Mo$K\alpha_1$) $=0.70926$ Å. A total of 5207 reflections was collected, of which the number of independent, non-zero reflections was 4972. The intensities of three standard reflections (070, 444, and 500) were measured every 50 reflections; no intensity decrease in these reflections was observed during the experiment. Usual Lorentz and polarization corrections were made, but the absorption correction was ignored ($\mu=8.57$ cm^{-1} for Mo$K\alpha$).

Solution and Refinement of the Structure

The structure was established by the heavy-atom method. A three-dimensional Patterson function was computed and interpreted to give the coordinates of palladium and phosphorous atoms. The remaining non-hydrogen atoms were easily located on the successive Fourier maps.

The block-diagonal, unit weight, least-squares refinement was carried out using the HBLS-V program,[5] the function minimized being $\Sigma(|F_o|-k\cdot|F_c|)^2$. Throughout the early stages of the refinement, the first set of data (4307 reflections of relatively lower

Table 1. Fractional atomic coordinates (estimated standard deviations in parentheses)

Atom	x	y	z	Atom	x	y	z
Pd	0.1305(1)	0.2160(1)	0.5227(1)	C(34)	0.2842(6)	0.1754(4)	1.1172(4)
P	0.0964(1)	0.3352(1)	0.7193(1)	C(35)	0.3593(5)	0.1619(4)	1.0276(5)
O(1)	−0.0646(2)	0.1712(2)	0.4537(2)	C(36)	0.3011(4)	0.2083(3)	0.9053(4)
O(2)	0.1732(2)	0.0987(2)	0.3513(2)	H(1A)	0.232(5)	−0.079(4)	0.197(5)
O(3)	0·4547(3)	0.0876(2)	0.6478(3)	H(1B)	0.105(5)	−0.111(4)	0.107(5)
O(4)	0.4622(3)	0.1226(2)	0.4505(3)	H(1C)	0.159(6)	−0.024(5)	0.080(7)
C(1)	0.1596(5)	−0.0560(3)	0.1596(5)	H(3)	−0.077(4)	−0.033(3)	0.195(4)
C(2)	0.0968(4)	0.0271(3)	0.2663(3)	H(5A)	−0.291(5)	0.034(4)	0.246(5)
C(3)	−0.0340(4)	0.0188(3)	0.2643(4)	H(5B)	−0.305(5)	0.139(4)	0.339(5)
C(4)	−0.1077(3)	0.0904(3)	0.3539(4)	H(5C)	−0.250(7)	0.014(6)	0.380(7)
C(5)	−0.2498(4)	0.0709(4)	0.3356(5)	H(6A)	0.363(4)	0.294(4)	0.686(5)
C(6)	0.3272(3)	0.2564(3)	0.5825(4)	H(6B)	0.324(4)	0.306(3)	0.523(4)
C(7)	0.4199(3)	0.1508(3)	0.5562(4)	H(O3)	0.494(5)	0.024(4)	0.623(5)
C(11)	−0.0890(3)	0.3824(3)	0.6989(3)	H(12)	−0.091(4)	0.543(3)	0.714(4)
C(12)	−0.1516(4)	0.4928(3)	0.7012(4)	H(13)	−0.341(5)	0.605(4)	0.685(5)
C(13)	−0.2956(4)	0.5250(4)	0.6812(4)	H(14)	−0.473(5)	0.470(4)	0.647(5)
C(14)	−0.3757(4)	0.4459(4)	0.6572(4)	H(15)	−0.365(4)	0.289(3)	0.645(4)
C(15)	−0.3139(4)	0.3370(4)	0.6551(5)	H(16)	−0.133(4)	0.230(3)	0.674(4)
C(16)	−0.1731(4)	0·3045(3)	0.6755(4)	H(22)	0.133(3)	0.478(3)	0.571(3)
C(21)	0.1708(3)	0.4621(2)	0.7759(3)	H(23)	0.229(4)	0.638(4)	0.639(5)
C(22)	0.1682(4)	0.5113(3)	0.6697(4)	H(24)	0.319(4)	0.725(3)	0.880(4)
C(23)	0.2199(5)	0.6089(3)	0.7065(4)	H(25)	0.323(5)	0.638(4)	1.051(5)
C(24)	0.2768(6)	0.6574(4)	0.8506(5)	H(26)	0.237(4)	0.478(3)	0.998(4)
C(25)	0.2822(6)	0.6084(4)	0.9562(5)	H(32)	0.000(4)	0.336(3)	0.956(4)
C(26)	0.2280(5)	0.5113(3)	0.9197(4)	H(33)	0.106(4)	0.244(3)	1.147(4)
C(31)	0.1684(4)	0.2727(2)	0.8782(3)	H(34)	0.321(5)	0.148(4)	1.200(5)
C(32)	0.0939(4)	0.2868(3)	0.9712(4)	H(35)	0.449(5)	0.125(4)	1.034(5)
C(33)	0.1531(6)	0.2370(4)	1.0895(4)	H(36)	0.351(4)	0.197(3)	0.840(4)

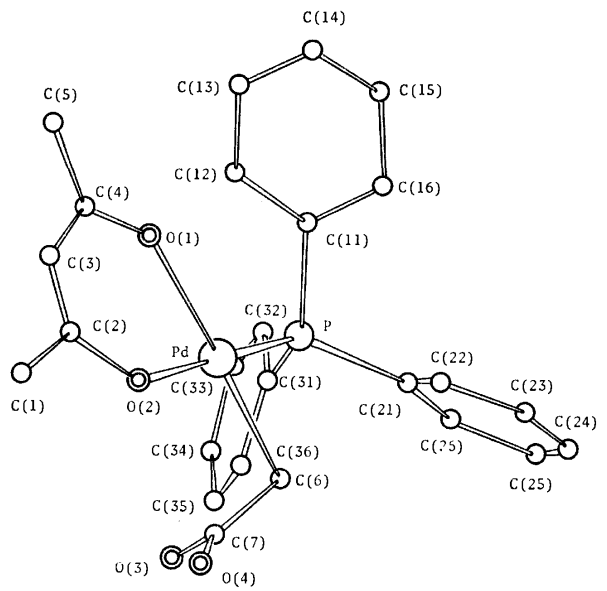

Fig. 1. Molecular structure of [(acac)(PPh_3)$PdCH_2COOH$] and numbering scheme of atoms.

diffraction angles) was used. After several cycles of isotropic refinement, $R_1=\Sigma||F_o|-|F_c||/\Sigma|F_o|=0.068$ for non-zero reflections. A further four cycles of refinement with anisotropic thermal parameters for all the non-hydrogen atoms reduced R_1 to 0.040. The difference synthesis could locate all the hydrogen atoms except the one attached to the carboxyl group; they were assigned to have equal thermal parameters, $B=3.0$ Å^2. The remaining 900 reflections were added to the first set of data. The difference Fourier map, computed after a few cycles of refinement, could locate the remaining hydrogen atom of the carboxyl group. Several cycles of refinement of all the atoms were carried out. The maximum shifts of the positional and thermal parameters for non-hydrogen atoms were about 0.14 σ and 0.08 σ respectively. The final R_1 is 0.032 ($R_2=\{\Sigma||F_o|-|F_c||^2/\Sigma|F_o|^2\}^{1/2}=0.041$) for 4972 non-zero reflections ($R_1=0.037$ for 5207 all reflections).

The atomic scattering factors used in all the calculations were those of Hanson *et al.*[6] The final positional and thermal parameters, along with their estimated standard deviations, are listed in Tables 1 and 2.*

Description of the Structure

Molecular Structure. The molecular structure of [(acac)(PPh_3)$PdCH_2COOH$] is shown in Fig. 1, which also indicates the numbering scheme. Figure 2 shows a stereoscopic view of the molecule, while the coordination geometry around the palladium atom is shown in

* The Table of structure factors is kept as Document No. 7621 at the Chemical Society of Japan.

TABLE 2. THERMAL PARAMETERS

a) Anisotropic thermal parameters ($\times 10^4$) expressed in the form: $\exp\{-(\beta_{11}h^2+\beta_{22}k^2+\beta_{33}l^2+\beta_{12}hk+\beta_{13}hl+\beta_{23}kl)\}$ for non-hydrogen atoms (estimated standard deviations in parentheses)

Atom	β_{11}	β_{22}	β_{33}	β_{12}	β_{13}	β_{23}
Pd	80.8(2)	48.8(1)	83.2(2)	−36.7(3)	57.2(4)	17.1(3)
P	84.3(8)	44.3(5)	74.5(8)	−34(1)	54(1)	20(1)
O(1)	92(3)	69(2)	121(3)	−61(3)	78(4)	−3(4)
O(2)	117(3)	72(2)	109(3)	−74(4)	106(5)	−20(4)
O(3)	131(3)	84(2)	133(3)	22(4)	123(5)	66(4)
O(4)	114(3)	87(2)	143(3)	−26(4)	144(5)	51(4)
C(1)	160(6)	75(3)	153(5)	−67(6)	160(9)	−39(6)
C(2)	121(4)	54(2)	97(4)	−40(5)	80(6)	17(4)
C(3)	121(4)	61(2)	125(4)	−76(5)	80(7)	−10(5)
C(4)	97(4)	60(2)	115(4)	−55(4)	55(6)	23(5)
C(5)	117(5)	100(4)	224(8)	−108(4)	133(10)	−38(8)
C(6)	87(3)	58(2)	136(4)	−41(4)	90(6)	18(5)
C(7)	74(3)	65(2)	117(4)	−44(4)	62(6)	23(5)
C(11)	92(3)	64(2)	80(3)	−36(4)	68(5)	15(4)
C(12)	105(4)	68(2)	110(4)	−23(5)	70(6)	30(5)
C(13)	108(4)	93(3)	149(5)	13(6)	78(8)	56(7)
C(14)	96(4)	129(4)	137(5)	−36(7)	76(8)	34(7)
C(15)	119(5)	110(4)	154(6)	−98(6)	115(8)	13(7)
C(16)	121(4)	75(3)	132(5)	−60(5)	123(7)	16(6)
C(21)	91(3)	49(2)	91(3)	−31(4)	63(5)	18(4)
C(22)	118(4)	60(2)	103(4)	−39(5)	60(6)	42(5)
C(23)	184(6)	69(3)	151(5)	−79(7)	114(9)	60(6)
C(24)	270(9)	76(3)	187(7)	−182(9)	147(13)	8(7)
C(25)	302(10)	112(4)	119(5)	−233(11)	118(12)	−37(7)
C(26)	193(6)	79(3)	96(4)	−126(7)	104(8)	−5(5)
C(31)	120(4)	48(2)	83(3)	−48(4)	44(6)	26(4)
C(32)	173(5)	71(3)	98(4)	−79(6)	102(8)	30(5)
C(33)	260(8)	87(3)	101(4)	−116(8)	131(10)	39(6)
C(34)	277(9)	83(3)	101(5)	−113(9)	26(10)	80(6)
C(35)	179(6)	89(3)	144(6)	−29(7)	4(10)	92(7)
C(36)	137(5)	78(3)	112(4)	−38(6)	50(7)	54(6)

b) Isotropic thermal parameters for hydrogen atoms (estimated standard deviations in parentheses)

Atom	B	Atom	B	Atom	B
H(1A)	4.9(12)	H(1B)	4.6(11)	H(1C)	7.8(16)
H(3)	2.6(8)	H(5A)	4.6(11)	H(5C)	4.6(11)
H(5C)	9.5(20)	H(6A)	3.3(9)	H(6B)	2.7(8)
H(O3)	5.2(12)	H(12)	1.7(7)	H(13)	3.6(10)
H(14)	4.4(11)	H(15)	3.1(9)	H(16)	1.9(7)
H(22)	0.6(6)	H(23)	3.4(9)	H(24)	2.7(9)
H(25)	5.0(12)	H(26)	2.3(8)	H(32)	2.7(9)
H(33)	3.1(9)	H(34)	3.8(10)	H(35)	3.8(10)
H(36)	1.9(12)				

Fig. 3. Tables 3 and 4 list the bond lengths and bond angles respectively. The least-squares best planes of several groups of atoms and the deviations of atoms from these planes are listed in Table 5.

The most remarkable feature of the overall molecular configuration is that the palladium atom is σ-bonded to the methylene group of acetic acid, as is to be expected from the IR and NMR studies.[2] A second feature is that this compound is dimeric, with intermolecular hydrogen bonding between carboxylic acid moieties. The palladium atom has a square-planar geometry established by one phosphorus, two enolate oxygen (O(1) and O(2)), and one carbon (C(6) in acetic acid) atoms; the mean and maximum deviations from the least-squares plane are 0.04 and 0.05 Å respectively.

The acetic acid moiety (C(6), C(7), O(3) and O(4)) is approximately planar, nearly perpendicular to the coordination plane; the dihedral angle between these planes is 88.5° (Fig. 3). The Pd–C(6)–C(7) angle (105.5(3)°) is slightly smaller than the tetrahedral

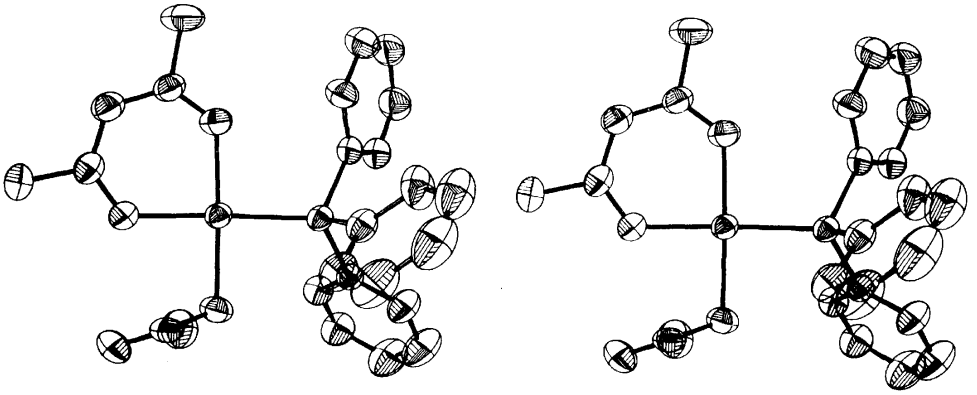

Fig. 2. Stereoscopic view of the molecule.

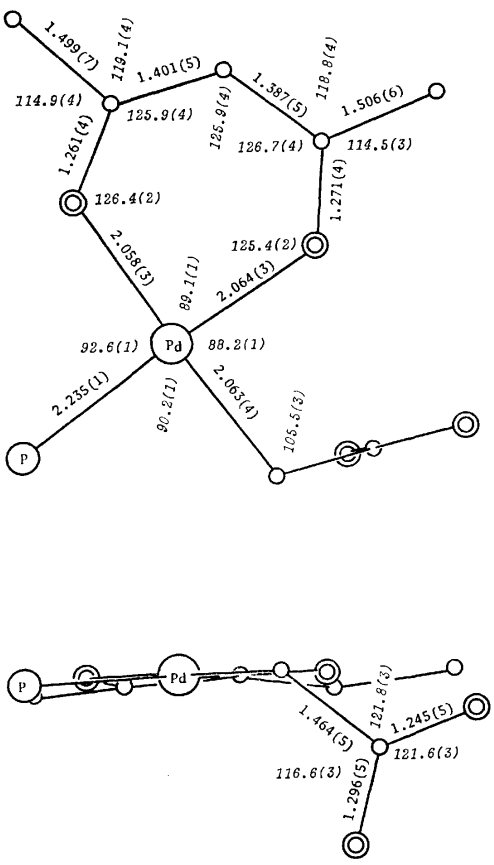

Fig. 3. The coordination geometry around the palladium atom.

Table 3. Bond lengths (l/Å) with estimated standard deviations in parentheses

Pd-P	2.235(1)	Pd-O(1)	2.058(3)
Pd-O(2)	2.064(3)	Pd-C(6)	2.063(4)
P-C(11)	1.820(3)	P-C(21)	1.822(3)
P-C(31)	1.829(4)	O(1)-C(4)	1.261(4)
O(2)-C(2)	1.271(4)	O(3)-C(7)	1.296(5)
O(4)-C(7)	1.245(5)	C(1)-C(2)	1.506(6)
C(2)-C(3)	1.387(5)	C(3)-C(4)	1.401(5)
C(4)-C(5)	1.499(7)	C(6)-C(7)	1.464(5)
C(11)-C(12)	1.389(5)	C(12)-C(13)	1.402(6)
C(13)-C(14)	1.381(7)	C(14)-C(15)	1.370(7)
C(15)-C(16)	1.370(6)	C(16)-C(11)	1.401(5)
C(21)-C(22)	1.389(5)	C(22)-C(23)	1.379(6)
C(23)-C(24)	1.380(8)	C(24)-C(25)	1.371(9)
C(25)-C(26)	1.387(8)	C(26)-C(21)	1.381(6)
C(31)-C(32)	1.391(6)	C(32)-C(33)	1.385(7)
C(33)-C(34)	1.360(8)	C(34)-C(35)	1.368(8)
C(35)-C(36)	1.394(7)	C(36)-C(31)	1.385(6)
O(3)-H(O3)	0.83(5)	C(1)-H(1A)	0.73(5)
C(1)-H(1B)	0.93(5)	C(1)-H(1C)	1.01(7)
C(3)-H(3A)	0.88(4)	C(5)-H(5A)	0.89(5)
C(5)-H(5B)	0.90(5)	C(5)-H(5C)	0.96(8)
C(6)-H(6A)	1.00(5)	C(6)-H(6B)	0.99(4)
C(12)-H(12)	0.96(4)	C(13)-H(13)	1.01(5)
C(14)-H(14)	0.96(5)	C(15)-H(15)	0.87(5)
C(16)-H(16)	0.93(4)	C(22)-H(22)	0.94(3)
C(23)-H(23)	0.92(5)	C(24)-H(24)	0.99(4)
C(25)-H(25)	0.91(5)	C(26)-H(26)	0.97(4)
C(32)-H(32)	1.00(4)	C(33)-H(33)	0.87(5)
C(35)-H(34)	0.91(5)	C(35)-H(35)	0.92(5)
C(36)-H(36)	0.96(4)		

angle, and the acetic acid moiety is bent away from the triphenylphosphine ligand. The Pd–C(6) bond length is 2.063(4)Å, which is a normal value and which is in agreement with the sum of the covalent radii (2.07 Å). The carboxyl group is hydrogen-bonded to the carboxyl group of the adjacent molecule related by the center of symmetry. These hydrogen bonds are moderately strong. The hydrogen bond distance is O(3)–H···O(4)=2.621(4) Å (H···O(4)=1.81(5) Å), which is comparable with those found in the majority of the carboxylic acid dimers. The C–O bond lengths are unequal (C(7)–O(3) 1.296(5) and C(7)–O(4) 1.245(5) Å), as is normally observed in most of the carboxylic acid dimers and also in $[(\pi\text{-}C_5H_5)Mo(CO)_3CH_2\text{-}COOH]$.[7]

The acetylacetonate ligand takes a typical enolate-type coordination; the bond lengths and bond angles have normal values, implying that the π-electrons are completely delocalized, as are those in other metal chelates of acetylacetone. This ligand is approximately

TABLE 4. BOND ANGLES (φ/°) WITH ESTIMATED STANDARD DEVIATIONS IN PARENTHESES

P-Pd-O (1)	92.6(1)	P-Pd-C (6)	90.2(1)
O (1)-Pd-O (2)	89.1(1)	O (2)-Pd-C (6)	88.2(1)
Pd-C (6)-C (7)	105.5(3)	C (6)-C (7)-O (3)	116.6(3)
C (6)-C (7)-O (4)	121.8(3)	O (3)-C (7)-O (4)	121.6(3)
Pd-O (1)-C (4)	126.4(2)	Pd-O (2)-C (2)	125.4(2)
O (2)-C (2)-C (1)	114.5(3)	O (2)-C (2)-C (3)	126.7(4)
C (1)-C (2)-C (3)	118.8(4)	C (2)-C (3)-C (4)	125.9(4)
O (1)-C (4)-C (3)	125.9(4)	O (1)-C (4)-C (5)	114.9(4)
C (3)-C (4)-C (5)	119.1(4)		
Pd-P-C (11)	112.7(1)	Pd-P-C (21)	116.3(1)
Pd-P-C (31)	112.3(1)	C (11)-P-C (21)	104.8(2)
C (11)-P-C (31)	104.4(2)	C (21)-P-C (31)	105.3(2)
P-C (11)-C (12)	122.3(3)	P-C (11)-C (16)	119.2(3)
C (12)-C (11)-C (16)	118.5(3)	C (11)-C (12)-C (13)	120.4(4)
C (12)-C (13)-C (14)	119.6(4)	C (13)-C (14)-C (15)	120.0(5)
C (14)-C (15)-C (16)	121.0(4)	C (11)-C (16)-C (15)	120.5(4)
P-C (21)-C (22)	118.4(3)	P-C (21)-C (26)	122.4(3)
C (22)-C (21)-C (26)	119.1(4)	C (21)-C (22)-C (23)	120.8(4)
C (22)-C (23)-C (24)	119.6(5)	C (23)-C (24)-C (25)	120.1(6)
C (24)-C (25)-C (26)	120.6(6)	C (21)-C (26)-C (25)	119.8(5)
P-C (31)-C (32)	122.1(3)	P-C (31)-C (36)	118.5(3)
C (32)-C (31)-C (36)	119.3(4)	C (31)-C (32)-C (33)	119.8(4)
C (32)-C (33)-C (34)	120.8(5)	C (33)-C (34)-C (35)	120.0(6)
C (34)-C (35)-C (36)	120.5(5)	C (31)-C (36)-C (35)	119.5(4)

TABLE 5. LEAST-SQUARES PLANES THROUGH VARIOUS GROUPS OF ATOMS AND THE DEVIATIONS (l/Å) OF THE ATOMS FROM THE PLANE

Equation of the plane is of the form $AX+BY+CZ+D=0$, where X, Y, Z and D are measured in Å unit. (Atoms marked by * are not included in the least-squares calculation.)

(a) Coordination around Pd							
		$-0.0058X+0.8397Y-0.5430Z+1.2894=0$					
Pd	0.027	P	−0.050	O (1)	0.037	O (2)	−0.044
C (6)	0.034	C (1)*	−0.362	C (2)*	−0.212	C (3)*	−0.276
C (4)*	−0.130	C (5)*	−0.200	C (7)*	−0.886		
(b) Acetic acid moiety							
		$-0.7640X-0.3323Y-0.5530Z+5.1556=0$					
O (3)	0.001	O (4)	0.001	C (7)	−0.003	C (6)	0.001
Pd*	1.923						
(c) Acetylacetone moiety							
		$-0.3242X+0.7569Y-0.6528Z+1.7571=0$					
O (1)	−0.005	O (2)	0.005	C (1)	0.004	C (2)	0.001
C (3)	−0.017	C (4)	0.004	C (5)	0.008	Pd*	−0.170
(d) Phenyl ring 1 (C (11)-C (16))							
		$0.1603X+0.0513Y-0.9857Z+6.5805=0$					
C (11)	0.002	C (12)	0.005	C (13)	−0.003	C (14)	0.002
C (15)	0.00	C (16)	−0.002	P*	0.056		
(e) Phenyl ring 2 (C (21)-C (26))							
		$0.8373X-0.5468Y+0.0062Z+1.9984=0$					
C (21)	0.002	C (22)	0.007	C (23)	−0.008	C (24)	0.002
C (25)	0.006	C (26)	−0.008	P*	−0.022		
(f) Phenyl ring 3 (C (31)-C (36))							
		$-0.4242X-0.7203Y-0.5489Z+5.2825=0$					
C (31)	−0.005	C (32)	−0.005	C (33)	0.006	C (34)	0.003
C (35)	−0.012	C (36)	0.013	P*	−0.011		

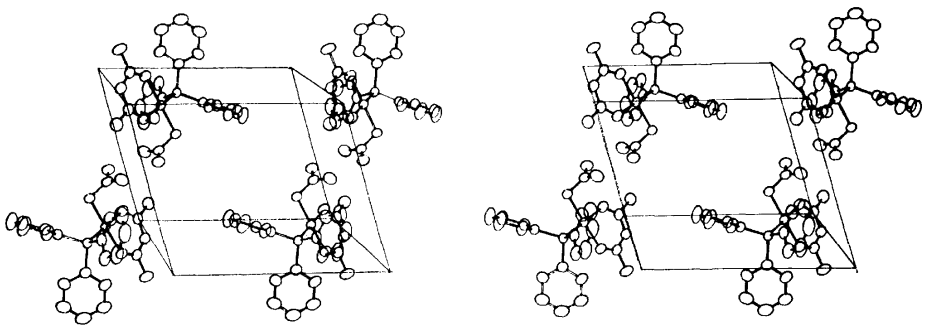

Fig. 4. Stereo drawing of the molecular packing in the unit cell.

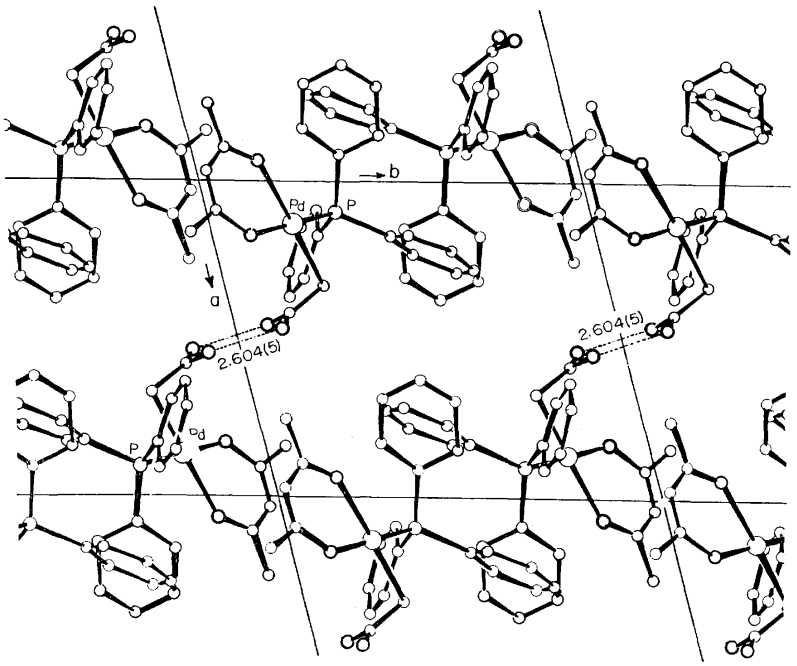

Fig. 5. Crystal structure projected along the c axis. Hydrogen bonds are shown by dotted lines.

Table 6. Intermolecular atomic contacts within 3.5Å

O(3)···O(4)[a]	2.621(4) Å	(Hydrogen bond)
O(3)···C(7)[a]	3.422(5)	
O(3)···O(3)[a]	3.499(6)	Code for superscript
O(4)···C(7)[a]	3.374(5)	a) $1-x, -y, 1-z$
C(12)···C(33)[b]	3.496(7)	b) $-x, 1-y, 2-z$
O(3)···C(5)[c]	3.373(6)	c) $-x, -y, 1-z$
O(1)···C(23)[d]	3.381(6)	d) $-x, 1-y, 1-z$

planar, and has a pseudo-symmetry of C_{2v} with the unique direction along the Pd–C(3) axis. The dihedral angle between the least-squares planes of this ligand and the coordination plane is 8.0 °. Two Pd–O bond lengths are approximately equal, 2.058(3) and 2.064(3) Å; they are also equal, within the limits of error, to those found in $[Pd(acac)_2(PPh_3)]$ (2.048(10) and 2.062(10) Å).[4]

The Pd–P bond length is 2.235(1) Å, which is close to those in $[Pd(C_2H_2O_2)(PPh_3)(py)]$[2,8] (2.232(3) Å) and $[Pd(acac)_2(PPh_3)]$[4] (2.258(4) Å). However, the values are different from those in $[Pd(C_4H_4O_3)(PPh_3)_2]$[2,9] (2.320(2) and 2.349(2) Å). The bond angles around the phosphorus atom are much distorted from the tetrahedral angle. Similar distortions are generally observed in triphenylphosphine complexes.

Crystal Structure. Figure 4 shows a stereoscopic view of the molecular packing along the c axis. In Fig. 5, the crystal structure projected along the same c axis is given; the intermolecular hydrogen bonds being shown by the dotted lines. The crystal is composed of hydrogen-bonded dimers related by the center of symmetry. Intermolecular atomic short contacts within 3.5 Å are listed in Table 6; some of them are slightly shorter than the usual van der Waals distances.

Computations throughout the present study were carried out on a NEAC 2200-700 computer at Osaka University. Figures 2 and 4 were drawn on a NUMERICON 7000 system at Osaka University with a local version of ORTEP.[10]

The authors wish to express their thanks to Professor Shinichi Kawaguchi and his co-workers of Osaka City University for their kindness in supplying crystals and for their many helpful discussions.

References

1) S. Baba, T. Ogura, and S. Kawaguchi, *Inorg. Nucl. Chem. Lett.*, **7**, 1195 (1971).
2) S. Baba, T. Ogura, S. Kawaguchi, H. Tokunan, Y. Kai, and N. Kasai, *J. Chem. Soc., Chem. Commun.*, **1972**, 910.
3) S. Baba and S. Kawaguchi, *Inorg. Nucl. Chem. Lett.*, **9**, 1287 (1973).
4) M. Horike, Y. Kai, N. Yasuoka, and N. Kasai, *J. Organometal. Chem.*, **72**, 441 (1974).
5) T. Ashida, The Universal Crystallographic Computing System, Osaka, The Computation Center, Osaka University (1973), p. 55.
6) H. P. Hanson, F. Herman, J. D. Lea, and S. S. Skillman, *Acta Crystallogr.*, **17**, 1040 (1964).
7) M. L. H. Green, J. K. P. Ariyarante, A. M. Bjerrum, M. Ishag, and C. K. Prout, *J. Chem. Soc., Chem. Commun.*, **1967**, 430.
8) N. Kasai and Y. Kai, unpublished data.
9) Y. Zenitani, H. Tokunan, Y. Kai, N. Yasuoka, and N. Kasai, unpublished data.
10) C. K. Johnson, ORTEP, Report ORNL-3794, Oak Ridge National Laboratory, Tenn., 1965.

Extrinsic Carrier Photogeneration in Poly(*N*-vinylcarbazole) Films Doped with Dimethyl Terephthalate

Masaaki YOKOYAMA, Yoshihiro ENDO, and Hiroshi MIKAWA

Department of Applied Chemistry, Faculty of Engineering, Osaka University, Suita, Osaka 565

(Received February 21, 1976)

Based upon the previously reported experimental results that the exciplex fluorescence of poly(*N*-vinylcarbazole) films doped with dimethyl terephthalate is partly quenched by an electric field, a model is proposed for the extrinsic carrier photogeneration mechanism. Interaction between a migrating singlet exciton and an electron acceptor ("encounter complex") produces an electron-hole ion pair having a rather large separation through a charge-transfer process between the components and a thermalization process of the excess energy. This ion pair dissociates into free carriers with Onsager's probability of escaping the geminate recombination which gives a "relaxed fluorescent exciplex state". The field dependence of the initial separation of the ion pair is also discussed.

Poly(*N*-vinylcarbazole) (PVCz) films exhibit only excimer fluorescence, while PVCz films doped with dimethyl terephthalate (DMTP), a weak electron acceptor, give a broad exciplex fluorescence. In the previous letter,[1] we reported that this exciplex fluorescence is partly quenched by applying an electric field in the solid film state, and suggested that this quenching is due to a field-assisted thermal dissociation of the exciplex into free carriers:

$$D^* + A \longrightarrow (D^+\cdots A^-)^* \longrightarrow D^+ + A^-, \qquad (1)$$

where D and A represent donor (PVCz) and acceptor (DMTP) molecules, respectively.

The possibility of such extrinsic carrier photogeneration process in PVCz–DMTP system had been proposed by Okamoto *et al.*[2] from their observation that the exciplex formation in PVCz films doped with DMTP enhanced the photocurrent in the lowest π-π^* absorption region.

Our observation of the quenching of exciplex fluorescence by an electric field provided direct evidence for the above-mentioned exciplex mechanism in the extrinsic photogeneration of carriers, and also is believed more generally to provide an insight into the mechanism of an extrinsic photogeneration in organic molecular crystals. In the previous paper, however, no explanation was presented for the observed quadratic field-dependence of the fluorescence decrement. In the present paper, we present a mechanism of the field-assisted thermal dissociation of an exciplex, by which the observed field-dependence of the fluorescence decrement will be successfully explained.

Mechanism

The mechanism represented by process (1) assumes the formation of exciplex state and its dissociation into free ions (carriers). Nothing is known hitherto concerning the dissociation process of an exciplex in the solid state. We have, however, some informations in the dissociation process of an exciplex in solution.[3–5]

According to the recent time-resolved spectroscopic investigations of the photoionization processes of DA systems, it is believed that (a) when an excited donor (acceptor) molecule approaches to an acceptor (donor) molecule, the interaction occurs at comparatively large distance resulting in a formation of so-called "encounter complex"; (b) this state converts immediately into "charge transfer state" (ionic state) by a rapid electron transfer; (c) this ionic state is a "nonrelaxed exciplex" with respect to the orientation of the solvent molecules; (d) this state relaxes into the ordinary "fluorescent relaxed exciplex state" being assisted by reorientation of the solvent molecules which liberates polarization energy; (e) in favorable cases, this relaxation process accompanies emission of exciplex fluorescence of somewhat shorter wavelength, main part of the exciplex fluorescence being, however, from the relaxed state; (f) if solvent polarity is large enough, dissociation of relaxed and/or nonrelaxed exciplex state into solvated ions becomes possible.

In our present PVCz–DMTP system in a film, however, the lowering of the ionization or dissociation energy by solvent orientation is impossible. From a simple estimation of the energy relation, the fluorescent relaxed exciplex state, in which D^+ and A^- are separated only about 3—4 Å, is found to be so tightly bound by

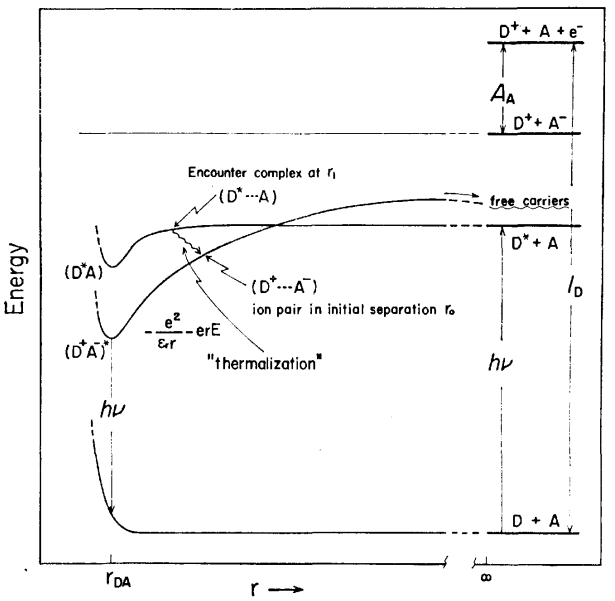

Fig. 1. Schematic energy diagram for the extrinsic photogeneration in DMTP-PVCz exciplex system. The abscissa indicates the separation of donor (D) from acceptor molecule (A), and an asterisk represents the excited state.

Coulombic force that its dissociation into free ions is impossible by the external field in the present experimental range. It is thus certain that any mechanism which involves the field-assisted thermal dissociation from the fluorescent relaxed exciplex state must be excluded in explaining our present results.

Photogeneration of an Ion Pair

Taking into account that (i) the singlet excited state of PVCz migrates effectively through the carbazole chromophores along the polymer chain,[6] and (ii) the major carrier is a hole, D^+, in a DMTP doped PVCz film as well as in a PVCz film, we propose that an electron-hole pair (ion pair), to which an external electric field is effective in assisting its dissociation, is not the relaxed fluorescent exciplex state, $(D^+A^-)^*$, but the one which is produced from the "*encounter complex*," $(D^*\cdots A)$, between a migrating singlet excition, D^*, and an electron acceptor, A, through a charge-transfer process between the components and a thermalization process of the excess energy. This mechanism is summarized in the following scheme and is depicted schematically in Fig. 1.

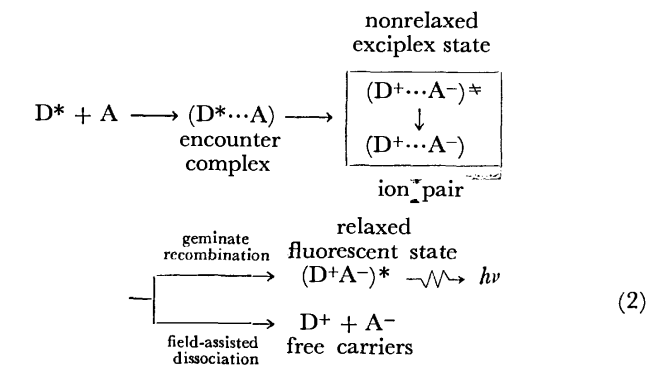

(2)

The "*nonrelaxed exciplex state*" named here is the one which is produced from an encounter complex through a rapid electron transfer at somewhat larger separation between the components in an encounter complex than in relaxed fluorescent exciplex state. Such a nonrelaxed exciplex state has the excess kinetic energy, and undergoes a thermalization of the excess energy to give an electron-hole ion pair at a separation r_0. This process is possible since the carbazole chromophores locate around an acceptor in high concentration and D^+ is mobile from molecule to molecule in the neighborhood of A^-. An electron-hole pair thus produced will either recombine geminately to give a "*relaxed fluorescent exciplex state*," or dissociate into free carriers being assisted by an external electric field. The field-assisted dissociation process will be treated in the next section.

Dissociation Process of an Ion Pair

As mentioned above, our model shown by Scheme (2) involves a field-assisted dissociation process of an ion pair state. To this process we have attempted to apply Onsager's theory[7] which predicts the field dependent probability of the dissociation of an ion pair into free ions.

Since this dissociation process is competing with geminate recombination into the relaxed fluorescent exciplex state in our case, we obtain the expression that predicts the ratio of the decrement of the exciplex fluorescence by an electric field to its zero field intensity, $\Delta F/F$, as follows:

$$\frac{\Delta F}{F} = \frac{F(0)-F(E)}{F(0)} = \frac{\eta\phi[1-P(0)]-\eta\phi[1-P(E)]}{\eta\phi[1-P(0)]} = \frac{P(E)-P(0)}{1-P(0)}, \tag{3}$$

where $F(E)$ is the exciplex fluorescence intensity in a field E, ϕ the quantum yield of the electron-hole pairs (field-independent), η the fluorescence quantum efficiency from the relaxed exciplex state, and $P(E)$ the efficiency as a function of E that an electron-hole pair will escape geminate recombination. Using the notation introduced by Geacintov and Pope[8] according to Onsager's theory, this efficiency will be expressed as,

$$P(E) = \int g(r)f(r,\theta,E)\,d\tau$$
$$g(r) = (4\pi r_0^2)^{-1}\delta(r-r_0)$$
$$f(r,\theta,E) = (\exp(-2q/r))\exp(-\beta r(1+\cos\theta)) \times \sum_{m,n=0}^{\infty} \frac{(2q)^m\beta^{m+n}r^n(1+\cos\theta)^{m+n}}{m!(m+n)!} \tag{4}$$

Here r_0 is the initial separation of electron and hole; θ, the orientation of the ion pair relative to the field direction; $q=e^2/2\varepsilon_r kT$; $\beta=eE/2kT$; e, electronic charge; ε_r, relative permittivity; kT, the thermal energy.

In Fig. 2 are shown the calculated curves $[P(E)-P(0)]/[1-P(0)]$ for various initial separations r_0 with $\varepsilon_r=3.0$ and $T=300$ K, together with the experimental data of $\Delta F/F$. Fitting of the experimental data with the theoretical curves gives approximately $r_0=26-30$ Å, although some discrepancies can be seen from a single r_0 value. This discrepancy will be discussed later. This r_0 value is in good agreement with the values obtained from the photocurrent measurements, *i.e.*, $r_0=35$ Å for 2,4,7-trinitro-9-fluorenone (TNF)–PVCz system by Melz[9] and $r_0=30$ Å for acid doped PVCz film by Pfister and Williams.[10]

Thus the quadratic field dependence in the decrement of the exciplex fluorescence is successfully explained on the basis of Onsager's model.

Field Dependence of Initial Separation of an Ion Pair

The deviation of experimental results from the prediction based upon Onsager's theory for the single r_0 value, was also pointed out by Melz[9] in his analyses of the carrier photogeneration from photocurrent measurements in TNF–PVCz films. However, any explanations have not yet been presented for this point.

We have attempted to explain this deviation with

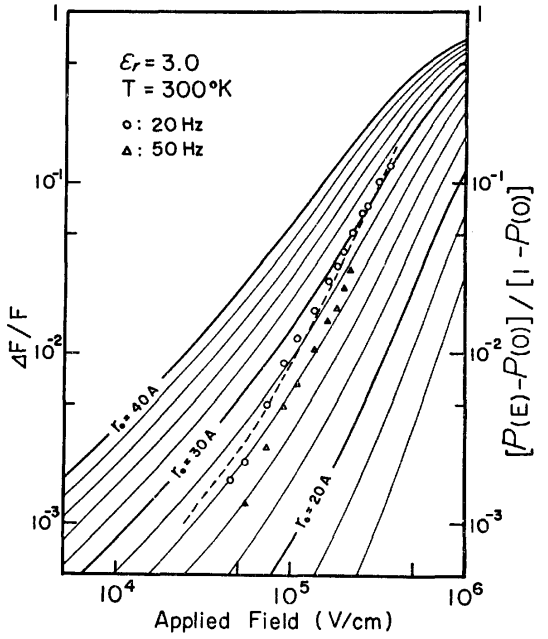

Fig. 2. Field dependence of fluorescence decrement in a 0.5 mol% DMTP doped PVCz film (12 μm thick) with square-wave applied voltage at 20 Hz (○) and 50 Hz (△), and theoretical prediction curves by Onsager's theory for an isotropic initial distribution of electron-hole pairs at various separations; $\varepsilon_r=3.0$, $T=300$ K; A dashed line represents the prediction curve including the field dependence of the initial separation r_0.

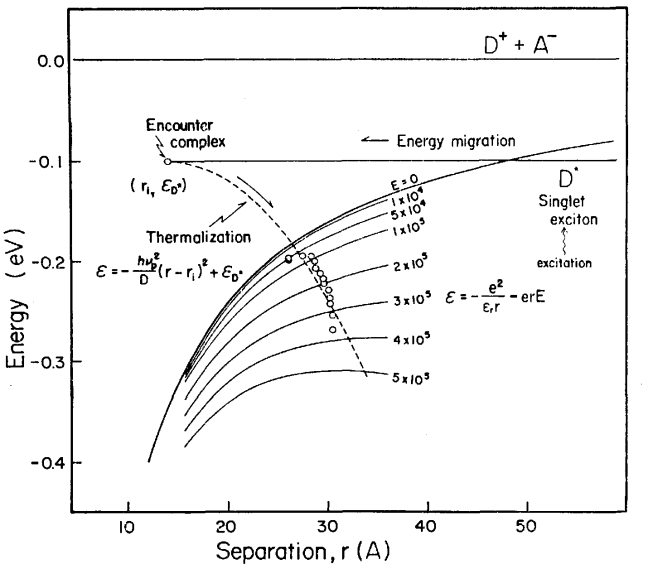

Fig. 3. Schematic representation for field dependence of the initial separations read from Fig. 2 (data at 20 Hz) plotted on the Coulomb potential curves for the corresponding field strengths.

the idea that the initial separation r_0 of the ion pair produced through the thermalization from nonrelaxed exciplex state might be field dependent.

The thermalization process from nonrelaxed exciplex state at the distance r_1 is considered to involve the separation process of an electron-hole pair dissipating the excess kinetic energy by phonon emission as is assumed in Knights-Davis' model.[11] The distance r_1 means the separation between a migrating excited donor and an acceptor at which the electron exchange interaction occurs. In our model, the thermalization begins to occur from this point r_1, but not from $r=0$ as in the case of the autoionization in an anthracene crystal. Therefore, the separation of the ion pair will be given by

$$r_0 - r_1 = \sqrt{Dt}, \tag{5}$$

where D is the diffusion coefficient, t the thermalization time, and r_0 the separation at the end of the thermalization, respectively. In the present case, the diffusion process involves only D^+, because D^+ is mobile from chromophore to chromophore while A^- is localized on an acceptor molecule.

The excess kinetic energy to be dissipated is taken to be equal to the energy difference between the singlet excition energy level (ε_{D^*}) and the Coulomb potential energy at r_0:

$$\varepsilon_{\text{excess}} = \varepsilon_{D^*} + \frac{e^2}{\varepsilon_r r_0} + er_0E, \tag{6}$$

Using the same treatment as described by Knights and Davis,[11] the time to be necessary to dissipate this energy is given by

$$t = \frac{\varepsilon_{\text{excess}}}{h\nu_p^2}, \tag{7}$$

where ν_p is a phonon frequency.

From Eqs. 5—7, we obtain the following equation for r_0 to be satisfied:

$$\frac{(r_0-r_1)^2}{D} = \frac{\varepsilon_{D^*} + \dfrac{e^2}{\varepsilon_r r_0} + er_0E}{h\nu_p^2}. \tag{8}$$

Hence,

$$-\frac{h\nu_p^2}{D}(r_0-r_1)^2 + \varepsilon_{D^*} = -\frac{e^2}{\varepsilon_r r_0} - er_0E. \tag{9}$$

The electron-hole initial separation r_0 at the end of the thermalization process, therefore, should be given as a crossing point of the following two curves in the energy diagram.

$$\varepsilon_1 = -\frac{h\nu_p^2}{D}(r-r_1)^2 + \varepsilon_{D^*}, \tag{10}$$

$$\varepsilon_2 = -\frac{e^2}{\varepsilon_r r} - erE. \tag{11}$$

Equation 10 represents the variation of the ion pair separation during the thermalization, which is given by a quadratic function of r with a curvature $h\nu_p^2/D$ and an apex at (r_1,ε_{D^*}). This equation is inherent to the system chosen. On the other hand, the Coulomb potential curve represented by Eq. 11 at an electric field E is field dependent. Thus, the crossing point, *i.e.*, the initial separation r_0 is field dependent.

In Fig. 3 the open circles represent the initial separations obtained from the experimental data (data at 20 Hz in Fig. 2) plotted on the Coulomb potential curves for the corresponding field strengths. Data points seem to trace something like a quadratic curve.

The thermalization curve is drawn so as to give a good fit by assuming ε_{D^*} to be 0.1 eV ($\Delta\varepsilon$) below the ($D^+ + A^-$) level and $r_1 = 14$ Å, taking into account that the electron exchange interaction in the triplet-triplet energy transfer occurs at the distance of ~15 Å between donor and acceptor molecules.[12] The value 0.1 eV for $\Delta\varepsilon$ gives the electron affinity (A_e) of DMTP to be about 1.0 eV, since the ionization potential (I_p) of PVCz in solid film would be about 4.7 eV[13] and the energy of the singlet exciton (E_{D^*}) of PVCz is estimated to be 3.55 eV from the fluorescence measurements (*i.e.*, $\Delta\varepsilon = I_p - A_e - E_{D^*}$). The value $A_e \sim 1.0$ eV seems to be fairly reasonable from our experience, although unfortunately we have no exact value at present.

Thus, we developed an expression to the field dependence of the initial separation of ion pair, and also showed that it gave a good fit with the experimental data. In Fig. 2 is shown also a prediction curve (dashed line) of the fluorescence quenching including the field dependence of the initial separation of ion pair given by the dashed curve in Fig. 3. As can be seen, the field dependence of the initial separation successfully explains the deviation of the experimental data from a single curve calculated on the basis of Onsager's theory as well as the quadratic field-dependence of fluorescence quenching.

We have developed a mechanism of the extrinsic carrier photogeneration due to a field-assisted thermal dissociation of an exciplex into free carriers. The ion pair which undergoes the dissociation with the assistance of an electric field, is produced through the electron transfer process and the thermalization process from an encounter complex between a migrating singlet exciton and an acceptor. The deviation of the experimental data from Onsager's theory can be explained taking into accout that the initial separation of the ion pair should be field dependent. We believe that the present model for the extrinsic carrier photogeneration would be applicable not only to the present DMTP–PVCz system, but also to organic molecular crystals. Experimental works on the temperature effect and the frequency dependence are now in progress.

Note added in proof. Slightly observed frequency dependence of $\Delta F/F$ values has turned out to be an instrumental artifact due to unexpected partial damage of a load resistance. With a correct resistance, no frequency dependence is observed and the correct values of $\Delta F/F$ are obtained as multiplied by 0.15 for each value at 20 Hz reported.

Since, however, among the curves predicted from the Onsager's theory shown in Fig. 2 the quadratic field-dependence is best reproduced in the case of $r_0 \cong 16$ Å for the initial separation of the ion pair,[9] we must slide down a prediction curve for $r_0 = 26$ Å so as to fit with the corrected values of $\Delta F/F$. Such shifting indicates the presence of a direct leak process from the nonrelaxed exciplex state $(D^+\cdots A^-)^*$ to the relaxed fluorescent state $(D^+A^-)^*$ not through the ion pair state in Eq. 2.

Thus, in more general form Eq. 3 should be corrected as follows:

$$\frac{\Delta F}{F} = \frac{\eta\phi[1-P(0)] - \eta\phi[1-P(E)]}{\eta\phi[1-P(0)] + \eta(1-\phi)} = \frac{\phi[P(E)-P(0)]}{1-\phi P(0)} \qquad (3)'$$

According to Eq. 3′ the fitting of the corrected values of $\Delta F/F$ with the theoretical curve for $r_0 = 26$ Å gives $\phi \cong 0.3$. Even in this case, however, some deviation from the prediction curve for the single $r_0 = 26$ Å value does exist. This deviation can be explained as well by the field-dependent initial separation of r_0 as described in the text.

The detailed analysis based upon the corrected experimental data will be published in this journal as soon as possible.

References

1) M. Yokoyama, Y. Endo, and H. Mikawa, *Chem. Phys. Lett.*, **34**, 597 (1975).
2) K. Okamoto, S. Kusabayashi, and H. Mikawa, *Bull. Chem. Soc. Jpn.*, **46**, 2613 (1973).
3) H. Knibbe, K. Röllig, F. P. Schafer, and A. Weller, *J. Chem. Phys.*, **47**, 1184 (1967).
4) Y. Taniguchi, Y. Nishina, and N. Mataga, *Bull. Chem. Soc. Jpn.*, **45**, 764 (1972).
5) H. Masuhara, T. Hino, and N. Mataga, *J. Phys. Chem.*, **79**, 994 (1975).
6) W. Klöpffer, *J. Chem. Phys.*, **50**, 2337 (1969).
7) L. Onsager, *Phys. Rev.*, **54**, 554 (1938).
8) N. E. Geacintov and M. Pope, "Proceedings of 3rd International Conference on Photoconductivity," ed. by E. M. Pell, Pergamon, Oxford (1971), p. 289.
9) P. J. Melz, *J. Chem. Phys.*, **57**, 1694 (1972).
10) G. Pfister and D. J. Williams, *J. Chem. Phys.*, **61**, 2416 (1974).
11) J. C. Knights and E. A. Davis, *J. Phys. Chem. Solids*, **35**, 543 (1974).
12) C. A. Parker, "The Triplet State," Cambridge University, Cambridge (1967), p. 353.
13) J. H. Sharp, *J. Phys. Chem.*, **71**, 2587 (1967).

Spectral Smoothing in Correlation NMR Spectroscopy

Hiroshi OZAWA and Yoji ARATA*

Computer Center, The University of Tokyo, Bunkyo-ku, Tokyo 113

**Department of Chemistry, The University of Tokyo, Bunkyo-ku, Tokyo 113*

(Received February 26, 1976)

A method has been proposed to eliminate a baseline oscillation which appears in a correlation NMR spectrum when one wants to observe peaks on the tilted baseline. An interpolation process in correlation NMR spectroscopy is also discussed which minimizes the number of sampling points.

In correlation NMR,[1,2] only a necessary portion of the spectrum can be scanned, and therefore, dynamic range problems which are frequently encountered in pulse FT NMR is much less serious. We have described in previous papers[3-6] a system for correlation NMR and some of its applications. In the present system, the theoretical function method[2] has been used to compensate the effect of the linear sweep; a rapid scan response is Fourier transformed, and then multiplied by $\exp(-ibt^2/2)$ where b is the sweep rate in radians per second to obtain the free induction decay, which is Fourier transformed again to give the correlation NMR spectrum. In the Fourier transform of a discrete, finite sequence of values, the sequence is assumed to be periodic; the last point of a sequence is assumed to be followed by the first point of the next sequence. As a result of this, when the baseline of the rapid scan response is tilted to a great extent and the first and the last points of a data sequence are quite different in magnitude, the correlation NMR spectrum obtained by the process involving multiplication by $\exp(-ibt^2/2)$ may show an oscillation of the baseline. This situation is actually encountered when one wants to observe small peaks which lie on the shoulder of large one.

One possible way to circumvent the above difficulty is application of an exponential window to the free induction decay which is derived from the rapid scan response. However, this could improve the situation only at the expense of additional line broadening. Another possibility is to apply an apodization window to the rapid scan response. This procedure may cause distortion near either end of the spectrum. In the present paper, we will report a method involving a *wing processing* which was found to be quite useful in observing peaks on the tilted baseline.

Experimental

A JEOL PS-100 NMR spectrometer operating at 100 MHz was modified for correlation spectroscopy as previously described.[3,5] A general program CORNMR was written to process the rapid scan response with the theoretical function method described by Gupta, Ferretti, and Becker.[2]

Results and Discussion

Figure 1a shows a rapid scan response for 2 mM ethanol in H_2O where ethanol peaks are on the shoulder of the large water signal. The conventional correlation NMR procedure leads to a spectrum as reproduced in Fig. 1b. In the present method, the rapid scan response with N data points is provided on its both ends with *wings*; the first point is provided with a *wing* with $N/2$ identical values which is equal to that of the first point, and the last point with a *wing* with $N/2$ identical values equal to that of the last point. The *winged* rapid scan response with $2N$ data points thus obtained is processed by the theoretical function method, and the spectrum is cut out of the relevant part of the final result. The rapid scan response given in Fig. 1a is treated with the above method, and the *winged* rapid scan response (Fig. 2a) was used to obtain the final spectrum shown in Fig. 2b.

Although the oscillation of the baseline is considerably decreased, there is still some residual fine oscillation in Fig. 2b. As discussed above, this comes from the fact that there is a difference in magnitude between the first and the $2N$-th points of the *winged* rapid scan response. A quarter of each *wing* is then replaced by a quarter cycle of the sine function to smoothly connect the *wings*, giving rise to a repetition of smoothly connected rapid scan response. The *winged* rapid scan response obtained by this procedure (Fig. 3a) gave the spectrum which is reproduced in Fig. 3b,

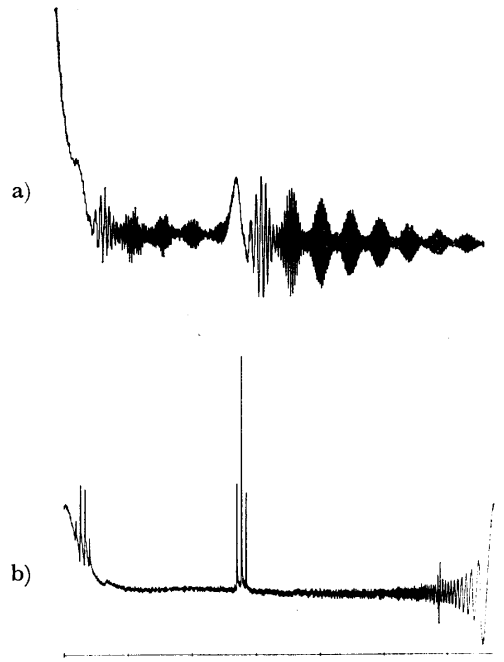

Fig. 1. (a) A rapid single scan response and (b) the correlation NMR spectrum at 100 MHz of 2 mM ethanol in H_2O. Sweep rate, 328.2 Hz/s; sampling time, 2.048 s; number of sampling points, 4096. One division is equal to 100 Hz.

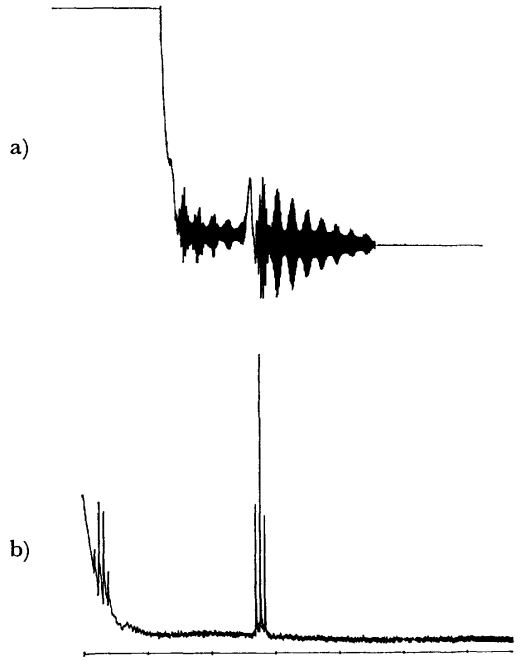

Fig. 2. (a) A rapid scan response in Fig. 1a supplemented with *wings* with 2048 points on its both ends, and (b) the correlation NMR spectrum obtained from it.

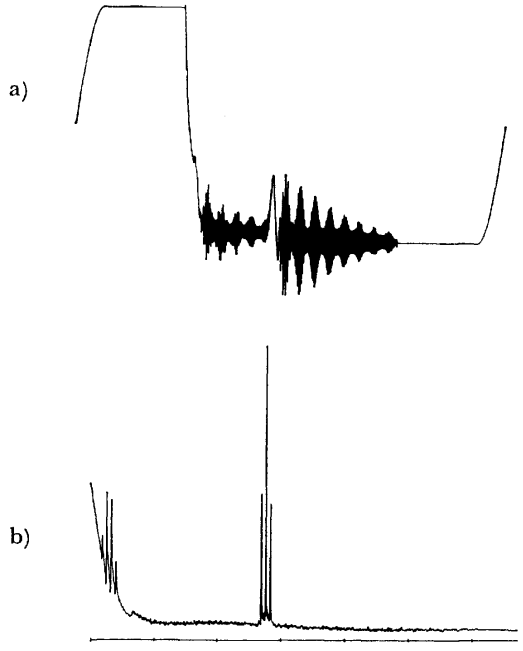

Fig. 3. (a) A rapid scan response in Fig. 2a with *wings* modified by replacing a quarter of each of them by the sine function, and (b) the correlation NMR spectrum obtained from it.

where the undesirable oscillation of the baseline is clearly eliminated. It should be noted that the procedure described here does not give rise to any distortion of the spectrum such as line broadening.

The resonance conditions are met sequentially in correlation NMR spectroscopy. Therefore, if only a necessary portion of the spectrum is scanned, the number of sampling points can be made very small without violating the sampling theorem. Sometimes, the final spectrum obtained using the minimum number of sampling points may not be smooth enough, so that it is quite difficult to find the peak maxima. However, interpolation can easily be done by supplementing a sufficient number of zeroes at the end of the free induction decay which is derived from the rapid scan response. Bartholdi and Ernst[7] have discussed the effect of supplementing zeroes at the end of the free induction decay obtained in the case of pulse FT NMR. In correlation NMR, this feature should especially be important when one wants to observe, for example, carbon-13 spectra where signals scatter over a wide range of frequency.

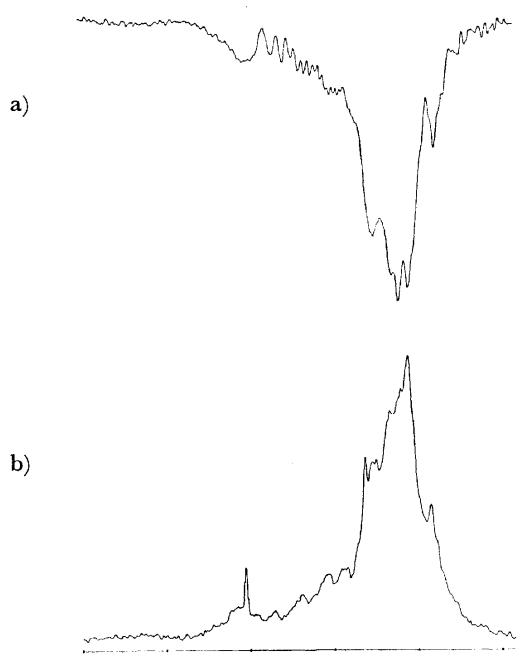

Fig. 4. (a) Rapid scan response and (b) the correlation NMR spectrum at 100 MHz of the aromatic region of hen egg white lysozyme in D_2O (10% (w/v) in 99.8% D_2O, pH=1.73, 35 °C). Sweep rate, 530.0 Hz/s; sampling time, 0.9728 s; number of sampling points, 2048; number of accumulations, 256; phase correction angle to obtain the spectrum, 180°. One division is equal to 100 Hz.

Figure 4a shows a rapid scan response for the aromatic region of hen egg white lysozyme in D_2O, where the sweep rate, sampling time, and number of sampling points are 530.0 Hz/s, 0.9728 s, and 2048, respectively. The spectrum obtained from this rapid scan response is given in Fig. 4b. Since the narrowest signal has a width of approximately 5 Hz, 256 data points should have been sufficient under the experimental condition to acquire all necessary information. The total of 256 data points which have been picked out of every eight points of the rapid scan response was used to obtain the free induction decay, from which the correlation NMR spectrum was derived; the histidine C-2 proton part of the spectrum is reproduced

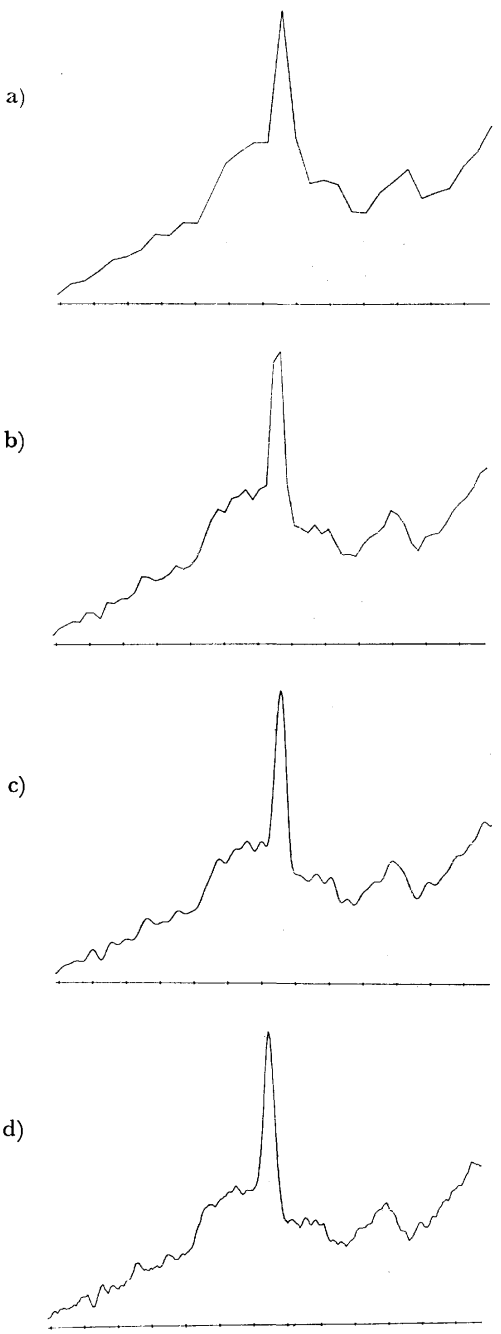

Fig. 5. Correlation NMR spectra of the histidine C-2 proton of hen egg white lysozyme in D_2O. Spectrum (a) was obtained by using 256 data points which are picked out of every eight points of the rapid scan response in Fig. 4a. The free induction decay used to obtain the spectrum (a) was made twice and eight times in length by supplementing zeroes at its end, from which spectra (b) and (c) were derived, respectively. The corresponding part of the spectrum shown in Fig. 4b is reproduced in (d). One division is equal to 10 Hz.

in Fig. 5a. The spectra in Figs. 5b and 5c are obtained when the number of data points of the free induction decay is made twice and eight times respectively in length by supplementing zeroes at its end. Figure 5c is quite similar with the exception of high-frequency noise to Fig. 5d which is a part of the spectrum in Fig. 4b derived using 2048 data points.

In conclusion, the present techniques to achieve spectral smoothing should allow additional freedom in using correlation NMR spectroscopy.

The authors wish to thank Professor S. Fujiwara for his continual encouragement.

References

1) J. Dadok and R. F. Sprecher, *J. Magn. Reson.*, **13**, 243 (1974).
2) R. K. Gupta, J. A. Ferretti, and E. D. Becker, *J. Magn. Reson.*, **13**, 275 (1974).
3) Y. Arata and H. Ozawa, *Chem. Lett.*, **1974**, 1257.
4) H. Ozawa and Y. Arata, *Chem. Lett.*, **1975**, 239.
5) Y. Arata and H. Ozawa, *J. Magn. Reson.* **21**, 67 (1976).
6) Y. Arata, *J. Magn. Reson.* (in press).
7) E. Bartholdi and R. R. Ernst, *J. Magn. Reson.*, **11**, 9 (1973).

Kinetic Study of Poly(acrylic acid)-Copper(II) Complex Formation

Hiroshi NISHIKAWA and Eishun TSUCHIDA

Department of Polymer Chemistry, Waseda University, Tokyo 160

(Received July 19, 1975)

The kinetics of poly(acrylic acid)–copper(II) (PAA–Cu) complex formation has been studied by a relaxation method. It was found that the greater stability of PAA–Cu complex than that of a monomeric analog is due to the increase of forward rate constant (k_f(PAA)/k_f(GA)=4) and decrease of the reverse rate constant (k_r(PAA)/k_r(GA)=1/4) in the polymer system. The results are explained in terms of an electrostatic effect of polyelectrolyte and a conformational change of the polymer ligand.

Several reports have appeared on the kinetics of complexation reactions of labile metal ions.[1–4] However, reaction with a polymer ligand has not been studied due to the complexity of the polymer system. Although polymer metal complexes, in particular polymer–copper(II) complexes exhibit high activity in the catalytic reaction in solution,[5,6] the mechanism of the catalysis has not been elucidated. In order to study the polymer–copper(II) complex catalyzed reaction in detail, it is necessary to clarify the effect of the polymer ligand on the complexation reaction. Static studies have been carried out on formation reaction of the polymer–copper(II) complexes by several investigators,[7–10] but the kinetics remains unclarified. The complexation reaction of copper(II) being very rapid, a relaxation method can be utilized for determining the reaction rate constant.

This paper deals with a kinetic study of the reaction of copper(II) ion with poly(acrylic acid) by means of the temperature-jump method. Discussion is given on the effect of polymer ligands in the kinetics of the complexation reaction.

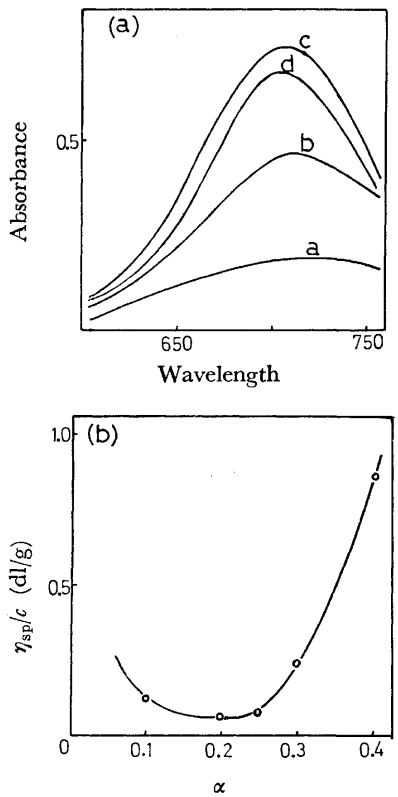

Fig. 1. Viscometric and spectroscopic change of poly(acrylic acid)-copper(II) solution with neutralization. [PAA]=1.0×10^{-2} unit·mol/l, [Cu]/[PAA]=1/10
(a) a: α=0.05, b: α=0.15, c: α=0.25, d: α=0.35

Experimental

Materials. Poly(acrylic acid) (PAA) was prepared by radical polymerization of acrylic acid, its average molecular weight being 1.2×10^5 as determined by viscometric measurement.

Commercial $CuCl_2\cdot H_2O$, gultaric acid, malonic acid, and other salts were used. The concentration of Cu(II) ion in solution was determined by chelate titration with use of EDTA.

All the solutions were prepared with freshly distilled water.

Methods. The acid dissociation constant of poly(acrylic acid) was determined by Henderson-Haselbach's method[7] by potentiometric titration with a Hitachi-Horiba M-1 pH-meter.

The viscosity of the polymer complex solution was measured at 25 °C with an Ubbelohde viscometer. Visible spectra of the polymer complex solutions were observed with a Shimadzu MPS50 spectrophotometer.

The complexation reaction of Cu(II)–PAA was followed with a temperature-jump apparatus (Union Giken RA-1200), the optical change in the indicator added (bromocresol green and bromochlorophenol blue) being observed. The rise-time of the temperature-jump apparatus is below 1 μs as confirmed from the discharge-curve, the other functions of the apparatus being checked through the reaction of proton exchange on trepaeolin 0,

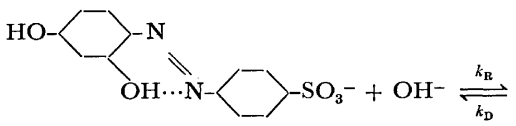

Trepaeolin O + H_2O

k_R: 3.8×10^5 $M^{-1}\cdot s^{-1}$ (3.6×10^5 $M^{-1}\cdot s^{-1}$)
k_D: 7.6×10^3 s^{-1} (8×10^3 s^{-1})

where the values in parentheses were taken from the work of Eigen *et al.*[11]

The complexation reaction of each monomeric analog was studied by the same way as in the polymer system.

Result and Discussion

The spectroscopic result showing that the maximum wavelength of d-d absorption spectra of poly(acrylic acid)–copper(II) (PAA–Cu) complex is observed at 700 nm (Fig. 1(a)), near that of malonato copper(II) (MA–Cu) complex (659 nm), suggests that two acrylate units of PAA coordinate to a copper(II) ion, a chelate complex being formed. Thus the complexation re-

action of PAA with copper(II) can be expressed by Eq. 1, where L is a coordination unit consisting of two acrylate anions, and HL one consisting of an acrylate anion and an undissociated acrylic acid.

$$M^{2+} + L^{2-} \underset{k_r}{\overset{k_f}{\rightleftharpoons}} ML \qquad k_f/k_r = K$$

$$M^{2+} + HL^{-} \underset{k_r'}{\overset{k_f'}{\rightleftharpoons}} ML + H^{+} \tag{1}$$

Analysis of the temperature-jump data requires a prior knowledge of appropriate equilibrium constants. The stability constant of polymer metal complex was determined by a modified Bjerrum's method reported by Gregor *et al.*[7] The acid dissociation constant of polyacid being affected by the charge on the partially dissociated polymer chain, the dissociation constant of PAA was determined by the following equations,

$$K' = \frac{[H^+][A]}{[N]}(Z)^{n-1} \qquad Z = \frac{\text{charged unit}}{\text{uncharged unit}}$$

$$K_1^a = \frac{[H^+][HL^-]}{[H_2L]} \qquad K_2^a = \frac{[H^+][L^{2-}]}{[HL^-]} \tag{2}$$

$$[A] = 2[L^{2-}] + [HL^-], \quad [N] = [HL^-] + 2[H_2L],$$

$$[L^{2-}] = \left[\frac{[A]}{[N] + [A]}\right]^2 [L]_t$$

where K' and n are given by Henderson-Haselbach plots, and [A], [N], and $[L]_t$ are concentration of acrylate anion unit, undissociated acrylic acid unit, and total concentration of uncoordinated ligand unit, respectively. Average coordination number, $\bar{n}$, is given by Eq. 3, where $[H_2L]_t$ and $[Cu(II)]_t$ are initial concentrations of ligand unit and copper(II) ion, the stability constant K of each system being given by the $\bar{n}$ *vs.* $p[L^{2-}]$ plots according to Bjerrum's theory.

$$\bar{n} = \frac{[H_2L]_t - [H_2L] - [HL^-] - [L^{2-}]}{[Cu(II)]_t} \tag{3}$$

The equilibrium constants used for analysis of PAA–Cu(II) system and its monomeric analog are given in Table 1.

The ranges of pH and concentrations of PAA and copper(II) ion available are strictly restricted by three factors: (1) decomposition of the chelate structure due to the electrostatic repulsion between carboxylate anions (Figs. 1(a) and 1(b)), (2) olation of the complex or copper ion, and (3) relatively small absorption change in the lower pH region.

By applying standard techniques for deriving relaxation time expressions,[3,12] we have

$$1/\tau = Ak_f + Bk_f'$$

$$A = \frac{[M^{2+}]}{1+\alpha} + [L^{2-}] + \frac{1}{K}$$

$$B = \frac{[M^{2+}]}{1+\alpha} + [HL^-] + \frac{1}{K \cdot K_2^a}\left([H^+] + \alpha\beta\frac{[ML]}{1+\alpha}\right) \tag{4}$$

$$\alpha = \frac{K_1^a[H^+] + \beta[H^+][HL^-] + [H^+]^2}{K_1^aK_2^a + 4\beta K_2^a[HL^-] + \beta K_2^a[L^{2-}]}$$

$$\beta = \frac{K_{In} + [H^+]}{K_{In} + [H^+] + [In^-]}$$

Since acid dissociation "constant" K_1^a or K_2^a changes in the polymer system with the charge on the polymer, K_1^a and K_2^a were calculated separately by Eq. 2 for each experimental point.

Plots $(\tau B)^{-1}$ *vs.* AB^{-1} for PAA–Cu(II) at the concentrations of PAA 1.0×10^{-2} M and 0.5×10^{-2} M (Fig. 2). The plots are almost linear, indicating that the standard relaxation techniques can be used for the polymer system. The same plots for the monomeric analog, glutarato–copper(II) (GA–Cu) and malonato–copper(II) (MA–Cu) complexes are illustrated in Figs. 3 and 4. The slopes give k_f's and intercepts k_f' respectively. The rate constants obtained are summarized in Table 2.

When the k_f values of Cu–PAA were compared with those of monomeric analog, the order acetic acid(AA)–Cu>MA–Cu>PAA–Cu>GA–Cu, was observed, which

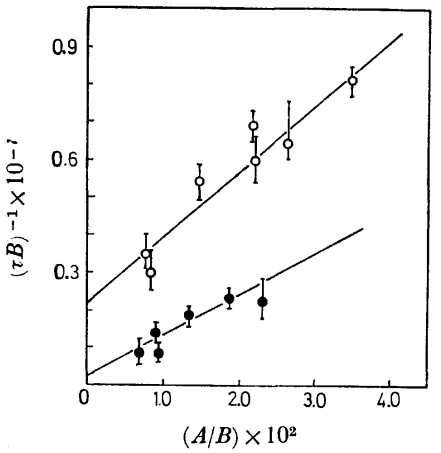

Fig. 2. Plots of $(\tau B)^{-1}$ *vs.* A/B for Cu(II)-PAA system. ○: [PAA]$=0.5\times10^{-2}$ M, ●: [PAA]$=1.0\times10^{-2}$ M.

TABLE 1. EQUILIBRIUM CONSTANTS ($\mu=0.1$, 25 °C)

Ligand[a]	Equilibrium constant	
PAA(5.0×10^{-3} M)	$pK'=5.91$, $n=1.83$	$\log K=3.6$
PAA(1.0×10^{-2} M)		$\log K=3.1$
GA[b]	$pK_1^a=4.1$	$\log K=2.4$
	$pK_2^a=5.0$	
MA[b]	$pK_1^a=2.8$	$\log K=5.0$
	$pK_2^a=5.3$	

Indicator	pK_{In}
Bromocresol green	4.7
Bromochlorophenol blue	4.0

a) PAA: Poly(acrylic acid), GA: Glutaric acid, MA: Malonic acid. b) *Cf.* M. Yasuda, K. Yamasaki, and H. Ohtaki, *Bull. Chem. Soc. Jpn.*, **33**, 1067 (1960).

TABLE 2. RATE CONSTANTS FOR COMPLEXATION OF Cu(II) WITH CARBOXYLIC ACIDS

Ligand	$k_f(M^{-1}s^{-1})$	$k_r(s^{-1})$	$k_f'(M^{-1}s^{-1})$
PAA(5.0×10^{-3} M)	1.7×10^8	4.5×10^4	2.2×10^6
PAA(1.0×10^{-2} M)	9.3×10^7	6.8×10^4	4.2×10^5
GA	4.1×10^7	1.6×10^5	3.0×10^5
MA	1.2×10^9	1.2×10^4	3.2×10^7
AA[a]	1.5×10^9	—	—

a) AA: Acetic acid; *cf.* G. Maass, *Z. Phys. Chem., Fraukfurt*, **60**, 131 (1968).

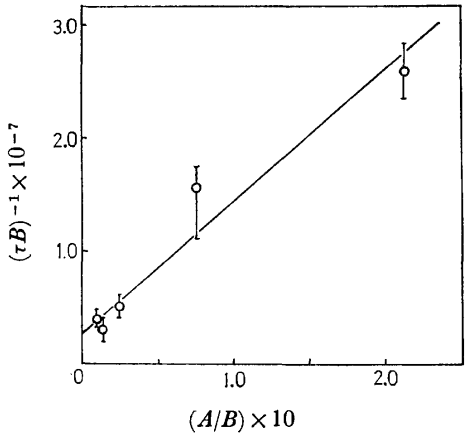

Fig. 3. Plots of $(\tau B)^{-1}$ *vs.* A/B for Cu(II)-GA system.

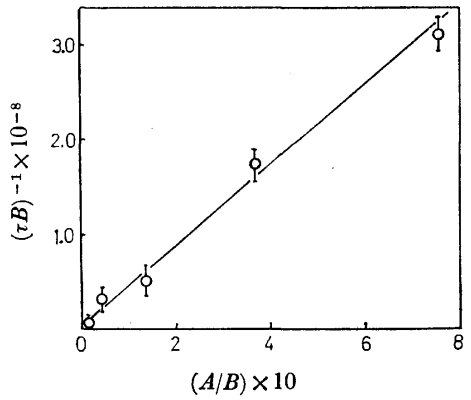

Fig. 4. Plots of $(\tau B)^{-1}$ *vs.* A/B for Cu(II)-MA system.

agrees with that of the stability constants except for the AA–Cu system.

Eigen and Wilkins proposed the following mechanism for bidentate complex formation.[1]

$$\underset{\text{I}}{W_2M\ W_1} + \text{A-B} \overset{K_{os}}{\rightleftharpoons} \underset{\text{II}}{W_2M\ W_1A\text{-B}}$$

$$\underset{\text{II}}{W_2M\ W_1A\text{-B}} \underset{k_1'}{\overset{k_1}{\rightleftharpoons}} \underset{\text{III}}{W_2M\text{-A-B}} + W_1 \qquad (5)$$

$$\underset{\text{III}}{W_2M\text{-A-B}} \underset{k_2'}{\overset{k_2}{\rightleftharpoons}} \underset{\text{IV}}{M\langle \overset{A}{B}) } + W_2$$

The first outer sphere complex formation step is very fast and diffusion controlled. If we assume that the outer sphere complex formation is in an equilibrium the forward rate constant k_f is given by

$$k_f = K_{os}k_1\frac{1}{1+(k_1'/k_2)} \qquad (6)$$

The equilibrium constant K_{os} for the outer sphere complex formation is affected by charge on both the metal ion and the ligand, the approximate value being given by[13]

$$K_{os} = 4Na^3/3000 \exp\frac{z_M z_L e_0^2}{\varepsilon a \kappa T} \qquad (7)$$

where N, a, κ and ε are the Avogadro number, the distance of the closest approach of the two ions, the Boltzmann constant and the dielectric constant, respectively, z_M and z_L being the corresponding net charges of metal and ligand.

Comparing the K_{os} value of each system calculated by Eq. 7, we find that the K_{os} values for MA–Cu and GA–Cu are about 7.5 times larger than that for AA–Cu. The K_{os} value of copper with PAA could not be calculated since the net charge of the ligand was not definite. However, it is certain that the K_{os} value for PAA–Cu is greater than that for the monomeric analog due to increase of ligand's net charge by carboxylate anions on the same chain. The large k_f value for PAA–Cu can be explained partially by the electrostatic effect of the neighboring carboxylate anions on the outer sphere complex formation.

The II→III step of each system examined is the substitution of water by carboxylate anion. If we assume that the k_1 values are the same for all the systems, the k_f/K_{os} value gives a measure of the difficulty of the chelate formation. The stability of the chelate ring is dependent on the number of atoms constituting the chelate and 5-(unconjugated system); 6-(conjugated system) membered ring is the most stable. Since the ligands in the complexes we examined are not conjugated, the chelate ring formation is considered to be rather slow in MA–Cu where a six-membered ring is formed, and much slower in GA–Cu where an eight-membered ring is formed. This is in line with the results obtained by means of Eq. 6 where the k_1'/k_2 value of GA–Cu is 30 times larger than that of MA–Cu.

The reduced viscosity of the polymer solution changes with the complexation (Fig. 1 (b)). This suggests that the conformation of the polymer ligand changes with chelate formation or dissociation. A larger k_1'/k_2 value and a smaller k_f/K_{os} value for polymer system as compared with those of monomeric analog are reasonable. However, the k_f value of PAA–Cu we obtained was larger than that of the GA–Cu system. This can not be explained by the effect of polymer ligand on the chelate formation step (III→IV).

The k_f value decreased with the increase of the polymer concentration. This might be due to the formation of intermolecular complex at higher polymer concentration since the anion concentration per one polymer molecule is lowered.

This work was partially supported by a Grant in Aid for Scientific Research from the Ministry of Education (No. 011011).

References

1) M. Eigen and R. G. Wilkins, "Mechanisms of Inorganic Reactions," Advance on Chemistry Series, No. 49, American Chemical Society, Wasington, D. C. (1965).

2) W. B. Makinen, A. F. Pearlmutter, and J. E. Stuehr, *J. Am. Chem. Soc.*, **91**, 4083 (1971).

3) R. F. Pasternack, E. Gibbs, and J. C. Cassatt, *J. Phys. Chem.*, **73**, 3814 (1969).

4) R. E. Shepherd, G. M. Hodgson, and D. W. Margerum, *Inorg. Chem.*, **10**, 989 (1971).

5) N. A. Vengerova, Yu. E. Kirsh, and V. A. Kabanov, *Vysokomol. Soed.*, *A*, **13**, 2509 (1971).
6) E. Tsuchida, H. Nishide, and T. Nishiyama, *J. Polym. Sci., Symp.* **47**, 45 (1974).
7) H. P. Gregor, L. B. Luttinger, and E. N. Lobel, *J. Phys. Chem.*, **59**, 34 (1955).
8) H. Nishikawa and E. Tsuchida, *J. Phys. Chem.*, **79**, 2072 (1975).
9) Yu E. Kirsh, V. Ya Kovner, A. I. Kokorin, K. I. Zamaraev, V. Ya Chernyak, and V. A. Kabanov, *Europ. Polym. J.*, **10**, 671 (1974).
10) M. Hatano, T. Nozawa, T. Yamamoto, and S. Kambara, *Makromol. Chem.*, **15**, 1 (1968).
11) M. Eigen, W. Kruse, G. Maass, L. De Maeyer, "Progress in Reaction Kinetics," Vol. II. ed. by G, Porter Pergamon Press (1964), p. 287.
12) R. F. Pasternack and H. Sigel, *J. Am. Chem. Soc.*, **92**, 6146 (1970).
13) R. Fuoss, *J. Am. Chem. Soc.*, **80**, 5059 (1958).

The Dissolution of Titanium Minerals in Hydrochloric and Sulfuric Acids

Masayuki IMAHASHI and Nobuki TAKAMATSU

Department of Chemistry, Toho University, Miyama-cho, Funabashi, Chiba 274

(Received July 23, 1975)

Kinetic dissolution experiments of powdered ilmenite and rutile were carried out in sulfuric and hydrochloric acids (0.03—1 M) at temperatures of 40, 65, and 90 °C in order to study the physico-chemical factors and the mechanism for the leaching of titanium and iron from these minerals and rocks under acidic conditions. The dissolution rate of ilmenite was strongly affected by the acidity and temperature of the acid solutions; the rate changes in the H_2SO_4 solutions were greater than those in the HCl solutions. The dissolution rate of rutile was much slower than that of ilmenite. Ilmenite was decomposed by the dissolution of titanium and iron in a nearly stoichiometric ratio under strongly acidic conditions such as 0.3—1 M. But under milder conditions, such as 0.03—0.1 M at 90 °C, the dissolution rate of titanium dropped rapidly in the initial step and the curved line for iron dissolution was nearly parabolic, suggesting the diffusion of iron through the residual layer of titanium.

Titanium is relatively abundant in the earth's crust: igneous rocks contain an average of approximately 0.44% of this element by weight.[1] Titanium is usually found in igneous and metamorphic rocks as titanomagnetite (Fe_2TiO_4–Fe_3O_4), ilmenite ($FeTiO_3$), and rutile (TiO_2), and is also found in pyroxene, hornblend, and biotite. Generally titanium remains undissolved in its host rocks even through the process of weathering and hydrothermal alteration of igneous rocks,[2] not only because it is present in the form of resistant minerals but also because it tends to form insoluble hydroxides in aqueous solutions. One of the authors[3] reported the titanium content of hydrothermally-altered rocks from the Tateyama Jigokudani area; while most of the titanium had remained immobile in the rocks, a part of it had been leached out under the strongly acid conditions. According to Noguchi *et al.*,[4] acid hot spring waters in Japan contain about $0.001n$—$0.1n$ mgTi/l and the titanium content of the waters tends to increase with increasing acidity. The titanium in the acid spring waters is likely to be derived from wall rocks by the attack of acid thermal solutions containing sulfuric and hydrochloric acids. The interaction between thermal solutions and rock-forming minerals may result in alterations of rocks, which would proceed through complicated processes: *i.e.*, hydration, ion exchange, dissolution, deposition, and recrystallization. All these processes should be affected by various physico-chemical factors, such as acidity, temperature, type of acid, *etc.* Some studies of the dissolution kinetics of rock-forming minerals have been reported,[5–8] but few reports on titanium minerals have been presented, except for the mineralogical studies of the alteration of ilmenite and other minerals.[9] In this study kinetic dissolution experiments on the decomposition of powdered ilmenite and rutile were carried out to examine the influence of the chemical character of active solutions and to analyze the mechanism of the decomposition of the minerals.

Experimental

Ilmenite and rutile were used in this study as titanium minerals. The dissolution experiments of powdered ilmenite (*cf.* Table 1) were carried out in H_2SO_4 and HCl solutions of 0.03—1 M at 40, 65, and 90 °C, and the experiments of rutile were also carried out in 1 M H_2SO_4 and HCl at 90 °C. The experiments were performed according to the procedure of Kamiya *et al.*[10] The acid concentration of the leaching solutions was adjusted by the addition of sulfuric and hydrochloric acid into distilled water, and at the same time the pH value of the solutions was measured in the range from 40 to 90 °C with a pH meter for high temperatures. Slight differences were found in the pH values of the initial and final solutions. 1 g of ilmenite (120—200 mesh) and/or rutile (under 120 mesh) was suspended in 250 ml of leaching solution, temperature-regulated at 40, 65, or 90 °C, which was stirred continuously with a magnetic stirrer coated with polyethylene. The dissolution rate of titanium and iron was determined by periodically pipetting a 10 ml aliquot from the bottle, centrifuging for a few minutes to remove the titanium minerals, and chemically analyzing the supernatant solution. Titanium and iron were determined colorimetrically by DAM (diantipyrylmethane) and *o*-phenanthroline respectively.

Results and Discussion

The amounts of titanium and iron leached from the powdered ilmenite at different times are shown in Figs. 1 to 6 and Figs. 9 and 10 respectively. These figures show that the leached amounts of titanium and iron are strongly affected by the acidity and temperature of the leaching solutions, and that these amounts in H_2SO_4 solutions are larger than those in HCl solutions at the same molality and temperature. As seen in Fig. 7, the amount of titanium leached from powdered rutile was very small compared with the ilmenite; the amount in the H_2SO_4 solutions was also larger than that in the HCl solutions. It can be seen from these figures that the titanium and iron ions are transported to the solution when hydrated protons diffuse into the solid, as indicated by Sanemasa and Katsura,[8] and that the dissolution rate of the ions from the minerals in the H_2SO_4 solutions is faster than that in the HCl solutions. Packter *et al.*[11] observed that the dissolution rate of gibbsite in the H_2SO_4 solutions was markedly faster than the rates in the HCl and $HClO_4$ solutions. They attributed the rate-promoting effect of sulfuric acid to the dipole interaction between the HSO_4^- ion or $H^+\cdots\cdots SO_4^{2-}$ ion pairs and the active sites on the solid surface. The study of olivine dissolution[7] also showed an effect from sulfuric acid similar to the case of gibbsite.

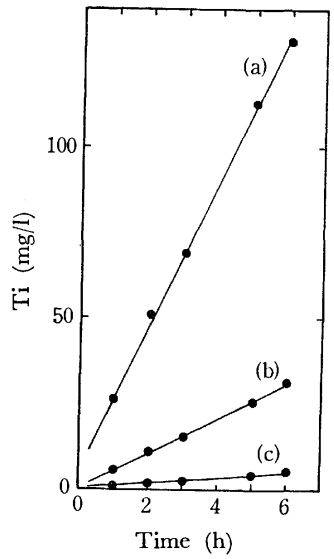

Fig. 1.

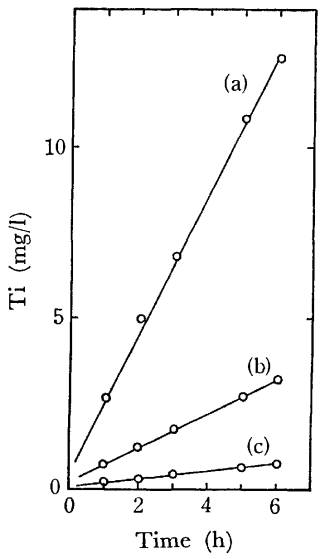

Fig. 2.

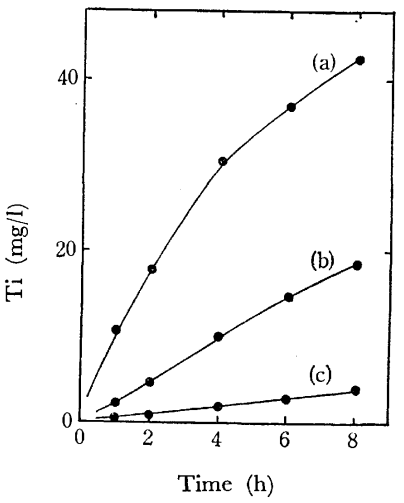

Fig. 3.

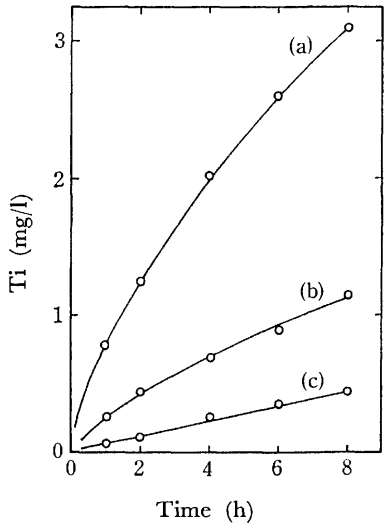

Fig. 4.

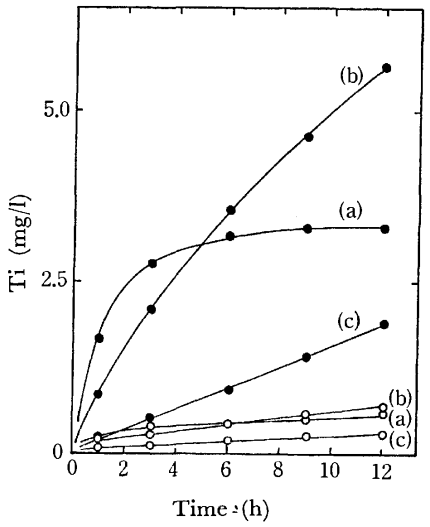

Fig. 5.

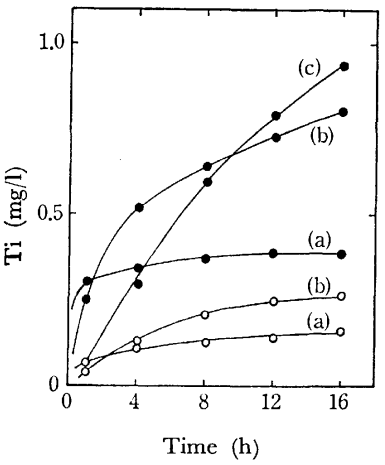

Fig. 6.

Figs. 1—6. Change in concentration of titanium dissolved in H_2SO_4 and HCl solutions from ilmenite at 40, 65 and 90 °C with the time of reaction.
(a): 90 °C, (b): 65 °C, (c) 40 °C, —●—: H_2SO_4, —○—: HCl.
Figs. 1 and 2: 1 M, Figs. 3 and 4: 0.3 M, Fig. 5: 0.1 M, Fig. 6: 0.03 M.

TABLE 1. CHEMICAL COMPOSITION OF ILMENITE

Constituent	Content (wt%)
TiO_2	52.96
FeO	46.06
MnO	1.58
$H_2O(-)$	0.00
$H_2O(+)$	0.18
Total	100.78

On the other hand, Kamiya *et al.*[10] reported that the dissolution of powdered quartz was catalyzed by sulfate and chloride ions and that the catalytic activity of the divalent sulfate ion was higher than that of the monovalent chloride ion. As described previously, the dissolution rates of titanium and iron from ilmenite were affected more highly by sulfate ions (and HSO_4^-) than by chloride ions, but the effect of sulfate ions on iron was not so large as on titanium. This may be due to the differences of valences and ionic radii between titanium and iron. Furthermore, the dissolution experiments of microcline[12] showed that Al^{3+} dissolution from the mineral was accelerated in the presence of sulfuric acid. These experiments, however, do not enable us to determine whether the interaction between titanium and sulfate (HSO_4^-) ion resulted from an electrostatic force or from an electronic force such as the bonding in coordination compounds. In any event, it is evident that sulfate and hydrogensulfate ions play an important role in the dissolution of ilmenite and rutile.

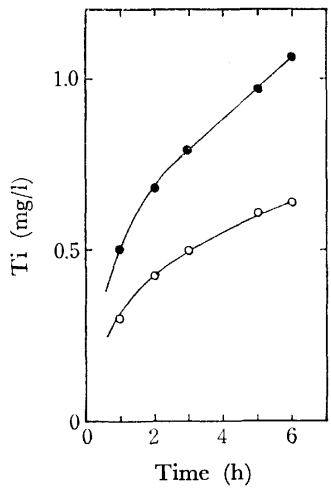

Fig. 7. Change in concentration of titanium dissolved in 1 M H_2SO_4 and HCl solutions from rutile at 90 °C with the time of reaction.
—●—: H_2SO_4, —○—: HCl.

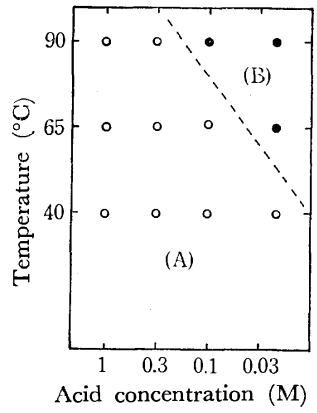

Fig. 8. Temperature and acid concentrations used in this experiment.

Figures 11 and 12 show the values of the molar ratio for the amount of titanium and iron dissolved at different times. The values were always smaller than 1, but these tended to become larger or smaller with time according to the conditions. Therefore, we have divided the conditions into the two groups shown in Fig. 8. Under the conditions of group A, the dissolution rate of iron from ilmenite was larger than that of titanium during the initial step of the dissolution, and over a very long time period the ratio of titanium to iron approached the stoichiometric ratio, *i.e.* Ti/Fe=1. On the other hand, under the conditions of group B, the values of the ratio tended to become smaller with time, and the amount of titanium leached in the course of the leaching experiments at high temperatures became less than that at low temperatures.

If we assume that the change in the surface of powdered ilmenite brings about the depression of the dissolution rate with time, we get the following approximate equations[10] for the A group:

$$m = K_1St + m_0 \qquad S = S_0(1-K_2t)$$
$$m - m_0 = K_1S_0 - K_1K_2S_0t^2$$

Fig. 9.

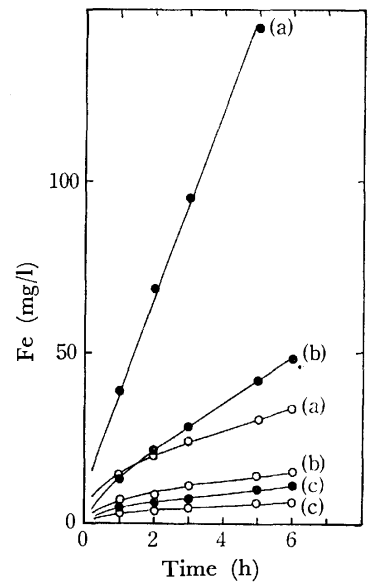

Fig. 10.

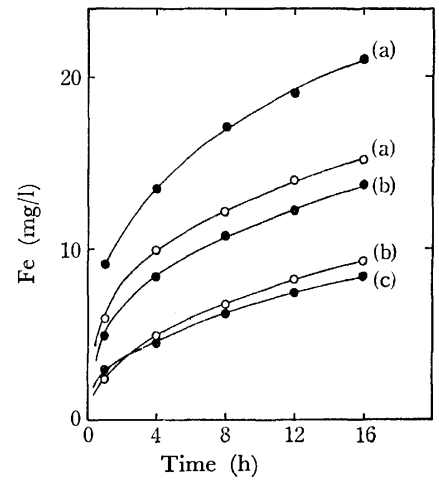

Figs. 9 and 10. Change in concentration of iron dissolved in H_2SO_4 and HCl solutions from ilmenite at 40, 65 and 90 °C with the time of reaction.
(a): 90 °C, (b): 65 °C, (c): 40 °C,
—●—: H_2SO_4, —○—: HCl.
Fig. 9: 1 M, Fig. 10: 0.03 M.

where m and m_0 are the amounts of dissolved titanium at time t and at the beginning, S and S_0 are the surface areas of powdered ilmenite at time t and at the beginning, and K_1 and K_2 are the constants for dissolution of titanium and for decrease in surface area, respectively. As the surface area of powdered ilmenite was not measured in our experiments, K_1S_0 represents the apparent dissolution rate of titanium at time zero. Figure 13 shows the values for K_1S_0 at different acid concentrations; the values tend to become smaller with decreasing temperature under the A conditions. On the other hand, under the B conditions (*e.g.*, 0.03 M at 90 °C) the amount of titanium leached at intervals of one hour was reduced rapidly in the initial step of the dissolution, as shown in Fig. 14. Therefore, under the B conditions it must be considered that some other factor besides the decrease of surface area brought about the depression of the dissolution rate. It might be thought to be the formation of insoluble

Fig. 11.

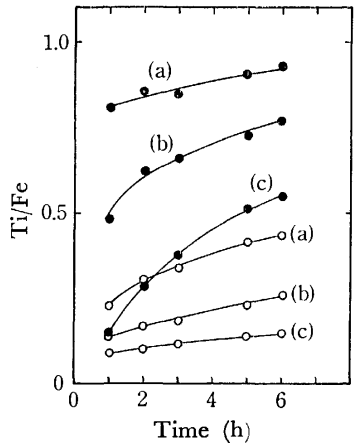

Fig. 12.

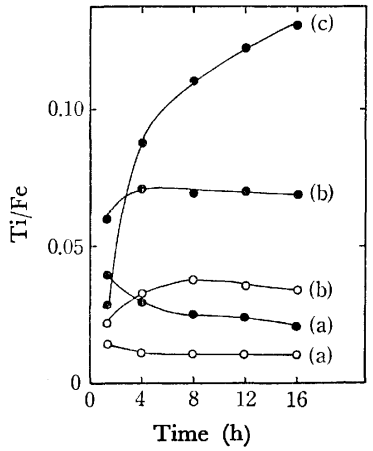

Figs. 11 and 12. Change in the Ti/Fe ratio dissolved in H_2SO_4 and HCl solutions from ilmenite at 40, 65 and 90 °C with the time of reaction.
(a): 90 °C, (b): 65 °C, (c): 40 °C
—●—: H_2SO_4, —○—: HCl.
Fig. 11: 1 M, Fig. 12: 0.03 M.

materials on the surface. And in fact, under the A conditions the curved line for iron dissolution was nearly linear, while the line was nearly parabolic under the B conditions. As shown in Figs. 15 and 16, an approximately linear relationship exists between the square of the leached amount of iron and time, *i.e.*, $m^2=kt+k'$, where m=leached amount of iron, t=time, and k=constant; this relationship is presumed to show that the iron ion diffuses through the residual layers into the solution. However, we could not discover any change of the structure of ilmenite by X-ray diffraction analysis after the 36 h leaching experiment at 90 °C in 0.1 M H_2SO_4. The amount of residual materials, therefore, is likely to be slight and the layer, if present, to be amorphous.

It may be concluded that ilmenite is decomposed by the dissolution of titanium and iron in a nearly stoichiometric ratio in the H_2SO_4 and HCl solutions ranging from 0.3 to 1 M, but in the solutions ranging from 0.03 to 0.1 M (pH 1—1.5) at 65—90 °C the dissolution rate of titanium decreases rapidly in the initial step. Consequently, the iron ion may diffuse into the acid solution through the insoluble residual layer of titanium. The insoluble materials of titanium

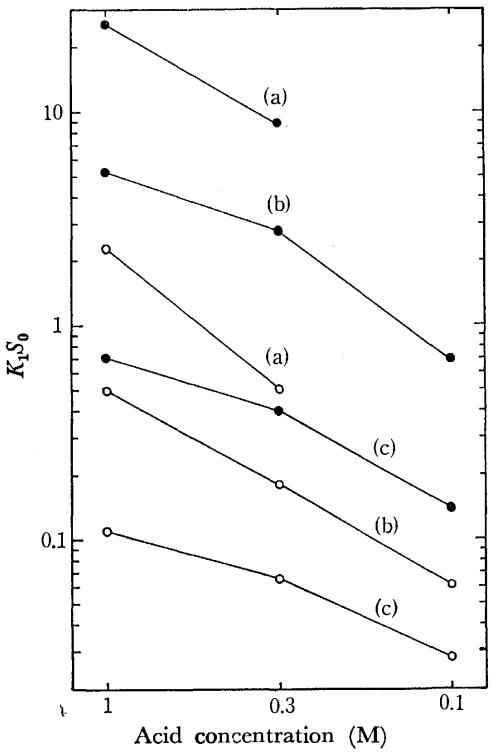

Fig. 13. Apparent dissolution rate of titanium from ilmenite at different acidities.
(a): 90 °C, (b): 65 °C, (c): 40 °C
—●—: H_2SO_4, —○—: HCl.

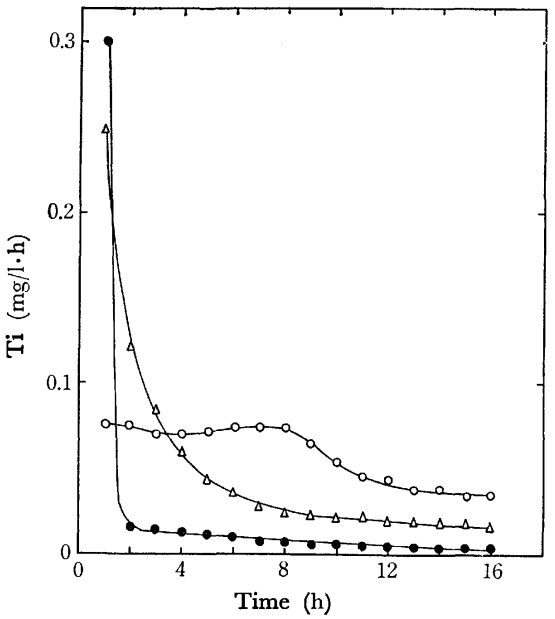

Fig. 14. Change in amount of titanium dissolved in 0.03 M H_2SO_4 from ilmenite at intervals of one hour.
—●—: 90 °C, —△—: 65 °C, —○—: 40 °C.

seem to be changed into resistant oxide minerals such as rutile over a long period, although we could not identify the minerals in this experiment in the limited time of 16 h. As described previously, the solubility of rutile in 1 M H_2SO_4 and HCl solutions was very much smaller than that of ilmenite, and rutile, therefore, does not seem to dissolve very much in acid

Fig. 15.

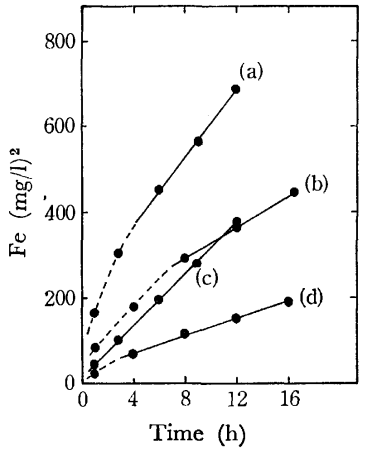

Fig. 16.

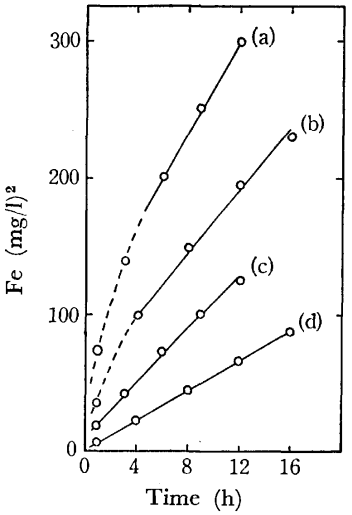

Figs. 15 and 16. Change in square of dissolved amount of iron from ilmenite at 65 and 90 °C.
—●—: H_2SO_4, —○—: HCl.
(a): 0.1 M at 90 °C, (b): 0.03 M at 90 °C
(c): 0.1 M at 65 °C, (d): 0.03 M at 65 °C.

solutions having concentrations below 0.1 M or pH 1. This supports the view that rutile is a fairly common alteration product of other titanium minerals, chiefly ilmenite, titanomagnetite, sphene, and perovskite, as well as of its polymorphs anatase.[13] It is reasonable to expect, moreover, that titanium minerals such as ilmenite and titanomagnetite in igneous rocks are changed into a titanium oxide mineral during the hydrothermal alteration at high temperature for pH 1.5 or above. The high content of titanium in hydrothermally-altered rocks from acid hot spring areas[3] seems to be due to the insolubility of the oxide minerals described above.

The authors wish to express their deep gratitude to Professor Hiroshi Kamiya of Nagoya Institute of Technology for his valuable advice and for his critical reading of the manuscript. The authors also wish to express their thanks to Professor Kimio Noguchi of Toho University for his encouragement throughout this work.

References

1) K. Rankama and Th. G. Sahama, "Geochemistry," University of Chicago Press, Chicago (1950), p. 558.
2) *E.g.*, J. Ossaka, *Chinetsu*, **17**, 65 (1968).
3) M. Imahashi, *Bull. Chem. Soc. Jpn.*, **43**, 2475 (1970).
4) K. Noguchi, M. Imahashi and N. Takamatsu, *General Edu. Review Toho Univ.*, **6**, 39 (1974).
5) R. Wollast, *Geochim. Cosmochim. Acta*, **31**, 635 (1967).
6) R. W. Luce, R. W. Bartlett, and G. A. Parks, *Geochim. Cosmochim. Acta*, **36**, 35 (1972).
7) I. Sanemasa, M. Yoshida, and T. Ozawa, *Bull. Chem. Soc. Jpn.*, **45**, 1741 (1972).
8) I. Sanemasa and T. Katsura, *Bull. Chem. Soc. Jpn.*, **46**, 3416 (1973).
9) *E.g.*, J. W. Gruner, *Econ. Geol.*, **54**, 1315 (1959).
10) H. Kamiya, A. Ozaki, and M. Imahashi, *Geochem. J.*, **8**, 21 (1974).
11) A. Packter and H. S. Dhillon, *J. Chem. Soc.*, **1969**, 2588.
12) M. Imahashi, H. Kamiya, and K. Watanuki, *Geochem. J.*, **9**, 177 (1975).
13) W. A. Deer, R. A. Howie, and J. Zussman, "Rock-forming Minerals," vol. 5, Longmans, London (1962), p. 38.

Polarographic Anodic Wave of Hydrogen Peroxide in Alkaline Solutions

Kenji KIKUCHI and Teisuke MURAYAMA*

Shiga Prefectural Junior College, Hikone, Shiga 522

**Department of Industrial Chemistry, Faculty of Engineering, Shizuoka University, Johoku, Hamamatsu 432*

(Received August 1, 1975)

The anodic reaction of hydrogen peroxide in alkaline solutions has been studied by the polarographic method. Polarograms were recorded in solutions with pH values ranging from 10.0 to 13.5. Hydrogen peroxide in alkaline solutions shows a one-step anodic wave at the dropping mercury electrode. The plot of half-wave potential against pH consists of three segments, each corresponding to a different value of $d(E_{1/2})/d(pH)$: -57 mV for the values of pH below 11.6, -29 mV for the pH range from 11.6 to 13.2, and 0 mV for the values of pH above 13.2 The limiting current is controlled by diffusion. It is concluded that the anodic wave corresponds to the formation of the species $[Hg(O_2H)(OH)]$.

Recently Honda *et al.* reported on the anodic reaction of hydrogen peroxide in alkaline solutions at the dropping mercury electrode.[1] They proposed a reaction mechanism given by:

$$H_2O_2 \rightleftharpoons H^+ + HO_2^- \quad (1)$$

$$HO_2^- \rightleftharpoons HO_2(a) + e^- \quad (2)$$

$$OH^- \rightleftharpoons OH(a) + e^- \quad (3)$$

$$HO_2(a) + OH(a) \rightleftharpoons O_2 + H_2O \quad (4)$$

where (a) denotes the adsorbed state. Based on experimental observation, they concluded that the rate-determining step is Reaction 4. The present study, however, indicates that another interpretation is more appropriate.

Experimental

All chemicals used were of reagent grade. The water used for all solutions was prepared by distillation of deionized water with potassium permanganate. The concentration of hydrogen ions in solutions was controlled with acetate buffer (pH 3.5 to 5.6), phosphate buffer (pH 6.0 to 7.7 and 11.0 to 12.0), ammonia buffer (pH 8.8 to 11.0), and sodium hydroxide solution (above pH 12.0). Five one-thousandths of 1% gelatin was added as the maximum suppressor. The ionic strength of the test solutions was adjusted to 0.1 or 0.5 M with either sodium nitrate or sodium chloride. The pH value of the test solutions was measured by use of a TOA HM-5B pH meter with a TOA HG-4005 glass electrode. The concentration of hydrogen peroxide in the stock solution was determined by iodometry.[2]

Polarograms were recorded by a Yanagimoto Model P8 polarograph. The cell used was of a beaker type. A saturated calomel electrode (SCE) was used as a reference electrode. The dropping mercury electrode (DME) had the following characteristics (in 0.5 M sodium chloride solution at zero applied potential *vs.* SCE and at a mercury head of 80.0 cm): the rate of flow of mercury (m), 2.338 mg/s; the drop time (t), 3.88 s; the capillary constant ($m^{2/3}t^{1/6}$). 2.15 $mg^{2/3}s^{-1/2}$. All potentials reported in this paper were corrected for iR drop. The test solution was freed from oxygen by bubbling nitrogen through the solution for 50 minutes and thermostated at 20.0±0.1 °C. As soon as the DME was introduced into the test solution, the recording of polarograms was started; each was completed within 10 minutes. Changes in the concentration of hydrogen peroxide during the bubbling and the recording were found to be within 1% of the initial concentration.

Results

The anodic wave of hydrogen peroxide observed in the solutions with pH values below 10 was accompanied by a maximum, making any quantitative discussion impossible. Figure 1 shows typical polarograms obtained in solutions with pH values above 10. It illustrates that hydrogen peroxide produces a single anodic wave and that the wave shifts to negative potentials with increasing pH. Logarithmic plots of the wave are given in Fig. 2, where the experimental points form good straight lines with a reciprocal slope of 29 to 30 mV. In the construction of the plots the current was corrected by the residual current determined in the 0.1 or 0.5 M sodium nitrate solution, not by the one determined in a buffer solution as is usual. The reason for this procedure is that the buffer solution produces an anodic current due to the hydroxide ion which also participates in the anodic reaction of hydrogen peroxide, as will be shown later.

Figure 3 shows variations of the half-wave potential and limiting current with pH. The former consists of three segments with different slopes: -57 mV for values of pH below 11.7, -29 mV for the pH range from 11.7 to 13.2, and 0 mV for values of pH above 13.2. The limiting current decreases with increasing pH until the value of the pH becomes 11.7, then remains unchanged.

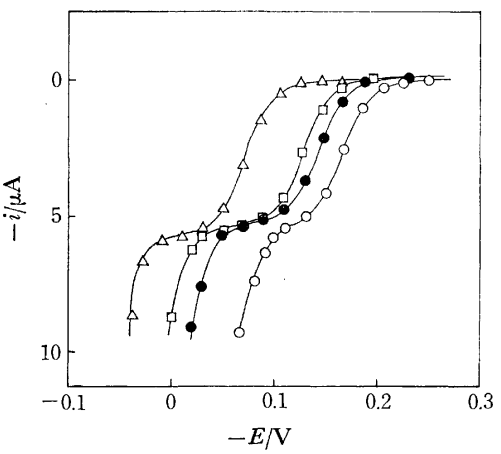

Fig. 1. Polarograms of 0.512 mM hydrogen peroxide. Ionic strengh, 0.5 M. pH: △, 10.08; □, 12.08; ●, 12.45; ○, 13.43.

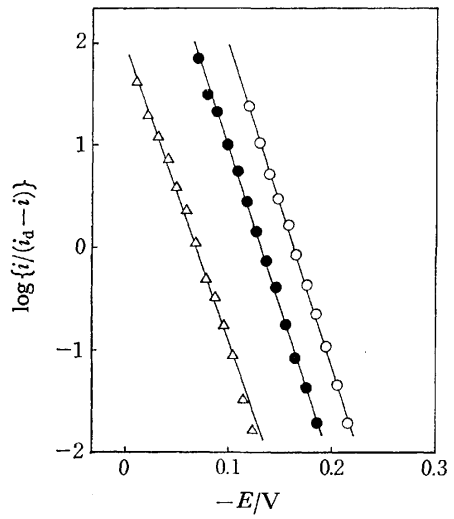

Fig. 2. Plot of $\log\{i/(i_d-i)\}$ *vs.* E.
Ionic strength, 0.5 M. Concentration of H_2O_2, 0.512 mM. pH: △, 10.82; ●, 12.26; ○, 13.43.

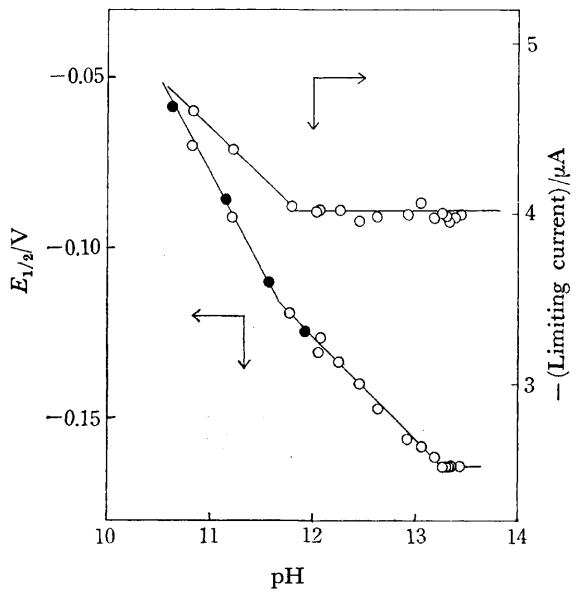

Fig. 3. Effect of pH on the half-wave potential and the limiting current.
Concentration of H_2O_2, 0.512 mM. Ionic strength: ○, 0.5 M; ●, 0.1 M.

When the pH of the solution was kept constant, the limiting current increased in proportion to the concentration of hydrogen peroxide and to the square root of the height of the mercury column. The temperature coefficient of the limiting current was 1.5×10^{-2} K^{-1}. These facts indicate that the limiting current is controlled by diffusion. The diffusion current of 0.512 mM hydrogen peroxide, i_d (μA), can be represented by

$$i_d = -5.07 + 0.57\ (\mathrm{pH}-10) \tag{5}$$

for pH values below 11.7, as shown in Fig. 3.

Discussion

Honda *et al.* considered that the oxidation reaction of HO_2^- is responsible for the anodic wave of hydrogen peroxide. It is, however, much more natural to assume that this wave corresponds to the dissolution of electrode mercury and the formation of a mercury(II) complex, as given by

$$Hg \rightleftharpoons Hg^{2+} + 2e^- \tag{6}$$

$$Hg^{2+} + HO_2^- + OH^- \rightleftharpoons [Hg(O_2H)(OH)] \tag{7}$$

The species HO_2^- is supplied by the acid dissociation reaction of H_2O_2.

$$H_2O_2 \rightleftharpoons HO_2^- + H^+ \tag{8}$$

The potential of DME may be written as

$$E = E^\circ + \frac{RT}{2F}\ln[Hg^{2+}]y \tag{9}$$

where E° is the standard potential of a mercuric-mercury electrode, R the gas constant, T the absolute temperature, F the Faraday constant, and y the activity coefficient of the mercuric ion. The concentration of mercuric ions at the electrode surface is given by

$$[Hg^{2+}] = \frac{\left(\frac{[H^+]}{K_a}+1\right)[H^+][Hg(O_2H)(OH)]}{\beta K_w([H_2O_2]+[HO_2^-])} \tag{10}$$

where K_a is the acid dissociation constant of H_2O_2, K_w the ionic product of water, and β the equilibrium constant of Reaction 7. Three equilibrium constants, K_a, K_w, and β, are defined as follows:

$$K_a = \frac{[H^+][HO_2^-]}{[H_2O_2]}$$

$$K_w = [H^+][OH^-]$$

$$\beta = \frac{[Hg(O_2H)(OH)]}{[Hg^{2+}][HO_2^-][OH^-]}$$

Introduction of Eq. 10 into Eq. 9 gives

$$E = E^\circ + \frac{RT}{2F}\ln\left\{\frac{y\left(\frac{[H^+]}{K_a}+1\right)[H^+]}{\beta K_w}\sqrt{\frac{D_1}{D_2}}\right\} + \frac{RT}{2F}\ln\frac{i}{i_d-i} \tag{11}$$

where i is the anodic current, i_d the anodic diffusion current, D_1 the common diffusion coefficient of species H_2O_2 and HO_2^-,[3] and D_2 the diffusion coefficient of the complex $[Hg(O_2H)(OH)]$. Equation 11 shows that a logarithmic plot should produce a straight line with the reciprocal slope of 29 mV if the solution is well-buffered with respect to hydrogen ions. Figure 2 shows that this is the case. The limiting current decreases with increasing pH in the range of pH values below 11.7. This indicates that the diffusion coefficient of HO_2^- is smaller than that of H_2O_2. A strong hydration caused by the charge on the HO_2^- ion may be responsible for this difference between the diffusion coefficients.

By introduction of the relation $i=i_d/2$ into Eq. 11 the half-wave potential at 20 °C becomes

$$E_{1/2} = E^\circ + \frac{0.058}{2}\log\left\{\frac{y\left(\frac{[H^+]}{K_a}+1\right)[H^+]}{\beta K_w}\sqrt{\frac{D_1}{D_2}}\right\} \tag{12}$$

When $[H^+]\gg K_a$, Eq. 12 becomes

$$E_{1/2} = E^\circ + \frac{0.058}{2}\log\frac{y}{\beta K_a K_w}\sqrt{\frac{D_1}{D_2}} - 0.58\,\mathrm{pH} \quad (13)$$

where the activity coefficient of the hydrogen ion is assumed to be unity. Because of Eq. 5 and the proportionality of $D_1^{1/2}$ to i_d, Eq. 13 may be rewritten as

$$E_{1/2} = E^\circ + \frac{0.058}{2}\log\frac{\alpha y}{\beta K_a K_w D_2^{1/2}} - 0.059\mathrm{pH} \quad (14)$$

In this equation α is a proportionality constant. When $[H^+] \ll K_a$, Eq. 12 becomes

$$E_{1/2} = E^\circ + \frac{0.058}{2}\log\frac{y}{\beta K_w}\sqrt{\frac{D_1}{D_2}} - \frac{0.058}{2}\mathrm{pH} \quad (15)$$

When pH is chosen as the independent variable, Eqs. 14 and 15 represent two straight lines. These straight lines intersect at the point whose pH value is equal to pK_a.

Equations 14 and 15 agree well with the experimental results shown in Fig. 3, except for a few points obtained in the solutions with pH values above 13.2. The abscissa of the intersection is 11.65, consistent with the value 11.65 reported for pK_a of hydrogen peroxide by Evans and Uri.[4]

Figure 3 shows that the half-wave potential deviates from the linear relation given by Eq. 13 above pH 13.2, although the points measured in this range are very few. Experimental difficulty prevented any measurements in solutions with higher pH values. Hence it is impossible to speculate on the electrode process above pH 13.2, at least at present.

References

1) M. Honda, T. Kodera, and H. Kita, *J. Res. Inst. Catal. Hokkaido Univ.*, **18**, 77 (1970).

2) F. P. Treadwell, "Analytical Chemistry," Vol. 2, John Wiley and Sons, New York (1955), p. 609.

3) J. Heyrovsky and J. Kuta, "Principles of Polarography," Academic Press, New York (1966), p. 350.

4) M. Evans and N. Uri, *Trans. Faraday Soc.*, **45**, 230 (1949).

Kinetics of the Proton-Transfer Reactions of Some *ortho*-Hydroxy Derivatives of Azo and Azomethine Compounds in Dioxane-Water Medium*

Noboru YOSHIDA and Masatoshi FUJIMOTO

Department of Chemistry, Faculty of Science, Hokkaido University, Sapporo 060

(Received December 11, 1975)

The kinetics of the proton-transfer reactions between hydroxide ion and *o*-hydroxy azo and *o*-hydroxy azomethine compounds having a strong O–H···N or an O–H···π intramolecular hydrogen-bond are studied in 50% (v/v) dioxane–water by means of temperature-jump method. The forward and the backward rate constant k_f and k_r for the overall reactions $OH^- + HA \underset{k_r}{\overset{k_f}{\rightleftharpoons}} H_2O + A^-$ are evaluated to be in the range between 4.4×10^4 and 6.1×10^8 $M^{-1}s^{-1}$ and between 1.5×10^3 and 6.2×10^4 s^{-1} respectively. The values of the k_f for the azomethines are by several orders of magnitude higher than those of the corresponding azo compounds. The values of k_f and k_r in dioxane–water are found to be smaller than those in aqueous medium.

Eigen and coworkers have extensively investigated the kinetics of the proton-transfer reactions in aqueous media using chemical relaxation methods.[1-3] The protolytic reactions between so-called "normal" Brønsted acids and bases which can readily form hydrogen-bonded structure with solvent water molecules proceed almost diffusion-controlled. Thus the characteristic recombination rate constants k_f between hydrogen ion and normal bases are reported to be in the order of 10^{11} $M^{-1}s^{-1}$ and those between hydroxide ion and normal acids almost 10^{10} $M^{-1}s^{-1}$. The differences are attributed to the higher mobility of the hydrogen ion in aqueous solution.

Considerable decrease in the recombination rate constants k_f is observed, however, because of the following factors on the side of Brønsted acids and/or bases;[1-3] (1) the charge type, the size, and the shape of the reactants, (2) the liquid structure of the solvent water around the reacting species, (3) existence of the intramolecular hydrogen-bond at the periphery of the reaction site, and (4) intramolecular electronic rearrangement and/or the conformational orientation that activate the donor groups as CH acids and pseudo acids.[4]

The proton-transfer reactions in aqueous solutions between some *o*-hydroxy azo compounds and hydroxide ion have been reported in detail.[1-3),5),6] It was noted that the slowness of the recombination reaction would reflect the strength of the intramolecular hydrogen-bond. Eyring *et al.* reported the kinetics on the proton transfer between hydroxide ion and a number of Brønsted acids.[6-9] They suggested on the basis of the kinetic data the following order of the relative strength for intramolecular hydrogen-bonds:

O–H···N>O–H···O>N–H···N>N–H···O,

which is similar to that proposed by Freedman.[10]

Eigen pointed out that hydroxide ion can hardly approach the proton in the hydrogen-bridged structure of the Brønsted acid molecule and suggested a detailed mechanism involving pre-equilibrium between two states of the proton in Brønsted acids.[3]

Only a few attempts, however, have so far been made for the kinetic studies on the proton-transfer reactions in mixed solvents[11] as compared with equilibrium studies.[12] With respect to the reaction mechanism, the extensive kinetic studies are needed. Nevertheless, there prevail many complicated situations.

The dioxane–water medium has often been used for the determination of the acid dissociation constants and/or the complex formation constants of water-insoluble Brønsted acids. 1,4-Dioxane, a typical water-miscible dipolar aprotic solvent, can cover the wide range of the dielectric constant of the medium by mixing with water. These characteristics are convenient also in the fast proton-transfer reactions to evaluate the solvent effects such as electrostatic effects *etc.* In the present study we report the proton-transfer reactions between hydroxide ion and five *o*-hydroxy azo and four *o*-hydroxy azomethine compounds in 50% (v/v) dioxane–water system.

In general *o*-hydroxy azomethines are known to be weaker as acids than the corresponding azo derivatives.[13] Since *o*-hydroxy azomethines are only sparingly soluble and gradually hydrolyzed in water, it was difficult to measure the reaction rate in aqueous solutions.[14] Furthermore *o*-hydroxy azomethines are often unstable even in the mixed solvent containing water, so that we used a stopped-flow-temperature-jump technique.

It should be noted that the rate constants k_f and k_r obtained for the proton transfer in the mixed solvent are always lower than those in aqueous system. This tendency could not generally be observed in the reactions between "normal" acids and bases.[1]

Experimental

Materials. Reagents: All chemicals used were of analytical grade, unless otherwise specified. Water was deionized and distilled. Dioxane was distilled and the water content was determined to be 2.97 mg/ml by Karl Fischer titration. 10^{-3} M stock solutions of azomethines were prepared by dissolving in dioxane. The solutions were kept only for three weeks at room temperature.

o-Hydroxy Azo and o-Hydroxy Azomethine Compounds: The compounds used here are: Tropaeolin-O (I; TPO), 4-(2-pyridylazo)resorcinol (II; PAR), 1-(2-pyridylazo)-2-naphthol (III; PAN), *N*-salicylidene-2-aminopyridine (IV; SAP), *N*-(2-pyridylmethylene)-*o*-aminophenol (V; PMA), *N*-(2-hydroxy-1-naphthylidene)-2-aminopyridine (VI; NAP), *N*-salicylidene-2-aminothiazole (VII; SAT), 4-(2-thiazolylazo)-resorcinol (VIII; TAR), and 1-(2-thiazolylazo)-2-naphthol

* Presented in part at 25th Annual Meeting on Coordination Chemistry, Tokyo, October 8, 1975, Abstract, p. 123.

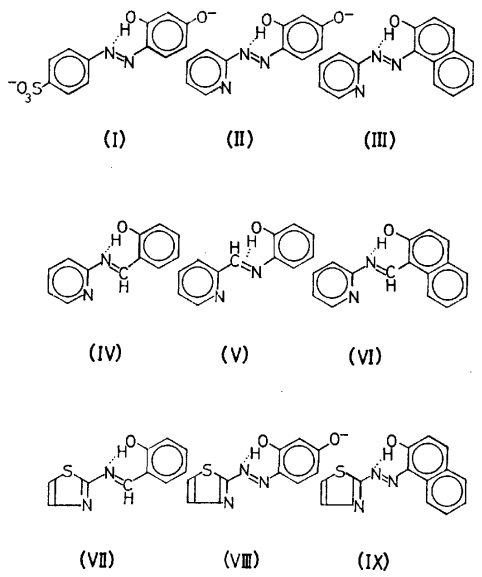

Fig. 1.

(IX; TAN). (See Fig. 1.)

The azo compounds (Dojindo) were purified by repeated recrystallization from 99.5% ethanol or ethanol-water. The azomethine compounds were prepared by condensation of aldehydes with amines, and recrystallized from 99.5% ethanol. As for the compound V, it was necessary to purify sufficiently the starting materials to prepare the pure crystalline compound.[15] Found: C, 72.8; H, 5.0; N, 13.9%. Calcd. for PMA, $C_{12}H_{10}N_2O$: C, 72.7; H, 5.1; N, 14.1%.

Measurements. *pH in the Mixed Solvents*: The analytical concentration C_H of the solvated proton in 50%(v/v) dioxane-water was determined titrimetrically. The pH* of the solution was measured with Hitachi-Horiba pH-meters, Model-P and Model M-7. For the potentiometric titrations of perchloric acid in the mixed solvent the ionic strength was adjusted with pure sodium perchlorate.[16] All measurements were carried out in nitrogen atmosphere.

Assuming the complete dissociation for the perchloric acid in the mixed solvent,[17] we used the following relation derived by Van Uitert and Haas[18] between the pH-meter readings (pH*) and $-\log C_H$ ($=pC_H$):

$$\log U_H = pC_H - pH^*,$$

where the function $\log U_H$ contains the term of activity coefficients γ_H's of the solvated proton and the liquid junction potential ΔE_j:[17]

$$-\log U_H = -\log \gamma_H^s \cdot \gamma_H^m + \Delta E_j.$$

The medium effect term γ_H^m depends on the solvent composition and the interionic attraction term γ_H^s varies with the ionic strength. The plot of pH* *vs.* pC_H gave an excellent linear relationship both in the acid and the alkaline region. The values of $\log U_H$ are thus evaluated in the range of pH*=3—12 at 25.0±0.1 °C to be −0.14±0.02 (μ=0.1) and +0.05±0.02 (μ=0.01).

Spectrophotometric Measurements of the Acid-Base Equilibria in the Mixed Solvent: The acid dissociation constants were determined spectrophotometrically with a Hitachi recording spectrophotometer Model EPS-3T. As for the Schiff bases, we used a Union Giken rapid-mixing apparatus Model MX-7 to avoid undesired hydrolysis. In the spectrophotometric measurements, potassium nitrate was used for the adjustment of the ionic strength to avoid the undesired behavior of the $NaClO_4$ as often observed on the wall of the optical cell in the case of the mixed solvents.

Kinetics of the Proton-Transfer Reactions: All measurements were carried out with a Union Giken co-axial-cable temperature-jump apparatus Model RA-105 equipped with a rapid-mixing device Model MX-7. The dead time of the mixer was about 5 ms. A temperature-rise of about 7 °C was attained within 2 μs (μ=0.1) by discharging a 0.0204 F capacitor, a co-axial cable of 200 m long, charged to 30 kV. The reaction was followed on the storage screen of an oscilloscope at the absorption maximum of the conjugated base of the Brønsted acid. All measurements were made at 25±0.1 °C.

Results

Equilibria of the Reaction. The potentiometric titrations were carried out at 25 °C and μ=0.1 and 0.01. The apparent ionic product K_w^c of water in dioxane–water medium was measured using the value of $\log U_H$ as mentioned above. A mixture of 2 V ml of the perchloric acid containing equal volume of water and dioxane was titrated with v ml of 0.1 M aqueous NaOH and v ml of dioxane in order to maintain the solvent composition at 50%(v/v). According to the fundamental theory of the acid-base equilibrium $C_H - C_{OH} = (VC_H^\circ - VC_{OH}^\circ)/2(v+V)$. Before the end point, $C_H \simeq VC_H^\circ(v_e - v)/2v_e(v+V)$ and after the end point, $C_{OH} \simeq VC_H^\circ(v - v_e)/2v_e(v+V)$, where C_H° and C_{OH}° denote the analytical concentrations of $HClO_4$ and NaOH added, respectively. The values of K_w^c are calculated to be $K_w^c = C_H \cdot C_{OH} = 4.23 \times 10^{-16}$ M^2 at μ=0.1 and 2.09×10^{-16} M^2 at μ=0.01.[19]

Since compounds IV, V, and VI are readily hydrolyzed in the mixed solvent in a few minutes, the absorption spectra were rapidly scanned immediately after mixing the solutions thermostated beforehand at 25±0.1 °C. The absorption spectra of PMA are shown in Fig. 2. The slow hydrolysis reaction did *not* affect the spectrophotometric measurement of pK_a^c as revealed by a definite isosbestic point. The stoichiometric

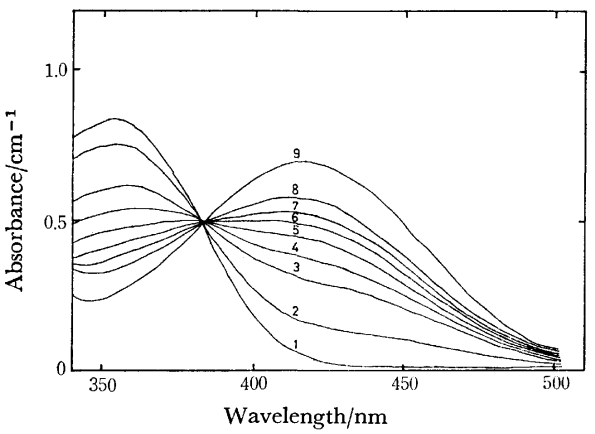

Fig. 2. Absorption spectra of *N*-(2-pyridylmethylene)-*o*-aminophenol (PMA; V) at various pH* values in 50%-(v/v) dioxane–water.
C_{HA}° (after mixing) = 1.279×10^{-4} M.
pH*: (1) about 6, (2) 8.82, (3) 10.71, (4) 11.21, (5) 11.45, (6) 11.88, (7) 12.09, (8) 12.30, (9) 0.1 M NaOH, at 25±0.1 °C, and μ=0.01 (KNO_3).

relation of the reactants is shown in the Scheme 1:

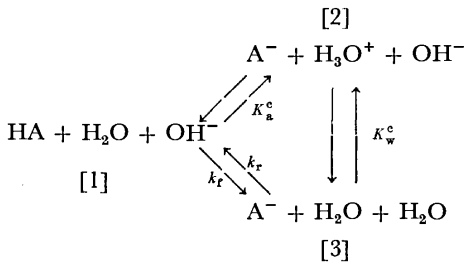

Scheme 1.

$$K_a^c = [H][A]/[HA] \quad (1)$$

$$K_b^c = k_f/k_r = [A]/[HA][OH] \quad (2)$$

$$K_w^c = [H][OH], \quad (3)$$

where [ ] represent the concentration, and charges are omitted. From Eqs. 1, 2, and 3 the following relationship is obtained:

$$K_a^c = (k_f/k_r)[H][OH] = K_b^c \cdot K_w^c. \quad (4)$$

The acid dissociation constants K_a^c's obtained spectrophotometrically are summarized in Table 1. As for PAR, the value of pK_a^c has so far been reported by several authors.[15,20]

In the present study it was found that the values of pK_a^c of the Brønsted acids increase with increasing dioxane content in the medium. The linear relationship between pK_a^c of weak acids such as acetic acid and the mole fraction of dioxane has been pointed out by Van Uitert and Haas[18] and Harned and Owen.[22] However the systematic kinetic study is needed in order to obtain the more useful information on the proton-transfer reactions in mixed solvents.

The equilibrium constant K_b^c and the rate constants for the reaction [1]⇄[3] were evaluated from the data of the temperature-jump study:

$$\tau^{-1} = k_f(\bar{C}_{OH} + \bar{C}_{HA}) + k_r. \quad (5)$$

Kinetics. Figure 3 shows a typical relaxation signal for SAT. The linear dependences of the reciprocal relaxation time on the sum of the equilibrium concentrations of the hydroxide ion and the Brønsted acid are given in Fig. 4. Serious deviation from the linear dependence of the observed τ^{-1} for the compound V at higher concentrations would be ascribed to the rising time of the temperature at $\mu=0.01$ comparable to the relaxation time of the reaction. The measure-

Table 1. Acid dissociation constants K_a^c determined from the spectrophotometric data at 25 °C

Brønsted acid	$pK_a^c(=-\log K_a^c)$[a]	
	in water	in 50%(v/v) dioxane-water
TPO	12.20	14.25
PAR	12.66; 12.31[b]	13.95; 13.60[b]
PAN	—	12.30[c]
SAP	—	10.48
PMA	—	11.10
SAT	—	9.10

a) $K_a^c=[A][H]/[HA]$, $\mu=0.1$ (KNO_3) for the azo derivatives and $\mu=0.01$ (KNO_3) for the azomethines. b) At 25 °C and $\mu=0.1$ ($NaClO_4$). See Ref. 15. c) At 25 °C and $\mu=0.1$($NaClO_4$). See Ref. 21.

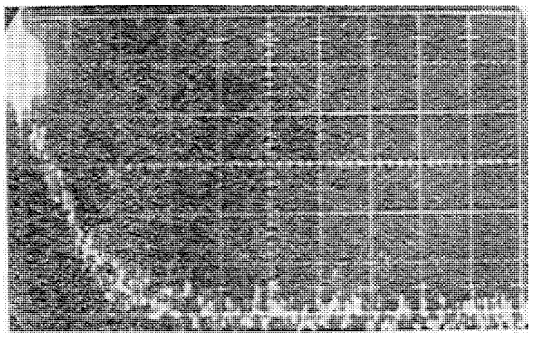

Fig. 3. A stopped-flow-temperature-jump signal for the proton-transfer reaction between *N*-salicylidene-2-amino-thiazole and OH^- ion in 50%(v/v) dioxane-water. $\bar{C}_{OH}$ (after mixing)$=7.78\times10^{-6}$ M (pH*= 10.52), $\bar{C}_{SAT}=1.05\times10^{-5}$ M, at 25±1 °C and $\mu=$ 0.01 (KNO_3). Abscissa: 50 μs/div., ordinate: 0.1 V/div.

Table 2. Rate constants for $HA + OH^- \underset{k_r}{\overset{k_f}{\rightleftharpoons}} A^- + H_2O$ in aqueous solution at 25 °C

Brønsted acid	$k_f/M^{-1}s^{-1}$	k_r/s^{-1}	K_b^c $(=k_f/k_r)/M^{-1}$	pK_a^c $(=-\log K_a^c)$[a]
TPO	6.9×10^5	1.6×10^4	4.5×10	12.4
PAR	6.4×10^5	6.2×10^3	1.0×10^2	12.0[b]

a) $K_a^c=K_b^c\cdot K_w^c$ at $\mu=0.1$(KNO_3). b) At 25 °C and $\mu=0.1$ ($NaClO_4$). See Ref. 23.

Table 3. Rate constants for $HA+OH^- \underset{k_r}{\overset{k_f}{\rightleftharpoons}} A^-+H_2O$ in 50%(v/v) dioxane-water solution at 25 °C

Brønsted acid	$k_f/M^{-1}s^{-1}$	k_r/s^{-1}	K_b^c $(=k_f/k_r)/M^{-1}$	pK_a^c $(=-\log K_a^c)$[a]
TPO	3.2×10^5	5.8×10^3	5.5×10	14.2
PAR	4.4×10^4	1.4×10^3	2.9×10	14.5
PAN	9.7×10^5	2.4×10^3	4.0×10^2	13.3
PMA	2.8×10^8	6.2×10^4	4.5×10^3	12.0
SAP	4.4×10^7	1.3×10^4	3.2×10^3	12.2
SAT	6.1×10^8	3.6×10^3	1.7×10^5	10.5

a) $K_a^c = K_b^c\cdot K_w^c$, $\mu=0.1$(KNO_3) for the azo compounds and $\mu=0.01$ (KNO_3) for the azomethines.

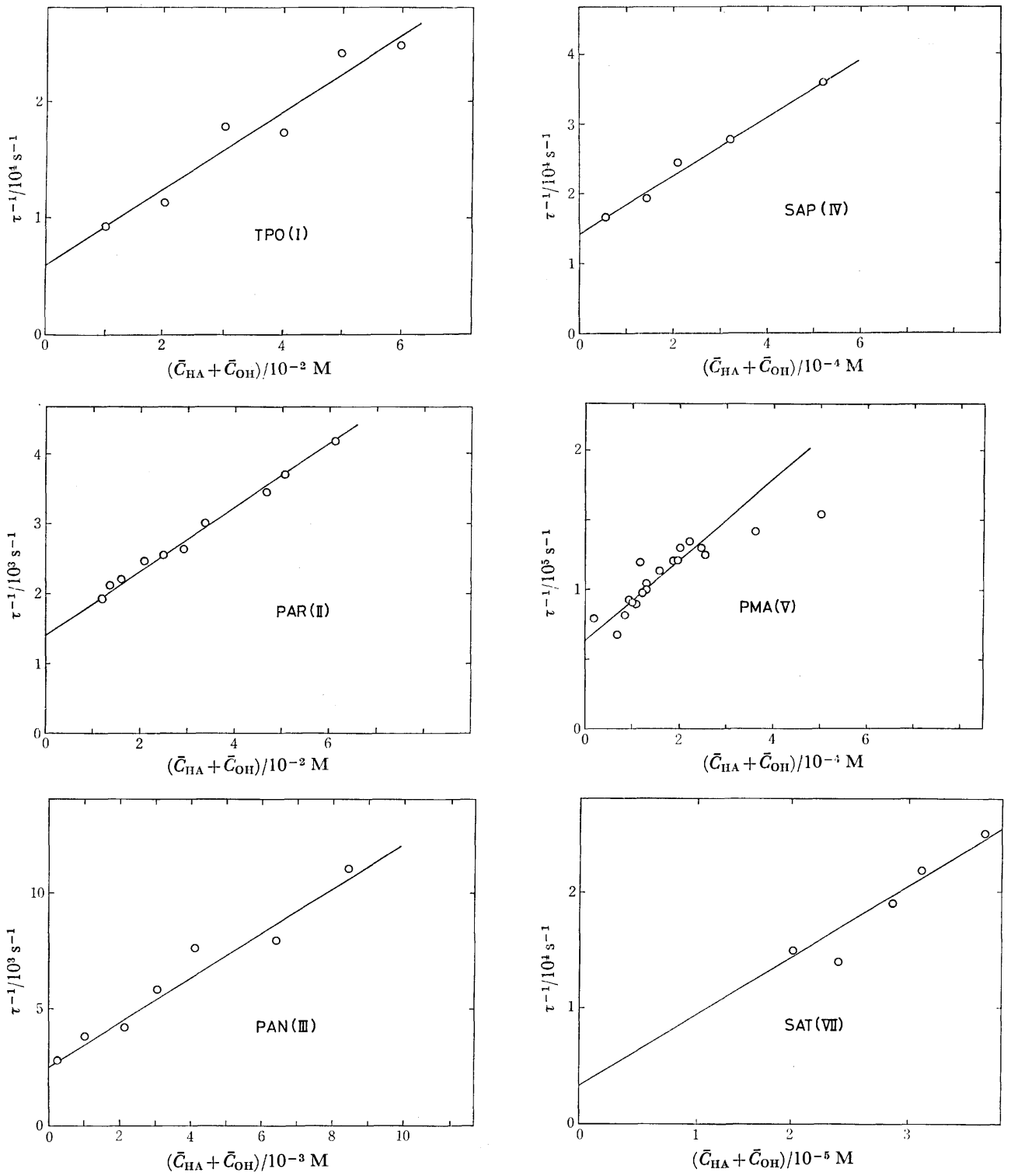

Fig. 4. Dependence of τ^{-1} on $(\bar{C}_{HA}+\bar{C}_{OH})$ for the proton-transfer reaction in 50%(v/v) dioxane-water. At 25 °C. μ=0.01 (KNO_3) for azomethines (IV, V, VII) and μ=0.1 (KNO_3) for azo derivatives (I—III).

ments of the rate of the proton-transfer reactions for TAN, TAR, and NAP were tried, but the observed signal-amplitude was too small.

The rate constants given in Tables 2 and 3 were calculated from the slope and the intercept of the straight lines in Fig. 4. The equilibrium constants K_a^c evaluated as $K_a^c=K_b^c\cdot K_w^c$ from the kinetic data are compared with those from the equilibrium data given in Table 1. The values are in good agreement with each other for the aqueous media, whereas in 50%(v/v) dioxane–water, the values of K_a^c derived from the *kinetic* data are always 1—2 orders of magnitude smaller than the corresponding spectrophotometric *equilibrium* constants K_a^c. As for the water-soluble Brønsted acid such as TPO these differences are quite small. The reason will be discussed in detail elsewhere.

Discussion

The overall reaction of the proton transfer is shown in Scheme 1. Equation 7 indicates that the observed increase in pK_a^c derived from the kinetic data is due to both the kinetic term $k_f/k_r=K_a^c$ and to the calculated ionic product K_w^c of water in the bulk mixed solvent. On the basis of the suggestion by Eigen *et al.*[3] concerning the proton-transfer reactions in aqueous solution, we propose the following reaction mechanism also in the mixed solvent for the recombination with OH^- ion of the Brønsted acid having an intramolecular hydrogen-bond.[24]

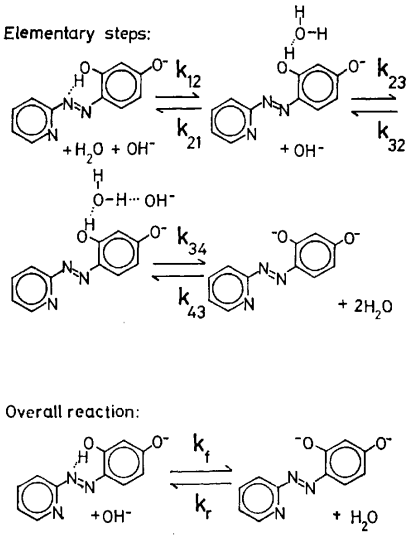

In the step of the intramolecular rearrangement HA$\rightleftarrows$HA* the hydrogen-bonded proton sets free from the azo-nitrogen atom and interacts with a solvent *water* molecule. The second step $HA^*+OH^-\rightleftarrows HA^*\cdots OH^-$ involves the formation and the dissociation of an encounter complex between OH^- ion and an activated Brønsted acid HA* caused by thermal motion. The third step $HA^*\cdots OH^-\rightleftarrows A^-+H_2O$ is the net chemical transformation involving the proton-transfer through the intervening *water* molecule and the charge-neutralization or the charge-separation.

A rate equation for such a reaction is derived as follows. In general, the stationary-state approximation is applied for HA* and the encounter complex:

$$dC_{HA^*}/dt = 0 \tag{6}$$

$$C_{HA^*} = (k_{12}C_{HA} + k_{32}C_{enc})/(k_{21} + k_{23}C_{OH}), \tag{7}$$

and

$$dC_{enc}/dt = 0 \tag{8}$$

$$C_{enc} = (k_{12}C_{HA^*}C_{OH} + k_{43}C_A)/(k_{32} + k_{34}). \tag{9}$$

The rate equation is expressed as:

$$-dC_{HA}/dt = k_{12}C_{HA} - k_{21}C_{HA^*}. \tag{10}$$

For the small perturbation ΔC_{HA} near the equilibrium, it can be approximated as:

$$-dC_{HA}/dt = -d\Delta C_{HA}/dt \tag{11}$$

$$= \Delta C_{HA}\cdot\frac{k_{12}k_{23}k_{34}(\bar{C}_{OH} + \bar{C}_{HA}) + k_{21}k_{32}k_{43}}{k_{32}k_{21} + k_{34}k_{21} + k_{34}k_{23}\bar{C}_{OH}} \tag{12}$$

with the reciprocal relaxation time:

$$\tau^{-1} = \frac{k_{12}k_{34}k_{23}(\bar{C}_{OH} + \bar{C}_{HA}) + k_{21}k_{32}k_{43}}{k_{32}k_{21}+k_{34}(k_{21}+k_{23}\bar{C}_{OH})} \tag{13}$$

Assuming the second step is the rate-determining for the bimolecular reaction:

$$k_{21} \gg k_{23},\ k_{34} \gg k_{32}, \tag{14}$$

and considering the larger value for $k_{21}>10^{10}\ s^{-1}$ ($k_{23}=10^{10}\ M^{-1}\ s^{-1}$ and $\bar{C}_{OH}=10^{-4}-10^{-2}\ M$):

$$k_{23}\bar{C}_{OH} \ll k_{21}, \tag{15}$$

the reciprocal relaxation time is reduced to

$$\tau^{-1} = K_{12}k_{23}(\bar{C}_{OH} + \bar{C}_{HA}) + k_{32}/K_{34}, \tag{16}$$

where K_{12} and K_{34} represent k_{12}/k_{21} and k_{34}/k_{43} respectively. Equations 5 and 16 lead to the most important relation:

$$k_f = K_{12}k_{23} \tag{17}$$

and

$$k_r = k_{32}/K_{34}. \tag{18}$$

The values of k_f and k_r for the proton transfer in the dioxane–water media are found to be smaller than those in aqueous media. This effect is especially remarkable in the case of PAR. If as a first approximation the k_{23} in the mixed solvent also be equal to that of $k_{23}=10^9-10^{10}\ M^{-1}\ s^{-1}$ in aqueous system, this decrease in the overall rate constant k_f in the mixed solvent may primarily be attributed to the decrease in the value of the equilibrium constant K_{12}. Similarly the decrease in the k_r value is attributed to the increase in the value of equilibrium constant K_{34} assuming the change in the value of k_{32} is also small. With respect to these assumptions direct evidence is needed, which will be reported in the near future.

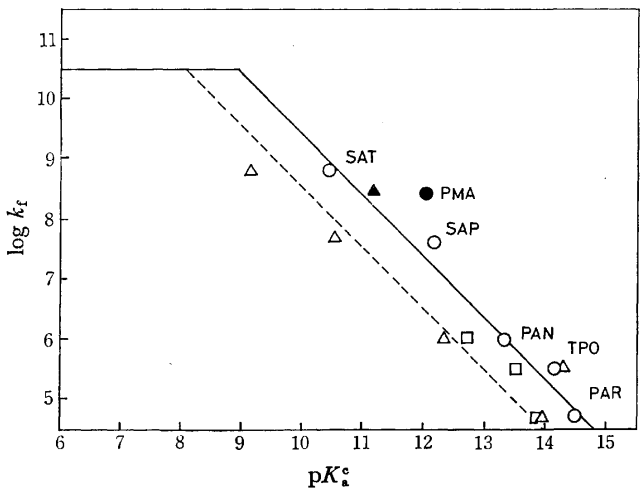

Fig. 5. Dependence of the recombination rate constants log k_f on the acid dissociation constants pK_a^c in 50%-(v/v) dioxane–water.
A full line shows the curve based on the value of $pK_w^c=15.68$ ($\mu=0.01$) and $pK_w^c=15.37$ ($\mu=0.1$). A broken line is the curve reproduced on the basis of the value measured for the azo compounds in aqueous solution. △ is the plot of log k_f *vs.* spectrophotometric pK_a^c. ○ is the plot of log k_f *vs.* kinetic pK_a^c using $pK_w^c=15.68$ ($\mu=0.01$). □ is the plot of log k_f *vs.* kinetic pK_a^c using $pK_w^c=15.37$ ($\mu=0.1$).

Figure 5 gives the Brønsted-plots with the slope $-\mathrm{d}\log k_f/\mathrm{d}\,pK_a^c=1$. If the reaction approaches the diffusion-controlled limit, the rate constants k_f do not reflect the thermodynamical stability of the hydrogen-bond. For the higher pK_a^c than 9.0, the recombination rate constants k_f show the linear dependence on the basicity of the Brønsted acid. This implies that the linear-free-energy relationship holds in this system. The intramolecular hydrogen-bonds in the azomethines are weaker than those in the corresponding azo compounds even for the same type of the intramolecular hydrogen-bonds O–H···N. Therefore the value of k_f for the azomethines is by 2—3 orders of magnitude larger than that for the azo compounds. The plot for PMA having an O–H···π-type intramolecular hydrogen-bond deviates from the straight line in Fig. 5.

Since the solvation on the given Brønsted acids with dioxane is involved, in particular, on the encounter-complex species in the transition state of the proton-transfer reaction, at present we allow for a possibility for a branched path involving a more or less preferential solvation of the reaction site with dioxane molecule to inhibit the formation of the hydrogen-bridged encounter complex available as a precursor of the proton-jump step. Further studies using the mixed solvent of various dioxane contents would give valuable informations on the liquid structure of the mixed solvent which may affect the protolytic behavior of the Brønsted acids.

Finally, it would be noteworthy from the biochemical standpoints[25] that the hitherto unknown data on the rate constants k_f and k_r for the proton-transfer reactions of the Schiff base were obtained in the present work.

The present work was supported by a grant-in-aid for Scientific Research from the Ministry of Education.

Note Added in Proof:

Recently Liphard and Jost reported the mechanism of the proton-transfer reaction of Brønsted acid Alizarin Yellow GG, which has an intramolecular hydrogen bond -COO$^-$···HO-, with hydroxide ion OH^- in aqueous solution. From the activation volumes of the overall reaction determined by the temperature-jump study under pressure they directly proved the existence of the first step $HA \rightleftharpoons HA^*$ and pointed out the significant role of *this* step in the proton-transfer reaction $HA + OH^- \rightleftharpoons A^- + H_2O$. [K. Q. Liphard and A. Jost, *Ber. Bunsenges. Physik. Chem.*, **80** (2), 125 (1976)].

References

1) M. Eigen, *Angew. Chem.*, **75**, 489 (1963).
2) M. Eigen and L. DeMaeyer, "Technique of Organic Chemistry," Vol. 8, Part 2, ed. L. Fries and A. Weissberger, Interscience, New York, N. Y. (1963), Chapter 18.
3) M. Eigen and W. Kruse, *Z. Naturforsch.*, **18b**, 857 (1963); M. Eigen, W. Kruse, G. Maass, and L. DeMaeyer, *Progr. Reaction Kinetics*, **2**, 287 (1964).
4) M. L. Ahrens, M. Eigen, W. Kruse, and G. Maass, *Ber. Bunsenges. Physik. Chem.*, **74**, 380 (1970); M. Eigen, G. Ilgenfritz, and W. Kruse, *Chem. Ber.*, **98**, 1623 (1965).
5) M. C. Rose and J. Stuehr, *J. Am. Chem. Soc.*, **90**, 7205 (1968); **93**, 4350 (1971).
6) J. C. Haslam and E. M. Eyring, *J. Phys. Chem.*, **71**, 4470 (1967); W. H. Inskeep, D. L. Jones, W. T. Silfvast, and E. M. Eyring, *Proc. Natl. Acad. Sci. U. S. A.*, **59**, 1027 (1967).
7) M. H. Miles, E. M. Eyring, W. W. Epstein, and R. E. Ostlund, *J. Phys. Chem.*, **69**, 467 (1965); M. H. Miles, E. M. Eyring, W. W. Epstein, and M. T. Anderson, *ibid.*, **70**, 3490 (1966).
8) J. L. Haslam, E. M. Eyring, W. W. Epstein, R. P. Jensen, and C. W. Jaget, *J. Am. Chem. Soc.*, **87**, 4247 (1965).
9) J. L. Haslam, E. M. Eyring, W. W. Epstein, G. A. Christiansen, and M. H. Miles, *J. Am. Chem. Soc.*, **87**, 1 (1965).
10) H. H. Freedman, *J. Am. Chem. Soc.*, **83**, 2900 (1961).
11) E. F. Caldin and J. F. Crooks, *J. Sci. Instr.*, **44**, 449 (1967); *J. Chem. Soc. B*, **1967**, 959; M. W. Massey, Jr. and Z. A. Schelly, *J. Phys. Chem.*, **78**, 2450 (1974).
12) H. P. Marshall and E. Grunwald, *J. Am. Chem. Soc.*, **76**, 2000 (1954); D. J. Glover, *ibid.*, **87**, 5257, 5279 (1965); H. Ohtaki, *Inorg. Chem.*, **7**, 1205 (1968).
13) L. G. Sillén and A. E. Martell ed., "Stability Constants," Special Publication No. 17, The Chemical Society, London (1964).
14) E. H. Cordes and W. P. Jencks, *J. Am. Chem. Soc.*, **84**, 832 (1962); R. L. Reeves, *ibid.*, **84**, 3332 (1962); B. E. Leach and D. L. Leussing, *ibid.*, **93**, 3377 (1971); R. Herscovitch, J. J. Charette, and E. de Hoffman, *ibid.*, **95**, 5135 (1973).
15) W. J. Geary, G. Nickless, and F. H. Pollard, *Anal. Chim. Acta*, **27**, 71 (1962).
16) M. Yamada and M. Fujimoto, *Bull. Chem. Soc. Jpn.*, unpublished data. "The Solution Chemistry for Complexes of Nickel(II) and Cobalt(II) with 3,3′-Bis[*N*,*N*-bis(carboxymethyl)aminomethyl]-*o*-cresolsulfonphthalein."
17) R. G. Bates, "Determination of pH," 2nd ed., Wiley, New York, N. Y. (1973), p. 176.
18) L. G. Van Uitert and C. G. Haas, *J. Am. Chem. Soc.*, **75**, 451 (1953).
19) Freiser recommended the value 15.38 at 25 °C and $\mu=0.1$ for pK_w^c. S. Takamoto, Q. Fernando, and H. Freiser, *Anal. Chem.*, **37**, 1249 (1965).
20) M. Hniličková and L. Sommer, *Collection Czecho. Chem. Commun.*, **26**, 2189 (1961); T. Iwamoto, *Bull. Chem. Soc. Jpn.*, **34**, 605 (1961).
21) A. Corsini, I. M. L. Yih, Q. Fernando, and H. Freiser, *Anal. Chem.*, **34**, 1090 (1962).
22) H. S. Harned and B. B. Owen, "The Physical Chemistry of Electrolytic Solutions," 3rd ed., Reinhold Publishing Corp., New York, N. Y. (1958).
23) T. Onodera and M. Fujimoto, *Bull. Chem. Soc. Jpn.*, **44**, 2003 (1971).
24) Even if dioxane is involved in the solvation of an acid proton, the proton-jump from the acid to OH^- ion would proceed only through the formation of an encounter-complex involving the hydrogen-bridge of water. Therefore concerning the recombination step between the Brønsted acid and OH^- ion, it is evident that the reaction *does* proceed in accordance with this mechanism.
25) W. A. Newton and E. E. Shell, *Proc. Natl. Acad. Sci. U. S.*, **51**, 382 (1964); Y. Morino and E. E. Snell, *J. Biol. Chem.*, **240**, 1211 (1965); D. E. Metzler, *J. Am. Chem. Soc.*, **79**, 485 (1957).

Color and Structural Changes of Bis(hexamethylenetetramine)cobalt(II) and nickel(II) Complexes in the Course of Thermal Dehydration in Solid State

Kenzo NAGASE, Hiroko YOKOBAYASHI, and Kozo SONE*

Colloge of General Education, Tohoku University, Kawauchi, Sendai 980

**Department of Chemistry, Faculty of Science, Ochanomizu University, Otsuka, Bunkyo-ku, Tokyo 112*

(Received December 18, 1975)

The stoichiometry of thermal dehydration of $MX_2(hmta)_2 \cdot nH_2O$ (hmta=hexamethylenetetramine; X= Cl^-, Br^-, I^-, NO_3^-, NCS^-; n=4—10) was established by the TG-DTA methods. The nature of the structural changes caused by complete or partial dehydration was studied on the basis of the accompanying changes in the electronic and vibrational spectra. Anions and hmta in general get into the coordination sphere with a decrease in the number of the coordinated water, but the bulky and weakly basic amine often gets coordinated in the last stage.

It has been known for a long time that hexamethylenetetramine (hmta=1,3,5,7-tetraazatricyclo[3.3.1.1.^{3,7}]decane) forms a number of peculiar complexes with various metals, among which those of cobalt(II) and nickel(II) are of special interest because their colors change strikingly in the course of dehydration. For example, the color of $Co(hmta)_2Cl_2 \cdot 10H_2O$ turns from pink to blue, while the corresponding nickel(II) complex changes first from bluish green to yellow, and then from yellow to violet, when they are heated up to about 423 K.[1] More recently these phenomena were studied by Lodzinskaya *et al.*,[2] who showed that the octahedral cobalt(II) complexes obtained from aqueous solutions are transformed into tetrahedral complexes by heating or treatment with ethanol. Kovacs *et al.*[3] found by X-ray analysis that the crystals of $Mg(hmta)_2Cl_2 \cdot 10H_2O$ and $Ca(hmta)_2Br_2 \cdot 10H_2O$ belong to the triclinic system and these complexes are formulated as $[M(H_2O)_6]X_2 \cdot 2hmta \cdot 4H_2O$. Buhannic and Guerchais[4] successfully assigned the IR bands of the complexes $MX_2(hmta)$ and $MX_2(hmta)_2$ (M=Co(II), Zn(II); x=halide or pseudohalide ions) to various vibrational modes of hmta, indicating that the T_d symmetry of free hmta is lowered to C_{3v} in $MX_2(hmta)_2$ and C_{2v} in MX_2 (hmta). Allan *et al.*[5] obtained the complexes of Mn(II), Fe(II), Co(II), Ni(II), Cu(II), Zn(II) and Cd(II) with different numbers of H_2O and hmta from ethanolic solutions, which they attempted to characterize on the basis of the electronic and vibrational spectra and magnetic moments.

Examining these previous works, the present authors came to the conclusion that a proper combination of thermal analyses with visible and infrared spectroscopy would lead to a better understanding on the nature of the dehydration process. The results of studies with some new information are presented in this paper.

Experimental

Materials. The complexes were crystallized at room temperature from aqueous solutions containing MX_2 and hmta in the molar ratio 1 : 2.5. Their compositions were checked by elemental analyses for C, H and N and weight-loss values in dehydration (Table 1).

Measurements. The infrared absorption spectra (400—4000 cm^{-1}) were measured with a Hitachi 215 spectrophotometer by the Nujol mull method. A Hitachi EPS-3T spectrophotometer equipped with a standard integrating sphere attachment was used for the measurements of the diffuse reflectance spectra (14000—30000 cm^{-1}). Deeply colored samples were diluted with finely powdered MgO. The X-ray diffraction charts were obtained with a Toshiba ADG-101 diffractometer using a manganese-filtered Fe$K\alpha$ radiation.

The TG-DTA curves were obtained with a Shinku Riko TGD-3000 differential thermal microbalance with a heating rate of 5K/min in static air. In each measurement, 15—20 mg of powdered sample in a platinum crucible was used.

Results and Discussion

Structures before Heating. A cobalt complex and the corresponding nickel complex (*i.e.* that with the same

TABLE 1. ANALYSES OF COMPLEXES

Complex	Found(%)				Calcd(%)			
	C	H	N	H_2O	C	H	N	H_2O
$CoCl_2(hmta)_2 \cdot 10H_2O$	24.36	7.46	18.93	30.7	24.42	7.52	18.99	30.5
$CoBr_2(hmta)_2 \cdot 9H_2O$	21.88	6.69	17.32	24.6	21.79	6.41	16.95	24.5
$CoI_2(hmta)_2 \cdot 8H_2O$	19.07	5.66	15.18	20.4	19.55	5.49	15.21	19.6
$Co(NO_3)_2(hmta)_2 \cdot 10H_2O$	22.21	7.05	21.95	27.3	22.40	6.90	21.78	28.0
$Co(NCS)_2(hmta)_2 \cdot 4H_2O$	31.99	6.35	26.68	14.1	31.88	6.12	26.57	13.7
$NiCl_2(hmta)_2 \cdot 10H_2O$	24.42	7.72	19.14	29.8	24.43	7.52	18.99	30.5
$NiBr_2(hmta)_2 \cdot 9H_2O$	21.39	6.61	16.87	24.6	21.79	6.41	16.96	24.5
$NiI_2(hmta)_2 \cdot 8H_2O$	19.49	5.73	15.38	19.7	19.56	5.50	15.33	19.7
$Ni(NO_3)_2(hmta)_2 \cdot 10H_2O$	22.17	6.96	21.85	27.3	22.41	6.90	21.79	28.0
$Ni(NCS)_2(hmta)_2 \cdot 4H_2O$	31.98	6.14	26.60	14.0	31.89	6.12	26.58	13.7

hmta=$C_6H_{12}N_4$

anion) have always the same composition (Table 1). Powder X-ray diffraction analyses indicate that, except for the cobalt iodide complex which was too poor in crystallinity to calculate the lattice constants, the crystals of all the complexes belong to the tetragonal system. As an example, the X-ray diffraction lines of the cobalt chloride complex and their assignments are given in Table 2. The lattice constants also indicate that the value of c/a is almost the same for each pair of a cobalt complex and a nickel complex with the same X (Table 3).

Table 2. X-Ray diffraction lines of $CoCl_2(hmta)_2 \cdot 10H_2O$ and their assignments

d/Å	I/I_0	hkl	$\sin^2\theta_{obsd}$	$\sin^2\theta_{calcd}$
8.97	100	001	0.0117	0.0119
7.78	5	101	0.0155	0.0158
6.96	30	111	0.0194	0.0197
5.84	10	201	0.0275	0.0275
5.49	40	220	0.0311	0.0311
4.49	10	301	0.0465	0.0469
4.09	40	112	0.0561	0.0554
3.45	30	222	0.0788	0.0787

Table 3. Lattice constants obtained from powder X-ray diffraction lines of $MX_2(hmta)_2 \cdot nH_2O$
Rad. Fe$K\alpha$, *Filter* Mn, *Syms.* Tetragonal

MX	a/Å	c/Å	c/a
CoCl	15.5	8.88	0.57
CoBr	16.4	9.19	0.56
$CoNO_3$	13.0	13.9	1.07
CoNCS	13.4	13.7	1.02
NiCl	15.6	8.84	0.57
NiBr	16.3	9.24	0.57
NiI	15.2	13.9	0.92
$NiNO_3$	12.9	13.9	1.08
NiNCS	12.5	13.8	1.11

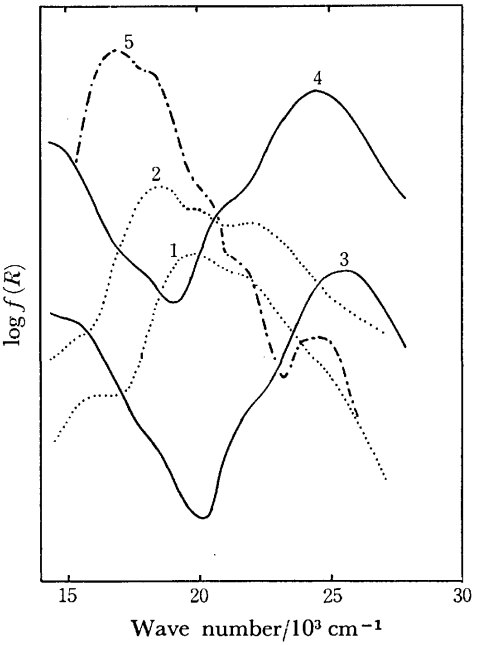

Fig. 1. Visible reflectance spectra of (1) $CoCl_2(hmta)_2 \cdot 10H_2O$, (2) $CoCl_2 \cdot 6H_2O$, (3) $NiCl_2(hmta)_2 \cdot 10H_2O$, (4) $NiCl_2 \cdot 6HO$ and (5) $CoCl_2(hmta)_2$.

The outlook of the visible reflectance spectra, the $\tilde{\nu}_{max}$ values of which are summarized in Table 4, show the existence of essentially octahedral coordination structures in all the complexes. The infrared spectra indicate that in all the complexes except the nickel thiocyanate complex, hmta molecules are not coordinated to the metals, since their symmetry was found to be T_d according to the criterion proposed by Buhannic and Guerchais.[4,6]

As examples, the visible reflectance spectra of $CoCl_2(hmta)_2 \cdot 10H_2O$, $NiCl_2(hmta)_2 \cdot 10H_2O$ and the anhydrous cobalt chloride complex are given in Fig. 1, together with those of $CoCl_2 \cdot 6H_2O$ and $NiCl_2 \cdot 6H_2O$

Table 4. Color and structural changes of $MX_2(hmta)_2 \cdot nH_2O$ caused by thermal dehydration

MX	Dehydration range/K	Loss of H_2O	Color[a] ($\tilde{\nu}_{max}/10^3$ cm^{-1})	C.N.	Sym. of hmta[c]
CoCl	324—402	10	*pink*(19.7)→blue(15.7)	6→4[b]	$T_d \rightarrow C_{3v}$
CoBr	327—377	9	*pink*(19.6)→blue(15.2)	6→4	$T_d \rightarrow C_{3v}$
CoI	326—384	8	*pink*(19.5)→green(15.2)	6→4	$T_d \rightarrow C_{3v}$
$CoNO_3$	322—373	6	*pink*(19.6)→*pink*(19.0)	6→6	$T_d \rightarrow T_d$
	374—389	2	→violet(17.4)	→6	→T_d
	397—417	2	→violet(17.4)	→6	→C_{3v}
CoNCS	356—400	4	*orange*(19.8)→bluish violet(16.1)	6→4	$T_d \rightarrow C_{3v}$
NiCl	330—381	8	*bluish green*(25.4)→*yellow*(22.8)	6→6	$T_d \rightarrow T_d$
	395—427	2	→violet(16.4, 18.8)	→4	→C_{3v}
NiBr	341—397	9	*bluish green*(25.3)→blue(15.5)	6→4	$T_d \rightarrow C_{3v}$
NiI	334—401	8	*bluish green*(25.3)→green(15.3)	6→4	$T_d \rightarrow C_{3v}$
$NiNO_3$	320—373	6	*bluish green*(25.3)→*yellowish green*(25.3)	6→6	$T_d \rightarrow T_d$
	373—405	2.5	→*yellowish green*(25.1)	→6	→T_d
	405—433	1.5	→*green*(24.7)	→6	→$T(C_{3v})$
NiNCS	334—387	1.5	*blue*(25.1)→*green*(25.4)	6→6	$(T_d+C_{3v}) \rightarrow C_{3v}$
	387—438	2.5	→yellowish green(26.3)	→6	→$(C_{3v}+C_{2v})$

a) Italics indicate pale color. b) Tetracoordinated species are all tetrahedral. c) Notations in parentheses are uncertain.

which were found, by X-ray analyses,[7] to be formulated as $[MCl_2(H_2O)_4]\cdot 2H_2O$. In general, the visible reflectance spectra of $CoX_2(hmta)_2\cdot nH_2O$ ($X=Cl^-$, Br^-, I^-, NO_3^-; $n=8$—10) are similar to each other, *i.e.*, they are essentially independent of the nature of X^-. The same can be said of the spectra of $NiX_2(hmta)_2\cdot nH_2O$. The spectra of $MCl_2(hmta)_2\cdot 10H_2O$ differ somewhat from those of $MCl_2\cdot 6H_2O$ (Fig. 1). In the case of the nickel compounds the difference seems to be rather small, but the $\bar{\nu}_{max}$ value of the hmta complex is somewhat higher. These facts suggest that X^- in these hmta complexes are not coordinated to the metals. This is supported by the fact that, in the case of the nitrate complexs, the infrared spectra indicate the presence of ionic NO_3^-. Moreover, the $\bar{\nu}_{max}$ values of these complexes (Table 4) are very close to those of the $[M(H_2O)_6]^{2+}$ ions (Co: 19600 cm^{-1}, Ni: 25300 cm^{-1}) observed in the absorption spectra of cobalt(II) and nickel(II) salts in aqueous solutions. These complexes are thus all hexaaqua complexes, and can be described as $[M(H_2O)_6]\cdot 2hmta\cdot(n-6)H_2O$.

$Co(NCS)_2(hmta)_2\cdot 4H_2O$ is characterized by the fact that it gives ν(O–H) at 3150 cm^{-1} which is considerably lower than that of an ordinary crystalline water (3400—3500 cm^{-1}), and that it begins to lose its water molecules at a temperature 20—30 K higher than the corresponding temperatures of the other complexes (Table 4). For this complex, the formulation as $[Co(NCS)_2(H_2O)_4]\cdot 2hmta$ seems to be the most probable.

On the other hand, $Ni(NCS)_2(hmta)_2\cdot 4H_2O$ seems to contain two sets of waters since it gives ν(O–H) bands, which can probably be attributed to both crystalline and coordinated water (3450 cm^{-1} and 3150 cm^{-1}), and loses about 1.5 water molecules at low temperature as in the case of the halides. The infrared bands of hmta in this complex seems to consist of two sets which correspond to two types of hmta having T_d and C_{3v} symmetries, respectively. The complex gives a single δ(NCS) at 482 cm^{-1}, indicating the presence of M–NCS bonds as in the case of the cobalt thiocyanate complex (Fig. 6).

Color and Structural Changes Caused by Thermal Dehydration. The TG and DTA curves of the complexes investigated are shown in Fig. 2. The curves of the cobalt complexes (except for the thiocyanate complex) have been published by Rodzinskaya *et al.*,[2] but their data differ somewhat from ours.

Except for the nickel chloride and bromide complexes, the complexes with halide ions give a smooth TG-DTA curve, although they contain both crystalline and coordinated water, all of which are lost in succession. If we compare the reflectance spectra of anhydrous products with the absorption spectra of typical cobalt and nickel complexes,[8] and their infrared spectra with the data of Buhannic and Guerchais,[4] we come to the conclusion that dehydration is accompanied with the changes octahedral→tetrahedral for the coordination structure and $T_d\rightarrow C_{3v}$ for the symmetry of hmta (Table 4), and that the metals are surrounded tetrahedrally by two X and two hmta in the final anhydrous products (*cf.* curve 5, Fig. 1, which shows characteristic features of a tetrahedral cobalt(II) complex[8]).

The nickel chloride and bromide complexes are dehydrated in two steps, although no distinct plateau could be observed on the TG curve in the case of the bromide complex. The nickel chloride complex gives a stable intermediate with the composition of $NiCl_2(hmta)_2\cdot 2H_2O$ in the first step, during which the T_d symmetry of hmta and the octahedral structure were retained. The visible spectrum of this dihydrate ($\bar{\nu}_{max}$: 22800 cm^{-1}) is now very close to that of $NiCl_2\cdot 2H_2O$ ($\bar{\nu}_{max}$: 22800 cm^{-1}), which is obtained by heating $NiCl_2\cdot 6H_2O$ at 383 K in the air (Fig. 3). Since the nickel in $NiCl_2\cdot 2H_2O$ was found by X-ray analysis[9] to be surrounded octahedrally by two water molecules

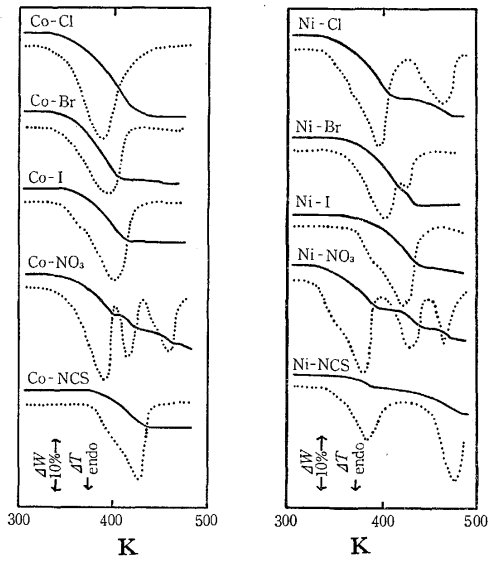

Fig. 2. TG(solid line), DTA(dotted line) curves of $MX_2(hmta)_2\cdot nH_2O$ in air.

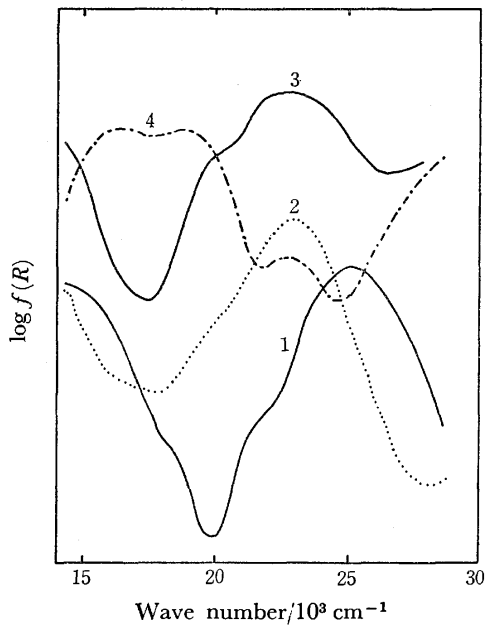

Fig. 3. Visible reflectance spectra of (1) $NiCl_2(hmta)_2\cdot 10H_2O$, (2) $NiCl_2(hmta)_2\cdot 2H_2O$, (3) $NiCl_2\cdot 2H_2O$ and (4) $NiCl_2(hmta)_2$.

TABLE 5. SUGGESTED STRUCTURE CHANGES
(L=hmta, X^-=anion)

CoCl, CoBr, CoI, NiBr, NiI:
$[M(H_2O)_6]X_2 \cdot (2—4)H_2O \cdot 2L \rightarrow [ML_2X_2]$
$CoNO_3$:
$[M(H_2O)_6]X_2 \cdot 4H_2O \cdot 2L \rightarrow [M(H_2O)_4X_2] \cdot 2L \rightarrow$
$[M(H_2O)_2X_2{*}] \cdot 2L \rightarrow [MX_2{*}L_2]$
CoNCS:
$[M(H_2O)_4X_2] \cdot 2L \rightarrow [MX_2L_2]$
NiCl:
$[M(H_2O)_6]X_2 \cdot 4H_2O \cdot 2L \rightarrow$ (Fig. 4) $\rightarrow [MX_2L_2]$
$NiNO_3$:
$[M(H_2O)_6]X_2 \cdot 4H_2O \cdot 2L \rightarrow [M(H_2O)_4X_2] \cdot 2L$
$\rightarrow$ (1.5 hydrate) $\rightarrow [MX_2{*}L_2]$

* Bidentate.

NO_3^- and two unidentate hmta.

$Co(NCS)_2(hmta)_2 \cdot 4H_2O$ loses four water molecules in one step to form the tetrahedral anhydrous complex. The infrared spectrum of the anhydrous complex indicates the presence of the unidentate hmta, and its ν(CN) and δ(NCS) are split into two by dehydration (Fig. 6). The anhydrous complex might thus be described as $[Co(NCS)_2(hmta)_2]$.

On the other hand, $Ni(NCS)_2(hmta)_2 \cdot 4H_2O$ loses its water molecules in two steps, the octahedral structure being kept through the dehydration steps. In the first step, the symmetry of hmta changes clearly to C_{3v}, a single band of δ(NCS) being observed at 480 cm^{-1} (Fig. 6). In the next step, the C_{3v} symmetry of hmta changes to C_{3v} or $C_{2v}+C_{3v}$ and δ(NCS) is split into two as in the case of the cobalt thiocyanate complex, although ν(CN) does not change. The nickel thiocyanate complexes formed at each of these dehydration steps can not be formulated at present because of incomplete data.

The color and structural changes caused by thermal dehydration of all the complexes investigated are summarized in Tables 4 and 5. We see that the decrease in the number of coordinated water molecules brings about the coordination of anions and hmta. However, in many cases the coordination of anions takes place first, and that of hmta only in the last stage of dehydration. This apparent reluctance of an amine, which usually shows a stronger coordination tendency than anions and water, toward coordination is probably due to the bulkiness of hmta and its weak basicity (pK_b=8.87). This might be the reason why hmta forms no amine complex and gives no hydroxide precipitate in aqueous solution, when a cobalt or nickel salt is mixed with hmta in it, precipitating only a "*complex*" which contains uncoordinated hmta molecules between hydrated cations and anions (or aqua-anion complexes such as $[M(H_2O)_4X_2]$). The only possible exception to this rule found in this study is the thiocyanate complex of nickel, but its actual structure is not known. Heating, however, drives out the water from the coordination sphere of each cation, enabling the reluctant amine to be coordinated, but this change can only occur after all the more avid anions have got their seats in the coordination sphere.

References

1) M. Harmelin and C. Duval, *Microchim. Acta*, **1962**, 275.
2) A. Lodzinskaya, A. Grodzicki, and T. Grodzicka, *Rocz. Chem.*, **46**, 1017 (1972).
3) P. De Santis, A. L. Kovacs, A. M. Liquori, and L. Mazzarella, *J. Am. Chem. Soc.*, **87**, 4965 (1965); A. L. Kovacs and L. Mazzarella, *Ric. Sci.*, **6**, 466 (1966).
4) M. M. Buhannic and M. J. E. Guerchais, *Rev. Chim. Miner.*, **8**, 111 (1971).
5) J. R. Allan, D. H. Brown, and M. Lappin, *J. Inorg. Nucl. Chem.*, **32**, 2287 (1970).
6) Although such a prediction of the symmetries of hmta in the complexes can be made in various regions of the spectra, the band of Δ_{cage} (ν_7) around 510 cm^{-1}, which is single in T_d and splits into two in C_{3v} and three in C_{2v}, can be used as the most convenient criterion.
7) J. Mizuno, *J. Phys. Soc. Jpn*, **15**, 1412 (1960); **16**, 1574 (1961).
8) A. B. P. Lever, "Inorganic Electronic Spectroscopy," Elsevier (1968), pp. 318—349.
9) B. Morosin, *Acta Crystallogr.*, **23**, 630 (1967).
10) N. F. Curtis and Y. M. Curtis, *Inorg. Chem.*, **4**, 804 (1965).
11) A. B. P. Lever, E. Mantovany, and B. S. Ramaswamy, *Can. J. Chem.*, **49**, 1957 (1971).

Bivalent Metal Complexes of *N,N*-Bis(2-hydroxyethyl)glycine

Yoshie INOMATA, Toshio TAKEUCHI, and Takao MORIWAKI

Department of Chemistry, Faculty of Science and Technology, Sophia University, Chiyoda-ku, Tokyo 102

(Received December 20, 1975)

Complexes of *N,N*-bis(2-hydroxyethyl)glycine(BHEG) with a bivalent cation (Cu(II), Ni(II), Co(II), Zn(II), Fe(II), Cd(II), and Pb(II)) have been prepared and investigated by means of infrared absorption spectra, powder surface diffuse reflection spectra, electronic spectra, magnetic susceptibility, and thermal analysis. They can be classified into two types: (A) $ML_2 \cdot nH_2O$ and (B) $ML \cdot X \cdot nH_2O$, (M: metal, L: BHEG$^-$, X: Cl^- or NO_3^-). Ni(II), Co(II), Zn(II), and Fe(II) complexes are of type A, and those of Cd(II) and Pb(II) of type B. In the case of Cu(II) complexes, a blue A type complex (Cu(II)-A) has been prepared from a basic solution and a green B type one (Cu(II)-B) from an acidic solution. From detailed assignments of IR spectra, BHEG is found to have a zwitter ion structure. From magnetic moment data and reflection spectra, we presume that the A type complexes have a *trans* octahedral structure and the B type complexes a tetrahedral structure.

BHEG seems to have the properties of both an amino acid and an amino alcohol, since it has a *N*-substituted amino, a carboxyl, and two hydroxyl groups as coordinating groups in one molecule. Chaberek *et al.*[1] investigated bivalent metal chelates of BHEG in aqueous solution and discussed the coordination of the hydroxyl group, besides the amino and carboxyl groups. However, no metal complex of BHEG in solid state has yet been studied. Krause[2] synthesized nickel(II) and cobalt(II) complexes with *N*-(2-hydroxyethyl)imino diacetic acid, which is similar to BHEG, and reported that there are complexes in which the metal is coordinated with a hydroxyl and one carboxyl group, in addition to the normal complexes in which the metal is coordinated with a imino nitrogen and two carboxyl groups.

Many studies have been carried out on amino alcohol complexes.[3-5] Kida[6] studied the influence of pH on the coordination of a hydroxyl group.

In the present work, the bivalent metal complexes of BHEG have been prepared and investigated, and detailed assignments for the infrared absorption bands of BHEG and its complexes have been made. Discussion is given on how the hydroxyl group influences the coordination with the metal.

Experimental

Preparation of Compounds. Nickel(II) complex was prepared by adding 0.005 mol of nickel chloride hexahydrate to a hot solution containing 0.005 mol of BHEG and 0.005 mol of sodium hydrogencarbonate. The mixture was then stirred in a water bath. After the solution was condensed, a blue precipitate formed was filtered, washed with ethyl alcohol several times, and dried.

Cobalt(II) and copper(II)-B (green) complexes were prepared by the same procedure as for the nickel(II) complex.

Zinc(II), cadmium(II), lead(II), iron(II), and copper(II)-A(blue) complexes were prepared by means of almost the same procedure as that for the nickel(II) complex, except that: a) the condensed solution was poured into ethyl alcohol in the case of the zinc(II) and cadmium(II) complexes and into acetone in the case of the lead(II) complex; b) the iron(II) complex was prepared from iron(II) sulfate heptahydrate at room temperature and dried *in vacuo*; and c) in the case of the copper(II)-A complex, sodium hydroxide was used instead of sodium hydrogencarbonate in order to keep the pH of the solution high.

Deuteration of Compounds. The deuterated BHEG and its complexes were prepared by dissolving these compounds in 99.9% deuterium oxide and drying *in vacuo*. The NH and OH groups were deuterated by this method.

Thermal Analysis. Thermal analysis was carried out in the air with a Rigaku Denki TG-DTA M-8075 from room temperature to 400 °C. It was found that cadmium(II), lead(II), and iron(II) complexes have one molecule of water.

Magnetic Studies. Magnetic moments were obtained for the solid samples by the Gouy method at room temperature, using $Hg[Co(SCN)_4]$ as a calibration standard.

Powder Diffuse Reflection Spectra. Powder diffuse reflection spectra were observed from 700 nm to 400 nm for copper(II)-A, copper(II)-B, nickel(II), and cobalt(II) complexes with a Hitachi 624 digital spectrophotometer equipped with a standard Hitachi reflection attachment.

Electronic Spectra. Electronic spectra of metal complexes in 1M $NaClO_4$ solution were obtained from 900 nm to 190 nm with the same spectrophotometer described above. Since nickel(II) complex is insoluble in 1 M $NaClO_4$ solution, its spectra could not be obtained. The results of the elemental analysis and the values of magnetic moments, reflection spectra, and electronic spectra are given in Table 1.

Infrared Absorption Spectra. Infrared absorption spectra from 4000 cm^{-1} to 300 cm^{-1} were obtained with Hitachi EPI-G2 and EPI-L spectrophotometers, which were calibrated with polystyrene and atmospheric water vapor. Samples were prepared as potassium bromide discs and Nujol mulls. The observed absorption frequencies and the assignments for BHEG and the metal complexes are given in Table 2.

Results and Discussion

From the results of elemental analysis and infrared spectra, the eight complexes prepared can be divided into two types, nickel(II), cobalt(II), zinc(II), iron(II) complexes belonging to type A ($ML_2 \cdot nH_2O$), and cadmium(II) and lead(II) complexes to type B ($ML \cdot X \cdot H_2O$). As for copper(II) complexes, a blue A type complex (copper(II)-A) can be prepared from a basic solution and a green B type one (copper(II)-B) from an acidic solution.

Electronic Spectra and Magnetic Moments. Copper(II)-A and copper(II)-B complexes have magnetic moments of 1.86 B.M. and 1.90 B.M. respectively, which are the same as those for $Cu(gly)_2 \cdot H_2O$.[7]

In copper(II)-A, the reflection spectrum shows a band at 630 nm, and the electronic spectrum in 1M

Table 1. Analytical data and physical properties of BHEG complexes

Complex	Found (calcd) %					Magnetic moment	Color	Reflection spectra	Electronic spectra
	C	H	N	M	Cl	μ_{eff}		nm	nm
$Ni[C_6H_{12}O_4N]_2$	36.64 (37.63)	6.23 (6.32)	7.02 (7.31)	15.50 (15.33)	0 0	3.36 B.M. (2.83)[a]	blue	752, 615, 365	
$Co[C_6H_{12}O_4N]_2$	37.33 (37.61)	5.74 (6.31)	7.31 (7.31)	15.39 (15.38)	0 0	4.56 (3.87)	pink	480, 463, 440	505, 487
$Zn[C_6H_{12}O_4N]_2$	37.26 (36.98)	6.09 (6.21)	7.16 (7.19)	16.50 (16.78)	0 0	dia (0)	white	—	—
$Fe[C_6H_{12}O_4N]_2\cdot H_2O$	36.17 (36.20)	6.88 (6.58)	6.88 (7.04)	14.03 (14.03)	0 0	5.52 (4.90)	pale green	>700	
$Cu[C_6H_{12}O_4N]_2$	36.66 (37.16)	6.10 (6.24)	7.07 (7.22)	16.02 (16.38)	0 0	1.86 (1.73)	blue	630	610, 602
$Cu[C_6H_{12}O_4N]Cl$	27.17 (27.59)	4.53 (4.63)	5.40 (5.36)	23.77 (24.33)	13.40 (13.57)	1.90 (1.73)	green	>700	760
$Cd[C_6H_{12}O_4N]Cl\cdot H_2O$	22.06 (21.97)	4.21 (4.30)	4.36 (4.27)	34.61 (34.26)	11.57 (10.81)	dia (0)	white	—	—
$Pb[C_6H_{12}O_4N]NO_3\cdot H_2O$	16.09 (16.04)	3.08 (3.14)	6.27 (6.23)	45.61 (46.11)	0 0	dia (0)	white	—	—

a) Spin only value.

$NaClO_4$ solution shows a peak at 610 nm assigned to $^2E_g \rightarrow {}^2T_{2g}$. Laurie[8] investigated the reflection spectra of several forms of bis(tyrosinato)copper(II) complexes and concluded that the blue form of Cu(II)-DL-tyrosine complex, which shows a peak at 625 nm, has a *trans* configuration. Graddon[9] studied the electronic spectra for anhydrous copper(II) complexes of amino acids and found that copper(II) complexes, which have a peak in the region near 621 nm, have *trans* octahedral configurations. Therefore, we can assume that the copper(II)-A complex has a *trans* octahedral configuration.

It was found that the reflection spectrum of copper(II)-B has a peak above 700 nm and the electronic spectrum in 1 M $NaClO_4$ solution has an absorption maximum at 760 nm. Hare *et al.*[10] studied the effect of pH on the electronic spectra of a number of copper(II)-amino acid complexes and found that all species of Cu(aminoacidato)$^+$ have maximum extinction coefficients of about 30 at 724 nm, while those of bis(amino acidato)copper(II) have maximum extinction coefficients between 60 and 75 at 621 nm. We can thus assume that the copper(II)-B complex has a Cu(aminoacidato)$^+$ ion.

Nickel(II) complex has a magnetic moment of 3.36 B.M. The three peaks in its reflection spectrum are given in Table 1. The spectrum is similar to that of $Ni(gly)_2\cdot H_2O$[11] in solution and the absorption peaks are assigned to $^3A_{2g} \rightarrow {}^1E_g$, $^3A_{2g} \rightarrow {}^3T_{1g}$ (F), and $^3A_{2g} \rightarrow {}^3T_{1g}$ (P).

Cobalt(II) complex is a high spin complex with a magnetic moment 4.56 B.M. It seems that these nickel(II) and cobalt(II) complexes have the same octahedral structure as that of copper(II)-A complex.

The iron(II) complex is pale green and has a magnetic moment of 5.52 B.M., which is the same as that of the iron(II) ion itself.

It seems that the iron(II) complex is a high spin complex. Zinc(II), cadmium(II), and lead(II) complexes are diamagnetic and their electronic spectra show no peaks in the visible region. These eight complexes in 1 M $NaClO_4$ solution have absorption peaks below 300 nm, which are assigned to the electron transfer of BHEG.

Infrared Absorption Spectra. The assignments for BHEG and its metal complexes have been based on a comparison of the observed spectra with those of glycine,[12,13] betaine,[14] other α-amino acid,[15,16] NTA,[17] triethanolamine,[3] HIDA,[2] and their metal complexes, which have been throughly studied.

BHEG: The broad bands at 3186 and 3089 cm^{-1} are assigned to the OH stretching vibrations, because of their disappearance on deuteration and the absence of bands in this region for betaine. Since these OH vibrations have lower frequencies than those of free OH vibration, it seems that OH forms a hydrogen bonding.[18]

The fine bands from 2985 to 2843 cm^{-1} are due to CH_2 stretching vibrations. The N^+–H stretching vibration which is supposed to appear at about 3000 cm^{-1} is difficult to distinguish as it overlaps the OH and CH_2 stretching vibrations.

The very strong band at 1639 cm^{-1} is assigned to the COO^- antisymmetric stretching and N^+–H deformation vibrations. On deuteration, the N^+–H deformation vibration shifts to 1275 cm^{-1} and appears as the N^+–D deformation vibration. Moreover, BHEG has no carboxy(C=O) stretching vibration at 1700 cm^{-1}, which is characteristic of acid. Thus BHEG, like glycine, has a zwitter ion structure in solid state.

The bands at 1401 and 699 cm^{-1} are due to the COO^- symmetric stretching and scissors vibrations. The bands at 1207 and 737 cm^{-1}, which shift on deuteration, are assigned to OH in plane and out of plane deformation vibrations, since they are not observed in betaine and glycine.

Metal Complexes: Nickel(II), cobalt(II), and zinc(II) complexes show similar spectra. The spectrum of lead(II) complex differs slightly from the spectrum of cadmium(II) complex, because of the presence of a NO_3^- ion.

TABLE 2. ASSIGNMENTS OF INFRARED ABSORPTION SPECTRA OF BHEG COMPLEXES (cm^{-1})

BHEG	Ni(II)	Co(II)	Zn(II)	Fe(II)	Cu(II)-A	Cu(II)-B	Cd(II)	Pb(II)	Assignments
				3361ssh			3526 s		
3186vsb	3271vs	3283vs	3271vs	3287sb	3306vs		3346sb	3272sb	OH str.
				3169mb	3160 s		3272sb		
3089vs	3063mb	3046mb	3072mb	3053mb		3025sb			
2985w	2984wsh	2976wsh	2980wsh	2976wsh	2993w				
					2979vw				
2973w	2964m	2963m	2962m	2964vw	2968w	2960 s	2974wsh		
	2954m	2954w	2954w	2957vw	2955w		2955w	2957w	
	2922w	2920w	2927w	2944w	2940w	2935 s	2930w		
2904m	2893w	2889w	2894sh	2914w	2923w	2891wsh	2913w		
2843m	2841w	2851w	2847w	2866w	2894w	2817w	2892w	2899w	CH_2 str.
				2830wb	2840w		2853w	2851w	
				2761wb	2797wsh	2779w			
2742w	2723mb	2717mb	2727mb			2720m			
2660w	2673wsh	2667w	2657w	2697w		2662w			
	2627wsh	2627w				2607w			
1639vsb	1599vsb	1586vsb	1605vsb	1583vsb	1621vsb	1578vsb	1570vsb	1593vsb	COO^- asym. str., N^+-H def. (for ligand)
					1611vsb				
1495w	1486w	1488w	1487w	1485w	1487w	1489m	1479w	1484w	
1487sh					1462sh	1480sh			CH_2 scissors
1453m	1453msh	1455msh	1454msh	1454msh	1450w	1463w	1448m	1468m	
1444sh	1435 s	1434 s	1433 s	1434m	1430m	1452m	1438m		
1401 s	1412 s	1410 s	1408 s	1413 s	1402 s	1406 s	1409 s	1406vsb	COO^- sym. str.
1387 s	1387m	1389m	1383m	1389m			1383sh	1385 s	NO_3^- asym. str. for Pb
1358 s	1368w	1370w	1369w		1367w	1376m			
						1369sh			
1314sb	1326m	1327m	1327w	1330m	1328w	1337m	1332 s		CH_2 wagging and
	1304 s	1311 s	1309m	1304m	1300m	1320m	1306w	1315w	CH_2 twisting
	1290sh	1299sh	1299sh	1288w	1281m	1283m	1283w	1289 s	
	1277m	1282m	1280m	1268vw	1271vwsh	1266m	1262m		
				1252vw					
1237vw				1245w					
1207m	1223m	1230m	1226m	1225w	1219m	1235w	1230m		OH in plane def. +C-OH str.
1139vw	1160vw	1160vw	1158vw	1159m	1150vw	1156w	1142m	1153w	C-N str.
1115w	1135w	1138w	1132w	1136w	1124w	1121m	1128m	1127m	
1096 s		1096sh	1093sh	1103w				1088 s	C-C str.
1077w	1070 s	1072 s	1071 s	1074 s	1074 s	1080m		1079 s	CCN asym. str.
		1068wsh	1067wsh						
	1061 s	1061 s	1060 s	1064 s	1057 s	1061 s	1064 s	1059m	
1046 s	1045 s	1047 s	1044 s	1048 s	1054 s	1042m	1050vw	1049vw	
					1041 s	1035m	1033m	1039m	
1026w	1028 s	1031 s	1029 s	1029 s	1023 s	1016 s	1011 s	1008m	C-OH str. for ligand
1003m									
972m	980m	984m	981m	995m	975w	985w	984w	981vw	
				987w					
				975vw					
	959 s	961 s	959 s	964m	955 s		959vw	938m	
				938vw					
933m	932 s	936 s	929m	930m	934 s		937m	911m	CH_2 rocking
903m						908m	905m	901m	
887m	892 s	893 s	891 s	889m	883m	895 s	881m	891sh	
856w				840w			862w	844w	
								829m	CCN sym. str.
	822m	827m	823w	812w				821m	
	807sh	811sh	806vw	801vw	818w	804m	793wb	802wsh	
797wb					793w				
699m	749 s	755 s	753 s	741m	748 s	739m	734m	715mb	COO^- scissors
					703m				
737mb	642w	633w	638w	637w	645w	620m	604w		OH out of plane def.
				615m					
583m				583w					
565w	563w	562w	563w	564w	567m	565m	577w		COO^- wagging

TABLE 2. (Continued)

BHEG	Ni(II)	Co(II)	Zn(II)	Fe(II)	Cu(II)-A	Cu(II)-B	Cd(II)	Pb(II)	Assignments
546m	536m	521m	530m	539w	537m		546w	545w	COO^- rocking
	522m	516m	514m	516m	512m	511m		507w	
				488vw					
477m				458w		480m			
424m	443w	436vw	435vw	432vw	444w	421w	448wb	443w	
	420vw	419vw	420vw	407w			430w	420w	
387w	387m	385w	376w	365sh	393m	372w	390w		M–N str. for Cu-A
	354m	356m	358w	360sh	360m				CCN asym. def.
	345m	346m	329m	345m		340m			M–N str. for Ni, Co, Zn, Fe and Cu-B
	338sh								
	330w	335vw	335sh	337m					
303w	313m	302m	304w	305w	308w	317m	303w		

Abbreviations: s=strong, m=medium, w=weak, sh=shoulder, b=broad.

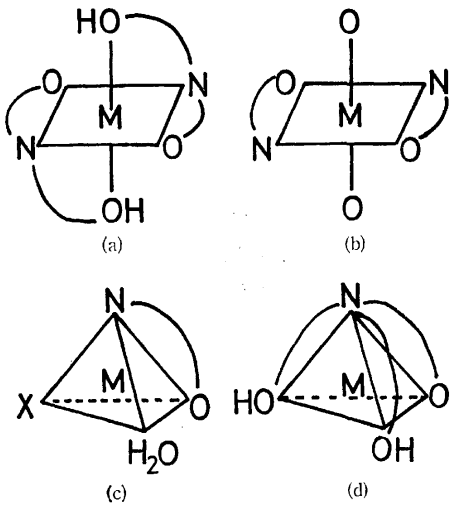

Fig. 1. Four possible configurations for BHEG complexes.
(a) Ni(II), Co(II), Zn(II), and Fe(II). (b) Cu(II)-A. (c) Cd(II) and Pb(II) ($X=Cl^-$ for Cd(II), NO_3^- for Pb(II)). (d) Cu(II)-B.

The broad bands above 3000 cm^{-1} for all complexes are assigned to OH stretching vibrations. In nickel(II), cobalt(II), zinc(II), and iron(II) complexes, one of these two OH stretching vibrations shifts *ca.* 100 cm^{-1} towards higher frequencies and the others towards lower frequencies as compared with those of the ligand. In the case of copper(II)-A, cadmium(II), and lead(II) complexes, all the vibrations shift to higher frequencies. This can be explained as follows. The OH vibration, which is at a lower frequency in the ligand due to hydrogen bonds, seems to become strong by the breaking of the hydrogen bonding when a complex is formed. When the OH group coordinates to a metal, the OH bond becomes weak and the OH stretching vibration shifts to lower frequencies. Therefore, in nickel(II), cobalt(II), zinc(II), and iron(II) complexes, one of these two OHs in one molecule does not coordinate, and the other slightly coordinates and forms a *trans* octahedral structure (Fig. 1-a).

On the other hand, in copper(II)-A, cadmium(II), and lead(II) complexes, neither of the OH groups coordinates. Copper(II)-A has a *trans* octahedral structure which extends above and below the basal plane like the alanine copper(II) complex[15] (Fig. 1-b), while cadmium(II) and lead(II) complexes take a tetrahedral structure with ligand, water, and anion (Fig. 1-c). In the copper(II)-B complex, the OH vibration markedly shifts to a lower frequency and the two OH groups seem to be coordinated to the metal to form a tetrahedral structrue with only one ligand (Fig. 1-d).

The bands at 1600 cm^{-1} assigned to COO^- antisymmetric stretching vibrations are observed at frequencies lower than those of the ligand. In the ligand the vibration shifts to higher frequencies because of the hydrogen bond, while in the complexes the hydrogen bonds are broken and the O–M bonds have a stronger ionic character. Fairly strong ionic coordination bonds are observed in NTA complexes.[17]

From 500 to 300 cm^{-1}, absorption bands which cannot be observed in the ligand appear in the complexes and are assigned to M–N stretching vibrations by comparison of the spectrum of the ligand with those of the metal complexes with glycine[12] and betaine.[14]

The frequency separation of the COO^- antisymmetric and symmetric stretching vibrations of the complexes in the same physical state increases in the order cobalt(II)<nickel(II)<zinc(II)<copper(II)-A (Table 1). The trend is the same as that in the corresponding series of complexes with various aliphatic α-amino acids, showing the corresponding order in the strengths of the metal-oxygen bond.

The copper(II)-A complex has a octahedral structure, like the glycine–copper(II) complex.[12] Nickel(II), cobalt(II), zinc(II) and iron(II) complexes have a *trans* octahedral structures, since BHEG acts as a tridentate ligand. However, cadmium(II) and lead(II) complexes have a four-coordinated structure with a 1 : 1 ratio of ligand to metal, differing from the *trans* octahedral structure of alanine–cadmium(II) complex.[15] The size and position of the CH_2CH_2OH group and the ionic radius of Cd^{2+} and Pb^{2+} seem to affect the formation of complexes.

References

1) S. Chaberek, Jr., R. C. Courtney, and A. E. Martell, *J. Am. Chem. Soc.*, **75**, 2185 (1953).
2) R. A. Krause, *Inorg. Chem.*, **2**, 297 (1963).
3) D. G. Brannon, R. H. Morrison, J. L. Hall, G. L. Humphrey, and D. N. Zimmerman, *J. Inorg. Nucl. Chem.*, **33**, 981 (1971).
4) Y. Kuge and S. Yamada, *Bull. Chem. Soc. Jpn.*, **42**, 2552 (1969).
5) M. N. Hughes and K. J. Rutt, *J. Chem. Soc., A*, **1968**, 2788.
6) S. Kida, *Nippon Kagaku Zasshi*, **85**, 428 (1964).
7) S. Kubo, *Kagaku To Kogyo*, **12**, 494 (1959).
8) S. H. Laurie, *Aust. J. Chem.*, **20**, 2609 (1967).
9) D. P. Graddon and L. Munday *J. Inorg. Nucl. Chem.*, **23**, 231 (1961).
10) C. R. Hare, B. S. Manhas, T. G. Mecca, W. Mungall, and K. M. Wellman, *Proc. IX Intl. Conf. Coord. Chem.*, **1966**, 199.
11) G. R. Brubaker and D. H. Busch, *Inorg. Chem.*, **5**, 2110 (1966).
12) T. J. Lane, C. S. C., J. A. Durkin, and R. J. Hooper, *Spectrochim. Acta*, **20**, 1013 (1964).
13) M. Tsuboi and T. Takenishi, *Kagaku No Ryoiki, Zokan*, **37**, 41 (1959).
14) J. V. Quagliano, S. Kida, and J. Fujita, *J. Am. Chem. Soc.*, **84**, 724 (1962).
15) J. F. Jackovitz, J. A. Durkin, and J. L. Walter, C. S. C., *Spectrochim. Acta*, **23A**, 67 (1967).
16) Y. Inomata, T. Inomata, and T. Moriwaki, *Bull. Chem. Soc. Jpn.*, **44**, 365 (1971).
17) F. J. M. Rajabalee, *Spectrochim. Acta*, **30A**, 891 (1974).
18) L. J. Bellamy, "The Infrared Spectra of Complex Molecules," John Wiley & Sons., New York (1958), p. 96.

Circular Dichroism of Cobalt(III) Complexes of the Type *cis*-$[CoN_2O_4]$ and *cis*-$[CoN_4O_2]$ Containing Acetylacetonate Ion, 2,2'-Bipyridine and 1,10-Phenanthroline

Kazuo KASHIWABARA (née KONYA),*[1] Kozo IGI,[2] and Bodie E. DOUGLAS
*Department of Chemistry, Faculty of Science, Tohoku University, Aramaki, Sendai 980
Department of Chemistry, University of Pittsburgh, Pittsburgh, Pa. 15260, U.S.A.
(Received February 16, 1976)

Two new cobalt(III) complexes, $[Co(acac)(bpy)_2]^{2+}$ and $[Co(acac)(phen)_2]^{2+}$ (acac=acetylacetonate ion, bpy=2,2'-bipyridine and phen=1,10-phenanthroline) were prepared from the reaction of $[Co(CO_3)(bpy)_2]^+$ and $[Co(CO_3)(phen)_2]^+$, respectively, with acetylacetone, and converted to the partially resolved optically active forms using a SP-Sephadex ion-exchange column. $[Co(acac)_2(bpy)]^+$ was also resolved partially with a SP-Sephadex column. $[Co(acac)_2(phen)]^+$ was resolved with a combination of silver dibenzoyl-*d*-tartrate and dibenzoyl-*d*-tartaric acid. The circular dichroism (CD) spectra for these four complexes and for $[Co(acac)_2(en)]^+$ and $[Co(acac)_2(tn)]^+$ (en=ethylenediamine, tn=trimethylenediamine) were measured. A marked solvent effect was observed in the d-d transition region for the CD spectra of the $[Co(acac)_2L]^+$ complexes. The absolute configurations for all these complexes were assigned on the basis of their CD spectra.

The preparation of mixed-ligand cobalt(III) complexes containing ligands which have strong coordinating ability to a cobalt(III) ion, *e.g.*, bipyridine, phenanthroline, acetylacetonate ion and cyanide ion *etc.*, is not easy because of disproportionation to form complexes for which all of the ligands are the same. Archer *et al.*[3,4] found $[Co(acac)_2(NO_2)_2]^-$ to be a good starting material for preparing $[Co(acac)_2(bpy)]^+$ and $[Co(acac)_2(phen)]^+$ complexes. A preliminary report of the mixed acac-bpy and acac-phen complexes has been made.[5] Here the preparation, optical resolution and circular dichroism (CD) of these complexes are reported.

Marked solvent effects were observed for the CD spectra in the d-d transition region for $[Co(acac)_2L]^+$ (L=bpy, phen, en, tn), but not for $[Co(acac)L_2]^{2+}$ (L=bpy, phen).

The assignments of the absolute configurations for these complexes were attempted on the basis of the CD spectra in the region of the d-d transitions and of the exciton bands. Both approaches have been applied to a variety of optically active metal complexes.[6] We assigned the absolute configurations of the $[Co(acac)L_2]^{2+}$ complexes from the CD in the exciton band region, and of the $[Co(acac)_2L]^+$ complexes using the d-d transition region.

Experimental

Preparation of Complexes. *1) Carbonatobis(2,2'-bipyridine)cobalt(III) Chloride Dihydrate*: Cobalt chloride hexahydrate, 4.7 g (0.02 mol) in 10 cm³ of water and 4 cm³ of 30% H_2O_2 were mixed in an ice-bath and added dropwise to a slurry of 12.0 g of $KHCO_3$ (0.12 mol) in 12 cm³ of water at 0 °C. After the addition, the mixture was stirred at 0 °C for 30 min. To this solution 6.25 g (0.04 mol) of 2,2'-bipyridine and 2 cm³ of ethanol were added and stirred for 1 h at 20 °C. The temperature was raised to 30—35 °C and stirring was continued for 3 h. Glacial acetic acid 2.4 g (0.04 mol) in 10 cm³ of water was added dropwise to the solution over a period of 15 min. After stirring for an additional 2 h at 50 °C, glacial acetic acid 2.4 g (0.04 mol) in 10 cm³ of water was again added over a period of 15 min. The solution was stirred for an additional 30 min at 50 °C and then cooled in an ice-bath for 2 h. The red crystals were filtered. The filtrate was concentrated to about half volume to obtain a second crop of crystals and then cooled overnight in a refrigerator to obtain another crop of crystals. These crude products were recrystallized from a small amount of hot water (80 °C), then filtered and washed with an acetone-water mixture, then acetone, and dried in air. If the filtrate is concentrated to half volume, more crystals are obtained. Total yield 8.4 g (90%). Found: C, 48.63; H, 4.29; N, 10.58%. Calcd for $[Co(CO_3)(bpy)_2]Cl\cdot 2H_2O$: C, 48.61; H, 3.90; N, 10.79%.

2) Carbonatobis(1,10-phenanthroline)cobalt(III) Chloride 4.5-Water: Cobalt chloride hexahydrate (4.7 g, 0.02 mol) in 10 cm³ of water and 4 cm³ of 30% H_2O_2 were mixed in an ice-bath and added dropwise to a slurry of 12.0 g of $KHCO_3$ (0.12 mol) in 12 cm³ of water at 0 °C. After the addition, the mixture was stirred at 0 °C for 30 min. To this solution 10 cm³ of 50% aqueous ethanol and 7.2 g (0.04 mol) of 1,10-phenanthroline were added and the resulting solution was stirred for 1 h at 20 °C. The temperature was raised to 30—35 °C and the stirring was continued for 2 h. After the addition of 10 cm³ of water, the stirring was continued for 1 h at 50 °C. Glacial acetic acid 2.4 g (0.04 mol) in 10 cm³ of water was added dropwise to the solution over a period of 15 min. After stirring for another 2 h at 50 °C, glacial acetic acid 2.4 g (0.04 mol) in 10 cm³ of water was again added over a period of 15 min. The reaction mixture was stirred for 30 min longer at 50 °C and filtered without suction. The filtrate was concentrated to half volume and cooled in a refrigerator overnight. The red crystals were filtered and washed with an acetone-water (small amount) mixture and then with acetone and dried in air. Yield 9.0 g (90%). Found: C, 50.66; H, 4.28; N, 8.83%. Calcd for $[Co(CO_3)(phen)_2]Cl\cdot 4.5H_2O$: C. 50.39; H, 4.22; N, 9.40%.

3) Acetylacetonatobis(2,2'-bipyridine)cobalt(III) Iodide 1.5 Water: Acetylacetone (0.6 g in 6 cm³ of water) and 1M HCl 6 cm³ were added to 2.3 g of $[Co(CO_3)(bpy)_2]Cl\cdot 2H_2O$ and the solution was warmed with stirring at 50—55 °C for 5 h. The solution was cooled to room temperature and filtered. Sodium iodide, 1.4 g in 2 cm³ of water, was added to the solution with stirring and the solution was cooled overnight in a refrigerator. The brownish-red product was filtered and washed with 2 cm³ of cold water and then with 4 cm³ of acetone. This crude product was recrystallized from 20 cm³ of hot water (80—85 °C). The red crystals were filtered and washed with a small amount of water-acetone mixture, then with acetone, and dried in air. Yield 0.6 g (17%). Found: C, 41.46; H, 3.20; N, 7.74%. Calcd

for $[Co(acac)(bpy)_2]I_2$: C, 41.16; H, 3.10; N, 7.95%.

The perchlorate of the complex was obtained by the addition of $NaClO_4$ to the filtrate from the recrystallization. It was filtered and washed with a small amount of cold water. Yield 0.4 g. Found: C, 42.94; H, 3.80; N, 7.75%. Calcd for $[Co(acac)(bpy)_2](ClO_4)_2 \cdot 1.5H_2O$: C, 43.12; H, 3.76: N, 8.04%.

4) Acetylacetonatobis(1,10-phenanthroline)cobalt(III) Iodide: This complex was prepared by using the same method as that for the 2,2'-bipyridine complex except that 2.6 g of $[Co(CO_3)(phen)_2]Cl \cdot 4.5H_2O$ was used. Fifty cm^3 of hot water was used for recrystallization. Yield 0.8 g (20%). Found: C, 43.21; H, 3.03; N, 7.24%. Calcd for $[Co(acac)(phen)_2]I_2 \cdot 1.5H_2O$: C, 43.57; H, 3.28; N, 7.14%.

The perchlorate was precipitated by the addition of $NaClO_4$ to the filtrate from the recrystallization. Yield 0.4 g. Found: C, 47.99; H, 3.43; N, 7.55%. Calcd for $[Co(acac)(phen)_2](ClO_4)_2 \cdot 0.5H_2O$: C, 47.95; H, 3.33; N, 7.71%.

5) Bis(acetylacetonato)(2,2'-bipyridine)cobalt(III) Iodide and Bis(acetylacetonato)(1,10-phenanthroline)cobalt(III) Perchlorate: These complexes were prepared according to the method reported by Archer *et al.*[3,4]

Optical Resolution of the Complexes. 1) $[Co(acac)(bpy)_2]^{2+}$: A solution of $[Co(acac)(bpy)_2]I_2$ (100—150 mg) was adsorbed on a SP-Sephadex C-25 resin (Pharmacia Fine Chemicals) column (2.5×120 cm) and eluted with 0.04 M sodium d-tartrate at a rate of 15—20 cm^3/h over a period of about 1 month. During this time, the red layer did not form separate bands although the band broadened considerably. Each fraction (100—150 cm^3) of the effluent was passed through a column of an anion exchange resin (Dowex 1-X8, 100—200 mesh) in ClO_4^- form, then evaporated to a small volume at 30 °C under reduced pressure, and then cooled overnight in a refrigerator. The red crystals of the perchlorate were filtered and washed with a small amount of cold water and dried under vacuum. Fifty mg of the perchlorate of the fast running fractions was again treated on the SP-Sephadex resin in the same way. The perchlorate of the fast running fraction (20 mg) was used for the CD measurement. Found: C, 42.94; H, 3.80; N, 7.75%. Calcd for $[Co(acac)(bpy)_2](ClO_4)_2 \cdot 1.5H_2O$: C, 43.12; H, 3.76; N, 8.04%.

2) $[Co(acac)(phen)_2]^{2+}$: The method was exactly the same as that for the 2,2'-bipyridine complex. Found: C, 47.99; H, 3.43; N, 7.55%. Calcd for $[Co(acac)(phen)_2](ClO_4)_2 \cdot 0.5H_2O$: C, 47.95; H, 3.33; N, 7.71%.

3) $[Co(acac)_2(bpy)]^+$: $[Co(acac)_2(bpy)]I$ (100—150 mg) was adsorbed on a SP-Sephadex C-25 column (2.5×120 cm) and eluted with 0.01 M sodium d-tartrate at a rate of 10—15 cm^3/h over a period of 2—3 weeks. During this time, the gray-violet layer did not form separate bands although the band broadened considerably. Each fraction (100—150 cm^3) of the effluent, to which a small amount of $NaClO_4$ was added, was evaporated to a small volume at 30 °C under reduced pressure. The resulting gray-violet product was filtered, washed with water, and dried under vacuum. Fifty mg of the perchlorate of the fast running fraction was again treated on the SP-Sephadex resin in the same way. The perchlorate of the fast running fraction (20 mg) was used for the CD measurement. Found: C, 46.25; H, 4.49; N, 5.18%. Calcd for $[Co(acac)_2(bpy)]ClO_4 \cdot 0.5H_2O$: C, 46.03; H, 4.44; N, 5.37%.

4) $[Co(acac)_2(phen)]^+$: The racemate, $[Co(acac)_2(phen)]ClO_4$ (5 g) and an anion exchange resin (Dowex 1-X8, Cl^- form, 20 g) were combined and stirred for 20 min in 250 cm^3 of methanol. The resin was filtered and washed with 20 cm^3 of methanol. The combined filtrate and washings were treated with a second portion (6 g) of resin. The resin was filtered and washed with 20 cm^3 of methanol. To the combined filtrate and washings were added silver dibenzoyl-*d*-tartrate (2.67 g) and dibenzoyl d-tartaric acid monohydrate (1.75 g) and the mixture was stirred for 10 min at 60 °C. Silver chloride was removed and washed with 30 cm^3 of hot methanol. To the combined filtrate and washings was added 90 cm^3 of ether and the resulting solution was cooled in a refrigerator. Fraction 1 (4.19 g) was separated by filtration. Fraction 2 (1.66 g) and fraction 3 (0.42 g) were obtained by further addition of ether and subsequent cooling. The filtrate (A) after the separation of the third fraction was used for the isolation of the opposite enantiomer. The solid fraction 1 (4.19 g) was dissolved in 560 cm^3 of methanol and 840 cm^3 of ether was added and the resulting solution was cooled in a refrigerator. The fraction 1—1 (1.99 g) was separated by filtration and the fractions 1—2 (0.85 g) and 1—3 (0.42 g) were obtained by the same method described above. The filtrate (B) after the separation of fraction 1—3 was also used for the isolation of the opposite enantiomer. Fraction 1—1 (1.99 g) was dissolved in 300 cm^3 of methanol and 500 cm^3 of ether was added and the resulting solution was cooled in a refrigerator. Two fractions were separated by fractional crystallization. Then, the various fractions with similar $\Delta\varepsilon$ values were combined and purified. Again, fractions of similar $\Delta\varepsilon$ were combined and purified. This kind of purification was repeated many times. Finally, 1.04 g of one diastereomer was obtained. This diastereomer was treated with an anion exchange resin (Dowex 1-X8, Cl^- form) in methanol to obtain the chloride salt. The resin was separated and ether was added to the methanol solution. Two fractions with low $\Delta\varepsilon$ value were separated, and the filtrate was evaporated to dryness under an air stream. The solid obtained by evaporation was purified twice by dissolving in methanol, adding ether and subsequent cooling in a refrigerator. Finally, brownish-violet flaky crystals were separated. Yield 92 mg. $\Delta\varepsilon_{523} = -2.30$ (solvent : water). Found: C, 53.69; H, 4.62; N, 5.24%. Calcd for $[Co(acac)_2(phen)]Cl \cdot H_2O$: C, 53.83; H, 4.93; N, 5.71%.

The filtrates (A) and (B) described above were combined and concentrated to 75 cm^3 using a rotary evaporator, and 150 cm^3 of ether was added. The resulting solution was cooled in a refrigerator. The first fraction (0.63 g) was separated by filtration. The filtrate was concentrated to 50 cm^3 with a rotary evaporator, 150 cm^3 of ether was added, the resulting solution was cooled in a refrigerator. Fraction 2 (0.34 g) and the fraction 3 (0.34 g) were separated in the same way. Fraction 1 was dissolved in 40 cm^3 of methanol, 70 cm^3 of ether was added and the resulting solution was kept in a refrigerator. The less active diastereomer (1—1) separated first and was filtered. This filtrate was evaporated to dryness to yield fraction 1—2 (0.19 g). The fractions 2, 3, and 1—2 were combined and treated in the same way as that of the other isomer. Finally, brownish-violet flaky crystals were obtained. Yield 0.28 g. $\Delta\varepsilon_{523} = +2.15$ (solvent : water). Found: C, 50.49; H, 5.55; N, 5.57%. Calcd for $[Co(acac)_2(phen)]Cl \cdot 3H_2O$: C, 50.15; H, 5.35; N, 5.31%.

The increase of $\Delta\varepsilon$ with each purification of the diastereomer was very small. Therefore, many purification steps were necessary.

5) $[Co(acac)_2(en)]^+$ and $[Co(acac)_2(tn)]^+$: These optical resolutions were carried out according to the methods reported.[7]

Measurements. Absorption spectra were obtained with a HITACHI 323 Recording Spectrophotometer and a Cary

14 spectrophotometer. CD spectra were measured with a J-20 Spectropolarimeter of Japan Spectroscopic Company and a Cary 61 recording spectropolarimeter. Optical isomers are identified by the sign of the CD in water at a specified wavelength. PMR spectra were measured with a Varian A-60 Spectrometer in a deuterium oxide solution containing sodium trimethylsilylpropanesulfonate(DSS) as the internal standard.

Ethanol and dimethyl sulfoxide for the measurements of absorption and CD spectra were spectroscopic grade.

Results and Discussion

Preparation and Properties. So far much attention has been paid to the tris-type complexes of cobalt(III) with identical bidentate ligands which have $\pi^*\leftarrow\pi$ ligand transitions, *e.g.*, $[Co(phen)_3]^{3+}$, for CD studies.[6] The complexes with two different ligands, *e.g.*, $[Co(bpy)_2(phen)]^{3+}$, have not been reported, presumably because of the difficulty of their preparation and optical resolution. Archer *et al.*[3,4] prepared $[Co(acac)_2(bpy)]^+$ and $[Co(acac)_2(phen)]^+$ by the reaction of bpy and phen, respectively, with $[Co(acac)_2(NO_2)_2]^-$. We attempted to prepare $[Co(acac)(bpy)_2]^{2+}$ and $[Co(acac)(phen)_2]^{2+}$ by the same reaction using increased amounts of bpy and phen, but disproportionation occurred. Then we tried the reactions of $[Co(CO_3)(bpy)_2]^+$ and $[Co(CO_3)(phen)_2]^+$ with acetylacetone instead of acetylacetonate ion. The yields were raised to about 20% by improving the reaction conditions, especially the reaction temperature and the amount of alcohol.

The optical resolution of these four complexes proved to be very difficult. To resolve $[Co(acac)(bpy)_2]I_2$ and $[Co(acac)_2(bpy)]I$, we used six resolving agents unsuccessfully: silver *d*-tartrate, silver dibenzoyl-*d*-tartrate, silver antimonyl *d*-tartrate, silver arsenyl-*d*-tartrate, silver *d*-α-bromocamphor-π-sulfonate and $(+)_{580}$-Ag[Co(edta)] (edta=ethylenediaminetetraacetate ion). For the optical resolution of $[Co(acac)_2(phen)]ClO_4$ five resolving agents were tried: silver *d*-α-bromocamphor-π-sulfonate, $(+)_{580}$-Ag[Co(edta)], $(-)_{561}$-Ag[Co(tmdda)(ox)][8] (tmdda = trimethylenediamine-*N*,*N*′-diacetate, ox=oxalate), a combination of silver *d*-tartrate and *d*-tartaric acid, and a combination of silver dibenzoyl *d*-tartrate and dibenzoyl *d*-tartaric acid monohydrate. In all trials the racemate was changed into the chloride salt using an anion exchange resin (Dowex 1-X8, Cl^- form) before the addition of resolving agents. The first four resolving agents were not effective at all, even though a mixture of both diastereomers was obtained. The last resolving agent showed the possibility of the separation of diastereomers, but the resolution was very laborious and took a long time. Therefore, the resolutions of the other complexes using these resolving agents were not tried. We attempted to use a SP-Sephadex resin which has been used for the isolation and optical resolution of cobalt(III) complexes.[9] The optically active forms for the other three complexes were obtained in this way, but complete resolution was not achieved. Low yields were obtained because of the small capacity of the resin. Although we tried to elute the complexes two times as described (Experimental), the increase of $\Delta\varepsilon$ for the complexes the second time was small.

PMR spectra of $[Co(acac)(bpy)_2]Cl_2\cdot 6H_2O$ and $[Co(acac)(phen)_2]Cl_2\cdot 4.5H_2O$ were measured. The chloride salts, which are more soluble than the perchlorates, were obtained using anion exchange columns. The former complex shows a methyl resonance at 2.28 ppm and a methine resonance at 6.11 ppm (δ relative to DSS). The latter complex shows a methyl resonance at 2.55 ppm and a methine resonance at 6.47 ppm. These signals show significant downfield shifts, especially for the methine resonances, compared to $[Co(acac)(en)_2]I_2$ (a methyl resonance at 2.17 ppm and a methine resonance at 5.78 ppm in D_2O solution[10]). This may be a consequence of the magnetic aniostropy of bpy and phen. The resonances of the bpy and phen ligands were observed at 7.7—9.7 ppm although these regions were not analyzed. The spectral pattern of $[Co(acac)(phen)_2]^{2+}$ in the region of the phenanthroline ligand is slightly different from that of $[Co(en)(phen)_2]^{3+}$.[11]

Circular Dichroism and Absolute Configuration. Figures 1 and 2 show the CD spectra and visible and ultraviolet absorption spectra in water and in ethanol for $[Co(acac)(bpy)_2](ClO_4)_2\cdot 1.5H_2O$ and $[Co(acac)(phen)_2](ClO_4)_2\cdot 0.5H_2O$, respectively, in the first eluates from a Sephadex column. For the absorption spectrum of $[Co(acac)(bpy)_2]^{2+}$, the first d-d band (~20000 cm^{-1}) and $\pi^*\leftarrow\pi$ ligand bands (33000—34000 cm^{-1}) are evident. The split exciton CD bands at about 34000 cm^{-1} are positive and then negative from lower energy, indicating a *A* configuration.[12] The positions of the exciton CD bands are similar to those of $[Co(bpy)_3]^{3+}$ (at 32500 cm^{-1}) and $[Co(bpy)_2(ox)]^+$ (at 33000 cm^{-1}).[13] The corresponding $\pi^*\leftarrow\pi$ absorption peaks for the

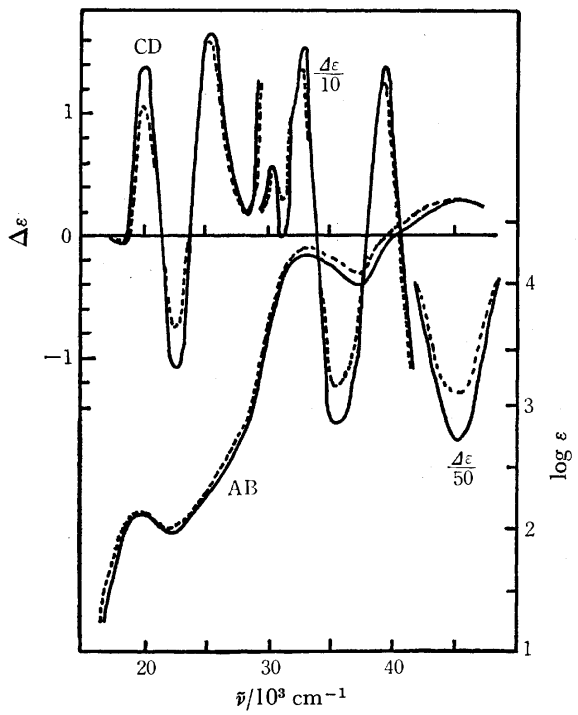

Fig. 1. Absorption (AB) and CD spectra of $(+)_{495}$-$[Co(acac)(bpy)_2]^{2+}$, in water (—) and in ethanol (---).

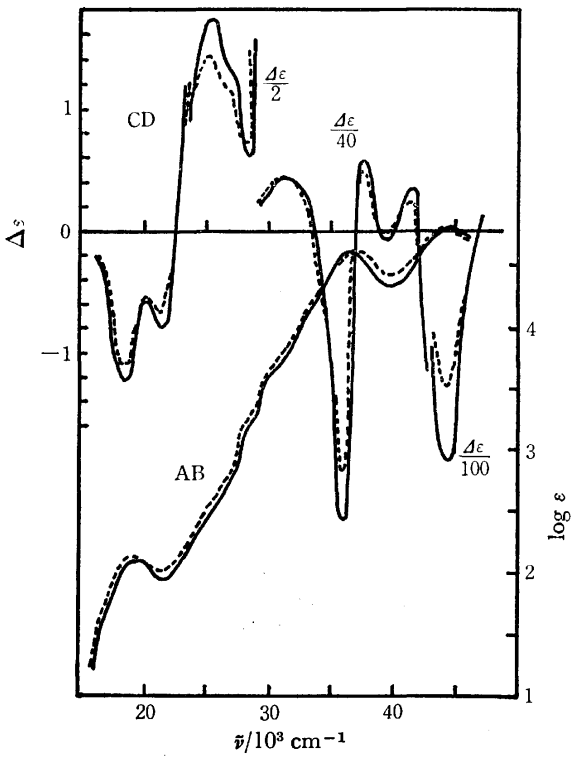

Fig. 2. Absorption (AB) and CD spectra of $(-)_{543}$-$[Co(acac)(phen)_2]^{2+}$, in water(—) and in ethanol(---).

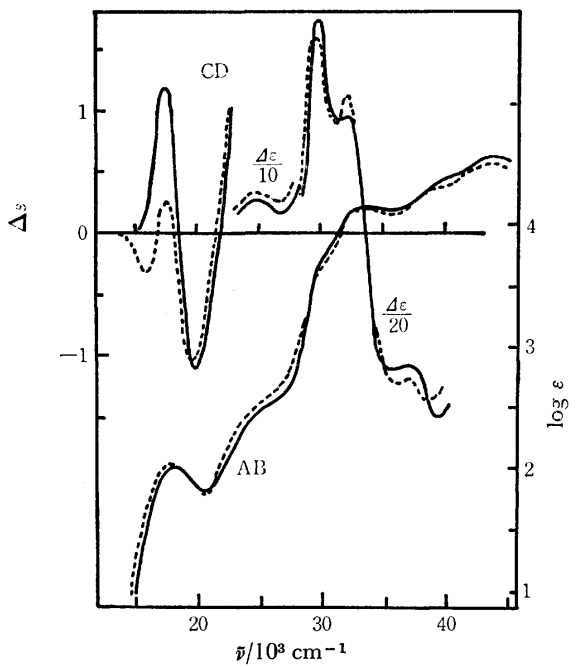

Fig. 3. Absorption (AB) and CD spectra of $(-)_{505}$-$[Co(acac)_2(bpy)]^+$, in water(—) and in ethanol(---).

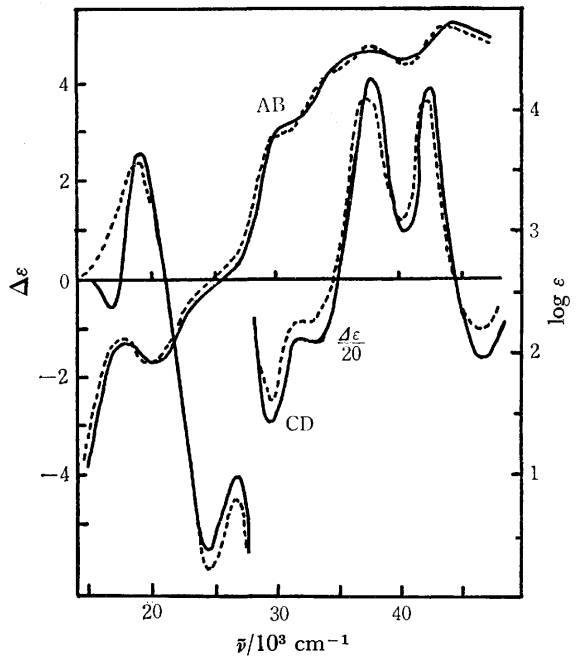

Fig. 4. Absorption (AB) and CD spectra of $(+)_{523}$-$[Co(acac)_2(phen)]^+$, in water (—) and in ethanol(---).

$[Co(acac)(phen)_2]^{2+}$ ion are observed at 36600 cm^{-1}, where the CD spectrum gives a negative and a positive band from lower energy, indicating the opposite or *Δ* configuration. The split exciton CD bands at about 37000 cm^{-1} correspond to those of $[Co(phen)_3]^{3+}$ (at 36300 cm^{-1}) and $[Co(phen)_2(ox)]^+$ (at 36800 cm^{-1}).[13] The CD curves in the visible region are quite different for the bpy and phen complexes. In each case one CD peak appears near the trough between the first d-d absorption band $[T_{1g}(O_h)]$ and the shoulder at higher energy, where the $T_{2g}(O_h)$ band is expected. Although assignments of the individual CD components cannot be made, the signs of the dominant CD peak (or the net rotational strength) in the T_{1g} region are consistent with the *Λ* configuration for $[Co(acac)(bpy)_2]^{2+}$ (Fig. 1, net positive) and **Δ** for $[Co(acac)(phen)_2]^{2+}$ (Fig. 2, net negative). The absorption spectra for $[Co(acac)(bpy)_2]^{2+}$ and $[Co(acac)(phen)_2]^{2+}$ in ethanol show slight red shifts relative to those in water. The CD spectral patterns in these solvents are almost the same, although the intensities of the peaks are slightly different.

In the case of the complexes containing two acetylacetonate ligands, the absorption spectra are very similar in water and in ethanol (Figs. 3, 4, 6. and 7). The CD spectra are also affected only to a small extent except in the region of the first absorption band. The CD spectrum of $[Co(acac)_2(bpy)]^+$ (Fig. 3, the isomer shown is from the first eluate from a Sephadex column) in ethanol shows three well-defined peaks of alternating signs in the first absorption band region, while in water there are only two peaks. For $[Co(acac)_2(phen)]^+$ (the enantiomer shown in Fig. 4 is from the more soluble diastereoisomer with hydrogen dibenzoyl *d*-tartrate) only one CD peak appears in ethanol in this spectral region, while two peaks appear in water. Note that the CD spectra throughout the d-d absorption region (Figure 5) are similar for $[Co(acac)_2(phen)]^+$ in dimethyl sulfoxide and in a KBr disc to that in ethanol. The solvent effects appear to be more remarkable in the case of $[Co(acac)_2(en)]^+$ and $[Co(acac)_2(tn)]^+$ (Figs. 6 and 7). In both cases there are two CD peaks in the first absorption band region for each solvent, but the lowest energy peak appears to change sign. It

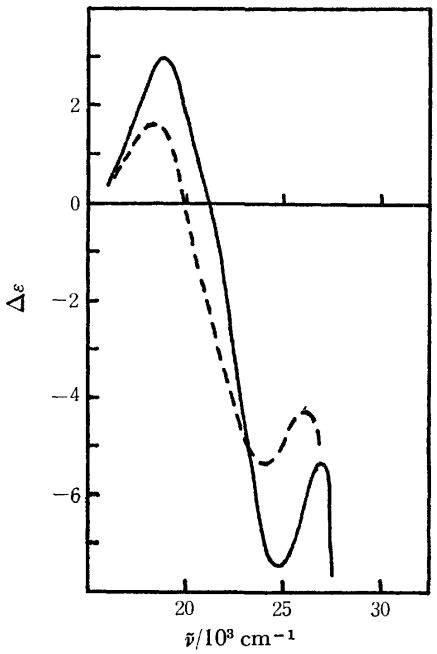

Fig. 5. CD spectra of $(+)_{523}$-$[Co(acac)_2(phen)]^+$, in dimethyl sulfoxide (—) and KBr disc(---) (arbitrary scale).

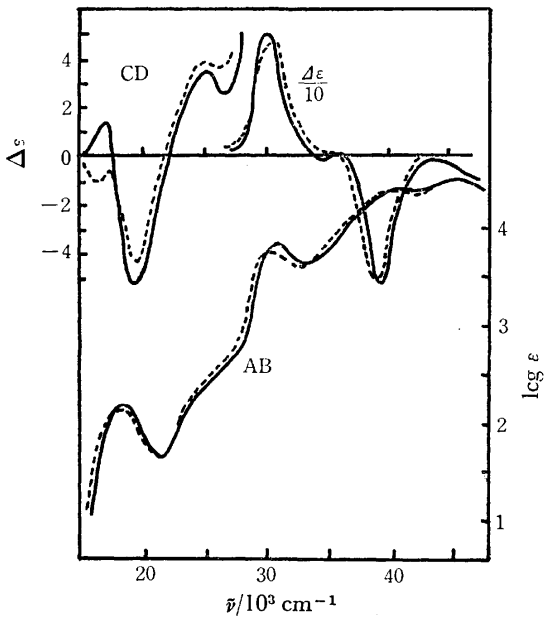

Fig. 6. Absorption (AB) and CD spectra of $(-)_{510}$-$[Co(acac)_2(en)]^+$, in water (—) and in ethanol(---).

should be noted that for both complexes the lowest energy (negative) CD peak is at lower energy in ethanol than the lowest energy (positive) peak in water.

The patterns of the CD spectra in the region of the first absorption band (Figs. 3, 4, 6, and 7) are not so erratic as might appear at first. For each of the four complexes, two CD peaks of opposite sign appear in water. The number of peaks and their signs vary in ethanol, except that the curves are similar for $[Co(acac)_2(en)]^+$ and $[Co(acac)_2(tn)]^+$. The variations are more

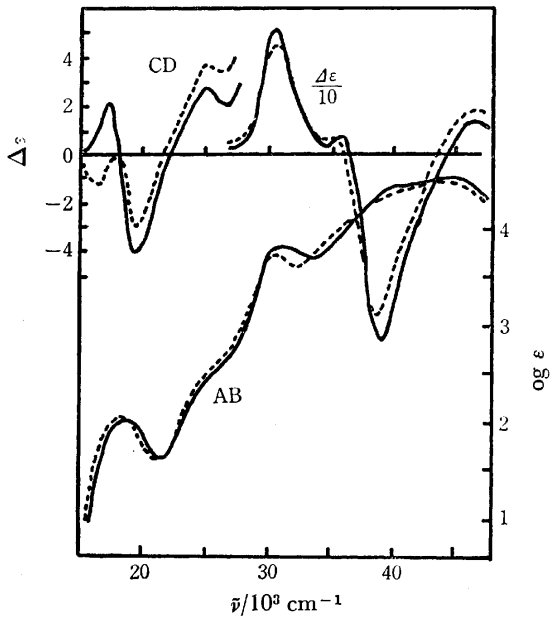

Fig. 7. Absorption (AB) and CD spectra of $(-)_{512}$-$[Co(acac)_2(tn)]^+$, in water (—) and in ethanol(---).

comprehensible if one considers the actual symmetry of the complexes, C_2. Three CD components are expected in the first absorption band region for C_2 symmetry, although often fewer components appear because of overlap resulting from small splittings. Three CD peaks actually appear for $[Co(acac)_2(bpy)]^+$ in ethanol. If one considers that there are actually three closely spaced components of alternating signs in each case, all of the spectra can be understood. It is expected that solvent changes or the addition of electrolytes will affect the relative intensities of the component and, to a lesser extent, their energies. The dominant component at highest energy in the first absorption band region, however, shows very slight solvent effect. For $[Co(acac)_2(bpy)]^+$ a lowering of the intensity of the lowest energy (negative) CD peak, or an increase of the intensity of the center (positive) CD peak, in going from ethanol to water would result in the two CD peaks observed in water (Fig. 3). The slight shift in the position of the positive peak toward lower energy in water would result from less cancellation by the lower energy negative peak. In the case of $[Co(acac)_2(phen)]^+$ (Fig. 4), the dominant CD peak in the first absorption band is positive, opposite in sign to that of $[Co(acac)_2(bpy)]^+$. In ethanol it would appear that the lowest energy component (also positive) for $[Co(acac)_2(phen)]^+$ completely cancels the middle (negative) component, resulting is a single positive CD peak. The middle (negative) peak shows up in water, because of lowering of intensity of the lowest energy component (or increase in intensity of the middle component). The CD curves for both $[Co(acac)_2(en)]^+$ and $[Co(acac)_2(tn)]^+$ (Figs. 6 and 7) in the first absorption band show two peaks of the same sign in ethanol, presumably the lowest and highest energy components, with the middle positive component being cancelled completely. For these complexes, two peaks of opposite sign appear in

water, with the lowest energy (negative) peak being cancelled completely.

The similarity of the CD patterns in the first band region in water for all complexes and the sign of the solvent insensitive intense peak on the higher energy side of the first absorption band provide a basis of relating the absolute configurations of the complexes. The sign of this peak is the same as the sign of the net rotational strength for the first absorption band region in each case. The CD spectral pattern for $(+)_{510}$-$[Co(acac)_2(en)]^+$ (the enantiomer of the isomer in Fig. 6) in water is strikingly similar up to 40000 cm^{-1} to that of Λ-$[Co(acac)_3]$, whose absolute configuration was determined by X-ray analysis.[14] Accordingly, $(+)_{510}$-$[Co(acac)_2(en)]^+$ should have the Λ configuration, as also assigned by Boucher[15] based on the sign of the dominant CD peak in the first band region. The enantiomers $(-)_{510}$-$[Co(acac)_2(en)]^+$ (Figure 6), $(-)_{512}$-$[Co(acac)_2(tn)]^+$ (Fig. 7), and $(-)_{505}$-$[Co(acac)_2(bpy)]^+$ (Fig. 3) have the Δ configuration and $(+)_{523}$-$[Co(acac)_2(phen)]^+$ (Fig. 4) has the Λ configuration. These assignments, based on the spectral sign pattern of Λ-$[Co(acac)_3]$, agree with those made based on the sign of the net rotational strength or of the intense solvent insensitive CD peaks in the first absorption band region.

The ultraviolet CD curves for $[Co(acac)_2(bpy)]^+$ and $[Co(acac)_2(phen)]^+$ are not very helpful in confirming the assignment of absolute configurations. The CD peaks for $[Co(acac)_2(bpy)]^+$ in the 32000—35000 cm^{-1} region (Fig. 3) overlap other peaks, so one cannot make reliable distinctions between charge transfer and possible exciton bands in this region. The $\pi^*\leftarrow\pi$ excition CD bands for other bis(acac) complexes have been observed at 40000 cm^{-1} or higher energy.[15] The characteristic split exciton CD bands require the coupling of two or more ligands with π-electron systems. No splitting of the $\pi^*\leftarrow\pi$ CD band occurs for $[Co(en)_2(phen)]^{3+}$ where there is only one ligand with a π-electron system.[17] The $\pi^*\leftarrow\pi$ transitions differ in energy for acac and bpy and it appears that such coupling between these ligands is not effective. If the absorption peak for $[Co(acac)_2(phen)]^+$ at *ca.* 43000 cm^{-1} corresponds to the $\pi^*\leftarrow\pi$ transition for acac, then the two CD peaks in this region, positive (at lower energy) and negative, could be the split exciton bands. This sign pattern is consistent [16] with the Λ configurations assigned from the first d-d band.

The encouragement and support of Professor Kazuo Saito during the part of the work carried out at Tohoku University are gratefully acknowledged.

References

1) Research Associate 1972—1973, University of Pittsburgh. Present Address: Department of Chemistry, Tohoku University, Sendai 980 Japan. Author to whom correspondence should be addressed.
2) Present Address: Department of Chemistry, The University of Tsukuba, Ibaraki 300—31 Japan.
3) R. D. Archer and B. P. Cotsoradis, *Inorg. Chem.*, **4**, 1584 (1965).
4) R. J. York, W. D. Bonds, Jr., B. P. Cotsoradis, and R. D. Archer, *Inorg. Chem.*, **8**, 789 (1969).
5) K. Konya and B. E. Douglas, *Inorg. Nucl. Chem. Lett.*, **10**, 491 (1974).
6) C. J. Hawkins, "Absolute Configuration of Metal Complexes," Wiley-Interscience, London (1971).
7) B. J. Brennan. K. Igi, and B. E. Douglas, *J. Coord. Chem.*, **4**, 19 (1974).
8) K. Igi and B. E. Douglas, *Inorg. Chim. Acta*, **10**, 109 (1974).
9) Y. Yoshikawa and K. Yamazaki, *Bull. Chem. Soc. Jpn.*, **46**, 3448 (1973).
10) L. J. Boucher, E. J. Battis, and N. G. Paez, *J. Inorg. Nucl. Chem.*, **33**, 1373 (1971).
11) H. Ito, J. Fujita, and T. Ito, *Bull. Chem. Soc. Jpn.*, **44**, 723 (1971).
12) B. Bosnich, *Acc. Chem. Res.*, **2**, 266 (1969).
13) J. Ferguson, C. J. Hawkins, N. A. P. Kane-Maguire, and H. Lip, *Inorg. Chem.*, **8**, 771 (1969).
14) R. B. Von Dreele and R. C. Fay, *J. Am. Chem. Soc.*, **93**, 4936 (1971).
15) L. J. Boucher, *Inorg. Chem.*, **9**, 1202 (1970).
16) S. Kaizaki, J. Hidaka, and Y. Shimura, *Inorg. Chem.*, **12**, 135 (1973).
17) J. Hidaka and B. E. Douglas, *Inorg. Chem.*, **3**, 1180 (1964).

Spectral Properties of Mixed Ligand Copper(II) Complexes Containing L-α-Amino Acids

Takeshi SAKURAI, Osamu YAMAUCHI, and Akitsugu NAKAHARA

Institute of Chemistry, College of General Education, Osaka University, Toyonaka, Osaka 560

(Received March 4, 1976)

Absorption and circular dichroism (CD) spectral behaviors of ternary copper(II) complexes containing two L-α-amino acids or an L-α-amino acid and iminodiacetate (ida), 2,2′-bipyridine (bpy), 2-pyridinecarboxylate (pca), or 2,6-pyridinedicarboxylate (pdca), have been studied comparatively, and synthetic studies have given as crystals the mixed ligand complexes, [Cu(ida)(L-arg)]·$2H_2O$, [Cu(ida)(L-orn)]·$2H_2O$, [Cu(ida)(L-lys)]·$1/4H_2O$, [Cu(pdca)(L-arg)]·H_2O, and [Cu(pdca)(L-orn)]·$2.5H_2O$, where L-arg, L-orn, and L-lys denote L-arginine, L-ornithine, and L-lysine, respectively. The CD magnitudes of the systems Cu(ida)(L-arg), Cu(ida)(L-orn), and Cu(ida)(L-lys) were found to be enhanced appreciably as compared with the magnitudes estimated from the values for the corresponding binary systems. These ternary systems showed further magnitude enhancements in 50% aqueous ethanol. The enhanced magnitudes observed for Cu(L-glu)(L-arg), where L-glu is L-glutamate, were also intensified in 10, 20, and 50% aqueous ethanol, whereas they were weakened nearly to the estimated values in aqueous solutions with higher ionic strengths (μ=0.1 and 0.5($NaClO_4$)). These observations support the view that the pairs of ligands constituting the above ternary complexes are fixed around copper(II) by electrostatic ligand-ligand interactions between the oppositely charged side chains. Pyridine-containing ligands, bpy, pca, and pdca, in the ternary systems with L-α-amino acids affected the signs and the magnitudes of the CD spectra.

Mixed ligand complexes as potential biological models have been studied most extensively by the potentiometric method, which has made available valuable information about the stabilities and distributions of complex species in solution.[1,2] Because of the biological importance of copper, a great deal of attention has been paid to the ternary copper(II) complexes containing optically active amino acids and peptides, where circular dichroism (CD) has often proved to be a more direct and effective source of information.[3,4]

In our previous studies on the ternary copper(II) systems composed of α-amino acids and related compounds,[5,6] the synthetic and spectroscopic findings have been interpreted as supporting the existence of the intramolecular electrostatic ligand-ligand interactions between the oppositely charged side groups around the central copper(II) ion as tentatively shown in Scheme 1. Facile isolation of the corresponding

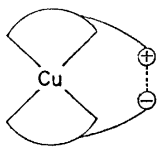

Scheme 1.

mixed ligand complexes implicated that such electrostatic bondings served as a driving force leading to the formation of mixed ligand complexes. While the ternary systems without the possibility of the ligand-ligand interactions exhibited the CD magnitudes equal to those estimated from the corresponding binary systems, most of the ternary systems expected to involve such interactions were accompanied by magnitude enhancements probably due to the structural rigidity.[5,6]

Martin and Prados[7] detected a CD magnitude enhancement and sign inversions for the systems Cu(2,2′-bipyridine)(L-phenylalanine) and Cu(2,2′-bipyridine)(L-alanine or L-leucine), respectively, and they ascribed the behaviors to the presence of the pyridine ring as a π-acceptor. On the other hand, Tsangaris and Martin[8] observed that the magnitudes were additive in the Cu(dipeptide) series.

Interests in the structural and spectral properties of the ternary systems and the demand for the relevant information prompted us to investigate the visible absorption and CD spectra of various ternary copper(II) systems containing two L-α-amino acids or an L-α-amino acid and iminodiacetate (ida), 2,2′-bipyridine (bpy), 2-pyridinecarboxylate (pca), or 2,6-pyridinedicarboxylate (pdca) under different conditions. We isolated for the present purpose several copper(II) complexes, Cu(A)(B), containing iminodiacetate or 2,6-pyridinedicarboxylate as ligand A and L-arginine (L-arg), L-ornithine (L-orn), or L-lysine (L-lys) as ligand B. The present paper describes the results obtained therefrom and the discussion of the structures and spectral behaviors of the ternary systems.

Experimental

Materials. L-Arginine, L-lysine dihydrochloride, L-ornithine monohydrochloride, L-glutamic acid (L-glu), L-aspartic acid (L-asp), L-alanine (L-ala), L-valine (L-val), iminodiacetic acid, 2,2'-bipyridine, 2-pyridinecarboxylic acid, and 2,6-pyridinedicarboxylic acid were purchased from Nakarai Chemicals, Ltd. All the chemicals used were of reagent grade or of highest grade available.

Synthesis of Mixed Ligand Copper(II) Complexes. [*Cu(ida)(L-lys)*]·*1/4H₂O.* Iminodiacetic acid (0.67 g, 5 mmol), L-lysine dihydrochloride (1.10 g, 5 mmol), and copper(II) perchlorate hexahydrate (1.85 g, 5 mmol) were dissolved in 30 ml of water, and the pH of the solution was adjusted at 7 with aqueous sodium hydroxide. After stirring for 1 h at room temperature the solution was concentrated *in vacuo* and filtered. Methanol was added to the filtrate to give blue crystals, which were recrystallized from aqueous methanol. Found: C, 34.88; H, 5.62; N, 12.25%. Calcd for $C_{10}H_{19}N_3O_6Cu \cdot 1/4H_2O$: C, 34.77; H, 5.69; N, 12.17%.

The following complexes were prepared at pH 7—10 in similar manners.

[Cu(ida)(L-arg)]·2H₂O. Found: C, 29.38; H, 5.58; N, 17.39%. Calcd for $C_{10}H_{19}N_5O_6Cu\cdot 2H_2O$: C, 29.66; H, 5.70; N, 17.30%.

[Cu(ida)(L-orn)]·2H₂O. Found: C, 29.88; H, 5.41; N, 11.41%. Calcd for $C_9H_{17}N_3O_6Cu\cdot 2H_2O$: C, 29.79; H, 5.84; N, 11.58%.

[Cu(pdca)(L-arg)]·H₂O. Found: C, 37.29; H, 4.70; N, 16.34%. Calcd for $C_{13}H_{17}N_5O_6Cu\cdot H_2O$: C, 37.10; H, 4.55; N, 16.64%.

[Cu(pdca)(L-orn)]·2.5H₂O. Found: C, 35.19; H, 5.15; N, 10.22%. Calcd for $C_{12}H_{15}N_3O_6Cu\cdot 2.5H_2O$: C, 35.51; H, 4.97; N, 10.35%.

Measurements of Absorption and CD Spectra. The spectroscopic measurements were performed in water or in aqueous ethanol at room temperature for the systems with the copper(II) : A : B ratios of 1 : 1 : 1 (ternary systems) and 1 : 2 : 0 and 1 : 0 : 2 (binary systems) at pH 5—11 at a copper(II) concentration of 5×10^{-3} M. The spectral samples were prepared from 0.1 M stock solutions of the ligands and copper(II) perchlorate. Because of the low solubility of 2,2′-bipyridine in water, a Cu(II)-bpy solution was used for preparation of the bpy-containing samples. The pH values were roughly adjusted with aqueous sodium hydroxide and dilute perchloric acid and finally determined after the spectroscopic measurements. The spectra of the Cu(L-glu)(L-arg) system were measured at different ionic strengths (μ) adjusted with sodium perchlorate. For the rest of the systems the ionic strengths of the solutions were not adjusted (μ= variable). Absorption spectra were recorded in the range 400—800 nm on a Union Giken SM-401 High Sensitivity recording spectrophotometer. CD spectra were measured in a 1- or 2-cm path length quartz cell in the range 350—800 nm with a JASCO MOE-1 spectropolarimeter.

Results and Discussion

Preparation of Mixed Ligand Copper(II) Complexes. Since iminodiacetate has a flexible molecular structure, it can be coordinated to copper(II) as a bidentate ligand, forming through the remaining carboxylate group electrostatic bondings with the positive group of the basic amino acid coordinated to the same copper(II) ion (**1**). Thus, iminodiacetate and the amino

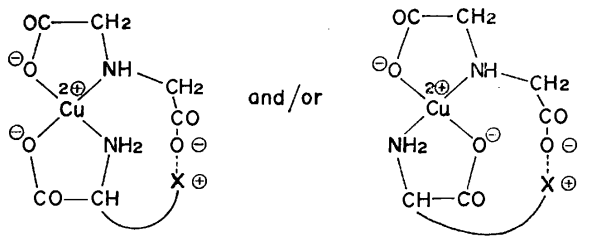

1

acids afforded the complexes [Cu(ida)(L-arg)], [Cu(ida)(L-orn)], and [Cu(ida)(L-lys)]. Although isolation of a ternary complex depends both on the stability and the solubility, it gives evidence of occurrence of a considerable amount of the ternary complex.

On the other hand, the inflexibility of the structure of pdca seems to affect the ternary complex formation, because attempts to prepare [Cu(pdca)(L-lys)] resulted in isolation of $Na_2[Cu(pdca)_2]$ under the conditions employed. Molecular models suggest that the interactions as illustrated in Scheme 1 are sterically unlikely to occur, so that the successful preparation of [Cu(pdca)(L-arg)] and [Cu(pdca)(L-orn)] might be ascribed to the statistical effect[9] and the complex-stabilizing effect of the pyridine ring as a π-acceptor.[7,10] The absorption spectral data of the ternary systems in the visible region (Table 1) apparently indicate the presence of rather large amounts of the binary species $Cu(pdca)_2$ and $Cu(B)_2$ in consequence of the lower stabilities of the ternary complexes.

Effects of Ionic Strength and Polarity of Solvent on the CD Magnitude. For the ternary systems with possible ligand-ligand interactions, the CD magnitudes expressed in terms of the relative magnitude, which assumes as unity the sum of the half magnitude ($1/2\Delta\varepsilon$) exhibited by each of the optically active ligands in the complex, have been found to be larger than unity.[5,6] In accordance with the observation about the Cu(edma)(B) systems,[5] where edma refers to ethylenediamine-*N*-monoacetate, the enhanced magnitude for the Cu(L-glu)(L-arg) system[6] has now been shown to be affected by the ionic strength of the solution and the polarity of the solvent used. The relative magnitude thus decreased from 1.3 (μ=variable) to 1.1 (μ=0.1) and 1.05 (μ=0.5) (Table 2). It might be suspected that the magnitude decrease at higher ionic strengths would result from the enhanced magnitudes for the binary systems to be compared. However, the molar extinction coefficients (ε) for the binary and ternary systems remain constant at different μ values (Table 2), indicating that the observed decrease is not due to the shifts of the equilibria. We may therefore infer that the decrease is caused by the weakened ligand-ligand interactions at higher salt concentrations. The magnitude increase in 10, 20, and 50% aqueous ethanol confirms that the interactions are electrostatic attractions which are favored in non-aqueous solvent.

L-orn-Containing Ternary Systems. The δ-amino group of ornithine is known to form an apical bonding with copper(II).[5,11,12] We observed in the previous study[6] that the systems Cu(L-asp)(L-orn) and Cu(L-glu)(L-orn) suffered complex CD spectral changes at pH>8. Figure 1 illustrates the pH dependence of their spectra, whose numerical data are summarized in Table 3. Since aspartate binds with copper(II) as a terdentate ligand with the β-carboxylate group at the apical position,[13] the spectral behaviors suggest that L-asp and possibly L-glu compete with the δ-amino group of L-orn for the apical coordination.

ida-Containing Ternary Systems. Table 4 shows that the absorption maxima of the Cu(ida)(B) systems ($\approx$665 nm) are between those of $Cu(B)_2$ ($\approx$620 nm) and $Cu(ida)_2$ (682 nm) and expectedly at longer wavelengths than those observed for the systems Cu(edma)(B) ($\approx$620 nm).[5]

The relative CD magnitudes for the Cu(ida)(B) systems in aqueous solution are 1.2—2.0 and are enhanced up to >1.7 in 50% aqueous ethanol (Table 4). These values are comparable with those of the systems containing two L-amino acids with charged side chains[6] but somewhat lower than those exhibited by the Cu(edma)(B) systems.[5] Both edma and ida may affect the CD spectra through molecular asymmetry originat-

TABLE 1. ABSORPTION SPECTRAL DATA FOR THE PYRIDINE-CONTAINING TERNARY SYSTEMS Cu(A)(B) (μ=variable)

Ligand B	Ligand A: pca			bpy			pdca		
	pH	ε	λ_{max}(nm)	pH	ε	λ_{max}(nm)	pH	ε	λ_{max}(nm)[a]
L-arg	9.9	48	636	10.0	59	611	9.9	38	739
	10.2[a]	60	638				10.5[a]	39	748
L-lys	9.8	49	632	9.2	58	608	10.0	38	710
	9.8[a]	61	636				10.0[a]	37	713
L-orn	not measured			7.5	58	607	7.9	37	737
				10.1	61	619	8.0[a]	38	746
							10.0	40	734
							10.2[a]	43	730
L-ala	8.9	49	633		59[b]	604[b]	9.9	37	740
	8.0[a]	59	636				10.7[a]	37	750
L-val	9.9	50	631		60[b]	604[b]	9.8	38	741
	10.1[a]	58	635				10.2[a]	38	750
L-glu	9.9	50	632	9.8	60	596	not measured		
	10.6[a]	59	638						
L-asp	not measured			8.7	53	614	not measured		

a) Measured in 50% aqueous ethanol. The pH values are pH meter readings. b) Taken from Ref. 7. c) The peaks were usually broad with a shoulder at 620—630 nm, which is indicative of the binary species Cu(L-amino acid)$_2$.

TABLE 2. EFFECTS OF IONIC STRENGTH AND POLARITY OF SOLVENT ON THE ABSORPTION (AB) AND CD SPECTRA FOR THE Cu(L-glu)(L-arg) SYSTEM

Medium[a]	Cu(L-glu)$_2$ pH	CD $\Delta\varepsilon$	CD λ_{max} (nm)	AB ε	AB λ_{max} (nm)	Cu(L-arg)$_2$ pH	CD $\Delta\varepsilon$	CD λ_{max} (nm)	AB ε	AB λ_{max} (nm)	Cu(L-glu)(L-arg) pH	CD $\Delta\varepsilon$	CD λ_{max} (nm)	AB ε	AB λ_{max} (nm)	Relative CD magnitude[b]
water (μ=var.)	8.5	-0.12_2	613	56	622	8.5	-0.11_1	598	56	622	8.5	-0.14_7	598	56	622	1.2_6
10% aq. ethanol	8.3	-0.12_3	612	59	619	7.9	-0.10_0	580	57	622	8.1	-0.15_6	601	59	621	1.3_4
20% aq. ethanol	8.2	-0.12_6	614	61	620	8.0	-0.10_1	580	58	620	8.5	-0.15_7	602	61	620	1.3_8
50% aq. ethanol	7.8	-0.13_8	616	62	620	8.1	-0.10_3	568	61	620	7.9	-0.17_3	600	63	620	1.4_4
water (μ=0.1)	7.7	-0.11_9	612	57	622	7.7	-0.12_0	592	55	622	7.6	-0.13_4	599	57	622	1.1_2
10% aq. ethanol (0.1 M $NaClO_4$)	8.7	-0.12_3	612	59	620	8.1	-0.12_0	586	56	622	8.3	-0.14_4	598	59	621	1.1_8
water (μ=0.5)	7.8	-0.13_2	615	57	622	7.7	-0.14_1	590	56	622	7.7	-0.14_3	607	57	622	1.0_5

a) Ionic strengths were adjusted with $NaClO_4$. The pH values in aqueous ethanol are pH meter readings.
b) Relative CD magnitude refers to $\Delta\varepsilon_{max}$(found)/$\Delta\varepsilon_{max}$(calcd).

ing from their fixation in a geometrical structure around copper(II) by the ligand-ligand bonding. The difference between edma and ida is that the imino nitrogen atom of the former can be asymmetric in the absence of the ligand-ligand interactions if it is coordinated to copper(II),[14-16] whereas the nitrogen atom of the latter cannot.

For the systems without the mentioned interactions, the CD magnitudes were found to be close to the estimated values and insensitive to addition of ethanol. The unexpectedly small magnitude for Cu(ida)(L-val) may partly be attributable to incomplete complex formation under the present conditions, in addition to the change in the spectral pattern in 50% aqueous ethanol.

These comparisons as well as those made earlier[5,6] indicate that the CD magnitudes are considerably enhanced when the ligand-ligand interactions occur and otherwise are reasonably additive even in some different ligand fields.[5,12]

Ternary Systems Involving a Pyridine Ring. (1) bpy-Containing Systems. The ternary systems Cu(bpy)(L-arg), Cu(bpy)(L-lys), and Cu(bpy)(L-glu) exhibited positive CD extrema around 560 nm, contrary to the negative peaks observed for the binary systems Cu(L-amino acid)$_2$ (Table 5). As Martin and Prados[7] reported for Cu(bpy)(L-phenylalanine), these anomalous spectral behaviors are probably caused by the electronic effects due to π-back donation, which has been pointed out in many ternary systems involving pyridine rings.[10]

Figure 2 shows that the CD spectral pattern of the

Table 3. Absorption and CD spectral data for the systems Cu(L-glu)(L-orn) and Cu(L-asp)(L-orn) at various pH values (μ=variable)

System	pH	CD				Absorption	
		Found		Estimated[a]			
		$\Delta\varepsilon$	λ_{max}(nm)	$\Delta\varepsilon$	λ_{max}(nm)	ε	λ_{max} (nm)
Cu(L-glu)(L-orn)	7.5	-0.12_6	598	-0.09_0	604	55	625
	8.3	-0.10_0	590	-0.08_4	600	56	622
	8.8	-0.07_2	560	-0.04_6	554	58	624
	9.2	-0.04_5	538	-0.03_2	542	58	624
		$+0.03_6$	670	$+0.03_6$	≈740		
	9.5	$+0.15_7$	623	$+0.07_5$	631	57	627
	10.2	$+0.20_6$	623	$+0.15_6$	633	60	633
Cu(L-asp)(L-orn)	7.1	-0.07_1	630	-0.04_8	630	51	628
	9.4	$+0.03_6$	624	$+0.05_2$	630	54	631
	10.8	$+0.20_1$	618	$+0.21_0$	620	57	636

a) Estimated from the data for the corresponding binary systems (Refs. 5 and 6).

Table 4. Absorption and CD spectral data for the systems Cu(ida)(L-amino acid) (μ=variable)

L-Amino acid	pH	CD				Absorption[c]		Relative CD magnitude[b]	Medium
		Found		Estimated[a]					
		$\Delta\varepsilon$	λ_{max}(nm)	$\Delta\varepsilon$	λ_{max}(nm)	ε	λ_{max} (nm)		
L-arg	8.1	-0.07_8	632	-0.05_9	590	45	665	1.3	water
	10.9	-0.11_3	646	-0.05_3	575	49	676	2.1	50% aqueous ethanol
L-lys	9.2	-0.07_6	625	-0.06_4	604	45	664	1.2	water
	8.8	-0.10_5	643	-0.06_1	580	48	699	1.7	50% aqueous ethanol
L-orn	8.3	-0.06_6	638	-0.03_3	558	46	664	2.0	water
	9.1	-0.04_0	645	$+0.07_2$	635	46	664		water
	10.5	$+0.07_0$	620	$+0.23_1$	631	49	663		water
L-ala	8.2	-0.04_1	633	-0.04_0	633	46	666	1.0	water
	11.2	-0.04_0	640	-0.02_9	600	47	670	(1.4)[d]	50% aqueous ethanol
L-val	9.0	-0.09_0	638	-0.13_9	590	42	656	0.7	water
	9.1	-0.03_9	627	-0.12_4	580	50	622	(0.3)[d]	50% aqueous ethanol

a) Estimated from the data for the systems Cu(L-amino acid)$_2$ (Ref. 5). b) Relative CD magnitude refers to $\Delta\varepsilon_{max}$(found)/$\Delta\varepsilon_{max}$(calcd). c) The data for the Cu(ida)$_2$ system are as follows: λ_{max}=682 nm; ε=38(at pH 8.1 and 9.3). d) The anomalous value is probably due to the increase of the positive extremum at >700 nm.

Cu(bpy)(L-asp) system at pH 9.6 appears to be similar to that of the Cu(bpy)(L-orn) system at pH 10.1 with the sign inverted. The fact may be explained as arising from the octahedral distortion, which allows L-asp to coordinate as a terdentate ligand through its α-amino and β-carboxylate groups occupying the planar position as expressed by **2**, where the α-carboxylate group of L-asp appears as if it assumed the same arrangement as that of D-ornithine. This explanation is in line with the argument that has been made by Wilson *et al.*[12] for the CD spectra of the Cu(L-orn)$_2$ system in alkaline solution. Based on the calculations by the crystal field approximation, Gil *et al.*[17] recently suggested the distorted octahedral coordination around copper(II) for Cu(bpy)(L-amino acid) and Cu(phenanthroline)(L-amino acid). They indicated the possibility that the two chelate rings formed by the ligands might be perpendicular to each other.

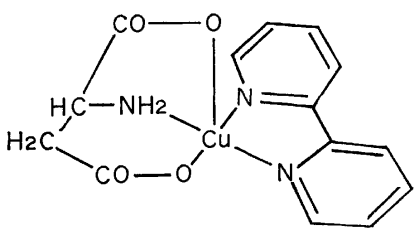

2

(2) pca- and pdca-Containing Systems. The pca-containing systems exhibited the absorption maxima centered around 635 nm (Table 1), from which formation of the ternary complexes may be inferred. For every L-amino acid employed, presence of pca in

TABLE 5. CD SPECTRAL DATA FOR THE PYRIDINE-CONTAINING SYSTEMS Cu(A)(B) (μ=variable)

Ligand	Ligand A: pca			bpy			pdca		
	pH	$\Delta\varepsilon$	λ_{max}(nm)	pH	$\Delta\varepsilon$	λ_{max}(nm)	pH	$\Delta\varepsilon$	λ_{max}(nm)
L-arg	9.9	-0.04_5	614	10.0	$+0.01_0$	560	9.9	-0.04_9	610
	10.2[a]	-0.04_5	590		$+0.00_7$	685	10.5[a]	-0.04_2	605
L-lys	9.8	-0.05_2	610	9.2	$+0.02_0$	578	10.0	-0.05_5	615
	9.8[a]	-0.05_5	600		$+0.01_3$	660	10.0[a]	-0.06_1	610
L-orn	not measured			7.5	$+0.05_6$	588	7.9	-0.01_8	580
				10.1	$+0.04_7$	603	10.0	$+0.09_7$	624
					-0.02_1	640	8.0[a]	-0.02_7	585
							10.2[a]	$+0.11_2$	622
L-ala	8.9	-0.02_9	626		$+0.02_4$[b]	570[b]	9.9	-0.03_3	630
	8.0[a]	-0.03_4	610		$+0.01_2$[b]	660[b]	10.7[a]	-0.03_2	625
L-val	9.9	-0.12_1	604		-0.06[b]	588[b]	9.8	-0.13_3	595
	10.9[a]	-0.12_7	584				10.2[a]	-0.10_9	585
L-glu	9.9	-0.05_0	620	9.8	$+0.02_4$	560	not measured		
	10.6[a]	-0.06_7	615		$+0.00_8$	680			
L-asp	not measured			8.7	$+0.01_0$	530	not measured		
					-0.05_4	628			

a) Measured in 50% aqueous ethanol. b) Taken from Ref. 7.

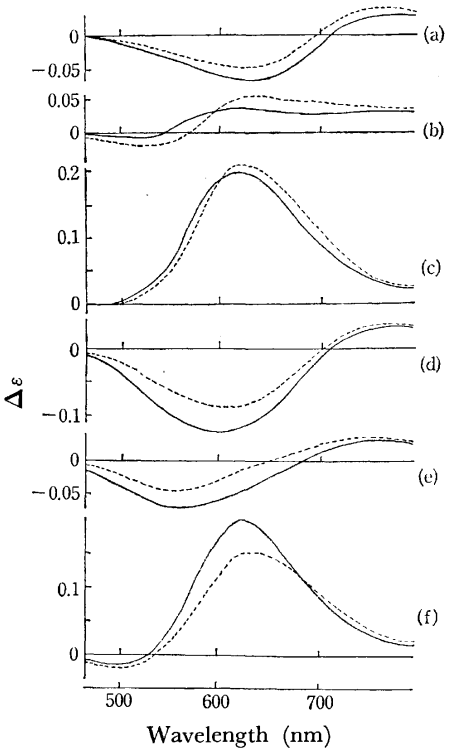

Fig. 1. Circular dichroism spectra of the systems Cu(L-asp)(L-orn) and Cu(L-glu)(L-orn).
Experimental curves: ——; Estimated curves: ----. The estimated curves were obtained by plotting against wavelength the sums of the half magnitudes ($1/2\Delta\varepsilon$) exhibited by Cu(L-orn)$_2$ and Cu(L-asp)$_2$ or Cu(L-glu)$_2$ (Ref. 6).
(a) Cu(L-asp)(L-orn) pH 7.1; (b) Cu(L-asp)(L-orn) pH 9.4; (c) Cu(L-asp)(L-orn) pH 10.8; (d) Cu(L-glu)(L-orn) pH 7.5; (e) Cu(L-glu)(L-orn) pH 8.8; (f) Cu(L-glu)(L-orn) pH 10.2.

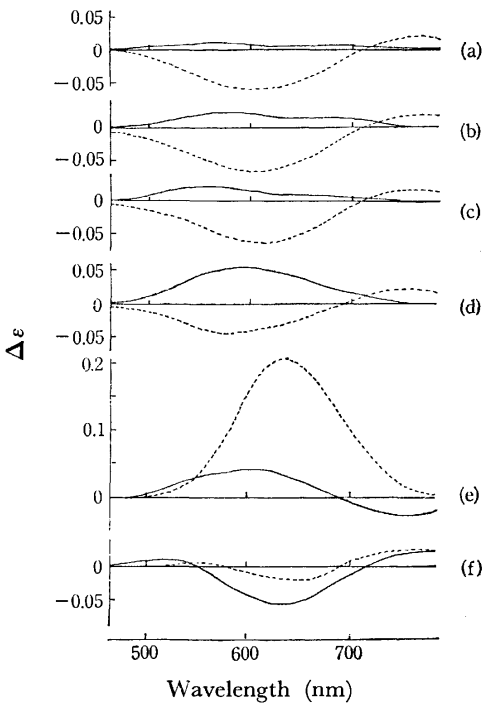

Fig. 2. Circular dichroism spectra of the systems Cu(bpy)(L-amino acid).
Experimental curves: ——; Estimated curves: ----. The estimated curves were obtained by plotting against wavelength the half magnitudes ($1/2\Delta\varepsilon$) exhibited by Cu(L-amino acid)$_2$.
(a) Cu(bpy)(L-arg) pH 10.0; (b) Cu(bpy)(L-lys) pH 9.2; (c) Cu(bpy)(L-glu) pH 9.8; (d) Cu(bpy)(L-orn) pH 7.5; (e) Cu(bpy)(L-orn) pH 10.1; (f) Cu(bpy)(L-asp) pH 8.7.

the ternary system decreased the CD magnitude, but the effects were not so remarkable as to invert the CD sign.

The absorption spectra of the pdca-containing systems showed a broad peak with a shoulder, and the wavelengths of their CD peaks (Table 5) were very close to those of Cu(L-amino acid)$_2$.[5] These spectra are compatible with the view that the binary species contribute much to the observed spectral patterns. Considering that it is difficult to construct a molecular model having ligand-ligand interactions depicted in Scheme 1, pdca does not seem to provide a favorable condition for the intramolecular bonding, and the stabilities of the ternary complexes may be lower than those containing edma or ida in place of pdca.

Small CD magnitudes of the pdca series may indicate that L-amino acids are coordinated to copper(II) through the amino group in the tetragonal plane, whereas pdca occupies the rest of the coordination sites.[18] Murakami *et al.*[19] reported that L-amino acids in the mixed ligand complexes, Cu(diethylenetriamine)(L-amino acid), are bonded to copper(II) in neutral solution through the amino group in the square plane and the carboxylate group interacting at the apical position, which is occupied by a hydroxyl ion in alkaline solution.

The present observations demonstrate that the pyridine ring in the ternary systems studied does change the CD patterns probably through the π-back donation associated with the copper(II)-pyridine bonding and thus may affect the formation of mixed ligand complexes.

We wish to express our thanks to Miss Tazuko Ikebata for technical assistance and to Miss Teruko Kuroe for elemental analysis. This work was supported by a grant from the Ministry of Education.

References

1) Y. Marcus and I. Eliezer, *Coord. Chem. Rev.*, **4**, 273 (1969).

2) R. -P. Martin, M. M. Pettit-Ramel, and J. P. Scharff, "Metal Ions in Biological Systems," Vol. 2, ed. by H. Sigel, Marcel Dekker, New York (1973), p. 1.

3) C. J. Hawkins, "Absolute Configuration of Metal Complexes," Wiley-Interscience, New York (1971), p. 148.

4) R. B. Martin, "Metal Ions in Biological Systems," Vol. 1, ed. by H. Sigel, Marcel Dekker, New York (1974), p. 129.

5) O. Yamauchi, Y. Nakao, and A. Nakahara, *Bull. Chem. Soc. Jpn.*, **48**, 2572 (1975).

6) T. Sakurai, O. Yamauchi, and A. Nakahara, *Bull. Chem. Soc. Jpn.*, **49**, 169 (1976).

7) R. B. Martin and R. Prados, *J. Inorg. Nucl. Chem.*, **36**, 1665 (1974).

8) J. M. Tsangaris and R. B. Martin, *J. Am. Chem. Soc.*, **92**, 4255 (1970).

9) a) R. DeWitt and J. I. Watters, *J. Am. Chem. Soc.*, **76**, 3810 (1954). b) S. Kida, *Bull. Chem. Soc. Jpn.*, **29**, 805 (1956).

10) H. Sigel, "Metal Ions in Biological Systems," Vol. 2, ed. by H. Sigel, Marcel Dekker, New York (1973), p. 63.

11) K. M. Wellman, T. G. Mecca, W. Mungall, and C. R. Hare, *J. Am. Chem. Soc.*, **90**, 805 (1968).

12) E. W. Wilson, Jr., M. H. Kasperian, and R. B. Martin, *J. Am. Chem. Soc.*, **92**, 5365 (1970).

13) S. Kirschner, *J. Am. Chem. Soc.*, **78**, 2372 (1956).

14) T. Yasui, *Bull. Chem. Soc. Jpn.*, **38**, 1746 (1965).

15) T. Yasui, J. Hidaka, and Y. Shimura, *J. Am. Chem. Soc.*, **87**, 2762 (1965).

16) C. J. Hawkins and C. L. Wong, *Aust. J. Chem.*, **23**, 2237 (1970).

17) L. Gil, E. Moraga, H. Bobadilla, S. Bunel, and C. A. Bunton, *J. Inorg. Nucl. Chem.*, **37**, 2509 (1975).

18) The mixed ligand complex, [Cu(pdca)(pyridine)], isolated as crystals (O. Yamauchi, H. Benno, and A. Nakahara, *Bull. Chem. Soc. Jpn.*, **46**, 3458 (1973)) may serve as evidence supporting that pdca can be coordinated to copper(II) as a terdentate ligand.

19) T. Murakami, T. Nozawa, and M. Hatano, *Bull. Chem. Soc. Jpn.*, **46**, 2456 (1973).

Photoreactions of Cyclic Benzylidene Acetals with Ketones in the Presence and Absence of Dissolved Oxygen

Morio SUZUKI, Toshimi INAI, and Ryoka MATSUSHIMA

Department of Industrial Chemistry, Faculty of Engineering, Shizuoka University, Hamamatsu 432

(Received September 4, 1975)

Photoreactions of 2-phenyl-1,3-dioxane (**1**) and 4,6-*O*-benzylidene-1,2,3-tri-*O*-acetylglucopyranose (**10**) in the presence of benzophenone, acetophenone, or acetone have been studied in both deoxygenated and aerated benzene solutions at room temperature. Photolysis of **1** with ketone in deoxygenated solution gave a dimeric product of **1** (**8**), cross adduct, and pinacol, while in aerated solution an oxidative ring cleavage product, *i.e.*, trimethylene glycol monobenzoate (**9**), was obtained instead of **8**, besides smaller amounts of pinacol and cross adduct. The yields of pinacol and cross adduct decreased with the change in ketone in the order benzophenone>acetophenone>acetone, while the yield of **8** or **9** was in the reverse order. Photolysis of **10** with ketone led to results parallel to those of **1**: photolysis under nitrogen atomosphere gave pinacol, cross adduct, and a dimeric product of **10** (**14**), while under bubbling air 4-*O*-monobenzoate and 6-*O*-monobenzoate derivatives of **10** were obtained instead of **14**, besides pinacol and cross adduct. The effects of temperature, oxygen, and structure on the course of the reaction, to produce dimeric or ring opening products, have been discussed.

Recently photoreactions of carbohydrate derivatives have been extensively studied.[1] Photochemical hydrogen abstraction from 2-alkyl-1,3-dioxanes[2] or from benzylidene derivatives of L-ribose[3] with acetone gives ring opening (β-cleavage) products, while photolysis of *o*-nitrobenzylidene derivatives of glucose gives oxidative ring opening products *via* intramolecular hydrogen abstraction followed by oxidation of the intermediate radicals.[4] Photoreactions of 2-aryl-1,3-dioxanes with ketone seem to have been little studied, though hydrogen abstraction from 2-phenyl-1,3-dioxanes by thermally generated *t*-butoxyl radicals[5] or NBS[6] produces ring opening products. In this work studies on the photoreactions of 2-phenyl-1,3-dioxane and its derivative of triacetylglucopyranose with ketone have been carried out, showing some different features from those referred to above.

Results

Photolysis of 2-Phenyl-1,3-dioxane with Ketone. Irradiation of a benzene solution of 2-phenyl-1,3-dioxane (**1**) in the presence of benzophenone, acetophenone, or acetone, at 15 °C under oxygen-free nitrogen atomosphere, gave the corresponding pinacol (**2**, **3**, or **4**, respectively), cross adduct (**5**, **6**, or **7**, respectively), and a dimer (**8**).

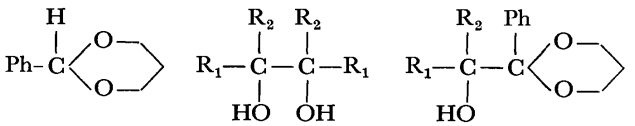

1 Pinacol Cross adduct

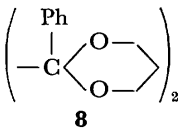

8

2: $R_1=R_2=Ph$ **5**: $R_1=R_2=Ph$
3: $R_1=Ph$, $R_2=Me$ **6**: $R_1=Ph$, $R_2=Me$
4: $R_1=R_2=Me$ **7**: $R_1=R_2=Me$

On the other hand, photolysis of the same solution under bubbling air gave trimethyleneglycol monobenzoate (**9**) instead of the dimer **8**, besides pinacol and cross adduct.

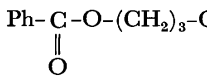

9

The results are summarized in Table 1. We see a significant change in the product distribution: the yields of pinacol and cross adduct decrease with the change in the ketone in the order benzophenone> acetophenone>acetone, while the yield of **8** or **9** is in the reverse order.

Photolysis of 4,6-O-Benzylidene-1,2,4-tri-O-acetyl-β-D-glucopyranose with Ketone. Irradiation of benzene solution of 4,6-*O*-benzylidene-1,2,3-tri-*O*-acetyl-β-D-glucopyranose (**10**) in the presence of benzophenone, acetophenone, or acetone, at 15 °C under oxygen-free nitrogen atomosphere, gave the corresponding pinacol (**2**, **3**, or **4**, respectively), cross adduct (**11**, **12**, or **13**, respectively), and a dimer (**14**). Photolysis of the same solution as above under bubbling air gave 4- and 6-*O*-benzoyl-1,2,3-tri-*O*-acetylglucopyranose (**15**) and (**16**), instead of the dimer **14**, besides pinacol and cross adduct. The results are summarized in Table 2.

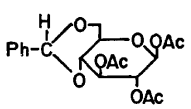

10

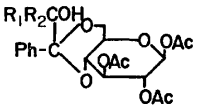

Cross adduct

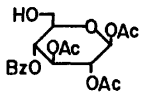

15

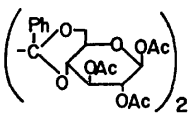

14

	R_1	R_2
11	Ph	Ph
12	Ph	Me
13	Me	Me

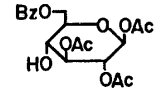

16

Quantum Yields for Hydrogen Abstraction. In order to see the structural factors affecting the efficiency for the abstraction of tertiary hydrogen atoms by excited state ketones, quantum yields for the hydrogen abstraction process have been measured for various substrate-ketone systems. On the basis of the following scheme

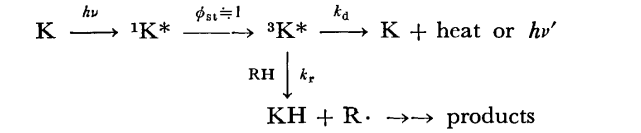

assumed for the photoreaction of a ketone (K) with a hydrogen donor (RH), the rate expression is given by

Table 1. Yields of the products by the photolysis of **1** (0.1 M) with ketone

Conditions			Products and yields[a]				Recovery of **1**, %
Atmosphere	Ketone, M		Pinacol, %	Adduct, %	**8**, %	**9**, %	
N_2	Benzophenone,	0.1	**2**, 28	**5**, 36	9.5	0	trace
N_2	Acetophenone,	0.1	**3**, 18	**6**, 30	13	0	20[b]
N_2	Acetone,	1.3	**4**, trace	**7**, 17	17	0	45
Air	Benzophenone,	0.1	**2**, 19	**5**, 27	0	35	10[c]
Air	Acetone,	1.3	**4**, 0	**7**, 5	0	70	40

a) Based on the consumed amount of **1**. b) Recovered yield of acetophenone was 19%. c) Recovered yield of benzophenone was 48%.

Table 2. Yields of the products of the photolysis of **10** (0.05 M) with ketone

Conditions			Products and yields[a]					Recovery of **10**, %
Atomosphere	Ketone, M		Pinacol, %	Adduct, %	**14**, %	**15**, %	**16**, %	
N_2	Benzophenone,	0.05	**2**, 26	**11**, 38	trace	0	0	15[b]
N_2	Acetophenone,	0.05	**3**, 16	**12**, 33	7	0	0	20[c]
N_2	Acetone,	1.3	**4**, trace	**13**, 23	9	0	0	46
Air	Benzophenone,	0.05	**2**, 19	**11**, 17	0	27	19	23[d]
Air	Acetone,	1.3	**4**, 0	**13**, trace	0	41	23	37

a) Based on the consumed amount of **10**. b) Recovered yield of benzophenone was 10%. c) Recovered yield of acetophenone was 17%. d) Recovered yield of benzophenone was 70%.

Table 3. Rate parameters for the abstraction of tertiary hydrogen atoms by excited state ketones[a]

Substrate	Ketone	ϕ	k_d/k_r, M
1	Benzophenone	0.64	0.056
1	Acetophenone	0.37	0.17
1	Acetone	0.11	0.77
$(EtO)_2CHPh$	Benzophenone	0.52	0.093
Ph_2CHOH	Benzophenone	0.67[b]	0.05
Me_2CHOH	Benzophenone	0.71[c]	0.18
Me_2CHPh	Benzophenone	0.30	0.23

a) Quantum yields at initial substrate concentration of 0.1 M. Initial concentrations of benzophenone and acetophenone were 0.1 M while that of acetone was 1.3 M. b) Ref. 7, p. 3. c) Data from S. G. Cohen, *Tetrahedron Lett.*, **1968** 4823.

$1/\phi = 1 + k_d/k_r[RH]$,[7] where, ϕ is the quantum yield of disappearance of RH or K. If the equation is multiplied by the quantum yield ϕ_s of the disappearance of K, known for a standard system such as ketone–benzhydrol,[8] we have

$$\frac{\phi_s}{\phi} = \phi_s + \frac{k_d\phi_s}{k_r[RH]}$$

Thus, ϕ and k_d/k_r can be obtained from the slope and intercept of a plot of the relative disappearance ratio *vs.* 1/[RH], using a value of $\phi_s = 0.68$ for 0.1 M benzophenone and 0.1 M benzhydrol.[8] The results are given in Table 3.

Discussion

Effects of Temperature and the Substrate Structure on the Course of the Reaction. The variation in the product yields with the change in ketone (Tables 1 and 2) might be related to the relative stability of ketyl radicals (K·). The yields of pinacols (K-K) and cross adducts (S-K) would decrease in the decreasing order of relative stability of ketyl radicals; the yield of the dimer (S-S), whose formation process *d* being competitive with the process *c*, would increase.

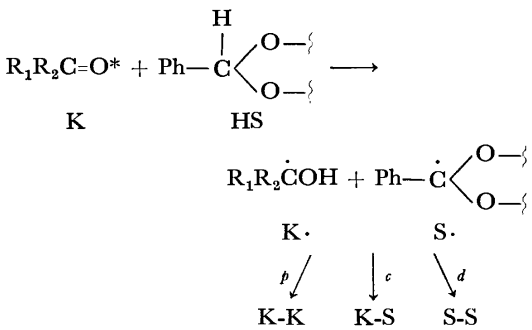

Acetone ketyl radical would rapidly react with solvent, though no further investigation was made on the products. The product ratio of the photolysis of **1** with acetophenone, 3 : 6 : 8 = 1 : 2.3 : 1.4 (Table 1), is close to the statistical ratio 1 : 2 : 1 which is inferred for the two radicals with similar stability, suggesting that S· is as stable as the acetophenone ketyl radical.

The reaction of S· shows a remarkable temperature dependence: at 15 °C S· (produced by hydrogen atom abstraction by excited state acetone) gives a dimer and cross adduct without ring opening (Table 1), while at 135 °C S· (produced by thermal hydrogen atom abstraction with *t*-butoxyl radical) gives a ring opening product.[5]

At low temperature, S· is stable enough to undergo collisional encounters with other radicals, resulting in dimerization and cross coupling reactions which are assumed to involve no significant activation processes and to be highly exothermic. At high temperature,

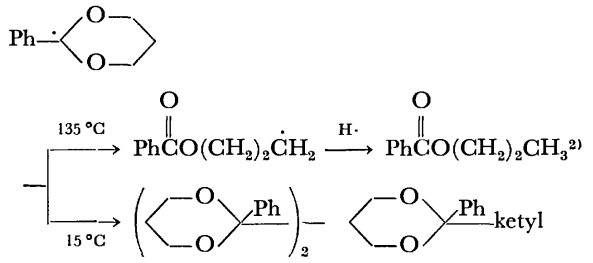

S· is somewhat activated or destabilized and unimolecular ring opening (β-cleavage), assumed to involve more or less activation process, would occur before bimolecular encounter of radicals.

A significant structural effect is observed on the features of the following intermediate radical:

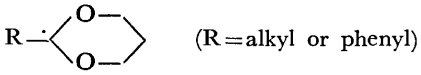

Upon irradiation in the presence of acetone at room temperature 2-alkyl-1,3-dioxane undergoes ring opening to give $RC(=O)O(CH_2)_2CH_3$ as the main product,[2] in contrast with the present results of 2-phenyl-1,3-dioxane (Table 1). The difference might be correlated to the relative stability of the intermediate radicals: the radical with R=alkyl is not so stabilized as that with R=phenyl whose resonance stabilization energy due to the benzyl group is *ca.* 18 kcal/mol.[9] Thus, the ring opening process of 2-phenyl-1,3-dioxane is expected to be much more endothermic than that of 2-alkyl-1,3-dioxane.

The product yields of the photolysis of **10** with benzophenone, acetophenone, or acetone are almost the same as those of the photolysis of **1** under similar conditions. The yields of the dimer **14** are lower and those of the cross adducts are slightly higher in Table 2 than the yields of the corresponding products in Table 1. This may reflect a larger steric hindrance of the intermediate radical derived from **10** as compared to that from **1**. Mutual coupling of bulky radicals to form **14** would sterically be less favorable as compared to the cross coupling with less bulky benzophenone ketyl radical.

Effects of the Dissolved Oxygen. The yields of pinacols, cross adducts and dimers decrease in the presence of oxygen. Oxidative ring opening products (benzoates) are formed in a significant yield (Tables 1 and 2). This shows a high reactivity of oxygen with the intermediate radicals.[3,4]

The fact that the benzoate derivatives are formed by the photoreaction in the presence of oxygen whereas they are not formed under purified nitrogen atmosphere, indicates that the source of oxygen (necessary for the formation of the benzoates) is the dissolved oxygen. It is likely that the source of oxygen required for the formation of methyl-2(or 3)-*O*-benzoyl-β-D-ribofuranoside in acetone-sensitized photolysis of methyl-2,3-*O*-benzylidene-β-D-ribofuranoside under nitrogen (commercial nitrogen without further purification[3]), is the small amount of oxygen which might be contained in the commercial nitrogen.

Since the yields of the benzoate derivatives relative to those of the cross adducts or dimers depend on the concentration of the dissolved oxygen,[11] it seems that the formation of the benzoate derivatives takes place through the reaction of the radical S· with the dissolved oxygen and that this process is competitive with processes *c* and *d*.

When the consumption of **1** is 90%, that of benzophenone is only 52%, upon irradiation of an air-saturated benzene solution containing equimolar amount of **1** and benzophenone. The discrepancy in the consumption rates of **1** and benzophenone might be related to the reformation of benzophenone by the reaction of the benzophenone ketyl radical with the dissolved oxygen, according to the report by Pitts *et al.*:[12]

$$Ph_2\dot{C}OH + O_2 \longrightarrow Ph_2C{=}O + HOO\cdot$$

$$HOO\cdot + RH \text{ (substrate or solvent)} \longrightarrow H_2O_2 + R\cdot$$

However, the mechanism for the formation of the benzoate derivatives, *e.g.*, as to whether or not the reaction proceeds through radical chain process, is not clarified as yet. The radical chain mechanism does not seem to be supported by the apparent rate; the photoreaction in the presence of the dissolved oxygen seems to proceed less efficiently than that under nitrogen atmosphere, though the quantum yields for the photoreaction in the presence of the dissolved oxygen have not been measured.

Structural Effects on the Rates of Hydrogen Abstraction. We see a significant change in ϕ (Table 3) with the change in structure of the substrate or the ketone. The lowest triplet lifetimes (τ_T) of acetone, acetophenone, and benzophenone in benzene at room temperature are 0.94, 3.5, and 12 μs, respectively.[13] The results in the first three runs in Table 3 show that ϕ and k_d/k_r are closely related to τ_T, k_r/k_d being nearly proportional to τ_T. Thus, the efficiency of the hydrogen abstraction from the substrate **1** by different ketones is mainly controlled by the lowest triplet lifetimes of the ketones.

Since the bond dissociation energies of the benzylic hydrogen atoms of **1** and $(EtO)_2CHPh$ are assumed to be similar, the slightly low photoreactivity of $(EtO)_2$-CHPh as compared to that of **1** may be attributed to the steric hindrance due to the free rotation of the two ethoxyl groups in $(EtO)_2CHPh$. The intermediate radical $Ph_2\dot{C}OH$ is expected to be stabilized to a greater extent by the two phenyl groups as compared to $Me_2\dot{C}HO$. Nevertheless the efficiency for the hydrogen abstraction of Ph_2CHOH is not higher than that of Me_2CHOH. This may partly be due to a saturation effect (selectivity will be poor when hydrogen abstraction occurs on highly reactive substrates), as well as the steric hindrance.

Experimental

Materials. 2-Phenyl-1,3-dioxane[5] and 4,6-*O*-benzylidene-1,2,3-tri-*O*-acetyl-β-D-glucopyranose[14,15] were prepared according to methods in literature. Guaranteed benzophenone, acetophenone, and acetone (Wako Chemicals) were used.

*Photolysis of 2-Phenyl-1,3-dioxane (**1**) with Benzophenone.* After deoxygenation with purified nitrogen current for 1 h,

a 125 ml benzene solution containing **1** (0.1 M) and benzophenone (0.1 M) was irradiated at 15 °C under purified nitrogen atmosphere with a 100 W high pressure mercury lamp for 5 h. The photolyzed solution was condensed and chromatographed over silica gel to give **2** (1.25 g), **5** (1.59 g) and **8** (0.39 g). **2** gave mp, NMR and IR spectra identical with those of authentic benzpinacol. **5**: colorless crystal, mp 189—190 °C; IR: 1580, 3520 cm^{-1}; NMR ($CDCl_3$): δ 1.0—1.4 (m, 1H, H_{5e}), 1.9—2.7 (m, 1H, H_{5a}), 3.12 (s, 1H, OH), 3.5—4.1 (m, 4H, H_4H_6), 6.8—7.7 (m, 15H, phenyl). Found: C, 79.25; H, 6.47%. Calcd for $C_{13}H_{18}O_3$: C, 79.74; H, 6.40%. **8**: colorless prism, mp 235—236.5 °C; IR: 2850, 2950 cm^{-1}; NMR ($CDCl_3$): δ 0.8—1.3 (m, 2H, $H_{5e}H_{5e}'$), 1.5—2.3 (m, 2H, $H_{5a}H_{5a}'$), 3.0—3.4 (m, 8H, $H_4H_4'H_6H_6'$), 7.1—7.3 (m, 10H, phenyl). Found: C, 73.68; H, 6.95%. Calcd for $C_{20}H_{22}O_4$: C, 73.60; H, 6.79%. Upon irradiation under bubbling air for 7.5 h, a 125 ml solution of the same as that above gave **9** (0.71 g), **2** (0.21 g) and **5** (1.06 g), besides recovered **1** (0.20 g) and benzophenone (1.18 g). **9** showed IR and NMR spectra identical with those of authentic trimethyleneglycol monobenzoate.

*Photolysis of 2-Phenyl-1,3-dioxane (**1**) with Acetophenone.* A 125 ml benzene solution containing **1** (0.1 M) and acetophenone (0.1 M) was irradiated in a similar way for 6 h under nitrogen atmosphere. Separation of the photolyzed solution by column chromatography over silica gel gave **3** (0.45 g), **6** (0.84 g), **8** (0.41 g), besides recovered **1** (0.41 g) and acetophenone (0.27 g). **3**: colorless prism, mp 121—122.5 °C (lit, 123—124 °C)[16]; IR: 1600, 2960, 3550 cm^{-1}: NMR ($CDCl_3$): δ 1.43 (s, 6H, Me), 2.72 (s, 2H, OH), 7.0—7.3 (m, 10H, phenyl). **6**: mp 114—116 °C; IR: 1590, 2850, 2950, 3560 cm^{-1}; NMR: δ 0.84—1.4 (m, 1H, H_{5e}), 1.63 (s, 3H, Me), 1.8—2.5 (m, 1H, H_{5a}), 2.96 (broad s, 1H, OH), 3.4—4.0 (m, 4H, H_4H_6), 6.8—7.3 (m, 10H, phenyl). Found: C, 76.14; H, 7.22%. Calcd for $C_{18}H_{20}O_3$: C, 76.03; H, 7.09%.

*Photolysis of 2-Phenyl-1,3-dioxane (**1**) with Acetone.* A 125 ml benzene solution containing **1** (0.1 M) and acetone (1.3 M), after previous deoxygenation, was irradiated at 15 °C under purified nitrogen atmosphere with a 100 W high pressure mercury lamp for 20 h. Separation of the photolyzed solution by column chromatography over silica gel gave **7** (0.26 g), **8** (0.38 g) and **4** (a trace), besides recovered **1** (0.93 g). **7**: mp 90.5—92 °C; IR: 2900, 3550 cm^{-1}; NMR ($CDCl_3$): δ 1.10 (s, 6H, Me), 1.0—1.4 (m, 1H, H_{5e}), 1.6—2.4 (m, 1H, H_{5a}), 2.48 (s, 1H, OH), 3.4—4.0 (m, 4H, H_4H_6), 7.3—7.5 (m, 5H, phenyl). Found: C, 70.71; H, 8.42%. Calcd for $C_{13}H_{18}O_3$: C, 70.24; H, 8.16%. Upon irradiation under bubbling air for 30 h, 125 ml of the same solution as that above gave **7** (0.09 g), and **9** (0.95 g), besides recovered **1** (0.82 g).

*Photolysis of 3,6-O-Benzylidene-1,2,3-tri-O-acetyl-β-D-glucopyranose (**10**) with Benzophenone.* A 100 ml benzene solution containing **10** (0.05 M) and benzophenone (0.05 M) was deoxygenated with purified nitrogen current, and then irradiated at 15 °C under purified nitrogen atmosphere for 15 h. Separation of the photolyzed solution by column chromatography over silica gel gave **2** (0.43 g), **11** (0.93 g) and **14** (a trace), besides recovered **10** (0.30 g) and benzophenone (0.09 g). **11**: mp 235—236.5 °C; IR: 1750, 3520 cm^{-1}; NMR ($CDCl_3$): δ 1.99, 2.06 (2s, 9H, AcO), 3.05 (s, 1H, OH), 3.3—4.3 (m, 4H), 4.8—5.6 (m, 2H, H_2H_3), 5.72 (d, 1H, J=7.7 Hz, H_1), 6.7—7.9 (m, 15H, phenyl). Found: C, 66.57; H, 5.60%. Calcd for $C_{32}H_{32}O_{10}$: C, 66.66; H, 5.59%. Upon irradiation under bubbling air for 15 h, 100 ml of the same solution as that above gave **2** (0.10 g), **15** (0.43 g) and **16** (0.30 g), besides recovered **10** (0.45 g) and benzophenone (0.64 g). **15**: mp 152.5—153.5 °C; IR: 1708, 1740, 3550 cm^{-1}; NMR ($CDCl_3$): δ 1.90, 2.00, 1.10 (3s, 9H, AcO), 2.6 (broad s, 1H, OH), 3.4—4.0 (m, 3H, H_5H_6), 5.0—5.6 (m, 3H, $H_2H_3H_4$), 5.80 (d, 1H, J_{12}=7.5 Hz, 1H), 7.8—8.1, 7.8—8.2 (m, 5H, phenyl). Found: C, 55.82; H, 5.48%. Calcd for $C_{19}H_{22}O_{10}$: C, 55.61; H, 5.40%. **16** showed mp, IR and NMR spectra identical with those of an authentic sample of 6-*O*-benzoyl-1,2,3-tri-*O*-acetyl-β-D-glucopyranose which was prepared separately.

*Photolysis of 4,6-O-Benzylidene-1,2,3-tri-O-acetyl-β-D-glucopyranose (**10**) with Acetophenone.* A 100 ml benzene solution containing **10** (0.05 M) and acetophenone (0.05 M) was deoxygenated with purified nitrogen current for 1 h, and then irradiated at 15 °C under purified nitrogen atmosphere for 30 h. Separation of the photolyzed solution by column chromatography over silica gel gave **3** (0.16 g), **12** (0.68 g) and **14** (0,68 g), besides recovered **10** (0.39 g) and acetophenone (0.10 g). **12**: mp 209.5—210.5 °C; IR: 1740, 3510 cm^{-1}, NMR ($CDCl_3$): δ 1.72 (s, 3H, Me), 1.99, 2.09 (2s, 9H, AcO), 2.51 (s, 1H, OH), 3.4—3.8 (m, 3H, H_5H_6), 4.0—4.3 (m, 1H, H_4), 4.8—5.5 (m, 2H, H_2H_3), 5.71 (d, 1H, J_{12}=7.7 Hz, H_1), 7.0—7.4 (m, 10H). Found: C, 58.18; H, 5.68%. Calcd for $C_{38}H_{42}O_8$: C, 58.01; H, 5.38%.

*Photolysis of 4,6-O-Benzylidene-1,2,3-tri-O-acetyl-β-D-glucopyranose (**10**) with Acetone.* A 100 ml benzene solution containing **10** (0.05 M) and acetone (1.3 M) was deoxygenated with purified nitrogen for 1 h, and then irradiated at 16 °C under nitrogen atomosphere for 60 h. Separation of the photolyzed solution by column chromatography over silica gel gave **4** (a trace), **13** (0.28 g) and **14** (0.19 g), besides recovered **10** (0.91 g). **13**: mp 183—184.5 °C; IR: 1740, 3500 cm^{-1}; NMR ($CDCl_3$): δ 1.02 1.17 (2s, 6H, Me), 2.00—2.10 (2s, 9H, AcO), 2.00—2.15 (s, 1H, OH), 3.4—3.8 (m, 3H, H_5H_6), 4.0—4.3 (m, 1H, H_4), 4.7—5.3 (m, 2H, H_2H_3), 5.52 (d, 1H, J_{12}=7.7 Hz, H_1), 7.3—7.4 (m, 5H, phenyl). Found: C, 58.85; H, 6.44%. Calcd for $C_{22}H_{18}O_{10}$: C, 58.40; H, 6.24%. Upon irradiation under bubbling air, 100 ml of the same solution as that above gave **12** (a trace), **15** (0.53 g) and **16** (0.30 g), besides recovered **10** (0.72 g).

Quantum Yields. Quantum yields were estimated from the plot of relative disappearance ratio *vs.* the reciprocal concentration of **1**. Benzene solutions containing ketone and various concentrations of **1** in identical pyrex tubes were irradiated with a merry-go-round irradiation apparatus with a 400 W high pressure mercury lamp. Initial concentrations of **1** were 0.08, 0.10, 0.15, 0.20 and 0.25 M, while that of benzophenone or acetophenone was 0.1 M and acetone 1.3 M. Each solution was deoxygenated before irradiation. The irradiation time was 15 min for the **1**-benzophenone system, 40 min for the **1**-acetophenone system, and 7 h for the **1**-acetone system: the extent of reaction for each system was nearly 15%. The colorimetric method was used to determine the disappearance of benzophenone or acetophenone, while for the **1**-acetone system NMR signal intensity at δ=5.4 of **1** was measured to determine the disappearance of **1**.

References

1) (a) K. Matsuura, Y. Araki, and Y. Ishido, *Bull. Chem. Soc. Jpn.*, **47**, 1197 (1974); **46**, 2261, 2538 (1973); *Carbohyd. Res.*, **29**, 459 (1973); *Kagaku No Ryoiki*, **27**, 35 (1972); (b) P. M. Collins and B. R. Whitton, *J. Chem. Soc. Perkin Trans. I*,

1974, 1069; **1973**, 1470; **1973**, 1670; (c) G. O. Phillips and T. Rickards, *J. Chem. Soc., B*, **1969**, 455; G. O. Phillips, *Adv. Carbohyd. Chem.*, **18**, 9 (1963).

2) D. Elad and R. D. Youssofych, *Tetrahedron Lett.*, **1963**, 2189.

3) K. Matsuura, S. Maeda, Y. Araki, and Y. Ishido, *Bull. Chem. Soc. Jpn.* **44**, 292 (1971).

4) P. M. Collins and N. N. Operaeche, *J. Chem. Soc., Chem. Commun.*, **1972**, 532.

5) E. S. Huyaer and Z. Garcia, *J. Org. Chem.*, **27**, 2716 (1962).

6) S. Hanessian and N. R. Plessas, *J. Org. Chem.*, **34**, 1035 (1969).

7) S. L. Murov, "Handbook of Photochemistry," Marcel Dekker, New York, N. Y. (1973), p. 73.

8) W. M. Moore, G. S. Hammond, and R. P. Foss, *J. Am. Chem. Soc.*, **83**, 2789 (1961).

9) A. Streitwieser, Jr., "Molecular Orbital Theory for Organic Chemists," John Wiley & Sons, Inc., New York, N. Y. (1961), p. 393.

10) K. Maruyama, "Yuuriki," Kagaku Dojin, Tokyo (1972), p. 63.

11) Unpublished data.

12) J. N. Pitts, Jr., R. L. Lestinger, R. P. Taylor, J. M. Patterson, G. Recktenwald, and R. B. Martin, *J. Am. Chem. Soc.*, **81**, 1068 (1959).

13) Ref. 7, p. 3.

14) R. L. Whistler and M. L. Wolfarm, "Method in Carbohydrate Chemistry," Vol. 2, Academic Press, New York and London (1963), p. 231.

15) L. Zervas, *Ber.*, **64**, 2289 (1931).

16) S. G. Cohen, *J. Am. Chem. Soc.*, **86**, 3060 (1964).

A Study on the Photochemistry of α,β-Unsaturated γ-Lactones. III. Photodimerization of 2-Penten-4-olide[1]

Kazuya OHGA* and Taku MATSUO**

Departmnt of Organic Synthesis, Faculty of Engineering, Kyushu University, Hakozaki, Higashi-ku, Fukuoka 812

(Received September 23, 1975)

Irradiation of 2-pentene-4-olide (I) with 254 nm light afforded three anti dimers; two *head-to-tail* isomers and one *head-to-head* isomer. The photodimerization proceeds *via* the lowest triplet state. The quantum yields for the formation of the photodimers were determined as a function of the concentrations of I. Addition of I in the excited state to cyclopentene gave two isomeric cyclobutane derivatives. The photocycloaddition took place more rapidly than the photodimerization of I. The photodimerization was also quenched by anisole, probably through formation of an exciplex between I and anisole.

In a previous paper,[2] we reported an interesting photochemical behavior of α,β-unsaturated γ-lactones with a carbon-carbon double bond exocyclic to the lactone ring: the *cis-trans* isomerization proceeds *via* the lowest π,π* triplet, while the β,γ-isomer arises from the second n,π* triplet. On the other hand, no mechanistic detail of the photochemical behavior of an α,β-unsaturated γ-lactone with an endocyclic carbon-carbon double bond has been available partly due to experimental difficulties.[3] We have succeeded, for the first time, in obtaining the kinetic parameters by the use of 2-pentene-4-olide as a typical α,β-unsaturated γ-lactone with an endocyclic carbon-carbon double bond.

Results and Discussion

Structures of Photodimers. Irradiation of 2-penten-4-olide (I) in acetonitrile with 254 nm light afforded three products, Ia, Ib, and Ic (relative yields, 1 : 0.9 : 3). Each product was isolated by the use of both column chromatography on silica-gel and preparative VPC. The molecular weights, results of elementary analyses, characteristic IR bands, and the NMR spectroscopic data indicate that the isolated products are isomeric cycloadducts of I as in the case of 2-buten-4-olide[3] (Table 1).

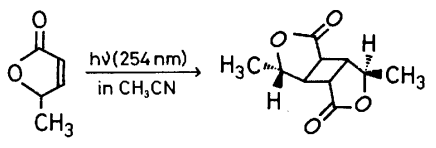

I Ia

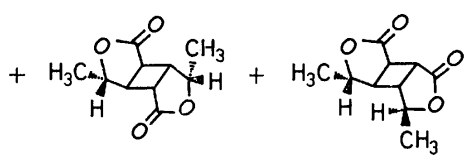

Ib Ic

Since no *trans*-fused photodimer with a five-four ring junction has been reported, the photodimers of I also are assumed to have a *cis*-fused structure. The proposed structures of the photodimers are supported by the NMR spectra. Each one doublet was observed for the methyl protons of Ia and Ic indicating that the two methyl groups in the respective dimer are at equivalent positions. Thus the signals due to the methine protons on the cyclobutane ring can be analyzed as a AA'BB'-system. The results of simulation are compared with the observed spectra (Fig. 1). The coupling constants obtained are summarized in Table 2.

In the case of cyclobutane ring protons, the *cis* vicinal coupling constants are generally larger than the *trans* couplings.[4] In the case of coumarine and carbostyryl photodimers, the long range coupling constants are positive in the *syn* configuration, while they are negative in the *anti* configuration.[4a] We thus conclude that Ia is an *anti*, *head-to-tail* dimer, while Ic is an *anti*, *head-to-head* dimer.

In the VPC (N_2, 55 ml/min) of the photodimers, the retention time of Ia (12.9 min) is shorter than that of Ic (18.1 min). This is in good agreement with the deduced structures, since it is suggested that a *head-to-tail* dimer has a shorter retention time than the corresponding *head-to-head* isomer due to the smaller dipole moment of the former.[5]

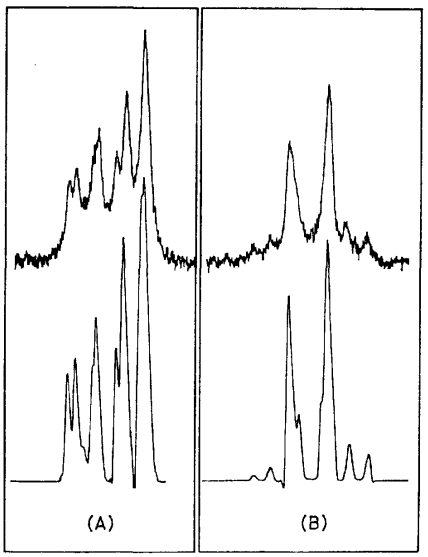

Fig. 1. NMR spectra of the cyclobutane protons: (A) Ia, (B) Ic. The simulated spectra are shown below the actually observed spectra.

* Present address: Department of Environmental Chemistry and Engineering, Faculty of Engineering, Oita University, Dannoharu, Oita 870-11.

** To whom inquiries should be addressed.

Table 1. Analytical data of photodimers

Isomer	Molecular weight[a]	Elementary analyses[b] C, %	H, %	Characteristic IR bands,[c] cm^{-1}	NMR Data[d] δ, ppm
Ia	196	61.04	6.10	1752(C=O) 1170(C-O-C)	1.37(d, J=6.3 Hz, 6H) 2.87(m, 2H)[e] 3.26(m, 2H)[e] 4.82(quartet-d, J=6.3 and 1.8 Hz, 2H)
Ib	196	61.26	6.15	1764(C=O) 1180(C-O-C)	1.41(d, J=6.3 Hz, 3H) 1.53(d, J=6.3 Hz, 3H) 2.6—3.5(m, 4H) 4.6—5.1(m, 2H)
Ic	196	61.45	6.17	1768(C=O) 1158(C-O-C)	1.32(d, J=6.3 Hz, 6H) 2.82(m, 2H)[e] 3.32(m, 2H)[e] 4.69(quartet, J=6.3 and 0 Hz, 2H)

a) Obtained from m/e value for the parent peak of the mass spectra. b) Calculated values for $C_{10}H_{12}O_4$: C, 61.21; H, 6.17%. c) KBr pellet. d) In $CDCl_3$. e) Obtained by the simulation of the cyclobutane ring proton signals (AA'BB' system).

Table 2. NMR parameters estimated by simulation (Hz)

	Ia	Ic
$\Delta\delta\nu$	23.5	29.6
$J_{AA'}$	−0.9	1.9
$J_{BB'}$	−0.9	5.0
J_{AB}	7.4	6.8
$J_{AB'}$	3.4	−1.0

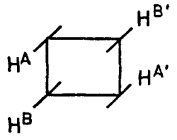

Ia

$J_{AB} > J_{AB'}$

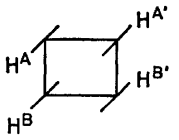

Ic

$J_{AB} > J_{AA'}$, $J_{BB'}$

The solvent effects on the relative formation yields in acetone-photosensitized reactions are also in favor of the above assigned structures. On going from acetonitrile to benzene, Ic/Ia decreases rapidly (from 3.0 to 1.0) while Ib/Ia remains almost constant (0.93 and 1.1). Since Ib/Ia is little affected by the change in solvent polarity, it may be reasonable to assign an *anti, head-to-tail* structure to Ib and Ia. The shorter retention time in VPC for Ib (15.0 min) than Ic (18.1 min) is also in agreement with a less polar structure of the former. The assignment is further supported by the fact that the mass-spectrum of Ib is much closer to that of Ia than to that of Ic.

The configurations of the methyl groups were determined by means of NMR spectroscopy. The two methyl groups in either Ia or Ic are in equivalent positions. The vicinal coupling constants between the proton on the lactone ring and that on the cyclobutane ring are close to zero in both isomers (Table 1); 1.8 Hz for Ia and 0 Hz for Ic. It seems that the vicinal protons are roughly at right angle to each other. We see from the molecular model that such dihedral angles

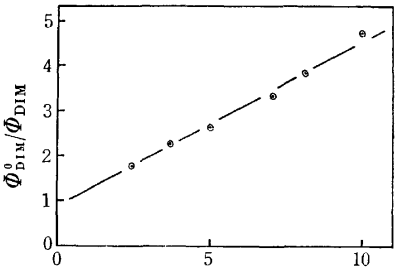

Fig. 2. Quenching of the photodimerization by 1,3-pentadiene.

can be obtained when the methyl groups are at the *exo* positions. If the methyl groups were at the *endo* positions, the dihedral angles should be nearly zero, and the vicinal coupling constants should be much larger. The methyl groups of Ib, on the other hand, are not equivalent as shown by the NMR spectra. Accordingly, Ib is concluded to be an *endo, exo*-isomer.

Reaction Scheme and Kinetic Parameters. The photodimerization of I can be sensitized by ketones (Table 3) with triplet energies higher than that of xanthone, and the reaction is quenched by 1,3-pentadiene. The relative yields of the photodimers in both the sensitizing and quenching experiments are the same as those in the case of the direct irradiation with 254 nm light. Moreover, the Stern-Volmer plot is linear, and the intercept is close to unity (Fig. 2). These results suggest that all of the three photodimers are formed through an identical excited triplet state.

On the basis of a series of sensitization experiments, the energy level of the excited triplet state is estimated to be about 70 kcal/mol in acetonitrile, since neither benzophenone nor fluorenone could sensitize the photodimerization any more as shown in Table 3. The energy level is close to that of the $T_1(\pi,\pi^*)$ state of 2-ethylidene-4-butanolide.[2]

The variations of the quantum yields for the formations of the dimers with the concentrations of I on

Table 3. Photosensitized dimerization in acetonitrile

Sensitizer	E_T kcal/mol	Dimer ratio	
		Ib/Ia	Ic/Ia
Acetone	80	0.93	3.0
Acetophenone	74	0.93	2.9
p-Methylacetophenone	73	0.96	3.0
p-Methoxyacetophenone	72	0.90	2.9
Xanthone	71	0.83	—[a)]
Benzophenone	69	—	—
Fluorenone	53	—	—
(Direct irradiation)		0.94	3.0

a) Not determined because of the overlapping of the VPC peaks for Ic and xanthone.

Table 4. Dimer quantum yields at various concentrations of I in acetonitrile

Concn M (10^{-1})	Quantum yield		
	Ia(10^{-2})	Ib(10^{-2})	Ic(10^{-2})
0.79	5.7	5.1	1.7
1.00	5.8	5.1	1.7
1.12	6.0	5.5	1.8
1.25	5.9	5.6	1.9
1.44	6.2	5.5	1.9
1.62	6.2	6.1	1.9
2.23	6.4	6.3	2.1
4.08	6.6	6.4	2.1
10.00	6.6	6.5	2.2

irradiation with 254 nm light in acetonitrile are shown in Table 4. The relative yields of the photodimers are independent of the concentrations of I in the concentration ranges investigated. It has been proposed by Wagner[6] and also by de-Mayo and his coworkers[7] that photodimers and/or photocycloadducts to olefins of α,β-unsaturated cyclic ketones are formed through metastable intermediates from the excited triplet states. The same mechanism may be used to explain the concentration dependence of the quantum yield for I:

$$I_0 \xrightarrow{h\nu} {}^1I^* \xrightarrow{\Phi_{ISC}} {}^3I^*$$

$${}^3I^* \xrightarrow{k_1} I_0$$

$${}^3I^* + I_0 \xrightarrow{k_r} {}^*I\text{-}I^*$$

$${}^*I\text{-}I^* \xrightarrow{k_e} \text{dimer}$$

$${}^*I\text{-}I^* \xrightarrow{k_{-r}} 2I_0$$

In this case, the relation between the quantum yield for the photodimerization, Φ_{DIM}, and the concentration of I, [I], may be given by the following equation:

$$\Phi_{DIM}^{-1} = \Phi_{ISC}^{-1}\Phi_P^{-1}(1+k_1/k_r[I])$$

where Φ_{ISC} and Φ_P denote the intersystem crossing yield for I and branching ratio for the decay to the final product from the metastable dimeric species, *I-I*. The rate constant for the unimolecular radiationless decay of the triplet I, $^3I^*$, and that for the addition of $^3I^*$ to I at the ground state are denoted by k_1 and k_r, respectively.

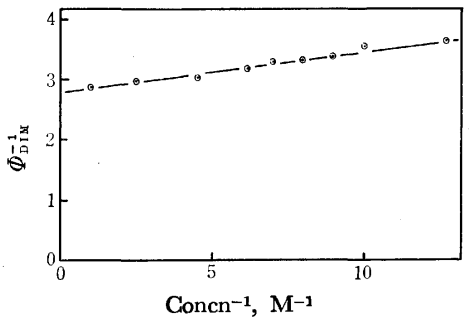

Fig. 3. Variations of the dimer quantum yield in acetonitrile as a function of the concentration of I.

Table 5. Kinetic parameters for the photodimerization of I in acetonitrile

Compound	k_r, $M^{-1}s^{-1}$	k_1, s^{-1}	$\Phi_{ISC}\cdot\Phi_P$
I	2.2×10^3	5.5×10^3	0.36
Cyclopentenone	6.6×10^8	0.4×10^8	0.36

The experimental data were accordingly plotted (Fig. 3), and the kinetic parameters were evaluated (Table 5) on the assumption that a rate constant for quenching by 1,3-pentadiene is $1.0\times10^{10}\,M\,s^{-1}$ in acetonitrile.[6] While the values for k_r and $\Phi_{ISC}\cdot\Phi_P$ are almost the same between I and 2-cyclopentenone, the k_1-value for the former is only one-sevenths of that for the latter. It is surprising that replacement of methylene alpha to the carbonyl group with etherial oxygen atom caused a remarkable decrease in k_1. It is also interesting that the value for $\Phi_{ISC}\cdot\Phi_P$ is more than ten times as that for either thymine or uracil.[8] As a net result of these variations in the kinetic parameters, the photodimerization yield of I turned out to be one of the highest among the related compounds.

Photocycloaddition to Cyclopentene. On the irradiation of I in acetonitrile in the presence of excess cyclopentene with a 30 W low-pressure mercury lamp for 19 h, two isomeric 1 : 1 cycloadducts were obtained: Id(36%) and Ie(24%). In analogy to the case of 2-buten-4-olide,[9] the steric structures of the adducts were concluded to be *cis-anti-cis* form. Analysis of the NMR spectra indicates that the difference between the two isomers are due to the stereochemistry of the methyl group. On the basis of the vicinal coupling constants, Id(J_{BC}=1.8 Hz) and Ie(J_{BC}=6.3 Hz) were assigned to an *exo*- and *endo*-isomers, respectively.

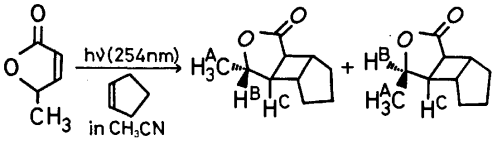

I Id Ie

Acetonitrile solution of I(0.1 M) was irradiated at 254 nm in the presence of various amounts of cyclopentene. The relative yields between the photodimers, as well as the ratio of cycloadducts (Id/Ie), were independent of cyclopentene concentration. The photodimerization reaction itself was partly quenched by

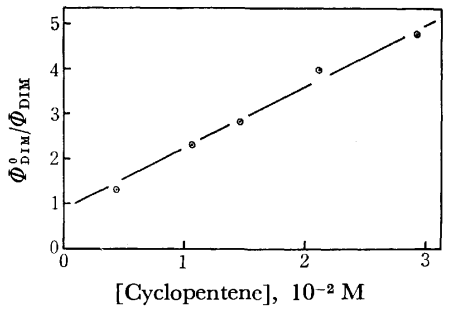

Fig. 4. Quenching of the photodimerization by cyclopentene in acetonitrile ([I])=0.1 M).

the addition of cyclopentene (Fig. 4). It is clear that both photodimerization and photocycloaddition proceed *via* the same excited species of I.

The rate constant (k_{ra}) for the reaction between ^{3}I* and cyclopentene is evaluated from the slope of the Stern-Volmer plot ($k_{ra}\tau=136$ M^{-1}) and the lifetime of ^{3}I* obtained in the analysis of the photodimerization (3.7×10^{-8} s at 0.1 M solution of I). The k_{ra}-value (3.7×10^9 s^{-1} M^{-1}), thus obtained, is more than ten times as large as k_r. The difference in the rate constants may be due to electrophilic property of ^{3}I*, which should favor more nucleophilic cyclopentene rather than I. In agreement with this suggestion, the photodimerization of I was quenched much more effectively by the use of 1,4-dioxene.

Interaction with Benzene Homologues. The above suggested electrophilic character of ^{3}I* was also varified by the investigation of interactions between ^{3}I* and benzene homologues. The photodimerization yields were measured in the presence of benzene, toluene, and anisole (Table 6). The amount of 254 nm light absorbed by the added benzene homologue was subtraced from the total intensity of light in evaluating the quantum yield. In other words, Φ_{DIM}/Φ^0_{DIM} should remain unity as far as the benzene homologues do not affect the reaction. In the case of benzene, however, the quantum yield increased, the photodimerization being apparently sensitized. A similar photosensitization would be expected to take place in the case of toluene and anisole. The experimental results indicate that the quantum yield was significantly reduced by anisole while it was hardly affected by toluene. It is clear that quenching and sensitization compete with each other in the presence of the benzene homologue. The highest quenching effect observed with anisole may be associated with the fact that the ionization potential of anisole is the lowest among the benzene homologues investigated. Quenching is quite likely to take place due to charge-transfer interactions between ^{3}I* and benzene homologues, which lead to the formation of exciplexes as an intermediate responsible for radiationless decay.

Table 6. Variations of the relative values, Φ_{DIM}/Φ^0_{DIM}, by the addition of benzene homologues

Compound	Concn 10^{-2} M	Light absorbed by I,[a] %	Φ_{DIM}/Φ^0_{DIM} Ia	Ib	Ic
Benzene	1.50	52.4	1.5	1.2	1.4
Toluene	1.47	52.2	0.98	0.93	0.95
Anisole	0.541	55.4	0.67	0.80	0.74

a) The fractions of 254 nm light absorbed by I.

Experimental

The NMR spectra were obtained on a Varian Model A-60 analytical spectrometer with tetramethylsilane as an internal standard. The IR and mass spectra were recorded on a JASCO Model DS-301 spectrometer and JEOL Model JMS-01SG mass spectrometer respectively. VPC analysis was carried out on a Shimadzu Model GC-3BF gas chromatograph equipped with a flame ionization detector, with the use of a column (2 m×3 mm) packed with 2% polyphenyl ether (six rings) on Diasolid L 60/80. The column temperature was 220 °C for the analysis of the dimers, 190 °C for that of the cyclopentene cycloadducts. The melting points were measured on a Yanagimoto micro melting-point measurement apparatus and are uncorrected.

Materials. The starting material, I, was prepared as described previously[10] and distilled under reduced pressure; bp 62.0 °C (3 mmHg). The distillate showed a single peak by VPC (10% polyphenyl ether (five rings) on Chamelite CS 60/80). *p*-Methylacetophenone (reagent grade) was purified by fractional distillation under reduced pressure just before use. Extra pure xanthone and fluorenone obtained from Tokyo Kasei Co. were used without further purification. Another ketone-sensitizers were purified as described previously.[2] 1,3-Pentadiene (76 : 24 *trans/cis* isomer ratio) was distilled at atmospheric pressure just before use, its purity being found to be 99.5% by VPC (20% benzyl cyanide and 12% silver nitrate on Chamelite CK 60/80). Cyclopentene was purified with ferric sulfate, followed by fractional distillation just before use. The distillate showed a single peak on inspection by VPC under the same conditions as those for 1,3-pentadiene.

Isolation of the Photodimers. The acetonitrile solution of I was irradiated with a 30 W low-pressure mercury lamp under the same conditions as those for the photodimerization of 2-buten-4-olide.[3] The three photodimers, Ia, Ib, and Ic were isolated from the reaction mixture by means of chromatography on silica gel with benzene–ethyl acetate (10 : 1) as an eluent, and successive preparative VPC with the use of a column packed with 1.5% polyphenyl ether (six rings) on Diasolid L. The photodimers were then recrystallized; mp : Ia, 194.0—195.0 °C (from benzene); Ib, 145.0—146.0 °C (from benzene–hexane); Ic, 222.5—224.0 °C (from ethyl acetate). MS(75 eV) : Ia, 196 (M^+, 19%), 181(M^+-CH_3, 38%), 108(M^+-2CO_2, 33%), 97(33%), 93($M^+-2CO_2-CH_3$, 88%), 80(74%), 79($M^+-2CO_2-2CH_3+H$, 100%); Ib, 196(12%), 181(15%), 108(44%), 97(24%), 93(94%), 80(63%), 79(100%); Ic, 196(3%), 181(5%), 108(9%), 97(12%), 93(100%), 80 (37%), 79(59%).

Quantum Yields for Photodimerization. Appropriate amounts of I were dissolved in acetonitrile of spectrograde purity ($0.79\times10^{-1}-10.00\times10^{-1}$ M). Eight ml of each acetonitrile solution was pipetted into the same sample tube[2] which was degassed by three freeze-pump-thaw cycles at less than 10^{-4} mmHg. The samples and the potassium ferrioxalate actinometer solution (6×10^{-3} M) were irradiated with light filtered through an aqueous solution containing $NiSO_4\cdot6H_2O$ (450 g/l), $CoSO_4\cdot7H_2O$ (150 g/l), and 5,7-dimetyl-1H-2,3-dihydro-1,4-diazepinium perchlorate (175 mg/l).[11] The irradiation apparatus used was described previously.[2] After irradiation at 20.0±0.1 °C for

1.5 h, the amount of each dimer was determined by VPC analysis with 4,4′-dimethoxydiphenylmethane as an internal standard. The yield of all dimers did not exceed 5%.

Photosensitized Dimerization of I. A solution of I and a sensitizer in acetonitrile was sealed after flushing with nitrogen and irradiated externally with a high-pressure mercury lamp (Riko-Sha UVL-700P) through Pyrex filter at near 21 °C for 3 h. The reaction was carried out in an ordinary glass sample tube except for the case of acetone sensitization where a Pyrex tube was used. Under such conditions, incident light is absorbed almost by the sensitizer alone. Dimer ratio was analyzed by means of VPC.

Quenching of the Photodimerization by 1,3-Pentadiene. The degassed samples containing I (1.00×10^{-1} M) and varying concentrations of 1,3-pentadiene in acetonitrile were irradiated with a merry-go-round apparatus. The relative quantum yields were determined with the same procedure as in the case of the determination of dimerization quantum yield except that an aqueous solution containing only 5,7-dimethyl-1*H*-2,3-dihydro-1,4-diazepinium perchlorate (177 mg/l) was used as a filter solution. By the use of the extinction coefficients measured at 254 nm on a Shimadzu Model UV-200 spectrophotometer, the amount of light absorbed by I was estimated after correcting the absorption due to 1,3-pentadiene.

Photocycloaddition of I to Cyclopentene. A 0.063 M solution of I in acetonitrile (160 ml) containing 0.56 M cyclopentene was irradiated with a 30 W low-pressure mercury lamp through quartz for 19 h under nitrogen gas. The VPC analysis of the irradiated sample, with oxanthrene as an internal standard, indicated that the cycloadduct, Id and Ie were formed in 36 and 24% yields, respectively. Preparative VPC was applied to isolate each cycloadduct. The cycloadduct Id was the sole adduct, but Ie was still contaminated by 3% Id after preparative VPC had been carried out twice. Id, Found: C, 71.99; H, 8.54%. Calcd for $C_{10}H_{14}O_2$: C, 72.26; H, 8.49%. IR(neat): 1776 (C=O), 1170 (C–O–C), 1450, 1471 cm^{-1} (cyclopentane ring). NMR($CDCl_3$): 1.27 (d, J_{AB}=6.3 Hz, 3H), 1.2—2.3 (m, 7H), 2.5—3.0(m, 3H), 4.66 (quartet-d, J_{AB}=6.3, J_{BC}=1.8 Hz, 1H). MS(75 eV): 166(M^+, 18%), 121 (M^+-CO_2-H, 27%), 99($C_5H_6O_2^+$+H, 75%), 68($C_5H_8^+$, 100%). Ie, Found: C, 71.95; H, 8.61%. Calcd for $C_{10}H_{14}O_2$: C, 72.26; H, 8.49%. IR(neat): 1770(C=O), 1175(C–O–C), 1450, 1469 cm^{-1} (cyclopentane ring). NMR($CDCl_3$): 1.43 (d, J_{AB}=6.3 Hz, 3H), 1.3—2.0(m, 6H), 2.1—3.0(m, 4H), 4.69(quintet, $J_{AB}=J_{BC}$=6.3 Hz, 1H). MS(75 eV): 166 (M^+, 14%), 121(M^+-CO_2-H, 26%), 99($C_5H_6O_2^+$+H, 66%), 68($C_5H_8^+$, 100%).

Quenching of the Photodimerization by Cyclopentene. The degassed samples containing I (1.00×10^{-1} M) and varying concentrations of cyclopentene (from 0.438×10^{-2} to 2.92×10^{-2} M) in acetonitrile were irradiated for 2 h under the same conditions as in the case of quenching by 1,3-pentadiene.

References

1) Contribution No. 381 from the Department of Organic Synthesis, Faculty of Engineering, Kyushu University.
2) K. Ohga and T. Matsuo, *Bull. Chem. Soc. Jpn.*, **46**, 2181 (1973).
3) K. Ohga and T. Matsuo, *Bull. Chem. Soc. Jpn.*, **43**, 3505 (1970).
4) a) L. Paolillo, H. Ziffer, and O. Buchsrdt, *J. Org. Chem.*, **35**, 38 (1970). b) I. Fleming and D. H. Williams, *Tetrahedron*, **23**, 2747 (1967).
5) H. Ziffer, H. M. Fales, G. W. A. Milne, and F. H. Field, *J. Am. Chem. Soc.*, **92**, 1597 (1970).
6) P. J. Wagner and D. J. Bucheck, *J. Am. Chem. Soc.*, **91**, 5090 (1969).
7) P. de Mayo, A. A. Nicholson, and M. F. Tchir, *Can. J. Chem.*, **47**, 711 (1969).
8) a) P. J. Wagner and D. J. Bucheck, *J. Am. Chem. Soc.*, **92**, 181 (1970). b) G. Marsh, D. R. Kearns, and K. Schaffner, *ibid.*, **93**, 3129 (1971).
9) M. Tada, T. Kokubo, and T. Sato, *Tetrahedron*, **28**, 2121 (1972).
10) K. Ohga and T. Matsuo, *J. Org. Chem.*, **39**, 106 (1974).
11) B. M. Monroe and S. A. Weiner, *J. Am. Chem. Soc.*, **91**, 450 (1969).

Study of the Synthesis of Histidine Peptides. II. Use of N^{im}-Tosylhistidine Derivatives in Conventional Solution Synthesis of Peptides[1,2]

Toshiyuki FUJII,* Terutoshi KIMURA, and Shumpei SAKAKIBARA**

Peptide Institute, Protein Research Foundation, 476 Ina, Minoh, Osaka 562

(Received September 29, 1975)

His–Gly and Ala–His–Gly were synthesized by the conventional solution methods using various N^{α}-protected-N^{im}-tosyl-L-histidines as the key intermediates, and handling conditions of these His(Tos)-derivatives were examined. During treatment of an Nps-peptide with HF, the formation of a strongly photosensitive by-product was observed when anisole alone was used as the scavenger, however the side reaction was completely suppressed when skatole was added to the reaction mixture. In order to evaluate the usefulness of these His(Tos)-derivatives in general peptide synthesis, TRH and LH–RH were synthesized, and both products were obtained in pure form without any difficulty. Thus, it can be emphasized that the use of these His(Tos)-derivatives is efficient and convenient for introducing His-residues into peptides even in solution procedures.

Previously, the present authors published the basic ideas on the use of the tosyl group for the protection of histidyl residues in peptide synthesis,[1] and the usefulness of Aoc–His(Tos) was demonstrated in the solid-phase synthesis of IIe^5-Angiotensin II.[3] Since then, this procedure has been tested by many other researchers, and it is widely recognized that the procedure is the most promising one for the incorporation of histidyl residues into peptides by the solid-phase method.[4] In a preceding paper,[5] detailed conditions for the synthesis of various N^{α}-protected His(Tos)-derivatives were presented, and the behavior of the tosyl group was examined under ordinary conditions which are generally used for peptide synthesis. The present study is the evaluation of the N^{im}-protection method in conventional peptide synthesis.

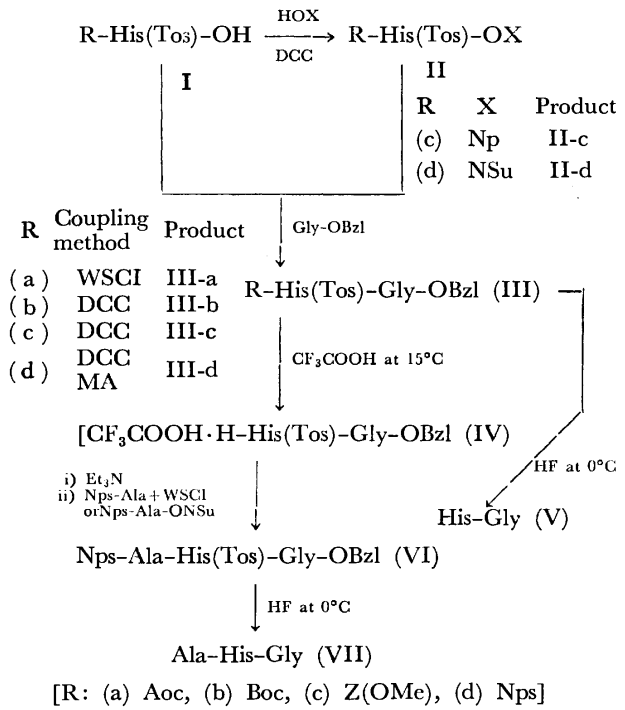

Scheme 1. Peptide Synthesis.

First, the coupling conditions of various N^{α}-protected His(Tos)-derivatives with glycine benzyl ester were examined applying different coupling methods (Scheme 1). From these experiments, it was confirmed that the mixed anhydride method, the dicyclohexylcarbodiimide (DCC) method, and the active ester method gave reasonable results, but the application of the azide method was impractical because of the instability of the tosyl group during the conversion of the hydrazide to the azide followed by the coupling reactions with amine components.

In the case of applying DCC as the coupling reagent, methylene chloride gave the most promising results as the reaction solvent. When tetrahydrofuran (THF), *N,N*-dimethylformamide (DMF), or acetonitrile was used as the reaction solvent under ordinary conditions, the formation of acyl urea was not negligible; particularly the use of an excess amount of base is known to enhance acyl urea formation.

There was no problem in synthesizing the active esters of N^{α}-protected N^{im}-tosylhistidines such as *p*-nitrophenyl ester and *N*-hydroxysuccinimide ester, as far as the DCC method was applied. However, an attempt to synthesize Aoc–His(Tos)–ONSu by the trifluoroacetate method[6] was unsuccessful; in the reaction, the *N*-hydroxysuccinimide ester of *p*-toluenesulfonic acid was formed as the major product.

Aoc– or Z(OMe)–His(Tos)–Gly–OBzl which was obtained by the above-mentioned procedures was treated with trifluoroacetic acid to remove the N^{α}-protecting group, and the product was further coupled with Nps–Ala using 1-ethyl-3-(3-dimethylaminopropyl)-carbodiimide (WSCI)[7] as the reagent or with Nps–Ala–ONSu. Both procedures gave the same product, Nps–Ala–His(Tos)–Gly–OBzl, in reasonable yields.

The removal of the protective groups from His(Tos)-containing peptides was tested under several different conditions, and the most promising results were obtained using the HF-method.[8] As had been expected, a single treatment of Z(OMe)–His(Tos)–Gly–OBzl with HF in the presence of anisole gave His–Gly without any problem. However, a peculiar phenomenon was observed when Nps–His(Tos)–Gly–OBzl or Nps–Ala–His(Tos)–Gly–OBzl was treated with HF using anisole as the scavenger: during processing of the reaction mixture, the formation of a yellow-colored material was observed, which was water-soluble and extremely

* Present address: Tanabe Seiyaku Co., Ltd., Yodogawa-ku, Osaka.

** To whom requests for reprints should be addressed.

photosensitive. This side product had a solubility similar to free peptide, quickly turned to brownish violet, and finally became black within two or three hours during the purification process of the peptide. Removal of the colored material from the principal product was not impossible, but the purification procedures reduced the yield of the final product considerably. The primarily-formed photo-sensitive material should be an Nps–anisole adduct, and it may have further changed to a complex compound through intermediates such as nitrosophenyl sulfoxide in an ordinary lighted room. The addition of excess skatole together with anisole in the HF-reaction mixture completely suppressed the formation of the black; a yellow compound was also formed in the reaction, but this colored material was soluble in chloroform and not so sensitive to visible light. This material was isolated from the reaction mixture as crystals, and the structure was confirmed to be 2-Nps-skatole. Recovery of His–Gly from Nps–His(Tos)–Gly–OBzl using the HF-reaction using skatole as the scavenger was about 80% efficient. The efficiency of the HF-Skatole procedure was also confirmed by obtaining Ala–His–Gly from Nps–Ala–His(Tos)–Gly–OBzl in a 64% yield after final purification.

As shown above, the introduction of a tosyl group into the histidyl residue is advantageous not only in reducing the formation of side products during the coupling reactions, but also in enhancing the solubility of the histidine derivatives in organic solvents. On the other hand, the tosyl group is known to be susceptible to HOBT, HBr, HCl, NaOH, NH_3 and even to the amine-components to be coupled.[5] Therefore, partial

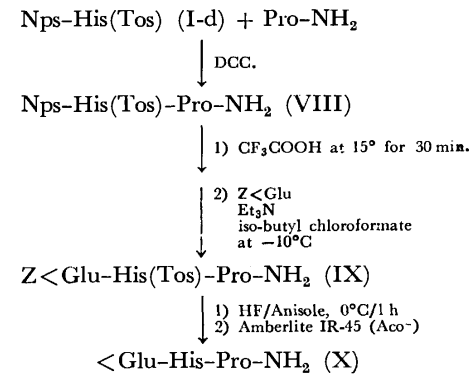

Scheme 2. Synthesis of Thyrotropin-releasing Hormone

cleavage of the tosyl groups is frequently observed during coupling reactions. Thus, in such cases, it may be favorable to remove all of the tosyl groups after the incorporation of the His-residues into peptides, because the major purpose of the protection of the histidyl residue will have been fulfilled after it has been incorporated into a peptide without forming considerable side products. These techniques were applied to the synthesis of biologically-active peptides, thyrotropin-releasing hormones (TRH)[9] and luteinizing-hormone releasing hormones (LH-RH),[10] in order to determine its efficiency.

The synthesis of TRH was carried out as shown in Scheme 2. Nps–His(Tos)[5] was coupled with proline amide[11] in a mixture of acetonitrile and DMF using DCC as the reagent. The Nps-dipeptide amide thus obtained was then treated with trifluoroacetic acid to remove the Nps-group, and the N^{α}-deprotected

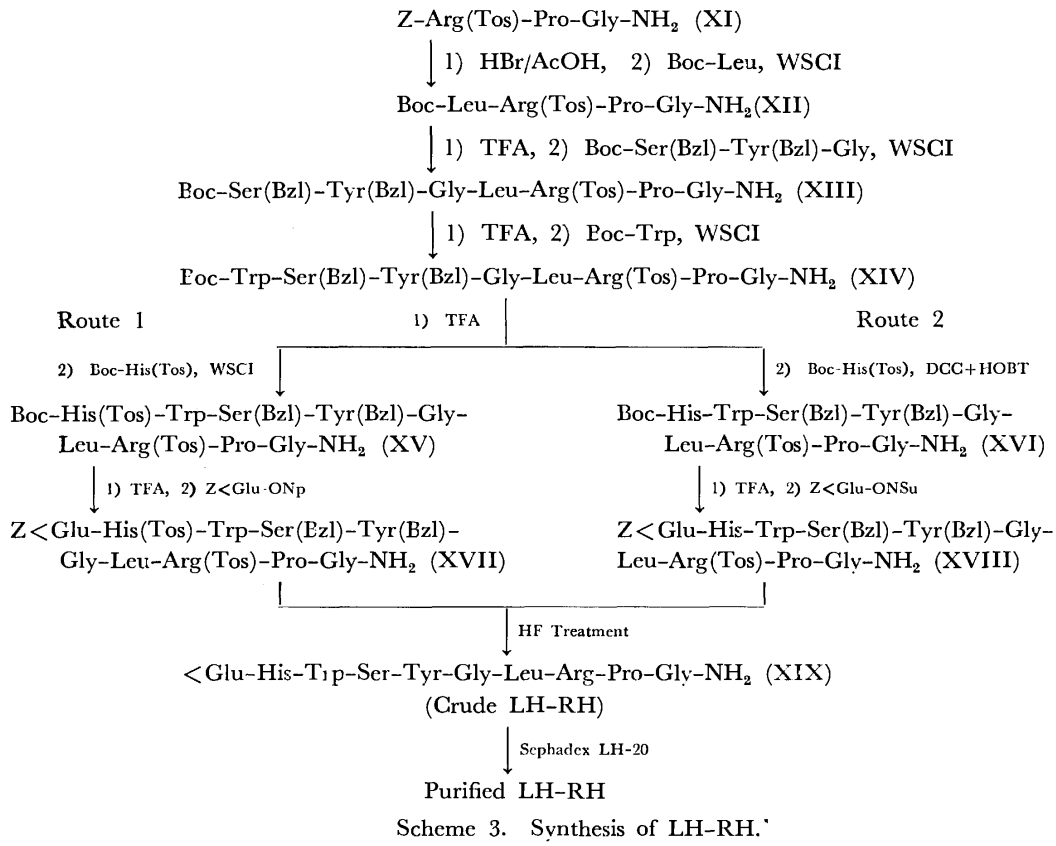

Scheme 3. Synthesis of LH-RH.

dipeptide amide was coupled with Z<Glu using the mixed anhydride method. Since the N^{im}-tosyl group had been kept stable throughout the synthesis, the final protected tripeptide could be purified simply by means of silica-gel column chromatography. The purified, fully-protected tripeptide was treated with HF in the presence of anisole, the excess HF was removed under reduced pressure, and the residue was treated with a short column of Amberlite IR-45 (AcO^- form) to remove the remaining HF. Then, the final product was obtained by lyophilization as an amorphous powder which proved to be homogeneous without the application of any additional purification procedures.

The synthesis of LH-RH was carried out *via* two different routes as shown in Scheme 3. In route 1, Boc–His(Tos)[5] was coupled with Trp–Ser(Bzl)–Tyr-(Bzl)–Gly–Leu–Arg(Tos)–Pro–Gly–NH_2 using WSCI[7] alone as the coupling reagent. The reaction proceeded smoothly, and Boc–His(Tos)–Trp–Ser(Bzl)–Tyr(Bzl)–Gly–Leu–Arg(Tos)–Pro–Gly–NH_2 was obtained as the major product, but partially formed de-tosylated material had to be removed to obtain a single product. Then, the Boc-group was removed by treatment with trifluoroacetic acid, and Z< Glu–ONp was coupled to obtain fully-protected LH-RH. In route 2, the same reaction was carried out in the presence of HOBT analogously to the Geiger procedure.[12] In this case, the tosyl group was completely removed during the coupling reaction,[5] and detosylated nonapeptide was obtained in a high yield. Since no problem was observed in the final coupling reaction with Z<Glu–ONSu,[13] route 2 was considered to be more practical for large-scale synthesis of LH-RH. The final protected decapeptide amide was treated with HF, in the presence of anisole together with tryptophan, followed by purification on Sephadex LH-20, and highly-purified LH-RH was obtained in good yield. The chromatogram of the HF-reaction product indicated the formation of a side product (Fraction II in Fig. 1.). Amino acid analysis of an acid hydrolyzate of the side product indicated a remarkable decrement in the recovery of Tyr. Thus, this material was considered to be modified LH-RH at the Tyr-residue, which should form during the HF-treatment.

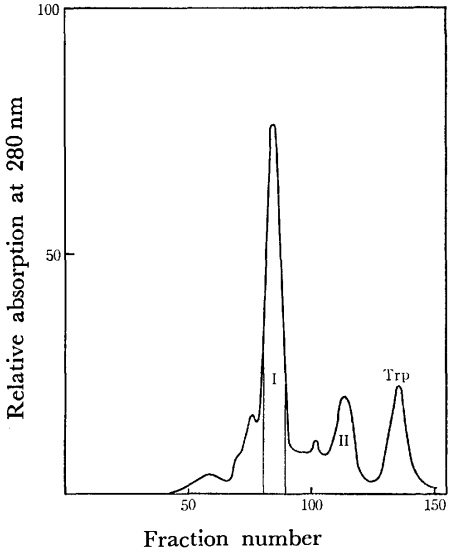

Fig. 1. Purification of crude LH-RH on Sephadex LH-20 column. Column size: 2.8×130 cm (Resin volume, 800 ml). Sample, 0.6 g; Eluent, 1% AcOH; Fraction volume, 6.3 ml; Flow rate, 75 ml/h.

As demonstrated above, the present method for the protection of histidyl residues by the tosyl group has proved to be useful not only in solid-phase synthesis, but also in conventional solution procedures.

Experimental

Melting points were measured by the capillary method and are uncorrected. Paper chromatography was carried out on Toyo filter paper No. 51, and thin layer chromatography on cellulose powder using the following solvent systems: R_f^1; 1-butanol : acetic acid : water (4 : 1 : 1), R_f^2; chloroform : methanol : 30% acetic acid (3 : 2 : 1), R_f^3; 1-butanol : acetic acid : water (4 : 1 : 5, upper phase). All materials obtained were dried over P_2O_5 *in vacuo* for 24 h at room temperature before being applied to the analysis. The IR spectra were recorded on a Shimadzu IR-27G spectrometer, and the UV spectra on a Hitachi EPS-2U spectrometer. The NMR spectra were recorded at 60 MHz with tetramethylsilane as the internal standard using a Hitachi R-20A spectrometer. The HF reactions were carried out using a PRF HF-Reaction Apparatus Type I.

Z(OMe)-His(Tos)–ONp (II-c). DCC (4.4 g, 21 mmol) was stirred into a solution of I-c[5] (9.5 g, 21 mmol) and *p*-nitrophenol (2.8 g, 21 mmol) in THF (100 ml) at −5 °C. The stirring was continued for 1 h at −5—0 °C and for additional 2 h at room temperature. After adding a few drops of glacial acetic acid at 0 °C, the mixture was stirred for 30 min, and then *N,N'*-dicyclohexylurea was removed by filtration; the parent solution was concentrated to a residue under reduced pressure. The residual oil was dissolved in ethyl acetate, the solution was washed successively with 5% aqueous sodium hydrogencarbonate and a saturated sodium chloride solution, and dried over magnesium sulfate. The dried solution was concentrated under reduced pressure, and the residue was recrystallized from methanol to obtain needles; wt. 10.0 g (84.7%), mp 93—5 °C, $[\alpha]_D^{23}$+ 41° (*c* 1, THF). Found: C, 56.43; H, 4.49; N, 9.48; S, 5.40%. Calcd for $C_{28}H_{26}O_9N_4S$: C, 56.56; H, 4.40; N, 9.42; S, 5.38%.

Nps–His(Tos)–ONSu (II-d). DCC (700 mg, 3.4 mmol) was stirred into a solution of I-d[5] (1.4 g, 3 mmol) and *N*-hydroxysuccinimide (350 mg, 3 mmol) in a mixture of ethyl acetate (50 ml) and THF (50 ml) at −5 °C. The stirring was continued for 1 h at −5—0 °C and for additional 2 h at room temperature, and then a few drops of glacial acetic acid were added to the reaction mixture at 0 °C. After 30 min, *N,N'*-dicyclohexylurea was removed by filtration, and the filtrate was concentrated under reduced pressure. The residue was dissolved in a small amount of ethyl acetate, the solution was charged at the top of a column (0.9×75 cm) of silica gel which had been equilibrated with a mixture of benzene and ethyl acetate (5 : 3). The column was developed using the same solvent mixture and fractions containing the second yellow band were collected and evaporated. The residue was treated with hexane producing amorphous solid; wt 1.5 g (89%).

Reaction of I-a with N-(Trifluoroacetoxy)succinimide (Formation of N-Tosyloxy-succinimide). *N*-(Trifluoroacetoxy)succinimide[6] (1.2 g, 5 mmol) was stirred into a solution of compound I-a[5] (2.1 g, 5 mmol) in dry pyridine (5 ml), and

the mixture was allowed to react overnight at room temperature. Then, the reaction mixture was poured into ice-water which precipitated colorless plates which were collected by filtration, washed with ice-water and dried. Then, the dried crystals were recrystallized from ethyl acetate; wt. 0.85 g (60.5%), mp 142.5—145 °C. IR (in Nujol) 1745 (C=O), 1595 (p-CH_3-C_6H_4), 1390, 1180 (SO_2-O-) cm^{-1}. NMR ($CDCl_3$, δ) 2.0—2.2 (d, 2H), 2.55—2.75 (d, 2H), 7.2 (s, 4H), 7.5 (s, 3H). Found: C, 49.10; H, 4.00; N, 5.29%. Calcd for $C_{11}H_{11}O_5NS$: C, 49.07; H, 4.12; N, 5.20%. An authentic sample was synthesized as follows: A solution of tosic anhydride[14] (3.2 g, 10 mmol) and *N*-hydroxysuccinimide (2.3 g, 20 mmol) in dry THF (30 ml) was refluxed for 5 h. Then, the solvent was evaporated out under reduced pressure, the residue was dissolved in ethyl acetate, the solution was washed well with water, and dried over anhydrous sodium sulfate. Concentration of the dried solution gave colorless plates; wt. 1.3 g (24%) mp 142—144 °C. This material showed the same IR and NMR spectra as the above obtained material.

Aoc-His(Tos)-Gly-OBzl (III-a). WSCI (190 mg, 1.2 mmol) was stirred into a solution of I-a (423 mg, 1 mmol) and Gly-OBzl·Tos-OH[15] (400 mg, 1.2 mmol) in THF (13 ml) at −5 °C; the mixture was allowed to react for 1 h at −5—0 °C and then for additional 15 h at room temperature. The solvent was exchanged with ethyl acetate, the solution was washed with 0.5 M sulfuric acid, 5% aqueous sodium hydrogencarbonate and water, and dried over anhydrous magnesium sulfate. Evaporation of the solvent under reduced pressure gave an oil; wt. 540 mg.

Boc-His(Tos)-Gly-OBzl (III-b). DCC (2.1 g, 10 mmol) was stirred into a mixture of compound I-b***,[5] (4.1 g, 10 mmol), Gly-OBzl·Tos-OH[15] (4.0 g, 12 mmol) and triethylamine (1.7 ml), in methylene chloride (40 ml) at −5—0 °C; the stirring was continued for 1 h at the same temperature and then for additional 15 h at room temperature. The *N,N'*-dicyclohexylurea formed was removed by filtration, and washed well with chloroform (100 ml); the solution and the washing were combined, washed successively with 0.5 M sulfuric acid, 5% aqueous sodium hydrogencarbonate and water, and dried over anhydrous magnesium sulfate. The dried solution was concentrated to dryness under reduced pressure, and the residue was washed with a mixture of ether and hexane, and dried. Recrystallization from ethyl acetate-hexane gave colorless needles; wt. 4.4 g (77.7%), mp 51—54 °C, $[\alpha]_D^{22}$ −1.1° (*c* 2, DMF); Found: C, 58.39; H, 6.27; N, 9.60%. Calcd for $C_{27}H_{32}O_7N_4S$: C, 58.26; H, 5.80; N, 10.07%.

Z(OMe)-His(Tos)-Gly-OBzl (III-c). *The DCC Method*: Compound I-c[5] (1.4 g, 3 mmol) and Gly-OBzl·Tos-OH[15] (1.2 g, 3.6 mmol) were coupled in chloroform (30 ml) at −5—0 °C in the presence of triethylamine (0.5 ml) using DCC (680 mg, 3.6 mmol) as described above. The reaction mixture was treated in the same manner, and the final product was recrystallized from methanol-ethyl acetate producing needles; wt. 1.5 g (80%), mp 166—167 °C, $[\alpha]_D^{22}$ +4.6° (*c* 2, DMF); Found: C, 60.13; H, 5.08; N, 9.12%. Calcd for $C_{31}H_{32}O_8N_2S$: C, 59.99; H, 5.20; N, 9.12%.

The Active Ester Method: A mixture of II-c (1.2 g, 2.1 mmol), Gly-OBzl·Tos-OH[15] (1.0 g, 3 mmol) and triethylamine (0.42 ml) in DMF (10 ml) was allowed to react for 15 h at room temperature. Then, it was diluted with chloroform (50 ml), and the solution was washed and treated as in the case of the synthesis of III-b; wt. 950 mg (76.6%), mp 166—167 °C, $[\alpha]_D^{22}$ +4.3° (*c* 1, DMF). The melting point of this compound showed no depression upon mixing with the product synthesized by the DCC method.

Nps-His(Tos)-Gly-OBzl (III-d). *The Mixed Anhydride Method*: A solution of isobutyl chloroformate (137 mg, 1 mmol) in toluene (1 ml) was stirred for 10 min into a mixture of compound I-d[5] (462 mg, 1 mmol) and triethylamine (0.14 ml) in chloroform (2 ml) and toluene (1 ml) at −10 °C. After stirring for additional 10 min, the solution was mixed slowly with a mixture of Gly-OBzl·Tos-OH[15] (350 mg, 1.05 mmol) and triethylamine (0.15 ml) in chloroform (2 ml) at −10—−5 °C. The stirring was continued for 2 h at room temperature; the reaction mixture was treated similarly to the case of the synthesis of III-b. Recrystallization of the final product from ethyl acetate gave yellow needles; wt. 470 mg (77.2%), mp 162—163 °C, $[\alpha]_D^{18}$ +56.7° (*c* 1, DMF). Found: C, 55.16; H, 4.19; N, 11.24; S, 10.44%. Calcd for $C_{28}H_{27}O_7N_7S_2$: C, 55.16; H, 4.46; N, 11.48; S, 10.51%.

The DCC Method: Compound I-d[5] (925 mg, 2 mmol) was subjected to a DCC reaction with Gly-OBzl·Tos-OH[15] (700 mg, 2.1 mmol) in methylene chloride as described above for the synthesis of III-b, and the same compound was obtained; wt. 850 mg (69.9%), mp 164—165 °C, $[\alpha]_D^{18}$ +57.5° (*c* 1, DMF). The melting point of this compound showed no depression upon mixing with the compound obtained by the MA method.

The Active Ester Method: Compound II-d (1.2 g, 2.1 mmol) was coupled with Gly-OBzl·Tos-OH (700 mg, 2.1 mmol) in DMF as in the case of the synthesis of II-c; wt. 910 mg (74.5%), mp 164—165 °C, $[\alpha]_D^{18}$ +57.7° (*c* 1, DMF). The melting point of this compound showed no depression upon mixing with the compound synthesized by the MA method.

Nps-Ala-His(Tos)-Gly-OBzl (VI). *The WSCI Method*: Compound III-a (450 mg, 0.8 mmol) was dissolved in trifluoroacetic acid (1 ml) at 15 °C. After 30 min, excess trifluoroacetic acid was evaporated out under reduced pressure, the residue was treated with dry ether (50 ml) to obtain an amorphous solid. After drying over sodium hydroxide *in vacuo*, this material was dissolved in methylene chloride (10 ml) together with Nps-Ala (160 mg, 1.1 mmol), and WSCI (100 mg, 0.7 mmol) was stirred into the solution at −5—0 °C for 30 min. The stirring was continued overnight at room temperature, then the solvent was removed by evaporation under reduced pressure, and the residue was dissolved in ethyl acetate. The solution was washed successively with 0.5 M sulfuric acid, aqueous 5% sodium hydrogencarbonate and water, and dried over anhydrous magnesium sulfate. The dried solution was concentrated under reduced pressure, the residue was triturated with hexane, and then recrystallized from ethyl acetate and hexane to obtain yellow needles; wt. 338 mg (62%), mp 88—89 °C, $[\alpha]_D^{17}$ −30.0° (*c* 1, AcOEt). Found: C, 54.34; H, 4.53; N, 12.35; S, 9.43%. Calcd for $C_{31}H_{32}O_8N_6S_2$: C, 54.69; H, 4.73; N, 12.34; S, 9.42%.

The Active Ester Method: Compound III-c (609 mg, 1 mmol) was treated with trifluoroacetic acid (1.2 ml) in the presence of anisole (0.4 ml) at 15 °C for 30 min. Excess trifluoroacetic acid was evaporated out under reduced pressure, the residue was treated with dry ether (50 ml) resulting in its solidification, and the solid (IV) was further washed with dry ether. The solid was dissolved in DMF (2 ml) together with Nps-Ala-ONSu (680 mg, 2 mmol)[16] and *N,N*-diethylglycine ethyl ester[17] (1 g), and the mixture was allowed to react overnight at room temperature. The reaction mixture was treated as described above, and the final product was recrystallized from ethyl acetate and hexane;

*** The melting point presented in the Table 1 in Ref. 5 should read 123—125 °C.

wt. 538 mg (79%), mp 87—88 °C, $[\alpha]_D^{18}$ −30.5° (*c* 1, AcOEt). The melting point of this compound showed no depression upon mixing with the compound synthesized by the WSCI method.

His–Gly (V). *A) The HF Treatment of III-c with Anisole*: Compound III-c (1.24 g, 2 mmol) was mixed well in an HF reaction vessel together with anisole (2.8 ml), and anhydrous HF (5 ml) was added to the vessel at −70 °C using an HF-reaction apparatus. The mixture was allowed to react at 0 °C for 1 h, and then excess HF was removed under reduced pressure. After remaining under vacuum for 3 more hours at 0 °C, the residue was extracted with water (10 ml), and the extract was washed well with ether (10 ml). The aqueous layer was treated with a small amount of active charcoal, and then the solution was passed through a column of Amberlite IR-45 (OH^- form) (10 ml), which was washed with water and with aqueous 5% acetic acid. The eluate and washing were combined and lyophilized, and the residue was crystallized from aqueous ethanol to obtain colorless needles; wt. 355 mg (84%), mp 190 °C (decomp.), $[\alpha]_D^{17}$ +24.7° (*c* 1, water). Reported:[18] mp 190 °C (decomp.), $[\alpha]_D$ +25±1° (*c* 2, water). The material showed a single spot of both ninhydrin and Pauly positive on paper chromatography (R_f^1 0.115), and on paper electrophoresis using a pyridine-acetate buffer (pH 4.8) as the solvent. Found: C, 43.61; H, 5.76; N, 25.4%. Calcd for $C_8H_{12}O_3N_4 \cdot {}^1/_2H_2O$: C, 43.43; H, 5.92; N, 25.32%.

B) The HF Treatment of III-d with Anisole: Compound III-d (1.22 g, 2 mmol) was treated in the same manner as described above except that the charcoal treatment was repeated until colorless material was obtained. Yield; 250 mg (56.6%), mp 190 °C (decomp.), $[\alpha]_D^{17}$ +24.5° (*c* 1, water), R_f^1 0.115.

C) The HF Treatment of III-d with Skatole: Compound III-d (1.22 g, 2 mmol) was treated with anhydrous HF (5 ml) in the presence of anisole (2 ml) together with skatole (600 mg, 4 mmol), as in the case of the synthesis of V, at 0 °C for 1 h. After removal of the excess HF under reduced pressure, the residue was dissolved in a mixture of water and chloroform. The aqueous phase was washed with ether, and then passed through a column of Amberlite IR-45 (OH^- form) (10 ml). The column was eluted with water and then washed with aqueous 5% acetic acid; the eluate and washing were combined and lyophilized. The residue was washed with methanol, and recrystallized from aqueous ethanol to obtain colorless needles; wt. 340 mg (80.5%), mp 189 °C (decomp.), $[\alpha]_D^{17}$ +24.3° (*c* 1, water), R_f^1 0.115.

Separation of the Side Product, 2-Nps-skatole: The chloroform layer, which was separated from the water-chloroform extract of the HF-reaction mixture, was washed with water and dried over anhydrous magnesium sulfate. The dried solution was concentrated to dryness, the residue was dissolved in a small amount of ethyl acetate, and the solution was charged at the top of a silica gel column (0.7×70 cm) which had been equilibrated with a solvent system of ethyl acetate and benzene (1 : 1). The column was developed with the same solvent mixture, the fractions containing the main peak were collected and evaporated. The residue was recrystallized from aqueous methanol; wt. 380 mg (67%), mp 139—141 °C, UV λ_{max}^{EtOH} 224 nm (ε 55200), 283 (ε 21400), 261 nm (ε 5600): NMR ($CDCl_3$, δ) 2.20—2.60 (s, 3H), 6.57—6.82 (m, 1H), 7.00—7.50 (m, 5H), 7.53—7.75 (m, 1H), 7.95—8.32 (m, 2H). Found: C, 63.60; H, 4.16; N, 9.60; S, 10.94%. Calcd for $C_{15}H_{12}O_2N_2S$: C, 63.38; H, 4.26; N, 9.89; S, 11.25%.

Ala–His–Gly (VII). Compound VI (1.36 g, 2 mmol) was mixed well with anisole (2 ml) and skatole (600 mg, 4 mmol) in an HF reaction vessel, and the mixture was treated with HF (7 ml) as above at 0 °C for 1 h. After removal of the excess HF, the residue was treated in the same manner as in the case of the synthesis of V (Procedure C). Compound VII thus obtained was recrystallized from aqueous ethanol producing colorless needles; wt. 360 mg (63.4%), mp 230 °C (decomp.), $[\alpha]_D^{18}$ +36.3° (*c* 1, AcOH). The homogeneity of this material was confirmed by ninhydrin and Pauly reagent on paper electrophoresis and paper chromatography; R_f^1 0.23. Amino acid ratios in an acid hydrolyzate: Ala 1.00, His 1.00, Gly 1.00. Ratio in an APM digest: Ala 1.00, His 1.00, Gly 0.98. Found: C, 46.87; H, 6.00; N, 24.70%. Calcd for $C_{11}H_{17}O_5N_4$: C, 46.63; H, 6.05; N, 24.72%.

Nps–His(Tos)–Pro–NH_2 (VIII). DCC (1.1 g, 5.3 mmol) was stirred into a solution of I-d[5] (2.3 g, 5 mmol) and Pro–NH_2[10] (0.57 g, 5 mmol) in a mixture of acetonitrile (50 ml) and DMF (20 ml) at −5 °C. Stirring was continued for 1 h at −5—0 °C and for additional 15 h at room temperature. The *N,N'*-dicyclohexylurea formed was removed by filtration, the filtrate was evaporated under reduced pressure, and the residue was redissolved in ethyl acetate. The ethyl acetate solution was washed successively with 0.5 M sulfuric acid, aqueous 5% sodium hydrogencarbonate, and water, and dried over anhydrous magnesium sulfate. The dried solution was concentrated to dryness, and the residue was washed with a mixture of methanol and ether, and dried. Recrystallization of the dried residue from ethyl acetate gave yellow needles; wt. 2.0 g (72%), mp 188 °C, $[\alpha]_D^{20}$ +15.1° (*c* 0.5, DMF). Found: C, 51.78; H, 4.62; N, 14.85; S, 11.07%. Calcd for $C_{24}H_{26}O_6N_6S_2$: C, 51.59; H, 4.69; N, 15.04; S, 11.47%.

Z<Glu–His(Tos)–Prc–NH_2 (IX). Compound VIII (0.79 g, 1.5 mmol) was dissolved in a mixture of trifluoroacetic acid (1.5 ml) and methylene chloride (1.5 ml) together with anisole (2 ml) at 15 °C. After 30 min, the methylene chloride and excess trifluoroacetic acid were removed by evaporation under reduced pressure, and the residue was treated with dry ether (50 ml) to give an amorphous powder. To a solution of Z<Glu (0.4 g, 1.5 mmol) and triethylamine (0.21 ml) in THF (4 ml), a solution of isobutyl chloroformate (0.21 g, 1.5 mmol) in toluene (2 ml) was added drop by drop at −10 °C for 10 min. After additional 10 min, the reaction mixture was stirred at once into an aqueous 5% sodium hydrogencarbonate solution of the powder obtained above at −5—0 °C; the pH of the solution was confirmed to be 7. After stirring for 1 h at room temperature, the solution was evaporated under reduced pressure, and the residue was extracted with chloroform (20 ml). The chloroform extract was washed successively with 0.5 M sulfuric acid, aqueous 5% sodium hydrogencarbonate, and dried over anhydrous magnesium sulfate. The solvent was evaporated to dryness, and the residue (0.63 g) was charged at the top of a column of silica gel (0.8×50 cm) which had been equilibrated with a solvent system of chloroform, ethyl acetate and ethanol (5 : 4 : 2). The column was developed with the same solvent mixture, and fractions containing the main band were combined and evaporated to dryness. The residue was washed well with dry ether to obtain an amorphous powder; wt. 450 mg (52.3%), mp 113—116 °C (decomp.), $[\alpha]_D^{15}$ −29.1° (*c* 1, DMF). Found: C, 57.09; H, 5.17; N, 12.86%. Calcd for $C_{31}H_{34}O_8N_6S$: C, 57.22; H, 5.27; N, 12.92%.

<Glu–His–Pro–NH_2 (X) (TRH). Compound IX (65 mg, 0.1 mmol) was treated with anhydrous HF (1 ml) in the presence of anisole (0.15 ml) at 0 °C for 1 h, as in the case of the synthesis of V, and then the excess HF was removed

under reduced pressure. After being kept under vacuum for 4 h at 0 °C, the residue was dissolved in water, the solution was washed with ether, and the aqueous layer was passed through a column (0.5×10 cm) of Amberlite IR-45 (AcO^- form). The column was eluted with water and washed with aqueous 5% acetic acid. The eluate and washing were combined and lyophilized to obtain a residual powder; wt. 37.6 mg (96.5%), $[\alpha]_D^{25}$ −44.8° (*c* 1, 95% AcOH). Reported:[19] $[\alpha]_D^{15}$ −45.1° (*c* 1, AcOH). The homogeneity of this material was confirmed by paper electrophoresis using a 0.1 M pyridine-acetic acid buffer (pH 4.7) and by paper chromatography, which were located using the Pauly reagent; R_f[2] 0.55. The amino acid ratio in an acid hydrolyzate: Glu 1.00, His 1.06, Pro 0.94. Found: C, 49.40; H, 6.34; N, 21.54%. Calcd for $C_{16}H_{22}O_4N_6 \cdot {}^3/_2H_2O$: C, 49.34; H, 6.47; N, 21.58%.

Z–Arg(Tos)–Pro–Gly–NH$_2$ (XI). A solution of Z–Arg(Tos)–Pro–Gly–OEt[20] (6.5 g, 0.01 mol) in methanol (150 ml) was saturated with ammonia gas at 0 °C. After being kept for 2 days at room temperature, the solution was concentrated to dryness and was triturated with ethyl acetate to obtain an amorphous powder: wt. 5.3 g (82%) mp 145.5—147 °C; $[\alpha]_D^{23}$ −20.2° (*c* 1, DMF). Found: C, 54.52; H, 6.13; N, 15.69; S, 5.13%. Calcd for $C_{28}H_{37}O_7N_7S$: C, 54.60; H, 6.05; N, 15.92; S, 5.20%.

Boc–Leu–Arg(Tos)–Pro–Gly–NH$_2$ (XII). Compound XI (3.7 g, 6 mmol) was dissolved in a 25% HBr solution in acetic acid (17 ml), and the solution was allowed to react for 50 min at room temperature. Then, the product was precipitated by adding a large volume of dry ether. The supernatant was removed by decantation, the precipitates were washed several times with dry ether, and dried over sodium hydroxide *in vacuo*. The dried material was dissolved in DMF (10 ml), the pH of the solution was adjusted to 7 with *N*-ethylmorpholine, and Boc–Leu–ONSu[21] (2.4 g, 7.2 mmol) was added to the solution. After being kept for 2 days at room temperature, the solution was diluted with excess chloroform. The chloroform solution was washed with 1 M hydrochloric acid, 10% sodium carbonate, and a saturated solution of sodium chloride, successively, and dried over anhydrous magnesium sulfate. The dried solution was concentrated under reduced pressure to a residue, which was crystallized from ethanol–hexane: wt. 3.1 g (75%), mp 152—153 °C, $[\alpha]_D^{27}$ −33° (*c* 1, DMF). Found: C, 52.81; H, 7.33; N, 15.78%. Calcd for $C_{31}H_{50}O_8N_8S \cdot {}^1/_2H_2O$: C, 52.89; H, 7.31; N, 15.92%.

Boc–Ser(Bzl)–Tyr(Bzl)–Gly–Leu–Arg(Tos)–Pro–Gly–NH$_2$ (XIII). Compound XII (3.1 g, 4.4 mmol) was dissolved in trifluoroacetic acid (10 ml) at 0 °C, and the solution was allowed to react for 1 h at room temperatdre. The solution was concentrated to a residue under reduced pressure; and the residue was dried over sodium hydroxide *in vacuo*. The dried material was dissolved in 30 ml of dried THF, and Boc–Ser(Bzl)–Tyr(Bzl)–Gly[22] (2.4 g, 4 mmol) was added to the solution together with HOBT (0.6 g, 4.4 mmol). Then, WSCI (0.8 ml, 4.4 mmol) was added to the mixture at 0 °C. The whole mixture was allowed to react overnight, and then, the solvent was evaporated out under reduced pressure. The residue was dissolved in chloroform (100 ml), the solution was washed well with water and dried for a short time over anhydrous magnesium sulfate. The dried solution was concentrated to a residue, which was purified by reprecipitation from chloroform-ethyl acetate; 4.6 g (97%), mp 118.5—123 °C, $[\alpha]_D^{20}$ −29.5° (*c* 1, DMF). Found: C, 59.35; H, 6.97; N, 12.22%. Calcd for $C_{60}H_{82}O_{13}N_{11}S \cdot 2H_2O$; C, 59.29; H, 6.97; N, 12.67%.

Boc–Trp–Ser(Bzl)–Tyr(Bzl)–Gly–Leu–Arg(Tos)–Pro–Gly–NH$_2$ (XIV). Compound XIII (3.8 g, 3.1 mmol) was dissolved in trifluoroacetic acid (12 ml) at 0 °C, and the mixture was allowed to react for 30 min at room temperature. Then, it was concentrated to a residue, which was washed with ether and dried over sodium hydroxide *in vacuo*. The dried material was dissolved in DMF (5 ml) together with HOBT (0.2 g), the pH of the solution was adjusted to 7 by adding triethylamine, and then, Boc–Trp–ONSu[21] (1.9 g, 4.7 mmol) was stirred into the solution. The whole mixture was allowed to react for 3 days, and then the product was precipitated out as a gelatinous powder by adding ethyl acetate. The product was collected by filtration, reprecipitated twice from DMF–ethyl acetate, washed with ether, and dried; wt. 3.9 g (90%), mp 142—149 °C (decomp.), $[\alpha]_D^{29}$ −27.4° (*c* 1, DMF). Found: C, 59.67; H, 6.60; N, 12.71%. Calcd for $C_{70}H_{89}O_{14}N_{13}S \cdot 2H_2O$: C, 59.85; H, 6.67; N, 12.96%.

Boc–His(Tos)–Trp–Ser(Bzl)–Tyr(Bzl)–Gly–Leu–Arg(Tos)–Pro–Gly–NH$_2$ (XV). Compound XIV (2.8 g, 2 mmol) was mixed well with 0.5 ml each of anisole and mercaptoethanol, and 10 ml of trifluoroacetic acid was added to the mixture at 0 °C; then, the solution was allowed to react for 30 min at room temperature. The solution was concentrated to a residue, which was triturated with dry ether and dried over sodium hydroxide *in vacuo*. The dried material was dissolved in a mixture of DMF and THF (10 ml each) together with I-b[5] (1.6 g, 4 mmol), and 0.62 ml of WSCI (4 mmol) was stirred into the mixture at 0 °C. Then, the mixture was allowed to react overnight at room temperature. THF was removed by distillation under reduced pressure, and the product was precipitated by the addition of water, which was collected by filtration and purified by reprecipitation from DMF-ethyl acetate; wt. 2.7 g (80%), mp 156—158.5 °C (decomp.), $[\alpha]_D^{20}$ −36.8° (*c* 1, DMF). Found: C, 58.40; H, 6.11; N, 13.00%. Calcd for $C_{83}H_{103}O_{17}N_{16}S_2 \cdot 2H_2O$: C, 58.74; H, 6.35; N, 13.2%.

Z<Glu–His(Tos)–Trp–Ser(Bzl)–Tyr(Bzl)–Gly–Leu–Arg(Tos)–Pro–Gly–NH$_2$ (XVII). Trifluoroacetic acid (3 ml) was stirred into a mixture of compound XV (252 mg, 0.15 mmol) and mercaptoethanol (0.05 ml) at 0 °C, and then the whole mixture was allowed to react for 40 min at room temperature. Excess trifluoroacetic acid was removed by distillation under reduced pressure, and the residue was treated with ether to precipitate the product as a powder, which was collected by filtration, washed with ether and dried over sodium hydroxide *in vacuo*. The dried material was dissolved in 1 ml of DMF, the pH of the solution was adjusted to 7 with *N*-methylmorpholine, and Z<Glu–ONp[23] (86 mg, 0.22 mmol) was stirred into the solution; the mixture was allowed to react for 2 days at room temperature. The reaction mixture was diluted with chloroform, the solution was washed successively with 1 M hydrochloric acid, water, 1 M sodium carbonate, and water, and dried over anhydrous magnesium sulfate. The dried solution was concentrated to a residue, which was purified by passage through a column of silica gel using a mixture of chloroform, methanol and acetic acid (95 : 5 : 3) as the solvent. Fractions containing the main band were collected and concentrated to a residue, which was purified by reprecipitation from chloroform–ether; wt. 150 mg (54.3%), mp 133.5—138.5 °C (decomp.), $[\alpha]_D^{20}$ −40.5° (*c* 1, DMF). Found: C, 59.39; H, 5.89; 13.41%. Calcd for $C_{91}H_{106}O_{19}N_{17}S_2 \cdot 3H_2O$: C, 59.33; H, 6.02; N, 12.93%.

Boc–His–Trp–Ser(Bzl)–Tyr(Bzl)–Gly–Leu–Arg(Tos)–Pro–Gly–NH$_2$ (XVI). Compound (XIV) (2.8 g, 2 mmol) was treated with trifluoroacetic acid as in the case of the synthesis of XV. The des-Boc-product was dissolved in

DMF (10 ml); HOBT (0.544 g, 4 mmol), Boc–His(Tos) (1.6 g, 4 mmol) and WSCI (0.62 ml, 4 mmol) were stirred successively into the DMF solution at 0 °C. After being allowed to react overnight at room temperature, the mixture was diluted with water to precipitate the product, which was collected by filtration and dried. Finally, the dried product was purified by reprecipitation twice from DMF–ethyl acetate; wt. 2.7 g (90%), mp 143.5—147.5 °C (decomp.), $[\alpha]_D^{25}$ −26.9° (*c* 1, DMF). Found: C, 58.95; H, 6.76; N, 14.23%. Calcd for $C_{76}H_{96}O_{15}N_{16}S \cdot 2H_2O$: C, 59.21; H, 6.54; N, 14.54%.

Z < Glu–His–Trp–Ser(Bzl) – Tyr(Bzl) – Gly–Leu–Arg(Tos)–Pro–Gly–NH_2 (XVIII). Compound XVI (2.3 g, 1.5 mmol) was treated with trifluoroacetic acid to remove the Boc-group as shown in the case of the synthesis of XVII. The des-Boc-compound thus obtained was dissolved in DMF (4 ml), together with HOBT (0.3 g, 2.2 mmol), the pH of the solution being adjusted to 7 by the addition of *N*-ethylmorpholine at 0 °C, and then Z<Glu–ONSu[12] (0.81 g, 2.25 mmol) was added. The whole mixture was allowed to react for 3 days at room temperature, and then excess water was added to precipitate the product, which was collected by filtration and dried. The dried material was reprecipitated twice from DMF–ethyl acetate for purification: wt. 2.2 g (88%), mp 132—138.5 °C (decomp.), $[\alpha]_D^{25}$ −25.4° (*c* 1, DMF). Found: C, 60.19; H, 6.18; N, 14.0%. Calcd for $C_{84}H_{99}O_{17}N_{17}S \cdot H_2O$: C, 60.45; H, 6.10; N, 14.27%.

<Glu–His–Trp–Ser–Tyr–Gly–Leu–Arg–Pro–Gly–NH_2 (LH–RH). (a): Compound XVIII (1 g, 0.58 mmol) was mixed well with tryptophan (0.1 g), phenol (0.5 g) and anisole (1 ml) in an HF reaction vessel; then, the mixture was treated with HF (10 ml) for one h at 0 °C as in the case of the synthesis of V. After removel of the excess HF under reduced pressure, the residue was extracted with 0.1 M acetic acid, the extract was washed with ether, and then passed through a Dowex 1×2 column (AcO^- form, 3×10 cm). The column was washed well with 0.1 M acetic acid, and the effluent and washing were combined and lyophilized to obtain 0.6 g of the crude product. The crude material was charged at the top of a column of Sephadex LH-20 (2.8×130 cm) which had previously been equilibrated with 1% acetic acid, and the column was eluted with the same solvent. Fractions containing the major product (Peak I in Fig. 1) were collected and lyophilized; the residue was further fractionated on the same type of column under the same conditions to obtain a homogenous product; wt. 220 mg, $[\alpha]_D^{25}$ −49.4° (*c* 0.4, H_2O), −51.0° (*c* 0.3, 1% AcOH). Reported: $[\alpha]_D^{28}$ −50.5° (*c* 1, 1%AcOH).[24] The homogeneity of this material was confirmed by paper electrophoresis using a 0.1 M pyridine-acetic acid buffer (pH 4.7) and by thin layer chromatography on cellulose powder, which were located using the Pauly reagent; R_f[3] 0.41. Found: C, 51.37; H, 6.58; N, 17.59%. Calcd for $C_{65}H_{75}O_{13}N_{17} \cdot 2C_2H_4O_2 \cdot 4H_2O$: C, 51.55; H, 6.67; N, 17.33%. The amino acid ratio in an acid hydrolyzate: His 1.00, Arg 0.96, Ser 1.00, Glu 1.04, Pro 1.01, Gly 1.98, Leu 0.96, Tyr 1.00, NH_3 1.06, Trp 0.97. The average recovery rate of the amino acids was 95%; Trp was determined by spectrophotometry. The amino acid ratio in an acid hydrolyzate of Fraction II: His 0.93, Arg 0.96, Ser 0.94, Glu 1.03, Pro 1.01, Gly 1.88, Leu 1.00, Tyr 0.28. *(b)*: Compound XVII (1 g, 0.53 mmol) was treated with HF in the same manner as described above. No major difference was observed at each step of the production of the final product; wt. 230 mg, $[\alpha]_D^{23}$ −48.7° (*c* 0.4, H_2O). Paper electrophoresis and thin layer chromatography showed this compound to be homogeneous and identical with the compound obtained above. Found: C, 51.74; H, 6.65; N, 17.67%. The amino acid ratio in an acid hydrolyzate: His 0.91, Arg 0.98, Ser 0.99, Glu 1.03, Pro 1.01, Gly 2.00, Leu 0.95, Tyr 1.00, NH_3 1.15, Trp 0.94. The average recovery rate of the amino acids was 94%.

References

1) Preliminary report: S. Sakakibara and T. Fujii, *Bull. Chem. Soc. Jpn.*, **42**, 1466 (1969).

2) The abbreviations used in this report are those recommended by the IUPAC-IUB: *J. Biol. Chem.*, **247**, 977 (1972); Aoc, *t*-amyloxycarbonyl; DCHA, dicyclohexylamine; HOBT, 1-hydroxybenzotriazole; APM, Amino Peptidase M.

3) T. Fujii and S. Sakakibara, *Bull. Chem. Soc. Jpn.*, **43**, 3954 (1970).

4) J. M. Stewart, M. Knight, A. C. M. Paiva, and T. Paiva, Reported on the Second American Peptide Symposium, Aug. 17, 1970, Cleveland, Ohio; G. P. Schwartz and P. G. Katsoyannis, *J. Chem. Soc., Perkin Trans. 1*, **1973**, 2894, B. W. Erickson and R. B. Merrifield, *Israel J. Chem.* **12**, 79, (1974).

5) Part I; T. Fujii and S. Sakakibara, *Bull. Chem. Soc. Jpn.*, **47**, 3146 (1974).

6) S. Sakakibara and N. Inukai, *Bull. Chem. Soc. Jpn.*, **38**, 1979 (1965).

7) J. C. Sheehan, J. Preston, and P. A. Cruickshank, *J. Am. Chem. Soc.*, **87**, 2492 (1965).

8) S. Sakakibara, Y. Shimonishi, Y. Kishida, M. Okada, and H. Sugihara, *Bull. Chem. Soc. Jpn.*, **40**, 2164 (1967); S. Sakakibara, Y. Kishida, R. Nishizawa, and Y. Shimonishi, *ibid.*, **41**, 438 (1968).

9) K. Forkers, F. Enzmann, J. Fölter, C. Y. Bowers, and A. V. Schally, *Biochem. Biophys. Res. Commun.*, **37**, 123 (1969); R. Burgus, T. F. Dunn, D. Desiderio, and R. Gullemin, *Compt. Rend.*, **269**, 1870 (1969); R. Burgus, T. F. Dunn, D. Desiderio, D. N. Ward, W. Vale, and R. Guillemin, *Nature*, **226**, 321 (1970); R. Burgus, T. F. Dunn, D. M. Desiderio, D. N. Ward, W. Vale, and R. Guillemin, *Endocrinology*, **86**, 573 (1970).

10) H. Matsuo, Y. Baba, R. M. G. Nair, A. Arimura, and A. V. Schally, *Biochem. Biophys. Res. Commun.*, **43**, 1334 (1971); R. Burgus, M. Butcher, M. Amos, N. Ling, M. Monanan, J. Riviere, R. Fellows, R. Blackewll, W. Vale, and R. Guillemin, *Proc. Natl. Acad. Sci. U. S. A.*, **69**, 278 (1972).

11) K. Strum, R. Geiger, and W. Siedel, *Ber.*, **96**, 609 (1963).

12) W. König and R. Geiger, *Ber.*, **103**, 788 (1970).

13) P. Kurath and A. M. Thomas, *Helv. Chim. Acta*, **56**, 1656 (1973); N, Yanaihara, C. Yanaihara, K. Tsuji, and T. Hashimoto, *J. Med. Chem.*, **16**, 373 (1973).

14) L. Field, *J. Am. Chem. Soc.*, **74**, 394 (1952).

15) L. Zervas, M. Winitz, and J. P. Greenstein, *J. Org. Chem.*, **22**, 1515 (1957).

16) J. Meienhofer, *Nature*, **205**, 73 (1965).

17) S. Sakakibara and M. Itoh, *Bull. Chem. Soc. Jpn.* **40**, 656 (1967).

18) G. Amiard, R. Heymes, and L. Vellus, *Bull. Soc. Chim. Fr.*, **1955** 1464.

19) D. Gillessen, A. M. Felix, W. Lergier, and R. O. Studer, *Helv. Chim. Acta*, **53**, 63 (1970).

20) E. Schnable, *Justus Liebigs Ann. Chem.*, **688**, 238 (1965).

21) G. W. Anderson, J. E. Zimmerman, and F. M. Callahan, *J. Am. Chem. Soc.*, **86**, 1839 (1964).

22) R. Matsueda, J. Maruyama, E. Kitagawa, H. Takahagi, and T. Mukaiyama, *Bull. Chem. Soc. Jpn.* **46**, 3240 (1973).

23) H. Gibian and E. Klieger, *Justus Liebigs Ann. Chem.*, **640**, 145 (1961); E. Klieger and H. Gibian, *ibid.*, **649**, 183 (1961).

24) R. Geiger, W. König, H. Wissmann, K. Geisen, and F. Enzmann, *Biochem. Biophys. Res. Commun.* **45**, 767 (1971).

Stereochemistry of the C and D Rings of C-Nor-D-homosteroids. II.[1] Synthesis of Etiojervane Analogs of Pregnan-3β-ol[2]

Akio MURAI, Takeshi NISHIMURA, and Tadashi MASAMUNE

Department of Chemistry, Faculty of Science, Hokkaido University, Sapporo 060

(Received September 30, 1975)

The synthesis of C/D *trans*- and *cis*-fused C-nor-D-homo-5α-pregnan-3β-ol 3-acetates (**13a** and **32**) from jervine (**1**) is described. The configurations of both the compounds and the synthetic intermediates were determined on the basis of chemical and spectral evidence.

During the past decade synthetic studies of C-nor-D-homosteroid hormones have been reported by several groups.[3-7] In the present paper we describe the transformation of jervine (**1**) into etiojervane analogs of 5α-pregnan-3β-ol, which include both C/D *cis*- and *trans*-fused ring systems. In connection with the study on the synthesis and NMR spectra of (22S, 23R, 25S)-12α(not 12β)- and Δ^{12}-jervanines,[8] the results of the present work are useful for discussion[9] on conformations of the rings in etiojervanes.

In 1953, Fried and Klingsberg[10] isolated 17-ethyletiojervan-3β-ol-11-one 3-acetate (**2**) in 33% yield from the hydrogenation product of the corresponding $\Delta^{5,12,17(20)}$-triene derivative (**3**), obtained from jervine (**1**) by one-step fragmentation. Later, Mitsuhashi and Shimizu[5a] prepared the compound (**2**) in 80% yield by the same reaction of 17β-ethyletiojerv-12-en-3β-ol-11-one 3-acetate (**4**), which had been derived from hecogenin, and correlated both the alkaloid and sapogenin, elucidating the configurations of C_3, C_8, C_9, C_{10} and C_{14} in jervine (**1**). However, the spatial arrangement at C_{12} and C_{13} of the compound (**2**), a key intermediate for the correlation, has not been determined yet. The present work was undertaken with an aim to clarify these configurations.

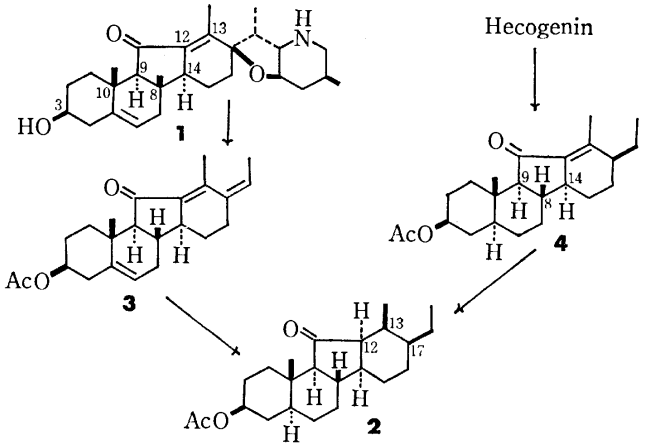

Scheme 1.

Hydrogenation of 12β-etiojerv-5-ene-3β,11β-diol-17-one 17-ethylene acetal[3b] (**5**), prepared from **3** by a four-stage process, over platinum in acetic acid afforded its 5α,6-dihydro derivative (**6**), mp 192—193 °C, in 88% yield along with triol (**7**), mp 235—236 °C (5%). Compound (**7**), with a molecular formula of $C_{19}H_{32}O_3$, is considered to be a hydrogenolysis product at C_{17}. On partial acetylation of compound (**7**) with acetic anhydride and pyridine afforded 3,17-diacetate (**7a**), mp 142—143 °C, which was oxidized with Jones' reagent to give 11-ketone (**8**), mp 120—121 °C. The ketone (**8**) was identified as 5α,12β-etiojervane-3β,17β-diol-11-one 3,17-diacetate by derivation from the corresponding 5,6-dehydro compound[11] with a well-defined configuration, indicating that triol **7** could be formulated as 3β,11β,17β-triol. In view of the fact that no hydrogenolysis product was isolated by the same treatment of the corresponding 11-deoxy (compound **15**) and 11-oxo derivatives,[9] the formation of **7** would reveal specific participation of the 11-hydroxy group to the catalytic reaction.

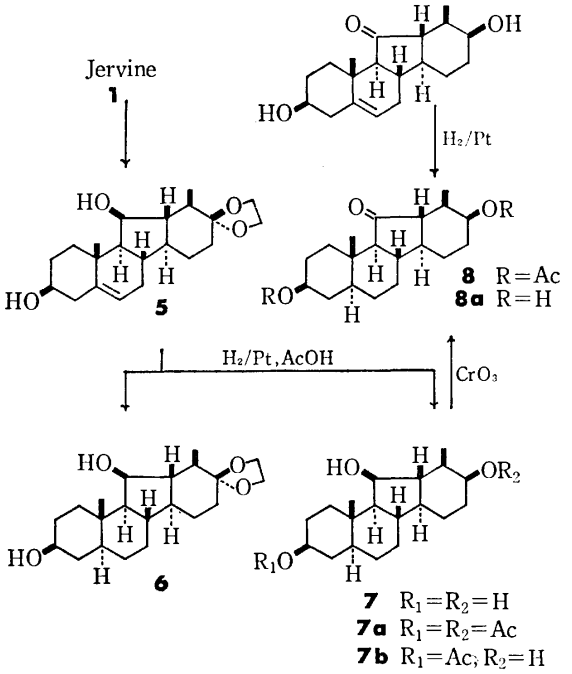

Scheme 2.

Treatment of 17-acetal **6** with acid produced 17-ketone (**9**), mp 188—190 °C, in 85% yield, whose NMR spectrum (19-C$\underline{H}_3$, δ 1.04) and ORD curve (Cotton effect, $a=-115°$) were consistent with the assigned configurations. The Witting reaction of **9** with ethylidenetriphenylphosphorane[12] proceeded smoothly and, after acetylation, gave the 17-ethylidene derivative (**10**), mp 156—157 °C, in a good yield (crude 82% and pure 41%). Compound **10**, when hydrogenated over platinum and then oxidized with chromium(VI) oxide, was transformed into a mixture of 17-epimeric 11-ketones (**11** and **12**), which showed a single spot differing from that of compound **2** on various solvent

systems on TLC and resisted further purification. However, treatment of the mixture with sodium methoxide in refluxing methanol effected epimerization at the carbon atom(s) adjacent to the 11-oxo group and, on acetylation and subsequent purification by preparative TLC, led to isolation of the relevant compound (**2**) in 15% yield. Judging from chemical shifts of the 19-methyl protons of the mixture (**11** and **12**, δ 0.84) and the epimerized product (**2**, δ 0.90), this isomerization took place with configurational inversion only at C_{12}.[13] The transformation from compound **5** into the mixture (**11** and **12**) involves no epimerization at C_{12} and C_{13} (all compounds, 12βH and 13αH). The present result, combined with the Mitsuhashi work,[5a] confirms the compound in question to be represented correctly by formula **2** (12αH, 13αH and 17αH).

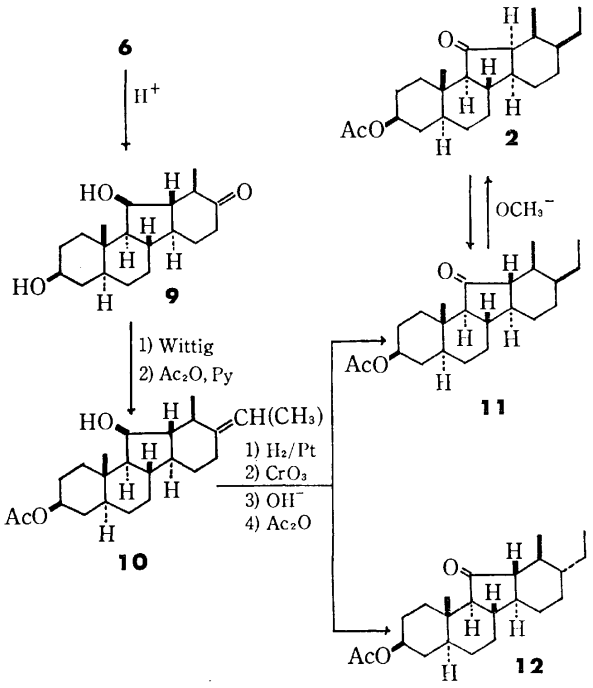

Scheme 3.

The afore-mentioned result suggests that a 12β-epimer of **2** with a 17β-ethyl group must be contained in the mixture. In fact, treatment of **2** with alkali in refluxing methanol followed by acetylation resulted in formation of a nearly 1 : 1 equilibrium mixture of **2** and the 12β-epimer, from which the latter (**11**), mp 121—123 °C, was isolated in 35% yield (crude 46%) by preparative TLC, showing practically the same IR spectrum as that of the mixture. In accordance with the assigned configurations, these 12-epimeric 11-ketones (**2** and **11**) exhibited negative Cotton effects with amplitudes of −82° and −170°, respectively, in the ORD curves.[14] On the other hand, the relevant hydrogenation mixture of **11** and **12** was treated with the base and then acetylated repeatedly, when most of one (**11**) of the two 12α-epimers was epimerized to the 12β-epimer (**2**), the other (**12**) being left as the main component of the mixture. This treatment led to isolation of compound **12** in 14% yield (crude 40%), mp 109—109.5 °C, suggesting that the mixture in question would contain almost equal amounts of 17-epimers (**11** and **12**). It is to be noted that, while the hydrogenation of double bonds at C_{12}—C_{13}, C_{13}—C_{17}, and C_{16}—C_{17} proceeded with the *cis*-addition mainly from the rear side, as illustrated by those of **4** and other compounds,[14] the hydrogen addition to a double bond at C_{17}–C_{20} took place from both sides.

The Wolff-Kishner reduction of 11-ketone **2** by a modification of the Huang-Minlon[15] or the Barton procedure[16] effected removal of the 11-oxo group, giving 3β-alcohol (**13**), mp 124—125 °C, as the sole isolable product in a moderate yield. Compound **13** was also obtained from 12-epimeric 11-ketone **11** in almost the same yield by the same treatment. This compound was readily acetylated to 3β-acetate (**13a**), mp 94.5—95 °C, or oxidized to 3-ketone (**14**), mp 119—121 °C, in good yield, the latter being further transformed into the ethylene acetal (**14a**), mp 98—100 °C. The following experiments were undertaken with a view to clarify the configuration at C_{12} of this compound (**13**).

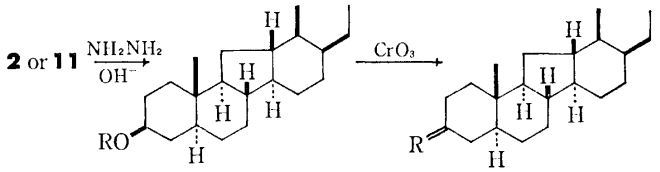

13 R=H **14** R=O
13a R=Ac **14a** R=$-OC_2H_4O^-$

Hydrogenation of 12β-etiojerv-5-en-3β-ol-17-one 17-ethylene acetal[4d] (**15**) over platinum gave its 5α,6-dihydro derivative (**16**), mp 177—179 °C, in 80% yield, along with its 5β-isomer (**17**), mp 107—109 °C. The major product (**16**) on acid hydrolysis formed 17-ketone (**18**), mp 179—180 °C, in 90% yield, which was readily derived into 3β-acetate (**18a**), mp 134.5—135 °C. The assigned configurations (5αH, 12βH and 13αH) at C_5, C_{12} and C_{13} of these 17-ketones were confirmed by the NMR spectra (19-methyl protons, **18**, δ 0.75 and **18a**, 0.78) and the ORD curves (Cotton effect, both **18** and **18a**, $a=-105°$). Compound **18** was then submitted to the Wittig reaction[12] to give an oily mixture of the 17-ethylidene derivatives (**19**) in 97% yield, which exhibited two sharp singlets with relative intensity of 4 to 3 due to the 19-methyl protons at δ 0.73 and 0.76 in the NMR spectrum. However, the mixture (**19**) and also its hydrogenation product, 17-ethyletiojervan-3β-ols, again resisted further purification, showing a single spot on TLC. Thus the mixture **19**, after being converted into 3-acetates (**19a**), amorphous, in 79% yield, was submitted to hydroboration[17] and subsequent oxidation with sodium dichromate in sulfuric acid,[18] giving a 4 : 3 mixture of 17β- and 17α-acetyletiojervan-3β-ol 3-acetates (**20**), mp 189—191 °C, and (**21**), mp 110.5—111 °C, which were isolated in 28 and 18% yields, respectively, along with the unreacted starting material (**19a**) (9%). The configurations at C_{17} of these compounds were assigned on the basis that the former (**20**) (17β(axial)-acetyl] was epimerized quantitatively with base to the latter (**21**)

[17α(equatorial)-acetyl].

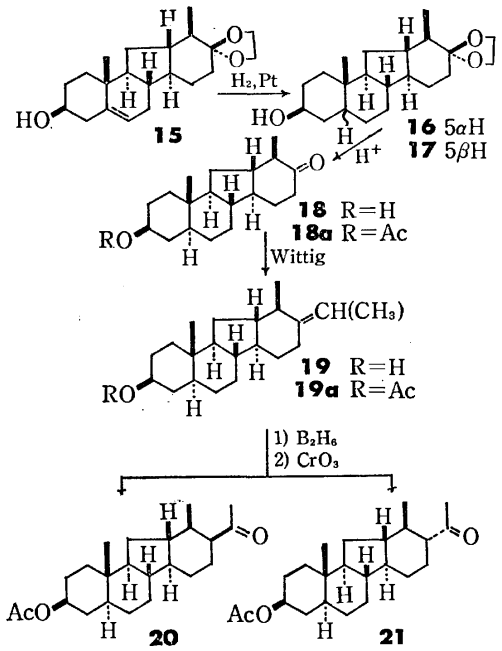

Scheme 4.

Reduction of 20-ketone (**20**) with sodium borohydride (NBH) in ethanol produced nearly equal amounts of 20α-(*S*)- and 20β-(*R*)-alcohols (**22**), mp 150—151 °C, and (**23**), mp 117—118 °C, which were readily isolated by preparative TLC. The configurational assignment to C_{20} of these epimeric alcohols was deduced from chemical shifts of the respective 18-methyl protons (**22**, δ 0.94 and **23**, 1.04); in each of these compounds the respective 21-methyl groups would be located at the most remote position from the D-ring as shown in **22A** and **23A**, and hence the 21-hydroxy group in **23** would be disposed 1,3-diaxial to the 18-methyl and deshield the 18-methyl protons more seriously in **23** than those in **22** in the NMR spectra. On the other hand, reduction of the isomeric 20-ketone (**21**) with sodium borohydride under comparable conditions gave an inseparable mixture of the corresponding 20-alcohols (**24**), mp 115—118 °C, in a moderate yield. The R_f values of these alcohols (**24**) on TLC clearly differed from those of alcohols **22** and **23**, indicating that the afore-mentioned hydride reduction took place without any configurational change at C_{17}.

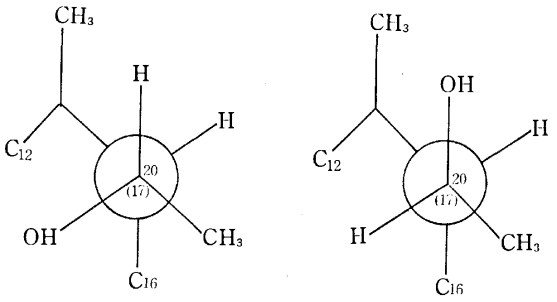

Attempted removal of the 20-hydroxy groups in compounds **22** and **23** did not proceed as expected. 20α-(*S*)-Alcohol (**22**), when treated with *p*-toluenesulfonyl chloride in pyridine, formed no tosylate but produced olefin (**25**), mp 92—92.5 °C, with a molecular formula of $C_{23}H_{36}O_2$ in 94% yield. The structure [one of 17-ethylideneetiojervanes (**19a**)] and configuration were assigned on the basis of the spectral data [Mass, *m/e* 344; NMR, δ 0.77 (3H, s, 19-C<u>H</u>$_3$), 1.66 (3H, d J= 6 Hz, 21-C<u>H</u>$_3$), and 5.15 (1H, q J=6 Hz, <u>H</u> at C_{20})] and the conformation (**22A**) of the starting alcohol (**22**). Naturally, the NMR spectrum of **25** closely resembled that of **19a**. On the other hand, 20β-(*R*)-alcohol (**23**) was converted under the same conditions as **22** into the corresponding tosylate (**23a**), amorphous, showing a single spot on TLC. Treatment of **23a** with lithium aluminium hydride gave two products (**26**), amorphous, and (**27**), mp 190—191 °C, which were isolated in 24 and 37% yields, respectively, by preparative TLC. The latter (**27**) was derived by simple hydrolysis of **23** and hence identified as 3,20-glycol, resulting only from hydrogenolysis of the O–S bond. The former (**26**) displayed three methyl proton signals, one singlet (19-C<u>H</u>$_3$) and two doublets (both J=

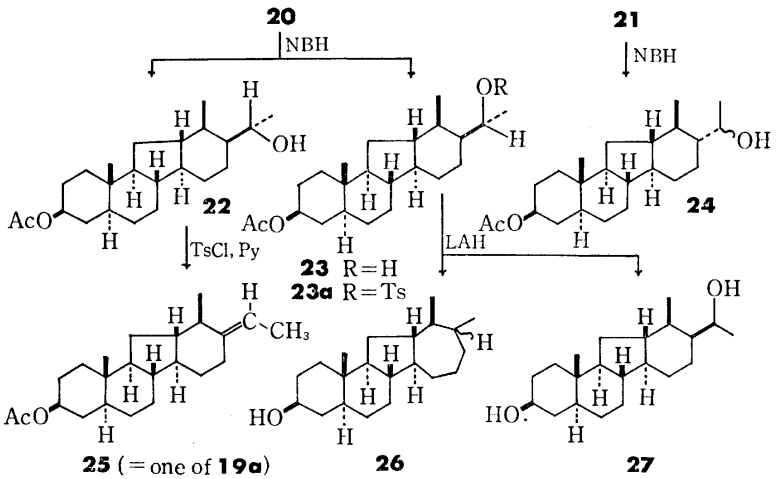

Scheme 5.

6 Hz) at δ 0.75, 0.97 and 1.19 in the NMR spectrum. These spectral data, as combined with consideration of the conformation (**23A**) of the starting alcohol, led to tentative assignment of formula **26** to the amorphous product.

The configuration at C_{12} of compound **13** was finally elucidated as follows. Reduction of 5α,12α-etiojervan-3β-ol-11-one 3-acetate (**2**) with sodium in isopropyl alcohol afforded 3β,11α-alcohol (**28**), mp 158—161 °C, in a good yield, whose configuration at C_{11} was consistent with the NMR spectrum: δ 0.775 (3H, s, 19-CH_3) and 4.00 (1H, br W_H=12 Hz). Treatment of **28** with acetic anhydride and pyridine gave a four-component mixture, from which the corresponding 3-acetate (**28a**), mp 128—129 °C, was isolated as the main product by preparative TLC in a moderate yield (pure 35%, and crude 65%). This compound (**28a**), when oxidized with chromium(VI) oxide, gave 5α,12β-etiojervan-3β-ol-11-one 3-acetate (**11**) in a good yield. Reduction of the 11-ketone (**11**) with lithium aluminium hydride in refluxing dioxane led to formation of the corresponding 3β,11β-alcohol (**29**), mp 186—188 °C, showing the following NMR spectrum: δ 1.02 (3H, s, 19-CH_3) and 4.06 (1H, do d J=6 and 8 Hz). This alcohol (**29**) underwent monoacetylation to give 3-acetate (**29a**), mp 151—152 °C, which was reconverted by oxidation into 12β*H*-11-ketone (**11**). The results indicate that 11-alcohols **28** and **29** are epimeric to each other only at C_{11} and the reduction of 11-ketone (**2**) to 11α-alcohol (**28**) is accompanied by configurational inversion at C_{12} (12αH to 12βH). The hydride reduction of 12α*H*-11-ketone (**2**) under the same conditions as that of 12β*H*-11-ketone (**11**) resulted only in hydrolysis of the 3-acetoxy group owing to severe steric hindrance due to β-oriented methyl and ethyl groups at C_{13} and C_{17}, respectively, leading to the recovery of the starting ketone after acetylation.

Treatment of 12α*H*-11α-alcohol (**28a**) with phosphoryl chloride in pyridine gave olefin (**30**), oil, in 90% yield. The same treatment of 12β*H*-11β-alcohol (**29a**) also produced olefin (**31**), oil, in quantitative yield, which was evidently different from olefin **30**. The structure of these olefins was assigned as shown in formulas **30** and **31**, respectively, on the basis of chemical shifts of the respective 19-methyl protons (**30**, δ 0.77 and **31**, 0.92) as well as the reaction mode. The chemical shift difference (0.15 ppm) in question between olefins was in good accord with that (0.175 ppm) in the corresponding normal steroid olefins,[19] and the formation of these olefins was interpreted by assuming that the dehydration proceeds in an E2-type *trans*-elimination manner. Hydrogenation of the latter olefin (**31**), 12β*H*-$\Delta^{9(11)}$-olefin, over platinum in acetic acid led to formation of the compound (**13a**) in question, mp 92—94 °C, establishing all the configurations of **13a** (5αH, 12βH, 13αH and 17αH). The same reaction of another olefin (**30**), 9α*H*-Δ^{11}-olefin, produced an isomeric compound (**32**), amorphous, formulated as 5α,12α-etiojervan-3β-ol 3-acetate. These compounds (**13a** and **32**) are regarded as C/D *trans*- and *cis*-etiojervane analogs of 5α-pregnan-3β-ol 3-acetate.

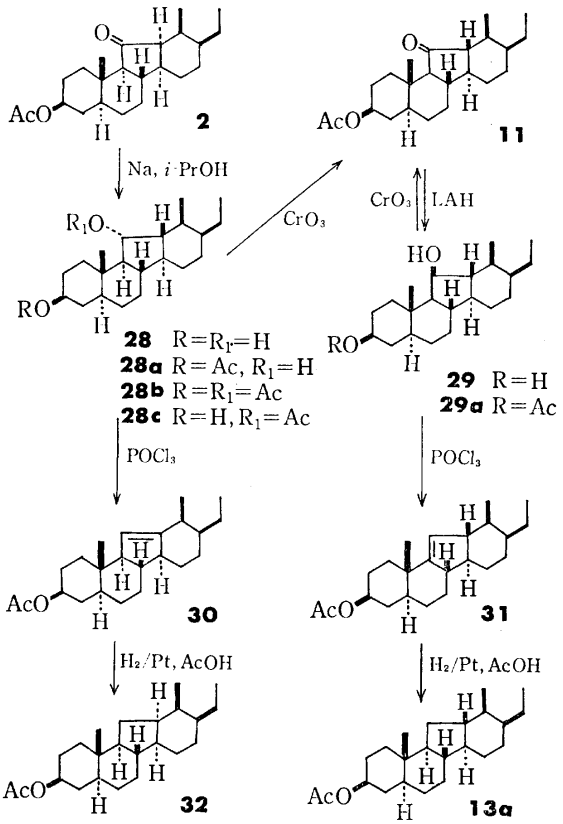

Scheme 6.

Experimental

All the melting points are uncorrected. The homogeneity of each compound was always checked by TLC on silica gel (Wakogel B-5) using various solvent systems, and the spots were developed with ceric sulfate in dil sulfuric acid and/or iodine. The optical rotations, ORD curves and IR spectra were measured in chloroform, dioxane and Nujol, respectively, unless otherwise stated. The NMR spectra were obtained in deuteriochloroform at 60 and/or 100 MHz, and the chemical shifts were given in δ-values, TMS being used as an internal reference. The abbreviations "s, d, t, q, br, m and do" in the NMR spectra denote "singlet, doublet, triplet, quartet, broad, multiplet and double," respectively.

17β-Ethyl-5α,12α-etiojervan-3β-ol-11-one 3-Acetate (2). a) A solution of 17-ethyletiojerv-5,12,17(20)-trien-3β-ol-17-one 3-acetate[10] (**3**, 8.33 g), mp 183—185 °C, in acetic acid (AcOH, 700 ml) was hydrogenated over Adams platinum (Pt, 5.76 g as $PtO_2 \cdot H_2O$) at room temperature (temp) for 16 h, when 2060 ml of hydrogen (3.5 mol) had been consumed. After removal of the catalyst by filtration and the solvent *in vacuo* by azeotropization with benzene, the residue was dissolved in methanol, and the methanol solution was concentrated to 70 ml and cooled to yield a crystalline substance, which was collected by filtration. Recrystallization from methanol afforded **2** (3.02 g), mp 115.5—116.5 °C (lit,[10] 114—116 °C); $[\alpha]_D$ −15.8° (lit,[10] −8.6°); ORD, $[\Phi]^{trough}_{334}$ −4520°, $[\Phi]^{trough}_{323}$ −2180°, $[\Phi]^{peak}_{293}$ +3680°, a=−82°; IR, ν_{max} 1730, 1260 and 1025 cm^{-1}; NMR, δ 0.72 (3H, d J=7 Hz, 18-CH_3), 0.90 (3H, s, 19-CH_3), 2.01 (3H, s, OCO-CH_3) and 4.65 (1H, br, H at C_3). This compound proved to be identical with a sample[5a], mp 118.2—118.9 °C and $[\alpha]_D$ −15.5°, obtained from hecogenin by direct comparison (IR, mixed mp and TLC). The mother liquors obtained on the concentration and recrystallization consisted of a

multicomponent mixture and resisted further purification.

b) A solution of **10** (156 mg), in AcOH (10 ml) was hydrogenated over Adams Pt (204 mg) at room temp, and 1.1 mol of hydrogen was consumed for 45 min. The reaction mixture gave an amorphous substance (142 mg) after usual work up; NMR, δ 0.84 (3H, t J=6 Hz, 21-C$\underline{H}_3$), 0.97 (3H, d J=6.5 Hz, 18-C$\underline{H}_3$), 1.06 (3H, s, 19-C$\underline{H}_3$), 2.01 (3H, s, OCOC$\underline{H}_3$), 4.01 (1H, br W_H=15.5 Hz, $\underline{H}$ at C_{11}) and 4.67 (1H, br, $\underline{H}$ at C_3). This was mixed with a complex prepared from chromium(VI) oxide (CrO_3, 215 mg) and pyridine (Py, 2 ml) under cooling and stirred at room temp overnight. The mixture was poured into water and extracted with ether, and the ether solution was washed with 1 M hydrochloric acid, 5% aqueous sodium hydrogencarbonate and saturated brine, dried and evaporated to leave a crystalline mixture (140 mg) of **11** and **12**, which showed a single spot on TLC.

The mixture was treated with 1 M sodium methoxide in refluxing methanol (15 ml) under nitrogen for 2 h. The solution was evaporated *in vacuo* and shaken with chloroform and water, and the chloroform solution was washed, dried and evaporated to leave amorphous residue (132 mg), which was acetylated with acetic anhydride (Ac_2O, 1 ml) and Py, (1.3 ml) at room temp overnight. The reaction mixture gave amorphous residue (143 mg) after usual work up, which showed two spots and was separated by preparative TLC (7 plates) with a 3 : 2 mixture of benzene and chloroform. The less mobile fraction gave a crystalline substance (18 mg), which on trituration with methanol had mp 114—117 °C. The more mobile fraction gave an amorphous material (84 mg), showing the same spot as the starting mixture, which was again treated in the same manner as the aforementioned mixture to give the crystalline substance (10 mg) besides the main amorphous material (73 mg). The crystalline substances were combined and recrystallized from methanol to yield **2** (9 mg), mp 118—119 °C, which was identical with an authentic sample (TLC, IR, NMR and optical rotation). The main amorphous material (73 mg) was treated twice in the same manner as described above and after usual work-up, gave a new crystalline substance (56.5 mg) with the same R_f value as the more mobile part. The substance was triturated with methanol to yield **12** (20 mg), mp 106—107 °C, and was recrystallized repeatedly from methanol to give an analytical sample, mp 109—109.5 °C; $[\alpha]_D$ −94.6°; ORD, $[\Phi]_{334}^{trough}$ −11350°, $[\Phi]_{323}^{trough}$ −6370°, $[\Phi]_{315}$=0°, $[\Phi]_{291}^{peak}$ −10520°, a=−219°; IR, ν_{max} 1732, 1234 and 1022 cm^{-1}; NMR, δ 0.85 (3H, s, 19-C$\underline{H}_3$). Found: C, 76.53; H, 10.04%. Calcd for $C_{23}H_{36}O_3$: C, 76.62; H, 10.07%.

*5α,12β-Etiojervane-3β,11β-diol-17-one 17-Ethylene Acetal (**6**) and 5α,12β-Etiojervane-3β,11β,17β-triol (**7**).* A solution of etiojerv-5-ene-3β,11β-diol-17-one 17-ethylene acetal[3b] (**5**, 2.50 g), mp 173—174 °C, in AcOH (50 ml) was hydrogenated over the Adams Pt (0.80 g) at room temp for 1 h, when 445 ml of hydrogen had been taken up. After removal of the catalyst and solvent, the residue was dissolved in chloroform, and the chloroform solution was washed with 5% aqueous sodium hydrogencarbonate and water, dried over anhydrous sodium sulfate and evaporated to leave an amorphous substance (3.08 g), which crystallized on trituration with acetone and was collected by filtration to yield **6** (1.36 g), mp 182—184 °C. The filtrate, showing two spots, was separated by preparative TLC (30 plates) over silica gel (Wakogel B-5, 10 g per plate) with ether as solvent. More mobile fractions, eluted with acetone, gave amorphous residue (0.60 g), which crystallized as needles on trituration with acetone to give **6** (0.35 g), mp 183—188 °C. Two recrystallizations from acetone gave an analytical sample, mp 192—193 °C; $[\alpha]_D$ +39.4°; IR, ν_{max} 3490, 3340, 1108 and 1031 cm^{-1}; NMR, δ 0.98 (3H, d J=6 Hz, 18-C$\underline{H}_3$), 1.03 (3H, s, 19-C$\underline{H}_3$), 1.50 and 2.01 (each 1H, s, $\underline{OH}$) and 3.85 (4H, s, $OC_2\underline{H}_4O$). Found: C, 71.88; H, 9.81%. Calcd for $C_{21}H_{34}O$: C, 71.96; H, 9.78%.

Less mobile fractions, eluted with chloroform, gave crystalline triol (**7**, 0.64 g), which on recrystallization from acetone had mp 231—234 °C and amounted to 0.11 g. This was recrystallized from acetone for analysis: mp 235—236 °C; $[\alpha]_D$ +63.3° (MeOH); IR, ν_{max} 3340, 1715 (acetone ?) and 1044 cm^{-1}. Found: C, 73.76; H, 10.47%. Calcd for $C_{19}H_{32}O_3$: C, 73.98; H, 10.46%.

*5α,12β-Etiojervane-3β,17β-diol-11-one 3,17-Diacetate (**8**).*

a) A solution of etiojerv-5-ene-3β,17β-diol-11-one[11] (107 mg) in AcOH (4 ml) was hydrogenated over Adams Pt (59 mg) at room temp for 1 h, when 1.27 mol of hydrogen had been consumed. After removal of the catalyst by filtration and the solvent *in vacuo* by evaporation, the residue was diluted with water and the solution was extracted with chloroform. The chloroform extracts were washed with 5% aqueous sodium hydrogencarbonate and water, dried, and evaporated to leave an amorphous residue (111 mg), which showed three spots and was separated by preparative TLC (8 plates) with ether. The most mobile part gave an amorphous substance (10 mg), which would be 5β,12β-etiojervane-3β,17β-diol-11-one from its NMR data, but was not further examined: δ 0.97 (3H, s, 19-C$\underline{H}_3$), 1.26 (3H, d J=4 Hz, 18-C$\underline{H}_3$), 3.77 (1H, br s W_H=8 Hz, $\underline{H}$ at C_{17}) and 4.07 (1H, br s W_H=9 Hz, $\underline{H}$ at C_3).

The middle part gave a crystalline substance (66 mg), which on trituration with acetone–isopropyl ether gave **8a** (61 mg), mp 179.5—180.5 °C. Recrystallization from the same solvent mixture afforded an analytical sample, mp 180.5—181 °C; $[\alpha]_D$ −44.2° (MeOH); IR, ν_{max} 3290, 1727 and 1028 cm^{-1}; NMR, δ 0.83 (3H, s, 19-C$\underline{H}_3$), 1.25 (3H, d J=5.5 Hz, 18-C$\underline{H}_3$), 3.59 (1H, br W_H=24 Hz, $\underline{H}$ at C_3) and 3.76 (1H, br s W_H=8 Hz, $\underline{H}$ at C_{17}). Found: C, 74.48; H, 9.91%. Calcd for $C_{19}H_{30}O_3$: C, 74.47; H, 9.87%. The least mobile part gave a crystalline substance (11 mg). The NMR spectrum indicated the compound to be etiojerva-3β,11β,17β-triol-11-one, but this was not further examined: NMR, δ 1.02 (3H, s, 19-C$\underline{H}_3$), 1.24 (3H, br s W_H=5 Hz, 18-C$\underline{H}_3$), 1.56 (s, disappeared on addition of D_2O, $\underline{OH}$), 6.43 (1H, br W_H=27 Hz, $\underline{H}$ at C_3), 3.81 (1H, br s W_H=8 Hz, $\underline{H}$ at C_{17}) and 4.08 (1H, do d J=6 and 10 Hz, $\underline{H}$ at C_{11}).

Compound **8a** (45 mg) was acetylated with Ac_2O (1 ml) and Py (1 ml) at room temp for 22 h. The reaction mixture gave amorphous residue (61 mg) after usual work up, which was crystallized from dil methanol to yield a crystalline substance (**8**), mp 123—125 °C; IR, ν_{max} 1743—1724, 1251, 1234 and 1024 cm^{-1}; NMR, δ 0.86 (3H, s, 19-C$\underline{H}_3$), 1.14 (3H, d J=6 Hz, 18-C$\underline{H}_3$), 1.99 and 2.04 (each 3H, s, 2OCOC$\underline{H}_3$), 5.42 (1H, br W_H=24 Hz, $\underline{H}$ at C_3) and 4.94 (1H, br s W_H=7.5 Hz, $\underline{H}$ at C_{17}).

b) Compound **7** (72 mg) was acetylated with Ac_2O (1 ml) and Py (1 ml) at room temp for 3 h. The reaction mixture was worked up as usual to give an amorphous residue (91.5 mg), showing two spots, which was separated by preparative TLC (2 plates) over silica gel using a 1 : 1 mixture of ether and benzene. More mobile fractions, eluted with acetone, gave an amorphous residue (45 mg), which crystallized on trituration with isopropyl ether to give 3,17-diacetate **7a** (12 mg), mp 138—139 °C. Recrystallization from isopropyl ether gave an analytical sample, mp 142—143 °C; $[\alpha]_D$ +64.8°; Mass, m/e 332 (M^+-CH_3COOH), 314, 299, 272 and 254; IR, ν_{max} 3515, 1729, 1715, 1254, 1241 and 1025

cm^{-1}; NMR, δ 0.99 (3H, d J=5 Hz, 18-C$\underline{H}_3$), 1.07 (3H, s, 19-C$\underline{H}_3$), 1.99 and 2.02 (each 3H, s, 2OCOC$\underline{H}_3$), 4.10 (1H, do d J=8 and 5.5 Hz, $\underline{H}$ at C_{11}), 4.70 (1H, br, $\underline{H}$ at C_3) and 5.00 (1H, br s W_H=6Hz, $\underline{H}$ at C_{17}). Found: C, 69.51; H, 9.55%. Calcd for $C_{23}H_{36}O_5$: C, 70.37; H, 9.24%.

Less mobile fractions, eluted with acetone, gave a crystalline residue (42 mg), which on trituration with acetone–isopropyl ether afforded triol 3-monoacetate (**7b**, 24 mg), mp, 172.5—173 °C. Recrystallization from the same solvent mixture gave an analytical sample: mp 173—173.5 °C; $[\alpha]_D$+35.6°; Mass, *m/e* 332 (M^+-H_2O), 314 and 272; IR, ν_{max} 3465, 3305, 1734, 1243, 1026 and 1018 cm^{-1}; NMR, δ 1.06 (3H, s, 19-C$\underline{H}_3$), 1.09 (3H, d J=7 Hz, 18-C$\underline{H}_3$), 2.02 (3H, s, OCOC$\underline{H}_3$), 3.81 (1H, br s W_H=6 Hz, $\underline{H}$ at C_{17}), 4.08 (1H, do d J=8.5 and 5 Hz, $\underline{H}$ at C_{11}) and 4.71 (1H, br W_H=24 Hz, $\underline{H}$ at C_3). Found: C, 71.82; H, 9.71%. Calcd for $C_{21}H_{34}O_4$: C, 71.96; H, 9.78%.

A solution of **7a** (40 mg) in acetone (4 ml) was treated with Jones' reagent (0.2 ml) in an ice-bath under stirring for 1 h. After addition of ethanol and evaporation of the solvent *in vacuo*, the resulting residue was diluted with water and extracted with chloroform. The chloroform solution was washed with 5% aqueous sodium hydrogencarbonate and water, dried and evaporated to give an amorphous residue (41 mg), which showed a single spot on TLC. Trituration with dil methanol afforded a crystalline substance (**8**, 19 mg), mp 120—121 °C, which was identical with an authentic sample.

*5α,12β-Etiojervane-3β,11β-diol-17-one (**9**).* Compound **6** (1.314 g) was dissolved in a solution of acetone (130 ml) and water (13 ml) containing *p*-toluenesulfonic acid (PTS, 146 mg), and refluxed for 3 h under stirring. After evaporation of the solvents below 25 °C the residue was made alkaline with 5% aqueous sodium hydrogencarbonate and extracted with chloroform repeatedly. The chloroform solution was washed with water, dried and evaporated to leave a crystalline material (1.497 g), which on recrystallization from acetone–isopropyl ether gave **9** (977 mg), mp 187—189 °C. Two recrystallizations from the same solvent mixture afforded an analytical sample, mp 188—190 °C; $[\alpha]_D$ +11.2° (MeOH); ORD, $[\Phi]_{318}^{trough}$ −4440°, $[\Phi]_{310}^{trough}$ −4080°, $[\Phi]_{274}^{peak}$ +7090°, a=−115°; IR, ν_{max} 3410, 1701 and 1037 cm^{-1}; NMR, δ 1.04 (3H, s, 19-C$\underline{H}_3$), 1.12 (3H, d J=7 Hz, 18-C$\underline{H}_3$), 3.55 (1H, br, $\underline{H}$ at C_3) and 4.12 (1H, br W_H=15 Hz, $\underline{H}$ at C_{11}). Found: C, 74.56; H, 9.76%. Calcd for $C_{19}H_{30}O_3$: C, 74.47; H. 9.87%.

*17-Ethylidene-5α,12β-etiojervane-3β,11β-diol 3-Acetate (**10**).* A suspended mixture of sodium hydride (Wako, 309 mg, *ca.* 50% in oil) in pentane (10 ml) was stirred for 2 min and then decanted, and the procedure was repeated five times to remove the oil. After removal of the pentane *in vacuo* the residual hydride was mixed with dimethyl sulfoxide (DMSO, 5 ml), which had been dried over calcium hydride and distilled, in a stream of nitrogen, stirred at room temp for 15 min and then at 70—73 °C for 50 min, and cooled, when the mixture became homogeneous and gray. To the solution was added dropwise a solution of ethyltriphenylphosphonium bromide (2.232 g, 6 mmol) in dry DMSO (12 ml) at room temp during 3 min under nitrogen, and the solution was stirred at room temp for 15 min. To the resulting dark red solution was added a solution of **9** (464 mg, 1.5 mmol) in dry tetrahydrofuran (THF, 5.5 ml) at room temp during 5 min under nitrogen. The whole mixture was further stirred at room temp for 15 min and then at 50—51 °C (bath temp) for 22 h. The reaction mixture was poured into ice-water and after being salted out, extracted with ether repeatedly. The ether solution was washed with saturated brine, dried and evaporated to leave oily residue (2.165 g). This was treated with Ac_2O (5 ml) and Py (10 ml) at room temp for 3 h and then worked up as usual to give an amorphous substance (1.908 g), showing two spots, which was separated by preparative TLC (25 plates) with benzene. The minor fraction amounted to 75 mg but was not further examined.

The main, less mobile fraction gave a crystalline substance (380 mg), which on recrystallization from acetone afforded **10** (191 mg), mp 152—154 °C. This was recrystallized twice from isopropyl ether for analysis: mp 156—157 °C; $[\alpha]_D$ +53.3°; IR ν_{max} 3505, 1713, 1267 and 1031 cm^{-1}; NMR, δ 1.04 (3H, s, 19-C$\underline{H}_3$), 1.19 (3H, d J=5.5 Hz, 18-C$\underline{H}_3$), 1.61 (3H, d J=6 Hz, 21-C$\underline{H}_3$), 2.01 (3H, s, OCOC$\underline{H}_3$), 4.10 (1H, br W_H=14.5 Hz, $\underline{H}$ at C_{11}), 4.64 (1H, br, $\underline{H}$ at C_3) and 5.17 (1H, q J=6 Hz, $\underline{H}$ at C_{20}). Found: C, 76.52; H, 10.08%. Calcd for $C_{23}H_{36}O_3$: C, 76.62; H, 10.07%.

*17β-Ethyl-5α,12β-etiojervan-3β-ol-11-one 3-Acetate (**11**).* a) Compound **2** (730 mg) was dissolved in methanol (48 ml) containing 5% potassium hydroxide and refluxed for 1 h under nitrogen. The solution was diluted with water under stirring to yield an amorphous substance (650 mg), which was collected, dried and treated with Ac_2O (4 ml) and Py (7 ml) at room temp overnight. After removal of the solvents by azeotropization with benzene, the residue crystallized on trituration with methanol. This crystalline material, showing two spots on TLC (chloroform : benzene=1 : 1), was dissolved in benzene and chromatographed on a mixture of silicic acid (22 g) and celite (1.5 g). Fractions eluted with benzene gave crystals (245 mg), which showed a single spot on TLC. Recrystallization from methanol afforded an analytical sample of **11**, mp 121—123 °C; $[\alpha]_D$ −66.8°; ORD, $[\Phi]_{334}^{trough}$ −9930°, $[\Phi]_{323}^{trough}$ −5810°, $[\Phi]_{293}^{peak}$ +7120°, a=−170°; IR, ν_{max} 1730, 1245 and 1025 cm^{-1}; NMR, δ 0.84 (3H, s, 19-C$\underline{H}_3$), 0.94 (3H?, t J=7 Hz, 21-C$\underline{H}_3$?), 1.16 (3H?, d J=6.5 Hz, 18-C$\underline{H}_3$), 2.02 (3H, s, OCOC$\underline{H}_3$) and 4.65 (1H, br, $\underline{H}$ at C_3). Found: C, 76.78; H, 10.32%. Calcd for $C_{23}H_{36}O_3$: C, 76.62; H, 10.07%.

b) A solution of compound **28a** (34 mg) in acetone (3.5 ml) cooled in an ice-bath was treated with Jones' reagent (0.05 ml) for 1 h under stirring. After addition of ethanol to decompose excess of chromium(VI) oxide (CrO_3), the solution was evaporated *in vacuo* below 40 °C, and then shaken with water and chloroform. The chloroform solution was worked up as usual to give a crystalline substance (35 mg), which on recrystallization from methanol afforded **11** (24 mg), mp 120—121 °C. This was identical with an authentic sample obtained by epimerization of **2**.

Equilibrium Measurements. Compound **2** (51 mg) in methanol (1 ml) was mixed with methanol (4 ml) containing 5% potassium hydroxide and allowed to stand at room temp for 60 h. After removal of methanol *in vacuo* the residue was shaken with chloroform and water. The chloroform solution gave a mixture (46 mg) of 12-epimeric alcohols, which was acetylated with Ac_2O (0.24 ml) and Py (0.48 ml) at room temp overnight. The reaction mixture was mixed with water (100 ml) under stirring to give an amorphous substance, which was collected by filtration and dried thoroughly. The resulting mixture (44 mg) of **2** and **11** had an optical rotation of $[\alpha]_D$ −43.2°.

Compound **11** (51 mg) was treated in the same manner as **2** produced a mixture of **2** and **11**, which showed an optical rotation of $[\alpha]_D$ −44.3°. The specific rotations in both experiments were practically the same, indicating that the equilibrium mixture consisted of 45% of the former (**2**) and 55% of the latter (**11**).

*17β-Ethyl-5α,12β-etiojervan-3β-ol (**13**) and Its 3-Acetate (**13a**).* a) Freshly-distilled diethylene glycol (DEG, 75 ml) containing sodium (2.0 g) was heated to 180 °C, and anhydrous hydrazine[20] (40 ml) was added to the solution, and refluxed for a while and cooled. After addition of compound **2** (3.52 g) the mixture was refluxed (at *ca.* 145 °C) for 16 h, cooled and the condenser was removed. The solution was heated to 180 °C to distill off excess of the hydrazine, and a new condenser was then set up. The solution was again refluxed at the temp for 24 h, cooled and mixed with water (450 ml), giving an amorphous powder (3.08 g), which was collected, dried and crystallized from methanol. Recrystallization from methanol afforded **13** (1.72 g), mp 124—125 °C; $[\alpha]_D$ + 75.9°, IR, no absorption near 1700 cm^{-1}; NMR, δ 0.74 (3H, s, 19-C$\underline{H}_3$), 0.84 (3H?, d J=6 Hz, 18-C$\underline{H}_3$) and 3.64 (1H, br, $\underline{H}$ at C_3). Found: C, 82.68; H, 11.45%. Calcd for $C_{21}H_{36}O$: C, 82.83; H, 11.33%.

Compound **13** (52 mg) was treated with Ac_2O (0.7 ml) and Py (1 ml) at room temp overnight. After usual work up the residue (57 mg) afforded **13a** (29 mg), 94.5—95 °C, on trituration with acetone and subsequent recrystallization from acetone; $[\alpha]_D^{14}$ + 55.3°; IR, ν_{max} 1742 and 1244 cm^{-1}; NMR, δ 0.76 (3H, s, 19-C$\underline{H}_3$), 0.83 (3H, d J=6.5 Hz, 18-C$\underline{H}_3$), 0.85 (3H, t J=6.5 Hz, 21-C$\underline{H}_3$), 2.03 (3H, s, OCOC$\underline{H}_3$) and 4.72 (1H, br, $\underline{H}$ at C_3). Found: C, 79.98; H, 11.13%. Calcd for $C_{23}H_{38}O_2$: C, 79.71; H, 11.05%.

b) The Wolff-Kishner reduction of compound **11** (240 mg) was carried out in the same way as mentioned above and produced crude **13** (221 mg), having mp 108—120 °C. Recrystallization from methanol afforded **13** (93 mg), mp 120—122 °C, in pure state, which was identical with that prepared from **2**.

*17β-Ethyl-5α,12β-etiojervan-3-one (**14**) and Its Ethylene Acetal (**14a**).* To a pasty complex prepared from Py (15 ml) and CrO_3 (1.5 g) was added **13** (1.50 g) dissolved in Py (15 ml), and the mixture was stirred at room temp for 15h. After removal of the solvent the mixture was extracted with chloroform, and the chloroform solution was washed with 1 M hydrochloric acid, 10% aqueous sodium hydroxide and water, dried and then evaporated to leave an oily substance, which crystallized on trituration with methanol and recrystallized from the same solvent to yield **14** (1.16 g), mp 118—119 °C. This sample was recrystallized from methanol for analysis: mp 119—121 °C; $[\alpha]_D$ +113.5°; IR, ν_{max} 1707 cm^{-1}; NMR, δ 0.85 (3H, d J=6 Hz, 18-C$\underline{H}_3$) and 0.94 (3H, s, 19-C$\underline{H}_3$). Found: C, 83.51; H, 11.20%. Calcd for $C_{21}H_{34}O$: C, 83.38; H, 11.33%.

A solution of **14** (352 mg) in benzene (60 ml) containing PTS (18 mg) and ethylene glycol (1.75 ml) was refluxed for 8 h under a Dean-Stark apparatus and then cooled, when the solution was separated into two layers. The upper layer was separated, washed with 5% aqueous sodium hydrogencarbonate (60 ml) and water (60 ml), dried and evaporated *in vacuo* to leave a crystalline residue. Recrystallization from acetone gave **14a** (247 mg), mp 98—100 °C; $[\alpha]_D$ +63.5°; IR, ν_{max} 1110, 1080 and 1066 cm^{-1}; NMR, δ 0.77 (3H, s, 19-C$\underline{H}_3$), 0.85 (3H?, d J=7 Hz, 18-C$\underline{H}_3$) and 3.93 (4H, s, $OC_2\underline{H}_4O$). Found: C, 79.96; H, 11.02%. Calcd for $C_{23}H_{38}O_2$: C, 79.71; H, 11.05%.

*5α,12β-Etiojervan-3β-ol-17-one 17-Ethylene Acetal (**16**) and Its 5β-Isomer (**17**).* A solution of 12β-etiojerv-5-en-3β-ol-17-one 17-ethylene acetal[4d] (**15**, 777 mg), mp 175—177 °C, in AcOH (20 ml) was hydrogenated over Adams Pt (150 mg) at room temp and 95 ml of hydrogen was consumed for 30 min. The reaction mixture was worked up as usual to give an amorphous substance (860 mg), which crystallized on trituration with isopropyl ether and was collected by filtration. This crystalline substance (**16**, 612 mg), mp 177—179 °C, was recrystallized twice from isopropyl ether for analysis: mp 177—179 °C; $[\alpha]_D$ +50.4°; IR, ν_{max} 3445, 1110, 1077 and 1043 cm^{-1}; NMR, δ 0.74 (3H, s, 19-C$\underline{H}_3$), 0.83 (3H, d J=6 Hz, 18-C$\underline{H}_3$), 3.55 (1H, br, $\underline{H}$ at C_3) and 3.87 (4H, s, $OC_2\underline{H}_4O$). Found: C, 75.21; H, 10.15%. Calcd for $C_{21}H_{34}O_3$: C, 75.40; H, 10.25%.

The filtrate, obtained on crystallization of **16**, was evaporated and then separated into three parts by preparative TLC (10 plates) with a 1 : 2 mixture of ether and benzene. The middle part (77 mg) showed the same IR spectrum and R_f value as **16**. The most mobile part (46 mg) crystallized on trituration with isopropyl ether, had mp 107—109 °C and amounted to 9 mg. The NMR and IR spectra indicated this compound to be a 5β-isomer of **16**; $[\alpha]_D$ +43.5°; IR, ν_{max} 3340, 1086, 1042 and 1031 cm^{-1}; NMR, δ 0.82 (3H, d J=5 Hz, 18-C$\underline{H}_3$), 0.89 (3H, s, 19-C$\underline{H}_3$), 3.91 (4H, s, $OC_2\underline{H}_4O$) and 4.06 (1H, br W_H=8.5 Hz, $\underline{H}$ at C_3). Found: C, 75.28; H, 10.40%. Calcd for $C_{21}H_{34}O_3$: C, 75.40; H, 10.25%

*5α,12β-Etiojervan-3β-ol-17-one (**18**) and Its 3-Acetate (**18a**).* Compound **16** (560 mg) was dissolved in acetone (50 ml) and water (5 ml) containing PTS (53 mg) and refluxed for 3 h. After removal of most of the solvents the residue was made alkaline with 5% aqueous sidium hydrogencarbonate and extracted with chloroform repeatedly. The resulting solution was washed with water, dried and evaporated to leave a crystalline residue, which was recrystallized from acetone-isopropyl ether (1 : 1) to yield **18** (439 mg), mp 176—179 °C. Recrystallization from the same solvent mixture afforded an analytical sample: mp 179—180 °C; $[\alpha]_D$ +5.0°; ORD, $[\Phi]_{318}^{trough}$ −4300°, $[\Phi]_{310}^{trough}$ −3500°, $[\Phi]_{273}^{peak}$ +6200°, a=−105°; IR, ν_{max} 3500, 3430, 1691 and 1035 cm^{-1}; NMR, δ 0.75 (3H, s, 19-C$\underline{H}_3$), 0.97 (3H, d J=6.5 Hz, 18-C$\underline{H}_3$) and 3.52 (1H, br, $\underline{H}$ at C_3). Found: C, 78.39; H, 10.34%. Calcd for $C_{19}H_{30}O_2$: C, 78.57; H, 10.41%.

Compound **18** (206 mg) was treated with Ac_2O (1 ml) and Py (2 ml) at room temp for 5 h, and the mixture was mixed with water under cooling and extracted with ether repeatedly. The ether solution gave a crystalline residue, which was recrystallized from isopropyl ether to yield **18a** (207 mg), mp 132—134 °C. This was recrystallized from the solvent for analysis: mp 134.5—135 °C; $[\alpha]_D$ −1.84°; ORD, $[\Phi]_{318}^{trough}$ −4900°, $[\Phi]_{309}^{trough}$ −4200°; $[\Phi]_{274}^{peak}$ +5600°, a=−105°; IR, ν_{max} 1736, 1702, 1244 and 1024 cm^{-1}; NMR, δ 0.78 (3H, s, 19-C$\underline{H}_3$), 0.99 (3H, d J=6.5 Hz, 18-C$\underline{H}_3$), 1.99 (3H, s, OCOC$\underline{H}_3$) and 4.68 (1H, br, $\underline{H}$ at C_3). Found: C, 75.92; H, 9.66%. Calcd for $C_{21}H_{32}O_3$: C, 75.86; H, 9.70%.

*17-Ethylidene-5α,12β-etiojervan-3β-ol (**19**) and Its 3-Acetate (**19a**).* The Wittig reaction of **18** was conducted in practically the same manner as that of **9**. To a red-brown solution, prepared from sodium hydride (313 mg, *ca.* 50% in oil) and ethyltriphenylphosphonium bromide (2.137 g, 5.76 mmol) in DMSO (14 ml), was added **18** (412 mg, 1.42 mmol) in THF (5.5 ml) at room temp during 2 min under stirring in a stream of nitrogen, and the mixture was stirred at room temp for 20 min and then at 50 °C (bath temp) for 22 h under nitrogen. The reaction mixture gave an amorphous residue (1.983 g) after usual work up, which was submitted to column chromatography over alumina (Merck, acidic 25 g, 20.5 cm in length and 1.6 cm in diameter), using hexane as solvent, to remove triphenylphosphine oxide. Fractions eluted with hexane-benzene (1 : 2, 150 ml), benzene (600 ml), benzene-ether (1 : 1. 800 ml) and ether (750 ml) were collected, evaporated and purified by preparative TLC (21 plates), using a 1 : 2 mixture of ether and

benzene. The main fraction was extracted with acetone and, after evaporation, dissolved in chloroform. The chloroform solution was worked up as usual to leave an oily mixture (**19**, 413 mg); IR, ($CHCl_3$), ν_{max} 3420 and 1027 cm^{-1}; NMR, δ 0.73 and 0.76 (total 3H, each s, intensity ratio 4 : 3, 19-CH_3), 0.95 (3H, d J=6 Hz, 18-CH_3), 1.60 (3H, d J=6 Hz, 21-CH_3), 3.56 (1H, br, H at C_3) and 5.15 (1H, q J=6 Hz, H at C_{20}).

The mixture (**19**, 410 mg) was treated with Ac_2O (2 ml) and Py (4 ml) at room temp for 12 h; it afforded the acetates (**19a**, 385 mg), amorphous, showing only a single spot on TLC; IR (film), ν_{max} 1738, 1241 and 1026 cm^{-1}; NMR, δ 0.74 and 0.77 (total 3H, each s, intensity ratio 4 : 3 19-CH_3), 0.97 (3H, d J=6.5 Hz, 18-CH_3), 1.58 (3H, d J=7.5 Hz, 21-CH_3), 2.00 (3H, s, $OCOCH_3$), 4.67 (1H, br, H at C_3) and 5.15 (1H, q J=7.5 Hz, H at C_{20}).

Hydrogenation of ***19***. A solution of **19** (315 mg) in AcOH (14 ml) was hydrogenated over Adams Pt (109 mg) at room temp for 40 min, when 25 ml (1 mol) of hydrogen had been consumed. After usual work up the reaction mixture gave a gelatinous substance, which was purified by preparative TLC (18 plates) with a 1 : 2 mixture of ether and benzene. The main fraction gave an oily substance (294 mg), showing a single spot, which exhibited an NMR spectrum superimposable over that of **13** and crystallized partially on standing in hexane. The crystalline material thus obtained amounted to 21 mg, had mp 83—88 °C (*cf.*, **13**, mp 124—125 °C) and showed an IR spectrum almost the same as that of **13**. The hydrogenation product would be a mixture of **13** and its 17-epimer but resisted further purification.

*17β-Acetyl-5α,12β-etiojervan-3β-ol 3-Acetate (**20**) and Its 17α-Isomer (**21**).* a) Diborane was generated by addition of boron trifluoride etherate (4 ml) in diglyme (22 ml) to excess of sodium borohydride (NBH) in diglyme, and was passed through a solution of **19a** (1.258 g) in ether (65 ml) at room temp during 25 min under stirring in a stream of nitrogen, and the resulting solution was stirred at room temp for 45 min and then heated at 70—80°C for 1 h. To the solution was added water (10 ml) and then an aqueous solution (25 ml) containing sodium dichromate (5.0 g as dihydrate) and conc sulfuric acid (3.7 ml) during 10 min under stirring and cooling with an ice-bath, and the whole mixture (two layers) was further stirred at room temp for 18 h. The aqueous layer was shaken with ether, and the ether and diglyme solutions were combined, washed with 5% aqueous sodium hydrogencarbonate repeatedly and then with saturated brine, dried and evaporated to leave amorphous residue (1.241 g), showing absorption maxima at 3435, 1735 and 1717 cm^{-1} in the IR spectrum (neat), wihch gave four spots on TLC and was separated by column chromatography with silica gel (Mallinckrodt, 26 g) with benzene.

The first fraction (115 mg) showing the largest R_f value proved to be the unreacted starting material (**19a**). The second fraction yielded crystalline substances (**20**, 269 mg), mp 189—190.5 °C. The third fraction yielded oily substances (226 mg). The fourth (389 mg) with the least R_f value was again dissolved in ether (6 ml), oxidized with the acidic chromate solution (6 ml) for 14 h and separated by preparative TLC (20 plates) with benzene. Each fraction was detected with iodine, eluted with acetone and, after evaporation, dissolved in chloroform and the chloroform solution was washed with 5% aqueous sodium hydrogencarbonate and water, treated with active carbon to remove iodine, dried and evaporated. The first fraction yielded crystalline substances (**20**, 80 mg), but the second fraction, which would be boron adducts (241 mg), was not examined further. The crystalline substances were combined and recrystallized from methanol to yield an analytical sample of **20**, mp 189—191 °C; $[\alpha]_D$ +36.8°; ORD, $[\Phi]_{309}^{peak}$ +2700°; $[\Phi]_{289}$=0°, $[\Phi]_{252}^{trough}$ −2560°, a=+52.6°; Mass, *m/e* 360 (M^+); IR, ν_{max} 1729, 1709, 1253 and 1021 cm^{-1}; NMR, δ 0.77 (3H, s, 19-CH_3), 0.93 (3H, d J=6 Hz, 18-CH_3), 1.98 (3H, s, $OCOCH_3$), 2.09 (3H, s, 21-CH_3), 2.83 (1H, br W_H=11 Hz, H at C_{17}) and 4.70 (1H, br, H at C_3). Found: C, 76.64; H, 10.10%. Calcd for $C_{23}H_{36}O_3$: C, 76.62; H, 10.07%.

The oily substances (the third fraction, 226 mg) were triturated with aqueous methanol to yield the crystalline substances (**21**, 136 mg), mp 92—110 °C. Recrystallization from the same solvent afforded an analytical sample, mp 110.5—111 °C; $[\alpha]_D$ +24.3°; ORD, $[\Phi]_{322}^{trough}$ −2110°; $[\Phi]_{302}$=0°, $[\Phi]_{255}^{peak}$ +6050°; a=−81.6°; Mass *m/e* 360 (M^+); IR ($CHCl_3$), ν_{max} 1722, 1258 and 1027 cm^{-1}; NMR, δ 0.76 (3H, s, 19-CH_3), 0.81 (3H, d J=6 Hz, 18-CH_3), 1.99 (3H, s, $OCOCH_3$), 2.09 (3H, s, 21-CH_3) and 4.68 (1H, br, H at C_3). Found: C, 76.85; H, 10.03%. Calcd for $C_{23}H_{36}O_3$: C, 76.62; H, 10.07%.

b) A solution of **20** (25 mg) was refluxed with 1 M sodium methoxide in methanol (10 ml) for 25 h under nitrogen. After removal of the solvent *in vacuo* the residue was mixed with water and extracted with chloroform. The chloroform solution was washed with water, dried and evaporated to leave a crystalline substance (27 mg), which was treated with Ac_2O (0.5 ml) and Py (0.5 ml) at room temp for 16 h. The reaction mixture gave **21** (13 mg), mp 110.5—111 °C, after being worked up as usual, which was identical with the afore-mentioned sample **21** [IR ($CHCl_3$) and TLC]. The starting material (**20**) could not be detected by TLC.

*17β-Ethyl-5α,12β-etiojervane-3β,20α-diol 3-Acetate (**22**) and Its 20β-Isomer (**23**).* A solution of **20** (212 mg) in ethanol (30 ml) was treated with NBH (622 mg) at room temp for 16 h under stirring. After dropwise addition of AcOH (2.4 ml) under cooling with ice-bath during 15 min, the solution was evaporated below 30 °C *in vacuo*, and the residue was mixed with water and extracted with chloroform repeatedly. The chloroform solution gave amorphous material (232 mg), which was separated by preparative TLC (10 plates) with a 1 : 10 mixture of ether and benzene. The most mobile part (81 mg) crystallized on trituration with acetone-isopropyl ether to give **22** (77 mg), mp 149.5—150 °C. This was recrystallized from the same solvent mixture for analysis: mp 150—151 °C; $[\alpha]_D$ +48.7°; IR, ν_{max} 3520, 1725, 1267 and 1028 cm^{-1}; NMR, δ 0.76 (3H, s, 19-CH_3), 0.94 (3H, d J=5 Hz, 18-CH_3), 1.22 (3H, d J=6.5 Hz, 21-CH_3), 2.01 (3H, s, $OCOCH_3$), 4.07 (1H, br m W_H=10 Hz, H at C_{20}) and 4.67 (1H, br, H at C_3). Found: C, 76.17; H, 10.37%. Calcd for $C_{23}H_{38}O_3$: C, 76.19; H, 10.57%.

The middle part (96 mg) crystallized on trituration with hexane to give **23** (73 mg), mp 117—118 °C. Recrystallization from hexane afforded an analytical sample: mp 117—118 °C; $[\alpha]_D$ +44.8°; IR ν_{max} 3530, 1726, 1260 and 1031 cm^{-1}: NMR, δ 0.78 (3H, s, 19-CH_3), 1.04 (3H, d J=5 Hz, 18-CH_3), 1.21 (3H, d J=6 Hz, 21-CH_3), 2.02 (3H, s, $OCOCH_3$), 3.99 (1H, br m, W_H=16 Hz, H at C_{20}) and 4.70 (1H, br, H at C_3). Found: C, 76.43; H, 10.63%. Calcd for $C_{23}H_{38}O_3$: C, 76.19; H, 10.57%.

The least mobile part gave a crystalline substance (42 mg) which would be a mixture of 3-alcohols but was not further examined.

*17α-Ethyl-5α,12β-etiojervane-3β,20ξ-diol 3-Acetate (**24**).* A solution of **21** (62 mg) in ethanol (10 ml) was treated with NBH (209 mg) at room temp and the reduction was practically complete after 3 h (*cf.*, the same reduction of **22**).

The reaction mixture was worked up as mentioned above to leave an amorphous residue (61 mg), which was purified by preparative TLC (3 plates) with a 10 : 1 mixture of benzene and ether. The crystalline, main fraction (39 mg), which showed a single spot differing from those of **22** and **23**, was recrystallized from isopropyl ether-hexane to give **24** (13 mg), mp 115—118 °C; $[\alpha]_D$ +21.2°; IR, ν_{max} 3410, 1733, 1710 (shoulder), 1245 and 1040 cm^{-1}; NMR, δ 0.78 (3H, s, 19-C$\underline{H}_3$), 0.91 (3H?, d J=5 Hz, 18-C$\underline{H}_3$), 1.10 (3H?, t J=6 Hz, 21-C$\underline{H}_3$), 2.13 (3H, s, OCOC$\underline{H}_3$), 4.07 (1H, br m W_H=15 Hz, $\underline{H}$ at C_{20}) and 4.65 (1H, br, $\underline{H}$ at C_3). Found; C, 76.10; H, 10.41%. Calcd for $C_{23}H_{38}O_3$: C, 76.19; H, 10.57%.

Treatment of **22** *with* p-*Toluenesulfonyl Chloride.* To a solution of **22** (74 mg) in Py (1.2 ml) was added *p*-toluenesulfonyl chloride (168 mg) and the mixture was stirred at room temp for 42 h. Water was poured onto the mixture and the resulting suspension was extracted with ether. The extracts were worked up as usual to give a crystalline substance (76 mg), showing a single spot on TLC, which was triturated with methanol to give **25** (66 mg), mp 92—92.5 °C. This was recrystallized from methanol for analysis: mp 92—92.5 °C; $[\alpha]_D$ +55.4°; Mass, *m/e* 344 (M^+); IR, ν_{max} 1738, 1657 (w), 1237 and 1024 cm^{-1}; NMR, δ 0.77 (3H, s, 19-C$\underline{H}_3$), 0.99 (3H, d J=6 Hz, 18-C$\underline{H}_3$), 1.66 (3H, d J=6 Hz, 21-C$\underline{H}_3$), 2.00 (3H, s, OCOC$\underline{H}_3$), 4.70 (1H, br W_H=24 Hz, $\underline{H}$ at C_3) and 5.15 (1H, q J=6 Hz, $\underline{H}$ at C_{20}). Found: C, 79.05; H, 10.26%. Calcd for $C_{23}H_{36}O_2$: C, 80.18; H, 10.53%.

*Reaction of 20-Tosylate (***23a***) of* **23** *with Lithium Aluminium Hydride (LAH).* A solution of **23** (67 mg) in Py (1 ml) was treated with *p*-toluenesulfonyl chloride (158 mg) at room temp for 42 h under stirring. The reaction mixture was worked up in the same manner as **22** and afforded oily tosylate (**23a**, 96 mg), which gave a single spot on TLC and showed absorption maxima at 1724, 1600, 1492, 1380, 1257, 1176, 1027 and 900 cm^{-1} in the IR spectrum ($CHCl_3$); NMR, δ 0.77 (3H, s, 19-C$\underline{H}_3$), 0.88 (3H, d J=7 Hz, 18-C$\underline{H}_3$), 1.31 (3H, d J=7 Hz, 21-C$\underline{H}_3$), 2.00 (3H, s, OCOC$\underline{H}_3$), 2.43 (3H, s, C$\underline{H}_3$C$_6$H$_4$) and 4.80 (2H, br, 2$\underline{H}$ at C_3 and C_{20}). This tosylate, without further purification, was refluxed with LAH (160 mg) in THF (15 ml) for 24 h and gave oily residue (75 mg) after usual work up, which showed two spots on TLC and was separated by preparative TLC (7 plates) with a 1 : 2 mixture of ether and benzene. The more mobile part (17 mg) gave an oily substance (**26**); NMR, δ 0.75 (3H, s, 19-C$\underline{H}_3$), 0.97 and 1.19 (each 3H d J=6 Hz, 2C$\underline{H}_3$ at C_{13} and C_{17a} or *vice versa*) and 3.68 (1H, br, $\underline{H}$ at C_3). The less mobile part (25 mg) crystallized on trituration with acetone-isopropyl ether to give **27** (8 mg), mp 182—185 °C. This was recrystallized from the same solvent mixture for analysis: mp 190—191 °C; $[\alpha]_D$ +46° (MeOH); IR, ν_{max} 3400, 3340, 1042 and 1030 cm^{-1}; NMR, δ 0.75 (3H, s, 19-C$\underline{H}_3$), 1.02 (3H, d J=6 Hz, 18-C$\underline{H}_3$), 1.19 (3H, d J=6 Hz, 21-CH$_3$), 3.65 (1H, br, $\underline{H}$ at C_3) and 4.00 (1H, br m W_H=17 Hz, $\underline{H}$ at C_{20}).

*17β-Ethyl-5α,12β-etiojervane-3β,11α-diol (***28***) and Its Acetates (***28a—28c***).* To a refluxing solution of **2** (241 mg) in isopropyl alcohol (40 ml) were added sodium pellets (1.6 g) in small portions during 1 h, and the mixture was further refluxed for 1 h.[21] After being cooled the mixture was diluted with water (20 ml) and evaporated below 42 °C *in vacuo*. The residue was mixed with water and extracted with chloroform repeatedly. The chloroform solution gave oily substance (263 mg), which crystallized on trituration with acetone-isopropyl ether to yield **28** (160 mg), mp 145—146.5 °C. Recrystallization from acetone afforded an analytical sample: mp 158—161 °C; $[\alpha]_D$ +0.42°; IR, ν_{max} 3355, 3295 and 1041 cm^{-1}; NMR, δ 0.775 (3H, s, 19-C$\underline{H}_3$), 0.89 (3H?, t J=6 Hz, 21-C$\underline{H}_3$?), 0.98 (3H, J=6 Hz, 18-C$\underline{H}_3$), 3.65 (1H, br, $\underline{H}$ at C_3) and 4.00 (1H, br W_H=12 Hz, $\underline{H}$ at C_{11}). Found: C, 78.57; H, 11.30%. Calcd for $C_{21}H_{36}O_2$: C, 78.69; H, 11.32%.

Compound **28** (112 mg) was acetylated with Ac_2O (0.4 ml) and Py (1.2 ml) at 17 °C for 2 h. The product (133 mg) was separated into 4 fractions (oil 35 mg, amorphous 72 mg, oil 12 mg, and crystalline 22 mg) by preparative TLC (7 plates) with a 1 : 5 mixture of ether and benzene. The last fraction afforded the unreacted material (**28**, 12 mg), which had mp 176—177 °C and 158—160 °C on recrystallization from acetone-isopropyl ether and acetone, respectively. The first and third fractions proved to be 3,11-diacetate (**28b**) and 11-acetate (**28c**), respectively, on the basis of the IR and NMR spectra: **28b**; oil, IR ($CHCl_3$), ν_{max} 1726, 1255 and 1027 cm^{-1}; NMR δ 0.84 (3H, d J=5 Hz, 18-C$\underline{H}_3$), 0.885 (3H, s, 19-C$\underline{H}_3$), 1.99 (6H, s, 2OCOC$\underline{H}_3$), 4.70 (1H, br, $\underline{H}$ at C_3) and 5.24 (1H, br W_H=12 Hz, $\underline{H}$ at C_{11}): **28c**; oil, IR ($CHCl_3$), ν_{max} 3600, 3400, 1727, 1253 and 1031 cm^{-1}; NMR, δ 0.84 (3H, d J=5 Hz, 18-C$\underline{H}_3$), 0.875 (3H, s, 19-C$\underline{H}_3$), 1.98 (3H, s, OCOC$\underline{H}_3$), 3.65 (1H, br, $\underline{H}$ at C_3) and 5.28 (1H, br W_H=13 Hz, $\underline{H}$ at C_{11}).

The second, main fraction crystallized on trituration with isopropyl ether to give **28a**, which on recrystallization from the same solvent afforded a pure sample (40 mg), mp 128—129 °C; $[\alpha]_D$ +42.0°; IR, ν_{max} 3570, 1724, 1255 and 1031 cm^{-1}; NMR, δ 0.79 (3H, s, 19-C$\underline{H}_3$), 0.98 (3H, d J=6 Hz, 18-C$\underline{H}_3$), 2.00 (3H, s, OCOC$\underline{H}_3$), 3.98 (1H, br W_H=11 Hz, $\underline{H}$ at C_{11}) and 4.68 (1H, br, $\underline{H}$ at C_3). Found: C, 76.16; H, 10.47%. Calcd for $C_{23}H_{38}O_3$: C, 76.19; H, 10.57%.

Attempted Hydride Reduction of **2**. a) A solution of **2** (51 mg) in dry THF (10 ml) was refluxed with NBH (30 mg) for 11.5 h and cooled. After addition of acetone (4 ml) the mixture was evaporated *in vacuo* and the residue was mixed with water and extracted with chloroform. The chloroform solution was washed with water, dried and evaporated to leave an amorphous substance, which crystallized on trituration with methanol, had mp 112—114 °C, and amounted to 32 mg. This was identified as the starting material **2** (IR, mixed mp and TLC).

b) A solution of **2** (51 mg) in THF (15 ml) was refluxed with LAH (260 mg) for 2.5 h under stirring. After addition of ice-water the mixture was acidified with 2 M hydrochloric acid (15 ml) and extracted with chloroform. The chloroform solution gave an oily substance (54 mg), which showed absorption maxima at 3615, 3440, 1728, 1031 and 1016 cm^{-1} in the IR spectrum. Treatment of **2** with the same reagent under more vigorous conditions (reflux in dry dioxane for 13 h) gave practically the same result.

*17β-Ethyl-5α,12β-etiojervane-3β,11β-diol (***29***) and Its 3-Acetate (***29a***).* A solution **11** (263 mg) in dioxane (20 ml) was refluxed with LAH (513 mg) for 45 h under stirring. After decomposition of excess reagent with methanol and water, the resulting precipitate was removed by filtration and washed with methanol. The filtrate and washings were combined and concentrated to dryness under reduced pressure. The residue was dissolved in chloroform and worked up as usual to give a crystalline substance (250 mg), which on trituration with acetone afforded **29** (220 mg), mp 185—186 °C. This was recrystallized from acetone for analysis: mp 186—188 °C; $[\alpha]_D$ +52°; IR, ν_{max} 3330, 1077, 1043 and 1033 cm^{-1}; NMR, δ 1.02 (3H, s, 19-C$\underline{H}_3$), 3.60 (1H, br, $\underline{H}$ at C_3) and 4.06 (1H, do d J=6 and 8 Hz, $\underline{H}$ at C_{11}). Found: C, 78.75; H, 11.22%. Calcd for $C_{21}H_{36}O_2$: C,

78.69; H, 11.32%.

Compound **29** (207 mg) was acetylated with Ac_2O (1 ml) and Py (2 ml) at 18 °C for 3 h. The product (235 mg) was triturated with acetone–isopropyl ether to yield **29a** (115 mg), mp 149—151 °C. This was recrystallized from the same solvent mixture for analysis: mp 151—152 °C; $[\alpha]_D$ +44°; IR, ν_{max} 3490, 1713, 1260 and 1033 cm^{-1}; NMR δ 1.04 (3H, s, 19-C$\underline{H}_3$), 2.01 (3H, s, OCOC$\underline{H}_3$) and 4.07 (1H, do d J=6 and 8 Hz, $\underline{H}$ at C_{11}). Found: C, 75.92; H, 10.30%. Calcd for $C_{23}H_{38}O_3$: C, 76.19; H, 10.57%.

*17β-Ethyl-5α-etiojerv-11-en-3β-ol Acetate (**30**).* To a solution of **28a** (101 mg) in freshly distilled Py (1 ml) was added freshly distilled phosphoryl chloride (0.1 ml) at 0 °C under stirring. A white salt was immediately precipitated. After being stirred at room temp for 1 h, the mixture was poured onto ice–water (30 ml). The resulting suspension was extracted with chloroform repeatedly. The extracts were washed with 1 M hydrochloric acid, 5% aqueous sodium hydrogencarbonate and water, dried, and evaporated to leave oily residue (111 mg), which showed a single spot on TLC and was chromatographed on silica gel (5 g) impregnated with 10% silver nitrate with benzene to afford pure oily substrance (**30**, 85 mg). Mass, *m/e* 344 (M^+), 315 ($M^+-C_2H_5$) and 255 ($M^+-C_2H_5-AcOH$); IR ($CHCl_3$), ν_{max} 1725, 1257 and 1022 cm^{-1}; NMR, δ 0.77 (3H, s, 19-C$\underline{H}_3$), 0.88 (3H, t J=7 Hz, 21-C$\underline{H}_3$), 1.02 (3H, d J=6 Hz, 18-C$\underline{H}_3$ 2.04 (3H, s, OCOC$\underline{H}_3$), 4.72 (1H, br, $\underline{H}$ at C_3) and 5.33 (1H, br s W_H=6 Hz, $\underline{H}$ at C_{11}).

A solution of **30** (6 mg) in AcOH (1 ml) was allowed to stand at room temp for 1 h. The mixture was diluted with water and extracted with chloroform. The extract was worked up as usual to give oily substance (6 mg), which was identical with the starting material substance (NMR and TLC).

*17β-Ethyl-5α,12β-etiojerv-9(11)-en-3β-ol Acetate (**31**).* To a solution of **29a** (192 mg) in freshly-distilled Py (2 ml) was added freshly-distilled phosphoryl chloride (0.3 ml) at 0 °C under stirring. The mixture was stirred at room temp for 1 h and poured onto ice–water (30 ml). After usual work up, the mixture afforded oily residue (235 mg), which was purified by column chromatography on silica gel (5 g) with benzene to give pure oily substance (**31**, 188 mg); Mass, *m/e* 344 (M^+), 329 (M^+-CH_3), 315 ($M^+-C_2H_5$), 284 (M^+-AcOH), 269 ($M^+-AcOH-CH_3$) and 255 ($M^+-AcOH-C_2H_5$); IR ($CHCl_3$), ν_{max} 1725, 1253 and 1024 cm^{-1}; NMR, δ 0.87 (3H, t J=8 Hz, 21-C$\underline{H}_3$), 0.92 (3H, s, 19-C$\underline{H}_3$), 0.98 (3H, d J=6.5 Hz, 18-C$\underline{H}_3$), 2.03 (3H, s, OCOC$\underline{H}_3$), 4.71 (1H, br, $\underline{H}$ at C_3) and 4.61 (1H, br s W_H= 6 Hz, $\underline{H}$ at C_{11}).

A solution of **31** (11 mg) in AcOH (1 ml) was stirred at room temp for 2 h. The mixture was worked up as usual to afford an oily residue (11 mg), which was identical with the starting material (NMR and TLC).

*17β-Ethyl-5α,12α-etiojervan-3β-ol Acetate (**32**).* A solution of compound **30** (76 mg) in AcOH (3.5 ml) was hydrogenated over Adams Pt (151 mg) at room temp for 55 min, when 5.9 ml of hydrogen (1.11 mol) had been consumed. The product (77 mg), oil, showed a single spot on TLC: $[\alpha]_D$ +0.5°; Mass, *m/e* 286 (M^+-AcOH, base); IR ($CHCl_3$), ν_{max} 1728, 1256 and 1025 cm^{-1}; NMR, δ 0.81 (3H, s, 19-C$\underline{H}_3$), 2.01 (3H, s, OCOC$\underline{H}_3$) and 4.73 (1H, br, $\underline{H}$ at C_3).

*17β-Ethyl-5α,12β-etiojervan-3β-ol Acetate (**13a**).* A solution of compound **31** (171 mg) in AcOH (4 ml) was hydrogenated over Adams Pt (118 mg) at room temp for 35 min, when 8.8 ml of hydrogen (0.74 mol) had been consumed. The catalyst (101 mg) was further added to the reaction mixture and hydrogenation was continued for 30 min, when 24.4 ml of hydrogen had been taken up. The product (164 mg) crystallized on trituration with methanol, had mp 74—75 °C, and amounted to 125 mg. It was recrystallized twice from aqueous methanol and then from acetone to give a pure material, mp 92—94 °C, which was identical with compound **13a** in all respects.

References

1) Part I, A. Murai, K. Arita, and T. Masamune, *Bull. Chem. Soc. Jpn.*, **46**, 3536 (1973).

2) Part XXIII of "C-Nor-D-homosteroids and Related Alkaloids"; Part XXII, A Murai, C. Sato, H. Sasamori, and T. Masamune, *Bull. Chem. Soc. Jpn.*, **49**, 499 (1976).

3) a) T. Masamune, K. Orito, and A. Murai, *Bull. Chem. Soc. Jpn.*, **39**, 2503 (1966). b) T. Masamune, A. Murai, and S. Numata, *Tetrahedron*, **25**, 3145 (1969). c) T. Masamune and K. Orito, *ibid.*, **25**, 4551 (1969). d) T. Masamune and T. Orito, *Bull. Chem. Soc. Jpn.*, **45**, 1888 (1972).

4) a) S. M. Kupchan and S. D. Levinc, *J. Am. Chem. Soc.*, **86**, 701 (1964). b) S. M. Kupchan, T. Masamune, and G. W. A. Milne, *J. Org. Chem.*, **29**, 755 (1964). c) S. M. Kupchan and M. J. Abu El-Haj, *ibid.*, **33**, 647 (1968). d) S. M. Kupchan, A. W. By, and M. S. Flom, *ibid.*, **33**, 911 (1968).

5) a) H. Mitsuhashi and Y. Shimizu, *Tetrahedron*, **19**, 1027 (1963). b) H. Mitsuhashi and N. Kawahara, *ibid.*, **21**, 1215 (1965). c) Y. Shimizu and H. Mitsuhashi, *ibid.*, **24**, 4207 (1968), and references cited therein.

6) a) W. F. Johns and I. Laos, *J. Org. Chem.*, **30**, 123, 4220 (1965), and references cited there. b) W. F. Johns, *ibid.*, **36**, 711 (1971).

7) J. W. Huffman, D. M. Alabran, and A. C. Ruggles, *J. Org. Chem.*, **33**, 1060 (1968).

8) T. Masamune, N. Sato, K. Kobayashi, I. Yamazaki, and Y. Mori, *Tetrahedron* **23**, 1591 (1967).

9) T. Masamune, A. Murai, K. Nishizakura, T. Orito, S. Numata, and H. Sasamori, *Bull. Chem. Soc. Jpn.*, **49**, 1622 (1976).

10) J. Fried and A. Klingsberg, *J. Am. Chem. Soc.*, **75**, 4929 (1953).

11) A. Murai, T. Nishimura, and T. Masamune, *Bull. Chem. Soc. Jpn.*, **49**, 1612 (1976).

12) *Cf.*, R. Greenwald, M. Chaykovsky, and E. J. Corey, *J. Org. Chem.*, **28**, 1128 (1963).

13) If the epimerization takes place at C_9, the difference in the chemical shift would be very large; D. M. Bailey, D. P. G. Hamon, and W. S. Johnson, *Tetrahedron Lett.*, **1963**, 555; J. P. Kutney, A. By, T. Inaba, and S. Y. Leong, *ibid.*, **1965**, 2911.

14) T. Masamune, A. Murai, K. Orito, H. Ono, S. Numata, and H. Suginome, *Tetrahedron*, **25**, 4853 (1969).

15) Huang-Minlon, *J. Am. Chem. Soc.*, **71**, 3301 (1949).

16) D. H. R. Barton, D. A. J. Ives, and B. R. Thomas, *J. Chem. Soc.*, **1955**, 2056.

17) G. Zweifel and H. C. Brown, *Org. Reactions*, **13**, 1 (1963).

18) H. C. Brown and C. P. Carg, *J. Am. Chem. Soc.*, **83**, 2951, 2952 (1961).

19) N. S. Bhacca and D. H. Williams, "Applications of NMR Spectroscopy in Organic Chemistry," Holden-Day, Inc., San Francisco (1964), p. 19.

20) L. I. Smith and K. E. Howard, *Org. Synth.*, **24**, 53 (1944).

21) *Cf.*, W. A. Jacobs and L. C. Craig, *J. Biol. Chem.*, **148**, 51 (1943); W. A. Jacobs and C. F. Huebner, *ibid.*, **170**, 635, (1947).

Stereochemistry of the C and D Rings of C-Nor-D-homosteroids. III.[1] The Synthesis of Etiojervane Analogs of Androstan-3β-ol[2]

Akio MURAI, Takeshi NISHIMURA, and Tadashi MASAMUNE
Department of Chemistry, Faculty of Science, Hokkaido University, Sapporo 060

(Received September 30, 1975)

The synthesis of C/D *trans*- and *cis*-fused C-nor-D-homoandrostan-3β-ol 3-acetates (**11a** and **34a**) from jervine (**1**) is described. The configurations of both the compounds and the synthetic intermediates are defined clearly on the basis of the chemical and spectral evidence.

As one of the continuing studies of C-nor-D-homosteroid hormones, we describe herein the transformation of jervine (**1**) into etiojervane analogs of androstan-3β-ol, which include both C/D *cis*- and *trans*-fused ring systems. This synthetic study has also been carried out with an aim to clarify the conformation of C and D rings of etiojervanes on the basis of the NMR and other spectra,[3] and the titled compounds will be useful as reference compounds for a series of these researches.[4,5]

The synthesis of C/D *trans*-fused C-nor-D-homoandrostan-3β-ol (**11**), and its derivatives started from 12β-etiojerv-5-en-3β-ol-11,17-dione 3-acetate[6,7] (**2**), prepared from jervine (**1**) *via* a five-step process. Treatment of **2** with sodium borohydride or with hydrogen over platinum in ethanol effected only reduction of the 17-oxo group to give a 30 : 1 or 2 : 1 mixture[8] of readily separable 17α- and 17β-alcohols (**3a** and **4a**), mp 208.5—209 °C and 173.5—174 °C, in which the hydroxy group at C_{17} was assigned α- and β-configurations, respectively, on the basis of signal patterns of the protons at C_{17}: **3a**, δ 3.08 and W_H=16 Hz; **4a**, δ 3.78 and W_H=6 Hz.[9] In fact, compound **3a** was transformed by the Wolff-Kishner reduction to a known compound, 12β-etiojerv-5-ene-3β,17α-diol[8] (**5**), in good yield. These alcohols, which on acetylation formed the respective 3,17-diacetates (**3b** and **4b**), mp 176—177 °C and 187—188 °C, were reconverted quantitatively into the original ketone (**2**) by oxidation, respectively, confirming the configurational retention at C_{12} and C_{13} during these reactions.

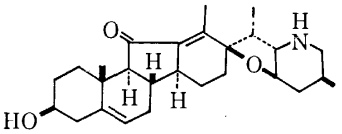

1

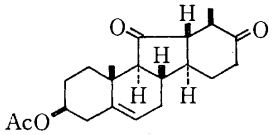

2

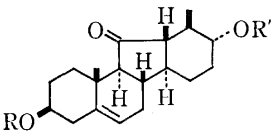

3 R=R′=H
3a R=Ac, R′=H
3b R=R′=Ac
3c R=Ac, R′=Ts

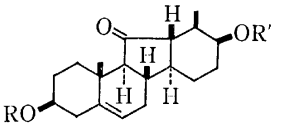

4 R=R′=H
4a R=Ac, R′=H
4b R=R′=Ac

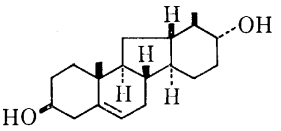

5

In order to remove the oxygen function at C_{17} and C_{11}, compound **3a** was converted into 17-tosylate (**3c**), mp 106—108 °C, which on treatment with lithium aluminium hydride afforded 3β, 11β-alcohol (**6**), mp 181—183 °C, in good yield. The chemical shift (δ 1.26) of 19-methyl protons in **6** was consistent with the assigned β-configuration to the 11-hydroxy group. Hydrogenation of **6** over platinum in acetic acid gave its 5α,6-dihydro derivative (**7**), mp 148—150 °C, in 83% yield, which was also obtained by the Wolff-Kishner reduction of a well-defined compound **8**,[1] indicative of the retention at C_{12} during the hydride reduction. This glycol **7**, on partial acetylation followed by oxidation with chromic anhydride, produced 11-ketone (**9**), mp 114—114.5 °C, in 70% yield. The transformation of **6** to **9** by the reverse process proceeded in almost the same yield; step 1, partial acetylation of **6** followed by oxidation to Δ^5-11-ketone (**10**), mp 156—157 °C, 69%, and step 2, hydrogenation of **10** to **9**, 76%.

Reduction of 11-ketone **9** by a modification[10] of the Wolff-Kishner reaction produced an aimed compound, 5α,12β-etiojervan-3β-ol (**11**), mp 119—120 °C, in 62% yield, which on acetylation formed 3-acetate (**11a**), mp 72.5—73.5 °C. The β-configuration at C_{12} of this compound (**11**) was determined in an unambiguous manner described below. 5α,12β-Etiojervan-3β-ol-17-one 3-acetate[1] (**12**) with the established configurations at C_{12} and C_{13} was treated with sodium borohydride to give a mixture of 17-alcohols, from which 17α- and 17β-alcohols (**13** and **14**), mp 119—119.5 °C and 96—96.5 °C, were isolated by preparative TLC in 75 and 24% yields, respectively. Treatment of **13** with *p*-toluenesulfonyl chloride followed by reduction with lithium aluminium hydride resulted in formation

of 3-alcohol, mp 118—119 °C, with a small amount of 3β,17α-glycol[8] (**13a**), mp 166—168 °C. The former was completely identical with compound **11** in all respects.

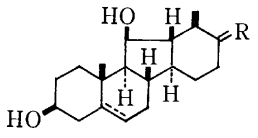

6 Δ^5, R=H_2
7 5αH, R=H_2
8 5αH, R=O

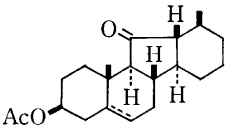

9 5αH
10 Δ^5

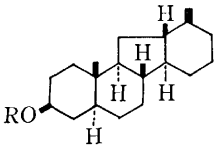

11 R=H
11a R=Ac

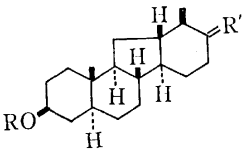

12 R=Ac, R'=O
13 R=Ac, R'=−H, ···OH
13a R=H, R'=−H, ···OH
14 R=Ac, R'=···H, −OH

5α,12α-Etiojervan-3β-ol-11-one 3-acetate (**25**), a 12-epimer of **9**, was synthesized as described below. Treatment of etiojerva-5,12-dien-3β-ol-11,17-dione 3-acetate[6b,7] (**15**) with sodium borohydride in methanol led to only reduction of the 17-oxo group to give a mixture of 17α- and 17β-alcohols (**16** and **17**), mp 170—171 °C and 236—238 °C, which were isolated in 78 and 5% yields, respectively. The configurations at C_{17} of these alcohols were decided on the basis of signal patterns of the protons at C_{17} (**16**, δ 4.20 with W_H of 20 Hz, and **17**, δ 4.06 with W_H of 7 Hz) and optical rotations (**16**, $[\alpha]_D$=−128 °C, and **17**, $[\alpha]_D$=−211°). The assigned configurations were in good accord with the fact that the allylic equatorial proton in cyclohexene systems is more shielded than the corresponding axial,[11] and also with the Mills rule.[12]

Hydrogenation of compound **16** over Adams platinum in acetic acid produced four stereoisomeric tetrahydro derivatives (**18**—**21**), mp 154—156 °C, 178.5—179 °C, 141—142 °C, and 132—133 °C, in 22, 27, 16, and 25% yields, respectively. The configuration of each product was deduced as described below. Compound **18**, when treated with sodium methoxide in refluxing methanol for 24 h, gave 3,17-alcohol (**18a**), mp 174.5—175 °C, which formed 3,17-diacetate (**18b**), mp 174.5—175 °C. This diacetate (**18b**) was also derived by direct acetylation of monoacetate **18**, indicating that the compound (**18**) was stable under the alkaline conditions. Moreover, glycol **18a** was also obtained by hydrogenation of compound **3** with established configurations in 54% yield. This fact, as coupled with the spectral data (a broad signal at δ 4.65 with W_H of 23 Hz due to the proton at C_3, and a negative Cotton effect with a=−160°,[13]), indicated that compound **18** possessed 5αH, 12βH, 13αH and 17βH configurations. Compound **19** was determined to be a 5-epimer of **18** on the basis of the spectral data: NMR, δ 0.97 (3H, s, 19-C$\underline{H}_3$), 1.27 (3H, d J=6 Hz, 18-C$\underline{H}_3$), and 5.01 (1H, br s W_H=6 Hz, $\underline{H}$ at C_3); ORD, a negative Cotton effect, a=−145°. On the other hand, compound **20** was found to be a 12-epimer of **18** on the following evidence. While compound **20** gave 3,17-diacetate (**20a**), mp 106—109 °C, it was epimerized at C_{12} by treatment with alkali under the same conditions as **18** to give glycol having mp 172—173 °C, quantitatively, which was identical with the afore-mentioned glycol (**18a**) in all respects. These results led to assignment of 5αH, 12αH, 13αH and 17βH configurations to **20**, which was supported by the NMR (19-C$\underline{H}_3$, **20** δ 0.88 and **18** δ 0.84) and ORD spectra (a negative Cotton effect, a=−83°).[13] Finally, the configurations of compound **21** were assigned as shown in the formula (5βH, 12αH, 13αH and 17βH) on the spectral data: NMR, δ 0.88 (3H, d J=7.5 Hz, 18-C$\underline{H}_3$), 1.01 (3H, s, 19-C$\underline{H}_3$), and 5.01 (1H, br s W_H=6 Hz, $\underline{H}$ at C_3); ORD, a negative Cotton effect, a=−77°. As reported previously,[13] hydrogenation of jervine (**1**) under the same conditions as **16** led to formation of C/D *trans*- and *cis*-fused tetrahydro derivatives with α-oriented hydrogens at C_5. The present result was of interest as compared with the hydrogenation result of jervine, because compounds **19** and **21** with β-hydrogens at C_5 were produced in better yields than those **18** and **20** with α-hydrogens at C_5.

5α,12α-Etiojervane-3β,17α-diol-11-one 3-acetate (**20**) was then treated with *p*-toluenesulfonyl chloride in pyridine, and the resulting 17-tosylate (**20b**), amorphous, was refluxed with lithium aluminium hydride in ether to give a single product (**22**), mp 213—214 °C, in 59% yiels from **20**. Contrary to the expectation that the oxygen function at C_{17} would be removed by these reactions, compound **22** had a molecular formula of $C_{19}H_{30}O_2$ and resisted hydrogenation over platinum in acetic acid. The IR spectrum showed the presence of both hydroxy and ether groups at 3405, 1150, 1075, 1060 and 1028 cm^{-1} and the NMR spectrum revealed the existence of three protons on carbon atoms bearing the oxygen functions at δ 3.55 (br W_H=19 Hz, $\underline{H}$ at C_3), 3.90 and 4.31 (each 1H, br s W_H=7 and 5 Hz, 2$\underline{H}$ at C_{17} and C_{11} or *vice versa*). Acetylation of **22** with acetic anhydride in pyridine afforded only monoacetate (**22a**), mp 123—125 °C, which exhibited no hydroxy group in the IR spectrum. All these results indicated this compound to be represented by formula

22. Likewise, the 5β-isomer (**21**) was treated in the same manner as **20** to give 17-tosylate (**21a**), mp 120—121 °C, which was submitted to the hydride reduction to yield the corresponding ether compound (**23**), mp 153—154 °C, in moderate yield (crude 89%, pure 24%). Compound **23** also had the same molecular formula, $C_{19}H_{30}O_2$, as **22**, and formed monoacetate (**23a**), mp 128—130 °C, showing the absence of a hydroxy group in the IR spectrum.

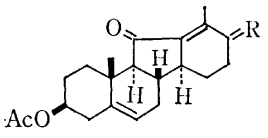

15 R=O
16 R=—H, ···OH
17 R=···H, —OH

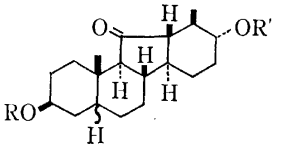

18 5αH, R=Ac, R′=H
18a 5αH, R=R′=H
18b 5αH, R=R′=Ac
19 5βH, R=Ac, R′=H

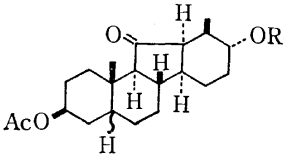

20 5αH, R=H
20a 5αH, R=Ac
20b 5αH, R=Ts
21 5βH, R=H
21a 5βH, R=Ts

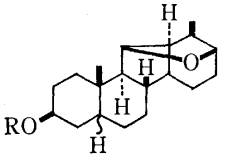

22 5αH, R=H
22a 5αH, R=Ac
23 5βH, R=H
23a 5βH, R=Ac

In order to remove the oxygen function at C_{17}, compound **20** was treated with phosphoryl chloride in pyridine to give olefin (**24**), mp 77—78 °C, in 56% yield, as an only isolable product. The assigned structure with a double bond at C_{16} and C_{17} was deduced from the NMR spectrum; δ 5.84 (2H, t J=5.5 Hz). Hydrogenation of **24** over platinum in acetic acid afforded quantitatively 12α-etiojervan-3β-ol-11-one 3-acetate (**25**), amorphous, which showed a negative Cotton effect of a=—70° in the ORD curve, indicating the configurational retention at C_{12} during the aforementioned reactions. It is to be emphasized that the 19-methyl protons (δ 0.89) of **25** were deshielded 0.04 ppm more than those (δ 0.85) of the corresponding C/D *trans*-fused compound (**9**),[14] and the same difference in chemical shift was observed between the respective 17β-ethyl derivatives.[1] Compound **25**, when treated with alkali in refluxing methanol and then acetylated, gave a quantitative yield of crystalline substance having mp 109—110 °C. This compound was identical with compound **9** in all respects, confirming the 12αH configuration of **25**.

Compound **21** was also treated in the same manner as **20** to give 16,17-olefin (**26**), mp 150—152 °C, in 69% yield, which on hydrogenation produced 5β,12α-etiojervan-3β-ol-11-one 3-acetate (**27**), mp 110—110.5 °C, in 70% yield. Treatment of these 12α-etiojervanes (**26** and **27**) with sodium methoxide in methanol under reflux followed by acetylation effected epimerization at C_{12} to give the corresponding C/D *trans*-fused (12βH) etiojervanes (**28** and **29**), mp 119.5—121 °C and 106—107.5 °C, in quantitative yields, respectively. As expected, the 19-methyl protons of the 12α-epimers (**26** and **27**) were deshielded slightly but definitely (0.02—0.04 ppm) as compared with those of the respective 12β-epimers.

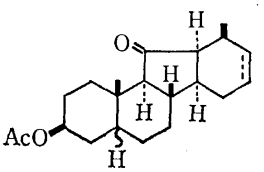

24 5αH, Δ^{16}
25 5αH, no Δ^{16}
26 5βH, Δ^{16}
27 5βH, no Δ^{16}

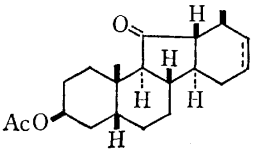

28 Δ^{16}
29 no Δ^{16}

The synthesis of 5α,12α-etiojervan-3β-ol 3-acetate (**34a**), a 12-epimer of compound **11a**, started from 17α-acetyl-5α,12α-etiojervan-3β-ol[4,15] (**30**). The Baeyer-Villiger oxidation of **30** with perbenzoic acid afforded 17-acetate (**31**), amorphous, which on oxidation and subsequent hydrolysis of the resulting 3-ketone (**32**), amorphous, gave 17-hydroxy-3-ketone (**32a**), mp 145—147 °C, in 35% yield from **30**. This compound (**32a**), when oxidized with Jones' reagent, was converted into 3,17-diketone (**33**), mp 173—175 °C, which was identical with the known sample,[16] confirming the 12αH and 13αH configurations of **32a**. This keto-alcohol (**32a**) was transformed smoothly into 17-tosylate (**32b**), amorphous, which on reduction with lithium aluminium hydride in refluxing ether gave rise to the 17-deoxy derivative (**34**), mp 122—124 °C, in 48.5% yield from **32a**. The β-configuration was assigned to the hydroxy group at C_3 on the basis of the NMR spectrum; δ 3.60 (1H, br W_H=20 Hz,

H at C_3). Hence compound **34**, which readily formed 3-acetate (**34a**), mp 97—97.5 °C, was identified as 5α,12α-etiojervan-3β-ol, because the transformation from **30** to **34** involved no epimerization at all asymmetric centers other than C_3. The 19-methyl protons of these C/D *cis*-fused etiojervanes (**34** and **34a**) were observed at lower fields (δ 0.80 and 0.81) than those (δ 0.75 and 0.75) of the corresponding C/D *trans*-fused (**11** and **11a**). These chemical shift differences of 19-methyl protons will be discussed with those of 18-methyl protons in the following paper.[3]

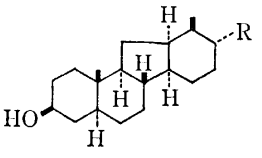

30 R=Ac
31 R=OAc

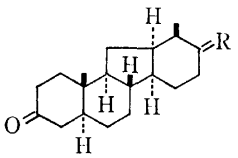

32 R=−H, ···OAc
32a R=−H, ···OH
32b R=−H, ···OTs
33 R=O

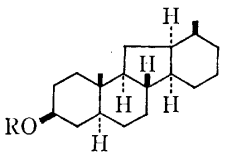

34 R=H
34a R=Ac

Experimental

All the melting points were uncorrected. The homogeneity of each compound was always checked by TLC over silica gel (Wakogel B-5), using various solvent systems, and the spots were developed with ceric sulfate in dil sulfuric acid and/or iodine. The optical rotations, ORD curves and IR spectra were measured in chloroform, dioxane and Nujol, respectively, unless otherwise stated. The NMR spectra were obtained in deuteriochloroform at 60 and/or 100 MHz, and the chemical shifts were given in δ-values, TMS being used as an internal reference. The abbreviations "s, d, t, q, br, m, and do" in the NMR spectra denote "singlet, doublet, triplet, quartet, broad, multiplet, and double," respectively.

*12β-Etiojerv-5-ene-3β,17α-diol-11-one (**3**), 12β-Etiojerv-5-ene-3β,17β-diol-11-one (**4**), and Their Derivatives (**3a—3c**, **4a** and **4b**).* a) A solution of 12β-etiojerv-5-en-3β-ol-11,17-dione 3-acetate[6,7] (**2**, 344 mg) in ethanol (32 ml) was hydrogenated over Adams platinum (Pt, 181 mg as $PtO_2 \cdot H_2O$) at room temperature (temp), when 24 ml (1.1 mol) of hydrogen had been consumed for 1 h. The amorphous product (397 mg) showed two main and two minor spots on TLC, the latter two (total 40 mg) being not examined further. The two major components were separated by preparative TLC (16 plates) with a 2 : 3 mixture of ether and benzene. More mobile fractions gave crystalline substance (90 mg), which on recrystallization from acetone-isopropyl ether afforded 17β-alcohol (**4a**, 72 mg), mp 172—173 °C. This was recrystallized twice from the same solvent mixture for analysis: mp 173.5—174 °C; $[\alpha]_D$ −169°; ORD, $[\Phi]_{332}^{trough}$ −10,000°, $[\Phi]_{321}^{trough}$ −6600°, $[\Phi]_{291}^{peak}$ +5800°, a=−158°; IR ν_{max} 3590, 1723, 1244, and 1038 cm^{-1}; NMR δ 1.03 (3H, s, 19-C$\underline{H}_3$), 1.29 (3H, d J=5 Hz, 18-C$\underline{H}_3$), 2.01 (3H, s, OCOC$\underline{H}_3$), 3.78 (1H, br s W_H=6 Hz, H at C_{17}), 4.50 (1H, br, H at C_3), and 5.43 (1H, br d J=4 Hz, H at C_6). Found: C, 72.83; H, 8.64%. Calcd for $C_{21}H_{30}O_4$: C, 72.80; H, 8.73%.

Less mobile fractions gave crystalline material (219 mg), which on trituration with acetone-isopropyl ether afforded 17α-alcohol (**3a**, 158 mg), mp 208—209 °C. This was recrystallized twice from the same solvent mixture for analysis: mp 208—209 °C; $[\alpha]_D$ −173.6°; ORD, $[\Phi]_{334}^{trough}$ −12900°, $[\Phi]_{332}^{trough}$ −8800°, $[\Phi]_{292}^{peak}$ +5500°, a=−184°; IR, ν_{max} 3340, 1733, 1247, and 1040 cm^{-1}; NMR δ 1.03 (3H, s, 19-C$\underline{H}_3$), 1.32 (3H, d J=4 Hz, 18-C$\underline{H}_3$), 2.01 (3H, s, OCOC$\underline{H}_3$), 3.08 (1H, br m W_H=16 Hz, H at C_{17}), 4.56 (1H, br, H at C_3), and 5.39 (1H, br d J=5 Hz, H at C_6). Found: C, 72.74; H, 8.74%. Calcd for $C_{21}H_{30}O_4$: C, 72.80; H, 8.73%.

Compound **3a** (54 mg) was treated with acetic anhydride (Ac_2O, 1 ml) and pyridine (Py, 1 ml) at room temp overnight and gave **3b** (50 mg), mp 176—177 °C, on trituration with acetone-isopropyl ether. This was recrystallized from the same solvent mixture for analysis: mp 176—177 °C; $[\alpha]_D$ −168.2°; IR, ν_{max} 1733, 1723, 1649, and 1242 cm^{-1}; NMR, δ 1.04 (3H, s, 19-C$\underline{H}_3$), 1.21 (3H, d J=6 Hz, 18-C$\underline{H}_3$), 2.02 and 2.04 (each 3H, s, 2OCOC$\underline{H}_3$), 4.49 (2H, br m, 2H at C_3 and C_{17}), and 5.43 (1H, br d J=4 Hz, H at C_6). Found: C, 70.99; H, 8.22%. Calcd for $C_{22}H_{32}O_5$: C, 71.10; H, 8.30%.

Compound **3a** (53 mg) was refluxed with 1 M sodium methoxide in methanol (5.3 ml) for 2 h under a stream of nitrogen. The solvent was evaporated *in vacuo* and the residue was diluted with water and extracted with chloroform, repeatedly. The chloroform solution was washed with water, dried and evaporated to leave crystalline residue (66 mg). The residue showed a single spot on TLC and was triturated with acetone to give **3** (35.5 mg), mp 209—212 °C. Recrystallization from the same solvent afforded an analytical sample, mp 212.5—213 °C; $[\alpha]_D$ −158.2° (MeOH); ORD, $[\Phi]_{333}^{trough}$ −11000°, $[\Phi]_{321}^{trough}$ −7360°, $[\Phi]_{291}^{peak}$ +5700°, a=−167°; IR, ν_{max} 3510, 3310, 3230, 1731, and 1044 cm^{-1}. Found: C, 75.00; H, 9.31%. Calcd for $C_{19}H_{28}O_3$: C, 74.96; H, 9.27%.

Compound **3** (18 mg) was treated with Ac_2O (1 ml) and Py (1 ml) at room temp overnight and gave **3b** (12 mg), mp 175—176 °C, on recrystallization from acetone-isopropyl ether. This sample was identical with the afore-mentioned **3b** (mixed mp, IR and TLC).

A solution of **3a** (708 mg) in Py (10 ml) containing *p*-toluene-sulfonyl chloride (TsCl, 413 mg) was stirred at room temp for 18 h. After further addition of the chloride (534 mg) the whole mixture was allowed to stand at room temp for additional 24 h and poured into ice-water. The resulting precipitates crystallized on trituration with ether-isopropyl ether, had mp 88—90 °C (dec) and amounted to 988 mg. Recrystallization from ether afforded an analytical sample of **3c**, mp 106—108 °C (dec); $[\alpha]_D$ −109.4°; IR, ν_{max} 1733, 1598, 1249, 1190, and 1180 cm^{-1}; NMR, δ 1.03 (3H, s, 19-C$\underline{H}_3$), 1.16 (3H, d J=4.5 Hz, 18-C$\underline{H}_3$), 2.01 (3H, s, OCOC$\underline{H}_3$), 2.44 (3H, s, $C_6H_4C\underline{H}_3$), 4.00 (1H, br, H at

C_{17}), 4.55 (1H, br, H at C_3), and 5.38 (1H, br d J=5 Hz, H at C_6). Found: C, 67.20; H, 7.27, S, 5.78%. Calcd for $C_{28}H_{36}O_6S$: C, 67.18; H, 7.25; S, 6.40%.

Compound **4a** (53 mg) was acetylated in the same manner as mentioned above and afforded **4b** (40 mg), mp 186—187 °C, on trituration with acetone–isopropyl ether. This was recrystallized from the same solvent mixture for analysis: mp 187—188 °C; $[\alpha]_D$ −111.6°; IR, ν_{max} 1734, 1723, 1651, and 1242 cm^{-1}; NMR, δ 1.06 (3H, s, 19-CH_3), 1.20 (3H, d J=5 Hz, 18-CH_3), 2.01 and 2.06 (each 3H, s, 2OCOCH_3), 4.61 (1H, br, H at C_3), 4.99 (1H, br s W_H=6 Hz, H at C_{17}), and 5.44 (1H, br d J=5 Hz, H at C_6). Found C, 71.07; H, 8.32%. Calcd for $C_{22}H_{32}O_5$: C, 71.10; H, 8.30%.

A solution of **4a** (202 mg) was refluxed with 1 M sodium methoxide in methanol (20 ml) for 2 h under nitrogen. After removal of the solvent *in vacuo*, the residue was diluted with water and extracted with chloroform. The chloroform solution was washed with water, dried and evaporated to leave crystalline substance (227 mg), which showed two spots on TLC and crystallized on trituration with acetone–isopropyl ether. This substance (165 mg), mp 168—170 °C, showed a single spot on TLC, and was recrystallized from the same solvent mixture to give an analytical sample of **4**, mp 168—170 °C; ORD, $[\Phi]_{331}^{trough}$ −11060°, $[\Phi]_{319}^{trough}$ −6900°, $[\Phi]_{290}^{peak}$ +6700°, a=−177.6°; IR, ν_{max} 3220 and 1722 cm^{-1}; NMR, δ 1.03 (3H, s, 19-CH_3), 1.33 (3H, br s, 18-CH_3), 3.52 (1H, br, H at C_3), 3.79 (1H, br s W_H=7 Hz, H at C_{17}), and 5.38 (1H, br, H at C_6). Found: C, 75.07; H, 9.42%. Calcd for $C_{19}H_{28}O_3$: C, 74.96; H, 9.27%.

Compound **4** (20 mg) was treated with Ac_2O (1 ml) and Py (1 ml) at room temp overnight and gave its 3,17-diacetate (13 mg), mp 184—185 °C, on trituration with methanol. This compound was identical with the afore-mentioned sample (**4b**) in all respects.

b) To a solution of **2** (1.104 g) in methanol (130 ml) cooled at −7 °C (bath temp) was added sodium borohydride (NBH, 202 mg), and the mixture was stirred at the temp for 1 h. After addition of acetic acid (AcOH, 0.4 ml) the mixture was stirred at room temp for 15 min and concentrated below 30 °C *in vacuo*. The residue was diluted with water and extracted with chloroform repeatedly, and the chloroform solution was washed with 5% aqueous sodium bicarbonate and water, dried and evaporated to leave crystalline residue (1.23 g). Recrystallization from acetone afforded 17α-alcohol (**3a**, 786 mg), mp 206—207 °C, which was identical with the afore-mentioned sample (method a) in all respects.

The filtrate, obtained on recrystallization, was evaporated and separated into three fractions by preparative TLC (10 plates) with a 2 : 3 mixture of ether and benzene. The most mobile part gave amorphous substance (81 mg), which crystallized on trituration with isopropyl ether, had mp 171—173 °C and amounted to 27 mg. This compound was identified as 17β-alcohol (**4a**). Likewise, the middle part (104 mg) afforded **3a** (42 mg), mp 202—204 °C, on trituration with acetone. The least mobile part gave amorphous material (80 mg), which crystallized on trituration with isopropyl ether to give a new 17-alcohol (41 mg), mp 167—171 °C. Recrystallization from acetone–isopropyl ether afforded an analytical sample, mp 173—174 °C; $[\alpha]_D$ −217.1°; ORD, $[\Phi]_{328}^{trough}$ −12400°, $[\Phi]_{317}^{trough}$ −8600°, $[\Phi]_{289}^{peak}$ +5100°, a=−175°; IR, ν_{max} 3520, 1722, 1247, 1038 and 1026 cm^{-1}; NMR, δ 0.83 (3H, d J=7 Hz, 18-CH_3), 1.04 (3H, s, 19-CH_3), 2.02 (3H, s, OCOCH_3), 3.75 (1H, br W_H=16 Hz, H at C_{17}), 4.61 (1H, br, H at C_3), and 5.43 (1H, d J=5 Hz, H at C_6). Found: C, 72.79; H, 8.86%. Calcd for $C_{21}H_{30}O_4$: C, 72.80; H, 8.73%. The ORD curve and NMR spectrum of this alcohol indicated that this compound would be a 13-epimer of 17α-alcohol (**3a**) and formed from the corresponding 17-ketone included in the starting material as an impurity. This was supported by the spectral data of its 17-acetate described below.

Treatment of the alcohol (50 mg) with Ac_2O (1 ml) and Py (1 ml) at room temp overnight produced its 17-acetate (40 mg), mp 196—198 °C, after trituration with acetone–isopropyl ether. This was recrystallized from the same solvent mixture for analysis: mp 198—199 °C; $[\alpha]_D$ −163.4°; IR, ν_{max} 1734, 1652, 1253, and 1044 cm^{-1}; NMR, δ 0.84 (3H, d J=7 Hz, 18-CH_3), 1.04 (3H, s, 19-CH_3), 2.03 (6H, s, 2OCOCH_3), 4.70 (2H, br m, 2H at C_3 and C_{17}), and 5.43 (1H, br d J=4.5 Hz, H at C_6). Found: C, 71.07; H, 8.42%. Calcd for $C_{23}H_{32}O_5$: C, 71.10; H, 8.30%.

*Oxidation of **3a** and **4a** to **2**.* Compound **3a** (21 mg) was stirred with a complex prepared from chromic anhydride (CrO_3, 104 mg) and Py (1 ml) at room temp for 14 h. The mixture was diluted with water and extracted with ether, and the ether solution was washed with 1 M hydrochloric acid, 5% aqueous sodium bicarbonate and saturated brine, dried and evaporated to yield amorphous material (24 mg), which crystallized on trituration with isopropyl ether. Recrystallization from the solvent afforded **2** (13 mg), mp 170—171 °C, which was identical with an authentic sample in all respects.

Compound **4a** (25 mg) was treated in the same manner as mentioned above and gave **2** (13 mg), mp 172—173 °C.

*12β-Etiojerv-5-ene-3β,17α-diol (**5**).* To freshly distilled diethylene glycol (DEG, 15 ml) was added sodium (400 mg); the mixture was then heated for a while and cooled. To this solution was added anhydrous hydrazine (6.5 ml), and the mixture was stirred at room temp for a while. After addition of compound **3a** (201 mg), the whole mixture was heated under reflux for 24 h. The excess hydrazine was then removed by distillation and the mixture was again refluxed for additional 17 h. The cooled solution was poured into water (100 ml) and extracted with chloroform. The extracts were washed with 1 M hydrochloric acid, 5% aqueous sodium bicarbonate and water, dried and evaporated to leave oil (446 mg), which was purified by preparative TLC (9 plates) with a 3 : 7 mixture of ethyl acetate and benzene. Main fractions were extracted twice with methanol to give crystalline substance (122.5 mg). This was recrystallized from acetone to afford a pure sample of **5**, mp 180—182 °C, which was identical with an authentic sample[8] in all respects.

*12β-Etiojerv-5-ene-3β,11β-diol (**6**).* 17-Tosylate (**3c**, 921 mg) was treated with lithium aluminium hydride (LAH, 2.0 g) in refluxing tetrahydrofuran (THF, 150 ml) for 18 h under stirring and then cooled with ice–water. After careful addition of water to decompose excess of the hydride, the mixture was submitted to filtration, and the filtrate was evaporated below 30 °C *in vacuo* and then extracted with chloroform. The chloroform solution was worked up as usual to yield amorphous substance (498 mg), which crystallized on trituration with acetone to give **6** (431 mg), mp 180—181 °C. Recrystallization from acetone afforded an analytical sample, mp 181—183 °C; $[\alpha]_D$ −54.5°; IR, ν_{max} 3430 and 1058 cm^{-1}; MNR, δ 1.02 (3H, d J=4 Hz, 18-CH_3), 1.26 (3H, s, 19-CH_3), 3.54 (1H, br, H at C_3), 4.19 (1H, br, m, H at C_{11}), and 5.24 (1H, br s W_H = 9 Hz, H at C_6). Found: C, 78.38; H, 10.25%. Calcd for $C_{19}H_{30}O_2$: C, 78.57; H, 10.41%.

*5α,12β-Etiojervane-3β,11β-diol (**7**).* a) A solution of **6** (662 mg) in AcOH (30 ml) was hydrogenated over Adams Pt (205 mg) for 30 min, when 57 ml (1.1 mol) of hydrogen had been consumed. The reaction product (870 mg),

obtained on usual work up, crystallized on trituration with isopropyl ether to give **7** (557 mg), mp 148—150 °C, which showed a single spot. Recrystallization from acetone–isopropyl ether afforded an analytical sample, mp 148—150 °C; $[\alpha]_D$ +34.8°; IR, ν_{max} 3380, 1033, and 1024 cm^{-1}; NMR, δ 1.00 (3H, d J=7.5 Hz, 18-C$\underline{H}_3$), 1.03 (3H, s, 19-C$\underline{H}_3$), 3.52 (1H, br, $\underline{H}$ at C_3), and 4.04 (1H, br m, $\underline{H}$ at C_{11}). Found: C, 77.84; H, 11.10%. Calcd for $C_{19}H_{32}O_2$: C, 78.03; H, 11.03%.

b) To a solution of ethylene glycol (10 ml) containing potassium hydroxide (1.1 g) was added 80% hydrazine hydrate (1 ml) and the solution was refluxed for 10 min. To the cooled solution was added compound **8**[1] (74 mg), and the mixture was refluxed for 17 h. After removal of excess of the hydrazine by distillation for 4 h, the reaction mixture was cooled, poured into ice–water (100 ml), and extracted with chloroform. The chloroform extracts gave crystalline substance (90 mg), showing a single spot. Tirturation with acetone–isopropyl ether afforded **7** (55 mg), mp 137—141 °C, which was identical with the afore-mentioned sample (method a).

*5α,12β-Etiojervan-3β-ol-11-one 3-Acetate (**9**).* a) Compound **7** (503 mg) was treated with Ac_2O (2.5 ml) and Py (5 ml) at room temp for 3 h and then poured into ice–water. After being salted out the mixture was extracted with ether, and the ether solution was worked up as usual to yield amorphous residue (655 mg), showing a single spot, which was dissolved in Py (10 ml) and oxidized by careful addition of CrO_3 (1 g) under cooling during 2 min and subsequent stirring at room temp for 12 h. The mixture was dissolved in water (50 ml) under cooling and extracted with ether repeatedly. The ether solution was shaken with 2 M hydrochloric acid to remove the resulting insoluble material by filtration, washed again with 2 M hydrochloric acid, 5% aqueous sodium bicarbonate and saturated brine, dried and evaporated to leave amorphous residue (664 mg), which crystallized on trituration with hexane to give **9** (407 mg), mp 113.5—114 °C. This was recrystallized from hexane for analysis: mp 114—114.5 °C; $[\alpha]_D$ −89.6°; ORD, $[\Phi]_{334}^{trough}$ −9600°, $[\Phi]_{323}^{trough}$ −5400°, $[\Phi]_{293}^{peak}$ +7900°, a=−175°, IR, ν_{max} 1730, 1238, and 1031 cm^{-1}; NMR, δ 0.85 (3H, s, 19-C$\underline{H}_3$), 1.16 (3H, d J=5 Hz, 18-C$\underline{H}_3$), 2.00 (3H, s, OCOC$\underline{H}_3$), and 4.69 (1H, br, $\underline{H}$ at C_3). Found C, 75.74; H, 9.63%. Calcd for $C_{21}H_{32}O_3$: C, 75.86; H, 9.70%.

b) A solution of compound **10** (382 mg), described later, in AcOH (18 ml) was hydrogenated over Adams Pt (204 mg) at room temp for 1 h, when 25 ml (1.1 mol) of hydrogen had been taken up. The reaction product (405 mg) crystallized on trituration with hexane, had mp 112—113 °C and amounted to 291 mg. Recrystallization from hexane afforded a pure sample of **9**, needles, mp 114—114.5 °C, which was identical with the afore-mentioned sample.

*12β-Etiojerv-5-en-3β-ol-11-one 3-Acetate (**10**).* Compound **6** (411 mg) was treated with Ac_2O (2 ml) and Py (4 ml) at room temp for 3 h, and the resulting crude acetate (517 mg), showing a single spot, was dissolved in Py (6 ml) and poured onto a complex, prepared from CrO_3 (1.05 g) and Py (10 ml), under cooling. The mixture was stirred at room temp for 20 h and, after addition of ethanol (20 ml), evaporated below 30 °C *in vacuo*. The residue was shaken with ether and water, and then filtered to remove insoluble material formed. The ether filtrate gave crystalline residue (516 mg), which was recrystallized from aqueous acetone to yield **10** (364 mg), mp 153—155 °C. Recrystallization from the same solvent afforded an analytical sample, mp 156—157 °C; $[\alpha]_D$ −162.9°; ORD, $[\Phi]_{334}^{trough}$ −12200°, $[\Phi]_{322}^{trough}$ −8300°, $[\Phi]_{292}^{peak}$ +5600°, a=−178°; IR, ν_{max} 1732, 1647, 1248, 1240, and 1043 cm^{-1}; NMR, δ 1.05 (3H, s, 19-C$\underline{H}_3$), 1.19 (3H, d J=5 Hz, 18-C$\underline{H}_3$), 2.01 (3H, s, OCOC$\underline{H}_3$), 4.57 (1H, br, $\underline{H}$ at C_3), and 5.39 (1H, br d J=5 Hz, $\underline{H}$ at C_6). Found: C, 76.46; H, 9.27%. Calcd for $C_{21}H_{30}O_3$: C, 76.32; H, 9.15%.

*5α,12β-Etiojervan-3β-ol (**11**) and Its 3-Acetate (**11a**).* a) To freshly distilled DEG (15 ml) was dissolved sodium (400 mg) by heating, and to the solution were added anhydrous hydrazine (8 ml) and **9** (193 mg). The solution was refluxed for 22 h and, after removal of the condenser, heated to 230 °C to remove excess of the hydrazine. A new condenser was set up and the solution was again refluxed at the temp for 22 h. After being cooled the solution was poured into water (100 ml) and extracted with chloroform. The chloroform solution gave oily substance, which was purified by preparative TLC (8 plates) with a 3 : 1 mixture of benzene and chloroform. The main fraction was extracted with acetone and, after evaporation, dissolved in chloroform. The chloroform solution was washed with 5% aqueous sodium bicarbonate and water, dried and evaporated to leave crystalline residue (118 mg), which on recrystallization from hexane afforded **11** (89 mg), mp 117.5—118 °C. Further recrystallization from hexane gave an analytical sample, mp 119—120 °C; $[\alpha]_D$ +54.2°; Mass, *m/e* 276 (M^+) and 258; IR, ν_{max} 3360, 3320, and 1033 cm^{-1}; NMR, δ 0.75 (3H, s, 19-C$\underline{H}_3$), 0.84 (3H, d J=5 Hz, 18-C$\underline{H}_3$), and 3.61 (1H, br, $\underline{H}$ at C_3). Found: C, 82.60; H, 11.72%. Calcd for $C_{19}H_{32}O$: C, 82.54; H, 11.66%.

Acetylation of **11** (62 mg) with Ac_2O (1 ml) and Py (1 ml) at room temp overnight gave **11a** (68 mg), mp 72—72.5 °C, on recrystallization from aqueous methanol. This was recrystallized from the same solvent mixture for analysis: mp 72.5—73.5 °C; $[\alpha]_D$ +40.5°; Mass, *m/e* 258 (M^+); IR, ν_{max} 1742, 1240, and 1029 cm^{-1}; NMR, δ 0.75 (3H, s, 19-C$\underline{H}_3$), 0.83 (3H, d J=6 Hz, 18-C$\underline{H}_3$), 1.99 (3H, s, OCOC$\underline{H}_3$) and 4.74 (1H, br, $\underline{H}$ at C_3). Found: C, 79.12; H, 10.64%. Calcd for $C_{21}H_{34}O_2$: C, 79.19; H, 10.76%.

b) Compound **13** (50 mg), described later, was mixed with TsCl (54 mg) in Py (1 ml) under cooling with ice–water and stirring, and the mixture was continuously stirred at room temp for 42 h and then dissolved in chloroform. The chloroform solution, after being worked up as usual, yielded amorphous residue (84 mg), which gave only a single spot and showed absorption maxima at 1722, 1263, and 1174 cm^{-1} in the IR spectrum. This was then dissolved in dry THF (10 ml) and refluxed with LAH (288 mg) for 12 h. After careful addition of water to decompose the hydride, the mixture was extracted with ether repeatedly. The ether solution, on usual work up, gave amorphous residue (68 mg), showing two spots, which was separated by preparative TLC (2 plates) with benzene. The more mobile part (31 mg) crystallized on trituration with hexane to yield **11** (15 mg), mp 118—119 °C, which was identical with the afore-mentioned sample.

The less mobile part (18 mg) gave **13a** (7 mg), mp 166—168 °C, which was identical with an authentic sample of 5α,12β-etiojervane-3β,17α-diol.[8]

*5α,12β-Etiojervane-3β,17α-diol 3-Acetate (**13**) and 5α,12β-Etiojervane-3β,17β-diol 3-Acetate (**14**).* Compound **12**[1] (155 mg) was treated with NBH (74 mg) in methanol (15 ml) at 0 °C for 1 h under stirring. After addition of AcOH (0.2 ml) the mixture was stirred for 10 min, evaporated below 30 °C *in vacuo* and extracted with chloroform repeatedly. The chloroform solution gave amorphous material (173 mg), which was separated into two parts by preparative TLC (7 plates) with a 1 : 3 mixture of ether and benzene. The

more mobile part (38 mg) crystallized on trituration with hexane, had mp 94—94.5 °C and amounted to 10 mg. Recrystallization from hexane afforded an analytical sample of **14**, mp 96—96.5 °C; $[\alpha]_D$ +47.7°; IR, ν_{max} 3535, 3490, 1724, 1239, and 1036 cm^{-1}; NMR δ 0.76 (3H, s, 19-C$\underline{H}_3$), 0.94 (3H, d J=5 Hz, 18-C$\underline{H}_3$), 1.98 (3H, s, OCOC$\underline{H}_3$), 3.78 (1H, br s W_H=5 Hz, $\underline{H}$ at C_{17}), and 4.69 (1H, br, $\underline{H}$ at C_3). Found: C, 75.59; H 10.25%. Calcd for $C_{21}H_{34}O_3$: C, 75.40; H, 10.25%.

The less mobile part (117 mg) gave **13** (84 mg), mp 119—119.5 °C, on trituration with isopropyl ether. This was recrystallized from isopropyl ether for analysis: mp 119—119.5 °C; $[\alpha]_D$ +26.7°; IR, ν_{max} 3370, 1736, 1241, and 1032 cm^{-1}; NMR, δ 0.76 (3H, s, 19-C$\underline{H}_3$), 0.97 (3H, d J=5 Hz, 18-C$\underline{H}_3$), 1.98 (3H, s, OCOC$\underline{H}_3$), 3.17 (1H, br m W_H=17 Hz, $\underline{H}$ at C_{17}), and 4.68 (1H, br, $\underline{H}$ at C_3). Found: C, 75.68; H, 10.11%. Calcd for $C_{21}H_{34}O_3$: C, 75.40; H, 10.25%.

*Etiojerva-5,12-diene-3β,17α-diol-11-one 3-Acetate (**16**) and Etiojerva-5,12-diene-3β,17β-diol-11-one 3-Acetate (**17**).* To a solution of **15**[6b,7] (2.01 g, mp 180—181 °C) in methanol (200 ml) was added NBH (400 mg) under stirring. After being stirred at room temp for 3 min, the yellow mixture became colorless, and to this mixture was added AcOH (1.5 ml) to decompose excess of the hydride. After being kept at room temp for 10 min, the mixture was concentrated below 35 °C *in vacuo*, and the resulting residue was diluted with water (100 ml) and extracted with chloroform. The chloroform solution, after being worked up as usual, left crystalline residue (2.05 g), which was separated into two parts by preparative TLC (43 plates) with a 1 : 2 mixture of ether and benzene. The more mobile part (143 mg) crystallized on trituration with acetone, had mp 236—237 °C and amounted to 133 mg. Recrystallization from acetone-isopropyl ether afforded an analytical sample of **17**, mp 236—238 °C; $[\alpha]_D$ −211.0°; IR, ν_{max} 3535, 1726, 1703, 1633, 1239, 1231, and 1041 cm^{-1}; NMR, δ 1.05 (3H, s, 19-C$\underline{H}_3$), 2.00 (3H, s, OCOC$\underline{H}_3$), 2.23 (3H, s, 18-C$\underline{H}_3$), 4.06 (1H, br s W_H=7 Hz, $\underline{H}$ at C_{17}), 4.58 (1H, br W_H=18 Hz, $\underline{H}$ at C_3), and 5.38 (1H, br s W_H=9 Hz, $\underline{H}$ at C_6). Found: C, 73.33; H, 8.23%. Calcd for $C_{21}H_{28}O_4$: C, 73.22; H, 8.19%.

The less mobile part (1.837 g) gave **16** (1.622 g), mp 170—171 °C, on trituration with acetone-isopropyl ether. This was recrystallized from the same solvent mixture for analysis: mp 170—171 °C; $[\alpha]_D$ −128.0°; IR, ν_{max} 3320, 1738, 1710, 1639, 1243, and 1045 cm^{-1}; NMR, δ 1.06 (3H, s, 19-C$\underline{H}_3$), 2.00 (3H, s, OCOC$\underline{H}_3$), 2.18 (3H, s, 18-C$\underline{H}_3$), 4.20 (1H, br W_H=20 Hz, $\underline{H}$ at C_{17}) 4.57 (1H, br W_H=20.5 Hz $\underline{H}$ at C_3), and 5.38 (1H, br s W_H=8.5 Hz, $\underline{H}$ at C_6). Found: C, 73.24; H, 8.26%. Calcd for $C_{21}H_{28}O_4$: C, 73.22; H, 8.19%.

*Hydrogenation of **16**.* A solution of **16** (1.401 g) in AcOH (50 ml) was hydrogenated over Adams Pt (504 mg) in AcOH (10 ml) at room temp for 10 h, when 2.2 mol of hydrogen had been consumed. The reaction product (1.613 g), after being worked up as usual, showed four spots on TLC and was separated by preparative TLC (77 plates) with a 1 : 1 mixture of ether and benzene. The most mobile fraction, extracted with acetone, gave crystalline substance (306 mg), which on recrystallization from acetone-isopropyl ether afforded 5α,12β-etiojervane-3β,17α-diol-11-one 3-acetate (**18**, 155 mg), mp 154—156 °C. This was recrystallized from the same solvent mixture for analysis: mp 155—156 °C; $[\alpha]_D$ −74.6°; ORD, $[\Phi]_{333}^{trough}$ −8200°, $[\Phi]_{323}^{trough}$ −4500°, $[\Phi]_{292}^{peak}$ +7800°, a=−160°; IR, ν_{max} 3375, 1732, 1244, and 1034 cm^{-1}; NMR, δ 0.84 (3H, s, 19-C$\underline{H}_3$), 1.27 (3H, d J=5.5 Hz, 18-C$\underline{H}_3$), 1.98 (3H, s, OCOC$\underline{H}_3$), 3.11 (1H, br W_H=20.5 Hz, $\underline{H}$ at C_{17}), and 4.65 (1H, br W_H=23 Hz, $\underline{H}$ at C_3). Found: C, 72.27; H, 9.18%. Calcd for $C_{21}H_{32}O_4$: C, 72.38; H, 9.26%.

The second mobile fraction gave crystalline substance (390 mg), which on recrystallization from acetone-isopropyl ether afforded 5β,12β-etiojervane-3β,17α-diol-11-one 3-acetate (**19**, 312 mg), mp 177—178 °C. This was recrystallized from the same solvent mixture for analysis: mp 178.5—179 °C; $[\alpha]_D$ −80.6°; ORD, $[\Phi]_{331}^{trough}$ −7500°, $[\Phi]_{322}^{trough}$ −4700°, $[\Phi]_{289}^{peak}$ +6900°, a=−144°; IR, ν_{max} 3505, 1723, 1229, and 1045 cm^{-1}; NMR, δ 0.97 (3H, s, 19-C$\underline{H}_3$), 1.27 (3H, d J=6 Hz, 18-C$\underline{H}_3$), 2.01 (3H, s, OCOC$\underline{H}_3$), 3.06 (1H, br W_H=20.6 Hz, $\underline{H}$ at C_{17}), and 5.01 (1H, br s W_H=6 Hz, $\underline{H}$ at C_3). Found: C, 72.09; H, 9.26%. Calcd for $C_{21}H_{32}O_4$: C, 72.38, H, 9.26%.

The third fraction gave crystalline material (317 mg), which afforded 5α,12α-etiojervane-3β,17α-diol-11-one 3-acetate (**20**, 152 mg), mp 139.5—140.5 °C, on trituration with acetone-isopropyl ether. This was recrystallized from the same solvent mixture for analysis: mp 141—142 °C; $[\alpha]_D$ −10.1°; ORD, $[\Phi]_{331}^{trough}$ −3500°, $[\Phi]_{290}^{peak}$ +4800°, a=−83°; IR, ν_{max} 3505, 1729, 1240, and 1031 cm^{-1}; NMR, δ 0.88 (3H, s, 19-C$\underline{H}_3$), 0.89 (3H, d J=7 Hz, 18-C$\underline{H}_3$), 1.98 (3H, s, OCOC$\underline{H}_3$), 3.81 (1H, br s W_H=9 Hz, $\underline{H}$ at C_{17}), and 4.67 (1H, br W_H=20 Hz, $\underline{H}$ at C_3). Found: C, 72.77; H, 9.47%. Calcd for $C_{21}H_{32}O_4$: C, 72.38; H, 9.26%.

Compound **20** (18 mg) was acetylated with Ac_2O (0.2 ml) and Py (0.2 ml) at room temp for 38 h, and gave crystalline substance (21 mg), which showed a single spot on TLC and yielded **20a**, mp 106—109 °C, on trituration with isopropyl ether: NMR, δ 0.88 (3H, s, 19-C$\underline{H}_3$), 0.92 (3H, d J=7 Hz, 18-C$\underline{H}_3$), 2.00 (6H, s 2OCOC$\underline{H}_3$), 4.68 (1H, br W_H=26 Hz, $\underline{H}$ at C_3), and 4.80 (1H, br s W_H=10.5 Hz, $\underline{H}$ at C_{17}).

The least mobile fraction (393 mg) was triturated with acetone-isopropyl ether to give 5β,12α-etiojervane-3β-17α-diol-11-one 3-acetate (**21**, 237 mg), mp 130—132 °C. Recrystallization from the same solvent mixture afforded an analytical sample, mp 132—133 °C; $[\alpha]_D$ −17.4°; ORD, $[\Phi]_{330}^{trough}$ −3900°, $[\Phi]_{290}^{peak}$ +3800°, a=−77°; IR, ν_{max} 3530, 1731, 1240, and 1024 cm^{-1}; NMR, δ 0.88 (3H, d J=7.5 Hz, 18-C$\underline{H}_3$), 1.01 (3H, s, 19-C$\underline{H}_3$), 2.01 (3H, s, OCOC$\underline{H}_3$), 3.80 (1H, br s W_H=9.5 Hz, $\underline{H}$ at C_{17}), and (1H, br s W_H=6 Hz, $\underline{H}$ at C_3). Found: C, 72.46; H, 9.26%. Calcd for $C_{21}H_{32}O_4$: C, 72.38; H, 9.26%.

*5α,12β-Etiojervane-3β,17α-diol-11-one (**18a**) and Its 3,17-Diacetate (**18b**).* a) Compound **3** (95 mg) was dissolved in AcOH (6 ml) and hydrogenated over Adams Pt (60 mg) at room temp, when 1 mol of hydrogen had been taken up for 1 h. The resulting amorphous product (112 mg) was purified by preparative TLC (4 plates) with ether to give amorphous substance (84 mg), which on trituration with acetone-isopropyl ether crystallized, had mp 168—170 °C and amounted to 46 mg. This was recrystallized from the same solvent mixture to give **18a** in pure state, mp 175—176 °C; $[\alpha]_D$ −66.6°; IR, ν_{max} 3420, 1725, and 1029 cm^{-1}; NMR, δ 0.83 (3H, s, 19-C$\underline{H}_3$), 1.29 (3H, d J=5 Hz, 18-C$\underline{H}_3$), 3.07 (1H, br W_H=18 Hz, $\underline{H}$ at C_{17}), and 3.60 (1H, br W_H=22 Hz, $\underline{H}$ at C_3). Found: C, 73.33; H, 10.02%. Calcd for $C_{19}H_{30}O_3 \cdot 0.5CH_3COCH_3$: C, 73.39; H, 9.92%.

Compound **18a** (32 mg) was treated with Ac_2O (0.2 ml) and Py (0.2 ml) at room temp overnight and gave **18b** (33 mg), mp 226—226.5 °C, on trituration with acetone-isopropyl ether. This was recrystallized from the same solvent mixture for analysis: mp 226—226.5 °C; IR, ν_{max} 1731, 1244, and 1025 cm^{-1}; NMR, δ 0.86 (3H, s, 19-C$\underline{H}_3$), 1.18 (3H, d

J=6 Hz, 18-CH_3), 1.99 and 2.02 (each 3H, s 2OCOCH_3), and 5.50 (2H, br m, 2H at C_3 and C_7). Found: C, 70.98; H, 8.78%. Calcd for $C_{23}H_{34}O_5$: C, 70.74; H, 8.78%.

b) A solution of **18** (50 mg) in methanol (10 ml) was refluxed with 1 M sodium methoxide under a stream of nitrogen. Ths solution was concentrated *in vacuo* and the resulting residue was diluted with water and then extracted with chloroform. The chloroform solution was washed with water, dried and evaporated to leave amorphous substance (60 mg), which showed a single spot on TLC and gave diol (36 mg), mp 174.5—175 °C, on trituration with acetone–isopropyl ether. This compound was identical with the afore-mentioned sample of **18a**.

Compound **18** (30 mg) was also treated with Ac_2O (0.5 ml) and Py (0.5 ml) at room temp overnight and gave its 17-acetyl derivative (32 mg), mp 225.5—226 °C, on trituration with acetone–isopropyl ether. This was identical with an authentic sample of **18b**, described in the section a.

c) A solution of compound **20** (22 mg) in methanol (10 ml) was refluxed with 1 M sodium methoxide under a stream of nitrogen for 24 h. The solution was worked up as usual to leave foamy residue (26.5 mg). This showed a single spot on TLC and was triturated with acetone–isopropyl ether to give crystalline substance (12 mg), mp 172—173 °C, which was identical with an authentic sample of **18a** in all respects.

*11β,17β-Oxido-5α,12α-etiojervan-3β-ol (**22**) and Its 3-Acetate (**22a**).* A solution of **20** (40 mg) in Py (1 ml) containing TsCl (102 mg) was stirred at room temp for 40 h and poured into ice–water, and then extracted with chloroform repeatedly. The chloroform solution was washed with 1 M hydrochloric acid, 5% aqueous sodium bicarbonate and water, dried and evaporated below 30 °C to leave 17-tosylate (**20b**, 56.5 mg), amorphous, which showed a single spot on TLC; IR ($CHCl_3$), ν_{max} 1730, 1600, 1492, 1253, 1177, and 1027 cm^{-1}; NMR, δ 0.79 (3H, d J=6 Hz, 18-CH_3), 0.87 (3H, s, 19-CH_3), 1.98 (3H, s, OCOCH_3), 2.42 (3H, s, $C_6H_4CH_3$), 4.55 (2H, br W_H=15 Hz, 2H at C_3 and C_{17}), and 7.30 and 7.75 (each 2H, d J=8 Hz, $C_6H_4CH_3$).

Tosylate **20b** (56.5 mg) was treated with LAH (170 mg) in refluxing ether (15 ml) for 5 h under stirring and then cooled with ice–water. After careful addition of water, the mixture was extracted with ether repeatedly. The ether solution gave crystalline material (41.5 mg), which showed practically a single spot and was purified by preparative TLC (2 plates) with a 2 : 1 mixture of ether and benzene. The main fraction, extracted with acetone, gave crystalline substance (19.5 mg), which on recrystallization from isopropyl ether afforded **22** (13 mg), mp 207—208 °C. Recrystallization from acetone–isopropyl ether yielded an analytical sample, mp 213—214 °C; $[\alpha]_D$ −18.5 °; IR, ν_{max} 3405, 1150, 1075, 1060, and 1028 cm^{-1}; NMR, δ 0.95 (3H, d J=6 Hz, 18-CH_3), 0.98 (3H, s, 19-CH_3), 3.55 (1H, br W_H=19 Hz, H at C_3), 3.90 and 4.31 (each 1H, br s W_H=7 and 5 Hz, 2H at C_{11} and C_{17} or *vice versa*). Found: C, 78.73; H, 10.42%. Calcd for $C_{19}H_{30}O_2$: C, 78.57; H, 10.41%.

Compound **22** (15 mg) was acetylated with Ac_2O (0.4 ml) and Py (0.4 ml) at room temp overnight to give **22a** (9 mg), mp 123—125 °C, on trituration with aqueous methanol: Mass, *m/e* 332 (M^+); IR, ν_{max} 1741, 1246, 1146, 1060, 1023, and 1005 cm^{-1}; NMR, δ 0.94 (3H, d J=6 Hz, 18-CH_3), 0.99 (3H, s, 19-CH_3), 1.99 (3H, s, OCOCH_3), 3.92 and 4.31 (each 1H, br s W_H=7 and 6 Hz, 2H at C_{11} and C_{17} or *vice versa*), and 4.68 (1H, br W_H=26 Hz, H at C_3).

*11β,17β-Oxide-5β,12α-etiojervan-3β-ol (**23**) and Its 3-Acetate (**23a**).* A solution of **21** (103 mg) in Py (1.5 ml) containing TsCl (204 mg) was stirred at room temp for 40 h and poured into ice–water and then extracted with chloroform repeatedly. The chloroform solution gave crystalline substance (185 mg), which showed a single spot and afforded 17-tosylate (**21a**, 130 mg) mp 120—121 °C, on trituration with isopropyl ether: IR, ν_{max} 1732, 1602, 1351, 1245, 1188, 1177, 1030, 1021, 840, and 819 cm^{-1}; NMR, δ 0.80 (3H, d J=7.5 Hz, 18-CH_3), 0.99 (3H, s, 19-CH_3), 2.03 (3H, s, $OCOCH_3$), 2.44 (3H, s, $C_6H_4CH_3$), 4.59 (1H, br s W_H=8.5 Hz, H at C_{17}), 5.04 (1H, br s W_H=7 Hz, H at C_3), and 2.65 and 2.21 (each 2H, d J=8 Hz, $C_6H_4CH_3$).

Tosylate **21a** (129 mg) was treated with LAH (238 mg) in refluxing ether (10 ml) for 4 h under stirring and then cooled with ice–water. After careful decomposition of excess of the hydride with water, the mixture was extracted with ether repeatedly. The ether solution gave crystalline substance (74 mg), which showed a single spot and afforded **23** (20 mg), mp 153—154 °C, on trituration with isopropyl ether: IR ($CHCl_3$), ν_{max} 3600, 3390, 1146, 1090, and 1003 cm^{-1}; NMR, δ 0.95 (3H, d J=7 Hz, 18-CH_3), 1.10 (3H, s, 19-CH_3), and 3.92, 4.04 and 4.30 (each 1H, br s W_H=8, 6 and 5 Hz, 3H at C_{11}, C_3 and C_{17} or *vice versa*).

Compound **23** (75 mg) was acetylated with Ac_2O (1 ml) in Py (1 ml) at room temp overnight and gave **23a** (70 mg), mp 121—123 °C, on trituration with aqueous methanol. Recrystallization from the same solvent mixture afforded an analytical sample, mp 128—130 °C; $[\alpha]_D$ −11.0°; Mass, *m/e* 332 (M^+); IR, ν_{max} 1741, 1247, 1096, and 1027 cm^{-1}; NMR, δ 0.96 (3H, d J=6.5 Hz, 18-CH_3), 1.11 (3H, s, 19-CH_3), 2.01 (3H, s, OCOCH_3), and 3.91, 4.33 and 5.04 (each 1H, br s W_H=7, 6 and 6 Hz, 3H at C_{11}, C_{17} and C_3 or *vice versa*). Found: C, 75.95; H, 9.66%. Calcd for $C_{21}H_{32}O_3$: C, 75.86; H, 9.70%.

*5α,12α-Etiojerv-16-en-3β-ol-11-one 3-Acetate (**24**).* A solution of **20** (77 mg) in dry Py (1.5 ml) was treated with phosphoryl chloride (0.3 ml) at room temp for 15.5 h. The mixture was poured into crushed ice and extracted with chloroform. The chloroform solution gave oily substance (61 mg), which was purified by preparative TLC with a 1 : 10 mixture of ether and benzene. The resulting oily residue (41 mg) was triturated into aqueous methanol to yield **24** (19 mg), mp 77—78 °C; $[\alpha]_D$ +53.7°; IR, ν_{max} 3010 (sh), 1735, 1722 (sh), 1640, 1240, 1027, and 695 cm^{-1}; NMR, δ 0.87 (3H, s, 19-CH_3), 0.92 (3H, d J=6.5 Hz, 18-CH_3), 2.00 (3H, s, OCOCH_3), 4.66 (1H, br W_H= 31 Hz, H at C_3), and 5.84 (2H, t J=5.5 Hz, 2H at C_{16} and C_{17}).

*5α,12α-Etiojervan-3β-ol-11-one 3-Acetate (**25**).* Compound **24** (53 mg) was hydrogenated over Adams Pt (31 mg) in AcOH (3 ml) at room temp for 30 min, when 1.2 mol of hydrogen had been consumed. The catalyst was removed by filtration and the filtrate was concentrated below 30 °C under reduced pressure and dissolved in chloroform. The chloroform solution was worked up at usual to give **25** (50 mg), amorphous, which resisted crystallization: $[\alpha]_D$ −11.1°; ORD, $[\Phi]_{333}^{trough}$ −3010°, $[\Phi]_{316}$ 0°, $[\Phi]_{290}^{peak}$ +3980°, a= −69.9°; Mass, *m/e* 332 (M^+); IR ($CHCl_3$), ν_{max} 1728 and 1245 cm^{-1}; NMR, δ 0.90 (3H, s, 19-CH_3), 0.92 (3H, d J= 6 Hz, 18-CH_3), 2.02 (3H, s, OCOCH_3), and 4.67 (1H, br W_H=24 Hz, H at C_3).

*Epimerization of **25** to **9**.* A solution of compound **25** (33 mg) in methanol (15 ml) containing 5% potassium hydroxide was refluxed under nitrogen for 2 h. The solution was evaporated, diluted with water and extracted with chloroform. The extracts were washed with water, dried and evaporated to leave amorphous residue (27.4 mg), which was acetylated with Ac_2O (0.5 ml) in Py (0.5 ml) at room temp overnight. After usual work up, the amorphous

reaction mixture (31 mg) crystallized on trituration with aqueous methanol to give crystalline substance (7 mg) having mp 108.5—110 °C, which was identical with an authentic sample of **9** in all respects.

5β,12α-Etiojerv-16-en-3β-ol-11-one 3-Acetate (26). A solution of compound **21** (144 mg) in dry Py (2.5 ml) was treated with phosphoryl chloride (0.5 ml) at room temp for 14 h. The mixture was worked up in the same manner as the corresponding 5α-mixture to leave oily residue (141 mg), which was purified by preparative TLC (9 plates) with a 1 : 10 mixture of ether and benzene. The main fraction was extracted with acetone and afforded crystalline residue (94 mg), which on trituration with aqueous methanol yielded **26** (63 mg), mp 146—152 °C. Recrystallization from the same solvent mixture gave an analytical sample, mp 150—152 °C; $[\alpha]_D$ +47.4°; IR, ν_{max} 3010, 1729, 1640, 1240, 1023, and 699 cm^{-1}; NMR, δ 0.92 (3H, d J=7 Hz, 18-C$\underline{H}_3$), 1.02 (3H, s, 19-C$\underline{H}_3$), 2.03 (3H, s, OCOC$\underline{H}_3$), 5.04 (1H, br s W_H=7.5 Hz, $\underline{H}$ at C_3), and 5.86 (2H, t J= 6 Hz, 2$\underline{H}$ at C_{16} and C_{17}). Found: C, 76.13; H, 9.18%. Calcd for $C_{21}H_{30}O_3$: C, 76.32; H, 9.15%.

Epimerization of 26 to 28. Compound **26** (32 mg) in methanol (12 ml) was treated with 1 M sodium methoxide under reflux for 17 h. After evaporation of the solvent, the mixture was diluted with water and extracted with chloroform. The chloroform solution left crystalline substance (25.5 mg), showing a single spot on TLC, which was acetylated with Ac_2O (0.4 ml) and Py (0.4 ml) at room temp overnight to give crystalline material (30 mg). This was triturated with aqueous methanol to give **28** (20 mg), mp 119.5—121 °C; NMR, δ 1.00 (3H, s, 19-C$\underline{H}_3$), 1.30 (3H, d J= 6 Hz, 18-C$\underline{H}_3$), 2.04 (3H, s, OCOC$\underline{H}_3$), 5.04 (1H, br s W_H=7 Hz, $\underline{H}$ at C_3), and 5.49 (2H, br s W_H=10 Hz, 2$\underline{H}$ at C_{16} and C_{17}).

5β,12α-Etiojervan-3β-ol-11-one 3-Acetate (27). A solution of compound **26** (50 mg) in AcOH (1 ml) was hydrogenated over Adams Pt (30 mg) at room temp for 2 h, when 1.2 mol of hydrogen had been consumed. The reaction mixture, after being worked up as usual, gave amorphous substance (54 mg), which showed a single spot on TLC and was triturated with aqueous methanol to yield **27** (35 mg), mp 106—109 °C. Recrystallization from the same solvent mixture gave an analytical sample, mp 110—110.5 °C; $[\alpha]_D$ −15.9 °; IR, ν_{max} 1727, 1250, 1240, and 1029 cm^{-1}; NMR, δ 0.91 (3H, d J=7.5 Hz, 18-C$\underline{H}_3$), 1.03 (3H, s, 19-C$\underline{H}_3$), 2.02 (3H, s, OCOC$\underline{H}_3$), and 5.02 (1H, br s W_H= 8 Hz, $\underline{H}$ at C_3). Found: C, 75.77; H, 9.59;% Calcd for $C_{21}H_{32}O_3$: C, 75.86; H, 9.70%.

Epimerization of 27 to 29. Compound **27** (39 mg) in methanol (17 ml) was treated with 1 M sodium methoxide under reflux for 17 h. After being worked up as usual, the mixture gave crystalline substance (29.5 mg), which was acetylated with Ac_2O (0.4 ml) and Py (0.4 ml) at room temp overnight. The resulting amorphous acetate crystallized on trituration with aqueous methanol to yield **29** (20 mg), mp 106—107.5 °C; IR, ν_{max} 1743, 1725, 1237, 1028, and 1017 cm^{-1}; NMR, δ 1.00 (3H, s, 19-C$\underline{H}_3$), 1.17 (3H, d J=5 Hz, 18-C$\underline{H}_3$), 2.03 (3H, s, OCOC$\underline{H}_3$), and 5.02 (1H, br s W_H=6 Hz, $\underline{H}$ at C_3).

5α,12α-Etiojervan-17α-ol-3-one (32a). To compound **30** (809 mg) in chloroform (10 ml) was added a chloroform solution (10 ml) containing perbenzoic acid (activity 83.3%, 611 mg) at 0 °C, and the mixture was allowed to stand at room temp for 86 h. The perbenzoic acid solution (10 ml) was again added to the mixture, and the whole solution was kept at room temp for additional 71 h. The solution was washed with 0.1 M aqueous sodium thiosulfate (4×20 ml), 5% aqueous sodium bicarbonate (2×10 ml) and water (2×20 ml), dried and evaporated to leave amorphous residue (**31**, 863 mg), which showed almost a single spot on TLC; IR ($CHCl_3$), ν_{max} 3620, 3460, 1720, 1252, and 1029 cm^{-1}.

To a cooled solution of the whole residue in acetone (20 ml) was added Jones' reagent (1 ml) under stirring, and the mixture was stirred at 0 °C for 50 min. After addition of ethanol (1.2 ml) the mixture was stirred for another 15 min and concentrated *in vacuo*. The residue was worked up as usual to give resinous substance (802 mg), which without purification was refluxed in a methanol solution (16 ml) containing 5% potassium hydroxide under nitrogen for 1 h. The resulting amorphous product (614 mg) showed two spots and was separated by preparative TLC (25 plates) with a 1 : 3 mixture of ether and benzene. More mobile fractions gave oily substance (204 mg), which on trituration with a mixture of acetone and isopropyl ether afforded crystalline substance, mp 82.5—84 °C, which would probably be the unreacted starting material: Mass, *m/e* 316 (M^+); NMR, δ 0.80 (3H, d J=6 Hz, 18-C$\underline{H}_3$), 0.99 (3H, s, 19-C$\underline{H}_3$), and 2.16 (3H, s, 21-C$\underline{H}_3$). Less mobile fractions gave crystalline material (318 mg), which on recrystallization from acetone-isopropyl ether afforded **32a** (248 mg), mp 143—145 °C. This was recrystallized from the same solvent mixture for analysis: mp 145—146.5 °C; $[\alpha]_D$ −5.5°; Mass, *m/e* 290 (M^+); IR, ν_{max} 3497, 1708, 1065, and 1036 cm^{-1}; NMR, δ 0.96 (3H, s, 19-C$\underline{H}_3$), 1.00 (3H, d J=6 Hz, 18-C$\underline{H}_3$), and 3.45 (1H, do t J=10, 10 and 4 Hz, $\underline{H}$ at C_{17}). Found: C, 78.40; H, 10.32%. Calcd for $C_{19}H_{30}O_2$: C, 78.57; H, 10.41%.

5α,12α-Etiojervane-3,17-dione (33). To a cold solution of compound **32a** (50 mg) in acetone (2 ml) was added Jones' reagent (0.2 ml) under stirring, and the mixture was stirred at 0 °C for 70 min. After addition of ethanol (0.3 ml), the mixture was concentrated *in vacuo*, and the residue was diluted with water and then extracted with chloroform. The chloroform solution was worked up as usual to yield oily substance (54 mg), which on trituration with acetone gave **33** (27 mg), mp 160—162 °C. This was recrystallized twice from ether to give a pure sample, mp 173—175 °C, which was identical with an authentic sample, prepared by the procedure of Johns and Laos (lit,[16] mp 169—170 °C).

5α,12α-Etiojervan-3β-ol (34) and Its 3-Acetate (34a). To a cold solution of compound **32a** (100 mg) in Py (2 ml) was added TsCl (100 mg), and the mixture was stirred at room temp for 48 h, diluted with water and extracted with chloroform. The chloroform solution gave oily substance (146 mg); IR ($CHCl_3$), ν_{max} 1707, 1601, 1176, 918, and 894 cm^{-1}.

The oily substance was dissolved in dry ether (20 ml) and refluxed with LAH (300 mg) under stirring for 13 h. After careful decomposition of excess of the hydride with water, the resulting heterogeneous mixture was shaken with 1 M hydrochloric acid and extracted with ether. The ether extracts left amorphous residue (97 mg), showing a single spot on TLC, which was triturated with acetone to give **34** (46 mg), mp 121—123 °C. This was recrystallized twice from aqueous acetone for analysis: mp 129.5—130 °C; $[\alpha]_D$ −31.0°; Mass, *m/e* 276 (M^+), 258, and 243; IR, ν_{max} 3380, 1045, and 1030 cm^{-1}; NMR, δ 0.79 (3H, s, 19-C$\underline{H}_3$), 0.79 (3H, d J=6 Hz, 18-C$\underline{H}_3$), and 3.58 (1H, br W_H= 22 Hz, $\underline{H}$ at C_3). Found: C, 82.68; H, 11.28%. Calcd for $C_{19}H_{32}O$: C, 82.54; H, 11.66%.

Compound **34** (42 mg) was acetylated with Ac_2O (1 ml) and Py (1 ml) at room temp overnight and gave oily substance (46 mg), which on trituration with methanol crystallized to yield **34a** (32 mg), mp 95.5—96 °C. This was recrystallized from the same solvent to give an analytical

sample, mp 97—97.5 °C; $[\alpha]_D$ −47.4°; Mass, *m/e* 258 (M^+); IR, ν_{max} 1738, 1234, and 1022 cm^{-1}; NMR, δ 0.80 (3H, d J=6 Hz, 18-CH_3), 0.81 (3H, s, 19-CH_3), 2.00 (3H, s, $OCOCH_3$), and 4.71 (1H, br W_H=27 Hz, H at C_3). Found: C, 79.23; H, 10.52%. Calcd for $C_{21}H_{34}O_2$: C, 79.19; H, 10.76%.

References

1) Part II, A Murai, T. Nishimura, and T. Masamune, *Bull. Chem. Soc. Jpn.*, **49**, 1602 (1976).

2) Part XXIV of "C-Nor-D-homosteroids and Related Alkaloids"; Part XXIII, Ref. 1.

3) T. Masamune, A. Murai, K. Nishizakura, T. Orito, S. Numata, and H. Sasamori, *Bull. Chem. Soc. Jpn.*, **49**, 1622 (1976).

4) A. Murai, K. Arita, and T. Masamune, *Bull. Chem. Soc. Jpn*, **46**, 3536 (1973).

5) T. Masamune, N. Sato, K. Kobayashi, I. Yamazaki, and Y. Mori, *Tetrahedron*, **23**, 1591 (1967).

6) a) T. Masamune, A. Murai, and S. Numata, *Tetrahedron.*, **25**, 3145 (1969). b) S. M. Kupchan and S. D. Levine, *J. Am. Chem. Soc.*, **86**, 701 (1964).

7) J. Fried and A. Klingsberg, *J. Am. Chem. Soc.*, **75**, 4929 (1953).

8) T. Masamune and K. Orito, *Tetrahedron*, **25**, 4551 (1969).

9) N. S. Bhacca and D. H. Williams, "Application of NMR Spectroscopy in Organic Chemistry," Holden-Day, Inc., San Francisco (1964), p. 79.

10) D. H. R. Barton, D. A. J. Ives, and B. R. Thomas, *J. Chem. Soc.*, **1955**, 2056.

11) The allylic equatorial proton of cyclohexene system is more shielded than the corresponding axial proton; G. F. H. Green, J. E. Page, and S. E. Staniforth, *J. Chem. Soc., B*, **1966**, 807.

12) J. A. Mills, *J. Chem. Soc.*, **1952**, 4976; A. K. Bose and G. Chatterjee, *J. Org. Chem.*, **23**, 1425 (1958); R. K. Hill and J. W. Morgan, *ibid.*, **33**, 927 (1968); J. H. Brewster, *J. Am. Chem. Soc.*, **81**, 5493 (1959).

13) T. Masamune, A. Murai, O. Orito, H. Ono, S. Numata, and H. Suginome, *Tetrahedron*, **25**, 4853 (1969).

14) If epimerization occurred at C_9, the 19-methyl protons of **20** had to appear in much lower field than those of **18**. *Cf.*, D. M. Bailey, D. P. G. Hamon, and W. S. Johnson, *Tetrahedron Lett.*, **1963**, 555; J. P. Kutney, A. By, T. Inaba, S. Y. Leong, *ibid.*, **1965**, 2911.

15) H. Suginome, N. Sato, and T. Masamune, *Tetrahedron Lett.*, **1969**, 2671.

16) W. F. Johns and I. Laos, *J. Org. Chem.*, **30**, 123 (1965).

Stereochemistry of the C and D Rings of C-Nor-D-homosteroids. IV.[1] The Relative Stabilities and NMR Spectra of 17-Substituted C/D *trans*- and *cis*-Fused Etiojervanes[2]

Tadashi MASAMUNE, Akio MURAI, Kouichi NISHIZAKURA, Takako ORITO, Satoshi NUMATA, and Hiroshi SASAMORI

Department of Chemistry, Faculty of Science, Hokkaido University, Sapporo 060

(Received September 30, 1975)

(1) The relative stabilities between 17-substituted C/D *trans*- and *cis*-fused 11-oxoetiojervanes were investigated by treatment of both or either one of these 12-epimeric compounds under equilibrating conditions. The equilibrium ratios thus obtained were estimated qualitatively in terms of the configuration and bulkiness of substituent(s) at C_{17}. (2) The chemical shifts of 19- and 18-methyl protons in a number of etiojervanes were examined collectively. The "principle of additivity" holds satisfactorily for the 19-methyl protons of all etiojervanes, with two exceptional cases, irrespective of the configuration at C_{12} and also for the 18-methyl protons of 12β-etiojervanes. However, the principle is not applicable for the latter protons of 12α-etiojervanes, suggesting that the D ring would take different conformations depending on the 17-substituents.

The Relative Stabilities. The relative stabilities of *trans*- and *cis*-hydrindanone systems have been investigated extensively and found to depend delicately upon structural change.[3] This variety has been illustrated by simple[4] and complex hydrindanone systems[5] as well as normal (D ring) and modified (A and B rings) steroidal ketone.[3,6,7] Qualitative, sometimes temporizing, explanations have been given for these results, but no general understanding appears to be available. Recently, a few of attempts to rationalize the observed relative stabilities by calculational methods have been reported and applied successfully to a variety of these compounds.[8,9] Nevertheless, it is still desirable to accumulate experimental results concerning the stabilities of hydrindanone systems incorporated into large and complex natural products.[10] For example, House and Rasmusson have reported that the *trans*-fused isomer (**1**) of 7-methyl-3a,4,7,7a-tetrahydro-1-indanone is greatly stable as compared with the *cis*-fused isomer (**2**),[11] while the situation has become completely opposite with the corresponding etiojervane analogs with a bulky substituent (S) at C_{17} (**3** and **4**).[12] This fact, as combined with the previously observed results, has led us to have interest in more detailed examination of the relative stabilities of the titled compounds. Recently, we reported the summarized result concerning this stability relationship as a preliminary communication.[13] We describe herein the details and also, in connection with this, discuss the NMR spectra of C/D *trans*- and *cis*-fused etiojervanes.

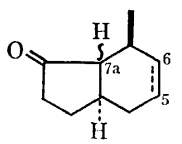

1 Δ^5, 7aβH
2 Δ^5, 7aαH
20 no Δ^5, 7aβH
21 no Δ^5, 7aαH

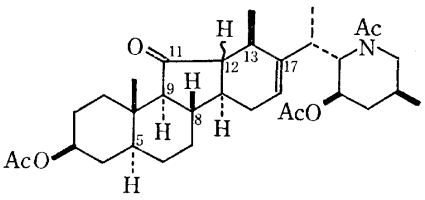

3 12βH
4 12αH

Prior to the epimerization studies, several 17-substituted etiojervanes were newly prepared, and syntheses of two representative compounds, 17-methyl- and 17-hydroxy-17-isopropyl-11-oxoetiojervanes, are described below. 5α,12β-Etiojervane-3β,11β-diol-17-one[14] (**5**) underwent the Wittig reaction[15] and subsequent acetylation to give the 17-methylene derivative (**6**), mp 172—173 °C, in 67% yield. Hydrogenation over Adams platinum produced a mixture of the 17β- and 17α-methyl compounds (**7** and **8**) in 84% yield, which was oxidized with chromic anhydride to mixture of the corresponding 11-oxo derivatives (**9** and **10**). While each of these mixtures showed a single spot on various TLC and resisted further purification, the mixture of compounds **9** and **10**, on treatment with sodium methoxide in refluxing methanol and subsequent acetylation, gave a product, which consisted mainly of the unreacted starting material but showed two spots clearly on TLC. Repeated epimerizations followed by acetylation effected isolation of a 12α-epimer (**11**), mp 163.5—164 °C, in 16% yield. Conversely, the same treatment of the 12α-epimer (**11**) produced the 12β-epimer (**9**), mp 140—141 °C, in good yield. As expected, these 12-epimeric 11-ketones (**9** and **11**) displayed negative Cotton effects with amplitudes of −157° and −77° in the ORD curves[12a] and signals due to the 19-methyl protons at δ 0.86 and 0.90 in the NMR spectra. The β-configuration of 17-methyl groups in both compounds was deduced from the fact that the epimerization of compound **9** to **11** took place, as discussed later.

17-Hydroxy-17-isopropyl-11-oxoetiojervanes were prepared from 12β-etiojerv-5-en-3β-ol-11,17-dione 17-ethylene acetal[16] (**12**). Hydrogenation of **12** over platinum in acetic acid produced the 5α,6-dihydro derivative (**13**), mp 172—174 °C, in 97% yield, which on hydrolysis with acid gave 11,17-diketone (**14**), mp 159—162 °C, in good yield. Treatment of **14** with

isopropylmagnesium bromide in ether produced a complex mixture, from which four compounds (**15**—**18**), having mp 180—182 °C, 168—170 °C, 136—138 °C and 193—195 °C, could be isolated by repeated preparative TLC in 16, 19, 1.5 and 4% yields (crude 40, 41, 3 and 5.5%), respectively. Contrary to the expectation, two major products (**15** and **16**) were formulated as 3β,11β,17β-triol and 3β,11β-diol-17-one, respectively, on the basis of the spectral data, indicating that reduction of the sterically hindered 11-carbonyl group occurred as a main reaction. While the former **15** revealed no absorption maximum in the carbonyl region, the latter **16** exhibited the maxima at 3400 and 1700 cm^{-1} and also a negative Cotton effect (a= −88°).[16,17] On the other hand, two minor products (**17** and **18**) were expected 17-isopropyl adducts. In accordance with the assigned structures, both the compounds (**17** and **18**) showed absorption maxima at 1732 and 1733 cm^{-1} in the IR spectra and also negative Cotton effects (a= −151° and −157°) in the ORD curves. Moreover, the configurations of two substituents at C_{17} were assigned as shown in the formulas (**17** and **18**) by epimerization experiments in the same manner as that compound **9**.

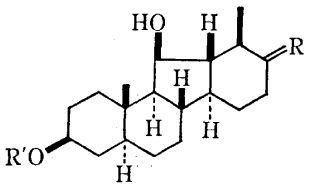

5 R=O R′=H
6 R=CH_2 R′=Ac
7 R=-CH_3, ···H R′=Ac
8 R=-H, ···CH_3 R′=Ac

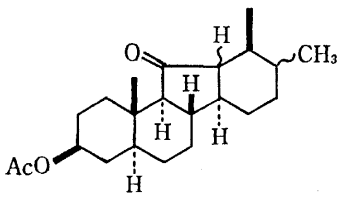

9 12βH, 17βCH_3
10 12βH, 17αCH_3
11 12αH, 17βCH_3

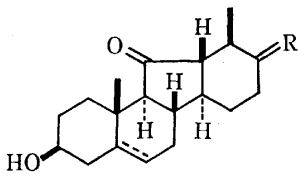

12 Δ^5, R=OC_2H_4O
13 5αH, R=OC_2H_4O
14 5αH, R=O

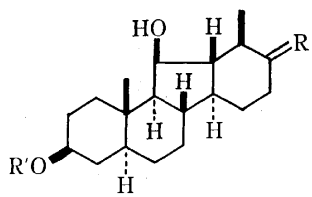

15 R=-H, ···OH, R′=H
15a R=-H, ···OH, R′=Ac
16 R=O, R′=H

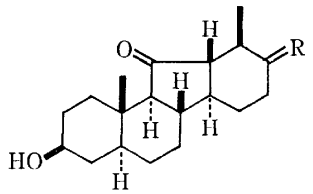

17 R=-C_3H_7, ···H
18 R=-H, ···C_3H_7

Equilibration studies were carried out by treatment of both or either one of C/D *trans*- and *cis*-fused 17-substituted 11-oxo-etiojervanes (**19** in Table 1) with 1 M sodium methoxide in refluxing methanol for several hours, and the summarized result, including the reported ones, is listed in Table 1.

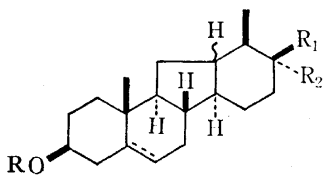

19 A=12βH
B=12αH

As shown in Table 1, 17-unsubstituted 12β-etiojervanes (IA and IIA in Table 1), regarded as reference compounds, were not epimerized completely, and the corresponding 12α-epimers (IB and IIB) could not be detected even by repeated TLC. Conversely, compounds IB and IIB were transformed quantitatively into IA and IIA, respectively. In view of the small equilibrium ratio (3 : 1) between *trans*- and *cis*-methylhydrindanones[11] (**20** and **21**), the present result would be rationalized by assuming that the five-membered C ring in etiojervanes **19** is fused in a *trans*-manner with the B ring and would therefore take a half-chair form rather than an envelope form. This conformation would lead to remarkable stabilization of *trans*-fused isomers (IA), as compared with *trans*-methylhydrindanone (**20**), and would also explain well the result that 12β-etiojervanes [IIIA (=**13**), IVA (=**12**) and VA[17]] with the same two substituents were much more stable than the corresponding 12α-epimers. Naturally, 12β-etiojervanes (VIA—IXA) with only one α-oriented (equatorial) substituent, apart from that (XA) with a bulky substituent,[12] were extremely favored under the equilibrating conditions over the respective 12α-epimers.

On the other hand, 17β-substituted 12β-etiojervanes (XIA—XIVA) would be destabilized by the axially disposed substituents, as compared with the refernce compounds (IA and IIA). This destabilization would increase in passing from the small[18] (OH, XIA), medium (CH_3, XIIA=**9** and C_2H_5, XIIIA) to the large(S, XIVA) substituent, leading to decrease of the

Table 1. Equilibration of 17-substituted 11-oxo-12β- and 12α-etiojervanes compounds (**19**)[a] and equlibrium ratio[b]

No.	C_5	R	R_1 (β)	R_2 (α)	12βH (A)	Ratio[b]	12αH (B)
I	5αH	Ac	H	H	(1)	⇄	(1)
II	Δ^5	Ac	H	H	(1)	⇄	(1)
III	5αH	H	OC_3H_4O		**13** (16)	—//→	
IV	Δ^5	H	OC_2H_4O		**12** (16)	—//→	
V	Δ^5	Ac	$CHCH_3$		(17)	←	(18)
VI	5αH	Ac	H	OH	(1)	⇄	(1)
VII	5βH	Ac	H	OH	(1)	⇄	(1)
VIII	Δ^5	H	H	OH	(1)	—//→	
IX	5αH	Ac	H	C_2H_5	(14)	—//→	
X	5αH	Ac	H	S	(12)	13 : 1	(12)
XI	Δ^5	H	OH	H	(1)	40 : 1	Exp
XII	5αH	Ac	CH_3	H	**9**	6 : 1	**11**
XIII	5αH	Ac	C_2H_5	H	(14)	11 : 9	(14)
XIV	5αH	Ac	S	H		←//—	(12)
XV	Δ^5	H	OH	C_2H	(19)	—//→	
XVI	Δ^5	H	C_2H	OH	(19)	—//→	
XVII	Δ^5	Ac	OH	C_2H_5	(19)	—//→	
XVIII	Δ^5	Ac	C_2H_5	OH	(19)	11 : 1	Exp
XIX	5αH	H	OH	C_3H_7	**18**	—//→	
XX	5αH	H	C_3H_7	OH	**17**	3 : 1	Exp

a) The symbols "A and B" refer to the configuration of C_{12}, and the numbers on parentheses to the references in which the compounds are cited. The symbols "**13** (=IIIA) and Exp" denote "compound **13** described in the text and compounds characterized in Experimental part in this paper." The formulas "$CHCH_3$, C_2H, C_3H_7 and S" mean "ethylidene, ethinyl, isopropyl groups, and a 17-substituent of **3** and **4**," respectively. b) The equilibrium ratio was obtained by measuring the amounts of isolated products.

ratio (12βH : 12αH) in question. The observed result was indeed in good accord with this presumption. Fortunately, a 12α-isomer (XIB), mp 237—239 °C, of XIA could be isolated by repeated epimerizations, showing a negative Cotton effect with amplitude of −69°. It is to be noted that the equilibrium ratio between XIIIA and XIIIB with a 17β-ethyl group was found to be about 1 : 1, suggesting that the energy difference between the reference compounds (IA and IB or IIA and IIB) would nearly equal the conformational energy (1.8 kcal)[18] of an ethyl group.

The afore-mentioned results indicated that the relative stabilities between 12-epimeric etiojervanes (XV—XX) with two substituents at C_{17} would depend on the relative bulkiness of β- and α-substituents. 12β-Etiojervanes (XVA and XVIA)[19] with two similar or those (XVIIA[19] and XIXA) with larger α-oriented substituents must be much more stable than the corresponding 12α-epimers. Indeed it was the case. On the other hand, the relative stabilities between 12-epimeric etiojervanes (XVIII and XX) with larger β-substituents must become comparable, and the unstable epimers might be isolable. The observed results were completely in accordance with this expectation, and 17β-ethyl-17α-hydroxy- and 17β-isopropyl-17α-hydroxy-12α-etiojervanes (XVIIIB and XXB), mp 149—150 °C and amorphous, could be isolated from the epimerization mixtures of the respective 12β-epimers (XVIIIA[19] and XXA (=**17**)].

In summary, the relevant stabilities depend upon the configuration and bulkiness of substituents at C_{17} and the equilibrium ratios are estimated roughly on the basis of these factors. This rationalization not only holds for both reactants and products, as mentioned in this paper, but also is applicable to reaction intermediates, as reported in the previous papers.[20,21] Moreover, the result suggests that both the C and D rings would probably take a somewhat fixed conformation at least in 12β-etiojervanes, and this conformational rigidity will be supported by the NMR spectra described in the following sections.

The NMR Spectra. During synthetic studies on C-nor-D-homo-steroid hormones, we have synthesized a number of etiojervanes. In view of the close similarities of structure within these etiojervanes, an intercomparison of the NMR spectra of a series of these compounds would be valuable in confirming certain stereochemical points as well as promoting the structure determination of new derivatives. In the previous papers on the NMR spectra of 22,27-imino-17,23-oxidojervanes [(22S,23R,25S)jervanines][22] and etiojerva-12,14,16-trienes with an aromatic D ring,[23] we have reported that the effects of many different substituents on the chemical shifts of 19-methyl protons are additive. However, these data have been confined to the correlation of the chemical shifts with changes of substituents only at C_3, C_4, C_5 and C_{11}. Moreover, it has not been reported whether or not the "principle of additivity" is applicable to the chemical shifts of 18-methyl protons. Hence we examined collectively the NMR spectra of a series of stereochemically well-established 17-substituted 12β- and 12α-etiojervanes, paying special attention to the influence due to the difference of C/D ring junctures and the

Table 2. The contribution ($\Delta\delta$) of functional groups to the chemical shift of the 19-methyl protons of etiojervanes

Groups	A (12βH, Δ^{11}, Δ^{12})				B (12αH)			
	T (5αH, Δ^4, Δ^5)		C (5βH)		T (5αH, Δ^4, Δ^5)		C (5βH)	
Reference shifts[a]	0.74	(176)[b]	0.87	(7)[b]	0.79	(116)[b]	0.92	(13)[b]
Functional groups	$\Delta\delta$[c]		$\Delta\delta$[c]		$\Delta\delta$[c]		$\Delta\delta$[c]	
Δ^1, 3=O					0.23	(4)		
Δ^1, 3=O, Δ^4	0.43	(2)	—		0.43	(2)	—	
2α-Br					0.08	(3)		
2α-Cl					0.07	(1)		
3β-OH	0.02	(58)	0.02	(3)	0.02	(25)	0.02	(2)
3β-OAc	0.03	(90)	0.03	(3)	0.03	(51)	0.03	(3)
3-OCH_2CH_2O-	0.03	(10)			0.03	(3)	0.04	(1)
3=O	0.21	(1)	0.09	(1)	0.21	(16)	0.09	(3)
3=O, Δ^4	0.40	(22)	—		0.40	(18)	—	
3=O, Δ^4, Δ^6			—		0.34	(3)	—	
4α-Br					0.04	(1)		
Δ^5	0.21	(92)	—		0.21	(12)	—	
6α-SAc					0.00	(4)		
Δ^8					0.17	(1)		
Δ^8, 11=O					0.28	(4)	0.40	(2)
$\Delta^{9(11)}$	0.15	(1)						
Δ^{11}	0.00	(2)			—		—	
Δ^{11}, $\Delta^{13(17)}$	0.02	(1)			—		—	
11β-OH	0.29	(30)			0.27	(6)		
11β-OAc	0.20	(3)						
11α-OH	0.02	(2)						
11α-OAc	0.12	(3)						
11=O	0.07	(52)	0.08	(4)	0.07	(27)	0.08	(9)
11=O, Δ^{12}	0.07	(10)	0.08	(1)	—		—	
11=O, Δ_{12}, $\Delta^{17(20)}$	0.12	(4)			—		—	
11=O, Δ^{12}, 17=O	0.12	(3)			—		—	
11β-ONO					−0.05	(1)		
11β,17β-O-					0.16	(2)	0.16	(2)
Δ^{12}	0.00	(14)			—		—	
13α,17α-O-					0.05	(1)		
13β,17β-O-					−0.02	(1)		
$\Delta^{13(17)}$	0.08	(1)			−0.10	(22)	−0.10	(5)
Δ^{16}	0.00	(8)	0.00	(1)	0.00	(4)	0.00	(1)
16β-OR					0.00	(3)		
16=O					0.06	(3)		
$\Delta^{17(20)}$	−0.01	(7)			0.01	(1)		
17=O	0.00	(16)			−0.10	(10)		
17β-C≡CH[d]	0.07	(2)						

a) The shifts refer to the assigned chemical shifts for 19-methyl protons of hypothetical compounds without any substituent. Solvent, $CDCl_3$. b) The figures in the parentheses refer to numbers of examples. c) The negative sign denotes shielding effect. d) The $\Delta\delta$ values of a number of 17-substituents, 0.00.

contribution of substituents at C_{17}. The result follows as.

19-Methyl Protons: In order to examine both additivity and magnitude of the shielding effects, all the compounds were first classified into two groups, A and B. The group A includes compounds having a C/D *trans*-fused ring (12βH) and those having an unsaturated carbon atom at C_{12} (Δ^{11} or Δ^{12}), and the group B compounds possessing a C/D *cis*-linkage (12αH). Each group was further divided into two groups, T (5αH, Δ^4 and Δ^5) and C (5βH), according to the mode of A/B ring juncture, as usually done in the normal steroid series. While reference compounds of the respective groups, 5- and 12-epimeric etiojervanes without any substituent, are not known, 5α,12β- and 5α,12α-etiojervan-3β-ols (**22** and **23**) and their acetates[1] (**22a** and **23a**) have recently been prepared and, moreover, a number of pairs of etiojervanes differing only by the configuration at C_5 have also been reported. In view of the well-known deshielding effects (0.02 and 0.03 ppm) of 3β-hydroxy and 3β-acetoxy groups for the chemical shift of 19-methyl protons,[22,23] the reference chemical

Table 3. The chemical shift of the 18-methyl protons of 12β-etiojervanes. substituents and chemical shifts (δ)[a]

C_{17}		C_{11}					
β	α	H_2	(44)[b]	O	(36)[b]	β-OH	(18)[b]
H	H	0.84±0.01	(2)	1.18±0.02	(3)	1.01±0.02	(2)
OH	H	0.95±0.04	(3)	1.29±0.04	(3)	1.09	(1)
H	OH	0.96±0.02	(2)	1.30±0.03	(5)		
OAc	H	0.89	(1)	1.17±0.03	(2)	0.99	(1)
H	OAc	0.90	(1)	1.20±0.02	(3)		
Ac	H	0.93[c]	(1)				
H	Ac	0.83±0.02	(6)				
CH_3	H			1.14	(1)	1.01	(1)
C_2H_5	H	0.84±0.01	(5)	1.16	(1)		
H	OTs			1.16	(1)		
H	NHAc	0.96±0.02	(3)				
H	$C(=NOH)CH_3$	0.81	(1)				
H	$C_4H_9O_3$[d]					1.02	(1)
H	$CH(CHO)CH_3$					0.975	(1)
H	$C_5H_9O_2$[e]					1.14±0.01	(2)
H	$COCH_2OAc$					0.95	(1)
OCH_2CH_2O		0.85±0.03	(5)	1.18±0.02	(2)	1.01±0.03	(3)
=O		1.00±0.03	(6)	1.34±0.02	(4)	1.14±0.02	(3)
$=CH_2$						1.15	(1)
$=CH(CH_3)$		0.97±0.02	(3)	1.32	(1)	1.18	(1)
Ac	OH			1.31	(1)		
OH	Ac			1.26	(1)		
$COCH_2OAc$	OAc			1.28	(1)		
C≡CH	OH			1.44	(1)		
OH	C≡CH			1.46	(1)		
$CH=CH_2$	OH			1.22	(1)		
OH	$CH=CH_2$			1.17	(1)		
C_2H_5	OH			1.23	(1)		
OH	C_2H_5			1.22	(1)		
Others[f]							

a) Solvent, $CDCl_3$. b) The figures in the parentheses refer to number of examples. c) The calculated δ-value, 0.89. d) $C_4H_9O_3=CH(OH)COOC_2H_5$. e) $C_5H_9O_2$=acetonide of a $-CH(OH)CH_2OH$ group. f) 11=H_2, 17β-$CH(OH)CH_3$ 0.93±0.02 (3) and 1.03±0.01 (3); 11=H_2, 17β-$CH(OTs)CH_3$ 0.88 (1); $\Delta^{9(11)}$, 17β-C_2H_5 0.98 (1); Δ^{11}, 17β-C_2H_5 1.02 (1); 11β-OAc, 17α-$CH(OH)CH_3$ 0.90 (1) and 0.84 (1); 11β-OAc, 17α-Ac 0.87 (1); 11α-OH, 17β-C_2H_5 0.98 (2); 11α-OAc, 17β-C_2H_5 0.84 (2).

shifts in the respective groups were assigned as shown in Table 2. The contributions of various functional groups were obtained by pairing compounds which differed only by the single group in question and by taking the average of difference of the chemical shifts. The calculated values, having available the reference shifts and the contributions listed in Table 2, were in good agreement, usually within 0.02 ppm (the deviation of 30 examples among 430 compounds examined, 0.03 ppm) except two exceptional cases, with the observed chemical shifts, indicating that the shielding effects are really active.

On the results given in Table 2, some comments are presented in the following. (1) The reference 19-methyl protons (δ 0.74 and 0.87) of the C/D *trans*-fused groups (A-T and A-C) appear at lower field than the corresponding protons (δ 0.71 and 0.83) in the iminooxidojervane series,[22] but still at higher field than those (δ 0.792 and 0.925) in the normal steroid series.[24] However, the difference (0.13 ppm) between their

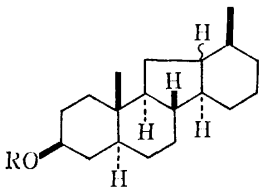

22 12βH, R=H **23** 12αH, R=H
22a 12βH, R=Ac **23a** 12αH, R=Ac

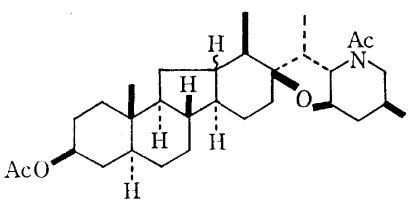

24 12βH
25 12αH

chemical shifts is equal to those (0.12 and 0.133 ppm) in the latter two series. (2) The 19-methyl protons of compounds in the C/D *trans*-fused groups (A-T and A-C) were observed at about 0.05 ppm high fields as compared with those in the corresponding C/D *cis*-fused groups (B-T and B-C). This chemical shift difference is represented by the reference shifts of two paired groups in Table 2: A-T and B-T, δ 0.74 and 0.79; A-C and B-C, δ 0.87 and 0.92. This difference is also almost the same as that (0.07 ppm) between diacetyl-5α,6,12β,13-tetrahydrojervine (**24**) and its 12α-epimer[12a] (**25**), a sole compound known as 12α-iminooxidojervane, supporting the 12α-configuration of the latter (**25**). (3) Each functional group in the A, B and C rings of compounds included in the C/D *trans*-fused groups (A-T and A-C) provides almost the same deshielding effect as the same group in the iminooxidojervane system, and it would not be necessary to repeat the previous discussions on the contribution of these groups. However, it is emphasized that this result, as coupled with the afore-mentioned reference shifts, implies that the chemical shifts of 19-methyl protons in the iminooxidojervane series can be estimated from Table 2, by assuming the contribution of 17-substituents of iminooxidojervane to be −0.04 ppm (up-field shift). (4) Each functional group in the C/D *cis*-fused groups (B-T and B-C) displays the contribution similar to the same group in the C/D *trans*-fused (A-T and A-C), as far as the functional groups in question exist in the A, B, and C rings. This indicates that the steric relation of these groups to the 19-methyl group hardly suffers change in passing from the *trans*-fused C/D linkage to the *cis*-fused, though the C-ring is expected to undergo distortion owing to the different C/D ring junctures. (5) Most of the functional groups in the saturated D ring exert no influence on the chemical shifts of 19-methyl portons. This has been demonstrated by a number of substituents at C_{17} in the C/D *trans*-fused as well as *cis*-fused compounds. Only exceptional functions are a 17β-ethinyl group in the group A-T and two 13,17-epoxy in that B-T. The deshielding effect of the former 17β-ethinyl group would be explained well by assuming that the substituent is oriented axial on the D ring with a slightly deformed chair conformation, though no reasonable interpretation is given for the effect of the two groups owing to obscure conformations of the D ring. (6) Several unsaturated functional groups (Δ^{12}, $\Delta^{13(17)}$, $\Delta^{17(20)}$ and 17=O) in the D ring of compounds with an unsaturated carbon atom at C_{12} provide deshielding effects, which would result from deformation of the C and D rings. On the other hand, unsaturated groups in the D ring in the C/D *cis*-fused groups (B-T and B-C), specially a double bond at C_{13}–C_{17} and a 17-carbonyl group, make important contributions to the relevant chemical shifts. According to a molecular model, the D ring in these compounds is disposed on the upper side of the molecule and the carbon atom at C_{17} approaches the 19-methyl group. These shielding effects would therefore be understood well as a result of the magnetic anisotropy of suchlike unsaturated groups. (7) Two exceptional cases for which the "additivity rule" does not hold were observed for a few of isojervine derivatives. This abnormality had already been discussed in the previous paper.[25]

Table 4. The chemical shift of the 18-methyl protons of 12α-etiojervanes

Substituents and chemical shifts (δ)[a]					
C_{17}		C_{11}			
β	α	H_2	(59)[b]	O	(15)[b]
H	H	0.80±0.01	(2)	0.92±0.01	(2)
OH	H	1.04±0.02	(7)		
H	OH	1.03±0.04	(9)	0.89±0.01	(2)
OAc	H	0.91±0.02	(6)	0.93	(1)
H	OAc	0.92±0.01	(10)	0.92	(1)
Ac	H	0.82±0.02	(3)		
H	Ac	0.83±0.02	(3)		
CH_3	H			0.88	(1)
C_2H_5	H			0.72	(1)
H	OTs			0.80±0.01	(2)
=O		1.00±0.02	(7)		
$=CH(CH_3)$				0.95	(1)
$COCH_2OAc$	OH			0.83	(1)
C_2H_5	OH			0.71	(1)
Others[c]					

a) Solvent, $CDCl_3$. b) The figures in the parentheses refer to numbers of examples. c) 11=H_2, 11β,17β-oxido 0.95±0.01 (4); 11=H_2, 17β-CH(OH)CH_3 0.87 (1); 11=H_2, 17α-CH(OH)CH_3 0.92 (1) and 0.90 (1); 11=H_2, 17β-CH(OAc)CH_3, 0.79 (1); 11=H_2, 17α-CH(OAc)CH_3 0.87 (1) and 0.83 (1); 11=H_2, 17β-CH(OH)CH_3, 17α-OH 0.92 (1); 11=H_2, 17β-CH(ONO)CH_3, 17α-OH 0.79 (1); 11=O, Δ^{16} 0.92 (2); 11=O, 17β-CH(OH)CH_2OAc, 17α-OH 0.82 (1); 11=O, 17β-CH(OAc)CH_2OAc, 17α-OH 1.03 (1).

18-Methyl Protons: In Tables 3 and 4 are summarized the chemical shifts of 18-methyl protons of a number of 12β- and 12α-etiojervanes with a β-methyl group at C_{13} (not with an unsaturated carbon atom at C_{13}). The signals due to the 18-methyl protons were distinguished without difficulty in most of the spectra, but the chemical shifts were given not so exactly as those due to the sharp 19-methyl protons, because the protons usually appeared as relatively indistinctly resolved doublets or overlapping signals above the background of methylene and methine protons. This inaccuracy was observed in many cases when the substituents at C_{17} were complex and, specially, the "S" group containing secondary methyl groups, and these undiscernible chemical shift data were not included in Tables 3 and 4. The present data seem at first to be confined to the correlation of the chemical shifts only with changes of substituents in the C and D rings. However, it must be emphasized that various functional groups in the A and B rings exert no important influence on the relevant chemical shifts, as far as the B and C rings are fused in a *trans*-manner (8βH and 9αH).

On the basis of the data summarized in Table 3, we examined the contributions of substituents at C_{11} and C_{17} for the 18-methyl protons of 12β-etiojervanes in the same manner as those for the 19-methyl protons, and found that the "additivity rule" holds roughly

Table 5. The contribution ($\Delta\delta$) of functional groups to the chemical shift of the 18-methyl protons of 12α-etiojervanes

Reference chemical shift[a] Functional groups at C_{11}		$\Delta\delta$[b]	δ 0.84 Functional groups at C_{17}		$\Delta\delta$[b]
$=H_2$	0.00	(44)	$=H_2$	0.00	(7)
=O	0.33	(36)	=O	0.16	(13)
β-OH	0.15	(19)	$=CH(CH_3)$	0.16	(5)
α-OH	0.16	(2)	$=CH_2$	0.16	(1)
β-OAc	−0.05	(3)	$-OCH_2CH_2O-$	0.01	(10)
α-OAc	−0.02	(2)	β-OH	0.11	(12)
Δ^{11}	0.20	(2)	α-OH	0.12	(12)
$\Delta^{9(11)}$	0.16	(1)	β-OAc	0.02	(4)
			α-OAc	0.05	(5)
			β-Ac	0.04	(2)
			α-Ac	0.00	(10)
			β-CH_3	0.00	(2)
			β- and α-C_2H_5[c]	−0.02	(13+1)
			β- and α-$COCH_2OAc$[c]	−0.04	(1+1)
			β- and α-$CH=CH_2$[c]	0.03	(1+1)
			β- and α-$C\equiv CH$[c]	0.18	(1+1)
			α-OTs	−0.01	(1)
			α-NHAc	0.12	(3)
			α-$C(=NOH)CH_3$	−0.03	(1)

a) The chemical shift of 18-methyl protons of compounds without any substituent in the C and D rings. Solvent, $CDCl_3$. b) The figures in the parentheses refer to numbers of examples. The negative sign denotes shielding effect. c) The contributions due to these 17α-substituents were assumed to be the same as those due to the corresponding 17β-substituents.

for the relevant shifts; namely, the observed chemical shifts are in good agreement (within 0.04 ppm) with the calculated values, assuming the chemical shift (δ 0.84) of compounds containing no substituents in the C and D rings to be the reference shift and having available the contributions of functional groups at C_{11} and C_{17} listed in Table 5. The following points are noted from Table 5. (1) In contrast to the contributions for the 19-methyl protons, 11β-hydroxy and acetoxy groups exhibited almost the same deshielding and shielding effects ($\Delta\delta$ 0.15 and −0.05 ppm) for the 18-methyl protons as the corresponding 11α-groups ($\Delta\delta$ 0.16 and −0.05 ppm). These effects are nearly equal to those in the iminooxidojervane series.[22] To the contrary, the deshielding effect ($\Delta\delta$ 0.33 ppm) of the carbonyl group at C_{11} is remarkably large as compared with that ($\Delta\delta$ 0.02 ppm) in the iminooxidojervane series,[22] indicating that the methyl group is oriented equatorial in the D ring with a fixed, slightly deformed chair form and hence located in the plane of the trigonal carbon atom in question. (2) The chemical shifts of 18-methyl protons depend largely on the β- and/or α-substituent(s) and extend from δ 0.84 to 1.46. Interestingly, the relevant signals of two compounds having the same substituents at C_{11} and/or C_{17} but differing only in the configuration at C_{17}, apart from the functional groups in the A and B rings, were found in almost the same fields except in the case of 17-acetyl-12α-etiojervanes (see Table 3). It follows that a substituent at C_{17}, whether the configuration is β or α, provides almost the same contribution (see Table 5). (3) The deshielding effects ($\Delta\delta$ in Table 5) of several 17-substituents (=O, β- and α-OH, and β- and α-OAc) are roughly the same as those ($\Delta\delta$ 0.22, 0.15, 0.21?, 0.00 and 0.05) of the corresponding substituents at C_1 in 5β-androstane series,[26] but completely different from those in 5α-androstane series.[26] This similarity in the deshielding effect between the first two series would support the afore-mentioned conformation in respect to the D ring.

The following comments are given for the chemical shifts of 18-methyl protons of 12α-etiojervanes in Table 4. (1) Contrary to the previous results, the "additivity rule" does *not* hold for the chemical shifts in question. This was exemplified clearly by the variety of shelding effects of a 11-carbonyl group ($\Delta\delta$ −0.14—+0.12 ppm), indicating that the D ring would not take a fixed conformation in the C/D *cis*-fused etiojervanes. (2) The 18-methyl protons in 12α-etiojervanes having no substituents at C_{11} were observed in higher or lower fields than those in the corresponding 12β-etiojervanes. These up- and down-field shifts ($\Delta\delta$ −0.04—+0.09 ppm) naturally depend on the functional groups at C_{17} as well as on the conformations of D ring and are therefore too difficult to be estimated. However, it is noteworthy that several β-oriented substituents (OH, OAc and Ac) at C_{17} exhibit essentially the same contributions ($\Delta\delta$ 0.24, 0.11 and 0.02 ppm) as the corresponding α-oriented, although this does not always imply that the 18-methyl group would have the similar steric relation for the respective 17β- and 17α-grops. (3) The 18-methyl protons in 11-oxo-12α-etiojervanes appeared at remarkably high field ($\Delta\delta$ −0.26—−0.52 ppm) as compared with those in the corresponding 12β-etiojervanes. This large up-field shift evidently results from the conformational change of the D ring

in passing from C/D *trans*-fused compounds to *cis*-fused; the D ring would assume a twist boat or more probably a half-chair conformation, and the β-methyl group at C_{13} would become equatorial in either of the conformations and hence located on the upper side of the C ring and in the conical region extending above the plane of the trigonal carbon atom of a 11-carbonyl group.

Experimental

All the melting points were uncorrected. The homogeneity of each compound was always checked by TLC on silica gel (Wakogel B-5) with various solvent systems, and the spots were developed with ceric sulfate in dil sulfuric acid and/or iodine. The optical rotations, ORD curves and IR spectra were measured in chloroform, dioxane, and Nujol, respectively, unless otherwise stated. The NMR spectra were obtained in deuteriochloroform at 60 and/or 100 MHz, and the chemical shifts were given in δ-values, TMS being used as an internal reference. The abbreviations "s, d, t, m, br, and do" in the NMR spectra denote "singlet, doublet, triplet, multiplet, broad, and double," respectively.

*17-Methylidene-5α,12β-etiojervane-3β,11β-diol 3-Acetate (**6**).* A suspended mixture of sodium hydride (Wako, 510 mg, *ca.* 50% in oil) in pentane (20 ml) was stirred for a while and then decanted under a stream of nitrogen. This procedure was repeated several times to remove the oil. After removal of the pentane *in vacuo* the residual hydride was mixed with fresh dimethylsulfoxide (DMSO, 6 ml), which had been dried over calcium hydride and distilled twice under nitrogen, stirred at 62—72 °C for 1 h and cooled, when the mixture became homogeneous and gray. To the solution was added dropwise a solution of dry methyltriphenylphosphonium bromide (2.863 g) in DMSO (10 ml) at room temperature (temp), and the whole solution was stirred at room temp for 20 min. To the resulting yellow, gel-like mixture was added a solution of 5α,12β-etiojervane-3β,11β-diol-17-one (**5**, 610 mg) in tetrahydrofuran (THF, 10.5 ml) at room temp under nitrogen during 10 min. The whole mixture was stirred at 50 °C (bath temp) for 22 h, cooled and poured into ice-water and, after being salted out, extracted with ether repeatedly. The ether solution was washed with saturated brine, dried over sodium sulfate and evaporated to leave oily residue (2.667 g). The residue was treated with acetic anhydride (Ac_2O, 5.5 ml) and pyridine (Py, 10 ml) at room temp for 3 h, poured onto crushed ice, salted out, and extracted with ether repeatedly. The ether extracts were washed with 2M hydrochloric acid, 5% aqueous sodium bicarbonate and saturated brine, dried and evaporated to give amorphous substance (2.164 g). A suspended mixture of the substance in hexane containing a trace of benzene was passed through an alumina column (Merck, acidic) with a 5 : 1 mixture of hexane and benzene to remove resin, and the whole eluate was then purified by preparative TLC over silica gel (Wakogel, 32 plates) with benzene to give crystalline substance (511 mg), showing a single spot, as a main fraction. This was triturated with acetone-isopropyl ether, collected by filtration to give **6** (409 mg), mp 171.5—172 °C. This was recrystallized twice from the same solvent mixture for analysis: mp 172—173 °C; $[\alpha]_D$ +40.9°; IR, ν_{max} 3600, 3080, 1724, 1640, 1262, 1024, and 891 cm^{-1}; NMR, δ 1.04 (3H, s, 19-C$\underline{H}_3$), 1.15 (3H, d J=6 Hz, 18-C$\underline{H}_3$), 1.97 (3H, s, OCOC$\underline{H}_3$), 4.15 (1H, br W_H=16 Hz, $\underline{H}$ at C_{11}), and 4.65 (3H, br m, 2$\underline{H}$ at C_{20} and $\underline{H}$ at C_3). Found: C, 76.28; H, 9.97%. Calcd for $C_{22}H_{34}O_3$: C, 76.26; H, 9.89%.

*Hydrogenation of **6**.* A solution of **6** (354 mg) in acetic acid (14 ml) was hydrogenated over pre-reduced Adams platinum (232 mg as $PtO_2 \cdot H_2O$) for 1 h, when 1.02 mol of hydrogen had been consumed. After removal of the catalyst, the solution was evaporated *in vacuo* below 40 °C and then treated with benzene (azeotropization) to give crystalline residue, which was dissolved in chloroform. The chloroform solution, after being worked up as usual, gave crystalline residue (355 mg), which on trituration with acetone afforded a mixture (295 mg) of 17β- and 17α-methyl-5α,12β-etiojervane-3β,11β-diol 3-acetates (**7** and **8**), mp 184—187 °C, showing a single spot. This was recrystallized from acetone-isopropyl ether and had mp 189—190 °C; $[\alpha]_D$+36.1°; IR, ν_{max} 3480, 1704, 1263, and 1031 cm^{-1}; NMR, δ 0.84 (3H, d J=7 Hz, 17-C$\underline{H}_3$), 1.01 (3H, d J=5.5 Hz, 18-C$\underline{H}_3$), 1.04 (3H, s, 19-C$\underline{H}_3$), 1.98 (3H, s, OCOC$\underline{H}_3$), 4.07 (1H, do d J=5 and 8 Hz, $\underline{H}$ at C_{11}), and 4.68 (1H, br m W_H=23 Hz, $\underline{H}$ at C_3). Found: C, 75.86; H, 10.52%. Calcd for $C_{22}H_{36}O_3$: C, 75.81; H, 10.41%.

*Oxidation of a Mixture of **7** and **8**.* A solution of a mixture of **7** and **8** (the preceding section, 248 mg) in Py (3 ml) was added chromic anhydride (CrO_3, 344 mg) under stirring during 30 min, and the whole mixture was further stirred at room temp for 14 h. The mixture was poured into ice-water (50 ml), extracted with ether (4×50 ml), and the ether solution was washed with 1M hydrochloric acid (3×20 ml), 5% aqueous sodium bicarbonate (2×20 ml) and saturated brine, dried and evaporated to leave crystalline residue (263 mg), showing a single spot. This was triturated with methanol-isopropyl ether to give a mixture of 17β- and 17α-methyl-5α,12β-etiojervan-3β-ol-11-one (**9** and **10**); the first crop (145 mg), mp 137—138 °C, the second (50 mg), mp 134—135 °C, and the third (11 mg), mp 130—131 °C. These were collected and recrystallized from methanol to give a mixture having mp 138.5—139 °C; $[\alpha]_D$ −74.1°; ORD, $[\Phi]_{334}^{trough}$ −9940°, $[\Phi]_{322}^{trough}$ −5510°, $[\Phi]_{293}^{peak}$ +8320°, a=−182.6°: IR, ν_{max} 1732, 1727, 1241, and 1027 cm^{-1}; NMR, δ 0.81 (3H, d J=6 Hz, 17-C$\underline{H}_3$), 0.87 (3H, s, 19-C$\underline{H}_3$), 1.14 (3H, d J=5.5 Hz, 18-C$\underline{H}_3$), 2.01 (3H, s, OCOC$\underline{H}_3$), and 4.68 (1H, br W_H=23 Hz, $\underline{H}$ at C_3). Found: C, 76.26; H, 9.90%. Found: C, 76.26; H, 9.89%.

*17β-Methyl-5α,12α-etiojervan-3β-ol-11-one 3-Acetate (**11**).* A solution of the mixture of **9** and **10** (the preceding section, 186 mg) was treated with 1M sodium methoxide in refluxing methanol (20 ml) for 2 h under nitrogen. After being cooled, the solution was evaporated, poured into water (30 ml) and extracted with chloroform repeatedly. The chloroform solution was worked up as usual to give crystalline residue (188 mg), which was treated with Ac_2O (1 ml) and Py (2 ml) at room temp for 3 h. The product (196 mg), showing two spots on TLC, was separated by preparative TLC with a 2 : 3 mixture of chloroform and benzene into two fractions; the starting crystalline mixture (168 mg) with larger R_f value and a new crystalline substance (17 mg) with smaller R_f. These treatments (epimerization, acetylation and subsequent purification by TLC) were repeated three times for the recovered starting mixture and led to isolation of 56 mg of the new material with 125 mg of the recovered, unchanged material. The latter had mp 127—129 °C on recrystallization from methanol-isopropyl ether and amounted to 116 mg. The former was recrystallized from isopropyl ether to give **11** (31 mg), mp 163—164 °C. This was recrystallized from the same solvent for analysis: mp 163.5—164 °C; $[\alpha]_D$ −18.2°; ORD, $[\Phi]_{334}^{trough}$ −4350°, $[\Phi]_{323}^{trough}$ −2210°, $[\Phi]_{292}^{peak}$ +3350°, a=−77°; IR, ν_{max} 1726, 1239, 1036, and 1027 cm^{-1}; NMR, δ 0.74 (3H, d J=7 Hz, 17-

CH_3), 0.88 (3H, d J=5 Hz, 18-C$\underline{H}_3$), 0.90 (3H, s, 19-C$\underline{H}_3$), 1.99 (3H, s, OCOC$\underline{H}_3$), and 4.69 (1H, br W_H=23 Hz, $\underline{H}$ at C_3). Found: C, 76.32; H, 9.92%. Calcd for $C_{22}H_{34}O_3$: C, 76.26; H, 9.89%.

*17β-Methyl-5α,12β-etiojervan-3β-ol-11-one 3-Acetate (**9**).* A solution of compound **11** (46 mg) was refluxed with 1M sodium methoxide in methanol (7 ml) for 2 h under nitrogen, cooled and then evaporated to leave oily residue. The residue was mixed with water (30 ml) and extracted with chloroform. The chloroform extracts gave a crystalline mixture (36.5 mg), which was treated with Ac_2O (0.5 ml) and Py (0.5 ml) at room temp for 3 h and then worked up as usual to give a crystalline acetate mixture (37 mg), showing two spots. This was separated by preparative TLC over silica gel (3 plates) with a 3 : 2 mixture of benzene and chloroform into two fractions; one (29 mg) with larger R_f value and the other (5 mg) with smaller R_f. The latter had mp 155—158 °C on trituration with isopropyl ether, amounted to 2.5 mg, and was identified as the starting material (**11**). The former was recrystallized from isopropyl ether–methanol to give **9** (21 mg), mp 138.5—139 °C. This was recrystallized from the same solvent mixture for analysis: mp 140—141 °C; $[\alpha]_D$ −80.2°; ORD, $[\Phi]_{334}^{trough}$ −8150°, $[\Phi]_{324}^{trough}$ −4450°, $[\Phi]_{292}^{peak}$ −7600°, a=−156.5°; IR, ν_{max} 1732, 1727, 1241, and 1027 cm^{-1}; NMR, δ 0.81 (3H, d J=5.5 Hz, 17-C$\underline{H}_3$), 0.86 (3H, s, 19-C$\underline{H}_3$), 1.14 (3H, d J=5.5 Hz, 18-C$\underline{H}_3$), 2.02 (3H, s, OCOC$\underline{H}_3$), and 4.67 (1H, br W_H=28 Hz, $\underline{H}$ at C_3). Found: C, 76.13; H, 9.95%. Calcd for $C_{22}H_{34}O_3$: C, 76.26; H, 9.89%.

*5α,12β-Etiojervan-3β-ol-11,17-dione 17-Ethylene Acetal (**13**).* A solution of 12β-etiojerv-5-en-3β-ol-11,17-dione 17-ethylene acetal (**12**, 3.56 g) in acetic acid (220 mg) was hydrogenated over Adams platinum (1.78 g) at room temp for 1.5 h, when 340 ml (1.21 mol) of hydrogen had been consumed. The reaction mixture was worked up as usual to give oily residue, which crystallized on trituration with isopropyl ether, had mp 162—164 °C and amounted to 3.33 g. This was recrystallized from isopropyl ether and then from acetone–isopropyl ether to give **13**, mp 172—174 °C; $[\alpha]_D$ −47°; ORD, $[\Phi]_{334}^{trough}$ −7310°, $[\Phi]_{278}^{peak}$ +6960°, a=−143°, IR, ν_{max} 3480, 3350, 1731, 1099, 1077, 1064, and 1030 cm^{-1}; NMR δ 0.83 (3H, s, 19-C$\underline{H}_3$), 1.16 (3H, d J=6.5 Hz, 18-C$\underline{H}_3$), 3.65 (1H, br, $\underline{H}$ at C_3), and 3.91 (4H, s, OC$\underline{H}_2$C$\underline{H}_2$O). Found: C, 71.91; H, 9.21%. Calcd for $C_{21}H_{32}O_4$: C, 72.38; H, 9.26%.

*5α,12β-Etiojervan-3β-ol-11,17-dione (**14**).* A solution of compound **13** (756 mg) in acetone (62 ml) and water (10 ml) was refluxed with *p*-toluenesulfonic acid (150 mg) for 4 hr. The solution was made neutral with 5% aqueous sodium bicarbonate, evaporated and extracted with chloroform. The chloroform solution was worked up as usual to give oily residue, which crystallized on trituration with acetone, had mp 159—162 °C, and amounted to 516 mg. This was recrystallized from acetone–isopropyl ether to give **14**, mp 169—172 °C; $[\alpha]_D$ −81°; ORD, $[\Phi]_{334}^{trough}$ −9980°, $[\Phi]_{332}^{trough}$ −8070°, $[\Phi]_{280}^{peak}$ +11430°, a=−214.1°; Mass, *m/e* 304 (M^+); IR, ν_{max} 3470, 1732, 1712, 1694, and 1033 cm^{-1}; NMR, δ 0.83 (3H, s, 19-C$\underline{H}_3$), 1.29 (3H, d J=6.5 Hz, 18-C$\underline{H}_3$), and 3.51 (1H, br, $\underline{H}$ at C_3).

*Reaction of **14** with Isopropylmagnesium Bromide.* To a mixture of dried magnesium ribbons (10.0 g) in dry ether (450 ml) was added dropwise isopropyl bromide (57.6 g) during 40 min, and the mixture was further stirred at room temp for 40 min. To the cooled, suspended mixture was added compound **13** (1.10 g) in ether containing a small amount of THF under stirring, and the whole mixture was refluxed for 4.5 h under nitrogen. After addition of saturated aqueous ammonium chloride (80 ml), the ether layer was separated and the aqueous layer was extracted with ether repeatedly. The ether solutions were combined and then worked up as usual to give oily residue (1.18 g), which was separated by preparative TLC over silica gel (45 plates) with a 1 : 1 mixture of benzene and ethyl acetate into four fractions, named fractions A—D in the order of R_f value. Fraction D (448 mg), the least mobile fraction showing a single spot, was crystallized on trituration with acetone–isopropyl ether and then recrystallized from the same solvent mixture to give 5α,12β-etiojervane-3β,11β,17α-triol (**15**, 189 mg), mp 180—182 °C; IR, ν_{max} 3380, 1098, 1058, 1023, and 970 cm^{-1}. This was converted into the diacetyl derivative (**15a**), amorphous; $[\alpha]_D$ 0.0°; Mass, *m/e* 332 (M^+−60), 314, 272, and 254; NMR, δ 1.04 (3H?, d J=6 Hz, 18-C$\underline{H}_3$), 1.06 (3H, s, 19-C$\underline{H}_3$), 2.00 and 2.03 (total 6H, each s, 2O-COC$\underline{H}_3$), 4.17 (1H, br W_H=15 Hz, $\underline{H}$ at C_{11}), and 4.65 (2H, br m, 2$\underline{H}$ at C_3 and C_{17}). Fraction C (455 mg), showing a single spot, crystallized on trituration with acetone–isopropyl ether and was then recrystallized from the same solvent mixture to yield **16** (204 mg), mp 168—170 °C; $[\alpha]_D$ −4.0°; ORD, $[\Phi]_{318}^{trough}$ −3300°, $[\Phi]_{276}^{peak}$ +5510°, a=−88°; Mass, m/e 306 (M^+); IR, ν_{max} 3560, 3440, 1700, 1100, 1053, and 864 cm^{-1}; NMR, δ 1.06 (3H, s, 19-C$\underline{H}_3$), 1.14 (3H?, d J=6.5 Hz, 18-C$\underline{H}_3$), 3.58 (1H, br W_H=24 Hz, $\underline{H}$ at C_3), and 4.18 (1H, br W_H=13 Hz, $\underline{H}$ at C_{11}). Fraction A (29 mg), the most mobile fraction, was identified as the starting material (IR and TLC). Fraction B (335 mg) were further separated by repeated preparative TLC over silica gel (18 plates), 8 : 1, 4 : 1 and 2 : 1 mixtures of benzene and ether being used successively as solvents, into several fractions. One (55 mg) of the two major fractions crystallized on trituration with acetone–isopropyl ether and was recrystallized from the same solvent mixture to give **17** (26 mg), mp 136—138 °C; $[\alpha]_D$ −11.7°; ORD, $[\Phi]_{327}^{trough}$ −9590°, $[\Phi]_{287}^{peak}$ +5500°, a=−151°; Mass, *m/e* 348 (M^+); IR, ν_{max} 3460, 1732, 1042, and 972 cm^{-1}; NMR, δ 0.83 (3H, s, 19-C$\underline{H}_3$), 0.92 [6H?, d J=6.5 Hz, CH(C$\underline{H}_3$)$_2$], 1.21 (3H?, d J=7 Hz, 18-C$\underline{H}_3$), and 3.65 (1H, br m, $\underline{H}$ at C_3). The other (127 mg) of the two major fractions was crystallized and recrystallized from acetone–isopropyl ether to yield **18** (60 mg), mp 193—195 °C; $[\alpha]_D$ −5.6°; ORD, $[\Phi]_{332}^{trough}$ −8330°, $[\Phi]_{290}^{peak}$ +7370°, a=−157°; Mass *m/e* 348 (M^+); IR, ν_{max} 3570, 1733, 1050, and 988 cm^{-1}; NMR, δ 0.84 (3H, s, 19-C$\underline{H}_3$), 0.93 [6H, d J=6 Hz, CH(C$\underline{H}_3$)$_2$], 1.23 (3H?, d J=6.5 Hz, 18-C$\underline{H}_3$), and 3.58 (1H, br m, $\underline{H}$ at C_3).

Equilibration Experiments. The studies were carried out for all the compounds listed in Table 1. Each reactant was treated with 1M sodium methoxide in methanol under reflux for several hours, and the product, after acetylation when necessary, was separated by preparative TLC, as had been illustrated in the sections of the preparation of compounds **9** and **11**. The equlibrium ratio was determined by measuring the amounts of isolated products and the result is summarized in Table 1. Each epimerzation experiment is not described here, and only new compounds, obtained during these studies, are characterized in the following.

12β-Etiojerv-5-ene-3β,17α-diol-11-one. Mp 212.5—213 °C (from acetone); $[\alpha]_D$ −158.2° (CH_3OH); ORD, $[\Phi]_{333}^{trough}$ −10990°, $[\Phi]_{321}^{trough}$ −7360°, $[\Phi]_{291}^{peak}$ +5710°, a=−167°; Found: C, 75.00; H, 9.31%. Calcd for $C_{19}H_{28}O_3$: C, 74.96; H, 9.27%.

12α-Etiojerv-5-ene-3β,17β-diol-11-one (XIB). Mp 237—239 °C (from methanol). The 3,17-diacetate. Mp 140—141 °C (from methanol); ORD, $[\Phi]_{333}^{trough}$ −3750°, $[\Phi]_{322}^{trough}$ −5520°, $[\Phi]_{294}^{peak}$ +1290°, a=−68.1°; IR, ν_{max} 1732, 1241, and 1056 cm^{-1}; NMR, δ 0.93 (3H, d J=7 Hz, 18-C$\underline{H}_3$),

1.12 (3H?, s, 19-C$\underline{H}_3$), 2.06 (6H, s, 2OCOC$\underline{H}_3$), and 4.83 (2H, br W_H=21 Hz, 2$\underline{H}$ at C_3 and C_{17}), and 5.50 (1H, br s, $\underline{H}$ at C_6).

17β-Ethyl-12α-etiojervane-3β,17α-diol-11-one 3-Acetate (XVIIIB) Mp 149—150 °C (from acetone–isopropyl ether); $[\alpha]_D$ −60°; ORD, $[\Phi]_{332}^{trough}$ −5290°, $[\Phi]_{291}^{peak}$ +1840°, a=−71.3°; IR, ν_{max} 3546, 1725, 1258, and 1032 cm^{-1}; NMR, δ 0.71 (3H, d J=7.5 Hz, 18-C$\underline{H}_3$), 0.91 (3H, t J=7 Hz, 21-C$\underline{H}_3$), 1.11 (3H?, s, 19-C$\underline{H}_3$), 2.02 (3H, s, OCOC$\underline{H}_3$), 4.58 (1H, br m, $\underline{H}$ at C_3), and 5.42 (1H, br s, $\underline{H}$ at C_6). Found: C, 73.71; H, 9.29%. Calcd for $C_{23}H_{34}O_4$; C, 73.76; H, 9.15%.

17β-Isopropyl-5α,12α-etiojervane-3β,17α-diol-11-one (XXB). Amorphous, $[\alpha]_D$ −5.6°; ORD, $[\Phi]_{334}^{trough}$ −2330°, $[\Phi]_{296}^{peak}$ +4640°, a=−69.7°; IR ($CHCl_3$), ν_{max} 3500, 1730, and 1043 cm^{-1}; Mass, m/e 348 (M^+); NMR, δ 0.80 (3H, d J= 7 Hz, 18-C$\underline{H}_3$), 0.89 (3H?, s, 19-C$\underline{H}_3$), and 3.54 (1H, br m, $\underline{H}$ at C_3).

References

1) Part III, A. Murai, T. Nishimura, and T. Masamune, *Bull. Chem. Soc. Jpn.*, **49**, 1612 (1976).

2) Part XXV of "C-Nor-D-homosteroids and Related Alkaloids"; Part XXIV, Ref. 1.

3) For reviews, see, G. Quinkert, *Experientia*, **13**, 381 (1975); D. H. R. Barton and G. A. Morrison, "Progress in the Chemistry of Organic Natural Products," Vol. 19, ed. by L. Zechmeister, Springer-Verlag, Wien (1961), p. 165.

4) W. Hückel, M. Sachs, J. Yantschulewistch, and F. Nerdel, *Justus Liebigs Ann. Chem.*, **518**, 155 (1935); W. Hückel, W. Egerer, and F. Mossner, *ibid.*, **645**, 162 (1961); H. O. House, V. Paragamian, R. S. Ro, and D. J. Wluka, *J. Am. Chem. Soc* **82**, 1457 (1960).

5) H. O. House and D. G. Melillo, *J. Org. Chem.*, **38**, 1398 (1973), and their previous papers.

6) N. L. Allinger, R. B. Hermann, and C. Djerassi, *J. Org. Chem.*, **25**, 922 (1960); J. F. Bielmann, D. Francetic, and G. Ourisson, *Tetrahedron Lett.*, **1960**, 4.

7) a) N. L. Allinger and L. Greenberg, *J. Org. Chem.*, **25**, 1399 (1960). b) W. G. Dauben, G. A. Boswell, Jr., W. Templeton, and J. W. McFarland, *J. Am. Chem. Soc.*, **85**, 2302 (1963), and references cited there.

8) F. V. Brutcher, Jr. and W. Bauer, Jr., *J. Am. Chem. Soc.*, **84**, 2233, 2236 (1962).

9) N. L. Allinger and M. T. Tribble, *Tetrahedron*, **28**, 1191 (1972), and references cited there.

10) Allinger's calculational results by the force field method were in good accord with the experimental results. However the calculation was not applied to the systems including a five-membered ring fused with two six-membered rings such as etiojervanes. *Cf.*, Ref 9.

11) H. O. House and G. Rasmusson, *J. Org. Chem.*, **28**, 31 (1963).

12) a) T. Masamune, A. Murai, K. Orito, H. Ono, S. Numata, and H. Suginome, *Tetrahedron*, **25**, 4853 (1969). b) O. Wintersteiner and M. Moore, *ibid.*, **20**, 1947 (1964).

13) T. Masamune, *Nippon Kagaku Zasshi*, **91**, 407 (1970).

14) A. Murai, T. Nishimura, and T. Masamune, *Bull. Chem. Soc. Jpn.*, **49**, 1602 (1976).

15) Cf., R. Greenwald, M. Chaykovsky, and E. J. Corey, *J. Org. Chem*,. **28**, 1128 (1963).

16) S. M. Kupchan, A. W. By, and M. S. Flom, *J. Org. Chem.*, **33**, 911 (1968).

17) S. M. Kupchan and M. J. A. El-Haj, *J. Org. Chem.*, **33**, 1947 (1968).

18) The words "similar, small, large or bulky" refer to conformational energies of each substituent in cyclohexane system. *Cf.*, E. L. Eliel, N. L. Allinger, S. J. Angyal, and G. A. Morrison, "Conformational Analysis," Interscience Publishers, New York (1965), p. 435.

19) T. Masamune, A. Murai, and S. Numata, *Tetrahedron*, **25**, 3145 (1969).

20) Ref. 17, formation of compound VI from IV.

21) Ref 19, formation of compound XIV from XIII.

22) T. Masamune, N. Sato, K. Kobayashi, I. Yamazaki, and Y. Mori, *Tetrahedron*, **23**, 1591 (1967).

23) T. Masamune, I. Yamazaki, K. Orito, and M. Takasugi, *Tetrahedron*, **27**, 3337 (1971).

24) N. S. Bhacca and D. H. Williams, "Application of NMR Spectroscopy in Organic Chemistry," Holden-Day, Inc., San Francisco (1964), p. 19.

25) T. Masamune, M. Takasugi, M. Gohda, H. Suzuki, S. Kawahara, and T. Irie, *J. Org. Chem.*, **29**, 2282 (1964).

26) T. Goto and K. Tori, "Zikken Kagaku Koza," Vol. 12, ed by M. Kotake, Maruzen Co., Tokyo (1967), p. 333.

Retardation of Autoxidation in the Presence of Water, Alcohols and Carboxylic Acids

Koji UKEGAWA and Yoshio KAMIYA*

National Research Institute for Pollution and Resources, Kawaguchi, Saitama 332

**Faculty of Engineering, The University of Tokyo, Hongo, Bunkyo-ku, Tokyo 113*

(Received October 11, 1975)

The oxidation of alcohols and α-substituted toluenes in water, methanol and acetic acid was studied at 60—70 °C in the presence of 0.040 M AIBN. The rate of oxidation of alcohol, $k_p/(2k_t)^{1/2}$, considerably increases when the alcohol is diluted with an inert solvent. The rate remarkably decreases with the addition of water, methanol or various carboxylic acids. However in the presence of tetralyl hydroperoxide, *viz.*, when the hydroperoxyl radical is replaced by the tetralyl peroxyl radical, no further inhibition effect due to water, methanol or carboxylic acids is observed. The rate of oxidation of 1,4-cyclohexadiene decreases with the addition of water or acetic acid. However in the presence of 0.20 M tetralyl hydroperoxide, no further inhibition effect is observed. The rate of oxidation of 1-phenylethanol decreases with the addition of benzoic acid but not with that of methylbenzoate. The rate of oxidation of (2-chloroethyl)benzene, ethylbenzene and isopropylbenzene does not decrease with the addition of 0.224 M acetic acid, but that of *N,N*-dimethylbenzylamine, *N,N*-diethylbenzylamine, benzyl alcohol, 1-phenylethanol and methyl benzyl ether decreases. It is concluded that hydroperoxyl and alkylperoxyl radicals with α-substituents such as hydroxyl, carbonyl, alkoxyl or amino groups undergo deactivation due to hydrogen bonding with water, alcohols and carboxylic acids.

Although the autoxidation of hydrocarbons has been studied thoroughly by a number of workers,[1–5] many points are still left unclarified. Hendry and Russell,[6] and Howard and Ingold[7] reported that the solvent effect on the rate of autoxidation can be correlated as a function of dielectric constant and neither π-complex formation nor hydrogen bonding of alkylperoxyl radical is observed.

Zaikov and Maizus[8] suggested that the deactivation of peroxyl radical occurrs owing to hydrogen bonding with water in the autoxidation of methyl ethyl ketone. Imamura *et al.*[9] reported that the autoxidation of acetaldehyde is considerably retarded in the presence of vaious carboxylic acids. Bimolecular interaction of hydroperoxyl radicals is known to be strongly retarded in the presence of water.

In the course of studies on the autoxidation of alcohols, we found that hydroperoxyl radicals can be deactivated by water, alcohol and carboxylic acids. Furthermore, peroxyl radicals with α-substituent containing nitrogen or oxygen atoms were found to be deactivated by hydroxyl compounds. The deactivation effect, which is hardly observed in the case of alkylperoxyl radicals, can be explained only in terms of hydrogen bonding.

Experimental

The technique of oxidation was described elsewhere.[10] All the experiments were carried out at 60—70 °C in the presence of α,α'-azobisisobutyronitrile as an initiator under atmospheric pressure of oxygen. Hydroperoxide produced was determined by iodometric titration, where hydroperoxide was treated with KI in 80% aqueous acetic acid at room temperature in the dark.

Tetralyl hydroperoxide obtained by the autoxidation of tetralin was purified several times by recrystallization from heptane. The other materials were used after distillation or recrystallization of extra pure reagents.

Results and Discussion

Peroxyl radicals formed in the autoxidation of alcohols decompose to ketones and a hydroperoxyl radical, the hydroperoxyl radical being the chain carrier in the autoxidation of alcohols.[11] However, the α-hydroxyperoxyl radical can also be the chain carrier in the oxidation of some alcohols.[12]

The oxidation of an alcohol initiated by AIBN (α,α'-azobisisobutyronitrile) proceeds according to the following mechanisms.

Initiation reaction:

$$\mathrm{AIBN} + \mathrm{RH} + \mathrm{O_2} \xrightarrow{R_i} \mathrm{RO_2\cdot(HO_2)}$$

Propagation reaction:

$$\mathrm{RO_2\cdot} + \mathrm{RH} \xrightarrow{k_p} \mathrm{ROOH} + \mathrm{R\cdot}$$

$$(\mathrm{HO_2\cdot} + \mathrm{RH} \longrightarrow \mathrm{HOOH} + \mathrm{R\cdot})$$

$$\mathrm{R\cdot} + \mathrm{O_2} \xrightarrow{\text{fast}} \mathrm{RO_2\cdot}$$

Termination reaction:

$$2\mathrm{RO_2\cdot}(2\mathrm{HO_2\cdot}) \xrightarrow{k_t} \text{non-radical products}$$

When the concentration of oxygen is sufficiently high, the rate of oxidation can be expressed by

$$-\mathrm{dO_2}/\mathrm{d}t = (\mathrm{RH})R_i^{1/2}k_p/(2k_t)^{1/2}$$

where k_p and k_t are the rate constants of chain propagation reaction and chain termination reaction, respectively, and R_i is the rate of initiation reaction. When (RH) and R_i are given, $k_p/(2k_t)^{1/2}$ can be calculated by measuring the rate of oxidation:

$$k_p/(2k_t)^{1/2} = -\mathrm{dO_2}/\mathrm{d}t/(\mathrm{RH})R_i^{1/2}.$$

It has been reported[13] that the value of $k_p/(2k_t)^{1/2}$ of hydrocarbon solution remains constant when the substrate is diluted with an inert solvent having a dielectric constant similar to that of the hydrocarbon. $k_p/(2k_t)^{1/2}$ was not constant in the oxidation of 1-phenylethanol, when the alcohol was diluted chlorobenzene having a dielectric constant similar to that of the alcohol. As shown in Fig. 1, $k_p/(2k_t)^{1/2}$ of 1-phenylethanol decreases markedly with the increase in the concentration of alcohol. This does not seem to have been reported in the autoxidation of hydrocarbons.

$k_p/(2k_t)^{1/2}$ increased with decreasing substrate concentration when other alcohols such as benzyl alcohol

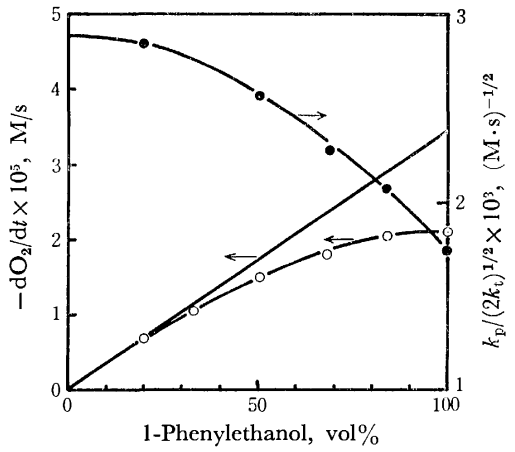

Fig. 1. The rate of oxidation of 1-phenylethanol as a function of alcohol concentration, 70 °C, $P_{O_2}=760$ mmHg, (AIBN) = 0.040 M, Solvent: chlorobenzene.

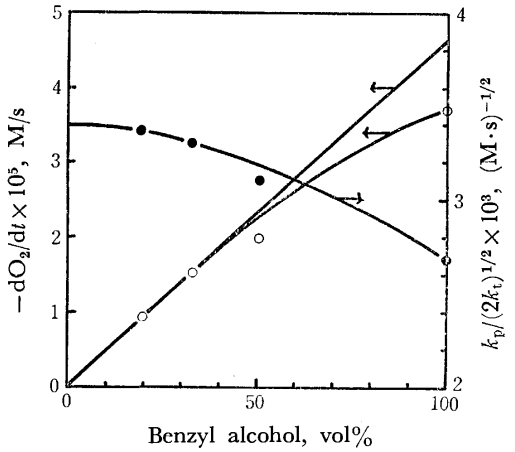

Fig. 2. The rate of oxidation of benzyl alcohol as a function of alcohol concentration, 70 °C, $P_{O_2}=760$ mmHg, (AIBN) = 0.040 M, Solvent: chlorobenzene/acetophenone = 1/2 by vol.

(Fig. 2) and 2-propanol were diluted with inert solvents whose dielectric constants were approximately equal to those of alcohols.

The values indicate that the hydrogen abstraction of alcohols is retarded by the hydrogen bonding between two hydroxyl compounds or by the hydrogen bonding of peroxyl radical with hydroxyl compound. The hydrogen bonding between alcohol molecules has no significant effect on the rate of hydrogen abstraction, since water no more retards the oxidation when a hydroperoxyl radical is replaced by a tetralylperoxyl radical.

The extrapolated values of $k_p/(2k_t)^{1/2}$ to zero alcohol concentration are given in Table 1. The ratio of $k_p/(2k_t)^{1/2}$ at 0% alcohol to $k_p/(2k_t)^{1/2}$ at 100% alcohol is between 2.0 and 1.3.

The effect of hydroxyl compounds on the rate of oxidation of 1-phenylethanol is shown in Fig. 3. *t*-Butyl alcohol accelerated the rate of oxidation, but water and methanol strongly retarded it; methanol did not retard the oxidation of tetralin (Table 2).

The result of *t*-butyl alcohol is probably due to steric hindrance for hydrogen bonding. Similarly,

Table 1. Effect of alcohol concentration on the rate of oxidation of alcohol

70 °C, $P_{O_2}=760$ mmHg, (AIBN) = 0.040 M

Alcohol	Solvent	$\frac{(k_p/(2k_t)^{1/2})(RH)=0\%}{(k_p/(2k_t)^{1/2})(RH)=100\%}$
2-Propanol	Chlorobenzene	2.0
1-Phenylethanol	Chlorobenzene	1.6
Benzyl alcohol	Chlorobenzene + acetophenone	1.3

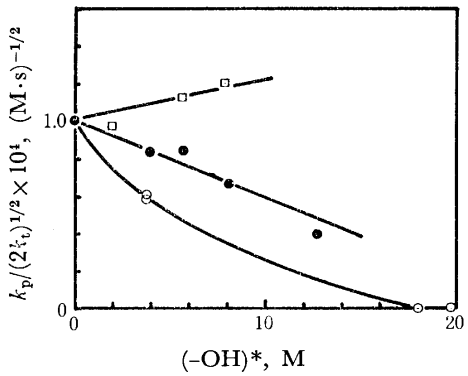

Fig. 3. Oxidation of 1-phenylethanol in the presencs of H_2O (○), methanol (●) or *t*-butyl alcohol (□), 60 °C, $P_{O_2}=760$ mmHg, (AIBN) = 0.040 M, * (-OH) = (H_2O) × 2.

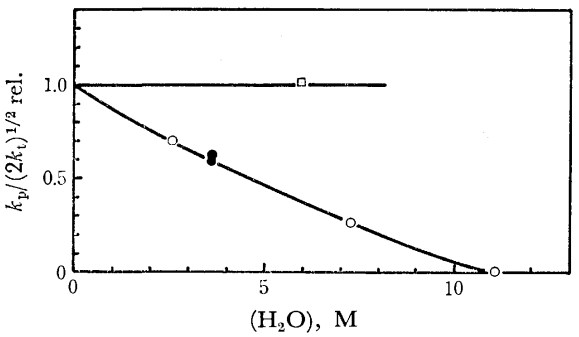

Fig. 4. Oxidation of 2-propanol, 1-phenylethanol or *p*-isopropyltoluene in the presence of H_2O.
○: 2-propanol at 60 °C, (AIBN) = 0.040 M. ●: 1-phenylethanol at 60 °C, (AIBN) = 0.040 M, H_2O/*t*-butyl alcohol = 1/2 by vol. □: *p*-isopropyltoluene at 70 °C, (AIBN) = 0.040 M, H_2O/*t*-butyl alcohol = 3/20 by vol.

the rate of oxidation of 2-propanol was inhibited in the presence of water, but the rate of oxidation of *p*-isopropyltoluene (Fig. 4) was not affected by the addition of methanol and water.

The rate of oxidation of 2-propanol in the presence of 0.20 M tetralyl hydroperoxide is plotted against water concentration (Fig. 5). The hydroperoxide method was proposed by Howard *et al.*[14] In the presence of tetralyl hydroperoxide, the chain carrier completely changes from the hydroperoxyl radical to the tetralylperoxyl radical at hydroperoxide concentrations above 0.1 M (Fig. 6). In the presence of tetralyl hydroperoxide, *viz.*, when the hydroperoxyl radical

Table 2. Effect of methanol on the rate of oxidation of tetralin

60 °C, $P_{O_2}=760$ mmHg, (AIBN) = 0.040 M

(Tetralin) M	(Methanol) M	$-dO_2/dt$ $\times 10^5$, M/s	$k_p/(2k_t)^{1/2}$ $\times 10^3$, $(M\cdot s)^{-1/2}$
6.58	0.0	3.13	6.23
5.06	5.70	2.86	7.41
4.39	8.23	2.61	7.79

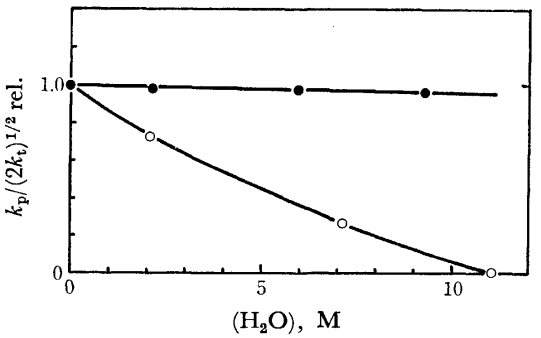

Fig. 5. Effect of water concentration in the autoxidation of 2-propanol.
○: Hydroperoxyl radical, in the presence of H_2O, 60 °C, (AIBN) = 0.040 M. ●: Tetralylperoxyl radical, in the presence of THP and H_2O, 50 °C, (AIBN) = 0.040 M, (THP) = 0.20 M.

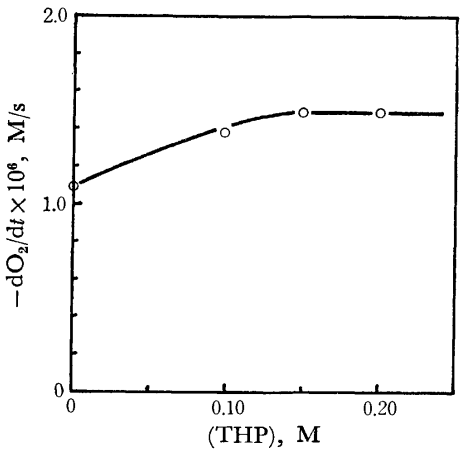

Fig. 6. Oxidation of 2-propanol in the presence of tetralyl hydroperoxide.
50 °C, (AIBN) = 0.040 M, $P_{O_2}=760$ mmHg, (2-propanol) = 13.1 M.

is replaced by the tetralylperoxyl radical, no further inhibition effect due to water is observed.

Thus it can be concluded that hydroxyl compounds such as water and alcohols except *t*-butyl alcohol, deactivate by hydrogen bonding only hydroperoxyl and α-hydroxyalkylperoxyl radicals and not ordinary alkylperoxyl radical.

The hydrogen bonding of peroxyl radical with hydroxy compound lowers both k_p and k_t. It is suggested that $k_p/(2k_p)^{1/2}$ decreases because the extent of decrease of k_p is greater than that of $\sqrt{2k_t}$.

The relative rate constant of oxidatikn of 1-phenylethanol, $k_p/(2k_t)^{1/2}{}_{rel.}$, is plotted against the concentration of carboxylic acids (Fig. 7). We see that the rate constant of oxidation of 1-phenylethanol, $k_p/(2k_t)^{1/2}{}_{rel.}$, is not affected by the addition of oxalic acid, decreasing remarkably by the addition of *p*-nitrobenzoic acid, decreasing to a similar extent by the addition of various carboxylic acids such as acetic, benzoic, butyric, chloroacetic acids. The effect of

Table 3. Effect of acetic acid on the rate of tetralin

60 °C, $P_{O_2}=760$ mmHg, (AIBN) = 0.040 M

(Tetralin) M	(Acetic acid) M	$-dO_2/dt$ $\times 10^5$, M/s	$k_p/(2k_t)^{1/2}$ rel.
7.35	0.0	3.13	1.00
6.68	1.59	2.80	0.984
5.65	4.04	2.50	1.04

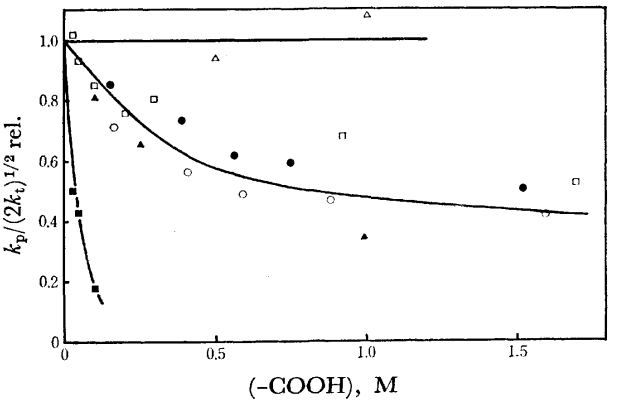

Fig. 7. Oxidation of 1-phenylethanol in the presence of carboxylic acids.
70 °C, $P_{O_2}=760$ mmHg, (AIBN) = 0.040 M.
○: acetic acid, ●: monochloroacetic acid, □: benzoic acid, ■: *p*-nitrobenzoic acid, ▲: butyric acid, △: oxalic acid.

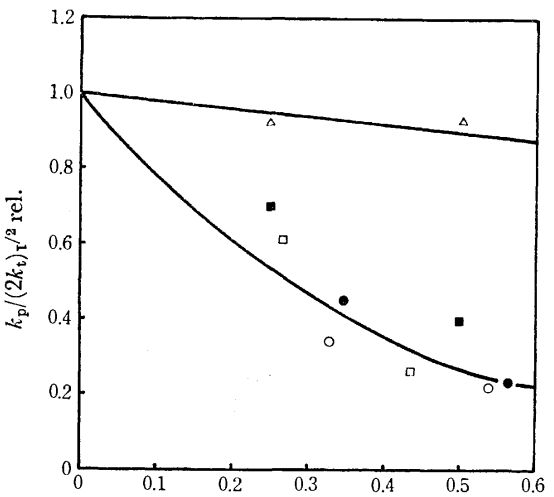

Fig. 8. Oxidation of 2-propanol in the presence of carboxylic acids.
60 °C, $P_{O_2}=760$ mmHg, (AIBN) = 0.040 M.
●: Acetic acid, ○: monochloroacetic acid, □: propionic acid, ■: benzoic acid, △: oxalic acid.

fatty acid and benzenecarboxylic acid seems to be independent of acid strength. The very small effect of oxalic acid may be due to intramolecular hydrogen bonding of oxalic acid. A similar solvent effect was observed in the oxidation of 2-propanol in the presence of carboxylic aicds (Fig. 8).

Acetic acid has no retardation effect on the hydrogen abstraction step by alkyl peroxyl radical (Table 3). This was confirmed by the hydroperoxide method, since the retardation effect due to acetic acid on the oxidation of 2-propanol is almost eliminated in the presence of tetralyl hydroperoxide (Fig. 9).

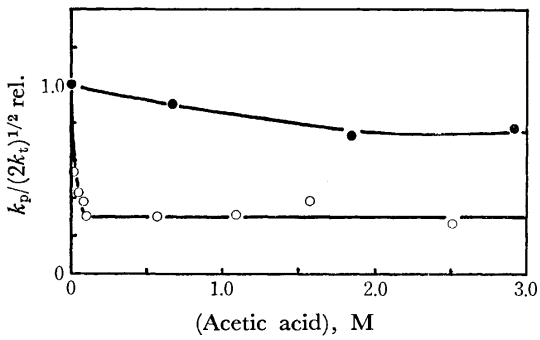

Fig. 9. Effect of acetic acid in the oxidation of 2-propanol.
50 °C, P_{O_2}=760 mmHg, (AIBN)=0.040 M
○: in the presence of acetic acid, ●: in the presence of acetic acid and THP, (THP)=0.20 M.

Table 4. Effect of acetic acid on the rate of oxidation of 1,4-cyclohexadiene
40 °C, P_{O_2}=760 mmHg, (AIBN)=0.040 M
(1,4-cyclohexadiene)=0.964 M, solvent: chlorobenzene

(Acetic acid) M	$-dO_2/dt$ $\times 10^6$, M/s	$k_p/(2k_t)^{1/2}$ rel.
0.0	7.13	1.00
0.0223	4.89	0.686
0.0520	3.02	0.424

Denisov and Solyanikov[15] reported that the decreasing rate of formation of hydrogen peroxide during the oxidation of 2-propanol is attributable to decomposition of hydrogen peroxide by the carboxylic acid formed during the course of oxidation. However, from our results it can be concluded that the rate of oxidation of 2-propanol decreases due to the deactivation of peroxyl radicals.

The effect of acetic acid on the hydroperoxyl radical is also confirmed in the autoxidation of 1,4-cyclohexadiene (Table 4), because in this case the chain carrier is hydroperoxyl radical[16].

The rate of oxidation of 1,4-cyclohexadiene was remarkably decreased by the addition of acetic acid (Table 4). The effect of association of hydroxyl compounds on the rate of oxidation of alcohol can be disregarded since 1,4-cyclohexadiene does not associate with acetic acid.

The rate of oxidation of 1-phenylethanol in the presence of phthalic acid or isophthalic acid is given in Table 5. It is clear that the rate of oxidation of 1-phenylethanol in the presence of isophthalic acid is smaller than that in the presence of phthalic acid. Phthalic acid has a greater dissociation constant than isophthalic acid, and the stability of intramolecular hydrogen bonding of phthalic acid should be higher than that of isophthalic acid.[17]

The relative rate constant of oxidation of 1-phenylethanol in the presence of 0.05 M isophthalic acid (0.815) is nearly equal to that in the presence of 0.1 M benzoic acid (0.798). It is concluded that the rate of oxidation of alcohols in the presence of dicarboxylic acid, which can form an intramolecular hydrogen bond, is greater than the rate in the presence of dicarboxylic acid, which has difficulty to form an intramolecular hydrogen bond.

The very small effect of oxalic acid on the autoxidation of 1-phenylethanol can be explained on the basis of intramolecular hydrogen bonding (Fig. 7).

Table 5. Effect of phthalic acid or isophthalic acid on the rate of oxidation of 1-phenylethanol
60 °C, P_{O_2}=760 mmHg, (AIBN)=0.040 M, solvent: *t*-butyl alcohol

(1-Phenylethanol) M	(Phthalic acid) M	(Isophthalic acid) M	$-dO_2/dt$ $\times 10^5$, M/s	$k_p/(2k_t)^{1/2}$ rel.
3.32	0.00	0.00	4.26	1.00
3.32	0.10	0.00	3.34	0.784
3.32	0.00	0.10	2.03	0.475

Table 6. Effect of benzoic acids on the rate of oxidation of 1-phenylethanol
60 °C, P_{O_2}=760 mmHg, (AIBN)=0.040 M, (-COOH)=0.10 M

Substituted benzoic acid	σ^+ [18]	1-Phenylethanol M	$-dO_2/dt$ $\times 10^5$, M/s	$k_p/(2k_t)^{1/2}$ $\times 10^3$, $(M\cdot s)^{-1/2}$	$k_p/(2k_t)^{1/2}$ rel.
p-CH_3O	−0.778	8.30	6.23	0.983	0.793
p-CH_3	−0.311	8.30	6.36	1.01	0.811
p-H	0.00	8.30	6.26	0.989	0.798
p-Cl	+0.114	8.30	6.54	1.03	0.834
m-COOH	+0.322	3.32	3.46	1.37	0.815
p-NO_2	+0.790	8.30	0.36	0.057	0.046

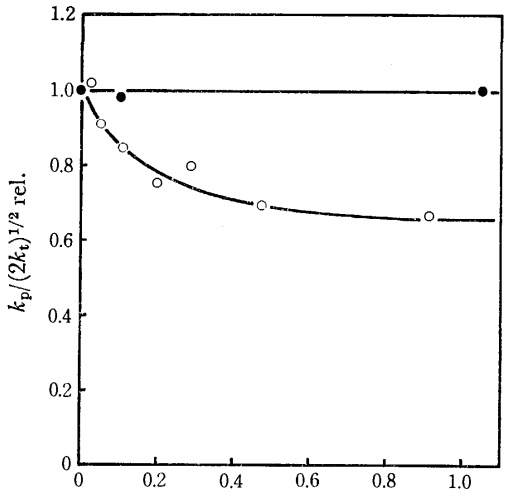

(Benzoic acid or methyl), (benzoate), M

Fig. 10. The rate of oxidation of 1-phenylethanol in the presence of benzoic acid (○) or methyl benzoate (●).
70 °C, $P_{O_2}=760$ mmHg, (AIBN) = 0.040 M.

TABLE 7. AUTOXIDATION OF *N,N*-DIMETHYLBENZYLAMINE AND DIBENZYL ETHER IN THE PRESENCE OF WATER IN *t*-BUTYL ALCOHOL

70 °C, $P_{O_2}=760$ mmHg, (AIBN) = 0.040 M

Substrate M	H_2O M	$-dO_2/dt \times 10^6$, M/s	$k_p/(2k_t)^{1/2}$ rel.
N,N-Dimethylbenzylamine			
4.51(in *t*-butyl alcohol)	0.0	73.1	1.00
4.51(in *t*-butyl alcohol)	3.71	10.3	0.14
Dibenzyl ether			
3.48(in *t*-butyl alcohol)	0.0	98.3	1.00
3.48(in *t*-butyl alcohol)	1.68	77.3	0.79

The effect of substituent on the benzene nucleus was studied using substitued benzoic acid in the autoxidation of 1-phenylethannol (Table 6). Except for the nitro group, no significant difference was observed in the retardation effect of benzoic acids.

The rate of oxidation of 1-phenylethanol, plotted against the concentration of benzoic acid or methyl benzoate (Fig. 10) apparently decreases with carboxylic acid and not ester. It can be said that carboxylic acids deactivate the chain carrier of alcohol, *viz.*, hydroperoxyl and α-hydroxyalkylperoxyl radicals, due to a hydrogen bonding, but not alkylperoxyl radicals.

The effect of α-substituent of toluene on the rate of autoxidation in the presence of hydroxyl compounds should be investigated.

Addition of water to *N,N*-dimethylbenzylamine and benzyl ether decreased the rate of oxidation by factors of 0.14 and 0.79, respectively (Table 7).

The effect of acetic acid in the autoxidation of ten kinds of α-substituted toluenes is given in Table 8.

The rate of oxidation of *N,N*-dimethylbenzylamine, benzyl alcohol, *N,N*-diethylbenzylamine, 1-phenylethanol and methyl benzyl ether decreased with the addition of acetic acid. On the other hand, the rate of oxidation of (2-chloroethyl)benzene, ethylbenzene, cumene and diphenylmethane was unaffected.

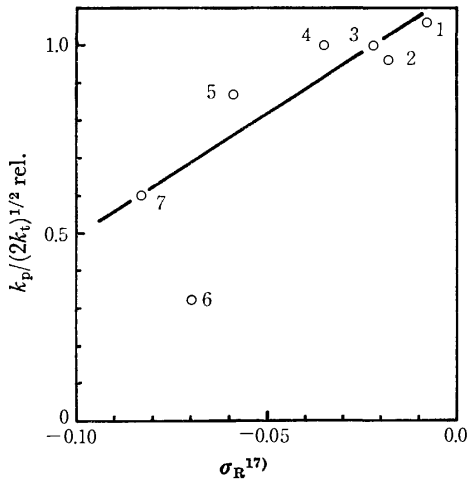

Fig. 11. Plots of $k_p/(2k_t)^{1/2}$ rel. against σ_R.
1: (2-chloroethyl)benzene, 2: diphenylmethane, 3: ethylbenzene, 4: isopropylbenzene, 5: methyl benzyl ether, 6: benzyl alcohol, 7: 1-phenylethanol.

TABLE 8. $k_p/(2k_t)^{1/2}$ rel. OF AUTOXIDATION OF α-SUBSTITUTED TOLUENES IN THE PRESENCE OF ACETIC ACID

70 °C, $P_{O_2}=760$ mmHg, (AIBN) = 0.040 M
(acetic acid) = 0.224 M, solvent: chlorobenzene

Substrate	$\{k_p/(2k_t)^{1/2}\}(AcOH)=0.224\ M$ / $\{k_p/(2k_t)^{1/2}\}(AcOH)=0.0\ M$
(2-Chloroethyl)benzene	1.06
Ethylbenzene	1.00
Isopropylbenzene	1.00
Diphenylmethane	0.96
Dibenzyl ether	0.93
Methyl benzyl ether	0.87
1-Phenylethanol	0.60
N,N-Diethylbenzylamine	0.60
Benzyl alcohol	0.32
N,N-Dimethylbenzylamine	0.19

It can be concluded that the hydroperoxyl radical and alkylperoxyl radicals with α-substituents such as hydroxyl, alkoxyl and amino groups are capable of forming hydrogen bonding with hydroxyl compounds.

We tried to correlate these results in terms of substituent effect. It is suggested that resonance effect takes part and increases the electron density of the peroxyl radical accelerating the formation of hydrogen bonding (Fig. 11).

According to Zaikov and Maizus,[8] the oxidation of methyl ethyl ketone is remarkably inhibited in the presence of water, and according to Imamura *et al.*[9] the rate of oxidation of acetaldehyde is retarded by the addition of various carboxylic acids.

Thus, alkylperoxyl radicals should have α-substituent such as hydroxyl, carbonyl, amino and alkoxyl groups for the formation of hydrogen bonding with water, alcohols and carboxylic acids. These results also indicate that the structure of hydrogen bonding of peroxyl radicals is very complex and it is difficult to

present any quantitative explanation. Solvation of peroxyl radical and association of hydroxyl compounds should take part. However, a bridged cyclic structure involving nitrogen or oxygen atoms of α-substituents can be proposed for hydrogen bonding between water and peroxyl radicals.

It seems that the results[2] showing that the termination rate constant of the hydroxyl radical is markedly affected by the solvent, *viz.*, 10^9 (l/mol·s) in neutral solvent but 10^6 in aqueous solution, and also that the hydroperoxyl radical is inactive in aqueous solution can be explained convincingly on the basis of hydrogen bonding effect.

References

1) K. U. Ingold, *Acc., Chem. Res.*, **2**, 1 (1969); *7th World Petrol Congress, Proceedings*, **5**, 15 (1967), Elsevier.
2) J. A. Howard, "Advances in Free Radical Chemistry," Logos (1972), Chap. 2, p. 49.
3) Y. Kamiya, "Organic Oxidation Reaction," Gihodo (1973).
4) N. M. Emanuel, E. T. Denisov, and Z. K. Maizus, "Liquid Phase Oxidation of Hydrocarbons," Plenum Press (1967).
5) J. Betts, *Quart, Rev.*, **25**, 265 (1971).
6) D. G. Hendry and G. A. Russel, *J. Am. Chem. Soc.*, **86**, 2368 (1964).
7) J. A. Howard and K. U. Ingold, *Can, J. Chem.*, **42**, 1044, 1250 (1964).
8) G. E. Zaikov and Z. K. Maizus, "Adv. Chem. Series," No. 75, Am. Chem. Soc. (1968), p. 150.
9) J. Imamura, T. Matsuzaki, M. Ando, N. Ohta, T. Saito and T. Ishikawa, Oxidation Symposium in Japan, Osaka, Preprint p. 1 (1969).
10) Y. Kamiya, S. Beaton, F. Lafortune, and K. U. Ingold, *Can. J. Chem.*, **44**, 2020, 2034 (1963).
11) F. Mashio and S. Kato, "Advances of Mechanisms of Organic Reactions (II)," Maki Shoten (1963), p. 65.
12) J. A. Howard, S. Korcek, and K. U. Ingold, *Can. J. Chem.*, **48**, 2165 (1970).
13) E. Niki, Y. Kamiya, and N. Ohta, *Bull. Chem. Soc. Jpn.*, **40**, 583 (1967).
14) J. A. Howard, W. J. Schwalm, and K. U. Ingold, "Adv. Chem. Series," No. 75, Am. Chem. Soc. (1968) p. 6.
15) E. T. Denisov and V. M. Solyanikov, *Neftekhimiya*, **3**, 360 (1963).
16) J. A. Howard and K. U. Ingold, *Can. J. Chem.*, **45**, 785 (1967).
17) Pimentel and McClellan, "The Hydrogen Bond," W. H. Freeman and Company, San Francisco and London (1960).
18) M. Imoto, "Yūki Hanno no Riron (I)," Kyoritsu Shuppan (1960).

Ring-opening Reactions of Cyclic Ethers. IX.[1] Molecular Weight Distribution of Adducts in the Acid-catalyzed Reactions of Epichlorohydrin with Alcohols

Shizen SEKIGUCHI,* Yasushi HASEGAWA, Kenji NAKAMURA, Kohji MATSUI, and Kensuke NAGAHAMA

Department of Synthetic Chemistry, Gunma University, Tenjincho, Kiryu, Gunma 376

(Received November 21, 1975)

It was found that the molecular weights of adducts in the acid-catalyzed reactions of epichlorohydrin with alcohols obey the Weibull-Nycander distribution but not the Flory distribution. The distribution constants ($C=k_i/k_0$) were found to be smaller than 1, indicating that the reaction rate of the initial stage (k_0), *i.e.*, the reaction of epichlorohydrin with a starting alcohol, is greater than the rates of the later stages (k_i), *i.e.*, the reactions of epichlorohydrin with its adducts. The results indicate that the reaction proceeds *via* an "borderline" A-2 mechanism.

Nonionic surface active agents, prepared from the successive addition reaction of alkylene oxides to aliphatic carboxylic acids, aliphatic amines, and esters of polyhydric alcohols, have recently attracted much attention. They are used as commercial surfactants to a greater extent than anionic ones.

Several papers have appeared dealing with basic studies on the preparation of surfactants. The molecular weight distribution (MWD) of the adducts in the sodium hydroxide-catalyzed addition reaction of ethylene oxide (EO) or propylene oxide to lower alcohols was determined by Shigematsu *et al.*,[2,3] who indicated that it obeys the Weibull-Nycander distribution.[4] Shoda *et al.*[5] studied the MWD of the products in the sodium hydroxide-catalyzed addition reaction of EO to the reduced alcohol of coconut oil and showed that it obeys the Flory distribution,[6] that is, the Poisson one. Nagase and Sakaguchi[7] indicated that the MWD of the adducts in the sodium-catalyzed addition reaction of EO to dodecyl alcohol obeys the Weibully-Nycander distribution better than the Flory one. Karabinos and Quinn[8] studied the potassium hydroxide-catalyzed reactions of EO with lauryl alcohol and showed that the MWDs of the adducts deviate from the Flory distribution. Tischbirek[9] discussed the effects of reaction temperature, pressure of reaction systems, concentration of EO, rate of stirring, and kinds of alcohols and catalysts on the MWD of the adducts in the acid- or base-catalyzed reactions of EO with alcohols (C_2, C_6, and C_{12} alcohols). Thus few papers have appeared on the MWD of adducts in the acid-catalyzed reactions of epoxides with alcohols.

On the other hand, the mechanism of the acid-catalyzed ring-opening reactions of epoxides has been discussed by many workers.[10-13] Briggs *et al.*[14] discussed the mechanism of the acid-catalyzed alcoholysis of epoxides in detail, criticizing our previous work.[11]

In order to confirm the mechanism of the acid-catalyzed alcoholysis of epichlorohydrin (EpCl), we have determined the distribution constant (C), which is the ratio of the rate constant of the later stages (k_1, k_2, ...) to that of the initial stage (k_0), and which distribution the MWD in these reactions would obey.

Experimental

Materials. Methyl, propyl, butyl, *s*-butyl, and isobutyl alcohols were purified by the usual method. Boron trifluoride etherate ($BF_3\cdot Et_2O$) and EpCl were repeatedly distilled through a rectifying column (Kyowa VI-DL Concentric Tube Fractionater, theoretical plate number 80); $BF_3\cdot Et_2O$ bp 125 °C; EpCl 114—115 °C, d_4^{30} 1.1682, n_D^{30} 1.4326.

Synthes is of 1 : 1 (EpCl·ROH) and 2 : 1 (3EpCl·ROH) Adducts. Epichlorohydrin reacts with an alcohol in the presence of an acid to give the following adducts.[11,15,16]

$$\mathrm{ClCH_2\text{-}\underset{\backslash O /}{CH}\text{-}CH_2} + \mathrm{ROH} \longrightarrow \underset{(\mathrm{EpCl\cdot ROH})}{\mathrm{ClCH_2CH(OH)CH_2OR}} \quad (1)$$

Table 1. Syntheses of 1 : 1 and 2 : 1 adducts

Run	Adduct	ROH[a] g(mol)	EpCl g(mol)	Catalyst g(mol)	React temp (°C)	React time (h)	Bp (°C/mmHg)	Yield[b] (%)
1	EpCl·*n*-C_4H_9OH	1280(17.3)	200 (2.16)	8 (0.078)[c]	117—121	12	72.6—74.6/2	60
2	EpCl·*i*-C_4H_9OH	1280(17.3)	200 (2.16)	8 (0.078)[c]	108—112	17.5	74.0—76.0/4	72
3	EpCl·*s*-C_4H_9OH	1280(17.3)	200 (2.16)	8 (0.078)[c]	99—103	26	86—88/8	80
4	2EpCl·*n*-C_4H_9OH	298(1.78)	20.8(0.224)	1.18(8.37×10^{-3})[d]	110—130	31	140—144/1	34
5	2EpCl·*i*-C_4H_9OH	238(1.42)	16.3(0.176)	1.13(7.99×10^{-3})[d]	110—130	30	145—150/4	52
6	2EpCl·*s*-C_4H_9OH	284(1.70)	19.8(0.211)	1.16(8.17×10^{-3})[d]	110—130	34	168—170/12	29
7	EpCl·CH_3OH	480(15.0)	140 (1.5)	2.8 (2.7×10^{-2})[c]	67—68	12	93.2—93.5/48—50	83.3
8	EpCl·*n*-C_3H_7OH	520(8.65)	100 (1.08)	1.6 (1.5×10^{-2})[c]	96—98	10	73—75/8	56.3

a) Alcohols used are *n*-, *i*-, and *s*-C_4H_9OH, CH_3OH, and *n*-C_3H_7OH in the case of Runs 1—3, 7 and 8, respectively; EpCl·ROH(1 : 1 adduct) in the case of Runs 4—6. b) Based on initial EpCl. c) 95% H_2SO_4 used as a catalyst. d) $BF_3\cdot Et_2O$ used as a catalyst.

Table 2. Refractive indices and elemental analyses of adducts

Run	Adduct	Ref. index[a] (n_D^t)	Elemental anal. (%) Calcd C	Calcd H	Found C	Found H
1	EpCl·*n*-C_4H_9OH	1.4437 (23.8) [1.4441 (23.5)][11a]	50.45	9.07	50.31	9.22
2	EpCl·*i*-C_4H_9OH	1.4399 (23.8)	50.45	9.07	50.37	9.06
3	EpCl·*s*-C_4H_9OH	1.4420 (23.2) [1.4425 (23.8)][11a]	50.45	9.07	50.30	9.09
4	2EpCl·*n*-C_4H_9OH	1.4652 (25.0)	46.33	7.77	46.50	7.71
5	2EpCl·*i*-C_4H_9OH	1.4597 (26.5)	46.33	7.77	46.31	7.74
6	2EpCl·*s*-C_4H_9OH	1.4593 (25.4)	46.33	7.77	46.48	7.67
7	EpCl·CH_3OH	1.4488 (15.4) [1.4488 (15.4)][11a]	38.57	7.28	38.58	7.42
8	EpCl·*n*-C_3H_7OH	1.4443 (15.4) [1.4447 (19.5)][11a]	47.22	8.58	47.08	8.39

a) Figures in parentheses indicate the temperature of measurement.

$$ClCH_2\text{-}\underset{\backslash O /}{CH}\text{-}CH_2 + ClCH_2CH(OH)CH_2OR \rightarrow ClCH_2CH(OH)CH_2OCH(ClCH_2)CH_2OR \quad (2)$$
(2EpCl·ROH)

Higher adducts are formed, depending on the reaction conditions, especially on the molar ratio of EpCl to alcohol. These adducts were synthesized for the preparation of calibration curves in vapor phase chromatography (VPC).

In the case of EpCl·CH_3OH, a typical procedure is described below. One hundred and forty grams (1.5 mol) of EpCl was added dropwise at room temperature to a stirred solution of 480 g (15 mol) of methyl alcohol and 2.8 g (2.7×10^{-2} mol) of H_2SO_4. EpCl had to be carefully added to prevent bumping. After addition of EpCl the mixture was further refluxed for 12 h. After the mixture had been neutralized with a concentrated sodium hydroxide solution, and dried over anhydrous sodium sulfate, methyl alcohol was distilled off and the residue was distilled under reduced pressure.

The reaction conditions, boiling points and yields for the preparation of the adducts are shown in Table 1, and the physical properties and results of elemental analyses in Table 2.

Determination of Unreacted Alcohols and Epichlorohydrin, and Adducts. The amount of the unreacted EpCl and Alcohols, and adducts were determined by VPC on a column packed with 10% polydiethylene glycol succinate (2 m) on Diasolid M at 100 °C for unreacted EpCl and alcohols (toluene used as an internal standard), 190 °C for 1 : 1 adducts and 200 °C for 2 : 1 adducts (in these cases, nitrobenzene used as an internal standard). Helium was used as a carrier gas.

Theoretical

Theories on molecular weight distribution have been worked out by several workers, the Flory[17] and Weibull-Nycander distributions[18] being often used. Molecular weight distribution can be calculated if certain assumptions are made on the relative reactivities of a starting alcohol and its adducts.

The reaction path of addition is expressed as follows:

$$ROH \xrightarrow[ClCH_2\text{-}\underset{\backslash O /}{CH}\text{-}CH_2]{k_0} ClCH_2\text{-}\underset{OH}{\underset{|}{CH}}\text{-}CH_2\text{-}OR \xrightarrow[ClCH_2\text{-}\underset{\backslash O /}{CH}\text{-}CH_2]{k_1}$$
(EpCl·ROH)

$$ClCH_2\text{-}\underset{\backslash O /}{CH}\text{-}CH_2\text{-}OR \xrightarrow[ClCH_2\text{-}\underset{\backslash O /}{CH}\text{-}CH_2]{k_2} ClCH_2\text{-}\underset{\backslash O /}{CH}\text{-}CH_2\text{-}O\text{-}CH_2\text{-}\underset{OH}{\underset{|}{CH}}\text{-}CH_2Cl$$
(2EpCl·ROH)

$$ClCH_2\text{-}\underset{\backslash O /}{CH}\text{-}CH_2\text{-}OR \xrightarrow[ClCH_2\text{-}\underset{\backslash O /}{CH}\text{-}CH_2]{k_3} ClCH_2\text{-}\underset{\backslash O /}{CH}\text{-}CH_2\text{-}O\text{-}CH_2\text{-}\underset{\backslash O /}{CH}\text{-}CH_2\text{-}O\text{-}CH_2\text{-}\underset{OH}{\underset{|}{CH}}\text{-}CH_2Cl$$
(3EpCl·ROH) (3)

Flory distribution (or Poisson distribution)

If $k_0=k_1=k_2=\cdots=k_n=\cdots$ in Eq. 2, we obtain

$$\frac{n_i}{n_{00}} = e^{-v}\cdot\frac{v^i}{i!} \quad (4)$$

Weibull-Nycander distribution

If $k_0=k_1=k_2=\cdots=k_n=\cdots$ in Eq. 1 we have

$$v = C\cdot\ln\frac{n_{00}}{n_0} - (C-1)\left(1-\frac{n_0}{n_{00}}\right) \quad (5)$$

and

$$\frac{n_i}{n_{00}} = \frac{C^{i-1}}{(C-1)^i}\left\{\frac{n_0}{n_{00}} - \left(\frac{n_0}{n_{00}}\right)^C \sum_{j=0}^{i-1}\frac{1}{j!}\left[(C-1)\ln\frac{n_{00}}{n_0}\right]^j\right\} \quad (6)$$

n_{00}; mole of a starting alcohol
n_i; mole of i-th mer (iEpCl·ROH)
v; average mole of added EpCl per one mole of the starting alcohol
C; distribution constant (k_i/k_0)

Thus we can calculate the v-value if the amount of unreacted EpCl is determined. Once the v-value is determined, the expected amounts of i-th mers formed in the Flory distribution can be calculated by means of Eq. 4. Furthermore, if the amount of unreacted alcohol is also determined, a C-value can be calculated by means of Eq. 5. Using the C-value and Eq. 6, one can estimated the expected amounts of i-th mers in the Weibull-Nycander distribution.

Table 3. Determination of adducts[a)]

Run	Alcohol	Catalyst[b)]	(mol%)	React. temp (°C)	v	Observed values n_0/n_{00}	n_1/n_{00}	n_2/n_{00}	C
9		$BF_3 \cdot Et_2O$	0.108	50	0.996	0.154	0.761	0.103	0.14
10		$BF_3 \cdot Et_2O$	0.109	70	1.000	0.160	0.743	0.101	0.16
11	n-C_4H_9OH	$BF_3 \cdot Et_2O$	0.054	70	0.917	0.200	0.754	0.079	0.14
12		$SnCl_4$	0.109	70	1.000	0.112	0.845	0.031	0.08
13		$ZnCl_2$	1.99	70	0.845	0.239	0.779	0.025	0.12
14		H_2SO_4	2.00	70	0.184	0.814	0.180	trace	0.10
15		$BF_3 \cdot Et_2O$	0.108	50	0.994	0.150	0.716	0.113	0.13
16	i-C_4H_9OH	$BF_3 \cdot Et_2O$	0.106	70	1.000	0.155	0.699	0.117	0.15
17		$SnCl_4$	0.109	70	1.000	0.129	0.733	0.097	0.10
18		$BF_3 \cdot Et_2O$	0.109	50	1.000	0.157	0.701	0.124	0.15
19	s-C_4H_9OH	$BF_3 \cdot Et_2O$	0.109	70	1.000	0.169	0.650	0.127	0.17
20		$SnCl_4$	0.109	70	1.000	0.129	0.733	0.097	0.10
21		$ZnCl_2$	2.00	70	0.902	0.167	0.712	0.067	0.07
22	CH_3OH	$BF_3 \cdot Et_2O$	0.063	55	0.980	0.158	0.725	0.108	0.13
23	n-C_3H_7OH	$BF_3 \cdot Et_2O$	0.035	70	0.882	0.235	0.678	0.108	0.17

a) Thirty grams (0.324 mol) of EpCl was used. The molar ratio of each alcohol to EpCl is one. b) Based on the amount of EpCl.

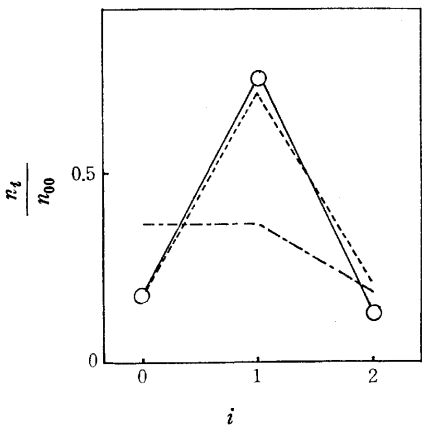

Fig. 1. The relationship between n_i/n_{00} and i.
——: observed, – – –: Flory distribution, ----: Weibull-Nycander distribution.

Results and Discussion

The results of determination of the adducts are given in Table 3. Through all runs, the recovery of initial EpCl summing up unreacted and transformed EpCl ranged from 95 to 100%, and, moreover, most of it was found to be transformed EpCl. Thus it seems that a very small amount of initial EpCl changed into unidentified products.[19)]

The results indicate that the distribution constant was smaller than 1, the 1 : 1 adduct being produced to a greater extent than the 2 : 1 one in every case. The observed values (n_i/n_{00}) in the case of Run 9 are compared with those calculated on the basis of the Flory and Weibully-Nycander distributions by use of C (0.14) (Fig. 1). The MWD in Run 9 clearly obeys the Weibully-Nycander one. Similar results were also obtained in the other runs.

The mechanism of acid-catalyzed ring-opening reactions of epoxides have been discussed by several workers. Long *et al.*[10)] concludedthat the acid-catalyzed hydrolysis of epoxides proceeds *via* a "borderline" A-1 mechanism,[10,20)] *viz.*, the carbonium ion formed through the co-ordination of an acid (catalyst) to the oxygen atom of epoxides reacts with nucleophiles.

On the other hand, Koskikallio and Whalley[12)] and leNoble and Duffy[13)] found that the volume of activation ($\Delta V^{\neq}$) is negative in the acid-catalyzed hydrolyses of epoxides and they concluded that the hydrolysis proceeds *via* an A-2 mechanism. Briggs *et al.*[14)] reported that the acid-catalyzed alcoholysis of styrene oxide proceeds *via* a "borderline" A-2 mechanism.

Entropy of activation as a criterion for reaction mechanism is discussed by many workers.[21)] Whalley[22)] deduced that (i) if $\Delta S^{\neq}$ is less than zero the reaction was probably A-2 and (ii) if $\Delta S^{\neq}$ is greater than zero the mechanism can be either A-1 or A-2. And, Stimson[23)] and Stimson and Watson[24)] showed that the hydrolysis of *t*-butyl benzoate and *t*-butyl formate in acidified 60% aqueous acetone gives $\Delta S^{\neq}$ values of +9.5 and −23.7 e.u., respectively, indicating that the former hydrolysis proceeds by an A-1 mechanism and the latter by an A-2 mechanism and that the hydrolysis of *t*-butyl 2,4,6-trimethylbenzoate in acidified 90% ethanol–water gives $\Delta S^{\neq}$ value of +8.1 e.u. by an A-1 mechanism.

We reported that the acid-catalyzed reaction of EpCl with alcohols or their adducts (nEpCl·ROH; n=1,2,3) proceeds via an "borderline" A-2 mechanism with $\Delta S^{\neq}$ values of −20∼−10 e.u., which were greater

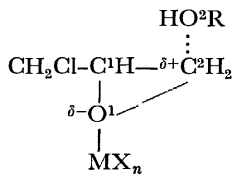

to some extent than those of usual A-2 mechanism and proposed the following transition state.[11)] The distribution constants of *ca.* 0.10 correspond to this

proposition, since if this transition state is assumed, the reaction rate of the first stage will be greater than those of the later ones owing to the steric crowding of the bulkier adducts (RO^2H) at C^2 atom. If the carbonium ion such as $ClCH_2(\bar{O}MX_n)\overset{+}{C}H_2$ were formed, the 1 : 1 adducts should be produced less than as shown in Fig. 1 and the MWD should obey the Flory distribution since this situation indicates that $k_0=k_1=\cdots$.

Although Briggs *et al.* stated that the choice of EpCl is not appropriate for the elucidation of the mechanism or ring-opening reaction of epoxides, we found that the determination of MWD of adducts in the acid-catalyzed reaction of EpCl with alcohols is very useful. It is concluded that in the presence of acidic catalysts EpCl reacts with alcohols *via* an "borderline" A-2 mechanism.

References

1) Part VIII; S. Sekiguchi, K. Matsui, and Y. Yasuraoka, *Bull. Chem. Soc. Jpn.*, **43**, 2523 (1970).

2) H. Shigematsu, Y. Miura, and Y. Ishii, *Kogyo Kagaku Zasshi*, **65**, 64 (1962).

3) H. Shigematsu, Y. Nishikawa, and Y. Ishii, *Kogyo Kagaku Zasshi*, **65**, 111 (1962).

4) B. Weibull and B. Nycander, *Acta Chem. Scand.*, **8**, 847 (1954).

5) Y. Shoda, T. Yamamoto, and T. Shimojima, *Yukagaku Kyokai Shi*, **7**, 8 (1958).

6) P. Flory, *J. Am. Chem. Soc.*, **62**, 1561 (1949).

7) K. Nagase and K. Sakaguchi, *Kogyo Kagaku Zasshi*, **63**, 588 (1960).

8) J. V. Karabinos and E. J. Quinn, *J. Am. Oil Chemists Soc.*, **33**, 223 (1956).

9) G. Tischbirek, *Vortraege Originalfass. Intern. Kongr. Grenzflaechenaktive Stoffe*, 3, Cologne, **1**, 126 (1960).

10) (a) F. A. Long and J. G. Pritchard, *J. Am. Chem. Soc.*, **78**, 2663 (1956); (b) J. G. Pritchard and F. A. Long, *ibid.*, **78**, 2667 (1956); (c) J. G. Pritchard and F. A. Long, *ibid.*, **78**, 6008 (1956); F. A. Long, J. G. Pritchard, and F. E. Stafford, *ibid.*, **79**, 2362 (1957); (d) L. L. Ingraham and S. Winstein, *ibid.*, **74**, 1160 (1952).

11) (a) S. Sekiguchi, I. Takase, and K. Matsui, *Kogyo Kagaku Zasshi*, **66**, 1827 (1963); *ibid.*, **68**, 286, 945, 2414 (1965); (b) S. Sekiguchi, S. Ishii, and K. Matsui, *ibid.*, **68**, 286 (1965); (c) S. Sekiguchi and S. Ishii, *ibid.*, **70**, 47 (1967).

12) J. Koskikallio and E. Whalley, *Trans. Faraday Soc.*, **55**, 815 (1959).

13) W. J. leNoble and M. Duffy, *J. Phys. Chem.*, **68**, 614 (1964).

14) (a) J. Briggs, N. B. Chapman, A. F. Finch, and V. Wray, *J. Chem. Soc., B*, **1971**, 55; (b) J. Briggs, N. B. Chapman. and V. Wray, *ibid.*, **1971**, 63, 66, 71.

15) F. G. Ponomarev, *Zhur. Obshchei. Khim.*, **22**, 128, 9291 (1952); *Chem. Abstr.*, **46**, 11105 (1952); *ibid.*, **47**, 3794 (1953).

16) (a) J. Novák, *J. Chromatogr.*, **31**, 137 (1967); (b) J. Novák and J. Reznicek, *ibid.*, **43**, 437 (1969).

17) P. Flory, *J. Am. Chem. Soc.*, **62**, 1561 (1940).

18) B. Weibull and B. Nycander, *Acta Chem. Scand.*, **8**, 847 (1954).

19) Unidentified products may be considered to involve higher adducts or isomeric adducts such as [$ClCH_2CH(OR)$-CH_2OH) and its higher ones. However, as their amounts were very small, they were neglected.

20) R. E. Parker and N. S. Isaacs, *Chem. Rev.*, **59**, 768 (1959).

21) (a) M. L. Bender, "Technique of Organic Chemistry," Vol. VIII, Part II, ed. by S. L. Friess, E. S. Lewis, and A. Weissberger, Interscience, New York, N. Y. (1963), p. 1427; (b) R. W. Taft, Jr., *J. Am. Chem. Soc.*, **74**, 5374 (1952); (c) R. W. Taft, Jr., E. L. Purlee, P. Riesz, and G. A. DeFrazio, *ibid.*, **77**, 1584 (1955); (d) G. Kohnstam, *Adv. Phys. Org. Chem.*, **5**, 121 (1967); (e) E. H. Cordes, *Prog. Phys. Org. Chem.*, **4**, 1 (1967).

22) E. Whalley, *Trans. Faraday Soc.*, **55**, 798 (1959).

23) V. R. Stimson, *J. Chem. Soc.*, **1955**, 4020.

24) V. R. Stimson and E. J. Watson, *J. Chem. Soc.*, **1954**, 2848.

Syntheses and Reactions of Fluorine-containing Aromatic Ketones

Hiroshi KIMOTO, Hiroshige MURAMATSU, and Kan INUKAI

Government Industrial Research Institute, Nagoya, Hirate-machi, Kita-ku, Nagoya 462

(Received November 27, 1975)

Phenyl 1,1,2,3,3,3-hexafluoropropyl ketone(I) and 2,2,3-trifluoro-3-(trifluoromethyl)indanone(II) were synthesized by the radical-addition reaction of benzaldehyde to hexafluoropropene. The reduction with $NaBH_4$ and the Grignard reaction with methylmagnesium iodide of these ketones gave the corresponding secondary and tertiary alcohols respectively. A Clemmensen reduction, alkaline hydrolyses, and reactions with hydroxylamine and with diazomethane were also carried out.

Fluorine-containing ketones have become of interest for their characteristic chemical properties due to the presence of an electron-deficient carbonyl group. Especially hexafluoroacetone and its chlorine-substituted derivatives have been widely studied and found to have unique reactivities.[1] However, few investigations of the syntheses and reactions of phenyl fluoroalkyl ketones are known.

In previous papers, we reported that the radical-addition reaction of alkylbenzenes to hexafluoropropene gave the 1 : 1 adducts, together with the cycloadducts,[2] and that the ratio of the products could be controlled by the reaction conditions.[3]

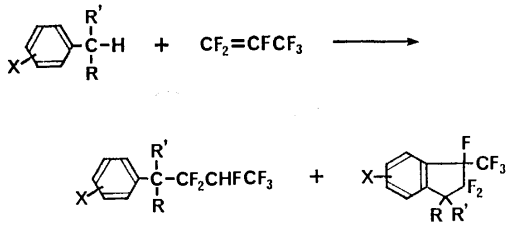

(R, R′=H, CH_3)

To ascertain the applicability of the above-mentioned radical reaction to the preparation of phenyl fluoroalkyl ketones, we attempted the addition of benzaldehyde to hexafluoropropene and obtained phenyl 1,1,2,3,3,3-hexafluoropropyl ketone(I) as a 1 : 1 adduct and 2,2,3-trifluoro-3-trifluoromethylindanone(II) as a cycloadduct.

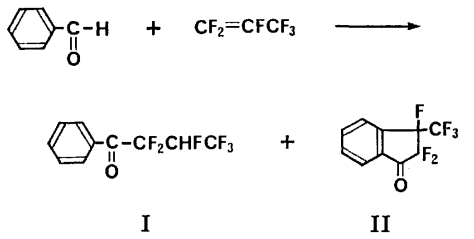

I II

Since the carbonyl group of these ketones conjugates with the aromatic ring, and since its electron density is decreased by the adjacent highly electronegative fluorine atoms, these ketones seem to have a high reactivity toward the nucleophiles. Therefore, we attempted some reactions of these ketones.

Results and Discussion

Addition Reaction of Benzaldehyde to Hexafluoropropene. The addition reaction of benzaldehyde to hexafluoropropene (HFP) was carried out in the presence of di-*t*-butyl peroxide in a stainless steel autoclave. Four kinds (A—D) of reaction conditions were employed: to investigate the effect of dilution with a solvent, 1,1,2-trichlorotrifluoroethane was used as an inert solvent in Methods B and C, and to study the effect of the molar ratio, an excess of HFP was used in Methods A and B, whereas an excess of benzaldehyde was used in Methods C and D. The reaction conditions and product yields are given in Table 1.

TABLE 1. THE RADICAL ADDITION REACTION OF BENZALDEHYDE TO HEXAFLUOROPROPENE

Method	A	B	C	D
C_6H_5CHO (mol)	0.400	0.400	0.800	1.201
HFP (mol)	0.575	0.563	0.333	0.467
DTBP (mol)	0.410	0.410	0.100	0.041
$C_2Cl_3F_3$ (mol)	—	1.000	0.535	—
[I]/[II][a]	2.8	1.6	5.5	
Yield[b] [I] (%)	21.5	18.5	8.8	trace
Yield[b] [II] (%)	7.4	8.4	1.8	—
Higher boiling products (g)	59	56	22	2

a) Determined by the peak areas of GLC. b) Yields are calculated on the basis of the amounts of benzaldehyde consumed.

The I/II ratios could be controlled by changing the reaction conditions. As compared with Method A, Method B gave a smaller value of I/II due to the effect of dilution. As compared with Method B, Method C gave a larger value of I/II due to the excess of benzaldehyde. These results can be explained in the same manner as in the addition reaction of alkylbenzenes described previously;[3] the I/II ratio is determined by the competition between the intermolecular hydrogen abstraction and the intramolecular cycloaddition, followed by the loss of a hydrogen radical. Only a trace of I was obtained by Method D, although the alkylbenzenes gave the 1 : 1 adducts in good yields under the same conditions.[2] In the cases of the addition reaction of benzaldehyde, a relatively larger amount of the initiator was required because it was consumed by the reaction with benzaldehyde yielding *t*-butyl benzoate.

The structures of I and II were elucidated by means of their IR, NMR, and mass spectra, which are shown in Table 2. The mass spectrum of I is very different from that of II. A large molecular ion peak was observed in II, whereas a very small one appeared in I. The large ions of I, *m/e*: 105 C_6H_5CO and *m/e*:

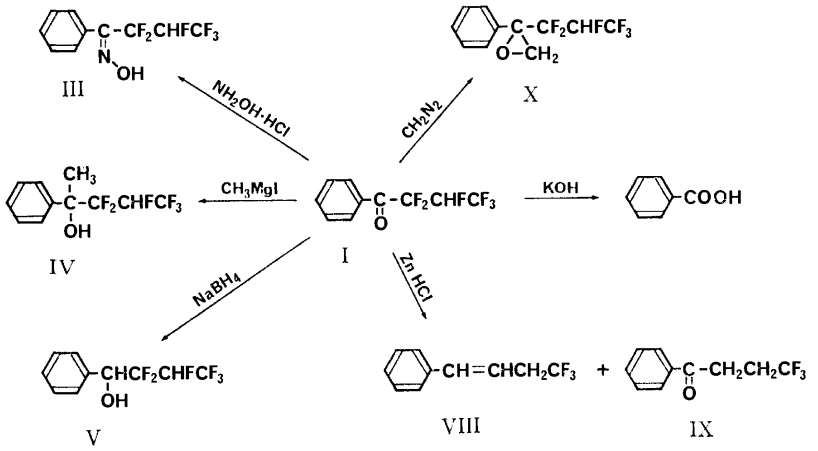

Fig. 1.

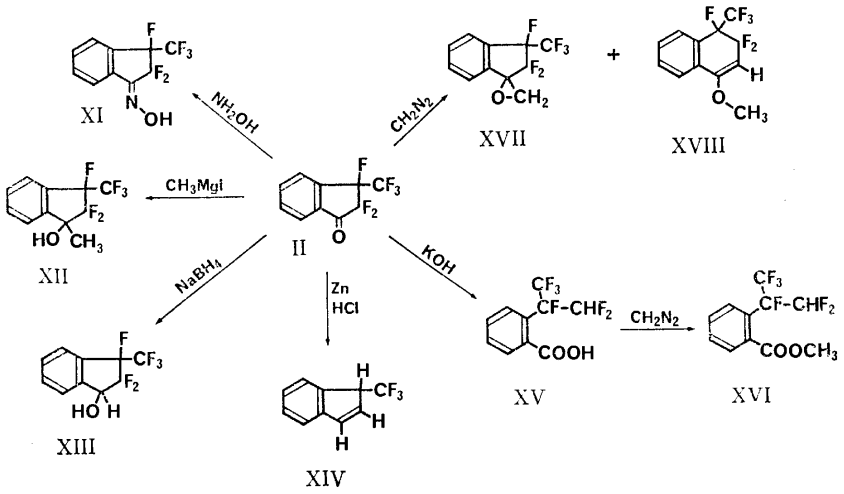

Fig. 2.

77 C_6H_5, are generated by the cleavage of the C–C bond connected to the carbonyl group.

In the NMR spectra, the signals of the fluorines of each CF_2 group on both I and II have AB patterns. For I, the non-equivalence is due to the adjacent asymmetric carbon atom. The configurations of the non-equivalent fluorines (^aF and ^bF) of II were estimated by means of the fluorine-fluorine coupling constants with a CF_3 group. From a consideration of the through-space coupling, it is assumed that the fluorine (^aF, δ= 41.7) with a smaller value (J=3.6 Hz) is on the opposite side of the indanone framework from the CF_3 group, whereas the fluorine (^bF, δ=47.1) with a larger value (J=14.0 Hz) is on the same side.

Some Reactions of Fluorine-containing Ketones. The reactions of I and II are summarized in Fig. 1 and Fig. 2 respectively. The corresponding ketoximes (III and XI) were prepared in high yields from I and II under acidic conditions, but under basic conditions haloform cleavages were competitive with the formation of oximes, III was not obtained, and the yield of XI fell to 45.3%.

Although the Beckmann rearrangement of these ketoximes was attempted under refluxing in trifluoroacetic acid or by heating at 100 °C in concentrated sulfuric acid, no corresponding acid amides were obtained; only ketoximes were recovered unchanged. In the reaction with 2,4-dinitrophenylhydrazine, II gave the corresponding hydrazone (mp 176 °C), but I did not yield the hydrazone under the same conditions. Some fluorinated ketones have been reported not to react with substituted hydrazines.[4]

The Grignard reaction of I with methylmagnesium iodide gave the corresponding tertiary alcohol (IV) in a 94% yield. GLC and the ^{19}F NMR spectrum indicated the presence of two diastereoisomers in the ratio of 65 : 35. On the other hand, the reaction of II with methylmagnesium iodide gave XII, which contained only one stereoisomer, in a 78% yield. The methyl group of XII seems to be on the opposite side of the trifluoromethyl group in the indane framework. In the reaction of cyclic fluoroketone(II), methylmagnesium iodide might attack the carbonyl carbon from a sterically favorable side, that is, opposite to the trifluoromethyl group.[5]

The reductions of I and II with sodium tetrahydroborate gave the corresponding secondary alcohols (V and XIII) in almost quantitative yields. The GLC of V indicated the formation of equal amounts of two diastereoisomers, whereas XIII consisted of two

Table 2. Spectral data of fluorine-containing ketones

Compound	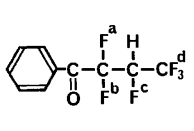	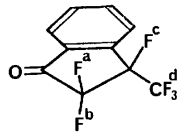
IR		
$\nu_{C=O}$ (cm^{-1})	1708	1762
NMR[a]		
Chemical shifts (ppm)		
$\tau_{C_6H_5(4)}$	1.9—2.9 m	2.0—2.2 broad s
τ_{CH}	4.73 d-d-d-q	
δ_{CF^a}	33.1 AB m	41.7 AB q
δ_{CF^b}	38.4 m	47.1 d-q
δ_{CF^c}	137.0 d-t-q	90.9 d-q
$\delta_{CF_3{}^d}$	−3.5 d-d-d-d	−1.8 d-d-d
Coupling constants (Hz)		
$J_{F^a-F^b}$	306.0	283.4
$J_{F^a-F^c}$	11.5	0.7
$J_{F^a-F^d}$	11.2	3.6
$J_{F^b-F^c}$	11.5	3.0
$J_{F^b-F^d}$	9.0	14.0
$J_{F^c-F^d}$	11.1	10.6
J_{H-F^a}	6.8	
J_{H-F^b}	13.1	
J_{H-F^c}	43.6	
J_{H-F^d}	6.0	
Mass spectra		
m/e (relative abundance)	256(0.3) M+	254(100) M+
	237(2.0) $C_{10}H_6F_5O$	235(22.8) $C_{10}H_4F_5O$
	217(3.3) $C_{10}H_5F_4O$	185(84.5) $C_9H_4F_3O$
	105(100) C_7H_5O	157(42.7) $C_8H_4F_3$
	77(58.6) C_6H_5	

a) Neat liquid; using TMS as an internal standard for ^1H and CF_3COOH as an external standard for ^{19}F. The signals being denoted by s(singlet), d(doublet), t(triplet), q(quartet), and m(multiplet).

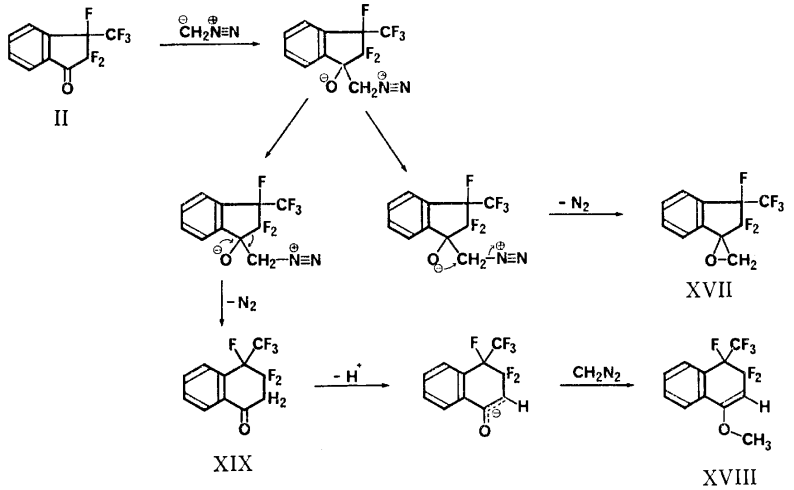

Fig. 3.

stereoisomers in the ratio of 90 : 10. The predominant isomer isolated by recrystallization was found to have a hydroxyl group on the same side of the trifluoromethyl group in the indane framework. The predominance of this isomer showed that the reduction proceeded mainly by the nucleophilic attack of the BH_4^- ion which, in effect, transferred H^- to the carbon[6] from the opposite side of the trifluoromethyl group.

The substitution of the hydroxyl group of V for bromine was carried out *via* the formation of tosylate

TABLE 3. MAIN MASS SPECTRAL BANDS

III

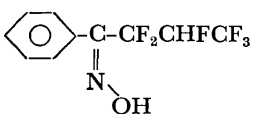

m/e	Abundance (%)	Ion
271	33.0	M^+
120	33.7	C_7H_6NO
103	20.7	C_7H_5N
77	100	C_6H_5
69	15.1	CF_3
51	23.0	C_4H_3

IV

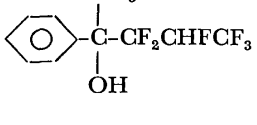

m/e	Abundance (%)	Ion
272	0.5	M^+
255	1.2	$C_{11}H_9F_6$
235	1.3	$C_{11}H_8F_5$
151	5.3	C_3HF_6
121	100	C_8H_9O
77	16.0	C_6H_5

V

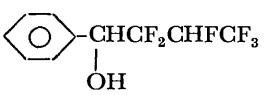

m/e	Abundance (%)	Ion
258	0.8	M^+
107	100	C_7H_7O
79	65.6	C_2HF_2O
77	35.5	C_6H_5
69	13.2	CF_3

VII

m/e	Abundance (%)	Ion
320	9.8	M^+
241	100	$C_{10}H_7F_6$
221	21.4	$C_{10}H_6F_5$
171	24.0	$C_9H_6F_3$
159	44.7	$C_8H_6F_3$
140	77.1	$C_8H_6F_2$

VIII

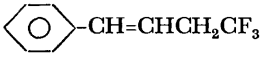

m/e	Abundance (%)	Ion
186	25.9	M^+
147	9.2	$C_{10}H_8F$
117	100	C_9H_9
115	58.5	C_9H_7
91	32.6	C_7H_7

IX

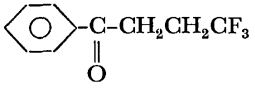

m/e	Abundance (%)	Ion
202	3.7	M^+
183	2.4	$C_{10}H_9F_2O$
105	100	C_7H_5O
77	55.6	C_6H_5
51	23.8	C_4H_3

m/e	Abundance (%)	Ion
188	4.6	M^+
168	10.4	$C_{10}H_{10}F_2$
91	100	C_7H_7
65	11.0	C_5H_5
51	6.8	C_4H_3

X

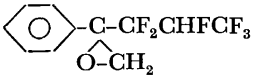

m/e	Abundance (%)	Ion
270	25.2	M^+
269	9.6	$C_{11}H_7F_6O$
151	23.6	C_3HF_6
119	14.3	C_8H_7O
91	100	C_7H_7

XI

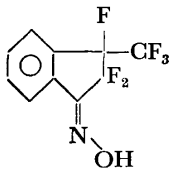

m/e	Abundance (%)	Ion
269	60.1	M^+
200	49.7	$C_9H_5F_3NO$
183	41.3	$C_9H_4F_3N$
169	20.9	$C_9H_4F_3$
152	100	$C_8H_4F_2N$

XII

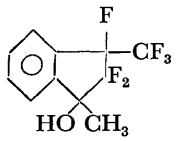

m/e	Abundance (%)	Ion
270	7.9	M^+
255	50.9	$C_{10}H_5F_6O$
250	67.2	$C_{11}H_7F_5O$
235	100	$C_{10}H_4F_5O$
207	30.5	$C_9H_4F_5$

XIII

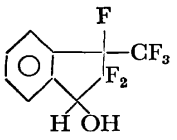

m/e	Abundance (%)	Ion
256	25.3	M^+
236	17.1	$C_{10}H_5F_5O$
167	100	$C_9H_5F_2O$
107	34.3	C_7H_4F
105	40.4	C_7H_5O

XIV

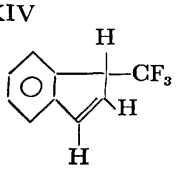

m/e	Abundance (%)	Ion
184	67.2	M^+
165	4.2	$C_{10}H_7F_2$
164	6.6	$C_{10}H_6F_2$
133	9.1	C_9H_6F
115	100	C_9H_7

XV

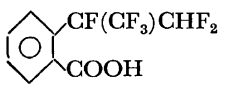

m/e	Abundance (%)	Ion
272	10.7	M^+
255	10.0	$C_{10}H_5F_6O$
204	45.8	$C_9H_4F_4O$
151	100	C_3HF_6

XVI

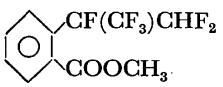

m/e	Abundance (%)	Ion
286	9.7	M^+
266	20.4	$C_{11}H_7F_5O_2$
255	100	$C_{10}H_5F_6O$
235	20.3	$C_{10}H_4F_5O$
207	14.5	$C_9H_4F_5$

XVII

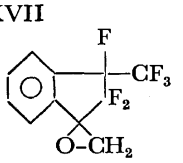

m/e	Abundance (%)	Ion
268	35.6	M^+
248	17.0	$C_{11}H_5F_5O$
219	14.1	$C_{10}H_4F_5$
171	17.0	$C_9H_6F_3$
169	100	$C_9H_4F_3$
151	76.3	$C_9H_5F_2$

XVIII

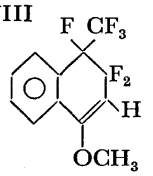

m/e	Abundance (%)	Ion
282	100	M^+
239	30.6	$C_{10}H_5F_6$
219	23.4	$C_{10}H_4F_5$
213	44.4	$C_{11}H_8F_3O$
169	32.8	$C_9H_4F_3$
151	40.0	$C_9H_5F_2$

(VI) as an intermediate. Bromide(VII) was obtained in a 60.2% overall yield. The same product was also synthesized by the photobromination of the 2,2,3,4,-4,4-hexafluorobutylbenzene obtained by the radical addition of toluene to hexafluoropropene.[2)]

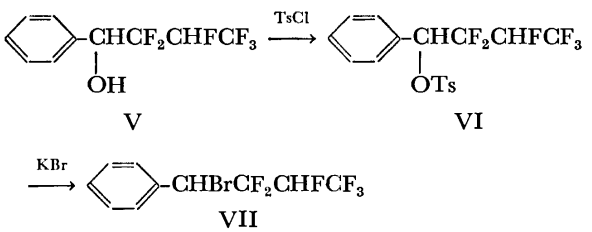

V VII

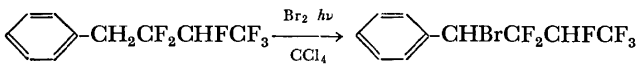

VII

The Clemmensen reduction of I gave several products, 1-phenyl-4,4,4-trifluorobutane, *trans*-1-phenyl-4,4,4-trifluoro-1-butene(VIII) and phenyl 3,3,3-trifluoropropyl ketone(IX), whose composition varied with the reaction conditions. Whereas the reduction at 70—80 °C for 2 h gave VIII as the main product in a 63.3% yield, the reduction at 0 °C gave IX in a 54.5% yield. The reduction of I in the presence of toluene at 90—100 °C gave a mixture of about equal amounts of four products,

TABLE 4. NMR SPECTRA

Compound	Absorption type	τ (ppm)	δ (ppm)	Splitting	J (Hz)	
III 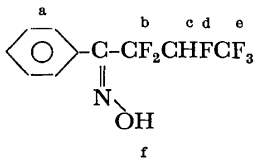	a (5H)	2.7		broad s	H_c-F_d	42
	b (1F)		27.1 } AB	d-d-q	F_b-$F_{b'}$	282
	b′ (1F)		32.9 } AB	t-q	H_c-F_e	6
	c (1H)	4.68		d-m	F_b-F_e	12
	d (1F)		131.4	d-m	$F_{b'}$-F_e	9
	e (3F)		−4.9	d-d-d-d	F_d-F_e	18
	f (1H)	2.7		overlapped with a		
V 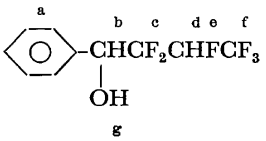	a (5H)	2.77		s	H_b-F_c	12
	b (1H)	5.20		t-m	H_d-F_c	10
	c (2F)		44.7	m	H_d-F_e	44
	d (1H)	5.31		d-m	H_d-F_f	6
	e (1F)		134.9	d-d-q	F_c-F_f	11
	f (3F)		−4.0	d-d-t	F_e-F_f	11
	g (1H)	6.63		broad s		
VIII 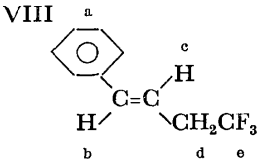	a (5H)	2.82		s	H_b-H_c	16
	b (1H)	3.55 } AB		s	H_c-H_d	6
	c (1H)	4.03 } AB		t	H_d-F_e	11
	d (2H)	7.12		d-q		
	e (3F)		−12.3	t		
IX 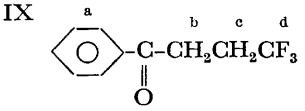	a (5H)	1.9—2.8		m	H_c-F_d	11
	b (2H)	6.0—6.9 } A_2B_2		m		
	c (2H)	7.0—7.9 } A_2B_2		m		
	d (3F)		−12.1	t		
XI 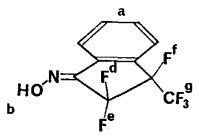	a (4H)	2.2—2.4		m	F_d-F_e	261
	b (1H)	1.4—1.5		m	F_d-F_f	3
	d (1F)		31.3 } AB	d-q	F_d-F_g	4
	e (1F)		36.5 } AB	d-q	F_e-F_f	2
	f (1F)		89.0	q-m	F_e-F_g	14
	g (3F)		−2.4	d-d-d	F_f-F_g	11
XII 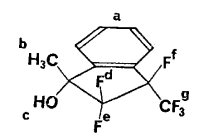	a (4H)	2.50		broad s	F_d-F_e	240
	b (3H)	8.45		broad s	F_d-F_g	6
	c (1H)	6.93		broad s	F_e-F_g	11
	d (1F)		48.4 } AB	m	F_f-F_g	10
	e (1F)		46.1 } AB	q-m		
	f (1F)		77.9	q-m		
	g (3F)		−4.7	d-d-d		
XIII 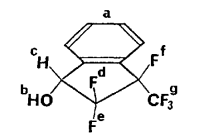	a (4H)	2.4—2.9		m	H_c-F_d	8
	b (1H)	5.17		broad s	H_c-F_e	8
	c (1H)	4.80		t	F_d-F_g	3
	d (1F)		41.4 } AB	m	F_e-F_g	14
	e (1F)		51.2 } AB	m	F_f-F_g	11
	f (1F)		82.6	d-q	F_d-F_e	241
	g (3F)		−3.9	d-d-d		
XIV 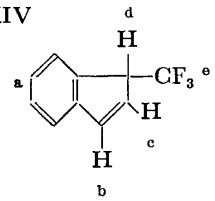	a (4H)	2.81		broad s	H_b-H_c	6
	b (1H)	3.16 } AB		broad s	H_c-H_d	2
	c (1H)	3.73 } AB		d	H_d-F_e	9
	d (1H)	6.00		q-m		
	e (3F)		−11.2	d-d-d		

Table 4. Continued

Compound	Absorption type	τ (ppm)	δ	Splitting	J (Hz)	
XVI	a (4H)	2.1—2.7		m	H_d-F_e	52
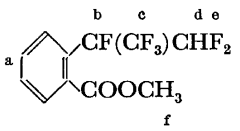	b (1F)		101.3	d-q	H_d-F_b	8
	c (3F)		−4.7	d-t	F_b-F_c	6
	d (1H)	3.35		d-t	F_b-F_e	9
	e (2F)		52.6	d-d-q	F_c-F_e	9
	f (3H)	6.18		s		
XVII	a (4H)	2.0—3.1		m	H_b-H_c	5
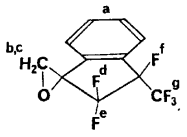	b (1H)	6.46	AB	s	F_d-F_e	279
	c (1H)	6.80		d	F_d-F_g	5
	d (1F)		41.9 AB	d-q	F_e-F_g	12
	e (1F)		45.6	t-q	F_f-F_g	10
	f (1F)		94.9	q-m		
	g (3F)		−0.8	d-d-d		
XVII	a (4H)	2.0—3.1		m	H_b-H_c	5
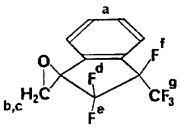	b (1H)	6.50	AB	s	F_d-F_e	281
	c (1H)	6.74		d	F_d-F_g	4
	d (1F)		41.3 AB	d-q	F_e-F_g	13
	e (1F)		46.2	t-q	F_f-F_g	11
	f (1F)		84.6	q-m		
	g (3F)		−3.2	d-d-d		
XVIII	a (4H)	2.4—3.1		m	H_c-F_d	3
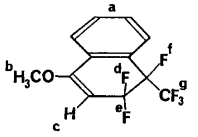	b (3H)	6.21		s	H_c-F_e	5
	c (1H)	4.37		d-d	F_d-F_e	281
	d (1F)		30.3 AB	m	F_d-F_f	15
	e (1F)		55.3	d-d-q	F_d-F_g	5
	f (1F)		115.6	d-d-q	F_e-F_f	10
	g (3F)		−2.6	d-d-d	F_e-F_g	18
					F_f-F_g	7

50% CCl_4 solution; using TMS as an internal standard for ^1H and CF_3COOH as an external standard for ^{19}F.

Table 5. Physical properties and analytical data

Compound	Bp (°C)	n_D^{20}	d_4^{20}	Formula	Elemental analysis C (%) Found	C (%) (Calcd)	H (%) Found	H (%) (Calcd)
[I]	194	1.4298	1.418	$C_{10}H_6F_6O$	46.51	(46.89)	2.41	(2.36)
[II]	205	1.4485	1.502	$C_{10}H_4F_6O$	47.48	(47.26)	1.74	(1.59)
[III]	Mp 79—84 °C			$C_{10}H_7F_6NO$	44.34	(44.29)	2.63	(2.60)
[IV][a]	214	1.4374	1.401	$C_{11}H_{10}F_6O$	48.37	(48.54)	3.46	(3.70)
[V][a]	213	1.4325	1.434	$C_{10}H_8F_6O$	46.61	(46.53)	3.00	(3.12)
[VII][a]	62—64/4[b]	1.6475	1.456	$C_{10}H_7F_6Br$	37.23	(37.41)	2.20	(2.20)
[VIII]	polymel. (180 °C)	1.4807	1.196	$C_{10}H_9F_3$	64.34	(64.51)	4.70	(4.87)
[IX]	Mp 59.8 °C			$C_{10}H_9F_3O$	59.63	(59.41)	4.57	(4.49)
[X][a]	208	1.4311	1.392	$C_{11}H_8F_6O$	48.99	(48.90)	3.04	(2.98)
[XI]	Mp 118.1 °C			$C_{10}H_5F_6NO$	44.52	(44.63)	2.05	(1.87)
[XII]	Mp 99.8 °C			$C_{11}H_8F_6O$	48.95	(48.90)	3.15	(2.98)
[XIII][a]	Mp 36—39 °C			$C_{10}H_6F_6O$	47.13	(46.89)	2.63	(2.36)
[XIV]	187	1.4859	1.280	$C_{10}H_7F_3$	65.32	(65.22)	3.76	(3.83)
[XVI]	226	1.4372	1.480	$C_{11}H_8F_6O_2$	46.58	(46.17)	2.84	(2.82)
[XVII][a]	decomp. (180 °C)	1.4493	1.483	$C_{11}H_6F_6O$	49.03	(49.27)	2.16	(2.26)
[XVIII]	Mp 75.7 °C			$C_{12}H_8F_6O$	50.92	(51.08)	2.85	(2.86)

a) Mixture of stereoisomers.
b) °C/mmHg; decomposed at 200 °C and atmospheric pressure.

1-phenyl-4,4,4-trifluorobutane, VIII, IX, and an unidentified compound. The reduction of cyclic ketone (II) at 60—70 °C gave 1-trifluoromethylindene(XIV) in a 42.3% yield.

Both the elimination of α-halogen and the formation of olefin are known to be side reaction in the Clemmensen reduction.[7] The formation of olefin was especially enhanced when a double bond formed conjugated with a phenyl group. In the treatment of the fluorinated ketones, I and II, with zinc amalgam and hydrochloric acid, the reduction of the fluorines on the α- and β-carbons of the ketones seemed to occur first, followed by the reduction of the carbonyl or olefin formation, which were dependent on the reaction conditions.

The haloform cleavage of these ketones was observed. The reaction of I with aqueous potassium hydroxide gave benzoic acid, whereas the reaction of the cyclic ketone(II) gave *o*-(hexafluoroisopropyl)benzoic acid (XV), which was isolated as the methyl ester(XVI) in a 50.3% yield. The mechanism of the alkaline degradation of II is as follows:

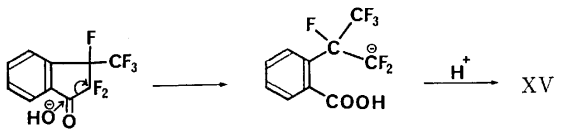

The reaction of I with diazomethane gave only the epoxide (X) in a 75.9% yield. On the other hand, the reaction of II gave ring-expanded enol ether(XVIII), together with the epoxide (XVII). The postulated mechanism of the formation of XVII and XVIII is shown in Fig. 3. The reaction of ketones with diazomethane has been extensively studied; non-fluorinated ketones react in three alternative ways, yielding epoxide and/or ketones in which a methylene group has been inserted.[8] The presence of electronegative substituents on ketones has been reported to enhance the reactivity with diazomethane and to give mainly oxides instead of the expanded ketones. α-Fluoroketones have been reported to give only epoxides in high yields.[9] In agreement with the information in the literature, the linear ketone(I) gave only epoxide. The cyclic fluorinated ketone(II), however, gave the ring-expanded product (XVIII) together with the epoxide(XVII). The reaction of II and diazomethane, with the migration of the difluoromethylene carbon, seems to lead to the ring-expanded ketone(XIX). Since the methylene group of XIX is adjacent to the electron-withdrawing difluoromethylene and carbonyl group, the acidic hydrogen dissociates as a proton and an enolate anion is generated. Another molecule of diazomethane reacts with the enolate anion to give enol ether(XVIII). The intermediate ketone (XIX) was not isolated. The NMR showed that both epoxides, X and XVII, were mixtures of two stereoisomers, in the ratios of 50 : 50 and 60 : 40 respectively.

The mass and NMR spectral data of the products are shown in Table 3 and Table 4 respectively. The physical properties and analytical data are shown in Table 5.

Experimental

The IR and mass spectra were measured using a Hitachi Model EPI-G3 grating spectrometer and a Model RMU-7 double-focussing mass spectrometer at 70 eV respectively. The NMR spectra were obtained on a Hitachi Model R-20B (^{1}H : 60 MHz; ^{19}F : 56.45 MHz), using TMS as an internal standard for ^{1}H and trifluoroacetic acid as an external standard for ^{19}F. The analytical GLC was carried out in a stainless steel column (3 m long × 3 mm diameter) packed with 20% Silicone DC550-Celite 545 or 20% Silicone DCQF-1-Chromosorb W on a Shimadzu GC-3AH. In the preparative scale work, an aluminum column (6 m long × 10 mm diameter) was used on a Varian Model 920.

Addition Reactions of Benzaldehyde to Hexafluoropropene. General Procedure: A mixture of benzaldehyde, HFP, DTBP, and 1,1,2-trichlorotrifluoroethane in the molar ratio shown in Table 1 was heated in a stainless steel autoclave at temperatures gradually rising from 130 °C to 160 °C. The products were separated by vacuum distillation. Phenyl 1,1,2,3,3,3-hexafluoropropyl ketone(I) and 2,2,3-trifluoro-3-trifluoromethylindanone(II) were obtained as colorless liquids, together with a large amount of a tarry residue.

Preparation of Oximes. Phenyl 1,1,2,3,3,3-Hexafluoropropyl Ketone Oxime (III): To a solution of I (2.5 g, 0.01 mol) in 4 ml of ethanol, 2 ml of a 50% aqueous hydroxylamine hydrochloride solution was added; the mixture was then refluxed for 8 h. After the ethanol had then been allowed to evaporate, 20 ml of water was added and the organic products were extracted with ether. After the solvent had been removed, III was obtained as an oily residue (1.9 g, 70.1%), which crystallized on standing overnight. Recrystallization from chloroform gave pale yellow needles (mp 84 °C).

2,2,3-Trifluoro-3-(trifluoromethyl)indanone Oxime (XI): In a similar proceddre, II (1.25 g, 0.005 mol) gave XI (1.3 g, 98.2%) as colorless needles (mp 118 °C).

Grignard Reactions with Methylmagnesium Iodide. 2-Phenyl-3,3,4,5,5,5-hexafluoro-2-pentanol (IV): Methylmagnesium iodide was prepared from methyl iodide (1.5 g, 0.011 mol) and magnesium turnings (0.25 g, 0.010 atom) in 20 ml of ether. Then a solution of I (2 g, 0.008 mol) in 10 ml of ether was added, drop by drop, with cooling in an ice bath. The mixture was stirred for one hour at room temperature and then poured into dilute hydrochloric acid. The ether layer was separated and dried over magnesium sulfate. After the removal of the solvent, the residue was distilled *in vacuo*; IV (2.0 g, 94.2%) was thus obtained as a colorless liquid.

1-Methyl-2,2,3-trifluoro-3-(trifluoromethyl)-1-indanol (XII): By a similar procedure, XII (1.0 g, 78.4%) was obtained from II (1.2 g, 0.005 mol). Recrystallization from chloroform gave colorless prisms (mp 100 °C).

Reduction with $NaBH_4$. 1-Phenyl-2,2,3,4,4,4-hexafluoro-1-butanol (V): Sodium borohydride (4.0 g, 0.106 mol) and 60 ml of anhydrous ether were placed in a 200 ml Erlenmeyer flask; a solution of I (20.5 g, 0.08 mol) in 30 ml of ether was then added, drop by drop at room temperature. After the addition had been completed, stirring was continued for 3 h. The mixture was then poured into ice water, and the ether layer was separated and dried. After the removal of the solvent, the residue was distilled *in vacuo*; V was thus obtained as a colorless liquid (16.6 g, 80.4%).

2,2,3-Trifluoro-3-(trifluoromethyl)-1-indanol (XIII): By a similar procedure, XIII (3.6 g, 89.5%) was obtained from II (4.0 g, 0.015 mol) as a colorless liquid. Crystallization from chloro- form gave colorless prisms (mp 39 °C).

Clemmensen Reductions. trans-*1-Phenyl-4,4,4-trifluoro-1-butene (VIII)*: Zinc ribbon (20 g, 0.306 atom) was added to a 10 ml aqueous solution of mercuric chloride (2 g, 0.007 mol). After 5 minutes' shaking, the water layer was decanted and 5 ml of water and 20 ml of concentrated hydrochloric acid were added. A solution of I (5 g, 0.020 mol) in 10 ml of ethanol was then added, drop by drop, the temperature rose to 70—80 °C, after which stirring was continued for 2 h. The mixture was extracted with 20 ml of toluene, and then the organic layer was washed with water and dried. Vacuum distillation gave VIII (2.3 g, 63.3%) as a colorless liquid which was proved by GLC to contain small amounts of 1-phenyl-4,4,4-trifluorobutane and phenyl 3,3,3-trifluoropropyl ketone.

Phenyl 3,3,3-trifluoropropyl ketone (IX): A reduction similar to that described above was carried out at 0 °C under cooling in an ice bath. IX (2.2 g, 54.5%) was thus obtained as the main product from I (5 g, 0.020 mol).

1-*Trifluoromethylindene (XIV)*: By a procedure similar to that described above, II (2.6 g, 0.010 mol) gave XIV (0.8 g, 42.3%) as a colorless liquid.

Alkaline Hydrolysis. Benzoic Acid: Powdered potassium hydroxide (2 g, 0.036 mol) and 10 ml of hexane were placed in a 50 ml Erlenmeyer flask, and then a solution of I (3 g, 0.012 mol) in 10 ml of hexane was added. After 1 hour's stirring, the mixture was acidified with dilute hydrochloric acid. Benzene (30 ml) was then added, and the organic layer was separated. The solvent was allowed to evaporate to give a white solid (1.5 g). Recrystallization from hexane gave benzoic acid (1.0 g) as colorless needles (mp 123 °C).

o-*(Hexafluoroisopropyl)benzoic Acid (XV) and Its Methyl Ester (XVI)*: By a similar procedure, II (3 g, 0.012 mol) gave a pale yellow oil XV (1.9 g, 59.2%). A solution of XV in 20 ml of absolute ether was cooled in an ice bath, and then a freshly prepared diazomethane solution in ether was added. After the mixture had stood for 30 min, the solvent was removed. The vacuum distillation of the residue gave XVI (1.7 g, 50.3%) as a pale yellow liquid.

Reaction with Diazomethane. 2-Phenyl-3,3,4,5,5,5-hexafluoro-1,2-epoxypentene (X): A solution of I (2.0 g, 0.008 mol) in 20 ml of absolute ether was cooled in an ice bath; subsequently a freshly prepared diazomethane ether solution was added until the yellow color was no longer discharged. After the mixture had stood at room temperature for 3 h, the solvent was removed to give a pale yellow oily residue (1.6 g, 75.9%). Further purification was done by preparative GLC.

2,2,3-Trifluoro-1,1-methyleneoxy-3-trifluoromethylindane (XVII) and 1,2,2-Trifluoro-1-trifluoromethyl-4-methoxy-1,2-dihydronaphthalene (XVIII): By a similar procedure, II (2.0 g, 0.008 mol) gave a pale yellow residue (1.5 g) which contained XVII and XVIII in a ratio of 3 : 4 (GLC). They were separated by preparative GLC. Recrystallization from ethanol gave XVIII as colorless prisms (mp 76 °C).

Bromine Substitution of the Alcohol (V). 4-Bromo-1,1,1,-2,3,3-hexafluoro-4-phenylbutane (VII): To a mixture of V (10.4 g, 0.04 mol) and *p*-toluenesulfonyl chloride (10 g, 0.05 mol), 20% aqueous sodium hydroxide (15 ml) was added, drop by drop. After the reaction mixture had been heated at 100 °C for 6 h, it was poured into 100 ml of water and extracted with dichloromethane. The evaporation of the solvent gave tosylate(VI) (12.1 g, 73.4%) as colorless prisms (mp 106 °C), which were then recrystallized from ethanol.

A solution of VI (10 g, 0.024 mol) and potassium bromide (12 g, 0.10 mol) in ethylene glycol (20 ml) was heated at 160 °C for 6 h. The reaction mixture was poured into water and extracted with dichloromethane. After the solvent had been removed, the oily residue was distilled *in vacuo*. Bromide (VII) (6.4 g, 82.1%) was obtained as a colorless oil.

References

1) C. G. Krespan and W. J. Middleton, Fluorine Chemistry Reviews, **1**, 145 (1967); H. P. Braendlin and E. T. McBee, "Advances in Fluorine Chemistry," **III**, Butter Worths, London (1963), p. 1.

2) H. Kimoto, H. Muramatsu, and K. Inukai, *Nippon Kagaku Kaishi*, **1975**, 112.

3) H. Kimoto, H. Muramatsu, and K. Inukai *Nippon Kagaku Kaishi* **1975**, 665; *Chem. Lett.*, **1974**, 791.

4) E. T. McBee, O. R. Pierce, H. W. Kilbourne, and E. R. Wilson, *J. Am. Chem. Soc.*, **75**, 3152 (1953).

5) McBee and co-workers proposed a mechanism for Grignard reaction of fluorine-containing carbonyl compounds. The carbonyl compounds with weak carbonyl oxygen basicity do not complex with alkylmagnesium halides and the reaction is promoted by the attack of the Grignard reagent to the electropositive carbonyl carbon. E. T. McBee, O. R. Pierce, and D. D. Meyer, *J. Am. Chem. Soc.*, **77**, 83 (1955).

6) O. R. Vail and D. M. S. Wheeler, *J. Org. Chem.*, **27**, 3802 (1962).

7) Y. Ogata, "Yuki Kagobutsu no Sanka to Kangen," Nankodo, Tokyo (1963) p. 668; E. L. Martin, *Org. React.*, Vol. I, p. 155.

8) C. D. Gutsche, *Org. React.*, Vol. VIII., p. 364.

9) H. E. Simmons and D. W. Wiley, *J. Am. Chem. Soc.*, **82**, 2288 (1960).

Thermolysis of Phenyl 3-Guaiazulenecarboxylate and the *p*-Acetyl and *p*-Methoxy Derivatives[1]

Shinji KUROKAWA and Arthur G. ANDERSON, Jr.*

Department of Chemistry, Faculty of Education, Saga University, Honjo-machi, Saga 840

**Department of Chemistry, University of Washington, Seattle, Washington 98195, U.S.A.*

(Received Dcember 8, 1975)

Thermolysis of *p*-acetylphenyl 3-guaiazulenecarboxylate (**1**) results in loss of the ester group. In contrast, thermolysis of phenyl 3-guaiazulenecarboxylate (**2**) or *p*-methoxyphenyl 3-guaiazulenecarboxylate (**3**) gives (i) loss of the ester group, (ii) loss of the 1-methyl group with concomitant rearrangement of the ester group to the 1-position, (iii) interchange of the ester and 1-methyl groups, and (iv) cyclization to 5-isopropyl-7-methyl-1,2-dihydrocyclopenta[*c*,*d*]azulen-1-one (**9**).

Previous studies[2-5] showed that thermolysis of 3-acylguaiazulenes at 200—260 °C resulted in loss of the acyl group, migration of the acyl group to the 2-position, and/or interchange of the acyl and the 1-methyl groups. It was observed that the nature of the acyl substituent determined the course of the reaction. Thus formyl gave deacylation, acetyl and benzoyl gave migration, and methoxycarbonyl gave acyl-methyl interchange as the main reactions. The mode of reaction in these cases varies with the electron density at the acyl carbons and with the relative stabilities of the corresponding acylium ions. Thus the ability of the acyl substituent to stabilize a positive charge on the carbonyl carbon seemed to be important. To test this hypothesis further, we have prepared *p*-acetylphenyl- (**1**), phenyl- (**2**), and *p*-methoxyphenyl (**3**) 3-guaiazulenecarboxylates and examined their thermolytic behavior. Differences in the products from **1** to **3** due to steric factors would be small.

Results and Discussion

Esters **1**—**3** were prepared by the reaction of S-guaiazulene (**4**) with phosgene to form S-guaiazulene-3-carbonyl chloride, and the latter was treated with the corresponding phenol.[6] Compounds **1** and **3** are new and were characterized by their UV, IR, NMR and mass spectra. During the isolation of **3** a crystalline by-product was obtained which was shown to be bis(*p*-methoxyphenyl) carbonate. This indicates that the acid chloride product contained phosgene in this case.

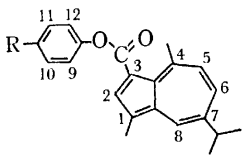

1: R=Ac
2: R=H
3: R=OMe

Thermolysis of the esters was carried out at 250 °C for one hour. As anticipated, differences in the products formed or in their relative amounts were found. Only elimination of the carbonyl moiety to give **4** was observed with the *p*-acetylphenyl ester (**1**). In sharp contrast, the phenyl (**2**) and *p*-methoxyphenyl (**3**) esters formed four azulenic products resulting from (i) loss of the ester group (**4**) (ii) migration of the ester group to C-1 with concomitant loss of the 1-methyl group (**5** or **6**), (iii) interchange of the 1-methyl and 3-ester group (**7** or **8**), and (iv) cyclization of the 4-methyl group (**9**). The NMR spectra of compounds **5**—**8** exhibited a characteristic marked low field chemical shift of 8-hydrogen due to the peri ester function. The structures of **5**—**8** were confirmed by conversion to the corresponding known methyl esters (**10** and **11**) by the method of Reimer and Downes.[7] The yield data are summarized in Table 1. There is a definite correlation between the yields of rearranged products and the ability of the aryl portion of the ester function to supply electrons to the carbonyl carbon. This supports the hypothesis of an ionic mechanism wherein an increase in positive charge on the carbonyl carbon is involved. In that the loss of the ester group to form **4** demonstrates the presence

TABLE 1. YIELDS OF THERMOLYSIS PRODUCTS

Ester	Products (%)			
1	**4**(29.3)			
2	**4**(11.8)	**5**(3.4)	**7**(1.6)	**9**(1.4)
3	**4** (5.1)	**6**(3.3)	**8**(6.1)	**9**(5.6)

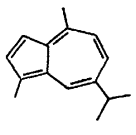

4

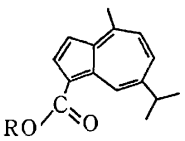

5: R=C_6H_5
6: R=*p*-$MeOC_6H_5$
10: R=Me

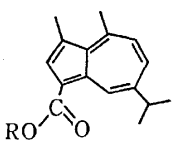

7: R=C_6H_5
8: R=*p*-$MeOC_6H_5$
11: R=Me

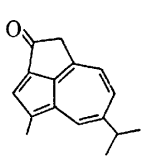

9

of a source of protons (perhaps in a decomposition product), reversible electrophilic substitution processes provide the simplest explanation for these reactions. The intermediacy of pi-complexes[8] can explain the formation of the rearrangement products. It is to be noted that all of the products have less steric hindrance than the starting esters and this is presumably the principal driving force. Of interest is the inverse correlation of the yields of **4** with those of the rearranged products. A possible explanation is that **4** is formed, for the most part, directly from the conjugate acid (**12**) through reaction with a nucleophile (*e.g.* the anion of the proton acid). The stability of **12** in terms of the tendency of the ester function to dissociate as a positive ion, or migrate *via* a pi-complex would decrease with the electron-donating ability of the ester aryl group, in agreement with the results obtained.

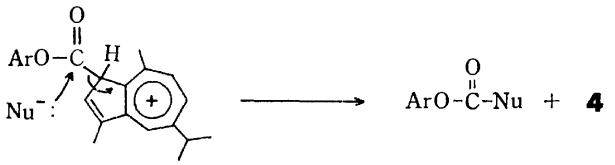

12

The formation of **9** is explicable in terms of the juxta-position of the acidic 4-methyl group[9] and a basic carbonyl oxygen. A simplified scheme is shown. The decreased oxygen basicity in **1** would correlate with the absence of **9** as a product in this case.

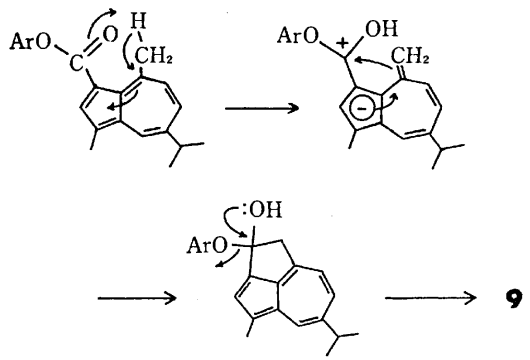

Experimental

NMR spectra were taken in $CDCl_3$, unless otherwise specified, on a JEOL MH-100 spectrometer (100 MHz) with TMS as internal standard. Mass spectra (MS) were obtained at 70 eV with a Hitachi-RMS-4 instrument. UV spectra were recorded in cyclohexane on a Hitachi 624 Digital Spectrophotometer with a Hitachi 056 Recorder, and IR spectra (liquids as films; solids as KBr disks) on a Hitachi EPI-S2 spectrophotometer. Mps are uncorrected. Kanto-Kagaku silica gel was used for chromatography unless otherwise specified. GLC was carried out on a Shimadzu GC-3AH instrument.

*p-Acetylphenyl 3-Guaiazulenecarboxylate (**1**), Phenyl 3-Guaiazulenecarboxylate (**2**), and p-Methoxyphenyl 3-Guaiazulenecarboxylate (**3**)* were prepared from guaiazulene according to the method of Treibs[6] in 44.3%, 31.4% and 29.8% crude (one spot on TLC) and 31.2%, 6.65% and 22.4% pure overall yields, respectively. Ester **1** was obtained from hexane as reddish-purple needles, mp 117.2—117.7 °C. TLC (benzene) R_f 0.11. λ_{max}: 251 (log ε 4.70), 305 (4.70), 318 (4.69), 388 (4.36), 524 (sh ε 612), 562 (755), 613 (sh 570), 673 (sh 175). IR: 1668 and 1702 cm^{-1}. NMR (δ): 1.38 (6H, d, J= 7.0 Hz $(CH_3)_2CH$), 2.57 (6H, s, 1-CH_3 and $COCH_3$), 3.02 (3H, s, 4-CH_3), 3.12 (1H, m, J=7.0 Hz, $(CH_3)_2CH$), 7.27 (2H, d, J=8.0 Hz, 9-H and 12-H), 7.30 (1H, d, J=11 Hz, 5-H), 7.5 (1H, dd, J=11.0 and 2.0 Hz, 6-H), 7.95 (2H, d, J=8.0 Hz, 10-H and 11-H), 8.11 (1H, s, 2-H), and 8.20 (1H, d, J=2.0 Hz, 8-H). MS: *m/e* 360 (M^+ for $C_{24}H_{24}O_3$) and 225 ($M^+ - CH_3COC_6H_5O$).

Ester **2** was isolated as violet plates from ethanol mp 62—63 °C (lit,[6] 69—70.5 °C). TLC (benzene) R_f 0.38. λ_{max}: 249 (log ε 4.40), 304.5 (4.53), 315 (sh 4.46), 386 (4.02), 482 (sh ε 190), 567 (527), and 650 (sh 404). IR: 1718 cm^{-1}. NMR (δ): 1.39 (6H, d, J=7.5 Hz, $(CH_3)_2CH$), 2.66 (3H, s, 1-CH_3), 3.12 (3H, s, 4-CH_3), 3.18 (1H, m, J=7.5 Hz, $(CH_3)_2CH$), 7.36 —7.56 (6H, 4 lines, C_6H_5 and 5-H), 7.68 (1H, dd, 6-H, J=2.0 and 10.9 Hz), 8.35 (1H, s, 2-H) and 8.42 (1H, d, J=2.0 Hz, 8-H). MS: *m/e* 318 (M^+ for $C_{22}H_{22}O_2$) and 225 ($M^+ - C_6H_5O$). NMR (δ) (CF_3COOH) of the conjugate acid: 1.60 (6H, d, J=6.8 Hz, $(CH_3)_2CH$), 2.55 (3H, m, J=1.4 and 2.7 Hz, 1-CH_3), 3.17 (3H, s, 4-CH_3), 3.57 (1H, m, J=6.8 Hz, $(CH_3)_2CH$), 5.48 (1H, m, 3-H), 6.8—7.6 (6H, C_6H_5 and 2-H), 8.71 (2H, s, 5-H and 6-H), and 8.75 (1H, s, 8-H) showing ring protonation at C-3.

Ester **3** separated from hexane as violet crystals, mp 96.8—97.3 °C. TLC (benzene) R_f 0.29. λ_{max}: 247 (log ε 4.85), 303 (4.89), 315 (sh 4.54), 387 (4.22), 531 (sh ε 586), 569 (728), 621 (sh 549), 684 (sh 193). IR: 1110 (C–O–C), 1170 (C–O–C) and 1703 cm^{-1} (C=O). NMR (δ): 1.35 (6H, d, J=7.0 Hz, $(CH_3)_2CH$), 2.57 (3H, s, 1-CH_3), 3.02 (3H, s, 4-CH_3), 3.08 (1H, m, J=7.0 Hz, $(CH_3)_2CH$), 3.75 (3H, s, OCH_3), 6.88 (2H, d, J=8.9 Hz, 10-H and 11-H), 7.10 (2H, d, J=8.9 Hz, 9-H and 12-H), 7.25 (1H, d, J=10.9 Hz, 5-H), 7.48 (1H, dd, J=10.9 and 2.1 Hz, 6-H), 8.11 (1H, s, 2-H) and 8.20 (1H, d, J=2.1 Hz, 8-H). MS: *m/e* 348 (M^+ for $C_{23}H_{24}O_3$) and 2.25 ($M^+ - CH_3OC_6H_4O$).

In the preparation of **3**, the treatment of the crude ester product with petroleum ether — 1% benzene afforded an insoluble crystalline product which was chromatographed on silica gel (benzene) and then recrystallized from methanol. The colorless needles, mp 98.1 °C, TLC (benzene) R_f 0.51 (spot developed with HNO_3–H_2SO_4), had spectral properties consistent with those expected for bis(*p*-methoxyphenyl) carbonate. IR: 1234 (C–O), 1763 (C=O) and 2830 cm^{-1} (ether C–H). NMR (δ): 3.77 (6H, s, OCH_3), 6.84 and 7.11 (8H, A_2B_2, J_{AB}=9.0 Hz, C_6H_4).

*Thermolysis of Esters **1**, **2** and **3**.*[10] The general procedure was to heat the ester (deoxygenated under high vacuum) sealed in a glass tube under nitrogen at 250 °C for 1 h. The treatment of the glass tube with acid or alkali gave no notable effect on thermolysis. The material was chromatographed on silica gel using a Toyo Kagaku Sangyo SF-160K automatic fraction collector. Benzene eluted S-guaiazulene (**4**) in the first fraction, then in the case of **1**, unchanged starting material. In the cases of **2** and **3**, a mixture of isomerized products, phenyl or *p*-methoxyphenyl 4-methyl-7-isopropyl-1-azulenecarboxylate (**5** or **6**) and the corresponding 3,4-dimethyl-7-isopropyl-1-azulenecarboxylate (**7** or **8**) was eluted after **4**, then unchanged starting material and, finally, benzene–ether (10 : 1) eluted 5-isopropyl-7-methyl-1,2-dihydrocyclopenta[*c*,*d*]azulen-1-one (**9**). Some tary material was obtained as the last fraction in the cases of **1** and **2**. The purity of the starting ester and of each product was checked by GLC

(SE 30 on Chromosorb W at 170—270 °C). The properties (R_f on TLC, IR, NMR and MS) of **4** were shown to be the same as those of an authentic sample. The complete separation of **5** and **7** and of **6** and **8** were very difficult and the yields reported include small correction factors based on GLC and NMR peak ratios.

From 151.8 mg of **1** were obtained 44.5 mg (29.3%) of **4** and 17.7 mg (11.7%) of tary material.

From 1.169 g of **2** were isolated 137.5 mg (11.8%) of **4**, 51.2 mg (4.4%) of unchanged **2**, and 636.8 mg (54.5%) of tar. The mixture of ester products was separated by chromatography on Amberlite IRC-50 (CG-50 Type 2) with 80% ethanol to give 39.6 mg (3.4%) of **5** and 18.8 mg (1.6%) of **7**. Ester **5** was obtained as a reddish violet oil. TLC (benzene) R_f 0.51. λ_{max}: 241 (log ε 4.43), 298 (4.62), 304 (4.64), 336.5 (3.72), 344 (3.75), 364 (3.99), 377 (4.09), 510 (sh ε 677), 532 (827), 570 (749) and 623 (300). IR: 1696 cm^{-1} (C=O). NMR (δ): 1.38 (6H, d, J=7.4 Hz, $(C\underline{H}_3)_2CH$), 2.93 (3H, s, 4-CH_3), 3.19 (1H, m, J=7.4 Hz, $(CH_3)_2C\underline{H}$), 7.23—7.51 (7H, m, C_6H_5, 3-H and 5-H), 7.70 (1H, dd, J=10.7 and 2.2 Hz, 6-H), 8.46 (1H, d, J=4.6 Hz, 2-H), and 9.84 (1H, d, J=2.2 Hz, 8-H). MS: *m/e* 304 (M^+ for $C_{21}H_{20}O_2$) and 78 ($C_6H_6^+$). Ester **7** was obtained as a violet oil. TLC (benzene) R_f 0.51. λ_{max}: 248 (log ε 4.48), 302 (4.64), 309 (4.66), 314 (sh 4.57), 377 (4.05), 389 (4.14), 562 (ε 887), 602 (sh 730) and 665 (258). IR: 1690 cm^{-1} (C=O). NMR (δ): 1.33 (6H, d, J=7.5 Hz, $(C\underline{H}_3)_2CH$), 2.82 (3H, s, 3-CH_3), 3.06 (3H, s, 4-CH_3), 3.15 (1H, m, J=7.5 Hz, $(CH_3)_2C\underline{H}$), 7.12—7.32 (6H, m, C_6H_5 and 5-H), 7.47 (1H, dd, J=10.7 and 2.0 Hz, 6-H), 8.21 (1H, s, 2-H), and 9.72 (1H, d, J=2.0 Hz, 8-H). MS: *m/e* 318 (M^+ for $C_{22}H_{22}O_2$), 225 ($M^+-C_6H_5O$) and 211 ($M^+-C_6H_5OCH_2$). Ketone **9** (16.6 mg, 1.4%) crystallized from hexane as dark violet needles, mp 99—100 °C. TLC (10 : 1 benzene–ether) R_f 0.13. λ_{max}: 235 (log ε 4.44), 242 (4.44), 258 (4.26), 268 (4.35), 300 (sh 4.36), 304 (4.47), 312 (4.51), 318 (4.62), 350 (sh 3.86), 362 (3.98), 375 (sh 3.96), 381 (4.03), 524 (sh ε 425), 544 (sh 538), 559 (659), 584 (616), 609 (692), 640 (sh 316) and 674 (324). IR: 1651 cm^{-1} (C=O). NMR (δ): 1.42 (6H, d, J=7.5 Hz, $(C\underline{H}_3)_2CH$), 2.65 (3H, s, 7-CH_3), 3.22 (1H, m, J=7.5 Hz, $(CH_3)_2C\underline{H}$), 4.04 (2H, s, CH_2), 7.32 (1H, d, J=12.8 Hz, 3-H), 7.68 (1H, s, 8-H), 7.82 (1H, dd, J=12.8 and 1.7 Hz, 4-H) and 8.29 (1H, d, J=1.7 Hz, 6-H). MS: *m/e* 224 (M^+ for $C_{16}H_{16}O$), 209 (M^+-CH_3), and 165 ($M^+-C_3H_7O$).

From 814.0 mg of **3** were obtained 41.5 mg (5.1%) of **4** and 437.3 mg (53.7%) of unchanged **3**. The mixture of ester products was treated as described above for the isolation of **5** and **7** and gave 26.9 mg (3.3%) of **6** and 49.8 mg (6.1%) of **8**. Ester **6** was obtained as a red oil. TLC (benzene) R_f 0.32. λ_{max}: 241 (log ε 4.45), 299 (4.59), 304 (4.61), 309 (sh 4.51), 364 (3.94), 377 (4.03), 513 (sh ε 738), 535 (888), 569 (715) and 623 (301). IR: 1692 (C=O) and 2830 cm^{-1} (O–CH_3). NMR (δ): 1.35 (6H, d, J=6.6 Hz, $(C\underline{H}_3)_2CH$), 2.85 (3H, s, 4-CH_3), 3.10 (1H, m, J=6.6 Hz, $(CH_3)_2C\underline{H}$), 3.72 (3H, s, OCH_3), 6.78 (2H, d, J=9.3 Hz, H-10 and H-11), 7.01 (2H, d, J=9.3, H-9 and H-12), 7.08 (1H, d, J=4.3 Hz, 3-H), 7.22 (1H, d, J=10.7 Hz, 5-H), 7.48 (1H, dd, J=10.7 and 2.2 Hz, 6-H), 8.24 (1H, d, J=4.3 Hz, 2-H) and 9.60 (1H, d, J=2.2 Hz, 8-H). MS: *m/e* 334 (M^+ for $C_{22}H_{22}O_3$) and ($M^+-CH_3OC_6H_4O$). Ester **8** crystallized from hexane as dark violet crystals, mp 91—92 °C. TLC (benzene) R_f 0.32. λ_{max}: 249 (log ε 4.57), 289 (sh 4.53), 300 (4.71), 308 (4.73), 314 (sh 4.66), 373 (4.14), 388 (4.21), 526 (sh ε 760), 562 (990), 604 (sh 826) and 666 (301). IR: 1700 cm^{-1}. NMR (δ): 1.35 (6H, d, J=7.2 Hz, $(C\underline{H}_3)_2CH$), 2.83 (3H, s, 3-CH_3), 3.05 (3H, s, 4-CH_3), 3.08 (1H, m, J=7.2 Hz, $(CH_3)_2C\underline{H}$), 3.80 (3H, s, OCH_3), 6.94 (2H, d, J=9.6 Hz, H-10 and H-11), 7.16 (2H, d, J=9.6 Hz, H-9 and H-12), 7.19 (1H, d, J=10.5 Hz, 5-H), 7.48 (1H, dd, J=10.5 and 2.0 Hz, 6-H), 8.23 (1H, s, 2-H) and 9.76 (1H, d, J=2.0 Hz, 8-H). MS: *m/e* 348 (M^+ for $C_{23}H_{24}O_3$) and 225 ($M^+-CH_3OC_6H_4O$). The yield of ketone **9** was 45.8 mg (5.6%).

*Methyl 4-Methyl-7-isopropyl-1-azulenecarboxylate (**10**).* *A. From **5**.* A solution of 20.98 mg of **5** in an excess (0.7 ml) of 0.03 M potassium methoxide in methanol was shaken in a sealed tube for 20 h. The mixture was then diluted with water (30 ml) and extracted with ether (3×10 ml). Chromatography of the concentrate from the ether extract on silica gel (benzene) separated 12.60 mg (75.4%) of **10** identical (UV, IR and NMR) with an authentic specimen.[11]

*B. From **7**.* The procedure given in *A* afforded 8.97 mg (85.4%) of **10**, identical (IR, NMR) with that from *A*, from 14.43 mg of **7**.

*Methyl 3,4-Dimethyl-7-isopropyl-1-azulenecarboxylate (**11**).* A. *From **6**.* In the manner described for the preparation of **10**, 4.42 mg of **6** was converted to 2.05 mg (57.6%) of **11** identical (UV, Vis, TLC) with an authentic specimen.[4]

*B. From **8**.* The procedure indicated in *A* gave from 5.96 mg of **8** a yield of 3.98 mg (90.9 %) of **11** identical with that from *A*.

References

1) Work performed at Saga University.
2) S. Kurokawa, *Bull. Chem. Soc. Jpn.*, **43**, 509 (1970).
3) S. Kurokawa, *Tetrahedron Lett.*, **1969** 3567.
4) S. Kurokawa, M. Hashimoto, and S. Hayashi, *Bull. Chem. Soc. Jpn.*, **45**, 3559 (1972).
5) S. Kurokawa, T. Safo, T. Noguchi, and K. Yano, *Bull. Chem. Soc. Jpn.*, **48**, 1559 (1975).
6) W. Treibs, Ch. Vollrad, and M. Reimann, *Justus Liebigs Ann. Chem.*, **648**, 164 (1961).
7) M. Reiner and R. H. Downes, *J. Am. Chem. Soc.*, **43**, 945 (1921).
8) M. J. S. Dewar, "Molecular Rearrangements," Vol. 1, ed. by Paul de Mayo, John Wiley, Interscience, New York, N.Y. (1963), Chapt 5.
9) K. Hafner, H. Pelster, and H. Patselt, *Justus Liebigs Ann. Chem.*, **650**, 80 (1961). This acidity would be enhanced in the 1–(3) protonated conjugate acid.
10) Each experiment was performed several times and a representative run is reported.
11) K. Kohara, *Bull. Chem. Soc. Jpn.*, **42**, 3229 (1969).

Synthesis of Eriostoic Acid and Eriostemoic Acid[1]

Masao TSUKAYAMA

Department of Applied Chemistry, Faculty of Engineering, University of Tokushima, Tokushima 770

(Received December 8, 1975)

A 1,8-dioxaanthracenepropionic acid derivative (**5**), after being converted into methyl ester-methyl ether (**6**), was reduced with sodium borohydride to give methyl eriostate (**7**). Hydrolysis of the ester (**7**) with alkali afforded eriostoic acid (**1**). On the other hand, eriostemoic acid (**2**) was synthesized from methyl eriostemate (**10**), which was obtained from a 1,5-dioxaphenanthrenepropionic acid derivative (**8**) *via* four steps.

Eriostoic acid has been isolated from *Eriostemon difformis* and the structure has been elucidated to be a linear-type benzodipyran (10-methoxy-2,2,7,7-tetramethyl-2*H*,7*H*-1,8-dioxaanthracene-9-propionic acid) (**1**) on the basis of degradation and spectral evidence.[2] On the other hand, eriostemoic acid isolated from *Eriostemon tomentellus* has been shown to be an angular-type benzodipyran derivative (9-methoxy-2,2,6,6-tetramethyl-2*H*,6*H*-1,5-dioxaphenanthrene-10-propionic acid) (**2**) which is closely related to **1**.[3] The present paper reports on the synthesis of **1** and **2** for confirmation of the proposed structures of natural eriostoic and eriostemoic acids.

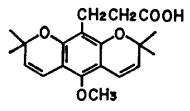

1

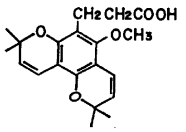

2

The condensation of a 1,8-dioxaanthracene derivative (**3**)[4] with acrylic acid in the presence of polyphosphoric acid gave a 1,8-dioxaanthracenepropionic acid derivative (**5**). The exhaustive methylation of **5** with dimethyl sulfate afforded the corresponding methyl ester-methyl ether (**6**). The reduction of **6** with an excess of sodium borohydride[5] in dry methanol containing a small amount of pyridine gave directly methyl eriostate (**7**). The NMR spectrum showed the presence of four vinylic protons as two overlapping doublets at δ 5.45 (2H) and 6.48 (2H) ppm, and the IR spectrum showed an olefinic group at 1630 cm^{-1} and the disappearance of the carbonyl group. Hydrolysis of **7** with 4% aqueous methanolic sodium hydroxide smoothly produced the desired acid (**1**) (mp 173—174 °C),[2] which was shown to be identical with natural eriostoic acid on the basis of a mixed-melting-point determination and by NMR, IR, and UV spectral comparisons.

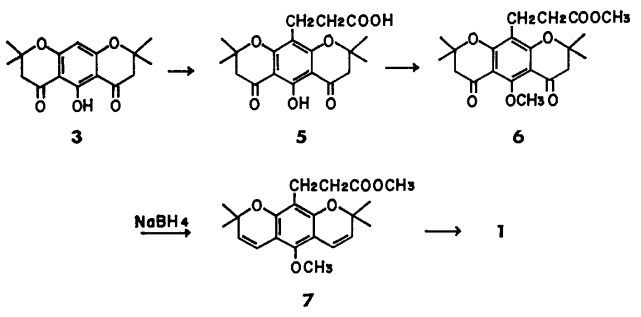

3 5 6 7

Scheme 1.

In a similar manner, the 1,5-dioxaphenanthrenepropionic acid derivative (**8**), which was obtained by the condensation of a 1,5-dioxaphenanthrene derivative (**4**)[4] with acrylic acid and whose structure was confirmed by NMR and IR spectra, was converted into the corresponding methyl ester-methyl ether (**9**). The reduction of **9** with sodium borohydride gave methyl eriostemate (**10**) in a poor yield. Hydrolysis of **10** with dilute alkali afforded the desired acid (**2**) (mp 101—102 °C),[3] which was shown to be identical with natural eriostemoic acid on the basis of a mixed-melting-point determination and by NMR, IR, and UV spectral comparisons.

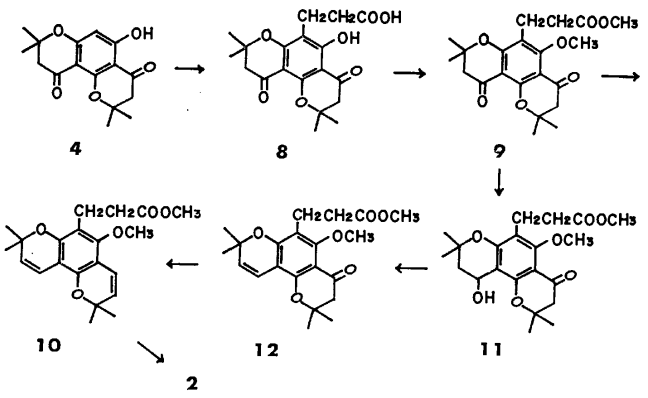

4 8 9 10 12 11 2

Scheme 2.

In view of the low yield of methyl eriostemate, an alternate method of preparing this compound was further investigated. The methyl ester-methyl ether (**9**) was converted into an alcohol derivative (mp 114—115 °C) (**11**) by catalytic reduction with Raney nickel in methanol under atmospheric conditions. The dehydration of the alcohol (**11**) with freshly-fused potassium hydrogensulfate in dry toluene was smoothly effected to give the corresponding dihydro-1,5-dioxaphenanthrenepropionic acid derivative (**12**). The NMR spectrum showed the presence of one vinyl group as a pair of doublets at δ 5.37 and 6.48 ppm and one methylene group as a singlet at δ 2.51 ppm, and the IR spectrum showed the presence of an olefinic group at 1637 cm^{-1} and the disappearance of the hydroxyl group. The reduction of **12** with sodium borohydride in dry tetrahydrofuran gave methyl eriostemate (**10**) in a 37% yield, which was identical with the sample synthesized in the manner described above.

The reduction of **12** with palladium charcoal in methanol gave the corresponding tetrahydro-1,5-dioxaphenanthrenepropionic acid derivative (**15**), which was identical with that derivative (**15**) obtained from

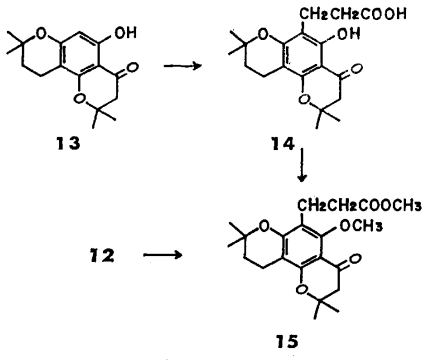

Scheme 3.

a tetrahydro-1,5-dioxaphenanthrene derivative (**13**)[4] *via* two steps, as shown in Scheme 3. Therefore, structure of the alcohol derivative (**11**) was elucidated on the basis of the facts described above.

Experimental

The melting points are uncorrected. The IR spectra were taken with a Hitachi 215 Spectrophotometer, and the UV spectra with a Hitachi 124 Spectrophotometer. The NMR spectra were determined with a JOEL PS-100 Spectrometer (100 MHz) using tetramethylsilane as an internal standard (δ, ppm). Column chromatography was carried out on Kieselgel 60 (70—230 mesh) (Merck).

*10-Hydroxy-2,2,7,7-tetramethyl-4,5-dioxo-3,4,5,6-tetrahydro-2*H,*7*H-*1,8-dioxaanthracene-9-propionic Acid (**5**).* 10-Hydroxy-2,2,7,7-tetramethy-4,5-dioxo-3,4,5,6-tetrahydro-2*H*,7*H*-1,8-dioxaanthracene (**3**) (5.6 g), which was prepared according to a procedure described by Jefferson *et al.*,[4] and acrylic acid (3 g) were heated in the presence of freshly-prepared polyphosphoric acid (90 g) with stirring at 80—85 °C for 2 h and then poured into ice-cold water (300 ml). The diluted reaction mixture was allowed to stand overnight at room temperature to afford a white precipitate. The precipitate, after being dissolved in chloroform (200 ml), was extracted with 5% aqueous sodium carbonate (50 ml×3), and the alkalin solution was acidified with dilute hydrochloric acid to give acid **5** (3 g, 43%), which produced a light brown ferric chloride reaction in ethanol and which was obtained as colorless needles upon recrystallization from methanol: mp 190—191 °C; IR ν_{max}^{KBr}: 1610, 1675, 1735 cm^{-1}; NMR ($CDCl_3$) δ: 1.46 (s, 12H, CH_3 × 4), 2.66 (s, 4H, CH_2CO × 2), 2.37—2.92 (m, 4H, CH_2CH_2), 13.76 (s, 1H, OH). Found: C, 62.73; H, 6.19%. Calcd for $C_{19}H_{22}O_7$: C, 62.97; H, 6.12%.

*Methyl 10-Methoxy-2,2,7,7-tetramethyl-4,5-dioxo-3,4,5,6-tetrahydro-2*H,*7*H-*1,8-dioxaanthracene-9-propionate (**6**).* A mixture of acid **5** (3 g), dimethyl sulfate (7 g), and anhydrous potassium carbonate (8 g) was heated under reflux in dry acetone (100 ml) for 25 h. The resulting product was recrystallized from methanol to give methyl ester-methyl ether (**6**) (2.5 g, 77%) as colorless needles: mp 121.5—122.5 °C; IR ν_{max}^{KBr} 1693, 1730 cm^{-1}; NMR ($CDCl_3$) δ 1.43 (s, 12H, CH_3 ×4), 2.63 (s, 4H, CH_2CO×2), 2.34—2.96 (m, 4H, CH_2CH_2), 3.67 (s, 3H, OCH_3), 3.87 (s, 3H, OCH_3). Found: C, 64.61; H, 6.73%. Calcd for $C_{21}H_{26}O_7$: C, 64.60; H, 6.71%.

*Methyl Eriostate (**7**).* Sodium borohydride (0.16 g) was added portionwise to a solution of methyl ester-methyl ether **6** (0.39 g) in a mixture of dry methanol (15 ml) and pyridine (3.5 ml) with stirring for 1 h at room temperature, and the mixture was further warmed at 45 °C for 9 h. The reaction mixture was then cooled, acidified with dilute hydrochloric acid and extracted with ether, and the ethereal solution was washed with a saturated aqueous solution of sodium chloride and dried, and the solvent was evaporated. The residue was purified by column chromatography with silica gel and benzene to give an oil (**7**) (61 mg, 17%), which was crystallized from hexane as colorless prisms (mp 96—97 °C, lit, mp 94 °C[2]): IR ν_{max}: 1630, 1735 cm^{-1}; NMR ($CDCl_3$) δ: 1.39 (s, 12H, CH_3×4), 2.36—2.94 (m, 4H, CH_2-CH_2), 3.66 (s, 3H, OCH_3), 3.70 (s, 3H, OCH_3), 5.45 and 6.48 (each d, 2H, J=10 Hz, CH=CH). Found: C, 70.13; H, 7.40%. Calcd for $C_{21}H_{26}O_5$: C, 70.37; H, 7.31%.

*Eriostoic Acid (**1**).* Methyl eriostate (**7**) (22 mg) was hydrolyzed with 4% aqueous methanolic sodium hydroxide (20 ml) at 80 °C for 30 min. The reaction mixture was then acidified with dilute hydrochloric acid to afford eriostoic acid (**1**) as white precipitates, which was recrystallized from ethyl acetate as colorless prisms (20 mg, 95%) (mp 173—174 °C, lit, mp 173—174 °C,[2]) no depression in a mixed-melting-point determination with natural eriostoic acid): IR ν_{max}^{KBr}: 1630, 1718 cm^{-1}; NMR ($CDCl_3$) δ: 1.40 (s, 12H, CH_3×4), 2.43—2.97 (m, 4H, CH_2CH_2), 3.70 (s, 3H, OCH_3), 5.45 and 6.48 (each d, 2H, J=10 Hz, CH=CH); UV λ_{max}^{EtOH} nm (log ε): 259 (4.60), 268 (4.59), 340 (3.52). Found: C, 69.87; H, 7.18%. Calcd for $C_{20}H_{24}O_5$: C, 69.74; H, 7.02%.

*9-Hydroxy-2,2,6,6-tetramethyl-4,8-dioxo-3,4,7,8-tetrahydro-2*H,*6*H-*1,5-dioxaphenanthrene-10-propionic Acid (**8**).* 9-Hydroxy-2,2,6,6-tetramethyl-4,8-dioxo-3,4,7,8-tetrahydro-2*H*,6*H*-1,5-dioxaphenanthrene (**4**)[4] (6 g) and acrylic acid (3 g) were heated in the presence of freshly-prepared polyphosphoric acid (90 g) with stirring at 80—85 °C for 2 h. The reaction mixture was similary treated as described for the preparation of **5** to give acid **8** (3.4 g, 45%), which showed a light brown ferric chloride reaction in ethanol, as colorless needles: mp 192—193 °C; IR ν_{max}^{KBr}: 1632, 1687, 1706 cm^{-1}; NMR ($CDCl_3$) δ: 1.45 (s, 6H, CH_3×2), 1.53 (s, 6H, CH_3×2), 2.63 (s, 2H, CH_2CO), 2.72 (s, 2H, CH_2CO), 2.44—2.96 (m, 4H, CH_2-CH_2), 12.94 (s, 1H, OH). Found: C, 62.83; H, 6.12%. Calcd for $C_{19}H_{22}O_7$: C, 62.97; H, 6.12%.

*Methyl 9-Methoxy-2,2,6,6-tetramethyl-4,8-dioxo-3,4,7,8-tetrahydro-2*H,*6*H-*1,5-dioxaphenanthrene-10-propionate (**9**).* A mixture of acid **8** (4 g), dimethyl sulfate (7 g), and anhydrous potassium carbonate (8 g) was heated under reflux in dry acetone (100 ml) for 25 h. The product was recrystallized from methanol to give methyl ester-methyl ether **9** (3.5 g, 81%) as colorless needles: mp 105—106 °C; IR ν_{max}^{KBr}: 1683, 1725 cm^{-1}; NMR ($CDCl_3$) δ: 1.45 (s, 6H, CH_3×2), 1.49 (s, 6H, CH_3×2), 2.64 (s, 4H, CH_2CO×2), 2.36—2.94 (m, 4H, CH_2CH_2), 3.65 (s, 3H, OCH_3), 3.81 (s, 3H, OCH_3). Found: C, 64.45; H, 6.77%. Calcd for $C_{21}H_{26}O_7$: C, 64.60; H, 6.71%.

*Methyl Eriostemate (**10**).* Sodium borohydride (0.24 g) was added portionwise to a solution of methyl ester-methyl ether **9** (0.5 g) in a mixture of dry methanol (20 ml) and pyridine (4 ml) with stirring for 1 h at room temperature, and the mixture was maintained at 45 °C for 9 h. The reaction product thus obtained was purified by column chromatography with silica gel and benzene to give methyl eriostemate (liquid) (**10**) (28 mg, 6%): IR ν_{max}: 1635, 1735 cm^{-1}; NMR (CCl_4) δ: 1.38 (s, 6H, CH_3×2), 1.40 (s, 6H, CH_3×2), 2.28—2.79 (m, 4H, CH_2CH_2), 3.60 (s, 3H, OCH_3), 3.67 (s, 3H, OCH_3), 5.33 (d, 2H, J=10 Hz, CH=CH), 6.38 and 6.48 (each d, 1H, J=10 Hz, CH=CH). Found: C, 70.24; H, 7.40%. Calcd for $C_{21}H_{26}O_5$: C, 70.37; H, 7.31%.

*Eriostemoic Acid (**2**).* Methyl eriostemate (**10**) (25 mg) was hydrolyzed with 4% aqueous methanolic sodium hydro-

xide (20 ml) at 80 °C for 30 min. The reaction mixture, after being acidified with dilute hydrochloric acid, was extracted with ether and the ethereal solution was washed with water and dried, and the solvent was evaporated. The residue was eluted over a silica gel column with chloroform–ethyl acetate (4 : 1) to give the desired acid (**2**) (20 mg, 83%), which was recrystallized from hexane as colorless prisms (mp 101—102 °C, lit, mp 101 °C,[3]) no depression in a mixed-melting-point determination with natural eriostemoic acid): IR ν_{max}^{KBr}: 1640, 1708 cm^{-1}; NMR ($CDCl_3$) δ: 1.39 (s, 12H, $CH_3\times4$), 2.43—2.93 (m, 4H, CH_2CH_2), 3.69 (s, 3H, OCH_3), 5.45 (d, 2H, $J=10$ Hz, CH=CH), 6.46 and 6.59 (each d, 1H $J=10$ Hz, CH=CH). UV λ_{max}^{EtOH} nm (log ε): 206 (4.29), 254 (4.33), 258 (4.33), 280 (4.13), 331 (3.39), 347 (3.29). Found: C, 70.03; H, 7.09%. Calcd for $C_{20}H_{24}O_5$: C, 69.74; H, 7.02%.

*Methyl 4-Hydroxy-9-methoxy-2,2,6,6-tetramethyl-8-oxo-3,4,7,8-tetrahydro-2H,6H-1,5-dioxaphenanthrene-10-propionate (**11**).* Methyl ester-methyl ether **9** (0.95 g) was hydrogenated over Raney nickel (6 g) in methanol (30 ml) under atmospheric pressure at room temperature. After the uptake of hydrogen ceased, the solution was filtered and the solvent was evaporated under reduced pressure. The residue thus obtained was purified in column chromatography with silica gel and chloroform–ethyl acetate (20 : 1) to afford a colorless solid, showing lower R_f value (0.32) than that (0.39) of the starting material. The solid was recrystallized from light petroleum ether (40—50 °C) to give alcohol derivative **11** (0.44 g, 46%) (mp 114—115 °C) as colorless prisms: IR ν_{max}^{KBr}: 1665, 1738, 3460 cm^{-1}; NMR ($CDCl_3$) δ: 1.39 (s, 3H, CH_3), 1.47 (s, 6H, $CH_3\times2$), 1.53 (s, 3H, CH_3), 2.04 (d, 2H, CH_2), 2.68 (s, 2H, CH_2CO), 2.37—2.95 (m, 4H, CH_2CH_2), 3.68 (s, 3H, OCH_3), 3.78 (s, 3H, OCH_3), 4.92 (t, 1H, CHOH). Found: C, 64.12; H, 7.28%. Calcd for $C_{21}H_{28}O_7$: C, 64.27; H, 7.19%.

*Methyl 9-Methoxy-2,2,6,6-tetramethyl-8-oxo-7,8-dihydro-2H,6H-1,5-dioxaphenanthrene-10-propionate (**12**).* Alcohol **11** (0.45 g) was refluxed with freshly-fused potassium hydrogensulfate (2 g) in toluene (5 ml) for 7 h. The mixture was then filtered and the filtrate was evaporated under reduced pressure to give a colorless oil, which was purified over a silica gel column with chloroform–methyl ethyl ketone (50 : 1) to give colorless needles **12** (0.4 g, 93%) (mp 85—86 °C, crystallization from light petroleum ether): IR ν_{max}: 1637, 1678, 1735 cm^{-1}; NMR (CCl_4) δ: 1.45 (bs, 12H, $CH_3\times4$), 2.51 (s, 2H, CH_2CO), 2.27—2.83 (m, 4H, CH_2CH_2), 3.61 (s, 3H, OCH_3), 3.73 (s, 3H, OCH_3), 5.37 and 6.48 (each d, 1H, $J=10$ Hz, CH=CH). Found: C, 67.09; H, 7.11%. Calcd for $C_{21}H_{26}O_6$: C, 67.36; H, 7.00%.

*Another Synthesis of Methyl Eriostemate (**10**).* Sodium borohydride (90 mg) was added portionwise to a solution of methyl ester **12** (0.145 g) in dry tetrahydrofuran (15 ml) with stirring for 1 h at room temperature, and the mixture was refluxed for 6 h. The reaction mixture was cooled and treated as described above to give an oil. The oil was eluted over a silica gel column with benzene to give methyl eriostemate (liquid) (**10**) (52 mg, 37%), the identity of which was confirmed by spectroscopic comparison with the methyl eriostemate synthesized above. The starting material **12** (90 mg) was also recovered.

*9-Hydroxy-2,2,6,6-tetramethyl-8-oxo-3,4,7,8-tetrahydro-2H,6H-1,5-dioxaphenanthrene-10-propionic Acid (**14**).* 9-Hydroxy-2,2,6,6-tetramethyl-8-oxo-3,4,7,8-tetrahydro-2*H*,6*H*-1,5-dioxaphenanthrene (**13**)[4] (1.9 g) and acrylic acid (1.5 g) were heated in the presence of polyphosphoric acid (45 g) with stirring at 60—65 °C for 1.5 h, and the reaction mixture was poured into ice-cold water (200 ml). The mixture was allowed to stand overnight at room temperature, and a white precipitate was collected and purified by column chromatography with silica gel and a mixed solvent of chloroform–methanol (190 : 9) to give an acid **14** (0.5 g, 21%) (mp 202—203 °C; recrystallization from methanol as colorless prisms). It gave a dark blue ferric chloride reaction in ethanol: IR ν_{max}^{KBr} 1635, 1708 cm^{-1}; NMR ($CDCl_3$) δ 1.33 (s, 6H, $CH_3\times2$), 1.44 (s, 6H, $CH_3\times2$), 1.74 and 2.53 (each t, 2H, $J=6$ Hz, CH_2), 2.43—2.95 (m, 4H, CH_2CH_2), 2.65 (s, 2H, CH_2CO), 12.17 (s, 1H, OH). Found: C, 65.50; H, 7.04%. (s, 2H, CH_2CO), 12.17 (s, 1H, OH). Found: C, 65.50; H, 7.04%. Calcd for $C_{19}H_{24}O_6$: C, 65.50; H, 6.94%.

*Methyl 9-Methoxy-2,2,6,6-tetramethyl-8-oxo-3,4,7,8-tetrahydro-2H,6H-1,5-dioxaphenanthrene-10-propionate (**15**).* A mixture of acid **14** (0.13 g), dimethyl sulfate (0.3 g), and anhydrous potassium carbonate (2 g) was heated under reflux in dry acetone (50 ml) for 24 h. The product was purified by column chromatography on silica gel with chloroform–ethyl acetate (20 : 1) to give a colorless oil (**15**). The oil was crystallized from light petroleum ether (40—50 °C) as colorless prisms (70 mg, 50%) (mp 79—80 °C): IR ν_{max}: 1673, 1735 cm^{-1}; NMR ($CDCl_3$) δ: 1.33 (s, 6H, $CH_3\times2$), 1.43 (s, 6H, $CH_3\times2$), 1.75 and 2.52 (each t, 2H, $J=6$ Hz, CH_2), 2.36—2.94 (m, 4H, CH_2CH_2), 2.60 (s, 2H, CH_2CO), 3.68 (s, 3H, OCH_3), 3.77 (s, 3H, OCH_3). Found: C, 66.97; H, 7.59%. Calcd for $C_{21}H_{28}O_6$: C, 67.00; H, 7.50%.

*Additional Synthesis of **15**.* Methyl ester **12** (0.11 g) was hydrogenated over palladium charcoal (95 mg) in methanol (20 ml) at room temperature. After the uptake of hydrogen ceased within 40 min, the solution was filtered and the filtrate was evaporated under reduced pressure. The residue was purified by column chromatography on silica gel with chloroform–ethyl acetate (20 : 1) to give a colorless oil (0.10 g, 90%). The oil was crystallized from light petroleum ether to give colorless prisms **15** (mp 79—80 °C; not depressed upon mixture with the sample synthesized above).

The author wishes to express his deep gratitude to Professor Shūichi Hayashi and Dr. Mitsuru Nakayama, Hiroshima University, for their guidance and encouragement throughout the course of this work, and also to Professor P. R. Jefferies, Department of Chemistry, University of Western Australia, Nedlands, W. A., for supplying the samples of natural eriostoic acid and eriostemoic acid.

References

1) This has previously been reported in preliminary form: M. Nakayama, S. Hayashi, M. Tsukayama, T. Horie, and M. Masumura, *Chem. Lett.*, **1975**, 55.

2) A. M. Duffield, P. R. Jefferies, and P. H. Lucich, *Aust. J. Chem.*, **15**, 812 (1962).

3) A. M. Duffield and P. R. Jefferies, *Aust. J. Chem.*, **16**, 123 (1963).

4) A. Jefferson, I. Moor, and F. Scheimann, *J. Chem. Soc., C*, **1967**, 151.

5) J. Nickl, *Chem. Ber.*, **92**, 1989 (1959).

A Facile Method for the Oxidation of Alcohols

Kazuhiko SAIGO, Anri MORIKAWA, and Teruaki MUKAIYAMA

Department of Chemistry, Faculty of Science, The University of Tokyo, Hongo, Bunkyo-ku, Tokyo 113

(Received December 19, 1975)

Trialkyltin alkoxides, prepared from alcohols and trialkyltin methoxide by azeotropical removal of methanol, are easily oxidized by bromine in the presence of trialkyltin methoxide, a hydrogen bromide captor, to give the corresponding aldehydes or ketones in good yields. Alcohols are oxidized directly in one step to the corresponding carbonyl compounds by utilizing bis(tributyltin) oxide and bromine.

Selective oxidation of alcohols to the corresponding aldehydes or ketones is important in organic synthesis, and a number of methods have been reported. Reagent such as aluminum triisopropoxide (the Oppenauer oxidation),[1] CrO_3–AcOH complex (Jones reagent),[2] CrO_3–pyridine complex (Collins reagent),[3] dicyclohexylcarbodiimide–dimethyl sulfoxide,[4] dimethyl sulfide–chlorine or *N*-chlorosuccinimide[5] and others[6] are commonly employed for oxidizing alcohols to aldehydes or ketones, but they bring about certain difficulties. For example, further oxidation of the desired aldehyde to carboxylic acid and of carbon–carbon double bonds or isomerization of carbon–carbon double bonds sometimes takes place reducing the yields of the desired aldehydes or ketones. This prompted us to look for efficient reagents for the oxidation of alcohols to the corresponding aldehydes or ketones.

The study was initiated to examine the effective combination of a metal alkoxide ($R^1R^2CHOMX_{n-1}$) and an oxidant (Y-Z) based on the following consideration: If oxidant Y has a strong affinity to alkoxide M and oxidant Z also has an affinity toward hydride, the oxidation would be effectively promoted *via* 6-membered cyclic intermediate to give the desired carbonyl compound accompanied by the formation of $MX_{n-1}Y$ and HZ as illustrated in the following scheme.

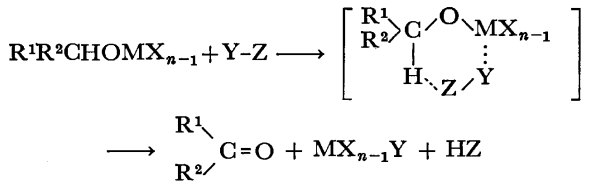

After several trials with cinnamyl alcohol as a model alcohol, cinnamaldehyde was obtained in a moderate yield when triethyltin cinnamyl oxide was treated with bromine[7] as briefly reported in a previous communication.[8] In this report, details of the oxidation are described with additional results.

The starting materials, triethyltin alkoxides, were prepared according to a modification of the method in literature.[9] Alcohol was allowed to react with triethyltin methoxide[10] in toluene under refluxing, the methanol formed being removed continuously. The corresponding triethyltin alkoxide was obtained in a good yield after distillation under reduced pressure (Table 1).

It was found that, in the absence of the hydrogen bromide captor, the starting triethyltin alkoxide was destroyed by the rapid reaction with hydrogen bromide to form triethyltin bromide and the alcohol, and that in order to improve the yield of the carbonyl compound it is necessary to capture hydrogen bromide produced at the same time. Of several hydrogen bromide captors examined, the best result was obtained when

Table 1. Preparation of triethyltin alkoxides

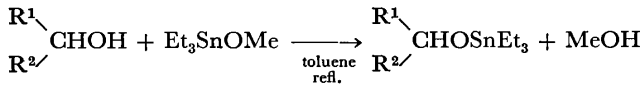

Alcohol	Reaction time (h)	Isolated yield (%)	Bp (mmHg)
Geraniol	8	92	134—6 °C (1.0)
Cinnamyl alcohol	2	84	145—7 °C (0.75)
(*E*)-2-Hexen-1-ol	14	78	105—7 °C (2.4)
Piperonyl alcohol	6	86	153—6 °C (0.8)
Benzyl alcohol	9	78	108 °C (0.7)
1-Phenylethanol	5	78	108—9 °C (1.4)
2-Octanol	4	86	108—9 °C (1.8)

Table 2. Examination of hydrogen bromide captors

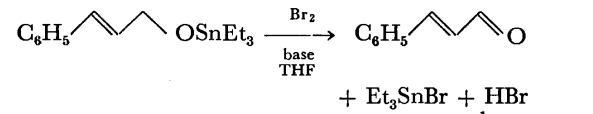

Base	Yield (%)[a]	Base	Yield (%)[a]
Et_3SnOMe	82	K_2CO_3	33
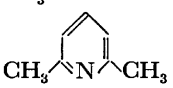	47	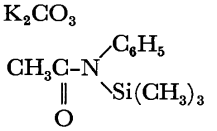	trace
NaH	43		trace

a) Yield determined by GLC.[11]

Table 3. Oxidation of triethyltin alkoxides

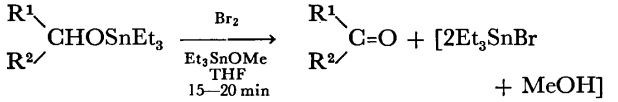

Alcohol	Yield (%)
Geraniol	94[a]
Cinnamyl alcohol	92[b]
(*E*)-2-Hexen-1-ol	71[b]
Piperonyl alcohol	96[a]
Benzyl alcohol	81[b]
1-Phenylethanol	79[b]
2-Octanol	85[b]

a) Isolated yield. b) Yield determined by GLC.[11]

triethyltin methoxide was employed as a captor (Table 2).

The effect of the solvent on the oxidation of triethyltin 1-phenylethoxide with bromine was studied in tetrahydrofuran (THF), dichloromethane and benzene, and the corresponding ketone, acetophenone, was obtained in 78%, 70% and 66% yields, respectively.

Optimum yield was obtained when a THF solution of bromine was added dropwise to a THF solution of triethyltin alkoxide in the presence of triethyltin methoxide as a hydrogen bromide captor. The oxidation of various triethyltin alkoxides was attempted and the corresponding aldehydes or ketones were obtained in good yields (Table 3).

Similarly, tributyltin alkoxide, easily prepared from bis(tributyltin) oxide and an alcohol, was oxidized with bromine in the presence of tributyltin methoxide as a hydrogen bromide captor. As an example, tributyltin benzyl oxide was oxidized to give benzaldehyde in 82% yield.

$$C_6H_5CH_2OSnBu_3 \xrightarrow[Bu_3SnOMe,\ THF]{Br_2} C_6H_5CHO + [2Bu_3SnBr + MeOH]$$

The yield decreased when chlorine or iodine was employed as an oxidant instead of bromine.

It is remarkable that the reaction is completed as soon as the titration of a bromine solution is over. It is noteworthy that the oxidation of geraniol affords geranial in a high yield, no by-products such as a further oxidized product (geranic acid), an isomerized product (neral) and brominated products formed by the addition of bromine to the olefinic linkages being detected.

The present method involves the following two processes: (1) Preparation of trialkyltin alkoxides from alcohols and trialkyltin methoxide or bis(trialkyltin) oxide, and (2) oxidation of trialkyltin alkoxides to the carbonyl compounds with bromine in the presence of trialkyltin methoxide. In order to find a one step procedure for the oxidation of alcohols, oxidation with bromine utilizing bis(tributyltin) oxide[12] was studied on the basis of the following: Bis(tributyltin) oxide reacts with alcohols to give the corresponding tributyltin alkoxides and tributyltin hydroxide,[13] and with hydrogen halide to give tributyltin halide and tributyltin hydroxide. Thus tributyltin alkoxides would be formed *in situ* from alcohols and bis(tributyltin) oxide, and the alkoxides would be similarly oxidized with bromine in the presence of bis(tributyltin) oxide, a hydrogen bromide captor.

Actually, cinnamaldehyde was obtained in 84% yield by adding a bromine solution into a solution of an equimolar amount of cinnamyl alcohol in the presence of bis(tributyltin) oxide. It was found that THF is also better than benzene or dichloromethane as a solvent similarly to the case of oxidation of isolated trialkyltin alkoxides (Table 4).

In the case of the oxidation of 2-octanol, 2-octanone was obtained only in 60% yield under these conditions. After several trials it was found that the optimum yield is obtained for 2-octanone when the mole ratio of alcohol, bis(tributyltin) oxide and bromine is 1 : 2 : 2. In the case of hindered alcohols such as 1-phenylethanol, benzhydrol and 3β-cholestanol, the yields were improved by treatment of alcohol with bis(tributyltin) oxide in the presence of molecular sieves[14] at 50—60 °C for several hours before the addition of bromine. The oxidation of several alcohols was examined under these conditions and the corresponding aldehydes or ketones were obtained in good yields (Table 5).

Table 4. Solvent effect in the oxidation of alcohols with bromine using bis(tributyltin) oxide

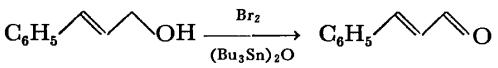

Solvent	Yield (%)[a]
THF	84
CH_2Cl_2	53
C_6H_6	47

a) Yield determined by GLC.[11]

Table 5. Direct oxidation of alcohols with bromine in the presence of bis(tributyltin) oxide

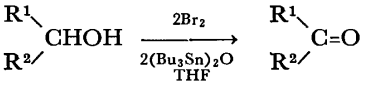

Alcohol	Yield (%)	
Cinnamyl alcohol	85[b]	
2-Octanol	90[b]	
(*E*)-2-Hexen-1-ol	81[b]	
Benzyl Alcohol	89[b]	
Piperonyl alcohol	83[a]	
1-Phenylethanol	62[b]	(88)[b]
Benzhydrol		(62)[b]
3β-Cholestanol		(89)[a]

a) Isolated yield. b) Yield determined by GLC.[11] Values in parentheses indicate the yields when alcohols were allowed to react with bis(tributyltin) oxide in the presence of molecular sieves before the addition of bromine.

By this procedure, alcohols are directly oxidized by bromine in the presence of bis(tributyltin) oxide without isolation of the intermediates, trialkyltin alkoxides, which was necessary in the former procedure.

The present procedures utilizing organotin derivatives and bromine as an oxidant provides convenient and efficient methods for the oxidation of alcohols to the corresponding aldehydes or ketones. It is expected that these methods will find widespread use.

Experimental

Preparation of Triethyltin Alkoxides. A solution of an alcohol (20 mmol) and triethyltin methoxide (24 mmol) in toluene (50 ml) was refluxed for 2—14 h (Table 1) under an argon atmosphere, and methanol formed was azeotropically removed. After removal of the solvent, the corresponding triethyltin alkoxide was obtained by distillation under reduced pressure.

General Procedure for Oxidation of Triethyltin Alkoxides with Bromine. To a THF solution of triethyltin alkoxide (1 M) and triethyltin methoxide (1.2—1.7 M) was added dropwise a THF solution of bromine (1 M) at room tem-

perature under an argon atmosphere. As soon as the addition of bromine was over, the reaction mixture was quenched with a 5% aq. $Na_2S_2O_3$ solution and a 5% aq. NaOH solution, and the resulting mixture was extracted with ether. The ethereal layer was washed with a 5% aq. NaOH solution and brine, and dried over anhydrous Na_2SO_4. The yields of the corresponding carbonyl compounds were determined by vapor phase chromatographic analysis or by isolation using thin layer chromatography (silica gel).

Oxidation of Triethyltin Geraniloate with Bromine. To a solution of triethyltin geraniolate (679 mg, 1.89 mmol) and triethyltin methoxide (754 mg, 3.18 mmol) in THF (20 ml) was added drop by drop a solution of bromine (310 mg, 1.94 mmol) in THF (10 ml) over a period of 15 min at room temperature under an argon atmosphere. The reaction mixture was then quenched with a 5% aq. $Na_2S_2O_3$ solution (5 ml) and a 5% aq. KOH solution (20 ml). The resulting mixture was extracted with ether (60 ml), and the ethereal layer was washed with a 5% aq. KOH solution (20 ml) and with brine (20 ml). After evaporation of the solvent, geranial (269 mg, 94%), identified by NMR spectrum and GLC analysis on comparison with an authentic graphy.

Preparation of Tributyltin Benzyl Oxide. A solution of benzyl alcohol (2.67 g, 25.5 mmol) and bis(tributyltin) oxide (7.61 g, 12.8 mmol) in benzene (70 ml) was refluxed for 4 h under an argon atmosphere; water was continuously removed. After removal of the solvent, tributyltin benzyl oxide was isolated by distillation under reduced pressure (7.61 g, 75%, bp 140—142 °C/0.9 Torr).

Oxidation of Tributyltin Benzyl Oxide with Bromine. To a THF (20 ml) solution of tributyltin benzyl oxide (461 mg, 1.16 mmol) and tributyltin methoxide (374 mg, 1.17 mmol) was added a THF (10 ml) solution of bromine (185 mg, 1.16 mmol) within a period of 20 min at room temperature under an argon atmosphere. After a similar work-up, GLC analysis indicated a yield of 82% of benzaldehyde (pentylbenzene as an internal standard with 10% Carbowax 20 M column).

General Procedure for the Oxidation of Alcohols with Bromine Utilizing Bis(tributyltin) Oxide. A solution of alcohol (1 M) and bis(tributyltin) oxide (2 M) in THF was stirred for 30 min at room temperature or for 1—2 h at 50—60 °C in the presence of molecular sieves (3 A) (in the case of hindered alcohols) under an argon atmosphere. To the mixture was added dropwise a THF solution of bromine (2 M) in the course of 30 min at room temperature. *Work-up (a) Isolation of the Product*: To the reaction mixture was added powdered $Na_2S_2O_3$, and the resulting suspension was stirred for 30 min. After filtration, the solvent was evaporated under reduced pressure. To the remaining residue were added NH_4F, H_2O and ether. The mixture was stirred for 30 min, and the precipitate formed was filtered off. The ethereal layer was washed with water and dried over anhydrous Na_2SO_4. After removal of the solvent, the corresponding carbonyl compound was isolated by preparative thin layer chromatography or column chromatography (silica gel). *(b) Determination of the Product by GLC*: The reaction mixture was quenched with a 5% aq. NaOH solution and a 5% aq. $Na_2S_2O_3$ solution, the resulting mixture being extracted with ether. The ethereal layer was washed with a 5% aq. NaOH solution and brine, and dried over anhydrous Na_2SO_4. The yield was indicated by GLC analysis with an internal standard.

Oxidation of 2-Octanol with Bromine Utilizing Bis(tributyltin) Oxide. A solution of 2-octanol (127 mg, 0.97 mmol) and bis(tributyltin) oxide (1260 mg, 2.17 mmol) in THF (20 ml) was stirred for 30 min at room temperature under an argon atmosphere. To the solution was added dropwise a solution of bromine (347 mg, 2.17 mmol) over a period of 30 min. After quenching with a 5% aq. $Na_2S_2O_3$ solution (5 ml) and a 5% aq. NaOH solution (20 ml), the mixture was extracted with ether, and the ethereal layer was washed with a 5% aq. NaOH solution (20 ml) and dried over anhydrous Na_2SO_4. GLC analysis indicated a yield of 90% of 2-octanone (ethylbenzene as an internal standard).

Oxidation of 3β-Cholestanol with Bromine Utilizing Bis(tributyltin) Oxide. A THF (20 ml) solution of 3β-cholestanol (379 mg, 0.975 mmol) and bis(tributyltin) oxide (1169 mg, 1.961 mmol) was heated at 50—60 °C in the presence of molecular sieves for 1 h. A THF (10 ml) solution of bromine (313 mg, 1.96 mmol) was then added drop by drop within a period of 30 min at room temperature. The reaction mixture was quenched with powdered $Na_2S_2O_3$ (1.0 g), stirred for 30 min and filtered. After concentration of the filtrate under reduced pressure, NH_4F (10 g) in water (10 ml) and ether (10 ml) were added to the remaining residue. The mixture was stirred for 30 min, and the resulting precipitate was filtered off. The ethereal layer was washed with removal of the solvent, 3-cholestanone (337 mg, 89%) was isolated by column chromatography (silica gel).

References

1) C. Djerassi, *Org. React.*, **6**, 207 (1951).

2) K. Bowden, I. M. Heilbron, E. R. H. Jones, and B. C. L. Weedon, *J. Chem. Soc.*, **1946**, 39 : A. Bowers, T. G. Halsall, E. R. H. Jones, and A. J. Lemin, *ibid.*, **1953**, 2555.

3) J. C. Collins, W. W. Hess, and F. J. Frank, *Tetrahedron Lett.*, **1968**, 3363.

4) K. E. Pfitzner and J. F. Moffatt, *J. Am. Chem. Soc.*, **87**, 5661 (1965); *ibid.*, **88**, 1762 (1966).

5) E. J. Corey and C. U. Kim, *J. Am. Chem. Soc.*, **94**, 7586 (1972); *Tetrahedron Lett.*, **1973**, 919; *J. Org. Chem.*, **38**, 1223 (1973); E. J. Corey, C. U. Kim, and M. Takeda, *Tetrahedron Lett.*, **1972**, 4339.

6) E. J. Corey and W. J. Fleet, *Tetrahdron Lett.*, **1973**, 4499; J. D. Albright, *J. Org. Chem.*, **39**, 1997 (1974).

7) David independently reported that selective conversion of cycloalkalne-1,2-diols into acyloins took place by treatment of their dibutyltin derivatives with bromine. S. David, *C. R. Acad. Sci., Ser. C*, **278**, 1051 (1974); *Chem. Abstr.*, **81**, 77507a (1974).

8) K. Saigo, A. Morikawa, and T. Mukaiyama, *Chem. Lett.*, **1975**, 145.

9) G. P. Mack and E. Parker, U.S. 2727917 (1955); *Chem. Abstr.*, **50**, 10761 (1956); M. F. Shostakovskii, V. M. Vlasov, and R. G. Mirskov, *Zh. Obshch. Khim.*, **34**, 1354 (1964); *Chem. Abstr.*, **61**, 677 (1964).

10) E. Amberger and M. R. Kula, *Chem. Ber.*, **96**, 2560 (1963).

11) 2 m, 10% Carbowax 20 M column.

12) G. J. M. van der Kerk and J. G. A. Luiten, *J. Appl. Chem.* **6**, 53 (1956).

13) T. Harada, *Sci. Papers Inst. Phys. Chem. Research*, **35**, 290 (1939); *Chem. Abstr.*, **33**, 5357 (1939). A G. Davies, D. C. Kleinschmidt, P. R. Palan, and S. C. Vasishtha, *J. Chem. Soc., C*, **1971**, 3972.

14) 3A type molecular sieves constructed by Union Showa Co.

Liquid-phase Oxidation Catalyzed by Cu(II)-Cl. III. Oxidation of 1,2,3,4-Tetrahydronaphthalene

Sei-ichiro IMAMURA, Masaaki TERAMOTO, Takao SUMI, Hideki AOMI, Hiroshi TERANISHI, and Yoshinobu TAKEGAMI*

Department of Chemistry, Kyoto Institute of Technology, Matsugasaki, Sakyo-ku, Kyoto 606

**Department of Hydrocarbon Chemistry, Kyoto University, Yoshida, Sakyo-ku, Kyoto 606*

(Received January 11, 1976)

1,2,3,4-Tetrahydronaphthalene was oxidized in the presence of copper(II) acetate in glacial acetic acid. An addition of lithium chloride which formed complexes with copper(II) ion highly accelerated the reaction, and the initiating process was found to be the decomposition of 1,2,3,4-tetrahydro-1-naphthyl hydroperoxide by the copper(II)-chloride ion complexes. However, only about 8% of the decomposition contributed the initiation, and it was suggested that the larger part of the decomposition proceeded through a non-ionic mechanism. Spectrophotometric and ESR experiments suggested that one of the accelerating effects of the chloride ion was due to its action to decompose the inactive copper(II) acetate dimer and form active copper(II)-chloride ion complexes and that the order of the activity of the complexes was $CuCl^+ < CuCl_2 < CuCl_3^-$, $CuCl_4^{2-}$.

Copper(II) salts are well-known to form complexes with alkali chloride in glacial acetic acid, in aqueous solutions, or in acetonitrile, and extensive data on these complexes are available.[1-6]

Previously we carried out the oxidation of cyclohexene catalyzed by copper(II) salts in glacial acetic acid and found that the reaction was highly accelerated by an addition of various alkali chlorides.[7] During the reaction, however, the chloride ion was consumed by a chlorination of cyclohexene or of the oxidation products and a rapid deactivation of the catalyst occurred.[8] However, the mechanism of the oxidation has not been discussed in detail.

This paper deals with the oxidation of 1,2,3,4-tetrahydronaphthalene and the decomposition of 1,2,3,4-tetrahydro-1-naphthyl hydroperoxide by copper(II) acetate–lithium chloride for the investigation of the catalytic action and of the effect of the chloride ion.

Experimental

Commercial 1,2,3,4-tetrahydronaphthalene (tetralin) was washed with 5% aqueous sodium hydroxide and concentrated sulfuric acid, and distilled twice under a reduced pressure. 1,2,3,4-Tetrahydro-1-naphthyl hydroperoxide (THP) was obtained by an autoxidation of tetralin and purified twice by recrystallization from petroleum ether.[9] Glacial acetic acid and acetonitrile were purified by the usual methods, and anhydrous copper(II) acetate was obtained by a dehydration of copper(II) acetate dihydrate. 1,2,3,4-Tetrahydro-1-naphthol (α-tetralol) was prepared by the reduction of 1,2,3,4-tetrahydro-1-naphthalenone (α-tetralone) followed by a fractional distillation.[10] Commercial α-tetralone and other G. R. grade reagents were used without further purification.

The apparatus used in the oxidation and the procedures were the same as described in the previous paper.[7] The rate of the oxidation was confirmed not to be controlled by the diffusion of oxygen into the liquid phase.

The decomposition of THP was carried out under a nitrogen atmosphere. In a 100 ml reaction vessel immersed in a constant temperature water bath, acetic acid and a known amount of THP were stirred until a desired temperature (usually 37 °C) was reached. Then a known amount of the catalyst solution was added and the reaction started. The reaction was followed by an iodometry of the remaining THP.

The analysis of the products was carried out using a Hitachi 063 gas chromatograph. The conditions were as follows: (1) Column packing-PEG 6000 (1 m); Carrier gas-N_2 (30 ml/min); Column temperature-150 °C, 180 °C, and (2) Column packing-Chromosorb 101 (1 m); Carrier gas-He (30 ml/min); Column temperature-150 °C.

The ESR and electronic spectra of the catalyst were observed at room temperature by the use of a JES-PE spectrometer and a Hitachi 125 spectrophotometer, respectively.

Results and Discussion

Visible Spectra of Copper(II) Acetate–Lithium Chloride in Glacial Acetic Acid. Visible spectra of the copper(II) acetate–lithium chloride were observed in glacial acetic acid varying the concentration of lithium chloride and the result is shown in Table 1. As the concentration of lithium chloride is increased, the absorption maximum shifts from 680 nm to the higher wavelength region, and the color of the solution gradually changes from blue to green and finally to yellow. The result suggests that the acetate anion of copper(II) acetate is replaced by the chloride ion and complexes which posess copper–chloride ion bondings are formed.[1] In the subsequent sections, we

$$Cu^{2+} \underset{K_1}{\overset{Cl^-}{\rightleftharpoons}} CuCl^+ \underset{K_2}{\overset{Cl^-}{\rightleftharpoons}} CuCl_2 \underset{K_3}{\overset{Cl^-}{\rightleftharpoons}} CuCl_3^- \underset{K_4}{\overset{Cl^-}{\rightleftharpoons}} CuCl_4^{2-} \quad (1)$$

call these complexes Cu(II)–Cl.

Table 1. Absorption spectra of Cu(II)-Cl in AcOH

$LiCl/Cu(OAc)_2$[a]	λ_{max}/nm
1	680
2	690
3	700
4	710
5	750
6	>800
10	>800

$[Cu(OAc)_2] = 2.0 \times 10^{-3}$ M.

a) Molar ratio.

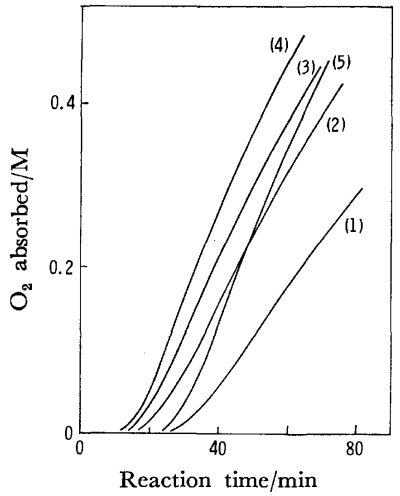

Fig. 1. Oxidation of tetralin catalyzed by Cu(II)-Cl in AcOH at 80 °C.
$[Cu(OAc)_2]=2.0\times10^{-3}$ M, [Tetralin]=1.25 M.
[LiCl]/(M$\times10^{-3}$) : (1) 2.0, (2) 6.0, (3) 8.0, (4) 10.0, and (5) 20.0.

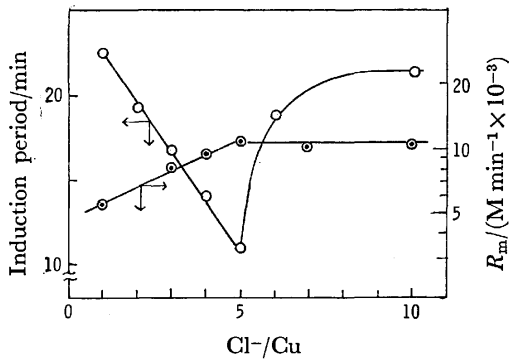

Fig. 2. Effect of LiCl in the oxidation of tetralin in AcOH at 80 °C.
$[Cu(OAc)_2]=2.0\times10^{-3}$ M, [Tetralin]=1.25 M.

Oxidation of Tetralin Catalyzed by Cu(II)-Cl at 80 °C. Tetralin was oxidized at 80 °C in the presence of Cu(II)-Cl. Figure 1 shows that the chloride ion has an accelerating effect on the reaction, while copper(II) acetate itself was inactive in the absence of lithium chloride. In Fig. 2 the maximum rate of oxidation (R_m) and the induction period are plotted against the molar ratio of chloride ion to copper(II) ion at the constant concentration of copper(II) ion. It is shown that, with the increase in the concentration of chloride ion, R_m increases and reaches a maximum at the molar ratio near five and, then, remains constant. The induction period also takes a minimum at the molar ratio of five and is rather prolonged in the higher concentration region of chloride ion.

In Fig. 3 the accumulation of the oxidation products is shown. The yield of α-tetralone is much higher than that of α-tetralol. The yield of THP is considerably low and there is no steady state concentration of THP. The low yield of THP suggests the high activity of Cu(II)-Cl to decompose THP.

The color of the solution changed in the course of the reaction from yellow to green and finally to blue, which suggested that the state of the catalyst gradually changed. The visible spectra of the reaction mixture were observed during the reaction and the result is given in Table 2. We see that the absorption maximum of the catalyst shifts to the shorter

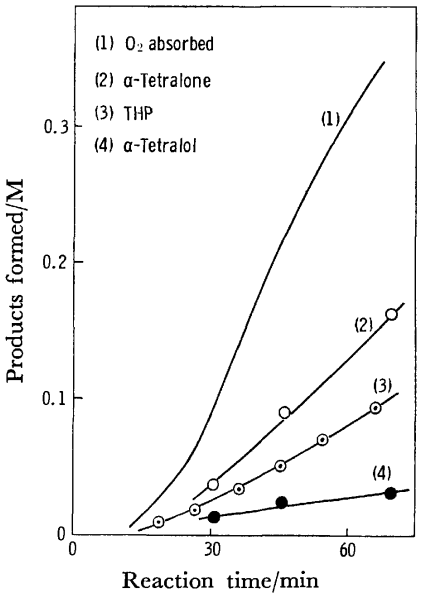

Fig. 3. Product distribution in the oxidation of tetralin catalyzed by Cu(II)-Cl in AcOH at 80 °C.
$[Cu(OAc)_2]=2.0\times10^{-3}$ M, [Tetralin]=1.25 M, $[LiCl]=1.0\times10^{-2}$ M.

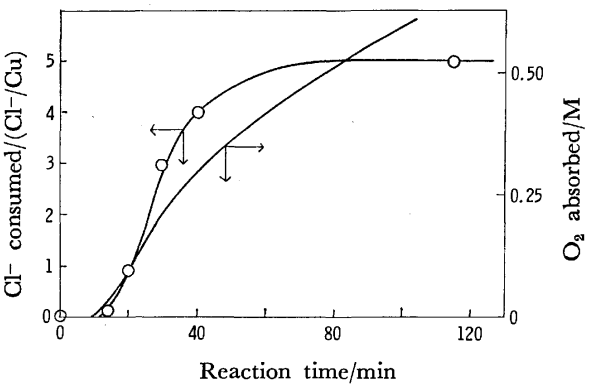

Fig. 4. Consumption of Cl^- during the reaction at 80 °C.
$[Cu(OAc)_2]=2.0\times10^{-3}$ M, $[LiCl]=1.0\times10^{-2}$ M, [Tetralin]=1.25 M.

TABLE 2. TIME DEPENDENCE OF ABSORPTION SPECTRUM IN THE OXIDATION OF TETRALIN IN AcOH AT 80 °C

Reaction time/min	λ_{max}/nm
0	750
15	740
20	710
30	690
40	680
55	680
115	680
180	680

$[Cu(OAc)_2]=2.0\times10^{-3}$ M; $[LiCl]=1.0\times10^{-2}$ M.

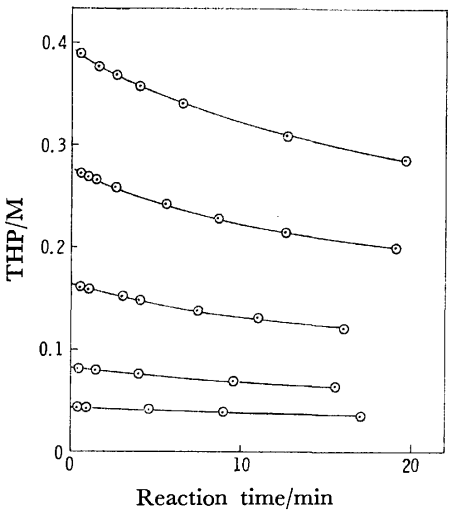

Fig. 5. Decomposition of THP catalyzed by Cu(II)-Cl in AcOH at 37 °C.
$[Cu(OAc)_2]=2.0\times10^{-3}$ M, $[LiCl]=2.0\times10^{-2}$ M.

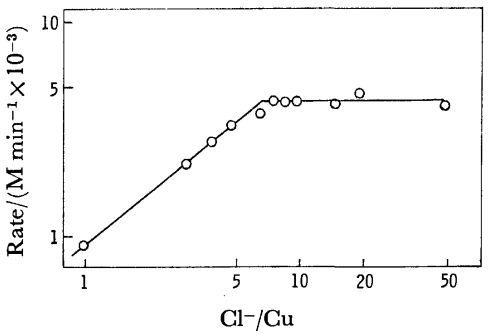

Fig. 6. Effect of LiCl in the decomposition of THP catalyzed by Cu(II)-Cl in AcOH at 37 °C.
$[Cu(OAc)_2]=8.0\times10^{-3}$ M, [THP]=0.10 M.

wavelength region as the reaction proceeds, and after 40 min the absorption at 680 nm begins to appear. The chloride ion seems to be consumed during the reaction and change to inactive organic chlorine compounds.[7,8,11] The quantity of the chloride ion consumed during the reaction was roughly estimated from Table 2 by the use of the chloride ion to copper(II) ion molar ratio *vs.* absorption maxima data listed in Table 1, and the result is shown in Fig. 4. It may be seen that the consumption of chloride ion occurs as soon as the induction period is over. The state of the catalyst changes in this manner during the reaction, so, it is impossible to carry out a kinetic discussion from the measurement of R_m's.

Decomposition of THP Catalyzed by Cu(II)-Cl. THP was decomposed by Cu(II)-Cl in glacial acetic acid at 37 °C and the result is shown in Fig. 5.[12] Copper(II) acetate without lithium chloride was found to be inactive as in the oxidation of tetralin. Kochi reported that copper(II) salts do not decompose hydroperoxides directly and that an induction period exists at the initial stage of the reaction.[13] In the present result, however, no induction period exists, indicating that Cu(II)-Cl decomposes THP directly.

Figure 6 shows the rate dependence on the concentration of chloride ion at the constant concentration of copper(II) ion. The rate increases with the increase of chloride ion up to the molar ratio of chloride ion to copper(II) ion of eight, after which it remains almost constant. It was found that Cu(II)-Cl gradually changed to inactive copper(II) acetate during the reaction, and the amount of THP decomposed before the catalyst was deactivated increased with the increase of the concentration of chloride ion. The accelerating effect of chloride ion shown in Fig. 6 resembles to that in the oxidation of tetralin (Fig. 2), which indicates that the catalytic action of Cu(II)-Cl in the decomposition of THP is correlated to that in the oxidation of tetralin.

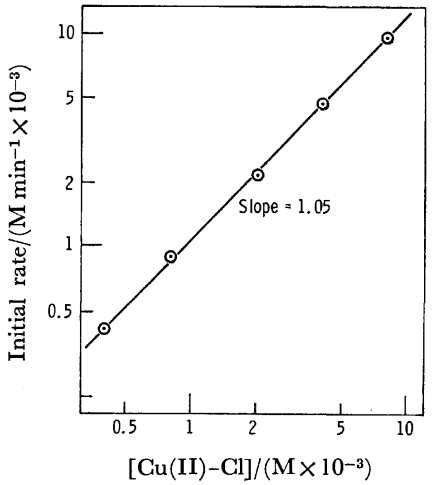

Fig. 7. Decomposition of THP catalyzed by Cu(II)-Cl in AcOH at 37 °C.
[THP]=0.17 M, $Cl^-/Cu=10$.

Table 3. Product distribution in the decomposition of THP catalyzed by Cu(II)-Cl[a]

Solvent	Temp. /°C	ϕ_3CH	α-Tetralone /%[b]	α-Tetralol /%[b]	H_2O /%[b]
AcOH	50	0	79.6	7.2	93.4
AcOH	50	0.34	71.0	5.0	
AcOH	70	0	66.8	7.5	
CH_3CN	37	0	79.5	12.6	

[THP]=0.17 M; $[Cu(OAc)_2]=8.0\times10^{-3}$ M; $[LiCl]=8.0\times10^{-2}$ M.
a) The Products were analyzed after the decomposition was completed. b) Based on the initial concentration of THP.

Figure 7 shows the rate dependence on the concentration of Cu(II)-Cl ($Cl^-/Cu=10$). From this and the result shown in Fig. 5, the initial rate of the decomposition of THP by Cu(II)-Cl ($Cl^-/Cu=10$) is expressed as

$$-d[THP]/dt=k[Cu(II)\text{-}Cl]^{1.05}[THP]^{1.28} \quad (2)$$

The products in the decomposition of THP were α-tetralol, α-tetralone, α-tetralyl acetate, water, and a high-boiling unknown product. In Table 3 the yields of α-tetralone and α-tetralol after the reaction was completed are shown. The yield of α-tetralone is much higher than that of α-tetralol, and water is producuced almost quantitatively. Triphenylmethane,

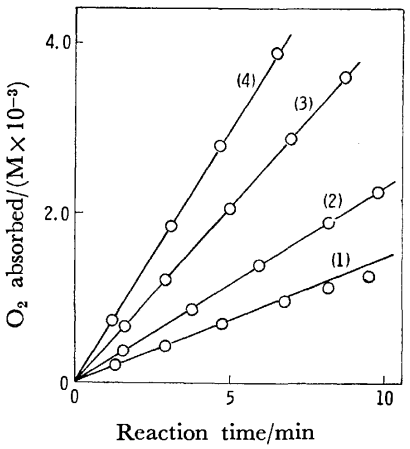

Fig. 8. Oxidation of tetralin catalyzed by Cu(II)–Cl–THP in AcOH at 37 °C.
[Tetralin]=1.26 M, [THP]=0.1 M, $Cl^-/Cu=10$, $[Cu(OAc)_2]/(M\times10^{-3})$: (1) 0.5, (2) 1.0, (3) 3.0, and (4) 6.0.

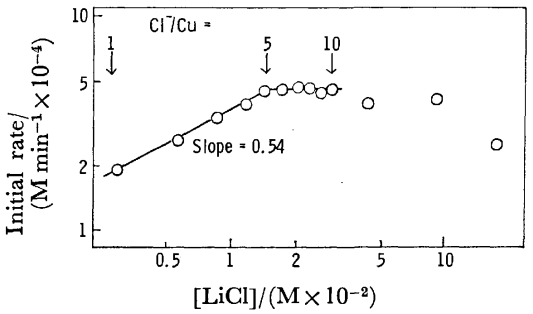

Fig. 9. Effect of LiCl in the oxidation of tetralin catalyzed by Cu(II)–Cl–THP in AcOH at 37 °C.
$[Cu(OAc)_2]=3.0\times10^{-3}$ M, [THP]=0.1 M, [Tetralin]=1.26 M.

which is a good hydrogen donor in radical reactions, does not increase the yield of α-tetralol, suggesting that the reaction proceeds mainly by an ionic or a molecular mechanism. In the case of acetonitrile solvent, chloride ion also accelerated the decomposition of THP catalyzed by copper(II) acetate and the product distribution was similar to that in glacial acetic acid. (see Table 3). Although the unknown product was not analyzed and the amount of α-tetralyl acetate was not determined, the disagreement in the material balance shown in Table 3 is considered to be due to the formation of these by-products.[7,8]

Oxidation of Tetralin Initiated by Cu(II)–Cl–THP at 37 °C. As shown in the previous sections, the catalytic activity of Cu(II)–Cl in the oxidation of tetralin was correlated to that of the decomposition of THP; the decomposition of THP by Cu(II)–Cl is suggested to be effective in initiating the oxidation. Therefore, a series of experiments was carried out as described below, assuming that the intiation step is the decomposition of THP by Cu(II)–Cl. A known amount of THP was added at the beginning of the oxidation and the rate dependences on the concentrations of THP, tetralin, copper(II) acetate, and chloride ion were observed. Figure 8 shows an example of

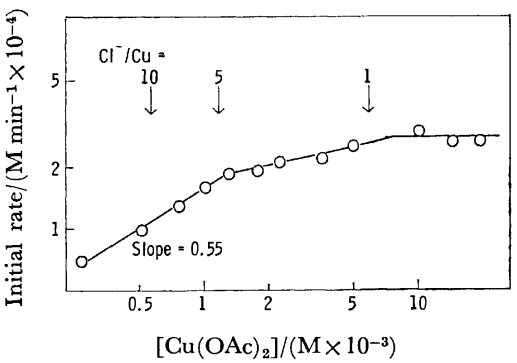

Fig. 10. Effect of $Cu(OAc)_2$ in the oxidation of tetralin catalyzed by Cu(II)–Cl–THP in AcOH at 37 °C.
$[LiCl]=6.0\times10^{-3}$ M, [THP]=0.1 M, [Tetralin]=1.26 M.

the oxidation catalyzed by Cu(II)–Cl–THP at 37 °C. The reaction proceeds without any induction period and at a constant rate, which enables us to carry out the kinetic investigation from the measurement of the initial rates. The change of the catalyst state due to the consumption of chloride ion will be neglected in the initial stage of the reaction.

The effect of chloride ion was investigated again and the results are shown in Figs. 9 and 10. Figure 9 shows the rate dependence on the chloride ion concentration at a constant concentration of copper(II) ion. The rate is proportional to $[Cl^-]^{0.54}$ up to the chloride ion to copper(II) ion molar ratio of five, then remains constant, and is rather decreased by an addition of excess chloride ion. As Fig. 10 shows, at the constant concentration of chloride ion, the rate is proportional to $[Cu(II)]^{0.55}$ unless the molar ratio becomes less than five. In the molar ratio range below five, the rate does not increase so much with the increase in the copper(II) ion concentration. When the concentration of copper(II) ion exceeds that of chloride ion, the rate becomes independent of the copper(II) ion concentration; that is, an excess copper(II) ion over chloride ion does not take part in the oxidation. The effect of chloride ion shown above is the same as that in the decomposition of THP except that an excess chloride ion (more than ten molar ratio) retards the oxidation. These observations indicate clearly that the presence of copper–chloride ion bonds is inevitable for the catalyst to be active and that the most active catalyst is formed in the chloride ion to copper(II) ion molar ratio range from five to ten.

The rate dependences on the concentrations of tetralin, Cu(II)–Cl ($Cl^-/Cu=10$), and THP are shown by dotted lines in Figs. 11—13. From these results, the apparent rate equation for the oxidation of tetralin is obtained as shown below.

$$-dO_2/dt = k_1[RH]^{1.05}[Cu(II)\text{-}Cl]^{0.53}[THP]^{0.68} \quad (3)$$

RH : Tetralin

Oxidation Mechanism. On the basis of the results obtained in the preceding sections, it is suggested that Cu(II)–Cl produces active radicals by an interaction with THP in the initiation step. Therefore, the mechanism of the oxidation of tetralin is

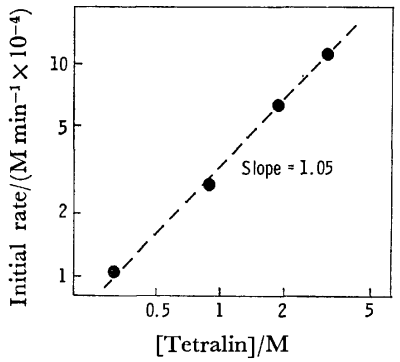

Fig. 11. Oxidation of tetralin catalyzed by Cu(II)-Cl-THP in AcOH at 37 °C. Rate dependence on [Tetralin].
$[Cu(OAc)_2]=3.0\times10^{-3}$ M, $[LiCl]=3.0\times10^{-2}$ M, [THP]=0.1 M.

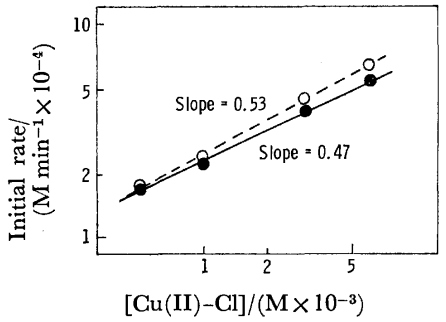

Fig. 12. Oxidation of tetralin catalyzed by Cu(II)-Cl-THP in AcOH at 37 °C. Rate dependence on [Cu(II)-Cl]. [THP]=0.09 M, [Tetralin]=1.26 M, $Cl^-/Cu=10$.

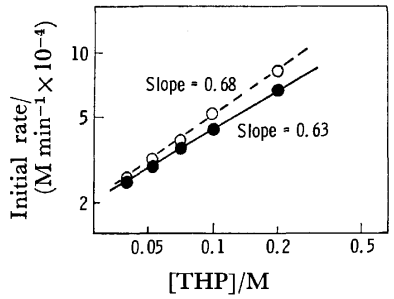

Fig. 13. Oxidation of tetralin catalyzed by Cu(II)-Cl-THP in AcOH at 37 °C . Rate dependence on [THP].
$[Cu(OAc)_2]=3.0\times10^{-3}$ M, $[LiCl]=3.0\times10^{-2}$ M, [Tetralin]=1.26 M.

represented as follows.

$$\mathrm{THP} + \mathrm{Cu(II)\text{-}Cl} \xrightarrow{\mathrm{RH}} \mathrm{R}\cdot \qquad (4) \quad R_i$$

$$\mathrm{R}\cdot + \mathrm{O_2} \longrightarrow \mathrm{ROO}\cdot \qquad (5)$$

$$\mathrm{ROO}\cdot + \mathrm{RH} \longrightarrow \mathrm{THP} + \mathrm{R}\cdot \qquad (6) \quad k_p$$

$$2\mathrm{ROO}\cdot \longrightarrow \text{Inactive products} + \mathrm{O_2} \qquad (7) \quad 2k_t$$

When the kinetic chain length is short, the amount of oxygen evolved in step (7) cannot be neglected. Taking this into consideration and by the use of a steady state approximation, the rate of the oxygen absorption is expressed as

Table 4. Dependence of R_i on THP concentration[a)]

[THP]/M	R_i/M min^{-1}
0.050	3.78×10^{-5}
0.068	5.31×10^{-5}
0.090	8.07×10^{-5}
0.130	1.30×10^{-4}
0.260	2.88×10^{-4}

a) Reaction condition is the same as described in Fig. 13.

Table 5. Dependence of R_i on catalyst concentration[a)]

[Cu(II)-Cl]/M	R_i/M min^{-1}
5.0×10^{-4}	1.75×10^{-5}
1.0×10^{-3}	3.45×10^{-5}
3.0×10^{-3}	8.07×10^{-5}
6.0×10^{-3}	1.78×10^{-4}

a) Reaction condition is the same as described in Fig. 12.

$$-dO_2/dt = k_p/\sqrt{2k_t}[RH]\sqrt{R_i} + R_i/2 \qquad (8)$$

From this rate expression, the dependences of R_i on the concentrations of Cu(II)-Cl and THP were investigated as follows. The value of $k_p/\sqrt{2k_t}$ was obtained as $4.0\times10^{-3}\,l^{1/2}\,s^{-1/2}$ in the oxidation of tetralin initiated by AIBN at 37 °C.[14] This value was substituted into Eq. 8, and the values of R_i are calculated at each concentration of the reactants from the data shown in Figs. 12 and 13. The results are listed in Tables 4 and 5, and afford R_i expressed as

$$R_i = k_2[\mathrm{Cu(II)\text{-}Cl}]^{0.98}[\mathrm{THP}]^{1.25} \qquad (9)$$

We see that the rate dependences on the concentrations of Cu(II)-Cl and THP are similar to those in the decomposition of THP by Cu(II)-Cl. (Eq. 2)

As mentioned before, when the kinetic chain length is short, the contribution of $R_i/2$ cannot be neglected in Eq. 8. Therefore, the values of $R_i/2$ are calculated from Tables 4 and 5, and substracted from the overall rates of the oxidation shown by dotted lines in Figs. 12 and 13. The solid lines thus obtained afford the following rate expression in which the contribution of $R_i/2$ is excluded.

$$-dO_2/dt = k_3[RH]^{1.05}[\mathrm{Cu(II)\text{-}Cl}]^{0.47}[\mathrm{THP}]^{0.63} \qquad (10)$$

This is in good agreement with rate relation (11) which is obtained by substituting Eq. 9 into the first term of the right of Eq. 8.

$$-dO_2/dt \propto k_p/\sqrt{2k_t}[RH]^{1.0}[\mathrm{Cu(II)\text{-}Cl}]^{0.49}[\mathrm{THP}]^{0.63} \qquad (11)$$

From the discussion shown above, it can be concluded that the formation of active radicals by the interaction of Cu(II)-Cl with THP is the main initiating step in the oxidation of tetralin.

Efficiency of the Initiation by Cu(II)-Cl-THP. In order to investigate the nature of the decomposition of THP by Cu(II)-Cl, the efficiency of the initiation by Cu(II)-Cl-THP was investigated. As described in the previous sections, the rate of the initiation (R_i) was expressed by Eq. 9. Under the same condition, the rate of the decomposition of THP (R) was observed.

Table 6. Efficiency of radical production in the decomposition of THP catalyzed by Cu(II)-Cl in AcOH at 37 °C

Cu(II)-Cl/M	R/M s^{-1}	R_i/M s^{-1}	Efficiency/%[a]
5.0×10^{-4}	2.25×10^{-4}	1.75×10^{-5}	7.8
8.0×10^{-4}	3.70×10^{-4}	2.80×10^{-5}	7.6
1.0×10^{-3}	4.70×10^{-4}	3.45×10^{-5}	7.3
			a. v. 7.6

a) Efficiency $=R_i/R\times100$

In Table 6 the values of R_i and R are listed. The fourth column in the table shows the values of $R_i/R\times100$ which indicate the efficiency of the production of active radicals in the reaction of Cu(II)-Cl with THP shown by Eq. 4. We see that only 7—8% of the decomposition contributes to the initiation. From this and the effect of triphenyl methane upon the product distribution shown in Table 3, it is suggested that the larger part of the decomposition proceeds through an ionic or a molecular mechanism such as a dehydration of THP to produce ketone and water as the product distribution shows.

$$\text{THP} \xrightarrow{\text{Cu(II)-Cl}} \begin{cases} \text{Non-radical mechanism} \\ \vee \qquad (H_2O+R{=}O) \qquad (12) \\ \text{Radical mechanism} \qquad (13) \end{cases}$$

ESR and Electronic Spectra of Cu(II)-Cl in Glacial Acetic Acid. Copper(II) ion forms various chloro complexes in glacial acetic acid as shown by Eq. 1. To clarify the active species both in the oxidation of tetralin and in the decomposition of THP, and also to investigate the effect of chloride ion, ESR and electronic spectra of Cu(II)-Cl were observed

As copper(II) ion has an unpaired electron in its 3d-orbitals, its ESR signal must be observed. However, as shown in Fig. 14, copper(II) acetate in glacial acetic acid has no signal. This phenomenon can be explained by the following fact. That is, copper(II) acetate has a dimer structure as indicated by Fig. 15 and the distance between each copper atom is only 2.64 Å, indicating an extensive quenching of the

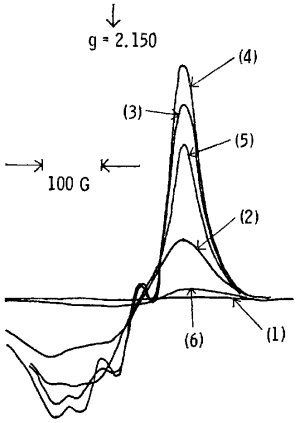

Fig. 14. ESR spectra of Cu(II)-Cl in AcOH measured at room temperature.
$[Cu(OAc)_2]=2.8\times10^{-3}$ M, Cl$^-$/Cu: (1) 0, (2) 1, (3) 3, (4) 5, (5) 10, and (6) 200.

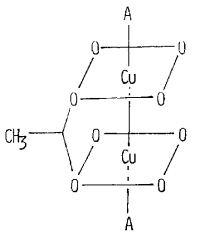

Fig. 15. Structure of $Cu(OAc)_2$. Only one bridging group is shown.[17]

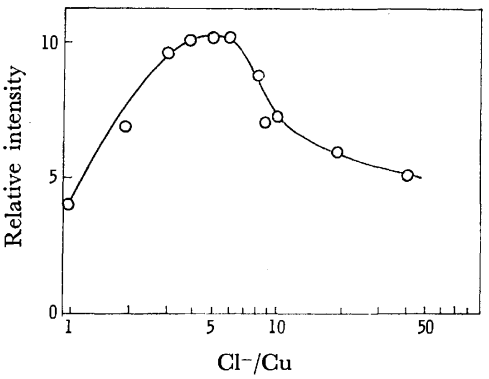

Fig. 16. Relative intensity of the ESR spectrum of Cu(II)-Cl in AcOH measured at room temperature. $[Cu(OAc)_2]=2.8\times10^{-3}$ M.

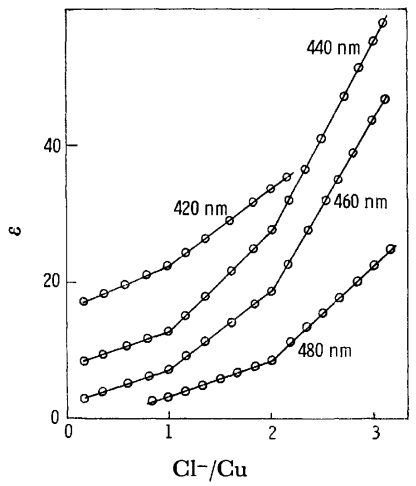

Fig. 17. Molar ratio plot for Cu(II)-Cl in AcOH measured at room temperature.

spin moments of the copper(II) ions.[17] When lithium chloride is added, an asymmetric signal with two small peaks near the center appears, which suggests that the copper(II) acetate dimer is decomposed and monomer species are formed. By means of spectrophotometry and magnetic susceptibility measurement, Sawada *et al.*, also reported that copper(II) acetate is dimerized in glacial acetic acid and that an addition of chloride ion affords monomer species which have copper–chloride ion bonds.[18] In Fig. 16 the intensity of the signal relative to that of the Mn^{2+} external standard is plotted against the molar ratio of chloride ion to copper(II) acetate. The intensity increases with the increase of the concentration of chloride ion

and reaches a maximum at the molar ratio from four to eight. In the oxidation of tetralin, the active catalyst was formed in the molar ratio range from five to ten, and, in the decomposition of THP, the maximum rate is attained at the molar ratio of eight and, then, remains constant. Although a slight discrepancy in the effect of chloride ion exists between these two cases, it is clear that one of the accelerating effects of the chloride ion is to decompose the dimer structure of copper(II) acetate (inactive) and to form monomer species (active) by coordinating to the copper(II) ion.

The formation of Cu(II)–Cl was investigated spectrophotometrically on the basis of the molar ratio method. Figure 17 shows the plots of ε, the absorption coefficient of Cu(II)–Cl, at 420, 440, 460, and 480 nm against the chloride ion to copper(II) acetate molar ratio. At the molar ratios of one and two, the slopes of the ε-molar ratio lines change. This indicates that the equilibrium constants, K_1 and K_2, are large enough to afford mono- and dichloro complexes almost quantitatively at the corresponding molar ratios. However, the catalytic activity of Cu(II)–Cl continues to increase up to the molar ratio of five or above both in the oxidation of tetralin and in the decomposition of THP. This indicates clearly that the order of the activity of Cu(II)–Cl is $CuCl^+ < CuCl_2 < CuCl_3^-$, $CuCl_4^{2-}$.

Thanks are given to Mr. Nobuaki Onishi for his assistance in the experimental work.

References

1) S. E. Manahan and R. T. Iwamoto, *Inorg. Chem.* **4**, 1409 (1965).
2) M. Tamura and A. Yasui, *Kogyo Kagaku Zasshi*, **72**, 557 (1969).
3) H. McConell and N. Davidson, *J. Am. Chem. Soc.*, **72**, 3168 (1950).
4) D. F. Morris and E. L. Short, *J. Chem. Soc.*, **1962**, 2672.
5) T. E. Moore, F. W. Burtch, and C. E. Miller, *J. Phys. Chem.*, **64**, 1454 (1960).
6) J. R. Bell, T. L. Tyvoll, and D. L. Wertz, *J. Am. Chem. Soc.*, **95**, 1456 (1973).
7) S. I. Imamura, T. Banba, and Y. Takegami, *Bull. Chem. Soc. Jpn.*, **46**, 856 (1973).
8) S. I. Imamura, T. Otani, and H. Teranishi, *Bull. Chem. Soc. Jpn.*, **48**, 1245 (1975).
9) H. Hock and W. Susemihl, *Chem. Ber.*, **66**, 61 (1933).
10) S. W. Chailin and E. G. Brown, *J. Am. Chem. Soc.*, **71**, 122 (1949).
11) The organic chlorine compounds were not analyzed.
12) The reaction at the higher temperature was too rapid to be followed accurately.
13) J. K. Kochi, *J. Am. Chem. Soc.*, **86**, 1958 (1963).
14) Alagy's rate equation[15] for the initiation by AIBN, $R_i = 2e \times 1.58 \times 10^{15} \exp(-30800/RT)[AIBN]$, was used. The value of e was taken as 0.43 at 37 °C, taking the effect of the viscosity of the reaction mixture into consideration.[16]
15) J. Alagy, G. Clement, and J. C. Balaceanu, *Bull. Soc. Chim. Fr.*, **1960**, 1495.
16) S. Kato and M. Shizuki, *Preprint of the 8th Oxidation Symposium, Osaka* (1974), p. 51.
17) F. A. Cotton and G. Wilkinson, "Advanced Inorganic Chemistry," A Comprehensive Text, Interscience Publishers, New York (1962), p. 754.
18) K. Sawada, H. Ohtaki, and M. Tanaka, *J. Inorg. Nucl. Chem.*, **34**, 3455 (1972).

The Photoreaction of Benzyl 1-Cycloalkenyl Ketone in Acidic or Protic Media*

Masaru TADA, Hiroshi SAIKI, Kyo MIURA, and Hiraku SHINOZAKI

Department of Chemistry, School of Science and Engineering, Waseda University, Shinjuku, Tokyo 160

(Received January 12, 1976)

Three benzyl 1-cycloalkenyl ketones, I—III, were irradiated in the presence of boron trifluoride–diethyl ether (0.05 mol/l) in benzene to give the products V—VII, formed by the bonding between the β-position of $\alpha\beta$-unsaturated ketone and the *ortho* position of the benzene ring. Benzyl 1-cyclooctenyl ketone (IV) was inactive to the photocyclization because of the preferential geometrical isomerization of the olefin moiety. Trifluoroacetic acid promotes the reaction exceedingly, but the reaction takes place also in methanol. The reaction in methanol was deduced from quenching experiments to be a triplet process. The reaction takes both singlet and triplet processes when irradiation is carried out in the presence of boron trifluoride–diethyl ether. The participation of the complex between benzyl 1-cycloalkenyl ketone and boron trifluoride is proposed for the singlet process.

It has been reported that a photochemical Friedel-Crafts reaction takes place upon the irradiation of cycloalkene and benzene derivatives in the presence of a catalytic amount of Lewis acid.[1] A strained *trans*-cycloalkene has been considered to be an active intermediate which gives a carbonium ion in the presence of an acid catalyst. In this paper we will report the photochemical cyclization of benzyl 1-cycloalkenyl ketones (I—III) under various reaction conditions.

The external irradiation (a 450-W medium pressure Hg lamp) of solutions of I, II, and III in benzene containing boron trifluoride–diethyl ether (0.05 mol/l) through a Pyrex tube for 3 h gave the reaction products of V, VI, and VII in 79, 87, and 90% yields respectively. However, the starting material was recovered when benzyl 1-cyclooctenyl ketone (IV) was irradiated. These experimental results are in sharp contrast with the fact that an attempted thermal cyclization of benzyl 1-cyclohexenyl ketone (II) with Lewis acid recovered the starting material.[2-4] Elemental analyses and the molecular peaks of mass spectra due to the products V (m/e=186), VI (m/e=200), and VII (m/e=214) show the products to be the isomers of the starting ketones. All the products show the infrared absorption for the saturated ketone at 1720 (V), 1710 (VI), and 1717 cm^{-1} (VII) and the absorptions for *ortho*-disubstituted benzene ring at 750 (V), 755 and 765 (VI), and 753 cm^{-1} (VII). NMR spectra of the

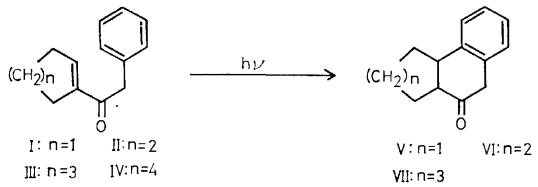

I: n=1 II: n=2
III: n=3 IV: n=4

V: n=1 VI: n=2
VII: n=3

products V, VI, and VII show signals (singlet) due to the methylene adjacent to the carbonyl group at δ= 3.62 (V), 3.48 (VI), and 3.50 ppm (VII). These spectral data define unequivocally the structures of the products except for the stereochemistry of the ring junction. The V and VII products were found to be homogeneous by GLC analyses (SE-30 and OV-17 on Chromosorb W), but the VI product consisted of two isomers, VIa and VIb. VIa was deduced to be *cis*-1,2,3,4,4a,10a-hexahydro-10-phenanthrone by the transformation of VIa into *cis*-1,2,3,4,4a,9,10,10a-octahydrophenanthrene.[1,5] The thioketal obtained by the action of 1,2-ethanedithiol–borontrifluoride–diethyl ether to VIa was reduced by Raney-Ni, and the reduced product was identified with the authentic octahydrophenanthrene by a comparison of their GLC and IR spectra. The formation of VIa and VIb was not due to the isomerization of the product under the present reaction conditions. The acid or base treatment of the VI product with varying ratios of the two isomers did not change the original ratio, and the base-catalyzed deuteration of the VI product by deuterium oxide gave only the dideuterated derivative, indicating that the enolization took place only in the direction of the benzylic position. The reaction occurs in reaction systems other than boron trifluoride–diethyl ether as will be described below, and the ratio of VIa and VIb is dependent on the solvent of the reaction, VIa : VIb=*ca.* 1 : 1 for boron trifluoride–diethyl ether/benzene, 4 : 1 for methanol, and 5 : 1 for acetonitrile. Base-catalyzed enolization takes place only in the direction of the benzylic position, and no epimerization can be expected for V and VII. The stereochemistry of these products, therefore, remains undetermined.

The benzyl 1-cyclohexenyl ketone (II) was subjected to a wide variety of the reaction conditions for the purpose of understanding the nature of the reaction. Trifluoroacetic acid is as effective a catalyst as boron trifluoride–diethyl ether for the photocyclization of II, and enol ethers of VIa and VIb were isolated from the reaction using methanol as the solvent. Polar solvents, such as methanol and acetonitrile, provide a good reaction system for the photo-cyclization even without

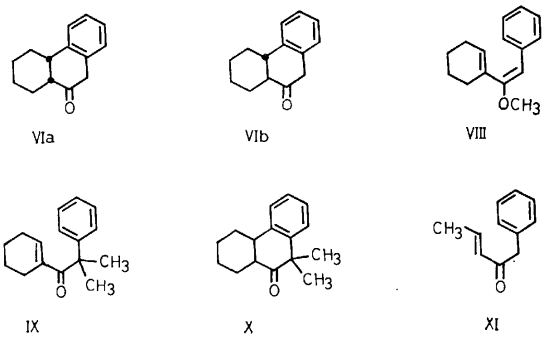

VIa VIb VIII

IX X XI

* Part of this work was reported as a preliminary report: *J. Chem. Soc., Chem. Commun.*, **1975**, 55.

acid catalyst. The reactivity in various reaction systems decreases in the following sequence, judging by the time required for the completion of the reaction: 0.05 M boron trifluoride–diethyl ether/benzene≈0.05 M trifluoroacetic acid/benzene ≈ methanol>0.05 M boron trifluoride–diethyl ether/acetonitrile≫acetonitrile>benzene.

One possible mechanism is an electrocyclization of the formal triene system in the enol form of the II ketone, however, this possibility was eliminated by the following observations. The enol ether VIII caused only geometrical isomerization upon irradiation, and the dimethyl derivative, IX, gave the cyclized product, X (molecular peak m/e=228, IR 1709 cm^{-1}), which was difficult to isolate in a practical yield due to its photo-lability.

The failure of the photocyclization of VI must be due to the rapid relaxation of the excited state by isomerization to the *trans*-cyclooctene system.[6] This was further supported by the irradiation of the benzyl 1-propenyl ketone (XI), which caused no cyclization, but only geometrical isomerization. In methanol, compound I, which has a cyclopentene moiety was converted smoothly into V (the conversion was completed within 120 min), while compound II, with a cyclohexene moiety, reacted more slowly to give VI. Compound III, with a cycloheptene moiety, was not, however, converted into VII under the same reaction conditions. The cyclization of I in methanol was quenched effectively by 1,3-pentadiene to give linear Stern-Volmer plot, $k_q\tau$=16 M^{-1}. This quenching experiment shows that the photocyclization proceeds by means of a triplet process. In contrast to the reaction in methanol, all three compounds, I, II, and III, caused a facile cyclization to give V, VI, and VII in benzene containing boron trifluoride–diethyl ether (0.05 mol/l). The Stern-Volmer plots of the quenching experiments of the reaction in the boron trifluoride–diethyl ether/benzene system using 1,3-pentadiene as the quencher are shown in Fig. 1. The curvatures of the plots and plateaus at Φ_0/Φ=1.8 for I and Φ_0/Φ= 1.3 for II show that both singlet and triplet processes are encountered in the reaction of I and II. In the region showing the plateaus, the triplet process is almost completely quenched, and the following relation exists: $\Phi_0=(\Phi_S+\Phi_T)$ and $\Phi=\Phi_S$, where Φ_S and Φ_T denote the quantum yield of the reaction by the use of a singlet and a triplet process respectively. This analysis reveals that 56% and 77% of the reactions of I and II respectively proceed through a singlet process.[7] On the contrary, the reaction of compound III is essentially not quenched by 1,3-pentadiene and gives a linear Stern-Volmer plot with a small negative slope. This means that the cyclization of III takes place *via* only a singlet process. The negative slope is accounted for by the quenching of the triplet decay of the cyclized product, VII, which was substantiated by the irradiation of the isolated product.

Carbonyl compounds form complexes with boron trifluoride–diethyl ether,[8] and the UV absorption of II in hexane containing boron trifluoride–diethyl ether (0.05 mol/l) shows a new absorption around 270 nm, with concomitant decrease in the intensity

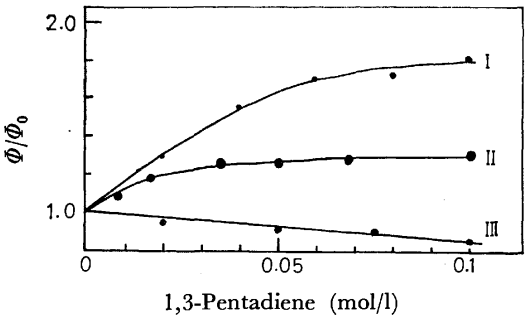

Fig. 1. Quenching of photocyclization of I, II, and III (0.1 mol/l) in benzene containing BF_3-etherate (0.05 mol/l).

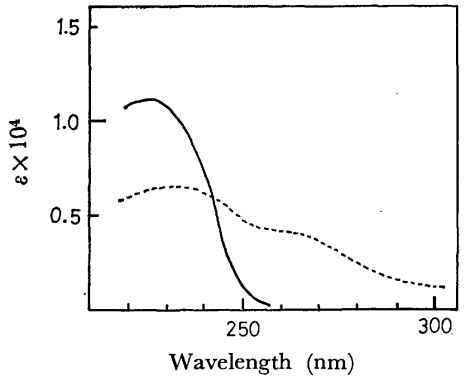

Fig. 2. UV spectra of benzyl 1-cyclohexenyl ketone (II) in hexane (——) and in hexane containing BF_3-etherate (0.05 mol/l) (----).

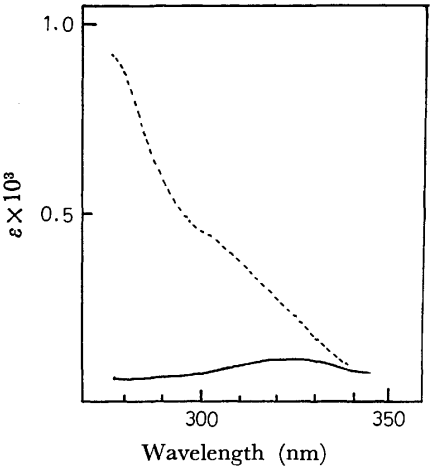

Fig. 3. UV spectra of benzyl 1-cyclohexenyl ketone (II) in benzene (——) and in benzene containing BF_3-etherate (0.05 mol/l) (----).

of the π-π^* absorption at 224 nm (Fig. 2); the absorption in benzene containing boron trifluoride–diethyl ether (0.05 mol/l) is very different from the absorption in the absence of the acid in n-π^* region (Fig. 3). This spectroscopic behavior, in conjunction with the quenching experiments, suggest that the excitation of the complex between the corbonyl compound and boron trifluoride is reponsible for the photochemical cyclization by a singlet process. This conclusion is supported by the facts that compound III reacts in the presence

of boron trifluoride–diethyl ether, but no reaction takes place in methanol, and that the importance of the singlet process decreases with the decrease in the ring size of the cycloalkene moiety of compounds III (100%), II (77%), and I (56%).

The most important process in the energy dissipation of the triplet excited state is a geometrical isomerization of the double bond in the cycloalkene moiety. With compound I, with a cyclopentene moiety, in which the geometrical isomerization is impossible, the triplet cyclization in methanol is an effective process, whereas compound III, with a cycloheptene moiety, preferentially deactivates to the *trans* isomer of III and no cyclization takes place in methanol. On the same ground, the relative importance of the triplet process for the cyclization in benzene containing boron trifluoride–diethyl ether increases in the order of compound III (0%), compound II (23%), and compound I (44%). As has been described earlier, the benzyl 1-cyclooctenyl ketone (IV) and the benzyl 1-propenyl ketone (IX) do not undergo the photocyclization in either methanol or benzene containing boron trifluoride–diethyl ether. This means that the energy dissipation by the geometrical isomerization of the cycloalkene moiety is also important in the singlet excited state of the complex. The geometrical isomerization from the excited state of the complex is an important competitive process with photocyclization in the cases of compounds IV and XI.

The importance of the acidic function in the photocyclization is demonstrated by the fact that the reaction proceeds more rapidly in methanol than in acetonitrile, which is a more polar solvent than methanol. These facts prompt us to propose the reaction mechanism depicted in Scheme 1, where S* and T* denote a singlet and a triplet excited state respectively. The reaction in an aprotic solvent such as acetonitrile must proceed in a fassion similar to the reaction in methanol, but without a protonated intermediate.

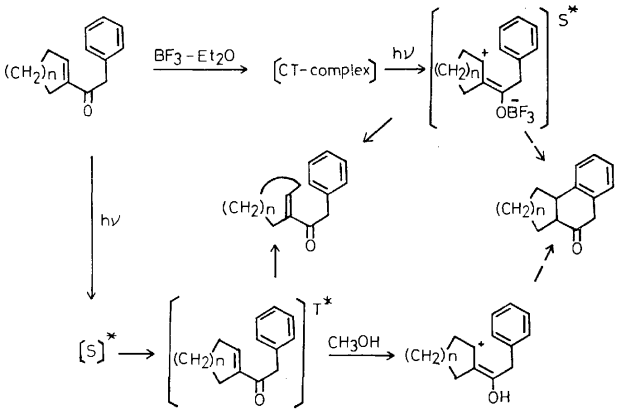

Scheme 1.

The excitation of the complex between the carbonyl compound and boron trifluoride may be expected to produce a more polar state which accumulates a more positive charge on the β-position of the unsaturated carbonyl compound.[9] On the other hand, the carbonyl compound can be expected to acquire an intensified basicity in its triplet excited state and to abstract a proton from a protic solvent, and the increase in the positive charge on β-position can also be expected.[10] Thus, the β-carbons of compounds I, II, and III must become more electrophilic by excitation to attack the benzene ring intramolecularly.

The irradiation of a mixture of 1-acetylcyclohexene and toluene in the presence of boron trifluoride–diethyl ether does not bring about an intermolecular reaction of a type similar to that of the benzyl 1-cycloalkenyl ketone. This implies an interaction between the enone system and the benzene ring in the excited state. The participation of the benzene ring in the excited state and the oriented structure of this intramolecular exciplex, XII, may be essential factors in making possible the facile intramolecular cyclization (Scheme 2).

The stereochemistry of the product must be governed by the mode of protonation to the intermediate enol derivative, XIII, and must be dependent on the polarity of the solvent in the case of the reaction of the benzyl 1-cyclohexenyl ketone (II).

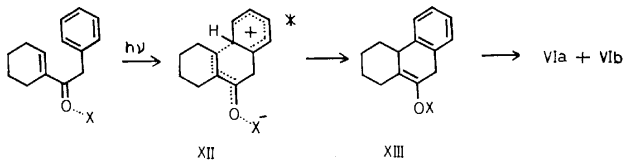

Scheme 2.

Experimental

Syntheses of Starting Materials. A) Benzyl 1-Cycloalkenyl Ketones (I—IV): Ketones I—IV were synthesized by the method of Cook and Hawett for the synthesis of the II ketone,[2] using carbon disulfide as the solvent. The benzyl 1-cyclopentenyl ketone (I), the benzyl 1-cyclohexenyl ketone (II), the benzyl 1-cycloheptenyl ketone (III), and benzyl 1-cyclooctenyl ketone (IV) were obtained in 16, 54, 21, and 35% yields respectively. The $\alpha\alpha$-dimethylbenzyl 1-cyclohexenyl ketone (IX) was synthesized by a similar method, but using dichloromethane as the solvent and at a reaction temperature of −60 °C. The crude product (IX) obtained by distillation contained three isomeric impurities; the material for the photoreaction was purified by succesive chromatography on silica gel eluted by benzene and preparative GLC (8% Carbowax 20 M on Chromosorb P, He). I: mp 64 °C. Mass: M^+=186. IR(CCl_4): 1660 cm^{-1}. Found: C, 83.63; H, 7.64%. Calcd for $C_{13}H_{14}O$: C, 83.83; H, 7.58%. II: mp 46 °C.[2] Mass: M^+=200. IR(CCl_4): 1655 cm^{-1}. III: bp 120 °C/0.9 mmHg. Mass: M^+=214. IR(neat): 1650 cm^{-1}. Semicarbazone; mp 171—172 °C. Found: C, 71.10; H, 7.92; N, 15.75%. Calcd for $C_{16}H_{21}ON_3$: C, 70.82; H, 7.80; N, 15.49%. IV: bp 170—172 °C/0.65 mmHg. Mass: M^+=228. IR(neat): 1560 cm^{-1}. Semicarbazone; mp 170—172 °C. Found: C, 71.46; H, 8.33; N, 14.73%. Calcd for $C_{17}H_{23}ON_3$: C, 71.54; H, 8.12; N, 14.73%. IX: bp 170—172 °C/0.35 mmHg. Mass: M^+=228.1499. Calcd for $C_{16}H_{20}O$: 228.1513. IR(neat): 1650 cm^{-1}

B) Benzyl 1-Propenyl Ketone (XI): Benzylmagnesium chloride prepared from benzyl chloride (12.6 g, 0.1 mol) and magnesium (2.4 g, 0.1 mol) in 60 ml of ether was added to crotonaldehyde (7.0 g, 0.1 mol) diluted with ether (60 ml) over a 1-h period under cooling in an ice-bath. The reaction

mixture was then agitated for a further hour at the ambient temperature. The reaction mixture was then treated with a saturated solution of ammonium chloride (22 ml), and the organic layer was condensed after drying over sodium sulfate to give crude 1-phenyl-3-penten-2-ol. This alcohol was oxidized by means of the Saret reagent (CrO_3 10 g/pyridine 100 ml) at room temperature for 24 h. Ether was added to the reaction mixture, and it was filtered; the filtrate was then washed with water and a saturated solution of cupric sulfate. The condensate of the solution, after drying over sodium sulfate, gave a rather complex mixture. The Benzyl 1-propenyl ketone (200 mg) was isolated from the mixture by repeated chromatography on silica gel eluted with a mixed solvent of chloroform and hexane. Mass: M^+= 160.0886. Calcd for $C_{11}H_{12}O$: 160.0888. IR(neat): 1660 and 1680 cm^{-1}. NMR(CCl_4): 1.40 (3H, double doublet, J=6 and 2 Hz), 3.63 (2H, singlet), 6.05 (1H, double doublet, J=13 and 2 Hz), and 6.80 ppm (δ) (1H, double quartet, J=13 and 6 Hz).

General Procedure of Photocyclization. The solvents and reagents used in the photochemical reaction were purified in the following ways. The methanol was refluxed over magnesium methoxide and distilled. The benzene was washed with concd H_2SO_4 and distilled after refluxing over sodium. The acetonitrile was purified by distillation after drying over phosphorus pentoxide. Boron trifluoride-diethyl ether was distilled under a nitrogen atomosphere and stored in a sealed tube in a cold and dark place. The trifluoroacetic acid was a commercially available reagent, and used without purification. The irradiation of the starting ketones, placed in a Pyrex tube, was carried out using a 450-W USHIO medium-pressure Hg lamp mounted in an imersion jacket and using a RIKOSHA merry-go-round-type irradiation apparatus—the distance between lamp and reaction tube was *ca.* 5 cm. The progress of the reaction was monitored by means of an IR spectrum of the aliquot; we observed the disappearance of the absorptions due to unsaturated carbonyl groups.

Photochemical Reaction in the Presence of Boron Trifluoride-Diethyl Ether. The starting ketones, I—IV, IX, and XI (1—1.5 mmol), in 10 ml of benzene containing boron trifluoride-diethyl ether (0.05 mol/l) were placed in Pyrex tubes, and the air was replaced by nitrogen or argon. Irradiation was then continued until the starting materials had completely disappeared. The reaction mixtures were then passed through an alumina column (10×100 mm, Merck activity II—III) to remove the boron trifluoride; the benzene eluate was condensed under reduced pressure to give the cyclized ketones in yields of 79% (V), 87% (VI), and 90% (VII). The yield of the X ketone was poor due to its photo-lability, which was proved by the irradiation of the isolated X ketone. Some improvement in the yield was, however, achieved by using a soft glass filter instead of a Pyrex filter. The irradiation of the benzyl 1-cyclooctenyl ketone (IV) and the benzyl 1-propenyl ketone (IX) recovered the starting materials even after a prolonged reaction period (8 h). V: bp 105—110 °C (bath)/1.0 mmHg. Mass: M^+= 186.1034. Calcd for $C_{13}H_{14}O$, 186.1045. IR(CCl_4): 1720 cm^{-1}. NMR (CCl_4): 3.62 ppm(δ) (2H, singlet). VI: bp 145—155 °C (bath)/0.9 mmHg. Mass: M^+=200. IR (CCl_4): 1710 cm^{-1}. NMR(CCl_4): 3.48 ppm (δ) (2H, singlet). Found: C, 84.16; H, 8.32%. Calcd for $C_{14}H_{16}O$: C, 83.96; H, 8.05%. VII: bp 145—150 °C (bath)/0.2 mmHg. Mass: M^+=214. IR(neat): 1717 cm^{-1}. NMR (CCl_4): 3.50 ppm (δ) (2H, singlet). Found: C, 84.31; H, 8.58%. Calcd for $C_{15}H_{18}O$: C, 84.07; H, 8.47%. X: bp 100 °C (bath)/0.2 mmHg. Mass: M^+=228. IR(neat): 1709 cm^{-1}. NMR(CCl_4): 1.40 (6H, singlet), 3.00 (1H, multiplet), and 2.40 ppm (δ) (1H, multiplet). Found: C, 84.18; H, 8.94%. Calcd for $C_{16}H_{20}O$: C, 84.16; H, 8.83%.

GLC analyses (5% OV-17 and Carbowax 20 M on Chromosorb W, N_2) showed the V and VII ketone to consist essentially of one stereoisomer. VI ketone, however, showed two peaks due to the isomers (VIa and VIb) *cis* and *trans* with respect to the ring junction, and the IR and NMR spectra of VI were identical with those of 1,2,3,4,4a,10a-hexahydro-10-phenanthrone obtained by Parham *et al.*[11] The two isomers were separated by preparative GLC and have similar spectroscopic properties in every respect. The faster moving isomer, VIa, was deduced to be *cis*-1,2,3,4,4a,10a-hexahydro-10-phenanthrone.

Photochemical Reaction in Methanol. Irradiations were carried out in the manner described above except for the use of methanol instead of boron trifluoride-diethyl ether/benzene as the solvent system. The benzyl 1-cyclopentenyl ketone (I) and the benzyl 1-cyclohexenyl ketone (II) were consumed within 2 and 3 h respectively, and they gave the cyclized products, V and VI, in 90 and 80% yields respectively. The benzyl 1-cycloheptenyl ketone (III), however, does not cyclize to VII under those reaction conditions.

Photochemical Reactions in Other Solvent Systems. The irradiation of II ketone was carried out in acetonitrile, in acetonitrile containing boron trifluoride-diethyl ether (0.05 mol/l), in benzene, and in benzene containing trifluoroacetic acid (0.05 mol/l). The ratio of VIa to VIb was dependent upon the solvent used, VIa : VIb were 1 : 1 in the boron trifluoride-diethyl ether/benzene, 5 : 1 in the acetonitrile, and 8 : 1 in the methanol.

Transformation of VIa into cis-*1,2,3,4,4a,9,10,10a-Octahydrophenanthrene.* The VI ketone (VIa : VIb=8 : 1), dissolved in 3 ml of 1,2-ethanedithiol, was treated with 2 ml of boron trifluoride-diethyl ether, after which the reaction mixture was stirred for 15 min at room temperature. An excess amount of saturated aqueous sodium hydrogencarbonate was then added to the mixture and it was extracted with hexane. The hexane extract was condensed after drying over sodium sulfate to give a yellow residue. The residue was dissolved in 10 ml of ethanol containing 1.5 g of Raney-Ni, and the mixture was stirred for 15 h at the ambient temperature. The subsequent evaporation of the ethanol after filtration gave 55 mg of the product (62%). GLC and NMR analyses of the product identified it as *cis*-1,2,3,4,4a,-9,10,10a-octahydrophenanthrene[1] containing a small amount of the *trans* isomer.

Attempted Equilibration of VI. The VI ketone (VIa : VIb=1 : 1 and 8 : 1, 50 mg) was dissolved in 10 ml of methanolic potassium hydroxide (1 mol/l), after which the solution was stirred for 24 h at room temperature under nitrogen. The reaction mixture was then neutralized with dil H_2SO_4, diluted with water, and extracted with ether. The evaporation of ether after drying over sodium sulfate recovered the starting material. GLC analysis of the recovered material showed an identical peak ratio due to the two components of the starting ketones. The attempted equilibration of the VI ketone using H_2SO_4 instead of the base catalyst gave the same result.

Deuteration of the VI Ketone. The VI ketone (5 mg) was dissolved in 1 ml of a mixed solvent of deuterium oxide and tetrahydrofuran (1 : 4) and 20 μl of pyridine was added to it, after which the mixture was kept at the ambient temperature for 45 h. After the evaporation of tetrahydrofuran under reduced pressure, the aqueous mixture was extracted with hexane. The mass spectrum of the ketone, VI, recoverd from the hexane extract showed intensified (M+1) and

$(M+2)$ peaks, $(M+1)/M=2.07$ and $(M+2)/M=1.50$, whereas the ratio of $(M+3)$ to $(M+2)$ was the one expected from the natural abundance of ^{13}C, $(M+3)/(M+2)=0.15$.

Irradiation of Enol Ether, VIII. The *Z* and *E*-forms of enol ether, VIII, were isolated in pure forms from a mixture of enol ether prepared from the II ketone and trimethyl orthoformate by the catalysis of H_2SO_4. The *Z* or *E*-form of the enol ether in 2 ml of benzene was placed in a Pyrex tube and was externally irradiated. GLC analysis (5% OV-17 on Chromosorb W, N_2) of either solution showed only a geometrical isomerization of the enol ether at the double bond, and a photo-equilibrated mixture of the same composition resulted from the irradiation of either isomer for 2 h, 58% *Z* and 42% *E*.

Quenching of the Photoreaction in Boron Trifluoride-Diethyl Ether/Benzene by 1,3-Pentadiene. The I, II, and III ketones (0.5 mmol each) were dissolved in 5 ml of benzene containing boron trifluoride-diethyl ether (0.05 mol/l) and 1,3-pentadiene (0.01—0.1 mol/l). Pyrex tubes containing the reaction mixture with varying amounts of 1,3-pentadiene were placed in a merry-go-round-type irradiation apparatus and irradiated in the same manner as in the preparative experiments for 5—15 min when more than 70% of the starting materials persisted. After irradiation, the same quantity of the internal standard was added to each reaction tube for the measurement of the peak intensity of the product by GLC analysis (5% OV-17 on Chromosorb W, N_2). In the case of the reaction of II, the GLC peak due to one of the products (VIa) was not well separated from that of the starting material, and so the peak due to VIb was employed for the quenching experiments. The experimental results are shown in Fig. 1. 1,3-Pentadiene was not consumed in the presence of boron trifluoride-diethyl ether to an extent detectable by the NMR analysis of the reaction mixture under the present reaction conditions.

Quenching of the Photoreaction in Methanol-Benzene by 1,3-Pentadiene. The I ketone (20 mg) was dissolved in 40 ml of a mixed solvent of methanol and benzene (1 : 4) containing varying amounts of 1,3-pentadiene (0.01—0.1 mol/l); an experiment similar to that described above was then performed. Benzene was added to the solvent system to get a homogeneous solution of 1,3-pentadiene. Stern-Volmer plot of this experiment showed a straight line with the slope of $k_q\tau=16\ M^{-1}$.

The authors wish to thank Professor Yasuji Yamade for the measurement of the high resolution mass spectra and Professor W. E. Parham for giving us the spectroscopic data for VIa and VIb. The financial support by Matsunaga Science Foundation is greatefully acknowledged.

References

1) M. Tada and H. Shinozaki, *Chem. Lett.*, **1972**, 1111.
2) J. W. Cook and C. L. Hawett, *J. Chem. Soc.*, **1933**, 1098.
3) W. S. Johnson and C. D. Gutsche, *J. Am. Chem. Soc.*, **68**, 2239 (1946).
4) One successful result has been reported for the thermal cyclization of benzyl 2,6-dimethyl-1-cyclohexenyl ketone by the catalysis of polyphosphoric acid; C. Schmidt and J. Thazhuthaveetil, *Tetrahedron Lett.*, **1970**, 2653.
5) J. W. Cook, N. A. McGinnis, and S. Mitchel, *J. Chem. Soc.*, **1944**, 286.
6) R. Noyori, H. Inoue, and M. Kato, *J. Am. Chem. Soc.*, **92**, 6699 (1970).
7) N. J. Turro and P. A. Wriede, *J. Am. Chem. Soc.*, **90**, 6863 (1968).
8) A. Pagliardini, G. Torri, L. Elegant, and M. Azzaro, *Tetrahedron Lett.*, **1972**, 4241.
9) R. S. Muliken and W. B. Person, "Molecular Complex," Wiley Interscience, New York (1969), p. 5.
10) Professor O. L. Chapmann suggested us the more basic nature of the excited state of carbonyl compound and intervention of the protonated species as an intermediate. We appreciate his suggestion.
11) W. E. Parham and C. S. Roosewelt, *J. Org. Chem.*, **37**, 1975 (1972).

Thermal Decarbonylation of Tropone[1)]

Akira AMANO, Toshio MUKAI,* Tomoo NAKAZAWA,*,** and Kiyoaki OKAYAMA*,***

Department of Applied Chemistry, Faculty of Engineering, Tohoku University, Aoba-Aramaki, Sendai 980

**Department of Chemistry, Faculty of Science, Tohoku University, Aoba-Aramaki, Sendai 980*

(Received January 30, 1976)

Thermal reaction of tropone has been studied at temperatures ranging from 420 to 490 °C and at residence times ranging from 1.5 to 6.9 s using a conventional flow apparatus. Tropone undergoes first-order unimolecular decarbonylation. The value of kinetic parameters for this reaction are evaluated as being: $A=10^{14.2}$ s^{-1}, $E_a=54.1$ kcal mol^{-1}, $\Delta S^{\neq}=2.8$ eu, $\Delta H^{\neq}=52.6$ kcal mol^{-1}, and $\Delta G^{\neq}=50.6$ kcal mol^{-1}. These values indicate that the decarbonylation takes place by one-step concerted mechanism *via* a norcaradienone-like transition complex. The latter complex is characterized by a partial transannular C_2–C_7 bond formation and concerted elongation of C_1–C_2 and C_1–C_7 bonds in tropone. The proposed transition complex is in conformity with reported thermal behavior of 1,3,5-cycloheptatriene as well as with molecular orbital symmetry theory.

A considerable attention has been directed to the pyrolysis of seven-membered conjugate systems. They include 1,3,5-cycloheptatriene,[2)] 7,7-dicyanonorcaradiene,[3)] 7-cyano-7-(trifluoromethyl)norcaradiene,[3)] 7,7-dimethoxycycloheptatriene,[4)] tropone ethylene acetal,[5)] thiepine derivatives,[6)] thiepine 1,1-dioxide,[7)] and azepine.[8)]

Concerning thermal reactivities of troponoid compounds, Dauben and his coworkers suggested in 1960 on the basis of their mass-spectroscopic observation that in the pyrolysis of 7-methoxycycloheptatriene benzene and carbon monoxide could be produced through an intermediary formation of tropone.[9)] It was supposed along with Woodward-Hoffmann Rule[10)] that the troponoid compounds exhibited the behavior to heat different from that to photoirradiation, on which bicyclo[3.2.0]hepta-3,6-dien-2-ones were formed.[11)] As our expectation, we have found quite unique, thermally induced rearrangements of troponoid compounds such as quantitative decarbonylation of tropone and comprehensive transformation of tropones and tropolones leading to benzenoid compounds.[1,12)] It has been expected then that further investigations on this novel reaction would provide with valuable informations as to norcaradiene skeleton frequently assumed but still controversial intermediate for the reactions of seven-membered conjugate system. The investigations should also be reckoned important, since the reaction may serve as an example of the thermal reaction of seven-membered compounds to test molecular orbital theory advanced by Woodward and Hoffmann.[10)] This paper deals with the kinetics for the decarbonylation reaction of tropone in details.

Experimental

Materials. Tropone of sufficient purity for use with the present kinetic measurements was prepared from an authentic sample of tropone picrate (mp 99—100 °C, yellow needles). The picrate was treated with aqueous ammonia and tropone was extracted with chloroform. After the extract was washed with water and dried over anhydrous sodium sulfate, chloroform was evaporated off from the extract and the residual oil was distilled at 80 °C under 5 mmHg. Gas chromatographic analysis of the distillate revealed no evidence of contamination of tropone. Toluene used as solvent was of reagent grade and of not less than 99.95 mol% purity. Cylinder helium used as carrier gas was of not less than 99.9 mol% purity. Both of these were used as received.

Kinetic Measurements. Toluene carrier technique was employed using a conventional all-glass flow apparatus. A touelne solution of 11.04 mol% tropone was introduced into the apparatus from a glass syringe of 19.3 mm in inside diameter. Reaction vessel was made of a quartz tubing, 20 mm in inside diameter and 140 mm in length, and was equipped with a thermo-sheath placed along its central axis. The vessel was fitted in an electrically heated aluminum-bronze block furnace, the temperature of which was controlled electronically within ±0.1°. Temperature profiles of the reaction vessel were determined, during each run while the reaction was taking place, by a movable Pt-Pt·Rh thermocouple in the sheath. Annular space of the vessel was filled with quartz tips, leaving a free volume of 14.30 ml. Injection of the solution was maintained at a rate of 20.75 $ml \cdot min^{-1}$ by a microfeeder to which the syringe was mounted. The tropone–toluene vapor was then carried into the reaction vessel along with a stream of helium dried over magnesium perchlorate. Rate of the latter stream, varying from 16 to 90 $ml \cdot min^{-1}$ (STP), was controlled by a needle valve and was measured by a soap-film flow meter within ±0.5%. Tropone in the reaction vessel was thus doubly diluted both by toluene and by helium that the pressure of tropone was kept below 30 mmHg throughout the present investigation. The pressure limitation such as described above was found important to eliminate carbonaceous materials formed otherwise. The reaction was carried out under conditions varied over the following ranges: temperature, 420—490°; residence time, 1.5—6.9 s. Product gases were passed through a train of traps, chilled by ice and methanol-Dry Ice, in which condensable components were collected for analysis. Non-condensable components were first led to a gas sampling tube immersed in liquid nitrogen to separate carbon monoxide, and were then purged after measurements of their flow velocities.

Definition of Temperature and Residence Time. From the observed temperature profiles of the reaction vessel, the following approximation was found valid. Where z is the length in mm along the reactor axis and other symbols

$$\int_{z=0}^{z=140} \exp(-E/RT)\,dz \approx \int_{z=20}^{z=100} \exp(-E/RT)dz$$

** Present address, Department of Chemistry, Faculty of Science, Osaka University, Toyonaka, Osaka 560.

*** Present address, Yokkaichi Work, Mitsubishi Petrochemical Co. Yokkaichi, Mie 510.

have their usual significances. Effective reactor length was therefore 80 mm, corresponding to an effective reactor volume, V, of 8.17 ml. The average reaction temperature, T_{av} could then be defined by a graphic integration according to the following equation. The value of activation energy,

$$T_{av} = \frac{2.303E}{R} \log \left\{ \int_{z=20}^{z=100} \exp(-E/RT)\mathrm{d}z/80 \right\}$$

E, used with the above equation should coincide with the resulting value, E_a, determined from temperature dependence of specific reaction rate. This match was attained by trial-and-error calculations. Residence time, t, in s was calculat-

$$t = PVT/760\ T_{av}F$$

ed by the equation, where F is the corrected total flow rate of the reactant gas mixture in ml s^{-1}, T the room temperature, and P the atmospheric pressure in mmHg.

Analysis. Condensable components collected in the traps, consisting of benzene, toluene and unreacted tropone, were analyzed gas chromatographically using a combined column composed of 3 m Thermol-3 and 3 m Silicone Grease DC-550 at 150° with 40 ml min^{-1} of helium as a carrier gas. Under the given conditions, retention volumes were: benzene, 352 ml; toluene, 456 ml. Error involved in the analysis was estimated to be approximately ±2% of recorded values. Carbon monoxide collected in the gas sampling tube was also analyzed by gaschromatograph using a 5 m Molecular Sieve 5A column at 0° with 40 ml min^{-1} of helium as a carrier gas. In a few runs, results obtained by the gas-chromatographic analysis were confirmed by a mass-spectrographic analysis.

Results

Thermal Reaction of Tropone and the Related Compounds. Threshold temperature of tropone pyrolysis was found to be approximately 400°C, and as will be shown later the rate of the reaction could be most conveniently measured at temperatures between 420 and 500 °C. Besides tropone unreacted and toluene used as solvent, the pyrolyzates were consisted exclusively of benzene and carbon monoxide. Neither polymerization nor condensation products were detected both in the pyrolyzates and on the wall of the reaction vessel. Analysis of the products revealed that the amount of benzene was consistently in equi-molar with that of carbon monoxide. Therefore the reaction can be characterized simply by the following stoichiometry:

$$\text{Tropone} \rightarrow \text{Benzene} + \text{Carbon Monoxide}$$

In a few preliminary runs, however, a considerable amount of biphenyl was formed at temperatures exceeding 800°. Since an entirely different principle may operate in the pyrolysis at extremely high temperatures, the biphenyl forming reaction will be ignored in our present discussion.

Order and Molecularity of the Reaction. Summarized in Table 1 are the results of twenty-six kinetic measurements carried out under the specified conditions. In each of these runs, conversion of tropone was kept below 25% and was usually in the range of 1—15%. This precaution was taken to avoid data which were inadequate for use with the following kinetic analysis. Illustrated in Fig. 1 are the plots of $-\log(1-x)$ *vs.* t, where x denotes fraction of tropone consumed. With exceptions of runs where conversions were higher, experimental data are all fitted with well-defined straight line passing the origin. The reaction is, therefore, first order in tropone with no induction period. These together with the fact that bibenzyl

Table 1. Pyrolysis of tropone

Temperature (K)	Residence time (s)	Conversion (mol%) × 10^3	Rate constant (s^{-1})
691.6	4.11	0.42	1.027
692.0	3.66	0.30	0.819
696.0	5.02	0.57	1.160
709.2	5.27	2.28	4.391
711.6	6.60	2.55	3.904
714.5	6.02	2.73	4.589
715.6	3.07	1.66	5.453
733.0	2.92	3.92	13.69
733.0	3.77	4.98	13.56
733.0	4.78	5.59	12.03
734.0	5.13	6.81	13.75
734.0	6.32	8.08	13.33
734.0	7.49	12.31	17.53
734.0	8.91	14.35	17.63
739.6	5.98	11.47	34.59
745.0	2.99	7.61	26.51
745.0	4.55	10.26	23.78
745.3	3.82	8.47	23.16
745.4	2.02	4.77	24.17
745.4	8.97	17.33	21.22
746.1	5.93	13.84	25.11
750.0	2.25	8.78	40.86
750.4	3.39	8.36	25.73
754.3	5.73	15.50	29.38
754.6	6.59	25.65	44.98
756.7	4.73	12.55	28.36

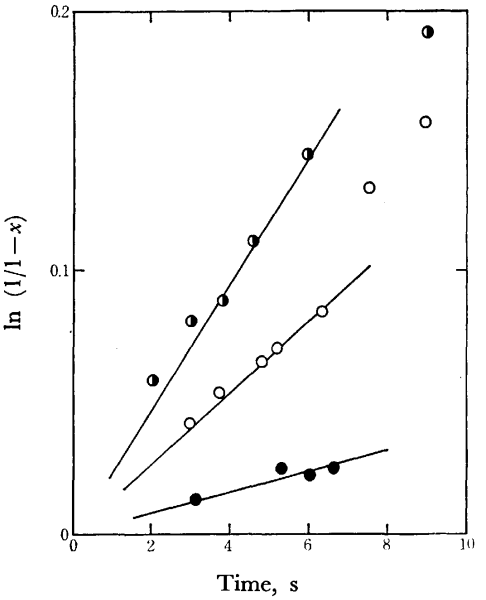

Fig. 1. First-order plots for the decarbonylation of tropone. Filled circles, 438 °C; half-filled circles, 472 °C; empty circles, 461 °C.

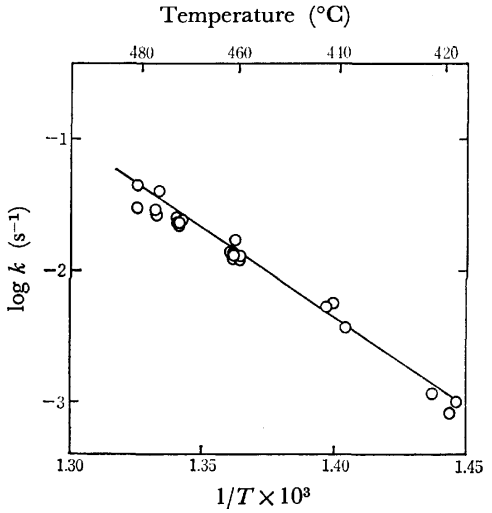

Fig. 2. Arrhenius plots for the decarbonylation of tropone.

Table 2. Rate constants

Temperature (K)	Rate constant $\times 10^3$ (s^{-1})
711.6	4.2±0.27
734.0	13.4±0.93
745.4	23.6±0.80
754.6	41.7±5.5

was not formed would strongly suggest that the decarbonylation takes place *via* a simple unimolecular splitting off of carbonyl group.

Kinetic Parameters. Listed in Table 2 are the values of rate constant calculated from the slope of the lines in Fig. 1. Error limits, estimated from uncertainties involved in measured quantities, are also indicated for each value of the rate constants. Arrhenius plots based on the values listed in the table are given in Fig. 2. Thus, rate constant can be expressed by the following equation:

$$\log k(s^{-1}) = (14.22\pm0.67) - (54100\pm2000)/4.575\,T$$

Thermodynamic properties of the transition complex can therefore be characterized by the following values: $\Delta S^{\ddagger}=2.8\pm3.0$ eu, $\Delta H^{\ddagger}=52.6\pm2$ kcal·mol^{-1}, and $\Delta G^{\ddagger}=50.6\pm2$ kcal·mol^{-1}.

Discussion

Mechanism of Decarbonylation. Illustrated in Fig. 3 are feasible pathways through which tropone may undergo unimolecular decarbonylation.

Of the three paths, Path A, proposed for the reaction of 2-azidotropone,[13] can be ruled out for the present case in view of strong C_1–C_2 linkage. Recent investigations on tropone by use of X-ray analysis,[14] gas phase electron diffraction,[15] NMR spectroscopy, [16,17d] and on the basis of theoretical calculations[17] reveal its structure, as being planar, with pronounced bond alternation. Dipole moment of 4.17—4.30 D reported

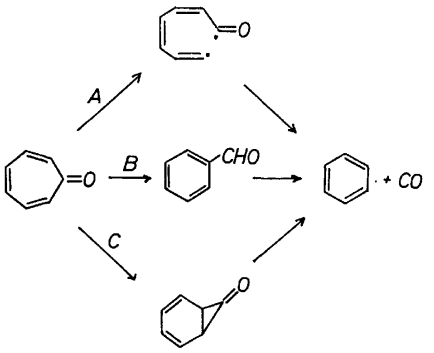

Fig. 3. Mechanism for the decarbonylation of tropone.

for tropone,[18] exhibits, along with the presence of carbonyl stretching band in lower frequency region,[19] π-stabilization to a considerable extent.[20] The stabilization energy for tropone measured from the heat of hydrogenation is higher than that for nonplanar cycloheptatriene[21,22] by 3 kcal mol^{-1}. All these structural evidences definitely indicate that the energy required for α-cleavage of tropone ring is no less than 78 kcal·mol^{-1}, the value usually assigned for D(CH_3CO-CH_3) in acetone.[23] The value of $E_a\approx54$ kcal·mol^{-1} observed in the present work is too low for the decarbonylation to take place *via* Path A. The value of $\Delta S^{\ddagger}\approx2.8$ eu observed is also incompatible with this path. Biradical formation would remove restrictions of internal motions, resulting in an increase of entropy by a considerable amount. The argument is quite similar to that given for the isomerization of cyclobutenes.[24] In this latter case, experimentally observed value of $\Delta S^{\ddagger}\approx-0.7$ eu was taken as an evidence against the biradical mechanism. Mention should also be made of the fact that bibenzyl was not detected in the present work.

Intermediary formation of benzaldehyde *via* α-cleavage concerted with hydrogen atom migration is assumed in Path B. The assumption is based on a somewhat superficial interpretation of the reactions of a similar type such as isomerizations of cycloheptatriene[2] and 2-chlorotropone.[12] This path is clearly ruled out on the following experimental grounds. According to our preliminary examinations, benzaldehyde was not detected in the pyrolyzates and benzene was not formed from benzaldehyde under conditions comparable with those in the present work.

Only Path C is now left for consideration. As will be seen later, it is concluded in our present discussion that Path C with slight modification is in accord with a bulk of the latest informations. Since norcaradienone assumed in this path bears an intimate relation with norcaradiene intermediate in the isomerization of cycloheptatriene, the mechanism *via* Path C will be discussed separately in the subsequent paragraph with special reference to that of the latter compound.

Norcaradiene Skeleton as Transient Structure. As has been mentioned earlier, cycloheptatriene isomerizes to the corresponding benzene derivatives at temperatures around 100 °C.[2] The values of kinetic parameters have been assigned as being $E_a\approx51$ kcal mol^{-1} and $A\approx10^{13.5}$ s^{-1}. The reaction, therefore, takes place

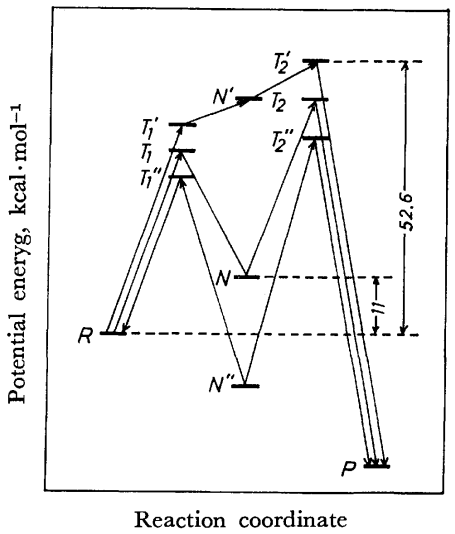

Fig. 4. Potential energy diagram for reactions involving norcaradiene skeleton.

Table 3. Symmetry of HOMO and LVMO of tropone

Orbital numbers	1	2	3	4	5	6	7	8
HOMO	−	+	+	−	−	+	+	−
LVMO	0	+	−	−	+	+	−	0

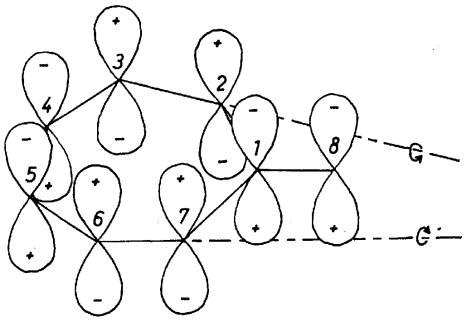

Fig. 5. Orbital symmetry and steric course for the decarbonylation of tropone.

at a rate comparable with that of tropone. Klump and Chesick discussed the reaction in terms of a metastable norcaradiene intermediate in equilibrium with cycloheptatriene.[2b] Energetics of the Klump-Chesick mechanism can best be expressed by the steps, R→T_1 →N→T_2→P, illustrated in Fig. 4. In this figure, R, P and N (also N′ and N″) represent energy levels of reactant, product and transient complex having norcaradiene skeleton, respectively. Those of the first and the second transition-states are also represented by T_1 and T_2 (also T_1', T_1'', T_2' and T_2''). Although mechanistic similarity does exist between the pyrolyses of cycloheptatriene and tropone as to the tendency toward the formation of norcaradiene skeletone, norcaradienone formed from tropone is believed to be far less stable than norcaradiene assumed in the Klump-Chesick mechanism.

Referred to below are some indirect evidences in support of the above statement. Valence isomerization between the cycloheptatrienes and norcaradienes has been extensively studied[25] and many norcaradiene derivatives were found to exist even at room temperatures.[3,26] Norcaradiene in equilibrium with cycloheptatriene has never been observed spectroscopically but the Diels-Alder reaction of cycloheptatriene with dienophiles such as maleic anhydride affords an adduct derived from norcaradiene as an only product.[27] Contrary to these, an isolation of norcaradienone has never been documented and there is no evidence for its existence. The Diels-Alder reaction of tropone gives rise not to an adduct derived from norcaradienone but to that obtained by direct addition to 2 and 5 positions of tropone nucleus.[28] Furthermore, higher reactivity found in cyclopropanone which undergoes ring opening quite readily[29] and the higher π-stabilization found in planar tropone than that in nonplanar cycloheptatriene[21,30] suggest that the process from tropone to norcaradienone is energetically less favorable than that from cycloheptatriene to norcaradiene. Thus, for the case of tropone, N in Fig. 4 would be raised to N′, and consequently T_1 to T_1' and T_2 to T_2'. The reaction now takes place through Path C comprizing the steps: R→T_1'→N′→T_2'→P. The level N′ no longer stands for an intermeidate in its usual terminology, but is more like a transient complex between two transition-states. The assumption of such norcaradienone-like complex does not conflict with the observed normal *A*-factor and moderate E_a value. Steric course of the proposed mechanism will be discussed in more detail on the light of the rule advanced by Woodward and Hoffmann.[10]

It should be mentioned that 7,7-dicyanonorcaradiene and 7-cyano-7-(trifluoromethyl)norcaradiene have been recognized in stable form.[3] In these compounds, electrophilic substituents on C_7 must have strong stabilization effect toward norcaradiene.[31] The net effect in this case is, therefore, to lower the intermediate level from N to N″, and hence the transition-state levels from T_1 and T_2 to T_1'' and T_2'', respectively. The isomerization would then take place in two ways: N″→T_1''→R and N″→T_2''→P. Results obtained by Giganek support this view.

Molecular Orbital Symmetry Theory. Molecular orbital symmetry theory provides a clear-cut account for stereochemical consequences observed in thermal as well as photochemical valence isomerizations of polyolefins.[10] The decarbonylation of tropone appears to be a newer addition to those for which this theory is obeyed. Listed in Table 3 are the reported symmetry factors of the highest occupied and the lowest vacant molecular orbitals of tropone.[32] For thermal reactions where HOMO determines the steric course, the theory predicts the overlap between orbitals of the C_2 and C_7 positions by disrotatory process as illustrated in Fig. 5. As the C_2–C_3 and C_6–C_7 bonds rotate in the directions indicated by curved arrows in Fig. 5, a partial bond is formed between the C_2 and C_7 positions, and carbonyl group is squeezed out from the plane of the ring. This can only take place at the expense of the weakening of the C_1–C_2 and C_1–C_7 bonds. The compensation described above as to the rigidity of the molecule as a whole is in con-

formity with the small value of $\Delta S^{\neq}$ 2.8 eu observed in the present study. The resulting structure is identical with the norcaradienone-like transient complex brought up earlier in connection with Path C.

In sharp contrast with thermally induced reactions, photolysis of tropones has been known to form $\Delta^{3,6}$-bicyclo[3.2.0]hepta-3,6-dien-1-one.[11] Since the steric course of photochemical reactions is determined by the symmetry of LVMO, the photolyzate of tropones is again in conformity with the theory. Thus, it appears that the molecular orbital symmetry theory can be extended to cover reactions of seven-membered conjugate system at elevated temperatures.

References

1) Organic Thermal Reactions XXXV. Part XXXIV, Ref. T. Mukai and T. Nakazawa, "Topics in Nonbenzenoid Aromatic Chemistry," Vol. II, ed. by T. Nozoe, Hirokawa Pub. Co., Inc., Tokyo, in Press.

2) a) W. G. Woods, *J. Org. Chem.*, **23**, 110 (1958); W. G. Herndon and L. L. Lowry, *J. Am. Chem. Soc.*, **86**, 1922 (1964); b) K. N. Klump and J. P. Chesick, *ibid.*, **85**, 130 (1963); c) K. W. Egger, *ibid.*, **90**, 6 (1968); d) R. Atkinson and B. A. Thrush, *Proc. R. Soc. London., Ser. A*, **316**, 131 (1970).

3) E. Ciganek, *J. Am. Chem. Soc.*, **87**, 1149 (1965); E. Ciganek, *ibid.*, **89**, 1454, 1458 (1967).

4) R. W. Hoffmann and J. Schneider, *Tetrahedron Lett.*, **1967**, 4347.

5) T. Fukunaga, T. Mukai, Y. Akasaki, and R. Suzuki, *Tetrahedron Lett.* **1970**, 2975.

6) a) D. N. Reinhoudt and C. G. Kouwenhoven, *J. Chem. Soc., Chem. Commun.*, **1972**, 1233; b) I. Murata and T. Tatsuoka, *Tetrahedron Lett.*, **1975**, 2697.

7) W. L. Mock, *J. Am. Chem. Soc.*, **89**, 1281 (1967).

8) a) K. Hafner, D. Zinster, and K-L. Moritz, *Tetrahedron Lett.*, **1964**, 1733: b) L. A. Paquette, D. A. Kuhla, and J. H. Barret, *J. Org. Chem.*, **34**, 2879 (1969).

9) A. G. Harrison, L. R. Honnen, H. J. Dauben, Jr., and F. P. Lossing, *J. Am. Chem. Soc.*, **82**, 5593 (1960).

10) R. Hoffmann and R. B. Woodward, *Acc. Chem. Res.*, **1**, 17 (1968); R. B. Woodward and R. Hoffmann, "The Conservation of Orbital Symmetry," Verlag Chemie GmbH, Academic Press (1970).

11) O. L. Chapman, "Advances in Photochemistry," Vol. 1, ed. by W. A. Noyes, G. S. Hammond, and J. N. Pitts, John Wily & Sons, Inc., New York (1963), p. 323.

12) T. Mukai, T. Nakazawa, and T. Shishido, *Tetrahedron Lett.*, **1967**, 2465; T. Mukai, T. Nakazawa, and K. Okayama, *ibid.*, **1968**, 1695.

13) J. D. Hobson and J. R. Malpass, *Chem. Commun.*, **1966**, 141

14) M. L. Barrow, O. S. Mills, and G. Hilippino, *J. Chem. Soc., Chem. Commun.*, **1973**, 66.

15) M. Ogasawara, T. Iijima, and M. Kimura, *Bull. Chem. Soc. Jpn.*, **45**, 3277 (1972).

16) A. C. Veracini and F. Pietra, *J. Chem. Soc., Chem. Commun.*, **1972**, 1262.

17) a) M. J. Z. Dewar and T. Morita, *J. Am. Chem. Soc.*, **91**, 802, (1969); M. J. S. Dewar and N. Trinajstic, *Croat. Chem. Acta*, **42**, 1 (1970); b) B. A. Hess, Jr., L. J. Schaad, and C. W. Holyoke, *Tetrahedron*, **28**, 5299 (1972); c) D. J. Bertelli and T. G. Andrews, Jr., *J. Am. Chem. Soc.*, **91**, 5280 (1969); d) D. J. Bertelli and T. G. Andrews, *ibid.*, **91**, 5286 (1969).

18) a) Y. Kurita, S. Seto, T. Nozoe, and M. Kubo, *Bull. Chem. Soc. Jpn.*, **26**, 272 (1953); Y. Kurita, *Sci. Repts. Tohoku Univ.*, **I**, **38**, 85 (1954); b) A. DiGiacomo and C. P. Smyth, *J. Am. Chem. Soc.*, **74**, 4411 (1952); c) D. J. Bertelli and T. G. Andrews, Jr., *Tetrahedron Lett.*, **1967**, 4467.

19) a) H. J. Dauben and H. Ringold, *J. Am. Chem. Soc.*, **73**, 876 (1951); b) W. von E. Doering and F. L. Detert, *ibid.*, **73**, 876 (1951); c) S. Kinumaki, K. Aida ,and Y. Ikegami, *Sci. Repts. Res. Inst. Tohoku Univ.*, **A**, **8**, 263 (1956).

20) H. Hosoya and S. Nagakura, *Bull. Chem. Soc. Jpn.*, **39**, 1414 (1966).

21) a) R. B. Turner, W. R. Meador, and R. E. Winkler, *J. Am. Chem. Soc.*, **79**, 4116 (1967); b) R. B. Turner, W. R. Meador, W. von E. Doering, L. H. Knox, J. R. Mayer, and D. W. Wiley, *ibid.*, **79**, 4127 (1957).

22) F. A. L. Anet, *J. Am. Chem. Soc.* **86**, 458 (1964).

23) E. O'Neal and S. W. Benson, *J. Chem. Phys.*, **36**, 2196 (1962).

24) H. M. Frey, "Advances in Physical Organic Chemistry," Vol. 4, ed. by V. Gold, Academic Press, London and New York (1966), p. 148.

25) G. Maier, "Valenzisomerierierungen," Verlag Chemie, Weinheim/Bergstr. (1972), p. 105 and references cited therein.

26) a) T. Mukai, H. Kubota, and T. Toda, *Tetrahedron Lett.*, **1967**, 3581; b) F. -G. Klärner, *ibid.*, **1974**, 19.

27) a) K. Alder, K. Kaiser, and M. Schumacher, *Ann.*, **602**, 80 (1957); b) M. J. Goldstin and A. H. Gevirtz, *Tetrahedron Lett.*, **1965**, 4417.

28) T. Nozoe, T. Mukai, K. Takase, and T. Nagase, *Proc. Jpn. Acad.*, **28**, 477 (1952); T. Nozoe, T. Mukai, T. Nagase, and Y. Toyooka, *Bull. Chem. Soc. Jpn.*, **33**, 1247 (1960).

29) N. J. Turro, *Acc. Chem. Res.*, **2**, 25 (1969) and references cited therein.

30) The degree of aromaticity of tropone has been controversial over the years. Many workers calculated resonance energy for tropone; 16—24 kcal mol^{-1} [W. N. Hubbard, C. Katz, G. B. Guthrie, and G. Waddington, *J. Am. Chem. Soc.*, **74**, 4456 (1952)]; 8—11 kcal mol^{-1} (ref. 21b); 0.74 kcal mol^{-1} [M. J. S. Dewar, A. J. Harget, and N. Trinajstic, *J. Am. Chem. Soc.*, **91**, 6321 (1969)].

31) R. Hoffmann, *Tetrahedron Lett.*, **1970**, 2907.

32) H. Yamaguchi, Y. Amako, and H. Azumi, *Tetrahedron*, **24**, 268 (1968).

The Crystal and Molecular Structure of (+)-1-Bromo-2-hydroxy-2-phenylethyl *p*-Tolyl Sulfoxide: The Bromohydrin of (+)-*trans*-β-Styryl *p*-Tolyl Sulfoxide

Fujiko Iwasaki, Shuichi Mitamura,* and Gen-ichi Tsuchihashi*

Department of Materials Science, The University of Electro-Communications, Chofu-shi, Tokyo 182

**Sagami Chemical Research Center, Nishi-Ohnuma, Sagamihara, Kanagawa 229*

(Received February 2, 1976)

The crystal structure of (+)-1-bromo-2-hydroxy-2-phenylethyl *p*-tolyl sulfoxide, a major isomer formed by the electrophilic addition of BrOH to (+)-*trans*-β-styryl *p*-tolyl sulfoxide (**1**), has been determined by the X-ray diffraction method. The crystal is hexagonal; space group, $P6_2$; $a=15.61$, $c=10.82$ Å, and $Z=6$. The final R value is 0.079. A helical chain of the hydrogen bond between hydroxyl and sulfinyl groups (O···O, 2.63 Å) is formed around the threefold screw axis. The absolute configuration has been determined to be S_S, $S_{C(1)}$, $S_{C(2)}$ from the Mo Kα anomalous scattering of bromine and sulfur atoms. The bromine atom is *gauche* to the sulfinyl oxygen across the C(1)–S bond and *trans* to the hydroxyl oxygen across the C(1)–C(2) bond. Based on the established absolute configuration of the title compound, a mechanism which involves the preferential formation of an intermediary bromonium ion is proposed for the addition of BrOH to **1**.

The electrophilic addition of BrOH to (+)-*trans*-β-styryl *p*-tolyl sulfoxide (**1**) results in a dominant formation of a diastereomer, (+)-1-bromo-2-hydroxy-2-phenylethyl *p*-tolyl sulfoxide (**2a**) as shown in Scheme 1. The absolute configuration of **2a** was determined chemically.[1] We have recently reported the crystal structure and the absolute configuration of 1,2-dibromo-2-phenylethyl *p*-tolyl sulfoxide (**3**), a dominant isomer formed by the ionic bromination of **1**, by X-ray analysis.[2] The high selectivity of these additions is attributed to the preferential formation of a bridged bromonium ion by the electronic demand of the adjacent chiral sulfinyl group.

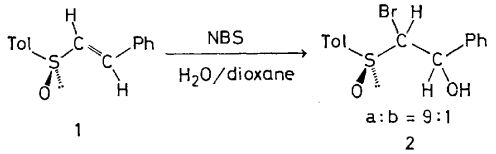

1 2

Scheme 1.

An X-ray diffraction study was undertaken to establish the absolute configuration and the molecular conformation of **2a** in order to elucidate such a specific reaction mechanism.

Experimental

The dominant isomer of **2** was recrystallized from hexane–ethanol solution. The crystals are colorless needles elongated along the c axis. They are unstable in air, and more unstable in a thin glass capillary. Therefore the intensity measurement was carried out without coating.

The cell dimensions were calibrated with copper powder lines superposed on Weissenberg photographs (Cu K, $\bar{\alpha}=1.5418$, $\beta=1.3920$ Å). The crystal data are: $C_{15}H_{15}BrSO_2$, MW=339.25; hexagonal, $a=15.61\pm0.01$, $c=10.82\pm0.01$ Å, $U=2281$ Å^3, $Z=6$, $D_x=1.48$, $D_m=1.50$ g cm^{-3}; $F(000)=1032$, μ(Mo Kα)=27.8 cm^{-1}; mp 149—151 °C; $[\alpha]_D^{26}$ +222.4° (c 0.526, MeOH). Laue symmetry and systematic absences ($l\neq3n$ for $00l$) indicated the possible space group $P6_2$ or $P6_4$. The former was proved to be correct by the analysis for the absolute configuration.

Intensity data were collected on a RIGAKU automatic diffractometer, using MoKα radiation monochromatized with a graphite monochromator. An ω-2θ scan technique was used to obtain the intensities with width of $\Delta\omega=1.0°+0.5°\tan\theta$ and a scanning speed of 2° min^{-1}. At both ends of the scan range for each reflection, 10 s background counts were taken. The intensities of three standard reflections, measured after every 50 reflections, decreased over the period of data collection. Their final intensities were 85% of the original values. The data were corrected for decomposition. Reflections in the range $2\theta<55°$ and $-13\leq l\leq7$ were measured, and 1043 of these had $F_o>3\sigma(F)$, which were considered as observed reflections. This set included the reflections with indices hkl and $hk\bar{l}$ which were treated as independent because of the anomalous scattering of Mo Kα radiation by bromine and sulfur atoms.

Structure Determination

The position of the bromine atom was found by inspection of a three-dimensional Patterson map. For a heavy atom alone, the R value was 0.43. Successive cycles of Fourier syntheses revealed the location of the remaining non-hydrogen atoms. The atomic parameters were refined by block-diagonal least-squares method, first with isotropic temperature factors to an R value of 0.17 and then with anisotropic temperature factors for all the non-hydrogen atoms to an R value of 0.10. A difference Fourier map showed positive density at the expected hydrogen atom positions except those of the methyl group. The coordinate of the hydroxyl-hydrogen atom H(O1) was estimated from this map. But the positions of other hydrogen-atoms, except those of the methyl group, were calculated with C–H distance of 1.08 Å. These parameters were included in the structure-factor calculations though they were not refined. The isotropic thermal parameters for hydrogen atoms were assumed to be 7.0 Å^2. Further cycles of refinement were carried out on two enantiomorphic structures taking the anomalous dispersion effect into consideration. The lowest R values for the two enantiomers were 0.079 and 0.089, respectively. The former corresponded to the space group $P6_2$ and the latter to $P6_4$. The difference of the R values is significant,[3] so that the true space group is assigned as $P6_2$ and the molecule has an absolute configuration illustrated in Fig. 1.

The weighting scheme used was: $w=0.3$ if $|F_o|<15$, $w=1.0$ if $15\leq|F_o|\leq60$ and $w=(60/|F_o|)^2$ if $|F_o|>60$. The atomic scattering factors were taken from "International Tables for X-ray Crystallography".[4] The

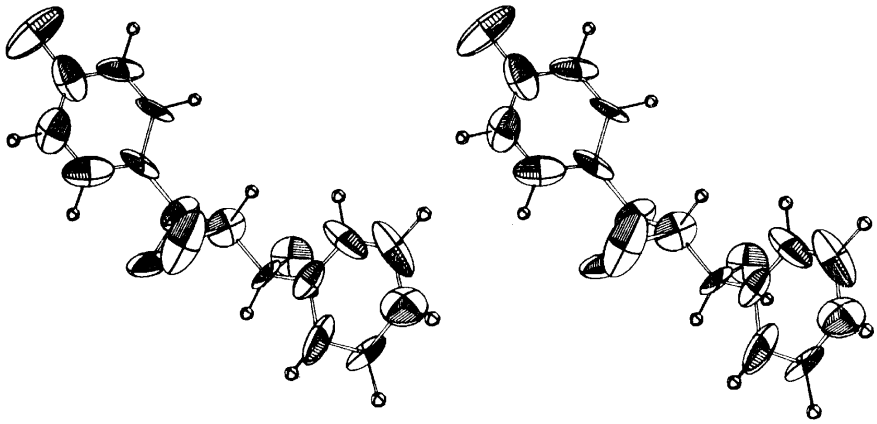

Fig. 1. Stereoscopic view of the molecule.

TABLE 1. FINAL ATOMIC PARAMETERS

(a) Atomic coordinates ($\times 10^4$) and anisotropic thermal parameters ($\times 10^3$) of non-hydrogen atoms with their estimated standard deviations.[a] The anisotropic temterature factors are of the form:

$$\exp\{-2\pi^2(U_{11}h^2a^{*2}+U_{22}k^2b^{*2}+U_{33}l^2c^{*2}+2U_{12}hka^*b^*+2U_{13}hla^*c^*+2U_{23}klb^*c^*)\}$$

The B_{eq} values are the equivalent isotropic temperature factors.[b]

Atom	x	y	z	U_{11}	U_{22}	U_{33}	U_{12}	U_{13}	U_{23}	B_{eq}
Br	1700(3)	3463(3)	3333(4)	285(5)	154(3)	81(2)	171(3)	−58(2)	−31(2)	11.5
S	1327(5)	4664(4)	1344(5)	106(5)	68(4)	37(3)	10(4)	1(3)	7(3)	6.7
O(1)	2404(11)	5115(14)	1060(14)	55(10)	140(15)	91(12)	−40(11)	18(9)	−45(11)	10.7
O(2)	1351(11)	5918(10)	3427(15)	103(12)	72(10)	111(12)	57(10)	−8(10)	19(10)	7.1
C(1)	1244(16)	4363(16)	3042(17)	100(19)	87(16)	23(10)	14(14)	21(12)	31(10)	6.7
C(2)	1788(15)	5317(15)	3737(14)	72(15)	86(17)	20(11)	−4(13)	−2(10)	−35(10)	6.2
C(3)	1593(15)	5032(13)	5132(18)	106(17)	49(12)	63(13)	42(13)	−17(13)	−27(12)	5.6
C(4)	713(16)	4501(18)	5723(26)	45(15)	111(21)	137(22)	28(15)	42(14)	28(16)	8.1
C(5)	566(19)	4327(22)	6992(25)	98(19)	163(27)	114(23)	52(19)	100(18)	65(19)	10.3
C(6)	1425(17)	4755(16)	7676(21)	86(18)	54(16)	98(17)	13(14)	3(14)	7(12)	7.1
C(7)	2343(16)	5306(13)	7171(19)	96(17)	23(12)	85(15)	15(12)	−29(13)	−43(11)	5.9
C(8)	2465(22)	5446(18)	5868(19)	166(26)	114(23)	40(13)	56(21)	2(16)	−35(13)	8.9
C(9)	638(14)	3449(17)	722(16)	26(12)	122(19)	52(12)	20(13)	28(10)	42(12)	5.9
C(10)	−328(13)	2931(18)	646(17)	14(12)	137(21)	67(14)	29(14)	−4(10)	7(13)	6.1
C(11)	−818(14)	2015(16)	66(22)	42(14)	91(17)	79(15)	−18(13)	8(13)	26(15)	7.4
C(12)	−333(17)	1539(18)	−353(20)	105(19)	157(23)	67(15)	102(19)	13(13)	28(15)	7.4
C(13)	666(18)	2019(16)	−248(22)	136(20)	96(17)	88(17)	94(17)	−24(16)	−8(15)	7.2
C(14)	1179(17)	2990(17)	237(22)	78(16)	86(17)	90(18)	16(14)	−34(14)	28(14)	7.7
C(15)	−887(28)	525(17)	−869(27)	256(39)	35(15)	126(23)	48(20)	−70(23)	−14(14)	11.9

(b) Atomic coordinates for hydrogen atoms ($\times 10^3$).

Atom	x	y	z	Atom	x	y	z
H(O1)	183	645	400	H(7)	298	565	778
H(1)	48	402	332	H(8)	321	588	547
H(2)	258	576	360	H(10)	−77	323	104
H(4)	4	417	518	H(11)	−161	166	−4
H(5)	−14	393	746	H(13)	108	167	−56
H(6)	141	458	855	H(14)	198	339	26

a) The e.s.d.'s are in parentheses and refer to the last significant digits of the respective values in Tables 1 and 3 and in Fig. 3. b) W. C. Hamilton, *Acta Crystallogr.*, **12**, 609 (1959).

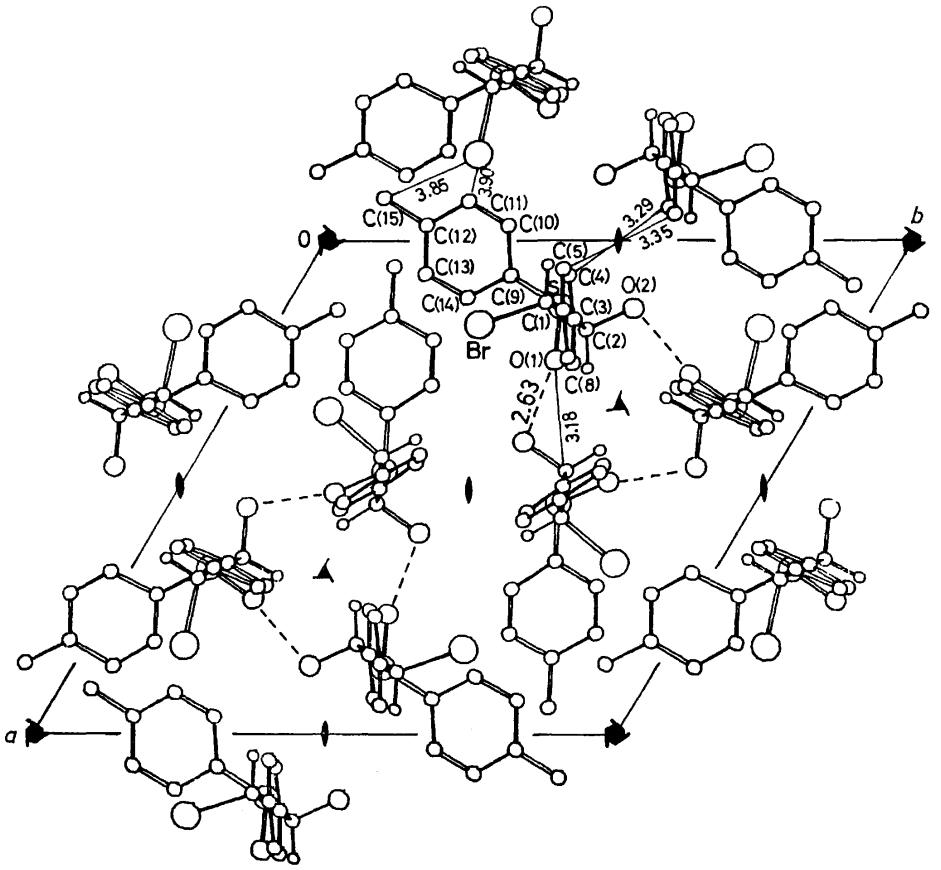

Fig. 2. Projection of the structure along the c axis.

Table 3. Intermolecular distances less than 4.0Å

Symmetry code			
Superscript			
None	x	y	z
i	x	y	$z-1$
ii	y	$y-x$	$z-1/3$
iii	y	$y-x$	$z+2/3$
iv	$-x$	$-y$	z
v	$-x$	$1-y$	z
vi	$y-x$	$1-x$	$z-2/3$
vii	$1-y$	$1-y+x$	$z-1/3$

S···C(6^{i})	3.97 (3) Å	O(2)···C(1^{v})	3.87 (3) Å
O(1)···C(6^{i})	3.90 (3)	O(2)···C(4^{v})	3.86 (3)
C(9)···C(6^{i})	3.74 (4)	C(4)···C(4^{v})	3.29 (3)
C(14))···C(6^{i})	3.79 (4)	C(4)···C(5^{v})	3.59 (5)
Br···C(5^{ii})	3.90 (4)	C(5)···C(5^{v})	3.35 (4)
C(13)···C(11^{ii})	3.75 (4)	O(1)···C(7^{vi})	3.66 (3)
Br···C(11^{iii})	3.90 (3)	O(1)···C(8^{vi})	3.96 (4)
Br···C(15^{iii})	3.85 (4)	O(1)···O(2^{vii})	2.63 (3)
C(6)···C(11^{iii})	3.71 (4)	O(1)···C(2^{vii})	3.18 (3)
C(7)···C(10^{iii})	3.74 (4)	O(1)···C(3^{vii})	3.57 (3)
C(7)···C(11^{iii})	3.67 (4)	O(1)···C(8^{vii})	3.56 (4)
C(8)···C(11^{iii})	3.90 (4)	C(2)···C(7^{vii})	3.95 (3)
C(15)···C(15^{iv})	3.86 (4)	C(2)···C(8^{vii})	3.99 (4)
O(2)···O(2^{v})	3.73 (4)	C(8)···C(7^{vii})	3.80 (4)
		O(1)···H(3^{vii})	1.68

final atomic parameters and their estimated standard deviations are given in Table 1. The observed and calculated structure factors are listed in Table 2.[5]

Results and Discussion

Figure 2 shows the crystal structure viewed along the c axis. The methyl groups are arranged around the sixfold screw axis. A helical chain of the hydrogen bonds between hydroxyl and sulfinyl groups is formed around the threefold screw axis: thus the structure consists of infinite columns parallel to the c axis. The O···O hydrogen-bond distance is 2.63 Å. Intermolecular contacts between adjacent columns are of van der Waals' type; those less than 4 Å are shown in Table 3.

The bond distances and angles are shown in Fig. 3 with their estimated standard deviations. The C(1)–S–O(1), C(9)–S–O(1) and C(1)–S–C(9) angles are 104, 111, and 100°; the corresponding angles in 1,2-dibromo-2-phenylethyl *p*-tolyl sulfoxide (**3**) are 105, 107, and 100°, respectively.[2] The S–O(1) distance is 1.49 Å, which agrees well with those in other sulfoxides.[6,7] The S–C(1) and S–C(9) distances are 1.88 and 1.78 Å. They are different from each other, while in (+)-methyl *p*-tolyl sulfoxide the corresponding S–C lengths are 1.796 and 1.797 Å, respectively.[6] The longer distance of S–C(1) is attributed to the presence of the bromine atom. The corresponding length in **3** is 1.82 Å. The non-bonding intramolecular distances of S···Br is 3.09 Å in **2** and also 3.09 Å in **3**, respectively.

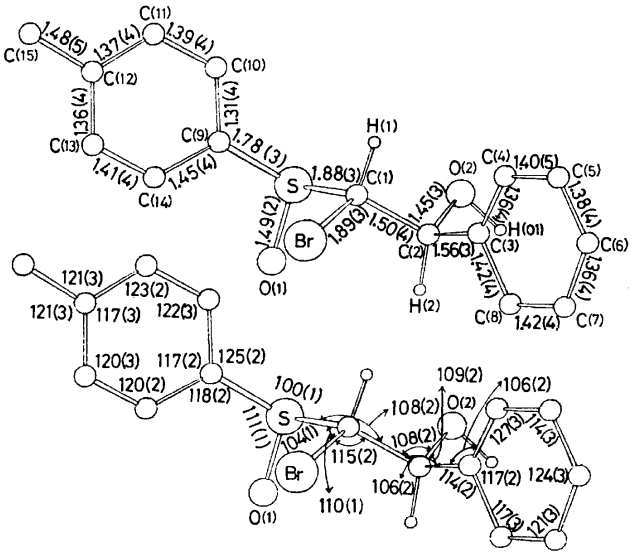

Fig. 3. Bond lengths (Å) and angles (°) with their estimated standard deviations.

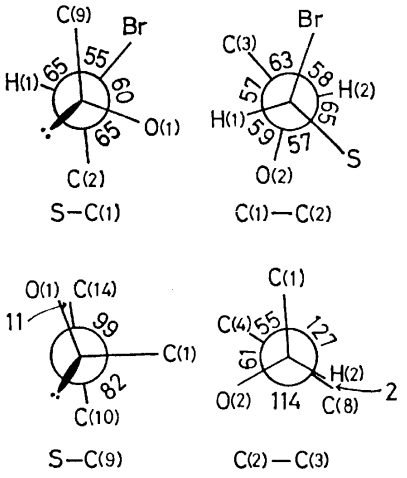

Fig. 4. Torsion angles in the molecule.

The length for C(1)–Br is 1.89 Å, which is slightly shorter than those of **3** (2.00 and 1.98 Å). The average values for C–C bonds in aromatic rings are 1.39 (phenyl) and 1.38 Å (tolyl), respectively. The length of C(12)–C(15) is 1.48 Å. The length of C(2)–O(2) is 1.45 Å, which is very similar to the corresponding values for methanol[8] and 1-hexadecanol.[9]

The least-squares planes are listed in Table 4. The dihedral angle between these planes is 70°.

The torsion angles of groups around the bonds, S–C(1), C(1)–C(2), S(1)–C(9), and C(2)–C(3) are shown in Fig. 4. The sulfinyl oxygen atom is *gauche* to Br across the S–C(1) bond. The torsion angle, O(1)–S–C(1)–Br is 60° and non-bonding distance O(1)···Br is 3.33Å; the corresponding values for **3** is 45° and 3.13 Å, respectively. The bromine atom is *trans* to the hydroxyl oxygen O(2) across the C(1)–C(2) bond. The non-bonding distances, Br···C(3), Br···C(9), S···O(2), and O(1)···C(14), are 3.20, 3.27, 2.97, and 3.02 Å, respectively.

The absolute configuration was unequivocally determined to be *S* at the sulfur atom, *S* at C(1), and *S* at C(2). Therefore the structure of the dominant isomer derived from the electrophilic addition of BrOH to **1** is (+)-(S_S, $S_{C(1)}$, $S_{C(2)}$)-1-bromo-2-hydroxy-2-phenylethyl *p*-tolyl sulfoxide (**2a**). The same assignment has been made earlier on the basis of chemical evidence.[1] Based on the assigned structure of (+)-(S_S, $S_{C(1)}$, $S_{C(2)}$)-**2a**, it can be concluded that the electrophilic addition of BrOH proceeds in the *trans* manner, giving a product in which the bromine atom is in the *gauche* position to the sulfinyl oxygen atom in the adjacent sulfinyl group. A similar result has been obtained for the ionic bromination of **1**. (+)-(S_S, $S_{C(1)}$, $S_{C(2)}$)-1,2-Dibromo-2-phenylethyl *p*-tolyl sulfoxide is formed as a dominant isomer.[2] The selectivity for these additions can be explained in terms of the preferential formation of intermediary bromonium ion (**4a**) rather than **4b**, as is shown in Scheme 2.

Table 4. Least-squares planes

Equation of the plane: $AX+BY+CZ+D=0$, where X, Y and Z are the coordinates in Å referred to the orthogonal axes a, b* and c.

	A	*B*	*C*	*D*
(1) Phenyl ring C(3)—C(8)	0.548	−0.831	−0.100	6.986
(2) *p*-Tolyl ring C(9)—C(14)	0.161	−0.409	0.898	1.473

Deviations (Å×10³) of atom the least-squares planes.

Plane 1		Plane 2	
C(3)	−8	C(9)	−3
C(4)	−2	C(10)	31
C(5)	5	C(11)	−32
C(6)	2	C(12)	3
C(7)	−13	C(13)	30
C(8)	15	C(14)	−27
C(2)[a]	−132	C(15)[a]	51
		S[a]	−48

a) Atoms not used to define the least-squares plane.

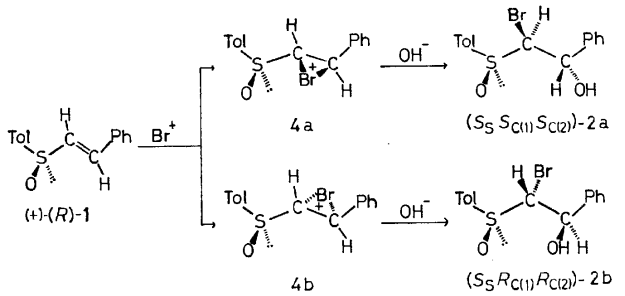

Scheme 2.

All the crystallographic computations were performed on a HITAC 8800 computer of the Computer Center of the University of Tokyo, using the UNICS program system.[10] Figures 1, 2, and 3 were drawn by using the program ORTEP[11] on a CDC 6600 computer at the Century Research Center.

The authors wish to express their thanks to Mr. T. Hori and Mr. K. Ogawa of Rigaku Denki Co. Ltd.

for the use of the diffractometer and for their assistance in the data collection.

References

1) G. Tsuchihashi, S. Mitamura, and K. Ogura, *Tetrahedron Lett.*, **1974**, 455.
2) F. Iwasaki, S. Mitamura, and G. Tsuchihashi, *Bull. Chem. Soc. Jpn.*, **43**, 944 (1975).
3) W. C. Hamilton, *Acta Crystallogr.*, **18**, 502 (1965).
4) "International Tables for X-ray Crystallography," Vol. IV, Kynoch Press, Birmingham (1974), p. 71.
5) Table 2 has been submitted to, and is kept by the Office of the Chemical Society of Japan, 1—5, Kanda-Surugadai, Chiyodaku, Tokyo 101. (Document No. 7622)
6) U. de la Camp and H. Hope, *Acta Crystallogr.*, **B26**, 846 (1970).
7) D. Tranqui and H. Fillion, *Acta Crystallogr.*, **B28**, 3306 (1972); B. Dahlén, *ibid.*, **B29**, 595 (1973).
8) K. J. Tauer and W. N. Lipscomb, *Acta Crystallogr.*, **5**, 606 (1952).
9) S. Abrahamsson, G. Larsson, and E. von Sydow, *Acta Crystallogr.*, **13**, 770 (1960).
10) T. Sakurai, Ed., The Universal Crystallographic Computation Program System, The Crystallographic Society of Japan (1967); T. Sakurai, T. Ito, H. Iwasaki, Y. Watanabe, and M. Fukuhara, *Rep. Inst. Phys. Chem. Res.*, **43**, 62 (1967).
11) C. K. Johnson, ORTEP, Report ORNL-3794, Oak Ridge National Laboratory, Oak Ridge, Tennessee (1965).

Kinetics on the Formylation of Iodobenzene Catalyzed by Palladium(II) Chloride in a Pyridine Solution

Hajime YOSHIDA, Nobuyuki SUGITA,* Kiyoshi KUDO*, and Yoshimasa TAKEZAKI*

Research Institute, Mitsubishi Oil Co., Ltd. ; *Ôgi-machi Kawasaki-ku, Kawasaki-shi 210*

**Institute for Chemical Research, Kyoto University, Gokanosho, Uji-shi 611*

(Received January 31, 1976)

Benzaldehyde was obtained in good yields by the formylation of iodobenzene with carbon monoxide and hydrogen catalyzed by palladium(II) chloride in a pyridine solution. The effect of following variables on the rate of producing benzaldehyde was examined kinetically : initial catalyst and iodobenzene concentrations, partial pressure of carbon monoxide and hydrogen, and temperature. A probable reaction mechanism *via* formyl- and benzoyl-palladium(II) intermediates is discussed on the basis of this kinetic study.

The formylation of halobenzene with carbon monoxide and hydrogen has been recently reported to produce benzaldehyde in the presence of tertiary amine and a catalytic amount of dihalogenobis-(triphenylphosphine)palladium(II)[1] or palladium-black.[2] In both reactions, palladium(0) complex was suggested to be the active species. The formylation of halobenzene differs from the earlier hydroformylation of olefin in respect to the applicable substrate, though both reactions react with carbon monoxide and hydrogen to produce aldehyde. As an example of hydroformylation catalyzed by palladium-(II) chloride or metallic palladium, the production of propanal from ethylene has been known[3] but the yield was low and a considerable amount of ethane was simultaneously produced. In our previous paper,[4] methyl benzoate has been obtained from iodobenzene, carbon monoxide and methanol in the presence of such a tertiary amine as pyridine and a catalytic amount of palladium(II) chloride. In this reaction, the mechanism *via* methoxycarbonyl-palladium(II) intermediate was proposed on the basis of the kinetic study. The formylation is rather analogous to the methoxycarbonylation although hydrogen is placed of methanol, because both reactions demand the addition of amine capable of removing hydrogen halide generated during the reactions.

The formylation of iodobenzene according to Eq. 1, was examined kinetically in a pyridine solution using palladium(II) chloride as the catalyst. Benzaldehyde was obtained in good yields,

$$PhI + CO + H_2 \longrightarrow PhCHO + HI \qquad (1)$$

but the reaction mechanism of the formylation differed from that of methoxycarbonylation.

The purpose of this paper is to describe the results on the formylation of iodobenzene and to discuss its mechanism on the basis of the kinetic study.

Results

Preliminary Investigations. The formylations of some halobenzene were attempted under much the same conditions and the results are shown in Table 1. The maximum yield was obtained when iodobenzene was used as the substrate.

The reactivities of some palladium(II) halide were examined under the same conditions and the results are shown in Table 2. The yield increased to some extent in the order $PdCl_2 < PdBr_2 < PdI_2$. If the active species is palladium(0) complex, the difference of reactivities among palladium(II) halides is difficult to be explained.

In addition to benzaldehyde and pyridine hydroiodide salt, traces of benzene, biphenyl and chlorobenzene were detected in the reaction solutions; refer to the footnote of Table 1. But the sum of amounts of remaining iodobenzene and produced benzaldehyde accounted for over 96% of initial iodobenzene at each reaction time. Thus, the amounts of these by-products were neglected in this study.

The reaction proceeded rapidly in the early stage and then progressed linearly as the time went on; refer to Fig. 1 as an example. The equation $Y = At + B$, where Y and t represent respectively the produced benzaldehyde concentration ($mol \cdot l^{-1}$) and reaction time (min) while A ($mol \cdot l^{-1} \cdot min^{-1}$) and B ($mol \cdot l^{-1}$) are constants, can be applied as the empirical equation for expressing the relationship between time and the produced benzaldehyde concentration after 5—10 min.

The effect of stirring speed on the values of A and B in the empirical equation was examined and the

Table 1. Reaction of Ph-X with CO and H_2

$PdCl_2$ 0.5 mmol, C_5H_5N 20 ml, Initial P_{CO} 50 $kg \cdot cm^{-2}$, Initial P_{H_2} 50 $kg \cdot cm^{-2}$, 140 °C, 90 min, 750 rpm

Ph-X (mmol)	Yield of PhCHO (%)[a]
-Cl (49.1)	10[b]
-Br (47.6)	4.4[c]
-I (44.7)	99[c]

a) Based on the amount of initial Ph-X. b) Trace of PhH was also produced. c) Traces of PhH, Ph-Ph and PhCl were also produced.

Table 2. Reactivity of catalyst PdX_2

PdX_2 0.40 mmol, PhI 49.4 mmol, C_5H_5N 50 ml, P_{CO} 50 $kg \cdot cm^{-2}$ (const.), P_{H_2} 50 $kg \cdot cm^{-2}$ (const.), 130 °C, 60 min, 750 rpm

Catalyst PdX_2	Yield of PhCHO (%)[a]
$PdCl_2$	43
$PdBr_2$	51
PdI_2	61

a) Based on the amount of initial PhI.

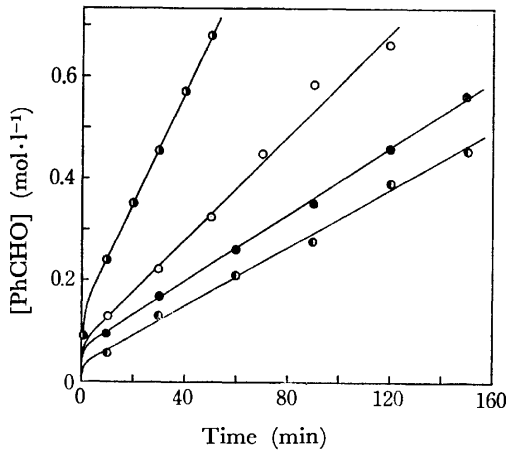

Fig. 1. Relation between time and benzaldehyde concentration.
PhI 0.745 mol·l^{-1}, C_5H_5N 50 ml, P_{CO} 50 kg·cm^{-2} (const.), P_{H_2} 50 kg·cm^{-2}(const.), 130 °C, 750 rpm. Anal. points; ◑ 1.68×10^{-2}, ○ 8.28×10^{-3}, ● 4.49×10^{-3}, ◐ 3.62×10^{-3} mol·l^{-1} initial $PdCl_2$ concn. Curves show the calculated relationships between time and produced benzaldehyde concentration according to Eq. 18.

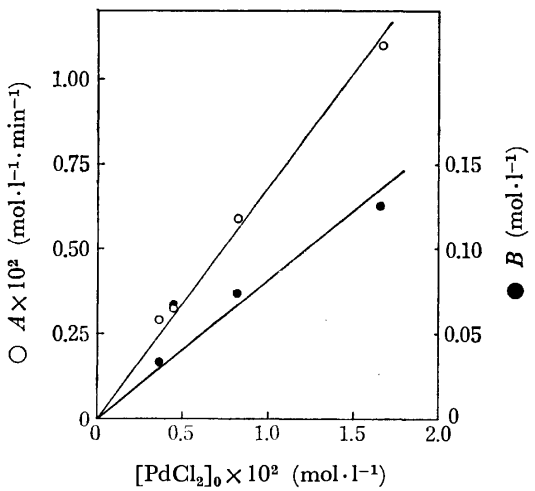

Fig. 2. Relation between $[PdCl_2]_0$ and A or B.
Reaction conditions were shown in the footnote of Fig. 1.

result is shown in Table 3. The value of A was independent of the stirring speeds and the value of B also seemed to be independent of the stirring speeds within an experimental error. Therefore, the reaction may be regarded not to be diffusion-controlled as far as it is carried out under milder conditions than those of Table 3. Henceforwared, the total volume was calculated as the sum of amounts of initial iodobenzene and pyridine.

Kinetic Results. The effects of following variables on the values of A and B in the empirical equation were examined and the results are written in order.

At first, the effect of initial palladium(II) chloride concentration was examined and the result is shown in Fig. 2. Both values of A and B were proportional to the palladium(II) chloride concentration, though the value of B was somewhat insufficient.

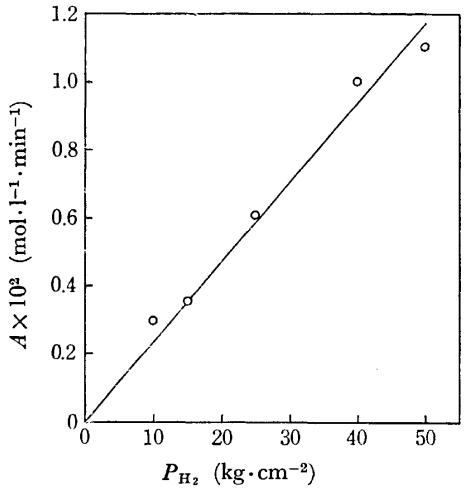

Fig. 3. Relation between P_{H_2} and A.
Reaction conditions were shown in the note of Table 5.

Table 3. Effect of stirring speed
$PdCl_2$ 1.68×10^{-2} mol·l^{-1}, PhI 0.745 mol·l^{-1}, C_5H_5N 50 ml, P_{CO} 50 kg·cm^{-2} (const.), P_{H_2} 50 kg·cm^{-2} (const.), 130 °C

Stirring speed (rpm)	Empirical eq. $Y=At+B$	
	$A\times10^2$ (mol·l^{-1}·min^{-1})	B (mol·l^{-1})
600	1.08	0.140
750	1.09	0.135
750	1.10	0.125
900	1.08	0.113

Table 4. Effect of partial pressure of CO
$PdCl_2$ 1.67×10^{-2} mol·l^{-1}, PhI 0.745 mol·l^{-1}, C_5H_5N 50 ml, P_{H_2} 50 kg·cm^{-2} (const.), 130 °C, 750 rpm

P_{CO} (kg·cm^{-2})	Empirical eq. $Y=At+B$	
	$A\times10^2$ (mol·l^{-1}·min^{-1})	B (mol·l^{-1})
50	1.10	0.125
25	1.18	0.123
10	1.08	0.094

Next, the effect of partial pressure of carbon monoxide was examined and the result is shown in Table 4. The variation in the partial pressure of carbon monoxide did not affect both values of A and B, *i.e.*, the rate is independent of the partial pressure of carbon monoxide. In case of the methoxycarbonylation of iodobenzene the rate was dependent on the carbon monoxide pressure.[4] Thus, this result suggests that the mechanism of formylation is not analogous to that of methoxycarbonylation.

Next, the effect of partial pressure of hydrogen was examined and the result is shown in Fig. 3 and Table 5. The value of A was proportional to the partial pressure of hydrogen irrespective of the other partial pressure of carbon monoxide, as shown in Fig. 3. This result again shows that the rate is independent of the

Table 5. Effect of partial pressure of H_2
$PdCl_2$ 1.68×10^{-2} mol·l^{-1}, PhI 0.745 mol·l^{-1}, C_5H_5N 50 ml, 130 °C, 750 rpm

P_{H_2} (kg·cm^{-2})	P_{CO} (kg·cm^{-2})	Empirical eq. $Y=At+B$	
		$A\times10^2$ (mol·l^{-1}·min^{-1})	B (mol·l^{-1})
50	50	1.10	0.125
40	20	1.00	0.118
25	50	0.609	0.096
15	45	0.353	0.077
10	50	0.296	0.095

Table 6. Effect of initial PhI concentration
$PdCl_2$ 3.66×10^{-3} mol·l^{-1}, C_5H_5N 50 ml, P_{CO} 50 kg·cm^{-2} (const.), P_{H_2} 50 kg·cm^{-2} (const.), 130 °C, 750 rpm

PhI concn (mol·l^{-1})	Empirical eq. $Y=At+B$	
	$A\times10^3$ (mol·l^{-1}·min^{-1})	B (mol·l^{-1})
0.745	2.96	0.041
0.447	3.04	0.049
0.303	2.86	0.047

Table 7. Effect of temperature
$PdCl_2$ 1.70×10^{-2} mol·l^{-1}, PhI 0.745 mol·l^{-1}, C_5H_5N 50 ml, P_{CO} 50 kg·cm^{-2} (const), P_{H_2} 50 kg·cm^{-2} (const.), 750 rpm

Temp (°C)	Empirical eq. $Y=At+B$	
	$A\times10^2$ (mol·l^{-1}·min^{-1})	B (mol·l^{-1})
140[a)]	1.77	0.045
130	1.10	0.125
115	0.577	0.076
100	0.290	0.045

a) P_{CO} 100 kg·cm^{-1} (const.).

partial pressure of carbon monoxide. On the other hand, the value of B hardly changed though the partial pressure of hydrogen changed, as seen in Table 5.

As the reaction proceeded linearly as the time went on except for the early stage, the rate is supposed to be independent of remaining iodobenzene concentration; refer to Fig. 1. The effect of initial iodobenzene concentration was examined and the result is shown in Table 6. The rate was remained constant by the change of initial iodobenzene concentration and this result also differed from that in case of the methoxycarbonylation of iodobenzene.[4)]

Finally, the effect of temperature was examined and the result is shown in Table 7. The rise in temperature caused the increase in the value of A while little affected the value of B.

Discussion

Reaction Mechanism. The following mechanism is assumed;

$$\underset{\mathbf{1}}{PdCl_2(C_5H_5N)_2} + H_2 \xrightarrow{k_2} \underset{\mathbf{2}}{HPdCl(C_5H_5N)_2} + HCl \quad (2)$$

$$\mathbf{2} + CO \xrightarrow{\text{fast}} \underset{\mathbf{3}}{HCOPdCl(C_5H_5N)_2} \quad (3)$$

$$\mathbf{3} + PhI \xrightarrow{\text{fast}} \underset{\mathbf{4}}{PdClI(C_5H_5N)_2} + PhCHO \quad (4)$$

$$\mathbf{4} + H_2 \xrightarrow{k_5} \mathbf{2} + HI \quad (5)$$

$$\mathbf{4} + H_2 \xrightarrow{k_6} \underset{\mathbf{5}}{HPdI(C_5H_5N)_2} + HCl \quad (6)$$

$$\mathbf{5} + C_5H_5N + CO \xrightarrow{\text{fast}} \underset{\mathbf{6}}{Pd(CO)(C_5H_5)_3} + HI \quad (7)$$

$$\mathbf{6} + PhI \xrightarrow{\text{fast}} \underset{\mathbf{7}}{PhCOPdI(C_5H_5N)_2} + C_5H_5N \quad (8)$$

$$\mathbf{7} + H_2 \xrightarrow{k_9} \mathbf{5} + PhCHO \quad (9)$$

$$HCl \text{ or } HI + C_5H_5N \longrightarrow C_5H_6Cl \text{ or } C_5H_6I \quad (10)$$

where k_2, k_5, k_6 and k_9 represent the rate constants of elementary processes (2), (5), (6) and (9), respectively. The elementary processes (3), (4), (7) and (8) are assumed to proceed rapidly, because the rate was independent of iodobenzene concentration and partial pressure of carbon monoxide. The catalytic cycle from (7) to (9) is the same one proposed by Schoenberg and Heck[1)] and Ito *et al.*[2)] The reaction (8) is well known[5,6)] in case of the analogous triphenylphosphine complexes. However, this catalytic cycle cannot explain the following results mentioned before: the difference of reactivities among palladium(II) halides, the production of chlorobenzene and the rapid reaction in the early stage. Thus, the other catalytic cycle from (3) to (5), which bears a resemblance to the mechanism of methoxycarbonylation of iodobenzene,[4)] is assumed to produce benzaldehyde before the catalytic cycle from (7) to (9) proceeds. The existence of complex **2** is known[7)] in case of triphenylphosphine being used as a ligand. On the other hand, the formylpalladium(II) complex **3** is unknown but is probably possible to form during the reaction, because acylpalladium(II) complex is well known[8)] to be formed by the carbonylation of alkylpalladium(II) complex. The catalytic cycle from (3) to (5) corresponds to the part of rapid reaction in the early stage and the other cycle from (7) to (9) corresponds to the most part of reaction which proceeds linearly as the time goes on. The reaction (8) may proceed essentially *via* phenylpalladium intermediate of short lifetime, because the analogous reaction (triphenylphosphine was used in place of pyridine) has been reported[5)] to proceed *via* five co-ordinated phenyl-palladium intermediate. Benzene and biphenyl detected as by-products are probably formed by the attack of hydrogen and iodobenzene on the phenyl-palladium intermediate, respectively. But the reaction (8) is here assumed to be one elementary process, since the amounts of benzene and biphenyl were little enough to be negligiable. Similarly, the reaction (4) too may not always proceed as one ele-

mentary process, because detected chlorobenzene is probably formed by the exchange of halides between the chloride in the intermediate **3** and the iodide in iodobenzene.

Rate Equation. From the reaction mechanism proposed above, the rate equation of producing benzaldehyde can be derived in the following way.

The material balance for palladium can be expressed as,

$$C_1 + C_4 + C_7 = [PdCl_2]_0 \tag{11}$$

where C_n represents the concentration of intermediate ***n*** and $[PdCl_2]_0$ the initial palladium(II) chloride concentration. The rates of decreasing concentration of intermediates **1** and **4** are respectively expressed as,

$$-\frac{dC_1}{dt} = k_2HPC_1 \tag{12}$$

$$-\frac{dC_4}{dt} = k_6HPC_4 - k_2HPC_1 \tag{13}$$

where H and P represent the Henry's constant and partial pressure of hydrogen. From Eqs. 12 and 13, C_1 and C_4 can be obtained as,

$$C_1 = [PdCl_2]_0 e^{-k_2HPt} \tag{14}$$

$$C_4 = \frac{k_2[PdCl_2]_0}{k_{2-6}}(e^{-k_6HPt} - e^{-k_2HPt}) \quad (k_{2-6} \equiv k_2 - k_6) \tag{15}$$

and C_7 can also be obtained from Eqs. 11, 14 and 15.

$$C_7 = [PdCl_2]_0\left(1 + \frac{k_6}{k_{2-6}}e^{-k_2HPt} - \frac{k_2}{k_{2-6}}e^{-k_6HPt}\right) \tag{16}$$

The rate equation of producing benzaldehyde can be given from Eqs. 14, 15 and 16 as,

$$\frac{d[PhCHO]}{dt} = k_2HPC_1 + k_5HPC_4 + k_9HPC_7$$
$$= [PdCl_2]_0HP\left(k_9 - \frac{k_6k_{2-9} - k_2k_{2-5}}{k_{2-6}}e^{-k_2HPt} + \frac{k_2k_{5-9}}{k_{2-6}}e^{-k_6HPt}\right) \tag{17}$$

$(k_{2-9}, k_{2-5}, k_{5-9} \equiv k_2 - k_9, k_2 - k_5, k_5 - k_9)$

where [PhCHO] represents the produced benzaldehyde concentration. Finally, the relationship between time and the produced benzaldehyde concentration is derived from Eq. 17 as follows.

$$[PhCHO] = k_9HP[PdCl_2]_0t + \frac{k_2k_{5-9} + k_6k_{2-9}}{k_2k_6}[PdCl_2]_0 + \frac{k_6k_{2-9} - k_2k_{2-5}}{k_2k_{2-6}}[PdCl_2]_0e^{-k_2HPt} - \frac{k_2k_{5-9}}{k_6k_{2-6}}[PdCl_2]_0e^{-k_6HPt} \tag{18}$$

Analysis of Kinetic Results. The kinetic results are compared with the derived rate equation (18).

Since $\exp(-k_2HPt)$ and $\exp(-k_6HPt)$ in Eq. 18 are quickly drawn close to zero as the time goes on, they are assumed to be zero after about 10 minutes. On this assumption, Eq. 18 can be rewritten as,

$$[PhCHO] = k_9HP[PdCl_2]_0t + \frac{k_2k_{5-9} + k_6k_{2-9}}{k_2k_6}[PdCl_2]_0 \tag{19}$$

and Eq. 19 has the same shape as the empirical equation $Y = At + B$, giving the following relationships.

$$A = k_9HP[PdCl_2]_0 \tag{20}$$

$$B = \frac{k_2k_{5-9} + k_6k_{2-9}}{k_2k_6}[PdCl_2]_0 \tag{21}$$

As seen in Eq. 20, the value of A must be of the first order with respect to the palladium(II) chloride concentration and the partial pressure of hydrogen, as shown in Figs. 2 and 3. On the other hand, as seen in Eq. 21, the value of B must be of the first order with respect to the palladium(II) chloride concentration, as shown in Fig. 2. Accordingly, the kinetic results are sufficiently consistent with the relationships of Eq. 19.

Determination of Rate Constants. The value of k_9H is determined as 1.37×10^{-2} kg^{-1}·cm^2·min^{-1} at 130 °C as the average between 1.35×10^{-2} from the gradient in Fig. 2 and 1.39×10^{-2} in Fig. 3. The value of k_9H at the other temperatures are determined according to Eq. 20 as follows; 2.08×10^{-2}, 6.70×10^{-3} and 3.45×10^{-3} kg^{-1}·cm^2·min^{-1} at 140, 115 and 100 °C, respectively. The temperature coefficient of k_9H is obtained as 14.4 kcal·mol^{-1} from the Arrhenius plot shown in Fig. 4.

The values of other rate constants cannot be determined, but the values of k_2H and k_6H can be estimated roughly in the following way. As the produced benzaldehyde concentration 0.093 mol·l^{-1} at 1 min was observed as seen in Fig. 1, the value of 0.093 mol·l^{-1}·min^{-1} can be regarded to be nearly equal to the initial rate at the palladium(II) chloride concentration 1.7×10^{-2} mol·l^{-1}, the partial pressure of hydrogen 50 kg·cm^{-2} and 130 °C. On the other hand, the initial rate equation can be given from Eq. 17 as,

$$\left\{\frac{d[PhCHO]}{dt}\right\}_0 = k_2HP[PdCl_2]_0 \tag{22}$$

and the value of k_2H is estimated as 0.1 kg^{-1}·cm^2·min^{-1} at 130 °C. Next, the following equation can be

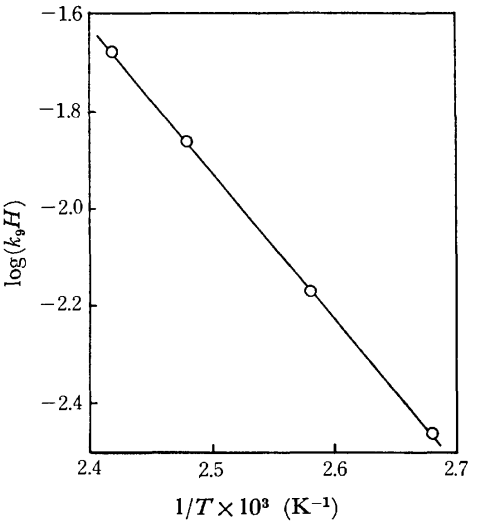

Fig. 4. Arrhenius plot of k_9H.
Reaction conditions were shown in the note of Table 7.

derived from Eq. 21 and the gradient of linear plot between palladium(II) chloride concentration and B in Fig. 2.

$$\left\{\frac{k_2k_{5-9}+k_6k_{2-9}}{k_2k_6}\right\} = 7.4 \quad (23)$$

By assuming that the value of k_5H is equal to that of k_2H because the reaction (5) has a resemblance to the reaction (2), the value of k_6H is estimated as 0.015 $kg^{-1}\cdot cm^2\cdot min^{-1}$ at 130 °C.

From the obtained values of k_2H and k_6H, the values of $\exp(-k_2HPt)$ and $\exp(-k_6HPt)$ can be regarded to be nearly equal to zero after about 10 min.

Calculated Relationship between Time and Benzaldehyde Concentration. Finally, the relationships between time and the produced benzaldehyde concentration which are calculated according to the derived rate equation (18), are compared with the observed ones. As an example, Fig. 1 shows that the calculated relationships are consistent with the observed ones including the part of rapid reaction in the early stage.

As discussed above, the proposed mechanism explains sufficiently the experimental results over the range of this study. Thus, the reaction mechanism is supposed to represent one of possible mechanisms.

Experimental

Materials. Palladium(II) chloride, palladium(II) bromide, palladium(II) iodide and biphenyl were commercially obtained and used without further purification. Iodobenzene, bromobenzene, chlorobenzene, benzaldehyde, benzene, pyridine and tetralin were distilled by means of ordinary methods. Hydrogen was commercial material and was over 99.9% pure. Carbon monoxide was prepared by decomposing formic acid in hot sulfuric acid, and was over 98% pure.

Procedure. Reactions were carried out in a glass-tube placed in a stainless-steel autoclave (*ca.* 200 cm^3) equipped with a Teflon stirrer and a Teflon sampling line. Palladium(II) chloride (0.2—1 mmol), iodobenzene(2—5 ml) pyridine (50—53 ml) and tetralin (5 ml) were placed in the autoclave, which was then purged with nitrogen three or four times. The autoclave was heated up to 100—140 °C within 60 min and then maintained over 20 min at the reaction temperature. Immediately after carbon monoxide and hydrogen mixture was added up to 20—100 $kg\cdot cm^{-2}$, the stirring (750 rpm) was started and this time was marked as zero time. The stirring was stopped from time to time and a sample (*ca.* 1 ml) was withdrawn through the sampling line into a trap chilled in a ice-bath within 30 s. To keep the pressure constant during the reaction, carbon monoxide and hydrogen mixture gas was supplied from the reservoir in which carbon monoxide and hydrogen were mixed beforhand in each fixed ratio.

Analysis. Products were identified by the comparison of their retention times in the gas chromatography with those of authentic samples. An Apiezon Grease L column (2 m, 3 mmϕ) with nitrogen carrier was used at 160 °C for the determination of the amounts of benzaldehyde and iodobenzene with tetralin as an internal standard.

References

1) A. Schoenberg and R. F. Heck, *J. Am. Chem. Soc.*, **96**, 7761 (1974).
2) T. Ito, K. Mori, T. Mizoroki, and K. Ozaki, *Bull. Chem. Soc. Jpn.*, **48**, 2091 (1975).
3) J. Tsuji, N. Iwamoto, and M. Morikawa, *Bull. Chem. Soc. Jpn.*, **38**, 2213 (1965).
4) H. Yoshida, N. Sugita, K. Kudo, and Y. Takezaki, *Nippon Kagaku Kaishi*, **1974**, 1386.
5) K. Kudo, M. Sato, M. Hidai, and Y. Uchida, *Bull. Chem. Soc. Jpn.*, **46**, 2280 (1973).
6) M. Hidai, T. Hikita, Y. Wada, Y. Fujikura, and Y. Uchida, *Bull. Chem. Soc. Jpn.*, **48**, 2075 (1975).
7) K. Kudo, M. Hidai, T. Murayama, and Y. Uchida, *J. Chem. Soc., Chem. Commun.*, **1970**, 1701.
8) G. Booth and J. Chatt, *J. Chem. Soc., A.*, **1966**, 634.

Branched-chain Sugars. VIII. On the Configuration of Branched-chain Sugars from Methyl 3-*O*-Benzoyl-4,6-*O*-benzylidene-α-D-*arabino*-hexopyranosid-2-ulose[1]

Juji YOSHIMURA, Kazutoshi MIKAMI,* Ken-ichi SATO, and Chung-gi SHIN*

Laboratory of Chemistry for Natural Products, Faculty of Science, Tokyo Institute of Technology, Ookayama, Meguro-ku, Tokyo 152

**Laboratory of Organic Chemistry, Faculty of Technology, Kanagawa University, Rokkakubashi, Kanagawa-ku, Yokohama 221*

(Received February 16, 1976)

Stereoselectivities in the Grignard, diazomethane and nitromethane reaction of methyl 3-*O*-benzoyl-4,6-*O*-benzylidene-α-D-*arabino*-hexopyranosid-2-ulose (**1**) were examined. In contrast to the Grignard reaction of **1** using methylmagnesium iodide to give a single 2-*C*-methyl derivative (**4**), the diazomethane reaction followed by reduction afforded another epimer (**6**). The nitromethan condensation product (**10**) of **1** was converted into the corresponding 2-*C*-acetaminomethyl derivative (**13**). The NMR spectrum of 2-*O*-acetate of **4** and comparison of the optical rotations of **4**, **6**, **10** and **13** in cuprammonium solution indicated that **4** and others have D-*gluco*- and D-*manno*-configuration, respectively. Discussions were made on the stereoselectivties of these reactions.

In a previous paper,[2] we reported that the Grignard and nitromethane reaction of methyl 2-*O*-benzoyl-4,6-*O*-benzylidene-α-D-*ribo*-hexopyranosid-3-ulose gave D-*allo*-type branched-chain sugars, while diazomethane reaction afforded a D-*gluco*-type product. In this paper, these reactions of the corresponding 2-ulose were carried out, and the complemental stereoselectivities of the Grignard and diazomethane reaction and a new evidence for the stereoselectivity of nitromethane reaction are described.

Results and Discussion

The starting material; methyl 3-*O*-benzoyl-4,6-*O*-benzylidene-α-D-*arabino*-hexopyranosid-2-ulose (**1**) was synthesized in 87% yield by the oxidation of methyl 3-*O*-benzoyl-4,6-*O*-benzylidene-α-D-glucopyranoside,[3] which was separated in 7% yield as a by-product in the selective synthesis of the corresponding 2-*O*-benzoate reported by Carey and Hodgson.[4] The structure of **1** was clearly supported by the presence of a sharp singlet of H_1 (δ 4.80) and a doublet of H_3 (δ 5.98, $J_{3,4}=10.0$) in the NMR spectrum.

Reaction of **1** with equimolar methyl magnesium iodide at room temperature gave the corresponding 2-*C*-methyl derivative (**2**) in 50% yield, which was then acetylated in the presence of acid catalyst to give 2-*O*-acetate (**3**) quantitatively. The chemical shift (δ 1.91) of methyl protons of the tertiary acetoxy group in **3** indicated that **3** has D-*gluco*-configuration.[5] Treatment of **2** in methanol with barium oxide gave the de-*O*-benzoylated product (**4**) in 37% yield.

On the other hand, reaction of **1** with diazomethane in benzene–ethanol–ether gave quantitatively the corresponding spiro-epoxide (**5**) which was characterized by the presence of an AB quartet of epoxy-methylene protons (δ 2.82 and 2.74, $J=4.0$) in the NMR spectrum. Reduction of **5** with lithium aluminium hydride gave the corresponding 2-*C*-methyl derivative (**6**) in 67% yield. The compound was determined to be 2-epimer of **4** from the physical constants and the optical rotation change in cuprammonium solution[6] (Table 1). Treatment of **5** with barium oxide in methanol gave the corresponding de-*O*-benzoylated product (**8**), and the ring-opening product; methyl 4,6-*O*-benzylidene-2-*C*-methoxymethyl-α-D-mannopyranoside (**7**). These results offer a new instance of the complemental stereoselectivity of the Grignard and diazomethane reactions.[2,7]

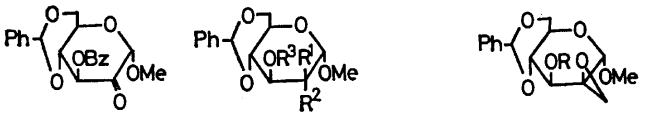

(**1**) (**2**) $R^1=CH_3$ $R^2=OH$ $R^3=Bz$ (**5**) R=Bz
(**3**) $R^1=CH_3$ $R^2=OAc$ $R^3=Bz$ (**8**) R=H
(**4**) $R^1=CH_3$ $R^2=OH$ $R^3=H$
(**6**) $R^1=OH$ $R^2=CH_3$ $R^3=H$
(**7**) $R^1=OH$ $R^2=CH_2OCH_3$ $R^3=H$
(**9**) $R^1=OH$ $R^2=CH_2NO_2$ $R^3=Bz$
(**10**) $R^1=OH$ $R^2=CH_2NO_2$ $R^3=H$
(**11**) $R^1=OH$ $R^2=CH_2NO_2$ $R^3=Ac$
(**12**) $R^1=OH$ $R^2=CH_2NH_2$ $R^3=H$
(**13**) $R^1=OH$ $R^2=CH_2NHAc$ $R^3=H$

Reaction of **1** with nitromethane in tetrahydrofuran at room temperature gave the corresponding 2-*C*-nitromethyl derivative (**9**) and its de-*O*-benzoylated product (**10**) in 12% and 63% yield, respectively. Acid catalyzed acetylation of **10** gave only 3-*O*-acetate (**11**) in 80% yield. Catalytic hydrogenation of **10** gave the corresponding 2-*C*-aminomethyl derivative (**12**), which was then converted into 2-*C*-acetamidomethyl derivative (**13**) quantitatively. In order to determine the configuration of the nitromethane condensation product, optical rotations of **10** and **13** in cuprammonium solution were measured, together with **4** and **6**. The results shown in Table 1 clearly indicate that the epimeric correlation between the Grignard and nitromethane reaction products and also the same configuration of the nitromethane and diazomethane reaction products. From these results, the stereoselectivity of nucleophilic additions indicated that the Grignard reagent attacked the carbonyl group from the less hindered site, while diazomethane and nitromethane from the hindered site.

Excepting a few instances in which an additive attractive factor to magnesium atom is included in the substrate,[8] the same stereoselectivity between the

Table 1. Rotational change of compounds **4**, **6**, **10** and **13** in cuprammonium solution

Compound	$[\alpha]_D^{50\%\ MeOH}$		$[\alpha]_D^{Cupra\ A}$
4	+136°	⟶	+ 60°
6	+ 84°	⟶	+248°
10	+ 94°	⟶	+148°
13	+ 34°	⟶	+144°

Grignard reagent and simple catalytic reductions are generally accepted. As was pointed out in our previous paper,[2] the stereoselectivity of diazomethane reaction is mainly controlled by the attractive force between vicinal (or neighboring) axial-hydroxyl oxygens and diazomethylene cation of zwitterionic intermediate, and consequently, the Grignard and diazomethane reactions show sometimes complemental stereoselectivities.

Concerning the nitromethane condensation, it is known that the stereoselectivity is the same as the reduction or the Grignard reaction in the cases of methyl 4,6-*O*-benzylidene-2-substituted-α-D-*arabino*-hexopyranosid-3-uloses,[2] methyl 3,4-*O*-isopropylidene-β-L-*erythro*-pentopyranosid-2-ulose,[9] 1,2;5,6-di-*O*-isopropylidene-α-D-*ribo*-hexofuranos-3-ulose,[10] while, reversely in the case of methyl 6-deoxy 3,4-*O*-isopropylidene-α-L-*lyxo*-hexopyranosid-2-ulose.[11] Consequently, the last instance and the result obtained here imply the exceptional stereoselectivity of nitromethane condensation. However, it is known that nitromethane condensation gave the epimeric mixtures in various ratios depending upon the conditions used.[9,12] Moreover, similar phenomena in the addition of nucleophiles to enoses[13] and a furanos-3-ulose[14] are explained by isomerization of the kinetically-controlled product into thermodynamically-controlled product. A similar interpretation will be applied to the result of the nitromethane reaction.

In order to pursue the kinetically-controlled D-*gluco*-type product, the reaction was carried out at a lower temperature (−20 °C——78 °C) under monitoring with TLC. The starting material (R_f=0.46 with the solvent system; benzene/acetone=8/1) changed into a compound of R_f=0.18, and then gradually into **9** (R_f=0.35). However, the amount of the intermediate product (R_f=0.18) gradually diminished during the treatment of the reaction mixture at room temperature even after acidification, whereas that of **9** increased. Moreover, the intermediate product isolated with preparative TLC was always contaminated with the monohydrate of **1**. In one instance, a doublet of H_3 (δ 5.04, $J_{3,4}$=11.0) and a quartet of $C_{2'}$-methylene (δ 4.75 and 4.54, J=10.0) and a singlet of H_1 (δ 5.14) were observed in the NMR spectrum of such a product, in addition to the signals of the monohydrate. These chemical shifts are higher than that of **9** (H_3; δ 5.85; $J_{3,4}$=11.0, $C_{2'}$-methylene; δ 4.98 and 4.81, J=11.7, H_1; δ 5.20), and seems to be rational to assign to D-*gluco*-type product.

Experimental

All melting points were uncorrected. The solutions were evaporated under reduced pressure at a bath temperature not exceeding 50 °C. Optical rotations were measured in a 0.5-dm tube with a Carl Zeiss LEP-Al polarimeter. IR spectra were recorded with a Hitachi Model EPI-G2 spectrometer. NMR spectra were taken with JEOL 4H-100 spectrometer in deuteriochloroform containing TMS as an internal reference. Chemical shifts and coupling constants were recorded in δ and Hz units, and IR frequencies in cm^{-1}.

*Methyl 3-O-Benzoyl-4,6-O-benzylidene-α-D-arabino-hexopyranosid-2-ulose (**1**).* The starting material, methyl 3-*O*-benzoyl 4,6-*O*-benzylidene-α-D-glucopyranoside was obtained, from the mother liquor of the corresponding 2-*O*-benzoate prepared by the method of Carey and Hodgson,[4] in 7% yield which was recrystallized from acetone (mp 216—218 °C). The structure was confirmed by elemental analysis and the NMR spectrum of the corresponding 3-*O*-acetate (mp 154 °C, lit,[3] mp 153—154 °C); NMR: 1.9—2.8 (Ph, m), 5.82 (H_3; t, $J_{2,3}$=9.2), 5.48 (methine H; s), 5.11 (H_2; q; $J_{2,3}$=10.0), 4.96 (H_1; d, $J_{1,2}$=4.0), 4.31 ($H_{5,6e}$=4.0), 3.98 (H_5; sex, $J_{5,6a}$=10.0), 3.78 (H_4; t, $J_{4,5}$=9.2), 3.86 (H_{6a}; t, $J_{6a,6e}$=9.2), 3.42 (OMe), 1.96 (OAc).

A solution of the starting material (5.0 g, 12.9 mmol) in DMSO (50 ml) and acetic anhydride (30 ml) was kept at room temperature for 10 h, and then poured into ice-water. The resulting solution was neutralized with 2 M potassium carbonate, and then extracted with chloroform. Treatment of the chloroform extract in a usual manner gave a sirup, which was crystallized and recrystallized from acetone–water to give needles (4.5 g, 86.9%) of the monohydrate of **1**. Mp 136—137 °C; $[\alpha]_D^{17}$ +36.4° (*c* 0.75, $CHCl_3$); IR; 3530 and 3500 (OH), 1720 (ester).

Found: C, 63.08; H, 5.45%. Calcd for $C_{21}H_{20}O_7 \cdot H_2O$; C, 62.68; H, 5.51%.

Dehydration of the above hydrate at 100 °C/15 mmHg for 2 h gave again a sirupy **1**. $[\alpha]_D^{16}$ +35.0° (*c* 1.15, $CHCl_3$); IR: 1750 (C=O), 1720 (ester); NMR: 2.0—2.8 (Ph; m), 5.98 (H_3; d, $J_{3,4}$=10.0), 5.53 (methine H; s), 4.80 (H_1: s), 4.44 (H_{6e}; q, $J_{6a,6e}$=11.5), 4.26 (H_5: sex, $J_{5,6e}$=4.2), 4.05 (H_4; t, $J_{4,5}$=10.0), 3.83 (H_{6a};t,$J_{5,6a}$=11.5), 3.47 (OMe).

Found; C, 65.26; H. 5.35%. Calcd for $C_{21}H_{20}O_7$; C, 65.61; H, 5.24%.

*Methyl 3-O-Benzoyl-4,6-O-benzylidene-2-C-methyl-α-D-gluco-pyranoside (**2**).* To a solution of methylmagnesium iodide in ether (5 ml) prepared from magnesium turnings (60 mg, 2.47 mmol) and methyl iodide (5 ml) was added **1** (1 g, 2.6 mmol) in benzene (5 ml), and the reaction mixture was refluxed for 1.5 h, poured into cold ammonium chloride solution, and the resulting solution was extracted with methylene chloride. The extract was washed with water and evaporated to give a white powder which was crystallized from methanol–petroleum ether. Yield, 510 mg(49%). Mp 150—152 °C; $[\alpha]_D^{22}$ +17.6° (*c* 0.5, 50% MeOH); IR: 3610 (OH), 1750 (ester), 1595 (Ph); NMR: 8.2—7.2 (Ph; m), 5.67 (H_3; d, J=10.5), 5.51 (methine; s), 4.48 (H_1, s), 4.33 (H_{6e}; q, $J_{6e,5}$=4.0, $J_{6e,6a}$=10.0), 4.10—3.65 (H_4, H_5, H_{6a}; m), 3.46 (OMe), 2.74 (OH, broad s), 1.44 (*C*-Me; s).

Found; C, 66.18; H, 6.08%. Calcd for $C_{22}H_{24}O_7$: C, 65.99; H, 6.04%.

Acetylation of **2** with acetic anhydride in the presence of catalytic amount of *p*-toluenesulfonic acid gave the corresponding 2-*O*-acetate (**3**) in a quantitative yield, which was recrystallized from ethanol–hexane. Mp 163—165 °C; $[\alpha]_D^{22}$ +32.7° (*c* 0.5, acetone); IR: 1730 and 1720 (ester), 1600 (Ph); NMR: 8.2—7.2 (PH; m), 5.86 (H_3; d, $J_{3,4}$=10.0), 5.49 (methine; s), 5.46 (H_1; s), 4.30 (H_{6a}; q, $J_{6e,5}$=4.0, $J_{6a,6e}$=9.0), 4.15—3.65 (H_4, H_5, H_{6a}; m), 3.39 (OMe), 1.91 (OAc), 1.76 (*C*-Me; s).

Found: C, 65.29; H, 6.19%. Calcd for $C_{24}H_{26}O_8$: C, 65.15; H, 5.92%.

Methyl 4,6-O-Benzylidene-2-C-methyl-α-D-glucopyranoside (4). A suspension of **2** (400 mg, 1 mmol) and barium oxide (400 mg, 2.5 mmol) in methanol (20 ml) was refluxed for 30 min, filtered, and then evaporated. The residue was extracted with methylene chloride, and the extract was treated in a usual manner to give a sirup which was purified on a silica gel column (benzene/methanol/etheyl actate=5/1/1). The purified sirup (110 mg, 37.2%) crystallized slowly on standing. Mp 55—56 °C; $[\alpha]_D^{21}$ +92.2° (*c* 0.25, 50% MeOH); IR: 3450 (OH); NMR: 7.6—7.2 (Ph, m), 5.46 (methine, s), 4.36 (H_1; s), 4.22 (H_{6e}; q, $J_{6e,5}$=2.5, $J_{6e,6a}$=7.5), 3.95—3.3 (H_3, H_4, H_5, H_{6a}; m), 3.37 (OMe), 3.05 and 2.75 (2× OH; each broad s), 1.28 (*C*-Me, s).

Found: C, 60.54; H, 6.78%. Calcd for $C_{15}H_{20}O_6$; C, 60.80; H, 6.80%.

Methyl 2,2'-Anhydro-3-O-benzoyl-4,6-O-benzylidene-2-C-hydroxymethyl-α-D-mannopyranoside (5). To a suspension of **1** (200 mg, 0.52 mmol) in benzene (40 ml)–ethanol (6 ml) was added dropwise a solution of diazomethane (1 mmol) in ether (30 ml) at O °C. With proceeding the reaction, the mixture turned to be homogeneous. After standing the mixture at 0 °C for 3 h, the solution was evaporated, and the resulting sirup crystallized gradually. The crystals were recrystallized from ethanol to give colourless needles in a quantitative yield. Mp 144 °C; $[\alpha]_D^{23}$ +13.1° (*c* 1.0, acetone); IR: 1720 (ester), 1590 and 710 (Ph); NMR: 8.12—7.22 (Ph and PhCO; m), 6.01 (H_3; d, $J_{3,4}$=10.0), 4.34 (H_{6e}; q, $J_{6e,6a}$=8.8, J_{6e}=3.7), 4.23 (H_1, s), 4.10 (H_4; t, $J_{4,5}$= 8.2), *ca.* 4.08 (H_5, m), 3.88 (H_{6a}; q, $J_{6a,5}$=9.8), 3.41 (OMe), 2.82 and 2.74 (CH_2; ABq, J=4.0).

Found: C, 66.13; H, 5.62%. Calcd for $C_{22}H_{22}O_7$: C, 66.32; H, 5.57%.

Methyl 4,6-O-Benzylidene-2-C-methyl-α-D-mannopyranoside (6). To a solution of **5** (200 mg, 0.5 mmol) in ether (20 ml) was added lithium aluminium hydride (60 mg), and the mixture was stood at room temperature for 1 h. The excess hydride was carefully decomposed with water, and the water layer was extracted with ether. The combined ether extract was washed with water, dried, and evaporated to give a colorless needles which were recrystallized from ethanol–hexane. Yield, 100 mg (67.2%); mp 149—150 °C; $[\alpha]_D^{22}$ +39.1° (*c* 0.5, 50% MeOH); IR: 3450 and 3370 (OH), 1450 and 700 (Ph).

Found: 61.14; H, 6.78%. Calcd for $C_{15}H_{20}O_6$: C, 60.80; H, 6.80%.

Methyl 2,2'-Anhydro-4,6-O-benzylidene-2-C-hydroxymethyl- (8) and 4,6-O-benzylidene-2-C-methoxymethyl-α-D-mannopyranoside (7). A suspension of **5** (200 mg, 0.5 mmol) and barium oxide (200 mg, 1.25 mmol) in methanol (20 ml) was refluxed for 30 min, filtered, and then evaporated. A solution of the residue in methylene chloride was washed with water, dried, and evaporated to give a sirup which showed two spots on tlc (R_f=0.4 and 0.2; benzene/methanol/ethyl acetate= 5/1/1). The two products were separated on a silica gel column, to give **8** (R_f=0.4; 35 mg, 23.7%) and **7** R_f=0.2; 30 mg, 18.3%).

Compound **8**: mp 160—162 °C; $[\alpha]_D^{21}$ +77.4° (*c* 0.25, CH_2Cl_2); IR: 3300 (OH), 3000 (epoxy methylene); NMR: 7.5—7.2 (Ph; m), 5.52 (methine; s), 4.35—4.15 (H_{6e}, H_4; m), 4.19 (H_1; s) 3.77 (H_5; sex, $J_{6e,5}$=4.0, $J_{5,6a}$=$J_{5,4}$=10.0), 3.82 (H_3; d, $J_{3,4}$=9.5), 3.16 (H_{6a}; t, $J_{6a,6e}$=8.0), 3.36 (OMe), 3.13 and 2.70 (CH_2; ABq, J=5.0), 2.05 (OH).

Found; C, 61.09; H, 6.35%. Calcd for $C_{15}H_{18}O_6$: C, 61.21; H, 6.17%.

Compound **7**: mp 163—165 °C; $[\alpha]_D^{22}$ +50.6° (*c* 0.58, CH_2Cl_2); IR: 3470 (OH); NMR: 7.5—7.2 (Ph, m), 5.53 (methine, s), 4.55 (H_1; s), 4.3—4.2 (H_4), 3.9—3.75 (H_{6e}, H_{6a}, H_5, H_3; m), 3.70 and 3.51 (CH_2; ABq, J=11.0), 3.36 and 3.35 (2×OMe), 3.08 and 2.85 (2×OH).

Found: C, 58.69; H, 6.68%. Calcd for $C_{16}H_{22}O_7$; C, 58.88; H, 6.80%.

Methyl 3-O-Benzoyl-4,6-O-benzylidene-2-C-nitromethyl-α-D-mannopyranoside (9). To a solution of nitromethane (5 ml) in tetrahydrofuran (5 ml) were added successively sodium methoxide (Na; 0.07 mmol) and **1** (1 g, 2.6 mmol) with stirring, and the resulting solution was stirred for 6.5 h at room temperature, neutralized with acetic acid (70%), extracted with chloroform. The extract was washed with water, dried, and evaporated to give colorless prisms which were recrystallized from ethanol, and **9** was separated from the corresponding de-*O*-benzoylated compound (**10**) by fractional crystallization from ethanol. Yield, 140 mg (12.1%); mp 221—223 °C; $[\alpha]_D^{22}$ +90.0° (*c* 1.0, acetone); IR: 3450 (OH), 1750 (ester), 1545 (NO_2); NMR; 8.10—7.20 (Ph and PhCO; m), 5.85 (H_3; d, $J_{3,4}$=11.0), 5.49 (CH_2; s), 5.20 (H_1; S), 4.98 and 4.81 (CH_2; ABq, J=11.7), 4.35 (H_{6e}; q, $H_{6a,6e}$=10.0, $J_{6e,5}$=5.0), 4.02 (H_5; m), 3.82 (H_4; t, $J_{4,5}$=11.0), 3.60 (H_{6a}; t, $J_{6a,5}$=10.0), 3.52 (OMe), 3.16 (OH).

Found: C, 59.66; H, 5.25; N, 3.17%. Calcd for $C_{22}H_{23}NO_9$: C, 59.32; H, 5.21; N, 3.14%.

Methyl 4,6-O-Benzylidene-3-C-nitromethyl-α-D-mannopyranoside (10): Yield, 55.5 mg (62.5%); mp 244—245 °C; $[\alpha]_D^{22}$ +40.0° (*c* 1.0, acetone); IR: 3500 and 3400 (OH), 1560 (NO_2).

Found: C, 52.80; H, 5.60; N, 3.91%. Calcd for $C_{15}H_{19}NO_8$: C, 52.78; H, 5.61; N, 4.10%.

Methyl 3-O-Acetyl-4,6-O-benzylidene-2-C-nitromethyl-α-D-mannopyranoside (11). Acid Catalyzed acetylation of **10** (100 mg) at room temperature and recrystallization of the product from ethanol–hexane gave the 3-*O*-acetate in 80.1% (90 mg) yield. Mp 196—197 °C; $[\alpha]_D^{22}$ +22.8° (*c* 0.5, acetone); IR: 3400 (OH), 1708 (ester), 1542 (NO_2); NMR: 7.5—7.25 (Ph; m), 5.51 (methine, s), 5.35 (H_3; d, J= 10.0), 4.76 (H_1; s), 4.72 and 4.43 (CH_2; ABq, J=12.0), 4.4—3.8 (H_4, H_5, H_{6a}, H_{6e}; m), 3.43 (OMe), 2.10 (OAc), 1.63 (OH).

Found: C, 52.99; H, 5.47; N, 3.60%. Calcd for $C_{17}H_{21}NO_9$: C, 53.26; H, 5.52; N, 3.65%.

Methyl 2-C-Aminomethyl-4,6-O-benzylidene-α-D-mannopyranoside (12). Hydrogenation of **10** (500 mg) in ethanol in the presence of palladium-charcoal (10%), and cryrestallization of the product from ethanol–hexane gave prisms in 57% (260 mg) yield. Mp 170 °C; $[\alpha]_D^{22}$ +55.2° (*c* 1.0, acetone); IR: 3500 and 3600 (OH), 3290 (NH_2).

Found: C, 57.98; H, 6.87; N, 4.63%. Calcd for $C_{15}H_{21}NO_6$: C, 57.86; H, 6.80; N, 4.50%.

Methyl 2-C-Acetamidomethyl-4,6-O-benzylidene-α-D-mannopyranoside (13). Acetylation of **12** with acetic anhydride in ethanol and recrystallization of the product from ethanol–hexane gave the *N*-acetate in a quantitative yield. Mp 204—205 °C; $[\alpha]_D^{22}$ +34.0° (*c* 0.5, 50% MeOH); IR: 3540 (OH), 3300 (NH), 1635 and 1540 (amide).

Found: C, 58.31; H, 6.69; N, 3.79%. Calcd for $C_{17}H_{23}NO_7$: C, 57.78; H, 6.56; N, 3.96%.

The authors are grateful to Mr. Hitoshi Matsumoto for NMR measurements, and members of Laboratory of Organic Analysis for elemental analysis.

References

1) Part VII, *Carbohyd. Res.*, **44**, 275 (1975).

2) J. Yoshimura, K. Sato, K. Kobayashi, and C. Shin, *Bull. Chem. Soc. Jpn.*, **46**, 1806 (1973).
3) G. W. Jeanloz and D. A. Jeanloz, *J. Am. Chem. Soc.*, **79**, 2579 (1957).
4) F. A. Carey and K. O. Hodgson, *Carbohyd. Res.*, **12**, 463 (1970).
5) F. W. Lichtenthaler and P. Emig, *Tetrahedron Lett.*, **1967**, 577.
6) R. E. Reeves, *Adv. Carbohyd. Chem.*, **6**, 131 (1951).
7) J. P. Horwitz, N. Mody, and R. Gasser, *J. Org. Chem.*, **35**, 2335 (1970).
8) J. Yoshimura, Y. Ohgo, K. Ajisaka, and Y. Konda, *Bull. Chem. Soc. Jpn.*, **45**, 916 (1972); M. L. Wolfrom and S. Hanessian, *J. Org. Chem.*, **27**, 1800 (1962); J. S. Burton, W. G. Overend, and N. R. Williams, *J. Chem. Soc.*, **1965**, 3433.
9) S. W. Gunner, R. D. King, W. G. Overend, and N. R. Williams, *J. Chem. Soc.*, **1970**, 1954; R. J. Ferrier, W. G. Overend, G. A. Raffery, H. M. Wall, and N. R. Williams, *ibid.*, **1968**, 1091.
10) J. Yoshimura, K. Kobayashi, K. Sato, and M. Funabashi, *Bull. Chem. Soc. Jpn.*, **45**, 1806(1972); H. P. Albrecht and J. G. Moffatt, *Tetrahedron Lett.*, **1970**, 1063; A. Rosenthal, K. S. Ong, and D. Baker, *Carbohyd. Res.*, **13**, 111 (1970).
11) P. M. Collins and W. G. Overend, *J. Chem. Soc.*, **1965**, 1912.
12) F. W. Lichtenthaler, *Angew. Chem.*, **76**, 84 (1964); J. C. Sowden *Adv. Carbohyd. Chem.*, **6**, 291 (1951).
13) T. Sakakibara and R. Sudo, *J. Org. Chem.*, **40**, 2823 (1975); *J. Chem. Soc., Chem. Commun.*, **1974**, 69.
14) J. M. Bourgeois, *Helv. Chim. Acta*, **56**, 2880 (1973).

Mechanism of the Reaction of Methoxycarbonylcarbene as Revealed by CIDNP. V. Thermal Reaction of Methyl Diazoacetate with Benzyl Ethers

Hiizu IWAMURA, Yuzo IMAHASHI, Katsuhiko KUSHIDA,* Kiyoshi AOKI,* and Shiroh SATOH*

Department of Chemistry, Faculty of Science, The University of Tokyo, 7-3-1 Hongo, Bunkyo-ku, Tokyo 113

**Application Laboratory, Nippon Electric Varian, Ltd., 5-8-1 Yotsuya, Fuchu, Tokyo 183*

(Received February 26, 1976)

When methyl diazoacetate is allowed to react thermally with dibenzyl, benzyl phenyl and benzyl ethyl ethers, insertion into the benzylic carbon-oxygen bonds takes place *inter alia* to give $PhCH_2CH(OR)CO_2CH_3$(**3**, R=$PhCH_2$, Ph, and CH_3CH_2, respectively). Strongly polarized signals due to the insertion products **3** were observed in the ^1H and ^{13}C NMR spectra of the reacting mixture. Application of Kaptein's rules to the CIDNP signals demonstrates the formation of **3** by the cage recombination of radical pairs $\overline{PhCH_2\cdot\cdot CH(OR)CO_2CH_3}$ (**2**). Product analyses by VPC have also been performed and escape products toluene and $ROCH_2CO_2CH_3$ (**4**) inherent to the radical pairs were detected. In the reaction with benzyl ethyl ether, **4** (R=$PhCH_2$) without noticeable CIDNP is produced about six times more than **4** (R=CH_3CH_2). No methyl α-benzyloxybutyrate is formed. The results indicate that the ethyl group is more easily cleaved than the benzyl *via* a non-radical path. Formation of an ylide intermediate $(PhCH_2)R\overset{\oplus}{O}-\overset{\ominus}{C}HCO_2CH_3$ (**1**, R=CH_3CH_2) followed by the Hoffmann type β-elimination of ethylene is the most reasonable explanation. Homolysis of the same ylide **1** is considered to give the radical pair **2** (R=CH_3CH_2). A similar process appears to lead solely to radical pairs **2** (R=$PhCH_2$, Ph) in the case of ylides lacking β-hydrogen. The potentiality of this ylide mechanism in the reactions of ethers is discussed.

In contrast to nearly random insertion of methylene into various C–H bonds, the reaction of electrophilic alkoxycarbonylcarbene with ethers is characterized by two types of reactions, namely, the insertion reaction into the C–O bonds and the displacement reaction of one of the alkyl groups. There are several *a priori* mechanisms conceivable for these reactions. A widely quoted one is the electrophilic attack of the carbene at the lone pair of electrons to form an ylide intermediate which then undergoes the Stevens rearrangement and/or the Hoffmann type β-elimination of an olefin (Scheme 1). However, the experimental supports so far obtained for the mechanism are limited and not conclusive.[1)]

Recent mechanistic studies disclosed the mechanism of the Stevens rearrangement of ammonium and sulfonium ylides;[2)] it is not a simple ionic intramolecular process but a homolysis-recombination one. Accordingly radical pairs $\overline{R\cdot\ \cdot CH(OR')CO_2R''}$ might play an important role in the present case and the inserted and/or displaced products might be derived from recombination and/or disproportionation or hydrogen abstraction after diffusion (broken lines, Scheme 1).

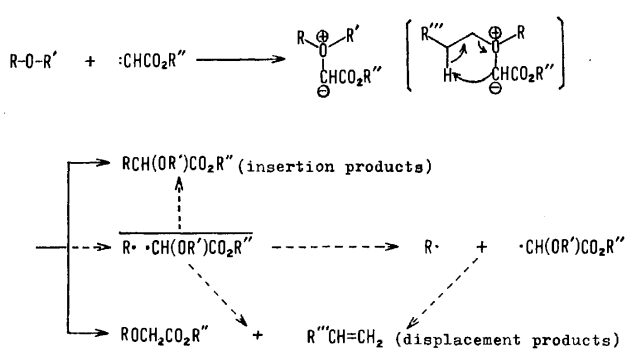

Scheme 1.

In order to confirm these possibilities, we chose the CIDNP technique which is considered to provide direct verification of intermediacy of radical pairs for a particular product of interest. A minor preference was given to the ESR method by which we can prove the presence of radical species but can not obtain anything definite about the manifold reaction paths. Methyl diazoacetate was allowed to react with benzyl ethers in the heated NMR probe. Benzyl ethers were selected because of their simple NMR spectra and their high boiling points sufficient to generate the carbene thermally, in spite of the complexity of the reaction caused by the addition of the carbene to the aromatic ring. Standard product analyses by means of VPC were also made to determine the composition of the products.

Results

CIDNP Spectra. The 60 MHz proton NMR spectra obtained during the course of thermal decomposition of *ca.* 10 vol % solutions of methyl diazoacetate (MDA) in dibenzyl, benzyl phenyl, and benzyl ethyl ethers at 180 °C are shown in Figs. 1a, 1b, and 1c, respectively. A strong emissive signal (denoted by E) is seen in the δ 2.9—3.1 region in each ether solution. By comparison of the chemical shifts with those of authentic samples, these emission signals are assigned to the *C*-benzyl methylene protons (A_2 parts of approximately A_2X patterns) of insertion products, methyl α-benzyloxyhydrocinnamate (**3a**), α-phenoxyhydrocinnamate (**3b**), and α-ethoxyhydrocinnamate (**3c**). The large difference in intensity of the lower and higher field halves is due to the superposition of multiplet effect of E/A phase on net emission. The enhanced absorption singlet (denoted by A) at higher field is assigned to the methyl protons of toluene. In addition we see enhanced abosprtion at the shoulder on the high-field side of the benzylic methylene proton signals of the solvent (Fig. 1a) and the corresponding

Table 1. Product analyses of the reactions of methyl diazoacetate with dibenzyl, benzyl phenyl, and benzyl ethyl ethers by VPC

Types of products	Products	Yields (%) R=CH_2Ph	R=Ph	R=CH_2CH_3
Recombination	$PhCH_2CH(OR)CO_2CH_3$	6.9	2.7	9.4
	$RCH(OCH_2Ph)CO_2CH_3$	—	≪0.1	≪0.1
Escape	$PhCH_3$	2.8	0.6	2.1
	$ROCH_2CO_2CH_3$	3.1	0.2	0.9
Hoffmann-type	$PhCH_2OCH_2CO_2CH_3$	—	—	5.6
C-H insertion	$PhCH(OR)CH_2CO_2CH_3$	4.2	0.8	3.0
	$CH_3CH(OCH_2Ph)CH_2CO_2CH_3$	—	—	5.4
	$PhCH_2O(CH_2)_3CO_2CH_3$	—	—	1.6

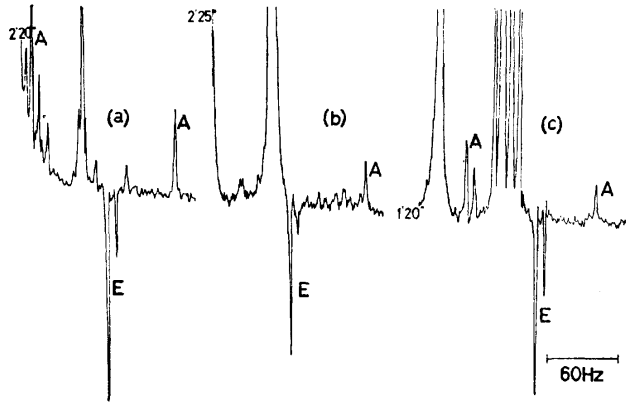

Fig. 1. The 60 MHz ^1H NMR spectra taken during thermal decomposition at 180 °C of *ca.* 10 vol% methyl diazoacetate in (a) dibenzyl ether, (b) benzyl ethyl ether, and (c) benzyl ethyl ether. The time when cw scanning of 600 Hz/200 s was started after insertion of the samples into the NMR probe is indicated.

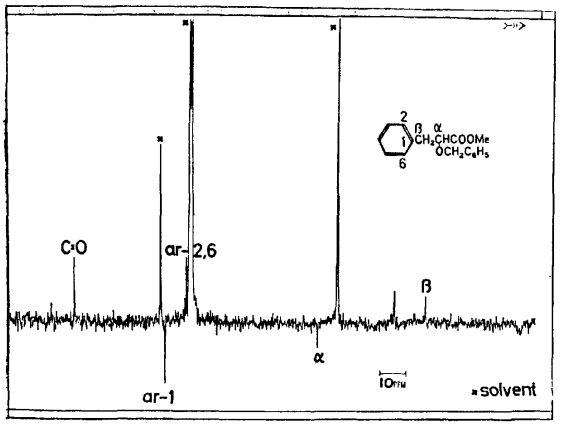

Fig. 2. The 20.1 MHz ^{13}C spectrum taken during the thermolysis at 170 °C of a 15 wt% solution of methyl diazoacetate in dibenzyl ether. The free induction decay signal was accumulated 1200 times on three portions of the batch solution.

enhanced absorption between the solvent signals (Fig. 1c). Their chemical shifts correspond to those of methine protons (X part of A_2X spins) of **3a** and **3c**. In the latter case, the lowest-field signal out of the triplet almost disappears as a result of the superposition of E/A multiplet effect. When the reactions are over,

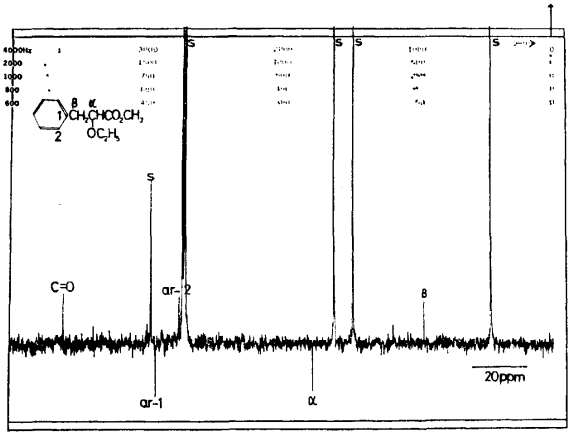

Fig. 3. The 20.1 MHz ^{13}C spectrum taken during the thermolysis at 170 °C of a 6 wt% solution of methyl diazoacetate in benzyl ethyl ether. The free induction decay signal was accumulated 2000 times on four portions of the batch solution. S denotes solvent signal.

all the polarized signals collapse and nothing can be seen except those of the solvents unless the H_1 level and sensitivity of a spectrometer are increased.

The pulse Fourier transform ^{13}C spectra (20.1 MHz) taken during the course of thermolysis of MDA in dibenzyl and benzyl ethyl ethers are reproduced in Figs. 2 and 3, respectively. The spectra are time-averaged for *ca.* 800 s from 500 s after the start of the reaction (see Experimental). The emission signals at 10.8 and 68.5 ppm (down field from the benzylic carbon signal of solvent dibenzyl ether) are assigned to the α and aromatic C-1 carbon atoms of **3a** (Fig. 2). The enhanced absorption signals at −33.2, 56.9, and, 99.1 ppm are found to be due to the β, aromatic C-2 (C-6), and carbonyl carbon atoms of **3a**. Relatively high intensity of polarized signals in spite of the low yield of **3a** (*vide infra*) as compared with those of solvent indicates a considerably large enhancement ($\sim 10^2$). The emission signals at 65.5 and 7.9 ppm (down field from the benzylic carbon signal of solvent benzyl ethyl ether) are due to aromatic C-1 and α-carbons of **3c** (Fig. 3). The enhanced absorption signals at 99.3, 56.8 and −33.1 ppm are assigned to the carbonyl, aromatic C-2 (C-6), and β-carbons, respectively, of **3c**.

Reaction Products. Table 1 shows the results of product analyses by VPC for the reaction of MDA in

Table 2. Theoretical and observed signs of CIDNP

Product	Nucleus	μ	ε	Δg	A_i	Signs	
						Theoret	Observed
$PhCH_2CHCO_2CH_3$ | OR	CH	−	+	+	−	A (+E/A)	A (+E/A)
	CH_2	−	+	−	−	E (+E/A)	E (+E/A)
	α-C	−	+	+	+	E	E
	β-C	−	+	−	+	A	A
	ar C-1	−	+	−	−	E	E
	ar C-2	−	+	−	+	A	A
	C=O	−	+	+	−	A	A
$PhCH_3$	CH_3	−	−	−	−	A	A

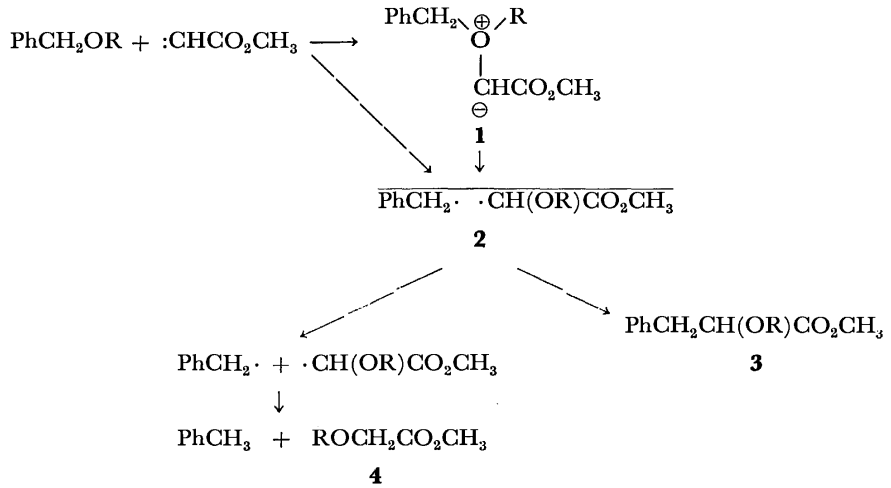

Scheme 2.

dibenzyl, benzyl phenyl, and benzyl ethyl ethers, respectively, at 170 °C for 1 h. The products are classified with respect to the type of reaction from which they were derived. All the possible C–H insertion products are formed in moderate yields.[3] The mass balance is not satisfactory since the main reaction of methoxycarbonylcarbene to give norcaradiene or cycloheptatriene derivatives *via* the addition to the aromatic rings is not taken into account. Peaks probably due to these products appear near or beyond the peaks due to the products analysed. Most values are accurate within 10%, some exceeding the limit because of the low yield and/or incomplete separation of the VPC peaks.

Discussion

All the spectral results are consistent with the formation of the singlet geminate radical pairs $\overline{PhCH_2\cdot\ \cdot CH(OR)CO_2CH_3}$ (**2**, **a**; R=$PhCH_2$, **b**; R=Ph, **c**; R=CH_3CH_2) followed by cage recombination to give the C–O insertion products **3**. The signs of net polarization (Γ_{ne}+ for absorption and−for emission) are given by $\Gamma_{ne}=\mu\varepsilon\Delta g A_i$ according to the first order treatment of Kaptein,[4] where μ, ε and A_i labels indicate the multiplicity of the precursor (−for singlet precursor), the type of the products (+for cage recombination) and the sign of hyperfine coupling of the nucleus i under consideration, respectively. Radicals $\cdot CH(OR)CO_2CH_3$ are assumed to have a *g*-value not far from 2.0036 of analgous radical $\cdot CH(OH)CO_2H$,[5] while the *g*-value of benzyl radical is 2.0025.[6] The methylene protons of insertion products **3**, for example, reside in the component of the pair which has a smaller *g*-value, their hyperfine coupling constant being negative (−16.3 gauss).[7] Their polarization is predicted to be emission when the insertion products are formed by the cage recombination (ε, +) of the singlet radical pair (μ, −). Similarly the polarization of the carbonyl carbons of **3** which are on the component with larger *g*-value of the radical pairs and possess negative hyperfine coupling constants[8] is considered to be an ehnanced absorption (Γ_{ne}=−−+−=+). The agreement between the theory and the observed signs of CIDNP is satisfactory (Table 2). There is no doubt about the intermediacy of radical pairs **2** for the formation of the insertion products.

The product distributions also support the above conclusion. Toluene and $ROCH_2CO_2CH_3$ (**4**) are formed in less than one fourth the amount of the insertion products **3** and are quite natural as escape products of radical pairs **2**. Their formation is difficult to justify by other routes. The observed enhanced absorption of the methyl protons of toluene is consistent with such a mode of formation (Table 2). Emission is expected for the methylene protons of $ROCH_2CO_2CH_3$ but can not be detected. The question is now where the radical pairs **2** come from.

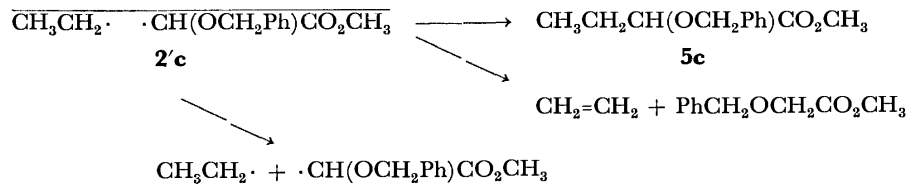

Scheme 3.

Two alternatives are possible, namely, direct abstraction of an alkoxy group OR by the carbene or homolysis of the oxonium ylides **1** which in turn are formed by electrophilic attack of the carbene at the lone pair of electrons (Scheme 2). A clue to the proper selection can be found from Table 1.

Benzyl phenyl ether gives each type of products in fairly lower yields as compared with those of other ethers. The reduced reactivity corresponds to the lower nucleophilicity of the lone pair of electrons of the oxygen atom and to the higher reactivity at the aromatic rings of phenyl ethers. Actually the reactions of dichlorocarbene with phenoxides and anisoles at the ring give phenol aldehydes and tropone derivatives, respectively.[9] Products derived from insertion into the O–R bond (R≠CH_2Ph) are not detected.

The yields of insertion products **3a** and **3c** do not differ much in dibenzyl and benzyl ethyl ethers. However, methyl benzyloxyacetate is formed in the latter nearly twice as much as in the former (Table 1). Methyl benzyloxyacetate is produced in a greater amount as compared with methyl ethoxyacetate (**4c**) in benzyl ethyl ether even if the lower yield of the latter than that of toluene may partly be an artefact.[10] The results indicate that the ethyl group is more easily cleaved than benzyl. The apparent cleavage of the benzyl group is actually due to diffusion of the radical pairs **2** (*vide supra*). However, cage disproportionation of radical pair $\overline{CH_3CH_2\cdot \cdot CH(OCH_2Ph)CO_2CH_3}$ (**2'c**) and/or hydrogen abstraction by $\cdot CH(OCH_2Ph)CO_2CH_3$ after diffusion from **2'c** (Scheme 3) can not be the origin of cleavage of the ethyl group for the following reasons.

First of all, the cage recombination product methyl α-benzyloxybutyrate (**5c**) of the radical pair **2'c** is absent (*vide supra*). If **2'c** were formed, it could have recombined to give **5c** in a detectable amount as judged from the amount of the disproportionation and/or escape product, methyl benzyloxyacetate. The radical pair **2'c** is, therefore, considered not to be formed.

In order to find a rationale, let us have recourse to thermochemical data. From the standard heats of formation of radicals,[11] the dissociation energy of O–benzyl bond is estimated to be smaller by *ca.* 15 kcal/mol than that of the O–alkyl bond in benzyl alkyl ethers or benzyl dialkyl oxonium ions:

$$\begin{aligned} &D(PhCH_2\overset{\oplus}{O}R_2) - D(PhCH_2\overset{\oplus}{R}O\text{-}R) \\ &\approx D(PhCH_2\text{-}OR) - D(PhCH_2O\text{-}R) \\ &= \Delta H_f^\circ(PhCH_2\cdot) + \Delta H_f^\circ(RO\cdot) - \Delta H_f^\circ(PhCH_2O\cdot) \\ &\quad - \Delta H_f^\circ(R\cdot) \\ &\approx -15 \text{ kcal/mol} \end{aligned} \quad (1)$$

The cleavage of the O–benzyl bond to give **2c** is, therefore, considered to be easier than that of the O–alkyl bond to give **2'c**, whether they occur at the same time with the attack of the carbene at oxygen or in oxonium ylide **1c**.

Secondly no CIDNP of methyl benzyloxyacetate and ethylene expected to arise in the cage disproportionation of **2'c** is observed. Thus, formation of the ylide intermediate **1c** followed by the Hoffmann type β-elimination of ethylene by a non-radical path gives a reasonable explanation for the easy cleavage of the ethyl group. Homolysis of the same ylide is considered to give the radical pair **2c** (Scheme 4).

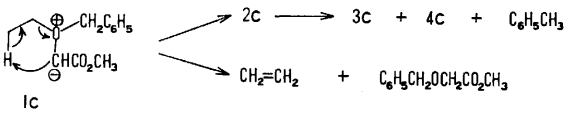

Scheme 4.

Similarly in dibenzyl and benzyl phenyl ethers the carbene attacks at oxygen to give ylide intermediates **1a** and **1b**. However, a possible path for their disappearance is restricted to the dissociation to the radical pairs **2a** and **2b**, respectively. Formation of methyl benzyloxyacetate in benzyl ethyl ether is only an additional pathway of dissipation of oxonium ylide which becomes available for **1c** because of the presence of hydrogen at β-carbon.

Path **1→3** is formally [1,2]sigmatropy to the anionic center. The process is forbidden as a concerted reaction with respect to orbital symmetry. Prior dissociation to radical pairs may be favored. The same rationale is widely used to explain the general radical nature of the Stevens rearrangement.[2] In contrast, path **1c** to methyl benzyloxyacetate *via* Hoffmann-type β-elimination of ethylene is formally [2,3]sigmatropy including anionic center. Six electrons are involved in a cyclic array of orbitals, the reaction being allowed as a concerted reaction. This may be the reason for the path being effectively competitive with path **1c→3c**.[12]

While chemical yields of the C–O insertion products are not necessarily high for the benzyl ethers, the insertion reaction is often of preparative value. The mechanistic information we obtained above together with the survey on the successful reaction types for insertion[1] reveal that there are three structural features governing the C–O insertion reaction.

Firstly it is small ring ethers which lead effectively to ring-enlarged products as a result of the C–O insertion of the carbene. Relief of the ring strain is considered to be responsible for the weak C–O bond. In contrast, displacement products and the corresponding olefins are almost exclusively formed in the case of acyclic ethers, especially when there are β-hydrogen

atoms available. In small ring ethers, the β-hydrogen atoms, if present, can not take part in conformation **1c** necessary for the displacement reaction. Lower steric demand for electrophiles of the oxygen atom in small ring ethers as compared to acyclic ethers should also be taken into account. There are many examples of higher reactivity or basicity of tetrahydrofuran when compared to diethyl ether.[13] Attempt to detect CIDNP for these high-yield insertion products of cyclic ethers has been unsuccessful. As an example the CH_2CH moiety of product **6**[14] appears in the δ 4.1—4.9 region as an approximate A_2X pattern, showing normal increase in its absorption signals during the course of formation in an NMR probe. The negative result does not necessarily rule out the homolysis-recombination mechanism of the intermediate oxonium ylide. Singlet 1,6-biradicals are formed instead of radical pairs. Exchange coupling between the unpaired electrons in **7** is estimated to be too large to allow the appearance of CIDNP.[15] On the other hand, internal recombination to give the C–O insertion product is expected to be efficient, resulting in a high yield of **6**.

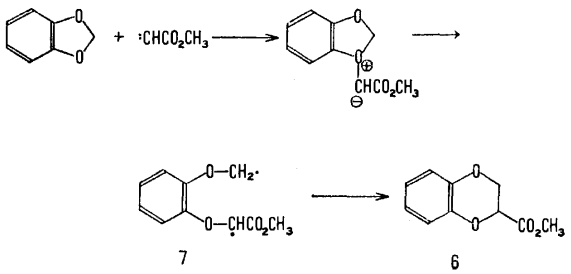

7 6

Secondly, a high yield of C–O insertion is found in allyl ethers. The C–O insertion is accompanied by allyl inversion as shown in the following.[1c]

8

The transition state is aromatic with 6π electrons in a cyclic array of five atomic orbitals; the reaction is rationalized to be efficient.

Thirdly, phenyl ethers are disfavored with respect to reactivity to give insertion products. In addition to the enhanced reactivity at the aromatic ring and the β-elimination of the alkyl chain, if structurally possible, displacement of the methyl group takes place indicating the inertness of the C(aryl)–O bond towards carbene insertion.[16]

$$PhOCH_3 + :CHCO_2R \longrightarrow PhOCH_2CO_2R$$

Experimental

General Procedure for Measuring CIDNP Spectra. ^1H NMR spectra were measured on a Hitachi R-20B Spectrometer (60 MHz). Cw sweep of 200 or 400 s/600 Hz was employed. The pulse Fourier transform ^{13}C NMR spectra were obtained on a Varian CFT-20 spectrometer (20.1 MHz). The free induction decay signals, obtained by application of a short radio frequency pulse of 8 μs width, acquisition time of 1.023 s and 8K data points over the 4000 Hz spectral width, were accumulated a few thousand times on several portions of a batch solution (400—500 times for each portion). Pulse delay of 1 s was taken in the case of dibenzyl ether. As an internal lock, a capillary of dimethyl sulfoxide-d_6 was fixed concentrically at the center of a sample tube of 8 mm o.d. The reaction was started by introducing the sample tube containing *ca.* 5—15 wt or vol% solution of MDA in ethers to the NMR probe preheated at 170—180 °C. Under these conditions the half-life of MDA is less than 5 min. The assignment of the signals was made by comparison of their chemical shifts with those of the authentic samples under the experimental conditions.

VPC Analyses. VPC analyses were carried out on a Shimadzu GC-4A instrument equipped with an FID detector under nitrogen flow rate of 60 ml/min. A 3 m glass column of 4 mm i.d. packed with 10% polyethylene glycol 20 M on 60/80 mesh Uniport B and a 1.5 m glass column of the same diameter packed with 20% diethylene glycol stearate on 60/80 mesh Uniport B were used. The samples for VPC analyses were prepared separately from those for NMR study by heating the sample solutions in glass ampoules in an oil bath at 170 °C for a longer period (1 h) to ensure the completion of the reactions and to avoid the loss of low boiling materials. Molar ratios of dibenzyl, benzyl phenyl, and benzyl ethyl ethers to MDA were 12.9, 12.8, and 13.3, respectively. Identification of VPC components was carried out by comparison of the retention time with that of authentic samples. All the quantitative analyses were carried out by using an internal standard, bromobenzene in most cases. The C–H insertion product was not sufficiently separated from other components of unknown origin to determine the yield accurately, and the same detector response as for the corresponding C–O insertion product was assumed.

Starting Materials. Commercial dibenzyl and benzyl phenyl ethers were purified by distillation. Benzyl ethyl ether was prepared from benzyl chloride and ethanol by the standard method to give clear liquid; bp 183 °C (lit,[17] 189 °C). MDA was obtained by the same procedure as for the corresponding ethyl ester.[18]

Authentic Samples for Identification of Reaction Products. Methyl Benzyloxy-, Phenoxy- and Ethoxyacetates. Free acids were prepared according to literature[19-21] and esterified with methanol and sulphuric acid. Their boiling points are 112 °C/3 mmHg, 130 °C/5 mmHg (lit,[22] 245 °C) and 57—58 °C/29 mmHg (lit,[23] 148 °C/734 mmHg), respectively.

Most insertion products into the C–O or C–H bonds were prepared by the coupling of appropriate hydroxy and halogen compounds promoted by silver oxide.[24] The general procedure is as follows. To a water cooled mixture of 50 mmol of a hydroxy compound and 150 mmol of a halide was added portionwise 75 mmol of silver oxide under vigorous stirring. In some cases exothermic reactions took place. The mixture was gradually heated up to *ca.* 100 °C and maintained at the temperature for 6 h under stirring. Its color turned grey from black due to the formation of silver halide. With the aid of diethyl ether the solid was filtered off and the concentrated filtrate was chromatographed on silica gel with hexane–ether as an eluent. Further purification was performed by preparative TLC. 10—80% Yields were obtained based on hydroxy compounds. Reactants, bp's, NMR spectra, and the results of elemental analyses are summarized in Table 3.

Commercially unavailable reactants were prepared as follows. α-Hydroxyhydrocinnamic acid was prepared from phenylacetaldehyde[25] and esterified with methanol and

Table 3. Authentic samples prepared by the silver oxide-promoted alkylation of alcohols with halides ($ROH + R'X \xrightarrow{Ag_2O} ROR'$) and their boiling points, analytical and ^1H NMR data

ROR′	ROH	R′X	Bp (°C/mmHg)	NMR (CCl_4, δ)	Elemental analyses (%) Found C	Found H	Calcd C	Calcd H
$PhCH_2CH(OCH_2Ph)CO_2CH_3$	$PhCH_2CH(OH)CO_2CH_3$	$PhCH_2Br$	—	2.95(d, 2H), 3.61(s, 3H), 3.98(q, 1H), 4.40(ABq, 2H, J=15 Hz), 7.11(s, 10H)	75.63	6.60	75.53	6.71
$PhCH(OCH_2Ph)CH_2CO_2CH_3$	$PhCH(OH)CH_2CO_2CH_3$	$PhCH_2Br$	147/3	2.26—3.15(m, 2H), 3.59(s, 3H), 4.30 (ABq, 2H, J=12 Hz), 4.75(q, 1H), 7.18(s, 5H), 7.27(s, 5H)	75.77	6.94		
$PhCH(OPh)CH_2CO_2CH_3$	PhOH	$PhCHBrCH_2CO_2CH_3$	—	2.45—3.22(m, 2H), 3.63(s, 3H), 5.56 (q, 1H), 6.6—7.5(m, 10H)	74.68	6.37	74.98	6.29
$PhCH(OCH_2Ph)CO_2CH_3$	$PhCH(OH)CO_2CH_3$	$PhCH_2Br$	151/3	3.61(s, 3H), 4.51(ABq, 2H, J=12 Hz), 4.81(s, 1H), 7.0—7.6(m, 10H)	75.10	6.32		
$PhCH_2CH(OCH_2CH_3)CO_2CH_3$	$PhCH_2CH(OH)CO_2CH_3$	CH_3CH_2I	—	1.13(t, 3H, J=7 Hz), 2.90(d, 2H), 3.1—3.7(m, 2H), 3.61(s, 3H), 3.88 (q, 1H), 7.15(s, 5H)	69.47	7.81	69.31	7.74
$PhCH(OCH_2CH_3)CH_2CO_2CH_3$	$PhCH(OH)CH_2CO_2CH_3$	CH_3CH_2I	124/12	1.18(t, 3H, J=7 Hz), 2.18—2.93 (m, 2H), 3.33(q, 2H, J=7 Hz), 3.60 (s, 3H), 4.64(q, 1H), 7.24(s, 5H)	69.09	7.51		
$CH_3CH(OCH_2Ph)CH_2CO_2CH_3$	$CH_3CH(OH)CH_2CO_2CH_3$	$PhCH_2Br$	106/4	1.21(d, 3H), 2.16—2.78(m, 2H), 3.59 (s, 3H), 3.91(m, 1H), 4.45(s, 2H), 7.21(s, 5H)	69.04	7.79		
$CH_3CH_2CH(OCH_2Ph)CO_2CH_3$	$CH_3CH_2CH(OH)CO_2CH_3$	$PhCH_2Br$	106/5	0.8—1.1(m, 3H), 1.4—2.1(m, 2H), 3.67(s, 3H), 3.77(t, 1H), 4.46(ABq, 2H, J=12 Hz), 7.24(s, 5H)	69.10	7.69		

sulphuric acid to give methyl α-hydroxyhydrocinnamate, an oil, bp 99 °C/3 mmHg. Methyl β-hydroxyhydrocinnamate was obtained by the same procedure as for the corresponding ethyl ester.[26] Bromination with phosphorous tribromide gave methyl β-bromohydrocinnamate, an oil, bp 115 °C/4 mmHg. Reduction of methyl acetoacetate with sodium borohydride gave methyl β-hydroxybutyrate, an oil, bp 82 °C/26 mmHg. Propionaldehyde cyanohydrin prepared according to the method of Letch and Linstead[27] was hydrolyzed with concd hydrochloric acid. Esterification of the resulting acid with methanol and sulphuric acid gave methyl α-hydroxyburyrate, an oil, bp 58 °C/18 mmHg.

Methyl α-Phenoxyhydrocinnamate. To a stirred suspension of 50 mmol sodium phenoxide in 70 ml of benzene was added dropwise a solution of 50 mmol of methyl α-bromohydrocinnamate (an oil obtained by esterification of the free acid,[28] bp 100 °C/2.5 mmHg) in benzene, and the mixture was refluxed for 4 h. The cooled mixture was treated as usual and purified by column chromatography on silica gel and preparative TLC to give an oil, bp 144 °C/3 mmHg. NMR(CCl_4, δ); 3.15(d, 2H), 3.57(s, 3H), 4.41(t, 1H), *ca.* 6.2—6.7 (m, 5H), 7.18(s, 5H). Anal. Found: C, 75.63; H, 6.60. Calcd for $C_{17}H_{18}O_3$; C, 75.53; H, 6.71%.

Methyl γ-Benzyloxybutyrate. γ-Benzyloxybutyric acid was prepared by a procedure similar to that of Reppe *et al.*.[29] Esterification with diazomethane gave a clear oil, bp 112 °C/5 mmHg. NMR(CCl_4, δ): *ca.* 1.6—2.6(m, 4H), 3.44 (t, 2H, J=6 Hz), 3.58(s, 3H), 4.42(s, 2H), 7.22(s, 5H). Treatment of the ester with ammonia in a methanol gave the corresponding amide, mp 81—82 °C (benzene-cyclohexane). Anal. Found: C, 68.52; H, 7.97; N, 7.39%. Calcd for $C_{11}H_{15}NO_2$: C, 68.37; H, 7.82; N, 7.25%.

This work was partly supported by the Ito Science Foundation.

References

1) (a) W. Kirmse, "Carbene Chemistry," 2 nd ed., Chapter 11, Academic Press, New York, N. Y. (1971); (b) M. Jones, Jr. and A. R. Moss, Ed., "Carbenes," Vol. 1, Chapter 1, Wiley, New York, N. Y. (1973); (c) W. Ando, Y. Saiki, and T. Migita, *Tetrahedron*, **29**, 3511 (1973); W. Ando, S. Kondo, K. Nakayama, K. Ichibori, H. Kohoda, H. Yamato, I. Imai, S. Nakaido, and T. Migita, *J. Am. Chem. Soc.*, **94**, 3870 (1972).

2) (a) A. R. Lepley and G. L. Closs, Ed., "Chemically Induced Magnetic Polarization," Chapter 8, Wiley, New York, N. Y. (1973); (b) A. R. Lepley and A. G. Giumanini, "Mechanism of Molecular Migrations," Vol. 3, B. S. Thyagarajan, ed., Wiley, New York, N. Y. (1971), p. 297; (c) H. Iwamura, M. Iwamura, T. Nishida, M. Yoshida, and J. Nakayama, *Tetrahedron Lett.*, **1971**, 63; W. D. Ollis, M. Rey, I. O. Sutherland, and G. L. Closs, *J. Chem. Soc. Chem. Commun.*, **1975**, 543; U. H. Dolling, G. L. Closs, A. H. Cohen, and W. D. Ollis, *ibid.*, **1975**, 545.

3) The C–H insertion products do not show any CIDNP. This is in harmony with the widely accepted view that singlet carbenes insert into the C–H bonds in one step.[30] In the contrast, the insertion of triplet carbenes into the C–H bonds is considered to occur by abstraction-recombination mechanism[30] and CIDNP has been observed.[31]

4) R. Kaptein, *J. Am. Chem. Soc.*, **94**, 6251 (1972).

5) D. V. G. L. N. Rao and W. Gordy, *J. Chem. Phys.*, **35**, 362 (1961).

6) Reference 2a, Chapter 3, p. 108.

7) J. A. Pople, D. L. Beveridge, and P. A. Dobosh, *J. Am. Chem. Soc.*, **90**, 4201 (1968).

8) R. Livingston, J. K. Dormenn, and H. Zeldes, *J. Chem. Phys.*, **53**, 2448 (1970); G. P. Laroff and R. W. Fessenden, *ibid.*, **55**, 5000 (1971).

9) Reference la, pp. 394, 429.

10) The yields of $ROCH_2CO_2CH_3$ are expected to be nearly equal to the yield of toluene but they are considerably lower except in dibenzyl ether.

11) J. K. Kochi, ed., "Free Radicals," Vol. 2, Chapter 17, Wiley, New York, N. Y. (1973); Compilation of J. H. S. Green, *Quart. Rev. (London)*, **15**, 125 (1961); *Circ. Natl. Bur. Standards(U.S.)*. **1952**, 500.

12) Methyl benzyloxyacetate and methyl ethoxyacetate are both "displaced" products but are formed in a completely different fashion. The duality has not been fully recognized. Furthermore cage disproportionation is apparently able to produce a displaced product, though its occurrence is doubtful in the present case as judged from the failure to observe CIDNP due to methyl ethoxyacetate.

13) A. Amaro and K. Grohmann, *J. Am. Chem. Soc.*, **97**, 3830 (1975).

14) C. D. Gutsche and M. Hillman, *J. Am. Chem. Soc.*, **76**, 2236 (1954).

15) G. L. Closs and C. E. Doubleday, *J. Am. Chem. Soc.*, **95**, 2735 (1973); Reference 2a, Chapter 3.

16) G. B. R. de Graaf, J. H. Van Dijk-Rothuis, and G. van de Kolk, *Rec. Trav. Chim. Pays-Bas*, **77**, 224 (1958) and references cited therein.

17) J. V. Braun., *Ber.*, **43**, 1351 (1910).

18) G. S. Marvel, *Org. Synth.*, Coll. Vol. II, 310 (1943); N. E. Searle, *ibid*, Coll. Vol. IV, 424 (1963).

19) K. M. Hammond, N. Fisher, E. M. Tanner, and G. S. Franklin, *J. Chem. Soc.*, **1957**, 1062.

20) P. Giacosa, *J. Prak. Chem.*, **19**, 396 (1879).

21) R. C. Fuson and B. H. Wojcik, *Org. Synth.*, Coll. Vol. II, 260 (1943).

22) P. Fritzsche, *J. Prak. Chem.*, **20**, 267 (1879).

23) A. Fölsing., *Ber.*, **17**, 486 (1884).

24) W. A. Cowdrey, E. D. Hughes, and C. K. Ingold, *J. Chem. Soc.*, **1937**, 1228.

25) R. Biquard. *Ann. Chim.*, **20**, 97, 144 (1933).

26) C. R. Hauser and D. S. Breslow, *Org. Synth.*, Coll. Vol. III, 408 (1955).

27) R. A. Letch and R. P. Linstead, *J. Chem. Soc.* **1932**, 443.

28) G. S. Marvel, *Org. Synth.*, Coll. Vol. III, 705 (1955).

29) W. Reppe und Mitarbeitern, *Justus Liebigs Ann. Chem.*, **596**, 158 (1955).

30) Reference la, Chapter 7.

31) G. L. Closs and A. D. Trifunac, *J. Am. Chem. Soc.*, **92**, 2 186 (1970); M. L. Kaplan and H. D. Roth, *J. Chem. Soc., Chem. Commun.*, **1972**, 970; D. Bethell, M. R. Brinkman, and J. Hayes, *ibid.*, **1972**, 475.

the quenching of benzonitrile by triethylamine was accompanied by the appearance of a new emission at longer wavelength (Fig. 1), which may be assigned to an exciplex formed between the two components, while no exciplex emission was observed in the quenching of benzonitrile by diethylamine in benzene.

Hydrogen Isotope Exchange in Benzonitrile. Irradiation of a mixture of benzonitrile and diethylamine-[N^2H] with a 1 kW high pressure mercury arc lamp for 20 h resulted in minor amounts of deuterium incorporation (0.9%) in the recovered benzonitrile as determined by mass spectrometry. When a solution of benzonitrile in acetonitrile was irradiated in the presence of diethylamine[N^2H] under the same conditions, the amino-deuterium is transferred to benzonitrile to the extent of 4.5%. A labelling experiment of benzonitrile with triethylamine in acetonitrile was carried out in the presence of deuterated water to elucidate the mechanism. It is of interest to note that the deuterium was involved in the starting material recovered (4.1%).

In view of the incorporation of deuterium in benzonitrile the light induced tritiation of benzonitrile was undertaken with diethylamine[N^3H] or with triethylamine–tritiated water to determine the tritium distribution in the nucleus and the relative rate of tritiation.

A mixture of diethylamine[N^3H], benzene, and benzonitrile was irradiated with a high pressure mercury arc lamp. After a usual work-up, the aromatic compounds were recovered by distillation. Benzene fraction was purified by fractional distillation and submitted to tritium assay. Benzonitrile was degraded by the known procedures[8] in order to determine the tritium distribution. Similarly, a solution of benzonitrile in acetonitrile was irradiated with a high pressure mercury arc lamp in the presence of triethylamine and tritiated water. The benzonitrile was recovered in a similar way and degraded.

The tritium distribution in the recovered benzonitrile and the relative rate of tritiation (per C–H bond) are shown in Table 2 together with related data. The tritium distribution pattern is very similar to that obtained with 1-propanethiol[S^3H] and acetic acid[O^3H],[3] but differs greatly from that reported for the addition of tritium atoms[2] (Table 2). The order of reactivity among the nuclear positions is *para*$\gg$*ortho*$>$*meta* in the present study, whereas it is *meta*$\approx$*ortho*$>$*para* for the addition of tritium atoms.[2] The relative rate of the tritiation on benzonitrile to benzene is extremely high with diethylamine[N^3H] and its value is larger than that with 1-propanethiol-[S^3H] by a factor of seven, although the tritium distribution is similar in patterns in both reagents. The decrease in the relative rate with 1-propanethiol could readily be accommodated in terms of a slight inclusion of tritium atoms generated by the photolysis of the thiol in the tritiation process, since tritium atoms add more easily to benzene than to benzonitrile.

The observed difference in results between tritiation with 1-propanethiol and that reported by Pryor[2] using benzenethiol requires some discussion. Benzenethiol would be photolyzed more easily than 1-propanethiol, because the former has a much smaller S–H bond strength (75 *versus* 88 kcal/mol).[9] In addition, the high pressure mercury arc lamp in a Pyrex immersion well was employed in this work, whereas Rayonette lamps (nominally 300 nm) were used in the earlier experiments,[2] in which hydrogen atoms could be produced more efficiently. In order to confirm this view the photolysis of benzenethiol[S^3H] in a mixture of benzonitrile and benzene was re-examined under the present conditions and the results are listed in Table 2. The tritium distribution takes intermediate values between those with 1-propanethiol and those reported by Pryor[2] with benzenethiol, and the relative rate is decreased to 21. These observations suggest that the tritiation by tritium atoms in the present study occurs moderately with benzenethiol, but not so seriously as in the photolysis using the Rayonette lamps. Thus, it is probable that the values of tritium distribution reported by Pryor are evaluated as the results for the hydrogen atom reactions.

TABLE 2. LIGHT INDUCED TRITIATION OF BENZONITRILE

Triton donor	Tritium distribution (%)[a]			k_{rel}[b]
	Ortho	*Meta*	*Para*	
Diethylamine[N^3H]	18.9	1.4	79.7	1740
Triethylamine and tritiated water	10.0	0.2	89.8	
1-Propanethiol[S^3H][c]	17.4	2.0	80.8	254
Acetic acid[O^3H][c]	12.4	1.0	86.7	
Benzenethiol[S^3H]	31.0	5.0	64.0	21
Benzenethiol[S^3H][d] (Pryor *et al.*)	42.0	45.2	12.8	

a) Average values of data obtained by duplicate runs. b) Rate (per C–H bond) of nuclear tritiation relative to benzene. c) Data taken from Ref. 3. d) Data taken from Ref. 2.

Mechanism for Hydrogen Isotope Exchange. In recent years light induced hydrogen isotope exchange of aromatic compounds has been investigated in acidic media.[10] The previous studies[10] showed that the excited states are much more basic than the ground states, and the exchange takes place through prototropic equlibria of the excited state. As to the multiplicity of the excited state,[10] the first excited singlet states were suggested to be responsible for the exchange from fluorescence quenching experiments, but in some cases a triplet state or a higher excited singlet state was demonstrated to participate in the reaction. Previously, we have shown that the rate of tritium incorporation into benzonitrile is lower in tritiated acetic acid than in tritiated 1-propanethiol by a factor of 10^{-3} in spite of the higher acidity of acetic acid.[3] This fact indicates that proton transfer is not involved in the rate determining step and the basicity of the excited states is irrelevant to the exchange.

The UV spectra of benzonitrile–diethylamine and –triethylamine mixture in hexane were the sums of the absorption spectra of each component, indicating that charge-transfer interaction in the ground state is absent or very weak. Thus, a possible role of a charge-transfer complex in the ground state is ruled out.

As mentioned above, fluorescence of aromatic

nitriles was quenched efficiently by the amines and the quenching of benzonitrile by triethylamine was accompanied by the appearance of a new exciplex emission (Fig. 1). In view of these findings the most plausible mechanism for the exchange reaction seems to involve an exciplex possessing charge-transfer nature between singlet excited benzonitrile and the amines.[11]

The exciplex either deactivates to each component in the ground state *via* exciplex emission or undergoes electron transfer from the quencher to the quenchee to give a radical cation and a radical anion, respectively. With diethylamine[N^3H], the radical cation contains an acidic triton and the triton transfer from the radical cation to the radical anion may occur to give a radical pair, which may disproportionate to result in the hydrogen exchange. On the other hand, the radical cation from triethylamine does not contain an acidic proton (triton) and tritiated water in the system functions as a triton donor to the anion radical.

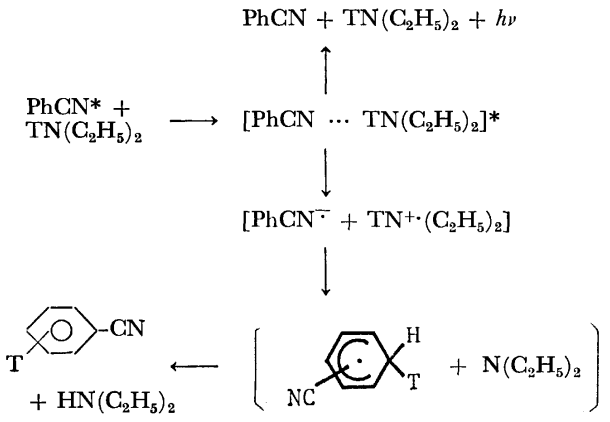

The suggested reaction pathway is compatible with the observation that the order of the tritiation among the nuclear positions is *para*≫*ortho*>*meta*. The triton transfer to the anion radical of benzonitrile occurs to the *ortho*- and *para*-positions to give cyclohexadienyl radicals, I_o and I_p, in preference to the *meta*-positions to give I_m, because the greater electronic stabilization is achieved in I_o and I_p than I_m. This trend is kept in the subsequent disproportionation reactions to give the *ortho*- and *para*-tritiated benzonitrile in higher portion than the *meta*-substituted one.

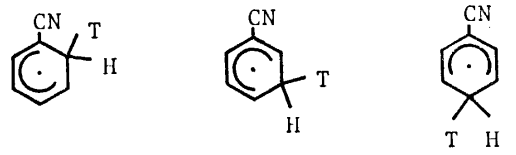

I_o I_m I_p

Inspection of the tritium distribution pattern in Table 1 indicates that there is an overall similarity between 1-propanethiol, acetic acid, and the amines. It is, therefore, suggested that similar intermediates participate in the distribution determining step. The decrease in the rate of the tritiation with acetic acid and scarce quenching of benzonitrile fluorescence by acetic acid are rationalized as a reflection of the difference in ionization potential between acetic acid,[12] 1-propanethiol,[13] and the amines.[7] The formation of the charge transfer exciplex and following electron transfer from quencher to aromatic substrate would be hard in quenchers having higher ionization potential such as acetic acid.

Experimental

Materials. Benzene, diethylamine, triethylamine, and benzonitrile were purified by distillation or vacuum distillation. Terephthalonitrile was recrystallized three times from benzene. α-Naphthonitrile was purified by distillation under reduced pressure followed by twice recrystallizations from ligroin.

Diethylamine[N^2H]: Diethylamine was fractionally distilled from deuterated water. The distillation was repeated until no signal due to the amino proton was observed in the NMR spectrum.

Diethylamine[N^3H]: Diethylamine (15.0 ml) was mixed with tritiated water (0.1 ml, 5 Ci/ml), stirred for 30 min, dried over artificial zeolite, and purified by bulb to bulb distillation to give the tritiated amine (2.90 Ci/mol).

Benzenethiol[S^3H]: benzenethiol was tritiated in a way similar to the above and purified by distillation.

Deuteration of Benzonitrile. *(a) With Diethylamine*[N^2H]: A mixture of benzonitrile (19.4 mmol) and diethylamine-[N^2H] (58.4 mmol) was irradiated for 20 h under nitrogen atmosphere with a 1 kW high pressure mercury arc lamp (RIKO Rotary Photochemical Reactor, Model RH 400—10W). After irradiation, the deuterated benzonitrile was recovered by fractional distillation under reduced pressure. Irradiation of a solution of benzonitrile (9.7 mmol) and the amine (19.5 mmol) in 10 ml of acetonitrile was carried out under the same conditions and benzonitrile was recovered by distillation.

(b) With Triethylamine and Deuterated Water: A solution of benzonitrile (9.7 mmol), triethylamine (14.3 mmol), and deuterated water (100 mmol) in 10 ml of acetonitrile was irradiated for 15 h with the high pressure mercury arc lamp and the deuterated benzonitrile was fractionated.

The isotopic content was determined by mass spectral analysis using a Hitachi RMU-6 mass spectrometer.

Tritiation of Benzonitrile with Diethylamine[N^3H]. Tritiated diethylamine (42.0 mmol, 6.38×10^{12} dpm/mol), benzonitrile (218 mmol), and benzene (218 mmol), all of which were degassed by the usual freeze-thaw cycles, were mixed in Pyrex tubes under nitrogen atmosphere. Irradiation was carried out for 20 h under nitrogen atmosphere with the 1 kW high pressure mercury arc lamp. The reaction mixture was washed with 1 M sulfuric acid and water to remove the amine and the aromatic compounds were recovered by distillation. Benzene was further purified by fractional distillation and submitted to tritium assay. Benzonitrile (17.5 g) recovered was hydrolyzed by refluxing with a solution of potassium hydroxide (14.5 g) in 68 ml of water for 5 h. After the usual work-up, the tritiated benzoic acid isolated was purified by recrystallization from water until reproducible specific activities were obtained and submitted to tritium assay.

A reference solution, identical to the irradiated solution but stored in the dark for the corresponding period, was subjected to the same procedure and the incorporation of tritium in the substrate was confirmed to be negligible.

Tritiation with Triethylamine and Tritiated Water. A solution of benzonitrile (291 mmol), triethylamine (43 mmol), and tritiated water (6.0 ml, 3.61 mCi/ml) in 30 ml of acetonitrile was placed in Pyrex tubes, deoxygenated by purging with argon, and irradiated for 10 h with the 1 kW lamp.

After the irradiation, triethylamine and water were removed by distillation. The residue was washed with water and hydrolyzed as described above.

Tritiation with Benzenethiol[S^3H]. A mixture of benzenethiol[S^3H] (99 mmol, 4.45×10^{11} dpm/mol), toluene (501 mmol), and benzonitrile (486 mmol) was placed in Pyrex tubes, degassed by the usual freeze-thaw cycles, and irradiated for 6 h with the 1 kW lamp. After irradiation, benzenethiol was removed by washing with 10% NaOH and water, and the aromatic compounds were recovered by fractional distillation. Toluene was oxidized to benzoic acid by refluxing with aq. $KMnO_4$. Benzonitrile was converted to benzoic acid as described above.

The relative rate of nuclear tritiation of benzonitrile to toluene was determined as 5.9 from the specific activities of each benzoic acid derived from benzonitrile and toluene. The relative rate of benzonitrile to benzene (per C-H bond) was calculated to be 21 using the reported value of toluene (3.6),[3] which was obtained by competitive tritiation of toluene and benzene with 1-propanethiol[S^3H]. Since the relative rate of toluene to benzene for the addition of hydrogen atoms (1.7)[14] is small and photolysis of benzenethiol is supposed to generate much more amounts of hydrogen atoms than that of 1-propanethiol under the present condition, the relative rate of toluene would be diminished if it were determined with benzenethiol[S^3H]. Thus, the estimated value for benzonitrile would be larger than the value determined experimentally.

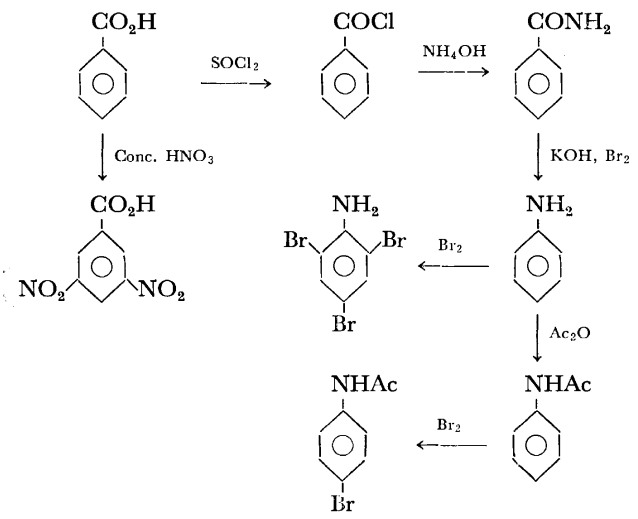

Degradation. The tritiated benzoic acid was diluted, if necessary, with inactive specimen for convenience in chemical manipulations, and then degraded in order to determine the tritium distribution according to the preceding schemes.[8]

The degradation products were purified by means of recrystallization until reproducible specific activities were obtained. Tritium activity was measured with a Packard Tri-Carb liquid scintillation spectrometer Model 3380. Each sample was counted for a period sufficient to reduce the randam error to 1% or less.

Quenching studies. Fluorescence measurements were made on a Hitachi fluorescence spectrophotometer MPF-2A.

References

1) W. A. Pryor and J. P. Stanley, *Intra-Science Chemistry Reports*, **4**, 99 (1970).
2) W. A. Pryor, T. H. Lin, J. P. Stanley, and R. W. Henderson, *J. Am. Chem. Soc.*, **95**, 6993 (1973), and references cited therein.
3) H. Takiguchi, K. G. Yoshida, H. Ouchi, M. Yoshida, N. Morikawa, and O. Simamura, *Chem. Lett.*, **1974**, 593.
4) P. Neta and R. H. Schuler, *J. Am. Chem. Soc.*, **94**, 1056 (1972).
5) M. Yoshida, H. Sakuragi, I. Tanaka, K. Tokumaru, and N. Morikawa, *Bull. Chem. Soc. Jpn.*, **48**, 2399 (1975).
6) See for example: A. Lablache-Combier, *Bull. Soc. Chim. Fr.*, **1972**, 4791.
7) S. L. Murov, "Handbook of Photochemistry," Marcel Dekker, Inc., New York, N. Y. (1973).
8) W. A. Bonner, *J. Am. Chem. Soc.*, **79**, 2469 (1957); R. M. White and F. S. Rowland, *ibid.*, **82**, 4713 (1960).
9) J. A. Kerr, *Chem. Rev.*, **66**, 465 (1966); M. Mackle, *Tetrahedron*, **19**, 1159 (1963).
10) See for a critical discussion: W. J. Spillane, *Tetrahedron*, **31**, 495 (1975).
11) An excited charge-transfer complex between *p*-chlorobiphenyl and triethylamine has been proposed as an intermediate in the photoreduction of the former by the latter; M. Ohashi, K. Tsujimoto, and K. Seki, *J. Chem. Soc., Chem. Commun.*, **1973**, 384.
12) K. Watanabe, *J. Chem. Phys.*, **26**, 542 (1957).
13) *Monograph Ser. Res. Instit. Appl. Elect. Hokkaido Univ.*, No. 4 (1954—7), Appendix.
14) C. I. Brett and V. Gold, *Chem. Commun.*, **1971**, 148.

Preparation of Matsutake Alcohol (1-Octen-3-ol) from a Butadiene Telomer

Jiro TSUJI, Katsuhiko TSURUOKA, and Keiji YAMAMOTO

Department of Chemical Engineering, Tokyo Institute of Technology, Ookayama, Meguro-ku, Tokyo 152

(Received March 15, 1976)

A simple preparation of 1-octen-3-ol so called Matsutake alcohol using a butadiene telomer is described: selective hydrogenation of the terminal double bond of 2,7-octadienyl acetate gave 2-octenyl acetate which was converted *via* palladium-catalyzed allylic rearrangement and hydrolysis into 1-octen-3-ol.

Naturally occurring *l*-1-octen-3-ol is known as Matsutake alcohol.[1] The racemic form of this alcohol has been prepared by a reaction of pentylmagnesium bromide with acrylaldehyde, and resolved.[1,2] Two other procedures have been reported which involve Friedel-Crafts reaction of hexanoyl chloride with ethylene[3] and Grignard reaction of vinyl bromide with hexanal.[4]

As part of studies on the utilization of butadiene telomers[5] for organic synthesis, we wish to describe a simple preparation of *dl*-1-octen-3-ol starting from 2,7-octadienyl acetate(**1**), which is readily obtained, along with 1-vinyl-5-hexenyl acetate(**2**), by the palladium-catalyzed telomerization of butadiene with acetic acid (Eq. 1).[6]

$$2CH_2{=}CH{-}CH{=}CH_2 + AcOH \xrightarrow{(Pd)} CH_2{=}CHCH_2CH_2CH_2CH{=}CHCH_2OAc \quad \mathbf{1}$$
$$+ CH_2{=}CHCH_2CH_2CH_2CH(OAc)CH{=}CH_2 \quad \mathbf{2} \qquad (1)$$

The compound **2** seemed to be the most suitable precursor of 1-octen-3-ol. However, attempted homogeneous hydrogenation of **2** catalyzed by chlorotris(triphenylphosphine)rhodium(I) in a benzene solution did not proceed selectively, and a mixture of three possible hydrogenation products was formed even at 40% conversion.

It has been found that **1** is readily equilibrated with **2** in a ratio of *ca.* 3 : 1 by way of an allylic rearrangement under the influence of the palladium catalyst. Therefore, **1** may be a suitable starting material for 1-octen-3-ol, if a sequence of partial hydrogenation and the rearrangement of the acetoxyl group shown below is possible.

$$CH_2{=}CH(CH_2)_3CH{=}CHCH_2OAc \longrightarrow \mathbf{1}$$
$$CH_3(CH_2)_4CH{=}CHCH_2OAc \quad \mathbf{3}$$
$$CH_3(CH_2)_4CH(OAc)CH{=}CH_2 \quad \mathbf{5}$$

Thus **1** was hydrogenated at room temperature in the presence of chlorotris(triphenylphosphine)rhodium(I) (0.5—1.0 mol%) in purified benzene under hydrogen pressure (17.5 kg/cm² initial pressure). Analysis of the reaction mixture by GLC showed the formation of 2-octenyl acetate(**3**) as a main product and octyl acetate(**4**) as a minor product in a ratio of 80 : 20 at about 90% conversion. This result is satisfactory for preparative purpose.

The selectivity for partial hydrogenation of **1** apparently depends on the conversion as shown in Table 1. The results indicate that the rate difference is rather small in the consecutive hydrogenation of the terminal and the internal olefinic bonds of **1**. Attempts to improve the selectivity for partial hydrogenation of **1** by using a cationic rhodium complex, $[(NBD)Rh(PPhMe_2)_2]^+ClO_4^-$ (NBD=norbornadiene),[7] were fruitless.

The distilled product containing both **3** and **4** was then subjected to allylic 1,3-shift of the acetoxyl group. When palladium acetate (3 mol%) combined with three equivalents of triphenylphosphine was used as a catalyst in the presence of potassium acetate in *t*-butyl alcohol, **3** was readily equilibrated with 3-acetoxy-1-octene(**5**) in 3 h at 70 °C in a ratio of 1.9 : 1.0 on the basis of GLC, while **4** remained intact. The lower boiling **5** was isolated by distillation, further purified by preparative GLC and characterized by NMR and IR spectra (see Experimental). The mixture of **3** and **4** undistilled was again subjected to the conversion into **5** under the same conditions as above. In preparative scale synthesis, the lower boiling product **5** can be continuously distilled out by fractionation, while the rearrangement of the higher boiling **3** to **5** proceeds in the vessel containing the active catalyst system to completion.

Finally, **5** was hydrolyzed in aqueous methanolic alkali to give 1-octen-3-ol in a high yield.

TABLE 1. SELECTIVE PARTIAL HYDROGENATION OF 2,7-OCTADIENYL ACETATE (**1**) CATALYZED BY $ClRh(PPh_3)_3$ AT ROOM TEMPERATURE

Conditions		Conversion of **1** (%)	Product ratio[a]	
Catalyst concentration (mol%)	Initial pressure of H_2 (kg/cm²)		**3**	**4**
1.0	6.0	39	96	4
1.0	17.5	47	92	8
1.0	—[b]	52	94	6
0.5	17.5	79	85	15
0.5[c]	17.5	89	82	18
0.5	17.5	91	79	21
0.5	17.5	95	75	25

a) Determined by GLC. b) Normal pressure. c) $(1/2[(C_6H_{10})RhCl]_2 + Ph_2PCH_2CH_2PPh_2)$ prepared *in situ*.

Experimental

Materials. Fractionally distilled 2,7-octadienyl acetate(**1**) (bp 106.5 °C/24 mmHg) was still contaminated with a small amount (*ca.* 6%) of unidentified material,

whereas 1-vinyl-5-hexenyl acetate(**2**) (bp 92.0 °C/24 mmHg) was pure by GLC.

GLC Analysis. A column (3 mm×3 m) packed with 20% UCON oil (50 HB-2000) on Celite (60—80 mesh) was used at 140 °C with 0.8 kg/cm² (40 ml/min) of hydrogen as a carrier gas. Under these conditions, **1** eluted in 11.3 min while **2** in 5.7 min, and all hydrogenation products were satisfactorily separated from each other.

Attempted Partial Hydrogenation of 2. In a 100 ml glass vessel flushed with dry nitrogen was placed a solution of 0.45 g (2.7 mmol) of **2**, 25 mg (2.7×10^{-2} mmol) of $ClRh(PPh_3)_3$ in 5 ml of purified benzene. The mixture was shaken at room temperature under hydrogen atmosphere for 4 h. GLC analysis showed that the product contains **2**, **5** (and/or 1-ethyl-5-hexenyl acetate, and 1-ethylhexyl acetate in the ratio 62 : 21 : 18. 3-Octyl acetate was obtained independently by thorough hydrogenation of **2** using 5% Pd-C in benzene–ethanol solution.

Partial Hydrogenation of 1. The following is typical: In a 100 ml-micro autoclave were placed 9.09 g (54 mmol) of **1**, 250 mg (0.27 mmol, 0.5 mol%) of $ClRh(PPh_3)_3$, and 30 ml of pure benzene. Hydrogen (17.5 kg/cm²) was charged after purging air twice with hydrogen and the mixture was magnetically stirred for 5 h. GLC analysis of the reaction mixture indicated the presence of **3** and **4** in a ratio of 75 : 25 at 95% conversion of **1**. Two other very minor unidentified products were detected by GLC. Another run under 40 kg/cm² of initial hydrogen pressure gave exactly the same results as above. The product ratio of **3** to **4** decreased with the increasing conversion of **1** as shown in Table 1. Benzene was removed by evaporation and the residue was distilled *in vacuo* to give 7.52 g of a mixture of **3** and **4**, bp 96—97 °C/17 mmHg.

Rearrangement of 3 to 5. To a mixture of 0.297 g (1.3 mmol) of palladium acetate, 1.04 g (4.0 mmol) of triphenylphospine, 4.32 g (44 mmol) of potassium acetate and 2.65 g (44 mmol) of acetic acid in 50 ml of *t*-butyl alcohol was added 7.52 g of the above distillate in one portion. The mixture was heated at 70 °C with stirring for 3 h, during which time **3** gradually rearranged into **5** to attain an equilibrium. The reaction mixture was poured into 50 ml of water, extracted three times with hexane. GLC showed the extracts to contain **5** and **3**, in the ratio 1 : 1.9, in addition to **4**. The acetates (5.20 g) were obtained by flush-distillation (~60 °C/4 mmHg). The combined distillate (10.38 g) of two runs was fractionally distilled to give 2.50 g of almost pure **3**, bp 82—84 °C/13 mmHg, which was further purified by preparative GLC. NMR(CCl_4, δ) 0.89 (deformed t, 3H, $\underline{CH_3}CH_2$), 1.34 (br, s, 8H, $(\underline{CH_2})_4$), 1.99 (s, 3H, $\underline{CH_3}CO$), and 4.97—6.04 ppm (m, 4H, $\underline{CH}OAc$ and $\underline{CH}=\underline{CH_2}$). IR (film) 1750($\nu_{CO}$) and 1240 cm^{-1}(δ_{CO}).

The remainder in the pot-still (7.50 g), containing **3**, **4**, and **5** in a ratio of 53 : 40 : 7, was again treated with palladium acetate (3 mol%) in the same manner as indicated above to give **3** by equilibration. Higher temperature (90 °C) for the catalyzed 1,3-shift was found to cause considerably the elimination of the acetoxyl group from **5** to form 1,3-octadiene.

Hydrolysis of **5** with 1 M potassium hydroxide in aqueous methanol (1/1) gave nearly quantitatively 1-octen-3-ol, which was purified by preparative GLC. NMR and IR spectra of 1-octen-3-ol were in good accord with those reported previously.[4] NMR (CCl_4, δ) 0.90 (deformed t, 3H, $\underline{CH_3}$-CH_2), 1.36(br.s, 8H, $(\underline{CH_2})_4$), 2.15 (s, 1H, $\underline{OH}$), 4.00 (m, 1H, $\underline{CH}OH$), 4.95—5.25 (m, 2H, $\underline{CH_2}$=), and 5.56—6.10 ppm (m, 1H, -$\underline{CH}$=). IR(film) 3400 (ν_{OH}) and 920 cm^{-1} ($\delta_{CH_2=}$).

References

1) S. Murahashi, *Sci. Papers Inst. Phys. Chem. Res. (Tokyo)*, **34**, 1525 (1938); *Chem. Abst.*, **32**, 3755⁶ (1938).
2) P. A. Levene and A. Walti, *J. Biol. Chem.*, **94**, 593 (1931).
3) T. Ueda, *Nippon Kagaku Kaishi*, **83**, 338 (1962).
4) H. Fujita and Y. Ohata, *Yuki Gosei Kagaku Kyokai Shi*, **33**, 645 (1975).
5) J. Tsuji, *Acc. Chem. Res.*, **6**, 8 (1973).
6) S. Takahashi, T. Shibano, and N. Hagihara, *Tetrahedron Lett.*, 2451 (1967).
7) R. R. Schrock and J. A. Osborn, *J. Am. Chem. Soc.*, **93**, 2397 (1971).

A Study of the Removal of Oily Soil by Rolling up in Detergency

Keizo OGINO and Wataru AGUI

Faculty of Science and Technology, Science University of Tokyo, Noda, Chiba 278

(Received December 11, 1975)

The removal of simply constituted oily soil from a low-energy surface such as polypropylene (PP) has been examined in aqueous solutions of sodium dodecylbenzenesulfonate and its builders. Oleic acid, olive oil, lauryl alcohol, oleyl alcohol, and liquid paraffin were used as model oily soils. Rolling-up was observed in all the soils except oleyl alcohol and liquid paraffin. The rolling-up of the soil occurred in the contact angle range of $0°<\theta<90°$(θ is contact angle) when the soil was removed incompletely from PP. Apparent activation energies for rolling-up were derived, *i.e.*, 8 kcal/mol for oleic acid and 11.9 kcal/mol for olive oil. Complexes were formed for oleic acid, lauryl alcohol, and oleyl alcohol. The effects of the surfactant in various concentrations at various temperature, and with various builders were studied in view of the interfacial tension and the contact angle.

Although cleaning systems have in practice, complicated constitutions (*i.e.*, multicomponent soils in multiphase adhering to substrates which are immersed in a multicomponent cleaning both), it is known that there are three basic mechanisms by which liquid oily soil may be removed in detergent solutions: rolling-up, emulsification, and solubilization.[1,2]

Adam first pointed out that oily soil originally present as a thin layer coating the substrate is pushed into a sphere, together with the substrate, when immersed in a detergent solution; then, it can be removed from the substrate.[3] He also adopted Young's equation to relate the contact angle to the interfacial tension. Thereafter, many investigators reported microscopic studies of similar processes with various kinds of textile fibers and oily soils in the surfactant solutions.[4-7] Kling *et al.* showed some quantitative results on a process using nonpolar oily soil such as liquid paraffin.[8-10]

In the present paper, oleic acid (*cis*-9-octadecanoic acid), olive oil, lauryl alcohol(1-dodecanol), oleyl alcohol(*cis*-9-dodecen-1-ol), and liquid paraffin were used as model oily soils, and the removal of these oily materials from low-energy solid surfaces was studied.

Experimental

Materials. *Substrate*: Sheets of polypropylene (Mitsui Nobulene JHG) ($100\times40\times1.2$ mm) were prepared under a projecting pressure of 475/cm² at 250 °C and were pressed with a pressure of 200 kg/cm² at 180 °C. The sheets were then cut into specimens of $10\times10\times1.2$ mm: the surface was cleaned with a commercial detergent solution at 35 °C several times, rinsed with distilled water for 60 min, soaked in absolute ethanol for 5 min, dried in a vacuum for 3 h, and stored in a desiccator at room temperature before use.

Surfactant: The sodium dodecylbenzenesulfonate (NaDBS) was of an extra pure reagent grade, purchased from the Tokyo Kasei Co., and was purified by extraction with absolute ethanol.

Builders: The anhydrous sodium sulfate and sodium carbonate were of a guaranteed reagent grade, obtained from the Hikotaro Shudzui Co. and the Showa Chemical Co. respectively. The sodium tripolyphosphate was from the Mitsui Toatsu Chem. Co., it was the commercial grade.

Model Oily Soils: The oleic acid and lauryl alcohol were of a reagent grade from the Tokyo Kasei Co. The oleyl alcohol and liquid paraffin of an extra pure reagent grade were from the Wako Pure Chem. Co. The olive oil was commercially purchased from the Kozakai Seiyaku Co.

Apparatus and Procedure. An oily soil droplet of 1.5 μl was put on the surface of PP by means of a microsyringe connected with a micrometer. The sheet of PP was then set in a glass cell ($40\times25\times15$ mm). The glass cell was placed on the table of the Goniometer, M-2010, A-a, G-I type of the Erma Kogaku Co. Ltd., and then the detergent solution was poured slowly onto it. The contact angle of the droplet, its change, and the radius of the contact area between the droplet and the PP plate were measured in the solution, and the appearance of the droplet was photographed.

A polarizing microscope with crossed nicols (PFM type of the Nippon Kogaku Co. Ltd.) was used to observe the state of the droplets in the solution at 30 °C. The time required to remove oily soils from the PP by rolling-up was measured at 25, 30, 40, 50, and 55±1 °C. The interfacial tension of the system was measured by a Wilhelmy-type Surface Tensiometer, ST-1, of the Shimadzu Seisakusho Co. at 30 °C.

Results and Discussion

Observation of the Rolling-up Process. Figure 1 shows the behavior of oily soils adhering on PP in the

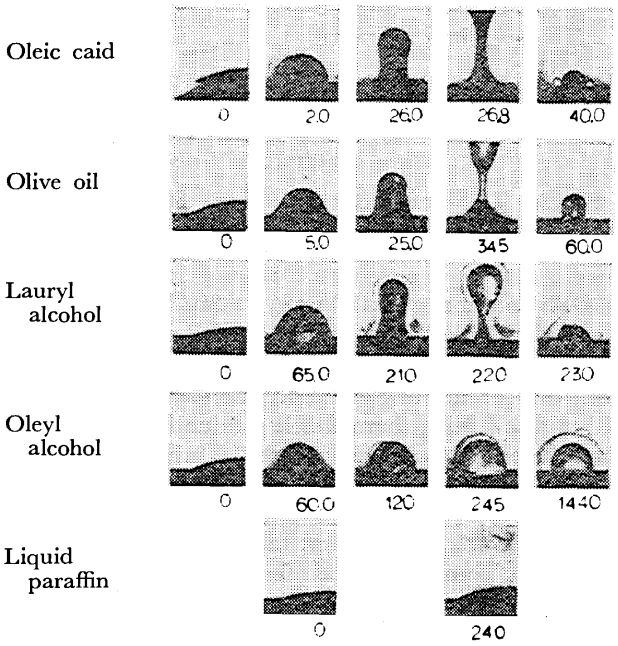

Fig. 1. Behavior of oily soils in 0.150% NaDBS solution at 30 °C. (Numbers show the time in minutes after immersion into the solution.)

Table 1. Removal of oily soils

Oily soil	Contact[a] angle in air	Contact angle in water	In NaDBS 0.150% solution			
			Contact[b] angle	Complex[c] formation	Rolling up[d]	Rolling up[e] time
Oleic acid	27.5°	7.0°	81.7°	○	○	26.9
Olive oil	28.3°	5.0°	81.0°	×	○	34.5
Lauryl alcohol	17.0°	38.0°	67.0°	○	○	222.2
Oleyl alcohol	26.8°	6.9°	54.5°	○	×	—
Liquid paraffin	18.0°	0.0°	26.5°	×	×	—

a) Measured in air at room temperature. b) Angle quoted is final contact angle in the surfactant solution. c) ○: Complex formed visibly, ×: No complex formed visibly. d) ○: Rolling up occured, ×: No rolling up occured. e) The figures show the time (min), required to remove soils by rolling up.

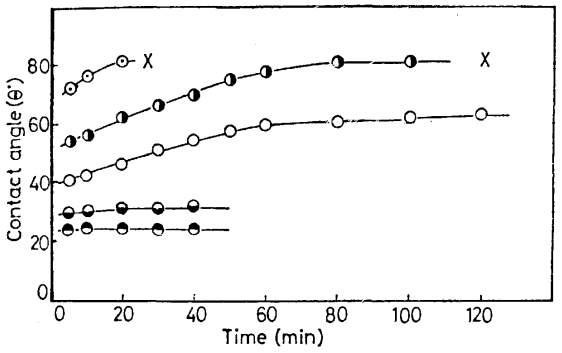

Fig. 2. The change of contact angle of oleic acid at varying concentration of NaDBS solution (30 °C).
⊙: 0.150%, ◑: 0.125%, ○: 0.100%,
◒: 0.050%, ◓: 0.025%, ×: shows Rolling up.

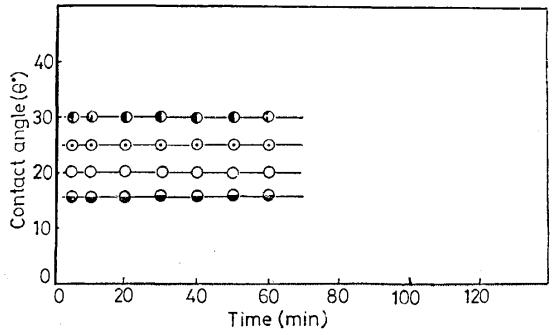

Fig. 3. The change of contact angle of liquid paraffin in NaDBS solution (at 30 °C).
◐: 0.200%, ⊙: 0.150%, ○: 0.100%, ◒: 0.050%.

NaDBS solution of 0.150 wt% at 30 °C. The contact angle of the oleic acid droplet on PP was 27.5° in air. As soon as the droplet came into the surfactant solution, the contact angle rapidly increased from 27.5° to 68° in a few min; thereafter it gradually increased with the time until it reached 81° after 20 min. Accordingly, the contact area between the droplet and PP decreased, and the droplet was constricted and floated away after about 26 min. Thereafter, a transparent layer, the so-called "complex," was formed at the remaining droplet/solution interface after about 40 min.

The olive oil droplet was removed incompletely from the PP surface after 34.5 min by the same process as that used for the oleic acid droplet, but in this case the complex was not formed. Lauryl alcohol behaved

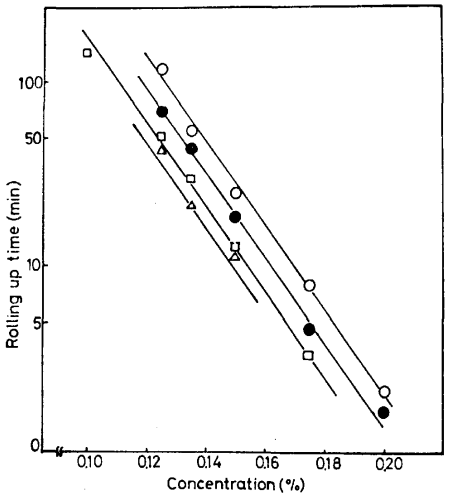

Fig. 4. The effect of NaDBS concentration of the time required for rolling up of oleic acid droplet.
○: 30 °C, ●: 40 °C, □: 50 °C, △: 55 °C.

like oleic acid in the earlier stages, but the complex was formed on the surface of the droplet after 60 min and the droplet coated with the complex gradually grew and then was incompletely detached and floated away after 220 min. The oleyl alcohol droplet was kept for 50 h. The complex began to form after 150 min; it grew gradually with the time and covered the droplet, but no rolling-up occurred. A rigid complex seemed to form between oleyl alcohol and NaDBS. On liquid paraffin, little change was recognized within 50 min.

Figure 2 shows the dependence of the contact angle of oleic acid on PP on the time in the solutions of NaDBS at various concentrations. Similar relations were also obtained for olive oil, lauryl alcohol, and oleyl alcohol, but, as is shown in Fig. 3 no distinct change was recognized with the time for liquid paraffin in the solutions of NaDBS. Table 1 summarizes the results obtained above.

The contact angle of the soils in air decreased in this order: olive oil > oleic acid > oleyl alcohol > liquid paraffin>lauryl alcohol. These results agree approximately with Zisman's;[11] that is, the contact angle of the same series of organic liquids on a low-energy surface decreases with the decrease both the molecular weight and the surface tension. However, when oily soils are placed in the NaDBS solution, the

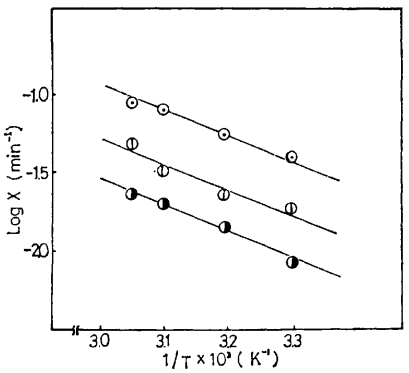

Fig. 5. Arrhenius plot for rolling up of oleic acid droplet in NaDBS solution.
⊙: 0.150%, ⓘ: 0.135%, ◑: 0.125%.

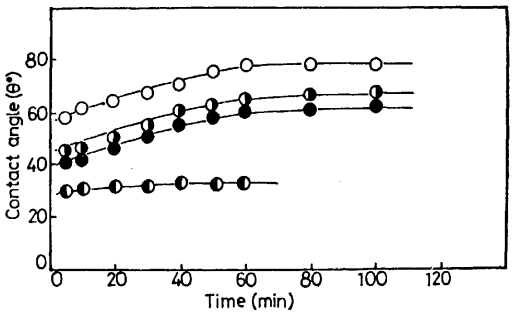

Fig. 6. The contact angle of oleic acid droplet in NaDBS–Na_2SO_4 solution (total solid 0.100%, at 30 °C). Surfactant: builder ratio, ●; 1 : 0, ○; 3 : 1, ◑; 1 : 1, ◐; 1 : 3.

contact angle of the oil/substrate interface gradually increases, and substantially the contact angle increases with the increase in the surfactant concentration. The rolling-up was observed in all the soils except oleyl alcohol and liquid paraffin; the time required for the rolling-up of soils from PP decreased in this order: lauryl alcohol>olive oil>oleic acid. Visible complexes were formed for oleic acid, lauryl alcohol, and oleyl alcohol at the surface of the droplets.

Effect of Concentration of NaDBS and Temperature. Figure 4 shows the effect of the concentration of the NaDBS solution on the time required for the rolling-up of an oleic acid droplet between 30 and 55 °C. It may be seen in Fig. 4 that the time required for the removal of the oleic acid droplet by rolling-up becomes shorter exponentially with the increase in the concentration at each temperature. A similar result was also obtained for olive oil.

In Fig. 5, the logarithms of the reciprocal rolling-up time (log X) are plotted as functions of the reciprocal absolute temperature($1/T$) for oleic acid. The relation gives a straight line. Consequently, the apparent activation energies for rolling-up are derived, *i.e.*, 8 kcal/mol for oleic acid and 11.9 kcal/mol for olive oil.

Effect of Neutral Builders. Figure 6 shows the time dependence of the contact angle of oleic acid against PP in the surfactant solutions containing

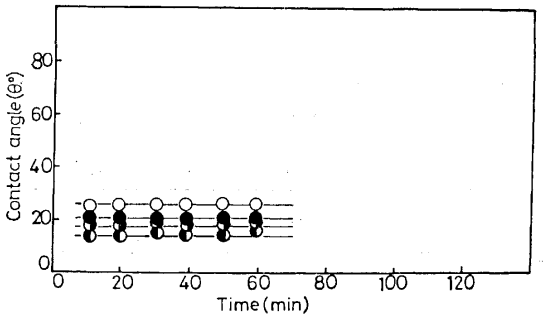

Fig. 7. The contact angle of liquid paraffin droplet in NaDBS–Na_2SO_4 solution (total solid 0.100%, at 30 °C). Surfactant : builder ratio, ●; 1 : 0, ○; 3 : 1, ◑; 1 : 1, ◐; 1 : 3.

Table 2. The time required for rolling up of oleic acid droplet in NaDBS–Na_2SO_4 solution at 30 °C (min)

Surf. : builder	Total concn (%)				
	0.100	0.125	0.150	0.175	0.200
1 : 0	—	120.2	26.9	7.9	2.2
3 : 1	—	92.0	14.5	6.3	2.4
1 : 1	—	—	88.3	70.6	17.4
1 : 3	—	—	—	—	—
0 : 1	—	—	—	—	—

Table 3. The time required for rolling up of olive oil droplet in NaDBS–Na_2SO_4 solution at 30 °C (min)

Surf. : builder	Total concn (%)				
	0.100	0.125	0.150	0.175	0.200
1 : 0	—	—	34.5	8.5	In.
3 : 1	39.0	8.6	In.	In.	In.
1 : 1	—	9.4	3.5	In.	In.
1 : 3	—	—	—	10.0	8.6
0 : 1	—	—	—	—	—

In: Instantaneous.

neutral builder sodium sulfate (0.100 wt%). Similar figures were also obtained for olive oil, lauryl alcohol, and oleyl alcohol, but, as is shown in Fig. 7, no distinct change was observed for liquid paraffin. It was found that, when the ratio of NaDBS to Na_2SO_4 was 3 to 1 by weight, the increase in the contact angle with the time became the largest at each oily soil. The effect of the total concentration of NaDBS and Na_2SO_4 on the rolling-up of the oily soils was further studied. The results are shown in Tables 2 and 3 for oleic acid and olive oil droplets respectively at 30 °C. As is evident from these results, the time required for rolling-up decreases most remarkably in the solution containing NaDBS and Na_2SO_4 at the ratio of 3 to 1, while the time required for the rolling-up of oleic acid was shorter than that of olive oil in the solution containing the neutral builder Na_2SO_4, but the result was the inverse in the surfactant solution

Table 4. Removal of oily soils

	In 0.150% NaDBS solution		In NaDBS : Na_2SO_4=1 : 1 (total solid 0.200%) solution		In NaDBS : Alkaline builder= 1 : 1(total solid 0.200%) solution	
	Rolling up	Liquid crystal	Rolling up	Liquid crystal	Rolling up	Liquid crystal
Oleic acid	○	○	○	○	×	◎
Olive oil	○	×	◎	×	◎	×
Lauryl alcohol	○	○	×	○	×	◎
Oleyl alcohol	×	○	×	○	×	◎
Liquid paraffin	×	×	×	×	×	×

◎; Rolling up occurred instantly. ○; Rolling up occurred. ×; No rolling up occurred.
◎; Liquid crystal formed strongly. ○; Liquid crystal formed. ×; No liquid crystal formed.

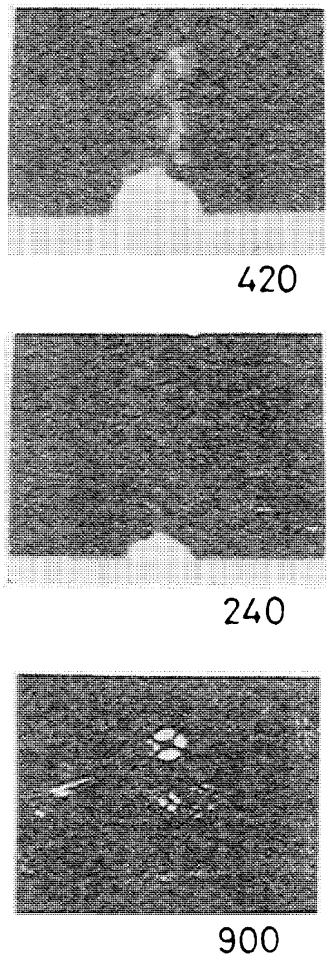

Fig. 12. The behavior of oily soil in the NaDBS containing alkaline builder.
a) oleic acid (NaDBS : STPP=1 : 1, total concn 0.200%, after 420 min).
b) lauryl alcohol (at the same condition of above, after 240 min).
c) myelinic figure for oleyl alcohol (NaDBS : Na_2CO_3=1 : 1, total concn 0.200%, after 900 min).

buoyancy of the oily soil, the cohesive force of the oil itself, and the adhesive force between oil and substrate. When these three forces are unbalanced and the buoyancy overcomes the other forces as a result of the adsorption and the desorption of surfactant molecules at the substrate/soil/solution interfaces under the hydrodynamic fluctuation or the convection of the solution, the incomplete detachment and floatation of the oily soil, the process from Stage 5 to Stage 7 in Fig. 8 will take place. We assume that the complex formation may also contribute to the rolling-up of lauryl alcohol [Fig. 8(b)].

Observation of Liquid Crystals. As is shown in Fig. 1, we observed complexes on the surface of soils, especially a distinct complex layer on lauryl and oleyl alcohol droplets. Figure 11 shows the appearance of complexes for oily soils in a 0.150 per cent NaDBS solution; we made the observation by means of the polarizing microscope with crossed nicols. Complexes from oleic acid (remaining droplet after rolling-up), lauryl alcohol, and oleyl alcohol show optical anisotropy around the original oily soil. Therefore, we assumed that these complexes might be regarded as ternary liquid crystalline phases composed of an oil–water–surfactant.[4,12]

We studied further the behavior of oily soils in the NaDBS solution containing builders. Table 4 summarizes the results. With respect to oleic acid, in the solution containing only NaDBS and NaDBS with Na_2SO_4, rolling-up occurred before the formation of the liquid-crystalline phase. As is shown in Fig. 12(a), though in the solution containing NaDBS and alkaline builders such as sodium tripolyphosphate(STPP) or sodium carbonate, no rolling-up occurred. Oleic acid is considered to react with the alkaline builder to form sodium oleate at the solution/soil interface; as a result, the oleic acid would be removed from the PP surface by a spontaneous emulsification.

Olive oil forms no liquid crystal; nevertheless, it is remarkably rolled up by the addition of builders to a surfactant. For higher alcohols, such as lauryl and oleyl alcohol, the time required to form a liquid crystal is shorter in the solution of NaDBS containing an alkaline builder than in the other solutions. As is shown in Fig. 12(b), lauryl alcohol was removed continuously in small droplets from PP in the solution of NaDBS containing STPP, while oleyl alcohol showed a myelinic appearance after about 900 min in the solution of NaDBS containing Na_2CO_3 [Fig. 12(c)]. With respect to liquid paraffin, no distinct change was recognized, not even in the solution of NaDBS containing builders.

References

1) A. M. Schwartz, *J. Am. Oil Chem. Soc.*, **48**, 566 (1971).
2) J. T. Davies, "Interfacial Phenomena," Academic

Press, New York and London (1961), p. 418.
3) N. K. Adam, *J. Soc. Dyestuff Col.*, **53**, 121 (1937).
4) D. G. Stevenson, *J. Textile Inst.*, **44**, T12 (1953).
5) R. E. Wagg and G. D. Mrs. Fairchild, *J. Textile Inst.*, **48**, 455 (1958).
6) R. P. Harker, *J. Textile Inst.*, **50**, Y189 (1959).
7) T. Tsunoda and Y. Oba, *Yukagaku*, **18**, 41 (1969).
8) W. Kling, *Kolloid-Z.*, **115**, 37 (1949).
9) W. Kling and H. Kopp, *Melliand Textilber.*, **30**, 23 (1949).
10) W. Kling and H. Lang, *Kolloid-Z.*, **142**, 1 (1955).
11) W. A. Zisman, *J. Colloid Sci.*, **5**, 514 (1959); *ibid.*, **7**, 109 (1952).
12) A. S. C. Lawrence, *Nature*, **183**, 1491 (1959).

NOTES

BULLETIN OF THE CHEMICAL SOCIETY OF JAPAN, VOL. 49 (6), 1709—1710 (1976)

The Crystal Structure and the Absolute Configuration of (+)-2,3 : 6,7-Dibenzobicyclo[3.3.1]nona-2,6-diene-4,8-diyl Bis(*p*-bromobenzoate)

Tsuguhiro KANEDA, Chuji KATAYAMA, and Jiro TANAKA

Department of Chemistry, Faculty of Science, Nagoya University, Chikusa, Nagoya 464

(Received February 26, 1976)

Synopsis. The crystal and the molecular structure of the titled compound was investigated by the X-ray diffraction method. The absolute configuration was determined by the Bijvoet method as 1*R*4*S*5*R*8*S*.

The titled compound was synthesized, optically resolved, and crystallized by Tatemitsu, Ogura, Nakagawa, Nakagawa, Naemura, and Nakazaki.[1] The optical properties of related compounds to it were investigated, and it was desired to determine the absolute configuration of the compound by the X-ray method.

Experimental

The space group of the crystal was determined from oscillation and Weissenberg photographs. The cell dimensions were determined by the least-squares method, using 12 reflections which had been carefully measured on a Hilger-Watts four-circle diffractometer with Ni-filtered Cu$K\alpha$ radiation (λ=1.5418 Å). Crystal data : $C_3H_{22}O_4Br_2$, *M. W.* =618.34, orthorhombic $P2_12_12_1$, a=12.391(1), b=19.802(1), c=10.595(1)Å, z=4, D_m=1.576, D_c=1.580 g·cm^{-3}, μ=46.79 cm^{-1} (for Cu$K\alpha$ radiation). Intensity data were collected with the diffractometer in the θ-2θ scanning mode ($2\theta \leqq 144°$) with the same radiation using a crystal whose size was 0.2×0.2×0.4 mm. No correction was made for absorption or extinction.

TABLE 1. ATOMIC PARAMETERS (×10^4) AND THEIR STANDARD DEVIATIONS

The anisotropic thermal factors are of the form $\exp\{-(h^2B_{11}+k^2B_{22}+l^2B_{33}+hkB_{12}+hlB_{13}+klB_{23})\}$.

	x	y	z	B_{11}	B_{22}	B_{33}	B_{12}	B_{13}	B_{23}
Br(1)	3939(2)	9820(1)	−4144(1)	133(1)	25(1)	103(1)	−1(1)	17(3)	−2(1)
Br(2)	2612(1)	2943(1)	4721(2)	100(1)	23(1)	230(3)	17(1)	24(4)	−5(2)
O(1)	3584(7)	8581(4)	1814(8)	64(6)	16(2)	78(8)	−14(6)	−34(13)	−2(7)
O(2)	4216(10)	9599(4)	2303(9)	165(13)	21(2)	119(11)	−33(9)	−145(22)	10(9)
O(3)	1961(7)	6342(4)	4439(8)	97(8)	18(2)	84(10)	0(7)	73(16)	3(8)
O(4)	1209(9)	6168(4)	6345(8)	139(11)	22(2)	94(10)	22(9)	82(19)	10(8)
C(1)	3008(12)	7349(6)	5027(11)	113(13)	22(3)	39(10)	−10(11)	40(22)	−6(11)
C(2)	3870(10)	7186(5)	4072(12)	56(8)	20(3)	88(12)	−8(9)	−8(22)	5(11)
C(3)	4141(9)	7662(6)	3147(12)	42(8)	23(3)	83(12)	−2(9)	−3(19)	−9(11)
C(4)	3683(10)	8369(5)	3129(12)	67(10)	16(3)	74(12)	−4(9)	−11(20)	−3(10)
C(5)	2597(11)	8410(5)	3792(11)	67(10)	19(3)	79(13)	−21(10)	19(21)	10(10)
C(6)	1706(10)	8046(5)	3149(13)	60(9)	12(3)	113(15)	−5(8)	28(22)	−6(11)
C(7)	1392(10)	7388(6)	3512(12)	48(9)	21(3)	84(13)	2(9)	18(19)	1(11)
C(8)	1848(11)	7067(5)	4671(13)	97(11)	12(2)	105(15)	−25(10)	44(24)	−4(11)
C(9)	2827(13)	8139(6)	5148(13)	128(15)	23(3)	80(14)	6(12)	43(27)	−15(12)
C(10)	4399(10)	6564(6)	4139(14)	55(9)	23(3)	106(14)	5(9)	−34(23)	1(13)
C(11)	5173(11)	6391(7)	3273(14)	67(10)	27(4)	122(17)	−28(11)	−30(26)	7(14)
C(12)	5427(12)	6835(7)	2291(16)	68(11)	32(4)	139(19)	14(12)	−35(26)	−23(16)
C(13)	4924(11)	7470(6)	2234(12)	62(10)	24(3)	85(15)	−15(10)	6(22)	−3(12)
C(14)	1176(11)	8368(6)	2163(13)	50(9)	22(3)	129(17)	15(10)	−13(23)	−4(13)
C(15)	313(12)	8042(8)	1517(15)	73(11)	36(5)	139(19)	27(13)	−6(27)	−1(18)
C(16)	12(13)	7380(8)	1847(18)	75(12)	35(5)	204(26)	−19(13)	13(35)	12(21)
C(17)	555(11)	7068(7)	2842(16)	72(11)	29(4)	155(21)	−23(13)	16(26)	−20(17)
C(18)	3889(11)	9193(5)	1563(12)	75(10)	15(3)	111(15)	−6(10)	−75(25)	−10(11)
C(19)	3902(10)	9332(5)	137(11)	72(9)	13(2)	82(12)	1(9)	−22(23)	−8(10)
C(20)	3148(11)	9020(6)	−639(12)	74(10)	28(4)	82(15)	−12(11)	−34(23)	−19(13)
C(21)	3119(12)	9171(6)	−1926(13)	88(12)	23(4)	91(14)	5(11)	40(24)	−7(13)
C(22)	3910(11)	9627(6)	−2354(12)	58(9)	21(3)	100(14)	3(10)	−6(23)	−13(11)
C(23)	4681(12)	9939(7)	−1643(14)	92(13)	26(4)	122(17)	−20(12)	−9(27)	14(15)
C(24)	4668(11)	9802(6)	−318(13)	88(11)	23(3)	100(14)	−13(12)	3(23)	−3(14)
C(25)	1638(10)	5956(6)	5419(13)	54(9)	22(3)	98(14)	−10(9)	−4(20)	10(12)
C(26)	1843(10)	5218(6)	5176(12)	58(8)	22(3)	89(13)	1(10)	−9(20)	29(13)
C(27)	2408(14)	5001(6)	4083(13)	99(12)	23(3)	105(14)	6(11)	35(29)	−6(12)
C(28)	2652(13)	4300(7)	3946(15)	94(13)	27(4)	130(18)	13(13)	22(3)	17(15)
C(29)	2305(10)	3868(5)	4900(12)	57(9)	18(3)	106(15)	7(9)	−13(22)	−13(11)
C(30)	1735(12)	4070(7)	5929(16)	80(11)	25(4)	138(18)	12(11)	30(28)	20(16)
C(31)	1483(11)	4752(6)	6055(12)	95(12)	25(4)	79(13)	4(12)	26(23)	13(13)

Structure Determination

The structure was determined by the symbolic addition method using the program coded by Dr. Furusaki in Hokkaido University. An E-map revealed all the atoms except hydrogen atoms. The block-diagonal least-squares refinement was proceeded with anisotropic thermal parameters for all non-hydrogen atoms by using 1929 independent reflections with $|F^\circ| > 3\sigma$. The final R-index was converged to 0.062 with an equal weight for each reflection. The program HBLS-IV coded by Prof. Ashida was utilized for the block-diagonal least-squares refinement. The final atomic parameters with their standard deviations are shown in Table 1.

The atomic scattering factors for all atoms and $\Delta f'$ and $\Delta f''$ values for bromine atom were taken from International Tables for X-ray Crystallography.[2] The computations were carried out on a FACOM 230-60 computer at Nagoya University Computation Center. The table of the observed and calculated structure factors is kept at the office of this Bulletin. (Document No. 7623).

Results and Discussion

Figure 1 shows the atomic labelings, bond distances and angles with their standard deviations. The molecule has a bicyclo[3.3.1]nonadiene ring skeleton, and the bicyclo ring seems to be distorted by the

TABLE 2. DETERMINATION OF THE ABSOLUTE CONFIGURATION

h	k	l	$100\times\{I(hkl)-I(\overline{hkl})\}/I(hkl)$ Obsd	Calcd
1	6	4	−6.0	−8.5
2	2	1	5.3	7.1
2	10	1	9.0	9.3
3	4	2	−6.7	−5.1
4	11	1	−8.7	−9.6
5	8	2	8.2	6.5
6	5	5	−9.1	−7.6
6	6	5	5.3	5.9

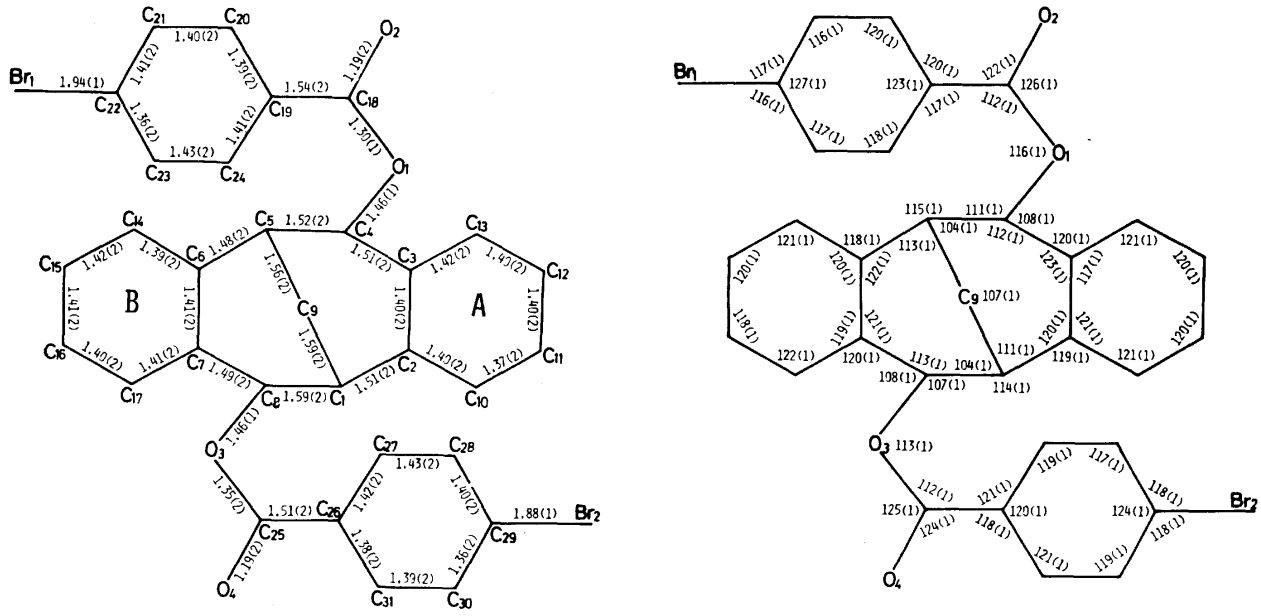

Fig. 1. Bond distances (l/Å), bond angles (ϕ/°) and atomic labelings. The e.s.d.'s are shown in the parentheses. Symbols, A and B, in the benzene rings are the names of the corresponding rings.

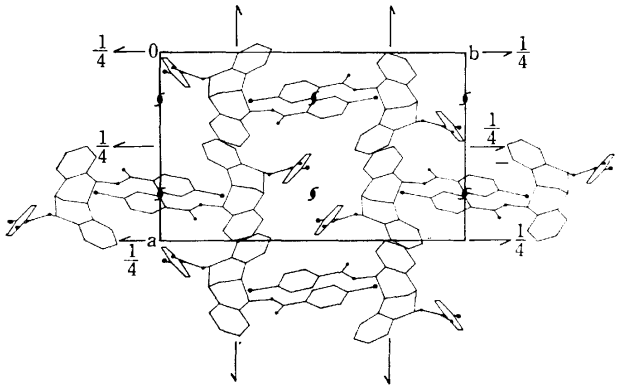

Fig. 2. Projection of the structure along c axis.

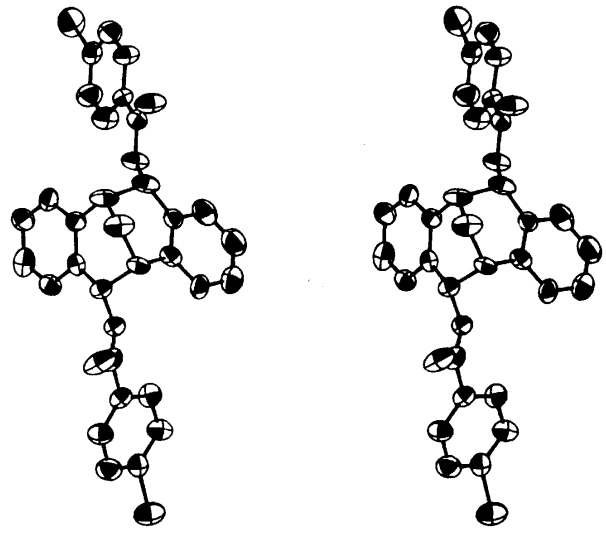

Fig. 3. Stereoscopic view of the molecule. The atoms are represented as thermal ellipsoids of a size such that the vibrating atoms have a 50% probability of being found within them.

presence of the bridge. Bond angles C(2)–C(1)–C(8) and C(4)–C(5)–C(6) are larger by 4.5° and 5.5°, respectively, than the normal tetrahedral angle. On the other hand, C(8)–C(1)–C(9) and C(4)–C(5)–C(9) are both smaller by 5.5° than the normal value. The planarities of two benzene rings, A and B, are good with the maximum deviations by 0.02 and 0.01 Å, respectively, while C(4) deviates by 0.16 Å from the A plane and C(8) by 0.19 Å from the B plane. These considerable deviations are not noticed in (−)-argemonine methiodide which also has bicyclo[3.3.1]nonadiene skeleton.[3] The bond distances and the remaining bond angles show the normal values for the respective bond types. Dihedral angle between the A and B planes is 86.9°, which was 90.4° in (−)-argemonine methiodide. Projection of the structure along the c axis is shown in Fig. 2. No particularly short intermolecular contact was found in this crystal.

The absolute configuration was determined by the Bijvoet method using the anomalous scattering by the bromine atom. The observed and calculated intensity differences between 8 pairs are listed in Table 2. The signs of observed values are in good agreement with those calculated based on the positional parameters of Table 1 in the right-handed coordinate system. The absolute configuration thus determined is 1*R*4*S*5*R*8*S* for (+)-enantiomer (Fig. 3).

References

1) H. Tatemitsu, F. Ogura, Y. Nakagawa, M. Nakagawa, K. Naemura, and M. Nakazaki, *Bull. Chem. Soc. Jpn.*, **48**, 2473 (1975).

2) "International Tables for X-ray Crystallography," Vol. III, Birmingham : Kynoch Press (1968), p. 201.

3) T. Kaneda, N. Sakabe, and J. Tanaka, *Bull. Chem. Soc. Jpn.*, **49**, 1263 (1976).

BULLETIN OF THE CHEMICAL SOCIETY OF JAPAN, VOL. 49 (6), 1711—1712 (1976)

Viscosity *B* Coefficients for Di- and Trialkylammonium Chlorides in Aqueous Solutions

Kunio TAMAKI, Mitsuyoshi KUSHIDA, and Yōko ŌHARA
Department of Chemistry, Yokohama City University, Kanazawa-ku, Yokohama 236
(Received March 11, 1976)

Synopsis. The viscosity *B* coefficients of the Jones-Dole equation for di-*n*-alkylammonium chlorides (methyl to butyl) and tri-*n*-alkylammonium chlorides (methyl to propyl) in water at 25 °C were determined, and the effect of structural changes in the solvent water induced by the alkyl-substituted ammonium ions is discussed.

The behavior of electrolytes with nonpolar groups in water may be interpreted approximately by a balance of two types of interaction; hydrophobic hydration due to the nonpolar parts, and electrostrictive hydration due to the ionic parts.[1] In a previous paper,[2] the role of the alkyl groups in the coordination of the charge-bearing nitrogen atom in the series of *n*-alkylammonium salts RNH_3X, di-*n*-alkylammonium salts R_2NH_2X, tri-*n*-alkylammonium salts R_3NHX, and tetra-*n*-alkylammonium salts R_4NX was discussed on the basis of the changes in the heat capacity upon dissolution in water. The study of the viscosity of aqueous electrolyte solutions provides a useful method of obtaining information on ion-solvent interactions.[3,4] The viscosity *B* coefficients for RNH_3X[1,5] and R_4NX[6-9] are found in the literature. In this paper, we will report our experimental study of the viscosity *B* coefficients for R_2NH_2Cl (methyl to butyl) and R_3NHCl (methyl to propyl) in aqueous solutions.

Experimental

R_2NH_2Cl and R_3NHCl salts used in this work were the same samples as those described in a previous paper.[2] The viscosities were measured at 25±0.007 °C by a method similar to that described in our previous papers.[1,10]

Results and Discussion

The viscosity of aqueous electrolyte solutions is given by the Jones-Dole equation:[11]

$$\eta/\eta_0 = 1 + Ac^{1/2} + Bc \quad (1)$$

where η and η_0 are the viscosity of the solution and the solvent respectively; c, the molar concentration; A, the constant arising from the interaction between the ions, and B, the viscosity *B* coefficient. Equation 1 may be converted to:

$$(\eta/\eta_0-1)/c^{1/2} = A + Bc^{1/2} \quad (2)$$

By plotting $(\eta/\eta_0-1)/c^{1/2}$ against $c^{1/2}$, as is shown in Fig. 1, the *B* coefficient can be determined from the slope of the straight line. The values of the *B* coefficient so determined are summarized in Table 1.

The *B* value obtained in this procedure is considered to be the sum of the contributions from a cation and an anion. Taking the ionic *B* value, B_{ion}, of Cl^- ion to be −0.007 according to the separation basis of Gurney,[3] the B_{ion} values of $R_2NH_2^+$ and R_3NH^+ ions

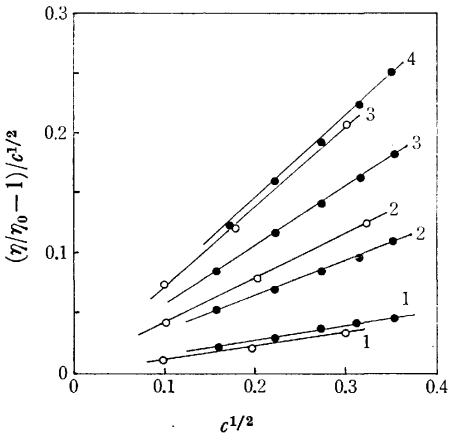

Fig. 1. Plots of $(\eta/\eta_0-1)/c^{1/2}$ against $c^{1/2}$. ● R_2NH_2Cl salts, ○ R_3NHCl salts. 1, methyl; 2, ethyl; 3, propyl; 4, butyl.

TABLE 1. ESTIMATION OF THE ION-SOLVENT INTERACTION EFFECTS

R	*B* (l/mol)	B_{ion} (l/mol)	$\overline{V}^\circ$ (cm³/mol)	$\overline{V}^\circ_{ion}$ (cm³/mol)	B_{solv} (l/mol)
			R_2NH_2Cl		
Me	0.105	0.112	72.5	49.3	−0.011
Et	0.286	0.293	106.7	83.5	0.084
Pr	0.490	0.497	138.7	115.5	0.208
Bu	0.687	0.694	170.7	147.5	0.325
			R_3NHCl		
Me	0.110	0.117	90.59	67.3	−0.051
Et	0.378	0.385	138.6	115.4	0.097
Pr	0.681	0.688	186.8	163.6	0.279

can be obtained; they are listed in Table 1.

The viscosity *B* coefficient is usually interpreted as consisting of two terms; the first is the effect of the ionic size, B_{size}, and the second is the contribution arising from the ion-solvent interaction, B_{solv};[4]

$$B_{ion} = B_{size} + B_{solv} \quad (3)$$

If we assume that the Einstein equation derived for the case of spherical colloid may be applied approximately to the aqueous electrolyte solutions, B_{size} may be obtained from this equation:

$$B_{size} = 0.0025\,\overline{V}^\circ_{ion} \quad (4)$$

where $\overline{V}^\circ_{ion}$ is the ionic partial molal volume expressed in cm³/mol. Thus, B_{solv} can be derived by ths use of this equation:[7]

$$B_{solv} = B_{ion} - 0.0025\overline{V}^\circ_{ion} \quad (5)$$

The values of the partial molal volume, $\overline{V}^\circ$, of R_2NH_2Cl and R_3NHCl salts have been reported by Conway and

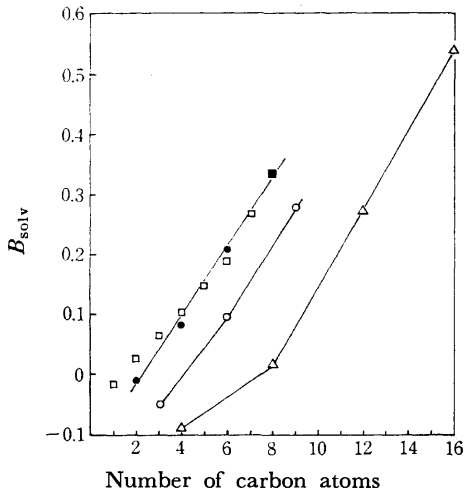

Fig. 2. Plots of B_{solv} against number of carbon atoms in the ions. □ RNH_3^+, ● $R_2NH_2^+$, ○ R_3NH^+, △R_4N^+.

his collaborators.[12,13] The $\overline{V}^\circ_{ion}$ values of $R_2NH_2^+$ and R_3NH^+ ions may be obtained by subtracting 23.2 cm^3/mol, the $\overline{V}^\circ_{ion}$ value of Cl^- ion[14], from the $\overline{V}^\circ$ values of R_2NH_2Cl and R_3HNCl salts. The B_{solv} values obtained for $R_2NH_2^+$ and R_3NH^+ ions are summarized in Table 1.

As may be seen in Table 1, the B_{solv} values of $Me_2NH_2^+$ and Me_3NH^+ ions are negative; both the methyl salts are, then, to be classified as simple salts. This implies that the interaction of the charge-bearing nitrogen atom with water surpasses the hydrophobic hydration due to methyl groups; thus, the overall behavior of these methyl salts in water is governed by electrostrictive hydration.

Table 1 indicates the positive B_{solv} values for $Et_2NH_2^+$, $Pr_2NH_2^+$, $Bu_2NH_2^+$, Et_3NH^+, and Pr_3NH^+ ions; they are all classifiable as the hydrophobic structure-making ions in water.

The B_{solv} values of RNH_3^+ and R_4N^+ ions may also be obtained using the viscosity and partial molal volume data in the literature.[1,5–9,15] Thus, in the cases of RNH_3^+, $R_2NH_2^+$, R_3NH^+, and R_4N^+ series, the dependence of the B_{solv} values on the total number of carbon atoms in the ions is shown in Fig. 2. It is found that the B_{solv} values for the alkyl-substituted ammonium ions with the same number of carbon atoms will be in this order: $RNH_3^+ \fallingdotseq R_2NH_2^+ > R_3NH^+ > R_4N^+$. The Behavior of the B_{solv} values obtained in this paper for the alkyl-substituted ammonium ions is consistent with the inclination of the changes in the heat capacity upon dissolution of these salts in water reported in a previous paper.[2]

References

1) K. Tamaki, Y. Ōhara, H. Kurachi, M. Akiyama, and H. Odaki, *Bull. Chem. Soc. Jpn.*, **47**, 384 (1974).
2) K. Tamaki, S. Yoshikawa, and M. Kushida, *Bull. Chem. Soc. Jpn.*, **48**, 3018 (1975).
3) R. W. Gurney, "Ionic Processes in Solution," McGraw-Hill, New York (1953).
4) R. H. Stokes and R. Mills, "Viscosity of Electrolytes and Related Properties," Pergamon, Oxford (1965).
5) J. E. Desnoyers, M. Arel, and P-A. Leduc, *Can. J. Chem.*, **47**, 547 (1969).
6) R. L. Kay, T. Vituccio, C. Zawoyski, and D. F. Evans, *J. Phys. Chem.*, **70**, 2336 (1966).
7) J. E. Desnoyers and G. Perron, *J. Solution Chem.*, **1**, 199 (1972).
8) D. Eagland and G. Pilling, *J. Phys. Chem.*, **76**, 1902 (1972).
9) P. K. Mandall, B. K. Seal, and A. S. Basu, *Z. Phys. Chem. Neue Folge*, **89**, 41 (1974).
10) K. Tamaki, Y. Ōhara, and Y. Isomura, *Bull. Chem. Soc. Jpn.*, **46**, 1551 (1973).
11) G. Jones and M. Dole, *J. Am. Chem. Soc.*, **51**, 1950 (1929).
12) L. H. Laliberté and B. E. Conway, *J. Phys. Chem.*, **74**, 4116 (1970).
13) R. E. Verrall and B. E. Conway, *J. Phys. Chem.* **70**, 3961 (1966).
14) F. J. Millero, *Chem. Rev.*, **71**, 147 (1971).
15) F. J. Millero, "Water and Aqueous Solutions, Structure, Thermodynamics, and Transport Processes," ed. by R. A. Horne, Wiley-Interscience, New York, N. Y. (1972), p. 565.

BULLETIN OF THE CHEMICAL SOCIETY OF JAPAN, VOL. 49 (6), 1713—1714 (1976)

The Catalytic Hydroboration of Ethylene with Diborane in the Gas Phase — The Acidity of Catalysts and the Reaction Activity —

Tsuneo MATSUDA, Isao SETO,* and Toyosuke TANAKA

Faculty of Engineering, Saitama University, Shimoohkubo, Urawa, Saitama 338

**Bridgestone Tire Co. Ltd., Kyobashi, Chuo-ku, Tokyo 104*

(Received December 8, 1975)

Synopsis. The catalytic hydroboration of ethylene with diborane to triethylborane in the gas phase was studied in the presence of various catalysts. The acidity of catalysts and the reaction activity were measured; the increase in the activity can be related to surface acidity of the catalysts.

The hydroboration of olefin in the liquid phase using diglyme (diethylene glycol dimethyl ether), tetrahydrofuran (THF), diethyl ether and so on as solvent was widely investigated.[1] Very few investigations of the noncatalytic hydroboration in the gas phase have, however, been reported.[2-5] We previously found that Pd–carbon was a active catalyst for the vapor-phase hydroboration of ethylene.[6] In this paper the activity of various catalysts in the hydroboration of ethylene was investigated, and it was found that the surface acidity of catalysts is correlated with its activity.

Experimental

The reaction was carried out in a closed circulation apparatus equipped with two small traps in which the product was collected. One of the traps was cooled with a salt–ice bath during the reaction.

Diborane was produced by allowing $NaBH_4$ in a diglyme solution or $LiAlH_4$ in an ether solution to react with $BF_3 \cdot C_2H_5OC_2H_5$ at room temperature under a nitrogen atmosphere.[7] The diborane was purified by freezing it with liquid nitrogen, by then pumping off any impurities, and finally by distilling it. The ethylene was also purified by low-temperature distillation. The catalysts used were Pd-carbon (Pd 3 wt.%), α- and γ-Al_2O_3 (kindly provided by Kawaken Fine Chemicals and the Tōkai Kōnetsu Co., Ltd.), active carbon, Ni-γ-Al_2O_3, and silica gel and its pretreated species with an acidic or alkaline medium. Before the reaction the catalysts were treated at 450 °C for 1 h under a vacuum (about 10^{-3} mmHg). The reaction conditions were as follows: molar ratio: 6 (C_2H_4; 4.58, B_2H_6; 0.758 mmol); catalyst used: 0.5 g; temperature: 50 °C, and time: 1 h. After the reaction, the residual gases in the apparatus were condensed by the liquid nitrogen into another trap containing THF, which was then isolated from the reactor system during the reaction, in order to recover the unreacted diborane. Then the dry nitrogen was admitted into the apparatus and the reaction vessel, and the traps in which the product had condensed were removed from the reactor system. Immediately the catalyst in the reaction vessel was washed with the purified ether several times in order to extract the reaction product adhering on the catalyst, after which the extract was added to the trap containing the product. The product thus collected was analyzed by gas chromatography, with a 10 wt% Silicone oil on Celite 545 column,[8] and using toluene as the internal standard. The unreacted diborane in THF was converted to boric acid with water. The boric acid was then titrated with a sodium hydroxide solution in the presence of glycerol, using phenolphtalein as an indicator.

The surface acidity of the catalysts was determined by the measurement of the irreversibly adsorbed amount of ammonia at 50 °C.

Results and Discussion

The only hydroboration product of ethylene under the conditions described above was triethylborane. It has been reported that, in a high molar ratio of diborane to olefins, mono- and dialkylborane were produced in the gas phase without any catalyst,[4] but in this study no such products were detected. The pressure changes during all the catalytic reactions were almost the same as in the previous paper;[6] an induction period in the initial stage was observed in every case. The catalyst properties and the results of the hydroboration of ethylene on the various catalysts are summarized in Table 1. A good correlation between the catalytic activity (yield) and the acidity was found, as is indicated in Fig. 1.

The γ-Al_2O_3, both supported and non-supported, was active, and in the hydroboration with the Ni-γ-Al_2O_3 catalyst tributylborane was detected in a small yield as well as triethylborane. The tributylborane may be formed by the reaction of diborane and the butenes which are produced by the dimerization of ethylene, since Ni or NiO supported on a silica and (or) an alumina catalyst showed catalytic activity in the dimerization of ethylene.[9] The addition of nickel

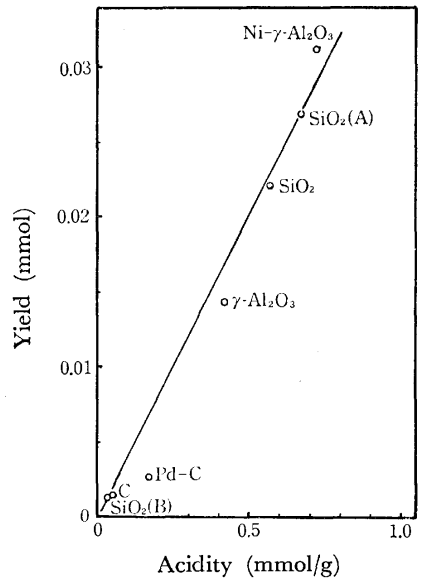

Fig. 1. A correlation of the yield and the acidity of the various catalysts.

TABLE 1. PROPERTIES OF CATALYSTS AND THIER CATALYTIC BEHAVIOR FOR HYDROBORATION OF ETHYLENE

Catalyst	Pd-carbon (Pd 3%)	Active carbon	α-Al_2O_3	Pd-α-Al_2O_3[a] (Pd 1%)	Pd-α-Al_2O_3[a] (Pd 3%)	γ-Al_2O_3	Ni-γ-Al_2O_3[b]	SiO_2[c]	SiO_2 (A)[d]	SiO_2 (B)[e]
Surface area[f] (m^2/g)	1030	1206	1.6	—	—	212	228	594	560	—
Acidity (mmol/g)	0.165	0.045	0	—	trace	0.427	0.725	0.567	0.674	0.035
Yield × 10 mmol[g]	0.354	0.167	0	trace	trace	1.45	3.15	2.33	2.69	0.160
(%)	4.7	2.2	—	—	—	19.1	41.6	30.7	35.5	2.1
Conversion[h] (%)	83.9	81.1	—	—	—	60.8	67.5	—	—	—
Selectivity[i] (%)	5.6	2.7	—	—	—	31.4	61.6	—	—	—

a) The α-Al_2O_3 was dipped in palladium chloride hydrochloric acid solution and then calcined at 400 °C for several hours in H_2 atmosphere. b) The catalyst containing 2.8 wt% Ni on γ-Al_2O_3 was prepared by the impregnation of γ-Al_2O_3 with $Ni(NO_3)_2$ solution and calcined at 400 °C for several hours in H_2 atmosphere. c) Commercial SiO_2 from Wakō Junyaku Co., Ltd. d) The silica gel in c) was boiled in 1M-HCl for 30 min and then washed with distillated water until no acid was detected. e) The silica gel in c) was treated in 1M-NaOH in stead of HCl by the same way as described in d). f) The surface area was determined by BET method at −196 °C with nitrogen. g) Percentage yield was calculated on the basis of both the amount of $B(C_2H_5)_3$ produced and the initial amount of diborane, $[B_2H_6]_0$. h) Conversion was calculated as the following equation; $\frac{[B_2H_6]_0-[B_2H_6]}{[B_2H_6]_0}\times 100$ $[B_2H_6]$; amount of unreacted diborane. i) $(\text{selectivity})=\frac{(\text{yield }\%)}{(\text{conversion})}\times 100$.

TABLE 2. THE DISTRIBUTION OF THE ACIDIC STRENGTH OF SOME CATALYST (unit; mequ./g)

Catalyst	pK_a		
	below 6	6.8—4.0	4.0——3.0
γ-Al_2O_3	0.082	0.225	0.038
SiO_2	0.383	0.157	0
SiO_2 (A)	0.536	0.338	0.134
SiO_2 (B)	0	0.064	0

to γ-Al_2O_3 increases the acidity by the interaction of the nickel with the support, as was also indicated by Aonuma *et al.*[10] In order to further ascertain the effect of the acidity on the catalytic activity, hydroboration with silica gel treated with acid or alkali was carried out. As is shown in Table 1 and Fig. 1, the acid-treated silica gel caused increases in the yield and the acidity. The percentage yield of the product with respect to the admitted amount of diborane at the initial stage are shown in Table 1. On the basis of the results of the titration of the boric acid, the conversion of diborane was calculated to be as is shown in Table 1.

The greater conversion on the Pd–C and active carbon than on the other catalysts may be ascribed to the large surface area of the former, much unreacted diborane being adsorbed.[6] This is probably the reason for the great discrepancy between the percentage yield and the conversion of diborane. As another reason, the reacted diborane calculated on the basis of the results of the titration does not always proceed to triethylborane, because a gas (perhaps H_2) uncondensable by liquid nitrogen, which may be due to the reaction of diborane with the hydroxylic surface of γ-Al_2O_3 and Ni-γ-Al_2O_3,[12] was detected. Because of the small surface area of α-Al_2O_3, the supported and non-supported α-Al_2O_3 would have little of either activity of acidity.

The distribution of the acidic strength of several catalysts was measured by the titration of the butylamine–benzene solution, using Netral Red (pK_a=6.8), 1-phenylazo-2-naphtylamine (pK_a=4.0), and dicinnamylideneacetone (pK_a=−3.0) as indicators.[11] Table 2 indicates the results of the distribution with respect to the strength of the acidity. As is shown in Table 2, relatively weak acidic sites seem to catalyze the hydroboration.

The hydroboration proceeds with the migration of the hydrogen atom in diborane to olefin and the B–C bond being newly constructed. It is known that diborane dissociatively absorbs on the catalyst surface.[6, 12] The acidic site on the catalysts seems to be related to the migration of the hydrogen of BH_3, by which the olefin atom can easily attack the boron atom.

References

1) H. C. Brown "Hydroboration," W. A. Benjamin, Inc., New York, (1962).
2) D. T. Hurd, *J. Am. Chem. Soc.*, **70**, 2053 (1948).
3) A. T. Whatley and R. N. Peace, *J. Am. Chem. Soc.*, **76**, 835 (1954).
4) H. H. Lindner and T. Onak, *J. Am. Chem. Soc.*, **88**, 1886 (1966).
5) T. P. Fehlner, *J. Am. Chem. Soc.*, **93**, 6366 (1971).
6) T. Matsuda, H. Kawashima, and M. Ojima, *Bull. Jpn. Petro. Inst.*, **18** (1976). in press.
7) I. Shapio, H. G. Weiss, M. Schmich, Sol'Skolnik, and G. B. L. Smith, *J. Am. Chem. Soc.*, **74**, 901 (1952).
8) S. Schomburg, R. Koester, and D. Henneberg, *Z. Anal. Chem.*, **170**, 285 (1959).
9) for instance, K. Morikawa, *Kogyo Kagaku Zasshi*, **41**, 694 (1938); M. Koizumi, *Osaka City University*, **4**, No. 1, Series C (1953), A. Ozaki, *Shokubai*, No. 14, 65 (1957).
10) M. Sano, Y. Kageyama, T. Ōtsuka, and K. Aonuma, *Shokubai*, **13**, 73 (1971).
11) K. Tanabe, "Shokubai Kōgakukōza," Vol. 4, Chijin Shokan, Tokyo (1964), p. 169.
12) J. J. Fripita and M. Van Tongelen, *J. Catal.*, **5**, 158 (1965).

BULLETIN OF THE CHEMICAL SOCIETY OF JAPAN, VOL. 49 (6), 1715—1716 (1976)

The Reaction of a Stable Free Nitrogen-centered Radical, 3,4-Dihydro-2,4,6-triphenyl-2*H*-1,2,4,5-tetrazin-1-yl, with Organolithium Compounds

Yozo MIURA, Yuzo MORIMOTO, and Masayoshi KINOSHITA

Department of Applied Chemistry, Faculty of Engineering, Osaka City University, Sumiyoshi-ku, Osaka 558

(Received December 5, 1975)

Synopsis. 3,4-Dihydro-2,4,6-triphenyl-2*H*-1,2,4,5-tetrazin-1-yl (**1**) reacted with ethyl- and butyllithiums to give 1-ethyl- and 1-butyl-2,4,6-triphenyl-1,2,3,4-tetrahydro-1,2,4,5-tetrazines respectively. On the other hand, biphenyl and 1-benzyl-2,4,6-triphenyl-1,2,3,4-tetrahydro-1,2,4,5-tetrazine were given by the reaction of **1** with phenyllithium in toluene. Thus, the results indicate that these reactions proceed through a homolytic process.

In a previous report it was shown that the reactions of 3,4-dihydro-2,4,6-triphenyl-2*H*-1,2,4,5-tetrazin-1-yl (**1**, 1,3,5-triphenylverdazyl) with Grignard reagents[1] or organoaluminum compounds[2] in toluene or in THF proceed through a homolytic process, affording 1-alkyl-2,4,6-triphenyl-1,2,3,4-tetrahydro-1,2,4,5-tetrazines (**2**) and biaryls.

In the course of the preparation of polymers containing stable free radicals,[3] the reaction of **1** with butyllithium used as an initiator was examined, and it was found that a coupling compound (**2b**) was formed. In this report, the reactions of **1** with several organolithium compounds are studied, and a reasonable reaction mechanism is presented.

Experimental

All the melting points are uncorrected. Butyllithium in hexane was obtained from the Mitsuwa Pure Chemicals Co., Ltd. Ethyllithium was prepared by treating diethylmercury with lithium in anhydrous ether,[4] while phenyllithium was prepared by treating bromobenzene with lithium in the same solvent.[5] The concentrations of the reagents were determined by the method of Gilman.[6] 3,4-Dihydro-2,4,6-triphenyl-2*H*-1,2,4,5-tetrazine-1-yl (**1**) was prepared according to the procedure of Kuhn and Trischmann,[7] and was recrystallized from methanol, mp 141—142 °C (lit,[7] 139—140 °C). THF and toluene were distilled from $LiAlH_4$ before use.

The reactions of **1** with organolithium compounds were performed in THF and in toluene according to a procedure similar to that described in a previous report.[1] The amounts of **1** recovered and the coupling compounds (**2**) formed in the reactions with alkallithiums were determined by a similar procedure.[1] The coupling compounds were recrystallized from methanol. 1-Ethyl-2,4,6-triphenyl-1,2,3,4-tetrahydro-1,2,4,5-tetrazine (**2a**): 0.19 g (0.55 mmol); mp 133—134 °C (lit,[1] 133—134 °C). 1-Butyl-2,4,6-triphenyl-1,2,3,4-tetrahydro-1,2,4,5-tetrazine (**2b**): 0.21 g (0.57 mmol); mp 109—111 °C (isolated from the reaction in THF); 0.26 g (0.70 mmol); mp 108—110 °C (from the reaction in toluene, lit,[1] mp 109—111 °C).

The compounds formed in the reaction of **1** with phenyllithium were isolated by column chromatography, using benzene/hexane (1/1 in volume) as the eluent. The isolated compounds were as follows: biphenyl 0.15 g (0.79 mmol), mp 69—71 °C (lit,[7] 71 °C); 1-benzyl-2,4,6-triphenyl-1,2,3,4-tetrahydro-1,2,4,5-tetrazine (**2d**) 0.060 g (0.15 mmol), mp 167—169 °C (recrystallized from methanol, lit,[8] 172 °C), and two unidentified compounds (0.058 and 0.010 g).

The amount of biphenyl which arose from the preparation procedure of phenyllithium was determined by a procedure similar to that used for the arylmagnesium bromides,[1] to be 0.047 g (0.31 mmol, 0.53% based on the amount of bromobenzene used for the preparation of phenyllithium). The yield of biphenyl described in Table is corrected for the amount in the starting phenyllithium solution.

Results and Discussion

When an organolithium compound was added to a THF or toluene solution of **1** at 0 °C, the dark green color of **1** faded rapidly to be replaced with light brown. This brown solution maintained its color in the absence of moisture. However, when the solution was poured into water, its color immediately returned to green, indicating the regeneration of **1**. This reaction behavior is similar to that of the reaction of **1** with Grignard reagents or organoaluminum compounds, but the reactions with organolithium compounds proceed more rapidly than those with Grignard

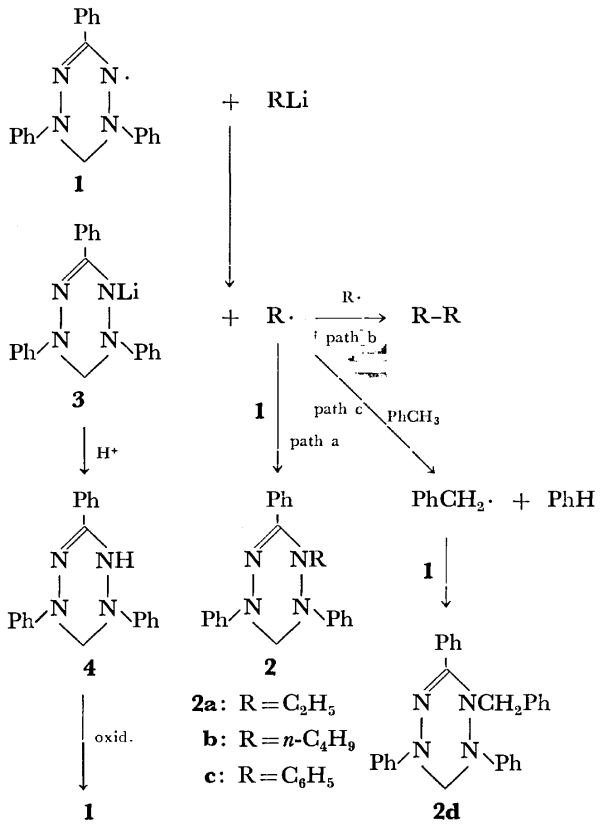

Scheme.

Table. The results of the reactions of 3,4-dihydro-2,4,6-triphenyl-2*H*-1,2,4,5-tetrazin-1-yl (**1**) with organolithium compounds

Organolithium compound	mmol[a]	**1**[b] mmol	Recovered **1** %	Isolated coupling compounds	
				2 (%)[c]	Other (%)[c]
Ethyllithium[d]	1.6	1.6	38	**2a** (35)	
Butyllithium[d]	1.5	1.6	39	**2b** (36)	
Butyllithium[e]	1.4	1.6	30	**2b** (44)	
Phenyllithium[f]	4.0	3.2	70	**2d** (5)	Biphenyl(42)

a) Molar amount required for the completion of the reaction. b) Molar amount used in the reaction. c) Based on the amount of **1** used. d) Solvent, tetrahydrofuran: 15 ml. e) Toluene: 20 ml. f) Toluene: 30 ml.

reagents.

The amounts of **1** recovered were determined by the measurement of the absorbance at 720 nm in a benzene solution extracted from the reaction mixture. Next, the benzene solution was concentrated and subsequently subjected to column chromatography to give the coupling products (**2**) and biphenyl. The results are given in Table.

The results of the reactions with the alkyllithiums are similar to those of the reactions with alkylmagnesium halides or alkylaluminums. In the reaction with phenyllithium in toluene, however, the corresponding coupling compound (**2c**) was not isolated, though biphenyl and a small amount of 1-benzyl-2,4,6-triphenyl-1,2,3,4-tetrahydro-1,2,4,5-tetrazine (**2d**) were isolated. The formation of biphenyl was expected from the results of the reaction of **1** with arylmagnesium bromides. It is very interesting that **2d** was isolated from the reaction mixture, because the formation of this compound indicates the presence of benzyl radical in the reaction system.

On the basis of these results, a reasonable reaction mechanism may be illustrated as is shown in Scheme. In the reaction of **1** with alkyllithiums, **1** and an alkyllithium are converted into the corresponding lithium salt (**3**) and an alkyl radical. The radical is captured exclusively by another **1** to give **2** (path a). The salt (**3**) is stable under anhydrous conditions, and it decomposes immediately in contact with water to give a leuco compound (**4**), which is the oxidized gradually by atmospheric oxygen to **1**.

On the other hand, the phenyl radical formed in the reaction of **1** with phenyllithium is not captured by **1**; it either couples with itself to give biphenyl (bath b) or abstracts a hydrogen from the solvent (toluene) to give benzene and a benzyl radical (path c). The benzyl radical is captured immediately by **1** to give **2d**.

References

1) Y. Miura, Y. Morimoto, and M. Kinoshita, *Bull. Chem. Soc. Jpn.*, **49**, 253 (1976).
2) Y. Miura, Y. Morimoto, and M. Kinoshita, *Bull. Chem. Soc. Jpn.*, **48**, 3765 (1975).
3) Y. Miura, Y. Morimoto, and M. Kinoshita, *Makromol. Chem.*, **175**, 3487 (1974).
4) W. Schlenk and J. Holtz, *Chem. Ber.*, **50**, 262 (1917).
5) R. G. Jones and H. Gilman, *Org. React.*, **6**, 339 (1951).
6) H. Gilman, E. A. Zoellner, and J. B. Dickey, *J. Am. Chem. Soc.*, **51**, 1576 (1929).
7) R. Kuhn and H. Trischmann, *Monatsh. Chem.*, **95**, 457 (1964).
8) M. Kinoshita, N. Yoshizumi, and M. Imoto, *Makromol. Chem.*, **127**, 185 (1969).
9) R. Fittig, *Ann.*, **121**, 361 (1862).

BULLETIN OF THE CHEMICAL SOCIETY OF JAPAN, VOL. 49 (6), 1717—1718 (1976)

The Thermal Decomposition of Cyanodiphenylmethyl *t*-Butyl Peroxide: An Example of C–O Bond Scission

Masao Ōkubo, Emiko Iba-Imai, Hiroko Mizuta, and Takumi Kawamoto

Department of Chemistry, Faculty of Science and Engineering, Saga University, Honjō-machi, Saga 840

(Received June 9, 1975)

Synopsis. The thermal decomposition of cyanodiphenylmethyl *t*-butyl peroxide was investigated. The peroxide is abnormally stable and decomposes slowly at 130—135 °C, and the main reaction product is tetraphenylsuccinonitrile. A main reaction path including the C–O bond scission, in contrast to the case of triphenylmethyl *t*-butyl peroxide, is proposed.

It has been reported that cyanodiphenylmethyl *t*-butyl peroxide(I)[1] is unaffected by treatment with two molar equivalents of phenylmagnesium bromide.[2] The stability of the α-cyano group and that of the O–O bond of I attracted our attention. This peroxide resembles triphenylmethyl *t*-butyl preoxide(II) in its molecular structure as well as its stability towards the Grignard reagent. Upon thermal decomposition in cumene, II yields 1-phenoxy-1,1,2-triphenyl-2-methylpropane (60%) as a result of the rearrangement of the triphenylmethoxyl radical, followed by recombination with the cumyl radical.[3] The preferential migration of the *p*-nitrophenyl group in *p*-nitrophenyldiphenylmethoxyl radical has also been reported.[3,4] These facts led the present authors to study the thermal decomposition of I.

Peroxide I was also unaffected by treatment with iodide ions in both the absence[5] and presence[6] of ferric ions at room temperature.[2] Treatment in boiling acetic acid[7] liberated iodine, but the thiosulfate-titer went up to extraordinarily high values (250—500 mol%) and fluctuated seriously. Thus, no iodometric search for the decomposition course of I was not made in this work.

When peroxide I was decomposed in some alkylbenzenes (toluene, ethylbenzene, *p*-xylene, mesitylene, and cumene) at their boiling temperatures, acetone and *t*-butyl alcohol were produced. The manner of the variation in the molar ratio of the two products (Table 1) is consistent with the reactivities of these aromatics towards the hydrogen abstraction by the *t*-butoxyl radical.[8]

After a solution of I(1.0 M) in cumene had been heated at 130—135 °C for 5 h, the yields of acetone and *t*-butyl alcohol were 5 and 16% respectively. From the viscous oily mixture obtained after the complete evaporation of cumene under reduced pressure, a large amount of unreacted I (53%) and a small amount of dicumyl(III) were detected by NMR spectroscopy on the basis of the *t*-butyl- and methyl-proton signals. Tetraphenylsuccinonitrile(IV), the main reaction product, was separated from the unreacted I by the elution of the mixture with petroleum ether–benzene through a silica-gel column. A small amount of benzophenone (V, 7%), accompanied by a trace of benzhydrol (VI), was detected by GLC. The yields of III and IV were estimated to be 9 and 31% respectively from the integrated NMR spectrum of the mixture (See Experimental Section).

The results of the product analysis imply that I is remarkably stable and that it decomposes in a novel manner. The stability of I is evident in comparison with II; it was reconfirmed that the latter decomposed completely after 5 h under the same reaction conditions.[3] The substantially high yield of IV (67%) suggests that the main reaction path begins with the cleavage of the C–O bond (Scheme 1).

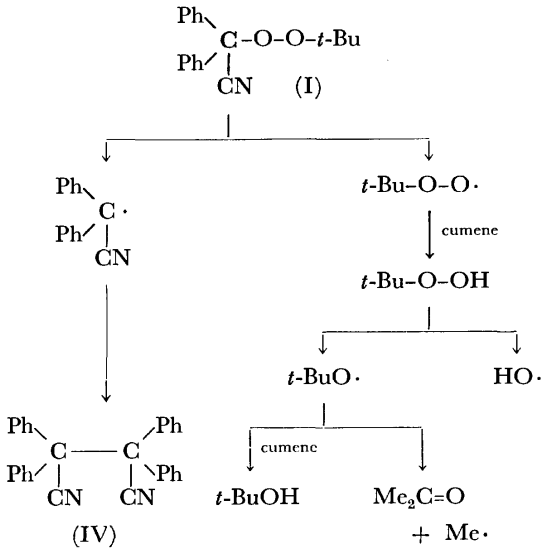

Scheme 1.

Table 1. Variation of the molar ratio of *t*-butyl alcohol and acetone with aromatics

Aromatics	[*t*-BuOH]/[Acetone]
Mesitylene	0.1
Cumene	3.1
Fluorene (ArH/I=1.0)[a]	1.1
(ArH/I=2.0)	1.6

a) Peroxide I and fluorene (0.004 mol), dissolved in chlorobenzene (50 ml), were heated in an oil bath maintained at 180—185 °C.

The yield of V did not exceed 7 mol% in any of the aromatics used. Hydrogen cyanide (VII) was detected by the use of a piece of test paper impregnated with an aqueous solution of cupric acetate–benzidine acetate.[9] The formation of V, VI, and VII suggests a concurrent minor reaction path beginning with the ordinary O–O bond scission, as is shown in the following:

$$\underset{\text{(I)}}{Ph_2C(CN)-O-O-t\text{-}Bu} \longrightarrow Ph_2\dot{C}(CN) + t\text{-}BuO\cdot$$

$$Ph_2C(CN)-O\cdot \longrightarrow [Ph_2\dot{C}-OCN] \longrightarrow \underset{\text{(V)}}{Ph_2C=O} + \underset{\text{(VII)}}{\cdot CN(\rightarrow HCN)}$$

Though no direct evidence was obtained, the migration of the cyano group in the cyanodiphenylmethoxyl radical should be taken into account.[3,4]

Another example of the C–O bond scission of organic peroxide has been found in the thermal decomposition of *N*-cyclohexyl-1-*t*-butylperoxycyclohexylamine, which afforded the corresponding imine by the loss of *t*-butyl hydroperoxide,[10] but this manner of decomposition is probably due to the existence of the neighboring NH group. Though the reason for the unexpected stability of peroxide I remains obscure, its C–O bond scission can be ascribed to the stabilization of the cyanodiphenylmethyl radical by the spin-delocalization[11]; this is consistent with the absence of diphenylacetonitrile, which shows the low hydrogen-abstracting ability of the radical.

Experimental

Materials. The peroxide I was prepared by the treatment of diphenylacetonitrile with *t*-butyl hydroperoxide; mp 52 °C.[1] The peroxide II was prepared by the reported method.[3] Dicumyl(III) was prepared by the thermal decomposition of di-*t*-butyl peroxide in cumene.[12] Tetraphenylsuccinonitrile(IV) was prepared from diphenylacetonitrile.[1]

Procedures. Thermal decomposition was carried out using 1.0 M solution of I under a N_2 atmosphere. After the oil bath had been removed, a few milliliters of the aromatic solvent of the reaction mixture were distilled into an ice-cooled receiver and the ratio of the contents of acetone and *t*-butyl alcohol in the distillate was then determined by means of GLC.

In order to obtain a mixture of high-boiling products for the NMR measurement, the cumene was completely removed by the repeated dissolution of the oily mixture into CCl_4 and by evaporation under reduced pressure; the resulting pale yellow viscous oil was free from cumene (checked by GLC) and could be analyzed by the integration of the NMR spectrum. The contents of I and III were estimated on the basis of the intensities of the *t*-butyl- and methyl-proton signals; the intensities corresponding to the phenyl-protons of I and III were substracted from the overall intensity in the same region. The result gave the sum of the contents of IV and V, the latter of which had been determined by the use of GLC.

References

1) M. S. Kharasch and G. Sosnovsky, *Tetrahedron*, **3** 105 (1958).
2) M. Ōkubo, H. Saitō, and T. Tomiyoshi, *Bull. Chem. Soc. Jpn.*, **47**, 1289 (1974).
3) M. S. Kharasch, A. C. Poshkus, A. Fono, and W. Nudenberg, *J. Org. Chem.*, **16**, 1458 (1951).
4) J. I. G. Cadogan, D. H. Hey, and W. A. Sanderson, *J. Chem. Soc.*, **1961**, 5234.
5) J. P. Wibaut, H. B. van Leewen, and B. van der Wal, *Rec. Trav. Chim. Pays-Bas*, **73**, 1033 (1954).
6) L. S. Silbert and D. Swern, *Anal. Chem.*, **30**, 385 (1958).
7) R. D. Mair and J. Graupner, *Anal. Chem.*, **36**, 194 (1964).
8) C. Walling and P. J. Wagner, *J. Am. Chem. Soc.*, **85**, 2333 (1963).
9) A. Sieverts and H. Hermsdorf, *Z. Angew. Chem.*, **34**, 3 (1921); *Chem. Abstr.*, **15**, 1269 (1921).
10) E. G. E. Hawkins, *J. Chem. Soc., C*, **1969**, 2686.
11) C. D. Cook and M. Fraser, *J. Org. Chem.*, **29**, 3716 (1964).
12) K. M. Johnston and G. H. Williams, *J. Chem. Soc., C*, **1960**, 1168.

BULLETIN OF THE CHEMICAL SOCIETY OF JAPAN, VOL. 49 (6), 1719—1720 (1976)

A Proton Magnetic Resonance Study of the Molecular Configurations of 2′,5′-Dichloroacetoacetanilide in Various Solvents

Michio KONDO

Central Research Laboratories, Sankyo Co., Ltd., Hiromachi 1-2-58, Shinagawa-ku, Tokyo 140

(Received September 25, 1975)

Synopsis. It has been found by ^{1}H NMR spectroscopy that 2′,5′-dichloroactoacetanilide (**1**) exists predominantly in the *keto* form containing an intramolecular hydrogen bond between the amide proton and the carbonyl oxygen at the γ-position in chloroform solutions. In pyridine, the line broadening of signals suggests a rapid interconversion between the *keto* and *enol* forms. Configurations of the *enol* form are discussed.

It is well known that β-diketones undergo *keto-enol* tautomerism in solution. ^{1}H NMR studies of such tautomerism have been carried out for a number of derivatives of acetylacetone and acetoacetic acid,[1] but only a few studies have been done on acetoacetamide derivatives.[2]

The *keto-enol* equilibrium is sensitive to many factors, such as the temperature, the concentration, and the solvent, as well as to the presence of substituents. Acetylacetone, *N*,*N*-dimethylacetoacetamide, and ethyl acetoacetate show a successively decreasing contribution of *enol* form.[1,2]

It is an interesting subject to determine which of the many possible conformations are actually reallized in the case of each compound. This paper will be concerned with the molecular configuration of 2′,5′-dichloroacetoacetanilide (**1**), which is revealed to exist predominantly in the *keto* form in $CDCl_3$.

Experimental

Commercial 2′,5′-dichloroacetoacetanilide (**1**) was purified by recrystallization from CCl_4.

The ^{1}H NMR spectra were recorded on a Varian T-60A spectrometer, using TMS as the internal standard. The concentrations of the samples were 6% (w/v) unless otherwise noted.

The IR and UV spectra were measured on a Hitachi infrared spectrophotometer, Model G-3, and a Hitachi spectrophotometer, Model 356, respectively.

Results and Discussion

The ^{1}H NMR spectra of **1** in various solvents are relatively simple and seem to be composed of two kinds of signals. Raising the temperature of a DMSO solution of **1** up to 100 °C caused no new signals to appear, but there was a slight upfield shift of the amide proton signal.

The signal at δ 3.64 (in $CDCl_3$, for example) corresponding to *ca.* 2H can be ascribed to the methylene protons in *keto* forms on the basis of its chemical shift. The broad signal at δ 9.77 corresponding to *ca.* 1H may be attributed to the amide proton. The alternative assignment of this signal to an enolic OH in the G structure can be eliminated on the basis of the close resemblance in the IR spectra of **1** and 2′, 5′-dichloroacetanilide (**2**) in $CDCl_3$ (Table 1). The amide bands at about 1600 and 1700 cm^{-1} were clearly observed at about same positions. The UV spectra of **1** and **2** in 1,2-dichloroethane solutions are very similar to each other. These facts seem to allow us to rule out the contribution of G in the present case.

The ABX spectral pattern of the aromatic ring protons permits an unequivocal assignment of H-6′ because of the presence of two chlorine atoms. The similarity in the δ values for the ring protons of **1** and **2** enables us to assign forms A to D with the *trans* configuration about the amide bond to *keto* tautomers for **1**, because the *trans* configuration of **2** has been proved on the basis of the diagnostic acetylation-deshielding shift.[3] The corresponding *cis* configurations were dificult to realize, judging from the generally known fact that amide bonds (or peptide bonds) predominantly exist in the *trans* form.[4]

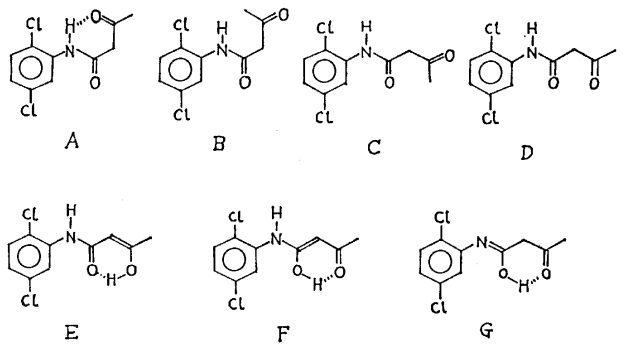

The amide proton of **1** resonates at a field lower by about 2.14 ppm than does that of **2**. This pronounced downfield shift can be interpreted in terms of the A configuration, wherein an intramolecular hydrogen bond is formed between the amide proton and the γ-carbonyl oxygen, though the contributions of B, C, and D can not be neglected. The concentration dependence of the amide proton signal was negligible, as was to be expected from the intramolecular hydrogen bond formed. The broad band at 2900—3400 cm^{-1} in the IR spectrum of **1** may also be ascribed to the amide proton intramolecularly hydrogen-bonded.

An analogous situation was observed in CCl_4 solutions. In DMSO, it is not clear from only the position of the amide proton signal whether or not this configuration remains unchanged, because that of **2** also resonates at a low field due to the intermolecular hydrogen bonding with a DMSO molecule. However, the molecular planarity is considered to be lowered in DMSO, as suggested by the diagnostic upfield shift of the H-6′ signal as compared with that in $CDCl_3$.[5]

TABLE 1. SPECTRAL DATA FOR 2′,5′-DICHLOROACETOACETANILIDE (**1**) AND 2′,5′-DICHLOROACETANILIDE (**2**) IN VARIOUS SOLVENTS

NMR: Chemical shift in ppm										
Compd			CCl_4[a]		$CDCl_3$		DMSO-d_6		C_5D_5N	
	keto	enol	keto	enol	keto	enol	keto	enol	keto	enol
1	CH_3	CH_3	2.31	1.97	2.33	1.99	2.23	1.96	2.18	
	CH_2	CH	3.56	5.01	3.64	5.07	3.71	5.45	4.00	
	NH		9.73		9.77		9.87		10.47	
	H-3′	H-3′	7.30		7.33		7.53		7.35	
	H-4′	H-4′	6.99		7.03		7.25		7.07	
	H-6′	H-6′	8.52	8.58	8.47		8.05	7.93	8.60	
		OH		13.3		13.3		13.4		
Population			77	23	92	8	92	8		
2		CH_3			2.24		2.13			
		NH			7.63		9.60			
		H-3′			7.30		7.56			
		H-4′			7.02		7.26			
		H-6′			8.47		7.98			
UV (in dichloroethane) nm(ε)										
1	300(s)[b], 292(2400), 283(3040), 248(13500)									
2	— 292(1200), 283(1200), 246(14000)									
IR (in $CDCl_3$)[c] cm^{-1}										
1	3392, 3400—2900, 1712, 1690, 1587, 1525									
2	3400, 3100, 1710, 1693, 1587, 1581, 1510									

a) Saturated solution. b) Shoulder. c) Lower frequency bands are omitted.

In pyridine it is noted that the linewidths of the signals of the methyl and methylene protons are much broader than those in chloroform. Although no apparent signal ascribable to *enol* forms were observed, the broadening in the methylene proton signal suggests a rather rapid interconversion between the *keto* and *enol* forms. This could be ascribed to catalytic actions of pyridine.[1d]

The population of the *keto* form is much greater in this compound than in *N,N*-dimethylacetoacetamide.[2] The intramolecular hydrogen bonding between the amide proton and the γ-carbonyl oxygen may be responsible for this.

It is possible to imagine four configurations (E and F and the corresponding *cis* forms, E′ and F′) as *enol* forms. The fact that the chemical shift of H-6′ in the *enol* tautomer is very close to that for the *keto* tautomer favors the E and F structures, which have the oxygen atom in close proximity to H-6′, rather than E′ and F′, which have the olefinic proton in such proximity. The methyl signals of the *enol* tautomers were observed at fields higher than those of the *keto* tautomers in the solvents examined, as was also observed for a series of β-diketones and β-keto esters.[1e] The difference between the chemical shifts of the two tautomers of **1** is almost the same as that in the case of ethyl acetoacetate, but it is clearly larger than that of acetylacetone. If the *enol* molecule assumes the F form, the chemical shift of the acetyl protons should not be very different from that in the *keto* form. Furthermore, if a rapid interconversion between E and F is supposed, the chemical shift difference between the *keto* and *enol* forms should be equal to the corresponding difference in acetylacetone. The argument given above leads one to the conclusion that the molecular configuration of the *enol* tautomer is E.

The olefinic proton signal of the *enol* tautomer was observed at δ 5.07 in $CDCl_3$, higher by -0.51 ppm than that of acetylacetone, but almost the same as that of ethyl acetoacetate. The enolic OH proton resonates at δ 13.3 in $CDCl_3$. The corresponding values for acetylacetone and ethyl acetoacetate are δ 15.6 and 12.2 in pure liquid respectively.[1e] These facts also support the argument presented above.

References

1) a) H. S. Jarrett, M. S. Sadler, and J. N. Schoolery, *J. Chem. Phys.*, **21**, 2092 (1953). b) L. W. Reeves, *Can. J. Chem.*, **35**, 1351 (1957). c) L. W. Reeves and W. G. Schneider, *ibid.*, **36**, 793 (1958). d) M. T. Rogers and J. L. Burdett, *ibid.*, **43**, 1516 (1965). e) J. L. Burdett and M. T. Rogers, *J. Am. Chem. Soc.*, **86**, 2105 (1964). f) J. L. Burdett and M. T, Rogers, *J. Phys. Chem.*, **70**, 939 (1966). g) G. Allen and R. A. Dwek, *J. Chem. Soc., B*, **1966**, 161. h) J. G. Dawber and M. M. Crane, *J. Chem. Educ.*, **44**, 150 (1967).

2) R. F. Hobson, L. W. Reeves, and R. C. Shaddick, *Org. Mag. Res.*, **6**, 129 (1974).

3) R. F. C. Brown, L. Radom, S. Sternhell, and I. D. Rae, *Can. J. Chem.*, **46**, 2577 (1968).

4) G. N. Ramachandran and V. Sosisekharan, "Conforma- of Polypeptides," in Advances in Protein Chemistry, Vol. 23, Academic Press, New York (1968).

5) I. D. Rae, *Can. J. Chem.*, **46**, 2589 (1968).

BULLETIN OF THE CHEMICAL SOCIETY OF JAPAN, VOL. 49 (6), 1721—1722 (1976)

Reaction of Thiocarbonyl Compounds with Tributylphosphine[1)]

Yoshiro OGATA, Mitsuji YAMASHITA, and Makoto MIZUTANI

Department of Applied Chemistry, Faculty of Engineering, Nagoya University, Chikusa-ku, Nagoya 464

(Received October 6, 1976)

Synopsis. The reaction of thiobenzophenone (**1**) with tributylphosphine (**3**) gives an oligomer at room temperature, but it gives tributylphosphine sulfide (**4**), 1,1,2,2-tetraphenylethane, and tetraphenylethylene (**6**) at 100 °C. The reaction of thiofluorenone with **3** gives **4**, bifluorenylidine (**8**), and bifluorenyl (**9**) at room temperature. These possible mechanisms are discussed by carbene intermediates.

The deoxygenation and desulfurization of organic compounds by trivalent phosphorus compounds is well known.[2)] Some of these reactions may proceed *via* carbene intermediates, but there have been only a few attempts to identify carbenes in the reaction with trivalent phosphorus compounds.[3)] The reaction of benzophenone with triisopropyl phosphite to give a mixture of diisopropyl benzhydrylphosphonate, triisopropyl phosphate, tetraphenyl–ethylene, and propylene, probably proceeds *via* an ionic path.[4)]

On the other hand, it was postulated[5)] that hexafluoroacetone reacts with phosphite *via* a carbene intermediate to give trialkoxybis(trifluoromethyl)methylene phosphorane. The reaction of cyclic 1,2-thiocarbonates with trimethyl phosphite gives olefinic product, together with a small amount of orthoformate derivative formed by carbene reaction.[6)] Also the formation of fluorene, bifluorenyl, and tribiphenylenepropane by the reaction of fluorene with tributylphosphine in hydrogen donating solvents[7)] suggests the intermediacy of carbene.

The thiophilicity of trivalent phosphorus compounds should be higher than the oxophilicity in the reaction of ketonic compounds, and we reported previously the facile reaction of thiobenzophenone with phosphite.[8)] This paper deals with evidence for carbene formation during the desulfurization of some thioketones by phosphine, and their higher reactivities.

Results and Discussion

No reaction of thiobenzophenone (**1**) with triphenylphosphine (**2**) occurred even at 160 °C for 24 h. An apparent reaction of **1** on addition of tributylphosphine (**3**) proceeds at room temperature, but the reaction gave only an oligomer of **1** in good yield without desulfurization. When the oligomer was dissolved in inert solvents, the dark blue color of the monomer was reappeared, and it strongly suggests that the formation of the oligomer is reversible.

The acid-catalyzed dimerization and trimerization of thioaldehydes, dialkyl thioketones, and alkyl aryl thioketones are well known.[9,10)] On the other hand, cyclization of monothiobenzil and dithiobenzil derivatives to four-membered ring including one or two sulfur atoms was recently reported.[11,12)]

But only a few report was known concerning the formation of polymeric thiobenzophenone.[13)] This is the first report on the reversible formation of oligomer.

$$n\text{-}Ph_2CS(\mathbf{1}) \xrightarrow{n\text{-}Bu_3P} (Ph_2CS)_n \qquad (n=2 \text{ or } 3)$$

However, the reaction of **1** with **3** under N_2 at 100 °C for 10 h gives mainly tributylphosphine sulfide (**4**, 89%), 1,1,2,2-tetraphenylethane (**5**, 65%), and tetraphenylethylene (**6**, 28%). The formation of **5** and **6** suggests the intermediacy of carbene in the reaction, i.e., these products may be produced by the coupling of diphenyl carbene or diphenylmethyl radical arising from abstraction of sulfur from **1** by phosphine, followed by hydrogen atom abstraction.

$$\underset{\mathbf{1}}{Ph_2CS} + \underset{\mathbf{3}}{n\text{-}Bu_3P} \rightarrow \underset{\mathbf{4}}{n\text{-}Bu_3PS} + \underset{\mathbf{5}}{(Ph_2CH\text{-})_2} + \underset{\mathbf{6}}{Ph_2C{=}CPh_2} \quad (2)$$

The photochemical reaction of diphenyldiazomethane in some solvents gives benzophenonazine and tetraphenylethane, those yields depending upon solvents used[14)] where the formed diphenylcarbene couples with starting material to give benzophenonazine, and/or abstracts hydrogen atom from the solvent followed by coupling to give tetraphenylethane. In our present reaction, the formed carbene may react with thiobenzophenone to give tetraphenylethylene, and/or may abstract a hydrogen atom from phosphine followed by coupling to give tetraphenylethane. (See Scheme 1).

The reaction of thiofluorenone (**7**) with tributylphosphine (**3**) proceeds at room temperature. The products are mainly **4** (95%), bifluorenylidine (**8**, 63%), and bifluorenyl (**9**, 23%). It is known that the reaction of fluorenone with tributylphosphine at 155—165 °C for 76 h affords bifluorenylidene (40%),[7)] and that the photochemical reaction of diazofluorene in cyclohexane affords bifluorenyl (24%).[14)] Hence following reaction pathways are conceivable for our reaction of thiofluorenone to form **4**, **8** and **9**.

Fluorenyl carbene abstracts a hydrogen atom from tributylphosphine (**3**), then couples each other to form bifluorenyl (**9**), because **9** was obtained even in the reaction in neat. Three pathways are concievable for the formation of **8**, i.e., (i) coupling of two molecules of fluorenyl carbene (path a), (ii) formation of episulfide followed by desulfurization (path b), and (iii) formation of phosphorane followed by Wittig reaction with thiobenzophenone (path c).[3b,15)] Phosphines have been utilized as carbene acceptors,[16)] but path c is less probable in this reaction because of the little effect on the product distribution by adding benzaldehyde to the reaction mixture.[17)] The desulfurization from episulfide by phosphine and coupling of carbene is very fast, so that both paths a and b cannot be ruled out. The analogous reaction mechanism may be applicable for the reaction of **1** with **3**.

The facile reaction of thiofluorenone with tributylphosphine at room temperature for 3 h in comparison

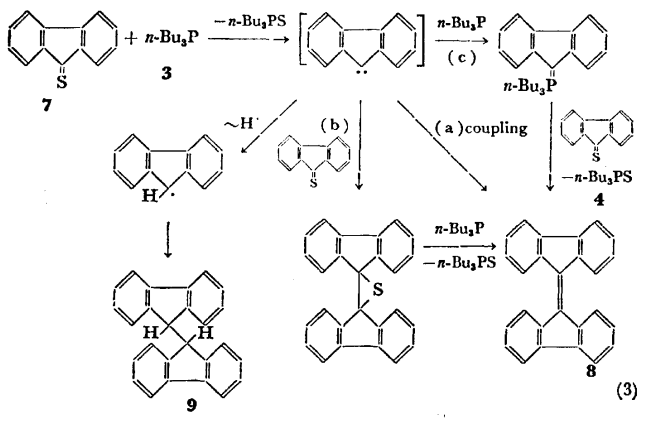

Scheme 1.

with the reaction of thiobenzophenone, which required 10 h reaction at 100 °C, is attributable to the driving force due to the stability of the formed carbene; *i.e.* fluorenyl carbene may be more stable than diphenyl carbene in view of its resonance forms. Gas phase reaction of diphenyl carbene gives about 30% yield of fluorene.[18]

The thiophilicity of trivalent phosphorus compounds towards thiocarbonyl compounds surpasses the oxophilicity towards the corresponding carbonyl compounds.[8,19] The reaction of **7** with **3** proceeds at room temperature, while the reaction of fluorenone with **3** necessitates the higher temperature of 155—165 °C,[7] and the reaction of benzophenone with triisopropyl phosphite needs more drastic conditions, *i.e.*, 72 h reaction at 170 °C, while those of thiobenzophenone with trialkyl phosphites can proceed at 100 °C for 10 h.[4,8]

Experimental

All melting points and boiling points were uncorrected. A Yanagimoto GCG 550F and Hitachi K53 gas chromatographs were used with a 1 m×3 mm column packed with Silicone GE SE 30 (8%) coated on Chromosorb W. IR spectra were measured by a Perkin-Elmer Model 337 spectrophotometer. NMR spectra were measured by a JNM-C60-HL NMR instrument of Japan Optics Laboratory. Mass spectra were measured by a Hitachi RMS-4 mass spectrometer.

Reaction of Thiobenzophenone with Tributylphosphine. The reaction of thiobenzophenone (**1**) with excess tributylphosphine (**3**) (*ca.* 3 equivalents) at room temperature for 10 min gave oligomer of **1** (quantitative), which was dissociated to its monomer on dissolving in benzene and chloroform, mp 130 °C.

The NMR spectra show only aromatic protons (δ= 7.18—7.72), and IR spectra show C-S absorption (651 cm^{-1}), but no C=S absorption. The reported mp of polymeric thiobenzophenone is 146.5 °C[13]

The mixture of **1** (0.67 g) and **3** (1.7 g) was heated under N_2 for 10 h at 100 °C. The products were tetraphenylethylene (28%), tetraphenylethane (65%), and tributylphosphine sulfide (89%), which were identified by NMR, IR, VPC. and mp by comparison with the authentic samples. In addition to these compounds, other two minor unidentified products were obtained.

Reaction of Thiofluorenone (7) with Tributylphosphine(3). The reaction of thiofluorenone (**7**) with **3** was carried out for 3 h at room temperature. Bifluorenylidine (63%), bifluorenyl (23%), and tri-*n*-butylphosphine sulfide (95%) were separated from the reaction mixture by TLC (Kiesel gel G/benzene) and identified by VPC analysis by comparison with the authentic samples. The formation of 9-diphenylenephenanthrone was also observed, and was identified by IR (KBr, C=O, 1700 cm^{-1}), NMR ($CDCl_3$, δ=6.2—7.9, aromatic protones), mp 201.5—203 °C (recrystallized from petroleum ether–benzene), and elemental analysis. Found: C, 90.90; H, 5.06%. Calcd for $C_{26}H_{16}O$: 90.70; H, 5.13%.

Reaction of **1** *with* **2**. A mixture of **1** (0.71 g) with **2** (3.71 g) was heated in a sealed tube under N_2 for 24 h at 160 °C, but no reaction product was observed by VPC analysis.

References

1) Contribution No. 216.
2) a) A. J. Kirby and S. G. Warren, "The Organic Chemistry of Phosphorus," Elservier, Amsterdam (1967) Chapter 3; b) R. F. Hudson, "Structure and Mechanism in Organo-Phosphorus Chemistry," Academic Press, London (1965) Chapter 6; c) G. M. Kosolapoff and L. Maier, "Organic Phosphorus Compounds," Vol. 1, Wiley Interscience, New York, N.Y. (1972) Chapter 1.
3) a) F. Ramirez, H. Yamanaka, and O. H. Basedow, *J. Am. Chem. Soc.*, **83**, 173 (1961); b) E. J. Corey and G. Markl, *Tetrahedron Lett.*, 3201 (1967).
4) A. C. Poshkus and J. E. Herweh, *J. Org. Chem.*, **29**, 2567 (1964).
5) W. J. Middleton and W. H. Sharkey, *J. Org. Chem.*, **30**, 1384 (1965).
6) D. Horton and C. G. Tindall, Jr., *J. Org. Chem.*, **35**, 3558 (1970).
7) I. J. Borowitz, M. Anschell, and P. D. Readio, *J. Org. Chem.*, **36**, 553 (1971).
8) Y. Ogata, M. Yamashita, and M. Mizutani *Tetrahedron*, **30**, 3709 (1974).
9) a) E. Campaigne and M. P. Georgardis, *J. Heterocyclic Chem.*, **6**, 339 (1969); b) J. Ashby and H. Suschitsky, *Tetrahedron Lett.*, 1315 (1971); c) J. W. Greidanus, *Can. J. Chem.*, **48**, 3530 (1970); d) P. Metzner and J. Viable, *Bull. Soc. Chem. Fr.*, 3739 (1970).
10) a) S. Oae, A. Nakanishi, and N. Tsujimoto, *Chem. Ind. (London)*, **1972**, 575; b) T. Kitazume and N. Ishikawa, *Chem. Lett.*, **1973**, 267.
11) B. Saville and M. Steer, *J. Chem. Soc., Chem. Commun.*, **1972**, 616.
12) W. Kusters and P. de Mayo, *J. Am. Chem. Soc.*, **95**, 2383 (1973).
13) C. Engler, *Chem. Ber.*, **11**, 922 (1878).
14) W. Kirmse, L. Horner, and H. Hoffmann, *Justus Liebigs Ann. Chem.*, **614**, 19 (1958).
15) W. Kirmse, "Carbene Chemistry," 2nd ed., Academic Press, New York, N.Y. (1971) Chapters 1, 2, and 11.
16) a) D. Lloyd and M. I. C. Singer, *Chem. Ind. (London)*, **1967**, 1042; b) D. Lloyd and M. I. C. Singer, *ibid.*, 787 (1967); c) D. Lloyd and M. I. C. Singer, *Chem. Commun.*, **1967**, 510.
17) A. W. Johnson, "Ylide Chemistry," Academic Press, New York, N.Y. (1966) p. 138.
18) a) H. D. Hanison and F. P. Lossing, *J. Am. Chem. Soc.*, **82**, 1052 (1960); b) J. A. Myers, R. C. Joines, and W. M. Jones, *ibid.*, **92**, 4740 (1970).
19) a) M. Fukuyama and A. Ono, *Kagaku No Ryoiki*, **22**, 977 (1968); b) M. Fukuyama and A. Ono, *ibid.*, **22**, 1091 (1968).

BULLETIN OF THE CHEMICAL SOCIETY OF JAPAN, VOL. 49 (6), 1723—1724 (1976)

The Photochemical Reaction of Iron Pentacarbonyl and 1,3-Butadiene-1,1,4,4-d_4. The Lack of Secondary Isotope Effects

Ryoji Noyori and Keiichi Yokoyama

Department of Chemistry, Nagoya University, Chikusa, Nagoya 464

(Received March 2, 1976)

Synopsis. No significant deuterium isotope effects have been noticed in the formation of the 1,3-butadiene–iron tricarbonyl complex, in contrast to the olefin complexation of Ag^+ or Rh(I) species.

Deuterated olefins and 1,3-dienes are known to form complexes with silver nitrate more readily than their undeuterated analogs.[1] The same trend has been observed with the reaction of Rh(I) complexes.[2] In connection with a mechanistic study of the iron carbonyl-promoted reaction of 1,3-dienes and α,α'-dibromo ketones,[3] we have now examined the reaction of a deuterated butadiene and iron pentacarbonyl [$Fe(CO)_5$].

Intermolecular competition experiments were carried out using an approximate 1 : 1 mixture of 1,3-butadiene (**1**) and 1,3-butadiene-1,1,4,4-d_4 (**2**). A mixture of $Fe(CO)_5$ and a 10-fold excess of **1** and **2** was placed in a sealed Pyrex tube and exposed to a high-pressure mercury arc. The resulting iron carbonyl complexes, **3** and **4**, were isolated, and the isotopic composition

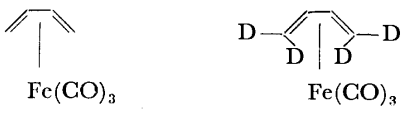

3 **4**

was analyzed carefully on a 100 MHz NMR machine with a CAT system. The correction of the rate constant of the d_4 substrate to a per deuterium basis was done in order to determine the secondary deuterium isotope effect, k_H/k_D. The results, given in Table 1, indicate that the deuterium substitution does not exert any significant influence on the rate of butadiene–iron tricarbonyl complex formation.

The photochemical reaction between $Fe(CO)_5$ and butadiene is considered to proceed through the pathway outlined in Scheme 1.[4] Since the butadiene ligand in **3** is not displaced by free butadiene under the present reaction conditions, the negligible deuterium isotope effect is associated with the stage of iron tetracarbonyl–butadiene (as a monoolefinic ligand) complex formation. In iron carbonyl–olefin complexes, the σ-donative ability of the olefinic ligand is less

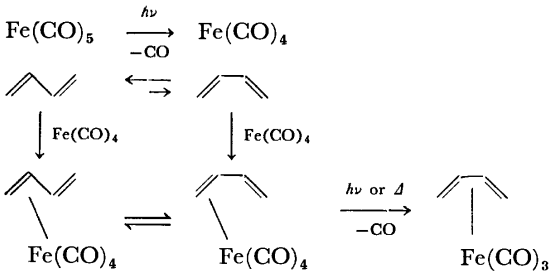

Scheme 1.

Table 1. Secondary deuterium isotope effect in the formation of butadiene–$Fe(CO)_3$ complex

Run	Butadiene composition, d_4/d_0[a]	$Fe(CO)_3$ complex composition, d_4/d_0[a,b]	(k_H/k_D)[4], obsd	k_H/k_D
1	0.898[c]	0.899	0.999	1.00
2	1.19[d,e]	1.24	0.964	0.992
3	1.19[d]	1.21	0.983	0.996
			Av 0.982	0.996

a) Determined by NMR analysis. b) Average of 50 integrations. c) Average of 39 integrations. d) Average of 100 integrations. e) Recovered butadiene $d_4/d_0=1.20$.

important than the π-acceptor capacity;[5] accordingly, unlike the cases of Ag^+ and Rh(I),[1,2] subtle difference in electronic properties between deuterium and protium does not affect the relative complex stabilities. In addition, this observation may imply that carbon atoms of the butadiene–iron tetracarbonyl complex are little distorted from the sp^2-hybridized structures.[6]

Experimental

The NMR spectra were recorded on a Varian Associates Model HA-100D spectrometer equipped with a Model C-1024 time-averaging computer. 1,3-Butadiene (**1**) (Tokyo Kasei) was used after distillation. 1,3-Butadiene-1,1,4,4-d_4 (**2**) was prepared by the method of Cope[9] and stored at −20 °C on Molecular sieves 3A before use. The NMR spectrum (CCl_4 solution, tetramethylsilane as the internal standard) exhibited a very small signal due to $=CH_2$ protons, indicating that the butadiene was *ca.* 96% labeled. An approximate 1 : 1 mixture of **1** and **2** was prepared, and the ratio of the d_0 substrate to the d_4 substrate was determined on the basis of integrated relative intensities for the $=CH_2$ (δ 5.10) and =CH– (δ 6.25) signals in the NMR spectrum (CCl_4 solution), using factors obtained from the spectrum of undeuterated diene, **1**. The values in Table 1 are averages of 39 or 100 integrations. The isotopic composition of the iron tricarbonyl adduct was determined in the same manner; **3** (benzene-d_6 solution) showed signals at δ (benzene signal taken as δ 7.37) 0.09, 1.55 ($=CH_2$), and 4.88 (=CH–).

A typical experiment was executed as follows. A Pyrex tube (1 cm × 20 cm) equipped with a rubber septum was flushed with nitrogen and cooled at −78 °C. To this vessel we then introduced $Fe(CO)_5$ (Strem Chemicals, 79 mg, 0.4 mmol) and a mixture of **1** and **2** (220 mg, 4 mmol, $d_0/d_4=1.00/0.898$) by means of microsyringes. The tube was sealed, warmed to room temperature, and exposed to a 200 W high-pressure mercury lamp from a distance of 2 cm. After a 40-min irradiation, the tube was opened and the unreacted butadiene was removed under atmospheric pressure. The short-path distillation of the residue (20 mmHg; bath

temperature, 70—100 °C) gave a mixture of **3** and **4** as a yellow oil (61 mg, 78% yield). The product was recrystallized from pentane at −90 °C under nitrogen and immediately subjected to the NMR analysis under an argon atmosphere (benzene-d_6); this analysis indicated the production of **3** and **4** in a 1 : 00 : 0.999 ratio.

References

1) R. J. Cvetanović, F. J. Duncan, and W. E. Falconer, *Can. J. Chem.*, **41**, 2095 (1963); R. J. Cvetanović, F. J. Duncan, W. E. Falconer, and R. S. Irwin, *J. Am. Chem. Soc.*, **87**, 1827 (1965).

2) V. Schurig and E. Gil-Av, *Chem. Commun.*, **1971**, 650.

3) R. Noyori, S. Makino, and H. Takaya, *J. Am. Chem. Soc.*, **93**, 1272 (1971); R. Noyori, Y. Baba, S. Makino, and H. Takaya, *Tetrahedron Lett.*, **1973**, 1741; R. Noyori, S. Makino, T. Okita, and Y. Hayakawa, *J. Org. Chem.*, **40**, 806 (1975); R. Noyori, Y. Baba, and Y. Hayakawa, *J. Am. Chem. Soc.*, **96**, 3336 (1974); R. Noyori, S. Makino, Y. Baba, and Y. Hayakawa, *Tetrahedron Lett.*, **1974**, 1049; R. Noyori, T. Souchi, and Y. Hayakawa, *J. Org. Chem.*, **40**, 2681 (1975); Y. Hayakawa, M. Sakai, and R. Noyori, *Chem. Lett.*, **1975**, 509.

4) E. Koerner von Gustorf, Z. Pfajfer, and F. -W. Grevels, *Z. Naturforsch.*, **26b**, 66 (1971).

5) Olefins bearing electron-withdrawing group(s) form the stable iron tetracarbonyl complexes; E. Koerner von Gustorf and F. -W. Gravels, *Fortschr. Chem. Forsch.*, **13**, 366 (1969).

6) The diene framework in **3** remains planar.[7] On the other hand, olefinic carbons in iron tetracarbonyl—electron-deficient olefins are considerably distorted from the sp^2 structures.[8]

7) O. S. Mills and G. Robinson, *Acta Crystallogr.*, **16**, 758 (1963); P. Crews, *J. Am. Chem. Soc.*, **95**, 636 (1973).

8) A. R. Luxmoore and M. R. Truter, *Proc. Chem. Soc. (London)*, **1961**, 466; P. Corradini, C. Pedone, and A. Sirigu, *Chem. Commun.*, **1966**, 341.

9) A. C. Cope, G. A. Berchtold, and D. L. Ross, *J. Am. Chem. Soc.*, **83**, 3859 (1961).

BULLETIN OF THE CHEMICAL SOCIETY OF JAPAN, VOL. 49 (6), 1725—1726 (1976)

The Cycloaddition of 1,2,4,5-Tetrazines with Indoles. The Formation of 5*H*-Pyridazino[4,5-*b*]indoles

Masahiko TAKAHASHI, Hiroyuki ISHIDA, and Masao KOHMOTO

Department of Industrial Chemistry, Faculty of Engineering, Ibaraki University, Hitachi, Ibaraki 316

(Received March 13, 1976)

Synopsis. The cycloaddition of 3,6-disubstituted 1,2,4,5-tetrazines (**1**) with indoles (**2**) gave 1,4-disubstituted 5*H*-pyridazino[4,5-*b*]indoles (**4**).

It is well known[1] that indoles add at the C_2 or C_3 position to certain olefins and acetylenes substituted by electron-withdrawing substituents. On the other hand, the cycloaddition at the C_2 and C_3 positions of indoles with some dipolarophiles has been reported. The cycloaddition of indoles with acetylenedicarboxylate[2] has been studied in detail, and the ring-expansion of the adducts has been observed to give benzoazepines. The 1 : 2 adducts were obtained by the reaction with *p*-benzoquinone and 1,4-naphtoquinone.[3] 1,3-Dipolar cycloaddition to indoles has been reported in the cases of azides[4] and nitrilimines.[5]

Previously, we have described the reaction of 1,2,4,5-tetrazines with 2-phenyl-1-azirine.[6] In this paper we wish to report the cycloaddition of 1,2,4,5-tetrazines with indoles. Heating a toluene solution of 3,6-di-(2-pyridyl)-1,2,4,5-tetrazine (**1a**) and indole (**2a**) gave a crystalline product (35% yield). The elemental analysis and the mass spectral measurement supported the molecular formula of $C_{20}H_{13}N_5$. The IR spectrum showed an NH absorption at 3220 cm^{-1}, but the NMR spectrum did not show the methine protons anticipated for compound (**3a**). From these data it was concluded that the product was not the expected compound, **3a**, but the further-dehydrogenated compound, 1,4-di(2-pyridyl)-5*H*-pyridazino[4,5-*b*]indole (**4a**). The same product, **4a**, was also obtained in a low yield by the treatment of **1a** with 3-methylindole (**2b**). When **1a** was treated with 2-methylindole (**2c**), two products were obtained. One product was identical with **4a**, while the other was (**3d**), an intermediate to **4a**. From these results it has become apparent that the primary cycloadducts, **3a—d**, immediately aromatize on the extrusion of R^1R^2 (H_2, CH_4) to form **4a—b**. Similar results have been reported recently by Seitz *et al.*[7] for the reaction of dimethyl 1,2,4,5-tetrazine-3,6-dicarboxylate with thiophene, *N*-methylimidazole, 2,5-dimethylfuran, or *N*-methylpyrrole.

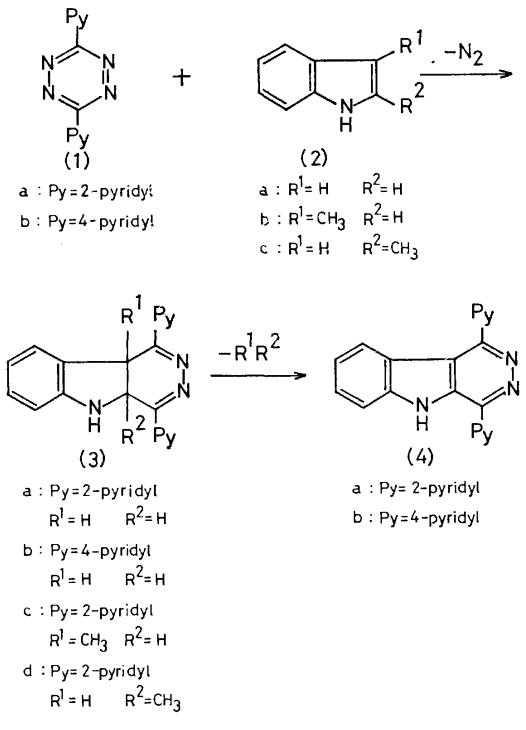

Experimental

The IR, UV, and NMR spectra were measured with a JASCO Model IRA-2 spectrometer, a Shimadzu Model MPS-501 spectrometer, and a Hitachi Model R-20 spectrometer respectively. A Shimadzu Model UM-3B apparatus was used for the elemental analysis.

*Reaction of **1a** with **2a**.* A toluene solution (20 ml) of **1a** (1.44 g, 6.1 mmol) and **2a** (0.68 g, 5.8 mmol) was refluxed for 3 h. After cooling, the precipitates were filtered off and then washed with methanol to remove a by-product, 3,5-di(2-pyridyl)-1,2-dihydro-1,2,4,5-tetrazine, to give 1,4-di-(2-pyridyl)-5*H*-pyridazino[4,5-*b*]indole **4a** (0.65 g, 35% yield). Recrystallization from benzene afforded pale yellow prisms; mp 202—204 °C. Found: C, 74.11; H, 3.76%. Calcd for $C_{20}H_{13}N_5$: C, 74.29; H, 4.05%. IR (KBr, cm^{-1}): 3220, 1615, 1587, 1579, 1538. UV (MeOH, nm (log ε)): 270 (sh, 4.45), 286 (4.52), 358 (3.85). NMR ($CDCl_3$, δ): 11.95 (s, 1H, NH), 7.10—9.15 (m, 12H, aromatic H). MS *m/e* (%): 323 (M^+, 90), 322 (100), 294 (7.8), 293 (11), 266 (5.4), 245 (30), 219 (4.6), 192 (3.5), 161 (11).

*Reaction of **1b** with **2a**.* 1,4-Di(4-pyridyl)-5*H*-pyridazino [4,5-*b*]indole **4b** (0.88 g, 24% yield) was obtained by refluxing a xylene solution (30 ml) of **1b** (2.4 g, 10 mmol) and **2a** (2.7 g, 23 mmol) for 7h. Recrystallization from pyridine afforded pale yellow prisms; mp>300 °C. Found: C, 74.22; H, 4.40%. Calcd for $C_{20}H_{13}N_5$: C, 74.29; H, 4.05%. IR (KBr, cm^{-1}): 3360, 3030, 2930, 2880, 2780, 1600, 1585, 1566, 1549. UV (MeOH, nm (log ε)): 224 (4.54), 272 (4.45), 352 (3.58).

*Reaction of **1a** with **2b**.* A toluene solution (40 ml) of **1a** (0.94 g, 4.0 mmol) and **2b** (0.84 g, 6.4 mmol) was refluxed for 68 h. After cooling, the precipitates were filtered, washed with methanol, and recrystallized from methanol to give a pale yellow product (0.18 g, 15% yield). Its mp and IR spectrum were identical with those of **4a**.

*Reaction of **1a** with **2c**.* A toluene solution (30 ml) of **1a** (0.71 g, 3.0 mmol) and **2c** (0.57 g, 3.6 mmol) was refluxed for 22 h. After cooling, the precipitates were filtered, washed with methanol, and recrystallized from methanol to give **4a** (0.13 g, 13% yield). The filtrate was concentrated *in vacuo* to give a small amount of precipitates, which were then recrystallized from methanol to afford red needles;

mp 177—183 °C. Found: C, 74.33; H, 4.80%. Calcd for $C_{21}H_{17}N_5$: C, 74.31; H, 5.05%. MS *m/e* (%): 339 (M^+, 9.3), 325 (25), 324 (100), 261 (11), 78 (12).

The authors wish to express their thanks to Dr. Masatoshi Hirayama for the NMR measurements and to the Sankyo Co., Ltd., for the mass measurements.

References

1) R. J. Sundberg, "The Chemistry of Indoles," Academic Press, New York and London (1970).

2) a) R. M. Acheson, "Advances in Heterocyclic Chemistry," Vol. 1, p. 125, Academic Press, New York and London (1963); b) H. Plieninger and D. Wild, *Chem. Ber.*, **99**, 3063 (1966); c) L. Knorr, *ibid.*, **36**, 1272 (1903); d) W. E. Noland, W. C. Kuryla, and R. F. Lange, *J. Am. Chem. Soc.*, **81**, 6010 (1959); e) R. M. Acheson and J. N. Bridson, *Chem. Commun.*, **1971**, 1225; f) F. Fried, J. B. Taylor, and R. Westwood, *ibid.*, **1971**, 1226; g) R. M. Acheson, J. N. Bridson, T. R. Cecil, and A. R. Hands, *J. Chem. Soc., Perkin Trans. I*, **1972**, 1569.

3) a) W. E. Noland and F. J. Baude, *J. Org. Chem.*, **31**, 3321 (1966); b) J. D. Bu'Lock and J. Harley-Mason, *J. Chem. Soc.*, **1951**, 703; c) K. K. Prasad, *Tetrahedron Letters*, **1974**, 1361.

4) A. S. Bailey and J. E. White, *J. Chem. Soc., B.*, **1966**, 821.

5) a) M. Ruccia, N. Vivona, F. Piozzi, and M. C. Aversa, *Gazz. Chim. Ital.*, **99**, 588 (1969); b) M. Ruccia, N. Vivona, G. Cusmano, M. L. Marino, and F. Piozzi, *Tetrahedron*, **29**, 3159 (1973).

6) M. Takahashi, N. Suzuki, and Y. Igari, *Bull. Chem. Soc. Jpn.*, **48**, 2605 (1975).

7) G. Seitz and T. Kaempchen, *Chem. -Ztg.*, **99**, 292 (1975); *Chem. Abstr.*, **83**, 114325d (1975).

Foamy Complex Formation for Removing and Recovering of Heavy Metal Ions in Dilute Solutions with *N*-Monodecanoyl Diethylenetriamine

Gaku IZUMI, Makoto SATO, Sakae SHOJI, and Kanenao OIKAWA
Government Industrial Research Institute, Tohoku, Nigatake, Harano-machi, Sendai 983
(Received June 28, 1975)

In order to highly selectively remove and recover heavy metals, usually harmful, from wastewater, a modified foam-separating method using a fatty compound, *i.e.* *N*-monodecanoyl diethylenetriamine, was investigated on real and model wastewater, containing several kinds of metals. This agent forms soluble and foamy complexes with the metals.

As methods for removing harmful heavy metals from wastewater, precipitation, floatation after deposition, absorption, extraction, *etc.* have been employed. However, these methods are accompanied by difficult problems, especially, in the case where a small amount of heavy metals is dissolved in a large quantity of wastewater.[1] Therefore, in order to solve these problems, the authors proposed an effective method[2] based on the foam-separating principle.[3]

Generally, such compounds as fatty acid amido-amines which contain amino- or imino-groups in the molecule react with heavy metal salts and produce organic complexes.[4] The authors have found that, if a fatty acid amino-amine having a suitable structure is added to an aqueous solution of heavy metal salts, even in a very dilute solution, the amido-amine reacts instantly with the metal ions and produces complexes which are considerably water-soluble, very foamy and very absorbable in bubbles.[2,5] Also, the authors have successfully applied this to the removal and recovery of harmful heavy metals from wastewater.[2] In the present paper, the results for an effective typical amido-amine type agent, *N*-monodecanoyl diethylenetriamine hydrochloride, are reported.

Experimental

N-Monodecanoyl diethylenetriamine hydrochloride (C_{10}-ODT) was prepared by the direct aminolysis of methyl decanoate with diethylenetriamine and neutralization with hydrochloride.

After C_{10}ODT was added to the aqueous solution containing heavy metal ions, the pH of the solution was adjusted. Then, the foam treatment was carried out by bubbling air, passed through a water-washing bottle, into the solution at a constant flow rate (200—250 ml/min) until foaming almost ceased.

The batch foaming column consisted of a glass tube (28 mm i.d., 500 mm long) with a glass filter (2G, 20 mm i.d.) fixed in a rubber stopper at the bottom of tube. Into this column, 50 ml of the solution for foam treatment was poured. The foam which ran over the top of the column was recovered and the amount of metal ions in the residual water was analysed after the treatment.

The continuous multistage foam treatment was carried out using a trial apparatus (Fig. 1). After the treatment, the amount of metal ions in the residual water was analyzed.

Solutions containing 10 ppm of single metal ions were prepared with sulfates, chlorides or acetates of copper, lead, zinc and iron.

Solutions containing mixtures of 10 ppm of each metal ion were prepared with copper sulfate, lead nitrate, zinc sulfate, and calcium sulfate or with copper sulfate, zinc sulfate, lead nitrate, cadmium chloride, cobalt sulfate, and manganese sulfate.

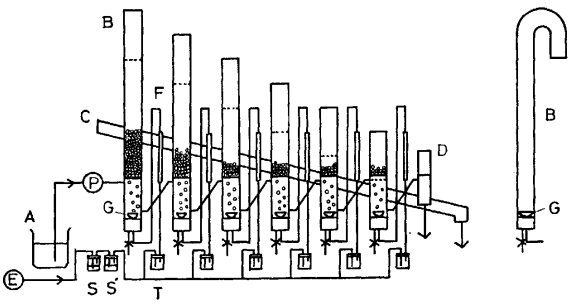

Fig. 1. The trial apparatus for the multistage foam treatment.
C_{10}ODT was added into the wastewater and the pH of the solution was adjusted. This solution was sent by the fluid pump P from the beaker A to the first foaming column B. Every column also consists of glass tube (ϕ 32, L 360—220 mm) with a glass filter G fixed in the rubber stopper at the bottom of tube, and the top of the column is bent in a shape of a half circle and is connected to the foam assembling pipe C. The six foaming columns are all connected in series and the last column is connected to the fluid level meter D. Air is blown into B at the flow rate of about 300 ml/min through the blower E, the humidity chamber S, S', the trap T, the flow meter F and G. The water is sent at the flow rate of 23—25 ml/min.

For application to real wastewater, several kinds of wastewater were sampled at non-ferrous metal mines, an electroplating factory, a spinning factory and an antiseptic factory.

The amounts of heavy metals in the solutions were analyzed for hydrochloric acidity with an atomic absorption spectrophotometer (Shimadzu-AA600).

Results

The result of the elementary analysis of C_{10}ODT is as follows. Found: C, 51.00; H, 9.94; N, 12.44%. Calcd for $C_{14}H_{33}N_3OCl_2$: C, 51.00; H, 10.33; N, 12.60%.[5]

Foaming Ability of the Solution Containing a C_{10}ODT–Metal Complex. An aqueous solution of C_{10}ODT has little foaming ability, but when C_{10}ODT is added to a dilute aqueous solution containing heavy metal ions, the foaming ability of the solution greatly increases due to the rapid formation of water-soluble and foaming C_{10}ODT–metal complex over a suitable pH range (Fig.

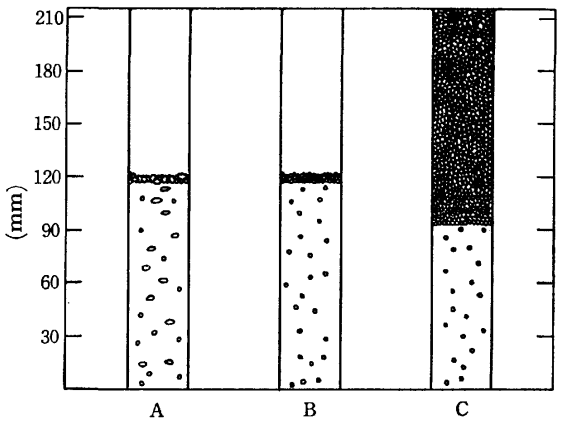

Fig. 2. The foaming ability of the solution of C_{10}ODT–metal complex.
A: Air was blown at the flow rate of 250 ml/min into the aqueous solution of ferrous sulfate at pH 7.
B: Air was blown into the aqueous solution of C_{10}-ODT on the same conditions as A.
C: After C_{10}ODT was added to the aqueous solution of ferrous sulfate at the addition ratio of 2 mol of C_{10}ODT/ gram-atom of iron, air was blown into this solution on the same conditions as A.

2). The foaming ability of the C_{10}ODT–metal complex differs according to the kind of heavy metal, with the C_{10}ODT–copper complex having a particularly high foaming ability.

The effect of the addition of C_{10}ODT to an aqueous solution containing an amount of ferrous sulfate equivalent to 10 ppm of iron is shown in Fig. 2. C_{10}ODT and ferrous sulfate solutions have little foaming ability separately, but a solution of the C_{10}ODT–iron complex has a great foaming ability.

Foam Treatment of Prepared Solution. As an example of batch foam treatment of solutions containing a single kind of metal ion with C_{10}ODT, the case of a solution containing copper ions is shown in Fig. 3.[5]

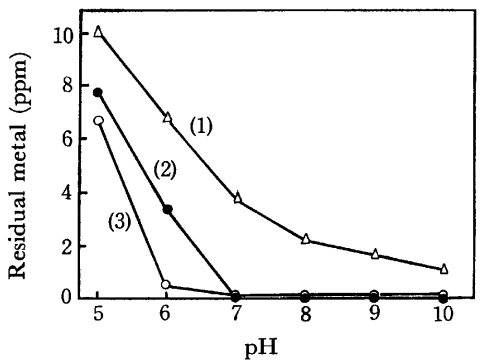

Fig. 3. The result of the batch foam treatment of the aqueous solution of copper sulfate equivalent to 10 ppm of copper with C_{10}ODT.
(1): 1/1; (2): 2/1; (3): 3/1 (C_{10}ODT/Cu).

For the foam treatments of aqueous solutions of copper sulfate, copper chloride, and copper acetate, there was no significant difference between the removing and recovering effects of copper ions. In each case, with a proportional addition of 2 mol of C_{10}ODT/gram-atom of copper, the residual copper after foam treatment at pH 7—10 was 0.05—0.4 ppm.

In the case of zinc, at a proportional addition ratio of more than 2 mol of C_{10}ODT/gram-atom of zinc, the residual zinc after foam treatment at pH 9—10 was less than 1 ppm (Fig. 4).

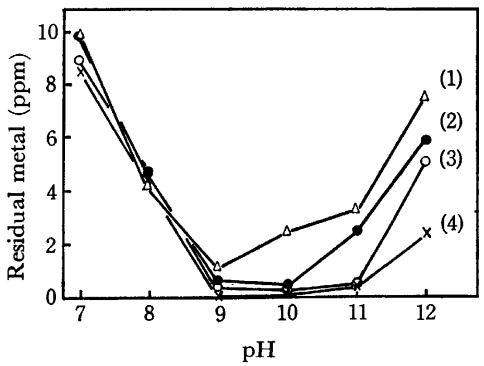

Fig. 4. The result of the batch foam treatment of the aqueous solution of zinc sulfate equivalent to 10 ppm of zinc with C_{10}ODT.
(1): 1/1; (2): 2/1; (3): 3/1; (4): 4/1 (C_{10}ODT/Zn).

As is shown in the above instances, it is seen that the optimum pH value for foam treatment with C_{10}ODT is considerably different for each heavy metal.

In the case of an equimolar mixed solution of several kinds of heavy metal ions, the metal ion content in the residual water after foam treatment differed for each metal (Figs. 5—7).

The results of Figs.5—7suggest that, if the proportional addition of C_{10}ODT to metal ions is selected properly, the specific metal may be removed and recovered over a definite pH range. Thus, by utilizing such properties of C_{10}ODT, the specific metal ion can be removed and recovered selectively (Fig. 8). Thus,

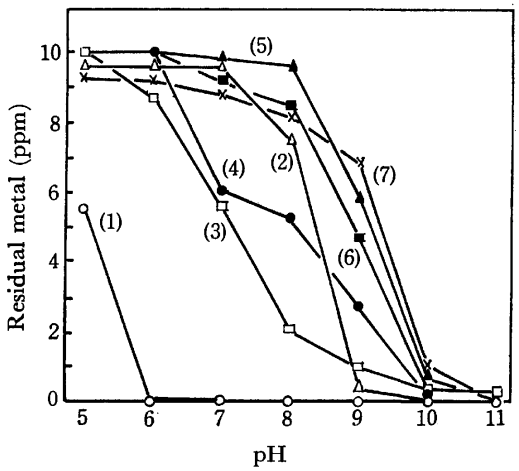

Fig. 5. The result of the foam treatment of the mixed aqueous solution of heavy metal ions.
After C_{10}ODT was added to the solution at the addition ratio of 0.5 mol of C_{10}ODT/ gram-atom of each metal, the pH of the solution was adjusted and the foam treatment was carried.
(1): Cu; (2): Zn; (3): Pb; (4); Ni; (5): Cd; (6): Co; (7): Mn.

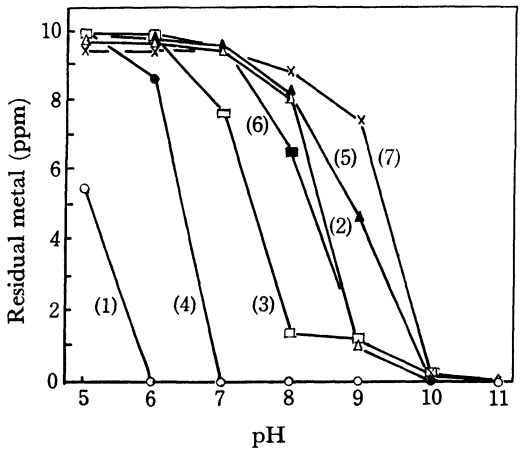

Fig. 6. The result of the foam treatment of the mixed aqueous solution of heavy metal ions.
The similar treatment, at the addition ratio of 1 mol of C_{10}ODT/ gram-atom of each metal, was carried.
(1): Cu; (2): Zn; (3): Pb; (4): Ni; (5): Cd; (6): Co; (7): Mn.

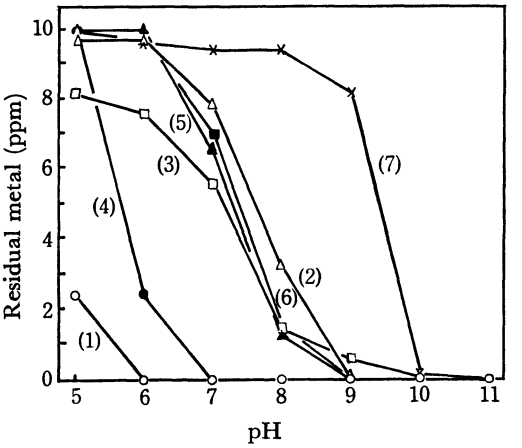

Fig. 7. The result of the foam treatment of the mixed aqueous solution of heavy metal ions.
The similar treatment, at the addition ratio of 2 mol of C_{10}ODT/ gram-atom of each metal, was carried.
(1): Cu; (2): Zn; (3): Pb; (4): Ni; (5): Cd; (6): Co; (7): Mn.

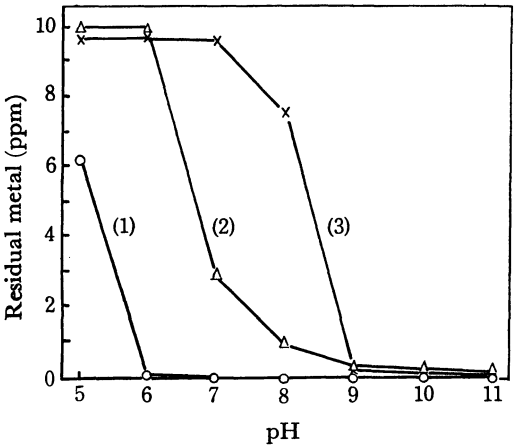

Fig. 8. The selective foam treatment of the mixed aqueous solution of heavy metal ions.
(1): Cu; (2): Pb; (3): Zn.

after 200 ppm of C_{10}ODT was added to a mixed solution of copper sulfate, lead nitrate, and zinc sulfate which was equivalent to a mixture of 10 ppm of each metal ion, batch foam treatment was carried at various pH values of the solution. Consequently, at first, nearly 100% of the copper ions at pH 6, next, about 70% of the lead ions at pH 7 and finally, about 98% of the zinc ions at pH 9 were selectively removed and recovered. However, for a foam treatment beginning at pH 9 resulted in the simultaneous recovery of more than 96% of all heavy metal ions. Calcium sulfate (equivalent to 200 ppm of calcium) did not influence these results.

Foam Treatment of Real Wastewater. Batch foam treatment was carried out on wastewater from a mine A (Table 1), after the addition of C_{10}ODT to the water at ratios of 0.5, 1.0 or 2.0 mol/gram-atom of zinc and copper with the pH of the solution adjusted. The result is shown in Table 1. 100% of the copper and zinc were removed and recovered by the foam treatment at pH 9 for a proportional addition of 1—2 mol of C_{10}ODT/gram-atom of copper and zinc.

Table 1. Batch foam treatment of a sample from a non-ferrous metal mine A

Sample	pH	Addition ratio (C_{10}ODT/Metal)	(ppm) Zinc	Copper	Iron
A	2.9	—	30.78	8.84	5.60
Treated A	9.0[a)]	1/1	0.15	0.00	0.00
		2/1	0.00	0.00	0.00

a) pH directly before foam treatment.

The batch foam treatment was carried on wastewater from a mine B (Table 2) for a proportional addition of 0.1 mol of C_{10}ODT/gram-atom of zinc and the results are shown in Table 2. All heavy metals were completely removed and recovered within limited values, and moreover, no reduction of the efficiency of the treatment by the coexisting abundant calcium ions was observed.

Table 2. Batch foam treatment of samples from a non-ferrous metal mine B

Sample	pH	(ppm) Zinc	Cadmium	Copper	Lead	Iron	Calcium
B	2.3	679.39	4.02	0.18	1.29	111.69	250.0
Treated B	8.0[a)]	6.64	0.17	0.00	0.00	0.00	
	9.0[a)]	1.46	0.07	0.00	0.00	0.00	
	10.0[a)]	8.54	0.07	0.00	0.00	0.00	

Addition Ratio (C_{10}ODT/Zinc)=0.1/1.
a) pH directly before foam treatment.

After C_{10}ODT was added to the wastewater from a mine C (Table 3) for a proportional addition of 1 mol of C_{10}ODT/gram-atom of each metal, the foam treatment was carried at pH 6. As shown in Table 3, about 99% of the copper was removed and recovered selectively. The cadmium and zinc in the residual water were removed and recovered within limited values by

Table 3. Batch foam treatment of samples from a non-ferrous metal mine C

Sample	pH	(ppm)			
		Copper	Zinc	Cadmium	Iron
C	6.2	9.5	68.5	3.2	0.9
1 (Treated C)	6.0[a)]	0.1	63.6	3.2	0.2
Treated 1	9.0[a)]	0.1	0.5	0.1	0.1

Addition Ratio (C_{10}ODT/Each Metal) = 1/1.
a) pH directly before foam treatment.

the form treatment of the residual water at pH 9 (Table 3).

After C_{10}ODT was added to the wastewater of an electroplating factory E (Table 4) for a proportional addition of 1 or 1.5 mol of C_{10}ODT/gram-atom of each metal, the pH of the solution was adjusted and continuous multistage foam treatment was carried out. A better removal and recovery yield of the metal ions was obtained when 1.5 mol of C_{10}ODT was added (Fig. 9). When the foam treatment was applied at pH 6, 99.5% of the copper was removed and recovered selectively, but 90.1% of the zinc and 100% of the nickel remained in the residual water. When the foam treatment was carried out initially at pH 9, the copper, zinc and nickel were removed and recovered simultaneously with a yields of 100, 93.6, and 93.7%, respectively.

When C_{10}ODT was added to the wastewater from a spinning factory S (Table 4) for a proportional addition of 0.5 mol of C_{10}ODT/gram-atom of zinc and continuous multistage foam treatment was applied at pH 10, 99.7% of the zinc ions were removed and recovered.

Of course, by bubbling air into the real wastewater and the model solution, both without C_{10}ODT, almost no foam was produced, and consequently, none of the metal dissolved in the water could be removed and recovered.

Table 4. Analysis of wastewater from an electroplating factory E and a spinning factory S

Sample	pH	(ppm)			
		Copper	Zinc	Nickel	Calcium
E	1.9	50.46	24.88	3.15	—
S	1.9	—	128.7	—	1.1

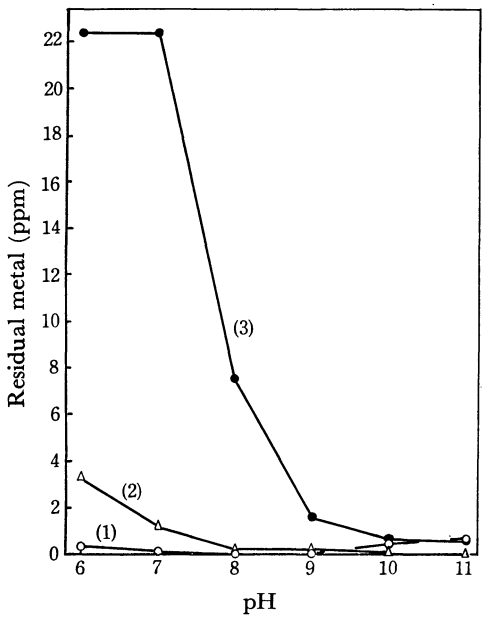

Fig. 9. The result of the continuous multistage foam treatment of the wastewater of an electroplating factory.
(1): Cu; (2): Ni; (3): Zn.

Discussion

For the foam treatment of aqueous solutions containing heavy metal ions, the optimum pH for good foaming varies with the metal. This may be due to the differences of the conditional stability constant[6)] of the C_{10}ODT–metal complex.

Also, when the C_{10}ODT addition ratio was varied, even when good foaming was observed upon the application of the foam treatment, in some cases the residual metal concentration varies considerably. For instance, for the foam treatment of copper sulfate (Fig. 3), at pH values above about 6.5, good foaming was observed. But in this foam treatment for a proportional addition ratio of 1 mol of C_{10}ODT/gram-atom of copper, the removal and recovery yield of the copper was lower in comparison with other cases. Such differences due to the variation of the C_{10}ODT ratio were similarly observed in cases involving other heavy metals and were thought to be due to the structural differences of the complexes.

When a tridentate ligand co-ordinates over a suitable pH range to a copper ion having a co-ordination number of four, one of two types of complexes, *i.e.*, a 1 : 1 hydroxo chelate (A) or a 2 : 1 chelate (B), is obtained[7)] and one of the copper co-ordination bonds in the former complex A co-ordinates with the water.[7)] Thus, C_{10}-ODT, a tridentate ligand, may co-ordinate with copper ions similarly in the above-mentioned case. The authors have previously determined that when C_{10}ODT was added exessively to a solution containing copper ions, a 2 : 1 chelate was produced.[5)] The difference in the structures of the complexes which are formed by adding 1 or 2 mol of C_{10}ODT per gram-atom of copper may be inferred by the fact that the colors of the solutions in these two cases are considerably different from each other, that is, the color in the former case is blue and that of the latter is purple. However, concerning the structures of the complexes, no further investigation was attempted.

As mentioned above, in the case of a small amount of harmful heavy metals dissolved in a large quantity of wastewater, by applying the usual methods, especially, the precipitation method, it is not easy to remove effectively the metals. But, by the present simple method utilizing complex formation of the amido-amines, the problem can be solved.

If necessary, from the complexes recovered by this method, almost all the amido-amine can be easily regenerated by electrolysis.[8)]

The structure of the ligand of a metal complex has influence on not only the solubility,[7] but also the effect of the foam treatment. The authors found that among the acyl groups of C_8–C_{12} involved in these water-soluble metal complexes, the decanoyl group acted as the most desirable hydrophobic group for the foam treatment.[9]

It is interesting that for wastewater containing a high concentration of heavy metal ions, even with a small amount of C_{10}ODT, the foam treatment can be applied (Table 2). The reason for this may be that the complexes formed by the co-ordination of the metal ions with C_{10}ODT are also water-soluble and foamy, and the foam absorbs not only the dissolved complexes but also the deposited particles consisting of the hydroxides of the heavy metals and the complexes which have formed beyond their solubilities.

(September 5, 1974, reported at the 12th World Congress of the International Society for Fat Research in Milano, Italy)

References

1) G. Izumi, *Kankyo Gijutsu*, **3**, 10 (1974); G. Izumi, *Kagaku*, **29**, 282 (1974).

2) G. Izumi, T. Kimura, M. Sato, T. Goto, K. Mori, S. Shōji, M. Koizumi, S. Ujiie, K. Oikawa, S. Sasaki, and T. Suzuki, *Nippon Kagaku Kaishi*, **1973**, 1247.

3) I. Koizumi, *Kogyo Kagaku Zasshi*, **65**, 1343 (1962);K. Yoshida and T. Takeuchi, *Hyomen*, **8**, 65 (1970); F. Sebba, *J. P. Journal*, Showa 36—8717 (1961); F. Sebba, "Ion Floatation," Elsevier Pub. Comp., New York (1962), p. 6; T. Sasaki, "Jikken Kagaku Koza (Sequel)," Vol. 2, ed. by Nippon Kagaku Kai, Maruzen (1967), p. 570.

4) T. Takeshita and S. Maeda, *Yukagaku*, **17**, 354 (1968); T. Tsumaki and M. Yoshino, "Dai Yuki-kagaku (Organic Metal Compound)," Vol. 18, ed. by M. Kotake, Asakura Shobo (1962), p. 424.

5) T. Suzuki, M. Sato, S. Shoji, T. Kimura, and G. Izumi, *Kogyo Yosui*, **195**, 18 (1974).

6) K. Ueno, "Nyumon Kireto-kagaku," Nankodo (1972), pp. 226, 238.

7) T. Sakaguchi and K. Ueno, "Kinzoku-kireto," Vol. 1, Nankodo (1965), pp. 30, 32.

8) T. Suzuki, S. Ujiie, T. Kimura, and G. Izumi, "Abstracts of Lectures at The 31th Annual Meeting of The Chemical Society of Japan," Vol. 1, Nippon Kagaku Kai (1974), p. 607.

9) G. Izumi, unpublished.

The Catalytic Reduction of Nitrogen Oxide by Carbon Monoxide over Metal Oxide Catalysts —The Correlation of the Activities with the Surface States of Metal Oxides—

Katsumi SAKURAI, Yasuaki OKAMOTO, Toshinobu IMANAKA, and Shiichiro TERANISHI

Department of Chemical Engineering, Faculty of Engineering Science, Osaka University, Toyonaka, Osaka 560

(Received July 21, 1975)

In the catalytic NO–CO reaction over metal oxide catalysts, the surface states of reduced metal oxides were studied with ESCA, and the correlation of the activities of the reduced metal oxide catalysts for the NO–CO reaction with their surface states was investigated. The surfaces of the catalysts were studied with ESCA after treatments *in situ*. It was revealed that the surface states of the metal oxides did not always agree with their bulk constituents. For example, it was found that the oxygen in the surface layer of the cobalt oxide after a proper reduction treatment by CO was richer than in its bulk. Moreover, the correlation between the surface states and the activities of those oxides was successfully explained. It was also concluded that, in the NO–CO reaction, the metal states were most active for the cobalt, iron, and nickel oxides, while the Cu^+ state was more active than the Cu metal state for the copper oxide.

The investigation of the catalytic reduction of NO by CO has advanced as part of an effort to prevent the air pollution caused by automobile exhaust, for this reaction can simultaneously change two noxious species, that is, nitrogen oxide and carbon monoxide, to innoxious species, that is, nitrogen and carbon dioxide. Many studies of catalyzed reactions over metal oxide catalysts have been reported.[1–4] However, the study of the correlation of the activities of the metal oxide catalysts with their surface states has rarely been reported. Therefore, it would be very interesting to investigate such a correlation. In the NO–CO reaction, great interest is focussed on what the surface states of the catalysts are during the reaction and on what valence states of the metal ions in the catalysts are most active. Accordingly, the surface states of the metal oxides were studied with ESCA in an attempt to solve these problems.

The phenomenon that the surface of the catalysts was reduced after the NO–CO reaction was observed, so the metal oxides were treated with CO gas in order to reduce them to some degree. Subsequently, the surface states of those reduced oxides were studied with ESCA in order to investigate the correlation of the activities of the catalysts for the NO–CO reaction with the surface states of the catalysts, and also the correlation of their surface states with the degree of reduction of the bulk catalysts.

Experimental

Fe_2O_3, Co_2O_3, Ni_2O_3, and CuO were used as metal oxide catalysts. The Co_2O_3 and Ni_2O_3 were supplied by Nakarai Chemicals, Ltd., while the CuO was supplied by Wako Pure Chemical Industries, Ltd. Only the Fe_2O_3 was prepared by the decomposition, at 600 °C for 4 h in air, of $Fe(OH)_3$, which had itself been produced from iron(III) nitrate and aqueous ammonia. The BET surface areas of Fe_2O_3, Co_2O_3, and Ni_2O_3 were 4.7, 24.8, and 141.3 m^2/g respectively.

The reduction of these catalysts and the reactions between CO and NO were carried out in a usual closed circulating system apparatus, the volume of which was about 340 cm^3. The amount of the catalyst used in each run was 0.020 g for Co_2O_3, Ni_2O_3, and CuO, and 0.100 g for Fe_2O_3. The catalyst, set in the closed circulating apparatus, was evacuated for 4 h at 400 °C, and then it was reduced by CO for a given time at 300 °C. Subsequently, after the evacuation, a reactant gas was introduced into the system, and the reaction between CO and NO was carried out at 300 °C. The partial pressures of NO, CO, and Ar in the gas mixture at about 4.7 cmHg were 1.8, 1.9, and 1.0 cmHg respectively. The product gas mixture was analyzed by means of a Hitachi RMS-4 mass spectrometer calibrated for pure gases. The concentrations of the product gas constituents (CO_2, N_2, and so on) were calculated by comparing their peak intensities with that of Ar. The reaction rates were calculated from the rates of the increases in the peak intensity at $m/e=44$.

The degree of reduction of the bulk catalysts, which is represented by x, is defined by the ratio of the amount of oxygen in the catalyst lost by reduction to that of oxygen in the catalyst before reduction. That is, $M_2O_{3(1-x)}$ shows the composition of the bulk at x for sesquioxides, and $MO_{(1-x)}$, that for monoxides. The conversion of CO into CO_2 was estimated by means of analysis with the mass spectrometer. The CO disproportionation ($2CO \rightarrow CO_2 + C$) occurred at the same time in the reduction by CO. The extent of the disproportionation can be estimated by the amount of the pressure decrease in the closed system. Thus, the above reduction degree was corrected.

The photoelectron spectra were measured on a Hitachi 507 photoelectron spectrometer using Al $K\alpha_{1,2}$ radiation. Powdered samples were mounted on a sample holder made of stainless steel. The oxide catalysts were reduced by CO in a closed treatment chamber which was directly linked to the analysis part. After evacuation, the reduced catalysts were immediately introduced into the adjacent analysis part and were measured with ESCA. Also, in this case the reduction degree was determined in the same way as in the above closed circulating system. The binding energies were corrected by using the value of 285.0 eV for the C 1s level resulting from the contaminated carbon. The reproducibility of this value was within ± 0.2 eV.

Results and Discussion

Figure 1 shows the dependence of the initial reaction rate on the degree of reduction of the catalysts. Initial reaction rates were used to represent the activity, since the catalysts were reduced by the progress of the reaction. Figure 1 indicates that the activities increase as the degree of reduction increases for three oxides of Fe,

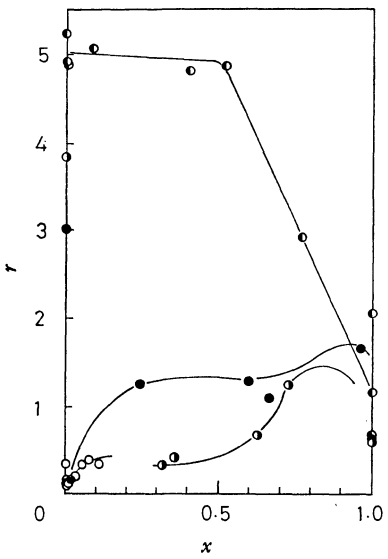

Fig. 1. Dependence of the initial reaction rate on the degree of the reduction.
x: Degree of reduction; $M_2O_{3(1-x)}$ for Fe, Co, and Ni; $MO_{(1-x)}$ for Cu.
r: Initial reaction rate (cmHg/min·g)
●: Co_2O_3, ○: Fe_2O_3, ◑: Ni_2O_3, ◐: CuO

Co, and Ni, and that no very marked change occurs at a moderate degree of reduction (x=0.2—0.6) for the cobalt oxide. The oxides of Co and Ni have comparably high activities near the degree of x=1. That is, they are supposed to have high activities near the metal state. At the degree of x=1, the oxides of both Co and Ni have low activities; this may be caused by the deposited carbon produced by the incidental CO disproportionation. The oxides of Co and Ni, which were not reduced before the reaction, have considerably high activities. These high activities are considered to be attributable to the excess oxygen adsorbed originally on the surfaces of the oxides used. That is, in the case of these catalysts, CO rapidly reacts with the excess oxygen in the initial stage of the reaction; hence, the formation

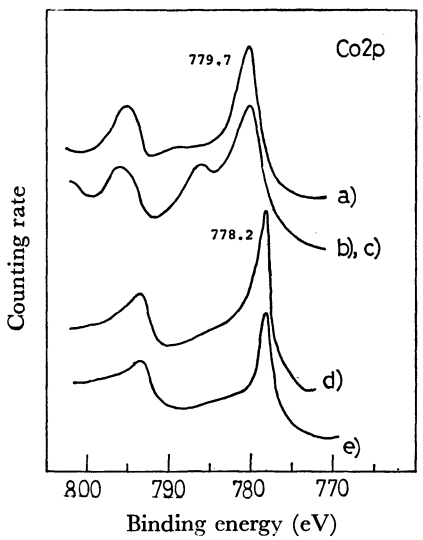

Fig. 2. Co2p ESCA spectra of Co_2O_3 reduced by CO.
a) x=0, b) x=0.37, c) x=0.65, d) x=0.99, e) x=1.

of CO_2 increases upon the additional reaction. Therefore, the activities are considered to be very high.

The behavior of the copper oxide is markedly different from the other three oxides. In Fig. 1 the curve for the copper oxide shows a break at the degree of x=0.5; below this point a high activity is maintained. while above it the activity descends linearly with the degree of reduction. It is obvious that the activity of the copper oxide is higher than those of the other three oxides used in almost all the range of the degrees of reduction.

Table 1. Assignment of the ESCA spectra of the metal oxides in Figs. 2, 4, 5, and 7

Oxide	Spectra	x (Degree of reduction)	Bulk constituent	Surface species
Co_2O_3	a)	0	$CoO_{1.5}$	Co^{3+}
	b)	0.37	$CoO_{0.95}$	Co^{2+}
	c)	0.65	$CoO_{0.53}$	Co^{2+}
	d)	0.99	$CoO_{0.02}$	Co^{0}
	e)	1	Co	Co^{0}
Fe_2O_3	a)	0	$FeO_{1.5}$	Fe^{3+}
	b)	0.04	$FeO_{1.44}$	Fe^{3+}, Fe^{2+}
	c)	0.11	$FeO_{1.33}$	Fe^{3+}, Fe^{2+}
Ni_2O_3	a)	0	$NiO_{1.5}$	Ni^{2+}
	b)	0.52	$NiO_{0.72}$	Ni^{2+}
	c)	0.58	$NiO_{0.63}$	Ni^{2+}, Ni^{0}
	d)	0.74	$NiO_{0.39}$	Ni^{2+}, Ni^{0}
CuO	a)	0	CuO	Cu^{2+}
	b)	0.02	$CuO_{0.98}$	Cu^{2+}
	c)	0.16	$CuO_{0.84}$	Cu^{2+}, Cu^{+}
	d)	0.40	$CuO_{0.60}$	Cu^{+}
	e)	0.76	$CuO_{0.24}$	Cu^{0}

Then we studied, by means of ESCA, the correlation of the surface states of the metal oxides with the reduction degree of the bulk oxides. Figure 2 shows the ESCA spectra of Co 2p for the cobalt oxide. The a), b), and c) spectra in Fig. 2 roughly correspond to Co_2O_3, CoO, and $CoO_{0.5}$ respectively in terms of bulk. Therefore, both the d) and e) spectra correspond to the metal state in bulk. The assignment of the spectra of the cobalt oxide and of the other metal oxides is shown in Table 1. In Fig. 2, it may be observed that the b) spectrum is the same as the c) spectrum, though the degree of the bulk reduction of the former (x=0.37) is different from that of the latter (x=0.65). The b) and c) both spectra correspond to CoO.[5] From these facts it may be considered that the surface state of the cobalt oxide remains CoO over a considerably wide range of the degree of reduction and that the oxygen in the surface layer is richer than in the bulk at a moderate degree of reduction. This fact is consistent with the constant activity at a moderate degree of reduction for the cobalt oxide in Fig. 1. Figure 3 shows the dependence of the peak intensities of O1s and C1s on the cobalt oxide surface upon the degree of reduction. This dependence agrees well with the above facts that the intensity of the O1s peak on the surface is constant at a moderate degree of reduction. When the cobalt oxide at the degree of x=1 was further reduced, it was found

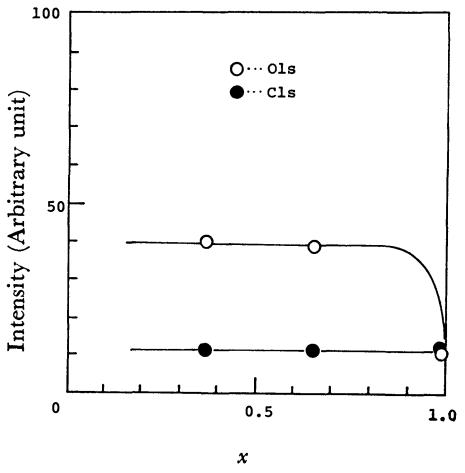

Fig. 3. Dependence of the peak intensity of O1s and C1s for Co_2O_3 on the degree of reduction.
x: Degree of reduction.

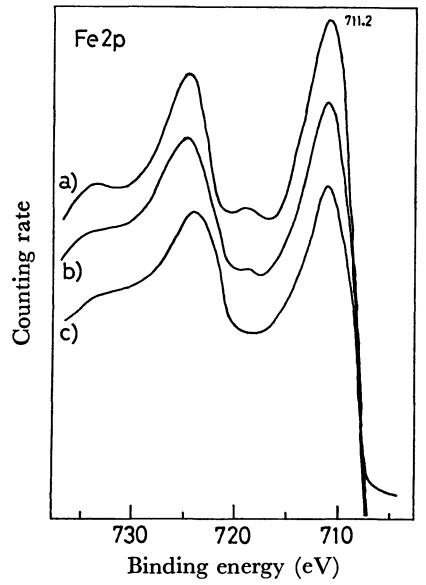

Fig. 4. Fe 2p ESCA spectra of Fe_2O_3 reduced by CO.
a) $x=0$, b) $x=0.04$, c) $x=0.11$.

that the intensity of the C1s peak on the cobalt surface increased suddenly; this suggests that the disproportionation of CO occurs when the oxygen in the cobalt oxide is exhausted.

Fe_2O_3 is more difficult to reduce than Co_2O_3. The spectra of the iron oxide show no remarkable change, as is shown in Fig. 4, but the main peaks of Fe2p tend to become broader and its satellite peaks disappear as the oxide is reduced. It may be supposed that the spectra accompanied by the satellite peaks correspond to Fe^{3+} and that the spectra without them correspond to the mixed state of Fe^{2+} and Fe^{3+} in Fe_3O_4. Therefore, it may be concluded that, in the case of the iron oxide, the divalent and trivalent states of iron can not definitely be differentiated on the basis of the Fe 2p-spectral data.

As is shown in Fig. 5, the spectra of Ni 2p vary around the degree of $x=0.5$. It may be considered from Fig. 5 that the surface constituent of the nickel oxide is NiO

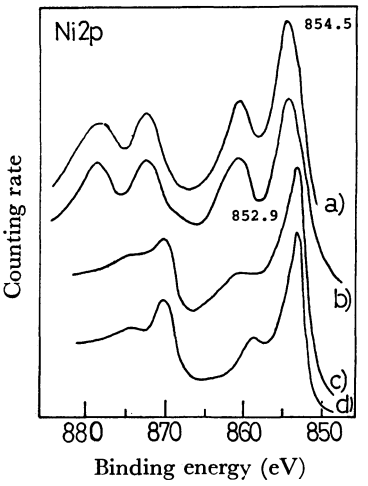

Fig. 5. Ni 2p ESCA spectra of Ni_2O_3 reduced by CO.
a) $x=0$, b) $x=0.52$, c) $x=0.58$, d) $x=0.74$.

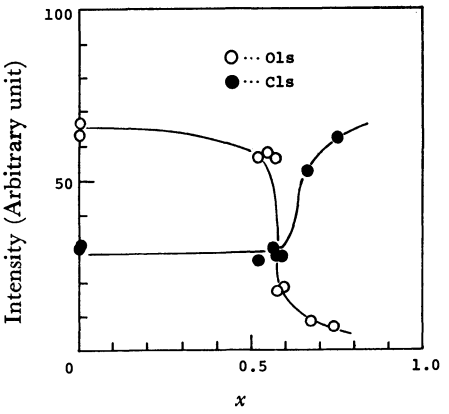

Fig. 6. Dependence of the peak intensity of O1s and C1s for Ni_2O_3 on the degree of reduction.
x: Degree of reduction.

below the degree of $x=0.5$ and is a mixture of NiO and nickel metal above the degree of $x=0.5$. Figure 6 shows the dependence of the intensity of the O1s and C1s spectra for the nickel oxide surface on the degree of reduction. The amount of the surface oxygen is roughly constant below the degree of $x=0.5$, while it decreases sharply near the degree of $x=0.5$; this coincides with the above reduction tendency of the nickel oxide. Figure 1 indicates that the activity of the nickel oxide is roughly constant below the degree of $x=0.5$ and increases above the degree of $x=0.5$; this increase in the activity corresponds with the appearance of nickel metal on the catalyst surface. Thus, the behavior of the nickel oxide is similar to that of the cobalt oxide, except that the former produces the metal states at a lower reduction degree than does the latter.

In Fig. 5, the a) spectrum at the degree of $x=0$ after the evacuation treatment, which is accompanied by satellite peaks, may be supposed to correspond to the Ni^{2+} state in spite of the Ni^{3+} bulk constituent, but the binding energy of the Ni $2p_{3/2}$ peak of the spectrum (854.5 eV) is considerably smaller than that of NiO (855.4 eV). This finding suggests that the surface of the oxide may be almost covered with the noncrystal

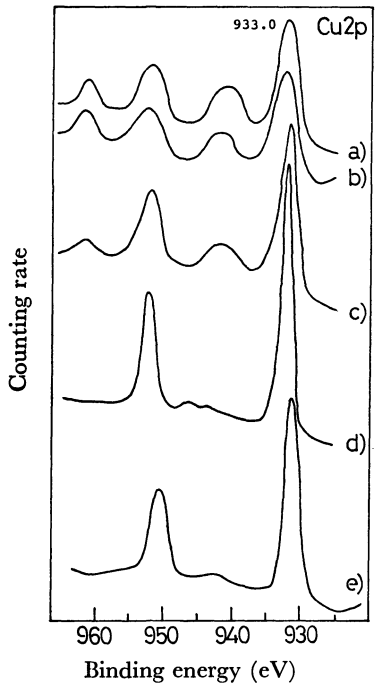

Fig. 7. Cu 2p ESCA spectra of CuO reduced by CO.
a) $x=0$, b) $x=0.02$, c) $x=0.16$, d) $x=0.40$, e) $x=0.76$.

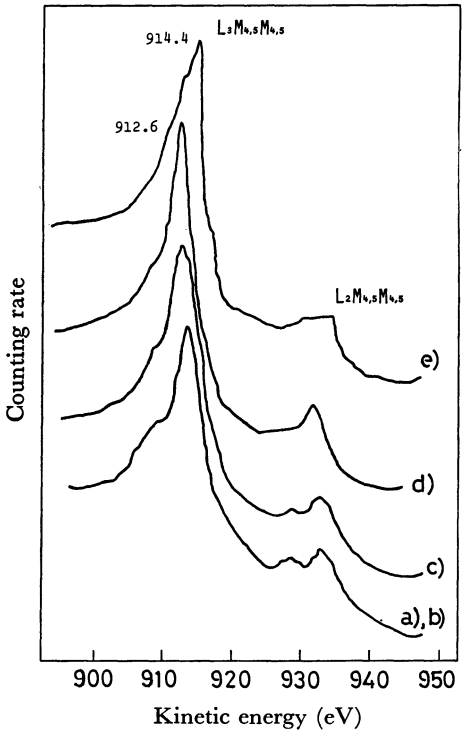

Fig. 8. Auger spectra of CuO reduced by CO.
a) $x=0$, b) $x=0.02$, c) $x=0.16$, d) $x=0.40$, e) $x=0.76$.

Ni^{2+} oxide with defects upon evacuation at a high temperature.

Figure 7 shows the ESCA spectra of Cu 2p for the copper oxide, while the Cu LMM Auger spectra are shown in Fig. 8. The spectra of Cu 2p start to vary around the degree of $x=0.16$, and the satellite peaks almost disappear at the degree of $x=0.40$, as is shown in Fig. 7. The a) and b) spectra, with the satellite peaks, are assigned to the Cu^{2+} state.[6] In Fig. 7, the ESCA d) spectrum is almost the same as e), while, as is shown in Fig. 8, the kinetic energy of the $L_3M_{4,5}M_{4,5}$ peak of the corresponding Auger spectrum, d), is smaller than that of e) by 1.8 eV. Accordingly, the ESCA spectra in Fig. 7, d) and e), can be assigned to the Cu^+ and Cu metal states respectively.[7] This fact indicates that CuO on the oxide surface may decrease as Cu_2O increases below the degree of about $x=0.40$, and that CuO may almost disappear at the degree of $x=0.40$. Therefore, it may be supposed that the copper oxide catalyst has a high activity when CuO coexists with Cu_2O on the catalyst surface, and that the activity decreases as the copper metal increases above the degree of about $x=0.5$, where CuO disappears entirely. In conclusion, for the copper oxide the active species in the NO–CO reaction is mainly Cu^+, and the Cu metal is a much lower active species than Cu^+.

It may be concluded that, in the NO–CO reaction, the metal states are most active for the cobalt, iron, and nickel oxides, while the Cu^+ state is more active than the Cu metal state for the copper oxide. As has been mentioned above, the differences between the bulk constituents and the surface states of some reduced metal oxides were revealed by ESCA. Moreover, the correlation between the surface states and the activities of those metal oxides was successfully explained. By using ESCA, useful information on the above problem could also be obtained for other metal compounds which are not dealt with in this paper.

References

1) M. Shelef and K. Otto, *J. Catal.*, **12**, 361 (1968).
2) J. F. Roth and R. C. Doerr, *Ind. Eng. Chem.*, **53**, 293 (1961).
3) G. L. Bauerle, G. R. Service, and Nobe Ken, *Ind. Eng. Chem. Prod. Res. Develop.*, **11**, 54 (1972).
4) M. Shelef and K. Otto, *J. Catal.*, **10**, 408 (1968).
5) Y. Okamoto, H. Nakano, T. Imanaka, and S. Teranishi, *Bull. Chem. Soc. Jpn.*, **48**, 1163 (1975).
6) D. C. Frost, A. Ishitani, and C. A. McDowell, *Mol. Phys.*, **24**, 861 (1972).
7) P. E. Larson, *J. Electron Spectrosc.*, **4**, 213 (1974).

A Study on the Anode Effect in KF-2HF System. II. Difference in Anodic Behavior between Edge Plane and Layer-plane of Pyrolytic Graphite

Hiroki IMOTO and Nobuatsu WATANABE

Department of Industrial Chemistry, Faculty of Engineering, Kyoto University, Yoshida, Sakyoku Kyoto 606

(Received August 18, 1975)

The anodic behavior of pyrolytic graphite has been studied by voltammetry and ESCA analysis in the molten KF-2HF system at 100 °C, attention being given to the difference in anodic behavior between the edge plane and layer-plane of the pyrolytic graphite. The polarization current obtained by a linear potential sweep experiment decreased rapidly with increasing potential after the onset of the anode effect. When the edge plane was used as a working electrode surface the current density was recovered on the subsequent sweep toward negative potentials, whereas the current density was hardly recovered on the layer-plane surface of the electrode. The difference in polarization behavior was interpreted on the basis of the difference in the rate of decomposition reaction of graphite fluoride, $(CF)_n$, formed on the electrode surface. ESCA spectra of the electrodes polarized at various potentials indicate that $(CF)_n$ was formed even at 2.0 V *vs.* Pt, below the fluorine evolution potential, on the edge plane of the pyrolytic graphite and that its amount did not increase appreciably with increasing potential. On the layer-plane, however, no formation of $(CF)_n$ was observed at 2 V *vs.* Pt, its amount increasing appreciably with potential at the potentials above 3 V *vs.* Pt.

The anodic behavior of graphite and carbon in molten fluorides is of importance since the cell operation during the course of electrolysis at high current density is remarkably restricted by the occurrence of anode effect.[1-3] In the preceding paper,[4] it was reported that the onset of the anode effect is due to a significant decrease in the wettability of the anode surface by the electrolyte caused by the formation of graphite fluoride, $(CF)_n$, having very low surface energy, and that the compound is formed even under normal electrolysis conditions. In the present investigation, the anodic behavior of the two distinct planes of pyrolytic graphite, edge plane and layer-plane, was studied by the potential sweep and potentiostatic methods, and by ESCA analysis of the electrodes polarized potentiostatically at various potentials and the electrodes after the anode effect.

The following reactions are considered to occur simultaneously on the anode surface.

1) Fluorine evolution

$$2F^- \longrightarrow F_2 + 2e^- \quad (1)$$

2) Formation of $(CF)_n$ film

$$nF^- + nC \longrightarrow (CF)_n + ne^- \quad (2)$$

3) Decomposition of $(CF)_n$ film

$$(CF)_n \longrightarrow C + CF_4,\ C_2F_6,\ etc. \quad (3)$$

The results obtained were interpreted by considering the kinetic balance between the formation and the decomposition reaction of the $(CF)_n$ film on the anode surface.

Experimental

Voltammetry and preparation of the samples for ESCA analysis were carried out in the cell shown in Fig. 1. The cell was made of iron and its temperature was maintained at 100 °C in an oil bath. The wall of the cell was used as a cathode and the bottom of the cell was covered with a Teflon plate. The brass leads and all parts of the electrodes A, B, and C directly in contact with the vapor of hydrogen fluoride or KF-2HF melt were coated with Teflon. The molten KF-2HF was dehydrated by pre-electrolysis by using the carbon electrode

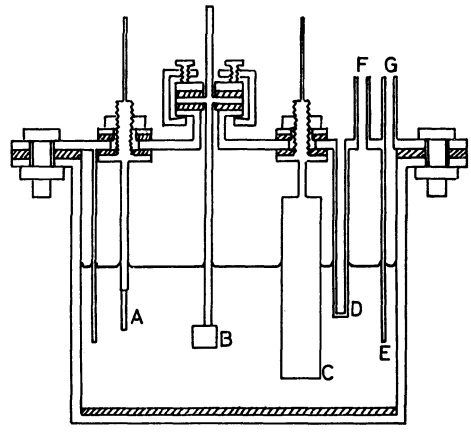

Fig. 1. Electrolytic cell.
A: Reference electrode (Pt), B: anode, C: carbon electrode for dehydration, D: well for thermometer, E: skirt, F: anode gas outlet, G: cathode gas outlet. The hatched parts are made of Teflon.

C. The potentials of working electrode B were measured with respect to the reference electrode A of a Pt rod. The pyrolytic graphite used was supplied by Nihon Carbon Co., Ltd.. The pyrolytic graphite was heat-treated at 2200 °C for 1 h before use. Its crystallographic properties determined by X-ray analysis were as follows: lattice parameters $a=2.457$ Å and $c=6.831$ Å, crystallite size La (110)$>$1000 Å, crystallite height Lc (002)$=$240 Å, degree of crystalline alignment P (Franklin's *P*-value)*$=0.84$. The apparent density was 2.08 g/cm^3. The specific resistances parallel and perpendicular to the c axis were 0.52 and 3.9×10^{-5} ohm·cm, respectively. The layer-plan electrode was *ca.* 14 mm$\times$ *ca.* 9 mm and *ca.* 1 mm in thickness. The edge plane electrode was *ca.* 10 mm$\times$5 mm and *ca.* 6 mm in thickness. The apparent surface area was used for the calculation of current density. The surface of the edge plane electrode was polished with fine sandpaper Emery #600, the powder of graphite being removed by washing with distilled water.

* *P*-value was calculated by the equation

$$d(002) = 3.340 - 0.086(1-P^2),$$

where P is a ratio of the misoriented parts to the sum of the oriented and misoriented parts.

The electrodes were connected with the brass leads by winding fine copper wire on to them. Only one face of the pyrolytic graphite, the edge plane or the layer-plane, was used as a working electrode surface, the other faces being covered with Teflon tape. The edge plane electrodes polarized at various potentials were washed with anhydrous hydrogen fluoride in order to remove KF-2HF before ESCA analysis.

Results and Discussion

Polarization Curves. Figure 2 shows a polarization curve obtained by sweeping potential 1—10 V *vs.* Pt for the layer-plane electrode. Three peaks were observed on the *I—V* curve. An explanation for these peaks was given in a previous paper[5] in which the anodic behavior of carbon, graphite, and glassy carbon electrodes was dealt with. The first peak corresponds to the discharge reaction of trace water in the electrolyte and the second and third peaks to the discharge reaction of fluoride ion. Current density decreased rapidly at 5 V due to the onset of the anode effect. Restoration of the current density was hardly observed on the subsequent sweep from 10 to 3 V. The observed current density was as small as 2 mA/cm², when the anode potential was swept again from 3.5 to 10 V at the same sweep rate. Thus it is indicated that

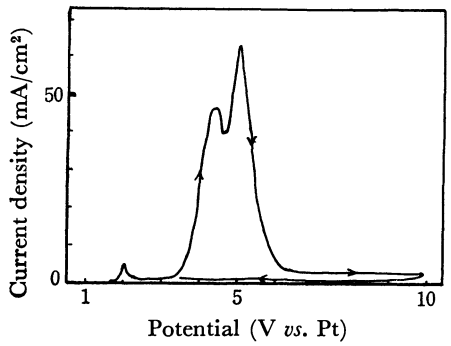

Fig. 2. *I—V* curve (potential sweep) in KF-2HF at 100 °C. Anode: layer-plane of pyrolytic graphite, sweep rate: 12.5 mV/s.

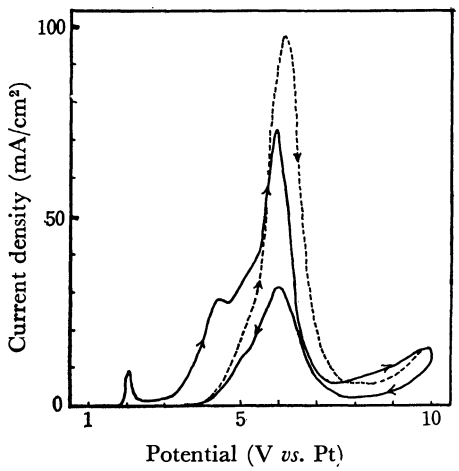

Fig. 3. *I—V* curves (potential sweep) in KF-2HF at 100 °C. Anode: edge plane of pyrolytic graphite, sweep rate: 12.5 mV/s.
——: First sweep, ------: second sweep.

if $(CF)_n$ film is once formed on the layer-plane of pyrolytic graphite by reaction (2), the anode surface is hardly restored.

Figure 3 shows the polarization curves obtained by the potential sweep method for the edge plane electrode. On the first sweep from 1 to 10 V, the polarization curve for the edge plane electrode was similar to that for the layer-plane electrode. However, in contrast to the case for the layer-plane electrode, the restoration of current was observed on the subsequent sweep toward negative potentials, the peak current density on the second sweep toward positive potentials (a dotted line) being comparable to the third peak on the first sweep. The restoration in current indicates that the decomposition of $(CF)_n$ takes place much faster on the edge plane than on the layer-plane.

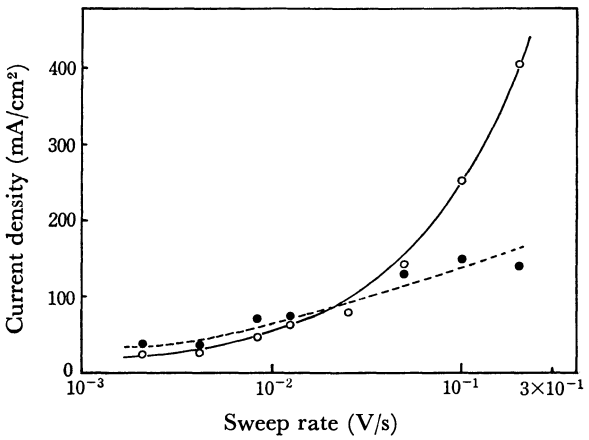

Fig. 4. Dependence of peak current densities on sweep rate.
○: Layer-plane of pyrolytic graphite,
●: edge plane of pyrolytic graphite.

The third peak current density in the polarization curve on the first sweep toward positive potential depends upon the rates of reactions (2) and (3). The peak current densities are plotted against the sweep rate for both layer-plane and edge plane electrodes in Fig. 4. The peak current density increased noticeably with increasing sweep rate for the layer-plane electrode, while it increased only slightly for the edge plane electrode. It is supposed in general that the peak current density becomes less dependent on the sweep rate with an increase in the rate of deactivation of electrode surface, since the relatively fast deactivation reaction of electrode surface with respect to the sweep rate leads to a nearly steady-state condition of the electrode surface irrespective of the sweep rate. Thus, it might be suggested that the rate of deactivation of the anode surface, which depends upon the difference in rates between reactions (2) and (3), is smaller at the layer-plane electrode than at the edge plane electrode, if it is assumed that the potential dependence of the current density due to the fluorine evolution reaction (1) at both the plane is equal to each other.

When the layer-plane and edge plane electrodes were polarized potentiostatically at various potentials, the current densities reached stationary values within 30

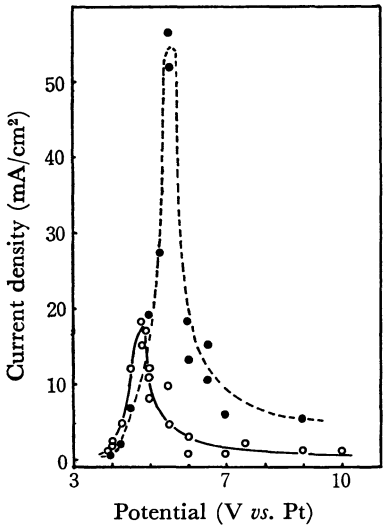

Fig. 5. *I—V* curves (potentiostatic) in KF-2HF at 100 °C.
○: Layer-plane of pyrolytic graphite,
●: edge plane of pyrolytic graphite.

min. These values are plotted against potentials in Fig. 5. Maximum current densities are observed at 4.8 V and 5.5 V for the layer-plane and edge plane, respectively. Since the maximum current densities are observed at 5.5 V for carbon and graphite,[4] it seems that the critical current densities at graphite and carbon anodes are attributable to those at their edge plane.

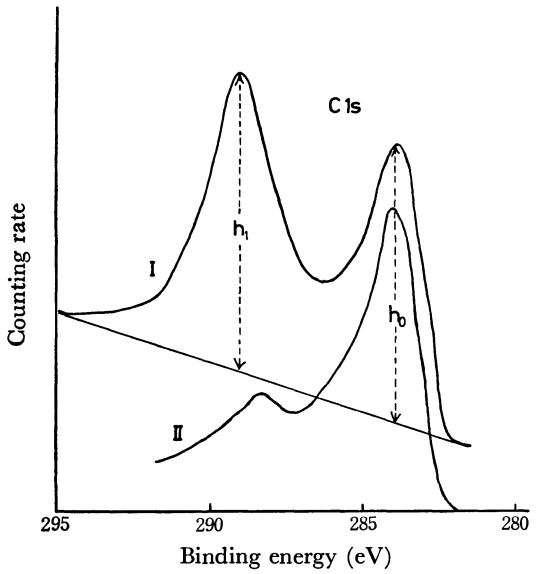

Fig. 6. ESCA spectra of pyrolytic graphite anodes immediately after the anode effect.
I: Layer-plane,
II: edge plane.

ESCA Spectra. When the layer-plane and edge plane electrodes were polarized at a constant current density of 400 mA/cm², the anode effect took place within 10 s and the circuit was opened immediately after the onset of the anode effect. Figure 6 shows the ESCA spectra of the carbon 1s electron for the above samples. The peak at 284 eV corresponds to the binding energy of the carbon 1s electron for the carbon which has only the C–C bond. The peak at 288.5 eV corresponds to the one for the carbon atom with the C–F bond.[4] The height of the peaks at 284 eV and 288.5 eV is denoted by h_0 and h_1, respectively.

In order to investigate the potential dependence of the amount of $(CF)_n$ on the anode surface, the ESCA spectra of the fluorine 1s electron as well as carbon 1s electron were obtained for the layer-plane and edge plane electrodes polarized potentiostacitally at various potentials for 30 min. The height of the peaks at 688

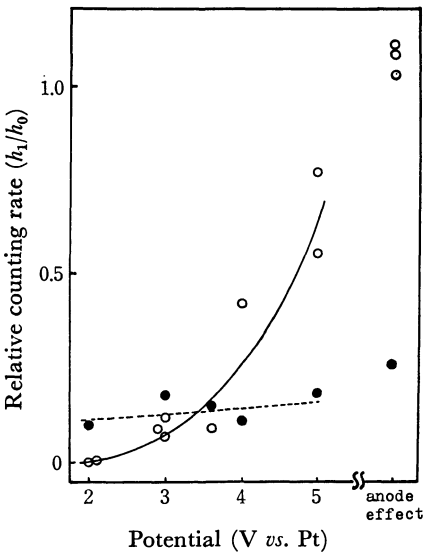

Fig. 7. Potential dependence of ESCA spectra. C 1s (288.5 eV).
○: Layer-plane of pyrolytic graphite,
●: edge plane of pyrolytic graphite.

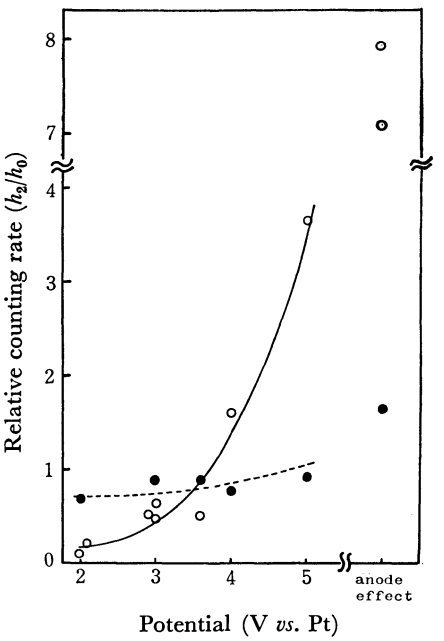

Fig. 8. Potential dependence of ESCA spectra. F 1s (688 eV).
○: Layer-plane of pyrolytic graphite,
●: edge plane of pyrolytic graphite.

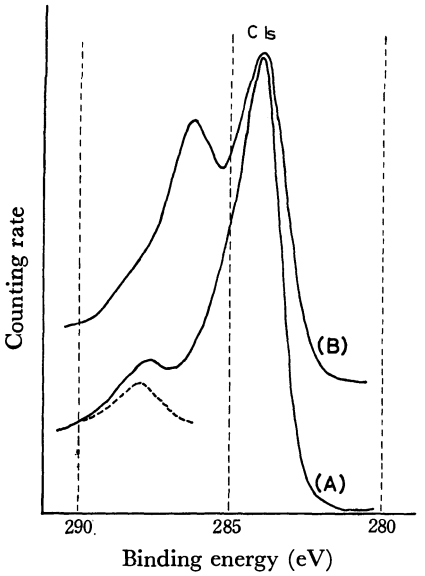

Fig. 9. ESCA spectra of anode surfaces.
(A): Edge plane of pyrolytic graphite polarized at 2.0 V *vs.* Pt in KF–2HF at 100 °C.
(B): Graphite polarized at constant current density of 500 mA/cm^2 in 2M-H_2SO_4 at room temperature.

eV corresponding to the binding energy of F 1s electron is represented by h_2. The ratios h_1/h_0 and h_2/h_0 plotted against potentials are illustrated in Figs. 7 and 8, respectively.

The equilibrium potential of reaction (1) is 3.4 V *vs.* Pt in KF–2HF at 100 °C.[6] A peak was observed at 288.5 eV in the carbon 1s spectra for the edge plane electrode polarized at 2 V, at a more negative potential than 3.4 V. The following experiments were carried out in order to confirm the view that the peak at 288.5 eV observed for the edge plane electrode polarized at 2 V is attributable to the C–F bond, but not to the C–O bond formed by the discharge reaction of the trace water.

Sample A: the edge plane electrode polarized at 2.0 V for 30 min at 100 °C in KF–2HF.

Sample B: the graphite anodically polarized at constant current density of 500 mA/cm^2 in 2M-H_2SO_4, for 10 min at room temperature.

Figure 9 shows the ESCA spectra of C 1s electron for samples A and B. A peak was observed at 286 eV for sample B, which is identical with that for the graphite oxide in the binding energy.[7] Since the peak at 288.5 eV for sample A is attributable to the C–F bond, but not to the C–O bond, it becomes apparent that reaction (2) proceeds at a more negative potential than the equilibrium potential of reaction (1).

The same tendency is shown in Fig. 7 as in Fig. 8. It is thus evident that the peak at 288.5 eV is associated with the carbon bound with fluorine atom. No detectable amount of $(CF)_n$ exists on the layer-plane electrode polarized at 2 V in Fig. 7, but the amount of $(CF)_n$ increases noticeably as the potential becomes higher than 2 V. On the other hand, a considerable amount of $(CF)_n$ is detected on the edge plane electrode polarized at 2 V, above which the amount of $(CF)_n$ increases slightly with increasing potential.

The values of h_1/h_0 for the layer plane electrode are much larger than those for the edge plane under the conditions of the anode effect, which is in line with the view that the rate of the decomposition of the $(CF)_n$ film is larger on the edge plane than on the layer-plane.

It is concluded that the amount of $(CF)_n$ formed on the surface of carbon and graphite anode increases with an increase in the polarization potential and that the restoration of current at these electrodes during the polarization toward negative potentials after the onset of anode effect is attributed to the fast decomposition reaction of the $(CF)_n$ film on the portions of these electrodes where the edge plane is in contact with the electrolyte.

The authors are greatly indebted to Shimadzu Seisakusho Co., Ltd. for permission to use their electron spectrometer.

Refenceers

1) N. Watanabe, M. Ishii, and S. Yoshizawa, *Denki Kagaku*, **29**, 492 (1961).
2) N. Watanabe, M. Ishii, and S. Yoshizawa, *Denki Kagaku*, **29**, 497 (1961).
3) A. Tasaka, K. Nakanishi, and N. Watanabe, *Denki Kagaku*, **38**, 376 (1970).
4) H. Imoto, T. Nakajima, and N. Watanabe, *Bull. Chem. Soc. Jpn.*, **48**, 1633 (1975).
5) M. Nishimura, A. Tasaka, K. Nakanishi, and N. Watanabe, *Denki Kagaku*, **38**, 294 (1970).
6) A. Tasaka, Thesis (Kyoto University) (1970), p. 54.
7) J. B. Donnet, H. Dauksch, J. Escard, and C. Winter, *C. R. Acad. Sci., Paris, Ser. C*, **275**, 1219 (1972).

ESR Study of γ-Ray Irradiated Potassium Hexacyanocobaltate $K_3[Co(CN)_6]$

Naoki FURUTA,* Tokuko WATANABE, and Shizuo FUJIWARA

Department of Chemistry, Faculty of Science, The University of Tokyo, Hongo, Bunkyo-ku, Tokyo 113

(Received October 2, 1975)

ESR results for γ-irradiated $K_3[Co(CN)_6]$ in powder and single crystal forms are reported. The main paramagnetic species detected at 77 K were diisocyanide $[Co^{II}(CN)_4(NC)_2]^{4-}$ and pentacyanocobaltate(II) $[Co^{II}(CN)_5]^{3-}$. On annealing, diisocyanide was lost and pentacyanocobaltate was formed. In Part I the reaction mechanism is discussed from the results of the powdered sample and in Part II the noncollinear structure is presented as the plausible molecular form of diisocyanide from the results of the single crystal.

The central diamagnetic transition metal ions in inorganic complex compounds are transformed into paramagnetic ones by high energy radiation, leaving the mother lattice almost unchanged. The products have been referred to as the hot ions.[1] Hot ions of Zn and Cd in cyanocomplexes have recently been investigated extensively as single crystals.[2-5] The cyanocomplexes are useful as the samples of the investigation of hot ions because they easily form good single crystals and show interesting features, such as the dimer formation and the high ligand lability; thus, cyanocobaltate(III) has been taken as the sample of the present experiment. The cyanocabaltate(II) complexes are dimerized when synthesized by the usual chemical methods, forming a diamagnetic compound. Also, the hot ion Co(II) presents ESR data which refer to the low spin state of d^7, in contrast to the usual method. It has been reported that the paramagnetic diisocyanide $[Co^{II}(CN)_4(NC)_2]^{4-}$, (to be referred to as species I),** and the pentacyanocobaltate $[Co^{II}(CN)_5]^{3-}$ (species II) are produced by the high energy irradiation of cyanocobaltate.[6-9] However, those investigations in the literature are preliminary and leave several problems to be investigated. For example, when the sample is annealed from 77 K to room temperature, only species II can be observed, and not I. Also, the mechanisms of the formation and the temperature dependence of the stability of these species have not been clarified. Hence, we decided to investigate these problems more in detail; we found that species I and species II are stable at 77 K, but, on annealing, an electron is released from species I resulting in the formation of species II. The first part of this paper is concerned with the investigation of the powdered sample, and the second part, that of the single crystal.

Part I Powdered Sample

Experimental

Potassium hexacyanocobaltate(III) was prepared with cobalt(II) chloride hexahydrate and potassium cyanide.[10] The reagents used were of the reagent grade and no further putification was done. The purity of the synthesized sample was checked by elemental analyses: Calcd for $K_3[Co(CN)_6]$: C, 21.68; H, 0; N, 25.29%. Found: C, 21.65; H, 0; N, 25.74 % mol wt 332.25. The powdered samples were exposed to γ-rays from a ^{60}Co source of the University of Tokyo at room temperature and at 77 K. ESR spectra were obtained with a JEOL 3BS Type X-band spectrometer using 100 kHz field modulation. The magnetic field was calibrated by Mn^{2+} (doped in MgO) and the resonance position of DPPH (g= 2.0036). The ESR spectrum was measured for each specimen before irradiation and it was confirmed that the sample did not contain any ESR-active paramagnetic species. The number of the hot ions was determined by comparing the integrated intensity of hot ions with that of the standard sample $[Co^{III}(NH_3)_6]$ $[Cu^{II}Cl_5]$ which contained 1.3×10^{18} Cu(II) ions. The sample was sealed *in vacuo* (4.2×10^{-6} Torr), and this was compared to the sample in air in order to see the atmospheric effect. The sample irradiated at 77 K was annealed gradually, and ESR was measured during this procedure. The effect of the total dose applied to the sample was also examined. When the sample was kept at constant temperature, species I decayed and II was formed. The rate of this decay and that of the formation were also measured.

Results

Figure 1 shows the ESR spectra of the sample after irradiation at 77 K (referred to as I in the figure) and that at room temperature (II). In both spectra $g_{//}$ and $g_{\perp}$ are split into eight lines by Co(II) with a nuclear spin of 7/2. The spectral patterns are different, with the different parameters shown in Table 1. Apparently,

Table 1. ESR parameters of hot ions formed in γ-irradiated powder $K_3[Co(CN)_6]$.

	$g_{//}$	$A_{//}$(G)	$g_{\perp}$	$A_{\perp}$(G)
Irradiated at 77 K (Spectrum I)				
$[Co^{II}(CN)_4(NC)_2]^{4-}$	2.001 (±0.002)	61.7 (±0.3)	2.091 (±0.001)	−70.0 (±0.3)
$[Co^{II}(CN)_5]^{3-}$	2.004 (±0.005)	89 (±2)	2.170 (±0.003)	−29.3 (±1)
Irradiated at room temperature (Spectrum II)				
$[Co^{II}(CN)_5]^{3-}$	2.004 (±0.005)	89 (±2)	2.170 (±0.003)	−29.3 (±1)

the features of the spectrum in Fig. 1 are complicated and cannot be analysed by simple observation. After the analysis of the angular dependence of the ESR spectra of the single crystal, it was revealed that the tensors of g and A for species I were orthogonal to each other, and $g_{//}$ was split by $A_{\perp}$ and $g_{\perp}$ by $A_{//}$ and $A_{\perp}$. More details of the latter finding will be described in Part II of this article. For species II the $A_{//}$ can be observed as

* Present address: Department of Chemistry and Physics, National Institute for Environmental Studies, P. O. Yatabe, Tsukuba, Ibaraki 300-21.

** With respect to the real form of the molecule, it is not clear whether two of the cyanide ligands are inversed[14] or twisted.[8,9] We use the formula $[Co^{II}(CN)_4(NC)_2]^{4-}$ for convenience.

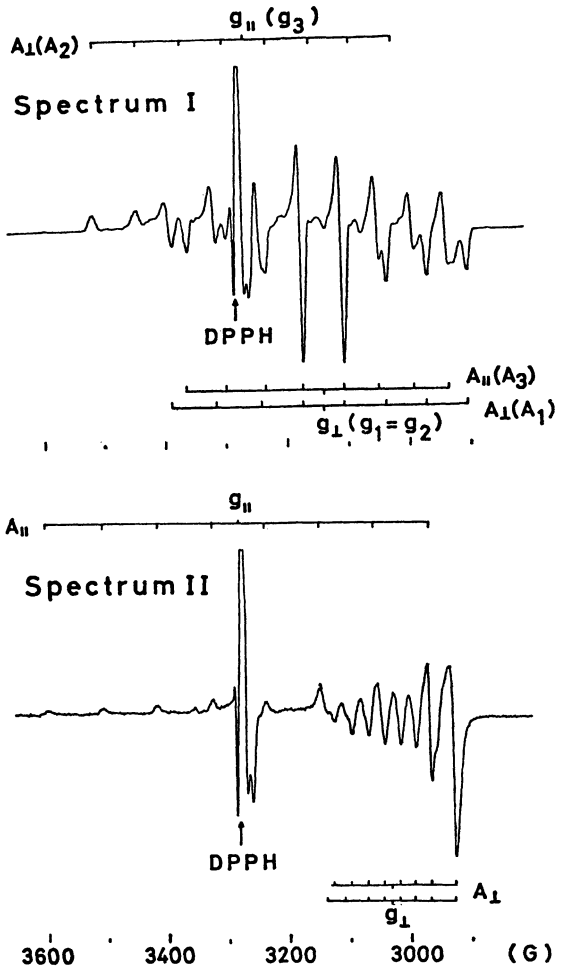

Fig. 1. ESR spectra of γ-irradiated powder $K_3[Co(CN)_6]$ at 77 K (Spectrum I) and room temperature. (Spectrum II).

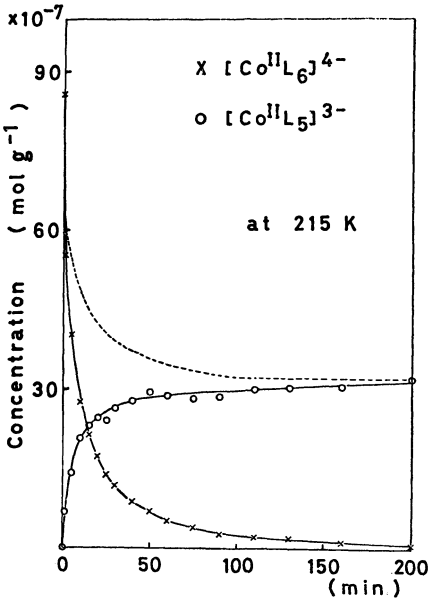

Fig. 2. The process of the decay and the formation of hot ions at 215 K.
(×: Species I, ○: species II, ----: total paramagnetic species.)

Table 2. Dose effect ($\times 10^{-7}$ mol g^{-1})
I: $[Co^{II}(CN)_4(NC)_2]^{4-}$
II: $[Co^{II}(CN)_5]^{3-}$
III: diamagnetic species

Total dose (rad)	Irradiated at 77 K				At r.t.
	I	II	After annealing		II
			II	III	
1×10^5	4.8	0.2	3.8	(1.2)	5.8
5×10^5	18	0.8	13	(5.8)	18
1×10^6	32	1.7	22	(12)	32
5×10^6	92	9.0	47	(54)	90
1×10^7	120	14	52	(82)	133
5×10^7	171	50	87	(134)	215

the split of the $g_{//}$ part, as usual. Species I can be assigned to the hexacoordinated species $[Co^{II}(CN)_4(NC)_2]^{4-}$ and species II to the pentacoordinated one $[Co^{II}(CN)_5]^{3-}$, by the comparison of the g and A values with those of the alkylisocyanide complexes.[11,12] The temperature dependence of the two species was noticeable. As the sample which has been irradiated at 77 K was annealed to room temperature, the formation of the species II was observed by ESR. During annealing both species I and II were observed simultaneously: I decreased and II increased. The results are shown in Fig. 2. Species I decreases and II increases with time. Besides species I and II, an ESR signal of narrow linewidth was observed in the center of the spectrum; this was attributed to the radical produced by irradiation. Since the intensity of the radical species was independent of the decay of I, hence, it was not taken into the consideration of the reaction mechanisms of I and II. No sizable difference was observed between the samples sealed *in vacuo* and that in the air.

The magnitudes of the total dose exerts a large influence on the yield of hot ions, as seen in Table 2. The experimental results can be summarized as: i) on irradiation of the same dosage, the total yield of I and II is independent of the temperature, and ii) on annealing, some part of species I changes into the diamagnetic species. Figures 3 and 4 present the process of the decay and formation of hot ions. The formations of species II and the diamagnetic species are second order reactions, and the activation energies of the two reactions were measured as 9 and 8 kcal/mol, respectively.

Discussion

Electronic States of Hot Ions. From the crystal field approximation, the ESR parameters of the d^7-low spin state in the C_{4v} (or D_{4h}) symmetry may be expressed as follows:[13]

$$g_{//} = 2.0023 \tag{1}$$

$$g_{\perp} = 2.0023 + 6\frac{\lambda}{\Delta} \tag{2}$$

$$A_{//} = P\left[-\kappa + \frac{4}{7} - \frac{6}{7}\frac{\lambda}{\Delta}\right] \tag{3}$$

Table 3. Some parameters derived from ESR measurements (using crystal field approximation)

	λ/Δ	$P(cm^{-1})$	κ	$\lambda(cm^{-1})$	$\Delta(cm^{-1})$	χ	$A_{iso}(G)$	$A_{aniso}(G)$
Species I	0.0148	0.0168	0.215	340	23000	0.04	−36.5	100
Species II	0.0279	0.0173	0.0654	352	12600	0.06	−9.8	103

$$A_{\perp} = P\left[-\kappa+\frac{2}{7}-\frac{45}{7}\frac{\lambda}{\Delta}\right] \quad (4)$$

where $\Delta=E(z^2)-E$ (xz or yz), κ is an isotropic term, and λ is the spin-orbit coupling constant. The values calculated for λ/Δ, P, and κ from the experimental results listed in Table 1 are shown in Table 3, where $A_{//}$ and $A_{\perp}$ are assumed to have opposite signs. A comparison of the value of P (see Table 3) to that of the free ion P_0 (0.0254 cm^{-1}) suggests that the unpaired electron is delocalized considerably in the orbital of the cyanide ligands (33%). This also gives rise to a smaller value of λ (see Table 3) than that for the free ion λ_0 (515 cm^{-1}). With the consideration of the delocalization, the value of Δ for hot ions can be estimated from λ/Δ. Values of A_{iso} and A_{aniso} can also be calculated from $-P\kappa$ and $4/7P$, respectively. Symons and Wilkinson[14] gave an equation to derive the spin density χ in Co(4s): $A_{iso}(G)=1320\chi-90\leftarrow(1-\chi)$, where 1320 G is the theoretical value of A_{iso} from Co(4s) and 90 G is the $3d_{z^2}$ contribution to A_{iso} *via* spin polarization. χ was calculated by applying this relation. The values of χ, A_{iso}, and A_{aniso} are shown in Table 3. From the molecular orbital approximation, the ESR parameters of the d^7-low spin state in a C_{4v} (or D_{4h}) symmetry can be obtained as follows:[15]

$$g_{//} = 2.0023 \quad (5)$$

$$g_{\perp} = 2.0023 + 6\frac{\alpha^2\beta^2\lambda_0}{E(^2E)-E(^2A_1)} \quad (6)$$

$$A_{//} = P_0\left[-\kappa+\frac{4}{7}\alpha^2-\frac{6}{7}\frac{\alpha^2\beta^2\lambda_0}{E(^2E)-E(^2A_1)}\right] \quad (7)$$

$$A_{\perp} = P_0\left[-\kappa+\frac{2}{7}\alpha^2-\frac{45}{7}\frac{\alpha^2\beta^2\lambda_0}{E(^2E)-E(^2A_1)}\right] \quad (8)$$

The molecular orbitals are

$$^2A_1(e^4b_2^2a_1^1) = \alpha d_{z^2} - d'\Phi_1(z^2) \quad (9)$$

$$^2E(e^3b_2^2a_1^2) = \beta d_{xz}\ (\text{or } d_{yz}) - \beta'\Phi_1\ (\text{xz or yz}) \quad (10)$$

The values of P_0 and λ_0 for a free Co ion are calculated from atomic spectral data. They depend on their Co charge[16-18] (Table 4). From the optical spectrum[13]

Table 4. The values of P_0 and λ_0 for a Co ion they depend on the charge on the Co ion

Assumed Co charge	$P_0(cm^{-1})$	$\lambda_0(cm^{-1})$
Co^0	0.022[16]	390[18]
$Co^{+0.52}$	0.0224	424
Co^+	0.0228[17]	455[18]
Co^{2+}	0.0254[17]	515[18]

of $[Co^{II}(CN)_5]^{3-}$, $E(^2E)-E(^2A_1)$ has been determined to be 10350 cm^{-1}. By substituting $E(^2E)-E(^2A_1)$, $\alpha^2\beta^2$, and the experimentally observed $g_{\perp}$ value into Eq. 6, λ_0, the charge of Co, and P_0 of hot ions are evaluated as 424 cm^{-1}, +0.52, and 0.0224, respectively. With the values of $E(^2E)-E(^2A_1)$, P_0, λ_0, and $\alpha^2\beta^2$ thus fixed, the orbital coefficients α^2 and β^2 and the isotropic hyperfine interaction $-P_0\kappa$ can be calculated from Eqs. 7 and 8.

In the case of the hot ion $[Co^{II}(CN)_4(NC)_2]^{4-}$, substituting $\alpha^2\beta^2$, λ_0, and the experimentally obtained $g_{\perp}$ value into Eq. 6, $E(^2E)-E(^2A_1)$ is evaluated as 18900 cm^{-1}. With the values of $E(^2E)-E(^2A_1)$, P_0, λ_0, and $\alpha^2\beta^2$ thus obtained, the orbital coefficients α^2 and β^2 and the isotropic hyperfine interaction $-P_0\kappa$ can be calculated from Eqs. 7 and 8. The calculated results are summarized in Table 5.

Table 5. Some parameters derived from ESR measurements (using molecular orbital approximation)

	$E(^2E)-E(^2A_1)$	α^2	β^2	$-P_0\kappa(cm^{-1})$
Species I	18900	0.783	0.847	−0.00395
Species II	10350	0.826	0.826	−0.00171

According to the results shown in Tables 3 and 5, it is concluded that: i) the λ values for penta and hexa coordinated species are the same (about 350 cm^{-1}); ii) the energy difference between the ground and the excited states is different for the two salts (about 10000 cm^{-1} for the pectacoordinated hot ion and about 20000 cm^{-1} for the hexacoordinated hot ion); and iii) the spin densities of hot ions are calculated as Co($3d_{z^2}$) 0.78 and Co(4s) 0.04 for species I, and Co($3d_{z^2}$) 0.83 and Co(4s) 0.06 for species II.

Mechanism of the Changes of Species I and II. *At 77K*: The mechanism of the reactions which take place in the γ-irradiated solid sample is assumed to take the scheme shown in Fig. 3. The secondary electrons which are formed by the γ-ray irradiation will hit Co^{III} in the complex of $[Co^{III}L_6]^{3-}$(1) in Fig. 3. With respect to the subsequent reactions, several different possible paths can be assumed. The first one is the case where the species(1) kicks out an electron, leaving itself as an positive hole. If the hole is stable, it will persist (3). If it is unstable, it may release one of the cyanide ligands,

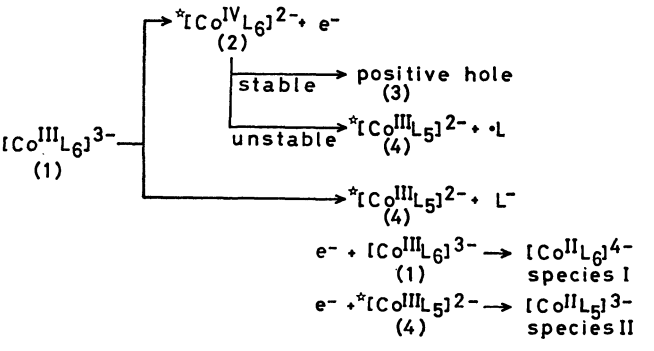

Fig. 3. The reaction mechanism at 77 K.
☆ stands for an excited species.

thus forming species (4). The latter can also be produced from species (1) directly. The active electron which is produced by the irradiation or by the process of the formation of (2) is trapped by (1) or (4), and produces hot ions.

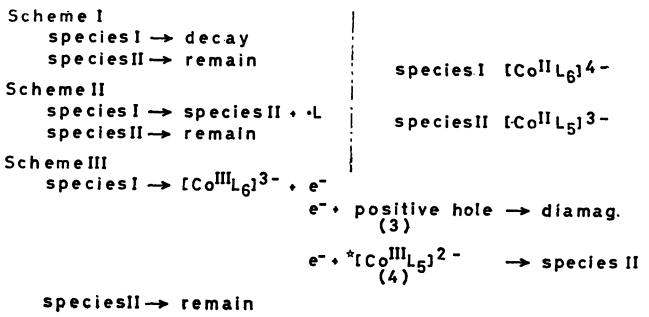

Fig. 4. The reaction mechanism on annealing.
☆ stands for an excited species.

On Annealing: From the experimental results, three processes of annealing can be imagined, as shown in Fig. 4. Among the processes shown in Fig. 4, we take scheme III as the most plausible. Scheme I cannot explain why the intensity of species II increases with temperature. Scheme II cannot explain the fact that some part of species I changes into the diamagnetic species. And of scheme II is the actual case, the formation of species II must be a first order reaction. In fact, this is against the experimental findings that both the formation of species II and that of the diamagnetic species are second order. But scheme III can explain the observed facts fairly well. According to this scheme, species I $[Co^{II}L_6]^{4-}$ releases an electron and returns to the original complex $[Co^{III}L_6]^{3-}$, and the electron thus released is trapped by another Co complex ion, such as $[Co^{IV}L_6]^{2-}$ (3) or $[Co^{III}L_5]^{2-}$ (4), forming either the diamagnetic ion or species II $[Co^{II}L_5]^{3-}$. Furthermore, the originally formed species II is kept unchanged according to this scheme.

Part II Single Crystal Experimental

Potassium hexacyanocobaltate(III) was prepared in the same way as in Part I from cobalt(II) chloride hexahydrate and potassium cyanide. Single crystals of $K_3[Co(CN)_6]$, approximately $3\times3\times1$ mm^3 in size, were obtained by slow evaporation of the aqueous solution. They were irradiated at 77 K with ^{60}Co γ-rays. 1×10^6 rads of γ-rays in total were applied to the sample at the rate of 5×10^4 rads/h. All conditions of the ESR measurements were the same as those in Part I. The crystals of $K_3[Co(CN)_6]$ exhibit polytypism.[19,20] Two unit cells occur in the structure of $K_3[Co(CN)_6]$: one, which is dominant, is orthorhombic (20 r) and the other monoclinic (1M,3M,7M). The ESR spectra observed in the present refer to the orthorhombic symmetry. The orthorhombic axes b and c of the crystal were easily identified with the aid of the crystallographic data,[21] and the axis of the right-handed orthorhombic system was unambiguously assigned. The ESR spectra were observed by rotating the sample at 15° intervals with the external magnetic field in the ab, ac, or bc plane.

Results

A typical example of the spectrum is shown in Fig. 5. It consists of one strong line due to the unidentified radicals, two wing lines (arrows) due to hydrogen atoms produced in the sample tube, and eight wing lines due to the Co(II) hot ions with a nuclear spin of 7/2. Two groups of octets are seen in the figure, which refer to two non-equivalent directions of the hyperfine tensor of the Co(II) hot ion. Each hyperfine line of cobalt is, furthermore, split into five lines, suggesting the coupling of cobalt with two equivalent nitrogen atoms. When the magnetic field was set parallel to the bc, ca, or ab planes, each spectrum became simple and revealed that it was formed of the two spectra shown in Figs. 5 and 6. Moreover, when the spectra taken at the arbitrary positions were analysed, taking this result into consideration, it was found that the spectra were produced by species I of the Co(II) hot ion located in four different sites in the unit cell. This means the produced hot ion is assigned as species I, which has been referred to in Part I, and is located at four sites in the unit cell of the mother lattice. The g-tensor was evaluated by measuring the central position between the first and the eighth peaks. The hyperfine coupling tensor was obtained as one-seventh of the separation between the first and eighth peaks. These results are shown in Fig. 7.

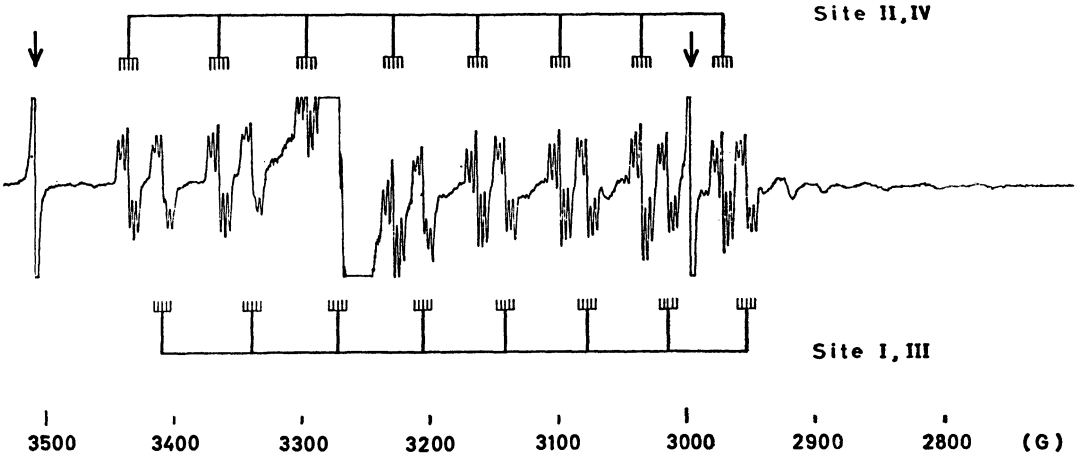

Fig. 5. An ESR spectrum of an irradiated single crystal of $K_3[Co(CN)_6]$ at 77 K.

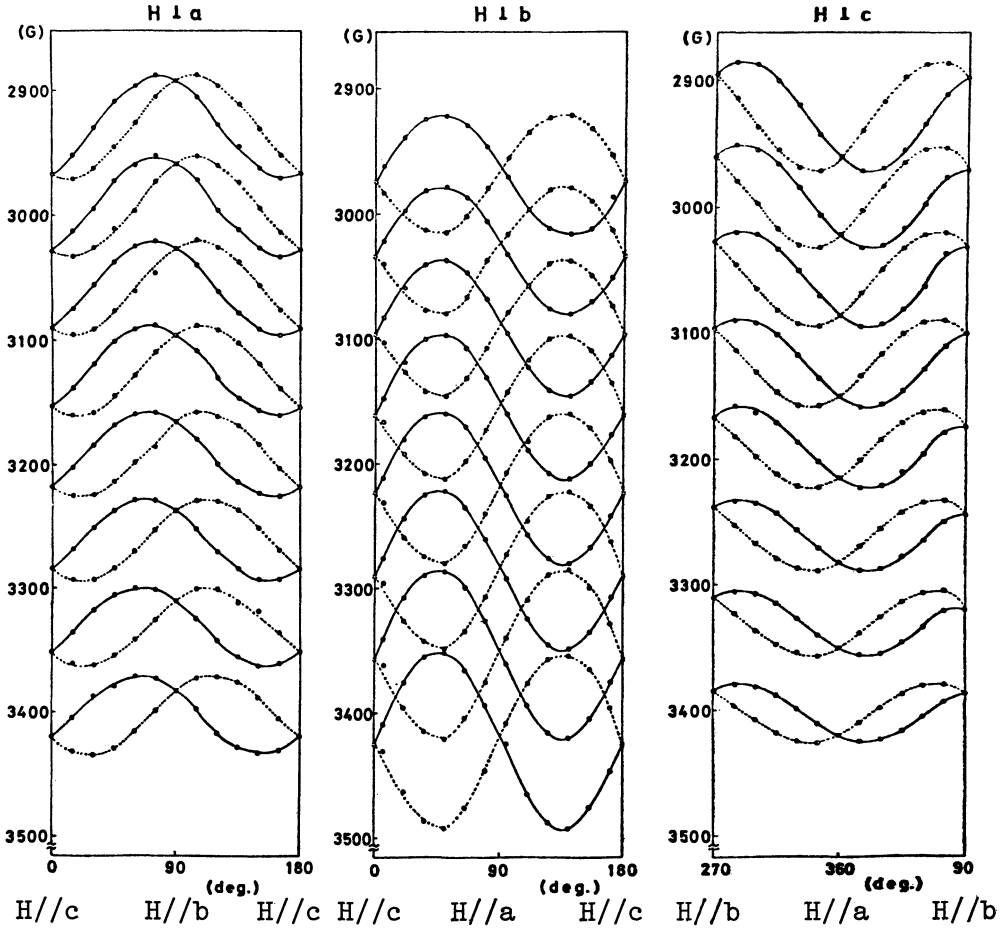

Fig. 6. The angular dependence of ESR spectra of irradiated single crystals of $K_3[Co(CN)_6]$ with orientation H being perpendicular to a, b, and c.

Discussion

Three different coordinate systems must be considered for the crystal of the sample: i) the crystallographic coordinate system (a, b, c), ii) the principal axis system of the g-tensor (α, β, γ), and iii) the principal axis system of the A-tensor (1, 2, 3). From the direction consines with respect to the magnetic field, the g values, and the hyperfine splitting K, the principal values and the principal of axes the g-tensor and the A-tensor are determined by the least-square method. The principal axes of the g-tensor do not necessarily coincide with those of the A-tensor. In the coordinates (α, β, γ), the g-tensor is diagonalized by

$$g^2 = (l_\alpha, l_\beta, l_\gamma) \begin{pmatrix} G_{\alpha\alpha} & 0 & 0 \\ 0 & G_{\beta\beta} & 0 \\ 0 & 0 & G_{\gamma\gamma} \end{pmatrix} \begin{pmatrix} l_\alpha \\ l_\beta \\ l_\gamma \end{pmatrix}$$

where $G_{\alpha\alpha}=g^2_{\alpha\alpha}$, $G_{\beta\beta}=g^2_{\beta\beta}$ and $G_{\gamma\gamma}=g^2_{\gamma\gamma}$
In the coordinates (1, 2, 3), the A-tensor can be diagonalized, but the g-tensor cannot.

$$g^2K^2 = (l_1, l_2, l_3) \begin{pmatrix} g_{11} & g_{12} & g_{13} \\ g_{21} & g_{22} & g_{23} \\ g_{31} & g_{32} & g_{33} \end{pmatrix} \begin{pmatrix} B_{11} & 0 & 0 \\ 0 & B_{22} & 0 \\ 0 & 0 & B_{33} \end{pmatrix} \begin{pmatrix} g_{11} & g_{21} & g_{31} \\ g_{12} & g_{22} & g_{32} \\ g_{13} & g_{23} & g_{33} \end{pmatrix} \begin{pmatrix} l_1 \\ l_2 \\ l_3 \end{pmatrix}$$

where $B_{11}=A^2_{11}$, $B_{22}=A^2_{22}$, and $B_{33}=A^2_{33}$.
In the crystallographic coordinates, the principal values

Table 6. The principal values and tne direction cosines of the principal axes of $[Co^{II}(CN)_4(NC)_2]^{4-}$, compared with the direction cosines of $Co-C_i$ bonds in undamaged complexes, $K_3[Co(CN)_6]$

direction cosines of $Co-C_i$ bonds in undamaged complexes, $K_3[Co(CN)_6]$, calculated from Curry and Runciman's data.[21]

	a	b	c
$Co-C_2$	0.678	0.237	0.696
$Co-C_1$	−0.421	0.906	0.044
$Co-C_3$	−0.642	−0.325	0.694

The principal values and the direction cosines of the principal axes of $[Co^{II}(CN)_4(NC)_2]^{4-}$.

Principal values (G)		a	b	c
A_1	68.4	0.66	0.22	0.72
A_2	70.3	−0.34	0.94	0.02
A_3	61.3	−0.67	−0.26	0.69

Principal values		a	b	c
g_3	2.009	0.70	0.25	0.67
g_1	2.089			
g_2	2.091		⊥ wrt above	

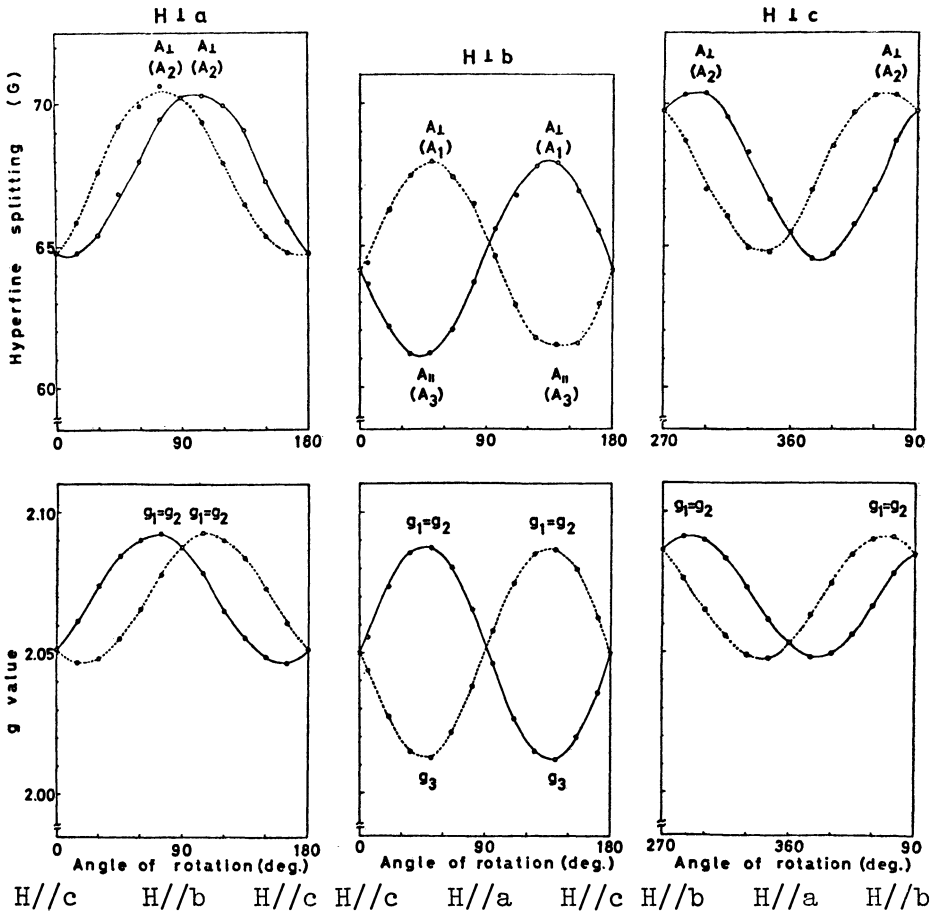

Fig. 7. The variation of hyperfine splitting and g values for irradiated single crystals of $K_3[Co(CN)_6]$ with the magnetic field H being perpendicular a, b, and c.

and the principal axes were determined (Table 6). The direction of the $A_{//}(A_3)$ axis coincides with Co–C_3 and the direction of the $g_{\parallel}(g_3)$ axis coincides with Co–C_2. Since $g_1 \simeq g_2 \simeq g_{\perp}$, the direction cosines of g_1 and g_2 cannot be determined exactly. Under the condition that the g-tensor and the A-tensor are axially symmetric, the parallel directions are orthogonal to each other. From the angular dependence of the superhyperfine splitting of nitrogen it is known that two cyanide ligands are inversed or twisted along the parallel direction of the g-tensor ($A^N_{//}=3.92$ G, $A^N_{\perp}=2.95$ G). Accordingly, the structure of the hot ion is axially symmetric along the $g_{//}$ axis. On the other hand, the distribution of the electron density is axially symmetric along the $A_{//}$ axis, *i. e.*, perpendicular to the $g_{//}$ axis. Similar noncollinear examples have been found in radicals,[22–24] but very rarely in metal complexes. Only five cases have been reported in the literature.[4,25–28] When the principal values and the principal axes of the g-tensor and the A-tensor are determined, the powder ESR spectrum can be assigned. As the parallel components of the g-tensor and the A-tensor are orthogonal, the $A_{\perp}$ can be seen at the $g_{//}$ part, and the $A_{//}$ and $A_{\perp}$ can be seen at the $g_{\perp}$ part (Fig. 8). Empirically it is known that $|A_{//}|<|A_{\perp}|$ for the hexacoordinated d^7-low spin complex, whereas $|A_{//}|>|A_{\perp}|$ for the pentacoordinated one.[1] Symons and his co-workers[8] reported that the g-tensor is

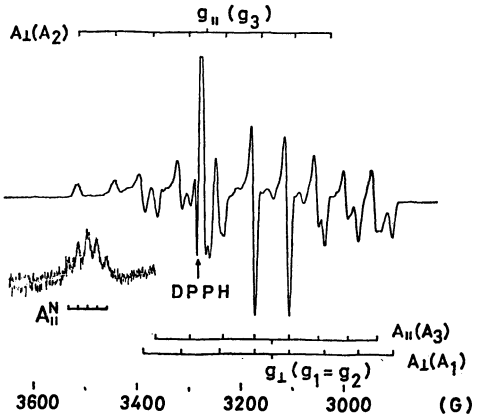

Fig. 8. An ESR powder spectrum of $[Co^{II}(CN)_4(NC)_2]^{4-}$. ESR parameters assigned by using the single crystal data. The superhyperfine structure at the $g_{//}$ part is caused by two equivalent nitrogen atoms of ligands.

axially symmetric ($g_x=g_y$) but the A-tensor is anisotropic ($A_x \neq A_y$). However, this statement is not right; both the g-tensor and the A-tensor are axially symmetric, and hence the principal axes do not coincide.

Other alkali metals were used instead of $3K^+$ to examine the effect of the mother lattice (Fig. 9). Species I can be measured only in the cases of $3K^+$ and $3Rb^+$.

References

1) S. Fujiwara, T. Watanabe, and H. Tadano, *J. Coord. Chem.*, **1**, 195 (1971).
2) J. Isoya and S. Fujiwara, *Bull. Chem. Soc. Jpn.*, **45**, 2181 (1972).
3) J. Isoya, H. Ishizuka, A. Yamasaki, and S. Fujiwara, *Chem. Lett.*, **1972**, 397.
4) N. S. Dalal, J. A. Hebden, and C. A. McDowell, *J. Magn. Resonance*, **16**, 289 (1974).
5) N. S. Dalal, J. A. Hebden, and C. A. McDowell, *J. Magn. Resonance*, **16**, 312 (1974).
6) J. Danon, R. P. A. Muniz, A. O. Caride, and I. Wolfson, *J. Mol. Struct.*, **1**, 127 (1968).
7) A. O. Caride, S. I. Zanette, and J. Danon, *J. Chem. Phys.*, **52**, 4911 (1970).
8) M. C. R. Symons and J. G. Wilkinson, *J. Chem. Soc., A*, **1972**, 1086.
9) J. R. Shock and M. T. Rogers, *J. Magn. Resonance*, **18**, 157 (1975).
10) W. C. Fernelius, *Inorg. Synth.*, Vol. II, McGraw-Hill New York (1946), p. 225.
11) J. P. Maher, *J. Chem. Soc., A*, **1968**, 2918.
12) M. E. Kimball, D. W. Pratt, and W. C. Kaska, *Inorg. Chem.*, **7**, 2006 (1968).
13) F. D. Tasay, H. B. Gray, and J. Danon, *J. Chem. Phys.*, **54**, 3760 (1971).
14) M. C. R. Symons and J. G. Wilkinson, *J. Chem. Soc., A*, **1971**, 2069.
15) R. J. Booth and W. C. Lin, *J. Chem. Phys.*, **61**, 1226 (1974).
16) A. Abragam and M. H. L. Pryce, *Proc. R. Soc. London*, **206**, 173 (1951).
17) B. R. McGarvey, *J. Phys. Chem.* **71**, 51 (1967).
18) T. M. Dunn, *Trans. Faraday Soc.*, **57**, 1441 (1961).
19) J. A. Kohn and W. D. Towns, *Acta Crystallogr.*, **14**, 617 (1961).
20) E. C. Reynfardt and J. C. A. Boeyens, *Acta Crystallogr.*, **B28**, 524 (1972).
21) N. A. Curry and W. A. Runciman, *Acta Crystallogr.*, **12**, 674 (1959).
22) R. W. Holmberg, *J. Chem. Phys.*, **51**, 3255 (1969).
23) E. L. Cochran, F. J. Adrian, and V. A. Bowers, *J. Chem. Phys.*, **44**, 4626 (1966).
24) R. M. Golding and W. C. Tennant, *Mol. Phys.*, **25**, 1163 (1973).
25) R. Byfleet, F. G. Herring, W. C. Lin, C. A. McDowell, and D. J. Ward, *Mol. Phys.*, **15**, 239 (1968).
26) J. G. Van Rens, C. P. Keijzers, and H. van Willigen, *J. Chem. Phys.*, **52**, 2858 (1970).
27) R. H. Borcherts and C. Kikuchi, *J. Chem. Phys.*, **40**, 2270 (1964).
28) J. R. Pilbrow and M. E. Winfield, *Mol. Phys.*, **25**, 1073 (1973).

The Theory of the Reverse Diffusion of Ions in Mixed Electrolyte Solutions and Experimental Results on the HCl-$CaCl_2$-H_2O Ternary System[1)]

Masayuki NAKAGAKI and Shuji KITAGAWA

Faculty of Pharmaceutical Sciences, Kyoto University, Sakyoku, Kyoto 606

(Received October 13, 1975)

Reverse diffusion is the migration of solutes in the direction opposite to that expected from the concentration gradient, that is, from a portion with a lower concentration to that with a higher concentration. This type of diffusion of ions in mixed electrolyte solutions was studied theoretically on the basis of nonequilibrium thermodynamics. For a solution containing two kinds of cations and one kind of anion, it has been concluded that the reverse diffusion occurs when the mobilities of the coexisting ions differ largely, because the effect of the diffusion potential is pronounced in such a case. It has also been concluded that the practical diffusion coefficient of an ion varies linearly with the ratio of the concentration gradient of a coexisting ion to that of the diffusing ion when the average concentration ratio of the ions is fixed. Moreover, the range of the concentration-gradient ratio, where the practical diffusion coefficient is negative, has been determined. These theoretical conclusions were tested experimentally for the HCl-$CaCl_2$-H_2O ternary system. The results satisfactorily verified that reverse diffusion actually occurred and that the relationship between the diffusion coefficient and the concentration-gradient ratio was linear, as has been expected.

The Fick law of diffusion predicts that a solute will migrate from a portion with a higher concentration to one with a lower concentration at a rate proportional to the concentration gradient. The diffusion through a membrane, that is, the so-called passive transport, also proceeds in the same direction. In contradiction to this, the active transport in biological membranes is transport against the concentration gradient. However, an ion can migrate against its concentration gradient passively in a system of mixed electrolytes, at least under certain limited conditions. This has already been pointed out theoretically in our previous paper.[2)]

According to nonequilibrium thermodynamics, the flux of the ion (i), J_i, is proportional to the gradient of the total potential of the component, $\tilde{\mu}_i$, which is the electrochemical potential in the present case. Thus, the rate of the diffusion of each ion is modified by the effect of the electric potential, the so-called diffusion potential, and, under certain conditions, the reverse diffusion of an ion can proceed, as has already been predicted both qualitatively[3)] and quantitatively.[2,4)] However, no precise experimental support of the reverse diffusion has so far been given. For the KCl-$MgCl_2$-H_2O system and the K(HAsp)-$Mg(HAsp)_2$-H_2O system, where $HAsp^-$ indicates the hydrogen aspartate anion, it has been reported[5)] that the diffusion coefficient of a cation becomes smaller with the addition of a faster cation, but the diffusion coefficient has not reached a negative value.

Theoretical

Practical Diffusion Coefficient of Ions. According to nonequilibrium thermodynamics, the flux of the ion (i), $[J_i]$ (mg-ion·cm^{-2}·s^{-1}), through a diffusion layer between two aqueous solutions, I and II, is given by the following equation,[2,4,6,7)] after the term of the electric potential gradient has been eliminated by using the condition that the diffusion current is zero in the steady state:

$$[J_i] = -D_i\left(\frac{\partial[i]}{\partial x}\right) + \frac{z_i B_i [i]}{\sum_j z_j^2 B_j [j]} \sum_j z_j D_j \left(\frac{\partial [j]}{\partial x}\right) \quad (1)$$

Here, $[i]$ (g-ion·l^{-1}) is the concentration of the i ion, while x is the coordinate taken in the direction of the flux. Moreover, B_i is the mobility of the ion, i, which is related to the radius of the ion, a_i, and the viscosity of the medium, η, by the Stokes law if the ion is considered to be spherical;

$$B_i = 1/6\pi\eta a_i \quad (2)$$

and D_i is the diffusion coefficient related to the mobility by the following equation:

$$D_i = kTB_i h_i \quad (3)$$

where k is the the Boltzmann constant, T is the absolute temperature, and h_i is the coefficient;

$$h_i = 1 + (\partial \ln f_i / \partial \ln [i]) \quad (4)$$

with f_i being the activity coefficient of the ion, i. If the concentration dependence of the activity coefficient can be neglected so that $h_i = 1$, then Eq. 3 is simplified to:

$$D_i = kTB_i \quad (5)$$

which gives the Einstein equation when Eq. 2 is used together with it.

The actual rate of diffusion of the ion, i, in a solution, however, can not be determined by D_i or, in other words, by the ionic radius and the solvent viscosity only, because of the electrostatic interaction between ions, or, we could say, because of the effect of the diffusion potential. The practical diffusion coefficient of the ion (i), D'_i, may then be defined by:

$$[J_i] = -D_i'(\partial[i]/\partial x) \quad (6)$$

Its theoretical expression is given by the following equation, which has been derived from Eq. 1, in the same approximation as was used for Eq. 5:

$$D_i' = kTB_i\left\{1 - \frac{z_i[i]\sum_j z_j B_j (\partial[j]/\partial x)}{(\sum_j z_j^2 B_j [j])(\partial[i]/\partial x)}\right\} \quad (7)$$

In the case of an electrolyte solution containing one cation, 1, and one anion, 3, only, Eq. 7 gives the Haskell

equation:

$$D_1' = D_3' = kT(z_1+|z_3|)B_1B_3/(z_1B_1+|z_3|B_3) \quad (8)$$

If, however, the electrolyte solution contains two cations, 1 and 2, and one anion, 3, the practical diffusion coefficients are given, on the basis of Eq. 7 and the equation of electrical neutrality;

$$z_1[1] + z_2[2] = |z_3|[3] \quad (9)$$

by the following equations:

$$D_1' = kTB_1\left\{1-z_1\frac{F(1/2)}{G(1/2)}H\right\} \quad (10a)$$

$$D_2' = kTB_2\{1-z_2H\} \quad (10b)$$

$$D_3' = kTB_3\left\{1+|z_3|\frac{1+G(1/2)}{1+F(1/2)}H\right\} \quad (10c)$$

where:

$$H = \frac{(B_2-B_3)+(B_1-B_3)G(1/2)}{(z_2B_2+|z_3|B_3)+(z_1B_1+|z_3|B_3)F(1/2)} \quad (10d)$$

Here, $F(i/j)$ is the ratio of concentrations (g-equiv$\cdot l^{-1}$);

$$F(i/j) = |z_i/z_j|\cdot[i]/[j] \quad (11)$$

and $G(i/j)$ is the ratio of the concentration gradients, the concentration being expressed again in g-equiv$\cdot l^{-1}$:

$$G(i/j) = |z_i/z_j|\cdot(\partial[i]/\partial x)/(\partial[j]/\partial x) \quad (12)$$

Equations 10a—d show that the practical diffusion coefficient, D'_i, is a function of the concentration ratio and the concentration-gradient ratio, and that D'_2 is linear and D'_1 and D'_3 are hyperbolic against $G(1/2)$ at a fixed $F(1/2)$. As for the 3 anion, Eqs. 10c, d may be rewritten, by using Eq. 9, as follows:

$$D_3' = kTB_3\left\{1+|z_3|[1+F(1/2)]\right.$$
$$\left.\times\frac{(B_2-B_3)+(B_1-B_2)G(1/3)}{(z_2B_2+|z_3|B_3)+(z_1B_1+|z_3|B_3)F(1/2)}\right. \quad (13)$$

Therefore, D'_3 is linear with $G(1/3)$ at a fixed $F(1/2)$.

Reverse Diffusion. As is obvious from Eq. 6, the reverse diffusion of the ion, i, takes place when the practical diffusion coefficient, D'_i, is negative; the condition for it is readily obtained from Eqs. 10a—d:

When the 1 cation is also present, the reverse diffusion of the 2 cation proceeds when Eq. 14 is fulfilled if $B_1>B_3$, or when Eq. 15 is fulfilled if $B_1<B_3$:

$$G(1/2) > \frac{(z_1/z_2)(B_1/B_3)+(|z_3|/z_2)}{(B_1/B_3)-1}F(1/2) + \frac{(|z_3|/z_2)+1}{(B_1/B_3)-1}$$
$$(B_1>B_3) \quad (14)$$

$$-G(1/2) > \frac{(z_1/z_2)(B_1/B_3)+(|z_3|/z_2)}{1-(B_1/B_3)}F(1/2) + \frac{1+(|z_3|/z_2)}{1-(B_1/B_3)}$$
$$(B_1<B_3) \quad (15)$$

Since the right side of Eq. 15 is positive, the reverse diffusion of the 2 ion can occur, if $B_1<B_3$, only in the case of counter diffusion, that is, in the case where the concentration gradients of the 1 and 2 cations are in the opposite direction so that $G(1/2)<0$.

Equation 14 will be fulfilled if $G(1/2)$ is large enough or if $F(1/2)$ is small enough and (B_1/B_3) is large enough, while Eq. 15 will be fulfilled if $-G(1/2)$ is large enough or if $F(1/2)$ is small enough and (B_1/B_3) is small enough. Therefore, both Eqs. 14 and 15 predict that the reverse diffusion of the 2 cation will be observed when the coexisting cation, 1, is at a smaller concentration but is of a greater concentration gradient and when the mobility of the coexisting cation, 1, differs more from that of the anion, 3.

This may be interpreted as follows: If the coexisting cation, 1, moves faster than the anion, 3, as in the case of Eq. 14, the diffusion potential is generated in such a way that the front part of the diffusion layer is positive and the rear part negative, so that the 2 cation is pulled back by this electric potential, even against its concentration gradient, if the latter is not very large. On the other hand, if the coexisting cation 1 moves much slower than the anion, 3, as in the case of Eq. 15, the direction of the diffusion potential will be opposite to the previous case, so that the 2 cation is pushed forth by this potential, irrespective of the direction of its concentration gradient; the reverse diffusion of the 2 cation results if the direction of its concentration gradient is opposite to those of the 1 cation and the anion, 3.

As for the reverse diffusion of the anion, 3, D'_3 of Eq. 10c or 13 becomes negative when Eq. 16 or 17 is fulfilled, where the use of the suffix 1 for the cation of greater mobility does not lose any generality:

$$1 > -G(1/2) > \frac{\{(z_2/|z_3|)+1\}+\{(z_1/|z_3|)(B_1/B_2)+1\}F(1/2)}{\{(B_1/B_2)+(z_2/|z_3|)\}+\{(z_1/|z_3|)+1\}(B_1/B_2)F(1/2)}$$
$$(B_1>B_2) \quad (16)$$

$$-G(1/3) > \frac{\{(z_2/|z_3|)+1\}+\{(z_1/|z_3|)(B_1/B_2)+1\}F(1/2)}{\{(B_1/B_2)-1\}\{1+F(1/2)\}}$$
$$(B_1>B_2) \quad (17)$$

According to Eqs. 16 and 17, it may be concluded that the reverse diffusion of the anion, 3, may be observed only when the concentration gradient of the faster cation, 1, is in the direction opposite to those of the coexisting cation, 2, and of the anion, 3.

Numerical Calculations on the HCl–$CaCl_2$–H_2O System. The numerical values of D'_i have been calculated for

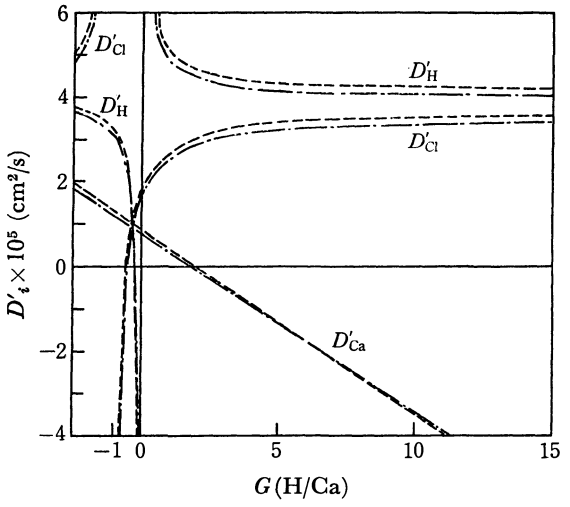

Fig. 1. Calculated values of D'_i against $G(H^+/Ca^{2+})$ at $F(H^+/Ca^{2+})=2$.
The broken lines indicate the values at $h_i=1$, while chain lines indicate the values obtained by using the Güntelberg equation.

the HCl–$CaCl_2$–H_2O system according to Eqs. 10a—d, with 1=H^+, 2=Ca^{2+} and 3=Cl^-. The results for the case of $F(H/Ca)=2$ as an example are shown in Fig. 1, where the concentration-gradient ratio $G(H/Ca)$ is taken on the abscissa.

The broken lines in Fig. 1 are the results obtained for $h_i=1$ by neglecting the concentration dependence of the activity coefficient, while the chain lines are the results obtained by using Eq. 4 and the Güntelberg approximation:[8]

$$\ln f_i = -Az_i^2\sqrt{J}/(1+\sqrt{J}) \quad (18)$$

where A is a constant at a given temperature:

$$A = \sqrt{2\pi N_A/1000}\cdot(e/\sqrt{D_0kT})^3 \quad (19)$$

Here, N_A is the Avogadro Number, e is the elementary charge, D_0 is the dielectric constant of the solvent, and J is the ionic strength:

$$J = (1/2)\sum_i z_i^2[i] \quad (20)$$

By comparing these curves, it may be concluded that the effect of the concentration dependence of the activity coefficient is small, at least in the concentration range studied in this paper.

The values of mobility, B_i, used in these calculations were obtained from the values of the equivalent conductance at an infinite dilution, λ^0_i, given in the literature[9], according to the well-known equation:

$$B_i = \lambda_i^\circ N_A/(|z_i|F_A^2) \quad (21)$$

The values of kTB_i and kTB_ih_i thus obtained are shown in Table 1.

Table 1. Values of D_i ($=kTB_ih_i$) in aqueous HCl–$CaCl_2$ solutions at 25 °C

Ion	λ_i° ($\Omega^{-1}\cdot cm^2\cdot g\text{-}eq^{-1}$)	$D_i\times10^5$ ($cm^2\cdot s^{-1}$)	
		($h_i=1$)	(Güntelberg)
H^+	349.82	9.315	8.990
Ca^{2+}	59.50	0.792	0.682
Cl^-	76.35	2.033	1.928

For the HCl–$CaCl_2$–H_2O system, Fig. 1 shows that the diffusion coefficients, D'_H, D'_{Ca}, and D'_{Cl}, become negative in their respective regions, so that each ion would cause a reverse diffusion in these regions. Figure 1 shows that D'_{Ca} decreases linearly with $G(H/Ca)$, as is to be expected from Eqs. 10b, d, and that D'_{Ca} becomes negative when $G(H/Ca)$ is greater than a certain value, as is to be expected from Eq. 14, since $B_H>B_{Cl}$, as is shown in Table 1.

Figure 1 also shows that the change in D'_H with $G(H/Ca)$ is hyperbolic, as is to be expected from Eqs. 10a, d, and that D'_H becomes negative in the region, which can be expected from Eq. 15a, since $B_{Ca}<B_{Cl}$, as is shown in Table 1. The region of $G(1/2)$, in which D'_1 is negative in the presence of the 2 cation, is derived readily from Eq. 15:

$$0<-G(1/2)<F(1/2)\Big/\left\{\frac{(z_2/z_1)(B_2/B_3)+|z_3|/z_1}{1-(B_2/B_3)}+\frac{1+(|z_3|/z_1)}{1-(B_2/B_3)}F(1/2)\right\} \quad (B_2<B_3) \quad (15a)$$

Instead of $G(H/Ca)$, however, if $G(Ca/H)$ is taken on the abscissa, as is shown in Fig. 5, D'_H is linear, as is to be expected from Eqs. 10b, d, with 1=Ca^{2+} and 2=H^+, and becomes negative when $-G(Ca/H)$ is greater than a certain value, as is to be expected from Eq. 15.

As for the Cl^- anion, the curves shown in Fig. 1 are hyperbolic, as is to be expected from Eqs. 10c, d, with 1=H^+, 2=Ca^{2+}, and 3=Cl^-. The value of D'_{Cl} becomes negative, as is shown in Fig. 1, in the region where $G(H/Ca)$ is negative but greater than -1, as is expected from Eq. 16, since $B_H>B_{Cl}$, as is shown in Table 1. If, however, $G(H/Cl)$ is taken on the abscissa, as is shown in Fig. 6, D'_{Cl} is linear at a fixed value of $F(H/Ca)$, as is to be expected from Eq. 13, and becomes negative when $-G(H/Cl)$ is large enough, as is to be expected from Eq. 17, since $B_H>B_{Cl}$.

Experimental

Diffusion Measurements. McBain's porous-plate method[10] was used for the diffusion measurements, with a diffusion cell modified as has been reported previously.[11] A glass cell divided into two compartments by a porous plate, as is shown in Fig. 2, was held vertically in a thermostat at 25±0.1 °C after each compartment had been filled with a mixed solution of HCl and $CaCl_2$. The solution with the higher density was placed in the upper compartment, I, and that with the lower density, in the lower one, II, in order to keep the concentration distribution in each compartment homogenous by means of convectional flow.[10]

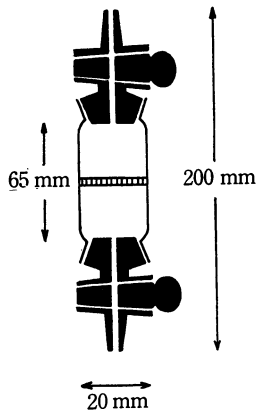

Fig. 2. Diffusion cell.

After a certain time, t, had passed, the concentration in each compartment was measured, and the practical diffusion coefficient, D_i', defined by Eq. 6, was calculated according to the following equations:

$$D_i' = (\langle m_i\rangle/Kt)/\langle[i]_I-[i]_{II}\rangle \quad (22)$$

where K is the cell constant, which depends on the porosity, area, and thickness of the porous plate, and where

$$\langle m_i\rangle = (1/2)\{V_I([i]_I^\circ-[i]_I^t)+V_{II}([i]_{II}^t-[i]_{II}^\circ)\} \quad (23)$$

$$\langle[i]_I-[i]_{II}\rangle = (1/2)\{([i]_I^\circ-[i]_{II}^\circ)+([i]_I^t-[i]_{II}^t)\} \quad (24)$$

where $[i]_I^\circ$ and $[i]_{II}^\circ$ are the initial concentrations of the ion, i, in the upper and lower compartments, $[i]_I^t$ and $[i]_{II}^t$ are those after the time, t, and V_I and V_{II} are the volumes of the compartments.

The diffusion time, t, was set at about 30 h. The values

Table 2. Constants of the diffusion cells used

Cell No.	V_I (ml)	V_{II} (ml)	K (cm)
1	6.9994	7.1516	0.626_1
2	6.4548	6.3961	0.404_5
3	6.6927	6.7142	0.553_4

of V_I and V_{II} are given in Table 2 together with the values of K measured with 0.05 N KCl, the diffusion coefficient of the latter being 1.863×10^{-5} ($cm^2 \cdot s^{-1}$), as is given in the literature.[12]

For the solutions containing only one electrolyte, the diffusion equation (6) can be integrated to obtain the equation to be used for the calculation of the diffusion coefficient.[2,5,11] Instead of this, however, the average amount of diffusion, $<m_i>$, and the average concentration difference, $<[i]_I-[i]_{II}>$, were used in this study, and the diffusion coefficient was calculated by means of Eq. 22, because the integration with time is complicated for mixed electrolyte solutions.[7] The discrepancy between the diffusion coefficients obtained by Eq. 22 and the usual integrated equation was not more than 10% for the one-electrolyte solutions used.

Parameter Values. In order to compare the experimental D_i' values with the theoretical ones, the values of $F(i/j)$ and $G(i/j)$ defined by Eqs. 11 and 12 are needed. The experimental values of $F(i/j)$ were calculated from:

$$F(i/j) = |z_i/z_j| \cdot \frac{([i]_I^\circ + [i]_{II}^\circ) + ([i]_I^t + [i]_{II}^t)}{([j]_I^\circ + [j]_{II}^\circ) + ([j]_I^t + [j]_{II}^t)} \quad (25)$$

where $([k]_I^\circ+[k]_{II}^\circ)$ and $([k]_I^t+[k]_{II}^t)$, k being i or j, take almost the same values, since V_I and V_{II} have almost the same value. The value of $F(i/j)$ is, therefore, kept almost contant during the diffusion experiment. For the experimental values of $G(i/j)$, the following equation was used with Eq. 24, since the concentration distribution in a diffusion layer had been found to be almost linear:[7]

$$G(i/j) = |z_i/z_j|\langle[i]_I-[i]_{II}\rangle/\langle[j]_I-[j]_{II}\rangle \quad (26)$$

Concentration Determination. The concentration of the H^+ ion was determined by titration with NaOH as the standard solution and with phenolphthalein as the indicator. The concentration of the Ca^{2+} ion was determined by chelatometry, with disodium-EDTA as the standard solution and Eriochrome Black T as the indicator. The concentration of the Cl^- ion was determined by precipitation titration, with $AgNO_3$ as the standard solution and fluorescein as the indicator.

Results and Discussion

Examples of Reverse Diffusion. Some examples of the data are shown in Table 3. Since the parameter values of the three cells used in the experiments are not the same, as is shown in Table 2, the values of $|z_i|[i]_I$ and $|z_i|[i]_{II}$ differ from cell to cell; only the average values are given in Table 3 in order to shorten the listing. The values of D'_i given in the Table are the averages of the values obtained for individual cells. A comparison of data for different cells is given in Figs. 3—6.

It may be seen from Table 3 that the reverse diffusion actually takes place; that is, the concentration increases in the solution with the higher concentration and decreases in that with the lower concentration, for Ca^{2+} in Example 1, for H^+ in Example 2, and for Cl^- in Example 3; the diffusion coefficients, D'_i, are negative in all these cases.

Table 3. Examples of data on the reverse diffusion

Ion	t (h)	$\|z_i\|[i]_I$ (mN)	$\|z_i\|[i]_{II}$ (mN)	$D'_i\times10^5$ ($cm^2 \cdot s^{-1}$)
		Example 1		
H^+	0	148.6	52.1	3.66
	30	125.8	74.5	
Ca^{2+}	0	52.6	48.4	−2.68
	30	53.7	47.1	
Cl^-	0	200.7	100.4	3.15
	30	179.7	121.3	
		Example 2		
H^+	0	97.2	103.3	−3.31
	30	94.8	105.7	
Ca^{2+}	0	100.5	0	0.87
	30	93.6	6.8	
Cl^-	0	197.8	103.0	1.29
	30	188.5	112.2	
		Example 3		
H^+	0	87.8	111.6	2.85
	30	92.4	107.0	
Ca^{2+}	0	65.4	35.3	1.05
	30	63.0	37.8	
Cl^-	0	153.1	146.8	−3.06
	30	155.3	144.6	

Reverse Diffusion of Ca^{2+}. The experimental D'_{Ca} values are plotted against G(H/Ca) in Fig. 3 for F(H/Ca) $=0.5$, 1, and 2. This figure also shows that the deviation of the experimental data due to the use of different cells is not large.

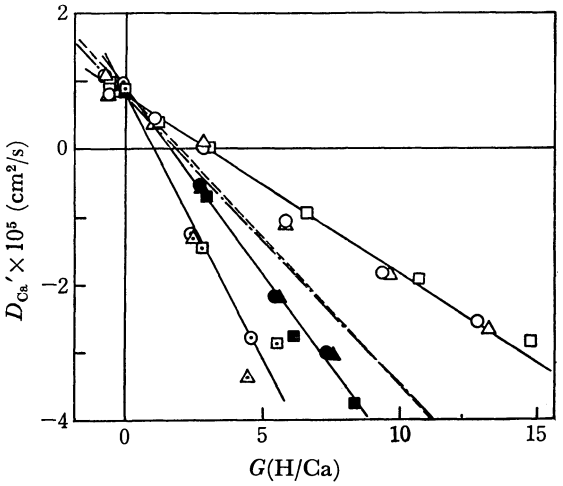

Fig. 3. Diffusion coefficient of Ca^{2+} at 25 °C as a function of G(H/Ca) when F(H/Ca) is fixed.
F(H/Ca)=0.5 (Cell #1, ⊙; #2, ⊡; #3, △), 1.0 (#1, ●; #2, ■; #3, ▲), and 2.0 (#1, ○; #2, □; #3, △).
Theoretical values for F(H/Ca)=2 are shown by a broken line for $h_i=1$, and by a chain line for Güntelberg approximation.

Figure 3 gives the experimental verifications of the theoretical conclusions that D'_{Ca} will be linear to G(H/Ca) and that the inclination will be the steeper when the value of F(H/Ca) is the smaller, as is to be expected from Eqs. 10b, d, with $1=H^+$, $2=Ca^{2+}$, and

3=Cl^-, and that the reverse diffusion of Ca^{2+} will proceed when G(H/Ca) is large, as is to be expected from Eq. 14.

The theoretical curves for F(H/Ca)=2 are also shown in Fig. 3. Neither of the theoretical curves fits in quantitatively with the experimental straight lines. This will be discussed later. It is, however, noticeable that the experimental results are in agreement, qualitatively, with the theoretical expectations mentioned above.

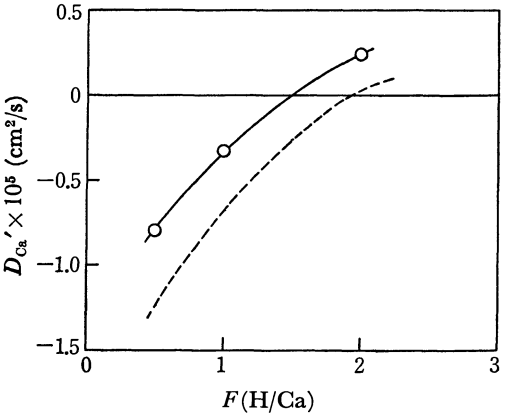

Fig. 4. Dependency of D_{Ca}' on F(H/Ca) for G(H/Ca)=2 at 25 °C.
The broken line is theoretical for $h_i=1$.

The dependency of D'_{Ca} on F(H/Ca) is shown in Fig. 4 for G(H/Ca)=2, where the experimental values are obtained by the interpolation of Fig. 3. It may be seen from Fig. 4 that the experimental curve satisfies qualitatively the trend of the theoretical broken line drawn for $h_i=1$. This result verifies that the reverse diffusion of Ca^{2+} takes place when F(H/Ca) is small, as is to be expected from Eqs. 10b, d.

Reverse Diffusion of H^+ and Cl^-. The dependency of D'_H on G(Ca/H) is shown in Fig. 5 for F(H/Ca)=2, that is, for F(Ca/H)=0.5. The results verify the theoretical conclusions that D'_H will be linear to G(Ca/H) at a fixed F(Ca/H), according to Eqs. 10b, d with

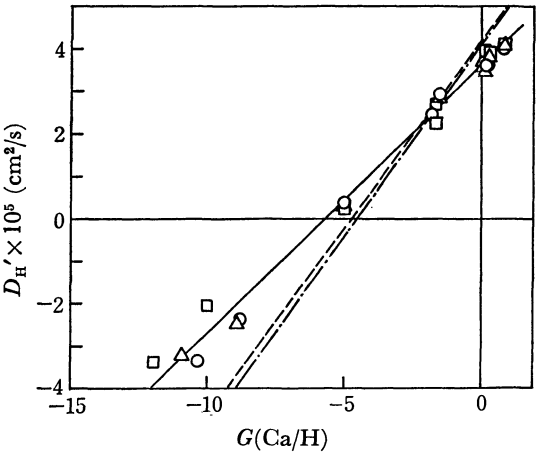

Fig. 5. Dependency of D_H' on G(Ca/H) for F(H/Ca)=2 at 25 °C.
Cell #1, ○; #2, □; #3, △.
Theoretical curves are shown by a broken line for $h_i=0$ and by a chain line for Güntelberg approximation.

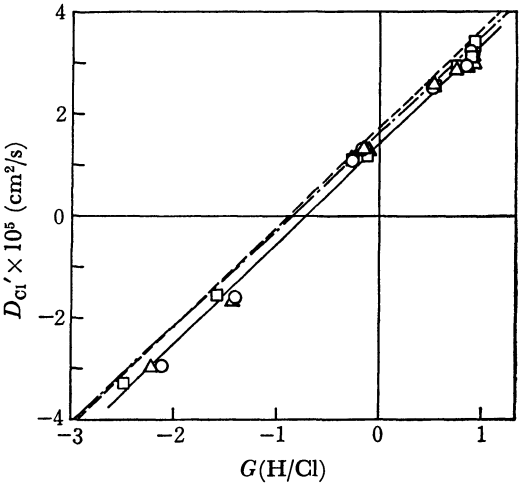

Fig. 6. Dependency of D'_{Cl} on G(H/Cl) for F(H/Ca)=2 at 25 °C.
Cell #1, ○; Cell #2, □; Cell #3, △.
Theoretical curves are shown by a broken line for $h_i=0$ and by a chain line for Güntelberg approximation.

1=Ca^{2+} and 2=H^+, and will be negative when $-G$-(Ca/H) is large, according to Eq. 15, where $B_{Ca}<B_{Cl}$, as is shown in Table 1. The theoretical curves shown in Fig. 5 show the same trend as the experimental results.

The result for D'_{Cl} against G(H/Cl) shown in Fig. 6 is quite similar to that shown in Fig. 5. The relation is linear at a fixed F-value, F(H/Ca)=2, as is to be expected from Eq. 13, and D'_{Cl} becomes negative when $-G$(H/Cl) is large, as is to be expected from Eq. 17, where $B_H>B_{Ca}$, as is shown in Table 1. The discrepancy between experimental and theoretical lines is not large in this case.

Approximation of a Constant Cation Ratio. In our previous papers,[2,4] theoretical equations have been derived, and compared with experimental data, by assuming the fraction of the cation concentrations to be constant throughout the diffusion layer. For a mixed electrolyte solution containing 1 and 2 cations and an anion, 3, the fraction of the equivalent concentration of the 2 cation, ξ_2, defined by:

$$\xi_2 = z_2[2]/(z_1[1]+z_2[2]) \tag{27}$$

may be used in place of $F(1/2)$ and $G(1/2)$ in Eqs. 10a—d, since

$$F(1/2) = G(1/2) = (1-\xi_2)/\xi_2 \tag{28}$$

according to the present assumption. Then, the following equation, which has been given in our previous paper,[4] is obtained:

$$D_2' = kTB_2\frac{(z_1-z_2)B_1(1-\xi_2)+(z_2+|z_3|)B_3}{z_1B_1(1-\xi_2)+z_2B_2\xi_2+|z_3|B_3} \tag{29}$$

The value of D'_2 becomes negative if $z_2>z_1$ and if ξ_2 is small enough, as is shown by the following equation:

$$\xi_2<1-(B_2/B_1)(1+|z_3|/z_2)/(1-z_1/z_2) \quad (z_1<z_2) \tag{30}$$

As for the HCl–$CaCl_2$–H_2O system, the experimental values of D'_i against average ξ_2-values are shown in Fig. 7, together with theoretical broken lines. It may be seen from Fig. 7 that the diffusion coefficient of the slower cation, D'_{Ca}, decreases, both experimentally

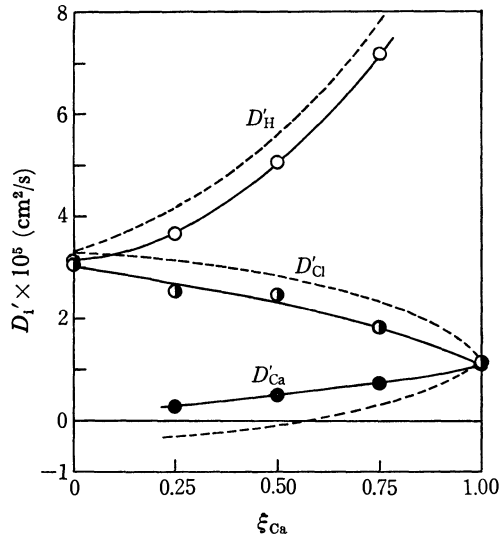

Fig. 7. Relation between D'_i and ξ_{Ca} for aqueous HCl–$CaCl_2$–H_2O solutions at 25 °C.
Experimental data for H^+, ○; Ca^{2+}, ●; Cl^-, ◑.
Broken lines are theoretical for $h_i=1$.

and theoretically, with the decrease in ξ_{Ca}, and that the theoretical curve goes down to negative, as has already been stated,[2,4] although the experimental data do not. This is because the condition $F(1/2)=G(1/2)$ in Eq. 28 is too severe for the accuracy of the present experiments, as may seen from Figs. 3 and 4, which show that D'_{Ca} takes distinctly negative values only in the region where $G(H/Ca)$ is larger than $F(H/Ca)$.

Phenomenological Coefficients. The phenomenological equations of the nonequilibrium thermodynamics are often written as follows for a mixed solution of two electrolytes, A and B[2,3,7,13]:

$$\left.\begin{aligned}[J_A] &= -D_{AA}\left(\frac{\partial[A]}{\partial x}\right) - D_{AB}\left(\frac{\partial[B]}{\partial x}\right)\\ [J_B] &= -D_{BA}\left(\frac{\partial[A]}{\partial x}\right) - D_{BB}\left(\frac{\partial[A]}{\partial x}\right)\end{aligned}\right\} \quad (31)$$

where x is the coordinate in the direction of the diffusion. If the A electrolyte consists of the 1 cation and the anion, 3, and the B electrolyte consists of the 2 cation and the anion, 3, the phenomenological coefficients, D_{AA}, D_{AB}, D_{BA}, and D_{BB}, are related to the mobilities of ions, B_i, according to Eq. 1, since

$$[J_1] = \nu_1[J_A],\quad [J_2] = \nu_2[J_B]$$
$$[1] = \nu_1[A],\quad [2] = \nu_2[B] \quad (32)$$

where ν_1 and ν_2 are the numbers of the respective cations contained in one mole of the electrolytes. The results are given by Eqs. 24—27 of Ref. 7.

This treatment is, however, rather formalistic, because what really exist in the solution of strong electrolytes are not the electrolytes, A and B, but the ions, 1, 2, and 3. For each ion, the phenomenological equation may be written as follows:

$$[J_i] = \sum_j L_{ij}(\partial[j]/\partial x) \quad (33)$$

According to Eq. 1, therefore,

$$L_{ii} = -D_i$$
$$L_{ij} = z_i z_j B_i D_j [i]/(\sum_k z_k^2 B_k [k]) \quad (34)$$

If, however, the phenomenological equations are written on the basis of the physico-chemical potentials of the ions, $\tilde{\mu}_i$, as in the following equation,[14]

$$[J_i] = -\sum_j l_{ij}(\partial\tilde{\mu}_j/\partial x) \quad (35)$$

then Eq. 1 corresponds to the case of $l_{ij}=0$ $(i\neq j)$. This means that the cross terms have not yet been taken into consideration, even though the L_{ij} of Eq. 34 and the D_{AB} and D_{BA} of Eq. 31 are not zero.

The possibility that the cross terms, l_{ij}, are not zero might be important in explaining the discrepancy seen in the quantitative comparisons between the theoretical and experimental results, as shown in Figs. 3—7 of this paper. In order to discuss this point further, however, the experimental problems which are related to taking the averages of the concentration gradients between the initial and final values must be settled first, although these expedients do not affect the facts that ions migrated from the lower to the higher concentrations and that the reverse diffusion was actually observed experimentally. Further studies will be reported separately.

References

1) This paper was presented at the 27 th Symposium on Colloid and Interface Chemistry, Akita, October 1974.
2) M. Nakagaki and M. Kobayashi, *Nippon Kagaku Kaishi*, **1973**, 635.
3) R. Flemming and L. J. Gosting, *J. Phys. Chem.*, **77**, 2371 (1973).
4) M. Nakagaki, "Zoku Seitaimaku to Makutoka", ed. by M. Nakagaki, Nankodo Co., Tokyo (1974), p. 1.
5) M. Nakagaki and M. Kobayashi, *Yakugaku Zasshi*, **92**, 1212 (1972).
6) M. Nakagaki, "Yakubutsu no Seitainai Iko", ed. by M. Nakagaki, Nankodo Co., Tokyo (1969), p. 1.
7) M. Nakagaki and M. Kobayashi, *Yakugaku Zasshi*, **93**, 287 (1973).
8) E. Güntelberg, *Z. Phys. Chem.*, **123**, 199 (1926).
9) G. C. Benson and A. R. Gordon, *J. Chem. Phys.*, **13**, 470, 473 (1945); Cf. "Landolt-Börnstein Tabellen", Vol. 2, Part 7, Springer-Verlag, Berlin, Göttingen, Heidelberg (1960), p. 257.
10) J. W. McBain and T. H. Liu, *J. Am. Chem. Soc.*, **53**, 59 (1931). *Cf.* also, J. W. McBain, "Colloid Science", D. C. Heath and Co., Boston (1950), p. 201.
11) M. Nakagaki, N. Koga, and S. Iwata, *Yakugaku Zasshi*, **82**, 1134 (1962).
12) R. H. Stokes, *J. Am. Chem. Soc.*, **73**, 3527 (1951).
13) P. J. Dunlop and L. J. Gosting, *J. Am. Chem. Soc.*, **77**, 5238 (1955); R. L. Baldwin, P. J. Dunlop and L. J. Gosting, *ibid.*, **77**, 5235 (1955); H. Fujita and L. J. Gosting, ibid., **78**, 1099 (1956); P. J. Dunlop, *J. Phys. Chem.*, **61**, 994 (1957); R. P. Wendt, *ibid.*, **69**, 1227 (1965); J. L. Duda and J. S. Vrentas, *ibid.*, **69**, 3305 (1965); and so forth.
14) D. G. Miller, *J. Phys. Chem.*, **71**, 616 (1967).

Solvation Effects on the Electron-Transfer Reaction of TCNQ Anion Radical and 2,3-Dichloro-5,6-dicyano-*p*-benzoquinone

Akihiko YAMAGISHI

Department of Chemistry, Faculty of Science, Hokkaido University, Sapporo 060

(Received October 15, 1975)

Rate constants were obtained with a temperature-jump apparatus for the electron-transfer reaction between 7,7,8,8-tetracyanoquinodimethane anion radical and 2,3-dichloro-5,6-dicyano-*p*-benzoquinone in acetonitrile/tetrahydrofuran (MeCN/THF) and in acetonitrile/water (MeCN/H_2O) mixtures. In MeCN/THF, the forward rate constant (k) was determined in three kinds of mixed solvents: $k=(5\pm2)\times10^9$ $M^{-1}s^{-1}$ (pure MeCN), $(2.2\pm0.2)\times10^9$ $M^{-1}s^{-1}$ (1:2 MeCN/THF), and $(6\pm2)\times10^8$ $M^{-1}s^{-1}$ (1:10 MeCN/THF) at 25 ± 2 °C. In MeCN/H_2O the forward rate constant increases with the square of the H_2O concentration in the range of $[H_2O]=2$—10 M; $k=k_0[H_2O]^2$ with $k_0=(1.0\pm0.2)\times10^6$ $M^{-3}s^{-1}$ at 25 ± 2 °C. The results are discussed in terms of the specific solvation and the ion-pairing of ion radicals.

Recent studies of electron-transfer reactions of ion radicals demonstrate that the solvation structure of an ion radical affects the reaction rate drastically.[1] The specific solvation and ion-pairing with counter ions reduce the electron-transfer rate by a few orders of magnitudes.[1] The conclusion has been deduced mostly from ESR studies of the electron exchange between an ion radical and its parent molecule.

$$R^{\ddagger}\ (\text{or } R^{-}) + R \rightleftharpoons R + R^{\ddagger}\ (\text{or } R^{-})$$

For a reaction of this kind, the free energy change of reaction, $\Delta F°$, is zero.

The present paper gives the results of the temperature-jump study of the reaction between 7,7,8,8-tetracyanoquinodimethane (TCNQ) anion radical and 2,3-dichloro-5,6-dicyano-*p*-benzoquinone (DDQ).

$$TCNQ^{-} + DDQ \rightleftharpoons TCNQ + DDQ^{-}, \qquad (1)$$

The electron affinity of DDQ is much greater than that of TCNQ, indicating that $\Delta F°$ of Reaction 1 is largely negative.[2,3] It was intended to see whether the specific solvation and the ion-pairing still cause an additional energy barrier even under the conditions of a negative free energy change, $\Delta F°<0$.

Experimental

Sodium (Na^+) and tetraethylammonium (NEt_4^+) salts of TCNQ and DDQ were prepared by the reduction with NaI and NEt_4I, respectively. $NaClO_4$ and $NaB(C_6H_5)_4$ were used without purification. NEt_4ClO_4 was prepared by the reaction of NEt_4OH with $HClO_4$. MeCN and THF were distilled with a distillation column of *ca.* 30 cm length, H_2O contents being 0.5 mg/ml (MeCN) and 1.7 mg/ml (THF). Both were stored under $CaCl_2$. H_2O was distilled after being deionized.

The instruments for equiliblrium, conductivity and rate measurements were described elsewhere.[4] As regards the temperature-jump apparatus, the rise time of temperature was determined by following the decrease of a DDQ^- dimer at 700 nm after the temperature-jump; *e.g.* for 1:10 MeCN/THF solvent containing 0.01 M NEt_4ClO_4 and *ca.* 10^{-3} M NEt_4^+-DDQ^-, the 90% temperature rise was attained within 10 μs. Equilibrium measurements were carried out at 25 ± 1 °C. For temperature-jump measurements, samples were kept at 20 ± 1 °C. The difference in temperature between static and kinetic results was neglected.

Results

Reactions in MeCN/THF. The apparent equilibrium constant of Reaction 1 in MeCN/THF was determined in the same way as for MeCN solvent.[5]

$$K_{ap} = [TCNQ][DDQ^-]_t/[TCNQ^-]_t[DDQ]$$

where $[\ ]_t$ denotes the total concentration of each ion radical, since an ion radical is present as either a free ion or an ion-paired ion. $[TCNQ^-]_t$ is calculated from the absorbance at 842 nm, assuming $\varepsilon=4.33\times10^4$ for all the solvents. $[DDQ^-]_t$ is equated to $[DDQ^-]_t=[DDQ^-]^0+\Delta[TCNQ^-]$, where $[DDQ^-]^0$ is the initial concentration of DDQ^- and $\Delta[TCNQ^-]$ the decrease of $TCNQ^-$ when DDQ is added. K_{ap} thus obtained is plotted against the volume percent of THF (Fig. 1).

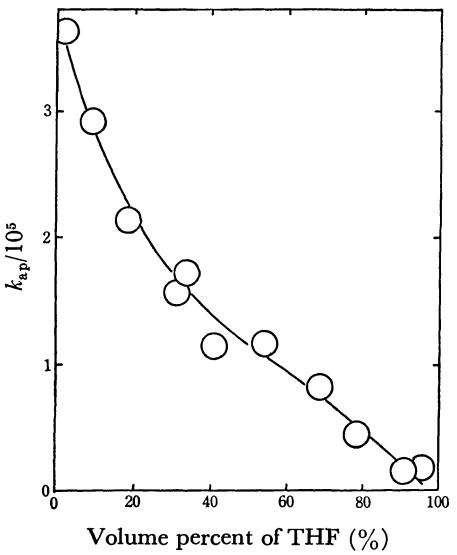

Fig. 1. K_{ap} obtained in MeCN/THF mixtures.

K_{ap} was also obtained in the presence of various amounts of added salts. The results are given in Table 1. The addition of $NaClO_4$ gives a negligible effect on K_{ap} in pure MeCN. In 1:2 MeCN/THF, however, K_{ap} increases as $[NaClO_4]$ increases. In 1:10 MeCN/THF, the small amount of $NaB(C_6H_5)_4$ increases K_{ap} remarkably, while further addition of the salt decreases K_{ap}.

Table 1. The effect of Na^+ on K_{ap}

a) In MeCN; $K^0_{ap}=3.6\times10^5$ [a]				
$[NaClO_4]$/M	0.012	0.041	0.12	0.21
K_{ap}/K^0_{ap} at 25 °C	1.0	1.0	1.0	1.0
b) In 1:2 MeCN/THF; $K^0_{ap}=8.2\times10^4$ [a]				
$[NaClO_4]$/M	0.0072	0.025	0.057	0.087
K_{ap}/K^0_{ap}	1.3	1.5	1.5	1.7
c) In 1:10 MeCN/THF; $K^0_{ap}=1.0\times10^4$ [a]				
$[NaB(C_6H_5)_4]$/M	0.0011	0.0022	0.0043	0.01
K_{ap}/K^0_{ap}	1.5	1.5	1.4	1.1

a) K^0_{ap} denotes K_{ap} at $[Na^+]=0$.

Table 2. The molar conductivity, λ, of $NEt_4^+TCNQ^-$ and $NEt_4^+DDQ^-$

a) $NEt_4^+TCNQ^-$ in MeCN				
$[NEt_4^+TCNQ^-]\times10^6$/M	2.2	4.5	8.8	14
λ	145	132	123	111
b) $NEt_4^+TCNQ^-$ in 1:2 MeCN/THF				
$[NEt_4^+TCNQ^-]\times10^6$/M	5.3	10	21	
λ	112	112	107	
c) $NEt_4^+TCNQ^-$ in THF				
$[NEt_4^+TCNQ^-]\times10^6$/M	2.1	3.7	5.9	9.1
λ	65.5	61.7	60.7	57.0
d) NEt_4^+ DDQ^- in MeCN				
$[NEt_4^+DDQ^-]\times10^5$/M	6.3	9.5	14	32
λ	240	238	240	232
e) $NEt_4^+DDQ^-$ in THF				
$[NEt_4DDQ^-]\times10^5$/M	1.2	2.5	4.9	9.3	16
λ	123	91.8	66.9	49.5	40.1

In order to obtain the dissociation constants of ion radical salts, the molar conductivities of $NEt_4^+TCNQ^-$ and $NEt_4^+DDQ^-$ were measured in MeCN/THF (Table 2). The dissociation constant, K_D, for

$$NEt_4^+R^- \rightleftharpoons NEt_4^+ + R^-$$

is roughly estimated by means of the equation.

$$K_D = \frac{C\lambda^2}{\lambda_\infty^2}. \quad (2)$$

Where C is the total concentration of an ion radical salt and λ_∞ the molar conductivity at infinite dilution. For $NEt_4^+DDQ^-$ in THF, K_D is obtained to be $(4.9\pm1.0)\times10^{-5}$ M at 25 ± 2 °C. In the other solvents, however, K_D defined by Eq. 2 gives no constant value, making the estimation of K_D impossible.

Temperature-jump studies were performed in MeCN, 1:2 MeCN/THF, and 1:10 MeCN/THF in order to obtain the rate constans of Reaction 1. With a temperature-rise, the trasient increase of $TCNQ^-$ is observed at 745 nm in all the solvents. k_{obs} defined by

$$-\frac{d\Delta[TCNQ^-]}{dt} = k_{obs}\Delta[TCNQ^-] \quad (3)$$

is related to the forward rate constant as follows.[5]

$$k_{obs} = k\{[TCNQ^-]_{t,e}+[DDQ]_e\}, \quad (4)$$

where $[\ ]_e$ denotes the equilibrium concentration at an elevated temperature. The k values determined at various concentrations of supporting electrolytes are given in Table 3.

Table 3. k at various concentrations of counter ions at 25 °C

a) MeCN				
$[NEt_4ClO_4]$/M	0.012			
$k\times10^{-9}/M^{-1}s^{-1}$	5 ± 2			
b) 1:2 MeCN/THF				
$[NEt_4ClO_4]$/M	0.0012	0.0024	0.0050	0.010
$k\times10^{-9}/M^{-1}s^{-1}$	2.6 ± 0.5	2.2 ± 0.5	2.2 ± 0.5	2.2 ± 0.5
c) 1:10 MeCN/THF				
$[NaB(C_6H_5)_4]$/M	0.006	0.012	0.024	
$k\times10^{-8}/M^{-1}s^{-1}$	7 ± 2	5 ± 2	6 ± 2	

Reactions in MeCN/H_2O: The apparent equilibrium constant of Reaction 1 in MeCN/H_2O was determined in the same way as in MeCN/THF. A large uncertainty in K_{ap} arises in the higher concentration of H_2O, since DDQ^- decomposes gradually in such regions and DDQ is reduced to DDQ^-. K_{ap} thus obtained is plotted against the volume percent of H_2O (Fig. 2).

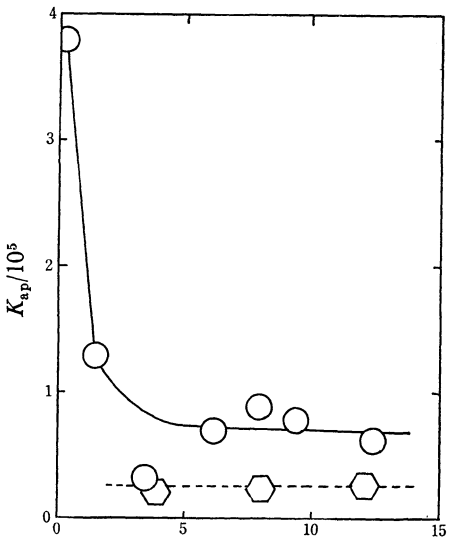

Fig. 2. K_{ap} obtained in MeCN/H_2O mixtures; A solid line is determined by spectrophotometric measurements and a dotted line by rate measurements.

The rates of Reaction 1 in MeCN/H_2O mixtures were determined using a temperature-jump apparatus. In MeCN/H_2O, the trasient increase of $TCNQ^-$ is observed at 745 nm with temperature-rise. k_{obs} defined by Eq. 3 is determined by varying the concentrations of $TCNQ^-$ and DDQ at constant concentrations of TCNQ and DDQ^-. Under these conditions, Eq. 4 is transformed into

$$k_{obs} = k\{[TCNQ^-]_e + C/[TCNQ^-]_e\}, \quad (5)$$

where C is a constant given by

$$C = [TCNQ]_e[DDQ^-]_{t,e}/K_{ap}.$$

The dependence of k_{obsd} on $[TCNQ^-]_e$ is shown in Fig. 3. As expected from Eq. 5, k_{obsd} becomes minimum for a certain value of $[TCNQ^-]_e$. This concentration is denoted by $[TCNQ^-]_e^*$. It is apparent from Eq. 5 that $[TCNQ^-]_e$ is equal to $[DDQ]_e$ at $[TCNQ^-]_e^*$. Using

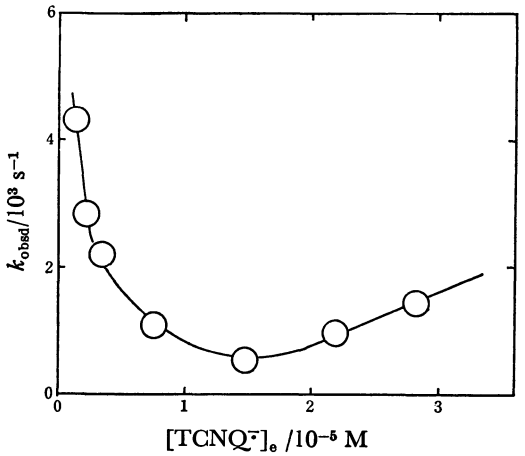

Fig. 3. Dependence of k_{obsd} on [TCNQ$^-$]$_e$ in 9: 1 MeCN/H_2O; [TCNQ] 1.1×10^{-3} M and [NEt_4^+DDQ$^-$] 4.1×10^{-4} M.

the value of [TCNQ$^-$]$_e$*, K_{ap} is determined by

$$K_{ap} = [TCNQ]_e[DDQ^-]_{t,e}/[TCNQ^-]_e{}^{*2}.$$

K_{ap} obtained in this way agrees with the one obtained by the equilibrium measurements within a factor of 5 (a dotted curve, Fig. 2).

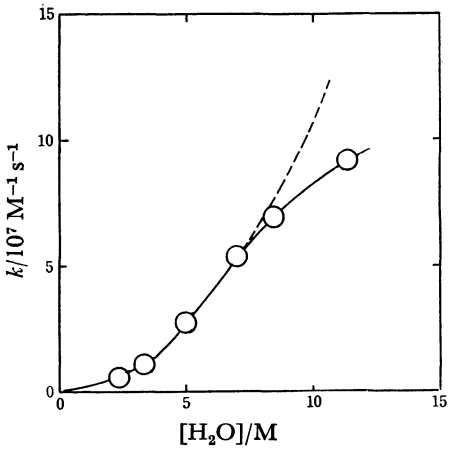

Fig. 4. Dependence of k on the H_2O concentration. A dotted curve denotes the calculated values according to Eq. 6.

Figure 4 gives the dependence of k on the concentration of H_2O. It is concluded that k increases with the square of the H_2O concentration from 2 to 10 M.[6]

$$k = k_0[H_2O]^2$$
$$k_0 = (1.0\pm0.2)\times10^6\ M^{-3}\ s^{-1} \text{ at } 25\pm2°C. \quad (6)$$

Discussion

The effect of THF on the equilibrium and the rates of Reaction 1 is interpreted in terms of the ion-pairing of ion radicals.

$$\begin{array}{ccc} TCNQ^- + DDQ & \overset{k_1}{\rightleftharpoons} & TCNQ + DDQ^- \\ M^+ \uparrow\downarrow & & \uparrow\downarrow M^+ \\ M^+TCNQ^- + DDQ & \underset{k_2}{\rightleftharpoons} & TCNQ + M^+DDQ^- \end{array} \quad (7)$$

K_{ap} is expressed in terms of the dissociation constants of M$^+$TCNQ$^-$ and M$^+$DDQ$^-$, K_D^T and K_D^P, respectively, as follows.

$$K_{ap} = K_0(1+[M^+]/K_D^P)/(1+[M^+]/K_D^T) \quad (8)$$

where K_0 is the equilibrium constant for the electron-transfer reaction of free ions.

$$K_0 = \frac{[TCNQ][DDQ^-]}{[TCNQ^-][DDQ]}$$

K_{ap} in MeCN only slightly varies with the addition of $NaClO_4$ (Table 1). This indicates that K_D^T is nearly equal to K_D^P previously determined to be 0.40 M.[4] On the other hand, K_{ap} in 1 : 10 MeCN/THF increases rapidly until it reaches a constant value. According to Eq. 8, this implies that K_D^P is smaller than K_D^T in this medium. From the limiting value of $K_{ap}/K^0_{ap}=1.5$ at the region of [$NaB(C_6H_5)_4$]=0.0011—0.0022 M, K_D^T is equated to 1.5 K_D^P. Assuming that K_D^P in 1 : 10 MeCN/THF does not differ from K_D^P in THF ($4.9\pm1.0\times10^{-5}$ M), K_D^P and K_D^T are roughly estimated to be 5×10^{-5} M and 8×10^{-5} M, respectively.

Under the scheme of Eq. 7, k is expressed in terms of K_D^T and K_D^P as follows.

$$k = k_1\left(\frac{K_D^T}{[M^+]+K_D^T}\right) + k_2\left(\frac{[M^+]}{[M^+]+K_D^T}\right), \quad (9)$$

where k_1 and k_2 are the forward rate constants for the reactions between TCNQ$^-$ and DDQ and between M$^+$TCNQ$^-$ and DDQ, respectively. In deriving the equation, the rate of ion-pairing of TCNQ$^-$ with M$^+$ is assumed to be much greater than that of electron-transfer. Taking [Na^+]≈[$NaB(C_6H_5)_4$]≈10^{-2} M and $K_D^T\approx8\times10^{-5}$ M in 1 : 10 MeCN/THF, k is simply equated to k_2 in this solvent. k_2 in 1 : 10 MeCN/THF is about one order smaller than in MeCN. It is concluded that the transfer process of Na^+ causes an additional energy barrier even under the conditions of a negative free energy change, $\Delta F° < 0$.

The effects of H_2O on the equilibrium and rate constants are most likely ascribed to the capacity of H_2O for hydrogen-bonding. As regards DDQ and its anion radical, the formation of hydrogen bond with H_2O has been confirmed by polarographic investigations.[3] The decrease of K_{ap} in MeCN/H_2O indicates that the free energy change of reaction, $\Delta F°$, becomes less negative. This seems closely related to the fact that the electron affinity of DDQ decreases in hydroxylic solvents like H_2O and ethanol.[3] The specific solvation of DDQ and DDQ$^-$ by H_2O is thus concluded from Fig. 2 to be completed at the concentration of [H_2O]= 6 vol. %.

The kinetic result shown in Fig. 4 implies that H_2O acts catalytically in electron-transfer. From the dependence of the forward rate on [H_2O] (Eq. 6), it is suggested that a part of DDQ is solvated by two H_2O molecules to form DDQ(H_2O)$_2$, and that electron-transfer takes place through this species.

$$TCNQ^- + DDQ(H_2O)_2 \rightleftharpoons TCNQ + DDQ^-(H_2O)_2 \quad (8)$$

It is assumed herewith that TCNQ does not form hydrogen-bond with H_2O in the investigated region of

[H_2O] since a carbon atom is a weaker proton acceptor than an oxygen atom.[7]

The author thanks Prof. Masatoshi Fujimoto for his encouragement. This work was supported by the ministry of Education.

References

1) N. Hirota, "Radical Ions," E. T. Kaiser and L. Kevan, Ed. Interscience, New York, N. Y. (1968), p. 35.
2) D. S. Acker and W. R. Hertler, *J. Am. Chem. Soc.*, **84**, 3370 (1962).
3) M. E. Peover, *Trans. Faraday Soc.*, **58**, 1656 (1962).
4) A. Yamagishi, *Bull. Chem. Soc. Jpn.*, **48**, 2440 (1975).
5) A. Yamagishi, *Chem. Lett.*, **1975**, 899.
6) Since the activity of H_2O in MeCN is not available, k is plotted against [H_2O]. At the higher concentration, the effect of aggregation of H_2O molecules should not be neglected. *Cf.* A. Rainis, R. Tung, and M. Szwarc, *J. Am. Chem. Soc.*, **95**, 659 (1973).
7) M. L. Ahrens, M. Eigen, W. Krusc, and G. Maaass, *Ber. Bunsenges. Phys. Chem.*, **74**, 382 (1970).

Photolysis of Formaldehyde in the Presence of Nitric Oxide

Kohji TADASA,* Naomi IMAI, and Tetsuo INABA

Faculty of Liberal Arts and Sciences, University of Osaka Prefecture, Sakai, Osaka 591

(Received October 31, 1975)

The photolysis of CH_2O has been studied in the absence and presence of NO from room temperature to 300 °C. In the photolysis of CH_2O alone, the CO and H_2 formation rates increase greatly with temperature. When NO is added, these rates vary and reach constant values with an increase in the amount of NO. These limiting rates are independent of the temperature to within the experimental error, in contrast to the rates observed for CH_2O alone. It is suggested that the limiting rate of CO formation corresponds to the sum of the rates of the two primary processes, the molecular and radical reactions, and that that of H_2 formation corresponds to the rate of the molecular process. For photolysis totally inhibited by NO, the rates of formation of CO, H_2, N_2, and N_2O were examined and a reaction mechanism is proposed which is consistent with that for the photosensitized reaction between hydrogen and nitric oxide previously studied in this laboratory.

The effect of the addition of nitric oxide on the pyrolysis of formaldehyde has been investigated in this laboratory and it was found that nitric oxide very effectively inhibits the radical chain process, while nitric oxide reacts with formaldehyde at high temperature forming CHO radicals.[1] Thus, NO has both inhibitive and accelerative effects on the free radical process, rendering the elucidation of the overall reaction mechanism very difficult.

In the work reported here, the photolysis of CH_2O was investigated in the presence of NO at lower temperatures, for which the thermal reaction between NO and CH_2O is negligible and NO reacts only with radicals formed photochemically.

Experimental

Materials. Formaldehyde was prepared from paraformaldehyde. The method of preperation and purification are same as those in a previous paper.[1] Nitric oxide was obtained from Takachiho Kagaku Co., Ltd. with a research-grade purity of 99.6%, and subjected to several trap-to-trap distillations.

Apparatus. The reaction was studied in a conventional static system, and was carried out in a cylindrical quartz vessel of 262 ml placed in an electric furnace, which was wrapped in asbestos and placed inside a cylindrical alminum collar 20 cm long and 9 cm in diameter with walls 1.6 cm thick, for the purpose of maintaining a constant temperature.

The light source was a medium pressure mercury arc. A glass filter was used to remove light of wavelength less than 2700 Å.

Procedure. Formaldehyde and nitric oxide were introduced into the vessel, which was maintained at the experimental temperature. For all experiments, the incident light intensity was the same. The photolytic products were separated by means of cold traps and a Toepler pump, and analyzed quantitatively by means of a gas chromatograph. The separation and analysis techniques are similar to those described in a previous paper.[1]

Results

The amounts of CO, H_2, N_2, and N_2O produced during the photolysis of CH_2O with NO were measured. A large amount of H_2O was found, but it was not measured. An unmeasurable amount of CO_2 was observed at room temperature. No methanol was detected, although it is important in the pyrolysis.

The yields of CO, H_2, N_2, and N_2O were measured at different reaction times during the uninhibited and inhibited photolysis. Some results are given in Fig. 1, which shows that the amount of each product increases linearly from the beginning of the photolysis. The initial rate of formation of each product, in all experiments, was determined by the amount produced after 10 min of photolysis.

Figure 2 shows the results of a series of runs carried out at a constant pressure of formaldehyde (100 Torr) and various pressures of NO (0—100 Torr) at (a) room temperature, (b) 100 °C, (c) 200 °C, and (d) 300 °C. On the other hand, Fig. 3 shows the effect of the CH_2O pressure (20—120 Torr) on the photolysis for a fixed amount of NO (50 Torr) at (a) 100 °C and (b) 200 °C.

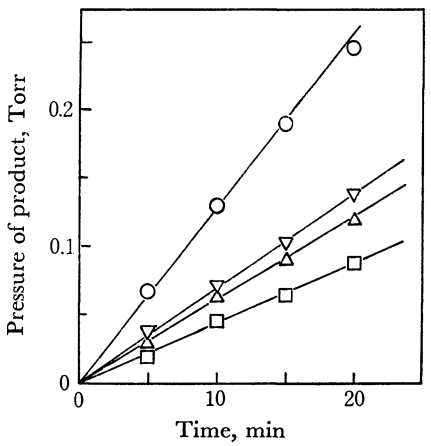

Fig. 1. Yields of products in the photolysis of 100 Torr CH_2O with 50 Torr NO at 100 °C.
○: CO, △: H_2, ▽: N_2, □: N_2O.

Discussion

The photodecomposition of CH_2O has been studied by a number of workers and it is well established that the photolysis occurs *via* two primary processes.[2-4]

* Present address: Department of Agricultural Chemistry, College of Agriculture, University of Shinshu, Ina, Nagano 396.

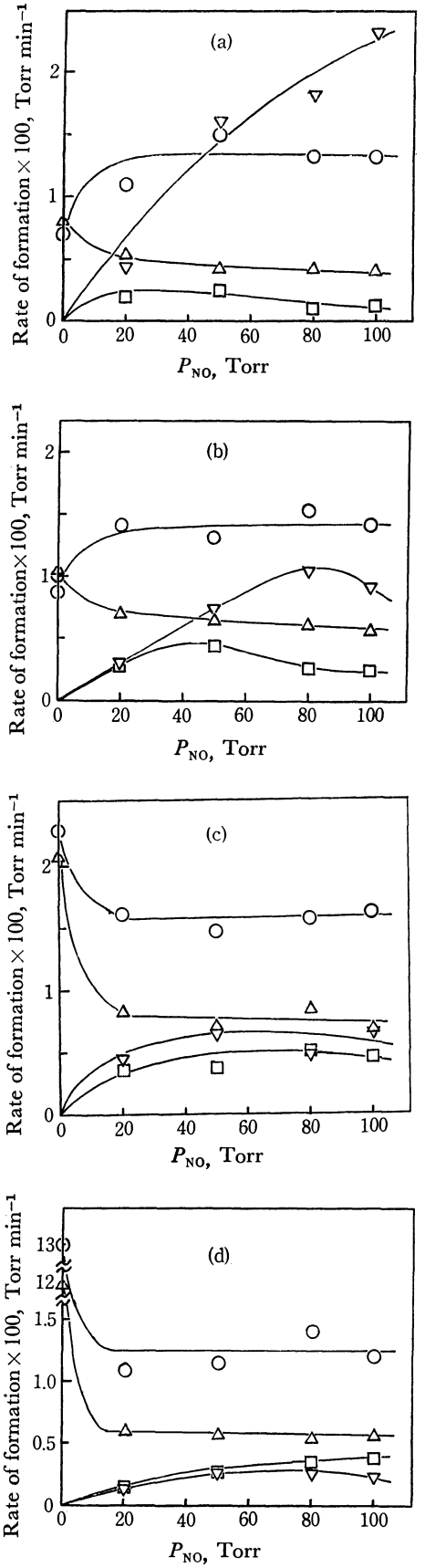

Fig. 2. Plot of rate of formation *vs.* NO pressure for the photolysis of 100 Torr CH_2O.
○: CO, △: H_2, ▽: N_2, □: N_2O.
(a) Room temperature, (b) 100°C, (c) 200°C, (d) 300°C.

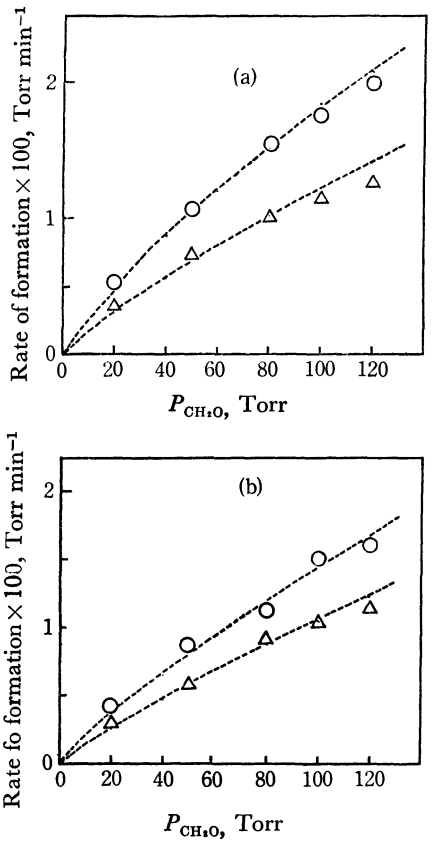

Fig. 3. Plot of rate of formation *vs.* CH_2O pressure for the photolysis with 50 Torr NO.
Data obtained were multiplied by factors in parentheses for the purpose of direct comparison with the dotted lines.
(a) 100°; ○: CO (1.35), △: H_2 (1.77).
(b) 200°, ○: CO (1), △: H_2 (1.5).

$$CH_2O + h\nu \longrightarrow H + CHO \quad (I)$$
$$\longrightarrow H_2 + CO \quad (II)$$

Sperling and Toby[4] observed that the quantum yields of the H_2 and CO formations do not vary with temperature between 80 and 120 °C. On the other hand, Akeroyd and Norrish,[2] and Calvert and Steacie[5] have found the quantum yield of CH_2O photolysis to increase with temperature at high temperatures, *e.g.*, $\phi_{CO}=1.0$ at 101 °C, 5.4 at 196 °C, and 69 at 295 °C.[5] In this work, the results shown in Fig. 2 (NO=0 Torr) indicate that the rates of H_2 and CO formation increase with temperature in a manner similar to that observed by them. Such a temperature dependency of the quantum yields, together with the fact that nearly equal amounts of H_2 and CO are produced in the photolysis indicates that Process I is followed by the chain process, which is assumed to proceed mainly *via* the following reactions:

$$H + CH_2O \longrightarrow H_2 + CHO$$
$$CHO + M \longrightarrow CO + H + M$$
$$CHO + (wall) \longrightarrow products + (wall)$$

When NO is added to the CH_2O during photolysis, the rates of CO and H_2 formation vary and attain limiting values for increasing amounts of NO, as is shown in Fig. 2. The limiting rates of CO and H_2

formation are approximately independent of the temperature, contrary to those for the photolysis of CH_2O alone.

Since, in the CH_2O pyrolysis, H_2 formation is almost totally inhibited by a small amount of NO, the rate of H_2 formation which occurs for photolysis with NO added can be attributed to the molecular Process II. The difference between the limiting rates of the CO and H_2 formations should be regarded as the rate of CO formation caused by Process I. The following discussion will, therefore, concern the radical process caused by Reaction I under conditions of sufficient inhibition by NO ($P_{NO}>30$ Torr).

The Hg-photosensitized reaction of H_2 and NO[6] has been studied in this laboratory in order to study the reactions in a system containing H atoms and NO at low temperature. In this photosensitization, it was found that the main products are H_2O and N_2, with the H_2O formation being of the zeroth order and the N_2 formation of the first order with respect to NO at room temperature. A third product is N_2O and its rate of formation decreases with the amount of NO. Although the amount of H_2O in the products was not measured in the work reported here, stoichiometry predicts that

$$R_{CO} - R_{H_2} = R_{H_2O}$$

i.e., the same amounts of CO and H_2O are formed by the radical process. The reaction orders of the H_2O, N_2, and N_2O formations with respect to NO are quite similar both for H_2–NO photosensitization and for the photolysis studied at room temperature, indicating that these products are formed by similar processes in both cases.

Thus, the following reaction scheme is proposed for the radical process of CH_2O–NO photolysis at room temperature, the scheme being consistent with that of H_2–NO photosensitization:

$$CH_2O + h\nu \longrightarrow CHO + H \quad (I)$$
$$CHO + M \longrightarrow CO + H + M \quad (1)$$
$$CHO + HO \longrightarrow CO + HNO \quad (2)$$
$$H + NO + M \longrightarrow HNO + M \quad (3)$$
$$2HNO \longrightarrow H_2O + N_2O \quad (4)$$
$$HNO + 2NO \longrightarrow N_2 + H + NO_3 \quad (5)$$
$$NO_3 + NO \longrightarrow 2NO_2 \quad (6)$$
$$NO_2 + HNO \longrightarrow OH + 2NO \quad (7)$$
$$OH + HNO \longrightarrow H_2O + NO \quad (8)$$

This reaction scheme leads to the following rate equations:

$$R_{CO} = R_1 + R_2 = I_{a(I)}$$
$$R_{H_2O} = R_4 + R_8 = I_{a(I)},$$

where $I_{a(I)}$ refers to the rate of the primary Reaction I.

The extinction coefficient of CH_2O has been estimated to be ε=4.84,[4] 1.87,[4] and 0.07[7] mol^{-1} l cm^{-1} at 313, 334, and 366 nm, respectively. In Fig. 3, the dotted lines are drawn since the rate is proportional to the intensity of light absorbed by CH_2O using the value of the extinction coefficient given above at 313 nm. Although the curvatures of the observed values are larger than those calculated, the differences are not as large. Thus, Figs. 2 and 3 show that R_{CO} and R_{H_2O} in the radical process ($=R_{CO(total)}-R_{H_2}$) are proportional to I_a and are independent of the NO pressure, supporting the above rate equations.

According to the above reaction scheme, N_2 is produced by the chain disproportionation of NO, Reactions 5 and 3,[8] and N_2O is produced by the disproportionation of HNO, Reaction 4.[9] Hence,

$$R_{N_2} = k_5[HNO][NO]^2$$
$$R_{N_2O} = k_4[HNO]^2,$$

where [HNO] can be obtained from the following equation

$$I_{a(I)} = k_4[HNO]^2 + k_7[NO_2][HNO].$$

As discussed in a previous paper on H_2–NO photosensitization,[6] the following relations hold if $R_4 \ll R_7 (= R_8)$** and $[NO_2] \propto [NO]$***, NO_2 being consumed by reaction with Hg in the reaction cell, the amount of which it is not possible to measure accurately:

$$R_{N_2} \propto I_a[NO]$$
$$R_{N_2O} \propto I_a^2/[NO]^2$$

Figure 2(a) indicates that these relations are approximately valid at room temperature.

At higher temperatures, however, the above rate expressions for N_2 and N_2O do not hold as is shown in Figs. 2(b), (c), and (d). As the temperature rises up to 200 °C, moreover, R_{N_2} decreases and R_{N_2O} increases, with the latter decreasing for temperatures above 200 °C. Such dependencies on the temperature were also observed for H_2–NO photosensitization and can be explained by a similar reaction mechanism. Since Reaction 5 is a termolecular reaction, its rate should decrease for a rise in temperature, causing a decrease of R_{N_2}. The increase of R_{N_2O} with the temperature increase is assumed to be caused by the following reaction:

$$HNO + NO \longrightarrow N_2O + OH \quad (9)$$

in addition to Reaction 4, which appears to have a small activation energy and a rate that should not depend greatly on the temperature. At temperatures higher than 200 °C, the following reaction will proceed:

$$2HNO \longrightarrow 2OH + N_2 \quad (10)$$

Thus, a great amount of HNO is consumed by Reactions 10 and 8, with the R_{N_2O} being decreased by Reactions 4 and 9. The relations $R_{CO}=I_{a(I)}$ and $R_{H_2O}=I_{a(I)}$, however, are valid even for the reaction scheme at high temperature.

References

1) K. Tadasa, N. Imai, and T. Inaba, *Bull. Chem. Soc. Jpn.*, **47**, 548 (1974).

2) E. I. Akeroyd and R. G. W. Norrish, *J. Chem. Soc.*, **1936**, 890.

3) E. Gorin, *J. Chem. Phys.*, **7**, 256 (1939); P. Klein and L. Schoen, *ibid.*, **24**, 1094 (1956); M. Venugopalan and K.O.

** This assumption is reliable because the N_2O yield is much smaller than that of H_2O at room temperature (Fig. 2(a)).

*** Since NO_2 is produced by chain disproportionation of NO, and its rate determining step should be (5), this assumption seems not to be very unprobable.

Kutschke, *Can. J. Chem.*, **42**, 2451 (1964); B. A. DeGraff and J. G. Calvert, *J. Am. Chem. Soc.*, **89**, 2247 (1967).

4) H. P. Sperling and S. Toby, *Can. J. Chem.*, **51**, 471 (1973).

5) J. G. Calvert and E. W. R. Steacie, *J. Chem. Phys.*, **19**, 176 (1951).

6) K. Tadasa, N. Imai, and T. Inaba, *Bull. Chem. Soc. Jpn.*, under contribution.

7) R. G. W. Norrish and F. W. Kirkbride, *J. Chem. Soc.*, **1932**, 1518.

8) E. A. Arden and L. Phillips, *Proc. Chem. Soc.*, **1962**, 354; E. A. Arden and L. Phillips, *J. Chem. Soc.*, **1964**, 5118.

9) P. Harteck, *Ber.*, **66**, 423 (1933); H. A. Taylor and C. Tanford, *J. Chem. Phys.*, **12**, 47 (1944); M. Z. Hoffman and R. B. Bernstein, *ibid.*, **64**, 1753 (1960); O. P. Strausz and H. E. Gunning, *Trans. Faraday Soc.*, **60**, 347 (1964); K. A. Wilde, *Combust. Flame*, **13**, 173 (1969); R. Atkinson and R. J. Cvetanović, *Can. J. Chem.*, **51**, 370 (1973).

10) K. Tadasa, N. Imai, and T. Inaba, *Bull. Chem. Soc. Jpn.*, **47**, 2979 (1974).

Excited-State Dipole Moments of Azulene and 3,5-Dimethylcyclopenta[*ef*]heptalene

Hiroyuki YAMAGUCHI, Teruki IKEDA,* and Hiroaki MAMETSUKA**

Department of Chemistry, Kumamoto University, Kumamoto 860

(Received November 6, 1975)

The dipole moments of the lower two singlet excited states of azulene (I) and 3,5-dimethyl derivative of cyclopenta[*ef*]heptalene (II) have been determined from the frequency shift of the absorption and emission spectra in various solvents. The direction of the excited-state dipole moments of molecules I and II is opposite to the direction of the ground-state dipole moments. The dipole moments of the two excited states of molecules I and II have been calculated by using the semi-empirical SCF-π-MO CI method. There is a general agreement between the theoretical results and the experimental results. This agreement shows that the polarization effect of the σ-electrons is almost identical in the ground and excited states of both molecules.

Many phenomena occurring in the electronically-excited states of molecules, such as photochemical reactions, are dependent on the changes in the electronic structures. Electronic excitation in molecules usually leads to a new electron density distribution and, consequently, to changes in dipole moments. Pariser[1] has calculated the dipole moments for the singlet excited states of azulene (I) and found that they increase in magnitude and reverse in sign with respect to the ground state. This behavior has been used to interpret the blue shift of the longest absorption band going from a nonpolar solvent to a polar solvent.

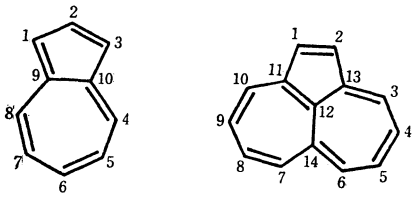

I II

Fig. 1. Numbering of carbon atoms.

The change in dipole moment for the excited state of a polar molecule could be measured by observing the absorption and emission spectra, as suggested by Mataga *et al.*,[2] Lippert,[3] and McRae.[4] By using the equations developed by McRae, Robertson *et al.*[5] have experimentally investigated the values of the change in dipole moment for each of the singlet excited states of I. However, they have not obtained the definitive values of the change in dipole moment for each of the excited states of I.

The electronic structures of cyclopenta[*ef*]heptalene (II) have been of interest since Hafner and Schneider[7] prepared its dimethyl derivative in 1958—59. The electronic spectra of II may be considered to be well understood as a result of the work of Ali and Coulson,[8] Julg and Francois,[9] and others.[10] Recently, Eaton *et al.*[11] have shown that the observed emission in the case of 3,5-dimethylcyclopenta[*ef*]heptalene corresponds to anomalous fluorescence due to a transition from the second excited singlet, as in the case of I.

The purpose of our research was to determine experimentally the dipole moments in the lower two electronic excited states of I and the dimethyl derivative of II and to compare the experimental results with the theoretical results obtained by using the semi-empirical SCF-π-MO CI method.[12,13] It may be possible to use the results of such investigations to deepen our understanding of the electronic properties for excited states of nonbenzenoid aromatic hydrocarbons containing an azulene nucleus.

Experimental

Chemicals. Substance I was purchased from Tokyo Kasei Chemicals Co. The 3,5-dimethyl derivative of II was received from Professor K. Hafner. These Substances were carefully purified by recrystallization from hexane and by subsequent sublimation *in vacuo*. Both compounds were spectroscopically pure, from comparison with published spectra.[11] The solvents used were carefully purified according to the descriptions in Ref. 14. The purity of solvents was established by checking for emission before use.

Measurements. The dielectric constants were determined with a home-made resonance-method apparatus. A dielectric constant measurement cell with cylindrical platinum electrodes was used. The refractive indices were measured by means of a Pulfrich refractometer. The static dielectric constant (ε) and the refractive index (n) at the sodium D line of the solvents agreed with the values cited in Ref. 14. The densities of the solutions were measured by the use of a pycnometer for volatile liquids. The absorption spectra were obtained with a Cary Model 14 recording spectrophotometer equipped with a thermostated cell holder. The fluorescence spectra were taken with a Shimadzu RF-502 recording spectrophotometer equipped with a thermostated cell holder. The wave numbers of the emission-band maxima were determined from the emission spectra, as corrected for the spectral sensitivity of the instrument. The concentration of I and 3,5-dimethyl derivative of II was kept less than 10^{-4} mol/l for all solutions prepared, so that the system was free from any undersired concentration quenching. All measurements were made on deaerated samples at 20 °C.

Determination of Excited-state Dipole Moments. If we ignore any changes in the solute polarizability on excitation, the solvent shifts can be written as follows:[4] for the wave number of the band maxima of absorption spectra (ν_a)

$$\nu_a = K\left[\frac{n^2-1}{2n^2+1}\right] + C\left[\frac{\varepsilon-1}{\varepsilon+2} - \frac{n^2-1}{n^2+2}\right] + \text{Const.}, \quad (1)$$

* Present address: Japan Spectroscopic Co. Ltd., Hachioji, Tokyo 192

** Present address: Research Institute of Industrial Science, Kyushu University, Fukuoka 812

and for the difference ($\Delta\nu_{af}$) between ν_a and the wave number ν_f of the corresponding fluorescence

$$\Delta\nu_{af} = C'\left[\frac{\varepsilon-1}{\varepsilon+2} - \frac{n^2-1}{n^2+2}\right] + \text{Const.} \quad (2)$$

The constants C and C' are given by Eqs. 3 and 4, respectively,

$$C = \frac{2m_0(m_0-m_i)}{a^3hc} \quad (3)$$

$$C' = \frac{2(m_0-m_i)^2}{a^3hc} \quad (4)$$

where a is the cavity radius in Onsager's theory[6] of the reaction field, and m_0 and m_i are the dipole moments of the ground state and the ith excited state of the solute molecule, respectively.

For the hydrocarbon solvents, the second term of Eq. 1 is zero and the constant K is the least-squares slope of the curve of ν_a against $(n^2-1)/(2n^2+1)$. It remains to evaluate the constants C and C' of Eqs. 1 and 2 for the lower two transitions observed in a range of polar solvents. By using the constant K determined from the nonpolar solvents, the constants C and C' are chosen to give the best reproduction of the observed frequency shifts. From the constants C and C', the excited-state dipole moments, m_i, for each transition of I and the 3,5-dimethyl derivative of II can be calculated using Eqs. 3 and 4 and the dipole moments m_0 determined experimentally.

MO Calculation

The method of calculation used for obtaining the energetically most stable structure in a conjugate molecule is the SCF formalism of the Pariser-Parr-Pople semiempirical MO method,[15,16] taken together with the variable bond-length technique. The C–C bond distances and, correspondingly, the resonance and Coulomb repulsion integrals are allowed to vary with bond orders at each iteration until self-consistency is achieved. Bond lengths are correlated with bond orders by the aid of the following formula:[17]

$$r_{\mu\nu}\,(\text{Å}) = 1.520 - 0.186p_{\mu\nu} \quad (5)$$

The Coulomb repulsion integrals are evaluated using the Mataga-Nishimoto formula.[18] The resonance integral is assumed to be of exponential form $\beta=A\exp(-br)$, the value of exponent b being taken as 1.7Å^{-1}.[12]

As the starting geometries for iterative calculation, we take all the possible structures in which bond lengths are distorted so that the set of displacement vectors may form a basis of an irreducible representation of the full symmetry group of a molecule.

In order to discuss the geometrical structures of electronically excited states, the procedure described above is used, except for the use of a different value, 3.3 Å^{-1}, for exponent b in the exponential form of the resonance integral.[13] This value of b was determined so that the predicted fluorescence energy from the lowest singlet excited state ($^1B_{2u}$) in benzene may fit the experimental value.

In discussing the properties of excited states, configuration mixing of all the singly excited states is included.

Results and Discussion

For the hydrocarbon solvents, the constants K for the first electronic transitions of I and the dimethyl derivative of II were obtained from the least-squares slopes of the curves of ν_a against $(n^2-1)/(2n^2+1)$ (see Figs. 2 and 3). By using the constants K, the constants C for these transitions were chosen to reproduce the frequency shifts observed in a range of polar solvents (see Figs. 4 and 5). The observed $\Delta\nu_{af}$ for the second electronic transitions against $[(\varepsilon-1)/(\varepsilon+2)-(n^2-1)/(n^2+2)]$ rela-

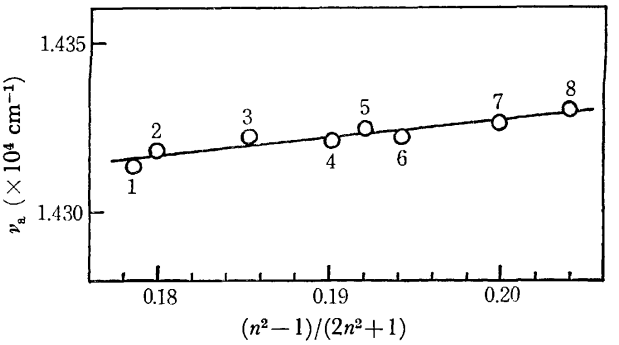

Fig. 2. The plot of ν_a against $(n^2-1)/(2n^2+1)$ for azulene. Here numbers denote the solvents as (1): isopentane, (2): pentane, (3): hexane, (4): heptane, (5): 2,2,4-trimethylpentane, (6): octane, (7): decane, (8): cyclohexane.

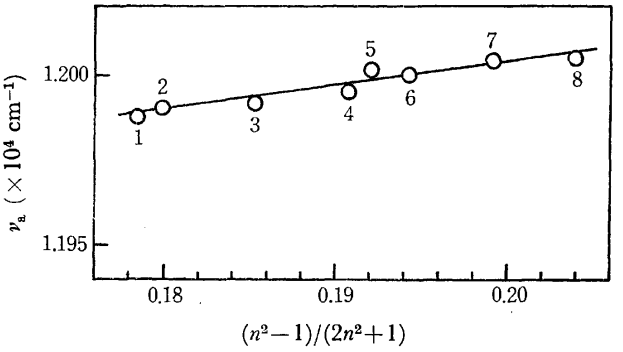

Fig. 3. The plot of ν_a against $(n^2-1)/(2n^2+1)$ for 3,5-dimethylcyclopenta[*ef*]heptalene. The numbers are the same as described in Fig. 2.

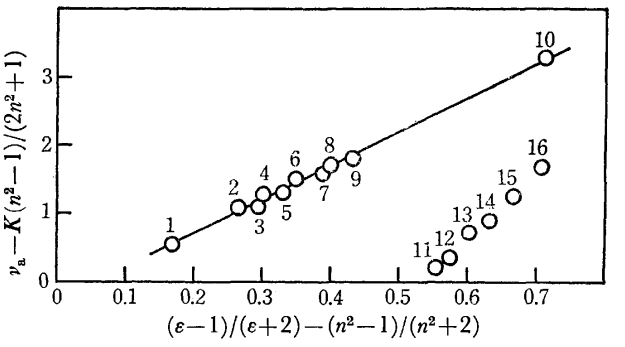

Fig. 4. The plot of $\nu_a - K(n^2-1)/(2n^2+1)$ against $(\varepsilon-1)/(\varepsilon+2)-(n^2-1)/(n^2+2)$ for azulene. Here numbers denote the solvents as (1): dibutyl ether, (2): diisopropyl ether, (3): chlorobenzene, (4): diethyl ether, (5): butyl acetate, (6): isobutyl acetate, (7): propyl acetate, (8): ethyl acetate, (9): methyl acetate, (10): acetonitrile, (11): pentyl alcohol, (12): isopentyl alcohol, (13): butyl alcohol, (14): isopropyl alcohol, (15): ethyl alcohol, (16): methyl alcohol.

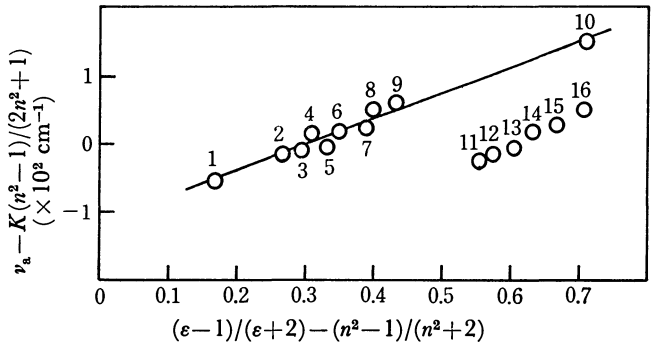

Fig. 5. The plot of $\nu_a - K(n^2-1)/(2n^2+1)$ against $(\varepsilon-1)/(\varepsilon+2)-(n^2-1)/(n^2+2)$ for 3,5-dimethylcyclopenta-[*ef*]heptalene. The numbers are the same as described in Fig. 4.

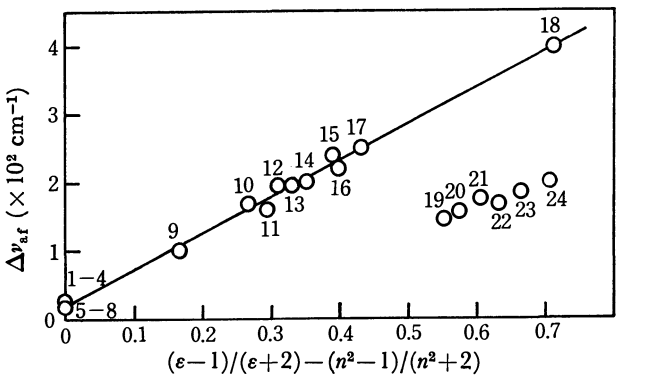

Fig. 6. The plot of $\Delta\nu_{af}$ against $(\varepsilon-1)/(\varepsilon+2)-(n^2-1)/(n^2+2)$ for azulene. Here numbers denote the solvents as (1): isopentane, (2): pentane, (3): hexane, (4): pentane, (5): 2,2,4-trimethylpentane, (6): octane, (7): decane, (8): cyclohexane, (9): dibutyl ether, (10): diisopropyl ether, (11): chlorobenzene, (12): diethyl ether, (13): butyl acetate, (14): isobutyl acetate, (15): propyl acetate, (16): ethyl acetate, (17): methyl acetate, (18): acetonitrile, (19): pentyl alcohol, (20): isopentyl alcohol, (21): butyl alcohol, (22): isopropyl alcohol, (23): ethyl alcohol, (24): methyl alcohol.

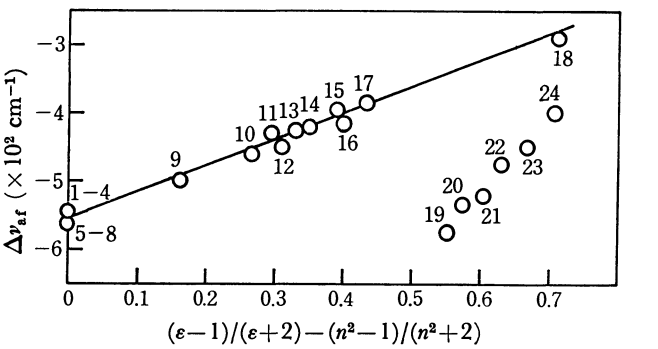

Fig. 7. The plot of $\Delta\nu_{af}$ against $(\varepsilon-1)/(\varepsilon+2)-(n^2-1)/(n^2+2)$ for 3,5-dimethylcyclopenta[*ef*]heptalene. The numbers are the same as described in Fig. 6.

tions are shown in Figs. 6 and 7. The straight lines in the figures were obtained by the least-squares method. The C' values for both molecules were determined by using the slopes of these lines. It was evident that the alcohol solvents had to be separated from the other polar solvents for Eqs. 1 and 2 to represent the frequency shifts successfully. These different results in the alcohol solvents are attributed to hydrogen bonding and to the resulting erroneous value of the local field expressed in terms of the solvent dielectric constant and refractive index in Eqs. 1 and 2. Thus, the constants C and C' were determined from frequency shifts observed in nonalcoholic solvents; these values are listed in Table 1. From Eqs. 3 and 4, the excited-state dipole moments, m_i, for each transition were obtained by using the constants C and C', the experimentally-determined m_0, and the value of a estimated from the apparent molal volume. The results are given in Table 2. Using $a=3$ Å and $a=4$ Å, Robertson *et al.*[5] have obtained the dipole moments for each transition of I. The agreement with the present results in the case of $a=4$ Å is satisfactory, but in the case of $a=3$ Å is less satisfactory.

Table 1. Constants of frequency shifts

Molecule	a (Å)[a]	Excited state	K (cm^{-1})	C (cm^{-1})	C' (cm^{-1})
I	3.65[b]	S_1	499	476	
		S_2			530
II	4.29[b]	S_1	509	399	
		S_2			351

a) Estimated from the apparent molal volume ϕ_v. The ϕ_v is defined by the relation: $\phi_v=1000(d_2-d_1)/(m_1d_2d_{12})+M_1/d_{12}$, where d_2 and d_{12} are the densities of the solvent and the solution of molality m_1 of the solute having molecular weight M_1, respectively. b) Measured in cyclohexane.

Table 2. Excited-state dipole moments

Molecule	Dipole moment (D)[a]	
	S_1	S_2
I	−1.30	−0.60
II	−1.13	−0.37

a) The negative sign represents the fact that the direction of the dipole moment is opposite to that of the ground-state dipole moment.

For molecules I and II, the starting bond distortions belonging to the irreducible representation, a_1 and b_2, of the full symmetry group, C_{2v}, are taken as the starting bond distortions for iterative calculation. It turns out that, in the ground state (S_0) and the two lower excited states (S_1 and S_2) of both molecules, all the starting bond distortions converge into a unique self-consistent set of electronic structures corresponding to C_{2v}. The dipole moments for S_0, S_1, and S_2 states of both molecules are calculated by using the theoretical electron densities and bond lengths. The calculated dipole moments for S_0, S_1, and S_2 of I are 2.82, −3.55, and −2.65 D, respectively, and those of II are 3.08, −3.27, and −1.30 D, respectively. The calculated dipole moment for S_0 of I is somewhat larger than the experimental value 1.0 D.[19] A similar difficulty has been met with in case of II: the calculated value is somewhat larger than the observed value 1.29 D for its 3,5-dimethyl-derivative.[20] Pariser[1] has shown that the disagreement between the theoretical and experimental values is attributable to the polarization effect of the σ-electrons. If the calculated dipole moment for S_0 of II is multiplied

by the correction factor, 1.0/2.82, which is derived from the fact that the calculated dipole moment for S_0 of I must agree with the experimental value, the dipole moment for II is predicted to be 1.09 D, in agreement with the experimental value. If the same procedure is carried out for the dipole moments of the excited states, the dipole moments for S_1 and S_2 states of molecules I and II become −1.26 and −0.94 and −1.16 and −0.46 D, respectively. Such obtained-theoretical values are in general agreement with the experimental values, except that the theoretical values of S_2 for I and II are slightly larger than the observed values. This discrepancy between the experimental moments and the theoretical moments indicates that the σ core is much more polarized in the second excited state than in the first. The methyl groups would not play any decisive role in the equilibrium structures of molecule II.[8]

Since the direction of the dipole moments of the excited states of I and II is opposite to the direction of the dipole moments of the ground states, it may be expected that in the excited states of both molecules the nucleophilic substitution occurs on the five-membered ring and the electrophilic substitution occurs on the seven-membered ring. Recently, Vink *et al.*[21] have shown that with molecule I a reaction starting from the excited state with a nucleophile leads to substitution at the same positions as an electrophilic substitution in the ground state.

One of the present authors (H. Y.) especially wishes to thank Professor T. Nakajima of Tohoku University for his fruitful discussions and to thank Professor K. Hafner of Technische Hochschule Darmstadt for the supply of 3,5-dimethylcyclopenta[*ef*]heptalene. The investigation was supported in part by a Scientific Research Grant from the Ministry of Education.

References

1) R. Pariser, *J. Chem. Phys.*, **25**, 1112 (1956).
2) N. Mataga, Y. Kaifu, and M. Koizumi, *Bull. Chem. Soc. Jpn.*, **28**, 690 (1955).
3) E. Lippert, *Z. Naturforsch.*, **A10**, 541 (1955).
4) E. G. McRae, *J. Phys. Chem.*, **61**, 562 (1957).
5) W. W. Robertson, A. D. King, Jr., and O. E. Weigang, Jr., *J. Chem. Phys.*, **35**, 464 (1961).
6) L. Onsager, *J. Am. Chem. Soc.*, **58**, 1486 (1936).
7) K. Hafner and J. Schneider, *Angew. Chem.*, **70**, 702 (1958); *Justus Liebigs Ann. Chem.*, **624**, 37 (1959).
8) M. A. Ali and C. A. Coulson, *Mol. Phys.*, **4**, 65 (1961).
9) A. Julg and P. Francois, *Theor. Chim. Acta (Berl.)*, **7**, 101 (1966).
10) H. Yamaguchi, T. Terasaka, and T. Nakajima, *Theor. Chim. Acta (Berl.)*, **18**, 255 (1970).
11) D. F. Eaton, T. R. Evans, and P. A. Leermarkers, *Mol. Photochem.*, **1**, 347 (1969).
12) H. Yamaguchi, T. Nakajima, and T. L. Kunii, *Theor. Chim. Acta (Berl.)*, **12**, 349 (1968).
13) Y. Fujimura, H. Yamaguchi, and T. Nakajima, *Bull. Chem. Soc. Jpn.*, **45**, 384 (1972).
14) J. A. Riddick and W. B. Bunger, "Organic Solvent," Vol. II, ed. by A. Weissberger, John Wiley & Sons, New York (1970).
15) R. Pariser and R. G. Parr, *J. Chem. Phys.*, **21**, 446, 767 (1953).
16) J. A. Pople, *Trans. Faraday Soc.*, **49**, 1375 (1953).
17) T. Nakajima and S. Katagiri, *Mol. Phys.*, **7**, 149 (1963).
18) N. Mataga and K. Nishimoto, *Z. Phys. Chem.*, **13**, 140 (1957).
19) G. W. Wheland and D. E. Mann, *J. Chem. Phys.*, **17**, 264 (1949).
20) K. Hafner and G. Schneider, *Justus Liebigs Ann. Chem.*, **672**, 194 (1964).
21) J. A. J. Vink, C. M. Lok, J. Cornelisse, and E. Havinga, *J. Chem. Soc., Chem. Commun.*, **1972**, 710.

Infrared Absorption Spectrum of Gaseous CF_3CO Radical; Recording on a Rapid-Scan Infrared Spectrometer

Muneteru KOZUKA and Taro ISOBE

Chemical Research Institute of Non-Aqueous Solutions, Tohoku University, Sendai 980

(Received November 27, 1975)

A rapid-scan infrared spectrometer capable of scanning the region from 5000 to 650 cm^{-1} in 200 μs was constructed and successfully applied to study CF_3CO radical produced by flash photolysis. Four absorption bands of the radical were detected at 1574, 1338, 1115, and 1024 cm^{-1} for scanning started 25 μs after the firing of a Xe flash tube. They were tentatively assigned to the CO stretching, CF_3 stretching (a species), CF_3 stretching (e species), and CC stretching vibrations, respectively.

The powerful technique of flash photolysis kinetic (UV-visible) spectroscopy, developed by Norrish and Porter[1] and Herzberg and Ramsey,[2] has been extended to the infrared spectral region by Pimentel and his collaborators.[3] They employed, for the first time, a zinc-doped germanium semiconductor detector[4] in their rapid-scan infrared spectrometer. The instrument was capable of scanning the region from 5000 to 650 cm^{-1} in several hundred micro-seconds. The scanning speed corresponded to about 100 times the speed of preceding systems developed by other workers.[5] Using this instrument, they succeeded not only in recording infrared absorption spectra of several new transient intermediates produced by flash photolysis,[3,6-8] but also in developing the first chemical laser[9] and the first photodissociation laser.[10] These new techniques have been successfully used for studying vibrational relaxation processes.[11]

Therefore, it is now possible to record vibrational spectra of tetratomic or larger transient intermediates, and consequently, to elucidate the mechanisms of many complex reactions. Nevertheless, such studies in the infrared spectral region are very few and many interesting chemical systems remain to be examined, while studies in the UV and visible regions are quite numerous.

The present authors constructed a rather conventional rapid-scan infrared spectrometer and succeeded in detecting CF_3CO radical produced by the flash photolysis of CF_3COI. It is hoped that this instrument will be successively improved by introducing the various new techniques developed in recent years.

Experimental

Materials. NH_3, $COCl_2$, and CO_2 gases were obtained commercially and purified by trap-to-trap distillations. CF_3COI (bp 7 °C) was prepared by a reaction of CF_3COBr (bp 2 °C) with KI. CF_3COBr was obtained by a reaction of CF_3COOH and PBr_3. Immediately before recording the spectra, CF_3COI was decolorized with Cu powder and distilled to eliminate the I_2 released.

Instrument. The instrument consists of a monochromator with a high-speed rotating Littrow mirror, a copper-doped germanium detector (Fujitsu Corp.), a Globar source, a 40-cm quartz gas cell, photolysis flash circuitry and a time base pulse control circuit.

The spectrometer optical path is shown in Fig. 1. In order to protect the detector from the discharge noise of the Xe flash tube, the optical bench of the detector and monochromator sections is separated from that of the Globar source and sample cell sections. This also facilitates the exchange of the light source unit and the sample cell. The collimator mirror, M_8, is an off-axis paraboloidal mirror 60 mm in diameter and with a 280-mm focal length. The rotating Littrow mirror which is made of glass in the form of a tetragonal prism (JASCO Corp.), is used for rapid scanning of the wavelength. Each of the four faces is 50 mm high and 60 mm wide; the face-to-face angles and the face-to-shaft angle are accurate to 6″ and 10″, respectively. The reflecting surfaces are aluminized. The mirror housing is installed on the spectrometer table, while, in order to reduce mechanical vibration, the drive motor (Matsushita Denki Corp., Model SCD-W 150) is set on an independent frame, and both are connected by means of a slender rubber tube (10 mm o.d., 8 mm i.d. and 30 mm long). Rotation at 3000 min^{-1} produces a slight mechanical vibration of the spectrometer table, while rotation at 6000 min^{-1} is well balanced on a frame for adjustment. The mirror scans the 4000—650 cm^{-1} region with a rotation of about 3.3°, so that a speed of 2750 min^{-1} permits the region to be scanned in about 200 μs.

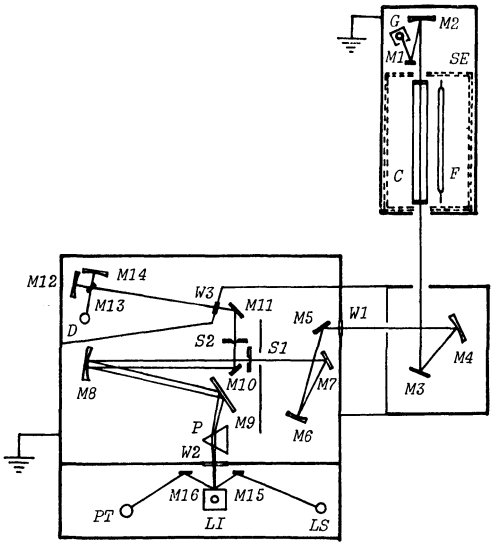

Fig. 1. Optical layout of rapid-scan infrared spectrometer. G: Globar source; SE: electro-magnetic shield; F: Xe flash tube; C: 40 cm quartz gas cell; W_1, W_2, and W_3: NaCl Windows; S_1: entrance slit; S_2: exit slit; P: NaCl prism; M_1, M_3, M_5, M_7, M_{10}, M_{11}, M_{13}, M_{15}, and M_{16}: planar mirrors; M_2, M_4, and M_{12}: spherical mirrors; M_6: troid; M_8: off-axis paraboloid; M_{14}: paraboloid; LI: littrow mirror (tetragonal prism); LS: trigger source (tungsten bulb); PT: phototransistor (OS-14). The light path length from the source to the detector is 4.4 m.

A copper-doped germanium crystal was chosen as the detector on the basis of three criteria: response time, sensitivity, and frequency range. The size is $2.5\times5.0\times6.0$ mm. One of the faces of area 5.0×6.0 mm is soldered onto a copper cooling holder in specially-designed helium cryostat,[12] using indium and Wood's metal (mp 75 °C). A detector temperature of 4 K was routinely maintained using 1.1 l of liquid helium at reduced pressure (15 mmHg) for 8 h. The temperature was measured with a gold-doped germanium resistor, Cryo Resistor Model CR-1000 (Cryo Cal. Inc.). The background radiation was minimized with a silver film shield maintained at 4 K, an outer copper-plate shield at 77 K, and a KBr plate filter at 77 K. The detector element is visible from the room temperature side through an angle of about 35°. The measured response time was less than 0.05 μs,[13] the detectivity D* (500 K, 1800) 3×10^{10} cm·$Hz^{1/2}\cdot W^{-1}$,[13] the dark resistance 160 kΩ at DC bias current of 50 μA, and the sensitive frequency range approximately 6000—350 cm^{-1}, with maximum sensitivity at about 500 cm^{-1}. The detector leads pass through insulated feed throughs to a small circuit board mounted on the outer wall of the cryostat. This circuit, designed to minimize lead capacitance, contains a power supply (22.5 V dry-cell battery), and a load resistor (100 kΩ carbon-deposited resistor). The signal is fed to a Keithley 102-B wide band preamplifier (2—1.7×10^6 Hz and 0.5—150×10^3 Hz bandpasses available), and then to a synchroscope (Iwasaki Tsushinki Corp., Model SS-5102) equipped with a *Multi-Trace* preamplifier plug-in unit (Iwasaki Tsushinki Corp., Model SP-05M-B). The detector system is shilded with copper and mu-metal screens in order to reduce the discharge noise.

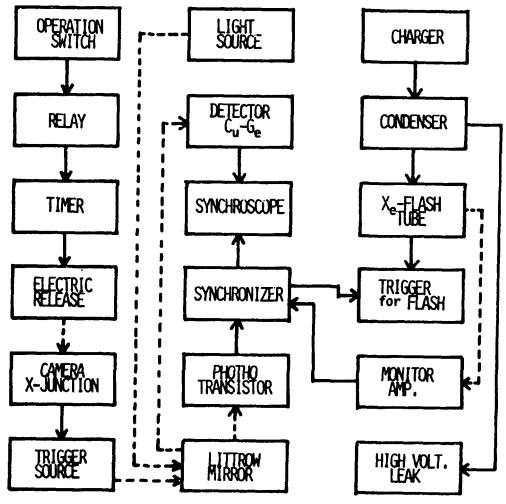

Fig. 2. Block diagram of whole electric system. Real and dotted lines denote electric and optical connections, respectively.

The flash photolysis lamp is a 10 i.d. × 440 mm quartz tube with concentric tungsten electrodes 2 mm in diameter. The lamp is filled with Xe to a pressure of 25 mmHg. The unit is capable of dissipating 600 J in about 20 μs. This energy is supplied by six 8.0 μF condensers charged to 5 kV.

A block diagram of the entire electrical system is shown in Fig. 2. Operation on a micro-second time scale raises special synchronization and recording problem. Firstly, the flash photolysis lamp must be fired, and, after a 25-μs delay for detector recovery, the Littrow mirror must be at the correct angular position to begin the spectral scan. During the next 200 μs, the voltage trace must be recorded. This is accomplished with the specially-designed time-base pulse-control

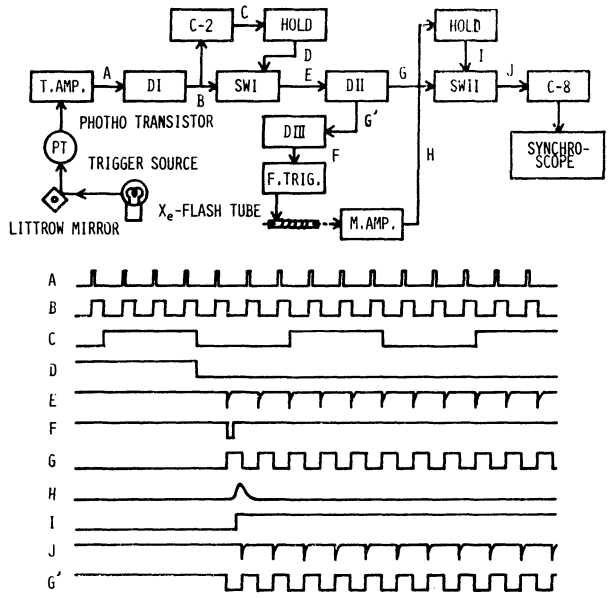

Fig. 3. Block diagram of time base pulse control system (synchronizer) and its timing chart. T. Amp.: amplifier for trigger pulse, F. Trig.: trigger for flash, M. Amp.: monitor amplifier.

circuit, *Synchronizer*, shown in Fig. 3. When the *Operation Switch* (in Fig. 2) is turned on, the *Electrical Release*, which is made of a speaker magnet coil, pushes the shutter of the camera. The *Trigger Source* bulb connected to the *X-junction* of the camera is lightes. The light beam is reflected by the rotating Littrow mirror and focused onto a silicon phototransistor (OS-14) which produces a pulse each time the mirror passes a given rotational position. The resulting pulse train is amplified, and fed to the *Synchronizer* circuit, where it is used to trigger the synchroscope and the Xe flash tube (point A in Fig. 3). Here, the infrared light and the light for the triggering pulse reflect on the same face of the Littrow mirror for synchronization. The phase relationship between the trigger pulse and the spectral wave length can be adjusted by changing the positions of the phototransistor and the bulb, or alternatively, by changing the delay time in the first delay circuit, DI, in Fig. 3 (point B). In order to obtain stable operation, the first three pulses (point A in Fig. 3) are discarded with the counter circuit, C-2 (point C). The fourth pulse releases the HOLD circuit from clamping (point D) and the fifth passes through the first switching circuit, SWI, to the second delay circuit, DII (point E). The voltage drop in one of the DII collectors (point G') forces the third delay circuit, DIII, to generate a delayed pulse (point F), and the voltage rise of the pulse, in turn, induces a 2 μF condenser (in *Trigger for Flash* circuit in Fig. 2) to discharge through a thyratron (Toshiba Corp., 1G50A). A fly-back transformer (Chuo Musen Corp., TV-304 CD 3) connected to the thyratron generates a trigger pulse of about 20 kV which fires the charged Xe flash tube. A portion of the flash light is fed to a photomultiplier (Hamamatsu Televi Corp., R-252) in the *Monitor Amp.* circuit in Fig. 2. The resultant signal is amplified and used to release the second switching circuit, SW-II, from clamping (point H and I in Fig. 3). Finally, the output signal of the DII (point G) arrives at the synchroscope either *via* a counter circuit, C-8, or directly (point J). The C-8 is used to thin out some pulses in the train for the purpose of recording the spectra of fairly long-lived intermediates (life time: 0.1—1.0 s). By adjusting the delay times of DII and DIII, one can set the sweep of the synchroscope to the moment desired after the flash terminates.

Results and Discussion

Instrument Performance. Reference spectra of air, $COCl_2$ and NH_3 were recorded on the instrument equipped with an NaCl prism and a Globar source. Immediately before every run, the light source was adjusted to a white glow (1300—1600 °C), and the Littrow mirror was set to high-speed rotation (about 3000 min^{-1}). Dried N_2 gas was blown through the light path, as necessary.

The 1.7 MHz amplifier bandpass increases the noise level by a factor of 1000 over that of narrow bandpass amplifiers normally used in thermocouple spectrometers. Therefore, reducing this noise is essential to rapid-scan infrared spectroscopy. To facilitate the estimation of the absolute value of this noise in various recording conditions, the narrowest possible slit width and the highest possible gain of the detector system were used throughout the experiment. Because of the resultant low S/N, it became very difficult to quantitatively control the influence of the following factors which dominate the spectral resolution, the band shape and the band intensity: the brightness of the light source, the rotating speed of the Littrow mirror, the selection of the wavelength region, the gain of the detector system, the sweep speed of the synchroscope, *etc.* The S/N may be estimated from the ratio of the intensity to the thickness of the voltage trace. Throughout the experiment, it was 38—43 at 3000 cm^{-1} and 4—8 at 1000 cm^{-1}.

The thickness of the voltage trace was investigated using a *wave analyser* (General Radio Company Concord, USA, Type 1900-A). It was found that the thickness was due to white noise of about 100 μV and not due to any hum. The noise increased exponentially below 100 Hz. This agrees well with the noise characteristics of a CuGe detector. The Keithley 102-B preamplifier has a noise level of 20 μV in case of short-input circuit, a gain of 60 dB and a 1.7 MHz bandpass. The noise signal appears as high as 50—60 μV on the synchroscope. This would build up the 100 μV white noise along with the noise contributions due to the CuGe detector and load resistor. Besides this high frequency noise, there was a microphonic noise of 50—100 μV and of about 100 Hz, which is caused by the mechanical vibration accompaning the rotation of the Littrow mirror.

Although the time constant of the entire detector system could not be measured precisely because of the microphonic noise, it was observed that the intensity of the voltage trace at a scanning speed of 1000 min^{-1} did not decrease at speeds up to 3000 min^{-1}.

Figure 4 shows the atmospheric absorption spectrum due to ν_{OH} (3654)* and δ_{OH} (1595) of H_2O, and due to ν_{CO} (2349) of CO_2. Each of the four voltage traces corresponds to scanning by each of the four faces of the Littrow mirror. Under the conditions, it may be said that the spectral resolution is independent of the face. The microphonic noise slightly shifts the starting point of the first (lowest) sweep in Fig. 4 with respect to the starting points of the other sweeps. Wave

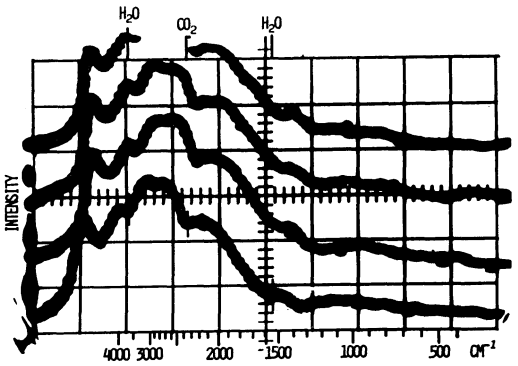

Fig. 4. Atmospheric absorptions. 150 μ slits, sweep 20 μs/div., 0.5 mV/div. The evacuated 40 cm qurtz gas cell was set in the light path.

number calibration was carried out on the basis of the absorption bands for which vertical short lines were drawn. Because the reflecting faces of the Littrow mirror are separated from the rotating axis by 25 mm, the nonlinearity in the wave number scale is emphasized, as compared with that in the case of a planar Littrow mirror. Figure 5 shows the absorption bands due to $COCl_2$. In addition to the two fundamental frequencies,

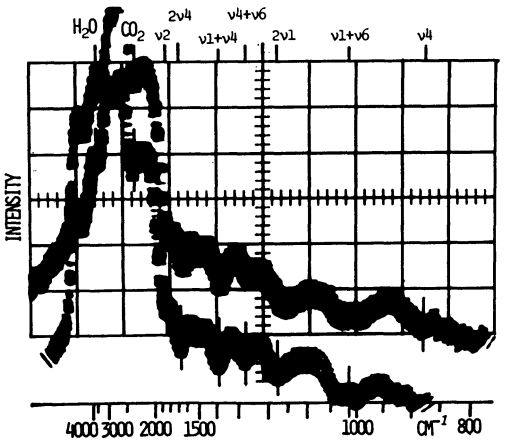

Fig. 5. Absorptions due to $COCl_2$ and atmosphere. 150 μ slits, sweep 50 μs/div., 0.2 mV/div., 40 cm gas cell, 30 mmHg $COCl_2$.

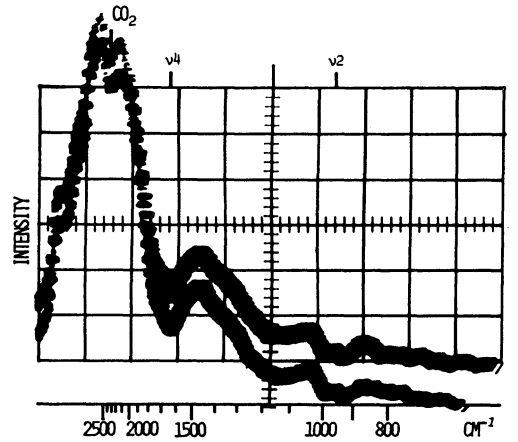

Fig. 6. Absorptions due to NH_3 and atmosphere. 300 μ slits, sweep 50 μs/div., 0.3 mV/div., 40 cm gas cell, 30 mmHg NH_3.

* Numerals in parentheses denote the wave numbers of the absorption bands.

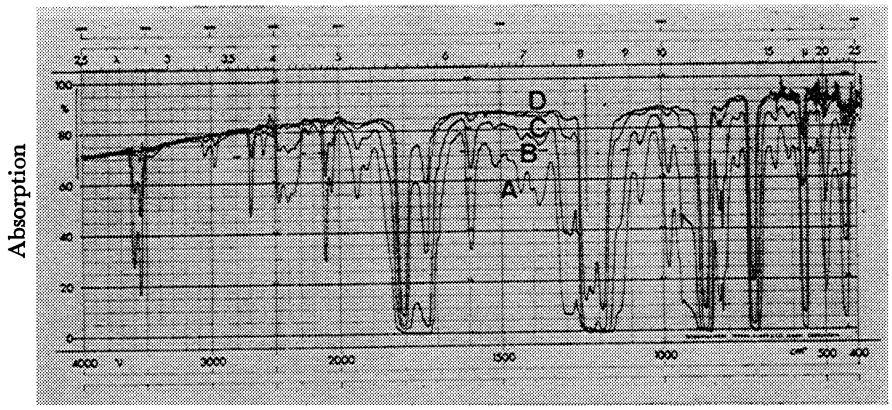

Fig. 7. Infrared spectrum of CF_3COI recorded on a Perkin-Elmer Model 125 Spectrometer with use of 10 cm gas cell: (A) 25 mmHg, (B) 15 mmHg, (C) 8 mmHg, (D) 3 mmHg.

ν_2 (1827) and ν_4 (849), five combination bands, $2\nu_4$ (1677), $\nu_1+\nu_4$ (1412), $\nu_4+\nu_6$ (1276), $2\nu_1$ (1159) and $\nu_1+\nu_6$ (1011), are recorded. Figure 6 shows the HNH deformation mode, ν_4 (1627.5), and the umbrella mode, ν_2 (931.58 and 968.08), of NH_3.[14]

From these spectra, it is seen that the instrument is quite adequate for qualitative low-resolution detection of transient intermediates with half-lives as short as 50 μs.

Application. CF_3COI was chosen as the first chemical system for exploration on the basis of the following criteria: (1) high infrared absorption coefficients of the CF and CO stretching vibrations, (2) a high photolytic yield for the breaking of the CI bond, (3) its chemical interest, and (4) an adequate vapor pressure at room temperature. Prior to the experiment, INDO calculations were carried out to estimate the minimum CC-bond distances for CF_3COF, CF_3COH, CF_3CN, and CF_3CO radicals, since sufficient information about these molecular parameters could not be obtained in other ways. The following assumptions were made: CF (in CF_3) 1.34 Å, CO 1.19 Å, CH 1.09 Å,[15] CN 1.15 Å, ∠FCF (in CF_3) 109°28′,[15] and ∠HCO 120°.[15] The calculated values were 1.50, 1.49, 1.47, and 1.42 Å, respectively. These values suggest that the CC stretching vibration in the CF_3CO radical couples strongly with the CF and CO stretching vibrations, and consequently the fundamental frequencies of the radical are fairly different from those of CF_3COI.

Since no IR spectrum of CF_3COI has yet been published, the one recorded on the Perkin-Elmer 125 spectrometer is shown in Fig. 7. Absorption bands at 1806, 1240, 1190, and 870 cm^{-1} were approximately assigned to ν_{CO}, ν_{CF_3}, $\nu_{FCF_2}(a')$, $\nu_{FCF_2}(a'')$, and ν_{CC}, respectively. When the sample pressure is high, the absorption maxima are shifted from the fundamental frequencies. This was taken into account in the wave number calibration in Fig. 8. Spectra (A), (B) and (C) in Fig. 8 were recorded on the instrument before, immediately after, and about two seconds after photolysis, respectively. ν_{CO} of CO_2 was recorded in (A), besides ν_{CO}, ν_{CF}'s, and ν_{CC} of CF_3COI. The first and the second traces are slightly shifted with respect to each other. This could also be because of microphonic noise as in the case of Fig. 4. In (B), dried N_2 gas was

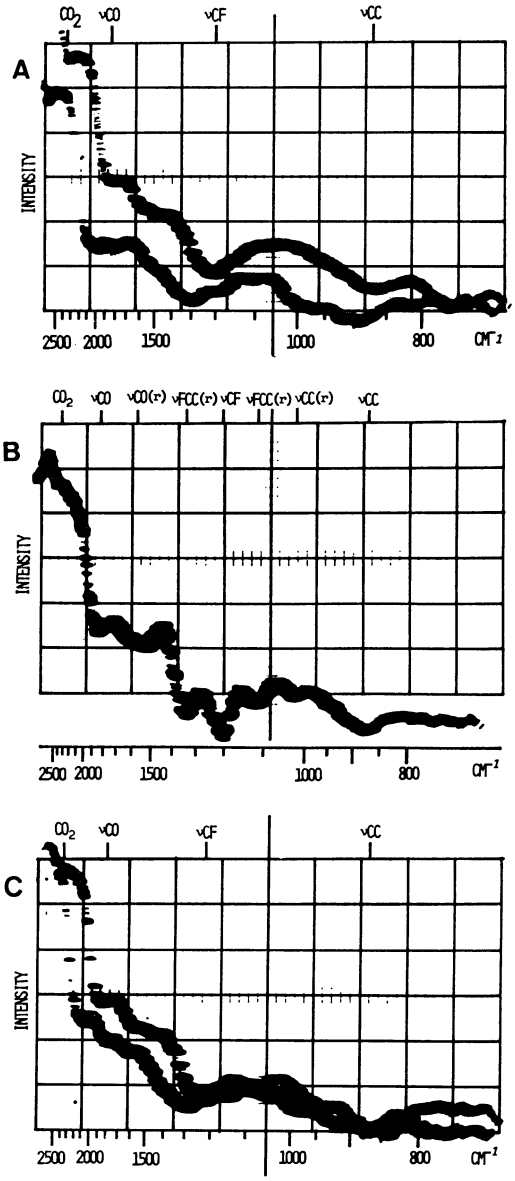

Fig. 8. Flash photolysis of CF_3COI: 200 μ slits, sweep 20 μs/div., 0.2 mV/div., 40 cm gas cell, 40 mmHg CF_3COI, N_2 700 mmHg, (A) Before Photolysis, (B) Immediately after photolysis, (r) denote radical, (C) About 2 s after photolysis.

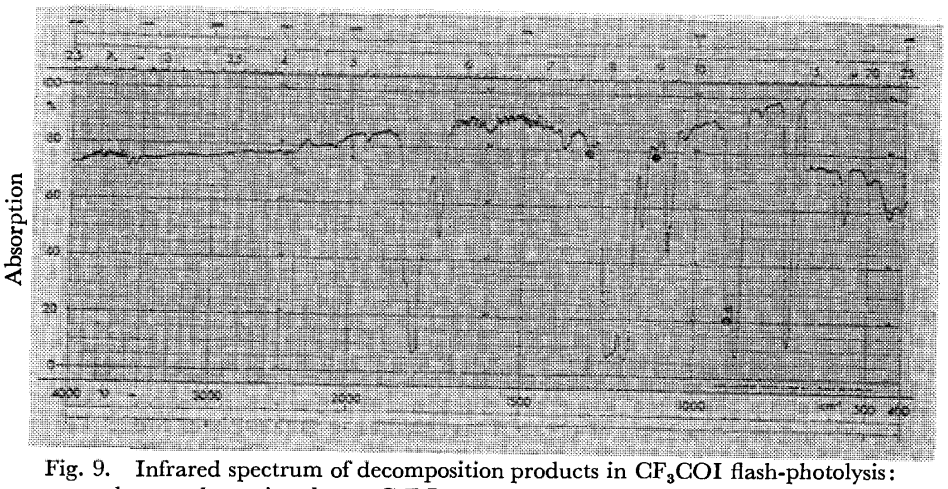

Fig. 9. Infrared spectrum of decomposition products in CF_3COI flash-photolysis:
* denote absorption due to C_2F_5I.

blown through the optical path. Spectrum (B) was swept 25 μs after trigger pulse was fed to the charged Xe flash tube. Although the *Multi Trace* unit was set to sweep twice, only one voltage trace was recorded. This could be caused by tailing of the flash noise. Prior to this experiment, it was ascertained that any single sweep, for which the *Multi Trace* unit acts only as an ordinary preamplifier, was performed normally and consistently at 25 μs after photolysis, but not at 13 μs. Therefore, the trace in (B) is undoubtedly the first sweep, but not the second (about 5 ms later). In addition to the absorption bands due to CO_2 and CF_3COI, four new absorption bands were detected at 1574, 1338, 1115 and 1024 cm^{-1}. They did not appear in (C). Their absolute intensities were difficult to estimate because of the microphonic noise, but the sensitivity of this instrument in the relevant spectral region is confirmed in Figs. 5 and 6. The CF_3CO radical population should be smaller than the $COCl_2$ and NH_3 populations, while the absorption coefficient of the radical should be larger than those of the combination bands and of the umbrella mode in the molecules. Therefore, it is thought that the data are quite adequate for qualitative discussion. The decomposition products were transfered into a 10 cm gas cell, and the infrared spectrum was recorded on a Perkin-Elmer 125 spectrometer (Fig. 9). The CF_3COI pressure decreased to one tenth of the value before photolysis. The absorption in the 1800 cm^{-1} region suggests that there is no perfluorobiacetyl, $(CF_3CO)_2$. The absorption bands at 1321, 1113, and 923 cm^{-1} should be due to C_2F_5I. In addition, there are uncondensed molecular species at liquid N_2 temperature. They are CO (2100), C_2F_6 (1113), CF_4, CF_3I, *etc.* The light intensity of the Xe flash tube has the peak in the wavelength region of 300—400 nm. The CI bond is usually ruptured by the light, but the CF, CC and CO bonds are not. All of these suggest that the photolysis produces, first, a CF_3CO radical in the electronic ground state, and then the radical decomposes into a CF_3 radical and CO, either due to room light or thermal collisions. This explanation is in good agreement with the results of Noda *et al.*[16] that the CH_3CO radical in an isolated matrix at liq. N_2 temperature is easily decomposed by visible light into a CH_3 radical and CO.

Consequently, it is concluded that the four weak and transient absorptions in Fig. 8 (B) are due to the CF_3CO radical. They were tentatively assigned to ν_{CO} (1574), ν_{CF_3} (1338, a species), ν_{CF_3} (1115, e species), and ν_{CC} (1024). They should be coupled strongly to each other.

The authors wish to thank the Ministry of Education for financial support for this study. They also wish to express their gratitude to the (late) Prof. Kozo Kamiryo, Dr. Katsuhiko Ishida, Messrs. Kiichi Sato and Setsuo Tamagawa of the Research Institute of Electrical Communication of this university, and to Messrs. Minoru Takahashi and Eijiro Yamazaki of this institute, who assigned in the construction of the liquid He cryostat. The authors also gratefully acknowledge Prof. Tsuneo Ikenoue and his collaborators of this institute for assistance in constructing the electric circuits, and the (late) Professors Susumu Kinumaki and Tetsuo Hata, Mr. Shinji Onodera and Mrs. Hamako Sato of this institute for their assistance in earlier stages of this work.

References

1) R. G. N. Norrish and G. Porter, *Nature*, **164**, 658 (1949).
2) G. Herzberg and D. A. Ramsey, *Discuss. Faraday Soc.*, **9**, 80 (1950).
3) G. C. Pimentel and K. C. Herr, *J. Chim. Phys.*, **1964**, 1509; K. C. Herr and G. C. Pimental, *Appl. Opt.*, **4**, 25 (1965).
4) M. E. Lasser, P. Cholet, and E. C. Wurst, *J. Opt. Soc. Am.*, **48**, 468 (1958); H. Levinstein, *Proc. Inst. Radio Engnrs.*, **47**, 1478 (1959); L. Johnson and H. Levinstein, *Phys. Rev.*, **117**, 1191 (1960).
5) B. W. Bullock and S. Silverman, *J. Opt. Soc. Am.*, **40**, 608 (1950); E. F. Daly, *Nature*, **166**, 1027 (1950); P. W. Wheatly, E. R. Vincent, D. L. Rotenberg, and G. R. Cowan, *J. Opt. Soc. Am.*, **41**, 665 (1951); D. A. H. Brown and V. Roberts, *J. Sci. Instr.*, **30**, 5 (1953).
6) R. J. Jensen and G. C. Pimentel, *J. Phys. Chem.*, **71**, 1803 (1967).
7) G. A. Carlson and G. C. Pimentel, *J. Chem. Phys.*, **44**, 4035 (1966).
8) L. Y. Tan, A. M. Winer, and G. C. Pimentel, *J. Chem. Phys.*, **57**, 4028 (1972).

9) J. V. V. Kasper and G. C. Pimentel, *Phys. Rev.*, **14**, 352 (1965).
10) J. V. V. Kasper and G. C. Pimentel, *Appl. Phys. Lett.*, **5**, 231 (1964).
11) R. D. Coombe and G. C. Pimentel, *J. Chem. Phys.*, **59**, 251 (1973).
12) Details will be reported elsewhere.
13) T. Yamaoka and Y. Ueda (Fujitsu Corp.), private communication.
14) H. Y. Sheng, E. F. Barker, and D. M. Dennison, *Phys. Rev.*, **60**, 786 (1941); *Sadtler* 95B.
15) R. H. Schwendeman, *Diss. Abs.*, **18**, 1645 (1958).
16) S. Noda, K. Fueki, and Z. Kuri, *J. Chem. Phys.*, **49**, 3287 (1968).

Heat of Adsorption from Solution. II. The Heat of Adsorption of Pyridine on Silica-Alumina from the Hexane Solution

Hiromitu NAONO,* Kazuko MOORI, and Tetsuo MORIMOTO

Department of Chemistry, Faculty of Science, Okayama University, Tsushima, Okayama 700

(Received December 19, 1975)

The amounts of physisorbed and chemisorbed pyridine on silica–alumina in the hexane solution were measured at 30 °C, and found to be 1.25 and 0.25 molecules/100 Å^2 respectively. The number of strong acid sites determined by Benesi's method are in good agreement with the chemisorbed molecules, which indicates that the ratio of the number of chemisorbed pyridine molecules to that of the strong acid sites on the surface of silica–alumina is equal. The adsorption calorimetry was carried out on the same system by means of a flow microcalorimeter which permits us to differentiate the heats of physisorption and chemisorption: the results showed that the heats of physisorption and chemisorption of pyridine are 11.3 ± 0.3 and 22 ± 4 kcal/mol respectively.

It is well known that silica–alumina is a typical solid acid; a number of efforts have been devoted to clarify the interaction between the silica–alumina surface and basic molecules.[1] The infrared spectroscopic studies using ammonia, butylamine, and pyridine as adsorbates have made it possible to distinguish the acid sites on silica–alumina into two types, *i.e.*, those of Brönsted and Lewis acid.[2,3] On the other hand, no exact measurements of the interaction energy between the acid surface and basic molecules have satisfactorily been carried out.[4–7]

The present work was undertaken in order to determine precisely the heat of adsorption of pyridine on silica–alumina from the hexane solution. For the calorimetric measurements, a flow microcalorimeter is used; it was found in the preceding paper to be suitable for the exact measurement of a small heat evolved in a solid–liquid system.[8] The present paper will also show the advantage of using flow calorimetry in order to differentiate the heat of the chemisorption of an adsorbate from that of the physisorption; this can be done by combining the heat of adsorption data with the chemisorbed and physisorbed amounts of the adsorbate.

Experimental

Materials. Silica–alumina powder (13 wt % alumina) presented by the Shokubaikasei Co., Ltd., was washed forty times by hot distilled water (*ca.* 80 °C) until the conductivity of the supernatant liquid was brought to a limiting value, 5×10^{-6} Ω^{-1}cm^{-1}. The powder was then dried at 100 °C in the atmosphere, and finally degassed at room temperature for 4 h at a reduced pressure of 10^{-3} Torr. The guaranteed-grade reagents of hexane, benzene, and pyridine were purified by passing them through a silica gel column. On the other hand, the guaranteed-grade reagent of butylamine and such indicators as anthraquinone, benzylideneacetophenone, 4-(phenylazo)diphenylamine, and *p*-dimethylaminoazobenzene were used without further purification.

Surface Area and Porosity of Silica–Alumina. The adsorption and desorption isotherms of nitrogen on silica–alumina were measured at −196 °C by the volumetric method. The surface area was calculated by the BET method, where the adsorbed area of a nitrogen molecule was assumed to be 16.2 Å^2. The pore volume of silica–alumina was estimated from the adsorbed amount of nitrogen at the saturated pressure. The pore-size distribution was calculated from the desorption branch of the isotherms by the method reported by Barret *et al.*, where the shape of pores was assumed to be cylindrical.[9]

Water Content of Silica–Alumina. The surface water content of silica–alumina was determined by the successive-ignition-loss method reported previously.[10]

Acidity of Silica–Alumina. The measurement of the surface acidity of silica–alumina was carried out by Benesi's method by using the indicators mentioned above.[11] Ten milliliters of a 4—12% solution of butylamine dissolved in benzene were mixed with 0.15—0.27 g of silica–alumina which had been pretreated *in vacuo* at room temperature. The mixture was shaken for 10 h at 30 °C. A few drops of a 0.1% indicator solution were then added to the mixture, and the color change of the silica–alumina was observed. The acidity was determined from the minimum amount of butylamine which did not bring about a color change.

Adsorption of Pyridine on Silica–Alumina from the Hexane Solution. The amounts of pyridine adsorbed on silica–alumina from the hexane solution were determined from the difference between the concentrations of the solution before and after the adsorption. Ten milliliters of the pyridine solution were poured into a 15 ϕ centrifugal tube with a cap, containing 0.35—0.65 g of silica–alumina. The tube was then shaken for 10 h at 30 °C. The equilibrium concentration of the pyridine was determined by means of absorption spectroscopy at the wavelength of 220 nm. In this experiment, the adsorption measurement of pyridine was carried out on the fresh and pyridine-chemisorbed surfaces. The latter surface was prepared by immersing the silica–alumina into a 0.1 M pyridine solution and by then washing the sample in a column with a sufficiently large quantity of hexane until no pyridine was detected in the hexane. The wet sample was then transferred to the centrifugal cell. After the residual hexane in the cell had been pipetted out, the pyridine solution of a known concentration was again poured into the cell. The effect of dilution due to the residual hexane was within an experimental error of adsorption (2%).

Adsorption Calorimetry of Pyridine on Silica–Alumina. A flow microcalorimeter was used for the adsorption calorimetry.[8] Silica–alumina (0.10—0.12 g) was set into the calorimeter. Hexane was forced to flow through at the flow rate of 0.21 ml/min by means of the pump. After a stable base line with no slope had been recorded, the hexane was replaced by a 0.1 M pyridine solution. A solution of the same concentration was then allowed to flow through until no heat evolved by the adsorption was detected; the temperature went

* Present address: Department of Chemistry, Faculty of Science, Kwansei Gakuin University, Uegahara, Nishinomiya 662.

down to the same level as the original base line (Fig. 6). In this stage, the adsorption equilibrium was established. In this calorimetry, the measurement was carried out at 30 °C; the two surfaces mentioned above were also used.

Results and Discussion

Characterization of Silica-Alumina Powder. Prior to the measurement of the interaction energy between the silica-alumina surface and the pyridine molecules, such properties of silica-alumina as the surface area, the pore volume, the pore-size distribution, the water content, and the surface acidity were examined.

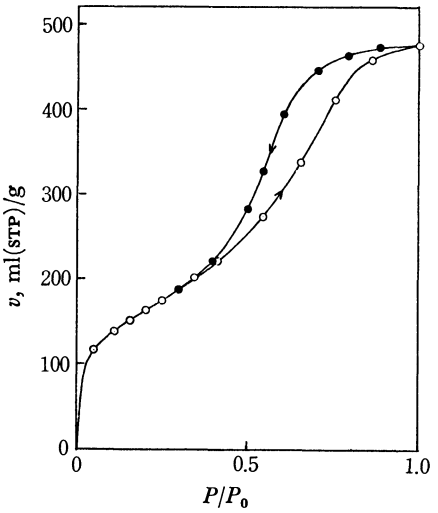

Fig. 1. Adsorption isotherm of nitrogen on silica-alumina at −196 °C. Pretreatment at 25 °C. ○: adsorption, ●: desorption.

Figure 1 shows the adsorption isotherm of nitrogen gas on silica-alumina. The facts that a distinct hysteresis appears in the isotherm and that the isotherm is of Type IV[12] reveal the sample used to be porous. From the isotherm, the BET surface area and the pore volume were estimated to be 596 m^2/g and 0.74 ml/g respectively. Assuming that the pores are cylindrical, we can calculate the average radius of the pores, $\bar{r}_p$, from the $\bar{r}_p=2v_p/S$ relation, where v_p is the pore volume, and S, the surface area. The calculated value of $\bar{r}_p$ is found to be 25 Å. The pore-size distribution curve given in Fig. 2 shows a peak at 21 Å, representing an asymmetric distribution extending to larger pores. It should be noted that most pores in silica-alumina are remarkably larger than the molecular size of butylamine or pyridine; this suggests that these molecules can easily diffuse into pores.

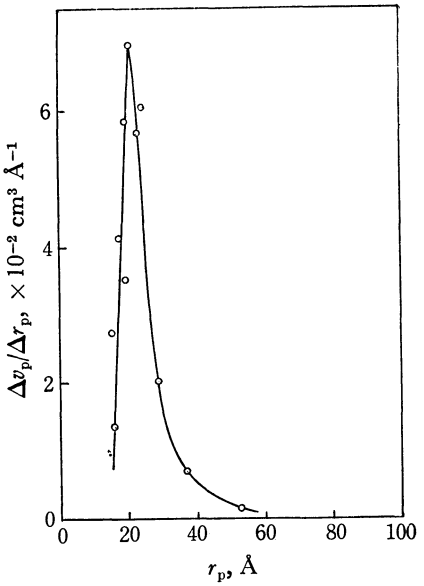

Fig. 2. Pore size distribution of silica-alumina.

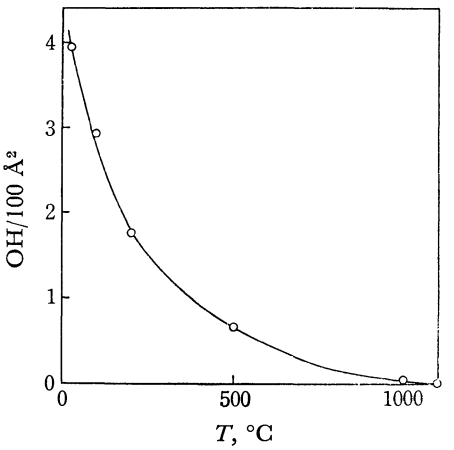

Fig. 3. Water content of silica-alumina.

In Fig. 3, the water content of silica-alumina, expressed by the number of surface hydroxyl groups per 100 Å², is given as a function of the pretreatment temperature. It may be seen from Fig. 3 that the water content of the silica-alumina used in the present experiment approximates that of pure silica,[13-15] but the dehydration behavior is greatly different from that in silica; that is, the surface water content of silica-alumina decreases rapidly with an increase in the pretreatment temperature.

In Fig. 4, the acidity is given as a function of the acid strength (H_0), expressed by the number of acid sites per 100 Å². The fact that the acidity goes nearly parallel to the abscissa leads to the conclusion that all the acid sites on silica-alumina are strongly acidic. Benesi reported a similar result for silica-alumina calcined at 550 °C.[11] On the other hand, the average

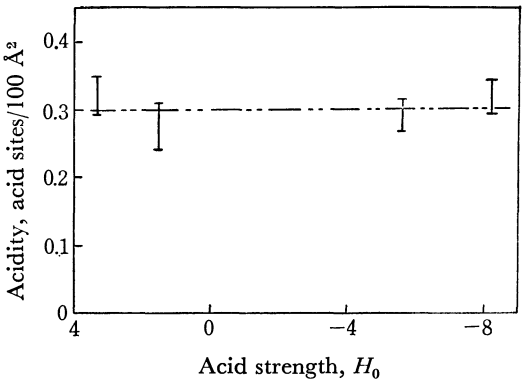

Fig. 4. Acidity *vs.* acid strength for silica-alumina.

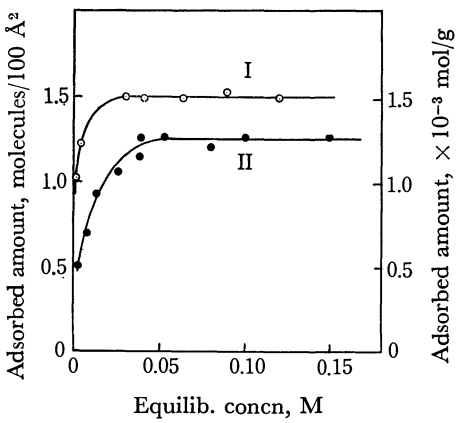

Fig. 5. Adsorption isotherm of pyridine on silica–alumina from *n*-hexane solution at 30 °C. I: fresh surface, II: pyridine-chemisorbed surface.

surface population of acid sites is only 0.3 sites/100 Å² (Fig. 4), indicating that the acid sites are very sparse on silica–alumina.

Adsorption of Pyridine on Silica–Alumina from the Hexane Solution. The adsorption isotherm of pyridine measured on silica–alumina from the hexane solution is shown in Fig. 5. Curves I and II correspond to the adsorption of pyridine on fresh and pyridine-chemisorbed surfaces of silica–alumina respectively; both curves are found to be of the Langmuir type. The difference between the two curves at saturation is read to be 0.25 molecules/100 Å² from Fig. 5, which indicates the amount of strongly adsorbed pyridine which could not be removed by washing the pyridine-preadsorbed surface with a large quantity of hexane, while the II isotherm represents the physisorption of pyridine, 1.25 molecules/100 Å² as a maximum (Fig. 5). Taking account of the magnitude of the heat of adsorption to be given later, these pyridine molecules may be considered to be chemisorbed on the surface of silica–alumina. Here, it is interesting to note that the acidity mentioned above is in fairly good agreement with the quantity of chemisorbed pyridine; this enables us to conclude that one molecule of chemisorbed pyridine interacts with one acid site.

One further question remains to be solved, whether pyridine molecules are chemisorbed on the Brönsted or Lewis acid sites. Shiba *et al.* determined both Brönsted and Lewis acid on silica-alumina as a function of the silica content.[16] On silica–alumina containing 13 wt % alumina, the amounts of Brönsted and Lewis acid were found to be *ca.* 80 and 20% respectively when treated at 500 °C. In our sample, the pretreatment temperature is 25 °C. As may be seen from Fig. 3, the water content decreases remarkably with the increase in the temperature from 25 to 500 °C. It is expected that, in the present silica–alumina, the greater part of the acid sites are of the Brönsted type, because the Brönsted acid sites increase with the water content. Thus, it may reasonably be considered that, in the present investigation, pyridine molecules react with the Brönsted sites to form pyridinium ions.[3]

Adsorption Calorimetry of Pyridine on Silica–Alumina. Figure 6 shows the response of the flow microcalorimeter to the adsorption of pyridine on silica–alumina from the hexane solution. Peaks I and II were obtained by the adsorption of pyridine on the fresh and pyridine-chemisorbed surfaces respectively. After Peak I was measured, the flowing liquid was converted from the solution to the solvent. In order to wash away the physisorbed pyridine, the solvent was forced to flow through the calorimeter for a prolonged period (15—20 h), until no pyridine was detected in the solvent flowing out of the calorimeter. Again, a pyridine solution of the same concentration was introduced into the calorimeter. Peak II was thus obtained. Pyridine molecules adsorbed on silica–alumina are composed of two part, *i.e.*, reversible and irreversible parts, as has been stated above; the corresponding heats of adsorption can be analyzed from the areas of the two peaks. As a matter of course, Peak II arises from the reversible or physical adsorption of pyridine, while Peak I should involve both kinds of adsorption. First, the reliability of adsorption calorimetry was confirmed by the measurements of twelve runs at the concentration of a 0.1 M pyridine solution; the data were calibrated by using electrical energy. The results obtained are listed in Table 1, giving the average values of 19.6 ± 0.2 and 14.1 ± 0.2 cal/g for Peaks I and II respectively.

Table 1. Calorimetric results on the pyridine adsorption on silica–alumina from 0.1 M solution at 30 °C

Run no.	Fresh surface (cal/g)	Pyridine-chemisorbed surface (cal/g)
1	18.3	13.5
2	19.0	12.6
3	19.8	14.2
4	20.2	15.7
5	20.2	14.6
6	19.6	13.7
7	18.7	12.3
8	19.9	14.9
9	20.5	15.8
10	19.8	14.3
11	18.8	13.0
12	20.1	14.4
av.	$19.5_8\pm0.2_1$	$14.0_8\pm0.2_0$

Next, on the basis of the calorimetric data (Table 1) and the adsorption isotherms (Fig. 5), the heat of adsorption of pyridine can be computed to be 11.3 ± 0.3 and 22 ± 4 kcal/mol for the physisorbed and chemisorbed pyridine respectively. In the present calorimetric measurements, the heat of dilution should be a factor in addition to the heat evolved by adsorption. The heat of dilution can be estimated from the dependence of the heat-of-mixing, ΔH_{mix}, on the concentration of the solution. The calorimetric measurement of ΔH_{mix} was carried out at 30 °C in a pyridine–hexane system by means of an adiabatic calorimeter. In the concentration range from 0.03 to 0.1 M pyridine, ΔH_{mix} was found to be 2.10 ± 0.02 kcal/mol. The fact that ΔH_{mix} is independent of the concentration indicates that the heat of dilution is less than the limits of experimental

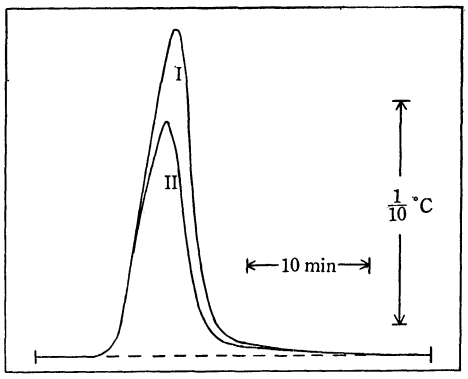

Fig. 6. Adsorption peaks of pyridine on silica–alumina from 0.1 M solution at 30 °C. I: fresh surface, II: pyridine-chemisorbed surface.

error, *i.e.*, ±0.02 kcal/mol. Accordingly, the heat of dilution is neglected compared with the heats of adsorption mentioned above.

The larger heat of chemisorption may be attributed to the strong interaction of strong Brönsted acid sites with pyridine molecules through the relation of 1: 1 between the site and molecule. In other words, the heat of chemisorption is considered to be the heat of the formation of pyridinium ions on the silica–alumina surface. On the other hand, the heat of the physisorption of pyridine is probably due to the interaction of the physisorbed molecules with possible surface sites other than the strong acid sites, *i.e.*, with surface silanol groups.

So far, several investigators have reported on the heat of adsorption in systems of basic molecules silica–alumina.[4–7] However, the direct calorimetric heats of physisorption and chemisorption in the system of pyridine–silica–alumina have not been measured. Roca *et al.* estimated indirectly the heats of physisorption and chemisorption of pyridine on silica–alumina by utilizing the adsorption isosters and the temperature-programmed desorption technique;[17] they obtained 8 kcal/mol for the heat of physisorption and 33 and 39 kcal/mol for the heat of chemisorption on two different sites. Their heat of physisorption is slightly lower than ours, while their heat of chemisorption is fairly larger than ours.

In considering the discrepancy between the two sets of data, it is necessary to compare the pretreatment conditions. In our sample degassed at 25 °C, there is a great possibility that the surface includes physisorbed water molecules, because of the remarkable decrease in water content with the temperature (Fig. 3), while in Roca's sample degassed at 400 °C, physisorbed water molecules are considered to be almost entirely removed from the surface. It may, therefore, be considered that the heat of chemisorption of pyridine may be greatly reduced by the existence of physisorbed water, while the heat of physisorption may not be influenced significantly by the existence of physisorbed water.

References

1) K. Tanabe, "Solid Acids and Bases," Kodansha, Tokyo and Academic Press, New York and London (1970), p. 58.
2) M. L. Hair, "Infrared Spectroscopy in Surface Chemistry," Marcel Dekker, Inc., New York (1967), p. 169.
3) T. Morimoto, J. Imai, and M. Nagao, *J. Phys. Chem.*, **78**, 704 (1974).
4) R. L. Richardson and S. W. Benson, *J. Phys. Chem.*, **61**, 405 (1957).
5) A. C. Zettlemoyer and J. J. Chessick, *J. Phys. Chem.*, **64**, 1131 (1960).
6) V. Kevorkian and R. O. Steiner, *J. Phys. Chem.*, **67**, 545 (1963).
7) P. L. Hsieh, *J. Catalysis*, **2**, 211 (1963).
8) T. Morimoto and H. Naono, *Bull Chem. Soc. Jpn.*, **45**, 700 (1972).
9) E. P. Barret, L. G. Joyner, and P. P. Halenda, *J. Am. Chem. Soc.*, **73**, 373 (1951).
10) T. Morimoto, K. Shiomi, and H. Tanaka, *Bull. Chem. Soc. Jpn.*, **37**, 392 (1964).
11) H. A. Benesi, *J. Phys. Chem.*, **61**, 970 (1957).
12) S. Brunauer, L. S. Deming, W. E. Deming, and E. Teller, *J. Am. Chem. Soc.*, **62**, 1723 (1940).
13) T. Morimoto, M. Nagao, and J. Imai, *Bull. Chem. Soc. Jpn.* **44**, 1282 (1971).
14) T. Morimoto and H. Naono, *Bull Chem. Soc. Jpn.*, **46**, 2000 (1973).
15) H. Naono, T. Kadota, and T. Morimoto, *Bull. Chem. Soc. Jpn.*, **48**, 1123 (1975).
16) T. Shiba, M. Sato, H. Hattori, and K. Yoshida, *Shokubai (Tokyo)*, **6**, 80 (1964).
17) F. F. Roca, P. Renard, L. de Mourgues, and Y. Trambouze, *J. Chim. Phys. Physicochim. Biol.*, **65**, 1555 (1968).

^{13}C-NMR Study of Aerosol OT in Chloroform

Masaharu UENO, Hiroshi KISHIMOTO, and Yoshimasa KYOGOKU*

Faculty of Pharmaceutical Sciences, Nagoya City University, Tanabe-dori, Mizuho-ku, Nagoya 467

**Institute for Protein Research, Osaka University, Suita, Osaka 565*

(Received December 24, 1975)

The dynamic structure of Aerosol OT molecules in micellar state was studied by measurements of ^{13}C-NMR spin-lattice relaxation time (T_1) and the effect of a lantanide shift reagent Yb(fod)$_3$ in chloroform at 25 MHz and 40 °C. The results were analyzed on the basis of the conformation and segmental motions of Aerosol OT molecules in micellar state, with the following conclusions: Aerosol OT molecules in the micellar state associate with each other by the polar head groups; their hydrocarbon chains are flexible; the mobility of side chain is restricted to a greater extent than that of the main chain; carbonyl carbon-(2′) is located nearer to the polar group than carbon-(2) in steric conformation.

Studies on the state of surface active agents in solution are of interest from a biological viewpoint, since the amphiphilic behavior of surface active agents such as micelle formation and hydrophobic interaction can also be observed in biological systems. As a suitable substance for the study, Aerosol OT was chosen and thermodynamical studies were carried out on its solution state in water[1] or in organic solvents[2] and also its two-phase distribution between water and an organic solvent.[3] Spectroscopic studies, however, are necessary for more extensive and detailed information.

Recently, solution states of surface active agents in water or organic solvents have been studied by means of NMR.[4] The dynamic structure of molecules have been studied in the last few years, since the use of Fourier transform NMR made the measurement of relaxation time practicable. Clifford and Pethica studied the properties of micellar solutions of sodium alkyl sulfates in D_2O by ^{1}H-NMR T_1 measurement.[5] Henriksson and Ödberg studied the micellar structure of heptafluorobutyric acid and sodium pentadecafluorooctanoate in H_2O and D_2O by ^{19}F-NMR T_1 measurement.[6] Podo *et al.* studied the dynamical structure and hydration of micelle by ^{1}H-NMR T_1 measurement.[7] However, the study of local mobility or segmental motions by means of ^{1}H- or ^{19}F-NMR is difficult because of the overlap of proton signals and the simplicity of the ^{19}F signal. For this study, ^{13}C-NMR would be most useful. Williams *et al.* and Levy *et al.* studied the local mobility of surface active agents in water and several organic solvents by ^{13}C-NMR.[8,9] We have applied it to the study of Aerosol OT molecules in the micellar state in chloroform.

Experimental

Materials. Aerosol OT (sodium 1,2-bis(2-ethylhexyloxycarbonyl)ethane-1-sulfonate, American Cyanamid Co., Ltd.) was used. The anhydrous material is claimed to be 99% pure and to contain about 1% of methanol insoluble impurity. The procedure by Higuchi and Misra[10] was used for purification. The solvents used were as follows: chloroform was distilled twice; chloroform-d_1 (Merck Co., Ltd.) was dried by passing through an alumina gel column. Yb(fod)$_3$ (tris(6,6,7,7,8,8,8-heptafluoro-2,2-dimethyl-3,5-octanedionato) ytterbium, Nagoya Katayama Kagaku-Kogyo KK).

Methods. ^{13}C nuclear magnetic resonace spectra were recorded on a JEOL-PFT-100 pulse Fourier transform NMR spectrometer at 25 MHz locked on deuterium using 10-mm sample tubes. Chemical shift, δ, was measured relative to tetramethyl silane used as an internal standard by data reduction. For ordinary FT NMR experiments (proton decoupled), pulse angle: 45°, repetition: 2.0 s, data point: 8192, frequency range: 6250 Hz, numbers of scans: 400 (time domain accumulation). For T_1 measurements (proton decoupled), pulse angle: 180°-τ-90°, repetition: 20.0 s, data point: 8192, frequency range: 6250 Hz, numbers of scans: 400. For off resonance experiment, pulse angle: 45°, repetition: 3.0 s, data point: 4096, frequency range: 1000 Hz, numbers of scans: 5000.

Vapor pressure depressions were measured with a molecular weight apparatus (Hitachi Perkin-Elmer Type 115) based on a thermister method.[11]

Results and Discussion

Vapor Pressure Depression Measurement. Vapor pressure depressions of the solvent were measured for the determination of CMC (critical micelle concentration) and association number of Aerosol OT in chloroform. The thermister bridge reading, ΔR, is plotted against solute concentration (molality) in Fig. 1. Open circles correspond to Benzil as a standard substance and solid circles to Aerosol OT. The insert shows the result of measurement in low concentration. The arrow indicates CMC, 4×10^{-4} M (mol kg^{-1}). By comparison of the slopes of the two straight lines for Benzil and for Aerosol OT, the number average association number was calculated to be 5.

^{13}C-NMR Spectra. ^{13}C-NMR spectra were measured for a solution at 2×10^{-1} M. We see from the results that a large part of Aerosol OT at this concentration is in a micellar state. Spectrum (a) was taken under ^{1}H noise decoupling conditions and spectrum (b) under ^{1}H partial decoupling conditions. Spectrum (c) shows the effect of the addition of a shift reagent and spectrum (d) that of 2-ethyl-1-hexanol whose signals were already assigned.[12] Almost all the signals in spectrum (a) were assigned to each carbon with reference to spectra (b), (c) and (d). Two peaks of carbonyl carbons at lower fields, however, could not be assigned to either C(2) or C(2′) from only the above reference. We took, therefore, the off resonance spectrum. If the two protons of methylene(1′) are assumed to be magnetically equivalent, it is expected

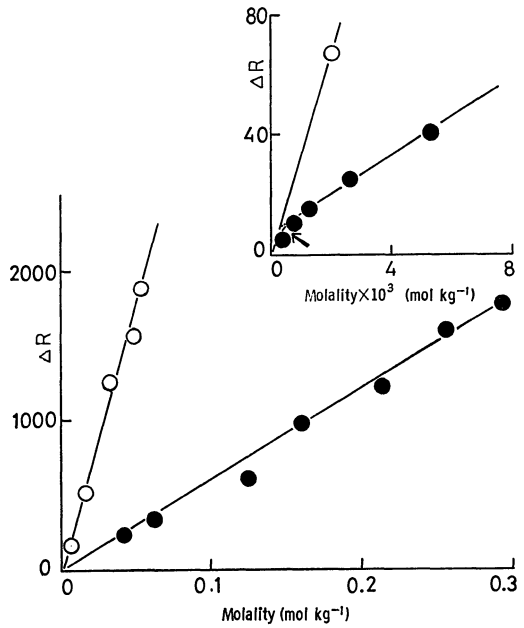

Fig. 1. Thermister bridge reading (ΔR) *vs.* solute concentration in $CDCl_3$.
●: Aerosol OT as solute, ○: Benzil as solute.
The figure inserted in upper right is the result of measurements in dilute concentration. The arrow in the figure indicates CMC.

that under the off resonance conditions the peak of C(2) is split into two peaks by the one proton of methine (1), and that of C(2′) into three peaks by the two protons of methylene (1′). As shown in Fig. 3, the lower-field signal of the two is split into two peaks and is assignable to C(2), while the higher-field signal is split into three peaks and assignable to C(2′). The two methylene carbons (3) and (3′) (Fig. 2-a) also exist in magnetic nonequivalence. However, it is difficult to assign the two signals. It was tentatively assumed that the peak at the lower-field is assigned to C(3) and that at the higher-field to C(3′), by taking into consideration the fact that the carbonyl-carbon peak near a polar group such as ($-SO_3^-$) appears at lower field.

The Influence of a Shift Reagent. The influence of a lantanide shift reagent, $Yb(fod)_3$, on the spectra was examined. Figure 2-(c) shows the spectrum of Aerosol OT on addition of $Yb(fod)_3$ at 0.1 mole ratio. Some peaks become broader and are shifted down field. The chemical shift is plotted against the ratio (La)/(AOT), the molal concentration ratio of lantanide shift reagent to Aerosol OT, in Fig. 6. The $Yb(fod)_3$-induced shift increases in the order of carbons-(2′>1>1′>2>3>3′). For the carbons-(4,4′, 5,5′, 6,6′, 7,7′, 8,8′, 9,9′, 10,10′), no induced shifts were observed. It is probable that the shift reagent coordinates to the polar group, and that carbons nearer the polar group in a spacial distance are more influenced by the shift reagent. It might be

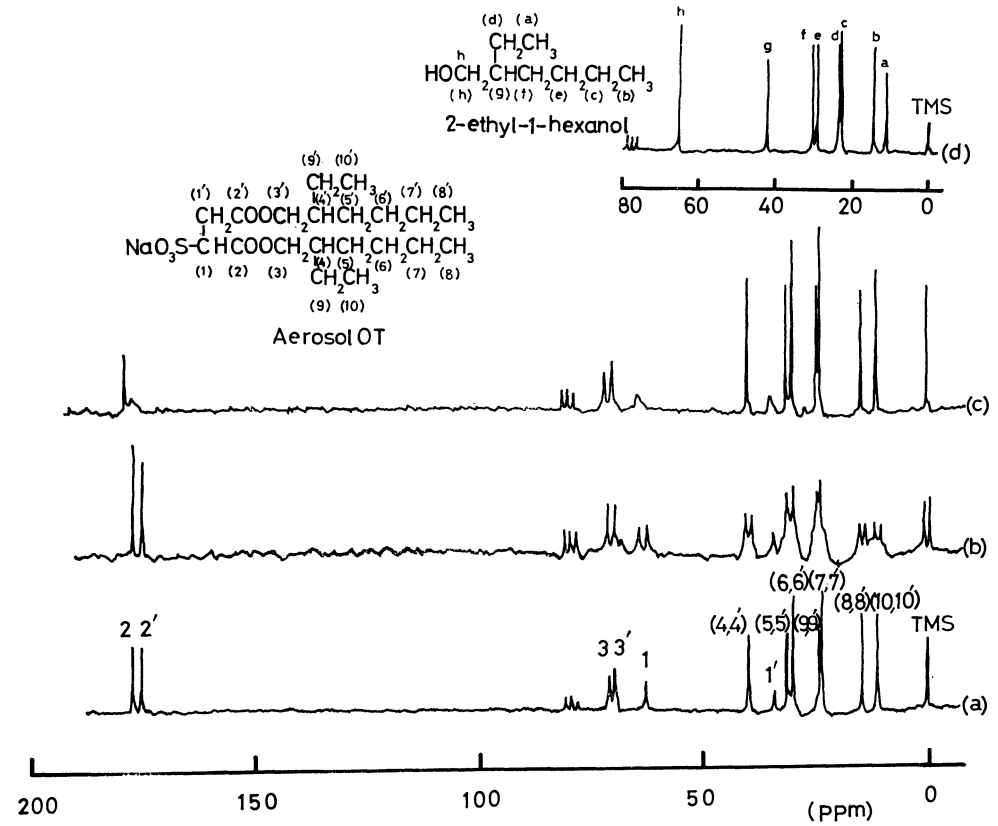

Fig. 2. Natural-abundance carbon-13 NMR spectra.
(a): Proton noise decoupled spectrum of 0.2 M Aerosol OT in $CDCl_3$.
(b): Proton partially decoupled spectrum of 0.2 M Aerosol OT in $CDCl_3$.
(c): Proton noise decoupled spectrum of 0.2 M Aerosol OT in the addition of $Yb(fod)_3$ at 0.1 mole ratio.
(d): Proton noise decoupled spectrum of 2-ethyl-1-hexanol.

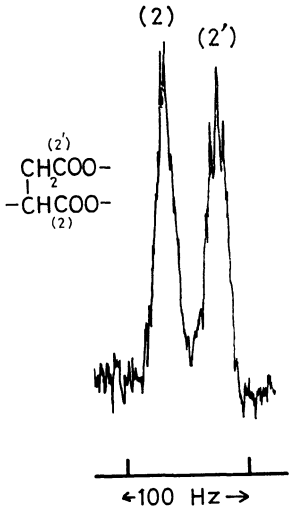

Fig. 3. Two carbonyl carbon signals at the condition of the off resonance.

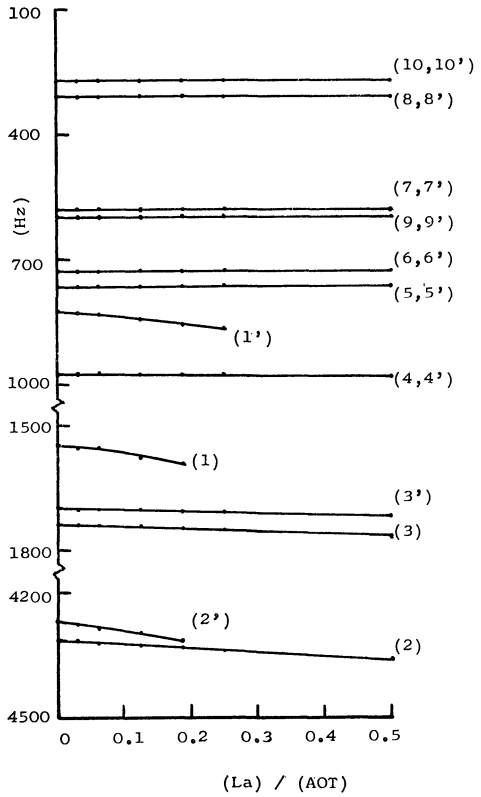

Fig. 4. The chemical shift (Hz) relative to TMS *vs.* the ratio of (La)/(AOT) (the mole ratio of lantanide shift reagent to Aerosol OT).

presumed that carbonyl carbon-(2') is located nearer the polar group in spacial distance than carbonyl carbon-(2) in spite of the longer distance through chemical bonds. On the contrary, methylene C(3) is nearer to the polar group than C(3'), as expected from the chemical sequence. Carbon-(4,4', 5,5', 6,6', 7,7', 8,8', 9,9', 10,10') are far from the polar group.

T_1 *Measurement.* Spin-lattice relaxation time T_1 was measured by the 180°-τ-90° pulse sequence method. The sample was dissolved in chloroform-d_1, and the

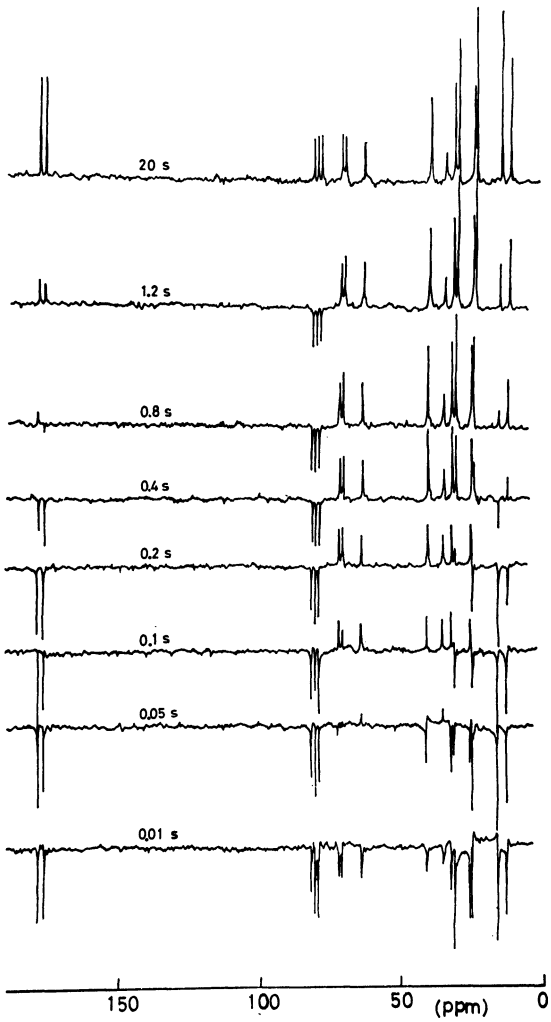

Fig. 5. Proton noise decoupled natural-abundance carbon-13 partially relaxed Fourier transform NMR spectra of 0.4 M Aerosol OT in $CDCl_3$ at 25 MHz and 40 °C. The time in seconds over each spectrum is τ, the interval between the 180° pulse and 90° pulse.

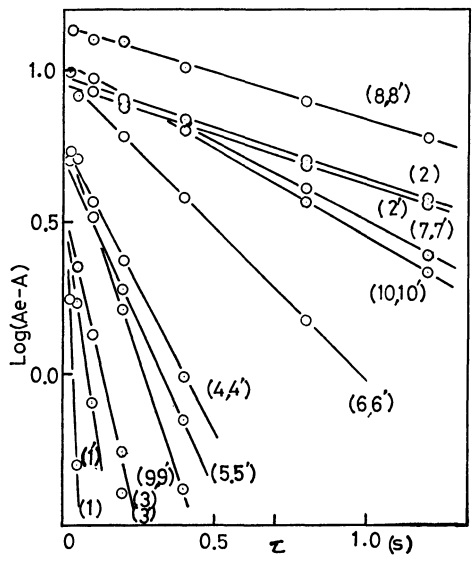

Fig. 6. $\mathrm{Log}(A_e - A)$ *vs.* interval τ, where A is the relative peak intensity and A_e is the limited peak intensity when interval τ is long enough.

Table 1. Spin-lattice relaxation time (T_1) and (NT_1) of the ^{13}C nuclei and ^{13}C chemical shift relative to TMS

		T_1(s)	NT_1(s)	δ(ppm)
C=O	(2)	1.39		171.6
	(2′)	1.51		169.7
CH	(1)	0.10	0.10	61.3
	(4,4′)	0.23	0.23	38.6
CH_2	(3)	0.08	0.16	68.5
	(3′)	0.08	0.16	67.5
	(1′)	0.05	0.10	33.1
	(5,5′)	0.21	0.42	30.3
	(6,6′)	0.42	0.84	28.9
	(9,9′)	0.15	0.30	23.5
	(7,7′)	0.85	1.70	23.0
CH_3	(8,8′)	1.39	4.17	14.1
	(10,10′)	1.02	3.06	10.8

* N: The number of protons attached to carbon.

solution was degassed. The concentration was 200 mg/ml, which is sufficiently high to neglect the existence of monomer. Repetition time was 20 s and the peaks were accumulated 400 times in time domain. The results are shown in Fig. 5. In the pulse sequence method, the relative peak intensity A is given by

$$A = A_e(1-2\exp(-\tau/T_1))$$

where τ is the interval between the 180° and 90° pulses and A_e is the limited peak intensity when interval τ is long enough (20 s). In Fig. 6, log (A_e-A) are plotted against τ. T_1 can be calculated from the slopes. The results are given in Table 1 with the corresponding chemical-shift values. The estimated errors in the T_1 measurement were within 10%. We found that when the relaxation was caused by magnetic dipole interaction, most of it was affected by the protons bonded directly to carbon. The relaxation becomes faster with an increase in the number of attached protons. In order to correlate relaxation time to segmental motion, the number of the proton time T_1, *i.e.*, NT_1, is more useful than T_1 itself.

With respect to the main chains, T_1 of carbons gradually becomes greater as they become located far from the polar group ($-SO_3Na$). This implies that segmental mobility increases as the segment becomes located farther from the polar group of the molecule in the miecllar state in chloroform. This is in line with the fact that Aerosol OT in chloroform forms reverse micelles with the aid of dipole interaction among intermolecular polar groups, the hydrocarbon parts far from the micellar core moving freely. This is interesting when compared with the behavior of micelle in water. The relaxation times of main and side chains were compared with each other. T_1 of C(8) is greater than that of C(10), the same relation holding for C(5) and C(9). This indicates that the side chains are restricted in mobility to a greater extent than the main chains in micellar state. It is concluded that (1) Aerosol OT molecules in the micellar state associate with each other by the polar head groups, hydrocarbon chains being flexible, (2) the mobility of side chains is more restricted than that of the main chain, and (3) carbonyl carbon-(2′) is located nearer in spacial distance to the polar group than carbonyl carbon-(2).

References

1) M. Ueno and H. Kishimoto, *Yakugaku Zasshi*, **94**, 724 (1974).
2) H. Kishimoto and M. Ueno, *Yakugaku Zasshi*, **94**, 1408 (1974).
3) Y. Sato, M. Ueno, and H. Kishimoto, *Yakugaku Zasshi*, **95**, 1286 (1975).
4) a) H. Inoue and T. Nakagawa, *J. Phys. Chem.*, **70**, 1108 (1966); b) S. G. Frank, Y. H. Shaw, and N. C. Li, *ibid.* **77**, 238 (1973); c) N. Muller and H. Simsohn *ibid.*, **75**, 942 (1971); d) J. C. Eriksson and G. Gillberg, *Acta Chem. Scand.*, **17**, 1478 (1963); e) R. E. Atkinson, G. E. Clint, and T. Walker, *J. Colloid Sci.*, **46**, 32 (1974); f) O. A. El Seoud, E. J. Fendler, J. H. Fendler, and R. T. Medary, *J. Phys., Chem.*, **77**, 1876 (1973); g) References cited there in.
5) a) J. Clifford and B. A. Pethica, *Trans. Faraday Soc.*, **60**, 1483 (1964); b) J. Clifford and B. A. Pethica, *ibid.*, **61**, 182 (1965); c) J. Clifford, *ibid.*, **61**, 1276 (1965).
6) U. Henriksson and L. Ödberg, *J Colloid Sci.*, **46**, 212 (1974).
7) F. Podo, A. Ray, and G. Némethy, *J. Am. Chem. Soc.*, **95**, 6164 (1973).
8) E. Williams, B. Sears, A. Allerhand, and E. H. Cordes, *J. Am. Chem. Soc.*, **95**, 4871 (1973).
9) G. C. Levy, R. A. Komoroski, and J. A. Halstead, *J. Am. Chem. Soc.*, **96**, 5456 (1974).
10) W. I. Higuchi and J. Misra, *J. Pharm. Sci.*, **51**, 455 (1962).
11) A. P. Brady, H. Huff, and J. W. Mcbain, *J. Phys. Colloid Chem.*, **55**, 311 (1951).
12) L. F. Johnson and W. C. Jankowski, "Carbon-13 NMR Spectra," John Wiley and Sons, Inc. (1972), p. 322.

Chemisorption of Nitrogen Oxide and Nitrogen on Tungsten

Teijiro TAMURA and Takuya HAMAMURA

Department of Chemistry, Faculty of Industrial Arts, Kyoto Technical University, Matsugasaki, Sakyo-ku, Kyoto 606

(Received December 25, 1975)

The chemisorption of nitrogen oxide and nitrogen on a polycrystalline tungsten filament was studied using flash desorption mass spectroscopy. The saturation coverage for nitrogen oxide and nitrogen on tungsten is 8.8×10^{14} molecules/cm^2 and 1.9×10^{14} molecules/cm^2, respectively. These saturation coverages on tungsten are about 1.7 times those on rhenium. The initial sticking probability of nitrogen oxide is very high compared with other gases. It is assumed that the nitrogen oxide adsorption is non-dissociative on tungsten, while the nitrogen is adsorbed dissociatively. When the temperature of the tungsten filament saturated with nitrogen oxide is raised, a small amount of nitrogen oxide molecules desorb at about 475 K, and dissociation occurs at more elevated temperatures. The greater part of the nitrogen desorbs before the temperature reaches 1500 K. No oxygen desorption was detected upon heating the tungsten saturated with nitrogen oxide. It appears that oxygen probably desorbs as tungsten oxide. Three states of nitrogen desorption, designated α, β_1, and β_2, on tungsten appeared at room temperature. The activation energy of the desorption for the strongly chemisorbed nitrogen of the β_1 and β_2 states on tungsten are 78 kcal/mol and 80.5 kcal/mol, respectively.

Fundamental to the understanding of heterogeneous reactions, such as catalytic reactions, is the determination of the role of the surface and the dependence of the reaction variables on the properties of the solid. Recently, detailed data of chemisorption studies have been presented taking advantage of the progress of ultra-high vacuum techniques and the development of modern methods,[1-5] such as the use of flash filaments, isotopic mixing, FEM, FIM, LEED and AES.

Many studies of chemisorption of common gases on tungsten have been made, but there have been only a few studies of the chemisorption of nitrogen oxide.[6-9]

In the present investigation, the chemisorption of nitrogen oxide and nitrogen on a tungsten filament was studied using flash desorption mass spectroscopy.

Experimental

The ultra-high vacuum apparatus used in this study is similar to that used in previous work[10,11] except that the reaction vessel with a volume of 1.0 l contained a polycrystalline tungsten filament with a geometrical surface area of 1.26 cm^2. The tungsten filament was analyzed spectroscopically. (Found: Mo, 0.08%; Mg, 0.004%)

The total pressure was measured by means of a Pirani gauge with a sensitivity of 7.2×10^{-8} Torr/μV for N_2 and NO, and 7.5×10^{-8} Torr/μV for O_2. An omegatron mass spectrometer was used for analyzing the gaseous component and for measuring the partial pressure in the reaction vessel; it has a sensitivity of 12 Torr^{-1} and 11.8 Torr^{-1} for N_2 and NO, respectively. A B-A gauge was used only for the ultimate-pressure measurement, because the nitrogen oxide was dissociated by the hot filament of the gauge.

The temperature of the tungsten filament was measured by the same method as that reported in a previous paper.[10] The nitrogen oxide and nitrogen were also prepared by the method described in that paper, and no impurities up to mass 200 were detected by means of the omegatron mass spectrometer.

The ultimate pressure, read on a B-A gauge, was 3×10^{-10} Torr in the reaction system after rigorous outgassing. Before the experiment, the tungsten filament was heated to 2200 K in an oxygen atmosphere of about 1×10^{-6} Torr for a long time, in order to remove carbonaceous surface contamination.

The procedure used for the present experiments are also similar to that previously described.[10] The number of molecules of nitrogen oxide or nitrogen that strike the tungsten filament during the adsorption process is calculated from the recorder trace of the omegatron or the Pirani gauge. The amount of adsorbed molecules is calculated from the pressure and the volume of the reaction vessel when the filament is flashed at 2200 K in the closed system. In the case of the adsorption of nitrogen oxide, the number of molecules adsorbed is twice the number of molecules desorbed, because the desorbed gas is nitrogen.

After the adsorbed layers were formed, the temperature of the tungsten filament was raised slowly with an approximately linear sweep rate while the system was being evacuated. During that period, the ion currents of the omegatron mass spectrometer for each mass were recorded on a chart recorder.

Results and Discussion

Sticking Probability and the Amount of Adsorbed Nitrogen Oxide and Nitrogen on Tungsten. The relation between the number of molecules impinging on the filament, $N_{(e)}$(exposure), at various temperatures and those adsorbed, N, is shown in Fig. 1. The saturation coverage for nitrogen oxide is 8.8×10^{14} molecules/cm^2 at 300 K, which is much higher in comparison with that on rhenium. For adsorption on a tungsten filament at elevated temperatures, the saturation coverage of nitrogen oxide decreases as shown in Fig. 1. There are 8.2×10^{14} and

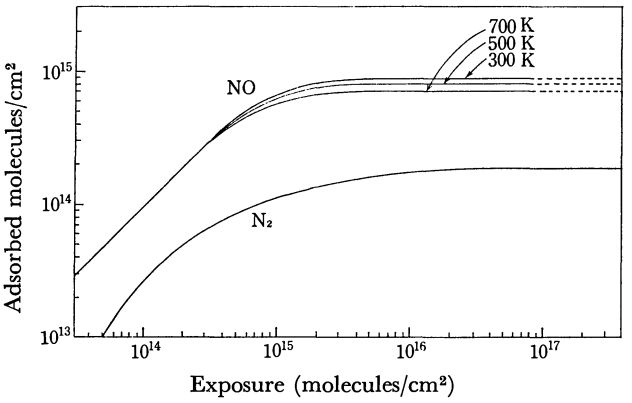

Fig. 1. Surface coverage as a function of exposure.

7.0×10^{14} molecules/cm^2 at 500 K and 700 K, respectively.

For the sake of comparison with nitrogen oxide adsorption, the adsorption of nitrogen was studied on the same tungsten filament. The saturation coverage of nitrogen on tungsten is 1.9×10^{14} molecules/cm^2, as is shown in Fig. 1. The saturation coverage for nitrogen oxide is 4.6 times as much as that for nitrogen. This ratio agrees with that on rhenium.[10] Assuming that the number of metal surface atoms is 1.5×10^{15} atoms/cm^2, this is equivalent to a W: NO ratio of about 2: 1. Yates *et al.*[6] state that the saturation coverage for nitrogen oxide on tungsten is 1.4×10^{15} molecules/cm^2, which is obtained from the ratio of the areas of the desorption spectrum of the nitrogen oxide monolayer to that of the nitrogen monolayer and from Ehrlich's data[12] for the adsorption of nitrogen on tungsten. Since saturation coverages of nitrogen on polycrystalline tungsten of 1.25 to 3.0×10^{14} molecules/cm^2 have been found by many investigators, as listed in Table 1, a comparison of the saturation coverage for nitrogen oxide and nitrogen should be made using the same tungsten filament.

Table 1. Comparison of initial sticking probabilities, saturation coverages and activation energies for nitrogen desorption

Investigator	s (initial)	Saturation coverage (molecules/cm^2)	E_d (kcal/mol)	Ref.
Schlier	0.42	1.8×10^{14}	—	13
Ehrlich	0.3	2.8×10^{14}	—	14
Hickmott	0.26	1.8×10^{14}	β: 81	15
Oguri	0.2	1.25×10^{14}	ε: 84 ζ: 69	16
Rigby	0.4	1.5×10^{14}	β_1: 73 β_2: 75	17
Yates, Jr.	—	1.6×10^{14}	β_1: 82 β_2: 84	18
Madey	—	—	β_1: 80 β_2: 82, 89	19
King	0.61	3.0×10^{14}	—	20
Tamura	0.35	1.9×10^{14}	β_1: 78 β_2: 80.5	This work

From the curve in Fig. 1, the sticking probability, s, can be calculated by means of the following equation:

$$s = \mathrm{d}N/\mathrm{d}N_{(e)}.$$

The relationship between the sticking probability and the surface coverage for nitrogen oxide is shown in Fig. 2. The initial sticking probability for nitrogen oxide adsorption on tungsten is close to unity up to $\theta\simeq0.4$ (θ is the monolayer fraction). This value agrees well with that found for the 110 surface of tungsten single crystals.[9] The initial sticking probability for nitrogen adsorption on tungsten obtained from Fig. 2 is 0.35, which is reasonable value in comparison with those of other papers.[13-17] Furthermore, the result obtained by the usual method, using flash desorption at a constant flow rate,[21] also agree with those of the present method. As in the case of the Re–NO system, one of reasons for such a high value of the initial sticking probability is that the ionization potential of nitrogen oxide (9.5 eV)[22] is lower than those of nitrogen ($\approx$16 eV), oxygen ($\approx$15 eV) and carbon monoxide ($\approx$14 eV).

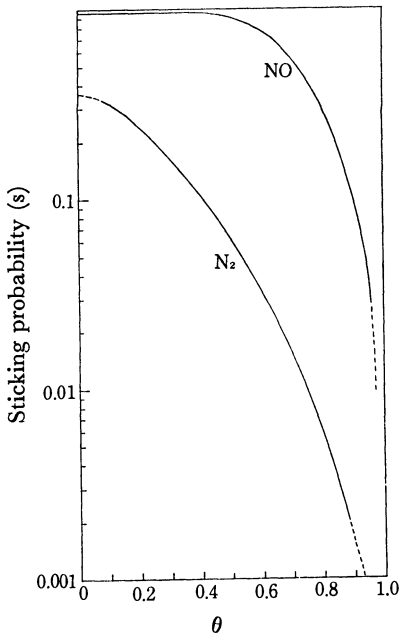

Fig. 2. Sticking probability as a function of surface coverage.

Rate of Adsorption and Desorption of Nitrogen Oxide and Nitrogen on Tungsten. It was confirmed that the rate of adsorption depends on the first power of the pressure. The rate of adsorption at constant pressure and temperature may, then, written as:

$$\mathrm{d}N/\mathrm{d}t = K\cdot P(1-\theta)^n,$$

where K and n are constants and P is the pressure of the nitrogen oxide or nitrogen. It was found that the rate of nitrogen oxide adsorption is proportional to $(1-\theta)$ as is shown in Fig. 3, and it seems that nitrogen oxide molecules are adsorbed non-dissociatively on tungsten. Nevertheless, for nitrogen adsorption, it may be shown that the adsorbed nitrogen was present in a dissociated form, because the rate of adsorption was proportional to $(1-\theta)^2$, as is shown in Fig. 3.

On the other hand, when the nitrogen oxide adsorbed is desorbed at definite temperature in a closed system,

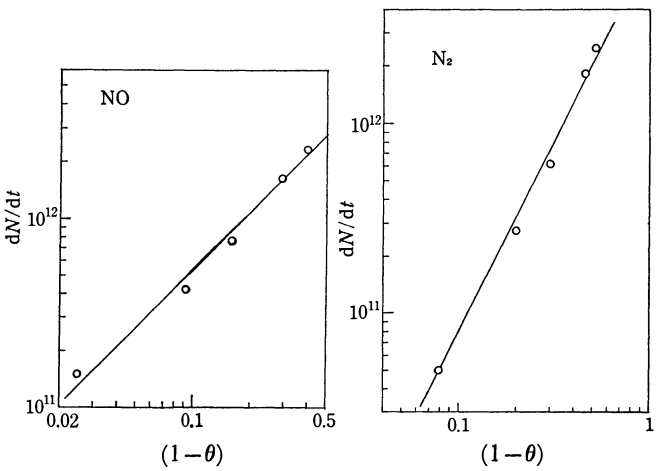

Fig. 3. The relation between the rate of adsorption and $(1-\theta)$.

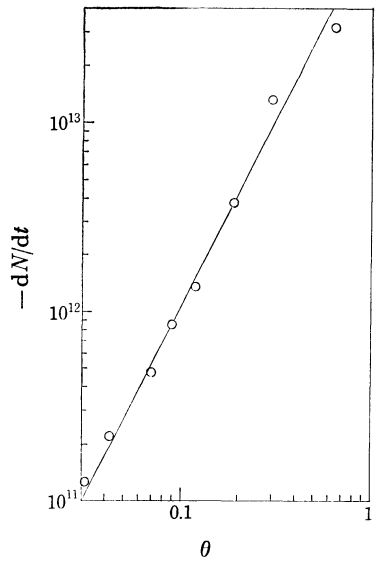

Fig. 4. The relation between the rate of nitrogen desorption and θ.

the rate of desorption may be expressed simply as:

$$-dN/dt = K'\theta^{n'},$$

where K' $[=\nu\exp(-E/RT)]$ is a constant and n' is the order of the desorption. In the W–NO system, the nitrogen oxide is decomposed for an increase in the tungsten temperature and is desorbed as in the case of nitrogen. The relation between the desorption rate and the surface coverage is shown in Fig. 4. As can be seen, the nitrogen desorption rate from a nitrogen oxide layer is roughly proportional to θ^2. At such high temperature, re-adsorption can be neglected.

Desorption Spectra. *1) Desorption from a Nitrogen Oxide Monolayer on Tungsten*: When tungsten saturated with nitrogen oxide was heated, nitrogen oxide and nitrogen from the tungsten surface due to decomposition of the nitrogen oxide desorbed, but neither molecular nor atomic oxygen were detected by means of the omegatron mass spectrometer. The desorption spectra from a nitrogen oxide monolayer on tungsten are shown in Fig. 5.

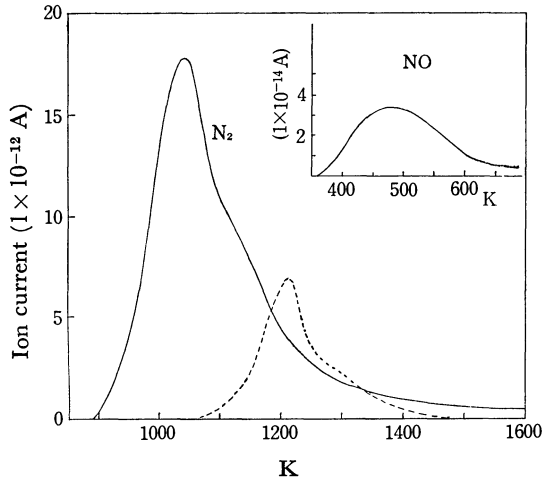

Fig. 5. The desorption spectra from nitrogen oxide monolayer. Dashed curve denotes nitrogen from nitrogen monolayer.

Table 2. The T_p of NO and N_2, and the amount of desorbed gas from a monolayer
(The percentages being calculated in terms of adsorbed NO)

	T_p (K)	%
NO	475	0.3
N_2	1045	99.7

The temperature of the desorption-peak maximum, T_p, for nitrogen oxide and nitrogen in each desorption spectrum, and the percentage calculated in terms of the adsorbed nitrogen oxide are shown in Table 2. Desorption of nitrogen oxide began at about 350 K, and above 900 K no further desorption of nitrogen oxide was observed. Moreover, when the initial coverage of nitrogen oxide was changed, no desorption of nitrogen oxide was observed below 0.75 nitrogen oxide monolayer. The greater part of the nitrogen from the nitrogen oxide monolayer desorbed before the temperature reached 1500 K. The T_p of the nitrogen desorption from a nitrogen oxide monolayer was lower than that from a nitrogen monolayer by about 170 K. Although Yates *et al.*[6] have observed the desorption of oxygen from a nitrogen oxide monolayer on tungsten, no oxygen desorption was seen in the present experiment. It appears that the oxygen from the nitrogen oxide monolayer evaporates as tungsten oxide.

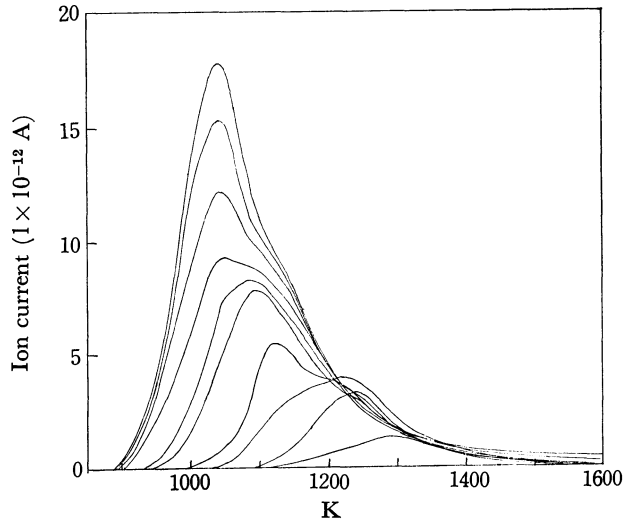

Fig. 6. The desorption spectra of nitrogen from various initial coverages of nitrogen oxide.

2) Desorption of Nitrogen from Various Initial Coverages of Nitrogen Oxide on Tungsten: The desorption spectra as a function of initial coverage of nitrogen oxide at 300 K are shown in Fig. 6. The desorption spectra for very low coverages of nitrogen oxide ($\theta<0.1$) resemble those for very low coverages of nitrogen. The T_p at $\theta=0.1$ and $\theta=0.2$—0.3 for nitrogen oxide adsorption correspond to the β_2 and β_1 peaks of the nitrogen desorption spectrum for a nitrogen layer on tungsten, respectively.

This behavior is reasonable, since the dissociation of nitrogen oxide for a very low coverage would produce a dilute layer of adsorbed nitrogen and oxygen (or oxide),

the desorption of nitrogen should be unaffected by the small amount of oxygen (or oxide) coverage. When the coverage of nitrogen oxide is increased, two new modes, ω_2(T_p: $\approx$1100 K) and ω_1 (T_p: 1045 K) peaks as designated by Yates *et al.*,[18] appeared which were formed beginning at about θ=0.3 and 0.7, respectively. However, no retrograde temperature behavior for the T_p of the ω_1 peak was observed in the present experiment.

Peng and Dawson, [23,26] and Matsushita and Hansen[24,25] have stated that these ω peaks resemble those for nitrogen desorption (λ state) from an adsorbed layer of ammonia on tungsten heated to 800 K or from that of activated nitrogen by electron bombardment, and that the number of total nitrogen atoms adsorbed is 8.6×10^{14} atoms/cm^2 because one nitrogen atom occupies a single vacancy site. Since one nitrogen oxide molecule may occupy a single vacancy site, a nitrogen oxide monolayer of 8.8×10^{14} molecules/cm^2 agrees with 8.6×10^{14} sites/cm^2 in the λ state of nitrogen adsorption.

The processes of adsorption, dissociation and desorption may be expressed as follows:

$$NO_{(g)} \longrightarrow NO_{(a)} \quad (1)$$
$$NO_{(a)} \longrightarrow N_{(a)} + O_{(a)} \quad (2)$$
$$2N_{(a)} \longrightarrow N_{2(g)} \quad (3)$$

Equations 2 and 3 are the reactions during the heating process. It is believed that the rate of process 2 is faster than that of process 3, since the rate of nitrogen desorption is roughly proportional to θ^2.

3) Desorption of Nitrogen from a Nitrogen Layer on Tungsten: The desorption spectra for various coverages of nitrogen are shown in Fig. 7. For nitrogen adsorption on tungsten at room temperature, three states, α, β_1, and β_2, were found in the desorption spectrum as has

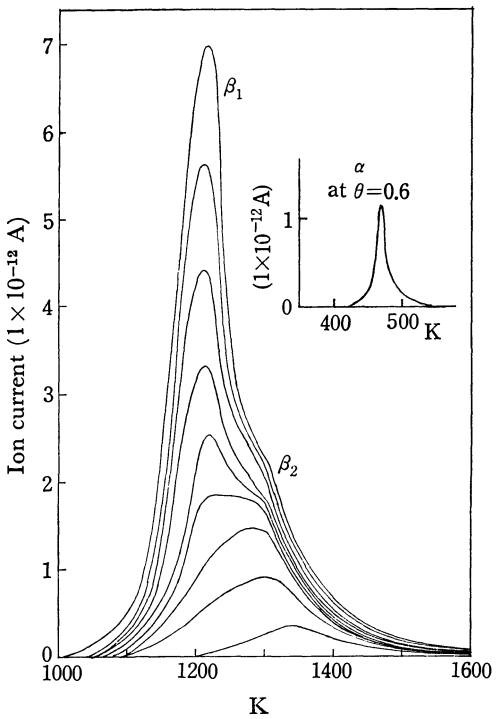

Fig. 7. The desorption spectra from various initial coverages of nitrogen.

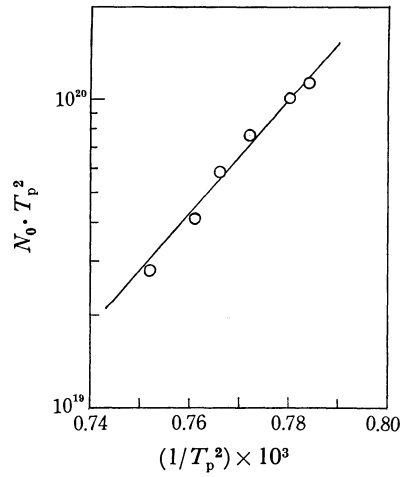

Fig. 8. A plot of log $N_0T_p^2$ *vs.* $1/T_p$.

been reported by other investigators.[16,17] The α state exhibits a maximum peak height (T_p: 470 K) at θ=0.6, and the α peak disappears for saturation coverage of nitrogen. The amount of α nitrogen desorbed corresponds to 5% of the β nitrogen at $\theta\simeq$0.6 (corresponding to 3% of a monolayer). Since the nitrogen from the α state desorbs at very low temperatures, it appears that the bond strength of W–$N_2(\alpha)$ is considerably weaker than those of the β states.

The β_1 peak appears beginning at $\theta\simeq$0.3. The T_p of the β_1 peak does not shift from the value of 1205 K as the coverage increases. According to Redhead's report,[27] and assuming that the desorption of the β_1 state follows first order kinetics and that the pre-exponential factor is 10^{13}/s, we obtain a value of 78 kcal/mol as the activation energy of β_1 nitrogen desorption.

On the other hand, the T_p of the β_2 peak shifts to a lower temperature with an increase in the coverage. Also, according to Redhead, when the desorption kinetics are 2nd order, the following equation should be valid:

$$E/RT_p^2 = (N_0\nu/\bar{\beta})\exp(-E/RT_p),$$

where N_0 is the initial coverage, ν is the rate constant, E is the activation energy for β_2 nitrogen desorption, and $\bar{\beta}$ is the rate at which the filament temperature is raised. A plot of $\log(N_0T_p^2)$ *vs.* $1/T_p$ is shown in Fig. 8. From the slope, the activation energy for desorption in the β_2 state is 80.5 kcal/mol. Data for the activation energy for nitrogen desorption on tungsten by other investigators are shown together in the Table 1.

References

1) J. A. Becker "Advances in Catalysis," Vol. 7, ed. by W. Frankenburg, V. I. Komarewsky, and K. E. Rideal, Academic Press, New York (1955), p. 135.
2) G. Ehrlich "Advances in Catalysis," Vol. 14, ed. by D. D. Eley, H. Pines, and P. B. Weisz, Academic Press, New York (1963), p. 255.
3) P. J. Estrap and E. G. McRae, *Surface Sci.*, **25**, 1 (1971).
4) C. C. Chang, *Surface Sci.*, **25**, 53 (1971).
5) T. E. Madey and J. T. Yates, Jr., *J. Vac. Sci. Technol.*, **8**, 525 (1971).
6) J. T. Yates, Jr. and T. E. Madey, *J. Chem. Phys.*, **45**,

1623 (1966).
7) J. T. Yates, Jr., T. E. Madey, and J. K. Payn, *Nuovo Cimento Suppl.*, **5**, 558 (1967).
8) T. E. Madey, J. T. Yates, Jr., and N. E. Erickson, *Surface Sci.*, **43**, 526 (1974).
9) R. Klein and J. T. Yates, Jr., "Proc. 2nd Internal. Conf. on Solid Surfaces," 1974, *Jpn. J. Appl. Phys.*, Suppl. 2, Pt. 2 (1974).
10) T. Tamura, *Bull. Chem. Soc. Jpn.*, **44**, 590 (1971).
11) T. Tamura, *Bull. Chem. Soc. Jpn.*, **44**, 2116 (1971).
12) G. Ehrlich, *J. Chem. Phys.*, **36**, 1171 (1962).
13) R. E. Schlier, *J. Appl. Phys.*, **29**, 1162 (1958).
14) G. Ehrlich, *J. Phys. Chem.*, **34**, 29 (1961).
15) T. W. Hickmott and G. Ehrlich, *J. Phys. Chem. Solids*, **5**, 47 (1958).
16) T. Oguri, *J. Phys. Soc. Jpn.*, **18**, 1280 (1963).
17) L. J. Rigby, *Can. J. Phys.*, **43**, 532 (1965).
18) J. T. Yates, Jr. and T. E. Madey, *J. Chem. Phys.*, **43**, 1055 (1965).
19) T. E. Madey and J. T. Yates, Jr., *J. Chem. Phys.*, **44**, 1675 (1966).
20) D. A. King and M. G. Wells, *Surface Sci.*, **29**, 454 (1972).
21) P. A. Redhead, *Trans. Faraday Soc.*, **57**, 641 (1961).
22) R. B. Heslop and P. L. Robinson, "Inorganic Chemistry," Elsevier Pub., Co., New York (1960), p. 319.
23) Y. K. Peng and P. T. Dawson, *J. Chem. Phys.*, **54**, 950 (1971).
24) K. Matsushita and R. S. Hansen, *J. Chem. Phys.*, **52**, 3619 (1969).
25) K. Matsushita and R. S. Hansen, *J. Chem. Phys.*, **52**, 4877 (1969).
26) P. T. Dawson and Y. K. Peng, *Surface Sci.*, **33**, 565 (1972).
27) P. A. Redhead, *Vacuum*, **12**, 203 (1962).

Finite Element Approach to the Vibrational Schrödinger Equation of Diatomic Species

Hideyuki ARAI, Isao KANESAKA,* and Yukio KAGAWA**

Computer Center of Toyama University, Toyama University, Gofuku, Toyama 930

(Received January 5, 1976)

The finite element approach was successfully applied to the vibrational Schrödinger equation of diatomic species. An O_2 molecule with a harmonic potential and an Ar_2 molecule with a Lennard-Jones potential were examined and their eigen values and the associated eigen function were obtained. The calculated eigen values of the O_2 molecule agree with those expected. In the case of the Ar_2 molecule the calculated eigen values agree with those experimentally obtained when Lennard-Jones parameters are $\varepsilon=115.1$ (cm^{-1}) and $\sigma=3.35$ (Å). This verifies the validity of the present approach.

The finite element method was originally developed for the analysis of structures and has been widely applied to various problems in engineering science because of its versatility.

The method has been successfully applied to the analysis of the field problems, Laplace, Poisson and Helmholts equations.[1,2] It is a variant of the Rayleigh-Ritz procedure, turning a continuum field discrete with the best possible approximation by means of variational calculus which minimizes the functional corresponding to the governing differential equation. The present procedure might be an extended approach of the variational calculus widely used in wave mechanics.[3]

The purpose of this paper is to present the finite element method for the vibrational Schrödinger equation with two body potential V which is expressed as follows:

$$\frac{d^2\Psi}{dQ^2}+\frac{2\mu}{\hbar^2}(E-V)\Psi=0 \tag{1}$$

where Ψ is a wave function, Q a normal coordinate, μ a reduced mass, and E an eigen value.

If V is given by

$$V(Q)=\frac{1}{2}kQ^2 \tag{2}$$

where k is a force constant, Eq. 1 is the Schrödinger equation of harmonic oscillator.

In the case of the Lennard-Jones potential, which is of interest to us, V is given by

$$V(Q)=4\varepsilon\left\{\left(\frac{\sigma}{r_e+Q}\right)^{12}-\left(\frac{\sigma}{r_e+Q}\right)^{6}+0.25\right\} \tag{3}$$

where ε is a potential energy in equilibrium distance r_e and σ a distance of two bodies at $V=\varepsilon$.

The eigen values and their associated wave functions for harmonic oscillators as well as those under the Lennard-Jones potential were numerically calculated by means of the finite element approach. The results are compared with those obtained analytically and experimentally.

Functional and Finite Element Formulation

According to variational calculus the solution of Eq. 1 is equivalent to finding the function Ψ which minimizes the following functional:[3]

$$\chi=\int_Q\left\{\frac{1}{2}\left(\frac{d\Psi}{dQ}\right)^2-\frac{1}{2}\frac{2\mu}{\hbar^2}(E-V)\Psi^2\right\}dQ \tag{4}$$

where the integration is taken over the whole region under consideration.

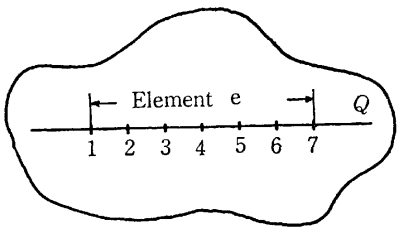

Fig. 1. The division of the region into the elements.

The region is divided into small elements (Fig. 1) for which the trial function was assumed to be:

$$\Psi=\sum_k^7\alpha_kQ^{k-1}=\mathbf{N}\boldsymbol{\alpha} \tag{5}$$

where the components of $\mathbf{N}$ are spatial functions and the α_s are seven unknown constants to be chosen so as to satisfy the nodal values at the element nodes.

Thus the function Ψ is uniquely specific within the element by the nodal values Ψ_1, Ψ_2, Ψ_3,……, Ψ_7, their associated coordinates being

$$\Psi^{(e)}=[\mathbf{N}_1\mathbf{N}_2\cdots\mathbf{N}_7]^T\boldsymbol{\alpha}=\mathbf{C}^{(e)}\boldsymbol{\alpha} \tag{6}$$

where (e) refers to the element and $\Psi^{(e)}$ indicates the values of Ψ at the nodes and is given by

$$\Psi^{(e)}=[\Psi_1\Psi_2\cdots\Psi_7]^T \tag{7}$$

T denotes transposition, and $\mathbf{N}_i$ consists of the coordinate value corresponding to node i, and is given by

$$\mathbf{N}_i=[1\,Q_i\,Q_i^2\cdots Q_i^6] \tag{8}$$

Premultiplying each side of Eq. 6 by $\mathbf{C}^{(e)-1}$ (inverse of $\mathbf{C}^{(e)}$ matrix) and substituting $\boldsymbol{\alpha}$ into Eq. 5, we obtain the trial function

$$\Psi=\mathbf{N}\mathbf{C}^{(e)-1}\Psi^{(e)} \tag{9}$$

Substituting Eq. 9 into Eq. 4, we get the functional for the element

$$\chi^{(e)}=\frac{1}{2}\Psi^{(e)T}(\mathbf{C}^{(e)-1})^T(\mathbf{P}^{(e)}-\mathbf{E}\mathbf{R}^{(e)})\mathbf{C}^{(e)-1}\Psi^{(e)} \tag{10}$$

where

$$\mathbf{P}^{(e)}=\int_e\frac{d}{dQ}\mathbf{N}^T\frac{d}{dQ}\mathbf{N}dQ+\frac{2\mu}{\hbar^2}\int_e V\mathbf{N}^T\mathbf{N}dQ \tag{11}$$

* *Faculty of Literature and Science, Toyama University, Gofuku, Toyama* 930.

** *Faculty of Engineering, Toyama University, Nakagawa, Takaoka* 933.

$$\mathbf{R}^{(e)} = \frac{2\mu}{\hbar^2}\int_e \mathbf{N}^T\mathbf{N}dQ \tag{12}$$

where the integration is taken over the element.

In order to minimize the functional $\chi^{(e)}$, we take the partial derivative with respect to $\Psi^{(e)}$ and obtain

$$\frac{d\chi^{(e)}}{d\Psi^{(e)}} = (\mathbf{C}^{(e)-1})^T\mathbf{P}^{(e)}\mathbf{C}^{(e)-1}\Psi^{(e)} - \mathbf{E}(\mathbf{C}^{(e)-1})^T\mathbf{R}^{(e)}\mathbf{C}^{(e)-1}\Psi^{(e)} = 0 \tag{13}$$

The equation holds for all the elements which divide the space.

The values of Ψ_1 at the interconnecting nodes between adjoining elements should be the same. Under these condition we obtain a linear algebraic equation of the form

$$(\mathbf{A}-\mathbf{EB})\Psi = 0 \tag{14}$$

The eigen values and the wave functions are calculated from Eq. 14.

Numerical Examples

The functional of Eq. 4 is defined in unbounded space where the integration should be carried out. This can not be achieved by numerical analysis. Since the lower eigen values are of interest, the potential is calculated for the lower well region, which is divided into elements.

The first example for calculation is of the O_2 molecule with harmonic potential. That is, Eq. 1 is to be solved under the conditions of Eq. 2. The eigen values and their eigen functions are resolved analytically.

Six elements divided the integrated region which was chosen so as to cover lower eigen values. Two schemes were considered for the method of division: Case 1, equal space division; Case 2, finer division employed for the vicinity of the potential well.

Table 1. The observed and calculated eigen values (cm^{-1}) of the O_2 and Ar_2 molecules

v	O_2			Ar_2		
	Anal[a]	Calcd		Obsd[b]	Calcd	
		Case 1	Case 2		[I]	[II]
0	791.3	794.0	791.2	15.1	13.9	14.7
1	2374.0	2458.6	2373.9	40.6	37.6	40.1
2	3956.7	4220.3	3959.0	60.7	56.4	60.7
3	5539.4	5984.7	5545.5	75.8	68.6	76.8
4	7122.0	9444.3	7169.9	86.4	79.3	87.3

a) Obtained from $k=11.8$ (mdyn/Å). b) From Refs. 4 and 6.

The calculated lower six eigen values are given in Table 1. The values obtained by the finite element approach agree reasonably with the analytical ones obtained on the basis of $\kappa=11.8$ (mdyn/Å). The results are not independent of the division method. Elements are not enough because of the limitation of the capacity of the computer. However, the present approach is promising if the division is proper by chosen (Case 2); the spacing of the i-th element from the origin is as follows: $\Delta Q^{(e_i)}=0.025|i|$, $i=\pm1$, ±2, ±3. The potential function used is shown in Fig. 2 with the eigen functions (not normalized) corresponding to the six lower eigen values.

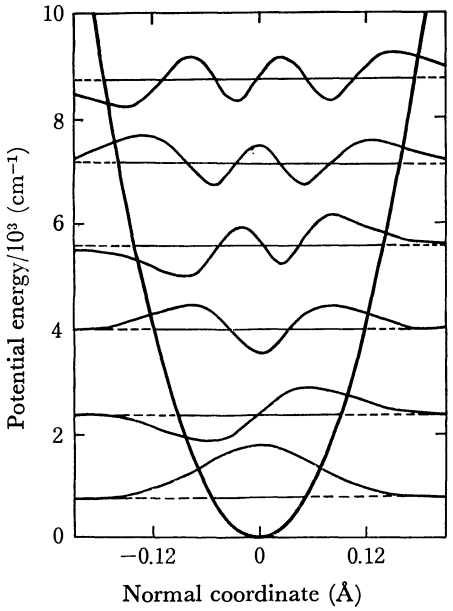

Fig. 2. The potential function and the calculated eigen functions (arbitrary unit) of the O_2 molecule. The solid horizontal lines show the level of the eigen values.

The next example of calculation is for the case with Lennard-Jones potential; it is to solve Eq. 1 under the conditions of Eq. 3. In this case the Ar_2 molecule is taken as an example. The experimental eigen values obtained by spectroscopic[4] and molecular beam[5] methods are given in Table 1. From the results we obtain: ε in Eq. 3 is 98.7 cm^{-1} and r_e 3.85 Å which gives the value of σ, 3.35 Å.

The region where the potential is negative in the

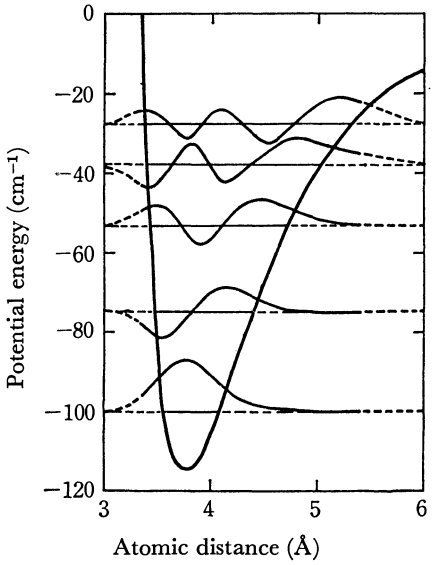

Fig. 3. The potential function and the calculated eigen functions (arbitrary unit) of the Ar_2 molecule. The solid horizontal lines show the level of the eigen values. The dotted lines are hypothetically drawn.

ordinary Lennard-Jones potential form was chosen for integration. Finer division was used for the vicinity of the potential well (Case 2); the spacing of the i-th element from the potential minimum is as follows: $\Delta Q^{(e_i)} = 2^{|i|-1}\{(2)^{1/6}\sigma - \sigma\}/3$, $i = \pm 1, \pm 2, 3, 4$. The calculated eigen values (Calcd I) are also given in Table 1. The agreement between the observed and calculated values is not satisfactory, the calculated ones being as a whole lower than the observed ones. We thus varied the value of ε. When ε is 115.1 cm^{-1}, the values of Calcd II are obtained, agreeing with those observed. This shows that since the Lennard-Jones potential explained the spectroscopic result,[4] this potential is proper for the bound state, though it has been unfavorable for the collision data.[5,6]

The potential function and the eigen functions for the Ar_2 molecule in the case of Calcd II are given in Fig. 3. The dotted lines for the eigen functions out of the region of integration are hypothetical.

Conclusion

The finite element approach is successfully applied to the vibrational Schrödinger equation. Simple examples of diatomic species are considered for verification of the approach. The method is promissing and seems to deserve further application.

The numerical calculations were performed at the Computer Center of Toyama University.

We wish to thank Professor K. Kawai, the Faculty of Literature and Science, Toyama University, for his valuable suggestions, and Professor S. Tanaka and Mr. S. Ishida of the Computer Center, Toyama University, for their help in the computation.

References

1) O. C. Zienkiewicz, "The Finite Element Method in Engineering Science," McGraw-Hill, London (1971).
2) H. N. Douglas and G. Vries, "The Finite Element Method," Academic Press, New York and London (1973).
3) L. I. Schiff, "Quantum Mechanics," McGraw-Hill, London (1968), p. 255.
4) Y. Tanaka and K. Yoshino, *J. Chem. Phys.*, **53**, 2012 (1970).
5) J. M. Parson, P. E. Siska, and Y. T. Lee, *J. Chem. Phys.*, **56**, 1511 (1972).
6) K. K. Docken and T. P. Schafer, *J. Mol. Spectry.*, **46**, 454 (1973).

Nature of Catalytically Active Sites over Solid Acids. I. Selective Poisoning of Lewis Acid Sites on Silica-Alumina with Pyridine and Its Application to Olefin Polymerization

Koichi MIZUNO, Masanori IKEDA, Toshiaki IMOKAWA, Jun-ichiro TAKE, and Yukio YONEDA

Department of Synthetic Chemistry, Faculty of Engineering, The University of Tokyo, Hongo, Bunkyo-ku, Tokyo 113

(Received February 4, 1976)

When pyridine chemisorbed on silica–alumina was evacuated at 350 °C, the 1460 cm^{-1} band due to Lewis-bound pyridine (LPY) remained while the 1540 cm^{-1} band due to Brønsted-bound pyridine (BPY) completely disappeared. This disappearance of the BPY band was revealed to accompany a loss of the Brønsted acid sites themselves besides their liberation. However, the lost Brønsted acid sites were regenerated by allowing the sample to stand overnight at 110 °C. Thus, strong Lewis acid sites of silica–alumina were able to be selectively poisoned by pyridine without any damage to the Brønsted acid sites. By poisoning catalysts *in situ* by controlled amounts in this way, the nature of the active site was investigated for polymerization of propylene or *cis*-2-butene at a low temperature of 30 °C. The initial activity declined sharply as the extent of pyridine poisoning of the Lewis acid sites increased. Therefore, it was concluded that strong Lewis acid sites (25—30% of the total Lewis acid content) were active in polymerization over silica–alumina.

The catalytic activities and selectivities in solid acid catalysts may be governed by the type of acid site, the acid strength, and the acid content. One of the characteristics of solid catalysts is that, in general, they have many kinds of chemisorption sites of different nature. Therefore, the determination of the role of these sites in reactions, especially the nature of catalytically active sites may be essential to the elucidation of reactions over solid acid catalysts. Infrared spectroscopy of chemisorbed pyridine has been recently proposed as a method for distinguishing between Brønsted and Lewis type surface acid sites.[1] Of a variety of methods so far proposed for the determination of the acidic properties of solid surfaces, this method is probably the most reliable. Only in a few studies[2,3] has this technique been applied to determine the nature of catalytically active sites. Even these determinations, however, require correlations between IR data on the acidic properties and reaction data, both obtained in separate experiments, and therefore, are rather indirect. If only a certain type of acid sites can be selectively poisoned with a base, the use of such a poisoned catalyst should permit a more direct determination of the nature of catalytically active sites. It has been found that upon evacuation at above 300 °C some Lewis-bound pyridine (LPY) over silica–alumina remains, whereas Brønsted-bound pyridine (BPY) disappears completely.[4,5] In the present study, it was attempted first, on the basis of this experimental fact, to prepare silica–alumina whose Lewis acid sites were selectively poisoned by pyridine without any poisoning of the Brønsted acid sites, and second, by using *in situ* such catalysts, to elucidate the nature of active sites for polymeric olefin formation reactions.

It is well known that an olefin such as propylene or butene forms an adsorbed residue giving rise to IR bands characteristic of a saturated hydrocarbon over silica–alumina[6] and deamminated ammonium Y (or HY) zeolite[7] at room temperature. Deuterium-tracer studies of butene isomerization over silica–alumina revealed that the residue is the active site for the isomerization.[8,9] Recently, the residue proved to consist of oligomers (about four monomer units, on the average).[10–12] However, the nature of active sites in the polymeric olefin formation has been controversial because of the lack of conclusive evidence. Ozaki and Kimura[8] have speculated that olefin was chemisorbed on Lewis acid sites as a monomer. Hirschler[10] concluded that Brønsted acid sites were active over silica–alumina on the basis of the similarity in composition of polymeric species formed over silica–alumina and those formed over deamminated Y zeolite. On the contrary, Weeks *et al.*[7] concluded that the active sites were dehydroxylated (surface Al^{3+} ions, *i.e.*, Lewis acid sites) over Y zeolite because no significant difference was found between products over deamminated and dehydroxylated zeolites. Peri[6] regarded an α-site, a pair consisting of an Al^{3+} ion (Lewis acid) and an oxide ion, to be active. Holm, Bailey, and Clark[13] and Sato, Aonuma, and Shiba[14] have reported that the catalytic activity of silica–alumina for propylene polymerization at an elevated temperature varied in proportion to the Brønsted acid content. However, reasonable objections have been presented to their determinations of the Brønsted acid content.[15] The present study employing silica–alumina, whose Lewis acid sites were selectively poisoned, revealed that the catalytic activity for the polymeric olefin formation declined sharply as the extent of pyridine poisoning of the Lewis acid sites increased. Therefore, it is concluded that strong Lewis acid sites are active in polymerization over silica–alumina.

Experimental

Materials. The silica–alumina (SA-1, 13% Al_2O_3, 540 m^2/g) was used in a previous study.[16] Pyridine distilled from a GR reagent was dried over KOH under vacuum, and finally vacuum-distilled into a vessel containing molecular sieve 5A evacuated at 350 °C before use. Propylene and *cis*-2-butene (Matheson Co.) were dried by circulation for 1.5 h over anhydrous magnesium perchlorate prepared freshly by evacuation up to 240 °C, and then were thoroughly degassed by the freeze-pump-thaw technique.

Sample Preparation. Self-supporting 20 mm diameter wafers of SA-1 were formed by pressing the oxide powder at 6200 kg/cm^2 in a conventional KBr die. For each wafer, 20—80 mg of sample was used.

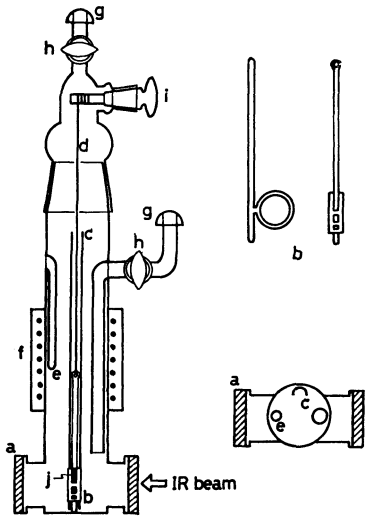

Fig. 1. Sketch of infrared cell. (a) CaF_2 window; (b) sample holder; (c) guideway; (d) Pt wire (0.2 mmϕ); (e) thermowell; (f) furnace; (g) ball joint; (h) stopcock; (i) reel; (j) sample wafer.

Infrared Cell. The cell used for IR-spectral measurements and as the reactor in reaction runs is shown in Fig. 1. The body was made of Pyrex or quartz, and equipped with CaF_2 windows (a) 40 mm in diameter and 5 mm thick. The middle of the cell was surrounded by a thermostatically controlled furnace (f).

A Pyrex or quartz sample holder (b), in which the wafer was mounted, was suspended with a Pt wire (d) from a reel (i), and could be moved through a guideway (c) up and down by winding up and off the Pt wire. This permitted reproducible positioning of the wafer in the analytical beam of the infrared spectrometer.

The cell could readily be connected through two ball joints (g) to a conventional vacuum manifold or to a closed circulation system (about 570 ml including the cell) for reaction runs.

Procedures. The wafer was inserted between two rings of the sample holder, pretreated in an oxygen stream as described earlier,[17] and finally activated in the cell by evacuation at 450 °C and about 10^{-4} mmHg usually for 15 h.

The amounts of Brønsted and Lewis acid sites were determined on the basis of IR absorption spectra of chemisorbed pyridine. The wafer was dosed with about 0.2 mmol/g of pyridine for 0.5 h at room temperature, and then evacuated for 1 h at 110 °C (referred to as the standard pyridine treatment) in order to eliminate hydrogen-bonded pyridine (HPY) which gives rise to the 1438 cm^{-1} band. The peak absorbances of the bands at 1540 and 1460 cm^{-1} (ascribable to BPY and LPY, respectively) were taken as the amount of acid sites of the corresponding type. The amount of acid sites thus obtained proved to agree excellently with that determined by means of the usual method in which a wafer was exposed to a large excess of pyridine vapor. By the use of such a small amount of pyridine, we were able to protect the wafer from surface contaminations with pyridine dissolved in the grease, as was evidenced, for example, by the absence of the slow reappearance of the HPY band after the 110 °C evacuation.

The polymeric olefin formation reaction was carried out in the closed circulation system provided with the cell at an initial olefin pressure of 10 mmHg and 30 °C. Its progress was followed by observing the IR spectrum of the polymeric species formed over the wafer after gaseous and physically-adsorbed olefin had been removed with a liquid nitrogen trap. During the course of this removal, the spectra of the polymeric species showed no significant change. The pressure decrease of the olefin was negligibly small for the period of the reaction.

Infrared spectra over the range of 4000 to 1300 cm^{-1} were recorded on a model DS-401G grating spectrometer (Japan Spectroscopic Co.) at room temperature. Attenuation of the reference beam with specially-designed screens was necessary to compensate for the energy loss due to light scattering by the wafer. Spectral slit widths were ~3 cm^{-1} at 1500 cm^{-1} and ~10 cm^{-1} at 3000 cm^{-1}.

Peak absorbances are all normalized so as to indicate the absorbance per unit optical thickness of the wafer. This normalized absorbance, AS/W (cm^2/g), corresponds to the quantity $\varepsilon M/W$, where A and ε are respectively the absorbance and the absorption coefficient of a band, M is the amount (mmol) of the responsible species, and S and W are the cross section (cm^2) and weight (g) of the wafer, respectively.

Results

Selective Poisoning of Lewis Acid Sites over Silica–Alumina. Figure 2 shows the IR spectra of pyridine chemisorbed on SA-1. The standard pyridine treatment of SA-1 produced spectrum (a), in which three bands appear at 1540, 1490, and 1460 cm^{-1} in accordance with spectra in the literature.[1,18] The bands at 1540, 1460, and 1490 cm^{-1} are ascribed to BPY, LPY, and to both species, respectively. Every band decreased in intensity when the wafer was evacuated at higher temperatures. On evacuation at 350 °C for 1 h (spectrum (b)), the LPY band remained while the BPY band completely disappeared. Seemingly this disappearance of the BPY band may indicate the desorption of BPY and hence mere liberation of the Brønsted acid sites. If this were true, the BPY band should reappear with the same intensity as the original when the standard pyridine treatment is repeated after the 350 °C evacuation.

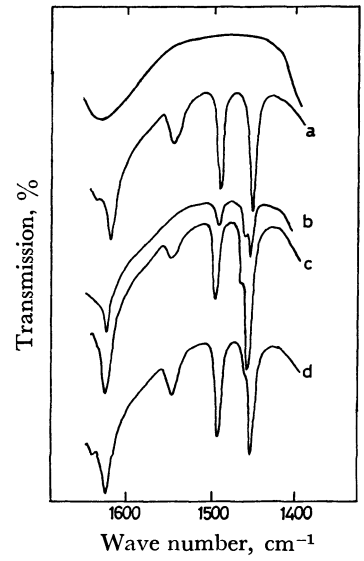

Fig. 2. IR-spectral changes of adsorbed pyridine induced by 350 °C-evacuation: (a) original; (b) after 350 °C evacuation for 1 h; (c) immediate standard pyridine treatment of (b); (d) standard pyridine treatment of (b) after 110 °C standing overnight.

Table 1. Changes of acidic properties induced by evacuation at 350 °C

Catalyst No.	1		2		3		4	
(Activation time, h)	(2)		(2)		(5)		(15)	
	Acid content[a]							
	B-	L-	B-	L-	B-	L-	B-	L-
Original	5.0	19.0	3.9	20.7	4.1	17.5	2.2	20.6
After 350 °C evacuation followed by standing								
110[b]	5.1	17.6	4.3	19.2	↓	↓	↓	↓
RT[c]	4.1	16.7	↓	↓	↓	↓	↓	↓
none	↓	↓	2.9	21.8	1.9	19.1	1.7	20.7
110	4.6[d]	17.7[d]	4.2	20.4	4.4	16.5	2.5	20.7
RT	4.5[d]	17.4[d]	3.1	19.9	↓	↓	↓	↓

a) cm^2g^{-1}. b) Overnight at 110 °C. c) Overnight at room temperature. d) After standing for 2 days.

Table 1 summarizes the results of an examination of this problem. The acid content of a fresh wafer, which is labelled "original," was determined first for both acid types. After the wafer had been successively evacuated at 350 °C for 1 h and allowed to stand under the conditions given in Table 1, its acid contents were determined again. Acidity data obtained from several cycles of this procedure, in which the conditions for standing were altered in the sequence cited, are given in the lines indicating the corresponding treatment. The arrows indicate the particular treatments that were not followed. The immediate standard pyridine treatment after the 350 °C evacuation ("none" in Table 1 and spectrum (c)) revealed that the intensity of the BPY band decreased definitely while the intensity of the LPY band did not significantly change. This indicates that evacuation at 350 °C gives rise to the loss of some Brønsted acid sites themselves over SA-1, in addition to the liberation of these sites resulting from the desorption of BPY. On the other hand, when the wafer was allowed to stand overnight at 110 °C after the 350 °C evacuation, spectrum (d) was observed to be identical to spectrum (a). This fact demonstrates that the Brønsted acid sites lost are regenerated by allowing the wafer to stand overnight at 110 °C. These observations are reproducible as is seen in Table 1. In conclusion, the selective poisoning of Lewis acid sites over silica–alumina is attainable without any damage to the Brønsted acid sites when the following treatment is employed: the wafer is dosed with pyridine, evacuated at 350 °C, and allowed to stand overnight at 110 °C.

The mechanism of the loss and regeneration of Brønsted acid sites is not completely clear at present. In view of the same absorption coefficients for the BPY and LPY bands,[19–21] inspection of Table 1 indicates that the total number of acid sites (Brønsted plus Lewis) remains sensibly constant at all stages. The loss of Brønsted acid sites is compensated with the generation of Lewis acid sites, and the regeneration of the former with the loss of the latter. This observation may be associated with the well-known interconversion of Brønsted and Lewis acid sites on silica–alumina:[5,18] the conversion of Brønsted to Lewis acid sites occurs on dehydration and the reverse occurs on hydration. Some empirical evidence was reported to suggest that the presence of bases such as pyridine facilitates dehydration or dehydroxylation of the surface.[22,23] However, the regeneration, especially of an exact amount, of the lost Brønsted acid sites after standing overnight at 110 °C is surprising in view of the experimental procedure employed in which no water was added. The hydroxylation may result from the action of water from the bulk of the catalyst. Table 1 also suggests that this regeneration includes a slow chemical process.

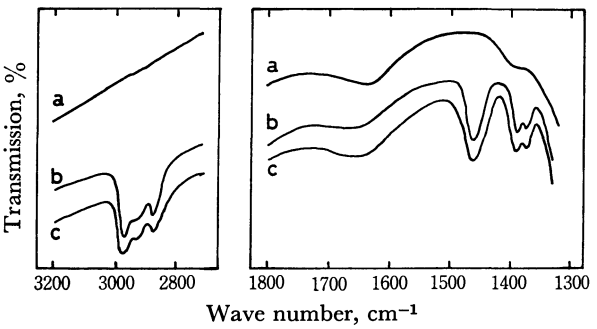

Fig. 3. IR spectra of polymeric *cis*-2-butene over SA-1. Background spectra (a); spectra of polymeric *cis*-2-butene 2 (b) and 20 h (c) after the reaction at 30 °C and 10 mmHg.

Polymeric Olefin Formation. Introduction of propylene or *cis*-2-butene onto SA-1 immediately produced the irreversibly adsorbed species giving rise to IR absorption bands at 2970—2960, 2930, and 2870 cm^{-1} in the C–H stretching region and at 1470, 1385, and 1370 cm^{-1} in the C–H deformation region. Figure 3 shows some spectra recorded, which are characteristic of saturated hydrocarbons. Each band grew steadily and reached a constant intensity 1—2 days after the introduction of the olefin (see Fig. 4). At any stage of the reaction, no olefinic species was detected, as evidenced by the absence of absorption in the unsaturated C–H stretching (3300—3000 cm^{-1}) and C=C stretching regions (1700—1600 cm^{-1}). The adsorbed species was not desorbed on evacuation at room temperature, and was desorbed by about 50, 80, and 95% on evacuation at 100, 200, and 450 °C, respectively, indicating that it is strongly held to the surface. Recently, the adsorbed species have been proven to be oligomers.[10–12]

The amount of polymeric propylene formed and its

Table 2. Distribution of desorption products of polymeric propylene (100 °C)

Reaction time, min	Amount of polymeric propylene,[a] μmol/g	H/C Ratio	Desorption products, mol %						
			C_3	C_4	C_5	C_6	C_7	C_8	C_9
1	70	1.9	26	44	18	7	1	1	2
5	142	—	19	46	21	11	1	1	1
30	223	1.9	6	52	22	14	2	1	3

a) On propylene basis.

H/C ratio were determined by means of the combustion method. The results are given in Table 2. The experiments were carried out in a separate closed circulation system (ordinarily, 1300 ml) with SA-1 powder (*ca.* 1 g) which had been pretreated and activated in the same manner as in the IR study. After exposure to olefin for the times described and removal of gaseous and physically-adsorbed hydrocarbons with a liquid nitrogen trap, dry oxygen at about 500 mmHg was circulated over the wafer at 450 °C overnight. The carbon dioxide and water produced were separated with a liquid nitrogen trap and a dry ice/ethanol trap, and the corresponding amounts were determined volumetrically. The amount of the polymeric species obtained by means of the present method, which is given on the olefin monomer basis, agreed well with that from the pressure decrease of the gaseous olefin. With either propylene or *cis*-2-butene, the peak intensity at 2970—2960 cm^{-1} was found to be proportional to the amount of the polymeric species. The intensity of this peak was therefore taken to be the amount of the polymeric species formed.

The distribution of desorption products of the polymeric propylene are also given in Table 2. After removal of gaseous and physically-adsorbed hydrocarbons with a liquid nitrogen trap, the sample was inserted into a furnace previously regulated thermostatically at 100 °C and maintained at the same temperature for 1 h. The desorbed products were collected into a trap maintained at −196 °C with or without evacuation, and analyzed with two FID gas chromatographs equipped with a VZ-7 column operating at room temperature and with a silicon DC-11 column temperature-programmed from room temperature to 150 °C at 6 °C/min, respectively. No hydrocarbons other than reactant propylene were detected in the gas phase. Neither C_1- nor C_2-hydrocarbons were detected in the desorption products. The C_3-hydrocarbons consisted only of propylene and the C_4-hydrocarbons contained mainly 1-butene and/or isobutylene. Although the VZ-7 column used could not separate 1-butene from isobutylene, this GLC peak may be due to isobutylene because of the absence of 2-butene. The C_4-, C_5-, C_7-, and C_8-hydrocarbons are probably cracking products of polymeric propylene. As the reaction proceeded, the amount of propylene (a C_3-hydrocarbon) decreased, whereas the amount of higher (C_4—C_9) hydrocarbons increased, suggesting that monomeric olefin changes successively into dimer, trimer, and higher oligomers over the surface.

Selective Poisoning Study of Polymeric Olefin Formation. Preliminary experiments revealed that the catalytic activity of SA-1 decreased in a drastic way when its Lewis acid sites were selectively poisoned with an amount of pyridine (*ca.* 0.2 mmol/g) similar to that in the acid content measurements, strongly suggesting that Lewis acid sites are active in the polymerization. Confirmation of this suggestion required that a series of more active, selectively poisoned wafers were prepared by using smaller amounts of pyridine. For this reason, it was necessary to determine the acid contents of a wafer after activity tests, assuming that the acid content was conserved for each acid type before and after the reaction.

Table 3. Conservation of acid contents before and after reaction

	Peak intensity, $cm^2\ g^{-1}$		
	BPY (1540)	LPY (1460)	BPY+LPY (1490)
Before reaction:			
a. acid content	2.2	20.7	7.4
b. selectively poisoned	0	5.6	1.6
After reaction:			
c. removal of gaseous propylene with a liq. N_2 trap	0	—	1.7
d. acid content	2.3	18.3	8.0

As is shown in Table 3, the validity of the assumption was confirmed by an examination with one wafer poisoned selectively with about 0.2 mmol/g of pyridine. The acid contents after reaction (d), which were determined by a method described below, agree with those before reaction (a) to within the experimental error. Table 3 also shows that no pyridine held on the Lewis acid sites migrates onto Brønsted acid sites during the course of the reaction (b and c). This is evidenced by the absence of the BPY band after the reaction and the invariability of the intensity of the 1490 cm^{-1} band. After the reaction, the LPY band overlapped with the strong 1470 cm^{-1} band assigned to the CH_2 and asymmetrical CH_3 deformations of the polymeric olefin.

On the basis of these results, the following procedure was employed for reaction experiments. An activated wafer was dosed with a small amount of pyridine for 0.5 h at room temperature, evacuated for 1 h at 350 °C, and allowed to stand overnight at 110°C. The poisoned state of the wafer surface was ascertained on the basis of its IR spectra. The reaction was conducted as described above. After the polymeric olefin had been removed by evacuation for 1 h at 350 °C, the wafer was dosed with about 0.2 mmol/g of pyridine, allowed to stand overnight at 110 °C, and finally evacuated

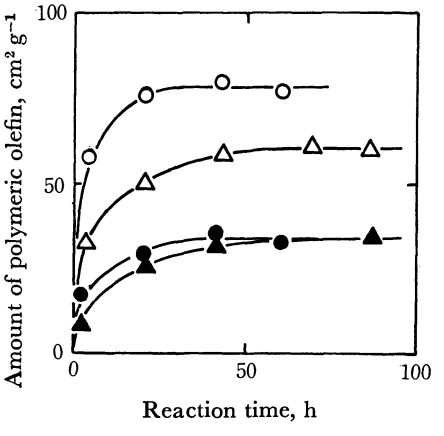

Fig. 4. Time-course of the formation of polymeric olefin: propylene over clean (△) and selectively poisoned (▲) SA-1; *cis*-2-butene over clean (○) and selectively poisoned (●) SA-1.

for 1 h at the same temperature, in order to determine its acid contents.

Figure 4 shows the time evolution of the formation of the polymeric olefin over a clean and a selectively poisoned wafer. On both wafers, the formation of the polymeric olefin took place rapidly in the early stage of the reaction, slowed down gradually, and finally ceased after 1—2 days. At any stage of the reaction, the amount of polymeric olefin formed was smaller on a selectively poisoned wafer than on a clean wafer. The amount of the polymeric olefin formed after 1 min was taken as the initial activity.

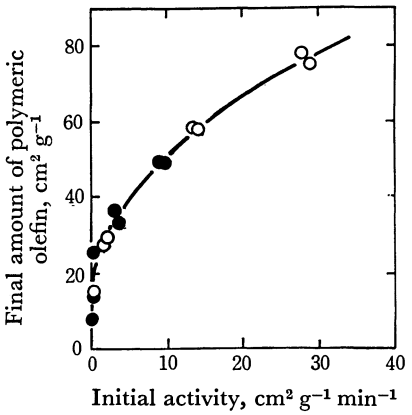

Fig. 5. Correlation between the initial activity and the final amount of formation of polymeric olefin: propylene (●) and *cis*-2-butene (○).

Figure 5 shows a correlation of the initial activity with the amount of polymeric olefin formed after 20 h (the final amount of formation). The final amount of formation of the polymeric olefin increased with an increase in the initial activity.

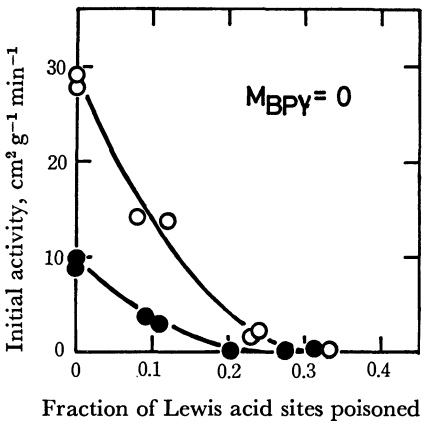

Fig. 6. Effect of pyridine poisoning on the initial activity for the formation of polymeric olefin: propylene (●) and *cis*-2-butene (○).

Figure 6 illustrates a relationship between the initial activity and the fraction of Lewis acid sites poisoned. The fraction of Lewis acid sites poisoned was calculated for each wafer from the amount of Lewis acid sites poisoned (the intensity of the LPY band) before the reaction and the Lewis acid content determined after the reaction. It should be noted here that for all the wafers used no Brønsted acid sites are poisoned, *i.e.*, $M_{BPY}=0$.

Discussion

Nature of the Polymeric Species. The polymeric species have characteristics of saturated hydrocarbons, as characterized in their IR spectra by the absence of unsaturated =C–H and C=C stretching bands and by the presence of saturated C–H stretching and bending bands. Unlike an adsorbed paraffin, however, the species is strongly held to the surface. Such characteristics are also evidenced by the finding that the H/C ratio is close to 2 for the polymeric species (Table 2) and that no materials other than reactant olefins were detected in the gas phase. This, as well as the absence of a band around 1600 cm^{-1} arising from a conjugated polyene structure, indicates that no dehydrogenation of the polymeric species occurs under the experimental conditions employed. It has been reported that dehydrogenation occurs at higher temperatures.[24-26]

IR bands in the C–H deformation region provide, in general, valuable structural information about hydrocarbons. Hirschler[10] characterized the extracted polymeric species as a mixture of highly-branched polymeric monoolefin on the basis of its IR spectrum. In the symmetrical CH_3 deformation region, the doublet at 1385 and 1370 cm^{-1} is an indication of the presence of a $(CH_3)_2CH$–, $(CH_3)_2CR$–, or $(CH_3)_3C$– group in the species.[27] Therefore, the polymeric species probably is branched and consists of saturated oligomers with a cationic property. Recent Raman and IR spectra[28] of butyl cations show that in the relevant frequency regions no significant difference is found between butyl cations and the corresponding neutral butyl groups. A cationic property of the polymeric species is also suggested by difference in the reactivity of various olefins (isobutylene$\gg$*cis*-2-butene$>$propylene $\gg$ethylene).

Nature of Active Sites. Figure 6 indicates that the initial activity of SA-1 declines sharply for polymeric olefin formation as the fraction of Lewis acid sites poisoned increases, in spite of the fact that the Brønsted acid sites remain unpoisoned for all the samples. Since the initial activity should depend directly upon the number of active sites, these results unequivocally demonstrate that some of the Lewis acid sites (25—30% of the total Lewis acid content) play a vital role in initiating the reaction over silica–alumina. The pyridine molecules held to Lewis acid sites of all samples are those which remain unremoved on the Lewis acid sites even by evacuation at a temperature as high as 350 °C. It can be stated, therefore, that such Lewis acid sites are strongly acidic. Consequently, the conclusion is drawn that strong Lewis acid sites are active in the formation of the polymeric olefin over silica–alumina. This conclusion is consistent with our recent results that added-back water sharply decreases the initial activity of SA-1 and to a slight extent the Lewis acid content, in spite of an increase in the Brønsted acid content.[21] Although the catalysts of Friedel-Crafts type have been thought to require a co-catalyst such as water

and alcohol,[29] recent studies of isobutylene polymerization in the liquid phase revealed that $AlBr_3$[30] and $AlCl_3$[31] both catalyzed the reaction even in the absence of a co-catalyst.

As expected from Fig. 5, a correlation similar to that in Fig. 6 was found between the final amount of formation of the polymeric olefin and the extent of pyridine poisoning of the Lewis acid sites. This correlation indicates that the final amount of formation decreases with a decrease in the number of the active sites. If polymeric olefin migrated onto sites other than the active sites, where it was formed, and liberated them, the final amount of formation of the polymeric olefin should ultimately become essentially the same for all the samples, independent of the number of unpoisoned active sites. Therefore, the above correlation is easily explained on the assumption that the polymeric olefin grows on the active sites that initiated the reaction and remains on them.

In view of this interpretation as well as the nature of the polymeric olefin described above, the formation of the polymeric olefin may be visualized as follows:

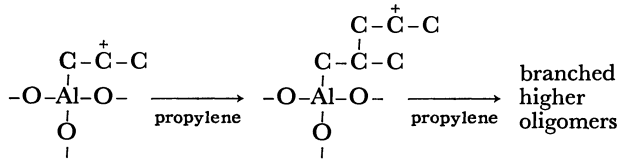

Polymerization may accompany isomerization resulting in further branching of the oligomers. Since the distribution of products shown in Table 3 is substantially the same as that found in the gas phase in the olefin polymerization over silica–alumina at higher temperatures,[25,26] the high-temperature polymerization may proceed *via* a polymeric olefin intermediate.

The authors are indebted to Drs. Yasukazu Saito, Toshio Uchijima, and Makoto Misono for valuable discussions.

References

1) E. P. Parry, *J. Catal.*, **2**, 371 (1963).
2) J. W. Ward and R. C. Hansford, *J. Catal.*, **13**, 154 (1969).
3) J. W. Ward, *J. Catal.*, **26**, 451 (1972).
4) D. Ballivet, D. Barthomeuf, and P. Pichat, *J. Chem. Soc. Faraday Trans. 1*, **1972**, 1712.
5) J. Take, T. Ueda, and Y. Yoneda, unpublished data.
6) J. B. Peri, *Proc. Int. Congr. Catal., 3rd, Amsterdam, 1964*, **2**, 1100 (1965).
7) T. J. Weeks, Jr., C. L. Angell, I. R. Ladd, and A. P. Bolton, *J. Catal.*, **33**, 256 (1974).
8) A. Ozaki and K. Kimura, *J. Catal.*, **3**, 395 (1964).
9) J. W. Hightower and W. K. Hall, *J. Am. Chem. Soc.*, **89**, 778 (1967).
10) A. E. Hirschler, *Am. Chem. Soc. Meet., Chicago, Sept. 1970*, Preprints, Div. of Petrol. Chem., **15**, No. 3, A97 (1970).
11) J. N. Finch and A. Clark, *J. Catal.*, **13**, 147 (1969).
12) A. Clark and J. N. Finch, *Proc. Int. Congr. Catal., 4th, Moscow, 1968*, **2**, 361 (1971).
13) V. C. F. Holm, G. C. Bailey, and A. Clark, *J. Phys. Chem.*, **63**, 129 (1959).
14) M. Sato, T. Aonuma, and T. Shiba, *Proc. Int. Congr. Catal., 3rd, Amsterdam, 1964*, **1**, 396 (1965).
15) L. Forni, "Catalysis Reviews," Vol. 8, ed. by H. Heinemann, Marcell Dekker, New York (1974), p. 65.
16) J. Take, H. Kawai, and Y. Yoneda, *J. Catal.*, **36**, 365 (1975).
17) J. Take, K. Mizuno, and Y. Yoneda, *J. Catal.*, in, press.
18) M. R. Basila, T. R. Kantner, and K. H. Rhee, *J. Phys. Chem.*, **68**, 3197 (1964).
19) J. W. Ward, *J. Catal.*, **11**, 271 (1968).
20) T. R. Hughes and H. M. White, *J. Phys. Chem.*, **71**, 2192 (1967).
21) J. Take, M. Ikeda, and Y. Yoneda, unpublished data.
22) M. Primet, P. Pichat, and M. V. Mathieu, *J. Phys. Chem.*, **75**, 1221 (1971).
23) A. E. Hirschler, *J. Catal.*, **6**, 1 (1966).
24) P. E. Eberly, Jr., *J. Phys. Chem.*, **71**, 1717 (1967).
25) F. E. Shephard, J. J. Rooney, and C. Kemball, *J. Catal.*, **1**, 379 (1962).
26) M. Misono and Y. Yoneda, *Bull. Chem. Soc. Jpn.*, **40**, 42 (1967).
27) L. J. Bellamy, "The Infra-red Spectra of Complex Molecules," Methuen & Co. London; John Wiley & Sons New York, 2nd ed. (1958).
28) G. A. Olah, J. R. DeMember, A. Commeyras, and J. L. Bribes, *J. Am. Chem. Soc.*, **93**, 459 (1971).
29) P. H. Plesch, "The Chemistry of Cationic Polymerization," ed. by P. H. Plesch, Pergamon Press (1963), p. 141.
30) M. Chmelvir, M. Marek, and O. Wichterle, *J. Polymer Sci., C*, **16**, 833 (1967).
31) J. H. Beard, P. H. Plesch, and P. P. Rutherford, *J. Chem. Soc.*, **1964**, 2566.

The Primary Process of the Photochemical Isomerization of Azanaphthalene *N*-Oxides

Norisuke HATA and Isao ONO

Department of Chemistry, College of Science and Engineering, Aoyama Gakuin University, Chitosedai, Setagaya, Tokyo 157

(Received February 12, 1976)

The quantum yields for the photochemical isomerization of azanaphthalene *N*-oxides, such as quinoline *N*-oxide and isoquinoline *N*-oxide, into lactam (Process I) or oxazepine (Process II) were determined in benzene (or carbon tetrachloride), in methanol, and in mixtures of the two solvents. Consequently, the reaction was revealed to be closely related to whether or not the *N*-oxide oxygen atom forms a hydrogen bond with the solvent molecule; that is, a strong hydrogen-bonding interaction between the excited singlet *N*-oxide and alcohol is essential for Process I, but not for Process II. It was further demonstrated that Process II occurred with the formation of powerful oxidants (probably oxaziridines) from the excited singlet *N*-oxide, whereas such an oxidizing species was not involved in Process I. The reaction mechanisms of Processes I and II were also discussed on the basis of the present experimental results.

It has been well established that the photochemical isomerization of quinoline *N*-oxide or isoquinoline *N*-oxide into lactam (Process I) or oxazepine (Process II)[1] occurs from the lowest excited singlet state (S_1).[2,3] In order to account for such a photoisomerization, oxaziridines have been customarily postulated as the primary photoproduct from which all the products were derived.[4] However, several experimental data conflicting with this idea have recently been documented in the literature. Lohse has concluded from the results of his laser photolysis and quantum-yield measurements of isoquinoline *N*-oxides that there was no common intermediate leading to both Processes I and II.[2] In view of the photochemical behavior of isoquinoline *N*-oxide in water at different pH values, we have also indicated that the intervention of an oxaziridine intermediate is extremely doubtful in Process I.[3]

In the present paper, we wish to report some new observations and interpretations of the primary process of the photochemical isomerization of azanaphthalene *N*-oxides, such as quinoline *N*-oxide and isoquinoline *N*-oxide.

Experimental

2-Phenyl-, 3-phenyl-, and 2-cyano-quinoline *N*-oxides, and isoquinoline *N*-oxide were synthesized and purified according to the method given in the literature.[5,6] In the irradiation experiments, reagent-grade benzene, methanol, and ethanol of Wako Pure Chemical Industries Co. and also spectro-grade carbon tetrachloride (Dojindo Co.) were used without further purification. The photolytic procedure was quite similar to that described in a previous paper.[3] Small-scale photolyses for the determination of the quantum yield were performed in a quartz cylindrical cell (5-cm in diameter and 1-cm in length), using a 250 W high-pressure mercury lamp (USH-250D) equipped with a filter combination of a nickel sulfate solution with UV-31 and UVD-25 Toshiba filters, while the light intensity was determined by means of a potassium tris-(oxalato)ferrate(III) actinometer. Large-scale photolyses were carried out in a Pyrex vessel (70 ml) using a 100 W high-pressure immersion mercury lamp (Riko Kagaku Sangyo Co.). All the photolytic experiments were undertaken in a nitrogen atmosphere. The UV absorption spectra were measured with a Hitachi recording spectrophotometer EPS-3T.

Results and Discussion

The photochemical isomerization of azanaphthalene *N*-oxides in solution is well known to be very sensitive to the nature of the solvent or substituent group.[4] That is, isoquinoline *N*-oxide **1**, quinoline *N*-oxide **2**, or 3-phenylquinoline *N*-oxide **3** isomerizes predominantly to the corresponding lactam, **1a**, **2a**, or **3a**, in a hydroxylic solvent, such as alcohol and water (Process I), whereas in a nonhydroxylic solvent, such as benzene and acetone, these *N*-oxides are primarily converted into the corresponding oxazepines **1b**, **2b**, and **3b** (Process II). In the case of 2-phenylquinoline *N*-oxide **4** or 2-cyanoquinoline *N*-oxide **5**, having an electron-withdrawing group at the 2-position of a quinoline nucleus, however, Process II occurs preferentially to give rise to a stable oxazepine, **4b** or **5b**, irrespective of the nature of the solvent, whether hydroxylic or nonhydroxylic. Table 1 lists the chemical yields of the main products of the photolyses of **1**—**5** in various solvents. Meanwhile, the intermolecular hydrogen-bonding in heterocyclic *N*-oxides has been investigated spectroscopically in detail.[12] It has been thus proved that the oxygen atom of the $N\rightarrow O$ group in **1**, **2**, or **3** formed a strong hydrogen bond to alcohol or water, whereas such a hydrogen-bonding interaction was negligibly small in the case of **4** or **5** because of the electron-withdrawing group at the 2-position of a quinoline nucleus.

It is inferred from the foregoing that the remarkable dependence of the photochemical isomerization of azanaphthalene *N*-oxides on the nature of the solvent or substituent is closely related to whether or not the *N*-oxide oxygen atom can form a hydrogen bond with a hydroxylic solvent. In order to clarify this point, we determined the qunatum yield of both the disappearance of *N*-oxide (Φ_{dis}) and the formation of lactam or oxazepine (Φ_{lac} or Φ_{oxa}) for **1**, **3**, and **4** in benzene (or carbon tetrachloride), in methanol, and in mixtures of the two solvents at room temperature.

Figure 1 shows the results when the quantum yield for the disappearance of **1** or **4** was plotted against the concentration of methanol in a carbon tetrachloride

TABLE 1. PRODUCT DISTRIBUTION IN PHOTOLYSES OF AZANAPHTHALENE *N*-OXIDES

N-Oxide	Solvent	Product (Yield, %)		Ref.
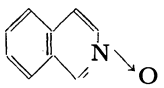 **1**	Ethanol	**1a** (67)		2
	Acetone	**1a** (8)	**1b** (unstable)	2
	Benzene	**1a** (10)	**1b** (unstable)	Present work
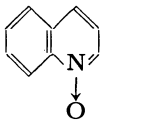 **2**	Ethanol	**2a** (49)	**2b** (unstable)	7
	Acetone	**2a** (15)	**2b** (unstable)	8
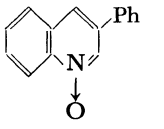 **3**	Ethanol	**3a** (98)		9
	Acetone	**3a** (20)	**3b** (unstable)	9
	Benzene	**3a** (21)	**3b** (unstable)	Present work
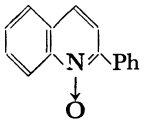 **4**	Ethanol	**4a** (8)	**4b** (80)	6, 10, 11
	Benzene		**4b** (95)	Present work
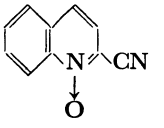 **5**	Ethanol		**5b** (84)	Present work
	Acetone		**5b** (90)	11
	Benzene		**5b** (88)	Present work

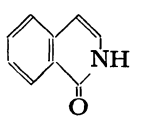

1a

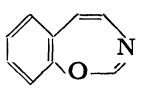

1b

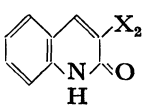

2a (X_2=H)
3a and **4a** (X_2=Ph)

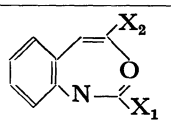

2b (X_1=H, X_2=H)
3b (X_1=H, X_2=Ph)
4b (X_1=Ph, X_2=H)
5b (X_1=CN, X_2=H)

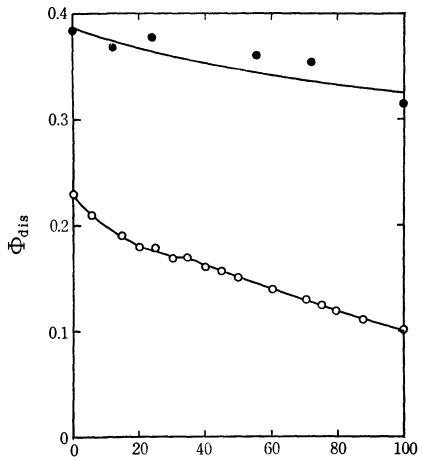

Fig. 1. Quantum yield of the disappearance of **1** or **4** in methanol–CCl_4 or methanol–benzene.
—○—: Isoquinoline *N*-oxide **1** in methanol–CCl_4 ([**1**]; 4.0×10^{-5} M), —●—: 2-Phenylquinoline *N*-oxide **4** in methanol–benzene ([**4**]; 1.0×10^{-4} M).

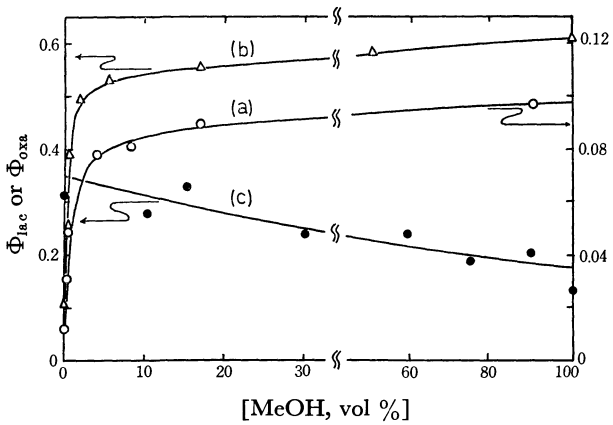

Fig. 2. Quantum yield of the formation of **1a**, **3a**, or **4b** in methanol–benzene ([*N*-oxide]; 2.0×10^{-3} M).
(a) —○—: **1a**, (b) —△—: **3a**, (c) —●—: **4b**.

or benzene solution, from which the quantum yield was noticed to decrease with an increase in the concentration of methanol.

Figure 2 shows the quantum yield of the formation of lactam or oxazepine determined as a function of the concentration of methanol in a benzene solution. As can be seen from Curve (a) or (b) in the figure, the value of Φ_{lac} in a benzene solution of **1** or **3** increased steeply upon the addition of a small amount of methanol until it became approximately a constant value at a concentration of methanol greater than 5 vol%. On the other hand, **4** showed a continuous decrease in Φ_{oxa} as the concentration of methanol increased (Curve (c) in Fig. 2).

As is shown in Scheme 1, such a dependence of the quantum yield on the concentration of the alcohol could be interpreted in terms of a hydrogen-bonding equilibrium between the *N*-oxide and alcohol;[13,14] in

this scheme it was assumed that Process I proceeds from the excited singlet *N*-oxide hydrogen-bonded to alcohol ($S_1\cdots HOR$), while the nonhydrogen-bonded excited singlet *N*-oxide (S_1) undergoes Process II.

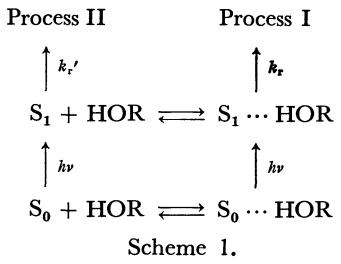

Scheme 1.

Assuming photostationary state conditions, the quantum yield for the formation of oxazepine or lactam is given by Eq. 1 or 2;

$$1/\Phi_{oxa} = K_e(k_r+k_d)[ROH]/k_{r'} + (k_{r'}+k_{d'})/k_{r'} \quad (1)$$

$$1/\Phi_{lac} = (k_{r'}+k_{d'})/K_e k_r[ROH] + (k_r+k_d)/k_r \quad (2)$$

where k_d or $k_{d'}$ is the sum of the rate constants of the deactivation of $S_1\cdots HOR$ or S_1 other than the reaction, k_r or $k_{r'}$ is the rate constant of the reaction of $S_1\cdots HOR$ or S_1 to give products responsible for Process I or Process II, and K_e is the equilibrium constant between $S_1\cdots HOR$ and S_1. Accordingly, if this scheme is correct, the reciprocal of Φ_{oxa} or Φ_{lac} should be directly proportional to the alcohol concentration or its reciprocal. In fact, as is shown in Figs. 3 and 4, the plot of Φ_{oxa} or Φ_{lac} against [MeOH] or its reciprocal was found to be linear, which was consistent with Eq. 1 or 2. This means that Process I proceeds through the S_1-species hydrogen-bonded to methanol, while the nonhydrogen-bonded S_1-species is responsible for Process II.

The first step in the photochemical isomerization of heterocyclic *N*-oxides has been supposed to be the formation of an oxaziridine intermediate common to both Processes I and II. However, all attempts to observe oxaziridine intermediates have been unsuccessful, except for the case of 9-cyano- or 9-chloroacridine *N*-oxide, where the isolation of oxaziridine has been effected in the form of the valence-tautomer.[15] If the photochemical isomerization of quinoline *N*-oxide or isoquinoline *N*-oxide proceeds *via* an oxaziridine intermediate, irradiations of the *N*-oxides in the presence of the iodide ion would have to bring about the liberation of iodine and the formation of parent amine at the same

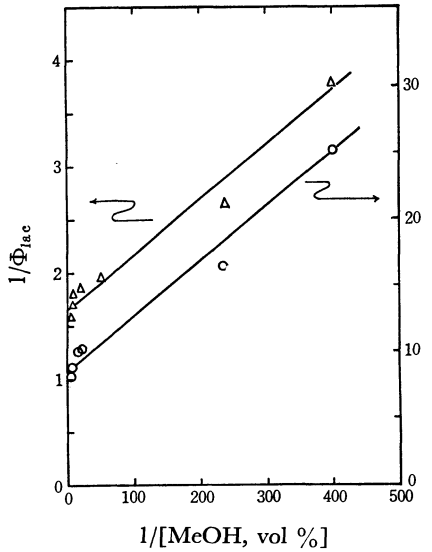

Fig. 3. Quantum yield of the formation of **1a** or **3a** *vs.* concentration of methanol.
—○—: **1a**, —△—: **3a**.

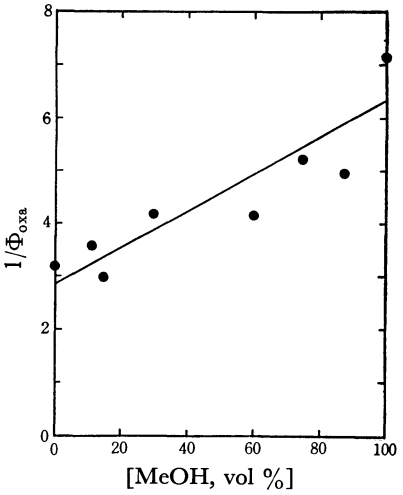

Fig. 4. Quamtum yield of the formation of **4b** *vs.* concentration of methanol.

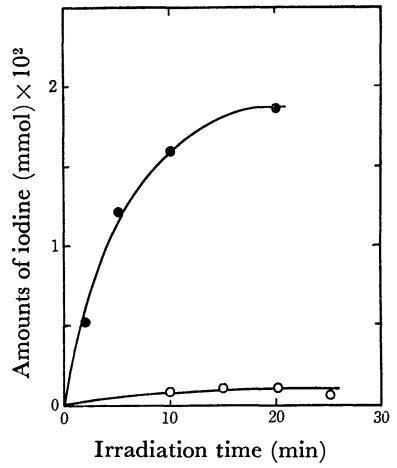

Fig. 5. Amounts of iodine liberated *vs.* irradiation time.
—○—: Isoquinoline *N*-oxide **1**, —●—: 2-Cyanoquinoline *N*-oxide **5**. [*N*-oxide]: 2.0×10^{-3} M, [KI]: 1.0 M, Solvent: 20 ml of ethanol–water (1: 1).

Table 2. The effect of iodide ion on photolyses of *N*-oxides **1** and **5**

N-Oxide	Concentration of KI	Product (Yield, %)
1	0 M	**1a** (66), Isoquinoline (trace)
	1.0 M	**1a** (52), Isoquinoline (trace)
5	0 M	**5b** (73), 2-Quinolinecarbonitrile (trace)
	1.0 M	2-Quinolinecarbonitrile (68)

Concentration of *N*-oxide; 5×10^{-3}M. Solvent; 40 ml of ethanol–water (1: 1). Irradiation Time; 20 min.

time, for oxaziridines are normally powerful oxidants. Figure 5 and Table 2 show the results when the photolysis of **1** or **5** was performed in aqueous ethanol containing potassium iodide in a nitrogen atmosphere, where iodine release was followed iodometrically as a function of the irradiation time. As may be seen from Fig. 5, iodine was detected in quantity in the case of **5**, but not in the case of **1**. In addition, in the case of **5** there was observed a complete quenching of the photoisomerization and a marked increase in the yield of the deoxygenation product (2-quinolinecarbonitrile), whereas the photochemical reaction of **1** was scarcely affected by iodide ions (Table 2). These results suggest that Process II takes place with the formation of a powerful oxidant (probably oxaziridine) from the excited singlet *N*-oxide, whereas such an oxidizing intermediate is not involved in Process I.

From the experimental results presented above, the following conclusions can be obtained regarding the primary process of the photochemical isomerization of azanaphthalene *N*-oxides: (i) When the *N*-oxide oxygen atom does not form a hydrogen bond with solvent molecules, the azanaphthalene *N*-oxide excited into the S_1 state may be initially converted into the oxaziridine and thereafter transformed into the oxazepine (Process II). This is quite consistent with the mechanism given by earlier investigators (Scheme 2).[4] (ii) When there

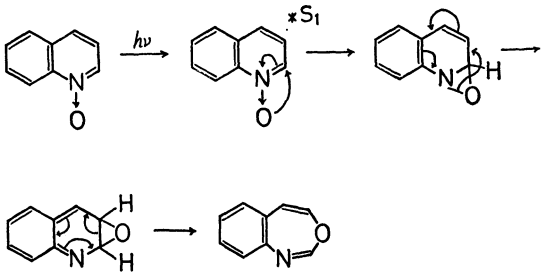

Scheme 2.

is a strong hydrogen-bonding interaction between the *N*-oxide oxygen atom and the solvent molecule, the azanaphthalene *N*-oxide may undergo photochemical rearrangement to the lactam without the formation of an oxaziridine intermediate (Process I), as we have deduced in a previous paper.[3] These conclusions also imply that the formation of oxaziridine from the excited singlet *N*-oxide is greatly diminished by the hydrogen-bonding interaction between the *N*-oxide oxygen atom and the hydroxylic solvent. A very similar conclusion has also been obtained by Tanaka *et al.* in the case of the photochemical isomerization of α,*N*-diphenylnitrone to oxaziridine (singlet reactions) in solution

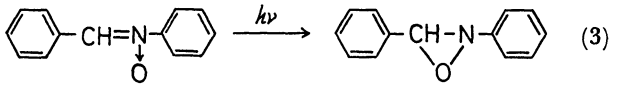

(3)

(Eq. 3),[16] where the drop in the quantum yield of the reaction has been shown to be produced either by changing the solvent from cyclohexane to ethanol or by introducing a hydroxyl group to the *ortho*-position of an α-phenyl ring.

As to the mechanism of Process I, Kaneko and Buchardt have independently presented the idea that the primary photoproduct was an oxaziridine which can be postulated to undergo a heterolytic cleavage to give a carbonium ion or a zwitterion[4] (*cf.* Schemes 1 and 2 in Ref. 3), but such a mechanism evidently conflicts with the conclusion described above. Therefore, we propose the following mechanism to account for Process I (Scheme 3): According to the concept of electron donor-acceptor interaction, hydrogen bond formation is generally accepted to be due to the stabilization caused by resonance interaction between the no-bond structure and the CT structure, *e.g.*, Eq. 4, which is shown for quinoline *N*-oxide, and the contribution of the CT structure may be important in strong

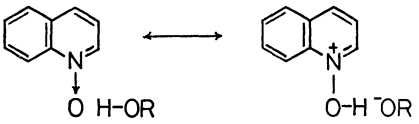

(4)

no-bond structure CT structure

hydrogen-bonding.[12c] Therefore, as is shown in Scheme 3, the photoexcitation of such a hydrogen-bonded *N*-oxide is presumed to cause a protonation of the N→O group to give ion-pairs, through which a conversion to the lactam could occur.[17]

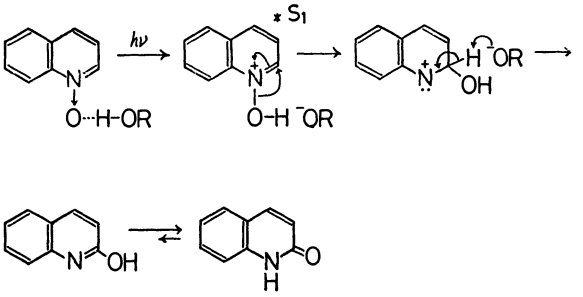

Scheme 3.

In conclusion, the authors wish to thank Professor Oyo Mitsunobu for his kind discussion and Miss Michiko Maniwa for her assistance.

References

1) According to the convention in the previous paper,[3] the photochemical isomerization to a lactam is referred to as Process I, and the photochemical conversion to an oxazepine is termed Process II.

2) C. Lohse, *J. Chem. Soc., Perkin Trans. 2*, **1972**, 229.

3) I. Ono and N. Hata, *Bull. Chem. Soc. Jpn.*, **46**, 3658 (1973).

4) G. G. Spence, E. C. Taylor, and O. Buchardt, *Chem. Rev.*, **70**, 231 (1970); S. Yamada, M. Ishikawa, and C. Kaneko *Chem. Pharm. Bull.*, **23**, 2818 (1975).

5) E. Ochiai, "Aromatic Amine Oxide," Elsevier (1967), Chap. 3.

6) O. Buchardt, B. Jensen, and I. K. Larsen, *Acta Chem. Scand.*, **21**, 1841 (1967).

7) O. Buchardt, *Acta Chem. Scand.*, **17**, 1461 (1963).

8) J. Streith, H. K. Darrah, and M. Weil, *Tetrahedron Lett.*, **1966**, 5555.

9) O. Buchardt, P. L. Kumler, and C. Lohse, *Acta Chem. Scand.*, **23**, 2149 (1969).
10) O. Buchardt, *Tetrahedron Lett.*, **1966**, 6221.
11) C. Kaneko and S. Yamada, *Chem. Pharm. Bull.*, **14**, 555 (1966).
12) a) E. Ochiai, "Aromatic Amine Oxide," Elsevier (1967), Chap. 4; b) A. R. Katritzky and J. M. Lagowski, "Chemistry of the Heterocyclic *N*-Oxides," Academic Press (1971), Chap. 1; c) N. Mataga and T. Kubota, "Molecular Interactions and Electronic Spectra," M. Dekker (1970), Chap. 7.
13) The existence of such a hydrogen-bonding equilibrium in the fluorescent state has been demonstrated in the case of acridine *N*-oxide by Kubota *et al.*[12c,14]
14) T. Kubota and H. Miyazaki, *Nippon Kagaku Zasshi*, **79**, 916 (1958).
15) S. Yamada, M. Ishikawa, and C. Kaneko, *J. Chem. Soc., Chem. Commun.*, **1972**, 1093.
16) K. Shinzawa and I. Tanaka, *J. Phys. Chem.*, **68**, 1205 (1964); K. Koyano and I. Tanaka, *ibid.*, **69**, 2545 (1965); N. Harada, Y. Mori, and I. Tanaka, *Mol. Photochem.*, **2**, 153 (1970).
17) Ion-pair formation in the excited states through hydrogen-bonding interaction has been well investigated on the system containing β-naphthol and amine. A. Matsuzaki, S. Nagakura, and K. Yoshihara, *Bull. Chem. Soc. Jpn.*, **47**, 1152 (1974) and also references cited therein.

The Crystal Structure of the Intermolecular Complex between 9-Ethyladenine and Indole

Tsuguhiro KANEDA and Jiro TANAKA

Department of Chemistry, Faculty of Science, Nagoya University, Chikusa, Nagoya 464

(Received February 12, 1976)

The crystal structure of a 1: 1 complex of 9-ethyladenine and indole has been determined by the X-ray method. The crystal system is monoclinic with the space group of $P2_1/c$. The cell dimensions are $a=15.712(2)$, $b=8.098(1)$, $c=11.838(1)$Å, and $\beta=103.90(1)°$. Adenines form walls made of double layer. An overlap of adenines is found between layers. The adenine molecule in the front layer is found to be joined by the hydrogen bond with the molecule in the back layer. An intermolecular hydrogen bond is found between adenine and indole rings. The significance of these observations in the interaction of adenine with tryptophan in biological systems is discussed.

The crystal structures of adenine derivatives and its complexes with uracil or thymine have been studied in order to find the intermolecular forces between DNA bases and other related molecules.[1-6] Adenine is also important as a constituent of many biologically significant molecules such as ATP, NAD and FAD. Voet and Rich,[7-9] and Tomita and his group[10] studied the structure of intermolecular complexes between adenine with other molecules such as riboflavin, barbiturate and nicotinic acid derivatives. The aim of these investigations is to find a specific interaction in enzymatic or biological reactions involving adenine group.

Helene and his co-workers[11-14] studied the interaction of aromatic residues of proteins with nucleic acids and their model system spectroscopically, and suggested the formation of complexes between purine or pyrimidine with aromatic amino acids, *e.g.*, adenosine with tryptophan. Morita *et al.*[15-17] studied a specific interaction between ATP with an enzyme, myosine-ATPase, and its model system by the UV absorption measurement. They suggested that a charge transfer force exists between adenine and indole rings through the stacking of molecules. The charge transfer force may be important between the donor and acceptor molecules. However, no such interaction has been confirmed in the crystal of the complex composed of adenine and indole. An X-ray study is desirable on the complex of these molecules.

In the present paper we give the crystal structure of a 1: 1 9-ethyladenine-indole complex. It was found that the hydrogen bonding is most important as an intermolecular force between adenine and indole rings as well as between adenines.

Experimental

Equimolar amounts of 9-ethyladenine and indole were dissolved in methanol. Pale yellow crystals were obtained by slow evaporation at room temperature. The ultraviolet spectrum of the dissolved crystals shows that they contain approximately equimolar amounts of 9-ethyladenine and indole.

The space group was determined from oscillation and Weissenberg photographs. The density was measured by the flotation method in the mixed solution of cyclohexane and carbon tetrachloride. The cell dimensions were determined by the least-squares method, using twelve reflections carefully measured on a Hilger-Watts four circle diffractometer with Zr-filtered Mo$K\alpha$ radiation ($\lambda=0.71069$ Å). The crystal was found to be not so unstable while being left to stand in the air, but the color changed to light brown. It was therefore mounted in a glass capillary for the X-ray measurements. Intensity data were collected with the same diffractometer in the ω-2θ scanning mode ($2\theta \leqq 52°$) with the same radiation. The size of the crystal used was $0.3\times0.3\times0.2$ mm. No absorption or extinction correction was made because of the smallness of the crystal. In order to confirm the stability of the crystal and the counter system, the intensities of three standard reflections were measured every 50 reflections. The fluctuation and the decay of standard reflections was within 5%. The crystal data are given in Table 1.

Table 1. Crystal data

$C_7H_9N_5 \cdot C_8H_7N$
F.W.: 280.33
Crystal system: monoclinic
Space group: $P2_1/c$
$a=15.712$ (2), $b=8.098$ (1),
$c=11.838$ (1) Å; $\beta=103.90$ (1)°,
$D_m=1.274$, $D_c=1.273$ g·cm^{-3}
$\mu=1.05$ cm^{-1} (for Mo$K\alpha$ radiation).

Determination and Refinement of the Structure

The structure was solved by the direct method with the program MULTAN[18] using 415 reflections with $|E| \geqq 1.20$. An E-map computed from the phase set with the highest figures of merit ($FOM=1.448$) revealed the positions of non-hydrogen atoms. The block-diagonal least-squares method was applied to the refinement of the structure parameters by using 1106 independent reflections with $|F^\circ| \geqq 5\sigma$. An R-index was reduced to 0.107. At this stage, a difference Fourier synthesis was performed. Two other peaks could be assigned to the disordered ethyl group of 9-ethyladenine, and eleven hydrogen atoms, other than those belonging to the ethyl groups, were found in this map. The occupancies for the differently oriented ethyl groups were also refined as a group by the least-squares method to be 0.65 and 0.35, respectively. Subsequent refinement was carried out with anisotropic thermal parameters for non-hydrogen atoms, and with isotropic ones for hydrogen atoms. The final R-index converged to 0.074 with an equal weight for each reflection.

The atomic scattering factors were taken from the work of Stewart, Davidson and Simpson[19] for the

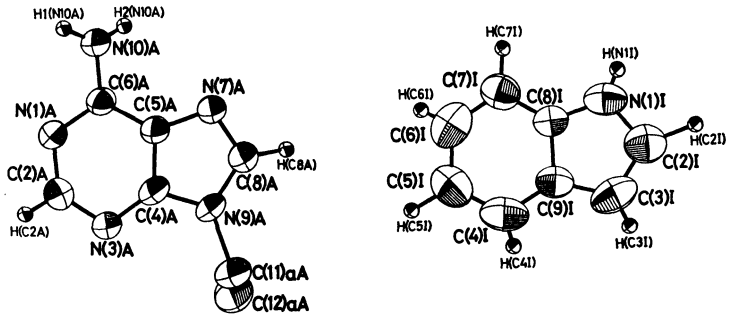

Fig. 1. The atomic labelings of 9-ethyladenine and indole. Nonhydrogen atoms are represented as thermal ellipsoids of a size such that the vibrating atoms have a 50% probability of being found within them. Hydrogen atoms are represented as spheres that are defined by the artificial isotropic thermal factor B of 1.0 Å^2.

hydrogen atom and from the International Tables for X-ray Crystallography[20] for other atoms. The program HBLS-IV coded by Ashida and the program written by Katayama and Wada were utilized for the block-diagonal least-squares refinements. The program ORTEP coded by Johnson was utilized for the drawings in Figs. 1, 4 and 5. All the computations were performed on a FACOM 230-60 computer at the Nagoya University Computation Center. The observed and calculated structure factors are listed in Table 2.[21]

Results and Discussion

The atomic labelings and thermal ellipsoids are shown in Fig. 1. The positional and thermal parameters with their standard deviations for non-hydrogen atoms are given in Tables 3 and 4, respectively. The coordinates and isotropic thermal parameters for hydrogen atoms, except for those belonging to ethyl groups, are given in Table 5.

Molecular Structure. The bond distances and bond angles with their standard deviations involving only heavy atoms are given in Tables 6 and 7, respectively. The covalent bond distances and angles of 9-ethyladenine are in good agreement with values found in other crystals.[2,8] The bond distances and angles around the disordered ethyl groups show somewhat abnormal values because of the disordered structure. The adenine molecule is highly planar with a maximum deviation of 0.028 Å for C(5)A from the least-squares plane (Table 8).

The bond distances and angles of indole agree with values found in crystals of L-tryptophan hydrobromide,[24] tryptamine picrate and D,L-tryptophan picrate.[25] The only exception is in the C(7)I–C(8)I bond distance, which is smaller by *ca.* 0.06 Å as compared with the values in the literature.[24,25] The indole molecule is also highly planar with a maximum deviation of 0.011 Å for C(5)I from the least-squares plane.

Crystal Structure. The crystal structure projected along the b axis is shown in Fig. 2. Adenines form walls consisting of a double layer. An overlap of adenines, related to a center of symmetry, is observed between the layers. Four hydrogen bonds are found between adenine molecules which connect the molecule in the front layer with the molecule in the back one (Fig. 3).

Table 3. Atomic coordinates and their standard deviations of heavy-atoms

	x	y	z
N(1)A	0.5394 (4)	−0.2711 (8)	0.3944 (6)
C(2)A	0.5873 (5)	−0.3077 (11)	0.5023 (8)
N(3)A	0.6376 (4)	−0.2102 (9)	0.5798 (6)
C(4)A	0.6358 (4)	−0.0550 (11)	0.5389 (7)
C(5)A	0.5893 (4)	0.0019 (10)	0.4320 (7)
C(6)A	0.5396 (4)	−0.1149 (10)	0.3558 (7)
N(7)A	0.6055 (4)	0.1677 (9)	0.4186 (6)
C(8)A	0.6601 (6)	0.2075 (12)	0.5180 (9)
N(9)A	0.6811 (5)	0.0773 (10)	0.5925 (7)
N(10)A	0.4945 (4)	−0.0801 (8)	0.2478 (6)
C(11)aA[a]	0.727 (1)	0.087 (2)	0.731 (1)
C(11)bA[a]	0.774 (1)	0.070 (3)	0.683 (2)
C(12)aA[a]	0.817 (1)	0.033 (2)	0.720 (1)
C(12)bA[a]	0.729 (2)	0.081 (5)	0.794 (2)
N(1)I	0.7783 (4)	−0.3929 (9)	0.7547 (7)
C(2)I	0.7949 (5)	−0.4117 (14)	0.8741 (9)
C(3)I	0.8688 (5)	−0.5067 (13)	0.9058 (8)
C(4)I	0.9681 (4)	−0.6378 (12)	0.7841 (9)
C(5)I	0.9789 (5)	−0.6512 (13)	0.6727 (10)
C(6)I	0.9168 (5)	−0.5753 (14)	0.5837 (9)
C(7)I	0.8473 (5)	−0.4849 (12)	0.6014 (8)
C(8)I	0.8399 (4)	−0.4743 (10)	0.7120 (7)
C(9)I	0.8990 (4)	−0.5481 (11)	0.8064 (8)

a) The symbols a and b were used for the disordered carbons, C(11) and C(12), to discriminate the major and the minor sites.

The hydrogen bond network is developed along the b axis. All the amino NH bonds participate in hydrogen bonds, N(10)A-H···N(7)A($1-x$, $1/2+y$, $1/2-z$) and N(10)A-H···N(1)A($1-x$, $-1/2+y$, $1/2-z$). The intermolecular distances and angles for the hydrogen bonds are given in Table 9. The overlapping mode of adenine molecules is shown in Fig. 4. The interplanar distance between adenine rings is 3.50 Å. A more extensive overlapping of adenine rings is found in 9-methyladenine,[1] ATP,[6] and (9-ethyladenine)-(1-methyl-5-fluorouracil) complex.[3] The interplanar distance is 3.31—3.40 Å.

The stacking and hydrogen bondings may influence the conformation of the ethyl group, namely the structure of methylene carbons. C(11)aA and C(11)bA bend

Table 4. Anisotropic thermal factors* ($\times 10^4$) and their standard deviations of heavy-atoms

	B_{11}	B_{22}	B_{33}	B_{12}	B_{13}	B_{23}
N(1)A	65 (4)	135 (12)	82 (6)	−9 (12)	−28 (8)	−6 (15)
C(2)A	68 (6)	162 (17)	94 (9)	−46 (17)	1 (11)	39 (21)
N(3)A	66 (4)	151 (14)	87 (6)	−21 (13)	−35 (8)	27 (16)
C(4)A	51 (5)	173 (17)	79 (7)	−14 (14)	−32 (9)	−18 (19)
C(5)A	44 (4)	133 (14)	78 (7)	13 (13)	−13 (8)	0 (18)
C(6)A	43 (4)	139 (15)	72 (7)	25 (13)	1 (8)	−17 (17)
N(7)A	64 (4)	146 (13)	105 (7)	−21 (13)	−61 (9)	35 (16)
C(8)A	102 (8)	170 (19)	140 (11)	−72 (20)	−118 (15)	71 (25)
N(9)A	105 (6)	182 (15)	111 (8)	−68 (17)	−124 (11)	14 (19)
N(10)A	67 (4)	139 (12)	80 (6)	3 (13)	−33 (8)	7 (16)
C(11)aA	66 (8)	231 (30)	90 (12)	2 (27)	−24 (16)	2 (33)
C(11)bA	38 (12)	128 (41)	61 (21)	10 (39)	−36 (26)	−4 (53)
C(12)aA	44 (7)	264 (34)	147 (16)	−7 (26)	−3 (17)	10 (39)
C(12)bA	121 (25)	448 (96)	15 (20)	48 (84)	16 (36)	−54 (74)
N(1)I	67 (5)	184 (16)	119 (8)	−6 (15)	−7 (9)	36 (18)
C(2)I	66 (6)	261 (23)	133 (11)	−29 (21)	30 (13)	10 (28)
C(3)I	85 (7)	261 (23)	97 (9)	−89 (22)	6 (12)	73 (25)
C(4)I	62 (6)	208 (20)	148 (11)	−38 (18)	−22 (13)	58 (26)
C(5)I	60 (6)	240 (22)	166 (13)	−6 (19)	18 (14)	−92 (28)
C(6)I	90 (7)	248 (23)	120 (10)	−116 (22)	51 (14)	−71 (26)
C(7)I	58 (5)	211 (20)	125 (10)	0 (18)	18 (12)	−1 (24)
C(8)I	49 (5)	163 (16)	88 (8)	−16 (14)	17 (9)	13 (19)
C(9)I	47 (5)	174 (17)	103 (8)	−21 (15)	7 (10)	23 (20)

* The anisotropic thermal factors are of the form $\exp\{-(h^2B_{11}+k^2B_{22}+l^2B_{33}+hkB_{12}+hlB_{13}+klB_{23})\}$.

Table 5. Hydrogen atom parameters and their standard deviations

	x	y	z	B
H(C2A)	0.568 (3)	−0.406 (9)	0.534 (6)	5.2 (18)
H(C8A)	0.716 (5)	0.307 (14)	0.499 (9)	13.2 (35)
H1(N10A)	0.437 (5)	−0.137 (16)	0.227 (10)	16.2 (42)
H2(N10A)	0.507 (4)	0.004 (10)	0.225 (7)	6.7 (21)
H(N1I)	0.740 (4)	−0.343 (11)	0.727 (7)	7.3 (23)
H(C2I)	0.735 (4)	−0.347 (11)	0.912 (7)	8.5 (25)
H(C3I)	0.889 (4)	−0.530 (11)	0.972 (7)	7.5 (24)
H(C4I)	0.991 (4)	−0.677 (11)	0.843 (7)	7.4 (23)
H(C5I)	1.038 (5)	−0.704 (13)	0.655 (8)	10.5 (30)
H(C6I)	0.930 (4)	−0.568 (10)	0.522 (7)	6.6 (21)
H(C7I)	0.802 (4)	−0.430 (11)	0.541 (7)	7.7 (23)

Table 6. Bond lengths and their standard deviations

9-Ethyladenine		Indole	
N(1)A–C(2)A	1.35 (1) Å	N(1)I–C(2)I	1.38 (1) Å
N(1)A–C(6)A	1.35 (1)	N(1)I–C(8)I	1.36 (1)
C(2)A–N(3)A	1.32 (1)	C(2)I–C(3)I	1.37 (1)
N(3)A–C(4)A	1.34 (1)	C(3)I–C(9)I	1.41 (1)
C(4)A–C(5)A	1.38 (1)	C(4)I–C(5)I	1.37 (2)
C(4)A–N(9)A	1.36 (1)	C(4)I–C(9)I	1.38 (1)
C(5)A–C(6)A	1.41 (1)	C(5)I–C(6)I	1.39 (1)
C(5)A–N(7)A	1.38 (1)	C(6)I–C(7)I	1.37 (1)
C(6)A–N(10)A	1.33 (1)	C(7)I–C(8)I	1.34 (1)
N(7)A–C(8)A	1.32 (1)	C(8)I–C(9)I	1.40 (1)
C(8)A–N(9)A	1.36 (1)		
N(9)A–C(11)aA	1.62 (1)		
N(9)A–C(11)bA	1.59 (2)		
C(11)aA–C(12)aA	1.51 (2)		
C(11)bA–C(12)bA	1.64 (4)		

Table 7. Bond angles and their standard deviations

9-Ethyladenine		Indole	
N(1)A–C(2)A–N(3)A	129.1 (8)°	N(1)I–C(2)I–C(3)I	106.3 (9)°
N(1)A–C(6)A–C(5)A	117.4 (6)	N(1)I–C(8)I–C(7)I	128.8 (7)
N(1)A–C(6)A–N(10)A	118.7 (6)	N(1)I–C(8)I–C(9)I	107.7 (7)
C(2)A–N(1)A–C(6)A	118.8 (6)	C(2)I–N(1)I–C(8)I	110.5 (7)
C(2)A–N(3)A–C(4)A	110.6 (7)	C(2)I–C(3)I–C(9)I	109.8 (8)
N(3)A–C(4)A–C(5)A	127.1 (7)	C(3)I–C(9)I–C(8)I	105.8 (7)
C(4)A–C(5)A–C(6)A	117.0 (7)	C(4)I–C(5)I–C(6)I	117.7 (9)
C(4)A–C(5)A–N(7)A	111.0 (6)	C(4)I–C(9)I–C(8)I	118.1 (8)
C(4)A–N(9)A–C(8)A	106.9 (7)	C(5)I–C(4)I–C(9)I	120.6 (8)
C(4)A–N(9)A–C(11)aA	124.5 (8)	C(5)I–C(6)I–C(7)I	123.9 (10)
C(4)A–N(9)A–C(11)bA	125.2 (11)	C(6)I–C(7)I–C(8)I	116.2 (8)
C(5)A–C(4)A–N(9)A	105.5 (7)	C(7)I–C(8)I–C(9)I	123.5 (7)
C(5)A–C(6)A–N(10)A	123.9 (7)		
C(5)A–N(7)A–C(8)A	103.5 (7)		
C(6)A–C(5)A–N(7)A	131.9 (7)		
N(7)A–C(8)A–N(9)A	113.1 (8)		
C(8)A–N(9)A–C(11)aA	126.4 (9)		
C(8)A–N(9)A–C(11)bA	120.5 (11)		
N(9)A–C(11)aA–C(12)aA	95.7 (10)		
N(9)A–C(11)bA–C(12)bA	92.2 (13)		

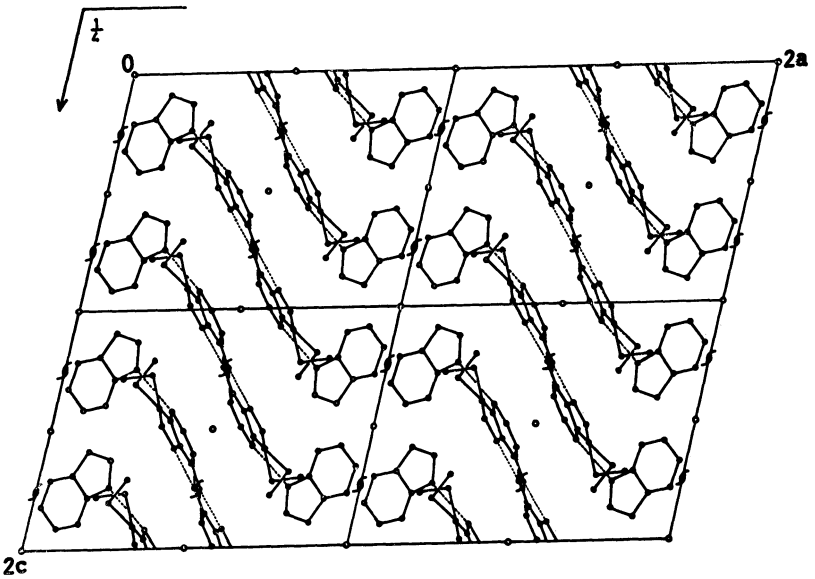

Fig. 2. Projection of the crystal structure along the b axis. Carbon atoms are depicted as open circles and nitrogen atoms as filled circles. Hydrogen bonds are represented with both dotted and broken lines. The atoms of 9-ethyladenines in both ends of the dotted line are related by the symmetry code (ii), and those of broken line are related by the symmetry code (iii) in Table 9.

TABLE 8. DEVIATIONS OF NONHYDROGEN ATOMS FROM THE LEAST-SQUARES PLANES

9-Ethyladenine plane[a]		Indole plane[b]	
N(1)A	0.012 Å	N(1)I	0.003 Å
C(2)A	0.001	C(2)I	0.004
N(3)A	−0.002	C(3)I	0.000
C(4)A	−0.017	C(4)I	−0.006
C(5)A	−0.028	C(5)I	0.011
C(6)A	0.009	C(6)I	−0.003
N(7)A	0.002	C(7)I	0.000
C(8)A	0.008	C(8)I	−0.006
N(9)A	0.015	C(9)I	−0.003
N(10)A[c]	0.064		
C(11)aA[c]	−0.32		
C(11)bA[c]	0.71		

a) Equation of the plane: $0.8971X-0.2178Y-0.3844Z'-5.320=0$. b) Equation of the plane: $0.5484X+0.8270Y+0.1244Z'-3.975=0$. c) Atoms not included in the least-squares calculation.

away to the opposite side from the adenine plane by 0.32 and 0.71 Å, respectively. A similar deviation from the plane of the adenine ring is observed for the carbon atoms of glycosidic bonds in adenosine-5′-phosphate[22] and deoxyadenosine[23] crystals, where the hydrogen bond network is developed extensively and the molecular packing is favorable to the bent conformation. Hydrogen bonds are also formed in the present crystal, the region around the disordered ethyl groups being crowded by the neighboring molecules. The distance between the terminal methyl carbon (C(12)aA) and the atoms of indole rings (C(4)I and C(5)I) is *ca.* 3.50 Å, and that between C(12)bA and hydrogen atoms of adenine rings, (H1(N10A) and H(C8A)), is *ca.* 2.60 Å (Table 9).

Indole molecules are sandwiched by the adenine

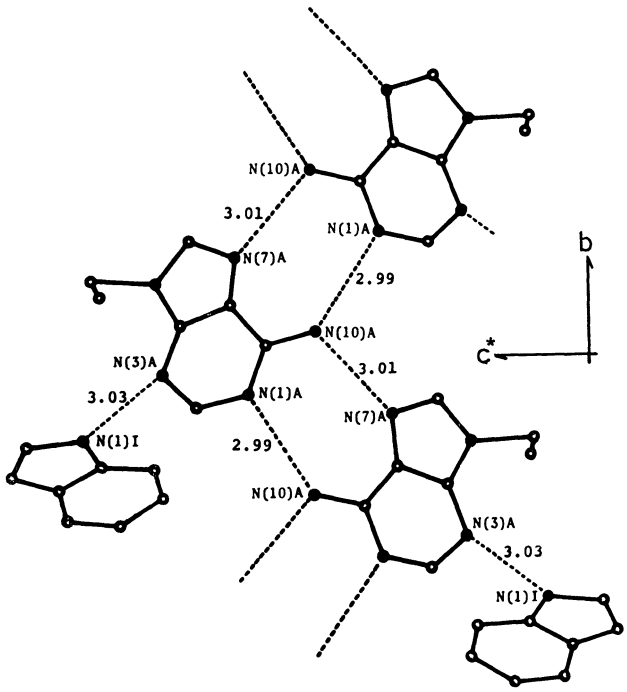

Fig. 3. Hydrogen bond network viewed along the a axis.

walls, sticking to the wall by the hydrogen bonding. A stereoscopic view along the a axis is shown in Fig. 5. No stacking interaction is found between indoles, nor between adenine and indole. Their arrangement in the crystal may be favored by the hydrogen bonding and the dipole-dipole interaction between neighboring molecules.

The most interesting feature of the crystal structure is the hydrogen bonding between adenine and indole. The N(1)I–H···N(3)A distance is 3.03 Å, which is not

Table 9. Hydrogen bonds and short van der Waals contacts
Roman numerals represent symmetry operators relevant to the atoms listed second.

Hydrogen bonds

Donor	Acceptor	Distance D···A	Distance H···A	Angle D—H···A
N(1)I —H (N1I)	···N(3)A$^{i)}$	3.03 (1) Å	2.33 (7) Å	159 (9)°
N(10)A—H1(N10A)···	N(7)A$^{ii)}$	3.01 (1)	2.32 (12)	126 (9)
N(10)A—H2(N10A)···	N(1)A$^{iii)}$	2.99 (1)	2.31 (8)	147 (6)

Short van der Waals contacts

C(4)A···	C(6)A$^{iv)}$ 3.56 (1) Å	N(10)A···	C(12)bA$^{iv)}$ 3.43 (3) Å
C(4)A···	C(2)I$^{v)}$ 3.53 (1)	C(4)I ···	C(12)aA$^{vii)}$ 3.53 (2)
C(5)A···	C(5)A$^{iv)}$ 3.55 (1)	C(5)I ···	C(12)aA$^{viii)}$ 3.49 (1)
C(5)A···	C(2)I$^{v)}$ 3.54 (1)	C(11)aA···	H1(N10A)$^{iv)}$ 2.8 (1)
N(7)A···	C(12)bA$^{vi)}$ 3.39 (3)	C(12)aA···	H(C5I)$^{ix)}$ 3.1 (1)
C(8)A···	C(12)bA$^{vi)}$ 3.54 (3)	C(12)bA···	H1(N10A)$^{iv)}$ 2.6 (1)
N(10)A···	C(11)aA$^{iv)}$ 3.55 (1)	C(12)bA···	H(C8A)$^{x)}$ 2.6 (1)

Symmetry code

superscript	Symmetry operator						
i)	x	y	z	vi)	x	$1/2-y$	$-1/2+z$
ii)	$1-x$	$1/2+y$	$1/2-z$	vii)	x	$-1+y$	z
iii)	$1-x$	$-1/2+y$	$1/2-z$	viii)	$2-x$	$-1/2+y$	$3/2-z$
iv)	$1-x$	$-y$	$1-z$	ix)	$2-x$	$1/2+y$	$3/2-z$
v)	x	$-1/2-y$	$-1/2+z$	x)	x	$1/2-y$	$1/2+z$

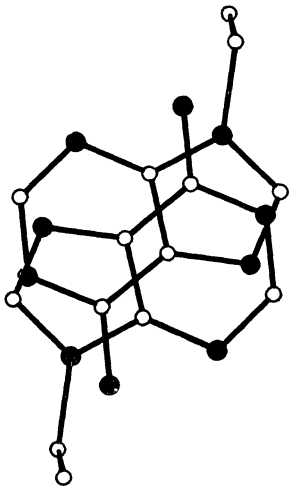

Fig. 4. A stacking pattern of the 9-ethyladenine pair. Carbon atoms are depicted as open circles and nitrogen atoms are filled circles.

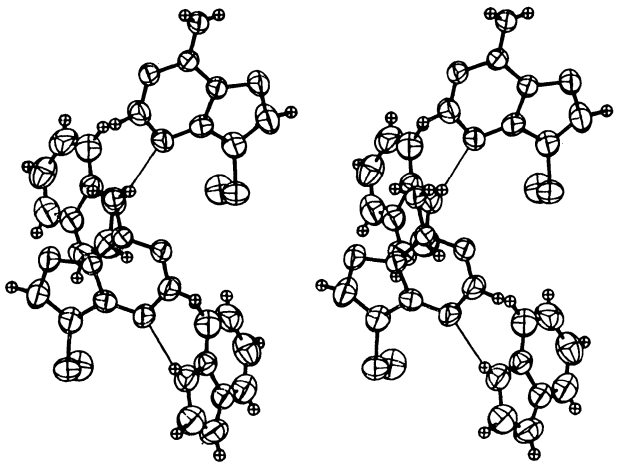

Fig. 5. A stereoscopic view of the 9-ethyladenine-indole pair. The criterion to thermal ellipsoids of nonhydrogen atoms and that of hydrogen atoms are the same in Fig. 1. The hydrogen bond between H(N1I) and N(3)A is represented in a thin solid line.

particularly small as compared with other NH···N hydrogen bond distances.[9] The molecular plane of indole tilts to that of the adenine ring with a dihedral angle of 74.7°. No particular stacking of adenine-indole pair is found in the crystal. It is therefore unlikely that the molecular association for this pair occurs through the overlapping of two rings.

The result is biologically significant in that the same mode of interaction is expected to exist between adenine and tryptophan in the biological system. It can be suggested that the hydrogen bonding is more important than the stacking of two rings in the pair. This seems reasonable since both molecules have an electron donating character contrary to the case in which one is electron donating and the other accepting. An alternative interpretation on the spectral change found in model biological systems should be worth considering by the result in this study.

References

1) R. F. Stewart and L. H. Jensen, *J. Chem. Phys.*, **40**, 2071 (1964).
2) K. Hoogsteen, *Acta Crystallogr.*, **16**, 907 (1963).
3) L. Katz, K. Tomita, and A. Rich, *Acta Crystallogr.*, **21**, 754 (1966).
4) K. Tomita, L. Katz, and A. Rich, *J. Mol. Biol.*, **30**, 545 (1967).
5) T. D. Sakore, S. S. Tavale, and H. M. Sobell, *J. Mol. Biol.*, **43**, 361 (1969).
6) O. Kennard, N.W. Isaacs, W. D. S. Motherwell, J. C. Coppola, D. L. Wampler, A. C. Larson, and D. G. Watson,

Proc. R. Soc. London, Ser. A, **325**, 401 (1971).
7) D. Voet and A. Rich, *Proc. Natl. Acad. Sci. U.S.A.*, **68**, 1151 (1971).
8) D. Voet, *J. Am. Chem. Soc.*, **94**, 8213 (1972).
9) D. Voet, *J. Am. Chem. Soc.*, **95**, 3763 (1973).
10) K. Tomita, S. Fujii, K. Fujiki, and T. Fujiwara, *Acta Crystallogr., Sect. A*, **31**, 43 (1975).
11) T. Montenay-Garestier and C. Helene, *Biochemistry*, **10**, 300 (1971).
12) C. Helene, J. L. Dimicoli, and F. Brun, *Biochemistry*, **10**, 3802 (1971).
13) C. Helene and J. L. Dimicoli, *FEBS Lett.*, **26**, 6 (1972).
14) F. Brun, J. J. Toulme, and C. Helene, *Biochemistry*, **14**, 558 (1975).
15) F. Morita, *J. Biol. Chem.*, **242**, 4501 (1967).
16) H. Yoshino, F. Morita, and K. Yagi, *J. Biochem.*, **71**, 351 (1972).
17) F. Morita, *Biochim. Biophys. Acta*, **343**, 674 (1974).
18) G. Germain, P. Main, and M. M. Woolfson, *Acta Crystallogr., Sect. A*, **27**, 368 (1971).
19) R. F. Stewart, E. R. Davidson, and W. T. Simpson, *J. Chem. Phys.*, **42**, 3175 (1965).
20) "International Tables for X-Ray Crystallography," Vol. III, Kynoch Press, Birmingham (1968), p. 201.
21) Table 2 is kept at the Chemical Society of Japan. Kanda, Surugadai, Chiyoda-ku, Tokyo 101. (Document No. 7624).
22) J. Kraut and L. H. Jensen, *Acta Crystallogr.*, **16**, 79 (1963).
23) D. G. Watson, D. J. Sutor, and P. Tollin, *Acta Crystallogr.*, **19**, 111 (1965).
24) T. Takigawa, T. Ashida, Y. Sasada, and M. Kakudo, *Bull. Chem. Soc. Jpn.*, **39**, 2369 (1966).
25) G. L. Gartland, G. R. Freeman, and C. E. Bugg, *Acta Crystallogr., Bect. B*, **30**, 1841 (1974).
26) C. E. Bugg, J. M. Thomas, M. Sundaralingam, and S. T. Rao, *Biopolymers*, **10**, 175 (1971).

Structure Analysis of a Collagen Model Polypeptide, (Pro-Pro-Gly)$_{10}$

Kenji OKUYAMA, Nobuo TANAKA,* Tamaichi ASHIDA,** and Masao KAKUDO*

Department of Applied Chemistry, Kyushu University, Fukuoka 812
**Institute for Protein Research, Osaka University, Suita, Osaka 565*
***Department of Applied Chemistry, Nagoya University, Nagoya 464*

(Received February 19, 1976)

A detailed conformation study of the polypeptide (Pro–Pro–Gly)$_{10}$, synthesized as a collagen model, has been done using X-ray diffraction. Several structures having the observed helical parameters (unit height=8.61 Å, unit twist=51.4°) together with standard bond lengths and angles were generated and tested in terms of an existence of intermolecular van der Waals contacts and least squares calculations using 49 equatorial reflections. It was found from these studies that three polypeptide chains make a three-stranded rope of which the helical parameters are similar to but significantly different from those of the collagen models proposed so far. There exist two possible models for (Pro–Pro–Gly)$_{10}$ according to the type of hydrogen bonding. One is the model having a hydrogen bond so-called 'standard' structure type, and the other has a hydrogen bond of collagen II type. The two-dimensional electron density map, synthesized with the observed structure factors, agrees well with these models. In the least squares calculations, atomic scattering factors were modified by taking into account of effects of amorphous water between the three-stranded ropes.

The first three-stranded coiled coil model for collagen was that suggested by Ramachandran and Kartha.[1] Since then, this structural model has been widely accepted as correct at least in its general features. The structure was derived from a prototype structure, shown in polyglycine II and polyproline II structures, by the introduction of a right handed rope twist so that the individual chains had a coiled coil conformation. It is almost impossible, however, to determine the detailed molecular structure from only the poor X-ray fiber patterns of native collagen; so various models for the molecular conformation have been suggested from the X-ray data. In order to obtain more decisive information to determine the structure of collagen precisely, a number of polypeptide models have been synthesized.[2,3] Since the features of the chemical compositions of the collagen are the occurrence of glycyl residues at every third positions in the sequence and a relatively high contents of proline and hydroxyproline residues, many of these synthetic polypeptides have the sequence in the form of (Gly–Pro–X)$_n$, in which X is a variety of amino acids. A number of structure analyses of these synthetic polypeptides have been reported so far,[4] although X-ray diffraction patterns obtained from these were also poor fiber patterns similar to those from collagen.

In the case of (Pro–Pro–Gly)$_{10}$, single crystals available for X-ray diffraction study were obtained by a dialysis from 10% acetic acid.[5] This is the first one that could be crystallized among the polypeptides belonging to collagen group proteins. The crystal is orthorhombic, space group $P2_12_12_1$, with twelve molecules per unit cell of dimensions: a=26.93, b=26.42 and c=100.4 Å. The crystal has a subcell structure with the c' dimension of one-fifth of the true period, c'=100.4/5=20.08 Å. Intensity data of 787 reflections (exclusive of reflections with $l \neq 5n$) were collected. It was given in the previous paper[6] that the crystal of (Pro–Pro–Gly)$_{10}$ consists of a three-stranded coiled coil structure, of which the helical parameters are similar to but significantly different from those of collagen models proposed so far. The long extended helix of the polypeptides lies parallel to the c axis. In this paper we will describe more detailed molecular structures found by a systematic evaluation of possible molecular conformations and crystal structures derived by a method of two-dimensional least squares refinement.

Structure Analysis

At the beginning of this study, we tried to crystallize a heavy atom derivative of (Pro–Pro–Gly)$_{10}$, that is 4-bromoprolylprolylglycyl-(Pro–Pro–Gly)$_9$. Although crystals of this derivative were obtained by a dialysis from acetic acid, these had a disorder along the c axis, and they were not suitable for X-ray study. Therefore, we built molecular models systematically as in fibrous protein research. These models were tested for acceptable intra- and intermolecular van der Waals contacts and also hydrogen bonds which stabilize the three-stranded coiled coil structure. Finally the structures were refined by the least squares calculations.

Relations among the Individual Chains in Triple Helix. As mentioned earlier,[6] the helical parameters of (Pro–Pro–Gly)$_{10}$ are considerably different from those of collagen models proposed so far.[7–9] There are 21 amino acid residues in one pitch of (Pro–Pro–Gly)$_{10}$ (Fig. 1, left). The vector from the first amino acid residue to the

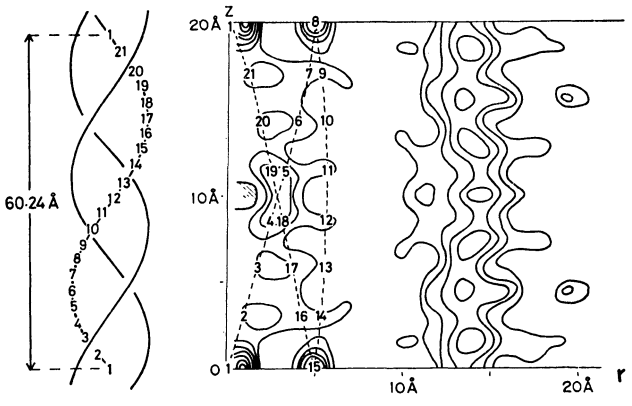

Fig. 1. Left: Three stranded helices. Each helix has 21 amino acid residues in one pitch. Right: Cylindrical Patterson map of (Pro–Pro–Gly)$_{10}$.

n-th amino acid residue is represented as a symbol n in the cylindrical Patterson map (Fig. 1, right). These vectors are connected with dashed lines. Peaks in the range of $0 \leq r \leq 10$ Å in this map are well interpreted by these 21 vectors.

The structure of $(Pro\text{–}Pro\text{–}Gly)_{10}$ consists of three equivalent helical molecules, and each of them has the above mentioned conformation. If these three chains are arranged in an antiparallel fashion, the repeat distance along the chain axis coincides with a pitch, 60.24 Å, rather than a pseudoperiod of 20.08 Å (=60.24/3), which is clearly shown in the $(0kl)$ precession photograph.[6] Therefore, these three are arranged in a parallel fashion. Electron microscopic study of this polypeptide has shown the same result.[10]

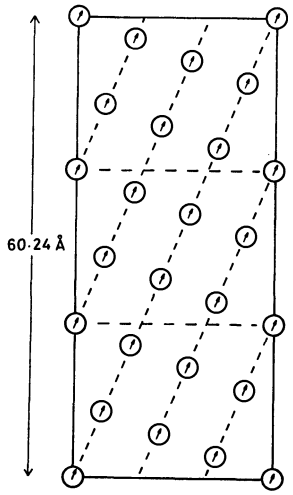

Fig. 2. Radial projection of $(Pro\text{–}Pro\text{–}Gly)_{10}$.

A radial projection of a right handed helix of $(Pro\text{–}Pro\text{–}Gly)_{10}$ is shown in Fig. 2, where an open circle represents a repeating unit, Pro–Pro–Gly, and an arrow in the circle represents a direction of the unit. It is easily shown that in order to have a pseudoperiod of 20.08 Å, the chains must be all parallel and also shifted by a distance of 2.87 Å or 5.74 Å which correspond to the heights of one-third or two-thirds of the unit along the chain axis, from the neighboring chains. Consequently, it is clear that the relation of the atomic coordinates of one chain and those of the corresponding in the other two chains are as follows;

$$(r,\ \phi,\ z)$$
$$(r,\ \phi-102.9°,\ z+2.87)$$
$$(r,\ \phi-205.8°,\ z+5.74)$$

If the polypeptide chain is a left handed helix, its radial projection is a mirror image of that of a right handed one and the relation of the atomic coordinates are as follows;

$$(r,\ \phi,\ z)$$
$$(r,\ \phi+102.9°,\ z+2.87)$$
$$(r,\ \phi+205.8°,\ z+5.74)$$

Analytical Procedure. Figure 3 (a) shows the structural formula of a tripeptide unit of $(Pro\text{–}Pro\text{–}Gly)_{10}$, together with its nine internal rotations. In

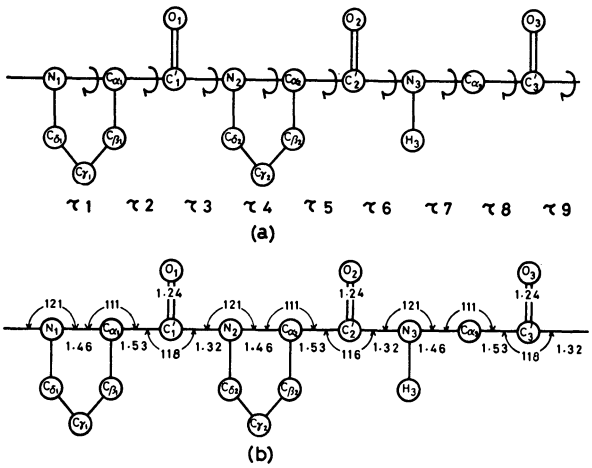

Fig. 3. (a) Structural formula and the notation of internal rotation angles in one tripeptide unit of $(Pro\text{–}Pro\text{–}Gly)_{10}$. (b) Standard stereochemistry of $(Pro\text{–}Pro\text{–}Gly)_{10}$.

building the various possible molecular conformations, we have made several stereochemically reasonable assumptions. Bond distances and angles of peptide backbone were fixed to the values shown in Fig. 3 (b). These are the mean values obtained from the results of structure analyses of oligopeptides. The value of $C_\alpha\text{–}C'\text{–}N$ angle is 118° in the peptide group followed by the prolyl residue, and 116° in that followed by the glycyl residue, because of the steric repulsion between the C_α atom of the preceding residue and the bulky C_δ methylene group of the pyrrolidine ring.[11] For the glycyl residue we have taken the values of 1.0 Å, 1.07 Å, 120° and 109.5° for the bond lengths of N–H and C–H and bond angles of $C_\alpha\text{–}N\text{–}H$ and $H\text{–}C_\alpha\text{–}H$, respectively. For the prolyl residue we have taken the dimension of *p*-bromocarbobenzoxy-glycyl-prolyl-leucyl-glycine.[12] It is known that *cis* as well as *trans* conformations are possible for the peptide bond of proline residues (*e.g.*, the structures of polyproline I and II). However, on the triple helix of $(Pro\text{–}Pro\text{–}Gly)_{10}$ at the lower temperatures, the study of proton magnetic spectra made it clear that the peptide bonds in Pro–Pro and Gly–Pro are all in *trans* conformations.[13] So, we also assumed that the six atoms of the peptide group in all three residues are coplaner, that is, $\tau 3 = \tau 6 = \tau 9 = 180°$. In this study, dihedral angles of the polypeptide chain are taken to be zero for a *cis* conformation and are taken to be positive for an anticlockwise rotation looking along the peptide backbone from the amino terminal to the carboxyl terminal. (This definition is different from that of a standard nomenclature[14] in the direction of rotation.)

Thus, the variable parameters reduced to only six dihedral angles, *i.e.*, $\tau 1$, $\tau 2$, $\tau 4$, $\tau 5$, $\tau 7$ and $\tau 8$. If we take into account of our finding that the structure of $(Pro\text{–}Pro\text{–}Gly)_{10}$ has 7 units (*i.e.*, 21 amino acid residues) in one turn of a single chain, there become not six but five independent parameters.[15] In our program the five parameters were varied systematically and a number of molecular models were built for each combination.[16] Intramolecular atomic coordinates for each model are

transformed into the cylindrical coordinates by using **T** and **L** matrices.[17] The unit height h and one of the six dihedral angles, which was $\tau 2$ in our calculations, were obtained simultaneously. The molecular conformations, whose h and $\tau 2$ are out of the ranges of criterion listed in Table 1, were eliminated in each stage. For the remaining conformations the atomic coordinates of the neighboring chains were given by the relations among the three-stranded chains. Further, the models which do not have a hydrogen bond, judged from a distance b(N, O) and an angle θ(H, N, O), were excluded. Finally the remainders were tested against intra- and intermolecular van der Waals contacts. The minimum van der Waals contacts are based on the "outer limit" values cited by Ramakrishnan and Ramachandran.[18] The various stages of the analysis and the regions found to have the reasonable structures are described in Table 1.

The validities of the molecular structure were tested by the two-dimensional least squares refinements using 49 equatorial reflections. The parameters are the position of the molecular axis (x, y), a rotation angle of a molecule about it, an over all temperature factor and a scale factor. In these calculations we have taken into account of the scattering by water molecules in the unit cell as described in the following section.

Effects of Water Molecules. The water content of (Pro–Pro–Gly)$_{10}$ crystals is 46% (by weight). Although several water molecules may be held at the definite positions by hydrogen bonds to the carbonyl oxygens of polypeptides, these positions may be clarified as the structure analysis proceeds. We took into account of the only water molecules which can be assumed to be uniformly distributed between the three-stranded ropes. For the first approximation we have assumed that all the atoms are spheres with van der Waals radii, 1.60, 1.35 and 1.40 Å for C, N and O, respectively. Each of the atomic scattering factors shown in Fig. 4 is calculated from the ordinary atomic scattering factors minus the scattering factor of water molecules which occupy uniformly the atomic volume with an electron

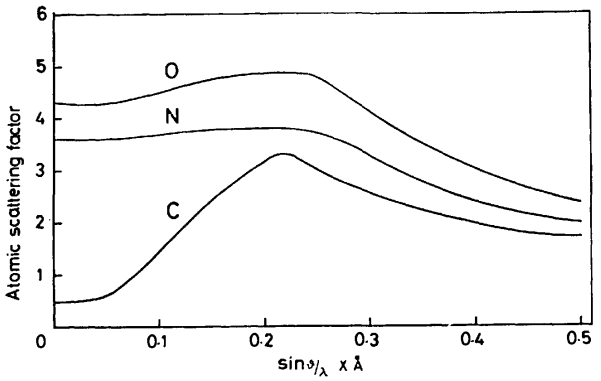

Fig. 4. Atomic scattering factors for atoms immersed in water.

density of 0.33 electrons/Å^3. This correction of atomic scattering factors decreased the R index about 10% in the least squares calculations. The temperature factor was not decreased so immediately as the cases without a correction. A similar method of correcting for background has been used already in the structural studies of DNA.[19]

Results of Analysis. Structures of the left handed helices as well as those of the right handed ones were examined. However, none of the structures of the left handed helices was acceptable in view of their intra- and intermolecular atomic contacts. As shown in Table 1, the ranges of five independent internal rotation angles became narrow at each cycle. In cycle 1, the dihedral angles, $\tau 1$ and $\tau 4$ in pyrrolidine rings were fixed to 60°, while the dihedral angles of glycine, $\tau 7$ and $\tau 8$, were searched over all ranges. From structure analyses of oligopeptides[11,20] and the energy calculations of prolyl oligomers,[21] the dihedral angles of C_α–C′ in proline residue, $\tau 2$ and $\tau 5$, were assumed to be in the ranges of 170~260°. There are some structures in which these angles are in the range of −50~40°, but the range is for the α-helix type dihedral angles.[11] Increments of the three parameters, $\tau 5$, $\tau 7$ and $\tau 8$, were 10° at the first cycle. The structures in the range of

Table 1. Computational details in structure analysis of (Pro–Pro–Gly)$_{10}$

	Parameters	Cycle 1	Cycle 2	Cycle 3	Cycle 4	
Region tested (Increments)	$\tau 1$	60°	45—85° (5)	50—85° (5)	53—77° (3)	
	$\tau 4$	60°	45—80° (5)	50—70° (5)	47—68° (3)	
	$\tau 5$	170—260° (10)	170—240° (10)	175—205° (5)	182—203° (3)	
	$\tau 7$	0—350° (10)	40—100° (10)	75—105° (5)	77—98° (3)	
	$\tau 8$	0—350° (10)	180—240° (10)	175—215° (5)	183—210° (3)	
Criteria	$\tau 2$	170—270°	170—270°	170—270°	170—270°	
	Unit height	6.61—10.61Å	8.44—8.78Å	8.51—8.71Å	8.58—8.64Å	
	H-bond					
	b(N, O)	—	3.2—2.6Å	3.2—2.6Å	3.2—2.6Å	
	θ(H, N, O)	—	—	0—35°	0—30°	
Region passed					Model 1	Model 2
	$\tau 1$	60°	55—85°	55—75°	53—68°	68—77°
	$\tau 2$	170—240°	177—209°	188—209°	186—202°	193—208°
	$\tau 4$	60°	50—65°	50—65°	53—68°	50—65°
	$\tau 5$	170—260°	180—200°	185—200°	185—188°	194—197°
	$\tau 7$	−20—140°	80—100°	80—95°	92—95°	83—86°
	$\tau 8$	180—240°	180—210°	185—210°	198—210°	183—192°

6.61～10.61Å of the unit height were selected in all combinations of these three parameters. After the first cycle it was shown that the angles of $\tau 7$ and $\tau 8$ of glycine residue were in the range of −20～140° and 180—240°, respectively. These ranges show that the glycyl residue has the left handed polyglycine II type structure, as in the collagen models. Therefore, taking into account of energy map of diglycine,[22] the range of $\tau 7$ was restricted to 40～100° at the second cycle.

In cycles 2, 3 and 4, structures without NH···O hydrogen bonds were eliminated. In the case of $(Pro–Pro–Gly)_{10}$, there were two possible types of hydrogen bonds, that is, $N_3(Gly)\cdots O_2(Pro)$ and $N_3(Gly)\cdots O_1(Pro)$. We call hereafter the structure having the former type hydrogen bond model 1 and that having the latter model 2. The ranges of parameters for model 1 and 2 at cycle 4 are shown in the last column of Table 1. Illustrations of a hydrogen bond between neighboring chains of each model are shown in Fig. 5.

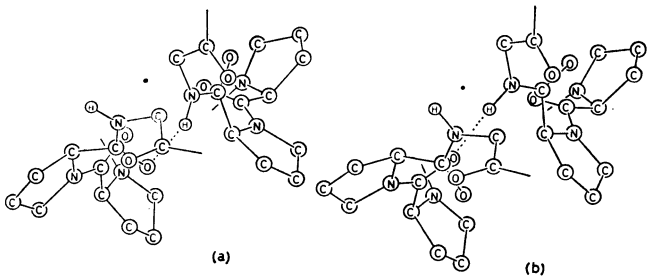

Fig. 5. An axial projection of segments of the two $(Pro–Pro–Gly)_{10}$ models. (a) Model 1, (b) Model 2. The filled circle represents the axis of the molecule for each model. The dashed line represents a hydrogen bond.

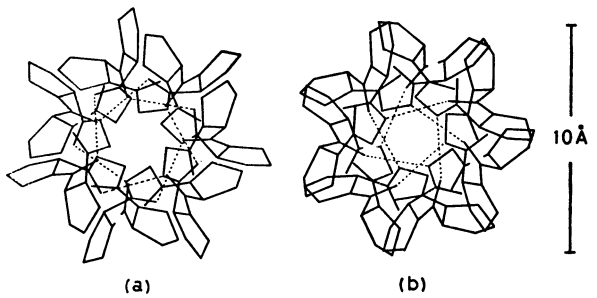

Fig. 6. The molecular structure viewed down the c axis. (a) Model 1, (b) Model 2.

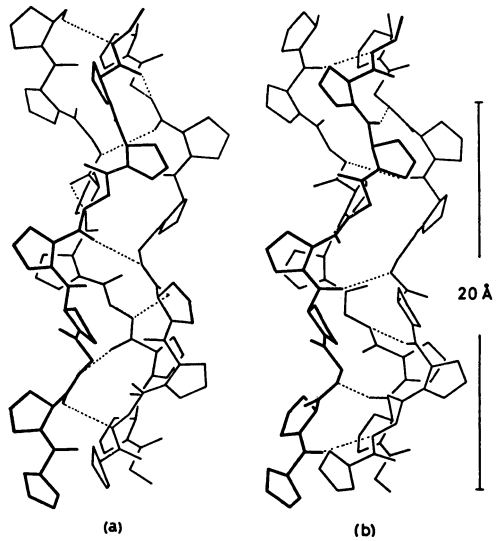

Fig. 7. The molecular structure viewed down the b axis. (a) Model 1, (b) Model 2.

Fifteen structures, which were chosen from different parts of regions for each model, have been tested by the two-dimensional least squares refinements. The R index $(\Sigma||F_o|^2-|F_o|^2|/\Sigma|F_o|^2)$ was calculated after three cycles with the same initial setting parameters for each structure. The dihedral angles and the hydrogen bond parameters of all the fifteen structures are listed in Table 2, together with their R indices.

As typical structures, the structure of No. 4 in Table 2 for model 1 and that of No. 13 for model 2 are shown in Figs. 6 and 7, since they had small R indices and good hydrogen bond parameters. Atomic coordinates for the repeating unit are given in Table 3. The intermolecular short contacts (less than 3.5 Å) of the structures are as follows;

$O_1\cdots C\delta_1$ 3.27, $N_3\cdots O_1$ 3.14, $N_3\cdots O_2$ 3.09, $C\alpha_3\cdots C\alpha_3$ 3.49, $C'_3\cdots C\alpha_3$ 3.38, $O_3\cdots C\alpha_3$ 3.28, $O_3\cdots C\delta_1$ 2.90, $O_1\cdots C\alpha_3$ 2.99 and $O_1\cdots C\delta_1$ 2.27 Å in model 1 (No. 4). $C\alpha_2\cdots O_1$ 2.96, $C\beta_2\cdots O_1$ 3.42, $C_2'\cdots O_1$ 3.41, $N_3\cdots O_1$ 2.97 and $O_3\cdots C\alpha_3$ 2.99 Å in model 2 (No. 13).

Since the molecule has 7 units in one turn (7/1 helix), there is a 7-fold rotational symmetry in Fig. 6. At the molecular center of this figure, there exists a hole surrounded by glycyl residues. The dimension of this

TABLE 2. PARAMETERS OF FIFTEEN STRUCTURES CHOSEN FROM THE DIHEDRAL ANGLE REGIONS FOR EACH MODEL

	Model 1							Model 2							
Number	1	2	3	4	5	6	7	8	9	10	11	12	13	14	15
$\tau 1$/°	54	56	58	60	62	64	66	67	69	71	73	73	75	75	77
$\tau 2$/°	193	195	192	193	197	199	199	199	198	202	202	202	205	199	207
$\tau 4$/°	62	60	62	60	56	54	54	60	60	58	54	58	52	58	50
$\tau 5$/°	185	185	188	186	186	186	188	194	197	196	194	197	194	198	194
$\tau 7$/°	95	95	91	94	94	94	92	86	82	83	86	82	86	82	86
$\tau 8$/°	209	207	207	205	203	201	199	192	192	188	188	186	186	186	184
b(N, O)/Å	2.95	2.95	2.93	3.09	3.03	3.02	3.14	3.08	2.74	2.99	2.94	3.07	2.97	3.12	3.01
θ(H, N, O)/°	22	20	29	30	27	25	22	29	30	28	30	28	29	27	28
θ'(180-NOC)/°	76	78	70	68	70	72	76	27	22	33	23	33	25	20	28
R index × 100	42	42	39	32	35	36	34	29	34	30	28	26	27	27	26

Table 3. Atomic coordinates of the repeating unit in the model structures of (Pro-Pro-Gly)$_{10}$

Residue	Atom	Model 1 (No. 4)			Model 2 (No. 13)		
		x/Å	y/Å	z/Å	x/Å	y/Å	z/Å
Pro	N_1	2.94	0.00	0.00	3.40	0.00	0.00
	$C\alpha_1$	3.88	−0.27	1.08	4.08	−0.52	1.18
	$C\beta_1$	4.68	1.06	1.13	5.05	0.64	1.50
	$C\gamma_1$	4.43	1.77	−0.08	5.14	1.48	0.37
	$C\delta_1$	3.17	1.27	−0.68	3.93	1.27	−0.49
	C_1'	3.14	−0.63	2.37	3.16	−0.52	2.39
	O_1	1.93	−0.42	2.39	2.23	0.30	2.38
Pro	N_2	3.85	−1.15	3.36	3.40	−1.38	3.36
	$C\alpha_2$	3.21	−1.52	4.62	2.56	−1.44	4.55
	$C\beta_2$	4.40	−2.13	5.40	3.19	−2.63	5.32
	$C\gamma_2$	5.44	−2.40	4.48	4.01	−3.35	4.42
	$C\delta_2$	5.23	−1.58	3.25	4.37	−2.47	3.27
	C_2'	2.55	−0.31	5.27	2.41	−0.05	5.17
	O_2	2.72	0.81	4.76	3.18	0.85	4.81
Gly	N_3	1.83	−0.55	6.36	1.46	0.08	6.08
	$C\alpha_3$	1.16	0.53	7.07	1.22	1.36	6.74
	C_3'	2.03	1.06	8.21	2.12	1.50	7.97
	O_3	2.87	0.28	8.67	2.81	0.52	8.27

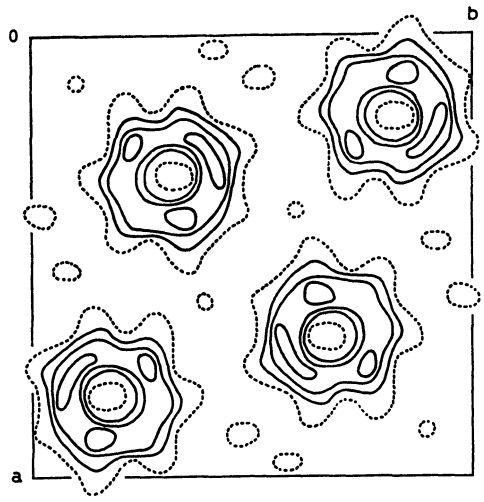

Fig. 8. Electron density map projected along the c axis.

hole is 2.0~2.5 Å for model 1 and 2.7~3.1 Å for model 2. The R index of the least squares refinements decreases as the dimension of this hole increase.

The electron density map, calculated from the observed structure factors $|F_o|$ and phases calculated by the fifteen structures of Table 2, is shown in Fig. 8. Only 38 ($hk0$) reflections whose signs were the same in all the fifteen structures were used in this calculation. In this map, the center portion of the triple helix has low electron density, and high electron density parts are distributed cylindrically with about 5.7 Å in diameter. Further, there are seven projections of electron density from this cylinder.

Discussion

It can be seen from the systematic study of molecular conformations that there exist two possible structures distinguished by hydrogen bonding. The structure of model 1 has the so called "standard" structure type hydrogen bond and that of model 2 has the collagen 11 type hydrogen bond. The difference between these two structures is illustrated in Fig. 5 and the values of hydrogen bond parameters are listed in Table 2. The angle θ(H, N, O), between N-H and H···O, is 20~30° in model 1 and 27~30° in model 2. The angle θ'(180−NOC'), between C=O and O···N, is about 70~80° in model 1 and 20~30° in model 2. These values as well as the hydrogen bond lengths are not extreme cases of hydrogen bonding parameters.[23]

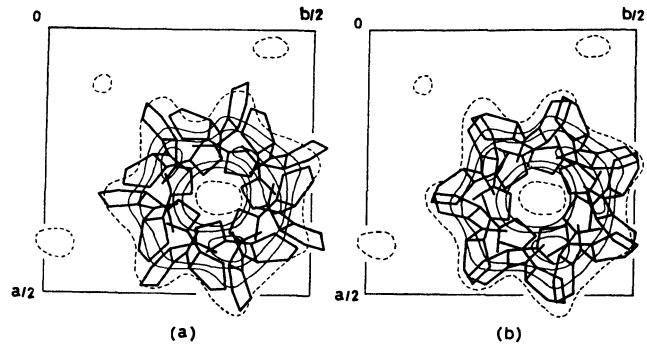

Fig. 9. Comparison of the electron density in an asymmetric unit with the molecular structures of (a) model 1 and (b) model 2 for (Pro-Pro-Gly)$_{10}$.

The two structures are supported by the electron density map as seen from Fig. 9. There is a remarkable coincidence, seven knobs of pyrrolidine rings being well fitted to those of the electron density distribution. The position of the molecular axis of the triple helix obtained from least squares refinements is x=8.57±0.06 Å and y=8.42±0.06 Å. Then, the distance between nearest neighbours of the triple helix is 13.7~12.9 Å, which agrees well with the peaks lined up at about r=14 Å in the cylindrical Patterson map (Fig. 1). The electron density map calculated from all the 49 ($hk0$) reflections for each model was somewhat different from the map in Fig. 8 if examined in detail. This may be due to the neglect of the water molecules which are at the definite positions in the unit cell. At this stage it cannot be decided which is more plausible for (Pro-Pro-Gly)$_{10}$, model 1 or 2.

A comparison of the hydrogen bond type and the helical parameters of (Pro-Pro-Gly)$_{10}$ with those of the several collagen models[7,9] and of a synthetic polypeptide (Pro-Gly-Pro)$_n$[4] is shown in Table 4. The amino acid sequence of (Pro-Gly-Pro)$_n$ is the same as that of (Pro-Pro-Gly)$_{10}$. The molecular weight is about 15000 for the former and 2528 for the latter. Our sample was practically monodispersed,[24] and single crystals available for X-ray study were obtained. On the other hand, molecular weights of (Pro-Gly-Pro)$_n$ seem to be polydispersed and only the fiber patterns similar to those of collagen could be obtained. Collagen 1 and "standard" structures can not be considered as good models for collagen because imino acids could not be incorporated in position R_3 or R_2, respectively,[25] while it is known that the amino acid sequence of collagen

Table 4. Comparisons of features for several collagen models and collagen model synthetic polypeptides

	Amino acid sequence $(Gly_1–R_2–R_3)_n$	Types of hydrogen bond	Helical parameters
Collagen I[7]	R_2 any residue R_3 Gly only	$N(Gly_1)\cdots O(Gly_1)$	10/1 helix, $h=2.86\times3$Å, $t=36°$
Collagen II[7]	R_2 any residue R_3 any residue	$N(Gly_1)\cdots O(R_2)$	10/1 helix, $h=2.86\times3$Å, $t=36°$
'Standard' structure[9]	R_2 Pro or Hypro imposible R_3 any residue	$N(Gly_1)\cdots O(R_3)$ $N(R_2)\cdots O(R_2)$	12/1 helix, $h=2.91\times3$Å, $t=30°$
$(Pro–Gly–Pro)_n$[4]	R_2 Pro R_3 Pro	$N(Gly_1)\cdots O(R_2)$	10/1 helix, $h=2.87\times3$Å, $t=36°$
$(Pro–Pro–Gly)_{10}$	R_2 Pro R_3 Pro	$N(Gly_1)\cdots O(R_2)$ or $N(Gly_1)\cdots O(R_3)$	7/1 helix, $h=2.87\times3$Å, $t=51.4°$

proteins obtained from several sources has many tripeptide sequences of Gly–Pro–X. Structures of collagen II and $(Pro–Gly–Pro)_n$ have the same type hydrogen bond and the same helical parameters with each other. And the structure of collagen II is considered to be the most favorable model for collagen so far.[25] In the model 1 of $(Pro–Pro–Gly)_{10}$, the hydrogen bond is the same type as that in "standard" structure and the other (model 2) is the same as that of collagen II structure, although the helical parameters of this polypeptide are significantly different from those of collagen models. The major difference of these structures is in the pseudoperiod along the fiber axis. The pseudo period of $(Pro–Pro–Gly)_{10}$ is 20.08 Å, which is clearly shown in the (0*kl*) precession photograph.[6] On the other hand, that of collagen II structure was considered to be 28.6 Å, since the meridional reflection with 2.86 Å spacing was considered to be 10 th order reflection. Bear[26] thought, however, that the pseudoperiod of kangaroo tail tendon collagen was 20.0 Å. He ascribed the meridional reflection of 2.86 Å as the 7-th, although the molecular structure suggested was incorrect. If this is true, the helical parameters of $(Pro–Pro–Gly)_{10}$ are the same as those of collagen.

During this study we have assumed that the molecule is an infinite chain, but actually the dimension of the molecules is 86.1 Å (2.87×30) and the number of turns in this peptide chain is only 1.4. Therefore, it should be taken into account of this molecular terminal effects in the least squares refinements. However, the results at this stage are the same, whether the molecule is assumed to be finite or infinite.

We are grateful to Prof. M. Takayanagi of Kyushu University for his encouragement throughout this work. We are indebted to Drs. S. Sakakibara and Y. Kishida of Protein Research Foundation for suppling the valuable samples. All the numerical computations were done on a FACOM 230-75 of the Computer Center of Kyushu University.

References

1) G. N. Ramachandran and G. Kartha, *Nature*, **176**, 593 (1955).
2) N. S. Andreeva, N. G. Esipova, M. I. Millionova, V. N. Rogulenkova, and V. A. Shibnev, "Conformation of Biopolymers," Vol. 2, Academic, New York (1967), p. 469.
3) D. M. Segal and W. Traub, *J. Mol. Biol.*, **43**, 487 (1969).
4) A. Yonath and W. Traub, *J. Mol. Biol.*, **43**, 461 (1969).
5) S. Sakakibara, Y. Kishida, K. Okuyama, N. Tanaka, T. Ashida, and M. Kakudo, *J. Mol. Biol.*, **65**, 371 (1972).
6) K. Okuyama, N. Tanaka, T. Ashida, M. Kakudo, S. Sakakibara, and Y. Kishida, *J. Mol. Biol.*, **72**, 571 (1972).
7) A. Rich and F. H. C. Crick, *Nature*, **176**, 915 (1955).
8) P. M. Cowan, S. McGavin, and A. C. T. North, *Nature*, **176**, 1062 (1955).
9) G. N. Ramachandran, "Treatise on Collagen," Vol. 1, ed. by G. N. Ramachandran, Academic, London (1967), p. 103.
10) B. R. Olsen, R. A. Berg, S. Sakakibara, Y. Kishida, and D. J. Prockop, *J. Mol. Biol.*, **75**, 589 (1971).
11) T. Ashida and M. Kakudo, *Bull. Chem. Soc. Jpn.*, **47**, 1129 (1974).
12) T. Ueki, T. Ashida, M. Kakudo, Y. Sasada, and Y. Katsube, *Acta Crystallogr.*, **B25**, 1840 (1969).
13) Y. Kobayashi and Y. Kyogoku, *J. Mol. Biol.*, **81**, 337 (1973).
14) IUPAC-IUB Commission on Biochemical Nomenclature, *J. Mol. Biol.*, **52**, 1 (1970).
15) M. Yokouchi, H. Tadokoro, and Y. Chatani, *Macromolecules*, **7**, 769 (1974).
16) S. Arnott and A. J. Wonacott, *Polymer*, **7**, 157 (1966).
17) H. Sugeta and T. Miyazawa, *Biopolymers*, **5**, 673 (1967).
18) C. Ramakrishnan and G. N. Ramachandran, *Biophys. J.*, **5**, 909 (1965).
19) R. Langridge, D. A. Marvin, W. E. Seeds, H. R. Wilson, C. W. Hooper, and M. H. F. Wilkins, *J. Mol. Biol.*, **2**, 38 (1960).
20) R. Balasubramanian, A. V. Lakshminarayanan, M. N. Sabesan, G. Tegoni, K. Venkatatesan, and G. N. Ramachandran, *Int. J. Protein Res.*, **3**, 25 (1971).
21) A. J. Hopfinger and A. G. Walton, *J. Macromol. Sci. Phys.*, **B3**, 171 (1969).
22) A. J. Hopfinger, Ph. D. thesis, Case Western Reserve University, Cleveland, Ohio (1970).
23) C. Ramakrishnan and N. Prasad, *Int. J. Protein Res.*, **3**, 209 (1971).
24) S. Sakakibara, Y. Kishida, Y. Kikuchi, R. Sakai, and K. Kakiuchi, *Bull. Chem. Soc. Jpn.*, **41**, 1273 (1968).
25) D. B. Fraser and T. P. MacRae, "Conformation in Fibrous Proteins," Academic, New York and London (1973), p. 371.
26) R. S. Bear, *Advan. Protein Chem.*, **7**, 69 (1952).

Topological Index as Applied to π-Electronic Systems. IV. On the Topological Factors Causing Non-Uniform π-Electron Charge Distribution in Non-Alternant Hydrocarbons*

Ivan GUTMAN,** Tamiё YAMAGUCHI,*** and Haruo HOSOYA***§

**Institute "Ruđer Bošković," Zagreb, Croatia, Yugoslavia

***Department of Chemistry, Ochanomizu University, Bunkyo-Ku, Tokyo 112

(Received February 25, 1976)

The topological factors which cause non-uniform π-electron charge distribution in non-alternant hydrocarbons (NAH's) are discussed. For estimating and analyzing the net-charge density a novel topological index, topological charge density, Q_r^T, is proposed. It is defined as $Q_r^T=\mathrm{Re}(F_{G,r}(1))$, the real part of $F_{G,r}(y)=\Delta_{r,r}(iy)/\Delta(iy)$, where $\Delta(x)$ is the secular determinant of graph G and $\Delta_{r,r}(x)$ is its adjunct with row r and column r struck out. This quantity Q_r^T, corresponding to the Coulson net charge density $Q_r=1-q_r$, is related with the topological indices $\tilde{Z}_G$ and $\tilde{Y}_G$ which are defined in terms of the coefficients of the characteristic polynomial of graph G. As all the newly proposed indices can be enumerated graphically, one can easily estimate the net-charge densities of NAH's.

Coulson and Rushbrooke[1] have proved that the Hückel MO theory predicts uniform π-electron charge distribution in all the alternant hydrocarbons (AH's). Although the structural requirements for uniform π-charge distribution are presently well understood,[1,2] it is not much known[3-6] on the same problem for non-alternant hydrocarbons (NAH's). A number of empirical rules which relate the π-electron charge distribution of NAH's with their structure are collected in Ref. 3, but with an incomplete mathematical justification.[4,7] In Ref. 5 some general consequences of the Coulson integral formula for charge density are presented.

Until recently it has not been recognized[5-11] that useful topological information can be deduced from the Coulson integral representation[12] of several π-electron characteristics of conjugated systems, although parallelism among the several reactivity indices derived from the Hückel MO theory were already proved.[13,14] According to Ref. 12, the total π-electron energy E_π, the bond order p_{rs} between atoms r and s and the charge density Q_r (not the π-electronic but net-charge density) on atom r can be expressed as:

$$E_\pi = \frac{1}{\pi}\int_{-\infty}^{+\infty} F_G(y)\mathrm{d}y, \tag{1}$$

$$p_{rs} = \frac{1}{\pi}\int_{-\infty}^{+\infty} F_{G,rs}(y)\mathrm{d}y, \tag{2}$$

$$Q_r = \frac{1}{\pi}\int_{-\infty}^{+\infty} F_{G,r}(y)\mathrm{d}y, \tag{3}$$

where

$$F_G^*(y) = N - iy\Delta'(iy)/\Delta(iy) \tag{4a}$$

$$F_{G,rs}(y) = -\Delta_{r,s}(iy)/\Delta(iy) \tag{5}$$

$$F_{G,r}(y) = \Delta_{r,r}(iy)/\Delta(iy). \tag{6}$$

Here $i=\sqrt{-1}$ is the imaginary unit and $\Delta(x)\equiv P_G(x)=\det(xI-A)$ is the characteristic polynomial of the molecular graph G with N vertices.[15] A and I are the adjacency matrix and the unit matrix, $(-1)^{r+s}\Delta_{r,s}$ denotes Δ with row r and column s struck out. Note that $\Delta_{r,r}=P_{G\ominus r}$, where $G\ominus r$ is the graph obtained by deletion of vertex r and all the edges incident to it from graph G. Equation 1 holds also for the integrand[9,10]

$$F_G^{**}(y) = y^{-2}\ln|y^N P_G(1/iy)|. \tag{4b}$$

A proof of this relation will be given in Appendix I.

Let us write $P_G(x)$ in the form

$$P_G(x) = \sum_{k=0}^{N} a_k x^{N-k}. \tag{7}$$

Since the relations between the coefficients a_k and the structure of the molecular graph G are nowadays completely elucidated,[16,17] by means of Eqs. 1—3 one can get insight into the topological factors determining E_π, p_{rs} and Q_r. However, this analysis is not simple[14] because of the complicated form of Eqs. 4—6.

We have shown that E_π of a number of conjugated hydrocarbons can be approximated fairly well by $\log\tilde{Z}_G$,[8]

$$E_\pi \doteq c\log\tilde{Z}_G \tag{8}$$

where

$$\tilde{Z}_G = \sum_{k=0}^{m}(-1)^k a_{2k} \tag{9}$$

with $m=[N/2]$. It was also found that the value of F_G^{**} for $y=1$ has an analogous behavior as $\tilde{Z}_G$.[18] In particular, numerical analysis shows that E_π is nearly linearly related to $F_G^{**}(1)$. The similar is valid for the function $F_{G,rs}$. That is, $F_{G,rs}(1)$ is shown to be used as a good index for bond orders.[11] This suggests[6] that $F_{G,r}(1)$ may also possess interesting properties for the study of Q_r. In the present paper we would like to demonstrate that this is indeed the case. In order to analyze this problem two different kinds of the topological indices for a given graph are to be defined.

Topological Indices $\tilde{Z}_G$ and $\tilde{Y}_G$

Let us consider the polynomial $P_G(x)$ for $x=i$. According to Eq. 7,

$$P_G(i) = i^N(\tilde{Z}_G + i\tilde{Y}_G) \tag{10a}$$

and

$$P_G(-i) = (-i)^N(\tilde{Z}_G - i\tilde{Y}_G), \tag{10b}$$

where two topological indices are defined as

$$\tilde{Z}_G = \sum_{k=0}(-1)^k a_{2k}^{8)} \tag{11a}$$

$$\tilde{Y}_G = \sum_{k=0}(-1)^{k+1} a_{2k+1}. \tag{11b}$$

* Part III: *J. Chem. Phys.*, **64**, 1065 (1976).

§ To whom all the correspondence should be made.

TABLE 1. THE CHARACTERISTIC POLYNOMIAL AND THE TOPOLOGICAL INDICES $\tilde{Z}_G$ AND $\tilde{Y}_G$ FOR TYPICAL NON-ALTERNANT HYDROCARBONS

$G^{a)}$	$P_G(x)$	$\tilde{Z}_G$	$\tilde{Y}_G$
I	x^4-4x^2+1	6	
	$-2x$		-2
II	$x^6-6x^4+8x^2-1$	16	
	$-2x$		2
III	$x^8-8x^6+19x^4-13x^2+1$	42	
	$-2x$		-2
IV	$x^6-7x^4+11x^2-4$	23	
	$-2x^3+2x$		-4
V	$x^8-9x^6+24x^4-20x^2$	54	
	$-4x^3+8x$		12
VI	$x^{10}-11x^8+41x^6-61x^4+31x^2-4$	149	
	$-2x^5+6x^3-2x$		10
VII	$x^{12}-13x^{10}+62x^8-134x^6+129x^4-45x^2$	384	
	$-4x^5+16x^3-12x$		-32
VIII	$x^6-7x^4+11x^2+3$	16	
	$-4x^3+12x$		-16
IX	$x^8-9x^6+22x^4-10x^2$	42	
	$-2x^5+10x^3-4x$		-16
X	$x^8-9x^6+24x^4-19x^2+5$	58	
	$-2x^5+8x^3-4x$		-14
XI	$x^{12}-14x^{10}+71x^8-165x^6+180x^4-82x^2+9$	522	
	$-2x^7+12x^5-24x^3+14x$		52
XII	$x^{12}-14x^{10}+71x^8-161x^6+158x^4-54x^2+5$	464	
	$-4x^7+22x^5-32x^3+8x$		66
XIII	$x^{14}-16x^{12}+98x^{10}-291x^8+434x^6-305x^4+86x^2-5$	1236	
	$-2x^9+12x^7-18x^5+4x$		28

a) See Chart 1.

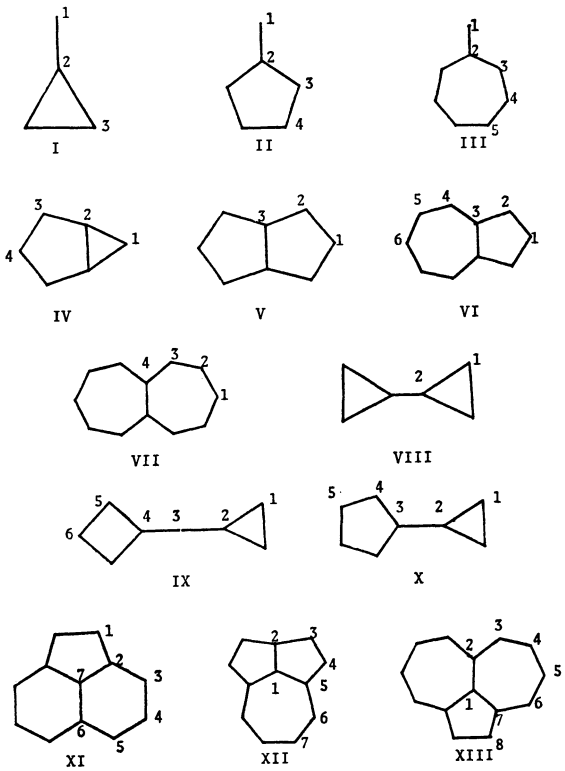

Chart 1

Hence we have

$$F_G^{**}(1) = \ln (\tilde{Z}_G^2 + \tilde{Y}_G^2)^{1/2}. \tag{12}$$

Note that $\tilde{Z}_G$ is always positive,[19] whereas $\tilde{Y}_G$ is zero for an AH and may take a positive or negative value according to the topology of a NAH as shown in Table 1, where the characteristic polynomial and the topological indices $\tilde{Z}_G$ and $\tilde{Y}_G$ for the typical NAH's are given. The following relation can be shown for almost all the NAH's (See the later discussions):

$$\tilde{Z}_G \gg |\tilde{Y}_G|. \tag{13}$$

Thus for an AH we have

$$F_G^{**}(1) = \ln \tilde{Z}_G \qquad (\boldsymbol{G}\in\mathrm{AH}) \tag{14}$$

and for a NAH the relation

$$F_G^{**}(1) \doteq c \ln \tilde{Z}_G \qquad (\boldsymbol{G}\in\mathrm{NAH}) \tag{15}$$

holds as expected.[8,18]

As the Sachs theorem states that[17]

$$a_0 = 1$$
$$a_n = \sum_{S_n}(-1)^{c(s)} \qquad (N\geq n\geq 1), \tag{16}$$

it follows that

$$\tilde{Z}_G = 1 + \sum_{k=1}^{m}(-1)^k \sum_{S_{2k}}(-1)^{c(s)}$$
$$= 1 + \sum_{S_{2k}}(-1)^{n(s)/2+c(s)}. \tag{17}$$

Here $c(s)$ and $n(s)$ denote the number of components and the number of vertices of the directed Sachs graph s. The summation in Eq. 16 runs over the set S_n of all the Sachs graphs with $n(s)=n$ vertices which are contained in the molecular graph $\boldsymbol{G}$, while in Eq. 17 over the set S_{2k} of all the Sachs graphs with even

number of vertices which are contained in G. In another terminology[21] a directed Sachs graph is called a linear graph.

If graph G has no cycle, namely if G is a tree, or an acyclic hydrocarbon, $n(s)=2c(s)$ and Eq. 17 leads to

$$\begin{aligned}\tilde{Z}_G &= 1+\sum_{k=1}\begin{pmatrix}\text{number of Sachs graphs}\\ \text{with } k \text{ disjoint edges}\end{pmatrix}\\ &= \sum_{k=0}^{m} p(G,k) \qquad (G\in\text{Tree})\\ &= Z_G, \end{aligned} \tag{18}$$

where $p(G, k)$ is the non-adjacent number and Z_G the orignal version of the topological index.[22]

For a non-tree graph Eq. 17 is expressed as

$$\tilde{Z}_G = Z_G + \Delta Z_G \tag{19}$$

$$\Delta Z_G = \sum_{S^{\circ}_{2k}}(-1)^{n(s)/2+c(s)}, \tag{20}$$

where S°_{2k} runs over all the even Sachs graphs containing at least one cycle, and ΔZ_G is called as the aromaticity index.[8] Figures 1 and 2 summarize all the indices,

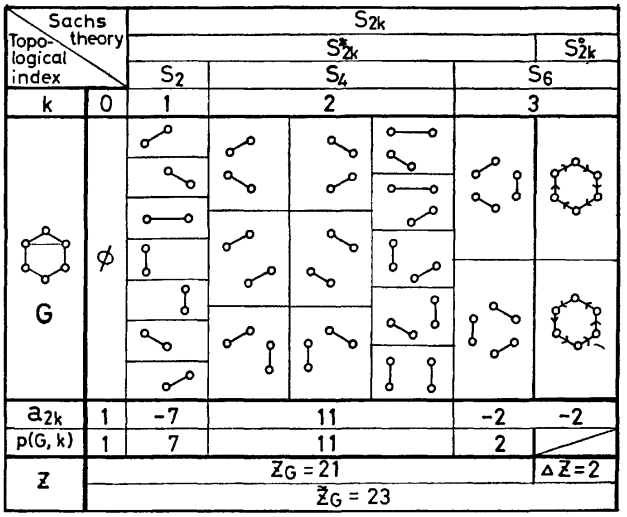

Fig. 1. Relation between the Sachs theorem and the topological indices. Even-Sachs graphs S_{2k} of graph $G\equiv$IV are given, which are divided into cycle-including (S°_{2k}) and cycle-excluding (S^{*}_{2k}) graphs. The symmetric part of $P_G(x)=(x^6-7x^4+11x^2-4)+(-2x^3+2x)$ is obtained from this figure. See Table 1 and Fig. 2.

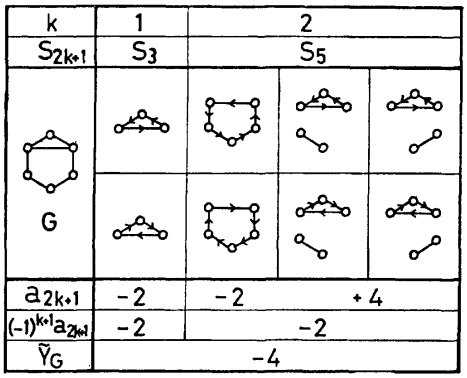

Fig. 2. Relation between $\tilde{Y}_G$ and odd-Sachs graphs, S_{2k+1}, of graph $G\equiv$IV. Note that the anti-symmetric part of $P_G(x)=(x^6-7x^4+11x^2-4)+(-2x^3+2x)$ is obtained from this figure. See Fig. 1 and Table 1.

Z_G, ΔZ_G, $\tilde{Z}_G$ and $\tilde{Y}_G$, and illustrates the relation between the Sachs theorem and the topological indices with graph IV as an example. In Ref. 8 it is shown how a combination of two or more cycles contributes to the sign of ΔZ_G. Here analysis will be developed in line with the Sachs formula.

Let s contain $p_0(s)$, $p_1(s)$, $p_2(s)$, and $p_3(s)$ cycles of the size, $4m$, $4m+1$, $4m+2$, and $4m+3$, respectively. Then[10]

$$n \equiv p_1 + 2p_2 + 3p_3 \pmod 4$$

$$c \equiv p_0 + p_1 + p_2 + p_3 \pmod 4$$

from which one deduces

$$n/2 + c \equiv p_0 + (p_3-p_1)/2 \pmod 2$$

or

$$\tilde{Z}_G = \sum_{S_{2k}}(-1)^{p_0+(p_3-p_1)/2} \tag{21}$$

One sees that $\tilde{Z}_G$ is closely related with the cycles contained in the molecular graph. For example, a couple of disjoint $4m$-membered cycles increase the $\tilde{Z}_G$ value as well as a combination of $(4m+1)$- and $(4m+3)$-membered cycles, whereas a couple of $(4m+1)$- or of $(4m+3)$-membered cycles decrease $\tilde{Z}_G$.[8]

If one uses the linear relation (8) the above statement is nothing else but the stability criterion, *i.e.* an extended Hückel rule,[8] for an arbitrary network of conjugated hydrocarbons.

As mentioned earlier, for AH's $a_{2k+1}=0$ for all k and we have $\tilde{Y}_G=0$. If the size of the smallest odd-cycle in G is $2g+1$, one gets $a_1=a_3=\cdots=a_{2g-1}=0$ and $a_{2g+1}=-2n_{2g+1}$, where n_{2g+1} is the number of such cycles.[15,16] Therefore the sign of $\tilde{Y}_G$ is equal to the sign of the term $(-1)^{g+1}a_{2g+1}$. That is,

$$\tilde{Y}_G = \begin{cases} >0 & \text{if the smallest odd cycle in } G \text{ is of the size } 4m+1\\ <0 & \text{if the smallest odd cycle in } G \text{ is of the size } 4m+3, \end{cases} \tag{22}$$

as shown in Table 1. Hence, $\tilde{Y}_G$ presents a topological index which in a particular way reflects the non-alternant character of a π-electron network. It is important to emphasize that $\tilde{Y}_G$ distinguishes the $(4m+1)$-rings from $(4m+3)$-ones, which seems to be the most important structural factor in determining Q_r.

A consideration analogous to that used for the derivation of Eq. 21 gives

$$\tilde{Y}_G = \sum_{S_{2k+1}}(-1)^{p_0+(p_3-p_1+1)/2} \tag{23}$$

showing that the indices $\tilde{Z}_G$ and $\tilde{Y}_G$ are algebraically closely related. S_{2k+1} is the set of all the directed Sachs graphs with odd number of vertices, which are contained in graph G. However, it is not necessary to draw all these graphs in order to determine the value of $\tilde{Y}_G$. A simple graphical method for the enumeration of $\tilde{Y}_G$ is given in Appendix II.

Topological Charge Density

Following the discussion above it is natural to use the $F_{G,r}$ value for $y=1$ as a kind of topological index for representing the net charge density on atom r in hydrocarbon G.

Substitution of Eq. 10a into Eq. 6 yields

$$F_{G,r}(1) = (\tilde{Z}_{G\ominus r}+i\tilde{Y}_{G\ominus r})/(i\tilde{Z}_G-\tilde{Y}_G), \quad (24)$$

whose real part is expressed as

$$Q_r^{\mathrm{T}} = \mathrm{Re}(F_{G,r}(1)) = \frac{\tilde{Z}_G\tilde{Y}_{G\ominus r}-\tilde{Y}_G\tilde{Z}_{G\ominus r}}{\tilde{Z}_G^2+\tilde{Y}_G^2} \quad (25)$$

and will be called as the topological (net-) charge density. Although all the quantities in the right-hand side of Eq. 25 are derived from the characteristic polynomial, they can easily be obtained graphically by hand calculation as in Appendix II even without knowing the characteristic polynomial.

TABLE 2. TOPOLOGICAL CHARACTERISTICS OF SUBGRAPHS OF GRAPH IV AND ITS TOPOLOGICAL CHARGE DENSITIES

r	$P_{G\ominus r}(x)$	$\tilde{Z}_{G\ominus r}$	$\tilde{Y}_{G\ominus r}$	Q_r^{T} a)	Q_r b)
1	x^5-5x^3+5x-2	11	2	0.165	0.300
2	x^5-4x^3+3x	8	0	0.059	0.073
3	$x^5-5x^3+4x-2x^2+2$	10	−4	−0.095	−0.215
4	$x^5-5x^3+3x-2x^2$	9	−2	−0.018	−0.072

a) $Q_r^{\mathrm{T}}=\frac{\tilde{Z}_G\tilde{Y}_{G\ominus r}-\tilde{Y}_G\tilde{Z}_{G\ominus r}}{\tilde{Z}_G^2+\tilde{Y}_G^2}$. b) $Q_r=1-q_r$, where q_r is the Coulson charge density calculated from the HMO's.

Examples are shown in Table 2 for graph IV, for which the topological charge density Q_r^{T} is correlated fairly well with the charge density calculated from the Hückel MO's. It is to be noted that the sign of the Q_r value is correctly predicted by Q_r^{T}. Correlation between Q_r and Q_r^{T} was extensively studied for typical NAH molecules. The results are summarized in Table 3, from which the following conclusions are drawn.

TABLE 3. COMPARISON BETWEEN THE TOPOLOGICAL CHARGE DENSITY Q_r^{T} AND THE HÜCKEL CHARGE DENSITY Q_r FOR TYPICAL NON-ALTERNANT HYDROCARBONS

G	r	$\tilde{Z}_{G\ominus r}$	$\tilde{Y}_{G\ominus r}$	a)	Q_r^{T}	Q_r b)
I	1	4	−2	−4	−0.100	−0.488
	2	2	0	4	0.100	0.123
	3	3	0	6	0.150	0.182
II	1	11	2	10	0.038	0.378
	2	5	0	−10	−0.038	−0.047
	3	8	0	−16	−0.062	−0.092
	4	7	0	−14	−0.054	−0.073
III	1	29	−2	−26	−0.015	−0.311
	2	13	0	26	0.015	0.024
	3	21	0	42	0.024	0.058
	4	18	0	36	0.017	0.038
	5	19	0	38	0.021	0.047
IV	1	11	2	90	0.165	0.300
	2	8	0	32	0.059	0.073
	3	10	−4	−52	−0.095	−0.215
	4	9	−2	−10	−0.018	−0.072
V	1	24	2	−180	−0.059	−0.173
	2	27	4	−108	−0.035	0.185
	3	21	0	−252	−0.082	−0.198
VI	1	63	−2	−928	−0.042	−0.047
	2	71	−4	−1306	−0.059	−0.173
	3	55	0	−550	−0.025	−0.027
	4	70	10	790	0.035	0.145
	5	64	6	254	0.011	0.014
	6	67	8	522	0.023	0.130
VII	1	176	−8	2560	0.017	−0.119
	2	168	−6	3072	0.021	0.118
	3	184	−10	2048	0.014	−0.125
	4	144	0	4608	0.031	0.133
VIII	1	10	−4	96	0.188	0.106
	2	8	−4	64	0.125	−0.211
IX	1	21	0	336	0.166	0.295
	2	16	0	256	0.127	0.252
	3	20	−10	−100	−0.050	−0.061
	4	18	−6	36	0.018	0.119
	5	26	−10	−4	−0.002	−0.503
	6	22	−8	16	0.008	0.106
X	1	27	4	610	0.171	0.281
	2	22	4	540	0.152	0.263
	3	20	−10	−300	−0.084	−0.181
	4	26	−10	−216	−0.061	−0.157
	5	24	−10	−244	−0.069	−0.165
XI	1	246	0	−12792	−0.046	−0.066
	2	182	0	−9464	−0.034	−0.044
	3	237	30	3336	0.012	0.091
	4	207	18	−1308	−0.005	−0.008
	5	242	24	−56	−0.000	0.073
	6	167	18	712	0.003	0.002
	7	199	−2	−11392	−0.041	−0.095
XII	1	199	−2	−14062	−0.064	−0.156
	2	173	−8	−15130	−0.069	−0.161
	3	219	20	−5174	−0.024	0.040
	4	220	6	−11736	−0.053	−0.148
	5	171	20	−2006	−0.009	0.060
	6	216	44	6160	0.028	0.114
	7	201	36	3438	0.016	0.093
XIII	1	521	2	−12116	−0.008	0.066
	2	443	50	49396	0.032	0.116
	3	589	22	10700	0.007	−0.048
	4	540	36	29376	0.019	0.101
	5	541	22	12044	0.008	−0.049
	6	587	50	45364	0.030	0.118
	7	448	−20	−37264	−0.024	−0.091
	8	568	−42	−67816	−0.044	−0.122

a) $\tilde{Z}_G\tilde{Y}_{G\ominus r}-\tilde{Y}_G\tilde{Z}_{G\ominus r}$. $\tilde{Z}_G$ and $\tilde{Y}_G$ are given in Tabe 1.
b) $Q_r=1-q_r$.

(1) The topological charge density Q_r^{T} is useful for estimating the relative magnitudes of Q_r in an individual NAH.

(2) The correlation gets worse but still satisfactory for the following three groups of NAH's with i) an NBMO (non-bonding) (V, VII, and IX), ii) an anti-bonding HOMO (highest occupied) (VIII), and iii) a

bonding LUMO (lowest unoccupied).

(3) For relatively small NAH's (I-IV, VI, X) excluding the above groups, both the relative orders and the signs of Q_r values are correctly predicted by Q_r^{T}.[23]

Discussion

As the mathematical form of Q_r^{T} is fairly simple a number of general conclusions are drawn straightforwardly. Equation 25 suggests one to consider Q_r^{T} as a competition between the two terms $\tilde{Z}_G\tilde{Y}_{G\ominus r}$ $(=A_r)$ and $-\tilde{Y}_G\tilde{Z}_{G\ominus r}$ $(=B_r)$. Inspection of Table 3 shows that for almost all the cases, the former term predominates over the latter. Since $\tilde{Z}_G$, as well as $\tilde{Z}_{G\ominus r}$, is always positive and the largest number among the four indices in the expression of Q_r^{T}, the relative magnitude of $\tilde{Y}_{G\ominus r}$ is in parallel with the Q_r^{T} value and hence Q_r. In this sense the first term A_r is local or atomic factor determining the Q_r value. On the other hand, the second term B_r is a global or molecular factor, since its sign is already determined by that of $\tilde{Y}_G$, *i.e.*, by the topology of G (See Eq. 22).

By using this logic one can prove that for a network G in which the only entry of $(4m+3)$-cycle is a triangle, this triangle is positively charged. Choose a vertex r in the triangle. According to Eq. 22 $\tilde{Y}_G$ is negative and B_r positive. If there is no other odd cycle in G, $\tilde{Y}_{G\ominus r}$ is zero and so is A_r. Thus Q_r^{T} is positive. If there is at least one $(4m+1)$-cycle, $\tilde{Y}_{G\ominus r}$ is positive and so are A_r and Q_r^{T}. Thus Q_r^{T} is always positive. If a heptagon or a higher-member of $(4m+3)$-cycle coexists with a triangle in network G, it can be shown that the electron repulsive power of a triangle is stronger than that of a larger $(4m+3)$-cycle.[24] Then unless the conflict between two or more triangles occurs a triangle is shown to be always positive. Although this is a well-known conjecture in the MO theory based on a huge collection of numerical data, there has never been given a general proof for an arbitrary network by conventional perturbation treatment. In order to make the proof complete it will be analyzed in detail in the forthcoming paper that the signs of Q_r^{T} and Q_r are expected to be the same for almost all the cases with a very few exceptions as XIII. Similarly one can conclude that a pentagon is negatively charged in almost all the cases.

In conclusion it will be worth noting that by using the relations (8), (13), and (25), one can get a novel relation

$$Q_r^{\mathrm{T}} \doteq \exp(-E_\pi(G)/c)[\tilde{Y}_{G\ominus r} - \tilde{Y}_G \exp(-L_r/c)]$$

where $L_r = E_\pi(G) - E_\pi(G\ominus r)$ is the localization energy[25,26] of atom r. This interesting relation shows that the value of Q_r is not independent of the stability of the molecule (E_π) and the reactivity of its considered site (L_r).

Appendix I

Proof of Eq. 4b

Given two different functions $F_G^*(y)$ and $F_G^{**}(y)$ for an AH as

$$F_G^*(y) = N - iy\Delta'(iy)/\Delta(iy) \tag{4a}$$

$$F_G^{**}(y) = y^{-2}\ln|y^N P_G(1/iy)|. \tag{4b}$$

and we will show the following equality

$$\int_{-\infty}^{+\infty} F_G^*(y)\mathrm{d}y = \int_{-\infty}^{+\infty} F_G^{**}(y)\mathrm{d}y. \tag{A1}$$

Integration of $F_G^{**}(y)$ by parts one gets

$$\begin{aligned} I &= \int_{-\infty}^{+\infty} F_G^{**}(y)\mathrm{d}y \\ &= [yF_G^{**}(y)]_{-\infty}^{+\infty} - \int_{-\infty}^{+\infty} y\{\mathrm{d}F_G^{**}(y)/\mathrm{d}y\}\mathrm{d}y \\ &= -\int_{-\infty}^{+\infty} y\{\mathrm{d}F_G^{**}(y)/\mathrm{d}y\}\mathrm{d}y \end{aligned} \tag{A2}$$

by noting that $F_G^{**}(y)$ is an even function for AH's.

Differentiation of $F_G^{**}(y)$ with respect to y gives

$$\begin{aligned} \mathrm{d}F_G^{**}(y)/\mathrm{d}y &= -2y^{-3}\ln|y^N P_G(1/iy)| + y^{-3}A(y) \\ &= -2y^{-1}F_G^{**}(y) + y^{-3}A(y), \end{aligned} \tag{A3}$$

where

$$A(y) = N - P_G'(1/iy)/\{iyP_G(1/iy)\}. \tag{A4}$$

Substitution of Eq. A3 into Eq. A2 gives

$$I = 2I - \int_{-\infty}^{+\infty} y^{-2}A(y)\mathrm{d}y. \tag{A5}$$

Thus we have

$$I = \int_{-\infty}^{+\infty} y^{-2}A(y)\mathrm{d}y \tag{A6}$$

Transformation of $y = -Y^{-1}$, $\mathrm{d}y = Y^{-2}\mathrm{d}Y$ gives the relation

$$\begin{aligned} \int_{-\infty}^{+\infty} y^{-2}\mathrm{d}y &= \left[\int_{-\infty}^{0} + \int_{0}^{+\infty}\right] y^{-2}\mathrm{d}y \\ &= \left[\int_{0}^{+\infty} + \int_{-\infty}^{0}\right]\mathrm{d}Y \\ &= \int_{-\infty}^{+\infty}\mathrm{d}Y. \end{aligned} \tag{A7}$$

From Eqs. A4, A6, and A7 one gets

$$I = \int_{-\infty}^{+\infty} F_G^*(y)\mathrm{d}y. \tag{A8}$$

(Q.E.D.)

Appendix II

Graphical enumeration of $\tilde{Y}_G$ value.

The coefficients of the characteristic polynomial $P_G(x)$ are related with the topological index of the parent graph G and its subgraphs $\{G\ominus R_i\}$, where R_i is a cycle or a set of r_i disjoint cycles with a total of n_i vertices, as[11,16]

$$\begin{aligned} P_G(x) = &\sum_{k=0}^{m}(-1)^k p(G, k)x^{N-2k} \\ &+ \sum_{i}^{R_i\subset G}\sum_{k=0}^{m_i}(-1)^k(-2)^{r_i}p(G\ominus R_i, k)x^{N-n_i-2k}. \end{aligned} \tag{A9}$$

Since the $\tilde{Y}_G$ value is a collection of the coefficients of the terms x^{N-2k-1}, only the contribution by the odd-membered cycles are counted. Then it is straightforward to have

$$\begin{aligned} \tilde{Y}_G &= \sum_{i}^{\substack{n_i=2l_i+1\\ R_i\subset G}}(-1)^{l_i+1}(-2)^{r_i}\sum_{k=0}^{m_i}(-1)^k p(G\ominus R_i, k) \\ &= \sum_{i}^{\substack{n_i=2l_i+1\\ R_i\subset G}}(-1)^{l_i+1}(-2)^{r_i}Z_{G\ominus R_i}, \end{aligned} \tag{A10}$$

which is to be compared with the expression for $\tilde{Z}_G$[8]

$$\tilde{Z}_G = Z_G + \sum_{i}^{\substack{n_i=2l_i\\ R_i\subset G}}(-1)^{l_i}(-2)^{r_i}Z_{G\ominus R_i}. \tag{A11}$$

TABLE A1. G

i	$n_i=2l_i+1$ R_i	l_i	r_i	$G\ominus R_i$	$Z_{G\ominus R_i}$ (A)	$(-2)^{r_i}\times(-1)^{l_i+1}$ (B)	$A\times B$
1		1	1		3	−2	−6
2		2	1	●	1	2	2

$P_G(x)=(x^6-7x^4+11x^2-4)+(-2x^3+2x)$ $\tilde{Y}_G=-4$

$\tilde{Z}_G=1-(-7)+11-(-4)=23$ $\tilde{Y}_G=(-2)-2=-4$

TABLE A2. G: 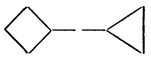

i	$n_i=2l_i+1$ R_i	l_i	r_i	$G\ominus R_i$	$Z_{G\ominus R_i}$ (A)	$(-2)^{r_i}\times(-1)^{l_i+1}$ (B)	$A\times B$
1		1	1		10	−2	−20
2		3	2	●	1	4	4

$P_G(x)=(x^8-9x^6+22x^4-10x^2)+(-2x^5+10x^3-4x)$ $\tilde{Y}_G=-16$

$\tilde{Z}_G=1-(-9)+22-(-10)=42$ $\tilde{Y}_G=(-2)-10+(-4)=-16$

In Tables A1 and A2, examples of obtaining $\tilde{Z}_G$ values for graphs IV and IX are given, respectively.

References

1) C. A. Coulson and G. S. Rushbrooke, *Proc. Cambridge Phil. Soc.*, **36**, 193 (1940).

2) G. G. Hall, *Proc. R. Soc., Ser. A*, **229**, 251 (1955); K. Ruedenberg, *J. Chem. Phys.*, **29**, 1232 (1958); *ibid.*, **34**, 1884 (1961); J. Koutecký, *ibid.*, **44**, 3702 (1966).

3) I. Gutman, N. Trinajstić, and T. Zivković, *Tetrahedron*, **29**, 3449 (1973).

4) I. Gutman and N. Trinajstić, *Chem. Phys. Lett.*, **20**, 257 (1973).

5) I. Gutman and N. Trinajstić, *Croat. Chem. Acta*, **48**, 19 (1976).

6) T. Yamaguchi and H. Hosoya, "Analysis of the regularity of the charge density of hydrocarbons," Presented at the Symposium on the Molecular Structure, Osaka, November 1975.

7) R. A. Marcus, *J. Chem. Phys.*, **43**, 2643 (1965).

8) H. Hosoya, K. Hosoi, and I. Gutman, *Theor. Chim. Acta*, **38**, 37 (1975).

9) A. Graovac, I. Gutman, and N. Trinajstić, *Chem. Phys. Lett.*, **35**, 555 (1975); *ibid.*, **37**, 471 (1976).

10) I. Gutman and N. Trinajstić, *J. Chem. Phys.*, to be pullished.

11) H. Hosoya and M. Murakami, *Bull. Chem. Soc. Jpn.*, **48**, 3512 (1975); H. Hosoya and K. Hosoi, *J. Chem. Phys.*, **64**, 1065 (1976).

12) C. A. Coulson, *Proc. Cambridge Phil. Soc.*, **36**, 201 (1940); C. A. Coulson and H. C. Longuet-Higgins, *Proc. R. Soc., Ser. A*, **191**, 39 (1947).

13) H. Baba, *Bull. Chem. Soc. Jpn.*, **30**, 154 (1957).

14) K. Fukui, T. Yonezawa, and C. Nagata, *J. Chem. Phys.*, **26**, 831 (1957).

15) I. Gutman and N. Trinajstić, *Topics Curr. Chem.*, **42**, 49 (1973).

16) H. Hosoya, *Theor. Chim. Acta*, **25**, 215 (1972).

17) A. Graovac, I. Gutman, N. Trinajstić, and T. Zivković, *Theor. Chim. Acta*, **26**, 67 (1972).

18) I. Gutman, unpublished.

19) This is an outcome of the general relations, $a_0=1$ and $(-1)^k a_{2k}\geq 0$, for which very few exceptions are known such as the case with 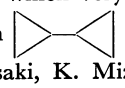 , 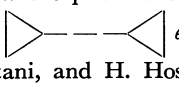 *etc.*[20]

20) K. Kawasaki, K. Mizutani, and H. Hosoya, *Natural Science Rept. Ochanomizu Univ.*, **22**, 181 (1971).

21) F. Harary, "Graph Theory," Addison-Wesley Publ. Co., Reading, Mass. (1969), pp. 150—155; see also I. Gutman and W. C. Herndon, *Chem. Phys. Lett.*, **34**, 387 (1975).

22) H. Hosoya, *Bull. Chem. Soc. Jpn.*, **44**, 2332 (1971).

23) Note that for these NAH's the inequality (13) no longer holds.

24) This is another feature of the Hückel $4n+2$ rule, which is not determined by the repulsion between electrons but attributable to the intrinsic stability of a $(4n+2)$-π ring system.

25) I. Gutman, Thesis, Univ. of Zagreb (1973).

26) G. W. Wheland, *J. Am. Chem. Soc.*, **64**, 900 (1942).

ESR of Hot Ions: Ni(I) Complex Ions Produced in Rigid Solutions by UV-Exposure

Chikara AMANO* and Shizuo FUJIWARA

Department of Chemistry, Faculty of Science, The University of Tokyo, Hongo, Bunkyo-ku, Tokyo 113

(Received March 8, 1976)

It has been shown that univalent nickel complex ions are produced in rigid solutions by electrons released on photo-ionization of *N,N,N',N'*-tetramethyl-*p*-phenylenediamine. These complexes have the same *g*-values as those obtained by γ-irradiation, suggesting that the univalent nickel complex ions produced on γ-irradiation can be formed as a result of the capture of near-thermal electrons by bivalent nickel complexes. Upon UV-exposure at various sample temperatures between -196 °C and -70 °C, a new chemical species with $g_{//}$ of 2.37 and $g_{\perp}$ of 2.128 has been observed, which appears to be an exchange-coupled dimer of the univalent hexaaqua nickel complex ions.

Paramagnetic ions which are produced in diamagnetic inorganic metal complexes upon γ-ray irradiation, are referred to as the hot ions.[1,2] Investigations have been carried out in this laboratory on metal ions such as Co, Ni, Pd, Pt, Rh, Ir, Cu, Zn, Cd, Hg, and Tl, in order to clarify the distortion of the lattice structure of the host compounds, which is caused by the formation of reduced or oxidized metal complex ions.

This paper deals with the hot ion of nickel which will be compared with the case of Pd and Co. From the viewpoint of the distortion of the ligand field, Pd(II), which takes a square planar structure, presents an extreme case where the hot ion is stabilized without appreciable change of the symmetry of ligand field in the process of one electron reduction. In the case of Ni(II), however, the original octahedral structure becomes distorted to the tetragonal one by the formation of Ni(I), which may be caused by the Jahn-Teller effect. The technique of investigation adopted in this experiment is almost the same as that in the case of Pd(II), *i.e.* the reaction of Ni(II) complex ions with the photoelectrons from *N,N,N',N'*-tetramethyl-*p*-phenylenediamine (TMPD) in rigid solutions. We have also examined the effect temperature of the rigid solutions on the formation of Ni(I) complex ions during and after UV-exposure.

Experimental

Nickel(II) chloride hexahydrate, purified by the anion exchange method, was dissolved into a glassy solvent, a mixture of ethylene glycol and water (2: 1 v/v). Ethylenediamine (en), 2,2'-bipyridyl (bpy), or 1,10-phenanthroline (phen) was added to the nickel(II) solution as a ligand. The molar ratio of nickel(II) chloride to each ligand was varied in the same way as in a previous experiment.[3] The concentration of nickel(II) complex ions was between 0.01 and 0.1 mol/l. *N,N,N',N'*-tetramethyl-*p*-phenylenediamine hydrochloride (TMPD·HCl) was added to the above solutions in an equal molar ratio to nickel(II) complex ions. Xylene, a mixture of *o*-, *m*-, and *p*-xylene, was also used as a glassy solvent in the case of nickel(II) ethyl xanthate complex, where hydrochloric acid free TMPD was used. Each solution was placed in the sample tube for ESR measurements and immersed in liquid nitrogen. The sample was exposed to UV-light through a quartz lens window of the ESR cavity for 10—60 min. An Ushio mercury lamp UI-501C (500 W) was used as a UV source. In order to suppress short wavelength light, a Corning color filter 7-54 was used which does not transmit UV-light with a wavelength smaller than 230 mμ. In the case of hexaaqua nickel(II) complexes, the effect of temperature during and after UV-exposure was closely checked by examining the relative amount of products. ESR experiments were performed in the temperature range -196 °C to -50 °C.

* Present address: Department of Engineering Physics, The University of Electro-communications, Chofugaoka, Chofu, Tokyo 182

Results and Discussion

Upon exposure to UV-light the sample turned blue, due to the formation of a TMPD cation radical. At the same time, two ESR signals became observable, one at the position of usual organic radicals, and the other at a few hundred gauss lower field (Fig. 1, 3). The

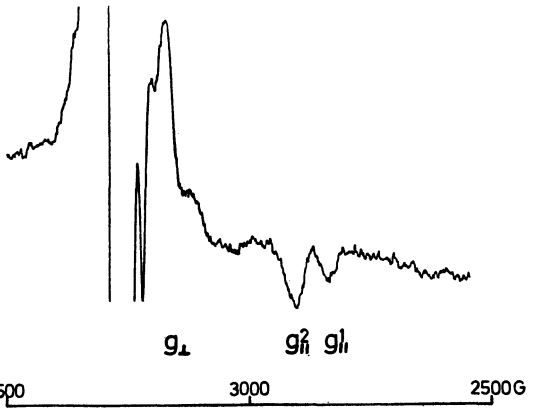

Fig. 1. ESR spectra of $[Ni(bpy)(H_2O)_4]^+$ ($g'_{//}$) and $[Ni(bpy)_2(H_2O)_2]^+$ ($g^2_{//}$). $NiCl_2 \cdot 6H_2O$: dipy = 1: 1.

line shape of the former signal suggests that some unidentified organic radicals are superimposed on the TMPD cation radical. By raising the temperature of the sample, the signal intensity decreased, only one signal with a characteristic structure remaining observable above -50 °C. The signal is identical with that of the TMPD cation radical which can be easily produced by adding sodium nitrite or lead tetracetate to a TMPD·HCl solution (Fig. 2). On the other hand, the latter signal can be assigned to a univalent nickel complex ion since the *g*-values are characteristic of the complex ion with d^9 electron configuration.[3] The results suggest

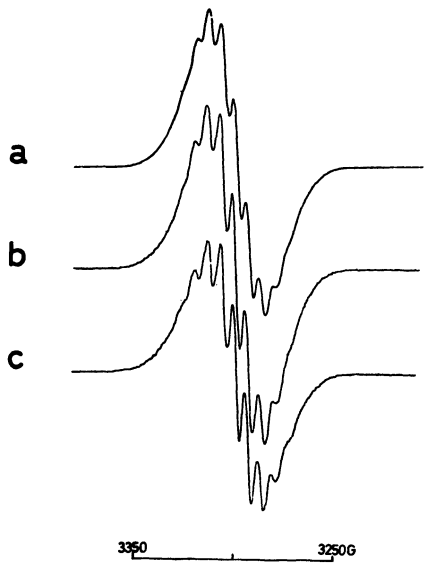

Fig. 2. ESR spectra of TMPD·H^{2+}. a) −196 °C. b) −160 °C. c) −90 °C. The strength is arbitrary.

a possible reaction scheme as follows:

$$TMPD\cdot H + h\nu\ (318\ m\mu) + h\nu\ (380\ m\mu) \longrightarrow TMPD\cdot H^{2+} + e^-$$

$$Ni^{2+}\ comp. + e^- \longrightarrow Ni^{+}\ comp.$$

$$H_2O \text{ or ethylene glycol} + e^- \longrightarrow \text{radicals}$$

The g-values of the univalent nickel complex ions are shown in Table 1. By comparing the g-values obtained in this experiment with those in the case of γ-irradiation, it can be concluded that the electronic state of the univalent nickel complex ions obtained in both these experiments are identical. This might suggest that the univalent nickel complex ions formed on γ-irradiation are produced by the capture of near-thermal electrons in a later stage of radiation-chemical processes. It seems that TMPD·H^+ does not participate in ligation to the nickel(II) ion, and the univalent nickel complex ions retain the ligand molecules originally bonded to the nickel(II) ions. ESR signals of the univalent nickel complex ions disappear above −50 °C and do not appear even if the sample temperature is lowered again.

Table 1. ESR parameters of nickel complexes

Complexes	Matrices	$g_{//}$	$g_\perp$
$[Ni(H_2O)_6]^+$	EG–H_2O	2.468 (2.466)[a,b]	2.078 (2.076)
$[Ni(H_2O)_6]^+$	EtOH	2.486 (2.471)	(2.078)
$[Ni(en)(H_2O)_4]^+$	EG–H_2O	2.36[c] (2.359)	2.07 (2.072)
$[Ni(en)_2(H_2O)_2]^+$	EG–H_2O	2.29 (2.282)	2.07 (2.064)
$[Ni(bpy)(H_2O)_4]^+$	EG–H_2O	2.32 (2.311)	2.09 (2.075)
$[Ni(bpy)_2(H_2O)_2]^+$	EG–H_2O	2.27 (2.259)	2.09 (2.074)
$[Ni(phen)(H_2O)_4]^+$	EG–H_2O	2.32 (2.317)	2.08 (2.076)
$[Ni(phen)_2(H_2O)_2]^+$	EG–H_2O	2.28 (2.271)	2.08 (2.074)
$[Ni(C_3H_5OS_2)_2]^-$	Xylene	2.275 (2.280)	2.084 (2.074)
$[Ni(H_2O)_6]^{3+}$	EG–H_2O	2.32 (2.308)	
$[Ni(H_2O)_6]_2^{2+}$	EG–H_2O	2.37	2.128

a) ±0.005. b) The g-values in parentheses are those obtained in the previous γ-irradiation experiment. c) ±0.01 (for g-values with two figures below decimal point).

In a previous experiment on γ-irradiation, an isotropic ESR signal with g-value of 2.308 which was tentatively assigned to a tervalent nickel complex ion was observed along with the univalent nickel complex ion having d^9 electron configuration. The isotropic signal observed in the present experiment on UV-light exposure gives the same g-value. In order to examine these signals more closely, rigid sample solutions were exposed to UV-light at several temperatures. Between −130 °C and −196 °C, a univalent nickel complex ion with g-values of 2.468($g_{//}$) and 2.078($g_\perp$) is strong in intensity. This is named low temperature signal. The isotropic signal with g-value of 2.308 is weak (Fig. 3). Between −125 °C and −100 C°, a new signal (a high temperature signal) with the g-values 2.37($g_{//}$) and 2.128($g_\perp$) appears and grows gradually at the expense of the low temperature signal, while the isotropic signal reaches the maximum strength at −115 °C and decays gradually beyond this temperature. The low temperature signal is not observed above −115 °C. In the range −95 °C to −70 °C, only the high temperature signal remains observable. The high temperature signal does not change to the low tempera-

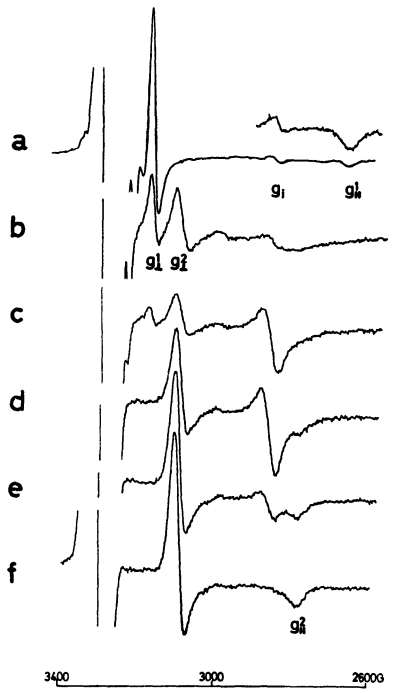

Fig. 3. Three ESR spectra are observed, as the temperature is raised: low temperature signal ($g^1_{//}$ and $g^1_\perp$), isotropic signal (g_i), and high temperature signal ($g^2_{//}$ and $g^2_\perp$). a) UV-exposure at −140 °C. b) −125 °C. c) −120 °C. d) −115 °C. e) UV-exposed at −115 °C and raised to −100 °C. f) UV-exposed at −115 °C and raised to −90 °C.

ture signal by cooling the rigid solution again to −150 °C, indicating two different chemical species.

The thermal stability of these species is in the order: high temperature signal>isotropic signal>low temperature signal. The low temperature signal and isotropic one are also observed in the previous γ-irradiation experiment. The high temperature signal appears to be due to nickel complex ion because of its relatively large g-shift. A large g-shift, say greater than 0.2, would be most likely caused by strong spin-orbit interaction, and is typical of heavy atoms, *i.e.* nickel ion in this case. From the relation $g_{//}>g_{\perp}>2$, which is characteristic of a d^9 electron configuration with D_{4h} symmetry elongated along one of the four fold axes of O_h, it can be concluded that the paramagnetic center is due to a univalent nickel complex ion. Since the average g-value $(g_{//}/3+2g_{\perp}/3)$ is nearly the same in both low and high temperature signals, these two species do not seem to differ much in electronic state. However, each component of the principal g-values differs a great deal. Copper(II) sulfate does not show one of its principal g-values in any direction in the crystalline state because of the presence of exchange interaction between the neighboring ions in the same unit cell.[4] Thus the apparent g-values differ in the rigid solution state from those in the crystalline state. It appears that the high temperature signal is due to an exchange-coupled dimer of the univalent nickel complex ions.

We would like to thank Dr. Yoji Arata for valuable discussions in the preparation of this paper.

References

1) S. Fujiwara, T. Watanabe, and H. Tadano, *J. Coord. Chem.*, **1**, 195 (1971).
2) J. Isoya and S. Fujiwara, *Bull. Chem. Soc. Jpn.*, **45**, 2182 (1972).
3) C. Amano and S. Fujiwara, *Bull. Chem. Soc. Jpn.*, **46**, 1379 (1973).
4) D. M. S. Bagguly and J. H. E. Griffiths, *Nature*, **162** 538 (1948).

Silver Ion Catalysed Oxidation of Primary Aliphatic Amines by Potassium Peroxydisulfate — A Kinetic Study

J. Sreekantha Babu, Km. Veena Joshi, and A. K. Bhattacharya
School of Studies in Chemistry, Vikram University, Ujjain, India

(Received May 28, 1974)

A detailed kinetic study of the oxidation of propyl-, isopropyl-, butyl- and isobutylamines by potassium peroxydisulfate in presence of silver ions has been carried out in aqueous medium. The effects of silver ion concentration and various neutral salts have been detected and the variation of the order of reaction with respect to amine had been explained. The activity of Ag^+ ion has been correlated with the amine structure and probable rate law and the mechanism has been proposed.

Marshall[1] observed the catalytic action of silver ions in the oxidation by peroxydisulfate. Agrawal and Mushran[2] and Srivastava and Hambir Singh[3] reported the silver ion catalysed oxidation of certain amides by peroxydisulfate while Khare and Bhattacharya[4] studied kinetically the morpholine–persulfate reaction. Beileryan *et al.*[5] studied certain aspects of the peroxydisulfate oxidation of some simple primary and secondary amines and amino alcohols. In the present investigation silver ion catalysed oxidation of propyl-, isopropyl-, butyl-, and isobutylamines has been studied kinetically and the effect of amine structure on the catalytic activity of silver ions has been discussed.

Experimental

All the chemicals used were of AnalaR or E. Merck's G. R. quality. The amines were distilled before use. The solutions were always freshly prepared in redistilled water. The amine solution and peroxydisulfate solution along with other required solutions were separately thermostated to attain constant temperature (accuracy ± 0.1 °C). The amine solution is added to peroxydisulfate to start the reaction. Aliquots (5 ml) of the reaction mixture were pipetted out in ice cold water to quench the reaction. The progress of the reaction has been studied by estimating the unreacted peroxydisulfate with use of Kolthoff and Carr's[6] iodometric method with necessary modifications.

Preliminary experiments showed that all the reactions follow pseudo first order kinetics in the presence of silver ion when the concentration of amine has been taken in excess. The self decomposition of peroxydisulfate was found to be negligible and therefore not taken into consideration. Since the boiling point of isopropylamine is 34 °C, all the results of the silver ion catalysed oxidation of isopropylamine have been given at 20 °C, while the oxidation of the other three amines have been carried out at 30 °C. The rate of uncatalysed oxidation was found to be quite small for all the four amines.

Results and Discussion

Effect of Silver Ion Concentration on the Rate of Oxidation. We see that the rate of reaction increases with increase in the concentration of Ag^+ ions for all the four reactions. Straight lines were obtained for the plots of pseudo first order rate constant k *versus* (Ag^+) and the values of intercepts are in good agreement with the rate of uncatalysed reaction (k_o).

Order with Respect to Each Reactant. Since the values of pseudo first order rate constants were found to be fairly constant during all the sets, the order with respect to peroxydisulfate is unity.

The values of order of reaction with respect to amine at different silver ion concentrations in each case are given in Table 2.

The order with respect to amine decreases with the increase in silver ion concentration.

According to Moelwyn-Hughes[7] the uncatalysed and catalysed reactions proceed simultaneously in the presence of a catalyst, and the relation $k=k_o+k_c$ (catalyst), holds, where in k is observed overall pseudo first order rate constant in the presence of catalyst silver ion.

k_o is pseudo first order rate constant for uncatalysed reaction and k_c, is catalytic constant.

The above relation holds for all the four amines, the k_c values for different concentrations of (Ag^+) being fairly constant within the limits of experimental error (Table 3).

Effect of Neutral Salts. The values of rate constants in the presence of different concentrations of

Table 1.
(Pot. peroxydisulfate) 0.005M (Amine) 0.20M

Isopropylamine		Propylamine		Butylamine		Isobutylamine	
(Ag^+) $\times 10^4$ M	$k\times 10^2$ min^{-1}	(Ag^+) $\times 10^5$ M	$k\times 10^2$ min^{-1}	(Ag^+) $\times 10^5$ M	$k\times 10^2$ min^{-1}	(Ag^+) $\times 10^5$ M	$k\times 10^2$ min^{-1}
—	0.1019	—	0.1300	—	0.1123	—	0.1327
2.5	0.6064	6.0	0.7196	5.0	0.6121	5.0	0.5058
5.0	1.156	10.0	1.141	10.0	1.131	10.0	0.8752
7.5	1.709	15.0	1.605	15.0	1.609	15.0	1.197
10.0	2.251	20.0	2.054	20.0	2.122	20.0	1.562
12.5	2.756	25.0	2.570	30.0	3.247	30.0	2.239

TABLE 2.
(Pot. peroxydisulfate) 0.005M

(Ag+) M	Concn of amine C′ (M)	Concn of amine C″ (M)	Rate Const. ×10² k′ min⁻¹	Rate Const. ×10² k″ min⁻¹	Order of reaction n
Isopropylamine					
—	0.40	0.20	0.2023	0.1019	0.9897
2.5×10^{-4}	0.40	0.20	1.120	0.6064	0.8870
5.0×10^{-4}	0.40	0.20	2.002	1.156	0.7920
10.0×10^{-4}	0.40	0.20	3.736	2.251	0.7308
Propylamine					
—	0.40	0.30	0.2505	0.1876	1.007
6.0×10^{-5}	0.20	0.10	0.7196	0.4683	0.6192
20.0×10^{-5}	0.20	0.10	2.054	1.569	0.3880
25.0×10^{-5}	0.20	0.10	2.570	2.010	0.3528
Butylamine					
—	0.30	0.20	0.1586	0.1123	1.002
5.0×10^{-5}	0.20	0.10	0.6121	0.4030	0.6332
10.0×10^{-5}	0.20	0.10	1.131	0.8090	0.4833
15.0×10^{-5}	0.20	0.10	1.609	1.200	0.4011
Isobutylamine					
—	0.30	0.20	0.1991	0.1327	1.000
5.0×10^{-5}	0.20	0.10	0.5058	0.3163	0.6774
20.0×10^{-5}	0.20	0.10	1.562	1.168	0.4192
30.0×10^{-5}	0.20	0.10	2.239	1.718	0.3817

neutral salts are given in Table 4.

Table 4 indicates that the rate of oxidation decreases with the addition of neutral salts, *i.e.* with increase in ionic strength.

The order of reaction with respect of amine was found to change with the amine concentration as well as with the temperature and it was not possible to calculate the over all rate constant and hence the energy parameters.

Rate Laws and Discussion. The experimental results show that all the four amines behave similarly. Hence, the following general rate law is proposed for all the four amines.

$$\frac{-d(S_2O_8^{2-})}{dt} = k_s(Am)(S_2O_8^{2-}) + k_c(Ag^+)(S_2O_8^{2-}) \quad (8)$$

Uncatalysed path Catalysed path

where k_s is second order rate constant for uncatalysed reaction and k_s (Am) $=k_o$ pseudo first order rate constant for uncatalysed reaction. The rate law suggests that in the presence of catalyst both uncatalysed and catalysed reactions proceed simultaneously. In the absence of a catalyst the reaction proceeds through the path involving the first term only and the order with respect to amine should be one. Similar results were reported by Chaltykyan and Beileryan,[8] during the course of their study of the uncatalysed oxidation of some simple primary and secondary amines. In the presence of high concentration of Ag^+ ions, k_o is negligible as compared with k_c (Ag^+), *i.e.* the reaction proceeds entirely along the second path and the order with respect to amine would be zero. Naturally, at moderate concentrations of Ag^+ which have been used in the present investigation, the order with respect to amine is fractional. This was found to be actually the case. With further increase

TABLE 3.
(Pot. peroxydisulfate) 0.005M (Amine) 0.20M

Isopropyl- (Ag+) ×10⁴ M	Isopropyl- k_c l·mol⁻¹·min⁻¹	Propyl- (Ag+) ×10⁵ M	Propyl- k_c l·mol⁻¹·min⁻¹	Butyl- (Ag+) ×10⁵ M	Butyl- k_c l·mol⁻¹·min⁻¹	Isobutyl- (Ag+) ×10⁵ M	Isobutyl- k_c l·mol⁻¹·min⁻¹
2.5	20.18	6.0	98.26	5.0	98.96	5.0	74.62
5.0	21.08	10.0	101.10	10.0	101.87	10.0	74.25
7.5	21.42	15.0	98.33	15.0	99.78	16.0	70.95
10.0	21.49	20.0	96.20	20.0	100.48	20.0	71.46
12.5	21.43	25.0	97.60	30.0	104.45	30.0	69.88
Average	21.08		98.30		101.31		72.33
From graph	21.22		100.00		102.52		71.27

TABLE 4.
(Pot. peroxydisulfate) 0.005M

	Isopropyl-		Propyl-		Butyl-		Isobutyl-	
Amine Concn M →	0.20		0.10		0.20		0.20	
(Ag+) M →	10.0×10^{-4}		20.0×10^{-5}		10.0×10^{-5}		10.0×10^{-5}	
Salt	Salt concn	$k\times10^2$ min⁻¹	Salt concn	$k\times10^2$ min⁻¹	Salt concn	$k\times10^2$ min⁻¹	Salt concn	$k\times10^2$ min⁻¹
—	—	2.251	—	1.569	—	1.182	—	0.8752
K_2SO_4	0.0075	2.004	0.015	1.271	0.010	0.8112	0.020	0.7399
K_2SO_4	0.0150	1.833	0.025	1.005	0.015	0.6997	0.025	0.7150
Na_2SO_4	0.0075	2.113	0.010	1.303	0.015	0.8015	0.004	0.8537
Na_2SO_4	0.0150	1.929	0.020	1.086	0.020	0.7187	0.008	0.8131
$NaClO_4$	0.0075	2.062	0.005	1.392	0.005	1.008	0.008	0.8220
$NaClO_4$	0.0150	1.871	0.030	1.112	0.012	0.8604	0.020	0.7511

in silver ion concentration the order should decrease, approaching zero. This is also in agreement with the observed data (Table 2).

The second term in the rate law also suggests that the reaction proceeding *via* catalysed path occurs between two oppositely charged ions, and negative salt effect should be observed. This was found also to be the case.

In the presence of excess amine as in the present study, Eq. 1 is reduced to

$$\frac{-d(S_2O_8^{2-})}{dt} = [k_o + k_c(Ag^+)](S_2O_8^{2-}) \quad (2)$$

At particular Ag^+ concentration,

$$[k_o + k_c(Ag^+)] = k, \text{ the over all rate constant} \quad (3)$$

Equation 3 is similar to that proposed by Moelwyn-Hughes, which has been experimentally found to hold good.

Effect of Amine Structure on the Oxidation Rate. Since the rate constants for the uncatalysed oxidation of all the four amines are of similar magnitude, the catalytic activity of Ag^+ ion has been compared for the values of k_c. To compare the results of isopropyl amine with propylamine, the value of k_c of propylamine was determined at 20 °C under identical conditions and found to be 47.52 l mol^{-1} min^{-1}.

Chaltykyan and Beileryan[9] suggested that the catalytic activity of silver ions in the oxidation of amines with peroxydisulfate increases with decreasing basicity of amines. Nikolaev and Sychev[10] and other workers have reported that the catalytic activity of the metal ion is directly proportional to the instability of metal amine complex.

The order of stability of the silver amine complex and P_{kb} values of the four amines are: butyl-<isobutyl-[11] and propyl-<isopropyl-. The catalytic activity of Ag^+ ions should therefore be in the reverse order which was actually the case.

Mechanism. Taking into consideration all the experimental evidences, the following mechanism has been proposed. Firstly Ag(III)[12,13] will form (rate determining step) which will readily oxidizes the amine to hydroxyl amine derivative

$$S_2O_8^{2-} \underset{k_2}{\overset{k_1}{\rightleftharpoons}} 2SO_4^{\cdot-} \quad (3a)$$

$$\frac{(SO_4^{\cdot-})^2}{(S_2O_8^{2-})} = k_o \text{ (Equilibrium constant)} \quad (3b)$$

$$2SO_4^{\cdot-} + Ag^+ \xrightarrow[\text{Rate determining step}]{\text{slow}} 2SO_4^{2-} + Ag^{3+} \quad (4)$$

$$Ag^{3+} + R\cdot NH_2 + H_2O \xrightarrow{\text{Rapid}} R\cdot NHOH + Ag^+ \quad (5)$$

This explains the rate law proposed for the catalysed path,

$$\frac{-d(S_2O_8^{2-})}{dt} = k_2(Ag^+)(SO_4^{\cdot-})^2$$

from Eq. 3b.

$$(SO_4^{\cdot-})^2 = k_e(S_2O_8^{2-}), \text{ then}$$

$$\frac{-d(S_2O_8^{2-})}{dt} = k_2k_e(Ag^+)(S_2O_8^{2-})$$

$$= k_c(Ag^+)(S_2O_8^{2-})$$

where $k_c = k_2k_e$ is catalytic constant.

The stoichiometric ratio determined for all the four amines is 1 : 1, showing that one molecule each of the oxidant and reductant have been consumed in the reaction.

The oxidation products have been isolated from the reaction mixture using solvent extraction technique. The presence of two compounds other than the excess of amine have been found by thin layer chromatography. From the samples obtained hydroxyl amine derivative and oxime have been detected.[14,15] The oximes formed were due to autooxidation of hydroxylamine derivatives[16,17] as the pH of the systems is above 7. This might be due to reduction of catalyst Ag^+ ion left in the system to Ag by the hydroxylamine derivatives.[18] Black particles of silver were observed when the system was left for a long time.

Lebedev and Kazarnovskii[19] also found oximes, hydroxyl amines of hydroxyamic acids as end products in their study on the catalytic oxidation of aliphatic amines with hydrogen peroxide. Bacon and Stewart[20] also reported aldoximes as the products of oxidation of the silver catalysed peroxydisulfate oxidation of amine.

The authors are thankful to Prof. M. M. Bokadia, Head, School of Studies in Chemistry, Vikram University, Ujjain, for providing laboratory and other research facilities. They are grateful to the Council of Scientific and Industrial Research, India for the award of Junior research fellowship to Km. Veena Joshi and Junior and Postdoctoral fellowships to J. Sreekantha Babu.

References

1) H. Marshall, *Proc. Roy. Soc. (Edinbourgh)*, **23**, 163 (1900).
2) M. C. Agrawal and S. P. Mushran, *Chem. Anal.*, **50**, 350 (1968).
3) S. P. Srivastava and Hambir Singh, *J. Indian Chem. Soc.*, **48**, 725 (1971).
4) B. P. Khare and A. K. Bhattacharya, *Proc. Nat. Acad. Sci. (India)*, Vol. XI, Sec. A, III, 247 (1970).
5) N. M. Beileryan, R. M. Akopyan, and O. A. Chaltykyan, *Dokl. Akad. Nauk Arm. SSR.*, **50**, 149 (1970).
6) I. M. Kolthoff and E. M. Carr, *Anal. Chem.*, **25**, 298 (1953).
7) E. A. Moelwyn-Hughes, "Kinetics of Reactions in Solution," Oxford University Press, London (1947), p. 297.
8) O. A. Chaltykyan and N. M. Beileryan, *Dokl. Akad. Nauk Arm. SSR.*, **30**, 225 (1960).
9) O. A. Chaltykyan and N. M. Beileryan, *Izvest. Akad. Nauk Arm. SSR Khim. Nauki.*, **14**, 209 (1961).
10) L. A. Nikolaev and A. P. Sychev, *Nauch. Dokal. Vysshei Shkoly, Khim. Khim. Teknol.*, **1**, 89 (1958).
11) J.L. Pauley and H. H. Hau, *J. Phys. Chem.*, **70**, 3363 (1966).
12) D. A. House, *Chem. Rev.*, **62**, 187 (1962).
13) M. C. Agrawal and S. P. Mushran, *J. Indian Chem. Soc.*, **42**, 629 (1965).
14) Endres and Kaufmann, *Ann.*, **530**, 184 (1937).

15) F. Feigl and Silva, *Analyst*, **82**, 583 (1957).
16) E. H. Rodd, "Chemistry of Carbon Compounds," Elsevier Publishing Co., Amsterdam (1966), p. 41.
17) S. Patai, Ed., "The Chemistry of the Carbon-Nitrogen Bond," Interscience Publications, New York (1970), p. 120.
18) C. P. Lloyd and W. F. Pickering, *J. Inorg. Nucl. Chem.*, **29**, 1907 (1967).
19) O. L. Lebedev and S. N. Kazarnovskii, *Zhur. Obshch. Khim.*, **30**, 1631 (1960).
20) R. G. R. Bacon and D. Stewart, *J. Chem. Soc., C*, **1966**, 1384.

Dielectric Study of the Intermolecular Association of Alcohols in Solutions of Benzene

Buta SINGH and J. K. VIJ
Department of Physics, Punjabi University, Patiala-147002, India
(Received September 2, 1975)

The relative permittivity at 1 MHz, the refractive index at the wavelength of sodium D-line and density of the nine alcohols, 1-propanol (A), 2-propanol (B), 1-butanol (C), 2-methyl-1-propanol (D), 1-pentanol (E), 1-hexanol (F), 1-heptanol (G), 3-methyl-2-hexanol (H), 3-methyl-3-hexanol (I), have been measured at 25 °C in benzene in the entire concentration range. The measurements for 1-dodecanol (J) have been made in dilute solutions only. The dipole moments of these molecules in dilute solutions, using Higasi's equation, and the apparent dipole moment for various solute concentrations, using Kirkwood-Fröhlich equation, have been calculated. The results suggest that at low concentrations the alcohols associate to form weakly polar multimers. At high concentrations and in pure liquids, the isomers in which the hydroxyl group is relatively free, favour the formation of highly polar multimers, whereas the isomers in which the hydroxyl group is sterically blocked by the methyl group, favour the formation of closed or ring dimers having low dipole moment.

The low frequency relative permittivity, the electric dipole moment, the Kirkwood correlation factor and dielectric relaxation measurements are useful for studying liquid structure.[1,2] Alcohols have probably been studied more extensively than any other group of compounds and their dielectric absorption is well established. Nevertheless a complete molecular model of the liquid structure capable of explaining the experimental results in alcohols is as yet incomplete. The position of the hydroxyl and the methyl groups on the hydrocarbon chain in alcohols greatly influence the relative permittivity and the correlation factor and consequently the degree and type of hydrogen bonding in these liquids.[3-5] In 1929, Smyth and Stoops[3] reported on the temperature dependence of the relative permittivity of twenty-two isomeric alcohols and also the dilute solution studies of two of these compounds in benzene. They concluded that there is a possibility of both parallel and antiparallel alignments of near-neighbour dipoles. The particular type depends on the molecular geometry, temperature and dilution in nonpolar solvents. Dannhauser made systematic studies on the temperature dependence of the relative permittivity of eight lower alcohols[6] and eight isomeric octanols.[4] He explained the results in terms of the alcohol association into highly polar linear chain n-mers ($n=1,2,3,4....$) and ring dimers having small or zero dipole moment.

Hydrogen bonding in aliphatic alcohols in dilute solution has also received considerable attention. However, most of the data available to date is limited to low concentrations only.[7-9] Rajala and Crossley[10] studied the association of butanols and 1-decanol in the concentration range from 0.2 to 1.0 mol fraction in different solvents and concluded that alcohol association is initially dominated by the formation of small, weakly polar multimers, and eventually large highly polar multimers predominate.

The present work reports the data of the relative permittivity for several alcohols in benzene as a nonpolar solvent in the entire concentration range. In these alcohols the alcohol molecular size and the steric environment of the hydroxyl group are the variables. The data is analysed in terms of the Kirkwood correlation factor, the liquid structure of these alcohols being discussed.

Experimental

Materials. The name and the specifications of the alcohols as given by the manufacturer are given in parentheses after each sample.

(A) 1-propanol (E. Merck A. G., pure grade),
(B) 2-propanol (B. D. H., A. R.),
(C) 1-butanol (B. D. H., A. R.),
(D) 2-methyl-1-propanol (B. D. H., A. R.),
(E) 1-pentanol (Riedel A. G.),
(F) 1-hexanol (Eastman, for chemical purposes),
(G) 1-heptanol (Fluka A. G., practical grade),
(H) 3-methyl-2-hexanol (Fluka A. G., purum),
(I) 3-methyl-3-hexanol (Fluka A. G., purum),
(J) 1-dodecanol (Eastman, for chemical purposes).

Alcohols A—E and G were all dried and distilled and the middle fraction for each sample was collected for use. Alcohols F and H—J were used as such. Benzene (B. D. H., A. R.) which was previously dried by passing sodium wire was subsequently distilled and the middle fraction thus obtained was used. The refractive indices of all the alcohols (except for 1-dodecanol) and of benzene were measured. The values were found to compare well with those given in literature. The melting point of 1-dodecanol was found to be distinct, its value of 23 °C coinciding closely with the literature value of 22.6 °C.

Measurements. Relative permittivity measurements at the frequency of 1 MHz were made with a dielectrometer based on the heterodyne beat method.[11] A two-terminal dielectric cell (type DFL 2, made in Germany), with air capacitance of 17.9 pF, was used. The refractive indices at the wavelength of the sodium D-line were measured with Abbey's refractometer (Andhra Scientific Company Ltd., Machilipatnam, India). The desity measurements were, made with a pycnometer having a volume of 11.563 ml. Temperature was maintained at 25 °C within 0.1 °C. The accuracy in the relative permittivity measurements was estimated to be $\pm 0.5\%$. The accuracy in the refractive indices measurements was estimated upto the fourth decimal place and that for the density measurements 0.03%.

Results of the Measurements. The values of the low frequency relative permittivity ε_0, the relative permittivity at infinite frequency ε_∞, and the square of refractive index n_D^2, at each concentration (mole fraction) for the alcohols C, G, H,

Table 1. Values of ε_0, ε_∞, n_D^2 μ_{eff} and g at different concentrations (mole fractions f_2) in benzene at 25 °C

$f_2\times10^2$	ε_0	ε_∞	n_D^2	μ_{eff} (D)	g	$f_2\times10^2$	ε_0	ε_∞	n_D^2	μ_{eff} (D)	g
		1-Butanol						3-Methyl-2-hexanol			
1.96	2.347	2.269	2.238	1.68	1.00	0.44	2.289	2.273	2.242	1.62	0.93
3.45	2.408	2.265	2.234	1.71	1.04	1.69	2.333	2.269	2.236	1.65	0.96
6.54	2.542	2.256	2.222	1.75	1.08	2.69	2.372	2.233	2.265	1.69	1.01
13.45	2.895	2.237	2.200	1.82	1.17	5.13	2.450	2.258	2.224	1.64	0.96
21.12	3.438	2.216	2.175	2.07	1.52	11.19	2.640	2.240	2.201	1.62	0.93
40.55	5.799	2.162	2.115	2.33	1.92	31.69	3.010	2.188	2.139	1.44	0.74
60.06	9.434	2.106	2.059	2.67	2.52	59.90	3.569	2.125	2.075	1.47	0.76
82.22	13.901	2.042	1.999	2.82	2.98	80.56	3.989	2.088	2.044	1.51	0.81
100.00	17.203	1.989	1.953	3.00	3.19	100.00	4.476	2.058	2.022	1.58	0.88
		1-Heptanol						3-Methyl-3-hexanol			
0.54	2.290	2.272	2.242	1.54	0.84	0.37	2.285	2.273	2.243	1.52	0.82
1.29	2.314	2.270	2.237	1.71	1.04	0.99	2.313	2.270	2.240	1.76	1.10
3.17	2.398	2.265	2.232	1.74	1.07	1.81	2.324	2.268	2.236	1.57	0.87
7.68	2.571	2.252	2.215	1.73	1.07	3.27	2.381	2.263	2.230	1.61	0.92
24.37	3.304	2.209	2.158	1.83	1.19	6.57	2.487	2.251	2.216	1.62	0.92
39.41	4.414	2.176	2.123	2.08	1.54	11.98	2.627	2.234	2.197	1.56	0.86
60.51	6.801	2.135	2.085	2.48	2.18	30.85	2.996	2.178	2.139	1.46	0.75
79.00	8.820	2.104	2.054	2.68	2.54	57.17	3.225	2.114	2.082	1.33	0.63
100.00	11.013	2.074	2.023	2.84	2.88	81.79	3.242	2.065	2.040	1.21	0.52
						100.00	3.248	2.034	2.019	1.16	0.48

and I, are given in Table 1. For the rest of the alcohols the data are not given here.

ε_∞ has been calculated by first calculating a_∞ by the method reported elsewhere[12,13] and then using the relation:

$$\varepsilon_\infty = \varepsilon_{1\infty} + a_\infty w_2 \quad (1)$$

Here $\varepsilon_{1\infty}$ is the relative permittivity of benzene and w_2 is the weight fraction of the solute. The effective dipole moment at each concentration was calculated using the Kirkwood-Fröhlich equation:[14]

$$\mu_{eff}^2 = g\mu_0^2 = \frac{9kT(\varepsilon_0-\varepsilon_\infty)(2\varepsilon_0+\varepsilon_\infty)}{4\pi N\varepsilon_0(\varepsilon_\infty+2)^2} \quad (2)$$

where kT is the thermal energy and N is the number of solute molecules per ml. The Kirkwood correlation factor g was estimated by taking the dipole moment of the alcohol molecules in vacuum μ_0 to be 1.68 D.[5] The values of μ_{eff} and g for the alcohols C, G, H, and I are given in Table 1.

The dipole moments of these molecules in dilute solutions were calculated using the modified Higasi equation[15] given below:

$$\mu = B\sqrt{(a_0-a_\infty)}, \quad (3)$$

where a_0 is given by the relation:

$$\varepsilon_0 = \varepsilon_1 + a_0 w_2 \quad (4)$$

Table 2. Values of ε_0 (pure liquid), a_0, a_∞, the dipole moment μ calculated by Higasi's method[15] in benzene and the values of μ_{eff} in the pure liquid calculated using the Kirkwood-Fröhlich equation at 25 °C

Material	ε_0 (pure liquid)		a_0	a_∞	μ (dilute solution)		μ_{eff} (pure liquid)	
	Expt. values	Lit. values			Expt. values (D)	Lit. values (D)	Expt. values (D)	Lit. values (D)
1-Propanol (A)	20.317	20.10[16] 20.33[8] 21.1[17] (20 °C)	5.440	−0.330	1.78	1.54—1.76	3.01	3.09[18] 2.97[6]
2-Propanol (B)	19.348	18.3[16] 19.41[6]	5.200	−0.391	1.75	1.64—1.80	3.00	2.94[6]
1-Butanol (C)	17.203	17.10[10,16] 17.51[6] 17.68[17] (20 °C)	4.047	−0.285	1.71	1.53—1.76	3.00	2.84[10] 2.85[8] 2.89[6]
2-Methyl-1-propanol (D)	17.224	17.12[10] 17.7[16] 17.936[6]	4.000	−0.305	1.71	1.59—1.81	3.03	2.85[10] 2.88[6] 2.96[18]
1-Pentanol (E)	14.883	13.9[16] 15.15[17] (20 °C)	3.400	−0.245	1.71	1.59—1.71	2.98	—
1-Hexanol (F)	12.829	13.3[16] 13.2[17] (20 °C)	3.000	−0.223	1.73	1.55—1.73	2.95	2.86[8]
1-Heptanol (G)	11.013	11.55[17] (20 °C)	2.674	−0.200	1.74	1.67—1.73	2.84	2.83[8]
3-Methyl-2-hexanol (H)	4.476	—	2.370	−0.216	1.65	—	1.58	—
3-Methyl-3-hexanol (I)	3.248	—	2.125	−0.240	1.58	—	1.16	—
1-Dodecanol (J)	—	—	1.515	−0.157	1.69	1.52	—	—

Values of μ_{eff} in the pure liquid form are calculated by taking the values of g at 27 °C and using the relation $\mu_{eff}^2 = g\mu_0^2$; $\mu_0 = 1.68$ D.

ε_0 and ε_1 are the relative permittivity of the solution and the solvent respectively, and w_2 is the weight fraction of the solute. a_∞ is the same as defined by Eq. 1. The constant B is given by:

$$B = \frac{1}{2(\varepsilon_1+2)}\sqrt{\frac{27kTM_2}{\pi N_A d_1}} \qquad (5)$$

where the different symbols have their usual meaning. Values of the dipole moment are given in Table 2.

Discussion

The values of the relative permittivity of alcohols in the pure liquid form are given in Table 2. There is a close agreement between the experimental and literature values. There is also an agreement between our values of the dipole moments calculated using Higasi's equation[15] in dilute solutions of benzene and the literature values (Table 2) except for the case of 1-dodecanol. For this alcohol our value of the dipole moment is 1.69 D whereas the literature value is 1.52 D. However, our value is quite close to the value of 1.68 D of the alcohol molecule in a vacuum. The values of the dipole moments for 3-methyl-2-hexanol and 3-methyl-3-hexanol are not found in literature. The dipole moments in the pure liquid for all the alcohols except 1-dodecanol are given in Table 2. These values compare within 3% to the literature value of the dipole moment for the alcohols where available.

The concentration dependence of the relative permittivity for the first nine alcohols is shown in Fig. 1. The curves for 1-butanol and 2-methyl-1-propanol almost overlap each other. The plots of the correlation factor g *versus* the alcohol mole fraction are shown in Figs. 2 and 3.

Effect of ε_∞ *on the Dipole Moment and the Correlation Factor.* Our results yield dipole moments μ_{eff} calculated using the Kirkwood-Fröhlich relation.[14] The values are listed in Table 1. The dipole moments are

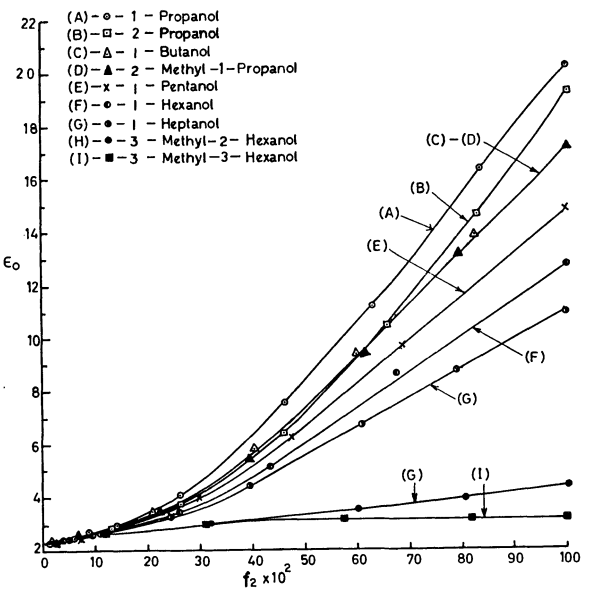

Fig. 1. Plots of ε_0 *versus* f_2 for the alcohols A—I in benzene at 25 °C.

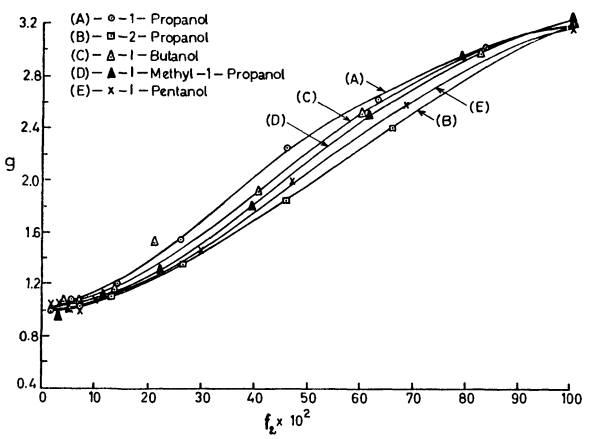

Fig. 2. Plots of g *versus* f_2 for the alcohols A—E in benzene at 25 °C.

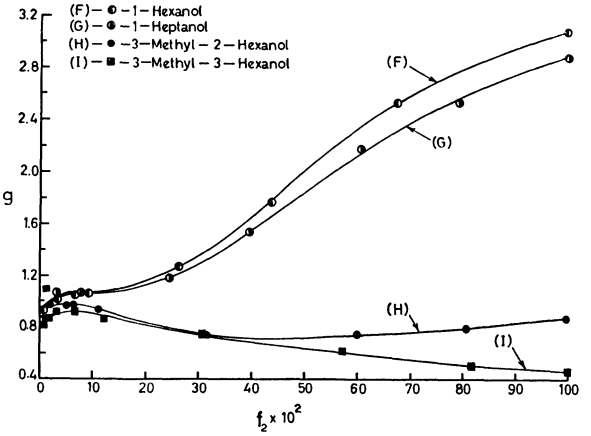

Fig. 3. Plots of g *versus* f_2 for the alcohols F—I in benzene at 25 °C.

compared with the literature values when available. Our values for 1-butanol in the concentration range 0.019—0.065 mole fraction lie within the range 1.68—1.75 D. It has been found that the discrepancy is due to different values of ε_∞ obtained by using different methods for its evaluation. Several authors[7-9] have calculated the value of ε_∞ by fitting the permittivity data to the Cole-Cole plots using a digital computer. We have calculated the values of ε_∞ using Eq. 1. On using the values of ε_∞ as given by Johari and Smyth[19] for 1-butanol in benzene in the same concentration range, we find that our values of dipole moments at about the same concentration range lie within 1.48—1.60 D and therefore, compare well with the values given by Crossley.[9] The comparison is shown in Table 3. The dipole moments calculated by using our values, are, therefore, higher by a factor of about 0.2 D at low concentrations in all the alcohols. Consequently, g values are also higher than those quoted in literature. For higher concentrations and in pure liquids the difference in the dipole moments is expected to be less for the alcohols A to G since the relative permittivity at infinite frequencies ε_∞ makes dipole moments less sensitive to slight changes in ε_∞. Since the relative permittivity of the alcohols H and I is of the order of magnitude as the square of refractive index, a small uncertainty in the

Table 3. Values of the dipole moments of 1-butanol by taking the values of ε_∞ (at about the same concentration range)

$f_2 \times 10^2$	ε_0	ε_∞	μ_{eff} (D)
From Johari and Smyth[19]			
1.96	2.347	2.286	1.48
3.45	2.408	2.296	1.51
6.54	2.542	2.296	1.60
From the data given by Crossley[9] in benzene[a]			
2.35	—	—	1.46
3.53	—	—	1.55
5.24	—	—	1.60

a) The author[9] did not give the values of ε_0 and ε_∞.

value of ε_∞ will greatly affect the values of the dipole moment, and consequently, the value of g.

Behaviour of alcohols A—G and effect of Chain-length. The correlation factor g is a measure of those short-range intermolecular forces that lead to the specific dipole-dipole orientations. According to the Kirkwood-Fröhlich theory[14] $g\mu_0^2$ is the square of the dipole moment of the spherical cavity so that its size is macroscopically small and microscopically large. The size should be such that the surroundings can be assumed to have relative permittivity of the liquid. The value of g greater than unity is interpreted in terms of predominantly parallel alignment of the near-neighbour dipoles and g less than unity corresponds to a structure such that its dipole moment is less than that of the monomer. A more specific interpretation depends on the introduction of a molecular model of the liquid structure.

The plots of g against the alcohol mole fraction for alcohols A—G are shown in Figs. 2 and 3. In the absence of the association of the neighbouring molecules, g should be unity for all concentrations. Strong self association is evident for large alcohol concentrations in benzene and in pure liquids. As concentration of alcohols increases from 0.15 to 0.90 mole fraction, values of g increase in the order 1-heptanol<1-hexanol<1-pentanol<2-methyl-1-propanol<1-butanol<1-propanol. Propanols and butanols attain almost the same value in pure liquid. The trend shows that self association (with the exception of 2-propanol) decreases with increase in the length of hydrocarbon chain.

Taking into account the effect of ε_∞ as discussed above, we can say that the values of g are about 20—25% less than unity at the concentration range of *ca.* 0.2 mole fraction. With the increase of alcohol concentration the values of g increase and approach unity at the concentration of *ca* 0.20 mole fraction. This leads us to the conclusion that the initial association involves the formation of multimers having smaller dipole moments than the free monomer. These multimers may be closed or open dimers and timers.[4,20,21] Above the concentration of 0.2 mole fraction g increases rapidly with the increase of the alcohol concentration for the alcohols. (Figs. 2 and 3). Dannhauser[4] and also, Gold and Perrine[22] suggest the association into linear chains as mechanism responsible for the large values of g. Some authors support the existence of highly polar cyclic tetramers.[23,24] In 2-propanol the values of g are lower (Fig. 2) than 1-propanol, 1-butanol and 1-pentanol in the concentration range 0.15—0.90 mole fraction. This is probably due to the chain-branching close to the –OH group which presents steric factors for the formation of large multimers.

Behaviour of 3-Methyl-2-hexanol and 3-Methyl-3-hexanol. The values of g decrease with the increase of the alcohol concentration for 3-methyl-3-hexanol in the entire concentration range. Whereas in the case of 3-methyl-2-hexanol it decreases initially with the increase of concentration in the range 0.10—0.35 mole fraction above which it again starts increasing with comparatively less slope. In these alcohols the –OH group is so effectively screened due to the presence of the neighbouring $-CH_3$ group that association is restricted to small weakly polar multimers, preferably ring dimers, the values of g for pure liquids being less than unity. Association into higher open chain n-mers or highly polar cyclic tetramers is not possible because of steric effects. The results are in agreement with those given by Dannhauser[4] and Crossley *et al.*[25] for 2-methyl-3-heptanol, 3-methyl-3-heptanol, and 4-methyl-3-heptanol in pure liquids.

It is evident that in a liquid alcohol for a given temperature and concentration, one has to assume equilibrium between different structures. The equilibrium constants between the various structures are strongly dependent on the nature of alcohol and its concentration in an inert solvent.

The research project was financed by the Department of Atomic Energy. One of the authors (Buta Singh) is grateful to Professor B. S. Sood, Head, Department of Physics, for the encouragement during the work.

References

1) J. Crossley, *Adv. Mol. Relaxation Process*, **2**, 69 (1970).
2) G. C. Pimental and A. L. McClellan, "The Hydrogen Bond," W. H. Freeman and Co., San Francisco, California (1960).
3) C. P. Smyth and W. N. Stoops, *J. Am. Chem. Soc.*, **51**, 3330 (1929).
4) W. Dannhauser, *J. Chem. Phys.*, **48**, 1911 (1968); *ibid.*, **48**, 1918 (1968).
5) C. P. Smyth, "Dielectric Behaviour and Structure," McGraw-Hill, New York (1955), pp. 83—85.
6) W. Dannhauser and L. W. Bahe, *J. Chem. Phys.*, **40**, 3058 (1964).
7) J. Crossley, L. Glasser, and C. P. Smyth, *J. Chem. Phys.*, **55**, 2197 (1971).
8) L. Glasser, J. Crossley, and C. P. Smyth, *J. Chem. Phys.*, **57**, 3977 (1972).
9) J. Crossley, *Can. J. Chem.*, **49**, 712 (1971).
10) G. E. Rajala and J. Crossley, *Can. J. Chem.*, **49**, 3617 (1971).
11) J. K. Vij and K. K. Srivastava, *Ind. J. Pure Appl. Phys.*, **7**, 391 (1969).
12) K. Higasi, K. Chitoku, and S. Ogata, *Denki Kenkyusho Iho*, **18**, 147 (1966).
13) B. Singh and J. K. Vij, *Bull. Chem. Soc. Jpn.*, **48**, 2551 (1975).

14) H. Fröhlich, "Theory of Dielectrics," 2nd ed., Clarendon Press, Oxford (1958), p. 52.
15) K. Higasi, *Denki Kenkyusho Iho*, **4**, 231 (1952).
16) "Handbook of Chemistry and Physics," 39th ed., 1957—1958.
17) S. K. Garg and C. P. Smyth, *J. Phys. Chem.*, **69**, 1294 (1965).
18) A. L. McClellan, "Tables on Experimental Dipole Moments," Freeman and Co., San Francisco (1963).
19) G. P. Johari and C. P. Smyth, *J. Am. Chem. Soc.*, **91**, 6215 (1969).
20) H. C. Van Ness, Jon Van Winkle, H.H. Richtol, and H. B. Hollinger, *J. Phys. Chem.*, **71**, 1483 (1967).
21) J. Malecki, *J. Chem. Phys.*, **43**, 1351 (1965).
22) P. I. Gold and R. L. Perrine, *J. Phys. Chem.*, **71**, 4218 (1967).
23) P. Bordewijk, F. Gransch, and C. J. F. Böttcher, *J. Phys. Chem.*, **73**, 3255 (1969).
24) A. N. Fletcher and C. A. Heller, *J. Phys. Chem.*, **71**, 3742 (1967).
25) J. Crossley, L. Glasser, and C. P. Smyth, *J. Chem. Phys.*, **52**, 6203 (1970).

Determination of the Dissociation Constants of Salicylic Acid in Water-Ethanol Mixtures by Modified Conductometric Methods

A. K. MANDAL and S. C. LAHIRI
Department of Chemistry, University of Kalyani, Kalyani, Nadia, West Bengal, India
(Received September 9, 1975)

The dissociation constants of salicylic acid in water and ethanol–water mixtures (8—87.6 wt % of ethanol), have been determined by the modified conductometric method as suggested by Gelb. The results have been checked independently from the plot ΛC *vs.* $1/\Lambda$ of salicylic acid in mixed solvents. $\Lambda^{\circ}_{HClO_4}$ and $\Lambda^{\circ}_{\text{salicylic acid}}$ have also been determined.

The importance and limitations of the determinations of the dissociation constants of acids and bases in mixed solvents have been well-discussed.[1-4] In order to explore a suitable method for the determination of the dissociation constants in mixed solvents which could avoid the uncertainties due to liquid-junction potential and changed sensitivity of the glass electrode, we found the conductometric method as suggested by Gelb[5] with suitable modification can be utilized with success. The method is handy and less time consuming and ensures high accuracy. The method involves the assumption of complete dissociation of $HClO_4$ in mixed solvents—an assumption on which the measurement of H^+ ion concentration in mixed solvents is generally based. Until now the assumption has been regarded as being valid in mixed solvents containing fairly high percentages of organic solvents.

We report in this communication the dissociation constants of salicylic acid in a series of ethanol–water mixtures by the modified conductometric method. We are particularly interested in the determination of pK values of comparatively weak acids which may be useful for the preparation of suitable buffers, the lack of which is one of the strong handicaps for the measurement of H^+ ion concentrations in mixed solvents.

Experimental

Absolute ethanol was treated with the requisite quantity of calcium oxide, kept overnight, and then distilled. The middle fraction was collected and used without further treatment. The slight traces of water, if any, in the organic solvents were neglected. The weight percentages of the organic solvent and the relative permittivities of the solvent mixtures were determined in the same way as described before.[6] Salicylic acid (G. R. E. Merck) was recrystallized from alcohol. Perchloric acid and other reagents used for standardization were of E. Merck's reagent grade.

Conductance measurements were done with the aid of a Leeds and Northrup Model 4959 conductance bridge with a sensitivity of $\pm 0.1\%$. A 50—60 cycle signal was employed. A dip-type Philips conductance cell with a cell-contant, $\theta = 0.815\ cm^{-1}$ was utilized. The cell constant was determined using accurately measured KCl (G. R. E. Merck) solutions and using the conductance values from the literature[7] and the value of the cell-constant was repeatedly checked during the course of the experiment. The measurements were done at 25 ± 0.05 °C.

The initial conductance of a certain amount of the acid solution was measured. Definite amounts of perchloric acid in appropriate solvents were added at regular intervals. The mixtures were allowed sufficient time to attain equilibrium and the conductance of each solution was measured. The experiment was repeated with different concentrations of the salicylic acid and also in different percentages of mixed solvents. The ionic strengths of the solutions were kept as low as practicable ($\approx 10^{-3}$ M) so that the ionic strength correction was almost negligible. The blank titrations were performed in the same way as described above, the experimental solutions being replaced by the same amount of the appropriate solvent. The conductances of the solvents were taken to apply appropriate corrections.

Results and Discussion

The dissociation constant K for the reaction

$$HA \rightleftharpoons H^+ + A^- \tag{1}$$

can be represented as

$$K = \frac{[H^+][A^-]}{[HA^-]} \times f_{\pm}^2 \tag{2}$$

(f_{HA} may be regarded as unity).

However, if we take a mixture of completely dissociated $HClO_4$ and partly dissociated HA, Eq. 2 can be written as

$$K = \frac{\alpha(\alpha C_{HA} + C_{HClO_4}) \times f_{\pm}^2}{(1-\alpha)} \tag{3}$$

C_{HA} = total concentration of HA
C_{HClO_4} = concentration of $HClO_4$ in the mixture
$f_{\pm}$ = mean activity coefficient
α = the degree of dissociation of HA in presence of $HClO_4$

The conductances of the mixtures (containing HA and $HClO_4$) and the blank solutions (containing $HClO_4$ only) are given by

$$\frac{1}{R} = \frac{1}{1000\theta}[C_{HClO_4}\Lambda'_{HClO_4} + \alpha C_{HA}\Lambda'_{HA}] \tag{4}$$

[where $\Lambda'_{HA} = \lambda_{H^+} + \lambda_{A^-}$ at the appropriate ionic strength and $\Lambda = \alpha\Lambda'$, $\alpha = 1$ in the case of $HClO_4$] and

$$\frac{1}{R^*} = \frac{1}{1000\theta} C^*_{HClO_4}\Lambda^{*\prime}_{HClO_4} \tag{5}$$

(* indicates quantities for blank solutions)

θ = cell constant.

When $1/R = 1/R^*$, we have

$$C^*_{HClO_4}\Lambda^{*\prime}_{HClO_4} = C_{HClO_4}\Lambda'_{HClO_4} + \alpha C_{HA}\Lambda'_{HA} \tag{6}$$

Since C_{HClO_4} and $C^*_{HClO_4}$ do not differ considerably and the ionic strengths of the solutions are equal, one can write $\Lambda'_{HClO_4}=\Lambda^{*\prime}_{HClO_4}$. However, approximations are made that $\Lambda'_{HClO_4}=\Lambda'_{HA}$ in aqueous as well as in mixed solvents. This is quite reasonable in view of the closeness of the mobility of ClO_4^- and anions on which the difference in equivalent conductances of $HClO_4$ and organic acids ultimately depends. Thus,

$$C_{HClO_4} + \alpha C_{HA} = C^*_{HClO_4} \quad (7)$$

from which α is obtained.

Modified equations[8] can be used to take into account the variations of Λ'_{HClO_4} and Λ'_{HA} due to variations in ionic strengths; this, however, is not necessary in our case as the ionic strengths are kept low ($\approx 10^{-3}$ M) and the variation of ionic strengths is also too small to vitiate the assumption $\Lambda^{*\prime}_{HClO_4}=\Lambda'_{HClO_4}$ to a measurable accuracy.

Further modifications of K values are possible taking

$$\alpha = (C^*_{HClO_4}-C_{HClO_4})/\beta C_{HA} \quad (8)$$

where $\Lambda'_{HClO_4}=\Lambda^{*\prime}_{HClO_4}$ and $\beta=\Lambda'_{HA}/\Lambda'_{HClO_4}$.
We have calculated β as suggested by Gelb but found the alternative procedure given below to be superior.

Equivalent conductance values of perchloric acid at different dilutions (5.0×10^{-2} M to 5.0×10^{-4} M) were obtained from conductance measurements. At low concentrations, Λ'_{HClO_4} values when plotted against $C^{1/2}$ gave good straight lines in aqueous as well as in mixed solvents. $\Lambda^\circ_{HClO_4}$ values were obtained by extrapolation to zero dilution. Λ_{HA}° and K values were obtained from the plot of $C\Lambda$ against $1/\Lambda$ of a number of dilute solutions of HA utilizing the equation[9]

$$C\Lambda = -K\Lambda^\circ + K\Lambda^{\circ 2}/\Lambda \quad (10)$$

where the intercept gives $(-K\Lambda^\circ)$ and the slope $(K\Lambda^{\circ 2})$. This, however, gives us an independent method of checking K values free from any assumption.

The β values were evaluated from $\Lambda^\circ_{HClO_4}$ and Λ°_{HA} values. Since the ionic strengths are very low, the slight differences of Λ' from Λ° values would not affect the value of β to any measurable extent. β value in water comes to be 400/415=0.96. The β values in mixed solvents also lie within 0.90 to 0.96, deviations occurring at higher percentages. However, evaluation of K and Λ° of the acid by the dilution method is liable to be erroneous at higher percentages of alcohols, where the dissociation constant decreases enormously.

The average values of $\Lambda^\circ_{HClO_4}$, $\Lambda^\circ_{salicyclic\ acid}$, and p$K$ measured from several sets of experiments (using both the titration method and the dilution method) for each percentage of organic solvent are given in Table 1. The agreement of the K values suggests the accuracy of the titration method. The activity correction term from the Debye-Hückel limiting equations, making appropriate corrections for the change in the dielectric constant values, comes out to be about 0.02 (in 8 wt % of alcohol) to 0.09 (87 wt% of alcohol).

The values from the spectrophotometric measurements were also incorporated in Table 1 for comparison.[10] The results are found to agree fairly well. The results obtained by the spectrophotometric method utilizing a glass–calomel electrode for measurement of H^+ ions give higher values at higher percentages of alcohol. This may be due to uncertainties in H^+ ion concentration measurements. The association of ions may be increasingly greater as the percentage of alcohol increases. However, it is noted that the pK values obtained by the modified conductivity method, when plotted against weight percentages and mole fractions of organic solvent, give excellent straight lines (up to 0.6 mole fraction); the plot of pK *vs.* $1/\varepsilon$ (ε=relative permittivity) gives deviations only at higher percentages of organic solvent.

The method however, cannot be used when the pK values are rather high (more than 4 or so). It is known that the dissociation constant is considerably suppressed with the addition of $HClO_4$; as a result α becomes too small. For such cases, however, it is possible to take a large number of $1/R$ values from fairly concentrated to dilute solutions of HA (as dilute as measurable without impairing the accuracy). Suitable blank curves are obtained by addition of a dilute solution of perchloric acid to the appropriate solvents and the interpolated values of $1/R^*$ are determined from these blank curves. Under this condition, the equation reduces to $\alpha C_{HA}=$

Table 1. Average values of Λ° and pK measured from several experiments (at 25 °C)

Wt % of ethanol	$1/\varepsilon\times10^2$	Mole fraction of ethanol	pK values: Titration method (a)	pK values: Titration method (b)	pK values: From plot of ΛC *vs.* $1/\Lambda$	Λ° in ohm^{-1}·cm^2: $HClO_4$	Λ° in ohm^{-1}·cm^2: Salicylic acid	Wt % of ethanol	pK[c]
0.0	1.27	—	3.09	3.04	3.04	415.0	400.0	0.0	2.97
8.0	1.35	0.033	3.14	3.10	3.08	372.0	344.8	15.3	3.32
16.4	1.42	0.071	3.29	3.25	3.19	301.5	289.6	30.5	3.65
25.3	1.53	0.117	3.44	3.39	3.38	250.0	240.0	45.3	3.97
34.4	1.71	0.170	3.55	3.52	3.47	196.0	186.0	61.9	4.10
44.0	1.90	0.235	3.77	3.72	3.71	172.6	154.8	69.0	4.50
54.1	2.14	0.315	3.98	3.95	3.97	142.0	132.0	82.0	5.24
64.7	2.92	0.418	4.23	4.20	4.13	118.0	94.0	—	—
76.0	3.41	0.556	4.55	—	—	102.0	—	—	—
87.6	—	0.740	4.97	—	—	92.0	—	—	—

a) The pK-values before β-correction. b) The pK-values after β-correction. c) pK-Values from spectrophotometric data.[10]

$C^*_{HClO_4}$, from which α and hence pK values are calculated. Further refinements as suggested above are possible.

The method has the advantage that the accurate determination of cell constants is not at all necessary, provided the same cell is used, as the θ terms cancel.

The $\Lambda^\circ_{HClO_4}$ in water has been found to be 415, in good agreement with the values in the literature ($\lambda^\circ_{H^+}$= 349.8 and $\lambda^\circ_{ClO_4^-}$=64.6[11] or 67.32)[12] at 25 °C. The $\Lambda^\circ_{HClO_4}$ values decrease with increasing percentages of alcohol, as expected. The reliability of the results may be obtained from the comparison of $\Lambda^\circ_{HClO_4}$ and Λ°_{HCl} values ($\lambda^\circ_{Cl^-}$=76.34 at 25 °C). The values of Λ°_{HCl} in ethanol reported in the literature vary from 81.7 to 89.1[13] where $\Lambda^\circ_{HClO_4}$ at 87.6 wt % of alcohol is 92.00. The values thus appear to be reasonable. The $\Lambda^\circ_{\text{salicylic acid}}$ (in water) comes out to be 400 ($\lambda^\circ_{\text{salicylate ion}}$= 35 at 25 °C).[11] A slight disagreement is thus apparent. It is, however, difficult to suggest the extent of reliability of the $\lambda^\circ_{\text{salicylate ion}}$ value. It is as yet inopportune to say something positively about the modified conductometric method. In comparison to the pH-metric method the assumptions involved in the determination of pK values by this method should not vitiate the result appreciably, even if association of $HClO_4$ takes place at higher percentages of alcohol, as we are concerned with the conductivities.

Systematic studies by different techniques are necessary to make a definite statement about the reliability of this method in different mixed solvents.

References

1) S. C. Lahiri and S. Aditya, *J. Ind. Chem. Soc.*, **51**, 319 (1974).
2) R. G. Bates, "Determination of pH," John Wiley and Sons, New York (1964).
3) H. S. Harned and B. B. Owen, "The Physical Chemistry of Electrolytic Solutions," 3rd ed., Reinhold Publishing Corporation, New York (1958).
4) T. Shedlovsky and R. L. Kay, *J. Phys. Chem.*, **60**, 151 (1956).
5) R. I. Gelb, *Anal. Chem.*, **43**, 1110 (1971).
6) S. C. Lahiri, G. Biswas, and S. Aditya, *Thermo Chim. Acta*, **9**, 369 (1974).
7) N. A. Lange, "Handbook of Chemistry," McGraw-Hill Book Company, New York, Toronto, London (1961).
8) T. Shedlovsky, *J. Am. Chem. Soc.*, **54**, 1405 (1932).
9) E. A. Moelwyn-Hughes, "Physical Chemistry," 2nd ed., Pergamon Press, Oxford (1964), p. 853.
10) S. K. Pal and S. C. Lahiri, *Z. Phys. Chem. (Leipzig)*, **246**, 81 (1971).
11) B. E. Conway, "Electrochemical Data," Elsevier Publishing Company, Amsterdam (1952), p. 45.
12) G. J. Janz and S. S. Danyluk, "Electrolytes," ed. by B. Pesce, Pergamon Press, Oxford, London (1962), p. 263.
13) G. Milazzo, "Electrochemistry," Elsevier Publishing Company, Amsterdam, London, New York (1963), pp. 60—61.

π-Electron Structure of Some Nonbenzenoid Hydrocarbons Using β-Variable Method

Subrata CHATTERJEE and Nanda K. DAS GUPTA*

Department of Chemistry, Visva-Bharati University, Santinikentan, West Bengal, India
**Department of Chemistry, The University of Alberta, Edmonton, Alberta, Canada*

(Received October 14, 1975)

The molecules pentaleno[*def*]heptalene, cyclohept[*fg*]acenaphthylene, naphth[*cde*]azulene and cyclohept[*bc*]-acenaphthylene have been studied using β-variable methods proposed by Dewar *et al.* and Yamaguchi *et al.* The predicted results are compared with experimental values and with other theoretical results.

The Pariser-Parr-Pople (PPP) semiempirical self-consistent antisymmetrized molecular orbital (SCF ASMO) method[1] is very useful in predicting the electronic structure of conjugated systems. From time to time the semiempirical nature of the method has been changed by several authors by changing the mode of evaluation of certain integrals. Among these are Nishimoto and Forster[2], Yamaguchi *et al.*[3] and Dewar and co-worker[4] who used exchange integrals $\beta_{\mu\nu}$ as functions of bond order $p_{\mu\nu}$ or bond length $r_{\mu\nu}$. These methods are known as the "β-variable" method. The former two methods were developed to calculate the electronic transitions and the latter one to calculate the ground state properties of conjugated systems. But we[5] have successfully applied the β-variable technique of Yamaguchi *et al.*[3] and Dewar *et al.*[4] to predict the electronic transitions of many nonbenzenoid hydrocarbons. In this paper we are going to report the results of calculations on some nonbenzenoid hydrocarbons shown in Fig. 1. However, these molecules were studied by several authors[6] using a different set of parameters. Our aim is to see how far the results calculated by the "β-variable" technique are in agreement with the experimental results.

Geometry of the Molecules. Although the β-variable technique is insensitive to the assumed geometry of the molecule, still for molecules **1**[7] and **2**[8] we used the actual structure and for the other two we assigned the

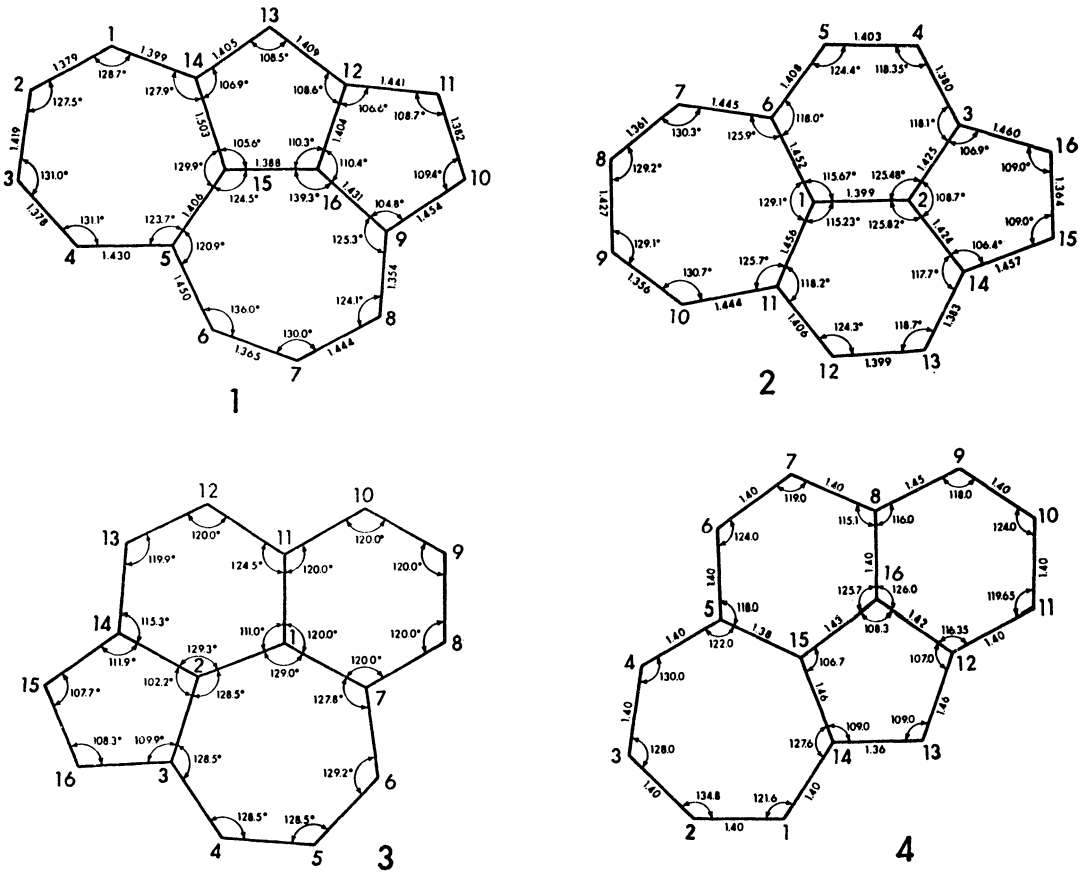

Fig. 1. Molecules.
(**1**) Pentaleno[*def*]heptalene. (**2**) Cyclohept[*fg*]acenaphthylene. (**3**) Naphth[*cde*]azulene.
(**4**) Cyclohept[*bc*]acenaphthylene.

* On leave of absence from: Department of Chemistry, Visva-Bharati University, Santiniketan, West Bengal, India.

TABLE 1. $\pi^*\leftarrow\pi$ TRANSITIONS (eV) AND OSCILLATOR STRENGTHS (f)

Molecule	Symmetry	Present work a eV	a f	b eV	b f	Experiment** eV	Experiment** log ε	Other work c eV	c f*	d eV	d f	e eV	e f	g eV	g f
1				1.89	0.06	1.8	2.1			1.81	0.004				
		2.35	0.15			2.2	3.1	2.2	0.016	2.38	0.05				
		3.27	0.36	2.84	0.45	2.8	3.8	2.9	0.21	3.11	0.3				
				3.00	0.39			3.0	0.55						
										3.20	0.09				
		3.32	0.42												
		3.41	0.48	3.47	0.64	3.4		3.4	0.53	3.66	1.1				
		3.62	0.44												
		3.96	0.27	3.97	0.39			3.8	0.37	4.07	0.9				
				4.19	0.36			4.1	0.31	4.30	0.2				
		4.51	0.28	4.24	0.24	4.3		4.3	0.22	4.43	1.1				
		4.93	0.33	4.91	0.46	4.9		5.0	0.20						
2						2.5	3.6			2.59	0.1			2.504	0.002
														2.553	0.056
										2.89	0.04				
	B_2	3.36	0.24	3.18	0.27	3.0		2.9	0.26	3.14	0.3	2.98	0.28	2.986	0.115
								3.1	0.31			3.15	0.026		
								3.3	0.98			3.32	0.066		
	B_2	3.91	0.40	4.06	0.51	3.8	4.6	3.9	0.43	3.45	1.5	3.87	0.025	3.998	1.715
		4.31	0.41	4.28	0.42			4.2	0.39	4.34	0.1			4.187	0.207
								4.4	0.51	4.58	0.03	4.50	0.96		
												4.67	0.16		
	A_1			4.59	0.0			4.6	0.0						
		4.86	0.02	4.83	0.0	4.8	4.3	4.7	0.01	4.76	1.2	5.09	0.87		
		4.94	0.01	5.11	0.0			5.0	0.0			5.13	0.010		
		5.03	0.44									5.26	0.021		
	B_2	5.58	0.23	5.58	0.25			5.4	0.01			5.64	0.021		
	B_2	5.80	0.0	5.92	0.0	5.8		5.84*	0.31			5.68	0.040		
3				2.69	0.42	2.2	2.8	2.6	0.46	2.10	0.08			1.803	
		3.10	0.43	3.17	0.25	3.0	3.4	2.9	0.24	2.89	0.3			2.792	
														3.496	
		3.43	0.21	3.85	0.72	3.6	3.9	3.7	0.73	3.61	0.6			3.722	
		3.92	0.65					3.8	0.35	3.90	0.1				
		4.03	0.33	3.99	0.42	4.0		4.1	0.49					4.153	
								4.2	0.18						
				4.27	0.55					4.31	0.2				
		4.47	0.55	4.40	0.22	4.6	4.5	4.7	0.42	4.51	1.3				
		4.50	0.19												
4						2.4	2.9			2.23	0.1			1.949	
								2.8	0.24						
		3.24	0.68	2.85	0.67	2.9	3.8	2.9	0.77	2.90	0.5			2.746	
		3.39	0.24	3.21	0.32	3.4		3.5	0.21					3.674	
		3.65	0.23	3.69	0.32					3.78	0.3				
		3.98	0.49	4.00	0.51			3.9		3.83	0.07			3.910	
		4.56	0.14	4.35	0.58	4.3	4.5	4.3	0.49	4.18	1.2			4.118	
				4.44	0.15			4.4	0.16						
										4.37	0.8				
		4.67	0.57	4.64	0.31			4.6	0.32						
		4.98	0.25	5.02	0.16	5.0	4.8	5.0	0.11	4.61	0.4				
		5.08	0.11					5.2	0.37						

(a) Present work using the methods of Dewar and Harget.[4] (b) Present work using the method of Yamaguchi *et al.*[3] (c) Ref. 6(a). (d) Ref. 6(b). (e) Ref. 6(d). (g) Ref. 6(c).

* and values of oscillator strengths (f) in Item c not included in Ref. 6(a).

** Experimental spectra: Molecule **1**, Ref. 6(b) and 18(a). **2**, Ref. 6(b) and 18(b). **3**, Ref. 6(b) and 18(c). **4**, Ref. 6(b) and 18(d).

geometry shown in Fig. 1 for our calculation.

Parameters. As usual the two-centre, two-electron repulsion integrals $\gamma_{\mu\nu}$ were computed from the initial geometry of the molecules using the formula of Ohno[9] for the method of Dewar and Harget and for the method of Yamaguchi *et al.* the formula of Mataga and Nishimoto[10] was used. For both the methods the integrals between non-bonded atoms were not varied throughout the calculation.

The one-centre, two-electron repulsion integrals were evaluated from the valence-state ionization energy I_μ (11.16 eV)[11] and electron affinity A_μ (0.026 eV)[11] of the carbon atom using the relation

$$\gamma_{\mu\mu} = I_\mu - A_\mu = 11.134 \text{ eV}.$$

For bonded atoms, $\gamma_{\mu\nu}$ and core resonance integrals $\beta_{\mu\nu}$ were adjusted at each iteration on the basis of bond-order bond length relations. For the method of Yamaguchi *et al.* the relations are

$$r_{\mu\nu}(\text{Å}) = 1.520 - 0.186 p_{\mu\nu}$$

and

$$\beta_{\mu\nu} = \beta_0 \exp\left[a(r_0 - r_{\mu\nu})\right]$$

where r_0 is the bond length of benzene, a is equal to 1.7 Å^{-1} and β_0 has been taken to be equal to -2.15 eV.[5] For the method of Dewar and Harget the relations are

$$\beta_{\mu\nu} = -6.927 S_{\mu\nu}$$

and

$$r_{\mu\nu}(\text{Å}) = 1.512 - 0.174 p_{\mu\nu}$$

where $S_{\mu\nu}$ is the overlap integral between two π_{2p} orbitals with orbital exponent 1.59. In both the methods $\beta_{\mu\nu}$ for non-bonded atoms was equal to zero.

The starting vectors were Hückel MO coefficients and the interation was continued until the self-consistency was achieved within the desired degree of accuracy.

Results and Discussion

Table 1 contains the calculated $\pi^* \leftarrow \pi$ transitions along with the oscillator strengths and experimental results. For comparison we have also included in the table the other theoretical results. Since the molecules are not simple it is very difficult to make point-to-point correlations. However, attempts have been made to do so. It is clear that except for a few cases the present work in which case no configuration interaction was performed is in good agreement with experiment and is also comparable to other theoretical results where, in some cases, configuration interaction was done.

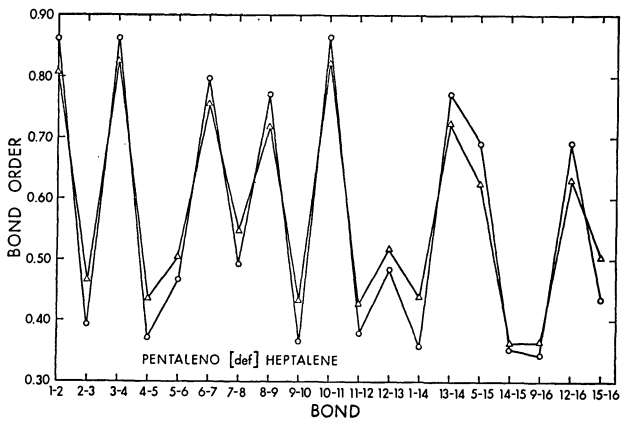

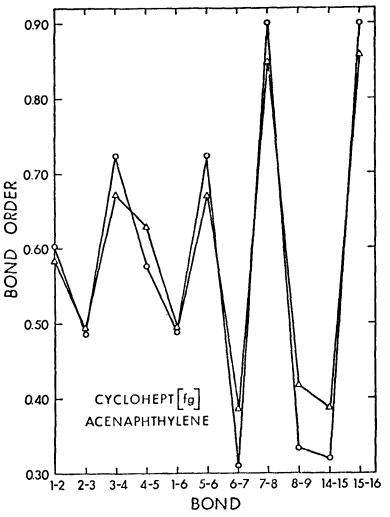

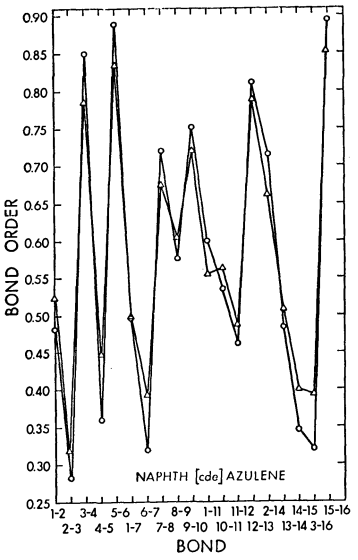

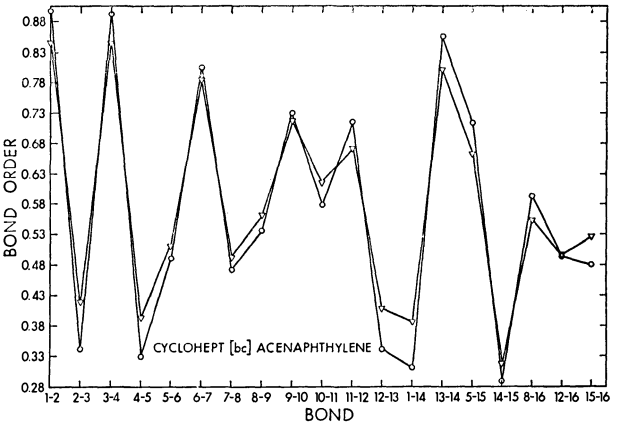

Fig. 2. Variation of bond order with bonds (SCF(a)—○; SCF (b)—△).

Figure 2 represents the variation of bond order with

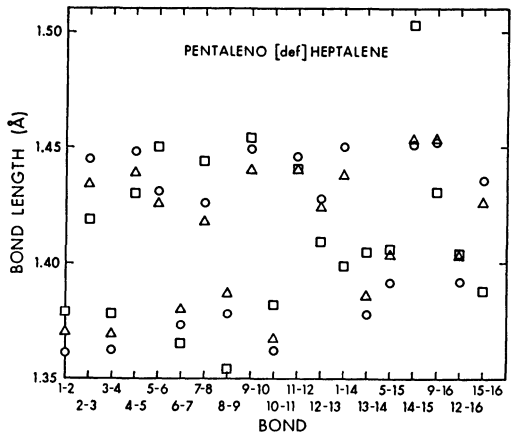

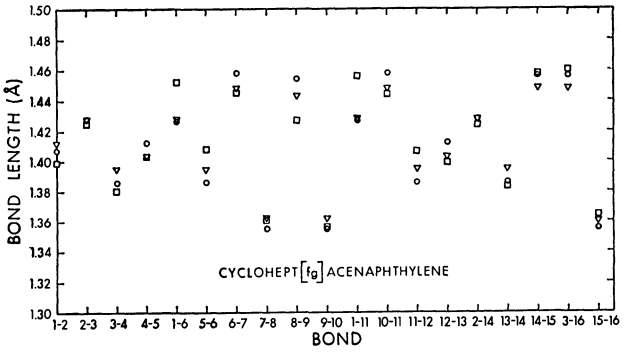

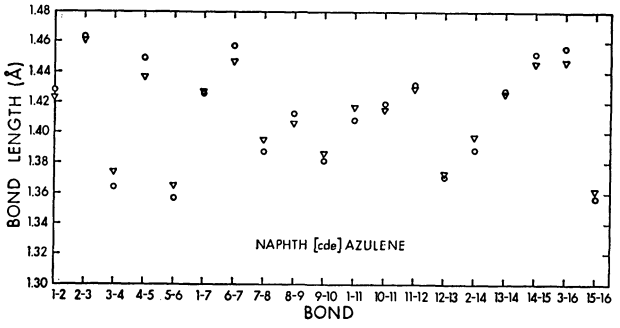

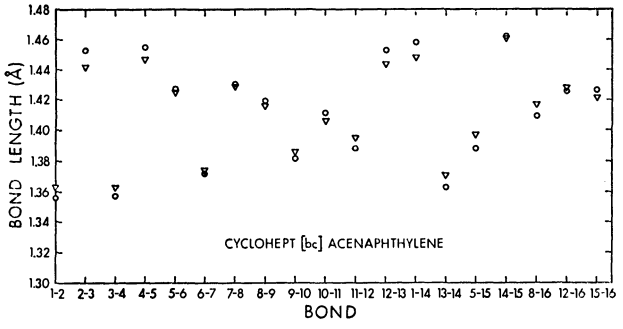

Fig. 3. Comparison between predicted bond lengths and experimental bond lengths (SCF (a)—○; SCF (b)—△; experimental—□).

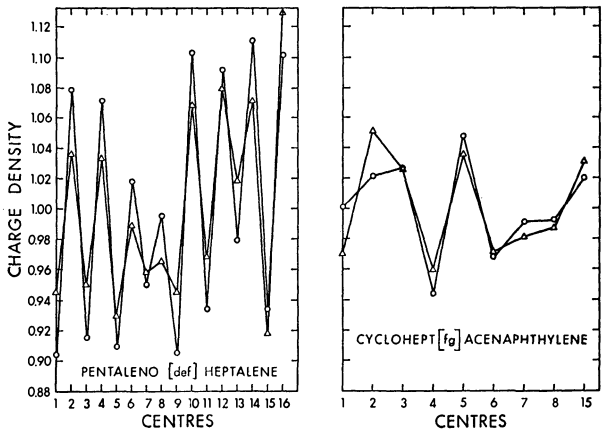

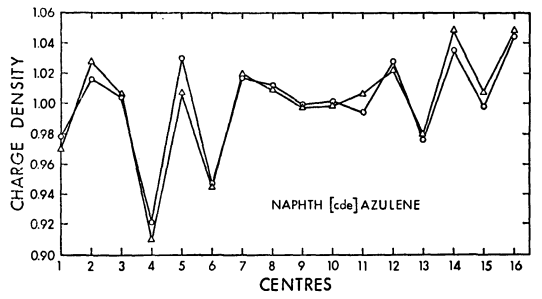

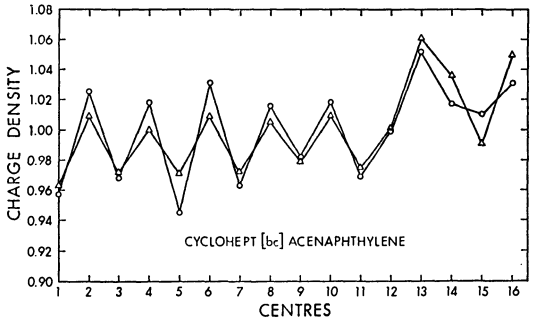

Fig. 4. Variation of charge density with centres (SCF(a) —○; SCF (b)—△).

bond. It is seen that the two methods maintain almost the same trend of variation in all the cases. Figure 3 compares the bond length calculated by the different methods. Experimental values, where available are also included in the figure. It is evident from Fig. 3 that in all the molecules the bond lengths calculated by the two methods are in very good agreement with each other. Except for a few cases, the agreement between the predicted bond lengths and the experimental values are good. Figure 4 represents the variation of charge density with different centres. Here also the two methods maintain the same trend.

It will be clear from the predicted bond lengths that when a bond is common to two different types of rings then the bond has a tendency to have single bond character. This is pronounced when the bond is common to five and seven membered rings and less pronounced when the bond is common to a six membered ring and seven or five membered ring. The range is from 1.43 to 1.46 Å. But the bond C_{15}–C_{16} of the molecule cyclohept[*bc*]acenaphthylene has a value of 1.422 Å calculated by the method of Yamaguchi *et al.* Although the bond is common to two different types of

TABLE 2. CALCULATED VALUES OF IONIZATION POTENTIAL, ELECTRON AFFINITY AND DIPOLE MOMENT

Molecule	Ionization potential (eV)				Electron affinity (eV)				Dipole moment (D)		
	Uncorrected		Corrected		Uncorrected		Corrected				
	a	b	b	c	a	b	b	c*	a	b	c
1	−8.99	−8.16	7.10	7.36	−2.21	−2.96	1.06	−2.45	1.75	2.68	1.51
2	−9.16	−8.45	7.39	7.61	−2.16	−2.82	0.92	−2.44	1.26	2.27	2.06
3	−9.16	−8.47	7.41	7.54	−2.13	−3.01	1.11	−2.23	1.09	1.77	1.70
4	−9.13	−8.34	7.28	7.42	−2.12	−2.81	0.91	−2.48	0.59	1.00	0.87

(a) Present work using the methods of Dewar and Harget. (b) Present work using the method of Yamaguchi *et al.* (c) Ref. 6(a). (* Measure of half-wave reduction potential)

rings, still its single bond nature is not exhibited as much. A similar situation is also seen in the case of C_1–C_2 bond, the value being 1.423 Å calculated by the method of Yamaguchi *et al.* of molecule **3**. This may be due to the fact that these molecules have three consecutive bonds, common to two different types of rings. As a result the tendency of single bond character for the middle one, C_1–C_2 for molecule **3** and C_{15}–C_{16} for molecule **4**, is not so pronounced. Again when a bond is in common to two of the same type of rings such as two seven membered, five membered and six membered rings the bond has a predicted bond length almost equal to that of an aromatic C–C bond. The examples are C_5–C_{15} (1.392, 1.404 Å) and C_{12}–C_{16} (1.392, 1.403 Å) of pentaleno[*def*]heptalene, C_1–C_2 (1.407, 1.412 Å) of molecule **2**, C_1–C_{11} (1.408, 1.417 Å) of naphth[*cde*]-azulene and C_8–C_{16} (1.409, 1.417 Å) of cyclohept[*bc*]-acenaphthylene. Moreover if we examine the predicted peripheral bond lengths of all the molecules, an interesting feature will be observed. The predicted peripheral bond lengths of one of the seven and five membered rings of pentaleno[*def*]heptalene has alternate single bond and double bond character. Thus the bonds C_{14}–C_1, C_2–C_3, C_4–C_5, C_9–C_{10}, and C_{11}–C_{12} have single bond character whereas the bonds C_1–C_2, C_3–C_4, and C_{10}–C_{11} have double bond character. The peripheral bonds of the other seven membered ring (C_5–C_6, C_6–C_7, C_7–C_8, and C_8–C_9) and five membered ring (C_{12}–C_{13} and C_{13}–C_{14}) have more or less bond length equal to an aromatic C–C bond length. Thus the peripheral bonds of this molecule are of two types— in one case the bonds are localized and in the other case they are delocalised. This is more clearly observed in the method of Yamaguchi *et al.* A similar situation is also seen in the case of other molecules. Thus the peripheral bonds of the naphthalene ring of molecule **2** are delocalised whereas those of five and seven membered rings are localized. In the case of naphth[*cde*]-azulene and cyclohept[*bc*]acenaphthylene the peripheral bonds of five and seven membered rings have alternate single and double bond character. Moreover the peripheral bonds of naphthalene moiety of these molecules are not predicted to be of similar type. It is found that the peripheral bonds of one of the benzene rings of the naphthalene nucleus is more delocalised than the other one which is joined with both five and seven membered rings. Thus the peripheral bonds of these molecules are either aromatic or polyolefinic in nature. Hence any definition of aromacity based on the global π-electron properties such as delocalization energy, magnetic properties or the standard deviation of bond length[12] is not adequate for these types of molecules.

Ionization Potential, Electron Affinity and π-Dipole Moment. According to Koopmans' theorem[13] the highest occupied orbital energy and the lowest unoccupied orbital energy represent ionization potential and electron affinity respectively of a molecule. But ionization potential and electron affinity calculated in this way is 1 or 2 eV higher than the true value. Hence we have used a relation of Kunii and Kuroda[14] for the calculation of ionization potential (I.P.) and electron affinity (E.A.). The relations are

$$\text{I.P.} = -(\varepsilon_i + 1.06)\ \text{eV}$$

and

$$\text{E.A.} = -\varepsilon_j - 1.90\ \text{eV}$$

where ε_i and ε_j are respectively the highest occupied and lowest unoccupied orbital energy. Table 2 contains uncorrected and corrected ionization potential and electron affinity respectively along with other theoretical values calculated in a similar way. It is seen that the present work is in good agreement with other theoretical results.

Table 2 also contains calculated values of π-dipole moment of these molecules along with other results. The dipole moment of molecule **2** has been determined experimentally and it is 0.49 D.[15] Theoretical values for the π-dipole moment have been obtained by Birss and Das Gupta,[6a] 1.15 and 2.06 D, by Pullman *et al.*,[16] 1.0 D, and by Francois *et al.*,[17] 0.9 D, compared with the present value of 1.26 and 2.27 D.

The authors express their gratitude to Professor F. W. Birss for many stimulating discussions and financial support. They are also thankful to the Computing Services, University of Alberta, for computational facilities.

References

1) R. Pariser and R. G. Parr, *J. Chem. Phys.*, **21**, 466, 767 (1953); J. A. Pople, *Trans. Faraday Soc.*, **49**, 1375 (1953).

2) K. Nishimoto and L. S. Forster, *Theor. Chim. Acta*, **3**, 407 (1965); **4**, 155 (1966).

3) H. Yamaguchi, T. Nakajima, and T. L. Kunii, *Theor. Chim. Acta*, **12**, 349 (1968).

4) M. J. S. Dewar and A. J. Harget, *Proc. Roy. Soc. (London)*, *A*, **315**, 443, 457 (1970) and other references therein.

5) A. Das Gupta and N. K. Das Gupta, *Can. J. Chem.*, **52**, 155 (1974); **53**, 915 (1975); *J. Mol. Struct.*, **27**, 113 (1975).
6) (a) F. W. Birss and N. K. Das Gupta, *Can. J. Chem.*, **49**, 2840 (1971); (b) P. Baumgartner, E. Weltin, G. Wagnière, and E. Heilbronner, *Helv. Chim. Acta*, **48**, 751 (1965); (c) J. Koutecky, P. Hochman, and J. Michl, *J. Chem. Phys.*, **40**, 2439 (1964); (d) H. Yamaguchi and T. Nakajima, *Bull. Chem. Soc. Jpn.*, **44**, 682 (1971).
7) Based on the structure of 4-methyl-pentaleno [6,6*a*,1,2-*def*] heptalene. H. J. Lindner, *Chem. Ber.*, **102**, 2456 (1969).
8) A. W. Hansen, *Acta Crystallogr.*, **13**, 215 (1960); **21**, 97 (1966).
9) K. Ohno, *Theor. Chim. Acta*, **2**, 219 (1964).
10) N. Mataga and K. Nishimoto, *Z. Phys. Chem.*, **13**, 140 (1957).
11) J. Hinze and H. H. Jaffe, *J. Am. Chem. Soc.*, **84**, 540 (1962).
12) (a) A. Julg and P. Francois, *Theor. Chim. Acta*, **7**, 249 (1967); (b) T. Nakajima, "Topics in Current Chemistry," **32**, 1 (1972).
13) T. Koopmans, *Physica*, **1**, 104 (1934).
14) T. L. Kunii and H. Kuroda, *Theor. Chim. Acta*, **11**, 97 (1968).
15) D. A. Pitt, A. J. Petro, and C. P. Smyth, *J. Am. Chem. Soc.*, **79**, 5633 (1957).
16) B. Pullman, A. Pullman, G. Berthier, and J. Pontis, *J. Chim. Phys.*, **49**, 20 (1952).
17) P. Francois and A. Julg. *J. Chim. Phys.*, **65**, 1180 (1968).
18) (a) K. Hafner, R. Fleischer, and K. Fritz, *Angew. Chem. Int. Ed. Engl.*, **4**, 69 (1965); (b) V. Boekelheide and G. K. Vick, *J. Am. Chem. Soc.*, **78**, 653 (1956); (c) P. D. Gardner, C. E. Wulfman, and C. L. Osborn, *ibid.*, **80**, 143 (1958); (d) D. H. Reid, W. H. Stafford, and J. P. Ward, *J. Chem. Soc.*, **1955**, 1193.

Effect of Solvent on Dipole Moment of Aliphatic Mercaptans

A. N. SRIVASTAVA and P. R. TALESARA
Chemistry Department, University of Jodhpur, Jodhpur-342001, India
(Received December 18, 1975)

Evidence of donor-acceptor complexes as a result of interaction between thiols and carbon tetrachloride has been obtained from the studies of dipole moment at 30 °C. Our polarisation data in other solvents except benzene are new. The results obtained have been discussed in terms of the influence of solvent on dipole moments in the light of general theory of Higasi.[1-3]

A survey of the literature reveals that only a few workers[4-6] have determined the dielectric-polarisation of alkanethiols, either to examine the equations derived from current theories of dielectric polarisation or to study the effect of sulfur replacing oxygen in an alcoholic group. The dipole moment value available[4,5] for these compounds are widely divergent. The present work has therefore been undertaken to re-examine the value of dipole moment as well as to assist in understanding the application of general theory of Higasi in case of aliphatic mercaptans.

Experimental

The method and technique have been described earlier.[7]

Purification. All the alkanethiols were purified[8] before use by distilling over anhydrous sodium sulfate in a quick fit apparatus where there was no possibility for the liquid to be in contact with atmospheric moisture or carbon dioxide. Table 1 contains the physical quantities experimentally measured for the liquids studied in the present paper.

The non polar solvents, benzene and carbon tetrachloride of grade E. Merck (G.R.) and dioxane of grade B.D.H. (A.R.) were used as such as the measured dielectric constants of these solvents agreed within ± 0.001 unit with the literature values.[6]

Table 1. Experimental physical constants

Name of substance	Density	Refractive index	Boiling point
Propyl mercaptan	0.82995	1.4330	66.1 °C
Butyl mercaptan	0.83134	1.4375	96.2 °C
Isobutyl mercaptan	0.82334	1.4340	40.0 °C
t-Butyl mercaptan	0.78888	1.4175	61.0 °C

Cyclohexane (B.D.H. Laboratory reagent) was distilled twice and the fraction boiling at 78 °C was used.

The solution moment values have been evaluated from the usual expression

$$\mu_S = 0.01281 \times 10^{-18}(P_{2\infty} - P_e)^{1/2} T^{1/2} \quad (1)$$

The solute-polarisation at infinite dilution *i.e.* $P_{2\infty}$ has been calculated by the method of Halverstadt and Kumler.[9] The values of the constants α, β, ε_1 and V_1 in Halverstadt and Kumler equation have been evaluated by the method of least squares and are given in Table 2. The electronic polarisation (P_e) is the same as molecular refraction for sodium D line and has been taken from literature.[10] Atomic polarisation (P_a) has not been taken into consideration according to the suggestion of Debye,[11] *viz.* the electronic polarisation calculated from sodium D line partly compensates the neglect of atomic polarisation.

Table 2. Evaluated constants in Halverstadt and Kumler pquation

Name of solvent	α	β	ε_1	V_1 (ml)	$P_{2\infty}$ (ml)	μ (in Debye)
		(Propyl mercaptan)				
Benzene	3.002	+0.0701	2.2533	1.1517	72.24	1.55
Carbon tetrachloride	2.8613	+0.2901	2.2041	0.6352	74.10	1.58
Dioxane	3.0222	+0.1988	2.2102	0.9788	70.57	1.52
Cyclohexane	2.0795	−0.1613	2.0023	1.3037	69.00	1.43
		(Butyl mercaptan)				
Benzene	3.0882	+0.0759	2.2448	1.1518	78.46	1.57
Carbon tetrachloride	2.8105	+0.3521	2.2086	0.6346	94.39	1.58
Dioxane	3.1333	+0.2440	2.2006	0.9790	77.33	1.56
Cyclohexane	2.1963	−0.0830	1.9961	1.3021	68.16	1.50
		(Isobutyl mercaptan)				
Benzene	2.7938	+0.0712	2.2635	1.1551	74.14	1.50
Carbon tetrachloride	2.6814	+0.3547	2.2112	0.6353	76.50	1.54
Dioxane	3.0023	+0.2494	2.2010	0.9788	75.53	1.53
Cyclohexane	2.5910	+0.6623	1.9860	1.3026	68.88	1.41
		(*t*-Butyl mercaptan)				
Benzene	3.1010	+0.1276	2.2534	1.1520	79.82	1.59
Carbon tetrachloride	3.0530	+0.3858	2.2082	0.6351	84.02	1.65
Dioxane	3.3553	+0.2760	2.2020	0.9796	81.41	1.61
Cyclohexane	1.6942	+0.0598	2.0174	1.2948	65.09	1.34

Table 3. Excess polarisation values (ml)

	(Propyl mercaptan+carbon tetrachloride)						
f_1f_2	0.0192	0.0374	0.0464	0.0541	0.0616	0.0695	0.0767
P^E	+0.329	+0.615	+0.717	+0.866	+1.034	+1.134	+1.260
	(Butyl mercaptan+carbon tetrachloride)						
f_1f_2	0.020	0.0388	0.0474	0.0556	0.0631	0.0710	0.0783
P^E	+0.366	+0.574	+0.744	+0.970	+0.992	+1.102	+1.125
	(Isobutyl mercaptan+carbon tetrachloride)						
f_1f_2	0.0201	0.0397	0.0478	0.0577	0.0658	0.0728	0.0931
P^E	+0.246	+0.400	+0.537	+0.687	+0.810	+0.822	+1.183

Table 4. Apparent dipole moment values of thiols in Debye units (μ_s)

Solute	Benzene $\varepsilon_1=2.2645$			Carbon tetrachloride $\varepsilon_1=2.2176$	Dioxane $\varepsilon_1=2.2015$	Cyclohexane $\varepsilon_1=2.0070$
	by Hunter and Partington	by Mathias and E. D. Carvalhofilho	by present authors	by present authors		
Propyl mercaptan	1.33	1.51	1.55	1.58	1.52	1.43
Butyl mercaptan	1.32	1.53	1.57	1.58	1.56	1.50
Isobutyl mercaptan	—	1.53	1.50	1.54	1.53	1.41
t-Butyl mercaptan	—	1.59	1.59	1.65	1.61	1.34

Results and Discussion

The solvent effect in mercaptan can be understood with reference to the structure of H_2S. Hydrogen sulfide is an asymmetrical top molecule and has two-fold axis of symmetry. The molecule may be considered to consist of two ellipsoids with a common axis 'c' and with a dipole in its axis of symmetry at a distance a_1 from one end of the diameter and a_2 from the other end (diameter along axis of symmetry $2a=a_1+a_2$). The value of a_1, a_2, and c have been calculated from the spectroscopic[12] data for the H–S bondlength (1.328 Å) and ∠HSH (92°2′). Thus

$$c = 0.9568\,\text{Å}, \quad a_1 = 0.0544\,\text{Å}, \quad a_2 = 0.8663\,\text{Å}$$

According to the theory of Higasi[1-3] if $a<c$, $a_1<c$ and $a_2<c$, the induced moment is evaluated by the expression

$$\mu_1 = 2\pi n\alpha\mu(B_1+B_2) \qquad (2)$$

where the value of B_1 and B_2 may be obtained from the expression

$$B = \frac{k'^2}{k'^2-1}\left|1-\frac{1}{(k'^2-1)^{1/2}}\sin^{-1}\frac{(k'^2-1)^{1/2}}{k'}\right|-\frac{1}{3} \qquad (3)$$

(where $k'=c/a>1$) by substituting $k'=c/a_1$ and $k'=c/a_2$ respectively. From the calculated values of $B_1=+0.5833$ and $B_2=0.0286$, it is observed that B_1 and B_2 are both positive and therefore as suggested by Higasi, the solvent effect would be positive *i.e.* $\mu_s>\mu_v$. Literature value[13] 0.97 D for μ_s of H_2S in benzene, appears to be much convincing and is greater than 0.93 D,[14] a value in the vapour state. The observed ratio for μ_s/μ_v is therefore 1.04. The value calculated for μ_s/μ_v on the basis of Higasi's treatment comes to be 1.09. This shows that theory of Higasi is correctly applicable[7] in case of H_2S molecule. If one of the hydrogen atom of H_2S is replaced by an alkyl group, this will lead to an increase in the value of 'c' and c would be further greater than a_1 and a_2. Therefore it is expected that k' would be greater than one and μ_s would be greater than μ_v in case of mercaptans studied here. Unfortunately the data in vapor state are not available in case of alkanethiols. However, in case of positive solvent effect, according to the suggestion of Higasi, the solution moment should be greater in the solvent having higher dielectric constant and as such μ_s (benzene) should be greater than μ_s in the other three solvents.

The unexpected higher values for last two mercaptans (Table 4) in dioxan than the values in benzene may be regarded due to hydrogen bonding between hydrogen atoms of the solute and the donor oxygen atoms of the solvent molecules, an effect which would give rise both to the lengthening of the S–H bond and polarisation of solvent molecules. The high values are therefore best considered as due to an "interaction polarisation." This is further supported by the observation of Taylor[15] reporting that smaller is the ionisation constant of the acid, the stronger is the hydrogen bond. The ionisation constant values,[16] 2.26×10^{-11}, 2.21×10^{-11} and 0.89×10^{-11} for propyl mercaptan, butyl mercaptan and *t*-butyl mercaptan respectively suggest therefore that the possibility of hydrogen bonding in the last case is more and as such a high value is expected. The decreasing order of ionisation constant leads to anticipate that isobutyl mercaptan (the ionisation constant of which is not available) has a greater tendency of hydrogen bonding in dioxane than the first two thiols. Consequently the solution moment value of isobutyl mercaptan happens to be greater than that in benzene but the value is certainly less than that of butyl mercaptan in dioxane, as expected.

The moment values in carbon tetrachloride has been examined in the light of Earp and Glasstone[17] theory. Accordingly it has been shown in Fig. 1 (data shown in Table 3) that for these systems the excess polarisation P^E is a linear function of f_1f_2 and passes through the origin, confirming that the contact pairs are exclusively

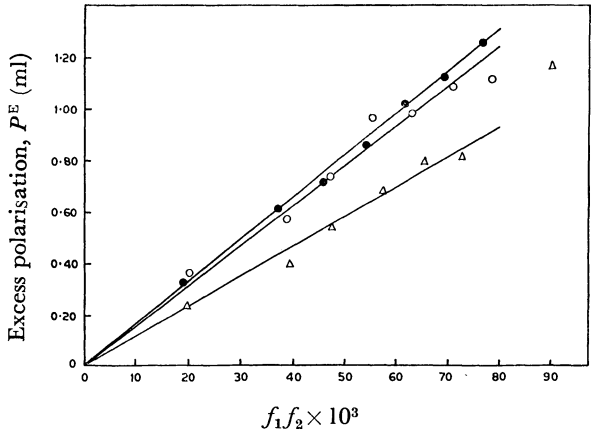

Fig. 1. P^E *vs.* f_1f_2.
Solvent: carbon tetrachloride.
●: Propyl mercaptan, ○: butyl mercaptan, △: isobutyl mercaptan.

formed. The unexpected higher values for all the four thiols in carbon tetrachloride than those in benzene may therefore be due to the formation of donor-acceptor type complexes. Praunitz and coworkers[18] have also adduced evidence that carbon tetrachloride behaves as an electron acceptor. Besides, the support for complex formation between benzene and carbon tetrachloride (acceptor) is recently[19] reported. Literature[20] also reports the behavior of mercaptans as donor.

The dipole moment value determined by Hunter and Partington[4] in Table 4 appears to be low. This observation is further supported by the data of Walls and Smith[21] and Mathias[5] who have found higher values. It is expected that with larger atoms or groups in place of hydrogen in H_2S, the bond angles would be larger and as such the dipole moment value for butyl mercaptan should be higher than that of propyl mercaptan. This contention is also supported by Mathias,[5] who observed that the dipole moment calculated by Debye's equation increases with the extention of the carbon chain in the normal thiols. It is pertinent to mention that out moment values fairly agree with those obtained by Mathias.[5] Our data in Table 4 amply demonstrate the above facts.

The authors are thankful to Prof. R. C. Kapoor, Head, Department of Chemistry for providing the necessary facilities. One of us (P.R.T.) is grateful to C.S.I.R. and U.G.C., Govt. of India for financing the project.

References

1) K. Higasi, *Bull. Inst. Phys. Chem. Jpn.*, **14**, 146 (1935).
2) K. Higasi, *Sci. Pap. Inst. Phys. Chem. Res. Jpn.*, **28**, 284 (1935).
3) K. Higasi, *Sci. Pap. Inst. Phys. Chem. Res. Jpn.*, **31**, 311 (1937).
4) C. E. Hunter and J. R. Partington, *J. Chem. Soc.*, **1932**, 1831, 2812.
5) S. Mathias and E. C. Filho, *J. Phys. Chem.*, **62**, 1427 (1958).
6) C. N. R. Rao, "A Handbook of Chemistry and Physics," (1967).
7) A. N. Srivastava, and B. Krishna, *Aust. J. Chem.*, **19**, 1851 (1966).
8) C. E. Hunter and J. R. Partington, *J. Chem. Soc., Pt. 2*, **1939**, 2812.
9) I. F. Halverstadt and W. D. Kumler, *J. Am. Chem. Soc.*, **64**, 2988 (1942).
10) J. R. Partington, "Advanced Treatise on Physical Chemistry," Vol. IV, Longmanns, London (1953), p. 60.
11) P. Debye, "Polar Molecules," Dover Publication, New York (1929), p. 51.
12) H. Sebert, "Anwendungen der Schwingungsspktroskopie in der Anorganischen Chemie," Springer Verlag, Berlin (1966), p. 50.
13) C. L. Angul and R. J. W. Le Fevre, *J. Chem. Soc., Pt. 2*, **1952**, 1951.
14) J. W. Smith, "Electric Dipole Moments," Butter-Worths Scientific Publications (1955), p. 86.
15) M. D. Taylor, and M. B. Templeman, *J. Am. Chem. Soc.*, **78**, 2950 (1956).
16) M. M. Kreevoy, E. T. Harper, R. E. Duvall, H. S. Wilgus, III, and L.T. Ditsch, *J. Am. Chem. Soc.*, **82**, 4899 (1960).
17) D. P. Earp and S. Glasstone, *J. Chem. Soc.*, **1935**, 1709.
18) R. Anderson and J. M. Praunitz, *J. Chem. Phys.*, **39**, 1225 (1963).
19) G. W. Chantry, H. A. Gebbie, and H. N. Mirza *Spectrochim. Acta*, **23A**, 2749 (1967).
20) M. Good, A. Major, J. N. Chaudhari, and S. P. McGlynn, *J. Am. Chem. Soc.*, **83**, 4329 (1961).
21) W. S. Walls and C. P. Smyth, *J. Chem. Phys.*, **1**, 337 (1933).

Chromium(III) Complexes with Amino Acids. I. Chromium(III) Complexes with Glycine and *dl*-α-Amino Acids

Hisaya Oki and Kiyoe Otsuka

Department of Chemistry, Faculty of Education, Fukui University, Fukui 910

(Received September 10, 1975)

A comparison has been made between the synthesis carried out by the isothermal matrix method in solid state and that by the usual method in solution for chromium(III) complexes with glycine and *dl*-α-amino acids (alanine, aminobutyric acid, norvaline, norleucine, valine, isoleucine and leucine). The effect of the length of the skeletal carbon chain or the presence of the side chain in α-amino acids on the formation of complexes was investigated. The complexes with α-amino acids which have a normal chain were obtained in *fac*-structure except for norleucine complexes, whereas the complexes with α-amino acids which have a side chain were obtained only in dimer-type by the matrix method in solid state. The chromium(III) complexes with *dl*-α-amino acids were all prepared as tris-type structure, except for α-aminobutyric acid and valine, whereas all the complexes of dimer-type structure were prepared in solution, except for alanine and norleucine.

A number of chromium(III) complexes with natural amino acids are known.[1-10] However, no systematic studies have been carried out on the effect of the length of the skeletal carbon chain or the presence of a side chain in α-amino acids upon the formation of complexes. No studies have been reported on the difference between racemic- and L-amino acids in the complexation. All the tris-type chromium(III) complexes with the natural α-amino acids are of *fac*-structure, no *mer*-form being obtained as crystals. The preparation of purple *mer*-$[Cr(gly)_3]$ has been claimed by Israily.[11] However, Gillard *et al.* reported that this purple fraction is a hydrated dihydroxobridged dimer, $[Cr_2(gly)_4(OH)_2]\cdot 6H_2O$.[12] In the present work, attempts were made to prepare chromium(III) complexes with glycine and racemic amino acids (where racemic amino acids= alanine, aminobutyric acids, norvaline, norleucine, valine, isoleucine and leucine) by the isothermal matrix method in solid state and by the method in solution where hexaamminechromium(III) nitrate was used as the starting material.

Experimental

Preparation of Chromium(III) Complexes. There are two methods for the preparation of chromium(III) complexes with natural α-amino acids according to the mode of starting.

a) Preparation by Solid State Reaction: Hexaamminechromium(III) nitrate was mixed with α-amino acids in a mortar. The mixture was heated at 135±1 °C in a Toyoroshi electronic drying oven. The mole ratios of the amino acids to the starting complex and the heating time applied are given in Table 1.

Table 1. Mole ratios of amino acids to the starting complex and the reaction times at 135±1 °C

α-Amino acid	Mole ratio	Reaction time (min)
Glycine	3	45
α-Alanine	2.5	60
α-Aminobutyric acid	3	60
Norvaline	4	60
Valine	3	60
Isoleucine	2	50
Leucine	3	40

The reaction products containing glycine and *dl*-α-alanine were dissolved in water and kept standing at room temperature overnight. $[Cr(gly)_3]\cdot H_2O$ and $[Cr(\alpha\text{-ala})_3]$ were obtained as red or pink crystals. The reaction products containing *dl*-α-alanine, *dl*-α-aminobutyric acid and *dl*-norvaline were dissolved in methanol. After removal of residues by filtration, the filtrates were kept standing at room temperature for one or two days. $[Cr(\alpha\text{-ala})_3]$, $[Cr(\alpha\text{-ambut})_3]\cdot H_2O$ and $[Cr(norval)_3]\cdot H_2O$ were gradually deposited as pink crystals. When the reaction products containing *dl*-valine, *dl*-isoleucine and *dl*-leucine were dissolved in methanol, the complexes could not be crystallized. However, when water was used as a solvent, *dl*-μ-hydroxo-tetrakis(amino acidato)dichromium(III) complexes were obtained as light purple crystals, where amino acids are *dl*-α-aminobutyric

Table 2. Analytical data (by the solid state reaction)

Complexes	C (%)		H (%)		N (%)	
	Calcd	Found	Calcd	Found	Calcd	Found
$[Cr(gly)_3]\cdot H_2O$	24.66	24.39	4.83	5.00	14.38	14.04
$[Cr(\alpha\text{-ala})_3]$	34.18	33.64	5.74	5.85	13.29	13.20
$[Cr(\alpha\text{-ambut})_3]\cdot H_2O$	38.18	37.40	6.96	7.03	11.17	11.07
$[Cr(norval)_3]\cdot H_2O$	43.06	42.20	7.71	7.79	10.04	10.48
$[Cr(norval)_3]\cdot 2H_2O$	41.28	41.11	7.39	7.81	9.63	9.61
$[Cr(OH)(\alpha\text{-ambut})_2]_2\cdot 3H_2O$	31.07	31.07	6.84	6.45	9.06	9.92
$[Cr(OH)(norval)_2]_2\cdot 2H_2O$	37.62	38.36	7.26	6.94	8.77	9.12
$[Cr(OH)(val)_2]_2\cdot 2H_2O$	37.62	38.57	7.26	7.18	8.77	8.74
$[Cr(OH)(leu)_2]_2\cdot 4H_2O$	39.45	40.73	8.00	7.82	7.67	8.12
$[Cr(OH)(isoleu)_2]_2\cdot 4H_2O$	39.45	38.58	8.00	7.54	7.67	7.70

Table 3. Analytical data (by the solution state reaction)

Complexes	C (%)		H (%)		N (%)	
	Calcd	Found	Calcd	Found	Calcd	Found
$[Cr(\alpha\text{-ala})_3]$	34.18	33.30	5.74	5.64	13.29	13.18
$[Cr(norval)_3]\cdot 3H_2O$	39.61	39.93	7.92	7.06	9.24	9.30
$[Cr(norleu)_3]\cdot 2H_2O$	45.18	44.19	8.43	7.98	8.78	8.74
$[Cr(leu)_3]\cdot 2H_2O$	45.18	44.99	8.43	7.99	8.78	8.46
$[Cr(OH)(gly)_2]_2$	22.13	21.70	5.83	5.82	10.81	10.23
$[Cr(OH)(\alpha\text{-ambut})_2]_2\cdot 2H_2O$	32.99	33.74	6.53	5.98	9.62	9.85
$[Cr(OH)(norval)_2]_2\cdot 2H_2O$	37.62	37.05	7.26	6.70	8.77	8.52
$[Cr(OH)(val)_2]_2\cdot 2H_2O$	37.62	38.10	7.26	6.90	8.77	9.10
$[Cr(OH)(isoleu)_2]_2\cdot 4H_2O$	39.45	39.02	8.00	7.72	7.67	7.80

acid, *dl*-norvaline, *dl*-valine, *dl*-isoleucine and *dl*-leucine. The reaction product containing *dl*-norvaline was washed with water and the residue was dissolved in DMF. After filtration, the filtrate was evaporated until its volume was reduced to one-third. To this was added water until pink crystals began to appear. The crystals have the same composition as that of the product deposited from the methanolic solution, but the amount of the water of crystallization contained is two, instead of one mole. The analytical data are given in Table 2.

b) *Preparation by the Reaction in Solution*: Hexaamminechromium(III) nitrate (345 mg) and glycine (225 mg) were dissolved in water (10 ml) and the mixture was heated on a waterbath until a small quantity of purple crystals began to appear. The purple crystals formed were removed by filtration while hot. When the filtrate was cooled to room temperature, red crystals were precipitated, which were contaminated by some amount of purple crystals. The red compound was separated by decantation in ethanol. The red and the purple crystals are considered to be tris- and binuclear-type chromium(III) complexes, respectively.

By the same method as described above, the complex with *dl*-alanine was precipitated only as of tris-type. The complexes with *dl*-aminobutyric acids, valine and isoleucine were precipitated as hydroxo bridging dimer complexes. The complexes with *dl*-norvaline was first precipitated as pink crystals. After they had been removed by filtration, water was added to the filtrate until the volume became equal to the original one. By heating the resulting solution on a waterbath, pink and purple crystals were precipitated. Pure $[Cr(OH)(dl\text{-norval})_2]_2\cdot 2H_2O$ was precipitated by repeating the same procedure. Pink crystals were dissolved in DMSO because of contamination by a small quantity of the purple crystals. After filtration, the filtrate was added dropwise to water, causing instant precipitation of $[Cr(dl\text{-norval})_3]\cdot 3H_2O$ as pink crystals. The complexes with norleucine and leucine were precipitated as red-purple crystals. The crystals were dissolved in DMF and after removal of residues by filtration, the filtrate was added dropwise into water. $[Cr(dl\text{-norleu})_3]\cdot 2H_2O$ and $[Cr(dl\text{-leu})_3]\cdot 2H_2O$ were precipitated almost instantly. The analytical data of these complexes are given in Table 3.

Apparatus. The UV spectra were measured with a Hitachi 139 spectrophotometer. The IR spectra were measured with a Hitachi EPI-G3 infrared spectrophotometer in Nujol mull.

Results and Discussion

UV Absorption Spectra. Mizuochi *et al.*[10] measured all the UV absorption spectra of the chromium(III) complexes of tris-type with amino acids in a 20% perchloric acid solution except the spectrum of tris(L-leucinato)chromium(III) complex which was measured in methanol and DMF. Gillard *et al.*[12] reported that the values found for the absorption maxima of *fac*-tris(glycinato)chromium(III) complex in solid state (530 nm) and in 70% $HClO_4$ solution (539 nm) differ from each other, suggesting the occurrence of some chemical reactions during the course of dissolution.

Table 4. Absorption maxima of tris-type chromium(III) complexes

	$\bar{\nu}_1$ (log ε)	$\bar{\nu}_2$ (log ε)	Solvent	Reflectance method	
				$\bar{\nu}_1$	$\bar{\nu}_2$
Solid state reaction					
Gly	18.6(1.63)	25.0(1.56)	60%$HClO_4$	19.8	26.0
Ala	18.7(1.76)	25.1(1.67)	20%$HClO_4$	19.4	25.7
Ambut	18.6(1.75)	25.0(1.64)	20%$HClO_4$	19.4	25.6
Norval	19.3(2.13)	25.4(2.06)	DMF	19.4	25.9
Solution state reaction					
Ala				19.4	25.7
Norval	19.3(2.11)	25.4(2.01)	DMSO	19.4	25.9
Norleu	19.3(2.39)	25.5(2.23)	DMSO		
Isoleu	19.1(2.26)	25.4(2.14)	DMSO		
Leu	19.3(2.19)	25.6(2.13)	DMSO		
				($\bar{\nu} \times 10^3$ cm^{-1})	

The UV absorption spectra of chromium(III) complexes of tris-type with glycine, alanine and aminobutyric acid were measured in both solid state and in perchloric solution. The absorption spectra of chromium(III) complexes with other amino acids of tris-type were measured in DMF or DMSO. Their maxima are summarized in Table 4. The spectra of tris(glycinato)chromium(III) complex in 60% perchloric acid and in solid state are shown in Fig. 1. These data suggest that this complex undergoes acid hydrolysis or chemical reaction on dissolution in perchloric acid. The spectra of tris(norvalinato)-chromium(III) complex in DMSO and in solid state are shown in Fig. 2. It can be seen that the absorption curve in DMSO is similar to that in solid state except for slight shifts of the peak to longer wave number region in solid state. This indicates that the latter complex is significantly stable even in DMSO solution.

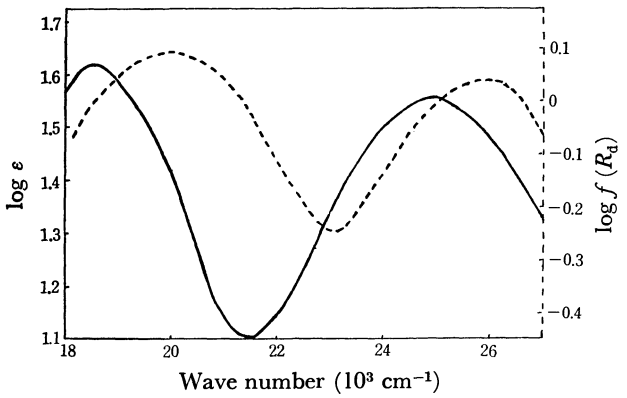

Fig. 1. The absorption spectra of tris-glycinatochromium(III) complex in 60% $HClO_4$ solution (—) and in solid state (---).

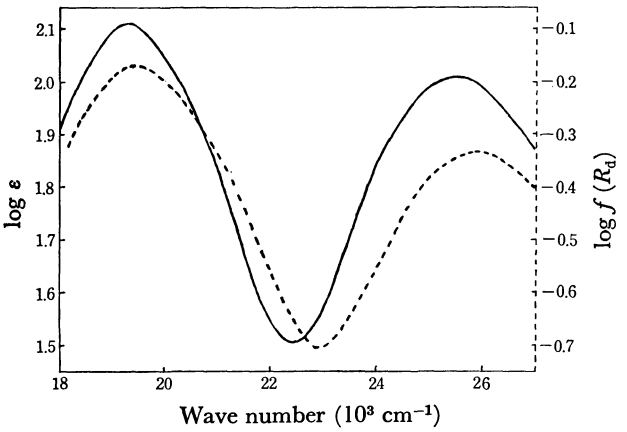

Fig. 2. The absorption spectra of tris-norvalinatochromium(III) complex in DMSO solution (—) and in solid state (---).

For all the $[Co(O)_n(N)_{6-n}]$ series, the predicted shift of the first and second absorption bands has been discussed by Matsuoka *et al.*[13] In the present paper, their calculations were applied to these chromium(III) complexes. The value 21.9×10^3 cm^{-1} and 28.3×10^3 cm^{-1} were obtained for the maxima of the first and the second bands, respectively, in the $[Cr(en)_3]^{3+}$ complex, and 17.5×10^3 cm^{-1} and 23.8×10^3 cm^{-1} for those in the $[Cr(ox)_3]^{3-}$ complex. The maxima of the first and the second absorption bands in *fac*-$[Cr(O)_3(N)_3]$ were calculated to be 19.7×10^3 cm^{-1} and 26.1×10^3 cm^{-1}, respectively. The absorption maxima of these chromium(III) complexes in solid state and in DMF or DMSO solution (Table 4) coincide with the wave numbers obtained by the above calculation. This suggests that the tris-type chromium(III) complexes we prepared have the *fac*-form. Although the absorption maxima of tris-glycinato, alaninato and aminobutyrato complexes in perchloric acid differ from those predicted, the values obtained by Gillard *et al.*,[12] Nakahara[14] (glycine) and Mizuochi *et al.*[10] (alanine and aminobutyric acid) agreed with those obtained in perchloric acid solution (Table 4).

The results indicate that *fac*-tris(amino acidato)-chromium(III) complexes are unstable in acid solution, the stability differing substantially from that of the corresponding cobalt(III) complexes in acid. Tris-(amino acidato)chromium(III) complexes become easily soluble in organic solvent, with increase in the length of the skeletal carbon chain of α-amino acid.

IR Spectra. Infrared absorption spectra were measured in the range 4000—400 cm^{-1}. The spectra of tris-type chromium(III) complexes with glycine, α-alanine and α-aminobutyric acid agree with those of the corresponding chromium(III) complexes of *fac*-form as reported by Mizuochi *et al.*[10] No *fac*-form of chromium(III) complexes with norvaline and norleucine could be found. The preparation of purple chromium-(III) complex with α-aminobutyric acids was reported but no spectrum. The spectrum of purple chromium(III) complex with aminobutyric acid agrees with that for the corresponding chromium(III) complex, *cis*-$[Cr(OH)(ambut)_2H_2O]$, which they prepared. However, it is doubtful whether the assignment of this structure is correct, since, the di-μ-hydroxotetrakis(glycinato)-dichromium(III) shown by X-ray diffraction analysis and magnetic measurement,[15] was assigned to hydroxo-aquo complex. The purple crystals with glycine and L-phenylalanine were confirmed to have the dimer structure by magnetic measurement.[16]

Table 5. Chromium(III) complexes with *dl*-α-amino acids

Amino acid	$[Cr(L)_3]$	$[Cr(OH)(L)_2]_2$
Glycine	◑	○
α-Alanine	◑	
α-Aminobutyric acid	●	◑
Norvaline	◑	◑
Norleucine	○	
Valine		◑
Isoleucine	○	◑
Leucine	○	◑

L=amino acid.
● Complexes prepared by the solid method.
◑ Complexes prepared by both methods.
○ Complexes prepared by the solution method.

The chromium(III) complexes with various *dl*-amino acids of the type $[CrL_3]$ and $[Cr(OH)L_2]_2$, where L denotes amino acid, were synthesized in the solid state and in solution (Table 5). Preparation of chromium(III) complexes with natural *dl*-α-amino acids carried out by the two methods may be charactrized as follows: i) Solid State Reaction. The complexes with *dl*-α-amino acids which have no side chain were prepared as tris-type structure, except for *dl*-norleucine. The complexes of dimer-structures were prepared with α-aminobutyric acid and norvaline. Taking account of the carbon skeleton in *dl*-amino acids, when the reaction product is dissolved in water, complexes with glycine and α-alanine are obtained as tris-type, but those with α-aminobutyric acid and norvaline in which the length of carbon chain is longer than that of alanine are obtained as the dimer type. When the reaction product is dissolved in methanol, the complex with glycine can not be crystallized, but the complexes with other amino acid are obtained as tris-type. The preparation of tris-type chromium(III) complex with norleucine

was not successful. However, the solid state reaction of norleucine was similar to that of other amino aicds. Thus, the complexes of *fac*-structure can be easily separated from the dimer type, when the solvent is changed. This is advantageous for the preparation of tris-type complexes in a solid method than in the solution method. The complexes with valine, isoleucine and leucine which have a side chain were obtained only as the dimer-type. ii) Solution State Reaction. The chromium(III) complexes with racemic α-amino acids have all been prepared with tris-type structure, except for α-aminobutyric acid and valine. All the complexes with dimer-structure have been prepared, except for alanine and norlecine. Preparation in solution method seems more convenient than that in solid state. A mixture of tris- and dimer-complexes is prepared by the solution method. It should be separated into components by another method.

Taking account of the carbon skeleton in racemic amino acids, we obtained dimer-type complexes containing glycine and α-aminobutyric acid and tris-type complexes containing α-alanine and norvaline. Complexes with racemic α-amino acids appear predominantly with dimer- and tris-structures, alternatively, depending on the length of the carbon skeleton. However, this can not always be applied to complexes with norleucine, since it gave only a tris-type structure.

Complexes with isoleucine and leucine which have a side chain were obtained with tris- and dimer-type structures. However, the complex with valine which has a methyl group in the β-position, as well as isoleucine, was obtained with only a dimer-type structure.

The present method in solution state using hexaamminechromium(III) nitrate is very simple as compared with the usual method in the same state, using chromium(III) hydroxide and chromium(III) chloride as a starting material. It is necessary to remove unreacted hydroxide using chromium(III) hydroxide and to neutralize the reactant solution in the method using chromium(III) chloride, but it is not necessary to separate unreacted substance in the dissolved state and the reactant solution naturally neutralized in the method using hexaamminechromium(III) nitrate.

No circular dichroism was observed for tris-type. All tris-type chromium(III) complexes were in *fac*-structure, no *mer*-form being obtained.

The authors wish to thank Professor R. Tsuchiya, Kanazawa University, for valuable discussions and suggestions.

References

1) H. Ley and H. Winkler, *Ber.*, **45**, 380 (1912).
2) L. M. Volshtein and V. P. Molosnova, *Doklady Akad. Neuk. SSSR.*, **92**, 479 (1952).
3) L. Tchougaeff and E. Serbin, *C. R. Acad. Sci.*, **151**, 1361 (1910).
4) L. Hugouneng and A. Morel, *C. R. Acad. Sci.*, **154**, 119 (1912).
5) L. M. Volshtein, *C. R. Acad. Sci. SSSR*, **54**, 321 (1946).
6) H. Ley and K. Ficker, *Ber.*, **45**, 377 (1912).
7) R. W. Green and V. P. Ang, *J. Am. Chem. Soc.*, **77**, 5482 (1955).
8) L. M. Volshtein and V. P. Molosnova, *Zh. Neorg. Khim.*, **4**, 1995 (1959).
9) L. M. Volshtein, *Zh. Neorg. Khim.*, **1**, 2378 (1956).
10) H. Mizuochi, A. Uehara, E. Kyuno, and R. Tsuchiya, *Bull. Chem. Soc. Jpn.*, **44**, 1555 (1971).
11) N. Israily, *C. R. Acad. Sci., Ser. C*, **262**, 1426 (1966).
12) R. D. Gillard, S. H. Laurie, D. C. Price, D. A. Phipps, and C. F. Weick, *J. Chem. Soc., Dalton Trans.*, **1974**, 1385.
13) N. Matsuoka, J. Hidaka, and Y. Shimura, *Bull. Chem. Soc. Jpn.*, **40**, 1868 (1967).
14) M. Nakahara, *Bull. Chem. Soc. Jpn.*, **35**, 782 (1962).
15) J. T. Veal, W. E. Hatfield, D. Y. Jeter, J. C. Hempel, and D. J. Hodgson, *Inorg. Chem.*, **12**, 342 (1973).
16) A. Earnshaw and J. Lewis, *J. Chem. Soc., A*, **1971**, 2271.

Isomerization of the (D-Aspartato)(L-2,4-diaminobutyrato)-cobalt(III) Complex

Masatoshi WATABE, Shigeji KAWAAI, and Sadao YOSHIKAWA*

General Education Department of Kogakuin University, Hachioji, Tokyo 193
**Department of Synthetic Chemistry, Faculty of Engineering, The University of Tokyo, Hongo, Bunkyo-ku, Tokyo 113*

(Received October 20, 1975)

The isomerization of two of the three possible geometrical isomers for the (D-aspartato)(L-2,4-diaminobutyrato)cobalt(III) complex afforded the residual third isomer which has not here to fore been obtained. The equilibrium mole fractions of these isomers in water in the presence of activated carbon were found for D-*cis*O_5*cis*N_5, D-*trans*O_5*trans*N_5, D-*fac* to 0.68, 0.11, 0.21, respectively. As the two ligands coordinated are considered to involve no intermolecular hydrogen bonding or steric hindrance, the relative positions of the six coordinated atoms around a cobalt atom may cause these unequal isomer ratios. These isomerisms are dealt with by means of a network of first-order reversible reactions and the relative values of the rate constants are determined.

The preparation and absorption and PMR spectra of [Co(L- or D-asp)(L-2,4-dba)] (asp=aspartate ion and dba=diaminobutyrate ion) have already been reported.[1] Though three possible isomers of [Co(L-asp)-(L-dba)] could be obtained, only two isomers of [Co(D-asp)(L-dba)] could be obtained (Figs. 1-a and c). The residual isomer (Fig. 1-b) could not be obtained though several preparative methods were attempted. The two ligands coordinated are considered to involve no intermolecular hydrogen bonding or steric hindrance. It is interesting to study the difficulty encountered in obtaining the third isomer of [Co(D-asp)(L-2,4-dba)]. In the work reported here, the present authors studied whether the third isomer of [Co(D-asp)(L-2,4-dba)] could be obtained by equilibrating the complex obtained earlier in the presence of activated carbon.

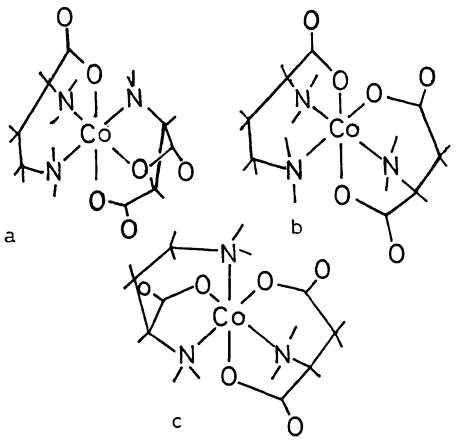

Fig. 1. The three possible geometrical isomers of the [Co(D-asp)(L-2,4-dba)] a: *cis*O_5*cis*N_5, b: *trans*O_5*trans*-N_5, c: *fac*. The isomers are named by considering 5-membered N and O atoms.

Experimental

The [Co(D-asp)(L-2,4-dba)] was prepared as described in a previous paper.[1] Two isomers were obtained and named D1 and D2 in their order of elution using a cation exchange column (Dowex 50 w X8, Na form). Activated carbon was purchased from Takeda-Yakuhin, Ltd, which was "Shirasagi," and dried at 100 °C before use.

The isomerization of D1 (D-*cis*O_5*cis*N_5) and D2 (D-*fac*) isomers using the activated carbon as a catalyst afforded the third isomer D3 (D-*trans*O_5*trans*N_5). When the resulting mixture was loaded on a cation exchange column (Dowex 50 w X8, 100—200 mesh Na form) the D3 isomer was found to closely follow the D1 isomer. As the D3 isomer was relatively less soluble, this fraction was concentrated and kept in a refrigerator overnight. A small quantity of the D3 isomer was precipitated. Found D3: C, 28.73; H, 5.26; N, 12.07%. Calcd for $CoC_8H_{14}O_6N_3 \cdot 1.5H_2O$: C, 28.75; H, 5.13; N, 12.57%.

A starting isomer (80 mg, 0.0024 mol) was dissolved in 100 ml water at 50 °C. To this solution, 20 mg of activated carbon was added. A reflux condensor was attached to the flask. The solution was stirred and maintained at 50 °C in a temperature-controlled reaction vessel. The reaction was timed with a stop clock whenever the carbon was introduced into the sample in the vessel. Since the isomerization is "frozen" upon the removal of the carbon from the sample solutions, rapid filtration is an excellent way to stop the reaction. The method adopted requires 7 mm glass tubing packed with a cotton filter. The packed tubes were placed, using a specially-prepared fitting, on the end of a 5 ml hypodermic syringe. The solution was examined for optical rotation immediately after withdrawal and at the end of the run. No loss of optical activity was noted. Sampling was continued for 24 h at intervals of 30 and 60 min. The concentrations of all isomers after sampling were determined as follows. First, the concentration of the D2 isomer was determined using high-speed liquid chromatography in comparison with a known concentration of the D2 isomer. The concentrations of the D1 and D3 isomers were determined using the molar rotation $[\phi]$ at 489 and 540 nm.

	489 nm	540 nm
D1	44.53	0.0
D2	8.20	−4.82
D3	0.0	−80.20

The concentrations of the D1 and D3 isomers were calculated using the following equation:

$$[\phi]_{D1}x + [\phi]_{D2}y + [\phi]_{D3}(1-x-y) = \alpha/c,$$

where $[\phi]_{D1}$, $[\phi]_{D2}$, and $[\phi]_{D3}$ are the molar rotations, x and y are the concentrations of the D1 and D2 isomers, respectively and c is the initial concentration of the isomer which is isomerized. α is the rotation of the plane of polarization, expressed in degrees. Since the concentration loss of the complex due to adsorption on the surface of the carbon and due to other reactions was less than 2 percent, it was possible

to treat the complex concentration as constant throughout a run. The concentration of cobalt was determined using nitrosonaphthol.

Measurements. The electronic absorption spectra and the optical rotatory dispersion spectra were measured with a JASCO ORD-UV-5 spectrometer. The wavelength correction was cheked using neodymium glass which is absorping at 589 nm. The chromatographic separation was carried out with a JASCO LCP-350 high-speed liquid chromatograph. A 500×2.3 mm glass column containing 50 w X8 Dowex and a 200—400 mesh Na form was used for all measurements. The complexes were eluted with water at a flow rate of 1.0 ml/min at a pressure of *ca.* 40 kg/cm^2.

Results and Discussion

Figure 1 shows the possible isomers of [Co(D-asp)(L-dba)]. The D-*trans*O_5*trans*N_5 isomer (Fig. 1 (b)) has not previously been prepared. Figure 2 shows the results of high-speed liquid chromatography for the equilibrated mixture, starting from the D2 isomer. The D-*mer* isomer was found to appear in front of the D2 isomer. After the isomerization of more than 2 grams of the D1 or D2 isomer in 100 ml of H_2O in the presence of activated carbon, the equilibrated mixture was loaded on a cation exchange column (30×700 mm Na form) and eluted with water. The fractions were taken in a fraction collector. The optical rotatory dispersion and visible spectra of the rear part of the D-*mer* fractions did not agree with those of the D-*cis*O_5*cis*N_5 isomer. These fractions were collected, concentrated and kept under refrigeration overnight. A small amount of precipitate appeared. The optical rotatory dispersion and visible spectra of the filtrate agreed well with those of the D-*cis*O_5*cis*N_5 isomer. The elemental analysis of this precipitate coincided with those of the other two isomers. This isomer was named D3, with the possible

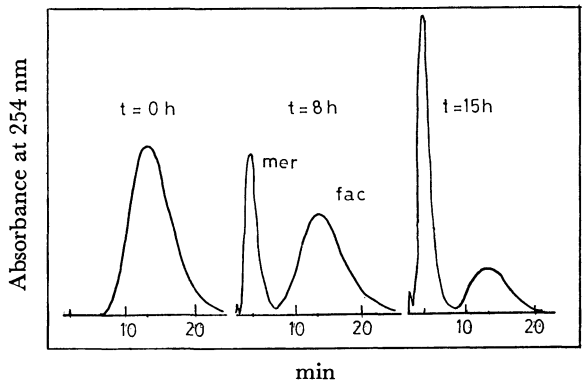

Fig. 2. High speed liquid chromatogram indicating the result of the isomerization for the D2 isomer (UV detector).

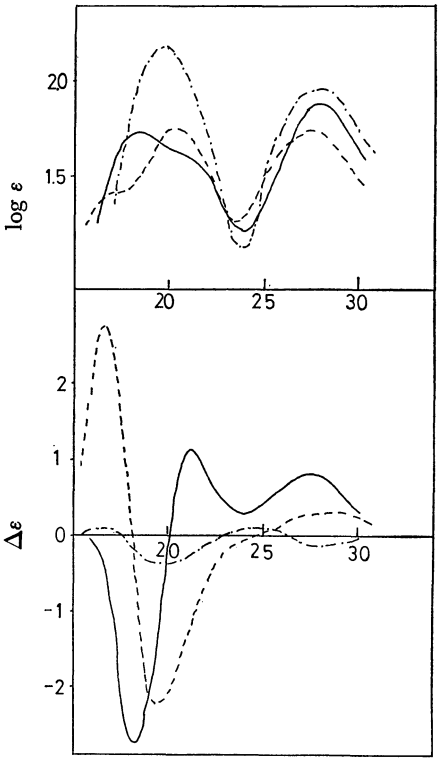

Fig. 3. The visible (upper) and the CD (lower) spectra of the [Co(D-asp)(L-2,4-dba)], —, D1 (*mer*); ---D3 (*mer*); -·-D2 (*fac*). The D3 isomer is eluted faster than the D2.

TABLE 1. NUMERICAL DATA FROM ABSORPTION AND CD SPECTRA OF [Co(L-or D-asp)(L-2,4-dba)]

Complex	I band				II band			
	Absorption		CD		Absorption		CD	
	$\bar{\nu}_{max}$ [a)]	log ε	$\bar{\nu}_{max}$	Δε	$\bar{\nu}_{max}$	log ε	$\bar{\nu}_{max}$	Δε
D-*cis*O_5*cis*N_5	18.3	1.75	18.4	−2.80	27.3	1.88	27.8	0.80
	20.8	1.55	21.3	1.08				
D-*trans*O_5*trans*N_5	16.8	1.38	16.7	2.75	27.4	1.73	28.0	0.26
	20.5	1.75	19.5	−2.25				
D-*fac*	19.3	2.18	16.7	0.10	27.2	1.95	24.8	0.10
			19.8	−0.40			28.0	−0.20
L-*trans*O_5*cis*N_5	18.2	1.92	18.7	−2.50	27.2	2.05	27.2	0.96
	20.0	1.92	21.8	4.80				
L-*cis*O_5*trans*N_5	16.7	1.44	17.5	2.28	27.2	1.99	26.8	0.33
	20.4	1.97	19.8	−0.22				
L-*fac*	19.3	2.23	18.2	1.48	27.3	1.90	*ca.* 27	−0.11
			20.6	−0.56				

a) In 10^3 cm^{-1} units.

configuration D-*trans*O_5*trans*N_5. Figure 3 shows the visible absorption and circular dichroism spectra of the [Co(D-asp)(L-2,4-dba)] complex. All numerical data together with those obtained for [Co(L-asp)(L-2,4-dba)] are listed in Table 1. The visible absorption spectrum of the D-*fac* isomer is similar to that of L-*fac*. This shows that for these complexes which are diastereoisomers of each other, whether D-asp or L-asp is coordinated does not seriously affect the electronic absorption patterns. The first absorption bands for all the *mer* isomers exhibit splittings, though that for the L1 isomer is not obvious.[1] The intensity of the lower energy side of the first absorption band for D3 is smaller than that of the higher energy side. But in the case of D1, this relation is reversed. The L2 spectrum pattern is almost the same as that of the D3 isomer. In order to study the above findings, molecular models are considered. When the L-2,4-dba coordinated for all the *mer* isomers are placed in the same coordinates, the positions of the carboxylate and amino groups of the D-asp of the *trans*O_5*trans*N_5 isomer are quite similar to those of L-asp of the *cis*O_5-*trans*N_5 isomer for [Co(L-asp)(L-2,4-dba)]. The only difference between the complexes lies in the alteration of the 5-membered and 6-membered chelate rings for the asp ligand. The same situation occurs in the relation between the coordinated ligands of the *cis*O_5*cis*N_5 and *trans*O_5*cis*N_5 isomers. From the visible spectra, the assignment of one series, for example, [Co(L-asp)(L-2,4-dba)], is found to serve as an assignment for the other diastereoisomeric series, for example, [Co(D-asp)(L-2,4-dba)]. The circular dichroism spectra of [Co(D-asp)-(L-2,4-dba)] can not at present be correlated with those of [Co(L-asp)(L-2,4-dba)].[2] The PMR spectrum of the D3 isomer was not compared with those of the other isomers because this isomer was only slightly soluble in water. The racemization of $[Co(en)_3]^+$ (en=ethylenediamine) and of $[Co(edta)]^-$ (edta=ethylenediaminetetraacetate ion) using activated carbon as a catalyst has been studied.[3-8] Particularly, the racemization of $[Co(edta)]^-$ has been examined in detail by Cooke *et al.* and Erdmann and Douglas.[6-8] In the present work, the isomerization of [Co(D-asp)(L-2,4-dba)] was studied using activated carbon. The optical rotatory dispersion spectral changes in the isomerization of [Co(D-asp)(L-2,4-dba)] are shown in Fig. 4. This

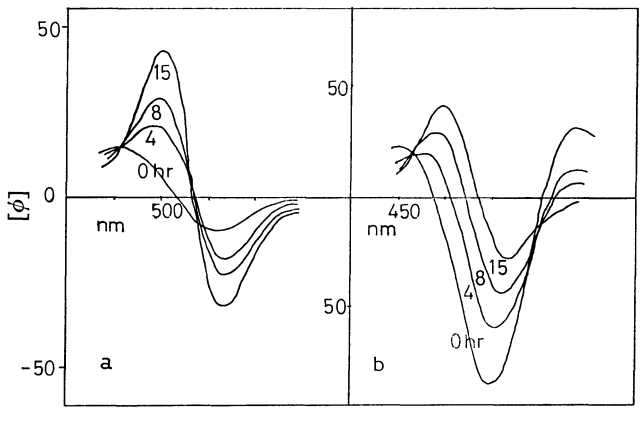

Fig. 4. The ORD spectral changes due to the isomerization for the D2 (left) and the D3 (right) isomers.

indicates that the last equilibrating molar fraction were equal for all kinds of isomers used as the starting material. The rate of isomerization was found to essentially follow second-order kinetics, first order for the complex and first order for the carbon. The activated carbon once used was washed with water and dried at 100 °C for 3 h. This activated carbon was not deactivated in contrast with the experiments reported Erdmann *et al.*[4] Isomerization without activated carbon was very difficult. Since no direct measure of the effective concentration of activated carbon was available, this isomerization was treated as first-order kinetics in the complex only. This isomerization was considered to occur for the three possible isomers. Consequently, the system of differential equations representing the behavior of this system is:

$$da_1/dt = -(k_{12}+k_{13})a_1 + k_{21}a_2 + k_{31}a_3$$
$$da_2/dt = k_{12}a_1 - (k_{23}+k_{21})a_2 + k_{32}a_3$$
$$da_3/dt = k_{13}a_1 + k_{23}a_2 - (k_{31}+k_{32})a_3,$$

where a_i is the molar fraction, and the rate constant of the reaction, for which the notation of the $D_i(i=1, 2, 3)$ isomers is transformed into D_j, is represented by k_{ij}. A method was easily applicable for obtaining the relative value of the rate constant but it was difficult to obtain absolute values. If k_{31} is taken to be unity, all the rate constants were determined as shown in Fig. 5. The values of the rate constants of this system

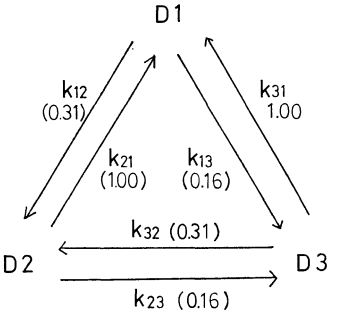

Fig. 5. A network of the isomerization system.

decrease in the order $k_{31},k_{21}>k_{12},k_{32}>k_{13},k_{23}$. D3 is isomerized most rapidly of the three isomers. The molar fractions at equiliblium are: a_1, a_2, a_3=0.68, 0.21, 0.11, respectively. Since these complexes are considered to involve no hydrogen bonding or steric hindrance between asp and 2,4-dba coordinated on the basis of the molecular model concept, such a distribution in favor of the D1 isomer is surprising. The free energy differences at 25 °C are as follows: $\Delta G_{12}=G(D1)-G(D2)=-RT\ln 68/21=-0.69$ kcal/mol and $\Delta G_{13}=-RT\ln 68/11=-1.08$ kcal/mol. The reason for this distribuion in favor of the D1 isomer may be ascribed to the relative site of the atoms coordinated (α- and γ-amino nitrogens and α- and γ-carboxylate oxygens, as is shown in Fig. 1). Recently, investigations of the *trans* effect for the cobalt(III) complex containing S-bonded sulfite ligands have been reported.[10] In cobalt(III) chemistry, S-bonded sulfite produces a specific and dramatic labilization of the ligands situated the *trans* position relative to it. This electronic effect which is transmitted through

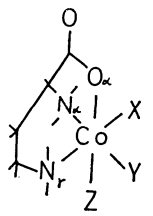

Fig. 6. Coordination axes to which L-2,4-dba ligand fixes.

the bonds may apply to our study. For example, L-2,4-dba coordinated axes (Fig. 6). The α-amino nitrogen seems to affect the atom of the D-asp which confirmly combines at the site y (Fig. 6). Similar relations arise for the other cases (N_γ-Co-site x and O_α-Co-site z). It cannot at present be estimated whether any of these bond relations affect the partial mole fraction because of the lack of data. Only a small amount of the *trans*N isomer of $[Co(L\text{-asp})_2]^-$ [11] could be prepared. In addition to the above results and the low molar fraction of the D-*trans*O_5*trans*N_5 isomer of [Co(D-asp)(L-2,4-dba)] in equilibrium using activated carbon, it is suggested that the two α-nitrogen atoms avoid the *trans* position.

This work was supported by a special grant from Kogakuin University.

References

1) M. Watabe, K. Onuki, and S. Yoshikawa, *Bull. Chem. Soc. Jpn.*, **48**, 687 (1975).
2) M. Watabe and S. Yoshikawa, *Bull. Chem. Soc. Jpn.*, **48**, 2185 (1975).
3) W. G. Gehman and W. C. Fernelius, *J. Inorg. Nucl. Chem.*, **9**, 71 (1959).
4) W. C. Erdman, H. E. Swift, and B. E. Douglas, *J. Inorg. Nucl. Chem.*, **24**, 1365 (1962).
5) C. H. Johnson, *Trans. Faraday Soc.*, **31**, 1612 (1935).
6) D. W. Cooke, Y. A. Im, and D. H. Busch, *Inorg. Chem.*, **1**, 13 (1962).
7) W. C. Erdmann and B. E. Douglas, *J. Inorg. Nucl. Chem.*, **24**, 1355 (1962).
8) W. C. Erdmann and B. E. Douglas, *J. Inorg. Nucl. Chem.*, **26**, 601 (1964).
9) M. Boudart, "Kinetics of Chemical Processes," Prentice-Hall, Inc., Englewood Cliffs, New Jersey (1968).
10) a) J. E. Byrd and W. K. Wilmarch, *Inorg. Chim. Acta. Rev.*, **5**, 7 (1975); b) J. M. Palmer and E. Deutsch, *Inorg, Chem.*, **14**, 17 (1975).
11) K. Hosaka, H. Nishikawa, and M. Shibata, *Bull. Chem. Soc. Jpn.*, **42**, 277 (1969).

Preparative and Magnetic Studies of Several Binuclear Copper(II) Alkanoate Complexes with Salicylideneamines

Tadashi Tokii and Yoneichiro Muto

Department of Chemistry, Faculty of Science and Engineering, Saga University, Saga 840

(Received October 27, 1975)

Compounds with the stoichiometry of Cu(5-R″-sal·N–R)R′COO (5-R″-sal·N–= ·$\overset{2}{O}$·C_6H_3($\overset{5}{R''}$)·$\overset{1}{C}$H=N–; R= methyl, phenyl, *o*-tolyl and *p*-tolyl; R′=ethyl, monochloromethyl and dichloromethyl; R″=H, CH_3 and Cl) have been prepared, and their magnetic and spectral properties have been studied. The magnetic and IR spectral data of the compounds where R=methyl and *o*-tolyl, R′=dichloromethyl, and R″=H indicate that they have phenolic oxygen-bridged dimer units in their crystals. On the other hand, a carboxylate-bridged binuclear structure is postulated for the other complexes on the basis of magnetic and IR spectral data. It has been observed that, in the latter group of complexes, both the $-2J$ (singlet-triplet separation) and ν_{max} (ligand-field transition energy) values decrease in the order of Cu(Sal·N–R)C_2H_5COO>Cu(Sal·N–R)$ClCH_2COO$>Cu(Sal·N–R)Cl_2CHCOO, where Sal·N–= ·$\overset{2}{O}$·C_6H_4·$\overset{1}{C}$H=N–. The preparation and characterization of the Cu(Sal·N–R)HCOO·DMF compounds (R=*p*-tolyl and *p*-chlorophenyl; DMF=*N*,*N*-dimethylformamide) are also reported.

Bis(N-R-salicylideneaminato)copper(II), Cu(Sal·N–$R)_2$, reacts with copper(II) halide or nitrate to yield binuclear complexes with the structure shown in I, $[Cu(Sal\cdot N\text{–}R)X]_2$, in which the phenolic oxygen atoms act as bridges, where R=alkyl or aryl and X=Cl,[1,2] Br[3] or NO_3.[4,5] These binuclear complexes display antiferromagnetic behavior, in conformity with the Bleaney-Bowers equation (1)[6] formulated for the magnetic susceptibility of an isolated pair of interacting ions of spin 1/2:

$$\chi_A = \frac{Ng^2\beta^2}{3kT}\left[1+\frac{1}{3}\exp\left(\frac{-2J}{kT}\right)\right]^{-1} + N\alpha \qquad (1)$$

where $-2J$ is equal to the energy separation between the singlet and triplet states, which gives the degree of strength of the magnetic interaction.

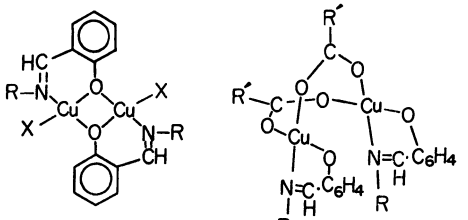

I

II

In the course of our studies of binuclear complexes of the I type, we found that, by the reaction of copper(II) alkanoates, $Cu(R'COO)_2$, with $Cu(Sal\cdot N\text{–}R)_2$, complexes with the Cu(Sal·N–R)R′COO stoichiometry were isolated when R=phenyl and *p*-tolyl and R′=ethyl.[7] On the basis of the magnetic and IR spectral data of these complexes, it was concluded that they possess the carboxylate-bridged binuclear structure represented in II.[7] It is noteworthy that the antiferromagnetic interaction in these propionate complexes ($-2J$=101 cm^{-1})[7] is much weaker than that in the corresponding chloride complexes ($-2J\approx$350 cm^{-1}),[7,8] $[Cu(Sal\cdot N\text{–}R)Cl]_2$, where R=phenyl and *p*-tolyl.

As a continuation of those studies, we have newly prepared seven compounds with the Cu(Sal·N–R)-R′COO stoichiometry and two compounds with the Cu(Sal·N–R)HCOO·DMF stoichiometry, where DMF =*N*,*N*-dimethylformamide. These new compounds have been characterized on the basis of elemental analyses, the IR and visible spectra, and the temperature dependences of the magnetic susceptibilities. Since no reasonable relationship between the magnitude of the antiferromagnetic interaction in dimeric copper(II) carboxylates and the acidity of the parent carboxylic acids has yet been established,[9–13] the observation of the $-2J$ values in the newly prepared complexes of the II type is of particular interest.

Experimental

Syntheses. Cu(Sal·N–R)R′COO Complexes: A typical synthetic method is as follows. A solution of an anhydrous copper(II) alkanoate (12 mmol) in ethanol (50 ml) was added, through a quantitative filter paper, to one of the parent $Cu(Sal\cdot N\text{–}R)_2$ complexes (10 mmol). The solution was stirred at *ca.* 70° C for 1/2 h and then concentrated to one-third of its volume. After the solution had been allowed to stand overnight at *ca.* 5 °C in a freezer, the separated crystals were collected and washed twice with a small quantity of ethanol and once with ether. They were all green in color.

Cu(Sal·N–R)HCOO·DMF Complexes: To a solution of the parent $Cu(Sal\cdot N\text{–}R)_2$ complex (10 mmol) in DMF (30 ml), we added copper(II) formate tetrahydrate (10 mmol). The mixture was stirred on a hot plate for 1/2 h. The green crystals thus precipitated were collected and recrystallized from DMF.

The data of the elemental analyses of the new compounds are summarized in Table 1.

Physical Measurements. The magnetic susceptibilities were determined by the Gouy method in the range from the temperature of liquid nitrogen to room temperature. The effective magnetic moments per copper ion at room temperature were calculated from this expression:

$$\mu_{eff} = 2.83\sqrt{(\chi_A - N\alpha)\cdot T} \qquad (2)$$

where χ_A is the molar magnetic susceptibility corrected for the diamagnetism of the constituted atoms using Pascal's constant[14] and where $N\alpha$ is the temperature-independent paramagnetism per gram-ion of copper(II). The $N\alpha$ was assumed to be 60×10^{-6} emu.[15] The results are given in Table 2. The ESR (X-band) spectra of polycrystalline samples were measured with a JEOL ESR-apparatus, model JES-ME-1X, at room temperature. The IR spectral measurements were made with a Hitachi EPI-G2 IR spectro-

Table 1. Analytical data of new compounds

Complex[a]	C%		H%		N%		Cu%	
	Found	Calcd	Found	Calcd	Found	Calcd	Found	Calcd
1. Cu(Sal·N-*p*-tol)HCOO·DMF	54.90	55.17	5.11	5.14	7.20	7.15	16.28	16.21
2. Cu(Sal·N-*p*-Clph)HCOO·DMF	49.47	49.52	4.29	4.16	6.78	6.79	15.43	15.41
3. Cu(Sal·N-CH_3)Cl_2CHCOO	36.69	36.89	2.80	2.79	4.26	4.30	19.59	19.51
4. Cu(Sal·N-*o*-tol)Cl_2CHCOO	47.92	47.84	3.32	3.26	3.47	3.49	15.80	15.82
5. Cu(5-CH_3sal·N-ph)C_2H_5COO	58.79	58.86	5.20	4.94	3.87	4.04	18.07	18.32
6. Cu(5-Clsal·N-ph)C_2H_5COO	52.44	52.32	4.08	3.84	3.82	3.81	17.30	17.30
7. Cu(Sal·N-*p*-tol)$ClCH_2COO$	52.23	52.32	3.86	3.84	3.86	3.81	17.60	17.30
8. Cu(Sal·N-ph)Cl_2CHCOO	46.43	46.47	2.90	2.86	3.54	3.61	16.46	16.39
9. Cu(Sal·N-*p*-tol)Cl_2CHCOO	47.82	47.84	3.22	3.26	3.50	3.49	15.92	15.82

a) Sal·N-=·$\overset{2}{O}$·C_6H_4·$\overset{1}{C}$H=N-, sal·N-=·$\overset{2}{O}$·C_6H_3·$\overset{1}{C}$H=N-, tol=tolyl, ph=phenyl, and DMF=*N*,*N*-dimethylformamide.

Table 2. Magnetic data of new compounds

Complex	μ_{eff} B. M. (°C)	$-2J$ (cm^{-1})	g[a]
1. Cu(Sal·N-*p*-tol)-HCOO·DMF	1.00 (18)	498	2.20
2. Cu(Sal·N-*p*-Clph)-HCOO·DMF	0.99 (24)	514	2.20
3. Cu(Sal·N-CH_3)-Cl_2CHCOO	0.84 (15)	572	2.18
4. Cu(Sal·N-*o*-tol)-Cl_2CHCOO	1.39 (12)	335	2.20
5. Cu(5-CH_3sal·N-ph)C_2H_5COO	1.72 (25)	96	2.14(2.18)
6. Cu(5-Clsal·N-ph)-C_2H_5COO	1.72 (22)	96	2.14(2.18)
7. Cu(Sal·N-*p*-tol)-$ClCH_2COO$	1.74 (14)	88	2.14(2.14)
8. Cu(Sal·N-ph)-Cl_2CHCOO	1.78 (17)	61	2.13(2.13)
9. Cu(Sal·N-*p*-tol)-Cl_2CHCOO	1.77 (16)	61	2.13(2.13)

a) The data in parentheses were determined by ESR measurements on the polycrystalline samples.

photometer in the 400—4000 cm^{-1} region on Nujol mulls. The reflectance spectra were measured with a Hitachi EPS-3T recording spectrophotometer.

Results and Discussion

Synthesis. It was observed that the dichloroacetate complexes, 8 and 9, listed in Table 1 were most readily obtainable, even though dichloroacetic acid has the lowest pK_a value among the parent carboxylic acids employed in the preparation in this study.[10,16,17] It was also found that, in the reaction of copper(II) formate with Cu(Sal·N-ph-Y)$_2$, where ph-Y=a monosubstituted phenyl group with the Y substituent, no formate complexes were isolated when Y=*o*-CH_3, *o*-Cl, *m*-CH_3, and *m*-Cl. This finding is in accord with the previous observation that, in a preparation of DMF adduct complexes of the [Cu(Sal·N-ph-Y)X·DMF]$_n$ type, where X=Cl[2] or NO_3,[5] the complexes with Y at the *p*-position of the phenyl ring were easily obtained, while a synthesis of complexes with Y at the *o*- or *m*-position was unsuccessful; *i.e.*, the Y substituent attached at the *o*- or *m*-position hinders the coordination of the DMF molecule to the central metal ion much more than the one at the *p*-position, since the former is present at a position closer to the metal ion than the latter.

Magnetic Susceptibility. The magnetic susceptibilities of the complexes were determined over the temperature range of 80—300 K; the data are shown in Figs. 1—3 as plots of the molar magnetic susceptibility (χ_A) *vs.* the temperature (T). The magnetic data for the complexes, except for Compound 4, are well represented by Eq. 1 (*cf.* Figs. 1 and 3). The $-2J$ and g values listed in Table 2 were evaluated from the best fit of the cryomagnetic data to Eq. 1, assuming $N\alpha = 60\times10^{-6}$ emu.[15] The g values for some of the complexes were in good agreement with the average g values determined from ESR measurements of the polycrystalline samples (*cf.* Table 2). The close agreement between the observed and calculated temperature dependences of the magnetic susceptibility is powerful evidence for a binuclear structure of these complexes. For Compound 4, the observed magnetic data could not satisfactorily fit Eq. 1 when the following values were used: J was estimated from the $-2J\approx1.6\,kT_C$ relation, where k is the Boltzmann constant, and T_C, the temperature of the maximum susceptibility; g ranged

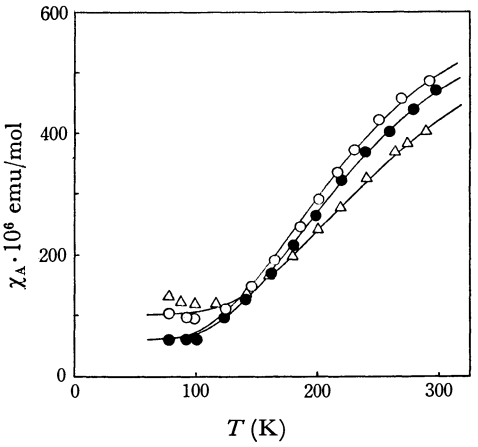

Fig. 1. Temperature dependence of magnetic susceptibilities of (○) Cu(Sal·N-*p*-tol)HCOO·DMF, (●) Cu(Sal·N-*p*-Clph)HCOO·DMF, and (△) Cu(Sal·N-CH_3)Cl_2CHCOO.
The solid curves represent the Bleany-Bowers equation.

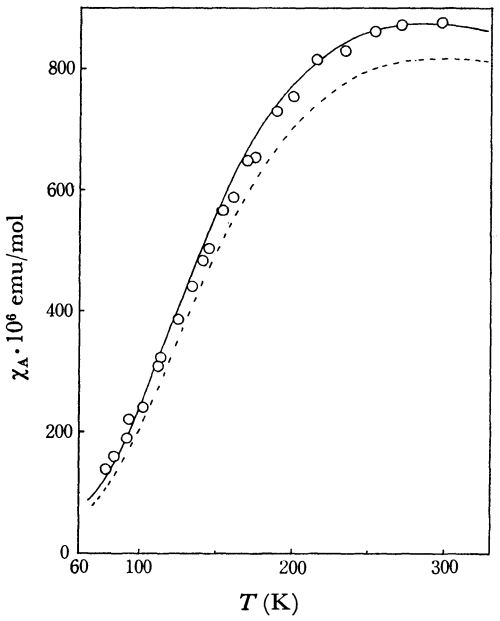

Fig. 2. Temperature dependence of magnetic susceptibilities of (○) Cu(Sal·N-*o*-tol)Cl_2CHCOO.
The broken curve was calculated from the Bleaney-Bowers equation (1) with $-2J=335$ cm^{-1}, $g=2.20$, and $N\alpha=60\times10^{-6}$ emu. The solid curve was calculated from the modified equation (3) with $-2J=335$ cm^{-1}, $g=2.20$, $N\alpha=60\times10^{-6}$ emu and $\theta=+20$ K.

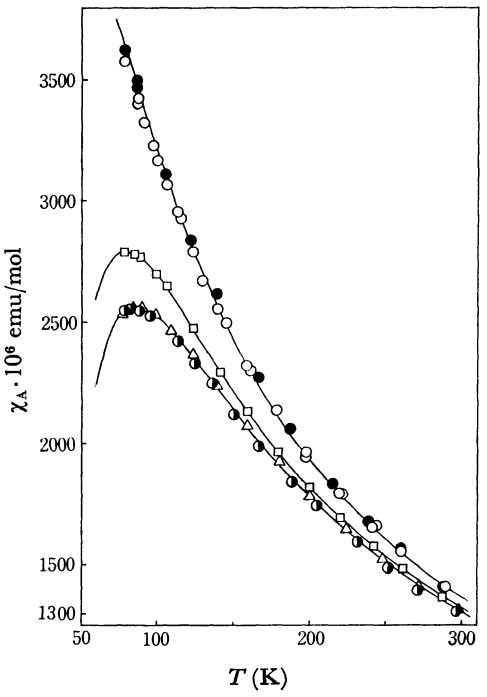

Fig. 3. Temperature dependence of magnetic susceptibilities of (△) Cu(5-CH_3sal·N-ph)C_2H_5COO, (◑) Cu(5-Clsal·N-ph)C_2H_5COO, (□) Cu(Sal·N-*p*-tol)-$ClCH_2$COO, (●) Cu(Sal·N-ph)Cl_2CHCOO, and (○) Cu(Sal·N-*p*-tol)Cl_2CHCOO.
The solid curves represent the Bleaney-Bowers equation.

from 2.10 to 2.20, and $N\alpha$ was 60×10^{-6} emu (*cf.* Fig. 2). However, a better fit was obtained for the data to the theoretical curve drawn based on a modification of the Bleaney-Bowers equation (3):[18]

$$\chi_A = \frac{Ng^2\beta^2}{3k(T-\theta)}\left[1+\frac{1}{3}\exp\left(\frac{-2J}{kT}\right)\right]^{-1} + N\alpha \qquad (3)$$

where the Weiss constant, θ, allows for intermolecular interaction between dimers (*cf.* Fig. 2). From a best-fitting procedure of the experimental data to Eq. 3, the $-2J$ and g values listed in Table 2 and the value of $\theta=+20$ K were evaluated. The positive value for θ suggests the presence of ferromagnetic spin interaction between the dimers.

The complexes described here can be classified into two groups based on the magnetic data. Group (A): in Compounds 1—4, the effective magnetic moments at room temperature are definitely smaller than the spin-only value, 1.73 B.M., for one unpaired electron, and the $-2J$ values are larger than 300 cm^{-1}. Group (B): in Compounds 5—9, the moments are close to the spin-only value, and the $-2J$ values are smaller than 100 cm^{-1}.

Electronic Spectra. The electronic spectra of all the complexes investigated were recorded by the diffuse reflectance technique. The frequencies of the ligand-field band maxima are collected in Table 3. Some of the spectral curves of the Group (A) and (B) complexes are shown in Fig. 4 and Fig. 5 respectively. It is apparent from Table 3 and Figs. 4 and 5 that there is a marked difference in the spectra between Group (A) and (B) complexes. This is indicative of a structural difference between them. The spectra of the Group (A) complexes are similar to one another and closely resemble those of DMF adducts of the I type complexes, [Cu(Sal·N-R)X·DMF]$_2$, to which a five-coordinated square pyramidal configuration with axially coordinated DMF molecules was assigned.[2,5] For comparison, the reflectance spectral curve of [Cu(Sal·N-*p*-tol)NO_3·DMF]$_2$, where *p*-tol=*p*-tolyl,[5] is given in Fig. 4. Group (B) complexes have a ligand-field band in an energy region ((15—16)$\times10^3$ cm^{-1}) much higher than that of Group (A) complexes. As can be seen in Fig. 5, the spectral features of Group (B) complexes are very similar to one another, indicating that they are isostructural.

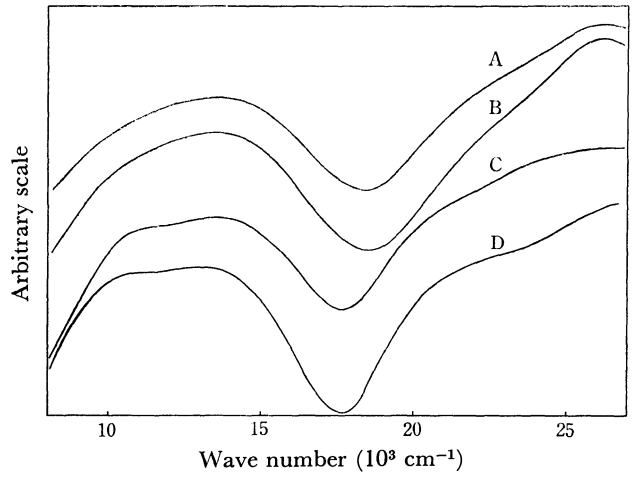

Fig. 4. Reflectance spectra of (A) Cu(Sal·N-*p*-tol)H-COO·DMF, (B) Cu(Sal·N-*p*-Clph)HCOO·DMF, (C) Cu(Sal·N-*o*-tol)Cl_2CHCOO, and (D) Cu(Sal·N-*p*-tol)NO_3·DMF.[5]

Table 3. Reflectance and IR spectral data of new compounds and the related compounds

Complex	Ligand field band maximum ν_{max}, kK[d]	IR absorption, cm^{-1} band maximum[e] near 1540 cm^{-1}	$\nu_{as}CO_2$	ν_sCO_2	Δ_{as-s}
1. $Cu(Sal\cdot N\text{-}p\text{-tol})HCOO\cdot DMF$	13.9, 10.9sh	1552 (+19)			
2. $Cu(Sal\cdot N\text{-}p\text{-Clph})HCOO\cdot DMF$	13.3, 10.5sh	1549 (+15)			
3. $Cu(Sal\cdot N\text{-}CH_3)Cl_2CHCOO$	13.5, 11.5sh	1553 (+19)	1641	1371	270
4. $Cu(Sal\cdot N\text{-}o\text{-tol})Cl_2CHCOO$	14.6, 11.1sh	1555 (+15)	1658 1650	1377	277
5. $Cu(5\text{-}CH_3sal\cdot N\text{-ph})C_2H_5COO$	15.8	1537 (+ 6)	1590	1426	164
6. $Cu(5\text{-}Clsal\cdot N\text{-ph})C_2H_5COO$	15.8	1529 (+ 2)	1590	1429	161
$Cu(Sal\cdot N\text{-ph})C_2H_5COO$[a]	15.8	1538 (+ 7)	1588	1428	160
$Cu(Sal\cdot N\text{-}p\text{-tol})C_2H_5COO$[a]	15.8	1538 (+ 5)	1589	1433	156
$Cu(C_2H_5COO)_2$[b]			1589	1420	169
7. $Cu(Sal\cdot N\text{-}p\text{-tol})ClCH_2COO$	15.5	1537 (+ 4)	1630	1414 1400	223
8. $Cu(Sal\cdot N\text{-ph})Cl_2CHCOO$	15.6	1536 (+ 5)	1657 1650	1410 1401	248
9. $Cu(Sal\cdot N\text{-}p\text{-tol})Cl_2CHCOO$	15.3	1540 (+ 7)	1653 1647	1406 1401	246
$Cu(Cl_2CHCOO)_2(\alpha\text{-picoline})_2$ (purple)[c]			1657 1643	1376	274

a) Ref. 7. b) Ref. 22. c) Ref. 24. d) sh=shoulder. e) The numerical values in parentheses indicate the increased wave numbers from the bands in the parent $Cu(Sal\cdot N\text{-}R)_2$ complexes.

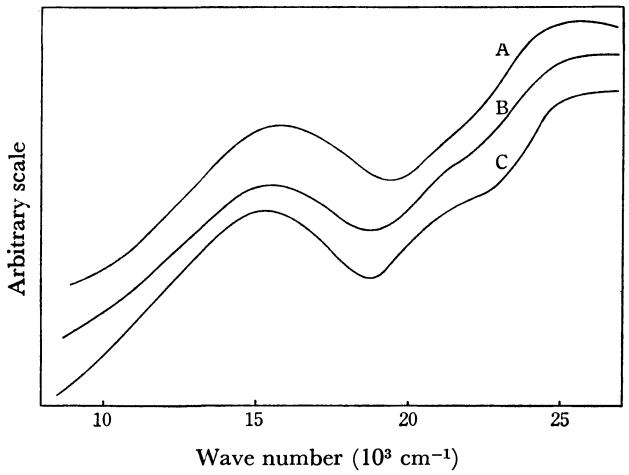

Fig. 5. Reflectance spectra of (A) $Cu(Sal\cdot N\text{-}p\text{-tol})C_2H_5COO$,[7] (B) $Cu(Sal\cdot N\text{-}p\text{-tol})ClCH_2COO$, and (C) $Cu(Sal\cdot N\text{-}p\text{-tol})Cl_2CHCOO$.

IR Spectra. For the present complexes and the previously reported propionate complexes, $Cu(Sal\cdot N\text{-}R)C_2H_5COO$, where R=phenyl and *p*-tolyl,[7] the absorption near 1540 cm^{-1}, and those due to antisymmetric($\nu_{as}CO_2$) and symmetric(ν_sCO_2) carboxylate stretching vibrations were measured to obtain information concerning the coordination mode of the phenolic oxygen atoms and carboxylate groups in the complexes. The assignment of the observed bands was made by comparing the bands of these complexes with those of the parent $Cu(Sal\cdot N\text{-}R)_2$ complexes and the corresponding binuclear chloro and nitrato complexes of the I type. The results are listed in Table 3, together with the data reported for the related alkanoate compounds.

Although there have been tentative assignments for the absorption near 1540 cm^{-1} in $Cu(Sal\cdot N\text{-}R)_2$ (*e.g.*, to $\nu C{=}N$,[19] $\nu C\text{–}O$(phenolic)[1,20] or to the skeltal vibration of the aromatic ring[21]), no definite conclusion has yet been reached as to the origin of the band. However, a shift of the band to higher energies by 10—20 cm^{-1} near 1540 cm^{-1} is now at least taken as an unambiguous criterion of the formation of a phenolic oxygen-bridging between metal ions in polymeric salicylideneamine complexes.[1-3,7,8,20,21] As is shown in Table 3, the band shift was observed for all the complexes of Group (A), indicating the presence of phenolic oxygen-bridges between the copper(II) ions in these complexes. On the other hand, no significant band shift was observed for any of the complexes of Group (B), indicating that, in these complexes, no phenolic oxygen-bridge exists.

For the carboxylate coordination, a comparison of the carboxylate stretching frequencies in the present complexes with those in the related copper(II) alkanoates is informative. All the propionate complexes described here exhibit $\nu_{as}CO_2$ and ν_sCO_2 bands in an energy region very similar to that reported for anhydrous copper(II) propionate,[22] $Cu(C_2H_5COO)_2$, which has a copper(II) acetate monohydrate type of binuclear structure[23] (*cf.* Table 3). The close similarity in absorption energy leads to the conclusion that the propionate complexes have carboxylate bridges of a syn-syn arrangement[16] between copper(II) ions, as is shown in II. In the case of the dichloroacetate complexes, the frequencies of $\nu_{as}CO_2$ and ν_sCO_2 and the separation between them, Δ_{as-s}, in the complexes belonging to Group (A), 3 and 4, markedly differ from those in the complexes belonging to Group (B), 8 and 9. The $\nu_{as}CO_2$, ν_sCO_2, and Δ_{as-s} in the Group (A) complexes are nearly the same as those reported for the purple isomer of bis(α-picoline)copper(II) dichloroacetate, $Cu(Cl_2CHCOO)_2(\alpha\text{-pic})_2$, for which the carboxylate coordination was identified as intermediate between a strictly unidentate type and a strictly bidentate-chelate type.[24] It seems, therefore, reasonable to conclude that, in the dichloroacetate complexes of Group (A), no carboxylate bridges of the syn-syn type

exist. No unambiguous assignment for carboxylate coordination in the dichloroacetate complexes, 8 and 9 (Group (B)), and in the monochloroacetate complex, 7, could be drawn from their IR data. However, the magnetic and reflectance spectral features of these chloroacetate complexes (7, 8 and 9) are very similar to those of the propionate complexes. The appearance of IR bands at *ca.* 1540 cm^{-1} indicates that the magnetic interaction in the chloroacetate complexes probably takes place through carboxylate bridging rather than through phenolic oxygen bridging. These facts suggest that the carboxylate coordination mode in these chloroacetate complexes is of a syn-syn bridging type, as is seen in the propionate complexes.

Structure and Magnetic Interaction. The magnetic and IR spectral data for Group (A) complexes clearly indicate that the complexes have phenolic oxygen-bridged dimer units of the I type in crystals. The reflectance spectra showed them to have a penta-coordinated square pyramidal configuration. Accordingly, the most probable structure for the formate complexes, 1 and 2, seems to be III, in which the DMF

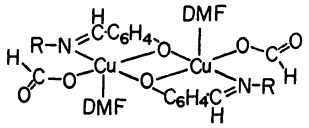

III

molecule occupies the fifth coordination site of the copper ion. The penta-coordination in the dichloroacetate complexes, 3 and 4, seems to be possible when the carboxylate group acts as a bidentate chelate or a bridging group (triatomic –O–C–O– or monoatomic –O(CO)–) between the dimer units. The presence of inter-dimer magnetic interaction observed for the Cu(Sal·N–*o*-tol)Cl_2CHCOO complex, 4, is indicative of the carboxylate bridges between the dimer units in this complex.

The $-2J$ values determined for Group (A) complexes are considerably larger than those reported for the I type complexes with a pseudo-tetrahedral configuration,[2,25] but they are comparable with those reported for the I type complexes with a square pyramidal configuration.[2] This can be seen in Table 4.

The carboxylate-bridged binuclear structure shown in II may be assigned to Group (B) complexes on the basis of their magnetic and spectral data. An analogous dimeric structure bridged by two carboxylate groups in the syn-syn manner exists in crystals of the *p*-toluidine adduct of copper(II) propionate, $[Cu_2(C_2H_5COO)_4(p\text{-toluidine})_2]_n$, the structure of which has recently been determined by X-ray analysis.[26] The structure is basically composed of carboxylate-bridged dimers which are linked into one-dimensional polymeric chains by relatively long monoatomic Cu–O(CO)–Cu carboxylate bridges. Yawney *et al.*[26] have interpreted the magnetic data conforming to Eq. 1 with $-2J=105$ cm^{-1} in terms of a superexchange interaction between copper ions through bridging two carboxylate groups of Cu–O–C–O–Cu linkages rather than in terms of a direct metal–metal interaction, since the Cu–Cu separation (3.197 Å) is too large to allow any significant interaction between them. The $-2J$ values (96—101 cm^{-1}) of the present propionate complexes, 5 and 6, and Cu(Sal·N–R)C_2H_5COO complexes, where R=phenyl and *p*-tolyl, are practically identical with that reported for $[Cu_2(C_2H_5COO)_4(p\text{-toluidine})_2]_n$. This also supports the assignment of the II structure for the present propionate complexes.

The magnetic properties of Group (B) complexes significantly differ from those of the corresponding dimeric carboxylates, $Cu_2(R'COO)_4$, or their adduct complexes with the structure shown in IV, $Cu_2(R'COO)_4L_2$, where L is an additional unidentate ligand:

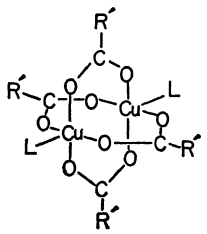

IV

(1) The magnitude of antiferromagnetic interaction observed in Group (B) complexes is considerably smaller than those found in $Cu_2(C_2H_5COO)_4$ ($-2J=300$ cm^{-1})[27] and $Cu_2(ClCH_2COO)_4(\alpha\text{-pic})_2$ ($-2J=322$ cm^{-1}).[24] Such a decrease in magnetic interaction can

Table 4. Comparison of $-2J$ values determined for phenolic oxygen-bridged binuclear copper(II) complexes with salicylideneamines

Complex	$-2J$, cm^{-1}	Structure type
Cu(Sal·N–CH_3)Cl (brown form)[a]	242[a]	Pseudo-tetrahedral[c]
	292[b]	
Cu(Sal·N–sec·C_4H_9)Cl	320[c]	Pseudo-tetrahedral[c]
Cu(Sal·N–$CH_2CH_2CH_2OH$)Cl·DMF	518[d]	Square-pyramidal[d]
Cu(Sal·N–*p*-tol)NO_3·DMF	528[e]	Square-pyramidal[e]
Cu(Sal·N–*p*-Clph)NO_3·DMF	516[e]	Square-pyramidal[e]
Cu(Sal·N–*p*-tol)HCOO·DMF	498[f]	Square-pyramidal[f]
Cu(Sal·N–*p*-Clph)HCOO·DMF	514[f]	Square-pyramidal[f]
Cu(Sal·N–$CH_2CH_2CH_2OH$)Cl	504[d]	Trigonal bipyramidal with some distortion[g]
Cu(Sal·N–CH_3)Cl (yellow-orange form)[a]	580[a]	Trigonal bipyramidal[d]
Cu(Sal·N–*p*-NO_2ph)Cl	563[d]	Trigonal bipyramidal[d]

a) Ref. 31. b) Ref. 1. c) Ref. 25. d) Ref. 2. e) Ref. 5. f) Present work. g) Ref. 32.

be explained in terms of a decrease in the number of the bridging carboxylate groups through which superexchange interaction is operative, from four in these dimeric copper(II) carboxylates[23,28] to two in the Group (B) complexes. (2) The degree of antiferromagnetic interaction in the Group (B) complexes is apparently reduced according as the number of the substituted chlorine atoms on the acetate group is increased; the order of decrease in $-2J$ is Cu(Sal·N–R)C_2H_5COO> Cu(Sal·N–R)$ClCH_2COO$> Cu(Sal·N–R)Cl_2CHCOO. This is the same as the order of decrease in the ligand-field transition energies observed for these complexes (*cf.* Table 3 and Fig. 5); *i.e.*, there exists a good linear relation between the $-2J$ and ν_{max} values. The effect of the chloro-substituent on the magnetic and spectral properties may be attributed to the electron-withdrawing nature of the substituent; *i.e.*, the electron-withdrawing effect causes a decrease in the overlap between the metal-ion orbitals and the orbitals of the bridging carboxylate oxygen atoms and, hence, leads to a weaker magnetic interaction and a lower ligand-field band energy. However, the same type of polar effect of the substituents does not appear in the dimeric copper(II) carboxylates as in $Cu_2(F_3C\text{-}COO)_4$(quinoline)$_2$ ($-2J=310$ cm^{-1}),[13] $Cu_2(ClCH_2\text{-}COO)_4$(α-pic) ($-2J=322$ cm^{-1}),[24] and $Cu_2(CH_3C\text{-}OO)_4(py)_2$ ($-2J=325$ cm^{-1}).[29] These complexes all show almost the same magnitude of $-2J$ values regardless of the nature of the substituents. Therefore, there must exist some different conditions in these two types of complexes which make the II-type complexes more sensitive to substitution than the IV-type compounds. The insensitivity of the IV complexes to substitution seems to be linked to the rigid framework of the dimer structure, composed of four carboxylate bridges. This is apparent in the Cu–O–C–O–Cu superexchange path length, which is almost the same for these adduct complexes, *ca.* 6.45 Å.[13,28,30] Such an extremely inflexible path length may lead to constancy in the magnitude of superexchange interaction. On the other hand, the II-type complexes, whose dimer structure is constructed by connecting a pair of copper(II) ions with two carboxylate bridges, is more flexible than that of the IV complexes; thus, it should be more sensitive to any change upon substitution. The different sensitivities could cause the different electronic states in these flexible and inflexible dimer systems, leading to the observed difference in the magnetic interaction. Another probable explanation can perhaps be given in terms of the steric effect of substituents. The flexible framework of the II complexes is considered to be more sensitive to any type of steric conditions than the inflexible framework of the IV compounds. Such steric conditions may come from the repulsion force between the electronegative halogen atoms on the adjacent dimeric molecules or some others. At present, it is difficult to decide which reason is the more important for the observed substituent effect. However, the authors hope that their observation of the effect will lead to the resolution of the unsolved problems regarding the magnetic interaction in copper(II) carboxylate systems.

References

1) E. Sinn and C. M. Harris, *Coord. Chem. Rev.*, **4**, 391 (1969), and references therein.
2) M. Kato, K. Imai, Y. Muto, T. Tokii, and H. B. Jonassen, *J. Inorg. Nucl. Chem.*, **35**, 109 (1973).
3) C. M. Harris, J. M. James, P. J. Milham, and E. Sinn, *Inorg. Chim. Acta*, **3**, 81 (1969).
4) M. Kato, Y. Muto, H. B. Jonassen, K. Imai, M. Kondo, K. Katsuki, and S. Ikegami, *Bull. Chem. Soc. Jpn.*, **42**, 3039 (1969).
5) K. Imai, M. Kato, Y. Muto, T. Tokii, and H. B. Jonassen, Proceedings of 26th Annual Meeting of the Chemical Society of Japan, Hiratsuka, April, 1972, Vol. I, p. 364.
6) B. Bleaney and K. D. Bowers, *Proc. Roy. Soc., Ser. A*, **214**, 451 (1952).
7) T. Tokii, S. Emori, and Y. Muto, *Bull. Chem. Soc. Jpn.*, **47**, 2887 (1974).
8) C. M. Harris and E. Sinn, *J. Inorg. Nucl. Chem.*, **30**, 2723 (1968).
9) M. Kato, H. B. Jonassen, and J. C. Fanning, *Chem. Rev.*, **64**, 99 (1964).
10) J. Lewis, Y. C. Lin, L. K. Royston, and R. C. Thompson, *J. Chem. Soc.*, **1965**, 6464.
11) J. Lewis, F. E. Mabbs, L. K. Royston, and W. R. Smail, *J. Chem. Soc., A*, **1969**, 291.
12) R. W. Jotham, S. F. A. Kettle, and J. A. Marks, *J. Chem. Soc., Dalton Trans.*, **1972**, 428.
13) J. A. Moreland and R. J. Doedens, *J. Am. Chem. Soc.*, **97**, 508 (1975).
14) P. W. Selwood, "Magnetochemistry," Interscience Publishers, New York (1956), pp. 78, 91.
15) B. N. Figgis and R. L. Martin, *J. Chem. Soc.*, **1956**, 3837.
16) R. L. Martin and H. Waterman, *J. Chem. Soc.*, **1959**, 1359.
17) S. Yamada, H. Nishikawa, and R. Tsuchida, *Bull. Chem. Soc. Jpn.*, **33**, 1278 (1960).
18) M. Inoue, M. Kishita, and M. Kubo, *Inorg. Chem.*, **6**, 900 (1967).
19) K. Ueno and A. E. Martell, *J. Am. Chem. Soc.*, **60**, 1270 (1956).
20) G. E. Batley and D. P. Graddon, *Aust. J. Chem.*, **20**, 877, 885 (1967).
21) H. Okawa and S. Kida, *Bull. Chem. Soc. Jpn.*, **45**, 1759 (1972).
22) Y. Kuroda, *Nippon Kagaku Zasshi*, **82**, 1624 (1961).
23) A. V. Ablov, Yu. A. Siminov, and T. I. Malinovskii, *Dokl. Akad. Nauk SSSR*, **171**, 854 (1966); *Chem. Abstr.*, **66**, 49992b (1967).
24) S. F. A. Kettle and A. J. P. Pioli, *J. Chem. Soc., A*, **1968**, 1243.
25) R. M. Countryman, W. T. Robinson, and E. Sinn, *Inorg. Chem.*, **13**, 2013 (1974).
26) D. B. W. Yawney, J. A. Moreland, and R. J. Doedens, *J. Am. Chem. Soc.*, **95**, 1164 (1973).
27) R. L. Martin and H. Waterman, *J. Chem. Soc.*, **1957**, 2545.
28) G. Davey and F. S. Stephens, *J. Chem. Soc., A*, **1970**, 2803.
29) E. Kokot and R. L. Martin, *Inorg. Chem.*, **3**, 1306 (1964).
30) G. A. Barclay and C. H. L. Kennard, *J. Chem. Soc.*, **1961**, 5244.
31) Y. Muto, M. Kato, T. Tokii, K. Imai, and H. B. Jonassen, *Bull. Chem. Soc. Jpn.*, **43**, 3962 (1970).
32) J. A. Bertrand, J. A. Kelley, and J. L. Breece, *Inorg. Chim. Acta*, **4**, 247 (1970).

Conditions for the Formation of Compounds Consisting of BaO and Fe_2O_3 from Aqueous Suspensions

Masao KIYAMA

Institute for Chemical Research, Kyoto University, Uji, Kyoto 611

(Received December 4, 1975)

Suspensions containing either iron(III) hydroxide or hydroxide oxide and barium ions were subjected to autoclaving at various temperatures from 100 to 300 °C, and the properties of the resulting products were studied. A ferromagnetic precipitate, $BaO \cdot 6Fe_2O_3$, consisting of hexagonal plate-like particles, was obtained by suitable combination of temperature, kind and particle size of iron(III) hydroxide oxide, and concentration of $Ba(OH)_2$. Nonferromagnetic precipitates, $BaO \cdot 4.5Fe_2O_3$ and $BaO \cdot 2Fe_2O_3$, were also formed depending on the conditions. The mechanism of their formation is discussed. The magnetic properties of the $BaO \cdot 6Fe_2O_3$ precipitates are investigated.

$BaO \cdot 6Fe_2O_3$ is widely used as a permanent magnet, and its properties have been thoroughly investigated.[1] The compound can be obtained as a polycrystalline substance when a mixture of iron(III) oxide and barium carbonate is ignited at high temperatures (>800 °C) in an oxidizing gas.[2] The hydrothermal synthesis of $BaO \cdot 6Fe_2O_3$ was achieved for the first time in 1969.[3] It was found that iron(III) hydroxide or hydroxide oxide can react with the barium ion in a suspension to form $BaO \cdot 6Fe_2O_3$ if we choose the proper pH, concentration of barium ion, and temperature; nonferromagnetic precipitates, $BaO \cdot 4.5Fe_2O_3$ and $BaO \cdot 2Fe_2O_3$, are also obtained depending on the conditions.[3]

This paper will deal with the conditions for the formation of compounds consisting of BaO and Fe_2O_3 and with the magnetic properties of $BaO \cdot 6Fe_2O_3$.

Experimental

Material. Chemicals of an analytical grade were used except for the iron(III) hydroxide oxides and oxide. α- and γ-FeO(OH), consisting of needle-like particles of different mean sizes, were prepared by the seed method. Acidic suspensions of very fine, needle-like particles of α- and γ-FeO(OH) (used as seeds) were obtained by the air oxidation of $Fe(OH)_2$ at 40 °C in a $FeSO_4$ solution and of $Fe(OH)_2$ at 15 °C in a $FeCl_2$ solution respectively.[4] A 20-g of iron powder (size<140 μm) was added to 1 l of the suspension. Oxidation to α-FeO(OH) was carried out at 70 °C and to γ-FeO(OH) at 50 °C by bubbling air into the suspension at the rate of 500 l/h.[5] In order to obtain α- and γ-FeO(OH) with different mean particle sizes, the particle growth of FeO(OH) in suspension was controlled by the amount of seed added.

β-FeO(OH), consisting of needle-like particles, was prepared by the air oxidation of mixtures of $FeCl_2$, $FeCl_3$ and NH_4Cl solutions at 70 °C with different concentrations with respect to the total amount of iron.[6] The mean particle size increased with an increase in the concentration.

Needle-like particles, each consisting of very fine particles of α-Fe_2O_3, were prepared by the calcination of α-FeO(OH) particles in air at 300 °C for 2 h.

Procedure. Suspensions containing barium ions and one of iron(III) hydroxide, hydroxide oxide, or oxide were prepared as follows: (1) An acidic solution was prepared in a cylindrical tetrafluoethylene bottle (40 ml) by mixing 12.8 mmol of iron(III) nitrate and 1.6 mmol of barium nitrate in 10—15 ml of conductivity water. To the acidic solution the required amount of NaOH was added in various mol ratios of NaOH to the total nitrate. Water was then added to make the total volume 25.0 ml. (2) Starting suspensions containing either iron(III) hydroxide oxide or oxide, and $Ba(OH)_2$ were also prepared in the cylindrical bottles by mixing 36.0 mmol of iron(III) hydroxide oxide or 18.0 mmol of oxide, and different amounts of $Ba(OH)_2 8H_2O$ in 25.0 ml of water.

In order to prevent carbonation, the preparation was carried out in a nitrogen atmosphere. The bottles containing the suspensions were stoppered with tetrafluoethylene caps and dipped in water contained in an autoclave* to prevent the reduction of the volume of the suspension during the course of autoclaving. Four suspensions were subjected to autoclaving in each run. The suspensions were heated to the desired temperature at the rate of 4 °C/min, and then kept at this temperature for 5 h.

The products were separated from the solution by filtration, treated with a dilute $HClO_4$ solution to remove the remaining $Ba(OH)_2$, washed thoroughly with water, treated with acetone, and dried at 80 °C.

Examination. The products and the iron(III) hydroxide oxides used as the starting materials were examined by means of X-ray powder diffraction using Mn filtered Fe$K\alpha$ radiation. The products and the iron(III) hydroxide oxides which were found to consist of only one phase were subjected to BET surface measurements and to optical or electron microscopic observation. Products consisting of only one phase were further washed with 3M-$HClO_4$ to remove the adsorbed barium ion. After they had been dissolved in a HCl solution by heating, the barium and iron(III) ion contents were determined by means of gravimetric analysis.

Results and Discussion

Conditions for the Formation of $BaO \cdot 6Fe_2O_3$. A brown precipitate was formed when the NaOH solution was added to an acidic solution containing iron(III) and barium nitrates. When the NaOH/total NO_3^- in mol ratio ($=R$) was 0.8, most of the iron(III) ions precipitated, the pH of the resulting suspension becoming 2.4—2.8. When $R \geqq 0.9$, the pH of suspensions became> 7 as a result of the formation of $Ba(OH)_2$ (no precipitation). By autoclaving, it turned out that pH≧11 for the suspensions with $R \geqq 0.9$ and pH≦1.1 for those with $R=0.8$.

The formation of the products is shown in Fig. 1 in terms of R and temperature. The concentration of

* Constructed of stainless steel.

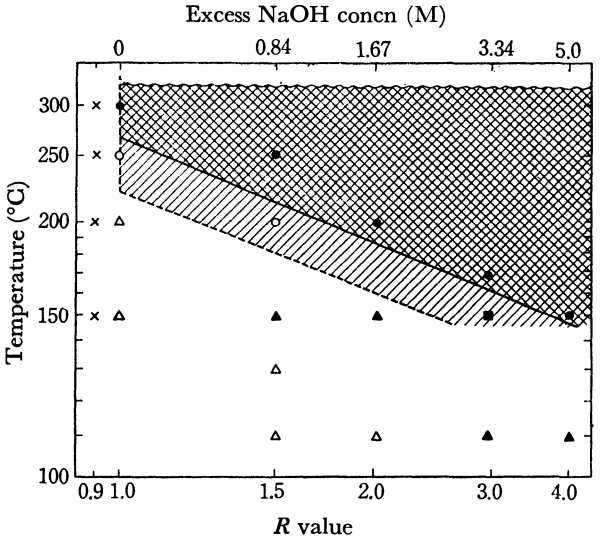

Fig. 1. Conditions for the formation of $BaO \cdot 6Fe_2O_3$ from suspensions containing 0.514 M-$Fe(NO_3)_3$, 0.064 M-$Ba(NO_3)_2$, and vairous amounts of NaOH.
● $BaO \cdot 6Fe_2O_3$, ○ $BaO \cdot 6Fe_2O_3 + \alpha\text{-}Fe_2O_3$, ▲ $BaO \cdot 4.5Fe_2O_3$, ■ $BaO \cdot 6Fe_2O_3 + BaO \cdot 4.5Fe_2O_3$, × $\alpha\text{-}Fe_2O_3$, △ $BaO \cdot 4.5Fe_2O_3 + \alpha\text{-}Fe_2O_3$.

excess NaOH in the suspension, as calculated from the R value, is also given. $BaO \cdot 6Fe_2O_3$, a brown ferromagnetic precipitate, is formed in the range of $R > 1.0$ at temperatures higher than those for the formation of $BaO \cdot 4.5Fe_2O_3$, a brown nonferromagnetic precipitate, or a mixture of $\alpha\text{-}Fe_2O_3$ and $BaO \cdot 4.5Fe_2O_3$. The temperature at which $BaO \cdot 6Fe_2O_3$ is formed decreases with the increase in R. When similar experiments were carried out with chlorides in place of nitrates, no remarkable difference were found in the conditions for the formation of $BaO \cdot 6Fe_2O_3$.

The physical and chemical properties of iron(III) hydroxide, formed by the addition of an alkaline solution to an iron(III) salt solution, were studied in detail by van der Giessen.[7] The precipitate consists of superfine particles (30—40 Å in size) stable in a neutral suspension medium. In an alkaline medium, however, the precipitate is transformed into α-FeO(OH) or $\alpha\text{-}Fe_2O_3$, or their mixture, depending on the temperature of aging.[8-10] $\alpha\text{-}Fe_2O_3$ is formed at temperatures higher than those at which α-FeO(OH) is formed. The temperature at which $\alpha\text{-}Fe_2O_3$ is formed depends on the time elapsed during the course of aging at room temperature and on the concentration of the excess alkali. It seems that $BaO \cdot 6Fe_2O_3$ is formed at such temperatures that iron(III) hydroxide is transformed into $\alpha\text{-}Fe_2O_3$, provided that the amount of $Ba(OH)_2$ in the suspension is suitable for $BaO \cdot 6Fe_2O_3$ formation. The content of barium ions in the product increases with the decrease in the solubility of $Ba(OH)_2$ at a given concentration of the total barium ions. The solubility might decrease with a rise in the temperature and with an increase in the NaOH concentration.[11]

Iron(III) hydroxide oxides in alkaline suspension media can be transformed into $\alpha\text{-}Fe_2O_3$ by autoclaving, the rate of transformation depending on the crystal structure of the iron(III) hydroxide oxides as well as on the particle size and shape. In order to examine the effects of the modification and particle size of iron(III) hydroxide oxide on the formation of $BaO \cdot 6Fe_2O_3$ in the presence of $Ba(OH)_2$, the following experiments were carried out by the use of iron(III) hydroxide oxides and oxide, similar in particle shape and size (Fig. 2). The suspensions containing 4.5 mmol of $Ba(OH)_2$ and either iron(III) hydroxide oxide or oxide were subjected to autoclaving at 150, 200, 250, and 300 °C. The products are given in Table 1, together with the BET surface area, S, of the starting material. We see that the temperature required for the transformation of α-, β-, and γ-FeO(OH) into $\alpha\text{-}Fe_2O_3$ decreases in this order, and that the use of α-FeO(OH) at higher temperatures favors the formation of $BaO \cdot 6Fe_2O_3$. The contents of $BaO \cdot 4.5Fe_2O_3$ and $BaO \cdot 6Fe_2O_3$ in the products obtained by autoclaving β-FeO(OH) suspensions at 200 and 300 °C were much smaller than those in the products from γ-FeO(OH) suspensions at corresponding temperatures. When $\alpha\text{-}Fe_2O_3$ was used as the starting material, autoclaving gave rise to the growth of fine particles in needle-like particles. A very small amount of hexagonal plate-like particles of $BaO \cdot 2Fe_2O_3$ besides $\alpha\text{-}Fe_2O_3$ was, however, found in the product obtained by autoclaving at 300 °C.

Similar experiments were carried out using powders

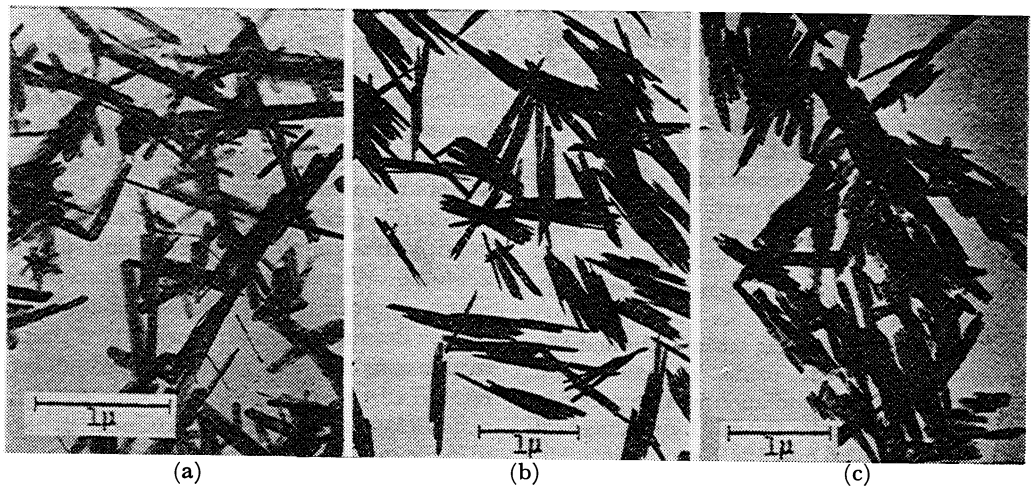

(a) (b) (c)

Fig. 2. Electronmicrographs of α-FeO(OH) (a), β-FeO(OH) (b), and γ-FeO(OH) (c) powders (Table 1).

TABLE 1. PRODUCTS OBTAINED BY AUTOCLAVING OF SUSPENSIONS CONTAINING 0.18M-$Ba(OH)_2$

Starting material	S(m^2/g)	Autoclaving temperature			
		150 °C	200 °C	250 °C	300 °C
α-FeO(OH)	23.2	α-FeO(OH)	α-FeO(OH)+B	α-Fe_2O_3+B	B
β-FeO(OH)	26.0	—	α-FeO(OH) +α-Fe_2O_3+A	α-Fe_2O_3	α-Fe_2O_3+B
γ-FeO(OH)	21.1	α-FeO(OH)+A	α-Fe_2O_3+A	α-Fe_2O_3+B	α-Fe_2O_3+B
α-Fe_2O_3[a)]	110.5	—	—	α-Fe_2O_3	α-Fe_2O_3+C

A=$BaO \cdot 4.5Fe_2O_3$, B=$BaO \cdot 6Fe_2O_3$, C=$BaO \cdot 2Fe_2O_3$.
a) Obtained from α-FeO(OH) with 23.2 m^2/g.

of α- and γ-FeO(OH) with different mean particle sizes. The results indicate that the decrease in the apparent density (g/ml) of iron(III) hydroxide oxide in the starting suspension was favorable for the formation of $BaO \cdot 6Fe_2O_3$. The apparent density decreased with a decrease in the mean particle size down to a size corresponding to about 20 m^2/g in S. When the size was too small (S>40 m^2/g), the apparent density increased as a result of the aggregation of very fine needle-like particles caused by drying during the course of the preparation of iron(III) hydroxide oxides.

In order to study the effect of the $Ba(OH)_2$ concentration on the formation of $BaO \cdot 6Fe_2O_3$, alkaline suspensions containing α-FeO(OH) particles (Table 1) and different amounts of $Ba(OH)_2$ (0.32—72 mmol, corresponding to 0.015—2.88 M $Ba(OH)_2$), were subjected to autoclaving at 300, 250, and 200 °C. The contents of $BaO \cdot 6Fe_2O_3$ in the products were determined by comparing the relative intensities of X-ray diffraction peaks of d(006) 3.86 Å for $BaO \cdot 6Fe_2O_3$, and d(104) 2.69 Å for α-Fe_2O_3, and d(103) 3.19 Å for $BaO \cdot 2Fe_2O_3$. The contents are plotted against the $Ba(OH)_2$ concentration at three reaction temperatures (Fig. 3). The content of $BaO \cdot 6Fe_2O_3$ in the products consisting of $BaO \cdot 6Fe_2O_3$ and α-Fe_2O_3 increases with an increase in the $Ba(OH)_2$ concentration and reaches 100% with 0.18—0.24 M $Ba(OH)_2$ for autoclaving at 300 °C, 0.24—0.28 M at 250 °C, and 0.36 M or more at 200 °C. A further increase in $Ba(OH)_2$ concentration at 300 and 250 °C resulted in the formation of $BaO \cdot 2Fe_2O_3$ besides $BaO \cdot 6Fe_2O_3$ and the content of $BaO \cdot 2Fe_2O_3$ reached 100% with 1.44 M $Ba(OH)_2$. At 200 °C, a further increase in $Ba(OH)_2$ concentration caused no formation of $BaO \cdot 2Fe_2O_3$, but only hindered the growth of $BaO \cdot 6Fe_2O_3$ particles.

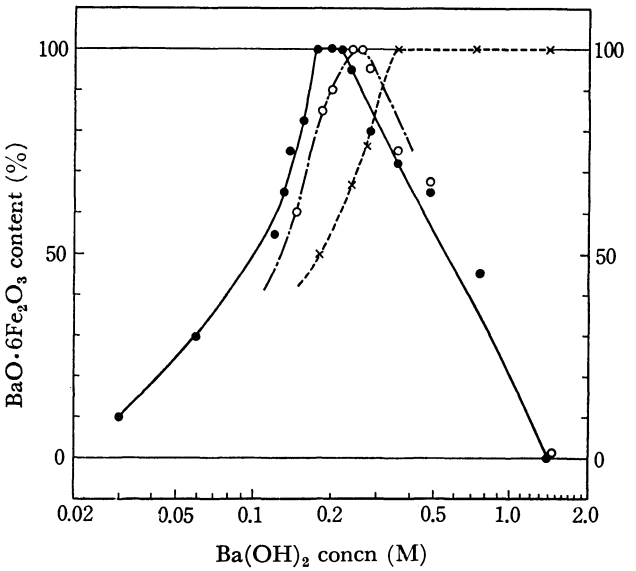

Fig. 3. Effect of $Ba(OH)_2$ concentration on $BaO \cdot 6Fe_2O_3$ formation at 200(×), 250(○), and 300 °C(●).

In order to examine the effect of reaction time on the content of $BaO \cdot 6Fe_2O_3$ in the product, the suspensions containing α-FeO(OH) (Table 1) and 0.14, 0.18, and 0.29 M $Ba(OH)_2$ were subjected to autoclaving at 250 and 300 °C for 5 min, 1/2, 2, and 8 h. In all cases, except for the reaction at 250 °C with 0.14 M $Ba(OH)_2$, α-FeO(OH) was completely transformed into $BaO \cdot 6Fe_2O_3$ or a mixture of $BaO \cdot 6Fe_2O_3$ and $BaO \cdot 2Fe_2O_3$ or α-Fe_2O_3 in 5 min. Under the conditions of 250 °C and 0.14 M $Ba(OH)_2$, $BaO \cdot 6Fe_2O_3$ was hardly formed in 5 min; however, α-FeO(OH) was completely transformed into a mixture of $BaO \cdot 6Fe_2O_3$ and a small amount of α-Fe_2O_3 in 2 h. The contents of $BaO \cdot 6Fe_2O_3$ in the products at complete transformation were not determined by the reaction time, but by the concentration of $Ba(OH)_2$ and the temperature, as is shown in Fig. 3.

γ-FeO(OH) as well as iron(III) hydroxide is unstable

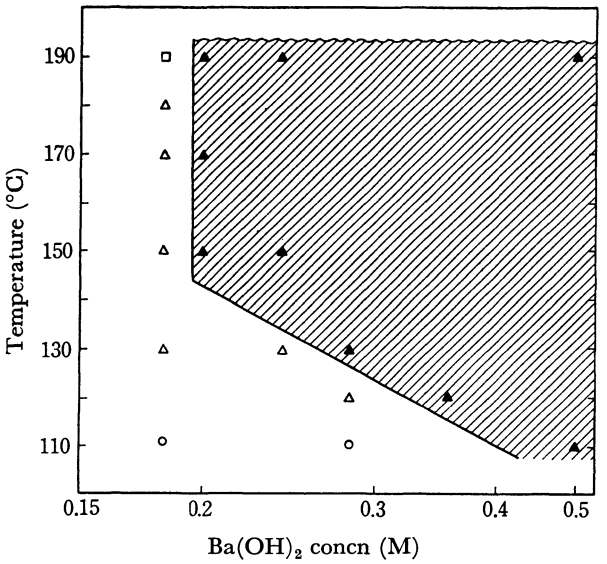

Fig. 4. The transformation products of γ-FeOOH in suspension media with various amounts of $Ba(OH)_2$. ▲ $BaO \cdot 4.5Fe_2O_3$, △ $BaO \cdot 4.5Fe_2O_3$+α-FeO(OH), ○ $BaO \cdot 4.5Fe_2O_3$+γ-FeO(OH), □ $BaO \cdot 4.5Fe_2O_3$+α-Fe_2O_3+α-FeO(OH).

in an alkaline medium and is transformed into α-FeO(OH) at temperatures lower than those needed for the transformation into α-Fe_2O_3.[12,13] The precipitate of $BaO \cdot 4.5Fe_2O_3$ seems to be formed in the presence of $Ba(OH)_2$ at temperatures at which γ-FeO(OH) is transformed into α-FeO(OH) (Table 1). In order to confirm this assumption, the following experiments were carried out using γ-FeO(OH) (Table 1). Alkaline γ-FeO(OH) suspensions containing different amounts of $Ba(OH)_2$ were subjected to autoclaving at temperatures in the range of 110—190 °C. The products are shown in Fig. 4 in relation to the temperature and the $Ba(OH)_2$ concentration (in M). Products consisting only of $BaO \cdot 4.5Fe_2O_3$ can be obtained by choosing the $Ba(OH)_2$ concentration and temperature.

In order to examine if $BaO \cdot 6Fe_2O_3$ is formed by the dissolution of the barium ion in the particles of $BaO \cdot 2Fe_2O_3$ or $BaO \cdot 4.5Fe_2O_3$ into a solution, two suspensions of $BaO \cdot 2Fe_2O_3$ (2 g) and $BaO \cdot 4.5Fe_2O_3$ (2 g) in water (25 ml) were subjected to autoclaving at 300 °C for 5 h. Some particles of $BaO \cdot 2Fe_2O_3$ were transformed into α-Fe_2O_3, while $BaO \cdot 4.5Fe_2O_3$ was completely transformed into a mixture of $BaO \cdot 6Fe_2O_3$ and α-Fe_2O_3. When 0.14 M-$Ba(OH)_2$ containing $BaO \cdot 4.5Fe_2O_3$ was used, the product consisted of only $BaO \cdot 6Fe_2O_3$. It may be considered from the experimental results that some or all of the $BaO \cdot 6Fe_2O_3$ particles in the products obtained from β- and γ-FeO(OH) suspensions are formed *via* $BaO \cdot 4.5Fe_2O_3$.

The transformation processes could be summarized as follows:

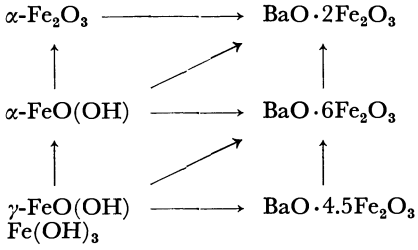

No direct transformations, such as α-$Fe_2O_3 \rightarrow BaO \cdot 6Fe_2O_3$ and α-FeO(OH)$\rightarrow BaO \cdot 4.5Fe_2O_3$, take place. Since β-FeO(OH) did not favor the formation of $BaO \cdot 6Fe_2O_3$, its yield being very small as compared with those of α-FeO(OH) and γ-FeO(OH), experiments using β-FeO(OH) were not sufficiently carried out.

The change in the shape and size of the particles before and after the transformation was observed in electronmicrographs. The change in particle shape and size suggests that the mechanism of formation takes place in the suspension medium. The barium ions in the alkaline suspension medium might react either with iron(III) ions on the surface of the particle of the intermediate product (the precursor of each product) or with iron(III) complexes formed by the dissolution of the intermediate product particle in the suspension medium to form a nucleus of $BaO \cdot 6Fe_2O_3$, $BaO \cdot 4.5Fe_2O_3$, or $BaO \cdot 2Fe_2O_3$. It is probable that the product formation takes place by the dissolution, followed by crystallization on suitable nuclei.

Properties of Precipitates. The ferromagnetic products, $BaO \cdot 6Fe_2O_3$, with a hexagonal crystal structure (a=5.88 and c=23.2 Å),[14] consisted o hexagonal plate-like particles. Their size increased with a rise in the reaction temperature; it depended also on the size of the particles in the starting suspension (Fig. 5). The diameter and thickness of the hexagonal plate-like particles obtained from the suspensions of iron(III) hydroxide did not exceed 1 and 0.05 μm respectively. The diameter of the particles obtained from the suspensions of α-FeO(OH) was 1—2 μm, the thickness depending on the conditions under which they were formed. These products** contained greater amounts of barium ions than those calculated from the $BaO \cdot 6Fe_2O_3$ formula. The relative heights of the X-ray diffraction peaks vary with the sample (Figs. 6(a)—(c)). This is because the hexagonal plate-like particles in the pressed powdery sample for X-ray measurement undergo alignment to some extent. The degree of alignment, F, depends on the thickness, d, of the particles (1—2 μm in diameter) and on the packing density P (Table 2). The d values were calculat-

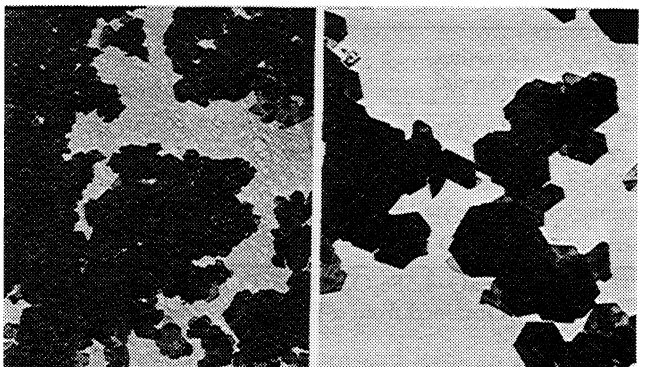

Fig. 5. Electronmicrographs of $BaO \cdot 6Fe_2O_3$ precipitates obtained by autoclaving of iron(III) hydroxide (a) and α-FeO(OH) (b) suspensions at 300 °C.

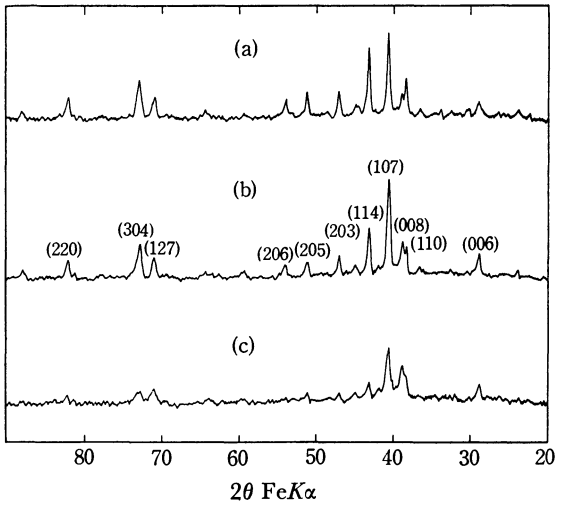

Fig. 6. X-Ray diffraction patterns of $BaO \cdot 6Fe_2O_3$ precipitates 1—2 μm in dia. and 0.17 (a), 0.08 (b), and 0.03 μm (c) in d.

** Contained less than 0.4 wt% of Fe^{2+}

Table 2. Alignment degree F and packing density P of compacts prepared by pressing $BaO \cdot 6Fe_2O_3$ powders with particle dia. 1—2 μm at pressures

S (m^2/g)	d (μm)	10 kg/cm^2		100 kg/cm^2		1000 kg/cm^2	
		F	P	F	P	F	P
9.65	0.041	0.09	0.98	0.26	1.64	0.37	2.67
6.75	0.060	0.23	1.09	0.48	2.06	0.56	2.72
5.25	0.079	0.26	1.27	0.36	1.90	0.49	2.72
2.69	0.168	0.09	1.50	0.21	2.20	0.35	2.78

$F = I_{d(008)}/I_{d(008)} + I_{d(107)}$, where $I_{d(008)}$ and $I_{d(107)}$ are relative intensities of X-ray diffraction on (008) and (107) crystal faces, respectively, of $BaO \cdot 6Fe_2O_3$.

ed by means of this formula;

$$d(\mu m) = 3(3)^{1/2}/1.5\rho S(3)^{1/2} - 6$$

assuming that the diameter of the circle circumscribing the hexagon is 2 μm, where $\rho = 6.3$ is the specific gravity of the $BaO \cdot 6Fe_2O_3$ crystal.

Since the c axis of the $BaO \cdot 6Fe_2O_3$ crystal is the easy direction of magnetization, all the hexagonal plate-like particles can be aligned by magnetic field when they are free to rotate. A brown suspension prepared by mixing the $BaO \cdot 6Fe_2O_3$ precipitates with an adequate amount of a liquid such as oil, water, or ethanol in a test tube, loses its color when brought near a magnet since light is reflected by the aligned basal planes perpendicular to the direction of the magnetic field.

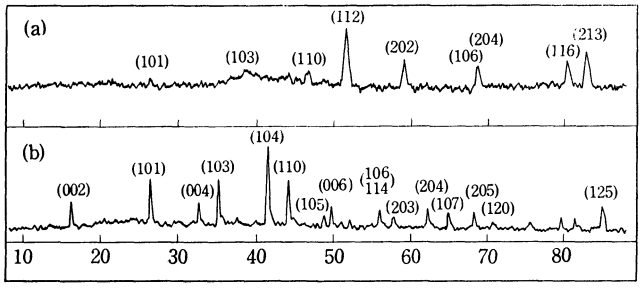

Fig. 7. X-Ray diffraction patterns of $BaO \cdot 4.5Fe_2O_3$ (a) and $BaO \cdot 2Fe_2O_3$ (b).

X-Ray diffraction patterns of the non-ferromagnetic products consisting of only one phase are shown in Figs. 7(a) and (b). Samples (a) and (b) contained barium and iron(III) ions in the Fe_2O_3/BaO mol ratios of 4.4—4.6 and 1.9—2.2 respectively. $BaO \cdot 4.5Fe_2O_3$ is estimated to have a hexagonal crystal structure with $a = 4.8$ and $c = 11.3$ Å. The particles were spherical (maximum size, 0.05 μm). It was difficult to obtain large particles. Particles of $BaO \cdot 2Fe_2O_3$ remarkably increase in size with increases in the temperature and in the concentration of $Ba(OH)_2$. Large particles with a hexagonal crystal structure with $a = 5.12$ and $c = 13.8$ Å were easily obtained by autoclaving at 300 °C. Their properties were then studied.[3,15]

When heated at 800 °C in the air for 4 h, the $BaO \cdot 4.5Fe_2O_3$ particles were decomposed into $BaO \cdot 6Fe_2O_3$ and a small amount of $BaO \cdot Fe_2O_3$, whereas the $BaO \cdot 2Fe_2O_3$ particles, 20—40 μm in diameter, were hardly decomposed at all. This difference might be due to the difference in their particle size.

Magnetic Properties of $BaO \cdot 6Fe_2O_3$ Precipitates. The products were obtained from α-FeO(OH) suspensions containing various amounts of $Ba(OH)_2$ at 200, 250 and 300 °C under the conditions shown in Fig. 3. The samples, consisting of hexagonal plate-like particles 1—2 μm in diameter, were selected, pressed in brass cylinders 15 mm in diameter and 5 mm in height, and sandwiched between the pole pieces of a magnet. After the sample had been magnetized at $H = 17$ kOe, the demagnetization curve was obtained from 5 kOe with a self-recording permeameter. The results are given in Table 3. As the d value increases to 0.044 μm, the values of $4\pi I/P$ and ${}_iH_c$ increase. The d dependence of $4\pi I/P$ and ${}_iH_c$ might indicate the presence of superparamagnetic particles in the samples with $d \leqq 0.044$ μm.

Table 3. Magnetic properties of $BaO \cdot 6Fe_2O_3$ precipitates

Preparation conditions		S (m^2/g)	d (μm)	P (g/ml)	$4\pi I/P$ (G)	${}_iH_c$ (Oe)	I_r/I
Autoclaving temp.	Concn $Ba(OH)_2$ (M)						
200 °C	0.72	20.8	0.016	0.92	210	286	0.41
	0.48	17.5	0.019	1.12	120	606	0.62
	0.36	8.1	0.041	0.86	230	813	0.57
250 °C	0.28	7.6	0.044	1.11	520	973	0.72
	0.24	6.7	0.050	0.95	480	942	0.59
	0.20	6.6	0.051	1.29	480	942	0.63
300 °C	0.20	5.2	0.066	0.93	510	1042	0.55
	0.18	4.1	0.085	0.92	490	1003	0.65

Samples 1—2 μm in diameter and 0.15 μm or less in d were prepared under various conditions. The saturation magnetization, σ_s, at 17 kOe and the ${}_iH_c$ were also measured in the P range of 0.9—2.2 g/ml at room temperature. The values of the samples with $0.05 \leqq d \leqq 0.15$ μm were 55 ± 4 in σ_s (emu/g) and 0.9—1.0 kOe in ${}_iH_c$. The samples were calcined in the air at ≈1000 °C. It was found that no remarkable difference in σ_s and ${}_iH_c$ occurred between the calcined and the original samples.

The author is indebted to Prof. T. Takada, Kyoto University, for suggesting the investigation, to Prof. N. Nakanishi, Konan University, for his valuable discussion, and Mr. T. Asai for his help in the experiments.

References

1) J. Smit and H. P. J. Wijn, "Ferrites," Wiley, New York (1959), p. 194.
2) Y. Goto and T. Takada, *J. Am. Ceram. Soc.*, **43**, 150 (1960); H. J. van Hook, *ibid.*, **47**, 579 (1964).
3) T. Takada, M. Kiyama, Y. Bando, and T. Shinjo, *Bull. Inst. Chem. Res., Kyoto Univ.*, **47**, 298 (1969).

4) M. Kiyama, *Bull. Chem. Soc. Jpn.*, **47**, 1646 (1974).
5) M. Kiyama, T. Akita, S. Shimizu, Y. Okuda, and T. Takada, *Bull. Chem. Soc. Jpn.*, **45**, 3422 (1972).
6) M. Kiyama and T. Takada, *Bull. Chem. Soc. Jpn.*, **45**, 1923 (1972).
7) A. A. van der Giessen, *J. Inorg. Nucl. Chem.*, **28**, 2155 (1966); *J. Phys. Chem. Solids*, **28**, 343 (1967).
8) K. Wefers, *Ber. deut. Keram. Ges.*, **43**, 677 (1966).
9) U. Schwertman, *Z. Anorg. Allgem. Chem.*, **298**, 23 (1959).
10) R. J. Atkinson, A. M. Posner, and J. P. Quirk, *J. Inorg. Nucl. Chem.*, **30**, 3271 (1968).
11) W. F. Linke, "Solubilities of Inorganic and Metal-Organic Compounds," 4th ed, Vol. 1, Am. Chem. Soc., Washigton, D. C. (1958), p. 379.
12) A. Krause, K. Moroniowna, and E. Przybylski, *Z. Anorg. Allgem. Chem.*, **291**, 203 (1934).
13) G. W. van Oosterhout, *J. Inorg. Nucl. Chem.*, **29**, 1235 (1967).
14) V. Adleskolt, *Arki. Kem. Mineralog Geol.*, **12A**, (29) 1 (1938).
15) S. Okamoto, H. Sekizawa, and S. I. Okamoto, *J. Phys. Chem. Solids*, **36**, 591 (1974).

Sterically Controlled Substitution of Copper(II) with 3,3′-Bis[*N*,*N*-bis(carboxymethyl)aminomethyl]-*o*-cresolsulfonphthalein

Mutsuo YAMADA

Department of Chemistry, Faculty of Science, Hokkaido University, Sapporo 060

(Received December 11, 1975)

The rate constants for the formation of the diprotonated bimetallic complex of copper(II) with 3,3′-bis[*N*,*N*-bis(carboxymethyl)aminomethyl]-*o*-cresolsulfonphthalein (XO) have been determined by the stoppedflow method. The results are interpreted in terms of the reactions, $Cu+LH_2 \rightleftharpoons CuLH_2 \overset{Cu}{\rightleftharpoons} Cu_2LH_2$ and $Cu+LH_3 \rightleftharpoons CuLH_2+H \overset{Cu}{\rightleftharpoons} Cu_2LH_2+H$. The over-all rate constants, k_1 and k_2 for both reactions are determined to be $k_1=(3.6\pm0.3)\times10^6 M^{-1}s^{-1}$ and $k_2=(8.7\pm1.3)\times10^3\ M^{-1}s^{-1}$ at 25.0 °C and I=0.1 M.

During a search for establishing the solution chemistry on the metal complexes with XO,[1-3] it has been found that copper(II) ion forms the diprotonated bimetallic complex Cu_2LH_2 with XO in solutions containing an excess of copper(II) ion to XO at pH 3.5—5.5. The structure of the complex has been proposed to be four nine-membered and two eight-membered rings.[2]

In the present paper it is examined by the stopped-flow method how the unfavorable large-membered chelate rings affect the complexation reaction of copper(II) ion with XO.

Experimental

Materials. *Reagents*: All chemicals used are of analytical grade, unless otherwise specified. Water is deionized and distilled.

Xylenol Orange: The acid form of the "*pure*" specimen[4,5] is used. 1×10^{-3} M stock solution of XO is prepared by weight.

Copper(II) Perchlorate: Copper(II) perchlorate is prepared from recrystallized copper(II) chloride by heating with a small excess of perchloric acid. Perchlorate is recrystallized twice from water. The solution is standardized by EDTA titration using PAN as indicator.

Sodium Perchlorate: The purified salt[1] is heated at *ca.* 200 °C to prepare anhydrous salt. The concentration of the solution is determined by weight. The ionic strength of the solution is adjusted to 0.1 M with the sodium perchlorate.

Buffer Solutions: They are prepared from 1.0 M acetic acid and 1.0 M sodium acetate.

Measurements. The rates of complexation reaction are measured at 574 nm, the maximum absorption of Cu_2LH_2 complex,[2] with a Union Giken stopped-flow rapid-scan spectrophotometer Model RA 1300 and their signals are stored in an image dissector and then recorded on a Rigaku Denki transient recorder.

The pH values of the solutions are measured with a Radiometer pH Meter 4d (Copenhagen) equipped with a glass electrode Type G 202B and a saturated calomel electrode Type K 401.

All measurements are made at 25.0±0.2 °C by circulating thermostated water from a Lauda Type K 2R Electronic with a circular Duplex pumps.

Results

Figure 1 shows the plot of k_{obsd}, the apparent first-order rate constant, against the total concentration of copper(II) ion for the total concentration of XO,

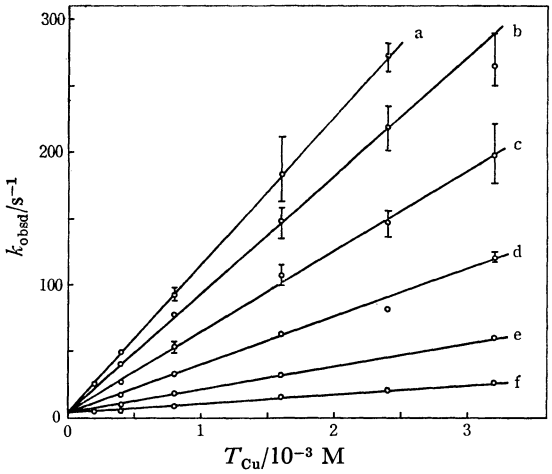

Fig. 1. Plot of k_{obsd} against the total concentration of copper(II) ion at various pH values in the formation of Cu_2LH_2 for $T_L=1.60\times10^{-5}$ M, at 25.0 °C and I=0.1 M. pH: a) 5.36±0.04, b) 5.17±0.03, c) 4.97±0.03, d) 4.70±0.04, e) 4.27±0.07, and f) 3.87±0.09.

$T_L=1.60\times10^{-5}$ M at pH 3.87—5.36 at 25.0 °C and I=0.1 M. As k_{obsd} is the first-order with respect to copper(II) ion at each value of pH, the following equation holds

$$k_{obsd} = k_f[Cu] + k_d, \quad (1)$$

where k_f and k_d are the forward and the reverse rate constants of the reaction, respectively.

In the above pH region, the protolytic equilibria of the ligand are

$$LH_2 + H \rightleftharpoons LH_3; \quad K_1 = 10^{6.74} \quad (2)$$

$$LH_3 + H \rightleftharpoons LH_4; \quad K_2 = 10^{2.85}, \quad (3)$$

where K_1 and K_2 are the acid-association constants[6] of the ligand at 25.0 °C and I=0.1 M.

The kinetic data are consistent with the assumption that the formation of Cu_2LH_2 proceeds *via* two paths in Eqs. 4 and 5 and that the protolytic reactions of Eqs. 2 and 3 reach equilibria much faster than the metal complex reactions

$$Cu + LH_2 \rightleftharpoons CuLH_2 \overset{Cu}{\rightleftharpoons} Cu_2LH_2; \ k_1 \quad (4)$$

$$Cu + LH_3 \rightleftharpoons CuLH_2 + H \overset{Cu}{\rightleftharpoons} Cu_2LH_2 + H; \ k_2, \quad (5)$$

where $CuLH_2$ is a terdentate intermediate **4** in Fig. 3.

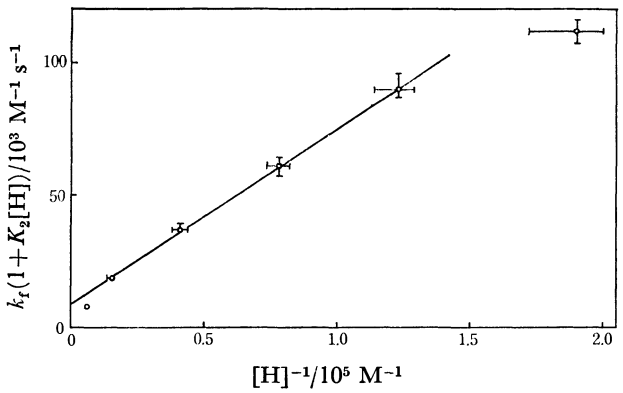

Fig. 2. Plot of $k_f(1+K_2[H])$ against the inverse of hydrogen ion concentration in the formation of Cu_2LH_2 at 25.0 °C and $I=0.1$ M.

The forward rate of the formation of Cu_2LH_2 is given by

$$d[Cu_2LH_2]/dt = k_f[Cu]C_L = k_1[Cu][LH_2] + k_2[Cu][LH_3], \quad (6)$$

where

$$C_L = [LH_4] + [LH_3] + [LH_2], \quad (7)$$

and k_1 and k_2 are the over-all forward rate constants of the reactions for (4) and (5), respectively.

From Eqs. 6 and 7, the formation rate constant k_f is expressed by the equation

$$k_f = (k_1+k_2K_1[H])/(1+K_1[H]+K_1K_2[H]^2). \quad (8)$$

Plot of $k_f(1+K_2[H])\times10^3$ against $[H]^{-1}\times10^5$ gives a straight line (Fig. 2). From Eq. 8 the relation $k_f(1+K_2[H])=k_2+k_1/K_1[H]$ holds in the experimental pH region. The intercept and the slope give the values of k_2 and k_1/K_1, respectively. The values of k_1 and k_2 are evaluated to be $k_1=(3.6\pm0.3)\times10^6\ M^{-1}s^{-1}$ and $k_2=(8.7\pm1.3)\times10^3\ M^{-1}s^{-1}$ at 25.0 °C and $I=0.1$ M.

Discussion

From equilibrium measurements it has been found that copper(II) ion forms the diprotonated *bimetallic* complex with XO,[2] while from kinetic measurements of the complexation reaction of copper(II) ion with XO, k_{obsd} is found to be the first-order with respect to copper(II) ion. These facts indicate that on complexation of copper(II) ion with XO two copper(II) ions do not simultaneously react with two different coordinating sites of XO but successively react with them to form the diprotonated *bimetallic* complex. Thus following mechanisms are considered (Fig. 3).

Using steady-state approximation for species **3** and **4** (**3'** and **4**), and assuming rapid equilibria between species **1** and **2** (**1'** and **2'**), and assuming $k_{45}[Cu]\gg k_{43}$ ($k'_{45}[Cu]\gg k'_{43}$) and $k_{32}\gg k_{34}$ ($k'_{32}\gg k'_{34}$) one gives the expression for the forward rate constant at each value of pH in Eq. 9

$$k_f = k_{34}K_{os}K_{12}K_{23}[Cu][LH_2] + k'_{34}K'_{os}K'_{12}K'_{23}[Cu][LH_3]. \quad (9)$$

From Eqs. 6 and 9,

$$k_1 = k_{34}K_{os}K_{12}K_{23} \quad (10)$$

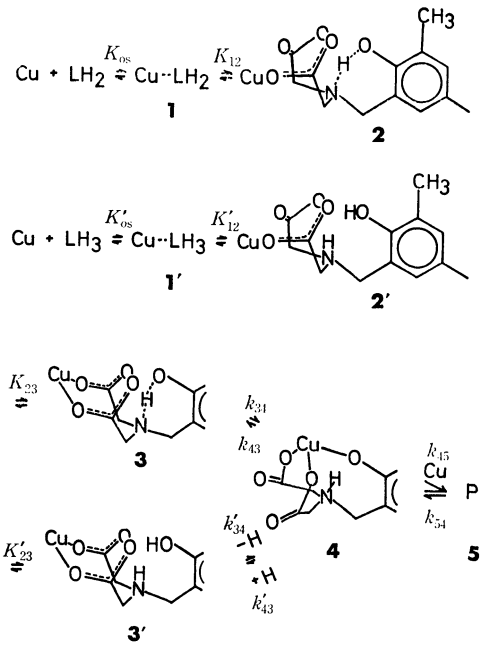

Fig. 3. Proposed mechanisms of the formation of Cu_2LH_2.

$$k_2 = k'_{34}K'_{os}K'_{12}K'_{23}. \quad (11)$$

As the value of the product $K_{os}K_{12}$ is approximately estimated to be 78 M^{-1} from the stability constant of the copper(II) acetate,[7] the value of the product $k_{34}K_{23}$ is calculated to be $4.6\times10^4\ s^{-1}$. If K_{23} is estimated from the ratio of the copper(II) complexes with malonic acid[7] and acetic acid,[7] K_{23} is calculated to be 4.6×10^3. Thus k_{34} is approximately evaluated to be $10\ s^{-1}$.

It is due to the small value of k_{34} that the value of k_1 ($3.6\times10^6\ M^{-1}s^{-1}$) is smaller by approximately 3 orders of magnitude than those of the rate constants of the normal substitution reaction of aquo copper(II) ion with the ligands.

It is found that the formation of large-membered chelate rings reduces the rate of the substitution reaction.

Kustin *et al.* have termed the reactions like this "*sterically controlled substitution,*" the rate has been shown to be ligand dependent.[8]

The author should like to thank Professor M. Fujimoto for general discussion and reading the manuscript.

References

1) M. Yamada and M. Fujimoto, *Bull. Chem. Soc. Jpn.*, to be published. "The Solution Chemistry for Complexes of Nickel(II) and Cobalt(II) with 3,3'-Bis[*N*,*N*-bis(carboxymethyl)aminomethyl]-*o*-cresolsulfonphthalein."

2) M. Yamada, *Bull. Chem. Soc. Jpn.*, to be published. "Diprotonated Bimetallic Complex between Copper(II) with 3,3'-Bis[*N*,*N*-bis(carboxymethyl)aminomethyl]-*o*-cresolsulfonphthalein."

3) M. Yamada and M. Fujimoto, *Bull. Chem. Soc. Jpn.*, to be published.

4) M. Yamada and M. Fujimoto, *Bull. Chem. Soc. Jpn.*, **44**, 294 (1971).

5) M. Yamada and M. Fujimoto, *Bull. Chem. Soc. Jpn.*, to be published. "Preparative Thin-Layer Chromatography

of Semi-Xylenol Orange and Xylenol Orange by Developing with Solvents Giving Discrete pH Change on the Plate."

6) M. Murakami, T. Yoshino, and S. Harasawa, *Talanta*, **14**, 1293 (1967).

7) L. G. Sillén and A. E. Martell, "Stability Constants of Metal-Ion Complexes, Supplement No. 1," Special Publication, No. 25, The Chemical Society, London (1970).

8) K. Kustin, R. F. Pasternack, and E. M. Weinstock, *J. Am. Chem. Soc.*, **88**, 4610 (1966); A. Kowalak, K. Kustin, R. F. Pasternack, and S. Petrucci, *ibid.*, **89**, 3126 (1967); R. F. Pasternack and K. Kustin, *ibid.*, **90**, 2295 (1968).

The Crystal Structure of $(+)_{350}$-Diammine-*N,N,N'*-trimethylethylenediamineplatinum(II) Di-μ-(+)-tartrato-(4-)bis(antimonate(III)) Monohydrate

Keiji Yokoho, Keiji Matsumoto, Shun'ichiro Ooi, and Hisao Kuroya

Department of Chemistry, Faculty of Science, Osaka City University, Sumiyoshi, Osaka 558

(Received January 14, 1976)

X-Ray structure analysis of the title compound has revealed that the asymmetric secondary nitrogen center in the complex cation has the *S* absolute configuration. The crystals are orthorhombic, with the space group $P2_12_12_1$ and with $Z=4$ in a unit cell with dimensions of: $a=18.783(6)$, $b=14.138(4)$, and $c=8.473(2)$Å. The crystal structure has been determined from three-dimensional diffractometer data and refined by the least-squares method to R of 0.030 for 1971 independent reflections with $I>3\sigma(I)$. The Pt atom has a square-planar coordination by four N atoms, and the methyl group bonded to the secondary nitrogen is equatorial with respect to the chelate ring. Each complex cation is surrounded octahedrally by six di-μ-(+)-tartrato(4-)-bis(antimonate(III)) anions.

Although an optical resolution has been made for a large number of octahedral Co(III) complexes, there have been few reports concerning the resolution of the planar Pt(II) complexes. In order to study the correlation between the circular dichroism and the structure in dissymmetric planar metal complexes, we have prepared several Pt(II) chelates of *N*-substituted diamine and have attempted to resolve each of them into enantiomeric forms.

Of these chelates, $[Pt(NH_3)_2(Me_3en)]^{2+}$ (Me_3en, *N,N,N'*-trimethylethylenediamine) exists in two optical isomers: the one has a secondary nitrogen with the *R* configuration, while the other involves *S* asymmetric nitrogen. By the use of silver di-μ-(+)-tartrato(4-)-bis(antimonate(III)) ($Ag_2[Sb_2(+)\text{-tart}_2]$) as the resolving agent, the seemingly diastereoisomeric salt, $(+)_{350}$-$[Pt(NH_3)_2(Me_3en)][Sb_2(+)\text{-tart}_2]\cdot H_2O$, could be obtained as a less soluble fraction in an acidic solution. The circular dichroism of this compound is different from that of $K_2[Sb_2(+)\text{-tart}_2]$ in the 250—350 nm region. Although this indicate that there is some resolution, it is uncertain whether or not the resolution is complete. Fortunately, if the diastereoisomeric salt contains only one antipode of the enantiomeric pair, it is necessary to elucidate the absolute configuration of the complex in order to advance our study. Therefore, an X-ray structure analysis was performed on this compound.

Experimental

Details of the preparation of the title compound will be reported in the near future.

X-Ray Data Measurement. *Crystal Data*: $C_{13}H_{26}N_4O_{13}Sb_2Pt$, $M=884.96$, Orthorhombic, $a=18.783(6)$, $b=14.138(4)$, $c=8.473(2)$Å, $U=2250(1)$Å^3, $Z=4$, $D_m=2.59$ (by flotation), $D_c=2.61$ gcm^{-3}, Mo$K\alpha$ radiation ($\lambda=0.71069$ Å), μ(Mo$K\alpha$) $=89.9$ cm^{-1}. Space group $P2_12_12_1$.

The Laue symmetry and the space group were determined from oscillation and Weissenberg photographs. The unit-cell parameters were obtained by the least-squares treatment of 19 θ values measured on a Philips diffractometer with Mo$K\alpha$ radiation.

Data Collection. The intensities were measured by means of the ω-2θ scan method on a Philips PW 1100 four-circle diffractometer using a graphite monochrometer and Mo$K\alpha$ radiation with a crystal with dimensions of $0.12\times0.13\times0.10$ mm. A scan speed of 0.017° s^{-1}, a scan width of $(0.9+0.2\tan\theta)$°, and two 20 s background counts were chosen. Three standard reflections (400, 0$\bar{6}$0, and 004), monitored every 4 h throughout the data collection, showed no significant

Table 1. Final atomic coordinates and temperature factors

	x	y	z	B (Å^2)
Pt	0.23028(2)	0.22925(3)	0.49010(6)	a)
N(1)	0.2206(6)	0.3731(8)	0.5321(13)	2.1(2)
N(2)	0.1903(6)	0.2155(9)	0.7156(15)	2.7(2)
N(3)	0.2364(6)	0.0840(8)	0.4547(13)	2.3(2)
N(4)	0.2647(6)	0.2452(8)	0.2579(13)	2.3(2)
C(1)	0.1754(11)	0.3865(15)	0.6779(26)	5.0(4)
C(2)	0.8171(10)	0.3128(15)	0.7857(26)	4.6(4)
C(3)	0.1778(10)	0.4201(15)	0.4050(24)	4.5(4)
C(4)	0.2926(10)	0.4183(14)	0.5392(23)	4.3(4)
C(5)	0.2292(9)	0.1505(12)	0.8234(21)	3.5(3)
Sb(1)	0.47727(5)	0.40889(7)	0.30078(12)	a)
Sb(2)	0.57461(5)	0.53830(7)	−0.22411(11)	a)
C(6)	0.4067(7)	0.3390(10)	0.0125(19)	2.5(2)
C(7)	0.4834(7)	0.3117(9)	−0.0057(18)	2.0(2)
C(8)	0.5128(7)	0.3497(10)	−0.1598(17)	2.1(2)
C(9)	0.5940(7)	0.3345(10)	−0.1600(17)	2.1(2)
C(10)	0.6017(7)	0.5352(10)	0.3194(16)	1.8(2)
C(11)	0.5431(7)	0.5929(11)	0.2342(17)	2.3(3)
C(12)	0.5725(7)	0.6340(10)	0.0837(16)	2.1(2)
C(13)	0.5108(7)	0.6768(9)	−0.0120(18)	2.1(2)
O(1)	0.3883(5)	0.3802(8)	0.1403(13)	2.8(2)
O(2)	0.3637(7)	0.3166(9)	−0.0928(15)	4.1(3)
O(3)	0.5252(5)	0.3412(7)	0.1285(12)	2.4(2)
O(4)	0.4975(5)	0.4486(7)	−0.1770(11)	2.3(2)
O(5)	0.6340(5)	0.4083(7)	−0.1825(12)	2.6(2)
O(6)	0.6195(5)	0.2548(7)	−0.1390(11)	2.2(2)
O(7)	0.5862(5)	0.4505(8)	0.3592(12)	2.8(2)
O(8)	0.6605(6)	0.5707(8)	0.3411(13)	3.1(2)
O(9)	0.4829(5)	0.5357(7)	0.1994(11)	2.3(2)
O(10)	0.6094(4)	0.5654(6)	−0.0096(13)	2.3(2)
O(11)	0.5006(5)	0.6415(7)	−0.1484(13)	2.8(2)
O(12)	0.4737(5)	0.7394(8)	0.0422(12)	3.1(2)
H_2O	0.0720(7)	0.4372(9)	0.0669(15)	4.3(3)

a) Anisotropic temperature factors ($\times10^5$) in the form $\exp[-(B_{11}h^2+B_{22}k^2+B_{33}l^2+B_{12}hk+B_{13}hl+B_{23}kl)]$, with parameters:

	B_{11}	B_{22}	B_{33}	B_{12}	B_{13}	B_{23}
Pt	104(1)	197(2)	564(6)	6(3)	13(5)	−33(8)
Sb(1)	151(2)	247(4)	847(13)	34(6)	184(11)	164(14)
Sb(2)	197(3)	271(4)	628(12)	−63(6)	50(10)	107(13)

variation in intensity. Of the independent reflections measured in the $5°\leq 2\theta \leq 50°$ range, 1971 reflections with $I>3\sigma(I)$ were considered to be observed and were used for the structure analysis ($\sigma^2(I)=CT+(t_c/t_b)(B_1+B_2)+(pI)^2$; CT, total integrated peak count obtained in a scan time t_c; B_1 and B_2, background counts each obtained in time $t_b/2$; $p=0.04$; $I=CT-(t_c/t_b)(B_1+B_2)$). The intensity data were processed with the computer program of Hornstra and Stubbe.[1] A spherical absorption correction ($r=0.05$ mm) was applied.

Structure Determination and Refinement. The crystal structure was solved by the heavy-atom technique. The positional and thermal parameters were refined by the least-squares method, the function minimized being $\sum w(F_o-|F_c|)^2$. The weight for each reflection, w, was unity in the initial refinement; in the final one $w=0.5$ for $F_o<25.1$, $w=1$ for $25.1\leq F_o\leq 150.8$, and $w=(150.8/F_o)^2$ for $F_o>150.8$. All the parameter shifts in the final cycle of the refinement were $<(1/10)\sigma$. The final R value was 0.030. The atomic scattering factors of the neutral Pt, Sb, O, N, and C were employed from Ref. 2. Real and imaginary parts of the anomalous dispersion correction were applied for Pt and Sb atoms.

The atomic coordinates listed in Table 1 correspond exactly to the absolute crystal structure, which was determined on the basis of the well-established absolute configuration of the $[Sb_2(+)\text{-}tart_2]$ anion. A complete list of the observed and calculated structure factors is preserved by the Chemical Society of Japan (Document No. 7625). All the computations were carried out by means of the FACOM 270-30 computer at Osaka City University. The computer programs used in the calculations were as follows: RSSFR-4 (Fourier synthesis), HBLS-4 (least-squares calculation), and DAPH (interatomic distances and angles, least-squares plane, and coordinates of H atoms), all of which were adapted to the FACOM 270-30 computer.

Results and Discussion

The absolute configuration of the complex cation and the absolute crystal structure viewed down the c axis are shown in Figs. 1 and 2 respectively. The bond lengths and angles in the complex, along with some selected interatomic distances, are presented in Table 2.

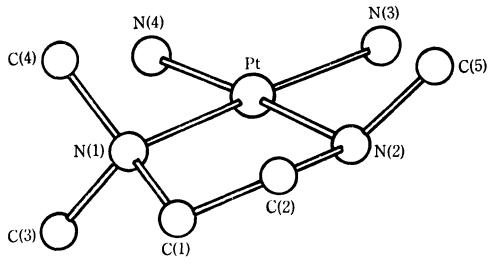

Fig. 1. The absolute configuration of the complex cation in $(+)_{350}$-$[Pt(NH_3)_2(Me_3en)][Sb_2\text{-}(+)\text{-}tart_2]\cdot H_2O$.

From the space group and the number of the formula units in the unit cell, it was inferred that the crystals involve only one antipode of the two optical isomers. The absolute configuration of the secondary nitrogen atom in the complex was elucidated to be *S* by the subsequent crystal structure analysis.

The Pt atom has a square-planar coordination by four nitrogen atoms. The equation of the plane defined by the 4 N atoms is:

$$0.9403X + 0.0138Y + 0.3400Z = 5.484^{3)}$$

The deviations (Å) of atoms from the plane are as follows: Pt, −0.040; N(1), −0.02; N(2), 0.02; N(3), −0.02; N(4), 0.02; C(1), 0.36; C(2), −0.15; C(3), 1.09; C(4), −1.32, and C(5), −0.97. The N–CH_3 bond in the secondary amino group is equatorial with respect to the five-membered chelate ring.

The Pt–NH_3 bond lengths agree with those in *trans*-

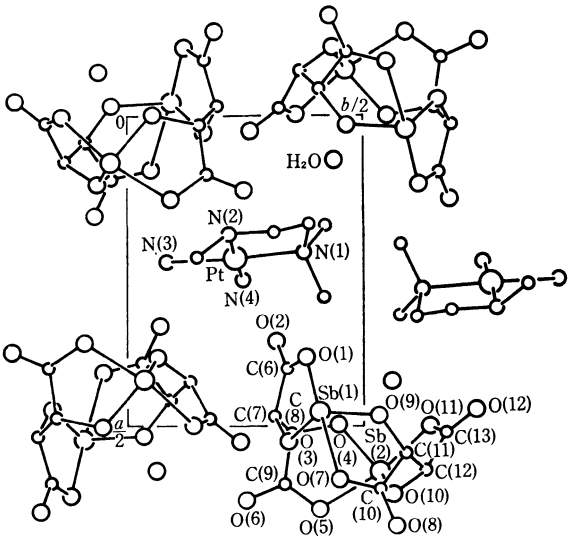

Fig. 2. The crystal structure viewed down the c axis.

Table 2. Interatomic distances and angles

Bond lengths (Å)		Bond angles (°)	
Pt–N(1)	2.07(1)	N(1)–Pt–N(2)	84.4(5)
Pt–N(2)	2.06(1)	N(3)–Pt–N(4)	87.4(5)
Pt–N(3)	2.08(1)	Pt–N(1)–C(1)	108(1)
Pt–N(4)	2.08(1)	Pt–N(1)–C(3)	111(1)
N(1)–C(1)	1.51(3)	Pt–N(1)–C(4)	110(1)
N(1)–C(3)	1.50(2)	C(1)–N(1)–C(3)	103(1)
N(1)–C(4)	1.50(2)	C(1)–N(1)–C(4)	115(1)
N(2)–C(2)	1.50(3)	Pt–N(2)–C(2)	107(1)
N(2)–C(5)	1.49(2)	Pt–N(2)–C(5)	117(1)
C(1)–C(2)	1.40(3)	C(2)–N(2)–C(5)	110(1)
		N(1)–C(1)–C(2)	111(2)
		C(1)–C(2)–N(2)	115(2)

Atom		Interatomic distance (Å)	Positions[a] of	
A	B		A	B
H[N(2)][b]	O(3)	2.23	1	3
N(3)	O(5)	3.01(2)	1	2
N(3)	O(8)	3.13(2)	1	3
N(3)	O(10)	2.95(2)	1	5
N(4)	O(6)	2.91(2)	1	2
N(4)	O(8)	2.96(2)	1	5
H_2O	O(4)	3.00(2)	1	4
H_2O	O(6)	2.92(2)	1	2

a) Numerals refer to the following equivalent positions; 1: x, y, z. 2: $-1/2+x, 1/2-y, -z$. 3: $-1/2+x, 1/2-y, 1-z$. 4: $1/2-x, 1-y, 1/2+z$. 5: $1-x, -1/2+y, 1/2-z$. b) The coordinates of H atom linked to N(2) were calculated on the assumption that the N–H bond length is 1.03 Å.

$[PtCl_2(NH_3)_2]$ (2.05(4) Å)[4] and $[Pt(NH_3)_4][Re_2O_3(CN)_8]$ (2.047—2.059(9) Å)[5] within the limits of experimental error, though they seem to be slightly longer than those cited for comparison. The bond lengths of Pt–N(1) (tertiary amino group) and Pt–N(2) (secondary) are almost equal, but are somewhat longer than those of Pt–N (primary) found in $[Pten_2][MoO(H_2O)(CN)_4]\cdot 2H_2O$ (2.024(6) and 2.036(4) Å).[6] The C–C single bond in the complex cation is unusually short. However, all the bond lengths and angles in the $[Sb_2(+)\text{-tart}_2]$ anion are normal and are in good agreement with the corresponding ones in $K_2[Sb_2(+)\text{-tart}_2]\cdot 3H_2O$.[7] The abnormal C–C bond length presumably results from errors in absorption correction for the intensity data.

The complex cation is surrounded octahedrally by six $[Sb_2(+)\text{-tart}_2]$ anions. Since no hydrogen atoms could be located, it is difficult to point out unequivocally the hydrogen bonds in which the NH_3 or H_2O molecule participates. Some possible hydrogen bonds are shown in Table 2. However, the hydrogen bonding in the present crystal seems to be rather weak from the viewpoint of the interatomic distance between proton donor and acceptor.

This research was supported by a Scientific Research Grant from the Ministry of Education. K. M. also acknowledges the financial support of the Matsunaga Science Foundation.

References

1) J. Hornstra and B. Stubbe, PW 1100 Data Processing Program, Philips Research Laboratories, Eindhoven Holland.
2) "International Tables for X-Ray Crystallography," Vol. III, Kynoch Press, Birmingham (1962), p. 202.
3) The *X*, *Y*, and *Z* are orthogonal coordinates (Å) referred to a, b and c axes.
4) G. H. W. Milburn and M. R. Truter, *J. Chem. Soc.*, *A*, **1966**, 1609.
5) R. Shandles, E. O. Schlemper, and R. K. Murmann, *Inorg. Chem.*, **10**, 2785 (1971).
6) P. R. Robinson, E. O. Schlemper, and R. K. Murmann, *Inorg. Chem.*, **14**, 2035 (1975).
7) M. E. Gress and R. A. Jacobson, *Inorg. Chim. Acta*, **8**, 209 (1974).

Proton Magnetic Resonance Spectra of Metal Ammine Complexes. VIII.* Hydrogen Isotopic Exchange in the $[Co(O)_2(N)_4]^+$ Complex Ions

Toshiaki TAURA, Ushio SAKAGUCHI, and Hayami YONEDA

Department of Chemistry, Faculty of Science, Hiroshima University, Hiroshima 730

(Received January 20, 1976)

The rates of amine hydrogen isotopic exchange in the $[Co(O)_2(N)_4]^+$ complex ions, where $(O)_2$ represents carbonate, oxalate, or malonate ions, and $(N)_4$, tetraammine, bis(ethylenediamine), or bis(trimethylenediamine), were measured in D_2O at 35 °C by the PMR technique. It was found that: (1) the rates for *trans* (to oxygen) amines are faster than those for *cis* amines; (2) the rates, especially for *trans* amines, in the carbonato complexes are slower than those in the oxalato and malonato analogs, and (3) the difference between the rates for *cis* and *trans* amines is smaller in the bis(diamine) complexes than in the tetraammine complexes. These results are discussed in terms of the influence of the chelate geometry in the complex on the exchange reaction.

In our previous papers,[1] it was reported that the *trans* amine hydrogen exchange in $[CoCN(NH_3)_5]^{2+}$, $[CoNO_2(NH_3)_5]^{2+}$, and *cis*-$[Co(CN)_2(en)_2]^+$ is unusually decelerated.** In general, coordinated ligand molecules are influenced by the electron-withdrawing effect of the positively charged metal ion. This effect leads to the decrease in the electron density on the nitrogen atom of the coordinated amine ligand and to a concomitant labilization of the hydrogen atom attached to this nitrogen. Therefore, if the Co–N bond is weakened, the electron density on the nitrogen atom will be restored and the amine ligand will approach its free state so that the hydrogen atom bound to this nitrogen atom becomes less labile. This is the reason for the deceleration in the above complexes. Thus, it was thought that the measurement of the rate of hydrogen exchange might serve as a convenient means of obtaining information on the chemical bonding in complexes.

On the other hand, it is known from the results of X-ray studies that the O–Co–O bond angles in the dicarboxylato complexes are *ca.* 70° for the carbonate ion,[2] *ca.* 84° for the oxalate ion,[3] and *ca.* 96° for the malonate ion.[4] The effect of the deviation of these angles from the ideal octahedral value (90°) has been studied through the circular dichroism spectra of the dicarboxylatobis(ethylenediamine) complexes[5] and the aquation reaction of the carbonato$(N)_4$ complexes.[6] Douglas *et al.*[5] reported that the T_{1g} rotatory strength decreases sharply, $CO_3^{2-} > ox^{2-} > mal^{2-}$, with an increase in the size of the carboxylato chelate ring. Dasgupta and Harris[6] discussed the relationship between this deviation and the aquation kinetics. These studies interested us in the effect of this deviation on the rate of amine hydrogen exchange.

To investigate the influence of the geometry of the dicarboxylato chelate, the rates of amine hydrogen exchange in the $[Co(O)_2(N)_4]^+$ complex ions, where $(O)_2=CO_3^{2-}$, ox^{2-}, or mal^{2-} and where $(N)_4=(NH_3)_4$, $(en)_2$, or $(tn)_2$, have been determined by the PMR technique.

* Part VII: U. Sakaguchi, S. Yamazaki, and H. Yoneda, *Bull. Chem. Soc. Jpn.*, **49**, 402 (1976).

** In this paper, en, tn, ox, or mal represent ethylenediamine, trimethylenediamine, the oxalate ion, or the malonate ion respectively.

Experimental

Preparation. The $[CoCO_3(NH_3)_4]Cl\cdot 1/4H_2O$, $[CoCO_3(en)_2]Cl$, and $[Coox(tn)_2]Cl\cdot H_2O$[7] complexes were prepared by the usual methods, and the number of molecules of the water of crystallization was determined by elemental analysis. $[Coox(NH_3)_4]Cl\cdot H_2O$, $[Comal(NH_3)_4]Cl\cdot 3/2H_2O$, and $[Coox(en)_2]Cl\cdot H_2O$ were obtained by adding an equimolar amount of oxalic and malonic acids to the corresponding carbonato complexes and then by heating the mixtures until the effervescence subsided. $[Comal(en)_2]Cl\cdot H_2O$ was obtained from the iodide salt[5] by trituration with AgCl. $[CoCO_3(tn)_2]Cl\cdot H_2O$ was prepared by a method similar to that used for the bis(ethylenediamine) analog. *cis*-$[Co(CH_3CO_2)_2(NH_3)_4]ClO_4$ was prepared by Kuroda's procedure.[8] All these complexes were recrystallized once or twice. The data of the spectrophotometric measurements are summarized in Table 1.

Table 1. First absorption maxima for the $[Co(O)_2(N)_4]^+$ complex ions (nm)

	CO_3	ox	mal	$(CH_3CO_2)_2$
$(NH_3)_4$	522	508	516	522
$(en)_2$	511	497	497	
$(tn)_2$	520	510		

Measurement. The rate of amine hydrogen exchange was determined by following the change in the PMR signal intensity with the time, which was measured at 35 °C with a Varian T-60 spectrometer. An adequate amount of the sample was dissolved in D_2O, and the pD was adjusted by HCl for the dicarboxylato chelate complexes and by $HClO_4$ for the diacetatotetraammine complex so that the exchange might be complete in an appropriate time. The PMR measurement was initiated a few minutes after the sample had dissolved, and the pD of the sample solution was measured at about 30 °C with a Hitachi Horiba Model F-7 pH meter using a microelectrode immediately after the PMR measurement. The absorption spectra were measured with a Shimadzu UV-200 double beam spectrophotometer.

The oxalato tetraammine complex is sparingly soluble in D_2O, and the *cis* and *trans* amine signals overlap.

The influence of counter ions on the rate seemed insignificant, because the change in the concentration of the complexes did not affect the rates, within the limits of experimental errors.

Results and Discussion

The PMR spectra of some samples in D_2O or HCl–D_2O are shown in Fig. 1. We have assigned the higher

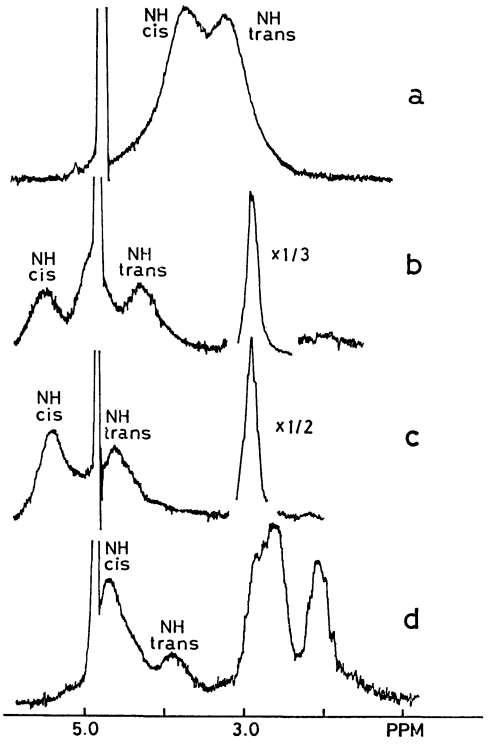

Fig. 1. The PMR spectra of (a) $[CoCO_3(NH_3)_4]^+$, (b) $[CoCO_3(en)_2]^+$, (c) $[Coox(en)_2]^+$, and (d) $[CoCO_3(tn)_2]^+$ in D_2O or HCl–D_2O.

field signal to the *trans* amine and the lower field signal to the *cis* amine based on the magnetic anisotropy of the cobalt ion.[9] In the tetraammine and bis(trimethylenediamine) complexes, both *trans* and *cis* amine proton signals appear at higher fields than the HDO signal, while the bis(ethylenediamine) complexes give the *trans* amine signal at a higher field, and the *cis* one at a lower field, than the HDO signal, except that $[Coox(NH_3)_4]^+$ has only one broad signal at a higher field than HDO.

Figure 2 shows the time change in the amine proton signal intensities for $[Comal(NH_3)_4]^+$ in D_2O. It may be noted in this figure that the *trans* amine signal disappears about ten minutes after dissolution, but the

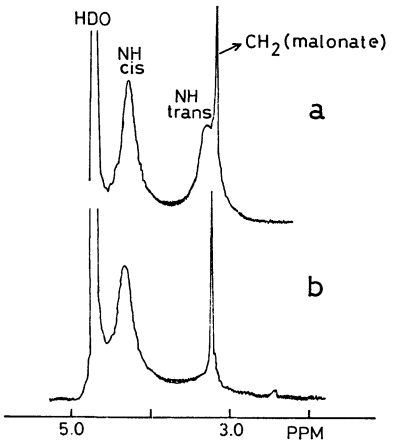

Fig. 2. The PMR spectra of $[Comal(NH_3)_4]^+$ in D_2O (a) immediately after dissolution, and (b) about ten minutes after dissolution.

cis one remains almost unchanged. Therefore, the exchange rate for the *trans* amine hydrogens is much faster than that for the *cis* ones.

The rate constant for the exchange is given by

$$\ln h_t = -kt + c$$

where h_t and k refer to the peak height of an amine proton signal at time t and the rate constant respectively, and where c is a constant. As is shown in Fig. 3, plots

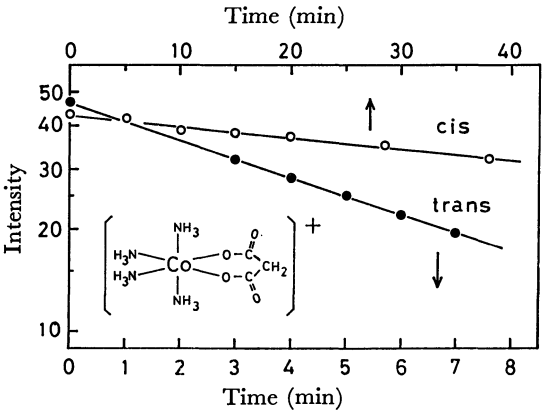

Fig. 3. Plots of log h_t *vs. t.* ●: *trans*, ○: *cis*. *Trans* and *cis* amines correspond to the downward and upward scales respectively.

of log h_t against the time gave straight lines. The rate constants for hydrogen exchange were obtained from the slopes of these plots. It is known[10] that the pseudo-first-order rate constant is directly proportional to the concentration of OD^- ions:

$$k_{obsd} = k_0[OD^-]$$

where k_{obsd} and k_0 refer to the observed and the second-order rate constant respectively.

The rate-constant data obtained in this manner are collected in Table 2. The data are also plotted in Fig. 4. A comparison of these data indicates that: (1) *trans* amine protons are more labile than *cis* ones; (2) the

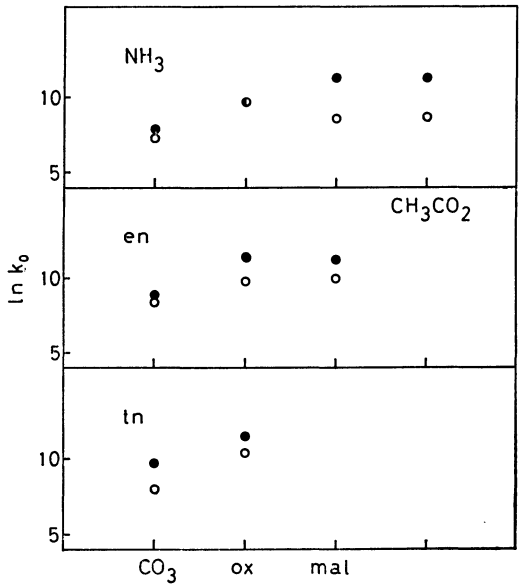

Fig. 4. Plots of ln k_0. ●: *trans*, ○: *cis*, ◐: not assigned.

Table 2. Rate constants for hydrogen exchange in $[Co(O)_2(N)_4]^+$ at 35 °C
k_{obsd}: observed rate constant ($s^{-1} \times 10^3$), k_0: second-order rate constant ($M^{-1}\,s^{-1} \times 10^{-4}$).

		CO_3			ox			mal			$(CH_3CO_2)_2$		
		pD[a]	k_{obsd}	k_0	pD	k_{obsd}	k_0	pD	k_{obsd}	k_0	pD	k_{obsd}	k_0
$(NH_3)_4$	*cis*	7.93	1.3	0.15	6.02	0.18	1.7[b]	6.41	0.14	0.54	6.75	0.34	0.60
	trans	7.93	2.2	0.26				6.41	2.1	8.2	6.75	4.6	8.2
$(en)_2$	*cis*	7.77	2.6	0.44	6.66	0.81	1.8	6.86	1.5	2.1			
	trans	7.77	4.1	0.70	6.66	4.0	8.8	6.86	5.4	7.5			
$(tn)_2$	*cis*	7.26	0.53	0.29	5.10	0.041	3.3						
	trans	7.26	3.0	1.7	5.10	0.13	9.9						

a) The pD was calculated using the formula pD=pH+0.4, in which pH is a value measured with a usual pH meter in D_2O. b) Not assigned to *cis* or *trans*.

rates for the carbonato complexes are slower than those for the oxalato and malonato analogs; (3) the difference between the rates for the *cis* and *trans* amines is much smaller in the carbonato complexes, and (4) this difference seems to be smaller in the complexes with chelated amines.

As has been mentioned before, the O–Co–O bond angle increases with an increase in the size of the dicarboxylato chelate ring. The deviation of the O–Co–O bond angle from the ideal octahedral value (90°) is greatest in the carbonato complex, and the coplanar N–Co–N bond angle is enlarged in comparison with the octahedral value. This effect will make the Co–N bond less stable, and the hydrogen exchange for *trans* amines will be decelerated. This is considered to be the reason why the rates for *trans* amines in the carbonato complexes are much slower than in the oxalato and malonato analogs. The rates for *trans* amines in the $[Coox(en)_2]^+$ and $[Comal(en)_2]^+$ ions are similar to each other, probably because the deviation of the O–Co–O bond angle is smaller in these complexes. Therefore, the difference in the steric effect between the oxalato and malonato ligands does not seem to be apparent in the hydrogen exchange, though this effect may play an important role in the base hydrolysis of these complex ions.[11]

If *cis* amines are not so much influenced by the carbonato chelate, the difference in the rates for *trans* and *cis* amines necessarily becomes smaller in the carbonato complexes. This seems to be the case with the tetraammine and bis(ethylenediamine) complexes.

The remarkable deceleration of the hydrogen exchange for *cis* amines in $[CoCO_3(tn)_2]^+$ is not clearly explicable. It may be due to the internal hydrogen bonding, as suggested by a study of the carbonate exchange in a basic medium.[12]

The difference between the rates for *trans* and *cis* amine protons is appreciably smaller in the bis(ethylenediamine) and bis(trimethylenediamine) complexes than in the tetraammine analogs. Though the origin of this difference is not known, it is probable that the alkyl bridge links the *cis* to the *trans* amine and imparts a similar bonding property to both amines. Therefore, the rate for *cis* amines will be more similar to the rate for *trans* amines in the chelate amine complexes than in the complexes with no chelated amines.

Factors other than steric ones which affect the rate of hydrogen exchange, will now be examined. The maxima of the first absorption bands are nearly equal. They are positioned at 522, 508, and 516 nm in, for example, the tetraammine complexes of the carbonate, oxalate, and malonate ions respectively, as is shown in Table 1; therefore, the ligand field effect seems insignificant. The ligand field of the carbonato ligand, however, is slightly weaker than that of the others, and one may think that the peculiarity of the rate for the carbonato complex is due to this slight difference in ligand field strength. To make it clear, the rate of amine hydrogen exchange in *cis*-$[Co(CH_3CO_2)_2(NH_3)_4]^+$ was measured, for which λ_{max} is almost equal to that for the corresponding carbonato complex, as is shown in Table 1. In contrast to this similarity in the ligand field strength, the rate for *cis*-$[Co(CH_3CO_2)_2(NH_3)_4]^+$ is much more analogous to that for the malonato complex than for the corresponding carbonato complex. This result supports our expectation that the ligand field effect is less important for the rate of amine hydrogen exchange.

Thus, it can be concluded that the difference in the rate of amine hydrogen exchange arises from the steric source and not from the ligand field effect, and that the peculiarity of the carbonato complexes probably originates from the remarkably strained chelate geometry, where the O–Co–O bond angle is *ca.* 70°. Then, this peculiarity leads us to expect that the *trans*-bond-weakening effect is larger in the carbonato complex than in the oxalato and malonato analogs, although this effect on the Co–N bond length is not clearly apparent in the reported crystal structures.[2] It was also found that the difference in the rate for *trans* and *cis* amines is smaller in the chelate amine complexes than in the complexes with no chelated amines. This suggests that the effect of a dicarboxylato ligand on *trans* and *cis* amines is averaged to some extent through the alkyl bridge of the amine chelate.

References

1) H. Yoneda, U. Sakaguchi, and K. Maeda, *Chem. Lett.*, **1975**, 107; U. Sakaguchi, K. Maeda, and H. Yoneda, *Bull. Chem. Soc. Jpn.*, **49**, 397 (1976).

2) G. A. Barclay and B. F. Hoskins, *J. Chem. Soc.*, **1962**, 586; G. J. Gene and M. R. Snow, *J. Chem. Soc., A*, **1971**, 2981; M. R. Snow, *Aust. J. Chem.*, **25**, 1307 (1972).

3) K. R. Butler and M. R. Snow, *J. Chem. Soc., A*, **1971**, 565.

4) K. Matsumoto and H. Kuroya, *Bull. Chem. Soc. Jpn.*, **45**, 1755 (1972).
5) W. T. Jordan, B. J. Brennan, L. R. Foebe, and B. E. Douglas, *Inorg. Chem.*, **12**, 1827 (1973).
6) T. P. Dasgupta and G. M. Harris, *J. Am. Chem. Soc.*, **93**, 91 (1971).
7) I. R. Jonasson, S. F. Lincoln, and D. R. Stranks, *Aust. J. Chem.*, **23**, 2267 (1970).
8) K. Kuroda and P. S. Gentile, *Bull. Chem. Soc. Jpn.*, **38**, 1362 (1965).
9) H. Yoneda and Y. Nakashima, *Bull. Chem. Soc. Jpn.*, **47**, 669 (1974); Y. Nakashima, U. Sakaguchi, and H. Yoneda, *Chem. Lett.*, **1974**, 503; Y. Nakashima, U. Sakaguchi, and H. Yoneda, *Bull. Chem. Soc. Jpn.*, **48**, 762 (1975); Y. Nakashima, *ibid.*, **48**, 766 (1975).
10) J. S. Anderson, H. V. A. Briscoe, and N. L. Spoor, *J. Chem. Soc.*, **1943**, 361.
11) M. E. Farago, *Coord. Chem. Rev.*, **1**, 66 (1966).
12) J. E. Boyle and G. M. Harris, *J. Am. Chem. Soc.*, **80**, 782 (1958).

Kinetic Study on Dimerization of Chlorotris(triphenylphosphine)-rhodium(I) in Benzene

Yoshimi OHTANI, Masatoshi FUJIMOTO, and Akihiko YAMAGISHI

Department of Chemistry, Fuculty of Science, Hokkaido University, Sapporo 060

(Received March 3, 1976)

The monomer-dimer equilibrium of $RhCl(PPh_3)_3$ in benzene has been studied with a stopped-flow apparatus under He gas pressure. The decomposition rate of a dimer, $[RhCl(PPh_3)_2]_2$, obeys pseudo-first-order kinetics with respect to the concentration of PPh_3, whereas the formation rate of a dimer obtained by diluting an equilibrium solution with benzene depends on the equilibrium concentration of a monomer, a dimer and PPh_3 in a complexed manner. The kinetic results are consistent with the following mechanism; $2RhCl(PPh_3)_3 \rightleftarrows RhCl(PPh_3)_2 + RhCl(PPh_3)_3 + PPh_3 \rightleftarrows [RhCl(PPh_3)_2]_2 + 2PPh_3$.

Chlorotris(triphenylphosphine)rhodium(I) first synthesized by Wilkinson and coworkers has been found to catalyze various kinds of reactions, such as hydrogenation, carbonylation and decarbonylation.[1-3] There have been, however, some disputes over the structures of the complexes in solution. Wilkinson and coworkers proposed the complete dissociation of $RhCl(PPh_3)_3$ into $RhCl(PPh_3)_2$ and PPh_3 on the basis of the molecular weight measurement:

$$RhClL_3 \rightleftarrows RhClL_2 + L \quad (L: PPh_3) \qquad (1)$$

Based on the deviations of the absorbance of $RhCl(PPh_3)_3$ from Beer's law and the effects of added PPh_3 on the spectra, Arai and Halpern estimated the dissociation constant of Reaction 1, K_{dissoc}, to be $(7 \pm 1) \times 10^{-5}$ M.[4] On the other hand, Tolman and coworkers recently observed that the ^{31}P NMR signal of chlorotris(tri-*p*-tolylphosphine)rhodium(I), $RhCl[P(p\text{-tolyl})_3]_3$, in toluene becomes weak on raising temperature with the appearance of other sharp resonances. The new resonances were identical with those of the dimer form of the complex, $[RhCl[P(p\text{-tolyl})_3]_2]_2$, which was prepared independently.[5,6] Thus it was concluded that $RhCl(PPh_3)_3$ reversibly dimerized according to

$$2RhClL_3 \rightleftarrows [RhClL_2]_2 + 2L. \qquad (2)$$

Tolman and coworkers determined the dimerization constant of Eq. 2, K_{dimer}, using the same results of the electronic spectra as obtained by Halpern *et al.*; $K_{dimer} = (3.3 \pm 0.4) \times 10^{-4}$ M in benzene.[6] Although ^{31}P NMR spectra unambiguously showed the reversible interconversion between a monomer and a dimer, a number of kinetic investigations on the catalytic actions of the complexes still suggests the presence of the intermediate, $RhClL_2$.[1] The present work describes the kinetics of the monomer-dimer equilibrium in benzene with the purpose to settle down the problems concerning the origin of the intermediate complex, $RhClL_2$.

Experimental

$RhCl(PPh_3)_3$ was prepared in the usual manner from $RhCl_3 \cdot 3H_2O$ and PPh_3.[1] Found: C, 70.12; H, 4.79; Cl, 3.94%. Calcd for $C_{54}H_{45}ClP_3Rh$: C, 70.10; H, 4.90; Cl, 3.83%. PPh_3 was recrystallized from ethanol. Reagent grade benzene was distilled. The solution was prepared by dissolving $RhCl(PPh_3)_3$ and PPh_3 under vacuum after rigorously excluding oxygen from solvents.

The absorbance of $RhCl(PPh_3)_3$ in benzene was measured by a Hitachi EPS-3T recording spectrophotometer. Ten ml of a PPh_3 solution (9.64×10^{-3} M) was added gradually to 10 ml of a $RhCl(PPh_3)_3$ solution (5.16×10^{-4} M). Equilibrium constant based on the dimerization equilibrium was calculated from the absorbance change at 430 nm. Equilibrium shift due to dilution was so small that it could be neglected.

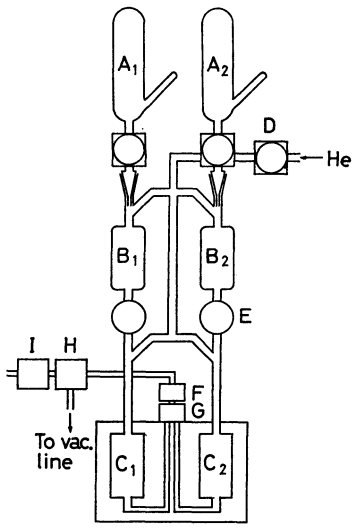

Fig. 1. Schematic diagram of the stopped-flow apparatus. A, B, and C, reservoir; D, Teflon stopcock; E, greaseless valve; F, cell; G, mixing chamber; H, three-way tap; I, air valve.

Kinetic measurements were made using a Union Giken RA 102 stopped-flow apparatus. The mixing part of the apparatus is made of glass and Teflon (Fig. 1). The samples were dissolved in (A) under vacuum. After filled with He gas, (A) was mounted on the body. The body was evacuated and the samples were dropped into (B). After raising the He gas pressure up to *ca.* 2 kg/cm^2, the samples were dropped into (C). The flow was started by opening the air valve. The flow period is about 40 ms. The reaction was followed spectrophotometrically, using a quartz cell of 2 mm optical path. The nominal purity of He gas is 99.8%, thus the effect of O_2 was negligibly small.

Results and Discussion

The variation of the absorbance at 430 nm by the addition of PPh_3 to a $RhClL_3$ solution is shown in Fig. 2. The dissociation equilibrium and the dimerization equilibrium could not be distinguished only from this result.[6] But from the reasons mentioned in the

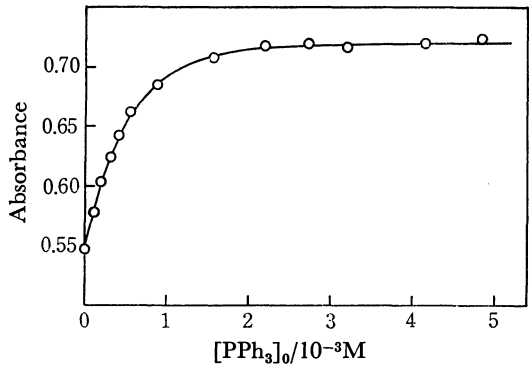

Fig. 2. Effect of added PPh_3 on the absorbance at 430 nm of a 5.2×10^{-4} M $RhCl(PPh_3)_3$ solution in benzene. 20 °C.

introduction, the dimerization equilibrium is considered to be more likely. Assuming equilibrium (2), Eq. 3 is obtained

$$K_{dimer} = [(RhClL_2)_2][L]^2/[RhClL_3]^2 = \frac{(A_\infty - A)\{[L]_0^2\Delta\varepsilon + (A_\infty - A)\}^2}{2\Delta\varepsilon\left\{A - A_\infty\left(1-\frac{\Delta\varepsilon}{\varepsilon_1}\right)\right\}^2} \quad (3)$$

where A is the absorbance, A_∞ the limiting absorbance at high PPh_3 concentrations, ε_1 and ε_2 are the extinction coefficients of $RhClL_3$ and $(RhClL_2)_2$, respectivery, $\Delta\varepsilon=\varepsilon_1-(1/2)\varepsilon_2$ and $[L]_0$ is the concentration of added PPh_3. The value of ε_1 was calculated from $\varepsilon_1 = A_\infty/[RhClL_3]_0$; $\varepsilon_1=1.4\times10^3$ 1 mol^{-1} cm^{-1}. K_{dimer} and $\Delta\varepsilon$ were determined using the curve-fitting method; $K_{dimer}=9\times10^{-5}$ M, $\varepsilon\Delta=7.1\times10^2$ 1 mol^{-1} cm^{-1} and $\varepsilon_2=2(\varepsilon_1-\Delta\varepsilon)=1.4\times10^3$ 1 mol^{-1} cm^{-1}. K_{dimer} is of the same order of magnitude as obtained by Tolman *et al.* $((3.3\pm0.4)\times10^{-4}$ M).[6]

When $RhCl(PPh_3)_3$ and PPh_3 are mixed, the time-course of the absorbance change at 430 nm gives a single exponential curve. The rate of the absorbance change at 430 nm is related to the decomposition rate of the dimer as below.

$$A_{430} = \varepsilon_1[RhClL_3] + \varepsilon_2[(RhClL_2)_2] = \varepsilon_1[RhClL_3]_0 - (2\varepsilon_1-\varepsilon_2)[(RhClL_2)_2] = -2\Delta\varepsilon[(RhClL_2)_2] + \text{const.}$$

Thus,

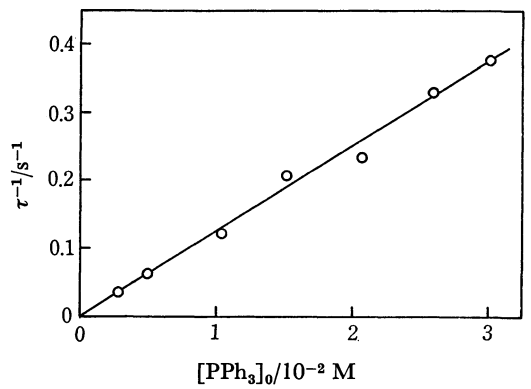

Fig. 3. The dependence of the decomposition rate of a dimer on the concentration of added PPh_3. $[RhCl(PPh_3)_3]_0=5.0\times10^{-4}$ M, at 430 nm and 20 °C.

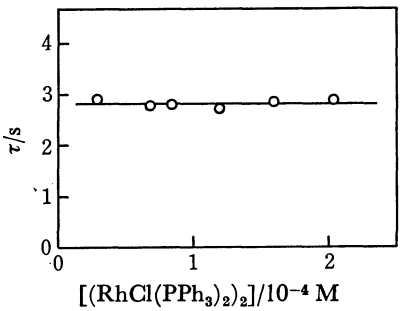

Fig. 4. The dependence of the decomposition rate of a dimer on the initial concentration of $[RhCl(PPh_3)_2]_2$. $[PPh_3]_{add}=3.0\times10^{-2}$ M, at 430 nm and 20 °C.

$$\frac{dA_{430}}{dt} = -2\frac{d[(RhClL_2)_2]}{dt}.$$

Figure 3 shows the dependence of the decomposition rate on the concentration of added PPh_3. Figure 4 shows the dependence of the decomposition rate on the concentration of a dimer. It shows the first-order dependence of the rate on $[RhCl(PPh_3)_2]_2$. Summarizing the above results, the decomposition rate is expressed by Eq. 4.

$$-\frac{d[(RhClL_2)_2]}{dt} = k[(RhClL_2)_2][L] \quad (4)$$

When the solution containing the equilibrium concentrations of a monomer and a dimer is diluted by pure benzene, the equilibrium (2) shifts to the right-hand side. Therefore the formation of a dimer can be followed by mixing the equilibrium solution with pure benzene. Figure 5 shows the dependence

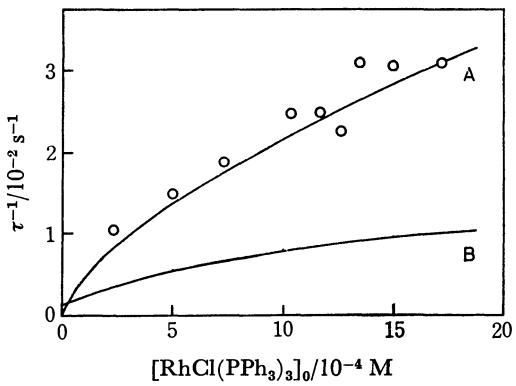

Fig. 5. The dependence of the reciprocal of the relaxation time for dilution experiments on the total concentration of $RhCl(PPh_3)_3$. 20 °C.
Solid lines show calculated curves; A from Eq. 6 and B from dissociation mechanism.

of the formation rate of a dimer on the concentration of added PPh_3. It shows that the formation rate of a dimer increases with the concentration of $RhCl(PPh_3)_3$. Equation 4 suggests that the rate-determining step in the dimer decomposition is the first attack by PPh_3 on a dimer. Thus the following mechanism is proposed in interpreting the present kinetic results:

$$2RhClL_3 \overset{K_1}{\rightleftharpoons} RhClL_2 + RhClL_3 + L \overset{k_2}{\underset{k_{-2}}{\rightleftharpoons}} (RhClL_2)_2 + 2L \quad (5)$$

The above mechanism assumes that the dissociation reaction (1) is present as a pre-equilibrium of the dimer formation. The rate of the concentration change of a dimer is given by Eq. 6.

$$\frac{d[(RhClL_2)_2]}{dt} = k_2[RhClL_3][RhClL_2] - k_{-2}[(RhClL_2)_2] \times \{[L]_0 + [RhClL_2] + 2[(RhClL_2)_2]\} \quad (6)$$

where $[L]_0$ is the added PPh_3 concentration. For the decomposition experiments $[L]_0$ is so large that the second term in Eq. 6 is predominant. That is,

$$\frac{d[(RhClL_2)_2]}{dt} = -k_{-2}[L]_0[(RhClL_2)_2]$$

$$\tau^{-1} = [L]_0 k_{-2}$$

This coincides with Eq. 4, leading to $k_{-2}=k=12\ M^{-1}\ s^{-1}$. As for the dilution experiments $[L]_0$ is zero, and Eq. 6 is modified to Eq. 7.

$$\frac{d[(RhClL_2)_2]}{dt} = k_2[RhClL_3][RhClL_2] - k_{-2}[(RhClL_2)_2] \times \{[RhClL_2] + 2[(RhClL_2)_2]\} \quad (7)$$

Applying the approximation of the vicinity of the equilibrium to each species, the pseudo-first-order rate constant for the rate of the concentration change of a dimer is given by

$$\frac{d\Delta[(RhClL_2)_2]}{dt} = -\tau^{-1}\Delta[(RhClL_2)_2]$$

where $\Delta[\ ]$ is the concentration change at dilution and τ^{-1} is expressed as below.

$$\tau^{-1} = \frac{[RhClL_3]_e\{[RhClL_3]_e + 4[(RhClL_2)_2]_e\}}{2[(RhClL_2)_2]_e^2} K_1 k_2 + 4[(RhClL_2)_2]_e k_{-2} \quad (8)$$

where $[\ ]_e$ denotes the equilibrium concentration of each species and $K_1=k_1/k_{-1}$. The value of τ^{-1} is calculated as a function of $[RhCl(PPh_3)_3]_0$, using Eq. 8. A solid curve in Fig. 5 is a calculated one, showing that Eq. 8 predicts the observed dependence of the rate on $[RhCl(PPh_3)_3]_0$ satisfactorily. Therefore, it is concluded that reaction mechanism (5) describes the monomer-dimer equilibrium of the complexes correctly. The present mechanism implies that an intermediate $RhClL_2$ is produced rapidly in a pre-equilibrium step leading to the dimer formation.

The present work was supported by the grant-in-aid for Scientific Research from the Ministry of Education.

References

1) J. A. Osborn, F. H. Jardine, J. F. Young, and G. Wilkinson, *J. Chem. Soc., A*, **1966**, 1711.
2) D. Evans, J. A. Osborn, and G. Wilkinson, *J. Chem. Soc., A*, **1968**, 3133.
3) K. Ohno and J. Tsuji, *J. Am. Chem. Soc.*, **90**, 99 (1968).
4) H. Arai and J. Halpern, *Chem. Commun.*, **1971**, 1571.
5) P. Meakin, J. P. Tesson, and C. A. Tolman, *J. Am. Chem. Soc.*, **94**, 3240 (1972).
6) C. A. Tolman, P. Z. Meakin, D. L. Linden, and J. P. Tesson, *J. Am. Chem. Soc.*, **96**, 2762 (1974).

Application of the Zone Melting Technique to Metal Chelate Systems. XII.[1] Computer-assisted Consideration on the Intermittent Zone Melting

Isao YOSHIDA, Hiroshi KOBAYASHI, and Keihei UENO[2]

Department of Organic Synthesis, Faculty of Engineering, Kyushu University, Hakozaki, Higashi-ku, Fukuoka 812

(Received March 13, 1976)

The solute distribution profile on a columned charge of length L after m-cycles of the intermittent zone melting with j zones of length l, was computed for a range of distribution coefficient, k. The effects of j, l and k upon the separation efficiencies by this method were investigated in terms of the fractional length, α, which was refined to an required purity level, γ, in a limited number of m, and the fractional ratio, σ, of a solute amount which was concentrated into a limited portion of a fractional column length, β. The intermittent method is superior in respect to the separation efficiencies, α as well as σ, over the usual method, if a columned charge was zone-melted with the same number of zones of the same length at the same zone-travelling speed. Results of theoretical calculation were confirmed on systems of azobenzene in naphthalene and those of some metal acetylacetonates in the beryllium chelate of the same ligand compound.

In usual practices of zone melting, more than one molten zone are produced on a columned charge for the sake of time-economy. Two basic modes are useful in the operation with multiple zones.

The first mode, in which all zones traverse through the charge from one end to another, is called a "normal" mode herein, and has been extensively studied in its theory as well as in its practices.[3-5]

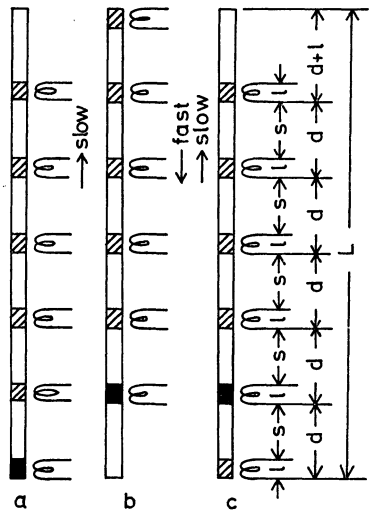

Fig. 1. Reciprocal zone travelling mode in the intermittent zone melting.

The second mode is what is called an "intermittent" method,[6-8] wherein the zones are produced at equal spacings on the charge as shown in Fig. 1(a), and each zone travels in phase to a direction along the charge. After travelling to the distance d between the centers of the nearest neighbor zones, as shown in Fig. 1(b), the heater assembly returns quickly to its initial position as shown in Fig. 1(c). In this cycle, the melt in the first zone is transferred into the second one, meantime the melt initially formed in the second zone transferred into the third one and so forth. In every cycle, the melt in each zone is transferred in a similar manner into its next neighbour in turn.

In the intermittent mode, therefore, the solute distribution is described in terms of the number of reciprocal cycles of the heater assembly, m, and the number of zones produced on a charge, j, in place of the number of zone passes, n, in the normal mode.

In this paper, we consider how the solute distributions vary depending upon m, j and each zone length, l. Also the separation efficiencies are compared between the two modes for systems of a range of distribution coefficient, k.

Results of the theoretical calculation are experimentally confirmed on the system of naphthalene containing azobenzene as a solute and those of bis(acetylacetonato)-beryllium(II), admixed with various metal chelates of the same ligand.

Calculating Procedures of the Solute Distribution. The solute distribution profile on the columned charge of length L after the intermittent zone melting with j zones of l long each, is calculated as follows: The whole columned charge is devided into j divisions of d long except the last one, which is $(d+l)$ long, where d is chosen longer than l. The divisions are assigned with serial numbers, i, in turn from the initial. Since i is defined as

$$i = \{x/d\} + 1$$

and $$L = jd + l, \text{ then } i = 1, 2, 3, \cdots, j,$$

where x is the distance from the initial end along the charge, and $\{x/d\}$ the integer part of the numerical value of x/d. Also variable y is defined as

$$0 \leqq y = (x - \{x/d\}d) = x - (i-1)d \leqq d,$$

where $i=1, 2, 3, \cdots\cdots, (j-1)$,
except the last division, wherein

$$0 \leqq y = x - (j-1)d \leqq d + l$$

In the region of $0 \leqq y \leqq d-l$ on a division, a basic equation in the course of zone melting is represented by Eq. 1 on the basis of mass balance,

$$\frac{dP_{m,i}(y)}{dy} = \frac{k}{l}[C_{m-1,i}(y+l) - P_{m,i}(y)] \qquad (1)$$

where $P_{m,i}(y)$ represents the solute concentration

redistributed into the solid at the position y in the i-th division in the course of m-th cycle, and $C_{m-1,i}(y+l)$ the concentration at $(y+l)$ in the same division after the completion of the $(m-1)$th cycle. The initial conditions for Eq. 1 are

$$P_{m,i}(0) = C_{m-1,i-1}(d)$$

except in the first division, where

$$P_{m,1}(0) = k\int_0^l C_{m-1,1}(y)\mathrm{d}y$$

and $C_{0,i}(y)$ is constant regardless to i and y. In the region of $(d-l)\leqq y\leqq d$ on each division except the j-th one, solute distribution is developed in the basis of distribution profile which has been formed by the preceding zone on the same cycle. A basic equation is, therefore, given by Eq. 2.

$$\frac{\mathrm{d}P_{m,i}(y)}{\mathrm{d}y} = \frac{k}{l}[P_{m,i+1}(y+l-d) - P_{m,i}(y)] \qquad (2)$$

In the corresponding region on the j-th division Eq. 1 is valid, where $C_{m-1,i}(y+l)$ is a constant regardless of y.

When a zone travels to the stroke d, its heating device returns quickly back to the initial position, the molten liquid being left as there it is. Thus after the completion of the m-th cycle, in the region of $0\leqq y\leqq l$ in each division except the first one, $C_{m,i}(y)$ is constant, being equal to the solute concentration of the melt which was equilibrated with the solid at the crystallizing interface therein, and therefore

$$C_{m,i}(y) = P_{m,i-1}(d)/k \qquad (3)$$

where $0\leqq y\leqq l$, $i=2, 3, 4, \cdots\cdots, j$.
Similarly in the region of $d\leqq y\leqq(d+l)$ in the j-th division, the solute concentration in the solid is constant after the completion of m-th cycle as indicated by Eq. 4.

$$C_{m,j}(y) = P_{m,j}(d)/k \qquad (4)$$

When the stroke d is more than twice as long as l, the distribution profile of each division after the completion of the m-th cycle is defined by Eqs. 3 and 5,

$$C_{m,i}(y) = P_{m,i}(y) \qquad (5)$$

in the region of $0\leqq y\leqq l$, and $l\leqq y\leqq d$, respectively, with the exception of the region of $0\leqq y\leqq l$ on the first division and that of $d\leqq y\leqq d+l$ on the j-th one, where the distribution being defined by Eqs. 4 and 5, respectively. If $d\leqq 2l$, then the distribution profile is defined by Eqs. 3 and 5 in the regions of $0\leqq y\leqq l$ and $d-l\leqq y\leqq d$, respectively. Those in the regions of length l at the both ends of the charge are represented by Eqs. 3 and 5 in the similar manner to the above case.

Results and Discussion

Solute Distribution Profile. Some examples of the solute distribution profiles after the intermittent zone melting by use of the six-stage of zones ($j=6$) are shown in Figs. 2, and 3, former of which indicates the effect of cycle number, m for the systems of k equal to 0.4, while the latter the effect of distribution coefficient, k, after 12 cycles of m.

One can readily notice that distribution profiles by the intermittent method are, as a whole, similar to those by the normal method given by Pfann,[3] except

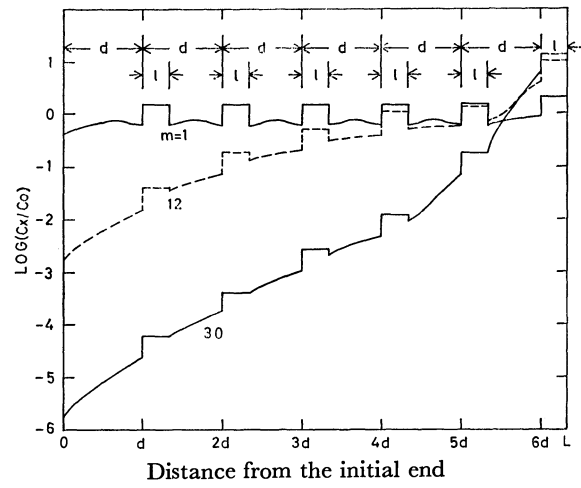

Fig. 2. The solute distributions by the intermittent zone melting after 1, 12, and 30 cyclex of m on the system of $k=0.4$ where $j=6$, $l=0.051L$, and $d=0.16L$. C_x is the solute concentration at x, defined as$C_x=C_{m,i}\{x-(i-1)d\}$ after the m-th cycle.

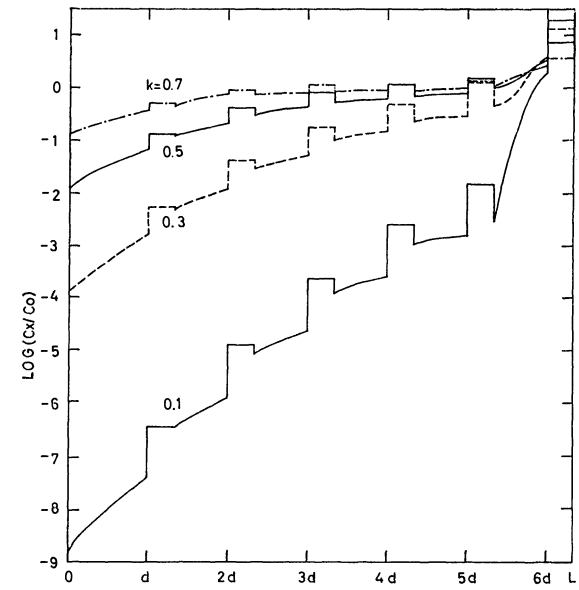

Fig. 3. The solute distributions by the intermittent zone melting after 12 cycles of m on the systems of $k=0.7$, 0.5, 0.3, and 0.1, where $j=6$, $l=0.051$ L, and $d=0.16L$. C_x means the same as in Fig. 2.

protuberant nodes at equal spacings on the curves. The node occurs at the region in which the stroke of a zone overlaps with that of the next neighbor, and the concentration level of a nodal region is equal to that of a molten zone left therein after each cycle. The height or depth of the protuberance decreases with an increase of m, and even in the ultimate stage there remain step-shaped nodes on the distribution curve.

Refining Efficiency. Refining effect can be compared in terms of the length of a refined fraction, of which average concentration decreases to a certain required purity level in a limited period of time. Suppose an α fraction of a columned charge is zone-refined to an average purity, γ, and this value is given as follows:

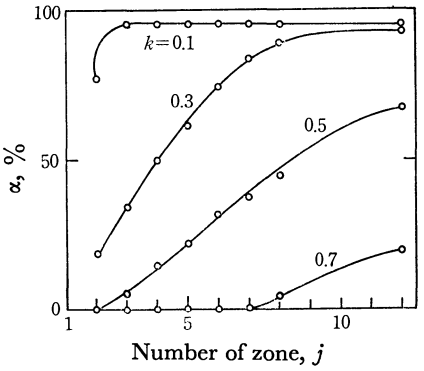

Fig. 4. Relationship between the refining efficiency, α, and the number of zone, j, when $m=2j$, and $l=0.05L$.

$$\gamma = \left[\int_0^{\alpha L} C_m(x)\,dx\right] \Big/ \alpha L C_0 \quad (k<1) \tag{6}$$

$$\gamma = \left[\int_{(1-\alpha)L}^{L} C_m(x)\,dx\right] \Big/ \alpha L C_0 \quad (k>1) \tag{7}$$

where $0 \leqq \alpha \leqq 1$

Figure 4 shows the relationships between the α-value and the zone number, j, when assumed to be $\gamma=0.01$ for a range of k, where m and l are to be $2j$ and $0.05L$, respectively. The higher j-value affords the more efficient refining as expected on the analogy of the effect by the number of zones in the normal mode.

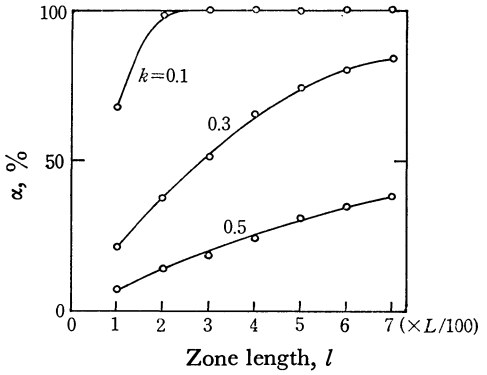

Fig. 5. Relationship between the refining efficiency, α, and zone length, l, when $m=2j$, $j=6$.

On a column of limited length, an increased number of zones leads inevitably to shorter zone-length. However, as shown in Fig. 5, the relationships between α and l indicate that shorter zones do not necessarily give higher refining efficiency in the early stage of the number of m such as in our cases. The column length L is related as $L=l(j+1)+js$, where s means the length of a solid part separating a zone from the next neighbor, and it is practical upon producing more than one zone on a column that the partition solid part is made to be longer than the diameter of the charge for most organic substances. In our case this corresponds to s longer than $0.02L$.

In Fig. 6, α-value after $2j$-cycles of m is plotted against l or j. Although the zone length with which the most efficient refining is attained, varied with k, molten zones of 14—19 stage and 0.03—0.05L long seem to be optimal in general for the range of k.

Concentrating Efficiency. In a similar manner to the

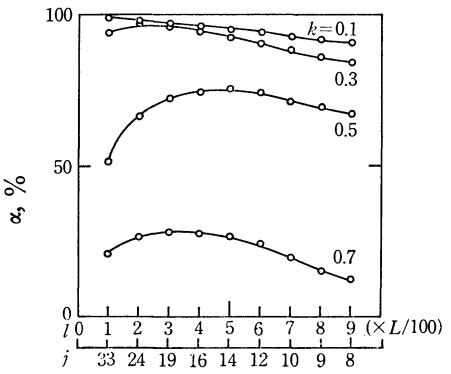

Fig. 6. Dependence of the refining efficiency, α, upon zone length, l, and the number of zone, j, when $m=2j$.

above, concentrating effect can be compared in terms of the fractional amount, σ, of a solute concentrated into the region of length βL as defined in Eqs. 8 and 9:

$$\sigma = \int_{(1-\beta)L}^{L} C_m(x)dx/C_0L \quad (k<1) \tag{8}$$

$$\sigma = \int_0^{\beta L} C_m(x)dx/C_0L \quad (k>1) \tag{9}$$

where $0<\beta<1$.

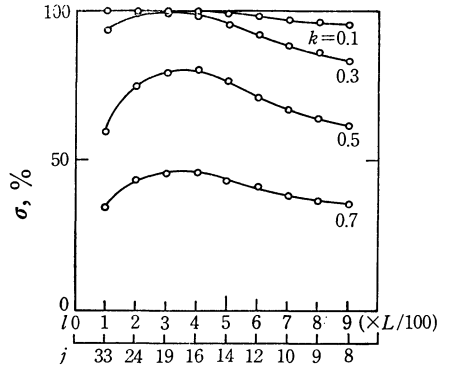

Fig. 7. Dependence of the concentrating efficiency, σ, upon zone length, l, and the number of zone, j, where $m=2j$.

Effects of j and l upon the concentrating efficiency are in a similar manner to those observed in the refining effect, and when s is chosen to be $0.02L$, as shown in Fig. 7, the maximum efficiency is attained with l of $0.03-0.04L$ long and j of between 16 to 19-stage, in accordance with those conditions under which the optimal refining efficiency is afforded.

Comparison of Separation Efficiency between the Normal and Intermittent Zone Melting. In the normal mode the heater assembly arranged as shown in Fig. 1, required the time of $[d(j-1)+L]/v$ to traverse through the whole columned charge, meanwhile j zones pass through, where v is travelling speed of the assembly. An apparent time, t, required for one zone to pass the charge is given as;

$$t = [(j-1)d+jd+l]/jv$$
$$= [(2j-1)d+l]/jv \tag{10}$$

In the intermittent mode, on the other hand, the

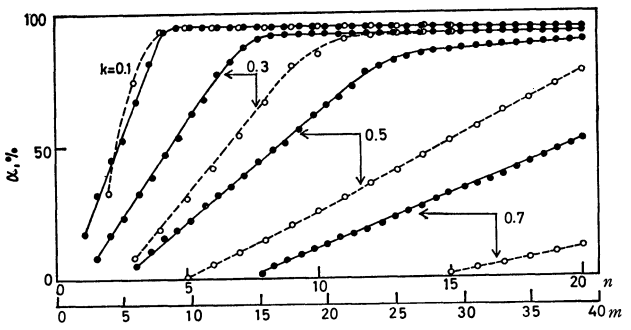

Number of zone passes, n, and strokes, m

Fig. 8. The refining effect, α, by the intermittent- (—●—) and normal (---○---) zone melting, where k less than unity, $j=6$, $l=0.051L$, and $d=0.16L$.

time, t', required for travelling to one stroke is

$$t' = d/v \tag{11}$$

When v is chosen to be constant in the both mode, elimination of v from Eqs. 10 and 11 gives

$$\frac{t}{t'} = \frac{(2j-1)d+l}{jd} \tag{12}$$

Using the relation of t/t' the separation efficiencies by the both methods can be compared on the same scale of operation time. Some comparisons in terms of α are illustrated in Fig. 8, in which α is plotted against n and m, when $\gamma=0.1$ for a range of k less than unity.

Evidently one can notice that the intermittent method affords to attain to the ultimate separation (plateau of the curves) much sooner than the normal method. Situation is the same on the systems of k higher than unity. The reverse situation in a system of lower k-value seems practically of no problem, because such a solute can be readily separated from the matrix in any way. Superiority of the former method is retained upon the comparison in terms of the concentrating efficiency, σ.

Intermittent Zone Melting of Azobenzene in Naphthalene and Metal Acetylacetonates in Beryllium Acetylacetonate. Experimental test of the calculations was performed on the systems of azobenzene in naphthalene and some metal acetylacetonates in bis(acetylacetonato)beryllium(II). The length of a zone, l, and of the partition

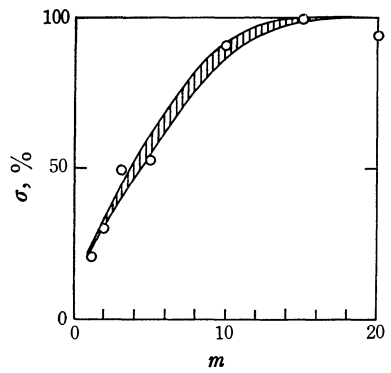

Fig. 9. Concentrated fractions, σ, of azobenzene on a naphthalene column against the number of reciprocal cycles, m. The shaded area indicates the theoretical σ-value for the system of $k=0.22\pm0.02$, when β is chosen to be 0.17.

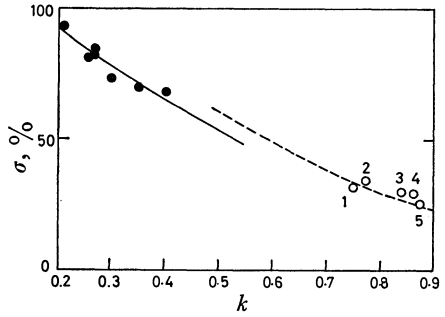

Fig. 10. The σ-value of azobenzene (●) in naphthalene after 10 cycles of m, and those of various metal acetylacetonates (○) in the $Be(AA)_2$ after 12 cycles of m: 1; $Cu(AA)_2$, 2; $Co(AA)_3$, 3; $Al(AA)_3$, 4; $Cr(AA)_3$, and 5; $Fe(AA)_3$, respectively. Dotted- and solid curves indicate the calculated σ-value as the function of k for the corresponding conditions, respectively.

solid part, s, were chosen to be $0.051L$ and $0.107L$, respectively, for procedural convenience. The k-value of azobenzene in naphthalene was determined according to Sorensen,[10] to give 0.22 ± 0.02 under the same operation conditions. The distribution of the solute on a columned charge forms a quite similar curve to those given in Fig. 3. Concentrating effect in terms of σ-value increases with an increased number of m, as shown in Fig. 9, in good agreement with the theoretical calculation for a system of k of 0.22 ± 0.02, which is indicated by a shaded area enclosed with two solid lines.

Figure 10 shows σ-values of the solutes of various k-values, where the effective k of azobenzene could be varied between 0.2 to 0.4 by controlling the stirring effect of molten zones on zone melting as well as the Sorensen's measurement of k-value, and k-values of the metal chelates differ depending upon the kind of the central metal ion. Experimental points stand in good agreement with the respective theoretical curves calculated under the corresponding conditions.

Calculating procedures described above were useful for prediction of experimental results of the intermittent method of zone melting.

Experimental

Materials. Bis(acetylacetonato)beryllium(II) and other metal acetylacetonates were prepared by standard procedures.

Apparatus and Procedures. A high speed zone melting apparatus, operation procedures for the intermittent mode and the determination of k according to Sorensen were essentially same as described previously.[9] A columned charge of 253 mm long and 4 mm in diameter was precessed with 6-stage zones of each 13 mm long, separated with solid parts of each 27 mm long. Zone travelling speed was chosen to be 864 mm/h.

Determination of Solute Concentration. Azobenzene in naphthalene was determined in methanol by use of spectrophotometry[9] on a Hitachi 139 instrument. Metal acetylacetonates were determined, after decomposed in a hot mixture (8 ml) of perchloric acid (3 parts), fuming nitric acid (3 parts) and hydrochloric acid (4 parts), in the form of metal ion by atomic absorption spectrophotometry on a Jarrel-Ash AA-1 instrument.

Computation of the Concentration Profiles. Differential equations (Eqs. 1 and 2) were not solved analytically, and

computed numerically by the Runge-Kutta-Gill method, with the grid spacing of $L/26000$. The computed concentration profile after each intermittent cycle was counterchecked by whether the Simpson's integration of the solute amount over the entire length of the column gave an amount equal to the initial one, where the integration step being equal to the grid spacing. Integral equations (Eqs. 7—10) were also computed in the similar manner. All computations were performed by use of FACOM 230-60 and 230-75 in the Computation Center of Kyushu University.

This work was supported by a grant from the Ministry of Education, to whom the authors are grateful. They are also indebted to Mr. Minato Ookawa for his assistance in FORTRAN programming of the computation.

References

1) Contribution No. 389 from the Department of Organic Synthesis, Kyushu University. Part XI; I. Yoshida, H. Kobayashi, and K. Ueno, *Talanta*, under submission.
2) To whom correspondences should be addressed.
3) W. G. Pfann, "Zone Melting" 2nd ed., John Wiley and Sons, New York (1966).
4) H. Schildeknecht, "Zone Melting," Academic Press, New York (1966).
5) E. F. G. Herington, "Zone Melting of Organic Compounds," Blackwell Sci. Publ., Oxford (1963).
6) Ref. 3, p. 77.
7) Ref. 4, p. 108.
8) K. Eckschlager, V. Ettel, P. Stopka, and Z. Kodejs, *Collect. Czech. Chem. Commun.*, **36**, 3900 (1971).
9) I. Yoshida, H. Kobayashi, and K. Ueno, *Bunseki Kagaku*, **23**, 769 (1974).
10) P. Sorensen, *Chem. Ind. (London)*, **1959**, 1593.

Isomers of *trans*-Dichlorocobalt(III) Complex with (2*S*,10*S*)-2,10-Diamine-4,8-diazaundecane

Masafumi GOTO,[1] Tadashi MAKINO, Masahiko SABURI, and Sadao YOSHIKAWA[2]

Department of Synthetic Chemistry, Faculty of Engineering, The University of Tokyo, Hongo, Bunkyo-ku, Tokyo 113

(Received March 15, 1976)

A novel complex, *trans*(*R*,*S*)-[$CoCl_2$((2*S*,10*S*)-Me_2-2,3,2-tet)]ClO_4((2*S*,10*S*)-Me_2-2,3,2-tet=(2*S*,10*S*)-4,8-diazaundecane-2,10-diamine) was prepared from the *trans*(*R*,*R*) isomer in basic methanol. The configuration of the *trans*(*R*,*S*) isomer was determined from the PMR and CD evidences. The equilibrium ratio of the *R*,*S* and *R*,*R* isomers in basic methanol was estimated to be 7.6±0.3: 1 (ΔG_{298}=1.20±0.03 kcal/mol), the former being in preference to the latter.

It has been demonstrated that the linear tetramine 3,7-diazanonane-1,9-diamine, $NH_2(CH_2)_2NH(CH_2)_3NH(CH_2)_2NH_2$ (abbreviated as 2,3,2-tet), tends to coordinate to metal ions with the *trans* geometry more easily than the triethylenetetramine.[3-5] The possible three isomers of *trans*-$CoCl_2$(2,3,2-tet)$^+$ arisen from the difference in the configurations of the asymmetric secondary nitrogen atoms *R*,*S*(*meso*), *R*,*R*, and *S*,*S* have been isolated.[5,7,8] Further, the thermodynamic advantage of the *R*,*S* configuration over the racemic forms (*R*,*R* and *S*,*S*) has been suggested, though any detailed evidences have not been reported yet.[9]

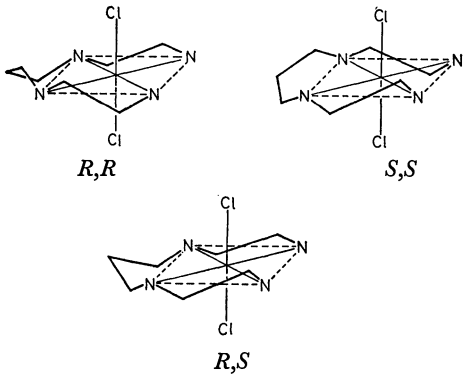

Fig. 1. Possible structures of *trans*-[$CoCl_2$(2,3,2-tet)]$^+$; *R*,*R*, *S*,*S*, and *R*,*S*.

The dominant difference between the *R*,*S* and *R*,*R* (or *S*,*S*) forms consists in the conformation of the central six-membered chelate ring. The chair conformation is adopted in the *R*,*S* form, while the skew-boat conformation in the *R*,*R* and *S*,*S*, as indicated in Fig. 1. The former should be fairly preferred over the latter in a similar manner as in the cyclohexane ring.

Recently, Alexander and coworkers reported some cobalt(III) complexes with (2*S*,10*S*)-4,8-diazaundecane-2,10-diamine (=(2*S*,10*S*)-Me_2-2,3,2-tet[10]), a methyl-substituted derivative of 2,3,2-tet. For the *trans*-dichlorocobalt(III) complex they obtained only one isomer, in which both of the methyl groups adopt the equatorial orientation and the absolute configurations of the secondary N atoms are *R*,*R*.

We have isolated the other *trans*-dichlorocobalt(III) complex of (2*S*,10*S*)-Me_2-2,3,2-tet and assigned the *R*,*S* configuration to it on the proton magnetic resonance (PMR) and other data, the results of which will be reported in the present paper.

Experimental

The ligand (2*S*,10*S*)-Me_2-2,3,2-tet was prepared in a similar way as reported by Harrington, Linke and Alexander,[9] and isolated by distillation. Bp 120—125 °C (4 mmHg).

Preparation of trans-[*$CoCl_2$*((2S,10S)-*Me_2*-2,3,2-tet)]*ClO_4* (*A Mixture of Two Isomers*). (2*S*,10*S*)-Me_2-2,3,2-tet (2.04 g) and $CoCl_2 \cdot 6H_2O$ (2.58 g) were dissolved in 1 M HCl (11 ml) and then water (10 ml) was added. The resultant solution was aerated for 6 h. Concentrated hydrochloric acid (10 ml) was added and the dark wine-red solution was evaporated on a water bath to a volume of 10 ml. To the violet solution was added 60% $HClO_4$ (4 ml), and the green crystals which separated were filtered off after cooling in an ice bath for 1 h, washed with ethanol and ether, and air-dried. Yield, 2.36 g. The product was revealed to be a mixture of two isomers from the PMR measurement.

Preparation of A-β(R,R)-[*$CoCO_3$*((2S,10S)-*Me_2*-2,3,2-tet)]-*$ClO_4 \cdot H_2O$*. The isomeric mixture of *trans*-[$CoCl_2$((2*S*,10*S*)-Me_2-2,3,2-tet)]ClO_4 (0.60 g)was dissolved in 18 ml of water containing 1 ml of 2 M $HClO_4$ with heating and 1.5 g of $NaHCO_3$ were added in small portions. The resultant red solution was concentrated on a water bath to a volume of 10 ml and, then, solid $LiClO_4 \cdot 3H_2O$ (2 g) was added. After cooling wine-red crystals which separated were collected, washed with ethanol and ether, and air-dried. Yield, 0.52 g. Found: C, 28.40; H, 6.29; N, 13.13%. Calcd for [$CoCO_3$-($C_9H_{24}N_4$)]$ClO_4 \cdot H_2O$: C, 28.28; H, 6.17; N, 13.19%.

Preparation of trans(R,R)-[*$CoCl_2$*((2S,10S)-*Me_2*-2,3,2-tet)]-*ClO_4*. *A-β*(*R*,*R*)-[$CoCO_3$((2*S*,10*S*)-Me_2-2,2,2-tet)]-ClO_4 (0.50 g) was added to a mixture of concentrated hydrochloric acid (2 ml) and water (1 ml). After the evolution of carbon dioxide had ceased, 60% $HClO_4$ (2 ml) was added, and the resultant red solution was warmed on a water bath until the separation of green crystals was almost completed. The contents were cooled and the crystals were filtered off, washed with ethanol and ether, and air-dried. Yield, 0.40 g. Found: C, 25.76; H, 5.94; N, 13.32%. Calcd for [$CoCl_2$-($C_9H_{22}N_4$)]ClO_4: C, 25.88; H, 5.80;N, 13.42%.

Preparation of trans(R,S)-[*$CoCl_2$*((2S,10S)-*Me_2*-2,3,2-tet)]-*ClO_4*. *trans*(*R*,*R*)-[$CoCl_2$((2*S*,10*S*)-Me_2-2,3,2-tet)]ClO_4 (0.86 g) was dissolved in 2% 2,6-lutidine in methanol, and the solution was heated under reflux for 2 h. The resultant solution was acidified with methanol saturated with hydrogen chloride gas at room temperature, and then, concentrated to about 10 ml on a rotary evaporator. Solid $LiClO_4$ (2.5 g) was added and the crystals which appeared were filtered off, washed with ethanol and ether, and air-dried. Yield, 0.52 g. A mixture of *trans*(*R*,*S*) and *trans*(*R*,*R*) isomers, thus

obtained, was carefully recrystallized from methanol, and the initial fraction composed of deep green crystals was collected, washed with ethanol and ether, and air-dried. Found: C, 25.74; H, 5.94; N, 13.48%. Calcd for $[CoCl_2(C_9H_{24}N_4)]ClO_4$: C, 25.88; H, 5.80; N, 13.42%.

Measurements. Visible absorption spectra were obtained on a Shimadzu UV-210 spectrophotometer. Circular dichroism spectra were recorded on a JASCO J-20 recording spectropolarimeter. The visible absorption and CD spectra of *trans*-dichloro complexes were obtained in a methanol solution, while the spectra for the carbonato complex was recorded in a aqueous solution. Proton magnetic resonance spectra were obtained on a Hitachi R-20B spectrometer using sodium 2,2-dimethyl-2-silapentane-5-sulfonate as an internal standard reference. The spectra of the *trans*-dichloro complexes were obtained in tetradeutetrated methanol immediately after treating with tetraphenylarsonium chloride and filtering the precipitates. The PMR spectrum of the carbonato complex was recorded in deuterium oxide.

Measurements of Isomerization and Equilibrium between the R,R *and* R,S *Isomers of* trans-$CoCl_2((2S,10S)$-Me_2-*2,3,2-tet*$)^+$. A weighed sample (about 15 mg) of *trans*(*R,R*)- or *trans*(*R,S*)-$[CoCl_2((2S,10S)$-Me_2-2,3,2-tet)$]ClO_4$ was dissolved in 8 ml of 2% lutidine in methanol in a 10 ml volumetric flask, and the solution was warmed to 50 °C for 40 min. After cooling to room temperature (25 °C), the solution was acidified by gentle bubbling of dry hydrogen chloride gas. The volume was adjusted to 10 ml by adding methanol and the CD curve of the resultant solution was recorded.

Results and Discussion

Harrington, *et al.* prepared the *trans*(*R,R*)-$[CoCl_2((2S,10S)$-Me_2-2,3,2-tet)$]ClO_4$ from the *Λ-cis-β*-$[CoCl_2((2S,10S)$-Me_2-2,3,2-tet)$]Cl$, which was isolated from the usual air oxidation products by means of cation exchange chromatography technique, and isomerized to the *trans*(*R,R*) in methanol solution.[9] We obtained the *trans*-dichloro complex by adding perchloric acid (60%) directly to a reaction mixture of the air oxidation procedure. The product, thus obtained, was revealed to be an isomeric mixture of two species from the PMR evidence (Fig. 2-a). The overlapped two doublets of unequal intensities were observed in the region of C-methyl resonance (1.3—1.5 ppm).

The isomeric mixture of *trans*-dichloro complex was converted to the carbonato complex, the PMR spectrum of which showed two overlapping methyl doublets (Fig. 3). This indicates that the carbonato complex has no C_2 symmetry axis and is assigned to the *β* topology. The CD curve (Fig. 4) exhibits a dominant positive band in the first absorption band region ($^1A_{1g} \rightarrow {}^1T_{1g}$ (O_h)), demonstrating the *Λ* configuration of the complex.

The *trans*-dichloro complex prepared from the above-mentioned carbonato complex under strongly acidic condition proved to be identical with the *trans*(*R,R*) isomer reported previously.[9] The PMR spectrum shows a single methyl doublet (Fig. 2-b), and coincides with that reported by Alexander *et al.* The CD spectrum is also the same as the curve previously assigned to the *R,R* isomer[9] (Fig. 5). These results indicates that the carbonato complex also adopts the *R,R* configuration with respect to the secondary N atoms, since the conversion from carbonato to *trans*(*R,R*) dichloro complexes should proceed with retention of secondary N configurations under the acidic condition employed.

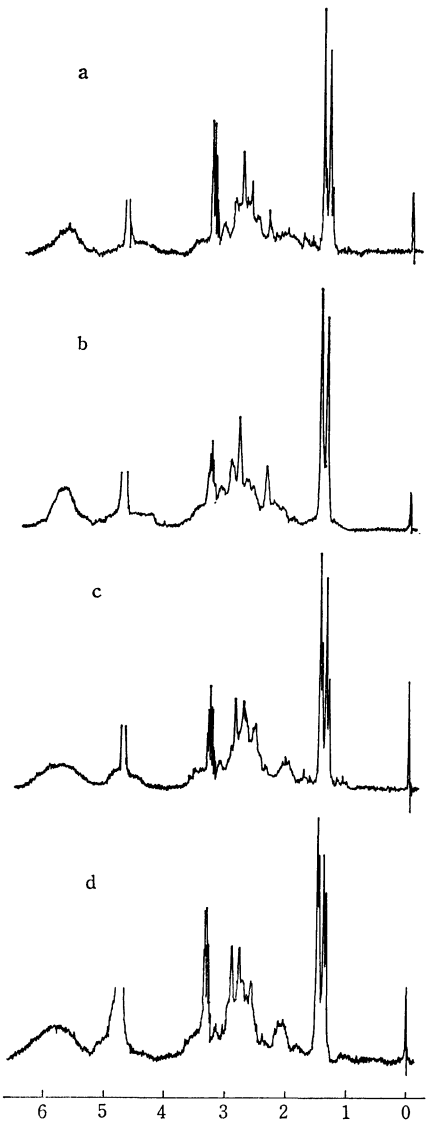

Fig. 2. PMR spectra of *trans*-$[CoCl_2((2S,10S)$-Me_2-2,3,2-tet)$]^+$; (a), a mixture of *R,R* and *R,S* initially obtained: (b), the pure *R,R* isomer; (c), a mixture of *R,R* and *R,S* (*R,R*<*R,S*)) recovered after the equilibration in basic methanol; and (d), the pure *R,S* isomer (in CD_3OD).

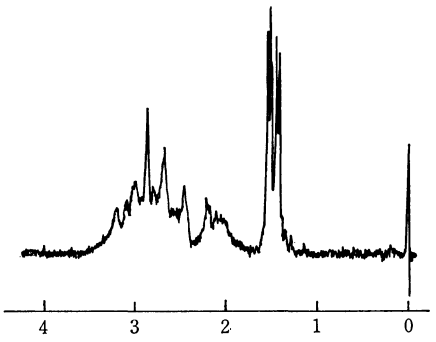

Fig. 3. PMR spectrum of *Λ-β*-$[CoCO_3((2S,10S)$-Me_2-2,3,2-tet)$]^+$ (in D_2O).

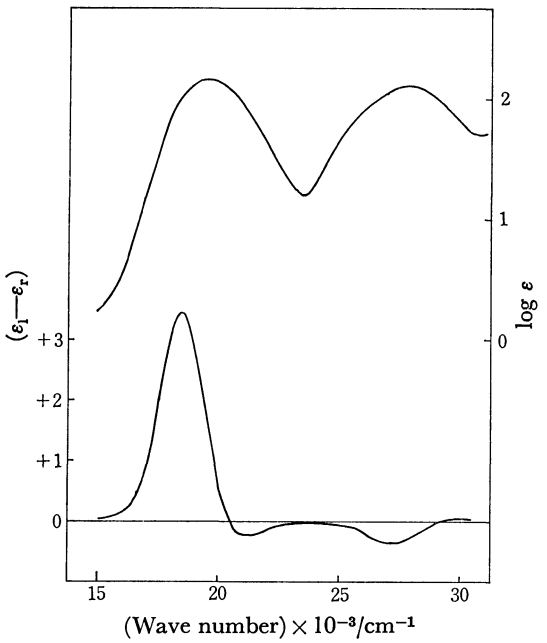

Fig. 4. Visible absorption and CD spectra of Λ-β-[$CoCO_3$((2*S*,10*S*)-Me_2-2,3,2-tet)]ClO_4.

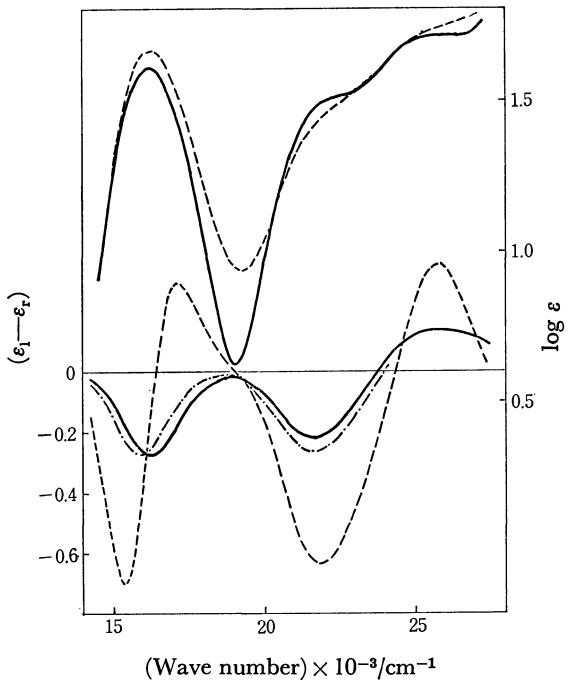

Fig. 5. Visible absorption and CD spectra of *trans(R,R)* (------) and *trans(R,S)* (——) isomers of [$CoCl_2$((2*S*, 10*S*)-Me_2-2,3,2-tet)]$^+$ and CD spectrum of the equilibrated mixture (-·-·-).

It was described that the *trans*(*R*,*R*)-dichloro complex exhibited no evident structural changes in slightly basic methanol solution.[9] We found, however, that the *trans*-dichloro complex obtained directly from an air-oxidation product composed of at least two isomers. So we attempted to isomerize the *trans*(*R*,*R*) form under strongly basic condition such as in 2% 2,6-lutidine in methanol under reflux. The CD curve obtained after the reflux for 2 h was found to be significantly different from the original curve. The *trans*-dichloro complex recovered from the above solution exhibited two methyl doublets with unequal intensities in the PMR spectrum (Fig. 2-c). The *trans*-dichloro isomer different from the *trans*(*R*,*R*) could be purified by carefully repeated recrystallization from methanol as prismatic crystals. The PMR and CD spectra of the present isomer are shown in Figs. 2-d and 5, respectively. The intensities of the two methyl doublets in this PMR can be regarded to be practically equivalent.

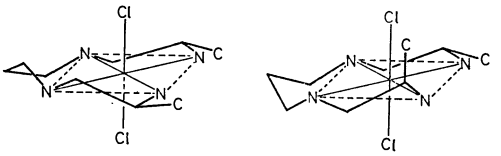

Fig. 6. Possible structures of *trans*-[$CoCl_2$((2*S*, 10*S*)-Me_2-2,3,2-tet)]$^+$: (a) *trans(R,R)*, and (b) *trans(R,S)*.

It is reasonable to consider that the possible structures for the *trans*-$CoCl_2$((2*S*,10*S*)-Me_2-2,3,2-tet)$^+$ ion are those depicted in Fig. 6. The structure shown in Fig. 6-a corresponds to the *trans*(*R*,*R*) configuration, which has the central six-membered chelate ring in the skew-boat conformation and the five-membered rings in the same δ conformation, and further two equivalent methyl groups oriented equatorially. The PMR and CD spectra given in Figs. 2 and 5 for *trans*(*R*,*R*) isomer are in accord with these structural features as described by Harrington, Linke, and Alexander.[9]

The other structure for the *trans*-dichloro complex (Fig. 6-b), which will be designated as *trans*(*R*,*S*) because the secondary nitrogen centers adopt the opposite configuration to each other, has the six-membered ring in the chair conformation and the five-membered rings in the conformation of opposite chirality. One of the methyl groups must have an axial position, while the other in an equatorial position. The PMR spectrum for *trans*(*R*,*S*) isomer should give rise to two methyl doublets of the equal intensities, since the axial methyl group will exhibit, in principle, a different chemical shift from that of the equatorial methyl group. The PMR spectrum of the novel *trans* isomer (Fig. 2-d) is in accord with the requirements from *trans*(*R*,*S*) geometry.

For the *trans*(*R*,*S*) isomer the conformational effects will not contribute to the optical activity for the first approximation because the five-membered rings has the opposite conformation. The vicinal effects from the two methyl groups should primarily be appeared in the CD curve. It is expected from the results on the CD of *trans*-[$CoCl_2(N)_4$]$^+$ type complexes with diamines[11] or tetramines[12] that the equatorial methyl group shows a relatively small vicinal effect. The vicinal effect from an axial methyl group which has not been estimated yet would not be much intense compared with that from the equatorial methyl group.

The CD curve of new *trans*-[$CoCl_2$((2*S*,10*S*)-Me_2-2,3,2-tet)]ClO_4 shown in Fig. 5 is fairly different from and apparently less intense than that of the *trans*(*R*,*R*) isomer. It will be reasonable that the *trans*(*R*,*S*) isomer of $CoCl_2$((2*S*,10*S*)-Me_2-2,3,2-tet)$^+$ gives such a CD

spectrum as indicated above. Consequently, we assign the novel *trans*-dichloro complex to the *R,S* configuration on the ground of characteristics of the PMR and CD data.

The reaction condition employed for obtaining the *trans*(*R,S*) isomer from the *trans*(*R,R*) isomer should promote the reverse change (*R,S*→*R,R*), and establish ultimately an equilibrium between the isomers. The CD curves of both of the *trans*-dichloro complexes obtained after heating under reflux for 1 h in a 2% 2,6-lutidine methanol solution found to agree with each other within the experimental error. The CD curve of the equilibrium mixture at room temperature shown in Fig. 5 crosses at the intersections of the CD curves for the *R,R* and the *R,S* isomer except in the higher energy region where the influences due to 2,6-lutidine are considered to occur. Assuming that only the two isomers, *R,R* and *R,S*, are equilibrated under the above condition, the ratio of these isomers was estimated to be 7.6 ± 0.3: 1 ($\Delta G = -1.20\pm0.03$ kcal/mol) in favor of the *R,S* isomer.

It is very interesting that the *trans*(*R,S*) isomer having the six-membered ring in the chair conformation and one of the methyl groups in an axial location is fairly stable than the *trans*(*R,R*) having the six-membered ring in the skew-boat conformation and both of the methyl groups in the equatorial situation. The energetic advantage of the chair conformation over the skew-boat conformation with respect to the six-membered ring exceeds significantly the disadvantage brought about by an axial methyl group.

Therefore, the most stable configuration for (2*S*,10*S*)-Me_2-2,3,2-tet complexes should be the *Λ-cis-β* geometry, in which the six-membered chelate ring adopts the chair conformation and both of the methyl groups can occupy equatorial positions. This is in accord with the observation that the dominant isomer obtained from the air-oxidation products by means of ion-exchange chromatography is the *Λ-cis-β* dichloro complex.[9]

Recently, an X-ray crystallographic study have demonstrated that the six-membered ring adopts the chair conformation in the *Λ-β*-[Coox(5*R*,7*R*)-Me_2-2,3,2-tet)]$^+$ ion, even though one of the methyl groups occupies an axial orientation at the six-membered ring.[13] On these findings we conclude that metal complexes coordinating methyl-substituted 2,3,2-tet derivatives will often give rise to isomers having an axial methyl group due to the higher preference of the chair conformation for the six-membered ring.

References

1) Present address: Faculty of Pharmaceutical Sciences, Nagoya-City University, Tanabe-dori, Mizuho-ku, Nagoya.

2) To whom all the correspondence should be addressed.

3) B. Bosnich, R. D. Gillard, E. D. McKenzie, and G. A. Webb, *J. Chem. Soc., A*, **1966**, 1331.

4) H. G. Hamilton and M. D. Alexander, *Inorg. Chem.*, **5**, 2060 (1966).

5) H. G. Hamilton and M. D. Alexander, *J. Am. Chem. Soc.*, **89**, 5065 (1967).

6) *R* and *S* refer to the absolute configuration of the coordinated secondary nitrogen atoms according to the rules devised by R. S. Cahn, C. K. Ingold, and V. Prelog, *Angew. Chem., Int. Ed. Engl.*, **5**, 385 (1966).

7) G. R. Brubaker and D. P. Schaefer, *Inorg. Chem.*, **9**, 2373 (1970).

8) G. R. Brubaker and D. P. Schaefer, *Inorg. Chem.*, **10**, 968 (1971).

9) P. C. Harrington, S. Linke, and M. D. Alexander, *Inorg. Chem.*, **12**, 168 (1973).

10) Alexander *et al.* abbreviated the ligand 4,8-diazaundecane-2,10-diamine simply as diMe-2,3,2-tet. We consider, however, that it is necessary to designate the positions of the methyl groups on the ligand skeleton for the sake of avoiding the confusions, since the other ligands such as (4*R*,6*R*)-4,6-dimethyl-3,7-diazanonane-1,9-diamine can be also abbreviated as diMe-2,3,2-tet. For convenience the rules we employed for the triethylenetetramine series are introduced in this report to the methyl-substituted 2,3,2-tet ligands regarding the 2,3,2-tet chain as 1,4,8,11-tetraazaundecane as in the case of 5-methyl derivatives: P. W. R. Corfield, J. C. Dabrowiak, and E. S. Gore, *Inorg. Chem.*, **12**, 1734 (1973). The following abbreviations will be used: (5*R*)-Me-2,3,2-tet (=(5*R*)-5-methyl-1,4,8,11-tetraazaundecane or (4*R*)-4-methyl-3,7-diazanonane-1,9-diamine), (5*R*,7*R*)-Me_2-2,3,2-tet (=(4*R*,6*R*)-1,9-diamino-4,6-dimethyl-3,7-diazanonane).

11) B. Bosnich and J. MacB. Harrowfield, *J. Am. Chem. Soc.*, **94**, 3425 (1972).

12) M. Goto, A. Okubo, T. Sawai, and S. Yoshikawa, *Inorg. Chem.*, **9**, 1488 (1970).

13) A. Fujioka, S. Yano, and S. Yoshikawa, *Inorg. Nucl. Chem. Lett.*, **11**, 341 (1975).

Precise Measurement of Ionic Diffusion Coefficients with a Hanging Mercury Drop Electrode

Haruko IKEUCHI, Yoshimi FUJITA(née AIHARA), Kyoichi IWAI,* and Gen P. SATÔ

Department of Chemistry, Faculty of Science and Technology, Sophia University, Kioicho, Chiyoda-ku, Tokyo 102

(Received April 19, 1976)

The diffusion coefficient and the product of the charge number of electrode reaction n and the concentration of depolarizer c can be determined simultaneously from the time dependence of the diffusion limiting current observed at a spherical electrode of known size. Nearly ideal spherical diffusion was realized by means of a mercury drop electrode hanging from the tip of a fine glass capillary (0.2 mm, outer diameter) which was kept at constant size by adjusting the mercury head. The diffusion coefficients of thallium(I), cadmium(II), bismuth(III), and hexamminecobalt(III) ions in 0.1 mol dm^{-3} potassium nitrate aqueous solutions were determined at 25 °C. The experimental nc values agreed with the corresponding known values within 3%.

The present paper deals with a method for determining the diffusion coefficients of ions by using a mercury drop electrode hanging from a thin-walled capillary.

The dropping mercury electrode (DME) has been widely used for measuring the ionic diffusion coefficients in solutions containing excess indifferent electrolytes.[1-6] Ikeuchi[4] measured the diffusion coefficients of amminenitrocobalt(III) complexes in potassium nitrate solutions by means of the instantaneous diffusion current observed at the first drops.[7] The diffusion coefficients in the same systems were measured also by the diaphragm cell method.[8] The two sets of data did not agree with each other except for triamminetrinitrocobalt(III). Similar disagreement has been reported in the cases of hydrogen ion[6] and cadmium ion.[9] Since the reason for such a discrepancy was not clear, further investigation was required to know whether the discrepancy reflected a mere experimental artefact or an essential difference in the physical nature of the diffusion processes in the electrochemical and non-electrochemical methods.

For this purpose, the mass transfer process at DME is not simple enough.[10] The effects of depletion[11] and shielding[12] can be circumvented or reduced by the first-drop method[13,7] and by the use of a thin-walled capillary,[3,7] respectively; but streaming of solution caused by the continuously falling drops is inevitable. The polarographic maximum often interferes and necessitates the addition of surfactants, which may alter the diffusion current in an unpredictable way.[1] Besides these experimental complications, the convective diffusion to DME itself is an involved mathematical problem. In spite of considerable theoretical and experimental work devoted to the subject, no general agreement on the details of the mathematical expression for the diffusion current-time relationship of DME has yet been established[10]; different values of diffusion coefficients may be calculated from the same experimental data by using different equations.

With a stationary, hanging mercury drop electrode (HMDE) the situation is much less complicated: the ideal diffusion current-time relationship is strictly described by a simple equation, no polarographic maximum interferes, no streaming of the bulk of solution is caused, and HMDE is as reproducible as DME. A planar electrode may be simpler and, when properly positioned, more stable than HMDE against disturbance due to the convection caused by the density gradient developed in the diffusion layer. However, the spherical electrode has an interesting feature, described below, which is not shared by the planar electrode.

Laitinen and Kolthoff[14] first examined the diffusion current at a spherical platinum electrode. The theoretical equation for spherical diffusion was verified by Shain and Martin[15] with a Gerischer type HMDE. They pointed out the influence of shielding by the glass tip supporting the mercury drop. Kao and Chang[16] made an extensive study on the diffusion at a mercury drop electrode hanging from a fine support and showed that the equation was followed for as long as 20 min in certain particular systems in which the convection due to the density change was expected to be very small. Recently Kojima and Bard[17] also used a fine-tipped Gerischer type HMDE in a.c. polarographic study.

The magnitude of the current $|I_d|$ at time t controlled by the ideal spherical diffusion is given by the following equation:[18,10]

$$|I_d| = FSncD[r^{-1} + (\pi Dt)^{-1/2}] \quad (1)$$

with

$$S = 4\pi r^2, \quad (2)$$

where r is the radius of the electrode; F, the Faraday constant; n, the charge number of the electrode reaction; c and D, the bulk concentration and diffusion coefficient of the depolarizer, respectively. The plot of $|I_d|$ against $t^{-1/2}$ results in a straight line whose intercept A and slope B are given by

$$A = 4\pi FrncD \quad (3)$$

and

$$B = 4\pi^{1/2}Fr^2ncD^{1/2}. \quad (4)$$

If r is known, D and nc can be determined from a single $|I_d|-t$ curve by solving Eqs. 3 and 4. This situation, essentially different from that in the case of the diffusion at DME and planar electrode where these quantities appear always as product $ncD^{1/2}$, implies an interesting application of HMDE.

When n is known or estimated, c and D can be obtained. Hence, the measurement of an $|I_d|-t$ curve

* Present address: Yamato Scientific Co., Ltd., Nihonbashihoncho, Chuo-ku, Tokyo 103.

at HMDE of known size enables one to determine the diffusion coefficient of the species whose concentration is uncertain, or to determine its concentration without referring to any standard solution. Alternatively, n and D can be obtained when c is known, thereby offering a method for evaluating the n values under polarographic conditions. This will be particularly useful in those cases in which the conventional coulometric method fails because of complications due to reactions subsequent to the charge transfer.

The values of n and D can be determined independently by a suitable combination of electrochemical methods; *e.g.*, rotating disk voltammetry and chronopotentiometry,[19] and/or chronoamperometry and stationary electrode voltammetry.[20] However, such a procedure is technically complicated or often limited by the reversibility of the system.

Simultaneous determination of n and D is possible by using a hemispherical[21] or a cylindrical[22] electrode. These methods, however, involve the difficulties inherent to construction of a solid electrode of precise geometry with known surface area. Furthermore, the diffusion current-time relationship at a cylindrical electrode of finite length is too complicated to be described by any simple equation. The usefulness of these electrodes for the accurate determination of diffusion coefficients seems questionable.

In order to realize the ideal spherical diffusion at HMDE, the mercury drop must be small enough to remain practically spherical, and the disturbance of the diffusion layer due to convection and to the shielding by the drop support must be minimized. In other words, the support should be as fine as possible, and the diffusion current should be measured within a relatively short time before the diffusion layer becomes disturbed. These conditions can be satisfied approximately by adequate experimental arrangement.

In the present experiment, the $|I_d|-t$ curves of depolarizer of known n and c were measured, and r was determined from the mass of the mercury drop. By means of Eqs. 3 and 4, D and $(nc)_{obsd}$ were calculated. The value of $(nc)_{obsd}$ should agree with the product of the known n and c. This fact, together with the linearity of the experimental $|I_d|-t^{-1/2}$ plot, provides a test of the extent to which the data are consistent with Eq. 1.

Experimental

Electrode System and Electrolytic Cell. The HMDE and the electrolytic cell system are shown schematically in Fig. 1. The electrode capillary was constructed from a glass capillary, 0.3 mm and 7 mm in inner and outer diameters, respectively. A piece of the capillary was drawn so that a fine capillary tip was formed at one end. The tip was cut at a suitable length. The cut end must be sharp and rectangular when examined under a microscope. A length of the bore of the upper part was constricted in order to provide a suitable slow flow of mercury.[23] A glass sheath with several holes was placed around the fine part. The sheath not only protected the fragile fine tip but also served to reduce mechanical disturbance of the solution in the vicinity of the mercury drop.[3] The mercury reservoir was held by a clamp which could move smoothly between two adjustable stoppers of a heavy stand column. When the electrode was not in use, a minimum

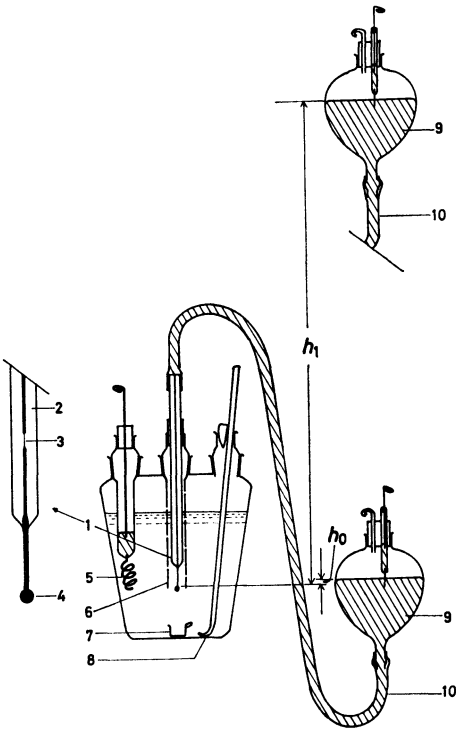

Fig. 1. HMDE and electrolytic cell.
(Reference electrode and nitrogen gas inlet and outlet are not shown.)
1: HMDE, 2: glass capillary, 3: constriction, 4: mercury drop, 5: Pt-spiral counter electrode, 6: glass sheath, 7: glass cup, 8: glass rod, 9: mercury reservoir, 10: Tygon tubing.

mercury head was applied to keep mercury flowing in order to avoid possible clogging. The characteristics of a typical capillary were as follows: radii of the capillary tip, 0.12 mm (outer) and 0.05 mm (inner); mercury flow rate, 6×10^{-2} mg·s^{-1} at mercury head of 40 cm.

The electrolytic cell (capacity, about 100 cm^3) was all of Pyrex. The counter electrode was a spiral of platinum wire, and the reference electrode was a saturated calomel electrode (SCE), which was connected to the electrolytic solution by means of a potassium nitrate bridge with an agar plug. The cell was placed in a thermostated water bath, the temperature of which was checked with a standard mecury thermometer. The temperature fluctuation in the cell solution was about $\pm$0.01 °C.

Instrumental. A potentiostat with a current follower was used. The output signal of the current follower was recorded by a high speed pen recorder (Riken Denshi Co. Ltd., SP-G3; response time, 0.2 s for full scale of 25 cm with auxiliary pen for recording reference time signal). The chart speed (16 mm s^{-1}) was checked by recording a reference signal (1 Hz) generated from a quartz crystal oscillator. The triangular wave generator for linear-sweep voltammetry was constructed according to Tsuji and Takahashi.[24]

Reagents. The purity of mercury was essential: traces of impurity tended to deposit on the constricted part of the capillary and eventually cause clogging. Mercury for polarographic use was repeatedly washed with 3—5% nitric acid and then with distilled water. After being dried, it was distilled under reduced pressure in an all-quartz distillator: the first two thirds of distillate was collected for use.

Thallium(I) nitrate (>99%: Yamada Kagaku Yakuhin, K. K.) was recrystallized from distilled water and dried in a

vacuum oven at 50 °C. Hexamminecobalt(III) nitrate was prepared according to the usual method,[25] recrystallized from dilute acetic acid, and dried over silica gel. The stock solution was prepared by dissolving a weighed amount of the nitrate. Cadmium(II) nitrate stock solution (10.59_3 mol m^{-3}) was prepared by dissolving 0.5953_5 g of the metal (99.999 % Wako Pure Chemical Industries, Ltd.) in reagent grade nitric acid and by diluting the solution to 500 cm^3. Bismuth-(III) nitrate stock solution (5.117_2 mol m^{-3}) was prepared similarly, from 0.5347_0 g of the metal (99.999%, Wako Pure Chemical Industries, Ltd.); but it contained about 0.7 mol dm^{-3} nitric acid in order to prevent hydrolysis. Potassium nitrate (reagent grade) was recrystallized from distilled water. The water used throughout was deionized water distilled in an all glass apparatus (Kinoshita Rikakogyo Co., Ltd., Model KR-70-AN). All the volumetric operations were performed in a water bath controlled at (25±0.1) °C.

Procedures. The hanging mercury drop was formed by letting a new drop grow at a fixed mercury head h_1 for a certain duration of time and then decreasing the head to h_0, the head necessary to balance the back pressure of the mercury drop. The mercury head h_1 was so chosen that a mercury drop 0.4—0.8 mm in diameter was produced in 5—10 min. The value of h_0 was determined for each capillary. The flow rates of mercury m were measured at several different mercury heads. By extrapolating the m-h plot to $m=0$, h_0 was estimated approximately. Then it was adjusted until the peak current of the linear-sweep voltammogram remained constant for 30 min. Once h_1 and h_0 were determined, the two stoppers on the supporting stand were fixed to these positions so that h_1 and h_0 were reproduced.

The cell solution was deoxygenated with nitrogen gas which had been passed through vanadium(II) sulfate solution and then distilled water; during the measurement nitrogen gas was flushed over the cell solution.

The diffusion current was recorded as follows. After a new mercury drop was formed, the lowest positive potential at which practically no electrolysis occurred was applied on it. Then the potential was switched to that at which the diffusion current was measured. These potentials were found by inspecting the d.c. polarogram of the depolarizer in question. After the current-time curve was recorded, the mercury drop was detached and taken out by means of a glass cup and rod (Figs. 1, 7, and 8). After rinsing and drying, it was weighed on a semimicro-balance. The radius r of the drop was calculated by assuming sphericity. The recorded current-time curve was corrected for the residual current, which was measured by repeating the above procedure with the corresponding supporting electrolyte solution.

The value of $|I_d|$ was plotted against $t^{-1/2}$, and A and B were calculated by the least squares method from the linear portion of the plot; deviating points (*vide infra*) were omitted. By inserting the value of r into Eqs. 3 and 4, D and $(nc)_{obs}$ were determined.

Results and Discussion

Some typical $|I_d|-t$ curves and the corresponding $|I_d|-t^{-1/2}$ plots are shown in Figs. 2 and 3, respectively. Two types of deviation are seen: one at shorter times and the other at longer times. The former, observed at $t<1.5$ s in all cases, was caused by the delay in response of the current measuring system, mainly of the recorder. The latter was dependent on the kind and temperature of the sample solution; for example, at 25 °C it began to appear at about 10 s for thallium ion

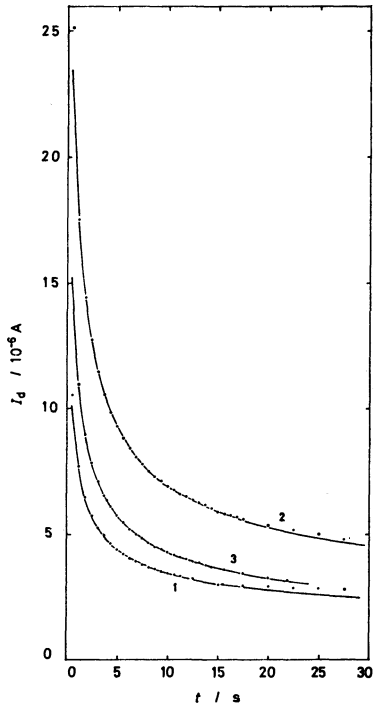

Fig. 2. Typical $|I_d|-t$ curves. In 0.1 mol dm^{-3} KNO_3 solution, at 25 °C.
Points represent observed $|I_d|$ values. Solid lines were calculated by Eq. 1 with A and B obtained from the straight lines in Fig. 3.
1) 1.000_0 mol m^{-3} Tl^+, −0.7 V *vs.* SCE, $r=0.484$ mm.
2) 1.059_3 mol m^{-3} Cd^{2+}, −0.7 V *vs.* SCE, $r=0.674$ mm.
3) 0.5117_2 mol m^{-3} Bi^{3+}, −0.2 V *vs.* SCE, $r=0.646$ mm.

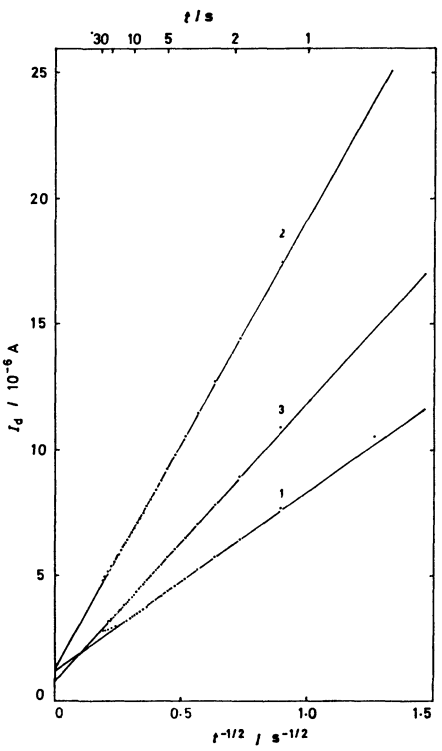

Fig. 3. $|I_d|-t^{-1/2}$ plots.
Conditions, the same as in Fig. 2.

Table 1. Diffusion coefficients in 0.1 mol dm^{-3} KNO_3 at 25 °C determined by thin-walled HMDE

Ion	Number of runs	Applied potential *vs.* SCE / V	r / mm	$(nc)_{calcd}$ / mol m^{-3}	$(nc)_{obsd}/(nc)_{calcd}$	$10^{10}D$ / $m^2\ s^{-1}$	Experimenter	Other data	$10^{10}D$ / $m^2\ s^{-1}$
Tl^+	3	−0.8, −0.9	0.6069	2.000	1.00	19.5	Y.F. (1970)	18.19[a]	
	6	−0.6, −0.7, −0.8, −0.9	0.6053	1.000	1.03 ±0.03	19.1 ±0.8	Y.F. (1970)	18.59[b] 19.9[c]	
	9	−0.7, −1.0, −1.3,	0.6406	1.000	0.997 ±0.024	19.3 ±0.7	H.I. (1971)	18.7[d]	
	7	−0.7, −1.0, −1.3	0.4853	1.000	1.01 ±0.02	19.7 ±0.6	H.I. (1972)		
	2	−1.0	0.4507	1.000	1.02	19.3	H.I. (1972)		
	5	−0.7, −1.0, −1.3	0.6307	1.001	0.999 ±0.028	19.6 ±0.9	K.I. (1972)		
	5	−0.6, −0.7, −0.8	0.6019	0.5000	0.984 ±0.021	20.7 ±1.0	Y.F. (1970)		
average	37				1.00 ±0.01	19.6 ±0.5			
$[Co(NH_3)_6]^{3+}$	2	−0.5, −0.6	0.6064	2.000	0.994	8.19	Y.F. (1970)	7.70[e]	
	3	−0.5, −0.7	0.6035	1.000	0.999	8.00	Y.F. (1970)	8.70[d]	
	1	−0.5	0.6071	0.5000	0.999	8.12	Y.F. (1970)		
average	6				0.997 ±0.031	8.08 ±0.34			
Cd^{2+}	4	−0.7	0.6720	2.119	0.990 ±0.032	7.41 ±0.04	H.I. (1974)	6.90[a], 6.87[b] 7.07[c], 7.24[d]	
Bi^{3+}	7	−0.1, −0.2, −0.4, −0.6	0.6469	1.540	1.01 ±0.01	6.32 ±0.12	H.I. (1974)		

The estimated uncertainty is 95% confidence limit.

a) von Stackelberg, Pilgram, and Toome,[1] with blunt DME, successive drops. b) Štráfelda and Šťastný,[3] with thin-walled DME, successive drops. c) Ikeuchi,[9] with blunt DME, first drop. d) Hashitani, Tanaka, and Tamamushi,[8] with glass diaphragm cell. e) Ikeuchi[4], with blunt DME, first drop.

(1 mol m^{-3}) and at about 17 s for cadmium and bismuth ions. The values for the thickness of the Nernst diffusion layer** at these time points fell around 0.15 mm, suggesting that the deviation was due to convection of the solution around the electrode: as the electrolysis proceeds, the diffusion layer thickens so that the density gradient in the thickening layer causes convection more easily.[14,1,26] Consequently, this deviation was strongly influenced by the concentration of the depolarizer, temperature fluctuation, and mechanical disturbance.

Apart from the above-mentioned deviations, the linearity of the $|I_d|-t^{-1/2}$ plots (Fig. 3) and the agreement between $(nc)_{obsd}$ and the corresponding known value $(nc)_{calcd}$ (Table 1) were satisfactory. The values of D and $(nc)_{obsd}/(nc)_{calcd}$ are independent of the concentration of the depolarizers at less than 2 mol m^{-3}, as shown for thallium(I) and hexamminecobalt(III) ions. Except for cadmium(II) ion, the values of D and $(nc)_{obsd}/(nc)_{calcd}$ are also independent of the potential at which the diffusion current was measured (at some potentials listed in Table 1, the diffusion current was accompanied by large polarographic maxima when DME was used in the absence of maximum suppressor). For cadmium(II) ion, the measurement was successful only at or near −0.7 V *vs.* SCE. At other potentials the current was not reproducible and in many cases $|I_d|-t^{-1/2}$ plot was not linear; if the plot happened to be linear, the value of $(nc)_{obsd}$ did not agree with $(nc)_{calcd}$. The cause of such behavior is not yet clear.

For the sake of comparison, Table 1 includes some D values in 0.1 mol dm^{-3} potassium nitrate solutions obtained by other methods.

Any actual hanging mercury drop cannot be strictly spherical; it is more or less pear-shaped and shielded by the capillary tip. For a small mercury drop hanging from a thin-walled capillary, however, the error due to these factors is not large. For example, microscopic observation[27] of a mercury drop 0.56 mm in radius hanging from a capillary 0.05 mm in inner radius with a wall thickness of 0.07 mm showed that the actual surface exposed to the solution was larger by 1.0% than that of a perfectly spherical drop of the same mass; the increase in surface area due to distortion of the drop shape outweighed the decrease in surface area due to the fact that a mercury thread is attached to the drop. The capillary tip, in this case, occupied 0.9% of the volume of the solution layer which was 0.15 mm thick. The increase in surface area and the shielding by the capillary tip influence the diffusion current in opposite directions and partially compensate each other. The effect of the change in curvature will be smaller, because the curvature is larger at the bottom of the drop and smaller at the top than that of the ideal sphere. Although quantitative analysis of the total effect of these factors on $(nc)_{obsd}$ and D values was too difficult, the

** The thickness of the Nernst diffusion layer δ for spherical diffusion was calculated by the equation:

$$\delta = \frac{SncFD}{|I_d|} = (\pi Dt)^{1/2} - \frac{\pi Dt}{r+(\pi Dt)^{1/2}}.$$

resultant error might scarecely amount to 1%.

Table 1 shows that the error in $(nc)_{obsd}$ is less than 3%. In view of this value the application of the present method to analytical purposes seems hopeful. The error involved in the D values will likely be of the same order of magnitude.

The data for thallium ion in Table 1 show remarkable agreement among the sets of measurements which were carried out by different experimenters on different solutions with different HMDE's over a long period of time. This fact confirms the validity of the present method.

The research was supported in part by a grant from the Ministry of Education. The financial support granted to H. I. by Matsunaga Science Foundation for the present work is gratefully acknowledged. The authors' thanks are due to Sr. Jean Michalec for correcting the manuscript.

References

1) M. von Stackelberg, M. Pilgram, and V. Toome, *Z. Elektrochem.*, **57**, 342 (1953).
2) D. S. Turnham, *J. Electroanal. Chem. Interfacial Electrochem.*, **10**, 19 (1965).
3) F. Štráfelda and M. Šťasthý, *Collect. Czech. Chem. Commun.*, **32**, 1836 (1967).
4) H. Ikeuchi, *J. Electroanal. Chem. Interfacial Electrochem.*, **16**, 405 (1968).
5) M. Šťasthý and F. Štráfelda, *Collect. Czech. Chem. Commun.*, **34**, 168 (1969).
6) N. K. Roberts and H. L. Northey, *J. Chem. Soc., Faraday Trans. 1*, **1972**, 1528.
7) for example, J. Kůta and I. Smoler in P. Zuman and I. M. Kolthoff (Eds.), "Progress in Polarography," Interscience, Vol. 1, New York (1962), Chap. 3.
8) T. Hashitani, K. Tanaka, and R. Tamamushi, *Rikenhokoku*, **51**, 69 (1975).
9) R. Tamamushi and G. P. Satô in P. Zuman, L. Meites, and I. M. Kolthoff (Eds.), "Progress in Polarography," Wiley-Interscience, Vol. 3, New York (1972), Chap. 1.
10) for example, J. Heyrovský and J. Kůta, "Principle of Polarography," Publishing House of the Czechoslovak Academy of Sciences, Prague; Academic Press, New York (1966), Chap. 6.
11) L. Airey and A. A. Smales, *Analyst (London)*, **75**, 287 (1950).
12) H. Matsuda, *Bull. Chem. Soc. Jpn.*, **26**, 342 (1953).
13) W. Hans, W. Henne, and E. Meurer, *Z. Elektrochem.*, **58**, 836 (1954).
14) H. A. Laitinen and I. M. Kolthoff, *J. Am. Chem. Soc.*, **61**, 3344 (1939).
15) I. Shain and K. J. Martin, *J. Phys. Chem.*, **65**, 254 (1961).
16) H. Kao and C. Chang, *Scientia Sinica*, **15**, 336 (1966).
17) H. Kojima and A. J. Bard, *J. Electroanal. Chem. Interfacial Electrochem.*, **63**, 117 (1975).
18) for example, I. M. Kolthoff and J. J. Lingane, "Polarography," 2nd ed., Interscience, New York (1952), Chap. 2.
19) L. W. Potts and H. S. Swofford, Jr., *Anal. Chem.*, **47**, 131 (1975).
20) D. Moller and J. D. Knaack, *J. Electroanal. Chem. Interfacial Electrochem.*, **63**, 303 (1975).
21) C. Biondi and L. Bellugi, *J. Electroanal. Chem. Interfacial Electrochem.*, **24**, 263 (1970).
22) O. R. Brown, *J. Electroanal. Chem. Interfacial Electrochem.*, **34**, 419 (1972).
23) Y. Yamazaki, *Rev. Polarography (Kyoto)*, **13**, 26 (1964).
24) K. Tsuji and K. Takahashi, *Anal. Chim. Acta*, **57**, 473 (1971).
25) J. Bjerrum *et al.*, *Inorg. Synth.*, **2**, 216 (1946).
26) J. J. Vogel, *Collect. Czech. Chem. Commun.*, **30**, 2452 (1955).
27) H. Ikeuchi, T. Yazaki, and G. P. Satô, *Bunseki Kiki*, **14**, 207 (1976).

The Electrochemical Fluorination of Aliphatic Primary Monohydric Alcohols and Aldehydes[1]

Takashi ABE, Shunji NAGASE, and Hajime BABA

Government Industrial Research Institute, Nagoya, Hirate-machi, Kita-ku, Nagoya 462

(Received January 27, 1975)

The perfluorocyclic ethers as well as the perfluoroalkanoyl fluorides were obtained by the electrochemical fluorination of primary monohydric alcohols and aldehydes containing 4—8 carbon atoms. The five-membered rather than the six-membered perfluorocyclic ethers were formed as the cyclic products. The over-all yields of the perfluorocyclic ethers and the perfluoroalkanoyl fluorides from the alcohols were in the range of 10—20%, and 3—12% respectively. Those from the aldehydes were poor because of the formation of a considerable amount of tarry by-products. The physical properties of the perfluorocyclic ethers obtained are also described.

The electrochemical fluorination of diols, which resulted primarily in the formation of the six-membered perfluorocyclic ethers, was studied previously.[2]

Commonly, perfluorocyclic ethers (I and II) are known to be formed as the cyclization products in the electrochemical fluorination of straight chain carboxylic acids and their acid halides,[3] or of cyclic ethers directly.[4] The corresponding perfluoroalkanoyl fluorides (III) are also formed in the former case

$$CH_3(CH_2)_nC(O)X \xrightarrow[\text{fluorination}]{\text{Electrochemical}} \left(\begin{matrix} n\geq 2 \\ X=OH, \text{ halogen}\end{matrix}\right)$$

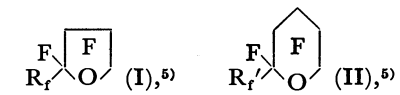

(I),[5] (II),[5]

$\left(R_f=C_{n-2}F_{2n-3},\ n\geq 2\right)$ $\left(R_f'=C_{n-3}F_{2n-5},\ n\geq 3\right)$

$CH_3(CF_2)_nC(O)F$ (III)

To investigate the behavior of alcohols upon electrochemical fluorination in more detail, we examined next the fluorination of several monohydric alcohols. It was found that primary monohydric alcohols also give the perfluorocyclic ethers as well as the perfluoroalkanoyl fluorides in considerable yields, which provides an additional useful route for the preparation of perfluorocyclic ethers.

This paper will deal with the electrochemical fluorination of alcohols and aldehydes having 4—8 carbon atoms, and with the characterization of the products and their related compounds.

Results and Discussion

The reaction conditions and the results of the fluorination of alcohols and aldehydes are shown in Tables 1 and 2 respectively.

The alcohols were dissolved in anhydrous hydrogen fluoride (AHF) to give a colorless electroconductive solution, while the aldehydes (butanal, pentanal, hexanal, heptanal, and octanal) gave a colored solution. The butyric aldehyde–AHF solution had a yellowish tint, and the others had a brownish one.

These solutions containing oxonium ion species were electrolysed smoothly and afforded perfluoroalkanes, perfluorocyclic ethers, and perfluoroalkanoyl fluorides as exhaustive fluorination products. On fluorination of most of the alcohols, only a very small amount of the perfluoroalkanes having the same number of carbon atoms as the starting materials was produced. However, there was a tendency for the formation of an increased amount of the perfluoroalkanes which comprise the same carbon skelton as the sample on fluorination of branched alcohols with an alkyl group on the β carbons, such as 2-ethyl-1-butanol and 2-methyl-1-pentanol.[6] The perfluoroalkanes having one fewer carbon atom than the starting materials and acyl fluorides were invariably formed as the principal cleaved products.

Fluorination of the Alcohols Having Linear Alkyl Groups (Runs 1—7 in Table 1). These alcohols afforded the perfluorocyclic ethers in fair yields. While the yields of the perfluoroalkanoyl fluorides decreased steadily with increase in the length of the carbon chain of the alcohols, the highest yield (21.7%) of the perfluorocyclic ethers was obtained in the case of 1-pentanol (Run 2). This may be due to the availability of the largest number of the C–H bonds on the δ and ε carbons of the alcohol, to create a carbon radical, and also due to the easier mobility of the alkyl group towards the carbonyl oxygen, which occurs intramolecularly, to form a 5-membered or 6-membered ring.

The perfluorocyclic ethers thus obtained consisted almost of the 5-membered and its isomeric 6-membered ring compounds. When the perfluorotetrahydrofurans contain side chains, they were on the 2-position of the ring. However, in the case of the perfluorotetrahydropyrans, ^{19}F NMR revealed that the side chain attached to the 3- or 4-positions of the pyran ring but not to the 2-position as has hitherto been reported.[3a]

The yields of the perfluorotetrahydrofuran from the alcohols with unsaturated bonds at γ carbon (Run 6 and 7) increased slightly, compared with the results in Run 1.

Fluorination of the Alcohols Having Side Chains (Runs 8—12 in Table 1). In Run 8, the perfluoro-2-methyltetrahydrofuran rather than the perfluoro-3-methyltetrahydrofuran was obtained as the major cyclization product. In Run 10, the yield of perfluoro-3,3-dimethyltetrahydrofuran, the expected cyclization product from fluorination of 3,3-dimethyl-1-butanol alcohol, was very poor (<1%), in spite of a sufficient number of available C–H bonds (9) of the starting material for the formation of the 5-membered ring. Instead, perfluoro-2,3-dimethyltetrahydrofuran, perfluoro-3-ethyltetrahydrofuran, perfluoro-2,5-dimethyl-

Table 1. Summary of the fluorination of monohydric alcohols

Anodic current density, 3.5 A/dm²; cell temp, 5—6 °C; volt, 5—10 V; sample, 0.20 mol

Run	Sample	Electricity passed (A h)	Fluorinated compounds obtained (g)	Ag salt of the perfluorocarboxylic acids obtained (g)	Perfluorocyclic ethers and perfluoroalkanoyl fluorides (Yield, mol %)
1	1-Butanol	119	16.3	11.8(11.8)[a]	$\overline{CF_2CF_2CF_2CF_2O}$ (IX) (11.7)
2	1-Pentanol	131	22.5	12.0(11.6)	$\overline{CF(CF_3)CF_2CF_2CF_2O}$ (X) (18.2), $\overline{CF_2CF_2CF_2CF_2CF_2O}$ (XI) (3.5)
3	1-Hexanol	143	25.3	6.9 (6.5)	$\overline{CF(C_2F_5)CF_2CF_2CF_2O}$ (XII) (8.6), $\overline{CF(CF_3)CF_2CF_2CF(CF_3)O}$ (XIII) (2.8), $\overline{CF_2CF(CF_3)CF_2CF_2CF_2O}$ + $\overline{CF_2CF_2CF(CF_3)CF_2CF_2O}$ (XIV)[b] (1.4), $\overline{CF_2CF_2CF_2CF_2CF_2CF_2O}$ (XV) (trace)
4	1-Heptanol[c]	151	34.5[d]	3.2 (2.3)	$\overline{CF(C_3F_7)CF_2CF_2CF_2O}$ (XVI) (10.3), $\overline{CF_2CF(C_2F_5)CF_2CF_2CF_2O}$+ $\overline{CF_2CF_2CF(C_2F_5)CF_2CF_2O}$ (XVII)[e] (0.9)
5	1-Octanol[c]	161	28.1[f]	3.2 (1.6)	$\overline{CF(C_4F_9)CF_2CF_2CF_2O}$ (XVIII) (10.3)
6	3-Buten-1-ol[g]	60	8.5	4.8 (4.8)	IX (14.1)
7	3-Butyn-1-ol[h]	59	9.7	5.3 (5.3)	IX (14.2)
8	3-Methyl-1-butanol	134	22.4	7.3 (4.8)	$\overline{CF_2CF(CF_3)CF_2CF_2O}$ (3.6), X (8.6), XI (2.6), $C_2H_5CF(CF_3)C(O)F$ (3.2)
9	3-Methyl-1-pentanol	163	28.8	3.8 (3.7)	$\overline{CF(CF_3)CF(CF_3)CF_2CF_2O}$ (XIX) (8.4), $\overline{CF_2CF(C_2F_5)CF_2CF_2O}$ (XX) (8.5), XIII (2.2), $\overline{CF_2CF_2CF(CF_3)CF_2CF_2O}$ (XXI)[i] (2.6), XV (0.5)
10	3,3-Dimethyl-1-butanol	173	30.8	3.2 (3.0)	$\overline{CF_2C(CF_3)_2CF_2CF_2O}$ (0.9), XIX (9.9), XX (6.1), XIII (3.0), XXI (2.3), XV (trace)
11	2-Ethyl-1-butanol	163	28.3	—	XX (6.4), $(C_2F_5)_2CFC(O)F$ (5.5)

a) Ag salt of the perfluoro carboxylic acid obtained, with the same carbon numbers as the samples (calculated by analysing the methyl ester derivatives of the corresponding perfluoro carboxylic acids). b) Bp 59.5—60.0 °C. Found: F, 72.2%. Calcd: F, 72.8%. c) Sample fed, 0.19 mol. d) 7.1 g were obtained as cell drainings. e) Bp 84.5—85.0 °C. Found: F, 72.7%. Calcd: F, 73.0%. f) 10.9 g were obtained as cell drainings. g) Sample fed, 0.11 mol. h) Sample fed, 0.13 mol. i) Contaminated with a considerable amount of perfluoro-3-methyltetrahydropyran.

Table 2. Summary of the fluorination of aldehydes

Anodic current density, 3.5 A/dm²; cell temp, 5—6 °C; volt, 5—10 V; sample, 0.20 mol

Run	Sample	Electricity passed (A h)	Fluorinated compounds obtained (g)	Ag salt of the perfluoro carboxylic acids obtained (g)	Perfluoro cyclic ethers (Yield, mol %)
1	Butanal	85	11.9	7.2(7.2)[b]	IX (5.9)
2	Pentanal	113	12.3	4.2(2.8)	X (3.9), XI (1.3)
3	Hexanal	136	12.8	2.1(1.4)	XII (3.0), XIII (1.3), XIV (0.6)
4	Heptanal[a]	137	19.1	2.8(1.4)	XVI (3.9), XVII (0.3)
5	Octanal[a]	143	9.8	1.5(—)	XVIII (trace)

a) Sample fed, 0.19 mol. b) Ag salt of the perfluoro carboxylic acid obtained, with the same carbon numbers as the samples.

tetrahydrofuran, and perfluoro-4-methyltetrahydropyran were obtained as cyclic products. On the other hand, the fluorination of 3-methyl-1-pentanol (Run 9) afforded almost the same kinds of products as in the case of 3,3-dimethyl-1-butanol (Run 10). Perfluorotetrahydrofurans with perfluoroalkyl groups attached to the expected position of the ring could be obtained satisfactorily in other Runs. Thus, the rearrangement which involves the 1,2-shift of the methyl group of the starting material (3,3-dimethyl-1-butanol) in competition with the cyclization is very likely to take place through the fluorination.

Although an unequivocal explanation has not yet been made of the mechanisms of the electrochemical fluorination,[7] a free radical type reaction is generally accepted. However, so far as the isomerization in the course of the fluorination is concerned, the rearrangement of alkyl groups *via* carbonium ion intermediate is more attractive rather than the free radical type rearrangement,[8] since the alkyl radicals do not generally rearrange.[9] The Hofer-Moest reaction, an example of Kolbe electrolysis, is known to proceed not only in the radical process but also mainly through the carbonium ion process.[9] Similarly, the fluorination by the electrochemical process may be interpreted in terms both of the free radical and the ionic reaction.

Thus, the acyl fluoride formed by the elimination of hydrogen fluoride from unstable α,α-difluoro alcohols (postulated initial fluorination product from alcohols) may be subjected to hydrogen abstraction by fluorine to give a free radical (IV). Then the expected 3,3-dimethyltetrahydrofuran may be created by the intramolecular cyclization. However, the major part of IV may rearrange competitively into other acyl fluorides *via* V, which resulted from further anodic oxidation of the radical of IV. The methyl group on the γ carbon of the intermediate compound (V) migrates favorably in such a way as to produce more stable tertiary carbonium ions. With a highly branched starting material, more opportunities will be given for such an rearrangement than for the cyclization.

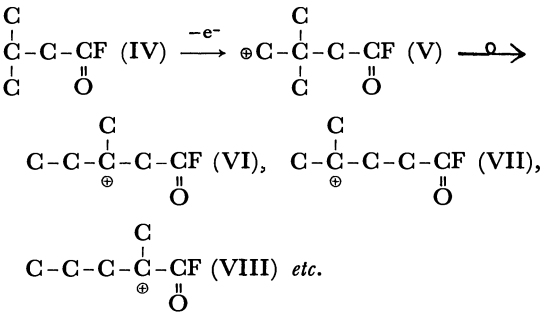

The carbonium ion of acyl fluoride (VI) can proceed to the corresponding perfluoroalkanoyl fluoride, but generally it will lead to the cyclic ethers by the intramolecular attack of one of the radicals formed on the three different carbons (denoted by a, b, and c) to the carbonyl oxygen atom. The cyclization which can proceed to the formation of three isomeric perfluorocyclic ethers is formulated as follows:

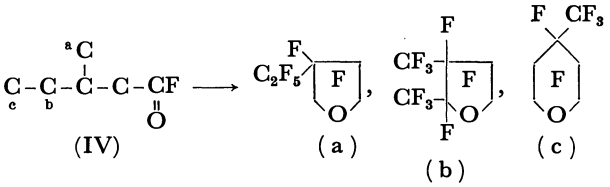

Table 3. Properties of perfluorocyclic ethers and perfluoroalkanoyl fluorides

Compound	Bp (°C)	d_4^{20}	Elemental analysis C (%)	Elemental analysis F (%)
$CF_2CF(CF_3)CF_2CF_2O$	28.5—29.0			71.5(71.3)[a]
$CF(C_2F_5)CF_2CF_2CF_2O$[b]	54.0—55.5	1.6944		72.1(72.2)
$CF(C_3F_7)CF_2CF_2CF_2O$[c]	75.2—75.5	1.7475	22.56(22.95)[a]	72.8(72.7)
$CF(C_4F_9)CF_2CF_2CF_2O$[d]	99.0—99.5	1.7847	22.96(23.08)	73.7(73.1)
$CF(CF_3)CF_2CF_2CF(CF_3)O$	53.5—54.0	1.7321		71.6(72.2)
$CF(CF_3)CF(CF_3)CF_2CF_2O$[e]	52.9—53.3	1.7063		72.3(72.2)
$CF_2CF(C_2F_5)CF_2CF_2O$	55.2—55.8	1.7200		72.3(72.2)
$CF_2C(CF_3)_2CF_2CF_2O$	57.2—57.7	1.7618	22.37(22.79)	72.2(72.2)
$CF_2CF(CF_3)CF_2CF_2CF_2O$[f]	58.2—59.0	1.7662	22.73(22.79)	72.5(72.2)
$C_2F_5CF(CF_3)C(O)F$[g]	29.5—31.5			71.0(71.3)
$(C_2F_5)_2CFC(O)F$	54.9—55.2	1.6721	22.98(22.79)	72.2(72.2)

a) Calculated values are given in parentheses. b) Reported bp 54—55 °C, d_4^{20} 1.6864, n_D^{20} 1.2640, see Ref. 4b. c) Reported bp 78—79 °C, d_4^{20} 1.7285, n_D^{20} 1.2724, Ref 4b. d) n_D^{20} 1.2795, reported bp 100—102 °C/741 Torr d_4^{20} 1.7660, n_D^{20} 1.2775, Ref 4b. see also the Technical Bulletin "Inert Fluorochemical Liquids FC-75," Minnesota Mining and Manufacturing Co., where extensive physical data are given. e) Mixed with small portions of perfluoro(2-ethyltetrahydrofuran). Estimated purity 80%. f) Isolated and purified from the products which were obtained by the fluorination of 2-methylamyl alcohol, see Ref. 6. g) Reported bp 23—26 °C, F. S. Fawcett, C. W. Tullock, and D. D. Coffman, *J. Am. Chem. Soc.*, **84**, 4275 (1962).

The perfluoro-3-methyltetrahydropyran, which is mixed with perfluoro-4-methyltetrahydropyran as an inseparable contaminant, is considered to be produced by the cyclization of VII and VIII. The properties of these perfluorocyclic ethers are shown in Table 3.

It is noteworthy that perfluoro-2-methylbutyryl fluoride $C_2F_5CF(CF_3)C(O)F$, and perfluoro-2-ethylbutyryl fluoride $(C_2F_5)_2CFC(O)F$, obtained in Runs 8 and 11 respectively, were collected safely in cold traps, after passing through a series of washing bottles containing 5% aqueous potassium hydroxide solution.

Some spectral data (^{19}F NMR and IR) of perfluoro-2-methylbutyryl fluoride and perfluoro-2-ethylbutyryl fluoride are shown in Table 4.

Table 4. ^{19}F NMR[a] and IR data of the perfluoro-2-methylbutyryl fluoride and perfluoro-2-ethylbutyryl fluoride

$CF_3-\overset{F'}{\underset{F''}{C}}-\overset{F}{\underset{C=O}{CF}}-CF_3$	$CF_3-\overset{F'}{\underset{F''}{C}}-\overset{F}{\underset{C=O}{CF}}-\overset{F'}{\underset{F''}{C}}-CF_3$
122.9 180.3	120.9 179.5
83.2 72.7	81.3
118.5 −32.5	118.0 −33.7
$J_{F'F''}=293$	$J_{F'F''}=298$
ν (C=O); 1890 cm^{-1} (vs), 1878 cm^{-1} (ms, sh)	ν (C=O); 1885 cm^{-1} (vs)

a) Chemical shifts and J values are given in ϕ (internal CCl_3F reference) and Hz respectively.

Generally, perfluoroalkanoyl fluorides of the type $R_fC(O)F$ (R_f=linear perfluoroalkyl group) hydrolyze very easily into the corresponding perfluoro carboxylic acids. The anomalies in hydrolytic stability of these perfluoroalkanoyl fluorides with the side chain on the α carbon may be ascribed to the spatial shielding of the carbonyl carbon by two perfluoroalkyl groups.

Fluorination of the Aldehydes. The fluorination of aldehydes gave a formation and distribution of the products similar to that obtained with the alcohols (Runs 1—5 in Table 1). However, the yields both of the perfluorocyclic ethers and the perfluoroalkanoyl fluorides were lower, and the formation of a considerable amount of tarry material in the cell was observed in each run. The polymerization of aldehydes in AHF, which gives a colored liquid of low-molecular weight, has been reported briefly in the literature.[11]

Experimental

Reagents and Apparatus. All reagents except 3,3-dimethyl-1-butanol, which was prepared by the reaction of 3,3-dimethylbutyryl chloride with lithium aluminium hydride in ether, were available from Tokyo Kasei Co.. Anhydrous hydrogen fluoride (AHF) was more than 99.5% pure. The electrolytic cell used was the same as that described in a previous paper.[12] A standard Pyrex vacuum line was used in the reaction of perfluoro-2,3-dimethyltetrahydrofuran with aluminum chloride for handling the volatile liquids and gaseous materials.

The IR spectrum measurements were made on a Hitachi EPI-G3 spectrometer, using a 6 cm gas cell with KBr windows. The ^{19}F NMR spectra were obtained on a Hitachi Model R-20B high resolution spectrometer operating at 56.46 MHz.

General Procedures for the Electrochemical Fluorination of Alcohols and Aldehydes. A typical example is the case of the fluorination of 3,3-dimethyl-1-butanol (Run 10 in Table 1). A 20.2 g portion of 3,3-dimethyl-1-butanol was dissolved in 1 l AHF in the cell. Then the electrolysis was carried out with an anodic current density of 3.5 A/dm^2, a cell temperature of 5—6 °C, and a cell voltage of 5 V, which rose gradually as the fluorination proceeded. The operation was continued until the voltage reached 10 V. Thus 173 Ahr of electrolysis was conducted.

The effluent gases from the cell were passed over NaF pellets, and then bubbled through two consecutive polyethylene bottles containing water (for collection of the perfluorocarboxylic acids resulting from the hydrolysis of the corresponding perfluoroalkanoyl fluorides). The gaseous products which did not react with water were further guided into an alkaline solution of potassium sulfite, and finally collected in traps immersed in liquid nitrogen.

(A) Analysis of the Perfluorocyclic Ethers: The products (30.8 g) condensed in the cold traps were initially subjected to low-temperature distillation, giving two fractions; fraction 1 (bp<0 °C, 3.3 g) and fraction 2 (25.7 g, 15.7 ml). The fraction 1 consisted mainly of CF_4, C_2F_6, and C_3F_8. The fraction 2 was carefully redistilled to collect the volatile compounds. Perfluoropentanes (a mixture of *n*- and isopentane, *n*-C_5F_{12}: *iso*-C_5F_{12}=57: 43) were obtained at about 25 °C as the main low boiling component. The distillation residue (16.7 g, 10.3 ml) was then further subjected to gas chromatographic analysis (compositions were calculated on the basis of chromatographic peak areas, assuming equal weight sensitivities for all components). Thus the following perfluorocyclic ethers were detected:

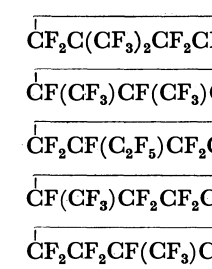

0.6 g,

6.3 g,

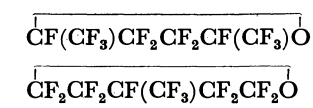

3.8 g,

1.9 g,

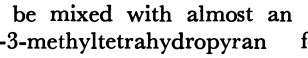

1.4 g.

The perfluoro-4-methyltetrahydropyran obtained was found to be mixed with almost an equal quantity of the perfluoro-3-methyltetrahydropyran from the ^{19}F NMR spectrum; 4-CF_3-*cyclo*-C_6F_9O: 3-CF_3-*cyclo*-C_6F_9O=50: 50. In addition to these perfluorocyclic ethers, the formation of perfluorohexamethylene oxide was also observed.[10] With the exception of perfluoro-2,3-dimethyltetrahydrofuran, the isolation and purification of these isomeric perfluorocyclic ethers were accomplished by means of repeated gas chromatography. The preparative-scale columns packed with Silicone QF-1 30% on Chromosorb PAW, diester of hexamethylene glycol with perfluorooctanoic acid 20% on Chromosorb PAW, and 1,6-bis(2,2,3,3,4,4,5,5,6,6,7,7-dodecafluoroheptyloxy)-hexane 30% on Chromosorb PAW were employed. These compounds were characterized by ^{19}F NMR, IR, and mass as well as elemental analyses. The perfluoro-2,3-dimethyltetrahydro furan obtained was found to be contaminated with a small amount of perfluoro-2-ethyltetrahydrofuran, from its spectrometric data (IR and ^{19}F NMR). However, it was not possible to separate them by the preparative gas chromatography. Therefore, the characterization of these compounds was subsequently achieved by converting them into the corresponding perfluoro-2,5,5-trichlorotetrahydrofuran

derivatives followed by the gas chromatographic separation according to a method described in the literature.[13]

Reaction of Perfluoro-2,3-dimethyltetrahydrofuran with $AlCl_3$: In a 30 ml stainless steel bomb, 1.0 g of anhydrous granular $AlCl_3$ and 1.57 g of perfluoro-2,3-dimethyltetrahydrofuran, which contained perfluoro-2-ethyltetrahydrofuran, were kept at 145 °C overnight. Purification was initially conducted by trap-to-trap distillation, using traps immersed in cold baths kept at −78 °C and −196 °C respectively. The gas chromatographic separation of the products which were retained in the −78 °C trap yielded two major fractions along with some unreacted starting material, carbon tetrachloride, and hexachloroethane. These fractions were assigned to be perfluoro-2,5,5-trichloro-2,3-dimethyltetrahydrofuran and perfluoro-2,5,5-trichloro-2-ethyltetrahydrofuran on the basis of their spectroscopic data and elemental analyses.

Perfluoro-2,5,5-trichloro-2,3-dimethyltetrahydrofuran: Yield: 0.82 g (52%), bp 132.5—133.5 °C, n_D^{20} 1.3627, d_4^{20} 1.7977. Found: C, 19.50; F, 46.8%. Calcd: C, 19.70; F, 46.8%.

Perfluoro-2,5,5-trichloro-2-ethyltetrahydrofuran: Yield: 0.21 g (13%), bp 131.0—131.5 °C (lit,: 136 °C),[13] n_D^{20} 1.3605 (lit,: n_D^{25} 1.3566),[13] d_4^{20} 1.7817. Found: C, 19.62; F, 46.7%. Calcd: C, 19.70; F, 46.8%.

(B) Analysis of the Perfluorocarboxylic Acids: The analysis of the perfluoroalkanoyl fluorides produced was performed through their methyl esters. The aqueous solution of the perfluoro carboxylic acids in the polyethylene bottles was neutralized by adding anhydrous Na_2CO_3, and the solution was evaporated to dryness, giving a white solid. It was extracted with alcohols and the extract was evaporated to dryness to give a pure sodium salt. Then the salt was acidified with 10% aqueous H_2SO_4, and free acid was extracted with ether. The ethereal solution of perfluoro carboxylic acid was treated with Ag_2O and filtered, and then the filtrate was evaporated to afford a dry silver salt. In a 50 ml three-necked flask fitted with a reflux condenser, a dropping funnel, and a thermometer, 3.3 g of the fine powdered silver salt and 20 ml of 1,1,2-trichloro-1,2,2-trifluoroethane were placed and heated to 70 °C, with stirring by a magnetic stirrer. Methyl iodide (3 g) was added to the mixture from the dropping funnel over a period of 30 min. The resulting mixture was kept with stirring for an additional 3 h. After removal of silver iodide by filtration, the solvent and unreacted methyl iodide were evaporated. Then, the preparative gas chromatography (column: Kel F #90 26% on Chromosorb PAW; carrier gas: He) of the residue evaporated gave 1.2 g of the mixtures of methyl esters of perfluoro carboxylic acid consisting of $C_3F_7C(O)OCH_3$ (3, peak area %), $C_4F_9C(O)OCH_3$ (2), and $C_5F_{11}C(O)OCH_3$ (95). A few shoulders, which suggested the presence of isomers, appeared on the peak of the gas chromatogram which corresponded to the methyl ester of perfluorohexanoic acid. No further analysis of these isomers was conducted.

The authors wish to thank Dr. Teruo Ueda for his technical assistance in this work and Mr. Kazuo Kodaira for the mass spectrometric measurements.

References

1) "Studies on the Cyclization upon Electrochemical Fluorination," part II.

2) Preceding paper in this series: T. Abe, S. Nagase, and H. Baba, *Bull. Chem. Soc. Jpn.*, **46**, 2524 (1973).

3) a) E. A. Kauck and J. H. Simons, U. S., 2644823 (1953); b) Saline Ludwigsshalle A. G., Germ. 1069639 (1959); c) Minnesota Mining and Manufacturing Co., Brit., 1007288 (1965); d) W. Blöchl, Fr., 1436269 (1966).

4) a) Minnesota Mining and Manufacturing Co., U. S., 2594272 (1952); Brit., 672720 (1952); b) I. P. Kolenko, N. A. Ryabinin, and B. N. Lundin, *Tr. Inst. Kim., Akad. Nauk SSSR, Ural Filial*, **1968**, 59.

5) The symbol(F) indicates perfluorinated alicyclic ring.

6) The fluorination of this compound gave the mixture of *cis*- and *trans*-perfluoro-2,4-dimethyltetrahydrofuran as the main cyclization product; this could be separated into almost pure *cis*- and *trans*-forms by gas chromatography. Detailed work will be published elsewhere by T. Abe.

7) N. Watanabe and M. Haruta, "Fussokagaku to Kogyo," Vol. II ed. by N. Watanabe, Kagakukogyosha, Tokyo (1973), p. 122.

8) J. Burdon and J. C. Tatlow, "Advances in Fluorine Chemistry," Vol. 1, ed. by M. Stacey, J. C. Tatlow, and A. G. Sharpe, Butterworth Scientific Publications, London (1960), p. 144.

9) C. Walling, "Molecular Rearrangement," Vol. I, ed. by P. D. Mayo, Interscience Publishers, New York (1963), p. 416.

10) To be published.

11) S. Murahashi and S. Sakakibara, *Yuki Gosei Kagaku*, **25**, 109 (1967).

12) T. Abe, S. Nagase, and H. Baba, *Bull. Chem. Soc. Jpn.*, **46**, 3845 (1973).

13) G. V. D. Tiers, *J. Am. Chem. Soc.*, **77**, 4837 (1955).

Solvolytic Ring-opening Reacions of *gem*-Dichloroaziridines in the Presence of Sulfuric Acid

Manabu SENŌ, Shinsaku SHIRAISHI, Yukio SUZUKI, and Teruzo ASAHARA

Institute of Industrial Science, University of Tokyo, Roppongi 7-22, Minato-ku, Tokyo 106

(Received July 1, 1975)

Solvolytic ring-opening reactions of *gem*-dichloroaziridines in the presence of sulfuric acid were investigated. The reaction products from 1-aryl-2,2-dichloro-3-phenylaziridines varied with the kind of substituent at 3-position of the aziridine ring. 2,2-Dichloro-1,3-diphenylaziridine gave α-chloro-α-phenylacetanilide, 2,2-dichloro-3-methyl-3-phenyl-1-(*m*-tolyl)aziridine gave *N*-(*m*-tolyl)atropamide and 2,2-dichloro-1,3,3-triphenylaziridine gave 3,3-diphenyloxindole. 1-Benzyl-2,2-dichloro-3,3-diphenylaziridine and 2,2-dichloro-1-phenethyl-3,3-diphenylaziridine gave 4,4-diphenyl-1,2,3,4-tetrahydroisoquinoline-3-one and 1,1-diphenyl-1,2,3,4,5-pentahydro-3-benzazepine-2-one, respectively. It was found that the substituent on C^3-carbon determines the mode of reaction.

gem-Dichloroaziridines have been prepared by various methods,[1-8] their reactivities being examined for hydrolysis,[1,2,3,6,8] isomerization[2,3] and aminolysis.[8] Ichimura and Ohta reported on the preparation of aromatic ketenimines from the reaction of 1,3,3-triaryl-2,2-dichloroaziridines with sodium iodide.[2] Klamann *et al.* observed that 1-(β-chloroethyl)-3,3-diphenyloxindole was produced by heating benzophenoneanil with chloroform and ethylene oxide in the presence of tetraethylammonium bromide, the reaction proceeding *via* the formation of 1,3,3-triaryl-2,2-dichloroaziridine.[7] On the other hand, Petyunin synthesized various lactams from *N*-aryl-α,α-diaryl-α-hydroxyacetamide in acetic acid in the presence of sulfuric acid.[9,10,11] These reports stimulated us to investigate in detail the reactivities of *gem*-dichloroaziridines in the medium containing sulfuric acid. It was found in the course of this study that atropamide, oxindole, isoquinoline and benzazepine derivatives are obtainable in good yields from the reactions of *gem*-dichloroaziridines in the presence of sulfuric acid. The results and analysis of the reaction scheme are presented in the present paper.

Results and Discussion

gem-Dichloroaziridines were prepared by addition of dichlorocarbene to the corresponding Schiff bases. Schiff bases were prepared by various methods Ph-CH=NPh was prepared from benzaldehyde and aniline, $Ph(CH_3)C{=}NAr$ from acetophenonediethylketal and *m*-toluidine, $Ph_2C{=}NPh$ from the reaction of sodium salt of aniline with benzophenone at 140—160 °C, and $Ph_2C{=}N(CH_2)_nPh$ (where $n=1,2$) by the reaction of $Ph_2C{=}O$ with $Ph(CH_2)_nNH_2$ at 150—180 °C in the presence of hydrobromic acid as a catalyst. *gem*-Dichloroaziridines prepared for the present investigation are listed in Table 1.

The *gem*-dichloroaziridines were treated with sulfuric acid in acetic acid. 2,2-Dichloro-1,3-diphenylaziridine (**1**) gave α-chloro-α-phenylacetanilide (**4**) in a 60% yield. The hydrolysis of **1** in a heterogeneous system

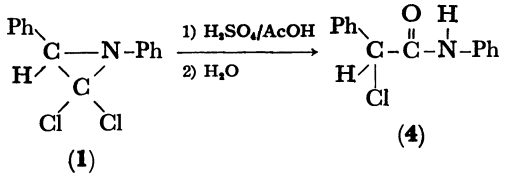

(1) (4)

TABLE 1. *gem*-DICHLOROAZIRIDINES

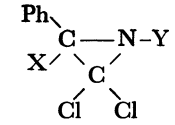

Aziridine compd no.	X	Y	Mp, °C (lit.)
1	H	C_6H_5	97—98 (99—100)[3]
2[a]	CH_3	*m*-$CH_3C_6H_4$	65—66
3a	C_6H_5	C_6H_5	96—97 (97—98)[2]
3b	C_6H_5	$C_6H_5CH_2$	138—145[b] (136—137)[8]
3c[c]	C_6H_5	$C_6H_5(CH_2)_2$	80—81.5

a) Found: C, 65.45; H, 5.21; N, 4.79; Cl, 24.55%. Calcd for $C_{16}H_{15}NCl_2$: C, 65.75; H, 5.13; N, 4.79; Cl, 24.32%. b) This compound shows exothermic peaks at 135—140 °C and 148—153 °C in DTA curve. Found: C, 71.55; H, 4.74; N, 3.87%. Calcd for $C_{21}H_{17}NCl_2$: C, 71.19; H, 4.80, N, 3.95%. c) Found: C, 72.17; H, 5.19; N, 3.66%. Calcd for $C_{22}H_{19}NCl_2$: C, 71.74; H, 5.16; N, 3.80%.

in water affords **4** and the hydrolysis in a water–dioxane homogeneous system gives an equimolar mixture of **4** and α-hydroxy-α-phenylacetanilide.[3]

2,2-Dichloro-3-methyl-3-phenyl-1-(*m*-tolyl)aziridine (**2**) gave *N*-(*m*-tolyl)atropamide (**5**) in a 61% yield. The product showed IR absorption at 1650 and 940 cm^{-1} and NMR absorption (δ value) at 6.24 (singlet) and 5.70 (singlet) which comfirmed the existence of methylene group. The hydrolysis of **2** in water–dioxane (1 : 3) mixture at reflux temperature for 1 h also gave the same product in a 62% yield. These reactions provide a novel convenient synthetic route to obtain atropamide. Meilahn *et al.* reported that 2,2-dichloro-3-ethyl-1,3-diphenylaziridines affords the hydrolysis product *via* a similar reaction.[8]

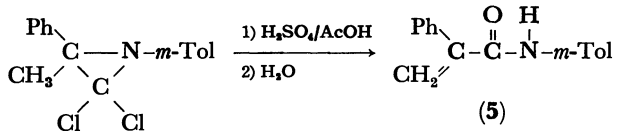

(2) (5)

When concentrated sulfuric acid was added dropwise to a solution of 2,2-dichloro-1,3,3-triphenylaziridine (**3a**) in acetic acid, red coloration appeared instantaneously and disappeared shortly. This indicates the

formation of carbonium ion as an intermediate. Concentrated sulfuric acid was added until no more coloration was observed. Working up the reaction mixture gave 3,3-diphenyloxindole (**8a**) in an 88% yield. On the other hand, by heating **3a** under anhydrous conditions, α-chloro-α,α-diphenyl-*N*-phenylacetimidoylchloride (**6a**) was obtained by thermal isomerization.* Compound (**6a**) thus prepared gave 3,3-diphenyloxindole (**8a**) quantitatively by treatment with sulfuric acid in acetic acid. Hydrolysis of **3a** in aqueous dioxane gave α-hydroxy-α,α-diphenylacetanilide (**7a**),[2] which also gave **8a** quantitatively by treatment with sulfuric acid.

In the presence of sulfuric acid as a catalyst, 1-benzyl-2,2-dichloro-3,3-diphenylaziridine (**3b**) gave 4,4-diphenyl-1,2,3,4-tetrahydroisoquinoline-3-one (**8b**) in a 99% yield. Hydrolysis of **3b** in aqueous dioxane gave *N*-benzylbenzilamide (**7b**),[8] which gave **8b** in an 80% yield by treatment with sulfuric acid. 2,2-Dichloro-1-phenethyl-3,3-diphenylaziridine (**3c**) gave 1,1-diphenyl-1,2,3,4,5-pentahydro-3-benzazepine-2-one (**8c**) in a 67% yield. Hydrolysis of **3c** gave *N*-phenethylbenzilamide (**7c**) in a 74% yield. Treatment of **7c** with sulfuric acid also gave **8c** in a 77% yield.

The reactions described above are summarized in the following scheme:

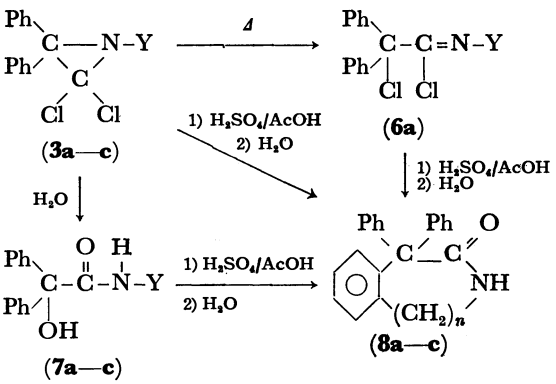

Y=Ph(CH$_2$)$_n$, a) n=0, b) n=1, c) n=2.

Petyunin *et al.* reported on the reaction from **7a** to **8a**[10-11] and Klamann *et al.* presented the reaction scheme to produce thermally oxindole from benzophenoneanil.[7] However, there is no report which gives the direct solvolytic rearrangement reactions of *gem*-dichloroaziridines to produce oxindole, isoquinoline derivatives and benzazepine derivatives. These reaction processes are rather moderate and give higher yields of products, as compared to the pyrolysis reaction at 150 °C reported by Klamann *et al.*

It was revealed from these experiments that the reaction proceeds through the cleavage of C^3–N bond. The existence of **9** and **10** was proposed for intermediates in the ring-opening reaction of *gem*-dichloroaziridines, where the chloride ion shifts intramolecularly, following C^3–N bond cleavage.[3] The nature of the intermediate (**10**) would be dependent on the substituent X.

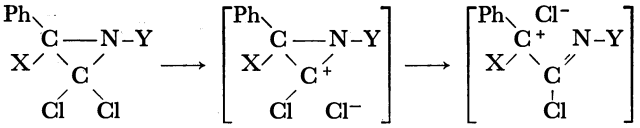

(**9**) (**10**)

In the case of X=H, Cl$^-$ is substantially bonding at C^3-atom, and the product (**4**) is formed in both the reactions with H_2SO_4–AcOH and aqueous dioxane through α-chloro-*N*-phenylacetimidoylchloride, as reported by Brook *et al.*[3]

In the case of X=CH$_3$, the hydrolysis product is easily converted into compound (**5**) by an elimination pathway in both the reactions with H_2SO_4–AcOH and aqueous dioxane.

In the case of X=phenyl, the C^3-carbonium ion is stabilized through the conjugation of adjacent phenyl groups and the counter Cl$^-$ ion becomes more free. Thus, the attack of carbonium ion to benzene ring at *ortho* position or the displacement of Cl$^-$ by OH$^-$ becomes more feasible. Compounds (**8a**), (**8b**), and (**8c**) are produced by the reaction of parent dichloroaziridine with H_2SO_4–AcOH and *N*-aryl-α-hydroxy-α,α-diphenylacetamide (**7a**), (**7b**), or (**7c**) by the reaction in aqueous dioxane. The difference in the mode of reaction between **1** and **3** is considered to reflect the stability of benzyl cation as compared with that of benzhydryl cation.

Experimental

Preparation of N-*(1-Phenethylethylidene)*-m-*toluidine.* A mixture of 38.8 g (0.2 mol) of acetophenonediethylketal and 21.4 g (0.2 mol) of *m*-toluidine was heated at 80—100 °C for 7 h. The resulting solution was distilled under reduced pressure to give 35 g (84%) of *N*-(1-phenylethylidene)-*m*-toluidine as yellow liquid; bp 150 °C (3 mmHg); IR (KBr) 1634 cm^{-1} (C=N); NMR (CDCl$_3$) δ (ppm) 6.3—8.1 (m, 9, aromatic), 2.30 (s, 3, CH$_3$-aromatic), 2.16 (s, 3, CH$_3$-C=N)

Preparation of N-*(Diphenylmethylidene)phenethylamine.* A mixture of 91 g (0.5 mol) of benzophenone, 60.5 g (0.5 mol) of phenethylamine and two drops of 2M hydrobromic acid was heated at 130—140 °C for 5 h under N$_2$ atmosphere. Distillation under reduced pressure gave 65 g (46%) of *N*-(diphenylmethylidene)phenethylamine as light yellow liquid; bp 190—195 °C (3 mmHg); IR (KBr) 1620 cm^{-1} (C=N); NMR (CDCl$_3$) δ (ppm) 7.75—6.50 (m, 15, aromatic), 3.55 (t, 2, -CH$_2$-N=C-), 2.94 (t, 2, -CH$_2$-phenyl)

Preparation of 2,2-Dichloro-3-methyl-3-phenyl-1-(m-*tolyl)aziridine* (*2*). To a mixture of 28 g (0.25 mol) of potassium *t*-butoxide, 13 g (0.0625 mol) of *N*-(1-phenylethylidene)-*m*-toluidine and 250 ml of hexane, 30 g (0.25 mol) of chloroform was slowly added dropwise under dry N$_2$ atmosphere at 0—5 °C with vigorous stirring. The reaction mixture turned from yellow to brown. Stirring was continued for 2 h at 0—5 °C and then 2 h at room temperature. The solution was filtered and the residue was washed with hexane. The combined solution of the filtrate and the washing was then evaporated in *vacuo* to leave crystals, which gave 11.2 g (61%) of 2,2-dichloro-3-methyl-3-phenyl-1-(*m*-tolyl)aziridine as a colorless crystal by recrystalization from hexane–chloroform; mp 64—65 °C; IR (KBr) 1350 cm^{-1} (symmetry stretching of aziridine ring); 840 cm^{-1} (antisymmetry stretching of aziridine ring); NMR (CDCl$_3$) δ (ppm) 6.6—7.6 (m, 9, aromatic), 2.31 (s, 3, CH$_3$-

* Thermal isomerization of **3b** and **3c** was carried out by heating them in a solvent such as benzene, toluene or *p*-xylene. However, no product like **6a** could be isolated under the limited condition employed.

Table 2. Reaction products of *gem*-dichloroaziridines in the presence of sulfuric acid

Product	Mp, °C (lit,)	IR, cm^{-1} KBr disk	NMR, ppm in $CDCl_3$	Formula	Anal., % Found (Calcd)		
					C	H	N
4	150—151 (146—148) [a]	3300 (ν_{NH}) 1670 ($\nu_{C=O}$)	8.40 (broad, 1) 7.40 (m, 10) 5.45 (s, 1)	$C_{14}H_{12}NOCl$	68.41 (68.43)	4.81 (4.89)	5.65 (5.70)
5	134—135	3250 (ν_{NH}) 1650 ($\nu_{C=O}$) 1615 ($\nu_{C=C}$) 940 ($\nu_{=C-H}$)	7.40 (m, 9) 6.95 (broad, 1) 6.24 (s, 1) 5.70 (s, 1) 2.30 (s, 3)	$C_{16}H_{15}NO$	80.23 (81.01)	6.77 (6.33)	5.60 (5.91)
8a	237—238 (225—226) [10]	3200 (ν_{NH}) 1700 ($\nu_{C=O}$)	8.00 (broad, 1) 7.30 (m, 14)	$C_{20}H_{15}NO$	84.10 (84.21)	5.18 (5.26)	4.99 (4.91)
8b	280—300 (d) [a]	3190 (ν_{NH}) 1680 ($\nu_{C=O}$)	8.90 (broad, 1) [b] 6.70 (m, 14) 4.00 (s, 2)	$C_{21}H_{17}NO$	83.86 (84.28)	5.71 (5.69)	4.48 (4.68)
8c	199—200 (187—189) [11]	3300 (ν_{NH}) 1650 ($\nu_{C=O}$)	7.35 (m, 14) 4.70 (s, 1) 3.33 (q, 2) 2.60 (t, 2)	$C_{22}H_{19}NO$	84.36 (84.35)	6.32 (6.07)	4.47 (4.47)

a) Mp was not observed. It was found by DTA measurement that this compound decomposes at 280—300 °C.
b) Since this compound was not soluble in the usual organic solvents, NMR was measured in sulfuric acid.

aromatic), 1.73 (s, 3, CH_3-aziridine ring); UV (cyclohexane) λ_{max} 236 nm, ε_{max} 12900.

Preparation of 2,2-Dichloro-1-phenethyl-3,3-diphenylaziridine (3c). To a mechanically stirred mixture of 9 g (0.08 mol) of potassium *t*-butoxide, 8 g (0.028 mol) of *N*-(diphenylmethylidene)phenethylamine, 60 ml of benzene and 60 ml of hexane, 9.5 g (0.08 mol) of chloroform was slowly added dropwise under N_2 atmosphere at 0 °C. The mixture was stirred for 10 h at room temperature and then treated with active carbon for decoloration. After removal of the solid part from the solution by filtration, the filtrate was evaporated *in vacuo* to leave a crystal, which was recrystalized from hexane to leave a crystal, which was recrystalized from hexane to afford 4 g (39 %) of 2,2-dichloro-1-phenethyl-3,3-diphenylaziridine; mp 80—81 °C; IR (KBr) 1322 cm^{-1} (symmetry stretching of aziridine ring), 840 cm^{-1} (antisymmetry stretching of aziridine ring); NMR ($CDCl_3$) δ (ppm) 7.3 (m, 15, aromatic), 3.05 (q, 4, $-CH_2-CH_2-$).

Reaction of gem-*Dichloroaziridine in the Presence of Sulfuric Acid.* The general procedure is as follows: 20 ml of concd H_2SO_4 was slowly added dropwise to a solution of *gem*-dichloroaziridine (0.006 mol) in 20 ml of glacial acetic acid. The solution was heated at 60 °C for 30 min. It was poured into 80 ml of water to precipitate crystals which were collected by filtration. The crystals were dissolved in chloroform and washed with 0.5 M sodium hydrogencarbonate solution and then with water. The chloroform solution was dried on anhydrous sodium sulfate. Evaporation of the solvent and recrystalization from an appropriate solvent gave a pure product. The results are summarized in Table 2.

*Reaction of α-Chloro-α,α-diphenyl-*N*-phenylacetimidoyl Chloride (6a) in the Presence of Sulfuric Acid.* 15 ml of concd H_2SO_4 was slowly added dropwise to a solution of 1.5 g of **6a** in 15 ml of acetic acid and then heated at 60 °C for 30 min. The reaction mixture was poured into 60 ml of water to give precipitates, which were treated as mentioned in the last section. 1.2 g (96%) of 3,3-diphenyloxindole (**8a**) was obtained.

Reaction of N*-Benzylbenzilamide (7b) in the Presence of Sulfuric Acid.* 15 ml of concd H_2SO_4 was added dropwise to a solution of 1.6 g of **7b** in 15 ml of acetic acid. The product was treated similarly as above, 1.2 g (80%) of 4,4-diphenyl-1,2,3,4-tetrahydroisoquinoline-3-one (**8b**) being obtained.

*Hydrolysis of 2,2-Dichloro-3-methyl-3-phenyl-1-(*m*-tolyl) aziridine (2).* A solution of 3 g of **2** in 15 ml of dioxane and 5 ml of water was refluxed for 2 h. Evaporation and recrystalization from ethanol gave 1.5 g (62%) of *N*-(*m*-tolyl)-atropamide.

Hydrolysis of 2,2-Dichloro-1-phenethyl-3,3-diphenylaziridine (3c). A solution of 3 g of **3c** in a mixture of dioxane and 5 ml of water was refluxed for 2 h. After evaporation and recrystallization from ethanol, 2 g (74%) of *N*-phenethylbenzilamide was obtained; mp 144—145 °C (lit. 139 °C); IR (KBr) 3225 cm^{-1} (NH), 1650 cm^{-1} (C=O); NMR ($CDCl_3$) δ (ppm) 7.3 (m, 15, aromatic), 3.93 (s, 1, OH), 3.60 (t, 2, $NH-C\underline{H}_2-CH_2-$), 2.80 (t, 2, $NH-CH_2-C\underline{H}_2-$); found: C, 80.12; H, 6.39; N, 4.26%, calcd for $C_{22}H_{21}NO_2$: C, 79.76; H, 6.34; N, 4.23%.

Pyrolysis of 2,2-Dichloro-1,3,3-triphenylaziridine (3a). A solution of 3.4 g of **3a** in *p*-xylene was refluxed for 1 h. Evaporation and recrystalization from hexane gave 2.4 g (70.6%) of α-chloro-α,α-diphenylacetimidoylchloride (**6a**); mp 68—69 °C (lit, 70—71 °C)[2]; IR (KBr); 1680 cm^{-1} (C=N); found: C, 70.54; H, 4.40; N, 3.94, calcd for $C_{20}H_{15}NCl_2$: C, 70.59; H, 4.41; N, 4.12%.

References

1) E. K. Fields and J. M. Sandri, *Chem. Ind. (London)*, **1959**, 1216.
2) K. Ichimura and M. Ohta, *Bull. Chem. Soc. Jpn.*, **40**, 1933 (1967).
3) R. E. Brooks, J. O. Edwards, G. Levey, and F. Smyth, *Tetrahedron*, **22**, 1279 (1966).
4) P. K. Kadaba and J. O. Edwards, *J. Org. Chem.*, **25**, 1431 (1960).
5) J. A. Derup and R. B. Greenwald, *Tetrahedron Lett.*, **1965**, 321.
6) A. G. Cook and E. K. Fields, *J. Org. Chem.*, **27**, 3686 (1962).

7) D. Klamann, H, Wache, K. Ulm, and F. Nerdel, *Chem. Ber.*, **100**, 1870 (1967).
8) M. K. Meilahn, L. L. Augenstein, and J. L. McManaman, *J. Org. Chem.*, **36**, 3627 (1971).
9) L. Ross and C. Barclay, "Friedel-Crafts and Related Reaction," Vol. 2, Part 2, ed. by G. A.Olah, Interscience Publischers, New York (1964), p. 847.
10) P. A. Petyunin and I. S. Berdinsky, *J. Gen Chem. U. S. S. R.*, **21**, 1877 (1951).
11) P. A. Petyunin, *J. Gen Chem. U. S. S. R.*, **22**, 761 (1952).

Asymmetric Hydrogenolysis of Hydrazones. Synthesis of Optically Active α-Alanine

Syun-ichi KIYOOKA, Keiko TAKESHIMA, Hidehumi YAMAMOTO, and Kojiro SUZUKI

Department of Chemistry, Faculty of Literature and Science, Kochi University, Asakura, Kochi 780

(Received July 23, 1975)

Optically active α-alanines have been synthesized by the asymmetric hydrogenolysis of the chiral hydrazones which were derived from chiral amines and ethyl pyruvate. Reduction of the C=N group in the hydrazones was carried out using PtO_2 catalyst in acetic acid at room temperature, followed by hydrogenolysis of the N–N linkage using the same catalyst in 1 M HCl at 100 °C (autoclave). The synthesis using (*S*)-bornylamine as a chiral reagent afforded L-alanine with optical purity of 46.5%. By using (*S*)-1,2-dimethylpropylamine as a simple chiral reagent, L-alanine was also obtained with optical purity of 32.2%. It has become apparent that the synthesis using (*S*)-alkylamine gave L-alanine, while D-alanine was obtained by using (*S*)-α-methylbenzylamine.

A number of methods for the asymmetric synthesis of α-amino acid have been reported and summarized in several reviews.[1] Among these, the reduction of hydrazide and hydrazone derivatives has the advantage of recovering the starting acids and amines without destruction of the optical activity. Akabori and his co-workers[2] reported the synthesis of L-alanine (8% e.e.) and L-phenylalanine (5% e.e.) using hydrazide of (*R*)-2-methyl-3-phenylpropanoic acid. Suzuki[3] also used hydrazide of *d*-tartaric acid to obtain L-alanine (12% e.e.). However, they did not recover the original optically active sources. On the other hand, Kost and his co-workers[4] used the hydrazone (**1**) derived from anabasine to obtain D-alanine (40% e.e., 10% yield) and recovered anabasine with optical purity of 90%. Corey and his co-workers[5] succeeded in an excellent asymmetric synthesis of D-alanine by using the compound (**2**) (96% e.e., 78% yield). Our present study deals with the asymmetric synthesis of α-alanine by the catalytic hydrogenolysis of the hydrazones derived from optically active hydrazines and ethyl pyruvate.

Results and Discussion

The reduction of *d*-camphoroxime with sodium in ethanol afforded the mixture of 70% of bornylamine (Ia) and 30% of isobornylamine (Ib). The mixture was separated into Ia and Ib by the treatment with glacial acetic acid in ether solution, using Hückel's method.[6] The optical purities of Ia and Ib were shown to be 99.7% and 98.6% by comparing their optical rotations with those in the literature.[7] Both amines, Ia and Ib, were respectively converted to the hydrazone derivatives, (Va) and (Vb), by the following procedures. I was condensed with benzaldehyde to give benzaldimine. The imine was treated with methyl iodide, followed by hydrolysis to give *N*-methyl compound (II). II was converted into hydrazine derivative (IV) through the reduction of its nitroso compound (III) with zinc dust. IV was condensed with ethyl pyruvate in a dry ether solution and gave the hydrazone (V). In the asymmetric reductions reported previously, Kost used zinc dust–hydrogen chloride and Corey used aluminum amalgam. Thus far the catalytic hydrogenolysis of the hydrazone has not been successful. The hydrogenation of Va and Vb did not proceed with 5% or 10% of palladium on carbon or platinum oxide in ethanol under the hydrogen pressure of 50 kg/cm² at room temperature or even at an elevated one. However, hydrogen was absorbed when the solvent was replaced with acetic acid using platinum oxide catalyst under atmospheric pressure. The colorless oil isolated from the above reaction was found to be the intermediate (VI) from its IR and NMR spectra. The NMR spectra of the diastereomers VI were so similar in their patterns of peaks that the optical yield of the asymmetric hydrogenation could not be calculated from the proportion of the NMR peaks of the particular protons, even with NMR shift reagents. Further, hydrogen was absorbed in the HCl solution of VI with PtO_2 when the temperature was elevated to 100 °C under a hydrogen

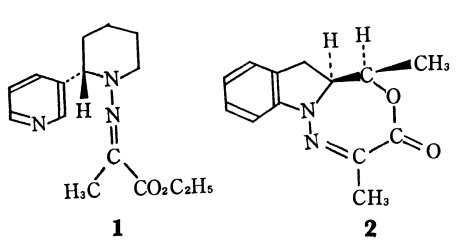

1

2

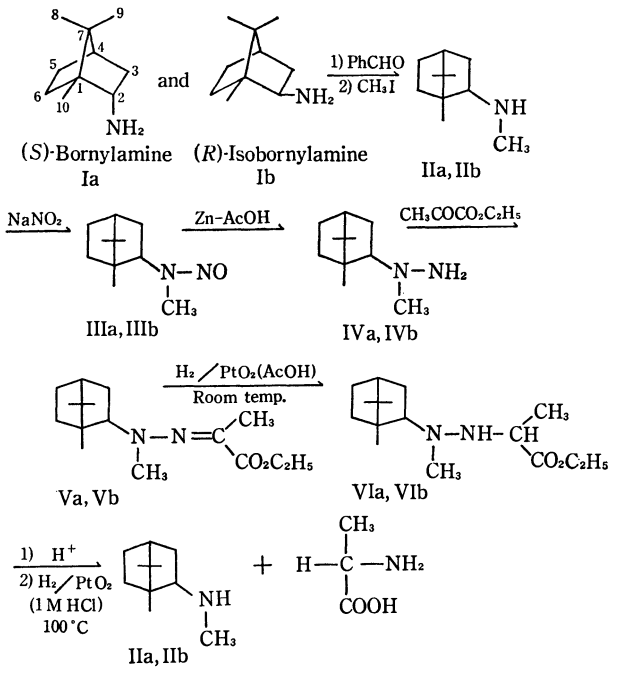

TABLE 1. ASYMMETRIC SYNTHESIS

Hydrazones	Methods	L-Alanine yield	Optical yield
Va (*S*)	Catalytic reduction	34%	46.5%
Va (*S*)	Chemical reduction	21%	10.9%
Vb(*R*)	Catalytic reduction	37%	9.2%

pressure of 50 kg/cm^2. Thus, the cleavage of the N–N linkage leading to α-alanine was carried out, and simultaneously *N*-methyl amine IV was recovered with 95% optical purity (38% yield). The reduction of the bornylhydrazone Va was also performed with zinc dust and hydrogen chloride in ethanol in order to compare the differences between the catalytic reduction and the "chemical" one (Zn–HCl). The resulting α-alanine was isolated by successive columns of an anion exchange resin (Amberlite IRA 410) and a cation exchange resin (Dowex 50W-X8) and the optical rotations of the eluted α-alanines were measured. The results of the asymmetric hydrogenolysis are shown in Table 1. Although the absolute configurations of the starting amines, Ia and Ib, were different at C-2 (asymmetric carbon), the catalytic reductions of Va and Vb, derived from the amines, gave alanines having the same configuration. This fact suggested that the conformation of the molecule adsorbed on the surface of the catalyst could not be predicted because of the difficulty in evaluating the extent of the intramolecular steric repulsions and the interactions between the molecule and the catalyst. What is known as the anchor effect[8] of the lone pair of nitrogen, the adsorption of the lone pair of the amino nitrogen on the surface of the catalyst, may be attributable to the fixing of the conformation of V and the amino nitrogen's tetrahedral character. However, the authors have been unable to find any detailed account of the asymmetric induction mechanism.

Next, as a simple alkylamine, (*S*)-1,2-dimethylpropylamine was chosen. The *dl*-1,2-dimethylpropylamine was synthesized and resolved into (*S*)-amine and (*R*)-amine with *d*-tartaric acid according to a recently reported method.[9] The synthetic method and experimental operation of the asymmetric synthesis using optically active 1,2-dimethylpropylamine was similar to that for (*S*)-bornylamine described above. L-Alanine (32.2% e.e.) was derived from the (*S*)-amine. As expected, from the (*R*)-antipode D-alanine was obtained in reasonable optical yield. Further, in order to examine the effect of an affinity[10] of the phenyl groups for the catalyst, (*S*)-α-methylbenzylamine was chosen and converted into its hydrazone derivative. The hydrazone absorbed two moles of hydrogen (PtO_2–AcOH) at ordinary temperature and pressure. Table 2 shows the results of the asymmetric reduction. Except for R_2= ethyl, the reductions of the hydrazones derived from (*S*)-α-methylbenzylamine gave D-alanine, contrary to the results for (*S*)-1,2-dimethylpropylamine. The cause of the low optical yields seemed to be a complex competition of the adsorption power between the lone pair of nitrogen and the phenyl group to fix the conformation of the molecule on the surface of the catalyst.

Experimental

Optical rotations were measured using an Applied Electric Lab. Automatic Polarimeter Model MP-IT and a Yanaco OR-50. IR spectra were recorded using a JASCO infrared spectrophotometer Model IRA-1. NMR spectra were measured using a JEOL-MH-100 spectrometer. The IR and NMR spectra supported the structures of all compounds used in this paper, but the data have not been written in the experimental section. Nitrogen was analyzed by the Kjeldahl method. Melting and boiling points are uncorrected. The α-alanines given by the asymmetric reductions were identified with pure L-alanine $[\alpha]_D^{21}$ +32.7° (*c* 0.5, acetic acid) by paper chromatography: the IR (KBr) spectra of the products agreed very closely with that of the authentic one.

(S)-*Bornylamine (Ia) and* (R)-*Isobornylamine (Ib).* *d*-Camphoroxime was prepared with *d*-camphor ($[\alpha]_D^{20}$ +44°, *c* 4.0, ethanol) and hydroxylamine.[11] The amines obtained on sodium metal–ethanol reduction[12] of the oxime were purified and separated into two parts (Ia and Ib) by fractional precipitation of their acetates, according to the procedure used by Hückel.[6] Bornylamine hydrochloride, $[\alpha]_D^{20}$ +23.1° (*c* 4.2, ethanol), (lit,[7] [α] +23.3°, *c* 4.0, ethanol) and isobornylamine hydrochloride, $[\alpha]_D^{20}$ −48.6° (*c* 4.0, ethanol), (lit,[7] [α] −49.4°, *c* 4.0, ethanol) were used in the following experiments.

(S)-N-*Methylbornylamine (IIa).* To a cooled solution of the *(S)*-bornylamine hydrochloride (50 g) in ethanol (350 ml), sodium hydroxide (30 g) was added with stirring. Benzaldehyde (30 g) was added to the solution containing the free amine. The mixture was heated under reflux for 4 h with stirring. The solvent was evaporated *in vacuo*. The concen-

TABLE 2.

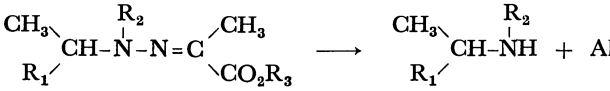

Hydrazone	Absolute configuration of starting amine	R_1	R_2	R_3	Alanine	Yield	Optical yield
IX	(*S*)-1,2-Dimethylpropylamine (VIIa)	Isopropyl	Methyl	Ethyl	L	40%	32.2%
X	(*R*) (VIIb)	Isopropyl	Methyl	Ethyl	D	43%	31.8%
XI	(*S*)-α-Methylbenzylamine (VIII)	Phenyl	Methyl	Ethyl	D	37%	0.9%
XI[a)]	(*S*) (VIII)	Phenyl	Methyl	Ethyl	D	32%	6.3%
XII	(*S*) (VIII)	Phenyl	Methyl	Isobutyl	D	35%	15.4%
XIII	(*S*) (VIII)	Phenyl	Ethyl	Ethyl	L	30%	3.2%
XIV	(*S*) (VIII)	Phenyl	Benzyl	Ethyl	D	38%	7.5%

a) Using the solvent of acetic acid–ethanol (1: 1), the temperature (0 °C) of the reaction was kept through reduction. In the other cases, the initial addition of one mole of hydrogen was carried out at room temperature using the catalyst of PtO_2 in acetic acid.

trate was cooled and diluted with water (100 ml), followed by extraction with ether. The extract after drying (sodium sulfate), on evaporation, gave the Schiff base quantitatively. The Schiff base obtained was heated with methyl iodide (36 g) in an autoclave (100 °C) for 24 h. The mixture was washed out with aqueous ethyl acetate (200 ml) from the autoclave and then the solution containing aqueous ethyl acetate was heated at 70 °C. The cooled mixture was added into a solution of 1 M hydrochloric acid (200 ml). After separation from the organic layer, the aqueous portion was made basic to litmus with 3 M sodium hydroxide with cooling, and extracted with ether. After drying (sodium sulfate) and evaporating the solvent, the oil obtained was distilled under reduced pressure (22 mmHg) at 95—110 °C (28 g). Found: N, 8.54%. Calcd for $C_{11}H_{21}N$: N, 8.37%.

(S)-N-*Nitroso*-N-*methylbornylamine (IIIa).* *N*-Methylbornylamine hydrochloride (25 g) was dissolved in water (200 ml) containing concd hydrochloric acid (0.5 ml). To the solution obtained, sodium nitrite (13 g) was added little by little at room temperature and then the mixture was heated to 70—80 °C for 3 h. After cooling to room temperature, the floating yellow oil was extracted with ether. The extract after drying (calcium chloride) gave on evaporation a yellow solid (mp 26 °C) (20 g).

(S)-N-*Methylbornylhydrazine (IVa).* To water (40 ml) maintained at 15 °C with zinc (30 g), IIIa (15 g) dissolved in acetic acid (32 ml) was added dropwise over 0.5 h with stirring. After this addition, the reaction mixture was stirred for 1 h at room temperature and heated for 1 more h at 80 °C. The unreacted zinc was filtered from the cooled mixture. Forty per cent solution of sodium hydroxide was added in large excess to the filtrate which was extracted with ether. After drying (potassium hydroxide), the residual oil on evaporation of the solvent was distilled at 195—200 °C to give a colorless oil (13 g). Found: N, 15.21%. Calcd for $C_{11}H_{22}N_2$: N, 15.37%.

Ethyl (S)-2-*(*N-*Methyl*-N-*bornylhydrazono)propionate (Va).* A cooled solution of IVa (4.7 g) in dry ether (300 ml) was added dropwise to a stirred ice-cooled solution of ethyl pyruvate (3 g) in dry ether (500 ml). The solution was kept at 5 °C for 12 h and then at room temperature for 5 h. Anhydrous magnesium sulfate was added to the ethereal solution. After evaporation of the solvent, a deep yellow oil (8 g) was obtained, which had $[\alpha]_D^{22}$ +278° (*c* 2.50, ethanol). Found: N, 9.99%. Calcd for $C_{16}H_{26}O_2N_2$: N, 10.51%.

The General Procedure for Catalytic Reduction. Hydrazone (1 g) and platinum oxide (150 mg) were placed in a 100 ml-round-bottomed flask, which was then filled with hydrogen under ordinary pressure. The solution obtained was hydrogenated at room temperature for 12 h. After filtration of the catalyst, the resulting solution was made alkaline to litmus with 1 M sodium hydroxide solution and extracted with ether. The ethereal solution was dried over anhydrous sodium sulfate. The evaporation of ether afforded a colorless oil (500 mg), which was assigned to a hydrazino compound by IR and NMR data. The hydrazino-compound was successively dissolved in 1 M hydrochloric acid (50 ml) with platinum oxide (100 mg) in a 200 ml-autoclave. The autoclave was then filled with hydrogen at 50 kg/cm² (room temperature) and stirred magnetically at 100 °C for 4 h. After cooling, the catalyst was filtered and the filtrate was evaporated *in vacuo* to dryness. The residue was redissolved in water (100 ml) and basified to pH 9 with 1 M ammonia. The *N*-methyl compound (optically active source) extracted with ether maintained its 95% optically activity (35% yield). The aqueous solution was passed through an ion exchange column packed with IRA-410. The elute was evaporated *in vacuo* to dryness. The residue obtained was redissolved in water (200 ml) and passed through a column packed with Dowex 50W-X8. The amino acid was eluted with 1 M ammonia. The basic solution was concentrated to dryness to give a white solid (30—40% yield). The IR (KBr) spectrum of the synthesized alanine was superimposable with that of an authentic sample. Paper chromatography of the synthesized alanine showed only the one spot having the R_f value as an authentic sample.

L-*Alanine from* (S)-*Hydrazone (Va) by Catalytic Reduction.* One gram of Va gave 109 mg (34% yield) of L-alanine of 46.5 % optical purity, $[\alpha]_D^{22}$ +15.21° (*c* 0.56, acetic acid).

L-*Alanine from Ethyl* (R)-*2*-(N-*Methyl*-N-*isobornylhydrazono) propionate (Vb) by Catalytic Reduction.* One gram of Vb, $[\alpha]_D^{20}$ −293° (*c* 2.7, ethanol), gave 118 mg (37% yield) of L-alanine of 9.2% optical purity, $[\alpha]_D^{22}$ +3.0° (*c* 0.56, acetic acid).

Zn–HCl Reduction of (Va). A mixture of Va (2.2 g), ethanol (40 ml), and zinc dust (2.7 g) was treated slowly with a saturated alcoholic solution of hydrogen chloride at 10 °C. When this zinc was completely dissolved, an additional amount (1.3 g) of zinc was added and the mixture was stirred at room temperature for 1 h. The filtered solution was evaporated *in vacuo* and the residue was dissolved in water. Hydrogen sulfide was introduced into the solution at pH 4. After precipitating ZnS, the mixture was separated by a centrifuge, then the supernatant was made alkaline at pH 9 with 1 M ammonia extracted with ether. The aqueous solution was passed through an ion exchange column packed with IRA-410 and the crude amino acid was eluted with 1 M acetic acid. The dried solid was disolved in water again and treated by passing through a Dowex-50W-X8 column. The L-alanine (140 mg), $[\alpha]_D^{21}$ +3.6° (*c* 0.55, acetic acid) of 10.9% optical purity, was obtained by elution with 1 M ammonia and evaporation.

Catalytic Reduction of Hydrazones (IX—XIV). The same procedure as in the experiment of bornylamine system Va was applied to the hydrazones IX—XIV, which were derived from *(S)*-1,2-dimethylpropylamine (VIIa): $[\alpha]_D^{20}$ −3.4° (neat) (lit,[13] $[\alpha]_D$ −3.45°); *(R)*-(VIIb): $[\alpha]_D^{20}$ +3.2° (neat); and *(S)*-α-methylbenzylamine (VIII): $[\alpha]_D^{22}$ −38.5° (neat).[14]

This work was supported in part by a Scientific Research Grant of the Ministry of Education (074192).

References

1) E. I. Klabunovskii, "Asymmetric Synthesis," Berlin, Deutscher Verlag der Wissenschaften (1963); J. D. Morrison and H. S. Mosher, "Asymmetric Organic Reactions," Prentice-Hall, Inc., New Jersey (1971).

2) S. Akabori and S. Sakurai, *Nippon Kagaku Zasshi*, **78**, 1929 (1957).

3) K. Suzuki and S. Kiyooka, unpublished results.

4) A. N. Kost, R. S. Sagitullin, and M. A. Yurovskaja, *Chem. Ind. (London)*, **1966**, 1496.

5) E. J. Corey, R. J. McCaully, and H. S. Sachdev, *J. Am. Chem. Soc.*, **92**, 2476 (1970); E. J. Corey, H. S. Sachdev, J. Z. Gougoutas, and W. Saenger, *ibid.*, **92**, 2488 (1970).

6) W. Hückel and P. Rieckmann, *Justus Liebigs Ann. Chem.*, **625**, 1 (1959).

7) J. Trojanek, J. Pospisek, and Z. Cekan, *Collect. Czech. Chem. Commun.*, **26**, 2602 (1961).

8) H. Kugita and E. L. May, *J. Org. Chem.*, **26**, 1954 (1961); C. P. Rader, G. E. Wicks, R. L. Young, and H. S. Aaron, *ibid.*, **29**, 2252 (1964).

9) R. H. Holm, A. Chakravorty, and G. O. Dudek, *J. Am. Chem. Soc.*, **86**, 379 (1964).

10) A. Kanai and S. Mitsui, *Nippon Kagaku Zasshi*, **87**, 183 (1966).

11) E. Nägeli, *Ber.*, **16**, 497 (1883).

12) D. V. Banthorpe, D. G. Morris, and C. A. Bunton, *J. Chem. Soc., B*, **1971**, 690.
13) R. H. Holm, A. Chakravorty, and G. O. Dudek, *J. Am. Chem. Soc.*, **86**, 379 (1964).
14) A. W. Ingersoll, *Org. Synth.*, Coll. Vol. II, 506 (1943).
15) XIV was derived from *(S)*-*N*-benzyl-α-methylbenzylamine, which was given by the reduction of *(S)*-*N*-benzilidene-α-methylbenzylamine with H_2/PtO_2 in ethanol at room temperature.

Iodination Reactions of Ketones in the Reversed Micellar Systems of Dodecylammonium Propionate in Hexane

Manabu SENŌ, Koji ARAKI, and Shinsaku SHIRAISHI

Institute of Industrial Science, The University of Tokyo, Roppongi 7-22, Minato-ku, Tokyo 106

(Received December 8, 1975)

The iodination reactions of ketones in the reversed micellar systems of dodecylammonium propionate (DAP) in hexane were studied at 25.0 °C in relation to the enzymatic function of aldolase or enolase. The reaction rate in the DAP reversed micellar system is 10^6—10^7 times greater than that in the system without DAP, 100 times greater even in comparison with that in DAP aqueous system at pH 6.8. As in the ammonium ion catalyzed reaction in aqueous media, the reaction in the presence of DAP proceeds *via* ketimine formation between ammonium groups of DAP and acetone and subsequent enolization of ketimine to enamine, which reacts very rapidly with iodine. The catalytic effect of DAP reversed micellar system in each reaction step was discussed. Further, this reversed micellar system shows a marked selectivity for acetone as compared with higher analogs.

Recently, Fendler *et al.* reported that the reversed micellar systems in nonpolar solvents catalyze several reactions and provide a favorable model for active sites of enzymes, and that the catalytic effect of these systems is related to the reaction field furnished with water pool in cores of reversed micelles, the polarity of which is lower than that of bulk water.[1,2] We also observed that the reversed micellar system of dodecylammonium propionate (DAP) in hexane shows an enzyme-like behavior in the hydrolysis of adenosine 5'-triphosphate (ATP).[3] We have studied the fundamental properties of this reversed micellar system, and shown that the catalytic effect is closely related to the properties of the water solubilized in the cores of reversed micelles.[4]

The functional groups of enzymes usually show their catalytic activities and specificities through some chemical interaction with substrates. It is of interest to demonstrate the reaction in which the functional groups of surfactant participate through the bond formation with substrate in the reversed micellar system, in order to clarify the enzymatic function.

In this paper, results of the studies on the iodination reaction of ketones in DAP reversed micellar system are given. The reaction is catalyzed by the conjugate acids of primary and secondary amines in aqueous media, proceeding *via* the formation of ketimine intermediate.[5] It has been proposed that at the active sites of aldolase and enolase their amine or ammonium groups participate in the reaction through the ketimine formation with carbonyl groups of a substrate. The ammonium group of DAP is expected to play a similar role in the iodination of ketones.

Experimental

Materials. Preparation and purification of DAP were described previously;[3] mp 55—56 °C (lit, 54—56 °C)[6]; Found (Calcd), C, 70.04 (69.44), H, 12.80 (12.82), N, 5.57 (5.40)%. Acetone was purified by the usual method. The other ketones were of reagent grade.

Iodination Rates of Ketones. A given amount of aqueous solution of iodine, containing a large excess of potassium iodide to suppress the formation of *N*-iodo derivatives,[5] was solubilized in hexane by DAP, the temperature of this reversed micellar solution being maintained at 25.0 °C. After the attainment of thermal equilibrium, the reaction was started by addition of ketone or a ketone/hexane solution in the UV cell of 10 or 2 mm in path length, and the decrease in absorption of triiodide ion at 363 nm was recorded with a Union stopped-flow spectrophotometer model RA-1100 with an RA-108s digital-memory unit. For slow reactions, a Hitachi 124 spectrophotometer was employed.

In DAP aqueous systems, the absorption band due to triiodide ion appears at 353 nm. The reaction in hexane in the absence of DAP, where the solution contains no potassium iodide, was traced by measuring the decrease in absorbance of iodine at 520 nm.

Ketimine Formation Reactions. The UV spectra of mixed solutions of DAP and acetone in hexane were recorded with a Union SM-401 spectrophotometer with an SM-4012 data-analyzer at 25.0 °C, at least half an hour after preparation of the sample solution in order to ensure the attainment of equilibrium. The absorption band of the ketimine intermediate was constructed from the spectra. The rates of ketimine formation were traced by recording the increase in absorption band of ketimine at 250 nm by the stopped-flow method.

Results

Mechanism of Iodination Reaction of Acetone in DAP Reversed Micellar Systems. The iodination reactions of acetone in DAP reversed micellar system were carried out under conditions where acetone concentration was

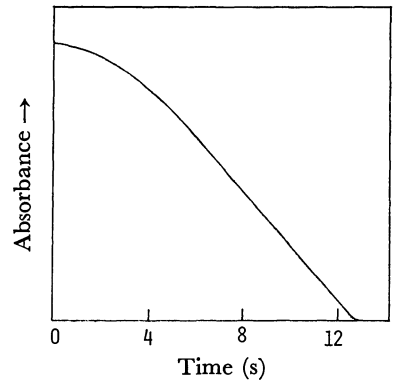

Fig. 1. The decrease in absorbance of triiodide ion at 363 nm. The typical instance of the initial stage and the subsequent steady state of the iodination reaction of acetone in the DAP reversed micellar system at 25.0 °C, where DAP, acetone, iodine and water concentrations are 1×10^{-1}, 5×10^{-4}, 1×10^{-4}, and 1.11×10^{-1} M, respectively.

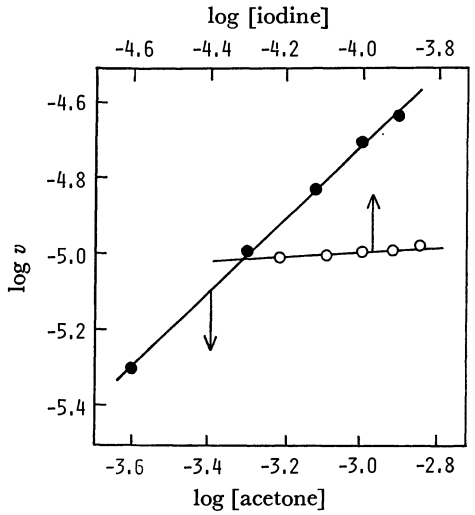

Fig. 2. Dependences of iodination rate of acetone (v) on concentrations of acetone (iodine concentration is 1×10^{-4} M) and iodine (acetone concentration is 5×10^{-4} M) in the DAP reversed micellar system at 25.0 °C, where DAP and water concentrations are 1×10^{-1} and 8.33×10^{-2} M, respectively.

much smaller than DAP concentration so that the reaction caused no large effect on micellar properties. A short induction period was observed, after which the reaction attained a steady reaction rate (Fig. 1). The dependence of the rates of the steady reaction, v, on the concentrations of various components was examined. The rate was proportional to acetone concentration and almost independent of iodine concentration (Fig. 2). A similar behavior was observed in the aqueous system.[7] The results indicate that the iodination step is very fast and the preceding steps, especially the enolization step of substrate, are slow and rate-determining. On the other hand, the dependence of v on DAP and water concentrations is complicated (Figs. 3 and 4). These results suggest that the effect of the reaction field in the reversed micellar system is not as simple as that in the aqueous ammonium ion catalyzed reaction, where the rate is proportional to the ammonium ion concentration

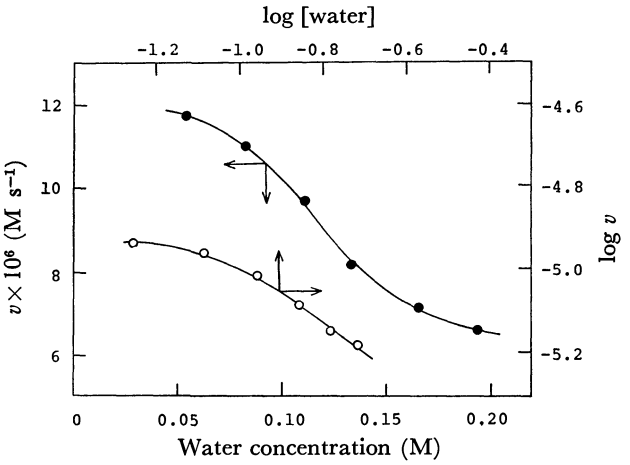

Fig. 3. Dependence of iodination rate of acetone (v) on water concentration in the DAP reversed micellar system at 25.0 °C, where DAP, acetone and iodine concentrations are 1×10^{-1}, 5×10^{-4}, and 1×10^{-4} M, respectively.

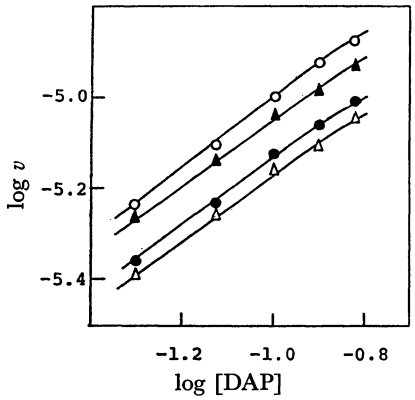

Fig. 4. Dependence of iodination rate of acetone (v) on DAP concentration at various [DAP]/[water] ratios; (○): 1.20, (▲): 0.901, (●): 0.719, and (△): 0.599, where acetone and iodine concentrations are 5×10^{-4} and 1×10^{-4} M, respectively.

together with the acetone concentration.[5]

The above results suggest also the existence of a reaction intermediate. For the sake of confirmation, the UV spectra of the DAP reversed micellar solution were measured in the presence of acetone. The result is shown in Fig. 5. Addition of acetone causes a broad

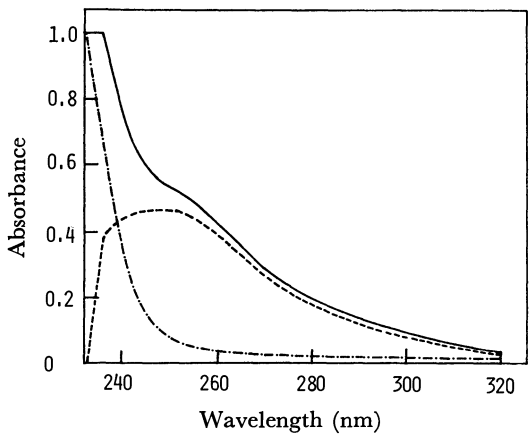

Fig. 5. UV spectra of the DAP reversed micellar solutions at 25.0 °C; (-·-·-): DAP (1.5×10^{-1} M) in the absence of acetone, (——): DAP (1.5×10^{-1} M) in the presence of acetone (7.5×10^{-3} M) and (------): the difference spectra of above two spectra.

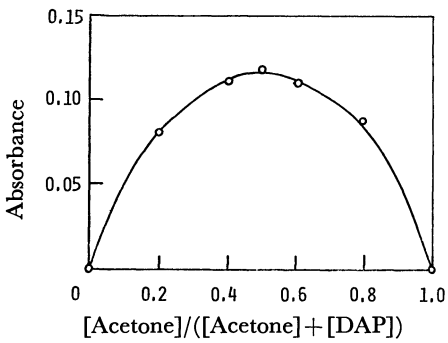

Fig. 6. Continuous variation method applied to the absorption band of the intermediate at 250 nm at 25.0 °C. Total concentration of acetone and DAP is kept constant at 2×10^{-2} M.

absorption band at 240—260 nm (λ_{max}=250 nm) as a shoulder of the DAP absorption band. The continuous variation method applied to this absorption band revealed that it should be ascribed to a 1 : 1 adduct of DAP and acetone (Fig. 6). The equilibrium constants of the formation of this intermediate, K_i, and its molar extinction coefficient, ε, were obtained by means of the equation

$$\frac{[A]_0}{d} = \frac{1}{\varepsilon K_i}\cdot\frac{1}{[D]_0} + \frac{1}{\varepsilon} \quad ([D]_0 \gg [A]_0) \qquad (1)$$

where d is the absorbance of the intermediate at 250 nm, and $[D]_0$ and $[A]_0$ are the initial concentrations of DAP and acetone, respectively. The analysis reveals that the reaction intermediate has an absorption maximum at 250 nm (ε=127), and this spectrum is not so different from that of *N*-isopropylidenebutylamine in cyclohexane (λ_{max}=246 nm, ε=140).[8]

These results, together with a comparison of the results on the aqueous ammonium ion catalyzed reaction, lead us to conclude that the iodination of acetone in DAP reversed micellar system in hexane proceeds *via* the formation of ketimine and subsequent enolization of ketimine, as proposed for the ammonium ion catalyzed reaction in aqueous media. The reaction mechanism can be written as follows.

$$(CH_3)_2C{=}O + DAP \underset{k_{-1}}{\overset{k_1}{\rightleftharpoons}}$$

$$[(CH_3)_2C{=}NR \text{ or } (CH_3)_2C{=}\overset{+}{N}(H)R] \xrightarrow{k_2}$$

$$CH_2{=}\overset{CH_3}{\overset{|}{C}}{-}NHR \xrightarrow{I_2} \text{product} \quad (R = n\text{-}C_{12}H_{25}) \qquad (2)$$

where k_1, k_{-1}, and k_2 are the rate constants of formation, decomposition and enolization, respectively, of ketimine. The step of formation of carbinolamine caused by addition of ammonium ion to acetone and the step of dehydration of carbinolamine to form ketimine could not be discriminated from each other. A combined step is given in terms of k_1 and k_{-1} in scheme (2). There is a possibility of direct enolization of acetone catalyzed by DAP. However, this pathway could be neglected, since the reaction rate during the induction period is much smaller than the steady rate. According to the above mechanism, the initial rate, v, and the apparent second-order rate constant, k_{app}, at the steady state are given under the conditions $[D]_0 \gg [A]_0$ as follows:

$$v = k_{app}[D]_0[A]_0 = \frac{k_2[D]_0[A]_0}{K_m + [D]_0} \qquad (3)$$

where $K_m = (k_{-1}+k_2)/k_1$.

Kinetic Analyses of Iodination Reaction of Acetone. The first-order rate constants, $k°$, and the second-order rate constants, k_{app}, in various reaction systems are given in Table 1. The values of K_m and k_2 could be estimated

Table 1. Iodination rate constants of acetone in various systems at 25.0 °C

Solvent	DAP(M)	Water(M)	$k°(s^{-1})$[e]	$k_{app}(M^{-1}\,s^{-1})$
Hexane[a]	1×10^{-1}	8.33×10^{-2}	2.02×10^{-2}	2.02×10^{-1}
Hexane[a]	1×10^{-1}	1.11×10^{-1}	1.75×10^{-2}	1.75×10^{-1}
Hexane[a]	1×10^{-1}	1.39×10^{-1}	1.50×10^{-2}	1.50×10^{-1}
Hexane[a]	1×10^{-1}	1.67×10^{-1}	1.38×10^{-2}	1.38×10^{-1}
Hexane[b]	0	0	5.2×10^{-9}	—
Water[c] (pH 6.8)	4×10^{-2}	—	7.6×10^{-5}	1.9×10^{-3}
Water[d] (pH 6.8)	0	—	2.1×10^{-9}	—

a) Acetone: 5×10^{-4} M, iodine: 1×10^{-4} M; b) acetone: 1×10^{-1} M, iodine: 2×10^{-3} M; c) acetone: 1×10^{-3} M, iodine: 2.5×10^{-5} M; d) acetone: 5×10^{-1} M, iodine: 2.5×10^{-5} M; e) $k°$ is defined by the following equation, $v=k°[A]_0$.

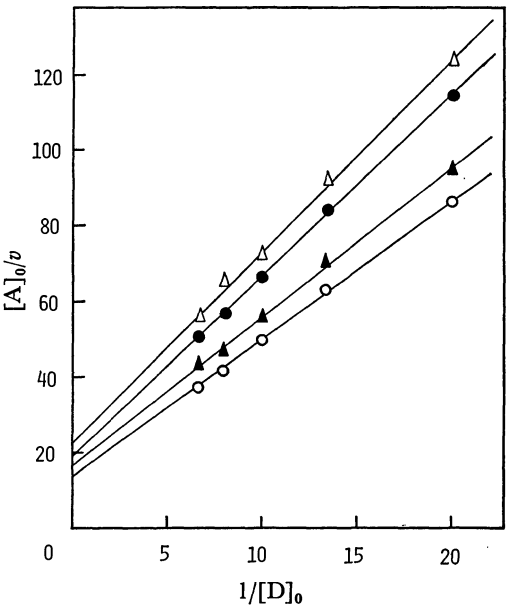

Fig. 7. Iodination reaction of acetone in the DAP reversed micellar system at 25.0 °C. Plot according to Eq. 4 at various [DAP]/[water] ratios; (○): 1.20, (▲): 0.901, (●): 0.719, and (△): 0.599; where acetone and iodine concentrations are 5×10^{-4} and 1×10^{-4} M, respectively.

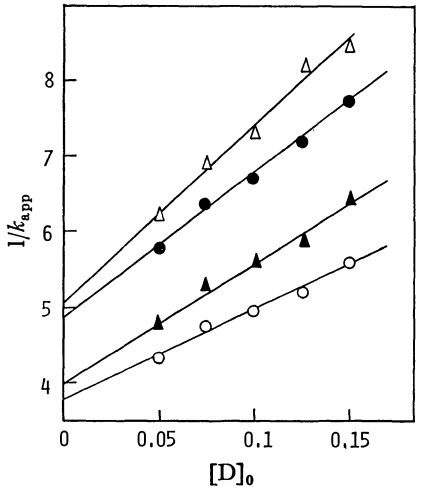

Fig. 8. Iodination reaction of acetone in the DAP reversed micellar system at 25.0 °C. Plot according to Eq. 5 at various [DAP]/[water] ratios; (○): 1.20, (▲): 0.901, (●): 0.719, and (△): 0.599; where acetone and iodine concentrations are 5×10^{-4} and 1×10^{-4} M, respectively.

Table 2. Iodination reaction of acetone in DAP reversed micellar systems at 25.0 °C

Substrate	[DAP]/[Water]	K_i (M^{-1})	k_1 (M^{-1} s^{-1})	k_{-1} (s^{-1})	k_2 (s^{-1})	K_m (K_m^{calcd}) (M)
Acetone	1.20	6.8	4.0×10^{-1}	5.8×10^{-2}	8.3×10^{-2}	0.31 (0.35)
Acetone	0.599	6.9	3.2×10^{-1}	4.7×10^{-2}	4.2×10^{-2}	0.21 (0.28)
Acetone-d_6	0.599	6.9	3.2×10^{-1}	4.6×10^{-2}	1.6×10^{-2}	0.16 (0.19)

Substrate: 5×10^{-4} M, iodine: 1×10^{-4}, DAP: 5×10^{-2} -1.5×10^{-1} M.

Table 3. Iodination rates of other ketones (R–CO–R′) in DAP reversed micellar and DAP aqueous systems at 25.0 °C

R	R′	Reversed Micellar[a] k_{aqq}^{r}[c]	Reversed Micellar[a] k_{rel}^{r}	Aqueous[b] k_{app}^{w}	Aqueous[b] k_{rel}^{w}	$\left(\frac{k_{app}^{r}}{k_{app}^{w}}\right)$	Values in Ref[d] k_{rel}^{OH}	Values in Ref[d] k_{rel}^{H}
Methyl	Methyl	1.4×10^{-1}	1	1.9×10^{-3}	1	74	1	1
Methyl	Ethyl	3.8×10^{-2}	0.27	1.3×10^{-3}	0.67	29	0.54	—
Ethyl	Ethyl	1.6×10^{-3}	0.011	5.3×10^{-4}	0.27	3.0	0.20	0.96
Isopropyl	Isopropyl	9.2×10^{-5}	0.00066	2.0×10^{-5}	0.010	4.6	0.014	0.064
Isobutyl	Isobutyl	2.6×10^{-4}	0.0019	3.0×10^{-4}	0.15	0.87	—	—
Methyl	Phenyl	2.5×10^{-4}	0.0018	2.5×10^{-4}	0.13	1.0	—	—
Ethyl	Phenyl	6.1×10^{-5}	0.00044	2.4×10^{-4}	0.12	0.25	—	—

a) DAP: 1×10^{-1} M, ketone: 5×10^{-4} M, iodine: 1×10^{-4} M, water: 1.67×10^{-1} M. b) DAP: 4×10^{-2} M, ketone: 1×10^{-3} M, iodine: 2.5×10^{-5} M. c) M^{-1} s^{-1}. d) See Refs. 8 and 9.

kinetically from the iodination rate, v. For this purpose, Eq. 3 is transformed into the following equations.

$$\frac{[A]_0}{v} = \frac{K_m}{k_2}\cdot\frac{1}{[D]_0} + \frac{1}{k_2} \quad (4)$$

$$\frac{1}{k_{app}} = \frac{1}{k_2}\cdot[D]_0 + \frac{K_m}{k_2} \quad (5)$$

The plots of $[A]_0/v$ against $1/[D]_0$ and of $1/k_{app}$ against $[D]_0$ give straight lines (Figs. 7 and 8), and the k_2 and K_m values can be determined from their slopes. The [DAP]/[water] ratio was kept constant so as not to affect the state of DAP reversed micelles in these experiments.[3,4]

The values of k_1 and k_{-1} can be determined by the measurements on the ketimine formation reaction between DAP and acetone; the k_1 value was obtained directly from the measurement on the increase in absorption of ketimine at 250 nm, and the k_{-1} value was estimated from k_1 and K_i values. The results are summarized in Table 2. The K_m values can be calculated from k_1, k_{-1}, and k_2 values, and the calculated values are given in Table 2 as K_m^{calcd} in parentheses. The values are close to those obtained experimentally, indicating the validity of the reaction mechanism.

Iodination Reactions of Other Ketones. The iodination rate constants of higher analogs of acetone in the DAP reversed micellar system, k_{app}^{r}, and those in the DAP aqueous system, k_{app}^{w}, are given in Table 3, where k_{rel}^{r} and k_{rel}^{w} represent the relative rates of higher ketones to acetone. For the sake of comparison the reported values of relative rates of higher ketones to acetone in the iodination reaction catalyzed by hydroxide anion, k_{rel}^{OH}, and by hydronium cation, k_{rel}^{H}, in aqueous system are also given.[9,10]

Discussion

Catalytic Effect of DAP Reversed Micellar Systems in Iodination Reaction of Acetone. The results given in Table 1 indicate that the rate constant of iodination of acetone in the DAP reversed micellar system is 10^6—10^7 times greater than that in the system without DAP, and about 100 times greater even in comparison with that in the DAP aqueous system. The second-order rate constants of the iodination reactions in aqueous solutions catalyzed by various catalysts are given in Table 4.[5,11]

Table 4. Iodination rate constants of acetone catalyzed by various acid-base catalysts at 25.0 °C[5,11]

Catalyst	k (M^{-1} s^{-1})
OH^-	1.7×10^{-1}
CH_3COO^-	2.4×10^{-7}
CH_3NH_2	1.9×10^{-2}
H_2O	8.3×10^{-12}
H_3O^+	2.5×10^{-5}
CH_3COOH	1.0×10^{-7}
$CH_3NH_3^+$	3.0×10^{-4}

These reactions proceed *via* prototropic mechanism catalyzed by general acid-base catalysts, the rate constants obeying the Brønsted relationship.[11] However, the ammonium ion catalyzed reaction is much faster than that expected from this relationship. As a reason for this acceleration, the reaction mechanism *via* ketimine formation has been proposed.[5]

Since the pK_a values of methylamine ($pK_a=10.26$) and dodecylamine ($pK_a=10.63$), or those of acetic acid ($pK_a=4.76$) and propionic acid ($pK_a=4.87$) are nearly equal to each other at 25.0 °C, no large difference should exist between them as general acid-base catalysts. Then, it could be anticipated that the contribution of DAP as a general acid-base catalyst would be very small in the DAP aqueous system of pH=6.8. In fact, the catalytic effect of DAP in aqueous media is very high, and the reaction is considered to proceed mainly *via* ketimine formation. This catalytic mechanism could

be applied to the DAP reversed micellar system, although a rate acceleration is enhanced by the micellar effect.

The catalytic effect of reversed micellar system can be discussed in detail by considering the role of micelles in each step of Scheme (2). The K_i value in DAP reversed micellar system is 6.8—6.9 (Table 2). In aqueous system the absorption band of ketimine was not clearly observed. However, the K_i value could be roughly estimated from the decrease in absorption band of acetone at 280 nm, where the absorption due to ketimine and DAP is negligibly small. The K_i value obtained for DAP and acetone in aqueous system is 0.2 ± 0.1 at 25.0 °C, close to the values 0.21—0.23 for methylamine and acetone, and 0.08 for butylamine and acetone.[12,13] The K_i value in aqueous system is much smaller than that in the reversed micellar system. It is therefore concluded that the stabilization of ketimine as a reaction intermediate would be one of the important factors for determining the catalytic effect of the reversed micellar system.

The results on hexadeuterated acetone are included Table 2. An isotope effect is observed only at the enolization step (k_2), ensuring also the reaction mechanism illustrated in Scheme (2).

Dependence of Iodination Rate on Water Concentration. The enolization rate, k_2, of ketimine is affected by water concentration. A major part of water in the DAP reversed micellar system in hexane is solubilized in the cores of reversed micelles,[4] iodine existing in the cores of reversed micelles. The k_2 value is nearly proportional to the [DAP]/[water] ratio (Fig. 9). A similar effect

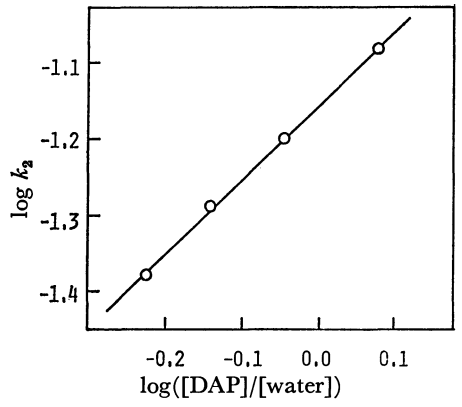

Fig. 9. Dependence of enolization rate constant of ketimine (k_2) on [DAP]/[water] ratio in the DAP reversed micellar system at 25.0 °C, where acetone and iodine concentrations are 5×10^{-4} and 1×10^{-4} M, respectively.

was observed for the ATP hydrolysis and was explained by a change in the microenvironment of substrate solubilized in the cores of reversed micelles.[3] This suggests that the enolization of ketimine occurs in the cores of reversed micelles to afford enamine, to which iodine adds rapidly.

We see from the rate Eq. 3 that, when the k_2 value increases, the K_m value increases and approaches the value of k_2/k_1, the k_{app} value becoming governed mainly by the k_1 value. On the other hand, it is clear from Table 2 that the water concentration largely affects the value of k_2, but not k_1. Therefore, it can be expected that the dependence of the reaction rate on water concentration becomes smaller with the lowering in water concentration or increase in the k_2 value. This expectation agrees with the results shown in Fig. 3.

Iodination Reactions of Other Ketones. It is supposed that the rate-determining step of the base-catalyzed reaction is the proton transfer from ketone, while that of the acid-catalyzed reaction is the proton transfer from protonated ketone.[14] Therefore, it could be expected that the acid-catalyzed reaction would be less affected by the electronic effect of substituents than the base-catalyzed reaction. The reaults in Table 3 show that k^{w}_{rel} values are similar to k^{OH}_{rel} values suggesting that the enolization of ketimine in the DAP aqueous system proceeds *via* proton transfer from the form $(CH_3)_2C{=}NR$.

On the other hand, in the DAP reversed micellar system the k^{r}_{rel} values of higher alkyl ketones are much smaller than the k^{w}_{rel} values. The ratio k^{r}_{app}/k^{w}_{app} is the largest for acetone, and decreases remarkably as the substituents become larger. The selectivity of the iodination reaction catalyzed by the reversed micellar system would be caused by the steric factor rather than the electronic factor of the substituents. Existence of the microscopic heterogeneous phase, *i.e.* a bulk hexane phase and a reversed micellar phase with core water, would play an important role in governing the selectivity through the distribution of substrate or intermediate between these two phases. The results are of interest in relation to the specificity of enzyme.

References

1) J. H. Fendler, F. Nome, and H. C. Van Woert, *J. Am. Chem. Soc.*, **96**, 6745 (1974).
2) J.H. Fendler and E.J. Fendler, "Catalysis in Micellar and Macromolecular Systems," Academic Press, New York, N. Y. (1975), p. 315.
3) M. Senō, S. Shiraishi, K. Araki, and H. Kise, *Bull. Chem. Soc. Jpn.*, **48**, 3678 (1975).
4) M. Senō, K. Araki, and S. Shiraishi, *Bull. Chem. Soc. Jpn.*, **49**, 899 (1976).
5) M. L. Bender and A. Williams, *J. Am. Chem. Soc.*, **88**, 2502 (1966).
6) A. Kitahara, *Bull. Chem. Soc. Jpn.*, **28**, 234 (1955).
7) R. P. Bell and K. Yates, *J. Chem. Soc.*, **1962**, 1927.
8) L. Sacconi, *Coord. Chem. Rev.*, **1**, 126 (1966).
9) C. F. Cullis and M. H. Hashimi, *J. Chem. Soc.*, **1956**, 2512; *ibid.*, **1957**, 1548.
10) J. Toullec and J.E. Dubois, *Tetrahedron Lett.*, **37**, 3377 (1971).
11) R. P. Bell and O. M. Lidwell, *Proc. R. Soc. London, Ser. A*, **176**, 88 (1940).
12) A. Williams and M.L. Bender, *J. Am. Chem. Soc.*, **88**, 2508 (1966).
13) R. E. Van Atta and D. R. Jamieson, *Anal. Chem.*, **31**, 1217 (1959).
14) K. Tanabe and T. Takeshita, "Acid-base Catalysis," Sangyo Tosho, Tokyo (1966), p. 36.

Reaction of Isocyanides with Mercuric Chloride

Hiroaki SAWAI and Takeo TAKIZAWA

Faculty of Pharmaceutical Sciences, The University of Tokyo, Bunkyo-ku, Tokyo 113

(Received November 17, 1975)

Isocyanides reacted with mercury(II) chloride in dry tetrahydrofuran upon heating to afford low molecular weight polymers and oligomers. Isocyanides without bulky groups underwent polymerization catalyzed by mercury(II) chloride. Various heterocyclic oligomers were obtained from the reaction of 2,6-xylyl isocyanide with mercury(II) chloride.

Isocyanides have been reported to polymerize by many kinds of catalysis,[1,2] (a) protonic acids catalysis, (b) certain Lewis acids catalysis, (c) group VIII metal catalysis and (d) ground glass catalysis. On the other hand, little has been known about the oligomerization of isocyanides in spite of its utility for the synthesis of heterocycles and oligomeric derivatives.

In the course of studying the reaction of isocyanides with mercury(II) compounds,[3-5] we found that isocyanides react with mercury(II) chloride to give labile isocyanide complexes, and to afford cyclic oligomers and low molecular weight polyisocyanides upon heating. Here we report the oligomerization and polymerization of isocyanides *via* isocyanide-mercury(II) chloride complexes.

Results and Discussion

Cyclo-oligomerization of 2,6-Xylyl Isocyanide (I). 2,6-Xylyl isocyanide reacted with mercury(II) chloride to give 2,6-xylyl isocyanide-mercury chloride complex (II) at room temperature.[3] When I and mercury(II) chloride in molar ratio of 4: 1 were heated in THF at reflux for 5 h, two heterocyclic tetramers (III and IV) and one pentamer (V) were isolated in 1, 4, and 1% yield based on I, respectively. The complex II was also obtained in good yield. The compound III was converted to IV easily by hydrolysis in aqueous THF solution or in silica gel column chromatography. Elemental analysis and mass spectrum of III indicate that compound III consists of four molecules of I, one chlorine and one hydrogen atom. IR spectrum of III shows absorptions at 3420 due to ν_{NH}, 1670, 1640, and 1625 cm^{-1} due to $\nu_{C=C}$ and $\nu_{C=N}$. NMR spectrum exhibited a singlet at δ 3.76 due to NH proton, four sharp singlets around δ 2.0 due to methyl protons and two broad singlets around δ 7.0 due to aromatic protons. Compound IV was found to have the composition of four molecules of I and one molecule of water on the basis of elemental analysis and mass spectrum. In the IR spectrum, IV shows absorptions at 3370 and 3296 due to two ν_{NH}. The NMR spectrum of IV shows characteristic singlets at δ 4.32 and 5.04 due to NH protons in addition to signals due to methyl protons and aromatic protons. UV absorption pattern is similar to that of pyrrolin-2-one derivatives.[6] From these data,

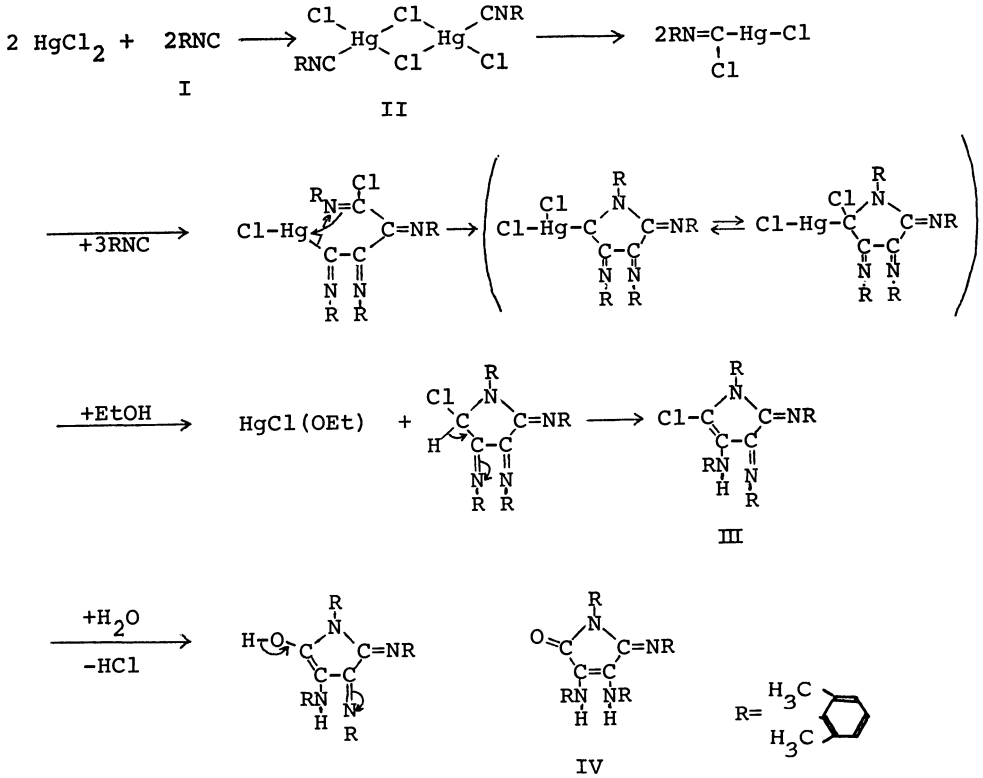

Fig. 1

III and IV were identified as 1-(2,6-xylyl)-2-chloro-3-(2,6-xylylamino)-4,5-bis(2,6-xylylimino)-2-pyrroline and 1-(2,6-xylyl)-3,4-bis(2,6-xylylamino)-5-(2,6-xylylimino)-3-pyrrolin-2-one, respectively. The formation of III and IV could be explained as following scheme. Insertion of I into Hg–Cl bond and successive insertion could form intermediate (A). Further insertion reaction presumably could hardly take place because of steric hindrance of I. Intramolecular addition of Hg–C bond to C=N forms complex (B), which converts to C. Subsequent proton shift of C could give III. The addition of ethanol to the reaction mixture enhanced the oligomerization. Thus, the oligomers III, IV, V, and blue crystalline hexamer (VI) were isolated in 4, 12, 3, and 0.2% yield, respectively. The reaction of phenylisocyanide–mercury(II) chloride complex with I gave small amounts of 1:1 co-oligomer (IV'), whose structure is similar to that of IV.

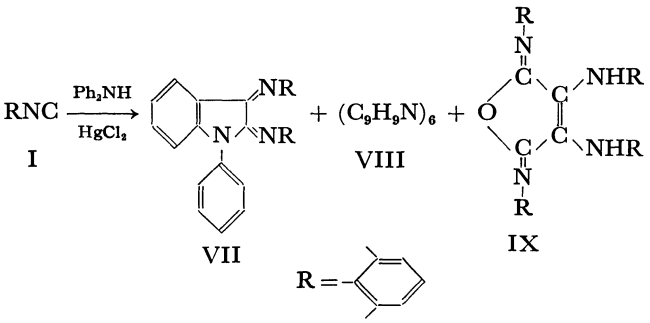

Fig. 2

Diphenylamine affected the oligomerization of I, though the role of diphenylamine is unclear. Heating a mixture of I, mercury(II) chloride and diphenylamine in THF solution gave red crystals (VII), brown crystalline hexamer (VIII) and orange yellow crystalline tetramer (IX) in 3, 21, and 31% yield, respectively. Elemental analysis and mass spectrum of VII indicate that VII is a 2:1 adduct of I and diphenylamine. IR and NMR spectra indicate that VII is an isatindiimine derivative. Compound IX was found to be an isomer of IV from elemental analysis and mass spectrum data. NMR spectrum exhibits that IX has a symmetrical molecular structure. Therefore, the compound IX was determined as 2,5-bis(xylylimino)-3,4-bis(xylylamino)furan. The compound I cannnot hold a polymer chain propagation and affords various heterocyclic oligomers.

Polymerization of Isocyanide. Isocyanides without bulky groups can polymerize in the presence of mercury(II) chloride. Heating a mixture of benzyl isocyanide and mercury(II) chloride in THF gave brownish powdery polymer In the similar manner, cyclohexyl and phenyl isocyanide gave brownish polymers. IR spectra of the polymers show absorptions at 1640—1650 and 3260—3370 cm^{-1} (weak) due to $\nu_{C=N}$ and ν_{NH}, respectively. Elemental analysis suggests that the polymers consist mainly of monomer unit and small amounts of water. The molecular weights of these polymers are 720—850. This indicates that the average degree of polymerization is seven to eight. These polymers are soluble in THF and chloroform, but insoluble

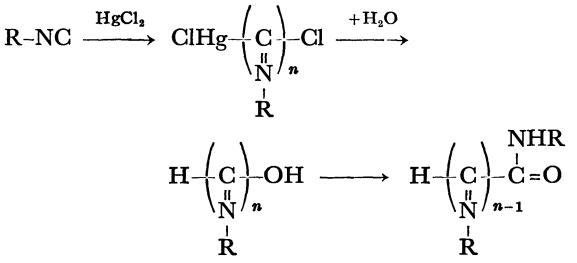

$n=(6), 7, 8, (9)$

Fig. 3

in ether. The molecular weights of the polymers are far lower than that of polyisocyanides obtained by $BF_3 \cdot OEt_2$ or $SnCl_4$ catalysis.[2] High reaction temperature and high molar ratio of isocyanides to mercury(II) chloride are also responsible for the low molecular weight.

Experimental

The melting points are uncorrected. The IR spectra were recorded with a JASCO DS-402 spectrometer. The NMR spectra were measured with a JEOL TMN-TS-100 spectrometer. The mass spectra were taken with a JEOL SG-01 apparatus. Molecular weights of the polymers are measured with Hitachi-Perkin Elmer 115 Molecular Weight Apparatus using chloroform solution. Isocyanides were prepared by the method of Ugi and coworkers.[7]

Reaction of I with Mercury(II) Chloride: Mercury(II) chloride (0.68 g, 25 mmol) **I** (1.31 g, 10 mmol) and dry THF (10 ml) were mixed in a 30 ml conical flask under nitrogen and stirred for 5 h at reflux. The reaction mixture was filtered to remove white powder (Hg_2Cl_2, 18 mg). The filtrate was concentrated and treated with 20 ml of ether to remove II (0.89 g) by filtration. The filtrate was concentrated *in vacuo* and subjected to column chromatography on silica gel. The crystalline oligomers, III, IV, and V were isolated by using hexane–ether as an eluent. Recrystallization of III from hexane–ether gave purified reddish purple crystals, (53 mg, 3.8%), mp 195—197°. Found: C, 77.02; H, 6.79; N, 10.16%. Calcd for $C_{36}H_{37}N_4Cl$: C, 77.05; H, 6.65; N, 9.98%. IR (KBr): 3420, 1670, 1645, 1625 cm^{-1}. NMR ($CDCl_3$): δ 1.99 (s, 6H), 2.02 (s, 6H), 2.12 (s, 6H), 2.36 (s, 6H), 3.76 (s, 1H), 6.70—6.90 (broad s, 9H), 7.12 (s, 3H). Mass spectrum: M^+= 561 (561).

Recrystallization of IV from hexane–dichloromethane gave purified orange yellow crystals, (14 mg, 1%), mp 201—203 °C. Found: C, 80.10; H, 7.33; N, 9.83%. Calcd for $C_{36}H_{38}ON_4$: C, 79.67; H, 7.06; N, 10.32%. IR (KBr): 3370, 3296, 1655, 1640 cm^{-1}. NMR ($CDCl_3$): δ 1.88 (s, 6H), 2.05 (s, 6H), 2.23 (s, 6H), 2.36 (s, 6H), 4.32 (s, 1H), 5.04 (s, 1H), 6.63 (s, 3H), 6.66 (s, 3H), 6.93 (s, 3H), 7.22 (s, 3H). UV $\lambda_{max}^{CH_2Cl_2}$: 263 (ε, 26×10^4), 452 nm (4.7×10^3). Mass spectrum: M^+=542 (542).

V was recrystallized from hexane–dichloromethane to give purple crystals, (13 mg, 1%) mp 159—161 °C. Found: C, 82.65; H, 7.14; N, 10.67%. Calcd for $C_{45}H_{45}N_5$: C, 82.40; H, 6.92; N, 10.68%. IR (KBr): 1666, 1612 cm^{-1}. NMR ($CDCl_3$): δ 1.36 (s, 9H), 1.67 (s, 3H), 1.93 (s, 6H), 2.09 (s, 3H), 2.18 (s, 3H), 2.27 (s, 3H), 2.44 (s, 3H), 5.2—5.6 (m, 2H), 6.0—6.15 (m, 1H), 6.60—6.90 (broad s, 9H), 7.05 (broad s, 3H). Mass spectrum: M^+=655 (655).

Reaction of I with Mercury(II) Chloride in the Presence of Ethanol: A mixture of I (2.62 g, 20 mmol), mercury(II) chlo-

TABLE 1. POLYISOCYANIDE OBTAINED FROM THE REACTION OF ISOCYANIDE AND MERCURY(II) CHLORIDE

Polyisocyanide	Yield (%)	Mp (°C)	MW	IR (cm^{-1})	Elemental analysis C%	H%	N%
Benzyl	67	90—93	850	1640, 1600, 3370 (W)	80.09 (80.30) [a]	5.90 (6.09) [a]	11.83 (11.70) [a]
Cyclohexyl	49	124—128	820	1650, 3260 (W)	73.80 (75.30) [b]	10.05 (10.11) [b]	12.40 (12.54) [b]
Phenyl	74	120—123	720	1638, 1600, 3360 (W)	78.68 (79.58) [c]	5.00 (5.00) [c]	13.27 (13.25) [c]

a) Calcd for $(C_6H_5CH_2NC)_7+H_2O$. b) Calcd for $(C_6H_{11}NC)_7+H_2O$. c) Calcd for $(C_6H_5NC)_7+H_2O$.

ride (1.36 g, 5 mmol), dry THF (20 ml) and ethanol (2 ml) was heated at reflux with stirring for 8 h under nitrogen. Hg_2Cl_2 (150 mg) and II (2.238 g) were removed by filtration. The oligomers, III (334 mg, 11.9%), IV (112 mg, 4.1%), V (81 mg, 3.1%) and VI (5 mg, 0.2%), were isolated from the reaction mixture with a chromatography on silica gel. The compound VI was recrystallized from hexane–dichloromethane to give purified blue crystalline hexamer, mp (decompose) 266—267 °C. Found: C, 81.83; H, 7.05; N, 10.50%. Calcd for $C_{54}H_{54}N_6$: C, 82.40; H, 6.92; N, 10.68%. IR (KBr): 1655, 1580, 1465 cm^{-1}. NMR ($CDCl_3$): δ 1.68 (s, 12H), 2.00 (s, 12H), 2.24 (s, 12H), 6.51 (s, 6H), 6.71 (broad s, 12H). Mass spectrum: $M^+=786$ (786).

Conversion of III to IV: The compound III (101 mg) was heated in aqueous THF at reflux for 0.5 h. The red color of the reaction mixture turned to orange yellow. The reaction mixture was dried over sodium carbonate, concentrated *in vacuo* and chromatographed on silica gel. The compound IV was isolated (92 mg, 94.5%).

The compound III was also completely hydrolyzed to IV, when keeping in silica gel column chromatography for 8 h.

Co-oligomerization of Phenyl Isocyanide with I. Phenyl isocyanide (0.42 g, 4 mmol) and mercury(II) chloride (550 mg, 2 mmol) were mixed in dry THF (10 ml) cooling with Dry Ice–methanol under nitrogen to prepare phenyl isocyanide–mercury(II) chloride complex.

I (1.053 g, 8 mmol) was added to the mixture. The reaction mixture was warmed to room temperature with stirring for 1 h, then heated at reflux for 4 h. The reaction mixture was concentrated *in vacuo*, treated with ether to remove polyphenyl isocyanide and II as precipitates. The filtrate was concentrated and subjected to column chromatography on silica gel to isolate orange yellow crystals (30 mg, 3.0%) and yellow crystals (8 mg). The orange yellow crystals were recrystallized from hexane–dichloromethane to give purified IV′, mp. 176—177 °C. Found: C, 78.76; H, 6.69; N, 11.28 %. Calcd for $C_{32}H_{30}ON_4$: C, 78.98; H, 6.21; N, 11.52%. IR (KBr): 3365, 3305, 1725, 1655, 1645, 1602 cm^{-1}. NMR ($CDCl_3$): δ 2.03 (s, 6H), 2.61 (s, 6H), 4.7 (broad s, 1H), 6.42 (broad s, 6H), 6.78 (s, 5H), 7.24 (s, 5H). Mass spectrum: $M^+=486$ (486).

Reaction of I with Mercury(II) Chloride in the Presence of Diphenylamine: Diphenylamine (0.85 g, 5 mmol) was added to the mixture of mercury(II) chloride (0.67 g, 2.5 mmol), I (1.31 g, 10 mmol) in dry THF (10 ml). The reaction mixture was heated at reflux for 5 h with stirring under nitrogen. The reaction mixture was concentrated and treated with 20 ml of ether to remove mercury(I) chloride, diphenylamine and II by filtration. The filtrate was concentrated and chromatographed on silica gel. Three compounds were isolated by using hexane–ether as an eluent. Recrystallization from hexane–ether gave the purified 2:1 adduct VII (36 mg, 3.3%), mp 178—180 °C. Found: C, 84.02; H, 6.50; N, 9.57%. Calcd for $C_{30}H_{27}N_3$: C, 83.88; H, 6.34; N, 9.78%. IR (KBr): 1672, 1637, 1589 cm^{-1}. NMR ($CDCl_3$): δ 1.91 (s, 6H), 2.11 (s, 6H), 2.11 (s, 6H), 6.4—6.85 (m, 5H), 6.93 (s, 3H), 7.20 (s, 3H), 7.25—7.60 (s, 4H). UV $\lambda_{max}^{CH_2Cl_2}$: 260 (ε, 4.1×10^4), 245 nm (2.85×10^3). Mass spectrum: $M^+=429$ (429).

Recrystallization of a brown compound from hexane–dichloromethane gave the purified VIII, (142 mg, 21.2%) mp. 295—298 °C. Found: C, 82.13; H, 7.06; N, 10.69%. Calcd for $C_{54}H_{54}N_6$: C, 82.40; H, 6.92; N, 10.68%. IR (KBr): 3380, 1671, 1625, 1507 cm^{-1}. NMR ($CDCl_3$): δ 1.84 (s, 6H), 2.15 (s, 6H), 2.24 (s, 6H), 3.98 (s, 1H), 6.59 (s, 3H), 6.73 (s, 3H), 6.83 (s, 3H). UV $\lambda_{max}^{CH_2Cl_2}$: 279 (ε, 49×10^5), 442 nm (5.8×10^5). Mass spectrum: $M^+=786$ (786).

Recrystallization of an orange compound from hexane–dichloromethane gave the purified IX, (213 mg, 30.7%), mp 211—212°. Found: C, 79.81; H, 6.62; N, 10.27%. Calcd for $C_{36}H_{38}ON_4$: C, 79.97; H, 7.06; N, 10.32%. IR (KBr): 3355, 1734, 1650, 1590 cm^{-1}. NMR ($CDCl_3$): δ 2.12—2.20 (broad m, 24H), 4.51 (s, 2H), 6.5—7.1 (broad m, 12H). UV $\lambda_{max}^{CH_2Cl_2}$: 276 (ε, 3.0×10^4), 487 nm (5.8×10^3). Mass spectrum: $M^+=542$ (542).

Polymerization of Isocyanides in the Presence of Mercury(II) Chloride. Benzyl isocyanide (1.20 g, 10 mmol) and mercury(II) chloride (0.672 g, 2.5 mmol) in 10 ml of dry THF was heated at reflux with stirring for 5 h under nitrogen. The reaction mixture was subjected to GLC analysis, and the formation of benzyl chloride (5% based on $HgCl_2$) was confirmed. White precipitates (Hg_2Cl_2, 280 mg) were removed from the reaction mixture by filtration. The filtrate was concentrated and 20 ml of ether was added to separate light brown powders, which were treated with $LiAlH_4$ in THF solution to remove mercury(II) by reduction. The brown powders were extracted with dichloromethane, dried over magnesium sulfate, concentrated and treated with ether–hexane to spectrate poly(benzyl isocyanide) as brown precipitates.

Poly(cyclohexy isocyanide) was obtained by the same procedure as that of poly(benzyl isocyanide).

The reaction of phenyl isocyanide (2.5 mmol, 20 mmol) with mercury(II) chloride (1.35 g, 5 mmol) was carried out at room temperature for 8 h and poly(phenyl isocyanide) was isolated by the similar manner as described in the reaction of benzyl isocyanide with mercury(II) chloride. Yield data, melting point, elemental analysis, IR data and molecular weight of these polymers are listed in Table 1.

References

1) F. Millich, *Chem. Rev.*, **72**, 101 (1972).
2) Y. Yamamoto, T. Takizawa, and N. Hagiwara, *Nippon Kagaku Zasshi*, **87**, 1335 (1966).
3) H. Sawai and T. Takizawa, *J. Organometal. Chem.*, **94**, 333 (1975).
4) H. Sawai and T. Takizawa, *Chem. Pharm. Bull.*, **23**, 374 (1975).
5) H. Sawai and T. Takizawa, *Tetrahedron Lett.*, **1972** 4263.
6) Y. Suzuki, Ph. D. Thesis, University of Tokyo (1973).
7) I. Ugi, U. Fetzer, U. Eholtzer, H. Knupfer and K. Offermann, *Angew. Chem. Int. Ed. Engl.*, **4**, 472 (1965).

α,β-Unsaturated Carboxylic Acid Derivatives. XI. Convenient Synthesis of *tert*-Butyl 2-Alkoxy- and Hydroxy-2-acetylamino-3-mono- or 3,3-dihaloalkanoates[1]

Chung-gi SHIN, Yoshiaki SATO, and Juji YOSHIMURA*

Laboratory of Organic Chemistry, Faculty of Technology, Kanagawa University, Rokkakubashi, Kanagawa-ku, Yokohama 221

**Laboratory of Chemistry for Natural Products, Faculty of Science, Tokyo Institute of Technology, Ōkayama, Meguro-ku, Tokyo 152*

(Received December 10, 1975)

It was found that the halogenation of *t*-butyl 2-acetylamino-3-bromo-2-alkenoate (**3**) by NBS or NCS gave *t*-butyl 2-acetylimino-3,3-dihaloalkanoate (**6** and **7**). The addition of water or several saturated, unsaturated and polyhydric alcohols to the carbon–nitrogen double bond of **6** or **7** was accomplished to give *t*-butyl 2-acetylamino-2-alkoxy- and hydroxy-3,3-dihaloalkanoate. Similarly, the treatment of *t*-butyl 2-bromoacetylamino-2-alkenoate in alcohol gave *t*-butyl 2-acetylamino-2-alkoxy-3-bromoalkanoate, *via* the addition of alcohol to the imino intermediate (**2**). The formation mechanism and the structural assignment are discussed.

Because of the possible synthetic utility of α-alkoxy and α-hydroxy-α-acylamino acids as an important skeleton moiety or starting material for the total synthesis of bicyclomycin,[2] 6-methoxypenicillins,[3] 7-methoxycephalosporins,[3] and ergotamine,[4] there have been several reports on the synthetic methods of the above α-acylamino acids,[5–9] but some limitations are present in the above methods.

On the other hand, the present authors have recently reported the facile synthesis of *tert* (*t*)-butyl 2-bromoacetylamino-2-alkenoate (**1**) by the reaction of *t*-butyl 2-acetylamino-2-alkenoate with *N*-bromosuccinimide (NBS),[10] and its bromine migration into *t*-butyl 3-bromo-2-acetylamino-2-alkenoate (**3**).

In this paper, we wish to report that a further reaction of **3** with NBS occurs to give *t*-butyl 2-acetylimino-3,3-dibromoalkanoate (**6**) as a stable intermediate in a quantitative yield, and that the subsequent addition of water or alcohols to the carbon-nitrogen double bond of **6** easily takes place to form *t*-butyl 2-acetylamino-2-alkoxy- or hydroxy-3,3-dibromoalkanoate (**8**). Furthermore, the latter reaction was extended to the direct reaction of **3** with *N*-chlorosuccinimide (NCS) in alcohol and that of **1** with alcohol to give *t*-butyl 2-acetylamino-2-alkoxy-3-bromo-3-chloroalkanoate (**9**) and *t*-butyl 2-acetylamino-2-alkoxy-3-bromoalkanoate (**10**), respectively.

Results and Discussion

Addition of Protic Solvent to the Carbon-nitrogen Double Bond. When the *E*- or *Z*-isomer of **3** separated[10] was treated individually with NBS in chloroform at room temperature for 20 min, an identical yellowish syrup was obtained in a quantitative yield. Since the expected *t*-butyl 2-(*N*-acetyl-*O*-alkylhydroxyamino)-3-bromo-2-alkenoate (**5**) could not be obtained by the reaction of the above syrup with sodium alkoxide in alcohol,[10] and from the following experimental facts, the structure of the syrup isolated was confirmed to be **6**. It was concluded that *t*-butyl 3-bromo-2-bromoacetylamino-2-alkenoate (**4**) formed initially as an unstable intermediate and the subsequent migration of bromine from **4** gave **6**.

It was found that the treatment of **6** (R=CH_3 and C_2H_5) with protic solvent, water or alcohols at temperatures below 60 °C for 2—24 h gave 8 in a *ca.* 60% yield by the addition reaction of water or alcohols to the carbon-nitrogen double bond of **6**. The saturated (methanol, ethanol and benzyl alcohols), unsaturated (allyl and propargyl alcohols) and polyhydric alcohols (ethylene glycol and glycerol) were applied in the above addition. However, it was found that no reaction of **6** with isopropyl alcohol occurred, due to the steric hindrance between the bulkyl bromine in the 3-position and the isopropyl group. Accordingly, the primary hydroxyl group of glycerol should preferentially be added to **6**, in the case of **8h**.

It was found that *t*-butyl 2-acetylamino-3,3-dibromo-2-ethoxybutanoate (**8c**; R=CH_3) was also obtained directly in a 69.3% yield by the reaction of *t*-butyl 2-acetylamino-3-bromo-2-butenoate (**3**; *E*+*Z*) with NBS in ethanol at room temperature for 6 h. To extend this reaction, when compound **3** was treated with NCS in alcohols (methanol and benzyl alcohols), the expected **9** was obtained in a *ca.* 70% yield.

Furthermore, in order to generalize the above reaction, the addition of alcohols (methanol and benzyl alcohols) to the intermediate **2** was attempted, by stirring **1** with alcohol at room temperature for 48 h to give the expected **10** in a *ca.* 30% yield. On the other hand, an independent preparation of **10** by the addition reaction of alcohol to the carbon-carbon double bond of **3** was unsuccessful.

All the new compounds were obtained in high purities as a pale yellow syrup (**6**) or colorless crystals (**8**, **9**, and **10**).

Structure and Formation Mechanism. The structures of all the new products were analyzed spectroscopically and the elemental analysis was satisfactory. From the NMR spectra, the NH proton peak signals of **8**, **9**, and **10** appeared in the δ=6.25—7.02 region as broad singlets, except for **8h** (R=CH_3, δ 8.02). On the other hand, the appearance of secondary amide absorption bands in the regions 3200—3380 (–NH) and 1600—1700 and 1490—1520 cm^{-1} (–NHCO) in the IR spectra of **8**, **9**, and **10**, and the disappearance of the tertiary amide (>NCO) bands in the regions 1720—1725 and

TABLE 1. *t*-BUTYL 2-ACETYLAMINO-2-ALKOXY- AND 2-HYDROXY-3,3-DIBROMOALKANOATES (**8**)

	Compound R	Compound R′	Yield %	Mp °C	Formula	Found (Calcd), % C	H	N	IR spectrum, cm^{-1}, in KBr OH	NH	COO	NHCO	C=C (C≡C)	NMR spectrum,[a] δ OH	NH
8a	CH_3	H	46.1	104[b]	$C_{10}H_{17}NO_4Br_2$	32.25 (32.03	4.64 4.57	3.91 3.73)	3400	3340	1735	1660	1510	5.88	6.83
8b	CH_3	CH_3	81.7	113—114[c]	$C_{11}H_{19}NO_4Br_2$	34.39 (33.96	4.96 4.92	3.48 3.60)		3350	1730	1690	1490		6.32
8b	C_2H_5	CH_3	65.3	105—106[b]	$C_{12}H_{21}NO_4Br_2$	35.92 (35.76	5.29 5.25	3.25 3.47)		3370	1740	1700	1490		6.44
8c	CH_3	C_2H_5	63.6	120—121[b]	$C_{12}H_{21}NO_4Br_2$	36.08 (35.76	5.26 5.25	3.36 3.47)		3370	1740	1695	1490		6.38
8c	C_2H_5	C_2H_5	52.6	109—110[b]	$C_{13}H_{23}NO_4Br_2$	37.54 (37.43	5.62 5.56	3.28 3.36)		3340	1730	1695	1515		6.48
8d	CH_3	$CH_2C_6H_5$	81.9	125—126[d]	$C_{17}H_{23}NO_4Br_2$	43.97 (43.89	4.96 4.98	3.06 3.01)		3320	1730	1680	1490		6.32
8d	C_2H_5	$CH_2C_6H_5$	80.2	120—121[b]	$C_{18}H_{25}NO_4Br_2$	45.14 (45.12	5.19 5.26	2.83 2.92)		3330	1735	1680	1500		6.44
8e	CH_3	$CH_2CH{=}CH_2$	48.5	96—97[b]	$C_{13}H_{21}NO_4Br_2$	37.77 (37.62	5.08 5.10	3.35 3.37)		3310	1740	1690	1490, 1640		6.37
8e	C_2H_5	$CH_2CH{=}CH_2$	37.5	75—76[b]	$C_{14}H_{23}NO_4Br_2$	39.25 (39.19	5.38 5.40	3.22 3.26)		3320	1740	1690	1500, 1650		6.44
8f	CH_3	$CH_2C{\equiv}CH$	38.9	137—138[b]	$C_{13}H_{19}NO_4Br_2$	37.95 (37.80	4.61 4.64	3.40 3.39)		3200	1740	1690	1495, (2100)		6.36
8f	C_2H_5	$CH_2C{\equiv}CH$	37.8	121—122[b]	$C_{14}H_{21}NO_4Br_2$	39.50 (39.37	4.87 4.96	3.23 3.28)		3230	1730	1690	1490, (2100)		6.44
8g	CH_3	CH_2CH_2OH	74.7	97—98[d]	$C_{12}H_{21}NO_5Br_2$	34.77 (34.39	5.22 5.05	3.44 3.34)	3360	3320	1740	1670	1510	2.73	6.45
8g	C_2H_5	CH_2CH_2OH	60.6	117—118[b]	$C_{13}H_{23}NO_5Br_2$	36.10 (36.05	5.20 5.35	3.29 3.23)	3360	3240	1750	1660	1520	2.27	6.63
8h	CH_3	CH_2CHCH_2OH OH	48.6	121—123[e]	$C_{13}H_{23}NO_6Br_2$	34.94 (34.77	5.31 5.16	3.12 3.13)	3380–3280		1740	1670	1500	4.09	8.02[g]
8h	C_2H_5	CH_2CHCH_2OH OH	37.1	112—115[f]	$C_{14}H_{25}NO_6Br_2$	36.37 (36.31	5.36 5.44	2.97 3.02)	3400–3150		1740	1670		2.93 3.25	6.64

a) Measured in $CDCl_3$. b) Colorless needles from ethanol–water. c) Colorless prisms from di-*n*-butyl ether. d) Colorless needles from di-*n*-butyl ether. e) Colorless prisms from chloroform. f) Colorless needles from carbon tetrachloride. g) Measured in DMSO-d_6.

TABLE 2. *t*-BUTYL 2-ACETYLAMINO-2-ALKOXY-3-BROMO-3-CHLORO- AND 3-MONOBROMOALKANOATES (**9** AND **10**)

	Compound R	Compound R′	Yield %	Mp °C	Formula	Found (Calcd), % C	H	N	IR spectrum, cm^{-1} in KBr NH	COO	NHCO	NMR spectrum,[a] δ NH
9b	CH_3	CH_3	78.0	96—97[b]	$C_{11}H_{19}NO_4BrCl$	38.47 (38.34	5.61 5.56	4.02 4.06)	3350	1740	1690, 1500	6.35
9b	C_2H_5	CH_3	61.3	94—95[c]	$C_{12}H_{21}NO_4BrCl$	40.59 (40.19	5.79 5.90	4.12 3.91)	3380	1745	1700, 1490	6.38
9d	CH_3	$CH_2C_6H_5$	78.5	121—122[c]	$C_{17}H_{23}NO_4BrCl$	48.56 (48.53	5.48 5.51	3.28 3.33)	3330	1740	1695, 1510	6.25 6.33
9d	C_2H_5	$CH_2C_6H_5$	50.8	119—120[b]	$C_{18}H_{25}NO_4BrCl$	49.91 (49.73	5.72 5.80	3.17 3.22)	3350	1740	1690, 1500	6.38 6.50
10b	CH_3	CH_3	28.3	90—91[d]	$C_{11}H_{20}NO_4Br$	42.41 (42.59	6.47 6.50	4.44 4.52)	3320	1730	1695, 1510	6.46 6.98
10d	CH_3	$CH_2C_6H_5$	25.7	115—116[b]	$C_{17}H_{24}NO_4Br$	52.86 (52.86	6.28 6.26	3.50 3.63)	3350	1730	1690, 1520	6.42 7.02

a) Measured in $CDCl_3$. b) Colorless needles from ethanol–water. c) Colorless needles from di-*n*-butyl ether. d) Colorless needles from hexane.

1655—1660 cm^{-1} of **1** and **6** indicate the formation of **8**, **9**, and **10**.

The yields, physical constants, and spectral data of **8**, **9**, and **10** are summarized in Tables 1 and 2.

In recent reports,[8,9] it has been assumed that the formation of methyl 2-acetylamino-2-methoxyalkanoate derived from methyl 2-acetylamino-2-acetylthio- or 2-chloroacetylaminoalkanoate proceeded *via* the addition reaction of methanol to the unstable intermediate, methyl 2-acetyliminoalkanoate. Here, however, the above assumption was proven by isolation of the stable intermediate (**6**) and the subsequent addition of water or alcohols to **6**. Consequently, it was also confirmed that **9** and **10** were derived from the addition reaction of

gel column using benzene–ethyl acetate (30: 1 V/V) as the eluent to give colorless crystals.

Preparation of ***8g.*** After treating **6** (R=CH_3, 0.0036 mol) with ethylene glycol (5 ml) with stirring at room temperature for 5 h, a similar work up gave a pale yellow syrup, which gradually crystallized to give colorless crystals of *t*-butyl 2-acetylamino-3,3-dibromo-2-(2-hydroxyethoxy)butanoate.

In a similar manner, *t*-butyl 2-acetylamino-3,3-dibromo-2-(2-hydroxyethoxy)pentanoate was obtained from the reaction of **6** (R=C_2H_5) with ethylene glycol.

Preparation of ***8h.*** After treating **6** (R=CH_3, 0.0036 mol) with glycerol (5 ml) with stirring at *ca.* 60 °C for 4 h, water (30 ml) was added to the reaction mixture, and then the aqueous mixture was extracted three times with chloroform (60 ml). The chloroform extracts were washed with water twice and then dried over anhydrous sodium sulfate. Concentration of the chloroform solution gave a colorless syrup, which gradually crystallized to give colorless crystals of *t*-butyl 2-acetylamino-3,3-dibromo-2-(2,3-dihydroxypropoxy)-butanoate.

In a similar manner, *t*-butyl 2-acetylamino-3,3-dibromo-2-(2,3-dihydroxypropoxy)pentanoate was obtained from the reaction of **6** (R=C_2H_5) with glycerol. The syrup obtained was purified on a silica gel column using benzene–ethyl acetate (1: 5 V/V) as the eluent to give colorless crystals.

Preparation of ***9b.*** Into a solution of **3** (R=CH_3, 0.0036 mol) in methanol (10 ml) was added NCS (0.004 mol) portion by portion with stirring at room temperature. After stirring for 10 h, the reaction solution was concentrated under reduced pressure to give a colorless syrup containing succinimide. The residue was dissolved in benzene (30 ml) and then the benzene solution was washed three times with water. The benzene layer was dried over anhydrous sodium sulfate and then evaporated under reduced pressure to give colorless crystals, which were identified to be *t*-butyl 2-acetylamino-3-bromo-3-chloro-2-methoxybutanoate.

In a similar manner, *t*-butyl 2-acetylamino-3-bromo-3-chloro-2-methoxypentanoate was obtained from the reaction of **3** (R=C_2H_5) with NCS in the presence of methanol, after stirring for 5 h.

Preparation of ***9d.*** After treating a solution of **3** (R=CH_3, 0.0036 mol) in benzyl alcohol (3 ml) with NCS (0.004 mol), a similar work up gave a colorless syrup, which gradually crystallized. The crystals were identified to be *t*-butyl 2-acetylamino-2-benzyloxy-3-bromo-3-chlorobutanoate.

In a similar manner, *t*-butyl 2-acetylamino-2-benzyloxy-3-bromo-3-chloropentanoate was obtained from the reaction of **3** (R=C_2H_5) with NCS in the presence of benzyl alcohol, after stirring for 20 h.

Preparation of ***10.*** After allowing a solution of **1** (R=CH_3, 0.0036 mol) in methanol (10 ml) to stand at room temperature for 2 days, a similar work up gave colorless crystals of *t*-butyl 2-acetylamino-3-bromo-2-methoxybutanoate.

In a simlar manner, *t*-butyl 2-acetylamino-2-benzyloxy-3-bromobutanoate was obtained from the reaction of **1** (R=CH_3) with benzyl alcohol.

References

1) Part X: C. Shin, Y. Yonezawa, H. Sakamoto, and J. Yoshimura, *Bull. Chem. Soc. Jpn.*, **48**, 2891 (1975). This work was presented at the 31st and the 32nd Annual Meetings of Chemical Society of Japan, Sendai, October, 1974; Fukuoka, October, 1975.

2) T. Miyoshi, N. Miyairi, H. Aoki, M. Kohsaka, H. Sakai, and H. Kamiya, *J. Antibiotics*, **25**, 569 (1972).

3) a) R. Nagarajan, L. D. Boeck, M. Gorman, R. L. Hamill, C. E. Higgens, M. M. Hoehn, W. M. Stark, and J. G. Whitney, *J. Am. Chem. Soc.*, **93**, 2308 (1971); b) E. O. Stapley, M. Jackson, S. Hernandez, S. B. Zimmerman, S. A. Currie, S. Mochales, J. M. Mata, H. B. Woodruff, and D. Hendlin, *Antimicrob. Ag. Chemother.*, **2**, 122 (1972); c) T. W. Miller, R. T. Goegelman, R. G. Weston, I. Putter, and F. F. Wolf, *ibid.*, **2**, 132 (1972); d) A. K. Miller, E. Celozzi, B. A. Pelak, E. O. Stapley, and D. Hendlin, *ibid.*, **2**, 281 (1972).

4) a) A. Stoll, *Helv. Chim. Acta*, **28**, 1283 (1945); b) A. Hofmann, A. J. Frey, and H. Ott, *Experientia*, **17**, 206 (1961).

5) M. M. Chemiakine, E. S. Tchaman, L. I. Denisova, G. A. Ravdel, and W. J. Rodionow, *Bull. Soc. Chim. Fr.*, **26**, 530 (1959).

6) C. Gallina, M. Maneschi, and A. Romeo, *J. Chem. Soc., Parkin Trans. 1*, **1973**, 1134.

7) S. Nakatsuka, H. Tanino, and Y. Kishi, *J. Am. Chem. Soc.*, **97**, 5008 (1975).

8) H. Poisel and U. Schmidt, *Chem. Ber.*, **108**, 2547 (1975).

9) R. K. Olsen and A. J. Kolar, *Tetrahedron Lett.*, **1975**, 3597.

10) C. Shin, K. Nanjo, T. Nishino, Y. Sato, and J. Yoshimura, *Bull. Chem. Soc. Jpn.*, **48**, 2492 (1975).

Chemistry of Nitrosoimines. XV.[1] Reactions of 3-Substituted 2-Nitrosoimino-2,3-dihydrobenzothiazoles with Lithium Aluminum Hydride and Diazo Compounds

Kin-ya AKIBA, Takayuki KAWAMURA, Masahide OCHIUMI, and Naoki INAMOTO

Department of Chemistry, Faculty of Science, The University of Tokyo, Hongo, Tokyo 113

(Received December 26, 1975)

3-Substituted 2-nitrosoimino-2,3-dihydrobenzothiazoles (**1**) were reduced with lithium aluminum hydride to give the corresponding thiazolone azines and bis[*o*-(*N*-substituted *N*-formylamino)phenyl] disulfides as major products. Reactions of **1** with some substituted diazomethanes gave the corresponding unsymmetrical azine *N*-monoxides (**16**) or azines (**17**) depending on the structure of the diazomethane.

We previously reported on the reactions of 3-substituted 2-nitrosoimino-2,3-dihydrobenzothiazoles (**1**) with Grignard reagents[2] and organolithiums.[3] In this paper, we report on the reactions of **1** with lithium aluminum hydride (LAH).[4] According to the report of Zimmerman and Paskovich on the preparation of the corresponding diazo compound by the reduction of bismesityl-*N*-nitrosoiminomethane with LAH,[5] the formation of the corresponding diazo compounds (**2**) or carbenes (**3**)[6] can be expected in the reaction, together with the products of nucleophilic attack of LAH on *C-2* and the sulfur of the thiazoline ring.

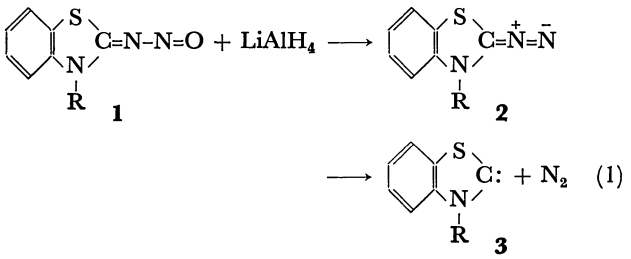

In order to know the reactivity of **1** toward diazo compounds or the corresponding carbenes, the reactions of **1** with some stable diazo compounds were examined under various conditions.

Reaction of 1 with LAH. The main products of reduction of **1** with an excess amount of LAH were 3-substituted 2,3-dihydrobenzothiazol-2-one azine (**4**), bis[*o*-(*N*-substituted *N*-formylamino)phenyl] disulfide (**5**), and bis[*o*-(*N*-substituted amino)phenyl] disulfide (**6**). The yields are given in Table 1.

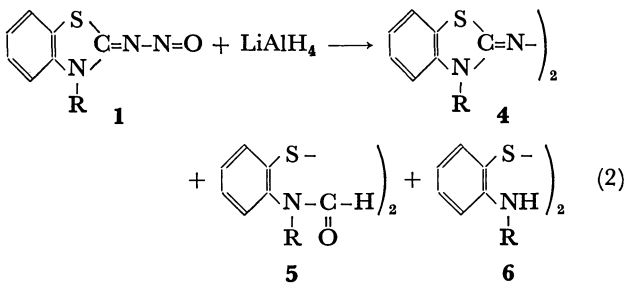

a) R=Ph, b) R=Me, c) R=Et

The formation of the azine (**4**) can be ascribed to the intermediacy of the diazo compound (**2**) produced by hydride attack on the nitrogen atom of the nitroso group (*path a*). On the other hand, the formation of the disulfide (**5**) can be explained by invoking the ring opened nitrosoimine (**7**) produced by hydride attack on the *C-2* of the ring (*path b*), **7** thus formed decomposing to the corresponding carbonyl compound and nitrogen gas.[7]

Table 1. Reduction of **1** with excess lithium aluminum hydride

1	4	5	6
a) R=Ph	16	30	20
b) R=Me	27	22	24
c) R=Et	30	28	18

Numerical values show yields (mole %) based on charged **1**.

When the reaction was carried out under argon atmosphere in a closed system, the evolved gas was only nitrogen as confirmed by mass spectrometry. This supports the proposed mechanism.

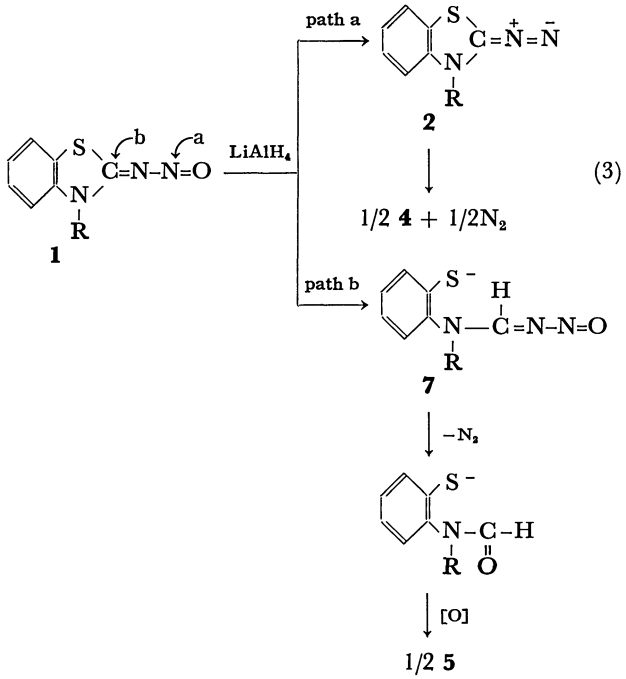

The products were scrutinized by column chromatography for the case of **1a**, two products (**8a** and **9a**)

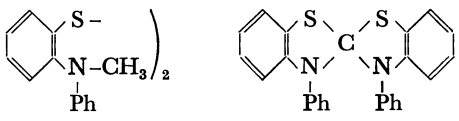

being obtained in very small amounts. The disulfide (**8a**) is a reduction product of **5a** with excess LAH, since **5a** was reduced with LAH in refluxing tetrahydrofuran (THF) to **6a** and **8a**. Formation of **9a** can be explained by means of the reaction of **1a** with *o*-anilinobenzenethiolate anion,[8] a precursor of **6**.

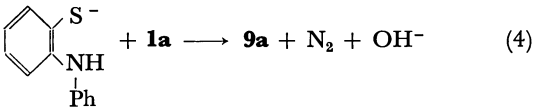

(4)

In order to prepare **2**, 2-hydrazono-3-phenyl-2,3-dihydrobenzothiazole (**10a**) was oxidized with mercury (II) oxide. The reaction took place very slowly at 0 °C as compared with that of benzophenone hydrazone, giving **4a** as the major product (*ca.* 70%). This shows that **2a** is too unstable to be isolated and gives **4a** easily. In order to study the nature of the corresponding carbene dimer, 3,3'-dimethylbi(2,3-dihydrobenzothiazolidene) (**11**) was prepared by the deoxygenation of **1** with triethyl phosphite.[9] It was found to be sensitive to air. Thus, air was bubbled into a benzene solution of **11**. Spiro-amide (**12**) was obtained as the major product (71%), which may be decomposition product of epoxide (**13**). Even if carbene dimer (**11**) were formed in the reduction reaction, **11** would be oxidized to **12** by air during the course of isolation. However, **12** could not be isolated from the reaction mixture of **1b** with LAH, indicating the absence of **11**, or fast reaction of **3** with **2**.

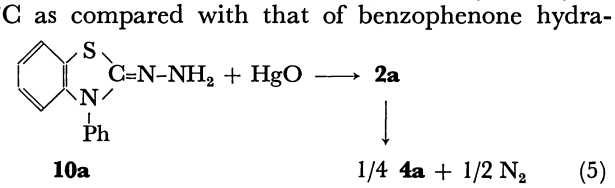

10a 1/4 **4a** + 1/2 N_2 (5)

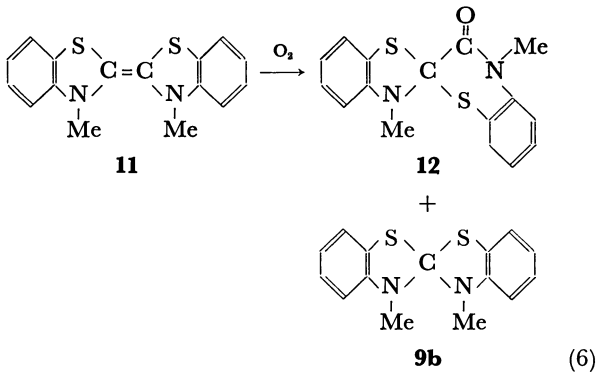

11 **12** **9b** (6)

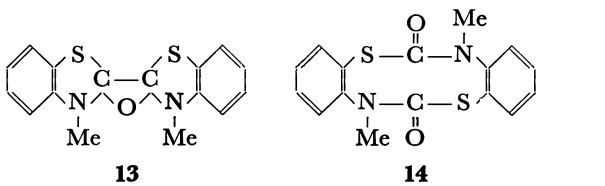

13 **14**

Wanzlick *et al.* reported that air-oxidation of **11** affords **14** in 75% yield. However, we could not substantiate the result. Our result is similar to that of the air-oxidation of naphthalene analog of **11**.[6c]

Reactions of 1 with Diazo Compounds. A dichloromethane solution of **1b** was refluxed for a week with diphenyldiazomethane (**15a**) and for one day with methylphenyldiazomethane (**15b**), and left to stand at room temperature for five days with phenyldiazomethane (**15c**). In the cases of **15a** and **15c**, the isolated products were unsymmetrical azine *N*-monoxides (**16**), whereas the product was unsymmetrical azine (**17b**) in the case of **15b**. The yields of the products are summarized in Table 2.

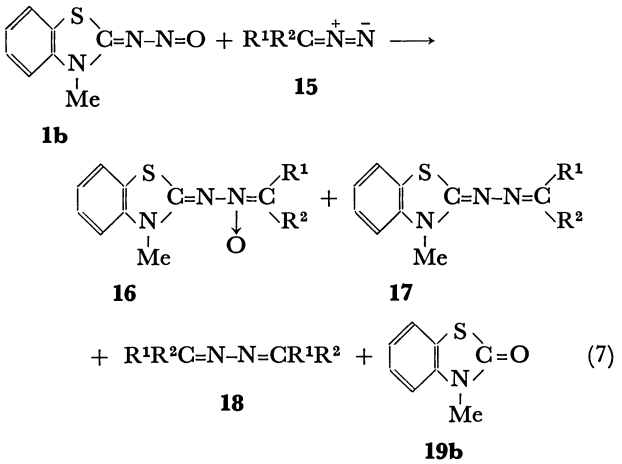

1b **15** **16** **17** **18** **19b** (7)

a) $R^1=R^2=Ph$, b) $R^1=Ph$, $R^2=Me$,
c) $R^1=Ph$, $R^2=H$

Table 2. Reaction of **1b** with diazo compounds[a]

15	16	17	18	19b	1b recovery
a) $Ph_2C=N_2$	16	—	42	80	—
b) $MePhC=N_2$	—	34	39	—	88
c) $PhHC=N_2$	11	—	46[b]	—	90

a) The yields (mol %) of **16**, **17**, and **19b** were calculated based on the amount of **1b** consumed. The yield of **18** was calculated based on the amount of charged **15**. b) PhCOCHPhN=NCHPhCOPh (11%), probably the by-product in the preparation of **15c**, was obtained.

The reaction of **1b** with **15a** was carried out in *N*,*N*-dimethylformamide (DMF) in the presence of copper-(I) chloride–triisopropyl phosphite complex (**20**) in order to generate carbene at low temperature (30 °C). However, the yields of **16a** and **17a** were low in spite of much effort to improve them and found to be *ca.* 7 and 4%, respectively.

The results indicate that the reactivity of **1** toward diazo compounds and carbenes is very low. This indicates that *path a* [Eq. 3] is the major route for the formation of **4**. Deoxygenation of **16a** with diphenylcarbene, generated from **15a** and **20**, gave **17a** in 75% yield under the same conditions. This shows that the primary product of the reaction of **1** with carbene is

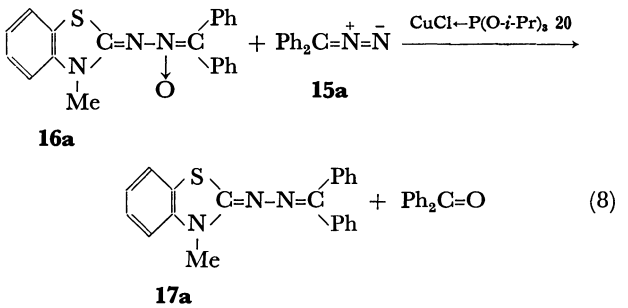

16a **15a** **17a** (8)

azine *N*-monoxide (**16**) which is deoxygenated by incident carbene to give unsymmetrical azine (**17**).

Experimental

Materials. 3-Substituted 2-nitrosoimino-2,3-dihydrobenzothiazoles (**1**) were prepared by the reported methods; 3-phenyl (**1a**), mp 140 °C (dec.),[10] 3-methyl (**1b**), mp 143 °C (dec.),[11] and 3-ethyl (**1c**), mp 143—144 °C (dec.).[12] Diphenyl-,[13] methylphenyl-,[13] and phenyldiazomethanes[14] were prepared by the reported methods. All the reactions were carried out under nitrogen.

*Reduction of 3-Methyl-2-nitrosoimino-2,3-dihydrobenzothiazole (**1b**) with LAH.* To a stirred solution of **1b** (10.0 g 47.8 mmol) in THF (700 ml) was added LAH (1.68 g, 47.0 mmol) portionwise at −70——40 °C during the period of 1 h. Vigorous gas evolution was observed upon the addition, and stirring was continued for 10 h at room temperature. Methanol (150 ml) was added to the solution and the resulting precipitates were filtered off. The filtrate was concentrated *in vacuo* and the residue was extracted with dichloromethane. The extract was concentrated and chromatographed on silica gel.

Bis(*o*-methylaminophenyl) disulfide (**6b**, 1.36 g, 24%) was eluted with benzene as a yellow oil, which was identified by comparison of IR and NMR spectra with those of an authentic sample.[15a] Bis[*o*-(*N*-formyl-*N*-methylamino)phenyl] disulfide (**5b**, 1.87 g, 22%) was also eluted with benzene, mp 107.0—108.5 °C (from ether) (lit,[8] 108 °C). 3-Methyl-2,3-dihydrobenzothiazolone azine (**4b**, 2.26 g, 27%) was eluted with dichloromethane, mp 259—260.5 °C (from benzene) (lit,[16] mp 260 °C).

*Reduction of 2-Nitrosoimino-3-phenyl-2,3-dihydrobenzothiazole (**1**) with LAH.* LAH (2.235 g, 59.0 mmol) and **1a** (10.0 g, 39.2 mmol) were used for the reaction, the reaction mixture being treated as described for **1b**. Yellow tar (*A*, 2.16 g), eluted with benzene, was chromatographed on silica gel three times using carbon tetrachloride, carbon tetrachloride–benzene and benzene as eluents. Fractions eluted with carbon tetrachloride–benzene (2: 1) were treated with preparative thin layer chromatography (TLC) to give a small amount of bis[*o*-(*N*-methyl-*N*-phenylamino)phenyl] disulfide (**8**), mp 120—123 °C (from ether); MS: *m/e* 428 (M^+, 1%) and 214 (1/2 M^+, 100). Yellow oil (1.6 g, 4.0 mmol, 20%), eluted with benzene, was identified as bis(*o*-anilinophenyl) disulfide (**6a**) by comparison of its IR spectrum with that of an authentic sample.[15b]

Pale yellow tar (*B*, 2.45 g), eluted also with benzene after elution of tar *A*, was chromatographed again on silica gel to give 3-phenyl-2,3-dihydrobenzothiazolone azine (**4a**, 1.41 g, 16%), mp 274—275 °C (from benzene). IR (KBr): 1610 cm^{-1} (C=N): MS: *m/e* 450 (M^+, 100%).

Found: C, 69.18; H, 3.96; N, 12.61; S, 14.33%. Calcd for $C_{26}H_{18}N_4S_2$: C, 69.32; H, 4.03; N, 12.44; S, 14.21%.

A small amount of spiro compound (**9a**, 60 mg) was also obtained from tar *B*, mp 187—189.5 °C (from ether). MS: *m/e* 410 (M^+, 100%).

Found: C, 72.79; H, 4.12; N, 6.65; S, 15.16%. Calcd for $C_{25}H_{18}N_2S_2$: C, 73.13; H, 4.41; N, 6.82; S, 15.61%.

Bis[*o*-(*N*-formyl-*N*-phenylamino)phenyl] disulfide (**5a**, 2.68 g, 30%) was eluted with chloroform–ether (1: 1), mp 161.5—162.0 °C (from ethyl acetate). IR (KBr): 1670 cm^{-1} (C=O); NMR ($CDCl_3$): δ 6.80—7.65 (m, 18H, Ar–H) and 9.5 (s, 2H, 2CHO); MS: *m/e* 456 (M^+, ≈1%) and 198 (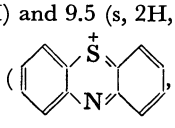 , 100).

Found: C, 68.52; H, 4.50; N, 5.99; S, 13.96%. Calcd for $C_{26}H_{20}N_2O_2S_2$; C, 68.41; H, 4.42; N, 6.14; S, 14.02%.

Red-brown tar (*ca.* 1 g), eluted finally with ether–chloroform (3: 1), could not be identified.

*Reduction of 3-Ethyl-2-nitrosoimino-2,3-dihydrobenzothiazole (**1c**) with LAH.* Reduction of **1c** (10 g, 44.8 mmol) with LAH (1.94 g, 51.1 mmol) was carried out as described for **1a**, and the corresponding products were obtained as follows: bis(*o*-ethylaminophenyl) disulfide (**6c**,[15a] 1.25 g, 18%), bis[*o*-(*N*-ethyl-*N*-formylamino)phenyl] disulfide (**5c**, 2.43 g, 28%), mp 113—114.5 °C (from ether) (lit,[8] 114—115 °C), and 3-ethyl-2,3-dihydrobenzothiazolone azine (**4c**, 2.59 g, 30%), mp 198.5—199.0 °C (from benzene) (lit,[17] 193—202 °C).

*Reduction of Bis[o-(N-formyl-N-phenylamino)phenyl] Disulfide (**5a**) with LAH.* Disulfide (**5a**, 1.7 g, 3.7 mmol) and LAH (0.442 g, 11.6 mmol) were refluxed in THF (50 ml) for 5 days. The reaction mixture was treated as above. Disulfides **6a** (0.33 g, 48%) and **8a** (0.18 g, 30%), mp 120—122.5 °C (from ether), were eluted with benzene. Unchanged **5a** (1.08 g, 63%) was recovered with chloroform–ether (2: 1). Thus the yields of **6a** and **8a** were calculated on the basis of the consumed **5a**.

*Air-oxidation of 3,3'-Dimethylbi(2,3-dihydrobenzothiazolidene) (**11**).* Air was bubbled for 3 h with stirring into a solution of **11**[9] (5.02 g, 16.2 mmol) in benzene (70 ml). After evaporation of the solvent, the brown residue was chromatographed on silica gel. 3,3'-Dimethylbi(2,3-dihydrobenzothiazolinyl) (0.16 g), which was an impurity contained in **11**, was eluted with benzene, mp 156.2—157.0 °C (from 2-propanol). NMR ($CDCl_3$): δ 3.00 (s, 6H, 2N–CH_3), 5.03 (s, 2H, 2C–H), and 6.4—7.4 (m, 8H, Ar–H); MS: *m/e* 300 (M^+, 20%) and 150 (M^+/2, 100). Spiro-amide (**12**, 20 mg) was eluted with dichloromethane–chloroform (1: 2) and brown tar (4.78 g) was eluted with dichloromethane–chloroform (1: 8). A portion of the brown tar was treated with preparative TLC (silica gel, benzene–dichloromethane (2: 1)). The major fraction was extracted with dichloromethane to give spiro compound (**9b**, 100 mg), mp 200—203 °C (lit,[8] 203.5—204 °C), *m/e* 286 (M^+), and **12** (3.5 g, 71%), mp 132—133.5 °C (from methanol). IR (KBr): 1670 cm^{-1}; δ 3.10 (s, 3H, N–CH_3), 3.55 (s, 3H, CONCH_3), and 6.7—7.4 (m, 8H, Ar–H); MS: *m/e* 298 (M^+−16, 10%), 165 (**19b**$^+$, 72) and 136 (*o*-S=C_6H_4=$\overset{+}{N}$=CH_2, 100).

Found: C, 61.44; H, 4.43; N, 8.96; S, 20.10%. Calcd for $C_{16}H_{14}N_2OF_2$: C, 61.14; H, 4.49; N, 8.91; S, 20.36%.

Essentially the same result was obtained by keeping a chloroform solution of **11** to stand in the air with stirring.

*Reaction of **1b** with Diphenyldiazomethane (**15a**).* Diphenyldiazomethane (5.17 g, 26.4 mmol) and **1b** (2.52 g, 13.1 mmol) in dichloromethane (150 ml) were refluxed for a week. After evaporation of the solvent, the residue was chromatographed on silica gel. Benzophenone azine (**18a**, 1.98 g, 42%) was eluted with benzene–dichloromethane (1: 1), mp 158—161 °C (from ethanol) (lit,[18] 162 °C). The thiazolone (**19b**, 1.73 g, 80%) was eluted with dichloromethane. Unsymmetrical azine *N*-monoxide (**16a**; 0.15 g, 16%) was eluted with dichloromethane–ether (1: 1), mp 188.5—189.5 °C (from ethanol). IR (KBr): 1540, 1435, 1350, and 1225 cm^{-1}; NMR ($CDCl_3$): δ 3.3 (s, 3H, N–CH_3) and 7.1—8.1 (m, 14H, Ar–H); MS: *m/e* 359 (M^+, 10%), 343 (M^+−16, 18), and 149 (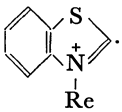 , 100).

Found: C, 70.35; H, 4.43; N, 11.50; S, 9.07%. Calcd for

$C_{21}H_{17}N_3OS$: C, 70.17; H, 4.77; N, 11.69; S, 8.92%.

Reaction of ***1b*** *with Methylphenyldiazomethane (****15b****).* Methylphenyldiazomethane (45 mmol) and **1b** (4.46 g, 23.1 mmol) in dichloromethane (150 ml) were refluxed overnight. After evaporation of the solvent, the residue was chromatographed on silica gel. Acetophenone azine (**18b**, 2.06 g, 39%) was eluted with hexane–benzene (1: 1), mp 118—122 °C (lit,[19] 121 °C). Unsymmetrical azine (**17b**, 0.26 g, 34%) was eluted with hexane–benzene (1: 1) and benzene, mp 115.0—116.0 °C (from ethanol). IR (KBr): 1610, 1575, 1550, and 1475 cm^{-1}; NMR ($CDCl_3$); δ 2.5 (s, 3H, C–CH_3), 3.6 (s, 3H, N–CH_3), and 6.8—8.1 (m, 9H, Ar–H); MS: *m/e* 281 (M^+, 100%).

Found: C, 68.13; H, 5.21; N, 15.17%. Calcd for $C_{16}H_{15}N_3S$: C, 68.30; H, 5.37; N, 14.93%.

Unchanged **1b** (3.92 g, 88% recovery) was eluted with benzene–dichloromethane (1: 1) and dichloromethane.

Reaction of ***1b*** *with Phenyldiazomethane (****15c****).* An ethereal solution (50 ml) of phenyldiazomethane was prepared from azibenzil (11.13 g, 50.1 mmol) by treatment with methanolic sodium hydroxide.[14] To the solution was added **1b** (4.83 g, 25.0 mmol) in dichloromethane (300 ml) and the mixture was stirred for 5 days at room temperature. After evaporation of the solvent, the residue was chromatographed on silica gel. Benzaldazine (**18c**, 2.35 g, 46%) was eluted with hexane–benzene (2: 1), mp 91—93 °C (from ethanol) (lit,[19] 93 °C). *trans*-Stilbene (0.27 g, 6%) was eluted with benzene, mp 122 °C (from ethanol). Azobis(α-benzoyl-α-phenylmethane) (0.90 g, 11%) was eluted with benzene, mp 201—202 °C (from ethanol). IR (KBr): 1680 cm^{-1}.

Found: C, 80.43; H, 5.06; N, 6.78%. Calcd for $C_{28}H_{22}N_2O_2$: C, 80.36; H, 5.30; N, 6.70%. Unsymmetrical azine *N*-monoxide (**16c**, 81 mg, 11%) was eluted with benzene, mp 178—179 °C (from ethanol). IR (KBr): 1550, 1130, and 1120 cm^{-1}; NMR ($CDCl_3$); δ 3.6 (s, 3H, N–CH_3), 7.3 (m, 7H, Ar–H), 7.6 (s, 1H, N–C–H), and 8.2 (m, 2H, Ar–H); MS: *m/e* 283 (M^+, 10%) and 90 ($PhCH^+$, 100).

Found: C, 63.56; H, 4.87; N, 14.54; S, 11.03%. Calcd for $C_{15}H_{13}N_3OS$: C, 63.58; H, 4.62; N, 14.83; S, 11.32%.

Residual **1b** (4.36 g, 90% recovery) was eluted with benzene and dichloromethane.

Unsymmetrical azines (**17**) as authentic samples were prepared by condensation of **10b** with the corresponding carbonyl compounds: **17a**, mp 151—152 °C; **17b**, mp 115—116 °C; **17c**, mp 163—164 °C (lit,[11] mp 163 °C).

Reaction of ***1b*** *with* ***15a*** *in the Presence of* ***20****.* Diphenyldiazomethane (**15a**, 5.17 g, 26.4 mmol) in DMF (50 ml) was added to **1b** (2.51 g, 13.0 mmol) and **20** (1.79 g, 6 mmol) in DMF (40 ml) and the mixture was left to stand overnight at 30 °C. The complex (**20**) was decomposed with a few ml of 30% aqueous hydrogen peroxide under cooling with ice-water. The solution was dried over anhydrous magnesium sulfate and filtered. After evaporation of the solvent under reduced pressure, the residue was chromatographed on silica gel. Benzophenone (3.25 g, 68%) was eluted with benzene and benzophenone azine (**18a**, 0.24 g, 10%) was eluted with benzene–dichloromethane (1: 1). Elution with dichloromethane gave **16a** (mp 186—188 °C, 0.325 g, 7%), **17a** (mp 147—148.5 °C, 0.18 g, 4%) and **19b** (0.24 g, 11%).

The reaction was carried out under various conditions and and **16a** and **17a** were determined by high speed liquid chromatography (HSLC) (Hitachi gel 3010: styrene–divinylbenzene copolymer) using methanol containing concd ammonia (1% v/v) as eluent. Results were essentially the same as described above.

Deoxygenation of Azine N*-Monoxide (****16a****) with Diphenylcarbene.* Diphenyldiazomethane (0.997 g, 5.1 mmol) in DMF (10 ml) was added dropwise to azine *N*-monoxide (**16a**, 0.171 g, 0.48 mmol) and the complex (**20**, 0.280 g, 0.91 mmol) in DMF (10 ml). Almost quantitative formation of azine (**17a**) was shown by HSLC, **17a** (0.21 g, 75%) being isolated by column chromatography.

References

1) For part XIV see: K. Akiba, T. Tsuchiya, I. Fukawa, and N. Inamoto, *Bull. Chem. Soc. Jpn.*, **49**, 550 (1976).

2) K. Akiba, T. Kawamura, M. Hisaoka, and N. Inamoto, *Bull. Chem. Soc. Jpn.*, **48**, 3262 (1975); M. Hisaoka, K. Akiba, and N. Inamoto, *ibid.*, **48**, 3266 (1975); K. Akiba, M. Hisaoka, T. Kawamura, and N. Inamoto, *ibid.*, **48**, 3270 (1975).

3) M. Hisaoka, K. Akiba, and N. Inamoto, *Bull. Chem. Soc. Jpn.*, **48**, 3274 (1975).

4) Preliminary report: K. Akiba, T. Kawamura, M. Ochiumi, and N. Inamoto, *Heterocycles*, **1**, 35 (1973).

5) H. E. Zimmerman and D. H. Paskovich, *J. Am. Chem. Soc.*, **86**, 2149 (1964).

6) a) H. Balli, *Angew. Chem.*, **76**, 995 (1964); b) H. Quast and S. Huenig, *Chem. Ber.*, **99**, 2017 (1966); c) H. W. Wanzlick, H. J. Kleiner, I. Lasch, H. U. Fueldner, and H. Steinmaus, *Justus Liebigs Ann. Chem.*, **708**, 155 (1967).

7) C. J. Thoman, S. J. and I. M. Hunsberger, *J. Org. Chem.*, **33**, 2852 (1968); K. Akiba, S. Matsunami, C. Eguchi, and N. Inamoto, *Bull. Chem. Soc. Jpn.*, **47**, 935 (1974).

8) W. H. Mills, L. M. Clark, and J. A. Aeschlimann, *J. Chem. Soc.*, **123**, 2358 (1923).

9) H. J. Kleiner, *Justus Liebigs Ann. Chem.*, **724**, 221 (1969).

10) H. Passing, *J. Prakt. Chem.*, [2] **153**, 1 (1939).

11) E. Besthorn, *Ber.*, **43**, 1519 (1910).

12) R. F. Hunter, *J. Chem. Soc.*, **1930**, 125.

13) L. I. Smith and K. L. Howard, *Org. Synth.*, Coll. Vol. III, 351 (1955); H. Staudinger and A. Gaule, *Ber.*, **49**, 1907 (1916).

14) P. Yates and B. L. Shapiro, *J. Org. Chem.*, **23**, 759 (1958).

15) a) A. I. Kiprianov and Z. N. Pazenko, *J. Gen. Chem.*, **19**, 1523 (1949); *Chem. Abstr.*, **44**, 3487 (1950); b) A. I. Kiprianov and I. K. Ushenko, *ibid.*, **17**, 2201 (1947); *Chem. Abstr.*, **42**, 5016 (1948).

16) R. Riemschneider, *Monatsh. Chem.*, **89**, 683 (1958); S. Huenig, H. Geiger, G. Kaupp, and W. Kniese, *Justus Liebigs Ann. Chem.*, **697**, 116 (1966).

17) S. Huenig, H. Balli, H. Conrad, and A. Schott, *Justus Liebigs Ann. Chem.*, **676**, 36 (1964).

18) T. Curtius and F. Rauterberger, *J. Prakt. Chem.*, [2] **44**, 192 (1891).

19) T. Curtius and L. Pflug, *J. Prakt. Chem.*, [2] **44**, 535 (1891).

Syntheses of Polymerizable Acetals. I. Vinylbenzaldehyde Acetals with Perfume Alcohols

Hiroyoshi KAMOGAWA, Shinya OKABE, and Masato NANASAWA

Department of Applied Chemistry, Yamanashi University, Takada, Kofu 400

(Received December 27, 1975)

Several acetal monomers and a hemiacetal monomer of vinylbenzaldehydes were synthesized from the reaction with some perfume alcohols in the presence of *p*-toluenesulfonic acid as an acid catalyst. It was found that primary alcohols such as citronellol and geraniol with the exception of cinnamyl alcohol afforded acetal monomers in high yields, secondary alcohols such as borneol and menthol in low yields, with the latter affording only hemiacetal monomer, and linalool, a tertiary alcohol, neither acetal nor hemiacetal monomers. The radical polymerizations of the acetal and hemiacetal monomers synthesized provided soluble polymers which easily release perfume alcohols under mild acidic conditions.

Acetals are well-known for their easily hydrolyzable properties under acidic conditions in spite of their stabilities in neutral or alkaline media. This outstanding characteristic can be utilized for the syntheses of the readily hydrolyzable polymers which might find their use in liberating their functional groups gradually under acidic conditions.

With such intentions, Kamogawa[1] prepared vinyl polymers containing the isoalloxazine functional group in side chains through hemiacetal linkage.

As the first attempt to incorporate functional groups into the side chains of vinyl polymers through pure acetal linkages for the above-mentioned purpose, vinylbenzaldehyde acetals with perfume alcohols were synthesized using *p*-toluenesulfonic acid (PTS) as a catalyst.

Acetal monomers were synthesized as follows:

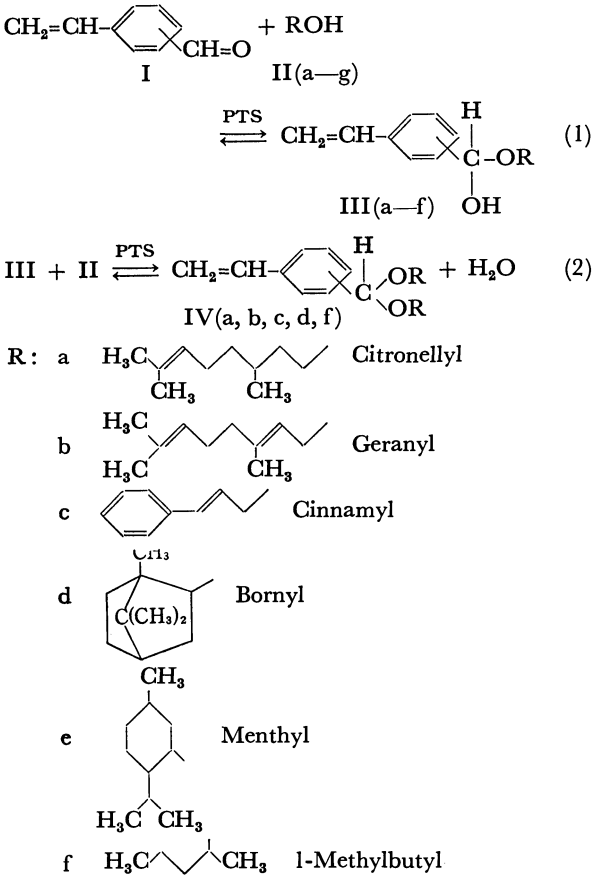

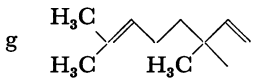

Table 1 shows the analytical results obtained for the acetal monomers synthesized. Since the starting chloromethylstyrene (I) was an unseparable mixture of para- and meta-isomers (40/60), the acetal monomers obtained should also be mixtures of para- and meta-isomers, presumably thereby having an oily appearance in spite of the absence of low-molecular weight impurities, as ascertained by gas chromatograph. The isomers could not be separated; the ratios of the para- to meta-isomers could not be determined.

As is generally recognized in acetal synthesis from aldehydes and alcohols under acidic conditions,[2] primary alcohols such as citronellol and geraniol gave high yields of acetals (IV-a and IV-b); secondary alcohols such as borneol and the reference, 2-pentanol, gave low yields (IV-d and IV-f). 3,7-Dimethyl-1,6-octadien-3-ol (linalool, II-g), a tertiary alcohol, gave neither acetal nor hemiacetal monomers, presumably due to the large steric hindrance exerted against the reaction. Similarly, *l*-menthol, a more sterically hindered secondary alcohol as compared with borneol, only gave a hemiacetal monomer (III-e). The fact that the yield of the monomer IV-c prepared with cinnamyl alcohol, a primary alcohol, was low (26.1%) may denote that steric hindrance is fairly large in this case, owing to the coplanar character of the styryl portion of the alcohol residue due to resonance.

The radical polymerization of acetal monomers appears to be almost unaffected by the kind of alcohol residue of the acetal monomers, as recognized from the results in Table 2. The polymer of III-e (a hemiacetal) is soluble in polar solvents such as alcohol due to the presence of pendant polar hydroxyl groups, but is insoluble in nonpolar petroleum ether, while the other polymers (acetals) are insoluble in alcohol but are soluble in petroleum ether.

The IR spectra of all polymers indicated no absorptions due to the double bond of the vinyl group (disappearance of the 910 cm^{-1} band) but indicated strong $-CH_2-$ absorption characteristic of the back-bone chains of vinyl polymers at 2930 and 2860 cm^{-1}.

The hydrolyses of the acetal polymers with liberation of perfume alcohol and the formyl group in the polymer during storage are dependent upon the extent of contact

TABLE 1. ANALYTICAL RESULTS OF THE SYNTHESIZED ACETAL MONOMERS

Monomer	Yield	Elemental analysis C[a)]%	Elemental analysis H[a)]%	IR (CCl_4) cm^{-1}	Mass peak *m/e*
IV-a	52.3	81.82 (81.69)	10.58 (10.79)	2860—2970(alkyl), 1610 (aryl), 1440 (CH), 1100 and 1060 (ether), 990 and 910 (vinyl)	426 (M^+)
IV-b	61.8	81.44 (82.46)	10.89 (9.95)	2850—2960 (alkyl), 1615 (aryl), 1430 (CH), 1100 and 1060 (ether), 985 and 905 (vinyl)	422 (M^+)
IV-c	26.1	85.51 (84.82)	6.72 (6.80)	3030 and 1610 (aryl), 2850—2950 (alkyl), 1440 (CH), 1120 and 1070 (ether), 980 and 910 (vinyl)	382 (M^+)
IV-d	22.4	81.90 (82.46)	9.98 (9.95)	2870—2980 (alkyl), 1610 (aryl), 1440 (CH), 1060 and 1040 (ether), 990 and 910 (vinyl)	422 (M^+)
IV-f	37.8	78.14 (78.62)	10.20 (10.34)	2870—2960 (alkyl), 1610 (aryl), 1440 (CH), 1080 and 1030 (ether), 990 and 910 (vinyl)	290 (M^+)

a) The figures in the parentheses indicate calcd values.

TABLE 2. POLYMERIZATION BEHAVIOR OF ACETAL MONOMER[b)]

Monomer	Precipitant for polymer	Conversion %	Polymer $[\eta]^{a)}$dl/g	Polymer Appearance	Polymer Solubility
IV-a	Methanol	92	0.32	Glassy	Sol. in pet. ether
IV-b	Methanol	34	0.22	Glassy	Sol. in pet. ether
IV-c	Methanol	84	0.25	White powder	Sol. in pet. ether
IV-d	Methanol	91	0.25	White powder	Sol. in pet. ether
III-e	Pet. ether	58	0.43	White solid	Sol. in ethanol
IV-f	Methanol	78	0.34	Glassy	Sol. in pet. ether

a) Intrinsic viscosity in THF at 30 °C. b) Initiator (AIBN), 0.005 g/l ml THF; monomer, 0.5 g/1ml THF; 70 °C × 48 h.

with moisture, as well as the acidity. Thus, a polymer of IV-a in a carbon tetrachloride solution indicated almost no change in the IR spectrum even after storage of several weeks in air; storage in the solid state, especially in a fluffy powder (*e.g.* the polymer of IV-d), caused considerable change in the IR spectrum even within a week with the appearance of a 1700 cm^{-1} band (formyl groups in polymer), thereby indicating that hydrolysis was in progress.

Experimental

IR, ^{1}H-NMR, and mass spectra were obtained with a Hitachi EPI-G spectrophotometer, a JNM-PMX 60 spectrometer, and a Hitachi RMU-6 MG spectrometer, respectively, under standard measurement conditions. Elemental analyses were carried out using a Perkin-Elmer 240 instrument.

Vinylbenzaldehyde (I). The Sommlet reaction[3,4] was applied for the synthesis. Thus, from chloromethylstyrene (Seibi Chem. Co., a 40/60% mixture of para- and meta-isomers) and an equimolar amount of hexamethylenetetramine vinylbenzaldehyde was obtained in 45—50% yields after refluxing in chloroform for 2—4 h and subsequent steam distillation of the resulting hexaminium salt in the presence of a polymerization inhibitor (*e.g.* 4-(*t*-butyl) catechol). Bp, 54—56 °C/0.2—0.3 mmHg. Elemental analysis, IR (CCl_4), and ^{1}H-NMR (CCl_4) demonstrated structure I. Para/meta= 40/60 by NMR.

Vinylbenzaldehyde Dicitronellyl Acetal (IV-a). A solution of 3.0 g (0.023 mol) of vinylbenzaldehyde, 7.2 g (0.046 mol) of citronellol, 0.03 g of 4-(*t*-butyl) catechol, and 0.15 g of *p*-toluenesulfonic acid (PTS) as a catalyst in 30 ml of anhydrous chloroform was refluxed with stirring for 7 h with the addition of a molecular sieve 3A (1/16) as dehydrating agent. Upon cooling the solution was evaporated *in vacuo* at 40 °C leaving an oil, which was extracted with aqueous sodium carbonate and 100 ml of ether. The organic layer was then dried over anhydrous potassium carbonate, filtered, and evaporated *in vacuo* at 40 °C to obtain a crude acetal monomer. The crude product was chromatographed on an alumina column eluted by petroleum ether to afford a colorless oil in a 52.3% yield. The product was soluble in common organic solvents, including petroleum ether, but was insoluble in water.

NMR (CCl_4, Me_4Si): δ 7.26 (d 4H aromatic), 6.77 (q, 1H vinyl), 5.78 (d 1H vinyl), 5.39 (s, 1H acetal), 5.29 (d 1H vinyl), 3.8—0.5 (b 38H dicitronellyl) ppm. [No -CHO peak].

Other acetal monomers, *i.e.*, vinylbenzaldehyde digeranyl acetal (IV-b), dicinnamyl acetal (IV-c), dibornyl acetal (IV-d), and bis(1-methylbutyl) acetal (IV-f), were synthesized in the same manner to provide oily products even after chromatographic purification (Table 1).

Vinylbenzaldehyde Menthyl Hemiacetal (III-e). The same reaction procedure was adopted as that for the synthesis of monomer IV-a, except that methanol was employed as the eluting agent of the alumina column. Thus, from 3.0 g (0.023 mol) of vinylbenzaldehyde and 7.4 g (0.046 mol) of *l*-menthol, a colorless viscous oil was obtained in a 22.4% yield. The product was soluble in common organic solvents and was insoluble in water.

Found: C, 79.31; H, 9.57%. Calcd for $C_{19}H_{28}O_2$ (hemiacetal): C, 79.16; H, 9.72%. IR (CCl_4): 3610 (OH), 2850—2960 (alkyl), 1610 (aryl), 990 and 910 cm^{-1} (vinyl). Mass spectrum *m/e* 288 (M^+). NMR (CCl_4, Me_4Si): δ 7.17 (d, 4H aromatic), 6.62 (q, 1H, vinyl), 5.63 (d, 1H, vinyl), 5.15 (d, 1H, vinyl), 4.53 (s, 1H, OH), 3.0—0.5 (b, 19H, menthyl) ppm. [No -CHO in IR and NMR].

Other acetal monomers synthesized also indicated characteristic peaks in NMR at δ 7.1—7.3 (aryl) and 5—7 (styrenic vinyl) together with peaks of the alcohol residues, the integrator calculations indicating that the monomers were

apparently pure, without any splitting of the singlet peaks due to the presence of isomers.

Polymerization. A conventional procedure for free-radical polymerizations was adopted. In a typical example conforming to the polymerization conditions in Table 2, 0.5 g of monomer IV-d and 0.005 g of α,α′-azobisisobutyronitrile (AIBN) were dissolved in 1 ml of tetrahydrofuran (THF). The solution was put into a glass ampoule, which was evacuated and sealed-off, and left standing for 48 h at 70 °C. Upon cooling, the viscous solution was poured into a large quantity of methanol to afford a white precipitate, which was freeze-dried from dioxane.

References

1) H. Kamogawa, *J. Poly. Sci. A-1*, **7**, 409 (1969).
2) C. A. Buehler and D. E. Pearson, "Survey of Organic Syntheses," Wiley, New York, N. Y. (1970), p. 515.
3) E. Campaigne and W. A. LeSuer, *J. Am. Chem. Soc.*, **70**, 1557 (1948).
4) S. J. Angyal, *Org. React.*, **8**, 197 (1954).

A Facile Synthesis of 2,5-Disubstituted Tetrazoles by the Reaction of Phenylsulfonylhydrazones with Arenediazonium Salts[1]

Suketaka Ito, Yumo Tanaka, Akikazu Kakehi, and Ken-ichi Kondo

Department of Industrial Chemistry, Faculty of Engineering, Shinshu University, Wakasato, Nagano 380

(Received January 28, 1976)

2,5-Disubstituted tetrazoles are obtained in good yields by the reaction of phenylsulfonylhydrazones of aromatic aldehydes (and cinnamaldehyde) with arenediazonium salts. From the synthetic viewpoint for tetrazoles, this method may be of high synthetic utility on account of the availability of starting materials, the simplicity of procedure, and higher yields.

The 1,5-dipolar cyclization[2] is a general method for synthesis of five-membered heterocycles; a typical example of this type of reaction is the cyclization of vinyldiazomethane to pyrazole.[3]

Azodiazomethane, an unknown diazalogue of vinyldiazomethane, can be expected to afford tetrazole through the 1,5-dipolar cyclization. As a synthetic route to azodiazomethane, the following scheme may be reasonable:

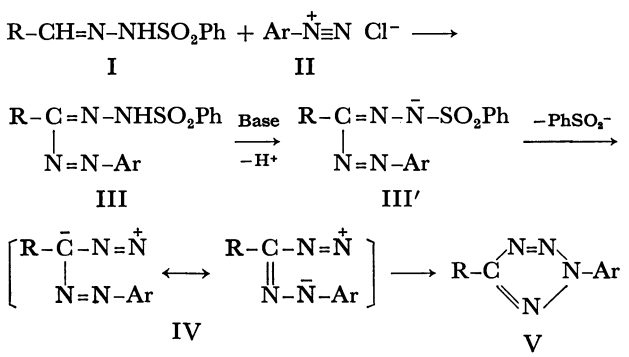

Scheme 1.

The first step is the well-known formazan formation[4] and the second is the Bamford-Stevens type reaction.[5] Although the Dimroth and Merzbacher method[6] is often employed for preparing 2,5-diaryltetrazoles, this method is troublesome, since it requires aryl azide as a starting material.

The present paper is concerned with an attempt to prepare 2,5-disubstituted tetrazoles[7] according to the above reaction scheme.[8]

Results and Discussion

As shown in Table 1, 2,5-disubstituted tetrazoles could be obtained as was expected, in good yields with a few exceptions. Phenylsulfonylhydrazones[9] were allowed to react with one equivalent of arenediazonium salt(II) in alkaline (NaOH) ethanol at 5—2 °C or in pyridine at −10——15 °C. Extraction of the reaction mixture with chloroform–water gave benzenesulfinic acid and tetrazole(V).[10] When 1.5 equivalents of diazonium salt were used, the yields of tetrazoles increased by a factor of about 1.1.

Attempts to isolate formazan (III) were unsuccessful: the overall reaction generally proceeded fast under these reaction conditions.[11] When the reaction of benzaldehyde phenylsulfonylhydrazone with benzenediazonium salt was carried out in aqueous alkali, there were separated brownish yellow precipitates, which were unstable and changed gradually to a deep red and then to brown mass. This product(mp 40—43 °C) could not be purified by crystallization, but gave 2,5-diphenyltetrazole (5%), 1,3,4,6-tetraphenyl-1,4-dihydro-1,2,4,5-tetrazine[12] (3%), and benzenesulfinic acid (16%) by treatment with hot sodium ethoxide–ethanol solution.

Although formazan(III) could not be isolated and confirmed in this study, the intermediacy of formazan (III) or formazanide anion (III′) should be reasonable from the reaction process.

Thus, the principal process of the reaction is identical with that of the reaction between *N*-phenylsulfonylbenzhydrazonoyl chlorides and arylhydrazines to yield 2,5-diaryltetrazoles.[7]

For the formation of tetrazole(V) from formazan

Table 1. 2,5-Disubstituted tetrazoles, 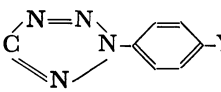 , from phenylsulfonylhydrazones and arenediazonium salts

Tetrazole[a,b] R	Y	Yield[c,d] (%)	Mp (°C)	Solvent[e]	Molecular formula	Calcd (%) C	H	N	Found (%) C	H	N
Ph	H	71 (51)	101—102[f]	E	$C_{13}H_{10}N_4$						
Ph	Me	72	104—105[g]	E	$C_{14}H_{12}N_4$						
Ph	MeO	71	101—102	E	$C_{14}H_{12}N_4O$	66.66	4.79	22.21	66.55	4.79	22.29
Ph	Cl	65	123—124[h]	E	$C_{13}H_9N_4Cl$						
Ph	NO_2	67	185—186 (dec.)[m]	B	$C_{13}H_9N_5O_2$						
p-MeC_6H_4	H	66 (37)	93— 95[i]	E	$C_{14}H_{12}N_4$						
p-MeC_6H_4	Me	69	137—138[m]	E	$C_{15}H_{14}N_4$						

TABLE 1. (Continued)

Tetrazole[a,b] R	Y	Yield[c,d] (%)	Mp (°C)	Solvent[e]	Molecular formula	Calcd (%) C	H	N	Found (%) C	H	N
p-MeC_6H_4	MeO	55	112—114	E	$C_{15}H_{14}N_4O$	67.65	5.30	21.04	67.55	5.28	20.98
p-MeC_6H_4	Cl	60	142—143	E	$C_{14}H_{11}N_4Cl$						
p-MeC_6H_4	NO_2	78	171—172 (dec.)[m]	B	$C_{14}H_{11}N_5O_2$						
p-*i*-PrC_6H_4	H	60 (42)	44— 45	M	$C_{16}H_{16}N_4$	72.70	6.10	21.20	72.81	6.04	20.88
p-*i*-PrC_6H_4	Me	65	50— 51	M	$C_{17}H_{18}N_4$	73.35	6.52	20.13	73.51	6.32	20.34
p-*i*-PrC_6H_4	MeO	51	84— 86	M	$C_{17}H_{18}N_4O$	69.37	6.16	19.03	69.63	6.20	19.04
p-*i*-PrC_6H_4	Cl	62	98— 99	M	$C_{16}H_{15}N_4Cl$	64.32	5.06	18.75	64.26	5.08	18.66
p-*i*-PtC_6H_4	NO_2	76	158—159 (dec.)	EB	$C_{16}H_{15}N_5O_2$	62.13	4.89	22.64	61.90	4.80	22.91
p-$MeOC_6H_4$	H	66 (44)	106—107[j]	E	$C_{14}H_{12}N_4O$						
p-$MeOC_6H_4$	Me	74	111—112[m]	E	$C_{15}H_{14}N_4O$						
p-$MeOC_6H_4$	MeO	59	123—125	E	$C_{15}H_{14}N_4O_2$	63.82	5.00	19.85	63.71	5.03	19.86
p-$MeOC_6H_4$	Cl	71	140—142[m]	EB	$C_{14}H_{11}N_4ClO$						
p-$MeOC_6H_4$	NO_2	69	182—184 (dec.)[m]	EB	$C_{14}H_{11}N_5O_3$						
p-$Me_2NC_6H_4$	H	38 (18)	111—112	M	$C_{15}H_{15}N_5$	67.91	5.70	26.40	67.94	5.73	26.41
p-$Me_2NC_6H_4$	Me	28	150—151	M	$C_{16}H_{17}N_5$	68.80	6.13	25.07	68.61	5.97	24.92
p-$Me_2NC_6H_4$	MeO	10	138—139	M	$C_{16}H_{17}N_5O$	65.07	5.80	23.71	64.82	5.80	24.06
p-$Me_2NC_6H_4$	Cl	52	177—178 (dec.)	EB	$C_{15}H_{14}N_5Cl$	60.10	4.71	23.36	59.96	4.68	23.36
p-$Me_2NC_6H_4$	NO_2	63	180—181 (dec.)	C	$C_{15}H_{14}N_6O_2$	58.06	4.55	27.08	57.90	4.61	26.86
p-ClC_6H_4	H	75 (50)	110—111[k]	E	$C_{13}H_9N_4Cl$						
p-ClC_6H_4	Me	65	141—142[m]	E	$C_{14}H_{11}N_4Cl$						
p-ClC_6H_4	MeO	73	156—157	E	$C_{14}H_{11}N_4ClO$	58.65	3.87	19.54	58.50	3.78	19.46
p-ClC_6H_4	Cl	68	176—177 (dec.)[m]	EB	$C_{13}H_8N_4Cl_2$						
p-ClC_6H_4	NO_2	75	184—185 (dec.)[m]	B	$C_{13}H_8N_5ClO_2$						
p-$O_2NC_6H_4$	H	82 (13)	199—201 (dec.)[l]	B	$C_{13}H_9N_5O_2$						
p-$O_2NC_6H_4$	Me	82	173—174[m]	B	$C_{14}H_{11}N_5O_2$						
p-$O_2NC_6H_4$	MeO	69	199—200 (dec.)	B	$C_{14}H_{11}N_5O_3$	56.57	3.73	23.56	56.24	3.70	23.63
p-$O_2NC_6H_4$	Cl	82	189—190 (dec.)[m]	B	$C_{13}H_8N_5ClO_2$						
p-$O_2NC_6H_4$	NO_2	71	202—203 (dec.)[m]	B	$C_{13}H_8N_6O_4$						
2-C_4H_3O	H	60 (19)	87— 88	M	$C_{11}H_8N_4O$	62.26	3.80	26.40	62.25	3.75	26.49
2-C_4H_3O	Me	63	83— 84	E	$C_{12}H_{10}N_4O$	63.71	4.46	24.76	63.76	4.49	24.87
2-C_4H_3O	MeO	59	92— 93	E	$C_{12}H_{10}N_4O_2$	59.50	4.16	23.13	59.45	4.13	23.29
2-C_4H_3O	Cl	68	120—122	E	$C_{11}H_7N_4ClO$	53.57	2.86	22.71	53.42	2.84	22.47
2-C_4H_3O	NO_2	30	163—164	B	$C_{11}H_7N_5O_3$	51.37	2.74	27.23	51.32	2.79	27.36
PhCH=CH	H	36 (21)	90— 91	E	$C_{15}H_{12}N_4$	72.56	4.87	22.57	72.78	4.98	22.60
PhCH=CH	Me	54	96— 97	E	$C_{16}H_{14}N_4$	73.26	5.38	21.36	73.29	5.39	21.46
PhCH=CH	MeO	48	123—124	E	$C_{16}H_{14}N_4O$	69.05	5.07	20.13	68.73	5.07	19.87
PhCH=CH	Cl	51	137—138	E	$C_{15}H_{11}N_4Cl$	63.72	3.92	19.82	63.56	3.87	19.93
PhCH=CH	NO_2	31	183—184 (dec.)	B	$C_{15}H_{11}N_5O_2$	61.43	3.78	23.88	61.55	3.75	23.84

a) Satisfactory analytical data (±0.3% for C,H,N) were also obtained for all known compounds in the table. b) 2-C_4H_3O: 2-Furyl. c) Yields (isolated) in the reaction of equimolar quantities of reactants. d) Figures in parentheses are yields in the reaction in sodium hydroxide–ethanol system, and others those in pyridine. e) Solvent for recrystallization. B: benzene, E: ethanol, EB: ethanol–benzene, C: chloroform, M: Methanol. f) Lit, mp 101.5—102.0°: O. Dimroth and S. Merzbacher, *Ber.*, **40**, 2402 (1907). g) Lit, mp 103°: D. Jercher and H. Fischer, *Chem. Ber.*, **89**, 563 (1956). h) Lit, mp 120.5—121.5°: Soon-Yung Hong and J.E. Baldwin, *Tetrahedron*, **24**, 3787 (1968). i) Lit, mp 92.0—93.0°: *idem., ibid.* j) Lit, mp 105.0—105.5°: *idem., ibid.* k) Lit, mp 108.0—108.5°: *idem., ibid.* l) Lit, mp 199.0—200.0°: E. Wedekind, *Ber.*, **31**, 478 (1898). m) The uncorrected mps of the identical tetrazoles prepared from *N*-phenylsulfonylbenzhydrazonoyl chlorides and arylhydrazines were reported in the preceding paper. (Ref. 7).

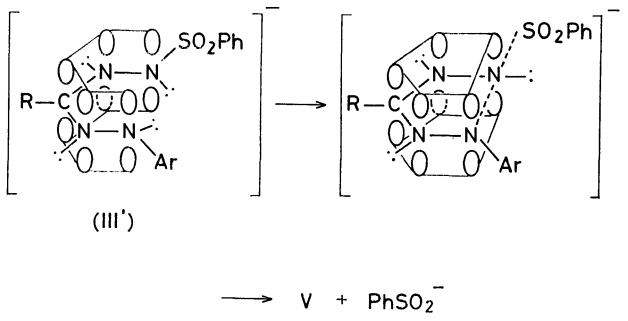

(III')

Scheme 2.

(III), a mechanism which involves the S_N1 type separation of benzenesulfinate ion from formazanide ion (III') and the 1,5-dipolar cyclization of arylazoaryldiazomethane (IV) to tetrazole (V), given in Scheme 1, may be possible. However, the possibility of neighboring-group participation by nitrogen may be conceivable as observed in substitution reactions of δ-haloalkylamines.[13] Thus, the intramolecular displacement may be represented as the most possible mechanism by considering the participation of the lone-pair orbital of arylazo α-nitrogen atom with a planar quasi-aromatic[14] configuration of formazanide anion in the transition state (Scheme 2). Since formazan and formazanide anion are isoelectronic with pentadienide anion, their most favored configuration should be the planar U-shaped form,[15] in which the π-system may gain some quasi-aromatic stabilization. This stabilization would compensate the weak nucleophilicity of azo group.

As shown in Table 1, pyridine resulted in higher yields of tetrazoles than sodium hydroxide–ethanol system. The principal reason for this results should be chiefly attributed to the fact that the hydrazones are not sufficiently soluble in cold alkaline ethanol in contrast in pyridine.

As for the reaction of benzaldehyde hydrazones in pyridine, it may be said that increase in the electrophilicity of diazonium ion generally increases the yields of tetrazoles.[16] The difficulty of obtaining triarylformazans with *p*-dimethylamino or *p*-hydroxyl substituent in the *C*-phenyl group was attributed to the preferential azo-coupling to the activated aromatic ring.[17] This might be questionable[18] and is not adoptable for the present results. The low yields in the case of *p*-(dimethylamino)benzaldehyde hydrazone can be accounted for by the antagonistic resonance effect of *p*-(dimethylamino)phenyl group on the azo-carbanion structure of hydrazonide anion.[19]

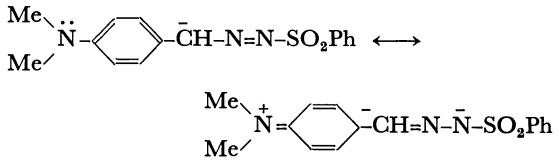

That is to say, the electron-donating nature of dimethylamino group should be responsible for the decreased nucleophilicity of α-carbon of aldehyde moiety of hydrazone.

In the present method, the starting materials are readily available, the procedure is simple, and the yield of product is high in general. In conclusion, this method possesses the higher synthetic utility for 2,5-diaryltetrazoles.

Experimental[20]

Preparation of Phenylsulfonylhydrazones (I). General Procedure: Aldehyde (0.1 mol) dissolved in a small amount of hot ethanol (liquid aldehydes were used directly) was mixed with the solution of phenylsulfonylhydrazine (17.2 g, 0.1 mol) in ethanol (100 ml). After being allowed to stand for 30 min, the mixture was cooled and diluted with water. The separated crystalline product was filtered, washed with aqueous ethanol, and air dried. Yield: 79—97%. *p*-Tolualdehyde hydrazone, 92%, mp 124—125 °C. Found: C, 61.32; H, 5.17; N, 10.17%. Calcd for $C_{14}H_{14}N_2O_2S$: C, 61.29; H, 5.14; N, 10.21%. *p*-Cumaldehyde hydrazone, 89%, mp 132—133 °C, Found: C, 63.38; H, 6.05; N, 9.16%. Calcd for $C_{16}H_{18}N_2O_2S$: C, 63.55; H, 6.00; N, 9.27%.

Reaction of Phenylsulfonylhydrazones (I) with Arenediazonium Salts(II). General Procedure: Diazonium salt solutions were prepared as follows: A cooled solution of sodium nitrite (5 mmol) in 2 ml of water was added to a solution of aniline (5 mmol) and 1.3 ml of concentrated hydrochloric acid in 8 ml of 50% ethanol below 5 °C.

(A) Reaction in Pyridine. The solution of arenediazonium chloride(II) was added dropwise over a period of 30 min to a stirred solution of I (5 mmol) in 30 ml of pyridine at −10—−15 °C. The reaction mixture was extracted with chloroform and water. The chloroform layer was washed with dilute hydrochloric acid followed by water and dried. After removal of the solvent from the chloroform extract, the resulting residue was chromatographed on a silica gel (10 g) column using benzene as the eluent to give the corresponding tetrazole, which was purified by recrystallization. The results are summarized in Table 1.

(B) Reaction in Sodium Hydroxide–Ethanol System. The diazonium salt solution was added to a cooled solution of sodium hydroxide (20 mmol) and I (5 mmol) in 40 ml of ethanol at 5—2 °C in a similar manner as above. The successive working-up was the same as that of (A). The results are summarized in Table 1.

The alkaline water layer was neutralized and extracted with chloroform to give unaltered I. The yields of recovered hydrazones (crude) were as follows: hydrazone of benzaldehyde, 38; *p*-tolualdehyde, 44; *p*-cumaldehyde, 35; *p*-anisaldehyde, 39; *p*-dimethylaminobenzaldehyde, 26; *p*-chlorobenzaldehyde, 38; *p*-nitrobenzaldehyde, 71%.

Identification of Benzenesulfinic Acid. The aqueous extract from the reaction mixture, in the reaction between benzaldehyde hydrazone and benzenediazonium chloride in sodium hydroxide–ethanol, was acidified, saturated with sodium chloride, and then extracted with dichloromethane. The dichloromethane extract was dried over sodium sulfate and treated with diphenyldiazomethane to afford phenyl benzhydryl sulfone,[21] mp 188—189 °C (Ref.[22] mp 188 °C), yield: 0.34 g (44% based on the 2,5-diphenyltetrazole obtained). (Found: C, 73.92; H, 5.17%).

References

1) A preliminary communication of portions of this study has appeared: S. Ito, Y. Tanaka, A. Kakehi, and K. Kondo, *Chem. Lett.*, **1973**, 1071.

2) For leading references, see (a) R. Huisgen, *Angew. Chem. Int. Ed. Engl.*, **7**, 321 (1968); b) H. Reimlinger,

Chem. Ber., **103**, 1900 (1970); (c) J. Elguero, *Bull. Soc. Chim. Fr.*, **1971**, 1925.

3) (a) D. W. Adamson and J. Kenner, *J. Chem. Soc.*, **1935**, 286. (b) C. D. Hurd and S. C. Lui, *J. Am. Chem. Soc.*, **57**, 2656 (1935). (c) G. L. Closs and W. Boll, *Angew. Chem.*, **75**, 640 (1963). (d) R. K. Bartlett and T. S. Stevens, *J. Chem. Soc., C*, **1967**, 1964.

4) H. von Pechmann, *Ber.*, **25**, 3175 (1892). *Cf.* A. W. Nineham, *Chem. Rev.*, **55**, 355 (1955).

5) W. R. Bamford and T. S. Stevens, *J. Chem. Soc.*, **1952**, 4735.

6) O. Dimroth and S. Merzbacher, *Ber.*, **40**, 2402 (1907). Concerning the synthetic methods for tetrazoles, see F. R. Benson in "Heterocyclic Compounds," Vol. 8, Chap. 1, R. C. Elderfield, Ed., John Wiley & Sons, Inc., New York (1967).

7) S. Ito, Y. Tanaka, and A. Kakehi, *Bull. Chem. Soc. Jpn.*, **49**, 762 (1976).

8) 2,5-Diaryltetrazoles were obtained by the oxidation of *N*-amidino- or *N*-carbamoylformazan with nitric acid, potassium permanganate, or NBS: E. Wedekind, *Ber.*, **31**, 473 (1898); V. A. Grakauskas, A. J. Tomasewski, and J. P. Horwits, *J. Am. Chem. Soc.*, **80**, 3155 (1958); W. Ried and H. Hillenbrand, *Justus Liebigs Chem. Ann.*, **590**, 128 (1954). These reactions should proceed *via* the formation of tetrazolium salts followed by their hydrolysis.

9) Since aliphatic aldehyde hydrazones could not be obtained in a pure state, none of them were used in the present study: aliphatic aldehydes such as propion- and butyraldehyde reacted with phenylsulfonylhydrazone to yield oily products, which decomposed with an evolution of gas on standing. Bartlett and Stevens also reported that formaldehyde *p*-tolylsulfonylhydrazone decomposed when crystallization was attempted: Ref. 3d.

10) The tetrazoles obtained were identified by their analytical and spectral data and, in the case of known compounds, by comparison with authentic specimens prepared by other synthetic methods. In the IR spectra, all the tetrazoles exhibit four characteristic peaks at 1260—1290 (weak), 1060—1080 (weak), near 1010 (medium to strong), and near 990 cm^{-1} (medium to strong). The absorption at 1260—1290 cm^{-1} can be assigned to the cyclic N–N=N group in analogy with other tetrazoles and triazoles [(a) E. Lieber and T. Enkoji, *J. Org. Chem.*, **26**, 4472 (1961); (b) E. Lieber, C. N. R. Rao, T. S. Chao, and H. Rubinstein, *Can. J. Chem.*, **36**, 1441 (1958)], and those at near 1070, 1010, and 990 cm^{-1} to the tetrazole ring system [(a) E. Lieber, D. R. Leverring, and L. J. Patterson, *Anal. Chem.*, **23**, 1594 (1951); (b) C. W. Roberts, G. F. Fanta, and J. D. Martin, *J. Org. Chem.*, **24**, 654 (1959); (c) C. W. Roberts and M. L. Maskaleris, *ibid.*, **24**, 926 (1959)].

11) The reaction was exothermic. When the diazonium salt solution was added all at once and the reaction mixture was worked up immediately, tetrazoles could be obtained in a decreased yield by a factor of only about 0.2. On the other hand, cinnamaldehyde phenylsulfonylhydrazone remained unchanged when treated with alkali under the same reaction condition as that in the present procedure.

12) The dimerized product of *N*-phenylbenzonitrilimine which might be formed directly from the intermediate precursor of formazan.

13) E. S. Gould, "Mechanism and Structure in Organic Chemistry," Henry Holt and Co., New York (1960), p. 570.

14) Lloyd and Marshall have proposed the definition of the term "quasi-aromatic": D. Lloyd and D. R. Marshall, *Angew. Chem. Int. Ed. Engl.*, **11**, 404 (1972). In the present paper, the term "quasi-aromatic....." is used in the usual sense.

15) R. Hoffmann and R. A. Olofson, *J. Am. Chem. Soc.*, **88**, 943 (1966).

16) This tendency is pronounced in the reaction with *p*-(dimethylamino)benzaldehyde hydrazone.

17) D. D. Libman, A. W. Nineham, and R. Slack, *J. Chem. Soc.*, **1954**, 1565.

18) Experimental data unfit for this explanation were reported: *e.g.* F. R. Fichter and J. Frohlich, *Chem. Zentr.*, **1903**, II. 426; Beilstein's "Handbuch der Organischen Chemie," Hw. Bd. XVI (1933), p. 27.

19) According to the recent study of the mechanism of formazam formation by the action of diazonium salt on arylhydrazone, the reaction intermediate is to be the *gem*-bis(arylazo) compound, ArCH(–N=NAr′)(–N=NAr″), whose rearrangement to formazan is an azo-hydrazone conversion: [A. F. Hegarty and F. L. Scott, *Chem. Commun.*, **1966**, 622].

$$ArCH{=}N{-}NHAr' + Ar''\overset{+}{N}{\equiv}N\ Cl^- \longrightarrow$$

$$ArCH(\underset{\displaystyle N{=}N{-}Ar'}{\underset{|}{}}){-}N{=}N{-}Ar' \longrightarrow ArC(\underset{\displaystyle N{=}N{-}Ar''}{\underset{|}{}}){=}N{-}NHAr'$$

20) Melting points were determined with a Yanagimoto micro-melting point apparatus Model MP-S3 and are corrected. The micro-analysis was performed on a Perkin-Elmer elemental analyzer Model 240. The IR spectra were recorded with a JASCO DS-301 spectrometer.

21) M. Kobayashi, H. Minato, and H. Fukuda, *Bull. Chem. Soc. Jpn.*, **46**, 1266 (1973).

22) R. Knoll, *J. Prakt. Chem.*, **113**, 40 (1926); *Chem. Abstr.*, **20**, 2669 (1926).

Reactions of 2,4-Dialkoxy-1,3-diphenyl-1,3,2,4-diazadiphosphetidines with Benzil, Benzalacetophenone, and α-Phenyliminobenzyl Phenyl Ketone

Takayuki KAWASHIMA and Naoki INAMOTO

Department of Chemistry, Faculty of Science, The University of Tokyo, Hongo, Tokyo 113

(Received February 3, 1976)

2,4-Diethoxy-1,3-diphenyl-1,3,2,4-diazadiphosphetidine (**1a**) reacted with benzil, benzalacetophenone, and α-phenyliminobenzyl phenyl ketone in refluxing *o*-dichlorobenzene to give 2-ethoxy-3,4,5-triphenyl-Δ^4-1,3,2-oxazaphospholine 2-oxide, 2-ethoxy-1,3,5-triphenyl-Δ^4-1,2-azaphospholine 2-oxide, and 2-anilino-3,4,5-triphenyl-Δ^4-1,3,2-oxazaphospholine 2-oxide, respectively. Under mild conditions, reaction of **1a** with benzil gave a Ramirez type 1 : 2 adduct, which thermally decomposed to give oxazaphospholine derivatives.

Mitsunobu and Mukaiyama[1] have used "iminophosphite," ArN=POR, in phosphorylation of alcohols to dialkyl phosphites. However, analogous compounds usually exist as cyclic dimers, 1,3,2,4-diazadiphosphetidines.[2] On heating, the dissociation of the dimer to the corresponding monomer may be expected to occur, the monomer being analogous to reactive intermediates such as phosphinylidenes (R–P=O) and phosphinothioylidenes (R–P=S).[3]

In order to get information on these points, we investigated the structure of "alkyl phenyliminophosphites" and the reactions with 1,3-dienes and carbonyl compounds such as benzil, benzalacetophenone, and α-phenyliminobenzyl phenyl ketone.

Structure of "Alkyl Phenyliminophosphites." "Alkyl phenyliminophosphites," prepared by the reported method,[1] were obtained as a viscous liquid, the ethyl derivative solidifying on standing for several weeks. No change of the spectral data was observed before and after solidification.

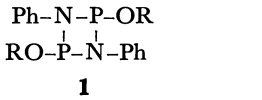

1

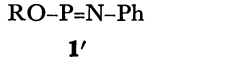

1′

a, R=Et; b, R=Me

The mass spectrum of the ethyl derivative showed parent and base peaks at *m/e* 334 and 167, respectively, supporting the view that the structure is a cyclic dimer, 2,4-diethoxy-1,3-diphenyl-1,3,2,4-diazadiphosphetidine (**1a**). The ^{1}H-NMR spectrum showed two triplets centered at δ 1.22 and 1.25. The ratio of peak area of the triplet of δ 1.25 to that of δ 1.22 was *ca.* 1.4, indicating the existence of two ethoxy group in a different environment.

If we assume a rapid inversion on the nitrogen atoms,[4] the existence of *cis* and *trans* isomers is possible with respect to two ethoxy groups. This was also supported by the ^{31}P-NMR spectrum. Two signals were observed at δ_P −134.9 and −182.0 ppm, the ratio of peak area being *ca.* 1.3. Since two phosphorus atoms are equivalent in this cyclic system, they should be assigned to signals of the phosphorus nuclei of *cis* and *trans* isomers.

Nielsen and Pustinger[5] observed two signals at δ_P −109.2 and −113.6 ppm in the ^{31}P-NMR spectrum of 2,4-dianilino-1,3-diphenyl-1,3,2,4-diazadiphosphetidine. It is expected in the *cis* isomer of **1a** that steric repulsion between two ethoxy groups causes repulsion of lone pair electrons on two phosphorus atoms and deshields the phosphorus nuclei. Thus, the signal in the *cis* isomer shifts considerably to a low field.

The ^{31}P-NMR spectrum of methyl derivative (**1b**) showed signals due to *trans* and *cis* isomers at δ_P −136.5 and −184.8 ppm, respectively.

Attempts to separate the *cis* and *trans* isomers of **1** were unsuccessful. The mixture was therefore used for reactions described below.

Attempted Reaction with Isoprene. If the dissociation equilibrium between **1** and **1′** was present, the resulting iminophosphite (**1′**) would be expected to undergo Diels-Alder type reaction with dienes analogously to R–P=S.[3a,c] However, the reaction with isoprene in *o*-dichlorobenzene at 190 °C for one day in a sealed tube gave neither Diels-Alder adduct nor Ramirez type adduct, indicating that **1** does not dissociate to **1′** at 190 °C.

Reaction with Benzil. Under nitrogen atmosphere, benzil reacted with **1a** in refluxing *o*-dichlorobenzene to give 2-ethoxy-3,4,5-triphenyl-Δ^4-1,3,2-oxazaphospholine 2-oxide (**2**) in 17% yield. The structure was determined by elemental analysis and spectral data.

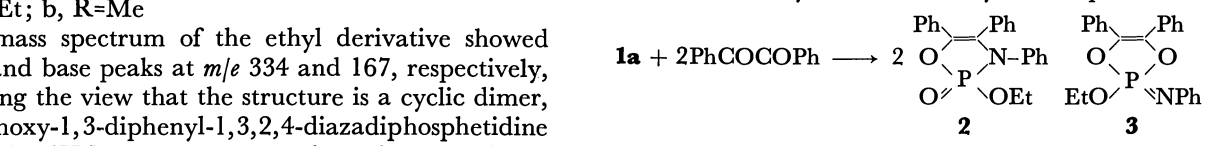

2 **3**

The IR and NMR spectra could not completely rule out another structure (**3**). However, the presence of peaks at *m/e* 268 (2,3-diphenylindole−H) and 180 (PhC≡N$^+$–Ph) in the mass spectrum supports the structure **2**.

Structure **2** was also confirmed by an unequivocal synthesis by another route. The following reaction is expected to take place:[1]

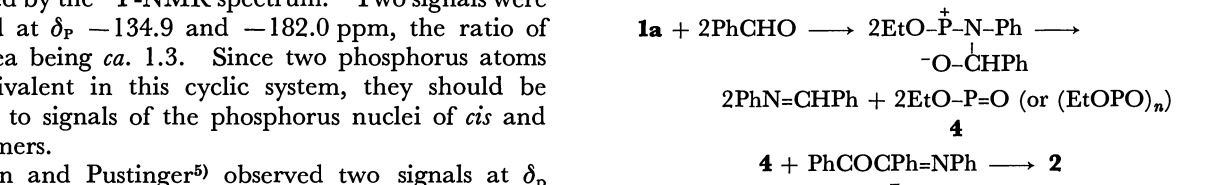

4

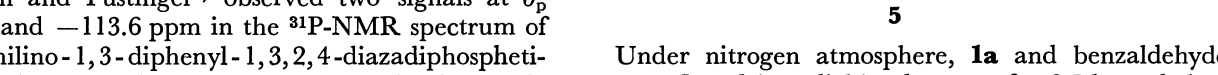

5

Under nitrogen atmosphere, **1a** and benzaldehyde were refluxed in *o*-dichlorobenzene for 3.5 h, and then

α-phenyliminobenzyl phenyl ketone (**5**) was added. After being refluxed for one day, **2** was obtained in 44% yield, the formation of *N*-benzylideneaniline being confirmed by NMR. Reaction of **4** with **5** is analogous to that of phosphinylidenes with benzil.[3b]

Under mild conditions, *viz.*, in boiling benzene or in acetonitrile at room temperature, **1a** reacted with benzil to afford 5,7-diethoxy-2,3,6,9,10,12-hexaphenyl-1,4,8,11-tetroxa-6,12-diaza-5,7-diphosphadispiro[4.1.4.1]-dodeca-2,9-diene (**6a**), a Ramirez type adduct, in 44 or 18% yield, respectively.

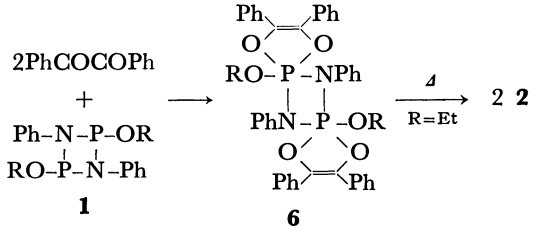

1 **6**

a, R=Et; b, R=Me

Similarly, **1b** reacted with benzil in acetonitrile at room temperature to give an analogous Ramirez type adduct (**6b**) in 12% yield. The ^{1}H-NMR spectrum showed complicated signals of methyl protons. These complexities can be attributed to virtual couplings observed in the ^{1}H-NMR spectra of some 2,2-diethoxy-1,3,5-triazatriphosphorine derivatives,[6] bis(dimethylamino)- and bis(methylthio)-1,3,2,4-diazadiphosphetidine 2,4-dioxides.[7]

Compound **6a** decomposed in refluxing *o*-dichlorobenzene to give **2** in 21% yield. It seems reasonable that **6** is an intermediate in the formation of **2**.

Reaction with Benzalacetophenone. Benzalacetophenone reacted with **1a** in refluxing *o*-dichlorobenzene to produce 2-ethoxy-1,3,5-triphenyl-Δ^4-1,2-azaphospholine 2-oxide (**7**) and an open-chain product (**8**), *O*-ethyl *N*-phenyl 1,3-diphenyl-3-hydroxy-1-propenylphosphonamidate, in 15 and 7% yields, respectively.

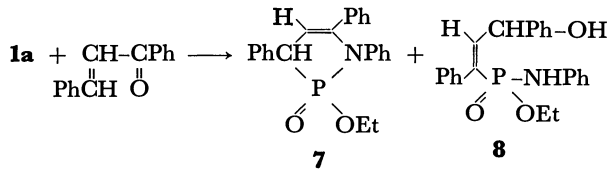

7 **8**

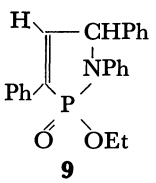

9

Another structure (**9**) is possible for **7**. The MS spectrum of **8** gave no parent peak, but the highest peak was observed at *m/e* 375 (M^+-H_2O), which seems to be due to **9** formed by intramolecular dehydration of **8**. The fragmentation pattern differed from that of **7**, the base peak of **7** being at *m/e* 282 ($M^+-EtOPO-H$), and that of **8** at *m/e* 193 ($Ph_2C_3H_3^+$). NMR signals due to ethoxy protons exhibited doubling. This is explained by the presence of asymmetric carbon at the 2-position of **7**.

From the results, structure **7** is favored over structure **9**.

Reaction with α-Phenyliminobenzyl Phenyl Ketone. Under similar conditions, **1a** reacted with α-phenyliminobenzyl phenyl ketone (**5**) to afford α,α′-bis(phenylimino)bibenzyl, **2**, and 2-anilino-3,4,5-triphenyl-Δ^4-1,3,2-oxazaphospholine 2-oxide (**10**) in 20, trace, and 40% yields.

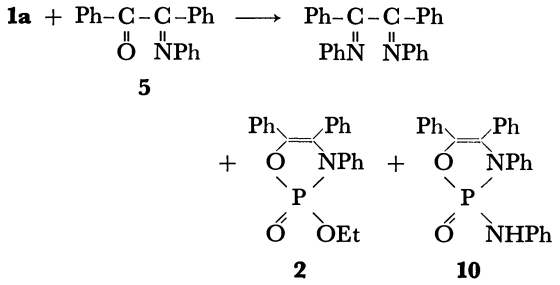

2 **10**

The expected product (**11**) corresponding to **2** and **7** was not obtained.

A possible mechanism is considered as follows, though an attempt to isolate the Ramirez type adduct (**12**) was unsuccessful.

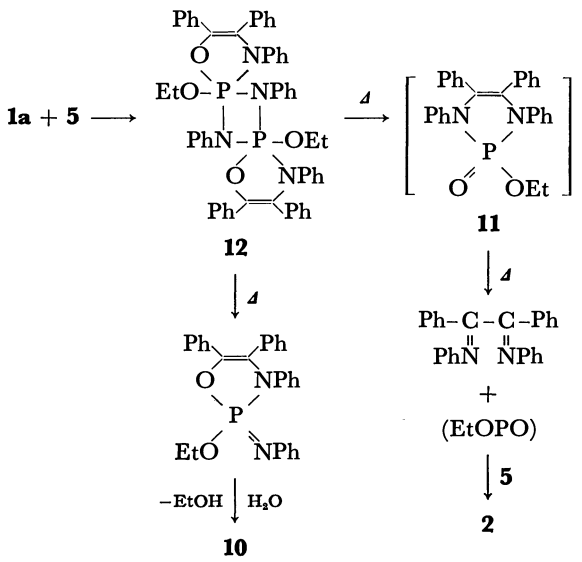

Compound **1a** did not react with α-methoxyiminopropiophenone in a refluxing acetonitrile.

Experimental

All melting and boiling points are uncorrected. IR and mass spectra were recorded on a Hitachi EPI-G2 spectrophotometer and a Hitachi RMU-6L mass spectrometer, respectively. ^{1}H-NMR spectra were measured with Hitachi R-20 B, R-24 (60 MHz) and R-22 (90 MHz) spectrometers using TMS as an internal standard. ^{31}P-NMR spectra were determined with a Hitachi R-20 B-R-204-PB spectrometer using 85% phosphoric acid as an external standard.

All reactions were carried out under nitrogen atmosphere.

Materials. Benzil,[8] α-phenyliminobenzyl phenyl ketone,[9] and benzalacetophenone[10] were prepared by the methods given in the literature.

2,4-Diethoxy-1,3-diphenyl-1,3,2,4-diazadiphosphetidine (1a). Compound (**1a**) was prepared by the reported procedure,[1]

bp 164 °C/0.2 mmHg (lit,[1] 145—147 °C/0.08 mmHg). The viscous liquid solidified on standing for several weeks, mp 45 °C. MS: *m/e* 334 (M^+, 53%) and 167 ($M^+/2$, 100); ^{1}H-NMR (CCl_4): δ 1.22 (t, J=7 Hz), 1.25 (t, J=7 Hz), 4.1 (m, 2H, >P-OC<u>H</u>$_2$Me), and 6.7—7.35 (m, 5H, Ph). The area ratio of the signal at δ 1.25 to that at δ 1.22 was *ca.* 1.4; ^{31}P-NMR (PhH): δ_P −182.0 and −134.9 ppm. The area ratio of the signal at δ_P −134.9 to that at δ_P −182.0 ppm was *ca.* 1.3.

*2,4-Dimethoxy-1,3-diphenyl-1,3,2,4-diazadiphosphetidine (**1b**).* Compound (**1b**) was prepared by a procedure similar to that for **1a**, but could not be distilled under reduced pressure because of thermal decomposition. Thus it was used without further purification. ^{31}P-NMR (PhH): δ_P −184.8 and −136.5 ppm.

*Reaction of **1a** with Benzil.* *a) In o-Dichlorobenzene*: To a solution of benzil (4.20 g, 20.0 mmol) in *o*-dichlorobenzene (30 ml) was added **1a** (3.34 g, 10.0 mmol) in *o*-dichlorobenzene (10 ml) and the mixture was refluxed for 2 h. After removal of the solvent, the residue was chromatographed on a silica gel dry column with dichloromethane to afford 1.32 g (17%) of **2**, mp 146.0—146.5 °C (from ether); IR (KBr): 1650 (C=C), 1240 (P=O), and 1025 cm^{-1} (POC); NMR ($CDCl_3$): δ 1.29 (t, J=7 Hz, 3H, Me), 4.25 (dp, J_{HCCH}=7, J_{POCH}=10 Hz, 2H, OCH_2^-), and 7.14—7.28 (m, 15H, 3Ph); MS: *m/e* 377 (M^+).

Found: C, 70.21; H, 5.11; N, 3.61%. Calcd for $C_{22}H_{20}NO_3P$: C, 70.02; H, 5.34; N, 3.71%.

b) In Benzene: To a solution of benzil (1.06 g, 5.0 mmol) in benzene (35 ml) was added **1a** (0.84 g, 2.5 mmol) in benzene (5 ml) with stirring. The mixture was refluxed for one day and the solvent was removed *in vacuo*. The residue was treated with ether to precipitate 0.835 g (1.1 mmol, 44%) of **6a**, mp 142—143 °C (dec) (from acetone). IR (KBr): 1650 (C=C) and 1020—1050 cm^{-1} (POC); ^{1}H-NMR ($CDCl_3$, 90 MHz): δ 1.11 (t, J=7 Hz, 3H, $POCH_2C\underline{H}_3$), 1.24 (t, J=7 Hz, 3H, $POCH_2C\underline{H}_3$), 3.96 (m, 4H, $POC\underline{H}_2Me$), and 7.1—7.6 (m, 30H, 6Ph); ^{31}P-NMR (PhH): δ_P +62.8 ppm; MS: *m/e* 754 (M^+).

Found: C, 70.27; H, 5.36; N, 3.60%. Calcd for $C_{44}H_{40}N_2O_6P_2$: C, 70.02; H, 5.34; N, 3.71%.

c) In Acetonitrile: A mixture of **1a** (1.69 g, 5.05 mmol) and benzil (2.11 g, 10.0 mmol) in acetonitrile (30 ml) was stirred for one day at room temperature. The resulting precipitates were recrystallized from acetone to give **6a** (0.693 g, 18%).

*Alternative Preparation of **2**.* A mixture of **1a** (1.18 g, 3.5 mmol) and benzaldehyde (0.76 g, 7.2 mmol) in *o*-dichlorobenzene (40 ml) was refluxed for 3.5 h. To the reaction mixture was added a solution of α-phenyliminobenzyl phenyl ketone (2.00 g, 7.0 mmol) in *o*-dichlorobenzene (10 ml). The mixture was then refluxed for one day. After evaporation of the mixture, the NMR spectrum of the residue showed the presence of *N*-benzylideneaniline at δ 8.40 (s, Ph-C<u>H</u>=). The residue was chromatographed on a silica gel dry column with dichloromethane to give crude **2** which was recrystallized from ether to give a pure sample (1.16 g, 3.1 mmol, 44%). Isolation of *N*-benzylideneaniline was unsuccessful because of the easy hydrolysis.

*Thermal Decomposition of **6a**.* A solution of **6a** (0.626 g, 0.83 mmol) in *o*-dichlorobenzene (30 ml) was refluxed for one day. After removal of the solvent under reduced pressure, the residue was chromatographed on a silica gel dry column to afford **2** (0.131 g, 0.35 mmol, 21%).

*Reaction of **1b** with Benzil.* A solution of crude **1b** prepared from aniline (4.185 g, 45 mmol) and methyl phosphorodichloridite (2.00 g, 15 mmol) in acetonitrile (10 ml) was added to a solution of benzil (3.16 g, 15 mmol) in acetonitrile (40 ml) and the mixture was stirred for 2 days at room temperature. The resulting crystals were recrystallized from acetone to give **6b** (0.648 g, 0.89 mmol, 12%), mp 158.0—158.5 °C. IR (KBr): 1640 (C=C) and 1020—1050 cm^{-1} (POC); NMR ($CDCl_3$): δ 3.65 (m, 6H, POMe) and 7.1—7.6 (m, 30H, 6Ph); MS: *m/e* 726 (M^+).

Found: C, 69.18; H, 4.72; N, 3.60%. Calcd for $C_{42}H_{36}N_2O_6P_2$: C, 69.42; H, 4.99; N, 3.85%.

*Reaction of **1a** with Benzalacetophenone.* A solution of **1a** (1.67 g, 5.0 mmol) and benzalacetophenone (2.08 g, 10.0 mmol) in *o*-dichlorobenzene (45 ml) was refluxed for 9 h. After removal of the solvent *in vacuo*, the residue was chromatographed on a silica gel dry column with dichloromethane–carbon tetrachloride (1:1). Elution with ether from the partition of R_f 0.5—0.7 gave **7** (0.555 g, 1.47 mmol, 15%), mp 179—180 °C (from ether). IR (KBr): 1640 (C=C), 1218 (P=O), and 1038 cm^{-1} (POC); NMR ($CDCl_3$): δ 1.08, 1.32 (dt, J=7 Hz, 3H, $POCH_2C\underline{H}_3$), 4.07 (m, 2H, $POC\underline{H}_2CH_3$), 5.72 (d, J_{PH}=20 Hz, 1H, =CH–), 6.70 (m, 1H, >CH–), and 7.0—7.7 (m, 15H, 3Ph); MS: *m/e* 375 (M^+, 75%) and 282 (PhC^+=CHCPh=NPh, 100).

Found: C, 73.84; H, 6.20; N, 3.87%. Calcd for $C_{23}H_{22}NO_2P$: C, 73.59; H, 5.91; N, 3.73%.

Elution with ethanol from the partition of R_f 0.7—0.9 gave 1.23 g of a tarry product. Treatment with a small amount of ethanol gave 0.284 g (7%) of **8**, mp 214 °C (from ethanol). An analytically pure sample could not be obtained. However, its structure was determined by the following spectral data. IR (KBr): 3260 (OH), 3100 (NH), 1630 (C=C), 1213 (P=O), and 1040 cm^{-1} (POC); NMR ($CDCl_3$): δ 1.00 (t, J=7 Hz, 3H, $OCH_2C\underline{H}_3$), 1.95 (s, 1H, OH), 3.64 (d, J=7 Hz, 1H, =CH–C<u>H</u>〈), 3.82 (dq, J_{HH}=7, J_{PH}=10 Hz, 2H, $POCH_3$), 6.10 (s, 1H, NH), 6.29 (t, J_{HH}=J_{PH}=7 Hz, 1H, =C<u>H</u>–CH〈), and 7.0—7.5 (m, 15H, 3Ph); MS: *m/e* 375 (M^+–H_2O, 47%) and 193 (100).

*Reaction of **1a** with α-Phenyliminobenzyl Phenyl Ketone.* A solution of **1a** (1.61 g, 4.8 mmol) and α-phenyliminobenzyl phenyl ketone (2.54 g, 8.9 mmol) in *o*-dichlorobenzene (40 ml) was refluxed for 24 h. After removal of the solvent under reduced pressure, the residue was chromatographed on a silica gel dry column. Elution with dichloromethane from the first partition of R_f 0.7—1.0 gave 0.644 g (1.8 mmol, 20%) of α,α′-bis(phenylimino)bibenzyl, mp 147—148 °C (from ethanol) (lit,[11] 142 °C); MS: *m/e* 360 (M^+). Elution with ether from the second partition of R_f 0.5—0.7 gave a trace of **2**. Elution with ether from the third partition of R_f 0.1—0.5 gave 1.66 g (3.9 mmol, 40%) of **10**, mp 164.5—165 °C (from ethanol). IR (KBr): 3150 (NH), 1640 (C=C), and 1235 cm^{-1} (P=O); NMR ($CDCl_3$): δ 6.7—7.1 (m, 10H, 2Ph), 7.24 (s, 10H, 2Ph), and 7.58 (bs, 1H, NH); MS: *m/e* 424 (M^+).

Found: C, 73.83; H, 4.95; N, 6.45%. Calcd for $C_{26}H_{21}N_2O_2P$: C, 73.58; H, 4.95; N, 6.60%.

This work was supported by a Grant-in-Aid from the Ministry of Education.

References

1) O. Mitsunobu and T. Mukaiyama, *J. Org. Chem.*, **29**, 3005 (1964).

2) H. W. Grimmel, A. Guenther, and J. F. Morgan, *J. Am. Chem. Soc.*, **68**, 539 (1946); J. Weiss and G. Hartmann, *Z. Naturforsch.*, **21b**, 891 (1966); E. H. M. Ibrahim, R. A. Shaw, B. C. Smith, C. P. Thakur, and M. Woods, *Phosphorus*, **1**, 153 (1971).

3) a) S. Nakayama, M. Yoshifuji, R. Okazaki, and N. Inamoto, *Chem. Commun.*, **1971**, 1186; b) M. Yoshifuji, S. Nakayama, R. Okazaki, and N. Inamoto, *J. Chem. Soc. Perkin Trans. 1* **1973**, 2065; c) S. Nakayama, M. Yoshifuji, R. Okazaki, and N. Inamoto, *Bull. Chem. Soc. Jpn.*, **48**, 546, 3733 (1975).

4) A. T. Bottini and J. D. Roberts, *J. Am. Chem. Soc.*, **80**, 5203 (1958).

5) M. L. Nielsen and J. V. Pustinger, Jr., *J. Phys. Chem.*, **68**, 152 (1964).

6) C. Hewlett and R. A. Shaw, *J. Chem. Soc., A*, **1966**, 56.

7) M. Green, R. N. Haszeldine, and G. S. A. Hopkins, *J. Chem. Soc., A*, **1966**, 1766.

8) R. Adams and C. S. Marvel, *Org. Synth.*, Coll. Vol. I, 94 (1941).

9) E. von Meyer and K. Voigt, *J. Prakt. Chem.*, **34**, 1 (1886).

10) E. P. Kohler and H. M. Chadwell, *Org. Synth.*, Coll. Vol. I, 78 (1941).

11) B. Lachowicz, *Monatsh. Chem.*, **14**, 283 (1893).

Optical Activation of Racemic α-Substituted Carbonyl Compounds Using Optically Active Amines

Hajime MATSUSHITA, Masao NOGUCHI, and Sadao YOSHIKAWA*

Central Research Institute, The Japan Tobacco and Salt Public Corporation, Umegaoka, Midori-ku, Yokohama, Kanagawa 227

**Department of Synthetic Chemistry, Faculty of Engineering, The University of Tokyo, Hongo, Bunkyo-ku, Tokyo 113*

(Received February 19, 1976)

Hydrolysis of immonium salts of enamines consisting of optically active amines and racemic α-substituted carbonyl compounds with hydrochloric acid gave the corresponding optically active carbonyl compounds. The NMR spectra showed that the immonium salt is a mixture of two diastereomeric isomers. The mechanism of the optical activation is discussed on the basis of an isotope labeling experiment and the NMR spectra.

Optically active carbonyl compounds with an asymmetric carbon atom at the α-position of the carbonyl group are widespread in nature as terpenoids, steroids and alkaloids, their synthesis being considered of interest by many workers.[1] The resolution of racemic carbonyl compounds,[2] asymmetric destruction,[3] asymmetric synthesis[4] and asymmetric transformation[5] has been reported. The asymmetric transformation by which racemic compounds are transformed into the corresponding optically active forms has not been much utilized, though nearly 100% yield of one enantiomer has been reported.[6] Compounds with an active proton at the asymmetric carbon are suitable for the asymmetric transformation, but it is difficult to isolate their optically active forms since they undergo racemization easily.[6] On the other hand, the compounds with an inactive proton at the asymmetric carbon are undesirable for their optical activation. The hydrolysis of the immonium salts of enamines of racemic α-substituted carbonyl compounds with optically active acids give the corresponding optically active carbonyl compounds and the original acids.[7] Conversion of the stable α-substituted carbonyl compounds into the labile immonium salts is a key step in the optical activation. This paper deals with another method of optical activation of racemic α-substituted carbonyl compounds. The enamines consisting of racemic α-substituted carbonyl compounds and optically active amines were treated with acid, and hydrolysis of the salts gave the optically active carbonyl compounds. This is a new method to obtain optically active α-substituted carbonyl compounds from their racemic forms.

Experimental

Optical rotations were determined with a JASCO Digital Automatic Polarimeter Model DIP 181. Gas chromatographic analyses were carried out on a 2 m column of 20% Carbowax 20 M on Cromosorb W with a Hitachi Gas Chromatograph, Model K 53. Nuclear magnetic resonance spectra were obtained with a JNM-PS-100 Spectrometer with tetramethylsilane as an internal standard.

S(+)-2-Methylpiperidine. *S*(+)-2-Methylpiperidine was obtained by resolution according to the method of Kostyanovsky *et al.*[8]

R(−)-2-Methylpyrrolidine. *R*(−)-*O*,*N*-Ditosyl-L-prolinol was prepared according to the method described by Kostyanovsky *et al.*[8] Anhydrous benzene (500 ml) and *R*(−)-*O*,*N*-ditosyl-L-prolinol (115 g, 0.28 mol) were placed in a 3 l four-necked round bottom flask equipped with a mechanical stirrer, a reflux condenser and a thermometer. Sodium bis(2-methoxyethoxy)aluminum hydride (700 g in benzene, 3.47 mol) was carefully added with vigorous stirring. The reaction mixture was refluxed and stirred for 5 days. It was then cooled, and ice-cold water was added with vigorous stirring. After separation of the benzene layer, the aqueous layer was made strongly basic with pellets of sodium hydroxide, and extracted with benzene. The separated benzene layer and the extracts were combined and extracted with three 100 ml portions of 6 M hydrochloric acid. The acid solution was made strongly basic with pellets of sodium hydroxide again, and extracted with ether. The ether solution was dried over anhydrous Na_2SO_4, and filtered. The solvent was distilled off and the residue was subjected to fractional distillation. All the fractions boiling up to 100 °C were collected (11.3 g, 47.7% yield based on the ditosylprolinol). This crude amine was subjected to the subsequent procedures without further purification.

Preparation of Enamines. Enamines of α-phenylpropionaldehyde (**1**), 2-methylcyclohexanone (**2**) and 2-ethylhexanal(**3**) were prepared by the usual azeotropic procedure using benzene as the solvent and purified by distillation. *R*(−)-2-methylpyrrolidine and *S*(+)-2-methylpiperidine were used as amine components of the enamines. *S*(+)-2-Methylpiperidine enamine of **1**: bp 129—130 °C (5 mmHg), 81% yield; MS *m/e* 215 (M^+), 200 (base); IR 1638 cm^{-1} ($\nu_{C=C}$); NMR ($CDCl_3$) mixture of two geometrical isomers (92: 8 at room temperature), major isomer, 1.03 (N–C–CH_3, d, J=6.7 Hz), 2.09 (C=C–CH_3, s), 6.40 (N–CH=C, s), 7.30 (phenyl, m), minor isomer, 5.81 (N–CH=C, s); $[\alpha]_D^{23}$ −426° (neat). *S*(+)-2-Methylpiperidine enamine of **2**: bp 136 °C (8.5 mmHg), 32% yield; MS *m/e* 193 (M^+), 178 (base); IR 1634 cm^{-1} ($\nu_{C=C}$); NMR ($CDCl_3$) 0.83 (N–C–CH_3, d, J=6.0 Hz), 1.70 (CH_3–C=C–N, s); $[\alpha]_D^{23}$ −89° (neat), $[\alpha]_D^{23}$ −71.2° (c=5, benzene). *S*(+)-2-Methylpiperidine enamine of **3**: bp 97—99 °C (6 mmHg), 91.9% yield; MS *m/e* 209 (M^+), 166 (base); IR 1664 cm^{-1} ($\nu_{C=C}$); NMR ($CDCl_3$) mixture of two geometrical isomers (60: 40 at room temperature), $[\alpha]_D^{23}$ −11.6° (neat). *R*(−)-2-Methylpyrrolidine enamine of **1**: bp 102—130 °C (5.5 mmHg), 76.1% yield; MS *m/e* 201 (M^+), 186 (base); IR 1631 cm^{-1} ($\nu_{C=C}$); NMR ($CDCl_3$) mixture of two geometrical isomers (89: 11 at room temperature), major isomer, 1.17 (N–C–CH_3, d, J=6.3 Hz), 2.15 (C=C–CH_3, s), 6.40 (N–CH=C, s), 7.3 (phenyl, m), minor isomer, 1.17 (N–C–CH_3, d, J=6.3 Hz), 2.04 (C=C–CH_3, s), 6.11 (N–CH=C, s), 7.17 (phenyl, m); $[\alpha]_D^{23}$ +398° (c=2.90, benzene). *R*(−)-2-Methylpyrrolidine enamine of **2**: bp 93.5 °C (7.5 mmHg), 78.7% yield; MS 179 (M^+), 164 (base); IR 1638 cm^{-1} ($\nu_{C=C}$);

NMR ($CDCl_3$) mixture of two geometrical isomers (85: 15 at room temperature), major isomer, 0.90 (CH_3–CH–C=C, d, J=6.0 Hz), 1.08 (CH_3–C–N, d, J=6.6 Hz), 4.30 (CH_3–CH–C=C, t, J=4.0 Hz), minor isomer, 1.66 (CH_3–C=C, s); $[\alpha]_D^{23}$ +190.5° (c=2.31, benzene).

The Hydrolysis of Enamines. To a solution of enamine (0.02 mol) in benzene (30 ml) was added an equivalent aqueous hydrochloric acid with vigorous stirring in an ice bath. The reaction was continued until the completion of hydrolysis which was confirmed gas chromatographically. The benzene layer was separated, successively washed with water and 5% aqueous sodium carbonate and water, and dried over anhydrous Na_2SO_4, the optical rotation being then measured. The recovery of carbonyl compound was determined with a gas chromatograph. The same results were obtained by another method: Dry HCl gas was bubbled into a benzene solution (50 ml) of enamine (0.02 mol), and the solvent was removed completely under reduced pressure. The residue was dissolved in benzene (30 ml), and to the solution in an ice bath was added water (15 ml) dropwise with vigorous stirring. The subsequent procedure was the same as mentioned above.

Results and Discussion

Hydrolysis of Enamines. The results are summarized in Table 1. The optical rotation of pure **1** is not known. Though the determination of the specific rotation of **1** was attempted by the method of Goering,[9] no pseudocontact-shift differences for enantiomers could be observed in the presence of tris-[3-(trifluoromethylhydroxymethylene)-*d*-camphorato]-europium(III). Cram reported the optical rotation of a mixture of **1** and acetophenone, α_{obs} +75.80°.[10] The optical rotation of the pure **2** was reported to be $[\alpha]_D^{18}$ +14.21° (l=0.5).[11] Calculating from this value, the optical yields are estimated to be 20.2% (in the case of *S*(+)-2-methylpiperidine) and 6.20% (in the case of *R*(−)-2-methylpyrrolidine). The optical activation of **3** was examined only in the case of *S*(+)-2-methylpiperidine. Optical rotations of the recovered **3** were determined at several other wave lengths as well as at 589 nm (D line): $[\alpha]_{577}^{23}$ −0.102°, $[\alpha]_{546}^{23}$ −0.138°, $[\alpha]_{435}^{23}$ −0.255°, $[\alpha]_{365}^{23}$ −0.499°. From the results in Table 1, six membered ring amine seems to contribute to the optical activation more effectively than the five membered amine. The difference in the ability of the optical activation can be attributed to the difference of the *exo* double bond stability. The higher degree overlapping of the lone pair on the nitrogen atom with the π-orbital of *exo* double bond and more favorable conformation of five membered ring with *exo* double bond seem to make the immonium salt with five membered amine more stable and less reactive than that with six membered amine.[12,13] Greater stability and smaller reactivity of the salt with five membered ring amine would be unfavorable for asymmetric transformation by proton exchange.

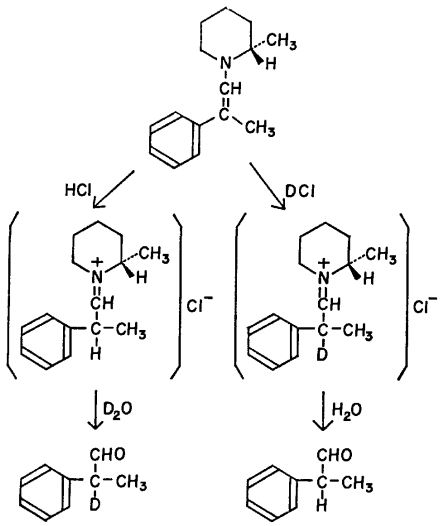

Fig. 1.

Isotopic Labeling Study. As shown in Fig. 1, hydrolysis of the immonium salt of HCl and 2-methylpiperidine enamine of **1** in D_2O gave deuterated **1**, but not that of the salt of DCl and the enamine in H_2O.

This suggests that the proton exchange at the asymmetric α-carbon of an immonium salt occurs easily. The reversible protonation in favor of one diastereomeric immonium salt results in an optically active **1**. Similar proton exchange reactions *via* enamine were reported by Leonard and Sauers.[14]

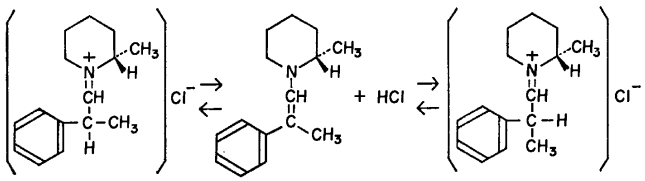

Immonium salts of enamines of racemic α-substituted carbonyl compounds with optically active acids gave, on hydrolysis with water, the corresponding optically active carbonyl compounds.[7] The mechanism of this optical activation was considered to be the same as the asymmetric transformation reported by Read and McMath.[15] The result of the isotopic labeling study also supports the mechanism.

NMR Spectra of Enamine and Immonium Salts. Dry HCl or DCl gas was bubbled into a solution of optically

Table 1. Optical rotation of some carbonyl compounds recovered from the immonium salts

Amine component	Carbonyl component	Recovered carbonyl compound $[\alpha]_D^{23}$	Optical yield %	Recovery %
S(+)-2-Methylpiperidine	**1**	−80.8 (c 25.0)		91
	2	−2.87 (c 42.2)	20.2[a]	77
	3	−0.098 (c 3.19)		85
R(−)-2-Methylpyrrolidine	**1**	+51.6 (c 8.11)		71
	2	+ 0.881 (c 15.5)	6.20[a]	60

a) Based on reported optically pure **2**, $[\alpha]_D^{18}$ +14.21.[11]

The Reactions of Polychloroethanes with Phenolate and Benzenethiolate Ions in Dipolar Aprotic Solvents

Shigeo TANIMOTO, Ryôzô TANIYASU, Tôru TAKAHASHI, Takatoshi MIYAKE, and Masaya OKANO

Institute for Chemical Research, Kyoto University, Uji, Kyoto 611

(Received February 26, 1976)

The reactions of several *gem*- and *vic*-polychloroethanes containing 3—5 Cl atoms with PhONa in dimethyl sulfoxide and with PhSNa in *N*,*N*-dimethylformamide were examined. Either the mono-, di-, or tetra-substituted compounds of polychloroethylenes were obtained as the main products, depending on the kinds of substrates as well as on the amounts of the bases. The reaction products from polychloroethylenes with 2—4 Cl atoms were also examined under similar conditions for the sake of comparison. Reasonable reaction paths leading to these products were given.

Though direct substitution reactions (S_N2) of primary alkyl halides have been widely utilized in the syntheses of various kinds of compounds,[1] the usefulness of alkylidene dihalides in this way is rather limited because of their low reactivities.[2] Thus ,it has been known that the basic substitution of the halogen atom(s) of less-reactive alkylidene dichlorides by nucleophiles other than thiolate ions proceeds only under severe reaction conditions; *e.g.*, the preparation of diphenoxymethane can be accomplished by heating dichloromethane with PhONa in 95% alcohol at 150 °C for 3 h in a sealed tube.[3] We have recently found, however, that this reaction can be conducted even at room temperature by the use of dimethyl sulfoxide (DMSO) as the solvent.[4] Since the basicity of a base is known to be greatly enhanced by the change in solvent from a hydroxylic solvent to DMSO because of the disappearance of a hydrogen-bonding interaction,[5] there is a possibility that, even with a less-basic nucleophile, an olefin-forming elimination might compete considerably with a substitution, at least in basic aprotic solvents. On the other hand, it has been reported that, in the reaction of an alkyl halide with a basic nucleophile, the introduction of an electron-withdrawing group, such as COR, SO_2R, and even Br or Cl, at the β-position results in a large increase in the rate of olefin formation.[6] With these points in mind, we examined the reactions of several *gem*- and *vic*-polychloroethanes containing 3—5 Cl atoms with PhONa in DMSO and with PhSNa in *N*,*N*-dimethylformamide (DMF). The products were mostly the mono- or disubstituted compounds of polychloroethylenes, probably formed by the dehydrochlo-

TABLE 1. REACTION OF POLYCHLOROETHANES WITH PhONa (IN DMSO)

Run	Polychloroethane	Equiv. of PhONa	Reaction temp (°C)	Reaction time (h)	Main products	Yield (%)
1	$CH_2ClCHCl_2$ (I)	2	70	10	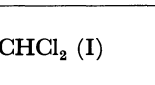	28
2	$CH_2ClCHCl_2$ (I)	3	70	10	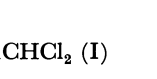	49
					$(PhO)_2C=CH_2$[b]	10
3	CH_3CCl_3 (II)	3	70	10	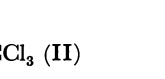	50
					$(PhO)_2C=CH_2$[b]	18
4	$CHCl_2CHCl_2$ (III)	4	70	5	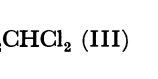	90
5	$CHCl_2CCl_3$ (IV)	2	70	10	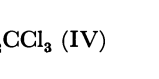	23
6	$CHCl_2CCl_3$ (IV)	5	70	10	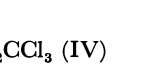	14
					$(PhO)_2C=CCl_2$[e]	52
7	$CH_2ClCHClCH_2Cl$	1	70	10	$CH_2=CCl-CH_2Cl$[f]	17
					$CH_2=CCl-CH_2OPh$[g]	41

a) Bp 74—77 °C/4 mmHg (lit,[8a] 80—81 °C/4 mmHg). b) Bp 148—152 °C/11.5 mmHg (lit,[10] 115—116 °C/1 mmHg). c) Bp 72—74 °C/4 mmHg (lit,[9] 98—99 °C/13.5 mmHg). d) Bp 91—93 °C/4 mmHg (lit,[8b] 112—113 °C/15 mmHg). e) A new compound. Bp 154—155 °C/4 mmHg. *Anal.* Found: C, 60.21; H, 3.62%. Calcd for $C_{14}H_{10}Cl_2O_2$: C, 59.86; H, 3.58%. f) Bp 92 °C (lit,[11] 92.5 °C). g) A new compound. Bp 68—69.5 °C/2.8 mmHg. *Anal.* Found: C, 63.97; H, H, 5.31%. Calcd for C_9H_9ClO: C, 64.00; H, 5.37%.

rination of the original polychlorides and by subsequent vinylic substitution(s) of the resulting olefins. Therefore, the reaction products from various polychloroethylenes with 2—4 Cl atoms were also examined under similar conditions for the sake of comparison.

The direct formation of substituted (chloro)ethylenes from polychloroethanes has never been reported so far as we know. However, there are several reports in the literature regarding vinylic substitution(s) of polychloroethylenes, where the reactions are mostly carried out in protic solvents or neat. Previous preparative data indicate that the substitution by RO^- [7] or ArO^- [8] can be achieved only under severe conditions, whereas the reaction with highly nucleophilic RS^- or ArS^- takes place readily under usual reaction conditions. The only study in a polar aprotic solvent was given by Normant; he found that, in DMF, the reaction of trichloroethylene with equimolar PhONa proceeded smoothly on heating at 65—70 °C.[9]

Results and Discussion

The reaction with PhONa was carried out by adding the chloroethanes to a solution of PhONa in DMSO (prepared by dissolving NaOH and PhOH in the solvent on heating) at an appropriate temperature. The reaction with PhSNa was conducted in a similar way, except for the use of DMF as the solvent under a nitrogen atmosphere, because the reaction in DMSO resulted in the formation of substantial amounts of diphenyl disulfide. The results for the two reactions are summarized in Tables 1 and 2. The reactions of the chloroethylenes with PhONa and PhSNa were similarly carried out in DMSO and DMF respectively. Some results are given in Table 3. The recorded yields in these tables are not always those obtained under optimum conditions. As can be seen from Tables 1 and 2, when more than an equivalent amount of the nucleophile was used, the substituted chloroethylenes and/or substituted ethylenes were isolated as the main products,

Table 2. Reaction of polychloroethanes with PhSNa (in DMF)

Run	Polychloroethane	Equiv. of PhSNa	Reaction temp. (°C)	Reaction time (h)	Main products	Yield (%)
1	$CH_2ClCHCl_2$ (I)	1	70	5	$CHCl_2CH_2SPh$[a]	49
2	$CH_2ClCHCl_2$ (I)	2	70	5		11
					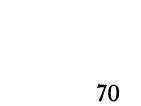	27
3	$CH_2ClCHCl_2$ (I)	3	70	5		58
4	$CHCl_2CHCl_2$ (III)	2	70	5	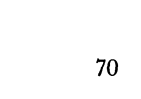	38
					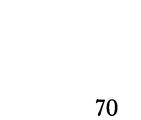	14
5	$CHCl_2CHCl_2$ (III)	4	70	5	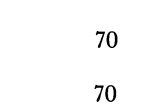	52
6	$CHCl_2CCl_3$ (IV)	5	70	5	$(PhS)_2C{=}C(SPh)_2$[f]	74
7	$CH_2ClCHCl_2$ (I)	1[g]	60	5	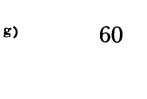	48
8	$CH_2ClCHCl_2$ (I)	3[g]	60	5	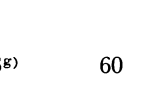	8
					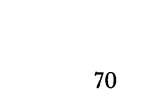	63
9	$CH_2ClCHClCH_2Cl$	1	70	5	$CH_2ClCHClCH_2SPh$[j]	58

a) A new compound. Bp 68—70 °C/3 mmHg. *Anal.* Found: C, 46.39; H, 3.97%. Calcd for $C_8H_8SCl_2$: C, 46.36; H, 3.89%. b) Bp 60—63 °C/3 mmHg (lit,[12] 92 °C/3 mmHg). *Anal.* Found: C, 56.05; H, 4.11%. Calcd for C_8H_7SCl: C, 56.31; H, 4.31%. c) Mp 30—31 °C (lit,[13] 30.5—31.5 °C). d) Bp 82—84 °C/3 mmHg (lit,[14] 140—142 °C/23 mmHg). e) A new compound. Mp 57—59 °C. *Anal.* Found: C, 60.81; H, 3.96%. Calcd for $C_{14}H_{11}S_2Cl$: C, 60.31; H, 3.98%. f) Mp 154—156 °C (Lit,[15] 154.5—155 °C). g) *n*-BuSNa is used in place of C_6H_5SNa. h) A new compound. Bp 80—82 °C/18 mmHg. *Anal.* Found: C, 47.51; H, 7.04%. Calcd for $C_6H_{11}SCl$: C, 47.83; H, 7.36%. i) Bp 88—92 °C/2 mmHg (lit,[16] 120—121 °C/2—3 mmHg). *Anal.* Found: C, 58.43; H, 9.48%. Calcd for $C_{10}H_{20}S_2$: C, 58.76; H, 9.86%. j) A new compound. Bp 92—94 °C/3 mmHg. *Anal.* Found: C, 49.02; H, 4.57%. Calcd for $C_9H_{10}SCl_2$: C, 48.88; H, 4.55%.

Table 3. Reaction of polychloroethylenes with PhONa (in DMSO) or with PhSNa (in DMF)

Run	Polychloroethylene	Equiv. of nucleophile	Reaction temp (°C)	Reaction time (h)	Main products	Yield (%)
1	$CH_2=CCl_2$ (V)	PhONa 2	30	40	PhO(H)C=C(H)Cl [a)]	11
2	$CH_2=CCl_2$ (V)	PhONa 2	70	5	PhO(H)C=C(H)Cl [a)] $(PhO)_2C=CH_2$ [b)]	15 53
3	Cl(H)C=C(H)Cl (VI$_c$)	PhONa 2	55	20	PhO(H)C=C(H)Cl [a)]	35
4	Cl(H)C=C(Cl)H (VI$_t$)	PhONa 2	55	50	No reaction	
5	$CHCl=CCl_2$ (VII)	PhONa 3	70	3	PhO(Cl)C=C(H)Cl [c)]	78
6	$CCl_2=CCl_2$ (VIII)	PhONa 4	70	10	PhO(Cl)C=C(Cl)Cl [d)] $(PhO)_2C=CCl_2$ [e)]	28 59
7	$CH_2=CCl_2$ (V)	PhSNa 1	60	5	PhS(H)C=C(H)Cl [f)] PhS(H)C=C(H)SPh [g)]	7 34
8	$CH_2=CCl_2$ (V)	PhSNa 2	60	5	PhS(H)C=C(H)SPh [g)]	52
9	Cl(H)C=C(H)Cl (VI$_c$)	PhSNa 1	60	5	PhS(H)C=C(H)Cl [h)] PhS(H)C=C(H)SPh [g)]	12 43
10	Cl(H)C=C(H)Cl (VI$_c$)	PhSNa 2	60	5	PhS(H)C=C(H)SPh [g)]	54
11	$CHCl=CCl_2$ (VII)	PhSNa 3	70	5	PhS(SPh)C=C(H)Cl [i)]	68
12	$CCl_2=CCl_2$ (VIII)	PhSNa 4	70	5	$(PhS)_2C=C(SPh)_2$ [j)]	78

a)—e) See a)—e) in Table 1, respectively. f) See b) in Table 2. g) See c) in Table 2. h) Bp 64—65 °C/3 mmHg (lit,[17] 85—86 °C/3.5 mmHg). *Anal.* Found: C, 56.25; H, 4.20%. Calcd for C_8H_7SCl: C, 56.31; H, 4.31%. i) See e) in Table 2. j) See f) in Table 2.

depending on the kinds of reactants and their molar ratios. These products are formed by the initial dehydrochlorination, followed by the vinylic substitution(s) of the resulting chloroethylenes once or several times successively. Indeed, a considerable similarity between some data in these tables and those in Table 3 was noted (compare the product for each pair: Runs 2 and 3, 4, and 6 in Table 1 *vs.* Runs 2, 5, and 6 in Table 3 respectively, and also Runs 2 and 3, 5, and 6 in Table 2 *vs.* Runs 7 and 8, 11, and 12 in Table 3 respectively). In only one case, where 1,1,2-trichloroethane (I) was treated with equimolar PhS^-, was the direct substitution product isolated as the main product (Run 1 in Table 2). On the contrary, the reaction with equimolar *n*-BuS^-, which is similarly nucleophilic but more basic than PhS^-,[18] mainly afforded the product with elimination, *i.e.*, *trans*-1-butylthio-2-chloroethylene (Run 7 in Table 2).

In connection with this, the following observation is also of interest. The reaction of 1,2,3-trichloropropane with equimolar PhS^- gave only the substitution product, 2,3-dichloropropyl phenyl sulfide, while the reaction with equimolar PhO^- (more basic than PhS^-[18]) yielded the elimination products, 2-chloroallyl chloride and 2-chloroallyl phenyl ether (Run 9 in Table 2 *vs.* Run 7 in Table 1).

The advantages of the method are the mild reaction conditions and the one-step synthesis of certain substituted (chloro)ethylenes from polychloroethanes. Representative is the synthesis of tetrakis(phenylthio)-ethylene from pentachloroethane (IV) or tetrachloroethylene (VIII). In contrast to our method, the reported one for the preparation of tetrakis(alkyl- or arylthio)ethylenes from VIII was carried out under

quite drastic conditions, even by means of a two-step synthesis.[19] Further, the formation of 1,1-dichloro-2,2-diphenoxyethylene from IV or VIII in DMSO is noteworthy, because the only reported product from VIII and PhO^- in a sealed tube is the monosubstituted chloroethylene.[20] Cope has reported that, when 1,1,1-trichloroethane (II) was treated with two moles of PhONa in water, a mixture of *o*- and *p*-hydroxyacetophenones was formed in a slight yield (by the Reimer-Tiemann reaction).[21] The reaction in DMSO, however, afforded 1-chloro-2-phenoxyethylene and 1,1-diphenoxyethylene as the main products.

Next, we will briefly consider a possible reaction path for each case. The reactions of both I and 1,1-dichloroethylene (V) with PhO^- yielded *cis*-1-chloro-2-phenoxyethylene and 1,1-diphenoxyethylene (Runs 1 and 2 in both Tables 1 and 3), while those with PhS^- (except for the case of Run 1 in Table 2) afforded *trans*-1-chloro-2-phenylthioethylene and *cis*-1,2-bis(phenylthio)ethylene (Runs 2 and 3 in Table 2 and Runs 7 and 8 in Table 3). Truce *et al.*[22] reported the formation of a similar monosubstituted *trans*-olefin and disubstituted *cis*-olefin from V and $p\text{-}CH_3C_6H_4S^-$, and proposed a sequence involving an addition-elimination mechanism and an elimination-addition mechanism for two successive substitutions. When I is used as the starting substrate, however, the first intermediate in this sequence, 1,1-dichloro-2-arylthioethane, is not necessarily formed *via* V, since we have observed the formation of this compound from I, without any accompanying elimination product, as has been described above. On the other hand, in the case of the more basic PhO^-, the formation of the monosubstituted *cis*-olefin from V can be explained by assuming an elimination-addition mechanism. The subsequent vinyl substitution leading to the disubstituted olefin may involve an elimination-addition mechanism, as in the case of PhS^-.

There is an additional remark to make on the dehydrochlorination of I with PhO^-. The generation of V rather than *trans*-1,2-dichloroethylene(VI_t) may be anticipated from electronic considerations; *i.e.*, the α-H of I is more acidic than the β-H because of the effect of the two electron-withdrawing Cl atoms. The reaction products from I were identical with those from II, supporting this expectation (Runs 1, 2, and 3 in Table 1 and Run 2 in Table 3). Further, VI_t did not react with PhO^- to afford any product. Therefore, a route *via* VI_t is unlikely.

$$\text{I or II} \xrightarrow[-HCl]{} \text{V} \xrightarrow[-HCl]{} CH{\equiv}CCl \xrightarrow{PhO^-} \begin{matrix} H & & H \\ & C=C & \\ PhO & & Cl \end{matrix}$$

$$\xrightarrow[-HCl]{} PhOC{\equiv}CH \xrightarrow{PhO^-} (PhO)_2C{=}CH_2 \quad (1)$$

$$\text{I or V} \xrightarrow{PhS^-} PhSCH_2CHCl_2 \xrightarrow[-HCl]{} \begin{matrix} H & & Cl \\ & C=C & \\ PhS & & H \end{matrix}$$

$$\xrightarrow[-HCl]{} PhSC{\equiv}CH \xrightarrow{PhS^-} \begin{matrix} H & & H \\ & C=C & \\ PhS & & SPh \end{matrix} \quad (2)$$

Here, the attack of the second PhS^- occurred exclusively at an electronically unexpected position. Such an unusual orientation may be ascribed to the resonance stabilization of the resulting carbanion with a S atom at the α-position:[23]

$$PhS\text{–}\bar{C}{=}CH\text{–}SPh \longleftrightarrow PhS\bar{}{=}C{=}CH\text{–}SPh$$

cis-1,2-Dichloroethylene (VI_c) has a favorable geometry for *trans* elimination, as has V, and both olefins afforded the identical *cis*-olefin as the monosubstituted product upon treatment with PhO^-, suggesting the involvement of a common intermediate. The reaction of VI_c with PhS^- also afforded *cis*-1-chloro-2-phenylthioethylene, which was isomeric with the product from V. Such a difference may arise from an increased sensitivity toward PhS^- at the β-C of V. The formation of the *cis*-products from VI_c in both reactions may be explained by assuming an elimination-addition mechanism:[24]

$$VI_c \xrightarrow[-HCl]{} CH{\equiv}CCl \xrightarrow{PhX^-} \begin{matrix} H & & H \\ & C=C & \\ PhX & & Cl \end{matrix} \quad (X=O, S) \quad (3)$$

1,1,2,2-Tetrachloroethane (III) reacted with excess PhO^- or PhS^- to give the *trans*-isomer of 1-substituted 1,2-dichloroethylene as the monosubstituted product, implying that both reactions proceed by the same sequence. Trichloroethylene (VII) also afforded the same *trans*-olefin in the reaction with excess PhO^-, but when PhS^- was used as the nucleophile the main product was a disubstituted one. A reaction path involving an elimination-addition sequence is probable. The same mechanism has already been proposed by Truce *et al.* for the reaction of VII with $p\text{-}CH_3C_6H_4SNa$:[25]

$$\text{III} \xrightarrow[-HCl]{} \text{VII} \xrightarrow[-HCl]{} ClC{\equiv}CCl \xrightarrow{PhX^-} \begin{matrix} Cl & & H \\ & C=C & \\ PhX & & Cl \end{matrix} \quad (X=O, S) \quad (4)$$

when X=S

$$\begin{matrix} Cl & & H \\ & C=C & \\ PhS & & Cl \end{matrix} \xrightarrow{PhS^-} PhSCHClCHClSPh$$

$$\xrightarrow{-HCl} \begin{matrix} Cl & & SPh \\ & C=C & \\ PhS & & H \end{matrix} \quad (5)$$

During the experiments of the reactions of III and VII, we occasionally experienced small explosions. This may be an indication of the intermediate formation of dichloroacetylene, since its exploding property has already been reported.[26]

In the reaction of excess PhO^- with IV as well as with VIII, the products were 1,1,2-trichloro-2-phenoxyethylene and 1,1-dichloro-2,2-diphenoxyethylene. Since VIII is incapable of dehydrochlorination, consecutive addition-elimination must take place for the formation of polysubstituted (chloro)ethylenes. Truce *et al.* previously proposed the same sequence for the reaction of VII with $p\text{-}CH_3C_6H_4S^-$:[27]

$$\text{IV} \xrightarrow[-HCl]{} \text{VIII} \xrightarrow{PhX^-} PhXCCl_2CHCl_2$$

$$\xrightarrow[-HCl]{} PhXCCl{=}CCl_2 \quad (X=O, S)$$

tion with CH_3ONa (in CH_3OH, at 50 °C), CH_3X: CH_2X_2= 1.0: *ca.* 10^{-3} and CH_2X_2: CH_2Cl_2=1.0: *ca.* 10^{-1}, where X=I or Br.

3) L. H. Backeland and H. L. Bender, *Ind. Eng. Chem.*, **17**, 236 (1925).

4) S. Tanimoto, R. Taniyasu, and M. Okano, *Yuki Gosei Kagaku Kyokai-shi*, **29**, 166 (1971).

5) J. R. Jones, *Chem. Brit.*, **7**, 336 (1971).

6) See J. Hine and P. B. Langford, *J. Am. Chem. Soc.*, **78**, 5002 (1956).

7) a) W. C. Kuryla and D. G. Leis, *J. Org. Chem.*, **29**, 2773 (1964); W. C. Kuryla, *ibid.*, **30**, 3926 (1965). b) E. Ziegler and W. Klementschitz, *Monatsh. Chem.*, **87**, 319 (1956).

8) a) Dow, U. S. P., 2135123 [*Chem. Abstr.*, **33**, 1412 (1939)]. For the structure of the product, see A. V. Kalavina *et al.*, *ibid.*, **62**, 6418 (1965). b) Ciba, Brit, P., 617820 [*Chem. Abstr.*, **43**, 7045 (1949)], E. Ziegler and W. Klementschitz, *Monatsh. Chem.*, **81**, 1113 (1950). For the structure of the product, see E. Ziegler and W. Klementschitz, *ibid.*, **83**, 1 (1952).

9) J. Normant, *Bull. Soc. Chim. Fr.*, **1963**, 1876.

10) S. M. McElvain and B. F. Pinzon, *J. Am. Chem. Soc.*, **67**, 650 (1945).

11) A. L. Henne and F. W. Haeckel, *J. Am. Chem. Soc.*, **63**, 2692 (1941).

12) L. M. Kataeva and T. G. Mannafov, *Zh. Strukt. Khim.*, **1969**, 830.

13) W. E. Truce and R. J. Mcmanimie, *J. Am. Chem. Soc.*, **76**, 5745 (1954).

14) F. Montanari and A. Negrini, *Boll. Sci. Fac. Chim. Ind. Bologna*, **15**, 27 (1957).

15) D. Seebach, *Angew. Chem. Int. Ed. Engl.*, **6**, 442 (1967).

16) H. J. Boonstra and J. F. Arens, *Rec. Trav. Chim. Pays Bas*, **79**, 866 (1960).

17) F. Montanari, *Gazz. Chim. Ital.*, **86**, 735 (1956).

18) pK_a at 25 °C in 23% aq. *t*-BuOH: *n*-BuSH 11.51, PhSH 7.47, PhOH 10.79 [W. H. Fletcher, *J. Am. Chem. Soc.*, **68**, 2726 (1946)].

19) a) H. Baganz and K. -E. Kräger, *Chem. Ber.*, **91**, 809 (1958). b) W. E. Truce and R. Kassinger, *J. Am. Chem. Soc.*, **80**, 6450 (1958); W. E. Truce, *et al.*, *Tetrahedron*, **21**, 2899 (1965).

20) A. Michael, *Ber.*, **19**, 846 (1886).

21) A. C. Cope, *J. Am. Chem. Soc.*, **57**, 572 (1935).

22) W. E. Truce and M. M. Boudakian, *J. Am. Chem. Soc.*, **78**, 2748 (1956).

23) S. Oae, "The Chemistry of Organic Sulfur Compounds," Part 1, Kagaku-Dojin, Kyoto (1968), p. 104.

24) W. E. Truce, M. M. Boudakian, R. F. Heine, and R. J. McManimie, *J. Am. Chem. Soc.*, **78**, 2743 (1956).

25) W. E. Truce and R. Kassinger, *J. Am. Chem. Soc.*, **80**, 1916 (1958).

26) See R. Riemschneider and K. Brendel, *Justus Liebigs Ann. Chem.*, **640**, 5 (1961); J. Siegel, R. A. Jones, and L. Kurlansik, *J. Org. Chem.*, **35**, 3199 (1970).

27) W. E. Truce and R. Kassinger, *J. Am. Chem. Soc.*, **80**, 6450 (1958).

Acid-catalyzed Rearrangements of Tetrahydroasatone and Tetrahydroisoasatone

Shosuke YAMAMURA and Yukimasa TERADA
Faculty of Pharmacy, Meijo University, Showa-ku, Nagoya 468
(Received March 2, 1976)

Tetrahydroasatone (**3**) and tetrahydroisoasatone (**4**) both are pretty unstable to various kinds of acid. Action of 6M·HCl–AcOH on the former converted it to the naphthalene-type compound (**5**) in high yield, whose structure was determined on the basis of its spectral data. In the case of tetrahydroisoasatone, twofold Wagner-Meerwein rearrangements take place, leading to the formation of the isomer-A (**9**), further rearrangements of which give rise to the bisnordiadamantane-type isomer-B (**10a**).

In the previous paper.[1] We reported the isolation and structures of two novel neolignans, asatone (**1**) and isoasatone (**2**). From a structural point of view, the former has a bicyclo[2.2.2]oct-5-en-2-one system as a part of the structure (**1**). In the case of isoasatone (**2**), it has a highly strained bicyclo[2.2.0]hexane system. Both of them are pretty unstable to various kinds of acid. In this paper, we wish to describe some interesting acid-catalyzed rearrangements of tetrahydroasatone (**3**) and tetrahydroisoasatone (**4**), both of which have been already produced on catalytic hydrogenation from **1** and **2**, respectively. Particularly, the structures of the reaction products are discussed in detail.

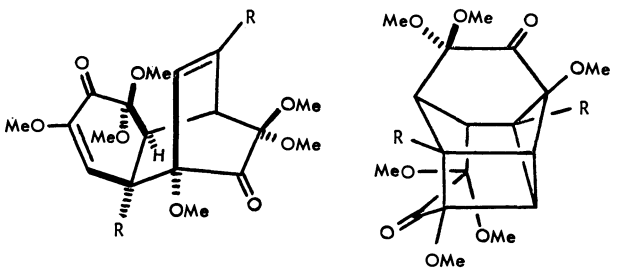

1 R=$CH_2CH=CH_2$ **2** R=$CH_2CH=CH_2$
3 R=*n*-Pr **4** R=*n*-Pr

Fig. 1.

As described above, asatone (**1**) and tetrahydroasatone (**3**) both are unstable in acidic solution, and many spots are found on an analytical TLC plate. However, when treated with 6 M·HCl-AcOH under vigorous conditions (100 °C, 1.5 h), tetrahydroasatone was converted in high yield (*ca.* 85%) into the yellow substance with a molecular formula (mp 181—182 °C; $C_{20}H_{22}O_5$), the structure (**5**) of which was elucidated on the basis of its spectral data (see Table 1), as follows.

The IR and UV spectra of this compound (**5**) suggest that it has a highly substituted naphthalene chromophore [ν_{max} 1605, 1570, and 1525 cm^{-1}: λ_{max} 415, 329, 289, and 226 nm]. This is also confirmed by the ^{13}C NMR spectral data of **5** [δ 99.42 (d) and 113.70 (s)—150.71 (s) ppm].[2]

This yellow substance (**5**) has two MeO groups (δ 3.60 and 4.00 ppm) in addition to two OH groups [ν_{max} 3400 br.cm^{-1}: δ 5.93 and 9.53 ppm], one of which has been readily converted into a MeO group on treatment of **5** with diazomethane in ether leading to the formation of the corresponding monomethyl ether (**6**), mp 138—139 °C; $C_{21}H_{24}O_5$; ν_{max} 3200 cm^{-1}; δ 3.72 (3H, s), 4.02 (3H, s) and 4.03 (3H, s) ppm. Of five oxygen atoms in **5**, the remaining one should be included in the CO group [ν_{max} 1640 (s)cm^{-1}; δ 206.55 ppm], the IR absorption band of which is shifted to 1665 cm^{-1} in the case of **6**. Furthermore, it is noted that **5** is proved to have two partial structures [A and B] on the basis of its ^1H and ^{13}C NMR spectral data [A: δ 1.20, 2.96, 13.87, and 24.51 ppm; B: δ 1.09, 2.24, 3.30, 6.76, 13.55, 17.85, 40.17, 134.68, and 113.70—150.71 ppm[2]].

$CH_3CH_2-\dot{C}=$ $CH_3CH_2CH=\dot{C}-CH_2-\dot{C}-$
[A] [B]

Table 1. The spectral data of the yellow substance

ν_{max}(Nujol)	3400br., 1640, 1605, 1570, and 1525 cm^{-1}
λ_{max}(MeOH)	415, 329, 289, and 226 nm (ε 5000, 11000, 28000, and 20000, respectively)
^{13}C NMR ($CDCl_3$)	13.55(q), 13.87(q), 17.85(t), 24.51(t), 40.17(t), 55.91(q), 61.11(q), 99.42(d), 113.70(s), 122.63(s), 122.88(s), 129.93 (s), 134.16(s), 134.68(d), 137.16(s), 142.19(s), 146.17(s), 148.85(s), 150.71 (s) and 206.55(s) ppm
^1H NMR ($CDCl_3$)	1.09(3H, t, J=7.0 Hz), 1.20(3H, t, J=7.8 Hz), 2.24(2H, quintet, J=7.0 Hz), 2.96 (2H, q, J=7.8 Hz), 3.30 (2H, d, J=1.7 Hz), 3.60(3H, s), 4.00(3H, s), 5.93(1H, s, OH), 6.76(1H, br.t, J=7.0 Hz), 6.95(1H, s) and 9.53(1H, s, OH) ppm

Finally, in the light of the structure of **3** consisting of two C_6-C_3 units, the structure of the yellow substance

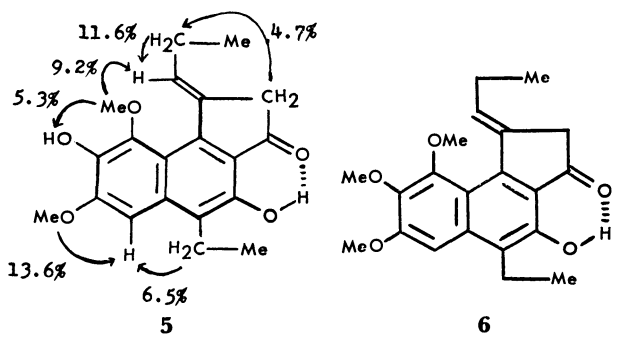

5 **6**

Fig. 2.

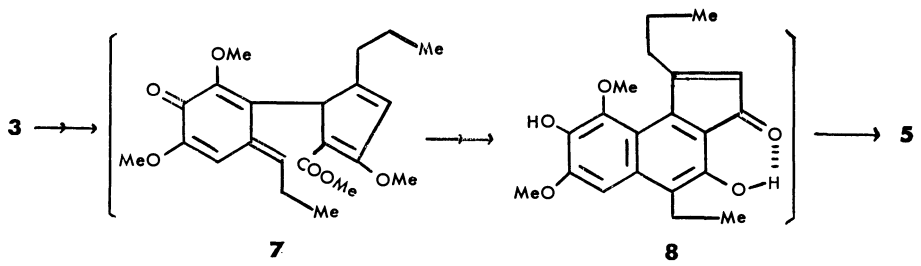

Scheme 1. A plausible reaction path-way from **3** to **5**.

(**5**) was determined by measurements of intramolecular nuclear Overhauser effects, and the final result was shown in Fig. 2.

Probably, the yellow substance (**5**) is produced from a plausible intermediate (**7**) *via* an α,β-unsaturated ketone (**8**) (see Scheme 1), although the formation process of **5** is not clear. In Scheme 1, it is quite reasonable that the conjugated ketone (**8**) is readily converted into the more stable ketone (**5**), for the former has an unstable cyclopentadienone system.

Isoasatone (**2**) and tetrahydroisoasatone (**4**) both are also unstable in acidic solution, and many spots are detected on an analytical TLC plate. However, when treated with dry ether saturated with HCl gas (room temp., 8 h),[3] tetrahydroisoasatone (**4**) with a symmetric structure was readily converted into an isomer-A (**9**) in 87.5% yield (mp 135.5—136.5 °C; $C_{24}H_{36}O_8$; ν_{max} 1755 and 1738 cm^{-1}). The NMR spectrum of **9** indicates that six MeO groups and four methine protons are all in different environment to one another. The IR absorption band at 1755 cm^{-1} indicates the presence of a five-membered ring CO group, which has been newly formed from one of the two six-membered ring CO groups (ν_{max} 1735 cm^{-1}) in **4**. On further treatment with zinc powder in MeOH containing one drop of concd HCl (room temp., 8 h), the isomer-A (**9**) afforded a mixture containing several compounds, from which another symmetrical isomer-B (**10a**) was obtained in *ca.* 10% yield (mp 152—153 °C; $C_{24}H_{36}O_8$; ν_{max} 1760 cm^{-1}). In the NMR spectrum of the isomer-B, only half of the total protons are observed as follows: δ 0.98 (6H, t, J=7.0 Hz), 1.2—2.3 (8H, complex), 2.52 (2H, dd, J=2.1 and 1.4 Hz), 2.89 (2H, dd, J=2.1 and 1.4 Hz), 3.23 (6H, s), 3.38 (6H, s) and 3.46 (6H, s) ppm. From the IR and NMR spectra of the isomer-B, two possible structures (**10a** and **10b**) are considered (see Scheme 2). As suggested by Yonemitsu and Witkop,[4] however, the cationic intermediate [C] at the initial step is unambiguously more favorable than another intermediate [D]. Therefore, the structures of two isomers A and B should be represented by **9** and **10a**, respectively.

In the course of the reaction (**4**—**10a**), twofold Wagner-Meerwein rearrangements take place after protonation of one of the two CO groups in **4**, leading to the formation of the isomer-A (**9**) which is a less strained cage-compound as compared with **4**. Further Wagner-Meerwein rearrangements released the strain energy due to the remaining cyclobutane ring in **9** to give the bisnordiadamantane-type isomer-B (**10a**). In the present study, the cage-compound (**9**) was first isolated as an intermediate between **4** and **10a**.

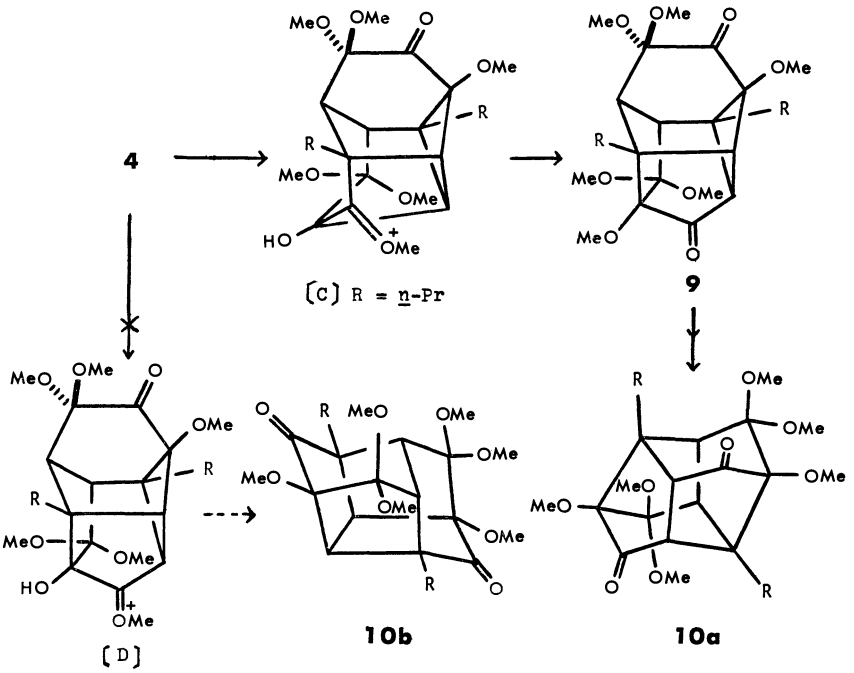

Scheme 2. Twofold Wagner-Meerwein rearrangements of **4**.

Experimental

All mps were uncorrected. The IR and UV spectra were obtained on a JASCO Model IR-S and on a Perkin-Elmer 202 spectrophotometer, respectively. The NMR spectra were taken on a JEOL JNM-PS 100 (100 MHz) using $CDCl_3$ as solvent. Chemical shifts are given in ppm from TMS as an internal standard. Coupling constants are given in Hz (s, singlet; d, doublet; t, triplet; q, quartet; m, multiplet). The mass spectra were obtained on a Hitachi RMU-6D mass spectrometer operating with an ionization energy (70 eV).

*Formation of the Yellow Substance (**5**).* A solution of tetrahydroasatone (200 mg) in 6 M·HCl (8 ml) and AcOH (1.5 ml) was heated at 100 °C for 1.5 h, and then poured into large amounts of water to give yellow crystals which were collected by filtration. Recrystallization from acetone–hexane afforded yellow plates of **5** (128 mg), mp 181—182 °C; *m/e* 342 (M^+) and 327 (Found: C, 70.23; H, 6.51%. Calcd for $C_{20}H_{22}O_5$: C, 70.16; H, 6.48%).

*Formation of the Methyl Ether (**6**).* To a solution of excess diazomethane in ether (50 ml) was added the compound (**5**) (15 mg) with stirring. The resulting solution was stirred at room temp. overnight, and then concentrated under reduced press. to give a crystalline solid (15 mg). Recrystallization from acetone–hexane afforded pale yellow crystals of **6**, mp 138—139 °C; ν_{max} (Nujol) 3200, 1665, 1605, 1565, and 1510 cm^{-1}; λ_{max} (MeOH) 416, 331, 291, and 225 nm (ε, 4600, 9000, 30000, and 19700, respectively); δ 1.15 (3H, t, J=7.5 Hz), 1.26 (3H, t, J=7.5 Hz), 2.31 (2H, quintet, J=7.5 Hz), 3.20 (2H, q, J=7.5 Hz), 3.39 (2H, d, J=2 Hz), 3.72 (3H, s), 4.02 (3H, s), 4.03 (3H, s), 6.92 (1H, br.t, J=7.5 Hz), 7.10 (1H, s), and 9.82 (1H, s, OH) ppm: *m/e* 356 (M^+) and 341 (Found: *m/e* 356.16336. Calcd for $C_{21}H_{24}O_5$: *m/e* 356.16236).

*Conversion of Tetrahydroisoasatone (**4**) to the Isomer-A (**9**).* A solution of **4** (20 mg) in anhydrous ether (5 ml) saturated with HCl gas was allowed to stand at room temp. for 8 h, and then carefully concentrated under reduced press. to give a colorless viscous liquid which was subjected to preparative TLC [Kieselgel PF_{254}; hexane–EtOAc (3: 1)]. From the most nonpolar fraction, a colorless viscous liquid was obtained and dissolved in small amounts of hexane to give white crystals of **9** (17.5 mg), mp 135.5—136.5 °C (from hexane); ν_{max} (Nujol) 1755 and 1738 cm^{-1} (no OH band); δ 0.90 (6H, t, J=6.5 Hz), 1.1—2.0 (8H, complex), 2.56 (1H, dd, J=2.2, and 1.6 Hz), 2.73 (1H, dd, J=6.8, and 1.6 Hz), 2.99 (1H, t, J=2.2 Hz), 3.13 (1H, dd, J=6.8, and 2.2 Hz), 3.24 (3H, s), 3.25 (3H, s), 3.32 (3H, s), 3.33 (3H, s), 3.34 (3H, s), and 3.48 (3H, s) ppm; *m/e* 452 (M^+), 437, 424, 420, 409, 405, and 392 (Found: *m/e* 452.24543. Calcd for $C_{24}H_{36}O_8$: *m/e* 452.24100).

*Further Rearrangement of **9** to the Isomer-B (**10a**).* The isomer-A (50 mg) was dissolved, with stirring, in a solution of MeOH (3 ml) containing one drop of concd HCl at −5 °C. To this solution was added activated zinc powder (500 mg) with vigorous stirring. The reaction mixture was allowed to stand at room temp. for 8 h with continuous stirring, and then poured into large amounts of water and extracted with ether. The ethereal extracts were washed with sat. NaCl aq. solution, and then dried over Na_2SO_4. Removal of the solvent afforded a pale brown oil, which was subjected to preparative TLC [Kieselgel PF_{254}; hexane–EtOAc (5: 1)]. From the most nonpolar fraction, a crystalline solid was obtained by elution with ether. Recrystallization from hexane afforded white crystals of the isomer-B (6 mg), mp 152—153 °C; ν_{max} (Nujol) 1760 cm^{-1} (no OH band); *m/e* 452 (M^+), 421, 406, and 390 (Found: *m/e* 452.24479. Calcd for $C_{24}H_{36}O_8$: *m/e* 452.24100).

The authors wish to thank Drs. M. Kurono and M. Toda (Ono Pharmaceutical Co., Ltd.) for measurements of high resolution mass spectra. They are also indebted to Prof. Y. Okumura and Dr. H. Irikawa (Shizuoka University) for measurements of ^{13}C NMR spectra.

References

1) K. Sasaki, Y. Hirata, S. Yamamura, Y. Chen, M. Hong, and H. Hsu, *Tetrahedron Lett.*, **1973**, 4881; S. Yamamura, Y. Terada, Y. Chen, H. Hsu, and Y. Hirata, *ibid.*, **1975**, 1903.

2) One of ten singlets (δ 113.70—150.71 ppm) is due to the quanternary carbon atom of a tri-substituted double bond in the partial structure [B].

3) This reaction should be carried out under completely anhydrous condition.

4) K. Hirao, M. Taniguchi, T. Iwakuma, O. Yonemitsu, J. L. Flippen, I. Karle, and B. Witokop, *J. Am. Chem. Soc.*, **97**, 3249 (1975), and references cited therein.

The Structures of Two Novel Neolignans, Asatone and Isoasatone

Shosuke YAMAMURA,† Yukimasa TERADA, Yuh-Pan CHEN,* Mina HONG,* Hong-Yen HSU,* Kyoyu SASAKI,** and Yoshimasa HIRATA**

Faculty of Pharmacy, Meijo University, Showa-ku, Nagoya 468

**Brion Research Institute of Taiwan, 116 Chung-Ching S. Rd., Sec. 3, Taipei, Taiwan*

***Chemical Institute, Nagoya University, Chikusa-ku, Nagoya 464*

(Received March 2, 1976)

Isolation and structures of two novel neolignans, asatone (**1**) and isoasatone (**2**), are described. The structure of the latter, established by means of an X-ray crystallographic analysis of its dihydroxy derivative, is in full agreement with its chemical and spectral data. From a biogenetic point of view, furthermore, thermal and photochemical reactions of these neolignans and their derivatives were carried out. In particular, asatone was photochemically converted into isoasatone.

The chemical constituents of many species of *Asarum* genus, *Aristolochiaceae*, have been investigated by many authors.[1] Particularly, chemotaxonomic studies on species of *Asarum*, *Asiasarum* and *Heterotropa* have been extensively carried out by Saiki and his co-workers.[2] In most cases, however, chemical constituents have been examined in steam-distillates of the fresh or air-dried whole herb of the plant.

The decoction of the stems and rhizomes of *Asarum taitonense* Hayata (Taiton Kanaoi in Japanese)[3] is used in Taiwan as a remedy for neuralgia by the local people.[4] In the course of our searching for physiologically active substances of this plant, we isolated two neoligans, named "asatone" and "isoasatone". In this paper, we wish to describe the isolation and structures of these neolignans. From a biogenetic point of view, thermal and photochemical reactions of these neolignans are also presented.

Isolation of Asatone (1) and Isoasatone (2). A sample of the dried and pulverized material of the whole herb of *Asarum taitonense* Hayata was directly refluxed with large amounts of hexane for 3 h, and then filtered. The filtrates were concentrated under reduced pressure to give a greenish yellow solid, which was chromatographed on silica gel and eluted with hexane–EtOAc (8: 1) to afford asatone (**1**), mp 101—102 °C, in *ca.* 0.2% yield. On the other hand, the residue was further extracted with $CHCl_3$ (under reflux, 3 h). The extracts were also chromatographed on silica gel, and eluted with hexane–EtOAc (8: 1) to give rise to white crystals of isoasatone (**2**), mp 156.5—158 °C, in *ca.* 0.001% yield. Asatone and isoasatone both have the same molecular formula ($C_{24}H_{32}O_8$). Furthermore, it should be noted that the mass spectra of these two neolignans are quite similar to each other [*m/e* 448 (M^+), 416, 384, 348, and 224]. However, the other spectral data are pretty different, as shown in Table 1.

The Structure of Asatone. As described above, asatone (**1**), a major component of *Asarum taitonense* Hayata, has a molecular formula [$C_{24}H_{32}O_8$ (*m/e* 448 (M^+))]. As cited in Table 1, the NMR methyl singlets at δ 3.0—3.6 ppm and IR absorption bands at 1740 and 1720 cm^{-1} indicate that asatone has six MeO and two CO groups, all of which are in different environment to one another. The presence of two allyl groups in **1** is based on its NMR spectrum [δ4.90—5.28, 5.50—6.20, 2.60—2.95, and 2.15 ppm] coupled with catalytic hydrogenation of **1**, which has been carried out over 10% Pd–C in EtOAc to afford tetrahydroasatone (**3**), mp 128—129 °C: $C_{24}H_{36}O_8$ [*m/e* 452 (M^+)]. The NMR spectrum of **3** has methyl triplet at δ 0.87 (6H, J=6.5 Hz) ppm and multiplets at δ 1.10—1.80 and 1.85—2.15 ppm corresponding to four methylene groups instead of multiplets at δ 4.90—5.28 and 5.50—6.20 ppm in **1**. Furthermore, it should be noted that at least one of the two allyl groups in **1** must be attached to an asymmetric quaternary carbon atom: irradiation at δ 5.85 ppm in **1** caused the quartet at δ 2.15 ppm to collapse to doublet, the large coupling constant (J=14.5 Hz) of which should be regarded as a J-value between geminal protons.

Asatone (**1**) has two CO groups, whose properties can be elucidated by $NaBH_4$ reduction, as follows. When treated with $NaBH_4$ in EtOH (room temp., 1.5 h), **1** afforded a mixture of three reduction products [hydroxyasatone-A (**4**): mp 127—128 °C, $C_{24}H_{34}O_8$,

Table 1. Spectral data of asatone (**1**) and isoasatone (**2**)

	Asatone (**1**)	Isoasatone (**2**)
ν_{max}(KBr)	1740, 1720, and 1635 cm^{-1}	1735 and 1640 cm^{-1}
λ_{max}(MeOH)	278 and 229 nm (ε 5660) and 5100, respectively)	221 nm (ε 2010)
δ($CDCl_3$)	2.15(1H, dd, J=7.5 and 14.5 Hz), 2.60—2.95(3H, m), 2.88(2H, br.s), 3.05(3H, s), 3.31 (3H, s) 3.38(3H, s), 3.42(3H, s), 3.47(3H, s), 3.60(3H, s), 4.90—5.28(4H, m), 5.39(1H, s), 5.55(1H, q, J=1.9 Hz) and 5.50—6.20(2H, m) ppm	2.56(2H, dd, J=8.6 and 14.3 Hz), 2.80(2H, s), 2.85(2H, dd, J=7.5 and 14.3 Hz), 3.00 (2H, s), 3.25(6H, s), 3.27(6H, s), 3.38(6H, s), 5.00(2H, br.d, J=15 Hz), 5.03(2H, br.d, J=11.5 Hz) and 5.35—5.80(2H, m) ppm

† To whom inquires should be addressed.

λ_{max} 218 nm (ε, 4500), ν_{max} 3500 cm^{-1} and δ 3.93 (1H, s) ppm; hydroxyasatone-B (**5**): mp 108—109 °C, $C_{24}H_{34}O_8$, λ_{max} 277 nm (ε, 4400), ν_{max} 3510 cm^{-1} and δ 3.92 (1H, s) ppm; dihydroxyasatone (**6**): mp 156—158 °C, $C_{24}H_{36}O_8$, ν_{max} 3550 and 3425 cm^{-1} (no CO band) and δ 3.80 (2H, br. s)]. In particular, each NMR spectrum of **4** and **5** has the sharp singlet corresponding to one proton attached to the carbon atom bearing the resulting OH group, indicating that the α- and α'-positions of each CO group in **1** must be fully substituted. Furthermore, the comparison of the spectral data between **1** and **4** indicates that asatone (**1**) has an α,β-unsaturated carbonyl system [A] in which only one olefinic proton is located at the β-position, since the NMR singlet at δ 5.39 (1H, s) ppm in **1** is shifted to δ 4.60 ppm in **4**. On the other hand, the α,β-unsaturated carbonyl system [A] is present in the isomer (**5**) and the resulting OH group must be derived from the isolated CO group in **1**. In the case of the third compound (**6**), which is further hydrogenated on 10% Pd–C to the corresponding tetrahydro-compound (**7**) (mp 151—152 °C, $C_{24}H_{40}O_8$), two CO groups are completely reduced to OH groups.

The partial structure [A] is further extended to [B], as follows. Catalytic hydrogenation of **1** in MeOH was carried out over 10% Pd–C (room temp., overnight) to afforded a mixture of **3** and hexahydroasatone (**8**) in *ca.* 70 and 10% yields, respectively. The UV and IR spectra of **8** [mp 133—134 °C; $C_{24}H_{38}O_8$: ν_{max} 1750 and 1745 cm^{-1}] indicate that conjugate double bond in [A] has been hydrogenated. Furthermore, the NMR spectrum of **8** has two new signals at δ 2.31 (2H, d, J= 5.5 Hz) and 3.63 (1H, t, J=5.5 Hz) ppm. Irradiation at δ 2.31 ppm caused the triplet at δ 3.63 ppm to collapse to singlet. This finding strongly supports the presence of the partial structure [B] in **1**.

Further information on the structure of asatone (**1**) was obtained by zinc reduction of **1** as well as of **3**.

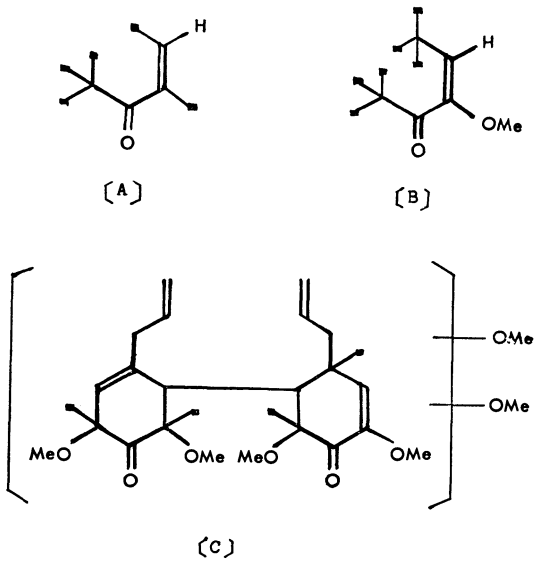

Fig. 1.

When treated with activated zinc powder in AcOH (under reflux, 6 h), tetrahydroasatone (**3**) was readily converted into 2,6-dimethoxy-4-propylphenol (**9**) and a biphenyl-type compound (**10**) in 57 (as 2eq.) and 23% yields, respectively. Further treatment of **9** with Ac_2O–pyridine gave the corresponding acetate (**11**), mp 88—88.5 °C (lit, 87 °C)[5]; $C_{13}H_{18}O_4$ [*m/e* 238 (M^+)]; ν_{max} 1765 cm^{-1}: λ_{max} 275 and 227 nm (ε, 790 and 6140, respectively). In connection with the formation of 9, the symmetric structure (**10**) of the biphenyl-type compound can be deduced on the basis of its spectral and chemical properties: $C_{22}H_{30}O_6$ [*m/e* 390 (M^+)]; ν_{max} 3460, 1610, 1585, and 1495 cm^{-1}; δ 0.81 (6H, t, J=7.0 Hz), 1.15—1.80 (4H, m), 2.22 (4H, td, J=7.0 and 1.5 Hz), 3.60 (6H, s), 3.95 (6H, s) and 6.60 (2H, br. s) ppm. Acetylation of **10** afforded in quantitative yield the corresponding diacetate (**12**), mp 117—118 °C;

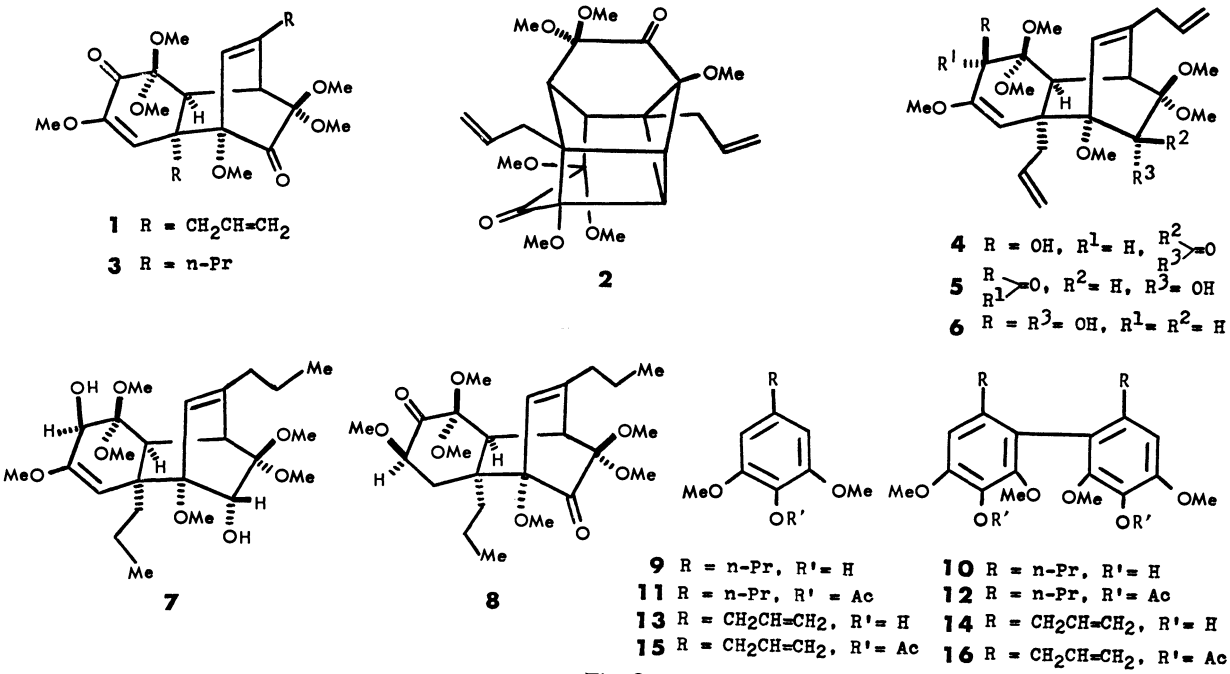

Fig. 2.

$C_{26}H_{34}O_8$: ν_{max} 1770 cm^{-1}; λ_{max} 279 and 232 nm (ε, 2470 and 13750, respectively). These two acetates (**11** and **12**) were also obtained directly from **3** in 51 (as 2 eq.) and 24% yields, respectively, on zinc reduction using Ac_2O (under reflux, 7 h) instead of AcOH. Under essentially the same condition, zinc reduction of asatone (**1**) in AcOH afforded a mixture of 2,6-dimethoxy-4-allylphenol (**13**) and a biphenyl-type compound (**14**) in 37 (as 2 eq.) and 19% yields, respectively. Acetylation of the former followed by catalytic hydrogenation (10% Pd–C in EtOAc) gave rise to **11** *via* 2,6-dimethoxy-4-allylphenyl acetate (**15**). Acetylation of **14** also afforded the corresponding diacetate (**16**), mp 125—125.5 °C; $C_{26}H_{30}O_8$ [*m/e* 470 (M^+)]; ν_{max} 1775 cm^{-1}. Clearly, two allyl groups are present in **16** [δ 3.10 (4H, d, J=6.7 Hz), 4.75—5.10 (4H, m) and 5.45—6.10 (2H, m) ppm]. The formation of these aromatic compounds in high yields strongly suggests that the carbon skeleton of asatone (**1**) consists of two C_6–C_3 units and **1** may have a partial structure [C]. Finally the structure of asatone (**1**) including its stereochemistry was elucidated on the basis of the photochemical reaction of asatone leading to the formation of isoasatone (**2**) in 64% yield,[6] whose structure had been unambiguously established by means of an X-ray crystallographic analysis of dihydroxyisoasatone (**17**),[7] as described later.

On the basis of the structure (**1**) thus obtained, the spectral data of asatone will be discussed below. As seen in Table 1, the UV absorption band [λ_{max} 278 nm (ε, 5100)] of **1** is observed at longer wavelength than calculated one. This is probably due to some effects of α',α'-dimethoxyl groups as well as of the isolated and tri-substituted double bond. Furthermore, the NMR broad singlet at δ 2.88 ppm in **1** (δ 2.84 ppm in **3**) is not due to one methylene group[8], but assignable to two methine protons which have the same chemical shift although these two protons are in different environment to each other. In fact, the ^{13}C NMR spectrum of asatone is in good agreement with the structure (**1**), and a tentative assignment of each signal is as follows: δ ($CDCl_3$) 39.0 (t), 41.3 (t), 116.9 (t), 118.2 (t), 133.4 (d), and 135.2 (d) [2×(CH_2=CH–CH_2)]; 43.9 (d) and 44.5 (d) [2×(>CH–)]; 49.8 (s) (>C<); 50.1—50.2[9], 54.8 (q) and 55.5 (q) (6×OMe); 92.1 (s) [>C(OMe)–]; 93.2 (s) and 98.7 (s) [2×(>C(OMe)$_2$)]; 116.6 (d) and 144.9 (s) (–HC=C<); 121.7 (d) 150.2 (s) and 188.7 (s) [(MeO)C=CH–C=O]; 201.4 (s) ppm (C=O).

The Structure of Isoasatone. Isoasatone (**2**) has been isolated, as a minor component, together with asatone (**1**) and has the same molecular formula ($C_{24}H_{32}O_8$) as that of the latter.

From a structural point of view, asatone and isoasatone both are quite similar to each other, as follows. They have two allyl and two CO groups in addition to six MeO groups. In fact, on catalytic hydrogenation with 10% Pd–C in EtOAc two allyl groups were reduced, giving the corresponding tetrahydro-compound (**18**), mp 161—162 °C; $C_{24}H_{36}O_8$; δ 0.90 (6H, t, J=5.5 Hz) and 1.70—2.30 (8H, complex) ppm. Furthermore, isoasatone was treated with $LiAlH_4$ in THF to give dihydroxyisoasatone (**17**), mp 153—154 °C; $C_{24}H_{36}O_8$; ν_{max} 3500 and 3430 cm^{-1} (no CO band); no UV absorption maximum; δ 3.71 (2H, s) ppm. Finally, this diol as colorless needles was subjected to an X-ray crystallographic analysis,[7] which proved it to have the complex structure (**17**), which is in good agreement with the physical data of dihydroxyisoasatone. Therefore, the

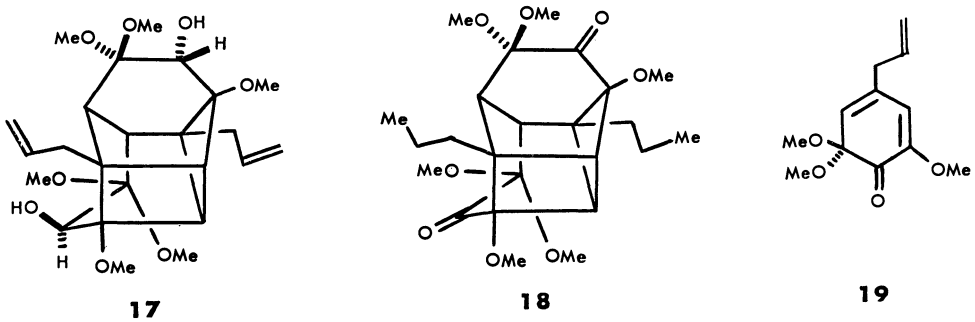

Fig. 3.

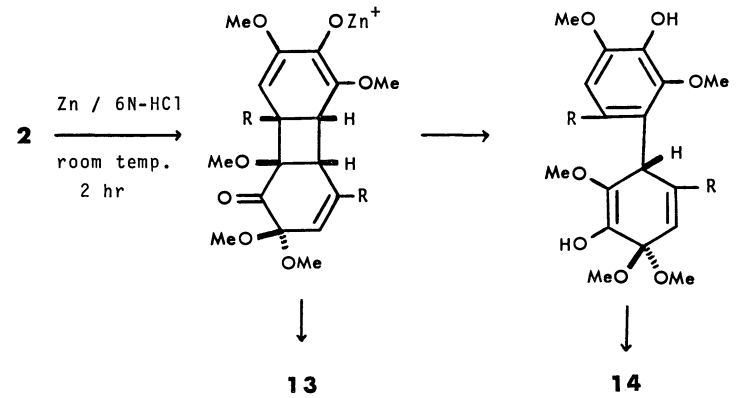

Scheme 1. Zinc reduction of isoasatone (**2**).

structure of isoasatone should be represented by **2**, in which the UV absorption maximum at 221 nm may be due to the conjugative overlap of the cyclobutane ring with the CO group, the α- and α′-positions of which are fully substituted with MeO groups.

As seen in the case of asatone (**1**), interestingly, zinc reduction of isoasatone (**2**) in 6 M·HCl–MeOH also gave a mixture of two phenolic compounds (**13** and **14**) in 46 (as 2 eq.) and 12% yields, respectively. On the basis of the structure (**2**), the formation process of these compounds is shown in Scheme **1**.

Biogenesis of Asatone and Isoasatone. Asatone (**1**) and isoasatone (**2**) both are optically inactive, and regarded as racemic compounds ($[\alpha]_D^{20}=\pm 0°$). From a biogenetic point of view, the carbon skeleton of these two neolignans consists of two C_6-C_3 units. Probably, 2,6-dimethoxy-4-allylphenol (**13**) is enzymatically oxidized to an optically inactive dienone (**19**), two molecules of which further react to each other to yield asatone (**1**). Further photochemical [π2+π2]cycloaddition of 1 may take place, leading to the formation of isoasatone (**2**) which has a bicyclo[2.2.0]hexane system.

Thermal and Photochemical Reactions of Asatone, Isoasatone and Related Compounds. In connection with the biogenesis of these two neolignans, thermal and photochemical reactions of these compounds were carried out, as follows.

The mass spectra of asatone (**1**) and its derivatives indicate that each base peak is observed at the position corresponding to half of the molecular weight [**1**, 224 ($C_{12}H_{16}O_4$); **3**, 226 ($C_{12}H_{18}O_4$); **4**, 226 ($C_{12}H_{18}O_4$); **5**, 226 ($C_{12}H_{18}O_4$); **6**, 226 ($C_{12}H_{18}O_4$); **7**, 228 ($C_{12}H_{20}O_4$)]. Clearly, the retro-Diels-Alder reaction in each compound must take place regardless of the presence of CO group, giving rise to the corresponding cyclohexadiene or dienone, to which the base peak is assignable. The mass spectra of isoasatone (**2**) and its derivatives are also found to be quite similar to that of asatone (**1**) [2, 224 ($C_{12}H_{16}O_4$); **17**, 226 ($C_{12}H_{18}O_4$); **18**, 226 ($C_{12}H_{18}O_4$)]. In the case of the isoasatone series, a highly strained bicyclo[2.2.0]hexane system of each compound is thermally decomposed in a stepwise manner and then further subjected to the retro-Diels-Alder reaction to give the corresponding cyclohexadiene or dienone, as shown in Scheme 2 (**18**→**20**). When heated in a sealed tube at 290—300 °C for 30 min, tetrahydroisoasatone (**18**) afforded 2,6-dimethoxy-4-propylphenol (**9**) in *ca.* 55% yield. As shown in Scheme 2, the thermal reaction of

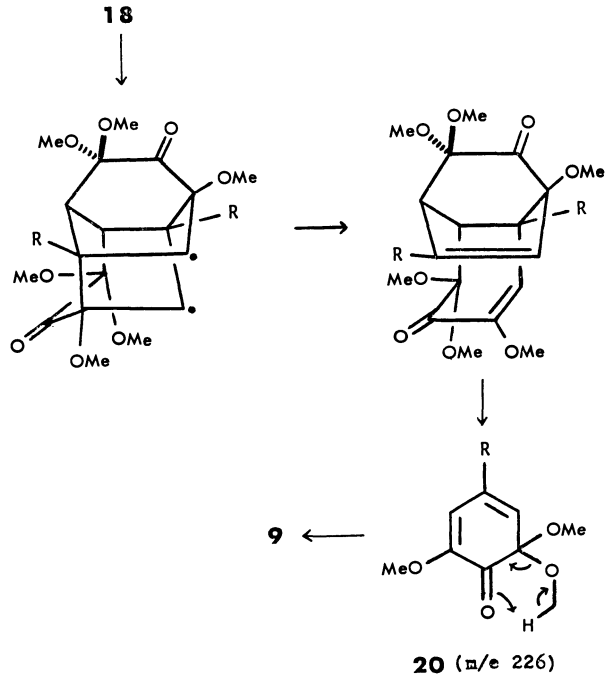

Scheme 2. Thermal reaction of tetrahydroisoasatone (**18**).

18 takes place in the same manner as that of the fragmentation reaction on electron impact, leading to the formation of the corresponding dienone (**20**), which must be further decomposed to **9**. In Scheme 2, it seems to be that the biradical formation process at the initial step requires more vigorous condition as compared with the others. In fact, tetrahydroisoasatone (**18**) is quite stable to acetic anhydride even under reflux conditions. On the other hand, when heated in acetic anhydride under reflux, tetrahydroasatone (**3**) afforded a mixture of 2,6-dimethoxy-4-propylphenyl acetate (**11**) and a diacetate (**21**), 14 and 49 (as 2 eq.) % yields, respectively. The structure of the latter was based on its spectral data: $C_{15}H_{20}O_6$ [m/e 296 (M^+)]; ν_{max} 1770 and 1740 cm^{-1}: λ_{max} 276 and 226 nm (ε, 970 and 9600, respectively); δ 0.90 (3H, t, J=7.5 Hz), 1.87 (2H, quintet, J=7.5 Hz), 2.08 (3H, s), 2.30 (3H, s), 3.78 (6H, s), 5.61 (1H, t, 7.5 Hz) and 6.58 (2H, s) ppm. In particular, the presence of a CH_3CH_2–CH(OAc)–grouping is confirmed by the NMR and IR spectra (δ 0.90, 1.87, 2.08 and 5.61 ppm; ν_{max} 1740 cm^{-1}). The formation process of these two acetates is shown in Scheme 3. It

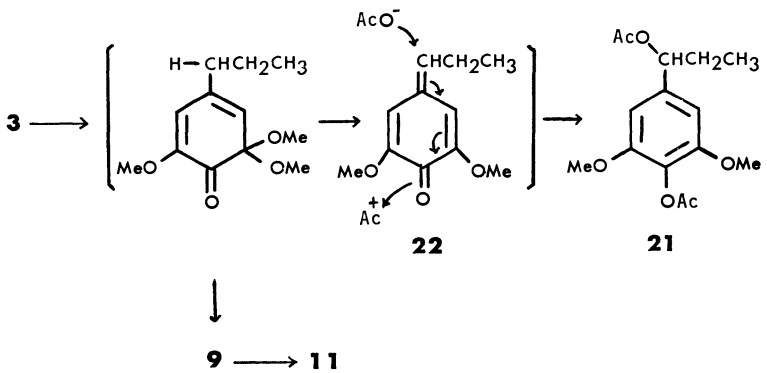

Scheme 3. The formation process of **11** and **21**.

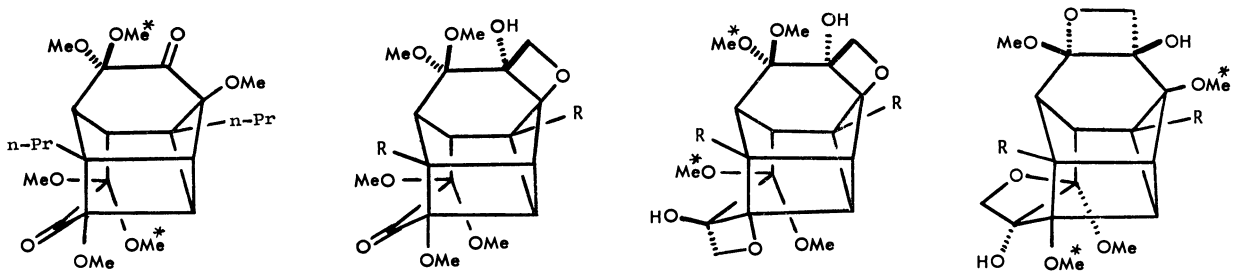

18a **23** **24a** **24b**

Fig. 4.

is noted that a methylene quinone (**22**) is regared as a plausible intermediate, from which the diacetate (**21**) can be produced.

From the above experiments, it is clear that the dienone (**19**) is the possible precursor for these neolignans.

Asatone (**1**) and isoasatone (**2**) both co-occur in the plant, and the former can be regarded as a plausible precursor of **2**. Thus, chemical correlation between them was successfully carried out by photochemical reaction of asatone, as follows.

When irradiated in hexane using 0.02% aq. K_2CrO_4 solution as a filter at 10 °C, asatone (**1**) was converted into isoasatone (**2**) in 64% yield. In the case of tetrahydroasatone (**3**), the corresponding tetrahydro-compound (**18**) was also obtained in 60% yield. On irradiation of **3** using pyrex filter, two oxetanes (**23** and **24a**) were produced in 47 and 20% yields, respectively, in addition to tetrahydroisoasatone (**18**) (*ca.* 30% yield). Clearly, the dihydroxyoxetane (**24a**) must be produced from **18** *via* the monohydroxyoxetane (**23**). In fact, these two compounds (**18** and **23**) were each subjected to further photochemical reaction to give **24a** in almost quantitative yields. The structures of these oxetanes are discussed below.

The monohydroxyoxetane is a colorless viscous liquid with a molecular formula ($C_{24}H_{36}O_8$), whose IR spectrum indicates the presence of each one OH and CO group (ν_{max} 3550 and 1730 cm^{-1}). This oxetane has five MeO groups (see Table 2) and a methylene group which constitutes a part of the oxetane ring [δ 4.33 (1H, d, J=5.5 Hz) and 4.67 (1H, d, J=5.5 Hz) ppm]. In the case of the dihydroxyoxetane (**24a**, mp 167—168 °C; $C_{24}H_{36}O_8$), which has four MeO groups and no CO group, two oxetane rings must be present [δ 4.11 (2H, d, J=5.0 Hz) and 4.49 (2H, d, J=5.0 Hz) ppm]. Furthermore, it should be noted that only half of the total protons are observed in the NMR spectrum of the dihydroxyoxetane. In connection with tetrahydroisoasatone (**18**), finally, the structure of dihydroxyoxetane (**24a**) was elucidated by measurements of intramolecular nuclear Overhauser effects (NOE), which were focused on the signals corresponding to MeO groups and methine protons (see Table 2).

In the NMR spectrum of **18**, low-intensity irradiation at δ 3.31 ppm caused **12** and 10% enhancements in the integrated intensities of two methine signals at δ 2.82 and 2.90 ppm, respectively. On the other hand, on irradiation at δ 3.22 ppm, any enhancement was not

Table 2. The NMR spectra of **18**, **23**, and **24**

Tetrahydro-isoasatone (**18**)	Monohydroxy-oxetane (**23**)	Dihydroxy-oxetane (**24a**)
2.82 (2H, s)	2.6—2.8 (3H, complex)	2.62(2H, s)
2.90(2H, s)	3.00(4H, s)[a]	2.65(2H, s)
3.22(6H, s)	3.23(3H, s)	2.97(6H, s)
3.31(12H, s)	3.32(3H, s)	3.31(6H, s)
	3.33(3H, s)	
	3.35(3H, s)	

a) One of the four methine protons is included.

detected in the signal intensities of the methine protons (δ 2.82 and 2.90 ppm). From the molecular model of **18**, it is clear that the methyl singlet at δ 3.22 ppm is assigned to one of the two α,α-dimethoxyl groups, that is marked by "asterisk" in **18a**. In the case of the dihydroxyoxetane, only low-intensity irradiation at δ 3.31 ppm caused 12% enhancement in the integrated intensity of the methine singlet at δ 2.62 ppm, and any interaction between the MeO group (δ 2.97 ppm) and two methine protons (δ 2.62 and 2.65 ppm) was not detected. From these data, the structure of the dihydroxyoxetane can be represented by **24a** or **24b**. However, the former is more favorable than **24b**, because the methyl singlet at δ 3.31 ppm is reasonably assigned to the MeO group marked by "asterisk" in **24a**. In the case of **24b**, the signal at δ 3.31 ppm must be assigned to the MeO group marked by "asterisk", although the NMR signal due to the remaining MeO group is expected to be observed in a lower magnetic field that that of the asterisked one, since this MeO group and the newly formed OH group on the oxetane ring both are in a *cis*-configuration to each other. The structure of the monohydroxyoxetane is represented by **23** on the basis of the structure of the dihydroxyoxetane (**24a**), which has been already derived from the former.

Experimental

All mps were uncorrected. The IR and UV spectra were recorded on a JASCO Model IR-S and on a Perkin-Elmer 202 spectrophotometer, respectively. The NMR spectra were (100 MHz) taken on a JEOL JNM-C60H (60 MHz) or JNM-PS 100 using $CDCl_3$ as solvent, unless otherwise stated. Only prominent peaks are cited. Chemical shifts are given in ppm from TMS as an internal standard. Coupling constants are given in Hz (s, singlet; d, doublet; t, triplet; q, quartet; m, multiplet). The mass spectra were obtained on

a Hitachi RMU-6D mass spectrometer operating with an ionization energy (70 eV). Preparative TLC were carried out on Kieselgel PF_{254} (E. Merk A.G., Germany).

Isolation of Asatone and Isoasatone. A sample of the dried and pulverized material of the whole herb (9 kg), which was collected at Chia-I, Taiwan, was extracted with large amounts of hexane (40 l) by refluxing for 3 h. The hot mixtures were filtered from the undissolved residue which was extracted with the same solvent (40 l, each time) for twice. The combined filtrates were concentrated under reduced press. to give a greenish yellow crude crystalline solid (32 g) besides a dark green jelly (140 g) after filtration. The resulting crystalline solid was treated with column chromatography using silica gel (Kieselgel, E. Merk A. G. Germany) (2 kg), and eluted with hexane–EtOAc (8: 1). From the eluates, after recrystallized from hexane, white crystals of asatone (17.6 g) were isolated: mp 101—102 °C; *m/e* 448 (M^+) and 224 (Found: C, 64.01; H, 7.26%. Calcd for $C_{24}H_{32}O_8$: C, 64.27; H, 7.19%).

The undissolved residue from hexane extractions was then extracted with $CHCl_3$ successively by refluxing for three times in the same way as hexane extractions. The combined $CHCl_3$ extracts were concentrated under reduced press. to give a dark green jelly (100 g). The resultant jelly was chromatographed on silica gel (Kieselgel, E. Merk A. G., Germany) (7 kg), and eluted with hexane–EtOAc (8: 1). From the eluates, after recrystallized from hexane, white crystals of isoasatone (120 mg) were isolated; mp 156.5—158 °C; *m/e* 448 (M^+) and 224 (Found: C, 64.55; H, 7.07%. Calcd for $C_{24}H_{32}O_8$: C, 64.27; H, 7.19%).

Catalytic Hydrogenation of Asatone (1). Catalytic hydrogenation of asatone (90 mg) in EtOAc (2.5 ml) was carried out over 10% Pd–C (10 mg) at room temp. overnight. After filtration of the catalyst, the solvent was evaporated under reduced press. to give a white crystalline solid, which was recrystallized from hexane to give white crystals of tetrahydroasatone (**3**) (85 mg), mp 128—129 °C; ν_{max} (Nujol) 1745, 1720, and 1635 cm^{-1}; λ_{max} (MeOH) 278 and 229 nm (ε, 5100 and 3940, respectively); δ 0.87 (6H, t, J=6.5 Hz), 1.10—1.80 and 1.85—2.15 (8H, m), 2.80 (2H, br.s), 3.05 (3H, s), 3.30 (3H, s), 3.37 (3H, s), 3.41 (3H, s), 3.46 (3H, s), 3.60 (3H, s), 5.41 (1H, s), and 5.51 (1H, q, J=1.5 Hz) ppm; *m/e* 452 (M^+), 420, 388, 356, 345, 226, and 211 (Found: *m/e* 452.2425. Calcd for $C_{24}H_{36}O_8$: *m/e* 452.2410. Found: *m/e* 226.1236. Calcd for $C_{12}H_{18}O_4$: *m/e* 226.1205).

$NaBH_4$ Reduction of Asatone (1). To a solution of of asatone (400 mg) in EtOH (3 ml) was carefully added $NaBH_4$ (40 mg), with stirring. The mixture was further stirred at room temp. for 1.5 h, and then decomposed with ice water. After addition of 1M·HCl aq. solution (*ca.* 0.5 ml), the aqueous solution was extracted with ether. The ethereal solution was washed with sat. NaCl aq. solution, and then dried over Na_2SO_4. Removal of the solvent afforded an oily substance, which was purified by preparative TLC using a mixed solvent [hexane–EtOAc (2: 1)] to give three crystalline compounds, namely, hydroxyasatone–A (**4**) (66 mg), hydroxyasatone–B (**5**) (108 mg) and dihydroxyasatone (**6**) (20 mg), respectively, after crystallized from hexane. The physical data of these three reduction products are described below.

Hydroxyasatone-A: Mp 127—128 °C; ν_{max} (Nujol) 3500, 3085, 1745, 1685, 1660, and 1640 cm^{-1}; λ_{max} (MeOH) 235 sh. and 218 nm (ε, 2640 and 4500, respectively); δ 3.93 (1H, s), 4.60 (1H, s), and 5.75 (1H, q, J=1.5 Hz) ppm; *m/e* 450 (M^+), 422, 418, 386, 381, 349, 345, 316, 307, and 226 (Found: *m/e* 450.2232. Calcd for $C_{24}H_{34}O_8$: *m/e* 450.2253. Found: *m/e* 226.1207. Calcd for $C_{12}H_{18}O_4$: *m/e* 226.1205).

Hydroxyasatone-B: Mp 108—109 °C; ν_{max} (Nujol) 3510, 3050, 1715, 1660, and 1635 cm^{-1}; λ_{max} (MeOH) 277 and 213 nm (ε, 4390 and 2510, respectively); δ 3.92 (1H, s), 5.50 (1H, q, J=1.5 Hz), and 5.60 (1H, s) ppm; *m/e* 450 (M^+), 422, 418, 386, 381, and 226 (Found: *m/e* 450.2232. Calcd for $C_{24}H_{34}O_8$: *m/e* 450.2253. Found: *m/e* 226.1197. Calcd for $C_{12}H_{18}O_4$: 226.1205).

Dihydroxyasatone: Mp 156—158 °C; ν_{max} (Nujol) 3550, 3425, 3060, 1685, 1665, and 1635 cm^{-1}; λ_{max} (MeOH) 222 nm (ε, 2590); δ 3.80 (2H, br.s), 4.78 (1H, s) and 5.72 (1H, q, J=1.5 Hz) ppm; *m/e* 452 (M^+ for $C_{24}H_{36}O_8$), 434, 420, 389, 379, and 226. High resolution mass spectrum of this compound has not been measured, but its structure can be supported by its physical data coupled with the next experiment.

Catalytic Hydrogenation of Dihydroxyasatone (6). Catalytic hydrogenation of **6** (15 mg) in EtOAc (3 ml) was carried out over 10% Pd–C (5 mg) at room temp. for 4 h. After filtration of the catalyst, the solvent was removed under reduced press. to give white crystals of dihydroxytetrahydroasatone (**7**) (15 mg), mp 151—152 °C (from hexane); ν_{max} (Nujol) 3500 and 1675 cm^{-1}; λ_{max} (MeOH) 217 nm (ε, 2400); δ 3.77 (2H, br.s), 4.80 (1H, s) and 5.71 (1H, q, J=1.5 Hz) ppm; *m/e* 456 (M^+) and 228 (Found: C, 63.11; H, 8.83%. Calcd for $C_{24}H_{40}O_8$: C, 63.13; H, 8.83%).

Reduction of Tetrahydroasatone (3) with $LiAlH_4$. To a solution of **3** (100 mg) in THF (1.5 ml) was added $LiAlH_4$ (20 mg) with stirring at 0 °C, and then the reaction temperature was elevated to room temp. The reaction mixture was further stirred at room temp. for 6 h, and then poured into ice-water and extracted with EtOAc. The extracts were washed successively with water and with sat. NaCl aq. solution, and then dried over $MgSO_4$. The solvent was removed under reduced press. to give almost colorless crystals of **7** (98 mg) (mp and IR spectrum).

Formation of Hexahydroasatone (8). Catalytic hydrogenation of asatone (200 mg) in MeOH (2 ml) was carried out over 10% Pd–C (40 mg) at room temp. for 12 h. After filtration of the catalyst, the solvent was removed under reduced press. to leave an almost colorless oil, which was separated by preparative TLC using hexane–EtOAc (3: 1) to afford two fractions. The upper fraction afforded white crystals of hexahydroasatone (20 mg), mp 133—134 °C (from hexane); ν_{max} (Nujol) 1750, 1745, and 1635 cm^{-1}; λ_{max} (MeOH) 221 nm (ε, 2812); δ 0.82 (3H, t, J=7.0 Hz), 0.90 (3H, t, J=7.0 Hz), 1.15—1.84 (6H, m), 1.95 (2H, t, J=7.0 Hz), 2.31 (2H, d, J=5.5 Hz)*, 2.78 (2H, s), 3.14 (3H, s), 3.28 (3H, s), 3.35 (6H, s), 3.43 (3H, s), 3.50 (3H, s), 3.63 (1H, t, J=5.5 Hz)*, and 5.85 (1H, q, J=1.9 Hz) ppm; *m/e* 426 (M^+−28), 395, 379, and 363 (Found: C, 63.22; H, 8.65%. Calcd for $C_{24}H_{38}O_8$: C, 63.41; H, 8.43%).

From the lower fraction, tetrahydroasatone (**3**) (144 mg) was isolated (mp and IR spectrum).

Zinc Reduction of Tetrahydroasatone (3) to Hexahydroasatone (8). A mixture of **3** (20 mg) and activated zinc powder (200 mg) in AcOH (2.5 ml) was stirred at room temp. for 14 h, and then poured into a lot of water, and extracted with EtOAc. The extracts were washed with water several times, and then dried over $MgSO_4$. Removal of the solvent under reduced press. afforded a brown oil (15 mg), from which hexahydroasatone (9 mg) was separated by preparative TLC using a mixed solvent [hexane–EtOAc (1: 2)] (mp and IR spectrum).

Formation of Two Phenolic Compounds (9 and 10). A mixture of tetrahydroasatone (100 mg) and zinc powder (450 mg) in AcOH (1.5 ml) was refluxed, with stirring, for

* Irradiation at δ 2.31 ppm caused the triplet at δ3.63 ppm to collapse to singlet. In the case of irradiation at δ 3.63 ppm, the doublet at δ 2.31 ppm was changed to singlet.

4.5 h. The cooled reaction mixture was poured into a lot of water, and then extracted with EtOAc. The extracts were washed with a lot of water several times, and then dried over $MgSO_4$. Removal of the solvent left a brown residue (83.6 mg), the preparative TLC of which was carried out using a mixed solvent [hexane–EtOAc (3: 1)] to afford two fractions. The upper fraction gave a colorless liquid of 2,6-dimethoxy-4-propylphenol (**9**) (49 mg); ν_{max} (Film) 3520, 1610, and 1515 cm^{-1}; δ 0.93 (3H, t, J=6.8 Hz), 1.20—1.85 (2H, m), 2.53 (2H, t, J=7.5 Hz), 3.86 (6H, s), 5.35 (1H, br.s, OH), and 6.37 (2H, s) ppm; *m/e* 196 (M^+ for $C_{11}H_{16}O_3$) and 168. This liquid was characterized as the corresponding acetate.

From the lower fraction, a colorless viscous liquid (**10**) (20 mg) was isolated; ν_{max} (Film) 3460, 1610, 1585, and 1495 cm^{-1}; δ 0.81 (6H, t, J=7.0 Hz), 1.15—1.80 (4H, m), 2.22 (4H, td, J=7.0 and 1.5 Hz), 3.60 (6H, s), 3.95 (6H, s) and 6.60 (2H, br.s) ppm; *m/e* 390 (M^+ for $C_{22}H_{30}O_6$), 329, 315, 301, 297, 287, 167, and 153. This oil was also acetylated with Ac_2O–pyridine.

Acetylation of 2,6-Dimethoxy-4-propylphenol (9). A solution of **9** (15 mg) in Ac_2O–pyridine (1: 1, 1 ml) was stirred at room temp. overnight, and then concentrated under reduced press. on a water-bath (*ca.* 80 °C) to leave white crystals of the acetate (**11**) in quantitative yield, mp 88.0—88.5 °C (from EtOH) (lit, 87 °C)[5]; ν_{max} (Nujol) 1765, 1600, 1510 sh, and 1505 cm^{-1}; λ_{max} (MeOH) 275 and 227 nm (ε, 790 and 6140, respectively); δ 0.95 (3H, t, J=7.5 Hz), 1.57 (2H, sextet, J=7.5 Hz), 2.32 (3H, s), 2.55 (2H, t, J=7.5 Hz), 3.80 (6H, s), and 6.42 (2H, s) ppm; *m/e* 238 (M^+) (Found: C, 65.05; H, 7.62%. Calcd for $C_{13}H_{18}O_4$: C, 65.53; H, 7.61%).

Acetylation of the Biphenyl-type Compound (10). A solution of **10** (19 mg) in Ac_2O–pyridine (1: 1, 1.5 ml) was stirred at room temp. overnight, and then worked up as usual to give pale yellow crystals of the diacetate (**12**) (20 mg), mp 117—118 °C (from EtOH); ν_{max} (Nujol) 1770, 1600, and 1585 cm^{-1}; λ_{max} (MeOH) 279 and 232 nm (ε, 2470 and 13750, respectively); δ 0.84 (6H, t, J=7.0 Hz), 1.10—1.80 (4H, m) 2.10—2.45 (4H, m), 2.31 (6H, s), 3.53 (6H, s), 3.87 (6H, s), and 6.67 (2H, s) ppm; *m/e* 474 (M^+) and 431 (Found: C, 65.38; H, 7.18%. Calcd for $C_{26}H_{34}O_8$: C, 65.80; H, 7.22%).

Zinc Reduction of Asatone in AcOH. A mixture of asatone (125 mg) and zinc powder (1 g) in AcOH (2.0 ml) was heated under reflux overnight with stirring, and then worked up as usual to give a brown oil, from which two aromatic compounds were separated by preparative TLC using a mixed solvent [hexane–EtOAc (3: 1)]. The upper fraction gave a colorless liquid of 2,6-dimethoxy-4-allylphenol (**13**) (38 mg); ν_{max} (Film) 3510, 3080, 1635, 1615, and 1513 cm^{-1}; δ 3.30 (2H, d, J=6.0 Hz), 3.82 (6H, s), 4.80—5.25 (2H, m), 5.39 (1H, br.s, OH), 5.55—6.25 (1H, m) and 6.40 (2H, s) ppm; *m/e* 194 (M^+ for $C_{11}H_{14}O_3$) and 166. This liquid was further used for the next experiment.

From the lower fraction, a colorless viscous liquid of the biphenyl-type compound (**14**) (21 mg) was isolated; ν_{max} (Film) 3460, 1640, 1613, 1585, and 1495 cm^{-1}; δ 3.00 (4H, d, J=6.0 Hz), 3.61 (6H, s), 3.90 (6H, s), 4.70—5.15 (4H, m), 5.52 (2H, br., OH), 5.45—6.20 (2H, m), and 6.60 (2H, s) ppm; *m/e* 386 (M^+ for $C_{22}H_{26}O_6$). This viscous liquid was characterized as the corresponding diacetate (**16**).

Conversion of 13 to 2,6-Dimethoxy-4-propylphenyl Acetate (11). A solution of **13** (30 mg) in Ac_2O–pyridine (1: 1, 1.5 ml) was allowed to stand at room temp. overnight, and then concentrated under reduced press. to afford a pale yellow oil of the corresponding acetate (**15**) (31 mg); ν_{max} (Film) 1775, 1640, 1608, and 1510 cm^{-1}; *m/e* 236 (M^+ for $C_{13}H_{16}O_4$), 194, 179, and 167.

Catalytic hydrogenation of the acetate (15 mg) in EtOAc (1.5 ml) was carried out over 10% Pd–C (3 mg) at room temp. overnight. After filtration of the catalyst, the solvent was removed under reduced press. to give white crystals of **11** (14 mg) (mp and IR spectrum).

Acetylation of the Biphenyl-type Compound (14). A solution of **14** (15 mg) in Ac_2O–pyridine (1: 1, 1 ml) was stirred at room temp. overnight, and then worked up as usual to give a crystalline solid (13 mg). Recrystallization from EtOH afforded white crystals of the diacetate (**16**), mp 125—125.5 °C; ν_{max} (Nujol) 1775, 1600, and 1585 cm^{-1}; λ_{max} (MeOH) 277 and 227 nm (ε, 2160 and 17750, respectively); δ 2.36 (6H, s), 3.10 (4H, d, J=6.7 Hz), 3.58 (6H, s), 3.90 (6H, s) 4.75—5.10 (4H, m), 5.45—6.10 (2H, m) and 6.70 (2H, s) ppm; *m/e* 470 (M^+) (Found: C, 66.32; H, 6.44%. Calcd for $C_{26}H_{30}O_8$: C, 66.37; H, 6.43%).

Conversion of 16 to 12. Catalytic hydrogenation of the diacetate (**16**) (10 mg) in EtOAc (1.5 ml) was carried out over 10% Pd–C (2 mg) at room temp. for 5 h, and then worked up as usual to give almost colorless crystals in quantitative yield. Recrystallization from EtOH gave the corresponding tetrahydro-compound (**12**) (mp, TLC and IR spectrum).

Zinc Reduction of Tetrahydroasatone (3) in Acetic Anhydride. A mixture of **3** (100 mg) and activated zinc powder (500 mg) in Ac_2O (2 ml) was heated under reflux for 7 h with stirring. After cooling, the reaction mixture was poured into water, and then extracted with large amounts of EtOAc. The extracts were washed well water and with sat. NaCl aq. solution successively, and then dried over $MgSO_4$. Removal of the solvent gave a brown oil, which was separated by preparative TLC using a mixed solvent [hexane–EtOAc (3: 1)] to give two fractions. The upper fraction afforded a pale yellow liquid, which was crystallized from EtOH to give slightly pale yellow crystals of **11** (54 mg) (mp and IR spectrum).

From the lower part, a pale yellow oil (25 mg) was separated and crystallized from EtOH to give the diacetate of the biphenyl-type compound (**12**) (mp and IR spectrum).

Reduction of Isoasatone (2) with $LiAlH_4$. To a solution of **2** (135 mg) in THF (3 ml) was added excess amounts of $LiAlH_4$ (135 mg) with stirring, and then the reaction mixture was further stirred at room temp. for 3 h. After decomposition of the remaining reagent with EtOH, the reaction mixture was diluted with water, and then extracted with EtOAc. The extract was washed with sat. NaCl aq. solution, and then dried over Na_2SO_4. Removal of the solvent afforded a crystalline solid (140 mg), which was recrystallized from hexane–ether to give white crystals of dihydroxyisoasatone (**17**), mp 153—154 °C; ν_{max} (Nujol) 3500, 3420, 3060, 1635, and 908 cm^{-1}; δ 2.39 (2H, br. dd, J=14.3 and 8.5 Hz), 2.41 (2H, s), 2.49 (2H, s), 2.55 (2H, br. dd, J=14.3 and 7.5 Hz), 3.24 (6H, s), 3.30 (6H, s), 3.35 (6H, s), 3.71 (2H, s), 5.01 (2H, br. d, J=11 Hz), 5.03 (2H, br.d, J=15 Hz), and 5.7—6.2 (2H, m) ppm; *m/e* 452 (M^+), 437, 421, 411, 403, and 226 (Found: C, 63.57; H, 8.20%. Calcd for $C_{24}H_{36}O_8$: C, 63.70; H, 8.02%).

Catalytic Hydrogenation of Isoasatone (2). Catalytic hydrogenation of **2** (15 mg) in EtOAc (2 ml) was carried out over 10% Pd–C (5 mg) at room temp. overnight. After filtration of the catalyst, the solvent was evaporated under reduced press. to give white crystals (15 mg), which were recrystallized from hexane to give white crystals of tetrahydroisoasatone (**18**), mp 161—162 °C; ν_{max} (Nujol) 1735 cm^{-1}; λ_{max} (MeOH) 222 nm (ε, 2070); δ 0.90 (6H, br.t, J=7.0 Hz), 1.7—2.3 (8H, complex), 2.82 (2H, s), 2.90 (2H, s), 3.22 (6H, s), and 3.31 (12H, s) ppm; *m/e* 452 (M^+), 437, 420, 389, and 226 (Found: C, 63.35; H, 8.00%. Calcd for $C_{24}H_{36}O_8$: C, 63.70; H, 8.02%).

Zinc Reduction of Isoasatone (2). Excess amounts of zinc powder (500 mg) were added to a solution of isoasatone (80

mg) in MeOH (5 ml) containing concd HCl (1.5 ml) with stirring. The reaction mixture was stirred vigorously at room temp. for 2 h, and then poured into large amounts of water and extracted with EtOAc. The extract was washed with sat. NaCl aq. solution, and then dried over Na_2SO_4. Removal of the solvent left a brown oil (65 mg), which was subjected to preparative TLC using a mixed solvent [EtOAc–hexane (1:2)]. From the upper fraction, 2,6-dimethoxy-4-allylphenol (**13**) (32 mg) was obtained (TLC and IR spectrum). The biphenyl-type compound (**14**) (8.2 mg) was also obtained from the lower fraction (TLC and IR spectrum).

Thermal Reaction of Tetrahydroisoasatone (18). Tetrahydroisoasatone (38 mg) in a sealed tube was heated at 290—300 °C for 30 min, and then extracted with EtOAc. Removal of the solvent gave a brown viscous liquid, whose analytical TLC showed eight spots. Preparative TLC of this liquid was carried out in hexane–EtOAc (2:1), and a colorless liquid (9 mg) was obtained from the less polar fraction corresponding to that of 2,6-dimethoxy-4-propylphenol (**9**) (TLC and IR spectrum).

Thermal Reaction of Isoasatone (2). Isoasatone (10 mg) in a sealed tube was heated at 280—290 °C for 20 min, and then dissolved in a small amount of $CHCl_3$, and then directly separated by preparative TLC using hexane–EtOAc (2:1) to give a colorless liquid (2 mg), which was isolated from the less polar fraction corresponding to that of 2,6-dimethoxy-4-allylphenol (**14**) (TLC and IR spectrum).

Reaction of Tetrahydroasatone (3) with Acetic Anhydride. A solution of **3** (240 mg) in Ac_2O (2.5 ml) was heated under reflux for 10 h, and then concentrated under reduced press. to give a brown residue, which was purified by preparative TLC using a mixed solvent [hexane–EtOAc (3:1)] to give pale yellow crystals (35 mg) from the upper fraction. Recrystallization from EtOH afforded 2,6-dimethoxy-4-propylphenyl acetate (**11**) in a pure state (mp and IR spectrum).

From the lower part, slightly brown liquid (155 mg)** was isolated. This liquid was further purified by preparative GLC to give a colorless liquid (**21**) [retention time: 2.8 min. (10% OV-17 (ϕ 0.25 inch × 3 m); at 230 °C; Carrier gas: Nitrogen (100 ml/min); Inlet pressure, 25.5 psi)]; ν_{max} (Film) 1770, 1740, 1608, 1510, 1235, and 1200 cm^{-1}; λ_{max} (MeOH) 276 and 226 nm (ε, 970 and 9600, respectively); δ 0.90 (3H, t, J=7.5 Hz), 1.87 (2H, quintet, J=7.5 Hz), 2.08 (3H, s), 2.30 (3H, s), 3.78 (6H, s), 5.61 (1H, t, J=7.5 Hz), and 6.58 (2H, s) ppm; *m/e* 296 (M^+), 254, 183, and 149 (Found: C, 61.10; H, 6.47%. Calcd for $C_{15}H_{20}O_6$: C, 60.80; H, 6.80%).

Reaction of Asatone (1) with Acetic Anhydride. A solution of **1** (104 mg) in Ac_2O (1.5 ml) was heated under reflux overnight. Removal of the excess Ac_2O under reduced press. afforded a brown oil, whose analytical TLC showed many spots. Preparative TLC using hexane–EtOAc (3:1) afforded only small amounts of 2,6-dimethoxy-4-allylphenyl acetate (**15**) (5.3 mg) (GLC, TLC, and IR spectrum).

Photochemical Conversion of Asatone (1) to Isoasatone (2). A solution of **1** (70 mg) in hexane (8 ml) was irradiated at 10 °C for 54 h, using 0.02% K_2CrO_4 aq. solution as a filter [Apparatus: Eiko-Sha PIH-100, high pressure Hg lamp (100W)]. The reaction solution was then evaporated under reduced press. to leave an almost colorless oil, which was purified by preparative TLC using hexane–EtOAc (3:1). From the less polar fraction corresponding to that of isoasatone, white crystals (44.8 mg) were isolated after recrystallized from hexane (mp and IR spectrum).

Photochemical Conversion of Tetrahydroasatone (3) to Tetrahydroisoasatone (18). Under essentially the same condition as that of asatone (**1**), a solution of **3** (65 mg) in hexane (8 ml) was irradiated. After removal of the solvent, a colorless oil was purified by preparative TLC using a mixed solvent [hexane–EtOAc (4:1)]. From the less polar fraction corresponding to that of tetrahydroisoasatone, white crystals (39 mg) were obtained after recrystallized from hexane (mp and IR spectrum).

Photochemical Reaction of Tetrahydroasatone (3) Using Pyrex Filter. A solution of **3** (45 mg) in hexane (4 ml) was irradiated at 10 °C for 8 hr, and then the solvent was removed under reduced press. to leave a colorless viscous liquid which was chromatographed on alumina (Nakarai Chem. Co. Ltd., 200 mesh) (1 g) and eluted with hexane–benzene (10:1) to give white crystals of tetrahydroisoasatone (**18**) (13.5 mg) (mp, TLC and IR spectrum). Further elution with hexane–benzene (5:1) afforded a colorless viscous liquid of the monohydroxyoxetane (**23**) (21 mg), ν_{max} ($CHCl_3$) 3550 and 1730 cm^{-1}; δ 0.88 (3H, t, J=6.0 Hz), 0.92 (3H, t, J=6.5 Hz), 1.4—2.1 (8H, complex), 2.6—2.8 (3H, complex), 3.00 (4H, s), 3.23 (3H, s), 3.32 (3H, s), 3.33 (3H, s), 3.35 (3H, s), 3.92 (1H, s, OH), 4.33 (1H, d, J=5.5 Hz), and 4.67 (1H, d, J=5.5 Hz) ppm; *m/e* 452 (M^+), 420, 405, and 226 (Found: *m/e* 452.24050. Calcd for $C_{24}H_{36}O_8$: *m/e* 452.24100). Further elution only with benzene gave white crystals of dihydroxyoxetane (**24a**) (9 mg), mp 167—168 °C (from hexane); ν_{max} (Nujol) 3500 sh. and 3450 cm^{-1}; δ (CCl_4) 0.90 (6H, t, J=6.5 Hz), 1.2—1.9 (8H, complex), 2.62 (2H, s), 2.65 (2H, s), 2.97 (6H, s), 3.31 (6H, s), 4.11 (2H, d, J=5.0 Hz), and 4.49 (2H, d, J=5.0 Hz) ppm; *m/e* 452 (M^+), 420, 404, and 226 (Found: *m/e* 452.24356. Calcd for $C_{24}H_{36}O_8$: *m/e* 452.24100).

The Formation of the Dihydroxyoxetane from Tetrahydroisoasatone (18). Tetrahydroisoasatone (10 mg) in a thin Pyrex NMR tube was dissolved in hexane (*ca.* 2 ml), and then irradiated at room temp. for 8 h [the NMR spectrum of the reaction solution indicated that **18** was completely converted into the oxetane (**24a**)]. Removal of the solvent gave white crystals of the dihydroxyoxetane in quantitative yield (mp and IR spectrum).

Photochemical Conversion of the Monohydroxyoxetane (23) to the Dihydroxyoxetane. Under essentially the same condition as described above, a solution of **23** (10 mg) in hexane (*ca.* 2 ml) was irradiated, and then concentrated under reduced press. to give white crystals of the dihydroxyoxetane in quantitative yield (mp and IR spectrum).

The authors wish to thank Drs. H. Harada and H. Yazawa (Fujisawa Pharmaceutical Co. Ltd.) for measurements of high resolution mass spectra. They are also indebted to Dr. K. Fujita (Nihondenshi Co. Ltd.) for measurements of ^{13}C NMR spectra.

References

1) Y. Asahina, *Yakugaku Zasshi*, **27**, 362 (1907); Y. Asahina, *Tokyo Kagaku Kaishi*, **28**, 921 (1907); T. Takahashi, *Nippon Kagaku Kaishi*, **51**, 432 (1930); T. Kaku and T. Kondo, *Yakugaku Zasshi*, **51**, 8 (1931); T. Kaku, C. Cho, and T. Orita, *ibid.*, **51**, 862 (1931); T. Kaku, N. Kutani, and J. Takahashi, *ibid.*, **56**, 361 (1936); T. Kaku and H. Ri, *ibid.*, **57**, 804, 1015 (1937); T. Kaku, K. Ittyoda, and H. Ri, *ibid.*, **58**, 687 (1938); M. Nagasawa, *ibid.*, **81**, 129 (1961); Huang-Minlon, *Ber.* **70**, 951 (1937); C. J. Cavallito and J. H. Bailey, *J. Am. Chem. Soc.*, **68**, 489 (1946); B. Spergely and N. G. Takacsi, *C.A.*, **56**, 8839 (1962); G. Staskiewicz, *ibid.*, **62**, 10817 (1965); Y. Fujita, *Bot. Mag. Tokyo*, **79**, 783 (1966).

2) Y. Saiki, T. Sato, H. Sasaki, and S. Fukushima, *J.*

** The purity of this liquid is more than 95%.

Pharm. Soc. Jpn., **87**, 1524 (1967); Y. Saiki, Y. Akahori, T. Noro, K. Morinaga, T. Taira, S. Fukushima, and T. Harada, *ibid.*, **87**, 1530, 1536, and 1540 (1967); Y. Saiki, S. Sano, and S. Fukushima, *ibid.*, **90**, 103 (1970) and references cited therein.

3) B. Hayata, "Incones Plantarum Formosanarum," Vol. V, Bureau of Productive Industries, Government of Formosa (1915), p. 148; A. T. Hsieh and T. I. Yang, "Nomenclature of Plants in Taiwan," College of Agriculture, National Taiwan University (1969), p. 402.

4) W. S. Kan, "Taiwan Yau-Yong-Tsu-Wu-Chi," Vol. I, National Institute of Chinese Medicine, Taiwan (1958), p. 102.

5) I. Heilbron, "Dictionary of Organic Compounds," Eyre and Spottiswoode Ltd. (1965), p. 1134.

6) S. Yamamura, Y. Terada, Y. Chen, H. Hsu, and Y. Hirata, *Tetrahedron Lett.*, **1975**, 1903.

7) K. Sasaki, Y. Hirata, S. Yamamura, Y. Chen, M. Hong, and H. Hsu, *Tetrahedron Lett.* **1973**, 4881; K. Sasaki and Y. Hirata, *Acta Crystallogr.*, **B30**, 1619 (1974).

8) Y. Chen, M. Hong, H. Hsu, S. Yamamura, and Y. Hirata, *Tetrahedron Lett.*, 1607 (1972).

9) Four MeO signals may be included.

Homolytic Aromatic Substitution by Iminyl Radicals. Photolysis of Aromatic Ketone *O*-Acyloximes in Aromatic Solvents

Hirochika SAKURAGI, Shun-ichi ISHIKAWA, Toshihiro NISHIMURA, Masayuki YOSHIDA, Naoki INAMOTO, and Katsumi TOKUMARU*

Department of Chemistry, Faculty of Science, The University of Tokyo, Hongo, Bunkyo-ku, Tokyo 113
**Institute of Chemistry, The University of Tsukuba, Sakura-mura, Nihari-gun, Ibaraki-ken 300-31*

(Received March 5, 1976)

Irradiation of benzophenone *O*-acetyloxime, *O*-phenylacetyloxime, *O*-benzoyloxime, and *O*-(*p*-chlorobenzoyl)-oxime in benzene, toluene, chlorobenzene, or *o*-xylene effected aromatic substitution on the solvent molecules by diphenylmethaniminyl radicals to give *N*-diphenylmethylenearylamines only when benzoxyl or *p*-chlorobenzoxyl radicals were generated concurrently. A mechanism involving a participation of the sufficiently long-lived acyloxyl radicals is proposed for the iminylation reaction on the basis of the reactivity patterns in this substitution reaction. *o*-Phenylbenzophenone *O*-benzoyloxime was also photolyzed in benzene to give 9-phenylphenanthridine, the intramolecular cyclization product of 2-biphenylylphenylmethaniminyl radicals.

Iminyl radicals are generated by various ways, among which thermal decomposition of oxime thionocarbamates[1] and hydrogen abstraction from imines[2] may be the most useful means. However, because of a lack of reactivity of iminyl radicals their chemistry has not received a great deal of attention and thus, recent interest has mainly been focused on their ESR spectra and electronic structure.[1a,b,2,3] Meanwhile, on irradiation of *O*-acyloximes formation of azines was reported and the results were rationalized by the intermediacy of iminyl radicals.[4-7] Recently it was found in our laboratory[5] that photolysis of benzophenone *O*-aroyloximes in benzene affords *N*-diphenylmethyleneaniline, the product formally derived from aromatic substitution of diphenylmethaniminyl radicals on the solvent molecule, together with benzophenone azine. Since there was no precedent for the aromatic substitution by iminyl radicals, we have undertaken to study the mechanism of this substitution reaction, and showed in a previous communication[6] that the above aromatic substitution occurs with an assistance of long-lived acyloxyl radicals. In the present paper we describe the details of our results.

Results

Products from Photolyses of O*-Acyloximes in Benzene.* The photolyses of benzophenone *O*-acetyloxime (Ia), *O*-phenylacetyloxime (Ib), and *O*-(*p*-chlorobenzoyl)-oxime (Ic) were carried out in benzene (0.1 M) so that a comparison could be made between the products from these *O*-acyloximes. The acyloxime Ic was the most feeble to light among them and decomposed completely within 20 h on irradiation with a 400 W high pressure mercury lamp. On the other hand the photolyses of Ia and Ib proceeded rather slowly. The products listed in Table 1 are readily interpretable in terms of the initial N–O bond homolysis followed by free-radical reactions of diphenylmethaniminyl radicals and acyloxyl radicals. Primarily, the results of the photolyses (Table 1) serve to point up the differences between the products resulting from the *O*-acetyloximes (Ia and Ib) and *O*-(*p*-chlorobenzoyl)oxime (Ic). The acetyloximes, Ia and Ib, yielded *N*-diphenylmethylene-methylamine (IIa) and *N*-diphenylmethylenebenzylamine (IIb), respectively, which would result from the coupling of diphenylmethaniminyl radicals (IV) with alkyl radicals derived from decarboxylation of the corresponding acyloxyl radicals, whereas the yield of such a coupling product, *N*-diphenylmethylene-*p*-chloroaniline (IIc), was negligible in the photolysis of Ic. The decomposition of Ib was highly accelerated with benzophenone, the addition of which did not

TABLE 1. PRODUCTS FROM IRRADIATION OF BENZOPHENONE *O*-ACYLOXIME (I), $Ph_2C{=}NOC(=O)R$, IN BENZENE (0.1 M) WITH A 400 W HIGH PRESSURE MERCURY LAMP

I	Ia	Ib	Ib[a)]	Ic
R in I	CH_3	$PhCH_2$	$PhCH_2$	*p*-ClC_6H_4
React. time (h)	40	40	3	20
I decomposed (%)	73	100	100	100
Products (%)[b)]				
$Ph_2C{=}O$	14	8		39
$Ph_2C{=}NH$		41	12	7
$Ph_2C{=}N{-}N{=}CPh_2$	15	14	8	19
$Ph_2C{=}NR$ (II)	23	30	51	1
$Ph_2C{=}NPh$ (III)	0	0	0	11
PhR	22	0		
R–R		13	15	
RCO_2Ph				4

a) Sensitized with benzophenone (0.1 M). b) Yield based on decomposed I.

TABLE 2. PRODUCTS FROM IRRADIATION OF FLUORENONE *O*-(*p*-METHYLBENZOYL)OXIME (V) IN BENZENE (0.1 M) WITH A 1 kW HIGH PRESSURE MERCURY LAMP[a)]

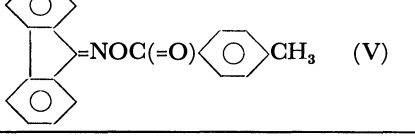

(V)

Products	Yield,[b)] %
Fluorenone	35
Fluorenone azine	18
N-Fluorenylideneaniline	4
N-Fluorenylidene-*p*-toluidine	1
4-Methylbiphenyl	35

a) 44% of V was decomposed on 20 h irradiation. b) Yield based on decomposed V.

Table 3. Total yields and isomer proportions of *N*-diphenylmethylenearylamines, $Ph_2C{=}NC_6H_4X$, formed in the iminylation of toluene and chlorobenzene[a]

Substrate (PhX)	Acyloxime	Total Yield of $Ph_2C{=}NC_6H_4X$ (%)	Proportion of $Ph_2C{=}NC_6H_4X$		
			o-$CH_3C_6H_4Y$[b]	*m*-$CH_3C_6H_4Y$	*p*-$CH_3C_6H_4Y$
$PhCH_3$	Id	9	28	66	5
	Ic	12	28	71	trace
			o-ClC_6H_4Y	*m*-ClC_6H_4Y	*p*-ClC_6H_4Y
PhCl	Id[c]	14	15	83	2

a) A 0.1 M solution of I in aromatic solvent was irradiated with a high pressure mercury lamp. b) Y stands for $Ph_2C{=}N$. c) Sensitized with benzophenone (0.1 M).

Table 4. Relative rates and partial rate factors for aromatic substitution of benzene derivatives by various radicals

Substrate (PhX)	Relative rate and partial rate factor[a]	Attacking radical (Source of radical)			
		$Ph_2C{=}N\cdot$		$Ph_3C\cdot$ (BPO+$Ph_3C\cdot$)[b]	$PhCO_2\cdot$ (BPO)[b]
		($Ph_2C{=}NOCOPh$)	($Ph_2C{=}NOCOC_6H_4Cl$-*p*)		
$PhCH_3$	k_{PhCH_3}/k_{PhH}	2.30	4.36	2.82	2.47
	F_o	2.1	4.1	0.90	4.1
	F_m	4.3	8.8	6.85	1.5
	F_p	1.1	0.5	1.32	3.7
PhCl	k_{PhCl}/k_{PhH}	0.77		0.60	0.51
	F_o	0.30		0.22	0.79
	F_m	1.91		1.10	0.24
	F_p	0.18		0.97	0.98

a) F_o is the reactivity at one *ortho* site in PhX relative to reactivity of one site in benzene; similarly for F_m and F_p. b) BPO stands for dibenzoyl peroxide.

change seriously the product distribution. *N*-Diphenylmethyleneaniline (III), which would be expected to be produced by the homolytic substitution with diphenylmethaniminyl radicals (IV) on the solvent benzene, was found in an appreciable amount only in the photolysis of Ic, but none was obtained in the photolysis of Ia and Ib.

Fluorenone *O*-(*p*-methylbenzoyl)oxime (V) was also irradiated in benzene (0.1 M) to afford *N*-fluorenylidene-*p*-toluidine, the coupling product, in a similar manner to Ic (Table 2).

Reactivity Patterns in Free-Radical Aromatic Substitution by the Iminyl Radicals (IV). Photolyses of benzophenone *O*-benzoyloxime (Id) and *O*-(*p*-chlorobenzoyl)-oxime (Ic) were carried out in toluene and chlorobenzene. The total yields and the isomer proportions of *N*-diphenylmethylenearylamines formed in the iminylation of toluene and chlorobenzene are given in Table 3. In toluene *N*-diphenylmethylenebenzylamine was also obtained, which is supposed to be formed by the coupling of the iminyl radicals with benzyl radicals derived from the solvent. Irradiation of Id in *o*-xylene gave also the substitution products, *N*-diphenylmethylene-2,3-dimethylaniline and -3,4-dimethylaniline, in 4.2 and 0.5% yield, respectively

Conventional competition experiments were carried out in which mixtures of benzene with toluene and with chlorobenzene were allowed to compete for the iminyl radicals (IV), and their relative reactivities were deduced from the composition of *N*-diphenylmethylenearylamines. The relative rates (k_{PhX}/k_{PhH}: the ratio of the total rate of substitution in PhX to that in benzene) and the partial rate factors for iminylation are summarized in Table 4 with similar data for the triphenylmethylation[8] and the benzoxylation.[9]

Photolysis of o-*Phenylbenzophenone* O-*Benzoyloxime (VI).* In addition to the quantitative study of the reactivity patterns of the iminyl radical IV, the reaction was employed to effect intramolecular cyclization onto an aromatic ring. Irradiation of *o*-phenylbenzophenone *O*-benzoyloxime (VI) in benzene in the presence of an equimolar amount of benzophenone resulted in the formation of 9-phenylphenanthridine (VIII, 74% in VPC yield) along with small amounts of *o*-phenylbenzophenone (3%) and 2-biphenylylphenylmethanimine (11%), but afforded none of substitution products, *N*-(2-biphenylylphenylmethylene)aniline (IX), on the solvent benzene by a corresponding iminyl radical (VII)

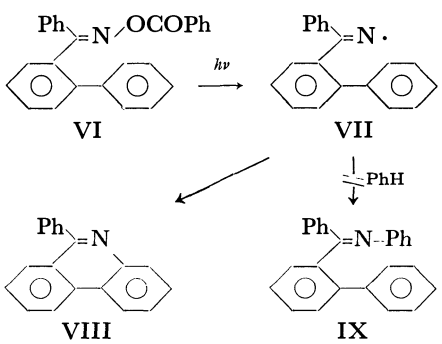

Scheme 1.

(Scheme 1). Isolated yield of the cyclization product (VIII) was 25% after purification.

Discussion

The principal reactions of iminyl radicals are dimerization to azines and β-scission to nitriles and alkyl radicals,[2,10] and only other reactions hitherto known are a hydrogen abstraction[11] and an intramolecular addition to an aromatic nucleus.[12] Thus, *N*-chloroketimines, on thermolysis in the presence of n-Bu_3SnH, gave ketimines, and the reduction was explained by a radical chain sequence involving hydrogen abstraction of iminyl radicals from n-Bu_3SnH.[11] When this reduction was carried out in the presence of 1-octene, no products derived from addition of iminyl radicals to 1-octene were observed.[11] Meanwhile, Forrester *et al.* reported that oxidation of *N*-substituted-methyleneaminooxy-acetic (XIV) or -propionic acids with peroxysulfate gave a phenanthridine (VIII), the product derived from intramolecular cyclization of iminyl radicals (VII) to an adjacent phenyl group[12] (Scheme 5).

In view of such an unreactive nature of iminyl radicals, it is highly notable that *N*-diphenylmethylenearylamines, the products of homolytic substitution by the iminyl radicals on the aromatic solvent, are formed only in the photolyses of benzophenone *O*-benzoyloxime (Id) and *O*-(*p*-chlorobenzoyl)oxime (Ic), whereas none was obtained in the photolyses of benzophenone *O*-acetyloxime (Ia) and *O*-phenylacetyloxime (Ib). These facts suggest that the aromatic substitution by the diphenylmethaniminyl radicals (IV) takes place only when the partner acyloxyl radicals are sufficiently alive like benzoxyl and *p*-chlorobenzoxyl radicals until they decarboxylate; the substitution does not occur when the iminyl radicals IV are generated together with short-lived acyloxyl radicals such as acetoxyl and phenylacetoxyl radicals. It is therefore likely that the aromatic substitution is not effected by IV alone, but is induced with an assistance of aroyloxyl radicals. These observations remind us of the role of benzoxyl radicals in the Wieland triphenylmethylation reaction,[13] in which tetraphenylmethane is a major product of the dibenzoyl peroxide-induced reaction of triphenylmethyl radicals with benzene. This reaction is now elucidated by the following reaction sequence (Scheme 2), in which induced decomposition of the peroxide is followed by attack of benzoxyl radicals on the solvent. The cyclohexadienyl radical formed is scavenged by a triphenylmethyl radical in a coupling reaction. Non-radical elimination of benzoic acid then gives tetraphenylmethane.

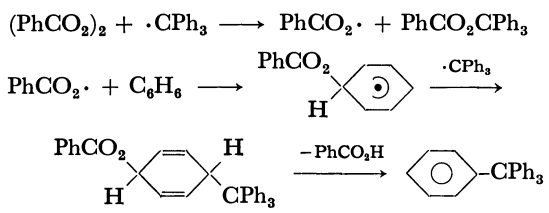

Scheme 2.

When toluene is used as a solvent, a major product is *m*-methyltetraphenylmethane, consistent with preferred *ortho* and *para* attack on toluene by a benzoxyl radical.

Consideration of the figures shown in Table 3 indicates that the proportions of substitutions at the *meta*-positions are unusually high irrespective of the polar character of the substituents. The results differ greatly from those obtained for usual homolytic substitution by free radicals such as alkyl and aryl radicals, which generally attack *ortho*- and *para*-positions of toluene or chlorobenzene in preference to *meta*-positions.[9] The unusual order of apparent reactivity among the nuclear positions ($m > o \gg p$) is again analogous to that of substitution by triphenylmethyl radicals or nitrogen dioxide in the presence of dibenzoyl peroxide. Anomaly in the same sense is also observed in the relative rates and the partial rate factors summarized in Table 4. It is worth noting that the relative rates and the partial rate factors for the iminylation of toluene and chlorobenzene with Id generally parallel those for the triphenylmethylation. With Ic the partial rate factor to toluene is considerably increased, although there is an overall similarity between Ic and Id. It is also observed in Table 4 that the relative rates of toluene and chlorobenzene for the benzoxylation are close to those for the iminylation with Id, but the benzoxylations occur preferentially at the *ortho*- and the *para*-positions. These findings suggest that the attack of the aroyloxyl radicals on the aromatic solvent is a key step in the aromatic substitution.

On the basis of the close correspondence with reactivity patterns in the iminylation and triphenylmethylation reactions as well as the above findings, it is concluded that the aromatic substitution by the iminyl radicals IV takes place through the following sequence of reactions (Scheme 3).

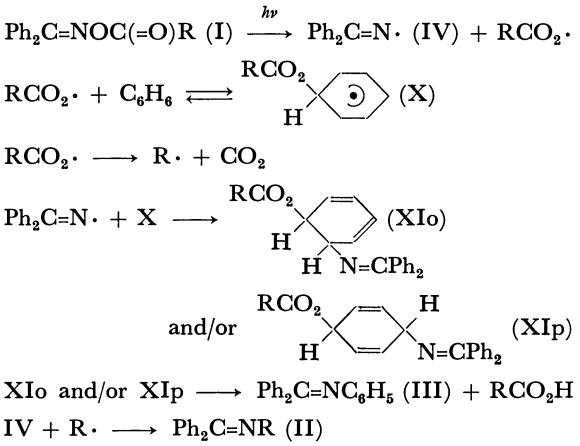

Scheme 3.

The acyloxyl radicals generated by photochemical cleavage of I either add reversibly to benzene to give cyclohexadienyl radicals (X) or decarboxylate. The resulting radicals, X, would combine with IV to give cyclohexadienes, XIo and/or XIp, which would subsequently decompose into III and carboxylic acid. In the irradiation of Ia or Ib, the intermediate acetoxyl or phenylacetoxyl radicals decarboxylate facilely before they add effectively to benzene. The formation of

N-fluorenylideneaniline in the photolysis of fluorenone *O*-(*p*-methylbenzoyl)oxime (V) in benzene is possibly explained in a similar manner.

Benzoxyl radicals are known[9] to add to the *ortho*- and *para*-positions of toluene to give cyclohexadienyl radicals, XIIo and XIIp, in preference to *meta*-positions to give XIIm (Scheme 4). The cyclohexadienyl radicals, XIIo and XIIp, would combine with IV exclusively at the position *meta* to methyl group to give *N*-diphenylmethylene-*m*-toluidine, XIIIm, and the cyclohexadienyl radical, XIIm, on the other hand, would combine necessarily at the positions *ortho* and *para* to methyl group to give *o*- and *p*-toluidine derivatives, XIIIo and XIIIp, respectively, the ratio of which would be regulated mainly by the steric factors of methyl and benzoxy groups on the cyclohexadienyl radical XIIm. This reaction scheme successfully explains the predominant production of XIIIm over XIIIo and XIIIp.

Taking account of the *ortho*- and *para*-orientation of benzoxyl radicals to chlorobenzene,[9] similar considerations can be applied to the preferential formation of *N*-diphenylmethylene-*m*-chloroaniline to *o*- and *p*-chloroaniline derivatives in the photolysis of Id in chlorobenzene.

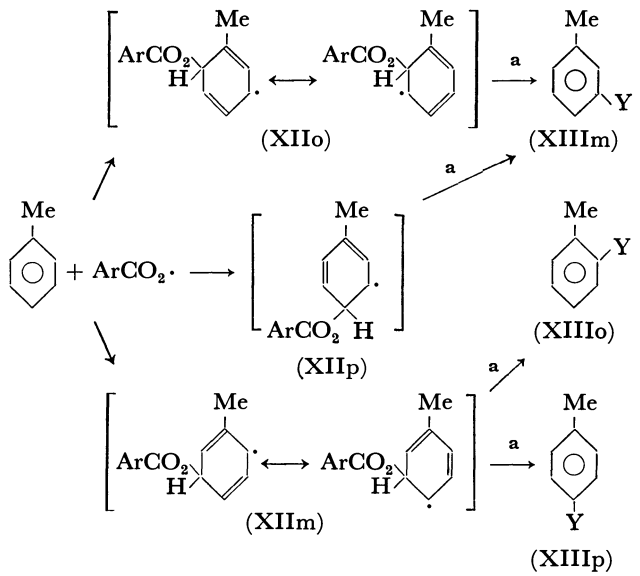

Y: $Ph_2C{=}N$; a: combination with Y· followed by elimination of $ArCO_2H$.

Scheme 4.

Instead of giving *N*-diphenylmethyleneaniline (III) irradiation of Ia and Ib in benzene afforded *N*-diphenylmethylenemethylamine (IIa) and *N*-diphenylmethylenebenzylamine (IIb), respectively, which would result from the combination of IV with the alkyl radicals derived from the decarboxylation of acyloxyl radicals (Scheme 3). We have reported previously[7] that the homolytic cleavage of *O*-acyloximes into iminyl and acyloxyl radicals takes place from the triplet states, in both direct and sensitized irradiation, with excitation energies comparable to those of their parent ketones. In view that the triplet pair of free radicals, in general, does not efficiently lead to a geminate product,[15] the formation of *N*-diphenylmethylenebenzylamine (IIb) from direct irradiation as well as from sensitization is not attributable to the geminate reaction between IV and benzyl radicals in a solvent cage, but to the combination between these radicals diffused out of the initial solvent cage. *A priori* it is reasonable to suppose that the production of *N*-diphenylmethylenemethylamine (IIa) from Ia is attributable to out-of-cage encounter of methyl and iminyl radicals.

Closely related to free-radical aromatic substitutions are intramolecular free-radical aromatic substitutions. The iminyl radicals (VII) produced by the photolysis of *o*-phenylbenzophenone *O*-benzoyloxime (VI) cyclize onto an adjacent phenyl group to give 9-phenylphenanthridine (VIII) (Scheme 1). Forrester *et al.* reported[12] that VII derived from the oxidation of the corresponding aminooxy-acetic acid (XIV) or -propionic acid gives 9-phenylphenanthridine (VIII) and hence the assistance of benzoxyl radicals is not necessarily required in the intramolecular cyclization. These results indicate that the iminyl radicals are sufficiently reactive in the addition to the benzene ring, provided the benzene nucleus is located adjacently to the radical center.

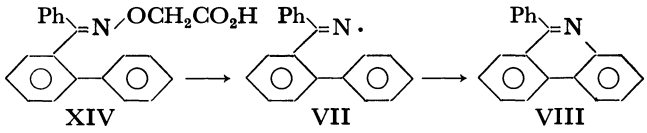

Scheme 5.

Experimental

All melting points are uncorrected. IR and UV spectra were recorded on a Hitachi EPI-G2 grating infrared spectrophotometer and a Hitachi EPS-3 recording spectrophotometer, respectively. NMR spectra were recorded with a Hitachi R-20B NMR spectrometer. Micro-analyses were performed by Organic Analytical Laboratory of our Department under supervision of Mr. S. Masuda. VPC analyses were performed on Hitachi 063 and K53 gas chromatographs equipped with flame ionization detectors. All quantitative results compared to internal standards were based on measured molar response factors determined from known mixtures of authentic materials. Irradiations were conducted with a Riko 400 W and a 1 kW high pressure mercury lamp in a water-cooled immersion well.

Materials. Special grade benzene, toluene, chlorobenzene, and *o*-xylene were distilled prior to use. Benzophenone (reagent grade) was crystallized from ethanol. Benzophenone *O*-acetyloxime,[16] *O*-benzoyloxime,[17] *O*-(*p*-chlorobenzoyl)oxime,[18] were prepared according to the methods described in literatures. Diphenylmethanimine,[19] *N*-diphenylmethylenemethylamine,[20] -benzylamine,[21] -aniline,[22] -*o*-toluidine,[23] -*m*-toluidine,[24] -*p*-toluidine,[22] -*p*-chloroaniline,[25] and -3,4-xylidine,[24] *N*-fluorenylidene-aniline,[22] and -*p*-toluidine,[26] 2-biphenylylphenylmethanimine,[27] and *N*-(2-biphenylylphenylmethylene)aniline[28] were prepared according to the methods described in literatures. Benzophenone azine[29] and fluorenone azine[30] were prepared according to the reported methods.

Benzophenone O-Phenylacetyloxime. Phenylacetic anhydride (14 g) was refluxed for 4 h with benzophenone oxime (6 g) in diethyl ether (100 ml). After cooling, the insoluble product was collected by filtration, and the ethereal filtrate was shaken with 10% sodium carbonate solution and then

water. A white crystalline solid precipitated was collected, combined with the above product, washed with ether, and dissolved in chloroform. To this solution was added hexane and the solution was cooled in an ice bath to afford white crystals (3 g), which were further purified on recrystallization from benzene–hexane; mp 112.5—113 °C (Found: C, 79.92; H, 5.30; N, 4.29%. Calcd for $C_{21}H_{17}NO_2$: C, 79.98; H, 5.43; N, 4.44%); IR (KBr) 1763 cm^{-1}; NMR ($CDCl_3$) δ 3.61 (s, 2H).

Fluorenone O-(p-*Methylbenzoyl*)*oxime.* Fluorenone oxime was acylated with *p*-methylbenzoyl chloride in the presence of pyridine according to the method of Renfrow *et al.*[18]; mp 143.5—144.5 °C (ethanol) (Found: C, 80.37; H, 4.90; N, 4.67%. Calcd for $C_{21}H_{15}NO_2$: C, 80.49; H, 4.83; N, 4.47%); IR (KBr) 1738 cm^{-1}; NMR ($CDCl_3$) δ 2.43 (s, 3H).

o-*Phenylbenzophenone* O-*Benzoyloxime.* *o*-Phenylbenzophenone oxime, prepared from *o*-phenylbenzophenone[31] by the method of Smith,[27] was acylated with benzoyl chloride in a way similar to fluorenone *O*-(*p*-methylbenzoyl)oxime; mp 115.5—116.5 °C (benzene–petroleum ether) (Found: C, 83.04; H, 4.96; N, 3.80%. Calcd for $C_{26}H_{19}NO_2$: C, 82.74; H, 5.07; N, 3.71%); IR (KBr) 1742 cm^{-1}.

N-*Diphenylmethylene*-o-*chloroaniline.* A mixture of 3 g of benzophenone, 3.5 ml of *o*-chloroaniline, and 1 drop of 48% hydrobromic acid was heated for 0.5 h at 250 °C under nitrogen. After cooling, 15 ml of ethanol was added to give light yellow crystals, which were recrystallized three times from ethanol to give pure specimen (1.8 g); mp 101—103 °C (Found: C, 78.04; H, 4.98; N, 4.78; Cl, 12.20%. Calcd for $C_{19}H_{14}ClN$: C, 78.21; H, 4.84; N, 4.80; Cl, 12.15%).

N-*Diphenylmethylene*-m-*chloroaniline.* A mixture of 3 g of benzophenone, 3.5 ml of *m*-chloroaniline, and 2 drops of 48% hydrobromic acid was heated for 1 h at 210 °C under nitrogen. After cooling, 15 ml of ethanol added to give light yellow crystals. Twice recrystallizations from ethanol gave pure specimen (2.4 g); mp 75.5—76.5 °C (Found: C, 77.95; H, 4.74; N, 4.72; Cl, 12.27%. Calcd for $C_{19}H_{14}ClN$: C 78.21; H, 4.84; N, 4.80; Cl, 12.15%).

N-*Diphenylmethylene*-*2,3-xylidine.* A solution of equivalent amounts of benzophenone and 2,3-xylidine in xylene was refluxed for 4 h in the presence of a few drops of 48% hydrobromic acid. The water formed during the reaction was removed as xylene azeotrope. After evaporation of the solvent, the residue was recrystallized from ethanol; mp 60—61 °C (Found: C, 88.50; H, 6.61; N, 4.75%. Calcd for $C_{21}H_{19}N$: C, 88.38; H, 6.71; N, 4.91%).

Photolyses of O-*Acyloximes.* A 0.1 M solution of benzophenone *O*-acyloxime in benzene was irradiated under nitrogen or argon in the absence or in the presence of benzophenone in a Pyrex immersion well with a 400 W mercury lamp. When toluene, chlorobenzene, or xylene was used as a solvent, irradiation was conducted in a Pyrex tube with a 1 kW mercury lamp using a Riko RH400—10 W rotary photochemical reactor.

Benzene solutions (0.1 M) of fluorenone *O*-(*p*-methylbenzoyl)oxime and *o*-phenylbenzophenone *O*-benzoyloxime were irradiated similarly by the 1 kW mercury lamp.

Volatile products other than starting acyloximes and ketazines were analyzed quantitatively by VPC using columns of Apiezon Grease L and Carbowax 20 M. Ketazines were separated by dry column chromatography on silica gel eluting with benzene, and analyzed quantitatively by UV spectrometry. In the photolyses of benzophenone *O*-acetyloxime the unreacted acetyloxime and the products, *N*-diphenylmethylenemethylamine and toluene, were analyzed also by NMR using an internal standard.

A solution of *o*-phenylbenzophenone *O*-benzoyloxime (0.377 g) in benzene (10 ml) in the presence of benzophenone (0.182 g) was irradiated by the 1 kW mercury lamp for 13.5 h. The reaction mixture was analyzed quantitatively by VPC using a column of Apiezon Grease L. 9-Phenylphenanthridine was separated by dry column chromatography on silica gel eluting with benzene as white crystals (0.064 g, 25%); mp 104—105 °C (lit,[32] 106 °C).

Competitive Experiments. A 0.1 M solution of benzophenone *O*-benzoyloxime or *O*-(*p*-chlorobenzoyl)oxime in a mixed solvent, benzene–toluene (22: 8 in a volume ratio) or in benzene–chlorobenzene (8 : 17), was irradiated by the 1 kW mercury lamp. The distributions of substituted products, *N*-diphenylmethylene-aniline, -toluidines, and -chloroanilines, were determined by VPC analysis using a column of Apiezon Grease L.

The authors wish to thank Professor T. Suehiro in Gakushuin University for his helpful discussions. Partial financial assistance through the Ministry of Education for K. T. is gratefully acknowledged.

References

1) a) R. F. Hudson, A. J. Lawson, and E. A. C. Lucken, *J. Chem. Soc., Chem. Commun.*, **1971**, 807; b) R. F. Hudson and A. J. Lawson, *ibid.*, **1972**, 721; c) C. Brown, R. F. Hudson, and A. J. Lawson, *J. Am. Chem. Soc.*, **95**, 6500 (1973).

2) D. Griller, G. D. Mendenhall, W. Van Hoof, and K. U. Ingold, *J. Am. Chem. Soc.*, **96**, 6068 (1974).

3) a) D. E. Wood, R. V. Lloyd, and D. W. Pratt, *J. Am. Chem. Soc.*, **92**, 4115 (1970); b) M. C. R. Symons, *Tetrahedron*, **29**, 615 (1973); c) R. F. Hudson, A. J. Lawson, and K. A. F. Record, *J. Chem. Soc., Chem. Commun.*, **1974**, 488.

4) a) J. -P. Vermes and R. Beugelmans, *Tetrahedron Lett.*, **1969**, 2091; b) R. Beugelmans and J. -P. Vermes, *Bull. Soc. Chim. Fr.*, **1970**, 342; c) T. Okada, M. Kawanisi, and H. Nozaki, *Bull. Chem. Soc. Jpn.*, **42**, 2981 (1969).

5) H. Ohta and K. Tokumaru, *Bull. Chem. Soc. Jpn.*, **48**, 2393 (1975).

6) S. Ishikawa, H. Sakuragi, M. Yoshida, N. Inamoto, and K. Tokumaru, *Chem. Lett.*, **1975**, 819.

7) M. Yoshida, H. Sakuragi, T. Nishimura, S. Ishikawa, and K. Tokumaru, *Chem. Lett.*, **1975**, 1125.

8) T. Suehiro, S. Igeta, O. Kuwabara, and M. Hirai, *Tetrahedron*, **26**, 963 (1970).

9) M. J. Perkins, "Free Radicals," Vol. II, ed. by J. K. Kochi, John Wiley and Sons, Inc., New York, N. Y. (1973) Chapter 16.

10) J. H. Wieringa, H. Wynberg, and J. Strating, *Tetrahedron*, **30**, 3053 (1974).

11) M. L. Poutsma and P. A. Ibarbia, *J. Org. Chem.*, **34**, 2848 (1969).

12) A. R. Forrester, M. Gill. J. S. Sadd, and R. H. Thomson, *J. Chem. Soc., Chem. Commun.*, **1975**, 291.

13) H. Wieland, T. Ploetz, and H. Indest, *Justus Liebigs Ann. Chem.*, **532**, 166 (1937).

14) T. Nakata, K. Tokumaru, and O. Simamura, *Tetrahedron Lett.*, **1967**, 3303.

15) For example, A. R. Lepley, and G. L. Closs, ed., "Chemically Induced Magnetic Polarization," John Wiley and Sons, Inc., New York, N. Y. (1973).

16) O. L. Brady and G. P. McHugh, *J. Chem. Soc.*, **127**, 2414 (1925).

17) A. W. Chapman and C. C. Howis, *J. Chem. Soc.*, **135**, 806 (1933).

18) W. B. Renfrow, J. F. Witte, R. A. Wolf, and W. R. Rohl, *J. Org. Chem.*, **33**, 150 (1968).

19) A. Lachman, *Org. Synth.*, Coll. Vol. **2**, 234 (1943).

20) C. R. Hayser, R. M. Manyik, W. R. Brasen, and P. L. Bayless, *J. Org. Chem.*, **20**, 1119 (1955).
21) G. Reddelien, *Chem. Ber.*, **53**, 334 (1920).
22) G. Reddelien, *Chem. Ber.*, **46**, 2718 (1913).
23) G. Reddelien, *Chem. Ber.*, **48**, 1462 (1915).
24) G. Reddelien, *Chem. Ber.*, **42**, 2759 (1909).
25) J. H. Billman and K. M. Tai, *J. Org. Chem.*, **23**, 535 (1958).
26) M. E. Taylor and T. L. Fletcher, *J. Org. Chem.*, **26**, 940 (1961).
27) P. A. S. Smith, *J. Am. Chem. Soc.*, **76**, 431 (1954).
28) H. H. Hatt, A. Pilgrim, and E. F. M. Stephenson, *J. Chem. Soc.*, **1941**, 478.
29) T. Curtius and F. Rauterberg, *J. Prakt. Chem.*, (2), **44**, 192 (1891).
30) T. Curtius and K. Kof, *J. Prakt. Chem.*, (2), **86**, 113 (1912).
31) W. Schlenk and E. Bergmann, *Justus Liebigs Ann. Chem.*, **464**, 1, 33 (1928).
32) C. L. Arcus and M. M. Coomb, *J. Chem. Soc.*, **1954**, 4319.

The Oxidation of 3-(2-Hydroxyphenyl)coumarins with Lead Tetraacetate

Kazu KUROSAWA and Keifumi NOGAMI

Department of Chemistry, Faculty of Science, Kumamoto University, Kurokami, Kumamoto 860

(Received March 10, 1976)

Five 3-(2-hydroxy-4-methoxyphenyl)coumarins (Ia—Ie) were oxidized with lead tetraacetate to the corresponding 6*H*-benzofuro[3,2-*c*][1]benzopyran-6-ones (IIa—IIe) and 3-(1-acetoxy-4-methoxy-2-oxo-3,5-cyclohexadienyl)coumarins (IIIa, IIIb, and IIId). Four 3-(3,4-dimethoxy-2-hydroxy-phenyl)coumarins (If—Ii) gave the corresponding 3-(1-acetoxy-3,4-dimethoxy-2-oxo-3,5-cyclohexadienyl)coumarins (IIIf—IIIi).

In the lead tetraacetate oxidations of phenolic compounds in which a hydroxyl group and a double bond are located in spatially suitable positions, an oxidative cyclization has often been observed.[1-5] A similar reaction of 3-(2-hydroxyphenyl)coumarin with lead tetraacetate is also expected to give 6*H*-benzofuro-[3,2-*c*][1]benzopyran-6-ones.

The 3-(2-hydroxyphenyl)coumarins (Ia—Ii) were prepared by the Perkin reaction of *o*-hydroxybenzaldehydes and *o*-hydroxyphenylacetic acids; the oxidations of Ia—Ii with lead tetraacetate were also carried out. The structures of the products were determined by examining their spectroscopic properties and by elemental analyses.

When the 3-(2-hydroxy-4-methoxyphenyl)coumarins (Ia—Ie) were oxidized, 6*H*-benzofuro[3,2-*c*][1]benzopyran-6-ones—(IIa)(10%), (IIb)(22%), (IIc)(12%), (IId)(14%), and (IIe)(5%)—were obtained, together with 3-(1-acetoxy-4-methoxy-2-oxo-3,5-cyclohexadienyl)coumarins-(IIIa)(32%), (IIIb)(16%), and (IIId)-(26%). IIc was found to be identical with dimethylcoumestrol[6] by a comparison of their melting points and their spectral data.

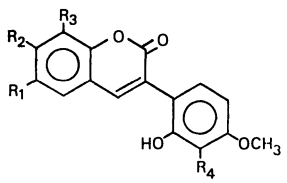

Ia~i

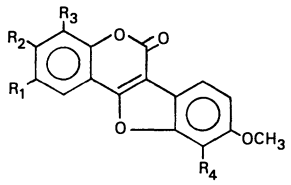

IIa~e

a $R_1=R_2=R_3=R_4=H$

b $R_1=OCH_3$, $R_2=R_3=R_4=H$

c $R_1=R_3=R_4=H$, $R_2=OCH_3$

d $R_1=R_2=R_4=H$, $R_3=OCH_3$

e $R_1=R_2=OCH_3$, $R_3=R_4=H$

f $R_1=R_2=R_3=H$, $R_4=OCH_3$

g $R_1=R_4=OCH_3$, $R_2=R_3=H$

h $R_1=R_3=H$, $R_2=R_4=OCH_3$

i $R_1=R_2=H$, $R_3=R_4=OCH_3$

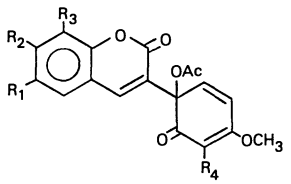

IIIa,b,d,f~i

When the 3-(3,4-dimethoxy-2-hydroxyphenyl)coumarins (If—Ii) were oxidized, 3-(1-acetoxy-3,4-dimethoxy-2-oxo-3,5-cyclohexadienyl)coumarins—(IIIf)(75%), (IIIg)(82%), (IIIh)(63%), and (IIIi)(84%)—were obtained. In the cases of the oxidation of Ia—Ie, there were considerable amounts of undefined products which could not be purified. It was found that the 6H-benzofuro[3,2-*c*][1]benzopyran-6-ones (IIa—IIe) were best prepared when a 1.5-equivalent of lead tetraacetate was used in boiling benzene.

In contrast to the oxidations of 2'-hydroxychalcones[2,3] and 2-hydroxybenzophenones,[4] which yielded aurones and xanthones respectively in fairly good yields, 3-(2-hydroxyphenyl)coumarins undergo angular acetoxylation in the cyclohexadienone ring rather than ring closure. This could be ascribed to the nature of the phenoxyl radical formed from the 2-hydroxyphenyl group with lead tetraacetate.[7] The phenoxyl radical has an electrophilic character and, therefore, favors an attack on the α-position to one on the carbonyl in the case of 2'-hydroxychalcones, and one on the *p*-position to one on a methoxyl group in the case of 2-hydroxybenzophenones. However, the carbon atom at the 4-position of 3-(2-hydroxyphenyl)coumarin is electron-deficient, as it is an α,β-unsaturated lactone; therefore, the phenoxyl radical is less reactive in this site.

Although several other syntheses of 6*H*-benzofuro-[3,2-*c*][1]benzopyran-6-ones have been reported,[8-10] the oxidative cyclization of 3-(2-hydroxyphenyl)coumarin can be used in the synthesis of 9-oxygenated 6H-benzofuro[3,2-*c*][1]benzopyran-6-ones.

Experimental

All the ^1H NMR spectra were recorded for the deuteriochloroform solution, unless otherwise stated, with a Hitachi R 24 NMR spectrometer, with tetramethylsilane as the internal reference. The IR spectra were recorded either for the chloroform solution or for the KBr disk with a JASCO IRA-1 grating spectrometer, while the UV spectra were measured for the methanol solution with a Hitachi EPS-3T spectrophotometer. The melting points were determined with a Yanagimoto hot-stage apparatus and were uncorrected.

Preparations of 3-(2-Hydroxyphenyl)coumarins (Ia—Ii). The general procedure for the preparation of 3-(2-hydroxyphenyl)coumarin was as follows: a mixture of *o*-hydroxybenzaldehyde (10 mmol), *o*-hydroxyphenylacetic acid (10 mmol), acetic anhydride (24 mmol), sodium acetate (50 mmol), and acetic acid (40 ml) was heated under reflux for 24 h. After the removal of the acetic acid, the resulting mixture was triturated with water, and the precipitates were collected by filtration. The crude product was purified by recrystallization.

3-(2-Hydroxy-4-methoxyphenyl)coumarin (Ia); mp 171—172 °C (EtOH), 62%, ν_{max}^{KBr}: 3180 (OH) and 1700 cm^{-1} (C=O), δ: 3.82 (s, OCH_3), 6.4—6.65 (m, 2H, $H_{(3')}$ and $H_{(5')}$), 7.1—7.7 (m, 5H), 7.82 (s, $H_{(4)}$), and 8.0 (broad s, OH). Found: C, 71.35; H, 4.68%. Calcd for $C_{16}H_{12}O_4$: C, 71.63; H, 4.51%.

3-(2-Hydroxy-4-methoxyphenyl)-6-methoxycoumarin (Ib); mp 179—180 °C (EtOH), 92%, ν_{max}^{KBr}: 3310 (OH) and 1710 cm^{-1} (C=O), δ: 3.80 (s, OCH_3), 3.85 (s, OCH_3), 6.4—6.7 (m, 2H, $H_{(3')}$ and $H_{(5')}$), 6.9—7.4 (m, 4H), 7.78 (s, $H_{(4)}$), and 8.20 (broad s, OH). Found: C, 68.24; H, 4.78%. Calcd for $C_{17}H_{14}O_5$: C, 68.45; H, 4.73%. 3-(2-Hydroxy-4-methoxyphenyl)-7-methoxycoumarin (Ic); mp 160—161 °C (EtOH), 79%, ν_{max}^{KBr}: 3330 (OH) and 1715 cm^{-1} (C=O), δ: 3.80 (s, OCH_3), 3.90 (s, OCH_3), 6.5—7.3 (m, 5H), 7.50 (d, $H_{(5)}$), 7.80 (s, $H_{(4)}$), and 8.1 (broad s, OH). Found: C, 68.25; H, 4.78%. Calcd for $C_{17}H_{14}O_5$: C, 68.45; H, 4.73%.

3-(2-Hydroxy-4-methoxyphenyl)-8-methoxycoumarin (Id); mp 182—183 °C ($CHCl_3$–EtOH), 83%, ν_{max}^{KBr}: 3260 (OH) and 1700 cm^{-1} (C=O), δ: 3.80 (s, OCH_3), 3.98 (s, OCH_3), 6.4—7.4 (m, 6H), 7.81 (s, $H_{(4)}$), and 8.1 (s, OH). Found: C, 68.21; H, 4.71%. Calcd for $C_{17}H_{14}O_5$: C, 68.45; H, 4.73%.

6,7-Dimethoxy-3-(2-hydroxy-4-methoxyphenyl) coumarin (Ie); mp 200—201 °C ($CHCl_3$), 84%, $\nu_{max}^{CHCl_3}$: 3240 (OH) and 1700 cm^{-1} (C=O), δ_{CF_3COOH}: 4.00 (s, OCH_3), 4.10 (s, $2\times OCH_3$), 6.7—7.5 (m, 5H), and 8.15 (s, $H_{(4)}$). Found: C, 65.56: H, 4.94%. Calcd for $C_{18}H_{16}O_6$: C, 65.85; H, 4.91%.

3-(3,4-Dimethoxy-2-hydroxyphenyl) coumarin (If); mp 203—204 °C ($CHCl_3$–EtOH), 95%, $\nu_{max}^{CHCl_3}$: 3500 (OH) and 1740 cm^{-1} (C=O), δ: 3.86 (s, OCH_3), 3.90 (s, OCH_3), 6.42 (s, OH), 6.52 (d, J=9 Hz, $H_{(5')}$), 7.0—7.6 (m, 5H), and 7.83 (s, $H_{(4)}$). Found: C, 68.35; H, 4.78%. Calcd for $C_{17}H_{14}O_5$: C, 68.45; H, 4.73%.

3-(3,4-Dimethoxy-2-hydroxyphenyl)-6-methoxycoumarin (Ig); mp 181—182°C (EtOH), 82%, $\nu_{max}^{CHCl_3}$: 3500 (OH) and 1735 cm^{-1} (C=O), δ: 3.82 (s, OCH_3), 3.88 (s, OCH_3), 392 (s, OCH_3), 6.55 (d, J=9 Hz, $H_{(5')}$), 6.55 (s, OH), 6.9—7.5 (m, 4H), and 7.82 (s, $H_{(4)}$). Found: C, 65.69; H, 4.98%. Calcd for $C_{18}H_{16}O_6$: C, 65.85; H, 4.91%.

3-(3,4-Dimethoxy-2-hydroxyphenyl)-7-methoxycoumarin (Ih); mp 136—137 °C (EtOH), 76%, $\nu_{max}^{CHCl_3}$: 3500 (OH) and 1730 cm^{-1} (C=O), δ: 3.88 (s, $2\times OCH_3$), 3.92 (s, OCH_3), 6.52 (d, J=9 Hz, $H_{(5')}$), 6.55 (broad s, OH), 6.8—7.5 (m, 4H), and 7.82 (s, $H_{(4)}$). Found: C, 65.58; H, 4.81%. Calcd for $C_{18}H_{16}O_6$: C, 65.85; H, 4.91%.

3-(3,4-Dimethoxy-2-hydroxyphenyl)-8-methoxycoumarin (Ii); mp 186—188 °C ($CHCl_3$–EtOH), 91%, $\nu_{max}^{CHCl_3}$: 3500 (OH) and 1740 cm^{-1} (C=O), δ: 3.88 (s, OCH_3), 3.92 (s, OCH_3), 3.96 (s, OCH_3), 6.51 (d, J=9 Hz, $H_{(5')}$), 6.50 (s, OH), 6.9—7.4 (m, 4H), and 7.84 (s, $H_{(4)}$). Found: C, 65.79; H, 4.91%. Calcd for $C_{18}H_{16}O_6$: C, 65.85; H, 4.96%.

Oxidation of 3-(2-Hydroxyphenyl)coumarins with Lead Tetraacetate. The general procedure for the oxidation of 3-(2-hydroxyphenyl)coumarin was as follows: to a solution of 3-(2-hydroxyphenyl)coumarin (1 mmol) in anhydrous benzene (30 ml), lead tetraacetate (1.5 mmol) was added; the mixture was then heated under reflux for 30 min. After the removal of the lead diacetate by filtration, the benzene was evaporated *in vacuo*. The resulting mixture was purified either by TLC or by recrystallization.

Ia yielded 9-methoxy-6*H*-benzofuro[3,2-*c*][1] benzopyran-6-one (IIa); mp 212—213 °C (EtOH), 10%, $\nu_{max}^{CHCl_3}$: 1740 cm^{-1}, λ_{max} (ε): 242 (35000), 334 (31100), and 345 nm (26900), δ: 3.88 (s, OCH_3) and 6.9—7.1 (m, 7H) (Found: C, 71.99; H, 3.74%. Calcd for $C_{16}H_{10}O_4$: C, 72.18; H, 3.79%); and 3-(1-acetoxy-4-methoxy-2-oxo-3,5-cyclohexadienyl) coumarin (IIIa); mp 184—186 °C (EtOH), 32%, $\nu_{max}^{CHCl_3}$: 1680 and 1740 cm^{-1}, λ_{max} (ε): 285 (14000) and 318 nm (10600), δ: 2.15 (s, OAc), 3.76 (s, OCH_3), 5.68 (d, J=2.5 Hz, $H_{(3)}$), 6.25 (dd, J=2.5, 10 Hz, $H_{(5)}$), 6.58 (d, J=10 Hz, $H_{(6)}$), 7.0—7.7 (m, 4H), and 7.84 (s, $H_{(4)}$) (Found: C, 65.95; H, 4.32%. Calcd for $C_{18}H_{14}O_6$: C, 66.25; H, 4.32%).

Ib gave 2,9-dimethoxy-6*H*-benzofuro[3,2-*c*][1]benzopyran-6-one (IIb)(mp 191—192 °C (EtOH), 22%, $\nu_{max}^{CHCl_3}$: 1740 cm^{-1}, λ_{max} (ε): 235 (38000), 320 (12300), and 345 nm (20200), δ: 3.90 (s, $2\times OCH_3$), 7.0—7.6 (m, 5H), and 7.90 (d, $H_{(7)}$) (Found: C, 68.81; 4.05%. Calcd for $C_{17}H_{12}O_5$: C, 68.91; H, 4.08%)) and 3-(1-acetoxy-4-methoxy-2-oxo-3,5-cyclohexadienyl)-6-methoxycoumarin (IIIb) (mp 176—177 °C (EtOH), 16%, $\nu_{max}^{CHCl_3}$: 1670 and 1740 cm^{-1}, λ_{max} (ε): 284 (20500) and 344 nm (10900), δ: 2.17 (s, OAc), 3.82 (s, $2\times OCH_3$) 5.71 (d, J=2.5 Hz, $H_{(3')}$), 6.26 (dd, J=2.5, 10 Hz, $H_{(5')}$), 6.45 (d, J=10 Hz, $H_{(6')}$), 6.9—7.3 (m, 3H), and 7.8 (s, $H_{(4)}$) (Found: C, 63.75; H, 4.52%. Calcd for $C_{19}H_{16}O_7$: C, 64.04; H, 4.53%).

Ic yielded 3,9-dimethoxy-6*H*-benzofuro[3,2-*c*][1]benzopyran-6-one (IIc); mp 198—199 °C (lit,[6] mp 197 °C), 12%.

Id gave 4,9-dimethoxy-6*H*-benzofuro[3,2-*c*][1]benzopyran-6-one (IId) (mp 250—251 °C (EtOH), 14%, $\nu_{max}^{CHCl_3}$: 1740 cm^{-1}, λ_{max} (ε): 242 (28800) and 335 nm (19900), δ: 3.99 (s, OCH_3), 4.05 (s, OCH_3) and 6.9—7.8 (m, 6H) (Found: C, 68.77; H, 4.11%. Calcd for $C_{17}H_{12}O_5$: C, 68.91; H, 4.08%) and 3-(1-acetoxy-4-methoxy-2-oxo-3,5-cyclohexadienyl)-8-methoxycoumarin (IIId) (mp 226—228 °C (EtOH), 38%, ν_{max}^{KBr}: 1670, 1740, and 1770 cm^{-1}, λ_{max} (ε): 257 (15400) and 301 nm (13500), δ: 2.15 (s, OAc), 3.77 (s, OCH_3), 3.80 (s, OCH_3), 5.65 (d, J=2.5 Hz, $H_{(3')}$), 6.13 (dd, J=2.5, 10 Hz, $H_{(5')}$), 6.6—6.9 (m, 3H), 7.30 (d, $H_{(5)}$), and 7.71 (s, $H_{(4)}$) (Found: C, 63.74; H, 4.47%. Calcd for $C_{19}H_{16}O_7$: C, 64.04; H, 4.53%)).

Ie yielded 2,3,9-trimethoxy-6*H*-benzofuro[3,2-*c*][1]benzopyran-6-one (IIe); mp 253—254 °C (EtOH), 5%, $\nu_{max}^{CHCl_3}$: 1740 cm^{-1}, λ_{max} (ε): 235 (32900) and 353 nm (29800), δ: 3.90 (s, OCH_3), 3.96 (s, OCH_3) 4.00 (s, OCH_3), 6.96 (s, 1H), 7.11 (s, 1H), 6.9—7.3 (m, 2H), and 7.88 (d, J=8.5 Hz, $H_{(7)}$) (Found: C, 66.44; H, 4.39%. Calcd for $C_{18}H_{14}O_6$: C, 66.25; H, 4.32%).

If gave 3-(1-acetoxy-3,4-dimethoxy-2-oxo-3,5-cyclohexadienyl)coumarin (IIIf); mp 145—146 °C (EtOH), 75%, $\nu_{max}^{CHCl_3}$: 1660 and 1740 cm^{-1}, λ_{max} (ε): 350 (12600) and 390 nm (inflection) (9720), δ: 2.15 (s, OAc), 3.52 (s, OCH_3), 3.80 (s, OCH_3), 5.53 (d, J=8.5 Hz, $H_{(5')}$), 7.1—7.6 (m, 4H), 7.74 (d, J=8.5 Hz, $H_{(6')}$), and 8.01 (s, $H_{(4)}$) (Found: C, 63.39; H, 4.76%. Calcd for $C_{19}H_{16}O_7\cdot 1/2C_2H_5OH$: C, 63.35; H, 5.02%.)

Ig yielded 2-(1-acetoxy-3,4-dimethoxy-2-oxo-3,5-cyclohexadienyl)-6-methoxycoumarin (IIIg); mp 190—192 °C (benzene), 82%, $\nu_{max}^{CHCl_3}$: 1650 and 1740 cm^{-1}, λ_{max} (ε): 376 nm (12700), δ: 2.18 (s, OAc), 3.49 (s, OCH_3), 3.80 (s, $2\times OCH_3$), 5.45 (d, J=8.5 Hz, $H_{(5')}$), 6.8—7.3 (m, 3H), 7.70 (d, J=8.5 Hz, $H_{(6')}$), and 7.94 (s, $H_{(4)}$) (Found: C, 62.19; H, 4.71%. Calcd for $C_{20}H_{18}O_8$: C, 62.14; H, 4.70%).

Ih yielded 3-(1-acetoxy-3,4-dimethoxy-2-oxo-3,5-cyclohexadienyl)-7-methoxycoumarin (IIIh); mp 178—179 °C (benzene–EtOH), 63%, $\nu_{max}^{CHCl_3}$: 1650 and 1740 cm^{-1}, λ_{max} (ε): 376 nm (12600), δ: 2.16 (s, OAc), 3.54 (s, OCH_3), 3.69 (s, OCH_3), 3.75 (s, OCH_3), 5.50 (d, J=8.5 Hz, $H_{(5')}$), 6.7—7.0 (m, 2H), 7.40 (d, $H_{(5)}$), 7.68 (d, J=8.5 Hz, $H_{(6')}$), and 7.92 (s, $H_{(4)}$) (Found: C, 62.27; H, 4.78%. Calcd for $C_{20}H_{18}O_8$: C, 62.17; H, 4.70%).

Ii gave 3-(1-acetoxy-3,4-dimethoxy-2-oxo-3,5-cyclohexadienyl)-8-methoxycoumarin (IIIi); mp 180—181 °C (benzene), 84%, $\nu_{max}^{CHCl_3}$: 1650 and 1740 cm^{-1}, λ_{max} (ε): 350 (11200) and 390 nm (inflection) (9100), δ: 2.15 (s, OAc), 3.47 (s, OCH_3), 3.75 (s, OCH_3), 3.91 (s, OCH_3), 5.43 (d, J=8.5 Hz, $H_{(5')}$), 6.9—7.3 (m, 3H), 7.80 (d, J=8.5 Hz, $H_{(6')}$), and 7.96 (s, $H_{(4)}$) (Found: 62.26; H, 4.73%. Calcd for $C_{20}H_{18}O_8$: C, 62.17; H, 4.70%).

References

1) F. F. Stephens and J. D. Bower, *J. Chem. Soc.*, **1949**, 2971.
2) K. Kurosawa, *Bull. Chem. Soc. Jpn.*, **42**, 1456 (1969).
3) K. Kurosawa and J. Higuchi, *Bull. Chem. Soc. Jpn.*, **45**, 1132 (1972).
4) K. Kurosawa, Y. Sasaki, and M. Ikeda, *Bull. Chem. Soc. Jpn.*, **46**, 1498 (1973).
5) K. Nogami and K. Kurosawa, *Bull. Chem. Soc. Jpn.*, **47**, 505 (1974).
6) W. J. Bowyer, A. Robertson, and W. B. Whally, *J. Chem. Soc.*, **1957**, 542.
7) D. Ferreira, E. V. Brandt, F. du R. Volsteedt, and D. G. Roux, *J. Chem. Soc. Perkin Trans. 1*, **1975**, 1438.
8) A. L. Livingston, E. M. Bickoff, R. E. Lundin, and L. Jurd, *Tetrahedron*, **20**, 1963 (1964).
9) O. H. Emerson and E. M. Bickoff, *J. Am. Chem. Soc.*, **80**, 4381 (1958).
10) H. W. Wanzlick, R. Gritzky, and H. Heidepriem, *Chem. Ber.*, **96**, 305 (1963).

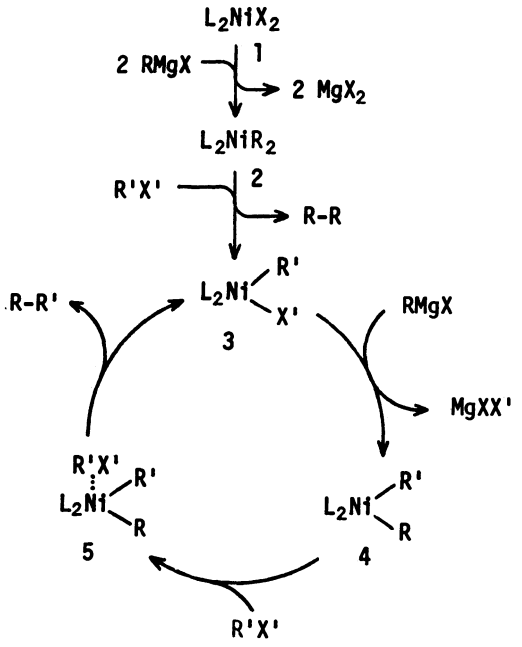

Scheme 1.

Reaction of **3** with the Grignard reagent then forms a new diorgano complex **4** from which the cross-coupling product is released by the attack of the organic halide, possibly *via* the pentacoordinated intermediate **5**, and thereby the original complex **3** is regenerated to complete the catalytic cycle.

The reaction, indeed, could be achieved by the addition of Grignard reagent to a vinylic or an aromatic halide in the presence of a catalytic amount of a dihalodiphosphinenickel and the yields were generally very high. Throughout this paper, the following phosphines and other ligands are described in their abbreviations shown here.

$Ph_2P(CH_2)_nPPh_2$

$n=1$, dppm
$n=2$, dppe
$n=3$, dppp
$n=4$, dppb

$Me_2P(CH_2)_2PMe_2$

dmpe

cis-$Ph_2PCH{=}CHPPh_2$

cis-dpen

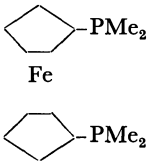

dmpf

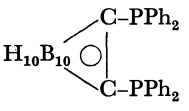

dppc

2,2′-Bipyridyl: bipy
Pyridine: py
Acetylacetonate: acac

II. Coupling of Butylmagnesium Bromide with Halobenzenes. To a mixture of chlorobenzene (1 part) and a catalytic amount of [Ni(dppp)Cl_2] (0.01—0.001 part) in anhydrous ether was added the butyl Grignard reagent (1.2 part) at 0 °C under nitrogen to give a tan clear mixture. The mixture was stirred at room temperature and a mildly exothermic reaction set in. After refluxing for 20 h and hydrolysis, GLPC analysis showed that the starting chlorobenzene was no longer present and butylbenzene was formed in quantitative yield. The product was easily isolated pure by simple distillation; there was no contamination with a structural isomer, such as *sec*-butylbenzene.

In the light of the fact that the above reaction readily goes to completion, the coupling of the butyl Grignard reagent with halobenzenes was chosen as a model reaction for the examination of the catalytic ability of various nickel–phosphine complexes and of the reactivity of halobenzenes.

Table 1. Catalytic activity of various [NiL_2Cl_2] for cross-coupling of *n*-C_4H_9MgBr with C_6H_5Cl[a]

L_2	Conversion (%)[b]	Yield (%) of *n*-$C_4H_9C_6H_5$[b]
dppp	100	100
dmpf	100	94
$2Ph_3P$	91	84[c]
$2Ph_3P$[d]	90	50[e]
dppe	73	79
dppe[f]	78	77
dmpe	53	47
dppc	30	28
dppb	38	28
cis-dpen	19	20
$2Et_3P$	63	6[g]
$2Ph_2MeP$	[h]	4[e]

a) Unless otherwise noted, to a mixture of C_6H_5Cl (~10 mmol), [NiL_2Cl_2] (~0.1 mmol) and anhydrous ether (10 ml) was added *n*-C_4H_9MgBr (~12 mmol), and then the mixture was heated for 20 h under nitrogen. b) Determined by GLPC using mesitylene as an internal standard based on the chlorobenzene used. c) Benzene 10%. d) Used as a mixture of PPh_3 (0.21 mmol) and anhydrous $NiCl_2$ (0.16 mmol). e) Benzene was not determined. f) Petroleum ether was used as additional solvent. g) Benzene 52%. h) GLPC showed the presence of a large amount of unchanged chlorobenzene.

Catalytic Activity of Various Nickel–Phosphine Complexes: Under the similar conditions, catalytic activity of various nickel(II) complexes was examined (Table 1). The catalytic activity of the nickel complexes depends strongly upon the nature of the ligands. This ligand-dependency clearly indicates that a catalytically active species does contain phosphine ligand(s) on nickel. In Table 1, the phosphine ligands are listed in the order of decreasing catalytic activity of their nickel complexes.

Bidentate phosphines as ligands exhibit much higher catalytic activity than unidentate ones; the efficiency of the bidentate phosphine ligands decreases roughly in the sequence: dppp>dmpf>dppe>dmpe>dppb>dppc>*cis*-dpen. It seems of particular interest to note that the catalytic activity depends on the length of the methylene bridge between two diphenylphosphino groups in a homologous series of $Ph_2P(CH_2)_nPPh_2$, *viz.*, $n=3>n=2>n=4$. The prominence of [Ni(dppp)Cl_2] as a catalyst is commonly observed also in different combinations of other Grignard reagents and halides (*vide infra*).

Of the unidentate phosphines as ligands, only triphenylphosphine is practically active for the coupling.

Although with $[Ni(PEt_3)_2Cl_2]$ chlorobenzene is consumed to the same extent as with $[Ni(PPh_3)_2Cl_2]$, benzene is formed as a major product.

The following nickel complexes and salts are practically inactive for the coupling: $[Ni(PPh_2Me)_2Cl_2]$, $[Ni(PPhMe_2)_2Cl_2]$, $[Ni(dppm)_2Cl_2]$, [Ni(bipy)Cl_2], $[Ni(py)_2Cl_2]$, $Ni(acac)_2$, and $NiCl_2$. With [Ni(bipy)Cl_2] as a catalyst the reaction mixture remained a deeply green color characteristic of diorganonickel complexes with the bipy ligand,[33] indicating that the intermediate is too stable to react further with chlorobenzene. It should be noted that an equimolar mixture of [Ni(dppe)Cl_2] and the dppe free ligand exhibited no catalytic activity, apparently owing to the blocking of catalytically active vacant sites on the nickel catalyst by the extra phosphine. Interestingly, $Ni(acac)_2$, which was reported to be efficient for the coupling of aryl Grignard reagents with aryl and alkenyl halides,[20] showed no activity at all for the coupling of simple alkyl Grignard reagents with chlorobenzene.

$[Pd(PPh_3)_2Cl_2]$, $[Pd(PEt_3)_2Cl_2]$, *cis*-$[Pt(PPh_3)_2Cl_2]$, and [Co(dppp)Cl_2] exhibited no catalytic activity, which may be attributable primarily to the fact that chlorobenzene hardly undergoes oxidative addition to the low valent species of these metals.[31d,34] The recently reported palladium(0)catalyzed Grignard coupling may be restricted to more reactive bromides.[22]

TABLE 2. EFFECT OF AGING ON THE CATALYTIC ACTIVITY IN THE COUPLING OF *n*-C_4H_9MgBr WITH C_6H_5Cl[a]

Aging time (h)	Reaction time after addition of C_6H_5Cl (h)	Conversion (%)	Yield (%) C_4H_9–C_6H_5	Yield (%) C_6H_6
		[Ni(dppp)Cl_2]		
1/30	3	>99	99	trace
1	3	>99	97	trace
3.5	3	>99	>99	trace
16	3	>99	98	trace
		[Ni(PPh_3)$_2Cl_2$]		
0[b]	3	63	52	N.d.
0[b]	20	87	72	N.d.
1/20	3	78	58	22
1	3	71	55	20
16	3	53	21	N.d.
16	20	94	69	35

a) To a mixture of the catalyst (0.05 mmol) and ether (5 ml) was added *n*-BuMgBr in ether (6 mmol) at 0 °C. The mixture was stirred at room temperature for a given period of aging time: [Ni(dppp)Cl_2] gave a yellowish clear solution, while [Ni(PPh_3)$_2Cl_2$] gave a dark brown mixture. Chlorobenzene (5 mmol) was then added at room temperature in one portion and the mixture was stirred at room temperature for 30 min and then refluxed for a given period of time. After hydrolysis the mixture was analyzed by GLPC. b) To a mixture of the catalyst, chlorobenzene and ether was added the *n*-C_4H_9MgBr solution.

Aging of Catalysts: Stability of the catalytically active species has been examined for [Ni(dppp)Cl_2] and [Ni(PPh_3)$_2Cl_2$] (Table 2). Thus, a catalytic amount of the nickel complex was firstly added to the butyl Grignard reagent, the resulting mixture was allowed to stand at room temperature under nitrogen for a given period of time, and then chlorobenzene was added. Rather surprisingly, the yellowish clear catalyst solution generated from [Ni(dppp)Cl_2] and the butyl Grignard reagent did not decrease in efficiency even after 16 h at room temperature. Upon addition of chlorobenzene at this point, an exothermic reaction set in and exactly the same results were obtained as the case where the Grignard reagent was finally added to a mixture of chlorobenzene and [Ni(dppp)Cl_2] (without aging).

In contrast with this result, a dark-brown mixture generated from [Ni(PPh_3)$_2Cl_2$] and the butyl Grignard reagent gradually diminished in activity with time. However, the prolonged coupling-reaction time led to essentially the same results as observed in experiments with no aging.

These results demonstrate a great stabilizing effect on the catalytically active species by, notably, the bidentate phosphine ligand.

Reactivity of Halobenzenes: Reactivity of halobenzenes, from fluoro- to iodo-benzene, was examined for the coupling with the butyl Grignard reagent in the presence of [Ni(dppp)Cl_2] or [Ni(dppe)Cl_2] as catalyst.

TABLE 3. REACTIVITY OF HALOBENZENES IN THE COUPLING WITH *n*-C_4H_9MgBr[a]

X in C_6H_5X	Reaction time (h)	Conversion[b] (%)	Yield (%)[b] *n*-$C_4H_9C_6H_5$	Yield (%)[b] C_6H_6
		[Ni(dppp)Cl_2]		
F	2	c)	31	c)
Cl	1	54	50	trace
Cl	2	80	81	trace
Cl[d]	3	93	95	trace
Br	1	47	39	6
Br	2	56	46	7
Br	4.5	62	54	9
I[d]	3[e]	99	80	19[f]
		[Ni(dppe)Cl_2]		
F	20	c)	18	c)
Cl	20	59	60	trace
Br	20	75	51	23

a) To a mixture of C_6H_5X (~5 mmol) and [NiL_2Cl_2] (~0.05 mmol) in 15 ml of ether was added a solution of *n*-C_4H_9MgBr (6.3 mmol) in ether at 0 °C and then refluxed for a given period of time, unless otherwise noted. b) Determined by quantitative GLPC based on C_6H_5X. c) Conversion and benzene could not be determined by GLPC, because C_6H_5F and benzene appeared in a single peak. d) Carried out in a 10-mmol scale. e) The reaction occurred vigorously even at 0 °C. Stirred at room temperature for 3 h. f) Biphenyl 2%.

The reactivity of halobenzenes appears to be dependent upon the nature of the catalyst. Thus, while with [Ni(dppp)Cl_2] a rather abnormal reactivity order PhI>PhCl>PhBr>PhF was observed, with [Ni(dppe)Cl_2] the order was normal: PhBr>PhCl>PhF (Table 3). However, from the competitive reactions (Table 4), the normal reactivity order was observed also with [Ni(dppp)Cl_2]. This strange behavior is difficult to

Table 4. Competitive reaction between two kinds of halobenzenes with n-C_4H_9MgBr[a]

Combination of C_6H_5X	Reaction time (h)	run	Conversion (%)[b] 1	2	3
		[Ni(dppp)Cl_2]			
C_6H_5F / C_6H_5Cl	1		25 / 52	24 / 58	26 / 47
C_6H_5Cl / C_6H_5Br	1		25 / 45	25 / 45	24 / 46
		[Ni(dppe)Cl_2]			
C_6H_5F / C_6H_5Cl	20		19 / 58	20 / 58	— / —
C_6H_5Cl / C_6H_5Br	20		29 / 78	30 / 80	29 / 75[c]

a) For the procedure, see footnote a) of Table 3: C_6H_5X, 5 mmol each; Grignard reagent, 6.4 mmol; catalyst, ~0.05 mmol; ether, 15 ml. b) Determined by GLPC. c) Benzene 22%.

explain, but implies that there are two or more rate-limiting steps in the reaction.

In view of the extremely low reactivity of organofluoro compounds toward metals, it seems of particular interest that even fluorobenzene, if not completely, does undergo the metal-catalyzed coupling reaction. To our knowledge, oxidative addition of a fluorine–carbon bond to a transition metal complex has not yet been reported.[31e] Iodobenzene reacts very vigorously even at 0 °C, with biphenyl being formed only in trace amounts. The formation of benzene also depends on the nature of the halides in the order: PhF<PhCl≪PhBr<PhI.

The foregoing results demonstrate that chlorobenzene exhibits a reasonable reactivity, gives a high yield of the cross-coupling product with no by-product, and hence is the halide that was chosen for the present reaction. The superiority of chlorobenzene as a halide is particularly worthy of note, because bromides or iodides have been used so far in almost all types of coupling reactions of organic halides using metals as coupling agents.

Table 5. Solvent effects on the coupling of C_2H_5MgBr with C_6H_5Cl[a]

Solvent	Reaction time (h)	Conversion[b] (%)	Yield (%)[b] $C_2H_5C_6H_5$	C_6H_6
		[Ni(dppe)Cl_2]		
$(C_2H_5)_2O$	16	99	98	trace
THF	22	78	66	11
		[Ni(PPh_3)$_2Cl_2$]		
$(C_2H_5)_2O$	16	86	59	20
THF	22	51	10	35

a) C_6H_5Cl, 12 mmol; C_2H_5MgBr, 12—14 mmol; catalyst, 0.1 mmol; solvent 20 ml. Refluxed for a given period of time. b) Determined by GLPC.

Solvent Effects: Grignard reagents are usually prepared either in diethyl ether or in THF, and hence these two solvents were examined in regard to solvent effects. The effects on the coupling of the ethyl Grignard reagent with chlorobenzene in the presence of [Ni(dppe)Cl_2] or [Ni(PPh_3)$_2Cl_2$] as catalyst are summarized in Table 5. For both of the catalysts used, the reactions tend to proceed considerably faster in diethyl ether than in THF and the undesired product, benzene, is formed in a larger amount in THF. Therefore, diethyl ether is better than THF as a solvent.

Although reasons for the observed solvent effects are not clear presently, it seems likely that a more basic solvent (THF>Et_2O) interacts more tightly with the nickel center to prevent the approach of the halide and/or the Grignard reagent to it.

III. Coupling of Other Alkyl, Aryl, and Alkenyl Grignard Reagents with Aryl and Alkenyl Halides. The generality of the nickel-phosphine complex-catalyzed Grignard cross-coupling is apparent from the results summarized in Tables 6 and 7.

Catalytic Activity of Nickel–Phosphine Catalysts: Table 6 summarizes a comparison of the catalytic activities of some selected nickel-phosphine complexes for several representative combinations of Grignard reagents and organic halides. The efficiency of the catalysts appears to be dependent mainly on the structur of the organic moieties of Grignard reagents and little on the nature of the organic halides. Several features are worthy of note.

Here again, [Ni(dppp)Cl_2] is the most effective for primary alkyl (regardless of the presence or absence of β-hydrogen(s) (*vide infra*)), secondary alkyl, and aryl Grignard reagents.

Two rather exceptional cases arise. Firstly, [Ni(dmpe)Cl_2], which contains a basic bidentate ligand, is the most suitable catalyst for allylic and vinylic Grignard reagents. Interestingly, both the Grignard reagents contain an unsaturated group potentially capable of coordination with the nickel center of the catalyst. This exceptional behavior may be related to the observations that basic ligands can cause π-σ conversion of an allyl-nickel complex, whereas less basic ligands form a relatively stable five-coordinate π-allyl-nickel complex, as exemplified by the following equations:[35]

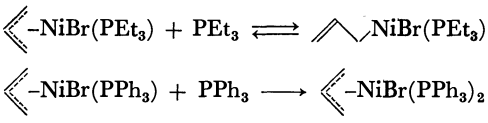

It should be noted that the former is coordinatively unsaturated, while the latter saturated.

The other exceptional case is observed in the coupling of the mesityl Grignard reagent for which a unidentate phosphine is better than bidentate phosphine ligands. It has long been recognized that *ortho*-substituted aryl-nickel complexes are of high kinetic stability[36] and hence the enhanced stability of a mesityl-nickel intermediate to be expected with a bidentate phosphine ligand may be responsible for the diminished reaction rates in this case. A reversible ligand dissociation from a dimesitylnickel complex of a unidentate phosphine has been observed.[37]

The pronounced differences in catalytic activity between [Ni(dppp)Cl_2] and [Ni(dppe)Cl_2] were observed for the coupling of the trimethylsilylmethyl Grignard reagent with chlorobenzene; with the former catalyst the coupling product was obtained in quantitative yield.

TABLE 6. CATALYTIC ACTIVITY OF $[NiL_2Cl_2]$ FOR THE COUPLING OF VARIOUS GRIGNARD REAGENTS WITH ORGANIC HALIDES[a]

RMgX	Halide	Yield (%) of coupling product[b]				
		dppp	dppe	dmpe	$2Ph_3P$	$2Et_3P$
n-PrMgBr	PhCl[c]	94	—	19	72[d]	—
i-PrMgCl	PhCl[c,e]	89	74	81	20[f]	trace
MeMgBr	PhCl[c]	100	65[g]	—	—	—
MeMgBr	Cl[c]	98	24	—	—	—
Me_3SiCH_2MgCl	PhCl[c]	100	0	16[h]	53[i]	95
CH_2=$CHCH_2MgBr$	PhBr[j]	trace	trace	63	36	37[k]
CH_3CH=$CHMgBr$	PhBr[l,m]	16	—	84	15	—
Mes–MgBr[n]	PhBr[c]	78	—	85	96	—
n-$C_8H_{17}MgCl$	CH_2=CHCl	—	95	—	72	48
PhMgBr	CH_2=CHCl	—	89	—	63	58

a) $[NiL_2Cl_2]$/RMgX/R′X′$\simeq 10^{-2}$/1.2/1.0. The reactions were carried out in a 5—10 mmol scale in diethyl ether, unless otherwise noted. b) Determined by quantitative GLPC based on the organic halide. c) Refluxed for 20 h. d) Benzene 20%. e) For the alkyl group isomerization, see Ref. 25. f) Benzene 24%. g) Recovered PhCl 24%. h) Refluxed for 37 h. i) Recovered PhCl 41%. j) Refluxed for 50 h. k) L_2=2*n*-Bu_3P. l) For 40 h at 50 °C in THF. m) Stereochemistry has been discussed in Ref. 26. n) Mes=mesityl.

TABLE 7. COUPLING OF ALKYL, CYCLOALKYL, ARYL, ALKENYL GRIGNARD REAGENTS WITH ARYL AND ALKENYL HALIDES:[a] CATALYST A; $[Ni(dppp)Cl_2]$, B; $[Ni(dppe)Cl_2]$, C; $[Ni(PPh_3)_2Cl_2]$, D; $[Ni(dmpe)Cl_2]$

Halide (mmol)	Grignard reagent (mmol)	Catalyst (mmol)	Time,[b] h	Product(s)	Yield[c] (%)
Aryl halide					
1,2-$Cl_2C_6H_4$ (200)	*n*-C_4H_9MgBr (500)	A (0.5)	6	1,2-$(C_4H_9)_2C_6H_4$	79—83
				1,2-$C_4H_9C_6H_4Cl$	*ca.* 10
1,2-$Cl_2C_6H_4$ (53)	*n*-C_4H_9MgBr (120)	B (0.38)	20	1,2-$(C_4H_9)_2C_6H_4$	89
				1,2-$C_4H_9C_6H_4Cl$	*ca.* 5
1,3-$Cl_2C_6H_4$ (51)	*n*-C_4H_9MgBr (120)	B (0.39)	20	1,3-$(C_4H_9)_2C_6H_4$	94
				1,3-$C_4H_9C_6H_4Cl$	< 5
1,4-$Cl_2C_6H_4$ (9.3)	*n*-C_4H_9MgBr (24)	B (0.04)	20	1,4-$(C_4H_9)_2C_6H_4$	95
				1,4-$C_4H_9C_6H_4Cl$	< 5
1,4-$Cl_2C_6H_4$ (102)	*n*-C_4H_9MgBr (224)	C (0.90)	26	1,4-$(C_4H_9)_2C_6H_4$	30[d]
1,2-$ClC_6H_4CH_3$ (49)	*n*-C_4H_9MgBr (72)	B (0.23)	20	1,2-$C_4H_9C_6H_4CH_3$	37
1,3-$ClC_6H_4CH_3$ (51)	*n*-C_4H_9MgBr (72)	B (0.22)	20	1,3-$C_4H_9C_6H_4CH_3$	48
1,4-$ClC_6H_4CH_3$ (48)	*n*-C_4H_9MgBr (72)	B (0.24)	20	1,4-$C_4H_9C_6H_4CH_3$	58
1,4-$ClC_6H_4CH_3$ (10)	*n*-C_4H_9MgBr (13)	A (0.05)	15	1,4-$C_4H_9C_6H_4CH_3$	(39)[e]
1,4-$ClC_6H_4OCH_3$ (24)	*n*-C_4H_9MgBr (38)	A (0.07)	6	1,4-$C_4H_9C_6H_4OCH_3$	(90)
1,4-$ClC_6H_4CF_3$ (12)	*n*-C_4H_9MgBr (13)	A (0.05)	15	1,4-$C_4H_9C_6H_4CF_3$	(56)[f]
1-Np-Br[g] (91)	*n*-C_4H_9MgBr (120)	B (0.42)	20	1-Np-C_4H_9	88
1-Np–Br (101)	*n*-C_4H_9MgBr (113)	C (0.91)	23	1-Np-C_4H_9	44[h]
1-Np–Br (99)	C_6H_5MgBr (125)	B (0.41)	20[i]	1-Np-C_6H_5	91
C_6H_5Br (92)	1-Np–MgBr[j] (126)	B (0.37)	20	1-Np-C_6H_5	98
C_6H_5Cl (5.5)	Mes–MgBr[k] (6)	A (0.04)	20	C_6H_5–Mes	(6)
1-Np–Br (4.1)	Mes–MgBr (6)	A (0.04)	20	1-Np–Mes	(45)
1,2-$CH_3OC_6H_4Br$ (5.2)	Mes–MgBr (6)	A (0.05)	20	1,2-$CH_3OC_6H_4$–Mes	(74)
Mes–Br[k] (4.2)	C_6H_5MgBr (6)	A (0.05)	20	C_6H_5–Mes	(48)
Mes–Br (4.7)	*n*-C_4H_9MgBr (6)	C (0.08)	20	Mes–H	(40)
C_6H_5Cl (9.6)	$(CH_3)_5Si_2CH_2MgCl$ (12)	A (0.03)	23	$(CH_3)_5Si_2CH_2C_6H_5$	(92)
1,2-$Cl_2C_6H_4$ (10)	$(CH_3)_3SiCH_2MgCl$ (24)	A (0.1)	20	1,2-$[(CH_3)_3SiCH_2]_2C_6H_4$	75
1,3-$Cl_2C_6H_4$ (30)	$(CH_3)_3SiCH_2MgCl$ (70)	A (0.3)	20	1,3-$[(CH_3)_3SiCH_2]_2C_6H_4$	83
1,4-$Cl_2C_6H_4$ (30)	$(CH_3)_3SiCH_2MgCl$ (70)	A (0.3)	20	1,4-$[(CH_3)_3SiCH_2]_2C_6H_4$	81
1-Np–Br (20)	$(CH_3)_3SiCH_2MgCl$ (24)	A (0.2)	21	1-Np–$CH_2Si(CH_3)_3$	66
9-Ant–Br[l] (4.0)	$(CH_3)_3SiCH_2MgCl$ (5)	C (0.05)	18[m]	9-Ant–$CH_2Si(CH_3)_3$	71

TABLE 7. Continued

Halide (mmol)	Grignard reagent (mmol)	Catalyst (mmol)	Time,[b] h	Product(s)	Yield[c] (%)
[Cl-C$_6$H$_4$-]$_2$ (2.4)	$(CH_3)_3SiCH_2MgCl$ (7.5)	A (0.02)	20	[$(CH_3)_3SiCH_2$-C$_6$H$_4$-]$_2$	65
C_6H_5Cl (30)	*c*-$C_6H_{11}MgBr$[n] (41)	A (0.15)	20	*c*-$C_6H_{11}C_6H_5$	(97)[o]
C_6H_5Cl (5.0)	*c*-$C_6H_{11}MgBr$ (7.3)	D (0.03)	20	*c*-$C_6H_{11}C_6H_5$	(80)
1,2-$Cl_2C_6H_4$ (9.6)	*c*-$C_6H_{11}MgBr$ (22)	A (0.02)	22	*c*-$C_6H_{11}C_6H_5$	(31)
				1,2-*c*-$C_6H_{11}C_6H_4Cl$	(8.5)[p]
1,3-$Cl_2C_6H_4$ (30)	*c*-$C_6H_{11}MgBr$ (66)	A (0.03)	20	1,3-(*c*-$C_6H_{11})_2C_6H_4$	73
1,4-$Cl_2C_6H_4$ (10)	*c*-$C_6H_{11}MgBr$ (22)	A (0.02)	22	1,4-(*c*-$C_6H_{11})_2C_6H_4$	63
1-Np-Br (30)	*c*-$C_6H_{11}MgBr$ (36)	A (0.03)	20	1-Np-*c*-C_6H_{11}	47
C_6H_5Cl (6.4)	*c*-C_3H_5MgBr[q] (7.3)	A (0.03)	81	*c*-$C_3H_5C_6H_5$	9
C_6H_5Br (4.0)	*c*-C_3H_5MgBr (4.8)	D (0.05)	70	*c*-$C_3H_5C_6H_5$	37
C_6H_5Br (8.4)	CH_2=$C(CH_3)MgBr$[r] (11)	D (0.08)	20[s]	$C_6H_5C(CH_3)$=CH_2	(85)
1,4-$ClBrC_6H_4$ (10)	CH_2=$C(CH_3)MgBr$[r] (11)	D (0.08)	20[s]	1,4-CH_2=$(CH_3)CC_6H_4Cl$	(68)
1,4-$Br_2C_6H_4$ (10)	CH_2=$C(CH_3)MgBr$[r] (22)	D (0.08)	20[s]	1,4-[CH_2=$(CH_3)C]_2C_6H_4$	(72)
				1,4-CH_2=$(CH_3)CC_6H_4Br$	(28)
1,2-$BrC_6H_4CH_3$ (10.6)	CH_2=$C(CH_3)MgBr$[r] (11.7)	D (0.04)	20[s]	1,2-$CH_3C_6H_4C(CH_3)$=CH_2	(30)
1,3,5-$Cl_3C_6H_3$ (5.6)	CH_2=$C(CH_3)MgBr$[r] (16.5)	D (0.04)	20[s]	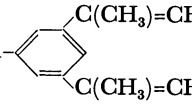	(25)
1,2,4,5-$Cl_4C_6H_2$ (4.6)	CH_2=$C(CH_3)MgBr$[r] (20.2)	D (0.08)	20	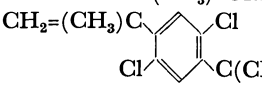	(70)
1-Np-Br (10)	CH_2=$C(CH_3)MgBr$[r] (11)	D (0.08)	20[s]	1-Np-$C(CH_3)$=CH_2	(78)
C_6H_5Br (55)	CH_2=$CHMgCl$[r] (12.5)	D (0.05)	20[m]	C_6H_5CH=CH_2	(28)[t]
Alkenyl halide					
CH_2=$CHCl$[u]	1-Np-$MgBr$[k] (55)	B (0.34)	20[m]	1-Np-CH=CH_2	80[t]
CH_2=$CHCl$[u]	*c*-$C_6H_{11}MgBr$ (10)	A (0.03)	2.5[m]	*c*-$C_6H_{11}CH$=CH_2	(47)[t]
CH_2=$CHCl$ (240)	4-ClC_6H_4MgBr (200)	A (0.1)	1.5[m]	4-ClC_6H_4CH=CH_2	79[t]
CH_2=$CHCl$[u]	$(CH_3)_3SiCH_2$-$MgCl$ (10)	A (0.1)	20	$(CH_3)_3SiCH_2CH$=CH_2	78[t]
CH_2=$CHCl$[u]	Mes-$MgBr$ (14)	A (0.1)	20[s]	Mes-CH=CH_2	(78)[t]
CH_2=CCl_2 (95.8)	C_6H_5MgBr (220)	B (0.62)	16.5	CH_2=$C(C_6H_5)_2$	82
CH_2=CCl_2 (50)	$C_6H_5CH_2MgCl$ (130)	B (0.20)	20	CH_2=$C(CH_2C_6H_5)_2$	43
CH_2=CCl_2 (20)	$(CH_3)_3SiCH_2MgCl$ (44)	A (0.40)	20	v)	
(*Z*)-ClCH=CHCl (5.0)	C_6H_5MgBr (12)	B (0.05)	2[m]	C_6H_5CH=CHC_6H_5 *Z*:*E*=90:10[w]	(91)
(*E*)-ClCH=CHCl (5.0)	C_6H_5MgBr (12)	B (0.05)	2[m]	C_6H_5CH=CHC_6H_5 *Z*:*E*=80:20[w]	(100)
(*E*)-ClCH=CHCl (7.2)	*n*-C_4H_9MgBr (32)	A (0.07)	24[m]	C_4H_9CH=CHC_4H_9	(23)
				C_8H_{18}	(48)
(*E*)-ClCH=CHCl (8.3)	$C_6H_5CH_2MgCl$ (38)	A (0.07)	63[m]	$(C_6H_5CH_2)_2$	(75)[x]
(*Z*)-ClCH=CHCl (12)	*c*-$C_6H_{11}MgBr$ (25)	A (0.02)	21	(*E*)-*c*-$C_6H_{11}CH$=CH-*c*-C_6H_{11}	(14)[y]
(*E*)-ClCH=CHCl (11)	*c*-$C_6H_{11}MgBr$ (23)	A (0.02)	21	(*E*)-*c*-$C_6H_{11}CH$=CH-*c*-C_6H_{11}	(43)[y]
CH_2=$C(CH_3)Br$ (12)	CH_2=$C(CH_3)MgBr$ (25)	A (0.1)	20	[CH_2=$C(CH_3)]_2$	(79)
CH_2=$C(Cl)CH$=CH_2[z] (108)	C_6H_5MgBr (125)	B (0.43)	20[m,z']	CH_2=$C(C_6H_5)CH$=CH_2	65
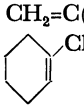 (83)	*n*-C_4H_9MgBr (120)	B (0.42)	20	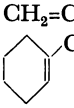	67

a) Carried out under nitrogen atmosphere. Unless otherwise mentioned, solvent is diethyl ether. The Grignard reagent was added to a mixture of a halide, a catalyst, and solvent. The reaction conditions are not necessarily optimum. b) Unless otherwise noted, refluxed for the given period of time. c) Isolated yield based on the halide, unless otherwise noted. Yields determined by quantitative GLPC are given in parentheses. d) Conversion 58%. e) Conversion 44%. f) Conversion 59%. g) Np=naphthyl. h) Naphthalene 43%. i) An exothermic reaction occurred. j) In a mixed solvent of benzene, ether, and THF (3:2:1). k) Mes=mesityl. l) Ant=anthryl. m) Room temperature. n) *c*-C_6H_{11}=cyclohexyl. o) Contaminated with a few per cent of dicyclohexyl. p) 1,2-Dicyclohexylbenzene was not formed. q) *c*-C_3H_5=cyclopropyl. r) In tetrahydrofuran. s) 40—50 °C. t) Based on the Grignard reagent. u) About 2 fold excess. v) A complex mixture of products were formed. w) For a detailed stereochemical aspects, see Ref. 26. x) Little $C_6H_5CH_2CH$=$CHCH_2C_6H_5$ was formed. y) Dicyclohexyl 8—9% yield. z) A *m*-xylene solution. z') A vigorous reaction occurred at 0 °C.

whereas with the latter no reaction occurred at all under similar conditions, the reaction mixture remaining a clear yellow solution. In view of the recently recognized concept that Me_3SiCH_2–transition metal complexes are the best examples of "elimination-stabilized alkyls,"[38] the lack of the catalytic activity of [Ni(dppe)Cl_2] in this case may be attributable primarily to the great stability of the initially formed bis(trimethylsilylmethyl)nickel intermediate. This hypothesis could be partially supported by the isolation of [Ni(dppe)$(CH_2SiMe_3)_2$] as a stable complex in high yield from the reaction of Me_3SiCH_2MgCl with [Ni(dppe)Cl_2] even in chlorobenzene as solvent.[39] However, with the experimental results at hand, it seems hard to find valid reasons for the higher efficiency of dppp as ligand as compared with dppe.[40]

Finally, of particular interest, but rather hard to understand, is that [Ni(dmpe)Cl_2] is among the poor catalysts for reactions with primary alkyl Grignard reagents, but one of the best ones for reactions with secondary alkyl Grignard reagents, although in the latter case extensive isomerization of the alkyl group from secondary to primary takes place during the cross-coupling.[25] This strange trend can not easily be interpreted in terms of the stability order of the organonickel intermediates involved.

Organic Halides and Grignard Reagents: Results summarized in Table 7 contain several features worthy of note.

(1) The present Grignard cross-coupling is equally applicable to substituted halobenzenes, polyhalobenzenes, and condensed aromatic halides. In these cases no positional scrambling is observed. Thus, the organic moiety of the Grignard reagent becomes bonded to the carbon atom which has borne the halogen atom. Therefore, the isomeric purity of the coupling products is very high.

(2) The reactivity order of substituted aryl halides has not yet been studied quantitatively, but judging from the exothermicity of reactions, dichloro- and dibromo-benzene and 1-bromonaphthalene are among the most reactive aryl halides examined, while chlorotoluenes are the least reactive ones. Interestingly, in spite of the low reactivity of monoalkylchlorobenzenes, dichlorobenzenes are smoothly *dialkylated* even in the presence of two-fold excess of dichlorobenzene over the alkyl Grignard reagent to give, for example, a 94: 6 mixture of dibutylbenzene and butylchlorobenzene. The result suggests that the second alkylation step in dichlorobenzene is mechanistically different from the alkylation of chlorotoluenes.

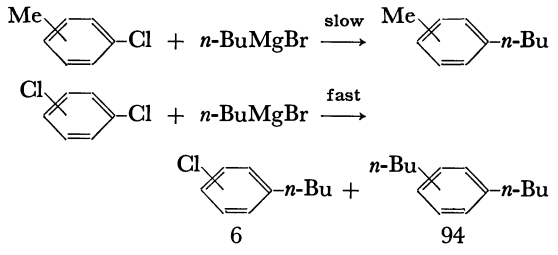

(3) Vinyl chloride is one of the most reactive halides and reacts with aryl and alkyl Grignard reagents with equal efficiency. The reactions using vinyl chloride are usually conducted either in a pressure glass-tube or in an ordinary reaction vessel, as described in Experimental section. These are strongly exothermic reactions and may proceed with violence unless controlled by the dropwise addition of Grignard reagents: care must be taken NOT to add a catalyst to a mixture of the halide and a Grignard reagent, particularly, in a large scale preparation. For example, the addition of a small amount of [Ni(dppp)Cl_2] to a mixture of vinyl chloride and 4-chlorophenylmagnesium bromide in ether at 0 °C led, after a few minutes' induction period, to an uncontrollable violent reaction.

While 1,1- and 1,2-dichloroethylenes react very smoothly with *aryl* Grignard reagents, reactions with *alkyl* Grignard reagents proceed sluggishly to give a mixture of products, usually the homo coupling product of the Grignard reagent predominating. The sluggish and complicated nature of these reactions constitutes, unfortunately, one of the most serious limitations of the present nickel–phosphine catalyzed Grignard coupling.

(4) Vinylic Grignard reagents exhibited relatively low reactivity and vinylmagnesium chloride in THF is one of the least reactive ones. Dihalobenzenes are not completely converted to dialkenylbenzenes even in the presence of [Ni(dmpe)Cl_2]. Therefore, from a synthetic viewpoint, styrene and its derivatives should be prepared from an aryl Grignard reagent and a vinylic halide rather than from an aryl halide and a vinylic Grignard reagent:

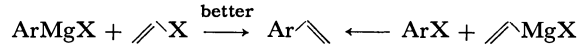

Stereochemical aspects of the coupling using vinylic halides or vinylic Grignard reagents have been reported briefly[26] and will be discussed in more detail elsewhere.

(5) The cyclohexyl Grignard reagent couples with almost all of the aryl halides studied, excepting 1,2-dichlorobenzene which gave no dicyclohexylbenzene, but a mixture of cyclohexylbenzene and cyclohexylchlorobenzene. The cyclopropyl Grignard reagent is reluctant to react with halobenzenes; a fair yield of cyclopropylbenzene was obtained with the [Ni(dmpe)-Cl_2] catalyst. It seems of interest to note that the relatively high activity of [Ni(dmpe)Cl_2] in this case is similar to the situation observed for vinylic Grignard reagents, and may be related partially to the special hybridization of cyclopropyl carbon atoms.[43]

(6) Sterically hindered, *ortho*-substituted aryl halides (especially bromides) and Grignard reagents also couple smoothly to afford *ortho*-substituted unsymmetrical biaryls. Chlorobenzene is reluctant to react with the mesityl Grignard reagent. Generally, better yields can be obtained from a combination of a hindered aryl Grignard reagent and a less hindered bromide rather than the reverse combination.

Unfortunately, the action of the *n*-butyl Grignard reagent on mesityl bromide resulted in the formation of mesitylene.

IV. Summary of General Scope and Limitations. The foregoing experimental results reveal that the present nickel–phosphine complex catalyzed Grignard coupling reaction is widely applicable to a variety of

Grignard reagents and various C(sp^2)-halides, with only a few limitations. Generally, for the direct alkylation and arylation of C(sp^2)-halides are required drastic reaction conditions, unless either they are strongly activated by some substituents or certain sophisticated reagents, such as organocuprates, are used.[44] The present reaction requires only a catalytic amount of a nickel–phosphine complex, uses mild reaction conditions, and gives high yields of cross-coupling products of high purity. It seems of interest to compare the present one-step preparation of, for example, the isomeric pure di-*n*-alkylbenzenes with the traditional multistep preparative methods starting with cyclohexenone or phthalic anhydride.[45]

The most serious limitation is that the substituents on the organic halides and on the Grignard reagents are restricted to those which cannot react with Grignard reagents. Reactions of appropriately masked halocarbonyl compounds are now being investigated with a view to overcoming the limitations.

V. A Brief Comment on the Mechanism. Although the mechanism of the present reaction has not yet been fully clarified, almost all of the foregoing results can be rationalized by Scheme 1. The most recent mechanistic studies by Morrell and Kochi[46] also provide results essentially consistent with this Scheme.

On the other hand, Felkin and Corriu and their coworkers have proposed a mechanism involving the oxidative addition of a Grignard reagent to Ni(0) species for a series of nickel-catalyzed Grignard reactions.[19,47]

We recently observed that organolithium reagents cannot be used in place of the corresponding Grignard reagents in the present coupling reaction.[48] Therefore, it seems likely that magnesium moieties of the Grignard reagents may play an important role in the high yield, selective cross-coupling reaction. While much remains to be studied for the elucidation of the mechanism, it seems apparent at least that diorganonickel intermediates are involved in this reaction.

In connection with these mechanistic aspects, it seems of interest to discuss a few special features of this reaction, based on the facts so far recognized concerning organonickel complexes. Firstly, the most remarkable feature of the present reaction is that even alkyl Grignard reagents containing the β-hydrogen(s) give selectively the cross-coupling products in high yields, because a transition metal alkyl containing β-hydrogen(s) is commonly unstable and tends to undergo β-elimination to form a metal hydride and an olefin;[38,49] nickel alkyls being also the case:

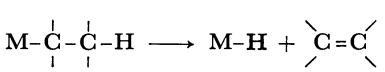

For the same reasons, no aging effect on the catalytic activity is also noteworthy. Here again, an important role of magnesium components may be envisaged, as well as the stabilizing effect of the phosphine ligands.

Secondly, the aforementioned reactivity of vinylic halides in striking contrast to vinylic Grignard reagents implies the importance of the interaction between the diorganonickel intermediate and the unsaturated organic component (*cf.* **5** in Scheme 1). Thus, a strong interaction between a vinylic halide and a diorganonickel intermediate favors the catalytic process. On the other hand, the vinylic Grignard reagent as an olefinic component may well compete with the organic halide of comparable or lower coordinating ability for coordination onto the diorganonickel intermediate. This type of interaction may be responsible for the inhibited catalysis encountered with [Ni(dppp)Cl_2] catalyst. The high efficiency of [Ni(dmpe)Cl_2] in this case may be attributable to the expected weak interaction between the electron-rich olefin in the vinylic Grignard reagent and the nickel species bearing the electron-donating phosphine.

Experimental

Materials. Phosphine–nickel(II), –palladium(II), –platinum(II), and –cobalt(II), and amine–nickel(II) complexes were prepared by known methods. In the following list, the references given after the compounds are to the source or method of preparation: [Ni(PPh_3)$_2Cl_2$],[50] [Ni(PPh_2Me)$_2Cl_2$],[51] [Ni($PPhMe_2$)$_2Cl_2$],[52] [Ni{P(*n*-Bu)$_3$}$_2Cl_2$],[53] [Ni(PEt_3)$_2$-Cl_2],[53] [Ni(dppm)$_2Cl_2$],[54] [Ni(dppe)Cl_2],[54] [Ni(dppp)-Cl_2],[54] [Ni(dppb)Cl_2],[55] [Ni(*cis*-dpen)Cl_2],[56] [Ni(dmpe)-Cl_2],[57] [Ni(dmpf)Cl_2],[58] [Ni(dppc)Cl_2],[59] [Ni(bipy)Cl_2],[30b,60] [Ni(py)$_2Cl_2$],[61] [Pd(PPh_3)$_2Cl_2$],[62] [Pd(PEt_3)$_2Cl_2$],[62] [Pt(P-Ph_3)$_2Cl_2$],[62] and [Co(dppp)Cl_2].[63] Cyclopropyl bromide,[64] 1-bromo-[65] and 2-bromo-propene,[65] mesityl bromide,[66] 1-chlorocyclohexene,[67] chloromethyl-trimethylsilane,[68] and -pentamethyldisilane[69] were prepared as reported previously. 9-Bromoanthracene was generously gifted by Dr. T. Kawamura, Department of Hydrocarbon Chemistry, Kyoto University. 4,4′-Dichlorobiphenyl and a solution of chloroprene in *m*-xylene were generously supplied by Kanegafuchi Chemical Industry Co., Ltd. and Toyo Soda Manufacturing Co., Ltd., respectively. Other organic halides were commercially available. Chlorobenzene, bromobenzene, and butyl bromide were purified by distillation before use, but others were used without further purification. Magnesium ribbons were commercially available (Nakarai Chemical). Ether was dried over sodium wire and distilled before use. Tetrahydrofuran (THF) was distilled from $LiAlH_4$ before use.

Grignard Reagents. Grignard reagents were prepared in a standard manner by adding a solution of an organic halide to magnesium ribbons which had been dried under a rapid stream of dry nitrogen by flaming. Magnesium was usually used in 10—20% excess over the halide in order to exhaust the latter. After completion of the addition the mixture was refluxed for about one hour to ensure the reaction. Concentrations of the Grignard reagents were determined by adding one ml of the solution to an excess of standard hydrochloric acid followed by back titration with a standard sodium hydroxide solution.

Coupling Reactions. Detailed procedure for coupling of 1,2-dichlorobenzene with *n*-butylmagnesium bromide will appear in Organic Syntheses,[23] and only several typical procedures are described in detail below. All other reactions were carried out in essentially the same manner. Conversions of reactions and yields of products were determined either by careful distillation or by quantitative GLPC using an appropriate internal standard calibrated against the pure samples. Quantitative GLPC was performed on a Hitachi GC 4B gas-chromatograph using a 3 m × 4 mm column 30% Silicone DC 550 on Celite (60—80). Preparative GLPC was performed on a Varian Aerograph Model 90-P gas-chromatograph, using a 3 or 6 m × 9 mm column packed with 30% Silicone DC 550

on Celite (60—80). Infrared spectra were obtained on a Hitachi EPI G3 Grating spectrophotometer, NMR spectra were obtained with a Varian T-60, EM-360, or HA-100 spectrometer in CCl_4 solutions with TMS, cyclohexane, or benzene as internal standard. Mass spectra were recorded on a Hitachi RMS-4 mass spectrometer.

The following coupling products were identified by spectral (NMR and/or IR) comparison with commercial authentic samples or established spectral data;[70] toluene, ethylbenzene, propylbenzene, cumene, 1,1-diphenylethylene, (*E*)- and (*Z*)-stilbene, styrene, cyclohexylbenzene, 1-phenylnaphthalene, vinylcyclohexane, cyclopropylbenzene, 1-decene, 1-, 2-, and 3-phenylpropene, 1,4-bis(isopropenyl)benzene, 4-isopropenylchlorobenzene and 2,3-dimethyl-1,3-butadiene. Authentic samples of 1-methylcyclohexene,[71] allyltrimethylsilane,[72] benzyltrimethylsilane,[73] and benzylpentamethyldisilane[74] were prepared by reported methods.

Other coupling products are listed below together with some physical constants, spectral and/or analytical data.

A. Procedure for the Examination of Catalytic Activity of Phosphine–Nickel Complexes, Reactivity of Halobenzenes and Solvent Effects. A catalyst was placed in a 50-ml two-necked flask equipped with a stirring bar, a serum cap and a reflux condenser fitted with a three way stopcock. The reaction vessel was then filled with nitrogen after evacuation and charged with an organic halide, anhydrous ether, and an appropriate internal standard (normal alkane) through the serum cap with a syringe. To the mixture was then added a Grignard reagent in a similar way at 0 °C with stirring. The resulting mixture was refluxed for a given period of time and hydrolyzed with a dilute acid. The organic layer was analyzed by GLPC.

B. Procedure for the Examination of Catalytic Activity on Aging. Essentially the same procedure was employed as above, excepting that to the catalyst were added first anhydrous ether and the butyl Grignard reagent at 0 °C, the resulting mixture was allowed to stand at room temperature under nitrogen for a given period of time (aging time), and finally chlorobenzene was added. After refluxing for a given period of time, the mixture was hydrolyzed and an internal standard was added. Data obtained by GLPC analysis are listed in Table 2.

C. Procedures for the Reaction of Aryl Halides. (a) Butylbenzene: In a 300-ml two-necked flask, equipped with a pressure-equalizing dropping funnel, a reflux condenser attached to a nitrogen line and a stirring bar, were placed 430 mg (0.81 mmol) of $[Ni(dppe)Cl_2]$, 10.78 g (95.8 mmol) and 100 ml of anhydrous ether; the nickel complex was insoluble in the mixture. To the mixture was added dropwise butylmagnesium bromide in ether (110 mmol; 40 ml of 2.8 M solution) at room temperature with stirring under nitrogen over 20 min. The mixture changed immediately to an yellow clear and then brown solution. After, 22 h-reflux the mixture was hydrolyzed with diluted hydrochloric acid under cooling with an ice bath. The organic layer and ether extracts from the aqueous layer were combined, washed with water, saturated sodium hydrogencarbonate solution and water, and then dried over calcium chloride. After evaporation of solvent distillation gave 9.80 g (76% yield based on the chlorobenzene) of butylbenzene boiling at 70 °C/19 mmHg;[75] n_D^{15} 1.4928. NMR (CCl_4, TMS): δ 7.11 (s, 5H), 2.59 (t, 7 Hz, 2H), 2.0—0.8 (m, 7H); IR: for monosubstituted benzene; 1945 (w), 1875 (w), 1802 (w), 1750 (w), 746 (s), 702 (s) cm^{-1}. Careful GLPC analysis and mass spectrometry, showing a base peak *m/e* 91 in addition to a parent peak *m/e* 134, but no *m/e* 105, clearly indicated no contamination with *sec*-butylbenzene.[76]

(b) 9-Trimethylsilylmethylanthracene: In a 50-ml two-necked flask equipped as described in A were placed $[Ni(PPh_3)_2Cl_2]$ (32 mg; 0.06 mmol), 9-bromoanthracene (1.017 g; 3.95 mmol) and 5 ml of anhydrous ether. To the stirred mixture was added dropwise an ether solution of trimethylsilylmethylmagnesium chloride (5.14 mmol) through a serum cap with a syringe at room temperature. Immediately an exothermic reaction occurred. The resulting brownish mixture was stirred at room temperature for 18 h. usual work-up and distillation afforded 0.74 g (71% yield based on the halide) of 9-trimethylsilylmethylanthracene as slightly yellow crystals, mp 59—60 °C, NMR (CCl_4) δ: 8.3—7.2 (m, 9H), 3.09 (s, 2H), −0.03 (s, 9H). Found: C, 81.62; H, 7.41. Calcd for $C_{18}H_{20}Si$: C, 81.75; H, 7.62%.

D. Procedures for the Reaction of Vinyl Chloride. (a) In a Pressure Glass Tube; 1-Vinylnaphthalene: Vinyl chloride (6 ml) was dried by passing the gas through a phosphorus pentoxide–calcium chloride column and condensed at −78 °C in a graduated, 100-ml pressure glass tube containing 178 mg (0.34 mmol) of $[Ni(dppe)Cl_2]$. To it were added at the same temperature 10 ml of anhydrous ether and a solution of 1-naphthylmagnesium bromide (55 mmol) in 50 ml of a mixed solvent of benzene, ether, and THF (3: 2: 1). The glass tube was stoppered and allowed to warm up to 0 °C. The resulting homogeneous solution was then kept standing at room temperature for 20 h. Work-up as above and distillation under reduced pressure gave 6.8 g (80% based on the Grignard reagent) of 1-vinylnaphthalene boiling at 89 °C/5 mmHg, n_D^{25} 1.6418 (lit,[78] bp 87 °C/2 mmHg, n_D^{25} 1.6436).

(b) In a Three-necked Flask; 4-Chlorostyrene: A solution of 4-chlorophenylmagnesium bromide was prepared in the usual manner from 4.9 g (0.20 g-atom) of magnesium and 38.3 g (0.20 mol) of 4-chloro-1-bromobenzene in 150 ml of anhydrous ether.

A 500-ml three-necked flask was equipped with a mechanical stirrer, a reflux condenser attached to a drying tube, and a gas inlet tube reaching the bottom. In the flask were placed about 50 mg (≈0.1 mmol) of $[Ni(dppp)Cl_2]$ and 100 ml of dry ether. The flask was cooled in an ice bath. Through the inlet tube was introdued 15 g (0.24 mol) of vinyl chloride which had been dried by passing the gas through a phosphorus pentoxide–calcium chloride column (about 40 cm × 2 cm diameter). The gas inlet tube was replaced by a pressure-equalizing dropping funnel, to which was transferred the Grignard solution prepared above under a nitrogen atmosphere. The Grignard solution was then added dropwise to the mixture containing the nickel catalyst, with stirring and cooling in an ice bath, over 45 min. The reaction mixture changed to yellow-brown with formation of two liquid layers. After completion of the addition the mixture was stirred at 0 °C for 30 min and then at room temperature for 1.5 h. The mixture was then cooled in an ice bath hydrolyzed by slow addition of about 150 ml of about 2 M-hydrochloric acid. After the usual work-up, distillation in the presence of a small amount of hydroquinone through a short Vigreux column under reduced pressure gave 21.5—22.0 g (78—79%) of 4-chlorostyrene, bp 78—80 °C/18 mmHg or 85—85.5 °C/25 mmHg, n_D^{20} 1.5664, (lit,[79] bp 38 °C/2.2 mmHg, n_D^{20} 1.5650), as a colorless to light yellow liquid.

1,2-Dibutylbenzene: bp 76—81 °C/3.5 mmHg, n_D^{20} 1.4920 (lit,[45a,b] n_D^{20} 1.4916). NMR: 7.00 (s, 4H), 2.60 (t, J=8.5 Hz, 4H), 1.7—0.7 (m, 14H). (Found: C, 88.31; H, 11.75%.) *1,3-Dibutylbenzene*: bp 84 °C/5 mmHg, n_D^{20} 1.4873 (lit,[45c] n_D^{25} 1.4860), d_4^{20} 0.8564. NMR: 7.1—6.8 (m, 4H), 2.57 (t, J= 8 Hz, 4H), 1.9—0.7 (m, 14H). (Found: C, 88.19; H, 11.41 %.) *1,4-Dibutylbenzene*: bp 93 °C/6 mmHg, n_D^{20} 1.4905 (lit,[80] n_D^{20} 1.4883). NMR: 6.93 (s, 4H), 2.54 (t, J=8 Hz, 4H), 1.8—0.6 (m, 14H). (Found: C, 88.65; H, 11.84%.) *2-Butyl-1-chlorobenzene*: n_D^{20} 1.5115 (lit,[81] n_D^{25} 1.5087). NMR: 7.4—6.9 (m, 4H), 2.70 (t, J=7.5 Hz, 2H), 1.9—0.7 (m, 7H). *3-Butyl-1-chlorobenzene*: n_D^{20} 1.5093. NMR: 7.3—6.88 (m, 4H), 2.60

(t, J=7.5 Hz, 2H), 1.9—0.7 (m, 7H). Found: C, 71.83; H, 8.15%. Calcd for $C_{10}H_{13}Cl$: C, 71.21; H, 7.77%. *4-Butyl-1-chlorobenzene*: n_D^{20} 1.5091. NMR: 7.11 (cent. of m, 4H), 2.56 (t, J=7.5 Hz, 2H), 1.9—0.7 (m, 7H). Found: C, 71.48; H, 7.86%. Calcd for $C_{10}H_{13}Cl$: C, 71.21; H, 7.77%. *2-Butyltoluene*: bp 85—86.5 °C/20 mmHg, $n_D^{18.5}$ 1.4981 (lit,[82] $n_D^{18.4}$ 1.49662). NMR: 7.03 (s, 4H), 2.58 (t, J=8 Hz, 2H), 2.11 (s, 3H), 1.8—0.8 (m, 7H). *3-Butyltoluene*: bp 90 °C/20 mmHg, $n_D^{18.5}$ 1.4937 (lit,[82] $n_D^{18.4}$ 1.49315). NMR: 7.2—6.8 (m, 4H), 2.55 (t, J=7 Hz, 2H), 2.33 (s, 3H), 1.8—0.7 (m, 7H). *4-Butyltoluene*: bp 81 °C/20 mmHg, n_D^{14} 1.4939 (lit,[82] $n_D^{14.2}$ 1.4912). NMR: 6.95 (s, 4H), 2.54 (t, J=8 Hz, 2H), 2.29 (s, 3H), 1.8—0.8 (m, 7H). (Found: C, 88.90; H, 10.99%.) *4-Butylanisole*: bp 165—170 °C/100 mmHg, n_D^{20} 1.5013 (lit,[83] bp 120 °C/19 mmHg, n_D^{15} 1.5027). NMR: 6.94, 6.66 (q, $A_2'B_2'$, 4H), 3.68 (s, 3H), 2.50 (t, J=7 Hz, 2H), 1.9—0.7 (m, 7H). (Found: C, 80.60; H, 10.06%.) *4-Butyl-1-trifluoromethylbenzene*: n_D^{20} 1.4402. NMR: 7.50, 7.21 (q, $A_2'B_2'$, 4H), 2.68 (t, J=7 Hz, 2H), 1.9—0.7 (m, 7H). Found: C, 65.00; H, 6.69%. Calcd for $C_{11}H_{14}F_3$: C, 65.04; H, 6.95%. *1-Butylnaphthalene*: bp 97.5—100.5 °C/5 mmHg (lit,[84] bp 287—288 °C/745 mmHg). NMR: 8.1—7.2 (m, 7H), 3.03 (t, J=9 Hz, 2H), 2.0—0.7 (m, 7H). *1,2-Bis(trimethylsilylmethyl)benzene*: mp 2—3 °C, n_D^{20} 1.4967 (lit,[85] mp 2—3 °C, n_D^{20} 1.4950). NMR: 6.87 (s, 4H), 1.99 (s, 4H), −0.01 (s, 18H). *1,3-Bis(trimethylsilylmethyl)-benzene*: mp 4—10 °C, n_D^{20} 1.4925 (lit,[86] mp 4 °C, n_D^{20} 1.4919). NMR: 7.17—6.47 (m, 4H), 1.97 (s, 4H), −0.02 (s, 18H). *1,4-Bis(trimethylsilylmethyl)benzene*: mp 64—64.5 °C (lit,[86] mp 61—63 °C). NMR: 6.80 (s, 4H), 1.93 (s, 4H), −0.02 (s, 18 H). *1-Trimethylsilylmethylnaphthalene*: n_D^{20} 1.5751. NMR: 8.04—6.98 (m, 7H), 2.52 (s, 2H), −0.02 (s, 9H). Found: C, 78.18; H, 8.39%. Calcd for $C_{14}H_{18}Si$: C, 78.44; H, 8.46%. *4,4'-Bis(trimethylsilylmethyl)biphenyl*: mp 82—83 °C. NMR: 7.22, 6.84 ($A_2'B_2'$ q, J=8 Hz, 8H), 1.95 (s, 4H), −0.09 (s, 18H). Found: C, 73.65; H, 9.20%. Calcd for $C_{20}H_{22}Si_2$: C, 73.54; H, 9.26%. *2-(o-Anisyl)mesitylene*: mp 55—56 °C. NMR: 7.3—6.8 (m, 4H), 6.76 (s, 2H), 3.67 (s, 3H), 2.24 (s, 3H), 1.89 (s, 6H). Found: C, 84.81; H, 7.76%. Calcd for $C_{16}H_{18}O$: C, 84.91; H, 8.01%. *2-(1-Naphthyl)mesitylene*: mp 70—72 °C. NMR: 7.9—7.05 (m, 7H), 6.88 (s, 2H), 2.33 (s, 3H), 1.85 (s, 6H). Found: C, 92.14; H, 7.71%. Calcd for $C_{19}H_{18}$: C, 92.63; H, 7.36%. *2-Phenylmesitylene*: NMR: 7.5—6.95 (m, 5H), 6.80 (s, 2H), 2.28 (s, 3H), 1.97 (s, 6H). *2-Cyclohexylchlorobenzene*: n_D^{20} 1.5421 (lit,[77] n_D^{20} 1.5436). (Found: C, 73.85; H, 7.64%.) *1,3-Dicyclohexylbenzene*: n_D^{20} 1.5370 (lit,[77] n_D^{20} 1.5356). NMR: 7.27—6.77 (m, 5H), 2.8—2.2 (br, 2H), 2.2—0.6 (m, 20H). *1,4-Dicyclohexylbenzene*: mp 103—103.5 °C (lit,[87] mp 101—102 °C). NMR: 7.05 (s, 4H), 2.8—2.2 (br, 2H), 2.2—0.6 (m, 20H). *1-Cyclohexylnaphthalene*: bp 172—174 °C/8 mmHg, n_D^{20} 1.6044 (lit,[88] bp 178—183 °C/12 mmHg, $n_D^{19.3}$ 1.6040). *4-Isopropenyl-1-bromobenzene*: n_D^{20} 1.5830 (lit,[89] n_D^{20} 1.5834). NMR: 7.57—7.17 (m, 4H), 5.31 (br, 1H), 5.06 (m, 1H), 2.13 (br, 3H). *2-Isopropenyltoluene*: n_D^{20} 1.5152 (lit,[90] n_D^{20} 1.5155). NMR: 7.06 (s, 4H), 5.13 (m, 1H), 4.83 (m, 1H), 2.18 (s, 3H), 2.03 (br, 3H). *3,5-Diisopropenyl-1-chlorobenzene*: n_D^{20} 1.5695. NMR: 7.40—7.23 (m, 3H), 5.37 (m, 2H), 5.11 (m, 2H), 2.13 (m, 6H). Found: C, 74.58; H, 6.89%. Calcd for $C_{12}H_{13}Cl$: C, 74.80; H, 6.80%. *1,4-Dichloro-2,5-diisopropenylbenzene*: n_D^{20} 1.5601. NMR: 7.25 (s, 2H), 5.13 (m, 2H), 5.03 (m, 2H), 2.03 (m, 6H). Found: C, 63.61; H, 5.47%. Calcd for $C_{12}H_{12}Cl_2$: C, 63.45; H, 5.32%. *1-Isopropenylnaphthalene*: n_D^{20} 1.6075 (lit,[91] n_D^{20} 1.6085). NMR: 8.10—7.13 (m, 7H), 5.37 (m, 1H), 5.07 (m, 1H), 2.20 (m, 3H). (Found: C, 92.55; H, 7.37%.) *2-Benzyl-3-phenylpropene*: bp 120—123 °C/5 mmHg, n_D^{20} 1.5652. NMR: 7.10 (br. s, 10H), 4.80 (s, 2H), 3.20 (s, 4H). Found: C, 92.00; H, 7.97%. Calcd for $C_{16}H_{16}$: C, 92.26; H, 7.74%. (E)-*1,2-dicyclohexylethylene*: n_D^{20} 1.4881. NMR: 5.04 (dd, J= 2 and 6 Hz, 2H), 2.5—2.0 (br, 2H), 2.0—0.7 (m, 20H). IR (neat): 965 cm^{-1} (*trans* olefin). Found: C, 87.33; H, 12.61%. Calcd for $C_{14}H_{24}$: C, 87.42; H, 12.58%. *2-Phenyl-1,3-butadiene*: bp 62.5 °C/20 mmHg, n_D^{20} 1.5487 (lit,[92] n_D^{20} 1.5489). NMR: 7.30 (s, 5H), 7.0—6.2 (m, 1H), 5.4—4.9 (m, 4H). *1-Butylcyclohexene*: bp 102 °C/65 mmHg, n_D^{20} 1.4610 (lit,[71] bp 180.8—182.9 °C, n_D^{20} 1.4591). NMR: 5.37 (br, 1H), 2.2—0.6 (m, 17H). IR (neat): 1670 cm^{-1} (trisubstituted olefin).

We thank the Ministry of Education for Grant-in-Aid (No. 911511, 011006, and 985156) and The Asahi Glass Foundation for the Contribution to Industrial Technology for financial support of this work. Our thanks are also due to Toshiba Silicone Co., Ltd. for a gift of chlorosilanes.

References

1) *E. g.*, (a) J. Tsuji, "Organic Synthesis by Means of Transition Metal Complexes," Springer-Verlag, Berlin, Heidelberg, New York (1975); (b) J. M. Swan and D. St. C. Black, "Organometallics in Organic Synthesis," Chapman and Hall, London (1974).
2) P. E. Fanta, *Synthesis*, **1974**, 9.
3) *A. E. Jukes, Adv. Organometal. Chem.*, **12**, *215 (1974).*
4) M. F. Semmelhack, *Org. React.*, **19**, 117 (1972).
5) R. Baker, *Chem. Rev.*, **73**, 487 (1973).
6) P. W. Jolly and G. Wilke, "The Organic Chemistry of Nickel," Vol. II, Academic Press Inc., New York, N. Y. (1975), Chapt. V, pp 246—293.
7) S. Takahashi, Y. Suzuki, and N. Hagihara, *Chem. Lett.*, **1974**, 1363.
8) G. H. Posner, *Org. React.*, **19**, 1 (1972); **22**, 253 (1975).
9) J. F. Normant, *Synthesis*, **1972**, 63.
10) J. P. Collman, *Acc. Chem. Res.*, **8**, 342 (1975).
11) T. Kauffman, *Angew. Chem., Internat. Edit. Engl.*, **13**, 291 (1974).
12) M. S. Kharasch and O. Reinmuth, "Grignard Reactions of Non-metallic Substances," Prentice-Hall, Englewood Cliffs, N. J. (1954), Chapt. 5.
13) M. Tamura and J. K. Kochi, *Bull. Chem. Soc. Jpn.*, **44**, 3063 (1971).
14) *E. g.*, L. E. Elsom, J. D. Hunt, and A. McKillop, *Organometal. Chem. Rev. A*, **8**, 135 (1972).
15) M. Tamura and J. K. Kochi, *Synthesis*, **1971**, 303.
16) M. Tamura and J. K. Kochi, *J. Am. Chem. Soc.*, **93**, 1483 (1971).
17) (a) M. Tamura and J. K. Kochi, *J. Am. Chem. Soc.*, **93**, 1487 (1971); (b) S. M. Neumann and J. K. Kochi, *J. Org. Chem.*, **40**, 599 (1975); (c) S. Smith and J. K. Kochi, *ibid.*, **41**, 502 (1976).
18) (a) M. Tamura and J. K. Kochi, *J. Organometal. Chem.*, **42**, 205 (1972); (b) L. Friedman and A. Shani, *J. Am. Chem. Soc.*, **96**, 7101 (1974); (c) J. F. Normant, A. Commercon, G. Cahiez, and J. Villieras, *C. R. Acad. Sci., Ser. C*, **278**, 967 (1974); (d) G. Fouquet and M. Schlosser, *Angew. Chem. Internat. Edit. Engl.*, **13**, 82 (1974); (e) K. Onuma and H. Hashimoto, *Bull. Chem. Soc. Jpn.*, **45**, 2582 (1972).
19) H. Felkin and G. Swierczewski, *Tetrahedron*, **31**, 2735 (1975).
20) R. J. P. Corriu and J. P. Masse, *J. Chem. Soc., Chem. Commun.*, **1972**, 144.
21) K. Tamao, K. Sumitani, and M. Kumada, *J. Am. Chem. Soc.*, **94**, 4374 (1972).
22) M. Yamamura, I. Moritani, and S. Murahashi, *J. Organometal. Chem.*, **91**, C39 (1975).

23) M. Kumada, K. Tamao, and K. Sumitani, *Org. Synth.*, in press.
24) M. Kumada, "Organotransition-Metal Chemistry," Ed. by Y. Ishii and M. Tsutsui, Plenum Publishing Corporation, New York, N. Y. (1975), p. 211.
25) (a) K. Tamao, Y. Kiso, K. Sumitani, and M. Kumada, *J. Am. Chem. Soc.*, **94**, 9268 (1972); (b) Y. Kiso, K. Tamao, and M. Kumada, *J. Organometal. Chem.*, **50**, C12 (1973).
26) (a) K. Tamao, M. Zembayashi, Y. Kiso, and M. Kumada, *J. Organometal. Chem.*, **55**, C91 (1973); (b) M. Zembayashi, K. Tamao, and M. Kumada, *Tetrahedron Lett.*, **1975**, 1719.
27) (a) G. Consiglio and C. Botteghi, *Helv. Chim. Acta*, **56**, 460 (1973); (b) Y. Kiso, K. Tamao, N. Miyake, K. Yamamoto, and M. Kumada, *Tetrahedron Lett.*, **1974**, 3; (c) K. Tamao, A. Minato, N. Miyake, T. Matsuda, Y. Kiso, and M. Kumada, *Chem. Lett.*, **1975**, 133; (d) T. Hayashi, M. Tajika, K. Tamao, and M. Kumada, *J. Am. Chem. Soc.*, **98**, 3718 (1976).
28) K. Tamao, S. Kodama, T. Nakatsuka, Y. Kiso, and M. Kumada, *J. Am. Chem. Soc.*, **97**, 4405 (1975).
29) (a) E. D. Thorsett and F. R. Stermitz, *J. Heterocycl. Chem.*, **10**, 243 (1973); (b) L. N. Pridgen, *ibid.*, **12**, 443 (1975); (c) K. Tamao, S. Kodama, I. Nakajima, A. Minato, and M. Kumada, The 8 th Congress of Heterocyclic Chemistry, Kyoto, Japan, Oct. (1975), Abstracts p. 174.
30) (a) M. Uchino, A. Yamamoto, and S. Ikeda, *J. Organometal. Chem.*, **24**, C63 (1970); (b) M. Uchino, K. Asagi, A. Yamamoto, and S. Ikeda, *ibid.*, **84**, 93 (1975).
31) (a) D. R. Fahey, *J. Am. Chem. Soc.*, **92**, 402 (1970); (b) D. R. Fahey., *Organometal. Chem. Rev. A*, **2**, 245 (1972); (c) M. Hidai, T. Kashiwagi, T. Ikeda, and Y. Uchida, *J. Organometal. Chem.*, **30**, 279 (1971); (d) D. H. Gerlach, A. R. Kane, G. W. Parshall, J. P. Jesson, and E. L. Muetterties, *J. Am. Chem. Soc.*, **93**, 3543 (1971); (e) G. W. Parshall, *ibid.*, **96**, 2360 (1974); (f) C. S. Cundy, *J. Organometal. Chem.*, **69**, 305 (1974).
32) P. W. Jolly and G. Wilke, "The Organic Chemistry of Nickel," Vol. I, Academic Press Inc., New York, N. Y. (1974), Chapt. IV, pp. 168—169.
33) (a) T. Saito, Y. Uchida, A. Misono, A. Yamamoto, K. Morifuji, and S. Ikeda, *J. Am. Chem. Soc.*, **88**, 5198 (1966); (b) G. Wilke and G. Herrmann, *Angew. Chem.*, **78**, 591 (1966);
34) P. Fitton and E. A. Rick, *J. Organometal. Chem.* **28**, 287 (1971).
35) D. Walter and G. Wilke, *Angew. Chem.*, **78**, 941 (1966).
36) (a) J. Chatt and B. L. Shaw, *J. Chem. Soc.*, **1960**, 1718; (b) G. E. Coates, M. L. H. Green, and K. Wade, "Organometallic Compounds," Vol. 2, Methuen and Co., London, 3rd ed. (1968), pp. 217—233.
37) Ref. 32, p. 160.
38) (a) G. Wilkinson, *Angew. Chem.*, **86**, 664 (1974); (b) G. Wilkinson, *Pure Appl. Chem.*, **30**, 627 (1972); (c) P. J. Davidson, M. F. Lappert, and R. Pearce, *Acc. Chem. Res.*, **7**, 209 (1974); (d) M. C. Baird, *J. Organometal. Chem.*, **64**, 289 (1974).
39) K. Tamao, A. Fujioka, and M. Kumada, unpublished studies (1972).
40) The preferencial catalytic activity of dppp–transition metal complexes has been observed also in olefin-oligomerization[41] and hydrogenation.[42]
41) *E. g.*, Y. Inoue, T. Kagawa, Y. Uchida, and H. Hashimoto, *Bull. Chem. Soc. Jpn.*, **45**, 1996 (1972).
42) J.-C. Poulin, T.-P. Dang, and H. B. Kagan, *J. Organometal. Chem.*, **84**, 87 (1975).
43) *E. g.*, J. D. Roberts and M. C. Caserio, "Basic Principles of Organic Chemistry," W. A. Benjamin, Inc., New York, N. Y. (1964), pp. 140—141.
44) *E. g.*, J. Mathieu and J. Weill-Raynal, "Formation of C–C Bond," Vol. II, Gierg Thieme Publishers, Stuttgart (1975).
45) (a) M. Ogawa and G. Tanaka, *Kogyo Kagaku Zasshi*, **58**, 696 (1955); (b) B. B. Elsner and H. E. Strauss, *J. Chem. Soc.*, **1957**, 583; (c) G. F. Woods and R. E. Plapinger, *J. Am. Chem. Soc.*, **73**, 5603 (1951).
46) D. G. Morrell and J. K. Kochi, *J. Am. Chem. Soc.*, **97**, 7262 (1975).
47) (a) R. J. P. Corriu, J. P. Masse, and B. Meunier, *J. Organometal. Chem.*, **55**, 73 (1973); (b) R. J. P. Corriu and B. Meunier, *ibid.*, **60**, 31 (1973); (c) E. Colomer, R. J. P. Corriu, and B. Meunier, *ibid.*, **71**, 197 (1974); (d) F. H. Carre and R. J. P. Corriu, *ibid.*, **74**, 49 (1974).
48) K. Tamao, Y. Kiso, M. Kumada, and A. Minato, The 32nd Meeting of the Chemical Society of Japan, Tokyo, April (1975), Abstracts III-1372.
49) *E. g.*, (a) Ref. 36b, Chapt. 7; (b) P. S. Braterman and R. J. Cross, *Chem. Soc. Rev.*, **2**, 271 (1973); (c) M. Tsutsui, M. Hancock, J. Ariyoshi, and M. N. Levy, *Angew. Chem., Internat. Edit. Engl.*, **8**, 410 (1969).
50) F. A. Cotton, O. D. Faut, and D. M. L. Goodgame, *J. Am. Chem. Soc.*, **83**, 344 (1961).
51) R. G. Hayter and F. S. Humiec, *Inorg. Chem.*, **4**, 1701 (1965).
52) E. C. Alyea and D. W. Meek, *J. Am. Chem. Soc.*, **91**, 5761 (1969).
53) K. A. Jensen, *Z. Anorg. Allg. Chem.*, **229**, 265 (1936).
54) G. R. Van Hecke and W. Dew. Horrocks, Jr., *Inorg. Chem.*, **5**, 1968 (1966).
55) S. S. Sandhu and M. Gupta, *Chem. Ind.* (London), **1967**, 1876.
56) C. A. McAuliffe and D. W. Meck, *Inorg. Chem.*, **8**, 904 (1969).
57) G. Booth and J. Chatt, *J. Chem. Soc.*, **1965**, 3238.
58) Y. Kiso, M. Kumada, K. Tamao, and M. Umeno, *J. Organometal. Chem.*, **50**, 297 (1973).
59) (a) R. P. Alexander and H. Schroeder, *Inorg. Chem.*, **2**, 1107 (1963); (b) M. Kumada, K. Sumitani, Y. Kiso, and K. Tamao, *J. Organometal. Chem.*, **50**, 319 (1973).
60) J. A. Broomhead and F. P. Dwyer, *Aust. J. Chem.*, **14**, 250 (1961).
61) D. M. L. Goodgame, M. Goodgame, and M. J. Weeks, *J. Chem. Soc.*, **1964**, 5194.
62) F. R. Hartley, *Organometal. Chem. Rev. A*, **6**, 119 (1970).
63) W. Dew. Horrocks, Jr., G. R. Van Hecke, and D. Dew. Hall, *Inorg. Chem.*, **6**, 694 (1967).
64) J. S. Meek and D. T. Osuga, *Org. Synth.*, Coll. Vol. 5, 126 (1973).
65) (a) G. B. Bachmann, *J. Am. Chem. Soc.*, **55**, 4279 (1933); (b) J. K. Farrell and G. B. Bachmann, *ibid.*, **57**, 1281 (1935).
66) L. I. Smith, *Org. Synth.*, Coll. Vol. 2, 95 (1943).
67) E. A. Braude and J. A. Coles, *J. Chem. Soc.*, **1950**, 2014.
68) F. C. Whitmore and L. H. Sommer, *J. Am. Chem. Soc.*, **68**, 481 (1946).
69) M. Kumada and M. Ishikawa, *J. Organometal. Chem.*, **1**, 411 (1964).
70) (a) F. A. Bovey, "NMR Data Tables for Organic Compounds," Vol. 1, Interscience Publishers, New York, N. Y. (1967); (b) "NMR Spectra Catalog," Varian Associates, 1962 and 1963; (c) C. J. Pouchert and J. R. Campbell, "The Aldrich Library of NMR Spectra," Vol. IV, Aldrich Chemical Company, Inc., Milwaukee, Wisconsin (1974); (d) C. J. Pouchert, "The Aldrich Library of Infrared Spectra," Aldrich Chemical Co., Inc. (1970).
71) F. K. Signaigo and P. L. Cramer, *J. Am. Chem. Soc.*, **55**, 3326 (1933).

72) L. H. Sommer, L. J. Tyler, and F. C. Whitmore, *J. Am. Chem. Soc.*, **70**, 2872 (1948).
73) C. R. Hauser and C. R. Hance, *J. Am. Chem. Soc.*, **73**, 5846 (1951).
74) E. A. Chernyshev, N. G. Tolstikova, A. A. Ivashenko, A. A. Zelenetskaya, and L. A. Leites, *Izv. Akad. Nauk SSSR, Otd. Khim. Nauk*, **1963**, 660; *Chem. Abstr.*, **59**, 7553 (1963).
75) R. R. Read, L. S. Foster, A. Russell, and V. L. Simril, *Org. Synth.*, Coll. Vol. 3, 157 (1955).
76) R. M. Silverstein and G. C. Bassler, "Spectrometric Identification of Organic Compounds," John Wiley & Sons, Inc., New York, N. Y. (1967).
77) J. Blackwell and W. J. Hickinbottom, *J. Chem. Soc.*, **1963**, 518.
78) D. T. Mowry, M. Renoll, and W. F. Huber, *J. Am. Chem. Soc.*, **68**, 1105 (1946).
79) *E. g.*, W. H. Saunders, Jr. and R. A. Williams, *J. Am. Chem. Soc.*, **79**, 3712 (1957).
80) *E. g.*, W. J. Mattox and A. V. Grosse, *J. Am. Chem. Soc.*, **67**, 84 (1945).
81) D. F. DeTar and C. Weis, *J. Am. Chem. Soc.*, **78**, 4296 (1956).
82) Beilstein, **5**, 437 (Syst. No. 470).
83) A. Klages, *Ber.*, **37**, 3987 (1904).
84) H. Gilman, C. G. Braumen, and R. K. Ingham, *J. Org. Chem.*, **22**, 685 (1957).
85) G. R. Wilson and G. M. Hutzel, *J. Org. Chem.*, **24**, 1791 (1959).
86) G. R. Wilson, G. M. Hutzel, and A. G. Smith, *J. Org. Chem.*, **24**, 381 (1959).
87) B. B. Corson and V. N. Ipatieff, *Org. Synth.*, Coll. Vol. 2, 151 (1943).
88) N. G. Rule and W. J. Hickinbottom, *J. Chem. Soc.*, **1959**, 2509.
89) D. Seymour and K. B. Wolfstirn, *J. Am. Chem. Soc.*, **70**, 1177 (1948).
90) Y.-R. Naves and A.-V. Gramploff, *Bull. Soc. Chim. Fr.*, **1961**, 1921.
91) W. M. Kutz, J. E. Nickels, J. J. McGovern, and B. B. Corson, *J. Am. Chem. Soc.*, **70**, 4026 (1948).
92) W. H. Carothers and G. J. Berchet, *J. Am. Chem. Soc.*, **55**, 2813 (1933).

Equilibrium and ^{31}P Chemical Shifts of the Adducts of Trialkylphosphines and Isothiocyanates, and Reactions of Triethylphosphine and Benzoyl Isothiocyanate

Kin-ya AKIBA, Toshio YONEYAMA, Hideaki HAMADA, and Naoki INAMOTO

Department of Chemistry, Faculty of Science, The University of Tokyo, Hongo, Tokyo 113

(Received April 13, 1976)

The adducts (**3**) of triethylphosphine (**1**) and several isothiocyanates (**2**) were prepared. Equilibrium constants of the adducts (**5**) from tributylphosphine (**4**) and phenyl (**2b**), benzoyl (**2e**), and *p*-toluenesulfonyl isothiocyanates (**2f**) were determined in some solvents. The ^{31}P chemical shifts of **5** were measured in DMF, and correlated with Hammett σ_p constants. Reactions of **3e** with **1** and **2e** gave phosphonium thiocyanates of **6** and **7**, and of **11**, respectively. Methylation of **3e** gave *S*-methyl *N*-benzoylmonothiocarbamate (**16**).

It has been known for 100 years that triethylphosphine forms the *1*:*1* adducts with carbon disulfide and isothiocyanates,[1] and the presence of *P–C* bond was exemplified by X-ray crystallographic study[2a] after much discussion. However, little is known on the reaction of the adducts and the formation of reactive alkylidenephosphoranes was recently reported by the reaction of tributylphosphine and carbon disulfide adduct with active acetylenes.[3]

This paper describes the general formation of the adducts of trialkylphosphines and several isothiocyanates, the equilibrium of the adducts in solution[4] and ^{31}P chemical shifts of the adducts,[4] and reactions of the adducts of triethylphosphine and benzoyl isothiocyanate.

Formation of the Adducts (3). An equimolar mixture of triethylphosphine (**1**) and isothiocyanates (**2**) gave adducts (**3**) in hexane and/or ether. The results are summarized in Table 1.

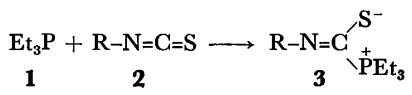

a, R=Me; **b**, R=Ph; **c**, R=α-$C_{10}H_7$; **d**, R=MeCO; **e**, R=PhCO; **f**, R=*p*-$MeC_6H_4SO_2$; **g**, R=Ph_2P(S)

The yields of **3** were high when the substituent (R) is electron-withdrawing. The adducts (**3b, e,** and **f**) gave correct elemental analyses, but it was not possible to obtain them for other adducts. Especially, **3d** and **3g** decomposed during recrystallization. The adducts of tributylphosphine and methyl and phenyl isothiocyanates could not be precipitated from the reaction mixture under similar conditions. These facts are compatible with observed equilibrium constants (see below).

Equilibrium of the Adducts in Solution. The equilibrium constants (*K*) of the adducts (**3** and **5**) from isothiocyanates (**2**) and tributylphosphine (**4**) or **1** were determined for the first time in some solvents spectrophotometrically, although the presence of the equilibrium was suspected before.[2c]

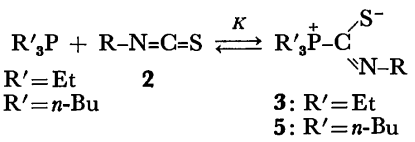

1: R′=Et **4**: R′=*n*-Bu **2** **3**: R′=Et **5**: R′=*n*-Bu

In the present systems, the extinction coefficients due to starting materials, phosphine and isothiocyanates, were negligible at 340 nm. Therefore, the extinction

TABLE 1. THE ADDUCTS (3) OF TRIETHYLPHOSPHINE AND ISOTHIOCYANATES

3	R	Mp (°C)	Yield (%)	Elemental analyses (%)[a] C	H	N	S
3a	Me	79.5—80.0	67	50.05 (50.24)	8.98 (9.49)	7.50 (7.32)	18.71 (16.76)
3b	Ph	62.0—63.0 (lit,[1e] 63)	53				
3c	α-$C_{10}H_7$	112—114 (dec)	77	68.46 (67.30)	7.72 (7.31)	4.85 (4.62)	
3d	MeCO	62—66	89	49.08 (49.30)	8.21 (8.27)	7.24 (6.39)	14.17 (14.62)
3e	PhCO	106.5—109.0 (dec)	96	59.74 (59.77)	7.21 (7.16)	5.06 (4.98)	11.31 (11.40)
3f	*p*-$MeC_6H_4SO_2$[b]	148.5—149.5	94	50.95 (50.74)	6.75 (6.69)	4.20 (4.23)	19.19 (19.35)
3g	Ph_2P (S)	99—101	69	59.21 (58.00)	6.62 (6.40)	3.56 (3.56)	15.88 (16.30)

a) The values in the parentheses are the calculated values. b) Mol wt: 329 (VPO method in dioxane) (calcd: 331.9), indicating almost no dissociation in dioxane.

coefficients due to the formation of the adducts at 340 nm were measured at several ratios of phosphine to the corresponding isothiocyanate, and the K value was calculated according to Drago's method.[5] In most cases, isosbestic points were observed, indicating the presence of equilibrium.[4] A typical example is shown in Fig. 1. The results are summarized in Table 2.

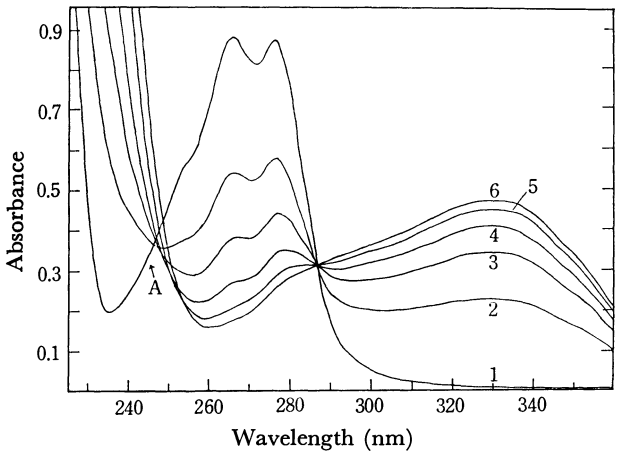

Fig. 1. UV Spectra of triethylphosphine (**1**) and phenyl isothiocyanate (**2b**) system in acetonitrile (24 °C). The ratio of **1** to **2b**: 2=4.22; 3=10.5; 4=21.1; 5=42.1; 6=84.3. 1 is the spectrum of **2b**. Concentration of **2b**, 7.42×10^{-5} M, was maintained constant throughout the measurement (*cf.* Table 4). A: One of isosbestic points should appear here, which is not observed due to absorption of excess **1**.

Table 2. Equilibrium Constants (K) at 24 °C

System	Solv.	K (1/mol)	ε (340 nm)	λ_{max} (nm)	Dielectric constant
4+**2b**	MeCN	840±43	6500	331	37.5
	Me_2CO	323±6	5600	337	20.7
	CH_2Cl_2	277±20	6400	334	8.9
	Et_2O	3.7—6.7		340	4.3
	n-C_6H_{14}	1.5—3.5		340	1.9
1+**2b**	MeCN	2910±120	6100	330	
4+**2e**	MeCN	$(3.4\pm1.0)\times10^4$		315	
4+**2f**	MeCN	$(2.4\pm0.5)\times10^4$		307	

The equilibrium constant becomes larger and hence the stability of the adducts increases according to the increase of polarity of solvents and the introduction of electron-withdrawing substituents. These effects are accompanied by blue shift of λ_{max} of absorption of the adducts. The result is consistent with $n\rightarrow\pi^*$ nature of the absorption but the molar extinction coefficient (*ca.* 6000) is very large for that. In the case of **5f**, the equilibrium lies completely to the adducts when two moles of **4** is added to one mole of **2f** in acetonitrile. The equilibrium constant of **2b** is smaller with **4** than that with **1**, probably because of the bulkiness of **4**, but this does not affect λ_{max} of the absorption. These results are consistent with the easiness of formation of the adducts during their preparation.

Since the attainment of the equilibrium between **4** and methyl isothiocyanate (**2a**) was very slow and isosbestic points could not be observed in the cases of allyl and diphenylphosphinothioyl isothiocyanates (**2g**), equilibrium constants for these systems could not be determined. Similar equilibrium of the betaine with *P–C* bond has been determined in the reaction of tributylphosphine (**4**) with benzylidenemalononitrile.[6a]

^{31}P Chemical Shifts of the Adducts (5). The ^{31}P-NMR chemical shifts (δ_P) of the adducts (**5**) were measured by mixing *N,N*-dimethylformamide (DMF) solutions of **4** and **2** to yield samples of about 0.83 M concentration for each reagent. The results are shown in Table 3.

Table 3. ^{31}P Chemical shifts of the adducts (**5**) in DMF at 34 °C

5	R	δ_P (ppm)	σ_p of R[a]
5a	Me	−18.3	−0.17
	CH_2=$CHCH_2$	−18.1	—
5b	Ph	−20.0	−0.01
5c	α-$C_{10}H_7$	−20.9	—
5g	Ph_2P (S)	−21.9 (J_{PP} 110 Hz)	0.28[8]
	Et_2NCS	−22.2	0.34[b]
5e	PhCO	−23.1	0.43[9]
5d	MeCO	−23.3	0.50
5f	p-$MeC_6H_4SO_2$	−26.8	0.72[c]

a) The σ_p values were taken from Ref. 7, unless otherwise stated. b) For MeNHCS group. c) For $MeSO_2$ group.

The δ_P values of the adducts (**5**) and the adduct of tributylphosphine with carbon disulfide (δ_P=−21.5 ppm in DMF) are similar to those of phosphonium salts (*cf.* $Bu_3\overset{+}{P}Et$ Br^-, δ_P=−35.5 ppm),[6b] supporting the betaine structure of **5** with *P–C* bond in solution.

Plots of the δ_P data against Hammett σ_p values of the R group gave a rather good straight line (ρ=−8.68, r=0.979), where two of σ_p values were quoted from those of the corresponding analogous substituents.

In these measurements, no residual **4** was detected except for **2a**, in which the rate of formation of the adduct should be slow. The equilibrium is shifted almost to the adducts (**5**) in the concentration used, as shown by a simple calculation using the K values shown in Table 2. However, when excess **4** was used for **2b**, two peaks were observed which correspond to **4** and **5b**, respectively, showing that the rate of equilibration is slow for observation by NMR.

Some Reactions of the Adducts (3). In the measurement of the equilibrium constant of the adduct (**3e**), a deviation from isosbestic points in UV spectra was observed when a large excess of **4** was used.

Therefore, a mixture of benzoyl isothiocyanate (**2e**) and two molar amounts of **1** was refluxed in acetone for 2 h. α-Triethylphosphonio-α-benzoylaminomethylenetriethylphosphorane thiocyanate (**6**), benzoylaminomethyltriethylphosphonium thiocyanate (**7**), triethylphosphine sulfide (**8**), and benzoic acid were obtained in 73, 14, 72, and 53% yields, respectively.

Two phosphorus atoms in **6** were equivalent in ^{31}P-NMR spectrum. Reaction of an equimolar mixture of **1** and **3e** gave a similar result.

The compound **7** is considered to be a hydrolysis product of **6** by moisture in acetone. In fact, standing of a mixture of **2e** and two molar amounts of **1** in acetone at room temperature for 71 h gave no **6**, but **7**, **8**, and benzoic acid in 61, 65, and 34% yields, respectively.

Their formation can be rationalized by the following scheme.

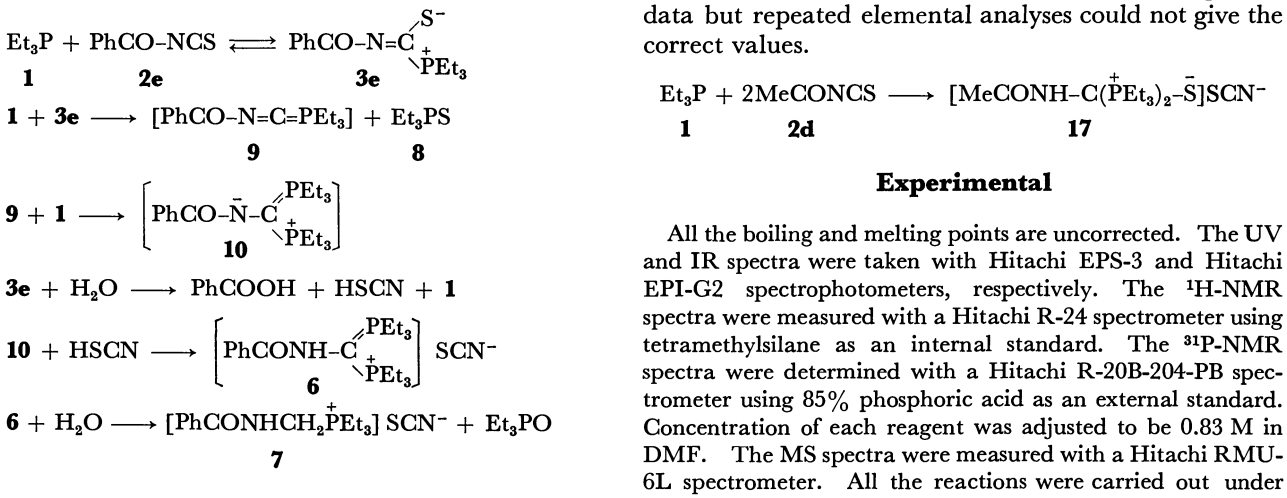

A facile desulfurization of **3e** by **1** to form a new heterocumulene (**9**) is assumed as a preceding step for formation of betaine (**10**), which is stabilized as the phosphonium salt (**6**).

On the other hand, reaction of **1** with two molar amounts of **2e** in refluxing acetone afforded benzamide (23%) and α-benzoylamino-α-benzoylthiomethyltriethylphosphonium thiocyanate (**11**) (27%). This reaction is explained as follows.

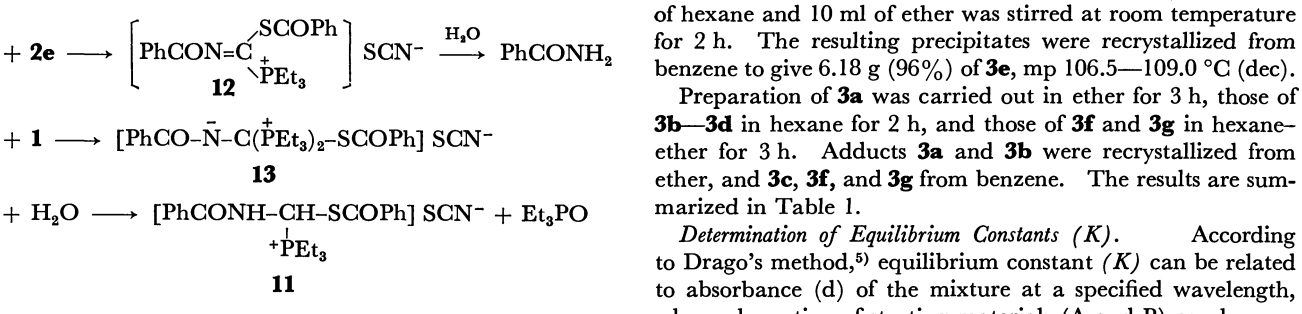

Methylation of **3a** with methyl iodide in ether gave triethyl-α-methylimino-α-methylthiomethylphosphonium iodide (**14**, 44%) at room temperature along with a small amount of triethylmethylphosphonium iodide (**15**).

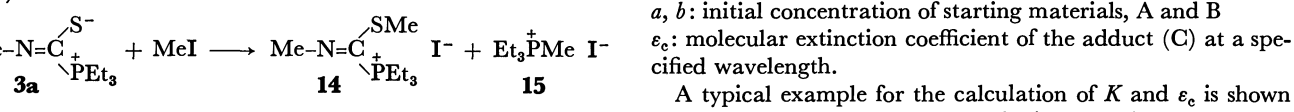

Similar methylation of **3b** gave only **15**. On the other hand, methylation of **3e** in refluxing acetone afforded 31% of *S*-methyl *N*-benzoylmonothiocarbamate (**16**) and 46% of benzamide. The formation mechanism is considered as follows.

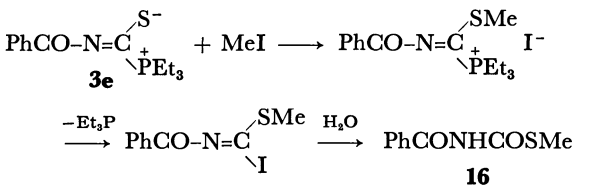

The adduct (**3f**) was stable in refluxing acetonitrile against **1** or methyl iodide, but gave 22% of **15** and 64% of *p*-toluenesulfonamide in refluxing methyl iodide.

Reaction of **1** with two molar amount of **2d** afforded a substance considered to be **17** based on the spectral data but repeated elemental analyses could not give the correct values.

Experimental

All the boiling and melting points are uncorrected. The UV and IR spectra were taken with Hitachi EPS-3 and Hitachi EPI-G2 spectrophotometers, respectively. The ^{1}H-NMR spectra were measured with a Hitachi R-24 spectrometer using tetramethylsilane as an internal standard. The ^{31}P-NMR spectra were determined with a Hitachi R-20B-204-PB spectrometer using 85% phosphoric acid as an external standard. Concentration of each reagent was adjusted to be 0.83 M in DMF. The MS spectra were measured with a Hitachi RMU-6L spectrometer. All the reactions were carried out under nitrogen.

Materials. Triethylphosphine,[10] acetyl,[11] benzoyl,[12] *p*-toluenesulfonyl,[13] diphenylphosphinothioyl,[14] and *N,N*-diethylthiocarbamoyl isothiocyanates[15] were prepared by the reported methods. The others were commercially available and used after purification.

Preparation of the Adducts (3). A typical procedure is described for **3e**.

A mixture of 2.72 g (23.0 mmol) of triethylphosphine (**1**) and 3.80 g (23.3 mmol) of benzoyl isothiocyanate (**2e**) in 60 ml of hexane and 10 ml of ether was stirred at room temperature for 2 h. The resulting precipitates were recrystallized from benzene to give 6.18 g (96%) of **3e**, mp 106.5—109.0 °C (dec).

Preparation of **3a** was carried out in ether for 3 h, those of **3b**—**3d** in hexane for 2 h, and those of **3f** and **3g** in hexane–ether for 3 h. Adducts **3a** and **3b** were recrystallized from ether, and **3c**, **3f**, and **3g** from benzene. The results are summarized in Table 1.

Determination of Equilibrium Constants (K). According to Drago's method,[5] equilibrium constant *(K)* can be related to absorbance (d) of the mixture at a specified wavelength, where absorption of starting materials (A and B) can be neglected.

$$A + B \overset{K}{\rightleftharpoons} C$$

$$1/K = d/\varepsilon_c + \varepsilon_c/d \times ab - (a+b)$$

a, b: initial concentration of starting materials, A and B

ε_c: molecular extinction coefficient of the adduct (C) at a specified wavelength.

A typical example for the calculation of K and ε_c is shown in Table 4, and the UV spectra of this system is shown in Fig. 1.

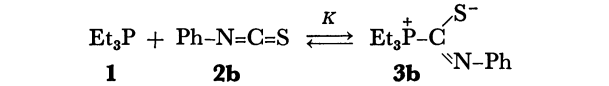

Table 4. Calculation of equilibrium constant of triethylphosphine (**1**) and phenyl isothiocyanate (**2b**) in acetonitrile (24 °C)

No. of the Solution	PhNCS ($\times 10^3$ M)	Et_3P ($\times 10^3$ M)	Absorbance (at 340 nm)
1	0.0742	0.000	0.000
2	0.0742	0.313	0.202
3	0.0742	0.782	0.309
4	0.0742	1.564	0.366
5	0.0742	3.128	0.407
6	0.0742	6.256	0.428

ε_c	$10^3/K$				
	2	3	4	5	6
6000	0.336	0.322	0.325	0.288	0.249
6100	0.347	0.340	0.356	0.344	0.357
6200	0.358	0.358	0.387	0.400	0.464
6300	0.369	0.376	0.418	0.456	0.571
6400	0.380	0.394	0.449	0.512	0.679
6500	0.391	0.412	0.479	0.568	0.786
6600	0.402	0.430	0.510	0.624	0.894
6700	0.413	0.448	0.541	0.680	1.001
6800	0.424	0.466	0.572	0.736	1.109

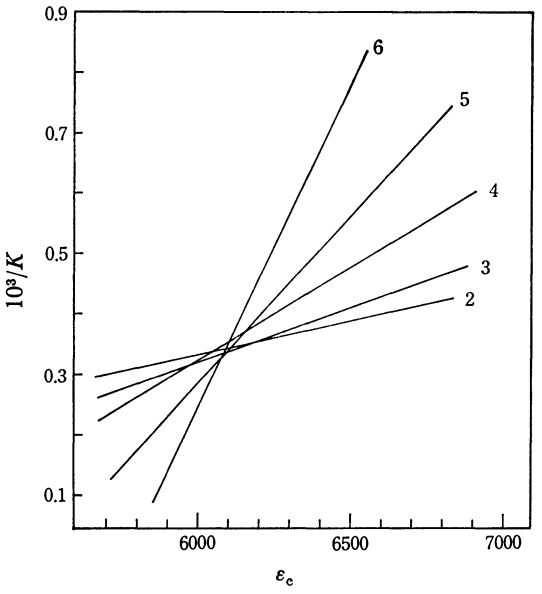

Fig. 2. Plot of ε_c against $10^3/K$ shown in Table 4.

Plot of $1/K$ *vs.* ε_c for each mixture gives a straight line, and $1/K$ and ε_c are determined at the cross point (Fig. 2).

Reactions of Triethylphosphine (1) with Benzoyl Isothiocyanate (2e). a) *2*: *1* reaction: 1) A mixture of 1.76 g (14.7 mmol) of **1** and 1.25 g (7.68 mmol) of **2e** in 30 ml of acetone was refluxed for 2 h. After evaporation of acetone, a small amount of benzene was added to the residue to precipitate 1.20 g (2.80 mmol, 73%) of **6**. Standing of the filtrate afforded 0.163 g (0.52 mmol, 14%) of **7**. The filtrate was chromatographed on silica gel. Elution with benzene–acetone (19: 1) gave 0.25 g (2.05 mmol, 53%) of benzoic acid and 0.415 g (2.76 mmol, 72%) of **8**, the separation of which was carried out using aqueous sodium carbonate. The spectral data of **8** were in agreement with those of an authentic sample.

6: mp 132.5—134.0 °C (from benzene–acetone); IR (KBr): 3240 (NH), 2050 ($^-$SCN), and 1660 cm^{-1} (CO). The ^{1}H-NMR spectrum in $CDCl_3$ showed a broad singlet at δ 8.65 due to NH (1H) proton and the signal disappeared by addition of D_2O; ^{31}P-NMR (DMF): δ_P −35 ppm.

Found: C, 59.13; H, 8.56; N, 6.65; S, 7.60%. Calcd for $C_{21}H_{36}N_2OP_2S$: C, 59.13; H, 8.51; N, 6.57; S. 7.52%.

7: mp 127.5—128.5 °C (from acetone); IR (KBr); 3210 (NH), 2050 ($^-$SCN), and 1650 cm^{-1} (CO). The ^{1}H-NMR spectrum in $CDCl_3$ showed signals at δ 4.51 (dd, J_{NHCH} 6.0, J_{PCH} 5.3 Hz, 2H, CH_2) and 9.35 (bs, 1H, NH). By addition of D_2O, the latter disappeared and the former changed to a doublet (J 5 Hz); ^{31}P-NMR (DMF): δ_P −28 ppm.

Found: C, 57.78; H, 7.75; N, 9.32; S, 10.18%. Calcd for $C_{15}H_{23}N_2OPS$: C, 58.04; H, 7.47; N, 9.02; S, 10.33%.

2) A mixture of 0.573 g (4.85 mmol) of **1** and 1.306 g (4.65 mmol) of **3e** in 50 ml of acetone was refluxed for 3 h. Similar treatment gave 0.543 g (1.27 mmol, 55%) of **6**, 0.133 g (0.43 mmol, 18%) of **7**, 0.283 g (1.9 mmol, 81%) of **8**, and 0.134 g (1.09 mmol, 47%) of benzoic acid.

3) Reaction of 0.959 g (8.11 mmol) of **1** and 0.721 g (4.42 mmol) of **2e** in 20 ml of acetone at room temperature for 71 h afforded 0.42 g (1.35 mmol, 61%) of **7**, 0.216 g (1.44 mmol, 65%) of **8**, and 91 mg (0.75 mmol, 34%) of benzoic acid.

b) *1*: *2* reaction. A mixture of 1.27 g (10.8 mmol) of **1** and 3.55 g (21.7 mmol) of **2e** in 50 ml of acetone was refluxed for 4.5 h. After evaporation, small amounts of benzene and acetone were added to precipitate 1.30 g (2.91 mmol, 54%) of **11**. The filtrate was chromatographed on silica gel. Elution with acetone gave 0.60 g (4.95 mmol, 23%) of benzamide. From other fractions, **8** and benzoic acid were identified by IR.

11: mp 151.0—152.0 °C (from benzene–acetone); IR (KBr): 3150 (NH), 2050 ($^-$SCN), 1652, and 1678 cm^{-1} (CO). The NMR spectrum in $CDCl_3$ showed signals at δ 6.97 (dd, J_{HNCH} 7.8, J_{PCH} 9.6 Hz, 1H, CH) and 10.3 (bd, 1H, NH). By addition of D_2O, the latter disappeared and the former changed to a doublet (J_{PCH} 9.6 Hz). Mol wt (VPO method in pyridine): 451.2 (calcd 477.8).

Found: C, 59.39; H, 6.18; N, 6.27; S, 14.75%. Calcd for $C_{22}H_{27}N_2O_2P_2S_2$: C, 59.17; H, 6.09; N, 6.27; S, 14.36%.

Methylation of 3. a) **3a**: A mixture of 0.761 g (3.98 mmol) of **3a** and 0.652 g of methyl iodide in 10 ml of ether was stirred overnight at room temperature to give 0.58 g (44%) of **14**, mp 101.5—103.0 °C (from 2-propanol).

Found: C, 32.51; H, 6.30; N, 4.06%. Calcd for $C_9H_{21}NPSI$: C, 32.44; H, 6.35; N, 4.20%.

Before the recrystallization of **14**, the presence of **15** was confirmed by NMR.

b) **3b**: A mixture of 1.08 g (4.27 mmol) of **3b** and 0.66 g of methyl iodide in 10 ml of ether was stirred overnight to precipitate **15** (1.01 g, 91%). The spectral data were in agreement with an authentic sample.

c) **3e**: A mixture of 0.622 g (2.21 mmol) of **3e** and 0.5 ml of methyl iodide in 30 ml of acetone was refluxed for 1 h. After evaporation, benzene was added to precipitate 37 mg of benzamide. The filtrate was chromatographed on silica gel. Elution with benzene–acetone (9: 1) gave 0.132 g (0.68 mmol, 31%) of **16**, mp 152 °C (from methanol) (lit,[16] 152—153 °C). IR (KBr): 3250 (NH), 1698 (SCO), and 1630 cm^{-1} (PhCO); MS: *m/e* 195 (M^+, 35%), 147 ($PhCONCO^+$, 95), 105 ($PhCO^+$, *ca.* 100), and 77 (Ph, 100).

Elution with benzene–acetone (3: 1) gave 74 mg of benzamide (46% in total).

d) **3f**: A solution of 0.978 g (2.96 mmol) of **3f** in 30 ml of methyl iodide was refluxed for 20 h. After evaporation, 0.171 g (22%) of **15** was obtained. The filtrate was chromatographed on silica gel. Elution with benzene–acetone (4: 1) gave 0.319 g (64%) of *p*-toluenesulfonamide.

Reaction of 1 and Acetyl Isothiocyanate (2d) in the Ratio of 1: 2.

A mixture of 0.68 g (5.75 mmol) of **1** and 1.15 g (11.4 mmol) of **2d** in 50 ml of acetone was stirred at room temperature for 6 days. The resulting precipitates were collected and recrystallized from methanol to give 0.279 g of **17**. The filtrate was chromatographed on silica gel. Elution with benzene–acetone (3: 1) gave 0.197 g (23%) of **8**. **17**: mp 158–159 °C (from MeOH); IR (KBr): 3150 (NH), 2050 (-SCN), and 1680 cm^{-1} (CO); NMR (D_2O): δ 2.2 (s, 3H, Me) and 0.9—3.0 (m, 30H, 6Et).

Found: C, 47.21—47.48; H, 8.18—8.48; N, 9.93—11.64; S, 14.51—19.09%. Mol wt: 372 (186×2: VPO method in pyridine). Calcd for $C_{16}H_{34}N_2OP_2S_2$: C, 48.46; H, 8.64; N, 7.06; S, 16.17%. Mol. wt.: 396.5.

This work was supported by a Grant-in-Aid from the Ministry of Education.

References

1) a) A. W. Hofmann, *Ann. Chem. Suppl.*, **1**, 25, 59 (1861); b) A. Hantzsch and H. Hibbert, *Ber.*, **40**, 1508 (1907); c) H. Staudinger and J. Meyer, *Helv. Chim. Acta*, **2**, 612 (1919); d) K. Issleib and A. Brack, *Z. Anorg. Allgem. Chem.*, **277**, 271, (1954); e) L. Horner and K. Klüpfel, *Justus Liebigs Ann. Chem.*, **591**, 69 (1955).

2) a) T. N. Margulis and D. H. Templeton, *J. Am. Chem. Soc.*, **83**, 995 (1961); b) M. Arshad, A. Beg, and M. S. Siddigui, *Can. J. Chem.*, **43**, 608 (1965); c) K. A. Jensen and P. H. Nielsen, *Acta Chem. Scand.*, **17**, 547 (1963).

3) H. D. Hartzler, *J. Am. Chem. Soc.*, **93**, 4961 (1971).

4) Preliminary report: K. Akiba, T. Yoneyama, and N. Inamoto, *Chem. Lett.*, **1974**, 561.

5) N. J. Rose and R. S. Drago, *J. Am. Chem. Soc.*, **81**, 6138 (1959).

6) a) Z. Rappoport and S. Gertler, *J. Chem. Soc.*, **1964**, 1360. b) S. Grim, W. Mcfarlane, E. Davidoff, and J. Harts, *J. Phys. Chem.*, **70**, 581 (1966).

7) D. H. McDaniel and H. C. Brown, *J. Org. Chem.*, **23**, 420 (1958).

8) R. A. Baldwin, M. T. Cheng, and G. D. Homer, *J. Org. Chem.*, **32**, 2176 (1967).

9) W. N. White, R. Schlitt, and D. Gwynn, *J. Org. Chem.*, **26**, 3163 (1961).

10) K. Sasse, "Methoden der Organischen Chemie," Band XII/1, Georg Thieme Verlag, Stuttgart (1963), p. 33.

11) R. Pohloudek-Fabini and E. Schroepl, *Pharm. Zentralk.*, **107**, 277 (1968); *Chem. Abstr.*, **69**, 43549c (1968).

12) A. Takamizawa, H. Hirai, and K. Matsui, *Bull. Chem. Soc. Jpn.*, **36**, 1214 (1963).

13) K. Hartke, *Arch. Pharm.*, **299**, 174 (1966); T. Kodama, S. Shinohara, and K. Hisada, *Yuki Gosei Kagaku Kyokaishi*, **24**, 310 (1966).

14) A. Schmidpeter and H. Groeger, *Chem. Ber.*, **100**, 3052 (1967).

15) R. H. Goshorn, W. W. Levis, Jr., E. Jaul, and E. J. Ritter, *Org. Synth.*, Coll. Vol. **4**, 307 (1963).

16) H. L. Wheeler and T. B. Johnson, *Am. Chem. J.*, **24**, 201 (1900).

Synthesis and Biological Activities of 2-Amino-2-deoxy- and 6-Amino-6-deoxy-α-D-glucopyranosyl-2,5-dideoxystreptamines

Seiichiro OGAWA, Yuji FUNAKI, Keiji IWATA, and Tetsuo SUAMI

Department of Applied Chemistry, Faculty of Engineering, Keio University, Hiyoshi, Yokohama 223

(Received April 17, 1976)

To investigate a relationship between structural features of aminocyclitols and biological activities of aminocyclitol antibiotics, 4-*O*-(2′-amino-2′-deoxy-α-D-glucopyranosyl)- and 4-*O*-(6′-amino-6′-deoxy-α-D-glucopyranosyl)-2,5-dideoxystreptamines (**8** and **15a**) have been synthesized, and their biological activities against several microorganisms were determined.

Chemical modification of aminocyclitol antibiotics[1] has so far been extensively carried out in order to elucidate a structure-activity relationship and to synthesize new antibiotics that are active against resistant bacteria. Most investigations have however been aimed at modification of aminosugar moieties of antibiotics, but few exploitations of a relationship between structural feature of aminocyclitol and biological activities of the corresponding antibiotics have been attempted.[2]

In continuation of the preceding report,[3] a synthesis of biologically active α-aminoglycosides of 2,5-dideoxystreptamine,[4] *viz.* 4-*O*-(2′-amino-2′-deoxy-α-D-glucopyranosyl)- and 4-*O*-(6′-amino-6′-deoxy-α-D-glucopyranosyl)-2,5-dideoxystreptamines (**8** and **15a**) is described in the present article.

Condensation of *N*,*N*′-dibenzyloxycarbonyl-2,5-dideoxystreptamine (**1a**)[4] with 3,4,6-tri-*O*-acetyl-2-deoxy-2-(2′,4′-dinitroanilino)-α-D-glucopyranosyl bromide (**2**)[5] was effected in the presence of mercuric cyanide and mercuric bromide in dry dioxane at reflux temperature for three days and afforded, after fractionation by a silica gel column chromatography, 4,6-di-*O*-[3′,4′,6′-tri-*O*-acetyl-2′-deoxy-2′-(2″,4″-dinitroanilino)-D-glucopyranosyl]-*N*,*N*′-dibenzyloxycarbonyl-2,5-dideoxystreptamine (**5**)[6] (5.2%) and a practically homogeneous 4-*O*-[3′,4′,6′-tri-*O*-acetyl-2′-deoxy-2′-(2″,4″-dinitroanilino)-α-D-glucopyranosyl]-*N*,*N*′-dibenzyloxycarbonyl-2,5-dideoxystreptamine (**6**) (13%), together with syrupy 3,4,6-tri-*O*-acetyl-1,2-dideoxy-2-(2′,4′-dinitroanilino)-D-arabino-hex-1-enopyranose (**3**)[7] (33.5% based on **2**) and 3,4,6-tri-*O*-acetyl-2-deoxy-2-(2′,4′-dinitroanilino)-D-glucose (**4**)[5] (6.7% based on **2**). Treatment of **6** with methanolic ammonia at room temperature gave crystalline 4-*O*-[2′-deoxy-2′-(2″,4″-dinitroanilino)-α-D-glucopyranosyl]-*N*,*N*′-dibenzyloxycarbonyl-2,5-dideoxystreptamine (**7**) in 41% yield. Removal of the protecting groups of **7** was then effected by treatment with Dowex 1×2 (OH^-), followed by hydrogenolysis in the presence of palladium black, giving **8** in 63% yield, as a homogeneous glassy product, which was characterized as the tri-*N*-acetyl derivative (**9**).

Biological activity of **8** was determined by a paper disk method comparing with that of antibiotic neamine, and the results were shown in Table 1. No direct proof to establish the absolute configuration of **8** has been done owing to a minute sample. However, on the basis of an empirical results that only 4-*O*-α-D-aminoglycosides of 2-deoxystreptamine have antibacterial activities,[9] **8** was tentatively assigned as 4-*O*-α-D-glucosaminide of

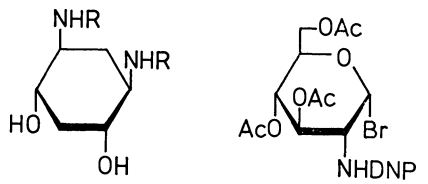

1a, R=Cbz
1b, R=Cbe

2

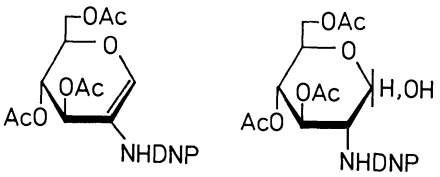

3 4

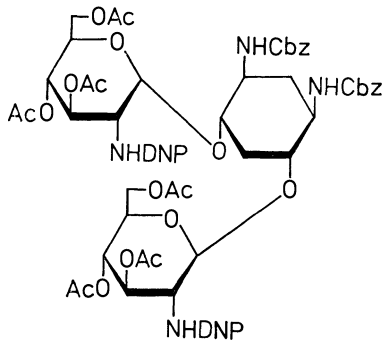

5

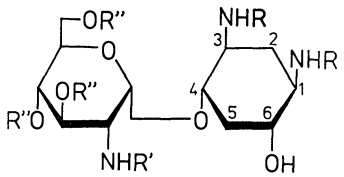

	R	R′	R″
6	Cbz	DNP	Ac
7	Cbz	DNP	H
8	H	H	H
9	Ac	Ac	H

Abbreviation:
Bn=benzyl, Cbe=ethoxycarbonyl,
Cbz=benzyloxycarbonyl,
DNP=2,4-dinitrophenyl

former had a remarkable antibacterial activity almost comparable to that of neamine, but the latter had no activity, confirming the absolute configuration deduced from the PMR data.

According to the present results, it has been presumed that aminocyclitol antibiotics which contain 2,5-dideoxystreptamine possess their antibacterial activities.

Experimental[13]

Modified Kõnigs-Knorr Reaction of N,N′-*Dibenzyloxycarbonyl-2,5-dideoxystreptamine (**1a**) and 3,4,6-Tri-*O-*acetyl-2-deoxy-2-(2′,4′-dinitroanilino)-α-*D*-glucopyranosyl Bromide (**2**).*[5] A mixture of **1a** (2.0 g), Drierite (6.0 g) and dry dioxane (150 ml) was heated at reflux to distil out some of the solvent. Then **2** (7.7 g), mercuric cyanide (7.7 g), and mercuric bromide (6.0 g) were added to this mixture in three portions every 24 h under gentle reflux and stirring. Three days after the last addition of the reagents, TLC (1 : 4 acetone–benzene) showed that all **1a** had been consumed and four main components (R_f 0.73, 0.50, 0.31, and 0.18) formed. An insoluble material was filtered off and the filtrate was evaporated to dryness. The residue was taken up in chloroform (300 ml), washed with a saline water, aqueous sodium hydrogencarbonate, and water, successively, dried over anhydrous sodium sulfate, and evaporated to give a crystalline residue (*ca.* 12 g). TLC indicated the presence of four main components, along with several minor components. The products were chromatographed on a silica gel column (300 g, Wako gel C-200) with 1 : 4 acetone–benzene as an eluant. Fractions were separated according to the results of TLC.

The first fractions (R_f 0.73) were evaporated to give 3,4,6-tri-*O*-acetyl-1,2-dideoxy-2-(2′,4′-dinitroanilino)-D-arabino-hex-1-enopyranose (**3**, 2.2 g, 33.5% yield based on **2** used) as a yellowish glass; $[\alpha]_D^{20}$ −115° (*c* 1, acetone); IR, 3340, 1750, 1670 cm^{-1}; PMR ($CDCl_3$) δ 2.02 (s, 3), 2.17 (s, 3), 2.21 (s, 3) (OAc), 5.44 (t, 1, $J_{3,4}=J_{4,5}=4.5$ Hz, H-4), 5.61 (dd, 1, $J_{1,3}=0.8$ Hz, H-3), 7.01 (d, 1, H-1).

Found: C, 47.57; H, 4.36; N, 8.86%. Calcd for $C_{18}H_{19}N_3O_{11}$: C, 47.69; H, 4.22; N, 9.27%.

The second fractions (R_f 0.50) were evaporated and crystallized from acetone–petroleum ether to give crystalline 3,4,6-tri-*O*-acetyl-2-deoxy-2-(2′,4′-dinitroanilino)-D-glucose (**4**, 0.45 g, 6.7% yield based on **2** used); mp 159—162 °C. This compound was identified with an authentic sample[5] by IR spectra and TLC.

The third fractions (R_f 0.31) were evaporated and crystallized from acetone–petroleum ether to give a crystalline 4,6-di-*O*-[3′,4′,6′-tri-*O*-acetyl-2′-deoxy-2′-(2″,4″-dinitroanilino)-D-glucopyranosyl-*N*,*N*′-dibenzyloxycarbonyl-2,5-dideoxystreptamine (**5**, 330 mg, 5.2% yield based on **1a** used); mp 291—294 °C; $[\alpha]_D^{21}$ +63° (*c* 0.3, pyridine); IR, 3340, 1750, 1520 cm^{-1}; PMR (DMSO-d_6) δ 1.76 (s, 3), 1.78 (s, 3), 1.98 (s, 3), 2.08 (s, 3), 2.10 (s, 3) (OAc), 5.18 (m, 4, C$\underline{H}_2$ of Cbz), 7.52 (s, 10, aromatic protons of Cbz).

Found: C, 52.73; H, 4.83; N, 8.48%. Calcd for $C_{58}H_{64}N_8O_{28}$: C, 52.73; H, 4.97; N, 8.29%.

The third fractions (R_f 0.18) were evaporated and crystal lized from acetone–petroleum ether to give crystalline product (821 mg). Recrystallization from acetone gave 4-*O*-[3′,4′,6′-tri-*O*-acetyl-2′-deoxy-2′-(2″,4″-dinitroanilino)-α-D-glucopyranosyl]-*N*,*N*′-dibenzyloxycarbonyl-2,5-dideoxystreptamine (**6**, 529 mg, 12.5% yield based on **1a** used) as homogeneous crystals; mp 286.5 °C; $[\alpha]_D^{20}$ +61.3° (*c* 0.75, pyridine); IR, 3340, 1740, 1690, 1520 cm^{-1}; PMR (DMSO-d_6), δ 1.77 (s, 3), 1.95 (s, 3), 2.10 (s, 3) (OAc), 5.16 (s, 4, C$\underline{H}_2$ of Cbz), 7.48 (s, 10, aromatic protons of Cbz).

Found: C, 54.98; H, 5.28; N, 7.71%. Calcd for $C_{40}H_{45}N_5O_{17}$: C, 55.36; H, 5.27; N, 8.07%.

*4-O-[2′-deoxy-2′-(2″,4″-dinitroanilino)-α-D-glucopyranosyl]-N,N′-dibenzyloxycarbonyl-2,5-dideoxystreptamine (**7**).* Compound **6** (567 mg) was treated with methanolic ammonia (100 ml) under stirring overnight at room temperature. The reaction mixture was evaporated to give a crystalline residue. Recrystallization from dioxane–methanol gave **7** (198 mg, 41%) as pale yellowish crystals; mp 277—279 °C; $[\alpha]_D^{16}$ +90° (*c* 0.3, *N*,*N*-dimethylformamide); IR, 3300, 1690, 1530 cm^{-1}.

Found: C, 54.51; H, 5.25; N, 9.17%. Calcd for $C_{34}H_{39}N_5O_{14}\cdot 1/2H_2O$: C, 54.39; H, 5.33; N, 9.33%.

*4-O-(2′-Amino-2′-deoxy-α-D-glucopyranosyl-2,5-dideoxystreptamine (**8**).* A solution of **7** (190 mg) in dioxane (30 ml) and water (6 ml) was treated with Dowex 1×2 (OH^-) (8 ml) under stirring overnight at room temperature. The resin was removed by filtration and the filtrate was evaporated to give a powder. The product was directly hydrogenolyzed in the presence of palladium black (30 mg) in a mixture of dioxane (10 ml) and water (10 ml) overnight at room temperature (the initial hydrogen pressure of 3.4 kg/cm^2). The crude product was crystallized from ethanol–ether to give **8** (50 mg, 63%) as a white powder; mp 151—155 °C (bubbling); $[\alpha]_D^{18}$+162° (c 0.8, H_2O); R_f Glucosamine Hydrochloride 0.31, R_f 2,5-Dideoxystreptamine Dihydrochloride 0.37.

Compound **8** (20 mg) was treated with two drops of acetic anhydride in methanol (2 ml) overnight at room temperature. The product was crystallized from ethanol–ether to give the tri-*N*-acetyl derivative (**9**, 20 mg, 71%) as crystals; mp 320—322 °C; $[\alpha]_D^{21}$ +140° (*c* 1.1, H_2O); IR, 1640, 1550 cm^{-1}.

Found: C, 48.58; H, 7.11; N, 9.13%. Calcd for $C_{18}H_{31}N_3O_9\cdot 1/2H_2O$: C, 48.86; H, 7.29; N, 9.49%.

*6-Azido-2,3,4-tri-*O*-benzyl-6-deoxy-α-D-glucopyranosyl Chloride (**10**).* This compound was prepared from crystalline methyl 2,3,4-tri-*O*-acetyl-6-azido-6-deoxy-α-D-glucopyranoside[14] by the direction of Umezawa and his coworkers;[9] syrup, $[\alpha]_D^{22}$ +117° (*c* 2.54, chloroform) (lit,[9] $[\alpha]_D^{24}$ +119° (*c* 0.94, chloroform)).

*N,N′-Diethoxycarbonyl-2,5-dideoxystreptamine (**1b**).* To a solution of 2,5-dideoxystreptamine dihydrochloride[4] (303 mg) in water (20 ml) was added sodium carbonate (1.1 g) and ethyl chloroformate (0.50 ml), and the mixture was stirred for 3 h at room temperature. The mixture was evaporated to dryness and the residue was extracted with hot dioxane (4×20 ml). The extracts were evaporated to give a syrup, which was crystallized from 2-propanol to give **1b** (250 mg, 62%) as crystals; mp 200—201 °C; IR, 3300, 1690, 1540 cm^{-1}; PMR (D_2O) δ 1.24 (t, 6, J=7 Hz, 2C$\underline{H}_3$ of Cbe), 4.15 (q, 4, 2C$\underline{H}_2$ of Cbe).

Found: C, 49.88; H, 7.55; N, 9.60%. Calcd for $C_{12}H_{22}N_2O_6$: C, 49.64; H, 7.64; N, 9.65%.

*Modified Kõnigs-Knorr Reaction of **1b** and **10**.* A mixture of syrupy **10** (4.86 g) and Drierite (6 g) in dry benzene (160 ml) and dry dioxane (54 ml) was magnetically stirred at 50—60 °C for 30 min. Then **1b** (1.98 g) and mercuric cyanide (4.92 g) were added to this mixture, and it was gently refluxed under vigorous agitation. After two days, a 5-g portion of mercuric cyanide was added to the mixture, and, after 9 days, **10** (1.32 g) and mercuric cyanide (1.3 g) were added. Twelve days after the last addition of the reagents, TLC (1: 12 acetone–benzene) indicated a disappearance of **1b**. The reaction mixture was cooled to room temperature and an insoluble matter was removed by filtration. The filtrate was evaporated to give a syrup which was taken up in chloroform (180 ml) and washed with aqueous sodium hydrogencarbonate and water, successively. The chloroform solution was dried over

anhydrous sodium sulfate and evaporated to give an amorphous solid (*ca.* 12 g). TLC showed that it contained three main components (R_f 0.31, 0.06, 0.03), together with several minor components. The products were throughly mixed with silica gel (11 g, Wako gel C-300) and the mixture was transfered to a top of a silica gel column (90 g, packed with benzene). The column was eluted with benzene, 10: 1 benzene–ethyl acetate, 5: 1 benzene–ethyl acetate, 1: 5 acetone–benzene, and 1: 3 acetone–benzene, successively. The fractions were separated according to the results of TLC.

The first fractions (R_f 0.31) were evaporated and crystallized from 2-propanol to give crystalline 4,6-di-*O*-(6′-azido-2′,3′,4′-tri-*O*-benzyl-6′-deoxy-D-glucopyranosyl)-*N*,*N*′-diethoxycarbonyl-2,5-dideoxystreptamine (**11**, 2.02 g, 24.6%). Recrystallized sample melted at 150—156 °C; $[\alpha]_D^{32}$ +57.5° (*c* 0.37, chloroform); IR, 3320, 2130, 1630, 1540 cm^{-1}; PMR ($CDCl_3$) δ 1.14 (t, 6, J=7 Hz, 2C$\underline{H}_3$ of Cbe), 4.07 (q, 4, 2C$\underline{H}_2$ of Cbe), 7.30 (s, 30, aromatic protons of Bn).

Found: C, 65.52; H, 6.41; N, 9.18%. Calcd for $C_{66}H_{76}N_8O_{14}$: C, 65.76; H, 6.36; N, 9.30%.

The second fractions (R_f 0.06) were evaporated and crystallized from ethanol to give crystalline 6-*O*-(6′-azido-2′,3′,4′-tri-*O*-benzyl-6′-deoxy-α-D-glucopyranosyl)-*N*,*N*′-diethoxycarbonyl-2,5-dideoxystreptamine (**12b**, 776 mg, 15%). Recrystallized sample melted at 204—205 °C; $[\alpha]_D^{32}$ +45.9° (*c* 0.47, chloroform); IR, 3320, 2120, 1680, 1540 cm^{-1}; PMR ($CDCl_3$) δ 1.16 (t, 3), 1.23 (t, 3) (J=7 Hz, C$\underline{H}_3$ of Cbe), 4.08 (q, 2), 4.24 (q, 2), (C$\underline{H}_2$ of Cbe), 7.30 (s, 5), 7.32 (s, 5), 7.35 (s, 5) (aromatic protons of Bn).

Found: C, 62.38; H, 6.53; N, 9.11%. Calcd for $C_{39}H_{49}N_5O_{10}$: C, 62.63; H, 6.60; N, 9.37%.

The third fractions (R_f 0.03) were evaporated and crystallized from ethanol to give crystalline 4- or 6-*O*-(6′-azido-2′,3′,4′-tri-*O*-benzyl-6′-deoxy-β-D-glucopyranosyl)-*N*,*N*′-diethoxycarbonyl-2,5-dideoxystreptamine (**13**, 162 mg, 3.2%). Recrystallized sample melted at 221—223 °C; $[\alpha]_D^{20}$ +43.5° (*c* 0.58, chloroform); IR, 3310, 2110, 1680, 1540 cm^{-1}; PMR ($CDCl_3$) δ 1.12 (t, 3), 1.23 (t, 3) (J=7 Hz, C$\underline{H}_3$ of Cbe), 4.13 (q, 4, 2C$\underline{H}_2$ of Cbe), 7.26 (s, 15, aromatic protons of Bn).

Found: C, 61.80; H, 6.52; N, 8.88%. Calcd for $C_{39}H_{49}N_5O_{10}\cdot H_2O$: C, 61.60; H, 6.71; N, 9.14%.

An unresolved mixture (*ca.* 2 g) was rechromatographed on a silica gel column (80 g) and eluted with the same solvents mixture to afford **12b** (86 mg, total yield 16.7%), **13** (67 mg, total yield 4.5%), and a mixture (964 mg) containing the 4-*O*-α-glycoside (**12a**) mainly, along with **12b** and **13**.

*6-O-(2′,3′,4′-Tri-O-benzyl-6′-deoxy-6′-ethoxycarbonylamino-α-D-glucopyranosyl)-N,N′-diethoxycarbonyl-2,5-dideoxystreptamine (**14b**).* A solution of **12b** (258 mg) in a mixture of dioxane (6 ml) and ethanol (6 ml) was hydrogenated in the presence of Raney nickel T-4[11] at room temperature for 24 h (the initial hydrogen pressure of 3.4 kg/cm²). The catalyst was removed by filtration and the filtrate was evaporated to dryness. The residue was dissolved in a mixture of 1: 1: 1 acetone–methanol–water (30 ml) and treated with an excess of ethyl chloroformate in the presence of sodium carbonate overnight at room temperature. An insoluble matter was filtered off and the filtrate was evaporated to dryness. The residue was taken up in chloroform (30 ml), and the solution was washed with aqueous sodium hydrogencarbonate and water, successively, dried over anhydrous sodium sulfate, and evaporated to give a product, which was crystallized from methanol to give crystalline **14b** (166 mg, 60.6%), mp 250—252 °C. Recrystallization from chloroform–ethanol gave an analytical sample, mp 256—258 °C; $[\alpha]_D^{22}$ +13.4° (*c* 0.84, chloroform); IR, no absorption due to an azido group was observed; PMR ($CDCl_3$) δ 1.15 (t, 3), 1.24) (t, 6) (J=7 Hz, C$\underline{H}_3$ of Cbe), 4.06 (q, 2), 4.12 (q, 4) (C$\underline{H}_2$ of Cbe), 5.67 (d, 1, $J_{1',2'}$=3.5 Hz, H-1′), 7.31 (s, 10), 7.34 (s, 5) (aromatic protons of Bn).

Found: C, 63.58; H, 7.01; N, 5.14%. Calcd for $C_{42}H_{55}N_3O_{12}$: C, 63.55; H, 6.98; N, 5.29%.

*4- or 6-O-(2′,3′,4′-Tri-O-benzyl-6′-deoxy-6′-ethoxycarbonylamino-β-D-glucopyranosyl)-N,N′-diethoxycarbonyl-2,5-dideoxystreptamine (**17**).* Compound **13** (136 mg) was hydrogenated in a mixture of dioxane (15 ml), ethanol (5 ml), and ethyl acetate (10 ml) similarly as described in the preparation of **14b**. The product was treated with ethyl chloroformate and sodium carbonate in 75% aqueous dioxane to give crude **17**, which was crystallized from ethanol to give crystalline **17** (108 mg, 74%), mp 254—256 °C; $[\alpha]_D^{21}$ +11.1° (*c* 0.39, chloroform); IR, no absorption due to an azido group was observed; PMR (DMSO-d_6) δ 1.00 (t, 3), 1.16 (t, 6) (J=7 Hz, C$\underline{H}_3$ of Cbe), 3.97 (q, 2), 4.01 (q, 4) (C$\underline{H}_2$ of Cbe), 7.26 (s, 5), 7.30 (s, 10) (aromatic protons of Bn).

Found: C, 63.05; H, 6.29; N, 5.11%. Calcd for $C_{42}H_{55}N_3O_{12}$: C, 63.55; H, 6.98; N, 5.29%, and, for hemihydrate: C, 62.83; H, 7.03; N, 5.23%.

*4-O-(2′,3′,4′-Tri-O-benzyl-6′-deoxy-6′-ethoxycarbonylamino-α-D-glucopyranosyl)-N,N′-diethoxycarbonyl-2,5-dideoxystreptamine (**14a**).* A mixture (964 mg) of **12a**, **12b**, and **13** obtained in the condensation reaction of **1b** and **10** was again fractionated by silica gel chromatography to give a fraction (492 mg) containing **12a** mainly. This product was hydrogenated in dioxane similarly as described in the preparation of **17**, and further converted into the tri-*N*-carboethoxy derivative in the usual manner. TLC (30:1 chloroform–ethanol) indicated that it consisted of a main component, along with two minor components identical with **14b** and **17**. The mixture was separated by the silica gel column (40 g) with 40: 1 chloroform–ethanol as an eluent to give a homogeneous syrup, which was crystallized from ethanol–hexane to give **14a** (268 mg, 5.0% yield based on **2b** used) as crystals, mp 189—190 °C; Recrystallized sample melted at 193—196 °C; $[\alpha]_D^{21}$ +31.7° (*c* 0.38, chloroform); PMR ($CDCl_3$) δ 1.14 (t, 3), 1.24 (t, 3), 1.26 (t, 3) (J=7 Hz, C$\underline{H}_3$ of Cbe), 4.07 (q, 2), 4.12 (q, 2), 4.15 (q, 2) (C$\underline{H}_2$ of Cbe), 7.29 (s, 5), 7.31 (s, 5), 7.33 (s, 5) (aromatic protons of Bn); (DMSO-d_6, 100 MHz) δ 0.91 (t, 3), 1.16 (t, 6) (J=7 Hz, C$\underline{H}_3$ of Cbe), 3.18 (q, 2), 4.01 (q, 4) (C$\underline{H}_2$ of Cbe), 5.06 (d, 1, $J_{1',2'}$=4 Hz, H-1′), 7.28 (s, 5), 7.30 (s, 5), 7.33 (s, 5) (aromatic protons of Bn).

Found: C, 63.75; H, 6.98; N, 5.23%. Calcd for $C_{42}H_{55}N_3O_{12}$: C, 63.55; H, 6.98; N, 5.29%.

*4-O-(6′-Amino-6′-deoxy-α-D-glucopyranosyl)-2,5-dideoxystreptamine (**15a**).* A solution of **14a** (244 mg) in ethanol (25 ml) containing a few drop of acetic acid was hydrogenated in the presence of freshly prepared palladium black at 50—60 °C for 24 h (the initial hydrogen pressure of 3.4 kg/cm²). The catalyst was removed by filtration and the filtrate was evaporated to give a syrup (165 mg), which was taken up in a small amount of methanol. The solution was added dropwise to aqueous barium hydroxide (5 ml, containing 1.3 g of $Ba(OH)_2\cdot 8H_2O$) at 60—70 °C, and the mixture was heated at 120 °C for 6 h. After having been neutralized with cabon dioxide, the reaction mixture was filtered centrifugally to remove barium carbonate and the filtrate was evaporated to give a syrup, which was chromatographed on Amberlite CG-50 (NH_4^+) column (4 ml). After having been washed with water, 0.05 M, and 0.1 M aqueous ammonia, successively, the column was then eluted with 0.2 M aqueous ammonia to give **15a** (69 mg, 74%) as a homogeneous glass; mp 153 °C; $[\alpha]_D^{21}$ +104.6° (*c* 1.39, H_2O); IR, 3350, 1570 cm^{-1}; PMR (D_2O) 5.14 (d, 1, $J_{1',2'}$=3 Hz, H-1′); R_f Glucosamine Hydrochloride 0.19, R_f 2-Deoxystreptamine Dihydrochloride 0.53.

Found: C, 45.15; H, 7.50; N, 12.51%. Calcd for $C_{12}H_{25}N_3$-

$O_6 \cdot 1/3H_2CO_3$: C, 45.16; H, 7.89; N, 12.81%.

Treatment of **15a** (18 mg) with acetic anhydride (1 ml) in methanol (1 ml) at room temperature for 3 h gave the tri-*N*-acetyl derivative (**16a**, 21 mg, 82%) as a glass, mp 235 °C (decomp); $[\alpha]_D^{22}$ +62° (*c* 1.05, H_2O); PMR (D_2O) δ 2.01 (s, 6), 2.05 (s, 3) (NAc), 5.08 (d, 1, $J_{1',2'}$=3 Hz, H-1').

Found: C, 48.56; H, 7.16; N, 9.70%. Calcd for $C_{18}H_{31}N_3O_9 \cdot 1/2H_2O$: C, 48.86; H, 7.29; N, 9.50%.

6-O-(6'-Amino-6'-deoxy-α-D-glucopyranosyl)-2,5-dideoxystreptamine (***15b***). A solution of **14b** (414 mg) in 90% aqueous 2-methoxyethanol (40 ml) containing a few drop of acetic acid was hydrogenated similarly as described in the preparation of **15a**. The product was digested with ethanol and the precipitates were collected by filtration to give a solid (182 mg). The mother liquor was shown to contain **15b** by TLC, and it was again hydrogenated similarly to give another crop of the solid (86 mg). The product was hydrolyzed with aqueous barium hydroxide as described above and purified by the resin column to give **15b** (106 mg, 67.5%) as a homogeneous glass, mp 140 °C (decomp); $[\alpha]_D^{21}$ +75.1° (*c* 0.9, H_2O); IR, 3350, 1570 cm^{-1}; PMR (D_2O) δ 5.10 (d, 1, $J_{1',2'}$ =3.5 Hz, H-1'); $R_{f\ \text{Glucosamine Hydrochloride}}$ 0.23, $R_{f\ \text{2-Deoxystreptamine Dihydrochloride}}$ 0.56.

Found: C, 41.20; H, 7.16; N, 10.77%. Calcd for $C_{12}H_{25}N_3O_6 \cdot 3/2H_2CO_3$: C, 40.49; H, 7.05; N, 10.50%.

Compound **15b** (16 mg) was converted into the tri-*N*-acetyl derivative (**16b**, 11 mg, 50%) as a white powder, mp 276 °C (decomp); $[\alpha]_D^{22}$ +57.9° (*c* 0.57, H_2O); PMR (D_2O) δ 1.98 (s, 3), 2.01 (s, 3), 2.04 (s, 3) (NAc), 5.03 (d, 1, $J_{1',2'}$=3.5 Hz, H-1').

Found: C, 47.83; H, 6.88; N, 8.68%. Calcd for $C_{18}H_{31}N_3O_9 \cdot H_2O$: C, 47.88; H, 7.37; N, 9.31%.

4- or 6-O-(6'-Amino-6'-deoxy-β-D-glucopyranosyl)-2,5-dideoxystreptamine (***18***). Compound **17** (105 mg) was hydrogenated and hydrolyzed similarly as described in the preparation of **15a**, and the product was purified by the resin column to give **18** (27 mg, 66%) as a glass, mp 144 °C (decomp); $[\alpha]_D^{21}$ +12.8° (*c* 1.33, H_2O); PMR (D_2O) δ 4.59 (d, 1, $J_{1',2'}$=7.5 Hz, H-1'); $R_{f\ \text{Glucosamine Hydrochloride}}$ 0.21, $R_{f\ \text{2-Deoxystreptamine Dihydrochloride}}$ 0.55.

This work has been supported financially in part by a grant of the Asahi Glass Foundation for the contribution to industrial technology.

References

1) S. Umezawa, *Adv. Carbohyd. Chem. Biochem.*, **30**, 164 (1974).

2) W. T. Shier, K. L. Rinehart, Jr., and D. Gottlieb, *Proc, Nat. Acad. Sci., U. S.*, **63**, 198 (1969); W. T. Shier, S. Ogawa. M. Hichens, and K. L. Rinehart, Jr., *J. Antibiot.*, **26**, 551 (1973).

3) T. Suami, S. Nishiyama, Y. Ishikawa, and S. Katsura, submitted for publication in *Carbohyd. Res.*

4) T. Suami, S. Ogawa, H. Uchino, and Y. Funaki, *J. Org. Chem.*, **40**, 456 (1975).

5) P. F. Lloyd and M. Stacey, *Tetrahedron*, **9**, 116 (1960).

6) The configurations of two glycoside bonds have not yet been established. Its configuration, together with the preparation of a free pseudo aminotrisaccharide will be reported elsewhere in future.

7) The structure was confirmed by an elementary analysis, and IR and PMR spectra. In PMR spectrum, a narrow doublet (δ 7.01) could be ascribed to a signal due to the vinyl proton, which is corresponding to that reported for the *N*-acetyl compound.[8]

8) N. Pravdic and H. G. Fletcher, Jr., *J. Org. Chem.*, **32**, 1806 (1967).

9) Y. Nishimura, T. Tsuchiya, and S. Umezawa, *Bull. Chem. Soc. Jpn.*, **44**, 2521 (1971).

10) Y. Takagi, T. Tsuchiya, and S. Umezawa, *Bull. Chem. Soc. Jpn.*, **46**, 1261 (1973).

11) S. Nishimura, *Bull. Chem. Soc. Jpn.*, **32**, 61 (1959).

12) A. Hasegawa, D. Nishimura, and M. Nakajima, *Agr. Biol. Chem.*, **36**, 1043 (1972); R. U. Lemieux, T. L. Nagabushan, K. L. Clemetson, and L. C. N. Tucker, *Can. J. Chem.*, **51**, 53 (1973).

13) Melting points were measured on a Mitamura Riken micro hot stage and are uncorrected. Decomposition points were determined in a capillary in a liquid bath and are uncorrected. IR spectra were measured on a Jasco IR-E spectrophotometer in KBr disks. PMR spectra were taken on a Varian A-60D (60 MHz) or HA-100D (100 MHz) in deuteriochloroform ($CDCl_3$), dimethyl sulfoxide-d_6 (DMSO-d_6), or deuterium oxide (D_2O) with tetramethylsilane or sodium 4,4-dimethyl-4-silapentane-1-sulfonate, respectively, as an internal standard. Chemical shifts are given in terms of δ-values, signals being denoted by s (singlet), d (doublet), t (triplet), q (quartet), or m (complex multiplet). Values given for coupling constants are of first-order. TLC was performed on silica gel (Wako gel B-10, Wako Pure Chemical Industries, Ltd.) and the spots were visualized by heating above 150 °C with 30% sulfuric acid. Paper chromatography used Toyo Roshi No. 52 paper, with the solvent system 6: 4: 3: 1 1-butanol–pyridine–acetic acid–water and with the reference compound D-glucosamine hydrochloride and appropriate aminocyclitol hydrochlorides. Elementary analyses were done by Mr. Saburo Nakada, to whom our thanks are due.

14) F. Cramer, H. Otterbach, and H. Springman, *Chem. Ber.*, **92**, 384 (1959).

Studies of Heterocyclic Compounds. VIII.[1] Synthesis and Tautomerism of 2-Hydroxypyrazolo[1,5-*a*]pyridine

Hisao Ochi, Tadashi Miyasaka, Kiyoshi Kanada,* and Kiichi Arakawa

School of Pharmaceutical Sciences, Showa University, 1-5-8 Hatanodai, Shinagawa-ku, Tokyo 142
**Research and Developing Section, Horiuchi Itaro Co. Ltd., Higashimurayama-shi, Tokyo 189*

(Received March 27, 1976)

2-Hydroxypyrazolo[1,5-*a*]pyridine (I) was synthesized by reaction of ethyl 2-pyridylacetate (IV) with hydroxylamine-*O*-sulfonic acid. I was shown to undergo nitrosation, nitration and bromination at C-3 position. Methylation of I with diazomethane gave 2-methoxypyrazolo[1,5-*a*]pyridine (V), while methylation of I with dimethyl sulfate gave a mixture of V and 1-methyl-1,2-dihydropyrazolo[1,5-*a*]pyridin-2-one (VI). The enol form was found to be predominant tautomeric species of I in solution. Treatment of I with acetic anhydride afforded 2-acetoxypyrazolo[1,5-*a*]pyridine (XIII) exclusively. 1-Acetyl-1,2-dihydropyrazolo[1,5-*a*]pyridin-2-one (XIV) dose not seem to intervene in the formation of thermally stable *O*-acetylated product (XIII).

In connection with the synthesis and reactivity of pyrazole derivatives[2,3] it seemed to us of interest to examine the chemical properties of 2-hydroxypyrazolo-[1,5-*a*]pyridine (I) as well as possible tautomerization including 1,2-dihydropyrazolo[1,5-*a*]pyridin-2-one (Ib), a pyrazolone form and a ylide form (Ic) (Scheme 1).

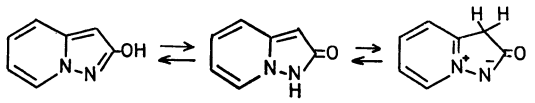

I I-b I-c

Scheme 1.

Although many papers have appeared on the synthesis of pyrazolo[1,5-*a*]pyridines,[4] only a few deal with the synthesis of condensed pyrazolone system functionalized at 2-position.[5-7]

2-Picoline is considered to be an easily available starting material for the synthesis. Attempts to form I by cyclization of 2-pyridylacetyl azide through the intermediacy of the nitrene (II) or by that of 2-pyridylacetohydrazide (III) with a strong base were unsuccessful. However, *N*-imination of ethyl 2-pyridylacetate (IV) with potassium salt of hydroxylamine-*O*-sulfonic acid (HAS)[8,9] afforded the desired bicyclic system as colorless fluorescent crystals (mp 127—128 °C), whose elemental analysis and mass spectrum agreed with the molecular formula $C_7H_6ON_2$.

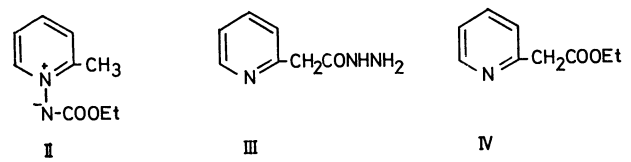

II III IV

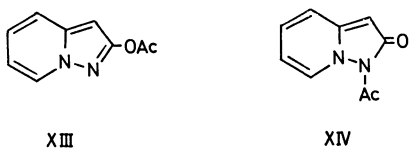

XIII XIV

The preparation of I was best carried out by adding an aqueous solution of HAS into 3 molar equivalents of 2-pyridylacetate (IV), extraction of the reaction product with a 10% aqueous sodium carbonate solution and recrystallization from benzene–hexane after stirring for 30 h at room temperature. The IR spectrum lacked an ester carbonyl band at around 1700 cm^{-1}, but showed a broad band at 3000 cm^{-1} (associated –O–H) and a strong band at 1635 cm^{-1} (–C=N–), indicating the presence of enol instead of carbonyl grouping. The NMR spectrum displayed a one proton singlet at δ5.83 ppm (C_3–H), a one proton broad doublet at δ 8.29 ppm (C_7–H, $J_{6,7}$=6 Hz) and other signals at δ 6.61 (C_6–H), 7.11 (C_5–H) and 7.34 ppm (C_4–H). Mass spectrum of this compound displayed molecular ion (*m/e* 134) which was the base peak and other ions of *m/e* 105 $[M–CHO]^+$, 91 $[C_6H_5N]^+$ and 79 $[C_5H_5N]^+$ (Fig. 1, Scheme 2).

Treatment of I with an ethereal solution of diazo-

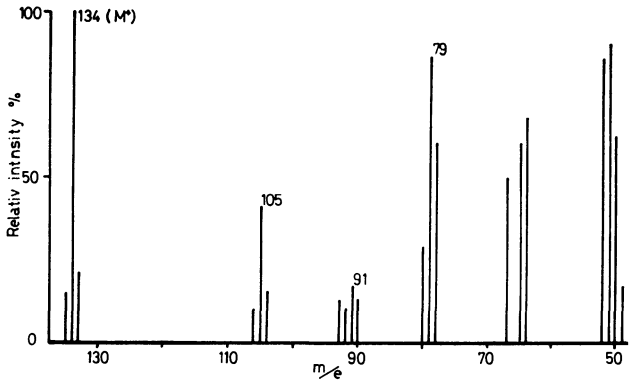

Fig. 1. Mass spectra of 2-hydroxypyrazolo[1,5-*a*]pyridine.

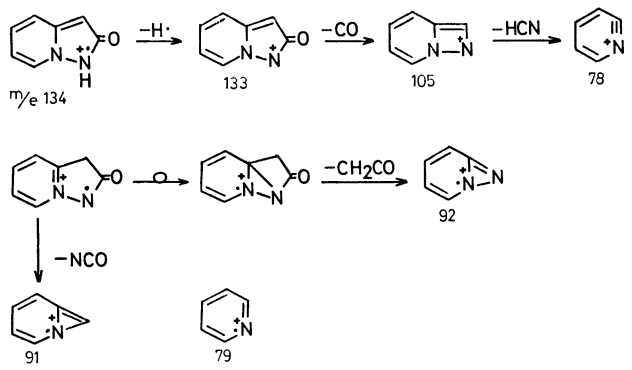

Scheme 2. Mass fragmentation pattern of 2-hydroxypyrazolo[1,5-*a*]pyridine.

methane gave an oily substance $C_8H_8ON_2$ which displayed a single spot on the TLC plate. The IR spectrum lacked a carbonyl band. The NMR spectrum showed an *O*-methyl signal at δ 3.98 ppm, indicating *O*-methylation of I to give 2-methoxypyrazolo[1,5-*a*]-pyridine exclusively. Methylation of I with dimethyl sulfate in aqueous sodium carbonate gave a (3: 1) mixture of two monomethyl derivatives. Separation through a silica gel column afforded the major component which was identical with the *O*-methyl derivative (V) and the minor component which was revealed to be 1-methyl-1,2-dihydropyrazolo[1,5-*a*]pyridin-2-one (VI) by the IR (>C=O 1660 cm^{-1}) and by the NMR spectra (δ 3.64 ppm, 3H, s) (Tables 2, 3).

Katritzky and Maine reported the tautomerism of substituted 3-hydroxypyrazoles.[10] The IR and the NMR spectra demonstrate that both keto and enol forms are present in nonprotic solvents such as chloroform in the case of 3-hydroxy-2-methylpyrazoles. However, enol form is present predominantly in the case of 3-hydroxy-1-methylpyrazoles. The UV spectrum of I in methanol as well as in cyclohexane had maxima at 232, 280 and 310 nm (log ε; 4.59, 3.09 and 3.10, respectively) and was very close to the spectrum of 2-methoxypyrazolo[1,5-*a*]pyridine (V). However, the UV spectrum of VI had maxima at the longer wave length: 241.5, 280.5, 288 and 341 nm (log ε: 4.47, 3.89, 3.88 and 3.32, respectively). By addition of a sodium hydroxide solution to the methanolic solution of I, the maxima shifted to the longer wave length of 260, 280 and 335 nm, respectively. This suggests a phenolic character of the hydroxyl group at 2-position. Thus the enol form was a predominant tautomeric species for I in solution.

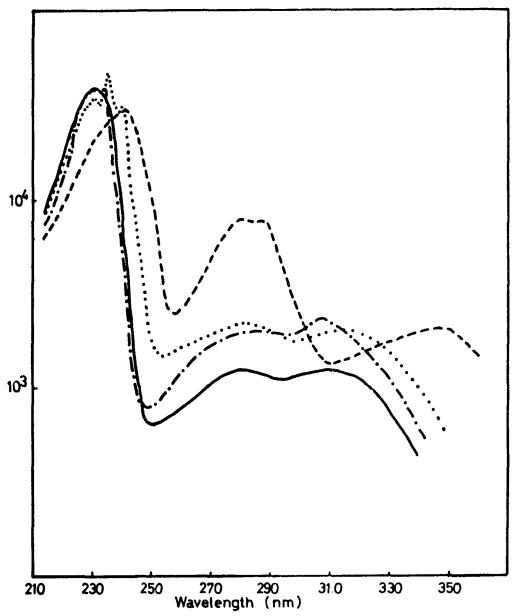

Fig. 2. UV spectra of I (——), V (-·-·-), and VI (------) in methanol and I (·····) in cyclohexane.

The electrophilic substitution of mono-cyclic 3-hydroxypyrazoles usually takes place at 4-position. Nitrosation, nitration and bromination of I afforded exclusively 3-monosubstituted products, 3-nitroso, 3-nitro- and 3-bromo-2-hydroxypyrazolo[1,5-*a*]pyridines (VII), (VIII) and (IX), respectively. The NMR spectra lacked the C_3-proton signals at δ 5—7 ppm (Table 2). Bromination of I with two molar equivalents of bromine gave dibromo compound (X) identical with the further brominated product of monobromide (IX). The IR and the NMR spectra indicated this to be 1,3-dibromo-1,2-dihydropyrazolo[1,5-*a*]pyridin-2-one.

Table 1. Derivatives of pyrazolo[1,5-*a*]pyridine

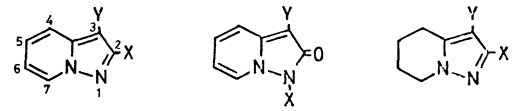

A B C

Compd	Form	X	Y	Mp °C
I	A	H	H	127—128
V	A	OCH_3	H	oil
VI	B	CH_3	H	165—167
VII	B	H	NO	>280
VIII	A	OH	NO_2	243 (decomp.)
IX	A	OH	Br	188.5—190.5
X	B	Br	Br	162 (decomp.)
XI	A	Cl	H	oil
XII	C	OH	H	172—174
XIII	A	$OCOCH_3$	H	oil

Table 2. NMR spectral data of pyrazolo-[1,5-*a*]pyridine

Compd	Solv.	3	4	5	6	7	$-CH_3$
I	$CDCl_3$	5.83	7.34	7.11	6.61	8.29	
V	$CDCl_3$	5.78	7.25	7.00	6.52	8.19	3.98
VI	$CDCl_3$	5.40	7.11	7.03	6.52	7.70	3.64
VII	DMSO-d_6		8.20	7.83	7.69	8.62	
VIII	DMSO-d_6		8.12	7.82	7.28	8.70	
IX	DMSO-d_6		7.25	7.20	6.72	8.38	
X	DMSO-d_6		8.24	8.02	7.78	8.69	
XI	CCl_4	6.28	7.32	7.02	6.62	8.25	
XIII	$CDCl_3$	6.38	7.42	7.11	7.72	8.26	2.36

Chemical shifts are expresed by δ ppm from TMS.

Table 3. Coupling constant

Compd.	$J_{4,5}$	$J_{4,6}$	$J_{4,7}$	$J_{5,6}$	$J_{5,7}$	$J_{6,7}$
I	8	1	1	7	1	6
V	8	1	1	7	1	7
VI						7
VII	7	1	1	7	1	6
VIII	8	1	1	7	1	7
IX						6
X	8.5	1	1	7	1	7
XI	8.5	1	1	7	1	7
XIII	9	1	1	7	1.5	7

Coupling constants, J, in terms of unit Hz.

Substitution of the hydroxy group of I with chlorine was carried out in the usual way by heating in refluxing phosphoryl chloride only to recover the starting material. By heating in a sealed tube at 145 °C for 6 h I was converted into 2-chloropyrazolo[1,5-*a*]pyridine (XI) in

72% yield.

Catalytic hydrogenation of I with platinum oxide in acetic acid gave colorless crystals (mp 172—174 °C) after sluggish absorption of two molar equivalents of hydrogen. The NMR spectrum (δ 1.90, 2.68, and 3.85 ppm, 8H) indicated that the hydrogenation took place upon the pyridine nucleus to furnish 2-hydroxy-4,5,6,7-tetrahydropyrazolo[1,5-*a*]pyridine (XII). The hydroxypyrazole moiety of I seems to be relatively electron-sufficient and the electron-deficient pyridine moiety seems reactive enough to undergo hydrogenation exclusively.

Arakawa *et al.* reported on the structure of the acetylated products of 3-hydroxy-5-methylpyrazole which had eight potential tautomeric forms[2] and also on the acetyl transfer reaction of 3-acetoxy-1-acetyl-5-methylpyrazole and the related compounds.[3] Among the four mono- and diacetyl derivatives the 2-acetyl-3-hydroxy-5-methylpyrazole formed initially were kinetically controlled products, which gave by thermal treatment 1-acetyl-3-hydroxy-5-methylpyrazole and 3-acetoxy-1-acetyl-5-methylpyrazole as the thermally more stable products (Scheme 3). We have tried acetylation of the bicyclic hydroxypyrazole (I) in order to examine the possible isomeric acetates responsible for the three conceivable tautomers (Scheme 1).

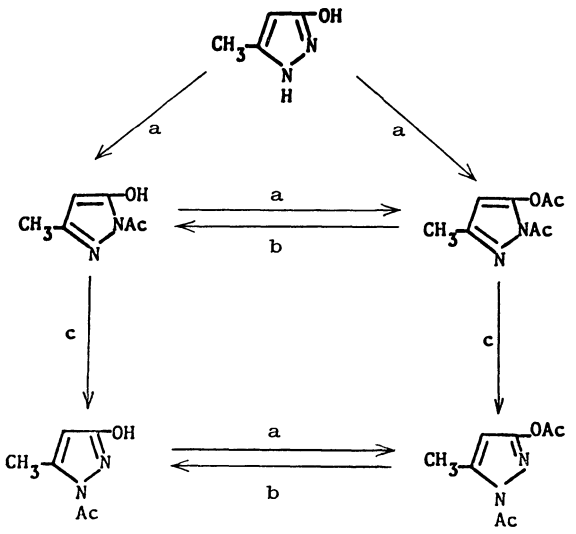

a : Acetylation
b : Basic Hydrolysis
c : Thermolysis

Scheme 3.

Hydroxypyrazole (I) gave an oily acetate (XIII) by heating in refluxing acetic anhydride for 2 h, which displyayed one spot on the TLC plate. The IR spectrum had one peak in the carbonyl region (ν_{max} 1780 cm^{-1}, $-\dot{C}=\dot{C}-O-COCH_3$). Elemental analysis and the NMR spectrum (δ 2.36 ppm, 3H, s) also indicate the compound to be 2-acetoxypyrazolo[1,5-*a*]pyridine. The time-course of acetylation was followed spectrophotometrically in a sample-tube for NMR measurement by observing the singlet signals at δ 5.78 and at δ 6.41 ppm of the C_3-protons of I and XIII, respectively. The signal at δ 5.78 ppm of the spectrum of I in acetic acid started diminishing slowly in its area-intensity as soon as acetic anhydride was added to the mixture. A new peak appearing at δ 6.41 ppm increased greatly in intensity, its spectrum changing completely into that of XIII after being heated 3 h at 35 °C (Fig. 3). Since no signal was observed in the region during the course of reaction, 1-acetyl-1,2-dihydropyrazolo[1,5-*a*]pyridin-2-one (XIV) did not seem to intervene in the formation of the thermally stable *O*-acetylated product (XIII).

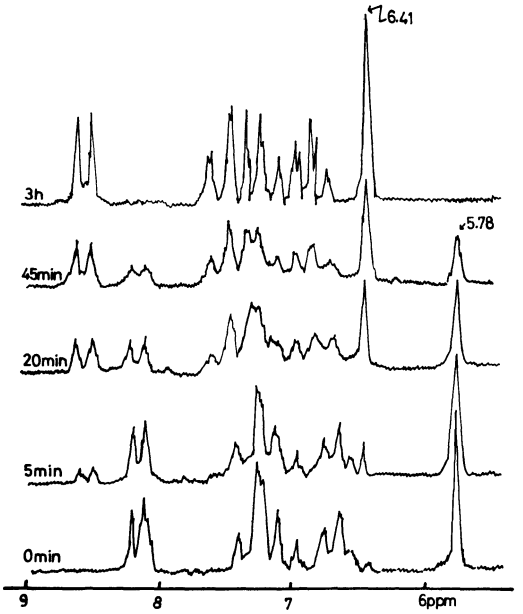

Fig. 3. NMR spectra during the time-course of changing I into XIII in a mixture of acetic acid and acetic anhydride at 35 °C.

Experimental

All the melting points were measured in capillary tubes and were uncorrected. The NMR spectra were measured on Hitachi R-20 60 MHz and Hitachi R-22 90 MHz spectrophotometers, using tetramethylsilane as an internal reference. The IR and the UV spectra were measured on a JASCO IRA-I spectrophotometer and a Hitachi EPS-3 spectrophotometer, respectively.

2-Hydroxypyrazolo[1,5-a]pyridine (I). After a mixture of ethyl 2-pyridylacetate (3.00 g), HAS (0.60 g) and water (3 ml) was stirred at room temperature for 30 h, it was extracted with CH_2Cl_2. The aqueous layer was made alkaline with 10% Na_2CO_3 to pH 9 and was extracted with CH_2Cl_2. The organic extracts were combined, and after drying over $MgSO_4$ the solvent was evaporated. The residual oil was shaken with Et_2O–10% Na_2CO_3. After the ether-layer was dried over $MgSO_4$, the solvent was evaporated to give the starting ethyl 2-pyridylacetate (2.11 g, 70.5% yield). The pH of the basic aqueous layer was adjusted to 5 by adding AcOH to precipitate brown powder (0.36 g, 45.9% yield, based upon the consumed starting material). Recrystallization from benzene–hexane gave 2-hydroxypyrazolo[1,5-*a*]pyridine (0.32 g, 40.7%) mp 127—128 °C, as colorless leaflets. UV λ_{max}^{MeOH} nm (log ε): 232 (4.59), 280.5 (3.09), 310 (3.10). IR $\nu_{max}^{CHCl_3}$ cm^{-1}: 3000, 1635, 1535, 1258. Found: C, 62.53; H, 4.48; N, 20.98%. Calcd for $C_7H_6ON_2$: C, 62.68; H, 4.51; N, 20.89%.

2-Methoxypyrazolo[1,5-a]pyridine (V). To a solution of

I (134 mg) in MeOH (5 ml) was added an excess solution of CH_2N_2 in ether[11] and the mixture was left to stand in an ice-box for a day. Evaporation of the solvent gave colorless oil (135 mg) which exhibited a single spot on a TLC plate (R_f= 0.89, 5% MeOH–$CHCl_3$ silica gel G. F. nach Stahl). Purification by passing a short column of SiO_2 gave colorless oil (118 mg, 80.5% yield). UV λ_{max}^{MeOH} nm (log ε): 234 (4.57), 282 (3.30), 307 (3.31). IR $\nu_{max}^{CHCl_3}$ cm^{-1}: 3000, 1640, 1540, 1360. Found: C, 64.57; H, 5.31; N, 18.71%. Calcd for $C_8H_8ON_2$: C, 64.85; H, 5.44; N, 18.91%.

Treatment of I with Dimethyl Sulfate–Sodium Carbonate, 2-Methoxypyrazolo[1,5-a]pyridine (V) and 1-Methyl-1,2-dihydropyrazolo-[1,5-a]pyridin-2-one (VI). After alternate portionwise addition of dimethyl sulfate (250 mg) and a solution of Na_2CO_3 (2.40 g) in H_2O (6 ml) to a stirred solution of I (268 mg) in EtOH (14 ml), the mixture was stirred at room temperature for 48 h. The precipitate was filtered off and the filtrate was evaporated *in vacuo* to give a brown residue, which was shaken with CH_2Cl_2 and H_2O. Drying and evaporation of the organic layer gave a brown residue, which was fractionated by passing through a SiO_2-column to first give colorless oil (186 mg, 62.8% yield) and next colorless prisms (48 mg, 16.2% yield). The former was found to be identical with V by comparison of TLC, IR and NMR spectra. The latter was recrystallized from benzene to give crystals (VI) melting at 165—167 °C. UV λ_{max}^{MeOH} nm (log ε): 241.5 (4.47), 280.5 (3.89), 288 (3.88), 341 (3.32). IR $\nu_{max}^{CHCl_3}$ cm^{-1}: 2960, 1660, 1630 (br). Found: C, 64.59; H, 5.32; N, 18.68%. Calcd for $C_8H_8ON_2$: C, 64.85; H, 5.44; N, 18.91%.

Nitrosation of I, 2-Hydroxy-3-nitrosopyrazolo[1,5-a]pyridine (VII). To an ice-cold stirred solution of I (100 mg) in a mixture of MeOH (2 ml) and 6M-HCl (2 ml) was added dropwise a solution of $NaNO_2$ (15 mg) in H_2O (0.7 ml). After stirring under ice-cooling for 30 min and at room temperature for 1 h the reaction mixture was cooled in ice-salt mixture to deposit a yellow precipitate, which was collected by filtration and washed with cold water. Recrystallization from MeOH gave golden feather-like crystals (63 mg, 52% yield). Mp>280 °C. UV λ_{max}^{MeOH} nm (log ε): 273 (4.30), 316.5 (3.76). IR ν_{max}^{KBr} cm^{-1}: 3040, 1700, 1680, 1635, 1020. Found: C, 51.53; H, 3.32; N, 27.50%. Calcd for $C_7H_5O_2N_3$: C, 51.54; H, 3.09; N, 27.60%.

Nitration of I, 2-Hydroxy-3-nitropyrazolo[1,5-a]pyridine (VIII). To an ice-cold stirred solution of I (70 mg) in concd HNO_3 (d=1.38) (1 ml) was added dropwise fuming nitric acid (d= 1.50) (0.5 ml). After stirring in an ice-bath for 30 min and at room temperature for 1 h the reaction mixture was poured onto ice–water to give a precipitate, which was collected by filtration. Recrystallization of the powder (61 mg) thus obtained from MeOH gave light brown leaflets (45 mg, 48.2 % yield) mp 243 °C (dec). UV λ_{max}^{MeOH} nm (log ε): 220 (4.30), 276 (3.51), 354 (4.16). IR ν_{max}^{KBr} cm^{-1}: 3440, 1645, 1580, 1360, 1220. Found: C, 46.71; H, 3.07; N, 23.21%. Calcd for $C_7H_5O_3N_3$: C, 46.93; H, 2.81; N, 23.46%.

Bromination of I with Equimolar Amount of Bromine, 3-Bromo-2-hydroxypyrazolo[1,5-a]pyridine (IX). To a stirred mixture of I (134 mg) and $NaOAc \cdot 3H_2O$ (140 mg) in AcOH (4 ml) was added dropwise a solution of Br_2 (160 mg) in AcOH (2 ml). After addition of ice–water the precipitated solid was collected by filtration. The pink-colored powder (146 mg) were recrystallized from MeOH to give prisms (126 mg, 56.3% yield), mp 188.5—190.5 °C. UV λ_{max}^{MeOH} nm (log ε): 235 (4.02). IR ν_{max}^{KBr} cm^{-1}: 1630, 1560 (br), 1520 (br). Found: C, 39.32; H, 2.32; N, 13.34%. Calcd for $C_7H_5ON_2Br$: C, 39.44; H, 2.35; N, 13.15%.

Bromination of I with Excess Brimine, 1,3-Dibromo-1,2-dihydropyrazolo[1,5-a]pyridin-2-one (X). To a stirred solution of I (134 mg) in AcOH (2 ml) was added dropwise at 15 °C a solution of Br_2 (320 mg) in AcOH (2 ml). After stirring for 1 h the reaction mixture was poured onto ice–water. The precipitate was collected by filtration and washed with cold water to give yellow powder (230 mg). Recrystallization from MeOH gave yellow scales (183 mg, 62.7% yield), mp 162 °C (dec). UV λ_{max}^{MeOH} nm (log ε): 249 (4.18), 308.5 (3.62), 350 (3.61). IR ν_{max}^{KBr} cm^{-1}: 1660, 1650, 1640. Found: C, 28.88; H, 1.55; N, 9.76%. Calcd for $C_7H_4ON_2Br_2$: C, 28.76; H, 1.71; N, 9.59%.

Attempted Chlorination of I by Refluxing in Phosphoryl Chloride. After a mixture of I (100 mg) and phosphoryl chloride (5 ml) was heated under reflux for 2 h the reaction mixture was treated in the usual way. The starting material (82 mg) was recovered unchanged.

Reaction of I with Phosphoryl Chloride at 145 °C, 2-Chloropyrazolo-[1,5-a]pyridine (XI). After a mixture of I (100 mg) and phosphoryl chloride (3 ml) was heated in a seald tube at 145 °C for 6 h, the reaction mixture was poured onto ice–water. Extraction with CH_2Cl_2, drying and evaporation of the solvent *in vacuo* afforded red oil (93 mg). Purification of the oil by passing through a column of SiO_2 gave colorless oil (82 mg, 72% yield). IR $\nu_{max}^{CHCl_3}$ cm^{-1}: 1640. Found: C, 54.91; H, 3.52; N, 18.52%. Calcd for $C_7H_5N_2Cl$: C, 55.08; H, 3.28; N, 18.36%.

Catalytic Hydrogenation of I, 2-Hydroxy-4,5,6,7-tetrahydropyrazolo-[1,5-a]pyridine (XII). A solution of I (134 mg) in AcOH (20 ml) was shaken in the presence of Pt which was prereduced from PtO_2 (100 mg) under atmospheric pressure. The absorption of hydrogen ceased after uptake of 2 mmol of hydrogen. After filtration of the solvent the residual colorless crystals (145 mg) were recrystallized from acetone–Et_2O to give colorless scales (89 mg, 69% yield), mp 172—174 °C. UV λ_{max}^{MeOH} nm (log ε): 228.5 (3.72), 260 (3.48). IR $\nu_{max}^{CHCl_3}$ cm^{-1}: 1540, 1035, 955. NMR δ ppm (in $CDCl_3$): 1.90 (4H, m), 2.68 (2H, t, J=5 Hz), 3.85 (2H, t, J=5 Hz), 5.26 (1H, s), 10.20 (1H, br. s, exchangeable with D_2O). Found: C, 60.62; H, 7.42; N, 20.09%. Calcd for $C_7H_{10}ON_2$: C, 60.85; H, 7.30; N, 20.28%.

Acetylation of I, 2-Acetoxypyrazolo[1,5-a]pyridine (XIII). A mixture of I (150 mg) in Ac_2O (10 ml) was heated under reflux for 2 h. After evaporation of solvent *in vacuo*, the residual oil was purified by passing through a column of SiO_2 to give colorless oil (188 mg, 97% yield). UV λ_{max}^{MeOH} nm (log ε): 222.5 (4.60), 286 (3.59). IR $\nu_{max}^{CHCl_3}$ cm^{-1}: 1780, 1645, 1380. Found: C, 61.48; H, 4.43; N, 16.12%. Calcd for $C_9H_8O_2N_2$: C, 61.36; H, 4.58; N, 15.90%.

The authors are grateful to the members of the Central Analysis Division of this school for the elemental analyses and the measurement of NMR spectra.

References

1) Part VII; H. Ohtsuka, T. Miyasaka, and K. Arakawa, *Chem. Pharm. Bull.*, **23**, 3254 (1975).

2) K. Arakawa, T. Miyasaka, and H. Ochi, *Chem. Pharm. Bull.*, **22**, 207 (1974).

3) K. Arakawa, T. Miyasaka, and H. Ochi, *Chem. Pharm. Bull.*, **22**, 214 (1974).

4) a) J. D. Bower and G. R. Ramage, *J. Chem. Soc.*, **1955**, 2834; b) J. D. Bower and G. D. Ramage, *ibid.*, **1957**, 4506; c) W. W. Paudler and D. E. Dunham, *J. Heterocycl. Chem.*, **2**, 410 (1965); d) M. Hamana, H. Noda, and J. Uchida, *Yakugaku Zasshi*, **90**, 991 (1970).

5) Reimlinger and co-workers reported preparation of condensed pyrazolones by the reaction of 3-amino-5-pyrazolone

with dimethyl acetylenedicarboxylate. *Cf.* H. Reimlinger, M. A. Peiren, and R. Meienyi, *Chem. Ber.*, **103**, 3252 (1970).

6) Okamoto and co-workers synthesized 3-hydroxypyrazolo[1,5-*a*]pyridine by the use of unique reaction of pyridine-*N*-imines. The authors are grateful to Prof. T. Okamoto, the University of Tokyo, for this information before publication. *Cf.* S. Suzue, M. Hirobe, and T. Okamoto, *Chem. Pharm. Bull.*, **21**, 2146 (1973).

7) For the synthesis of 3-acetyl-2-hydroxypyrazolo[1,5-*a*]-pyridine, see T. Kato and S. Masuda, *Chem. Pharm. Bull.*, **23**, 452 (1975).

8) R. Gösl and A. Meuwsen, *Chem. Ber.*, **92**, 2521 (1959).

9) T. Okamoto, H. Hirobe, C. Mizushima, and A. Osawa, *Yakugaku Zasshi*, **83**, 308 (1963).

10) A. R. Katritzky and F. W. Maine, *Tetrahedron*, **20**, 299 (1964).

11) Th. J. de Boer and H. J. Backer, *Recl. Trav. Chim. Pays-Bas*, **73**, 229 (1954).

A Potential Synthetic Intermediate of *dl*-Carnosic Acid

P. Kurian OOMMEN*

Department of Chemistry, McMaster University, Hamilton, Ontario, Canada

(Received January 22, 1975)

The Birch reduction of 2,7-dimethoxy-3-isopropylnaphthalene (IIb), which itself was made from IIa in five steps, followed by acid hydrolysis yielded the tetralone IIIa and the latter was carboxymethylated to IIIb by reaction with dimethyl carbonate and sodium hydride. Michael condensation of IIIb with methyl vinyl ketone yielded the unsaturated ketone IV. The tricyclic ketone IV on methylation followed by thioketalisation gave the thioketal IXa and the latter on Raney nickel desulfurisation yielded Ic.

Ever since Wenkert[1] established the structure of the naturally occuring oxygenated diterpene carnosic acid (Ia) the synthesis of this material with a rare C–20 carboxylic acid function presented great challenge. While the present work[2] was in progress Meyer and Schindler[3] reported the total synthesis of ethyl *dl*-carnosate dimethyl ether (Ib) following an A→B→C sequence. Later Mayer and Shew[4] developed a new method of constructing the 11,12-dihydroxylated C-ring of carnosic acid.

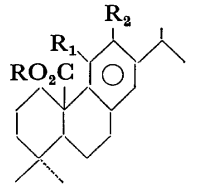

Ia, R=H, $R_1=R_2=OH$
b, R=Et, $R_1=R_2=OMe$
c, R=Me, $R_1=H$, $R_2=OMe$

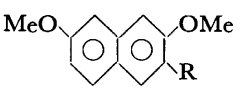

IIa, R=H
b, R=*i*-Pr
c, $R=CO_2H$
d, $R=CO_2Me$
e, $R=CMe_2(OH)$
f, $R=C(=CH_2)Me$

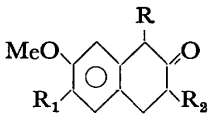

IIIa, $R=R_2=H$, $R_1=i$-Pr
b, $R=CO_2Me$, $R_1=i$-Pr, $R_2=H$
c, $R=R_1=H$, $R_2=i$-Pr

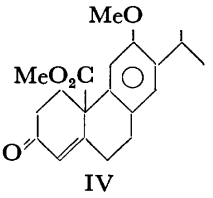

IV

Results and Discussion

The present work[2] is centred around the total synthesis of Ic following a C→B→A sequence. The known 2,7-dimethoxynaphthalene (IIa) was converted to IIb in five steps. This conversion involved (i) lithiation of IIa with butyl lithium and carbonation[5] of the lithiation product using Dry Ice, (ii) esterification of IIc, (iii) reaction of IId with methyl magnesium iodide, (iv) dehydration of the tertiary alcohol IIe and (v) hydrogenation of IIf. The procedure employed in the above reaction sequence was similar to Bergmann's method[6] of converting 2-acetylnaphthalene to 2-isopropylnaphthalene.

The next aim was to selectively reduce the less substituted ring and functionalise C–1 of the resultant tetralone. Thus the Birch reduction[7] of IIb using 2.45 equivalents of sodium in liquid ammonia followed by acid hydrolysis yielded the 2-tetralone IIIa. It is possible that some amount of reduction of the more substituted ring might have taken place at the same time resulting in the tetralone IIIc. Since the carbonyl group of IIIc is sterically hindered it cannot be expected to form a bisulfite adduct and hence this reaction can be used to separate IIIc from IIIa. The tetralone IIIa was carboxymethylated at the 1-position with dimethyl carbonate and sodium hydride in 80% yield by a modification of the procedure of Rhoads.[8,9] It is interesting to note that the reaction of methyl magnesium carbonate with 5-methoxy-2-tetralone has been reported[10] to result in carboxymethylation at the 3-position only. The highly enolic nature of the keto-ester IIIb obtained above implies that the steric interaction between the C–1 ester group and C–8 hydrogen was not sufficient to destabilise its enolic form.

To construct the tricyclic skeleton the Michael addition[11] of the keto-ester IIIb to methyl vinyl ketone was carried out in the presence of triton B methoxide and this resulted in the tricyclic ketone IV in 41.5% yield. The unsaturated ketone IV was methylated with methyl iodide and potassium tertiary butoxide according to the general procedure of Barton.[12] This procedure has been applied to systems similar to the one under study by Meyer[13] and by Stork.[14] The crude methylation product contained in addition to V, minor quantities of poly-methylation products as evidenced by the mass spectrum. Attempts to hydrogenate the crude methylation product at atmospheric pressure in the presence of 5% palladium-on-charcoal in glacial acetic acid resulted in a complex mixture of compounds containing products of reduction of the 5,6-double bond and/or the 3-keto group. Hydrogenation at high pressures yielded the saturated lactone VI. In hydrogenation of similar bicyclic ketone VII Meyer[13] obtained the lactone VIII.

In order to avoid the complicating effects of the 3-keto group during hydrogenation, the methylation product V was converted to the thioketal IXa by treatment with ethane-1,2-dithiol and boron trifluoride etherate in acetic acid. The procedure adopted was that of Stork.[14,15] Thioketalisation was accompanied by partial demethylation of the C–20 ester group. The thioketal acid (IXb)–thioketal ester (IXa) mixture on treatment with diazomethane in ether afforded the thioketal ester (IXa) in a pure form. The reaction proceeded in an overall yield of 80.4% from the unsaturated ketone IV. Desulfurisation of the thioketal IXa was effected by refluxing an alcoholic solution of

* Present address: Department of Chemistry, University of Tabriz, Tabriz, Iran.

IXa with an active variety of Raney nickel prepared by the method of Burgstahler.[16] Desulfurisation was accompanied by partial reduction of the 5,6-double bond. In similar tricyclic compounds with a C–20 methyl group the reduction of the 5,6-double bond has been found[14,15] to occur concomitantly with desulfurisation of the thioketal group. The rationalisation of the resistance of the 5,6-double bond to reduction in compounds with C–20 ester functions is rather difficult. The reduction of the 5,6-double bond was completed by refluxing the mixture obtained from the previous treatment with a large excess of the same active variety of Raney nickel in a current of hydrogen. Methyl *O*-methyl-11-desoxycarnosate (**1c**) was thus obtained in 62.4% yield from the thioketal IXa. An authentic sample of Ic was not available for comparison. But the authenticity of the synthetic sample was proved by the results of microanalysis, NMR and mass spectral data.

Since oxygenation of the C–11 position[3] of 11-desoxycarnosate has been achieved and demethylation of the C–20 ester[3] and the C–12 methyl ether[1] have been carried out, the total synthesis of Ic completes the synthesis of a potential synthetic intermediate of *dl*-carnosic acid.

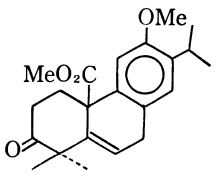

V

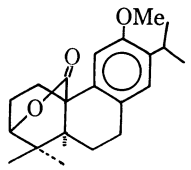

VI

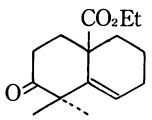

VII

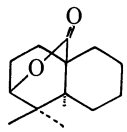

VIII

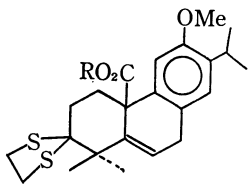

IXa R=Me
b R=H

Experimental

2,7-Dimethoxy-3-naphthoic acid (IIc). The preparation of 2,7-dimethoxynaphthalene (IIa) was effected by the reaction of 2,7-dihydroxynaphthalene with dimethyl sulfate and sodium hydroxide. The naphthoic acid IIc was obtained by carboxylation of IIa by the procedure of Gilman.[5] The reaction proceeded in 64.2% yield. Two crystallisations from 1:1 benzene–ethanol afforded an analytical sample, mp 185—186 °C; reported[5] mp 185.5 °C.

2,7-Dimethoxy-3-carbomethoxynaphthalene (IId). The esterification of the naphthoic acid IIc was carried out by the method of Fisher.[17] Refluxing a solution of the acid IIc in absolute methanol containing catalytic amounts of concentrated sulfuric acid gave the ester IId in 93% yield. Two crystallisations from 1:1 benzene–hexane yielded an analytical sample of IId, m.p. 101—102 °C; IR ($CHCl_3$) 1627, 1722 cm^{-1} (ester carbonyl); PMR δ ($CDCl_3$) 3.83 (s, C–7 methoxyl), 3.87 (s, C–2 methoxyl), 3.92 (s, C–3 ester methyl), 6.94 (q, C–6 H, $J_{5,6}$=9.5 Hz, $J_{6,8}$=2 Hz), 6.95 (d, C–8 H, $J_{5,8}$=2 Hz), 7.03 (s, C–1 H), 7.62 (d, C–5 H, $J_{5,6}$=9.5Hz), 8.19 (s, C–4H); Found: C, 68.32; H, 5.77%. Calcd for $C_{14}H_{14}O_4$: C, 68.28; H, 5.73%.

2,7-Dimethoxy-3-(2'-hydroxy-2'-propyl) naphthalene (IIe). A solution of 17.5 g of methyl 2,7-dimethoxynaphthalene-3-carboxylate (IId) in about 700 ml of anhydrous ether was added to 100 ml of a stirred solution of methyl magnesium bromide in ether containing 0.43 g of the reagent per ml. As the reaction progressed a white precipitate separated out. When all the ester was added the reaction mixture was refluxed for 1 h. The mixture was allowed to cool to room temperature and decomposed with 10% acetic acid. The reaction product was extracted with ether and the ether solution on evaporation yielded 17.3 g (99%) of naphthalene alcohol IIe, which was sufficiently pure for further reaction. A small portion of IIe was dissolved in hexane and filtered through a small column of alumina. The filtrate on evaporation yielded IIe as colourless crystals and two crystallisations from hexane and one from hexane–ether (3:1) mixture gave an analytical sample, mp 104.5—106 °C; IR ($CHCl_3$) 1630, 3533 (broad, intramolecularly hydrogen bonded OH), 3650 cm^{-1} (sharp, free OH); PMR δ ($CDCl_3$) 1.68 (s, isopropanol methyls), 3.77 (3H, s) and 3.81 (3H, s) (C–2 and C–7 methoxyl groups), 4.1 (1H, s, OH, $W^{h/2}$=7.5 Hz), 6.95 (q, C–6 H, $J_{5,6}$=9.5 Hz, $J_{6,8}$=2.5 Hz), 6.97 (d, C–8 H, $J_{6,8}$=2.5 Hz), 6.99 (s, C–1 H), 7.57 (d, C–5 H, $J_{5,6}$=9.5 Hz), 7.69 (s, C–4 H); Found: C, 73.21; H, 7.45%. Calcd for $C_{15}H_{18}O_3$: C, 73.14; H, 7.37%.

2,7-Dimethoxy-3-isopropylnaphthalene (IIb). A solution of the naphthalene alcohol IIe (17 g) in 150 ml of glacial acetic acid was refluxed for 30 min and the volume of the solution was reduced to about 25 ml by evaporation. The isopropenylnaphthalene IIf was not isolated and was hydrogenated in the presence of 1.8 g of 5% palladium on charcoal at 60 psi pressure for 24 h. The catalyst was removed by filtration and the filtrate evaporated to dryness. The residue on work up gave 16.3 g of IIb. A benzene solution of IIb was filtered through a column containing 60—65 g of alumina and this treatment resulted in 15.62 g (98.5%) of pure isopropylnaphthalene. Three crystallizations from hexane–petroleum ether, 30—60°C (3:1) gave an analytical sample, mp 95—96°C; IR ($CHCl_3$) 1602, 1623 cm^{-1}, PMR δ ($CDCl_3$) 1.28 (6H, C–3 isopropyl CH_3, d, J=7 Hz), 3.52 (1H, m, C–3 isopropyl methine H, J=7 Hz), 3.7 (3H) and 3.74 (3H) (s, C–2 and C–7 methoxyl groups), 6.85 (s, C–1 H), 6.88 (d, C–8 H, $J_{6,8}$=2.5 Hz), 6.89 (q, C–6 H, $J_{5,6}$=9.5 Hz, $J_{6,8}$=2.5 Hz), 7.43 (s, C–4 H), 7.51 (d, C–5 H, $J_{5,6}$=9.5 Hz); Found: C, 78.35; H, 7.86%. Calcd for $C_{15}H_{18}O_2$: C, 78.23; H, 7.88%.

1,2,3,4-Tetrahydro-7-methoxy-6-isopropylnaphthalen-2-one (IIIa). The 2-tetralone IIIa was prepared by the reduction of the naphthalene IIb using sodium in liquid ammonia solution. To a solution of the naphthalene IIb (6.4346 g) in a solvent mixture of 25 ml of absolute ethanol, 30 ml of tetrahydrofuran, 150 ml of anhydrous ether and 500 ml of liquid ammonia was added clean metallic sodium (1.572 g) in small pieces at a time. The reaction mixture was left overnight and the residue was acidified to pH 5 and extracted with ether. The

crude dihydronaphthalene (6.5 g) was hydrolysed by boiling with 30 ml of acetone and 6 ml of 3 M hydrochloric acid. The resultant solution was diluted with water, extracted with ether and the ether solution evaporated to dryness to yield 4.336 g of the crude tetralone IIIa. The crude product was purified by conversion to its bisulfite adduct and regeneration of the tetralone with sodium bicarbonate solution. Finally fractional distillation under reduced pressure afforded 4.0961 g (67.1%) of IIIa as a colorless liquid, bp 120—125 °C (0.33 mmHg); IR ($CHCl_3$) 1711 cm^{-1}; PMR δ ($CDCl_3$) 1.16 (6H, d, isopropyl methyls, J=6.5 Hz), 2.4 (t, C-3 H, $J_{3,4}$=6.5 Hz), 2.92 (t, C-4 H, $J_{3,4}$=6.5 Hz), 3.22 (m, isopropyl methine H, J=6.5 Hz), 3.38 (s, C-1 H), 3.75 (s, C-7 methoxyl), 6.46 (s, C-8 H), 6.88 (s, C-5 H); Found: C, 76.87; H, 8.19%. Calcd for $C_{14}H_{18}O_2$: C, 77.03; H, 8.31%.

1,2,3,4-Tetrahydro-7-methoxy-6-isopropyl-1-carbomethoxynaphthalen-2-one (IIIb). To a solution of 5.45 g of the 2-tetralone IIIa in 50 ml of dimethyl carbonate was added sodium hydride derived from 1.32 g of a sample of sodium hydride in mineral oil (51%) made free from mineral oil by washing with anhydrous ether. The reaction mixture was kept at ice-bath temperature for 15 min and at room temperature for 48 h in an atmosphere of nitrogen. It was then refluxed for 30 min, cooled to room temperature and the excess sodium hydride destroyed by pouring the reaction mixture in to ice-cold 10% hydrochloric acid. The organic material was extracted with ether and the solvents evaporated off. The residue on vacuum distillation afforded 5.52 g (80%) of the keto-ester IIIb as a colorless liquid, bp 150—160 °C (0.03 mmHg); IR ($CHCl_3$) 1587, 1629 (hydrogen bonded ester carbonyl), 1700 (weak), 1723 (weak) cm^{-1}; UV (MeOH) max. 212 (ε, 47200), 248 (ε, 15000), 255 (ε, 12400), 292 (ε, 6300), 300 (ε, 6200), 315 nm (ε, 3700); PMR δ ($CDCl_3$) 1.17 (6H, d, isopropyl methyls, J=7 Hz), 2.55 (m, C-3 and C-4 H, A_2B_2 system), 3.31 (m, isopropyl methine H, J=7 Hz), 3.75 (s, C-7 methoxyl), 3.85 (s, ester methyl), 6.81 (s, C-8 H), 7.17 (s, C-5 H), 12.96 (s, C-2 enolic H); Found: C, 69.66; H, 7.20%. Calcd for $C_{17}H_{20}O_4$: C, 69.54; H, 7.20%.

2,3,4,4a,9,10-Hexahydro-4a-methoxycarbonyl-6-methoxy-7-isopropylphenanthren-2-one (IV). To a solution of 5.52 g of the keto-ester IIIb in 200 ml of ice-cold absolute methanol under an atmosphere of nitrogen was added dropwise 1.68 g of methyl vinyl ketone. Triton B methoxide (470 mg) (40% solution of benzyl trimethyl ammonium methoxide in methanol) was then added and the reaction mixture cooled for a further 15 minutes and then left at room temperature for 24 h. The progress of the reaction was followed by periodic testing with ferric chloride. After 20—24 h a negative test was obtained. The reaction was stopped by addition of a few drops of 10% acetic acid until the solution was neutral. The methanol was evaporated under reduced pressure and the residue diluted with water and extracted with ether. The solution was evaporated to dryness and the IR and PMR spectra of the product indicated that it was a hydroxy ester.

It was, without further purification, refluxed with *p*-toluene sulfonic acid (5% by weight) in toluene solution using a Dean-Stark water separator. After 16 h the reaction mixture was evaporated to dryness and the residue chromatographed on alumina. In this way 2.722 g (41.5%) of the unsaturated ketone IV was obtained. Three crystallisations from hexane-ether (8: 1) mixture yielded an analytical sample, mp 94—95 °C: IR ($CHCl_3$) max. 1661, 1722 cm^{-1}; UV (MeOH) max. 230 (ε, 23000), 282 nm (ε, 3000); PMR δ ($CDCl_3$) 1.18 (6H, d, isopropyl CH_3, J=7 Hz), 3.23 (m, isopropyl methine H, J=7 Hz), 3.65 (s, C-6 methoxyl), 3.78 (s, ester methyl), 5.99 (s, C-1 H), 6.87 (s, C-5 H), 6.89 (s, C-8 H); Found: C, 73.17; H, 7.46%. Calcd for $C_{20}H_{24}O_4$: C, 73.14; H, 7.37%.

Methyl O-Methyl-3-keto-11-desoxy-Δ^5-carnosate (V). To a solution of 656 mg of the unsaturated ketone IV in 20 ml of anhydrous *t*-butanol was added a solution of 672 mg of potassium *t*-butoxide with stirring. During the addition of the butoxide the pale yellow solution turned deep orange in coloru. Methyl iodide (0.78 ml, 1.704 g) was then added and after a short interval the solution became turbid due to precipitated potassium iodide. The reaction mixture was left at room temperature under a nitrogen atmosphere for 48 h and the reaction was stopped by addition of 10% hydrochloric acid. The bulk of *t*-butanol was evaporated off under reduced pressure, and the residue extracted with ether after mixing with 50 ml of water. The ether solution on evaporation yielded 680 mg of an unstable dark brown liquid which was used directly to prepare IXa. *Thioketal IXa.* To a well-stirred solution of the methylation product V (680 mg) in 7 ml of glacial acetic acid kept at 5°C in an atmosphere of nitrogen was added 2 ml of ethane-1,2-dithiol and then dropwise 2 ml of boron trifluoride etherate over a 10 min period. The reaction mixture developed deep orange colour and the thioketal derivative separated out. Stirring was continued at 5 °C for 30 min and at room temperature for 1 h. The mixture was again cooled to 5°C and filtered under suction. The product was dissolved in 20 ml of ether and treated with excess of diazomethane solution in ether for 5 min and the ether evaporated off and this resulted in 695 mg (80.4%) of the thioletal IXa as colourless crystals. Three recrystallisations from acetone afforded an analytical sample of IXa, mp 206—207.5 °C; UV (MeOH) max. 238 (ε, 1850), 280 (ε, 1240), 285 nm (ε, 1240); PMR δ ($CDCl_3$) 1.18 (6H, d, C-16 and C-17 methyls, $J_{15,16}$=6.5 Hz), 1.22 (s, C-4 axial CH_3), 1.51 (s, C-4 equatorial CH_3), 3.2 (4H, m, C-3 thioketal $-CH_2-CH_2-$ group), 3.53 (C-20 ester CH_3), 3.77 (s, C-12 $-OCH_3$), 6.12 (m, C-6 H), 6.73 (s, C-11 H), 6.93 (s, C-14 H); Found: C, 66.52; H, 7.34; S, 14.82%. Calcd for $C_{24}H_{32}S_2O_3$: C, 66.65; H, 7.46; S, 14.80%.

Methyl O-Methyl-11-desoxycarnosate (Ic). A solution of 57.6 mg of the thioketal IXa in 20 ml of ethanol (absolute) was heated to reflux in an atmosphere of nitrogen. To the boiling solution was added 5 g of active Raney nickel prepared according to the procedure of Burgstahler.[16] The reaction mixture was refluxed for 30 min, cooled to room temperature and the catalyst filtered off under suction in an atmosphere of carbon dioxide. The filtrate was evaporated to dryness and a PMR spectrum of the product indicated partial reduction of 5,6-double bond. The material was dissolved in 20 ml of ethanol and refluxed with 5 g of active Raney nickel for a further 5 h in an atmosphere of hydrogen. The reaction mixture was cooled to room temperature, the catalyst filtered off and the filtrate evaporated to dryness. The residue on crystallisation from ethanol afforded 28.6 mg (62.4%) of methyl *O*-methyl-11-desoxycarnosate (Ic). Two crystallisations from ethanol yielded an analytical sample of Ic, mp 108—109.5 °C; IR ($CHCl_3$) max. 1605, 1707 cm^{-1}; UV (MeOH) max. 230 (ε, 5730), 280 (ε, 2400), 287 nm (ε, 2350); PMR δ ($CDCl_3$) 0.8 (s, C-4 axial CH_3), 0.98 (s, C-4 equatorial CH_3), 1.18 (6H, d, C-16 and C-17 methyls, J=6.5 Hz), 3.2 (1H, heptet, C-15 H, J=6.5 Hz), 3.55 (s, C-20 ester methyl), 3.75 (s, C-12 methoxyl), 6.72 (s, C-11 H), 6.86 (s, C-14 H); mass spectrum, mol wt calcd for $C_{22}H_{32}O_3$, 344.235; observed, 344.236; mass calcd for $C_{22}H_{31}O_3$, $(M-1)^+$ ion, 343.227; observed, 343.226; mass calcd for $C_{21}H_{29}O_3$, $(M-15)^+$ ion, 329.212; observed, 329.213. Found: C, 76.80; H, 9.43%. Calcd for $C_{22}H_{32}O_3$: C, 76.70; H, 9.36%.

The author wishes to thank Professor R. A. Bell for encouragement and help rendered during the course of this work and the Ontario Government for financial assistance.

References

1) E. Wenkert, A. Fuchs, and J. D. McChesney, *J. Org. Chem.*, **30**, 2931 (1965).
2) P. K. Oommen, Ph. D. Thesis, McMaster University, Hamilton, Ontario, Canada (1969).
3) W. L. Meyer and E. Schindler, *Tetrahedron Lett.*, **1966**, 4261.
4) D. C. Shew and W. L. Meyer, *Tetrahedron Lett.*, **1968** 2963.
5) S. V. Sunthankar and H. Gilman, *J. Org. Chem.*, **16**, 8 (1951).
6) F. Bergmann and A. Weizmann, *J. Org. Chem.*, **9**, 352 (1944).
7) W. Huckel and E. Vevera, *Chem. Ber.*, **89**, 2105 (1956).
8) S. J. Rhoads, J. C. Gilbert, A. W. Decora, T. R. Garland, R. J. Spangler, and M. J. Urbigkit, *Tetrahedron*, **19**, 1625 (1963).
9) J. A. Marshall, N. Cohen, and K. R. Arenson, *J. Org. Chem.*, **30**, 762 (1965).
10) a) S. W. Pelletier and P. C. Parthasarathy, *Tetrahedron Lett.*, **1964**, 103; b) S. W. Pelletier, R. L. Chapel, P. C. Parthasarathy, and N. Lewin, *J. Org. Chem.*, **31**, 1747 (1966).
11) P. R. Shafer, W. E. Loeb, and W. S. Johnson, *J. Am. Chem. Soc.*, **75**, 5963 (1953).
12) R. B. Woodward, A. A. Patchett, D. H. R. Barton, D. A. J. Ives, and R. B. Kelly, *J. Am. Chem. Soc.* **76**, 2852 (1954).
13) W. L. Meyer and A. S. Levinson, *J. Org. Chem.*, **28**, 2184 (1963).
14) G. Stork, A. Meisels, and J. E. Davies, *J. Am. Chem. Soc.*, **85**, 3419 (1963).
15) R. F. Church, R. E. Ireland, and J. A. Marshall, *J. Org. Chem.*, **31**, 2526 (1966).
16) L. F. Fieser and M. Fieser, "Reagents for Organic Synthesis," John Wiley and Sons, Inc., New York (1967), p. 729.
17) A. I. Vogel, "A Text Book of Practical Organic Chemistry," 3rd ed., Longmans Greene and Co., London (1956), p. 781.

Conversion of Alkyl Chlorides to Bromides, Selective Reactions of Mixed Bromochloroalkanes, and Halogen Exchange

W. Edward WILLY, Dennis R. McKEAN, and Barbara A. GARCIA

Chemistry Research Laboratory,[1] *Zoecon Corporation, 975 California Ave., Palo Alto, California 94304, USA*

(Received January 5, 1976)

Primary alkyl chlorides are quantitatively converted to their corresponding bromides in the presence of ethyl bromide, *N*-methyl-2-pyrrolidinone, and a catalytic amount of metal bromide. A variety of chlorides can be converted. Selective functionalization at bromine of several primary bromochloroalkanes was studied in conjunction with the chloride-bromide conversion for multistep syntheses. Methods for halogen exchange between chloride, bromide, and iodide in the octyl halide series are presented.

Alkyl bromides are often synthetically more useful than are their corresponding chlorides, as for example in the preparation of Grignard[2] and lithium reagents[3] and in copper-catalyzed alkylations.[4] Their convenience in these cases is due to their much higher reactivity.[5] For example, alkyl chlorides, other than for small molecules (*e.g.* butyl chloride), are often virtually inert under conditions for conversion to their Grignard reagents.[2] The reactivity difference between chlorides and bromides in copper-catalyzed alkylations is often large enough so that the chlorides are essentially useless.[4] There are other types of reactions in which the reactivity differences between bromides and chlorides are of practical significance.[6]

In view of the practical implications of these Br–Cl reactivity differences and because many alkyl chlorides are commercially available whereas their corresponding and often more reactive bromides are not, we were interested in a method of direct conversion of acyclic alkyl chlorides to their corresponding bromides. Many such attempts at direct conversion have been reported, for example with octyl chloride (**1**),[7] propargyl chloride (**4**),[8] and 4-chloromethyl-1,3-dioxolane (**11**)[9] (*cf.* Table 1), but in all cases[10] yields were low and the crude bromides were always contaminated with chlorides.[11]

We have discovered a simple, cheap, and efficient conversion of primary alkyl chlorides to their corresponding bromides. We wish to report the method (which can be generalized for all Cl, Br, and I interconversions) along with an indication of its synthetic utility.

Results and Discussion

Chloride-Bromide Equilibria. In our early work we sought a method of conversion of chlorides to bromides based upon the solubility difference between NaBr and NaCl. The utilization of the solubility differences (in acetone) between NaI and NaBr or NaCl to effect conversion of chlorides or bromides to iodides has long been known.[12] In all of our attempts, under various conditions, only partial conversion of chlorides to bromides was realized (see Table 3); in the best case (NaBr/*N*-methyl-2-pyrrolidinone)[13] we achieved an 84% conversion to bromide. In several cases the solvents reacted with the chlorides and bromides (Table 3, entries 2,3,11,17,18).

The limiting factor of this unsuccessful approach is that equilibrium is established between RCl and RBr (*cf.* Table 3, entries 27, 28), and a considerable amount of RCl always remains. We realized, then, that the Cl–Br conversion would have to be carried out in the presence of a solvent, or additive, which would react with Cl^- to yield a product which could easily be removed from the reaction mixture.

$$RCl \xrightarrow[\text{Solvent}\ \text{Additive}\ \Delta]{MBr} RBr \qquad (I)$$

M = metal, Li, K, Na, *etc.*
Additive = alkyl bromides

Scheme 1.

Conversion of Chlorides to Bromides. We found that the conversion (Eq. I) of RCl to RBr was quantitative if an alkyl bromide were added to the mixture of alkyl chloride (RCl), inorganic bromide (MBr), and solvent. We found ethyl bromide (bp 38 °C) to be most convenient since it (and ethyl chloride formed from it) is easily removed after the conversion.

We consider that *optimum conditions* on a large scale for the Cl–Br conversion (Eq. I) generally are with 0.2 equivalents of NaBr, 10 equivalents of EtBr, *N*-methyl-2-pyrrolidinone, and usually at 60—70 °C (see Table 1). Under these conditions the conversion is 97—99% complete and occurs within 3—10 days (exception: **11**). The optimum conditions can be varied if complete conversion (≥99.9%) to bromide is desired (*cf.* entry 1, Table 2).

N-Methyl-2-pyrrolidinone was selected as the reaction solvent based upon our preliminary studies (Table 3). *N*,*N*-Dimethylformamide (DMF) was utilized effectively in the Cl–Br conversion in the case of **4**,[8] but not for **7** (chlorohexyl formate forms in that case). The NaBr functions simply as a catalyst in the Cl–Br conversion since octyl chloride is nearly completely converted to octyl bromide with either four equivalents of NaBr or as little as 0.01 equivalents (*cf.* Table 2), although reaction time is considerably longer under catalytic conditions (NaBr is not a unique initiator here, and even if it were omitted, the conversion should eventually proceed if any trace impurities were present which react with ethyl bromide to liberate Br^-). The ethyl bromide additive is convenient, but 2-bromopropane and dibromomethane were found to be useful for the Cl–Br conversion. In principle, many other alkyl bromides could be used.

A general procedure for the conversion is described in the Experimental Section for compound **10**. Some

Table 1. Conversion of alkyl chlorides to bromides (60—70 °C)

	Chloride[a] RCl	% RBr Conv[b]	% RBr Yd[c]	EtBr Equiv	NaBr Equiv	*t* days	RCl (g), Sol (ml)[d]
1	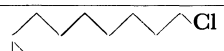	99.7	93	30	4	3	30.0, 550
2	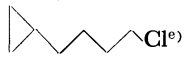	98	95	10	0.2	10	33.5, 335
3	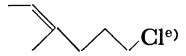	99		10	0.2	7	1, 7.5
4	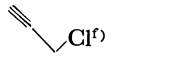	98	91	10	0.2	6	20.7, 300
5	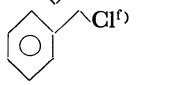	96		30	1	7	2, 45
6	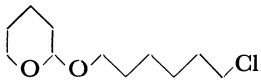	99	84[g]	30	1	5	11.0, 135
7	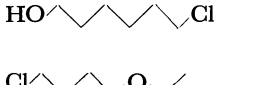	>99 98	h) 72[i]	30 20 (>-Br)	1 0.2	13 4	1, 20 26.8, 400
8	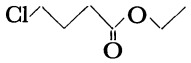	97	92	10	0.2	8	30.1, 200
9		99	90	10	0.2	2	20.0, 100
10	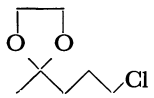	99	89	10	0.2	3	101.7, 617
11	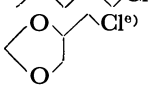	98	70	10	0.2	42	36.8, 300
12	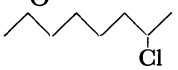	~20	j)	30	1	26	1, 18
13	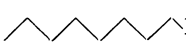	ROH 99.4	72	HOH 20		15	5, 75

a) All chlorides were purified to >98%. b) Conversion determined by GLPC. c) Yield of distilled product. d) Solvent was *N*-methyl-2-pyrrolidinone. e) For preparation, see Experimental Section. f) Conversion was at room temp. g) RBr (RCl prepared from **7**)[24] contained 4% HOBr. h) RBr contained 73% Br. i) RBr contained 9% >-OBr which was isolated by column chromatography over Silica Gel (RBr thermally unstable). j) RBr was a complex mixture containing mostly octene isomers, ~20% RBr, and very little **12** (GC/MS evidence).

Table 2. Effect of NaBr on octyl chloride conversion (60 °C)[a]

% Conversion[b] to Br	Equivalents EtBr	Equivalents NaBr[c]	*t* days
99.9	100	4	7
99.7	30	4	3
99.6	30	2	3
99.3	30	1	3
99.0	30	0.5	3
95.0	30	0.1	3
48.0	30	0.01	3
99.4	30	0.01	10

a) In each case 1 g of octyl chloride was in 18 ml of *N*-methyl-2-pyrrolidinone (exception: 50 ml for the first case). b) Determined by GLPC. c) Solubility in *N*-methyl-2-pyrrolidinone at 70 °C of NaBr=3.52 g/100 ml; of NaCl=0.16 g/100 ml (when EtBr is present the solubility of NaBr drops considerably).

advantages of the process are that it is very simple to carry out even on a large scale, ethyl bromide is inexpensive and easy to remove (and can be recycled), and no solvent is required to extract the product bromide.

The method appears to be general for *primary* alkyl chlorides (or dichlorides)[14] and several functional groups can be present in the chloride. Certain of the functions are mildly unstable to the conversion conditions; for example, the acetal function in **11** and the tetrahydropyranyl (THP) function in **6**. The hydroxyl function in **7** reacts with ethyl bromide so that 2-bromopropane was used to effect the conversion of **7**. Steric hindrance to the conversion was encountered for the acetal **11** and also for 2-chlorooctane (**12**). Note that although 2-bromopropane readily exchanges Cl^-, 2-chlorooctane (**12**) does not.[15] The tertiary ether 6-chloro-3-methoxy-3-methylhexane (prepared by methoxymercuration of **3**)[17] could not be converted to its bromide; under the conversion conditions it was quickly converted to a mixture of isomers of the unsaturated ether corresponding to **3** (Cl replaced by OCH_3) even in the presence of added sodium hydrogen carbonate, pyridine, 3A molecular sieves or the proton-sponge 1,8-bis(dimethylamino)naphthalene.

Selective Reactions with Mixed Halides. In addition to converting many commercially available chlorides to

TABLE 3. CHLORIDE-BROMIDE EQUILIBRIA[a] FOR OCTYL CHLORIDE (RCl)

MX[b]	Solvent[c]	T	t days	Composition of Mixture[d] RCl	RBr	Other
NaBr	THF/H_2O[e]	boil	23		<0.05	
NaBr	CH_3OH	boil	23	0.17	0.64	0.18 $ROCH_3$
NaBr	CH_3CH_2OH	70	19	0.49	0.34	0.17 $ROCH_2CH_3$
NaBr	CH_3COCH_3	70	21	0.88	0.12	
NaBr	CH_3COCH_3/H_2O[e]	boil	23	0.62	0.38	
LiBr	$CH_3COCH_2CH_3$	70	7	0.64	0.36	
LiBr	$CH_3COCH_2CH_3$, 2TMEDA[f]	70	2	no octyl halides remain		
NaBr	$CH_3COCH_2CH_3$	70	9		<0.05	
KBr	$CH_3COCH_2CH_3$	70	9		<0.05	
NaBr	CH_3CO_2H	70	10		<0.05	
NaBr	CH_3CO_2H	120	12	0.17	0.53	0.30 RO_2CH_3[g]
NaBr	$CH_3(CH_2)_4CO_2H$	120	4		0.05	
NaBr	$CH_3(CH_2)_4CO_2H$	150	8	0.20	0.80	high boiling impurity
NaBr	$HCON(CH_3)_2$ (DMF)	24	3 h		<0.05	
NaBr	DMF[h]	70	7 h	0.50	0.50	
		70	5	0.50	0.50	
		140	3	0.14	0.47	0.27 ROH, 0.12 RO_2CH
NaBr	DMF/H_2O[i]	70	20	0.29		0.35 ROH, 0.36 RO_2CH
3 NaBr, 0.2 KI	DMF	70	21	0.62	0.31	0.07 RI
NaBr[j]	DMF	70	10	0.66	0.34	
NaBr	$CH_3C{\equiv}N$	70	76	0.16	0.84	
3 NaBr, 1 NaI	$CH_3C{\equiv}N$	70	15	0.24	0.07	0.69 RI
NaBr	$CH_3C{\equiv}N$+0.2 18-crown-6[k]	70	28	0.15	0.85	
$CuBr_2$	$CH_3C{\equiv}N$	70	10		<0.05	
LiBr	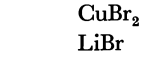 (PYRR)	70	28	0.81	0.19	
20 LiBr	PYRR+0.5 18-crown-6[k]	70	17	0.38	0.61	
NaBr	PYRR	70	3	0.13	0.87	
				0.16	0.84	corrected
3 NaBr, 1 NaCl[l]	PYRR	70	3	0.19	0.81	
4 NaBr, 4 LiBr	PYRR	70	2	0.16	0.84	
KBr	PYRR	70	25	0.41	0.59	
RbBr	PYRR	80	12	0.53	0.47	
RbBr	PYRR+0.2 18-crown-6[k]	80	12	0.53	0.47	
NaBr	HMPA	70	10		<0.05	
LiBr	DMSO	70	7		<0.05	
NaCl[m]	CH_3COCH_3	boil	40	0.09		0.91 RI

a) Equilibria here only implies reversibility except for entries 27 and 28 which are true equilibrium values. b) Four equivalents used in all cases except as noted. c) 7.5 ml solvent/mmol RCl. d) Values are mole fractions determined by GLPC and are uncorrected (except entry 27) for response ratio=(Br/Cl)=0.8. e) Biphasic. f) TMEDA=$Me_2N(CH_2)_2NMe_2$. g) *Cf.* S. Akabori and M. Ohtomi, *Bull. Chem. Soc. Jpn.*, **48**, 2991 (1975). h) After 7 h the mixture was filtered and 3 NaBr added; after additional 5 days, no change in RCl/RBr. i) Monophasic. j) Carried out on initial mixture of 0.8 RCl+0.2 RBr. k) 18-Crown-6=crown ether catalyst; see: C. J. Pederson, *J. Am. Chem. Soc.*, **89**, 7017 (1967); *cf.* also Ref. 22a, D. J. Sam and H. E. Simmons, *ibid.*, p. 2252, and C.L. Liotta and E. E. Grisdale, *Tetrahedron Lett.*, **1975**, 4203. l) Octyl bromide (RBr) used here. m) Octyl iodide (RI) used here.

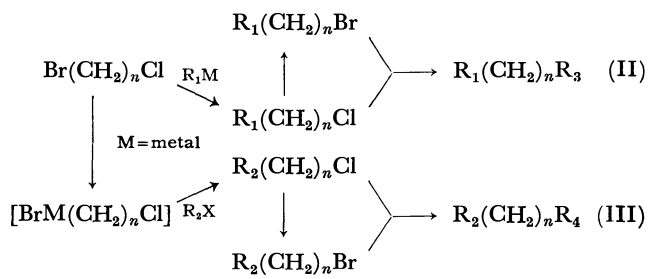

R_1, R_2, R_3, R_4=alkyl, aryl, other

Scheme 2.

their commercially unavailable and more reactive bromides we were interested in utilizing the Cl–Br conversion and the reactivity difference of bromide *vs.* chloride for multistep synthetic schemes (*cf.* Scheme 2).

We have found that certain bromochloroalkanes behave, *towards alkylation and metallation with magnesium*, as if they were simple bromoalkanes; in these cases the chlorine is essentially inert. For example, we found that 1-bromo-4-chlorobutane could be selectively functionalized at the bromine according to the plan of Scheme 2. Thus reaction of 1-bromo-4-chlorobutane with lithium dicyclopropylcuprate (Eq. IV)[18] yields

1-chloro-4-cyclopropylbutane exclusively and quantitatively; 1-bromo-3-chloropropane likewise yields 1-chloro-3-cyclopropylpropane.[26] (The corresponding reaction using bromochloromethane yields cyclopropylmethyl chloride but in low yield.) Chloride **3** (Table 1) was also selectively prepared from lithium di-2-butenylcuprate and 1-bromo-3-chloropropane. The

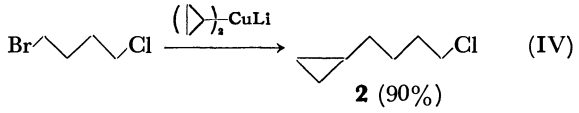

(IV)

2 (90%)

reaction of bromochlorobutane with magnesium yields chlorobutylmagnesium bromide[19] which, when treated with diethyl phenyl orthoformate (Eq. V)[20] yields 5-chloro-1,1-diethoxypentane (**9**); acetal **9** has previously

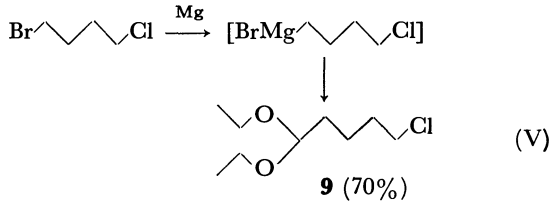

(V)

9 (70%)

been prepared (48% yield) from 5-chlorovaleryl chloride.[21a] The hexyl and heptyl chloroacetals corresponding to **9** were likewise formed from the five and six-carbon bromochloroalkanes, respectively (see Experimental Section). We found that for similar acetal functionalization (*cf.* Eq. V) of the chloro-THP **6** it was first necessary to convert to the bromide. Thus, while **6** (Table 1) was exceedingly unreactive with magnesium in tetrahydrofuran, the bromide of **6** reacted readily to yield $THPO(CH_2)_6MgBr$ which, after treatment with $PhOCH(OCH_2CH_3)_2$, yielded $THPO(CH_2)_6CH(OCH_2CH_3)_2$.

Treatment of 1-bromo-5-chloropentane with magnesium, followed by carbon dioxide, yielded high purity 6-chlorohexanoic acid (Eq. VI).

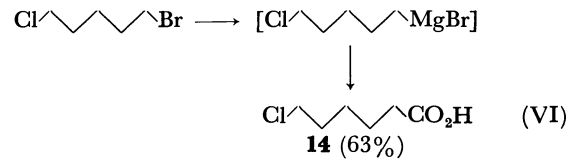

(VI)

14 (63%)

In an effort to find other metals which would selectively attack bromine (*cf.* Scheme 2), we attempted to selectively metallate 1-bromo-6-chlorohexane with lithium in ether; a complex mixture was obtained.

The products of reactions IV and V can be directly utilized for further reactions typical of alkyl chlorides, or can be converted to their corresponding bromides if more reactive molecules are desired for reactions typical of bromides (*cf.* Scheme 2). For example, 5-chloro-1,1-diethoxypentane (**9**, Eq. V) was converted to its bromide which was alkylated with lithium di-2-propenylcuprate to yield 1,1-diethoxy-6-methyl-6-heptene (Eq. VII).

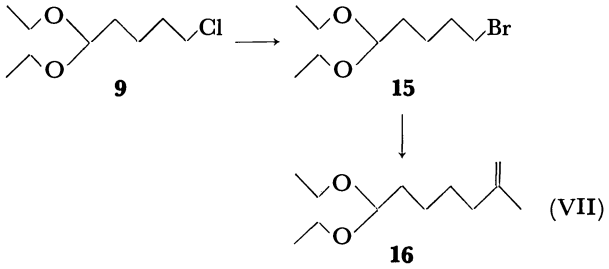

(VII)

Direct reaction of the cuprate with the chloride (**9**) was expected to be poor[18] since the corresponding reaction of lithium di-2-propenylcuprate with 6-chloro-3-methoxy-3-methylhexane (prepared from **3**) was very poor.

Hydrolysis. As part of our study we also found that octyl bromide (**13**) could be directly converted to 1-octanol (*cf.* Table 1). Under the conditions of this hydrolysis, 11-bromoundecanoic acid was completely converted to 11-hydroxyundecanoic acid (see Experimental Section).[29b] However, we were unable to convert ethyl 4-bromobutyrate (from **8**) to ethyl 4-hydroxybutyrate; butyrolactone was apparently formed in that case.

Halogen Exchange. We found that the conversion procedure (Scheme 1) used for the chlorides of Table 1 is also apparently general for all halogen exchanges involving *primary* Cl, Br, and I (see Table 4); similar exchanges to produce fluorides are also known.[22]

Experimental

Spinning-band distillations were with a Normagteflon

Table 4. Interconversion of octyl halides (60—70 °C)[12b]

$R_1X \xrightarrow[NaY]{R_2Y} R_1Y$ X, Y = Cl, Br, I; R_1 = octyl

R_1X[a]	R_2Y	NaY	% R_1Y	*t*/h
Cl	30 EtBr	0.5 NaBr	99.0	3 (days)
Cl[b,d]	10 MeI	0.2 NaI	99.7	10
Br	20 *i*-PrCl	0.2 NaCl	91	32 (days)
Br[c,d]	20 MeI	0.2 NaI	94	2
I	30 *n*-PrCl	0.2 NaCl	97	20 (days)
I	20 EtBr	0.2 NaBr	96	0.25

a) Except for entry 1 (*cf.* Table 2) all conversions were carried out with 1 ml *N*-methyl-2-pyrrolidinone/mmol R_1X, and % R_1Y was determined by GLPC (response ratios were taken as = 1.0). One gram samples of R_1X were used (except for the 2nd and 4th entries) and yields were not determined. b) Distilled yield of octyl iodide (bp 36.5—38 °C/0.01 mmHg) from 50 g of octyl chloride here was 98%. c) Distilled yield of octyl iodide (bp 80 °C/1.4 mmHg) from 50 g of octyl bromide here was 98%. d) This method in these two cases is more convenient, and of about equal expense (since most of the MeI is recovered and is recyclable: 93% by volume of MeI was recovered from the 4th entry) compared to the original Finkelstein method.[12]

apparatus (40 theoretical plates) from Norell Chemical Co. NMR spectra were recorded on a Varian T-60 instrument and infrared spectra on a Beckman Acculab 4 instrument. All solvents and organic reagents were dried over activated 4A molecular sieves prior to use. The bromochloroalkanes[23] were purchased from Fairfield Chemical Co., Blythewood, S.C. 29016, USA. All compounds not commercially available (described below) were characterized by their IR, NMR, and mass spectra.

Alkyl Bromides, General Procedure. The conversion of chloride **10** to its corresponding bromide is described as a representative example. A mixture of 101.7 g (0.62 mol) of 2-(3-chloropropyl)-2-methyl-1,3-dioxolane (**10**; Aldrich Chem. Co.), 617 ml of *N*-methyl-2-pyrrolidinone, 461 ml (6.2 mol) of ethyl bromide, and 12.7 g (0.124 mol) of sodium bromide (Mallinckrodt) was heated at 65 °C, in a 1-neck flask under a Friedrich condenser, for 3 days. The mixture was then cooled and poured into a mixture prepared from 1 liter each of ice, water, and brine, and contained in a separatory funnel. The lower layer, after shaking, was removed and washed with a mixture of 1 liter of water and 1 liter of brine. The organic phase was again removed and distilled (without drying) through a 45 cm Vigreaux column. Ethyl bromide (containing some ethyl chloride) was collected at 38—40 °C (1 atm). The remaining material was then distilled under vacuum. There was obtained 114.6 g (89%) of 2-(3-bromopropyl)-2-methyl-1,3-dioxolane, of 97% purity, bp 65 °C/3.5 mm Hg (lit,[25] 98—101 °C/13 mm Hg).

Highly volatile halides (*e.g.* **4**) were isolated by spinning-band distillation and thermally unstable ones (*e.g.* **7**) by column chromatography.

In the case of the chlorodioxolane **11** (Table 1) the total conversion time was shortened to 30 days by addition of the EtBr (at 0 °C) after the Cl–Br conversion had proceeded to *ca.* 67% RBr after 2 days at 65 °C in *N*-methyl-2-pyrrolidinone alone.

1-Chloro-4-cyclopropylbutane (2). A solution of 1.1 M cyclopropyllithium in ether (660 ml) was added over 45 min, at −35 °C, to a mixture of 73 g (0.38 mol) of copper (I) iodide and 660 ml of tetrahydrofuran (THF) After a Gilman test was negative, 1-bromo-4-chlorobutane (54 g, 0.32 mol) was rapidly added to the mixture which was held at −35 °C for 1.5 h. Aqueous satd. $(NH_4)_2SO_4$ (NH_4Cl yielded poor quality precipitates) was then added and the mixture was filtered. The product was extracted with 2 liters of 1:1 ether–pentane. The organic layer was washed several times with water, then with brine. After drying ($CaSO_4$) the extract was distilled through a 45 cm Vigreaux column to remove solvents. The pot residue was then short-path distilled to yield 37.4 g (90%) of 1-chloro-4-cyclopropylbutane (**2**):[26] bp 58—59 °C/17 mmHg; IR (neat): 3084 (▷), 3008, 2941, 2864, and 1024 cm^{-1}; NMR (CCl_4): δ 3.48 (t, J=6 Hz, 2H, C$\underline{H}_2$Cl); mass spectrum (70 eV): base peak *m/e* 55 ($\triangle^+$).

1-Chloro-3-cyclopropylpropane[26] was prepared from 1-bromo-3-chloropropane in the same manner as above, but was isolated by spinning-band distillation: bp 73 °C/85 mmHg.

Chloride **2** was converted to 1-bromo-4-cyclopropylbutane (as described above for **10**): bp 71—72 °C/15 mmHg; IR (neat): 3086 (▷), 3010, 2936, 2866, and 1023 cm^{-1}; NMR (CCl_4): δ 3.35 (t, J=6 Hz, 2H, C$\underline{H}_2$Br); mass spectrum (70 eV): base peak *m/e* 55 ($\triangle^+$).

Found: C, 47.39; H, 7.27; Br, 45.03%. Calcd for C_7H_{13}Br: C, 47.48; H, 7.40; Br, 45.12%.

6-Chloro-3-methyl-2-hexene (3). This compound was prepared from lithium di-2-butenylcuprate and 1-bromo-3-chloropropane as described above for **2**. The product (mixture of *cis/trans* isomers) was isolated in 80% yield by spinning band distillation: bp 51—52 °C/15 mmHg; IR (neat): 2874, 1449, 1382, 828, and 727 cm^{-1}; NMR (CCl_4): δ 3.47 (t, J=6 Hz, 2H, C$\underline{H}_2$Cl).

Found: C, 63.16; H, 9.88%. Calcd for $C_7H_{13}Cl$: C, 63.39; H, 9.88%.

Chloride **3** was converted to 6-bromo-3-methyl-2-hexene (as described above for **10**): bp 69—70 °C/17 mmHg; IR (neat): 2867, 1451, 1383, and 824 cm^{-1}; NMR (CCl_4): δ 3.34 (t, J=6 Hz, 2H, C$\underline{H}_2$Br).

Found: C, 47.42; H, 7.48; Br, 45.08%. Calcd for C_7H_{13}Br: C, 47.48; H, 7.40; Br, 45.12%.

5-Chloro-1,1-diethoxypentane (9). 1-Bromo-4-chlorobutane (77.1 g, 0.45 mol) was added to 12.1g (0.496 mol) of magnesium metal (10% excess) in 150 ml of THF as follows: about 2 ml of bromochlorobutane was added at 50 °C and when spontaneous reaction began the mixture was cooled to 0 °C and the rest of the bromochlorobutane was added in five equal portions, followed each time by 150 ml of THF, over a 1 h period. The mixture was stirred 2 h at 0 °C, 2 h at room temperature, then re-cooled to 0 °C. Diethyl phenyl orthoformate (88.4 g, 0.45 mol) was then added to the mixture which was stirred 2 h at 0 °C, overnight at room temperature, then filtered. The filter-cake was washed with 200 ml of ether and the filtrate was evaporated to remove solvents. The residue was diluted with ether (700 ml) and water (300 ml). The ether layer, after shaking, was removed and successively washed three times with aq. 50% sodium hydroxide (50 ml), twice with water (250 ml), once with brine (100 ml), then dried ($CaSO_4$) and evaporated to yield 83.0 g of colorless liquid which was purified by distillation through a 45 cm Vigreaux column. There was obtained from the product fraction 61.0 g (70%) of chloroacetal **9**, of 96% purity: bp 103—105 °C/15 mmHg (lit,[21a] 84—86 °C/5 mmHg); IR (neat): 2992, 2894, 1451, 1381, 1352, 1141, 1082, and 1018 cm^{-1}; NMR (CCl_4): δ 1.16 (t, J=7 Hz, 6H, $OCH_2C\underline{H}_3$) and 4.38 (t, J=5 Hz, 1H, C$\underline{H}$(OCH_2CH_3)$_2$); mass spectrum (70 eV): *m/e* (rel intensity) 151 (17), 149 (44), 121 (26), 103 (100, $CH_3CH_2OCH{=}OCH_2CH_3^+$), 85 (21), 75 (54, $HOCH{=}OCH_2CH_3^+$), and 47 (53).

Found: C, 55.67; H, 9.90; Cl, 18.10%. Calcd for $C_9H_{19}ClO_2$: C, 55.53; H, 9.77; Cl, 18.25%.

The pot residue (18.0 g, 15%) was high purity 1,1,6,6-tetraethoxyhexane: IR (neat): 2990, 2892, 1448, 1381, 1351, 1134, 1074, and 1019 cm^{-1}; NMR (CCl_4): δ 1.15 (t, J=6.5 Hz, 12H, $OCH_2C\underline{H}_3$) and 4.35 (t, J=4.5 Hz, 2H, C$\underline{H}$(OCH_2CH_3)$_2$); mass spectrum (70 eV): *m/e* (rel intensity) 170 (5), 127 (60), 103 (100), 81 (50), 75 (60), 73 (35), 59 (37), 47 (33), and 45 (33).

Found: C, 64.22; H, 11.29%. Calcd for $C_{14}H_{30}O_4$: C, 64.09; H, 11.52%.

The reactions of $Br(CH_2)_nCl$, where n=5 and n=6, with magnesium (10% excess) in THF (0 °C), followed by PhOCH(OCH_2CH_3)$_2$, according to the above conditions for preparation of **9**, similarly led to products in which the ratio of $(CH_3CH_2O)_2CH(CH_2)_nCl$: $(CH_3CH_2O)_2CH(CH_2)_nCH(OCH_2CH_3)_2$ was 89 : 11 for n=5 and 88 : 12 for n=6.

The reaction of 1 mole of $Cl(CH_2)_5Br$ with magnesium in THF (as above), followed by CO_2 gas (24 °C, 3 h),[2] yielded after distillation, 94.9 g (63%) of $Cl(CH_2)_5CO_2H$ (**14**) of 98% purity: mp 27.5—28 °C (lit,[27a] 24—26 °C); IR (neat): 3600—2400 (CO_2H), 1711 (C=O), 1463, 1416, 1283, and 946 cm^{-1}; NMR ($CDCl_3$): δ 2.39 (t, J=6 Hz, 2H, C$\underline{H}_2CO_2H$) and 3.56 (t, J=6.5 Hz, 2H, $ClC\underline{H}_2$).[30]

Chloride **9** was converted to 5-bromo-1,1-diethoxypentane (**15**; as described above for **10**): bp 98 °C/8 mmHg; IR (neat): 2988, 2894, 1448, 1380, 1351, 1138, 1072, and 1015 cm^{-1};

NMR (CCl_4): δ 1.17 (t, J=7 Hz, 6H, $OCH_2C\underline{H}_3$) and 4.39 (t, J=5 Hz, 1H, $C\underline{H}(OCH_2CH_3)_2$); mass spectrum (70 eV): *m/e* (rel intensity) 239 (1, M^+), 194 (41, $Br(CH_2)_4CH{=}OCH_2CH_3^+$), 166 (15, $Br(CH_2)_4CH{=}OH^+$), 148 (6), 103 (100, $CH_3CH_2OCH{=}OCH_2CH_3^+$), 85 (31), 75 (72), and 47 (65).

Found: C, 45.37; H, 8.01; Br, 33.69%. Calcd for $C_9H_{19}BrO_2$: C, 45.21; H, 7.95; Br, 33.44%.

4-Chloromethyl-1,3-dioxolane (11) was prepared, in 70% yield, from chloropropanediol and paraformaldehyde in dichloromethane:[28] bp 150—151 °C (lit,[9a] 144—146 °C; 150 °C[9b]).

1,1-Diethoxy-6-methyl-6-heptene (16) was prepared from the bromoacetal **15** and lithium di-2-propenylcuprate as described above for **2**. The product was isolated in 72% yield (94% purity by GLPC): bp 55 °C/0.3 mmHg; IR (neat): 3091 (>=), 1455, 1382, 1353, 1144, 1074, 1019, and 900 cm^{-1}; NMR (CCl_4): δ 1.17 (t, J=7 Hz, 6H, $OCH_2C\underline{H}_3$), 4.37 (t, J=4.5 Hz, 1H, $C\underline{H}(OCH_2CH_3)_2$) and 4.66 (br s, 2H, $=C\underline{H}_2$).

Found: C, 72.10; H, 12.06%. Calcd for $C_{12}H_{24}O_2$: C, 71.95; H, 12.08%.

11-*Hydroxyundecanoic Acid.* A mixture of 5.0 g (0.019 mol) of 11-bromoundecanoic acid, 7 ml (20×0.019 mol) of water, and 50 ml of *N*-methyl-2-pyrrolidinone was heated, at 60 °C, for 24 days. The mixture was then poured into 300 ml of water and extracted three times with 75 ml-portions of ether–pentane (1:1). The combined extracts were washed with water and brine, then dried ($CaSO_4$) and evaporated to yield a solid which was recrystallized from toluene. There was obtained 2.9 g (76%) of white solid, mp 66—67 °C (lit,[29a] 65.5—66 °C); IR (neat): 1708 (C=O) cm^{-1}; NMR ($CDCl_3$): δ 1.30 (br s, 16H, chain $\underline{H}$), 2.33 (t, J=6 Hz, 2H, $C\underline{H}_2CO_2H$) and 3.63 (t, J=6 Hz, 2H, $HOC\underline{H}_2$).

Hydrolysis of bromooctane (**13**) under similar conditions yielded 72% of 1-octanol (*cf.* Table 1).

We wish to thank John H. Jackson and Ralph A. Veit for performing the gas chromatographic analyses.

References

1) Contribution No. 47 from Zoecon Research Laboratories.

2) See: M. S. Kharasch and O. Reinmuth, "Grignard Reactions of Nonmetallic Substances," Prentice-Hall, New York, N.Y. (1954).

3) See: a) B. J. Wakefield, "The Chemistry of Organolithium Compounds," Pergamon Press, New York, N.Y. (1974); b) G. Wittig in "Newer Methods of Preparative Organic Chemistry," Interscience Publishers, New York, N.Y. (1948), pp. 572—575.

4) See: a) E. J. Corey and G. H. Posner, *J. Am. Chem. Soc.*, **89**, 3911 (1967); *ibid.*, **90**, 5615 (1968); b) G. H. Posner, *Org. Reac.*, Vol. 22, J. Wiley & Sons, New York, N.Y. (1975), p. 253ff, and Ref. 18.

5) Also alkyl iodides are often more reactive than their corresponding bromides and are very useful in alkylating organocopper compounds, generally less useful for Grignard reagent preparations, and ordinarily not useful for lithium reagent preparations (*cf.* Refs. 2—4).

6) See: a) "The Chemistry of the Carbon–Halogen Bond," ed. by S. Patai, Vol. 1, J. Wiley & Sons, New York, N.Y. (1973); b) *ibid.*, Vol. 2, (1973); c) J. F. Normant, G. Cahiez, C. Chuit, and J. Villieras, *Tetrahedron Lett.*, **1973**, 2407; d) J. Meijer, P. Vermeer, and L. Brandsma, *Rec. Trav. Chim. Pays-Bas*, **94**, 83 (1975); e) Ref. 23a; f) Ref. 23b; g) M. Larcheveque, P. Mulot, and T. Cuvigny, *J. Organometal. Chem.*, **57**, C33 (1973); h) W. Stoffel, *Ann. Chem.*, **673**, 26 (1964); i) A. S. Kovaleva, N. N. Borisov, A. V. Tysban, L. L. Ivanov, Yu. B. Pyatnova, and R. P. Evstigneeva, *Zh. Org. Khim. (USSR)*, **8**, 2474 (1972).

7) a) J. S. San Filippo, Jr., A. F. Sowiniski, and L. J. Romano, *J. Org. Chem.*, **40**, 3295 (1975); b) C. M. Starks, *J. Am. Chem. Soc.*, **93**, 195 (1971); c) E. V. Dehmlow, *Chem. Tech.*, **1975**, 210.

8) H. G. Peer and J. van Leeuwen, Belgium Patent 610219 (May 14, 1962).

9) a) J. Gelas and S. Michaud, *Bull. Soc. Chim. Fr.*, **1972**, 2445; b) L. Henry, *ibid.*, **1895**, 384.

10) See also: a) W. Dahlig, S. Pasynkiewicz, and L. Meszorer, *Roczniki Chem.*, **34**, 1519 (1960) [*Chem. Abstr.*, **61**, 5678c]; b) W. J. Bailey and E. Fujiwara, *J. Am. Chem. Soc.*, **77**, 165 (1955); c) W. Theilacker and G. Wendtland, *Ann. Chem.*, **570**, 50 (1950); d) E. D. Hughes, C. K. Ingold, and J. D. H. Mackie, *J. Chem. Soc.*, **1955**, 3173.

11) The Cl contaminations are reported in most, but not all cases; the methods reported involve conditions in which Cl–Br conversion is reversible and equilibrium can be obtained. In our studies equilibrium was never more favorable than 84% for the bromides (*cf.* Table 3).

12) a) H. Finkelstein, *Ber.*, **43**, 1528 (1910); b) C. K. Ingold, *Quart. Rev.*, **11**, 1 (1957).

13) Regarding anion solvation and the solvents of Table 3, see A. J. Parker, *Quart. Rev.*, **16**, 163 (1962).

14) 1,6-Dichlorohexane was converted (99% by GLPC) to 1,6-dibromohexane by the procedure described for **10**.

15) It should, therefore, be possible to selectively convert appropriate dichlorides to their corresponding bromochlorides. For example 1,3-dichlorobutane should be selectively converted to 1-bromo-3-chlorobutane under conditions described for **10** (*cf.* Refs. 7 and 16).

16) H. B. Hass and H. C. Huffman, *J. Am. Chem. Soc.*, **63**, 1233 (1941).

17) T. G. Traylor and A. W. Baker, *J. Am. Chem. Soc.*, **85**, 2746 (1963).

18) For a review of organocopper reactions, see J. F. Normant, *Synthesis*, **1972**, 63.

19) For Grignard derivatives of other dihalogens, see I. T. Millar and H. Heaney, *Quart. Rev.*, **11**, 109 (1957).

20) H. Stetter and E. Reske, *Chem. Ber.*, **103**, 643 (1970).

21) a) J. P. Ward and D. A. van Dorp, *Rec. Trav. Chim. Pays-Bas*, **88**, 177 (1969); b) Th. Cuvigny, J. F. LeBorgne, M. Larcheveque, and H. Normant, *J. Organometal. Chem.*, **1974**, 70 and A. I. Meyers, *et al.*, *J. Org. Chem.*, **38**, 36 (1973) report selective synthesis of 5-chloropentanal.

22) See, for example: a) C. L. Liotta and H. P. Harris, *J. Am. Chem. Soc.*, **96**, 2251 (1974); b) R. Stephens and J. C. Tatlow, *Quart. Rev.*, **16**, 44 (1962); c) A. L. Henne, *Org. React.*, II, 49 (1944); d) W. Bockemuller in "Newer Methods of Preparative Organic Chemistry," Interscience Publishers, New York, N.Y. (1948), p. 229ff and 593.

23) For preparation of $Br(CH_2)_nCl$ where n=4, 5, 6 see: a) M. S. Newman and J. H. Wotiz, *J. Am. Chem. Soc.*, **71**, 1292 (1949); b) J. A. Gautier, M. Miocque, and M. D. D'Engeniéres, *Bull. Soc. Chim. Fr.*, **1963**, 1368; c) J. Cason, L. Wallcave, and C. N. Whiteside, *J. Org. Chem.*, **14**, 37 (1949).

24) L. F. Fieser and M. Fieser, "Reagents for Organic Synthesis," Vol. I, J. Wiley & Sons, New York, N.Y. (1967), p. 256.

25) C. A. Grob and R. Moesch, *Helv. Chim. Acta*, **42**, 728 (1959).

26) A. A. Kamyshova, E. Ts. Chukovskaya, and R. Kh. Freidlina, *Izv. Akad. Nauk SSSR, Ser. Khim.*, **1974**, 896.

27) a) A. J. Hill and R. A. Shepard, *J. Org. Chem.*, **19**, 1802 (1954); b) T. Yamasaki, M. Nakai, and M. Oda, Japan

Patent *Kokai* 74 35326 (Apr. 1, 1974).
28) W. E. Willy, G. Binsch, and E. L. Eliel, *J. Am. Chem. Soc.*, **92**, 5394 (1970).
29) a) W. H. Lycan and R. Adams, *J. Am. Chem. Soc.*, **51**, 625 (1929); b) N. Rabjohn and M. S. Cohen, *ibid.*, **74**, 6290 (1952); c) P. Chuit and J. Hausser, *Helv. Chim. Acta*, **12**, 463 (1929).
30) *Cf.* J. P. Collman, S. R. Winter, and R. G. Komoto, U. S. Patent, 3872168 (Mar. 18, 1975).

A Novel Synthesis of 2-Trialkylphosphonio-1,3-dithiole-4-carboxylates

Charles U. PITTMAN, Jr. and Mitsuaki NARITA
Department of Chemistry, University of Alabama, University AL 35486 U.S.A.
(Received January 5, 1976)

Acetylene carboxylic acids reacted with trialkylphosphine–carbon disulfide ylides to produce fair to good yields of 2-trialkylphosphonio-1,3-dithiole-4-carboxylates (**4**) at temperatures as low as −20 to −30 °C. The formation of these zwitterionic products, by a prototropic shift in the ylide **3**, differs fron the known reaction of acetylenes, such as ethyl propiolate, with carbon disulfide and tributylphosphine to give tetrathiafuvalene derivatives. The structure of these zwitterionic products was confirmed by alkaline hydrolysis, reaction with benzaldehyde, and their IR and NMR spectra. Alkaline hydrolysis of **4** gave the corresponding carboxyl-substituted 1,3-dithioles (**7**). Treatment of 2-tributylphosphonio-1,3-dithiole-4-carboxylate (**4e**) with benzaldehyde in the presence of triethylamine resulted in the formation of 2-benzylidene-1,3-dithiole-4-carboxylic acid (**8**). The methine proton of the 1,3-dithiole ring of **4** in DMSO-d_6, appeared at δ 5.41—6.24 as a singlet peak. These methine protons were readily exchanged by deuterium in the presence of methanol-d_4, and disappeared from NMR spectra.

Electron deficient acetylenes and ring-strained acetylenes are known to react with carbon disulfide to give a variety of complex structures including tetrathiafulvalenes.[2-8] For example, perfluoro-2-butyne and carbon disulfide give perfluorotetramethyltetrathiafulvalene, quantitatively, in the presence of acid.[2] In the presence of sulfur, this reaction gave 4,5-bis(trifluoromethyl)-1,3-dithiole-2-thione.[3] In these reactions (shown in Eq. 1), 1,3-dithiolium carbenes, **1** were postulated as intermediates. The chemical properties of **1** have been discussed in the literatures.[8,9] Trialkylphosphine–

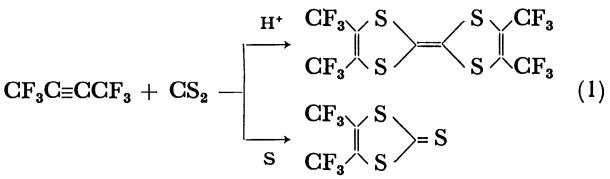

(1)

carbon disulfide ylides, **2**, known for 90 years, also react with electron deficient acetylenes to give tetrathiafulvalenes in poor yields.[4] When aromatic aldehydes were

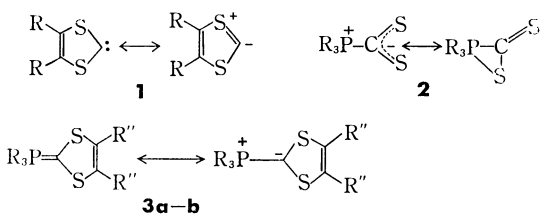

also present, excellent yields of 2-benzylidene-1,3-dithioles were obtained.[5] In these reactions, ylide **3** was presumed to be an intermediate. The unusually high reactivity of ylides, **3**, with aldehydes was attributed to the "antiaromatic" 1,3-dithiol ring. Since the negative charge at the 2-position is not readily accomodated by delocalization over the five-membered ring, the 2-carbon is a relatively strong nucleophile.

Results and Discussion

We now report that propiolic acid and acetylene dicarboxylic acid rapidly reacted with trialkylphosphine–carbon disulfide ylides, **2**, to give the zwitterionic 2-trialkylphosphonio-1,3-dithiole-4-carboxylates, **4** (see Eq. 2). These reactions proceeded at temperatures as low as −20 to −30 °C to give adducts **4a—e** which precipitated from THF. Acetylene dicarboxylic acid reacted more rapidly than propionic acid, as judged by the disappearance of the deep maroon color of the solution, and the former also gave better yields than the latter as shown in Table 1.

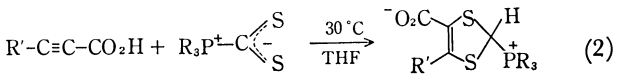

(2)

4a: R′=COOH, R=Me **4b**: R′=COOH, R=Et
4c: R′=COOH, R=*n*-Bu **4d**: R′=H, R=Et
4e: R′=H, R=*n*-Bu

The formation of **4**, instead of the acyclic compound **6** (Scheme 1) is surprising. The absence of **6** suggests the reaction proceeded *via* a concerted one-step addition similar to route A rather than by route B. Stepwise addition of **2** (route B) would initially generate acyclic zwitterion **5** with a vinyl carbanion center. It seems likely that **5** would undergo rapid C-protonation in the acidic media if it had been formed. However, rapid ring closure (**5** to **3**) cannot be definitively ruled out. A route similar to B was previously favored for the reaction of acetylenes with carbon disulfide.[2] In that work,[2] intermediates of the type **3** were implicated.

The formation of 2-trialkylphosphonio-1,3-dithiole-4-carboxylates **4**, contrasts sharply with the analogous reaction of ethyl propiolate with ylides of the type **2**.

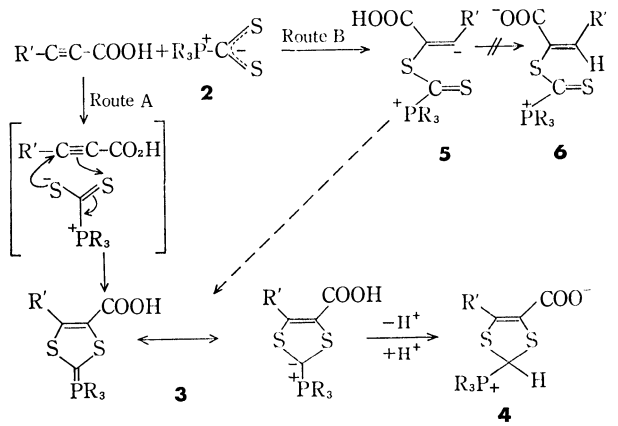

Scheme 1.

TABLE 1. RESULTS OF REACTION OF ACETYLENES WITH PHOSPHINE–CARBON DISULFIDE YLIDES AND AQUEOUS NaOH HYDROLYSIS PRODUCTS FROM 2-TRIALKYLPHOSPHONIO-1,3-DITHIOLE-4-CARBOXYLATES, **4**

Compound	Yield, %	Recrystallizing solvent	Mp, °C	Formula	C	H	S	P, %
					(Calcd)			
4a	100	water	156 (dec.)	$C_8H_{11}O_4PS_2$	35.41 (36.09	4.41 4.16	23.74 24.08	11.23 11.63)
4b	98	methanol	146 (dec.)	$C_{11}H_{17}O_4PS_2$	43.03 (42.85	5.58 5.56	20.70 20.79	10.15 10.05)
4c	87	acetone	122 (dec.)	$C_{17}H_{29}O_4PS_2$	51.61 (52.02	7.40 7.45	16.01 16.34	7.70 7.89)
4d	41	a)	136 (dec.)	$C_{10}H_{17}O_2PS_2$	45.30 (45.43	6.38 6.48	23.98 24.26	11.90 11.72)
4e	53	a)	116—118 (dec.)	$C_{16}H_{29}O_2PS_2$	55.30 (55.14	8.28 8.39	18.08 18.40	8.93 8.89)
7a	90	toluene	148—150 (dec.)	$C_4H_4O_2S_2$	33.09 (32.52	2.84 2.72	43.17 43.27)	
7b H_2O	95	toluene	158—160 (dec.)	$C_5H_6O_5S_2$	28.67 (28.57	2.83 2.88	30.21 30.50)	

a) Product was purified by washing with acetone.

For example where R=*n*-Bu, 2,6(7)-bis(ethoxycarbonyl) tetrathiafulvalene was formed in yields of 14 to 18% (Eq. 3).

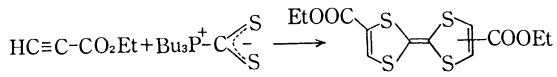

The structures of compounds **4a—e** were confirmed by their solubility, analyses, spectra, and hydrolysis reaction products. They were insoluble in benzene, ether, and THF, but soluble in water. Their analyses agreed with the assigned structures (see Table 1). The IR spectra of **4a—e** exhibited ν_{CO} bands at 1600, 1550 and 1350—1340 cm^{-1} ($-COO^-$), (see Table 2). Each compound exhibited a sharp melting (or decomposition) point (Table 1) and an NMR spectra (Table3) in accord with the assigned structure. Finally, the zwitterion structure of **4** was unequivocally confirmed by alkaline (NaOH) hydrolysis of **4e** and **4c**, followed by acidification, to give substituted 1,3-dithioles **7a** and **7b**, respectively (Eq. 4).

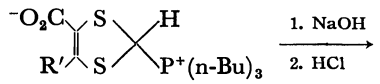

4e: R′=H
4c: R′=COOH

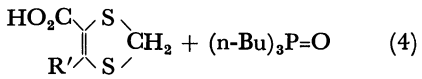

(4)

7a: R′=H
7b: R′=COOH

1,3-Dithiole-4,5-dicarboxylic acid, **7b**, contained a water of crystallization and was obtained as yellow needles which dehydrated at —80 °C to give orange crystals of **7b**. At 160—170 °C, **7b**, smoothly decarboxylated to monoacid **7a** (equation 5). This decarboxylation resembles that of 2-thioxo-1,3-dithiole-4,5-dicarboxylic acid.[11]

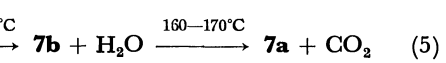

(5)

Compounds **4c** and **4e** did not react with benzaldehyde (See Scheme 2). However, when triethylamine

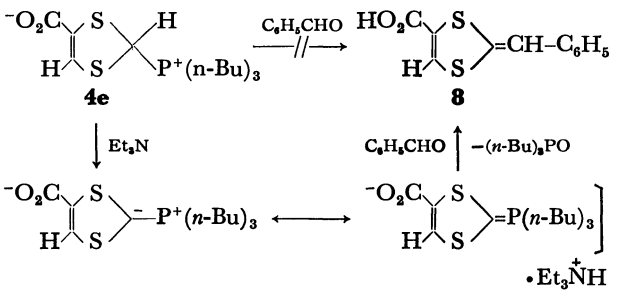

Scheme 2.

was added to **4c** or **4e**, ylides **3c** and **3e**, respectively, were formed. These ylides, as expected, rapidly reacted with benzaldehyde. For example, **4e** gave 2-benzylidene-1,3-dithiole-4-carboxylic acid, **8**, as shown in Scheme 2. This reaction further confirms the zwitterionic structure assigned to **4**.

The NMR spectra of zwitterion structures **4a—e** are summarized in Table 3. In DMSO-d_6, the methine proton of the 1,3-dithiole ring of **4a—e** appeared as a singlet at δ 5.41—6.24. In the case of **4e**, the methine proton

TABLE 2. IR SPECTRA OF 2-TRIALKYLPHOSPHONIO-1,3-DITHIOLE-4-CARBOXYLATES AND 1,3-DITHIOLE-4(5)-CARBOXYLIC ACIDS, **7**

Compound	IR Bands (cm^{-1}) (KBr)
4a	2980, 2900, 2860, 1680, 1635, 1550 1430, 1340, 1295, 1100, 1070
4b	2975, 2940, 2920, 1680, 1590, 1545 1440, 1340, 1100, 1070, 1050
4c	2960—2870, 1680, 1570, 1540, 1455 1340, 1095, 1075
4d	2940, 2910, 1595, 1555, 1465, 1450 1350, 1045, 1020
4e	2940—2870, 1595, 1460, 1345, 1230 1095, 1020, 1000
7a	1660, 1550, 1435, 1325, 1295, 1240 1040
7b	1660, 1520, 1450, 1270, 1085
7b H_2O	3600, 3400, 1630, 1570—1470, 1370 1225, 1160, 1085

hydrogens), respectively. The IR spectra of **7a, b** were similar to their corresponding 1,3-dithiole-2-thiones except for the absence of the 1070 cm^{-1} ($\nu_{C=S}$).

Pyrolysis of 1,3-Dithiole-4,5-dicarboxylic Acid Hydrate, (7b H_2O). 1,3-Dithiole-4,5-dicarboxylic acid, **7b** H_2O (1.05 g; 5 mmol) was heated for 15 min in an oil bath at 160—170 °C. An effervescing action was observed and fusing occurred to give a brown liquid. Cooling and grinding gave 0.72 g (97%) of 1,3-dithiole-4-carboxylic acid **7a**. Crystallization of **7a** from toluene gave pale pink-orange crystals, mp 148—150 °C.

2-Benzylidene-1,3-dithiole-4-carboxylic Acid, 8. To a solution of 1.01 g (10 mmol) of triethylamine in 20 ml of *N,N*-dimethylformamide, 1.75 g (5 mmol) of **4e** was suspended at room temperature. Benzaldehyde, 1.06 g (10 mmol) was then added. After *ca.* 20 min, it became homogeneous. The reaction mixture was stirred for 2 h. It was poured into 150 ml of 1 M hydrochloric acid to give orange crystals. Filtration and washing with small amounts of benzene gave 0.58 g (49%) of **8**: mp 150—152 °C (dec.). Recrystallization from toluene gave pure material: mp 152—154 °C (dec.); IR (KBr): 3100—2500, 1685, 1660, 1580, 1560, 1540, 1490, 1440, 1425, 1345, 1320, 1285, 1210, 1160, 1050 cm^{-1}; NMR (DMSO-d_6): δ 6.76 (s. broad, 1H, vinyl proton in 1,3-dithiole ring), 7.33 (m, 5H, phenyl protons), 7.64 (m, 1H, J 1 Hz).

Found: C, 55.64; H, 3.30; S, 26.81%. Calcd for $C_{11}H_8O_2S_2$: C, 55.91; H, 3.41; S, 27.13%.

The authors would like to thank the Office of Naval Research and the National Science Foundation for support of this work.

References

1) Preliminary communication: C. U. Pittman, Jr. and M. Narita, *J. Chem. Soc., Chem. Commun.*, **1975**, 960.
2) H. D. Hartzler, *J. Am. Chem. Soc.*, **95**, 4379 (1973).
3) C. G. Krespan and D. E. England, *J. Org. Chem.*, **33**, 1850 (1968).
4) L. R. Melby, H. D. Hartzler, and W. A. Sheppard, *J. Org. Chem.*, **39**, 2456 (1974).
5) H. D. Hartzler, *J. Am. Chem. Soc.*, **93**, 4961 (1971).
6) J. Nakayama, *J. Chem. Soc., Chem. Commun.*, **1974**, 166.
7) A. Krebs and H. Kimling, *Angew. Chem., Int. Ed. Engl.*, **10**, 509 (1971).
8) M. Narita and C. U. Pittman, Jr., *Synthesis*, **1975**, in press.
9) A. W. Hofmann, *Ann. Chem. Suppl.*, **1**, 26, 59 (1961); A. Hantzsch and H. Hibbert, *Chem. Ber.*, **40**, 1508 (1907).
10) H. Prinzbach and E. Futterer in "Advances in Heterocyclic Chemistry," Vol. 7, ed. A. R. Katritzky and H. J. Boulton, Academic Press, New York (1966), p. 103.
11) E. Klingsberg, *J. Am. Chem. Soc.*, **86**, 5290 (1964).

Alkaloids of *Rhazya stricta* Decaisne: Studies on Rhazinaline and Geissoschizine

Asima CHATTERJEE, Avijit BANERJI, Priyalal MAJUMDER, and Rekha MAJUMDER
Chemistry Department, University College of Science, Calcutta-700009, India

(Received January 5, 1976)

Chemical investigation of the basic principles of the leaves of *Rhazya stricta* Decaisne led to the isolation of a number of indolic bases. The studies on two of these, *viz.*, rhazinaline and geissoschizine are described. Rhazinaline, a new alkaloid, has been characterised as 16-formyl-16-epistrictamine. A detailed spectroscopical study of geissoschizine, which had not been previously isolated from a plant source, was carried out confirming the previous structural assignment. The isolation of this alkaloid from a plant source is important from a biogenetic viewpoint, since geissoschizine is one of the key preformed intermediates in the biosynthesis of C_{19}-C_{20} indole alkaloids.

The genus *Rhazya* comprises only two species, *viz.*, *R. stricta* Decaisne and *R. orientalis* A. DC., of which *R. stricta* grows profusely in the northwestern regions of the Indian subcontinent.[1,2] *R. stricta* is reputed in Indian folk medicine as a bitter tonic for sore throat, fever and general debility, and also as a curative for chronic rheumatism.[2] Recent investigations of *Rhazya* species have led to the isolation of a number of indole alkaloids, some of which have novel structural patterns.[3-8] In the present paper our work on the isolation and structure elucidation of two indole alkaloids from this source is described.[9,10]

Results and Discussion

Chemical investigation of the leaves of *R. stricta* Decaisne led to the isolation of five more indole alkaloids, in addition to (−)-quebrachamine,[11] rhazine (akuammidine),[11,12] strictamine[13] and rhazinine (antirhine).[11,20,21] Of these five indolic bases, designated rhazinaline, rhazinilam, R1, R2, and R3, the last two were obtained in very small amounts which precluded a detailed chemical investigation. The structure elucidation of rhazinilam, on which a preliminary report was made,[10] has been recently achieved by Smith *et al.*[14] The present paper reports in detail our studies on rhazinaline and alkaloid R1 (geissoschizine).

The dried powdered leaves of *R. stricta* were extracted successively with petrol (bp 60—80 °C) and chloroform in a Soxhlet apparatus. The marc was then percolated with ethanol. Fractionation of each of these extracts followed by repeated chromatography afforded the different alkaloids (*vide* Experimental).

The petrol extract yielded rhazinaline and an alkaloid R3 in addition to strictamine. Rhazinaline, $C_{21}H_{22}O_3N_2$ (M^+ 350), mp 137 °C, $[\alpha]_D^{25}$ +61° (EtOH) (0.002% yield) exhibited the UV spectrum characteristic of an indolenine chromophore, [λ_{max} (EtOH) 266 nm, log ε 3.78; λ_{min} (EtOH) 243 nm, log ε 3.60]. The presence of a four-proton multiplet in the PMR spectrum in the aromatic region (δ 7.06—7.73) showed the absence of further substitution in the benzenoid moiety. The PMR spectrum also revealed the presence of an ethylidene grouping (3H, double double at δ 1.78, J_1=8.5 Hz, J_2=2.5 Hz, 1H quartet around δ 5.51, J=8.5 Hz). The IR and PMR spectra of rhazinaline showed the absence of -OH or -NH- groups and the presence of a formyl [ν_{max} (Nujol) 1724 cm^{-1}; 1H singlet at δ 9.93] and methoxycarbonyl group [ν_{max} (Nujol) 1751 cm^{-1}; 3H singlet at δ 3.16]. The presence of both the formyl and methoxycarbonyl groups in rhazinaline was also indicated by the appearance of peaks at *m/e* 321 (M–CHO) and *m/e* 291 (M–CO_2Me) in its mass spectrum. Apart from these significant fragments, the mass spectrum of this alkaloid was uncharacteristic. Borohydride reduction of the base under controlled conditions afforded a dihydro compound, rhazinalinol, $C_{21}H_{24}O_3N_2$ (M^+ 352), mp 236 °C, whose IR spectrum lacked the carbonyl absorption at 1724 cm^{-1} but showed an hydroxyl band at 3333 cm^{-1}. The UV spectrum of this compound [λ_{max} (EtOH) 265 nm, log ε 3.78] indicated that the indolenine chromophore was unaffected. Reduction of both the formyl and methoxycarbonyl groups in rhazinaline was effected with lithium aluminium hydride. Rhazinalinediol, $C_{20}H_{24}O_2N_2$ (M^+ 324), mp 242 °C, which was obtained, lacked any carbonyl band in its IR spectrum, but showed an intense hydroxyl band at 3310 cm^{-1}. The presence of an indolenine chromophore in rhazinalinediol was indicated by its UV spectrum [λ_{max} (EtOH) 267 nm, log ε 3.71; λ_{max} (50% $HClO_4$/EtOH) 240, 244, 302 nm; log ε 3.78, 3.80, 3.75]. Attempts to reduce the indolenine double bond in rhazinalinediol by catalytic hydrogenation in ethanol and acetic acid failed. The formation of an acetonide by rhazinalinediol pointed to

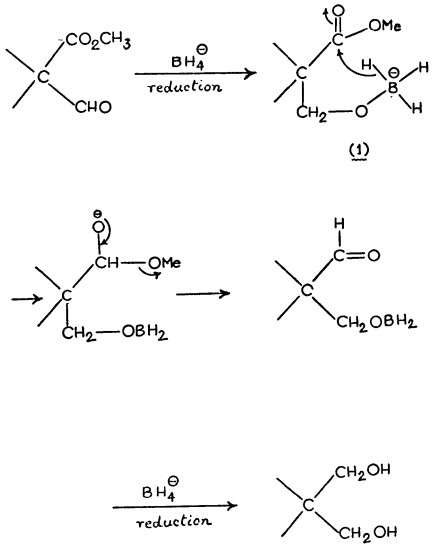

Chart 1.

the 1,3-relationship of the two hydroxyls, which in turn showed the presence of a OHC–C(–)–CO_2Me group in rhazinaline itself. Rhazinalinediol was also obtained as the sole product on prolonged action of excess sodium borohydride on rhazinaline. This rather of unexpected reduction of the ester group by borohydride might be explained by the mechanistic scheme shown in Chart 1, which assumes an intramolecular hydride transfer from the intermediate alkoxyborohydride (**1**).

On the basis of the observations outlined above, and from biogenetic considerations rhazinaline could be represented by structure **2**. The absolute configuration at C-15 is fixed from biogenetic considerations. The configuration at this center also determines those at C-3 and C-7, as otherwise the formation of the rigid pentacyclic system in **2** would not be possible. The appearance of the C-16 methoxycarbonyl signal at the high field value of δ 3.16 suggests shielding by a π-electron system and indicates that this group is situated towards the indolenine nucleus as in **2**. The various transformations of rhazinaline should therefore be represented as in Chart 2. The failure of the indolenine double bond in rhazinaline (**2**) and rhazinalinediol (**3**) to undergo reduction under conditions which normally affect reduction of this bond, *e.g.*, in strictamine,[13] was due to the steric hindrance effected by the C-22-methoxycarbonyl and C-22-hydroxymethyl groups respectively, as was apparent in an examination of Dreiding models.

Rhazinaline should therefore be identical with 16-formyl-16-epistrictamine isolated from *R. stricta* by Smith *et al.*[15] However, only the isolation of the substance was reported in their communication, and no account of its chemistry has been subsequently published. Non-availability of a sample of 16-formyl-16-epistrictamine precluded direct comparison with our alkaloid.

An amphoteric alkaloid, designated R1, was isolated from the ethanolic extract of the leaves of *R. stricta*. The properties of this indolic base, $C_{21}H_{24}O_3N_2$ (M^+ 352), mp 187 °C (dec), $[\alpha]_D^{25}$ +72° (chloroform), λ_{max} (EtOH) 221, 267, 280 (sh) (log ε 4.32, 3.88, and 3.57) suggested its identity with the compound geissoschizine (**4**).[16] This was confirmed by direct comparison (mmp, co-TLC, superimposable IR spectra and X-ray powder powder pattern) of our alkaloid with an authentic sample of giessoschizine. The structure of geissoschizine, known as a degradation product of the "dimeric," alkaloid geissospermine, was previously determined mainly on the basis of UV and IR spectral data and chemical correlations.[16] The PMR and mass spectra of geissoschizine are in conformity with structure (**4**). In its mass spectrum the characteristic peaks for tetrahydro-β-carboline alkaloids appeared at *m/e* 168, 169, 170, 171, and 184.[17] In addition significant peaks were observed at *m/e* 323 and *m/e* 251 corresponding to the loss of the formyl group and the C-15 side-chain, respectively, from the molecular ion peak. The 60 MHz PMR spectrum of the alkaloid, recorded in deuteriochloroform, was also consistent with structure (**4**). On borohydride reduction, geissoschizine furnished an amorphous dihydro-derivative, $C_{21}H_{26}O_3N_2$ (M^+ 354), which exhibited a typical tetrahydro-β-carboline UV spectrum [λ_{max} (EtOH) 224, 272, 282, 286 nm; log ε 4.26, 3.77, 3.72, 3.69]. The methoxycarbonyl band in the IR spectrum of this base appeared at the normal position, *viz.*, 1733 cm^{-1}, instead of at 1658 cm^{-1} as in geissoschizine. These observations are compatible with the reduction of the C-17 formyl group to a hydroxymethyl one.

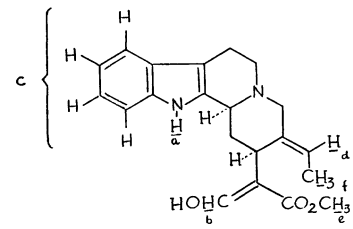

(**4**)
Geissoschizine

a δ 8.20 (1H, s, disappearing on deuteration)
b δ 7.91 (1H, s)
c δ 7.05—7.65 (4H, m)
d δ 5.42 (1H, q, J=7 Hz)
e δ 3.72 (3H, s)
f δ 1.81 (3H, d of d, J_1=7 Hz, J_2=1.5 Hz)

The isolation of geissoschizine, from *R. stricta* is of particular significance from the viewpoint of biogenesis, since it is one of the key preformed intermediates in the biosynthesis of indole alkaloids.[18,19]

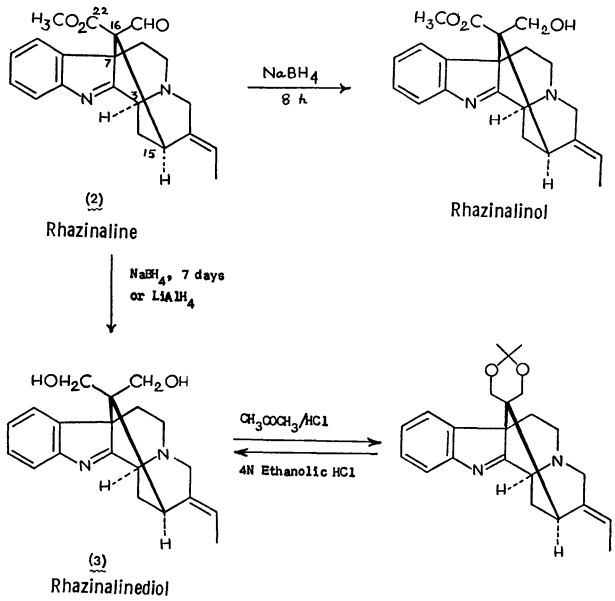

Chart 2. Reaction of rhazinaline.

Experimental

The melting points were determined on the Kofler block and are uncorrected. The analytical samples were routinely dried at 80 °C over P_2O_5 for 24 h *in vacuo*. Anhydrous sodium sulfate was used for drying the organic solutions. Chromatographic resolutions were carried out on Brockmann alumina (activity 1) and silica gel. TLC experiments were performed using silica gel G as adsorbent. Unless otherwise mentioned, the R_f values cited are those obtained using an ethyl acetate–ethanol mixture (3: 1) as the developing solvent.

The colors noted in brackets after the R_f values refer to those developed on spraying the chromatoplate with a 1% solution of ceric ammonium sulfate in 50% phosphoric acid. Those alkaloids which did not give any color with this reagent were visualised by spraying with Dragendorff's reagent.

Isolation and Characterisation of the Alkaloids. In a typical extraction 1 kg of the air-dried powdered leaves of *R. stricta* were defatted with petrol (bp 60—80 °C) (2.5 l) by extraction in a Soxhlet apparatus for 30 h. The defatted plant material was then exhaustively soxhletted with chloroform (2.5 l) for 30 h. The extracted marc was then soaked in ethanol (5 l) for 30 days.

Working-up of the Petrol Extract. The pale green petrol extract was concentrated (200 ml) and then churned for 10 h with 1.5 l of 5% aqueous citric acid solution. The mixture was filtered, and the residue thoroughly washed with 5% aqueous citric acid solution (2×100 ml). The combined aqueous solution was then extracted successively with benzene (4×250 ml) and chloroform (4×250 ml). The chloroform extract was washed with dilute ammonia solution and then with water, dried, concentrated and chromatographed on alumina. Strictamine was obtained from the petrol–benzene (1: 1) eluate and the earlier fractions of the benzene eluate, while the later fractions of the benzene eluate afforded rhazinaline. The combined mother liquor left after the crystallisation of rhazinaline (obtained from 10 kg of plant material) on concentration deposited an amorphous white solid R3, (0.0003% yield) which crystallised as granules, mp 217 °C R_f 0.27, from 30% methanolic chloroform. Alkaloid R3 exhibited a molecular ion peak at *m/e* 350.

Strictamine (0.005% yield), mp 105—106 °C (ether), $[\alpha]_D^{25}$ +60° (chloroform), R_f 0.25, λ_{max} (EtOH) 263 nm (log ε 3.72), was identified by comparison (MS, mmp, and TLC) with an authentic sample.

Rhazinaline (0.002% yield) crystallised from a petrol–benzene mixture (4: 1) as stout needles, mp 137 °C, $[\alpha]_D^{25}$ +61° (ethanol), R_f 0.31, UV: λ_{max} (EtOH) 266 nm (log ε 3.78); λ_{min} (EtOH) 243 nm (log ε 3.60) (λ_{max} and λ_{min} unaffected in 1 M KOH or 2% $HClO_4$/ethanol); IR ν_{max} (Nujol) (cm^{-1}); 1751 (-CO_2Me), 1724 (-CHO), 1621 (>C=C<), 1592 (aromatic), 774, 756, 745 (*o*-disubstituted benzene); PMR (60 MHz, $CDCl_3$) (δ): 9.93 (1H, s; -C<u>H</u>O), 7.06—7.73 (4H, m; aromatic Hs), 5.51 (1H, q; J=8.5 Hz; =C<u>H</u>-CH_3); 4.71 (1H, m; C-3-H), 4.03 (1H, m) and 3.80 (1H, m) ($N_{(b)}$-C<u>H</u>$_2$-C=C), 3.16 (3H, s, -CO_2C<u>H</u>$_3$), 1.78 (3H, d of d, J_1=8.5 Hz and J_2=2.5 Hz; =CH-C<u>H</u>$_3$); MS: *m/e* 350 (M^+), 321 (M—CHO), 291 (M—CO_2Me). Found: C, 71.50; H, 6.00; N, 7.94; -OCH_3, 8.75; -CCH_3, 4.10; active H, 0.00%. Calcd for $C_{21}H_{22}O_3N_2$: C, 72.00; H, 6.29; N, 8.00; -OCH_3 (one), 8.85; -CCH_3 (one), 4.29%.

Working up of the Chloroform Extract. The green chloroform extract was concentrated (100 ml) and the concentrate was churned with 5% aqueous citric acid solution (1 l) for 10 h and then left overnight. The yellow-brown supernatant solution was filtered and the residue thoroughly washed with 5% aqueous citric acid solution (2×200 ml). The combined acidic solution was basified (pH 10) with NH_3 solution and extracted with chloroform (5×200 ml). The combined chloroform extracts were washed with water, dried and then concentrated (50 ml). The concentrate was then chromatographed over alumina. Similar fractions were combined and rechromatographed over alumina and silica gel. In the latter case, mixtures of ethyl acetate–ethanol, in proportions varying from 9: 1 to 1: 1, were used as eluants. Six alkaloids, *viz.*, (−)-quebrachamine, rhazine, rhazinilam, R_2, rhazinine (antirhine) and rhazidine were isolated from this fraction. (−)-Quebrachamine, rhazine, rhazidine and rhazinine (antirhine) were identified by mass spectrometric and TLC comparisons, and mixed mp determinations with authentic samples.

(−)-Quebrachamine (0.002% yield) was crystallised from methanol as needles, mp 140—142 °C, $[\alpha]_D^{25}$ −96° (chloroform), R_f 0.24 (violet rimmed yellow spot), λ_{max} (EtOH) 228, 285, 292 nm (log ε 4.46, 3.78, 3.76). Rhazine (0.05% yield) was obtained by crystallisation from a benzene–chloroform (3: 1) mixture as fine needles, mp 236 °C, $[\alpha]_D^{25}$ +18° (ethanol), R_f 0.54 (pale grey), λ_{max} (EtOH) 227, 281, 288 nm (log ε 4.48, 3.78, 3.68). Rhazidine (0.02% yield) was purified by crystallization from 10% methanolic chloroform as granules, mp 278 °C, $[\alpha]_D^{25}$ −30° (ethanol), R_f 0.025 (red fading to yellow), λ_{max} (EtOH) 236, 292 nm (log ε 3.98, 3.51). Alkaloid R_2 (yield 0.0005%) formed needles, mp 176 °C, R_f 0.40 (red) from a mixture of cyclohexane–benzene (2: 1). It exhibited a molecular ion peak at *m/e* 350.

Rhazinilam (0.003% yield) was purified from ethyl acetate as plates, mp 208—210 °C, $[\alpha]_D^{25}$ −426° (chloroform), R_f 0.68 (orange-yellow), UV in 95% aldehyde free ethanol: End absorption at 213 nm (log ε 4.40); inflection points at 220, 274, 314 nm (log ε 4.31, 3.21, 1.94). Found: Mol wt 294.172705 (from mass spectrometry); C, 77.49; H, 7.41; N, 9.48; -CCH_3, 4.92; active H, 0.28%. Calcd for $C_{19}H_{22}ON_2$ (M^+ 294.1732): C, 77.45; H, 7.48; N, 9.53; -C-CH_3 (one), 5.10; active H (one), 0.34%.

Rhazinine (antirhine) (0.01% yield) crystallised from a benzene–chloroform mixture (1: 1) in fine needles, mp 118°C, $[\alpha]_D^{25}$ +4° (chloroform) and +1.3° (methanol), R_f 0.11. UV λ_{max} (EtOH): 227, 281, 289 nm (log ε 4.54, 3.88, 3.86); λ_{max} (0.1 M HCl/EtOH) 221, 274, 284 nm (log ε 4.62, 3.92, 3.90); IR ν_{max} (KBr) (cm^{-1}); 3630 (-OH), 3265 (-NH-), 1644 (>C=C<), 983 and 926 (-CH=C<u>H</u>$_2$), 1610 (aromatic), 762 and 730 (*o*-disubstituted benzene); PMR (100 MHz, $CDCl_3$) (δ): 8.14 (1H, broad s, disappearing on deuteration, indole -NH-) 6.90—7.54 (4H, m: aromatic Hs), 4.94—5.84 (C<u>H</u>=C<u>H</u>$_2$), 4.09 (1H, ill resolved t; C-3-H); 3.43—3.83 (2H, m; -C<u>H</u>$_2$-, OH). 2.23 (1H, broad s, disappearing on deuteration; -CH_2-O<u>H</u>); MS: M^+ 296.1827 (corresponds to $C_{19}H_{24}ON_2$, calculated 296.1889), 295, 265 (M-CH_2OH), 225, 223, 184, 170, 169, 168, 156.

Working-up of the Ethanolic Extract. The ethanolic extract (5 l) was concentrated to 250 ml under reduced pressure and then churned for 12 h with 5% aqueous citric acid olution (1.5 l). The mixture was filtered, and the filtrate was exhaustively extracted with chloroform (4×250 ml). The solution remaining after this processing was basified with NH_3 solution to pH 8 and extracted successively with ether (4×250 ml) and chloroform (4×250 ml). The ether solution was shaken with 2% aqueous sodium hydroxide solution (3×150 ml) to remove acidic and phenolic components. The ether extract after this treatment was concentrated and mixed with the concentrate obtained from the chloroform extract. The total extract was then chromatographed over alumina to yield rhazine, antirhine and rhazidine.

The alkaline solution containing the acidic and phenolic components was neutralised with dilute acetic acid solution and extracted with ether (3×250 ml). Concentration of this extract afforded crystals of geissoschizine (alkaloid R1).

Geissoschizine was purified by repeated crystallisation from methanol and ethyl acetate, when it was obtained as colourless granules, mp 187 °C, $[\alpha]_D^{25}$ +72° (chloroform). It was soluble in both acidic and alkaline aqueous solutions, UV: λ_{max} (EtOH) 221, 267, 290 (sh) nm (log ε 4.32, 3.88, 3.57); λ_{max} (0.1 M NaOH/EtOH) 280 nm (log ε 4.20); IR ν_{max} (Nujol) (cm^{-1}); 3311 (-OH/-NH), 1658 (>C=C-CO_2Me), 1642 (enolic >C=C<), 1600 (aromatic), 744 (*o*-disubstituted

benzene); PMR (60 MHz, $CDCl_3$) (δ): 8.20 (1H, broad s, disappears on deuteration, indole -NH-), 7.91 (1H, s; MeO_2C-C=CHOH), 7.05—7.65 (4H, m; aromatic Hs), 5.42 (1H, q, J=7 Hz; =CH-CH_3), 3.72 (3H, s, $-CO_2CH_3$), 1.81 (3H, d of d, J_1=7 Hz, J_2=1.5 Hz; =CH-CH_3); MS: *m/e* M^+ 352, 351, 323, 251, 184, 171, 170, 169, 168, 156, 155, 154, 144, 143, 130, 129. Found: C, 71.62; H, 6.70; N, 8.12; $-OCH_3$, 8.58; -C-CH_3, 4.02; active H, 0.52%. Calcd for $C_{21}H_{24}O_3N_2$: C, 71.59; H, 6.82; N, 7.95; $-OCH_3$ (one), 8.81; -C-CH_3 (one), 4.23; active H (two), 0.57%.

Sodium Borohydride Reduction of Geissoschizine. Excess sodium borohydride was added to a solution of geissoschizine (30 mg) in dry methanol (10 ml). The reaction mixture was kept at room temperature for 40 h. It was then evaporated, taken up with water (10 ml), and then extracted with chloroform (3×10 ml). The chloroform extract on evaporation yielded a gummy solid, which on dissolution in methanol followed by evaporation of the methanolic solution gave an amorphous solid (R_f 0.78). This compound exhibited a molecular ion peak at *m/e* 354, corresponding to the formula $C_{21}H_{24}O_3N_2$. UV: λ_{max} (EtOH) 228, 272, 282, 286 nm (log ε 4.26, 3.77, 3.73, 3.69); λ_{max} (0.2M HCl/EtOH) 220, 273 nm (log ε 4.44, 3.81); IR: ν_{max} (Nujol) (cm^{-1}): broad band around 3300 (-OH and -NH-), 1733 ($-CO_2Me$), 1600, 1580, 743 (*o*-disubstituted benzene).

Sodium Borohydride Reduction of Rhazinaline. Rhazialine (50 mg) was dissolved in methanol (10 ml) and treated with sodium borohydride (75 mg). The mixture was kept at room temperature for 8 h. The solution was then evaporated, water (10 ml) was added, and the resulting mixture extracted with chloroform (3×10 ml). The chloroform extract was dried, concentrated and chromatographed over alumina. The benzene–chloroform (3: 1) eluates on concentration yielded rhazinalinol as colorless granules (20 mg), mp 236 °C (R_f 0.22). UV: λ_{max} (EtOH) 265 nm (log ε 3.78); IR: ν_{max} (Nujol) (cm^{-1}); 3333 (-OH), 1750 ($-CO_2Me$); MS: *m/e* M^+ 352, 321 ($M-CH_2OH$), 293 ($M-CO_2Me$). Found: C, 71.20; H, 6.63; N, 7.84%. Calcd for $C_{21}H_{24}O_3N_2$: C, 71.59; H, 6.82; N, 7.95%.

The residue from the benzene–chloroform (1: 1) and the chloroform eluates upon crystallisation from 10% methanolic chloroform gave rhazinalinediol as fine needles (20 mg), mp 242 °C (R_f 0.18). UV: λ_{max} (EtOH) 267 nm (log ε 3.71); λ_{max} (50% $HClO_4$/EtOH) 240, 244, 302 nm (log ε 3.78, 3.80, 3.75); IR ν_{max} (Nujol) (cm^{-1}): 3310 (-OH), 1626, 1595, 745 (*o*-disubstituted benzene): MS: *m/e* M^+ 324, 293 ($M-CH_2OH$). Found: C, 73.96; H, 7.28; N, 8.48; active H, 0.51%. Calcd for $C_{20}H_{24}O_2N_2$: C, 74.07; H, 7.41; N, 8.64; active H (two), 0.62%.

Prolonged Treatment of Rhazinaline with Sodium Borohydride. Sodium borohydride (100 mg) was added to a solution of rhazinaline (25 mg) in methanol (3 ml), and the resulting mixture was allowed to stand at room temperature for 7 days. Working-up of the reaction mixture in the manner described previously gave rhazinalinediol (18 mg), mp 242 °C.

Lithium Aluminium Hydride Reduction of Rhazinaline. A solution of rhazinaline (40 mg) in dry ether (10 ml) was added to a slurry of lithium aluminium hydride (100 mg) in the same solvent (25 ml) at room temperature with stirring. The mixture was then refluxed for 6 h with continued stirring and then cooled. The excess reagent was decomposed by adding ice-cold water (2 ml), and the resulting mixture was refluxed for another 0.5 h. The mixture was filtered, and the residue washed with hot chloroform (5×5 ml). Chromatography of the extracted base over Brockmann alumina gave a solid which crystallised from 10% methanolic chloroform in fine needles (38 mg), mp 242 °C. This compound was found to be identical with rhazinalinediol (mixed mp, co-TLC and superimposable IR spectra).

Preparation of the Acetonide of Rhazinalinediol. To a solution of rhazinalinediol (30 mg) in acetone (25 ml) were added, 2 drops of concentrated hydrochloric acid and the mixture was left at room temperature for 40 h. Acetone was then removed under reduced pressure, and the residue was treated with water (10 ml), basified to pH 10 with dilute ammonia solution and extracted with chloroform (4×10 ml). The chloroform extract was dried and concentrated. The concentrate on TLC analysis showed to spots, one of which was identical with rhazinaline. The other compound (R_f 0.15) was separated by preparative TLC using silica gel G as adsorbent and an ethyl acetate–ethanol mixture (3: 1) as the developing solvent. This compound (12 mg) could not be crystallised. Found: M^+ 364; C, 75.58; H, 7.82; N, 7.61%. Calcd for $C_{23}H_{28}O_2N_2$: C, 75.77; H, 7.74; N, 7.69%.

Hydrolysis of the Acetonide. Rhazinalinediol acetonide (4 mg) was warmed on a water bath with 4M ethanolic hydrochloric acid (10 ml) for 3 h. The solution was then evaporated to a small volume (1—2 ml) under reduced pressure, taken up with water (5 ml), basified to pH 10 with ammonia solution and extracted with chloroform (3×5 ml). The dried and concentrated chloroform extract showed only one spot on TLC analysis, whose R_f value was equal to that of rhazinalinediol.

Catalytic Hydrogenation of Rhazinalinediol. Attempted hydrogenation of rhazinalinediol (20 mg) dissolved in ethanol (10 ml) in the presence of Adams catalyst (20 mg) failed and rhazinalinediol was quantitatively recovered.

Rhazinalinediol (15 mg), dissolved in glacial acetic acid (10 ml), was hydrogenated for 6 h in the presence of Adams catalyst (15 mg). There was no hydrogen uptake in the last two hours. The reaction mixture was filtered. The filtrate was diluted with water (10 ml), basified with ammonia solution and extracted with chloroform (3×10 ml). The chloroform extract on TLC showed the presence of two components (A) (R_f 0.24) and (B) (R_f 0.21) approximately in the same amount, their R_f values differing from that of rhazinalinediol. Separation of (A) and (B) was effected by preparative TLC using silica gel as adsorbent and a 3: 1 mixture of ethyl acetate–ethanol as the developing solvent. The qualitative UV spectra of (A) and (B) taken in ethanol showed maxima at 264 and 266 nm, respectively, indicating that the indolenine chromophore was unaffected. Paucity of material precluded further investigation of these substances.

The authors thank Dr. B. C. Das, Institut de Chimie des Substances Naturelle, France, Dr. G. F. Smith, Manchester University, Dr. S. C. Pakrashi, Institute of Experimental Medicine, Calcutta, and Dr. A. Hofmann, Zürich, for IR, PMR and mass spectra. Thanks are also due to Dr. J. A. Lamberton, CSIRO, Australia and Dr. A. A. Bertho, University of München for gifts of authentic samples of antirhine and geissoschizine, respectively. A Banerji and R. Majumder thank the CSIR (India) for financial assistance.

References

1) J. D. Hooker, "Flora of British India," Vol. III, Reeve & Co., London (1875), p. 640.

2) R. N. Chopra, S. L. Nayer, and I. C. Chopra, "Glossary of Indian Medicinal Plants," CSIR, New Delhi (1956), p. 212.

3) G. N. Smith, *Chem. Commun.*, **1968**, 912.

4) K. T. D. De Silva, G. N. Smith, and K. E. H. Warren,

Chem. Commun., **1971**, 905.

5) G. N. Smith, K. T. D. De Silva, and D. King, *Chem. Commun.*, **1971**, 908.

6) Y. Ahmad, P. W. Le Quesne, and N. Neuss, *J. Pharm. Sci.*, **60**, 1581 (1971).

7) G. A. Cordell, G. F. Smith, and G. N. Smith, *Chem. Commun.*, **1970**, 189, 191.

8) D. A. Evans, G. F. Smith, G. N. Smith, and K. S. J. Stapleford, *Chem. Commun.*, **1968**, 859.

9) A portion of the work described was presented at the 7th International Symposium on the Chemistry of Natural Products (IUPAC), Riga, USSR, 1970; Abstracts, p. 510.

10) A preliminary report on part of the work was previously published -A. Banerji, P. L. Majumder, and A. Chatterjee, *Phytochemistry*, **9**, 1491 (1970).

11) A. Chatterjee, C. R. Ghosal, N. Adityachaudhuri, and S. Ghosal, *Chem. Ind. (London)*, **1961**, 1034.

12) A. Chatterjee, C. R. Ghosal, and N. Adityachaudhuri, *Chem. Ind. (London)*, **1962**, 266.

13) H. K. Schnoes, K. Biemann, J. Mokry, I. Kompis, A. Chatterjee, and G. Ganguly, *J. Org. Chem.*, **31**, 1641 (1966).

14) K. T. D. De Silva, A. H. Ratcliffe, G. F. Smith, and G. N. Smith, *Tetrahedron Lett.*, **1972**, 913.

15) Z. Dabrowski, D. A. Evans, G. N. Smith, and G. F. Smith, "Abstracts, 5th International Symposium on the Chemistry of Natural Products," London (1968), p. 425.

16) M. -M. Janot, *Tetrahedron*, **14**, 113 (1961).

17) H. Budzikiewicz, C. Djerassi, and D. H. Williams, "Structure Elucidation of Natural Products by Mass Spectrometry," Vol. I, Holden-Day, San Francisco (1964), pp. 77—81.

18) A. Chatterjee, B. Mukherjee, and A. Banerji, *J. Sci. Ind. Res. (India)*, **29**, 29 (1970).

19) A. I. Scott, *Acc. Chem. Res.*, **3**, 151 (1970).

20) G. Ganguly, N. Adityachaudhuri, V. P. Arya, and A. Chatterjee, *Chem. Ind. (London)*, **1962**, 1623.

21) S. R. Johns, J. A. Lamberton, and J. L. Occolowitz, *Chem. Commun.*, **1967**, 229; *Aust. J. Chem.*, **20**, 1463 (1967).

NOTES

BULLETIN OF THE CHEMICAL SOCIETY OF JAPAN, VOL. 49 (7), 2005—2006 (1976)

The Franck-Condon Factor of the $\tilde{A}$-$\tilde{X}$ System of Ammonia

Isao KANESAKA, Mami USUI, and Kiyoyasu KAWAI

Faculty of Literature and Science, Toyama University, Gofuku, Toyama 930

(Received December 6, 1975)

Synopsis. The relative intensity of the $\tilde{A}$-$\tilde{X}$ system of ammonia was calculated by using the harmonic and devised harmonic wave functions. The calculated relative intensities do not agree completely with the observed ones. The relative intensity of the vibronic transition was also calculated. However further improvement was not obtained.

We reported an advanced method[1] for the calculation of the Franck-Condon factor of a polyatomic molecule and its application to the A-$\tilde{X}$ system of acetylene and dideuterioacetylene. Since the method might be utilized in other systems, it is desirable to clarify the extent of its potentiality. In the present paper we report on the calculated relative intensities of the A-$\tilde{X}$ system of NH_3 and ND_3.

The molecular structure of ammonia in the first excited state[2] is planar, having D_{3h} symmetry, with an N-H distance of 1.08 Å; that in the ground state[3] is pyramidal, having C_{3v} symmetry, with an N–H distance of 1.012 Å and an H–N–H angle of 106.7°. The long progressions of the A-$\tilde{X}$ system of NH_3[4] and ND_3[2] are represented in cm^{-1} by

$$\nu_{NH_3} = 46136 + 874v_2' + 4v_2'^2$$

$$\nu_{ND_3} = 46714 + 650v_2' + 4v_2'^2.$$

The frequency of 874[4] or 650[2] cm^{-1} has been assigned to the out-of-plane bending vibration ν_2' in the first excited state. The observed intensities relative to the 0 - 0 transition, which are directly estimated from the references,[5,6] are given in Table 1.

Ammonia in the ground state has a double minimum potential. This causes the splitting of vibrational levels. However, the Franck-Condon factor can be calculated with a high approximation without taking the double minimum potential into consideration.[1,7] We thus used the mean value of the two observed frequencies (Table 2).[6,8]

Table 1. Observed and calculated relative intensities of the $\tilde{A}$-$\tilde{X}$ system of ammonia

v'	NH_3				ND_3		
	Obsd[a]	Calcd			Obsd[b]	Calcd	
		[I]	[II]	R_v		[I]	[II]
0	1	1	1	1	1	1	1
1	3.9	6.6	6.5	6.4	4.0	8.3	8.1
2	10	22	21	20	10	34	31
3	17	48	42	41	20	91	75
4	24	77	66	62	35	181	135
5	27	95	83	76	50	277	194
6	30	87	89	80	60	329	240
7	27	81	105	94	80	357	302
8	26	32	85	75	110	227	307
9	21	4.4	62	55	160	83	297
10	16	0.12	41	37	200	8.2	278
11	11	0.65	25	24	160	1.8	258

a) From Ref. 5. b) From Ref. 6.

Table 2. Fundamental frequencies of ammonia in the ground state

Species		NH_3		ND_3	
		Obsd	$\Delta\nu$[a]	Obsd	$\Delta\nu$[a]
A_1	ν_1	3336.7	−3.1	2419.0	−3.4
	ν_2	950.4	0.0	748.8	0.0
E	ν_3	3443.8	3.0	2555.0	3.3
	ν_4	1627.5	0.0	1191.0	0.0

a) $\nu_{obsd} - \nu_{calcd}$. (cm^{-1})

The normal frequencies of NH_3 and ND_3 in the ground state were calculated by the method given by Shimanouchi,[9] by assuming a simplified force field with an interaction force constant between the bending coordinates. The difference between the observed and calculated frequencies can be seem in Table 2. The force constants are given in Table 3. The small difference between the force constants of NH_3 and ND_3 would scarcely affect the Franck-Condon factor.[1] The force constants for the out-of-plane bending modes of NH_3 and ND_3 in the excited state are 0.167 and 0.157 mdyn/Å, respectively.

Table 3. Force constants of ammonia in the ground state

	NH_3	ND_3
K(N-X)	6.424	6.484
H(X-N-X)	0.536	0.558
I(X-N-X, X-N-X)	−0.078	−0.071
(X=H or D)		(mdyn/Å)

Table 4. **L** matrix elements for z axis of nitrogen atom

	NH_3	ND_3
ν_2'	0.113	0.147
ν_1[a]	0.0467	0.0682
ν_2[a]	−0.102	−0.131

a) Designated in Table 2.

The normal coordinate vector of ν_2' is parallel to the C_3 axis. Thus only two normal coordinates of A_1 species in the ground state are taken into consideration. The values of the **L** matrix elements for the nitrogen

atoms are given in Table 4. The values of the overlap integral for the nitrogen atoms of NH_3 and ND_3 are 0.0224 and 0.0123, respectively, at $v'=0$, by considering the double minimum potential in the ground state.[1] Those for the hydrogen atom are the same as those for the nitrogen atom. Actually, the overlap integral for the hydrogen atom is two-dimensional, hence smaller than that for the nitrogen atom, and we therefore do not take it into consideration, since the overlap integral perpendicular to the C_3 axis is omitted in our approximation.[1] This scarcely alters the calculated relative intensities. The value of the oscillator-strength of the $A-\tilde{X}$ system of NH_3 has been reported to be 0.088.[5] This shows that the value of the observed oscillator-strength, f_v, is 4.42×10^{-5} for the 0 - 0 transition.

Calcd [I] and Calcd [II] were obtained by using the harmonic and devised harmonic[1] wave functions, respectively, in the excited state (Table 1). The calculated relative intensities do not agree completely with the observed ones. In higher levels the results of Calcd [II] are much better than those of Calcd [I]. Though the improvements seem to be satisfactory on the basis of our assumptions, the maxima of the observed and calculated relative intensities do not agree. This may be caused by the vibronic transition given by:

$$R_v(v', 0) = \int \Psi'_{v'} Q \Psi''_0 dQ$$

where Q is a normal coordinate, and Ψ' and Ψ'' are vibrational wave functions of the excited and ground states, respectively. We thus calculated $R_v(v', 0)$ by our method (Table 1). The variation in results is similar to that of Calcd [II]; similar results were obtained for ND_3. This shows that further improvement can not be expected from the vibronic transition. Precise wave functions for the excited state should be used.

In the present case the treatment of the overlap integral is essentially the same as that for a diatomic molecule, ammonia being one of the simplest molecules. The results given in Table 1 seem to show the limits of the applicability of our method.

References

1) I. Kanesaka and K. Kawai, *Bull. Chem. Soc. Jpn.*, **48**, 2745 (1975).
2) A. E. Douglas, *Discuss. Faraday Soc.*, **35**, 158 (1963).
3) E. D. Palik and E. E. Bell, *J. Chem. Phys.*, **26**, 1093 (1957).
4) A. D. Walsh and P. A. Warsop, *Trans. Faraday Soc.*, **57**, 345 (1961).
5) K. Watanabe, *J. Chem. Phys.*, **22**, 1564 (1954).
6) G. Herzberg, "Electronic Spectra and Electronic Structure of Polyatomic Molecules," Van Nostrand, Princeton (1966).
7) W. L. Smith and P. A. Warsop, *Trans. Faraday Soc.*, **64**, 1165 (1968).
8) G. Herzberg, "Infrared and Raman Spectra of Polyatomic Molecules," Van Nostrand, Princeton (1945).
9) T. Shimanouchi, "Computer Programs for Normal Coordinate Treatment of Polyatomic Molecules," Tokyo Univ. Press. (1968).

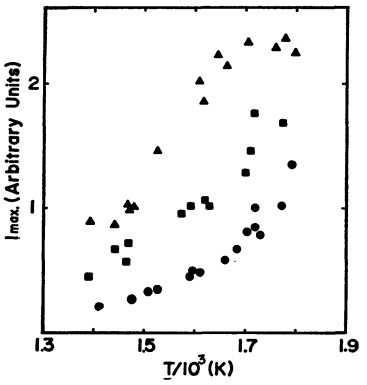

Fig. 2. Comparison of maximum intensity of total ionization at various temperatures.
●: 1.0% O_2+0.5% C_2H_4, ■: 1.5% O_2+0.5% C_2H_4, ▲: 2.0% O_2+0.5% C_2H_4.

and the H_3O^+ ion is not observed in the O_2-lean mixture; on the other hand, in the O_2-rich mixture, the $C_3H_3^+$ ion is rapidly succeeded by the H_3O^+ ion, which becomes the most abundant species.[1)]

From has been mentioned above, it may be considered that the increase in the total ions with the increase in the O_2 concentration is based on the increase in the number of H_3O^+ ions and that the most abundant ion is the H_3O^+ ion. The generally accepted steps for the $C_3H_3^+$ formation are:

$$CH + O \longrightarrow CHO^+ + e^- \qquad \Delta H = +20 \text{ kcal/mol} \qquad (1a)$$

or

$$CH^* + O \longrightarrow CHO^+ + e^- \qquad \Delta H = -46 \text{ kcal/mol} \qquad (1b)$$

$$CHO^+ + H_2O \longrightarrow H_3O^+ + CO \qquad \Delta H = -34 \text{ kcal/mol} \qquad (2)$$

However, there is controversy concerning the electronic state of CH in (1) reactions.[6-10)] Considering that the onset of the ion signal occurs earlier than that of CH* emission, and that the arrival time to the peak of the ion signal was earlier than that of the CH* emission, as has been mentioned above, it may be difficult for the (1b) reaction to be the main route of the CHO^+ formation in a lower-temperature region at comparatively O_2-lean mixtures. The CH* concentration increased with increases in the temperature and the O_2 concentration;[5)] the O concentration may also increase with increases in the temperature and the O_2 concentration. In a higher-temperature region and an O_2-rich mixture, it was found that the onset of the ion signal occurred later than that of the CH*emission, as has been mentioned above. Hence, in a higher-temperature region and an O_2-rich mixture, the (1b) reaction may occur.

The lag time in the total chemi-ionization was defined as the time elapsing between the reflected shock arrival and the time at which the probe current reached a constant value, 2.5×10^{-6} A. The lag time, τ_I increased with decreases in the temperature and O_2/C_2H_4 ratios. The plot of log τ_I *vs.* 1/T of each composition fit a single line, and the log τ_I increased with the decrease in the O_2 concentration. A plot of log $\tau_I[O_2]$ *vs.* 1/T for three compositions fits a single line, as is shown in Fig. 3. The temperature coefficient of the lag time can

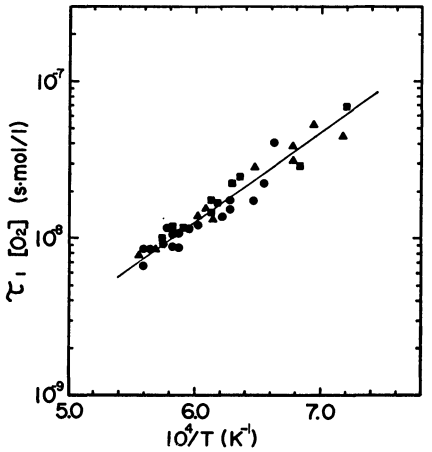

Fig. 3. A plot of log $\tau_I[O_2]$ *vs.* $1/T$ for reaction mixtures.
●: 1.0% O_2+0.5% C_2H_4, ■: 1.5% O_2+0.5% C_2H_4, ▲: 2.0% O_2+0.5% C_2H_4.

be obtained from the slope of the line; the value is 26.4 kcal/mol. Over the experimental temperature and concentration ranges we covered, the lag time can be represented as:

$$\log \tau_I[O_2] = -11.35 + 26.4 \times 10^3/4.58T$$

in units of s mol l^{-1}. This equation agrees with the following equation, which was determined from the measurements of the CH* emission in our previous work:[5)]

$$\log \tau_{CH^*}[O_2] = -11.45 + 27.5 \times 10^3/4.58T$$

Thus, we estimate that the following reaction is the rate-determining step for the ethylene oxidation in a shock tube:

$$C_2H_3 + O_2 \longrightarrow C_2H_3O + O \qquad (3)$$

also, the apparent activation energy obtained from our measurements in the total ionization is 26.4 kcal/mol, and the values, ΔH, of individual ionization reactions would be less than 20 kcal/mol.[6)] Hence, it may be concluded that Reaction 3 is the rate-determining step for chemi-ionization in the ethylene oxidation under the present experimental conditions.

References

1) I. D. Gay, G. P. Glass, R. D. Kern, and G. B. Kistiakowsky, *J. Chem. Phys.*, **47**, 313 (1967).
2) J. B. Homer and G. B. Kistiakowsky, *J. Chem. Phys.*, **47**, 5290 (1967).
3) L. J. Drummond, *Austr. J. Chem.*, **21**, 2641 (1968).
4) J. A. Baker and G. B. Skinner, *Combust. Flame*, **19**, 347 (1972).
5) Y. Hidaka, T. Kataoka, and M. Suga, *Bull. Chem. Soc. Jpn.*, **47**, 2166 (1974).
6) C. A. Arrington, W. Brennen, G. P. Glass, J. V. Michael, and H. Niki, *J. Chem. Phys.*, **43**, 1489 (1965).
7) A. Fontijn, W. J. Miller, and J. M. Hogan, *Symp. Combust. 10 th*, The Combustion Institute, Pittsburgh (1965), p. 545.
8) J. Peeters and A. Von Tiggelen, *Symp. Combust. 12 th*, The Combustion Institute, Pittsburgh (1969), p. 437.
9) T. Kinbara and K. Noda, *Symp. Combust. 13 th*, The Combustion Institute, Pittsburgh (1971), p. 333.
10) A. G. Gaydon and H. G. Wolfhard, "Flames" Chapman and Hall, London (1970) p. 323.

BULLETIN OF THE CHEMICAL SOCIETY OF JAPAN, VOL. 49 (7), 2009—2010 (1976)

Applicability of a Viscosity Formula of Liquid Mixtures to Gaseous Mixtures

Tetsuya ISHIKAWA

Seinan Gakuin University, Nishijin, Nishi-ku, Fukuoka 814

(Received November 22, 1975)

Synopsis. Since 1929, the writer has carried out an elaborate calculation on the viscosity of binary liquid mixtures,[1] using for an ideal mixture the formula

$$\eta = \frac{\eta_1}{1+\frac{k_2a_2}{k_1a_1}\frac{z_m}{1-z_m}} + \frac{\eta_2}{1+\frac{k_1a_1}{k_2a_2}\frac{1-z_m}{z_m}}$$

or that in hyperbolic form

$$\frac{(\eta-\eta_1)(1-z_m)}{(\eta_2-\eta)\cdot z_m} = \frac{k_2a_2}{k_1a_1} = K \text{ (a constant)}$$

where a is the degree of association, k the molecular field constant and z_m the formal mol fraction of component 2. However, if there occurs a maximum in $(\eta-z_m)$ diagram, we can not evaluate K from the formula, since negative values result in the neighborhood of the maximum. In this case the formula $K=\eta_1M_2a_2/\eta_2M_1a_1$ may be preferable provided that the equality $K=k_2/k_1=\eta_1M_2/\eta_2M_1$ holds for gaseous mixtures where $a_1=a_2=1$. The applicability of the formulas is discussed.

The writer tried to compare his formula for the ideal case[2] with that of Thiesen for gaseous mixtures:[3]

$$\eta = \frac{\eta_1}{1+A\frac{z_m}{1-z_m}} + \frac{\eta_2}{1+B\frac{1-z_m}{z_m}}, \quad A=\frac{a_{12}}{a_{11}}, \quad B=\frac{a_{21}}{a_{22}}$$

where a is an empirical constant defined as "Diffusions konstante".

Among the five mixtures, only the one He–H_2 satisfied conditions for the product A×B to be nearly unity: 0.991, 1.021, and 1.022 at 0, 15, and 100 °C, respectively. indicates that the writer's formula is available for gaseous ideal mixtures as well as liquid ideal mixtures.

The writer proposed another form of $K=\eta_1M_2a_2/\eta_2M_1a_1$ deduced from five liquid mixtures having equivalent association degrees or $a_1=a_2$ in his fundamental formula: C_2Cl_3H (0.99—1.02)-C_2Cl_5H (1.02—1.05), CCl_4 (1.09—1.00)-C_2Cl_4 (0.92—1.01), $C_2H_5COOC_2H_5$ (1.13—1.20)-$CH_3COOC_3H_7$ (1.16—1.21), $C_6H_5CH_3$ (1.16—1.14)-C_6H_5Br (1.19—1.05), *m*-$CH_3C_6H_4OH$ (1.81—1.60)-*p*-$CH_3C_6H_4OH$ (1.82—1.62), numbers in parentheses denoting association degrees.[4,5]

Precise measurements were carried out for ideal gaseous mixtures in a few cases: He–H_2 by Gille[6] and Kr–Ar by Kestin *et al.*[7]

TABLE 1. He–H_2, $\eta(\mu P)$

z_m–H_2	η_{obsd}			K(I)		
	0 °C	15 °C	100 °C	0 °C	15 °C	100 °C
0.00000	189.25	196.11	234.08			
0.03906	185.00	191.33	228.07	1.036	1.135	1.197
0.10431	175.96	183.19	220.32	1.242	1.143	1.020
0.13600	173.27	178.46	215.55	1.138	1.236	1.060
0.24913	160.32	165.28	198.60	1.144	1.199	1.136
0.40284	143.06	147.69	178.47	1.161	1.198	1.114
0.60143	122.67	126.52	151.74	1.144	1.190	1.155
0.81193	101.65	105.48	126.46	1.156	1.185	1.135
1.00000	84.10	87.76	104.50	1.146	1.187	1.117
			K(II)	1.133	1.125	1.128

Put as follows for the viscosity of an ideal gaseous mixture:

$$\frac{(\eta-\eta_1)(1-z_m)}{(\eta_2-\eta)\cdot z_m} = K \qquad \text{(I)}$$

Applying the relation to the mixtures He–H_2 and Kr–Ar, we obtain the results given in Tables 1 and 2, and Figs. 1 and 2. K(I) denotes the values calculated by means of (I), and K(II) the values obtained from the relation

$$K = \eta_1M_2/\eta_2M_1 \qquad \text{(II)}$$

We see in Tables 1 and 2 that the values of K(I) and K(II) coincide with each other, though all the values of

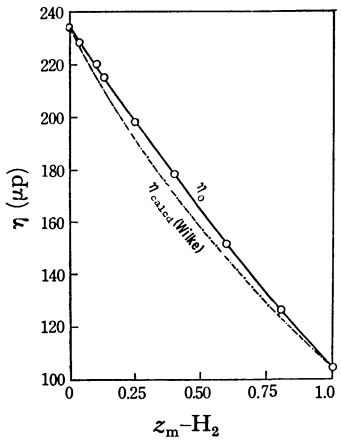

Fig. 1. He–H_2 (100 °C)

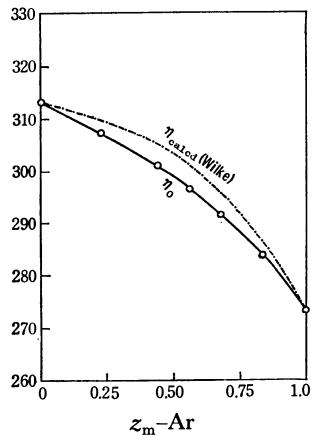

Fig. 2. Kr–Ar (100 °C)

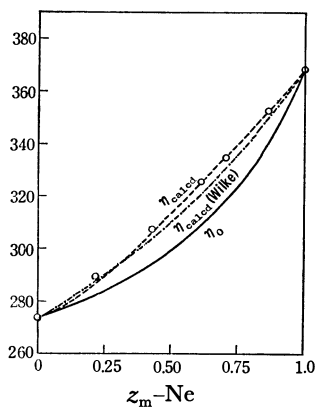

Fig. 3. Ar–Ne (100 °C)

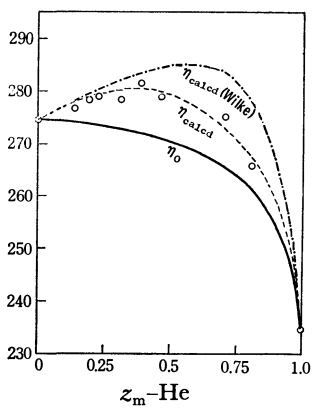

Fig. 4. Ar–He (99 °C)

TABLE 2. Kr–Ar, $\eta(\mu P)$

z_m–Ar	η_{obsd}							
	25 °C	100 °C	190 °C	300 °C	380 °C	510 °C	600 °C	700 °C
0.0000	254.79	312.97	375.58	442.57	490.08	557.75	602.68	652.61
0.2306	250.97	307.26	367.92	432.59	478.34	543.50	587.30	635.90
0.3915	247.46	302.42	361.23	423.95	468.29	531.62	574.27	622.35
0.5613	243.25	296.47	352.95	413.32	455.99	517.29	558.44	606.06
0.6793	239.59	291.49	346.22	404.89	—	—	—	—
0.8355	233.80	283.57	335.91	392.30	431.76	489.05	527.38	572.66
1.0000	226.29	273.25	323.08	377.22	414.34	468.48	505.05	547.76

z_m–Ar	K (I)							
	25 °C	100 °C	190 °C	300 °C	380 °C	510 °C	600 °C	700 °C
0.2306	0.5164	0.5554	0.5700	0.6014	0.6120	0.5893	0.6239	0.6326
0.3915	0.5378	0.5377	0.5846	0.6193	0.6278	0.6432	0.6379	0.6305
0.5613	0.5312	0.5602	0.5921	0.6333	0.6397	0.6479	0.6476	0.6243
0.6793	0.5395	0.5621	0.5990	0.6429	—	—	—	—
0.8355	0.5503	0.5609	0.6088	0.6563	0.6592	0.6576	0.6639	0.6322
1.0000	0.5350	0.5553	0.5909	0.6306	0.6347	0.6345	0.6433	0.6299
K(II)	0.5366	0.5459	0.5541	0.5592	0.5637	0.5674	0.5687	0.5678

K(I) are greater than those of K(II) at 380—700 °C, the divergence in $(\eta_{obs}-\eta_0)/\eta_0$ being at most 0.5%. If we take the relation

$$\eta_0 = \frac{\eta_1}{1+K\frac{z_m}{1-z_m}} + \frac{\eta_2}{1+\frac{1}{K}\frac{1-z_m}{z_m}}, \quad K = \frac{\eta_1 M_2}{\eta_2 M_1}$$

as a basic formula, any gaseous mixture can be analyzed as for liquid mixtures.[1]

As an example of non-ideal gaseous mixtures, two mixtures Ar–Ne (100 °C) and Ar–He (99 °C) are quoted from the measurements of Kestin, Wakeham and Watanabe[7] and Kalelkar and Kestin.[8]

The results are summarized in Tables 3 and 4 and Figs. 3 and 4. The curves denoted by η_{calcd} (Wilke) in Figs. 1—4 are plotted by use of Wilke's semi-theoretical formula for gaseous mixtures:[9]

$$\eta = \frac{\eta_1}{1+\phi_{12}\frac{z_m}{1-z_m}} + \frac{\eta_2}{1+\phi_{21}\frac{1-z_m}{z_m}},$$

$$\phi_{12} = \frac{[1+(\eta_1/\eta_2)^{1/2}\cdot(M_2/M_1)^{1/4}]^2}{2\sqrt{2}(1+M_1/M_2)^{1/2}},$$

$$\phi_{21} = \frac{[1+(\eta_2/\eta_1)^{1/2}\cdot(M_1/M_2)^{1/4}]^2}{2\sqrt{2}(1+M_2/M_1)^{1/2}}$$

TABLE 3. Ar–Ne, $\eta(\mu P)$, 100 °C

z_m–Ne	η_{obsd}	η_o	δ	$\delta/(1-z_m)z_m^2$
0.0000	273.25			
0.2093	289.14	281.88	7.26	(209.6)
0.4267	307.52	291.11	13.41	128.5
0.6145	325.34	308.93	16.41	112.7
0.7054	334.72	318.51	16.21	110.6
0.8639	352.41	340.67	11.74	115.6
1.0000	369.06			116.1
		K=0.3740		

TABLE 4. Ar–He, $\eta(\mu P)$, 99 °C

z_m–He	η_{obsd}	η_o	δ	$\delta/(1-z_m)z_m$
0.0000	273.07			
0.2270	276.27	271.68	4.59	28.16
0.4390	278.27	268.58	8.69	35.29
0.6308	276.35	266.13	10.22	43.88
0.7596	270.36	261.77	8.59	47.04
0.9048	253.99	251.21	2.78	32.27
1.0000	231.73			36.91
		K=0.1181		

Coincidence is satisfactory between η_0 and observed η_{obsd}(○) (Figs. 1 and 2), η_0 being less than η_{obsd}(Figs. 3 and 4). We can therefore apply any suitable functional form of z_m, generally $(1-z_m)^{\nu_1} z_m^{\nu_2}$ to the difference $\delta=(\eta_{obsd}-\eta_0)$, where ν_1 and ν_2 are the numbers of both component molecules which take part in a reaction to form a molecular compound or an aggregate or "embryo" as called by Lekenby and co-workers.[10]

References

1) T. Ishikawa, "The Theory on Viscosity of Liquid Mixtures," Maruzen, Tokyo (1968).
2) T. Ishikawa, *Bull. Chem. Soc. Jpn.*, **4**, 25 (1929).
3) M. Thiesen, *Verh. d. D. Phys. Ges.*, **4**, 348 (1902).
4) T. Ishikawa, *Bull. Chem. Soc. Jpn.*, **31**, 524 (1958).
5) E. C. Bingham and L. W. Spooner, *Physics*, **4**, 387 (1933).
6) A. Gille, *Ann. Phys.*, **48**, 799 (1915).
7) J. Kestin, W. Wakeham, and K. Watanabe, *J. Chem. Phys.*, **53**, 3773 (1970).
8) A. S. Kalelkar and J. Kestin, *J. Chem. Phys.*, **52**, 4248 (1970).
9) C. R. Wilke, *J. Chem. Phys.*, **18**, 517 (1950).
10) R. E. Leckenby, E. J. Robbins, and P. A. Trevalion, *Proc. Roy. Soc., Ser. A*, **280**, 49 (1964).

BULLETIN OF THE CHEMICAL SOCIETY OF JAPAN, VOL. 49 (7), 2011—2012 (1976)

On the Chemical Structure and Some Labile Hydrogens of 7-Methylguanosine

Mamoru NAKANISHI, Masamichi TSUBOI, and Iwao NAKAGAWA*

Faculty of Pharmaceutical Sciences, University of Tokyo, Hongo, Bunkyo-ku, Tokyo 113
**Laboratory of Chemistry for Natural Products, Faculty of Science, Tokyo Institute of Technology, Ookayama, Meguro-ku, Tokyo 152*

(Received April 19, 1976)

Synopsis. Proton magnetic resonance and infrared absorption studies indicate that 7-methylguanosine has 1-NH, 2-NH_2, and 8-CH groups in dimethylsulfoxide solution, while in an aqueous system of pH 6.0 these groups are subjected to rather rapid hydrogen exchange reactions with the solvent molecules, so that their life-times are respectively $\ll 10^{-2}$ s, $=0.025$ s and $=180$ s at 25 °C.

7-Methylguanosine has recently been found as a modified structure of the 5'-end of the messenger RNA in eukaryote system[1-4]. Its chemical structure may be strange and unique among nucleosides, because of the positively charged nitrogen atom at position 7. Thus, the following questions, for example, are to be answered: Is the hydrogen atom located on 1-N or 6-O? and how labile are the protons of the 1-NH, 2-NH_2, and 8-CH groups?

7-Methylguanosine was prepared by a modification of the procedure of Jones and Robins.[5] A solid sample obtained by lyophilization from a pH 4.0 aqueous solution was carefully dried in vacuum and dissolved in dry dimethylsulfoxide-d_6. The proton magnetic resonance spectrum of this solution is shown in the Figure. The 1-NH, 8-CH, and 2-NH_2 signals are observed at 11.9, 9.6, and 7.6 ppm, respectively (from tetramethylsilane). Thus, the structure shown in the Figure is now supported. The 7-NCH_3 signal is found at 4.2 ppm; this is lower than those of other usual N-CH_3, probably because of the positive charge on 7-N.

In aqueous solutions, 7-methylguanosine is found to be stable only in the pH range lower than its pK ($=7.1$[6] at 25 °C). In a H_2O solution of pH 4.0, as well as in that of pH 6.0, the 1-NH signal is not observed. This fact is attributable to a rapid hydrogen exchange reaction of this groups with the solvent molecule. The NH_2 signal (at 6.9 ppm) is broad and from its line width the rate constant of its hydrogen exchange with solvent is estimated to be 40 s^{-1} at 25 °C, pH 6. The hydrogen exchange reaction of 8-CH (at 9.2 ppm) is known to be faster than those of adenosine and guanosine.[7,8] We have followed the reaction not only by means of the proton magnetic resonance measurement but also by means of the infrared absorption measurement of the 8-CH stretching bands (two, at 3100 and 3170 cm^{-1}) in D_2O solutions. The reaction was found to be of the first-order. The rate constant k_e has been determined to be 6.4×10^{-5} s^{-1} at pH 4.0 (25 °C) and 5.5×10^{-3} s^{-1} at pH 6.0 (25 °C). Thus, k_e is proportional to the OH^- concentration. On the basis of the relation,

$$k_e = k_{OH}[OH^-] = \{k_d\, 10^{14-pK}/(10^{14-pK}+1)\}[OH^-],$$

(where k_d is the diffusion constant and was assumed to

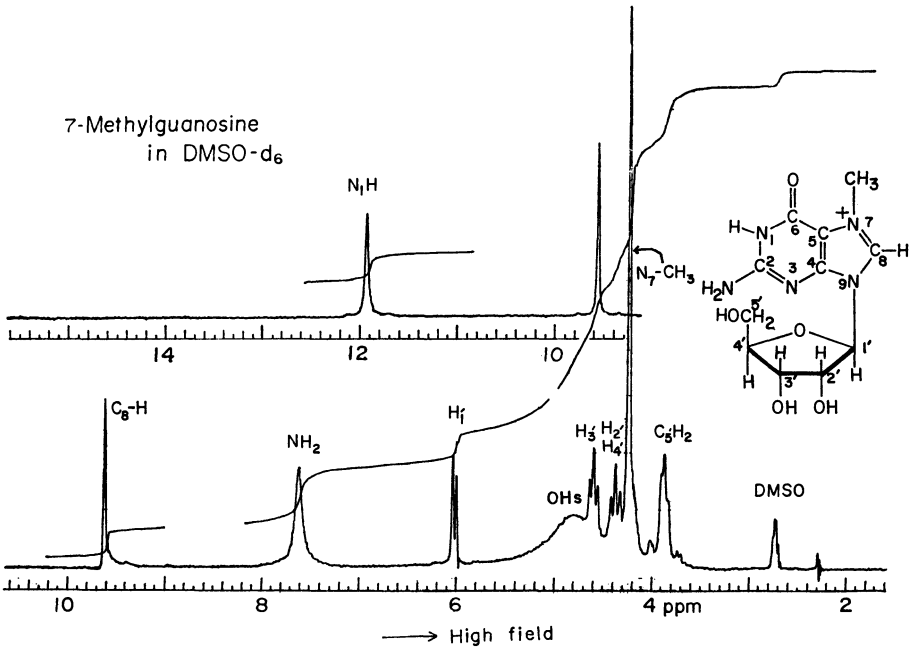

Fig. 100 MHz ^1H NMR spectrum of 7-methylguanosine in dimethylsulfoxide-d_6. The abscissa scale is the chemical shift in ppm from the tetramethylsilane resonance.

be equal to 10^{10} M^{-1} s^{-1}) the pK value of the 8-CH group has been estimated to be $18._3$ at 25 °C. The k_e value just determined would be useful in estimating the "fluctuation amplitude"[9] of the 7-methylguanine residue involved in a secondary structure of a messenger RNA or a transfer RNA.

This work was supported partly by a grant from the Ministry of Education.

References

1) Y. Furuichi and K. Miura, *Nature*, **253**, 374 (1975).
2) T. Urushibara, Y. Furuichi, C. Nishimura, and K. Miura, *FEBS Lett.*, **49**, 385 (1975).
3) Y. Furuichi, M. Morgan, S. Muthukrishnan, and A. J. Shatkin, *Proc. Nat. Acad. Sci. USA*, **72**, 362 (1975).
4) C. M. Wei and B. Moss, *Proc. Nat. Acad. Sci. USA*, **72**, 318 (1975).
5) J. W. Jones and R. K. Robins, *J. Am. Chem. Soc.*, **85**, 193 (1963).
6) J. A. Haines, C. B. Reese, and L. Todd, *J. Chem. Soc.*, **1962**, 5281.
7) M. Tomasz, J. Olson, and C. M. Mercado, *Biochemistry*, **7**, 1235 (1972).
8) M. Tomasz, *Biochim. Biophys. Acta*, **199**, 18 (1970).
9) M. Nakanishi, M. Tsuboi, and A. Ikegami, *J. Mol. Biol.*, **75**, 673 (1973).

BULLETIN OF THE CHEMICAL SOCIETY OF JAPAN, VOL. 49 (7), 2013—2014 (1976)

Ionization of Hydroxamic Acids in Aqueous Solutions

Shahid Abbas ABBASI* and Jameel AHMED**

Department of Chemistry, Indian Institute of Technology, Bombay-400076, India

(Received October 18, 1975)

Synopsis. Thermodynamic ionization constants of sixteen hydroxamic acids at 25 °C and 35 °C in aqueous solution and the corresponding $\Delta H°$ (standard enthalpy change) are presented.

Hydroxamic acids have extensive application in analytical[1] and medicinal chemistry.[2] The ionization of a hydroxamic acid has been found to have a strong bearing on its effectiveness as an analytical[1] or biological[3] reagent. This led to several studies on the determination of ionization constants of hydroxamic acids.[3-5] Most of these studies, however, were performed in media of high, constant ionic strength and at a single temperature (usually 25 °C) and the results are valid for only these conditions. The determination was carried out without taking necessary precaution to avoid carbon dioxide from the titration-solutions. The presence of dissolved atmospheric gases such as CO_2 in the hydroxamic acid solutions during pH titrations are liable to effect the ionization. In the present communication, thermodynamic ionization constants of a number of hydroxamic acids, determined under rigorously controlled conditions at 25 °C and 35 °C are reported.

Experimental

Hydroxamic Acids. The hydroxamic acids were prepared by following the general method of Blatt.[6] They were recrystallized repeatedly until they showed a sharp melting point. The purity was checked by microanalysis, gas-liquid chromatography and IR spectroscopy. Conductivity water was used throughout. All other reagents were of analytical grade.

Determination of Thermodynamic Ionization Constants. A weighed quantity of hydroxamic acid was placed in a thermostated titration vessel containing 50 ml of aqueous $HClO_4$ solution (1.00×10^{-3} M). Nitrogen, after being passed in succession through a train of guard tubes containing, pyrogallic acid, 3 M KOH solution and distilled water, was bubbled into the titration vessel. The rest of the experimental set-up for pH titration and the method of calculation of ionization constants was essentially the same as that described by Goldberg.[7] The expressions involved are:

$$K_a = \frac{[H^+][A^-]\gamma_{H^+}\cdot\gamma_{A^-}}{[HA]\gamma_{HA}} \quad (1)$$

where HA represents hydroxamic acid. It follows that

$$pK_a = -\log[H^+] + \log\frac{[HA]}{[A^-]} + 2\log\frac{1}{\gamma_\pm} \quad (2)$$

the activity coefficient of uncharged species being taken as unity.

The log $[H^+]$ values are read from the pH meter and $\gamma_\pm$, the mean activity coefficient, is obtained by interpolation of the data from Harned and Owen.[8] The titration was repeated until two sets of values differing within ±0.01 pH units were obtained.

Results and Discussion

The results for one representative titration, namely for salicylohydroxamic acid at 25 °C, are given in Table 1. The thermodynamic ionization constants of fourteen

TABLE 1. DETERMINATION OF THERMODYNAMIC IONIZATION CONSTANT OF SALICYLO HYDROXAMIC ACID AT 25 $\pm$0.1 °C
(Salicylohydroxamic acid) = 0.01 M, (KOH) = 0.1000 M.

I Titrant (0.1000 M KOH) ml	II pH	III Stoichiometric concentration HA	III Stoichiometric concentration A^-	IV HA/A^-	V log of column IV	VI $\log 1/\gamma_\pm$	VII pK_a
0.50	6.45	0.009	0.001	9/1	0.954	0.015	7.42
1.00	6.80	0.008	0.002	8/2	0.602	0.021	7.42
1.50	7.02	0.007	0.003	7/3	0.368	0.025	7.41
2.00	7.23	0.006	0.004	6/4	0.176	0.028	7.41
2.50	7.32	0.005	0.005	5/5	0.000	0.032	7.42
3.00	7.54	0.004	0.006	4/6	−0.176	0.035	7.40
3.50	7.75	0.003	0.007	3/7	−0.368	0.037	7.42
4.00	7.97	0.002	0.008	2/8	−0.602	0.040	7.41
4.50	8.33	0.001	0.009	1/9	−0.954	0.042	7.42
Result: Av. $pK_a = 7.41\pm0.01$							

pH values are accurate to ±0.01 units.

* To whom correspondance should be made.

** Department of Chemistry, Saifia College, Bhopal (M.P.), India.

Table 2. Thermodynamic ionization constants and standard enthalpy changes

No.	Hydroxamic acid	pK_a at 25 ±0.1 °C	pK_a at 35±0.1 °C	$\Delta H°$
1	Benzo-	8.89±0.01	8.79±0.02	4.21
2	*N*-Phenylbenzo-	8.41±0.01	8.30±0.01	4.62
3	Formo-	8.78±0.02	8.67±0.01	4.62
4	Glycine-	7.80±0.02	7.71±0.01	3.79
5	D-Tyrosine-	9.35±0.02	9.21±0.02	5.89
6	L-Tyrosine-	9.35±0.02	9.21±0.02	5.89
7	D-Lysine-	8.11±0.01	7.98±0.02	5.47
8	L-Lysine-	8.11±0.02	7.98±0.02	5.47
9	L-Lacto-	9.45±0.01	9.37±0.01	3.37
10	Chloroaceto-	8.53±0.01	8.42±0.01	4.62
11	*o*-Aminobenzo-	9.29±0.02	9.17±0.02	5.05
12	*p*-Hydroxybenzo-	9.06±0.01	8.95±0.02	4.62
13	Salicylo-	7.41±0.01	7.33±0.01	3.37
14	5-Nitrosalicylo-	6.89±0.01	9.01±0.01	3.37
15	*N*-Phenylcinnamo-	9.11±0.01	9.01±0.01	4.21
16	*N*-Furoylbenzo-	8.14±0.02	8.02±0.01	5.05

hydroxamic acids along with those of reference substance benzo- and *N*-phenylbenzohydroxamic acids are given in Table 2, together with the values of standard enthalpy change, $\Delta H°$, obtained by integrating van't Hoff's equation[9] at two temperatures, T_1 (298 K) and T_2 (308 K):

$$\log \frac{K_{a_2}}{K_{a_1}} = \frac{\Delta H°(T_2 - T_1)}{4.567 T_1 T_2}$$

where $\log K_a = -pK_a$.

Since the hydroxamic acids differ widely in structure and basicity (pK_a between 6.89 to 9.45 at 25 °C), it can be assumed that $\Delta H°$ is in general positive for the ionization of hydroxamic acids. There is, however, no definite trend in the magnitudes of change in values of $\Delta H°$ with change in the groups attached to the functional –C=O and –N–OH groups. It can be seen that while increase in the conjugation at the –C=O site (compound XV) increases the basicity of the compound relative to benzohydroxamic acid, introduction of π systems at the –N–OH fragment reduces the basicity (compounds II, XVI). With hydroxamic acids derived from amino acids, the pK_a values are in line with the basicity of the corresponding amino acids.[10]

The author is grateful to Dr. B. G. Bhat and Dr. R. S. Singh of I. I. T. Bombay, and the authorities of Saifia College, Bhopal, for providing necessary facilities, to Chandrashekharan and Unnikrishnan for technical help, and to the C. S. I. R., New Delhi, for a Senior Research Fellowship.

References

1) A. K. Majumdar, "*N*-Benzoylphenylhydroxylamine and its analogus," Pergamon Press, Oxford (1972), Chapters 2 and 3.
2) G. R. Gale and L. M. Atkins, *Arch. Int. Pharmacodyn.*, **180**, 289 (1969).
3) B. E. Hackley, Jr., R. Plapinger, M. Stolberg, and T. Wagner Jauregg, *J. Am. Chem. Soc.*, **77**, 3651 (1955).
4) R. L. Dutta and S. Ghosh, *J. Indian Chem. Soc.*, **44**, 820 (1967).
5) J. P. C. Jaimini and N. C. Sogani, *J. Indian Chem. Soc.*, **47**, 247 (1970).
6) A. H. Blatt, *Org. Synth.*, Coll. Vol. II, 67 (1943).
7) D. E. Goldberg, *J. Chem. Educ.*, **39**, 328 (1962); **40**, 341 (1963).
8) H. S. Harned and B. B. Owen, "The Physical Chemistry of Electrolytic Solutions," Reinhold, New York (1958).
9) G. N. Lewis and M. Randell, "Thermodynamics," McGraw Hill, New York (1961), Chapter 15.
10) L. G. Sillen, E. Hogfeldt, A. E. Martell, and R. M. Smith, Editors, "Stability Constants of Metal-Ion Complexes," Supplement No. 1, Special Publication No. 25, The Chemical Society, Burlington House, London (1970).

BULLETIN OF THE CHEMICAL SOCIETY OF JAPAN, VOL. 49 (7), 2015—2016 (1976)

Solvent Effect on the Raman Spectra of Mercury(II) Halides

Kozo Sone, Makiko Aritaki, Keiko Hiraoka, and Yutaka Fukuda

Department of Chemistry, Faculty of Science, Ochanomizu University, Otsuka, Bunkyo-ku, Tokyo 112

(Received April 15, 1976)

Synopsis. Raman spectra show that the Hg-X bond strengths in mercury (II) halides are remarkably weakened by the interaction with certain solvents. Relations between the degree of this weakening and (a) the Lewis basicity (Gutmann's donor number) of the solvent and (b) the ionic character of the Hg–X bond are pointed out, together with a simple explanation.

The Raman spectra of $HgCl_2$ in a number of organic solvents have been studied by Allen and Warhurst[1] and it was found that the frequency of the Cl–Hg–Cl stretching vibration is remarkably influenced by the nature of the solvent. They discussed their results chiefly on the basis of the dielectric constants of the solvents.

We have tried to study this kind of solvent effect further, using a larger variety of solvents, and comparing the obtained results with those of other halides, cyanide and methyl halides of mercury(II).

Experimental

Use was made of a JEOL-Sl Raman Spectrophotometer and an Argon laser (5145 Å). All the reagents (including solvents) used were Extra Pure or Spectro grade chemicals. Since the solubilities of the mercury(II) compounds in many of the solvents are low, the concentrations in many cases were much below 0.1 M.

Results and Discussion

The observed frequencies (ν) of the X–Hg–X symmetrical stretching vibration for the HgX_2 molecules are shown in Table 1,* and those of the Hg–X and Hg–CH_3 stretching frequencies for the CH_3HgX molecules in Table 2. The values of the apparent force constants(k) of the bonds, calculated by means of simple valence force models,[2] are also given. The ν values of $HgCl_2$ reported by Allen and Warhurst[1] were in general confirmed, except that in dioxane for which they reported 302 cm^{-1}.

The data in Table 1 clearly show that the ν and k values of a halide, *i.e.* the strength of the Hg–X bond in it, decrease in the order gas>benzene>acetone>water>methanol>dimethylformamide (DMF)>pyridine or, roughly speaking, with the increase of the coordination ability (Lewis basicity) of the solvent. It is also clear that the rates of this decrease are in the order $HgCl_2$>$HgBr_2$>HgI_2. This is the same as the order of the decrease of the ionic characters of Hg–X bonds which are estimated (from the classical electronegativity scale of Pauling) to be: Hg–Cl 26%, Hg–Br 19%, Hg–I 9%.

If we plot the values of k of the halides against the donor number (DN) of Gutmann,[3] which serves as a simple measure of the Lewis basicity of a solvent, these relations can be very clearly recognized. The results are shown in Fig. 1.

In the case of the methyl halides in Table 2,** there are also similar decreases of ν and k from methanol to pyridine, and the rates of this decrease are again in the order of chloride>bromide>iodide. However, it can

Table 1. Raman frequencies of HgX_2 (cm^{-1}) and apparent force constants of Hg–X bonds ($\times 10^5$ dyn cm^{-1})

	Gas[a]	Benzene	Nitromethane	Nitrobenzene	Benzonitrile	Acetonitrile
$HgCl_2$	335—360	340 (2.42)	335 (2.35)	335 (2.35)	330 (2.28)	330 (2.28)
$HgBr_2$	220—225	—	208 (2.05)	—	—	206 (2.01)
HgI_2	156	—	—	—	—	148 (1.64)
	Methyl Acetate	Acetone	Ethyl Acetate	Water	Methanol	Ethanol
$HgCl_2$	329 (2.27)	330 (2.28)	333 (2.33)	322 (2.17)	320 (2.15)	320 (2.15)
$HgBr_2$	206.5 (2.02)	209 (2.07)	209 (2.07)	—	209.5 (2.08)	207 (2.03)
HgI_2	149 (1.67)	—	151 (1.71)	—	151 (1.71)	153 (1.76)
$Hg(CN)_2$	—	—	—	415 (2.65)	411 (2.60)	—
	Dioxane	THF	DMF	DMSO	Pyridine	
$HgCl_2$	320 (2.15)	319.5 (2.14)	310 (2.02)	—	280 (1.64)	
$HgBr_2$	208 (2.05)	202 (1.93)	200 (1.89)	196 (1.82)	188 (1.67)	
HgI_2	154 (1.78)	148 (1.64)	145 (1.58)	142 (1.51)	140 (1.42)	

a) J. R. Ferraro, "Low-Frequency Vibrations of Inorganic and Coordination Compounds," Plenum, New York (1971), p. 142.

* In the case of $Hg(CN)_2$, a Raman line due to Hg–C≡N bending was observed at 270—272 cm^{-1} (in acetone, methanol, ethanol, dioxane and water) or at 267 cm^{-1} (in pyridine) and another due to C≡N stretching at 2195—2200 cm^{-1} (in methanol and ethanol) or at 2180 cm^{-1} (in pyridine). Insolubility of this compound in many of the solvents used, and overlapping with the Raman lines of the solvents, hindered closer study of the solvent effect in this case.

** The methyl halides showed two Raman lines, *i. e.* the Hg–X and Hg–CH_3 stretching frequencies; the line corresponding to X–Hg–CH_3 bending could not be located with certainty, probably because of its poor intensity.

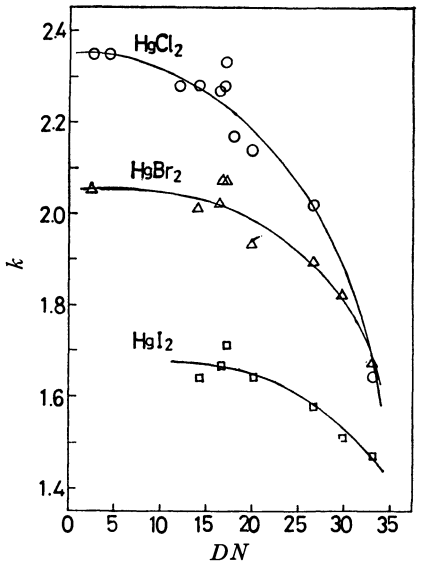

Fig. 1. *k vs. DN.*

Table 2. Raman frequencies of $(CH_3)HgX$ and apparent force constants of Hg–X and Hg–CH_3 bonds

	Methanol	Pyridine	
$(CH_3)HgCl$	328(1.95)	316(1.81)	(Hg–Cl)
	554(2.52)	547(2.46)	(Hg–CH_3)
$(CH_3)HgBr$	225(1.75)	212(1.56)	(Hg–Br)
	546(2.45)	535(2.35)	(Hg–CH_3)
$(CH_3)HgI$	178(1.50)	175(1.57)	(Hg–I)
	535(2.35)	528(2.27)	(Hg–CH_3)

be seen that the effect of solvent change is remarkably smaller than in the case of the simple halides.

All these results can probably be understood if we assume that the molecules of the donor solvents used tend to assemble around the central mercury atom of the linear HgX_2 molecule and to form coordinate bonds with it. If this kind of intetaction is assumed to be chiefly electrostatic in nature, it is easy to see that $HgCl_2$, which contains the most ionic bonds and therefore the most positively charged mercury atom, is the most susceptible to it, and the accumulation of the negative ends of the solvent molecules around the mercury atom will substantially weaken the Hg–Cl bond. This kind of solvent effect will naturally increase with increasing Lewis basicity of the solvent and decrease in the order of $HgCl_2 > HgBr_2 > HgI_2$, and from simple halides to methyl halides which are expected to be more covalent in nature.

It is now of interest to note that decrease of k of HgCl in going from gas to pyridine solution is as large as 30—40%, being comparable with the change of k observed when a double bond is converted into a single bond. This means that strong solvation can weaken a chemical bond to such a great degree. This effect will probably be an important reason for the fact that the Hg–X bond energies in the gas molecules decrease in the order $HgCl_2$ (54 kcal/mol)$\rightarrow HgBr_2$(44)$\rightarrow HgI_2$(35),[4] while the ease of formation of these molecules in aqueous solution increases in the opposite way (heats of formation: $HgCl_2$ (-13 kcal/mol)$\rightarrow HgBr_2(-21)\rightarrow HgI_2(-34)$).

Our thanks are due to Prof. Tsunetake Fujiyama of Tokyo Metropolitan University for his interest in this work and for his helpful discussions.

References

1) G. Allen and E. Warhurst, *Trans. Faraday Soc.*, **54**, 1786 (1958); J. R. Ferraro, "Low-Frequency Vibrations of Inorganic and Coordination Compounds," Plenum, New York (1971), p. 143.

2) G. Herzberg, "Infrared and Raman Spectra of Polyatomic Molecules," Van Nostrand, New York (1945), p. 172.

3) V. Gutmann, "Coordination Chemistry in Non-Aqueous Solutions," Springer, Wien (1968).

4) J. E. Huheey, "Inorganic Chemistry," Harper and Row, New York (1972), p. 698.

5) J. J. Christensen, *et al.*, "Handbook of Metal Ligand Heats", 2nd ed., Dekker, New York (1975).

BULLETIN OF THE CHEMICAL SOCIETY OF JAPAN, VOL. 49 (7), 2017—2018 (1976)

Rearrangement of 5-Isopropenyl-2-norbornene to 5-Methyl-3a,4,7,7a-tetrahydro-1*H*-indene

Shoji IWASE, Michihiro NAKATA, Sawako HAMANAKA, and Masaya OGAWA*

Department of Applied Chemistry, Faculty of Engineering, Kansai University, Senriyama, Suita, Osaka 564

(Received July 21, 1975)

Synopsis. The Diels-Alder reaction between cyclopentadiene and isoprene gave predominantly *endo*- and *exo*-5-isopropenyl-2-norbornenes and also *cis*-5-methyltetrahydro-1*H*-indene produced from the *endo*-product by Cope rearrangement.

In a previous paper,[1] the present have reported the reaction of isoprene (IP) with cyclopentadiene (CP). However, the stereochemical structure has not yet been established because of certain difficulties in the assignments of the ^{1}H-NMR spectra. Here, the authors report the chemical structures of the above reaction products confirmed by means of ^{13}C-NMR spectroscopy.

Experimental

Preparation of the Addition Products.[1,2] The co-dimers obtained in the reaction of IP with CP are both of methylvinylnorbornene (MVN) and methyltetrahydroindene (MTI). After the equi-molar reaction mixture had been stirred for 3 h at 145 or 160 °C in an autoclave and then cooled, the MVN produced was isolated by means of distillation and preparative gas chromatography. Following a similar procedure, MTI was also obtained under the reaction conditions at 145—220 °C for 3 h.

The co-dimer of the reaction of butadiene with CP, employed as a reference was prepared by a previously reported method.[2]

Rearrangement of MVN to MTI. The reaction of 0.1 ml of MVN was carried out in a 1-ml sealed tube in the range of the temperature from 145 to 170 °C. After the reaction had been completed and cooled, the product was analyzed by VPC.

Measurements. The ^{13}C-NMR spectra were recorded with a JNM-EC-100 Fourier transform spectrometer (25.15 MHz) with complete proton decoupling. The chemical shifts were determined in a CCl_4 solution of approximately 50 vol % using TMS as an internal standard. To all samples, the off-resonance proton decoupling technique was applied.

Preparative gas chromatography was carried out on a JEOL GC-750 with a 10 mmϕ × 3 m column packed with 25% silicon H. V. grease at 100 °C. The VPC analysis of the reaction products were made on a HITACHI KGL-2A gas chromatograph using a Golay column Q-90 (0.25 mmϕ × 90 m) at 134 °C.

Results and Discussion

Stereochemical Structure of MVN. The two possible structures for MVN are presented as follows:

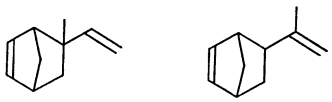

1 **2**

The result of the VPC analysis of the fractions of MVN showed the presence of the two components, **A** (R_t=22.4) and **B** (R_t=24.0). The molar ratio of **A** to **B** was found to be 14: 84 and 41: 59 in the fractions reacted at 145 and 160 °C, respectively. These two fractions were also examined by ^{13}C-NMR spectroscopy and the assignments of the signals in each fraction were easily determined. Furthermore, the numbers of protons attached to each carbon atom were obtained by means of the off-resonance proton decoupling technique. This result indicates that each of the components, **A** and **B**, has one nonprotonated sp^2 carbon atom. From this fact, the above structure **2** is in complete agreement with MVN, and thus **A** and **B** appear to be either the *endo*- or the *exo*-isomer of **2**.

TABLE 1. OBSERVED AND CALCULATED ^{13}C-NMR CHEMICAL SHIFTS[a] FOR VNB AND MVN

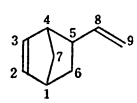

VNB

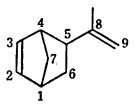

MVN

	Compound	C-2	C-3	C-6	C-7	C-8	C-9	CH_3	C-1,	4 or 5	
	Calcd VNB	137.2	134.2	36.5	37.0	145.3	114.9				
Obsd	*endo*-VNB	137.3	133.2	33.5	49.7	143.2	113.9		42.9	43.2	48.1
		(d)	(d)	(t)	(t)	(d)	(t)		(d)	(d)	(d)
	exo-VNB	137.3	136.8	33.5	45.9	143.6	112.6		42.2	42.6	48.1
		(d)	(d)	(t)	(t)	(d)	(t)		(d)	(d)	(d)
	Calcd MVN	136.2	134.5	33.9	37.0	149.5	112.4	20.1			
Obsd	*endo*-MVN	136.7	132.2	29.8	49.7	147.1	109.3	23.4	42.9	45.1	45.9
		(d)	(d)	(t)	(t)	(s)	(t)	(q)	(d)	(d)	(d)
	exo-MVN	136.7	135.9	31.5	45.3	149.5	107.9	23.4	42.3	45.5	44.7
		(d)	(d)	(t)	(t)	(s)	(t)	(q)	(d)	(d)	(d)

( ): off-resonance a) In ppm relative to internal TMS.

BULLETIN OF THE CHEMICAL SOCIETY OF JAPAN, VOL. 49 (7), 2019—2020 (1976)

Esterification of Alcohols with 1-Acylimidazole Assisted by *N*-Bromosuccinimide

Tsutomu KATSUKI

Department of Chemistry, Faculty of Science, Kyushu University, Higashi-ku, Fukuoka 812

(Received August 13, 1975)

Synopsis. Treatment of 1-acylimidazoles with alcohols in the presence of *N*-bromosuccinimide led to the rapid formation of the corresponding esters. The carboxylic acids with less than two hydrogen atoms at their α-positions generally gave good results. Even such a hindered ester as *t*-butyl pivalate could be prepared by this procedure.

The reaction between alcohols and 1-acylimidazoles[1] is known as one of the elegant esterification methods[2] under mild conditions. Though the above reaction is usually slow at room temperature, the esters of primary and secondary alcohols can be prepared by conducting the reaction at elevated temperatures.[3] For the preparation of hindered esters, however, the method is ineffective and the use of a strong base catalyst, such as sodium alkoxide or sodium amide, is indispensable.[4] *t*-Butyl pivalate, for example, has been prepared by the latter procedure in a 64% yield.[4] The author has found that when 1-acylimidazoles were treated with *N*-bromosuccinimide[5] in the presence of alcohols, rapid esterification took place at room temperature under neutral conditions. In most cases, the reaction terminated within sixty minutes. Hindered esters, such as *t*-butyl pivalate (**2**) and *t*-butyl 2,3,6-trimethylbenzoate (**3**) could be obtained in 48 and 65% yields, respectively, by refluxing the corresponding reactants in methylene chloride for twelve hours.

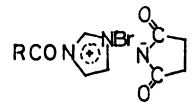

(1)

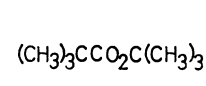

(2)

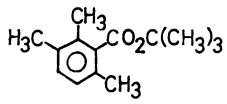

(3)

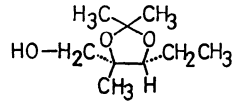

(4)

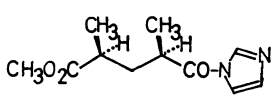

(5)

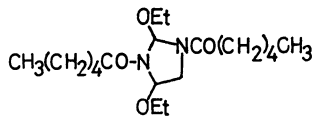

(6)

The esterification is considered to proceed *via* the intermediate represented by **1**. This method could be applied to the acylation of the acid-labile alcohol, 2,3-isopropyridenedioxy-2-methylpentanol (**4**).[6] The imidazolide (**5**) of methyl hydrogen meso-2,4-dimethylglutarate was converted into the corresponding *t*-butyl ester in a 70% yield without any detectable epimerization.

A limitation of the method is that the yield in the esterification of carboxylic acids having two or three hydrogen atoms on the α-carbon atoms, is fairly variable depending on the alcohols used. 1-Hexanoylimidazole was, for example, converted into its ethyl ester in only a 17% yield, and 80% of the product was an unexpected compound for which the tentative formula (**6**) has been given on the basis of spectral data. *s*-Butyl hexanoate was, however, obtained in a 80% yield.

A summary of the yields is given in Table 1 below.

Table 1. Per cent yields of esters

1-Acylimidazole	Alcohol	Solvent	Yield[a]
Pivaloyl	Ethanol	CH_2Cl_2	84
Pivaloyl	2-Methyl-2-propanol	CH_2Cl_2	48[b]
Pivaloyl	Cyclohexanol	THF	95[c]
Pivaloyl	(**4**)	THF	90
2-Methylpentanoyl	Ethanol	CH_2Cl_2	85
2-Methylpentanoyl	Cyclohexanol	CH_2Cl_2	81
2-Methylpentanoyl	2-Methyl-2-propanol	CH_2Cl_2	95
2,3,6-Trimethylbenzoyl	2-Methyl-2-propanol	CH_2Cl_2	65[b]
2,3,6-Trimethylbenzoyl	Benzyl alcohol	CH_2Cl_2	70[d]
Benzoyl	Ethanol	THF	80
Hexanoyl	Ethanol	CH_2Cl_2	17
Hexanoyl	2-Butanol	CH_2Cl_2	80
Hexanoyl	Benzyl alcohol	CH_2Cl_2	80[d]
Hexanoyl	2-Methyl-2-propanol	CH_2Cl_2	57
Acetyl	Cyclohexanol	THF	20

a) All yields are based on 1-acylimidazoles. b) These reactions were run under reflux for 12 h. c) The yield was determined by GLC. d) The yields were calculated from NMR spectra.

The analytical and NMR data of new compounds prepared in this study are given in Table 2.

Experimental

General. All the reactions were carried out in a nitrogen atmosphere. The quality of the reagents employed has a very marked effect upon the yield. Imidazole was purified by sublimation. *N*-Bromosuccinimide was recrystallized from water and dried at 25 °C under reduced pressure (5 mmHg). The alcohols employed were all absolute.

Tetrahydrofuran or dichloromethane was used as the solvent. But dichloromethane was preferable because tetrahydrofuran polymerized slowly under the reaction conditions.

Procedure. All the esters were prepared by almost the same procedure as exemplified by that of *t*-butyl 2-methyl-

Table 2. Analytical and NMR data of new compounds

Compound	Characteristic chemical shifts (δ) and analysis[a)]
1-(2-Methylpentanoyl)imidazole[b)]	0.93(m, 3H), 1.35(d, 3H), 3.13(m, 1H), 7.00(double-d, 1H), 7.12(double-d, 1H), 8.22(broad-s, 1H). Found: C, 64.77; H, 8.40. Calcd: C, 65.03; H, 8.49.
1-(2,3,6-Trimethylbenzoyl)imidazole[b)]	2.11(s, 3H), 2.17(s, 3H), 2.28(s, 3H), 6.95—8.00(m, 5H). Found: C, 72.51; H, 6.63. Calcd: C, 72.87; H, 6.59.
Benzyl 2,3,6-trimethylbenzoate	2.14(s, 3H), 2.20(s, 6H), 4.33(s, 2H), 6.97(qualtet, 2H), 7.30—7.46(m, 5H). Found: C, 79.85; H, 7.04. Calcd: C, 80.28; H, 7.13.
t-Butyl 2,3,6-trimethylbenzoate (**3**)	1.61(s, 9H), 2.23(s, 6H), 2.30(s, 3H), 6.98(qualtet, 2H). Found: C, 76.45; H, 9.28. Calcd: C, 76.32; H, 9.15.
Cyclohexyl 2-methylpentanoate	0.90(m, 3H), 1.11(d, 3H), 2.43(m, 1H), 4.75(m, 1H). Found: C, 72.33; H, 11.22. Calcd: C, 72.68; H, 11.18.
2,3-Isopropyridenedioxy-2-methylpentyl pivalate	1.05(m, 3H), 1.20(s, 9H), 1.30(s, 3H), 1.38(s, 3H), 1.41(s, 3H), 3.70(t, 1H), 3.93(s, 2H). Found: C, 64.01; H, 10.11. Calcd: C, 65.08; H, 10.14.

a) The C and H analyses were carried out on the samples which were obtained by the simple distillation of the reaction products by applying the micro pot-style molecular distillation apparatus at the appropriate bath temperature. b) The 1-acylimidazoles were prepared from the corresponding acyl chlorides and imidazole following the usual procedure.

pentanoate. The esters thus obtained were spectroscopically identified.

t-Butyl 2-Methylpentanoate (**7**): 1-(2-Methylpentanoyl)-imidazole prepared from 2-methylpentanoyl chloride (592 mg) and imidazole (610 mg) was dissolved in dichloromethane (25 ml). To this solution were added 2-methyl-2-propanol (422 mg) and then *N*-bromosuccinimide (814 mg) at one time at room temperature. After 1 h, the mixture was analyzed by GLC. GLC analysis indicated the formation of **7** in a 95% yield. The resulting mixture was distributed between water (20 ml) and pentane (100 ml). The organic layer was separated, washed successively with a saturated aqueous solution of citric acid, water, and a saturated aqueous solution of sodium hydrogencarbonate, dried over anhydrous sodium sulfate, and concentrated to a colorless oil (95%). The ester thus obtained was identified with an authentic sample by NMR spectroscopy.

The author is grateful to Professor Masaru Yamaguchi for his helpful advice and discussions. This work was supported in part by a grant from the Ministry of Education.

References

1) H. A. Staab and W. Rohr, "Newer Methods of Preparative Organic Chemistry," Vol. V, Academic Press, New York and London (1968), p.61.

2) The reagents employed are, for example, dimethylaminopyridine [G. Hofle and W. Steglich, *Synthesis*, **1972**, 620], triphenylphosphine–dipyridyldisulfide [T. Mukaiyama, R. Matsueda, and M. Suzuki, *Tetrahedron Lett.*, **1970**, 1901 and E. J. Corey and K. C. Nicolaou, *J. Am. Chem. Soc.*, **96**, 5614 (1974)], tosyl chloride–triethylamine [J. H. Brewster and C. J. Ciotti Jr, *J. Am. Chem. Soc.*, **77**, 6214 (1655)], and trifluoroacetylimidazole [H. A. Staab and G. Walther, *Chem. Ber.*, **95**, 2070 (1962) and H. D. Law, *J. Chem. Soc.*, **1965**, 3897].

3) H. A. Staab, *Angew. Chem.* **71**, 194 (1959).

4) H. A. Staab and A. Mannschreck, *Chem. Ber.*, **95**, 1284 (1962).

5) *N*-Chlorosuccinimide was also used but it was less effective than *N*-bromosuccinimide.

6) J. Inanaga, A. Takeda, N. Okukado, and M. Yamaguchi, *Mem. Fac. Sci., Kyushu Univ., C*, **9**, 293 (1975).

BULLETIN OF THE CHEMICAL SOCIETY OF JAPAN, VOL. 49 (7), 2021—2022 (1976)

The Nucleophilic Substitution of Dicarboxylic Imides on the Chelate Ring of Tris(3-bromo-2,4-pentanedionato)iron(III)

Yasuo YAMAMOTO, Kuninobu KASUGA, and Akira SUMITA

Department of Chemistry, Faculty of Literature and Science, Shimane University, Nishikawatsucho, Matsue 690

(Received September 16, 1975)

Synopsis. Succinimide and phthalimide were found to be capable of acting as a nucleophilic substituent on the chelate ring of tris(3-bromo-2,4-pentanedionato)iron(III) complex. No analogous reaction has been found between this complex and the other dicarboxylic imides, nor between other metal complexes and dicarboxylic imides including these two imides.

The electrophilic substitution on the chelate ring of acetylacetonato complexes is brought about by various reagents such as bromine,[1,2] iodine,[1] *N*-halosuccinimides,[1,5] nitro derivatives,[3,4] acyl derivatives[4] and chloride of iodine[1] or sulfur[6] *etc.*, while only a few reports have appeared on the further conversion of the substituted chelates.[6,7] The nucleophilic substitution reaction reported by Yoshida *et al.*[7] deserves the special attention. They found that the bromine atom on the chelate ring of 3-bromo-2,4-pentanedionato metal complexes is replaced by thiophenol or its para-substituted derivatives. During the course of our investigation on the mechanism of a similar reaction using mercaptanes, alcohols and alkoxides as substituents, we encountered in most cases the decomposition of chelate or the reduction of central metal and occasionally the formation of alkoxy bridged binuclear complexes.[8] In the present studies, we came across an unexpected result in which some dicarboxylic imides were substituted for bromine of tris(3-bromo-2,4-pentanedionato)iron(III).

3-Carbon of tris(2,4-pentanedionato)iron(III) was brominated by means of *N*-bromosuccinimide. Then the brominated compound, after isolation, was to be examined as to the substitution reaction of sodium methoxide. This reagent was accidentally added to the solution of complex without removal of succinimide, which is one of the byproducts of bromination. After being left to stand for three days, deposited white precipitates were separated by filtration, and the filtrate was evaporated in a vaccum. Orange plates thus obtained were recrystallized from dichlormethane–methanol solution. The results of elemental analysis. molecular weight and infrared spectrum indicate that this compound is tris(3-succinimido-2,4-pentanedionato)iron(III), the bromine atom at the 3-position of every chelate being replaced by succinimide, instead of the methoxide group. The departure of bromine was recognized by the fact that the white precipitates were soluble in water and silver bromide was formed by the addition of aqueous solution of silver nitrate. The analytical value and molecular weight were as follows. Found: C, 49.53; H, 4.66; N, 6.38%; mol wt, 631; mp 143—146 °C decomposed. Calcd for $FeC_{27}H_{30}N_3O_{12}$: C, 50.33; H, 4.69; N, 6.52%; mol wt, 644.4.

For the sake of confirmation, the brominated compound was isolated and examined. 1.97 g (0.003 mol) of tris(3-bromo-2,4-pentanedionato)iron(III) and 0.99 g (0.01 mol) of succinimide were dissolved in 180 ml of dichlormethane to which was added 0.54 g (0.01 mol) of sodium methoxide dissolved in 25 ml of methanol. After being left to stand for three days, an orange substance was obtained by the same procedure as above. This was also identified as tris(3-succinimido-2,4-pentanedionato)iron(III), A.

In a similar way, phthalimide reacted with tris(3-bromo-2,4-pentanedionato)iron(III), producing orange red crystals of hexagonal prism, which was confirmed to be tris(3-phthalimido-2,4-pentanedionato)iron(III), B. Found: C, 58.63; H, 3.91; N, 5.15%; mol wt, 750; mp 235—240 °C decomposed. Calcd for $FeC_{39}H_{30}N_3O_{12}$: C, 59.41; H, 3.84; N, 5.33%; mol wt, 788.5.

In the infrared spectra, product A and B show a peak at 1705 and 1725 cm^{-1}, respectively, both of them being attributed to the stretching vibration of carbonyl group vicinal to the imide nitrogen. The stretching vibration of the chelated carbonyl groups appears at 1545 cm^{-1} for the original brominated material. The peak shifts to 1580 cm^{-1} for product A and 1582 cm^{-1} for product B. In the region 1100—710 cm^{-1}, product B has peaks assigned to the benzene ring (Table 1).

Table 1. Characteristic absorption peaks of the original complex and the products in the infrared spectra, cm^{-1}

	$\nu(C=O)_1$	$\nu(C=O)_2$	ν (benzene ring)
Fe(Br–acac)$_3$		1545	
Product A	1705	1580	
Product B	1725	1582	1100 1090 880 800 720 710

$\nu(C=O)_1$: Carbonyl vicinal to the imide group.
$\nu(C=O)_2$: Chelated carbonyl.

The absorption peaks in the visible and ultraviolet region are given in Table 2 for the original material and products A and B. The metal reduction and

Table 2. Absorption maxima of the original complex and the product sin the electronic spectra, nm (log ε)

	$\pi-\pi^*$			$t_{2g}-\pi^*$	$\pi-e_g$[9]
$Fe(Br\text{-}acac)_3$	240[sh] (4.15)	292 (4.34)		375 (3.46)	470 (3.57)
Product A	244 (4.43)	268 (4.45)		347 (3.56)	432 (3.67)
Product B	244 (4.65)	270[sh] (4.48)	303[sh] (4.15)	347 (3.59)	433 (3.68)

oxidation bands and the band due to the intraligand transition of each one appear at an adequate position with reasonable extinction for the 1,3-diketone complexes. The shoulder at 303 nm of product B might originate from phthalimide residue, whose intense absorption at around 250 nm seems to hide the π—π^* transition band of product B.

These substitution reactions proceed also with the addition of potassium hydroxide instead of sodium methoxide. No change is observed in the absence of hydroxides or methoxides, in contrast to the substitution of thiophenol which is considerably inhibited by the addition of such a proton acceptor as pyridine or piperidine as well as in the basic solvent such as acetone, methanol, ether or dimethyl sulfoxide.[7] The disparity arises from the fact that the reaction depends on whether intermediate adducts exist in the case of thiophenol substitution or the coulombic attraction is dominant enough to promote the reaction.

The present reaction with succinimide or phthalimide seems to be characteristic of iron(III) complex. Aluminum(III), chromium(III), cobalt(III) and copper(II) complexes of the same ligand show no change with various dicarboxylic imides including these two imides. No other substituent has been found as regards the reaction involving this iron(III) complex.

The reaction seems to be a kind of Gabriel reaction. Bacon and Karim reported on the extension of copper-catalyzed reaction,[10] in which the substitution of phthalimide for halogen of aryl halide is catalyzed by copper(I) iodide. Application of this catalyst to the present reaction resulted in failure, suggesting a different mechanism.

Experimental

The electronic spectra and the infrared spectra were measured on a Hitachi 124 type Spectrophotometer and Hitachi 215 type Spectrophotometer, respectively. The elemental analyses were carried out by means of a Yanagimoto MT 2 CHN corder. A Hitachi 115 Vapour Pressure Osmometer was used for the determination of molecular weights. Reagents of guaranteed grade were used without further purification.

References

1) J. P. Collman, R. A. Moss, H. Malz, and C. C. Heindel, *J. Am. Chem. Soc.*, **83**, 531 (1961).
2) H. Reihlen, R. Ilig, and R. Wittig, *Ber.*, **58**, 12 (1925).
3) C. Djoidjeric, J. Lewis, and R. S. Nyholm, *Chem. Ind. (London)*, **1959**, 122.
4) J. P. Collman, R. A. Moss, S. D. Goldby, and V. S. Tvahanousky, *Chem. Ind. (London)*, **1960**, 1213.
5) R. W. Kluiber, *J. Am. Chem. Soc.*, **82**, 4839 (1960).
6) R. W. Kluiber, *J. Am. Chem. Soc.*, **83**, 3030 (1961).
7) Z. Yoshida, H. Ogoshi, and Y. Shimizu, *Kogyo Kagaku Zasshi*, **72**, 1648 (1969).
8) K. Kasuga, H. Itou, and Y. Yamamoto, *Bull. Chem. Soc. Jpn.*, **47**, 1026 (1974).
9) R. L. Lintvedt and L. K. Kernitsky, *Inorg. Chem.* **9**, 491 (1970).
10) R. G. R. Bacon and A. Karim, *J. Chem. Soc. Perkin Trans. 1*, **1973**, 272, 278.

BULLETIN OF THE CHEMICAL SOCIETY OF JAPAN, VOL. 49 (7), 2023—2024 (1976)

Reaction of Triethylphosphine with Dimethyl Acetylenedicarboxylate in the Presence of *p*-Chlorobenzaldehyde

Kin-ya AKIBA, Toshio YONEYAMA, and Naoki INAMOTO

Department of Chemistry, Faculty of Science, The University of Tokyo, Hongo, Tokyo 113

(Received April 13, 1976)

Synopsis. Reaction of triethylphosphine (**1**) with dimethyl acetylenedicarboxylate (**2**) in the presence of *p*-chlorobenzaldehyde gave dimethyl α-(*p*-chlorobenzoyl)-fumarate (**5**) and a bicyclic lactone (**6**). In the presence of water, reaction of **1** with **2** afforded dimethyl fumarate and triethylphosphine oxide.

Tertiary phosphines can add to acetylenic bonds.[1] The *1*:*1* adduct is considered to be a 1,3-dipole. Therefore, trapping of the 1,3-dipole with *p*-chlorobenzaldehyde was attempted, in order to check a possibility to prepare phosphorus-containing heterocycles.

Dimethyl acetylenedicarboxylate (**2**) was added dropwise to a mixture of triethylphosphine (**1**) and *p*-chlorobenzaldehyde (**3**) in ether at room temperature. The reaction products were dimethyl fumarate (**4**) (1.3%), dimethyl α-(*p*-chlorobenzoyl)fumarate (**5**) (13%), a bicyclic lactone (**6**) (1.2%), and triethylphosphine oxide (58%).

The structure of **5** was determined based on the spectral data, and the NMR data were essentially the same as those of dimethyl α-benzoylfumarate.[2] The structure of **6** was assigned by the spectral data. The carbonyl absorption band at 1760 cm^{-1} is in agreement with those of γ,δ-unsaturated δ-valerolactones.[3]

The methine proton at δ 6.50 is considerably broad, probably due to the presence of syn and anti protons to the bridgehead methoxycarbonyl group.

The formation of **4** is attributed to hydrolysis of a 1,3-dipolar intermediate (**7**) by moisture in the solvent, because the reaction of **1** with **2** in the presence of water gave 56% of **4** and 65% of triethylphosphine oxide. The formation of **4** exemplifies *trans* addition of **1** to **2** in accordance with *trans* structure of **5**.

The formation of **4**, **5**, and **6** is explained as follows.

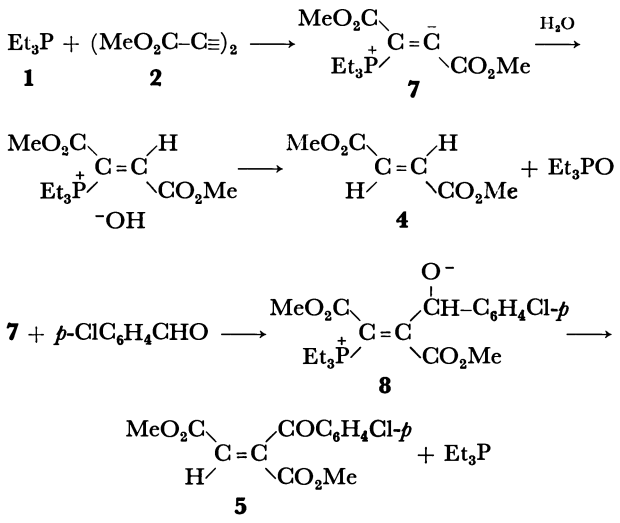

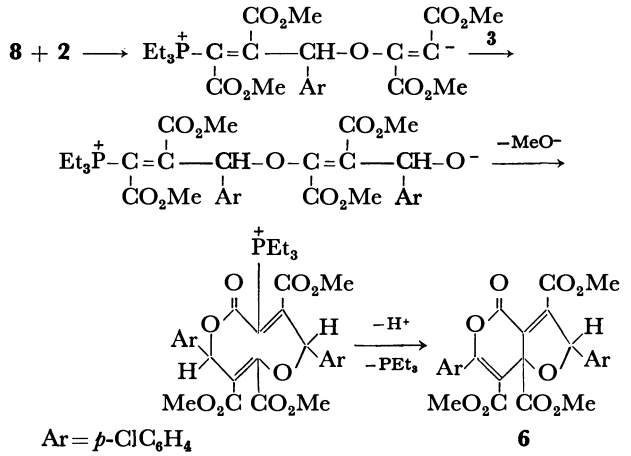

Although the yield of **6** is low, similar result was also obtained when the reaction was carried out at 0 °C. The present result indicates that the 1,3-dipole (**7**) can not afford phosphorus-containing heterocycles such as **9**, probably because of *trans* relation in the cationic and anionic centers of **7**.

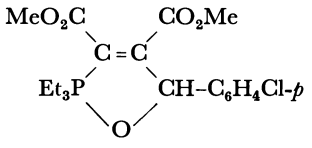

Experimental

Reaction of Triethylphosphine (1) with Dimethyl Acetylenedicarboxylate (2). a) In the presence of *p*-chlorobenzaldehyde (**3**): To a mixture of 2.33 g (19.7 mmol) of **1** and 13.3 g (95.1 mmol) of **3** in 20 ml of ether was added 5.23 g (36.8 mmol) of **2** in 40 ml of ether at room temperature over 6 h under nitrogen. Upon the addition of **2**, orange-red color developed in the solution. After evaporation of the solvent, the red tarry residue was chromatographed on silica gel. Elution with benzene recovered 0.372 g (7.1%) of **2** and 11.7 g (87.5%) of **3**. Fractions eluted with benzene–dichloromethane and dichloromethane–chloroform were rechromatographed on a silica gel dry column with dichloromethane to afford 1.35 g (13%) of **5**. Fractions eluted with dichloromethane–chloroform were rechromatographed on a silica gel dry column with dichloromethane to give 68 mg (1.3%) of **4**, mp 101.5—102.5 °C (lit,[4] 102.0 °C). Fractions eluted with chloroform were rechromatographed on a silica gel dry column with ether to give 0.239 g (1.2%) of **6**. Elution with methanol and distillation gave 1.52 g (58%) of triethylphosphine oxide. Red tar is polymerized **2**.

5: mp 79.5—80.5 °C (from ether); IR (KBr): 1730 (MeO-CO) and 1680 cm^{-1} (ArCO); NMR ($CDCl_3$): δ 3.65 (s, 3H, Me), 3.78 (s, 3H, Me), 7.08 (s, 1H, =CH–), 7.45, and 7.83

(A_2B_2, J_{HH}=8.4 Hz, 4H, C_6H_4); MS: *m/e* 282 (M^+, 3.7%) and 139 (ClC_6H_4CO, 100).

Found: C, 55.44; H, 3.73; Cl, 12.68%. Calcd for $C_{13}H_{11}O_5Cl$: C, 55.24; H, 3.92; Cl, 12.54%.

6: mp 203—205 °C (dec) (from acetone); IR (KBr): 1760 (sh) and 1740, 1660, and 1610 cm^{-1}; NMR ($CDCl_3$): δ 3.53 (s, 3H, Me), 3.87 (s, 3H, Me), 3.98 (s, 3H, Me), 6.50 (bs, 1H, CH), and 6.85—7.50 (m, 8H, $2C_6H_4$); MS: *m/e* 532 (M^+, 0.05 %) and 139 (ClC_6H_4CO, 100).

Found: C, 56.52; H, 3.10; Cl, 13.54%. Calcd for $C_{25}H_{18}O_9Cl_2$: C, 56.30; H, 3.40; Cl, 13.30%.

b) In the presence of water: To a mixture of 1.52 g (13.5 mmol) of **1** and 0.5 ml (27.8 mmol) of water in 30 ml of ether was added 2.11 g (27.8 mmol) of **2** in 20 ml of ether over 1.5 h at room temperature under nitrogen. Similar treatment afforded 1.17 g (56%) of **4** and 1.17 g (65%) of triethylphosphine oxide.

This work was supported by a Grant-in-Aid from the Ministry of Education.

References

1) L. Horner and H. Hoffmann, *Angew. Chem.*, **68**, 473 (1956); M. A. Shaw, J. C. Tebby, R. S. Ward, and D. H. Williams, *J. Chem. Soc. (C)*, **1967**, 2442; N, E. Waite, J. C. Tebby, R. S. Ward, and D. H. Williams, *ibid.*, **1969**, 1100; N. E. Waite, J. C. Tebby, R. S. Ward, M. A. Shaw, and D. H. Williams, *ibid.*, **1971**, 1620.

2) E. Winterfeldt and H. -J. Dillinger, *Chem. Ber.*, **99**, 1558 (1966).

3) F. Korte, K. H. Büchel, and K. Göhring, *Angew. Chem.*, **71**, 523 (1959).

4) S. Sugden and H. Whittaker, *J. Chem. Soc.*, **127**, 1873 (1925).

BULLETIN OF THE CHEMICAL SOCIETY OF JAPAN, VOL. 49 (7), 2025 (1976)

Origin of the Oxygen Atom in the Nitrosomesitylene Formed by the Oxidation of Mesidine with Fremy's Salt

Tomoji TAKAHASHI, Hiroshi MINATO, and Michio KOBAYASHI
Department of Chemistry, Tokyo Metropolitan University, Setagaya, Tokyo 158

(Received March 6, 1976)

Synopsis. The mechanism of the oxidation of aromatic amines with Fremy's salt was investigated by use of ^{18}O-labelled compounds. It was shown that the nitroso-oxygen atom originates not from water but from the nitroxide oxygen and sulfonate oxygen atoms of Fremy's salt.

Usually it is not possible to isolate nitroso compounds by the oxidation of aromatic amines, but such sterically hindered amines as mesitylenamine give nitroso compounds in good yields by the treatment with Fremy's salt.[1] However, the mechanism of this reaction has not been elucidated yet. We have investigated the mechanism of this reaction by use of ^{18}O-labelled Fremy's salt.

Fremy's salt[nitroxide-^{18}O] was prepared according to the following steps.

$$NaOH + H_2{}^{18}O \text{ (large excess)} \longrightarrow Na^{18}OH$$

$$2Na^{18}OH + NOCl \longrightarrow NaN^{18}OO + H_2{}^{18}O + NaCl$$

$$NaN^{18}OO + 2KHSO_3 \longrightarrow H^{18}O\text{-}N(SO_3K)_2 + NaOH$$

$$6H^{18}O\text{-}N(SO_3K)_2 + 2KMnO_4 \longrightarrow 3[{}^{18}O\text{-}N(SO_3K)_2]_2 + 2MnO_2 + 2KOH + 2H_2O$$

The excess ^{18}O atom% of Fremy's salt[nitroxide-^{18}O] prepared using $H_2{}^{18}O$ (excess ^{18}O, 1.3 atom%) was 0.104 ± 0.009%, and hence the excess ^{18}O atom% in the nitroxide oxygen must be 0.728 ± 0.06%, which roughly corresponds with the value calculated (0.65%) from the excess ^{18}O atom % of the heavy water used (1.3%). This shows that no oxygen exchange with solvents occurred during the above reactions.

The preparation of Fremy's salt[sulfonate-^{18}O] was attempted by the reaction between $NaNO_2$ and $KHS^{18}OO_2$ (obtained from $K^{18}OH$ and SO_2), but the salt prepared contained only 0.004 excess ^{18}O atom %. This suggests that rapid oxygen exchange with water took place. A separate experiment showed that sulfite ions readily exchange oxygen atoms with water under strongly alkaline conditions. Therefore, the above results can be rationalized by assuming that $KHS^{18}OO_2$ reacted with water faster than with $NaNO_2$.

The experimental results of the reaction between mesitylenamine and Fremy's salt may be summarized as follows:

1) When mesitylenamine was oxidized with unlabelled Fremy's salt in acetone–$H_2{}^{18}O$ (1.3 excess atom %), the nitrosomesitylene obtained possessed only 0.002 ± 0.001 excess ^{18}O atom %. Thus no ^{18}O-incorporation from $H_2{}^{18}O$ took place.

2) When mesitylenamine was oxidized with Fremy's salt[nitroxide-^{18}O] in acetone–H_2O, the nitrosomesidine obtained possessed 0.253 ± 0.03 excess ^{18}O atom %.

3) When mesitylenamine was oxidized with Fremy's salt[nitroxide-^{18}O] in dioxane–H_2O, the nitrosomesitylene obtained possessed 0.216 ± 0.005 excess ^{18}O atom %.

The above results clearly show that the oxygen atom of the nitrosomesitylene does not come from water but from Fremy's salt.

If the nitroxide oxygen atom of Fremy's salt directly becomes the nitroso oxygen of the nitrosomesitylene, the excess ^{18}O atom % of the nitrosomesitylene must be the same as that of the nitroxide oxygen of Fremy's salt (0.728 ± 0.06%). However, the value found was only about 1/3 of it. The possibility that the ^{18}O atoms of the nitrosomesitylene formed are lost by subsequent exchange with water can be rejected from our findings[2] that the oxygen atoms of aromatic nitroso compounds virtually do not exchange with water under neutral or strongly acidic conditions. Therefore, the oxygen atom of the nitrosomesitylene comes from both the nitroxide oxygen and the sulfonate oxygen atoms. A plausible mechanism is the following.

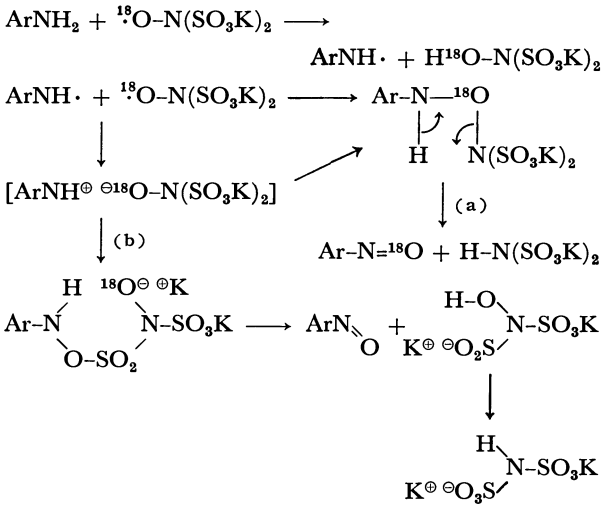

In the course (a) the nitroxide oxygen is converted directly into the nitroso group, whereas in the course (b) one of the sulfonate oxygen is converted to the nitroso oxygen. The excess ^{18}O atom % in the nitrosomesitylene found can be explained if course (a) and (b) take place in the ratio of 1 : 2.

References

1) H. -J. Teuber and G. Jellinek, *Chem. Ber.*, **85**, 95 (1952).
2) M. Aoyama, T. Takahashi, H. Minato, and M. Kobayashi, *Chem. Lett.*, **1976**, 245.

BULLETIN OF THE CHEMICBL SOCIETY OF JAPAN, VOL. 49 (7), 2026 (1976)

Synthesis of 2-Aminonaphthalene-1-thiol and Its Conversion into 8-Nitro-7*H*-benzo[*c*]phenothiazine

R. R. GUPTA* and S. K. JAIN

Department of Chemistry, University of Rajasthan, Jaipur, India

(Received **January** 5, 1976)

Synopsis. Synthesis of 2-Aminonaphthalene-1-thiol by hydrolytic cleavage of 2-aminonaphtho(2′,1′: 4, 5)thiazole and its conversion into 8-nitro-7*H*-benzo[*c*]phenothiazine *via* Smiles rearrangement *in situ* are reported.

Phenothiazines form an interesting series for Pharmaceutical and industrial uses[1,2] and physical studies.[3] A large number of phenothiazines have been synthesized, but there is no report on the synthesis of 7*H*-benzo-[*c*]phenothiazine and its substituted products. Phenothiazines are generally synthesized by condensation of *o*-aminobenzenethiols with *o*-halonitrobenzenes, but 2-aminonaphthalene-1-thiol has not been prepared so far and consequently 7*H*-benzo[*c*]phenothiazines have not been prepared. In the present investigation preparation of 2-aminonaphthalene-1-thiol and its conversion into 8-nitro-7*H*-benzo[*c*]phenothiazine are reported. The synthetic route is as follows:

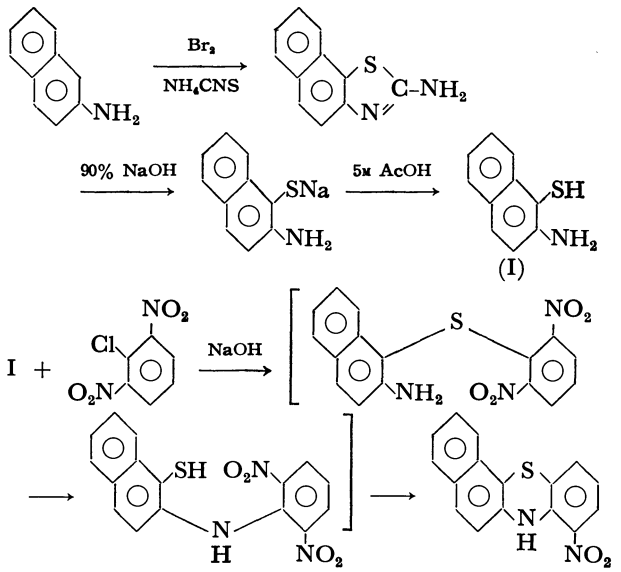

Schematic reaction.

Experimental

2-Aminonaphthalene-1-thiol was prepared by reacting *β*-naphthylamine (57.2 g, 0.4 mol) with Br_2 (80 ml) in 200 m of CH_3COOH and NH_4CNS (60.85 g) in 1 l of CH_3COOH and then refluxing 2-aminonaphtho(2′, 1′,: 4, 5)thiazole[4] thus formed with NaOH (550 g in 600 ml of H_2O) for 20 h. The reaction mixture was cooled, diluted with water (750 ml), filtered and neutralized with 5M-acetic acid. It was crystallized from ethanol as yellow crystals, mp 110 °C, yield 10 g (20%). Found: C, 68.50; H, 5.11; N, 7.97%, Calcd for $C_{10}H_9NS$: C, 68.57; H, 5.14; N, 8.00%. IR (KBr) 3330, 3510 (NH_2), and 2600 cm^{-1} (SH). 2-Aminonaphthalene-1-thiol (3.5 g, 0.02 mol) in 40 ml C_2H_5OH was converted into its sodium salt by refluxing with sodium hydroxide (0.8 g, 0.02 mol) in 10 ml H_2O and 20 ml of C_2H_5OH for five minutes. Sodium salt thus obtained was allowed to react with alcoholic solution of 2,6-dinitrochlorobenzene (4.0 g, 0.02 mol). The mixture was refluxed for 4 h and the product was crystallized from benzene–acetone mixture as violet crystals, mp 177 °C, yield 3.2 g (55%). IR (KBr) 3350 (NH), 1350, and 1500 cm^{-1} (NO_2). Found: C, 65.25; H, 3.38; N, 9.51%, Calcd for $C_{16}H_{10}N_2O_2S$: C, 65.30; H, 3.40; N, 9.52%.

The authors express their grateful thanks to Profs. R. C. Mehrotra and K. C. Joshi, for providing facilities in the department.

References

1) S. P. Massie, *Chem. Rev.*, **54**, (1954).

2) C. Bodea and I. Silberg, "Advances in Heterocyclic Chemistry," Vol. 9, ed. by A. R. Katritzky and A. J. Boulton, Academic Press, New York and London (1968), p. 321.

3) S. K. Jain, Ph. D. Thesis, Rajasthan University, Jaipur, India (1970).

4) R. Adams, *Org. React.*, **3**, 259 (1959).

BULLETIN OF THE CHEMICAL SOCIETY OF JAPAN, VOL. 49 (7), 2027—2028 (1976)

Synthesis of Succin-as-eins. III.[1] Dyes Derived from β-Benzoylpropionic, β-(3-Acenaphthoyl)propionic and β-(α-Thenoyl)propionic Acids

R. GOPAL,* P. C. GUPTA, and S. P. GARG**
Department of Chemistry, University of Allahabad, India

(Received October 14, 1975)

Synopsis. A number of succin-as-eins have been prepared by condensing β-benzoylpropionic, β-(3-acenaphthoyl)propionic and β-(α-thenoyl)propionic acids with phenol, resorcinol, catechol, quinol, phloroglucinol, pyrogallol and orcinol.

The γ-keto acids have been found to cyclize to their γ-hydroxylactones,[2] which yield acetyl derivatives[3-5] retaining their cyclic structures. The β-benzoylpropionic acid[6] (I: R=C_6H_5), β-(3-acenaphthoyl)propionic acid[7] (I: R=$C_{12}H_9$) and β-(α-thenoyl)propionic acid[8] (I: R=C_4H_3S) gave a new series of cyclic compounds succin-as-eins (IIIa—g)[1,9] on condensation with phenols such as phenol, resorcinol, catechol, quinol, phloroglucinol, pyrogallol and orcinol.

The IR (KBr) spectra of IIIa—g, IV and V show strong bands between 1760—1755 cm^{-1} (γ-lactone). The dye (IIIb: R=C_6H_5) (1760 cm^{-1}) on reduction with Zn-dust and acetic acid gave phenyl resorcinol succin-as-in (VI; IR (KBr) bands at 3600—3000 cm^{-1}, -OH in -COOH; 1700 cm^{-1}, >CO in -COOH) (*cf.*, methyl resorcinol succin-as-in[9]). The acid (VI) when left overnight was found changed into IIIb (R=C_6H_5).

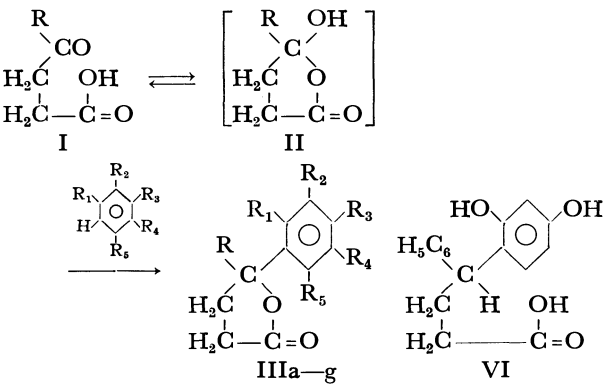

IIIa: $R_1=R_2=R_4=R_5=H$; $R_3=OH$
IIIb: $R_2=R_4=R_5=H$; $R_1=R_3=OH$
IIIc: $R_3=R_4=R_5=H$; $R_1=R_2=OH$
IIId: $R_2=R_3=R_5=H$; $R_1=R_4=OH$
IIIe: $R_2=R_4=H$; $R_1=R_3=R_5=OH$
IIIf: $R_4=R_5=H$; $R_1=R_2=R_3=OH$
IIIg: $R_2=R_4=H$; $R_5=CH_3$; $R_1=R_3=OH$
IV: $R_2=R_4=R_5=H$; $R_1=R_3=OCOCH_3$
V: $R_5=H$; $R_2=R_4=Br$; $R_1=R_3=OH$

Scheme 1.

TABLE 1. PREPARATION AND PROPERTIES OF PHENYL SUCCIN-AS-EINS (III: R=C_6H_5) AND ACENAPHTHYL SUCCIN-AS-EINS (R=$C_{12}H_9$)

Dyes	Condensation Temp (°C)	Condensation Time (h)	Mp (°C)	Appearance	λ_{max}^{EtOH} (mm); ε Neutral	λ_{max}^{EtOH} (mm); ε at (pH)	Found % C	Found % H	Calcd % C	Calcd % H
IIIa (R=C_6H_5)	150	5	280	Brown	—	412 (9.2); 4572	75.32	5.44	75.59	5.51
IIIb (R=C_6H_5)	170	6	>300	Shining red	460; 2943, 480; 2808	500 (9.1); 3294	70.86	5.04	71.11	5.18
IIIc (R=C_6H_5)	140	5	>300	Light brown	—	a)	70.90	5.20	71.11	5.18
IIId (R=C_6H_5)	140	5	206	Black	—	a)	71.14	4.92	71.11	5.18
IIIe (R=C_6H_5)	150	2	255	Dark red	—	475 (8.2); 2803	66.88	5.04	67.13	4.89
IIIf (R=C_6H_5)	140	4	300	Black	—	a)	66.92	5.16	67.13	4.89
IIIg (R=C_6H_5)	140	3½	185	Dirty yellow	—	495 (9.5); 2158	71.64	5.38	71.83	5.63
IIIa (R=$C_{12}H_9$)	150	3	>300	Brown	—	430 (9.8); 2719	79.64	5.18	80.00	5.45
IIIb (R=$C_{12}H_9$)	170	1/2	140	Deep red	530; 761	580 (9.5); 1041	75.90	5.60	76.30	5.20
IIIc (R=$C_{12}H_9$)	150	1	200	Light brown	—	a)	76.02	4.94	76.30	5.20
IIId (R=$C_{12}H_9$)	170	1	160	Dark yellow	—	a)	76.68	4.88	76.30	5.20
IIIe (R=$C_{12}H_9$)	180	1/4	170	Brown red	—	430, 450 (9.2); 4344	72.54	4.59	72.92	4.97
IIIf (R=$C_{12}H_9$)	180	1/4	>300	Dark brown	—	a)	73.30	4.61	72.92	4.97
IIIg (R=$C_{12}H_9$)	170	1/2	195	Dark red	—	a)	76.39	5.26	76.66	5.55
IV (R=C_6H_5)	140	5	128	Pale yellow	360; 6372	—	67.56	4.82	67.79	5.08
IV (R=$C_{12}H_9$)	140	3½	95	Pale yellow	370; 8600	—	72.88	4.84	72.56	5.11
V (R=C_6H_5)	130	2	>300	Red	530; 1849	530 (9.1); 2825	Br, 37.52%		Br, 37.35%	
V (R=$C_{12}H_9$)	30	5	125	Deep red	590; 2460	590 (9.0); 2460	Br, 31.50%		Br, 31.12%	

a) The alkaline solution decomposed during the measurement of λ_{max} values.

* Present address: Defence Laboratory, Jodhpur, India.

** Present address: Dept. of Chemistry, University of Jodhpur, Jodhpur, India.

Table 2. Preparation and properties of thenyl succin-as-eins (III; R = C_4H_3S)

Dyes	Condensation			Appearance	λ_{max}^{EtOH} (mm); ε		Found %			Calcd %		
	Temp (°C)	Time (h)	mp (°C)		Neutral	at (pH)	C	H	S	C	H	S
IIIa (R = C_4H_3S)	110	6	215	Brown	—	420 (9.0); 5200	64.29	4.32	12.01	64.61	4.60	12.30
IIIb (R = C_4H_3S)	120	3	210	Brown	475; 2153	500 (8.8); 3174	60.67	4.64	11.28	60.87	4.34	11.59
IIIc (R = C_4H_3S)	110	13	>300	Brown	—	a)	60.49	4.01	11.21	60.87	4.34	11.59
IIId (R = C_4H_3S)	140	6	>300	Brown	—	a)	61.13	4.62	11.23	60.87	4.34	11.59
IIIe (R = C_4H_3S)	120	1½	>300	Brown	—	480 (9.0); 2014	57.86	4.43	10.76	57.53	4.10	10.95
IIIf (R = C_4H_3S)	120	2	>300	Brown	—	a)	57.26	3.98	10.80	57.53	4.10	10.95
IIIg (R = C_4H_3S)	120	1	>300	Brown	—	500 (8.8); 3625	61.81	4.48	10.76	62.07	4.82	11.03
IV (R = C_4H_3S)	140	3	250	Light Brown	355; 5040	—	59.74	4.29	8.52	60.00	4.40	8.80
V (R = C_4H_3S)	30	120	>300	Orange Red	550; 868	550 (8.4); 868	Br, 36.48%			Br, 36.84%		

a) The alkaline solution decomposed during the measurement of λ_{max} values.

The absorption maxima (λ_{max}) of acenaphthyl succin-as-eins (IIIa—g, V: R = $C_{12}H_9$) have been found much higher than their analogous succineins and phthaleins but those of phenyl succin-as-eins (IIIa—g, V: R = C_6H_5) and thenyl succin-as-eins (IIIa—g, V: R = C_4H_3S) are comparable with their analogues.

Experimental

All melting points are uncorrected. The λ_{max} (UV and visible) have been recorded on Model DU-2 Beckmann Spectrophotometer and IR determined using a Perkin-Elmer Infracord Spectrometer.

The preparation and purification of the compounds (IIIa—g) taking respective acids (I) and phenols (yield, 40—45%), and diacetyl (IV), and dibromo (V) compounds were done in identical manner as described earlier.[1,9-11]

Zn-dust reduction of IIIb (R=C_6H_5). The dye (IIIb; R = C_6H_5) (1 g) was refluxed in glacial acetic acid (100 ml) with Zn-dust (5 g) for 15 min to yield a light yellow crystalline acid (VI; 0.9 g) mp 180 °C, which does not give fluorescence in alkaline solution. Found: C, 70.42; H, 5.64%. Calcd for $C_{16}H_{16}O_4$: C, 70.58; H, 5.88%.

The acid (VI) when left overnight changed to red compound IIIb (R = C_6H_5), superimposible IR and same λ_{max} values. The acetylation of the mixture of acid (VI) and red compound was carried out as in IV to give diacetyl (IV), mixed mp, identical IR, λ_{max} values and elemental analysis.

One of the authors (R.G.) thanks the C.S.I.R., New Delhi for a grant and fellowship and to Director, Defence Laboratory, Jodhpur for granting permission to publish the work.

References

1) R. Gopal and P. C. Gupta, *Bull. Chem. Soc. Jpn.*, **48**, 2227 (1975).
2) P. R. Jones, *Chem. Rev.*, **63**, 465 (1963).
3) S. Gabriel, *Ber.*, **14**, 919 (1881).
4) P. R. Jones and S. L. Congdon, *J. Am. Chem. Soc.*, **81**, 4291 (1959).
5) Biedermann, *Beilstein*, **24**, 4077. (Cyclic acetyl derivative of acid, I: R = C_6H_5).
6) L. F. Somerville and C. F. H. Allen, *Org. Synth.*, Coll. Vol. **2**, 81 (1943).
7) L. F. Fieser, *Org. Synth.*, Coll. Vol. **3**, 6 (1955).
8) L. F. Fieser and R. G. Kenelly, *J. Am. Chem. Soc.*, **57**, 1615 (1935).
9) R. Gopal, P. C. Gupta, and S. P. Garg, *Bull. Chem. Soc. Jpn.*, **47**, 1789 (1974).
10) R. Gopal, P. C. Gupta, and S. P. Garg, *J. Indian Chem. Soc.*, **50**, 410 (1973).
11) R. Gopal, P. C. Gupta, V. P. Aggarwala, and S. P. Garg, *Z. Naturforsch.*, **28b**, 468 (1973).

The Effect of Metal Oxides on the Transformation of Copper Phthalocyanine Crystals in Organic Solvents

Norimichi KAWASHIMA, Takao SUZUKI, and Kenjiro MEGURO

Department of Chemistry, Faculty of Science, Science University of Tokyo, Kagurazaka, Shinjuku-ku, Tokyo 162

(Received June 2, 1975)

The dimorphic transformation of copper phthalocyanine crystals was examined by means of X-ray diffraction analysis and electron-micrograph observation, for α-copper phthalocyayine and metal oxides of various mixing ratios with respect to weight were ground using a grinder and suspended in an organic solvent. The α-β transformation of copper phthalocyanine is accelerated by the presence of metal oxides such as alumina, magnesia, and zinc oxide. Particularly, alumina has a remarkable effect on the acceleration of β-copper phthalocyanine formation. The rate of transformation increases with the amount of metal oxide and the grinding time for a mixture of copper phthalocyanine and alumina. The activation energy for the α-β transformation in a (1 : 1) mixture of copper phthalocyanine and alumina ground for 30 min was calculated to be 12.0 kcal/mol.

The phthalocyanine pigments are some of the most important colored pigments owing to their excellent properties. They are remarkably resistant to alkalis and concentrated sulfuric acid and are stable under normal storing conditions. Since their tints have exellent durability in exterior finishes, they are used in paints, lacquers, enamels, and plastics. Their resistance to light, acids, and alkalis also makes them valuable pigments for printing on paper and textile goods.[1]

The polymorphic behavior of copper phthalocyanine was first found by German investigators.[2] Hamm and Norman[3] observed the dimorphic transformation of copper phthalocyanine by means of an electron microscope and electron diffraction. It is well known that the α-form crystal is transformed into the stable β-form either by treatment in various organic suspension media or by thermal treatment. The α-β transformation in organic suspensions is of greatest importance with respect to the decrease of tinting strength and the change of tone in the paint and ink industry. Many investigations have been reported on the transformation of copper phthalocyanine in organic suspensions from the viewpoints of practice and crystallography.[4–11]

Furthermore, in the paint industry, mixtures of several kinds of pigments are used to obtain various colors. Usually, mixtures of organic and inorganic pigments are used. In previous work, the grinding process of mixtures of copper phthalocyanine and inorganic pigments was examined.[12–14] There are no reports concerning the effect of inorganic pigments on the transformation of copper phthalocyanine in organic suspensions. In the work reported here, the effect of metal oxides on the transformation of copper phthalocyanine in organic solvents was investigated by means of X-ray diffraction analysis and electron microscopy.

Experimental

Materials. The α-form copper phthalocyanine (abbreviated α-CuPc) used here was supplied by the Dainippon Ink Chemical, Ltd. Metal oxides used were alumina, magnesia, and zinc oxide of a commercially available high purity (99.9%). The specific surface areas of the alumina, magnesia, and zinc oxide obtained using the BET method are about 170 m^2/g, 30 m^2/g, and 5 m^2/g, respectively. *p*-Xylene of commercial spectrograde quality was used as the organic solvent

Apparatus and Procedure. The mixtures of α-CuPc and metal oxides were ground using an Ishikawa-type grinder with an agate mortar in a closed chamber at room temperature at a (1 : 1) weight mixing ratio. Each mixture containing magnesia and zinc oxide was ground for 30 min after mixing. The mixture of α-CuPc and alumina was ground for 10, 30, and 60 min at weight mixing ratios of (2 : 1), (1 : 1), and (1 : 2). The mixtures were suspended in *p*-xylene to investigate the α-β transformation. The concentration of each suspension was always maintained within the range of 3 to 6 weight percent for *p*-xylene. About 30 cm^3 of the suspension was put in a glass tube with a glass stopper. The suspension was placed in a water bath at constant temperature to within ±0.05 °C. After the required interval of time had elapsed at a definite temperature, the suspension was rapidly cooled with cold water. After being quickly separated from the solvent, the precipitate was washed with a cold inert solvent such as methanol or acetone to remove any trace of the solvent. After being dried, these crystals did not tend to undergo further changes either in external appearance or in crystal structure. The immersion time was in the range of 10 min to 10 h depending on the treating temperature.

To determine the composition of each crystal form, X-ray diffraction analysis was employed using nickel-filtered copper radiation at 35 kV and 10 mA as the X-ray diffraction source, with a scanning speed of 1/2° per min, a time constant of 2 s, a divergence slit of 1° and a receiving slit of 0.2 mm. The X-ray diffraction diagrams were recorded by means of an X-ray diffractometer (Geigerflex). The observation of the powder surface was performed using a Hitachi HSM 2 electron microscope.

Results and Discussion

The X-ray diffraction patterns of original α-CuPc and β-CuPc are presented in Fig. 1. It is worth noting that a common characteristic of the X-ray diffraction patterns for the metastable and stable forms is that a pair of strong reflections appear at smaller angles, as indicated by the letters u and v for the α-form, and by s and t for the β-form crystals. These correspond to lattice spacing of 9 to 13 Å, which are closely related to the size and the stacking of the molecules in approximately 10 Å squares, as well as to the normal crystal arrangements of both forms.

The X-ray diffraction pattern of a (1 : 1) mixture of α-CuPc and β-CuPc is shown in Fig. 2(a). The

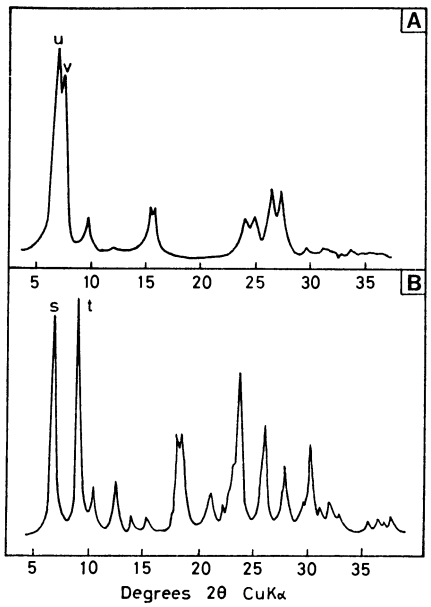

Fig. 1. X-Ray diffraction patterns of dimorphic forms of CuPc. (A): α-CuPc (Metastable form), u: 12.9 Å (200), v: 12.1 Å (002). (B): β-CuPc (Stable form), s: 12.6 Å (001), t: 9.8 Å ($20\bar{1}$).

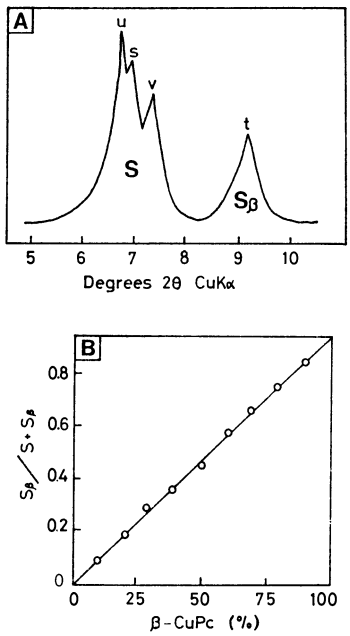

Fig. 2. (a): X-Ray diffraction pattern of a (1 : 1) mixture of α-CuPc and β-CuPc. (b): Calibration curve.

letter Sβ indicates the integral intensities of the reflection of β-CuPc, and S those of α-CuPc overlapping with β-CuPc. Sβ/S+Sβ is plotted against the composition of β-CuPc in mixtures of α-CuPc and β-CuPc of various mixing ratios in Fig. 2(b). The amount of β-CuPc in the samples can be determined from this calibration curve.

The α-β transformation of a mixture of α-CuPc and metal oxides was carried out in *p*-xylene at 50 °C. The reflections characteristic of α-CuPc are gradually

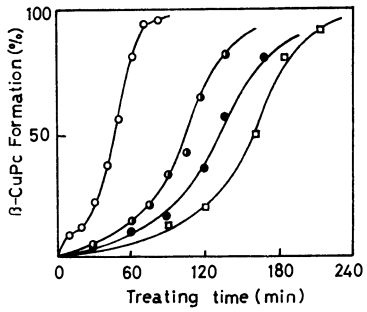

Fig. 3. The amount of β-CuPc formed in mixtures of α-CuPc and metal oxides *versus* the treating time in *p*-xylene at 50 °C.
(□): α-CuPc alone, (●): Mixture of α-CuPc and zinc oxide, (◑): α-CuPc and magnesia, (○): α-CuPc and alumina.

replaced by those of β-CuPc and the two sets of reflections are superimposed at the intermediate stages. By using the calibration curve, the amount of β-CuPc in the mixture of α-CuPc and metal oxide can be calculated. Figure 3 gives the relation between the amount of β-CuPc formed and the treating time. The effect of metal oxides on the transformation of α-CuPc increases in the order: alumina>magnesia>zinc oxide. The addition of alumina produced a remarkable effect on the rate of β-CuPc formation. This order is the same as the increasing order of the surface areas. Consequently, the rate of transformation is considered to depend on the specific surface areas of the oxides.

Our following discussion is mainly devoted to the effect of the addition of alumina on the transformation of α-CuPc.

Scanning electron micrographs of the original specimens and the mixtures of α-CuPc and alumina transformed in *p*-xylene at 40 °C are shown in Photo. 1. The horn-like crystals which formed on the surface of the alumina as shown in Photo. 1(D). It is obvious that almost all the α-CuPc crystals in Photo. 1(E) have transformed into flacky β-CuPc. The nuclei of the β-CuPc crystals formed in the solvent are considered to be adsorbed on the surface of the alumina, and then β-CuPc crystal growth is expected to proceed. The nuclei can be expected to increase with the amount of the addition and the grinding time.

The amount of β-CuPc formed in mixtures of α-CuPc and alumina of various mixing ratios is plotted against the treating time in Fig. 4. The amount of β-CuPc formed in mixtures of α-CuPc and alumina at each treating time increases with the amount of the addition.

This fact is explained by assuming that the adsorption of the nuclei on the surface of the alumina accelerates the β-CuPc crystal growth.

The amount of β-CuPc formed in the mixture ground for various periods is plotted against the treating time in *p*-xylene at 40 °C in Fig. 5. The amount of β-CuPc formed in the mixture increases with the grinding time. This fact indicates that the nuclei of β-CuPc crystals on the surface of the alumina can be formed more easily by mechanical treatment than by

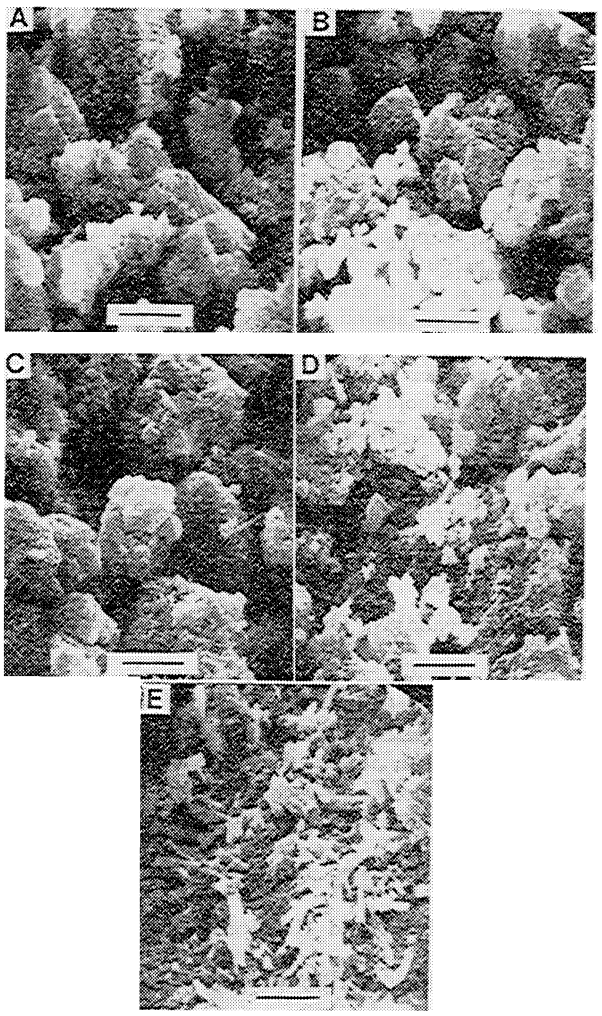

Photo. 1. Scanning electron micrographs of original specimens and the mixtures of α-CuPc and alumina undergoing transformation in *p*-xylene at 40 °C. The bars represent one micron.
(A): α-CuPc, (B): (1 : 1) mixture of α-CuPc and alumina ground for 30 min, (C); mixture treated for 60 min, (D): mixture treated for 75 min, (E): mixture treated for 90 min.

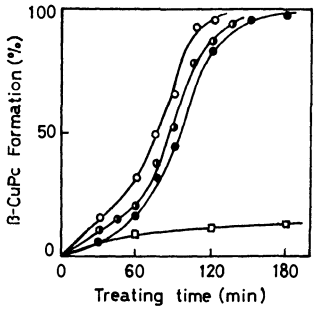

Fig. 4. The amount of β-CuPc formed in mixtures of α-CuPc and alumina ground for 30 min at various mixing ratios *versus* the treating time in *p*-xylene at 40 °C.
(□): α-CuPc alone, (●): (2 : 1) mixture, (◑): (1 : 1) mixture, (○): (1 : 2) mixture.

simple mixing. When the organic pigment is admixed with the inorganic one, the surface of inorganic pigment becomes covered with the former and grinding of the inorganic pigment is impeded by the lubricating action of the organic pigment.[12-14] Particularly, in the grinding of mixture of α-CuPc and inorganic powder, the transformation from α-CuPc to β-CuPc is considered to be accelerated by the absorption of the grinding energy.[14]

Figures 6 and 7 show the amounts of β-CuPc formed in α-CuPc alone and in a (1 : 1) mixture of α-CuPc and alumina, respectively, against the treating time

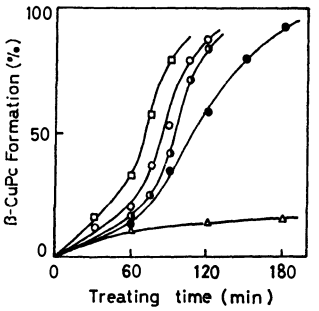

Fig. 5. The amount of β-CuPc formed in a (1 : 1) mixture of α-CuPc and alumina ground for various intervals *versus* the treating time in *p*-xylene at 40 °C.
(△): α-CuPc alone, (◑): Mixture ground for 10 min, (○): Mixture ground for 30 min, (□): Mixture ground for 60 min, (●): Simple mixing.

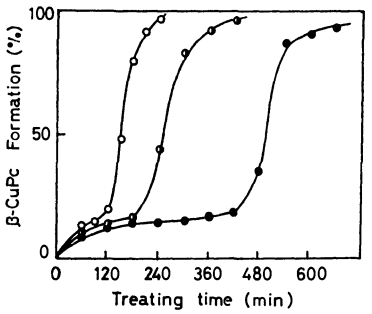

Fig. 6. The amount of β-CuPc formed in α-CuPc alone against the treating time in *p*-xylene at various temperatures.
(●): 30 °C, (◑): 40 °C, (○): 50 °C.

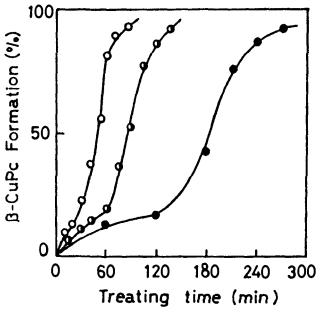

Fig. 7. The amount of β-CuPc formed in a (1 : 1) mixture of α-CuPc and alumina *versus* the treating time in *p*-xylene at various temperatures.
(●): 30 °C, (◑): 40 °C, (○): 50 °C.

in *p*-xylene at various temperatures. It appears difficult to explain the entire curve by a simple mechanism. In the earlier stages of the treatment, it is considered that crystals of meatstable form (α-CuPc) undergo preliminary growth without changing their crystal structure. The latter stages agree with first-order reaction kinetics.

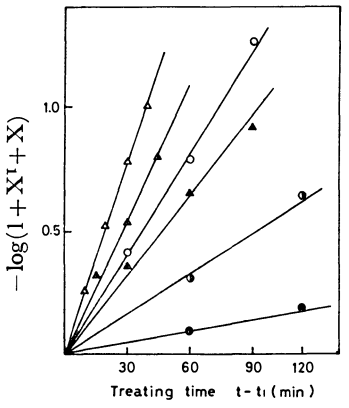

Fig. 8. The logarithm of the amount of β-CuPc formed in α-CuPc alone and the α-CuPc in the mixture *versus* the treating time in *p*-xylene at various temperatures.
(t_1): Induction time, (X_1): The amount of β-CuPc formed for a treating time t_1 in *p*-xylene.
(○): α-CuPc alone, (△): (1 : 1) mixture of α-CuPc and alumina.
(○): 50 °C X_1=0.286, t_1=150 min, (◑): 40 °C X_1=0.770, t_1=300 min, (●): 30 °C X_1=0.897, t_1=540 min, (△): 50 °C X_1=0.204, t_1=40 min, (◭): 40 °C X_1=0.323, t_1=90 min, (▲): 30 °C X_1=0.238, t_1=180 min.

Therefore, the logarithm of the amount of β-CuPc formed was plotted against the treating time, as is shown in Fig. 8. From the result, the activation energy for the transformation of α-CuPc alone and α-CuPc in a (1 : 1) mixture was calculated to be 17.6 kcal/mol and 12.0 kcal/mol, respectively. Other investigators[5,9] have found the activation energy for the transformation of α-CuPc alone in *p*-xylene to be 17.1 kcal/mol. This is in fairly good agreement with our results.

References

1) F. A. Moser and A. L. Thomas, "Phthalocyanine Compound," Reinhold Publishing Co., New York (1963), p. 2.
2) P. B. Report, 700336, p. 7945.
3) F. Hamm and E. van Norman, *J. Appl. Phys.*, **19**, 1097 (1948).
4) J. H. Beynon and A. R. Humphries, *Trans. Faraday Soc.*, **51**, 1065 (1955).
5) E. Suito and N. Uyeda, *Nippon Kagaku Zasshi*, **86**, 969 (1965).
6) E. Suito and N. Uyeda, *Proc. Jpn. Acad.*, **32**, 182 (1956).
7) N. Uyeda and E. Suito, *J. Electronmicroscopy*, **4**, 36 (1956).
8) E. Suito and N. Uyeda, *Kolloid Z.*, **193**, 97 (1963).
9) H. Takahashi, *Shikizai Kyokai Shi*, **36**, 550 (1961).
10) Y. Arai, *Senryo To Yakuhin*, **7**, 315 (1962).
11) S. Suzuki and Y. Bansho, *Kogyo Kagaku Zasshi*, **72**, 720 (1969).
12) N. Kawashima and K. Meguro, *Shikizai Kyokai Shi*, **46**, 670 (1973).
13) N. Kawashima and K. Meguro, *Shikizai Kyokai Shi*, **48**, 670 (1975).
14) N. Kawashima and K. Meguro, *Bull. Chem. Soc. Jpn.*, **48**, 1857 (1975).

Ion Cyclotron Resonance Study of Ion-molecule Reactions in Benzene: Mechanism of $C_3H_3^+$ Formation

Katsuyuki AOYAGI,[1a] Yoshinori HASUDA,[1b] Masahiro IRIE,[1c] Koichiro HAYASHI,[1c] and Junkichi SOHMA

Faculty of Engineering, Hokkaido University, Sapporo 060

(Received August 5, 1975)

Ion-molecule reactions in gaseous benzene, benzene-d_6, and their mixtures, particularly the formation process of $C_3H_3^+$, have been investigated using ion cyclotron single- and double-resonance techniques. Double-resonance experiments demonstrated that $C_3H_3^+$ is formed by the ion-molecule reaction: $C_6H_7^+ + C_6H_6 \rightarrow C_3H_3^+ +$ neutral product. In C_6H_6–C_6D_6 mixtures, not only $C_3H_3^+$ but also deuterium substituted ions, such as $C_3H_2D^+$ and $C_3HD_2^+$, are formed from $C_6H_7^+$. Quantitative analysis of the double-resonance intensity revealed that $C_3H_3^+$ is formed by the decomposition of the intermediate complex of $[C_6H_7^+–C_6D_6]$, which is a σ-type complex.

Ion-molecule reactions of aromatic hydrocarbons in the gas-phase have been studied using high-pressure mass spectrometry.[2–5] Ions generated from benzene by electron impact are mainly the molecular ion $C_6H_6^+$ and the characteristic fragment ions $C_3H_3^+$, $C_4H_2^+$, $C_4H_3^+$, $C_4H_4^+$, and $C_6H_5^+$.[2–5] It is well known that $C_3H_3^+$ is a stable ion appearing in the mass spectrum of benzene, as well as in a number of hydrocarbon compounds. 2-Propynyl[6] and cyclic[7] structures have previously been proposed as the structure of $C_3H_3^+$, however, at present, $C_3H_3^+$ is considered to be a cyclopropenyl cation.[8] The mechanism of $C_3H_3^+$ formation, however, has not yet been clarified. Ion-molecule reactions in gaseous benzene, especially the mechanism of $C_3H_3^+$ formation, were investigated using ion cyclotron single- and double-resonance (ICSR and ICDR) techniques.[9]

Results and Discussion

Reactions in Benzene. A single-resonance spectrum of benzene obtained at 2×10^{-5} Torr and electron energy of 70 eV is shown in Fig. 1. A number of fragment ions, as well as the molecular ion $C_6H_6^+$, are produced by electron impact on benzene. The spectrum is essentially the same as that obtained by an ordinary mass spectrometer at 1.1×10^{-5} Torr,[2] except for such

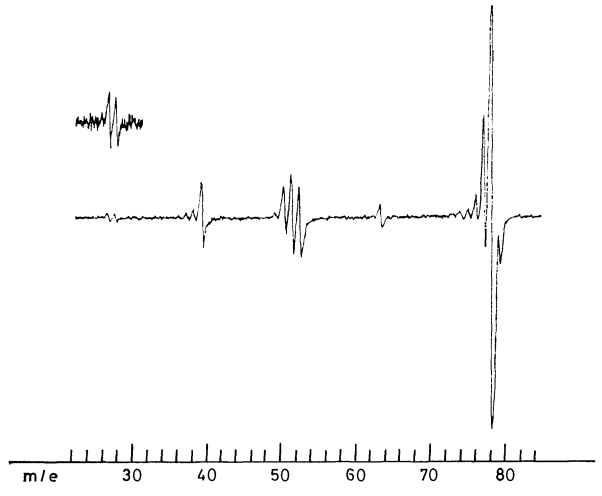

Fig. 1. Single-resonance spectrum of benzene at 2×10^{-5} Torr and 70 eV electron energy. Field modulation yields the derivative presentation.

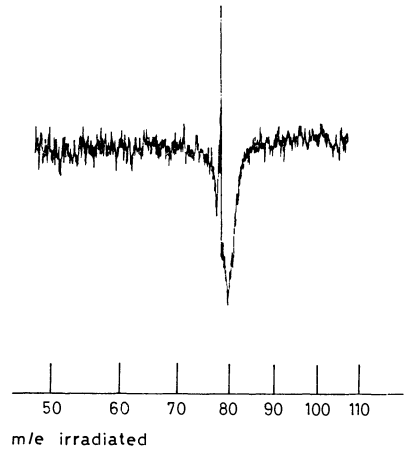

Fig. 2. Double-resonance spectrum of $C_3H_3^+$ in benzene. The sharp spike appearing the frequency (61.4 kHz) corresponding to *m/e* 78 is the first sub-harmonic of the observing frequency. This harmonic peak at double the observed ion mass serves as a convenient check on the mass assignment.

ions as $C_6H_7^+$, $C_7H_7^+$, $C_8H_7^+$, $C_9H_7^+$, $C_{10}H_7^+$, and $C_{11}H_9^+$. From among the many ions, the present double-resonance study concentrated on $C_3H_3^+$ which is one of the major product inos. Irradiation of $C_6H_7^+$ (*m/e* 79) caused on decrease in the intensity of $C_3H_3^+$ (*m/e* 39), as is shown in Fig. 2. This double-resonance indicates that $C_3H_3^+$ is not a primary ion produced by electron impact but is a product ion formed by the ion-molecule reaction:

$$C_6H_7^+ + C_6H_6 \rightarrow C_3H_3^+ + N, \quad (1)$$

where N denotes a neutral product. However, the ICDR peak of the precursor ion ($C_6H_6^+$) producing the reactant ion ($C_6H_7^+$) cannot be distinguished by the broadening of the $C_6H_7^+$ peak due to the strong irradiating field (the irradiating field is 4.8 times as strong as the observing field). The ICDR experiment indicates that if the velocity of the reactant ion R^+ is increased by means of irradiating field of resonance frequency at R^+, then a substantial change will occur in the concentration of product ion P^+, when the two ions are coupled chemically in the absence of irradiation. In reaction (1), a change of the $C_6H_7^+$ velocity reduces the abundance of $C_3H_3^+$, and therefore it is concluded that $C_6H_7^+$ should react with C_6H_6 to produce $C_3H_3^+$.

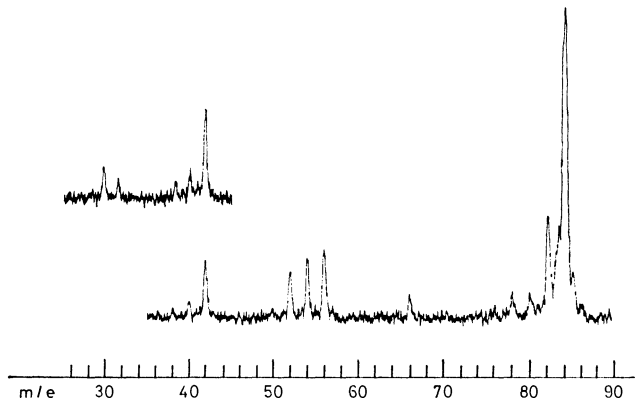

Fig. 3. Single-resonance spectrum of benzene-d_6 at 2×10^{-5} Torr and 70 eV electron energy. Energy modulation yields the absorption presentation.

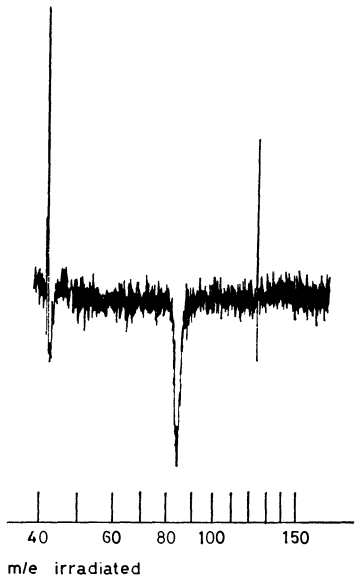

Fig. 4. Double-resonance spectrum of $C_3D_3^+$ in benzene-d_6. The large spike appearing at the frequency (122.8 kHz) corresponding to *m/e* 42 results from the interaction of the irradiating and observing oscillators, and the sharp feature at *m/e* 126 is due to the irradiaitng oscillator exciting the second subharmonic of the observing frequency.

A single-resonance spectrum of benzene-d_6 and a double-resonance spectrum of $C_3D_3^+$ (*m/e* 42) are shown in Figs. 3 and 4, respectively. These spectra are the same as those observed in benzene.

Reactions in Benzene and Benzene-d_6 *Mixtures.* Ionic reactions in a mixture of benzene and benzene-d_6 were investigated to clarify the reaction path for $C_3H_3^+$ formation in detail employing single- and double-resonance experiments. Figure 5 shows the single-resonance spectrum of a mixture of benzene and benzene-d_6 (ratio of 1 : 1). In addition to the spectra observed in benzene or benzene-d_6, the new product ions, $C_6HD_2^+$, $C_6H_5D_2^+$, $C_6H_3D_4^+$, and $C_6HD_6^+$, were observed. The single-resonance spectrum recorded with an increase in sensitivity around *m/e* 41 is shown in Fig. 6, for which the ions are identified as follows:

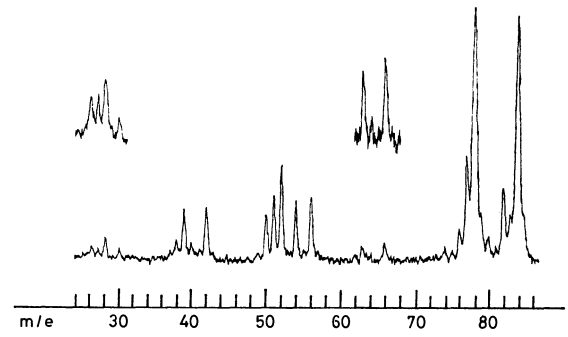

Fig. 5. Single-resonance spectrum of the 1 : 1 mixture of benzene and benzene-d_6 at 2×10^{-5} Torr and 70 eV electron energy.

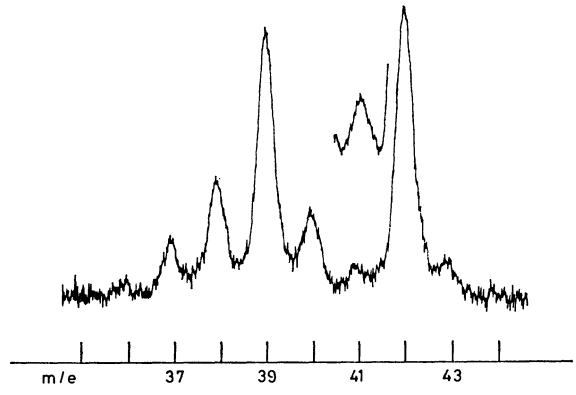

Fig. 6. Single-resonance spectrum recorded with the magnification of the 1 : 1 mixture of benzene and benzene-d_6 at 2×10^{-5} Torr and 70 eV electron energy.

$C_3H_3^+$ and C_3HD^+ at *m/e* 39, $C_3H_2D^+$ and $C_3D_2^+$ at *m/e* 40, $C_3HD_2^+$ at *m/e* 41 and $C_3D_3^+$ at *m/e* 42. The peak at *m/e* 41 is uniquely attributable to the ion which contain both hydrogen and deuterium. The formation of this ion suggests that $C_3H_3^+$ is formed not by the direct decomposition of $C_6H_7^+$ or C_6H_6, but by the decomposition of a mixture ion of the benzene and benzene-d_6 molecules.

Double-resonance experiments on a C_6H_6–C_6D_6 mixture (1 : 1 ratio) are shown in Figs. 7 and 8. The irradiation of $C_6H_7^+$ and $C_6D_7^+$ resulted in a decrease in the intensity of $C_3H_3^+$, as is shown in Fig. 7. This ICDR result predicts that the reactant ions which are coupled chemically with the product ion $C_3H_3^+$ are not only $C_6H_7^+$, but also $C_6D_7^+$. The contributions of $C_6H_6D^+$ and $C_6HD_6^+$ to the formation of $C_3H_3^+$ are scarcely observed. Similarly, the irradiation of $C_6H_7^+$ and $C_6D_7^+$ caused a decrease of the intensity of $C_3D_3^+$, as is shown in Fig. 8. The result indicates that the ions reacting with $C_3D_3^+$ are also $C_6H_7^+$ and $C_6D_7^+$. These ICDR results indicate that $C_3H_3^+$ and $C_3D_3^+$ are formed by the following processes:

$$C_6H_7^+ + \begin{Bmatrix} C_6D_6 \\ C_6H_6 \end{Bmatrix} \xrightarrow[[C_{12}H_{13}^+]]{[C_{12}H_7D_6^+]} C_3H_3^+ + N, \quad (2)$$

$$C_6D_7^+ + C_6H_6 \xrightarrow{[C_{12}H_6D_7^+]} C_3H_3^+ + N, \quad (3)$$

$$C_6D_7^+ + \begin{Bmatrix} C_6H_6 \\ C_6D_6 \end{Bmatrix} \xrightarrow[[C_{12}D_{13}^+]]{[C_{12}H_6D_7^+]} C_3D_3^+ + N, \quad (4)$$

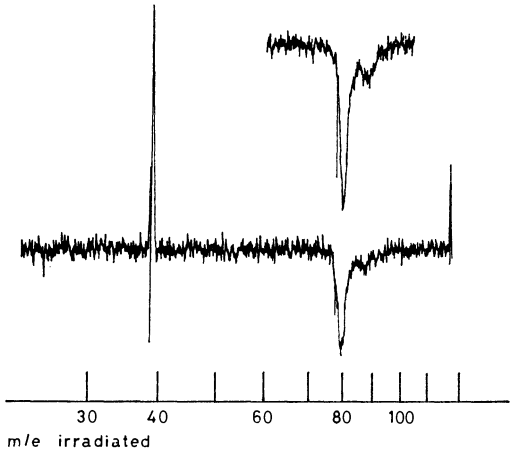

Fig. 7. Double-resonance spectrum of the species at *m/e* 39 in the 1 : 1 mixture of benzene and benzene-d_6. The large spike appearing at the frequency (122.8 kHz) corresponding to *m/e* 39 results from interaction of the irradiating and observing oscillators, and the sharp spikes at the frequencies (61 kHz and 41 kHz) corresponding to *m/e* 78 and *m/e* 117 are due to the irradiating oscillator exciting the first and second sub-harmonics of the observing frequency, respectively.

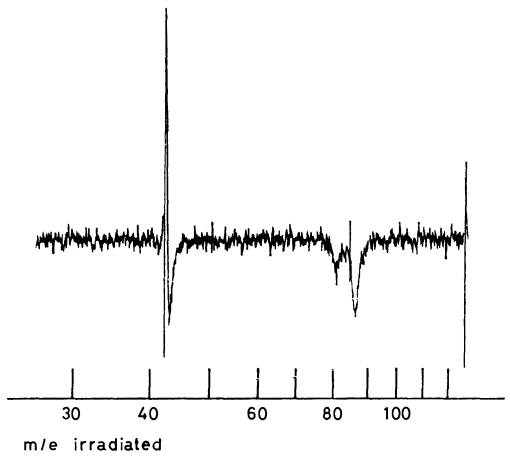

Fig. 8. Double-resonance spectrum of $C_3D_3^+$ in the 1 : 1 mixture of benzene and benzene-d_6. The large spike at *m/e* 42 results from interaction of the irradiating and observing oscillators, and the sharp spikes at *m/e* 84 and *m/e* 126 are due to the irradiating oscillator exciting the first and second overtones of the marginal oscillator, respectively.

$$C_6H_7^+ + C_6D_6 \xrightarrow{[C_{12}H_7D_6^+]} C_3D_3^+ + N. \quad (5)$$

In order to clarify the structure of the intermediate complex ion $[C_{12}H_{13}^+]$, the intensities of the ICDR peaks were quantitatively examined. The intensity ratio is considered to reflect quantitatively the degree of the contributions of the reactant ions. When the contribution of A ion to the formation of P ion is twice as high as that of B ion, the ICDR spectrum of P should be twice as high at resonance frequency of A than at that of B. Let us assume that the energy dependences of the rate constants for the reactions of $C_3H_3^+$ formation are almost equal, and let us also ignore the isotope effect of hydrogen and deuterium on the $C_3H_3^+$ formation reaction. The ratios of the intensities at the resonant frequencies of $C_6H_7^+$ and $C_6D_7^+$ were found to be $I_{79}/I_{86}=4/1$ and $I_{79}/I_{86}=1/2.7$ for the ICDR spectra of $C_3H_3^+$ and $C_3D_3^+$, respectively. These ratios are not in agreement with the simple ratio of the reactant ion and neutral molecules, which is usually expected for the addition reaction. This means that the ratio directly reflects the decomposition process.

As the intermediate complex for $C_3H_3^+$ formation, it is supposed that there are actually two intermediate complexes, a π-type complex and a σ-type complex:

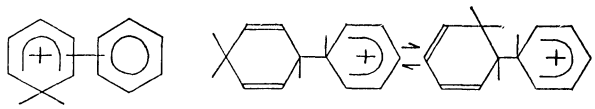

π-type complex σ-type complex

Here, it is defined that intramolecular exchange exists between H and D in the π-type compex, but does not exist in the σ-type complex. Figure 9 shows the I_{79}/I_{86} ratios of the observed value and the calculated value (see Appendix) in the case of $C_3H_3^+$. Here, I_{79} and I_{86} indicate the ICDR spectral intensities when $C_6H_7^+$ and $C_6D_7^+$ are irradiated, respectively. In the case of the σ-type complex, the I_{79}/I_{86} ratio of the calculated values is in good agreement with that of the observed values. In the case of the π-type complex, however, the calculated ratio does not agree with the observed ratio. This agreement between the observed and calculated ratios is evidence that $C_3H_3^+$ is formed by way of the σ-type complex in the ion-molecule reaction.

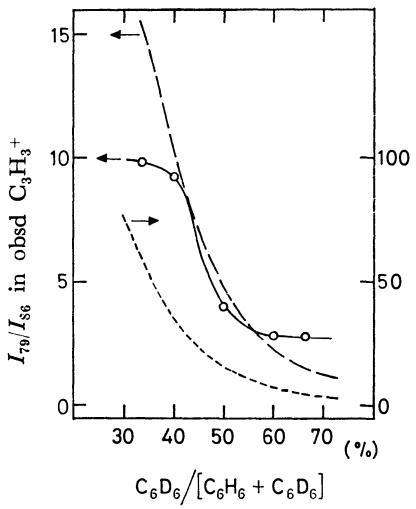

Fig. 9. Dependence of I_{79}/I_{86} on the ratio of the concentration of C_6D_6 to that of $C_6H_6 + C_6D_6$. Calculated (π-type complex), ----; calculated (σ-type complex), ——; observed, —○—.

On the other hand, the π-type complex is considered to dissociate into a protonated parent ion and a benzene molecule, and therefore, does not contribute to $C_3H_3^+$ formation.

In conclusion, the mechanism of $C_3H_3^+$ formation in gaseous benzene is explained by the following reaction path:

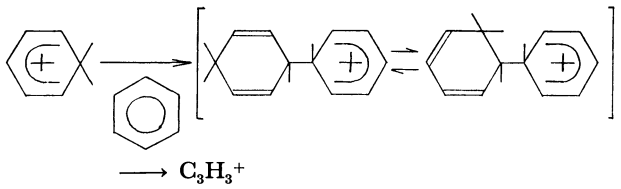

Experimental

The ICR spectra were obtained with a JEOL JIC-2M spectrometer, and the ICR cell was of a three-section square type similar to conventional ones.[9] Single-resonance spectra were obtained by fixing the frequency of the marginal oscillator and sweeping the magnetic field using field-modulation or energy-modulation phase-sensitive detection modes. Double-resonance experiments were performed by sweeping the frequency of the irradiating oscillator using a pulsed modulation mode for all reaction studies. The experimental conditions were as follows: energy of ionizing electrons 70 eV, trapping voltage 0.25 V, analyzer drift voltages −0.4 and 0.2 V, source drift voltages −2.5 and 0 V, observed of electric field and frequency 0.05 V/cm and 122.837 kHz and modulation frequency 80 Hz.

The analyzer chamber was baked at 150 °C for hours and evacuated below 2×10^{-7} Torr prior to performing the reported studies. Pressure was measured using an ionization vacuum gauge of the Bayard-Alpert type.

Benzene of special reagent grade (Wako Pure Chem. Ind., Ltd.) was purified by trap-to-trap distillation and the purity (>99.99%) was checked by gas-chromatography before use. Hexadeuterobenzene for spectroscopy (E. Merck, >99%D) was used without further purification. The samples were degassed under vacuum utilizing multiple freeze-pump-thaw cycles prior to introduction into the spectrometer.

Appendix

a) Formation of $C_6D_7^+$ in Benzene-d_6. For ICDR studies on benzene-d_6 and benzene, the following results were obtained. The irradiation of $C_6D_6^+$ at *m/e* 84 caused an increase in the intensity of $C_6D_7^+$. This ICDR result indicates that the $C_6D_7^+$ is formed by the ion-molecule reaction:

$$C_6D_6^+ + C_6D_6 \rightarrow C_6D_7^+ + N. \qquad (A1)$$

However, the ICDR peak of $C_6H_6^+$ corresponding to the reaction producing $C_6H_7^+$ was not confirmed due to the proximity of the observing $C_6H_7^+$ frequency to the irradiating $C_6H_6^+$ frequency. The reaction for $C_6H_7^+$ formation, however, could be considered to be the same as reaction (A1).

b) Calculation of the I_{79}/I_{86} Ratio of ICDR Spectral Intensities. $C_3H_3^+$ is formed by reactions (2) and (3). Then, the I_{79}/I_{86} ratio when $C_3H_3^+$ is observed is calculated to be

$$\frac{I_{79}}{I_{86}} = \frac{P(C_6H_7^+)\{C(C_6H_6)\times P[C_{12}H_{13}^+]+C(C_6D_6)\times P[C_{12}H_7D_6^+]\}}{P(C_6D_7^+)\times C(C_6H_6)\times P[C_{12}H_6D_7^+]}, \qquad (A2)$$

where

$$P(C_6H_7^+) = C(C_6H_6^+)\times C(C_6H_6)$$

with $P(C_6H_7^+)$ representing the probability that $C_6H_7^+$ is formed, $C(C_6H_6^+)$ the benzene ion concentration, $C(C_6H_6)$ the benzene concentration, $P[C_{12}H_{13}^+]$ the probability that $C_3H_3^+$ is formed from the complex $[C_{12}H_{13}^+]$ and the other symbols are defined in the same manner.

For example, in the case of a C_6H_6–C_6D_6 mixture in the ratio of 1 : 1, $C_6D_7^+$ is formed by reaction (A1). The concentration of C_6D_6 is 1/2, and that of $C_6D_7^+$ is also 1/2. Therefore, $P(C_6D_7^+)=1/4$. Similarly, $P(C_6H_7^+)=1/4$. Let us assume that $C_3H_3^+$ is formed by the random combination of three carbon and three hydrogen atoms in the π-type complex. The probability that $C_3H_3^+$ is formed from the complex $[C_{12}H_{13}^+]$ is

$$P[C_{12}H_{13}^+] = \frac{{}_{12}C_3\times{}_{13}C_3}{{}_{25}C_6} = \frac{286}{805}.$$

Similarly,

$$P[C_{12}H_7D_6^+] = \frac{{}_{12}C_3\times{}_{7}C_3}{{}_{25}C_6} = \frac{1}{23}$$

and

$$P[C_{12}H_6D_7^+] = \frac{{}_{12}C_3\times{}_{6}C_3}{{}_{25}C_6} = \frac{1}{161}.$$

By substituting the actual values into Eq. A2, we obtain

$$\frac{I_{79}}{I_{86}} = \frac{16.0}{1}.$$

In the case of a σ-type complex, let us assume that $C_3H_3^+$ is formed by a combination of the three adjoining carbon and the three adjoining hydrogen atoms in the σ-type complex. There are 16 combinations of the three adjoining carbon atoms. However, the number of combinations of the three adjoining hydrogen atoms differ for each complex. There are 19 combinations of the three adjoining hydrogen atoms in the complex $[C_{12}H_{13}^+]$, 9 such combinations in the complex $[C_{12}H_7D_6^+]$, and 6 such combinations in the complex $[C_{12}H_6D_7^+]$, respectively. Therefore, the probabilities that $C_3H_3^+$ is formed from each σ-type complex are equal to $P[C_{12}H_{13}^+]=19/16$, $P[C_{12}H_7D_6^+]=9/16$, and $P[C_{12}H_6D_7^+]=6/16$. By substituting the actual values into Eq. A2, we finally obtain $I_{79}/I_{86}=4.7/1$.

References

1) On leave of absence from the Division of Industrial Physical Chemistry, Faculty of Engineering, Hokkaido University, Sapporo 060. Present address: (a) JEOL Ltd., 1418 Nakagami, Akishima-shi, Tokyo 196; (b) Musashino Electrical Communication Laboratory, NTT, 3-9-11 Midoricho, Musashino-shi, Tokyo 180; (c) Institute of Scientific and Industrial Research, Osaka University, Suita-shi, Osaka 565.

2) F. H. Field, P. Hamlet, and W. F. Libby, *J. Am. Chem. Soc.*, **89**, 6035 (1967); *ibid.*, **91**, 2839 (1969).

3) S. Wexler and R. P. Clow, *J. Am. Chem. Soc.*, **90**, 3940 (1968).

4) A. Giardini-Guidoni and F. Zocchi, *Trans. Faraday Soc.*, **64**, 2342 (1968).

5) C. Lifshitz and B. G. Reuben, *J. Chem. Phys.*, **50**, 951 (1969).

6) J. Collin and F. P. Lossing, *J. Am. Chem. Soc.*, **79**, 5848 (1957).

7) J. L. Franklin and A. Mogenis, *J. Phys. Chem.*, **71**, 2820 (1967).

8) R. Breslow and J. T. Groves, *J. Am. Chem. Soc.*, **92**, 984 (1970).

9) (a) J. H. Futrell, "Dynamic Mass Spectrometry," Vol. 2, ed. by D. Price, Heyden & Son, New York (1971); (b) J. L. Beauchamp, *Ann. Rev. Phys. Chem.*, **22**, 527 (1971); (c) M. B. Comisarow and A. G. Marshall, *J. Chem. Phys.*, **62**, 293 (1975).

Triplet Excitation Energy Transfer in the Vinyl Polymers with Pendant Carbazolyl Groups

Akira ITAYA, Ken-ichi OKAMOTO, and Shigekazu KUSABAYASHI
Department of Chemical Engineering, Faculty of Engineering, Yamaguchi Universtity, Ube 755

(Received August 15, 1975)

The triplet energy transfer in poly(*N*-vinylcarbazole)(PVCz) prepared by radical and cationic polymerization (PVCz(r) and PVCz(c) respectively), poly[2-(*N*-carbazolyl)ethyl vinyl ether](PCzEVE), and brominated PVCz (BPVCz) has been investigated by measuring the delayed emission spectra in solid films and rigid solutions at 77 K. The prompt and delayed fluorescence spectra both in the solid film and in the rigid solution at 77 K were different for PVCz(r) and PVCz(c). This seems to be due to the difference in tacticity between them. PCzEVE, in which the Cz groups are connected from afar to the skeletal chains by means of $-O-CH_2-CH_2-$ bonds, showed the delayed fluorescence and the phosphorescence both in the rigid solutions and in the solid films at 77 K. The BPVCz film showed only the excimer phosphorescence. In the solid films of PVCz(r), PVCz(c), and PCzEVE, the Cz chromophore-delayed fluorescence increased with an increase in the concentration of triplet quenchers, such as naphthalene and fluorene. This phenomenon suggests the presence of a heterogeneous triplet-triplet annihilation in these aromatic vinyl polymer films. The quenching of the Cz chromophore phosphorescence both by the doping of the naphthalene in the solid films and by the doping of the 1,3-pentadiene in the rigid solutions obeyed the Stern-Volmer equation, and the migration coefficient, λ, and the mean exciton migration length, L, were obtained. The values of λ and L were in the following order; PVCz(r)>PVCz(c)>PCzEVE (>BPVCz) in the solid film and PVCz(r)>PVCz(c) in the rigid solutions. The order was explained by both the concentration of the intrinsic trap sites for triplet excitons and the distance between neighboring Cz chromophores in one polymer chain.

Recently, the emission spectra of aromatic vinyl polymers have been extensively investigated. The triplet energy transfer in a rigid solution at 77 K has been studied in detail on vinyl polymers with large aromatic rings, such as naphthyl and carbozolyl groups.[1-5] The investigations showed that the triplet excitons can migrate along the polymer chain, and that delayed fluorescence is caused by a homogeneous triplet-triplet (T-T) annihilation between two intramolecular migrating triplet excitons. Concerning the triplet energy transfer in the solid films, David *et al.* reported on vinyl polymers with small aromatic rings which emit only phosphorescence and no delayed fluorescence.[6,7] They showed that the triplet exciton migration frequencies in such polymer films were smaller than in the corresponding crystals. Concerning the vinyl polymer films with large aromatic rings, Fox *et al.* and Klöpffer *et al.* have qualitatively studied poly(1-vinylnaphthalene) and poly(*N*-vinylcarbazole) (PVCz) respectively.[5,8] Klöpffer *et al.* showed that the phosphorescence of PVCz films is governed by two kinds of traps, the concentration of which was estimated to be 5×10^{-3} (mol of trap/mol of basic unit) from the saturated concentration of the sensitized dopant phosphorescence, and that PVCz films emitted no delayed fluorescence. However, the triplet energy transfer in solid films has never hitherto been studied quantitatively on such vinyl polymers, to the knowledge of the authors.

Therefore, it seems that it would be interesting to investigate quantitatively the spectroscopic behavior of the triplet excitons in the vinyl polymers with large aromatic rings and to compare the difference between in rigid solutions and in solid films.

A preliminary short report has been published in *Chem. Lett.*[9] In the present work, the authors have investigated the changes in the delayed emission intensity of the vinyl polymers with pendant carbazolyl groups doped with various concentrations of a triplet quencher, such as naphthalene and 1,3-pentadiene, in rigid solutions as well as in solid films at 77 K.

Experimental

The following four vinyl polymers with pendant carbazole (Cz) chromophores were used.

The PVCz(r) was prepared by the polymerization of a 0.5 M benzene solution of purified *N*-vinylcarbazole (VCz) in the presence of 1 mol% azobisisobutyronitrile in an evacuated sealed tube at 70 °C for 7 h. The molecular weight ($\bar{M}_v$), as measured by the viscosimetrical method,[10] was 2×10^5.

The PVCz(c) was prepared by the polymerization of a 0.5 M toluene solution of purified VCz in the presence of 0.5 mol% BF_3–$(OC_2H_5)_2$ under a nitrogen atmosphere at 20 °C for 18.5 h. $\bar{M}_v=1\times10^5$. Both the PVCz(r) and the PVCz(c) were reprecipitated three times from the benzene solution with a methanol–acetone (1 : 1) mixture.

The poly[2-(*N*-carbazolyl)ethyl vinyl ether] (PCzEVE) has the Cz chromophores connected to the skeletal chain at a distance of about 4 Å by $-O-CH_2-CH_2-$ bonds. This was prepared by a method described previously.[11] $\bar{M}_n=$ 7800.

The brominated poly(*N*-vinylcarbazole)(BPVCz) was obtained by the bromination of PVCz(Luvican M170) with *N*-bromosuccinimide and was reprecipitated three times from the dichloroethane solution with acetone. The fraction of bromination was determined to be 0.9 from the elementary analysis.

Commercial naphthalene (NAPH) and fluorene of a scintillation grade were purified by zone-refining. Commercial 1,3-pentadiene (1,3-PD), a well-known triplet quencher, was used after repeated distillation. All the solvents used were purified by the usual methods. The solutions (donor concentration; 1×10^{-4} Cz unit M, solvent; 2 : 3 mixture of tetrahydrofuran and 2-methyltetrahydrofuran) for the measurements were deairated by means of freeze-pump-thaw cycles. Doped films were prepared by casting a dichloroethane solution of the polymer with a certain amount of the dopant onto quartz plates. The thicknesses of the films were about 7, 5, and 7 μm for PVCz, PCzEVE, and BPVCz respectively. The coated plates were immersed in liquid nitrogen for the measurement of the emission spectra.

The apparatus and techniques for measuring the delayed

emission spectra were described in a previous paper.[9] All the samples were excited by 345 nm light, which was not absorbed by the triplet quenchers. It was confirmed that the application of a phosphoroscope factor[12] was not necessary in the case of solid films. In the case of rigid solutions, the delayed fluorescence spectra were, however, corrected by using a phosphoroscope factor.

Results and Discussion

Delayed Emission Spectra in Rigid Solution and in Solid Film. The delayed emission spectra of PVCz(r), PVCz(c), and PCzEVE in rigid solutions and in solid films at 77 K are in Figs. 1 and 2 respectively. Concerning PVCz (r and c) in rigid solutions, Yokoyama *et al.*[4] and Klöpffer *et al.*[5] have reported as follows:

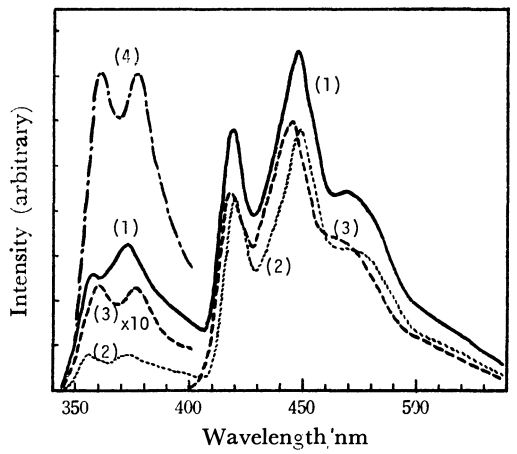

Fig. 1. Delayed emission spectra of (1) PVCz(r), (2) PVCz(c), and (3) PCzEVE in MTHF-THF rigid solutions at 77 K (uncorrected). The prompt fluorescence (4) of PCzEVE in MTHF-THF rigid solution at 77 K was also given for comparison.

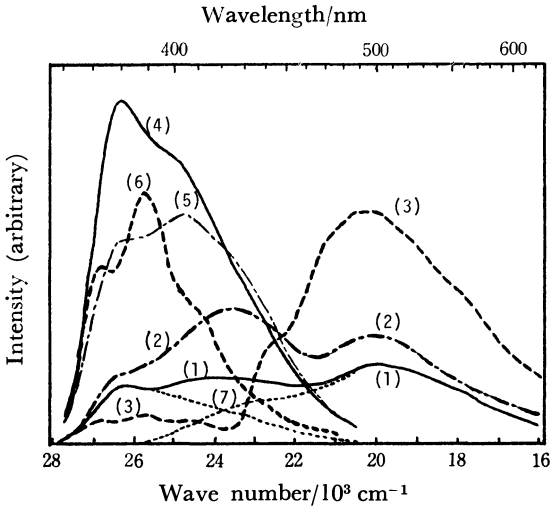

Fig. 2. Delayed emission spectra of (1) PVCz(r), (2) PVCz(c), and (3) PCzEVE films at 77 K. The prompt fluorescence spectra of (4) PVCz(r), (5) PVCz(c), and (6) PCzEVE films at 77 K were also given for comparison. The resolution spectra (7) of delayed emission spectum of PVCz(r) (1) were also given.

(1) The delayed emission spectrum consists of the delayed fluorescence and the phosphorescence; (2) the intensity and the lifetime of the delayed fluorescence are dependent on the molecular weight, and the delayed fluorescence is not observed for PVCz with a low molecular weight ($\overline{DP} \leqq 50$); (3) the phosphorescence is emitted from the trap site in the polymer chain because the phosphorescence (0-0 band; 420 nm) is located at a lower energy than that of the model compound (*N*-isopropylcarbazole) (0-0 band; 412 nm). However, they have not reported on the relationship of the spectra to the chemical preparation of the samples. In our present results, the delayed fluorescence spectra are a little defferent between PVCz(r) and PVCz(c), as is shown in Fig. 1, although the lifetimes (τ_{df}^{0}) are almost the same (11 ms for PVCz(r) and 12 ms for PVCz(c)). The phosphorescence spectra are almost the same between PVCz(r) and PVCz(c). The lifetime (τ_{ph}^{0}) is 1.8±0.2 s for PVCz(r and c).

In the case of solid films, Klöpffer *et al.*[5] showed that PVCz (r and c) films emitted only a phosphorescence governed by two traps (two component decay; 7.9±1 and 1.4 s), and no delayed fluorescence, and that two different types of spectra were observed in the phosphorescence and in the prompt fluorescence at 77 K, independent of the polymerization methods. In our present results, the delayed emission spectra of PVCz (r and c) consist of two emission bands, as is shown in Fig. 2. The prompt fluorescence spectra of the films and the example of the resolution spectrum (PVCz(r)) are also shown in Fig. 2. The further purification of the polymer (for example; reprecipitation up to ten times and/or extraction with hot methanol) gave no change in the spectra. The broad delayed emission in the longer wavelength region is invariably monophotonic in origin, and this lifetime consists of two components (7.9±0.7 and 1.6±0.5 s). Therefore, this emission is considered to be the phosphorescence emitted both from Trap I (excimer-forming site) and from Trap II, as has been described by Klöpffer *et al.*[5] On the other hand, both the position and profile of the delayed emission band in the shorter wavelength region are the same as those observed for the normal fluorescence at 77 K, as is shown in Fig. 2, and the emission intensity depends quadratically on the excitation light intensity. The lifetime of this emission is about 50 ms for PVCz (r and c). These facts indicate that this emission band can be assigned to the delayed fluorescence resulting from a homogeneous T-T annihilation between two migrating triplet exciton in films, as is the case with rigid solutions. The delayed fluorescence spectra also show two different types. One is rich in the excimer component and is observed for PVCz(c). The other is poor in the excimer component and is observed for PVCz(r). This was different from the results reported by Klöpffer *et al.*, but was confirmed using several samples prepared under different polymerization conditions. The difference between PVCz(r) and PVCz(c) is also observed for the prompt fluorescence in films at 77 K.[13] It has previously been reported that the tacticity of vinyl polymers with large aromatic rings was hardly sensitive at all to method of polymerization.[14] However,

recently we have found, by measuring their NMR spectra, that the PVCz, poly(*N*-vinyl-5*H*-benzo[*b*]-carbazole), and poly(*N*-vinyl-7*H*-benzo[*c*]carbazole) prepared by cationic polymerization have a higher isotacticity than those prepared by radical polymerization.[15] Frank *et al.* have found that the concentration of the excimer-forming site depends on the conformation of the polymer chain.[16] Judging from the above-mentioned discussion, the difference in the fluorescence spectra seems to be attributable to the different tacticity between PVCr(z) and PVCz(c).

The delayed emission spectra of PCzEVE in rigid solutions and in solid films at 77 K also consist of two bands, as is shown in Figs. 1 and 2. Both the position ($\bar{\nu}_{max}$; 360 or 376 nm in rigid solutions and 371, 388, or 409 (shoulder) nm in solid films) and the profile of the emission band in the shorter-wavelength region are nearly the same as is observed for the normal fluorescence ($\bar{\nu}_{max}$; 361 or 377 nm in rigid solutions and 370, 388.5, or 410 (shoulder) nm in solid films) at 77 K, and the emission intensity depends quadratically on the exciting-light intensity. Therefore, the emission bands of PCzEVE are identified as delayed fluorescence. It is interesting that PCzEVE in a rigid solution emits the delayed fluorescence, in spite of its short skeletal chain length ($\overline{DP}$=33). The τ_{df}^{0} of PCzEVE in a solid film is 45 ms, while that in a rigid solution could not be determined because of the low intensity. On the other hand, the delayed emission band at a longer wavelength ($\bar{\nu}_{max}$; 418, 446 nm in a rigid solution and about 495 nm in a solid film) is monophotonic in origin. Therefore, this emission band is identified as the phosphorescence emitted from the trap site, by analogy with PVCz(r and c). The τ_{ph}^{0} in a rigid solution is 6.6±0.1 s, while that in a solid film consists of two components (3.5±0.2 and 0.7±0.05 s), which is smaller than that of PVCz(r and c) by a factor of about two.

The BPVCz shows only one broad delayed emission band around 20730 cm^{-1}. This emission is invariably monophotonic in origin, and its position and profile are the same as the normal emission at 77 K. It shows a nonexponential decay with an apparent lifetime of 50 ms. The failure to observe a prompt fluorescence of BPVCz seems to be attributable to the high efficiency of the intersystem crossing from the excited singlet state to the triplet state due to the heavy atom effect of bromine. This delayed emission is considered, by analogy with poly(3,6-dibromo-*N*-vinylcarbazole) in a rigid solution at 77 K, to be the excimer phosphorescence.[18]

Triplet Energy Transfer in Solid Films and Rigid Solutions. The delayed emission spectra of PVCz(r), PCzEVE and BPVCz films doped with NAPH of various concentrations at 77 K are shown in Figs. 3—5. In Figs. 3 and 4, the prompt fluorescence spectra of the polymer films are also shown for the sake of comparison. In every polymer film studied, upon the doping of NAPH, the Cz chromophore-phosphorescence(I_{ph}) decreases significantly and is replaced by a sensitized NAPH phosphorescence(I_{sph}). Although the Cz phosphorescence lifetime(τ_{ph}) in PVCz(r and c) films could not be determined because of the overlapping of I_{ph} and

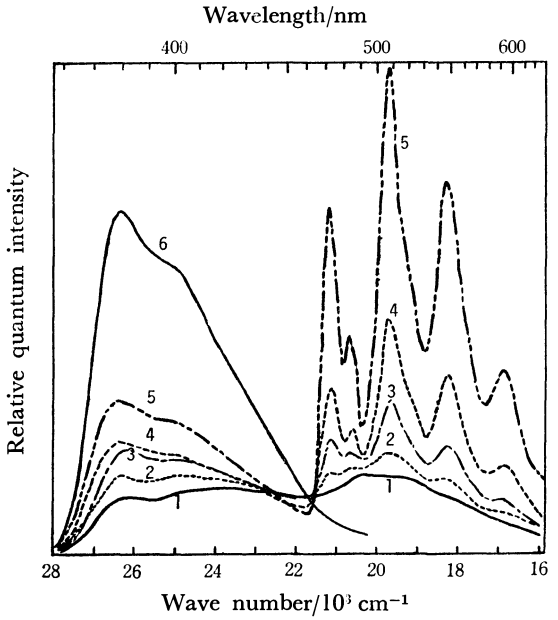

Fig. 3. Delayed emission spectra of PVCz(r) films doped with NAPH at 77 K. NAPH concentration; (1) 0, (2) 1.41×10^{-4}, (3) 7.04×10^{-4}, (4) 1.41×10^{-3}, and (5) 7.04×10^{-3} mol/VCz unit mol. The prompt fluorescence (6) of a PVCz(r) film was also given for comparison.

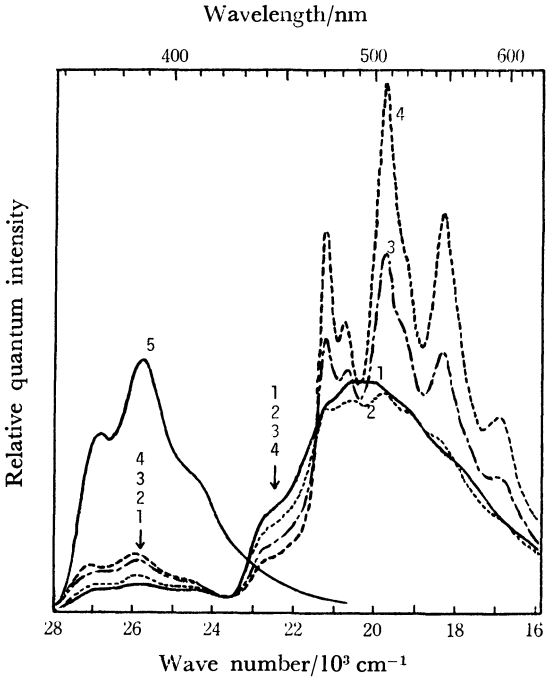

Fig. 4. Delayed emission spectra of PCzEVE films doped with NAPH at 77 K. NAPH concentration; (1) 0, (2) 2.62×10^{-4}, (3) 1.64×10^{-3}, and (4) 8.18×10^{-3} mol/CzEVE unit mol. The prompt fluorescence (5) of a PCzEVE film was also given for comparison.

I_{sph}, τ_{ph} in a PCzEVE film was found, by observing the decay curve at 444 nm, not to decrease upon the doping of NAPH. Therefore, in these films, the triplet energy seems to transfer from the freely migrating triplet exciton to the dopant, and I_{ph} seems to be emitted from the trapped triplet state.

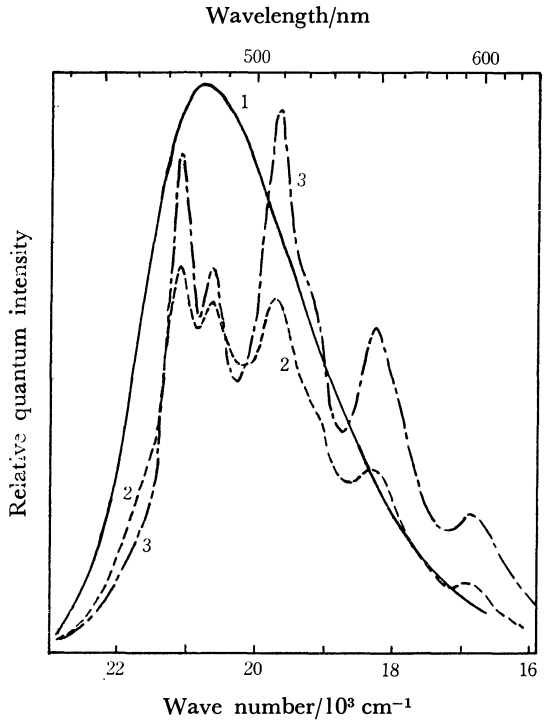

Fig. 5. Delayed emission spectra of BPVCz films doped with NAPH at 77 K. NAPH concentration; (1) 0, (2) 6.16×10^{-3}, and (3) 1.23×10^{-2} mol/BVCz unit mol.

The Cz chromophore-delayed fluorescence(I_{df}) increases with an increase in the concentration of NAPH. The changes in I_{df} and I_{sph} as a function of NAPH mole fraction in solid films are given in Fig. 6. In the case of the highest concentration of NAPH, the I_{ph} is quenched completely and I_{sph} reaches saturation, whereas I_{df} increases steeply and also second-order with respect to the exciting light intensity. The lifetime of the delayed fluorescence(τ_{df}) is gradually lengthened with an increase in the concentration of NAPH, as is shown in Fig. 7. Similar phenomena are observed for PVCz(c and r) and PCzEVE films doped with

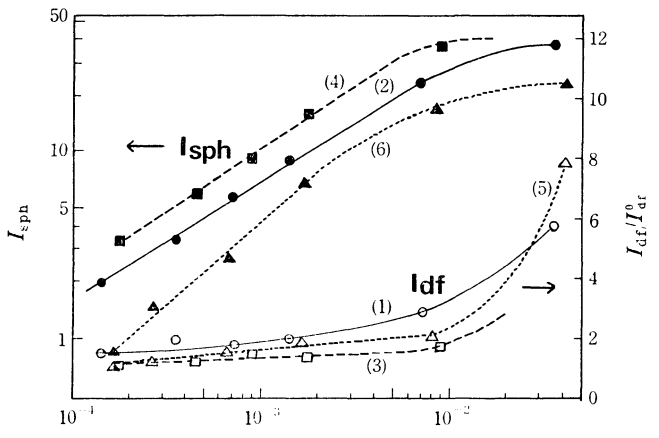

Fig. 6. Dependence of I_{df} and I_{sph} on concentration of NAPH in solid films at 77 K. (1), (2) ——; PVCz(r), (3), (4) ----; PVCz(c), and (5), (6) ……; PCzEVE.

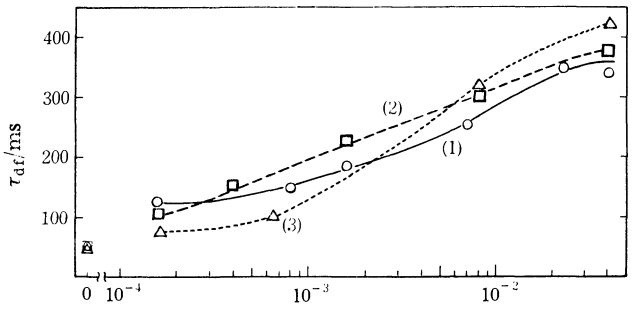

Fig. 7. Dependence of τ_{df} on concentration of NAPH in solid films at 77 K. (1) —○—; PVCz(r), (2) --□—; PVCz(c), and (3) ···△···; PCzEVE.

fluorene.

It is clear from the above-mentioned results that the dopants act as an effective triplet quencher for Cz chromophores in every film. The increase in I_{df} upon the doping of these triplet quenchers, therefore, strongly suggests that a heterogeneous T-T annihilation process occurs with a fairly good efficiency between freely migrating triplet excitons and either the triplet state of the dopant or a shallow trap site introduced by it.

In the case of PVCz(r and c) doped with NAPH in a rigid solution (Fig. 8), I_{ph} decreases and is replaced by I_{sph}, as is the case with solid films. On the other hand, the I_{df} shows an anomalous phenomenon, a little different from that in the solid films; it increases at low NAPH concentrations (up to 5×10^{-3} M) and decreases at higher concentrations. The change in the τ_{df} corresponds approximately to the change in the intensity; for example, the τ_{df} values of PVCz(r) are about 11, 12, 10, and 3 ms for 0, 8.40×10^{-4}, 2.10×10^{-3}, and 1.45×10^{-2} M respectively. In the case of PVCz(r and c) doped with NAPH, the heterogeneous T-T annihilation, therefore, seems to be present even in a rigid solution at 77 K.

In the case of PVCz(r and c) doped with 1,3-PD, a well-known triplet quencher in rigid solutions, both the I_{df} and the I_{ph} decrease significantly with an increase in the concentration of 1,3-PD, as is shown in Fig. 8, where I^0 and I are the Cz chromophore emission intensity in the absence and in the presence of the dopant respectively. The τ_{df} is decreased steeply ($\tau^0_{df}/\tau_{df}=4$—5 for 0.25×10^{-2} M). However, the τ_{ph} is hardly decreased by the doping of 1,3-PD ($\tau^0_{ph}/\tau_{ph}=1.0$—1.1 for 2.0×10^{-2} M). Therefore, it is considered that the triplet energy transfer mainly from freely migrating triplet excitons to the dopant, as is the case with solid films. The degree of quenching is much larger for the I_{df} than for the I_{ph}. This is the behavior usually observed for poly(1-vinylnaphthalene) (PVN) and poly(1-naphtyl methacrylate) (PNMA).[2,3] When 1,3-PD is used as the triplet quencher, the heterogeneous T-T annihilation is not present. No quenching experiment of PCzEVE has been done, because of its short chain length ($\overline{DP}=33$).

The I^0_{ph}/I_{ph} ratios are given in Fig. 9 as a function of the NAPH mole fraction in PVCz(r), PVCz(c), and PCzEVE films. Since the density of the vinyl polymers

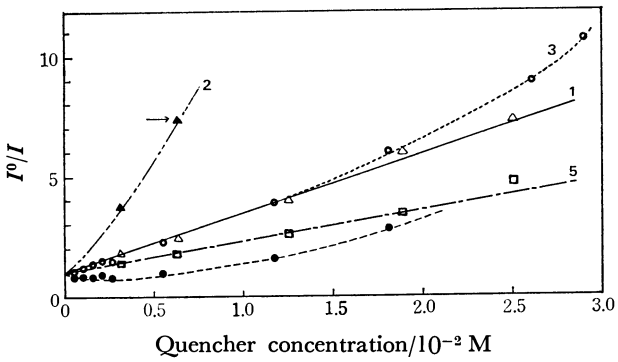

Fig. 8. Stern-Volmer plots (I^0_{ph}/I_{ph} and I^0_{df}/I_{df}) for the quenching of the delayed emission of PVCz(r) and PVCz(c) by NAPH and 1,3-PD in MTHF-THF rigid solution at 77 K.
(1) —△—; Phosphorescence in the PVCz(r)-1,3-PD system. (2) —▲——; Delayed fluorescence in the PVCz(r)-1,3-PD system. (3)···○···; Phosphorescence in the PVCz(r)-NAPH system. (4) —●—; Delayed fluorescence in the PVCz(r)-NAPH system. (5) —□-·-; Phosphoresceence in PVCz(c)-1,3-PD system. The point with arrow was corrected by the phosphoroscope factor which was estimated by assuming the lifetime to be 2 ms.

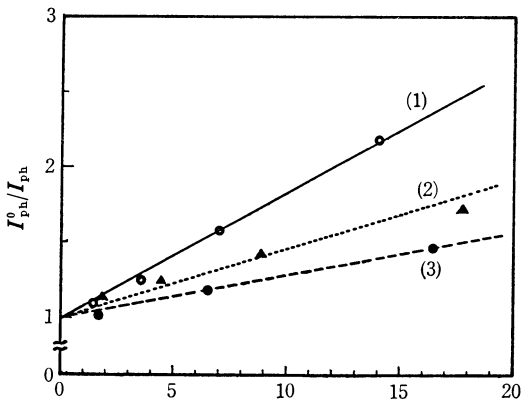

Fig. 9. Stern-Volmer type plots (I^0_{ph}/I_{ph}) for the quenching of the Cz chromophore phosphorescence of (1) PVCz(r), (2) PVCz(c), and (3) PCzEVE films by NAPH at 77 K.

was measured to be 1.19 g/cm^3, a conversion of the unit on the abscissa in Fig. 8 from mole fraction to molarity results in the Stern-Volmer polt;

$$I^0_{ph}/I_{ph} = 1 + k_t\tau[Q]$$

Here, k_t is the bimolecular quenching rate constant, τ is the excited state lifetime in the absence of a quencher, and [Q] is the quencher concentration of the molarity unit. In the case of PVCz(r and c) doped with 1,3-PD in a rigid solution, Stern-Volmer polts are also obtained, as is shown in Fig. 9. In the case of most aromatic vinyl polymers containing the present polymers, the phosphorescence is emitted not from the freely migrating triplet but from the trapped triplet state, so that the lifetime(τ_{ph}) is considered to be that of the trapped triplet state. Two times the τ_{df} value should, therefore, be used as the value of τ. The value of k_t were thus obtained from the slopes of the Stern-Volmer plots. The theory developed by Voltz *et al.*[19] was applied to the present results,

$$k_t = 4\pi N_0 \lambda R_0 \times 10^{-3}\ \mathrm{M^{-1}\,s^{-1}}$$

where N_0 is Avogadro's number, λ is the migration coefficient, and R_0 is the critical transfer distance between donor and acceptor, for which the transfer probability $p=1$ if $R \leq R_0$ and $p=0$ if $R>R_0$. The value of 15 Å is used as R_0.[20] The mean exciton migration length, L, is defined by;[21]

$L = \sqrt{2\lambda\tau}$ (for a one-dimensional random walk)

$L = \sqrt{6\lambda\tau}$ (for a three-dimensional random walk).

These values are listed in Table 1.

The values of λ and L are in the following order: PVCz(r)>PVCz(c)>PCzEVE in solid films and PVCz(r)>PVCz(c) in rigid solutions. If the distance between neighboring Cz rings is estimated to be 3.5 Å, the number of Cz rings which the triplet exciton can cause to migrate during the lifetime is estimated to be in the order of 400 from the values of λ listed in Table 1 both in solid films and in rigid solutions. Therefore, the difference in λ and L seems not to be attributable to the small difference in the degree of polymerization ($\overline{DP}$) between PVCz(r) ($\overline{DP}$=1000) and PVCz(c) ($\overline{DP}$=500).

It is well-known that the singlet exciton migration is limited by the intrinsic trap site (excimer-forming site).[22] Similarly, the triplet exciton migration seems to be limited by the intrinsic trap site, such as excimer-forming site in the polymers, because the observed phosphorescence was emitted only from the trap sites. Therefore, the difference in λ and L between PVCz(r) and PVCz(c) seems to be attributable to the difference in the concentration of the intrinsic trap site for the triplet exciton.

The value of λ in PCzEVE film is expected to be very small as compared with the case of PVCz(r and c), judging from the large distance between neighboring Cz chromophores. However, it is almost the same as the value for PVCz(c). The concentration of trap sites in PCzEVE film as smallest among the polymer films studied.[13] This is also supported by the facts that prompt fluorescence spectrum of PCzEVE film at 77 K (Fig. 2) is mainly monomeric in origin and that the phosphorescence shows a shoulder at about 440 nm. This is the reason for the relatively large λ value in PCzEVE film. This is also supported by the following consideration.

In using the published data on the triplet energy transfer in rigid solution at 77 K which have already been reported, where τ_{ph} was used as τ in the Stern-Volmer equation, we replace τ_{ph} by $2\tau_{df}$ as τ. Then, the migration coefficients λ of PVN[1] and PNMA[3] are estimated to be 3.3×10^{-13} and 4.6×10^{-13} cm^2/s respectively, although the molecular weights of these polymers are unknown. Judging from the structure of their polymer and their fluorescence spectra at room temperature, the concentration of intrinsic trap sites in PVN seems to be larger than that in PNMA. The comparable values in λ between PVN and PNMA seems to be explained by the overlap of two opposite

TABLE 1. SLOPES OF STERN-VOLMER PLOTS ($k_t\tau$), Cz PHOSPHORESCENCE AND DELAYED FLUORESCENCE LIFETIME (τ^0_{ph} and τ^0_{df}), BIMOLECULAR QUENCHING RATE CONSTANT (k_t), EXCITON MIGRATION COEFFICIENT (λ), AND MEAN EXCITON MIGRATION LENGTH (L) IN SOLID FILMS AND RIGID SOLUTIONS AT 77 K

Substance	$k_t\tau$/M^{-1}	τ^0_{ph}/s	τ^0_{df}/ms	k_t/M^{-1} s^{-1}	λ/cm^2 s^{-1}	L/Å[b]
PVCz(r)	134	7.9±0.7 1.6±0.5	50±3	1300	1.2×10^{-12}	85
PVCz(c)	74	7.9±0.7 1.6±0.5	50±5	740	6.5×10^{-13}	63
PCzEVE	57	3.5±0.2 0.7±0.05	45±5	630	5.6×10^{-13}	55
BPVCz	52	0.05[c]	—	—	—	—
PVCz(r)[a]	245	8.1±0.2	10±3	12000	1.1×10^{-11}	66
PVCz(c)[a]	128	8.1±0.2	11±2	5800	5.1×10^{-12}	47

a) In rigid solution. b) Three-dimensional random walk in solid film. c) Apparent lifetime.

effects—the concentration of the intrinsic trap site and the distance between neighboring naphthalene chromophores.

The $k_t\tau$ in BPVCz film is smallest among the polymers studied. This seems to be caused by the short triplet exciton lifetime resulting from the heavy atom effect of bromine.

In both PVCz(r) and PVCz(c), the lifetime of the triplet exciton in a solid film is larger than that in a rigid solution by a factor of about 5. On the contrary, the diffusion coefficient, λ, in a solid film is smaller than that in a rigid solution by a factor of 10. Although these phenomena are very interesting, a reasonable explanation cannot be offered at the present time. A further investigation of the other vinyl polymers is necessary and is now in progress.

References

1) R. F. Cozzens and R. B. Fox, *J. Chem. Phys.*, **50**, 1532 (1965).
2) C. David, M. Lempereur, and G. Geuskens, *Eur. Polym. J.*, **8**, 417 (1972).
3) A. C. Somersall and J. E. Guillet, *Macromolecules*, **6**, 218 (1973).
4) M. Yokoyama, T. Nakano, T. Tamamura, and H. Mikawa, *Chem. Lett.*, **1973**, 509; M. Yokoyama, T. Tamamura, T. Nakano, R. Ogawa, and H. Mikawa, Symposium on Molecular Structure, Nagoya, 8I21, October, 1973.
5) W. Klöpffer and D. Fischer, *J. Polym. Sci., Part-C*, **40**, 43, (1973).
6) C. David, W. Demarteau, and G. Geuskens, *Eur. Polym. J.*, **6**, 537 (1970).
7) C. David, W. Demarteau, and G. Geuskens, *Eur. Polym. J.*, **6**, 1405 (1970).
8) R. B. Fox, T. R. Price, R. F. Cozzens, and J. R. McDonald, *J. Chem. Phys.*, **57**, 2284 (1972).
9) A. Itaya, K. Okamoto, and S. Kusabayashi, *Chem. Lett.*, **1975**, 833.
10) N. Kuwahara, S. Higashida, M. Nakata, and M. Kaneko, *J. Polym. Sci., A-2*, **7**, 285 (1969).
11) K. Okamoto, M. Ozeki, A. Itaya, S. Kusabayashi, and H. Mikawa, *Bull. Chem. Soc. Jpn.*, **48**, 1362 (1975); K. Okamoto, A. Itaya, and S. Kusabayashi, *Polym. J.*, **7**, 662 (1975).
12) C. A. Parker and C. G. Hatchard, *Analyst*, **87**, 664 (1962).
13) A. Itaya, K. Okamoto, and S. Kusabayashi, 23rd Symposium on Macromolecules, Tokyo, G11E09, October, 1974. To be published elsewhere.
14) D. J. Williams, *Macromolecules*, **3**, 602 (1970); A. Kimura, S. Yoshimoto, Y. Akana, H. Hirata, S. Kusabayashi, H. Mikawa, and N. Kasai, *J. Polym. Sci., A-2*, **8**, 643 (1970).
15) K. Okamoto, M. Yamada, A. Itaya, T. Kimura, and S. Kusabayashi, *Macromolecules*, in press.
16) C. W. Frank and L. A. Harrah, *J. Chem. Phys.*, **61**, 1562 (1974).
17) S. Yoshimoto, Y. Akana, A. Kimura, H. Hirata, S. Kusabayashi, and H. Mikawa, *Chem. Commun.*, **1969**, 987.
18) M. Yokoyama, M. Funaki, and H. Mikawa, *J. Chem. Soc., Chem. Commun.*, **1974**, 372.
19) R. Voltz, A. Laustriat, and A. Coche, *J. Chim. Phys.*, **63**, 1253 (1966).
20) V. L. Ermolaev, *Soviet Phys. Ospekhi*, **80**, 333 (1963); R_0 value of Cz-1,3-PD system was not reported, so that the value was assumed to be the same as that of Cz-NAPH system.
21) J. B. Birks, "Photophysics of Aromatic Molecules," Wiley-Interscience, New York (1969), p. 532.
22) W. Klöpffer, *J. Chem. Phys.*, **50**, 2337 (1969); K. Okamoto, A. Yano, S. Kusabayashi, and H. Mikawa, *Bull. Chem. Soc. Jpn.*, **47**, 749 (1974).

Group Interactions in Polyelectrolytes. XII. Amination Kinetics of Chloromethylated Polystyrene in Binary Solvent Systems Composed of Dioxane and Dipolar Aprotic Solvents

Hiroshi KAWABE

The Institute of Physical and Chemical Research, Wako-shi, Saitama 351

(Received August 28, 1975)

The activation parameters ($\Delta G^{\ddagger}$, $\Delta H^{\ddagger}$, $\Delta S^{\ddagger}$) in the amination reaction of chloromethylated polystyrene (CMPS) and benzyl chloride with *s*-butylamine in *N,N*-dimethylformamide (DMF)–dioxanes mixtures and with 2-amino-1-butanol in dimethyl sulfoxide (DMSO)–dioxane mixtures were investigated as a function of x_1, the mole fraction of DMF or DMSO in the binary mixed solvents. A similar dependence of the parameters on x_1 was found in both systems, and the observed values of the parameters were in fair agreement with those calculated on the basis of Kondo and Tokura's theory concerning reaction rates in binary mixed solvents, assuming that the activated complex is solvated selectively with DMF or DMSO to form an addition product. The solvation in the DMSO–dioxane system was stronger than that in the DMF–dioxane system. Although $\Delta G^{\ddagger}$ decreases relatively uniformly with the increase in x_1, $\Delta H^{\ddagger}$ decreases sharply and reaches nearly a constant value at $x_1 \approx 0.2$. It was suggested that the increase of $T\Delta S^{\ddagger}$ in the range of $x_1 > 0.2$, which is approximately proportional to that of x_1, may be due to the relative increase in the configurational entropy change of the reaction system on transfer from dioxane to the dipolar aprotic solvents.

It has previously been reported that the amination rates of chloromethylated polystyrene (CMPS) and benzyl chloride with alkylamines and amino alcohols increase markedly on transfer of solvent from dioxane to such dipolar aprotic solvents as *N,N*-dimethylformamide (DMF) and dimethyl sulfoxide (DMSO).[1-3] This enhanced reactivity was ascribed to the solvation of the activated complex in the dipolar aprotic solvents. The dependence of the amination rate constants of CMPS and benzyl chloride with isobutylamine and *s*-butylamine on the composition of DMF–dioxane system was also investigated at a constant temperature;[4] the relation could be represented by curves calculated on the basis of Kondo and Tokura's theory concerning reaction rates in binary mixed solvents.[5]

In the present study, the amination with *s*-butylamine in the DMF–dioxane system has been surveyed at various temperatures in order to discuss the dependence of the activation parameters on the solvent composition. In the DMSO–dioxane system, since the polymer was precipitated in the initial stage of the amination with *s*-butylamine in pure DMSO, the amination kinetics has been investigated with 2-amino-1-butanol, the alkyl structure of which is the same as that of *s*-butylamine.

Experimental

Materials. The chloromethylated polystyrenes (CMPS-14, chlorine content: 20.30%, degree of chloromethylation: 0.829, mol wt: 1.17×10^5; CMPS-12, chlorine content: 21.83%, degree of chloromethylation: 0.914, mol wt: 1.04×10^5) were prepared and purified by the procedures described in previous papers.[6,7] The (*R*)-2-amino-1-butanol was also prepared as has been reported previously;[7] bp 92—93 °C/30 mmHg, n^{20} 1.457, $[\alpha]_D^{20}$ −9.96. The other chemicals and solvents were of a reagent grade and were distilled before use; they were proved to be pure by their refractive indices.

Kinetic Measurements. The procedures of the kinetic measurements in the amination of CMPS and benzyl chloride were the same as those described in previous papers.[1,6,7] The temperature of the reaction mixture was kept constant within ±0.1°. In the amination with *s*-butylamine in the DMF–dioxane system, the initial concentration of the amine (*a*) was about 0.400 M and that of the chloromethyl group (*b*) was about 0.040 M ($a/b=10$). The polymer used was CMPS-14. In the amination with 2-amino-1-butanol in the DMSO–dioxane system, *a* was about 0.21—0.22 M and *b* was about 0.044 M ($a/b=4.8$—5.0). The polymer used was CMPS-12.

Results and Discussion

Amination with s-Butylamine in DMF–Dioxane Systems. Chloromethylated polystyrene (CMPS) and benzyl chloride were aminated with *s*-butylamine in DMF–dioxane mixtures at 45, 60, and 75 °C. The rate constants in the mixed solvents, k_M, were computed on the basis of the second-order equation, as has been described previously.[4] The values of the activation energy, E_a, and the frequency factor, A, are listed in Table 1.

The plots of log k_M against x_1 are shown in Figs. 1 and 2, where the circles represent the observed values, while the solid and broken lines represent the

Table 1. Activation energy and frequency factor in the amination of CMPS and benzyl chloride with *s*-butylamine in DMF–dioxane mixture

x_1	Chloride	E_a, kcal/mol	log A[a]
0.1	CMPS	12.5±0.2	5.94±0.14
	Benzyl	12.5±0.7	5.73±0.32
0.20	CMPS	12.3±0.3	5.94±0.01
	Benzyl	12.4±0.0$_2$	5.99±0.02
0.35	CMPS	12.2±0.3	6.12±0.18
	Benzyl	12.3±0.3	6.28±0.28
0.50	CMPS	12.2±0.4	6.28±0.24
	Benzyl	12.2±0.4	6.40±0.24
0.60	CMPS	12.2±0.3	6.42±0.18
	Benzyl	12.3±0.2	6.61±0.13
0.80	CMPS	12.1±0.1	6.51±0.09
	Benzyl	12.2±0.4	6.68±0.25

a) A is expressed by l/mol min.

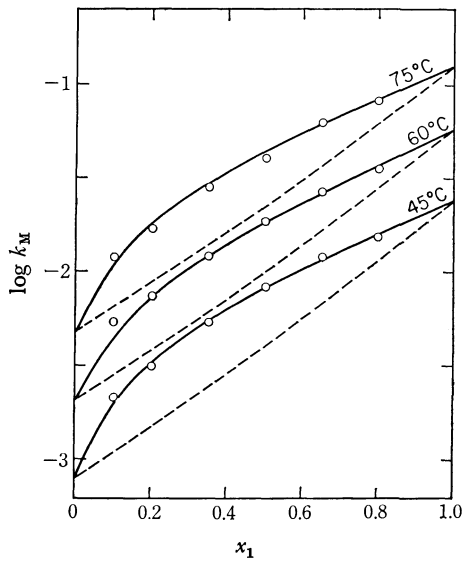

Fig. 1. Plot of log k_M *vs.* mole fraction of DMF, x_1, for the amination of CMPS with *s*-butylamine in DMF-dioxane mixture.
——: Calculated on the basis of Eq. 1.
----: Calculated on the basis of Eq. 2.

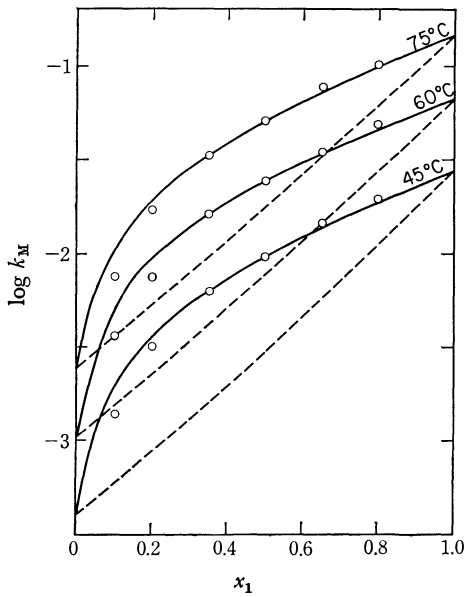

Fig. 2. Plot of log k_M *vs.* mole fraction of DMF, x_1, for the amination of benzyl chloride with *s*-butylamine in DMF-dioxane mixture.
——: Calculated on the basis of Eq. 1.
----: Calculated on the basis of Eq. 2.

values computed on the basis of Eq. 1 and of Eq. 2 respectively:

$$\log k_M = x_1 \log k_1 + x_4 \log k_4 - [x_1 \log (K+1) - \log (x_1K+1) + x_1x_4\,\alpha_{14}/2.303] \quad (1)$$

$$\log k_M = x_1 \log k_1 + x_4 \log k_4 - x_1x_4\,\alpha_{14}/2.303 \quad (2)$$

where x_1 and x_4 ($=1-x_1$) are the mole fractions of DMF and dioxane respectively in a DMF-dioxane system, where k_1 and k_4 are the rate constants in pure DMF and dioxane respectively, where K is the equilibrium constant of the specific interaction between the activated complex and DMF, expressed by the mole fractions of the species, and where α_{14} is an empirical coefficient which is related to the interaction between DMF and dioxane. The α_{14} may be evaluated by means of this relation:[4,8]

$$\Delta G_M^E/RT = x_1x_4\,\alpha_{14} \quad (3)$$

where ΔG_M^E represent the molar excess free energy of mixing in the binary system. The values of α_{14} and K were determined, by the procedures previously described,[4] to be:

α_{14}(at $x_1=0.5$) = 0.408(45 °C), 0.390(60 °C), 0.374(75 °C)

K(for CMPS) = 14.5(45 °C), 11.1(60 °C), 12.4(75 °C)

K(for benzyl chloride) = 37.6(45 °C), 38.1(60 °C), 31.4(75 °C)

The fact that the observed values shown in Figs. 1 and 2 are well expressed by Eq. 1 suggests that the activated complex is solvated selectively with DMF to form an addition product, as has been discussed previously.[4]

By differentiating Eq. 1, Kondo and Tokura gave the following expression for the activation energy in the binary system, ΔE_M^*:[5]

$$\Delta E_M^* = x_1\Delta E_1^* + x_4\Delta E_4^* + \frac{x_1x_4(\Delta E_1^* - \Delta E_4^*)}{x_1 + (1/K)} \quad (4)$$

where ΔE_1^* and ΔE_4^* represent the activation energies in the respective pure solvents.

The ΔE_M^* in the DMF-dioxane reaction system was computed on the basis of Eq. 4; the numerical values of E_a and log A in the pure solvents were given in

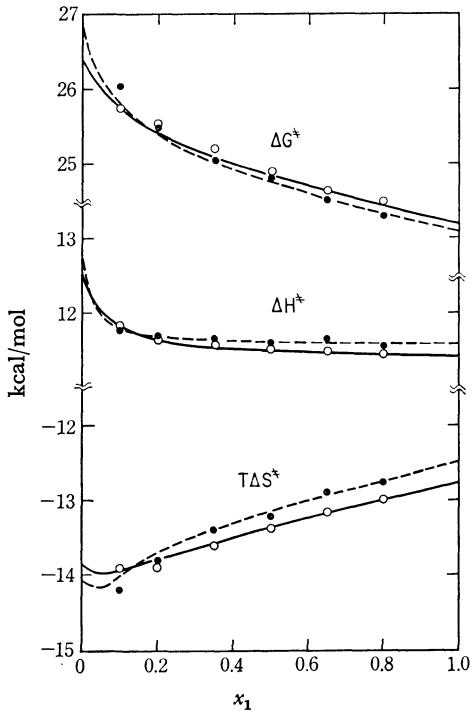

Fig. 3. Plot of the activation parameters *vs.* mole fraction of DMF, x_1, for the amination of CMPS (○) and benzyl chloride (●) with *s*-butylamine in DMF-dioxane mixture at 60 °C.
——: Calculated for CMPS.
----: Calculated for benzyl chloride.

Refs. 2 and 4. The activation parameters ($\Delta G^{\ddagger}_{M}$, $\Delta H^{\ddagger}_{M}$, and $\Delta S^{\ddagger}_{M}$) were calculated for 60 °C from the $\Delta E^{\ddagger}_{M}$ and log k_M values and plotted against x_1 in Fig. 3. The observed values of the activation parameters were obtained from the E_a and log A values listed in Table 1. The observed values expressed by the circles in Fig. 3 fall substantially on the calculated curves.

Amination with 2-Amino-1-butanol in the DMSO–Dioxane System. Although the amination of CMPS with *s*-butylamine in DMSO was heterogeneous because of the deposition of the polymer, the amination with 2-amino-1-butanol was throughly homogeneous in the overall range of the DMSO–dioxane system. Since the activated complex is also considered to be solvated with DMSO, the dependence of log k_M and $\Delta E^{\ddagger}_{M}$ on x_1, the mole fraction of DMSO, is expected to be similar to that in the DMF–dioxane system.

The amination of CMPS with 2-amino-1-butanol in pure dioxane was self-accelerated because of the neighboring group interaction;[7] however, this self-acceleration diminished upon the addition of a small amount of DMSO; the amination of CMPS in the DMSO–dioxane system conformed to the second-order equation in the range of x_1=0.16—1.0. Table 2 shows the values of E_a and log A computed by the least squares method from the observed k_M values at various temperatures.

The plots of log k_M at 60 °C against x_1 are shown in Fig. 4. The α_{14} value used for the calculation was evaluated in accordance with Eq. 3 by using the data on the DMSO–dioxane system given by Quitzsch *et al*:[9]

$$\alpha_{14}(\text{at } x_1=0.5) = 0.626(40\,^{\circ}\text{C})$$

Table 2. Activation energy and frequency factor in the amination of CMPS and benzyl chloride with 2-amino-1-butanol in DMSO-dioxane mixture

x_1	Chloride	E_a, kcal/mol	log A[a]
0.16	CMPS	13.2±0.4	6.70±0.25
	Benzyl	12.7±0.1	6.34±0.09
0.32	CMPS	12.8±0.2	6.74±0.14
	Benzyl	12.3±0.3	6.49±0.21
0.50	CMPS	12.7±0.3	6.92±0.05
	Benzyl	12.8±0.4	7.16±0.25
0.66	CMPS	12.5±0.3	7.00±0.27
	Benzyl	12.5±0.6	7.15±0.41
0.82	CMPS	12.7±0.2	7.24±0.10
	Benzyl	12.4±0.1	7.32±0.09

a) A is expressed by l/mol min.

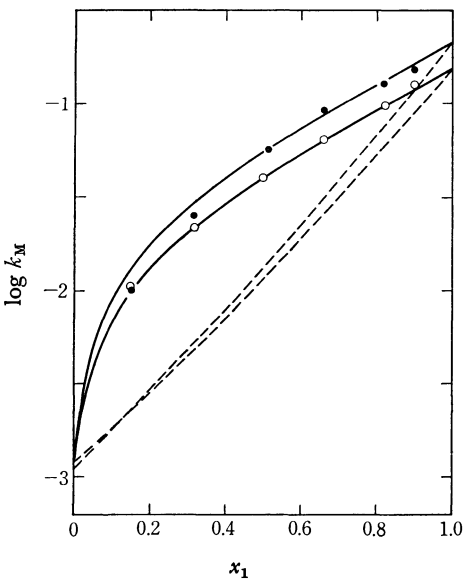

Fig. 4. Plot of log k_M *vs.* mole fraction of DMSO, x_1, for the amination of CMPS (○) and benzyl chloride (●) with 2-amino-1-butanol in DMSO-dioxane mixture at 60 °C.
——: Calculated on the basis of Eq. 1.
----: Calculated on the basis of Eq. 2.

The K values are shown in Table 3. The observed log k_M values fall substantially on the curves calculated on the basis of Eq. 1.

The $\Delta E^{\ddagger}_{M}$ values were calculated on the basis of Eq. 4. The observed values of the activation parameters for 60 °C are compared with the calculated values in Fig. 5. In the calculation of $\Delta E^{\ddagger}_{M}$, we used $\Delta E^{\ddagger}_{1}$= 12.5 ckal/mol for both CMPS and benzyl chloride by considering the E_a values in pure DMSO[1] and those given in Table 2. In the calculation of the solid lines in Fig. 5, we used $\Delta E^{\ddagger}_{1}$=13.5 kcal/mol for both CMPS and benzyl chloride in view of the E_a value in pure dioxane.[7] Recently, however, it has been found that both the k_0 of CMPS, the rate constant independent of the neighboring groups, and the k of benzyl chloride are linear functions of the molar concentration of amine, a, for the amination with 2-amino-1-butanol in dioxane, unlike the amination in DMSO.[10] The Arrhenius plot of the intrinsic rate constants, $k_{int}=\lim_{a\to 0}$ (k_0 and k), gave E_a=16.5 kcal/mol. We used this value for $\Delta E^{\ddagger}_{1}$ in the caluclation of the broken lines in Fig. 5, which indicated that $T\Delta S^{\ddagger}$ decreases in a lower range of x_1; a similar decrease in $T\Delta S^{\ddagger}$ is also shown in Fig. 3 for the DMF–dioxane system.

Table 3. Equilibrium constant in the solvation of the activation complex and thermodynamic quantities in the amination with 2-amino-1-butanol at 60 °C

Solvent	Chloride	K	K_c l/mol	$\Delta G^{\ddagger solv}$ kcal/mol	$\Delta H^{\ddagger solv}$ kcal/mol	$T\Delta S^{\ddagger solv}$ kcal/mol	$T\delta\Delta S^{\ddagger conf}$ kcal/mol
DMSO	CMPS	44.6	3.83	−0.9	−4.0	−3.1	2.5
	Benzyl	63.3	5.44	−1.1	−4.0	−2.9	2.5
DMF	CMPS			−0.6	−3.4	−2.8	1.9
	Benzyl			−0.8	−3.1	−2.3	1.9

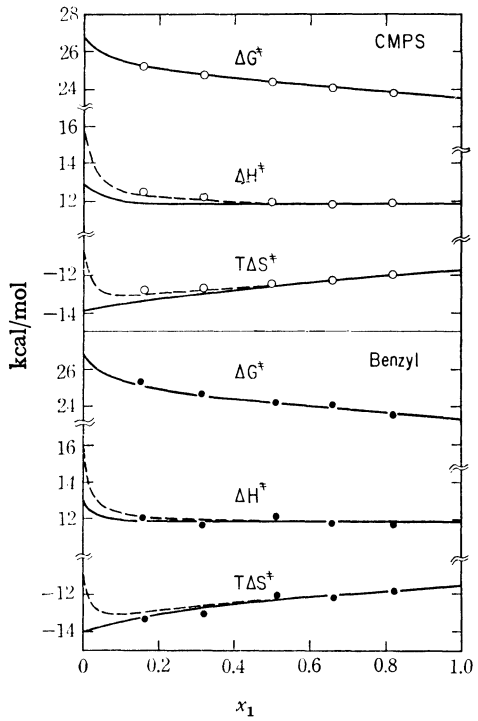

Fig. 5. Plot of the activation parameters *vs.* mole fraction of DMSO, x_1, for the amination of CMPS (○) and benzyl chloride (●) with 2-amino-1-butanol in DMSO-dioxane mixture at 60 °C.
——: Calculated by setting $E_4=13.5$ kcal/mol.
----: Calculated by setting $E_4=16.5$ kcal/mol.

Comparison between DMF–Dioxane System and DMSO–Dioxane System. The activation parameters of the amination change to various extents upon a change in solvent.[1-4] These changes are related to both the specific solvation of the activated complex in the dipolar aprotic solvents and the change in the configurational entropy of the reaction system from the initial state to the transition state, ΔS_1^{*conf}.

On the basis of the present amination data with 2-amino-1-butanol in the DMSO–dioxane system, we calculated the equilibrium constant of the solvation, expressed on the basis of the molar concentration ($K_c=KV_{sol}$), the thermodynamic quantities of the solvation (ΔG^{*solv}, ΔH^{*solv} and $T\Delta S^{*solv}$), and the difference between the configurational entropy change in DMSO and that in dioxane ($\delta\Delta S^{*conf}=\Delta S_1^{*conf}-\Delta S_4^{*conf}$), according to procedures described previously.[4] The value of $\Delta E_4^*=16.5$ kcal/mol was employed for this calculation, because the value of $\Delta E_4^*=13.5$ kcal/mol yielded $T\Delta S^{*solv}\approx 0$. The results listed in Table 3 suggest that the decrease in ΔG^* from dioxane to DMSO is caused not only by the negative ΔG^{*solv}, but also by the positive $T\delta\Delta S^{*conf}$. The $T\delta\Delta S^{*conf}$ value is the same for CMPS and benzyl chloride. Similar findings are obtained for the DMF–dioxane–*s*-butylamine reaction system (or isobutylamine) (*cf.* Table 4 of Ref. 4). Table 3 also shows the parameters of the DMF–dioxane–2-amino-1-butanol reaction system, which were calculated from the previously reported kinetic data in pure DMF[1] on the assumption that the ΔG^{*solv} value of benzyl chloride in this system equals that in the DMF–dioxane–*s*-butylamine (or isobutylamine) system and that the difference in ΔG^* between CMPS and benzyl chloride is based on the difference in ΔG^{*solv}. The $\delta\Delta S^{*conf}$ value in the former system thus obtained is almost the same as that in the latter system.

A comparison between the two systems in Table 3 indicates that the ΔG^{*solv} in the DMSO–dioxane system is lower than that in the DMF–dioxane system. It also indicates that the $T\delta\Delta S^{*conf}$ in the former system is higher than that in the latter system. These results may be ascribed to the fact that DMSO is more polar than DMF.

In view of Figs. 3 and 5, indicating a similar dependence of the activation parameters on x_1 for both DMF–dioxane and DMSO–dioxane systems, it seems that there is the same kind of solvation effect in both systems. Although ΔG^* decreases relatively uniformly with x_1, ΔH^* decreases sharply in the range of $x_1<0.2$ and then reaches an almost constant value. This may be ascribed to the selective solvation of the activated complex with the dipolar aprotic solvents; consequently, $T\Delta S^*$ may be expected to drop in this range. The relatively uniform increase in $T\Delta S^*$ in the range of $x_1>0.2$ may be ascribed to the relative increase in the $T\Delta S^{*conf}$ of the system, which is proportional to x_1.

The author wishes to express his thanks to Dr. Masaya Yanagita for his valuable discussions. He is also grateful to Mr. Yasunori Anami for his helpful assistance in carrying out the measurements.

References

1) H. Kawabe and M. Yanagita, *Bull. Chem. Soc. Jpn.*, **46**, 38 (1973).
2) H. Kawabe and M. Yanagita, *Bull. Chem. Soc. Jpn.*, **46**, 3627 (1973).
3) H. Kawabe, *Bull. Chem. Soc. Jpn.*, **47**, 2936 (1974).
4) H. Kawabe, *Bull. Chem. Soc. Jpn.*, **48**, 163 (1975). In this paper, the graphs in Figs. 2 and 3 should be replaced each other.
5) Y. Kondo and N. Tokura, *Bull. Chem. Soc. Jpn.*, **40**, 1433, 1438 (1967).
6) H. Kawabe and M. Yanagita, *Bull. Chem. Soc. Jpn.*, **41**, 1518 (1968).
7) H. Kawabe and M. Yanagita, *Bull. Chem. Soc. Jpn.*, **44**, 896 (1971).
8) V. K. Quitzsch, *J. Prakt. Chem.*, **28**, 59 (1965).
9) V. K. Quitzsch, H. Ulbrecht, and G. Geiseler, *Z. Phys. Chem.*, **234**, 33 (1967).
10) To be submitted to *Bull. Chem. Soc. Jpn.*

Infrared Studies of the Isocyanate Species Formed in the Reaction of NO with CO over Pt and Rh

Hiroo NIIYAMA, Motoo TANAKA, Hiroshi IIDA, and Etsuro ECHIGOYA

Department of Chemical Engineering, Tokyo Institute of Technology, Ookayama, Meguro-ku, Tokyo 152

(Received September 4, 1975)

The behavior of isocyanates formed on the surface of Rh and Pt in the reaction of nitrogen oxide with carbon monoxide was studied by means of IR spectroscopy using a flow reactor. The isocyanate species readily reacted with N_2O or H_2O, however, it did not decompose when dosed with NO or CO. The catalytic activity of Pt–Al_2O_3 in the reaction of NO+CO declined quickly with an increase in the amount of the surface isocyanate (–NCO). Accordingly, it is concluded that –NCO is not a reaction intermediate but an inhibitor of the reaction.

Recently, Unland[1] has observed the formation of isocyanate (–NCO) on the surface of Pt–Al_2O_3 in the reaction of NO with CO. He has stated that it is a reaction intermediate on the basis of the following findings. Firstly, Pt–NCO is produced when a mixture of NO and CO is dosed over Pt–Al_2O_3 at temperatures higher than 300 °C, where the reaction of NO with CO proceeds at an appreciable rate. Secondly, the amount of Pt–NCO changes with the gas phase composition and it disappears when an NO-rich mixture is dosed.

These findings are, however, not conclusive evidence that the species is a "true" intermediate in the reaction. Bell and London[2] have also observed the formation of –NCO on CuO catalyst, however, they considered that it was not a reaction intermediate but some by-product.

This paper reports the dynamic behavior of –NCO on the surface of Rh and Pt, which was especially studied confirm whether or not it is a reaction intermediate.

Experimental

Catalyst. Pt(1 wt %)–Al_2O_3 and Rh(1 wt %)–Al_2O_3 were prepared by impregnating γ-Al_2O_3 with an aqueous solution of either H_2PtCl_6 or $RhCl_3$. They were then dried at 100 °C for 24 h and calcined at 650 °C for 3 h. Pre-reduction was performed at 500 °C for 1 h in flowing H_2. Disks for IR studies were prepared after the prereduction. They were reduced again in an IR cell (at 300 °C for 1 h at 300 Torr or H_2) or in a flow reactor (at 500 °C for 1 h in flowing H_2) just before use.

The aluminas used as supports were obtained from two sources. Al_2O_3-I was prepared from Alumina Sol 200 (supplied by Nissan Chem. Co.) by drying at 100 °C for 24 h followed by calcination at 650 °C for 3 h. Al_2O_3-II was the commercially available alumina, Alon C.

IR Studies in a Vacuum. A conventional IR cell which was attachable to an appropriate vacuum and gas handling system was employed. The reactant mixture was in contact with the catalyst at 300 °C for 5 min and then was pumped off for 1 min at the same temperature. The isocyanate was produced on the surface of the catalyst by this procedure and was subjected to various treatments as described in the legends of the figures. IR measurements were made after the system had cooled to room temperature. The reactant, NO, CO or a mixture of the two, was introduced through a KOH-packed column into a gas handling system. They were stored in gas containers and were further purified by several freeze-thaw cycles before use.

NO+CO Reaction in a Flow System. Catalytic activity tests were made using a conventional flow system. A flow diagram is shown in Fig. 1. The reaction was occasionally interrupted by replacing the reactants in the system with pure helium (He). The reactor was then immersed in a fluidized thermal bath maintained at 500 °C in order to decompose or desorb surface residues. This procedure is tentatively termed "flash desorption", although not only desorption but also decomposition of the surface residue occurred simultaneously. Several bursts of O_2 were then introduced to establish complete combustion of the surface residues. This procedure is termed "combustion". Liberated gases were analyzed by gas chromatography. An IR cell, similar to that used in the vacuum studies but with slight modification for adaptation to the flow apparatus, was also employed as a reactor in order to observe the development of surface species for changes in catalytic activity.

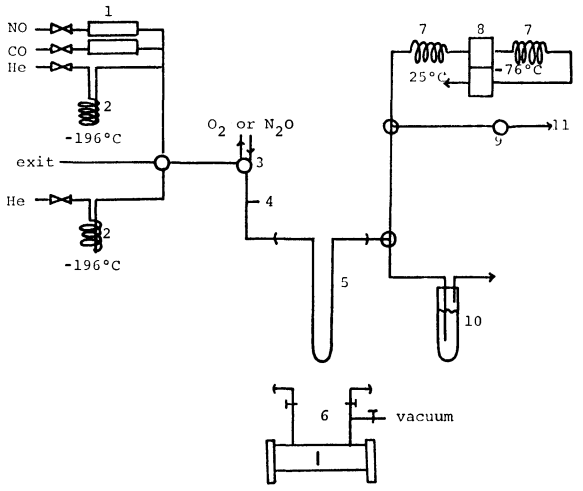

Fig. 1. Flow diagram.
1. KOH column. 2. MS-13X column. 3. O_2 or N_2O doser. 4. Liquid sample inlet. 5. Reactor. 6. IR cell. 7. Porapak Q. 8. T. C. Detecter. 9. Sampling cock. 10. Nessler's reagent. 11. Gas chromatography.

Results

Rh catalyst. The IR spectra of a mixture of NO and CO (NO=26 Torr, CO=59 Torr) which was dosed over Rh–Al_2O_3-II at 300 °C are given in Fig. 2. The spectra is quite similar, in general, to that reported by Unland,[1,3] as can be seen in Table 1. The small differences in the position of the peak maxima may be explained on the basis of the different histories of the catalysts. As has been pointed out by Primet *et al.*, the peak maximum changes, though slightly, depending

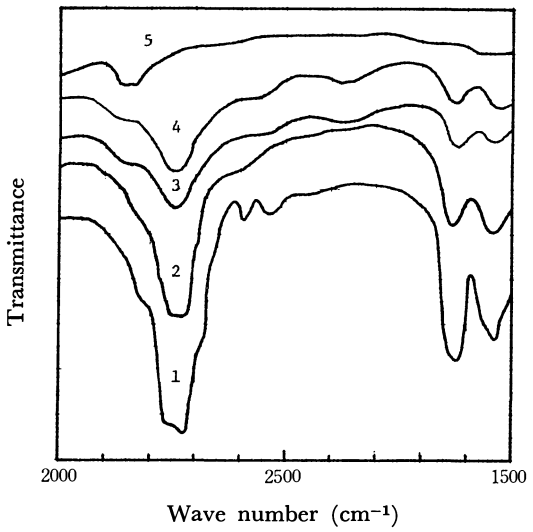

Fig. 2. Infrared spectra before and after the exposure of NO+CO mixture at 300 °C over Rh-Al_2O_3-II.
1. After the mixture (NO 26 Torr, CO 59 Torr) was exposed with following mild pumping. 2. After the subsequent pumping for 10 min. 3. After new mixture (NO 29 Torr, CO 8 Torr) was exposed over the -NCO formed catalyst. 4. After the new mixture was exposed over the fresh catalyst. 5. Back ground spectrum.

Table 1. Observed IR bands and their assignments

Present result	Unland (Rh)[3]	Unland (Pt)[1]	Assignment[1,3]
2250 vs[a]	2269	2261	-NCO
—	2175	2130	NCO^- or CN^-
2090 w	2106	2083	CO_{ad}
2020 w	2036	—	CO_{ad}
1900 w	—	—	CO_{ad} ?
1630 s	1635	1633	C=N ?
1560 s	1568	1564	CO_3^{2-} or NO_3^{2-}
1470 w	1475	1472	CO_3^{2-}

a) vs: very strong, s: strong, w: weak.

on the particle size of the metals dispersed on the supports. The band at 2250 cm^{-1} is due to -NCO[1,3] as is noted in Table 1. The results stated hereafter are mainly restricted to its behavior.

The band did not change after pumping for 10 min at 300 °C, indicating the high stability of the -NCO, however, it did drastically decrease when a new mixture with a higher NO/CO ratio was dosed. A new equilibrium was established within 5 min. The newly obtained spectrum is quite similar to that obtained when the new mixture was dosed over a fresh catalyst (Fig. 2, sp. 4). Quite interestingly, no such species was found when the same mixture (NO=26 Torr, CO=59 Torr) was introduced into the cell at room temperature and was then heated up to 300 °C. The quantitative reproducibility for bands other than -NCO was poor in this experiment mainly because of the difficulty in controlling the rate of temperature raise. However, in general, large amounts of gaseous N_2O were found. This was confirmed by both the IR spectrum in the gas phase and gas chromatographic analysis. This experiment suggests that N_2O might react with -NCO. More reproducible experiments which show the effect of N_2O on the surface -NCO are given below.

The quick response of the band intensity to changes in the gas-phase composition (Fig. 2) suggested that a reaction of -NCO with some other species readily occurred. The unimolecular decomposition or metathesis of -NCO was negligible because no significant change was observed after the -NCO had been held at the same temperature for 10 min in the absence of any gas.

The behavior of -NCO for the introduction of various gases are shown in Fig. 3. The amount of -NCO drastically decreased when N_2O was admitted, showing that the surface -NCO reacted with N_2O. Contact with CO_2 also resulted in a decrease in the -NCO although to a lesser extent in spite of the fact that larger amounts of CO_2 were admitted for longer times. In the latter case, enhancement of the band intensity at 2020 cm^{-1}, which was assigned to the absorbed CO, was also observed. No significant decrease was found when either NO or CO alone came into contact with the -NCO. The intensity of the -NCO was rather enhanced when NO was admitted.

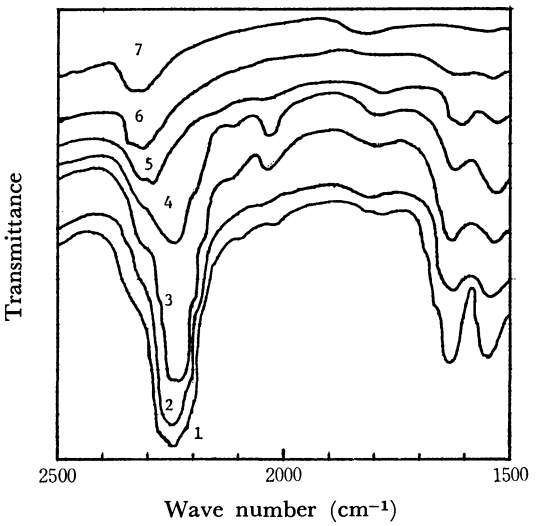

Fig. 3. Behaviors of -NCO and other species on the surface of Rh-Al_2O_3-II when various gases were admitted at 300 °C.
1. The spectrum of -NCO formed catalyst (the same as sp. 1 in Fig. 2) 2—6. After dosing, 2. NO (30 Torr for 5 min), 3. CO (50 Torr for 5 min), 4. CO_2 (50 Torr for 15 min), 5. N_2O (20 Torr for 5 min) and 6. H_2O (18 Torr for 5 min). 7. Back ground spectrum.

Pt Catalyst. The catalytic activity of Pt-Al_2O_3-I in the reaction of NO with CO declined in a rather curious fashion, as is shown in Fig. 4. The activity declined more rapidly when a reactant of lower NO/CO ratio was introduced as is indicated in Fig. 5. When the reactor containing such a deactivated catalyst in continuously flowing He was immersed in a thermal bath at 500 °C (flash desorption), CO_2 was liberated, as detected by a thermal conductivity cell located

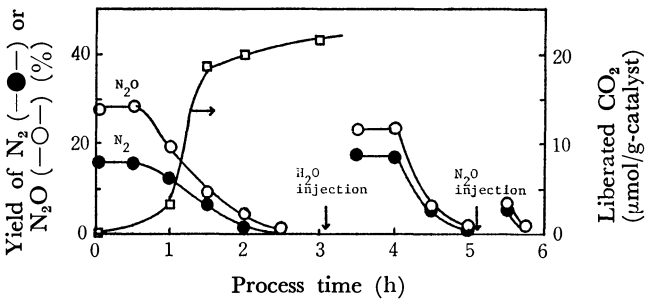

Fig. 4. The change of catalytic activity and the amount of surface residue, as expressed by liberated CO_2, with process time.
Catalyst; Pt-Al_2O_3-I, 0.3 g, reaction temperature; 300 °C, feed gas; NO: 3%, CO: 1% and He: balance, 100 cm³/min.

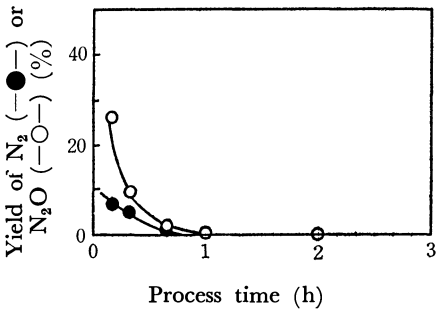

Fig. 5. The change of catalytic activity when the mixture of lower NO/CO ratio was fed.
Catalyst; Pt-Al_2O_3-I, 0.3 g, reaction temperature; 300 °C, feed gas; NO: 3%, CO: 2% and He: balance, 100 cm³/min.

downstream from the reactor. CO_2 was again found in some runs, as is noted later, when the O_2 bursts were subsequently introduced at the same temperature (combustion). The cumulative amount of CO_2 is also plotted in Fig. 4, as a function of the processing time. In the earlier stages of the processing time, all the CO_2 liberated was due to flash desorption. In the later stages, a considerable amount of CO_2 was liberated upon combustion, although, it was still to a smaller extent in comparison with that from flash desorption. It is evident from Fig. 4 that an inverse proportionality exists between the activity decline and the amount of CO_2 liberated. N_2 was also found for both the flash desorption and combustion processes, although with poor quantitative reproducibility.

The adsorption of CO_2 was independently studied by means of the burst technique. It was confirmed that no irreversible adsorption took place at 300 °C either on a fresh or on a deactivated catalyst. This indicates that the CO_2 liberated upon flash desorption was not due to simple "desorption" of adsorbed CO_2 but was due to some reaction (presumably decomposition or metathesis) of the surface complex producing CO_2. The activity was restored when either N_2O or H_2O was introduced over the deactivated catalyst, as is shown in Fig. 4. The formation of NH_3, when H_2O was introduced, was confirmed from the characteristic color change of Nessler's reagent. These findings can

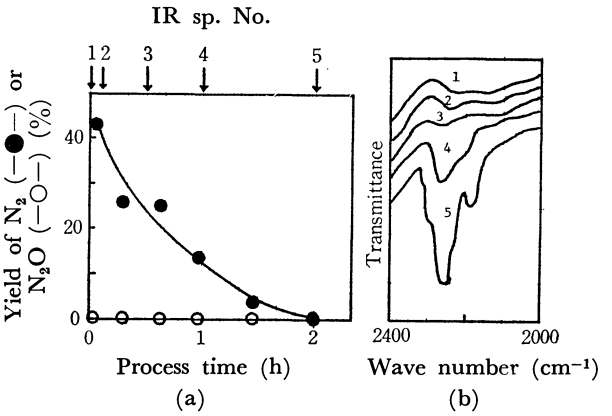

Fig. 6. The changes of catalytic activity (a) and the development of surface -NCO (b) with process time.
Catalyst; Pt-Al_2O_3-II, 0.025 g, reaction temperature; 350 °C, feed gas; NO: 12%, CO: 8% and He: balance, 25 cm³/min.

be summarized as follows: the species containing carbon, oxygen and nitrogen accumulates on the surface during the reaction of NO with CO and it retards the catalytic activity. If we assume that the retardation is attributed to a unique surface species, we can consider that the formation of –NCO is the primary cause for the deactivation.

In order to confirm the above expectation, the development of the surface species as a function of the processing time was studied. The catalytic activity was also simultaneously measured. This was done by attaching an IR cell to the flow system instead of the reactor. The results are given in Fig. 6. The reaction conditions were not the same as those for the former experiment (Figs. 4 and 5) primarily because of the small weight of catalyst disk. In spite of this, the activity declined with a general tendency similar to that of the former experiments. The IR spectrum above 2000 cm^{-1} was also similar to that obtained for the Rh catalyst in the vacuum experiments. It is apparent that the surface –NCO increases as the activity decreases. The IR spectrum below 2000 cm^{-1} was complex and its reproducibility was poor. As has been pointed out by Unland,[3] hydrogen, which might react with NO to form NH_3 or NH_4^+ in the course of the reaction of NO with CO, is strongly adsorbed on the surface during the pretreatment. Functional groups such as NO_3^-, CO_3^{2-} and C=N, which might be produced under these conditions, also have absorption bands in this region. Since the flow system is not adequate to completely isolate the system from the atmosphere, some effect of impurities, especially of H_2O or O_2, might also be expected. What the authors would like to emphasize here is that no band other than that of –NCO corresponds to the changes of catalytic activity with the processing time.

Discussion

It is well known that Pt and Rh have similar catalytic activities in many reactions. Unland[3] has reported that the adsorbed species in the reaction of NO with CO on several noble metals including Pt and Rh are

similar. The discussion hereafter can be applied, in many aspects, to both the Pt and Rh catalysts. This is an assumption, although it appears probable.

Unland has proposed[1] the following scheme for the formation and decomposition of –NCO.

$$Pt + NO + CO \rightarrow Pt\text{-}NCO + O_{ad} \quad (1)$$

$$CO + O_{ad} \rightarrow CO_2 \quad (2)$$

$$Pt\text{-}NCO + NO \rightarrow Pt + N_2 + CO_2 \quad (3)$$

The scheme explains why –NCO disappears or decreases when an NO-rich mixture is dosed. However, –NCO has been confirmed to be extremely stable when NO alone was introduced at high temperature. Accordingly, scheme of Unland, at least reaction (3), is not appropriate. All the present findings indicate that –NCO is not a typical reaction intermediate but an inhibitor which is produced under the reaction conditions. The quick response of the amount of –NCO to the change of gas-phase composition, which at first glance appears to be the characteristic behavior of a reaction intermediate, can be alternately explained as follows. Isocyanate is produced from NO and CO and reacts with N_2O. Then, the amount of –NCO reaches an equilibrium with the gas-phase components, NO, CO and N_2O. When a new mixture with a different NO–CO ratio is dosed, the gas-phase composition of NO, CO and N_2O also changes, resulting in changes of the amount of –NCO.

The main products in the reaction of NO with CO at lower temperatures were N_2O and CO_2.[5] A large amount of N_2O is expected to be produced upon the heating up of the reactant mixture with the catalyst from room temperature to 300 °C. This is the reason why no –NCO was observed for such a procedure.

It should be noted that –NCO may be a precursor of N_2. This is probable because N_2O is a typical oxygen atom donor. In spite of this, however, the reaction is of secondary importance because the main catalytic reaction is deactivated as the surface –NCO develops (Fig. 6). In addition, it was found in a separate experiment that a large amount of N_2 was produced when the mixture of NO and CO was passed as a burst through the bed of fresh catalyst on which no –NCO had been produced. These results indicate that path other than that through the –NCO intermediate exists for producing N_2.

To the authors' knowledge, no conclusive schemes had been proposed for the formation of –NCO. Arai *et al.* have found nitrosyl-carbonyl mixed adsorption on Rh, $Rh\langle^{NO}_{CO}$, at lower temperatures. They suggested that this is the precursor of –NCO.

The overall process for the deactivation may be written as follows:

$$NO + CO \xrightarrow{M} N_2,\ N_2O,\ CO_2 \cdots\cdots \text{main reaction} \quad (4)$$

$$NO + CO + M \rightarrow M\langle^{NO}_{CO} \rightleftharpoons M\text{-}NCO + O_{ad}$$

$$\xrightarrow{CO} M\text{-}NCO + CO_2 \quad (5)$$

$$M\text{-}NCO + N_2O \longrightarrow M + N_2 + NO + CO \quad (6)$$

$$2CO + M \longrightarrow CO_2 + M\text{-}C \quad (7)$$

$$M\text{-}NCO + H_2O \longrightarrow NH_3,\ CO_2,\ M \quad (8)$$

where M is a noble metal catalyst. The main catalytic reaction route, reaction (4), can be divided into several elementary steps. Since it is not the primary concern of this study to clarify them, the undefined formula (4) is tentatively written here. Reaction (5) appears to be reversible because the band of –NCO decreases upon the introduction of CO_2 (the results for the Rh catalyst, Fig. 3) and O_2 admission promotes the reaction of –NCO (the combustion procedure for the Pt catalyst). Reaction (6) is a tentative formula. What can be said with some certainty is that M–NCO reacts with N_2O to give N_2. Carbon deposition (disproportionation of CO) was also confirmed to take place at 300 °C and is therefore given in reaction (7), however, the rate is slower than that of –NCO formation.

In summary, –NCO is not considered to be an intermediate in the main catalytic reaction of NO with CO. However, the important roles of –NCO in the practical catalytic process of NO with CO, are emphasized here. Isocyanate is readily decomposed by water to form NH_3, which has already been pointed out by Unland[1,3] and also confirmed here. Most research work on the reaction were performed under water-free conditions. The catalytic activity under such conditions declines quickly because of –NCO formation. Under practical conditions, however, it will readily react with water which is always present in any combustion exhaust gases. This results in maintaining a high catalytic activity for a longer time. This is a very important point to be considered in selecting a practical catalyst for the reaction.

The authors are grateful to the Agency of Industrial Science and Technology for the financial support of this work.

References

1) M. L. Unland, *J. Phys. Chem.*, **77**, 1952 (1972).
2) J. W. London and A. T. Bell, *J. Catal.*, **31**, 32 (1973); *ibid.*, **31**, 96 (1973).
3) M. L. Unland, *J. Catal.*, **31**, 459 (1973).
4) M. Primet, J. M. Basset, E. Carbowski, and M. V. Mathieu, *J. Am. Chem. Soc.*, **97**, 3655 (1975).
5) A. Ebitani, H. Niiyama, and E. Echigoya, *Nippon Kagaku Kaishi*, **1974**, 1185.
6) H. Arai, M. Kameyama, H. Tominaga, and T. Kunugi, The 35th Meeting of Catalysis Society of Japan at Sendai, 1974; Preprint: *Shokubai*, **16**, 118 (1974).

The Study of the Raman Band Shape of Sulfuric Acid and Proton Transfer

Shun-ichi IKAWA and Masao KIMURA

Department of Chemistry, Faculty of Science, Hokkaido University, Sapporo 060

(Received September 18, 1975)

The Raman bands of sulfuric acid and ammonium sulfate in aqueous solutions were observed in the S–O stretching region and were resolved into components with a Voigt profile. The concentration dependence of the half band-widths was examined. The 980 cm^{-1} band of SO_4^{2-} in acidic solutions was determined to have a width of 8.0 ± 0.3 cm^{-1} when unbroadened by any chemical process. In the concentration-half-width curve for this band, two conspicuous bends were found, at about 2 M and 8 M stoichiometric concentrations of H_2SO_4. It seems that the former bend is attributable to the disappearance of water clusters, and the latter, to the partial defect of the primary hydration shell of the oxonium ion. The interrelation between the half-widths of the 980 cm^{-1} and 1050 cm^{-1} bands suggests that the formation of the $HSO_4^- \cdot H_3O^+$ ion pair is related to the spectroscopic lifetime of HSO_4^-.

It has been pointed out that the half-width of a Raman line of an anion, A^-, in acidic solutions yields the lifetime of A^-, which is determined by the rate of proton transfer between the A^- and H_3O^+ ions.[1,2] Chen and Irish reported, in their elaborate Raman spectral studies of hydrogensulfate–sulfate systems,[3,4] that the broadening of the 980 cm^{-1} line of SO_4^{2-} in acidic solutions is directly proportional to the oxonium ion concentration, $[H_3O^+]$, in the range lower than 2M, and that the proportionality changes abruptly at about $[H_3O^+]=2$ M. They evaluated the rate constant of proton transfer to be $5.5\times10^{11}M^{-1}s^{-1}$.

The resolution in these spectroscopic measurements was 10—15 cm^{-1}; such a low resolution might considerably affect the estimates of the band widths and the band shapes. The present study has been performed under a higher resolution in order to confirm or improve the previous results, or at least to gain some information.

Experimental

Solutions were prepared from H_2SO_4 (analytical reagent) and $(NH_4)_2SO_4$ (biochemical reagent) purchased from Wako Fine Chemicals. No impurity disturbing band analysis was detected from the observed spectra. The concentrations of sulfuric acid were determined from the specific gravity by referring to the standard table.[5] Raman lines excited by the 6328 Å line of a He–Ne gas laser were recorded on a JASCO R-300S Raman spectrophotometer at room temperature, 22 ± 2 °C. No temperature effect was appreciable on the observed spectra in this temperature range. Spectral slit widths were set at less than 2 cm^{-1} except for the 0.5 and 0.8 M sulfuric acid solutions, for which they were set at about 5 cm^{-1}.

Band Analysis

The observed spectral intensity, $I(\nu)=S(\nu)/(\nu-\nu_e)^4$, ranging from 850 to 1100 cm^{-1}, was resolved into components with the Voigt profile by the least-squares method, where $S(\nu)$ is the observed relative scattering intensity at a Raman shift of ν cm^{-1} and where ν_e is the wave number of the exciting line, 15803 cm^{-1}. The Voigt function is given by a convolution of the Lorentzian and Gaussian functions as follows:

$$V(\nu) = N\int_{-\infty}^{+\infty} \frac{\exp[-(\nu'/\beta_g)^2]}{(\nu-\nu')^2+\beta_l^2}d\nu' . \quad (1)$$

Practically, however, an approximate representation for $V(\nu)$ given by Kielkopf[6] was used to calculate the numerical values of $V(\nu)$. Extraneous scattering light, probably the wing of the Rayleigh scattering, overlaps in this region. It forms a nearly straight background. The $S(\nu)$ was then determined by subtracting the background from the observed total scattering intensity.

The effect of the finite slit width on the band shape cannot necessarily be neglected for the relatively fine band of SO_4^{2-} at 980 cm^{-1}. A spectral slit function is well approximated by a Gaussian function.[7] Therefore, for the 980 cm^{-1} bands of the salt and the 0.5 and 0.8 M sulfuric acid solutions, β_g's were fixed at values given by $\beta_g=S/2\sqrt{\ln 2}$,[8] where S is the spectral slit width. The appropriateness of this processing is shown in Fig. 1 for the salt solution. Twice the best fit values of β_l were then adopted as the true half-widths. They were smaller by about 10% than the apparent half-widths; for example, the apparent half-widths of 13.3 and 15.4 cm^{-1} for 0.5 and 0.8 M sulfuric acid solutions were diminished to 11.4 and 13.8 cm^{-1} respectively. As a band broadens out and as a slit width becomes narrow, the effect of the finite slit width decreases rapidly. Thus, in the analyses of bands other than those mentioned above, the effect of the finite slit width was not taken into account and the half-width of the best-fit Voigt profile was adopted as that of each component band.

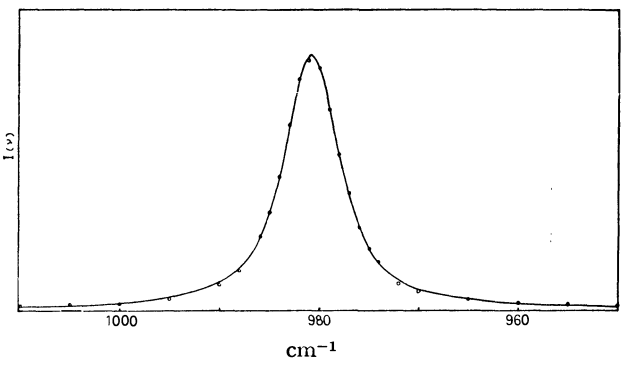

Fig. 1. Raman band of the 1.5 M ammonium sulfate solution.
° ° ° Observed intensity, —— calculated intensity with the Voigt profile: $\beta_g=1.0_2$ (fixed, $S=1.7$), $\beta_l=3.2$.

Results and Discussion

The spectra of sulfuric acid at all the concentrations studied could be well approximated by a superposition of four Voigt functions with peaks at about 900, 980, 1030, and 1050 cm^{-1}. The observed spectral intensities of sulfuric acid at several concentrations are shown in Fig. 2. Examples of the band resolution are shown in Figs. 3 and 4. Chen and Irish[3,4] reported that each component could be best approximated by a Lorentz-Gaussian product function whose wing falls much faster than that of the Voigt function. The bands observed in those studies might be deformed as a result of the larger slit widths.

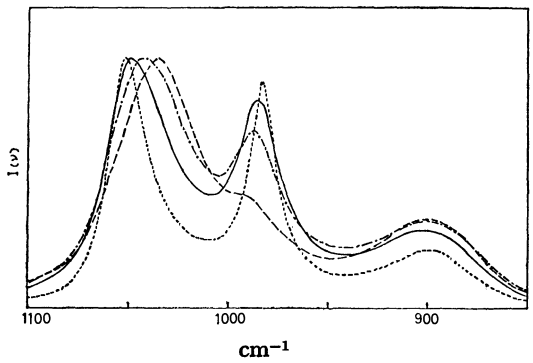

Fig. 2. Observed Raman bands of sulfuric acid. The intensities of the peaks at about 1050 cm^{-1} are normalized.
---- 1.4 M, —— 5.2 M, —·— 7.3 M, ——— 10.6 M.

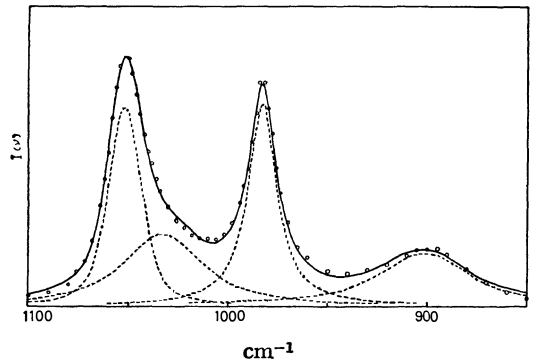

Fig. 3. Resolution of the band for 1.4 M sulfuric acid.
o o o Observed intensity, ---- calculated component intensity, —— calculated total intensity.

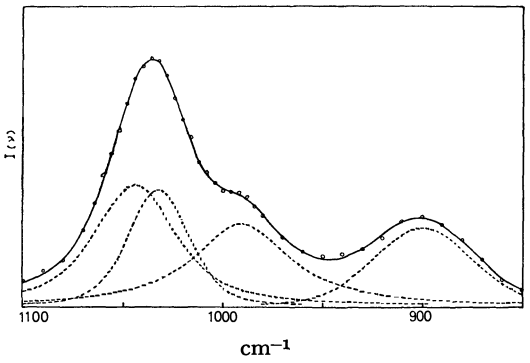

Fig. 4. Resolution of the band for 10.6 M sulfuric acid.
o o o Observed intensity, ---- calculated component intensity, —— calculated total intensity.

The band at about 980 cm^{-1} is assigned to the symmetric stretching vibration of SO_4^{2-}, while the bands at about 1050 cm^{-1} and 900 cm^{-1} are assigned to HSO_4^-.[9-11] The fourth band, at about 1030 cm^{-1}, was first found by Irish and Chen[3,4] and was assigned to the $H_3O^+ \cdot HSO_4^-$ ion pair. They identified an additional weak band near 950 cm^{-1}. However, its counterpart was not recognized in the present analysis.[12]

With an increase in the concentration of sulfuric acid from 0.5 to 10.6 M, the SO_4^{2-} band shifts from 982 to 991 cm^{-1}. On the other hand, the frequency of the HSO_4^- band near 1050 cm^{-1} is lowered from 1052 to 1044 cm^{-1}. These facts suggest that the S–O bond strength in SO_4^{2-} and HSO_4^- is affected by their ionic atmosphere in an opposite manner.

The concentration-half-width curves for the 980 and 1050 cm^{-1} bands are shown in Figs. 5 and 6 respectively. In the simulation of the bands, the uncertainty involved in the background line and the strong correlation between the bands at 1050 and 1030 cm^{-1} more or less obscure the best values of the half-widths. How-

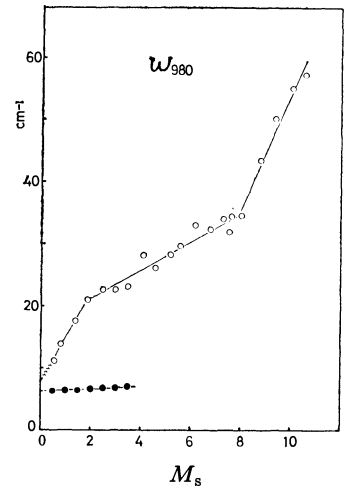

Fig. 5. Concentration dependence of the half-width of the 980 cm^{-1} band.
○: Sulfuric acid, ●: ammonium sulfate.

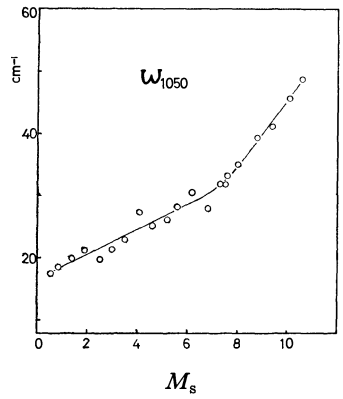

Fig. 6. Concentration dependence of the half-width o the 1050 cm^{-1} band of sulfuric acid.

ever, their influences are insignificant on the results obtained for the narrower bands appearing as plain peaks in the observed spectra. As for the 1050 cm^{-1} band, its half-width values in the range beyond 7 M probably have large errors.

The concentration-half-width curve for the 980 cm^{-1} band of H_2SO_4 in solutions has two conspicuous bends, at about 2 M and 8 M, in the stoichiometric concentration. The bend at the lower concentration has already been reported by Chen and Irish,[4] but the bend at 8 M has not been reported previously. The extrapolation of the curve to a zero concentration gives $\omega_0 = 8.0 \pm 0.3$ cm^{-1}. This value is close to that for the aqueous solutions of $(NH_4)_2SO_4$, 6.3 cm^{-1}. As for the 980 cm^{-1} band of the salt solutions, its half-width shows only a slight change, from 6.3 to 7.0 cm^{-1}, as the concentration increases from 0.5 to 3.5 M, and its band center is located almost consistently at 980.5 cm^{-1}. These half-widths are about half for $(NH_4)_2SO_4$ solutions and about 30% smaller for H_2SO_4 solutions as compared with the half-widths reported in the previous papers.[3,4]

Since the symmetry of SO_4^{2-} in aqueous solutions is regular tetrahedral,[13] the width of the totally symmetric stretching band at 980 cm^{-1} must not be affected by the reorientational motion of the ion.[14,15] Therefore, the broadening of the 980 cm^{-1} band is probably caused by the chemical process that extinguishes the SO_4^{2-} ion in the following equilibrium:

$$H_3O^+ + SO_4^{2-} \rightleftharpoons HSO_4^- + H_2O,$$

and by other mechanisms such as the vibrational relaxation.[16] Thus, the ω_0 may be considered to be the linewidth without the broadening due to the chemical process, and the value of $\omega - \omega_0$ for sulfuric acid is related to the mean lifetime, τ, of SO_4^{2-} by the equation:[14]

$$\omega - \omega_0 = 1/\pi c\tau \qquad (2)$$

where c is the velocity of light. The rate constant of proton transfer is given by:[1-4]

$$K_p = \pi c(\omega - \omega_0)/[H_3O^+]. \qquad (3)$$

By making use of values of $[H_3O^+]$ corresponding to the stoichiometric concentration of H_2SO_4, M_s, in the table presented by Chen and Irish[4], the K_p values were calculated; they are plotted against M_s in Fig. 7. The value of $K_p/\pi c$ at M_s values lower than 2 is 5.6 ± 0.2 M^{-1} cm^{-1} ($K_p = 5.3 \times 10^{11}$ M^{-1} s^{-1}), almost independent of the concentration. This value agrees well with that reported by Chen and Irish,[4] 5.8 M^{-1} cm^{-1}, in spite of the large differences in individual ω and ω_0 values between the two studies.[17] The value of K_p begins to decrease abruptly at about $M_s = 2$, corresponding to a bending in the concentration-half-width curve in Fig. 5. According to Eigen and collaborators,[18,19] the rate of proton transfer is much faster in ice than in liquid water because the chains of hydrogen bonds favorable for proton transfer are always arranged in ice. On the other hand, Robertson and Dunford[20] have pointed out, on the basis of their study of the Hammet acidity function of sulfuric acid, that the water clusters disappear rather abruptly at about $M_s = 2$. The results of the present study and the two earlier studies suggest that

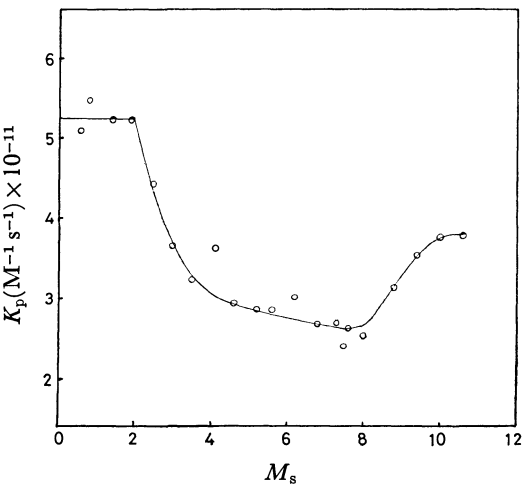

Fig. 7. Concentration dependence of the rate constant $K_p = \pi c(\omega - \omega_0)_{980}/[H_3O^+]$.

the water clusters participate actively in the proton transfer in aqueous solutions of H_2SO_4 because such clusters contain hydrogen-bond networks, even though their sizes are smaller than those in ice. Robertson and Dunford have also found that the average hydration number of the proton in sulfuric acid solutions becomes smaller than four at concentrations beyond $M_s = 8$. This means that a partial defect occurs in the primary hydration shell composed of the four water molecules which stabilize the proton in dilute solutions.[18] Such a defect may activate the proton to react rapidly with SO_4^{2-}. The rise of K_p in concentrated solutions beyond $M_s = 8$ may, then, be attributable to an increase in the defect of the hydration shells about the protons.

If the mean lifetime of HSO_4^- is limited only by the dissociation process,

$$HSO_4^- + H_2O \rightleftharpoons SO_4^{2-} + H_3O^+$$

then the following two relations hold[4]:

$$[1/\tau(HSO_4^-)] \cdot [HSO_4^-] = [1/\tau(SO_4^{2-})] \cdot [SO_4^{2-}] \qquad (4)$$

for the mean lifetime and:

$$(\omega - \omega_0)_{1050} = A(\omega - \omega_0)_{980} \qquad (5)$$

for the half-width, where

$$A = [SO_4^{2-}]/[HSO_4^-] = ([H_3O^+] - [H_2SO_4])/(2[H_2SO_4] - [H_3O^+]),$$

and where ω_0 is the broadening due to certain causes other than the above reaction. The ω_{1050} values in the $M_s < 7$ range, where they are fairly reliable, are plotted against the values of $A \cdot (\omega - \omega_0)_{980}$ in Fig. 8. If the value of $(\omega_0)_{1050}$ is independent of the concentration, the slope of the curve ought to be unity, as is shown by a broken line in Fig. 8. The observed curve has a slope of about 1.6; it can hardly be considered to have a slope of unity. Therefore, we cannot but consider that the value of $(\omega_0)_{1050}$ increases with the concentration. As has been described previously, the broadening of the SO_4^{2-} band due to any causes other than a chemical process does not vary remarkably with the concentration. Therefore, there seems to be another chemical process which serves

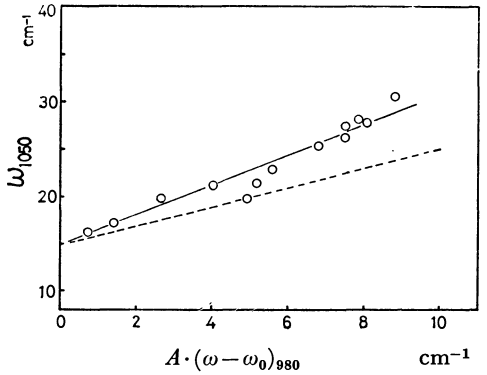

Fig. 8. Interrelation between ω_{1050} and $A\cdot(\omega-\omega_0)_{980}$. The broken line shows a slope of unity.

to shorten the spectroscopic lifetime of HSO_4^-. It seems that the process of forming the $HSO_4^-\cdot H_3O^+$ ion pair is related to the decrease in this spectroscopic lifetime and to the increase in the $(\omega_0)_{1050}$ with concentration.

The authors wish to thank Miss Michiko Kikuchi for her help in spectroscopic measurement. The calculations were performed on a FACOM 230-60 of the Computing Center of Hokkaido University.

References

1) M. M. Kreevoy and C. A. Mead, *J. Am. Chem. Soc.*, **84**, 4596 (1962); *Discuss. Faraday Soc.*, **39**, 166 (1965).
2) A. K. Covington, M. J. Tait, and W. F. K. Wynne-Jones, *Discuss. Faraday Soc.*, **39**, 172 (1965).
3) D. E. Irish and H. Chen, *J. Phys. Chem.*, **74**, 3796 (1970).
4) H. Chen and D. E. Irish, *J. Phys. Chem.*, **75**, 2672 (1971).
5) G. Lunge and M. Isler, *Z. Anorg. Chem.*, **3**, 129, 569 (1890); G. Lunge and P. Naef, *ibid.*, **3**, 90 (1890).
6) J. F. Kielkopf, *J. Opt. Soc. Am.*, **63**, 987 (1973).
7) R. E. Meredith, *J. Quant. Spectrosc. Radiat. Transfer*, **12**, 455, 485 (1972).
8) J. S. Seshadri and R. Norman Jones, *Spectrochim. Acta*, **19**, 1013 (1963).
9) L. A. Woodward and R. G. Hormer, *Proc. R. Soc. London, Ser. A*, **144**, 129 (1934).
10) G. E. Walrafen and D. M. Dodd, *Trans. Faraday Soc.*, **57**, 1286 (1961).
11) T. F. Young and G. E. Walrafen, *Trans. Faraday Soc.*, **57**, 34 (1961).
12) Since the dissociation process
$$H_3O^+\cdot SO_4^{2-} \rightleftharpoons H_2O + HSO_4^-$$
may proceed much faster than the process
$$H_3O^+\cdot HSO_4^- \rightleftharpoons H_2O + H_2SO_4$$
in aqueous solutions of sulfuric acid below 14 M (see Ref. 11), the $H_3O^+\cdot SO_4^{2-}$ ion pair is considered to be much more unstable than the $H_3O^+\cdot HSO_4^-$ ion pair assigned the 1030 cm^{-1} band at the concentrations employed in the present study. Therefore, a band due to the $H_3O^+\cdot SO_4^{2-}$ ion pair, if it exists, is possibly so weak and broad that it cannot be recognized.
13) See, *e.g.*, G. Herzberg, "Molecular Spectra and Molecular Structure. II. Infrared and Raman Spectra of Polyatomic Molecules," D. Van Nostrand and Company, Princeton, N. J. (1945).
14) I. I. Kondilenko, V. E. Pogorelov, and K. Khue, *Opt. Spectrosc.*, **28**, 367 (1970).
15) F. J. Bartoli and T. A. Litovitz, *J. Chem. Phys.*, **56**, 404 (1972).
16) The half-width of the 980 cm^{-1} band of the salt solutions should not be broadened by any chemical reaction, but in fact it changes slightly with an increase in the concentration, as was mentioned in the last paragraph. There seem to be several factors influencing the half-width in aqueous solutions in association with the concentration or the structure of aqueous solutions.
17) The observed band is expressed by a convolution of the spectral slit function and the true band-shape function; see Ref. 8. The observed half-width is, in general, smaller than the sum of the half-widths of the two functions. The ω and ω_0, and accordingly $\omega-\omega_0$, are influenced by the finite spectral slit width.
18) M. Eigen and L. De Maeyer in "The Structure of Electrolytic Solutions," W. J. Hamer, Ed., Wiley, New York, N. Y. (1959), p. 35.
19) M. Eigen and L. De Maeyer, *Proc. R. Soc. (London), Ser. A*, **247**, 505 (1958).
20) E. B. Robertson and H. B. Durfond, *J. Am. Chem. Soc.*, **86**, 5080 (1964).

CNDO/2 Calculations of Ionization Potentials of Some Fluorosubstituted Conjugated Hydrocarbons

Toshio HAYASHI and Takeshi NAKAJIMA

Department of Chemistry, Faculty of Science, Tohoku University, Sendai 980

(Received September 23, 1975)

The ionization potentials of the fluorosubstituted derivatives of ethylene, *trans*-1,3-butadiene, and benzene were calculated by using the modified CNDO/2 method. In agreement with the available experimental facts, the ionization potentials due to the π-electron were predicted to change little on fluorination, while those due to the σ-electron were predicted to suffer a more or less large change on fluorination. An explanation for this fact, called the perfluoro effect, can be given by a simple perturbational treatment.

One of the methods which can be of great help in the assignment of the photoelectron spectra of conjugated molecules is the perfluoro effect first studied by Robin *et al.*;[1] the substitution of the hydrogen atoms in a planar conjugated molecule by fluorine atoms will increase the ionization potentials (*IP*'s) of the σ-MO's by 2.5—5 eV, whereas the π-MO's are stabilized by only 0—1 eV.

Most of the molecular orbital calculations thus far made of ionization potentials of fluorosubstituted planar conjugated molecules have been confined to levels due to π-electrons. There have been very few systematic and quantitative studies of ionization potentials due to σ-electrons.

In order to identify the photoelectron spectra of monofluoro- and tetrafluoroethylene, Robin *et al.*[1] and Meza and Wahlgren[2] have performed the GTO calculations of ionization potentials due to π- and σ-electrons and compared the results with those for ethylene in order to examine the effect of fluorination on ionization potentials.

In this paper, we study systematically and quantitatively the fluorosubstituent effects by using a modified CNDO/2 method proposed in a previous paper.[3] In order to examine how the perfluoro effect holds for ethylene in particular, we draw a diagram showing the correlation of ionization potentials at various degrees of fluorination. The calculated ionization potentials are compared with the available experimental values and those obtained by other SCF MO methods. Further, we show that a simple perturbational treatment can give a satisfactory explanation of the perfluoro effect that the ionization potentials due to π-electrons of conjugated hydrocarbons suffer no substitutional change on fluorination.

Method of Calculation

Tajiri *et al.*[4] and Ohmichi *et al.*[5] have calculated the electronic spectra of a number of saturated and unsaturated compounds using a modified CNDO/2 method which is a compromise between the methods of Bene-Jaffé[6] and of Sichel-Whitehead.[7] Our method differs from those above in the following point; the local core matrix element, $U_{\mu\mu}$, of the atomic orbital, μ, is estimated as an additional empirical parameter and adjusted, together with selected values of the bonding parameters, β_A^0, and the separation constant, k, so that a wide range of ionization potentials of a certain molecule may be reproduced. The details of the method were described in a previous paper,[3] in which a good agreement between the calculated ionization potentials and electronic spectra and the experimental ones for several unsaturated hydrocarbons was obtained. The parameter values for the fluorine atom are determined so that they may reproduce a wide range of observed ionization potentials for mono-, 1,1-di-, and tetrafluoroethylene. The new parameter values, together with those of earlier workers, are given in Table 1.

TABLE 1. PARAMETER VALUES[a]

Parameter	Method	H	C	F
U_{ss}	CNDO/2[b]	−17.38	−70.30	−199.3
	Ohmichi *et al.*[c]	−13.60	−50.69	−130.1
	This method	−13.60	−42.0	−112.0
U_{pp}	CNDO/2		−61.8	−178.1
	Ohmichi *et al.*		−41.53	−108.9
	This method		−40.0	−110.0
β_A^0	CNDO/2	9	21	39
	Ohmichi *et al.*	8	15	
	This method	9	15	29
k	Ohmichi *et al.*		0.75	0.75
	This method		0.70	0.70

a) Values for U_{ss}, U_{pp}, and β_A^0 are in eV units.
b) Ref. 18. c) Ref. 5.

The geometrical structure of tetrafluoroethylene was taken from Sutton's tables.[8] For the other fluoroderivatives, the bond lengths of C–F and C–H are assumed to be 1.33 and 1.08 Å respectively, and all the bond angles are taken to be 120°. The bond lengths of all the formal C=C and C–C bonds are assumed to be 1.34 and 1.47 Å respectively. For the benzene derivatives, the C–C bond lengths of the benzene ring are assumed to be the same as those of benzene.

The calculations were carried out on the NEAC 2200, model 700, computer of Tohoku University.

Results and Discussion

The CNDO/2 Calculations for Fluoroderivatives. The high-resolution photoelectron spectra of ethylene, monofluoroethylene, 1,1-difluoroethylene, and tetrafluoroethylene have been investigated by Robin *et al.*[1] and by Lake and Thompson.[9] From the facts that the vibrational progression of the C=C bond stretching mode appears in the first bands observed at about 10.6 eV in these fluoroderivatives, and that in the

second bands no such progression is observed, it seems that the first *IP*'s are due to a π-electron, and the second *IP*'s, to a σ-electron. It is noted that the first *IP*'s of these fluoroderivatives are almost the same as that of ethylene, while the second *IP*'s suffer a large shift to a higher energy.

Table 2. Ionization potentials of monofluoroethylene (eV)

Vertical *IP*[10]	This work	*ab initio*[2]
10.58	10.58 $\pi a''$	10.27 a''
13.79	13.63 a'	14.85 a'
14.51	14.97 a'	15.71 a'
16.77	17.49 a'	18.09 a''
17.97	18.05 $\pi a''$	18.17 a'
	18.32 a'	19.71 a'
	20.22 a'	22.38 a'
	23.80 a'	28.86 a'
	28.18 a'	44.19 a'

Table 3. Ionization potentials of 1,1-difluoroethylene (eV)

Vertical *IP*[10]	This work
10.72	10.60 πb_1
14.79	14.92 a_1
15.73	15.17 b_2
	17.53 b_2
	17.75 πa_2
18.22	18.32 a_1
	18.56 b_2
19.68	18.71 a_1
	18.93 πb_1
	24.03 a_1
	25.94 b_2
	28.89 a_1

Table 4. Ionization potentials of tetrafluoroethylene (eV)

Obsd[1]	Calcd	
	This work	Robin *et al.*
10.52	10.55 $\pi 2b_{1u}$	10.86 $\pi 2b_{1u}$
15.95	15.53 $6a_g$	17.15 $6a_g$
16.4	17.68 $4b_{1g}$	17.40 $4b_{1g}$
16.6	17.68 $4b_{2u}$	17.77 $4b_{2u}$
16.9	18.05 $\pi 1a_u$	18.15 $\pi 1a_u$
17.60	18.08 $\pi 1b_{3g}$	18.32 $\pi 1b_{3g}$
18.21	18.21 $5b_{3u}$	18.82 $5b_{3u}$
	18.65 $3b_{1g}$	19.60 $\pi 1b_{2g}$
	18.89 $3b_{2u}$	19.90 $3b_{1g}$
	18.89 $\pi 1b_{2g}$	20.83 $\pi 1b_{1u}$
19.46	19.05 $5a_g$	21.50 $3b_{2u}$
21.0	19.05 $4b_{3u}$	22.15 $5a_g$
22.5	19.87 $\pi 1b_{1u}$	23.26 $4b_{3u}$
	22.29 $4a_g$	28.66 $4a_g$
	23.28 $2b_{1g}$	
	27.78 $2b_{2u}$	
	28.51 $3b_{3u}$	
	30.21 $3a_g$	

Tables 2, 3, and 4 show the calculated and observe ionization potentials of mono-, 1,1-di-, and tetrafluoroethylene respectively. It may be seen that the calculated ionization potentials of monofluoro- and difluoroderivatives and the calculated lower ionization potentials (<18.5 eV) of tetrafluoroethylene are in fairly good agreement with the experimental values. For the first seven levels of tetrafluoroethylene, the order of energy and the atomic populations are in good agreement with those obtained by a GTO calculation.[1]

Figure 1 shows the correlations of the MO's of ethylene with those of various fluoroderivatives of ethylene. The correlation diagram was drawn on the basis of the atomic and overlap population analyses and of the correspondence among the irreducible representations of various point groups. Comparing the atomic and overlap populations of ethylene with those of tetrafluoroethylene, we can correlate the $1b_{1u}$ π orbital and the $1b_{1g}$, $1b_{2u}$, $2b_{3u}$, and $2a_g$ σ orbitals of ethylene with the $2b_{1u}$ π orbital and the $2b_{1g}$, $2b_{2u}$, $3b_{3u}$, and $3a_g$ σ orbitals of tetrafluoroethylene respectively. This is because, in this correlation, the atomic populations on the carbon atoms in these orbitals of ethylene are least affected on fluorination. The $3a_g$ σ orbital of ethylene may be correlated with the $6a_g$ or $4a_g$ orbital of tetrafluoroethylene. The two other symmetrically possible correlations, $3a_g$ (ethylene)-$5a_g$ or $3a_g$ (tetrafluoroethylene), can be rejected, because the atomic population on carbon atoms in the $5a_g$ or $3a_g$ orbital of tetrafluoroethylene are substantially different from those in the $3a_g$ orbital of ethylene.

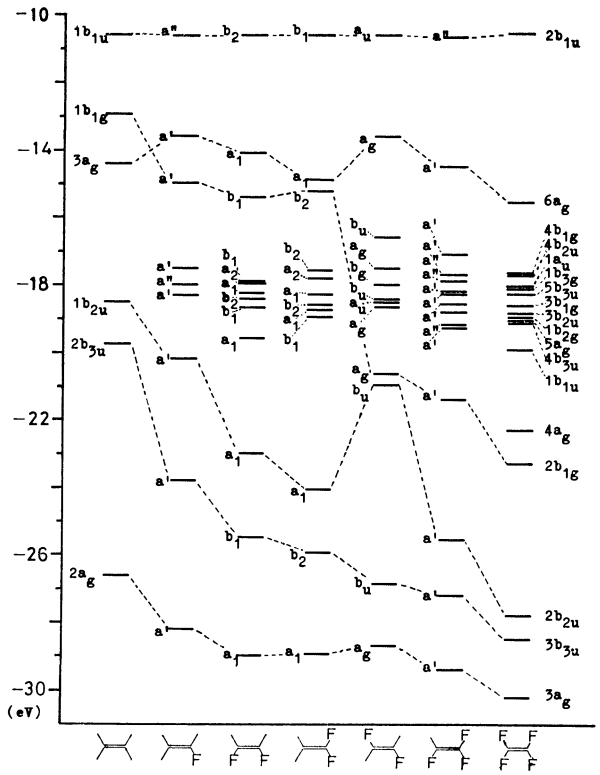

Fig. 1. MO correlation diagram of ethylene and its fluoro-derivatives.

Of the two possible correlations, we prefer the $3a_g$ (ethylene)-$6a_g$(tetrafluoroethylene) correlation. The reason for this preference is as follows; in the mono-, di- and tri-fluoroethylene examined, the orbitals related to the $3a_g$ orbital of ethylene turned out to have negative overlap populations on the C–F bonds, while in tetrafluoroethylene only the $6a_g$ orbitals has the negative overlap populations on the C–F bonds. The correlations of the σ-orbitals of ethylene with those of tetrafluoroethylene proposed by Robin *et al.*[1] are considerably different from the present correlations. For monofluoro- and trifluoroethylene, the correlations are less unambiguous because, for these molecules, the population analyses do not give sufficient information and their molecular symmetries are low.

It may be seen in Fig. 1 that the energy of the MO ($1b_{1u}$) due to π-electrons of carbon atoms of ethylene remains almost constant on fluorination, while the MO's due to σ-electrons are more or less markedly lowered in energy on fluorination, with the exception of the $3a_g$ σ orbital. This orbital is raised in energy in some fluoroderivatives and is lowered in some others, the change in energy being in all cases considerably small compared with those of other σ orbitals. It should be noted that the σ orbitals related to the $3a_g$ orbital of ethylene are characterized by the fact that, in these orbitals, the overlap population between the carbon and fluorine atoms is negative; that is, these orbitals are antibonding between the carbon and fluorine atoms. Furthermore, in these orbitals the atomic population on the fluorine atom is relatively small. On the other hand, all the other σ orbitals of the fluoroderivatives are bonding between the carbon and fluorine atoms, and in these orbitals the atomic populations on the fluorine atoms are relatively large.

Table 5. Ionization potentials of 1,1,4,4-tetrafluorobutadiene (eV)

Obsd[10]	This work
9.30	9.33 πb_g
12.04	12.34 πa_u
14.5	13.39 a_g
15.3	14.15 a_g
16.0	15.89 b_u
	17.37 b_u
	17.51 a_g
	17.75 πb_g
	17.76 πa_u
	17.93 a_g
18.0	18.08 b_u
19.6	18.58 a_g
21.0	18.68 b_u
21.9	18.73 a_g
	18.87 πb_g
	18.88 b_u
	19.03 πa_u
	22.09 b_u
	24.84 a_g
	26.40 b_u
	26.48 a_g
	28.67 b_u
	30.35 a_g

The assignment of the ionization potentials of *trans*-1,3-butadiene has not been uniquely determined. There remains the problem of where the two π *IP*'s lie. The earlier study by Robin *et al.*[10] of the photoelectron spectra of the fluorinated derivatives of this molecule indicated that the first three ionization potentials are due to π, σ, and π electrons respectively, but recent investigations[19–20] have suggested that the π, π, and σ sequence is also acceptable.

In order to examine this point, we calculated the ionization potentials of 1,1,4,4-tetrafluorobutadiene (Table 5) and compared them with those of the parent hydrocarbon calculated previously using the same method. In a previous paper[3] the experimental ionization potentials of 9.07, 11.27 and 12.17 eV were assigned to the calculated 9.07 (π), 11.75 (σ), and 12, 39 (π) eV respectively. The ionization potential calculated from the lowest π orbital of 1,3-butadiene (12.39 eV) shifts, though slightly, to a lower energy in its tetrafluoro derivative (12.34 eV). This result suggests that the third band observed at 12.17 eV in 1,3-butadiene corresponds to the second band observed at 12.04 eV in its tetrafluoro derivative, both the bands being due to π-electrons, because, in our calculations, the other two lower ionization potentials of the parent hydrocarbon shift to higher energies on tetrafluorination. Moreover, such an assignment is supported by the results of a simple perturbational treatment (*vide infra*).

Experimentally the intense bands observed at about 16 eV of the tetrafluobutadiene was attributed to the fluorine lone-pair electron. In our calculation this band is assigned to the b_u σ level, and the ionization potentials due to the fluorine lone-pair electrons are predicted to be 17—19 eV.

The photoelectron spectra of fluorobenzene, *p*-difluorobenzene, and 1,2,4-trifluorobenzene have been reported by Turner *et al.*[11] and Clark and Frost.[12] The absorption spectra of the lower energy region (9—14 eV) of fluorobenzene have also been investigated by other authors.[13–15] The calculated ionization potentials of monofluoro-, *p*-difluoro-, and 1,2,4-trifluorobenzene are listed in Tables 6, 7, and 8, together with the experimental values. In these tables the observed third bands are assigned to the calculated fifth ionization potentials (at about 13.8 eV) due to a π-electron. The reason for this assignment will be given below. The first three observed bands in these molecules are predicted to be due to π-electrons, the first two being related to the e_{1g} π levels of benzene observed at 9.3 eV, and the third one, to the a_{2u} π level of benzene observed at 12.1 eV. This assignment is in agreement with those proposed by Turner *et al.*,[11] Clark and Frost,[12] and Gilbert and Sandorfy.[13] On the other hand, Narayan and Murrell[16] have suggested that, in fluoro- and *p*-difluorobenzene, the π level, which is related to the a_{2u} level of benzene, should be preceded by a σ level, as in benzene itself, and that in the higher fluorides the highest σ level would lie below the third π level.

Table 6. Ionization potentials of fluorobenzene (eV)

Obsd		This work
Clark[12]	Turner[11]	
9.21	9.19	9.40 πb_1
9.87	9.82	9.54 πa_2
11.83	11.77	13.83 πb_1
12.98	12.8	11.37 b_2
13.89	13.68	12.00 a_1
14.55	14.2	14.07 b_2
	14.8	14.45 a_1
16.24	15.9	14.68 b_2
17.77	17.3	16.52 a_1
		17.74 b_2
19.02		18.11 πb_1
19.55		18.30 a_1
20.69		20.75 a_1
		21.53 b_2
		23.33 a_1
		25.46 b_2
		27.89 a_1
		33.23 a_1

Table 7. Ionization potential of *p*-difluorobenzene (eV)

Obsd		This work
Clark[12]	Turner[11]	
9.15	9.33	9.41 πb_{3g}
10.04	10.10	9.67 πb_{2g}
12.16	(12.3)	13.73 πb_{1u}
		11.42 b_{1g}
13.55	(13.6)	13.31 a_g
14.24	(14.3)	14.16 b_{3u}
15.01	(15.0)	14.37 b_{3u}
(15.44)	(15.3)	14.58 b_{2u}
(16.79)		16.87 b_{1g}
17.12	17.09	17.86 b_{2u}
		18.09 πb_{3g}
		18.27 a_g
17.93		18.31 πb_{1u}
19.74		18.73 b_{3u}
20.03		19.79 b_{2u}
		20.88 a_g
		22.12 b_{1g}
		25.70 b_{3u}
		26.92 a_g
		28.51 b_{2u}
		33.33 a_g

Table 8. Ionization potential of 1,2,4-trifluorobenzene (eV)

Obsd[12]	This work
9.30	9.50 $\pi a''$
10.05	9.72 $\pi a''$
12.26	13.67 $\pi a''$
12.93	11.84 a′
13.64	13.32 a′
14.35	14.18 a′
15.26	14.47 a′
(15.93)	16.04 a′
(16.92)	17.21 a′
	17.55 a′
	17.96 $\pi a''$
	18.13 a′
	18.23 $\pi a''$
17.05	18.35 a′
17.92	18.67 $\pi a''$
20.5	18.74 a′
	19.26 a′
	20.23 a′
	22.10 a′
	24.10 a′
	27.06 a′
	27.69 a′
	29.02 a′
	33.43 a′

Table 9. Differences of ionization potentials between benzene and its fluoro-derivatives

Calcd			
FB	PDFB	TFB	Symmetry of benzene
−0.01	0.00	0.09	$e_{1g}(\pi)$
0.13	0.26	0.31	
0.03	0.08	0.50	e_{2g}
0.66	1.97	1.98	
−0.10	−0.20	−0.09	$a_{2u}(\pi)$
Obsd			
FB	PDFB	TFB	Symmetry of benzene
−0.06	−0.12	0.03	$e_{1g}(\pi)$
0.6	0.77	0.78	
−0.1	−0.04	0.06	$a_{2u}(\pi)$
1.51	?	1.46	e_{2g}
2.42	2.08	2.17	

FB=Fluorobenzene, PDFB=*p*-Difluorobenzene, TFB=1,2,4-Trifluorobenzene.

Table 9 lists the calculated energy shifts, measured from the corresponding *IP*'s of benzene, of the first *IP*'s of the fluorobenzenes brought about on fluorination, together with the observed ones. In obtaining the observed shifts we have assumed that the observed third bands are related to the a_{2u} π-orbital of benzene, since the shifts of this band on fluorination are always very small. The energy shifts of the calculated fifth band are also quite small, so that the observed third band should be assigned to the calculated fifth one. The calculated third and fourth levels, predicted to be related to the e_{2g} σ orbitals of benzene, undergo relatively large blue shifts, and the observed fourth and fifth levels should be assigned to these levels.

Thus, the characteristic bands of the photoelectron spectra observed at 13.89 eV in fluorobenzene and at 13.55 eV in *p*-difluorobenzene should be assigned to the bands due to σ electrons. On the other hand, from a nonempirical LCAO MO SCF calculation,

Clark *et al.*[17] have assigned these bands to a fluorine 2p(σ) lone-pair orbital mixed with a benzene σ orbital. In our calculation, the ionization potentials due to fluorine lone-pair electrons are predicted to lie in the 15.5—18.5 eV range in fluorobenzene, the 16.5—19 eV range in *p*-difluorobenzene, and the 17.0—19.5 eV range in 1,2,4-trifluorobenzene.

A Perturbational Treatment of the Perfluoro Effect. In order to understand the origin of the perfluoro effect, we now use a simple perturbation theory in the framework of the Hückel MO approximation in calculating the energy change, due to fluorination, of π molecular orbitals. The energy change, brought about by a fluoro-substituent, of the i-th π molecular orbital of a conjugated molecule can be expressed as;

$$\Delta\varepsilon_i = C_{ir}^2\delta\alpha_C + \frac{C_{ir}^2}{\varepsilon_i-\varepsilon_F}\beta_{CF}^2$$

where C_{ir} is the molecular orbital coefficient of the carbon atom on which the fluoro-substituent is introduced; $\delta\alpha_C$, the change in the Coulomb integral brought about by the inductive effect of a fluorine atom on the attached carbon, and β_{CF}, the resonance integral between the carbon and fluorine 2p π orbitals.

In the Hückel MO approximation, for a fluoro-substituent $\delta\alpha_C$ and β_{CF} are taken usually to be 0.15—0.30 and 0.5—0.7 respectively in β (the standard resonance integral) units. The value of ε_F, the energy of the fluorine 2pπ atomic orbital, is taken to be about 3β (measured from the standard Coulomb integral, α), which corresponds to the ionization potential of the fluorine 2p electron, 17.34 eV. These parameter values indicate that, in case of fluorination, while the inductive effect gives rise to a lowering in the energy of the π molecular orbitals of the parent hydrocarbon, these orbitals are always raised by the conjugative (or mesomeric) effect, and suggest that, for π molecular orbitals which lie within a certain energy range of the parent hydrocarbon, the conjugative and inductive effects may cancel each other, with the result that these orbitals suffer no substantial energy change on fluorination. Actually, if we use $\delta\alpha_C=0.28$, $\beta_{CF}=0.7$, and $\varepsilon_F=2.8$, the sum, $\delta\alpha_C+\beta^2_{CF}/(\varepsilon_i-\varepsilon_F)$, is approximately equal to zero for π molecular orbitals which lie at about $\alpha+\beta$, *i.e.*, about 10 eV. The energies of the b_{1u} π orbital of ethylene and the e_{1g} π orbitals of benzene are equal to $\alpha+\beta$ in the Hückel MO approximation; thus, they can be predicted not to change on fluorination.

TABLE 10. DIFFERENCES OF π-IONIZATION POTENTIALS BETWEEN ETHYLENE AND ITS HALOGENO-DERIVATIVES (eV)[a]

	Mono-			Tetra-		
	F	Cl	Br	F	Cl	Br
Calcd[b]	0.012	−0.269	−0.722	0.049	−1.06	−2.89
Obsd	0.003	−0.34	−0.52	0.02	−1.01	

a) The standard β value is taken to be 3.1 eV.
b) Values for various parameters are taken as follows; $\delta\alpha$(Cl)=0.18, $\delta\alpha$(Br)=0.14, β(C-Cl)=0.6, β(C-Br)=0.5, $\varepsilon_{Cl}=1.8$, $\varepsilon_{Br}=1.4$.

The π molecular orbitals which are higher or lower in energy than $\alpha+\beta$ should, in principle, shift to a lower or a higher energy respectively on fluorination. For example, the b_g π orbital of butadiene, whose energy is $\alpha+0.618\beta$, is predicted to be lowered on fluorination, whereas the a_u π orbital, which lies at $\alpha+1.618\beta$, should be raised. This prediction is in qualitative agreement with the results obtained by the present calculation[3] and the experimental fact.[10]

On the basis of the simple perturbation theory, it is expected that, on halogenations other than fluorination, the π molecular orbitals which lie at about 10 eV of a conjugated hydrocarbon will be raised in energy. In the case, for example, of chlorination, the ionization potential of the chlorine 3p electron (12.95 eV) is considerably smaller than that of the fluorine 2p electron, and the chlorine atom is less electronegative than the fluorine atom, so that the conjugative effect overcomes the inductive effect, with the result that the π MO's of the parent hydrocarbon are raised in energy. In the case of bromination, the π MO's are predicted to be shifted further to a higher energy. Table 10 presents the differences, calculated by using the simple perturbation theory, of the π ionization potential between ethylene and its halogeno-derivatives. The predicted values are in fairly good agreement with the experimental ones[11] listed also in Table 10.

Finally, it may be added that, as for the σ MO's, there seems not to exist any simple way for predicting the amounts of energy change brought about by fluorination.

References

1) M. B. Robin, N. A. Kuebler, and C. R. Brundle, "Electron Spectroscopy," ed. by D. A. Shirley, North-Holland (1972), p 351; C. R. Brundle, M. B. Robin, and G. R. Jones, *J. Chem. Phys.*, **52**, 3383 (1970).; C. R. Brundle, N. B. Robin, and H. Bash, *ibid.*, **53**, 2196 (1970).

2) S. Meza and U. Wahlgren, *Theor. Chim. Acta.*, **21**, 323 (1971).

3) T. Hayashi and T. Nakajima, *Bull. Chem. Soc. Jpn.*, **48**, 980 (1975).

4) A. Tajiri, N. Ohmichi and T. Nakajima, *Bull. Chem. Soc. Jpn.*, **44**, 2347 (1971).

5) N. Ohmichi, A. Tajiri and T. Nakajima, *Bull. Chem. Soc. Jpn.*, **45**, 3026 (1972).

6) J. Del Bene and H. H. Jaffé, *J. Chem. Phys.*, **48**, 1807 (1968); *ibid.*, **48**, 4050 (1968); *ibid.*, **49**, 1221 (1969).

7) J. M. Sichel and M. A. Whitehead, *Theor. Chim. Acta.*, **7**, 32 (1967).

8) L. E. Sutton, "Tables of Interatomic Distances," The Chemical Society, London (1958).

9) R. F. Lake and H. Thompson, *Proc. R. Soc. London, Ser. A*, **315**, 323 (1970).

10) C. R. Brundle and M. B. Robin, *J. Am. Chem. Soc.*, **92**, 5550 (1970).

11) D. W. Turner, C. Baker, A. D. Baker, and C. R. Brundle, "Molecular Photoelectron Spectroscopy," John Wiley and Sons, Ltd., New York (1970).

12) I. D. Clark and D. C. Frost, *J. Am. Chem. Soc.*, **89**, 244 (1967).

13) R. Gilbert and C. Sandorfy, *Chem. Phys. Lett.*, **9**, 121 (1971).

14) C. Sluse-Goffart and J. Monigny, *Chem. Phys. Lett.*,

25, 231 (1974).
15) D. R. Smith and J. W. Raymonda, *Chem. Phys. Lett.*, **12**, 269 (1971).
16) B. Narayan and J. N. Murrell, *Mol. Phys.*, **19**, 169 (1970).
17) D. T. Clark, D. Kilcast, D. B. Adams, and I. Scanlan, *J. Electron Spectry.*, **1**, 153 (1972/1973).
18) J. A. Pople and D. L. Beveridge, "Approximate Molecular Orbital Theory," McGraw-Hill (1970).
19) C. R. Brundle, M. B. Robin, N. A. Kuebler, and Harold Basch, *J. Am. Chem. Soc.*, **94**, 1451 (1972).
20) E. Heilbronner, R. Gleiter, H. Hopf, V. Hornung, and A. de Meijere, *Helv. Chim. Acta*, **54**, 783 (1971); M. Beez, G. Bieri, H. Bock, and E. Heilbronner, *ibid.*, **56**, 1028 (1973).

Stability of Dextran Solutions

Masuo AIZAWA, Shuichi SUZUKI, Tatuo KUOKA,* Noriyasu NAKAJIMA,* and Yutaka IWAO
Research Laboratory of Resources Utilization, Tokyo Institute of Technology, Ookayama, Meguro-ku, Tokyo 152
**Morishita Pharmaceutical Co., Ltd., 418 Numakage, Urawa 336*

(Received December 8, 1975)

In order to clarify the accessibility of dextran to both water and dextran the onset of turbidity in dextran solution was studied by means of viscosimetry and near-infrared and PMR measurements. Mole fraction of monomeric and hydrogen-bonded water species in dextran solutions were calculated for various concentrations of dextran solutions from $2\nu_1+\nu_3$ and $\nu_1+\nu_2+\nu_3$ bands where ν_1, ν_2, and ν_3 are the fundamental vibrations of symmetric stretching, bending and asymmetric stretching, respectively. The extent of hydrogen bonds was estimated from PMR chemical shift of water proton. A dextran solution was characterized by a low concentration in monomeric water. An anomalous time dependence of viscosity and PMR chemical shift was observed for concentrated solutions. A mechanism has been proposed for gelation and the onset of turbidity, stress being laid on comparable accessibility of dextran to both water and dextran.

Certain molecular weight fractions of dextran are of significant use as blood plasma substitutes. This brings forward the hydration of dextran as an important physiological subject. However, little attention has been paid to the stability of dextran solutions. A 40% dextran 40 (a fraction of 40000 molecular weight) solution loses transparency with time and turns into a gel.[1] A 10% dextran 40 solution used as blood plasma substitute gives rise to the formation of insoluble substance in an injection vial during the course of sotrage.[2,3] This indicates peculiarity in the stability of a dextran solution. In this paper, the results of studies on the transition from a solution to a sol or a gel are given.

Onset of turbidity and gelation are generally accomapanied by an intermolecular cross-linking of polymer chains.[4] Accessibility of polymer chain to another one and water might play a key role to determine the state of a solution. Accessibility of dextran to water has been characterized by estimating the extent of hydrogen bonds in water by means of near-infrared and proton magnetic resonance (PMR) investigations. Intermolecular interaction of dextran has been evaluated from viscometric data.

Experimental

Dextran 40 from *Leuconostoc* strain cultured in sucrose media was obtained from Fison Ltd., Pharmaceutical Division (London). The average molecular weight was 40000.

Viscosity measurements were carried out with a Tokyo Keiki Type B Viscometer. A Shimadzu Model SV-20 automatic spectrophotometer was used for obtaining near-infrared spectra. A 1 cm-path of cell was jacketed with circulating temperature-controlled water. For PMR a JEOL Model MH-60 was used. Samples were injected in a standard tube and were kept at 25 °C for a fixed time. Measurements were conducted with and without spining a sample tube. Chemical shift was referred to external tetramethylsilane (TMS).

Results

Turbidity and Gelation of Dextran Solutions. Dilute dextran solution remains clear even after storage for a long time. Insoluble substance is formed in a 10% dextran solution during storage. When dextran concentration exceeds 20%, the solution gradually turns turbid. In the concentration range 40—50%, the occurrence of turbidity is followed by gelation. The change is accompanied by an increase in viscosity. The change of viscosity with time for a 48% dextran solution is shown in Fig. 1. Viscosity was determined at 25 °C with a Type B viscometer. Viscosity decreases at first, then increases, attaining more than ten times the initial value in 160 h after preparation.

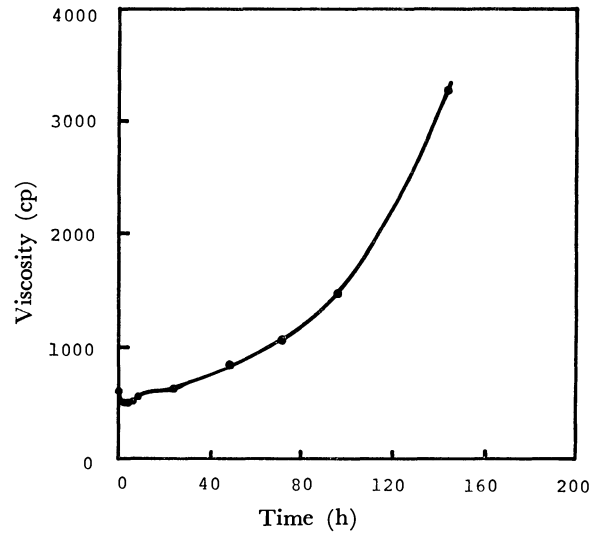

Fig. 1. Time dependence of viscosity of a dextran solution. Viscosity was determined for a 48% of dextran 40 solution at 25 °C.

Increase in viscosity is shown for solutions of various concentrations stored at 25 °C for 7 days. A marked increase is observed for the solution (concn>30%) which exhibited conspicious turbidity.

The results suggest that an increase in viscosity is induced by intermolecular cross-linking of dextran during the course of storage. Dextran might be dissolved in an unstable state, turning gradually to a stable state. Such a transition would be accelerated in a concentrated solution. The following investigation was performed in order to characterize the transition from an unstable solution to a stable solution.

Hydrogen-bonds in a Stable State of Dextran Solutions. In order to estimate the extent of hydrogen-bond formation, near-infrared and PMR investigations were carried out for a dextran solution stored for a long

time. An aqueous dextran solution contains several types of hydrogen-bond: (1) intra-dextran molecule, (2) inter-dextran molecule, (3) dextran–water molecule, and (4) inter-water molecule. Hydrogen-bonds related to water, (3) and (4), were studied with particular attention.

Hydrogen-bond formation of water molecules can be determined by various methods such as vibration spectroscopy and nuclear magnetic resonance (NMR). For an aqueous solution, near-infrared spectroscopy and NMR are effective.

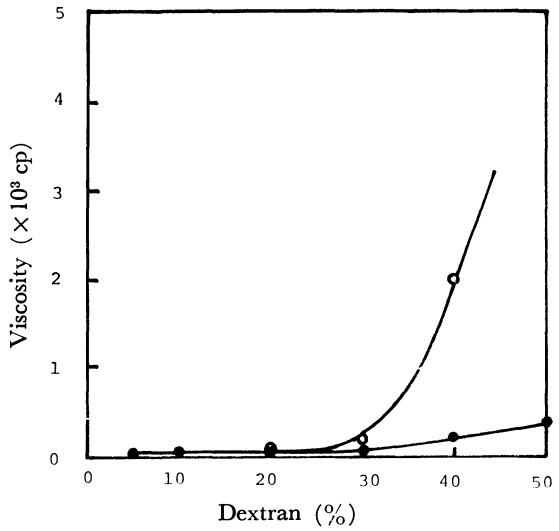

Fig. 2. Viscosity-concentration curves for dextran solutions. Viscosity was determined for a respective concentration of dextran 40 solution at 25 °C, 0 h (—●—) and 7 days (—○—) after preparation.

Water has three fundamental vibrations; ν_1 of symmetric stretching, ν_2 of bending and ν_3 of asymmetric stretching. Combination bands such as $\nu_1+\nu_2+\nu_3$ and $2\nu_1+\nu_3$ appear in near-infrared in the range 900—1300 nm. These two combination bands are sensitive to hydrogen-bond formation.

Water gives absorbance maximum at 977 nm for the $2\nu_1+\nu_3$ combination band at 25 °C. The peak is estimated to shift to 958 nm for monomeric water and 988 nm for entirely hydrogen-bonded water.[5] On the other hand, the $\nu_1+\nu_2+\nu_3$ combination band consists of three peaks, attributed to monomeric water (1160 nm), single hydrogen-bonded water (1200 nm) and double hydrogen-bonded water (1240 nm).[6] Relative intensity of these three peaks depends on the extent of respective hydrogen-bonded water species.

Near-infrared spectra at 25 °C are shown in Fig. 3 for water, 10% and 50% dextran solutions. The $2\nu_1+\nu_3$ peak shifted to a longer wavelength with an increase in the extent of hydrogen-bonded water species. A decrease in intensity for 50% dextran solution might be due to a decrease in the concentration of water.

A complicated change was observed for a $\nu_1+\nu_2+\nu_3$ combination band caused by addition of dextran to water. Absorbance at 1160 nm decreased a great deal for dextran solutions. The effect of dextran on relative intensity at 1160, 1200, and 1240 nm is more

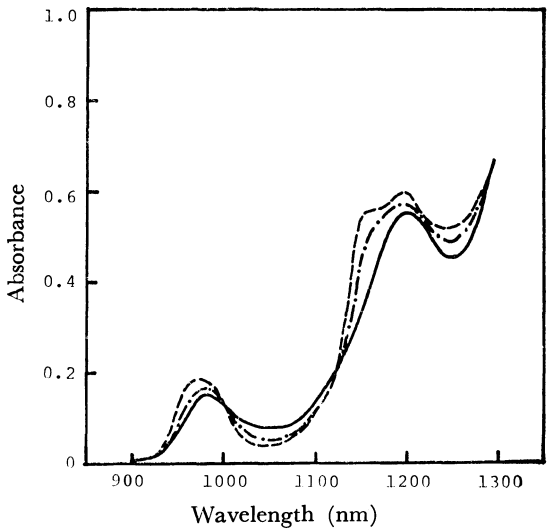

Fig. 3. Near-infrared spectra of water in dextran solutions. Spectra were obtained for a 50% (——), a 10% (—·—) of dextran solutions and water (----) at 25 °C.

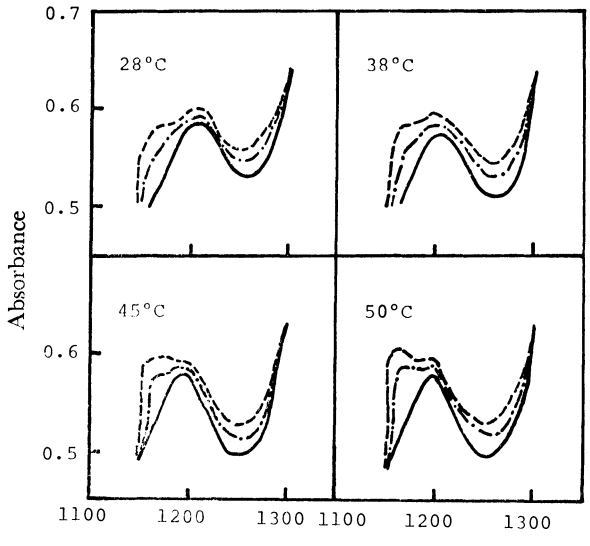

Fig. 4. Temperature dependence of near-infrared spectra of water in dextran solutions.
Spectran were determined for a 50% (——), a 10% (—·—) of dextran solutions and water (----) at respective temperature.

obvious with rise in temperature. Temperature dependence of the $\nu_1+\nu_2+\nu_3$ band is shown in Fig. 4 for water, 10% and 50% dextran solutions. For water, absorbance at 1160 nm increased markedly with an increase in temperature, which was caused by breakingdown of hydrogen-bonds. Formation of monomeric water species might be slightly depressed for the 10% dextran solution with increasing temperature. No obvious decrease in absorbance at 1160 nm was found for the 50% dextran solution even at 50 °C. This suggests that release of monomeric water species is extremely retarded, and that in concentrated solutions hydration becomes very stable against temperature.

The extent of monomeric and hydrogen-bonded

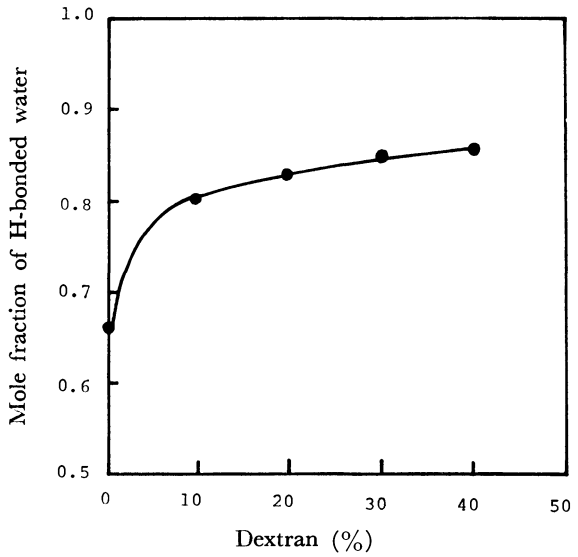

Fig. 5. Molar fraction of hydrogen bonded water species in various concentrations of dextran solutions.
Molar fraction of hydrogen bonded water species was calculated from absorbance at 1160 and 1200 mm at 28 °C.

water species can be estimated from intensity at 1160 and 1200 nm for dextran solutions.[7,8] Hydrogen-bonded water species should be classified into single and double hydrogen-bonded ones. We have calculated both types as hydrogen-bonded water species. Mole fraction of hydrogen-bonded water species is plotted for each concentration of dextran solution at 28 °C in Fig. 5. Hydrogen-bonds might be significantly formed with an increase in concentration of dextran. As an example the extent of monomeric water involved in 40% dextran solution is less than half in pure water at 28 °C.

A similar result was obtained from PMR studies on the state of water in dextran solution. Water proton gives a sharp single peak around 5 ppm *vs.* tetramethylsilane (TMS). Hydrogen-bond formation shifts the peak to lower magnetic field. A 10% dextran solution exhibited a slightly broadened but still sharp single peak at 6 ppm when a sample tube was spinned. Non-spinned sample, however, gave a very broadened signal. At 50% dextran concentration, another broad signal was detected at a higher magnetic field than that of the main signal. The broad signal at higher magnetic field was obtained either with or without spinning of the sample tube (Fig. 6). The signal was attributed to the protons of dextran. Broadening in water proton signal for a 50% dextran solution might be caused by immobilization of water.

The concentration dependence of PMR chemical shift is shown in Fig. 7 for water proton of dextran solutions of various concentrations. Measurements were carried out with a spinned sample tube 24 h after the samples had been prepared. Chemical shift moved sharply to lower magnetic field with an increase in concentration of dextran and reached a constant value at approximately 10%, which indicated a marked increase in the extent of hydrogen-bonds of water.

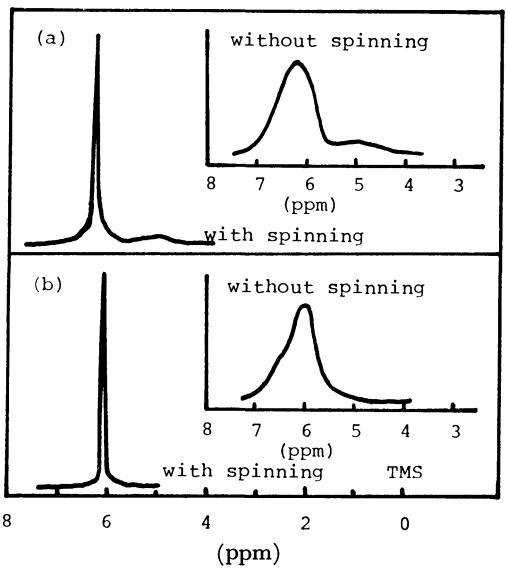

Fig. 6. Proton magnetic resonance spectra of water in dextran solutions.
Measurements were conducted for a 10% (b) and a 40% (a) of dextran solutions with and without spinning a sample tube at 25 °C using tetramethylsilane (TMS) as an external standard.

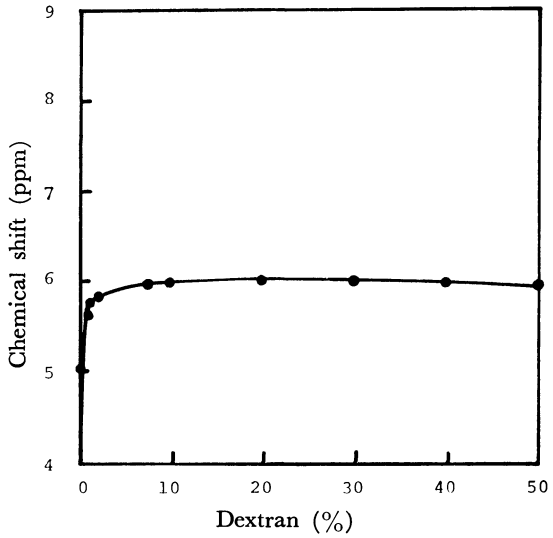

Fig. 7. Concentration dependence of PMR chamical shift for dextran solutions.
Chemical shift was determined from PMR spectrum for respective concentration of dextran solution measured with spinning a sample tube at 25 °C using TMS as an external standard.

Anomalous Time Dependence of Viscosity and PMR Chemical Shift. Investigations on the process of hydration of dextran are necessary to clarify the mechanism of the occurrence of turbidity and gelation. Time dependence of viscosity and PMR chemical shift was examined. An anomalous time dependence was observed in concentrated solutions.

Anomality in viscosity is shown in Fig. 8. Viscosity was measured at 25 °C for a 48% dextran solution. Viscosity was found to decrease sharply in the first few hours, reaching the minimum, and then to in-

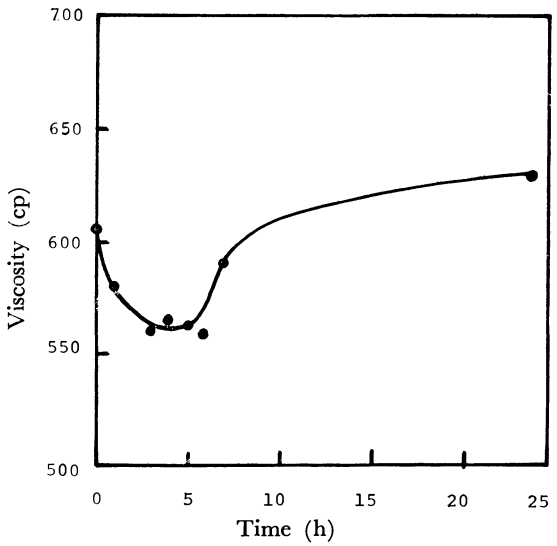

Fig. 8. Viscosity change of a dextran solution.
Measurements were made for a 48% of dextran solution at 25 °C.

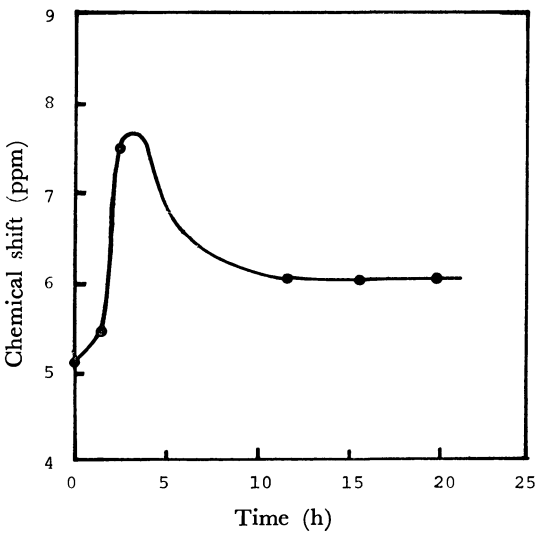

Fig. 9. Time dependence of PMR chemical shift of water in a dextran solution.
A 40% of dextran solution was injected into a standard sample tube with an external reference of TMS. The sample tube was spinned for measurement at 25 °C.

crease over the initial value. No such anomaly was observed for a dilute solution which showed constant viscosity irrespective of time. A 10% dextran solution showed a gradual increase in viscosity with no minimum. A minimum in viscosity–time curve was observed when the dextran concentration exceeds 30%.

Time dependence of PMR chemical shift is shown for a 40% dextran solution in Fig. 9. A marked shift to lower magnetic field in chemical shift took place in a few hours. This was followed by a sharp change to higher magnetic field up to a steady value. The steady value of chemical shift lies at fairly lower magnetic field as compared with that of the initial one. The maximum in a time–chemical shift curve appears in a solution with dextran concentration exceeding 30%. This is in line with viscosity.

Discussion

Maximum viscosity is associated with a PMR chemical shift *vs.* time curve for water proton of a dextran solution. Anomalous time dependences of viscosity and PMR chemical shift suggest that at least two competitive reactions such as hydration and dehydration take place simultaneously.

The viscosity of a dextran solution seems to be closely related to the states of polymer chains. The increase in viscosity might result from the intermolecular cross-linking of dextran, which causes turbidity and gelation. The decrease in viscosity in the first stage might be caused by an opposite reaction such as decoupling of intermolecular interaction followed by intermolecular linking. It seems that several processes such as (1) intermolecular cross-linking, (2) decoupling, (3) hydration, and (4) dehydration of dextran take place simultaneously and competitively. The combined effect of these processes might be determined by competitive accessibility of dextran to water and dextran. Dextran has comparable accessibility to both water and dextran. That is why a dextran solution exhibits a complicated behavior.

Dextrans are highly branched polymers of D-glucose. The linkages between D-glucose units at the branching points are α-1,6, α-1,4, and α-1,3. Taylor *et al.*[9,10] have extensively investigated the effects of variation in branching structure on the water sorption. Dextrans with a high α-1,4 content exhibited the greatest sorption, those with appreciable α-1,3 content exhibited intermediate sorption, while those with predominantly α-1,6 linkages were least hygroscopic. The results of powder X-ray diffraction measurements indicate that the structural correlation is related to the onset of crystalization or crystallinity. Linear polymers are crystallized with the greatest ease, while cross branching tends to prevent the alignment of proximal linear chains.

Dextran 40, in which the α-1,6 linkage predominates, can be characterized by the least hygroscopicity and the greatest ease in crystallization of dextran. Dextran is soluble in water because of an extreme accessibility to water. If dextran has a chance to associate with other polymer chains, intermolecular cross-linking through hydrogen-bonding would be induced due to high accessibility to dextran, giving rise to turbidity and gelation. Although a dextran solution displays turbidity and makes a gel, a neat and clear solution can be obtained by a small driving force to break intermolecular coupling, *e.g.*, heating, since the strength of intermolecular coupling would be no more than that of hydration. A turbid dextran solution can be transformed into a clear one by heating.

References

1) N. Nakajima, Y. Iwao, T. Kuoka, S. Suzuki, and M. Aizawa, *Yakugaku Zasshi*, **95**, 749 (1975).
2) R. A. Edwald, A. A. Young, and W. H. Crosby, *Military Med.*, **129**, 952 (1964).

3) D. E. Cadwallader, Jr., C. H. Becker, J. H. Winter, and D. Marcus, *J. Am. Pharm. Assoc.* (*Sci.*), **47**, 894 (1958).
4) M. Aizawa, M. Takahashi, and S. Suzuki, *Chem. Lett.*, **1974**, 193.
5) O. D. Bonner, G. B. Woolsey, *J. Phys. Chem.*, **72**, 899 (1968).
6) G. Herzberg, "Molecular Spectra and Molecular Structure. II," D. Van Northrand Co., Ind., Princeton, N. J. (1959), p. 281.
7) M. Aizawa, and S. Suzuki, *Bull. Chem. Soc. Jpn.*, **46**, 2634 (1973).
8) K. Buijs, and G. R. Choppin, *J. Chem. Phys.*, **39**, 2035 (1963).
9) N. W. Taylor, H. F. Zobel, N. N. Hillman, and F. R. Senti, *J. Phys. Chem.*, **63**, 599 (1959).
10) N. W. Taylor, J. E. Clusby, F. R. Senti, *J. Phys. Chem.*, **65**, 1810 (1961).

The Structure of the Cyclodextrin Complex. III. The Crystal Structure of the α-Cyclodextrin–Sodium Benzenesulfonate Complex

Kazuaki HARATA

Research Institute for Polymers and Textiles, Sawatari-4, Kanagawa-ku, Yokohama 221

(Received December 25, 1975)

The crystal structure of the α-cyclodextrin–sodium benzenesulfonate complex, which has a channel-type structure, was determined by X-ray analysis. The crystals were orthorhombic with the space group of $P2_12_12$, cell dimensions of $a=21.832(3)$, $b=16.529(2)$, and $c=8.356(1)$ Å, and $Z=2$. The structure was determined on the basis of 2894 diffractometer data and refined by the block-diagonal least-squares methods to the final R-value of 0.069. The benzenesulfonate anion is arranged in the channel which is formed by the stack of α-cyclodextrin rings along the c axis. The benzene ring is located in the cavity, while the sulfonato group is hydrogen-bonded to the primary hydroxyl groups of the adjacent α-cyclodextrin molecule. The space outside the channel is filled with water molecules and sodium ions, and the hydrogen-bonding network is formed. The energy of the complex formation was calculated for two possible structures of the 1 : 1 complex in an aqueous solution.

α-Cyclodextrin(α-CDx) forms a number of crystalline adducts with a variety of "guest" molecules.[1] Several types of crystal structures have been investigated by the X-ray method.[2-9] The cage-type structure[2-6] is formed when the "guest" molecule is sufficiently small to be enclosed in the cavity, both sides of which are blocked by adjacent α-CDx molecules. In the case of the *p*-iodoaniline complex,[7] the "guest" molecule is too large to be enclosed in the interior of the cavity; as a result, the amino group protrudes from an open end of the cavity.

In the channel-type structure,[8,9] the α-CDx molecules are stacked along two-fold axes to form endless channels and the "guest" molecules in the channels are hydrogen-bonded to the primary hydroxyl groups of α-CDx. A long molecule as well as a small molecule can be included in the channel. In the potassium acetate complex,[8] the acetate anion is so small that the two water molecules are located in the empty space of the cavity. In the Methyl Orange complex,[9] the "guest" molecule is twice as long as the cavity. Therefore, the "guest" molecule extends through two α-CDx rings. Sodium benzenesulfonate(BS) also forms an α-CDx complex with a channel-type structure. The benzenesulfonate anion is a part of the Methyl Orange anion, and it consists of hydrophobic and hydrophilic groups. It is of interest to know which group is included in the cavity, and whether or not the hydrophilic group forms hydrogen bonds with primary hydroxyl groups. In this paper we will present the crystal and molecular structure of the α-cyclodextrin–sodium benzenesulfonate (1 : 1) complex. The energy of the complex formation in an aqueous solution was also calculated in order to investigate the binding force of the complex.

TABLE 1. CRYSTAL DATA

$C_{36}H_{60}O_{30}\cdot C_6H_5O_3SNa\cdot 10H_2O$,		Orthorhombic
Molecular weight		1333.2
Cell dimensions	a	21.832(3) Å
	b	16.529(2)
	c	8.356(1)
Cell volume	V	3015.3 Å^3
Space group		$P2_12_12$
	Z	2
Density	D_m	1.47 g·cm^{-3}
	D_x	1.47

Experimental

Crystals which are colorless prisms elongated along the c axis were obtained by letting stand an aqueous solution containing α-CDx and BS with 1 : 1 molar ratio. The

TABLE 2. THE FINAL ATOMIC PARAMETERS ($\times 10^4$)

The anisotropic thermal factors are of the form: $\exp[-(B_{11}h^2+B_{22}k^2+B_{33}l^2+B_{12}hk+B_{23}kl+B_{31}lh)]$.

	x	y	z	B_{11}	B_{22}	B_{33}	B_{12}	B_{23}	B_{31}
C(1,G1)	1533(3)	2428(4)	3405(8)	8(1)	20(2)	77(10)	-6(3)	9(9)	1(6)
C(2,G1)	1269(3)	2821(4)	4882(8)	9(1)	22(2)	66(10)	-4(3)	-8(9)	-4(6)
C(3,G1)	595(3)	2557(4)	5051(9)	10(1)	22(2)	59(9)	3(3)	-5(8)	6(6)
C(4,G1)	252(3)	2770(4)	3518(8)	8(1)	18(2)	49(9)	-5(3)	3(8)	0(6)
C(5,G1)	564(3)	2389(4)	2070(8)	9(1)	22(2)	57(9)	-3(3)	8(9)	5(6)
C(6,G1)	284(3)	2644(4)	490(8)	14(2)	32(3)	56(10)	5(4)	-8(10)	4(7)
O(2,G1)	1618(2)	2621(3)	6265(6)	11(1)	34(2)	67(7)	2(3)	-15(7)	-20(5)
O(3,G1)	313(2)	2963(3)	6364(6)	11(1)	39(2)	54(7)	10(3)	-35(7)	-3(5)
O(4,G1)	-348(2)	2434(3)	3681(6)	6(1)	18(2)	73(7)	2(2)	14(6)	2(4)
O(5,G1)	1204(2)	2642(3)	2023(6)	9(1)	24(2)	58(7)	0(2)	18(6)	2(4)
O(6,G1)	538(2)	2213(3)	-816(6)	18(1)	39(2)	48(7)	2(3)	-14(8)	6(5)
C(1,G2)	2492(3)	-528(4)	3310(9)	8(1)	25(3)	91(11)	4(3)	29(10)	12(7)
C(2,G2)	2659(3)	-6(5)	4730(8)	10(1)	22(2)	80(10)	6(3)	9(10)	1(6)
C(3,G2)	2177(3)	644(4)	4950(9)	11(1)	23(3)	76(11)	3(3)	5(10)	-7(7)
C(4,G2)	2099(3)	1136(4)	3410(9)	10(1)	21(2)	69(11)	7(3)	8(9)	11(6)
C(5,G2)	2003(3)	576(4)	1954(9)	15(2)	22(3)	65(10)	10(3)	-4(9)	11(7)
C(6,G2)	2051(4)	1050(5)	373(9)	28(2)	23(3)	71(12)	14(4)	0(10)	-11(8)
O(2,G2)	2727(2)	-493(3)	6137(6)	17(1)	31(2)	84(8)	7(3)	35(7)	-18(6)
O(3,G2)	2332(2)	1196(3)	6201(6)	15(1)	27(2)	65(7)	5(3)	-11(7)	-11(5)
O(4,G2)	1541(2)	1584(3)	3639(6)	8(1)	19(2)	77(7)	3(2)	3(6)	8(5)
O(5,G2)	2468(2)	-32(3)	1909(5)	15(1)	19(2)	69(7)	8(3)	13(7)	29(5)
O(6,G2)	1903(4)	530(4)	-912(7)	46(3)	50(3)	77(9)	9(5)	-9(10)	6(9)
C(1,G3)	863(3)	-2936(4)	3359(9)	10(1)	20(2)	90(11)	4(3)	-4(9)	9(7)
C(2,G3)	1291(3)	-2872(4)	4788(9)	11(1)	28(3)	63(10)	4(3)	18(9)	0(6)
C(3,G3)	1507(3)	-2005(4)	4991(9)	10(1)	26(3)	60(10)	3(3)	21(9)	-4(7)
C(4,G3)	1811(3)	-1718(4)	3442(8)	10(1)	25(3)	41(9)	-3(3)	9(8)	-1(6)
C(5,G3)	1375(3)	-1840(4)	2014(8)	11(1)	25(3)	41(9)	1(3)	-9(9)	14(6)
C(6,G3)	1693(4)	-1663(5)	424(9)	19(2)	38(4)	56(11)	-13(4)	4(10)	14(7)
O(2,G3)	981(2)	-3156(3)	6205(6)	11(1)	39(2)	83(8)	-5(3)	59(8)	-1(5)
O(3,G3)	1934(2)	-1925(3)	6273(6)	12(1)	40(2)	51(7)	-9(3)	15(7)	-15(5)
O(4,G3)	1907(2)	-866(3)	3638(6)	8(1)	21(2)	74(7)	2(2)	3(6)	15(5)
O(5,G3)	1176(2)	-2676(3)	1958(6)	12(1)	22(2)	56(7)	-1(2)	-11(6)	8(5)
O(6,G3)	1281(3)	-1717(4)	-864(7)	22(1)	49(3)	74(9)	-8(4)	-8(9)	-10(6)
C(1,BS)	0(-)	0(-)	7088(12)	13(2)	31(4)	64(14)	10(6)	0(-)	0(-)
C(2,BS)	547(4)	-94(8)	6290(11)	10(2)	85(6)	128(14)	3(6)	-11(19)	-6(9)
C(3,BS)	538(4)	-87(9)	4619(11)	17(2)	91(7)	121(15)	9(7)	32(20)	37(10)
C(4,BS)	0(-)	0(-)	3797(14)	26(3)	44(5)	90(18)	12(8)	0(-)	0(-)
S(BS)	0(-)	0(-)	9206(3)	26(1)	26(1)	72(4)	7(2)	0(-)	0(-)
O(1,BS)	606(8)	-261(9)	9687(14)	49(5)	68(8)	63(17)	58(11)	-23(20)	-70(17)
O(2,BS)	-504(8)	-593(8)	9663(17)	57(6)	35(6)	152(25)	-40(10)	-7(20)	67(21)
O(3,BS)	-178(6)	832(7)	9708(14)	27(3)	33(5)	110(18)	7(6)	-22(17)	-6(13)
Na	1472(3)	4867(4)	9344(8)	22(2)	31(3)	108(10)	10(3)	-3(9)	16(7)
O(W1)	1170(6)	4885(7)	2255(14)	92(5)	86(6)	425(27)	38(11)	9(25)	-287(21)
O(W2)	0(-)	5000(-)	3634(17)	145(11)	56(6)	241(27)	35(16)	0(-)	0(-)
O(W3)	1377(3)	6306(4)	9145(8)	41(2)	40(3)	129(11)	31(4)	-7(10)	-26(9)
O(W4)	1712(3)	3383(4)	9290(7)	26(2)	45(3)	114(10)	-38(4)	4(10)	18(7)
O(W5)	1130(7)	4796(9)	9326(19)	31(4)	60(8)	22(29)	-9(10)	-37(28)	11(20)
O(W6)	303(7)	4571(9)	6846(22)	32(4)	53(7)	304(37)	16(9)	-1(31)	-45(24)
O(W6')	832(7)	4645(9)	7149(21)	28(4)	47(7)	271(34)	5(8)	-56(27)	-61(20)

	x	y	z	B		x	y	z	B
H(1,G1)	2029	2592	3166	1.8	H(6A,G2)	2518	1279	224	2.9
H(2,G1)	1299	3483	4838	1.9	H(6B,G2)	1733	1563	393	2.9
H(3,G1)	558	1912	5325	1.8	H(1,G3)	698	-3554	3101	1.9
H(4,G1)	218	3427	3360	1.7	H(2,G3)	1682	-3279	4631	2.5
H(5,G1)	529	1732	2207	2.2	H(3,G3)	1124	-1616	5353	2.1
H(6A,G1)	364	3293	310	2.2	H(4,G3)	2250	-2005	3216	2.1
H(6B,G1)	-209	2550	525	2.2	H(5,G3)	977	-1443	2166	2.1
H(1,G2)	2807	-1033	3056	2.4	H(6A,G3)	2067	-2080	250	2.8
H(2,G2)	3105	282	4580	2.4	H(6B,G3)	1888	-1047	465	2.8
H(3,G2)	1754	357	5329	1.8	H(2,BS)	969	-186	6964	4.4
H(4,G2)	2488	1540	3206	2.1	H(3,BS)	963	-145	3936	5.3
H(5,G2)	1560	287	2073	2.5	H(4,BS)	0	0	2485	4.2

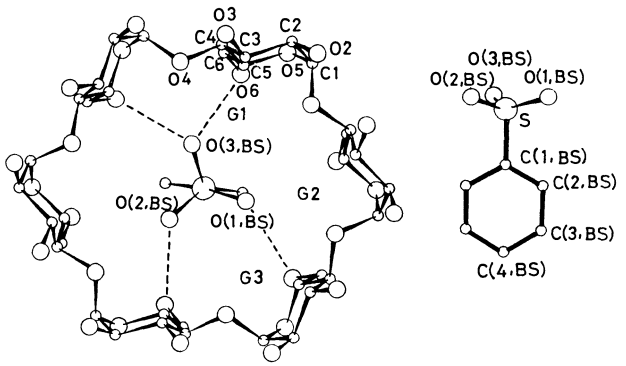

Fig. 1. The structure and numbering scheme of the complex. Dashed lines indicate hydrogen bonds between the sulfonato group and α-cyclodextrin.

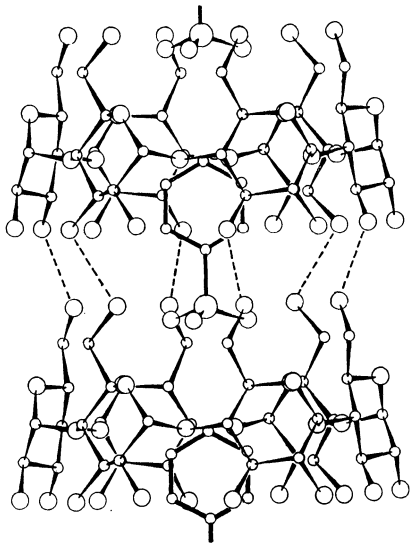

Fig. 2. The stacking feature of α-cyclodextrin rings. Dashed lines indicate O(3)---O(6) hydrogen bonds.

density was measured by the flotation method in a mixture of chloroform and dioxane. The crystal data are given in Table 1. The intensity data were collected on a Rigaku automated four-circle diffractometer using graphite monochromatized Cu$K\alpha$ radiation and the 2θ-ω scan technique. The crystal was enclosed in a quartz capillary with a small amount of water, since the crystal decomposes in air. 3064 independent reflections were obtained up to 150° in 2θ by using a specimen with dimensions of $0.4\times0.4\times0.4$ mm. 170 reflections with $|F_o|<3\sigma(F)$ were considered to be unobserved; $\sigma(F)$ is the standard deviation estimated according to the counting statistics. No corrections were made for absorption and extinction.

Determination and Refinement of the Structure

The structure was elucidated by assuming the same type of framework as that in the channel-type crystal. The positions and orientations of glucose residues were refined by the rigid-body least-squares method. A Fourier map calculated by using phases based on the glucose residues revealed the locations of BS and water molecules. The occupancy of 0.5 was assigned to the sodium ion, since there are only two BS molecules in the unit cell in spite of there being four equivalent positions. The BS anion was found on the two-fold axis with the statistical disorder of the sulfonato group. A water molecule (O(W5)) was found near the position of the sodium ion. The Na---O(W5) distance, however, is unreasonably short (Fig. 5). Therefore, O(W5) seems to occupy the position when the sodium ion is absent, having the average population of 0.5. O(W6) and O(W6′) are statistically disordered, and the distances of O(W5)---O(W6′) and O(W6)---O(W6′) are also absurdly short. These short distances can reasonably be explained by assigning 0.5 to the respective occupancies of O(W6) and O(W6′). The refinement of atomic parameters was carried out by the block-diagonal least-squares method. The positions of the hydrogen atoms attached to the carbon atoms were calculated and included in the structure factor calculation; the isotropic thermal factors used were equal to those of the carbon atoms to which the hydrogen atoms are bonded. The final R-value was 0.069. The quantity minimized was $\sum w(|F_o|-|F_c|)^2$, with $w=1.0$ for all reflections used. The atomic scattering factors were taken from "International Tables for X-ray Crystallography."[10] The atomic parameters are given in Table 2. The observed and calculated structure factors are listed in Table 3*.

Table 4. Bond distances (l/Å), angles (ϕ/°), and conformation angles (ϕ/°) in α-cyclodextrin

An asterisk (*) indicates the atom in the adjacent glucose residue.

	G1	G2	G3	AVERAGE
C(1)-C(2)	1.527(9)	1.512(10)	1.520(10)	1.520
C(1)-O(5)	1.429(8)	1.429(8)	1.422(8)	1.427
C(1)-O(4*)	1.408(8)	1.421(8)	1.422(8)	1.417
C(2)-C(3)	1.541(9)	1.514(10)	1.518(10)	1.524
C(2)-O(2)	1.424(8)	1.433(9)	1.442(9)	1.433
C(3)-C(4)	1.525(9)	1.531(10)	1.529(9)	1.528
C(3)-O(3)	1.425(8)	1.428(9)	1.426(8)	1.426
C(4)-C(5)	1.524(9)	1.543(10)	1.541(9)	1.536
C(4)-O(4)	1.430(7)	1.438(8)	1.432(8)	1.433
C(5)-C(6)	1.515(10)	1.539(11)	1.527(10)	1.527
C(5)-O(5)	1.458(8)	1.430(9)	1.448(8)	1.445
C(6)-O(6)	1.416(9)	1.412(11)	1.406(10)	1.411

	G1	G2	G3	AVERAGE
C(2)-C(1)-O(5)	109.3(5)	108.9(5)	109.3(5)	109.2
C(2)-C(1)-O(4*)	107.5(5)	106.8(5)	107.2(5)	107.2
O(5)-C(1)-O(4*)	110.3(5)	110.5(5)	111.1(5)	110.6
C(1)-C(2)-C(3)	110.0(5)	109.4(6)	110.2(6)	109.9
C(1)-C(2)-O(2)	109.8(5)	110.4(6)	109.5(6)	109.9
C(3)-C(2)-O(2)	111.9(5)	111.8(6)	111.3(6)	111.7
C(2)-C(3)-C(4)	109.0(5)	110.6(6)	109.5(6)	109.7
C(2)-C(3)-O(3)	110.4(5)	112.0(6)	112.0(6)	111.5
C(4)-C(3)-O(3)	109.1(5)	107.6(5)	108.9(5)	108.5
C(3)-C(4)-C(5)	110.6(5)	111.0(6)	110.3(5)	110.6
C(3)-C(4)-O(4)	106.2(5)	104.8(5)	105.8(5)	105.6
C(5)-C(4)-O(4)	109.0(5)	107.3(5)	107.9(5)	108.1
C(4)-C(5)-C(6)	113.4(5)	111.2(6)	111.5(6)	112.0
C(4)-C(5)-O(5)	109.3(5)	110.2(6)	109.6(5)	109.7
C(6)-C(5)-O(5)	106.5(5)	106.6(6)	106.9(5)	106.7
C(5)-C(6)-O(6)	111.9(6)	109.1(6)	111.2(6)	110.7
C(1)-O(5)-C(5)	114.8(5)	114.0(5)	113.9(5)	114.2
C(1)-O(4*)-C(4*)	118.3(5)	119.7(5)	118.7(5)	118.9

	G1	G2	G3	AVERAGE
C(1)-C(2)-C(3)-C(4)	-56.3	-55.5	-56.3	-56.0
C(2)-C(3)-C(4)-C(5)	55.8	50.8	54.1	53.6
C(3)-C(4)-C(5)-O(5)	-55.7	-50.8	-54.4	-53.6
C(4)-C(5)-O(5)-C(1)	59.2	58.5	59.6	59.1
C(5)-O(5)-C(1)-C(2)	-60.1	-63.6	-61.7	-61.8
O(5)-C(1)-C(2)-C(3)	57.3	60.4	59.0	58.9
O(4*)-C(1)-C(2)-O(2)	61.1	64.5	61.1	62.2
O(2)-C(2)-C(3)-O(3)	61.5	61.9	61.3	61.6
O(3)-C(3)-C(4)-O(4)	-65.4	-71.0	-66.7	-67.7
O(4)-C(4)-C(5)-C(6)	69.2	77.2	72.4	72.9
O(5)-C(5)-C(6)-O(6)	66.3	65.3	64.7	65.4
C(4)-C(5)-C(6)-O(6)	-173.5	-174.5	-175.5	-174.5
C(2)-C(1)-O(4*)-C(4*)	-129.0	-130.7	-129.6	-129.8
O(5)-C(1)-O(4*)-C(4*)	111.9	111.0	112.0	111.6
C(1)-O(4*)-C(4*)-C(3*)	127.6	130.3	130.5	129.5
C(1)-O(4*)-C(4*)-C(5*)	-114.3	-111.7	-110.2	-112.1

* Table 3 is kept as Document at the office of The Chemical Society of Japan. (Document No. 7626).

Description and Discussion of the Structure

The structure and numbering scheme of the complex are shown in Fig. 1. Bond distances, angles, and conformation angles in α-CDx(Table 4) are in good agreement with those of the Methyl Orange complex[9] and the potassium acetate complex.[8] The bond distances and angles of the BS anion are given in Table 5; they are in agreement with those observed in Methyl Orange.[11] The benzene ring has a good planarity (Table 6).

The geometrical data of the complex are shown in Table 7. The macro-cyclic conformation of the α-CDx ring is nearly the same as that in the Methyl Orange complex. The C(6)–O(6) bonds show a *gauche-trans* conformation, as is commonly observed in channel-type crystal. In the α-CDx cavity, the benzene ring is located at the same position as in the *p*-iodoaniline complex. The O(4, G3)---C(3, BS)

Table 5. Bond distances and angles in benzenesulfonate anion

(1) Bond distance (l/Å)			
C(1, BS)-C(2, BS)	1.376(14)	S(BS)-O(1, BS)	1.449(15)
C(2, BS)-C(3, BS)	1.396(15)	S(BS)-O(2, BS)	1.522(16)
C(3, BS)-C(4, BS)	1.369(16)	S(BS)-O(3, BS)	1.488(12)
C(1, BS)-S(BS)	1.770(10)		
(2) Bond angles (ϕ/°)			
C (1, BS) - C (2, BS) - C (3, BS)	118.2 (9)		
C (2, BS) - C (3, BS) - C (4, BS)	120.9 (10)		
C (2, BS) - C (1, BS) - S (BS)	119.0 (8)		
C (2-BS) - C (1, BS) - C (2, BS)*	122.0 (9)		
C (3, BS) - C (4, BS) - C (3, BS)*	119.7 (11)		
C (1, BS) - S (BS) - O (1, BS)	106.1 (8)		
C (1, BS) - S (BS) - O (2, BS)	104.5 (8)		
C (1, BS) - S (BS) - O (3, BS)	106.4 (6)		
O (1, BS) - S (BS) - O (2, BS)	113.6 (9)		
O (1, BS) - S (BS) - O (3, BS)	115.7 (8)		
O (2, BS) - S (BS) - O (3, BS)	109.5 (8)		

Table 6. Least-squares planes and deviations of atoms (d/Å)

An asterisk(*) indicates the symmetry related atom by the two-fold axis.

(1) Six O(4) atoms			
$0.0000X + 0.0000Y + 1.0000Z = 3.0517$			
O (4, G1)	0.024	O (4, G1)*	0.024
O (4, G2)	−0.012	O (4, G2)*	−0.012
O (4, G3)	−0.013	O (4, G3)*	−0.013
(2) Benzenesulfonate anion			
$0.1246X + 0.9922Y + 0.0000Z = 0.0000$			
C (1, BS)	−0.000	S (BS)	−0.000
C (2, BS)	−0.005	C (2, BS)*	0.005
C (3, BS)	0.005	C (3, BS)*	−0.005
C (4, BS)	0.000		

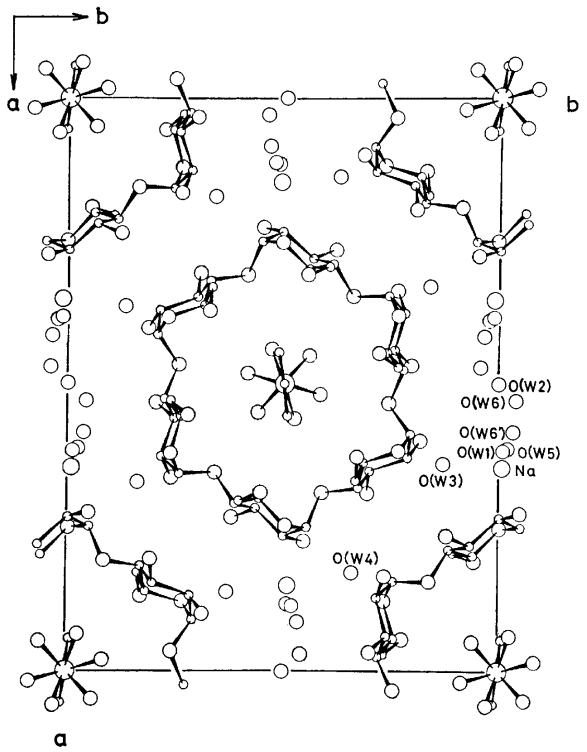

Fig. 3. The projection of the crystal structure along the c axis.

Table 7. Geometrical data for the complex (l/Å)

An asterisk(*) indicates the symmetry related atom by the two-fold axis.

(1) Diagonal distances of the cavity.				
O (4, G1)---O (4, G1)*	8.185		C (3, G1)---C (3, G1)*	8.837
O (4, G2)---O (4, G2)*	8.523		C (3, G2)---C (3, G2)*	9.739
O (4, G3)---O (4, G3)*	8.805		C (3, G3)---C (3, G3)*	9.337
O (6, G1)---O (6, G1)*	7.680		C (5, G1)---C (5, G1)*	8.269
O (6, G2)---O (6, G2)*	8.493		C (5, G2)---C (5, G2)*	8.950
O (6, G3)---O (6, G3)*	7.965		C (5, G3)---C (5, G3)*	8.544
(2) Distances between benzenesulfonate anion and α-CDx.				
C (3, G2)---C (3, BS)	3.785		O (6, G1)---O (3, BS)	2.800
C (3, G2)---C (2, BS)	3.925		O (6, G3)---O (1, BS)	2.857
C (3, G3)---C (2, BS)	3.943		O (6, G1)*---O (2, BS)	2.708
C (3, G3)---C (3, BS)	3.823		O (6, G3)*---O (3, BS)	2.857
O (4, G3)---O (2, BS)	3.919		O (6, G2)*---O (2, BS)	3.093
O (4, G3)---C (3, BS)	3.356		O (6, G2)---O (1, BS)	3.158

Table 8. Intermolecular distances (l/Å) less than 3.0 Å
Letters in the parentheses indicate the symmetry operation.

O (2, G1) - O (W4)		2.83	O (3, G3) - O (6, G3)	(b)	2.81
O (3, G1) - O (W6)		2.69	Na - O (W1)	(b)	2.52
O (W1) - O (W2)		2.81	O (6, G1) - O (3, BS)	(c)	2.80
O (W3) - O (W5)		2.56	O (6, G3) - O (3, BS)	(c)	2.86
Na - O (W3)		2.39	O (5, G1) - O (W4)	(c)	2.82
Na - O (W6′)		2.34	O (W1) - O (W5)	(c)	2.45
Na - O (W4)		2.51	O (5, G3) - O (W3)	(d)	2.92
O (W2) - O (W6)		2.85	O (W6) - O (W6′)	(e)	2.81
O (W5) - O (W6)		2.77	O (6, G1) - O (2, BS)	(f)	2.71
O (W4) - O (W5)		2.66	O (6, G3) - O (3, BS)	(f)	2.86
O (2, G3) - O (W3)	(a)	2.75	O (2, G2) - O (W1)	(g)	2.83
O (3, G1) - O (6, G1)	(b)	2.71	O (5, G2) - Na	(g)	2.55
O (3, G2) - O (6, G2)	(b)	2.81			

Symmetry code	Symmetry operator		
	x,	y,	z
a	x,	$-1+y$,	z
b	x,	y,	$1+z$
c	x,	y,	$-1+z$
d	x,	$-1+y$,	$-1+z$
e	$-x$,	$1-y$,	z
f	$-x$,	$-y$,	$-1+z$
g	$1/2-x$	$-1/2+y$,	$1-z$

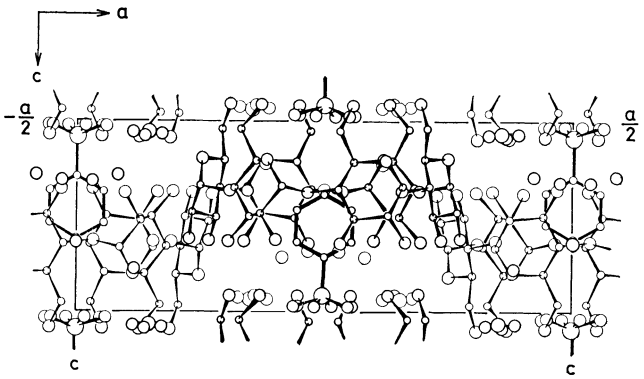

Fig. 4. The projection of the crystal structure along the b axis.

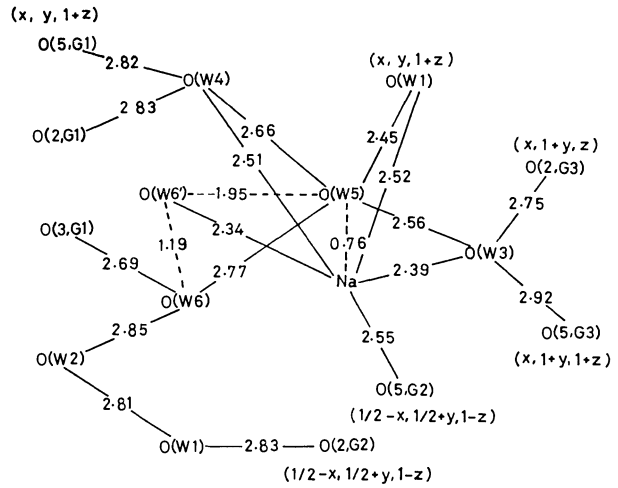

Fig. 5. The hydrogen-bonding scheme in the crystal. Dashed lines indicate the distances between the disordered atoms.

distance is 3.356 Å, while the corresponding distances are 3.25 and 3.35 Å in the *p*-iodoaniline complex.[7] The sulfonato group protrudes from the O(2), O(3) side of the cavity and is hydrogen-bonded to the primary hydroxyl groups of the adjacent α-CDx molecule; the distances of O(6, G1)---O(3, BS), O(6, G3)---O(1, BS), O(6, G1)*---O(2, BS), and O(6, G3)*---O(3, BS) are in the range of 2.708—2.857 Å, while the distances between the sulfonato group and the G2 residue are greater than 3.0 Å. In the water complex[4] and the 1-propanol complex,[6] which have cage-type structures, the hydrogen bonds are observed between the primary hydroxyl groups and the included "guest" molecule, and the hydroxyl groups involved in the hydrogen bonds have a *gauche-trans* conformation.

α-CDx molecules are stacked along the c axis with six O(3)---O(6) hydrogen bonds forming endless channels (Fig. 2). The BS anions are arranged in the channel, while the sodium cations are located outside the channel at nearly the same positions as those found in the other channel-type crystals (Figs. 3 and 4). The sodium ion is surrounded by O(W1), O(W3), O(W4), O(W6′), and O(5, G2), with Na---O distances between 2.34 and 2.55 Å. In the potassium acetate complex, a distorted octahedral coordination has been observed. In the Methyl Orange complex, five oxygen atoms are found around the sodium ion, but four of the Na---O distances are 2.86—2.90 Å, showing weak coordination. The hydrogen-bonding scheme is shown in Fig. 5. Intermolecular distances less than 3.0 Å are given in Table 8. The space outside the channel is filled with water molecules and sodium ions. Water molecules and hydroxyl groups

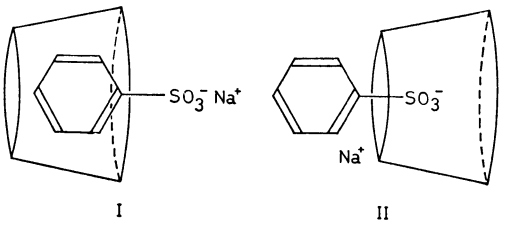

Fig. 6. Two possible structures of the 1 : 1 complex in an aqueous solution.

form the hydrogen-bonding network; O(W4) is hydrogen-bonded to O(2) and O(5) atoms of the Gl residue; O(W3) forms hydrogen bonds with O(2, G3) and O(5, G3); O(W6) and O(Wl) are also hydrogen-bonded to O(3, Gl) and O(2, G2) respectively. These four water molecules are linked to O(W5) by hydrogen bonds.

Formation Energy of the Complex in Aqueous Solution

In the crystalline state, the BS anion extends through two α-CDx rings. In an aqueous solution, the two structures shown in Fig. 6 are possible for the 1 : 1 complex. In the complex I, the hydrophobic benzene ring is located in the α-CDx cavity, while the hydrophilic sulfonato group is hydrogen-bonded to primary hydroxyl groups in the complex II. It has been emphasized[12,13] that the effect of solvation is important as well as the interaction between α-CDx and the "guest" molecule. The formation energy of the complex was calculated for these two complexes by using structural data in order to examine which structure is stable in an aqueous solution. That is, the heat of formation was estimated for the equilibrium in an aqueous solution;

$$\alpha\text{-CDx} + \text{BS} \rightleftharpoons \text{complex}. \tag{1}$$

The complex formation energy is expressed as follows:

$$\Delta E = E(\text{complex}) - E(\alpha\text{-CDx}) - E(\text{BS}) \tag{2}$$

$$E(\alpha\text{-CDx}) = E^{\text{sol}}(\alpha\text{-CDx}) \tag{2a}$$

$$E(\text{BS}) = E^{\text{sol}}(\text{BS}) \tag{2b}$$

$$E(\text{complex}) = E^{\text{sol}}(\text{complex}) + E^{\text{int}}(\text{complex}) \tag{2c}$$

E^{sol} is the solvation energy of the solute, and E^{int} is the interaction energy between α-CDx and the "guest" molecule. The solvation energy was calculated according to Halicioğlu and Sinanoğlu:[14,15]

$$E^{\text{sol}} = E^{\text{sol}}_{\text{cav}} + E^{\text{sol}}_{\text{e.s.}} + E^{\text{sol}}_{\text{vdw}} \tag{3}$$

where $E^{\text{sol}}_{\text{cav}}$, $E^{\text{sol}}_{\text{e.s.}}$, and $E^{\text{sol}}_{\text{vdw}}$ are the cavity term, the electrostatic term, and the van der Waals term respectively. The procedure of evaluating each term will be explained below.

Cavity Term. $E^{\text{sol}}_{\text{cav}}$ is the energy needed to create a cavity which will accomodate a solute molecule, A:

$$E^{\text{sol}}_{\text{cav}} = 4.836\kappa^{\text{e}}(\phi_{1\text{A}})V_{\text{A}}^{2/3}\gamma\left(1-\frac{\partial \ln\gamma}{\partial \ln T}-\frac{2}{3}\frac{1}{v}\frac{\partial v}{\partial T}T\right) \tag{4}$$

$$\kappa^{\text{c}}(\phi_{1\text{A}}) = 1 + \phi_{1\text{A}}^{2/3}(\kappa^{\text{e}}(1)-1) \tag{4a}$$

$$\phi_{1\text{A}} = V_1/V_{\text{A}} \tag{4b}$$

where V_1 and V_{A} are the molecular volumes of water and the solute A respectively, γ and $\kappa^{\text{e}}(1)$ are the surface tension and the cavity factor for water respectively. The values of $\kappa^{\text{e}}(1)$, γ, $\partial\ln\gamma/\partial\ln T$, and $1/v\ \partial v/\partial T$ were taken from Halicioğlu and Sinanoğlu.[14] The V_{A} of α-CDx was estimated from the X-ray data, and the volumes of a water molecule and the BS anion were estimated by means of the van der Waals volumes of atoms and molecules.[16] The parameters used are given in Table 9.

Table 9. Parameters for the calculation of solvation energy

Refractive index	n	1.333
Dielectric constant	ε	77.46
Surface tension	γ	72.00 dyn cm^{-3}
	$\frac{\partial \ln \gamma}{\partial \ln T}$	−0.157
Expansion coefficient	$\frac{1}{v}\frac{\partial v}{\partial T}$	0.257×10^{-3} K^{-1}
Cavity coefficient	κ^{c} (1)	1.277
Molecular volume		
Water		20.6 Å^3
BS anion		129.7
α-CDx		1330.0
Complex I		1381.0
Complex II		1376.0

Electrostatic Term. The electrostatic interaction energy between solute and solvent molecules was calculated by means of the following equation:

$$E^{\text{sol}}_{\text{e.s.}} = -\frac{D_{\text{d}}}{2}\sum_i \frac{\mu^2_{\text{A}i}}{V_{\text{A}i}(1-\bar{\alpha}_{\text{A}i}/r^3_{\text{A}i})} \tag{5}$$

$$D_{\text{d}} = \frac{2(\varepsilon-1)}{2\varepsilon+1} \tag{5a}$$

$$r^3_{\text{A}i} = \frac{3V_{\text{A}i}}{4\pi} \tag{5b}$$

where $\mu_{\text{A}i}$, $\bar{\alpha}_{\text{A}i}$, and $V_{\text{A}i}$ are the dipole moment, the average polarizability, and the volume of the i-th group in the solute molecule A, respectively, and where ε is the dielectric constant of the solvent. $\bar{\alpha}_{\text{A}i}$ was estimated as a sum of the atomic polarizabilities of the constituent atoms, while $V_{\text{A}i}$ was calculated by means of the van der Waals volumes of atoms and groups. Only the hydroxyl groups of α-CDx and the sulfonato group of BS were included in the calculation because these groups are in contact with solvent molecules. The effect of the sodium cation was neglected. The parameters are given in Table 10.

Table 10. Dipole moments, average polarizabilities, and volumes of C-SO_3^- and C-OH groups

	μ(Debye)	$\bar{\alpha}$	V
C-SO_3^-	5.07[a]	6.23 Å^3	51.3 Å^3
C-OH	1.69[b]	1.94	20.5

a) The value of the BS anion calculated on the basis of atomic charges. b) The value of methanol.

van der Waals Term. The van der Waals energy of solute-solvent interaction was expressed as follows:

$$E_{vdw}^{sol} = B_{1A}U_{1A} \tag{6}$$

$$B_{1A} = 1 - \frac{3}{4}D_r \tag{6a}$$

$$D_r = \frac{n^2-1}{n^2+1} \tag{6b}$$

where n is the refractive index of the solvent and U_{1A} the potential function used to express van der Waals interaction energy. Halicioğlu and Sinanoğlu[14] used the semi-empirical Kihara potential, but we have used the Lennard-Jones potential because it has an analytical form which is convenient for numerical calculation. We assumed that the molecules of the solute or solvent are rigid spheres. The energy of the interaction between a water molecule and the i-th atom in the solute molecule A (Fig. 7) is expressed as follows:

$$U_{1Ai} = \frac{\pi}{V_A}\int_{-l_i^0}^{l_i^0}\left[\frac{a_{1Ai}}{r_{1Ai}^{12}} - \frac{c_{1Ai}}{r_{1Ai}^{6}}\right](l_i^{02}-l^2)dl \tag{6c}$$

$$l_i^0 = R_A - l_{Ai} \tag{6d}$$

$$r_{1Ai} \approx R - l \tag{6e}$$

where a_{1Ai} and c_{1Ai} are coefficients of the potential function. By integrating from R_0 to ∞, the total van der Waals energy is found to be:

$$U_{1A} = \frac{4\pi}{V_1}\int_{R_0}^{\infty}(\sum_i U_{1Ai})R^2dR \tag{6f}$$

where $R_0 = R_A + R_1$. This integral equation was solved numerically.

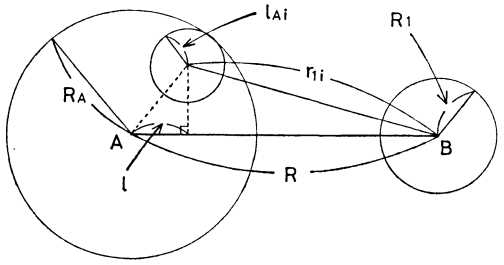

Fig. 7. A schematic drawing of interaction between water(B) and i-th atom in the solute(A).

α-CDx-"Guest" Interaction Term. In the calculation of the α-CDx-"guest" interaction energy, the non-bonded interaction betwwn non-hydrogen atoms was taken into account:

$$E^{int} = E_{e.s.}^{int} + E_{vdw}^{int} \tag{7}$$

$$E_{e.s.}^{int} = \sum_{i,j}\frac{q_iq_j}{\varepsilon r_{ij}} \tag{7a}$$

$$E_{vdw}^{int} = (1-K)\sum_{i,j}\left[\frac{a_{ij}}{r_{ij}^{12}} - \frac{c_{ij}}{r_{ij}^{6}}\right] \tag{7b}$$

$$K = \frac{3}{2}\left(\frac{n^2-1}{n^2+1}\right) \tag{7c}$$

where q_i and q_j are the atomic charges of the i-th and j-th atoms respectively. The atomic charges of the glucose residues and the BS anion were calculated by the CNDO/2 MO method[17] (Table 11). The charges of the C–H and O–H groups were used as those of the carbon and oxygen atoms respectively.

Table 11. Atomic charges

Glucose residue					
C (1)	0.24	C (2)	0.11	C (3)	0.11
C (4)	0.14	C (5)	0.14	C (6)	0.14
O (2)	−0.11	O (3)	−0.12	O (4)	−0.25
O (5)	−0.25	O (6)	−0.11		
BS anion					
C (1)	0.03	C (2)	0.01	C (3)	−0.03
C (4)	−0.04	S	0.52	O (1)	−0.49
O (2)	−0.49	O (3)	−0.49		

Coefficients of Potential Function. The coefficients of a_{ij} and c_{ij} were calculated by means of the following equation:[18]

$$c_{ii} = \frac{3e\hbar\alpha_i\alpha_j}{2m[(\alpha_i/N_i)^{1/2}+(\alpha_j/N_j)^{1/2}]} \tag{8}$$

$$a_{ij} = c_{ij}(r_{0i}+r_{0j})^6 \tag{8a}$$

where α_i and α_j are the atomic polarizabilities of the i-th and j-th atoms respectively, N_i and N_j are the numbers of electrons in the outer subshell, e and m are the charge and mass of the electron respectively, $\hbar$ is the Plank constant, and r_{0i} and r_{0j} are the van der Waals radii.[16] The values of α, N, and r_0 are given in Table 12, while a_{ij} and c_{ij} are listed in Table 13.

Table 12. Parameters for van der Waals potential function

Atom	N	r_0	α
C	4	1.70 Å	0.93 Å
O (Hydroxyl)	6	1.52	0.59
O (Ether)	6	1.52	0.64
O (Carbonyl)	6	1.52	0.84
S	6	1.80	3.09

Table 13. Coefficients for van der Waals potential function

		$a\times10^5$ mol/(kcal Å^{12})	$c\times10^2$ mol/(kcal Å^6)
C	C	4.948	3.203
C	O (H) [a]	2.745	2.463
C	O (E) [b]	2.930	2.628
C	O (C) [c]	3.632	3.258
C	S	15.73	8.555
O (H)	O (H)	1.565	1.982
O (H)	O (E)	1.663	2.107
O (H)	O (C)	2.032	2.574
O (H)	S	8.456	6.314
O (E)	O (E)	1.768	2.240
O (E)	O (C)	2.163	2.740
O (E)	S	9.058	6.764
O (C)	O (C)	2.658	3.368
O (C)	S	11.37	8.491
S	S	51.72	23.76

a) Oxygen atom in a hydroxyl group. b) Oxygen atom in ether. c) Oxygen atom in a carboxyl group.

Atomic Polarizability. The atomic polarizabilities of carbon and oxygen atoms were taken from Ketelaar.[19] For the sulfur atom, it was calculated by the following equation:[20]

$$\alpha = \frac{4}{9a_0}\sum_i (\bar{r}^2)^2 \tag{9}$$

$$(\bar{r}^2) = \left[\frac{n_i^*}{2(Z-S_i)}\right]^2 (2n_i^*+1)(2n_i^*+2)a_0^2 \tag{9a}$$

where n_i^* and $Z-S_i$ are the effective quantum number and the effective nuclear charge respectively, and where a_0 is the Bohr radius. In the case of the chlorine atom, the calculated atomic polarizability was twice the observed value; $\alpha_{calcd}=4.57$ and $\alpha_{obsd}=2.28$ Å^3. Therefore, the factor of 0.5 was multiplied to the calculated value for the sulfur atom.

Results and Discussion

The results are given in Table 14. The calculated formation energy of the complex I is larger by 8.74 kcal M^{-1} than that of the complex II, indicating that the inclusion of the hydrophobic group gives a more stable complex. The major part of the energy difference is $\Delta E^{sol}_{e.s.}$ of 7.06 kcal M^{-1}; this may be ascribed to the fact that the $E^{sol}_{e.s.}$ term is greatly reduced when the sulfonato group is included in the α-CDx cavity. The interaction energy between α-CDx and BS is larger in the complex I than in the complex II.

The α-CDx-BS interaction may involve the electrostatic, van der Waals, and hydrogen-bonding contacts. The van der Waals force between α-CDx and BS is an important component of the binding force. However, the contribution of the elcetrostatic interaction to the stability of the complex is small, since the interior of the α-CDx cavity is a relatively non-polar environment compared with the water environment. The effects of hydrogen bonds may also be small. In the complex II, the sulfonato group forms hydrogen bonds with primary hydroxyl groups of α-CDx, but it is also hydrogen-bonded to water molecules in the uncomplexed state.

TABLE 14. CALCULATED ENERGY FOR THE COMPLEX FORMATION (×mol/kcal)

(1) Solvation energy

	E^{sol}_{cav}	$E^{sol}_{e.s.}$	E^{sol}_{vdw}	E^{sol}
BS	22.22	−7.06	−0.65	14.52
α-CDx	98.71	−28.68	−5.36	64.67
Complex I	101.77	−35.63	−5.40	60.03
Complex II	100.93	−28.68	−5.12	67.13

(2) Solvation effects on the complex formation

	ΔE^{sol}_{cav}	$\Delta E^{sol}_{e.v.}$	ΔE^{sol}_{vdw}	ΔE^{sol}
Complex I	−19.76	0.0	0.61	−19.15
Complex II	−20.00	7.06	0.89	−12.05

(3) Interaction energy between α-CDx and BS

	E^{int}_{vdw}	$E^{int}_{e.s.}$	E^{int}
Complex I	−4.59	−0.03	−4.62
Complex II	−2.92	−0.06	−2.98

(4) Total association energy

	E(α-CDx)	E(BS)	E(complex)	ΔE
Complex I	64.67	14.52	55.41	−23.78
Complex II	64.67	14.52	64.15	−15.04

The stability of the complex in solution is determined by the α-CDx-"guest" interaction energy and the solvation energy. It is noteworthy that the effect of solvation on the complex formation is remarkably large; the ΔE^{sol} values are −19.15 kcal M^{-1} in the complex I and −12.05 kcal M^{-1} in the complex II, while the α-CDx-BS interaction energies are −4.62 and −2.98 kcal M^{-1} in the complex I and the complex II respectively. This indicates that the stability of the complex is largely determined by the difference in the solvation energies between the complexed state and the uncomplexed state. The change of the solvation energy is mainly ascribed to the cavity term. The cavity energy is proportional to the surface area of the solute molecule, and the solvation energy decreases when the "guest" molecule is included in the cavity of α-CDx.

The author wishes to thank Dr. Hisashi Uedaira for supporting this study and for his useful discussions. The author also wishes to acknowledge the helpful discussions and critical comments on the manuscript of Professor Jiro Tanaka of Nagoya University. The computation was carried out on a HITAC 8450 computer in our laboratory.

References

1) J. A. Thoma and L. Stewart, "Starch: Chemistry and Technology," Vol. I, ed. by R. L. Whistler and E. F. Pashall, Academic Press, New York (1965), pp. 209—249.
2) R. K. McMullan, W. Saenger, J. Fayos, and D. Mootz, *Carbohyd. Res.*, **31**, 37 (1973).
3) R. K. McMullan, W. Saenger, J. Fayos, and D. Mootz, *Carbohyd. Res.*, **31**, 211 (1973).
4) P. C. Manor and W. Saenger, *J. Am. Chem. Soc.*, **96**, 3630 (1974).
5) W. Saenger and M. Noltemeyer, *Angew. Chem.*, **86**, 594 (1974).
6) W. Saenger, R. K. McMullan, J. Fayos, and D. Mootz, *Acta Crystallogr., B*, **30**, 2019 (1974).
7) K. Harata, *Bull. Chem. Soc. Jpn.*, **48**, 2409 (1975).
8) A. Hybl, R. E. Rundle, and D. E. Williams, *J. Am. Chem. Soc.*, **87**, 2779 (1965).
9) K. Harata, to be published. Part II of this series.
10) "International Tables for X-Ray Crystallography," Vol. III, Birmingham: Kynoch Press (1965), pp. 202—208.
11) A. W. Hanson, *Acta Crystallogr., B*, **29**, 454 (1973).
12) E. A. Lewis and L. D. Hansen, *J. Chem. Soc. Perkin Trans. 2*, **1973**, 2081.
13) D. W. Griffiths and M. L. Bender, "Advances in Catalysis," **23**, 209 (1973).
14) T. Halicioğlu and O. Sinanoğlu, *Ann. N. Y. Acad. Sci.*, **158**, 308 (1969).
15) O. Sinanoğlu, "Molecular Associations in Biology," ed. by B. Pullman, Academic Press, New York (1968), pp. 427—445.
16) A. Bondi, *J. Phys. Chem.*, **68**, 441 (1964).
17) J. A. Pople and D. L. Beveridge, "Approximate Molecular Orbital Theory," McGraw-Hill, New York (1970).
18) K. S. Pitzer, "Advances in Chemical Physics," Vol. II, ed. by I. Prigogine, Interscience Publishers, New York (1965), pp. 59—83.
19) J. Ketelaar, "Chemical Constitution," Elsevier Publishing Co., New York (1958), p. 91.
20) J. O. Hirschfelder, C. F. Curtis, and R. B. Bird, "Molecular Theory of Gases and Liquids," John Willy & Sons, New York (1954).

Study of Metal–Polycarboxylate Complexes Employing Ion-Selective Electrodes. Cu(II) and Cd(II) Complexes with Poly(acrylic acid) and Poly(itaconic acid)

Fumitaka YAMASHITA, Tsuyoshi KOMATSU, and Tsurutaro NAKAGAWA
Department of Polymer Science, Faculty of Science, Hokkaido University, Sapporo 060

(Received December 25, 1975)

The complex formation of bivalent metal ions, Cu(II) and Cd(II), with poly(acrylic acid) and poly(itaconic acid) in aqueous solutions was studied by pH titration at 25 °C and at an ionic strength of 0.1, and at the same time the concentration of free metal ions was measured using ion-selective electrodes. In order to calculate the equilibrium constants of metal–polycarboxylate complex formation, a modified Gregor method is proposed and a more reasonable method for the determination of the formation constants of the complexes is also presented. The equilibrium constant of the metal–polycarboxylate complex formation involving two carboxylate groups was calculated from this method. The value for the Cu(II)–poly(itaconic acid) complex formation was $10^{-2.9}$, and was constant in the lower neutralization region. But constant values for the Cd(II) complexes were not obtained over the entire neutralization range.

In order to calculate the stability constants or the equilibrium constants of the complex formation of bivalent metal ions with polyelectrolytes by pH titration, the modified Bjerrum[1] method has been established by Gregor and co-workers,[2] and the reference plot method has been proposed by Mandel and Leyte.[3] In the scheme of Gregor and that of Mandel and Leyte, several hypotheses had to be taken into account, since the concentrations of ionic species for equilibrium in the complex formation cannot be determined at each stage of neutralization using only the equation of stoichiometric material balance.

Recently, ion-selective electrodes which are responsive to specific ions have been available for the investigation of ion activity. Rechnitz[4,5] has shown that the complex formation constants of Cu(II) with low molecular organic acids can be easily and precisely estimated using these electrodes.

In the present study, the equilibrium constants of metal–polycarboxylate complex formations were investigated using the pH titration method using ion-selective electrodes, and the data obtained were analyzed by the newly-proposed method.

Experimental

Material. The poly(itaconic acid)(PIA) sample used was material prepared by Dr. Muto[6] of this laboratory, and its molecular weight was estimated to be about 10^5. The sodium polyacrylate(PAA-Na) obtained commercially was manufactured by the Kishida Chem. Co. The acid form PAA solution was obtained from an aqueous solution of PAA-Na with the addition of hydrochloric acid and was purified by dialysis using cellophane tubing. Its molecular weight was estimated to be 7.6×10^5 by viscometric measurement. These solutions of polyacids were standardized by pH titration and stored in polyethylene containers at 5 °C.

All the chemicals used were of guaranteed reagent grade. The concentrations of the stock solutions of the bivalent metal ion salts, $Cu(NO_3)_2$ and $Cd(NO_3)_2$, were determined by the spectrophotometric chelatometric titration method. A carbonate-free NaOH solution was used as the titrant. The aqueous solutions were prepared using deionized water.

Potentiometric Titration. The pH measurements were carried out using a Yokogawa Model KPH-51A pH meter equipped with Toadenpa Model HG-4005 glass and HC-2005 calomel electrodes, and also with a Denkikagakukeiki Model HG-2 Digital pH meter equipped with Denkikagakukeiki Model MC-511 glass and Horiba Model 2050-05T calomel electrodes connected by a saturated KNO_3-agar salt bridge.

The concentrations of bivalent metal ions were measured with the pH meter equipped either with a Beckman Model 39612 cupric electrode or with a Toadenpa Model CD-125 cadmium electrode.

The titration, namely the measurements of the pH and the concentrations of the bivalent metal ions were carried out in a titration vessel with a water jacket maintained at 25.0 ± 0.05 °C in a nitrogen atmosphere.

Results and Discussion

Potentiometry Using Cu(II) and Cd(II) Ion-Selective Electrodes. The response of the cupric or cadmium electrode, the emf of the cell, was plotted linearly against the logarithm of the concentration for each ion and the corresponding slopes were 30.5 mV and 28.0 mV, respectively, in the concentration range from 10^{-6} to 10^{-2} mol/l at an ionic strength of 0.1 (KNO_3). These values of the slopes are very near to those expected from the Nernstian equation, and, according to their high reproducibility, the measurement of the concentrations of the ions was carried out with calibration at two points. The effect of pH on the response of the metal ions has to be taken into account because metal hydroxides are formed at values of pH more than 6. In the present work, however, the concentrations of the metal ions are much lower than those of the polyacids, therefore, all metal ions exist essentially as chelates in the pH region where the metal hydroxides are formed in the absence of chelating agents. It was shown by Rechnitz[4,5] that the activity measurement of the metal ion by the ion-selective electrode yields a reliable estimation of formation constants for a number of soluble copper complexes. In other words, the value of the electrode response is only due to the free metal ions, and their results suggest that metal ion chelates with polyacids have no effect on the response of the electrodes. Consequently, the activity values obtained for the present measurements were used without any special correction, except that of the activity coefficient of the concentrations.

Theory and Method of Calculation of the Equilibrium Constants of Complexation. Gregor and co-workers[2] have shown that the method of Bjerrum[1] for the evaluation of formation constants of metal complexes

may be adopted to elucidate the specific characteristics of polyelectrolytes.

By defining a reaction which does not cause any change in the charge of the polyacid, an equilibrium constant which can be expected to be independent of the charge on the polyacid was used by Gregor. Thus, the equilibrium exchange reaction between a proton and a metal ion is described as the equilibrium of the complex formation reaction.

A modification by Gregor of the calculation of the average coordination number $\bar{n}$ is as follows. Consider a solution in which the total acid concentration (dissociated, undissociated and chelated) is $[A_t]$ and the metal ion concentration is $[M_t]$. Using HA and A^- to designate a carboxylic group and a nonchelating carboxylate groups, respectively, $\bar{n}$ is given as follows:

$$\bar{n} = \frac{[A_t]-[HA]-[A^-]}{[M_t]}$$

Thus, if a relationship between $\bar{n}$ and $p([H^+]/[HA])$ can be obtained, the values of $\log B_2$ is determined by the following equation:

$$p\left(\frac{[HA]}{[H^+]}\right)_{\bar{n}=1} = \frac{1}{2}\log\left(\frac{[MA_2][H^+]^2[M^{2+}]}{[M^{2+}][HA]^2[MA_2]}\right)_{\bar{n}=1}$$

$$= \frac{1}{2}\log B_2, \quad B_2 = \frac{[MA_2][H^+]^2}{[M^{2+}][HA]^2}$$

where $[M^{2+}]/[MA_2]$ is equal to 1 at $\bar{n}=1$. But for any $\bar{n}$, the values of $[M^{2+}]/[MA_2]$ cannot be estimated, because there is, in general, no direct method for separately determining the values of $[M^{2+}]$ or $[MA_2]$.

Furthermore, in the case of polyacids, there is a difficulty in the determination of $[A^-]$. In order to estimate $[A^-]$, Mandel and Leyte[3] have devised the reference plot method instead of that of Gregor. The essential assumption of Mandel is based on the idea that in the Henderson-Hasselbach equation the α-dependent part of pK is only a function of the charge density on the polyacid. Thus,

$$pK = G + \zeta_\alpha$$

where G is a constant and ζ_α a function depending on α. Further,

$$p\left(\frac{[H^+]}{[HA]}\right) = G - p[A^-] + \zeta_\alpha.$$

On the basis of this equation Mandel and Leyte have suggested the reference plot method. A relationship between $p([H^+]/[HA])$ and $p[A^-]$ without metal ions is first plotted on a graph, and then, assuming that the metal ions added have no influence on this relationship, the values of $[A^-]$ can be obtained on the graph from the values of $p([H^+]/[HA])$ which can always be calculated.

In the present study, on the other hand, in addition to the pH values, the concentrations of free metal ions $[M^{2+}]$ can be determined simultaneously using ion-selective electrodes. Then, considering the relationship between the total metal ion concentration $[M_t]$ and the concentration of free metal ions $[M^{2+}]$, it can be easily seen that the difference between these two values is equal to the concentration of the truly complexed metal ions. Now, it is proposed that a real average coordination number $\bar{n}_r$ is introduced instead of $\bar{n}$ of Gregor (or Bjerrum), from which it can be shown how to calculate the equilibrium constant of the exchange reaction between protons and metal ions. The $\bar{n}_r$ is defined by the following equation:

$$\bar{n}_r = \frac{[A_t]-[HA]-[A^-]}{[M_t]-[M^{2+}]}$$

In contrast to the $\bar{n}$ of Gregor's method, $[M^{2+}]$ appears in the denominator of $\bar{n}_r$, and hence $\bar{n}_r$ is the average coordination number of the metal ions which are complexed with polyacids. Unfortunately, however, even when the value of $[M^{2+}]$ can be determined by the ion-selective electrode, the stoichiometric calculation of $[A^-]$ without any assumptions encounters difficulty. In the present study, the value of $[A^-]$

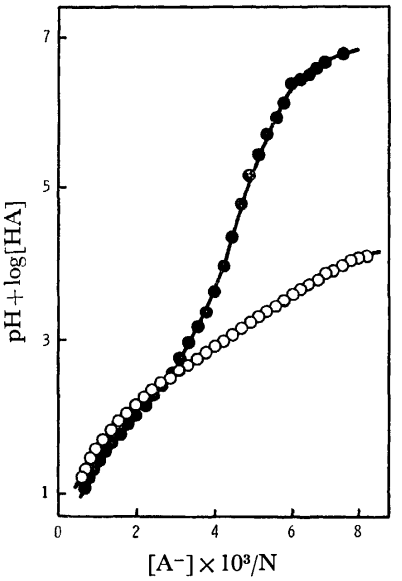

Fig. 1. The reference plots of 9.87×10^{-3} monomol/l PAA (○) and 4.75×10^{-3} monomol/l PIA ($=9.50\times10^{-3}$ N as carboxylic groups)(●) in 0.1 mol/l KNO_3.

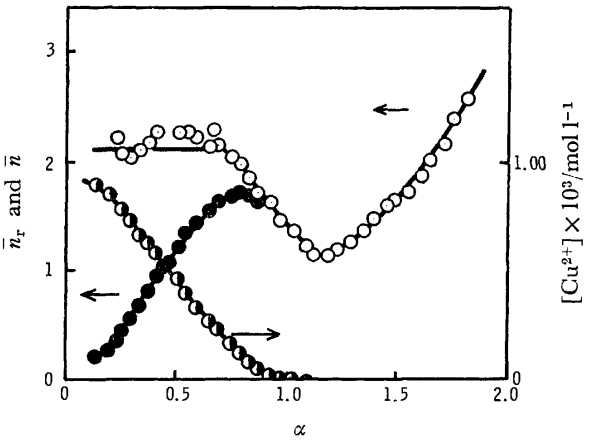

Fig. 2. The formation curves and the concentrations of Cu^{2+} at 4.75×10^{-3} monomol/l PIA and 1.09×10^{-3} mol/l $Cu(NO_3)_2$ in 0.1 mol/l KNO_3. ○: $\bar{n}_r$ by our method, ●: $\bar{n}$ by Gregor's method, and ◑: the concentration of Cu^{2+}.

is estimated by the reference plot method (Fig. 1).

In Fig. 2, not only $\bar{n}_r$ for Cu(II)-PIA, but also $\bar{n}$ and the concentrations of free Cu(II) ions [Cu^{2+}], are plotted against the degree of neutralization α. Comparing the $\bar{n}_r$ with $\bar{n}$, these average coordination numbers agree with each other at the point of zero [M^{2+}]. Consider a system where half of the [M_t] involves two ligands and the other half are free from complexation. Then, $\bar{n}$ is equal to 1, but $\bar{n}_r$ is 2. It is clear that the real coordination number of the metal ion is, in this case, two. This fact shows that $\bar{n}_r$ is more useful than $\bar{n}$. From $\bar{n}$ in Fig. 2, it can only be seen that some complexes whose "true" average coordination numbers are unknown are formed. On the other hand, from $\bar{n}_r$ the "true" average coordination number, and moreover, from the denominator of $\bar{n}_r$, the concentration of the complexes formed can be determined. As is shown in Fig. 2, at the low value of α, $\bar{n}_r$ shows clearly that the complex formed involves two carboxylate groups as ligands. Their equilibrium can be described by the following equation:

$$M^{2+} + 2HA \rightleftharpoons MA_2 + 2H^+;\ B_2 = \frac{[MA_2][H^+]^2}{[M^{2+}][HA]^2}$$

Then, in the region of α where the $\bar{n}_r$ is constant and equal to 2, the equilibrium constant B_2 can be stoichiometrically calculated with the assumption that only complexes involving two carboxylate groups are formed. In such a region of α, all the calculated values of log B_2 are constant, and are equal to -2.9. In comparison with the fact that the apparent acid-dissociation constants for polyacids are not constant, this result is interesting from the view point of chelation in polymeric systems.

Formation Curves and Stability of Complexes. In Figs. 3—5, the formation curves obtained using the present method for the Cd(II)–PIA, Cu(II)–PAA, and Cd(II)–PAA systems are shown. These curves are obtained under approximately the same conditions, and the concentration of polyacids is represented in the following way. Considering that all the carboxylic groups on the PAA and PIA chains are equivalent, concentrations of these groups are expressed in molarity,

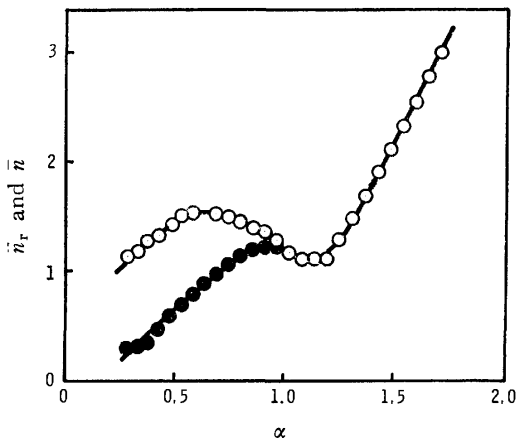

Fig. 3. The formation curves at 4.75×10^{-3} monomol/l PIA and 9.88×10^{-4} mol/l $Cd(NO_3)_2$ in 0.1 mol/l KNO_3. ○: $\bar{n}_r$ and ●: $\bar{n}$.

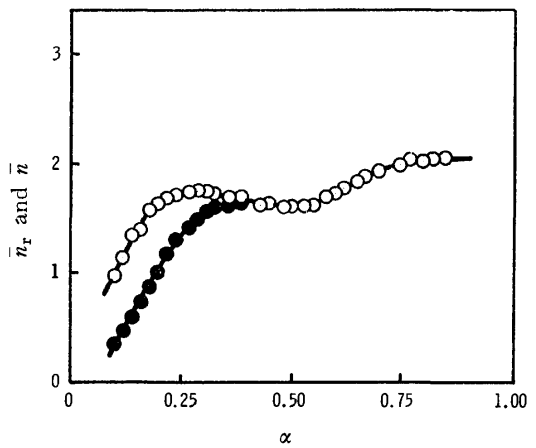

Fig. 4. The formation curves at 9.87×10^{-3} monomol/l PAA and 1.05×10^{-3} mol/l $Cu(NO_3)_2$ in 0.1 mol/l KNO_3. ○: $\bar{n}_r$ and ●: $\bar{n}$.

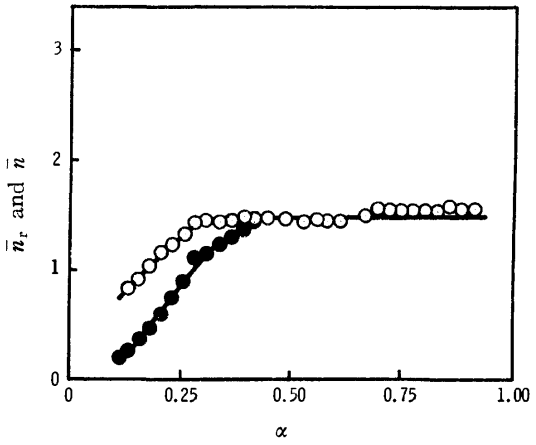

Fig. 5. The formation curves at 9.87×10^{-3} monomol/l PAA and 9.88×10^{-4} mol/l $Cd(NO_3)_2$ in 0.1 mol/l KNO_3. ○: $\bar{n}_r$ and ●: $\bar{n}$.

and hence the concentration of monomer units of PIA is equal to one half of the value of the present concentration of carboxylic groups.

From Fig. 3, it may be seen that no stable Cd(II)–PIA complex involving two carboxylate groups is formed, in contrast to the Cu(II)–PIA complex, and no constant value of log B_2 is obtained. Furthermore, for PIA complexes, Figs. 2 and 3 demonstrate that $\bar{n}_r$ begins to decrease at $\alpha=0.7$ and that for an increase in α, $\bar{n}_r$ increases passing through a minimum.

Figures 4 and 5 show $\bar{n}_r$ plots of PAA complexes of Cu(II) and Cd(II), which are similar in shape to those for $\bar{n}$ found by other workers, except that $\bar{n}_r$ begins from the value of 1. In spite of the existence of a flat region of $\bar{n}_r$ for the Cd(II)–PAA system, no constant value of log B_2 is obtained. For the Cu(II)–PAA system, there is a region $\bar{n}_r$ is equal to 2, but in this region no measurable free Cu(II) ions were present in the system, and therefore, a calculation of the equilibrium constant B_2 is impossible.

It is an interesting result that the stable Cu(II)–PIA complexes involving two carboxylate groups are formed but that no stable Cd(II)–PIA complexes are formed

at low values of α.

This fact can be explained by the fact that PIA is a polymer of dicarboxylic acid. Muto[6] has interpreted the specific counterion binding of alkali metal ions by taking into account the formation of a ring structure involving cooperative hydrogen bonding by two carboxylate groups. Now, we consider that the ring structure reacts with a free bivalent metal ion. If this bivalent ion must break this structure before forming the complex by entering between these two carboxylate groups and replacing a hydrogen ion. The difference in $\bar{n}_r$ between Cu(II)–PIA and Cd(II)–PIA in the region of α below 0.7 may be due to the difference of this ring-breaking ability for the Cu(II) and Cd(II) ions. This concept of hydrogen-bonded ring structure, however, seems not to be necessary, if we attribute the difference in the complexing ability of the Cu(II) and Cd(II) ions, irrespective of the structure of ligand groups.

The curves of $\bar{n}_r$ (and, of course, of $\bar{n}$) of PIA complexes in the region of α above 0.7 show strange behavior that the values of $\bar{n}_r$ increase more and more after a minimum has been reached. This tendency of the curves of the degree of binding for alkali metal ions was also shown by Muto. Therefore, this tendency need not result only from complex formation by bivalent metal ions. In connection with this fact several reasons are presented, for example, conformation change, the formation of metal hydroxides, and/or the formation of more complicated complexes, *etc.* It must be pointed out here that the method of calculation of $\bar{n}_r$ is more important. Thus, in the calculation of $\bar{n}_r$ (or of $\bar{n}$), the primary carboxylic groups are regarded as equivalent to secondary groups in the PIA monomer units and the concentrations of free carboxylate groups are estimated from the reference plot. Therefore, $\bar{n}_r$ shows some deviation due to uncertainty around the first neutralization step.

Calculating the formation constants by the present method, only the result of Cu(II)–PIA was obtained over a wide range of α, but other complexes, for example, Cd(II)–PAA, in spite of the existence of a flat region of $\bar{n}_r$, no constant value of the equilibrium constant is obtained for each value of α. In connection with this fact, in spite of taking into account 1–1 complex formation, the test was not successful. Some reasons may be given, such as unevaluated errors in the potentiometric measurements or the uncertainty in the estimation of the concentration of each ion which participates in the complex formation equilibrium (for example, employing the Mandel reference plot). In some cases, however, a series of values of equilibrium constants which vary monotonously with α has been obtained. This behavior as a function of the difference in the stability of the complexes is as follows. If the complexes formed, whose ligands are two carboxylate groups in a monomer unit, are very stable, the equilibrium of complex formation may not be influenced by, for example, the change of the polymer conformation, and this is the case of the Cu(II)–PIA system. On the other hand, when the complexes are not as stable, the equilibrium constants for complex formation must be influenced, if the conformation of the polymer chain is changed with α. Thus, it can be seen that the Cu(II)–PIA complexes involving two carboxylate groups in the low pH region are more stable than others and that both Cd(II) complexes with PAA and PIA are not so stable. These results are summarized in Table 1.

TABLE 1. $\log B_1$ AND $\log B_2$ VALUES OBTAINED FROM OUR METHOD IN Figs. 3—5

	Cu^{2+}	Cd^{2+}	
PAA complexes			
$\log B_1$	—	—	$(\bar{n}_r=1.5)$
$\log B_2$	-3.4 $(0.55<\alpha)$	—	$(\bar{n}_r=1.5)$
PIA complexes			
$\log B_1$	—	—	
$\log B_2$	-2.9 $(\alpha<0.66)$	—	

The authors wish to thank Dr. Muto for his offer of the PIA samples and for helpful suggestions and discussions.

References

1) J. Bjerrum, "Metal Ammine Formation in Aqueous Solution," P. Haase, Copenhagen (1941).
2) H. P. Gregor, L. B. Luttinger, and E. M. Loebl, *J. Phys. Chem.*, **59**, 34 (1955).
3) M. Mandel and J. C. Leyte, *J. Polym. Sci.*, **A2**, 2883 (1964).
4) G. A. Rechnitz and Z. F. Lin, *Anal. Lett.*, **1**, 23 (1967).
5) G. A. Rechnitz and N. C. Kenny, *Anal. Lett.*, **2**, 395 (1969).
6) N. Muto, *Bull. Chem. Soc. Jpn.*, **47**, 1122 (1974).

Temperature Dependence of the Dielectric Constants of Potassium-Chloranil Salt and Würster's Blue Perchlorate

Kikujiro Ishii,* Katsumi Kaneko,** and Haruo Kuroda

Department of Chemistry, Faculty of Science, University of Tokyo, Hongo, Tokyo 113

(Received January 22, 1976)

The dielectric constants of potassium-chloranil salt(K^+CA^-) and Würster's blue perchlorate (WBP) were measured around their phase-transition temperatures in the X-band microwave region. In the case of K^+CA^-, a sudden increase in the dielectric constant was observed accompanying a change to the low-temperature phase. This is interpreted to arise from the change in electronic polarization associated with a marked increase in the intensity of the charge-transfer band in the near-infrared region. An anomalous peak and associated gradual changes were observed in the temperature dependence of the dielectric constant of WBP around the phase transition temperature. The difference in dielectric behavior of these two cases is discussed in relation to the optical absorption spectra and other properties of the crystals.

Although the electronic polarizability of a molecular crystal is affected, more or less, by the electronic interaction between molecules, the effect on the dielectric behavior of molecular crystals has usually been regarded as being of minor importance. However, recent investigations on the dielectric properties of crystals of solid charge-transfer complexes and radical salts have revealed several examples where the charge-transfer interaction between molecules plays an important role in determining their dielectric properties.[1,2]

We previously reported the results of dielectric constant measurement on a series of solid molecular complexes containing tetracyanoquinodimethane (TCNQ) as an electron acceptor, pointing out that, when there is a strong low-energy charge-transfer band in the crystal spectrum of a molecular complex, the dielectric constant of the crystal is larger than the value expected by assuming the additivity of molecular polarizations of the constituent molecules.[1]

In the case of the potassium-chloranil salt (K^+CA^-), the crystal spectrum exhibits a near-infrared absorption band associated with the charge-transfer interaction between chloranil ions, the intensity of this charge-transfer band markedly increasing when the crystal is cooled down below the transition point where the crystal changes from the high-spin state to the low-spin state.[3] A similar temperature dependence of the intensity of low-energy charge-transfer band can be observed in the case of *N,N,N',N'*-tetramethyl-*p*-phenylenediamine(TMPD) perchlorate (Würster's blue perchlorate, WBP).[4] Thus it is of particular interest to examine the dielectric behavior of these solids in the vicinity of transition point to see if their dielectric constants increase with the increase of the intensity of low-energy charge-transfer band.

Experimental

The dielectric constants of K^+CA^- and WBP, in the X-band microwave region, were measured by the cavity perturbation method by using a variable-temperature cylindrical cavity of TM_{012} resonance mode with an operation frequency of 9.4 GHz. The structure of the apparatus is shown in Fig. 1. The sample, in the form of a fine crystalline powder, was packed in a thin fused-quartz tube (A in Fig. 1) which was inserted at the middle of the resonance cavity (H). The cavity was cooled by introducing cold nitrogen gas into the copper tube (B) wound around the copper block (E) installed at the top of the cavity. The temperature of the cavity was controlled by adjusting the flow rate of the cold nitrogen gas and/or by using an electric heater (F). We measured the resonance frequencies of the cavity without and with the sample, f_1 and f_2 respectively, at each temperature, and obtained the value $(f_1^2-f_2^2)/f_2^2$. The latter quantity can be assumed to be proportional to $(\varepsilon-1)$ in the first order approximation, where ε is the dielectric constant of the sample.[5,6] It was difficult to estimate the absolute value of dielectric constant from the above experiment because of the difficulty in avoiding the inhomogeneity as regards the packing of sample powder in the tube. Thus, we separately estimated the actual dielectric constant of the sample at room temperature by the method described previously,[5] using a rectangular cavity of TE_{105} mode.

The crystalline powder of WBP was prepared by the method of Michaelis and Granik.[7] The crystalline powder

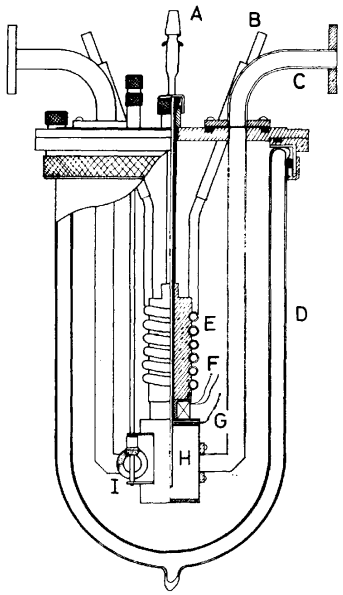

Fig. 1. A schematic drawing of the measuring apparatus.
A; sample tube, B; cold gas inlet, C; wave guide, D; Dewar's vessel, E; copper block, F; heater, G; thermocouple, H; TM_{012} cavity, I; coupling adjuster.

* Present adress: Institute for Molecular Science, Myodaiji-machi, Okazaki 444.

** Present adress: Department of Chemistry, Faculty of Science, Chiba University, Chiba 280.

of K^+CA^- was obtained by the method reported by Torrey and Hunter.[8] The results of elementary analysis agreed with the calculated values in both cases. Since K^+CA^- is known to form hydrate by absorbing moisture from the atmosphere,[9] the sample was carefully dried in a vacuum so that it was completely converted into anhydrous modification. The X-ray diffraction pattern of the powder sample thus obtained was confirmed to agree with that of the anhydrous state. In order to avoid a change of the sample into hydrous modification, the sample tube of dielectric constant measurement was pumped to the vacuum of 10^{-3} Torr soon after the sample powder had been packed into it.

Differential scanning calorimetry (DSC) was carried out on each sample with a Rigaku low-temperature DSC apparatus.

The polarized absorption spectra of single crystals were measured with a microspectrophotometer with a small cryostat at the specimen stage of the microscope system.

Results and Discussion

Figure 2a shows the plot of the frequency shift, $(f_1^2-f_2^2)/f_2^2$, against temperature in the case of K^+CA^-. An approximate scale of dielectric constant is given[10] on the right-hand side. This was determined by normalizing $(f_1^2-f_2^2)/f_2^2$ to the room temperature value of dielectric constant determined by the separate experiment.

On lowering the temperature, the frequency shift remains almost constant (at the value corresponding to the dielectric constant of about 3.5) from room temperature down to about 220 K, then exhibits a sudden increase in the 220—210 K region, and after showing a maximum at 210 K, it stays constant at lower temperatures.[11] On elevating the temperature, however, the frequency shift stays constant up to 260 K, where it shows a sudden decrease, showing a hysteresis in its temperature dependence.

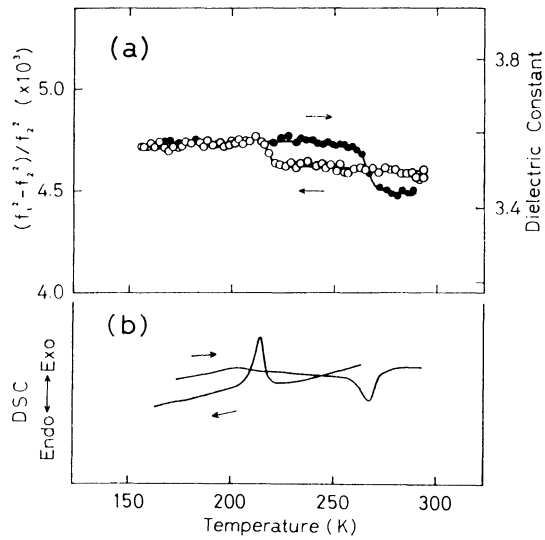

Fig. 2. (a) Temperature dependence of the dielectric constant of potassium-chloranil salt (K^+CA^-). $(f_1^2-f_2^2)/f_2^2$ is plotted as the ordinate, where f_1 and f_2 are the resonance frequencies of the microwave cavity without and with the sample respectively. An approximate scale of the dielectric constant is shown in the right hand side. (b) Differential scanning calorimetry curves of K^+CA^-.

The temperature dependence of the magnetic susceptibility is known to also exhibit an appreciable hysteresis between the heating and cooling processes; the phase transition occurs at 210 K on lowering the temperature, and at 260 K on elevating the temperature.[12,13] This difference of transition temperature is also clearly observable in the DSC curves (Fig. 2b). By comparing Figs. 2a and 2b, we note that the temperature, at which a sudden change of frequency shift occurs, exactly coincides with the transition point, for both the cooling process and heating process.

According to Konno *et al.*,[14] in the high-temperature phase of K^+CA^-, CA^- ions are stacked face-to-face on each other along the c-axis with uniform intermolecular separation, K^+ ions being located at the sites between CA^- columns. Although the details of the crystal structure of the low-temperature phase are not known, it has been inferred that the arrangement of CA^- ions in the CA^- column changes to a dimeric one in the low-temperature phase.[3,9]

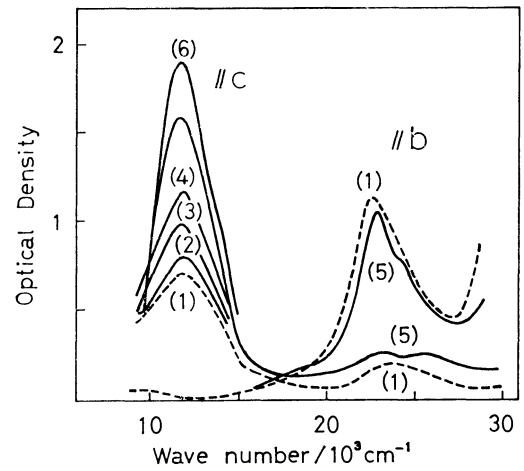

Fig. 3. Temperature dependence of the crystal spectra of the potassium-chloranil salt. (1); 297 K, (2); 280 K, (3); 240 K, (4); 218 K, (5); 209 K, (6); 163 K. (//b and //c denote the b- and c- axis spectrum, respectively).

The crystal spectrum of K^+CA^- is reproduced in Fig. 3.[3] The near-infrared absorption band, at 11.5×10^3 cm^{-1}, is almost completely polarized in the c-axis direction, and has been assigned to the band associated with the charge-transfer interaction between neighboring CA^- ions. As shown in Fig. 3, the intensity of this charge-transfer band markedly increases on lowering the temperature in the vicinity of transition point. Other absorption bands which are associated with the electronic transitions of the CA^- ion are not significantly affected by temperature.

The static electronic polarizability α_e of a semiconductive (or insulating) solid can be related to the electronic transitions of the solid as follows:

$$\alpha_e = \frac{e^2}{4\pi^2 m}\sum_j \frac{f_j}{\nu_j^2}, \qquad (1)$$

where ν_j and f_j are the frequency and oscillator strength, respectively, of the j-th electronic transition of the

solid.[15] We see that if there is any low-frequency electronic transition with a strong oscillator strength, it will make a considerable contribution to the electronic polarizability.

In order to consider the relation between the low-frequency charge-transfer band and the electronic polarizability of K^+CA^-, we rewrite Eq. 1 as follows:

$$\alpha_e = \frac{e^2}{4\pi^2 m}\frac{f_{CT}}{\nu_{CT}^2} + \frac{e^2}{4\pi^2 m}\sum_j \frac{f_j}{\nu_j^2} \qquad (2)$$

where the first term represents the contribution of the charge-transfer transition, and the second term those of other electronic transitions. The crystal spectrum of K^+CA^- exhibits a significant change in the vicinity of transition point only in the region of the charge-transfer band. Thus, one can reasonably assume that the second term of Eq. 2 must be almost the same at temperatures above and below transition point, so that the temperature dependence of the electronic polarizability in the vicinity of transition point will be determined mainly by the change in the first term. In other words, the electronic polarizability is expected to vary parallel to the intensity change of the charge-transfer band. Consequently, we can anticipate that the dielectric constant of K^+CA^- suddenly increases as the crystal changes from the high-temperature phase to the low-temperature phase if its change in the vicinity of transition point is primarily dependent on the variation of the electronic polarizability. This prediction is in agreement with observation. Naturally the dielectric constant of a solid depends not only on electronic polarization but also on atomic and lattice polarizations. At present, we can not exclude the possibility that the observed change of dielectric property of K^+CA^- in the vicinity of transition point is to some extent due to the change in the latter polarizations. But, as we will discuss later in comparison with the dielectric behavior of WBP, the electronic polarization is likely to play a dominant role in determining the observed dielectric behavior of K^+CA^- at transition point.

In the case of WBP, we obtained the results shown in Fig. 4a. The frequency shift, $(f_1^2-f_2^2)/f_2^2$, is almost constant down to 250 K, then gradually increases on lowering the temperature, and reaches a maximum value at 190 K. On undergoing the phase transition, it exhibits a sudden decrease, and thereafter, it gradually decreases on lowering the temperature.[16] In contrast to the corresponding plot of K^+CA^-, there appears no hysteresis in this case between the cooling and heating processes; the plot for both processes exhibits exactly the same temperature dependence. The situation is the same in the DSC experiment as shown in Fig. 4b.

Extensive investigasions have been carried out on the nature of the phase transition of WBP at 190 K, where WBP changes from the high-spin state at higher temperature to the low-spin state at lower temperature.[4,17-21] It was inferred from these studies that in the low-temperature phase the $TMPD^+$ column along the a-axis consists of a dimeric array of $TMPD^+$ ions, while it has a monomeric array of the ions in the high-temperature phase. The structural change was recently confirmed by crystal structure analysis.[22,23]

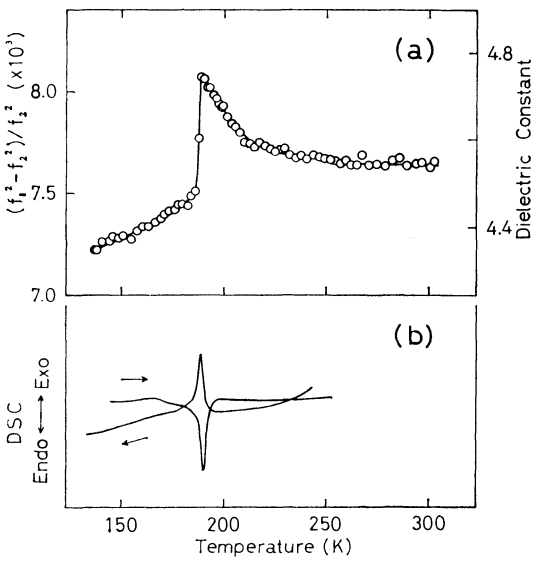

Fig. 4. (a) Temperature dependence of the dielectric constant of Würster's blue perchlorate (WBP). The change in the resonance frequency of the microwave cavity is plotted as the ordinate in the same manner with Fig. 2. An approximate scale of the dielectric constant is also shown in the right hand side. (b) Differential scanning calorimetry curves of WBP.

The polarized absorption spectrum of the WBP crystal is shown in Fig. 5. All the absorption bands in the b- and a-axes spectra at 297 K are attributable to the local-excitations associated with the electronic transitions of $TMPD^+$ ion. No strong absorption band can be found below 15×10^3 cm^{-1} at this temperature. However, as the temperature is lowered below the transition point, a new absorption band grows up at 12.5×10^3 cm^{-1} in the a-axis spectrum. The intensity of this band increases gradually over a wide temperature range on lowering the temperature. The corresponding absorption band has been observed at low temperatures also in the absorption spectrum of a polycrystalline sample of WBP, and attributed to the charge-transfer between $TMPD^+$

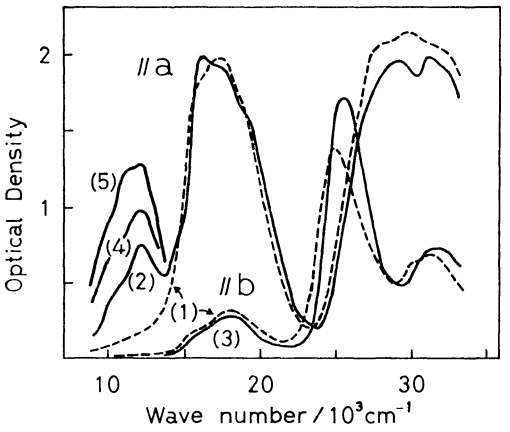

Fig. 5. Temperature dependence of the crystal spectra of Würster's blue perchlorate. (1); 285 K, (2); 138 K, (3); 134 K, (4); 122 K, (5); 83 K. (//a and //b denote the a- and b-axis spectrum, respectively.)

ions.[4] The fact that the above band is completely polarized in the direction of the $TMPD^+$ column, as revealed by the present study, indicates that it is indeed a charge-transfer band associated with the interaction between $TMPD^+$ ions in the $TMPD^+$ column.

Apparently, the change of the absorption spectrum of the WBP crystal accompanying the phase transition is very similar to that of the K^+CA^- crystal. Our discussion on the electronic polarizability of the K^+CA^- crystal should therefore be also applicable to the case of WBP. Since, as in K^+CA^-, the intensity of the low-frequency charge-transfer band of WBP markedly increases below the transition point while those of other absorption bands hardly change at all between above and below the transition point, it should be considered that the electronic polarizability of WBP increases in the low-temperature phase. The dielectric constant should thus be expected to increase as the temperature is lowered below the transition point, if the temperature dependence of dielectric constant is determined by the change in the electronic polarizability. However, the temperature dependence of frequency shift observed for WBP in the vicinity of transition point is just the contrary to that mentioned above (Fig. 4a), and quite different from that observed for K^+CA^-. This seems to indicate that the change of the dielectric constant of WBP is mainly determined by some other factor. The dielectric property of a solid is dependent not only on electronic polarization but also on atomic and lattice polarizations. However, it is very unlikely for atomic polarization to play the determining role for the relatively large change of dielectric constant as observed in the case of WBP at the transition point. In Fig. 4a, we note two features; a sudden decrease at the transition point, and gradual changes above and below this temperature. A similar type of temperature dependence of dielectric constant is known to occur in a crystal containing a component with an electric dipole when the rotational motion of the polar group (or molecule) is allowed above the transition point, but not in the low-temperature phase.[24] However, such a model associated with the orientational polarization can not be applied in the case of WBP.

Generally, in an ionic crystal, the lattice polarization arising from the displacement of ions makes a significant contribution to the static dielectric constant. The magnitude of this contribution is dependent on the frequency of lattice vibration. Recently, Terauchi[25] observed a diffuse X-ray reflection on the WBP crystal at temperatures above the transition point. As the temperature is lowered, the intensity of this reflection increases in proportion to $1/(T-T_c)$, where T_c is a critical temperature close to the transition point. The above reflection is interpreted to arise from the fluctuating dimerization of $TMPD^+$ ions in the $TMPD^+$ column. The fluctuation of β, the angle between the a- and c-axes, is also found to occur in the same temperature range. It is therefore inferred that some optical modes of lattice vibration are softened in the same temperature range. If this is the case, one could expect an anomaly concerning the lattice polarization. Seemingly, the increase of dielectric constant observed in the high-temperature phase of WBP on approaching the transition point is attributable to the above mechanism. On passing through the transition point, the lattice vibrational modes are considered to change suddenly, but the fluctuation of lattice may remain even in the low-temperature phase in the temperature region close to the transition point. The sudden decrease of the dielectric constant at the transition point and the gradual decrease below this point could be understood by this mechanism.

The dielectric behavior in the vicinity of transition point shows a marked difference between K^+CA^- and WBP although the phase transitions of these solids resemble each other in many respects. Two possible causes for the difference might be considered as follows. First, in the case of WBP the charge-transfer band appears at a frequency close to that of a strong local-excition band, while in the case of K^+CA^- it is very much lower than any of the local-excitation bands. The intensity change of the charge-transfer bands of WBP takes place gradually over a relatively wide temperature range, whereas that of K^+CA^- varies steeply on phase transition. Thus, the intensity change of charge-transfer band is expected to give a smaller effect on electronic polarizability in the case of WBP as compared with K^+CA^-. Second, we may consider that the contribution of lattice polarization is considerably larger in WBP than in K^+CA^-. In WBP, the heavy and bulky ClO_4^- ion is loosely bound to the $TMPD^+$ column, so that there can be a low-frequency lattice-vibrational mode giving a significant contribution to the lattice polarization. In K^+CA^-, the K^+ ion is rather tightly bound to the CA^- column through the interaction with the oxygen atoms of the neighboring CA^- ions. In effect, the dielectric constant of WBP, about 4.5 at room temperature, is much larger than that usually obtained for organic crystals composed of neutral molecules, and is comparable to those of inorganic ionic crystals. On the other hand, the dielectric constant of K^+CA^- at room temperature is 3.5, which is comparable to that obtained in the cases of non-ionic charge-transfer complexes involving polycyclic aromatic hydrocarbons as the donor and TCNQ as the acceptor. This indicates that lattice polarization makes a significant contribution to the dielectric constant in the case of WBP, but not in the case of K^+CA^-.

Refernces

1) K. Ishii, M. Kinoshita, and H. Kuroda, "Energy and Charge-Transfer in Organic Semiconductors," ed. by K. Masuda and M. Silver, Plenum Press, New York (1974), p. 183.

2) S. K. Khann, E. Ehrenfreund, A. F. Garito, and A. J. Heeger, *Phys. Rev. B*, **10**, 2205 (1974).

3) S. Hiroma and H. Kuroda, *Bull. Chem. Soc. Jpn.*, **46**, 3645 (1973).

4) T. Sakata and S. Nagakura, *Bull. Chem. Soc. Jpn.*, **42**, 1497 (1969).

5) K. Ishii, M. Kinoshita, and H. Kuroda, *Bull. Chem. Soc. Jpn.*, **46**, 3385 (1973).

6) The frequency shift $(f_1^2-f_2^2)/f_2^2$ is in reality proportional to (ε_a-1), where ε_a is the apparent dielectric constant of

powder sample. Since (ε_a-1) is proportional to $\delta\cdot(\varepsilon-1)$ when the volume fraction of crystals in the powder sample is expressed by δ, the frequency shift must be proportional to $(\varepsilon-1)/\rho$, where ρ is the crystal density. This means that, if there is an appreciable change in ρ, the observed variation of frequency shift does not directly show the actual change of dielectric constant which must be dependent of the change of crystal density, but shows the variation of polarization after correction has been done as regards the change of crystal density.

7) L. Michaelis and S. Granick, *J. Am. Chem. Soc.*, **65**, 1747 (1943).
8) H. A. Torrey and W. Hunter, *J. Am. Chem. Soc.*, **34**, 702 (1912).
9) S. Hiroma and H. Kuroda, *Bull. Chem. Soc. Jpn.*, **47**, 3014 (1974).
10) The scale should be taken only as a rough measure of dielectric constant, because of the reason mentioned in Ref. 6.
11) The changes are not due to the density change of crystal, because the observed frequency shift is proportional to $(\varepsilon-1)/\rho$ (see Ref. 6).
12) J. J. Andre and G. Weill, *Chem. Phys. Lett.*, **9**, 27 (1971).
13) T. Sugano, T. Ohta, and H. Kuroda, *Chem. Phys. Lett.*, **34**, 164 (1975).
14) M. Konno, H. Kobayashi, F. Marumo, and Y. Saito, *Bull. Chem. Soc. Jpn.*, **46**, 1987 (1973).
15) T. Nagamiya and R. Kubo, ed., "Solid State Physics," Iwanami, Tokyo (1961); See also, J. M. Ziman, "Principles of the Theory of Solid," Cambridge University Press, London (1964).
16) K. Ishii and H. Kuroda, *Chem. Phys. Lett.*, **32**, 607 (1975).
17) W. Duffy, *J. Chem. Phys.*, **39**, 490 (1962).
18) K. Okumura, *J. Phys. Soc. Jpn.*, **18**, 69 (1963).
19) D. D. Thomas, H. Keller, and H. M. McConnell, *J. Chem. Phys.*, **39**, 2321 (1963).
20) H. Chihara, M. Nakamura, and S. Seki, *Bull. Chem. Soc. Jpn.*, **38**, 1776 (1965).
21) G. T. Pott, C. F. van Bruggen, and J. Kommandeur, *J. Chem. Phys.*, **47**, 408 (1967).
22) J. L. De Boer and A. Vos, *Acta Crystallogr., Sect. B*, **28**, 835 (1972).
23) J. L. De Boer and A. Vos, *Acta Crstallogr., Sect. B*, **28**, 839 (1972).
24) See, for example; C. P. Smyth, "Dielectric Behavior and Structure," McGraw-Hill, New York (1955).
25) H. Terauchi, N. Sakamoto, and I. Shirotani, *J. Chem. Phys.*, **64**, 437, (1976).

Emission Spectra of the Vinyl Polymers with Pendant Carbazolyl Groups

Akira ITAYA, Ken-ichi OKAMOTO, and Shigekazu KUSABAYASHI

Department of Chemical Engineering, Faculty of Engineering, Yamaguchi University, Ube 755

(Received February 9, 1976)

The emission properties of poly(*N*-vinylcarbazole) (PVCz) prepared by radical and cationic polymerization (PVCz(r) and PVCz(c) respectively), the oligomers of *N*-vinylcarbazole, and poly[2-(*N*-carbazolyl)ethyl vinyl ether] (PCzEVE) were investigated in solutions. The fluorescence spectrum of PVCz(r) was different from that of PVCz(c). This seems to be attributable to the difference in the tacticity between them. On the basis of this result, the structure of the second excimer site is discussed. PCzEVE, in which the carbazolyl chromophores are widely spaced on the skeletal chains by $-O-CH_2-CH_2-$ bonds, showed an interesting, new, structureless emission band with a peak at 27000 cm^{-1}. This was different from both the monomeric structured fluorescence and the sandwich-like excimer one which were observed for the model compounds and the polymers. The emission properties of PCzEVE were unique among the vinyl polymers with aromatic chromophores widely spaced on the skeletal chain.

It is known that 1-ethylpyrene and 1-ethylnaphthalene show the excimer fluorescence in concentrated fluid solutions at room temperature. Poly(1-vinylpyrene)[1,2] and poly(1-vinylnaphthalene),[3,4] in which the pyrenyl and naphthyl groups are connected directly to the skeletal chains, show, almost entirely, only the excimer fluorescence in dilute solutions at room temperature. Poly(1-pyrenylmethyl vinyl ether) (PPyMVE),[1,5] poly-(1-naphthylmethyl vinyl ether) (PNMVE),[5] and ploy-(1-naphthyl methacrylate) (PNMA),[6] in which the pyrenyl and naphthyl groups are widely spaced on the skeletal chains by $-O-CH_2-$ and $-CO-O-$ bonds, show both the structured monomeric fluorescence and the excimer one in dilute solutions. On the other hand, *N*-ethylcarbazole(ECz) and 9-ethylacridine show no excimer fluorescence in the concentrated solutions.[1,7] Moreover, ECz shows no excimer fluorescence in either the molten state or the solid state.[7] Poly(9-vinylacridine) shows, almost entirely, only the excimer fluorescence in a dilute solution at room temperature.[1] Poly(*N*-vinylcarbazole) (PVCz), both in solution and in film, shows one broad fluorescence, which is not composed of only one component, but of two components. The broad emission at the longer wavelength(λ_{max}; *ca.* 23900 cm^{-1}) is assigned to the sandwich-like excimer fluorescence, which is the same as was mentioned above. On the other hand, the assignment of the broad emission in the shorter-wavelength region (λ_{max}; *ca.* 27000 cm^{-1}) is controversial because of the absence of the structure and of the large Stokes shift. David *et al.* and Yokoyama *et al.* have assigned it to the monomer fluorescence for PVCz in solution.[7,8] On the other hand, recently Johnson has assigned it to the second excimer fluorescence and reported that the polymer conformation appropriate for the formation of this state exists prior to the initial excitation step.[9] Offen *et al.*,[10] Klöpffer *et al.*,[11] and Powell *et al.*[12] have assigned the shorter-wavelength band to another intrinsic trap site, such as a dimer for PVCz films. However, the structure of the species emitting at *ca.* 27000 cm^{-1} has been amibguous thus far.

Recently, we have revealed, as a result of measuring the NMR spectra,[13] that cationic PVCz(c) have a higher isotacticity than radical PVCz(r). Therefore, it was of interest to investigate how the difference in the tacticity is reflected in the fluorescence spectra. In the present investigations, we have found that the difference influences the intensity of the second excimer fluorescence. On the basis of this result, the structure of the second excimer site, emitting at *ca.* 27000 cm^{-1}, was discussed.

Spectroscopic studies of the vinyl polymers with Cz chromophores widely spaced on the skeletal chains are of interest in connection with those of PVCz. In the present project, we investigated the spectroscopic behavior of poly[2-(*N*-carbazolyl)ethyl vinyl ether] (PCzEVE). It has already been found, from the absorption and NMR spectra,[14] that PCzEVE has no appreciable ground-state interaction among the Cz chromophores of PCzEVE.

Experimental

The vinyl polymers(PVCz(r), PVCz(c), PCzEVE), *N*-vinylcarbazole oligomers(VCz Olig. I and II; degrees of polymerization, 4 and 10 respectively), and the model compounds(*N*-isopropylcarbazole(*i*-PrCz), 1,3-bis(*N*-carbazolyl)-propane(DCzP)) were prepared by the methods described previously.[15,16] The dimethyl terephthalate(DMTP) was recrystallized twice from benzene and subsequently sublimed *in vacuo*. All of the solvents (2-methyltetrahydrofuran(MT-HF), tetrahydrofuran(THF), 1,2-dichloroethane) were purified by the usual methods. The solutions were completely degassed by freeze-pump-thaw cycles if necessary.

The emission spectra were measured with a spectrophotofluorometer constructed using a stabilized 500 W xenon lamp, monochromators, and a PM-55 (S-20) photomultiplier. The spectra were calibrated for the detector response by using a standard tungsten lamp. The fluorescence-decay times were measured with a pulsed N_2 gas laser as the exciting light source. Responses from the photomultiplier were led to a sampling oscilloscope(Tektronix 661) and recorded on a X-Y recorder, or led to a Tektronix 475 oscilloscope and the decay curve was photographed.

For the fluorescence polarization, two polarizers were used, and the data were corrected by the method described by Azumi and McGlynn.[17]

Results and Discussion

*Fluorescence in the Shorter-wavelength Region(*ca. *27000 cm^{-1}) of PVCz (r and c).* The fluorescence spectra of the various PVCz samples in aerated THF solutions at room temperature are shown in Fig. 1. The ratio of the second excimer fluorescence intensity to the

sandwich-like excimer one in PVCz(r) samples is remarkably larger than that in PVCz(c) samples. Figure 2 shows the fluorescence spectra of PVCz(r) and PVCz(c), which have almost the same concentrations in degassed THF–MTHF solutions at room temperature, and their resolution spectra. The resolutions were carried out on the assumption that the location of the sandwich-like excimer fluorescence

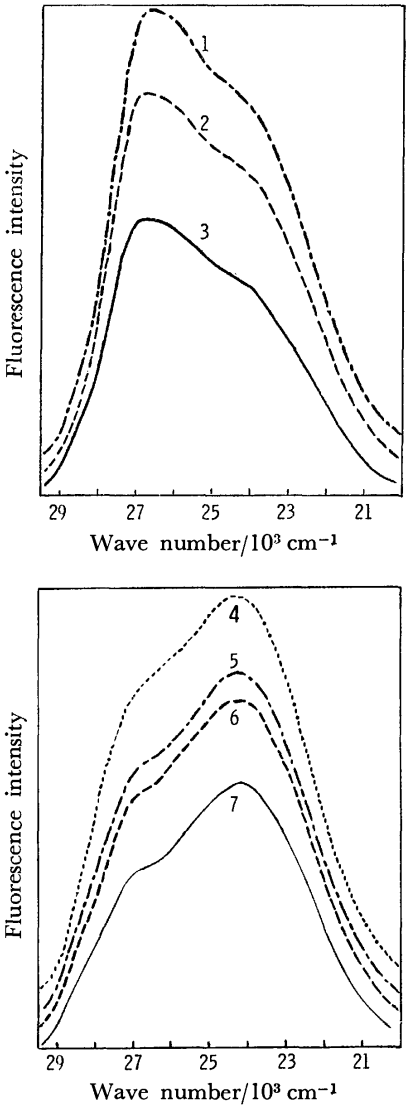

Fig. 1. Fluorescence spectra of PVCz and VCz-vinylnaphthalene(VN) copolymers polymerized by various methods in THF aerated solutions at room temperature. Excitation wavelength; 330 nm.
(1) VCz-VN(0.5 mol% in feed) copolymer polymerized by AIBN (1 mol%) in benzene (1 M) at 70 °C for 2 h, (2) PVCz(r) polymerized by AIBN (1 mol%) in benzene (1.3 M) at 70 °C for 4.5 h, (3) PVCz(r) polymerized by AIBN (1 mol%) in benzene (0.5 M) at 70 °C for 7 h, (4) PVCz(c) polymerized by BF_3OEt_2 (1 mol%) in toluene (0.26 M) at 20 °C for 1 h, (5) VCz-VN (1 mol% in feed) copolymer polymerized by BF_3OEt_2 (1 mol%) in toluene (0.86 M) at 15 °C for 3 h, (6) PVCz(c) polymerized by BF_3OEt_2 (1 mol%) in toluene (0.09 M) at −78 °C for 1 h, (7) PVCz(c) polymerized by BF_3OEt_2 (0.5 mol%) at 20 °C for 18.5 h.

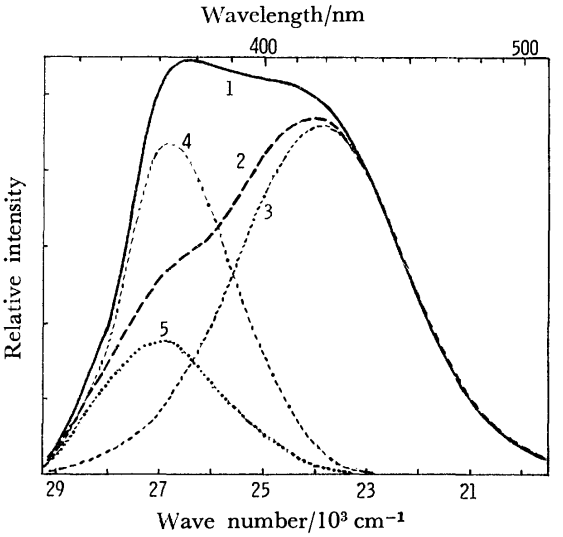

Fig. 2. Fluorescence spectra and the resolution spectra of PVCz(r) and PVCz(c) in MTHF-THF degassed solutions at room temperature. Optical densities at excitation wavelength (310 nm) are 0.132 and 0.131 for PVCz(r) and PVCz(c), respectively.
(1) ——; PVCz(r), (2) — —; PVCz(c), (3) ·····; the component of the sandwich-like excimer fluorescence of PVCz(r) and PVCz(c), (4) ----; the component of the second excimer fluorescence of PVCz(r), (5) ·····; the component of the second excimer fluorescence of PVCz(c).

band in solution was the same as that in film. The efficiency of the singlet-exciton migration along the polymer chain may be different between PVCz(r) and PVCz(c) because of their different tacticities. However, judging from the fact that no monomeric fluorescence is observed, their efficiencies seem to be very high, so that it seems not to be necessary to consider the difference in their efficiencies in the present case. It may safely be considered that the radiative rate constants of each fluorescence (second and sandwich-like excimer bands) of PVCz(r) are equal to those of PVCz(c). Therefore, Fig. 2 shows that the concentration of the sandwich-like excimer site in PVCz(r) is nearly equal to that in PVCz(c), and that the concentration of the second excimer site in PVCz(r) is higher than that in PVCz(c) by a factor of about 2.4. That is, the difference in the fluorescence spectra between PVCz(r) and PVCz(c) seems not to be attributable to any difference in the concentration of the sandwich-like excimer site, but to the difference in the concentration of the second excimer site.

In rigid glass at 77 K, a significant difference in the fluorescence spectra between PVCz(r) and PVCz(c) is found, as is shown in Fig. 3. The intensity of the 370 nm band of PVCz(r) is larger than that of PVCz(c). Johnson has pointed out a molecular-weight dependence of the emission spectrum of PVCz(r) in MTHF at 77 K.[9] The molecular weights of PVCz(r) and PVCz(c) used in this experiment are 1×10^5 and 2×10^5 respectively. Therefore, the difference in the fluorescence spectra between PVCz(r) and PVCz(c) in rigid glasses at 77 K seems not to be attributable to any difference in the molecular weight, but to the

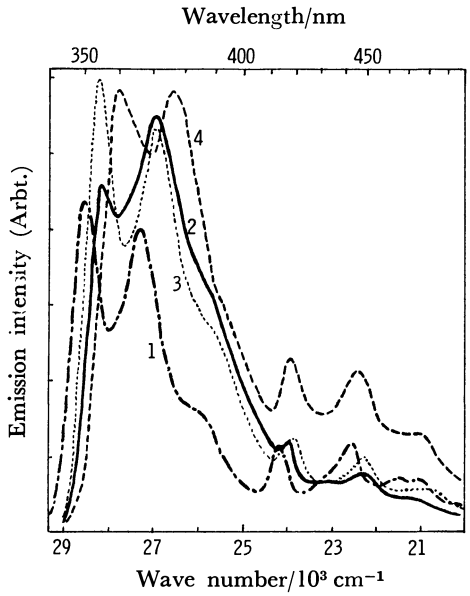

Fig. 3. Emission spectra of (1) ——; VCz Olig, II, (2)——; PVCz(r), (3)----; PVCz(c), and (4)———; PCzEVE in MTHF-THF rigid glasses at 77 K.

difference in their tacticities. The above-described results indicate that the fluorescence spectra both in fluid and in rigid solutions reflect the difference in the tacticity of PVCz and that the concentration of the second excimer site in syndiotactic-rich polymer-(PVCz(r)) is higher than that in isotactic-rich polymer-(PVCz(c)).

In the conformations for a three-skeletal carbon rotational dyad of syndiotactic and isotactic polymer-chain sequences based on a threefold rotational potential,[18] the conformational states with the lowest energy and those corresponding to the sandwich-like excimer site are shown in Fig. 4 (a) and (b). In the syndiotactic case there are a doubly degenerate ground state (g^+g^+,

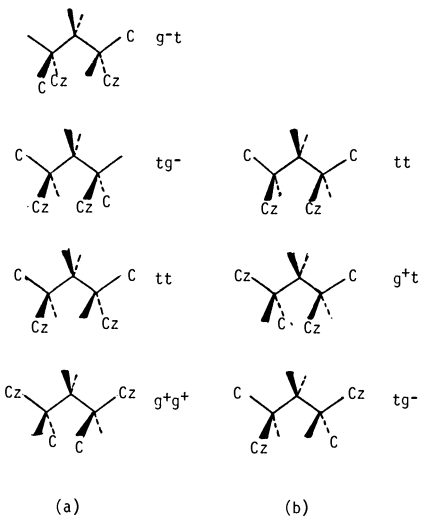

Fig. 4. The lowest energy conformations and excimer forming site ones for a three skeletal carbon rotational dyad of (a) syndiotactic and (b) isotactic polymer chain sequences based on a three fold rotational potential. This figure is quoted from Fig. 10 in Ref. 18.

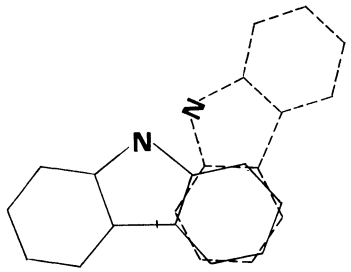

Fig. 5. The model of the second excimer of PVCz.

g^-t, tg^-) and a doubly degenerate excimer state (g^-t, tg^-). On the other hand, in the isotactic case there are a doubly degenarate ground state (g^+t, tg^-) and a singlet excimer state(tt). The formation of the sandwich-like excimer conformation from the ground-state conformation requires rotational motion about the carbon–carbon bond. In the ground-state conformations, we note that the tt conformation of the syndiotactic chain (Fig. 4(a)) has a shortest distance between neighboring Cz chromophores. Since the Cz chromophore is bulky, it seems to be easy to approach and mutually overlap the one benzene ring of the neighboring Cz chromophores in the excited state, as is shown in Fig. 5. The ground-state molecules corresponding to this reduced separation have a repulsive interaction.

It has been reported that 1,2-di(1-anthryl)ethane shows a broad excimer fluorescence in solution at room temperature at wavelengths shorter than the fluorescence of a sandwich-like excimer formed by the decomposition of its photodimer in rigid glass at 77 K, and that the structure of the excimer seems to be the overlap of only one benzene ring in the mutual anthracence chromophores.[19] Therefore, it seems reasonable to consider that the structure of the second excimer state may be the overlap of only one benzene ring in the neighboring chromophores. This structure seems to be supported by the fact that the formation of the sandwich-like excimer from the second excimer requires a rotational motion about the carbon-carbon bond.[9]

Concerning poly(α-methylstyrene) (PαMS)[20] andpolystyrene (PS),[20–22] it has been reported that the ratio of the sandwich-like excimer to the monomer fluorescence intensity, I_E/I_M, for the isotactic polymer is larger than that for the atactic polymer, although an opposite experimental result for PS has also been reported.[3] With regard to the relation between the tacticity of the polymer chain and I_E, Longworth[21] has reported that the I_E for isotactic PS is larger than that for atactic PS. In contrast to these results, in the case of PVCz, the concentration of the sandwich-like excimer site in the isotactic-rich polymer is nearly equal to that in the syndiotactic-rich polymer, as has been metioned above. The difference between the former (PαMS, PS) and the latter (PVCz) may be attributable to the existence of a second excimer resulting from the bulky Cz chromophore. No detailed explanation can, however, be offered at present.

Fluorescence Spectra of PCzEVE. The fluorescence spectra of the compounds with the Cz chromophores in MTHF–THF dilute solutions (2.0×10^{-4} M) at room temperature are shown in Fig. 6. The emission

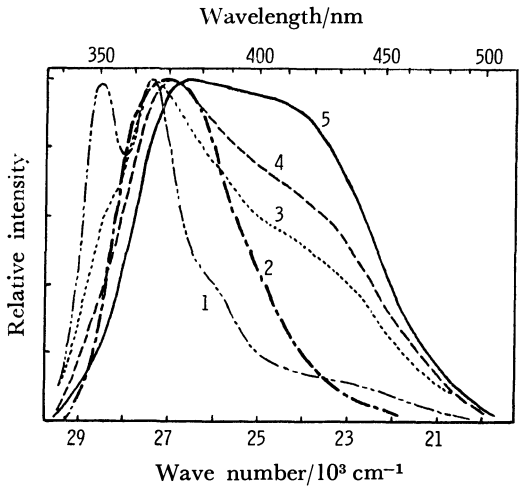

Fig. 6. Normalized fluorescence spectra of the model compound and vinylpolymers in MTHF-THF degassed solution at room temperature. Excitation wavelength; 310 nm.
(1) ——; DCzP, (2) ——; PCzEVE, (3) ----; VCz Olig. I, (4) ——; VCz Olig. II, (5) ——; PVCz(r).

spectrum of DCzP consists of a monomeric structured fluorescence and a sandwich-like excimer one with a peak at *ca.* 23900 cm^{-1}, as is well-known.[23-25] VCz Olig. I and II show a structureless fluorescence with a peak at 27000—27500 cm^{-1} and a sandwich-like excimer fluorescence, as in the case of PVCz, although VCz Olig. I also shows a monomer fluorescence as a shoulder. On the other hand, PCzEVE shows only a broad, structureless fluorescence with a peak at 27100 cm^{-1}. The Stokes shift (1990 cm^{-1}) is much larger than that of *i*-PrCz and DCzP (380 cm^{-1}). The fluorescence excitation spectra of PCzEVE, obtained by monitoring at several wavelength (350—450 nm) at room temperature, duplicate exactly the absorption spectrum of this solution at room temperature.

The fluorescence decay curve of PCzEVE in the MTHF-THF solution at room temperature is clearly two-component in all wavelength regions (370—430 nm), as is shown in Fig. 7. The decay constant of the long-lived component observed at 370 nm (33±1 ns) is longer than that of *i*-PrCz (17±2 ns) and shorter than that of the sandwich-like excimer fluorescence of PVCz (45±1 ns). The initial fast decay constant is 13±2 ns. This two-component decay of PCzEVE is also observed in rigid glass at 77 K (35±4 and 12±2 ns). The ratio of the short-decay component to the long one in rigid glass at 77 K is larger than that in a fluid solution at room temperature.

Table 1 shows the relative fluorescence quantum yields, taking the value of *i*-PrCz, which forms no excimer, as unity. The fluorescence quantum yield of PCzEVE is higher than that of DCzP, in which the sandwich-like excimer formation is the minimum among the materials used, as is shown in Fig. 6.

The fluorescence spectra of PCzEVE at various temperatures are shown in Fig. 8. At lower temperatures, two peaks appear, and they approach each other with an increase in the temperature. At tem-

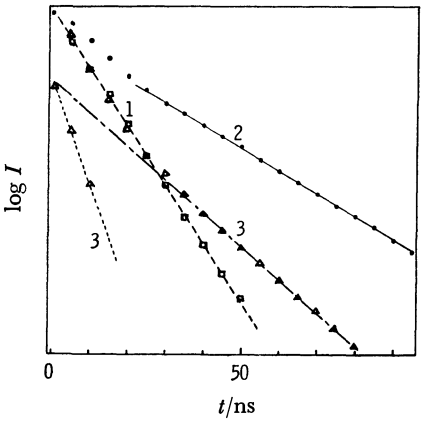

Fig. 7. Fluorescence decay curves of the model compound and vinylpolymers in MTHF-THF degassed solutions at room temperature.
(1) -□--□-; *i*-PrCz (λ_{obsd}=370 nm); τ_f=17 ns.
(2) • • •; PVCz(r) (λ_{obsd}=380 nm), —●—●—; the long-lived component; τ_f=46 ns.
(3) △△△; PCzEVE (λ_{obsd}=370 nm), —△--△—; the long-lived component; τ_f=31 ns, --△--△--; the short-lived compnent; τ_f=11 ns; the difference between the observed decay curve and the long-lived component.

Table 1. Relative fluorescence yields

Substance	η
i-PrCz	1.00
PCzEVE	0.79
DCzP	0.57
VCz Olig. I	0.40
VCz Olig. II	0.37
PVCz(r)	0.33
PVCz(c)	0.27

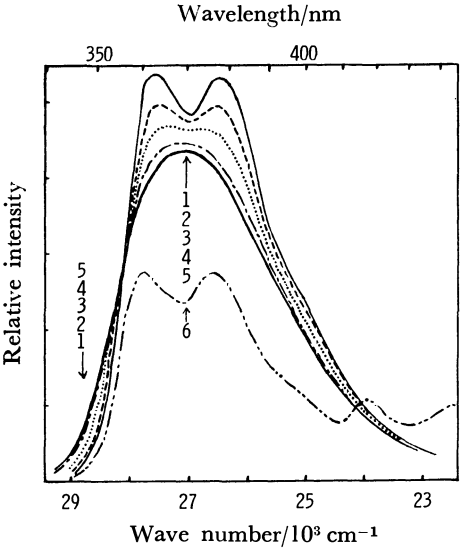

Fig. 8. Temperature dependence of the fluorescence spectra of PCzEVE in MTHF-THF degassed solution. Concentration of PCzEVE; 2.0×10^{-4} M. Excitation wavelength; 310 nm.
(1) 168 K, (2) 208 K, (3) 249 K, (4) 298 K, and (5) 318 K. The fluorescence (6) at 77 K was also given for comparison.

peratures higher than *ca.* 273 K, a structureless fluorescence spectrum with only one peak is observed. The fluorescence intensity decreases with an increase in the temperature. According to the measurement of the temperature dependence of the fluorescence spectra of the such compounds as PVCz(r and c), VCz Olig. I and II, and DCzP, the sandwich-like excimer formation has its maximum at *ca.* 293 K. On the other hand, in the case of PCzEVE, no appreciable change in the fluorescence spectra near 23900 cm^{-1} is observed over a wide temperature range, as is shown in Fig. 8. These facts indicate that PCzEVE does not form the sandwich-like excimer which is formed in PVCz(r and c), VCz Olig. I and II, and DCzP.

The emission spectrum of PCzEVE in rigid glass at 77 K is also shown in Fig. 3. The fluorescence spectrum of VCz Olig. II has, roughly, a so-called "mirror-symmetry" relation between the absorption and the fluorescence spectra (Fig. 3). However, PVCz(r and c) and PCzEVE do not have the mirror-symmetry relation. In particular, the fluorescence spectrum of PCzEVE is at a longer wavelength than that of PVCz(r and c) and has a different shape. The absorption spectra of PVCz(r and c) and PCzEVE in rigid glasses at 77 K are sharper than that in fluid solutions at room temperature, but no appreciable new band is observed. The fluorescence excitation spectra of these polymers in rigid glasses at 77 K are also in agreement with their absorption spectra. The resolution of the phosphorescence spectrum of PCzEVE is lower than those of *i*-PrCz and VCz Olig. I, the spectrum is very similar to that of PVCz(r and c), although its lifetime (6.6±0.1 s) is shorter than that of PVCz(r and c) (8.1±0.2 s).[16] Therefore, the excited-state interactions are present among the Cz chromophores in PCzEVE even at low temperatures, at which the solvent becomes rigid (*ca.* 102 K).

It has been reported that the triplet energy migration in PCzEVE occurs in rigid glass at 77 K.[16] The degrees of polarization of fluorescence for PVCz(r), PCzEVE, DCzP, and *i*-PrCz in rigid glasses at 77 K are shown in Fig. 9. The degrees are almost the same for PCVz(r) and for PCzEVE. This fact indicates that the singlet energy migration in PCzEVE occurs efficiently along the polymer chain, as is the case in PVCz.[7]

The concentrated THF solution of PCzEVE (0.5 M) shows the same spectra as in a dilute solution near 223 K and above.

As has been mentioned above, PPyMVE, PNMVE, and PNMA show both the normal structured monomeric fluorescence and the sandwich-like excimer fluorescence in dilute solutions. On the other hand, poly[2-(9-phenanthryl)ethyl vinyl ether] (PPhEVE), with phenanthryl chromophores widely spaced on the main chain by $-O-CH_2-CH_2-$ bonds, as does PCzEVE, shows, only the monomeric structured fluorescence in a dilute solution at room temperature.[26] The fluorescence structure and lifetime in a dilute solution are almost the same as those of 9-ethylphenanthrene. It is well-known that the excimer fluorescence of phenanthrene is not observed at room temperature.[27] In the case of PCzEVE, in which aromatic chromophores

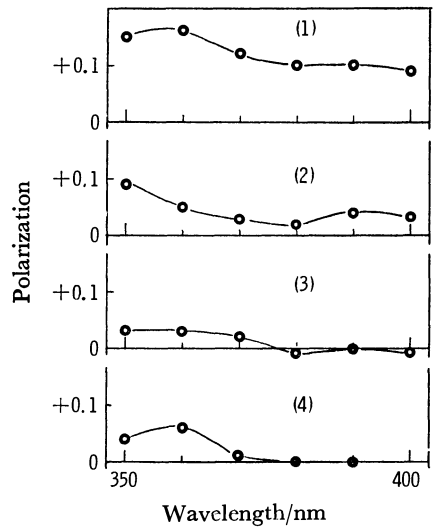

Fig. 9. Fluorescence polarizations of MTHF–THF rigid glasses of (1) *i*-PrCz (6.7×10^{-5} M), (2) DCzP (7.3×10^{-5} M), (3) PCzEVE (9.6×10^{-5} M), and (4) PVC(r) (1.0×10^{-4} M) at 77 K. Excitation wavelength; 334 nm.

are widely spaced on the skeletal chain than in PPyMVE, PNMVE, and PNMA, it is surprising that the normal structured monomeric fluorescence is not observed at all. The fact that the sandwich-like excimer fluorescence of PCzEVE is not observed in either dilute or concentrated solutions at room temperature also supports the idea that the sandwich-like excimer formation in PVCz is possible only between two adjacent chromophores.[7]

The above-described results indicate that the excited-state interaction among the Cz chromophores in PCzEVE is quite different from that is DCzP, VCz Olig. I and II, and PVCz(r and c), and that, in some vinyl polymers with aromatic chromophores widely spaced on the main chain, only PCzEVE is unique. This behavior of PCzEVE may reflect a characteristic of the bulky Cz chromophore.

The position of the PCzEVE fluorescence band in solution at room temperature is almost the same as that of the fluorescence in the shorter wavelength regions of PVCz(r and c) and VCz Olig. I and II, although the appearance of the structure below *ca.* 273 K is different. The initial fast decay constant of the PCzEVE fluorescence (11—14 ns) is nearly equal to the lifetime of the 370 nm fluorescence of PVCz in the polycrystalline THF matrix at 77 K (the order of 15 ns); at 370 nm the emission of PVCz is totally that due to the second excimer.[9] Therefore, one of the emitting species of PCzEVE in solution may be the same as a species emitting in the shorter-wavelength region of PVCz in solution (second excimer), although there remains the problems that the fluorescence lifetime of PCzEVE in solution at room temperature is nearly equal to that in rigid glass at 77 K and that the monomeric fluorescence of PCzEVE is not observed, in spite of the small binding energy of second excimer (*vide infra*).

Formation of an Exciplex. The fluorescence spectra

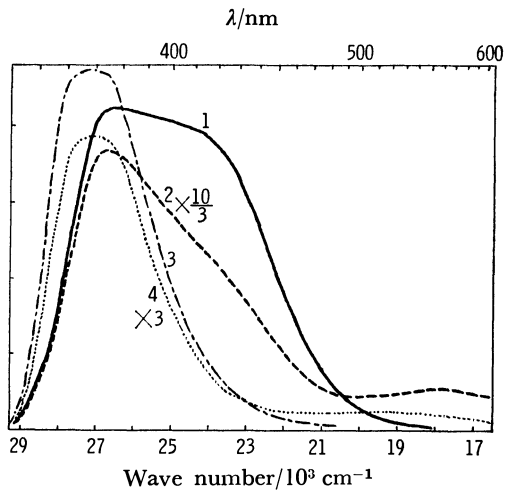

Fig. 10. Fluorescence spectra of PVCz(r) (3.9×10^{-4} M) and PCzEVE (1.9×10^{-4} M) in MTHF-THF degassed solutions in the absence and the presence of DMTP (1.9×10^{-2} M) at room temperature. The intensities of the spectra are not comparative for the different polymers.
(1) ——; PVCz(r) in the absence of DMTP, (2) ----; PVCz(r) in the presence of DMTP, (3) ——; PCzEVE in the absence of DMTP, and (4) ……; PCzEVE in the presence of DMTP.

of PVCz(r) and PCzEVE in degassed THF–MTHF solutions in the absence and in the presence of DMTP (6×10^{-2} M) are shown in Fig. 10. In the cases of PVCz (r and c) and VCz Olig. II, the fluorescence is nonuniformly quenched by DMTP, as in the case of PVCz(r) quenched by acids.[29] That is, the sandwich-like excimer fluorescence is quenched more effectively than the second excimer fluorescence. On the other hand, the fluorescence of PCzEVE is uniformly quenched by DMTP. In all cases, the exciplex fluorescence appears in the longer-wavelength region.

The quenching factor, Q, is defined by $Q=(I_0-I)/I$, where I_0 and I are the fluorescence intensity in the absence and in the presence of DMTP respectively. In determining the quenching factor, Q, of PVCz(r), the following equations have been used to separate the contribution of the second and sandwich-like excimer fluorescences at 370 and 420 nm:

$$I_{370} = I_s + 0.174I_E$$
$$I'_{420} = I_E + 0.064I_s$$
$$I_{420} = I'_{420} + 0.294I_{580}$$

where I_{370}, I_{420}, and I_{580} are the heights of the fluorescence intensity measured at 370, 420, and 580 nm respectively, I_E is the height corresponding to the sandwich-like excimer fluorescence intensity emitted at 420 nm, I_s is the height corresponding to the second excimer fluorescence intensity emitted at 370 nm, and I'_{420} is the height obtained by subtracting the contribution of the exciplex fluorescence intensity emitted at 420 nm from I_{420}. The contribution of the exciplex fluorescence intensity emitted at 420 nm has been estimated from the corrected spectrum of the THF solutions of PVCz(r) (9.2×10^{-5} M) and DMTP (0.155 M). The concentrations of the second excimer fluorescence intensity at 420 nm and the sandwich-like excimer fluorescence at 370 nm have been determined from the resolution spectra of PVCz(r) (Fig. 2). The dependence of the quenching factor, Q, of PVCz(r) on the concentration of DMTP is shown in Fig. 11. The second excimer band is linearly quenched, and the sandwich-like excimer band is superlinearly quenched. The quenching of the second and the sandwich-like excimer fluorescence seems to be described by the same reaction scheme as in the case of acid,[28] assuming that the monomer is replaced by the second excimer. Then,

$$K_s = k_a/(k_f+k_r+k_E) = k_a\tau_s = 57\ \mathrm{M^{-1}}$$
$$K_E = k_a'/(k_f'+k_r') = k_a'\tau_E = 13\ \mathrm{M^{-1}}$$

where k_f, k_r, and k_a are the radiative, nonradiative, and quenching rate constants respectively. The letters with prime and nonprime show the second and sandwich-like excimers respectively. The k_E is the rate constant of the conversion of the second excimer to the sandwich-like one. The τ_s and τ_E are the second and sandwich-like excimer fluorescence lifetimes, both in the presence of k_E and in the absence of DMTP respectively. From the measured fluorescence decay curves of PVCz(r) in an aerated THF solution at room temperature,[29] $\tau_s\sim4\times10^{-9}$ s and $\tau_E\sim17\times10^{-9}$ s. Then, $k_a\sim1\times10^{10}\ \mathrm{M^{-1}\,s^{-1}}$ and $k_a'\sim8\times10^{8}\ \mathrm{M^{-1}\,s^{-1}}$. Therefore, the quenching reaction is much more efficient for the second excimer than for the sandwich-like one.

If the PVCz–DMTP exciplex was formed between the migrating excited singlet state of the Cz chromophores and DMTP, the second excimer fluorescence would be also superlinearly quenched by DMTP, as is the case of the sandwich-like excimer fluorescence

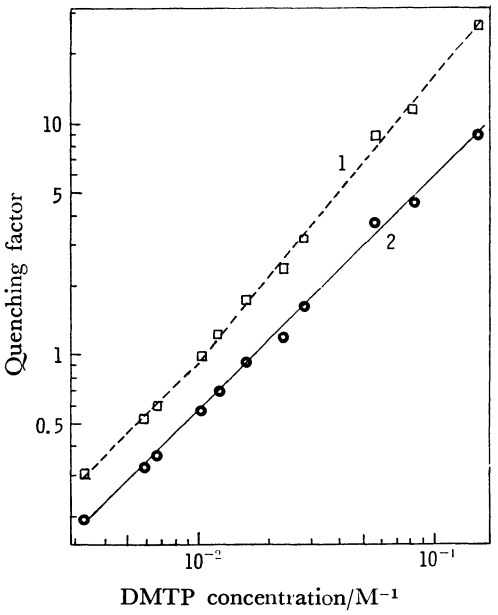

Fig. 11. Quenching of PVCz(r) by DMTP in THF aerated solutions at room temperature. Excitation wavelength; 345 nm.
(1) The sandwich-like excimer band, and (2) the second excimer band.

quenched by DMTP. Therefore, the PVCz–DMTP exciplex seems to be formed between the second excimer site and DMTP. This phenomenon seems to be supported by the fact that the intensity of the PVCz-(r)–DMTP exciplex is larger than that of the PVCz(c)–DMTP exciplex when the concentrations of the same donor and acceptor are the same. Therefore, the second excimer has a very binding energy, so it seems to dissociate to form the exciplex by the diffusive approach of DMTP.

The authors wish to express their thanks to Professor Noboru Mataga, Dr. Tadashi Okada, Dr. Hiroshi Masuhara, and Dr. Nobuaki Nakashima at Osaka University for helping us to measure the decay curve and to construct the N_2 gas laser.

References

1) M. Yokoyama, T. Tamamura, T. Nakano, and H. Mikawa, *Chem. Lett.*, **1972**, 499.
2) J. R. McDonald, W. E. Echols, T. R. Price, and R. B. Fox, *J. Chem. Phys.*, **57**, 1746 (1972).
3) M. T. Vala, J. Haebig, and S. R. Rice, *J. Chem. Phys.*, **43**, 886 (1965).
4) R. B. Fox, T. R. Price, R. F. Cozzens, and J. R. McDonald, *J. Chem. Phys.*, **57**, 534 (1972).
5) T. Yano, M. Yokoyama, and H. Mikawa, 22nd Annual Meeting on Macromolecules, (Kyoto) 29C09, May, 1973.
6) A. C. Sommersall and J. E. Guillet, *Macromolecules*, **6**, 218 (1973).
7) M. Yokoyama, T. Tamamura, M. Atsumi, M. Yoshimura, Y. Shirota, and H. Mikawa, *Macromolecules*, **8**, 101 (1975).
8) C. David, M. Piens, and G. Geuskens, *Eur. Polym. J.*, **8**, 1291 (1972).
9) G. E. Johnson, *J. Chem. Phys.*, **62**, 4697 (1975).
10) P. C. Johnson and H. W. Offen, *J. Chem. Phys.*, **55**, 2945 (1971).
11) W. Klöpffer and D. Fischer, *J. Polym. Sci. C*, **40**, 43 (1973).
12) G. E. Venikouas and P. C. Powell, *Chem. Phys. Lett.*, **34**, 601 (1975).
13) K. Okamoto, M. Yamada, A. Itaya, T. Kimura, and S. Kusabayashi, *Macromolecules*, in press.
14) K. Okamoto, A. Itaya, and S. Kusabayashi, *Chem. Lett.*, **1974** 1167.
15) K. Okamoto, M. Ozeki, A. Itaya, S. Kusabayashi, and H. Mikawa, *Bull. Chem. Soc. Jpn.*, **48**, 1362 (1975).
16) A. Itaya, K. Okamoto, and S. Kusabayashi, *Bull. Chem. Soc. Jpn.*, **49**, 2037 (1976).
17) T. Azumi and S. P. McGlynn, *J. Chem. Phys.*, **37**, 2413 (1962).
18) C. W. Frank and L. A. Harrah, *J. Chem. Phys.*, **61**, 1526 (1974).
19) T. Hayashi, T. Suzuki, N. Mataga, Y. Sakata, and S. Misumi, Symposium on Molecular Structure, (Osaka) 2A09, November, 1975.
20) H. Odani, *Bull. Inst. Chem. Res., Kyoto Univ.*, **51**, 351 (1973).
21) J. W. Longworth, *Biopolymers*, **4**, 1131 (1966).
22) T. Ishii, H. Matsushita, and T. Handa, *Kobunshi Ronbunshu*, **32**, 311 (1975).
23) W. Klöpffer, *Chem. Phys. Lett.*, **4**, 193 (1969).
24) W. Klöpffer and W. Liptay, *Z. Naturforsch.*, **25a**, 1091 (1970).
25) G. E. Johnson, *J. Chem. Phys.*, **61**, 3002 (1974).
26) A. Itaya, K. Okamoto, and S. Kusabayashi, to be published elsewhere.
27) J. B. Birks, "Photophysics of Aromatic Molecules," Wiley-Interscience (1969), p. 341.
28) G. Pfister, D. J. Williams, and G. E. Johnson, *J. Phys. Chem.*, **78**, 2009 (1974).
29) The decay curves were measured by using appropriate filters and a biplaner phototube R 617.

Heat Capacities and Some Vibrational Properties of Rubidium Chloride

Yoshiyuki HIGASHIGAKI and Hideaki CHIHARA

Department of Chemistry, Faculty of Science, Osaka University, Toyonaka 560

(Received March 1, 1976)

Molar heat capacities of RbCl were measured between 3 and 300 K with an adiabatic calorimeter and complete thermodynamic properties of the solids have been obtained. The nature of the lattice vibration spectrum of RbCl is examined in terms of the moments of spectrum. Values derived are $\theta_0=184.9\pm1.3$ K, $\theta_\infty=190.0\pm1.0$ K, E_z(zero-point energy)$=3.43\pm0.01$ kJ mol^{-1}. Those properties depend on the kind of cation rather than on the anion in alkali halides. Anharmonicity in the vibration is also discussed.

Because of their simple nature of crystal structure and atomic forces, alkali halides have been investigated by theory and experiment most extensively of all ionic solids. While the nature of lattice vibrations in these solids has been generally understood, the stability of crystal lattices, particularly the relative stability of structures, NaCl type and CsCl type, remains to be explored in relation to the difference in the vibrational properties.

Rubidium chloride occupies a special position among the alkali halide family because it exists in the two modifications, NaCl structure under ordinary conditions and CsCl structure under applied pressure.[1] The reason for the bimorphism lies in the fact that the ratios of radii of the cation and the anion assumes a value close to the critical value of 0.73 which separates the theoretical stability region of the two structures. Decreased stability of NaCl structure in the case of RbCl is expected to be seen in its vibrational properties.

Several papers[2,3,4] have been published to report the heat capacities of rubidium chloride since our measurements were concluded. However, those results are neither mutually consistent where they may be compared nor complete in that only derived quantities are given.

The purpose of the present paper is two fold: One is to provide complete thermodynamic properties of RbCl to help to understand its vibrational properties and the other is to provide heat capacity values of one of the components in the binary system NH_4Cl–RbCl which has been studied in this laboratory.

Experimental

Materials. Reagent grade rubidium chloride (Nakarai Chemicals, Ltd., stated minimum purity 99.5%) was dried *in vacuo* in a temperature-controlled quartz tube at 300 °C for 14 h. The high sensitivity DTA thermogram and the powder X-ray diffraction pattern showed no indications of trace of water or trace of the CsCl-type structure. Sample weight used for calorimetry was 69.0328 g (*in vacuo*) or 0.57980 mol.

Calorimeter and Cryostat. The calorimeter was of adiabatic type, the description of which has been reported elsewhere.[5,6] Helium exchange gas less then 1.6×10^{-6} mol was put into the calorimeter vessel to aid in thermal equilibration within it. No correction was made for the presence of the exchange gas in computing the heat capactiy values.

Temperature Scales. The working thermometer above 15 K is the Leeds & Northrup platinum resistance thermometer (model 8164), the temperature scale of which was fixed in our laboratory by comparison with another thermometer calibrated at the U. S. National Bureau of Standards, based on the IPTS-48 and the provisional NBS-55 scales. Below 15 K the thermometer was the germanium resistance thermometer (CryoCal, Inc., laboratory designation β), which had been calibrated in our laboratory.[7]

Results

Molar heat capacities at constant pressure are given in Table 1 and Fig. 1. The temperature rise in each measurement was small and therefore no curvature correction was necessary. Precision of the measurements was within 7.6% below 11 K, 1.0% from 11 to 20 K, and 0.6% above 20 K. Our results are compared with the results of Paukov and Khriplovich and Kirkham and Yates in Fig. 2, showing that our values lie intermediate between the two previous ones.

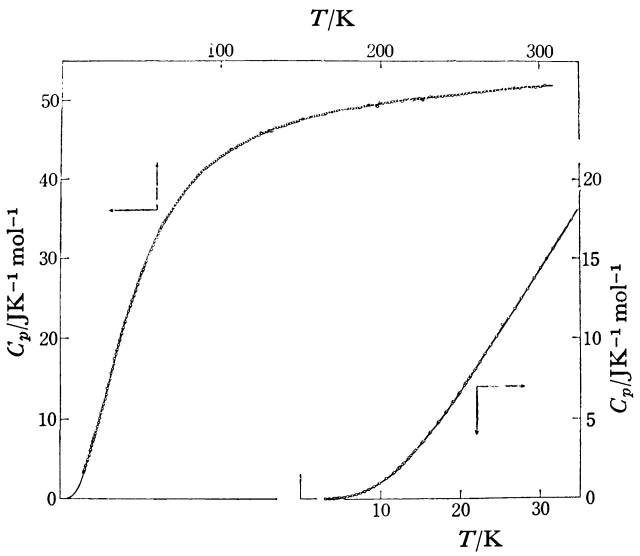

Fig. 1. Molar heat capacity of rubidium chloride.

Thermodynamic functions of rubidium chloride based on the smoothed heat capacity curve are given in Table 2.

Analysis of Experimental Results

Conversion of C_p to C_v and the Debye Temperature. The heat capacity at constant volume C_v was obtained from the heat capacity at constant pressure C_p by help of the standard thermodynamic equation,

$$(C_p-C_v)/C_p = \{1+(\chi_s C_p/\beta^2 VT)\}^{-1}$$

where χ_s is the adiabatic compressibility, β the volume expansion coefficient, V the molar volume, and T the absolute temperature.

TABLE 1. MOLAR HEAT CAPACITIES OF RUBIDIUM CHLORIDE

Weight of specimen 69.0328 g. Molecular weight 120.921, 1948 International Temperature Scales.

T/K	C_p/JK^{-1} mol^{-1}	T/K	C_p/JK^{-1} mol^{-1}	T/K	C_p/JK^{-1} mol^{-1}	T/K	C_p/JK^{-1} mol^{-1}	T/K	C_p/JK^{-1} mol^{-1}
Series I		20.497	7.072	43.807	24.09	Series XI		83.081	39.73
233.073	50.33	21.226	7.604	44.887	24.76	3.070	0.019	84.411	40.01
235.107	50.34	21.929	8.131	45.938	25.36	3.552	0.030	85.815	40.38
237.173	50.43			47.052	26.03	4.101	0.047	87.209	40.63
239.272	50.45	Series V		48.227	26.75	4.644	0.070	88.510	40.93
241.394	50.57	21.016	7.468					89.803	41.16
243.540	50.57	21.724	7.984	Series VIII		Series XII		91.091	41.35
245.739	50.56	22.416	8.504	192.281	49.25	6.918	0.289	92.379	41.57
247.946	50.63	23.098	9.010	196.475	49.30	7.456	0.380	93.668	41.74
250.161	50.65	23.790	9.537	198.090	49.12	7.975	0.475	94.955	41.93
252.399	50.75	24.510	10.09	199.763	49.68	8.536	0.593	96.233	42.14
254.662	50.85	25.261	10.77	201.504	49.54	9.157	0.767	97.503	42.37
256.933	50.92	26.042	11.27	203.402	49.64	9.870	0.993	98.373	42.53
261.400	51.00	26.843	11.87	205.425	49.61	10.687	1.261	100.042	42.70
263.588	50.96	27.646	12.53	207.468	49.75	11.532	1.579	101.311	42.87
265.903	51.10	28.453	13.11	209.529	49.00	12.363	1.927	102.587	43.04
268.266	51.26	29.266	13.78	211.634	49.90			103.868	43.26
270.462	51.17	30.066	14.41	213.776	49.80	Series XIII		105.154	43.42
272.723	51.30	30.870	15.01	215.928	49.99	48.627	27.00	106.542	43.67
275.080	51.26	31.685	15.64	218.092	49.57	49.643	27.57	107.102	43.63
277.447	51.44	32.480	16.24	220.281	50.00	50.650	28.21	108.412	43.77
279.841	51.41	33.262	16.86	222.473	50.08	51.638	28.66	109.725	43.85
282.265	51.47	34.037	17.45	224.662	50.10	52.618	29.16	111.047	44.15
284.710	51.52	34.808	18.01	226.872	49.92	53.596	29.66	112.374	44.25
287.185	51.45	35.583	18.58	229.082	50.28	54.582	30.11	113.716	44.37
		36.399	19.17	231.293	50.42	55.591	30.59	115.080	44.50
Series II		37.280	19.78	235.500	50.38	56.714	31.10	116.464	44.69
283.055	51.42	38.224	20.50			57.860	31.59	117.881	44.83
285.473	51.56	39.256	21.17	Series IX		58.939	32.12		
287.887	51.61	40.406	21.92	135.583	45.74	60.025	32.54	Sersies XVI	
290.302	51.71	41.602	22.71	137.216	46.46	61.114	33.03	125.446	45.57
292.733	51.72	42.757	23.44	138.856	46.58	62.196	33.46	127.137	45.76
295.161	51.63	43.874	24.16	140.476	46.63	63.281	33.88	128.828	45.82
297.853	51.65	44.966	24.83	142.051	46.83	64.370	34.27	130.508	45.96
300.806	51.71	46.036	25.47	143.621	46.91			132.178	45.94
303.746	51.91	47.094	26.07	145.200	47.05	Series XIV		133.840	46.35
		48.152	26.71	146.776	47.16	119.334	45.00	135.497	46.89
Seires III				148.347	47.20	120.826	45.17		
11.731	1.647	Series VI		149.919	47.32	122.361	45.31	Series XVII	
12.318	1.979	11.576	1.611	151.495	47.47	123.941	45.31	165.779	48.24
12.927	2.203	12.173	1.850	153.065	47.52	125.574	45.61	167.241	48.39
13.585	2.586	12.799	2.146	154.631	47.67	127.271	45.76	168.729	48.39
14.345	3.002	13.469	2.492	157.837	47.86	129.049	45.90	170.244	48.42
15.263	3.545	14.252	2.929	159.394	47.89			171.809	48.54
16.284	4.187	15.176	3.466	160.946	47.93	Series XV		173.499	48.61
17.286	4.836	16.225	4.122	162.499	47.99	63.819	34.06	175.258	48.70
18.210	5.438	17.286	4.815	164.054	48.09	64.924	34.46	176.996	48.75
19.060	6.062	18.239	5.440	165.608	48.16	66.036	34.85	178.731	48.78
19.846	6.589	19.106	6.063			67.156	35.25	180.461	48.92
20.580	7.139	19.925	6.634	Series X		68.281	35.59	182.188	48.88
21.270	7.653	20.726	7.225	4.281	0.052	69.413	35.94	183.914	49.00
				4.839	0.088	70.638	36.32	185.636	49.05
Series IV		Series VII		5.348	0.119	71.938	36.73	187.363	49.06
13.821	2.695	35.482	18.50	5.879	0.165	73.225	37.01	189.079	49.17
14.569	3.130	36.361	19.14	6.432	0.220	74.517	37.40	190.791	49.21
15.417	3.597	37.318	19.81	6.958	0.289	75.795	37.79	192.500	49.30
16.286	4.169	38.377	20.53	7.475	0.370	77.116	38.13	194.205	49.32
17.179	4.765	39.470	21.30	8.011	0.475	78.497	38.58		
18.078	5.350	40.562	22.01	8.577	0.601	79.864	38.92		
18.935	5.942	41.659	22.73	9.173	0.763	81.218	39.27		
19.737	6.511	42.729	23.43	9.837	0.967	82.558	39.61		

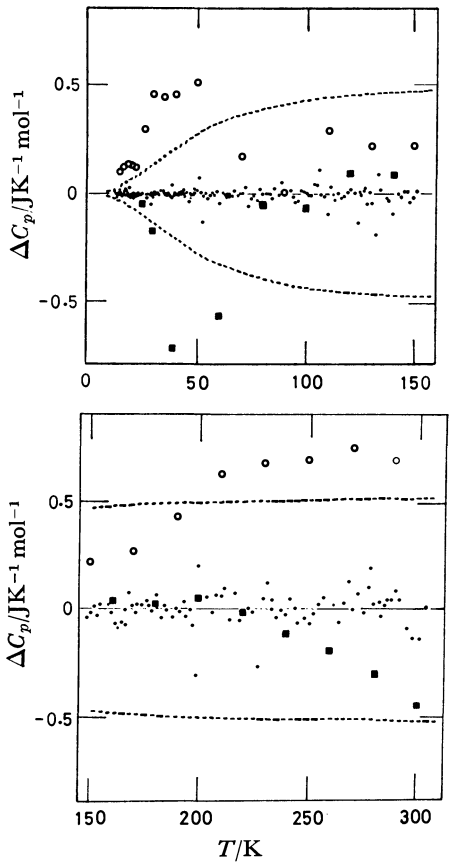

Fig. 2. Deviation plot based on our smoothed values. ----: 1% of C_p, ●: Present results, ■: Kirkham and Yates, ○: Paukov and Khriplovich.

To obtain values of the thermal expansion coefficient, we used Cooper and Yates' results[8] from 30 K to 260 K which were extrapolated to either temperature side in a manner consistent with other alkali halides.[9] Temperature dependence of adiabatic elastic constant of rubidium chloride was taken from the paper by Gluyas *et al.*,[10] because of better accuracy than others.[11,12] The χ_s values below 140 K were obtained by extrapolation. Density below room temperature was also obtained from the published values.[11,12]

The correction $C_p - C_v$ thus evaluated is negligibly small below 50 K, 0.1% of C_p at 100 K, 0.2% at 200 K, and 0.4% at 300 K.

The Debye characteristic temperature $\theta_D(V_T)$ derived from the C_v values depends on the crystal volume at the temperature T. $\theta_D(V_0)$ for the volume at 0 K can be approximated by[13]

$$\theta_D(V_0)/\theta_D(V_T) = (V_T/V_0)^\gamma$$

where γ is the Gruneisen constant. The values of $\theta_D(V_0)$ thus obtained are plotted against T in Fig. 3. The shallow basin at about 90 K is due to the inconsistency inherent in the temperature scale near the normal boiling point of oxygen. The shape of $\theta_D(T)$ curve appears quite normal for an alkali halide crystal with the NaCl-type structure; the rapid decrease at higher temperatures may be attributed to anharmonicity of lattice vibrations. A minimum occurs at about 11 K, showing the deviation of the actual frequency spectrum from the Debye spectrum. Similar minima for sodium chloride and for potassium chloride were explained theoretically by Kellerman[14] and by Jona,[15] respectively, applying the Born-von Karman theory.

Table 2. Thermodynamic functions of rubidium chloride

T / K	C_p° / JK^{-1} mol^{-1}	S° / JK^{-1} mol^{-1}	$(H^\circ - H_0^\circ)/T$ / JK^{-1} mol^{-1}	$-(G^\circ - H_0^\circ)/T$ / JK^{-1} mol^{-1}
5	0.091	0.025	0.022	0.003
10	1.017	0.293	0.218	0.075
15	3.380	1.113	0.818	0.294
20	6.712	2.539	1.862	0.677
25	10.47	4.442	3.246	1.196
30	14.35	6.697	4.757	1.940
35	18.15	9.192	6.405	2.787
40	21.65	11.85	8.100	3.754
45	24.84	14.60	9.786	4.810
50	27.76	17.37	11.45	5.920
60	32.58	22.88	14.59	8.288
70	36.12	28.18	17.44	10.75
80	38.96	33.21	19.95	13.25
90	41.15	37.93	22.19	15.73
100	42.70	42.35	24.17	18.18
110	43.98	46.49	25.91	20.58
120	45.06	50.37	27.47	22.90
130	45.97	54.01	28.85	25.16
140	46.69	57.45	30.10	27.35
150	47.35	60.69	31.22	29.46
160	47.95	63.77	32.26	31.51
170	48.43	66.69	33.20	33.50
180	48.84	69.47	34.05	35.42
190	49.19	72.12	34.84	37.28
200	49.48	74.65	35.57	39.09
210	49.75	77.07	36.24	40.84
220	50.01	79.39	36.86	42.53
230	50.26	81.62	37.44	44.18
240	50.49	83.76	37.98	45.78
250	50.72	85.83	38.49	47.35
260	50.94	87.83	38.96	48.87
270	51.17	89.77	39.42	50.35
280	51.39	91.64	39.85	51.79
290	51.61	93.45	40.25	53.20
300	51.82	95.20	40.64	54.57
273.15	51.24	90.36	39.56	50.80
298.15	51.78	94.88	40.57	54.32

The Debye characteristic temperature at 0 K, θ_0, was calculated from the intersection at $T^2=0$ of the C_pT^{-3} *versus* T^2 plot (Fig. 4) to give $\theta_0 = 18.49 \pm 1.3$ K. This value is compared with values determined by other measurements and also with the values for other alkali chlorides and rubidium halides in Table 3.

The θ_0 reported by Rallefson and Perssini is 168.5± 2.5 K, some 16 K lower than ours. However, their θ_D curve shows a peculiar behavior below 2 K which obscures the method by which their value was determined. Within the series of chlorides or the series of rubidium salts, it is seen the θ_0 decreases as the mass of constituent ion increases. This tendency agrees with

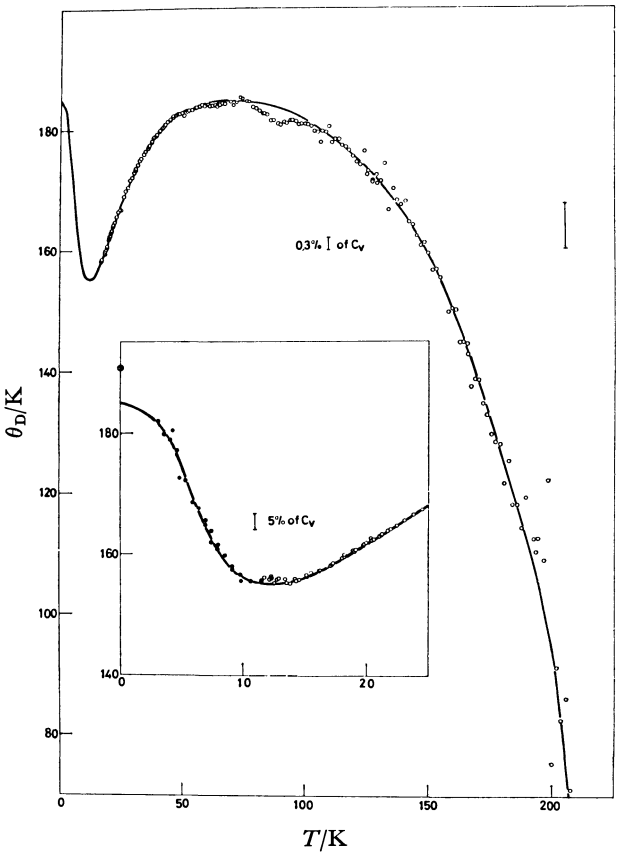

Fig. 3. Temperature dependence of the Debye characteristic temperature, $\theta_D(V_0)$.

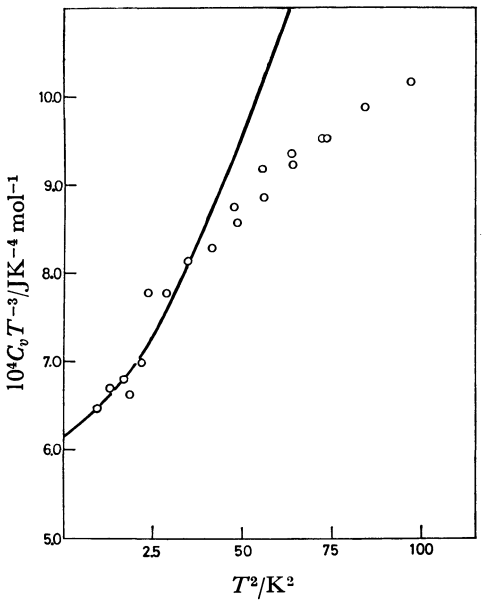

Fig. 4. Determination of θ_0 at 0 K.

the theoretical prediction that the θ_0^2 is inversely proportional to the molecular weight. An interesting feature in this connection is an empirical relation shown in Fig. 5 which is a plot of $\theta_0\sqrt{M}$ *vs.* $\sqrt{r}$ where M is the molecular weight and r the sum of constituent ionic radii.

Moments of Lattice Vibration Spectrum and Related Thermodynamic Properties. The accuracy with which

TABLE 3. COMPARISON OF θ_0 OF ALKALI CHLORIDE AND RUBIDIUM HALIDES

Alkali halide	Calorimetric	Ultrasonic	Inelastic
LiCl	422±6[e]	429±2.2[e] 424.7	
NaCl	320.6±1.5[f]	321.2±1.6[e]	325[b] 324[a]
KCl	235.1±0.5[f]	237.1[c]	238[b] 240[a]
RbCl	168.5±2.5[h] 184.9+1.3[g]	168.9±0.85[e] 168[i]	177[b] 171[a]
RbF		221.0[d]	
RbBr	134±2[h]	136.5±0.7[e]	139[i]
RbI	106.5±1.5[h]	108.0±0.55[e]	

a) Raunio and Rolandson.[16] b) Raunio and Rolandson.[16] c) Moyer.[17] d) Cleavelin, *et al.*[18] e) Lewis *et al.*[19] f) Barron, *et al.*[13] g) Present work. h) Rallefson and Peressini.[4] i) Rolandson and Raunio.[16]

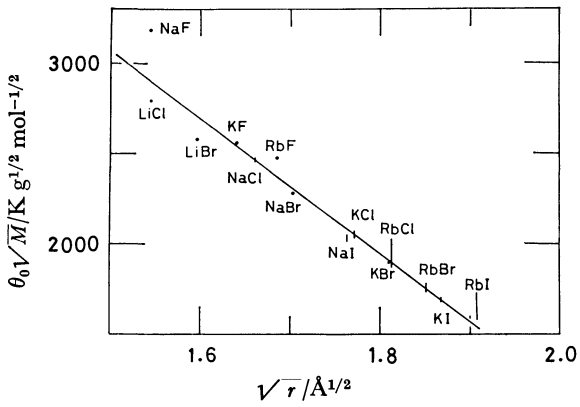

Fig. 5. Plot of $\theta_0\sqrt{M}$ *versus* $\sqrt{r}$.

the heat capacity may be determined for insulators does not permit to deduce the entire lattice vibration spectrum with a reasonable reliability. This was demonstrated by Barron and Morrison in the case of sodium chloride.[20] Instead, it is of more practical significance to derive the moments of vibration spectrum which are readier to compare for different alkali halides and which can be directly related to some thermodynamic properties.

The moment values were thus evaluated by using expansion formulae of the Debye temperature, the harmonic thermal energy, the harmonic entropy, and $C_v^{(h)}/T^n$. The results are summarized in Table 4 in the form of the $\nu_D(n)$ function.[13]

Now we shall attempt to compare the moment values of the thermodynamic properties derived therefrom with the values from other sources.

TABLE 4. VALUES OF $\nu_D(n)$

n	$\nu_D(n)$/10^{12}Hz	n	$\nu_D(n)$/10^{12}Hz
−3	3.85±0.03	1	3.82±0.02
−2	3.48±0.07	2	3.96±0.03
−1	3.41±0.04	4	4.10±0.04
0	3.62±0.02	6	4.17±0.11

The zero-th moment μ_0 is related to the geometric mean frequency $\nu_g=2.59\pm0.02$ THz, which may be compared with values 4.242 ± 0.013 THz for NaCl[13] and 3.412 ± 0.010 THz for KCl.[13] Similarly the zero point energy E_z decreases as the mass of the constituent ion increases; thus E_z of RbCl derived from the first moment in 3434 ± 10 J mol^{-1}, the smallest value for the alkali chloride having the NaCl structure.

The second moment is related to the high-temperature limit of the Debye temperature, $\theta_\infty=190.0\pm1.0$ K. This value agrees with 191 K obtained from inelastic scattering of neutrons[16] and also with 191 ± 1 K obtained from the Blackman's formula.

$$\theta_\chi=\frac{\hbar}{k}\left(\frac{5r_0}{\chi}\right)^{1/2}\left(\frac{1}{m_+}+\frac{1}{m_-}\right)^{1/2}$$

using the compressibility $\chi=5.54\times10^{-12}$ dynes cm^{-2} and the lattice constant $2r_0=6.581$ Å at 300 K.

Negative moments μ_{-1} and μ_{-2} are related to the Debye-Waller factors at $T=0$ and $T=\infty$ respectively, which appear in the diffraction intensity. However, no such information to compare with is available at the present time.

General shape of the $\nu_D(n)$ curve as shown in Fig. 6 is what one would expect for an ionic crystal although there are some differences in absolute values between ours and those by Cooper and Yates.

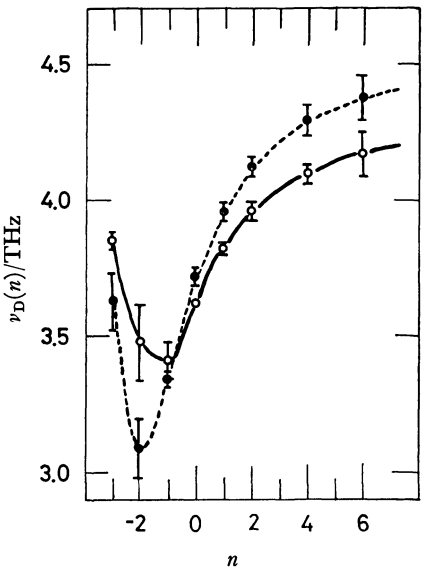

Fig. 6. Comparison of $\nu_D(n)$ function.

The differences come from the fact that Cooper and Yates gave smaller heat capacities than ours in the low temperature region.

Cation Effect and Anharmonicity. Figure 7 compares the reduced characteristic temperature $\theta_D(V_T)/\theta_\infty$ of the alkali chlorides.

It is clearly seen that as the mass of constituent ion increases, the value of θ_D/θ_∞ generally decreases and the temperature at which θ_D/θ_∞ becomes minimum goes lower. Similar tendency is also found in the case of potassium halides[13] although to a much smaller extent: thus this may be called the cation effect.

Blackman[21] showed that the ratio θ_0/θ_∞ should be

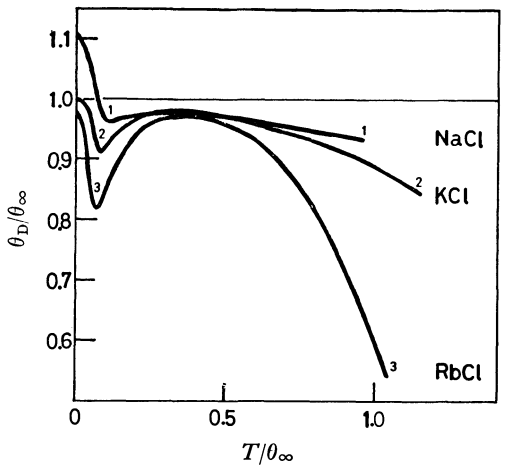

Fig. 7. Comparison of the reduced characteristic temperature.

proportional to $\sqrt{1-\eta^2}$, where $\eta=(m_+-m_-)/(m_++m_-)$. Table 5 suggests that the value of this proportionality constant is not really a constant but depends more critically on the alkali ion than on the halide ion. Barron *et al.*,[13] estimated the constant for RbBr and RbI to be probably within 10% of 0.95, in agreement with the value for RbCl. A simple calculation shows that the magnitude of this constant depends only on the elastic constants. Because the large effect of the alkali metal ion on the magnitude of the elastic anisotropy $c_{44}/(c_{11}-c_{12})$ was shown in Table X of Lewis, Lehoezky, and Briscoe's paper,[19] we may attribute the cation effect that has been demonstrated here also to that appearing in the elastic properties.

Table 5. Dependence of θ_∞/θ_0 upon mass ratio

Salt	θ_∞/θ_0	$\sqrt{(1-\eta^2)}$	$(\theta_\infty/\theta_0)\sqrt{(1-\eta^2)}$
NaCl[a]	0.905	0.977	0.88
NaI[a]	1.188	0.721	0.86
KCl[a]	1.002	0.999	1.00
KBr[a]	1.076	0.939	1.01
KI[a]	1.228	0.849	1.04
RbCl[b]	1.03	0.911	0.94
CsBr[c]	0.8816	0.9685	0.854
CsI[c]	0.8556	0.9997	0.855

a) Barron, *et al.*[13] b) Present work. c) Sorai.[22]

The cation effect also appears in anharmonicity of lattice vibrations. The anharmonic effect comes to be observable in thermodynamic functions such as heat capacity usually at temperatures higher than $(1/2)\theta_\infty$. In the case of RbCl, θ_∞ is 190 K and the maximum of θ_D occurs at 75 K. The magnitude of the anharmonic effect is represented and measured by the anharmonic coefficient A defined by

$$(F-F^h)/6Nk=-\frac{1}{2}AT^2+B+0(T^{-2})$$

or

$$(S-S^h)/6Nk=(C_v-C_v^h)/6Nk=AT$$

for the alkali halides, where $|AT|<1$.

Thus the quantity AT is the leading anharmonic contribution and its coefficient A depends on the volume only. Tosi and Fumi[23] gave more accurate formula for estimating the value of $A(V_0)$;

$$A = \frac{\theta_S - \theta_S^h}{T^2} \frac{d}{d(\theta_S^h/T)} \left(\frac{S^h}{6Nk} \right)$$

where θ_s is the experimental Debye temperature derived from the entropy for the volume at 0 K, θ_S^h the quasiharmonic Debye temperature computed from the ν_g and μ_n, S^h the quasiharmonic entropy, and $T \geqq \theta_\infty$. The coefficient for rubidium chloride was then estimated to be $A = (9.3 \pm 1.7) \times 10^{-5}\,K^{-1}$, using the Tosi-Fumi formula, and this is included in Table 6 for comparison of the anharmonic coefficients of various alkali halides.

Table 6. ANHARMONIC COEFFICIENT $A(V_0)$

Salt	$A(V_0)$ / $10^{-5}\,K^{-1}$	Salt	$A(V_0)$ / $10^{-5}\,K^{-1}$
KF[a]	-2.1 ± 0.5	NaCl[c]	-1.5 ± 0.9
KCl	3 ± 1	NaI[c]	-0.2 ± 0.5
KCl[c]	2.8 ± 0.7		
KBr[b]	2.5 ± 1	RbCl[d]	9.3 ± 1.7
KBr[c]	3.5 ± 1.0		
KI[b]	0.5 ± 0.5	CsBr[e]	-11.4 ± 0.3
		CsI[e]	-9.0 ± 0.3

a) Vieira and Hortal,[24] using a method different from Tosi-Fumi's method. b) Tosi and Fumi.[23] c) Leadbetter, *et al.*[25] d) Present work. e) Sorai.[22]

The coefficient for rubidium chloride is the largest among the alkali halides having the NaCl-type of structure and the sign and the magnitude of the coefficient is primarily determined by the kind of constituent cation.

The authors wish to express their gratitude to the assistance provided by Dr. T. Atake.

References

1) A. J. Darnell and W. A. McCallum, *J. Phys. Solids*, **31**, 805 (1970).
2) A. J. Kirkham and B. Yates, *Cryogenics*, **8**, 381 (1968).
3) I. E. Paukov and L. M. Khriplovich, *Zh. Fizi. Khim.*, **43**, 2678 (1969).
4) R. J. Rollefson and P. P. Peressini, *J. Appl. Phys.*, **43**, 727 (1972).
5) H. Chihara and M. Nakamura, *Bull. Chem. Soc. Jpn.*, **45**, 133 (1972).
6) T. Atake and H. Chihara, *J. Chem. Thermodynamics*, **3**, 51 (1971).
7) T. Atake and H. Chihara, *Bull. Chem. Soc. Jpn.*, **49**, 2126 (1974).
8) R. F. Cooper and B. Yates, *J. Phys. C., Solid St. Phys.*, **4**, L113 (1971).
9) B. Yates and C. H. Pauter, *Proc. Phys. Soc.*, **80**, 373 (1972).
10) M. Gluyas, F. D. Hughes and B. W. James, *J. Phys. D; Appl. Phys.*, **3**, 1451 (1970).
11) M. Ghafelhbashi, D. P. Dandekar, and A. L. Ruoff, *J. Appl. Phys.*, **41**, 652 (1970).
12) B. J. Marshall, D. O. Pederson, and G. G. Darris, *J. Phys. Chem. Solids*, **28**, 1061 (1967).
13) T. H. K. Barron, W. T. Werg, and J. A. Morrison, *Proc. R. Soc., Ser. A*, **242**, 478 (1959).
14) E. W. Kellerman, *Proc. R. Soc., Ser. A*, **178**, 17 (1940).
15) M. Jona, Jr., *Phys. Rev.*, **60**, 822 (1941).
16) a) NaCl, KCl, RbCl, and RbF, G. Raunio and S. Rolandson, *Phys. Rev.*, **B2**, 2098 (1970); b) RbCl and RbF, G. Raunio and S. Rolandson, *J. Phys. C, Solid St. Phys.*, **3**, 1013 (1970); c) RbBr, S. Rolandson and G. Raunio, *ibid.*, **4**, 958 (1971).
17) D. F. Moyler, *J. Phys. Chem. Solids*, **26**, 1459 (1965).
18) C. R. Cleavelin, D. O. Pederson, and B. J. Marshall, *Phys. Rev.*, **B5**, 3193 (1972).
19) J. T. Lewis, A. Lehoezky, and C. V. Briscoe, *Phys. Rev.*, **161**, 877 (1967).
20) T. H. K. Barron and J. A. Morrison, *Proc. R. Soc., Ser. A*, **256**, 427 (1960).
21) M. Blackman, *Proc. R. Soc., Ser., A*, **181**, 58, (1942).
22) H. Sorai, *J. Phys. Soc. Jpn.*, **25**, 421 (1968).
23) M. P. Tosi and F. G. Fumi, *Phys. Rev.*, **131**, 1458 (1963).
24) S. Vieira and H. Hortal, *J. Phys. C, Solid St. Phys.*, **4**, 1703 (1971).
25) A. J. Leadbetter, D. M. T. Newsham, and G. S. Settatree, *J. Phys. C, Solid St. Phys.*, **2**, 393 (1969).

MO-theoretische Untersuchung der Nucleophilen Substitution Einiger Silacycloalkane

Gernot FRENKING, Hiroshi KATO,* und Kenichi FUKUI

Department of Hydrocarbon Chemistry, Faculty of Engineering, Kyoto University, Sakyo-ku, Kyoto 606

**College of General Education, Nagoya University, Chikusa-ku, Nagoya 464*

(Received March 13, 1976)

CNDO/2 calculations have been carried out for $(CH_2)_{n-1}SiMeH$ and $(CH_2)_{n-1}CMeH$ with $n=3$, 4, 5, and 6. It is found that the electronic structure of the two classes of compounds shows principal differences in the ring-size dependence. It is suggested that this is the reason for the different ring dependence of the reactivity in the nucleophilic substitution reaction.

Die Ringgrößenabhängigkeit der cyclischen Organosilane $(CH_2)_{n-1}SiMeH$ wurde für die Substitutionsreaktion mit wässrigalkoholischem Alkali experimentell mit $n=4 \gg 5>6$ ermittelt.[1,2] Die wesentlich höhere Reaktivität der viergliedrigen Verbindung gegenüber fünfgliedrigen steht im Kontrast zu den Cycloalkanen, bei denen die Ringabhängigkeit von $(CH_2)_{n-1}CMeCl$ in der S_N2 Reaktion mit $n=3<4<5>6$ gefunden wurde.[3] Dabei übernimmt wegen des relativ elektropositiven Charakters des Silizium der damit verbundene Wasserstoff die Rolle des elektronegativen Substituenten im analogen Cycloalkan, im angeführten Beispiel die des Chlor. Zur Erklärung dieses Sachverhaltes wurden sterische Gründe angegeben, wonach für die Silacycloalkane in einem 'flank'-Angriff (Abb. 1a) der CH_2–Si–CH_2 Winkel α im Übergangszustand, 90°, demjenigen der viergliedrigen Ringverbindung im Grundzustand am nächsten kommt. Danach muß für die viergliedrige Ringverbindung zur Bildung des Übergangszustandes die geringste Ringspannung aufgewendet werden.[1] Unsere Berechnungen ergaben jedoch, daß der Wert für α in der fünfgliedrigen Verbindung näher an 90° liegt als der der viergliedrigen. Daher ist die gennante Erklärung fragwürdig.

Einzelheiten der Rechnungen

Die meisten Energieberechnungen wurden mit Hilfe der CNDO/2 Methode von Pople *et al.* durchgeführt.[4] Einige Berechnungen erfolgten im Rahmen von CNDO/2 unter Einschluß der d-Orbitale am Si.[5] Lokalisierte Orbitale wurden mit Hilfe der 'Energieminimisierungsmethode' von Edmiston und Ruedenberg[6] erhalten, basierend auf INDO MOs.[7] Berechnet wurden die Verbindungen $(CH_2)_{n-1}SiMeH$ und $(CH_2)_{n-1}CMeH$ mit $n=3$, 4, 5, und 6, welche von nun an mit Si(3) C(3), Si(4), usw. bezeichnet werden. Si(3) wurde aus Vergleichsgründen miteingeschlossen obwohl es noch nicht synthetisiert werden konnte.[8]

Für die Cycloalkane wurde die Geometrie der unsubstituierten Verbindungen übernommen,[9] und die CH_3-Gruppe wurde mit Tetraederwinkel am Kohlenstoff und einer C–C Bindungslänge von 1.52 Å plaziert.

Für die Geometrie der Silacycloalkane liegen keine experimentellen Daten vor. Für α wählten wir zunächst jene Werte, die entweder in der Literatur vorgeschlagen wurden,[10] oder an Hand von Analogbetrachtungen an Cycloalkanen am wahrscheinlichsten schienen. Fernerhin berechneten wir jedes Molekül mit einem abweichenden Wert. Tabelle 1 zeigt die Werte für α. Jene Geometrien die energetisch günstiger liegen sind mit 'normal', die anderen mit 'deformiert' bezeichnet. Bezüglich der Bindungslängen wurde der Si–C Abstand mit 1.85 Å für Si(6) und Si(5), und mit 1.94 Å für Si(4) als Wert für die Ringbindung eingegeben. Si(3) wurde mit beiden Werten berechnet. Die Bindungsabstände für die Si–CH_3 und Si–H Bindungen sind jeweils 1.85 Å und 1.48 Å. Si(4) wurde mit einer nichtplanaren Geometrie bei einem Biegungswinkel von 36°[11] berechnet; Si(5) wurde mit planarer Ringgeometrie berechnet, Si(6) in der Sesselform und einem Biegungswinkel von 54°45′. Die übrigen Geometriedaten wurden von den analogen Cycloalkanen unter Berücksichtigung der obigen Werte übernommen.

Tabelle 1. Werte des CH_2-Si-CH_2 Winkels α

	Si(3)	Si(4)	Si(5)	Si(6)
'Normal'	47°40′	83°	90°	83°
'Deformiert'	50°10′	90°	100°	120°

Ergebnisse und Diskussion

Die CNDO/2-Ergebnisse wurden auf Anhaltspunkte zur Erklärung des experimentellen Sachverhaltes untersucht. Tabelle 2 zeigt für die berechneten Verbindungen die Energielagen und wichtigsten AO-Koeffizienten der LUMOs (lowest unoccupied MO), die gemeinsam mit dem HOMO (highest occupied MO) des OH^- die dominierende Rolle in der Orbitalwechselwirkung spielen. Der antibindende Charakter in der X–H (X=Si, C) Bindung ist in den LUMOs der Si-Verbindungen wesentlich ausgeprägter als in denjenigen der C-Verbindungen. Fernerhin zeigt sich als wichtigster AO-Koeffizient des Si das isotrope s-AO, welches eine bedeutende Rolle in dieser Reaktion spielt, während dies im Falle der C-Verbindungen ein pσ-AO ist. Abgesehen von diesen Unterschieden zeigt sich daß die Energielagen der LUMOs mit der Ausnahme von Si(6) völlig mit der o.g. Reihenfolge der Reaktivität übereinstimmen; außerdem lassen sie für das hypothetische Si(3) eine geringe Reaktivität erwarten. Die Tatsache daß die Energielagen der Si-LUMOs deutlich niedriger als die der C-LUMOs liegen kann als eine Begründung für die höhere Reaktivität der Si-Verbindungen angesehen werden.

In Tabelle 3 ist die Ladungsverteilung an den Angriffszentren (Si bzw. C) und dem damit verbundenen Wasserstoff verzeichnet, sowie die E_{AB}-Werte für die Si–H und C–H Bindungen die während der Reaktion

Tabelle 2. Energielagen und einige AO-Koeffizienten der LUMO

n	Si(n) Koeffizient s(Si)	Si(n) Koeffizient s(H)[a]	Si(n) Energielage [eV]	C(n) Koeffizient p(C)[b]	C(n) Koeffizient s(H)[a]	C(n) Energielage [eV]
3	0.693	−0.528	1.88	0.315(p_z)[c]	−0.499[c]	7.27[c]
4	0.666	−0.508	1.73	0.243(p_z)	−0.420	6.80
5	0.657	−0.535	1.88	0.216(p_z)	−0.334	6.66
6	0.607	−0.534	1.69	0.286(p_y)[c]	−0.388[c]	7.41

a) Wasserstoff der X-H (X=Si, C) Bindung. b) Attackierter Kohlenstoff. c) 2. LUMO.

Tabelle 3. Ladung q und E_{AB} Werte der isolierten Moleküle

n	Si(n) q(Si)	Si(n) q(H)[a]	Si(n) E_{Si-H}[eV]	C(n) q(C)[b]	C(n) q(H)[a]	C(n) E_{C-H}[eV]
3	+0.333	−0.114	−11.31	+0.026	−0.004	−20.26
4	+0.554	−0.156	−11.40	+0.037	−0.004	−20.21
5	+0.539	−0.154	−11.45	+0.039	−0.016	−19.70
6	+0.535	−0.147	−11.46	+0.050	−0.028	−18.34

a) Wasserstaff der X-H (X=Si, C) Bindung. b) Attackierter Kohlenstoff.

aufbrechen. Obwohl die CNDO/2 Resultate eine unvernünftige C^+–H^- Polarisation angeben—mit allerdings recht kleinen Absolutwerten—ist der Trend in Abhängigkeit von der Ringgröße deutlich von dem der Si–H Bindung verschieden, und mit der Ausnahme von C(6) stimmt die Größenfolge mit derjenigen der Reaktivität uberein. Die E_{AB}-Werte zeigen mit steigender Ringgröße regelmäßig abnehmende Werte für die C–H Bindung und einen regelmäßigen Anstieg für die Si–H Bindung. Dies deutet einen prinzipiellen Unterschied in der Ringabhängigkeit der elektronischen Struktur für die Silacycloalkane zu den Cycloalkanen an, obwohl die unregelmäßige Ringabhängigkeit nicht reflektiert ist.

Bezüglich der lokalisierten MOs (LMOs) hatten wir in früheren Untersuchungen gefunden, daß in Cycloalkanen der %s Charakter der C–H Bindungen mit steigender Ringgröße abnimmt, während er in der C–C Bindung ansteigt, womit die Ringabhängigkeit der elektronischen Struktur wiedergegeben wird.[12] Obige Resultate lassen typische Unterschiede für silacycloalkane erwarten. In Tabelle 4 ist der %s Charakter am Si für die Si–H und Si–C Ringbindung der Silacycloalkane, sowie des attackierten Kohlenstoffs in der C–H und C–C Ringbindung verzeichnet. Es zeigen sich in der Tat deutliche Unterschiede im Trend zur Ringgröße. Die Reihenfolge für die Si–H Bindung ist $n=3>4<5<6$, und ein umgekehrter Ablauf ergibt sich für die Si–C Bindung, was völlig mit der experimentellen Reihenfolge übereinstimmt. Besonders die extremen Werte des Si(3) sind zu beachten. Der recht geringe %s Wert für die Si–C Bindung deutet eine schwache Ringbindung an und erklärt die Tatsache, daß diese Verbindung bis jetzt nicht synthetisiert werden konnte.

Die Übereinstimmung mit der experimentellen Ringgrößenabhängigkeit ist mit Ausnahme von C(6) auch für die Cycloalkane gegeben. Wie im Falle der Ergebnisse der Ladungsverteilung und der Energielagen der LUMOs ist es die sechsgliedrige Verbindung, bei der die berechneten Daten mit der experimentellen Reihenfolge nicht übereinstimmen und eine zu große Reaktivität angeben. Eine Erklärung liegt darin daß der recht voluminöse sechsgliedrige Ring eine zusätzliche sterische Hinderung der Reaktion bedeutet und die normal erwartete Übereinstimmung mit den theoretischen Daten unterbricht.

Zur Illustrierung der Ringbindungen in den berechneten Verbindungen ist in den Abbildungen 2 und 3 die LMO-Elektronendichteverteilung für die drei- und fünfgliedrigen Moleküle graphisch dargestellt. Es zeigt

Tabelle 4. LMO ergebnisse des %s-charakters einiger bindungen

n	Si(n) Si(Si-H)	Si(n) Si(Si-C)[a]	C(n) C(C-H)[b]	C(n) C(C-C)[c]
3	39.2%s	15.5%s	28.6%s	18.9%s
4	31.8%s	28.8%s	27.5%s	23.5%s
5	32.5%s	25.5%s	22.2%s	26.3%s
6	34.6%s	21.6%s	21.5%s	26.2%s

a) Si-C Ringbindung. b) Attackierter Kohlenstoff. c) Ringbindung des attackierten Kohlenstoffs.

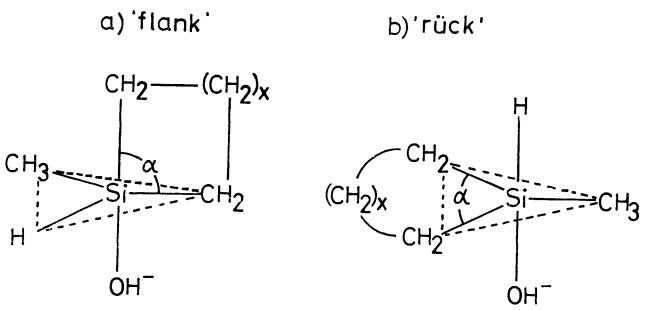

Abb. 1. Darstellung der beiden Angriffswege des OH^-.

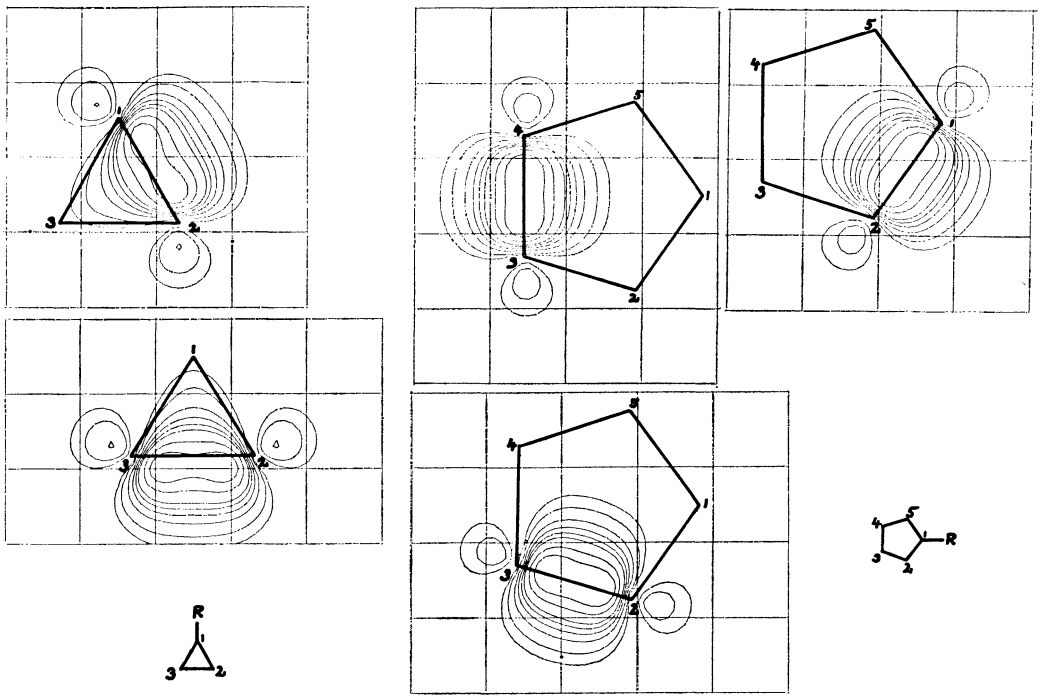

Abb. 2. Graphische Darstellung der Ringbindungs-LMOs von C(3) und C(5). Die Linien entsprechen Elektronendichten von 0.1; 0.2; 0.4; 0.6; 0.8; 1.0; 1.5; 2.0 Å^{-3}.

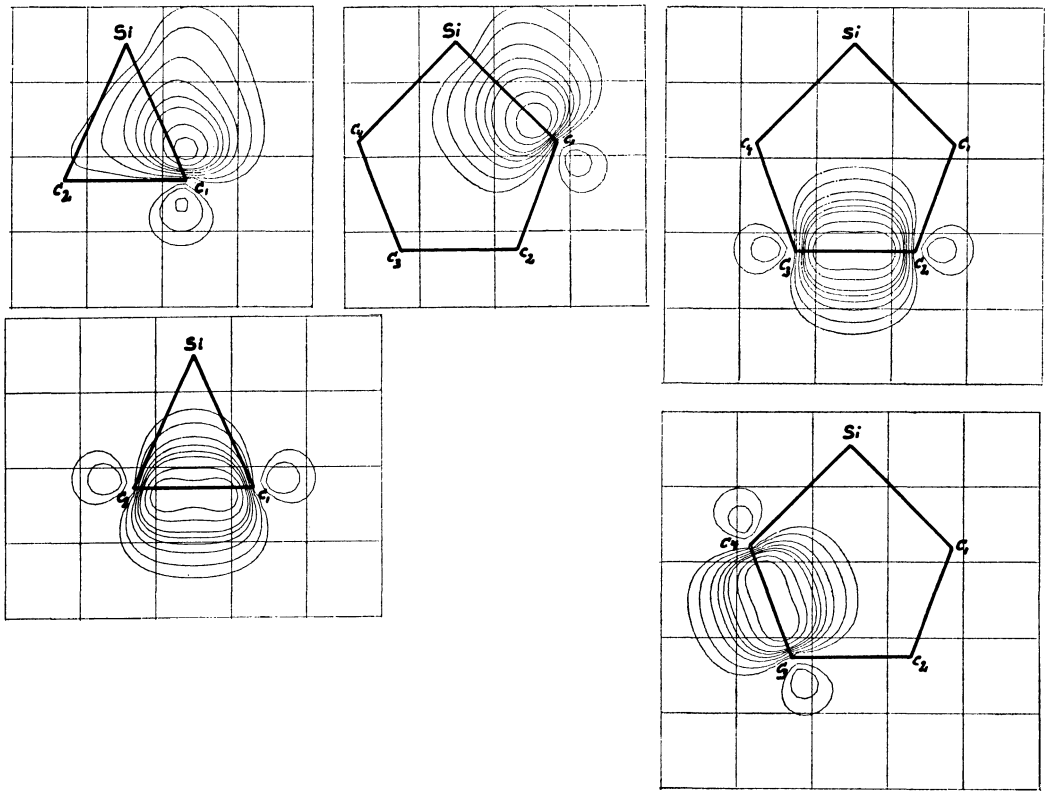

Abb. 3. Ringbindungs-LMOs von Si(3) und Si(5). Die Electronendichten sind die gleichen wie in Abb. 1.

sich daß die Ladungsverteilung in den C–C Bindungen durch den Methylsubstituenten bzw. das Siliziumatom kaum beeinflußt ist. Das Si–C LMO zeigt klar die größere Elektronegativität des Kohlenstoffs an. Fernerhin ist in den dreigliedrigen Verbindungen der Charakter der gebogenen Bindung ('bent bond') demonstriert.

Mit Hilfe des CNDO/2 Verfahrens berechneten wir die Energie des kombinierten Systems einer Cyclischen Verbindung und eines angreifenden OH^- Ions, welches einem Übergangszustand entspricht. In der Literatur sind .verschiedene Angriffswege bei der Substitution am

Tabelle 5. Energiedifferenz des Übergangszustandes mit verschiedener geometrischer Anordnung zur Summe der Grundzustände, in eV

	Si(n)			
Konfig.[a]	$n=3$	$n=4$	$n=5$	$n=6$
A	9.02 (0.04)[b]	7.76 (1.34)	7.46 (0.96)	10.15 (1.87)
B	10.53 (1.64)	7.69 (2.39)	11.80 (1.92)	13.72 (3.33)
C	7.87 (1.68)	7.18 (1.10)	7.43 (1.01)	7.34 (1.26)
D	9.57 (3.17)	8.56 (2.67)	7.31 (0.85)	9.11 (2.19)

a) A: 'normal flank'; B: 'deformiert flank'; C: 'normal rück'; D: 'deformiert rück'. b) Der Zahlenwert in der Klammer zeigt die Energiedifferenz von Si(n) mit verschiedener Geometrie zum Grundzustand, in eV.

Silizium vorgeschlagen.[1,13] Wir berechneten Übergangszustände für Silacycloalkan+OH^-, die einem 'flank' bzw. 'rück'-Angriff entsprechen; ihre Geometrie ist in Abb. 1 demonstriert. Die Übergangszustände von Cycloalkan+OH^- wurden lediglich mit 'rück'-Konfiguration berechnet, da dies dem normalen S_N2 Mechanismus entspricht. Der C–O Abstand wurde mit 2.00 Å, der Si–O Abstand mit der normalen Si–O Bindungslänge von 1.63 Å eingegeben. Der Grund für die Wahl der normalen Bindungslänge im Falle der Silacycloalkane liegt darin, daß die S_N2 Reaktion am Silizium unter Bildung eines relative stabilen Übergangskomplexes verläuft, dessen Bindungslängen nahe denen von normalen Werten liegen.[14] Die Berechnungen wurden mit linearer Anordnung des OH^- in Richtung auf das Angriffszentrum (Si bzw. C) durchgeführt. Die Energiewerte der Systeme mit dieser Geometrie lagen niedriger als bei einem X–O–H (X=Si, C) Winkel von 105°. Dieses physikalisch unsinnige Ergebnis dürfte auf die CNDO/2 Näherungen zurückzuführen sein.

Die Berechnungen der Si-Übergangszustände wurden mit beiden Werten für α, also 'normaler' und 'deformierter' Ringgeometrie durchgeführt. Die Ergebnisse in Tabelle 5 zeigen zum einen, daß der 'rück'-Angriff in allen Fällen günstiger ist als der 'front'-Angriff.[15] Mit Ausnahme von Si(5) ist auch im Übergangszustand in allen Fällen die 'normale' Ringgeometrie günstiger als die 'deformierte'; im Fall von Si(5) ergibt ein Wechsel zur 'deformierten' Geometrie einen energetisch günstigeren Wert. Berechnungen im Rahmen von CNDO/2 unter Einschluß von d-Orbitalen am Silizium ergaben die gleiche Reihenfolge. Die Werte in Tabelle 5 zeigen jedoch auch daß die Energiedifferenz zwischen der jeweils günstigsten 'rück' und 'flank' Geometrie besonders im Fall von Si(4) und Si(5) nicht sehr groß ist. Dies deutet die Möglichkeit eines 'flank'-Attacks besonders für jene Fälle an, bei denen der 'rück'-Angriff sterisch behindert ist wie etwa bei Brückenkopf-Silacycloalkanen.[3]

Auch die Energiedifferenz der Silacycloalkane in den verschiedenen Übergangsgeometrien zur Grundzustandsgeometrie ist in Tabelle 5 gezeigt. Die Werte ergeben eine geringere Bevorzugung für den 'rück'-Angriff als im Fall der kombinierten System (Tabelle 5); im Fall von Si(3) liegt der Wert für die 'normal flank' Geometrie sogar am günstigsten. Es ist also weniger die geometrische Veränderung des Silacycloalkans die auf Bevorzugung des 'rück'-Angriffs verursacht, als vielmehr die bessere Angriffsmöglichkeit für das OH^- Ion.

In Tabelle 6 sind die Energiedifferenzen der Übergangszustände mit der jeweils günstigstem Geometrie, sowie diejenigen der Cycloalkane zur Summe von (Grundzustand+OH^-) angegeben in Relation zu den Werten für die viergliedrigen Verbindungen. Es zeigt sich daß die Berechnung der Gesamtenergie der kombinierten Systeme die Ringabhängigkeit der Substitutionsreaktion perfekt wiedergibt. Auch von diesen Werten läßt sich auf eine sehr geringe Reaktivität des Si(3) schließen.

Tabelle 7 führt die Ladungsverteilung am zentralen Si—bzw. C—Atom sowie dem damit verbundenen Wasserstoff im Übergangszustand auf. Weiterhin ist die Ladungsdifferenz (Δq(H)) des abgehenden Wasserstoffs verglichen zum Grundzustand sowie der Ladungsübergang (CT) vom OH^- zum attackierten Molekül verzeichnet. Aus den Werten geht hervor daß der Ladungsübergang fast ausschließlich vom OH^- Ion zum abgehenden Wasserstoff stattfindet; im Falle der Cycloalkane sind die Δq(H) Werte in einigen Fällen sogar größer als die CT-Werte, was auf zusätzliche Ladungstrennung im cyclischen Molekül zurückzuführen ist.

Tabelle 6. Energiedifferenz des Übergangszustandes mit der jeweils günstigsten Geometrie zum Grundzustand, relativ zu den Werten für X(4) (X=Si, C), in eV

	$n=3$	$n=4$	$n=5$	$n=6$
Si(n)	+0.68	0	+0.12	+0.17
C(n)	+0.59	0	−0.13	−0.05

Ein +(−) Zeichen kennzeichnet einen größeren (kleineren) Wert relativ zum jeweiligen X(4).

Tabelle 7. Ladung q, Ladungsdifferenz des abgehenden Wasserstoffs, Δq(H), sowie Ladungsaustausch CT vom OH^- zum X(n) (X=Si, C) im Übergangszustand

X	n	q(X)	q(H)	Δq(H)	CT
Si(n)	3	+0.903	−0.466	0.352	0.378
	4	+1.137	−0.531	0.375	0.360
	5	+1.156	−0.507	0.353	0.338
	6	+1.146	−0.512	0.365	0.361
C(n)	3	+0.176	−0.147	0.143	0.092
	4	+0.194	−0.141	0.137	0.089
	5	+0.190	−0.139	0.123	0.086
	6	+0.172	−0.137	0.109	0.128

Tabelle 8. Ladungsbindungsmomente der LMOs für die X-H (X=Si, C) Bindung im Grund (G) und Übergangszustand (T), in D

n	Si(n)		C(n)	
	G	T	G	T
3	1.08	3.56	0.05	0.93
4	1.21	3.84	0.11	0.84
5	1.12	4.05	0.12	0.87
6	1.15	3.98	0.23	0.87

Eine Analyse der LMO-Ergebnisse der Übergangszustände mit linearer X–O–H (X=Si, C) Anordnung zeigt folgende Eigenschaften: Das X–H (X=Si, C) LMO ist im Vergleich zum Grundzustand stärker zum Wasserstoff hin polarisiert, was durch die Werte für die Ladungsbindungsmomente μ_{AB} in Tabelle 8 demonstriert ist. Sie wurden nach folgender Gleichung berechnet:[12]

$$\mu_{AB} = 4.804 R_m (Q_{Ai} - Q_{Bi})$$

$$Q_{Ai} = (2 \sum_{t}^{\text{on A}} C_{it}(A)^2) - 1$$

Dabei ist R_m der halbe AB Bindungsabstand in Einheiten von Å, wobei der Ursprungspunkt der Mittelpunkt der AB Bindung ist. Q_{Ai} ist die atomare Ladung des Atoms A im i-ten LMO, welches in der AB Bindung lokalisiert ist. C_{it} ist der Koeffizient des t-ten AO des Atoms A im i-ten LMO. Die Summierung t läuft über alle Valenz-AOs des Atoms A.

Fernerhin ergaben die LMO Resultate neben einem O–H LMO drei räumlich verschiedene, ansonsten gleichwertige LMOs welche nahezu lone-pair LMOs am Sauerstoff vom sp^3-Typ darstellen, dabei jedoch deutliche Koeffizienten am X-Atom (X=Si, C) aufweisen.

Zusammenfassung

Die Ringgrößenabhängigkeit der elektronischen Struktur der untersuchten Silacycloalkane zeigt deutliche Unterschiede zu derjenigen von analogen Cycloalkanen. Dies wird als Grund für die unterschiedliche Ringgrößenabhängigkeit der Reaktivität dieser beiden Verbindungsklassen in der Substitutionsreaktion vorgeschlagen. Der Trend in den Energielagen der LUMOs, in der Ladungsverteilung am Reaktionszentrum, in den E_{AB}-Werten der sich lösenden Si–H bzw. C–H Bindungen sowie im %s Charakter der Si–H, Si–C bzw. C–H und C–C Bindungen in Relation zur Ringgröße weist einen charakteristisch unterschiedlichen Verauf auf der mit wenigen Ausnahmen mit den experimentellen Ergebnissen übereinstimmt. Lediglich die Werte für die dreigliedrigen Verbindungen weisen ähnlich extreme Daten auf die eine geringe Reaktivität auch für das hypothetische Si(3) andeuten.

Einer der Autoren (G.F.) ist Herrn Tsutomu Minato für die Beschaffung der Computerprogramme und auch Herrn Kazuyoshi Tanaka für die Beihilfe des Maschineschreibens zu Dank verpflichtet. Er bedankt sich ebenfalls beim Japanischen Erziehungsministerium sowie dem Deutschen Akademischen Austauschdienst für die Gewährung eines Stipendiums. Alle drei Autoren möchten ihre Dankbarkeit gegenüber dem Rechenzentrum der Kyoto Universität für die Benutzung des FACOM 230-75 Computers ausdrücken.

Literatur

1) C. Eaborn, "Organosilicon Compounds," Butterworths, London (1960).
2) L. H. Sommer, U. F. Bennett, P. G. Campbell, and D. R. Weyenberg, *J. Am. Chem. Soc.*, **79**, 3295 (1957).
3) A. Streitwieser, Jr., *Chem. Rev.*, **66**, 571 (1966).
4) J. A. Pople, D. P. Santry, and G. A. Segal, *J. Chem. Phys.*, **43**, 129 (1965).
5) D. P. Santry and G. A. Segal, *J. Chem. Phys.*, **47**, 158 (1967).
6) C. Edmiston and K. Ruedenberg, *Rev. Mod. Phys.*, **35**, 457 (1963).
7) J. A. Pople, D. L. Beveridge, and P. A. Dobosh, *J. Chem. Phys.*, **47**, 2026 (1967).
8) Zur Stabilität von Silacyclopropanen vgl.: P. D. Mollere, and R. Hoffmann, *J. Am. Chem. Soc.*, **97**, 3680 (1975).
9) "Tables of Interatomic Distances", The Chemical Society, Spec. Publ. 11, London (1958).
10) L. H. Sommer and G. A. Baum, *J. Am. Chem. Soc.*, **76**, 5002 (1954).
11) J. Laane and R. D. Lord, *J. Chem. Phys.*, **48**, 1508 (1968).
12) G. Frenking, H. Kato, K. Hirao, and K. Fukui, *Bull. Chem. Soc. Jpn.*, **48**, 2769 (1975).
13) L. H. Sommer, "Stereochemistry, Mechanism and Silicon", McGraw-Hill, New York (1965).
14) P. Baybutt, *Mol. Phys.*, **29**, 389 (1975).
15) Hierzu vgl. MO-Untersuchungen an SiH_5^-: D. L. Wilheit and L. Spialter, *J. Am. Chem. Soc.*, **95**, 2100 (1973).

Preparation and Stereochemistry of a New Isomer (*Λ-cis-β*) of Cobalt(III) Complexes with (3*S*,8*S*)-3,8-Dimethyl-1,4,7,10-tetraazadecane[1)]

Masahiko SABURI, Teiji SATO, and Sadao YOSHIKAWA

Department of Synthetic Chemistry, Faculty of Engineering, University of Tokyo, Hongo, Bunkyo-ku, Tokyo 113

(Received October 17, 1975)

Carbonatocobalt(III) complex of (3*S*,8*S*)-3,8-dimethyl-1,4,7,10-tetraazadecane((3*S*,8*S*)-dimetrien) was prepared from *trans*-[$CoCl_2$((3*S*,8*S*)-dimetrien)]ClO_4 by treating with carbonate or hydrogencarbonate ion. The carbonato complex was assigned to the *Λ-cis-β* configuration, a novel geometry for the (3*S*,8*S*)-dimetrien complexes. The visible absorption, circular dichroism, and proton magnetic resonance data were obtained for the *Λ-β* and other carbonato complexes. Preparation and assignment of dinitrocobalt(III) complex with (3*S*,8*S*)-dimetrien are given. The relative stabilities of the four isomers of (3*S*,8*S*)-dimetrien complexes (*Λ-cis-α*, *Λ-cis-β*, *Δ-cis-β*, and *trans*) are discussed qualitatively.

Five stereoisomers are possible for the dianionocobalt(III) complexes of triethylenetetramine, one *cis-α*, two *cis-β*, and two *trans*. Of these isomers, the central metal ion is a chiral center except for one of the *trans* isomers (*meso-trans*). When a chiral tetramine obtained by introducing methyl group(s) into the carbon chain of trien is employed, the stereoisomers of cobalt(III) complex are sufficiently affected by the steric effects of the methyl substituents and give rise to the isomers of particular geometry and chirality.[2-5)] Three isolated isomers of dichloro- and dinitrocobalt(III) complexes with (3*S*,8*S*)-3,8-dimethyl-1,4,7,10-tetraazadecane (abbreviated as (3*S*,8*S*)-dimetrien), for instance, have the *Λ-cis-α*, *Δ-cis-β* and *trans* geometries, in which the absolute configurations of the two coordinated secondary nitrogen atoms have the combination of (*R*,*R*),[6)] (*R*,*S*), and (*S*,*S*), respectively.[2,3)]

The stereoselectivity found in the formation of the (3*S*,8*S*)-dimetrien complexes has been ascribed to the preferential equatorial orientation of the methyl groups with respect to the five-membered chelate rings.[2,3)] X-Ray diffraction studies demonstrated the preference of equatorial orientation of the methyl groups for the three isomers of dinitrocobalt(III) complexes.[7-9)] So far as the stereoisomers with the equatorial methyl groups are concerned, the possible isomers of (3*S*,8*S*)-dimetriencobalt(III) complex are those mentioned above (*Λ-cis-α*, *Δ-cis-β* and *trans*).

In the course of attempts to convert the *trans*-dichlorocobalt(III) of (3*S*,8*S*)-dimetrien into either of the *cis*-dichloro isomers, we have isolated a carbonato complex, which could be assigned to the *Λ-cis-β* configuration based on the data of circular dichloism (CD) and proton magnetic resonance (PMR). In the present report, the preparation and stereochemistry of the carbonatocobalt(III) complex of (3*S*,8*S*)-dimetrien will be described.

Experimental

Λ-β-Carbonato((3S,8S)-3,8-dimethyl-1,4,7,10-tetraazadecane)-cobalt(III) Perchlorate(Λ-β-[CoCO₃((3S,8S)-dimetrien)]ClO₄). To a solution of *trans*-[$CoCl_2$((3*S*,8*S*)-dimetrien)]ClO_4[2)] (0.50 g) in water (10 ml) was added lithium carbonate (0.20 g) and the mixture was heated for 30 min on a water bath (80 °C). Excess lithium carbonate was filtered off and the filtrate was evaporated to about 5 ml on a water bath. Five ml of methanol was added and the resultant precipitates were immediately removed by filtration. Solid lithium perchlorate (1.5 g) was added and dissolved. The sides of the vessel were scratched with a glass rod until red-violet crystals appeared. After being cooled in a refrigerator overnight, the crystals were collected, washed with methanol and ether, and air-dried. Yield, 0.25—0.30 g. The product was recrystallized from a small volume of water by adding methanol. Found: C, 27.32; H, 5.77; N, 13.75%. Calcd for [$CoCO_3(C_8H_{22}N_4)$]ClO_4: C, 27.57; H, 5.65; N, 14.27%.

This carbonato complex can be obtained in acidic condition as follows:

trans-[$CoCl_2$((3*S*,8*S*)-dimetrien)]ClO_4 (0.40 g) was dissolved in water (10 ml) and aquated for 30 min on a water bath (60 °C). To the resultant orange-red solution was added $NaHCO_3$ (0.20 g), the solution being left to stand at room temperature for 15 min. It was then evaporated to a volume of 5 ml, and methanol (5 ml) and solid lithium perchlorate (1.0 g) were added in succession. After being left to stand in a refrigerator overnight, the crystals which separated were filtered off, washed with methanol and ether, and air-dried. Yield, 0.25 g.

Λ-β-Carbonato((3S,8S)-3,8-dimethyl-1,4,7,10-tetraazadecane)-cobalt(III) Perchlorate (Λ-β-[CoCO₃((3S,8S)-dimetrien)]ClO₄·2H₂O. Crude *Λ-cis-β*-[$CoCl_2$((3*S*,8*S*)-dimetrien)]ClO_4[2)] (1.30 g) was added to 20 ml of 0.01 M $HClO_4$ and dissolved by vigorous shaking. After shaking for 3 min, the undissolved materials (mainly *Λ-cis-α*-[$CoCl_2$((3*S*,8*S*)-dimetrien)]ClO_4) were removed by filtration. The filtrate was heated for 5 min on a water bath (70 °C), and 0.60 g of $NaHCO_3$ was added in small portions. Solid sodium perchlorate (1.0 g) was added and the deep-red solution was kept in a refrigerator overnight. Deep-red crystals were collected, washed with cold water and ethanol, and air-dried. Yield, 0.58 g. More crystals were recovered from the above filtrate by evaporating on a rotary evaporator. (0.20 g). All the products were recrystallized from warm water. Found: C, 25.33; H, 6.08; N, 13.28%. Calcd for [$CoCO_3(C_8H_{22}N_4)$]$ClO_4 \cdot 2H_2O$: C 25.21; H, 6.11; N, 13.07%.

*Λ-β-[CoCO₃((3S,8S)-dimetrien)]ClO₄→*trans*-[CoCl₂((3S,8S)-dimetrien)]ClO₄.* *Λ-β*-[$CoCO_3$((3*S*,8*S*)-dimetrien)]ClO_4 (0.20 g) was dissolved in 5 M HCl (5 ml) and $LiClO_4$ (0.5 g) was added. Green needle-like crystals were obtained on standing at room temperature. The product was identified with *trans*-[$CoCl_2$((3*S*,8*S*)-dimetrien)]ClO_4.

Λ-β-[CoCO₃((3S,8S)-dimetrien)]ClO₄ → trans*-[Co(NO₂)₂((3S,8S)-dimetrien)]ClO₄.* *Λ-β*-[$CoCO_3$((3*S*,8*S*)-dimetrien)]ClO_4 (1.20 g) was added in small portions to 5 ml of 2 M $HClO_4$. The complex dissolved with effervescence to give an orange-red solution. Sodium nitrite (0.50 g) was added in small portions, and the solution was heated for 5 min on

a water bath (70 °C). After being cooled to room temperature, solid lithium perchlorate (1.0 g) was added and dissolved. The resultant solution was allowed to stand in a refrigerator overnight and the crystals separated were filtered off, washed with water, ethanol, and acetone. Yield, 0.50 g. The product recrystallized from warm water was identified with *trans*-$[Co(NO_2)_2((3S,8S)\text{-dimetrien})]ClO_4$.

Trans-$CoCl_2$((3S,8S)-dimetrien)$^+$→Λ-β-$CoCO_3$((3S,8S)-dimetrien)$^+$. A weighed sample (*ca.* 25 mg) of *trans*-$[CoCl_2((3S,8S)\text{-dimetrien})]ClO_4$ was dissolved in 20 ml of 0.01 M $HClO_4$ in a 25 ml volumetric flask. After the solution had been kept at room temperature for 1 h, 0.050 g of $NaHCO_3$ was added and dissolved. After 30 min the final volume was adjusted to 25 ml by adding water, and the visible absorption and CD spectra of the solution were recorded. The spectra agreed with those of the isolated Λ-β-$[CoCO_3((3S,8S)\text{-dimetrien})]ClO_4$ within experimental error.

Δ-cis-β-$CoCl_2$((3S,8S)-dimetrien)$^+$→Δ-β-$CoCO_3$((3S,8S)-dimetrien)$^+$. A weighed sample (*ca.* 17 mg) of Δ-*cis*-β-$[CoCl_2((3S,8S)\text{-dimetrien})]ClO_4$ was dissolved in 20 ml of 0.01 M $HClO_4$ in a 25 ml volumetric flask, and the solution was stood at room temperature for 15 min. 0.050 g of $NaHCO_3$ was added and the volume was adjusted to 25 ml by adding water. After being left to stand for 30 min, the visible absorption and CD spectra of the resultant solution were recorded. The spectral data were almost identical with those for the isolated Δ-β-$[CoCO_3((3S,8S)\text{-dimetrien})]ClO_4\cdot 2H_2O$.

Λ-cis-α-$CoCl_2$((3S,8S)-dimetrien)$^+$ → Λ-α-$CoCO_3$((3S,8S)-dimetrien)$^+$. A weighed sample (*ca.* 17 mg) of Λ-*cis*-α-$[CoCl_2((3S,8S)\text{-dimetrien})]ClO_4$ was dissolved in 20 ml of 0.01 M $HClO_4$ in a 25 ml volumetric flask. The solution was allowed to stand for 16 h at room temperature, followed by the addition of 0.050 g of $NaHCO_3$. The final volume was adjusted to 25 ml by adding water, and the visible absorption and CD spectra of the solution were measured.

Λ-cis-β-Dinitro((3S,8S)-3,8-dimethyl-1,4,7,10-tetraazadecane)-cobalt(III) Chloride (Λ-cis-β-$[Co(NO_2)_2$((3S,8S)-dimetrien)$]Cl\cdot 0.5H_2O\cdot 0.5CH_3OH$). (3*S*,8*S*)-Dimetrien·4HCl (1.60 g), $LiOH\cdot H_2O$ (0.63 g), $CoCl_2\cdot 6H_2O$ (1.09 g) and $NaNO_2$ (0.70 g) were dissolved successively in 50 ml of methanol and the resultant sulution was aerated for 1 h at room temperature. The white precipitates which appeared were filtered off, and the filtrate was transferred into a beaker and heated on a water bath at 80 °C. In a few minutes the solution began to boil and brown crystals began to separate. Boiling was continued for 30 min, with occasional addition of a few mililiters of methanol to maintain the volume at *ca.* 50 ml. The mixture was cooled to room temperature, and then stored in a refrigerator overnight. The crystals separated were collected and washed with methanol. Yield, 1.02 g. The crude product was dissolved in water (15—20 ml) at 70 °C, and the undissolved impurities were removed by filtration. An equal volume of methanol was added to the filtrate, and cooled in a refrigerator overnight. The brown crystals were filtered off, washed with methanol, and air-dried. Yield, 0.70 g. Found: C, 26.87; H, 6.43; N, 21.21%. Calcd for $[Co(NO_2)_2(C_8H_{22}N_4)]Cl\cdot 0.5H_2O\cdot 0.5(CH_4O)$: C, 26.50; H, 6.41; N, 21.82%.

Measurements. The absorption spectra were obtained with a Shimadzu MPS-50 L Spectrophotometer. The circular dichroism spectra were measured with a JASCO J-20 automatic spectropolarimeter. The 60 MHz proton magnetic resonance spectra were obtained with a Hitachi R-20 B spectrometer in D_2O solutions using sodium 2,2-dimethyl-2-silapentane-5-sulfonate (DSS) as an internal standard.

Results and Discussion

It is necessary to adopt basic reaction conditions in order to convert the *trans*(*S*,*S*)-$[CoCl_2((3S,8S)\text{-dimetrien})]^+$ ion into either the Λ-α(*R*,*R*)- or the Δ-β(*R*,*S*)-$[CoCl_2((3S,8S)\text{-dimetrien})]^+$ ion, since the reaction proceeds with the inversion of configuration at the coordinated secondary nitrogen center, which is usually promoted by base. We thus applied the method employed by Sargeson and Searle for the conversion of the *cis*-α-$[CoCl_2(trien)]^+$ into the β-$[CoCO_3(trien)]^+$ ion with carbonate ion.[10]

The carbonato complex, $[CoCO_3((3S,8S)\text{-dimetrien})]ClO_4$, complex (I), was obtained by the reaction of *trans*-$[CoCl_2((3S,8S)\text{-dimetrien})]ClO_4$ with excess Li_2CO_3. Its visible absorption and circular dichroism (CD) spectra are given in Fig. 1. The CD curve exhibits only a large positive band in the first absorption band region, which can be ascribed to the Λ configuration about the central cobalt(III) atom. This leads to the conclusion that complex (I) has the Λ-α configuration, if the possible isomers of *cis* geometry are restricted to Λ-α and Δ-β.

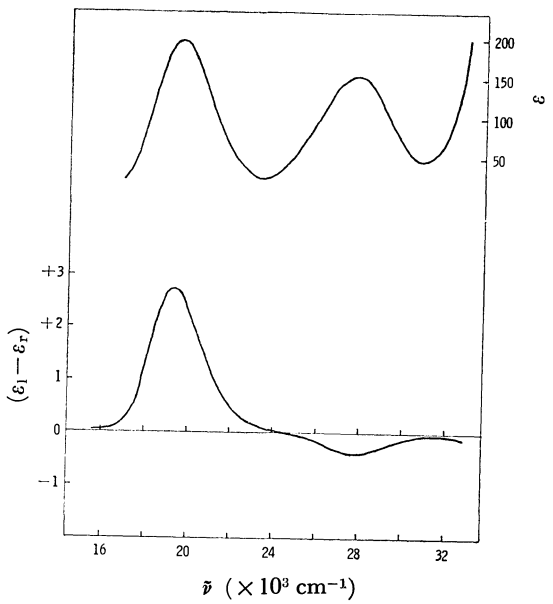

Fig. 1. Visible absorption and CD spectra of complex (I) (Λ-β-$[CoCO_3((3S,8S)\text{-dimetrien})]ClO_4$).

However, attempts to obtain the Λ-*cis*-α isomer of dichloro and dinitro complex, (Eqs. (1) and (2)), were found to give the corresponding *trans* isomer. Under the acidic conditions in (1) and (2), the configuration of the coordinated secondary N centers should be difinitely retained. This indicates that the secondary N atoms of complex (I) take the same configurations as the *trans* isomers, *i.e.* (*S*,*S*).

$$\text{Complex (I)} \xrightarrow{HCl} \xrightarrow{(LiClO_4)} trans\text{-}[CoCl_2((3S,8S)\text{-dimetrien})]ClO_4 \quad (1)$$

$$\text{Complex (I)} \xrightarrow{HClO_4} \xrightarrow{NaNO_2} \xrightarrow{(LiClO_4)} trans\text{-}[Co(NO_2)_2((3S,8S)\text{-dimetrien})]ClO_4 \quad (2)$$

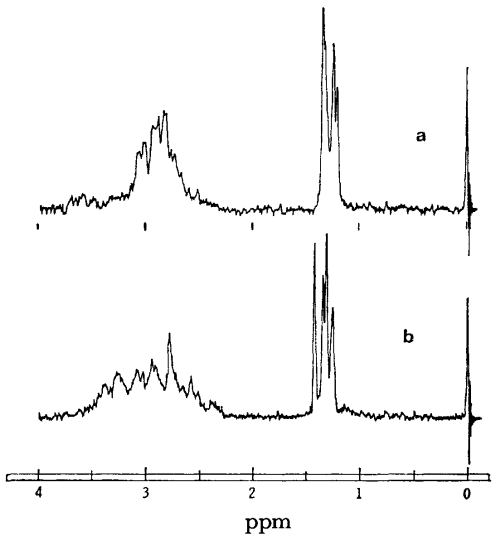

Fig. 2. PMR spectra of $[CoCO_3((3S,8S)\text{-dimetrien})]^+$ ion; (a) Λ-β isomer, and (b) Δ-β isomer.

The proton magnetic resonance (PMR) measurements would be useful for deciding whether (I) has C_2 axis or not. The PMR spectrum of (I) obtained in D_2O is given in Fig. 2(a), which exhibits two overlapped doublet in the 1.2—1.4 ppm region, assignable to the C-methyl groups of the ligand. The PMR spectrum corresponds, therefore, to that for the *cis*-β geometry and not for the *cis*-α form. Consequently, the absolute configuration of (I) can be determined to be the Λ-$\beta(S,S)$, which has been confirmed by X-ray crystallographic study.[11]

Sargeson and Searle provided an alternative method for preparing carbonatocobalt(III) complexes with trien.[10] The *cis*-α and *cis*-β-dichloro complexes were aquated completely and then treated with hydrogencarbonate ion with retention of the configurations. A similar treatment was carried out for the Λ-*cis*-α, Δ-*cis*-β and *trans* isomers of $CoCl_2((3S,8S)\text{-dimetrien})^+$ ion (Eqs. (3)—(5); L indicates the (3*S*,8*S*)dimetrien).

$$\Lambda\text{-}cis\text{-}\alpha\text{-}CoCl_2(L)^+ \xrightarrow{H_3O^+} \Lambda\text{-}cis\text{-}\alpha\text{-}CoCl(H_2O)(L)^{2+} \xrightarrow{HCO_3^-} \Lambda\text{-}\alpha\text{-}CoCO_3(L)^+ \quad (3)$$

$$\Delta\text{-}cis\text{-}\beta\text{-}CoCl_2(L)^+ \xrightarrow{H_3O^+} \Delta\text{-}cis\text{-}\beta\text{-}CoCl(H_2O)(L)^{2+} \xrightarrow{HCO_3^-} \Delta\text{-}\beta\text{-}CoCO_3(L)^+ \quad (4)$$

$$trans\text{-}CoCl_2(L)^+ \xrightarrow{H_3O^+} (\text{red complex}) \xrightarrow{HCO_3^-} \Lambda\text{-}\beta\text{-}CoCO_3(L)^+ \quad (5)$$

The carbonato complexes produced *in situ* according to Eqs. (3) and (4) have a positive and negative CD band, respectively, in the first absorption band region (Fig. 3). If we assume the complete retention of the configurations these CD curves can be ascribed to the Λ-α and Δ-β isomer of $[CoCO_3((3S,8S)\text{-dimetrien})]^+$ ion, respectively. The carbonato complex derived from the *trans* dichloro complex (Eq. (5)) showed the CD curve depicted in Fig. 3, which is identical with that of complex (I) (or Λ-β isomer)

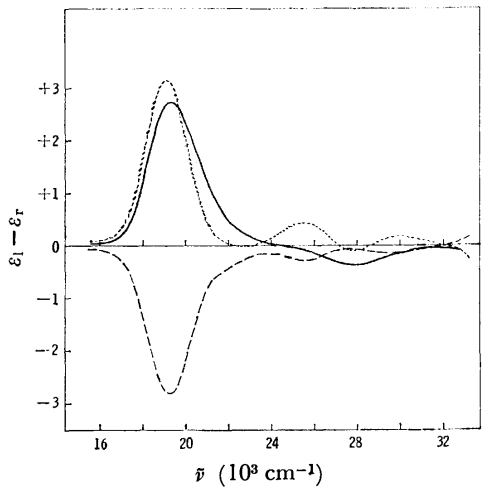

Fig. 3. CD curves for the carbonato complexes formed by the reactions of Eqs. (3) (----), (4) (——·), and (5) (——).

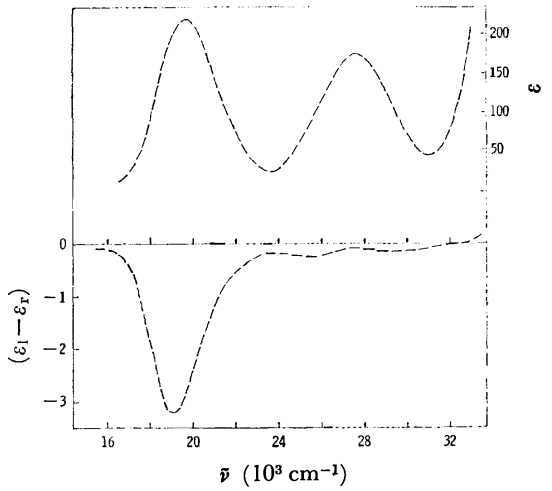

Fig. 4. Visible absorption and CD spectra of Δ-β-$[CoCO_3((3S,8S)\text{-dimetrien})]ClO_4 \cdot 2H_2O$.

shown in Fig. 1. Although both complexes, which result from reactions (3) and (5), have a CD pattern attributable to the Λ configuration, details of the curves apparently differ from each other.

Attempts to isolate the crystalline product of the Λ-α isomer, formed *in situ*, were unsuccessful because of high solubility of the complex. However, the Δ-β and Λ-β isomers could be easily obtained as perchlorate according to reactions (4) and (5). The Δ-β isomer exhibited the PMR spectrum which had two doublets due to the methyl groups in the 1.2—1.4 ppm region (Fig. 2(b)). The visible absorption and CD spectra of this complex are given in Fig. 4. The CD curve of the crystalline product of Δ-β isomer in Fig. 4 is slightly different from that in Fig. 3, probably due to a small contamination of the other complex in the latter case. The Λ-β isomer obtained under acidic condition (Eq. (5)) showed identical CD and PMR spectra for the Λ-$\beta(S,S)$ isomer obtained in the basic medium (complex (I)) (Figs. 1 and 2(a)).

The molecular structure of the Λ-β-$CoCO_3$ $((3S,8S)\text{-dimetrien})^+$ ion determined by the X-ray diffraction

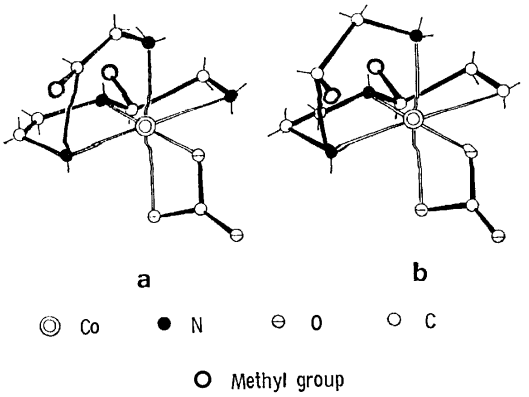

Fig. 5. Possible structures for *Λ*-*β*-[$CoCO_3$((3*S*,8*S*)-dimetrien)]$^+$ ion.

study is illustrated in Fig. 5(a), in which the methyl group on the chelate ring (A) which is not coplanar with the central chelate ring has an unusual axial orientation.[11] An alternative structure of the *Λ*-*β* configuration, both the methyl groups being equatorial, is also shown in Fig. 5(b). Chelate ring (A) in the latter structure takes the *δ* conformation, the methyl group being able to take an equatorial orientation. Chelate ring (A) in the former structure has alternatively the *Λ* conformation. It seems that in solution both conformers (a) and (b) undergo rapid interchange with each other, and are in an equilibrium governed by the free energy difference. The existence of two conformers similar to those in Fig. 5 has been demonstrated in the case of *β*$_2$-[Co(gly)(trien)]$^+$ ion.[12]

The existence of (3*S*,8*S*)-dimetrien complex with the *Λ*-*cis*-*β*(*S*,*S*) configuration was not taken into consideration in previous papers.[2,3] The assumption that the stereoisomers possible for the cobalt(III) complexes with methyl-substituted trien derivatives are restricted to those having the equatorial methyl groups has been found to be incorrect. It is of interest to note that the *Λ*-*β*(*S*,*S*)-[$CoCO_3$((3*S*,8*S*)-dimetrien)]ClO_4 is the sole product which can be isolated under basic preparative conditions. This suggests that the *Λ*-*cis*-*β*(*S*,*S*) geometry is more stable than the other *cis* forms *Λ*-*cis*-*α*(*R*,*R*) and *Λ*-*cis*-*β*(*R*,*S*).

No *Λ*-*cis*-*β*(*S*,*S*) isomer has been obtained for the dichloro and dinitro complexes with (3*S*,8*S*)-dimetrien.[2,5] The reactions carried out following Eqs. (1) and (2) should yield the corresponding dichloro or dinitro complex with *Λ*-*cis*-*β*(*S*,*S*) geometry, at least in the case of ordinary trien complexes.[10] The *trans*-(*S*,*S*) isomer, the actual products of reactions (1) and (2), and the *Λ*-*cis*-*β*(*S*,*S*) isomer are in common as regards the absolute configuration of the secondary N atoms. These isomers can be in an equilibrium in the acidic medium with retention of the secondary N configurations as indicated for the dichloro complexes in Eq. (6). When the perchlorate ion is present in a mixture of these isomers, the precipitation of only the

$$\begin{array}{ccc} \textit{Λ-cis-β}(S,S)\text{-}[CoCl_2(L)]^+ & \rightleftarrows & \textit{trans}(S,S)\text{-}[CoCl_2(L)]^+ \\ & & \downarrow ClO_4^- \\ & & \textit{trans}(S,S)\text{-}[CoCl_2(L)]ClO_4 \end{array} \quad (6)$$

less soluble salt of the *trans* isomer is induced, the *Λ*-*cis*-*β* isomer being highly soluble or hard to crystallize. A similar situation would occur for the *trans* and *Λ*-*cis*-*β* isomers of the dinitro complex.

*The dichlorocobalt(III) complex of (4R,5S)-4,5-*dimethyl-3,6-diazaoctane-1,8-diamine gave rise to the *cis*-*β*(*RS*,*SR*) isomer as the chloride form, while the *trans*(*R*,*S*) isomer was obtained as the perchlorate from a similar reaction mixture.[5] This suggests that either of two equilibrated isomers can be separately crystallized in pure state by use of different counter ions. However, an attempt to get crystalline product of *Λ*-*cis*-*β*-[$CoCl_2$((3*S*,8*S*)-dimetrien)]$^+$ by use of chloride or other anions was not successful and resulted in obtaining the trans isomer.

It was found unexpectedly that the chloride of *Λ*-*cis*-*β*-$Co(NO_2)_2$((3*S*,8*S*)-dimetrien)$^+$ ion crystallizes out in the course of the usual air-oxidation procedure, except that methanol was used as the solvent. The novel dinitro complex contains one half mole of methanol of crystallization per mole of the complex. The PMR and CD spectra of this isomer are shown in Figs. 6(a) and 7, respectively. The PMR spectrum indicates two kinds of doublet assignable to the C-methyl groups of the ligand in the 1.2—1.4 ppm region and can be attributed to the *cis*-*β* topology. The sharp signal at 3.40 ppm is assigned to the methyl group of methanol of crystallization. For the sake of comparison the PMR spectra of the *Λ*-*cis*-*β*, *Λ*-*cis*-*α*, and *trans* isomers are shown in Figs. 6(b), (c), and (d), which are appropriate to the specified geometries of the isomers. The CD curve of the present isomer shows a dominant positive and a minor negative peak in the first absorption band region, which establishes the *Λ* configuration.[3]

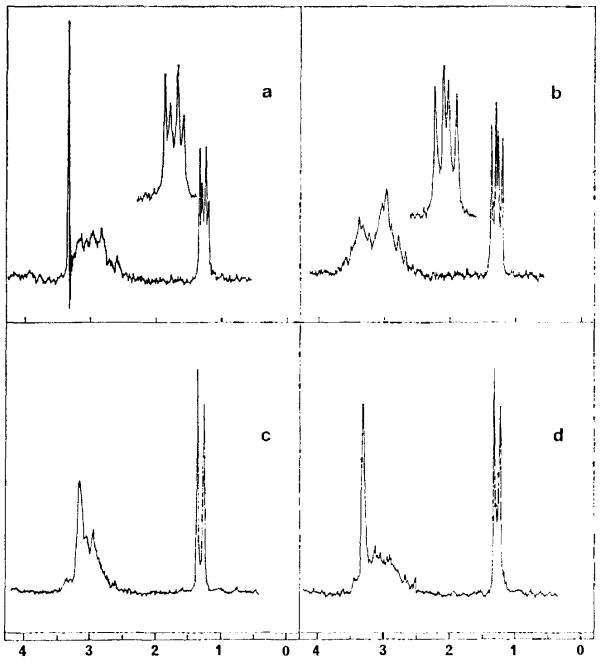

Fig. 6. PMR spectra of [$Co(NO_2)_2$((3*S*,8*S*)-dimetrien)]$^+$ isomers: (a) *Λ*-*cis*-*β*, (b) *Λ*-*cis*-*β*, (c) *Λ*-*cis*-*α*, and (d) *trans* (in D_2O).

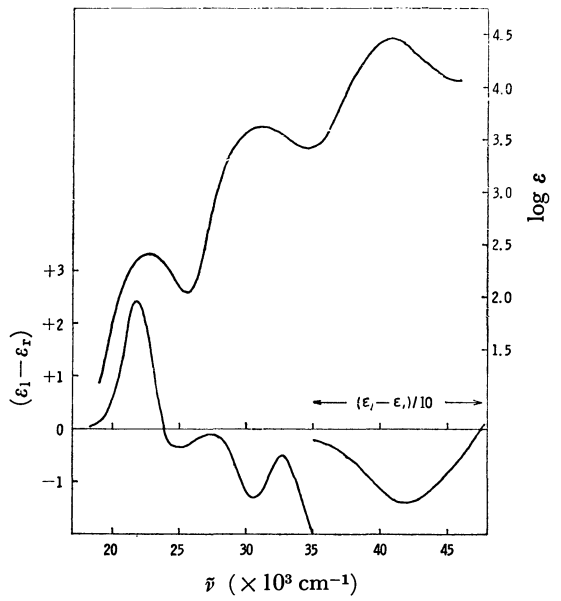

Fig. 7. Absorption and CD spectra of *Λ-cis-β*-[$Co(NO_2)_2$-((3*S*,8*S*)-dimetrien)]Cl·0.5 H_2O·0.5 CH_3OH.

A greyish violet solution was obtained on treating the *Λ-cis-β*-[$Co(NO_2)_2$((3*S*,8*S*)-dimetrien)]Cl with warm concentrated hydrochloric acid, no crystalline material being formed by concentration to near dryness. Addition of perchlorate ion to this solution resulted in the nearly quantitative formation of green crystals of the *trans*-(*S*,*S*)-[$CoCl_2$((3*S*,8*S*)-dimetrien)]ClO_4. The intermediate of the reaction should be highly soluble *Λ-cis-β*(*S*,*S*) dichloro complex which isomerizes into the *trans*(*S*,*S*) isomer in the same manner as in Eq. (6). It is therefore clarified that the *Λ-cis-β* dinitro complex adopts the (*S*,*S*) configuration with respect to the secondary N centers, since there is no possibility of inversion at the secondary N atoms under the conditions mentioned above.

The formation ratio of three isomers of [$CoCl_2$((3*S*,8*S*)-dimetrien)]$^+$ ion is *trans* : *Δ-cis-β* : *Λ-cis-α*= 15 : 5 : 1, when isolated as the perchlorate.[2] No exact estimation of the yields has been made, since it is difficult to isolate completely the materials in solution especially for highly soluble compounds such as the *Δ-cis-β* isomer. Furthermore, isomerization from the *Λ-cis-β* to the *trans* form should take place during the course of isolation, which affect the yield of the *trans* form. Thus, we can estimate the relative stability between the *Δ-cis-β* and *Λ-cis-α*, since these isomers would not undergo conversion or be obtained from the others in the acidic medium.

The strain energy minimization calculations applied to the isomers of [$Co(NO_2)_2$((3*S*,8*S*)-dimetrien)]$^+$ ion indicate that three isomers are in the order *Δ-cis-β*> *trans*>*Λ-cis-α* (according to the calculated enthalpy terms).[9] As far as the order of the *Δ-cis-β* and *Λ-cis-α* is concerned, the result of the calculation is in line with experimental results of the dichloro isomers. On the other hand, there is a distinct discrepancy between the calculated and experimental results with respect to the order of the *trans* isomer. We consider that the *trans* configuration is intrinsically unstable relative to the *Δ-cis-β* configuration due to the unfavorable bond angle distortions involved, as indicated by the strain energy minimization study.[9] Most part of the *trans* dichlorocomplex should be generated by the isomerization of the *Λ-cis-β*.

A preliminary study on the strain energy minimization calculation revealed that the *Λ-cis-β* form has an equivalent or more favorable stability as compared with the *Δ-cis-β* form.[13] It would be certain that higher yield of the *trans* isomer does not reflect its thermodynamic preference. For some metal chelate compounds the stereoisomers with an axially-oriented substituent with appreciable stability might be possible.

References

1) In IUPAC nomenclature rule, this ligand should be written as (2*S*,7*S*)-2,7-dimethyl-1,8-diamino-3,6-diazaoctane. In this paper, the ligand was termed as (3*S*,8*S*)-3,8-dimethyl-1,4,7,10-tetraazadecane in line with our previous reports: Refs. 2, 3.

2) M. Saburi and S. Yoshikawa, *Bull. Chem. Soc. Jpn.*, **45**, 806 (1972).

3) M. Saburi, T. Sawai, and S. Yoshikawa, *Bull. Chem. Soc. Jpn.*, **45**, 1086 (1972).

4) M. Goto, M. Saburi, and S. Yoshikawa, *Inorg. Chem.*, **8**, 358 (1969).

5) M. Goto, H. Matsushita, M. Saburi, and S. Yoshikawa, *Inorg. Chem.*, **12**, 1498 (1973).

6) The *R*, *S* nomenclature of the coordinated secondary nitrogen atoms follows that used in previous papers, *cf.* Refs. 2 and 3.

7) M. Ito, F. Marumo, and Y. Saito, *Acta Crystallogr., Sect. B*, **26**, 1408 (1970).

8) M. Ito, F. Marumo, and Y. Saito, *Acta Crystallogr., Sect. B*, **28**, 457 (1972).

9) M. Ito, F. Marumo, and Y. Saito, *Acta Cristallogr., Sect. B*, **28**, 467 (1972).

10) A. M. Sargeson and G. H. Searle, *Inorg. Chem.*, **6**, 787 (1967).

11) K. Toriumi and Y. Saito, *Acta Crystallogr., Sect. B*, **31**, 1247 (1975).

12) R. J. Dellaca, V. Janson, W. T. Robinson, D. A. Buckingham, L. G. Marzilli, I. E. Maxwell, K. R. Turnbull, and A. M. Sargeson, *J. Chem. Soc., Chem. Commun.*, **1972**, 57.

13) K. Toriumi and Y. Saito, private communication.

Thermal Change of Magnesium Highpolyphosphate Coacervates[1)]

Takao UMEGAKI, Yukihiro NAKAYAMA, and Takafumi KANAZAWA

Department of Industrial Chemistry, Faculty of Technology, Tokyo Metropolitan University, Fukazawa, Setagaya-ku, Tokyo 158

(Received December 17, 1975)

The thermal change of magnesium highpolyphosphate coacervates with various sodium contents was studied by means of DTA, TGA and high temperature X-ray diffraction technique. Most of the highpolyphosphates in the coacervates were degraded into hydrated orthophosphates up to about 100 °C, the pyrophosphates and tetrametaphosphates being formed at 200—300 °C and 300—500 °C, respectively. The formation temperature of "X" (a mixture of $Mg_2P_2O_7$ and $MgNa_2P_4O_{12}$) was lowered with an increase of sodium content in the coacervate samples. $Mg(H_2PO_4)_2 \cdot 2H_2O$, $Mg(H_2PO_4)_2$, $MgH_2P_2O_7$, "X" and $Mg_2P_4O_{12}$ were determined in the crystalline substances obtained by the isothermal heat treatment of coacervates at various temperatures.

Kingery[2)] found that various metal oxides react with phosphoric acid to form stable refractory compounds. Some commercial aluminum phosphates are used as binders for castable refractories.[3)] Bonding of basic refractories with sodium polyphosphates was studied by Lyon, Fox and Lyon.[4)] Some phosphate-bonded magnesite refractories of high hot modulus strengths were obtained by Foessel and Treffner.[5)]

In previous works, magnesium highpolyphosphate coacervates (MPC) were examined as potential binders,[6)] and their thermomechanical properties were described at temperatures from −120 to 100 °C.[7,8)] However, there seems to be no detailed report on the thermal change of magnesium highpolyphosphates, although the degradation of some highpolyphosphates in aqueous solutions was studied by Thilo and Wieker[9,10)] and Gill and Riaz.[11)]

This paper deals with the relationship between the sodium content of MPC and its thermal change. MPC always contains sodium, the presence of which in the coacervate is necessary for the formation of "X".[12,13)] We have studied the thermal change of the MPC containing various amounts of sodium by means of DTA, TGA and high temperature X-ray diffraction, in order to clarify the phosphate bonding formation.

Experimental

Preparation of Magnesium Highpolyphosphate Coacervates with Various Sodium Contents. The MPC samples were obtained from mixtures of the aqueous solutions of sodium metaphosphate and magnesium chloride by addition of ethyl alcohol. The sodium contents in the MPC samples are determined by those in sodium metaphosphate solutions. In order to prepare the coacervates of low sodium contents, the sodium metaphosphate solutions were passed through the ion exchange resin (Amberlite IR-120H) twice or more before being mixed with the chloride solutions. The sodium metaphosphate solutions were kept at −5—0 °C during the course of ion exchange to avoid the hydrolytic degradation of the highpolyphosphates. The chemical compositions of the MPC samples are given in Table 1.

Chemical Analysis of the Coacervates. The analytical methods for magnesium, sodium and phosphorus were described previously.[8)] Paper chromatography of the polyphosphate ions in the coacervate solutions was carried out according to the method by Kolloff.[14)]

Determination of the Average Chain Length of Coacervates. The end group titration[15)] was carried out in order to determine the average number of phosphorus atoms per chain in the polyphosphates of the coacervates. Solutions of the coacervate (*ca.* 1%) were titrated with 0.1 M sodium hydroxide with a pH meter (Denki Kagaku Keiki Model HG-2). Small amounts of 0.1 M sodium hydroxide were successively added to the coacervate solutions and the pH values of the solutions were recorded after each addition until the pH became 10.

In ^{31}P NMR spectra of polyphosphate, the chemical shifts of 9.5—12 ppm and of 20—27 ppm show the presence of terminal PO_4 and middle PO_4, respectively. Each integrated intensity represents the quantity of each PO_4 group in the phosphate chain.[16)] The chain length of the polyphosphates was also determined from the ratio of the integrated intensities for the two chemical shifts. All the NMR spectra were recorded on a Nichiden-Varian NMR Spectrometer Model NV-14 operating at 24.3 MHz at room temperature, using a dilute H_3PO_4 solution as an external reference of ^{31}P.

IR Absorption Spectra. The IR absorption spectra of the coacervates were recorded on a Hitachi IR spectrometer Model EPI-G2 in order to examine the presence of the P–O–P bonds.

Thermal Analysis of the Coacervates. DTA curves were recorded on a Shinku Riko AGNE Differential Thermal Analyzer DT-1500 up to 1100 °C at a heating rate of 5 °C/min. The coacervate samples were dried at 100 °C before DTA measurements in order to avoid swelling and foaming of the samples on abrupt dehydration in a platinum cell.

TGA was carried out by measuring the weight decrement of the coacervates with a quartz spring balance, heating rate being 5 °C/min.

X-Ray Analysis. X-Ray powder diffraction patterns were obtained with a Rigaku Denki Diffractometer Model D-3F, to which a device for high temperature measurements of some coacervates was attached.

Results

Average Chain Length of Highpolyphosphates in the Coacervates. The average chain length of highpolyphosphates in the MPC samples was calculated to be 19—23 from the titration curves, assuming that no sample contains cyclic phosphate ions.

The spectra of ^{31}P MNR for the coacervate solutions (Fig. 1) were almost the same as those of polyphosphates reported by Crutchfield *et al.*[16)] The two peaks in these spectra show the presence of the end PO_4 and the middle PO_4. Table 1 shows the average chain length calculated from the ratios of the integrated intensities of the two peaks. The values from the end group measurement coincide with those from the NMR spectra.

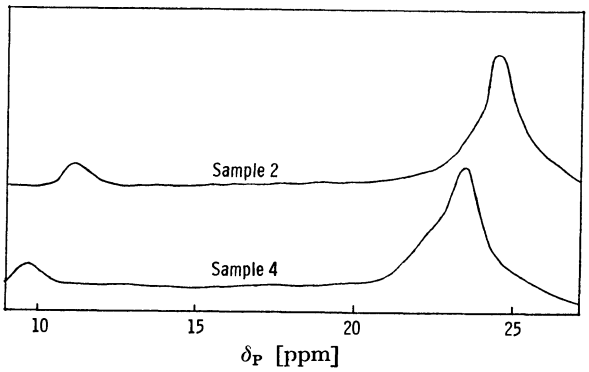

Fig. 1. ^{31}P NMR spectra of coacervates in aqueous solutions.

Table 1. Chemical composition of magnesium highpolyphosphate coacervates

No. of coacervate sample	Contents (%) NaO	MgO	P_2O_5	H_2O	Average chain length
1	1.07	11.8	39.2	53.0	
2	1.50	10.7	38.7	44.5	23
3	2.17	13.0	41.3	53.5	
4	3.46	6.65	34.6	61.1	22
5	7.46	5.60	29.0	58.0	

DTA and TGA of Magnesium Highpolyphosphate Coacervates. From the results of paper chromatography and IR, we see that most of the highpolyphosphates in the coacervates turn to hydrated orthophosphates after being heated at 100 °C. As shown in DTA and TGA curves (Fig. 2), two or more endothermic peaks at 100—200 °C suggest the occurrence of dehydration with various types. The endothermic peaks in the range 800—1000 °C appear due to the melting of some of the dehydrated coacervate samples, these melting temperatures being lowered with an increase in sodium content.

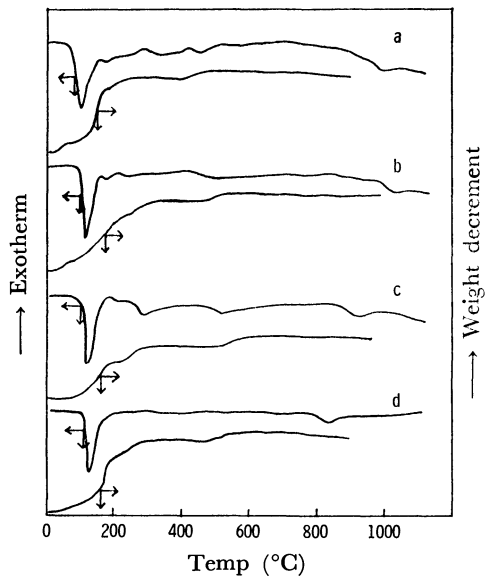

Fig. 2. TGA and DTA curves of coacervates.
a: Sample 1, b: sample 2, c: sample 3, d: sample 4.

Table 2. Products of the isothermal heat treatment of coacervates at various temperatures

No. of coacervate samples	Products[a)]
1	A(~100 °C), $Mg(H_2PO_4)\cdot 2H_2O$(120 °C), $Mg(H_2PO_4)_2$(130 °C), $MgH_2P_2O_7$(300 °C), X(400 °C), MTP(450 °C).
2	A(~100 °C), U(100—400 °C), X(460 °C), MTP(460 °C).
3	A(~100 °C), U(100—300 °C), X(350 °C), MTP(460 °C).
4	A(~100 °C), U(100—300 °C), X(320 °C).
5	A(~120 °C), U(120—300 °C), X(300 °C).

X[18]: a mixture of $Mg_2P_2O_7$ and $MgNa_2P_4O_{12}$, A: amorphous orthophosphates, U: a mixture of unknown crystalline substances, MTP: $Mg_2P_4O_{12}$.
a) Temperatures in parentheses represent those of formation of the products.

X-Ray Analysis of the Products Obtained by the Isothermal Heat Treatment. Taking the above results of DTA and TGA into account, the coacervates were isothermally dehydrated and heated at various temperatures. Table 2 shows the products obtained by the isothermal heat treatment of the coacervates.

After all the coacervates had been heated at 100 °C, orthophosphate ion was detected by paper chromatography and IR spectroscopy. No crystalline phosphate or ortho or pyro form other than $Mg(H_2PO_4)_2\cdot 2H_2O$, $Mg(H_2PO_4)_2$, and $MgH_2P_2O_7$ was found by X-ray diffraction analysis. It seems that the crystallization of magnesium ortho- and pyrophosphates was difficult in the coacervates rich in sodium.

By heat treatment at 300—400 °C most mixtures of the degraded phosphates turned into crystalline $Mg_2P_4O_{12}$ and "X", a new compound,[12,13] only "X" being found in Samples 4 and 5. The temperature for the formation of "X" was lowered with an increase of sodium content in the coacervate samples.

Discussion

The coacervate undergoes degradation, dehydration and condensation on heating as follows:[12,13]

$$\text{Coacervate} \xrightarrow{100°C} \text{Amorphous orthophosphates} \xrightarrow{120°C}$$
$$Mg(H_2PO_4)_2\cdot 2H_2O \xrightarrow{150—190°C} Mg(H_2PO_4)_2 \xrightarrow{210—290°C}$$
$$MgH_2P_2O_7 \xrightarrow{350°C} Mg_2P_4O_{12} \text{ and "X"} \xrightarrow{990°C}$$
Partial melting

The thermal change of the coacervates with various sodium contents seems to be as follows:

$$\text{Sample 1} \xrightarrow{100°C} \text{Amorphous orthophosphates} \xrightarrow{120°C}$$
$$Mg(H_2PO_4)_2\cdot 2H_2O \xrightarrow{130°C} Mg(H_2PO_4)_2 \xrightarrow{300°C}$$
$$MgH_2P_2O_7 \xrightarrow{400°C} MgH_2P_2O_7 \text{ and "X"} \xrightarrow{450°C}$$
$$Mg_2P_4O_{12} \text{ and "X"} \xrightarrow{990°C} \text{Partial melting}$$

Sample 3 $\xrightarrow{100°C}$ Amorphous orthophosphates $\xrightarrow{150—200°C}$
Unknown crystalline substances $\xrightarrow{350°C}$ "X" $\xrightarrow{460°C}$
$Mg_2P_4O_{12}$ and "X" $\xrightarrow{950\,°C}$ Partial melting

Sample 5 $\xrightarrow{120°C}$ Amorphous orthophosphates $\xrightarrow{150°C}$
Unknown crystalline substances $\xrightarrow{300°C}$ "X" $\xrightarrow{910°C}$
Partial melting

The temperature of formation of crystalline "X" is a little lower than that for the appearance of $Mg_2P_4O_{12}$. When the coacervates such as Samples 4 and 5 contain a large amount of sodium, no other crystalline substance than "X" is obtained by isothermal heat treatment. The formation of "X" is closely related to the presence of sodium ion.

The X-ray diffraction patterns of $MagN_2P_4O_{12}$[17] and "X" (Table 3) almost overlap each other. However, some peaks (d=3.0223, 2.9799 and 2.9107 Å), assigned to "X", disappear after the treatment of "X" with aqua regia.[18] Concerning the diffraction pattern of $MgNa_2P_4O_{12}$ there is no peak corresponding to the three peaks of "X". The highest and the next highest peaks of $Mg_2P_2O_7$ (d=3.015 and 2.976 Å) appear in the vicinity of the three peaks of "X" (ASTM X-Ray Powder Data File 8—38). This suggests that "X" is not a single compound but a mixture of $Mg_2P_2O_7$ and $MgNa_2P_4O_{12}$.

$MgNa_2P_4O_{12}$ is insoluble in acidic or alkaline solutions as well as $Mg_2P_4O_{12}$. If magnesium high-polyphosphates are used as binders, the principal bonding phase is expected to consist of chemically inert magnesium tetrametaphosphates.

Table 3. X-Ray powder diffraction data of "X"[12]

d(Å)	I/I_0	d(Å)	I/I_0
13.1	3	2.2553	8
6.43	12	2.2228	3
5.06	21	2.2004	9
4.76	9	2.1276	3
4.52	1	2.0993	1
4.29	4	2.0809	1
4.150	1	2.0368	4
3.695	4	2.0157	8
3.817	76	1.9733	1
3.572	100	1.9572	2
3.477	7	1.9324	6
3.281	5	1.9049	3
3.1114	7	1.8728	2
3.0223	9	1.8567	3
2.9799	5	1.8260	3
2.9107	12	1.8103	7
2.8536	5	1.7811	7
2.7790	4	1.7035	8
2.7493	3	1.6573	4
2.7281	2	1.6211	3
2.6473	3	1.6142	5
2.5974	3	1.5946	4
2.5230	25	1.5878	4
2.4242	2	1.5370	5
2.3131	5	1.4550	6

Conclusion

1) The thermal change is considered to take place in the following order:

a. degradation of polyphosphates into hydrated orthophosphates (≈100 °C).

b. dehydration of the hydrated orthophosphates (100—200 °C).

c. formation of pyrophosphates (200—300 °C).

d. formation of "X" and $Mg_2P_4O_{12}$ (300—500 °C).

e. melting of some phosphates obtained on heat treatment of the coacervate samples (800—950 °C).

2) The crystalline substances obtained by the progress of the thermal change of the coacervates are $Mg(H_2PO_4)_2\cdot 2H_2O$, $Mg(H_2PO_4)_2$, $MgH_2P_2O_7$, "X" and $Mg_2P_4O_{12}$.

3) The formation temperature of "X" is lowered with an increase of sodium content in the coacervate samples.

The authors wish to express their sincere thanks to the staff of Nichiden Varian Co., Ltd. for their co-operation in the NMR measurement.

This work was supported by a grant from Asahi Glass Foundation for Contribution to Industrial Technology.

References

1) Presented at the 26th National Spring Meeting of the Chemical Society of Japan, Hiratsuka, April, 1972. Some data were cited from Ref. 6.

2) W. D. Kingery, *J. Am. Ceram. Soc.*, **33**, 239 (1950).

3) A. D. F. Toy, "Comprehensive Inorganic Chemistry," Vol. 2, ed. by J. C. Bailar, H. J. Emeléus, R. Nyholm, and A. F. Trotman-Dickenson, Pergamon Press, New York, N. Y. (1973), p. 501.

4) J. E. Lyon, T. U. Fox, and J. W. Lyon, *Am. Ceram. Soc. Bull.*, **45**, 1078 (1966).

5) A. H. Foessel and W. S. Treffner, *Am. Ceram. Soc. Bull.*, **49**, 652 (1970).

6) T. Kanazawa, T. Umegaki, and H. Kawazoe *Asahi Garasu Kogyo Gijutsu Shoreikai Kenkyu Hokoku*, **21**, 81 (1972).

7) T. Umegaki and T. Kanazawa, *Bull. Chem. Soc. Jpn.*, **46**, 3587 (1973).

8) T. Umegaki and T. Kanazawa, *Bull. Chem. Soc. Jpn.*, **48**, 1452 (1975).

9) E. Thilo and W. Wieker, *J. Polym. Soc.*, **53**, 55 (1961).

10) E. Thilo and W. Wieker, *Z. Anorg. Allgen. Chem.*, **291**, 164 (1957).

11) J. B. Gill and S. A. Riaz, *J. Chem. Soc., A*, **1969**, 1803.

12) T. Kanazawa, H. Kawazoe, and T. Matsubara, *Kogyo Kagaku Zasshi*, **74**, 1784 (1971).

13) T. Kanazawa, H. Kawazoe, Y. Nogami, and T. Kawashima, *Nippon Kagaku Kaishi*, **1973**, 2084.

14) R. H. Kolloff, *Anal. Chem.*, **33**, 373 (1961).

15) J. R. van Wazer, E. J. Griffith, and J. F. McCullough, *Anal. Chem.*, **26**, 1755 (1954).

16) M. M. Crutchfield, C. F. Callis, R. R. Irani, and G. C. Roth, *Inorg. Chem.*, **1**, 813 (1962).

17) B. Thonnerieux, J. C. Grenier, A. Drif, and C. Martin, *Compt. Rend.*, **267**, 968 (1968).

18) T. Kanazawa, H. Kawazoe, T. Umegaki, and K. Isozaki, Abstracts of the Annual Meeting of the Ceramic Society of Japan, C7 (1975), p. 27.

The Synergistic Extraction of Cobalt Ion Fixed on the Ion Exchange Resin with a Mixture of 2-Thenoyltrifluoroacetone and Pyridine Bases

Tooru TAMURA, Kunio OHZEKI, and Tomihito KAMBARA
Department of Chemistry, Faculty of Science, Hokkaido University, Sapporo 060

(Received March 25, 1976)

The extraction of cobalt(II) on the ion exchange resin into a mixture of 2-thenoyltrifluoroacetone(Htta) with pyridine bases in various organic solvents has been studied. In the presence of pyridine bases(B), cobalt ions were extracted from the resin into the organic phase in the form of base adducts, $Co(tta)_2B_n$. The synergistic effect decreased in the order: pyridine>β-picoline>γ-picoline>α-picoline>γ-collidine$\simeq$isoquinoline$\simeq$piperidine>4-benzoylpyridine. This trend was related to its structure, particularly the steric effect of the *ortho*-substituent.

The synergistic effects of neutral ligands have been widely studied in the extraction of a metal ion with β-diketone.[1,2] The effect is well explained by the formation of the base adduct. Akaiwa *et al.* reported that nickel(II) and cobalt(II) ions were extracted synergistically by a mixture of 2-thenoyltrifluoroacetone(Htta) and pyridine base and that the extractability of their metal ions was dependent on the basicity of pyridine bases and the steric effect of their *ortho*-substituent.[3-5]

On the other hand, the conversion of a metal ion fixed on the ion exchange resin to a chelate compound based on the ion exchange reaction in organic medium has been studied.[6] The authors have reported that iron(III),[7] copper(II),[8] and nickel(II)[9] ions on Amberlyst 15 were quantitatively extracted with acetylacetone or Htta into organic medium by the aid of a small amount of pyridine–water mixture. The present paper deals with the synergistic extraction of cobalt ions fixed on Amberlyst 15 with Htta in the presence of pyridine bases.

Experimental

Apparatus and Reagents. A Hitachi 508 atomic absorption spectrophotometer was used for the cobalt absorption measurement at 240.1 nm in air-acetylene flame. Thenoyltrifluoroacetone, β-picoline, and trimetyl phosphate were obtained from Wako Pure Chemical Inc. (Tokyo) and used without further purification. Pyridine, α-picoline, γ-picoline, γ-collidine, isoquinoline, piperidine, 4-benzoylpyridine, tributyl phosphate and all other materials used were of guaranteed grade.

Preparation of Cobalt(II)-form Resin. The resin used was sulfonic acid cation exchanger, Amberlyst 15, with a macroreticular structure. The commercially available Amberlyst 15 was crushed and shieved to a fraction of 60—80 mesh. The resin was converted to Co(II)-form by treatment with a 0.1 M solution of cobalt nitrate and washed with water until the washings showed no color reaction with 1-nitroso-2-naphtol and dried over silica gel. The cobalt ions on the air-dried Co(II)-form resin were eluted by 4 M hydrochloric acid and determined by EDTA titration. It was found that 3.19±0.02 meq of cobalt ions were adsorbed onto 1.00 g of the air-dried Co(II)-form resin. The ratio of exchange capacity of cobalt ion to proton was 0.965 and so the cobalt ions were expected to be adsorbed on the resin in the form of Co^{2+}.

General Procedure. A portion of 5 cm^3 of 0.1 M Htta in organic medium was poured onto the 25 mg of air-dried Co(II)-form resin in a eggplant flask and varying amounts of pyridine were added. The mixture was shaken mechanically for 10 min at room temperature. After filtration, the resin was washed with ethanol and water. The cobalt ions remaining on the resin were eluted by 4 M hydrochloric acid and determined by atomic absorption spectrophotometry in air-acetylene flame.

Results and Discussion

Effect of Pyridine and Solvents. It was found that Htta or pyridine could not remove the cobalt ions fixed on the resin into organic medium, however, the mixture of them was highly effective, as Fig. 1 shows. Upon addition of pyridine, the red color was immediately developed in the organic phase, indicating the formation of a base adduct, $Co(tta)_2py_n$. Cobalt ions were quantitatively extracted into Htta-carbon tetrachloride and Htta–benzene solutions in the presence of pyridine of 4—14% and 4—6% (v/v), respectively. But in the case of Htta–chloroform solution, the extractability was less than 98%. The poor extraction of cobalt ions in ethanol is due to a probable interaction between the solvent and Htta. After all, the effect of the solvent natures on the extraction of cobalt ions from the resin decreased in the order: carbon tetrachloride>benzene>chloroform>ethanol. Except ethanol, this order agreed with that found in the solvent extraction study of cobalt–Htta–pyridine system by Akaiwa *et al.*[5]

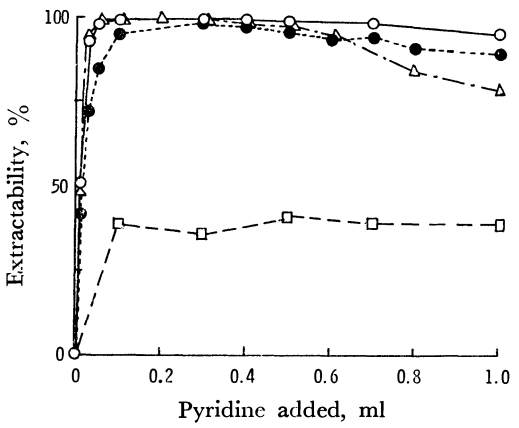

Fig. 1. Extractability of cobalt ions from the resin with 0.1 M Htta solutions in various solvents. Ethanol (□), chloroform (●), benzene (△), and carbon tetrachloride (○).

Composition of the Extracted Species. The composition of the extracted species in benzene was determined by the mole ratio method in the presence of pyridine and found to be Co(II) : Htta=1 : 2. The determination of the composition of a pyridine adduct was unsuccessful, because a considerable amount of pyridine might be adsorbed on the resin matrix.

Effect of Pyridine Bases. In place of pyridine, other neutral ligands were used as synergist. The extractability of cobalt ions from the resin with 0.1 M Htta and 0.245 M neutral ligands in benzene is given in Fig. 2, as a function of the shaking time. Pyridine was most effective and picolines except α-picoline followed it. The effect of α-picoline was inferior to that of other picolines. Pyridine bases such as γ-collidine, isoquinoline, piperidine, and 4-benzoylpyridine were less effective. In the case of trimethyl phosphate and tri-*n*-butyl phosphate, the extractability of cobalt ions was only about 10% after the 60-min shaking. Consequently, it is concluded that 2-substituted pyridine bases such as α-picoline and γ-collidine and those having a bulky structure such as isoquinoline and 4-benzoylpyridine were not effective. The synergistic effect of the neutral ligands on the ion exchange extraction decreased in the order of pyridine > β-picoline > γ-picoline > α-picoline > γ-collidine ≃ isoquinoline ≃ piperidine > 4-benzoylpyridine > trimethyl phosphate ≃ tri-*n*-butyl phosphate. On the other hand, it is reported that the synergistic effect of the pyridine bases on the solvent extraction of Ni(II)–Htta–benzene system decreases in the order of γ-picoline > β-picoline > pyridine > α-picoline, which is accordant with that of the basicity of pyridine bases.[3] The analogous conclusion is reported in the case of the solvent extraction of nickel(II) and cobalt(II) with thiodibenzoylmethane and *N*-phenyl-β-mercaptocinnamamide in the presence of pyridine bases.[10] It is explained that the poor effectiveness of α-picoline may be due to the steric influence by the *ortho*-methyl group. The disagreement of the results between ion exchange extraction and solvent extraction can be explained by the steric influence of the resin matrix with pyridine bases in the case of the ion exchange extraction. Namely, provided that the reaction occurs around cobalt ions on the resin, the pyridine bases must diffuse into the resin hole and so there appears a steric hinderance of the resin matrix with the large size molecule. The stability of adduct is related to the basicity of pyridine bases and has also an influence on the extractability of cobalt ions.

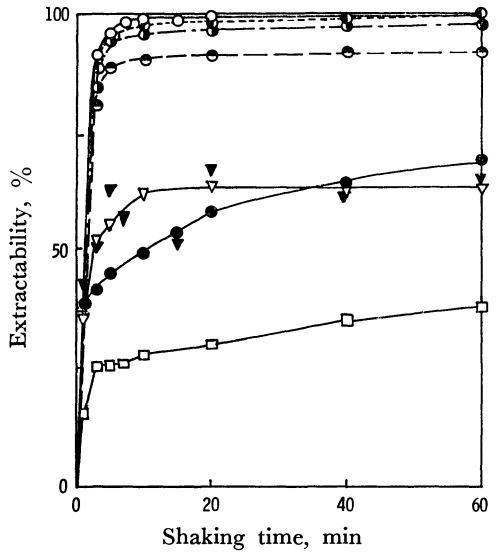

Fig. 2. Effect of shaking time on the synergism of the pyridine bases on the extraction of cobalt ions from the resin with 0.1 M Htta solutions in benzene, containing 0.245 M of pyridine (○), γ-picoline (◑), β-picoline (◐), α-picoline (◓), piperidine (●), isoquinoline (▲), 4-benzoylpyridine (□), and γ-collidine (△).

Effect of the Mesh Size of Co(II)-Form Resin. The Co(II)-form resins of 100—120 and 120—150 mesh ranges were prepared and the extractability of cobalt ions from each of them was compared with that from 60—80 mesh range. The γ-collidine having the *ortho*-substituent to the nitrogen atom of pyridine ring was used as synergist. The result is shown in Fig. 3. Though the extraction rate increased with decreasing mesh size of the resin, the extractability of cobalt ions after 10-min shaking was independent of the mesh size of the resin.

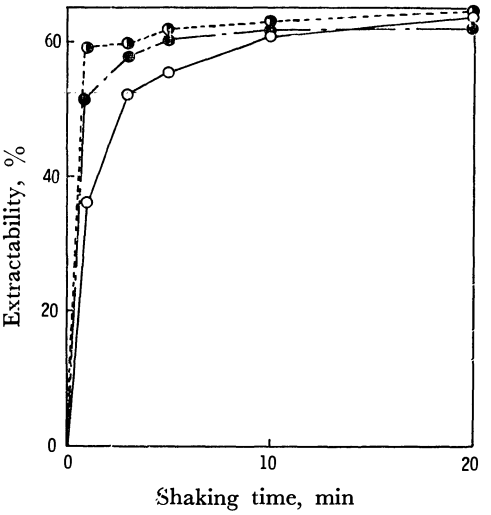

Fig. 3. Effect of the mesh size of Co(II)-form resin on the extraction of cobalt ions with a 0.1 M Htta solution in benzene, containing 0.245 M γ-collidine. The mesh range is 60—80 (○), 100—120 (●), and 120—150 mesh (◑).

Effect of Water Adsorbed to the Co(II)-Form Resin. It has been pointed out that the water played an important role in the reaction of β-diketone with metal ions fixed on the resin.[7-9] In the present case, the difference of the reactivities between the air-dried Co(II)-from resin and the oven-dried one, the latter being prepared by drying the former at 110 °C for 3 h, was investigated. After the 3 h drying at 110 °C. the color of the Co(II)-form resin changed from pink to violet. The water content on the air-dried Co-(II)-form resin was determined by the thermogravimetric analysis. It was found that the air-dried Co(II)-form resin adsorbed eight moles of water to

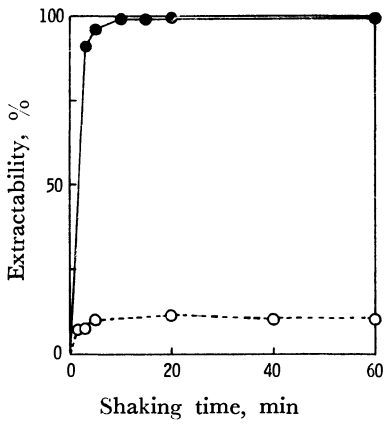

Fig. 4. The difference of the extractabilities between the air-dried Co(II)-form resin (●) and the oven-dried one (○). The extraction of cobalt ions from the resin was carried out with a 0.1 M Htta solution in benzene, containing 0.245 M pyridine.

a mole of cobalt ion on it, and six moles of those were removed by drying at 110 °C. Consequently, the form of the oven-dried Co(II)-form resin is expected to be $(RSO_3)_2Co \cdot 2H_2O$. It is supposed that this color change of the Co(II)-form resin is based on the removal of water molecules from cobalt ions. The use of oven-dried Co(II)-form resin gave a lower extractability in comparison with that of air-dried one, as Fig. 4 shows. Although the role of water remains not clarified, this indicates an importance of trace amounts of water in the extraction of cobalt ion fixed on the ion exchange resin with Htta into the organic medium.

References

1) H. Irving and D. N. Edgington, *J. Inorg. Nucl. Chem.*, **27**, 1359 (1965).
2) T. V. Healy, "Solvent Extraction Research," ed. by A. S. Kertes and Y. Marcus, Wiley-Interscience, New York (1969), p. 257.
3) H. Kawamoto and H. Akaiwa, *J. Inorg. Nucl. Chem.*, **31**, 1141 (1969).
4) H. Akaiwa and H. Kawamoto, *Anal. Chim. Acta*, **43**, 438 (1969).
5) H. Akaiwa, H. Kawamoto, and T. Saito, *Nihon Kagaku Zasshi*, **91**, 980 (1970).
6) C. E. Higgins, *J. Inorg. Nucl. Chem.*, **35**, 1941 (1973).
7) K. Ohzeki, M. Ikeuchi, and T. Kambara, *Bull. Chem. Soc. Jpn.*, **48**, 67 (1975).
8) T. Okamura, K. Ohzeki, and T. Kambara, *Bull. Chem. Soc. Jpn.*, **48**, 469 (1975).
9) K. Ohzeki, T. Tamura, and T. Kambara, *Bull. Chem. Soc. Jpn.*, **48**, 2829 (1975).
10) M. Chikuma, A. Yokoyama, and H. Tanaka, *J. Inorg. Nucl. Chem.*, **37**, 199 (1975).

The Coordinative Behavior of the Ethereal Oxygen Atom in Cobalt, Nickel and Copper Complexes with Schiff Bases Obtained from Salicylaldehyde Derivatives and 2-(Aminomethyl)furan

Shoichiro YAMADA, Kuniko YAMANOUCHI, Wasuke MORI, and Michihiko KISHITA

Institute of Chemistry, College of General Education, Osaka University, Toyonaka, Osaka 560

(Received March 26, 1976)

Cobalt(II), cobalt(III), nickel(II), and copper(II) complexes with *N*-(2-furylmethyl)salicylideneaminates (abbreviated as X-sal-fum) were synthesized. In addition to the M (X-sal-fum)$_2$ type complexes, those of the formula Cu(X-sal-fum)Cl were obtained in crystals. The complexes Co(X-sal-fum)$_3$ are six-coordinate, octahedral. The cobalt(II) complex is four-coordinate, tetrahedral and the nickel(II) complexes are four-coordinate, planar. In these complexes, the ligands X-sal-fum function as bidentates, the furan oxygen atom not being bound to the metal ions. The results are compared with those reported previously for related ligands. It is most likely that the complexes Cu(X-sal-fum)Cl consist of binuclear complexes with spin-spin interaction between copper(II) ions.

Ligands of the type (I), which bear a donor atom in Y, form various complexes with transition metal ions. The structure of these metal compleses is expected to vary in a delicate and complicated way. In previous papers, the present authors studied the synthesis and structure of transition metal complexes with ligands (II),[1] (III), (IV),[2] and (V).[3,4] As extension of these studies, various metal complexes with *N*-(2-furylmethyl)-salicylideneiminates (VI, abbreviated as X-sal-fum) have been synthesized and their structure has been examined in the present work. The results are compared with those of the corresponding complexes with related ligands.

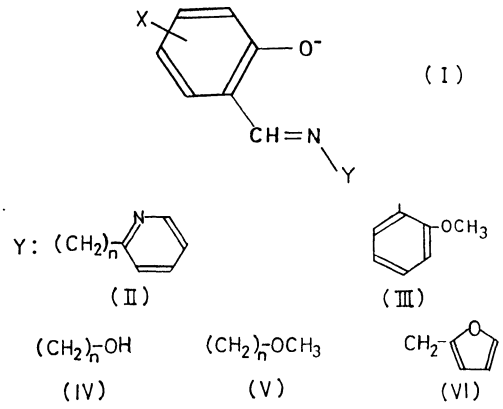

Experimental

Materials. Analytical data of new complexes obtained in the present work are shown in Table 1.

Bis[N-*(2-furylmethyl)salicylideneaminato)copper(II)*, *Cu(X-sal-fum)*$_2$. To a suspension of bis(salicylaldehydato)copper(II) (0.01 mol) in 90% ethanol (50 ml) was added 2-aminomethylfuran (0.02 mol) drop by drop at about 60 °C. The resulting suspension was heated at the same temperature with stirring for about 30 min. An olive green precipitate was recrystallized from acetone to yield olive green (X=H, 5-Cl and 5-Br) or yellow brown (X=3-CH$_3$O) crystals. They are soluble in chloroform, benzene and acetone and moderately soluble in ethanol. The solubility of the complexes with X=5-Br and 3-CH$_3$O is lower than that of the others with X=H and 5-Cl.

Cu(X-sal-fum)Cl (X=H, 5-Cl). A solution of the Schiff base (0.01 mol) in ethanol (50 ml) was added at about 60 °C to a solution of copper(II) chloride dihydrate (0.01 mol) in a small amount of water. The mixture was stirred at

TABLE 1. ANALYTICAL DATA OF METAL COMPLEXES WITH X-sal-fum

Compound	Calcd, %			Found, %			μ[a]
	C	H	N	C	H	N	
Cu(H-sal-fum)$_2$	62.13	4.35	6.04	62.10	4.42	6.16	1.89
Cu(5-Cl-sal-fum)$_2$	54.09	3.40	5.26	53.16	3.46	5.15	1.83
Cu(5-Br-sal-fum)$_2$	46.72	2.94	4.54	45.91	2.93	4.61	1.83
Cu(3-CH$_3$O-sal-fum)$_2$	59.59	4.62	5.35	59.11	4.56	5.32	1.95
Cu(H-sal-fum)Cl	48.17	3.37	4.68	47.59	3.42	4.60	1.31
Cu(5-Cl-sal-fum)Cl	43.19	2.72	4.20	42.99	2.90	4.34	0.92
Ni(H-sal-fum)$_2$	62.78	4.39	6.10	62.16	4.44	5.97	dia
Ni(5-Br-sal-fum)$_2$	46.72	2.94	5.54	46.13	3.03	4.74	dia
Ni(3-CH$_3$O-sal-fum)$_2$	60.15	4.66	5.40	59.42	4.66	5.35	dia
Co(5-Br-sal-fum)$_2$	46.70	2.94	4.54	46.42	3.00	4.57	4.35
Co(H-sal-fum)$_3$	65.55	4.58	6.37	65.46	4.59	6.43	dia
Co(5-Cl-sal-fum)$_3$	56.67	3.57	5.51	55.64	3.57	5.46	dia
Co(5-Br-sal-fum)$_3$	48.24	3.04	4.69	47.31	3.04	4.68	dia
Co(3-CH$_3$O-sal-fum)$_3$	62.48	4.84	5.61	62.29	4.83	5.59	dia

a) μ: BM at room temperature.

this temperature for about 30 min. A brown crystalline precipitate was filtered off and washed with ethyl ether. Any attempt to recrystallize was unsuccessful. The compounds are dark brown (X=H) and yellowish brown (X=5-Cl), respectively. They are insoluble in water, but are soluble in chloroform, benzene, acetone, diethyl ether and ethanol to undergo decomposition.

The corresponding 5-bromo-complex (X=5-Br) was obtained as dark brown microcrystals. Although the elemental analysis for carbon, hydrogen and nitrogen slightly deviates from the formula Cu(5-Br-sal-fum)Cl, its properties agree with those expected for this compound. For example, the electronic spectrum and temperature dependence of magnetic susceptibilities are remarkably similar to those of Cu(H-sal-fum)Cl. The ν(C-O) band appears at about 1558 cm^{-1}, a value which lies in the same region as those of Cu(H-sal-fum)Cl and Cu(5-Cl-sal-fum)Cl.

Bis[N-*(2-furylmethyl)salicylideneaminato]nickel(II), Ni(X-sal-fum)*$_2$. The complexes were prepared by a method similar to that for the corresponding copper(II) complexes. They are olive-green. Their solubility is similar to that of the copper(II) complexes.

Bis[N-*(2-furylmethyl)-5-bromo-salicylideneaminato]cobalt(II), Co-(5-Br-sal-fum)*$_2$. The complex was prepared as red crystals by a method similar to that for the corresponding copper(II) complexes. Its solubility is similar to that of the copper(II) complexes.

Tris[N-*(2-furylmethyl)-salicylideneaminato]cobalt(III), Co(X-sal-fum)*$_3$. The complexes were prepared as dark green crystals by a method similar to that for the copper(II) complexes, except that the ligand to metal ratio was 3 : 1 and that the reaction was conducted for about two to three hours. Addition of such an oxidizing agent as hydrogen peroxide accelerates the oxidation of cobalt(II) to cobalt(III). Their solubility is similar to that of the copper(II) and nickel(II) complexes.

Measurements. Electronic absorption spectra of the complexes were measured on a Shimadzu MPS-50L spectrophotometer. Infrared spectra were obtained from Nujol mulls using a Hitachi EPI-S2 infrared spectrophotometer.

Magnetic measurements at room temperature were carried out by the Gouy method using $CoHg(SCN)_4$ as a calibrant. Magnetic susceptibilities over a temperature range (76—320 K) were measured by the Faraday method. The temperature was controlled with an electric regulating system. For the complexes Cu(X-sal-fum)Cl, the Bleaney-Bowers Eq. 1 was found to hold,

$$\chi_A = g^2N\beta^2/3kT(1+1/3\exp(-2J/kT))^{-1} + N\alpha \quad (1)$$

where the symbols have their usual meanings.

Results and Discussion

Cobalt(II), Cobalt(III), and Nickel(II) Complexes. Both the bis(Schiff base)cobalt(II) and tris(Schiff base)cobalt(III) have been isolated. The cobalt(II) complex Co(5-Br-sal-fum)$_2$ is paramagnetic with a moment of 4.35 BM and shows an electronic absorption spectrum typical of the tetrahedral cobalt(II) complex, as shown in Table 2. The d-d band at about 8.2 kK may be assigned to a transition $^4T_1(F) \leftarrow {}^4A_2$. The cobalt(III) complexes Co(X-sal-fum)$_3$ are diamagnetic, and their electronic spectra are typical of the six-coordinate cobalt(III) complexes. The band at about 16.4—16.6 kK may be assigned to a transition $^1T_{1g} \leftarrow {}^1A_{1g}$, in the scheme of O_h field symmetry. Their d-d band maxima lie at almost the same frequencies as those of the corresponding *N*-alkylsalicylideneaminato-complexes.[5] In any of these complexes, the furan oxygen atom is not bound with the cobalt ion.

As shown in Table 1, complexes of the type Ni(X-sal-fum)$_2$ are diamagnetic in the solid state, indicating that they have a four-coordinate square-planar structure. They show electronic absorption spectra typical of the square-planar nickel(II) complex in non-donor solvents as well as in the solid state. The band at about 16 kK may be assigned to a $d_{x^2-y^2} \leftarrow d_{xy}$ transition. No absorption is observed at about 10—11 kK or lower frequencies, where the octahedral or tetrahedral nickel(II) complex is expected to absorb. Accordingly, it may be concluded that no association of the planar complexes occurs in solution at room temperature. In these nickel(II) complexes, the ligands X-sal-fum are found to function as bidentates, the furan oxygen atom not being bound to the nickel(II) ion.

It may be interesting to compare the results in the present work with those for related ligands as regards the coordination of the oxygen atom in the side chain Y. Of the ligands (III)—(VI), *n* being 2, (IV) has the highest ability to function as a terdentate ligand; the alcoholic oxygen atom is bound to the nickel(II) ion. Previous studies have shown that the nickel(II) complexes Ni(X-sal-Y)$_2$, Y being CH(R)CH(R)OH, have an octahedral configuration, in which the OH-group is bound to the nickel(II) ion.[6]

The oxygen atom in CH_3O has slightly lower capacity

TABLE 2. MAIN ABSORPTION MAXIMA OF M(X-sal-fum)$_2$ AND M(X-sal-fum)$_3$

Compound	Solvent	ν (log ε)
Ni(H-sal-fum)$_2$	$CHCl_3$	16.2(1.84), 23.7(3.66)
Ni(3-CH_3O-sal-fum)$_2$	$CHCl_3$	16.1(1.91), 23.6(3.62)
	Nujol	16.0
Ni(5-Br-sal-fum)$_2$	Nujol	16.0
Co(5-Br-sal-fum)$_2$	$CHCl_3$	8.2(1.67), 11.4(1.49), 26.4(3.93)
Co(H-sal-fum)$_3$	$CHCl_3$	16.6(2.48), 25.7(3.95)
Co(5-Cl-sal-fum)$_3$	$CHCl_3$	16.6(2.58), 25.2(3.95)
Co(5-Br-sal-fum)$_3$	$CHCl_3$	16.6(2.57), 25.2(3.92)
Co(3-CH_3O-sal-fum)$_3$	$CHCl_3$	16.4(2.62), 25.1(3.92)

ν: 10^3 cm^{-1}, sh: shoulder.

to be coordinated with the nickel(II) ion. It was revealed previously that Ni(H-sal-$CH_2CH_2OCH_3)_2$ is square-planar in the solid state, the OCH_3-group not being bound to the nickel(II) ion, although complexes of the type Ni(H-sal-$CH(R)CH_2OCH_3)_2$ have a six-coordinate, octahedral configuration with the CH_3O-group bound to the nickel(II) ion.

The present study shows that of the ligands (III)—(VI), n being 2, the furan oxygen atom in (VI) has the lowest tendency to be bound to the nickel(II) ion. In this respect, the ligand (III) seems to lie between (IV) and (VI). Previous studies have revealed that the CH_3O-group is bound to the metal ion in many of the Ni(X-sal-o-CH_3O-$C_6H_4)_2$ and Co(X-sal-o-CH_3O-$C_6H_4)_2$ type complexes.[3,7]

Summarizing the discussion given above, the following order may be derived as to the donor strength of the oxygen atom in Y of the ligands (I): CH_2CH_2-OH > $C_6H_4OCH_3$(o-) > $CH_2CH_2OCH_3$ > CH_2-furyl.

Copper(II) Complexes. Two types of copper(II) complexes have been isolated. The complexes Cu(X-sal-fum)$_2$ (X=H, 5-Cl, 5-Br, 3-CH_3O) in non-donor solvents show electronic absorption spectra with the first d-d band at about 17 kK, typical spectra being shown in Fig. 1. The absorption curves are similar to those of the complexes Cu(X-sal-n-alkyl)$_2$, the d-d band maxima being at nearly the same frequencies, a fact which implies that the complexes Cu(X-sal-fum)$_2$ may have an essentially planar, four-coordinate configuration.[8-10] Their magnetic moments also lie in the range from 1.83 to 1.95 BM, in agreement with the square-planar configuration. The spectra also show that the complexes in pyridine form pyridine adducts, in which the copper(II) ion assumes a coordination number exceeding four.

The complexes of the formula Cu(X-sal-fum)Cl (X=H, 5-Cl) at room temperature have subnormal magnetic moments of 1.31 and 0.92 BM, respectively,

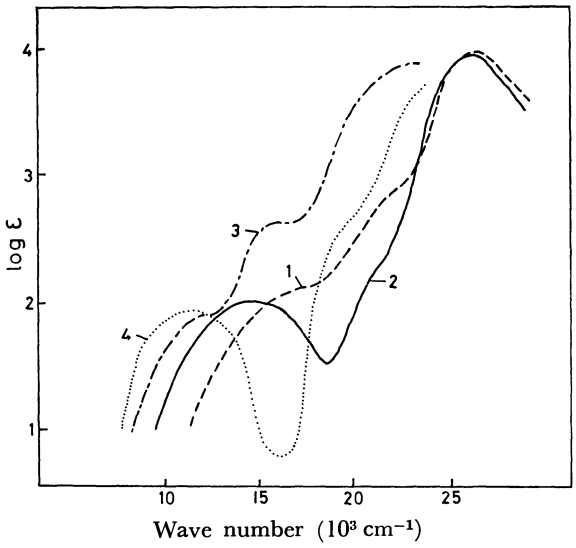

Fig. 1. Electronic absorption spectra of copper(II) complexes: 1, Cu(5-Br-sal-fum)$_2$, in $CHCl_3$; 2, Cu(5-Br-sal-fum)$_2$, in pyridine; 3, Cu(H-sal-fum)-Cl, in Nujol; 4, Cu(5-Cl-sal-fum)Cl, in Nujol.

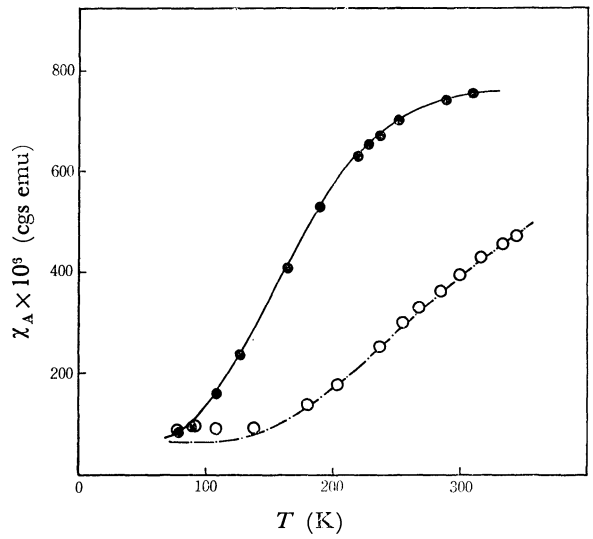

Fig. 2. Variation of magnetic susceptibilities, χ_A, with temperature: ●, Cu(H-sal-fum)Cl ($-2J$=550 cm^{-1}, g=2.26, $N\alpha$=60×10^{-6} emu); ○, Cu(5-Cl-sal-fum)Cl ($-2J$=1000 cm^{-1}, g=2.05, $N\alpha$=60×10^{-6} emu). The curves represent theoretical curves, which are calculated from Eq. 1, using values of J, g and $N\alpha$ given in parentheses.

which are much lower than the normal magnetic moments anticipated for the copper(II) complexes. A sort of interaction, therefore, may be expected to exist between two copper(II) ions. The magnetic susceptibility data over a temperature range 76—300 K, which are shown in Fig. 2, fit the Bleaney-Bowers Eq. 1, probably implying that these copper(II) complexes have a binuclear structure.

Their infrared ν(C-O) bands appear at 1555 (X=H) and 1550 cm^{-1} (X=5-Cl), respectively, which are found to be shifted toward higher frequencies than the typical bis(Schiff base)metal(II) complexes (1520—1530 cm^{-1}). Based on the criteria proposed previously,[11,12] the present finding seems to indicate that these complexes may have a structure with the phenolic oxygen atom bridging two cpoper(II) ions. The J value of Cu(Cl-sal-fum)Cl is significantly larger than that of Cu(H-sal-fum)Cl, a fact which suggests that the spin-spin interaction in the former is stronger than that in the latter.

As may be seen in Fig. 1, the spectrum of Cu(H-sal-fum)Cl widely differs from that of Cu(5-Cl-sal-fum)-Cl. Kato *et al.*[12] reported previously that the spectra of the Cu(X-sal-alkyl)Cl type complexes were classified into two groups, which were designated as B- and Y-type. The present study shows that the spectrum of Cu(H-sal-fum)Cl is similar to that of the B-type and that the spectrum of Cu(5-Cl-sal-fum)Cl is similar to that of the Y-type.

References

1) K. Yamanouchi and S. Yamada, *Inorg. Chim. Acta*, **12**, 105 (1975).

2) S. Yamada, Y. Kuge, and K. Yamanouchi, *Bull. Chem. Soc. Jpn.*, **43**, 406 (1970).

3) S. Yamada, E. Ohno, Y. Kuge, A. Takeuchi, K.

Yamanouchi, and K. Iwasaki, *Coord. Chem. Rev.*, **3**, 247 (1968).

4) A. Takeuchi and S. Yamada, unpublished.

5) H. Nishikawa and S. Yamada, *Bull. Chem. Soc. Jpn.*, **37**, 1154 (1964); L. Sacconi, P. L. Orioli, P. Paoletti, and M. Ciampolini, *J. Am. Chem. Soc.*, **85**, 411 (1963).

6) S. Yamada, Y. Kuge, and K. Yamanouchi, *Bull. Chem. Soc. Jpn.*, **40**, 1864 (1967); A. Chakravorty, J. P. Fennessey, and R. H. Holm, *Inorg. Chem.*, **4**, 26 (1965).

7) A. A. Diamantis, H. Weigold, and B. O. West, *J. Chem. Soc., A*, **1967**, 1281.

8) S. Yamada and H. Nishikawa, *Bull. Chem. Soc. Jpn.*, **36**, 755 (1963).

9) L. Sacconi and M. Ciampolini, *J. Chem. Soc.*, **1964**, 276.

10) D. Hall, R. H. Sumner, and T. N. Waters, *J. Chem. Soc., A*, **1959**, 1200.

11) R. B. Coles, C. M. Harris, and E. Sinn, *Inorg. Chem.*, **8**, 2607 (1969).

12) M. Kato, Y. Muto, H. B. Jonassen, K. Imai, and T. Tokii, *Bull. Chem. Soc. Jpn.*, **43**, 1066 (1970); M. Kato, K. Imai, Y. Muto, T. Tokii, and H. B. Jonassen, *J. Inorg. Nucl. Chem.*, **35**, 109 (1973).

Synthesis and Characterization of Aluminium(III) Complexes with Schiff Bases Obtained from Salicylaldehyde Derivatives and Alkylamines

Hiro KUMA and Shoichiro YAMADA

Institute of Chemistry, College of General Education, Osaka University, Toyonaka, Osaka 560

(Received April 2, 1976)

Aluminium(III) complexes with Schiff bases (abbreviated as X-sal-R) obtained from salicylaldehyde derivatives and amines (RNH_2) have been synthesized by a method starting from aluminium(III) isopropoxide. Complexes of the type Al(X-sal-*n*-alkyl)$_3$ have been isolated, but any attempt to obtain complexes of the types Al(X-sal-*i*-C_3H_7)$_3$ and Al(X-sal-aryl)$_3$ has not been successful. The tris-complexes obtained show similar electronic absorption spectra, regardless of R. Proton magnetic resonance spectra indicate that the aluminium(III) complexes may have a *fac*-configuration.

Tris(*N*-alkyl- or *N*-aryl-salicylideneaminato)-complexes of tervalent 3d transition elements, such as vanadium(III),[1] chromium(III),[2,3] cobalt(III),[4,5] and iron(III),[6] were studied previously. It seems interesting to study the corresponding complexes (abbreviated as M(X-sal-R)$_3$, I) of other tervalent metal ions having no d-electrons and compare the results with those previously reported for the complexes of the 3d ions. Along that line, yttrium(III) complexes with these ligands were examined in a previous paper.[7]

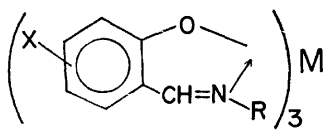

(I)

As extension of the previous studies, aluminium(III) was taken up as the central metal ion in the present work. No aluminium(III) complexes with these Schiff bases have ever been isolated.

Experimental

Materials. *Tris(N-alkylsalicylideneaminato)aluminium(III)*: To a suspension of aluminium(III) isopropoxide (0.01 mol) in 1-butanol or 2-propanol was added a Schiff base (0.033 mol), and the mixture was heated on an oil-bath at about 90 °C for 5 h. The solution was filtered and allowed to stand in a refrigerator overnight. A yellow, crystalline precipitate was collected by filtration and recrystallized from methanol or ethanol to yield pale-yellow crystals of Al(X-sal-R)$_3$. Difficulty was sometimes encountered in the recrystallization, since the complexes often undergo decomposition in the solution. The compounds are soluble in chloroform, methanol and ethanol, but insoluble in benzene. They undergo decomposition in water very readily.

Analytical data of the complexes are shown in Table 1.

Measurements. Electronic absorption spectra were measured on a Shimadzu MPS-50L spectrophotometer. Infrared spectra were obtained from Nujol mulls using a Hitachi EPI-S2 infrared spectrophotometer.

Proton magnetic resonance spectra were recorded on a JEOL Model C-NMR spectrometer using tetramethylsilane as an internal reference. Measurements at a temperature lower than −4 °C were not possible because of too low solubility.

Since the complexes underwent decomposition in solution, the spectral measurements were carried out as quickly as possible. Moreover, measurements were repeated after the spectra had once been determined, to see if any spectral change due to decomposition during the measurements occurred or not.

Results and Discussion

The reaction in ethylene glycol at a temperature higher than 100 °C was reported to be suitable in synthesizing the chromium(III) tris-complexes.[3,8] This method was employed successfully in the preparation of the tris(*N*-alkylsalicylideneaminato)iron(III) complexes, but did not yield the corresponding aluminium(III) complexes. The reaction of aluminium(III) isopropoxide with a Schiff base in a suitable anhydrous solvent, such as 1-butanol or 2-propanol, proved to be appropriate for synthesizing tris(*N*-alkylsalicylideneaminato)aluminium(III). This method may be considered to be applicable to preparation of the tris-complexes of other metal ions in high oxidation states.

It was not possible to synthesize complexes of the type Al(X-sal-*t*-C_4H_9)$_3$. The complexes of this type have never been reported for 3d elements, owing possibly to steric hindrance arising from the bulky *t*-butyl groups. Any attempt to isolate complexes of the type M(X-sal-*i*-C_3H_7)$_3$ has so far been unsuccessful

Table 1. Analytical data of the Al(X-sal-R)$_3$ type complexes

X	R	Calcd, %			Found, %			Mp °C	ν (C=N)	ν (C-O)
		C	H	N	C	H	N			
H	CH_3	66.66	5.59	9.72	66.77	5.61	9.58	205	1620	1540
H	C_2H_5	68.77	6.41	8.91	68.58	6.55	8.72	155	1620	1540
H	*n*-C_3H_7	70.15	7.07	8.18	69.65	6.96	8.04	187	1620	1540
5-Br	CH_3[a]	41.94	3.81	6.11	42.11	3.42	5.92	238	1620	1535
3-CH_3O	CH_3[a]	60.33	6.00	7.82	60.29	5.68	7.58	181	1625	1540

ν: cm^{-1}. a) With 1 H_2O.

for M=aluminium(III) and iron(III),[9] whereas the corresponding chromium(III),[3] manganese(III),[9] and cobalt(III)[10] complexes were obtained previously. The failure in isolating the aluminium(III) complexes of this type may be due mainly to the steric factor, since the ionic radius of Al^{3+} (0.57 Å) is much smaller than the other three ions. On the contrary, the radius of Fe^{3+}(0.67 Å) is slightly larger than those of Cr^{3+} (0.65 Å), Mn^{3+}(0.66 Å) and Co^{3+}(0.65 Å). Consequently, the reluctance of iron(III) to form the $Fe(X\text{-}sal\text{-}i\text{-}C_3H_7)_3$ type complexes may be due not to the steric factor alone, but to weaker iron(III)-to-ligand bond, as compared with that for chromium(III), manganese(III), and cobalt(III).

It may also be interesting to note that any aluminium(III) complexes with the neutral *N*-alkyl- or *N*-arylsalicylideneamines have not been isolated in the present work, in contrast to the yttrium(III) complexes.[7]

Main electronic absorption bands of the complexes $Al(X\text{-}sal\text{-}alkyl)_3$ are shown in Table 2. It is found that the electronic absorption bands due to internal transitions within the ligands are shifted very slightly toward higher frequencies on formation of the aluminium(III) complex. This slight band shift seems to show the weak aluminium(III)-to-ligand bond.

TABLE 2. ELECTRONIC ABSORPTION BANDS OF $Al(X\text{-}sal\text{-}R)_3$ IN CHLOROFORM

Compound	ν(log ε)	
$Al(H\text{-}sal\text{-}CH_3)_3$	24.6 (2.74),	31.8 (4.10)
$Al(H\text{-}sal\text{-}C_2H_5)_3$	24.6 (2.71),	31.8 (4.10)
$Al(H\text{-}sal\text{-}n\text{-}C_3H_7)_3$	24.5 (2.74),	31.8 (4.10)
$(H\text{-}sal\text{-}CH_3)H$[a]	24.5 (2.20),	31.6 (3.58)

ν: 10^3 cm^{-1}. a) Free Schiff base.

The complexes show an infrared ν(C=N) band at about 1620 cm^{-1}, indicating that the ligands are coordinated as bidentates in their deprotonated form with the metal ion. Previous studies have shown that the bidentate *N*-substituted salicylideneaminate anion bound with a metal ion exhibits the corresponding band at about 1610—1620 cm^{-1}, whereas the neutral salicylideneamines coordinated to a metal ion show the corresponding band at about 1640 cm^{-1}.[11]

The *fac* and *mer* isomers are possible in tris(chelate)-metal complexes, if the bidentate ligands are not symmetric. Pairs of such isomers have indeed been obtained with ligands, such as amino acids[12] and β-diketonates.[13] For the complexes of the type $M(X\text{-}sal\text{-}R)_3$, however, only the *mer* form has so far been isolated, and the *mer* form was found to be an exclusively predominant species in their solutions as well.[14] This result was ascribed to the steric disposition of the nitrogen substituents on one hand and to the electrostasic repulsion among the three oxygen atoms in the *fac* form on the other.

Main PMR spectral data of the complexes $Al(X\text{-}sal\text{-}CH_3)_3$ in chloroform-*d* are shown in Table 3. The $N\text{-}CH_3$ resonance appears as a sharp singlet at about 6.78 and 6.84 τ for X=H and 5-Br, respectively, at 50, 20, and −4 °C. It should be noted that the $N\text{-}CH_3$ resonance at 50 °C is as sharp as at −4 °C. The *mer* isomer, which has a lower symmetry than the *fac* isomer, would be unambiguously identified by three equally intense signals for the $N\text{-}CH_3$ groups, as was found to be the case with the corresponding cobalt(III) and vanadium(III) complexes.[1,14,15] Hence, the spectra of $Al(H\text{-}sal\text{-}CH_3)_3$ and $Al(5\text{-}Br\text{-}sal\text{-}CH_3)_3$ are found to be consistent with the *fac* form having three-fold symmetry, although their low solubility did not allow PMR spectral measurements at lower temperatures. A recent X-ray structural study[16] has revealed that $Al(H\text{-}sal\text{-}CH_3)_3$ consists of six-coordinate aluminium(III) complexes having a *fac* configuration. These aluminium(III) complexes seem to be the first examples of tris(*N*-substituted salicylideneaminato)metal(III) complexes having a *fac* configuration to be isolated.

TABLE 3. CHEMICAL SHIFTS, $\tau(N\text{-}CH_3)$, OF $Al(X\text{-}sal\text{-}CH_3)_3$ AT DIFFERENT TEMPERATURES

Compound	−4 °C	20 °C	50 °C
$Al(H\text{-}sal\text{-}CH_3)_3$	6.78	6.78	6.78
$Al(5\text{-}Br\text{-}sal\text{-}CH_3)_3$	6.84	6.84	6.84
$(H\text{-}sal\text{-}CH_3)H$[a]	—	6.87	—

a) Free Schiff base.

It is not clarified at the moment why the *fac* form of these aluminium(III) complexes is obtained much more readily than the *mer* form, in contrast to many 3d metal complexes. However, it may be true that the present finding would give rise to renewed controversies over the stability of the *mer* and *fac* isomers of the tris(bidentate)-metal complexes.

Financial support of this work by the Ministry of Education is gratefully acknowledged. Thanks are also due to Dr. Yoshiyuki Namba of Osaka College of Education for informing us of the results of the X-ray study prior to publication.

References

1) F. Röhrscheid, R. E. Ernst, and R. H. Holm, *J. Am. Chem. Soc.*, **89**, 6472 (1967).
2) M. J. O'Connor and B. O. West, *Aust. J. Chem.*, **21**, 369 (1968).
3) S. Yamada and K. Iwasaki, *Bull. Chem. Soc. Jpn.*, **41**, 1972 (1968).
4) B. O. West, *J. Chem. Soc.*, **1960**, 4944.
5) H. Nishikawa and S. Yamada, *Bull. Chem. Soc. Jpn.*, **37**, 1154 (1964).
6) A. van den Bergen, K. S. Murray, M. J. O'Connor, and B. O. West, *Aust. J. Chem.*, **21**, 1505 (1968).
7) H. Kuma and S. Yamada, *Inorg. Chim. Acta*, **15**, 213 (1975).
8) S. Yamada and K. Iwasaki, *Inorg. Chim. Acta*, **5**, 3 (1971); *Bull. Chem. Soc. Jpn.*, **42**, 1463 (1969).
9) S. Yamada and K. Yamanouchi, unpublished.
10) S. Yamada, E. Ohno, and K. Yamanouchi, *Bull. Chem. Soc. Jpn.*, **41**, 535 (1968).

11) H. H. Freedman, *J. Am. Chem. Soc.*, **83**, 2900 (1961); P. Teyssie and J. J. Charette, *Spectrochim. Acta*, **19**, 1407 (1963); L. Sacconi and U. Campigli, *Inorg. Chem.*, **5**, 606 (1966).
12) R. G. Denning and T. S. Piper, *Inorg. Chem.*, **5**, 1056 (1966).
13) R. C. Fay and T. S. Piper, *J. Am. Chem. Soc.*, **85**, 500 (1963).
14) R. H. Holm and A. Chakravorty, *Inorg. Chem.*, **3** 1521 (1964); M. Ciampolini, F. Maggio, and F. P. Cavasino, *Inorg. Chem.*, **3**, 1188 (1964).
15) R. H. Holm, *Acc. Chem. Res.*, **2**, 307 (1969).
16) Y. Namba, private communication.

Studies of the Mixed Amino Acid Complexes of Cobalt(III). IV.[1] Magnetic Circular Dichroism Spectra of the $[Co(ox)_x(gly)_y(en)_z]$ Complexes

Nobuko MATSUOKA and Yoichi SHIMURA

Department of Chemistry, Faculty of Science, Osaka University, Toyonaka, Osaka 560

(Received April 3, 1976)

Magnetic circular dichroism (MCD) spectra of a series of sixteen complexes of the $[Co(ox)_x(gly)_y(en)_z]$ type have been measured. The MCD intensity increases with increasing number of the coordinated carboxylato groups. A negative MCD band whose shape is similar to the corresponding absorption band was observed in the first d-d absorption band region. This negative band is assigned to the "B" term, in which the "A" term is swamped. A positive and a negative MCD band appear in the second d-d absorption band region. The origin of the positive band is discussed.

Only a few papers have reported the magnetic circular dichroism (MCD) spectra of cobalt(III) complexes; these results include $[Co(NH_3)_6]^{3+}$,[2,3] $[Co(CN)_6]^{3-}$,[2] $[CoCl(NH_3)_5]^{2+}$,[2] *trans*- and *cis*-$[CoCl_2(en)_2]^+$,[2] *cis*-$[Co(NH_3)_4(OH_2)_2]^{3+}$,[2] $[Co(en)_3]^{3+}$,[2,3] $[Co(ox)_3]^{3-}$,[2,4] $[Co(rac\text{-}pn)_3]^{3+}$,[3] $[Co(mal)_3]^{3-}$,[4] and $[Co(acac)_3]$.[5]* The purpose of the present work is to take a general view of the MCD spectra of a fundamental series of the sixteen cobalt(III) complexes, whose absorption spectra have been studied already.[6] The sixteen complexes form a complete series of the $[Co(ox)_x(gly)_y(en)_z]$ type,* where x, y, and z are 0, 1, 2, or 3 and $x+y+z$ equals 3. The oxalato, glycinato, and ethylenediamine ligands all produce a five-membered chelate ring; each complex is a tris-(chelate) type and belongs to one of the $[Co^{III}(O)_n(N)_{6-n}]$ types (n=0—6).

Experimental

The complexes were prepared by the methods described in the available literature.[6-13]

Visible and near-ultraviolet absorption spectra were measured by a Shimadzu UV-200 spectrophotometer. MCD spectra were recorded in a magnetic field of 15000 gauss with a Jasco MOE-1 spectropolarimeter. The MCD intensity is expressed in terms of the molar ellipticity per unit magnetic field in the direction of the light beam, $[\theta]_M$, which has the units of degree m^{-1} dm^3 mol^{-1} $gauss^{-1}$.

Measurements were made at room temperature in aqueous solutions, except for *fac*-$[Co(gly)_3]$, which was studied in 3 M H_2SO_4 solution.

Results and Discussion

Band shapes of MCD spectra have been generally interpreted as composed from three terms, A, B, and C, whose shapes are either dispersion type (for A) or absorption type (for B and C). The "A" term arises when at least one of the ground or the excited states is degenerate, while a "B" term is present in principle for every electronic transition. A "C" term exists only when the ground state is degenerate. This term may be disregarded in the present case, since the ground state of an octahedral cobalt(III) complex is nondegenerate, $^1A_{1g}$.

The sixteen complexes of $[Co(ox)_x(gly)_y(en)_z]$ series can be classified into ten types with respect to the coordinated atoms. They are $[Co(N)_6]$, $[Co(N)_5(O)]$, *cis(O)*- and *trans(O)*-$[Co(N)_4(O)_2]$, *mer(N)*- and *fac(N)*-$[Co(N)_3(O)_3]$, *trans(N)*- and *cis(N)*-$[Co(N)_2(O)_4]$, $[Co(N)(O)_5]$ and $[Co(O)_6]$, in which only the *mer(N)*-$[Co(N)_3(O)_3]$ type has no degenerate excited state in any approximation. Thus, the A term may be expected in most of the complexes, except in *mer(N)*-$[Co(gly)_3]$ and *mer(N)*-[Co(ox)(gly)(en)].

The observed MCD spectra of $[Co(ox)_x(gly)_y(en)_z]$ type complexes in the visible and near-ultraviolet region are shown in Figs. 1—6, together with their absorption spectra. The data are summarized in Table 1.

The First d-d Absorption Band Region. A negative band, whose shape resembles greatly the corresponding absorption band, appears in this region for all the present complexes. This result is in accordance with that from the magnetic rotatory dispersion studies of $[Co(en)_3]^{3+}$, $[Co(gly)(en)_2]^{2+}$, *etc.*[14] Thus it seems that only a negative B term is present, while the A

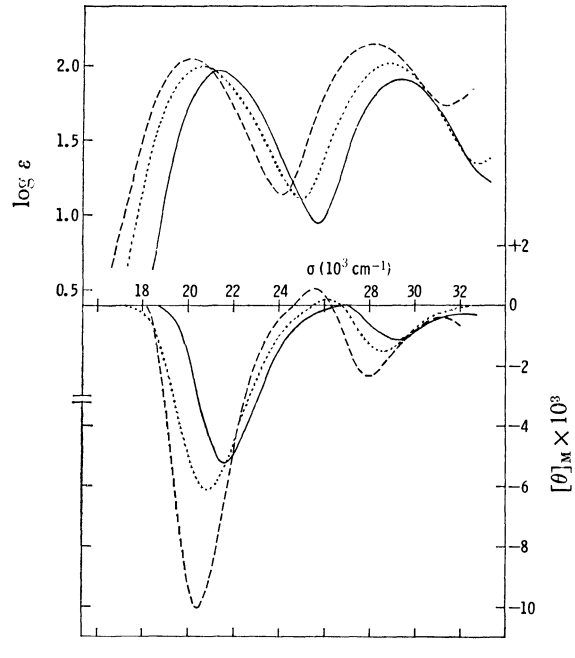

Fig. 1. Absorption and MCD spectra of $[Co(en)_3]^{3+}$ (——), $[Co(gly)(en)_2]^{2+}$ (……), and $[Co(ox)(en)_2]^+$ (----).

* Abbreviation of ligands: en=ethylenediamine, pn=propylenediamine, ox=oxalate(2−) ion, mal=malonate(2−) ion, acac=acetylacetonate(1−) ion, gly=glycinate(1−) ion, and ala=alaninate(1−) ion.

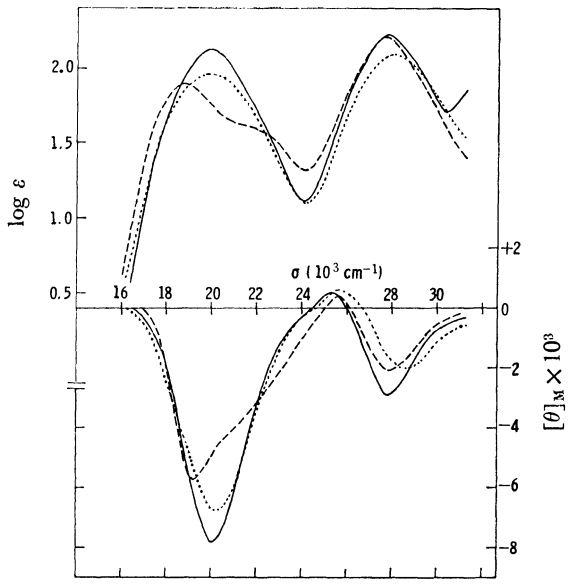

Fig. 2. Absorption and MCD spectra of three geometrical isomers of $[Co(gly)_2(en)]^+$: C_1-*cis*(*O*) (——), C_2-*cis*(*O*) (·····), and *trans*(*O*) (----).

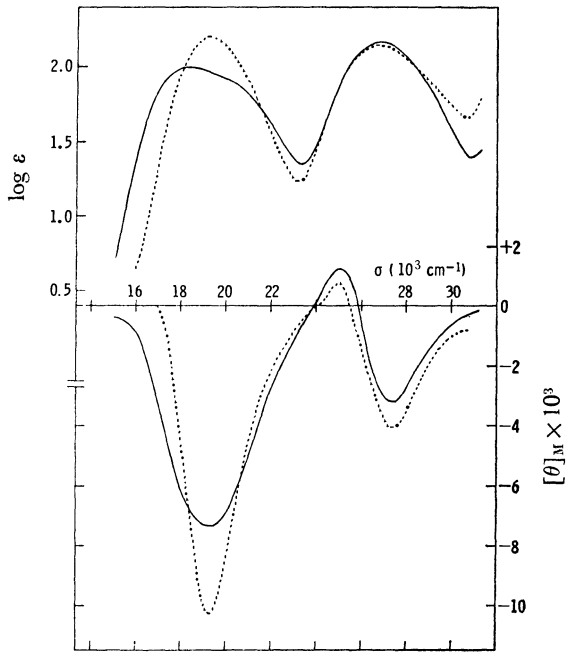

Fig. 3. Absorption and MCD spectra of two geometrical isomers of $[Co(gly)_3]$: *mer*(*N*) (——) and *fac*(*N*) (·····).

term is not to be seen. This is in agreement with the results of earlier workers, who interpreted the unobservable A term as a quenching of the orbital angular momentum in the excited state.[2]

It should be noted that the extremum of the MCD band has slightly higher energy than the maximum of the corresponding absorption band in most of the complexes (Table 1). This fact can be well explained by considering the presence of a small positive A term which is swamped by the large negative B term, as has been pointed out for $[Co(N)_6]$ type complexes

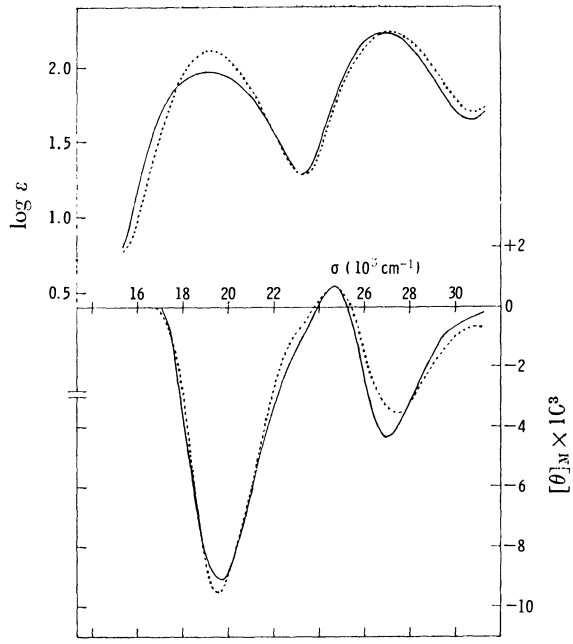

Fig. 4. Absorption and MCD spectra of two geometrical isomers of [Co(ox)(gly)(en)]: *mer*(*N*) (——) and *fac*(*N*) (·····).

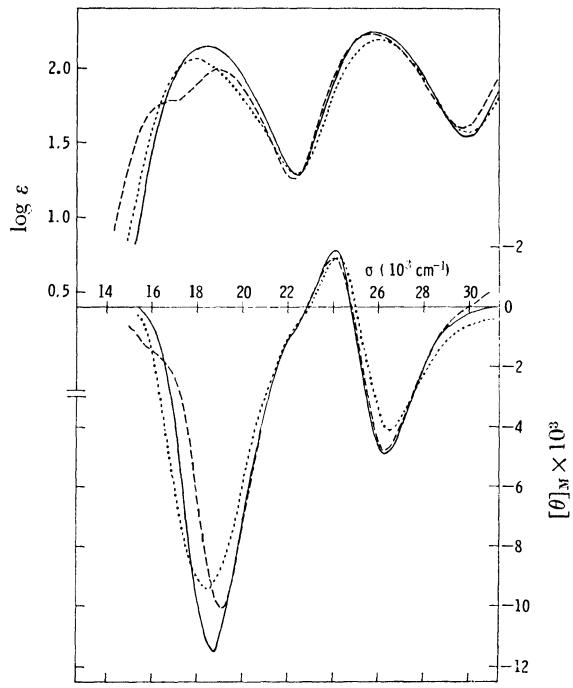

Fig. 5. Absorption and MCD spectra of three geometrical isomers of $[Co(ox)(gly)_2]^-$: *trans*(*N*) (----), C_2-*cis*(*N*) (·····), and C_1-*cis*(*N*) (——).

by Russell and Douglas.[3]

McCaffery and co-workers mentioned that the d d bands are much more resolved in MCD than in the absorption of *cis*- and *trans*-$[CoCl_2(en)_2]^+$.[2] We cannot detect such an effect, however, for the present complexes in comparing the *cis* and *trans* isomers of $[Co(gly)_2(en)]^+$ or $[Co(ox)(gly)_2]^-$, and the *mer* and *fac* isomers of $[Co(gly)_3]$ or [Co(ox)(gly)(en)] (Figs.

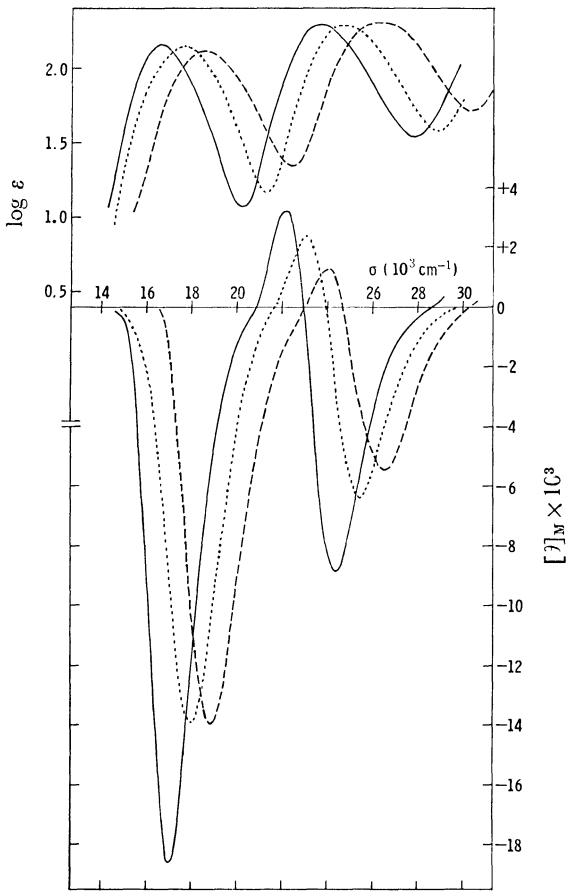

Fig. 6. Absorption and MCD spectra of $[Co(ox)_2(en)]^-$ (----), $[Co(ox)_2(gly)]^{2-}$ (·····), and $[Co(ox)_3]^{3-}$ (——).

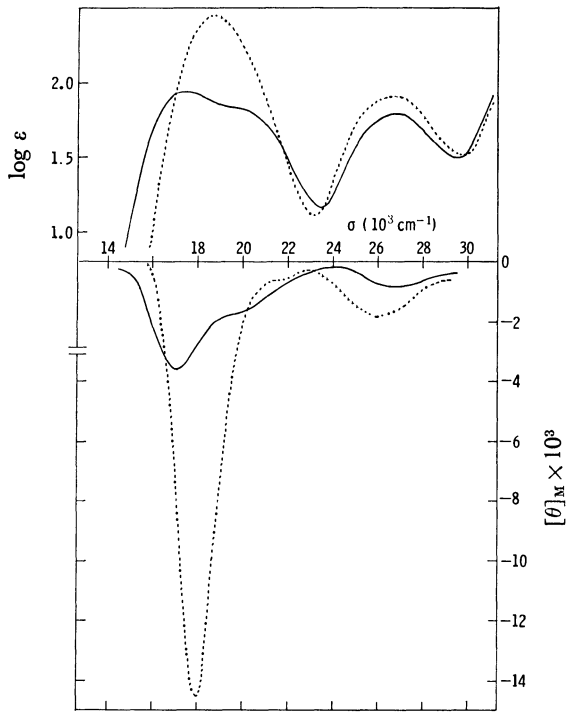

Fig. 7. Absorption and MCD spectra of two geometrical isomers of $[Co(\beta\text{-ala})_3]$: *mer*(*N*) (——) and *fac*(*N*) (·····).

2—5). Our sensitivity for the splitting into the component bands seems to be of the same order for both the MCD and the absorption spectra.

The Second d-d Absorption Band Region. It is a unique behavior of the present $[Co(ox)_x(gly)_y(en)_z]$

TABLE 1. ABSORPTION AND MCD DATA OF THE $[Co(ox)_x(gly)_y(en)_z]$ TYPE COMPLEXES
(Wave numbers are given $10^3\ cm^{-1}$)

Complex	First d-d band region			Second d-d band region		
	Absorption σ_{max}	MCD $\sigma_{ext}([\theta]_{Mext})$	$\lvert[\theta]_{Mext}\rvert$ a) / ε_{max}	Absorption σ_{max}	MCD $\sigma_{ext}([\theta]_{Mext})$	MCD $\sigma_{ext}([\theta]_{Mext})$
1. $[Co(en)_3]Br_3$	21.4	21.6(−0.0053)	5.8	29.3		29.2(−0.0011)
2. $[Co(gly)(en)_2](ClO_4)_2$	20.6	20.8(−0.0061)	6.3	28.8	26.0(+0.0002)	28.6(−0.0015)
3. $[Co(ox)(en)_2]Cl$	20.1	20.4(−0.0101)	9.2	28.1	25.6(+0.0005)	28.0(−0.0023)
4. C_1-*cis*-$[Co(gly)_2(en)]ClO_4\cdot 2H_2O$	19.9	20.1(−0.0079)	5.9	27.8	25.3(+0.0005)	27.8(−0.0030)
5. C_2-*cis*-$[Co(gly)_2(en)]I$	19.0	20.2(−0.0068)	7.4	28.1	25.6(+0.0006)	28.6(−0.0021)
6. *trans*-$[Co(gly)_2(en)]Br\cdot H_2O$	18.8	19.2(−0.0057)	7.3	27.7	25.6(+0.0004)	27.9(−0.0021)
7. *mer*-$[Co(ox)(gly)(en)]$	19.1	19.7(−0.0091)	9.8	27.0	24.7(+0.0007)	27.0(−0.0044)
8. *mer*-$[Co(gly)_3]\cdot 2H_2O$	18.4	19.4(−0.0074)	7.3	26.8	25.0(+0.0013)	27.4(−0.0033)
9. *fac*-$[Co(gly)_3]\cdot H_2O$	19.3	19.3(−0.0103)	6.5	26.7	25.0(+0.0008)	27.4(−0.0041)
10. *fac*-$[Co(ox)(gly)(en)]$	19.2	19.5(−0.0096)	7.5	27.2	24.7(+0.0007)	27.4(−0.0036)
11. *trans*-$Na[Co(ox)(gly)_2]$	19.0	19.1(−0.0101)	10.3	25.7	24.1(+0.0016)	26.3(−0.0048)
12. C_2-*cis*-$Na[Co(ox)(gly)_2]$	17.9	18.5(−0.0094)	8.2	26.0	24.2(+0.0017)	26.5(−0.0041)
13. C_1-*cis*-$Na[Co(ox)(gly)_2]$	18.4	18.8(−0.0115)	8.2	25.8	24.1(+0.0018)	26.3(−0.0049)
14. $Na[Co(ox)_2(en)]\cdot H_2O$	18.5	18.9(−0.0140)	10.9	26.1	24.1(+0.0013)	26.5(−0.0055)
15. $Na_2[Co(ox)_2(gly)]\cdot 1.5H_2O$	17.7	18.0(−0.0139)	10.1	24.8	23.0(+0.0024)	25.5(−0.0064)
16. $K_3[Co(ox)_3]\cdot 3H_2O$	16.6	17.0(−0.0186)	13.2	23.7	22.2(+0.0032)	24.4(−0.0089)

a) In the units of 10^{-5}.

complexes, except $[Co(en)_3]^{3+}$, that a positive MCD band is observed on the lower energy side of the main negative MCD band in the second d-d absorption band region (Figs. 1—6). No such positive band was reported for the cobalt(III) complexes studied previously, except for $[Co(ox)_3]^{3-}$.[2,4]

Alternative interpretations may be presented for the origin of the positive MCD band in the second d-d absorption band region. The first would to postulate that this band is a longer wavelength wing of an A term. McCaffery and co-workers interpreted the MCD spectrum of $[Co(ox)_3]^{3-}$ in this region by postulating an A term of trigonal splitting E transition in D_3 symmetry.[2] However, the fact that the *mer(N)*-$[Co(N)_3(O)_3]$ type complexes also have the positive band cannot be so explained, because these complexes do not have a degenerate excited state.

In the second explanation, the positive band is attributed to a positive B term arising from one of the splitting components of the $T_{2g}(O_h)$ transition in the lower symmetry. In this case, it is expected that the energy separation between the two components of the *trans* isomer of $[Co(N)_4(O)_2]$ or $[Co(N)_2(O)_4]$ type is larger than that of the *cis* isomer. This energy separation is $1/2\delta_\sigma - 1/2\delta_\pi$ for the *trans* isomer, and $1/4\delta_\sigma - 1/4\delta_\pi$ for the *cis*, using Yamatera's parameters.[15] Nevertheless, the observed separation between the positive and negative bands is virtually invariant for both isomers (Table 1).

It should be noted that the maximum of the second d-d absorption band is located at slightly higher energy than the negative MCD band for the complexes of $[Co(N)_6]$ and $[Co(N)_5(O)]$ type, while it lies in the intermediate region between the positive and negative MCD bands for the complexes having more carboxylato groups, *e.g.*, for the $[Co(N)_2(O)_4]$, $[Co(N)(O)_5]$, and $[Co(O)_6]$ type complexes. Moreover, the intensity ratio of the positive to the negative band increases in the above order, and in the limiting case the positive MCD band does not appear in the $[Co(en)_3]^{3+}$ complex. These results seem to indicate that the positive MCD band is related to the presence of coordinated carboxylato groups.

In order to confirm the above assumption, MCD spectra of the other complexes were measured. Unexpectedly, no positive band is observed in *mer(N)*- and *fac(N)*-$[Co(\beta\text{-ala})_3]$ (Fig. 7). Also $[Co(mal)_3]^{3-}$ and *cis*-$[Co(NH_3)_4(OH_2)_2]^{3+}$ did not exhibit this band, as was reported in the previous papers.[2,4] From these facts, it is concluded that the positive band is characteristic for the complex having a planar carboxylato chelate ring. It has been well established that the β-ala[16] and mal[17] chelate rings are not planar.

Intensity. It is interesting that the values of $|[\theta]_{Mext}|$ and also $|[\theta]_{Mext}|/\varepsilon_{max}$ increase with increasing number of coordinated carboxylato groups, in both the first and second d-d absorption band regions, as can be seen from Table 1.

The value of $|[\theta]_{Mext}|$ in the first d-d absorption band region is greater than that in the second d-d absorption band region for all the present complexes, although some exceptional complexes, such as $[CoCl(NH_3)_5]^{2+}$ and *cis*-$[CoCl_2(en)_2]^+$, have been reported previously.[2]

References

1) Part III of this series: N. Matsuoka, J. Hidaka, and Y. Shimura, *Bull. Chem. Soc. Jpn.*, **48**, 458 (1975).

2) A. J. McCaffery, P. J. Stephens, and P. N. Schatz, *Inorg. Chem.*, **6**, 1614 (1967).

3) R. L. Russell and B. E. Douglas, *Inorg. Chim. Acta*, **3**, 426 (1969).

4) R. L. Russell and B. E. Douglas, *Inorg. Nucl. Chem. Lett.*, **9**, 1251 (1973).

5) H. Kato and J. Gohda, *Bull. Chem. Soc. Jpn.*, **46**, 636 (1973).

6) N. Matsuoka, J. Hidaka, and Y. Shimura, *Bull. Chem. Soc. Jpn.*, **40**, 1868 (1967).

7) Y. Shimura and R. Tsuchida, *Bull. Chem. Soc. Jpn.*, **29**, 311 (1956).

8) N. Matsuoka, J. Hidaka, and Y. Shimura, *Bull. Chem. Soc. Jpn.*, **39**, 1257 (1966).

9) N. Matsuoka, J. Hidaka, and Y. Shimura, *Inorg. Chem.*, **9**, 719 (1970).

10) N. Matsuoka, J. Hidaka, and Y. Shimura, *Bull. Chem. Soc. Jpn.*, **45**, 2491 (1972).

11) F. P. Dwyer, I. K. Reid, and F. L. Garvan, *J. Am. Chem. Soc.*, **83**, 1285 (1961).

12) F. P. Dwyer, I. K. Reid, and A. M. Sargeson, *Aust. J. Chem.*, **18**, 1919 (1965).

13) M. B. Ćelap, S. R. Niketić, T. J. Janjić, and V. N. Nikolić, *Inorg. Chem.*, **6**, 2063 (1967).

14) Y. Shimura, J. Fujita, M. Kobayashi, and R. Tsuchida, Abstracts of papers presented at 7th Annual Meeting of the Chemical Society of Japan (1954), p. 201.

15) H. Yamatera, *Bull. Chem. Soc. Jpn.*, **31**, 95 (1958).

16) H. C. Freeman, *Adv. Protein Chem.*, **22**, 257 (1967).

17) K. R. Butler and M. R. Snow, *J. Chem. Soc., Dalton Trans.*, **1976**, 259.

Impurity Metal-Activated Crystal Growth of Niobium Monophosphide from Gas Phase

Seiji MOTOJIMA, Toyohiko IZUSHI,* Kohzo SUGIYAMA, and Yasutaka TAKAHASHI

Department of Synthetic Chemistry, Faculty of Engineering, Gifu University, Kakamigahara, Gifu 504

**Government Industrial Research Institute of Nagoya, Hirate-Machi, Kitaku, Nagoya 462*

(Received December 12, 1975)

Niobium monophosphide single crystals were obtained by chemical vapor deposition from a gas mixture of $NbCl_5$, PCl_3, H_2, and Ar on a quartz substrate using metallic impurity. The existence of Au, Pt, Pd, and Ni resulted in the growth of whiskers or pillar crystals. Maximum whisker length of 5 mm and thickness of 30 μm were obtained at 1150 °C for an hour with the use of Pt impurity. Platelet crystals ($400 \times 1000 \times 20$ μm, max.) were obtained with the use of Pt at 1240 °C. The growth directions of the whiskers and some platelet crystals were assigned to ⟨001⟩ and a direction in (001) plane, respectively. The optimum growth conditions for the pillar crystals in the case of Ni impurity: substrate temperature 1000—1020 °C, gas flow ratio $PCl_3/(NbCl_5+PCl_3)$ of 0.7—0.75. From observation of the tip and base of pillar crystals grown with Ni, the growth mechanism seems to be base VLS followed by VS.

Of the transition metal monophosphides, niobium monophosphide (NbP, niobium phosphide hereafter) is of interest as regards thermal stability. Niobium phosphide is a greyish black material having a metallic luster and good electrical conductor ($\approx 10^{-3}\,\Omega\cdot$cm),[1] and which is moderately hard (microhardness 599 kg/mm^2)[1] and is not attacked by water or dilute acids at room temperature.[2]

The existence of two equiatomic compounds (α- and β-NbP) proposed by Schönberg[3] was disproved by Bollar and Parthe,[4] who showed that there is a single compound with a range of homogeneity 44.7—50 a/o of phosphorus. The structure is body-centered tetragonal, four formulas per unit cell, space group $I4_1md$, the lattice parameter of c slightly varying from 11.40_0 (44.7 a/o P) to 11.37_8 (50 a/o P).[4]

Niobium phosphide has been prepared by heating niobium metal with red phosphorus in sealed tube at 650—1000 °C[1,5] with tricalcium diphosphide,[1] or by electrolyzing phosphate of metals.[6] The single crystal has been prepared by Schaefer and Fuhr[7] by means of chemical vapor transport. However, no work has been reported on whisker or pillar crystal growth from a vapor phase.

We have examined the growth conditions of whisker or pillar crystals with use of metallic impurity from a gas mixture of niobium pentachloride, phosphorus trichloride, hydrogen and argon, and also physical and chemical properties of the crystals. The results are given in this paper.

Experimental

A quartz tube (7 mm I. D. and 65 mm in length) containing a SiC heater was placed as a substrate in the center of a vertical reaction tube (quartz of 35 mm I. D.) heated from outside with a nichrome heater. The quartz substrate was abraded with emery papers, rinsed with deionized water and dried. A stream of niobium pentachloride (bp 240 5.°C) prepared by chlorination of niobium powder (14 mesh) at 500—600 °C and carried by argon, and another stream of hydrogen saturated by phosphorus trichloride at a given temperature were introduced from the upper inlet of the reaction tube. Argon was used for cleaning the reaction system before each experiment. The flow rates of each gas at room temperature were measured with an orifice-type flow meter. Flow rate of niobium pentachloride was calculated from that of chlorine stream to the niobium metal, where this chlorination reaction might be considered to proceed quantitatively in a steady state.

The surface temperature of the substrate was measured with an optical pyrometer through an observation window and was corrected by means of a CA thermocouple. The ambient temperature of the reaction atmosphere was controlled between 300 and 400 °C using the CA thermocouple to keep the niobium pentachloride in gas phase. As the source of impurities to promote the crystal growth, various metals such as Mn, Fe, Co, Ni, Pd, Pt, and Au were painted on the substrate in the form of aqueous solutions of sulphates or chlorides, and were subjected to decomposition or reduction into the corresponding metals inside the reactor at a temperature below that used for the niobium phosphide crystal growth. The surface concentration of the impurity was fixed at *ca.* 0.05 mg/cm^2 of substrate area.

The range of pillar crystal length and thickness in this paper refers to about twenty of the longest samples obtained in each experiment. Crystals were observed with a scanning electron microscope. An X-ray diffractometer, a micro-analyzer and an oscillation camera were used for analysis of the grown crystals, the base of pillar crystals and a well-formed whisker, respectively.

Conductivity of whisker and platelet crystal was measured by conventional two-probe method using a Wheatstone bridge in an argon flow.

Results and Discussion

Growth Conditions of the Pillar Crystals Using Ni Metal.

Effect of Substrate Temperature: Substrate temperature influences pillar crystal growth by a great deal as shown in Fig. 1. An average length of 1.2 mm was attained at 1000—1020 °C, the length decreasing abruptly at a temperature higher or lower than 1000—1020 °C. Above the optimum temperature, pillar crystals grew to a direction perpendicular to the growth axis resulting in considerable rough surface. The lowest temperature for the growth of pillar crystals was approximately 900 °C.

Effect of the Gas Composition: The effect of the gas flow ratio of $PCl_3/(NbCl_5+PCl_3)$ on the length and thickness of pillar crystals is shown in Fig. 2, where the sum of the flow rates of niobium pentachloride and phosphorus trichloride is kept at 0.20 cm^3/s.

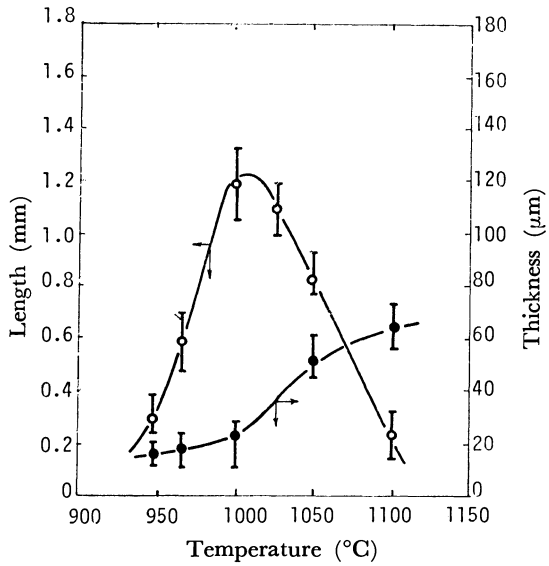

Fig. 1. Effect of substrate temperature on the length and the thickness of pillar crystals.
Impurity: Ni, reaction time: 10 min, $NbCl_5$ flow rate: 0.05 cm^3/s, PCl_3 flow rate: 0.15 cm^3/s, H_2 flow rate: 3.2 cm^3/s, Ar flow rate: 1.0 cm^3/s.

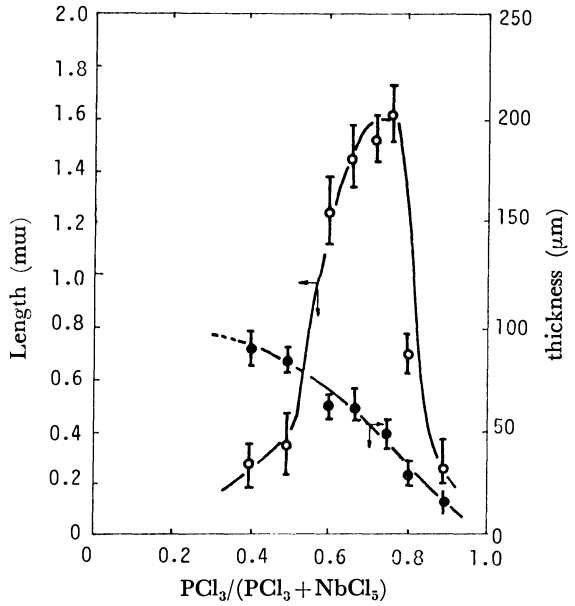

Fig. 2. Effect of gas flow ratio of $PCl_3/(NbCl_5+PCl_3)$ on the length and the thickness of pillar crystals.
Impurity: Ni, substrate temperature: 1050 °C, reaction time: 10 min, $NbCl_5+PCl_3$ flow rates: 0.20 cm^3/s, H_2 flow rate: 3.2 cm^3/s, Ar flow rate: 0.5 cm^3/s.

The length of crystals increased with increase in the ratio, and reached a maximum at a flow ratio of 0.70—0.75, decreasing abruptly above the ratio of 0.75. In contrast, the thickness of the crystals decreased linearly with increase in the ratio, pillar crystals with a well-formed and smooth surface growing preferably at the ratio of above 0.75 (Fig. 3). This optimum flow ratio declined to a PCl_3-rich region as compared with the expected reaction stoichiometry $PCl_3/(NbCl_5+PCl_3)$ of 0.5 and with the optimum flow ratio for the deposition of polycrystalline NbP by use of no impurity

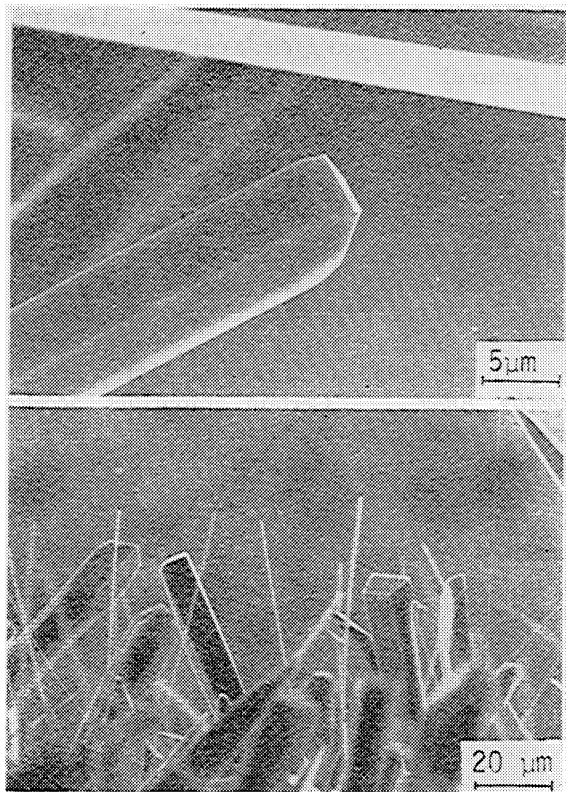

Fig. 3. Well-formed pillar crystals.
Impurity: Ni, substrate temperature: 1020 °C, reaction time: 10 min, $NbCl_5$ flow rate: 0.04 cm^3/s, PCl_3 flow rate: 0.15 cm^3/s, H_2 flow rate: 4.0 cm^3/s, Ar flow rate: 1.0 cm^3/s.

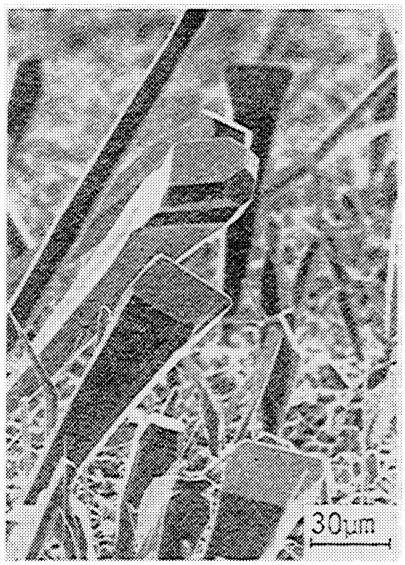

Fig. 4. Pillar crystals having a tapered form.
Impurity: Ni, substrate temperature: 1100 °C, reaction time: 30 min, $NbCl_5$ flow rate: 0.15 cm^3/s, PCl_3 flow rate: 0.15 cm^3/s, H_2 flow rate: 4.0 cm^3/s, Ar flow rate: 1.0 cm^3/s.

of 0.6. On the other hand, at a flow ratio of $PCl_3/(NbCl_5+PCl_3)$, crystals grew to a direction perpendicular to the growth axis; remarkable growth steps or a rough surface being observed. Tapered pillar crystals (Fig. 4) were obtained at 1100 °C and a flow

ratio $PCl_3/(NbCl_5+PCl_3)$ of about 0.8. The tips of the crystals were shaped a clear-cut square or a tetragonal pyramid.

Effect of the Growth Time: The effect of growth time on the crystal length and thickness is shown in Fig. 5. The length of the pillar crystals increased with increase in reaction time up to 15 min after an induction time of about 5 min, and levelled off after the elapse of 15 min. In contrast, the thickness remained constant 10—15 μm until 15 min, beyond which pillar crystals grew in thickness with time. This can be explained by rapid linear growth by VLS, followed by gradual thickening by VS mechanism.

Impurity Effect. Certain impurities accelerate the growth of whiskers or pillar crystals. The growth mechanism can be explained by "VLS mechanism." The impurity effects of various metals on the crystal growth of niobium phosphide at 900—1250 °C are summarized in Table 1. Iron, cobalt, chromium, and manganese give no influence on the whisker growth for all the temperatures examined, the deposition taking place in uniform coatings or polycrystals. Gold and nickel show a conspicuous effect at 1050 °C, giving straight whiskers and pillar crystals, respectively. Platinum gives well-formed straight whiskers and platelet crystals at 1100—1200 °C and 1250 °C, respectively. Palladium gives cubic crystals mixed with thin whiskers above 1100 °C.

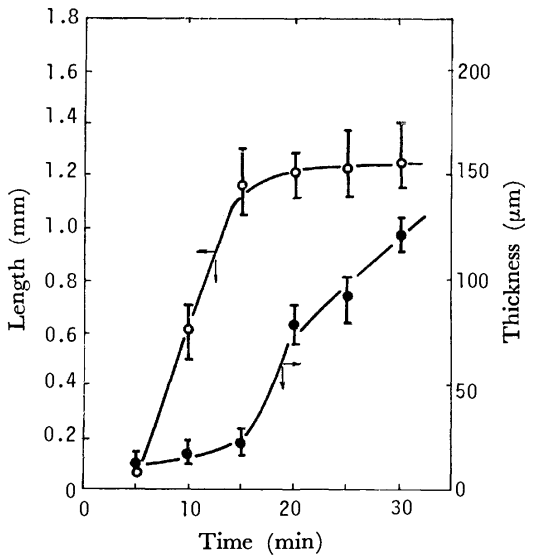

Fig. 5. Effect of reaction time on the length and the thickness of pillar crystals.
Impurity: Ni, substrate temperature: 1020 °C, $NbCl_5$ flow rate: 0.05 cm^3/s, PCl_3 flow rate: 0.15 cm^3/s, H_2 flow rate: 3.2 cm^3/s, Ar flow rate: 1.0 cm^3/s.

Table 1. Impurity effects

Impurity	Effect	Crystal morphology
Fe	−	Polycrystals
Co	−	Polycrystals
Ni	++	Pillars
Cr	−	Polycrystals
Mn	−	Polycrystals
Au	++	Whiskers
Pt	++	Whiskers and pillars (1100—1200 °C), and platelets (>1200 °C)
Pd	+	Cubic crystals (>1100 °C)

Crystal Morphologies. Typical whiskers grown with gold as an impurity are shown in Fig. 6. The whiskers have a square cross section and reach a maximum length of 1 mm and 5 μm in thickness after 2 h. Lateral surfaces are generally smooth, but a square-shaped growth depression appears occasionally (Fig. 6B). The tips of pillars is a clear-cut square (Fig. 6C). Figure 7 shows the appearance of pillar crystals grown on a platinum painted zone at 1150 °C for 15 min, polycrystal coatings depositing in the absence of platinum. Average pillar length reached 3 mm (5 mm max.) and thickness of 30 μm after

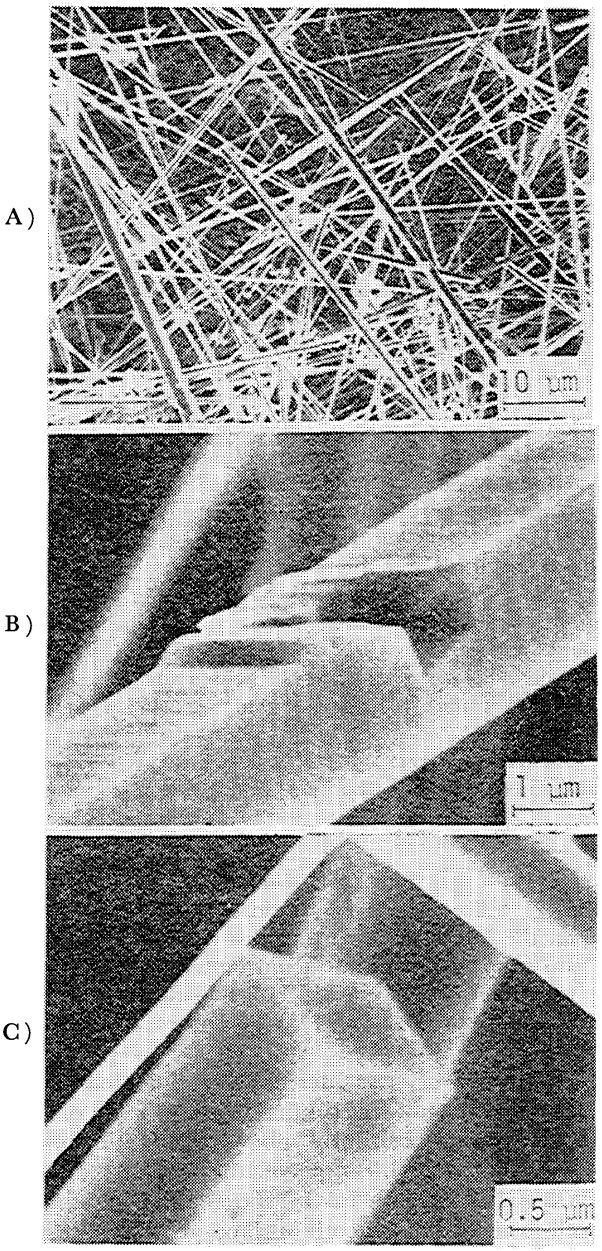

Fig. 6. Appearances of whiskers.
Impurity: Au, substrate temperature: 1050 °C, reaction time: 30 min, $NbCl_5$ flow rate: 0.04 cm^3/s, PCl_3 flow rate: 0.05 cm^3/s, H_2 flow rate: 3.5 cm^3/s, Ar flow rate: 0.5 cm^3/s.

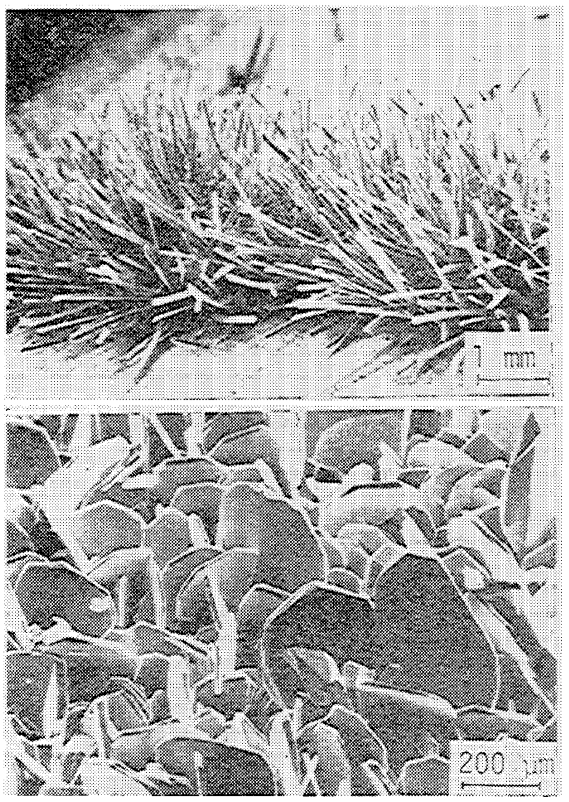

Fig. 7. Appearances of pillar and platelet crystals.
Impurity: Pt, reaction time: 15 min.
A) Substrate temperature: 1150 °C, $NbCl_5$ flow rate: 0.03 cm^3/s, PCl_3 flow rate: 0.03 cm^3/s, H_2 flow rate: 4.0 cm^3/s, Ar flow rate: 0.6 cm^3/s.
B) Substrate temperature: 1240 °C, $NbCl_5$ flow rate: 0.03 cm^3/s, PCl_3 flow rate: 0.04 cm^3/s, H_2 flow rate: 3.7 cm^3/s, Ar flow rate: 0.5 cm^3/s.

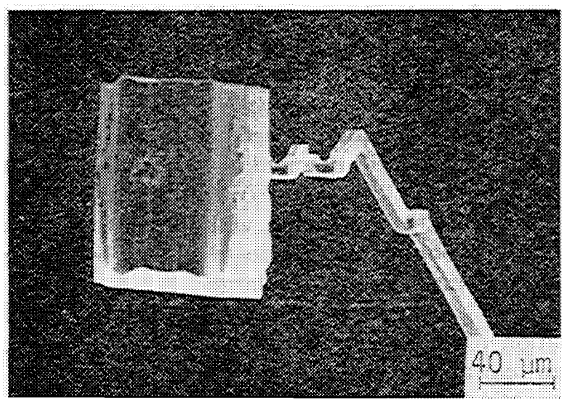

Fig. 8. Peculiar pillar crystals.
Impurity: Pt, substrate temperature: 1070 °C, reaction time: 15 min, $NbCl_5$ flow rate: 0.06 cm^3/s, PCl_3 flow rate: 0.04 cm^3/s, H_2 flow rate: 3.5 cm^3/s, Ar flow rate: 0.5 cm^3/s.

an hour. At a temperature higher than 1200 °C, thin platelet crystals $400 \times 1000 \times 20$ μm with a smooth surface grew on the platinum painted zone (Fig. 7B). Sometimes, peculiar pillar crystals with a deformed 120×100 μm cubic crystal at the middle or the tip of the crystal were observed (Fig. 8). Well-formed $100 \times 100 \times 50$ μm crystals deposited, sometimes mixed

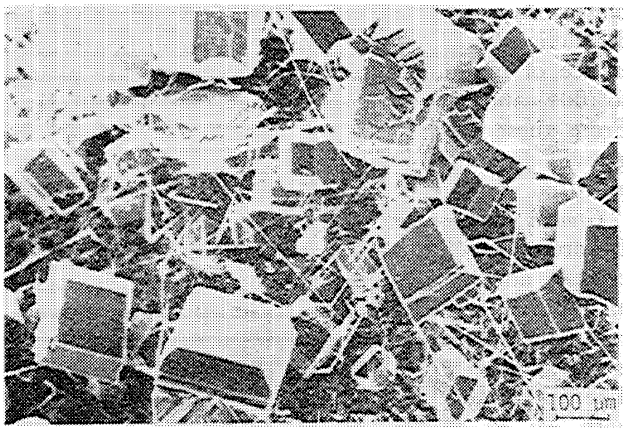

Fig. 9. Well-formed crystals.
Impurity: Pt, substrate temperature: 1145 °C, reaction time: 30 min, $NbCl_5$ flow rate: 0.04 cm^3/s, PCl_3 flow rate: 0.06 cm^3/s, H_2 flow rate: 4.1 cm^3/s, Ar flow rate: 0.6 cm^3/s.

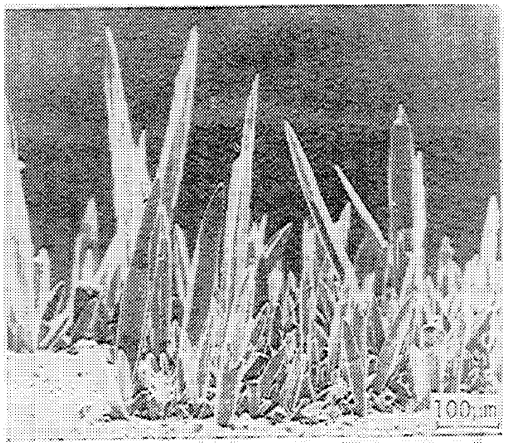

Fig. 10. Phylloid crystals.
Impurisy: Ni, substrate temperature: 1025 °C, reaction time: 15 min, $NbCl_5$ flow rate: 0.05 cm^3/s, PCl_3 flow rate: 0.10 cm^3/s, H_2 flow rate: 4.1 cm^3/s, Ar flow rate: 0.5 cm^3/s.

with thin whiskers on the platinum painted zone at 1145 °C for 30 min (Fig. 9). Similar crystals grew with palladium at 1070 °C.

Nickel impurity considerably accelerated the growth of phylloid crystals with a sharp tip, the maximum length reaching 2 mm and thickness 50 μm. A typical phylloid crystal grown at 1025 °C for 15 min is shown in Fig. 10.

The growth axis of the whisker was confirmed by full-rotation photograph. Indices of an X-ray diffraction photograph are shown in Fig. 11, in which one well-formed whisker (10 μm thick and 3 mm long) is mounted with the whisker axis perpendicular to the incident X-ray beam in an oscillation camera (diameter 57 mm).

X-Ray diffraction diagrams of whiskers (A), platelet crystals (B) and woolly whiskers (C) are shown in Fig. 12 together with that in reference (D),[8] where a collection of whiskers and platelet crystals were dispersed on a holder plate. Thus the axes of the whiskers and faces of platelets are mainly parallel to the holder

plate. A strong single peak is observed on whisker diffraction which corresponds to (200) of the tetragonal lattice of niobium phosphide. Strong peaks assinged to (004) and (008) are observed on platelet diffraction. From these results and the crystal morphologies, the growth direction of whisker is supposed to be ⟨001⟩ and that of platelet in some directions on (001) plane.

Growth Mechanism of Whiskers and Pillar Crystals. In order to clarify the growth mechanism of NbP crystals activated by metallic impurities, the location of impurity on the growing crystal plays an important role, since the evidence for the tip VLS mechanism is the existence of drops of impurity on their tips. The tip part of most whiskers and pillar crystals grown with Au, Pt, or Ni impurity is commonly shaped a clear-cut square or a long square pyramid, a drop like solid being seldom found on the tip, even in the initial stage of growth. The presence of Ni metal could not be confirmed by X-ray microanalysis of the tip of pillar crystals grown with Ni impurity. We might suppose that a tip VLS mechanism does not take part during the course of growth of whisker or pillar. The result of X-ray microanalysis on the cross section of the base of pillar crystals grown with Ni impurity is shown in Fig. 13. The layer is seen to consist of uniform composition of niobium–phosphorus–nickel. The eutectic temperatures[9] of the binary alloy of Nb–Ni and P–Ni are reported to be 1175 °C (40.2 a/o Nb) and 880 °C (19 a/o P), respectively. It seems that niobium atom is dissolved in the Ni–P melt to yield a melt of Nb–Ni–P mixture from which niobium phosphide can be crystallized. Pillar crystal growth was observed 2—5 minutes later after the substrate had been heated at a given temperature in a given reaction atmosphere. The "induction time" can be attributed to a slow diffusion rate of niobium and phosphorus into the nickel metal, or the time necessary for saturation of the drop with niobium and phosphorus. A possible mechanism for the pillar crystal growth of niobium phosphide activated by nickel metal may be base VLS mechanism at least during the course of the initial stage of growth. Appearance of a pillar crystal suggests the growth by VS mechanism. The pillar crystals might grow by base VLS mechanism followed by VS mechanism. However, another mechanism including a center axial screw dislocation mechanism or Chikawa's mechanism[10] cannot be excluded.

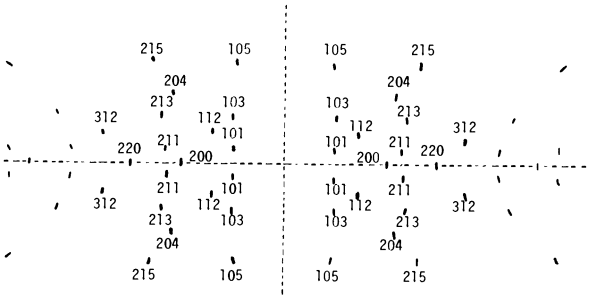

Fig. 11. Indices of the full-rotation photograph of a whisker.
Rotation axis was aligned with whisker axis (Cu$K\alpha$, diameter of camera: 57 mm).

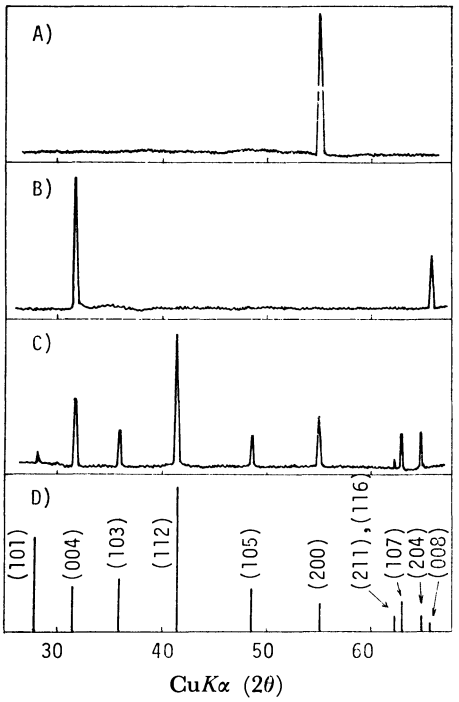

Fig. 12. X-Ray diffraction profiles.
A) A collection of whiskers placed on a holder plate along its growth direction.
B) A collection of platelet crystals dispersed on a holder plate.
C) Woolly whiskers as grown.
D) Data of NbP quoted from the Ref. 8.

Properties of Niobium Phosphide Crystals. Electrical Resistivity: Electrical resistivity of a well-formed whisker (10—20 μm in diameter and 2—3 mm in length) and a platelet crystal (200—300 μm in width and 10—20 μm in thickness) along the crystal axis and some directions in (001) plane was examined in argon atmosphere, respectively. The resistivity increased with a rise in temperature in the range 20—250 °C, characteristic of metallic conduction; 9×10^{-4} for a whisker and 1×10^{-2} Ω·cm for a platelet crystal. The former value is in line with 0.4×10^{-3} Ω·cm of powdered niobium phosphide reported by Ripley,[1] the latter being considerably larger.

Stability of Oxidation in Air: Resistivity against oxidation of niobium phosphide in air was examined at an elevated temperature. Figure 14 shows the change of weight ratio with time at various temperatures between 900 and 1100 °C. The weight ratio increased with a rise in temperature above 970 °C, until the ratio attained a limiting value of *ca.* 1.64. X-Ray diffraction profiles of the products obtained at 1100 °C for an hour exhibited only the peaks of niobium phosphate ($NbPO_5$). Niobium phosphate is a light fluffy white powder and can not form a tight protecting layer on the surface of niobium phosphide crystal. It may be concluded that niobium phosphide is very stable in air up to 950 °C, but oxidizes to the phosphate at above 970 °C. Oxidation products of TiP[11] and ZrP,[12] an analogous phosphide of NbP, are a mixture of titanium pyrophosphate and titanium

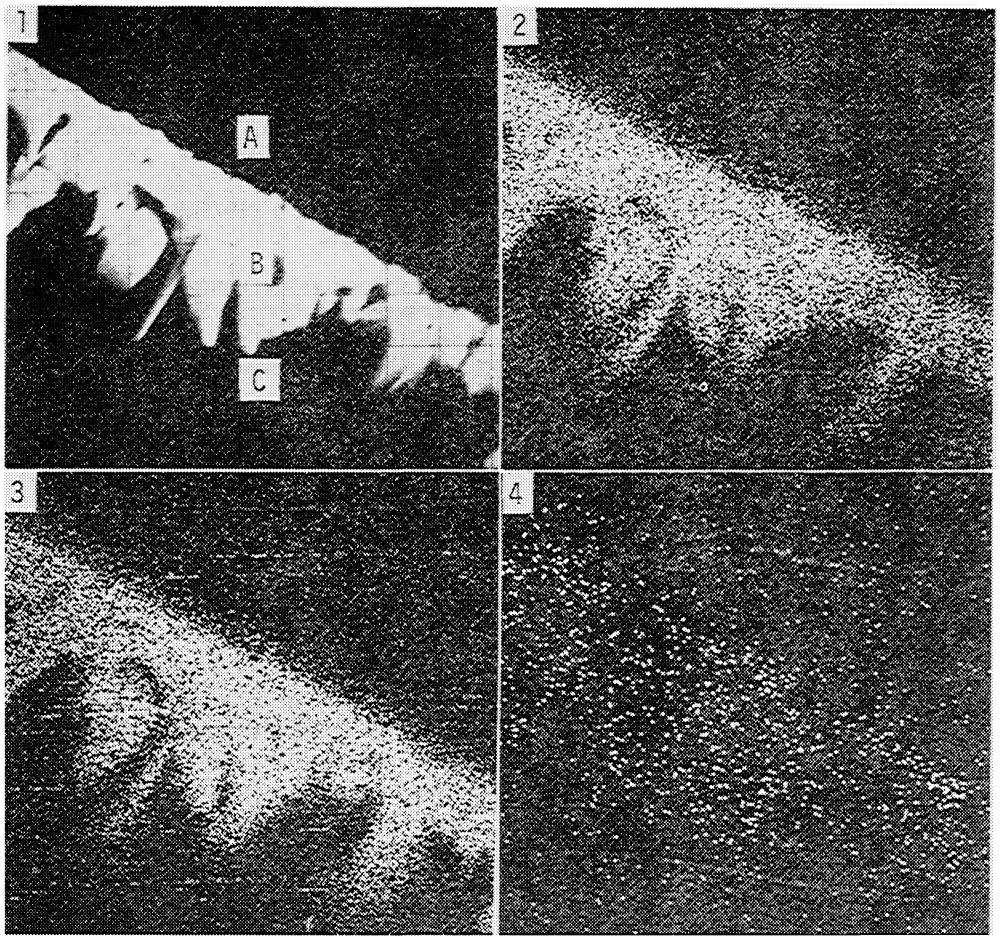

Fig. 13. Profiles of X-ray microanalysis.
(1) (A): quartz substrate; (B): NbP layer; (C): resin, (2) Nb$L\alpha$, (3) P$K\alpha$, (4) Ni$K\alpha$.

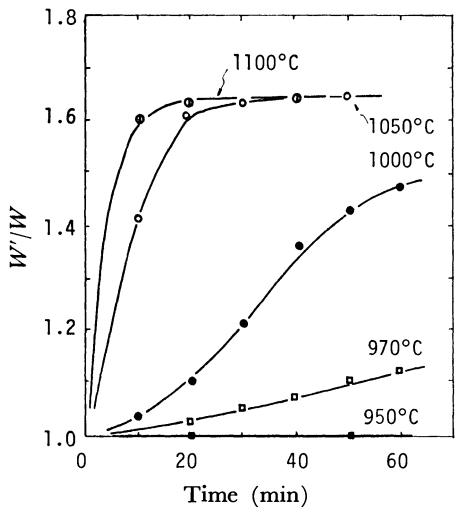

Fig. 14. Oxidation resistivity in the temperature range of 950—1100 °C

oxide, and zirconium oxide, respectively. It is of interest that oxidation products of the transition metal monophosphides differ from metal to metal.

Summary

Single crystals of NbP were obtained by the CVD method on a quartz substrate using metallic impurity.

1) Au, Pt, Pd, and Ni used as an impurity have an essential effect on whisker or pillar crystal growth. In the case of Pt, whisker (5 mm long $\times$ 30 μm thick, max.) and platelet crystals (400 $\times$ 1000 $\times$ 20 μm, max.) were obtained in an hour at 1150 and 1240 °C, respectively.

2) The growth directions of whiskers and platelet crystals were assigned to $\langle 001 \rangle$ and some direction in (001) plane, respectively.

3) In the case of Ni impurity, the longest pillar crystal was obtained at a substrate temperature of 1000—1020 °C, and $PCl_3/(NbCl_5+PCl_3)$ ratio of 0.7—0.75.

4) A drop-like solid was seldom found on the tip of most whiskers and pillar crystals, a layer with uniform Nb–P–Ni compositions being observed in the base of pillar crystals. It is presumed that base site VLS mechanism is responsible for the growth of NbP whiskers or pillar crystals rather than tip VLS mechanism.

References

1) R. L. Ripley, *J. Less-Common Met.*, **4**, 496 (1962).
2) E. Heinerth and W. Biltz, *Z. Anorg. Allg. Chem.*, **198**, 173 (1931).
3) N. Schönberg, *Acta Chem. Scand.*, **8**, 226 (1954).
4) H. Boller and E. Parthe, *Acta Crystallogr.*, **16**, 1095 (1963).

5) A. Reinecke, F. Wiechmann, M. Zumbusch, and W. Bilz, *Z. Anorg. Allg. Chem.*, **249**, 14 (1942).
6) H. Hartmann and W. Massig, *Z. Anorg. Allg. Chem.*, **266**, 98 (1951).
7) H. Schaefer and W. Fuhr, *J. Less-Common Met.*, **8**, 375 (1965).
8) L. G. Berry, "Inorg. Index to the Powder Diffraction File," Joint Committee on Powder Diffraction Standards, Pennsylvania (1971), Cards No. 17-882.
9) M. Hansen, "Constitution of Binary Alloys," McGraw-Hill, New York, Toronto, London (1958), pp. 1011, 1027.
10) J. Chikawa and T. Nakayama, *J. Appl. Phys.*, **35**, 2493 (1964).
11) S. Motojima, T. Wakamatsu, Y. Takahashi, and K. Sugiyama, *J. Electrochem. Soc.*, **123**, 290 (1976).
12) S. Motojima, Y. Takahashi, and K. Sugiyama, *J. Cryst. Growth*, **30**, 1 (1975).

The Crystal Structure of $(+)_{350}$-(*R*)-Propylenediamine-*N*,*N*′-dimethylethylenediamineplatinum(II) Di-μ-(+)-tartrato(4−)-bis(antimonate(III)) Dihydrate

Keiji MATSUMOTO, Shun'ichiro OOI, Masao SAKUMA, and Hisao KUROYA

Department of Chemistry, Faculty of Science, Osaka City University, Sugimotocho, Sumiyoshi-ku, Osaka 558

(Received March 11, 1976)

The crystal of the title compound is monoclinic, with $a=9.415(3)$, $b=15.767(7)$, $c=8.786(3)$ Å, $\beta=94.25(4)°$, the space group of $P2_1$, and $Z=2$. The structure was determined from the counter intensity data by heavy-atom techniques and was refined by the block-diagonal least-squares calculations to R 0.050 for 2604 non-zero reflections. The Pt atom has a square-planar coordination by 4N atoms, the secondary N atoms of which are of the *S* absolute configuration.

Few studies have been made of the optical resolution of the platinum(II) complexes as well as of the correlation between the optical activity and structure of the Pt(II) chelates. Ito *et al.*[1] studied the absorption and circular dichroism (CD) spectra of a number of Pt(II) chelates of optically active diamines. The resolution and racemization reaction of some *N*-methylethylenediamineplatinum(II) substances were investigated by Buckingham *et al.*[2] and Goddard *et al.*[3] Recently, Bosnich[4] reported on the conformational and vicinal effects which were observed in the CD spectra of *N*-methyl-substituted ethylenediamine and propylenediamine complexes of Pt(II). As a part of our studies of the CD-structure correlation, we have been attempting for several years to resolve several mixed ligand complexes of Pt(II). This report will describe the absolute configuration of the complex cation of $(+)_{350}$-[Pt(*R*-pn)(Me$_2$en)][Sb$_2$(+)-tart$_2$]·2H$_2$O (*R*-pn: (*R*)-(−)-propylenediamine; Me$_2$en: *N*,*N*′-dimethylethylenediamine; [Sb$_2$(+)-tart$_2$]: di-μ-(+)-tartrato(4−)-bis(antimonate(III))), which was obtained in the course of our studies; we will also show the crystal structure of this compound.

Experimental

Preparation of $(+)_{350}$-[*Pt*(R-*pn*)(*Me*$_2$*en*)][*Sb*$_2$(+)-*tart*$_2$]·2*H*$_2$*O*. [PtCl$_2$(Me$_2$en)] was prepared following a method which is analogous to that used for [PtCl$_2$en].[5] A mixture of [PtCl$_2$(Me$_2$en)] (0.57 g) and an excess of (*R*)-propylenediamine ((*R*)-(−)-pn) in water (15 ml) was heated at 90 ° until the solution became clear. The solution was evaporated to near dryness, whereby the excess of diamine was removed. The resulting [Pt(*R*-pn)(Me$_2$en)]Cl$_2$ is highly hygroscopic and could not be isolated. Ag$_2$[Sb$_2$(+)-tart$_2$] (1.05 g) was added to "[Pt(*R*-pn)(Me$_2$en)]Cl$_2$" in 20 ml of water, and the suspension was warmed for 0.5 h in the dark. The AgCl was then filtered off and washed with hot water (10 ml). The filtrate and washing were combined, and the resultant solution was evaporated to dryness under reduced pressure. The product was dissolved in 14 ml of hot water acidified with a drop of acetic acid. The solution was filtered, and a small amount of unidentified precipitates was removed; then the solution was allowed to stand at room temperature for two days. The colorless crystals thus obtained were recrystallized from hot water involving a drop of acetic acid. They were filtered, and subsequently washed with ethanol and acetone. Yield, 0.51 g (23%).

Found: C, 19.21; H, 3.38; N, 5.68%. Calcd for $(+)_{350}$-[Pt(*R*-H$_2$NCH$_2$CH(CH$_3$)NH$_2$)(H$_3$CNHCH$_2$CH$_2$NHCH$_3$)]-[Sb$_2$(+)-(C$_4$H$_2$O$_6$)$_2$]·2H$_2$O: C, 19.39; H, 3.23; N, 6.03%.

An optical rotation measurement was made on 0.0104 g of the compound in 10 ml of 0.02 M acetic acid at 350 nm, using a JASCO J-20 Automatic Recording Spectropolarimeter; $[\alpha]_{350}$, +510°.

X-Ray Data Collection. The crystals of $(+)_{350}$-[Pt(*R*-pn)(Me$_2$en)][Sb$_2$(+)-tart$_2$]·2H$_2$O are colorless, needle-shaped, and stable in the air. The specimen employed for data collection had dimensions of $0.23\times0.15\times0.13$ mm and was mounted on a glass fibre. Preliminary X-ray photographic studies, using oscillation, Weissenberg, and precession techniques, revealed the approximate unit cell dimensions, the Laue symmetry of 2/m, and the systematic absences of $0k0$ for $k=2n+1$. These extinctions indicate that the space group is $P2_1$, since the compound is optically active. Crystal data: $C_{15}H_{30}O_{14}N_4Sb_2Pt$, monoclinic, $a=9.415(3)$, $b=15.767(7)$, $c=8.786(3)$ Å, $\beta=94.25(4)°$, $U=1300.7$ Å^3, $Z=2$, $D_c=2.40$, $D_m=2.37$ g·cm^{-3}, space group $P2_1$, λ(Mo$K\alpha$)=0.71069 Å, μ(Mo$K\alpha$)=78.0 cm^{-1}.

The cell dimensions were determined by a least-squares fit using 2θ values measured accurately on a Philips PW1100 diffractometer. Intensity data with $6°\leqq2\theta\leqq55°$ were collected at room temperature by the use of graphite-monochromated Mo$K\alpha$ radiation. The ω-2θ scan technique was employed. The scan range was $(0.7+0.2\tan\theta)°$, and the scan speed, 1.0°/min; the background was counted for 20 s at each end of the scan. Three standard reflections, 600, $0\bar{4}0$, 003, measured every 240 min, showed no appreciable decay. A total of 2604 intensities with $I_{top}-2\sqrt{I_{top}}>I_{back}$ were classified as observed; I_{top} is the intensity (counts/s) measured at the top of the peak, and I_{back} is the mean background intensity (counts/s) obtained from the preliminary background measurements for 5 s on each side of the peak. Corrections for Lorentz-polarization and absorption effects were made, and the relative structure factors were derived.[6]

Structure Determination

The structure was solved by heavy-atom techniques. Six cycles of block-diagonal least-squares refinement with the isotropic temperature factor for each atom gave an R of 0.069. Nine cycles of the refinement, based on the anisotropic temperature factors for Pt and Sb atoms, resulted in $R=0.050$. The minimized function was $\Sigma w(F_o-|F_c|)^2$ $(=\Sigma w\Delta F^2)$. The weighting scheme, $w=(39.16/F_o)^2$ for $F_o>39.16$, $w=1$ for $23.30\leqq F_o\leqq39.16$, and $w=0.8$ for $F_o<23.30$, was used to make $w\Delta F_o^2$ approximately constant over the whole range of F_o. The corrections for the anomalous dispersion effect were applied for the Pt and Sb atoms.[7] The

Table 1. Final atomic coordinates and temperature factors, with estimated standard deviations in parentheses

	x	y	z	B(Å^2)
Pt	0.01070(5)	0	0.19076(6)	a)
N(1)	0.0269(16)	−0.0915(10)	0.0369(17)	2.8(2)
N(2)	0.0042(15)	−0.0773(9)	0.3409(16)	2.5(2)
N(3)	0.1746(18)	0.0890(11)	0.3458(19)	3.2(3)
N(4)	0.1963(18)	0.0766(11)	0.0355(19)	3.2(3)
C(1)	−0.0493(20)	−0.1621(13)	0.1155(22)	3.1(3)
C(2)	−0.1143(18)	−0.1258(11)	0.2537(20)	2.5(3)
C(3)	−0.1678(24)	−0.1959(15)	0.3545(26)	3.8(4)
C(4)	0.2883(24)	0.1433(15)	0.2719(26)	3.9(4)
C(5)	0.2317(24)	0.1590(15)	0.1080(26)	3.9(4)
C(6)	0.2410(37)	0.0550(23)	0.4950(39)	6.3(7)
C(7)	0.1111(26)	0.0854(16)	−0.1151(28)	4.2(4)
Sb(1)	0.55343(13)	0.36078(8)	−0.14028(15)	a)
Sb(2)	0.74737(14)	0.11255(9)	0.17924(16)	a)
O(1)	0.4116(14)	0.3521(9)	0.0388(15)	3.3(2)
O(2)	0.6900(12)	0.3538(8)	0.0405(14)	2.7(2)
O(3)	0.4087(15)	0.3560(11)	0.2915(16)	3.8(3)
O(4)	0.9057(15)	0.2097(10)	0.2373(18)	3.7(3)
O(5)	0.6235(13)	0.2050(8)	0.2373(15)	2.8(2)
O(6)	0.9194(17)	0.3402(11)	0.3379(18)	4.1(3)
O(7)	0.5094(13)	0.2395(9)	−0.1648(14)	2.9(2)
O(8)	0.7320(15)	0.3183(9)	−0.2646(16)	3.2(2)
O(9)	0.8176(18)	0.2063(11)	−0.3736(19)	4.3(3)
O(10)	0.5524(16)	0.0639(10)	0.0706(17)	3.8(3)
O(11)	0.7672(15)	0.1430(9)	−0.0327(16)	3.3(2)
O(12)	0.4361(18)	0.0460(11)	−0.1558(19)	4.2(3)
C(8)	0.4711(18)	0.3538(12)	0.1722(20)	2.8(3)
C(9)	0.6335(18)	0.3555(11)	0.1891(19)	2.5(3)
C(10)	0.6864(18)	0.2814(11)	0.2862(19)	2.4(3)
C(11)	0.8495(19)	0.2796(11)	0.2894(20)	2.7(3)
C(12)	0.7271(19)	0.2386(13)	−0.3000(21)	3.0(3)
C(13)	0.6054(20)	0.1869(13)	−0.2467(23)	3.1(3)
C(14)	0.6638(18)	0.1139(12)	−0.1458(19)	2.6(3)
C(15)	0.5394(21)	0.0715(13)	−0.0751(22)	3.2(3)
H_2O(1)	0.1240(26)	−0.4543(17)	0.4581(27)	7.1(5)
H_2O(2)	0.1452(16)	0.4229(10)	0.2471(18)	3.8(3)

a) Anisotropic temperature factors ($\times 10^5$) in the form of $\exp[-(B_{11}h^2+B_{22}k^2+B_{33}l^2+B_{12}hk+B_{13}hl+B_{23}kl)]$ with parameters:

	B_{11}	B_{22}	B_{33}	B_{12}	B_{13}	B_{23}
Pt	510(4)	195(2)	700(5)	3(7)	361(8)	−41(8)
Sb(1)	850(12)	234(4)	1136(16)	77(12)	−130(22)	104(13)
Sb(3)	932(14)	279(5)	1351(18)	303(13)	688(26)	365(15)

scattering factors for neutral Pt, Sb, O, N, and C atoms were taken from the International Tables for X-Ray Crystallography.[7] The hydrogen atoms could not be located in a difference Fourier synthesis computed at this stage. The maximum shift of parameters in the final cycle was $<0.1\,\sigma$. The absolute configuration of the complex cation was determined on the basis of the known configurations of the (+)-tartrate ion and (*R*)-propylenediamine molecule. The final atomic coordinates, which give the absolute structure of the crystal, are presented in Table 1, together with their temperature factors. The observed and calculated structure factors are preserved at the Chemical Society of Japan (Document Number 7627). All the calculations were performed on a FACOM 270-30 computer at Osaka City University. The programs used included a local version of the UNICS.[8]

Results and Discussion

The absolute configuration of the complex cation is shown in Fig. 1, while the crystal structure viewed along the b axis is presented in Fig. 2. The Pt atom has a square-planar coordination by 4 N atoms. The O(8)($1-x$, $-1/2+y$, $-z$) occupies the apical position of a square pyramid whose basal plane is defined by Pt, N(1), N(2), N(3), and N(4), the Pt···O(8) distance being 3.31 Å. Both of the asymmetric second-

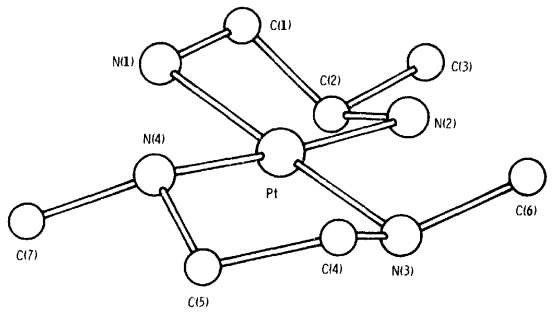

Fig. 1. The absolute configuration of the complex cation in $(+)_{350}$-[Pt(*R*-pn)(Me_2en)][$Sb_2(+)$-tart$_2$]·$2H_2O$.

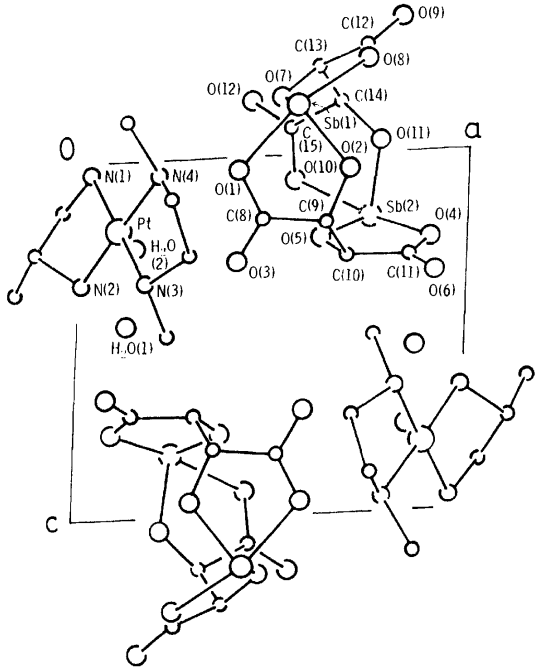

Fig. 2. The crystal structure viewed along the b axis.

ary N atoms of the Me_2en molecule have the *S* absolute configuration, and both the N–CH_3 groups are equatorial with respect to the 5-membered chelate ring (λ conformation) composed of the Me_2en ligand and the Pt atom.

In the solution of [Pt(*R*-pn)(Me_2en)]Cl_2 we prepared, the complex cation can exist in three isomers, (*R,R*), (*S,S*), and (*R,S*), where *R* or *S* denotes the absolute configuration of the asymmetric nitrogen center; the relative amounts of these isomers will be dependent upon the conformational energies of the respective isomers. The [$Sb_2(+)$-tart$_2$]$^{2-}$ anion chooses the (*S,S*) isomer to yield the least soluble diastereoisomer $(+)_{350}$-[Pt(*R*-pn)(Me_2en)][$Sb_2(+)$-tart$_2$]·$2H_2O$. The *S* isomer was also found in the least soluble diastereoisomer, $(+)_{350}$-[$Pt(NH_3)_2(Me_3en)$][$Sb_2(+)$-tart$_2$]·H_2O[9] (Me_3en: *N,N,N'*-trimethylethylenediamine). Thus, the dissymmetric [$Sb_2(+)$-tart$_2$]$^{2-}$ anion is likely to have a preference for the *S* and/or (*S,S*) isomer over the *R* and/or (*R,R*) isomer when the planar Pt(II) chelate of *N*-methyl-substituted ethylenediamine is given.

Table 2. Bond lengths (Å) and angles (°), with estimated standard deviations in parentheses

Pt-N(1)	2.06(2)	N(1)-Pt-N(2)	81.9(6)
Pt-N(2)	2.06(2)	N(3)-Pt-N(4)	84.2(7)
Pt-N(3)	2.04(2)	Pt-N(1)-C(1)	111(1)
Pt-N(4)	2.07(2)	Pt-N(2)-C(2)	109(1)
		Pt-N(3)-C(4)	108(1)
N(1)-C(1)	1.52(3)	Pt-N(3)-C(6)	116(2)
N(2)-C(2)	1.51(2)	Pt-N(4)-C(7)	114(1)
N(3)-C(4)	1.54(3)	Pt-N(4)-C(5)	109(1)
N(3)-C(6)	1.50(4)	C(4)-N(3)-C(6)	108(2)
N(4)-C(5)	1.48(3)	C(5)-N(4)-C(7)	113(2)
N(4)-C(7)	1.50(3)	N(1)-C(1)-C(2)	109(2)
		N(2)-C(2)-C(1)	106(1)
C(1)-C(2)	1.52(3)	N(2)-C(2)-C(3)	110(2)
C(2)-C(3)	1.53(3)	C(1)-C(2)-C(3)	111(2)
C(4)-C(5)	1.52(3)	N(3)-C(4)-C(5)	106(2)
		N(4)-C(5)-C(4)	109(2)

The bond lengths and angles are given in Table 2. The Pt–N bond lengths are in the range of 2.04—2.07 Å and seem slightly longer than the mean Pt–N bond length of 2.04 Å in [Pt en_2][Mo $O(H_2O)(CN)_4$]·$2H_2O$.[10] The coordination angle in the Pt—Me_2en chelate ring is 84.2°, while that in the Pt—(*R*)-pn chelate ring is 81.9°; the latter is smaller than the values reported in Refs. 9 and 10. The deviations of the atoms from the plane defined by 4 N atoms are as follows: Pt, −0.004; N(1), −0.007; N(2), 0.007; N(3), −0.007; N(4), 0.007; C(1), −0.045; C(2), 0.636; C(3), 0.402; C(4), −0.403; C(5), 0.324; C(6), −0.947; C(7), 0.893 Å. The equation of the plane is $-0.843X+0.512Y-0.168Z=-0.979$, where the coordinates are referred to the orthogonal axes, a, b, and c*. The geometry and dimensions of the [$Sb_2(+)$-tart$_2$]$^{2-}$ anion agree well with those in K_2[$Sb_2(+)$-tart$_2$]·$3H_2O$.[11]

The crystal consists of the [Pt(*R*-pn)(Me_2en)]$^{2+}$ cations, [$Sb_2(+)$-tart$_2$]$^{2-}$ anions, and water molecules. A [Pt(*R*-pn)(Me_2en)]$^{2+}$ cation (*x*, *y*, *z*) is surrounded trigonally by three [$Sb_2(+)$-tart$_2$]$^{2-}$ anions (*x*, *y*, *z*; $1-x$, $-1/2+y$, $-z$; $-1+x$, *y*, *z*). The possible

Table 3. Possible hydrogen bonds

Atoms A — H ··· B			Interatomic distances A···B	Interatomic distances H[b]···B	Positions[a] of A	Positions[a] of B
N(1)	H	O(2)	2.93(2)	1.95	1	2
N(1)	H	H_2O(2)	2.88(2)	1.97	1	3
N(2)	H	H_2O(1)	2.94(3)	1.93	1	4
N(4)	H	O(12)	2.95(2)	2.07	1	1
H_2O(1)		O(9)	2.71(3)		1	2
H_2O(1)		H_2O(2)	2.70(3)		1	6
H_2O(2)		O(1)	2.70(2)		1	1

a) The numerals refer to the following equivalent positions: 1 *x*, *y*, *z*; 2 $1-x$, $-1/2+y$, $-z$; 3 $-x$, $-1/2+y$, $-z$; 4 $-x$, $1/2+y$, $1-z$; 5 $-1+x$, *y*, *z*; 6 *x*, $-1+$y, *z*. b) The coordinates of the H atoms were calculated on the assumption that the N-H distance was 1.03Å.

hydrogen bonds are summarized in Table 3. Both primary amino groups take part in the formation of the N–H···O hydrogen bonds, while, with respect to the secondary amino groups, only one of the two participates in the N–H···O hydrogen bond, which is rather weak in view of the H···O distance (2.07 Å).

This research was supported by a Scientific Research Grant from the Ministry of Education. K. M. also wishes to acknowledge the financial support of the Matsunaga Science Foundation.

References

1) H. Ito, J. Fujita, and K. Saito, *Bull. Chem. Soc. Jpn.*, **40**, 2584 (1967).
2) D. A. Buckingham, L. G. Marzilli, and A. M. Sargeson, *J. Am. Chem. Soc.*, **91**, 5227 (1969).
3) J. B. Goddard and F. Basolo, *Inorg. Chem.*, **8**, 2223 (1969).
4) B. Bosnich and E. A. Sullivan, *Inorg. Chem.*, **14**, 2768 (1975).
5) G. L. Johnson, *Inorg. Synth.*, Vol. 8 (1966), p. 242.
6) J. Hornstra and B. Stubbe, PW1100 Data Processing Program, Philips Research Laboratories, Eindhoven, Holland.
7) "International Tables for X-Ray Crystallography," Vol. 3, Kynoch Press, Birmingham (1962), pp. 202, 215.
8) T. Sakurai, ed., "The Universal Crystallographic Computation Program System (UNICS)," The Crystallographic Society of Japan (1967).
9) K. Yokoho, K. Matsumoto, S. Ooi, and H. Kuroya, *Bull. Chem. Soc. Jpn.*, **49**, 1864 (1976).
10) P. R. Robinson, E. O. Schlemper, and R. K. Murmann, *Inorg. Chem.*, **14**, 2035 (1975).
11) M. E. Gress and R. A. Jacobson, *Inorg. Chim. Acta*, **8**, 209 (1974).

Stereoselectivities in Mixed Ligand Complexes of Cobalt(III), with L-Asparagine as a Ligand

Hideto TAKENAKA and Muraji SHIBATA

Department of Chemistry, Faculty of Science, Kanazawa University, Kanazawa 920

(Received March 26, 1976)

The [Co(ox)(L-aspNH$_2$)(en)] complex as well as the [Co(L-aspNH$_2$)$_{3-n}$(L-asp)$_n$]$^{n-}$ complexes (n=1,2) have been prepared and separated into their diastereoisomers by means of column chromatography. The structures of the isomers thus isolated have been characterized by their absorption, CD, and PMR spectra. Stereoselectivity in the [Co(ox)(L-aspNH$_2$)(en)] complex has been found for the *fac*-Λ and *mer*-Λ isomers, and those in the [Co(L-aspNH$_2$)$_{3-n}$(L-asp)$_n$]$^{n-}$ complexes, for the *fac*-Λ and *mer*-Λ isomers. These results have provided proof of the stereoselective effect due to the chelated L-asparaginate ion.

Metal complexes containing optically active ligands frequently exhibit stereoselective effects upon the formation of their diastereoisomers. In order to study such stereoselective formation, we previously examined the mixed amino acidato cobalt(III) complexes containing the L- or D-aspartate ion (L- or D-asp) as the primary ligand.[1-3] More recently we examined the complex consisting of the L-aspartate ion, the oxalate ion, and ethylenediamine, [Co(ox)(L-Hasp)(en)], in order to obtain proof of the stereoselective effect due to the chelated optically active aspartate ion.[4]

In the present work L-asparagine (L-HaspNH$_2$) was chosen as the primary ligand; a mixed complex [Co(ox)(L-aspNH$_2$)(en)] has been prepared in order to study the stereoselective influence due to the chelated L-asparaginate ion. Furthermore, a series of complexes, [Co(L-aspNH$_2$)$_{3-n}$(L-Hasp)$_n$] (n=1,2) have been prepared in order to study their stereochemistry and stereoselectivities. Related complexes, [Co(L-aspNH$_2$)$_3$] and [Co(L-aspNH$_2$)$_2$(D-Hasp)] have also been investigated.

Experimental

Preparation. Oxalato(L-asparaginato)ethylenediaminecobalt(III), [Co(ox)(L-aspNH$_2$)(en)]: The diastereoisomers of this complex were obtained much as were those of the corresponding L-aspartato complex.[4] The separation of the diastereoisomers was carried out by the use of a column containing 200—400 mesh Dowex 50WX8 resin in the Na-form (5.0×40.0 cm). During elution with water, six bands of non-charged species descended; the first and fourth bands, formed in very poor yields, were not the desired species. The other four bands corresponded to four isomers of the desired complex and were labeled A-1—A-4 according to the order of elution. These bands were collected in fractions, and each fraction was concentrated to a small volume with a rotary evaporator at *ca.* 35 °C. The concentrated solution was then kept in a refrigerator for a few days in order to crystallize the desired isomers. Recrystallization was performed from warm water (*ca.* 50 °C).

Bis(L-asparaginato)-L-hydrogenaspartato and L-Asparaginatobis(L-hydrogenaspartato)cobalt(III), [Co(L-aspNH$_2$)$_{3-n}$(L-Hasp)$_n$] (n=1, 2): To a green solution of tricarbonatocobaltate(III), (Co(NO$_3$)$_2$·6H$_2$O, 5.82 g, 0.02 mol scale) prepared by the usual method,[5] we added L-asparagine monohydrate (6.0 g, 0.04 mol); the mixture was then stirred at 40 °C for 2 h. To this solution we added L-aspartic acid (3.4 g, 0.025 mol) and activated charcoal (2.0 g), after which the mixture was stirred at *ca.* 50 °C for 1 h. The charcoal and a small amount of precipitates were removed by filtration, and then perchloric acid (60%) was added in order to neutralize the filtrate (pH *ca.* 7.0), whereupon the precipitation of KClO$_4$ and the evolution of CO$_2$ took place. The resulting solution was iced for a while and then filtered two or three times. A quarter of the final filtrate was diluted to *ca.* 1 l with water and then charged on a column of Sephadex QAE-A25 in the Cl-form (3.0×120.0 cm). After washing with water, the gradient elution with aqueous solutions of CaCl$_2$ prepared in 0.01 M and 0.03 M was employed at the rate of *ca.* 0.5 ml/min. The twelve bands completely separated were labeled L-1—L-12 according to the order of elution. The four bands from L-9 to L-12 corresponded to the *mer*-Λ, *mer*-Λ, *fac*-Λ, and *fac*-Λ isomers of the *tris*(L-aspartato)cobaltate(III) complex respectively, which had already been characterized.[6] The L-3 and L-4 bands were very poor in yield and were not the desired ones. The other six bands (L-1, L-2 and L-5—L-8) were collected in fractions, and every fraction was concentrated to a small volume with a rotary evaporator at *ca.* 35 °C. When the L-1 and L-6 concentrates were acidified with aqueous HCl (pH *ca.* 1.0), crude hydrogen compounds were obtained (Compounds L-1 and L-6). After the removal of the L-1 compound, the filtrate, which exhibited a minus CD sign in the first absorption-band region, was passed through a column containing Dowex 50 WX8 resin in the H-form (3.0×20.0 cm). The effluent was evaporated to a small volume, and ethanol was added until silky precipitates appeared. The precipitates (labeled L-1′) were collected by centrifuging. Similarly, after the removal of the L-6 compound the filtrate was also passed through a resin column in the H-form, and the effluent in the earlier stage, which exhibited a minus CD sign, was collected (L-6′). However, we failed to isolate crystals from that fraction because of the extremely poor yield. The L-2, L-5, L-7, and L-8 concentrates were also passed through the resin columns in the H-form. Each effluent was evaporated to a small volume, and a small amount of ethanol was added to precipitate each hydrogen compound. The desired compounds were obtained from the L-2, L-7, and L-8 fractions, but no compound was isolated from the L-5 fraction because of its great solubility and because it was obtained in the poorest yield. Recrystallization of each crude compound was performed by dissolving it in water containing a small amount of NaOH, and by then acidifying it with aqueous perchloric acid, and by finally adding a small amount of ethanol. Of these complexes, the L-6 complex was again recrystallized from a solution of pH *ca.* 4.0 in order to remove another isomer which still contaminated it.

Bis(L-asparaginato)-D-hydrogenaspartatocobalt(III), [Co(L-aspNH$_2$)$_2$(D-Hasp)]: This complex was prepared using D-aspartic acid in place of L-aspartic acid according to the procedure described above. Six bands of univalent anionic species separated on a Sephadex column were collected in

fractions (D-1—D-6). The D-4 and D-6 fractions were very poor in yield and were not the desired complexes. However, from the D-6 fraction a novel complex, *fac*(*N*)-[Co(L-aspNH$_2$)(D-asp)] in which both the ligands act as terdentate, was isolated.[7] The other four fractions (D-1—D-3 and D-5) were concentrated with a rotary evaporator at *ca.* 35 °C. Each of the D-1 and D-5 concentrates was passed through a column of Dowex 50 WX8 resin in the H-form (3.0×20.0 cm). The effluent was evaporated to a small volume. To the D-1 concentrate, methanol was added to give crystals of the desired hydrogen compound (D-1). The filtrate, which exhibited a minus CD sign, was further evaporated almost to dryness to obtain the residue (D-1′). The D-5 concentrate was stored in a refrigerator for a few days to obtain the hydrogen compound (D-5). The concentrated D-2 and D-3 fractions were acidified with aqueous HCl. The D-2 was then stored in a refrigerator for a few days to obtain the hydrogen compound (D-2), while the D-3 fraction, when treated similarly, gave the hydrogen compound (D-3) after the addition of ethanol. The recrystallization of each hydrogen compound was performed by dissolving it in an aqueous NaOH solution, by acidifying it with aqueous perchloric acid, and by then cooling it. As for the D-1′ compound, recrystallization was performed by dissolving it in a warm mixture of methanol and water and by then adding ethanol when cold.

Tris(L-asparaginato)cobalt(III), [*Co*(L-*asp*NH$_2$)$_3$]: The method used for the isolation of the four isomers of the [Co(L-Hasp)$_3$][6] complex was employed; to a green solution of tricarbonatocobaltate(III) (0.02 mol scale) we added L-asparagine monohydrate (9.0 g, 0.06 mol), and the solution was stirred at 60 °C for 2 h. Then the solution was adjusted to pH *ca.* 4.0 with aqueous HCl and stirred for a few min. The solution was again adjusted to pH *ca.* 8.0 with an aqueous solution of NaOH and then stirred at *ca.* 70 °C for 2 h. The resulting solution was kept in a refrigerator for a day in order to precipitate one of the desired isomers (*mer*-*Λ*). After the isomer had been collected by filtration, the filtrate was adsorbed on a column containing Dowex 50 WX8 resin in the Na-form (7.0×15.0 cm); two bands corresponding to non-charged species were collected in one fraction by elution with water. The fraction was concentrated to a small volume, and the concentrate was charged on another column in the Na-form (5.0×30.0 cm); after a while, two separate bands appeared. The fast-descending band was confirmed to be the *mer*-*Λ* isomer, and the slow-descending one, to be the *fac*-*Λ* species. Each band was collected in a fraction and concentrated to crystallize the isomer. Recrystallization was performed from warm water except for the *mer*-*Λ* isomer. The recrystallization of the *mer*-*Λ* isomer was performed by dissolving it in 30% perchloric acid and by then diluting it with water. The last isomer, *fac*-*Λ*, could not be isolated because of its poor yield.

Formation Ratios of the Isomers. Although asparagine is hydrolyzed to aspartic acid under certain conditions,[8] the hydrolysis was negligible in the reactions used in the present work. To every reaction mixture mentioned in *Preparation*, activated charcoal was added in order to favor the formation of an equilibrium mixture of diastereoisomers. From the spectral data on the fractions obtained by chromatographic separation, the formation ratios of the isomers were evaluated. For some isomers not isolated as crystals, the ε and the $|\Delta\varepsilon|$ values were assumed to be the same as those for the corresponding geometrical isomers isolated as crystals.

Measurement. The absorption (AB) spectra were measured with a Hitachi 323 Recording Spectrophotometer. The circular dichroism (CD) spectra were recorded on a JASCO Model ORD/UV-5 spectrophotometer with a CD attachment. The proton magnetic resonance (PMR) spectra were recorded on a JEOL JNM-PS-100 NMR spectrometer at *ca.* 23 °C, using D_2O as the solvent. The values of the chemical shifts were referred to internal sodium d_4-trimethylsilylpropionate (TMSP). The pH values of the solutions were measured with a Hitachi-Horiba M-7E pH meter. Sodium carbonate was used to adjust the pH values.

Results and Discussion

Characterization of Isomers. The [Co(ox)(L-aspNH$_2$)(en)] Complex: No work has been reported on cobalt(III) complexes containing asparagine as ligands except for the *tris*(asparaginato) complex.[9] The results of the elemental analyses for the isolated complexes are summarized in Table 1. The AB and CD spectral data in the d-d transition region are also given in Table 1. The *mer* or *fac* structure of each isomer was determined from the AB spectrum. The *Λ* or *Δ* configuration of the diastereomers was determined from the sign of the main CD peak in the first absorption-band region.

The PMR spectra of the four isomers of the [Co(ox)(L-aspNH$_2$)(en)] complex are shown in Fig. 1. Two protons of the CH$_2$ group and one proton of the CH group of L-aspNH$_2$ correspond to the AB and X portions respectively in an ABX system. The multiplet-like signals at 3.8—4.0 ppm are due to the CH moiety (X proton), and the separation width of the complicated signals is represented by the expression of $(J_{AX}+J_{BX})$.[10] Moreover, since the coupling constant of the vicinal protons, the J_{vic} value, depends on the dihedral angle,[11] the value of $(J_{AX}+J_{BX})/2$ gives information about the orientation of the side-chain of the chelated asparaginate ion, the X proton of the CH moiety being spatially fixed in the chelated state. The $(J_{AX}+J_{BX})/2$ values observed for the four isomers are: *mer*-*Λ*, 4.0 Hz; *mer*-*Δ*, 6.2 Hz; *fac*-*Λ*, 4.0 Hz; *fac*-*Δ*, 6.0 Hz. The corresponding value for the terdentate

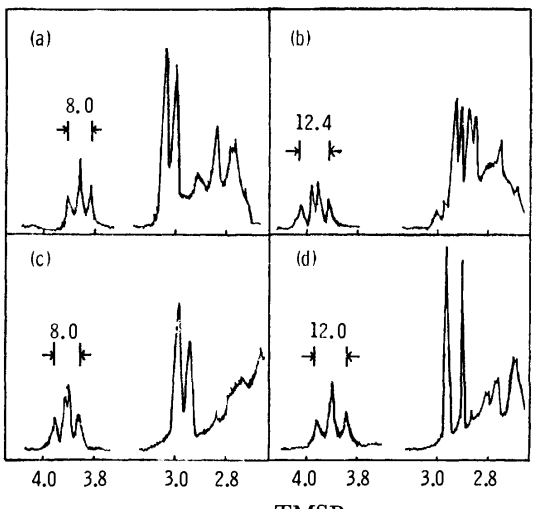

Fig. 1. PMR spectra of [Co(ox)(L-aspNH$_2$)(en)] in D_2O.
(a): *mer*-*Λ* Isomer, (b): *mer*-*Δ* isomer,
(c): *fac*-*Λ* isomer, (d): *fac*-*Δ* isomer.

TABLE 1. ELEMENTAL ANALYSES, ABSORPTION[a] AND CD[a] SPECTRAL DATA

Label	Complex	Elemental anal, %[b]			Band I		Band II		CD	
		C	H	N	$10^{-3}\tilde{\nu}_{max}$ cm^{-1}	ε_{max}	$10^{-3}\tilde{\nu}_{max}$ cm^{-1}	ε_{max}	$10^{-3}\tilde{\nu}_{max}$ cm^{-1}	$\Delta\varepsilon_{max}$
A-1	*mer*-*Λ*-[Co(ox)(L-aspNH$_2$)(en)]·H$_2$O	27.28 (26.96)	5.24 (4.81)	15.94 (15.73)	19.2	100	26.8	179	17.8 21.0	−2.07 −1.50
A-2	*mer*-*Λ*-[Co(ox)(L-aspNH$_2$)(en)]·H$_2$O	27.31 (26.96)	5.03 (4.81)	16.00 (15.73)	19.2	99	26.9	184	18.0 20.4	+1.97 +1.40
A-3	*fac*-*Λ*-[Co(ox)(L-aspNH$_2$)(en)]·2.5H$_2$O	25.31 (25.06)	5.41 (5.26)	14.50 (14.62)	19.2	152	27.2	170	18.9	+4.25
A-4	*fac*-*Λ*-[Co(ox)(L-aspNH$_2$)(en)]·0.5H$_2$O	27.98 (27.66)	4.84 (4.65)	15.83 (16.14)	19.2	149	27.0	162	19.0	−3.85
	mer-*Λ*-[Co(L-aspNH$_2$)$_3$]·1.5H$_2$O	29.86 (30.07)	5.35 (5.05)	18.06 (17.53)	18.5	106	26.8	159	18.8	+3.77
	mer-*Λ*-[Co(L-aspNH$_2$)$_3$]·3.5H$_2$O	28.06 (27.97)	5.87 (5.48)	15.98 (16.30)	18.4	110	26.7	166	18.6	−3.07
	fac-*Λ*-[Co(L-aspNH$_2$)$_3$]·2H$_2$O	29.47 (29.52)	5.62 (5.16)	17.31 (17.20)	19.3	204	26.7	154	19.1	−2.89
L-1	*mer*-*Λ*-[Co(L-aspNH$_2$)$_2$(L-Hasp)]·3H$_2$O	28.55 (28.41)	4.85 (5.17)	14.10 (13.81)	18.5	117	26.9	184	19.0	+3.41
L-1′	*mer*-*Λ*-[Co(L-aspNH$_2$)$_2$(L-Hasp)]·3H$_2$O	28.27 (28.41)	4.85 (5.17)	13.98 (13.81)	18.5	100	26.9	148	18.6	−2.10
L-2	*fac*-*Λ*-[Co(L-aspNH$_2$)$_2$(L-Hasp)]·2H$_2$O	30.30 (30.52)	4.32 (4.61)	11.66 (11.86)	19.4	197	26.7	165	19.3	−2.51
L-6	*mer*$_1$-*Λ*-[Co(L-aspNH$_2$)(L-Hasp)$_2$]·2H$_2$O	29.49 (29.40)	4.27 (4.73)	11.75 (11.42)	18.5	109	27.0	165	19.3	+3.12
L-7	*mer*$_2$-*Λ*-[Co(L-aspNH$_2$)(L-Hasp)$_2$]·4H$_2$O	26.95 (26.93)	5.46 (5.18)	10.67 (10.62)	18.5	113	27.0	179	19.3	+3.36
L-8	*fac*-*Λ*-[Co(L-aspNH$_2$)(L-Hasp)$_2$]	31.43 (31.73)	4.18 (4.22)	12.70 (12.33)	19.4	201	26.8	154	19.2	−2.76
D-1	*mer*$_1$-*Λ*-[Co(L-aspNH$_2$)$_2$(D-Hasp)]·5H$_2$O	26.14 (26.53)	5.04 (5.57)	13.01 (12.89)	18.4	115	26.9	181	18.7	+3.11
D-1′	*mer*-*Λ*-[Co(L-aspNH$_2$)$_2$(D-Hasp)]·4.5H$_2$O	26.81 (26.97)	4.82 (5.47)	13.16 (13.11)	18.3	107	26.9	168	18.6	−2.68
D-2	*mer*$_2$-*Λ*-[Co(L-aspNH$_2$)$_2$(D-Hasp)]·2H$_2$O	29.52 (29.46)	5.53 (4.95)	14.22 (14.31)	18.5	107	26.7	154	18.8	+3.29
D-3	*fac*-*Λ*-[Co(L-aspNH$_2$)$_2$(D-Hasp)]·2.5H$_2$O	29.10 (28.91)	5.37 (5.06)	13.80 (14.06)	19.2	207	26.6	174	18.7	+2.74
D-5	*fac*-*Λ*-[Co(L-aspNH$_2$)$_2$(D-Hasp)]·2.5H$_2$O	28.93 (28.91)	5.47 (5.06)	13.77 (14.06)	19.2	207	26.6	186	18.7	−2.56

a) Measured in alkaline solutions except for *mer*-*Λ*-[Co(L-aspNH$_2$)$_3$], which was measured in 60% HClO$_4$. b) ( ): Calcd.

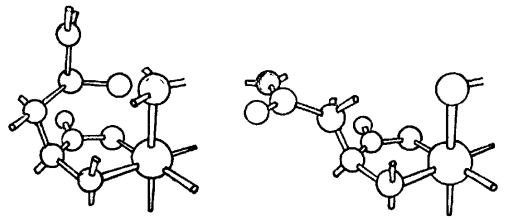

Fig. 2. Orientations of chelated L-aspNH$_2$ side-chain.

L-aspNH$_2$ ion in the [Co(L-aspNH$_2$)(D-asp)] complex is known to be 4.0 Hz.[7] This suggests that, in both the *mer*-*Λ* and *fac*-*Λ* isomers, the side-chain of the chelated L-aspNH$_2$ turns its *β*-acid amide group toward the apical site occupied by an NH$_2$ group of the chelated en, and that, in both the *mer*-*Λ* and *fac*-*Λ* isomers, the side-chain is far from the apical site occupied by an O group in the chelated $C_2O_4^{2-}$ ion (Fig. 2). Thus, these different orientations of the side-chain of chelated L-aspNH$_2$ are caused by the different inter-ligand interactions.

The [Co(L-aspNH$_2$)$_{3-n}$(L-Hasp)$_n$] Complexes: In a mixed tris-type complex with two kinds of amino acidate ion, three *mer* isomers can exist, each of them consisting of a pair of diastereomeric isomers: *cis*(*N*)-*cis*(*O*)-*Δ* and -*Λ*, *cis*(*N*)*trans*(*O*)-*Δ* and -*Λ*, and *trans*(*N*)-*cis*(*O*)-*Δ* and -*Λ*, according to the arrangements of two identical amino acidate ions. Previously, we characterized three isomers of *mer*-*Δ*-[Co(L-pro)(D-Hasp)$_2$] and one isomer of *mer*-*Λ*-[Co(L-pro)(L-Hasp)$_2$] on the basis of the PMR spectral data, the formation ratios, and an examination of the molecular models.[3] Yoneda *et al.*[12] characterized two isomers of *mer*-*Λ*-[Co(gly)$_2$(L-Hglu)][13] on the basis of a semiempirical consideration of the PMR spectrum.

Now, let us attempt to characterize two isomers of *mer*-*Λ*-[Co(L-aspNH$_2$)(L-Hasp)$_2$] on the basis of the PMR spectra. When we pay attention to three methine protons, namely, one proton for the chelated L-aspNH$_2$ ion and two protons for the two chelated L-asp ions, the following four criteria help in the characterization of the *mer*-*Λ* isomers concerned:

1. When an $NH_2CH(R)COO^-$ ion is chelating through a five-membered ring, the methine proton (*α*-hydrogen) shows no chemical shift in the range of pH 6—9.[14]

2. The methine proton adjacent to the coordinated N atom resonates at a higher magnetic field when the O atom occupies the site *trans* to the N atom than when the N atom occupies the same site.[15]

3. When the methine groups of both the chelating L-aspNH$_2$ and L-asp are present in the same types of chemical and magnetical environments, the methine proton of the L-aspNH$_2$ always resonates in a field lower by 0.10—0.12 ppm than that of the L-asp. This was confirmed by comparing the PMR spectra of complexes of the same type (Table 2).

4. The $(J_{AX}+J_{BX})/2$ values of the chelated L-aspNH$_2$ and L-asp give information about the orientations of the side-chains of both ligands.[3,4,16]

We first assign the signals of the methine protons in the spectrum of the *mer*-*Λ*-[Co(L-Hasp)$_3$] complex on the basis of the above criteria; the spectrum and the structure are shown in Figs. 3 and 4 respectively. The signals of the methine protons appear at 3.55, 3.80, and 3.98 ppm. From the second criterion, the two protons at B and C in Fig. 4 are expected to resonate in lower fields than that at A. Thus, the signals at 3.55 ppm are assignable to the methine proton at the A position. From the fourth criterion, the signals centered at 3.80 ppm with the value of $(J_{AX}+J_{BX})/2=$ 3.5 Hz, and those at 3.98 ppm with the value of $(J_{AX}+J_{BX})/2=5.8$ Hz, are assignable to the methine protons situated in the B and C positions respectively. When the L-asp ion chelating at the A position in Fig. 4 is replaced by a L-aspNH$_2$ ion to give *mer*-*Λ*-*trans*(*N*)*cis*(*O*) geometry, the chemical shift of the methine proton of the chelated L-aspNH$_2$ can be expected to be *ca.* 3.65—3.67 ppm from the third criterion, and the

Table 2. PMR Spectral data[a]

Complex	-CH (ppm)		-CH$_2$ (ppm)		$(J_{AX}+J_{BX})/2$ (Hz)		pD in D_2O soln
	aspNH$_2$	asp	aspNH$_2$	asp	aspNH$_2$	asp	
mer-*Λ*-[Co(ox)(L-aspNH$_2$)(en)]	3.86		3.04		4.0		5.0
mer-*Λ*-[Co(ox)(L-Hasp)(en)]		3.72		2.85		3.7	4.8
mer-*Λ*-[Co(ox)(L-aspNH$_2$)(en)]	3.98		2.90		6.2		6.4
mer-*Λ*-[Co(ox)(L-Hasp)(en)]		3.86		2.80		5.0	5.1
fac-*Λ*-[Co(ox)(L-aspNH$_2$)(en)]	3.90		2.96		4.0		6.5
fac-*Λ*-[Co(ox)(L-Hasp)(en)]		3.72		2.78		3.8	4.3
fac-*Λ*-[Co(ox)(L-aspNH$_2$)(en)]	3.94		2.90		6.0		5.2
fac-*Λ*-[Co(ox)(L-Hasp)(en)]		3.84		2.81		6.0	5.3
fac-*Λ*-[Co(L-aspNH$_2$)$_3$]	3.75		2.97		3.9		8.2[b]
fac-*Λ*-[Co(L-Hasp)$_3$]		3.61		2.78		3.9	9.0[b]
fac-*Λ*-[Co(L-aspNH$_2$)$_2$(L-Hasp)]	3.84 3.86		3.06 3.06		4.0 4.0		8.6[b]
		3.73		2.87		3.8	
fac-*Λ*-[Co(L-aspNH$_2$)(L-Hasp)$_2$]	3.78		3.00		4.0		
		3.66 3.67		2.82 2.82		3.6 3.6	8.8[b]

a) Measured in D_2O. b) Adjusted with Na_2CO_3.

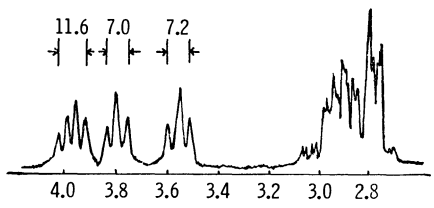

Fig. 3. PMR spectrum of *mer*-*Λ*-[Co(L-Hasp)$_3$] in D_2O (pD 9.1).

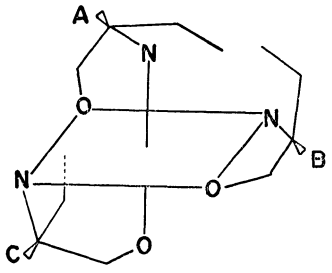

Fig. 4. Structure of *mer*-*Λ*-[Co(L-Hasp)$_3$].

chemical shifts of the two methine protons of the two chelated L-asp ions at the B and C positions can be expected to appear at *ca.* 3.80 ppm and *ca.* 3.98 ppm respectively from a comparison with the known signals for the *mer*-*Λ*-[Co(L-Hasp)$_3$] complex. By analogy, the chemical shifts of the methine protons of the chelating L-aspNH$_2$ and L-asp ions for the *mer*-*Λ*-[Co(L-aspNH$_2$)-(L-Hasp)$_2$] complex are expected to be *ca.* 3.55 ppm (L-asp at A), 3.90—3.92 ppm (L-aspNH$_2$ at B), and 3.80 ppm (L-asp at C) for the isomer of *cis*(*N*)*cis*(*O*) geometry, and *ca.* 3.55 ppm (L-asp at A), 3.80 ppm (L-asp at B), and 4.08—4.10 ppm (L-aspNH$_2$ at C) for the isomer of *cis*(*N*)*trans*(*O*) geometry. The spectra of the L-6 and L-7 isomers are partially shown in Fig. 5, as is that of the crude L-6 complex. From the values predicted above, the L-6 is identified as the *cis*(*N*)*cis*(*O*) isomer and the L-7, as the *trans*(*N*)*cis*(*O*) isomer. The crude L-6 complex shows a more complicated spectrum, indicating an overlapping of the signals arising from the *cis*(*N*)*cis*(*O*) isomer and contaminating *cis*(*N*)*trans*(*O*) isomer. The relative chemical shifts of methine protons for the present *mer*-*Λ* isomers and the *mer*-*Λ*-[Co(L-Hasp)$_3$] complex are illustrated in Fig. 6.

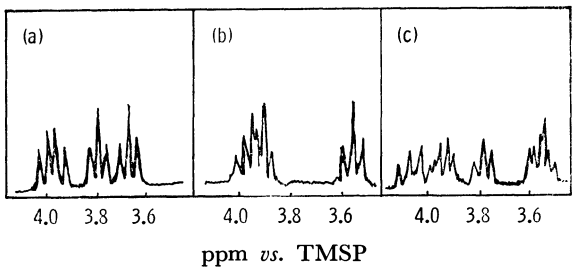

Fig. 5. PMR spectra of *mer*-*Λ*-[Co(L-aspNH$_2$)(L-Hasp)$_2$] in D_2O.
(a): L-7 Crystals (pD 9.3), (b): L-6 crystals (pD 8.3), (c): crude L-6 crystals (pD 9.5).

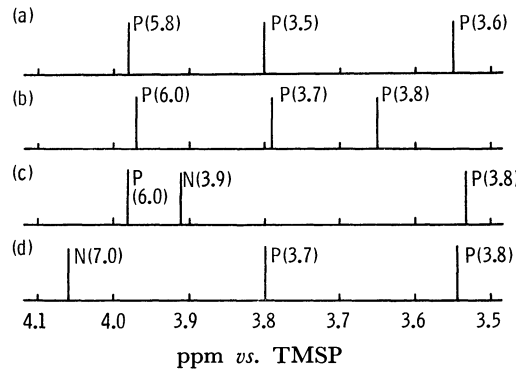

Fig. 6. Relative chemical shifts of methine protons in *mer*-*Λ*-[Co(L-aspNH$_2$)(L-Hasp)$_2$].
(a): Reference; *mer*-*Λ*-[Co(L-Hasp)$_3$], (b): *cis*(*O*)-*trans*(*N*), (c): *cis*(*O*)*cis*(*N*), (d): *cis*(*N*)*trans*(*O*).
P: L-Hasp, N: L-aspNH$_2$, ( ): $(J_{AX}+J_{BX})/2$, Hz.

Stereoselectivity. The [Co(ox)(L-aspNH$_2$)(en)] Complex: The percentage distribution of all the isomers for the [Co(ox)(L-aspNH$_2$)(en)] complex are given in Table 3, in which the values for related complexes[4] are also included for comparison. The percentage compositions of the diastereomeric pairs are summarized in Table 4. From Table 3 it is seen that the *mer*-(*Λ*+*Δ*) isomer existing in the present L-asparaginato complex and also those in the other complexes are more abundant than the *fac*(*Λ*+*Δ*) isomer, and that the abundances in the *mer* isomers are roughly 80%. Since the statistical weight of the L-amino acidate (L-am) ion upon chelation in such a reaction system is the same between the formation of the *mer* isomer and that of the *fac* isomer, the above fact suggests that the selective formation of the *mer* isomer in a [Co(ox)(L-am)(en)]-type complex takes place irrespective of the kind of L-am ligand. Table 4 shows that a significant stereoselectivity of over 70% is found in both the *mer*-*Λ* and *fac*-*Λ* isomers for the present L-aspNH$_2$ complex, while the selectivity for the L-asp complex is over 80%. The comparison of the stereoselectivities among the [Co(ox)(L-am)(en)]-type complexes suggests that the stereoselective formation of an isomer relates to the side-chain length and the existence of CO group in the side-chain of the chelated L-am ion. The marked stereoselectivity in the L-asp complex has been explained as a combined result of an interaction of the β-COO^- group in the chelated L-asp ion with an NH_2 group of the chelated en, which is favorable for the stereoselectivity, and an electrostatic repulsion of the β-COO^- with an O atom of the chelated $C_2O_4^{2-}$ ion, which is disadvantageous in the stereo-

Table 3. Percentage compositions of reaction mixtures

	mer-*Λ*	*mer*-*Λ*	*fac*-*Λ*	*fac*-*Λ*
[Co(ox)(L-aspNH$_2$)(en)]	62	19	14	5
[Co(ox)(L-Hasp)(en)][a)]	72	11	14	3
[Co(ox)(L-Hglu)(en)][a)]	48	32	11	9
[Co(ox)(L-leu)(en)][a)]	49	35	8	8
[Co(ox)(gly)(en)][a)]	42	42	8	8

a) Ref. 4.

Table 4. Percentage compositions of diastereoisomers

	[Co(ox)(L-aspNH$_2$)(en)]	[Co(ox)(L-Hasp)(en)][a)]	[Co(ox)(L-Hglu)(en)][a)]	[Co(ox)(L-leu)(en)][a)]	[Co(ox)(gly)(en)][a)]
mer-Λ	77	87	60	58	50
fac-Λ	74	82	55	51	50

a) Ref. 4.

selective formation.[4] For the stereoselectivity in the [Co(ox)(L-aspNH$_2$)(en)] complex, the following explanation can be offered; provided that the stereoselective formation of an isomer depends on the interaction of the CO group rather than on that of the NH_2 group of the free β-$CONH_2$ group with the adjacent group or donor atom in an apical position, for the *mer-Λ* or *fac-Λ* isomer, in which the apical position is occupied by an NH_2 group of the chelated en, the CO group tends to make a hydrogen bond with the NH_2 group to give favorable interaction. On the other hand, for the *mer-Λ* or *fac-Λ* isomer, in which the apical position is occupied by an O atom in the chelated $C_2O_4^{2-}$, the CO group tends to repel the O atom. This explanation is supported by the information about the orientation of the β-acid amide group mentioned before.

The [Co(L-aspNH$_2$)$_{3-n}$(L-asp)$_n$]$^{n-}$ Complexes: The results of the formation ratios through all the isomers of the [Co(L-aspNH$_2$)$_{3-n}$(L-asp)$_n$]$^{n-}$ complexes are given in Table 5. The minor component in each fraction in the chromatographic separations is evaluated as below 10% on the basis of the spectral data. The marked stereoselectivity was found in either the asparaginato complex (n=2) or the *bis*(asparaginato) complex (n=1); in either complex, the selective formation of the *Λ* isomer was found for the *fac* isomer, and that of the *Λ* isomer for the *mer* one. The stereoselectivities found in these complexes can be understood as the combined effects due to the two kinds of ligands. When a chelated L-asp ion is replaced by a D-asp ion to give the [Co(L-aspNH$_2$)$_2$(D-asp)]$^-$ complex, the formation ratio and the degree of the stereoselectivity are expected to vary from those of the [Co(L-aspNH$_2$)$_2$(L-asp)]$^-$ complex. Table 6 shows the results for the [Co(L-aspNH$_2$)$_2$(D-asp)]$^-$ complex. The fact that no appreciable selectivity is found in the [Co(L-aspNH$_2$)$_2$(D-asp)]$^-$ complex can be understood as the net result arising from the opposite stereoselective effects due to the chelated L-aspNH$_2$ and D-asp.

Table 5. Formation ratios and stereoselectivities in [Co(L-aspNH$_2$)$_{3-n}$(L-asp)$_n$]$^{n-}$ (n=1, 2, 3)

n	Label	Isomer	Ratio		Stereoselectivity
1	L-1	*mer-Λ*	11.5	..... *mer-Λ*	82%
	L-1′	*mer-Λ*	2.5		
	L-2	*fac-Λ*	16.3	*fac-Λ*	~95%
2	L-5	*mer-Λ*	0.4		
	L-6	*mer-Λ*	13.0	..... *mer-Λ*	83%
	L-6′	*mer-Λ*	3.3		
	L-7	*mer-Λ*	5.1		
	L-8	*fac-Λ*	39.8	*fac-Λ*	~100%
3	L-9	*mer-Λ*	1.5	..... *mer-Λ*	66%
	L-10	*mer-Λ*	2.9		
	L-11	*fac-Λ*	0.2	..... *fac-Λ*	95%
	L-12	*fac-Λ*	3.5		

Table 6. Formation ratios and stereoselectivities in [Co(L-aspNH$_2$)$_2$(D-asp)]$^-$

Label	Isomer	Ratio		Stereoselectivity
D-1	*mer-Λ*	21		
D-1′	*mer-Λ*	33	..... *mer-Λ*	58%
D-2	*mer-Λ*	21		
D-3	*fac-Λ*	7		
D-5	*fac-Λ*	18	..... *fac-Λ*	7%

References

1) K. Kawasaki, J. Yoshii, and M. Shibata, *Bull. Chem. Soc. Jpn.*, **43**, 819 (1970).
2) T. Matsuda, T. Okumoto, and M. Shibata, *Bull. Chem. Soc. Jpn.*, **45**, 802 (1972).
3) T. Matsuda and M. Shibata, *Bull. Chem. Soc. Jpn.*, **46**, 3104 (1973).
4) M. Takeuchi and M. Shibata, *Bull. Chem. Soc. Jpn.*, **47**, 2797 (1974).
5) M. Shibata, *Nippon Kagaku Zasshi*, **87**, 771 (1966).
6) M. Shibata, H. Nishikawa, and K. Hosaka, *Bull. Chem. Soc. Jpn.*, **40**, 236 (1967).
7) H. Takenaka and M. Shibata, *Chem. Lett.*, sumbitted for publication.
8) F. C. Steward and J. F. Tompson, *Nature*, **169**, 739 (1952).
9) P. Spacu, C. Gheorghice, M. Brezeanu, and S. Popescu, *Rev. Chim. Acad. Republ. Populaire Roum.*, **3**, 127 (1958).
10) J. W. Emsley, J. Feeney, and L. H. Sutcliffe, "High Resolution Nuclear Magnetic Resonance Spectroscopy," Pergamon Press, London (1965), p. 361.
11) M. Karplus, *J. Am. Chem. Soc.*, **85**, 2870 (1963).
12) H. Yoneda, U. Sakaguchi, and Y. Nakashima, *Bull. Chem. Soc. Jpn.*, **48**, 209 (1975).
13) K. Kawasaki and M. Shibata, *Bull. Chem. Soc. Jpn.*, **45**, 3100 (1972).
14) I. Legg and J. Steele, *Inorg. Chem.*, **10**, 2177 (1971).
15) M. Watabe, K. Onuki, and S. Yoshikawa, *Bull. Chem. Soc. Jpn.*, **48**, 687 (1975).
16) H. Ishizuka, T. Yamamoto, Y. Arata, and S. Fujiwara, *Bull. Chem. Soc. Jpn.*, **46**, 468 (1973).

The Extraction Spectrophotometric Determination of Palladium with Monothiodibenzoylmethane

B. N. PRABHU and S. M. KHOPKAR

Department of Chemistry, Indian Institute of Technology, Bombay 400076, India

(Received July 14, 1975)

Monothiodibenzoylmethane (HSDBM) was used for the quantitative extraction of palladium. It was extracted at pH 3.5—6.5, with 0.001 M HSDBM in benzene, as an orange-red colored complex and measured spectrophotometrically at 470 nm. Beer's law was valid in the concentration range of 0.6 to 3.6 μg of palladium per ml. The complex was stable for at least 144 h. Ten milliliters of 0.001 M HSDBM in benzene was adequate for quantitative extraction of palladium. The optimum period of equilibration was 10 min. It was possible to extract palladium in the presence of a large number of elements.

Monothiodibenzoylmethane (3-mercapto-1,3-diphenyl-2-propen-1-one) HSDBM, a monothio-substituted derivative of dibenzoylmethane was used for the extraction and photometric determination of several transition elements.[1] Further studies revealed that it is possible to extract palladium(II) at pH 3.5—6.5 as the orange-red colored complex and determine photometrically at 470 nm.

Amongst β-diketones, acetylacetone[3] was used for the extraction of palladium at pH 8.0. The extractions with benzoylacetone were complete between the pH range of 1.2 to 10.[3] The extractions with dibenzoylmethane were not only incomplete, but also the rate of equilibration was slow. With 2-thenoyltrifluoroacetone (HTTA), palladium was extracted as an orange-yellow complex, in methyl propyl ketone.[4] It was successfully separated from platinum in HTTA-butanol.[5] Monothiothenoyltrifluoroacetone[6,7] was used for the extractive spectrophotometric determination with some advantages. Recent methods for the solvent extraction[8] and photometric determination[9] are summarized in recent monographs.

The method proposed in this paper is simple, rapid and selective and is applicable at tracer concentrations; the special feature being, palladium can be separated from other noble metals by extraction.

Experimental

Apparatus and Reagents. Spektromom-204 spectrophotometer with matched 10 mm quartz cells. Type FEK-57 photoelectric filter photometer with 10 mm corex glass cuvettes. Cambridge pH-meter with glass and calomel electrodes. Wrist action flask shaker. Monothiodibenzoylmethane was prepared from dibenzoylmethane (Koch-light, England), by the procedure of Chaston *et al.*[10] About 0.001 M HSDBM in benzene was used. The reagent may be preferably preserved in the refrigerator.

A stock solution of palladium was prepared by dissolving 1.002 g of palladium chloride (Johnson Matthey and Co., London) in 500 ml distilled water containing 5% concentrated hydrochloric acid. The solution was standardized gravimetrically with dimethylglyoxime.[11] It contained 1.2 mg/ml of palladium. The dilute solution containing 6 μg/ml of palladium was prepared by appropriate dilution.

General Procedure. An aliquot of solution containing palladium (30 μg) was taken. The pH of the solution was adjusted to 5.0 on pH meter with 0.01 M hydrochloric acid or 0.01 M ammonium hydroxide. The total volume of the aqueous phase was made up to 25 ml. The solution was transferred to a separatory funnel. Ten ml of 0.001 M HSDBM in benzene was added to it. Then the solution was shaken on the wrist action flask shaker for about 10 min. The layers were allowed to settle and separate. The aqueous phase was carefully withdrawn. The orange-red colored palladium complex in the organic phase was transferred into a 10 ml volumetric flask. The absorbance of the complex was measured, at 470 nm, against the reagent blank. The amount of the palladium was computed from calibration curve.

Results and Discussion

Absorption Spectra. The absorption spectra of palladium-SDBM complex ($Pd=2.819\times10^{-5}$ M), against the reagent blank (A), is shown in Fig. 1. The spectrum of the reagent blank against benzene (B) is also shown. The complex showed maximum absorbance at 470 nm; with minimum absorbance for the reagent blank. Therefore this wavelength was selected for all measurements. The molar absorptivity at 470 nm was 8.868×10^3. The sensitivity (Sandell's definition) was 0.012 μg/ml/cm^2.

Extraction as the Function of pH. The extraction of palladium was carried out between the pH region of 1.0—10.0, with 10 ml of 0.001 M HSDBM in benzene. The results (Fig. 2) showed that the $pH_{1/2}$ was 3.0. The extraction was quantitative in the pH region of 3.5 to 6.5. The extraction was incomplete below and above this region. Hence pH 5.0 was used for all extractions.

Beer's Law. Different amounts of palladium, from 6 μg to 60 μg, were taken and were extracted with 10 ml of 0.001 M HSDBM in benzene. The absorbance of the complexes was measured at 460, 470, and 480 nm. The system conformed to Beer's law in the concentration range of 0.6 to 3.6 μg of palladium per ml at 470 nm. It is possible to expand this range provided, we use high reagent concentration.

Effect of Reagent Concentration. With all other factors kept constant, palladium was extracted with varying volumes and varying concentration of the reagent (Table 1). The results showed that 10 ml of 0.001 M HSDBM in benzene was adequate for quantitative extraction. The extraction was not quantitative at lower reagent concentration while at higher reagent concentration, there was negligible increase in extraction. The variation in volume of 0.001 M HSDBM showed that 10 ml of the reagent was ade-

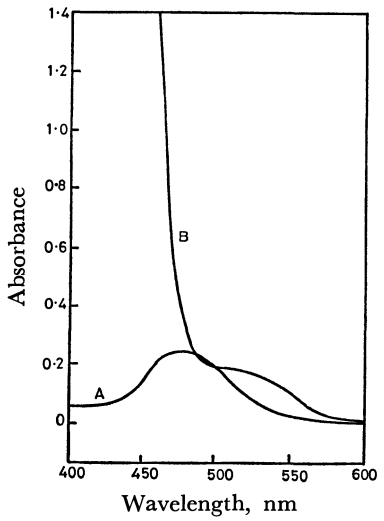

Fig. 1. Absorption spectra of palladium-SDBM complex.
(A): Pd(II)-SDBM complex *vs.* reagent blank. Pd(II)=2.818×10^{-5} M at pH=5.0.
(B): Reagent blank *vs.* benzene at pH=5.0, HSDBM=1.0×10^{-3} M in benzene.

Table 1. Effect of reagent concentration
Pd=30 μg; pH=5.0

Concentration of the reagent ($M\times10^{-3}$)	Amount added ml	Absorbance at 470 nm
0.25	10	0.090
0.50	10	0.180
0.75	10	0.240
1.00	10	0.250
1.25	10	0.250
1.50	10	0.250
2.00	10	0.250
2.50	10	0.250
1.00	2.5	0.120
1.00	5.0	0.150
1.00	7.5	0.195
1.00	15	0.250
1.00	20	0.250
1.00	25	0.250

quate for quantitative extraction of palladium. However, for very high metal ion concentration, it is preferable to use high reagent concentration.

Effect of Salting-out Agents. With all other conditions same, the chlorides of lithium, sodium, potassium, ammonium, magnesium and calcium in the concentration range of 0.5—5 M were used as salting-out agents. The results showed that none of them were effective, possibly on account of high ionic concentration. In few cases, the extraction substantially decreased due to competitive action of chloride ion with reagent anion for central metal atom to form complex. Similar phenomenon was also observed by previous workers.[6]

Stability of the Color of the Complex. The absorbance of the complex was measured at elapsed intervals

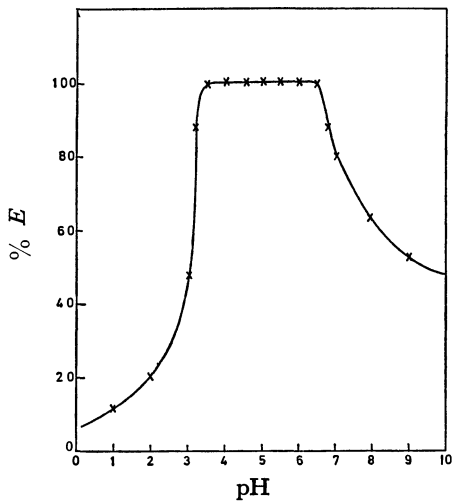

Fig. 2. Extraction as function of pH.

Table 2. Effect of diverse ions
Pd=30 μg; pH=5.0; SDBM=1×10^{-3} M in benzene

Tolerance limit (μg)	Foreign ion present
5.0×10^4	Ca^{2+}, Mg^{2+}, Na^+, K^+, Li^+, NO_3^-, SO_4^{2-}.
2.5×10^4	Sr^{2+}, $tart^{3-}$.
1.0×10^4	Tl^+, UO_2^{2+}, Cs^+, Rb^+, F^-, Cit^{3-}, thiourea, CrO_4^{2-}, $Mo_7O_{24}^{6-}$, ReO_4^-, SeO_3^{2-}, VO_3^-.
0.5×10^4	Ge^{4+}, Ba^{2+}, Be^{2+}, Br^-, AsO_3^-.
0.3×10^4	Sb^{3+}, Os^{8+}, Rh^{3+}, Pt^{4+}, Al^{3+}, Th^{4+}, Zr^{4+}, Y^{3+}, Mn^{2+}, Ga^{3+}, Ce^{4+}, SCN^-, TeO_3^{2-}, WO_4^{2-}.
0.1×10^4	Ti^{4+}, Bi^{3+}.
0.05×10^4	Pb^{2+}, Cd^{2+}, Cr^{3+}, Co^{2+}, Ru^{3+}, Ir^{4+}, Zn^{2+}, In^{3+}.
None	Hg^{2+}, Cu^{2+}, Au^{3+}, Fe^{3+}, Ni^{2+}, CN^-, $EDTA^{4-}$, $S_2O_3^{2-}$, mal^{2-}, $C_2O_4^{2-}$.

of 0, 1, 2, 4, 8, 16, 24, 48, 72, 96, 120, and 144 h. The complex was stable for at least 144 h. In other methods complex was not stable for such long duration.[12]

Period of Equilibration. The period of shaking was varied from 2.5 to 30 min. The extraction was incomplete up to a shaking period of 8 min, but was quantitative in 10 min of equilibration. This is more practicable in contrast to the method proposed by earlier workers.[3]

Composition of the Extractable Species. An attempt was made to ascertain the composition of the extractable species from the $\log C_{HSDBM}$ *vs.* $\log D$ plot.[13] The concentration of the reagent was varied from 1.0×10^{-4} to 5.0×10^{-4} M. The slope was 1.73, indicating that a di-solvated species is present. Therefore the composition of the extractable species is $Pd(SDBM)_2$.

Effect of Diverse Ions. The effect of several ions on the extraction behavior of palladium was studied (Table 2). The tolerance limit was calculated as described earlier.[1] The results showed that the alkali, alkaline earth metals were tolerated in high ratios (>1 : 1000). Thallium(I), uranium(VI) and common oxyanions were tolerated in the ratio of 1 : 300. The noble metals were tolerated in the ratio of 1 : 100. But, mercury, copper, gold, nickel, and iron showed

Table 3. Comparison of methods

Palladium taken (μg)	Palladium found by			
	HSDBM method	HSTTA method[6,7]	2-nitroso-1-naphthol method[14]	2-furildioxime method[15]
6.0	6.05	6.00	6.20	6.10
12.0	12.00	11.95	12.10	12.05
18.0	18.05	18.10	18.20	18.10
24.0	24.10	24.20	23.70	23.90
30.0	29.90	29.95	30.30	30.20

strong interference. The interferences due to some of the ions were eliminated using sequestering agents. Bismuth, chromium, thorium, titanium and gallium were masked with tartaric acid, while zirconium, antimony and aluminium were masked with fluoride. The interference due to osmium(VIII) and cobalt(II) were eliminated by selective extraction with carbon tetrachloride and 1-nitroso-2-naphthol respectively.[8]

Comparison with Other Methods. Four sets of five samples containing various amounts of palladium were taken. Then palladium from each sample was measured with monothiodibenzoylmethane, monothiothenoyltrifluoroacetone (HSTTA),[6,7] 2-furildioxime[14] and 2-nitroso-1-naphthol[15] methods. It was interesting to note (Table 3) that the amount of palladium found by HSDBM method, compares favorably well with other methods of extraction of palladium.

The absorbance of the solutions with 20 determinations was 0.250±0.001. The relative standard deviation was ±0.75%. It was possible to accomplish separation and spectrophotometric determination of palladium in a single operation. The overall process needed 30 min. As little as 0.12 μg of palladium per ml can be determined by this method. The method is selective, as it was possible to separate palladium from many elements including noble metals, with which it is associated.

Thanks are due to the Council of Scientific and Industrial Research (India), for awarding Junior Research Fellowship to one of the authors (B.N.P.).

References

1) R. R. Mulye and S. M. Khopkar, *Anal. Chim. Acta*, **76**, 204 (1975).
2) E. Uhlemann and H. Muller, *Anal. Chim. Acta*, **41**, 311 (1968).
3) J. Stary and E. Hladky, *Anal. Chim. Acta*, **28**, 227 (1963).
4) A. V. Rangnekar and S. M. Khopkar, *Bull. Chem. Soc. Jpn.*, **38**, 1696 (1965).
5) A. K. De and M. S. Rahaman, *Analyst*, **89**, 795 (1964).
6) A. V. Rangnekar and S. M. Khopkar, *Chem. Ind. (London)*, **1969**, 293.
7) A. V. Rangnekar and S. M. Khopkar, *Chem. Era*, **1970**, 42.
8) A. K. De, S. M. Khopkar, and R. A. Chalmers, "Solvent Extraction of Metals," Van Nostrand-Reinhold, London (1970).
9) F. F. Beamish and J. C. Van Loon, "Recent Advances in the Analytical Chemistry of Noble Metals," Pergamon, New York (1972), pp. 48, 332.
10) S. H. H. Chaston, S. E. Livingstone, T. N. Lockyer, V. A. Pickles, and J. S. Shannon, *Aust. J. Chem.*, **18**, 673 (1965).
11) A. J. Vogel, "The Text Book of Quantitative Inorganic Analysis," 3rd ed., Longmans Green, London (1961), p. 511.
12) V. K. Gustin and T. R. Sweet, *Anal. Chem.*, **34**, 44 (1963).
13) A. A. Yadav and S. M. Khopkar, *Bull. Chem. Soc. Jpn.*, **44**, 693 (1971).
14) O. Menis and T. C. Rains, *Anal. Chem.*, **27**, 1932 (1955).
15) K. L. Cheng, *Anal. Chem.*, **26**, 1895 (1954).

Ternary Complexs: Equilibrium Studies of Mixed-ligand Complexes of Neodymium Ion with Carboxylic and Phenolic Acids in Aqueous Medium

D. N. SHELKE and D. V. JAHAGIRDAR

Department of Chemistry, Marathwada University, Aurangabad 431002, India

(Received January 12, 1976)

The stability constants of simple and mixed ligand systems of neodymium ion with bidentate ligands such as carboxylic and phenolic acids are studied in an aqueous medium by pH metric titrations at 30±0.1 °C and at an ionic strength of 0.1 M ($NaClO_4$). Neodymium forms 1 : 1 complexes with succinic, adipic, itaconic, malonic, and 3,5-dinitrosalicylic acids and 1 : 1 and 1 : 2 complexes with phthalic, 5-sulfo-, and 4-hydroxysalicylic acids. Ternary complexes of neodymium with these acids when (i) both the ligands are carboxylic acids, (ii) one is carboxylic and the other a phenolic acid, (iii) both ligands are phenolic acids, are studied by potentiometry. The stability constants of these complexes are compared with those of binary complexes. The results have been discussed on the basis of the magnitudes of $\Delta \log K$, K_{DXY}, and $\log \beta_{XY} - 1/2[\log \beta_{XX} + \log \beta_{YY}]$, and also from the comparison of K_{2YX} and K_{MX_1} or K_{2XY} and K_{MY_1}. The values of K_{2YX} are directly related to the acid dissociation constant of the secondary ligand. The overall stability (β_{XY}) is found to be depending on the binary stabilities and the basicities of the ligands.

The simple chelates of lanthanoides with carboxylic and phenolic acids have been studied extensively, though not much work has been reported on the mixed ligand chelates of the lanthanides with these acids. As regards Nd(III), its mixed-ligand chelates with *meso*- and *dl*-tartaric acid have been investigated by Ramamoorthy and Manning.[1] We have reported earlier the formation of mixed-ligand chelates of UO_2^{2+} and Cu^{2+} with bidentate carboxylic and phenolic acids by simultaneous equilibria.[2,3] Nd(III) forms 1 : 1 complexes with carboxylic acids and 1 : 1 and 1 : 2 complexes with phenolic acids. The present work was undertaken to investigate whether the mixed-ligand chelates of Nd(III) with these acids are formed in a stepwise or a simultaneous equilibrium when (i) both the ligands are carboxylic acids, (ii) one is carboxylic and the other is phenolic acid, and (iii) both the ligands are phenolic acids. The calculations of various other factors were done, and the values obtained were utilized to understand some structural aspects of the mixed ligand chelates.

Experimental

Neodymium perchlorate was prepared by the standard procedure. The concentration of Nd(III) in original solution was estimated as Nd_2O_3. Succinic, adipic, itaconic, malonic, phthalic, 5-sulfo-, 3,5-dinitrosalicylic acids, and 4-hydroxysalicylic acids were of B.D.H.(AnalaR) grade. They were recrystallized and their purity was checked by their melting points. All the solutions were prepared in double-distilled water. The details of the measurements of pH are given in earlier paper.[4]

Titrations. The experimental procedure involved, the potentiometric titrations of carbonate-free solutions of (i) free $HClO_4$(4.40×10^{-3} M), (ii) free $HClO_4$(4.40×10^{-3} M)+ligand(X) (2.00×10^{-3} M), (iii) free $HClO_4$(4.40×10^{-3} M)+ligand(X) (2.00×10^{-3} M)+Nd(III) (2.00×10^{-3} M) (M), (iv) free $HClO_4$(4.40×10^{-3} M)+ligand(Y) (2.00×10^{-3} M), (v) free $HClO_4$(4.40×10^{-3} M)+ligand(Y) (2.00×10^{-3} M)+Nd(III) (2.00×10^{-3} M), (vi) free $HClO_4$(4.40×10^{-3} M)+ligand(X) (2.00×10^{-3} M)+ligand(Y) (2.00×10^{-3} M)+Nd-(III) (2.00×10^{-3} M), where the X and Y stands for two respective ligands. The ionic strength of solutions was maintained constant at 0.1 M by the addition of the appropriate amount of 1 M sodium perchlorate solution. The titrations were carried out in an inert atmosphere by bubbling oxygen-free nitrogen gas through an assembly containing the electrodes to keep out CO_2.

Results

Simple Systems. The proton-ligand formation number $\bar{n}_A$ was calculated by the method of Irving and Rossotti.[5] The preliminary values of pK_1 and pK_2 were calculated from the proton-ligand formation curves. The pointwise method was used for the calculations of accurate pK values. These are presented in Table 1. The metal-ligand formation number, $\bar{n}$ were calculated by the Irving and Rossotti's expression.[6] The maximum value of $\bar{n}$ before the pH of precipitation as observed in metal complex titration was 1.9 for phthalic, 5-sulfo-, and 4-hydroxysalicylic acids and 1.0 for succinic, adipic, malonic, and 3,5-dinitrosalicylic acids, showing thereby the ligands belonging to the first set form both 1 : 1 and 1 : 2 complexes and those to the other form only 1 : 1 complex. The pL values were calculated and the formation curves were constructed by plotting pL *vs.* $\bar{n}$. The log-K_1 and log K_2 were calculated initially by half-integral method and finally by the method of pointwise calculations. Since the difference in log K_1 and log K_2 was less than 1.7 in number of cases, their accurate values were calculated by the method of least squares. It is observed that neodymium forms only 1 : 1 complex with succinic, adipic, itaconic, malonic, and 3,5-dinitrosalicylic acids and both 1 : 1 and 1 : 2 complexes with phthalic, 5-sulfo-, and 4-hydroxysalicylic acids. The reported values of log K_1 and log K_2 for phthalic, 5-sulfo-, and 4-hydroxysalicylic acids[7,8] are in good agreement with our values.

In aqueous solution neodymium ion is present as $[Nd(H_2O)_6]^{3+}$, $[Nd(H_2O)_8]^{3+}$ and $[Nd(H_2O)_9]^{3+}$.[9] The metal chelate is formed due to the simultaneous replacement of water molecules from the coordination sphere of neodymium ion with formation of Nd–O bonds. The chelates formed are mainly entropy stabilized as the lanthanide chelates are generally supposed to be ionic in nature.

Table 1. Dissociation constants (pK_1 and pK_2) of ligands and stability constants ($\log K_1$ and $\log K_2$) of neodymium complexes
$t=30$ °C $\mu=0.1$ M ($NaClO_4$)

Ligand acid	pK_1		pK_2		$\log K_1$[a]		$\log K_2$[b]	
	Obsd	Lit	Obsd	Lit	Obsd	Lit	Obsd	Lit
Succinic	3.82±0.04	3.86(2) 4.00(7)	5.22±0.03	5.22(2) 5.21(7)	3.38	—	—	—
Adipic	4.14±0.02	4.12(2) 4.28(7)	5.06±0.03	5.03(2) 5.06(7)	2.90	—	—	—
Itaconic	3.62±0.04	3.68(7)	5.11±0.03	5.14(7) 5.06(7)	3.77	—	—	—
Malonic	2.86±0.02	2.66(7)	5.28±0.03	5.32(7) 5.27(7)	4.21	—	—	—
Phthalic	2.80±0.03	2.80(2)	4.92±0.04	4.92(2) 5.00(7)	4.22	4.22(7)	3.25	3.25(7)
5-Sulfosalicylic	2.63±0.02	2.49(7)	12.10±0.02	12.00(7)	7.39	7.39(7)	5.62	5.62(7)
3,5-Dinitrosalicylic	1.31±0.02	1.31(2)	7.02±0.02	7.00(2)	4.44	4.44(8)	—	—
4-Hydroxysalicylic	3.33±0.02	3.33(2) 3.31(7)	14.20	14.20(2)	10.91	—	9.75	—

a) $\log K_{MX_1}/\log K_{MY_1}$. b) $\log K_{MX_2}/\log K_{MY_2}$.

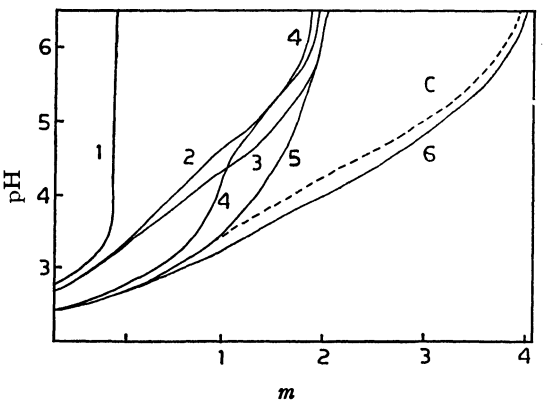

Fig. 1. Neodymium ion-succinic acid-malonic acid system. $\mu=0.1$($NaClO_4$), $t=30$ °C, pH titration curves of a system (i) $HClO_4$(1), (ii) $HClO_4$+succinic acid(2), (iii) $HClO_4$+succinic acid+neodymium ion(3), (iv) $HClO_4$+malonic acid(4), (v) $HClO_4$+malonic acid+neodymium ion(5), and (vi) $HClO_4$+succinic acid+malonic acid+neodymium ion(6) against 0.22 M sodium hydroxide, c=composite curve.

Mixed-ligand Systems. The formation of a mixed ligand complex was concluded initially from qualitative evidence by noting the pH of precipitation for MX, MY and MYX for the titration curves III, V and VI respectively. It was observed that the pH of precipitation for the mixed ligand system was either the same or higher than that of the simple ligand system. The formation of a mixed ligand chelate was confirmed by comparing the mixed ligand curve with the composite curve. The latter curve was drawn theoretically by the graphical addition of 1 : 1 MX curve to the titration curve of free ligand Y. If there is any interaction between NdX and Y the composite curve should be displaced from the experimental curve. The deviation of the composite curve from the mixed ligand titration one was observed in each case. The nature of the complex equilibrium was investigated according to the method suggested by Carey and Martell.[10]

The pH titration curves for a representative system are shown in Fig. 1. The moles of base added after the neutralization of $HClO_4$ are presented as m.

The procedure adopted to understand the complexation equilibria is discussed for a representative system. For all the remaining systems the conclusions drawn regarding the complexation were on the basis of the considerations given above. The final complexation reactions are given in a consolidated form.

Carboxylic–Carboxylic Acid Systems.

i) Neodymium-succinic (H_2Y)–adipic (H_2X) acid.
ii) Neodymium-succinic (H_2Y)–malonic (H_2X) acid.
iii) Neodymium-succinic (H_2Y)–itaconic (H_2X) acid.
iv) Neodymium-succinic (H_2Y)–phthalic (H_2X) acid.

The pH values of precipitation for four mixed ligand systems i—iv were 7.0, 6.8, 7.0 and 6.6 respectively, while those of Nd(III)–succinic acid, Nd(III)–adipic acid, Nd(III)–malonic acid, Nd(III)–itaconic acid, and Nd(III)–phthalic acid were 7.2, 7.1, 6.9, 7.0, and 6.8 respectively. All the carboxylic acids individually form 1 : 1 complex with neodymium except phthalic acid which forms both 1 : 1 and 1 : 2 complexes in the pH range 3—5. The deviation of the mixed ligand curve from the composite curve was from $m=0$—4 for the systems i, ii, and iii and $m=0$—3 for the system iv. The horizontal difference between the mixed ligand complex curve and the composite one remained nearly constant in all the systems, in the pH range 3—6, except in the case of succinic–phthalic acids, wherein the composite curve was towards right-hand side of the mixed ligand titration curve above pH 5. The formation of a mixed ligand chelate by a simultaneous equilibrium for i—iii can be shown as:

$$Nd^{3+} + H_2X + H_2Y \rightleftharpoons Nd(X)(Y)^- + 4H^+$$

In succinic–phthalic acid the mixed ligand titration curve was towards right hand side of the composite curve between $m=0$—3 and, therefore, the complexa-

TABLE 2. THE MIXED LIGAND SYSTEMS OF Nd^{3+}-ligand(Y)-ligand(X) WITH THE COMPLEXATION EQUILIBRIA $t=30\,^{\circ}C$; $\mu=0.1$ M ($NaClO_4$).

Acid system	Complexation equilibria
1. Malonic-adipic[a]	$Nd^{3+} + H_2X + H_2Y \rightleftharpoons Nd(X)(Y)^- + 4H^+$
2. Malonic-itaconic	
3. Phthalic-adipic	
4. Phthalic-itaconic	$Nd^{3+} + H_2X + H_2Y \rightleftharpoons Nd(HX)(Y) + 3H^+$
5. Phthalic-malonic	$Nd^{3+} + HX^- + HY^- \rightleftharpoons Nd(X)(Y)^- + 2H^+$
6. Succinic-3,5-dinitrosalicylic	$Nd^{3+} + HX^- + H_2Y \rightleftharpoons Nd(X)(Y)^- + 3H^+$
7. Malonic-3,5-dinitrosalicylic	$Nd^{3+} + HX^- + H_2Y \rightleftharpoons Nd(HX)(Y) + 2H^+$
8. Phthalic-3,5-dinitrosalicylic	$Nd^{3+} + HX^- + HY^- \rightleftharpoons Nd(X)(Y)^- + 2H^+$
9. Succinic-5-sulfosalicylic	$Nd^{3+} + H_2X^- + H_2Y \rightleftharpoons Nd(HX)(HY) + 2H^+$
10. Malonic-5-sulfosalicylic	
11. Phthalic-5-sulfosalicylic	
12. 5-sulfo-3,5-dinitrosalicylic	$Nd^{3+} + HX^- + HY^{2-} \rightleftharpoons Nd(X)(HY)^- + H^+$
13. 5-sulfo-4-hydroxysalicylic	$Nd^{3+} + H_3X + HY^{2-} \rightleftharpoons Nd(H_2X)(Y)^- + 2H^+$
14. 3,5-dinitro-4-hydroxysalicylic	$Nd^{3+} + H_3X + HY^- \rightleftharpoons Nd(H_2X)(Y) + 2H^+$

a) Y stands for malonic and X stands for adipic.

tion is represented as:

$$Nd^{3+} + H_2Y + H_2Y \rightleftharpoons Nd(X)(HY) + 3H^+$$

In the titrations of the neodymium ion mixed ligand systems against standard sodium hydroxide, the following possible equilibria along with disproportionation reactions are given in Table 2.

In all the cases the equilibria

$$K_{MX_1} = K(M+X \rightleftharpoons MX),$$
$$K_{MX_2} = K(MX+X \rightleftharpoons MX_2),$$
$$K_{MY_1} = K(M+Y \rightleftharpoons MY),$$
$$K_{MY_2} = K(MY+Y \rightleftharpoons MY_2),$$
$$K_{2XY} = K(MX+Y \rightleftharpoons MXY),$$
$$K_{2YX} = K(MY+X \rightleftharpoons MXY), \text{ and}$$
$$\beta_{XY} = K(M+X+Y \rightleftharpoons MXY),$$

must be involved.

The disproportionation constants

$$K_{DXY} = K(MX+MY \rightleftharpoons MXY+M),$$
$$K_{DXY} = K(MX_2+MY \rightleftharpoons MXY+MX),$$
$$K_{DXY} = K(MX+MY_2 \rightleftharpoons MXY+MY), \text{ and}$$
$$K_{DXY} = K(MX_2+MY_2 \rightleftharpoons 2MXY),$$

corresponding to the systems are calculated.

The distinguishable cases depend on the relative value of K_{MX_1}, K_{MX_2}, $\cdots$, β_{XY}. In all the cases $\beta_{XY} = K_{MX_1} \cdot K_{2XY} = K_{MY_1} \cdot K_{2YX}$.

The procedure adopted and the mathematical expressions used for the calculations of the stability constants of mixed-ligand chelates were given earlier.[11] All the mathematical calculations were done on the DCM Moscal 1400 electronic calculator. The β_{XY} values are presented in Table 3.

The stability of ternary complex is conveniently characterized by the following two ways. One is based on the difference of stability constants (logarithmic values), $\Delta\log K$, and the second on the disproportionation constant, $\log K_{DXY}$.

$$\Delta\log K = \log K_{MY_1} - \log K_{2XY}$$

Generally, $K_{MY_1} > K_{MY_2}$ because more coordinating positions are normally available for bonding of the first ligand to a metal ion than for the second ligand. The addition of ligand Y to MX should also show the same trend. Evidently, $K_{MY_1} > K_{2XY}$ or $\Delta\log K$ is positive. $\Delta\log K$ can also be calculated by the expression:

$$\Delta\log K = \log K_{MX_1} + \log K_{MY_1} - \log \beta_{XY}.$$

The positive $\Delta\log K$ value of ternary system indicates that primary ligand anion and secondary ligand anions preferentially form binary complexes to ternary complexes.

From the above expression it follows that the influence of both ligands in a ternary complex is mutual and of the same size. Both ligands are either stabilized or destablished in their coordination to the same metal ion. This is connected with the fact that the difference, $\Delta\log K$, is the result from the subtraction of two constants, and, therefore, also a constant which corresponds to the equation.

$$MX + MY \rightleftharpoons MXY + M$$

Obviously, the observation of positive values for $\Delta\log K$ would indicate that the equation is more on its right side.[12]

Based on the statistical considerations, mixed ligand chelate formation by these disproportionation reactions is favored, if $\log K_{DXY} > 0.6$ log units.[12] The comparison of equilibrium constants $\log K_{2XY}$ and $\log K_{MY_2}$, can be made to find out whether the primary diacid ligand prefers to coordinate to 1 : 1 binary complex of the same ligand. The factors concerning the higher or lower stability of ternary complexes as compared to the binary complexes can also be observed from the $\log \beta_{XY} - 1/2[\log \beta_{XX} + \log \beta_{YY}]$.

In short, the tendency of the formation of a ternary chelate can be examined from the magnitude of a) $\Delta\log K$, b) $\log K_{DXY}$, c) comparison of $\log K_{2XY}$ and $\log K_{MY_2}$ or $\log K_{2YX}$ and $\log K_{MX_2}$ and d) the magnitude of $\log \beta_{XY} - 1/2[\log \beta_{XX} + \log \beta_{YY}]$.

The mixed ligand chelate is formed due to the

TABLE 3. LOGARITHMS OF EQUILIBRIUM CONSTANTS OF TERNARY COMPLEXES OF NEODYMIUM ION
$t=30$ °C $\mu=0.1$ M ($NaClO_4$)

Acid systems	β_{XY}	K_{DXY}*	K_{2XY}	K_{2YX}	$\Delta\log K$	$\log\beta_{XY}-[\log K_{MX_1}+\log K_{MY_1}]$
Succinic-adipic	6.53	+0.25	3.26	3.15	−0.25	+0.25
Succinic-malonic	7.48	−0.11	3.27	4.10	+0.11	−0.11
Succinic-itaconic	7.41	+0.26	4.64	4.03	−0.26	+0.26
Succinic-phthalic	7.15	+0.52 −0.45**	2.93	3.77	+0.45	+0.03[a]
Malonic-itaconic	8.21	+0.23	4.44	4.00	−0.23	+0.23
Malonic-adipic	6.74	−0.37	3.84	2.52	+0.37	−0.37
Phthalic-malonic	7.39	−0.07 −1.05**	3.14	3.18	+1.03	−0.55[b]
Phthalic-itaconic	8.18	+1.16 +0.19**	3.96	4.41	−0.19	+0.68[b]
Phthalic-adipic	6.62	+0.47	2.40	3.72	+0.50	−0.02[b]
Succinic-5-sulfosalicylic	8.66	−0.35 −2.11**	1.27	5.28	+2.11	−1.22[a]
Malonic-5-sulfosalicylic	9.42	−0.42 −2.18**	2.03	5.21	+2.18	−1.29[a]
Phthalic-5-sulfosalicylic	8.74	−2.97 −3.00@	1.35	4.52	+2.87	−1.50[c]
Succinic-3,5-dinitrosalicylic	8.25	+0.43	3.81	4.87	−0.43	+0.43
Malonic-3,5-dinitrosalicylic	8.52	−0.14	4.08	4.31	+0.13	−0.13
Phthalic-3,5-dinitrosalicylic	8.22	+0.53 −0.44**	3.78	4.00	+0.44	+0.05[b]
5-Sulfo-3,5-dinitrosalicylic	11.58	+1.52 −0.25**	7.14	4.19	+0.25	+0.64[b]
5-Sulfo-4-hydroxysalicylic	17.56	−0.74 +2.39@	6.59	10.17	+0.80	+0.69[c]
3,5-Dinitro-4-hydroxysalicylic	12.45	−2.95 −1.74**	1.74	8.00	+2.96	−2.35[a]

The accuracy of β_{XY} values was between 0.05 to 0.10.
K_{DXY}*$=K(MX+MY\rightleftarrows MXY+M)$; $a=\log\beta_{XY}-[1/2\log\beta_{XX}+\log K_{MY_1}]$
K_{DXY}**$=K(MX_2+MY\rightleftarrows MXY+MX)$ $b=\log\beta_{XY}-[\log K_{MX_1}+1/2\log\beta_{YY}]$
$=K(MX+MY_2\rightleftarrows MXY+MY)$ $c=\log\beta_{XY}-1/2[\log\beta_{XX}+\log\beta_{YY}]$
K_{DXY}@$=K(MX_2+MY_2\rightleftarrows 2MXY)$.

simultaneous or stepwise replacement of four water molecules from the coordination sphere of the Nd^{3+} ion with the formation of four Nd–O bonds. The carboxylate oxygen is not directly bound to the benzene nucleus like the phenolate oxygen. The carboxylate oxygen may, therefore, adjust stereochemically more easily than the phenolate ion which is directly attached to the benzene nucleus. Greater strain in the Nd–O bond is, therefore, expected when the phenolate oxygen is coordinated to the metal ion than when the coordination takes place through the carboxylate oxygen. Further the electronegativity of phenolate oxygen will be higher than that of carboxylate oxygen. The Coulombic repulsion between the end oxygens will, therefore, be stronger when both ligands are phenolic acids than when they are carboxylic acids. Thus, the value of $\Delta\log K$ should be higher when both the ligands are phenolic acids than when both the ligands are carboxylic acids, and the intermediate value is expected when one is a carboxylic acid and the other a phenolic acid. The observed values of $\Delta\log K$ do not strictly fit into this pattern. This behavior can be scrutinized critically, if the values of the factors given in a, b, c and d are examined.

Carboxylic–Carboxylic Acid Systems. a) $\Delta\log K$ is negative for succinic–adipic, succinic–itaconic, malonic–itaconic, and phthalic–itaconic systems. The formation of the mixed-ligand chelates over the binary complexes in these cases is thus favored. On the other hand, systems like succinic–malonic, succinic–phthalic, phthalic–malonic, malonic–adipic, and phthalic–adipic have positive $\Delta\log K$. The value in the case of phthalic–malonic being significantly higher than the other remaining systems.

b) $\log K_{DXY}<0.6$ log units for all the systems except phthalic–itaconic acid system. The ternary complexation in the case of phthalic–itaconic acid system is thus favored by this equilibrium $MX+MY\rightleftarrows MXY+M$.

c) $\log K_{2XY}>\log K_{MY_2}$ for phthalic–malonic and phthalic–adipic acid systems.

d) $\log\beta_{XY}-1/2[\log\beta_{XX}+\log\beta_{YY}]$ is positive for succinic–adipic, succinic–itaconic, malonic–itaconic, and phthalic–itaconic which is complementary to the values of $\Delta\log K$ obtained for these systems and, therefore, confirm the conclusions drawn earlier.

In the series examined, the magnitude of $\Delta\log K$ is maximum for phthalic–malonic system. For this system $\log K_{DXY}$ is not favorable to the mixed ligand

chelate formation, similarly log K_{2XY}<log K_{MY_2}, but log K_{2YX}>log K_{MX_2}. This is the only factor which is favorable for the ternary complex formation. In the case of phthalic–itaconic the factors 'a' and 'b' are favorable to the formation of ternary complexes. For phthalic–adipic 'b' is favorable but 'c' is very much unfavorable giving a positive value of $\Delta\log K$. In the carboxylic–carboxylic acid systems, except phthalic acid, no other carboxylic acid forms 1 : 2 complex independently. The 1 : 1 : 1 mixed-ligand complexation occurs in a pH region where normally 1 : 1 complexes are formed by these acids. This may be probably the reason, for the presence of mixed chelate formation in these cases.

Carboxylic–Phenolic Acid Systems.

a) $\Delta\log K$ are all positive except succinic–3,5-dinitrosalicylic acid system.

b) log K_{DXY} is not favorable for ternary complex formation.

c) log K_{2YX}<log K_{MY_2} for ternary chelates with 5-sulfosalicylic acid is primary ligands. The value of $\Delta\log K$ is positive and higher than any of the systems belonging to group 1. In the case of succinic–3,5-dinitrosalicylic acid log $K_{DXY}=0.43$ which is quite close to 0.6 log units. These two ligands independently do not form 1 : 2 chelates. The value of $\Delta\log K$ and log $\beta_{XY}-1/2[\log\beta_{XX}+\log\beta_{YY}]$ are favorable to the ternary complex formation. In the case of phthalic–3,5-dinitrosalicylic acid system, phthalic acid forms a 1 : 2 complex. The factors a, b, and d are not favorable for malonic–3,5-dinitrosalicylic acid system. Similar is the case for phthalic–3,5-dinitrosalicylic acid system, but because of a positive value of a disproportionation reaction, a slightly higher value of $\Delta\log K$ was obtained for this system than malonic–3,5-dinitrosalicylic acid system.

Phenolic–Phenolic Acid Systems.

a) $\Delta\log K$ is positive for all the three systems. The magnitude of $\Delta\log K$ follows the order Nd^{3+}-3,5-dinitrosalicylic–4-hydroxysalicylic > Nd^{3+}-5-sulfosalicylic–4-hydroxysalicylic > Nd^{3+}-5-sulfosalicylic–3,5-dinitrosalicylic acid systems.

b) log $K_{DXY}>0.6$ for 5-sulfo-3,5-dinitrosalicylic acid and 5-sulfo–4-hydroxysalicylic acid system.

c) log $K_{2YX}>\log K_{MX_2}$ for 5-sulfo–4-hydroxysalicylic acid. log $K_{2YX}<\log K_{MX_2}$ for 3,5-dinitro–4-hydroxysalicylic and log $K_{2XY}>\log K_{MY_2}$ for 5-sulfo-3,5-dinitrosalicylic and 5-sulfo–4-hydroxysalicylic acid.

d) $\log\beta_{XY}-1/2[\log\beta_{XX}+\log\beta_{YY}]$ is positive for 5-sulfo–3,5-dinitrosalicylic and 5-sulfo–4-hydroxysalicylic acid and negative for 3,5-dinitro–4-hydroxysalicylic acid system.

In this series, except Nd^{3+}-3,5-dinitro–4-hydroxysalicylic acid the 'b' factor is much favorable to the remaining two systems, despite of $\Delta\log K$ being positive for them. The mixed-ligand chelation therefore, occurs mainly by the reaction

$$MX_2 + MY_2 \rightleftharpoons 2MXY, \text{ and}$$

$$MX + MY_2 \rightleftharpoons MXY + MY,$$

in the case of 5-sulfo–4-hydroxy- and 5-sulfo–3,5-dinitrosalicylic acid systems respectively. Only 3,5-dinitrosalicylic acid does not form a 1 : 2 complex. In the presence of 4-hydroxysalicylic acid it forms 1 : 1 : 1 chelate in a pH region at which it forms a 1 : 1 complex. In the case of 3,5-dinitrosalicylic acid, the absence of 1 : 2 complex may be due to the steric hindrance of the earlier attached ligand to the incoming ligand anion. The secondary ligand like 4-hydroxysalicylic acid or 5-sulfosalicylic acid which do not afford steric hindrance like 3,5-dinitrosalicylic acid may, therefore, attach to the 1 : 1 complex of Nd^{3+}-3,5-dinitrosalicylic acid to form a 1 : 1 : 1 complex.

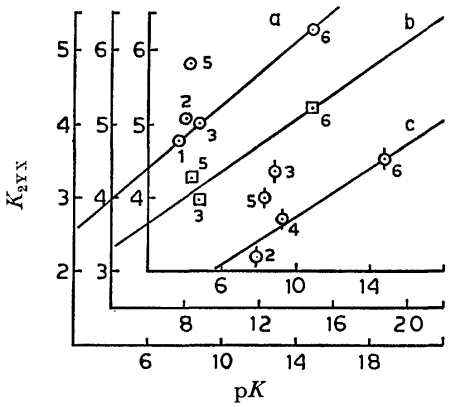

Fig. 2. Relation between log K_{2YX} and the product of the acid dissociation constants of the ligands for neodymium dibasic-dibasic systems.
(a) Neodymium ion-succinic acid(Y)-ligand(X),
(b) neodymium ion-malonic acid(Y)-ligand(X),
(c) neodymium ion-phthalic acid(Y)-ligand(X);
ligand(X): (1) phthalic acid, (2) malonic acid, (3) itaconic acid, (4) adipic acid, (5) 3,5-dinitrosalicylic acid, (6) 5-sulfosalicylic acid. $\mu=0.1$ M ($NaClO_4$), $t=30$ °C.

In the case of 3,5-dinitrosalicylic–4-hydroxysalicylic acid system the factors b, c, and d are not favorable which has resulted in a significantly large value of $\Delta\log K$.

The mixed-ligand chelates are formed in a simultaneous equilibria. The replacement of four water molecules from the hydration sphere of Nd^{3+} ion simultaneously by the two ligands would make the reaction 'entropy stabilized'. An additional factor in favor of the mixed ligand chelates, of some systems are the charge cancellation of the metal ion and the ligand to form a neutral complex.[11–14]

The order of log K_{2YX} is given as:

i) 5-sulfo>3,5-dinitro>itaconic>adipic when the primary ligands are succinic, malonic and phthalic acids.

ii) 4-hydroxy>3,5-dinitrosalicylic acid when 5-sulfosalicylic acid is a primary ligand. This is also the order of the basicities of the ligands. The plots of log K_{2XY} *vs.* ΣpK (Fig. 2) gave a satisfactory direct relationship between these two quantities. However, the points corresponding to adipic acid system deviated from the straight line, which may be due to the ring size effect.[11] We have already established the direct relationship between these two quantities for mixed-ligand chelates of vanadyl ion.[16] In the present investigation, the formation of ternary complexes of

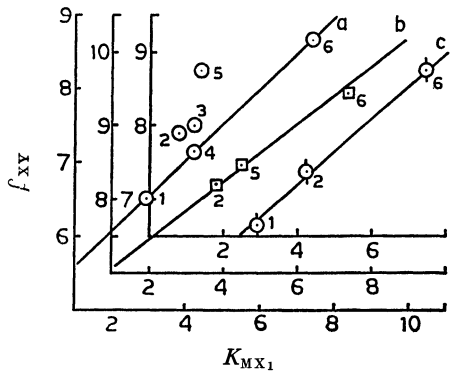

Fig. 3. Relation between β_{XY} and log K_{MX_1} of ternary complexes of neodymium ion. (a) neodymiun ion-succinic acid(Y)-ligand(X), (b) neodymium ion-malonic acid(Y)-ligand(X), (c) neodymium ion-phthalic acid(Y)-ligand(X), ligand(X): (1) adipic acid, (2) itaconic acid-malonic acid (c), (3) malonic acid (4) phthalic acid, (5) 3,5-dinitrosalicylic acid, (6)-5-sulfosalicylic acid. μ=0.1 M ($NaClO_4$), t= 30 °C.

the neodymium ion has been found to be depending on the basicities of the ligand.

The plots of β_{XY} *vs.* K_{MX_2} (Fig. 3) gave straight lines which are parallel. The values of overall stability constants β_{XY} for these systems are as:

5-sulfo > 3,5-dinitro > malonic > phthalic > itaconic > adipic when primary ligands are succinic, malonic and phthalic acids. This is in accordance to the stabilities of 1 : 1 binary complexes. This observation is in good agreement with the earlier work.[14-17].

The authors are grateful to Prof. D. D. Khanolkar, Head, Chemistry Department, Marathwada University, Aurangabad, for his valuable guidance and encouragement in the present work. One of the authors (DNS) thanks to UGC, New Delhi, for the award of a Junior Research Fellowship.

References

1) S. Ramamoorthy and P. G. Manning, *J. Inorg. Nucl. Chem.*, **34**, 1977 (1972).
2) V. D. Khanolkar, D. V. Jahagirdar, and D. D. Khanolkar, *J. Inorg. Nucl. Chem.*, **35**, 931 (1973).
3) E. G. Sase and D. V. Jahagirdar, *J. Inorg. Nucl. Chem.*, **37**, 985 (1975).
4) D. V. Jahagirdar and D. D. Khanolkar, *J. Inorg. Nucl. Chem.*, **35**, 921 (1973).
5) H. Irving and H. Rossotti, *J. Chem. Soc.*, **1953**, 3397.
6) H. Irving and H. Rossotti, *J. Chem. Soc.*, **1954**, 2904.
7) L. G. Sillen and A. E. Martell, "Stability Constants," Special Publication No. 17 and 25, Chemical Society, London (1964) and (1971), pp. 512, 534.
8) D. V. Jahagirdar and D. D. Khanolkar, Symposium in Chemistry, Chemists Convention, India, 1969, p. 303.
9) T. Moeller, "Comprehensive Inorganic Chemistry," Vol. 4, Pergamon Press, Oxford (1973), p. 1.
10) G. H. Carey and A. E. Martell, *J. Am. Chem. Soc.*, **89**, 2859 (1967).
11) M. S. Balakrishnan and M. Santappa, *J. Inorg. Nucl. Chem.*, **36**, 3813 (1974).
12) R. P. Martin, M. M. Petit-Ramel, and J. P. Scharff, "Metal-ions in Biological Systems, Vol. 2, Mixed Ligand Complexes," Marcel Dekker, New York (1973), p. 1.
13) W. B. Schaap and D. L. McMasters, *J. Am. Chem. Soc.*, **83**, 4699 (1961).
14) M. S. Balakrishnan and M. Santappa, *J. Inorg. Nucl. Chem.*, **37**, 1229 (1975).
15) H. Sigel and R. Griesser, *Inorg. Chem.*, **9**, 1238 (1970).
16) D. N. Shelke and D. V. Jahagirdar, paper communicated to *J. Inorg. Nucl. Chem.*
17) M. Koskinen, *Ann. Acad. Sci. Fenn.*, **A-155**, 7 (1970).

Melting and Solid–Solid Transition Temperatures at High Pressures for NH_4SCN, RbSCN, TlSCN, and CsSCN

William KLEMENT Jr.*

National Physical Research Laboratory, C.S.I.R., P.O. Box 395, Pretoria, South Africa

with an **Appendix—Lattice parameters of NH_4SCN and RbSCN at high temperatures**

by C. W. F. T. PISTORIUS†

(Received March 16, 1976)

Differential thermal analyses at high pressures have yielded the following trajectories for melting and solid-solid transitions in the several thiocyanates: (substance, transition, 1-bar transition temperature in °C, initial slope (dT/dp) in deg kbar^{-1}, initial curvature ($-d^2T/dp^2$) in deg kbar^{-2}, approximate maximum pressure in kbar) NH_4SCN, melting, ≈146, ~20 (tentative), —, ~3.5; NH_4SCN, (upper) solid-solid, 120±4, 12.6±1.5, —, 7.5; RbSCN, melting, 184±2, 15.7±0.3, 0.32±0.05, 36; RbSCN, solid-solid, 166±3, 13.5±1.0, 0.3±0.1, 30; TlSCN, melting, ≥234, ≥10 (tentative) >0, 34; TlSCN, solid-solid, 99±2, 9.6±1.0, ≈0.17, 34; CsSCN, melting, ≥206, ≈14±1.5, ~0.2—0.4, 33; CsSCN, solid-solid, ≥197, ≈11.8 ±1.0, ~0.2, 33. The solid-solid transitions investigated here for NH_4SCN, RbSCN and TlSCN appear to be closely-related, structurally, to the well-investigated transition in KSCN. The thermodynamics of the KSCN transition at 1-bar is discussed anew so as to be consistent with high pressure data. The transitions in these other thiocyanates are probably thermodynamically similar to the KSCN transition but the necessary data to establish the similarities are lacking. Lattice parameters for NH_4SCN and RbSCN show rapid variations with temperature below the solid–solid transition, as for KSCN. DSC and DTA results are presented for the 1-bar transition temperatures and entropy changes for NH_4SCN, RbSCN, TlSCN, CsSCN and also AgSCN. The entropy changes apparently associated with the structurally similar solid–solid transitions decrease with increasing cation polarizability.

Of the univalent thiocyanates, the phase relations[1] in KSCN are, thus far, the most complex, with 5 polymorphs having been postulated up to ~44 kbar, although there is only one rather thoroughly investigated[2,3] solid–solid transition at 1-bar. NaSCN shows[4] only one polymorph to ~40 kbar, which differs in structure from the 1-bar KSCN polymorphs, as do the low temperature phase of NH_4SCN,[5] the only known phase in AgSCN[6] and the CsSCN[7] phases. Besides data on the CsSCN phase relations at high pressures, this paper reports on the phase relations of NH_4SCN, RbSCN and TlSCN—all of which show phase transitions which apparently are similar to the KSCN transition. Also reported, in the Appendices, are a thermodynamic discussion of the KSCN transition more nearly in accord with existing data and lattice parameters for NH_4SCN and RbSCN at high temperatures.

Experimental

General Procedure. Transitions were detected by differential thermal analysis (DTA), using the piston-cylinder apparatus, furnace geometry and experimental procedures described previously.[8] Details of the runs for each substance are given below. After corrections for friction, pressures are believed accurate to ±0.5 kbar. Temperatures, as measured with Chromel-Alumel thermocouples, are believed accurate to ±2 °C.

NH_4SCN. In both runs, Merck reagent grade material was contained in aluminium capsules, which had been treated with HNO_3. The samples were dewatered by holding briefly above ~100 °C before sufficient pressure had been applied to seal the capsules. The lower solid-solid transition, investigated by Bridgman,[9] was not studied. In the first run, the upper solid-solid transition was observed by small but distinct breaks in the DTA signals, the corresponding temperatures agreeing to within ±1 °C on heating and cooling. At least two heating/cooling cycles were run at each pressure to demonstrate reproducibility and, where possible, this is usual in all of these experiments. After increasing pressure ≥8 kbar, signals could not be reproduced satisfactorily and the black contents of the capsule indicated decomposition. No efforts were made to investigate the details of the decomposition. In the second run, the solid-

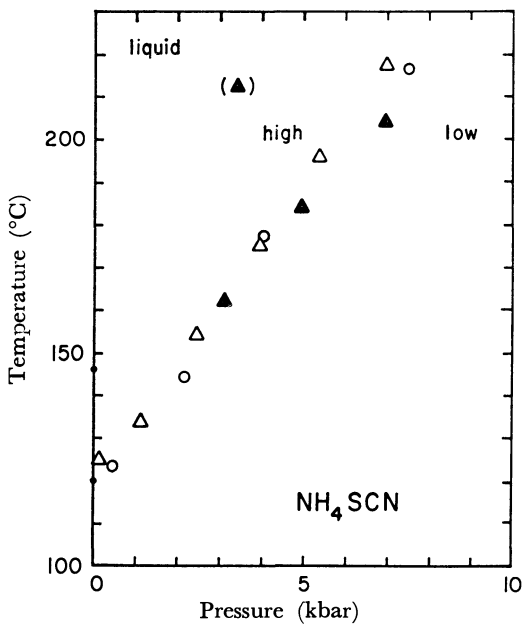

Fig. 1. Solid-solid and melting (point in parentheses and tentative) temperatures for NH_4SCN. Accepted 1-bar transition temperatures are indicated. Open symbols denote upstroke data; filled symbols denote downstroke data. Circles denote data from first run and triangles those from second run, both in aluminium capsules.

* On leave from School of Engineering and Applied Science, University of California, Los Angeles, California 90024, U.S.A.

† Deceased 12 XII 1975

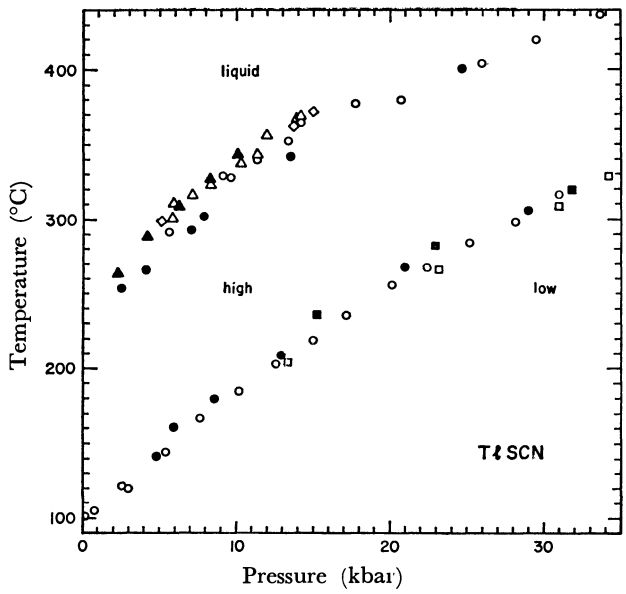

Fig. 4. Solid-solid and melting temperatures for TlSCN. Accepted 1-bar transition temperatures are indicated. Open symbols denote upstroke data; filled symbols denote downstroke data. Symbols for the several runs (capsule materials) are triangles-first (inconel); diamonds-second (copper); circles-third (aluminium); squares-fourth (tantalum). The melting data should be considered tentative.

the transition temperatures, which were the same, within experimental error, on heating and on cooling. The DTA signals for melting again showed only indistinct onsets and undercoolings were obvious from the freezing signals. The data (Fig. 4) for the solid-solid transition can be fitted by a power series with 1-bar intercept 99±2 °C, initial slope 9.6±1.0 deg kbar^{-1} and initial curvature ≈0.17 deg kbar^{-2}. The data (Fig. 4) for melting are disappointing, because of the poorly defined onsets (presumably due to impurities), and should only be considered as tentative. Only a poor fit is obtained with the usual power series but there may be estimated an initial slope≥10 deg kbar^{-1} and an initial curvature>0 for a 1-bar intercept of ~234 °C.

AgSCN. One exploratory run was made with BDH Laboratory Reagent material contained in an aluminium capsule. Large DTA signals were observed ≤2 kbar, with poorly defined onsets near ~180 °C on both heating and cooling. The run was abandoned after these signals disappeared and, subsequently, decomposition was indicated. No further work was attempted because of the lack of agreement with the DSC results (below).

DSC Results

Mr. S.J. Pretorius kindly made DSC runs on several substances. For NH_4SCN, the onset of the lower solid–solid transition was near 364 K, with a transition entropy of ≈2.2 cal mol^{-1} deg^{-1} (in good agreement with Bridgman[9]); the peak of the upper solid–solid transition was near 393 K, with a transition entropy ≥ 0.3_7 cal mol^{-1} deg^{-1}; the onset of melting was near 419 K, with a melting entropy of ≈$5._1$ cal mol^{-1} deg^{-1}; the latter temperatures agree satisfactorily with literature values.[10]

For Rb-SCN, one sample yielded the onset of melting near 455 K, with a melting entropy of ≈$5._9$ cal mol^{-1} deg^{-1}, and the peak of the solid–solid transition near 436 K, with a transition entropy≥0.6_3 cal mol^{-1} deg^{-1}; another sample showed the same transition temperatures but somewhat smaller entropies, which are within the accuracy of the technique—say ±10%; Wrzesnewsky[10] apparently obtained a slightly higher melting temperature. For TlSCN, the material used initially showed the onset of melting near 498 K, with a melting entropy of ≈$7._1$ cal mol^{-1} deg^{-1}, and only a poorly defined signal for the solid–solid transition; for the subsequent sample, the onset of melting was near 507 K, with a melting entropy of ≈$7._7$ cal mol^{-1} deg^{-1}, and the peak of the solid–solid transition was near 372 K, with a transition entropy of ≥0.3 cal mol^{-1} deg^{-1}; although the latter sample appears to be purer than the former, the onset of melting was not so sharp that impurities could be considered negligible. For AgSCN, a single run up from 330 K showed only what appeared to be melting, with onset near 534 K and the entropy ≈7.3 cal mol^{-1} deg^{-1}; decomposition appeared to occur a few degrees higher. Mr. R. A. Pacey kindly made several DTA-DSC runs on the CsSCN used here—which essentially corroborated the previous results[7] for transition temperatures and entropies.

Discussion

For melting, the Clausius-Clapeyron equation may be used to estimate the volume changes on fusion. With the absolute volume change in cm^3 mol^{-1} and the fractional volume change referred to the volume of the melting solid, there are estimated: for NH_4SCN, ~$6._4$ or ~11%; for RbSCN, ~$3._9$ or ≈$6._5$%; for TlSCN, ≥$3._2$ or ≥$6._1$%; for CsSCN, ≈$1._8$ or ≈$2._7$%; also for KSCN, 6.0—7.1[11] or $12._5$±1% and, for NaSCN, 4.3±0.5[4] or ≈9%. There appears to be a roughly linear correlation between the fractional volume change on fusion and the melting entropy for these compounds, the greatest deviations being for the least certain data (*e.g.*, NH_4SCN and TlSCN). The NaSCN datum can be brought into better agreement with this correlation by subtracting an orientational entropy term from the melting entropy since the $(SCN)^-$ ion is not disordered in the melting solid, as it presumably is for the other compounds. Such a correlation has not been discussed extensively for other sequences of chemically and structurally related compounds but then the present sequence offers a wider range of fractional volume changes and fusion entropies than is usually encountered for other sequences.

The solid–solid transition in CsSCN has an entropy change almost twice the melting entropy. The volume change for this transition is ≈1.6 cm^3 mol^{-1} from the X-ray diffraction results of Ref. 7, which leads to a calculated initial slope of ≈6.6 deg kbar^{-1}, in serious disagreement with the present experimental results. It is difficult to imagine how the experimental slope could be too high by some 5 deg kbar^{-1} and, since the entropy change has been corroborated, the data

for the change in volume must be considered further. In particular, the anomalously rapid increase in volume[7] of low-CsSCN with temperature is suspect because the entropy change at the transition is large enough to include all of the orientational entropy due to end-for-end disordering of the $(SCN)^-$ ion. It seems entirely possible that very little of the disordering takes place below the transition temperature and thus an obvious reason for the anomalous volume variation is eliminated. The high-low CsSCN transition is structurally dissimilar to the transitions in the other thiocyanates (which do show variations below the transition temperatures presumably due to progressive disordering) and it also shows hysteresis between transition temperatures on heating and cooling (in Fig. 2 of Ref. 7 and in Pacey's work, if not in the high pressure runs), unlike the other thiocyanate transitions. Correspondence with the senior author of Ref. 7 could not elicit any comment about the suspicions concerning the X-ray diffraction data on low-CsSCN at high temperatures.

Previously, the solid–solid transition in KSCN was discussed[3] entirely as a λ-transition, without any first-order component, *i.e.*, discontinuous volume or entropy change. This model[3], however, is inadequate because it cannot account for the experimental value of dT_λ/dp—which they[3] did not consider at all. Appendix A discusses the thermodynamics of the high-low KSCN transition in a way more nearly in accord with the high pressure data and it is concluded that the transition is mostly λ-like, although with a small first-order component.

Since the structures of the low-KSCN, NH_4SCN, RbSCN and TlSCN phases apparently are isomorphous, it may be assumed that the structures of the high phases are also isomorphous and also that the transitions are similar thermodynamically. Pistorius' data (Appendix B) show that the lattice parameters for low-RbSCN and also low-NH_4SCN vary rapidly with temperature upon approaching the transitions, akin to the analogous data[3] for KSCN; it is not unlikely that TlSCN shows similar behavior. If the estimates for transition entropies and the observed slopes are combined *via* the Clausius-Clapeyron equation to estimate the corresponding volume changes at the transitions in RbSCN and NH_4SCN, it is clear that these volume changes are larger than those which might be deduced by extrapolation of Pistorius' data (Appendix B). Hence, it is suggested that the transition entropies observed by DSC for RbSCN and NH_4SCN include both isothermal and nonisothermal contributions, as for KSCN. More painstaking calorimetric and volumetric determinations will be necessary to establish the variations below and near the high-low transitions for these substances.

Even more careful calorimetry is unlikely, however, to alter the present observation that, despite the uncertainties as to how to subtract the background, the transition entropies vary progressively as 1.30 ± 0.05,[2] $\geq 0.6_3$, $\geq 0.3_7$, and ≥ 0.3 cal mol^{-1} deg^{-1} for KSCN, RbSCN, NH_4SCN, and TlSCN, respectively. On one hand, this progression could be used to argue against the similarity of the transitions whilst, on the other hand, it could be used in an argument against the applicability of the molecular field model.[3] Taking the latter point of view, it is possible that the alternate formulation of Appendix A might be applicable but this is not demonstrable here for lack of necessary data.

It may be observed that the transition entropies decrease in order of increasing cation polarizability and that a similar progression has been recognized[11] for the discontinuous entropy changes attending the isostructural transitions in K_2SO_4, Rb_2SO_4, Cs_2SO_4, and Tl_2SO_4. For these sulfates, it is arguable that much of the disordering takes place gradually below the transition and this is especially well demonstrated by the enthalpy data[12] for Tl_2SO_4 as compared to K_2SO_4. The details of the disordering behavior in a sequence of isostructural compounds could be more conveniently investigated for these thiocyanates than for the sulfates because the temperatures are lower and the disordering more simply envisioned.

In the absence of data for microscopic order parameters, some consideration can be given to possible order parameters using available data and which can be devised from experience on transitions in other sequences of compounds. Thus, for instance, some M_2CO_3 transitions monoclinic→hexagonal with increasing temperature-proved describable[13] with the order parameter [monoclinic angle $-90°$], which became rigorously zero above the transition temperatures; it was also possible[13] to scale the order parameters onto the same curve *vs.* 'reduced temperature' T/T_λ. On heating to the transition temperature, the greatest thermal expansions are in the direction perpendicular to the planar carbonate ion and this also occurs for $NaNO_3$, $AgNO_3$, $CaCO_3$, *etc.* which have planar ions and λ-transitions. Likewise, for KSCN, NH_4SCN, RbSCN, and presumably TlSCN, the thermal expansion upon approaching the transition is greatest in the c-direction, which is perpendicular to the plane in which the $(SCN)^-$ ions are disordering end-for-end.[2,3] Also, it may be verified that the thermal expansions in the a-, b-, and c-directions for the orthorhombic phases are linked to one another by plotting the lattice parameters, at the same temperature, for each pair and observing that straight lines are obtained, within the precision of the data and independent of the uncertainty in temperature. As a possible order parameter for the thiocyanate transitions, one may consider [a−b] since this decreases monotonically with increasing temperature and is rigorously zero above the transition temperature. Comparing the KSCN and RbSCN data which are the most extensive, [a−b] *vs.* T/T_λ show different courses and this can be attributed to the different temperature dependences of the anion disordering, as postulated above.

An important generalization concerning the polymorphism in some structurally similar sequences of substances has emerged from the accumulating data[14] on phase transitions at high pressures. To wit, the larger the ionic radius of the cation the lower the pressure at which structurally identical polymorphs are

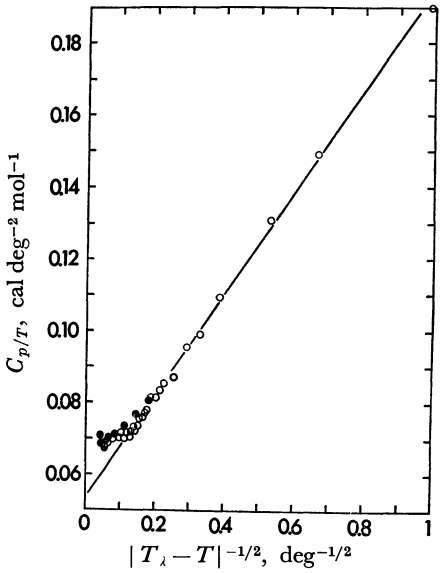

Fig. 5. Plots of $C_{p/T}$ *vs.* $(T_\lambda - T)^{-1/2}$ (open circles, for $T < T_\lambda$) and *vs.* $(1/4)(T - T_\lambda)^{-1/2}$ (filled circles, for $T > T_\lambda$) for KSCN.

encountered—and the validity of this empirical rule is surprisingly extensive.[14] Nevertheless, the lack of any new polymorphs in the present investigation of NH_4SCN, RbSCN, and TlSCN, compared with the several high pressure polymorphs of KSCN,[1] means that this empirical generalization is invalid for these thiocyanates.

Thanks are due to: the late C. W. F. T. Pistorius, P. W. Richter and J. B. Clark for encouragement and assistance; S. J. Pretorius and R. A. Pacey for the DSC and DTA-DSC runs. Much of the thinking about the KSCN transition was done whilst a Guggenheim Fellow at the Australian National University, Canberra, A. C. T.

Appendix A: Thermodynamics of the λ-like transition in KSCN

Yamada and Watanabé[3] have given a description of the KSCN transition in terms of a molecular-field model with a volume-dependent interaction energy. Unfortunately they did not consider that the initial variation of transition temperature with pressure, dT_λ/dp, was an important constraint on their correlations and it does not appear that their model is consistent with the experimental value[1,9] for $dT_\lambda/dp = 18._2 \pm 1._1$ deg kbar^{-1}. Here, the approach is more macroscopic and is along the lines of the discussion[15] of the nematic-isotropic transition in *p*-azoxyanisole, which has a small first-order transition superimposed on a λ-like transition.

The heat capacity data[2] for KSCN are represented (Fig. 5) as

$$C_{p/T} = (C_{p/T})_0 + A|T_\lambda - T|^{-1/2}, \qquad \text{(A-1)}$$

where $(C_{p/T})_0 \approx 0.054$ cal deg^{-2} mol^{-1} and $A \approx 0.14$ cal deg$^{-3/2}$ mol^{-1} for $T < T_\lambda$ and about a quarter of this for $T > T_\lambda$. As shown in Fig. 5, Eq. A-1 is valid down to $(T_\lambda - T)^{-1/2} \approx 0.10$ or $T \approx T_\lambda - 100$ °C and up to $1/4(T - T_\lambda)^{-1/2} \sim 0.1$ or $T \sim T_\lambda + 6$ °C. Within this temperature range and using $T_\lambda = 139.2_0$ °C[2], only the tabulated data[2] for 139.27 °C and 139.52 °C deviate much from Eq. A-1 and the accuracy

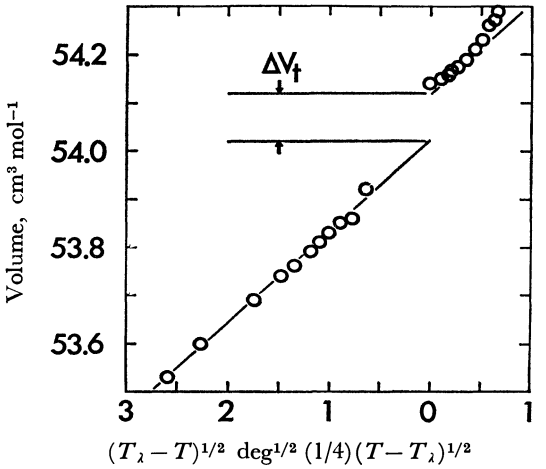

Fig. 6. Plot of molar volumes, for KSCN, *vs.* $(T_\lambda - T)^{1/2}$ for $T < T_\lambda$ and *vs.* $(1/4)(T - T_\lambda)^{1/2}$ for $T > T_\lambda$. The postulated volume discontinuity, ΔV_t, is indicated.

of these data very close to T_λ may be difficult to assess. The variation of thermal expansion with temperature may be anticipated from the Pippard relation[15-17] involving $C_{p/T}$, $(\partial V/\partial T)_p$ and dT_λ/dp. Thus plots of the thermal expansion data[3,18] *vs.* $|T_\lambda - T|^{-1/2}$ yield roughly linear fits over about the same temperature range for which Eq. A-1 is valid. Here, however, it is more accurate to describe the variation with temperature of the volumes—which were actually measured,[3,18] the thermal expansions being derived therefrom—and Fig. 6 shows the molar volumes[18] plotted *vs.* $(T_\lambda - T)^{1/2}$ for $T < T_\lambda$ and *vs.* $1/4(T - T_\lambda)^{1/2}$ for $T > T_\lambda$. For $T_\lambda = 142.7$ °C,[18] the slopes of the drawn lines (Fig. 6) are ≈ 0.19 cm^3 deg$^{-1/2}$ mol^{-1}, both above and below T_λ. It is inferred (Fig. 2) that there is a small, discontinuous volume change of ≈ 0.10 cm^3 mol^{-1} at the transition. Yamada and Watanabé[3] chose not to identify a discontinuous volume change there whereas Plester *et al.*[19] suggested a discontinuity of ~ 0.2 cm^3 mol^{-1}, almost certainly an overestimate due to inadequate data for the rapid variations near T_λ.

The Pippard relation together with the value of *A* (Eq. A-1) and the slope of the plot in Fig. 6 suggest $dT_\lambda/dp \sim 16._3$ deg kbar^{-1}, which compares well with the experimental values.[1,9] For the first-order component of the transition, the Clausius-Clapeyron equation suggests a discontinuous entropy change of ~ 0.14 cal deg^{-1} mol^{-1} and this may be within the uncertainties in the heat capacity data[2] near T_λ.

Appendix B: Lattice parameters of RbSCN and NH_4 SCN at high temperatures

by C. W. F. T. PISTORIUS

Diffractometer scans were made of RbSCN and NH_4SCN from the same stocks as used elsewhere in this paper. High temperature work was done with an MRC X-86-N attachment. For RbSCN at 23 °C, 54 reflections, up to (164), were observed and were consistent with Pbcm—as for KSCN[20] and TlSCN[21] below the solid-solid transition; the lattice parameters thus obtained were $a = 6.842$, $b = 6.895$, and $c = 8.019$ Å. For RbSCN at high temperatures, the following reflections were observed —(020), (200), (112), (022), (202), (122), (212), (130), (310), (224), (412)—and, above the transition, (112), (202), (220), (130), (224), (312). The lattice parameters deduced from these observed reflections are listed in Table B1, perhaps accurate to ±0.1%, at the various temperatures, accurate

Table B1. Lattice parameters of RbSCN and NH_4SCN at high temperatures

T(°C)	a(Å)	b(Å)	c(Å)	β(deg)
RbSCN				
23	6.842	6.896	8.017	
55	6.851	6.903	8.042	
75	6.856	6.909	8.060	
100	6.864	6.915	8.089	
120	6.872	6.922	8.114	
140	6.883	6.929	8.146	
161	6.901	6.938	8.179	
162		6.945	8.245	
180		6.948	8.264	
NH_4SCN				
22	4.247±3	7.146±5	13.022± 8	97.8_7
84	4.285±5	7.180±7	12.973±12	98.1_7
$88._5$	6.874±6	6.903±6	7.878± 8	
$102._5$	6.878±4	6.905±4	7.912± 6	
$117._5$	6.898±6	6.912±6	7.954± 8	
$140._5$		6.961±6	8.000± 8	

to ±5 °C. For NH_4SCN, lattice parameters were deduced from the (013), (102), (022), (112), (11$\bar{3}$), (121), (113), (12$\bar{2}$), and (015) reflections for the monoclinic phase, from the (121), (331), (042), (402), and several other reflections (all compatible with Pbcm) for the orthorhombic phase and from the (210), (112), (121), and (020) reflections for the tetragonal phase; the results are listed in Table Bl, at the various temperatures, accurate to ±5 °C above room temperature.

References

1) C. W. F. T. Pistorius, J. B. Clark, and E. Rapoport, *J. Chem. Phys.*, **48**, 5123 (1968).
2) M. Sakiyama, H. Suga, and S. Seki, *Bull. Chem. Soc. Jpn.*, **36**, 1025 (1963).
3) Y. Yamada and T. Watanabé, *Bull. Chem. Soc. Jpn.*, **36**, 1032 (1963).
4) C. W. F. T. Pistorius and J. C. A. Boeyens, *J. Chem. Phys.*, **48**, 1018 (1968).
5) Powder diffraction file-card No. 23—29.
6) I. Lindquist, *Acta Crystallogr.*, **10**, 29 (1957).
7) S. Manolatos, M. Tillinger, and B. Post, *J. Solid State Chem.*, **7**, 31 (1973).
8) C. W. F. T. Pistorius and J. B. Clark, *High Temp. High Press.*, **1**, 561 (1969); P. W. Richter and C. W. F. T. Pistorius, *J. Solid State Chem.*, **3**, 197 (1971).
9) P. W. Bridgman, *Proc. Am. Acad. Arts Sci.*, **51**, 55 (1915).
10) J. B. Wrzesnewsky, *Z. Anorg. Chem.*, **74**, 95 (1912).
11) H. F. Fischmeister, *Z. Phys. Chem. Neue Folge*, **7**, 91 (1959).
12) A. S. Dworkin and M. A. Bredig, *J. Phys. Chem.*, **74**, 3403 (1970).
13) W. Klement and L. H. Cohen, *Ber. Bunsenges. Phys. Chem.*, **79**, 327 (1975).
14) C. W. F. T. Pistorius, *Prog. Solid State Chem.*, in press.
15) W. Klement and L. H. Cohen, *Mol. Cryst. Liq. Cryst.*, **27**, 359 (1974).
16) A. B. Pippard, *Phil. Mag.*, **1**, 473 (1956).
17) W. Klement, *J. Phys. Chem.*, **74**, 2753 (1970).
18) T. Shinoda, H. Suga, and S. Seki, *Bull. Chem. Soc. Jpn.*, **33**, 1314 (1960).
19) D. W. Plester, S. E. Rogers, and A. R. Ubbelohde, *Proc. Roy. Soc. (London)*, **A235**, 469 (1956).
20) Powder diffraction file-card No. 9—388.
21) Powder diffraction file-card No. 8—65.

Free Radicals Produced by γ Irradiation of Nitroalkanes in Frozen Glassy Acidic Solutions

Masaru SHIOTANI, Alain FORCHIONI,* and Claude CHACHATY*

Faculty of Engineering, Hokkaido University, Sapporo 060

**Service de Chimie Physique, C.E.N. de Saclay, B.P.N° 2, 91190 Gif-sur-Yvette, France*

(Received October 29, 1975)

The scavenging of paramagnetic species by nitroalkanes formed during the γ irradiation of aqueous 6.4 molar sulfuric acid glasses has been studied by using ESR. Nitroalkanes give rise to RNO_2H radiclas, the nitrogen hyperfine coupling of which has the values $A_{//}^N=48$ G and $A_{\perp}^N=18$ G with $g_{//}=2.0035$ and $g_{\perp}=2.0075$. The RNO_2H yields for 0.5 molar solutions of nitromethane and 2-nitro-2-methyl-propanol are $G\simeq4$ and $G\simeq3$, respectively. $G(SO_4^- + OH\cdot)$ is roughly idenpendent of the nitroalkane concentration. These results are interpreted as the scavenging of hydrogen atoms due to the energetic recombination of non-hydrated primary species (H_2O^+, $OH\cdot$, e^-) according to an assumption of Hamill.

Since the first report by Livingston[1] of the possibility of trapping hydrogen atoms in glassy acidic matrices below 100 K, several ESR investigations have been made on the mechanism of formation, the spatial distribution and the thermal decay of trapped hydrogen atoms.[2] Only a few studies have been devoted to the radicals formed in the presence of electron and hydrogen atom scavengers. Among these radicals, the nitroalkanes are known to be particularly efficient as shown by ESR[3-6] and optical absorption studies[7,8] on liquid solutions of these compounds in polar solvents or in water.

The present work was carried out to identify the radicals from γ irradiated nitroalkanes at low temperature in glassy sulfuric acid aqueous solutions and to investigate their formation mechanism. The results of this study will be compared to those of a previous one in which nitroalkanes were irradiated in concentrated alkaline aqueous solutions[6] giving rise to unexpectedly high radical yields.

Experimental

Nitromethane (NM) was distilled at 72—74°C at pressure of 400 Torr in an argon atmosphere through a column containing a rotating helicoidal band. 2-Nitro-2-methyl-propanol (NMP) furnished by Aldrich Chemicals was used without further purification. Acidic solutions of nitroalkane were prepared just before degassing under vacuum. They were plunged into liquid nitrogen resulting in clear transparent glasses and stored at 77 K until they were irradiated. The irradiation dose rates were determined by ferrous sulfate dosimetry of the ^{60}Co source taking $G(Fe^{3+})=15.5$. The usual dose rates were 5.8×10^{19} eV mol^{-1} h^{-1} and 1.67×10^{20} eV ml^{-1} h^{-1}.

The ESR spectra were recorded with a Strand Labs 601 BX spectrometer operating at 9250 MHz with a 10 kHz field modulation. The microwave power level was kept below 0.1 mW to prevent saturation of the signals. The absolute yield of radicals trapped in the acidic matrix at 77 K was determined by double integration of the ESR spectra using $G(e_s^- + CH_3CHOH)=8$ for the reference sample of glassy ethanol irradiated under the same conditions and 1.3 for the ratio of the absorbed irradiation doses in 6.4 molar sulfuric acid glass and in ethanol.

The ESR experiments were completed by subsidiary gas chromatographic measurements of the molecular hydrogen yield by the method reported in Ref. 9.

Results and Discussion

Identification of the Free Radicals. Glassy Aqueous Solutions of H_2SO_4 without Additives: The ESR spectrum of γ irradiated H_2SO_4/H_2O glass consists of an asymmetrical singlet centered in the vicinity of $g=2.01$ and two lines separated by 505 G corresponding to trapped hydrogen atoms as shown in Fig. 1a. The singlet is attributed to either SO_4^- or HSO_4 radicals, but are hard to distinguished on account of the absence of hyperfine

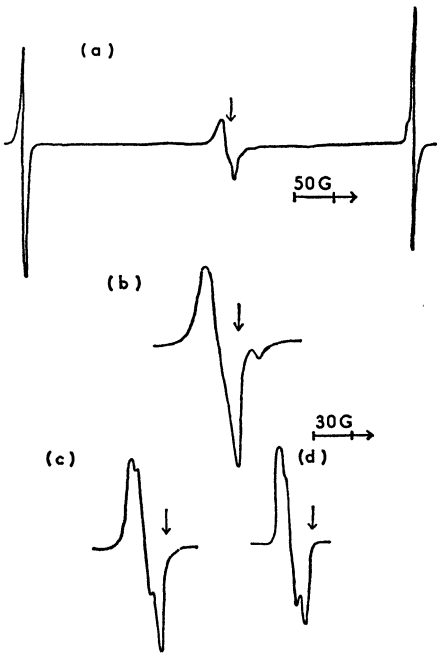

Fig. 1. ESR spectra of the radicals produced by γ irradiation of 6.5 mol dm^{-3} H_2SO_4 glassy solution of 77 K.
(a): Observed spectrum at 77 K immediately after γ irradiation.
(b): Extended spectrum of the central part of the spectrum (a).
(c): Observed spectrum at 77 K after warming above 150 K.
(d): Simulated spectrum corresponding to (c). The used parameters are given in the text. The vertical arrow indicates the position of $g=2.0036$.

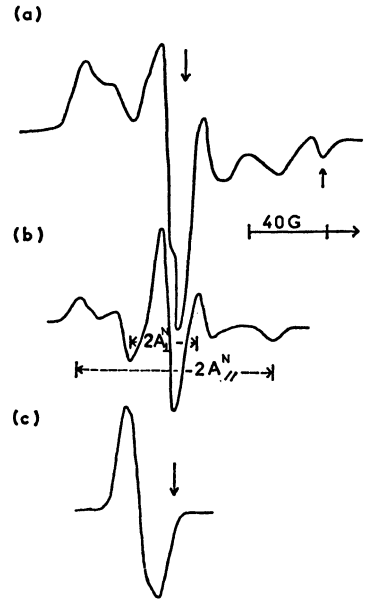

Fig. 2. ESR spectra of γ irradiated 0.5 molar solution of NMP in H_2SO_4/H_2O glasses at 77 K.
(a): Observed at 77 K.
(b) and (c): Simulated spectra of the radicals $(CH_3)_2=\dot{C}(CH_2OH)(NO_2H)$ and $SO_4^{\cdot-}$ (or $HSO_4^{\cdot}$) respectively.
The parameters used for this calculation are given in the text. The arrow shows (↑) a line assigned to $NO_2^{\cdot}$.

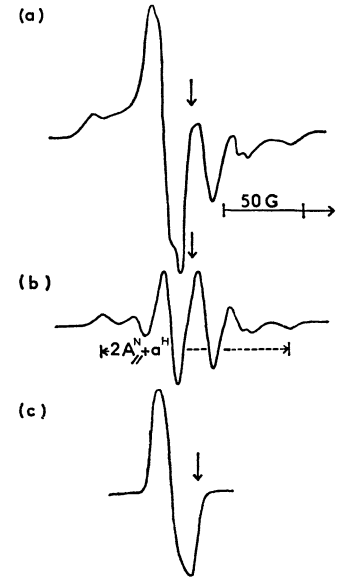

Fig. 3. ESR spectra of the radicals produced by γ irradiation of 0.5 molar solutions of CH_3NO_2 in H_2SO_4/H_2O glasses at 77 K.
(a): Spectrum observed at 77 K.
(b) and (c): Simulated spectra of radicals $CH_3\dot{N}O_2H$ and $SO_4^{\cdot-}$ (or $H\dot{S}O_4$) respectively.

structure (Fig. 1b). Here, it is assumed for the sake of simplicity that we are only dealing with $SO_4^{\cdot-}$. A weak peak is also seen on the high field side of the central asymmetric singlet. This peak belongs most likely to the asymmetrical doublet of the residual $OH^{\cdot}$ radicals (see, for instance, Ref. 2). The signal of $OH^{\cdot}$ is completely removed upon warming of the sample above 150 K, as is shown in Fig. 1c. The spectrum of $SO_4^{\cdot-}$ has been simulated using the program of Lefebvre and Maruani[10] and employing the optimized parameters $g_1=2.0064$, $g_2=2.0134$, $g_3=2.0192$ with a Gaussian line width $\lambda=5$ G (Fig. 1d). These principal values of the $\tilde{g}$ tensor are in good agreement with those given in Ref. 2c and the calculated second moment, $\langle\Delta H^2\rangle_{cal}=289\ G^2$, is fairly close to the experimental value, $\langle\Delta H^2\rangle_{exp}=297\ G^2$.

Radicals Formed in the Presence of Nitroalkanes: Nitromethane and NMP were irradiated in glassy sulfuric acid matrices in a concentration range from 0.01 to 0.5 mol. In both cases the yield of trapped hydrogen atoms is reduced drastically for scavenger concentrations above 0.25 mol dm^{-3}, as shown in Fig. 4d. The ESR spectrum of irradiated NMP in the H_2SO_4/H_2O glassy matrix is interpreted as the superposition of the spectra of $R\dot{N}O_2H$ and $SO_4^{\cdot-}$ radicals, as is shown in Fig. 2. Figure 2b shows that the computer simulation of the spectrum of the $R\dot{N}O_2H$ radical gives the best agreement with the experimental results when using $A_{//}^N=48$ G, $A_{\perp}^N=18$ G ($a_{iso}^N=28$ G) and $g_{//}=2.0035$ and $g_{\perp}=2.0075$ ($g_{iso}=2.0062$) where $A_{//}^N$, $A_{\perp}^N$, $g_{//}$ and $g_{\perp}$ are the principal values of the nitrogen hyperfine coupling tensor $\tilde{A}^N$ and of the $\tilde{g}$ tensor, respectively, the Gaussian line width being $\lambda=5$ G. The relevant second moment is $\langle\Delta H^2\rangle=694\ G^2$ with respect to 2.0036 (DPPH resonance). Exactly the same principal values of the $\tilde{A}_N$ and $\tilde{g}$ tensors as those previously reported for RNO_2H radicals trapped in alcohol matrices[3,4] were obtained, confirming that a species formed by direct hydrogen atom scavenging:

$$RNO_2 + H^{\cdot} \longrightarrow R\dot{N}O_2H \qquad (1)$$

and by electron scavenging followed by protonation of the anion radical:

$$RNO_2 + e^- \longrightarrow R\dot{N}O_2^- \xrightarrow{H_3O^+} H_2O + R\dot{N}O_2H \qquad (2)$$

is involved.

Figure 2a implies that in the case of 0.5 molar NMP in H_2SO_4/H_2O glass, there is a small contribution from the direct effect of γ irradiation to the formation of the $NO_2^{\cdot}$ radical which is detected by its high-field line. The other lines together with the spectrum of the radical $(CH_3)_2=\dot{C}-CH_2OH$, which are expected to be formed simultaneously, must be hidden under the much more intense spectra of the $R\dot{N}O_2H$ and $SO_4^{\cdot-}$ radicals.

In the case of CH_3NO_2 irradiated at 77 K, the ESR spectrum of CH_3NO_2 with $A_{//}^N=48$ G and $A_{\perp}^N=18$ G is observed and the coupling $a_{\beta}^H=22$ G of only one proton of the methyl group is resolved (Fig. 3). The rotation of the methyl group about the C–N bond is therefore hindered and the equilibrium positions of

Table 1. Radiochemical yields of radicals and molecular hydrogen

	G (H_2)	G ($H\cdot$)	G ($R\dot{N}O_2H$)	G ($SO_4^{-}+OH\cdot$)
H_2SO_4 6.4 mol. without additive	0.7 ±0.02	1.8±0.4	—	2.2±0.5
$HOH_2C-\overset{CH_3}{\underset{CH_3}{C}}-NO_2$ 0.5 mol in H_2SO_4/H_2O	0.22±0.02	≃0	2.7±1.0	2.3±0.3
CH_3NO_2 0.5 mol in H_2SO_4/H_2O	0.06±0.01	≃0	3.9±0.5	2.2±0.05

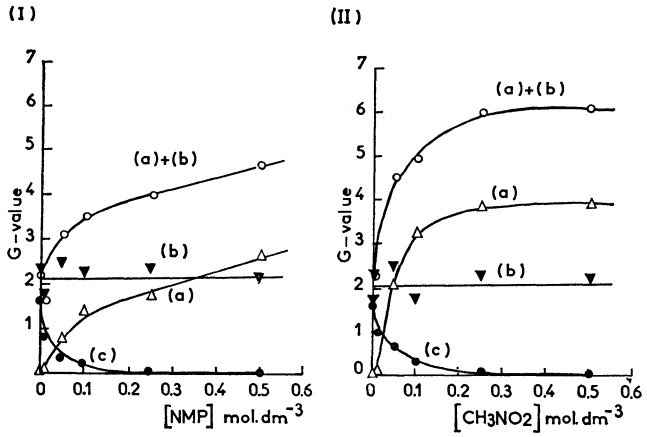

Fig. 4. G values of radicals measured at 77 K as a function of the concentration of nitroalkanes in H_2SO_4/H_2O glasses. (I) and (II) correspond to NMP and CH_3NO_2 respectively.

(a): △ $(CH_3)_2=C\overset{CH_2OH}{\underset{NO_2H}{\cdot}}$ or $CH_3\dot{N}O_2H$,

(b): ▼ SO_4^{-} (or $HSO_4\cdot$), (c): ● $H\cdot$.

Irradiation dose : 2.5×10^{20} eV ml^{-1}.

each proton correspond to the angles $\theta_1=0$ ($a_\beta^H=22.5$ G) and $\theta_2=\theta_3=\pm120°$ ($a_\beta^H=5.5$ G) where θ is the angle between the H_β–C–N plane and the axis of the nitrogen centered $2P\pi$ orbital of the unpaired electron. The spectrum of Fig. 3b was computed with these values of a_β^H, values of the $\tilde{A}^N$ and $\tilde{g}$ tensors which are given above and $\lambda=7$ G. The corresponding second moment is $\langle\Delta H^2\rangle=820$ G^2. The experimental spectrum of $CH_3\dot{N}O_2H$ recorded at 77 K is partially superposed on that of SO_4^{-} (Fig. 3a). Upon warming, the former shows a complex structure due to the release of the intermolecular rotation about the C–N bond, as previously reported for the same radical trapped in alcohol matrices.[3]

Determination of Radiochemical Yields. Measurements of radical and molecular hydrogen yields were carried out as a function of the concentration of nitroalkanes up to 0.5 mol and of irradiation doses up to 2.5×10^{20} eV ml^{-1}, as summarized in Figs. 4, 5, 6 and in Table 1. In the absence of nitroalkanes, the radiochemical yields for trapped hydrogen atoms and molecular hydrogen were $G(H_t)_0=1.8\pm0.4$ and $G(H_2)_0=0.7\pm0.02$, respectively. These values are in agreement with those given by Livingston and Weinberger,[11]

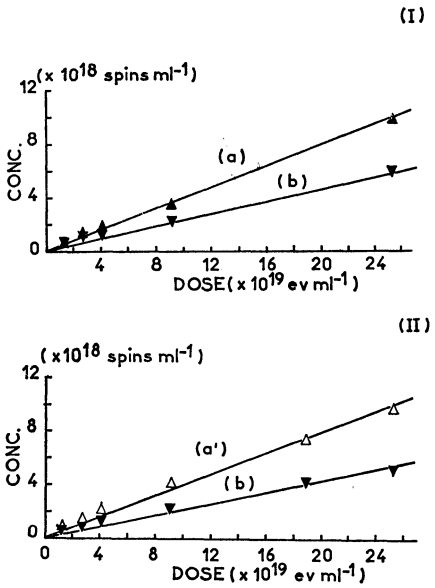

Fig. 5. Concentration of radicals as a function of irradiation dose. (I) and (II) correspond respectievly to NMP and to CH_3NO_2H 0.5 mol dm^{-3} in H_2SO_4/H_2O glassy solutions.

(a): ▲ $(CH_3)_2=C\overset{CH_2OH}{\underset{NO_2H}{\cdot}}$

(a'): △ $CH_3\dot{N}O_2H$, (b): ▼ SO_4^{-} ($HSO_4\cdot$).

$G(H_t)_0=1.5$ and $G(H_2)_0=0.6$, for an identical sulfuric acid concentration of 6.4 mol dm^{-3}. on the other hand, the sum of the G values of the SO^{-} and $OH\cdot$ radicals was found to be 2.2±0.5 and is in satisfactory agreement with the data of Henriksen and Köhnlein.[12,13] Taking into account the probable mechanisms of formation of atomic and molecular hydrogen, as well as that of $OH\cdot$ and SO_4^{-} radicals,[2] it may be assumed that $G(H_t)\sim G(SO_4^{-}+OH\cdot)\simeq2$ within the limits of experimental errors.

In the case of nitroalkane glassy solutions, the central part of the ESR spectra corresponds to SO_4^{-}, $R\dot{N}O_2H$ and $OH\cdot$. The relative yield of the $R\dot{N}O_2H$ radicals is estimated from the additivity rule of the second moments setting $\langle\Delta H^2\rangle=335$ G^2 for the composite spectrum of $SO_4^{-}+OH\cdot$ (Fig. 1b) and $\langle\Delta H^2\rangle=694$ G^2 and 820 G^2 for the $R\dot{N}O_2H$ radicals from NMP and CH_3NO_2, respectively (calculated values). Figure 5 shows that the concentration of free radicals

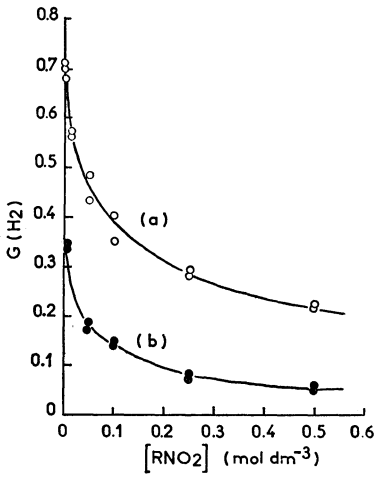

Fig. 6. G value of hydrogen molecules as a function of the concentration of nitroalkanes.
(a) and (b): Correspond respectively to the addition of NMP and CH_3NO_2. Irradiation dose : 4.2×10^{19} eV ml^{-1}.

induced by γ rays increases linearly with the irradiation dose and that no saturation tendency is observed under the present experimental conditions.

As shown in Fig. 4, the yield of $CH_3\dot{N}O_2H$ radicals increases rapidly with the nitromethane concentration up to 0.2 molar with a concomitant decay of hydrogen atoms which is no longer observed above $[CH_3NO_2]=0.25$ mol dm^{-3}. The yield of $CH_3\dot{N}O_2H$ reaches a limiting value of $G(CH_3\dot{N}O_2H)\simeq3.9$. It may be pointed out that the total limiting radical yield obtained in the presence of nitromethane is $G(R\cdot)\simeq6$, whereas in the absence of scavengers $G(R\cdot)\simeq4$. NMP is quite similar to CH_3NO_3 in following the trend that the trapped hydrogen atoms disappear completely when the concentration of the nitrocompound exceeds 0.25—0.3 mol dm^{-3}. However, NMP behaves as a less efficient electron and hydrogen atom scavenger than CH_3NO_2 since the total radical yield is $G(R\cdot)\simeq4$ at a maximum concentration of 0.5 mol dm^{-3}. The limiting yield of the $R\dot{N}O_2H$ radical from NMP could not be evaluated on account of the direct effect giving rise to $NO_2\cdot$ at higher concentrations of NMP. An important point is that the yield of $SO_4^{\cdot-}+OH\cdot$ is always of the order of 2 and independent of the concentration of added nitrocompounds (Fig. 4).

Chromatographic analysis of the molecular hydrogen yields shows that $G(H_2)$ is more efficiently reduced by CH_3NO_2 than by NMP and that it becomes negligibly small as $[CH_3NO_2]$ exceeds 0.3 mol dm^{-3}.

Discussion. It is interesting to point out that $G(H_t\cdot)\simeq G(SO_4^{\cdot-}+OH\cdot)\simeq2$ is just as in the case of alkaline glasses where $G(e^-_{solv.})\simeq G(O^{\cdot-})\simeq2$.[12] This suggests that the precursor of $H_t\cdot$ is the solvated electron and that the contribution of reaction 3 is unimportant:

$$H_2O \xrightarrow{\gamma} (H_2O)^* \longrightarrow H\cdot + OH\cdot \qquad (3)$$

The fact that $G(H_2)$ becomes negligibly small at nitroalkane high concentrations suggests that there is no direct formation of molecular hydrogen during γ radiolysis. On the other hand, the limiting yield of $G(CH_3\dot{N}O_2H)\simeq4$—5 obtained for nitromethane glassy solutions cannot be explained by assuming that this compound reacts directly with electrons before hydration (dry electrons). Otherwise, a concomitant increase of $G(SO_4^{\cdot-}+OH\cdot)$ which is produced by the precursor $(H_2O)^+$ should be observed. As in the case of nitroalkanes in alkaline glass,[6] we are led to the conclusion that the yield of $CH_3\dot{N}O_2H$ radicals which exceeds 2 may be due to the scavenging of hydrogen atoms from the entity ($H\cdot$, $H\cdot$, $OH\cdot$, $OH\cdot$) resulting from the energetic recombination of non-hydrated primary species.[14] The $R\dot{N}O_2H$ yield is actually the same as the total yield of the hydrated and dry electrons determined in previous work on the radiolysis of water.[14]

References

1) R. Livingston, H. Zeldes, and E. H. Taylor, *Phys. Rev.*, **94**, 725 (1954) and *Discuss. Faraday Soc.*, **19**, 166 (1955).
2) (a) P. N. Moorthy and J. J. Weiss, *Adv. Chem. Ser.*, **50**, 180 (1965); (b) L. Kevan, Radiation Chemistry of Aqueous Solution, Proc. 19th L. Farkas Memorial Symposium, Hebrew University, Jerusalem, 1967; (c) B. G. Ershow and A. K. Pikaev, *Radiat. Res. Rev.* **2**, 1 (1969).
3) C. Chachaty and C. Rosilio, *J. Chim. Phys. Phys.-Chim. Biol.*, **64**, 777 (1967).
4) C. Chachaty, Thèse de Doctorat ès Sciences, Université de Paris, 1968 (Rapport CEA, R3537, 1969).
5) E. Eiben and R. W. Fessenden, *J. Phys. Chem.*, **72**, 3387 (1968).
6) A. Forchioni and C. Chachaty, *Int. J. Radiat. Phys. Chem.* **2**, 231 (1970).
7) K. D. Asmus, A. Henglein, and G. Beck, *Ber. Bunsenges. Phys. Chem.*, **70**, 459 (1966).
8) K. D. Asmus and I. Taub, *J. Phys. Chem.*, **72**, 3382 (1968).
9) M. Faraggi and J. Desalos, *Int. J. Radiat. Phys. Chem.*, **1**, 335 (1969).
10) R. Lefebvre and J. Maruani, *J. Chem. Phys.*, **42**, 1480 (1965).
11) R. Livingston and A. J. Weinberger, *J. Chem. Phys.*, **33**, 499 (1960).
12) T. Henriksen, *Rad. Research*, **23**, 63 (1964).
13) W. Köhnlein and D. Schulte-Frohlinde, *Rad. Research*, **38**, 173 (1969).
14) W. H. Hamill, *J. Phys. Chem.*, **73**, 1341 (1969).

The Electronic Spectra of Some Phenylthiophenes. A Molecular Orbital Treatment

R. ABU-EITTAH† and R. HILAL*

Department of Chemistry, Faculty of Science, Kuwait University, Kuwait

**Department of Chemistry, Faculty of Science, Cairo University, Giza, Egypt*

(Received December 2, 1975)

The electronic absorption spectra of the thiophene derivatives: mono, di-, and poly-phenylthiophenes are studied in both polar and non-polar solvents. The interaction between thienyl and phenyl chromophores is investigated both experimentally and theoretically. Assuming planar and perpendicular conformers, molecular orbital calculations are carried out on 2-phenylthiophene and on 3-phenylthiophene using the Localized-Orbital Model. The results show: (i) the planar conformer is more adquate than the perpendicular one, (ii) the near UV spectra of the two isomers are similar though their degree of conjugation is different, and (iii) excited states arise from substantial configuration interaction. There is a good agreement between the observed and calculated spectra of the two isomers.

The electronic structures of the studied compounds are of interest since though aryl thiophenes are of chemical and biological importance, yet their chemistry has made no remarkable progress. Substitution in the thiophene ring affects the spectrum in a way which depends on the type of the substituent and position of substitution. Ostman[1] used the ω technique and the "p" and "d" models for the "π" orbitals and showed that α-position in thiophene is more active than the β-position. It is found that the position of the longest wavelength band of 2-substituted thiophenes is lineary related to the ^1L_a band of monosubstituted benzenes.[2]

Many molecular orbital calculations have been reported on the π-electron system of thiophene and related compounds.[3-6] The electronic spectra of some thiophene derivatives are interpreted *via* SCFMO calculations,[7-9] and the results agree with the experiment. It has been shown that d-orbital participation is considered trivial in correlation with the spectra of thiophene[4-10] as well as the spectra of composite molecules containing thiophene.[11,12]

The spectra and theoretical treatment of arylthiophenes are not thoroughly studied in the literature. The extended Hückel theory has been applied to 2- and 3-phenylthiophenes and showed that the molecules have an equilibrium conformation twisted by 37° from the planar conformer.[13] Elpern and Nachod[14] reported the spectra of 2- and 3-phenylthiophenes and interpreted them on the basis of linear and cross conjugated systems.

In this work, the electronic spectra of some phenylthiophenes are investigated. Results (experimental and theoretical) show that differentiation of phenylthiophene to linear and cross conjugated systems cannot be done on the basis of their spectra. The LOM has been applied successfully to conjugated hydrocarbons made up of two unsaturated residues joined by a single bond.[15]

Experimental

The studied phenylthiophenes were prepared by the methods reported in the literature,[16-18] the products were purified by repeated crystallization and the melting points correspond well with the reported values. The compounds, 2,4- and 3,4-diphenylthiophenes, were kindly provided by Prof. El-Gindy.

Solvents were purified as given before[19] and the spectra were scanned on a Beckman DK Spectrophotometer using 1.0 cm fused silica cells.

Results and Discussion

Interpretation of the Spectra. The electronic absorption spectra of 2-phenylthiophene are given in Fig. 1 using ethanol, 1- and 2-propanol as solvents. The shift in band maxima depends on both dipole moment and refractive index of the solvent as shown by Bayliss and McRae.[20] The spectrum in the 330—200 nm region includes three electronic transitions identified as I, II, and III (starting from lowest energy). Two transitions (I and II) are overlapping and appear as a broad asymmetric band in the 300—240 nm region and the third transition appears as an intense shoulder in the region of 220 nm. That the broad asymmetric band consists of two overlapping transi-

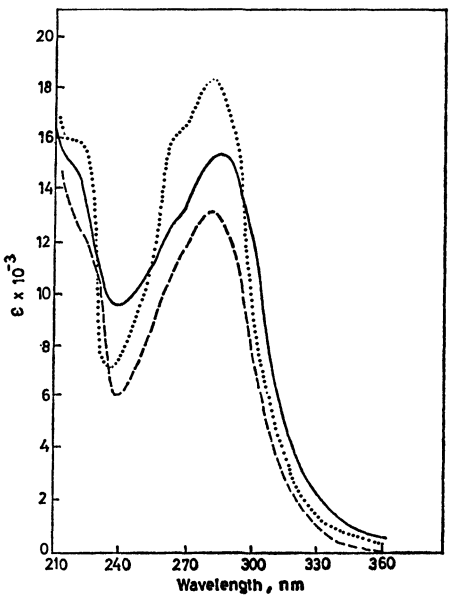

Fig. 1. Electronic absorption spectra of 2-phenylthiophene in 2-propanol (——), ethanol (----), and propanol (·····).

† To whom all correspondences should be addressed.

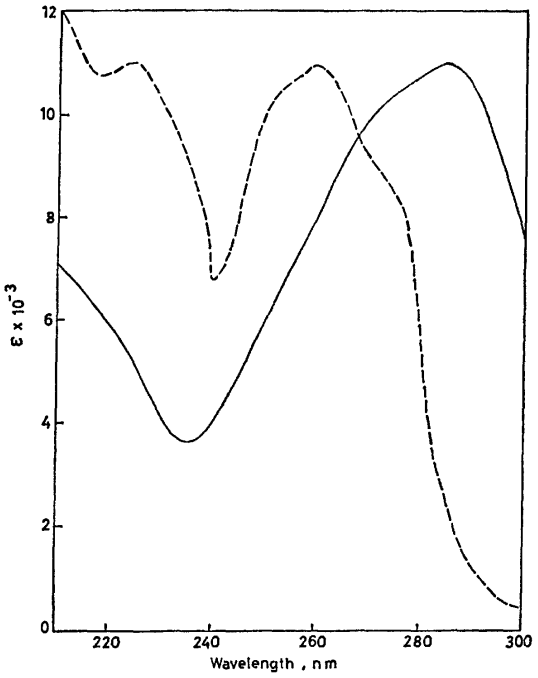

Fig. 2. Electronic absorption spectra of 2-phenylthiophene (——) and 3-phenylthiophene in ethanol (----).

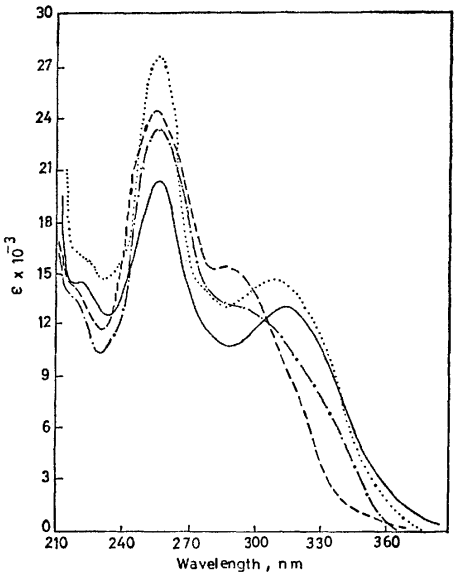

Fig. 3. Electronic absorption spectra of 2,4-diphenylthiophene in ethanol (——), 2,4-diphenylthiophene in cyclohexane (·····), 2,5-diphenylthiophene in ethanol (—·—), and 2,5-diphenylthiophene in cyclohexane (----).

tions is seen when comparing the spectra in ethanol and 1-propanol (Fig. 1). In the latter, the extent of overlap is decreased and transition II is easily traced. In ethanol and 2-propanol the extent of overlap of the first two electronic transitions is appreciable, yet careful examination of the band indicates that it comprises two overlapping transitions. Confirmation of this conclusion will be obtained *via* MO calculations.

The composite molecule, 2-phenylthiophene, can be considered to consist of two subsystems: thiophene and benzene. Since the two subsystems are separated by one single bond, interaction between the excited states of the two subsystems will be extensive. As a result, the excited states of the composite molecule will differ appreciably from the excited states of the separate subsystems. Hence it is not adequate to assign the transitions in 2-phenylthiophene to ones localized over the thiophene nucleus and others localized over the benzene nucleus especially if coplanarity of the molecule is not significantly distorted.

According to the resonance theory, the spectrum of 3-phenylthiophene should be different from that of the 2-phenyl derivative. However, this is not the case as Fig. 2 shows, and the two phenyl derivatives of thiophene have comparable spectra. The spectrum of the 3-phenyl derivative shows a broad band (300—240 nm) which also consists of two overlapping transitions (I and II) and the third transition appears as a shoulder. The dipole moments of 2- and 3-phenylthiophenes are 0.8 and 0.81 D respectively.[21] This shows that charge distribution in the two compounds are similar and consequently their spectra are expected to be similar. Substitution in the α-position of thiophene affects the spectrum but slightly and the resonance theory cannot adequately interpret the spectra of compounds as phenylthiophenes. The spectra of nitroanilines cannot be interpreted on the basis of the resonance theory. Contrary to the prediction of this theory, *ortho*- and *meta*-derivatives have similar spectra which differ from that of the *para*-derivative.[18,22]

Elpern and Nachod[14] reported the spectra of 2- and 3-phenylthiophene. They assigned the first transition of the two compounds to bands with λ_{max}=280 and 260 nm respectively and overlooked the fact that the first band in the spectra of the two compounds consists of two overlapping transitions. They attributed the difference in band maxima of the two compounds to the fact that the 3-phenyl isomer is cross conjugated. The results of this work indicate that 2-phenylthiophene has the first two electronic transitions at 282 and 264 nm whereas 3-phenylthiophene has the first two transitions at 275 and 260 nm which is quite comparable. The difference in transition energies of the two compounds is much less than that expected according to the resonance theory.

To confirm the above conclusion the spectra of 2,4-, 3,4-, and 2,5-diphenylthiophenes are investigated and shown in Figs. 3 and 4. The spectra of all diphenylthiophenes show three electronic transitions in the accessible ultraviolet region. In case of 2,5-diphenylthiophene the lowest energy transition (294 nm) appears as a shoulder at the long wavelength tail of the strong ~250 nm transition. The highest energy transition appears as a shoulder in the region of 220 nm. Band maxima are of the same value when the solvent is cyclohexane or ethanol, indicating that the bands are due to π–π^* transitions and charge transfer character is not apparent in the observed transitions.

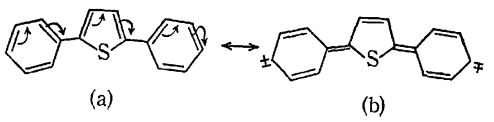

A comparison of the spectra of 2,5-diphenylthiophene and 2,4-diphenylthiophene is worthy. The extent of coplanarity is expected to be the same in the two compounds yet both have different sturctures (b) and (c).

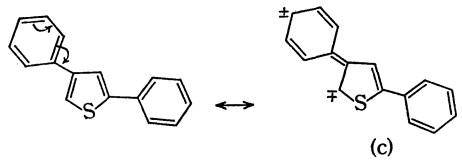

(c)

Accordingly, the two compounds ought to have different spectra and that the 2,5-diphenylthiophene absorbs light at longer wavelength than the 2,4-diphenyl derivative due to contribution of forms as (b) to the excited state. Experimentally, the spectra of the two compounds are comparable and 2,4-diphenylthiophene absorbs light at wavelength longer than the 2,5-diphenyl derivative. The bands observed for the studied compounds are assigned to excited states of the composite molecule and not to excited states of any of the subsystems (benzene and thiophene).

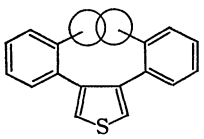

In case of 3,4-diphenylthiophene steric hindrance is significant and the spectrum of the composite molecule will be the additive spectra of the subsystems. This is seen in Fig. 4. The two benzene rings are not in one plane and probably not in the plane of thiophene

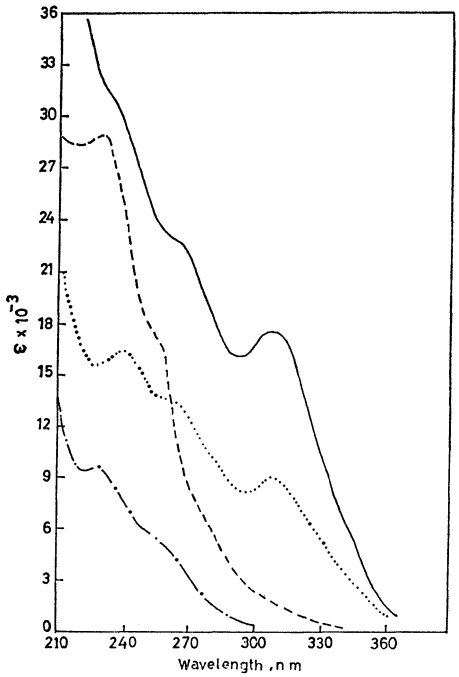

Fig. 4. Electronic absorption spectra of tetraphenylthiophene in ethanol (——), tetraphenylthiophene in cyclohexane (·····), 3,4-diphenylthiophene in ethanol (—·—), and 3,4-diphenylthiophene in cyclohexane (----).

Table 1. Band maxima and intensities of the studied phenylthiophenes in ethanol

Compound	λ_{max}, nm	ε M^{-1} cm^{-1}	f
2-Phenylthiophene	282	13 280	0.40
	264	6 500	0.19
	220	8 320	0.34
3-Phenylthiophene	275	6 350	0.07
	260	11 000	0.24
	222	11 000	0.22
2,5-Diphenylthiophene	294	13 265	0.32
	255	23 600	0.86
	220	14 189	—
2,4-Diphenylthiophene	312	13 147	0.44
	256	20 840	0.70
	222	14 430	0.59
3,4-Diphenylthiophene	255	5 200	0.13
	230	7 820	0.34
Tetraphenylthiophene	306	17 460	0.53
	258	23 280	1.05
	230	30 652	1.80

ring. If one benzene ring is coplanar with the thiophene ring the spectrum of 3,4-diphenylthiophene would be similar to that of 3-phenylthiophene, this is not the case.

The spectrum of tetraphenylthiophene is shown in Fig. 4. If one considers unsymmetric twist of the phenyl groups, the spectrum of tetraphenylthiophene will be that of the 2,4- and 3,4-isomers.

Table 1 gives the numerical values of band maximum, molar absorptivity and oscillator strength.

Molecular Orbital Calculations. The self-consistent molecular orbitals of the composite molecule A–B are those of the separate constituents A and B. If the subsystems are joined through atom u in A and atom v in B, then their extent of interaction is determined by the value of the resonance integral β_{uv}. If $\beta_{uv}=0$, the electronic excited states will be the locally excited ones A*, and B*, in addition to the charge transfer ones. The general expression for the interaction between two different singly excited configurations $^1\psi_{a-b}$ and $^1\psi_{c-d}$ is given by[23]:

$$\langle {}^1\psi_{a-b}|\hat{H}|{}^1\psi_{c-d}\rangle = 2(cd|ab) - (ca|bd)$$

where $\hat{H}$ is the Hamiltonian for the system for which $\beta_{uv}=0$

Application to Perpendicular Conformers. 2-Phenylthiophene: The effect of steric hindrance in 2-phenylthiophene will cause the rings of the constituents to be non-coplanar. The value of β will be small and in the case the two rings are perpendicular will be zero. The self consistent orbitals of benzene (θ's) and of thiophene (y's) subsystems are shown in Fig. 5, and a schematic energy level diagram is shown in Fig. 6. In case of thiophene, the d-orbitals are not included since its participation is considered trivial when dealing with the UV spectrum. The singly excited states of benzene are:

$$\theta_{\beta'} = (1/2^{1/2})(\theta_3^{-1}\theta_4 - \theta_2^{-1}\theta_5);\ \theta_{\beta} = (1/2^{1/2})(\theta_3^{-1}\theta_5 + \theta_2^{-1}\theta_4)$$

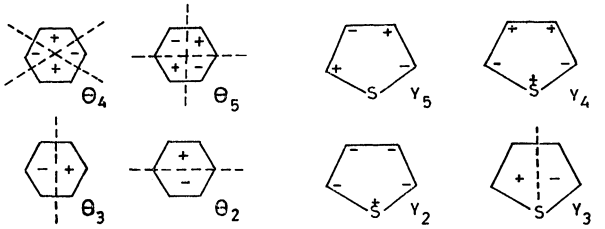

Fig. 5. The self consistent orbitals of benzene (θ) and thiophene (Y).

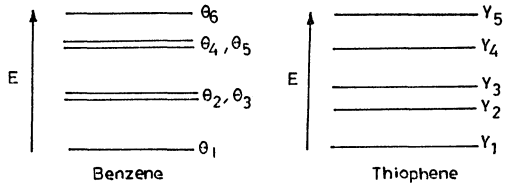

Fig. 6. A non scale energy level diagram for benzene and thiophene molecules.

$$\theta_p = (1/2^{1/2})(\theta_3^{-1}\theta_4 + \theta_2^{-1}\theta_5);\ \theta_\alpha = (1/2^{1/2})(\theta_3^{-1}\theta_5 - \theta_2^{-1}\theta_4)$$

The singly excited states of thiophene ring are constructed from the interaction between configurations of the same symmetry. The energy of the different configurations: $y_3^{-1}y_4$, $y_3^{-1}y_5$, $y_2^{-1}y_4$, $y_2^{-1}y_5$ are computed by the usual procedure,[24] and the configuration interaction matrix of thiophene is solved. The form of the first four singly excited states of thiophene are:

$$Y_I = (0.999y_3^{-1}y_4 - 0.009y_2^{-1}y_5);$$
$$Y_{II} = (0.893y_2^{-1}y_4 - 0.449y_3^{-1}y_5);$$
$$Y_{III} = (0.449y_2^{-1}y_4 + 0.893y_3^{-1}y_5);$$
$$Y_{IV} = (0.009y_3^{-1}y_4 + 0.999y_2^{-1}y_4).$$

Since orbitals θ and y are self consistent, the ground state will not interact with any of the singly excited configurations. There will be, however, interaction between the locally excited states of the thiophene and benzene rings. The molecule, 2-phenylthiophene, is not symmetric and as a result we consider interaction between all the excited states of the two subsystems. The matrix elements of the Hamiltonian between the locally excited states Y's and θ's are computed as follows:

$$\langle Y_I|\hat{H}|\theta_\alpha\rangle = \langle(0.999y_3^{-1}y_4 - 0.009y_2^{-1}y_5)|\hat{H}|(1/2^{1/2})(\theta_3^{-1}\theta_5 - \theta_2^{-1}\theta_4)\rangle \quad (1)$$

$$\langle y_3^{-1}y_4|\hat{H}|\theta_3^{-1}\theta_5\rangle = 2(\theta_3\theta_5|y_3y_4) - (\theta_3y_3|\theta_5y_5). \quad (2)$$

The second term in integral 2 is zero and to evaluate the first term of this integral, one expands[15] the MO in terms of the AO functions and using the ZDO approximation,

$$2(\theta_3\theta_5|y_3y_4) = 2(\sum_{u,\nu} C_{\theta_{3u}}C_{\theta_{5u}}C_{y_{4\nu}}C_{y_{3\nu}}\gamma_{u\nu}).$$

For the perpendicular conformers, only, electron repulsion integrals are considered between atom (1) in benzene (u), and atom (2) of thiophene (ν), and the terms $\gamma_{u\nu}$ are evaluated using the Nishimoto-Mataga[25] equation. Proceeding in this way the matrix elements of the Hamiltonian are computed between the eight states of 2-phenylthiophene. Solving this matrix, the energies and state wave finctions are obtained. The first three are:

(1) $0.765Y_I - 0.116Y_{II} + 0.182Y_{III} - 0.495\theta_\beta - 0.292\theta_p + 0.191\theta_\alpha$ ·····4.78 eV

(2) $\theta_{\beta'}$ ·····4.91 eV

(3) $0.184Y_I + 0.981Y_{II} - 0.022Y_{III} + 0.068\theta_p$ ···5.92 eV.

Comparison with experiment is postponed till we consider the planar conformer.

3-Phenylthiophene: Before considering the effect of conjugation between benzene and thiophene nuclei in 2-phenylthiophene it would be interesting to consider the perpendicular conformer of 3-phenylthiophene, computations are analogous to those of the 2-isomer. The matrix elements of the Hamiltonian between the locally excited states of the two subsystems are calculated as is done with the 2-phenyl isomer. The numerical values of these elements are much less than the corresponding ones of the 2-phenyl isomer. To this reason we attribute the difference in transition energies of the two isomers. Solving the interaction matrix of 3-phenylthiophene one gets the state functions and energies, of which:

(1) $\theta_{\beta'}$ ·····4.91 eV

(2) $0.726Y_I + 0.116Y_{II} + 0.229Y_{III} + 0.172\,Y_{IV} + 0.527\theta_\beta + 0.274\theta_p - 0.158\theta_\alpha$ ·····5.19 eV

(3) $0.343Y_I - 0.914Y_{II} - 0.089Y_{III} - 0.064Y_{IV} - 0.177\theta_\beta - 0.052\theta_p$ ·····6.91 eV.

Application to Planar Conformers. When considering the perpendicular conformers, interaction between singly excited configurations arises from electron repulsion alone. When considering the planar structures, resonance integrals, $\beta_{u\nu}$, between the two subsystems will not be zero. The resonance integral will mix together configurations which differ by the position of just one electron. The integrals to be evaluated are:

$$\int \psi_0 \hat{H}^{core} \psi_a^{-1}\psi_b d\tau = (2^{1/2}) \int \psi_a(i)\hat{H}_i^{core}\psi_b(i)d\tau_i \quad (3)$$

$$\int \psi_c^{-1}\psi_a \hat{H}^{core}\psi_c^{-1}\psi_b d\tau = \int \psi_a(i)\hat{H}_i^{core}\psi_b(i)d\tau_j \quad (4)$$

$$\int \psi_a^{-1}\psi_c \hat{H}^{core}\psi_b^{-1}\psi_c d\tau = -\int \psi_a(i)\hat{H}_i^{core}\psi_b(i)d\tau_i. \quad (5)$$

The three integrals 3—5 will be zero unless ψ_a belongs to one subsystem and ψ_b to the other.

2-Phenylthiophene: Following the above rules one has to consider the interaction between: (1) Ground state ψ_0, and charge transfer states, (2) charge transfer states to produce "charge resonance" wave functions, (3) locally excited configurations and charge resonance, and (4) locally excited configurations of the two subsystems.

To begin with, the charge transfer states: $\theta_2^{-1}y_4$, $y_3^{-1}\theta_5$, $\theta_3^{-1}y_4$, $y_3^{-1}\theta_4$ are combined to produce the following charge resonance wave functions:

$$CR_I = (1/2^{1/2})(\theta_2^{-1}y_4 + y_3^{-1}\theta_5)$$
$$CR_{II} = (1/2^{1/2})(\theta_2^{-1}y_4 - y_3^{-1}\theta_5)$$

$$CR_{III} = (1/2^{1/2})(\theta_3^{-1}y_4 + y_3^{-1}\theta_4)$$
$$CR_{IV} = (1/2^{1/2})(\theta_3^{-1}y_4 - y_3^{-1}\theta_4).$$

Since, 2-phenylthiophene is not symmetric we computed the interaction terms between thirteen different states, namely, the ground state, four charge resonance states, and eight locally excited states of the two subsystems (θ and Y's). Interaction integrals between the ground state and the charge resonance wave functions reduce to terms including the resonance integral β_{12} (between atom 1 in benzene and atom 2 in thiophene). The same thing applies to interaction integrals between the locally excited configurations of each subsystem and the charge resonance wave functions. The energies of "CR" are computed as such:

$$\langle\theta_2^{-1}y_4|\hat{H}|\theta_2^{-1}y_4\rangle = E_4 - E_2 - (y_4y_4|\theta_2\theta_2)$$

where E_4 is the ionization potential of the fourth MO of thiophene and is calculated by.[26]

$$E_4 = \sum_{u,\nu} C_{4u}C_{4\nu}F_{u\nu}$$

and

$$F_{u\nu} = \beta_{u\nu} - 1/2P_{u\nu}\gamma_{u\nu}.$$

The resonance integral, $\beta_{u\nu}$, between carbon atoms, in the benzene ring, is taken as -2.4 eV whereas that between carbon and sulfur atoms, in the thiophene ring, is taken as -1.63 eV. Other values of $\beta_{u\nu}$ are calculated using the relation[27]

$$\beta_{u\nu} = [S_{u\nu}/(1+S_{u\nu})][(I_u+I_\nu)/2].$$

The computed value of E_4 is 1.406 eV. The values of $E_2(E_{\theta_2})$ is considered equal to $E_3(E_{\theta_3})$ *i.e.* the ionization potential of benzene (9.76 eV). Also, (E_{y_3}) is taken as the ionization potential of thiophene (9.1 eV). The electron repulsion integrals are considered between all atoms (p π atomic orbitals) of benzene and all atoms of thiophene and calculated using the ZDO approximation The energies computed for the charge resonance wave functions and interaction terms are (eV):

$CR_I = 5.93$; $CR_{II} = 5.03$; $CR_{III} = CR_{IV} = 5.92$;

and

$(CR_I|CR_{II}) = -0.360$; $(CR_{III}|CR_{IV}) = -0.263$

$(CR_I|CR_{III}) = (CR_I|CR_{IV}) = (CR_{III}|CR_{IV}) =$ Zero.

The elements of the interaction matrix for the planar conformer of 2-phenylthiophene are thus calculated. Solving this martix (13×13) the energies and state wave functions of the compound are obtained. Those of the ground state and of the first three excited states are:

(1) $0.984\phi_0 - 0.103CR_I - 0.141CR_{III}$ ·····-0.2 eV

(2) $0.225\theta_{\beta'} + 0.341\theta_\beta + 0.162\theta_p - 0.07\theta_\alpha$
$- 0.608Y_I + 0.081Y_{II} - 0.091Y_{III}$
$- 0.211CR_I - 0.352CR_{II} - 0.498CR_{IV}$ ···4.46 eV

(3) $0.107\theta_\beta - 0.852\theta_{\beta'} - 0.111Y_I - 0.167Y_{III}$
$- 0.391CR_{II} + 0.160CR_{III} + 0.179CR_{IV}$ ···4.53 eV

(4) $0.175Y_{II} - 0.086Y_I - 0.293\theta_{\beta'} + 0.226\theta_p + 0.324\theta_\alpha$
$+ 0.611CR_I + 0.109CR_{II} + -0.481CR_{III}$
$- 0.320CR_{IV}$ ·····5.52 eV.

3-Phenylthiophene: Computations for this molecule are carried out similar to those of the 2-phenyl derivative. Interaction elements are of different values for the two isomers. On the other hand, β_{12} is taken equal to β_{13} (between atom 1 to benzene and atom 3 of thiophene). The following are the wave functions and the corresponding energies of the ground state and the first three excited states (covered by the spectrum in the 350—200 nm region):

(1) $0.993\phi_0 + 0.075CR_{II} + 0.094CR_{IV}$ ·····-0.097 eV

(2) $0.137Y_I - 0.138Y_{III} + 0.110Y_{IV} - 0.917\theta_{\beta'}$
$+ 0.076\theta_\beta + 0.292CR_I - 0.080CR_{II}$ ·····4.695 eV

(3) $0.141\theta_\alpha - 0.188\theta_p - 0.189\theta_\beta - 0.280\theta_{\beta'} - 0.424Y_{II}$
$- 0.475Y_I - 0.431CR_I - 0.388CR_{II}$
$- 0.291CR_{III}$ ·····4.87 eV

(4) $0.742Y_I - 0.528Y_{II} - 0.209\theta_\beta - 0.112\theta_p$
$- 0.300CR_{II}$ ·····5.61 eV.

Band Intensity. The intensity of a band is calculated by the equation

$$f = 1.085\times10^{-5}M^2\nu$$

where M is the transition moment and ν (cm^{-1}) the frequency. In the LOM, the ground state is described by the wave function $\psi_0 = a\Gamma + \sum_n b_n T_n$ and the excited state is described by:

$$\psi_{Ex} = \sum_n C_n \Lambda_n + \sum_{n'} d_{n'}T_{n'} + e\Gamma$$

then the transition moment, whithin the limits of zero overlap approximation, is calculated from:

$$\langle\psi_0|\hat{M}|\psi_{Ex}\rangle = a\sum_n C_n\langle\Gamma|\hat{M}|\Lambda_n\rangle + \sum_n\sum_{n'} b_nd_{n'}\langle T_n|\hat{M}|T_{n'}\rangle.$$

The first term reduces to the transition moment between two molecular orbitals and the second term is zero unless the charge transfer states (T_n and $T_{n'}$) are identical. It is calculated by expanding the wave function of the charge transfer state and considering integrals as $\langle y_i|y_j\rangle$, $\langle\theta_i|\theta_j\rangle$, and $\langle y_i|\theta_j\rangle$ to be zero. Also, the operator $\hat{M}$ is a one electron operator which does not depend on the electron spin.

Band intensities were calculated for the planar conformers. The origin of coordinates was assumed to be in midpoint of the bond joining the two subsystems.

Results are given in Table 2.

Comparison with Experiment. A comparison of the experimental and computed transition energies and band intensity is given in Table 2.

Discussion and Conclusions

According to the resonance theory, 2-phenylthiophene is expected to possess a spectrum different from that of the 3-phenyl isomer. The two compounds have different resonating structures and different resonance energy. Consequently, Elpern[14] assigned the first band in the spectra of the two compounds to one electronic transition with λ_{max} at 282 nm for 2-phenylthiophene and at 260 nm for 3-phenylthiophene.

Table 2. Calculated and experimental transition energies of 2- and 3-phenylthiophenes

Compound	Transition energy, eV			f	
	Perpendicular	Planar	Expt	Expt	Calcd
2-Phenylthiophene	4.78	4.66	4.40	0.40	0.40
	4.91	4.73	4.63	0.19	0.06
	5.92	5.72	5.64	—	0.14
3-Phenylthiophene	4.91	4.79	4.51	0.07	0.02
	5.19	4.97	4.77	0.24	0.10
	5.91	5.71	5.54	—	0.16

However, careful examination of the spectra (Fig. 2) shows that the first band comprises two electronic transitions whose energies are not widely separated. Calculation of band intensity confirms this conclusion. The calculated "f" for bands II in 2-phenylthiophene and I in 3-phenylthiophene is not zero. The calculated values are less than the experimental ones since they borrow some of their intensity from the stronger transitions with which they overlap. The resonance theory could not correlate the spectra of nitroanilines.

The results of computation of this work verify the following:

(1) The long wavelength band in the spectra of 2- and 3-phenylthiophene consists of two electronic transitions.

(2) The numerical values of the elements of the interaction matrix of 3-phenylthiophene are less than the corresponding ones of the 2-phenyl isomer. Due to this, we attribute the difference in transition energies of the two isomers.

(3) Contribution of the charge transfer wave function to the excited states of 2-phenylthiophene is more pronounced than in case of the 3-phenyl isomer. That is, dipolar resonating structures contribute substantially to the excited states of the 2-phenylthiophene.

(4) Results of the LOM treatment are reliable and correspondence between them and the experiment is quite satisfactory (Table 2).

(5) Excited states of phenylthiophenes arise from extensive interaction between the states of benzene and thiophene.

References

1) B. Ostman, *Foa Rep.*, **3**, 18 (1969); *Chem. Abstr.*, **71**, 48927a.
2) N. Sugimoto, S. Nishimura, and E. Imoto, *Bull. Univ. Osaka Prefecture*, **A8**, 71 (1959).
3) H. C. Longuet-Higgins, *Trans. Faraday Soc.*, **45**, 173 (1949).
4) J. Koutecky, *Tetrahedron Lett.*, **18**, 632 (1961).
5) C. B. Chowdhury and R. Basu, *J. Indian Chem. Soc.*, **46**, 779 (1969).
6) J. Fabian, A. Mehlhorn, and R. Zahradnik, *J. Phys. Chem.*, **72**, 3975 (1968).
7) D. T. Clark, *Tetrahedron*, **24**, 2663 (1968).
8) U. Gelins, B. Roos, and P. Siegbahn, *Theor. Chim. Acta*, **27**(3), 171 (1972).
9) J. Wam Reijendam and M. Janseen, *Tetrahedron*, **26**, 1303 (1970).
10) M. H. Palmer and R. H. Findlay, *Tetrahedron Lett.*, **41**, 4165 (1972).
11) R. Zahradnik, "Advances in Heterocyclic Chemistry," ed. by A. R. Katritzky, Vol. V, Academic Press, London (1965).
12) A. Tajiri, T. Asano, and T. Nakajima, *Tetrahedron Lett.*, **21**, 1785 (1971).
13) V. Galasso and G. DE Alti, *Tetrahedron*, **27**, 4947 (1971).
14) B. Elpern and F. G. Nachod, *J. Am. Chem. Soc.*, **72**, 3379 (1950).
15) H. C. Longnet-Higgins and J. N. Murrell, *Proc. Phys, Soc., Ser. A*, **68**, 601 (1955).
16) W. Kues and C. Paal, *Ber.*, **19**, 3142 (1886).
17) B. Böttcher and F. Bauar, *Ann.*, **544**, 218 (1951).
18) E. Baumann and M. Klett, *Ber.*, **24**, 3307 (1891).
19) R. Abu-Eittah and M. Hammed, *Bull. Chem. Soc. Jpn.*, **47**, 2576 (1974).
20) N. S. Bayliss and E, G. McRae, *J. Phys. Chem.*, **58**. 1002 (1954).
21) M. G. Gruntfest, Yu. V. Kolodyazhnyi, V. Undre, M. G. Voronkov, and O. A. Osipov, *Khim. Gelerotisk. Soedin*, **4**, 448 (1970); *Chem. Abstr.*, **73**, 87293b.
22) M. Godfrey and J. N. Murrell, *Proc. R. Soc., Ser. A*, **278**, 71 (1974).
23) J. A. Pople, *Proc. Phys. Soc., Ser. A*, **68**, 329 (1955).
24) S. P. McGlynn, L. Vanquicken, M. Kinoshito, and D. Carrol, "Introduction to Applied Quantum Chemistry," Holt, Reinhart and Winston, New York (1972).
25) K. Nishimoto and N. Mataga, *Z. Phys. Chem. (Frankfurt)*, **12**, 225 (1957).
26) J. A. Pople, *Trans. Faraday Soc.*, **49**, 1375 (1953).
27) G. Rasch, *Z. Chem.*, **2**, 347 (1962).

Semiempirical Molecular Orbital Considerations of the Electronic Structures of Transition Metal Complexes. I. Dioxygen Nickel Complexes

Kazuyuki TATSUMI, Takayuki FUENO,* Akira NAKAMURA, and Sei OTSUKA

Department of Chemistry, Faculty of Engineering Science, Osaka University, Toyonaka, Osaka 560

(Received October 28, 1975)

The electronic structure of $Ni(O_2)(HNC)_2$ as a model of "side-on" coordinated dioxygen nickel complexes has been investigated by the INDO method. Calculations show that the square-planar geometry is more stable than the pseudotetrahedral form in accord with the observed structure of $Ni(O_2)(t\text{-BuNC})_2$. The central nickel atom possesses an approximately zerovalent configuration: $(3d)^{8.5}$ $(4s)^{0.5}$ $(4p)^{1.0}$. The dioxygen–nickel bonding is effected primarily through the donation and back-donation of electrons in which the O_2 π_u and π_g^* orbitals parallel to the molecular plane participate. It is predicted that *both* the Ni–O and O–O bondings tend to have greater covalent bond strengths as the electron-attracting ability of the ligand isocyanide increases. Attempts are made to assign the electronic spectra.

A number of dioxygen complexes of transition metals have recently been isolated and characterized.[1–4] In connection with possible biochemical significance of these complexes, much of the current interest in this field is directed toward the understanding of the nature of the dioxygen–transition metal bondings.[5–8] The effect of such bondings upon the electronic structure of the dioxygen moiety is also receiving attention.[5]

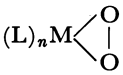

Molecular orbital theory has given several useful suggestions to these problems. Thus, the dioxygen–metal bond in "side-on" complexes has been described in terms of the Dewar-Chatt-Duncanson model,[9,10] in which the donation and back-donation of electrons between metal d orbitals and dioxygen are considered to be essential.[11] Ohkubo and co-workers[12] investigated the interaction between onium compounds and molecular oxygen; the catalytic activity of onium compounds in oxidation reactions was ascribed to an effective interaction of oxygen with the partially occupied d orbitals of the central atom in onium compounds. Recently, Norman[13] has dealt with $Pt(O)_2(PH_3)_2$ by the SCF-X_α scattered wave method to show that a building-up of an extra electron density in the antibonding $1\pi_g$ orbitals of dioxygen is not necessarily due to the direct Pt $d\pi \rightarrow O_2$ $1\pi_g$ back-donation. Apparently, however, characteristics of molecular oxygen coordinated to transition metal are still debatable.

The purpose of the present study is to discuss the nature of the dioxygen–nickel bonding of a "side-on" coordination complex $Ni(O_2)(t\text{-BuNC})_2$[14] in terms of an ASMO-SCF-MO method in the INDO approximation. Specifically, we examine the electronic structure of a model compound $Ni(O_2)(HNC)_2$ and the effects of its geometry and ligand structure on the dioxygen–nickel bonding as well as oxygen–oxygen bond. Assignment of the electronic spectra has also been attempted.

Method of Calculation

INDO Formalism. The approximation used in this work is basically that of the INDO method suggested by Pople *et al.*[15] Thus, all the two-electron integrals involving differential overlap are neglected, except for one-center exchange integrals of the type $(\mu\nu|\mu\nu)$.

However, our method differs somewhat from the original INDO method[15] in the evaluation of atomic integrals. First, both the one-center electron repulsion integrals $(\mu\mu|\nu\nu)$ and the one-center core attraction integrals $U_{\mu\mu}$ are obtained from the table by Oleari *et al.*[16–18] Second, the two-center repulsion integrals are approximated as:[19]

$$(\mu\mu|\nu\nu) = 14.3986/(R+a) \tag{1}$$

with

$$a = 28.7972/[(\mu\mu|\mu\mu)+(\nu\nu|\nu\nu)] \tag{2}$$

μ, on atom A; ν on atom B

where R is the distance (Å) between atoms A and B and $(\mu\mu|\mu\mu)$ *etc.* are represented in units of eV. The integrals $(\mu\mu|\nu\nu)$ for a given pair of atoms A and B may take on different values, depending on the type of the atomic orbitals, μ and ν. Third, the core resonance integrals $\beta_{\mu\nu}$ are evaluated by the Wolfsberg-Helmholtz expression:[20]

$$\beta_{\mu\nu} = -(\kappa/2)S_{\mu\nu}(I_\mu^{A}+I_\nu^{B}) \tag{3}$$

where I_μ^{A} and I_ν^{B} are the valence-state ionization potentials, $S_{\mu\nu}$ is the overlap integral between μ and ν, and the parameter κ is assumed to be 1.1.[21]

The attraction between an electron in atomic orbital μ of atom A and a core of atom B is assumed to be

$$(\mu|V_B|\mu) = -\sum_{\nu}^{B} N_\nu(\mu\mu|\nu\nu) \tag{4}$$

where N_ν refers to the number of valence electrons occupying ν. The elements of the Hartree-Fock matrix for a closed shell of electrons are then given by[22]

$$F_{\mu\mu}^{A,A} = U_{\mu\mu} + \sum_{\nu}^{A} P_{\nu\nu}\left[(\mu\mu|\nu\nu)-\frac{1}{2}(\mu\nu|\mu\nu)\right] + \sum_{\nu}^{B}(P_{\nu\nu}-N_\nu)(\mu\mu|\nu\nu) \tag{5}$$

$$F_{\mu\nu}^{A,A} = P_{\mu\nu}\left[\frac{3}{2}(\mu\nu|\mu\nu)-\frac{1}{2}(\mu\mu|\nu\nu)\right] \tag{6}$$

$$F_{\mu\nu}^{A,B} = \beta_{\mu\nu} - \frac{1}{2}P_{\mu\nu}(\mu\mu|\nu\nu) \tag{7}$$

where $P_{\mu\nu}$ *etc.* denote the bond orders.

The basis set of atomic orbitals used includes the following: 3d, 4s, and 4p of Ni; 2s and 2p of C, N,

* To whom correspondence should be addressed.

and O; and 1s of H. The initial electronic configurations of atoms assumed in the evaluation of the matrix elements (5)—(7) are $(3d)^{10}$ for Ni and $(2s)^2(2p)^m$ for C, N, and O, where m is 2, 3, and 4, respectively.

Evaluation of Integral Parameters. The one-center integrals appropriate to the present calculations are (i) core-electron attraction integrals U_{ss}, U_{pp}, and U_{dd}, (ii) Coulomb integrals $(\mu\mu|\nu\nu)$, and (iii) exchange integrals $(\mu\nu|\mu\nu)$. Oleari *et al.*[16,17] determined the one-center integrals by the least-squares fits of the total valence-state energies calculated therefrom for atoms as a function of their orbital occupation number. The calculations were based on the valence state energies taken from Moore's table.[23] The results are tabulated[18] for various valence-state quantities:[24]

U_{ss}, U_{pp}, U_{dd}, g_{ss}, g_{pp}, g_{dd}, g'_{sp}, $g'_{pp'}$, g'_{pd}, and $g'_{dd'}$

where

$$g_{\mu\mu} = (\mu\mu|\mu\mu) = J_{\mu\mu} \tag{8}$$

and

$$g'_{\mu\nu} = (\mu\mu|\nu\nu) - \frac{1}{2}(\mu\nu|\mu\nu) = J_{\mu\nu} - \frac{1}{2}K_{\mu\nu} . \tag{9}$$

In evaluating the individual one-center two-electron integrals, one must resolve $g'_{\mu\nu}$ into the components. We have made the resolution using the theoretical relationships between the individual integrals and the Slater-Condon parameters. The expressions for the Coulomb and exchange integrals in terms of the Slater-Condon parameters have been given by Clack.[25] The resolutions of g'_{sp}, g'_{sd}, and g'_{pd} necessitate evaluations of the Slater-Condon parameters G^1(sp), G^2(sd), G^1(pd), and G^3(pd). These parameters were taken from the data compiled by Hinze and Jaffé[26] for ligand atoms and by Oleari *et al.*[17] for the metal atom. The various two-electron integral values finally adopted for C, N, O, and Ni are summarized in Table 1.

The valence-state ionization potentials necessary for the evaluation of $\beta_{\mu\nu}$ were obtained from Oleari's $U_{\mu\mu}$ data and relevant Slater-Condon parameters. They are listed also in Table 1. The overlap integrals

Table 1. Atomic parameters[a] (eV)

	Ni	C	N	O	H
I_s	7.19	19.39	25.00	32.37	13.60
I_p	3.10	10.83	13.84	16.39	
I_d	5.02				
J_{sp}	6.872	11.410	12.583	14.480	
$J_{pp'}$	5.768	9.841	11.588	12.335	
J_{sd}	10.088				
$J_{z,zx}$	8.583				
J_{x,z^2}	8.331				
$J_{z,xy}$	8.215				
J_{z,z^2}	8.699				
$J_{z^2,xy}$	15.015				
$J_{z^2,xz}$	15.644				
J_{xy,x^2-y^2}	15.854				
$J_{xz,yz}$	15.225				

a) The other parameters, $U_{\mu\mu}$ and $g_{\mu\mu}$, are tabulated in Ref. 18. The $K_{\mu\nu}$ values can be obtained from Eq. 9.

Table 2. Orbital exponents of the basis set used

	s	p	d
H	1.0000		
C	1.6083	1.5679	
N	1.9237	1.9170	
O	2.2458	2.2266	
Ni	1.4730	1.4730	2.960

were calculated using single Slater orbitals. The orbital exponents were chosen from the data by Zerner and Gouterman[27] for nickel and from those by Clementi and Raimond[28] for ligand atoms. They are given in Table 2.

Electronic Excitation. The energies and moments for singlet excitations were calculated by the conventional virtual orbital approximation without configuration interaction. The configurational energy corresponding to one-electron excitation from molecular orbital i to virtual orbital j is given by

$$\Delta^1E = \varepsilon_j - \varepsilon_i - J_{ij} + 2K_{ij} \tag{10}$$

where ε_j and ε_i respectively denote the energies of orbitals j and i, and J_{ij} and K_{ij} are the molecular Coulomb and exchange integrals, respectively. The dipole moment length is given by

$$M_{i\to j} = \sqrt{2}\sum_{A}^{\text{atoms}}\sum_{\mu}^{A}\sum_{\nu}^{A} C_{i\mu}C_{j\nu}(\mu|\boldsymbol{r}_A|\nu) \tag{11}$$

where $\boldsymbol{r}_A$ is the coordinate vector operator of atom A and $C_{i\mu}$ *etc.* are the LCAO coefficients. In evaluating $M_{i\to j}$, a contribution from atomic polarization was taken into account. This latter contribution is denoted by $M'_{i\to j}$.

Results and Discussion

Geometry of $Ni(O_2)(HNC)_2$. Detailed X-ray structual information is available for $Ni(O_2)(t\text{-BuNC})_2$.[29] The two oxygen atoms lie on the plane containing the nickel and the two isocyanide groups.

To begin with, we have calculated the total energy of our model compound $Ni(O_2)(HNC)_2$ for two extreme geometries, in which the dihedral angle θ (Fig. 1) is 0 and 90°. The results are given in Table 3, together with the net charge on the oxygen atoms Q_O as well as the bond indices W[30] for the O–O and Ni–O bonds.

Table 3 indicates that the square-planar structure (θ=0°) is more stable than the pseudotetrahedral

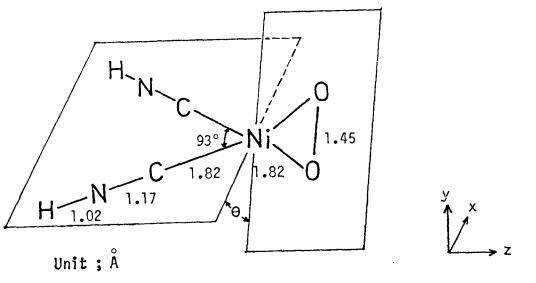

Fig. 1. Coordinate systems and structure for $Ni(O_2)(HNC)_2$.

Table 3. Total energy (E)[a], net charge on oxygen (Q), and bond indices (W) for the square-planar and pseudotetrahedral conformations of $Ni(O_2)(HNC)_2$

	Square-Planar	Pseudotetrahedral
E(eV)	−2201.2126	−2200.6274
Q_O	−0.4367	−0.4781
W_{O-O}	1.0495	1.0193
W_{Ni-O}	0.8346	0.7391

a) In calculating the total energy, the total core-core repulsion energy was approximated as

$$\sum_A \sum_B \sum_\nu^A \sum_\mu^B N_\mu N_\nu (\mu\mu|\nu\nu).$$

one ($\theta=90°$), a result compatible with the X-ray structure of $Ni(O_2)(t\text{-BuNC})_2$. Both the bond indices W_{O-O} and W_{Ni-O} are greater in the former geometry. Because the bond index can be regarded as a measure of the covalency of the bond in question,[30] the greater stability of the square-planar form can be ascribed to the greater covalent character of *both* the Ni–O and O–O bonds involved. The net charge Q_O, on the other hand, is smaller for the square-planar structure, implying a lesser extent of back-donation of electrons from Ni to O_2 as compared with the pseudotetrahedral structure. These two indications together suggest that the back-donation tends to reduce the covalency of the Ni–O as well as the O–O bond in the complex.

Electronic Structure. We have examined the electronic structure of $Ni(O_2)(HNC)_2$ of the square-planar form in detail. The magnetic susceptibility measurements of $Ni(O_2)(t\text{-BuNC})_2$ revealed a feeble magnetic moment of 0.13 BM.[14b] The PMR spectrum of the complex was also measured; the chemical shift falls in the range for diamagnetic isocyanide complexes. On the basis of these observations, we may assume that this complex is in a closed electronic structure.

The upper portion of the occupied molecular orbitals is diagrammatically shown in Fig. 2, together with low-lying vacant orbitals. Appended to the orbital levels are their numberings and symmetry representations for the C_{2v} point group instead of the higher symmetry D_{2h}. The omitted lower portion of the diagram consists merely of the essentially unperturbed O_2 $2\sigma_g$ and $2\sigma_u$ and isocyanide σ_g, σ_u, and π_u orbitals in the range from −45.4 to −16.5 eV.

The highest occupied level, $\phi_{21}(a_2)$, consists of 100% O_2 $\pi_g^*(\perp)$ orbital,[31] virtually no mixing between the Ni $3d_{xy}$ and O_2 $\pi_g^*(\perp)$ orbitals being involved. Thus, the back-donation to the O_2 $\pi_g^*(\perp)$ orbitals can be ignored. A similar conclusion was reached by the SCF-X_α scattered-wave calculation for $Pt(PH_3)_2(O_2)$.[13] The overlap integral between Ni $3d_{xy}$ and O p_y is considerably small (0.016). The lowest unoccupied level, ϕ_{22} (b_2), consists of Ni $4p_y$ and isocyanide $\pi^*(\perp)$ with an appreciable O_2 $\pi_u(\perp)$ character. The Ni–O_2 bonding is accomplished mainly through extensive mixings of the O_2 $\pi_u(\parallel)$ and σ_g orbitals with the Ni $3d_{z^2}$ and $3d_{x^2-y^2}$ orbitals, and of the O_2 $\pi_g^*(\parallel)$ with Ni $3d_{xz}$ orbital. The levels $\phi_{19}(a_1)$, $\phi_{17}(a_1)$, $\phi_{16}(a_1)$, and $\phi_{13}(a_1)$ involve the mixing

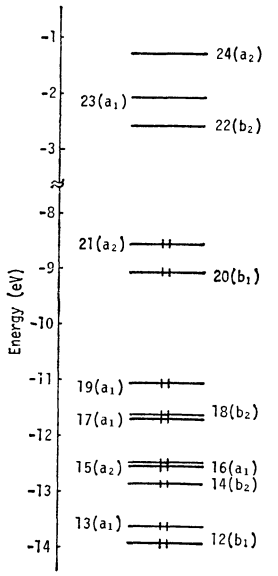

Fig. 2. Upper portion of the molecular orbital level diagram for $Ni(O_2)(HNC)_2$. The highest occupied level is $21(a_2)$.

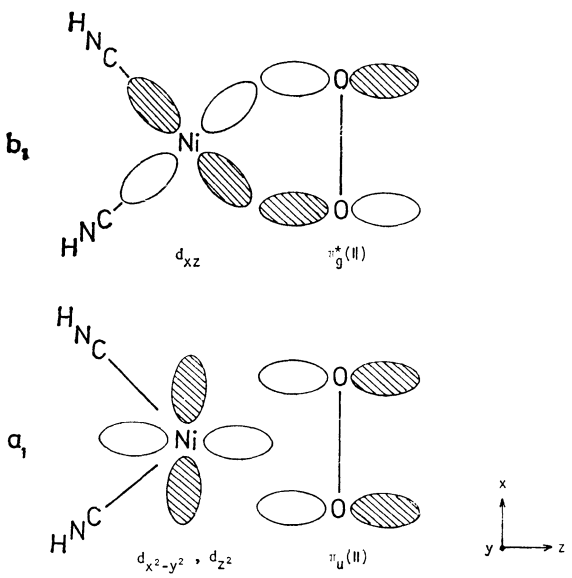

Fig. 3. Orbitals participating in the Ni–O_2 bonding of $Ni(O_2)(HNC)_2$.
b_1, the back-donation type; a_1, the donation type from O_2 to Ni.

of the former type while the level $\phi_{20}(b_1)$ is due to that of the latter. The two types of mixings, schematically shown in Fig. 3, are analogous to the donation and back-donation scheme in the Dewar-Chatt-Duncanson model.

The calculated valence-electron distributions over the atomic orbitals as well as the atoms present in the complex are summarized in Table 4. We see that the final electronic configuration of nickel is $(3d)^{8.49}$ $(4s)^{0.54}$ $(4p)^{0.98}$. Most of the d-orbital population resides in the d_{xy}, d_{yz}, $d_{x^2-y^2}$, and d_{z^2} orbitals. The 4p orbital is appreciably occupied. The net charge on nickel is nearly zero, even though its d-orbital occupation number is between 8 and 9. The isocyanide

Table 4. Calculated electron distributions for $Ni(O_2)(HNC)_2$

Atom	Atomic orbital	Charge density	
		on orbital	on atom
Ni	s	0.537	10.001
	p	0.975	
	d_{xz}	0.580	
	d_{yz}	1.978	
	d_{xy}	1.988	
	$d_{x^2-y^2}$	1.982	
	d_{z^2}	1.959	
O	s	1.744	6.437
	p	4.693	
C	s	1.313	3.860
	p	2.547	
N	s	1.244	4.923
	p	3.679	
H	s	0.780	0.780

ligands assume overall positive charges, as would be expected from the nature of isocyanide as a donating ligand. The net charge on each oxygen atom is *ca.* −0.44. The charge transfer from $Ni(HNC)_2$ to O_2 thus amounts to about one electron equivalent.

In order to gain a deeper insight into the O–O bonding nature, we calculated individual π orbital populations in the O_2 moiety as follows:

$$q(\pi_u(\perp)) = 4\sum_{i(a_2)}^{occ} C^2_{iO(p_y)} \quad (12)$$

$$q(\pi_u(\parallel)) = 4\sum_{i(a_1)}^{occ} C^2_{iO(p_z)} \quad (13)$$

$$q(\pi_g^*(\perp)) = 4\sum_{i(b_2)}^{occ} C^2_{iO(p_y)} \quad (14)$$

$$q(\pi_g^*(\parallel)) = 4\sum_{i(b_1)}^{occ} C^2_{iO(p_z)} \quad (15)$$

where $C_{iO(p_y)}$ *etc.* denote the LCAO coefficients of the i-th MO for the oxygen p orbitals specified, the summations extending over the MO's of a given symmetry a_1, a_2, b_1, or b_2. The various π orbital populations calculated for the $Ni(O_2)(HNC)_2$ complex are summarized in Table 5, together with the O–O bond length and the O–O stretching force constant.[32] For the sake of comparison, the corresponding values for molecular $O_2(^3\Sigma_g^-, {}^3\Sigma_u^\pm)$, superoxide O_2^-, and peroxide O_2^{2-} are also listed in Table 5.

The O–O bondings in dioxygen complexes have often been discussed on the basis of their analogy in bond length with those in O_2^{n-} anions ($n=1$ and 2) and excited-state O_2.[5,7,32,33] The electronic configuration of O_2 in the complex here calculated certainly reflects the effects of both the charge transfer to O_2 and the local excitation of O_2. Thus, the sum of the π^* orbital populations exceeds 3, indicative of a partial O_2^{2-} character while that of the π orbitals is less than 4, a result which would be expected if the coordinated dioxygen is assumed to partake of the character of excited $O_2(^3\Sigma_u^+$ or $^3\Sigma_u^-)$. The results can best be understood in terms of the intermolecular configuration interaction[34]; the ground state of the complex is represented by a superposition of the ground, charge-transfer, and locally-excited configurations made up of the molecular orbitals of the component molecules, $Ni(HNC)_2$ and $O_2(^3\Sigma_g^-)$.

Taking a step further, we will discuss the relative strengths of the O–O bondings of coordinated dioxygen, free oxygen anions, and various states of molecular oxygen. Since the π_u and π_g^* orbitals are, respectively, bonding and antibonding in nature, the population in the former orbitals should tend to strengthen the bond while the latter to weaken it. The O–O bond strength may be related, to a first approximation, with the differential population between them, defined as

$$\Delta q = q(\pi_u(\perp)) + q(\pi_u(\parallel)) - q(\pi_g^*(\perp)) - q(\pi_g^*(\parallel)) . \quad (16)$$

The values of Δq thus calculated for the various types of dioxygens are included in Table 5. They decrease in the order: $O_2(^3\Sigma_g^-) > O_2^- > Ni(O_2)(HNC)_2 > O_2^{2-} = O_2(^3\Sigma_u^\pm)$, in rough agreement with the decreasing order of the observed force constant f_{O-O} and the increasing order of bond length R_{O-O}. The f_{O-O} value used herewith for O_2^{2-} appears to be somewhat too large. Perhaps, dioxygen in Na_2O_2 is not adequate as a model for a free O_2^{2-}.

Polar Effect of Isocyanide Substituent. The strengths of the M–O and O–O bonds in the dioxygen complexes vary depending on the identity of the metal and auxiliary

Table 5. Calculated orbital populations (q) and observed bond lengths (R) and force constants (f) for dioxygen in various states

	$Ni(O_2)(HNC)_2$	O_2^-	O_2^{2-}	$O_2(^3\Sigma_g^-)$	$O_2(^3\Sigma_u^+, {}^3\Sigma_u^-)$
$q(\pi_u(\perp))$	1.88	2.00	2.00	2.00	(3.00)[a]
$q(\pi_u(\parallel))$	1.89	2.00	2.00	2.00	
$q(\pi_g^*(\perp))$	2.00	(3.00)[a]	2.00	1.00	(3.00)[a]
$q(\pi_g^*(\parallel))$	1.46		2.00	1.00	
Δq	0.30	1.00	0.00	2.00	0.00
R_{O-O}(Å)	1.45[b]	1.28[d]	1.49[d]	1.20[f]	1.42[f], 1.60[f]
f_{O-O}(mdyne/Å)	3.5[e]	6.2[e]	5.5[e]	11.5[f]	3.2[f], 2.3[f]

a) The values given in parentheses are the sums of two q values. b) Taken from Ref. 29. c) Taken from Ref. 32. d) N. -G. Vannerberg, *Prog. Inorg. Chem.*, **4**, 125 (1962). e) Obtained for KO_2 and Na_2O_2; E. J. Blunt, P. J. Hendra, and J. R. Mackenzie, *Chem. Commun.*, **1969**, 278. f) G. Herzberg, "Molecular Spectra and Molecular Structure," Vol. 2, D. Van Nostrand Co. Inc., Princeton, N. J. (1950).

Table 6. Net charge on oxygen (Q), bond indices (W), and oxygen orbital populations (q) for various I_s^H

I_s^H(eV)	15.6	13.6	11.6	9.6
Q_O	−0.4317	−0.4367	−0.4418	−0.4472
W_{O-O}	1.0514	1.0495	1.0476	1.0457
W_{Ni-O}	0.8384	0.8346	0.8305	0.8262
$q(\pi_u(\perp))$	1.8759	1.8764	1.8769	1.8774
$q(\pi_u(\parallel))$	1.8852	1.8857	1.8862	1.8867
$q(\pi_g^*(\perp))$	1.9999	1.9999	1.9999	1.9999
$q(\pi_g^*(\parallel))$	1.4535	1.4630	1.4728	1.4829
Δq	0.3077	0.2992	2.2904	0.2813

ligands. The O–O bond length ranges from 1.30 to 1.63 Å, while the M–O bond length from 1.82 to 2.09 Å. Also, the force constants of the O–O and M–O stretchings, determined by IR spectroscopy, range from 3.0 to 3.5 mdyn/Å and from 2.1 to 3.2 mdyn/Å, respectively.

In an attempt to elucidate the effect of the substituent of the isocyanide ligand on the O–O and M–O bond strengths, we have carried out model calculations by varying the ionization potential $I_s^H(=-U_{ss}^H)$ for the hydrogen atom of isocyanide, with the other parameters being fixed. When I_s^H is smaller than 13.6 eV, the hypothetical isocyanide ligand (CNH′) should be more electron-releasing than CNH, and *vice versa*.

The net charges on oxygen Q_O calculated with various I_s^H values are listed in the first line of Table 6. It can be seen that Q_O increases in magnitude as the isocyanide ligand becomes more electron-releasing. Thus, electropositive ligands tend to enhance the back-donation of electrons from nickel to dioxygen.

Also listed in Table 6 are the bond indices W_{O-O} and W_{Ni-O}, together with the values for q as well as Δq. The quantities Δq and W_{O-O}, both of which are the measures of the O–O covalent bond strength, decrease with decreasing I_s^H. The results indicate that the substitution of electron-releasing ligands leads to a decrease in the O–O bond strength. The trend can easily be accounted for in terms of the increasing back-donation from nickel to O_2 π_g^* orbital; $q(\pi_g^*(\parallel))$ increases considerably as I_s^H decreases. Similar situations are encountered in olefin and acetylene complexes.[35]

As for the strength of the nickel–oxygen bond, the W_{Ni-O} also decreases with the increasing electron-releasing character of the isocyanide ligand. The result might appear strange. With olefin and acetylene complexes, the relative strengths of metal–olefin (or metal–acetylene) π-bonding interaction reflect the amount of back-donation; a weaker C–C bond is usually accompained by a stronger metal–olefin bond.[35,36]

The most important difference between dioxygen and olefin (or acetylene) is that the former is much more electronegative than the latter, the half-occupied π_g^* orbital of the former being much lower in energy than the lowest vacant orbital of the latter. The nickel orbitals of the isocyanide complex may lie as high as or even higher than the π_g^* orbitals of dioxygen. In order to ascertain this possibility, the UHF-INDO calculations were performed for two isolated molecules, O_2 and $Ni(HNC)_2$. The latter molecule was assumed to be in the lowest triplet state, its geometry being assumed to be the same as in Fig. 1. The resulting HOMO (degenerate) of the α-spin orbital for O_2 is at −12.05 eV, while that for $Ni(HNC)_2$, at −6.21 eV. The former is significantly lower than the latter, indicative of the higher electronegativity of O_2. Indeed, the dioxygen–nickel bonding orbital $\psi_{20}(b_1)$ possesses a large dioxygen character, in harmony with the lower O_2 π_g^* orbital as compared with the HOMO of $Ni(HNC)_2$.

Under these circumstances, the covalency of the Ni–O bond and, hence, its bond strength should decrease as the nickel atom becomes more electron-releasing. The view is supported by the IR spectra, which show that the frequency of the rhodium–oxygen stretching ν_{Rh-O} for various dioxygen rhodium complexes[32] tends to increase in the order of electron-attracting ability of the substituents. This is in contrast with the results for Vaska's dioxygen complexes, where the reversibility of oxygen coordination was realized in the presence of electron-attracting ligands.[33] However, the reversibility may not necessarily be correlated with the dioxygen–metal bond strength.

Transition Energies and Dipole Moment Lengths. Ultraviolet and visible absorption spectra have been reported for $Ni(O_2)(t\text{-BuNC})_2$ both in a $CHCl_3$ solution and in the solid state.[14b] Assignment of the greatest wavelength absorption band was also given,[14b] where the ground electronic state of the complex was assumed to be $^3A_2$. However, the assumption is probably not valid in view of the data of magnetic susceptibility and PMR spectrum, as has already been

Table 7. Transition energies (Δ^1E) and transition moment lengths (M) for $Ni(O_2)(HNC)_2$

Transition	Symmetry	Calcd			Obsd[b]	
		Δ^1E(eV)	M(Å)	M'(Å)[a]	Δ^1E(eV)	ε
$\psi_{15}\rightarrow\psi_{26}$	$^1B_2$	1.80	0.008	0.008	2.07	38
$\psi_{16}\rightarrow\psi_{26}$	$^1B_1$	2.80	0.244	0.033		
$\psi_{21}\rightarrow\psi_{26}$	$^1B_2$	2.81	0.023	0.023		
$\psi_{21}\rightarrow\psi_{22}$	$^1B_1$	2.94	0.170	0.004	3.26[c]	316
$\psi_{13}\rightarrow\psi_{26}$	$^1B_1$	3.18	0.007	0.004		
$\psi_{20}\rightarrow\psi_{23}$	$^1B_1$	3.49	0.124	0.009		

a) Contribution from atomic polarization. b) Observed in $CHCl_3$ solution. See Ref. 13. c) Observed as a superposition of many peaks.

mentioned. Thus, we here attempt reassignments of the electronic spectra, assuming that the replacement of *t*-BuNC by HNC does not affect the spectra significantly.

Table 7 gives the energies Δ^1E and dipole moment lengths M calculated for the singlet transitions in the low-energy region, together with the experimental data. Considering the observed extinction coefficients ε and the calculated M, we may ascribe the band observed at 2.07 eV to the $\psi_{15}\rightarrow\psi_{26}$ ($^1A_1\rightarrow{}^1B_2$) transition. The transition has an appreciable d-d band character with a slight charge-transfer from nickel d orbitals to ligand π_g* orbitals. The band appearing at 3.26 eV can be ascribed primarily to the three $^1A_1\rightarrow{}^1B_1$ transitions, $\psi_{16}\rightarrow\psi_{26}$, $\psi_{21}\rightarrow\psi_{22}$, and $\psi_{20}\rightarrow\psi_{23}$. The $\psi_{16}\rightarrow\psi_{26}$ transition reveals a considerable mixing of the d-d excitation with charge-transfer from the oxygen $\pi_u(\parallel)$ orbital to the isocyanide $\pi^*(\parallel)$ orbital, the resulting M being large as compared with that for a d-d transition. On the other hand, the latter two transitions are almost completely of charge-transfer type. The $\psi_{21}\rightarrow\psi_{22}$ transition corresponds to the charge-transfer from the oxygen $\pi_g^*(\perp)$ orbital to the nickel p_z and the isocyanide $\pi^*(\perp)$ orbitals, while the $\psi_{20}\rightarrow\psi_{23}$ transition from the oxygen $\pi_g^*(\parallel)$ and the nickel d orbitals to the isocyanide $\pi^*(\parallel)$ orbitals.

It should be noted that the energies calculated for the $\psi_{15}\rightarrow\psi_{26}$ and $\psi_{16}\rightarrow\psi_{26}$ transitions are relatively small (1.80 and 2.80 eV, respectively) despite their large orbital energy gaps (12.01 and 11.89 eV, respectively). Apparently, this is a consequence of their interorbital Coulomb repulsions J_{ij} being relatively large (11.14 and 10.19 eV, respectively). That these particular transitions have large J_{ij} is not surprising, since both of them possess an appreciable d-d (and hence largely local) excitation character to which the contribution of one-center Coulombic repulsions should be dominant. It is also noteworthy that for these two transitions the contribution M' of atomic polarization to dipole moment length is not negligible.

Concluding Remarks

The results given above indicate that our modified INDO method can satisfactorily account for the structure of the nickel dioxygen complex studied. It can well serve as a tool in illuminating the nature of the chemical bondings involved.

One point that may be raised against the present treatment will be the accuracy of the INDO theory itself when extended to include d orbitals. However, recent success[37,38] of the theory in quantitative interpretation of the photoelectron spectra for several transition metal complexes does appear to warrant its reliability. Description of the ground-state properties of the nickel dioxygen complex studied herein is probably reliable enough at least qualitatively.

References

1) L. Vaska and D. L. Catone, *J. Am. Chem. Soc.*, **88**, 5324 (1966).
2) J. T. Mague and G. Wilkinson, *J. Chem. Soc., A*, **1966**, 1736.
3) G. Wilke, H. Schott, and P. Hembach, *Angew. Chem.*, **79**, 62 (1967).
4) C. D. Cook and G. S. Jauhal, *J. Am. Chem. Soc.*, **90**, 1464 (1968).
5) R. Mason, *Nature (London)*, **217**, 543 (1968).
6) J. A. McGinnety, N. C. Payne, and J. A. Ibers, *J. Am. Chem. Soc.*, **91**, 6301 (1969).
7) J. P. Collman, *Acc. Chem. Res.*, **1**, 136 (1968).
8) G. H. Olivé and S. Olivé, *Angew. Chem. Int. Ed.*, **13**, 29 (1974).
9) M. J. S. Dewar, *Bull. Soc. Chim. Fr.*, **18**, C79 (1951).
10) J. Chatt and L. A. Duncanson, *J. Chem. Soc.*, **1953**, 2939.
11) J. S. Valentine, *Chem. Rev.*, **73**, 236 (1973).
12) (a) K. Ohkubo and T. Yamabe, *Bull. Chem. Soc. Jpn.*, **44**, 1183 (1971); (b) K. Ohkubo and H. Kanaeda, *ibid.*, **45**, 11, 1550, 1571 (1972).
13) J. G. Norman, Jr., *J. Am. Chem. Soc.*, **96**, 3327 (1974).
14) (a) S. Otsuka, A. Nakamura, and Y. Tatsuno, *Chem. Commun.*, **1967**, 836; (b) S. Otsuka, A. Nakamura, and Y. Tatsuno, *J. Am. Chem. Soc.*, **91**, 6994 (1969); (c) S. Otsuka, A. Nakamura, Y. Tatsuno, and M. Miki, *ibid.*, **94**, 3761 (1972).
15) J. A. Pople, D. L. Beveridge, and P. A. Dobosh, *J. Chem. Phys.*, **47**, 2026 (1967).
16) L. Oleari, L. Di Sipio, and G. De Michelis, *Mol. Phys.*, **10**, 97 (1966).
17) E. Tondello, G. De Michelis, L. Oleari, and L. Di Sipio, *Coord. Chem. Rev.*, **2**, 65 (1967).
18) L. Di Sipio, E. Tondello, G. De Michelis, and L. Oleari, *Chem. Phys. Lett.*, **11**, 287 (1971).
19) K. Nishimoto and N. Mataga, *Z. Phys. Chem. N. F.*, **13**, 140 (1957).
20) M. Wolfsberg and L. Helmholtz, *J. Chem. Phys.*, **20**, 837 (1952).
21) K. Yamaguchi and T. Fueno, *Bull. Chem. Soc. Jpn.*, **44**, 43 (1971).
22) C. C. J. Roothaan, *Rev. Mod. Phys.*, **23**, 69 (1951).
23) C. Moore, "Atomic Energy Levels," Vol. 2, Nat. Bur. Stand. (1952).
24) Note that both g'_{pd} and $g'_{dd'}$ involve four different values, as are given in Table 1.
25) D. W. Clack, *Mol. Phys.*, **27**, 1513 (1974).
26) J. Hinze and H. H. Jaffé, *J. Chem. Phys.*, **38**, 1834 (1963).
27) M. Zerner and M. Gouterman, *Theor. Chim. Acta*, **4**, 44 (1966).
28) E. Clementi and D. L. Raimond, *J. Chem. Phys.*, **38**, 2686 (1963).
29) M. Matsumoto and K. Nakatsu, *Acta Crystallogr.*, **B31**, 2711 (1975).
30) K. B. Wiberg, *Tetrahedron*, **24**, 1083 (1968).
31) Throughout this paper, we use the notation $\pi(\parallel)$ and $\pi(\perp)$ to distinguish between the π orbitals which are parallel and perpendicular to the NiO_2 plane.
32) A. Nakamura, Y. Tatsuno, M. Yamamoto, and S. Otsuka, *J. Am. Chem. Soc.*, **93**, 6052 (1971).
33) S. J. LaPlaca and J. A. Ibers, *J. Am. Chem. Soc.*, **87** 2581 (1965).
34) T. Fueno, S. Nagase, K. Tatsumi, and K. Yamaguchi, *Theor. Chim. Acta*, **26**, 431 (1972); S. Nagase and T. Fueno, *ibid.*, **35**, 217 (1974).
35) (a) J. H. Nelson, K. S. Wheelock, L. C. Cusachs, and H. B. Jonassen, *J. Am. Chem. Soc.*, **91**, 7005 (1969); (b) *ibid.*, **92**, 5110 (1970).
36) F. R. Hartly, *Angew. Chem. Int. Ed.*, **11**, 596 (1972).
37) (a) D. W. Clack, *Mol. Phys.*, **27**, 1513 (1974); (b) D. W. Clack, *Theor. Chim. Acta*, **35**, 157 (1974).
38) K. Tatsumi and T. Fueno, *Bull. Chem. Soc. Jpn.*, **49**, 929 (1976).

Semiempirical Molecular Orbital Considerations of the Electronic Structures of Transition Metal Complexes. II. Acetylene- and Azo-Nickel Complexes

Kazuyuki TATSUMI, Takayuki FUENO, Akira NAKAMURA, and Sei OTSUKA
Department of Chemistry, Faculty of Engineering Science, Osaka University, Toyonaka, Osaka 560
(Received December 22, 1976)

The electronic structures of zerovalent nickel π complexes, Ni(HC≡CH)$(HNC)_2$ and Ni(*trans*-HN=NH)$(HNC)_2$, have been investigated by the INDO method. Both complexes are found to favor the square-planar geometry, in accord with the observed structures of Ni($C_6H_5C{\equiv}CC_6H_5$)(*t*-BuNC)$_2$ and Ni($C_6H_5N{=}NC_6H_5$)(*t*-BuNC)$_2$. Ni(*trans*-HN=NH)$(HNC)_2$ is predicted to be more stable than Ni(*cis*-HN=NH)$(HNC)_2$. The increment in the C–C and N–N bond lengths effected by the complexation seems to well reflect the net effects of σ donation and π back-donation. For the isocyanide N–C bond, an approximately linear relationship is found to hold between the calculated bond index and the observed force constant. It is suggested that both the Ni–C(of acetylene) and Ni–N(of diimide) bondings tend to have greater covalent bond strengths as the electron-releasing ability of the isocyanide ligand increases.

Since the discovery of Zeise's salt, transition metal π complexes have constituted an enormous, diversified field of chemistry.[1] Although the chemistry is well developed, theoretical inquiries to the field have still been limited to olefin complexes.[2] There have been very few attempts at coherent quantum-mechanical description of other π complexes.[3]

In our previous work,[4] we investigated the electronic structure of side-on coordinated nickel dioxygen complex Ni$(O_2)(HNC)_2$ by a modified INDO method. It was found that the greater the extent of back-donation of electrons from Ni to O_2, the weaker is the Ni–O_2 covalent bond strength. A unique substituent effect was predicted that *both* the Ni–O_2 and O–O bondings tend to have greater covalent bond strengths as the electron-attracting ability of the ligand isocyanide increases.

In this paper we will deal with the side-on isocyanide nickel complexes Ni(HC≡CH)$(HNC)_2$ and Ni(HN=NH)$(HNC)_2$ as model compounds for Ni($C_6H_5C{\equiv}CC_6H_5$)(*t*-BuNC)$_2$,[5] and Ni($C_6H_5N{=}NC_6H_5$)(*t*-BuNC)$_2$,[6] respectively. The purpose of the present study is to clarify the nature of the bondings involved in these complexes and the effects of their geometry and ligand structure on the bondings. A particular attention will be directed to comparisons between these complexes with a dioxygen nickel isocyanide complex, Ni$(O_2)(HNC)_2$.

Method of Calculation

The same ASMO SCF method at the level of the INDO approximation as described previously[4,7] was used. The basis set of atomic orbitals adopted in the calculation is: 3d, 4s, and 4p for Ni; 2s and 2p for both C and N; and 1s for H. The single-parameter functions of Zerner and Gouterman[8] have been used for the nickel atom while Clementi's functions[9] for ligand atoms. All the one-center integral parameters involved are the same as those used in our earlier paper.[4]

In calculating the core-core repulsion energy E_{AB}(core) between atoms A and B, we have used the following function:

$$E_{AB}(\text{core}) = (1-c)\sum_A\sum_B\sum_\mu^A\sum_\nu^B N_\mu N_\nu(\mu\mu|\nu\nu) + c\sum_A\sum_B\frac{14.399Z_AZ_B}{R_{AB}} \quad (1)$$

where N_μ and N_ν refer to the numbers of the valence electrons occupying AO's μ and ν, respectively; $(\mu\mu|\nu\nu)$ is the two-center repulsion integral; Z_A and Z_B are the core charge on atoms; and R_{AB} is the internuclear distance between A and B in units of Å. The parameter c has been determined to reproduce the experimental C–C bond length of acetylene (1.203 Å).[10] The resulting c value was 0.353.

Results and Discussion

A. Structure of Complexes. Precise structural information based on the X-ray data is available for Ni($C_6H_5C{\equiv}CC_6H_5$)(*t*-BuNC)$_2$[11] and Ni(*trans*-$C_6H_5N{=}NC_6H_5$)(*t*-BuNC)$_2$.[12] The dihedral angles θ between the bisisocyanide-nickel plane and the Ni–C–C (of acetylne) and Ni–N–N (of azobenzene) planes are 2.6°(7) and 1.2°(3), respectively, so that the complexes possess essentially the C_{2v} or C_2 symmetry. Acetylene, which is linear in the free state, takes a *cis*-bent structure (δ=31.4°) in the complex. Similarly, for the π-bonded azobenzene complex, there is a dihedral angle of 2ω= 26.8° between the two N–N–C (of phenyl) planes. This angle would be 0° if the C–N–N–C portion of the complex were coplanar as it is in free *trans*-azobenzene.

Conformation of the Complexes. In the first place, we will consider the conformations of our model compounds Ni(HC≡CH)$(HNC)_2$ and Ni(HN=NH)$(HNC)_2$. Calculations were carried out for a few extreme geometries of each compound. Figure 1 illustrates such geometries which can be characterized by two angles, θ and either δ or ω.

The total energies of Ni(HC≡CH)$(HNC)_2$ for three distinct conformations characterized by the symbol (θ, δ) are presented in Table 1, together with the bond indices W[13] for the Ni–C (of acetylene) and C–C bonds, the net charge Q on the acetylene moiety, and the electron populations q[4] in the acetylene π and π^* orbitals perpendicular ($\perp$) and parallel ($\parallel$) to the

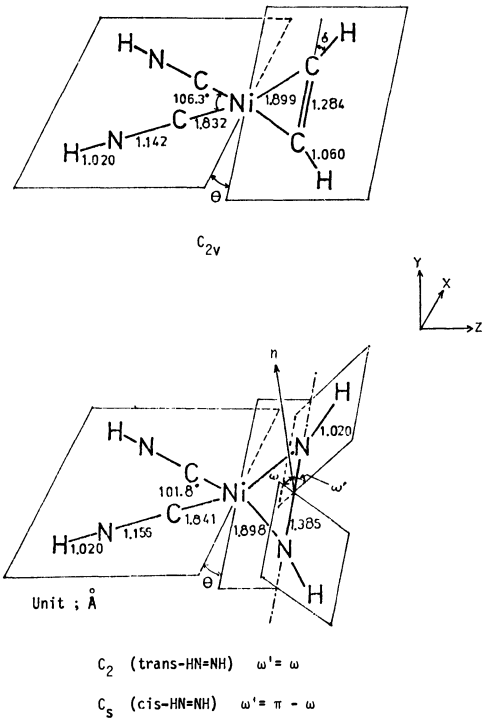

Fig. 1. Coordinate system and structures for Ni(HC≡CH)(HNC)$_2$ and Ni(HN=NH)(HNC)$_2$. The arrow n indicates the direction of the normal line on the plane which the nickel and diimide nitrogens are placed on.

Ni-acetylene plane.[14] Similar sets of data for conformations (θ, ω) of Ni(*trans*-HN=NH)(HNC)$_2$ are given in Table 2.

As can be seen in Tables 1 and 2, the square-planar bent ($\theta=0°$, $\delta>0°$) or twisted ($\theta=0°$, $\omega>0°$) form is more stable than either of the square-planar nonbent ($\theta=\delta=0°$) or untwisted ($\theta=\omega=0°$) structure and the pseudotetrahedral conformation ($\theta=90°$). The results agree well with the X-ray structures of Ni($C_6H_5C{\equiv}CC_6H_5$)-(*t*-BuNC)$_2$ and Ni(*trans*-$C_6H_5N{=}NC_6H_5$)(*t*-BuNC)$_2$.

The bond indices W for the Ni–C (of acetylene) and Ni–N (of diimide) bonds are the greatest for the square-planar bent (or twisted) structure. Since W can be regarded as a measure of covalent bond strength of the bond in question,[15] the greatest stability of the form may be ascribable to the greatest covalent character of the Ni–C or Ni–N bond. On the other hand, both W_{C-C} and W_{N-N} are the smallest for the square-planar bent and twisted structures. A stronger nickel-acetylene (or diimide) bonding is thus accompanied by a weaker C–C (or N–N) bond. A similar trend is noted in olefin complexes.[16]

Table 1. Total energy (E), bond indices (W), net charge on acetylene (Q), and various orbital populations (q) for Ni(HC≡CH)(HNC)$_2$

(θ, δ)	Square-Planar		Pseudo-tetrahedral
	Bent (0°, 31.4°)	Nonbent (0°, 0°)	Bent (90°, 31.4°)
E(eV)	−1424.097	−1417.332	−1422.003
W_{Ni-C}	0.8183	0.6949	0.7379
W_{C-C}	2.0838	2.2465	2.1702
$Q_{HC\equiv CH}$	−0.1421	−0.0080	−0.1993
$q(\pi_u(\perp))$	1.8630	1.8786	1.9557
$q(\pi_g^*(\perp))$	0.0043	0.0072	0.0021
$q(\pi_u(\parallel))$	1.6987	1.8618	1.6839
$q(\pi_g^*(\parallel))$	0.6329	0.4865	0.6313

We now attempt a more detailed analysis of the covalent bond strength of the Ni–C (of acetylene) and Ni–N (of diimide) bonds. Let us first discuss the problem of square-planar *vs.* pseudotetrahedral orientations of acetylene (bent) and diimide (twisted). As shown in Table 1, the net charge on the acetylene $Q_{HC\equiv CH}$ is smaller for the former structure. This has arisen primarily from the smaller value of $q(\pi_u(\perp))$, which implies a greater extent of electron donation from acetylene to nickel. To the contrary, the net charge on the diimide $Q_{HN=NH}$ is greater for the square-planar bent structure (Table 2). The increment of $Q_{HN=NH}$ has resulted mainly from the greater $q(\pi_g^*(\parallel))$ value,

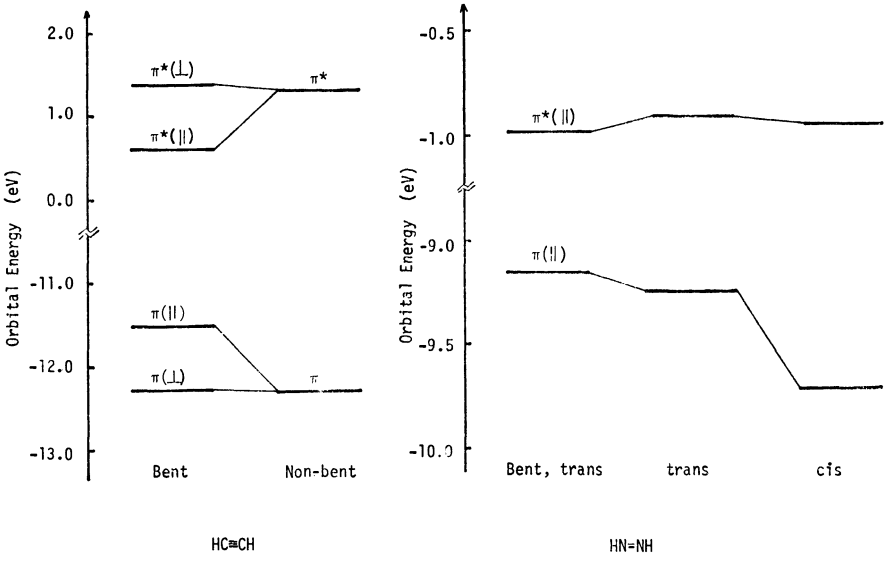

Fig. 2. Computed π and π^* energy levels for various geometries of HC≡CH and HN=NH. Bond lengths and angles are the same as those in the complexes.

Table 2. Total energy (E), bond indices (W), net charge on diimide (Q), and π orbital populations (q) for Ni(*trans*-HN=NH)$(HNC)_2$ and Ni(*cis*-HN=NH)$(HNC)_2$

(θ, ω)	*trans*-HN=NH			*cis*-HN=NH
	Square-Planar		Pseudo-tetrahedral	Square-Planar
	Twisted (0°, 13.4°)	Untwisted (0°, 0°)	Twisted (30°, 13.4°)	(0°, 13.4°)
E(eV)	−1515.275	−1513.445	−1515.243	−1515.049
W_{Ni-N}	0.8547	0.8338	0.8382	0.8476
W_{N-N}	1.1735	1.2059	1.1854	1.1762
$Q_{HN=NH}$	−0.3982	−0.3637	−0.3888	−0.3974
$q(\pi_u(\|\|))$	1.8057	1.8493	1.8023	1.8131
$q(\pi_g^*(\|\|))$	0.9367	0.9021	0.9078	0.9293

indicative of a greater extent of back-donation from nickel to diimide. Since a metal-unsaturated ligand bonding is accomplished by two independent interactions, σ donation and π back-donation, the greater extent of either process would strengthen the bond. Thus, the covalency of both the Ni–(HC≡CH) and Ni–(HN=NH) bonds is greater for the square-planar bent form as has been concluded on the basis of the bond index. However, it is noteworthy here that the origins of the greater stabilities for the square-planar forms differ between the acetylene- and azo-nickel complexes.

Next, we examine the bending (δ) and twisting (ω) effects of acetylene and diimide on the metal–π ligand bondings. Comparisons are now made between two extreme geometries, the square-planar bent ($\delta,\omega>0°$) and the square-planar nonbent ($\delta,\omega=0°$) structures. Both $q(\pi_u(\perp))$ and $q(\pi_u(\|))$ of the acetylene complex decrease in magnitude as the acetylene bends, while $q(\pi_g^*(\|))$ increases (Table 1). These results indicate greater extents of both σ donation and π back-donation for the bent form. The greater interaction means a greater Ni–(HC≡CH) bond strengthening. A change in the negligibly small $q(\pi_g^*(\perp))$ value need not be taken into account. In the diimide complex, $q(\pi_u(\|))$ is smaller for the twisted form, while $q(\pi_g^*(\|))$ is larger (Table 2). Thus the nickel–diimide bonding is also strengthened by the twisting of the diimide skeleton.

What brings about the increases in both the σ donation and π back-donation in the bent form? A possible answer can be obtained from the comparisons of the π and π^* orbital energy levels for the isolated HC≡CH and HN=NH fragments between the bent and nonbent structures (Fig. 2). In the case of acetylene, both occupied orbitals $\pi_u(\perp)$ and $\pi_u(\|)$ are more or less destabilized by the distortion while the unoccupied $\pi_g^*(\|)$ orbital lowers in energy. The destabilization of the occupied orbitals leads to a greater donor ability of the bent form while the stabilization of $\pi_g^*(\|)$ results in the greater acceptor ability. Contrary to this, the $\pi_g^*(\perp)$ orbital rises in energy as acetylene bends. However, this effect hardly exerts influence on the Ni–C (of acetylene) bonding because of the small overlap between Ni d_{xy} and C p_y orbitals (0.019). The diimide $\pi_u(\|)$ and $\pi_g^*(\|)$ orbitals show the same tendency as those of acetylene. The greater σ donor and π acceptor abilities of the twisted diimide can thus likewise be accounted for.

Configuration of HN=NH. For azo compounds two possible geometrical isomers, *cis* and *trans*, exist. We will focus our attention on the relative stabilities of the azo nickel complexes formed from the *cis* and *trans* isomers of HN=NH. We have calculated the total energy of our model compound Ni(*cis*-HN=NH)$(HNC)_2$, in which the bond lengths and angles are taken to be the same as those in *trans*-HN=NH complex. The result is given in the final column of Table 2, together with the bond indices W for the Ni–N and N–N bonds as well as the π and π^* orbital populations.

As Table 2 shows, the *trans* azo complex (square-planar bent) is more stable than the *cis*. The result may endorse the fact that the catalysis with low-valent diamagnetic metal complexes leads only to the *cis*→*trans* isomerization of *cis*-azobenzene; the reverse catalytic process hardly takes place.[17]

The greater stability of the *trans*-diimide complex as compared with the complex of the *cis* isomer is wholly compatible with the foregoing arguments on the effects of ligand deformation. Thus, the bond index W_{Ni-N} is larger in the *trans* isomer, indicative of a greater covalent character of the Ni–N bond. The π orbital population $q(\pi_u(\|))$ of the *trans*-diimide complex is smaller than that of the *cis* complex, while $q(\pi_g^*(\|))$ is greater in the former. The greater stability of the *trans* isomer would thus be a consequence of the greater extents of σ donation and π back-donation, which could immediately be rationalized from the π orbital level diagram shown in Fig. 2.

B. Ni-Ligand Bondings in the Square-Planar Conformer.

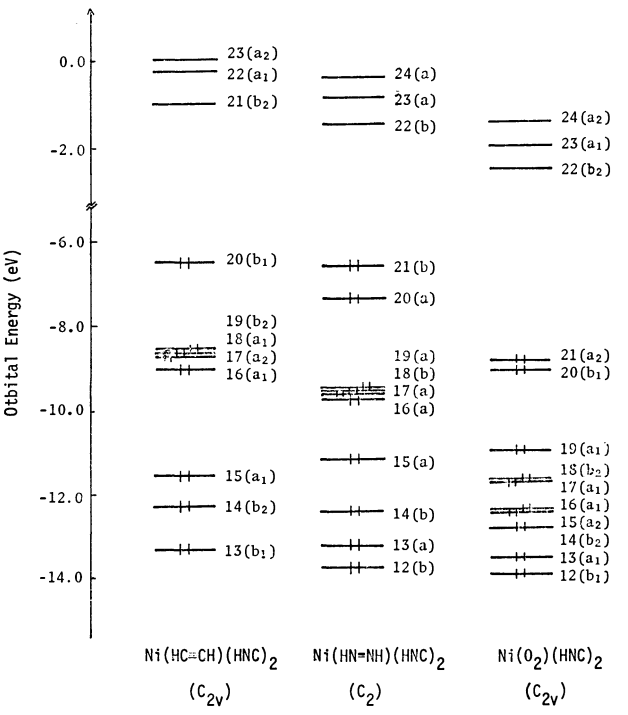

Fig. 3. Upper portions of the molecular orbital level diagrams for Ni(HC≡CH)$(HNC)_2$, Ni(HN=NH)$(HNC)_2$, and Ni$(O_2)(HNC)_2$. The highest occupied levels are 20 (b_1), 21(b), and 21(a_2), respectively.

In this section, we will describe the electronic structure of $Ni(HC{\equiv}CH)(HNC)_2$ and $Ni(trans\text{-}HN{=}NH)(HNC)_2$[18] for the square-planar form in detail. The level height and form of the bonding molecular orbitals are our specific concern here.

Molecular Orbitals. The molecular orbital energy levels are diagrammatically shown in Fig. 3, where those for the dioxygen complex $Ni(O_2)(HNC)_2$ are also shown for the sake of comparison. The levels are labeled according to the irreducible representations of the C_{2v} point group, except for the *trans*-diimide complex of the C_2 point group. Only the low-lying vacant orbitals and the upper portion of the occupied orbitals are included in the diagrams; lower orbitals which have been omitted in the diagrams consist merely of the essentially unperturbed ligand orbitals lying in the range -44.8 to -15.5 eV.

The lowest unoccupied levels, $\phi_{21}(b_2)$ for the acetylene complex and $\phi_{22}(b)$ for the azo complex, consist primarily of the isocyanide $\pi^*(\perp)$ orbital with an appreciable Ni $4p_y$ character. The highest occupied level $\phi_{20}(b_1)$ for the former complex is an admixture of the Ni $3d_{xz}$ with the $HC{\equiv}CH$ $\pi_g^*(\parallel)$ orbital. Similarly, $\phi_{21}(b)$ for the latter involves the mixing between the Ni $3d_{xz}$ and $HN{=}NH$ $\pi_g^*(\parallel)$ orbitals. These two bonding orbitals are of back-donation type which contribute to the Ni–$(HC{\equiv}CH)$ or Ni–$(HN{=}NH)$ bonding, corresponding to $\phi_{20}(b_1)$ for the dioxygen complex. Incidentally, the orbital $\phi_{21}(a_2)$ of the dioxygen complex is the lone-pair orbital $\pi_g^*(\perp)$ of O_2.

It is clear from Fig. 3 that the π-type bonding orbitals ascribable to the back-donation are more stabilized with the increase in the π acceptor ability of the unsaturated ligands. Figure 4 shows the contour maps of these back-donation type orbitals. The maps clearly show the delocalization of electrons from the Ni $3d_{xz}$ into the ligand $\pi_g^*(\parallel)$ orbital, which increases in the order $HC{\equiv}CH<HN{=}NH<O_2$, in harmony with the decreasing order of the π^* energy levels of the free molecules; 1.910 eV $(HC{\equiv}CH)$, 0.014 eV $(HN{=}NH)$, and -12.05 eV (O_2).[19]

The Ni–$(HC{\equiv}CH)$ and Ni–$(HN{=}NH)$ σ-type bondings are accomplished through donation type orbitals such as $\phi_{15}(a_1)$, $\phi_{16}(a_1)$, and $\phi_{18}(a_1)$ for the former complex and $\phi_{15}(a)$, $\phi_{16}(a)$, and $\phi_{19}(a)$ for the latter. However, each level is found to involve relatively small mixings between the Ni $d_{x^2-y^2}$ and d_{z^2} orbitals with the ligand $\pi_u(\parallel)$ orbital as compared to the back-donation type orbital.

All these results imply the relative importance of the π-type bonding in such basic zerovalent nickel complexes. Consistently, chemical and spectroscopic informations of zerovalent nickel olefin complexes show a considerable back-donation from nickel d to olefin π^* orbital.[21–24] The stability of the complexes is even governed entirely by the amount of back-donation.[23c,25] The trend forms a sharp contrast with the relative importance of σ donation in Zeise's anion $[Pt(C_2H_4)Cl_3]^-$ [26] as well as silver(I)-olefin complexes.[27]

Another type of Ni–$(HC{\equiv}CH)$ bonding is accomplished through the mixing of the $HC{\equiv}CH$ $\pi_u(\perp)$ orbital with the Ni d_{yz} orbital in $\phi_{14}(b_2)$. This is

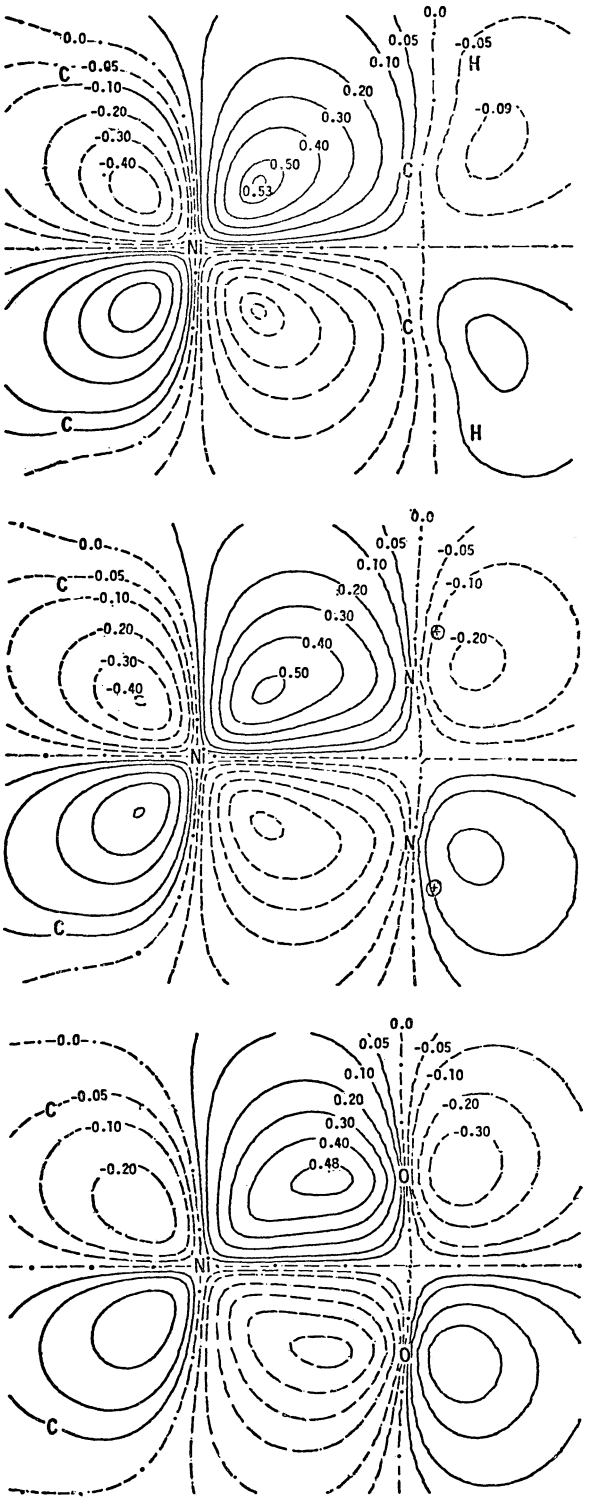

Fig. 4. Contour plots of the π-like bonding orbitals of (A) $Ni(HC{\equiv}CH)(HNC)_2$ [$20b_1$], (B) $Ni(HN{=}NH)(HNC)_2$ [21b], and (C) $Ni(O_2)(HNC)_2$ [$20b_1$]. The nitrogen and hydrogen atoms of the isocyanide ligand are excluded in the plots. The points marked with ⊕ are the projections of the hydrogen atoms onto the xz plane.

compatible with the model presented for platinum acetylene complexes by Nelson *et al.*[3a] A similar identification can be made for the dioxygen complex in the level $\phi_{14}(b_2)$.[4] The corresponding levels for the

azo complex are ψ_{20}(a) and ψ_{14}(b), which are the combinations of the two lone-pair orbitals on diimide. The mixing of the lone-pair with Ni d orbitals is practically zero.

Charge Distribution. Table 3 summarizes the calculated distributions of valence electrons over the nickel s, p, and d orbitals as well as the ligand atoms in the complexes. According to these results, the apparent electronic configurations of nickel are $(3d)^{8.90}(4s)^{0.52}(4p)^{1.07}$, $(3d)^{8.80}(4s)^{0.53}(4p)^{0.99}$, and $(3d)^{8.49}(4s)^{0.54}(4p)^{0.98}$ for Ni(HC≡CH)$(HNC)_2$, Ni(HN=NH)-$(HNC)_2$, and Ni$(O_2)(HNC)_2$, respectively. The net charge density on the nickel atom ranges from −0.49 to −0.01, increasing in the order Ni(HC≡CH)$(HNC)_2$< Ni(HN=NH)$(HNC)_2$<Ni$(O_2)(HNC)_2$. Their total d orbital occupation numbers lie between 8 and 9 and tend to increase in the reverse order. These trends are governed almost exclusively by the population on the d_{xz} orbital; nearly two electrons keep residing in each of the remaining four d orbitals. The above-mentioned order can be anticipated from the electronegativities of acetylene, diimide, and dioxygen. By a similar reasoning, positive charges on the donating isocyanide ligands should increase in the order Ni(HC≡CH)$(HNC)_2$< Ni(HN=NH)$(HNC)_2$<Ni$(O_2)(HNC)_2$. The charge transfer from the Ni$(HNC)_2$ identity to each unsaturated ligand amounts to 0.14 (acetylene), 0.41 (diimide), or 0.88 (dioxygen) of an electron.

TABLE 3. CALCULATED ELECTRON DISTRIBUTIONS FOR Ni$(C_2H_2)(HNC)_2$, Ni$(N_2H_2)(HNC)_2$, AND Ni$(O_2)(HNC)_2$

Atom	Atomic orbital	Charge density		
		Ni(C_2H_2)-$(HNC)_2$	Ni(N_2H_2)-$(HNC)_2$	Ni(O_2)-$(HNC)_2$
Ni	s	0.517	0.529	0.537
	p	1.065	0.991	0.975
	d_{xz}	1.151	0.966	0.580
	d_{yz}	1.928	1.957	1.978
	d_{xy}	1.960	1.974	1.988
	$d_{x^2-y^2}$	1.951	1.965	1.982
	d_{z^2}	1.912	1.933	1.959
C(C≡C)	s, p	4.155		
H	s	0.916		
N(N=N)	s, p		5.348	
H	s		0.851	
O(O=O)	s, p			6.437
C(CNH)	s, p	3.921	3.897	3.860
N	s, p	4.964	4.953	4.923
H	s	0.801	0.794	0.780

C. Bondings within the Ligands. The activation of unsaturated ligands by metal complexes has received considerable attention because of possible catalytic applications.[28,29] We will elaborate, in this section, on the properties of C≡C and N=N bondings as well as the isocyanide C≡N bond in the complexes.

The C≡C and N=N Bondings. In Table 4, the various π orbital populations for the acetylene and diimide complexes in the most stable forms are compared with those for free acetylene and diimide. The electron donation from nickel to the organic moiety upon complexation is reflected in the diminution in $q(\pi_u(\perp))$ or $q(\pi_u(\parallel))$ while the back-donation, in the increment in $q(\pi_g^*(\parallel))$. The following points are noteworthy in Table 4: (1) The back-donation to the acetylene $\pi_g^*(\perp)$ orbital is almost zero, in contrast to an appreciable donation from the acetylene $\pi_u(\perp)$ orbital; (2) despite the presence of the filled lone-pair orbitals, diimide acts as a fairly efficient π acceptor toward zerovalent nickel; and (3) the total π population in each complex is greater than that in the corresponding free unsaturated ligand. At any rate, both the diminution in $q(\pi_u)$ and the enhancement in $q(\pi_g^*)$ should lead to loosening of the C≡C and N=N bonds.

TABLE 4. CALCULATED ORBITAL POPULATIONS (q) AND OBSERVED BOND LENGTH (R)

	Ni(C_2H_2)-$(HNC)_2$	C_2H_2	Ni(N_2H_2)-$(HNC)_2$	N_2H_2
$q(\pi_u(\perp))$	1.86	2.00	—	—
$q(\pi_u(\parallel))$	1.70	2.00	1.81	2.00
$q(\pi_g^*(\perp))$	0.00	0.00	—	—
$q(\pi_g^*(\parallel))$	0.63	0.00	0.94	0.00
Δq	2.92	4.00	0.87	2.00
R_{L-L}(Å)	1.284[a]	1.19[b]	1.385[c]	1.243[d]

a) For Ni$(C_6H_5C{\equiv}CC_6H_5)(t\text{-BuNC})_2$, Ref. 11. b) For $C_6H_5C{\equiv}CC_6H_5$, J.M. Robertson and I. Woodward, *Proc. R. Soc., Ser. A*, **164**, 436 (1938). c) For Ni-$(C_6H_5N{=}NC_6H_5)(t\text{-BuNC})_2$, Ref. 12. d) For $C_6H_5N{=}NC_6H_5$, C. J. Brown, *Acta Crystallogr.*, **21**, 146 (1966).

We have previously introduced the quantity[4]

$$\Delta q = q(\pi_u(\perp)) + q(\pi_u(\parallel)) - q(\pi_g^*(\perp)) - q(\pi_g^*(\parallel)) \quad (2)$$

as a measure of the strength of the O–O π bond in the nickel dioxygen complex. The values of Δq calculated for HC≡CH and HN=NH, both complexed and uncomplexed, are included in Table 4. For either of the acetylene and azo complexes studied, Δq is much smaller than that for the corresponding free substrate. This would effect a considerable increase in the C≡C as well as N=N bond length R, as is actually the case.

The above-stated trend could be cast into a more quantitative generalization,[30,31] since conceptually our Δq is twice the π-bond order of the unsaturated ligand. Thus we consider the ratio of the increase in R upon complexation to that brought about on going from an unsaturated bond to a saturated one:[32]

$$r = \frac{R_{L=L}(\text{complex}) - R_{L=L}(\text{free})}{R_{L-L}(\text{saturated}) - R_{L=L}(\text{free})} \quad (3)$$

L = C, N, and O

The ratio r is now to be compared with the change in Δq effected by complexation:

$$\Delta(\Delta q) = \Delta q(\text{complex}) - \Delta q(\text{free}) \quad (4)$$

The $\Delta(\Delta q)$ takes on a value −2 when complexation involves a complete destruction of a π bond of the ligand. Needless to say, $\Delta(\Delta q)=0$ when complexation does not take place. The ratio r should respectively be 1 and 0 in these extreme cases.

Figure 5 is the plots of r against $\Delta(\Delta q)$ for the nickel isocyanide complexes of acetylene, diimide, dioxygen,

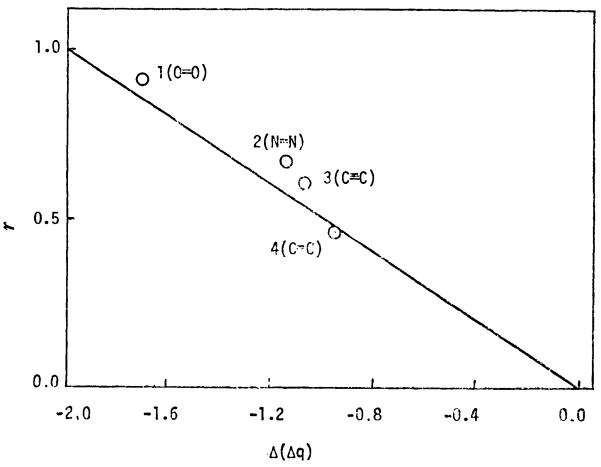

Fig. 5. Plots of the bond length ratio r of nickel complexes against the $\Delta(\Delta q)$ values calculated for the corresponding model compounds:
(1) $Ni(O_2)(t\text{-}BuNC)_2$
(2) $Ni(trans\text{-}C_6H_5N{=}NC_6H_5)(t\text{-}BuNC)_2$
(3) $Ni(C_6H_5C{\equiv}CC_6H_5)(t\text{-}BuNC)_2$
(4) $Ni(H_2C{=}CH_2)(P(C_6H_5)_3)_2$
The model compounds assumed are $Ni(O_2)(HNC)_2$, $Ni(trans\text{-}HN{=}NH)(HNC)_2$, $Ni(HC{\equiv}CH)(HNC)_2$, and $Ni(H_2C{=}CH_2)(PH_3)_2$, respectively. The bond length of O_2 in $Ni(O_2)(t\text{-}BuNC)_2$ was taken from M. Matsumoto and K. Nakatsu, *Acta Crystallogr.*, **B31**, 2711 (1975); for $Ni(H_2C{=}CH_2)(P(C_6H_5)_3)_2$, P.-T. Cheng, C. D. Cook, C. H. Koo, S. C. Nyburg, and M. T. Shimoni, *Acta Crystallogr.*, **B27**, 1904 (1971).

and ethylene. All the plots fall in the vicinity of the straight line which connects the two extreme points mentioned above. The results would make such plots for different atomic pairs meaningful.

N≡C Bonding. Infrared study[33] of a series of *cis*-planar nickel bisisocyanide complexes concludes that they possess two N≡C stretching bands assignable to the a and b modes with respect to the C_2 point group. We have applied the method of Cotton and Kraihanzel[34,35] to the two stretching frequencies observed, to derive a set of approximate force constants f_{N-C} and f_i. The former is the N≡C stretching force constant while the latter represents the *cis*-type (N≡C stretch)-(N≡C stretch) vibrational interaction force constant. Although there are several well-founded criticisms of the method,[36,37] it still seems to be useful for a comparative study of a family of analogous compounds.[38]

We here consider the N≡C stretching force constant f_{N-C}. Plotted in Fig. 6 are the f_{N-C} values for $Ni(C_6H_5C{\equiv}CC_6H_5)(t\text{-}BuNC)_2$, $Ni(C_6H_5N{=}NC_6H_5)(t\text{-}BuNC)_2$, and $Ni(O_2)(t\text{-}BuNC)_2$ against the bond indices W_{N-C} calculated for the N≡C bond of the corresponding model compounds. As can be seen in Fig. 6, there is a reasonably good linearity between f_{N-C} and W_{N-C} with a positive slope.

D. Polar Effect of Isocyanide Substituent. In dealing with the effects of substituent in isocyanide on the strengths of nickel-ligand bonds and the ligand C≡C and N=N bonds, we employ a similar model as has been

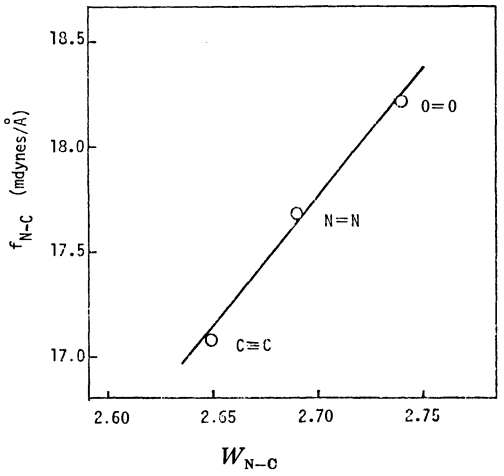

Fig. 6. Plots of the N≡C stretching force constants (f_{N-C}) *vs.* calculated bond indices (W_{N-C}) of the corresponding model compounds.

used previously.[4] That is, we assume a hypothetical isocyanide ligand (CNH′, for which the valence-state ionization potential I_S^H for the hydrogen atom H′ is allowed to vary, with the other parameters being fixed. When I_S^H is greater than 13.6 eV, CNH′ should be more electronegative than CNH, and *vice versa*. The differen-

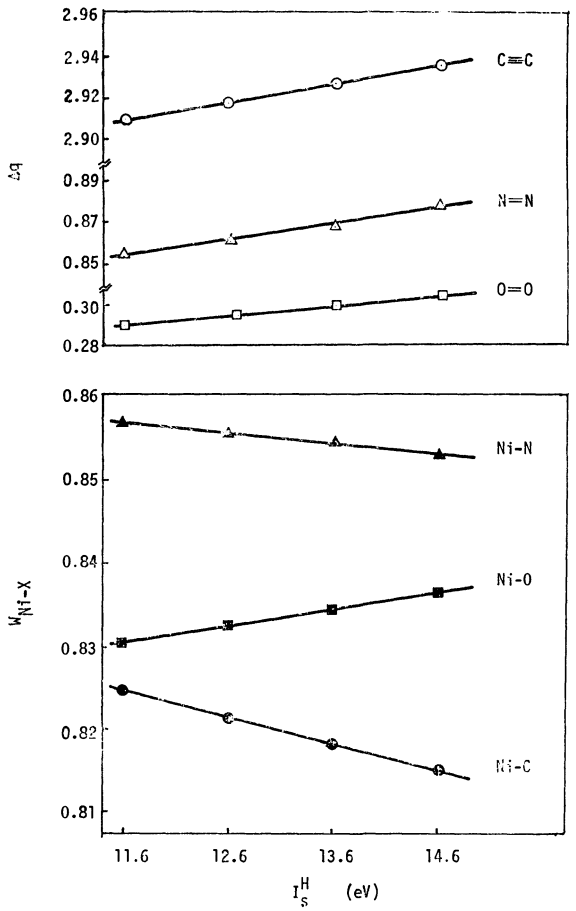

Fig. 7. Variations of the Δq values (top) and bond indices W (bottom) as the functions of I_S^H.
○, ●: $Ni(HC{\equiv}CH)(HNC)_2$, △, ▲: $Ni(HN{=}NH)(HNC)_2$, □, ■: $Ni(O_2)(HNC)_2$.

tial π orbital population Δq and bond indices W for the hypothetical complexes $Ni(HC{\equiv}CH)(H'NC)_2$ and $Ni(HN{=}NH)(H'NC)_2$ were calculated by varying I_S^H from 11.6 to 14.6 eV.

Figure 7 shows the variations in Δq and W_{Ni-L} as the functions of I_S^H. For the purpose of comparison, the calculated data for dioxygen complex $Ni(O_2)(H'NC)_2$ are also plotted. As Fig. 7 shows, the Δq-values for these three complexes altogether increase with the increasing I_S^H. Thus, as the isocyanide ligand becomes more electronegative, all the C≡C, N=N, and O=O bondings should be more and more strengthened. The trend can easily be accounted for in terms of the decreasing back-donation from nickel to the π^* orbital(s) of the unsaturated ligands.

As for the strength of the nickel–ligand bonds, both W_{Ni-C} and W_{Ni-N} decrease as the isocyanide ligand becomes more electron-withdrawing. The situation is analogous to the substitution effect on the metal–olefin π-bonding interaction in various olefin complexes.[16] By contrast, the W_{Ni-O} increases as I_S^H increases. That is, substitution of electronegative ligands tend to increase the nickel–oxygen bond strength.

The unique electronic effects of isocyanide substituents on the Ni–O bond strength can be rationalized from the type of orbital interactions involved. Figure 8 is a schematic level diagram for the highest occupied b_1 orbital of $Ni(HNC)_2(C_{2v})$ and the frontier π and π^* orbitals of the three isolated molecules, HC≡CH, HN=NH, and O_2. For the sake of convenience, the $Ni(HNC)_2$ b_1 and O_2 π levels are depicted as doubly occupied orbitals, although in reality calculations were performed by the UHF-INDO method. Note that the b_1 orbital in question lies below the π^* orbitals of HC≡CH and HN=NH but certainly above the π^* level of O_2.

The b_1 orbital which consists mainly of the Ni $3d_{xz}$ orbital interacts with the π^* levels, and this interaction contributes most dominantly to the back-donation. As the CNH is replaced by a more electron-releasing ligand, the b_1 level will be destabilized accordingly. This destabilization in turn should enhance the above-mentioned type of orbital interactions for the cases of HC≡CH and HN=NH whereas it should lead to a diminution in interaction in the case of O_2, as will be readily understood by a simple perturbation theory. The situations are wholly compatible with the trends noted in Fig. 7.

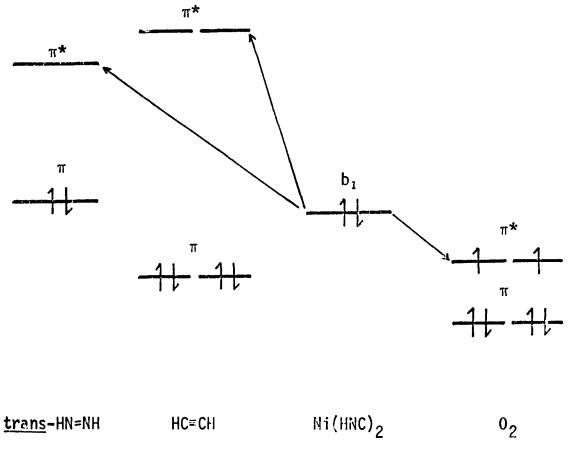

Fig. 8. Schematical level diagrams for the π and π^* orbitals of *trans*-HN=NH, HC≡CH, and O_2 as well as the highest b_1 orbitals of $Ni(HNC)_2$. The back-donation of electrons occurs in the direction of the arrows.

References

1) For a recent comprehensive review, R. F. Heck, "Organotransition Metal Chemistry," Academic Press, New York and London (1974).

2) a) J. W. Moore, *Acta Chem. Scand.*, **20**, 1154 (1966); b) H. Kato, *Bull. Chem. Soc. Jpn.*, **44**, 348 (1971); c) E. J. Baerends, D. E. Ellis, and R. Ross, *Theor. Chim. Acta (Berlin)*, **27**, 339 (1972); d) K. H. Johnson and F. C. Smith, Jr., *Phys. Rev.*, **B5**, 831 (1972).

3) a) J. H. Nelson, K. S. Wheelock, L. C. Cusacks, and H. B. Jonassen, *J. Am. Chem. Soc.*, **91**, 7005 (1969); *ibid.*, **92**, 5110 (1970); *Inorg. Chem.*, **11**, 422 (1972); *Chem. Commun.*, **1969**, 1019; b) J. G. Norman, Jr., *J. Am. Chem. Soc.*, **96**, 3327 (1974).

4) K. Tatsumi, T. Fueno, A. Nakamura, and S. Otsuka, *Bull. Chem. Soc. Jpn.*, **49**, 2164 (1976).

5) S. Otsuka, T. Yoshida, and Y. Tatsuno, *J. Chem. Soc., D*, **1971**, 42.

6) S. Otsuka, T. Yoshida, and Y. Tatsuno, *Chem. Commun.*, **1971**, 67.

7) K. Tatsumi and T. Fueno, *Bull. Chem. Soc. Jpn.*, **49**, 929 (1976).

8) M. Zerner and M. Gouterman, *Theor. Chim. Acta (Berlin)*, **4**, 44 (1966).

9) E. Clementi and D. L. Raimond, *J. Chem. Phys.*, **38**, 2686 (1963).

10) A. D. Mitchell ed., "Table of Interatomic Distances and Configuration in Molecules and Ions," The Chemical Society, London (1958).

11) R. S. Dickson and J. A. Ibers, *J. Organometal. Chem.*, **36**, 191 (1972).

12) R. Dickson and J. A. Ibers, *J. Am. Chem. Soc.*, **93**, 4636 (1971); *ibid.*, **94**, 2988 (1972).

13) K. B. Wiberg, *Tetrahedron*, **24**, 1083 (1968).

14) Strictly speaking, the π and π^* orbitals cannot be extracted from the molecular orbitals of the complexes in which HC≡CH and HN=NH are distorted in structure. However, since the distortion (δ or ω) is small, we may assume that both orbitals are constructed virtually of the $p_z(\parallel)$ and $p_y(\perp)$ (or $p_x(\perp)$) atomic orbitals alone.

15) T. Okada and T. Fueno, *Bull. Chem. Soc. Jpn.*, **48**, 2025 (1975).

16) F. R. Hartly, *Chem. Rev.*, **69**, 799 (1969); *Angew. Chem. Intern. Edit.*, **11**, 596 (1972).

17) A. Nakamura, K. Doi, K. Tatsumi, and S. Otsuka, *J. Mol. Catal.*, in press.

18) Hereafter in this paper, HN=NH denotes only a *trans* diimide unless otherwise noted.

19) These π_g^* orbital energies of acetylene and diimide were calculated using the INDO method. That of dioxygen was given by the UHF-INDO calculation. Molecular geometries are taken from the literature; see Refs. 10 and 20.

20) N. W. Winter and R. M. Pitzer, *J. Chem. Phys.*, **62**, 1269 (1975).

21) G. N. Schrauzer, *Chem. Ber.*, **94**, 6421 (1961).

22) H. B. Gray and C. J. Ballhausen, "Molecular Orbital Theory," W. A. Benjamin, New York, N. Y. (1964).

23) a) A. Yamamoto and S. Ikeda, *J. Am. Chem. Soc.*, **89**, 5989 (1967); b) A. Yamamoto, T. Shimizu, and S. Ikeda, *Polym. J.*, **1**, 171 (1970); c) T. Yamamoto, A. Yamamoto, and S. Ikeda, *J. Am. Chem. Soc.*, **93**, 3350, 3360 (1971).

24) a) C. A. Tolman, W. C. Seidel, and D. H. Gerlach, *J. Am. Chem. Soc.*, **94**, 2669 (1972); b) C. A. Tolman and W. C. Seidel, *ibid.*, **96**, 2774 (1974).
25) C. A. Tolman, *J. Am. Chem. Soc.*, **96**, 2780 (1974).
26) N. Rösch, R. P. Messmer, and K. H. Johnson, *J. Am. Chem. Soc.*, **96**, 3855 (1974).
27) H. Basch, *J. Chem. Phys.*, **56**, 441 (1972).
28) M. M. T. Khan and A. E. Martell, "Homogeneous Catalysis by Metal Complex," Vol. 1, Academic Press, New York and London (1974).
29) G. H. Olivé and S. Olivé, *Angew. Chem. Internat. Edit.*, **10**, 105 (1971); *ibid.*, **13**, 29 (1974).
30) C. A. Coulson, *Proc. R. Soc., Ser. A*, **169**, 413 (1939).
31) M. J. S. Dewar and H. N. Schmeising, *Tetrahedron*, **5**, 166 (1959); **11**, 96 (1960).
32) In the case of HC≡CH, the subscripts L–L and L=L should be read as indicating the C=C and C≡C bonds, respectively.
33) S. Otsuka, T. Yoshida, and Y. Tatsuno, *J. Am. Chem. Soc.*, **93**, 6462 (1971).
34) F. A. Cotton and C. S. Kraihanzel, *J. Am. Chem. Soc.*, **84**, 4432 (1962).
35) This method has widely been extended to various metal carbonyl and isocyanide systems. See for examples; W. Beck and K. Lottes, *Chem. Ber.*, **98**, 2657 (1965); A. C. Sarapu and R. F. Fenske, *Inorg. Chem.*, **14**, 247 (1975).
36) L. M. Bower and M. H. B. Stiddard, *Inorg. Chim. Acta*, **1**, 231 (1967).
37) L. H. Jones, *Inorg. Chem.*, **7**, 1681 (1968).
38) a) G. R. Van Hecke and W. DeW. Horrocks, Jr., *Inorg. Chem.*, **5**, 1960 (1966); b) F. A. Cotton, *ibid.*, **7**, 1683 (1968).

The Reaction of Singlet Methylene with Methane

Kazuhiko SHIBUYA, Kin-ichi OBI, and Ikuzo TANAKA
Department of Chemistry, Tokyo Institute of Technology, Ohokayama, Meguro-ku, Tokyo 152
(Received December 23, 1975)

Cyclopropane in an excess of methane was photolyzed at 1470 and 1634 Å. The decomposition rate constants of the resultant vibrationally excited ethane into methyl radicals were found to be 6.0×10^9 s^{-1} and 5.0×10^9 s^{-1} at 1470 and 1634 Å respectively. The following procedure was used in treating the results obtained in our and the other researchers' systems. The statistical calculation was made to estimate the internal energy of singlet methylene, $\bar{\varepsilon}_i$, which is initially acquired in the primary decomposition process. The RRKM theory was then used to estimate the internal energy of the excited ethane. According to these calculations, the fraction of excess photon energy carried into ethane decreases as the energy, $\bar{\varepsilon}_i$, increases.

The chemistry of methylene has received much attention in recent years. The difference in reactivity of the singlet and triplet species is well-known,[1] and the insertion of singlet methylene into C–H bonds of hydrocarbons has been extensively applied to chemical activation techniques.[2] The vibrationally excited ethane is formed by the insertion reaction of singlet methylene with methane;[3-7] it either decomposes into methyl radicals or is deactivated by collision. Ketene,[4,5] diazomethane,[3,7] and methane[6] have been used as the source of methylene.

We have previously reported that cyclopropane is the most suitable molecule to produce methylene in the vacuum ultraviolet region.[8] In this study, we carried out the photolysis of cyclopropane with methane and oxygen (or nitrogen oxide) (cyclo-C_3H_6/CH_4/O_2 or NO=1/10/0.1) at 1470 and 1634 Å. The decomposition rate constants of the vibrationally excited ethane were determined and compared with the results obtained from the experiments in which the other molecules were photolyzed to produce singlet methylene with different wavelengths.

Experimenta

Most of the experimental procedures used in the present study have been described previously.[8] A synthetic sapphire plate was used as the window of the xenon lamp to cut off the weak 1295 Å line. After irradiation, the products and the remaining reactants were vacuum-distilled at the temperature of solid nitrogen to rid the reaction cell of the excess methane and subsequently collected in a sample tube by means of a Toepler pump. Analyses were made by means of gas chromatography using a 3-m-long charcoal column.

Results and Discussion

In our system, the reaction scheme relating to singlet methylene is as follows:

$$\text{cyclo-}C_3H_6 + h\nu \longrightarrow {}^1CH_2 + C_2H_4, \quad \Delta H = 101 \text{ kcal mol}^{-1}, \tag{1}$$

$${}^1CH_2 + CH_4 \longrightarrow C_2H_6{}^*, \quad \Delta H = -100 \text{ kcal mol}^{-1}, \tag{2}$$

$$\longrightarrow {}^3CH_2 + CH_4, \tag{3}$$

$${}^1CH_2 + \text{cyclo-}C_3H_6 \longrightarrow \text{removal of } {}^1CH_2, \tag{4}$$

$$C_2H_6{}^* \xrightarrow{k_d} CH_3 + CH_3, \tag{5}$$

$$\xrightarrow{\sum k_s^i(M_i)} C_2H_6. \tag{6}$$

Reaction 1 is the major primary process in the photolysis of cyclopropane.[8] Singlet methylene reacts with methane to form vibrationally excited ethane, Reaction 2, or to be deactivated to the triplet, Reaction 3. The rate constants for Reactions 2 and 3 were found to be $(1.9\pm0.5)\times10^{-12}$ and $(1.6\pm0.5)\times10^{-12}$ cm^3 molecule^{-1} s^{-1} respectively from a flash photolysis study.[5] The energized ethane should be accompanied by decomposition to methyl radicals, Reaction 5, unless it is collisionally deactivated to a stable ethane molecule, Reaction 6. Both triplet methylene and methyl radicals will be removed by the added radical scavenger, oxygen or nitrogen oxide.[9]

A steady-state treatment of Reaction 1—6 leads to:

$$\frac{(C_2H_4)}{(C_2H_6)} = C \times (1+k_d\omega^{-1}), \tag{I}$$

$$C = 1 + \frac{k_3}{k_2} + \frac{k_4}{k_2}\frac{(\text{cyclo-}C_3H_6)}{(CH_4)}, \tag{II}$$

and

$$\omega = \sum_i k_s^i(M_i), \tag{III}$$

where C is constant under our experimental conditions of (cyclo-C_3H_6)/(CH_4)=1/10, and ω is the effective collision frequency of bath gas with the energized ethane. The collisional deactivation efficiencies (β) were taken to be 0.61 and 0.83 for methane and cyclopropane respectively.[10] The collision diameters of $\sigma_{C_2H_6}$=4.38 Å, σ_{CH_4}=3.81 Å, and $\sigma_{\text{cyclo-}C_3H_6}$=4.92 Å were used to calculate the collision frequencies (Z). The effective collision frequencies of bath gases in units of s^{-1}, $\omega=\beta Z$, are as follows: $\omega_{CH_4}=0.90\times10^7\ P_{CH_4}$ (Torr) and $\omega_{\text{cyclo-}C_3H_6}=1.20\times10^7\ P_{\text{cyclo-}C_3H_6}$ (Torr). The k_d values were determined from plots of $(C_2H_4)/(C_2H_6)$ *vs.* ω^{-1} at both wavelengths; these plots are illustrated in Fig. 1. We obtained $k_d=6.0\times10^9$ s^{-1} and C=3.2 at 1470 Å photolysis and $k_d=5.0\times10^9$ s^{-1} and C=3.2 at 1634 Å photolysis. The high-pressure intercept of 3.2, combined with k_3/k_2=0.8,[5] gives k_4/k_2=14 and leads to a value for the relative reactivity of methane and cyclopropane of $k_4/(k_2+k_3)$=7.8.

The k_d values are listed in Table 1, together with those obtained from the experiments in which ketene, diazomethane, and methane were used as the source of methylene. The variation in k_d apparently reflects the internal energy of methylene which is originally acquired in the primary decomposition process to form methylene. We tentatively used the following procedure to elucidate the dependence of k_d on the

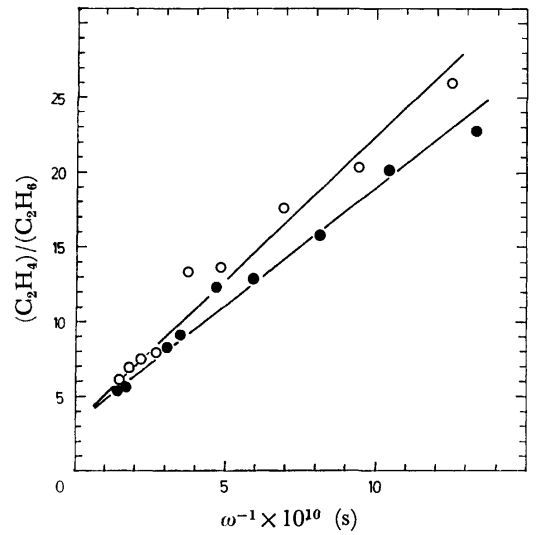

Fig. 1. Plot of $(C_2H_4)/(C_2H_6)$ *vs.* ω^{-1} at the 1470 and 1634 Å photolysis of cyclo-$C_3H_6/CH_4/O_2$ (or NO) mixtures.
○, 1470 Å Photolysis; ●, 1634 Å photolysis.

Table 1. Decomposition rate constants of C_2H_6* formed by the $^1CH_2 + CH_4$ reaction[a]

Source of methylene	$P_{1/2}$[c] (Torr)	k_d (s^{-1})	Ref.
CH_2CO (3130Å)[b]	240	2.6×10^9	4)
CH_2N_2 (4358Å)[b]	320	4.2×10^9	7)
cyclo-C_3H_6 (1634Å)	560	5.0×10^9	This work
cyclo-C_3H_6 (1470Å)	670	6.0×10^9	This work
CH_4 (1236 and 1048—1067Å)[b]	770	6.9×10^9	6)

a) Bell and Kistiakowsky[3] photolyzed CH_2N_2/CD_4 mixtures, from which a value for k_d of $\sim2\times10^9$ s^{-1} was deduced by Setser and Rabinovitch[11] after correcting for isotope effects, and Braun *et al.* flash-photolyzed CH_2CO/CH_4 mixtures, from which $k_d=4\times10^9$ s^{-1} was obtained. However, these values are not listed because their photolytic lamp was not monoenergetic. b) The following effective collision frequencies in units of s^{-1}, $\omega=\beta Z$, were used: $\omega_{CH_4}=0.90\times10^7$ P_{CH_4} (Torr), $\omega_{C_3H_8}=1.22\times10^7$ $P_{C_3H_8}$ (Torr), $\omega_{CH_2N_2}=1.61\times10^7$ $P_{CH_2N_2}$ (Torr), and $\omega_{iso\text{-}C_4H_{10}}=1.90\times10^7$ $P_{iso\text{-}C_4H_{10}}$ (Torr). c) The pressure at which the half of C_2H_6* is stabilized.

internal energy of methylene. First, the average internal energy of methylene, $\bar{\varepsilon}_i$, which is initially present in the primary decomposition process was estimated on the basis of the statistical model proposed by Campbell and Schlag.[12] Second, the average internal energy of methylene, $\bar{\varepsilon}_f$, which is carried into the insertion product (ethane) was calculated from the ordinary RRKM model.

Estimation of $\bar{\varepsilon}_i$. The methylene-forming processes besides Reaction 1 in Table 1 are:

$$CH_2CO + h\nu \rightarrow {}^1CH_2 + CO,\ \Delta H = 86\ \text{kcal mol}^{-1}, \quad (7)$$

$$CH_2N_2 + h\nu \rightarrow {}^1CH_2 + N_2,\ \Delta H = 52\ \text{kcal mol}^{-1}, \quad (8)$$

$$CH_4 + h\nu \rightarrow {}^1CH_2 + H_2,\ \Delta H = 117\ \text{kcal mol}^{-1}. \quad (9)$$

The maximum energy available for methylene can be obtained by means of:

$$\varepsilon_{max} = E_p - \Delta H, \quad (IV)$$

where E_p is the energy of the photon and ΔH, the heat of the reaction of each methylene-forming process. The energy, ε_{max}, may either be partitioned among each degree of freedom of methylene and the partner fragment more or less statistically or appear as the non-statistical kinetic energy of fragments.[13] To simplify the treatment, we neglected the non-statistical energy and assumed all the vibrational modes to be active. The fraction of methylene which retains a vibrational energy, ε, out of the maximum available energy, ε_{max}, can be written[12] as:

$$f(\varepsilon) = \frac{N_{CH_2}(\varepsilon)N_R(\varepsilon_{max}-\varepsilon)}{\sum N_{CH_2}(\varepsilon_j)N_R(\varepsilon_{max}-\varepsilon_j)}, \quad (V)$$

where $N_{CH_2}(\varepsilon)$ is the energy-level density of the methylene part of the molecule used as the source of methylene, and $N_R(\varepsilon_{max}-\varepsilon)$, that of the remaining part. The energy-level densities were calculated by means of Eq. IX; all the vibrational frequencies for ethylene and methylene are given in the Appendix. The average energy, $\bar{\varepsilon}_i$, was derived from:

$$\bar{\varepsilon}_i = \int \varepsilon f(\varepsilon)d\varepsilon. \quad (VI)$$

The resultant values are listed in Table 2. If methylene, with the internal energy of $\bar{\varepsilon}$, is inserted into the C–H bond of methane, the average internal energy of energized ethane, $\bar{E}$, is:

$$\bar{E} = \bar{\varepsilon} + \varepsilon_{thermal} - \Delta H \quad (VII)$$

where $\varepsilon_{thermal}$ is the thermal energy (≈2 kcal mol^{-1}) and ΔH, the heat of reaction of Reaction 2. The experimental values for k_d are plotted as a function of $\bar{E}(=\bar{\varepsilon}_i+\varepsilon_{thermal}-\Delta H)$ is Fig. 2. This plot may represent the dependence of k_d on the internal energy of ethane, assuming that all of $\bar{\varepsilon}_i$ is carried into the insertion product without any energy loss. In case singlet methylene without any internal energy is inserted into methane, the energized ethane possesses internal energies of 102 kcal mol^{-1}, corresponding to $\bar{\varepsilon}=0$ in Eq. VII. We obtained $k_d=1.7\times10^9$ s^{-1} at $E=102$ kcal mol^{-1} in Fig. 2.

Estimation of $\bar{\varepsilon}_f$. The specific rate constant, k_E, of the decomposition of ethane with an internal energy of E can be given by the RRKM theory[14,15]

Table 2. Internal energy of singlet methylene[a]

Source of methylene	ε_{max}[b] (kcal mol^{-1})	$\bar{\varepsilon}_i$[c] (kcal mol^{-1})	$\bar{\varepsilon}_f$[d] (kcal mol^{-1})	$\bar{\varepsilon}_f/\bar{\varepsilon}_i$
CH_2CO (3130 Å)	5	3	2	0.67
CH_2N_2 (4358 Å)	13	8	4	0.50
cyclo-C_3H_6 (1634)	74	14	5	0.37
cyclo-C_3H_6 (1470 Å)	93	17	6	0.35
CH_4 (1236 Å)	114	83	7	0.08
CH_4 (1048—1067 Å)	≈153	≈113	7	0.06

a) $\Delta H_f^\circ(^1CH_2)=101$ kcal mol^{-1} was assumed. b) Maximum energy carried by methylene to form C_2H_6*. c) Average energy of methylene calculated by means of $f(E)$. d) Calculated from the RRKM model.

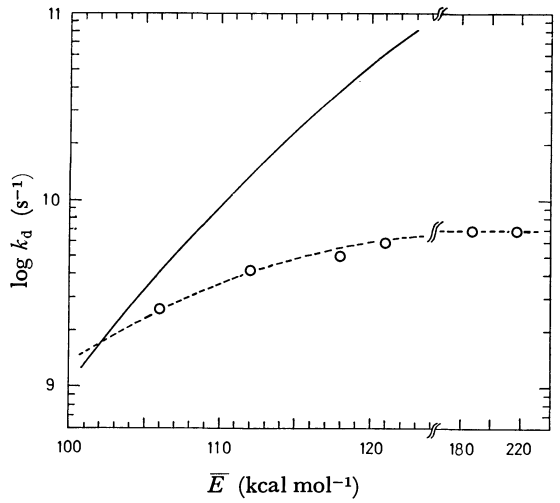

Fig. 2. Variation of k_d with $\bar{E}(=\bar{\varepsilon}_i+\varepsilon_{thermal}-\Delta H)$. Solid line represents the specific rate constant calculated from the RRKM treatment.

as follows:

$$k_E = \frac{1}{h}\frac{\sigma}{\sigma^\dagger}\left(\frac{I_A^\dagger I_B^\dagger I_C^\dagger}{I_A I_B I_C}\right)^{1/2}\frac{\sum P(E-E_0)}{N(E)}, \qquad \text{(VIII)}$$

where σ and $\sigma^\dagger$ are the symmetry numbers of the ethane molecule and the activated complex respectively. $N(E)$ is the energy level density for the ethane molecule at the energy of E, $\sum P(E-E_0)$, the energy-level sum for the activated complex, and E_0, the critical energy required for the decomposition of energized ethane into methyl radicals (85 kcal mol^{-1}).[15] In the absence of an internal free rotation, $N(E)$ and $\sum P(E-E_0)$ can be approximated by:

$$N(E) = \frac{(E+aE_z)^{s-1}}{\Gamma(s)\prod h\nu_i}, \qquad \text{(IX)}$$

and:

$$\sum P(E-E_0) = \frac{(E-E_0+a^\dagger E_z^\dagger)^{s^\dagger}}{\Gamma(s^\dagger+1)h\nu_i^\dagger}, \qquad \text{(X)}$$

as proposed by Whitten and Robinovitch.[16] In Eqs. IX and X, s and $s^\dagger$ are the numbers of the vibrational degrees of freedom, E_z and $E_z^\dagger$ are the zero point energies, and ν_i and $\nu_i^\dagger$ are the vibrational frequencies of ethane and the activated complex respectively. We assumed that $a=1$ and $a^\dagger=0.8$.[17] Our structural parameters for ethane are given in Table 3. The model used was similar to that adopted by Hase[18] except that we did not set the torsional mode (ν_4) at a free rotor in the activated complex. The frequency for $\nu_4^\dagger$ was taken to be 39 cm^{-1} because the model gave $k_E=1.7\times10^9$ s^{-1} at $E=102$ kcal mol^{-1} corresponding to $\varepsilon=0$. The calculated values for k_E are plotted as a function of the internal energy of ethane in Fig. 2 (solid line). The two curves in the figure apparently show different dependences on the energy, which implies that the internal energy, $\bar{\varepsilon}_f$, carried by methylene into the insertion product differs to a great extent from the energy, $\bar{\varepsilon}_i$, originally acquired in the methylene-forming process. We estimated the value for $\bar{E}(=\bar{\varepsilon}_f+\varepsilon_{thermal}-\Delta H)$ corresponding to each k_d value by virtue of the calculated curve for k_E. The average internal energy of singlet methylene which is carried into ethane, $\bar{\varepsilon}_f$, was calculated by introducing the average internal energy of energized ethane, $\bar{E}(=\bar{\varepsilon}_f+\varepsilon_{thermal}-\Delta H)$, into Eq. VII; the values for $\bar{\varepsilon}_f$ are listed in Table 2.

The ratios of $\bar{\varepsilon}_f$ to $\bar{\varepsilon}_i$ are also given in Table 2. The results show that only a fraction of $\bar{\varepsilon}_i$ (or ε_{max}) is carried into chemically activated ethane and that this fraction rapidly decreases as $\bar{\varepsilon}_i$ (or ε_{max}) becomes larger. The most likely explanation of this result is that singlet methylene suffers a number of inelastic collisions before reacting with methane and loses a considerable amount of the internal energy originally acquired in the primary decomposition process. In fact, a flash photolysis study[5] suggested that singlet methylene would undergo hundreds of collisions prior to insertion. The probability of the insertion reaction occurring, however, would be large to such an extent that the internal energy of singlet methylene is not fully thermalized before insertion.

TABLE 3. STRUCTURE PARAMETERS FOR ETHANE

	Molecule	Activated complex
Frequency (cm^{-1})	2915	2915
	955	—
	1388	1388
	260	39
	2915	2915
	1370	1370
	2950 (2)	2950 (2)
	1460 (2)	1460 (2)
	1190 (2)	273 (2)
	2974 (2)	2974 (2)
	1469 (2)	1469 (2)
	822 (2)	188 (2)
Zero-point energy (kcal mol^{-1})	45.1	38.9
r_{C-C} (Å)	1.54	3.6
Moment of inertia		
I_A =	10.8×10^{-40}	10.8×10^{-40}
$I_B = I_C$ =	42.0×10^{-40}	185.5×10^{-40}
(g cm^2)		
Number of symmetry	6	6

Appendix

The vibrational frequencies of ethylene are taken[19] to be 3000, 1600, 1350, 1000, 3100, 1250, 950, 950, 3100, 800, 3000, and 1450 cm^{-1} for ν_1 to ν_{12}.

The vibrational frequencies of methylene are estimated to be 2850, 1450, and 2925 cm^{-1} for ν_1, ν_2, and ν_3, respectively.

References

1) W. B. DeMore and S. W. Benson, *Adv. Photochem.*, **2**, 219 (1964).
2) H. M. Frey, *Prog. React. Kinet.*, **2**, 131 (1964).
3) J. A. Bell and G. B. Kistiakowsky, *J. Am. Chem. Soc.*, **84**, 3417 (1962).
4) M. L. Halberstadt and J. R. McNesby, *J. Am. Chem. Soc.*, **89**, 3417 (1967).

5) W. Braun, A. M. Bass, and M. Pilling, *J. Chem. Phys.*, **52**, 5131 (1970).
6) R. E. Rebbert, S. G. Lias, and P. Ausloos, *Chem. Phys. Lett.*, **12**, 323 (1971).
7) F. B. Growcock, W. L. Hase, and J. W. Simons, *Intern. J. Chem. Kinetics.*, **5**, 77 (1973).
8) K. Shibuya, K. Obi, and I. Tanaka, *Bull. Chem. Soc. Jpn.*, **48**, 1974 (1975).
9) R. L. Russell and F. S. Rowland, *J. Am. Chem. Soc.*, **90**, 1671 (1968).
10) S. C. Chan, B. S. Rabinovitch, J. T. Bryant, L. D. Spicer, T. Fujimoto, Y. N. Lin, and S. P. Pavlou, *J. Phys. Chem.*, **74**, 3160 (1970).
11) D. W. Setser and B. S. Rabinovith, *J. Chem. Phys.*, **40**, 2427 (1964).
12) R. J. Campbel and E. W. Schlag, *J. Am. Chem. Soc.*, **89**, 5103 (1967).
13) H. Akimoto, K, Obi, and I. Takana, *Bull. Chem. Soc. Jpn.*, **46**, 2267 (1973).
14) G. M. Wieder and R. A. Marcus, *J. Chem. Phys.*, **37**, 1835 (1962).
15) B. S. Rabinovitch and D. W. Setser, *Adv. Photochem.*, **3**, 1 (1964).
16) G. Z. Whitten and B. S. Rabinovitch, *J. Chem. Phys.*, **38**, 2466 (1963).
17) Y. Ogata, K. Obi, H. Akimoto, and I. Tanaka, *Bull. Chem. Soc. Jpn.*, **44**, 2671 (1971).
18) W. L. Hase, *J. Chem. Phys.*, **57**, 730 (1972).
19) T. Shimanouchi, "Table of Molecular Vibrational Frequencies," Part 1, U. S. Department of Commerce, National Bureau of Standards Washington, D. C. (1967).

A Study of Metal-Ligand Vibrations in Nickelocene and Ferrocene

Kenji YOKOYAMA, Shunsuke KOBINATA, and Shiro MAEDA

Research Laboratory of Resources Utilization, Tokyo Institute of Technology, O-okayama, Meguro-ku, Tokyo 152

(Received January 21, 1976)

Raman and infrared spectra of nickelocene and ferrocene were studied as regards metal-ligand vibrations. It was found that the C_5H_5-ring tilt vibration, $\nu_{16}(e_{1g})$, of nickelocene has considerably low frequency. This was discussed in view of metal-ligand binding between both metallocenes.

Nickelocene is a member of the ferrocene homologues but is thermally more unstable than ferrocene.[1] The Ni–cyclopentadienyl (Cp for short) distance is known to be greater than the Fe–Cp beyond the difference in covalent metallic radii of Ni and Fe.[2] This was accounted for by the difference in outer shell electron configurations, since $Ni(Cp)_2$ has two anti-bonding electrons in addition to the closed shell of $Fe(Cp)_2$ in MO representations.[3] In accordance with this, the infrared and Raman spectra[4,5] show that the metal–ligand vibrations of $Ni(Cp)_2$ have in general considerably lower frequencies than those of $Fe(Cp)_2$. Most striking is the difference observed for the Cp-ring tilt vibration $\nu_{16}(e_{1g})$[a], whose frequency is reduced as much as to half from $Fe(Cp)_2$ to $Ni(Cp)_2$, resulting in a reversed frequency order of ν_{16} and ν_4 (a_{1g} metal–Cp stretching) between both compounds. Since such behavior is evidently anomalous among other metal–ligand vibrations, a special mechanical condition associated with the ν_{16} mode of $Ni(Cp)_2$ may be found. As was suggested by Gächter *et al.*,[5] the antibonding electrons of $Ni(Cp)_2$ can be considered to be responsible for the anomaly. Since the problem is closely related to the nature of metal–Cp bindings, we have carried out a comparative study of the metal–ligand vibrations of $Fe(Cp)_2$ and $Ni(Cp)_2$ with particular attention to the behavior of ν_{16}.

The difference in metal–Cp bindings as above is expected to appear in the infrared and Raman intensities. The effect may be remarkable not only in the metal–Cp vibrations but also for such internal modes of Cp as appreciably perturb the electronic interaction between the metal and Cp-ring. These intensity features are also presented and discussed.

Experimental

Raman spectra were obtained for cyclohexane solutions of metallocenes, with 632.8 nm (He-Ne) exciting radiation for $Fe(Cp)_2$ and 514.5 nm (Ar^+) for $Ni(Cp)_2$. Since $Ni(Cp)_2$ slightly absorbs the latter radiation ($\varepsilon \approx 10$), the solution was prepared with a completely degassed solvent and irradiated in a vacuum sealed cell with a somewhat defocussed laser beam. Relative Raman intensity was determined by comparing the recorded band area with a solvent band at 426 cm^{-1}. Infrared intensities were determined in carbon tetrachloride, cyclohexane, and tetrahydrofuran solutions by means of Beer's law plots for integrated band area.

a) D_{5d} symmetry is assumed on the basis of crystalline data (J. D. Dunitz, L. E. Orgel, and A. Rich, *Acta Crystallogr.*, **9**, 373 (1956)). No essential change is necessary in the following considerations for D_{5h} or D_5 symmetries.

Results and Discussion

The observed Raman and infrared frequencies are given in Table 1 together with the frequencies and assignments previously given. Although Gächter *et al.*[5] tentatively assigned considerably higher frequencies than those of Lippincott and Nelson[4] to ν_{11} and ν_{21} of $Ni(Cp)_2$, it remains unexplained why they preferred these extremely weak Raman lines to the intense 355 cm^{-1} infrared band. On the other hand, the broad and asymmetric profile of 355 cm^{-1} absorption suggests a possibility of overlapping ν_{11} and ν_{21} which lie very close to each other in $Fe(Cp)_2$. Thus the assignment by Lippincott and Nelson[4] seems to be more reasonable, and can be adopted in the following discussion. The parenthesized frequencies of $Ni(Cp)_2$ in Table 1 are their estimated values based on the infrared frequencies and simple valence force field.

It is notable that the observed ν_{16} frquency of $Ni(Cp)_2$ is remarkably deviated from the above estimation, suggesting the presence of a special mechanical condition associated with the vibration of $Ni(Cp)_2$. Table 2 shows the ratios of force constants between $Ni(Cp)_2$ and $Fe(Cp)_2$ for some metal–ligand modes. Each vibration was assumed to be of an entirely metal–Cp character with no contribution of Cp-internal motions. Such an approximation may be sufficient for the present semi-quantitative discussion, since the changes of these metal–Cp frequencies from $Fe(Cp)_2$ to $Fe(C_5D_5)_2$ are generally as small as expected from the change of mass.

A number of theoretical studies have been devoted to the electronic structure of metallocenes.[6] They generally give the outer shell MO configurations:

$\cdots\cdots(e_{1g})^4(e_{2g})^4(a_{1g})^2$, $^1A_{1g}$ for $Fe(Cp)_2$

$\cdots\cdots(e_{1g})^4(e_{2g})^4(a_{1g})^2(e_{1g}^*)^2$, $^3A_{2g}$ for $Ni(Cp)_2$

where (e_{1g}) and (e_{1g}^*) are the metal–Cp bonding and anti-bonding orbitals, respectively, both of which are composed of the metal 3d(xz,yz) AO's and Cp-ring $\pi(e_1'')$ MO's. On the other hand, the (e_{2g}) and the (a_{1g}) orbitals are essentially non-bonding and represented by the metal $3d(x^2-y^2,xy)$ and $3d(z^2)$, respectively. A recent study by electron spectroscopy showed that the order of orbital energies in $Fe(Cp)_2$ is $(a_{1g})<(e_{2g})$.[7]

The perturbation theory gives the following expression for vibrational force constant[8]

$$k = k_1 - k_2$$

$$k_1 = \int \psi_o^{\circ *}(\partial^2 H/\partial Q^2)_o \psi_o^\circ d\tau$$

$$k_2 = 2\sum_{i \neq 0} |\int \psi_o^{\circ *}(\partial H/\partial Q)_o \psi_i^\circ d\tau|^2/(E_i^\circ - E_o^\circ).$$

Table 1. Vibrational frequencies of $Fe(Cp)_2$ and $Ni(Cp)_2$

Species		$Fe(Cp)_2$			$Ni(Cp)_2$			
		ν (cm^{-1})[a]	ν (cm^{-1})	ρ	ν (cm^{-1})[a]	ν (cm^{-1})[b]	ν (cm^{-1})	ρ
A_{1g}	1	3099	3112		(3100)	3108	3112	
	2	(804)	834[c]		(770)	780		
	3	1105	1105	≈0	(1105)	1109	1114	≈0
	4	303	306	0.22	(220)	255	245	0.33
A_{2u}	8	3085	3095		3075	3090	3100	
	9	811	809		773	776	763[c]	
	10	1103	1107		1110	1102	1111	
	11	478	476		355	420[d]	355	
E_{1g}	12	3085			(3085)	3102		
	13	1010	1006		(1010)	1002		
	14	(800)	816[c]		(770)			
	15	1408	1417		(1425)	1426		
	16	388	390	0.73	(275)	208	198	0.70
E_{1u}	17	3075	3095		3075	3078	3100	
	18	1002	1004		1000	997	1006	
	19	834	830		800	840	794[c]	
	20	1411	1410		1430	1404	1424	
	21	492	490		355	490[d]	355	
	22	170			(125)			

a) Data from Ref. 4. b) Data from Ref. 5. c) Observed in crystal. d) See text. ( ) Estimated value in Ref. 4. ρ Depolarization ratio.

k_1 is determined by the electronic wavefunction of the ground state at equilibrium configuration ϕ_0^0, so that its value for the Ni–Cp may be considerably smaller than that of the Fe–Cp owing to the anti-bonding electrons occupying (e_{ig}^*) orbitals. k_2 represents the relaxation of vibrational potential due to the vibronic mixing of excited state wavefunctions ϕ_i^0 into the ground state. k_2 may not be very important for other metal–Cp vibrations than $\nu_{16}(e_{1g})$, since the electronic spectra as well as theoretical studies[6,9,11] show that the excited states with a_{1g}, a_{2u}, e_{1u}, and e_{2u} symmetries, which can couple with the ground state through those vibrational perturbations, are all located at high energy, *viz.*, >40000 cm^{-1} in $Fe(Cp)_2$ and >30000 cm^{-1} in $Ni(Cp)_2$. On the other hand, there are several low-lying excited states of e_{1g} symmetry in both metallocenes, which have been assigned to the $(a_{1g})\rightarrow(e_{ig}^*)$ and $(e_{2g})\rightarrow(e_{ig}^*)$ excitations and are located at 22000 cm^{-1}—30000 cm^{-1} in $Fe(Cp)_2$ and at 14000 cm^{-1}—23000 cm^{-1} in $Ni(Cp)_2$, respectively. Thus the force constant of $\nu_{16}(e_{1g})$ may be considerably reduced from the k_1 value, which approximately corresponds to the classical valence force field, due to a large k_2 term involving these lower e_{1g} states. This is supported by the observation that the ν_{16} frequency is always considerably smaller than the related $\nu_{21}(e_{1u})$ ring tilt frequency.

The above fact is equally described as the vibrationally induced mixing of the (e_{ig}^*) orbital into the (e_{2g}) and (a_{1g}) orbitals. Such a mixing may modify the latter non-bonding orbitals so as to relieve the strain energy of the molecule (Fig. 1). This effect may be enhanced further on the (a_{1g}) orbital by the presence of $3d(z^2)$-4s hybridization, shown to be appreciable by an ESR study.[12] In $Ni(Cp)_2$, the above vibronic

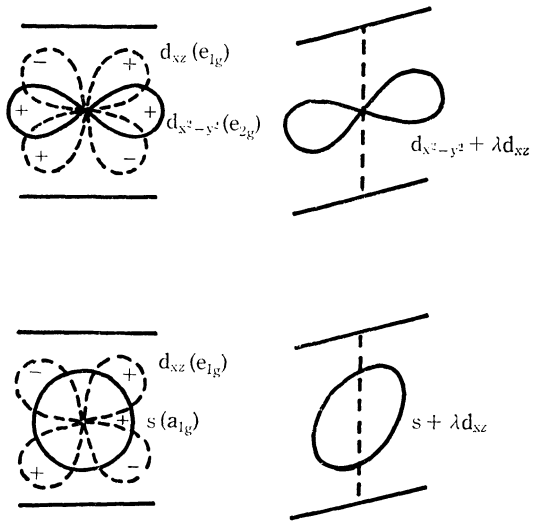

Fig. 1. Changes of the $3d(x^2-y^2)$ and the 4s orbital lobes due to a mixing 3d(xz) caused by $\nu_{16}(e_{1g})$ Cp-tilt vibration.

mixing effect on the force field may be partly cancelled by the opposite behavior of half-filled (e_{ig}^*) orbitals, but the $k_2[Ni(Cp)_2]$ may still be comparable to or even greater than that of $Fe(Cp)_2$ since the mixing orbitals are much closer to each other in energy than in $Fe(Cp)_2$.[10] On the other hand, the outer electron shell may be much less flexible for other modes, since each occupied MO can find partners of mixing only at very high energy.

In order to have an approximate idea, we consider a very simplified case in which k_2 is deliberately assumed to be significant only for the ν_{16} mode with equal values in both metallocenes. Then, k_1 of $Ni(Cp)_2$ may be

TABLE 2. RATIO OF FORCE CONSTANTS BETWEEN $Ni(Cp)_2$ AND $Fe(Cp)_2$ FOR METAL–Cp MODES

Mode[a]	$\nu_4(a_{1g})$	$\nu_{11}(a_{2u})$[b]	$\nu_{16}(e_{1g})$	$\nu_{21}(e_{1u})$[b]
$\frac{k[Ni(Cp)_2]}{k[Fe(Cp)_2]}$	0.64	0.57	0.26	0.53

a) Each mode was assumed to be of entirely metal-Cp character without the contribution of Cp-internal motions. b) Considerably higher $Ni(Cp)_2$ frequencies chosen in Ref. 5 give the ratios close to unity.

TABLE 3. VIBRATIONAL INTENSITIES OF $Fe(Cp)_2$ AND $Ni(Cp)_2$

Mode		$Fe(Cp)_2$	$Ni(Cp)_2$
IR	ν_8, ν_{17}	4.06×10^6 cm/M	3.13×10^6 cm/M
	ν_{20}	1.07	1.10
	ν_{10}	4.16	0.35
	ν_{18}	4.56	8.53
	ν_{21}	5.17	1.26
	ν_{11}	3.00	
Raman[a]	ν_4	1.0	5.6
	ν_{16}	0.2	1.5

a) Relative intensities.

estimated at about 60% of the $Fe(Cp)_2$ value from Table 2. Subsequently, we get the small $k[Ni(Cp)_2]/k[Fe(Cp)_2]$ value for ν_{16} in the table if we assume the common k_2 to be equal to 0.45 times of $k_1[Fe(Cp)_2]$. The essential fact is that the negative contribution from vibronic mixing, $-k_2$, affects the force constant of $Ni(Cp)_2$ more profoundly, since k_1 of $Ni(Cp)_2$, the minuend of the above equation, is considerably smaller than $k_1[Fe(Cp)_2]$.

A few remarks should be added to the results shown in Table 3. Most striking in the infrared is the extreme difference of ν_{10} (a_{2u} ring breathing) intensities between both metallocenes. The transition moment of this mode may mostly originate from the electron vibration[13] between Cp-rings *via* metal. Therefore, the observed difference indicates a much greater importance of charge transfer effect in the Fe–Cp bindings than in the Ni–Cp. As for Raman intensities, $Ni(Cp)_2$ is by far surpassing as far as the measured bands are concerned. On the basis of Raman intensity theory,[14] it may be understood as due to the fact that the allowed excited states of $Ni(Cp)_2$ are located at considerably lower energy than $Fe(Cp)_2$.

The authors are indebted to Professor M. Sato of Tokyo Institute of Technology for the gift of nickelocene crystals.

References

1) G. Wilkinson, P. L. Pauson, and F. A. Cotton, *J. Am. Chem. Soc.*, **76**, 1970 (1954).
2) L. Hedberg and K. Hedberg, *J. Chem. Phys.*, **53**, 1228 (1970).
3) W. Moffit, *J. Am. Chem. Soc.*, **76**, 3386 (1954).
4) E. R. Lippincott and R. D. Nelson, *Spectrochim. Acta*, **10**, 307 (1958).
5) W. Böhm, B. Gächter, M. Chouchani, J. A. Koningstein, E. M. Smirnova, Ya. M. Kimel'Feld, E. V. Bikova, and V. I. Aleksanyan, *Izv. Acad. Nauk SSSR, Ser. Khim.*, 572 (1975); B. F. Gächter, J. A. Konigstein, and V. T. Aleksanyan, *J. Chem. Phys.*, **62**, 4628 (1975).
6) Y. S. Sohn, D. N. Hendrickson, and H. B. Gray, *J. Am. Chem. Soc.*, **93**, 3603 (1971), where a series of references can be found.
7) J. W. Rabalais, L. O. Werme, T. Bermark, L. Karlsson, M. Hussain, and K. Siegbahn, *J. Chem. Phys.*, **57**, 1185 (1972).
8) H. F. Hameka, "Advanced Quantum Chemistry," Addison-Wesley Pub. Co., Reading, Mass., Chap. 4.
9) D. R. Scott and R. S. Becker, *J. Chem. Phys.*, **35**, 516 (1961).
10) I. Pavlik, V. Černý, and E. Maxová, *Collect. Czech. Chem. Commun.*, **35**, 3045 (1970).
11) A. T. Armstrong, D. G. Carroll, and S. P. Mcglynn, *J. Chem. Phys.*, **47**, 1104 (1967).
12) R. Prins and J. D. W. van Voorst, *J. Chem. Phys.*, **49**, 4665 (1968).
13) E. E. Ferguson and F. A. Matsen, *J. Chem. Phys.*, **29**, 105 (1958).
14) A. C. Albrecht, *J. Chem. Phys.*, **34**, 1476 (1961).

A Systematic Study of the Yields of γ-Radiolysis Products in C_1, C_2, and C_3-Chlorofluorocarbons

Takeshi TOMINAGA, Takefumi FUKUMIZU, Takashi AOYAMA, Akihiko OKUDA, and Yoshihiro MAKIDE

Department of Chemistry, Faculty of Science, The University of Tokyo, Bunkyo-ku, Tokyo 113

(Received March 19, 1976)

In the presence of bromine as a scavenger, the yields of the radiolysis products in eleven kinds of C_1—C_3 chlorofluorocarbons were investigated by means of gas chromatography. The *G*-values for the rupture of bonds in radiolysis were found to correlate with the halogen composition and the structure of their molecules. The *G*-values for the C–Cl (or C–F) bond rupture generally appear to increase with the number of chlorine (or fluorine) atoms in the chlorofluorocarbons; there was a marked difference between the *G*-values for the C–Cl rupture in each pair of structural isomers of chlorofluoroethanes. A striking selectivity in bond rupture was observed between the two C–C bonds in the chlorofluoropropanes.

Although the chlorofluorocarbons with three different types of bonds are interesting sytsems in radiation chemistry, only one work on the radiolysis of $CF_2ClCFCl_2$ (without scavengers) had been reported[1] before we initiated a systematic investigation of the radiolysis of chlorofluorocarbons as a preliminary step to the study of the radiolysis and radiation synthesis of various inorganic mixed halides. Our previous work on CF_2Cl_2, $CFCl_3$, CF_2ClCF_2Cl, and $CF_2ClCFCl_2$ with bromine as the scavenger, has revealed that the C–Cl and C–C bonds are generally more reactive than the C–F bond in the radiolysis reactions.[2,3] Recently we have studied the yields of the radiolysis products in C_1—C_3 chlorofluorocarbons and found that the reactivities of such bonds are largely influenced by the number of chlorine atoms and the structure concerning the C–Cl bonding in the molecule.[4,5] The object of the present article is to report the systematics in the reactivities of such bonds, derived from a detailed analysis of our recent data on the *G*-values of radiolysis products in the C_1, C_2, and C_3-chlorofluorocarbons, since the knowledge of the reactivities of the bonds in these compounds appears to be useful for elucidation of the mechanisms of radiolytic reactions and for the selection of procedures for the radiation synthesis of mixed halocarbons.

Experimental

Materials. Eleven kinds of chlorofluorocarbons were studied in the present work. Of these, CCl_4, $CFCl_3$, CF_2Cl_2, CF_2ClCF_2Cl, $CF_2ClCFCl_2$, and $CFCl_2CFCl_2$ were purchased from the Tokyo Chemical Industry Co., and CF_3CFCl_2, CF_3CCl_3, CF_2ClCCl_3, $CF_3CFClCF_2Cl$, and $CF_3CF_2CCl_3$, from P C R, Inc., U.S.A.; all were of a guaranteed reagent grade. These chlorofluorocarbons were purified three times by trap-to-trap distillation before use. The samples for γ-irradiation (all as liquid) were prepared by condensing mixtures of a chlorofluorocarbon and bromine into quartz capillary ampoules on a greaseless vacuum system equipped with Teflon needle valves. The bromine in the mixtures was determined by radioactivation analysis with thermal neutrons (15-s irradiation at a flux of 5×10^{11} n/cm^2 s).[6]

Gamma-ray Irradiation. The γ-irradiations were performed in a 16000-Ci ^{60}Co source for 5 to 25 h at an ambient temperature. The dose rates at the irradiation site were in the range of 2.27×10^{18}—2.73×10^{18} eV/g min, and the total energy absorbed in the system (0.82×10^{21}—3.40×10^{21} eV/g) was estimated on the basis of the electron densities of these compounds.

Gas Chromatographic Analysis of the γ-Irradiated Samples. The γ-irradiated samples were directly introduced into a gas chromatograph equipped with a thermal conductivity detector. The inorganic halogen in the mixtures was removed by means of a short stripping column packed with dehydrated potassium ferrocyanide powder, and then the organic species were analyzed on a 5-m Silicone DC 550 column. The unknown peaks on the gas chromatogram were mainly identified by (1) comparing their retention times with those of known compounds, or (2) by utilizing the known correlation between the logarithm of the retention volume and the composition of halogen atoms in mixed halocarbons.[7-9] Whenever it became necessary to confirm the identity of peaks of bromine-containing organic species, the γ-irradiated samples were further activated with thermal neutrons and their radiogas chromatograms were obtained by means of counting the ^{82}Br activities with an external γ-ray detector (NaI scintillation counter) placed after the thermal conductivity detector. The quantities of the products were determined from the TCD peak areas corrected for the detector sensitivities which had been obtained experimentally.[10]

Results and Discussion

Radiolysis of $CF_2ClCFCl_2$. Of the eleven chlorofluorocarbons studied in the present work, the radiolysis of $CF_2ClCFCl_2$ will be described here in detail as a typical example. In the presence of bromine, the major radiolysis products from $CF_2ClCFCl_2$ are $C_2F_3Cl_2Br$, CF_2ClBr, $CFCl_2Br$, and $C_2F_3ClBr_2$, which may be derived from the C–Cl and C–C bond rupture of the parent compound, followed by scavenging with bromine. The concentrations of the major products show a linear dose-dependence for the irradiation conditions used in this work (Fig. 1). The conversion of the parent compound was about 5% for a 10-h irradiation. As is illustrated in Fig. 2, the yields (in terms of *G*-values) of the bromine-scavenged products increase sharply with the increase in the bromine concentration and nearly level off at 0.1—0.2 mole fraction bromine. Table 1 summarizes the *G*-values for the formation of the major radiolysis products obtained from the plateau values of such scavenger curves. We can estimate, for example, the *G*-values for the rupture of the C–Cl or C–C bond on the assumption that the plateau *G*-value of $C_2F_3Cl_2Br$ or CF_2-

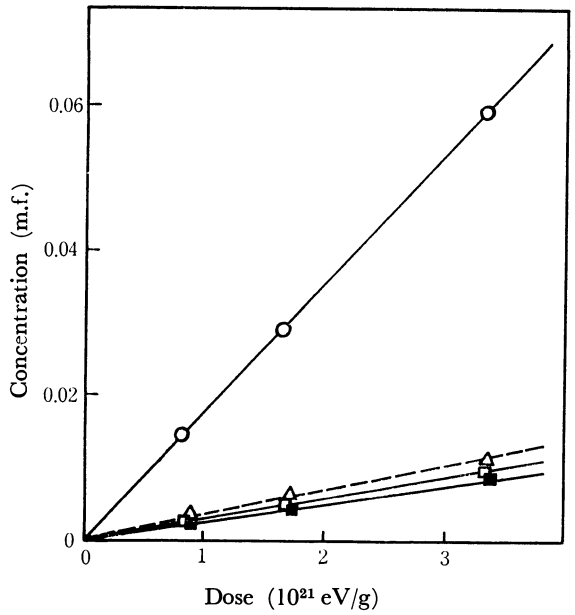

Fig. 1. The dose-dependence of the major radiolysis products from $CF_2ClCFCl_2$ containing 0.1 m. f. Br_2.
—○— $C_2F_3Cl_2Br$; —□— CF_2ClBr; —■— $CFCl_2Br$; --△-- $C_2F_3ClBr_2$.

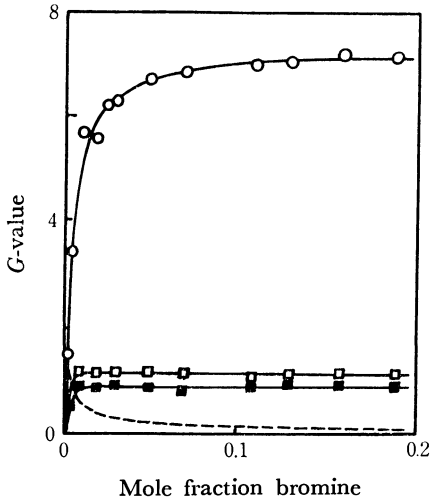

Fig. 2. The *G*-values for formation of major radiolysis products in the $CF_2ClCFCl_2$-Br_2 system as a function of bromine concentration.
—○— $C_2F_3Cl_2Br$; —□— CF_2ClBr; —■— $CFCl_2Br$; ---- CF_2Cl_2, $CFCl_3$

ClBr (or $CFCl_2Br$) corresponds to the *G*-value for the formation of the $C_2F_3Cl_2$ or CF_2Cl (or $CFCl_2$) radical (Table 1). Although the C_3 and C_4-chlorofluorocarbons resulting from the recombination or cross-combination of such radicals disappear quickly in the presence of bromine, the yields of CF_2Cl_2 and $CFCl_3$ decrease somewhat slowly with the increase in the bromine concentration (Fig. 2). The latter observation indicates that the chlorine accumulated in the system as the result of the C–Cl rupture during radiolysis may possibly compete with bromine for combination with the CF_2Cl and $CFCl_2$ radicals, thereby slightly reducing the bromine-scavenging effect

Table 1. *G*-values for the formation of the major radiolysis products in liquid $CF_2ClCFCl_2$ containing bromine

Product	Bond ruptured	*G*-value[a,b]
$C_2F_3Cl_2Br$	C–Cl	7.0 ±0.3
$CFCl_2Br$[c]	C–C	1.0 ±0.1
CF_2ClBr[c]	C–C	
$C_2F_3ClBr_2$	two C–Cl	1.3 ±0.1
$C_2F_2Cl_3Br$	C–F	0.16±0.01

a) *G*-value obtained at the plateau of the bromine-scavenger cure. b) Small amounts (*G*-value<0.1) of CF_2Br_2 and $CFClBr_2$, possibly derived from the rupture of both C–C and C–Cl bonds were also observed. c) The *G*-values for the formation of $CFCl_2Br$ and CF_2ClBr were 0.9 and 1.1 respectively.

on the formation of CF_2Cl_2 and $CFCl_3$.

The rupture of the single C–Cl bond in $CF_2ClCFCl_2$ can produce either of two isomers of $C_2F_3Cl_2Br$, *i.e.*, $CF_2ClCFClBr$ or $CF_2BrCFCl_2$. Although they could not be separated from each other by gas chromatography, the comparison of the yields of radiolysis products obtained from the re-irradiation of the $C_2F_3Cl_2Br$ fraction implies that the C(1)–Cl bond rupture was preferred by a factor of 3—4 to the C(2)–Cl bond rupture (the positions of carbon atoms are defined in the footnote to Table 2).

The product, $C_2F_3ClBr_2$, corresponding to the rupture of the two C–Cl bonds may not arise from the successive radiolysis process: $C_2F_3Cl_3+Br_2 \rightsquigarrow C_2F_3Cl_2Br$ and $C_2F_3Cl_2Br+Br_2 \rightsquigarrow C_2F_3ClBr_2$, since the *G*-value estimated for such a process can account for only a minor fraction of the observed *G*-value. It is likely that this product is mainly formed through the nearly simultaneous elimination of two chlorine atoms from adjacent carbon atoms (leading to the formation of an olefinic bond) and combination with bromine.[11]

Systematic Comparison of the G-values in C_1—C_3 Chlorofluorocarbons. Similar types of reactions and scavenging effects were observed for all the C_1—C_3 chlorofluorocarbons studied in the present work. In Table 2 are summarized the *G*-values for the rupture of various bonds, as estimated from the plateau *G*-values of the corresponding bromine-scavenged products, as has been described above.

The intra- and intermolecular comparison of the results listed in Table 2 indicates that the *G*-values for bond rupture in the C_1—C_3 chlorofluorocarbons tend to increase in the order: C–F<C–C<C–Cl, which is in accordance with the decreasing order of the bond dissociation energies of such bonds. Hence, we may consider that, in general, the weaker bond is more reactive. However, a more detailed analysis indicates that the *G*-values depend on the halogen composition and the structure of the parent molecules, as will be discussed below.

C–F Bond Rupture: For the compounds containing the same number of carbon atoms, the *G*-value for the C–F rupture tends to increase with the number of fluorine atoms in the molecule (Fig. 3). While there

TABLE 2. *G*-VALUES FOR RUPTURE OF VARIOUS BONDS IN CHLOROFLUOROCARBONS

No.	Compound	*G*-values for bond rupture[10]				
		C-Cl rupture	Double C-Cl rupture	C-F rupture	C(1)-C(2) rupture[a,b]	C(2)-C(3) rupture[a,b]
1	CF_2Cl_2	6.7	0.8	0.20		
2	$CFCl_3$	8.1	1.0	0.05		
3	CCl_4	7.7	0.3_3			
4	CF_3CFCl_2 (1,1-dichloro-)	5.9	0.15	0.5_1	1.0	1.0
5	CF_2ClCF_2Cl (1,2-dichloro-)	5.1	0.4_4	0.5_2	0.8	
6	CF_3CCl_3 (1,1,1-trichloro-)	9.3	0.3_1	0.15	0.9	
7	$CF_2ClCFCl_2$ (1,1,2-trichloro-)	7.0	1.3	0.16	1.0	
8	CF_2ClCCl_3 (1,1,1,2-tetrachloro-)	7.9	1.6	0.14	1.2	
9	$CFCl_2CFCl_2$ (1,1,2,2-tetrachloro-)	6.6	2.4	0.11	1.3	
10	$CF_3CFClCF_2Cl$ (1,2-dichloro-)	4.8	0.6_4	0.6_2	1.4	0.16
11	$CF_3CF_2CCl_3$ (1,1,1-trichloro-)	8.5	0.17	0.18	0.9	0·08

a) The positions of the carbon atoms are defined in the present article as follows: $CF_3CFClCF_2Cl$ as 1,2-dichlorohexafluropropane, and $CF_3CF_2CCl_3$ as 1,1,1-trichloropentafluoropropane. b) The *G*-values for the formation of the C-C scission products are as follows: CF_3Br (1.4) and $CFCl_2Br$ (0.6) from CF_3CFCl_2; CF_2ClBr (1.5) from CF_2ClCF_2Cl; CF_3Br (0.8) and CCl_3Br (1.0) from CF_3CCl_3; CF_2ClBr (1.1) and $CFCl_2Br$ (0.9) from $CF_2ClCFCl_2$; CF_2ClBr (1.2) and CCl_3Br (1.3) from CF_2ClCCl_3; $CFCl_2Br$ (2.6) from $CFCl_2CFCl_2$; $CF_3CFClBr$ (1.4) and $CF_2ClCFClBr$ (0.16) from $CF_3CFClCF_2Cl$; CCl_3Br (0.9) and CCl_3CF_2Br (0.08) from $CF_3CF_2CCl_3$. The values for the other products (CF_3Br, CF_2ClBr, and CF_3CF_2Br) from chlorofluoropropanes were omitted because, for analytical reasons, they could not be determined accurately.

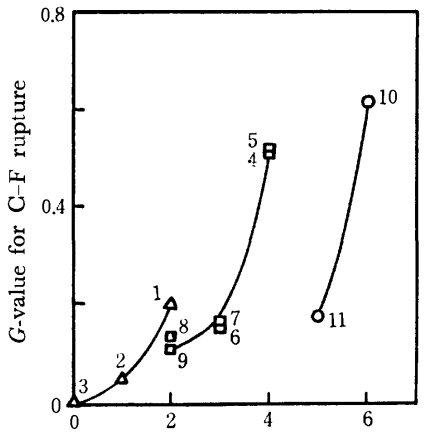

Fig. 3. The *G*-values for the C–F rupture as a function of the number of fluorine atoms in chlorofluoromethanes(△), chlorofluoroethanes(□), and chlorofluoropropanes(○).
(Keys to the numbers denoting compounds in Figs. 3—5 are given in Table 2).

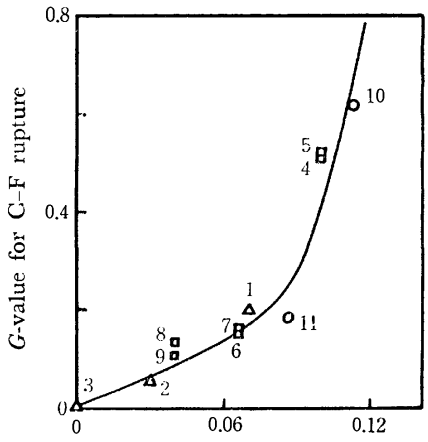

Fig. 4. The *G*-values for the C–F rupture as a function of the ratio of the number of electrons involved in the C–F bonding to the total number of electrons in the molecules of chlorofluoromethanes(△), chlorofluoroethanes(□), and chlorofluoropropanes(○).

are three isomeric pairs of chlorofluoroethanes, no significant difference was observed between the *G*-values for each pair of isomers. In Fig. 4, the *G*-value for the C–F rupture appears to correlate with the ratio of the number of electrons involved in the C–F bonding to the total number of electrons in the molecule. Thus, it is likely that the mechanism for the rupture of stable C–F bonds is possibly governed by a direct process, irrespective of small differences in the bond dissociation energies or structures of the molecules.

C–Cl Bond Rupture: As may be seen in Fig. 5, the *G*-value for the C–Cl rupture tends to increase slightly

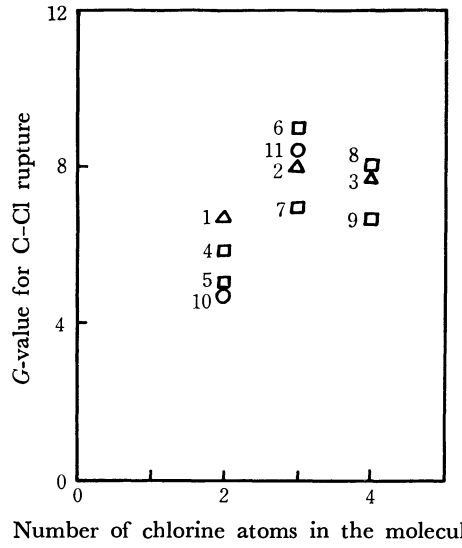

Fig. 5. The *G*-values for the C–Cl rupture as a function of the number of chlorine atoms in chlorofluoromethanes(△), chlorofluoroethanes(□), and chlorofluoropropanes(○).

with the number of chlorine atoms in the molecules containing the same number of carbon atoms, except for $CFCl_2CFCl_2$ and CF_2ClCCl_3. The difference between the *G*-values for each pair of isomers is large, and the isomer with a more asymmetrical structure concerning the C–Cl bonding (in which all or most chlorine atoms are bonded to one carbon atom) always gives a higher *G*-value for the C–Cl rupture. Such a trend may be accounted for tentatively by assuming that (1) the C–Cl bond dissociation energy may be slightly decreased with the increase in the total number of chlorine atoms in the molecule,[12] and that (2) the instability of the C–Cl bonding may be increased with the number of chlorine atoms attached to the same carbon atom as a result of the increased strain. When the *G*-value for the C–Cl rupture was plotted against the ratio of the number of electrons involved in the C–Cl bonding to the total number of electrons in the molecule, the correlation was not clear and was quite different from that observed for the C–F rupture in Fig. 4. Hence, the mechanism leading to the C–Cl rupture may be possibly controlled by processes which can be affected by small differences in the bond dissociation energies and structures of the molecules. While the radiolysis products in these systems are generally accountable in terms of the free radical processes, at least as intermediate steps, we should also examine the possibility that the dissociative electron attachment process involving electrons at low energies may contribute to the formation of such radicals (R):

$$RCl + e^- \longrightarrow R + Cl^-$$

However, only a few data on the dissociative attachment cross sections in the gas phase are available,[13] and the correlation between the *G*-value for the C–Cl rupture and the cross section for such a process in the liquid phase is still ambiguous.[14]

Besides the rupture of the single C–Cl bond, two C–Cl bonds in a molecule were often found to break, although the *G*-values for such a double C–Cl rupture were much smaller than for the single C–Cl rupture. For the chlorofluoroethanes, there is a marked difference between the *G*-values for each pair of isomers: in contrast to the single C–Cl rupture, the *G*-value is always larger for the symmetrical or less asymmetrical isomer (*i.e.*, 1,2-dichloro-, 1,1,2-trichloro-, and 1,1,2,2-tetrachloro-) than for the more asymmetrical counterpart (*i.e.*, 1,1-dichloro-, 1,1,1-trichloro-, and 1,1,1,2-tetrachloro-). Thus, the difference in the *G*-values for the single C–Cl rupture between the pair of isomers may be partly accounted for by the inverse difference in the *G*-values for the double C–Cl rupture. While the *G*-value for the double C–Cl rupture increases with the number of chlorine atoms in the series of the symmetrical or less asymmetrical isomers, it remains at low values in the series of the more asymmetrical isomers, except for the case of CF_2ClCCl_3. As has been indicated earlier, the large *G*-values for the double C–Cl rupture of the symmetrical and less asymmetrical isomers may be mainly ascribed to the nearly simultaneous elimination of two chlorine atoms from the adjacent carbon atoms, whereas the origin of the products corresponding to the double C–Cl rupture in the more asymmetrical isomers can be explained in terms of the successive radiolysis processes *via* monobromo compounds as intermediates (the simultaneous elimination process can also take place in CF_2ClCCl_3). These observations indicate that the *G*-values for the rupture of one or two C–Cl bonds in the chlorofluorocarbons are influenced by the number of chlorine atoms and the structure in the molecule: for the chlorofluorethanes and chlorofluoropropanes, the single C–Cl rupture occurs predominantly in the more asymmetrical isomers, while the double C–Cl rupture takes place appreciably in the symmetrical and less asymmetrical isomers.

C–C Bond Rupture: The *G*-values for the C(1)–C(2) rupture in the chlorofluoroethanes remain almost unchanged, or they increase only slightly with the increase in the number of chlorine atoms in the molecule; yet no significant difference is observed between the pair of isomers.

However, a striking selectivity in bond rupture is observed between the two C–C bonds in the chlorofluoropropanes: the *G*-values for the C(1)–C(2) rupture are about ten times those for the C(2)–C(3) rupture. Such a marked weakness of the C(1)–C(2) bond may be tentatively accounted for by the greater resonance stabilization obtainable in the formation of the C(1)–C(2) scission products than the C(2)–C(3) scission products.

a) In the case of $CF_3CF_2CCl_3$, the C(1)–C(2) rupture eventually yields CF_3CF_2 and CCl_3 radicals, while the C(2)–C(3) rupture produces CCl_3CF_2 and CF_3 radicals. The CCl_3 radical is near planar,[15] while the CF_3 radical has a deep pyramidal structure.[16] Thus, the strain energy in the ground state due to the proximity of halogen atoms in trihalomethyl groups may be more released in the formation of $\cdot CCl_3$ than in the formation of $\cdot CF_3$. This difference in shape between the two radicals may also lead to the larger interaction between the lone pair on halogen and the

p-orbital of carbon in the CCl_3 radical than in the CF_3 radical. Accordingly, a greater resonance stabilization may be acquired in the formation of $\cdot CCl_3$; thus, the C(1)–C(2) rupture will be favored. In addition, the steric interaction between the Cl atoms on C(1) and the F atoms on C(2) may elongate the C(1)–C(2) bond length and somewhat weaken the bond strength as compared with that of the C(2)–C(3) bond.

b) In $CF_3CFClCF_2Cl$, the C(1)–C(2) scission produces $CF_3CFCl\cdot$ and $\cdot CF_2Cl$, while the C(2)–C(3) scission yields $CF_2ClCFCl\cdot$ and $\cdot CF_3$. Since a greater resonance stabilization may be expected for the $\cdot CF_2Cl$ formation than for the $\cdot CF_3$ formation, the C(1)–C(2) rupture is favored. The elongation of the C(1)–C(2) bond as a result of the steric interaction between the Cl atoms on C(1) and C(2) atoms also tends to weaken the C(1)–C(2) bond.

In conclusion, the *G*-values for the rupture of various bonds in the chlorofluorocarbons are generally influenced by the halogen composition and the structure of the molecule. The systematic investigation of the *G*-values and the selectivity in bond rupture may provide us with important clues to an understanding of the mechanisms of radiolytic reactions as well as to establishing the systematics in radiation synthesis. Moreover, the present results may afford useful knowledge on the chemical reactivities of chlorofluorocarbons, which have not been fully studied in organic chemistry.

The present authors wish to express their thanks to Professor Nobufusa Saito, the University of Tokyo, for his encouragement and support. They are also greatly indebted to Dr. Masayuki Yoshida, the University of Tokyo, for many helpful discussions.

References

1) A. R. Kazanjian and D. R. Horrell, *J. Phys. Chem.*, **75**, 2217 (1971).
2) T. Tominaga, R. Iwata, and Y. Makide, *Chem. Lett.*, **1972**, 871.
3) T. Tominaga, T. Fukumizu, and Y. Makide, *Radiochem. Radioanal. Lett.*, **21**, 211 (1975).
4) T. Fukumizu, Y. Makide, and T. Tominaga, *Radiochem. Radioanal. Lett.*, **23**, 353 (1975).
5) T. Tominaga, Y. Makide, T. Fukumizu, and T. Aoyama, *Radiochem. Radioanal. Lett.*, **25**, 137 (1976).
6) The γ-dose absorbed during the neutron activation analysis was negligible, since it was less than 1/10000 of the dose absorbed in the ^{60}Co γ-irradiations.
7) T. Tominaga, R. Iwata, and Y. Makide, *Chem. Lett.*, **1973**, 485.
8) R. Iwata, Y. Makide, and T. Tominaga, *Bull. Chem. Soc. Jpn.*, **47**, 3071 (1974).
9) Y. Makide, T. Fukumizu, and T. Tominaga, *Bull. Chem. Soc. Jpn.*, **48**, 2387 (1975).
10) Since the sensitivity in the thermal conductivity detector appeared to correlate with the molecular weight for some chlorofluorocarbons, the sensitivities of most radiolysis products were estimated in our previous work by extrapolation based on such a correlation.[3-5] However, more extensive measurements of a number of bromochlorofluorocarbons have recently been carried out in our laboratory, and most bromine-containing compounds have been found to deviate appreciably from the above correlation (the details will be published elsewhere). Accordingly, the new sensitivity data determined experimentally have been used in the present work to re-calculate the *G*-values of the radiolysis products instead of the previous data mainly estimated by extrapolation.
11) The ^{19}F NMR spectrum of the $C_2F_3ClBr_2$ fraction revealed that $CF_2BrCFClBr$ was the predominant species.
12) R. Foon and K. B. Tait, *J. Chem. Soc., Faraday Trans. 1*, **68**, 1121 (1972).
13) S. Patai, Ed., "The Chemistry of the Carbon-halogen Bond," Interscience, New York (1973), p. 795.
14) On a hypothetical assumption that the ratio of the cross sections of the two chlorofluorocarbons in the liquid phase is similar to that in the gas phase, the dissociative attachment cross section of $CFCl_3$ may be about 100 times as large as that of CF_2Cl_2, whereas the difference in the *G*-values for the C–Cl rupture between these compounds is relatively small (1.4). Thus it seems unlikely that the dissociative electron attachment is the major process controlling the C–Cl bond rupture.
15) C. Hesse, N. Leray, and J. Rocin, *Mol. Phys.*, **22**, 137 (1971).
16) R. W. Fessenden and R. H. Schuler, *J. Chem. Phys.*, **43**, 2704 (1965).

Donor–Acceptor Interactions in the Ground State of the Systems Forming Heteroexcimers in the Excited State

Tadashi OKADA and Noboru MATAGA

Department of Chemistry, Faculty of Engineering Science, Osaka University, Toyonaka, Osaka 560

(Received March 22, 1976)

Several systems which form heteroexcimers in the excited state were forced to aggregate in low temperature rigid matrices, and their absorption, fluorescence excitation and emission as well as fluorescence rise and decay curves were determined. The results indicate the existence of several kinds of donor-acceptor pairs emitting heteroexcimer fluorescence at different wavelengths. Temperature dependence of absorption spectra of those systems in liquid solutions were examined, and collisional enhancement of the absorption intensity was observed.

Numerous investigations have been carried on the heteroexcimer formation between excited singlet aromatic hydrocarbons and various ground state amines or cyano compounds. However, spectroscopic studies of the charge transfer (CT) interaction in the ground state of the heteroexcimer forming systems are scarce. Since there is no observable absorption corresponding to the excimer or heteroexcimer emission, studies on these systems have been made nearly always in a liquid state where the exciplexes are formed by diffusional encounter between the excited and ground state partners.

For a study of the electronic processes in exciplexes at low temperatures, it would be advantageous to find a matrix of a saturated hydrocarbon having adjacent sites with orientations favorable for the formation of excimer or heteroexcimer. The phenomenon of association of pyrene or anthracene molecules was found first in a cyclohexane matrix and in 3 : 1 softened glasses of isopentane and methylcyclohexane (MP) by Ferguson,[1,2] detailed spectral studies on the dimer aggregates of aromatic hydrocarbons in the rigid matrices at low temperature being carried out.[2,3] By using the same technique, we found for the first time that the solutions of pyrene and aromatic amines in cyclohexane matrix show heteroexcimer fluorescence in addition to that of pyrene monomer at various temperatures.[4]

Concerning the ground state interactions of heteroexcimer forming systems, Itoh *et al.* have recently reported their studies on dicyanoanthracene–naphthalene system at various temperatures,[5] while Yoshihara *et al.* have examined the ground state absorption spectra of concentrated solutions of pyrene–*N,N*-dimethylaniline (DMA) system.[6] Ishida and Tsubomura suggested the existence of the CT absorption band due to the interaction between anthracene and various aliphatic amines adsorbed on a porous glass.[7]

In order to elucidate the CT interactions in the ground state of heteroexcimer forming systems, we have made detailed studies on the absorption, excitation, and emission spectra as well as fluorescence rise and decay curves of some systems in low temperature matrices. We have also measured the absorption spectra at various temperatures in liquid solution in order to examine the collisional CT interactions in these systems. The results are given in the following.

Experimental

Absorption spectra of rigid solutions at low temperature were measured with a Shimadzu MPS-50L spectrophotometer and those of liquid solutions with a Cary 15 spectrophotometer. Fluorescence spectra were measured with an Aminco-Bowman spectrophotofluorometer calibrated by means of a standard tungsten lamp. Excitation spectra were measured with a Nalumi RM 20-G spectrometer equipped with a 600 grooves/mm grating and a 500 W xenon lamp as a light source. Fluorescence was passed through a Bausch & Lomb high intensity monochromator and detected with a 1P28 photomultiplier. The fluorescence rise and decay curves were determined on an apparatus composed of a Bausch & Lomb high intensity monochromator, 1P28 or HTV-R213 photomultiplier, Tektronix 661 sampling oscilloscope, and a pulsed nitrogen gas laser.

Pyrene, anthracene, perylene, DMA, *N,N*-diethylaniline (DEA) and *N,N*-dimethyl-*p*-toluidine (*p*-DMT) were purified by the same method as reported.[8] Tributylamine[9] and 1,2,4,5-tetracyanobenzene (TCNB)[10] were also the same as before. 1-(2-or 9-anthryl)-3-(*p*-*N,N*-dimethylaminophenyl)-propane(2-or 9-A-$(CH_2)_3$–DMA) was supplied by Professor S. Misumi of this University. Spectrograde hexane, cyclohexane, methylcyclohexane, toluene and tetrahydrofuran (THF) were used without further purification. Isopentane and chlorobenzene were purified by the usual method.[11] All the solutions were carefully deareated by freeze-pump-thaw cycles.

The temperature of the sample was measured with a thermocouple placed on the sample tube. A thin quartz cell with 1 mm optical path was used for measuring the absorption spectra in cyclohexane matrix.

Results and Discussion

Interactions between Electron Donor and Acceptor in Low Temperature Matrices. The temperature dependence of the absorption spectrum of perylene (5×10^{-5} M)–DMA (2×10^{-3} M) system in cyclohexane is shown in Fig. 1. The dotted curve gives the absorption spectrum of perylene dimer observed in the cyclohexane matrix at 173 K, agreeing with that reported by Ferguson.[2] The absorption spectrum shows a gradual red shift and broadening with the lowering in temperature. A similar temperature dependence of the absorption spectrum was observed in the system of pyrene (2×10^{-5} M)–DEA (1×10^{-4} M) in cyclohexane (Fig. 2).

On the other hand, the absorption spectra of pyrene–aliphatic amine (triethylamine or tributylamine) systems in cyclohexane matrix were essentially the same as those of solution at room temperature, *i.e.* of pyrene. In the case of anthracene–DMA and DEA systems, no appreciable change of absorption band arising from the interaction between donor and acceptor was observed but the absorption spectra of stable dimer and higher aggregates of anthracene[3] were detected.

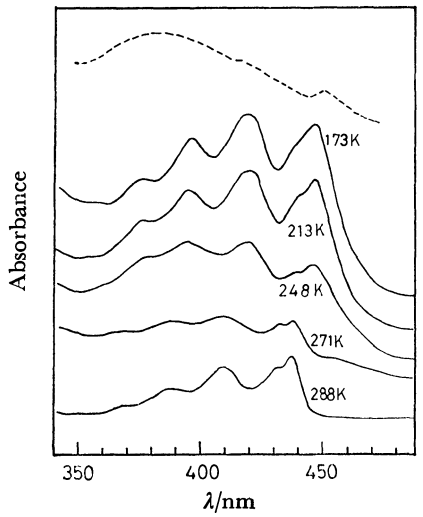

Fig. 1. Temperature dependence of the absorption spectrum of perylene (5×10^{-5} M)−DMA (2×10^{-3} M) system in cyclohexane. The dotted spectrum represents the absorption spectrum of perylene dimer observed at 173 K.

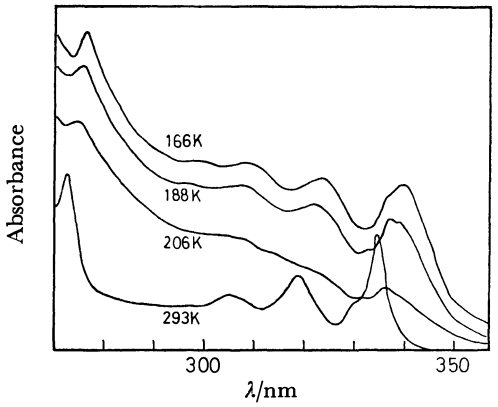

Fig. 2. Temperature dependence of the absorption spectrum of pyrene (2×10^{-5} M)-DEA (1×10^{-4} M) system in cyclohexane.

It was found that the dimer formation was a dominant process even in the case of pyrene or perylene solution with concentrations greater than 10^{-4} M in cyclohexane.

The excitation spectrum of the heteroexcimer fluorescence of the pyrene–DEA system monitored at 460 nm and that of the pyrene fluorescence monitored at 400 nm are shown in Fig. 3. The former is broadened and shifted to red as compared with the latter, similar to the absorption spectrum at low temperatures. The excitation spectrum of pyrene fluorescence is essentially the same as the absorption spectrum in solution at room temperature. In the system of high concentration of DEA (1×10^{-2} M), only the heteroexcimer fluorescence was observed throughout from room temperature to 77 K, the maximum of the excitation spectrum being observed at 342 nm in low temperature matrix as shown in Fig. 3. The same result was obtained in the case of the pyrene–DMA system. The broad excitation spectrum cannot be ascribed to the pyrene dimer since it differs notably from that of the pyrene excimer in low temperature cyclohexane matrix,[12]

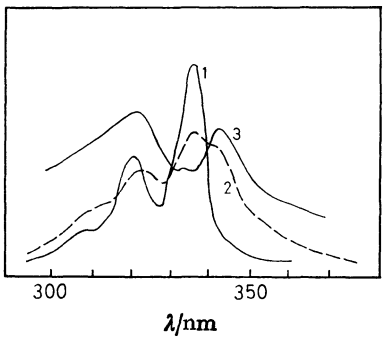

Fig. 3. Excitation spectra of pyrene-DEA system in cyclohexane matrix.
(1): [Pyrene]$=2\times10^{-5}$ M, [DEA]$=10^{-4}$ M, monitored at 400 nm.
(2): [Pyrene]$=2\times10^{-5}$ M, [DEA]$=10^{-4}$ M, monitored at 460 nm.
(3): [Pyrene]$=2\times10^{-5}$ M, [DEA]$=10^{-2}$ M, monitored at 460 nm.

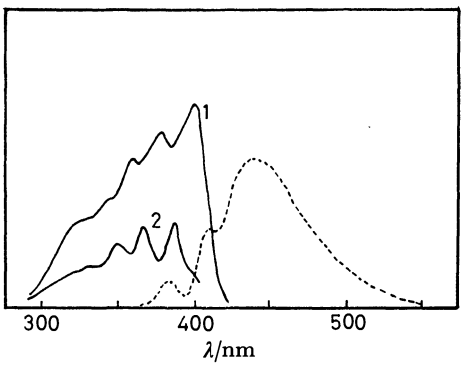

Fig. 4. Fluorescence (dotted) and excitation spectra of 2-A-$(CH_2)_3$-DMA in MP at 77 K monitored at 470 nm (1) and 400 nm (2).

Another clear-cut example of the ground state donor–acceptor interaction is the system of 2-A-$(CH_2)_3$–DMA in MP solution. The fluorescence and excitation spectra at 77 K are shown in Fig. 4. The excitation spectrum of the heteroexcimer fluorescence and that of the fluorescence from the anthracene part showed good correspondence with the absorption spectra at 77 K and room temperature, respectively.

The nature of the electronic transition responsibe for the excitation spectrum of the heteroexcimer fluorescence is not very clear at the present stage of the investigation. However, it seems that a loosely bound pair of donor and acceptor is formed in the low temperature matrix, the red shift of the absorption spectrum of which might be ascribed to the interaction between the locally excited state of the acceptor and the CT state which is situated higher than the former. When this donor–acceptor pair is excited by light absorption there occur some displacements of molecules in the pair leading to the heteroexcimer (CT state) formation.

Rise and Decay Curves of Heteroexcimer Fluorescence. In the systems described above, the rise curve of the heteroexcimer fluorescence in low temperature matrix was the same as the time-integrated function of exciting ns light pulse. This suggests that some stable

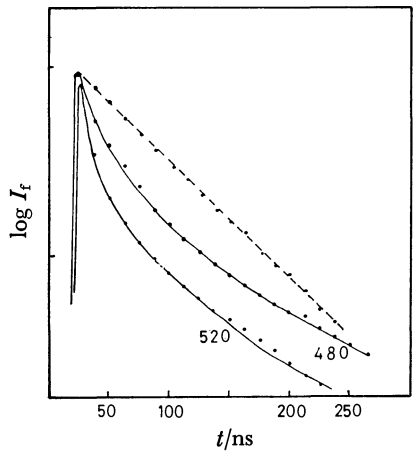

Fig. 5. Fluorescence decay curves of pyrene (1×10^{-5} M)—DEA (1×10^{-4} M) system in cyclohexane matrix at 196 K. See text.

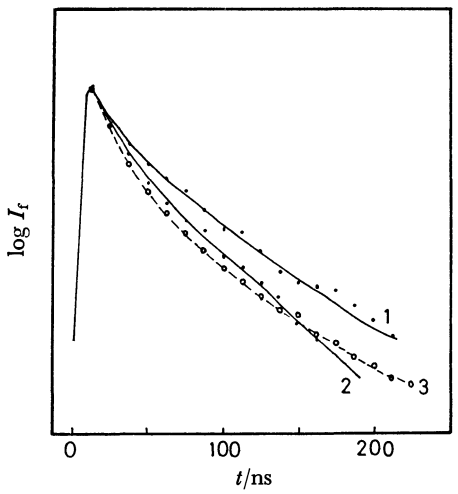

Fig. 6. Fluorescence decay curves of 9-A-$(CH_2)_3$-DMA in cyclohexane matrix at 196 K.
(1) Observed at 450 nm, (2) observed at 520 nm, (3) observed by detecting the whole emission band of heteroexcimer using a Toshiba VY-42 filter.

complex is already formed in the ground state, which agrees with the above results of absorption and excitation spectral measurements. However, it has been confirmed that the decay curve of the heteroexcimer fluorescence depends on the wavelength at which it is observed and shows a deviation from the simple exponential decay. The degree of deviation from exponential decay changes to some extent with temperature, depending also on the rate of heating or cooling. Roughly speaking, the longer the wavelength of observation, the greater the amount of the shorter decay component. This might be ascribed to the fact that there are several kinds of associated pairs emitting at different wavelengths. This phenomenon was observed in all the systems we studied but not in the case of excimer fluorescence band. As an example, the decay curves of some heteroexcimer systems are shown in Figs. 5 and 6. In the case of the pyrene–DMA or DEA system, the decay curve observed by detecting the whole emission band of heteroexcimer using an appropriate filter was accidentally single exponential (dotted line, Fig. 5). The apparent single exponential decay might represent the mean lifetime $\bar{\tau}_f$ if various kinds of heteroexcimers of the pyrene–DMA or DEA system. In the case of the pyrene (1×10^{-5} M)–DMA (1×10^{-2} M)–cyclohexane system, when the temperature is lowered, the band maximum of the heteroexcimer fluorescence shifts to red accompanied by a decrease both in the relative fluorescence intensity I_f and the mean lifetime at first, and then makes a blue shift, accompanied by increase in I_f and $\bar{\tau}_f$, to approximately the same position as it has at 300 K. The results of the temperature effects on the heteroexcimer fluoroscence are summarized in Table 1. It seems that some distribution of the associated donor–acceptor states differing with temperature might be forced to arise in the cyclohexane matrix. When the DMA concentration is small (1×10^{-4} M), the heteroexcimer fluorescence can be observed only in the wavelength region of 440—450 nm. One of the possible mechanisms for the appearance of the long wavelength fluorescence might be the formation of a more highly aggregated state than the 1 : 1 donor–aceptor pair.

Table 1. Temperature dependence of heteroexcimer fluorescence of pyrene (1×10^{-5} M)-DMA (1×10^{-2} M)-cyclohexane system

T/K	300	273	240	230—210	190-100
λ_{max}/nm	440	450	465	480	440
I_f	100	85	15	≈6	90
$\bar{\tau}_f$/ns	140	120	85	80	≈110

Absorption Spectra in Liquid Solutions. Yoshihara *et al.* studied the absorption spectra of the pyrene–DMA system in chlorobenzene, changing the DMA concentration in the range 0—7.89 M.[6] The absorption intensity in the wavelength region of 350—400 nm increases with an increase in concentration of DMA, the equilibrium constant of complex formation in the ground state being determined to be 0.2 M^{-1} with the aid of the Ketelaar plot. We also examined the anthracene–DMA system and obtained similar results.

In order to elucidate the electron donor–acceptor interactions in solution, it is worthwhile to measure the temperature dependence of the ultraviolet absorption spectra of donor–acceptor systems. The observed values of absorbance d for the THF solution of TCNB are plotted against the reciprocal of the temperature in Fig. 7. The value of d decreased at first with a rise in temperature from 298 K to 313 K, increasing with a further rise in temperature. A similar result was obtained for the system of perylene in *p*-DMT. The temperature dependence of $(d-d_0)$ of the pyrene (1×10^{-2} M)–DMA (1×10^{-2} M) system in hexane is shown in Fig. 8, where d and d_0 are the absorbance values observed for the ternary solution containing pyrene and DMA in hexane and for the equimolar hexane solution of pyrene, respectively. All of the d values are corrected for the volume change caused by temperature variation.

The observed increment of the absorption intensity at low temperatures can be explained by the very

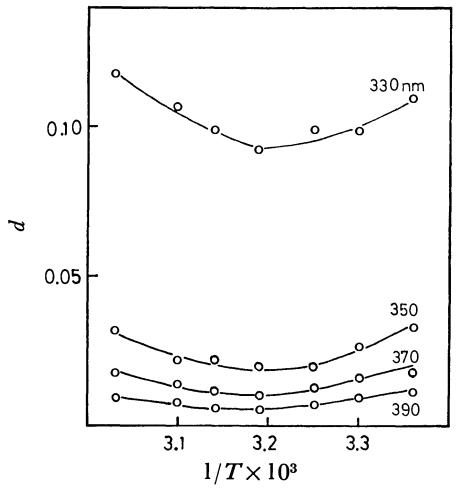

Fig. 7. Temperature dependence of d at various wavelengths in the TCNB-THF system.

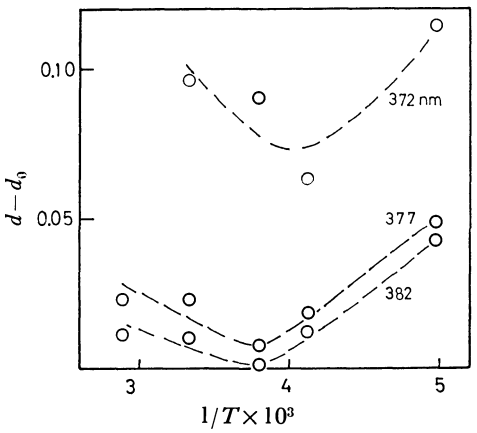

Fig. 8. Temperature dependence of $(d-d_0)$ at various wavelengths in the pyrene (1×10^{-2} M)-DMA (1×10^{2} M)-hexane system.

weak complex formation between donor and acceptor in the ground state which leads to the broadening and red shift of absorption band.

A collision induced CT interaction may arise at a high temperature leading to the enhancement of the absorption intensity, as it is actually observed in pyrene–DMA as well as TCNB–THF systems. Measurements of the collision induced absorption band would be difficult in the stable CT complex systems as compared with the heteroexcimer systems. Actually, in the case

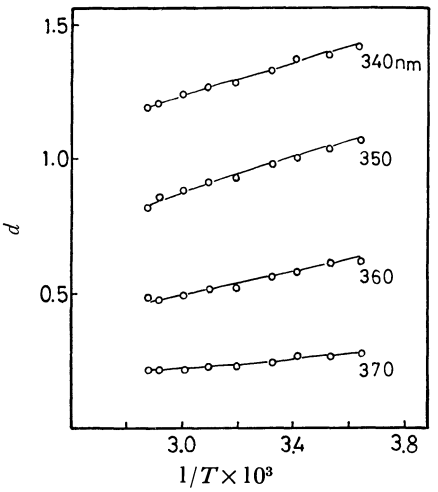

Fig. 9. Temperature dependence of d at various wavelengths in the TCNB-toluene system.

of the TCNB–toluene system, the intensity of the CT absorption band decreases monotonically with an increase in temperature up to 348 K (Fig. 9).

References

1) J. Ferguson, *J. Chem. Phys.*, **43**, 306 (1965).
2) J. Ferguson, *J. Chem. Phys.*, **44**, 2677 (1966).
3) E. A. Chandross, J. Ferguson, and E. G. McRae, *J. Chem. Phys.*, **45**, 3546 (1966); E. A. Chandross and J. Ferguson, *ibid.*, **45**, 3554 (1966).
4) N. Mataga, T. Okada, and H. Oohari, *Bull. Chem. Soc. Jpn.*, **39**, 2563 (1966).
5) M. Itoh, T. Mimura, H. Usui, and T. Okamoto, *J. Am. Chem. Soc.*, **95**, 4388 (1973); M. Itoh and T. Mimura, *Chem. Phys. Lett.*, **24**, 551 (1974); M. Itoh, *ibid.*, **26**, 505 (1974).
6) K. Yoshihara, K. Futamura, and S. Nagakura, *Chem, Lett.*, **1972**, 1243.
7) H. Ishida and T. Tsubomura, *Chem. Phys. Lett.*, **9**. 296 (1971).
8) N. Mataga and K. Ezumi, *Bull. Chem. Soc. Jpn.*, **40**, 1355 (1967).
9) N. Nakashima, N. Mataga, F. Ushio, and C. Yamanaka, *Z. Phys. Chem. N. F.*, **79**, 150 (1972).
10) N. Mataga and Y. Murata, *J. Am. Chem. Soc.*, **91**, 3144 (1969).
11) A. Weissberger, Ed., "Technique of Organic Chemistry," Vol. III, Interscience, New York (1955).
12) N. Mataga, Y. Torihashi, and Y. Ota, *Chem. Phys. Lett.*, **1**, 385 (1967).

The Viscosity of Tetraphenylphosphonium and -arsonium Halides in Water

Katsuko TAKAIZUMI and Toshiki WAKABAYASHI
The College of General Education, Tohoku University, Kawauchi, Sendai 980

(Received March 23, 1976)

A viscometer, the inside of which was thoroughly coated by silicon grease, was prepared because it is difficult to measure precisely the viscosities of aqueous solutions of tetraphenylonium salts by means of a usual flow-type viscometer because of the characteristic peculiar to these solutions, that they make the glass wall water-repellent and water droplets tend to adhere to it. By comparing the relative viscosities on sucrose and $LaCl_3$ in water obtained by the coated viscometer with those found in the literature, it was confirmed that the viscometer operates adequately. The viscosities of Ph_4PCl, Ph_4PBr, Ph_4PNO_3, Ph_4AsCl, and Ph_4AsBr in water have been measured at 15, 25, and 35 °C. The ionic *B*-coefficients determined at 25 °C are 1.09 mol^{-1} for both cations, while the ionic activation energies for viscous flow are +4.98 and +5.02 kJ/mol for Ph_4P^+ and Ph_4As^+ respectively.

The viscosity measurement of electrolyte solutions has been widely used as an important experimental method to provide information concerning the nature of ion–solvent interactions. Although no satisfactory interpretation for the viscosity *B*-coefficient has yet been established, its sign and magnitude and its temperature dependence are usually regarded as measures of the effects arising from the size of the ion and ion–solvent interactions.[1-3] Especially with aqueous solutions which are recognized as partly structured liquids, the *B*-coefficient has been discussed in connection with the water structure and the effects of ions or of neutral solutes upon it.[4-11]

On the other hand, in the studies of aqueous solutions of hydrophobic solutes, differences between the water-solute interactions of alkyl- and aryl-substituted ions have been illustrated. In these studies, tetraphenyl ions, such as Ph_4P^+, Ph_4As^+, and BPh^-_4, have often been examined as typical and important ions containing phenyl groups.[12-19] Furthermore, some indications that BPh^-_4 and Ph_4P^+ or Ph_4As^+ interact differently with water have been obtained.[14b-19]

However, it should be noted that no studies of the viscosity of aqueous solutions of tetraphenylphosphonium and -arsonium salts have appeared, except one[17] which dealt with Ph_4AsCl only at 25 °C, and concerning the temperature dependence no data are available. This may be attributed to the peculiar characteristics of the aqueous solutions of these salts that the solutions make the glass surface water-repellent, presumably because of the preferential adhesion[20] of these large cations on the glass surface, and that the solution tends to form droplets on the glass surface.[21] Thus, in this case it is difficult to measure the viscosity precisely by means of a usual flow viscometer.

The basic conditions for assuring the precise measurement of the viscosity of fluid by means of a flow viscometer are that the flow rate on the boundary surface of the capillary be zero and the flow in the capillary be laminar. As is well known, the former is fulfilled in the case of the mercury-glass surface though the angle of contact is larger than 90°, *i.e.*, *ca.* 140° at room temperature. It can, therefore, be expected that the viscosity measurement for an aqueous solution of Ph_4MX may be possible provided that a viscometer is available which is coated by a suitable hydrophobic substance to prevent the adhesion of water droplets on the surface.

The purposes of this work are the preparation of such a viscometer, the examination of its properties as a viscometer, and the determination of the viscosities and the temperature dependence of aqueous solutions of tetraphenylphosphonium and -arsonium halides.

Experimental

Viscometer. The outline of the viscometer is shown in Fig. 1. The inside of the viscometer and all the paths for sample solutions are thoroughly coated by silicon grease film. The coating procedure is as follows: a hexane solution containing silicon grease (Dow Corning Co., Ltd.) (about 2 ppm) was filtered several times by a glass filter; each part of the viscometer was then filled up with the solution and was dried at room temperature after the solution has been removed. This procedure was repeated ten times or more. Finally the apparatus was dried at 120 °C for 24 h. The inner wall thus prepared is completely water-repellent, and the water introduced in the apparatus flows out thoroughly without leaving any droplets on the wall.

The sample solution is introduced into the bulb, B, from B_1 through three filters and the B_2 and B_3 bulbs. The B_3 bulb is an automatic buret, with a volume of about 40 cm^3; it is used to measure out a constant volume of the solution. It was confirmed that the reproducibility of the measured volume was within an error of ±5 mg by the weight of water,

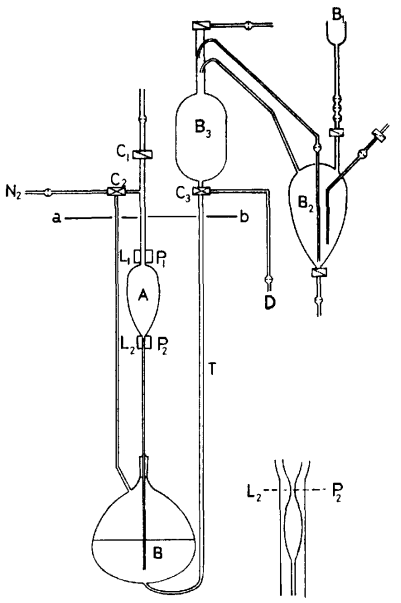

Fig. 1. The outline of the viscometer.

or 0.013%. The volume of the upper bulb, A, is about 20 cm^3; the length of the capillary, 18 cm; the diameter of the capillary, 0.06 cm.

The transit of the meniscus at each of the fixed points, P_1 and P_2 was detected as an electric pulse by means of a detector consisting of a small electric light (about 20 mW), a slit, and a phototransistor, PD 32H (NEC Co., Ltd.). The light was turned on for only a few seconds before and after the passing of the meniscus to minimize the heating. The pulse was introduced into a Takeda Riken universal counter, TR 5103, by which the flow time was recorded to the order of ms.

The viscometer was fixed in a stout frame made of brass, and, the main part was immersed in a thermostat maintaining its temperature within $\pm$0.0005 °C. The whole of the apparatus was mounted in air room, the temperature of which was controlled to within 0.1 °C. The thermostat consisted of inner and outer parts arranged concentrically. In the latter a cooling tube and a wire heater controlled automatically by a thermistor-regulator system were set, while in the former there was no heat source. The water in the bath was circulated between the two parts. Glass filters were set at all of the ends of the tubes of the apparatus opening to the atmosphere in order to keep the inside from dust.

The measured-out portion of the sample solution in B_3 is introduced slowly through the tube, T, into the bulb, B; the cock, C_3, is closed just when the meniscus passes C_3. The flow time was about 440 s for water at 25 °C. The reproducibility of the flow time is 10 ms, provided the variation in the bath temperature is kept within 0.0005 °C. After the timing, the inner solution is taken out thoroughly from an end, D, of the tube by suction. Since the removal of the solution is complete, there is no need to dry the inside after washing.

Density Measurements. The densities of the solutions at each temperature were measured by means of a pycnometer with a volume of 50 cm^3.

Chemicals. The tetraphenylphosphonium bromide was prepared by dissolving Ph_4PCl(Dotite TPPC) in dichloromethane and by shaking the solution with a 2 M aqueous solution of potassium bromide to change the chloride ion in the dichloromethane phase to the bromide ion. This extraction procedure was repeated with a fresh aqueous phase eight or more times. It was confirmed that the change of the anion from chloride to nitrate was completed by the time the process has been done five times. Considering the fact that the distribution ratio of Ph_4PBr is comparable to that of Ph_4PNO_3(200 or more) under the present conditions, the anion exchange is believed to be satisfactory. The organic phase was filtered with filter paper to remove the water, and then a small amount of ether was added to the filtrate to precipitate a small amount of a salt. The salt was filtered off from the organic solution. A crude Ph_4PBr was obtained from the solution by adding ether. The salt was recrystallized several times from dichloromethane by adding absolute ether to the solution. Ph_4AsBr was also prepared by a similar procedure. Ph_4PCl and Ph_4AsCl were purified by recrystallization.

The salts thus obtained were dried over P_2O_5 under atmospheric pressure because the aqueous solutions prepared from the salts dried for several days under a reduced pressure at 50 °C, or even at room temperature, have sometimes shown turbidity, though these drying processes are found in the literature. Also, the drying of the salts at a high temparature, 120 °C or more, should be avoided because it produces a substance which abnormally enhances the conductivity of the aqueous solution at a low concentration range, as was confirmed by conductivity measurements.[22]

Potentiometric titration with a standard iodine solution[23] to form Ph_4MI_3 showed a purity of 99.9% with respect to the tetraphenylonium ion in Ph_4PCl, Ph_4PBr, Ph_4PNO_3, Ph_4AsBr, and Ph_4AsCl, while potentiometric titration with silver nitrate showed a purity of 99.99% for the chlorides and bromides. No halide was found with Ph_4PNO_3.

The potassium chloride used in this study was of a Merck Suprapur. The sucrose was a specially prepared reagent grade for density gradient determination (Nakarai Kagaku Co.), and the aqueous solution was used within a day after preparation. Lanthanum chloride of a reagent grade (Wako Pure Chemical Ind.) was used with no further purification, and the concentration of the aqueous solution was determined by titration with a standard EDTA solution.

All of the solutions were prepared by weight with conductivity water.

Results and Discussion

The Nature of the Coated Viscometer. The viscometer was calibrated by the use of the equation: $\eta/d = at - b/t$, where a and b are regarded as instrumental constants of the viscometer. These constants were determined from the known densities and viscosities of aqueous solutions of potassium chloride[24] in the concentration range from 0.01 to 0.2 M. Although water is usually employed as a standard liquid, the potassium chloride solution was chosen here for the reason to be described below. The kinetic energy term can be connected with a and b by this relation:[3]

$$\frac{b}{a} = \frac{mV^2}{\pi^2 R^4 h_m g} \tag{1}$$

where V is the volume of liquid in the bulb, A, in Fig. 1, h_m is the mean height of the liquid column, R is the radius of the capillary, and m is a numerical coefficient introduced to take account of the particular shape of the capillary ends. For the present viscometer, m was estimated to be about 1.7, which is somewhat larger than usual values,[26] 0.5 to 1.2, for conventional flow viscometers.

It should be noted that the flow time of pure water, t_0, was longer by about 50 ms than that extrapolated to a zero concentration of potassium chloride. This suggests the presence of some interfacial effect due to the silicon grease film. For the flow time for water, therefore, we preferred the extrapolated one, which was determined by a quadratic equation of the molal concentration, to the observed one.

The relative viscosities of aqueous solutions of potassium chloride were reproduced with a standard deviation of 0.000023, which amounts to 0.002% of the relative viscosities, by means of the Jones and Dole equation;

$$\eta_r = 1 + Ac^{1/2} + Bc \tag{2}$$

with $A=0.0052_0$ and $B=0.014$.[24] A plot of $(\eta_r-1)/c^{1/2}$ against $c^{1/2}$ is shown in Fig. 2.

As a check, the viscosities of aqueous solutions of sucrose and lanthanum chloride were measured at 25 °C in the concentration region of 0.001 to 0.01 molar. The A- and B-coefficients determined by Eq. 2 are shown in Table 1, together with the values found in

TABLE 1. THE VISCOSITY *A*- AND *B*-COEFFICIENTS OF THE AQUEOUS SOLUTIONS OF SUCROSE AND $LaCl_3$

	A			*B*		
	Obsd	Ref.	Calcd	Obsd	p_B	Ref.
Sucrose	0	0[a]	0	0.89_0	0.004	0.878_6[a]
$LaCl_3$	0.031_6	0.0304[b]	0.0284	0.56_7	0.003	0.567_2[b]

a) Ref. 24. b) Ref. 25.

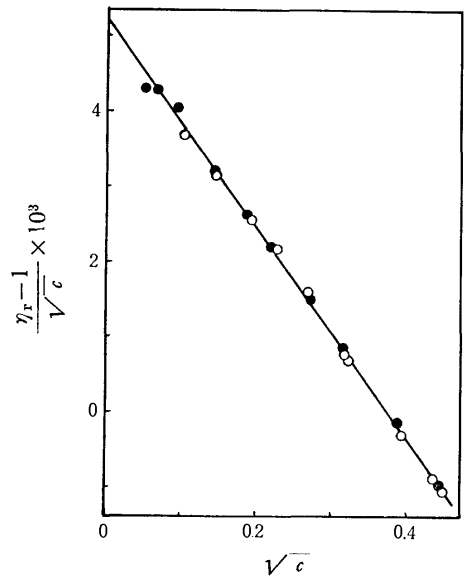

Fig. 2. Calibration of the coated viscometer with KCl in water at 25 °C.
○: Present data, ●: G. Jones and S. K. Talley.[24]

the literature. The probable errors expected in the *B*-coefficients, which are designated as P_B in the table, are 0.004 and 0.003 for sucrose and lanthanum chloride respectively. The agreement is fairly well, although with sucrose the present *B*-coefficient is slightly larger, beyond the probable error, than that found in the literature.[25]

Thus, it may be concluded that the coated viscometer can be used to determine the viscosities of aqueous solutions, provided that the extrapolated value for t_0 is used. One advantage of the present viscometer over the usual ones is that, since the sample solutions can be exchanged without removing the viscometer from the support, as has been described above, this viscometer is free from any error arising from the removal and resetting.

The Viscosities of Ph_4MX. The densities of aqueous solutions were calculated by Eq. 3, assuming a linearity of the density against the molal concentration of the salts;

$$d = d_0 + \alpha m \qquad (3)$$

where m is the molality and α is a constant for a given salt at a given temperature. The linearity was confirmed for Ph_4AsCl and Ph_4AsBr at 25 °C, at least in the low concentration range below 0.015 *m*, which was the highest concentration for the viscosity measurement. Table 2 lists the values of α for all of the salts and temperatures examined. The molar concentrations of the solutions were calculated from the molality and the density.

TABLE 2. DENSITY COEFFICIENTS OF Ph_4MX IN WATER AT 15, 25, AND 35 °C; α, IN Eq. 3

	Temp (°C)		
	15	25	35
Ph_4PCl	0.072_1	0.065_5	0.058_2
Ph_4PBr	0.108_1	0.098_1	0.088_1
Ph_4PNO_3	0.090_6	0.083_4	0.076_2
Ph_4AsCl	0.111_6	0.102_7	0.094_8
Ph_4AsBr	0.144_5	0.137_4	0.130_2

TABLE 3. THE RELATIVE VISCOSITIES OF THE AQUEOUS SOLUTIONS OF TETRAPHENYLONIUM BROMIDES AT 15, 25, AND 35 °C

Temp(°C)	15	$c(10^{-3}$ M)	25	$c(10^{-3}$ M)	35
$c(10^{-3}$ M)	η_r		η_r		η_r
			Ph_4PBr		
0.092_6	1.000210	0.799_2	1.001094	0.797_8	1.001017
0.569_7	1.000862	1.584_1	1.001982	1.595_6	1.001814
1.491_1	1.001996	2.461_4	1.003027	2.499_4	1.002826
2.836_0	1.003730	4.144_0	1.004707	4.007_5	1.004430
4.570_6	1.005875	6.301_6	1.007191	6.080_6	1.006461
7.531_3	1.009590	8.848_7	1.010156	8.036_2	1.008330
12.43_7	1.015526	10.61_3	1.011981	10.12_9	1.010524
			Ph_4AsBr		
0.801_2	1.001244	0.808_2	1.001081	0.781_2	1.001017
1.727_3	1.002361	1.622_3	1.002099	2.388_9	1.002668
2.525_6	1.003340	2.530_3	1.003094	4.021_3	1.004259
4.240_1	1.005620	4.275_1	1.005004	6.595_5	1.007078
6.568_0	1.008303	6.653_6	1.007664	8.813_6	1.009153
8.694_1	1.011168	9.171_3	1.010400	10.78_1	1.011089
11.25_2	1.014140	11.47_9	1.012991		

The vscosities of the aqueous solutions of Ph_4PCl, Ph_4PBr, Ph_4PNO_3, Ph_4AsBr, and Ph_4AsCl were measured at 15, 25, and 35 °C in the concentration range from 0.0005 to 0.012 M. The relative viscosities of aqueous solutions of these bromides are given in Table 3. Recently, it was stressed[20] that an extra term in c^2 should be added to the Jones and Dole equation in order to determine the *B*-coefficient precisely. In the present study, however, the Jones and Dole equation was employed to analyze the viscosity data. Taking account of the facts that the tetraphenyl ions have considerably large *B*-coefficients and that the measurement was carried out in a low concentration range below 0.012 M, no significant error will be introduced into the results by neglecting the extra term. As an example, the plots for Ph_4PBr at three temperatures are shown in Fig. 3. The *A*- and *B*-coefficients of Eq. 2 are obtainable from the intercept and the slope, as usual.

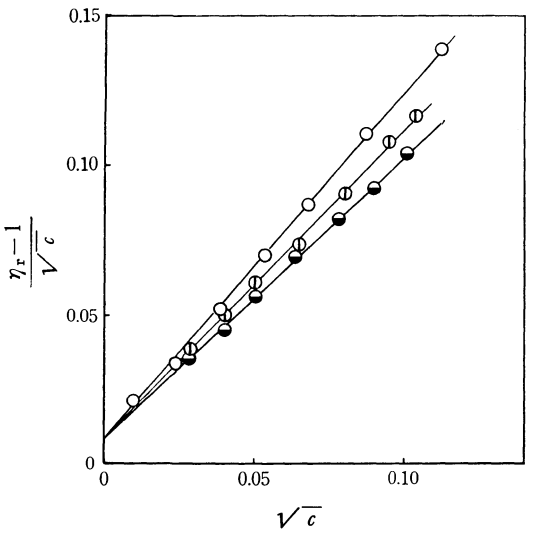

Fig. 3. Evaluation of the limiting slopes for relative viscosity of Ph_4PBr in water at 15°, 25°, and 35 °C. ○: 15 °C, ◑: 25 °C, ◒: 35 °C.

These coefficients were determined by the method of least squares and are listed in Table 3. The uncertainty in the B-coefficients is expected to be less than 0.02 mol^{-1}, as is shown in the column headed by p_B, which is the probable error. The A-coefficients found agree fairly well with the predicted ones, which are given in terms of the ionic equivalent conductivities by means of the relation derived by Falkenhagen and Vernon.[27] The splitting of the B-coefficient into the ionic components was carried out by the use of the scales introduced by Gurney[1] and by Kaminsky.[2] The ionic B-coefficients for the bromide ion at some temperatures were taken from the data by Kay, Vituccio, Zawoyski and Evans.[7] The ionic B-coefficients, B_i, thus obtained are given in the last column of Table 4. The consistency among the values of B_i for each cation obtained from different salts is satisfactory. No previous data to be compared with the present results are found in the literature except for one on Ph_4AsCl at 25 °C reported by Jolicoeur, Philip, Perron, Leduc, and Desnoyers,[17] this value is 1.08 mol^{-1}, the same as the value obtained here, though their value is based on a somewhat different equation, as has been mentioned above.

Table 4. The viscosity A- and B-coefficients of the aqueous solutions of tetraphenylonium halides

		A		B	p_B	B_i
		Obsd	Calcd			
15 °C	Ph_4PCl	0.0088	0.0089	1.20	0.015	1.22
	Ph_4PBr	0.0086	0.0087	1.17	0.014	1.22
	Ph_4AsCl	0.0085	0.0089	1.20	0.015	1.22
	Ph_4AsBr	0.0091	0.0087	1.17	0.014	1.23
25 °C	Ph_4PCl	0.0098	0.0091	1.08	0.013	1.09
	Ph_4PBr	0.0083	0.0090	1.05	0.014	1.09
	Ph_4PNO_3	0.0065	0.0094	1.04	0.014	1.08
	Ph_4AsCl	0.0085	0.0091	1.08	0.012	1.09
	Ph_4AsBr	0.0089	0.0090	1.04	0.003	1.08
35 °C	Ph_4PCl	0.010	0.0093	0.98	0.014	0.98
	Ph_4PBr	0.0085	0.0092	0.95	0.010	0.98
	Ph_4AsCl	0.0090	0.0093	0.98	0.013	0.98
	Ph_4AsBr	0.0092	0.0092	0.94	0.013	0.97

The temperature dependence of the viscosity can reasonably be expressed in terms of the activation energy for viscous flow, ΔE^*.[9,28] Assuming that the contribution of the salt to the ΔE^* is the sum of the activation energies for ionic components, it is possible to determine the ionic values for the 1 : 1 electrolyte by this equation:[9,28]

$$\Delta E^* - \Delta E_0^* = \Delta E_+^* + \Delta E_-^* \quad (4)$$

where ΔE_+^* and ΔE_-^* stand for the cationic and anionic activation energies respectively, and where ΔE_0^* is that for a pure solvent. With chloride and bromide ions,[9,28] values of −0.92 and −1.00 kJ/mol respectively for ΔE_-^* at a concentration of 1 M are assigned. The ionic activation energies thus obtained are listed in Table 5, together with those for other cations found in the literature, for comparison.

A widely accepted explanation for the viscosity B-coefficient of electrolytes, as summarized by Stokes and Mills,[3] is that the B-coefficient is a measure of the effects of (a) the size and shape of the ions, (b) the ordering of solvent molecules in the vicinity of ions as a result of the ionic field, and (c) the distortion of the solvent structure, leading to greater fluidity. The first two effects result in increasing the viscosity. One more effect is added with large hydrophobic ions such as tetraalkylammonium ions; that is, the "ice-like" structure of water at a distance from these ions is increased by their presence.[4,5] The size and sign of the B-coefficient can be determined as a result of the competition of these factors. Although the evaluation of each contribution of these effects is impossible at present, the effect of ionic size is usually estimated by the Einstein equation,[29] which was derived in the case of rigid spheres suspended in a viscous continuum. This effect results in a positive contribution to the B-coefficient by an amount of 0.0025 V,[3] where V is the hydrodynamic volume of the ion which may be equated with the standard partial molal volume of the ion, V_i^0($cm^3\,mol^{-1}$), at lower concentrations. The ionic

Table 5. Ionic activation energies of some tetra-substituted ions for viscous flow in water at 25 °C

	$\bar{V}_i^\circ$ (cm^3/mol)	B_i (mol^{-1})	ΔB_i	ΔE_i^* (kJ/mol)
Ph_4P^+	286.3[a]	1.09	0.37	4.98
Ph_4As^+	295.3[b]	1.09	0.35	5.02
		1.09[a]		
BPh_4^-	283.0[b]	1.12[a]	0.41	4.31[e]
Pr_4N^+	209.0[b]	0.86[c]	0.33	4.35[c]
		1.092[d]	0.57	2.60[d]
		0.780[f]	0.26	
Bu_4N^+	270.3[b]	1.28[c]	0.57	5.65[c]
		1.396[d]	0.71	5.15[d]
		1.168[f]	0.49	

a) Ref. 17. b) Ref. 31. c) Ref. 7. d) Ref. 9. e) Ref. 11. f) Ref. 20.

difference[20], $B_i - 0.0025\ V_i^0$, is considered as a measure of the effects arising from ion–solvent interactions other than the size effect, provided that it is reasonable to assume the ions to be spheres. These differences for tetraphenyl ions and some tetraalkylammonium ions are listed in the column designated as ΔB_i in Table 5. The ΔB_i values decrease in this order: $Bu_4N^+ > BPh^-_4 > Ph_4P^+ > Ph_4As^+ > Pr_4N^+$.

The ionic activation energies of tetraphenylonium ions for the viscous flow at 25 °C are given in Table 5, together with other tetrasubstituted ions. The ΔE_i^* values are all positive, since the sign of dB_i/dT is opposite to that of ΔE_i^*; this means that the dB_i/dT are all negative, and fairly large compared with most of the simple inorganic ions[9]. The order of the temperature dependence of the B-coefficient is somewhat uncertain because of the experimental errors, and more acculate data are required, but it is probably safe to speculate that the order is $Bu_4N^+ > Ph_4M^\pm > Pr_4N^+$.

The conclusion is reached that tetraphenyl ions, independent of the sign of the ionic charge, are classified into net "structure-makers" in water by reason of their positive and large values for ΔB_i[20] and the negative dependence of the B-coefficients on the temperature.[7–10] However, it will be necessary here to refer to the concept of the "structure" being made or broken by the solutes introduced in the water. The information found in the literature is contradictory if an attempt is made to classify the solutes into "structure-maker" and "-breaker" based on only the results obtained from a specific experimental technique. With respect to Ph_4P^+ and Ph_4As^+, a structure-breaking effect for the water structure has been inferred from osmotic coefficient measurements[13], while the reverse was suggested by a NMR study[15] and by an inspection of the partial molal heat capacities in water.[17] A marked effect on the water structure by Ph_4AsCl was not found in the near IR spectra.[16] Also, for the tetraphenylborate ion a similar situation holds. By the criterion[30] of the classification of solutes which is based on a thermodynamic relation, $(\partial \bar{C}_p/\partial p)_T = -T(\partial^2 \bar{V}_2/\partial T^2)_p$, both Ph_4AsCl and $NaBPh_4$ are "structure-breakers" because of the negative sign[32] of $(\partial^2 \bar{V}_2^0/\partial T^2)_p$ for them.

This inconsistency is not strange; as has already been mentioned by some authors,[30,31,33,34] it arises because we are still unable to define the structure as being either made or broken by solutes or to measure quantitatively the degree of the structure; also, the ion-water interactions are too complicated to explain in terms of structure-making or -breaking, though the concept has proven to be useful in some cases. Thus, it is inadequate to classify the tetraphenyl ions as either structure-makers or -breakers; at least the "structure" assumed in the present case should be different from the "iceberg" which is considered to be promoted by larger tetraalkylammonium ions.

To apply the Einstein equation to tetraphenyl ions (and also probably to R_4N^+ with long-chain alkyl groups) seems to be of doubtful value because tetraphenyl ions have a fairly open structure[15]; to regard them as a sphere can be only a very rough approximation. The specific interactions of water molecules with phenyl groups in Ph_4As^+, Ph_4P^+ and BPh^-_4 were indicated by a NMR study[15], and those with Ph_4As^+, by a laser-Raman study.[35] The authors of the latter pointed out the possibility that this ion is pentacordinate in water, with water entering the fifth coordination site, while in methanol it is tetracoordinate. Also by this coordination model the viscosity behavior of the tetraphenyl ions in water appears to be explicable, although it will be necessary to accumulate more precise and varied information in order to understand their states in water wholly.

References

1) R. W. Gurney, "Inoic Processes in Solution," McGraw-Hill Book Co., New York (1953).
2) M. Kaminsky, *Discuss. Faraday Soc.*, **24**, 171 (1957).
3) R. H. Stokes and R. Mills, "Viscosity of Electrolytes and Related Properties," Pergamon Press, New York (1965).
4) H. S. Frank and M. W. Evans, *J. Chem. Phys.*, **13**, 507 (1945).
5) H. S. Frank and W. Y. Wen, *Discuss. Faraday Soc.*, **24**, 133 (1957); H. S. Frank, *Proc. Roy. Soc., A*, **247**, 481 (1958).
6) H. S. Frank, "Chemical Physics of Ionic Solutions," ed. by B. E. Conway and R. G. Barradas, John Wiley & Sons, New York (1966), p. 53.
7) R. L. Kay, T. Vituccio, C. Zawoyski, and D. F. Evans, *J. Phys. Chem.*, **70**, 2336 (1966).
8) D. F. Evans, G. P. Cunningham, and R. L. Kay, *J. Phys. Chem.*, **70**, 2974 (1966).
9) E. R. Nightingale, Jr., "Chemical Physics in Ionic Solutions," ed. by B. E. Conway and R. G. Barradas, John Wiley & Sons, New York (1966), p. 87.
10) W. Y. Wen, "Water and Aqueous Solutions," ed. by R. A. Horne, Wiley-Interscience, New York (1972), p. 613.
11) R. L. Kay, "Water," Vol. 3, ed. by F. Franks, Plenum Press, New York and London (1973), p. 173.
12) J. F. Skinner and R. M. Fuoss, *J. Phys. Chem.*, **68**, 1882 (1964).
13) G. Kalfoglou and L. H. Bowen, *J. Phys. Chem.*, **73**, 2728 (1969).
14) (a) C. V. Krishnan and H. L. Friedman, *J. Phys. Chem.*, **73**, 3934 (1969); (b) C. V. Krishnan and H. L. Friedman, *ibid.*, **75**, 3606 (1971).
15) J. F. Coetzee and W. R. Sharpe, *J. Phys. Chem.*, **75**, 3141 (1971).
16) C. Jolicoeur, N. D. The, and A. Cabana, *Can. J. Chem.*, **49**, 2008 (1971).
17) C. Jolicoeur, P. R. Philip, G. Perron, P. A. Leduc, and J. E. Desnoyers, *Can. J. Chem.*, **50**, 3167 (1972).
18) H. L. Friedman and C. V. Krishnan, "Water," Vol. 3, ed. by F. Franks, Plenum Press, New York and London (1973), p. 1.
19) C. Jolicoeur and H. L. Friedman, *J. Phys. Chem.*, **75**, 165 (1971); *Ber. Bunsenges. Physik. Chem.*, **75**, 248 (1971).
20) J. E. Desnoyers and G. Perron, *J. Solution Chem.*, **1**, 199 (1972).
21) J. S. Fok, Z. Z. Hugus, and E. B. Sandell, *Anal. Chim. Acta*, **48**, 243 (1969).
22) Unpublished work; *cf.* the results in A. I. Popov and R. E. Humphrey, *J. Am. Chem. Soc.*, **81**, 2043 (1959).
23) H. H. Willard and G. M. Smith, *Ind. Eng. Chem., Anal. Ed.*, II, 186 (1939).
24) G. Jones and S. K. Talley, *J. Am. Chem. Soc.*, **55**, 624 (1933).
25) G. Jones and R. E. Stauffer, *J. Am. Chem. Soc.*, **62**,

335 (1940).
26) G. Barr, "A Monograph of Viscometer," Humphrey Milford, London (1931), p. 20.
27) H. Falkenhagen and E. L. Vernon, *Z. Phys.*, **33**, 140 (1932).
28) E. R. Nightingale, Jr., and R. F. Benck, *J. Phys. Chem.*, **63**, 1777 (1959).
29) A. Einstein, *Ann. Phys.*, **19**, 289 (1906).
30) L. G. Hepler, *Can. J. Chem.*, **47**, 4613 (1969).
31) F. J. Millero, "Water and Aqueous Solutions," ed. by R. H. Horne, Wiley-Interscience, New York (1972), p. 519.
32) F. J. Millero, *J. Chem. Eng. Data*, **15**, 562 (1970).
33) A. Ben-Naim, "Water," Vol. 2, ed. by F. Franks, Plenum Press, New York and London (1973), p. 585.
34) A. Holtzer and M. F. Emerson, *J. Phys. Chem.*, **73**, 261 (1969).
35) J. B. Orenberg, M. D. Morris, and T. V. Long, *Inorg. Chem.*, **10**, 933 (1971).

Proton Magnetic Resonance Study of Poly(*p*-chlorostyrene) of Low Molecular Weight

Yoshiyuki HIRAI, Yoshio NUNOMURA, and Yoshio IMAMURA

Department of Chemistry, Faculty of Science, Science University of Tokyo, Kagurazaka, Shinjuku-ku, Tokyo 162

(Received March 31, 1976)

Poly(*p*-chlorostyrne) samples of relatively low molecular weight (average degrees of polymerization($\overline{DP}$): 15, 24, and 46) were prepared by radical polymerization and their PMR spectra were observed in the temperature range 5—88 °C. When the temperature was elevated, the absorption of the methyne proton moved to lower field and the half height width for the absorption of the *ortho* proton decreased more remarkably than that of the *meta* proton. The absorption of the *ortho* proton of one polymer sample ($\overline{DP}$: 15) showed an anomalous broadening. These features of the observed spectra were interpreted in terms of ring current shielding by aromatic side groups, and the conformations of the polymer are discussed.

Many studies of proton magnetic resonance (PMR) spectra and proton relaxation times of polymers of low molecular weight have been made by various authors.[1-4] In many cases reported in the literature, the spectral patterns or spin-lattice relaxation times change with chain length in the region of short chains, and they become less sensitive to chain length as the chain becomes longer (*e.g.* average degrees of polymerization ($\overline{DP}$) : 20 for polystyrene).[2,5] These observations have been interpreted in terms of a so-called "polymeric effect". However, more precise discussion based on the viewpoint of conformations or internal motions of polymer chains has not been sufficiently developed. The present paper is concerned with the discussion of the conformations of polymers (poly(*p*-chlorostyrene)) of such low degrees of polymerization.

PMR spectra of polymers which contain aromatic side groups are always deformed by the ring current effect of the side groups. The extent of the ring current effect on each proton of the polymer would be influenced by the polymer conformation. Therefore, the PMR spectra of these polymers are accessible for conformational consideration. Poly(*p*-chlorostyrene) is one of the most favorable samples to this purpose, because this polymer gives well-resolved spectra in comparison with other polymers containing aromatic side groups, such as polystyrene and its *ortho* or *meta* derivatives.

The PMR spectra of poly(*p*-chlorostyrne)s ($\overline{DP}$: 15, 24, and 46) were observed in the temperature range 5—88 °C. The observed spectra were compared with each other in chemical shifts and in half height width, and the conformations are discussed in terms of the ring current shielding.

Experimental

p-Chlorostyrene was prepared by the procedure described in "Organic Syntheses".[6] Samples of poly(*p*-chlorostyrene) were obtained by polymerization of 10 ml of monomer in 50 ml of carbon tetrachloride for 5 h at 80 °C, using α,α'-azobisisobutyronitrile as an initiator. To obtain polymer samples of various molecular weights, the amount of the initiator was changed over the range from 0.5 g to 3 g. The polymers were precipitated in about 10 volumes of methanol in order to free them from any residual monomer and initiator, and were dried *in vacuo*. The number-average molecular weights of these polymers were determined using "KUNAUAR's Vapor Pressure Osmometer" in chloroform solution at 37 °C. The average degrees of polymerization of polymer samples were 14.8, 24.0, and 46.4 (they are denoted as 15-, 24-, and 46-polymer).

Polymer solutions for PMR spectral measurements were prepared by dissolving 0.1 g of the polymer in 1.0 ml carbon tetrachloride (spectral grade). Tetramethylsilane was added to each solution as an internal reference. The polymer solutions were transferred to 5 mm o.d. NMR tubes, which were sealed after the atmosphere was replaced with nitrogen gas. The PMR spectra of each polymer were observed over the range from 5 °C to 88 °C. These spectra were measured using a Japan Electric Optics Laboratory "JNM PS-100 Spectrometer" operated at 100 MHz.

Results and Discussion

Temperature Dependence of Chemical Shift. Figure 1 shows the PMR spectra of the phenyl protons of 24-polymer in carbon tetrachloride at 5 and 70 °C. The peaks at 2.95 τ and 3.59 τ are assigned to *meta* protons (*m*-H) and *ortho* protons (*o*-H) respectively. Figure 2 shows the spectra of aliphatic protons at various temperatures. The weak absorption near 7 τ corresponds

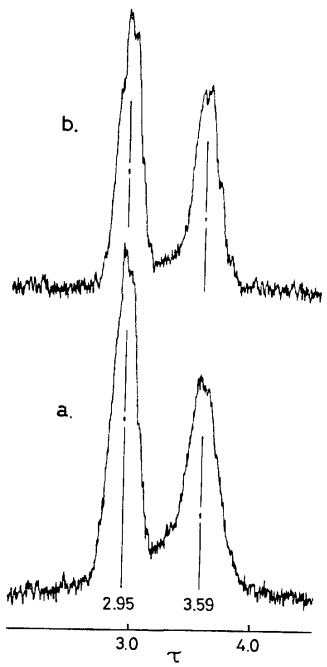

Fig. 1. PMR spectra of phenyl protons of poly(*p*-chlorostyrene) in carbon tetrachloride(0.1 g/ml). (a) 5 °C, (b) 70 °C.

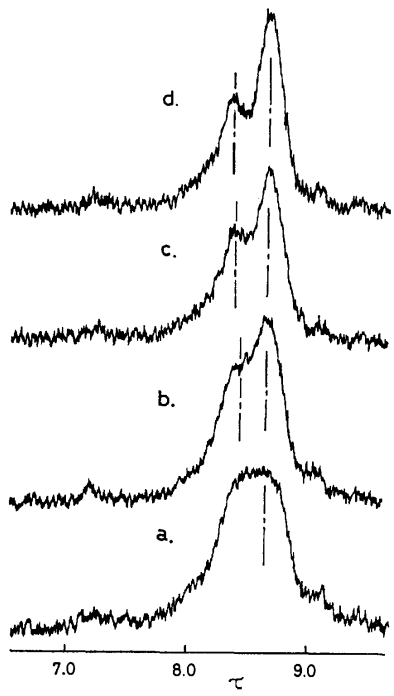

Fig. 2. PMR spectra of aliphatic protons of poly(*p*-chlorostyrene) in carbon tetrachloride(0.1 g/ml). (a) 5 °C, (b) 30 °C, (c) 50 °C, (d) 70 °C.

to the protons in terminal monomer units. The absorptions of the methyne proton (CH) and the methylene proton(CH_2) in nonterminal monomer units appear at about 8—9 τ. Figures 1 and 2 show that the peaks of the absorption of *o*-H, *m*-H, and CH_2 do not move, while that of CH moves to lower field as the temperature is raised.

The movement of peaks suggests a change of conformations. Indeed, chemical shifts are often influenced by conformations: for a change of conformations causes a change of environment at the position of the resonating proton, while the environment is governed by the effects of magnetic anisotropy or of electric field, *etc.* For poly(*p*-chlorostyrene), the effect of magnetic anisotropy is the most important factor. The magnetic anisotropy of the phenyl ring is significantly larger than that of the carbon–carbon (C–C) or carbon–chlorine (C–Cl) bond ($\chi_{//}-\chi_{\perp}$: 3.3×10^{-6} cm^3 mol^{-1} for C–C,[7] 3×10^{-7} cm^3 mol^{-1} for C–Cl[8] bond). Therefore, in this case, the changes of chemical shift caused by the conformational changes should be mainly governed by the effect of magnetic anisotropy (ring current effect) of the phenyl rings.

The extent of ring current shielding produced at the positions of CH_2, CH, *o*-H, and *m*-H was calculated for preferred conformations. The effects from the phenyl rings on either side of these protons were taken into account in this calculation. Phenyl-ring planes are assumed to be perpendicular to the plane defined by adjoining skeletal bonds. This assumption seems to be reasonable, as reported by Abe *et al.*[9,10] The ring current shieldings were estimated by the following equation:[11]

$$\Delta\sigma=\frac{\chi_{//}-\chi_{\perp}}{3R^3}(1-3\cos^2\theta)$$

where $\chi_{//}-\chi_{\perp}$ is the anisotropy of the magnetic susceptibility, R is the distance of the resonating proton from the center of the phenyl ring, and θ is the angular displacement from the symmetry axis. The bond length and bond angle are shown in Fig. 3. The value of $\chi_{//}-\chi_{\perp}$ for a *p*-chlorophenyl group would be somewhat different from the value for benzene. However, only a qualitative estimation is required in the present case: we used -59.7×10^{-6} cm^3 mol^{-1} [12] (benzene) as the value of $\chi_{//}-\chi_{\perp}$ for the *p*-chlorophenyl ring.

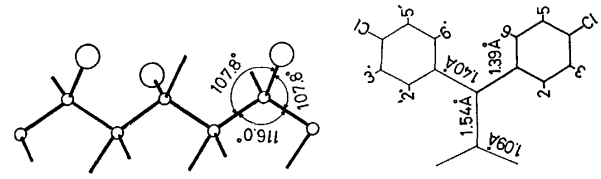

Fig. 3. Conformation and projection along the longitudinal axis of all-*trans* hypothetical syndiotactic poly(*p*-chlorostyrene).

Table 1. Comformations and ring current shielding (ppm unit)

Chain conform.		ΔE[a]	CH_2	CH	*o*-H	*m*-H
Meso	TG		−0.58			
	GT		−0.67			
Racemic	TT	0	−0.67			
	GG	1.66	−0.38			
Iso	TGTG	0		0.50	0.04	0.03
	GTGT			0.87	0.30	−0.07
	GTTG	1.06		0.48	−0.23	−0.16
Hetero	TTTG	0		1.45	0.33	−0.08
	TTGT	0.23		1.47	0.60	0.11
	GGTG	1.54		0.43	−0.17	−0.05
Syndio	TTTT	0		1.45	0.33	−0.08
	GGTT	1.10		0.58	0.51	0.09
	TTGG			0.43	−0.17	−0.05

a) Conformational energies (kcal/mol): Ref. 17.

The calculated results are given in Table 1, where the minus and plus signs represent paramagnetic and diamagnetic shielding, respectively. The results obtained from Table 1 follow: (a) Methylene protons experience approximately constant paramagnetic shelding, and *meta* protons experience only small paramagnetic shielding. (b) *Ortho* protons experience and indefinite amount of shielding, and the correlation to conformations is found to be irregular. (c) A methyne proton experiences diamagnetic shielding in any conformation, and the shielding was remarkably effective in the stable conformations in syndiotactic and heterotactic sequences (TTTT, GTTT, and TGTT).

Evidently, polymer chains occupy more stable conformations at low temperatures, and the rise of the temperature enables polymer chains to occupy conformations of higher energy. Table 1 demonstrates that such changes in conformations reduced the diamagnetic shielding produced at the position of CH in syndiotactic and heterotactic sequences, and cause the downfield shift of the peak of the methyne proton. Polystyrene or ring-substituted polystyrene by radical polymeri-

zation is known from NMR studies[13-15] to be syndio-rich. Therefore, the spectra of samples examined in this investigation should also reflect the characteristics of the ring current effect in syndiotactic and heterotactic sequences.

On the basis of a comparison of the observed results with the calculated ones, the following reasonable conclusions are drawn: (a) When the temperature is elevated, the fractions of the stable conformations (TTTT, GTTT, and TGTT) decrease. That decrease results in the decrease of diamagnetic shelding at the position of CH; consequently, the peak of CH moves to lower field. (b) The shielding produced at the positions of CH_2, *o*-H, and *m*-H is less sensitive to conformations, and the peaks of these protons do not move, even though the temperature is elevated and the fractions of stable conformations decrease.

Temperature Dependence of Half Height Width. Table 2 represents half height widths ($\Delta H_{1/2}$) for the absorptions of *o*-H and *m*-H of 24-polymer at various temperatures.

TABLE 2. HALF HEIGHT WIDTHS OF PMR PEAKS OF PHENYL PROTONS

Temp (°C)		5	20	30	40
$\Delta H_{1/2}$ (Hz)	*o*-H	31.3	29.3	28.3	27.3
	m-H	23.7	22.5	22.5	21.8
Temp (°C)		50	60	70	88
$\Delta H_{1/2}$ (Hz)	*o*-H	25.3	25.3	24.8	25.3
	m-H	21.5	21.3	20.5	20.0

The temperature dependence of the $\Delta H_{1/2}$ is shown in Fig. 4, together with those of 15- and 46-polymer. The $\Delta H_{1/2}$ for *o*-H absorption is apparently large at low temperatures, and decreases sharply up to 50 °C, and then decreases gradually with further rise in temperature. The abrupt small decrease between 40 °C and 50 °C may reflect an increase of the tortional oscillation of nonrotating phenyl rings, as Liu *et al.*[16] pointed out in the study of polystyrene. The $\Delta H_{1/2}$ for *m*-H absorption is small at low temperatures, and decreases gradually with the rise of temperature.

In general, the widths of spectra of polymers are caused by unresolved spin-spin splitting and by the time dependence of magnetic dipole interaction. However, this strong broadening observed only in *o*-H absorption at low temperatures cannot be interpreted in terms of these factors.

Table 3 represents the differences ($\Delta\sigma'$) of the ring current shielding on ortho protons and on meta protons: $\Delta\sigma' = |\Delta\sigma(H_2) - \Delta\sigma(H_6)|$ or $|\Delta\sigma(H_3) - \Delta\sigma(H_5)|$. The differences indicate the degree of difference in the chemical shifts of *ortho* protons or *meta* protons. The $\Delta\sigma'$ for *o*-H is great in any conformation, and it is particularly great at stable conformations (TTTT in syndiotactic, GTTT and TGTT in heterotactic sequence). On the other hand, the $\Delta\sigma'$ for *m*-H is relatively small in any conformation, and is less sensitive to conformations. The $\Delta\sigma'$ for *o*-H indicates that the *o*-H spectra consist of two absorptions (absorptions of H_2 and H_6) with different chemical shifts as the chains occupy the stable conformations.

TABLE 3. CONFORMATIONS AND DIFFERENCES ($\Delta\sigma'$) OF RING CURRENT SHIELDING (ppm unit)

Chain conform		$\Delta\sigma'$ $\lvert\Delta\sigma_{H_2}-\Delta\sigma_{H_6}\rvert$	$\lvert\Delta\sigma_{H_3}-\Delta\sigma_{H_5}\rvert$
Iso	TGTG	0.18	0.01
	GTGT	0.81	0.08
	GTTG	0.46	0.12
Betero	TTTG	1.03	0.03
	TTGT	1.30	0.16
	GGTG	0.11	0.24
Syndio	TTTT	1.03	0.03
	GGTT	0.78	0.04
	TTGG	0.11	0.24

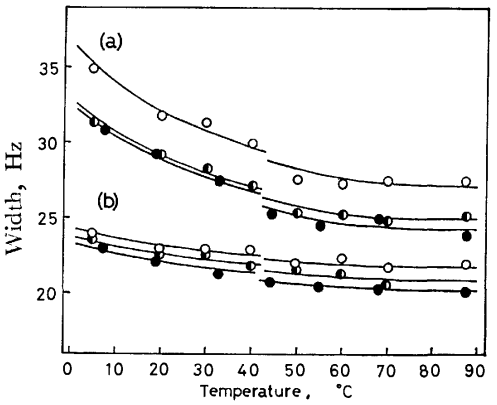

Fig. 4. Half height widths of Peaks of *ortho* protons(a) and *meta* protons(b) as a function of temperature. ○: 15-Polymer, ◐: 24-polymer, ●: 46-polymer.

From the above considerations, some interpretations for the temperature dependence of the width for phenyl absorptions can be drawn: (a) The polymer chains occupy stable conformations (TTTT, GTTT, and TGTT) at low temperatures; in these conformations the proton (H_2) has a different chemical shift from that of the proton (H_6). The overlap of the absorptions of H_2 and H_6 results in a broader absorption. (b) When the temperature is raised, the fractions of these conformations decrease, and the line widths decrease steeply. (c) The difference in the chemical shifts of *m*-H in any conformation is small, and such strong broadening as appeared in *o*-H is not observed.

These interpretations for the temperature dependence of the width are compatible with the conclusions drawn from the temperature dependence of chemical shifts.

Line Width and Molecular Weight. Figure 4 shows $\Delta H_{1/2}$ for phenyl absorptions of 15-, 24-, and 46-polymer as a function of temperature. The molecular weight dependence of $\Delta H_{1/2}$ for *m*-H absorption is small. While the $\Delta H_{1/2}$ values for *o*-H absorption of 24-polymer are similar to those of 46-polymer, those of 15-polymer are considerably different from those of 24- and 46-polymer and are anomalously large (the anomalous broadening was also observed in spectra of a polymer of lower molecular weight, $\overline{DP}$: 9.9). This phenome-

non is contrary to the well-known fact that line widths of spectra of polymers generally increase with the increase of molecular weights.

If the molecular weight distribution of 15-polymer sample is assumed to be broader than those of other samples, the sample would give a broader absorption. As shown in the absorption of aliphatic protons, if the chemical shift of phenyl protons in terminal monomer units differs from that of nonterminal monomer units and if these absorptions overlap, then the absorption of aromatic protons may become broad. This effect would be effective in the sample of low molecular weight (15-polymer). However, the anomalous broadening cannot be attributed to such effects as described above, because the anomalous broadening is observed only in *o*-H absorption and is not observed in *m*-H absorption.

As described in preceding sections, the ring current effect played an important role in understanding the PMR spectra of poly(*p*-chlorostyrene). The anomalous broadening observed in 15-polymer may also be related to the shielding effect. The temperature dependence of the chemical shift and the half height width was interpreted in terms of the preferred conformations listed in Table 1. The molecular weight dependence of the widths (the anomalous broadening) cannot be interpreted in terms of these conformations. The conformations listed in Table 1 are preferred conformations for polymers of low or high molecular weight; however, short chains could also occupy other conformations than these. For example, in shoft chains side groups are able to escape from each other, whereas in long chains such conformations are limited by steric restrictions. Since shielding is a function of conformations, the conformations which are permissible only in short chains ("permissible conformation"), produce somewhat different shielding from the shielding for the conformations listed in Table 1, and the existence of the permissible conformations must result in a broadening of spectra. As described in the preceding section, the ring current effect is effective for *o*-H and almost without effect for *m*-H; therefore, the broadening should be observed in the absorption of *o*-H.

On the basis of the above considerations, we can draw some reasonable interpretations for the PMR spectra of 15-, 24-, and 46-polymer. (a) The 15-polymer can occupy some conformations which are not permissible in polymers of higher molecular weight, and its *o*-H absorption shows the anomalous broadening owing to the absorptions arising from the so-called "permissible conformations"; the anomalous broadening can be interpreted only by the assumption of such conformations. (b) On the other hand, in the cases of 24- and 46-polymer, the conformations of the chains are just about limited to those listed in Table 1, and the anomalous broadening is not observed in the spectra of these polymers. The limitation of conformations in polymer chains might correspond to the phenomena called the "polymeric effect" cited at the beginning of this paper.

The assumption of permissible conformations does not disturb the interpretations for the temperature dependence of chemical shifts and half height widths given in preceding sections.

References

1) K. J. Liu and J. E. Anderson, *J. Macromol. Sci.*, **C5**, 1 (1970).
2) F. A. Bovey, G. V. D. Tiers, and G. Filipovich, *J. Polym. Sci.*, **38**, 73 (1958).
3) D. E. Woessner, *J. Chem. Phys.*, **41**, 84 (1964).
4) K. J. Liu and R. Ullman, *J. Chem. Phys.*, **48**, 1158 (1968).
5) F. A. Bovey, "High Resolution NMR of Macromolecules," Academic Press, New York and London (1972), p. 124.
6) R. L. Frank and J. R. Blegen, *Org. Synth.*, Coll. Vol. III, 200, 204 (1955).
7) A. A. Bothner-By and C. Naar-Colin, *Ann. N. Y. Acad. Sci.*, **70**, 833 (1958).
8) H. M. McConnell, *J. Chem. Phys.*, **27**, 226 (1957).
9) Y. Abe, A. E. Tonelli, and P. J. Flory, *Macromolecules*, **3**, 294 (1970).
10) A. E. Tonelli, Y. Abe, and P. J. Flory, *Macromolecules*, **3**, 303 (1970).
11) J. A. Pople, W. G. Schneider, and H. J. Bernstein, "High Resolution Nuclear Magnetic Resonance," McGraw-Hill, New York, N. Y. (1959), p. 176.
12) J. Hoarau, N. Lumbroso, and A. Pacault, *C. R. Acad. Sci.*, **242**, 1702 (1956).
13) L. F. Johnson, F. Heatly, and F. A. Bovey, *Macromolecules*, **3**, 175 (1970).
14) K. Matsuzaki, T. Uryu, K. Osada, and T. Kawamura, *J. Polym. Sci.*, **12**, 2873 (1974).
15) Y. Inoue, A. Nishioka, and R. Chujo, *Makromol. Chem.*, **156**, 207 (1972).
16) K. J. Liu and R. Ullman, *Polymer*, **6**, 100 (1967).
17) D. Doskočilová, J. Štokr, B. Schneider, H. Pivcová, M. Kolínský, J. Petránek, and D. Lím, *J. Polym. Sci., C*, **16**, 215 (1967).

Far Infrared Spectra of Solid 1,2-Dihalogenoethane

Jiro HIRAISHI

National Chemical Laboratory for Industry, Honmachi, Shibuya-ku, Tokyo 151

(Received April 7, 1976)

Far infrared spectra are measured for solid 1,2-dichloro-, dibromo-, and diiodoethane at several temperatures. The translational lattice vibrations of the crystals are observed for both high and low temperature phases. The observed frequencies of the low temperature phase of 1,2-dichloroethane agreed with the frequencies calculated by Mizushima *et al.* (Ref. 5). The nature of the phase transition is discussed on the basis of the temperature dependence of the spectra. The low frequency Raman spectrum of 1,2-diiodoethane is also reported.

Solid 1,2-dichloroethane and 1,2-dibromoethane undergo phase transitions at 177.0 and 249.49 K, respectively.[1] Lipscomb *et al.*[2] studied the X-ray diffraction of the high temperature phase (α phase) as well as the low temperature phase (β phase) of 1,2-dichloroethane and concluded that in the α phase either the molecule rotates freely or the orientation of the molecule around its Cl–Cl axis is disordered. The nature of the phase transition has been discussed in terms of Raman spectroscopy by several investigators.[3–6] For 1,2-dichloroethane, Ozora, *et al.* observed the low frequency Raman bands at several temperatures and concluded that the molecule rotates freely in the α phase.

For 1,2-dibromoethane, we reported the temperature dependence of the low frequeycy Raman bands due to the rotational lattice vibrations and showed that the nature of its phase transition is similar to that of 1,2-dichloroethane, although the crystal structure of its α phase is probably different from that of the β phase of 1,2-dichloroethane.[6]

The space group of the β phase of 1,2-dichloroethane is $C_{2h}{}^5$—$P2_1/c$; a unit cell contains two molecules.[2] The lattice vibrations at the center of the Brillouin zone are classified into $3a_g+3b_g+2a_u+b_u$. The vibrations of the a_g and b_g species are rotational modes and are Raman active, while those of the a_u and b_u species are translational modes and are infrared active. Ozora *et al.*[4] and Mizushima *et al.*[5] calculated the optically active lattice vibrations on the basis of Buckingham-type potentials between intermolecular atoms. They used the frequencies of the rotational lattice vibrations. No infrared study of the translational modes has been made in detail. Durig *et al.*[3] reported a very weak band at 50 cm^{-1} for 1,2-dichloroethane in the far infrared spectrum.

Hassel and Hveding[7] reported that solid 1,2-diiodoethane undergoes a rotational phase transition at 25.8 °C. However, no vibrational spectroscopic study has been made of the lattice vibrations of the crystal. In the present paper the far infrared spectra of solid 1,2-dichloroethane, 1,2-dibromoethane, their deuterated compounds, and 1,2-diiodoethane were studied at several temperatures in order to obtain information about the relation between translational lattice vibrations and the phase transition.

Experimental

Far infrared spectra were measured by use of a Hitachi model 070 interferometer. A cryostat equipped with a small refrigerator, Cryomech model GB03, was used for the measurements at low temperatures. Liquid samples were sealed into polyethylene cells of about 1 mm thickness. The translational lattice vibrations are very weak in the infrared spectra, because 1,2-dihalogenoethane molecules have a *trans* form in the solid state and have no dipole moment. For this cell thickness the bands due to intramolecular vibrations were completely saturated. The resolution used for the measurements was 0.65, 1.3, or 2.6 cm^{-1}, depending on the width of the bands. The temperature at the polyethylene cell was measured by use of an Au (with 0.07 atomic % Fe) chromel thermocouple obtained from Osaka Sanso Inc., which was calibrated by the calibrated GaAs thermometer of Lake Shore Cryogenics Inc. The temperature was kept constant within 0.5 K during the measurement of one interferogram. Although it reached approximately 13 K at the sample holder (made of copper), the temperature at the cell was about 65 K, because of the low thermal conductivity of the polyethylene plates.

The spectra of 1,2-diiodoethane was measured by use of a silicon plate with the cell thickness of about 0.5 mm. Commercially available 1,2-diiodoethane powder was used for the measurements, after subliming several times.

Results and Discussion

1,2-Dibromoethane. Figure 1 shows the far infrared spectra of 1,2-dibromoethane at several temperatures. At 69 K three bands at 51.1, 42.8, and 37.0 cm^{-1} were observed. The crystal structure of 1,2-dibromoethane has not yet been studied in detail. Reeds and and Lipscomb[2b] quoted the work by Meerman and

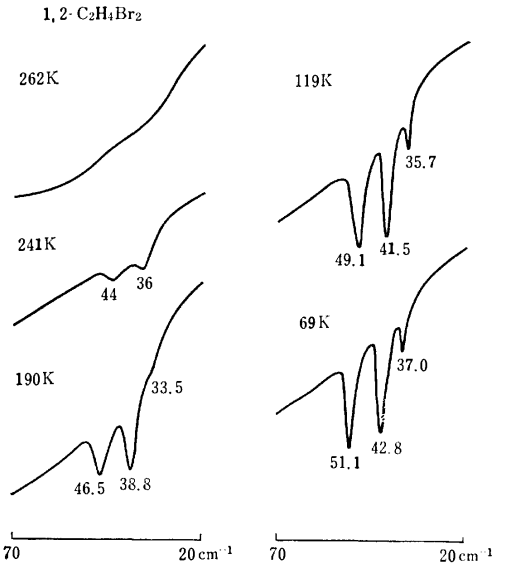

Fig. 1. Far infrared spectra of solid 1,2-$C_2H_4Br_2$.

stated that the crystal structure of the β phase of 1,2-dibromoethane was similar to that of 1,2-dichloroethane. Three bands owing to the translational lattice vibrations are expected to appear in the infrared spectra in the space group of C_{2h}^5 with two molecules in a unit cell. The present result does not contradict the statement by Reeds and Lipscomb. The spectra of 1,2-$C_2D_4Br_2$ were also measured and three bands at 50.8, 42.6, and 37.0 cm^{-1} were observed at 70 K. The small isotopic shifts are consistent with the assignments of the bands to translational lattice vibrations. The spectra of 1,2-dichloroethane show only two bands below 100 cm^{-1}, as will be seen later. The very weak band at 37.0 cm^{-1} may be assigned to an impurity. However, it did not decrease in intensity after the sample was purified by means of a spinning band fractional distillation column made by Tokyo Kagakuseiki Co., Ltd.

1,2-Dichloroethane. Two bands at 62.8 and 51.1 cm^{-1} were observed for 1,2-dichloroethane at 67 K (62.3 and 50.3 cm^{-1} for 1,2-$C_2D_4Cl_2$), as shown in Fig. 2, although three bands were expected, as noted above. Since the band of the lowest frequency of 1,2-dibromoethane is very much weaker than the others, it can be assumed, in the case of 1,2-dichloroethane, that the lowest frequency band is too weak to be observed.

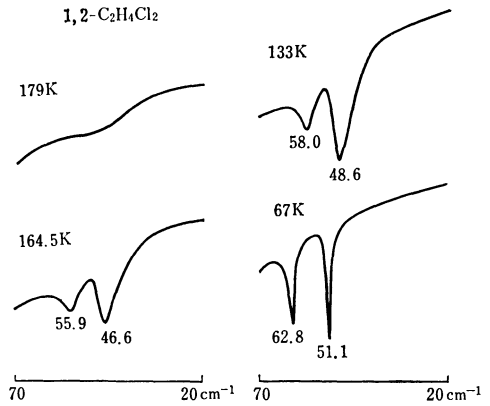

Fig. 2. Far infrared spectra of solid 1,2-$C_2H_4Cl_2$.

Ozora, *et al.*,[4] and Mizushima *et al.*[5] calculated the optically active lattice vibrations of 1,2-dichloroethane on the basis of the crystal structure at 133 K. According to their calculations, the third missing band may appear in the frequency region higher than 70 cm^{-1}. We could not detect the band in the frequency region lower than 150 cm^{-1}; here silicon plates were used instead of polyethylene sheets for the cell and windows, with the cell thickness of about 2 mm, to eliminate the interference of the band at 72 cm^{-1} from the polyethylene plates. In these calculations, the first derivatives of potential functions are neglected. Pomposiello *et al.* calculated the effect of the first derivatives on lattice vibrations of several molecular crystals including *trans*-1,2-dichloroethane.[8] Their result indicates that the frequencies of the translational lattice vibrations are not affected significantly by the first derivatives in the case of 1,2-dichloroethane and thus cannot eliminate the apparent discrepancy between the two possibilities concerning the assignment of the third missing band. In Table 1 the observed frequencies are assigned, tentatively, according to the calculation by Mizushima *et al.*

Table 1. Observed and calculated frequencies (cm^{-1}) of the β phase of 1,2-$C_2H_4Cl_2$

	Obsd	Calcd	
		a)	b)
a_g	117	109	111.6
	79	87	79.2
	55	58	50.4
b_g	—	99	97.0
	73	77	73.0
	(55)	60	49.9
a_u	—	98	83.8
	48.6	71	47.4
b_u	58.0	53	51.3

a) From Ref. 4. b) From Ref. 5.

1,2-Diiodoethane. Four bands (176, 136, 41.5, and 33.5 cm^{-1}) were observed below 200 cm^{-1} at 288.5 K. The bands at 176 and 136 cm^{-1} are assigned to the CCl bending (b_u species) and the torsional vibrations (a_u species), respectively. The other bands are very weak and are assigned to the intermolecular vibrations. The space group of solid 1,2-diiodoethane is C_{2h}^5 [7,9] and three translational lattice vibrations are infrared active. The spectra at various temperatures are shown in Fig. 3. Only two bands were observed

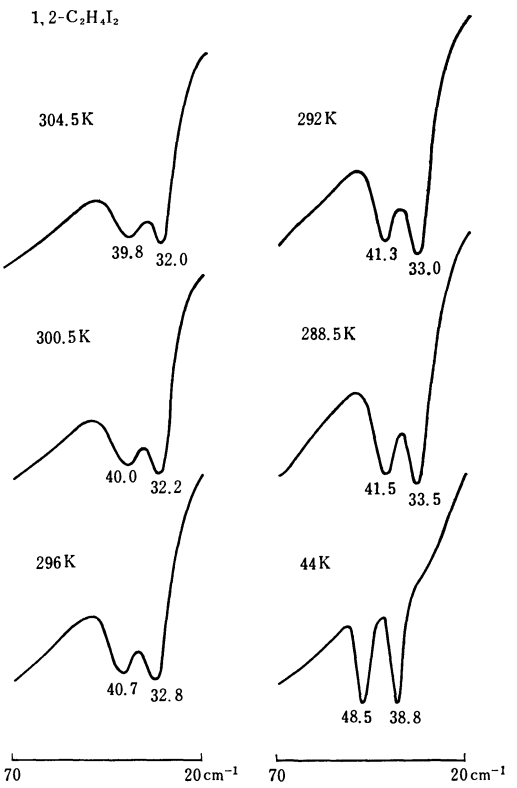

Fig. 3. Far infrared spectra of solid 1,2-$C_2H_4I_2$.

Table 2. Temperature dependence of the lattice vibrational frequencies (cm^{-1}) of 1,2-$C_2H_4Br_2$

Translational (in Far IR)			
69K	119K	190K	241K
51.1	49.1	46.5	44
42.8	41.5	38.8	36
37.0	35.7	33.5	—
Rotational (in Raman)[7]			
70K	116K	191K	245K
124.2	118.2	105.8	91.5
56.0	54.5	51.3	47
44.1	42.9	39.4	36
27.3	—	—	—

at the low temperature phase, as in the case of 1,2-dichloroethane.

Phase Transition and Translational Lattice Vibrations. Table 2 shows the frequencies of the lattice vibrations of 1,2-dibromoethane at several temperatures. The frequencies of the translational lattice vibrations in the β phase decrease upon approaching the transition temperature. Their behavior is similar to that of the lower frequency rotational modes. The highest frequency rotational mode is the libration around the Br–Br axis; this is the most unharmonic among the observed optically active lattice vibrations.

Above the transition temperature the absorption band is very broad for 1,2-dichloroethane as well as for 1,2-dibromoethane. As the crystal structure of the α phase of 1,2-dichloroethane is similar to that of the β phase, three translational lattice vibrations are also expected in the infrared spectra for the α phase, if the molecules rotate freely in the α phase. Figure 1 indicates that the spectra are not continuous at the transition temperature, which can be explained more plausibly in terms of the orientational disorder in the α phase. As Bertie and Whally discussed,[10] the $k=0$ selection rule is not applicable to an orientationally disordered crystal. Schwartz and Ron reported a similar discontinuity in the far infrared spectra at the transition temperature for acetylene[11] and cyclohexane crystals.[12] Chlorocyclopentane crystal also exhibits a very broad band in the disordered phase.[13]

1,2-diiodoethane crystal shows a continuous spectral change near the transition temperature, as given in Fig. 3. The transition temperature was confirmed to be 298.6 K, using DTA equipment from Rigaku Denki Co., Ltd.; this agreed well with the value reported by Hassel and Hveding.[7] The result of Fig. 3 is different from those of other crystals near the order-disorder transition, as discussed above; this can be explained in terms of free rotation of molecules in the high temperature phase of 1,2-diiodoethane.

Raman Spectrum of 1,2-Diiodoethane. The Raman spectrum of 1,2-diiodoethane was also measured by use of a Cary 82 spectrophotometer, with the 647.1 nm line of a Kr^+ laser as a source. Three bands at 43.5, 36.7, and 17 cm^{-1} were observed at approximately 290 K, as is shown in Fig. 4. 1,2-Dibromoethane and 1,2-dichloroethane[4] crystals show three rotational

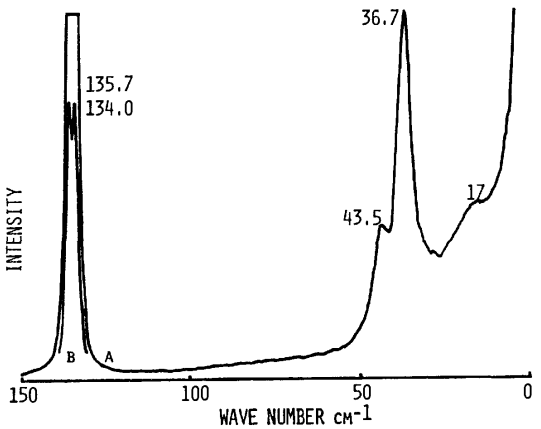

Fig. 4. Raman spectra of solid 1,2-$C_2H_4I_2$.
(A) $\Delta\nu=0.5\ cm^{-1}$. 5000 counts/full scale. (B) $\Delta\nu=0.2\ cm^{-1}$. 1000 counts/full scale. 134.0 and 135.7 cm^{-1} bands are assigned to the intramolecular CCI deformation vibrations (a_g and b_g species).

lattice vibrations in the Raman spectra, except for the rotational band around the halogen–halogen axis. Considering the results of 1,2-dichloro- and 1,2-dibromoethane crystals, the rotational band around the I–I axis is expected to be too weak and too broad to be observed at this temperature.

The author greatly acknowledges the measurement of the Raman spectrum of 1,2-diiodoethane by Dr. J. Shimada of Central Research Laboratory, Hitachi, Ltd. The author also acknowledges the help with the DTA measurement given by Dr. K. Hayamizu of National Chemical Laboratory for Industry.

References

1) K. S. Pitzer, *J. Am. Chem. Soc.* **62**, 331 (1940).
2) a) M. E. Milberg and W. N. Lipsomb, *Acta Crystallogr.*, **4**, 369 (1951); b) T. B. Reeds and W. N. Lipscomb, *ibid.*, **6**, 45 (1953); c) W. N. Lipscomb and F. E. Wang, *ibid.*, **14**, 1100 (1961).
3) J. R. Durig, K. K. Lau, S. E. Hannum, and F. G. Baglin, *J. Mol. Struct.*, **9**, 291 (1971).
4) A. Ozora, T. Nakagawa, and M. Ito, *Bull. Chem. Soc. Jpn.*, **45**, 95 (1972).
5) S. Mizushima, T. Shimanouchi, I. Harada, Y. Abe, and H. Takeuchi, *Can. J. Phys.*, **53**, 2085 (1975).
6) J. Hiraishi and T. Shinoda, *Bull. Chem. Soc. Jpn.*, **48**, 2732 (1975).
7) O. Hassel and J. A. Hveding, *Tidskr. Kjemi, Bergv. Met.*, **1**, 109 (1941). [Chem. Zentr. 113, 2115 (1942I).]
8) M. C. Pomposiello, H. Bonadeo, and E. D'Alessio, *Chem. Phys. Lett.*, **35**, 379 (1975).
9) H. P. Klug, *J. Chem. Phys.*, **3**, 747 (1935).
10) J. E. Bertie and E. Whalley, *J. Chem. Phys.*, **40**, 1637, 1646 (1964).
11) Y. A. Schwartz, A. Ron, and S. Kimel, *J. Chem. Phys.*, **51**, 1666 (1969).
12) Y. A. Sataty and A. Ron, *Chem. Phys. Lett.*, **25**, 384 (1974).
13) J. R. Durig, B. A. Hudgens, G. N. Zhizhin, V. N. Rogovoi, and J. M. Casper, *Mol. Cryst. Liq. Cryst.*, **31**, 185 (1975).

Magnetic Circular Dichroism Studies on *o*-, *m*-, and *p*-Nitroanilines and *o*-, *m*-, and *p*-Aminobenzoic Acids

Akira KAITO, Akio TAJIRI, and Masahiro HATANO

Chemical Research Institute of Non-aqueous Solutions, Tohoku University, Katahira, Sendai 980

(Received April 9, 1976)

The MCD and UV spectra of *o*-, *m*-, and *p*-nitroanilines and *o*-, *m*-, and *p*-aminobenzoic acids were measured. Some ambiguous absorption bands, which strongly overlap each other, can be separated in the MCD spectra. The Faraday *B* terms were calculated using wave functions obtained from the Pariser-Parr-Pople (PPP) method; the values are in good agreement with the experimental values derived from the MCD spectra. The spectral assignments are discussed not only by comparing the excited states of nitroanilines and aminobenzoic acids with those of benzene itself, but also by taking account of the electron migration between the benzene ring and the substituent groups. On the other hand, it turns out from the measurements of the MCD spectra that the zwitterion, $C_6H_4(NH_3^+)CO_2^-$, exists in aqueous solutions of *o*- and *m*-aminobenzoic acids.

The magnetic circular dichroism (MCD) technique has been shown to be useful for elucidating the magnetic moments in the degenerate electronic states and for analyzing the electronic spectra.[1-4] For highly symmetrical molecules, we can expect the Faraday *A* and *C* terms originating from the Zeeman splitting of the degenerate ground and excited states. On the other hand, only the Faraday *B* term, due to the mixing of the electronic states by the external magnetic field, is present for the molecules of lower symmetry.

The MCD spectra of substituted benzenes have been extensively investigated,[5-11] because the experimental results are sensitive to the substituents' effects. However, only slight attention has been paid to the MCD of the benzenes containing both electron-donating and electron-accepting substituents, whose electronic spectra are characterized by the appearance of an intense absorption band in the lower wave number region (25000—40000 cm^{-1}). The dissimilarity of the electronic spectra of these benzene derivatives from that of benzene itself is considered to be based on the fact that some intramolecular charge-transfer transitions have been found in the former along with the $\pi \rightarrow \pi^*$ transitions of the benzene ring. Tanaka[12] has given the spectral assignments of *p*-nitroaniline by measuring the polarized absorption spectrum of single crystals of *p*-nitroaniline. Some bands which are ambiguous and hidden in solution become evident in the crystalline spectrum.

On the other hand, the MCD technique is occasionally used for elucidating the complicated electronic spectra of ions and molecules. The strongly overlapping absorption bands of some aromatic organic compounds[13] have been separated, and the hidden transitions of substituted biphenyls[14] have been detected in the MCD spectra. It is one of the purposes of this work to apply the MCD technique to clarification of the ambiguous and complicated electronic spectra of *o*-, *m*-, and *p*-nitroanilines and *o*-, *m*-, and *p*-aminobenzoic acids.

In aqueous solutions of *o*-, *m*-, and *p*-aminobenzoic acids, there seem to exist four chemical species in equilibria, as shown in the diagram below.

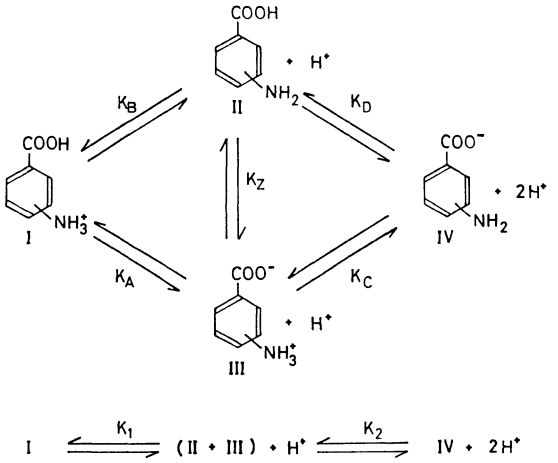

The ionization constants, K_1 and K_2, have been determined experimentally by the titration method.[15] Some investigators[15,16] have estimated the equilibrium constant, K_z, for ionization of neutral aminobenzoic acid (II) to the zwitterion (III). However, it is difficult to recognize the existence of the zwitterion (III) with the aid of the usual spectroscopic methods, such as absorption spectroscopy. This is because the absorption spectra of aminobenzoic acids are so complicated that the bands characteristic of the zwitterion (III) are hidden behind the bands due to other species of aminobenzoic acids. Another purpose of this work is to analyze the complicated electronic spectra of aminobenzoic acids in aqueous solutions in various pH ranges on the basis of the signs of the MCD spectra, and to show the existence of the zwitterion (III) in aqueous solutions.

Experimental

o-, *m*-, and *p*-Nitroanilines and *o*- and *p*-aminobenzoic acids were purified by recrystallization from water-ethanol. *m*-Aminobenzoic acid was sublimed after recrystallization from water. The MCD and UV spectra were measured with a JASCO J-20A recording spectropolarimeter equipped with a 12.5 kG electromagnet and with a Hitachi EPS-3T recording spectrophotometer, respectively. The experimental Faraday *B* terms were obtained by the use of the following equation:

$$B = -(1/33.53\nu_{max}) \int_{band} [\theta]_M d\nu \qquad (1)$$

Theoretical

The electronic transition energies and the Faraday *B* terms of nitroanilines and aminobenzoic acids were

calculated by the Pariser-Parr-Pople (PPP) approximation,[17] including configuration interactions (CI) among all singly excited configurations. One-center electron repulsion integrals and one-center core integrals were evaluated from valence state ionization potentials and electron affinities. The Nishimoto-Mataga[18] method was used for the estimation of two-center electron repulsion integrals. The resonance integrals were calculated in accordance with the Wolfsberg-Helmholtz equation.[19]

The Faraday B terms of a transition $j \leftarrow a$ is given by[1-4]

$$B_{a\to j} = \mathrm{Im}\{\sum_{k\neq a} (\langle k|\boldsymbol{\mu}|a\rangle/(E_k - E_a)) \cdot \langle a|\boldsymbol{m}|j\rangle \times \langle j|\boldsymbol{m}|k\rangle + \sum_{k\neq j} (\langle j|\boldsymbol{\mu}|k\rangle/(E_k - E_j)) \cdot \langle a|\boldsymbol{m}|j\rangle \times \langle k|\boldsymbol{m}|a\rangle\}, \quad (2)$$

where $\boldsymbol{m}$ and $\boldsymbol{\mu}$ stand for the magnetic and electric dipole moment operators, respectively, and E_a, E_j, and E_k are the energies of states, a, j, and k, respectively. The electric transition moments in Eq. 2 were evaluated by the use of the dipole length operator, $\boldsymbol{r}$, and the dipole velocity operator, $\boldsymbol{\nabla}$. The orthogonalized atomic orbital obtained by the Löwdin procedure[20] was used for the calculation of the magnetic and electric moments in Eq. 2.

It is known that the Faraday B terms calculated for a noncentric molecule using a limited basis set are origin dependent.[7,21] Caldwell and Eyring[7] have suggested that the error introduced by employing a limited basis set is minimized at the center of charge density. Accordingly, the origin is chosen at the center of charge of the ground state in this work.

Calculations were carried out using the NEAC 2200 computer in the computer center of Tohoku University.

Results and Discussion

The MCD (A) and UV (B) spectra of o- and m-nitroanilines are shown in Figs. 1 and 2. The single absorption band of m-nitroaniline observed in the higher wave number region (38000—48000 cm^{-1}) is split into two in the MCD spectrum, whereas the MCD spectrum of o-nitroaniline is weak and ambiguous in this spectral region.

The MCD and UV spectra of p-nitroaniline are shown in Fig. 3. In the region of 33000—39000 cm^{-1}, one can see a positive MCD band originating from the second $\pi\to\pi^*$ transition, which is obscured by the first intense $\pi\to\pi^*$ transition in the absorption spectrum. Two MCD bands appear with opposite signs in the higher wavenumber region (39000—48000 cm^{-1}), although these transitions are strongly overlapping in the absorption spectrum.

Figures 4—6 show the MCD and UV spectra of o-, m-, and p-aminobenzoic acids in heptane–dioxane (9 : 1 in volume) solution, in which only the neutral aminobenzoic acid (II) may be stable. p-Aminobenzoic acid exhibits negative and positive MCD bands at 33800 and at 36800 cm^{-1}, respectively, while a single absorption band appears in this spectral region. Each sign of the MCD spectra of o- and m-aminobenzoic acids is the same as that of p-aminobenzoic acid.

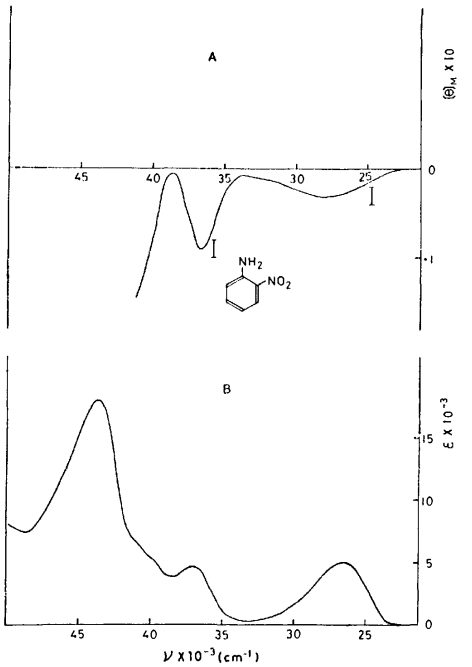

Fig. 1. MCD (A) and UV (B) spectra of o-nitroaniline in heptane solution at room temperature.

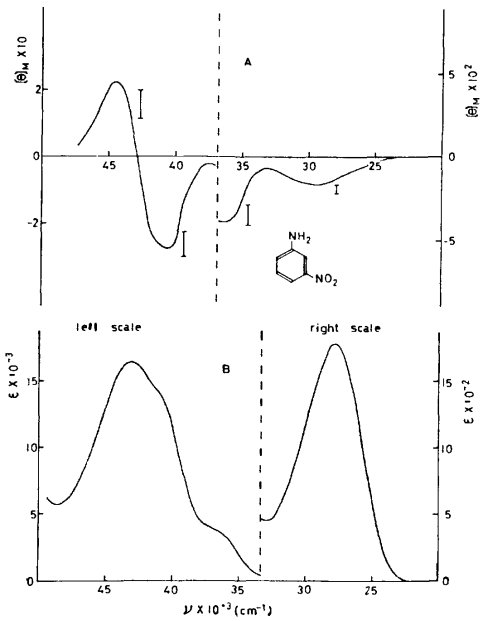

Fig. 2. MCD (A) and UV (B) spectra of m-nitroaniline in heptane-dioxane (9 : 1 in volume) solution at room temperature.

Thus, the MCD technique can be said to be a useful tool for elucidating the ambiguous absorption bands which are strongly overlapping in the absorption spectra. Three or four electronic transition scan be identified in the MCD and absorption spectra of nitroanilines and aminobenzoic acids.

The observed and calculated transition energies and Faraday B terms are summarized in Table 1, where

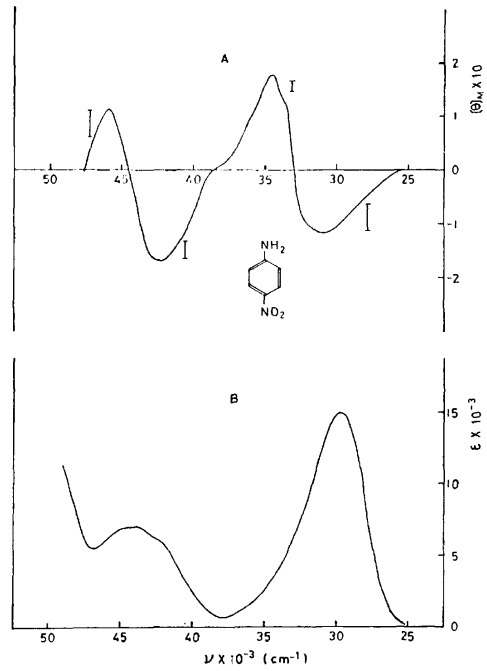

Fig. 3. MCD (A) and UV (B) spectra of *p*-nitroaniline in heptane-dioxane (9 : 1 in volume) solution at room temperature.

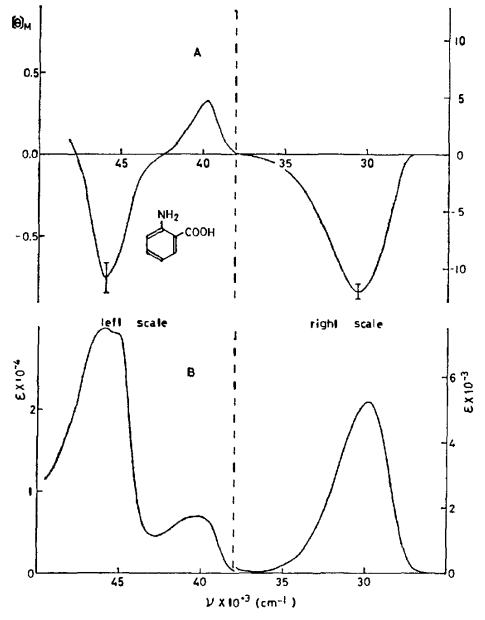

Fig. 4. MCD (A) and UV (B) spectra of *o*-aminobenzoic acid in heptane-dioxane (9 : 1 in volume) solution at room temperature.

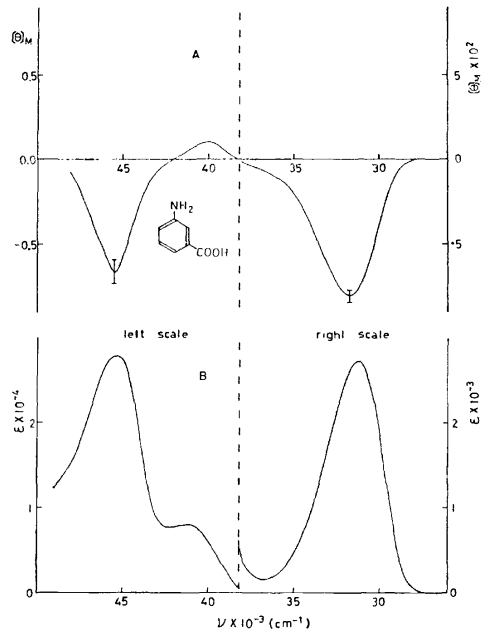

Fig. 5. MCD (A) and UV (B) spectra of *m*-aminobenzoic acid in heptane-dioxane (9 : 1 in volume) solution at room temperature.

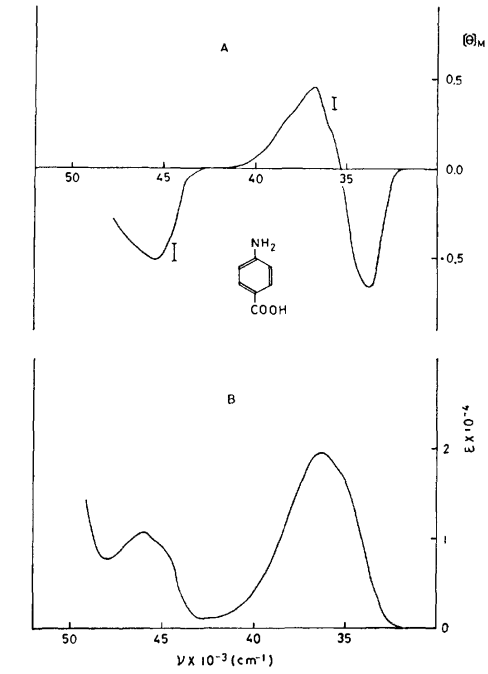

Fig. 6. MCD (A) and UV (B) spectra of *p*-aminobenzoic acid in heptane-dioxane (9 : 1 in volume) solution at room temperature.

$B_{\text{calcd}}(\boldsymbol{r})$ and $B_{\text{calcd}}(\boldsymbol{\nabla})$ denote the calculated Faraday B terms whose electric moment matrices are evaluated by the use of the dipole length and dipole velocity operators, respectively. The calculated transition energies are in good agreement with the observed values. The theoretical Faraday B terms also show fairly good agreement with the experimental values both in sign and in magnitude, except for the second $\pi \rightarrow \pi^*$ transitions of *o*- and *m*-nitroanilines. For these Faraday B terms of *o*- and *m*-nitroanilines, a large negative contribution from the mixing with the fourth excited state and a large positive contribution from the mixing with the first, third, and other higher excited states cancel each other. Therefore, it seems to be difficult to predict accurately the signs of these Faraday B terms of *o*- and *m*-nitroanilines.

It may be interesting to relate the excited states of nitroanilines and aminobenzoic acids to those of benzene

TABLE 1. OBSERVED AND CALCULATED TRANSITION ENERGIES (cm^{-1}) AND FARADAY B TERMS ($10^{-5}\beta D^2/cm^{-1}$) OF *o*-, *m*-, AND *p*-NITROANILINES AND *o*-, *m*-, AND *p*-AMINOBENZOIC ACIDS

Compound	ν_{obsd}	ν_{calcd}	B_{obsd}	$B_{calcd}(r)$	$B_{calcd}(f)$
o-Nitroaniline	26500	27600	20.8	18.9	13.5
	35300	38500	18.0	22.1	−6.3
	40800	42500	positive	65.0	39.1
	43200	44600		4.3	−2.0
m-Nitroaniline	27800	27700	9.7	12.1	6.4
	35100	38100	7.1	9.9	−8.6
	40300	41400	66.9	211.8	93.9
	44100	44800	−47.8	−186.9	−73.0
p-Nitroaniline	29700	32600	45.8	228.9	69.6
	34600	34700	−41.2	−248.6	−88.8
	42600	43100	44.9	93.3	37.7
	45700	48700	−16.2	−12.1	−12.7
o-Aminobenzoic acid	30500	30200	49.6	83.3	42.1
	39700	40200	−49.5	−117.7	−52.9
	45700	46000	126.9	97.9	52.5
		47600		181.8	68.2
m-Aminobenzoic acid	31700	31900	32.6	74.7	23.6
	40000	40800	−16.4	−120.0	−42.6
	45700	45200	118.7	210.3	91.0
p-Aminobenzoic acid	33800	34900	109.3	440.2	171.9
	36800	37100	−109.4	−500.6	−188.6
	45700	47500	111.4	245.5	92.0

itself. The lowest four excited states of benzene are expressed as

$$|^1B_{2u}\rangle = (1/\sqrt{2})[\Psi(\phi_x\rightarrow\phi_\xi) - \Psi(\phi_y\rightarrow\phi_\eta)], \quad (3)$$

$$|^1B_{1u}\rangle = (1/\sqrt{2})[\Psi(\phi_x\rightarrow\phi_\eta) + \Psi(\phi_y\rightarrow\phi_\xi)], \quad (4)$$

$$|^1E_{lux}\rangle = (1/\sqrt{2})[\Psi(\phi_x\rightarrow\phi_\xi) + \Psi(\phi_y\rightarrow\phi_\eta)], \quad (5)$$

$$|^1E_{luy}\rangle = (1/\sqrt{2})[\Psi(\phi_x\rightarrow\phi_\eta) - \Psi(\phi_y\rightarrow\phi_\xi)], \quad (6)$$

where $\Psi(\phi_x\rightarrow\phi_\xi)$ is a configuration in which one electron is excited from the molecular orbital, ϕ_x to ϕ_ξ, and ϕ_x, ϕ_y, ϕ_ξ, and ϕ_η stand for the highest occupied and the lowest vacant orbitals and transform like X, Y, $(X^2-Y^2)/2$, and XY, respectively. Nitroanilines and aminobenzoic acids have six occupied orbitals $\phi_1,\cdots,\phi_6$, and four vacant orbita ls$\phi_7,\cdots,\phi_{10}$. As shown in Fig. 7, the highest occupied orbital ϕ_6 consists of ϕ_y and the nonbonding orbital of the amino group. The molecular orbitals ϕ_5 and ϕ_8, correspond to ϕ_x and ϕ_η of benzene itself. The molecular orbitals ϕ_7 and ϕ_9, are expressed as linear combinations of ϕ_ξ and the lowest vacant orbital of the nitro or carboxyl group. Coefficients of the main configurations in each excited state are given in the third column of Table 2.

On the other hand, the displacement of the charge distribution associated with each transition should be taken into account. If the magnitude of the net charge density on a substituent group or on the benzene ring is larger than 0.5, the intramolecular charge-transfer configuration between the benzene ring and the substituent group is considered to be predominant. The calculated net charge densities on the phenyl, amino, and nitro or carboxyl groups in each excited state are listed in the fourth column of Table 2.

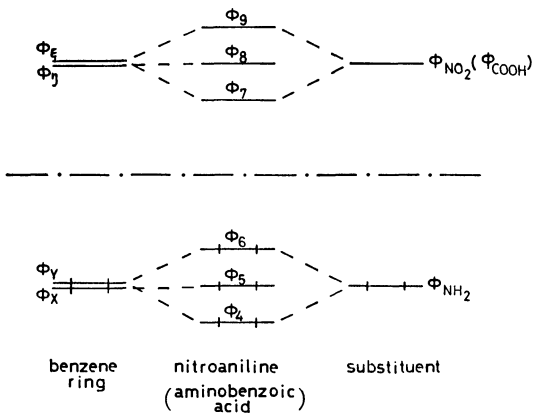

Fig. 7. Interaction of the highest occupied and the lowest vacant molecular orbitals of the benzene ring with the orbitals of the substituent groups.

The first $\pi\rightarrow\pi^*$ transitions of *o*-, *m*-, and *p*-nitroanilines can be assigned to the intramolecular charge-transfer band between the anilino and nitro groups; this can be also verified by the fact that large solvent effects are observed for these transitions. The first excited states of *o*- and *m*-aminobenzoic acids and the second excited state of *p*-aminobenzoic acid consist of the $^1B_{1u}$ state of benzene and the intramolecular charge-transfer state between the amino and carboxyphenyl groups. The first excited state of *p*-aminobenzoic acid and the second excited states of other compounds are said to be the $^1B_{2u}$ state of benzene with an appreciable contribution from the intramolecular charge-transfer configuration. The fourth excited state

TABLE 2. STATE FUNCTIONS AND NET CHARGE DENSITIES ON THE BENZENE RING AND SUBSTITUENT GROUPS

Compound	ν_{calcd} (cm^{-1})	State function[a]	Net charge density			Assignment
			$-NH_2$	$-Ph$	$-NO_2(-CO_2H)$	
o-Nitroaniline	27600	$0.98\Psi_{6\to7}+0.18\Psi_{5\to8}$	0.57	0.04	−0.61	CT
	38500	$0.75\Psi_{5\to7}-0.53\Psi_{6\to8}$	0.33	0.14	−0.47	$^1B_{2u}$
	42500	$0.58\Psi_{5\to7}-0.64\Psi_{6\to9}$	0.45	0.13	−0.58	CT
	44600	$0.71\Psi_{6\to8}+0.52\Psi_{6\to9}$	0.51	−0.28	−0.24	
m-Nitroaniline	27700	$0.96\Psi_{6\to7}+0.19\Psi_{5\to8}$	0.54	0.04	−0.58	CT
	38100	$0.77\Psi_{5\to7}-0.54\Psi_{6\to8}$	0.31	0.16	−0.46	$^1B_{2u}$
	41400	$0.58\Psi_{5\to7}+0.65\Psi_{6\to8}$	0.42	0.10	−0.52	CT, $^1E_{lux}$
	44800	$0.41\Psi_{6\to8}-0.85\Psi_{6\to9}$	0.49	−0.21	−0.28	
p-Nitroaniline	32600	$0.98\Psi_{6\to7}+0.12\Psi_{5\to8}$	0.47	0.16	−0.62	CT
	34700	$0.58\Psi_{5\to7}-0.78\Psi_{6\to8}$	0.38	−0.19	−0.19	$^1B_{2u}$
	43100	$0.79\Psi_{5\to7}+0.58\Psi_{6\to8}$	0.38	0.17	−0.55	CT, $^1E_{lux}$
	48700	$0.33\Psi_{5\to8}+0.90\Psi_{6\to9}$	0.47	−0.11	−0.36	$^1B_{1u}$
o-Aminobenzoic acid	30200	$0.96\Psi_{6\to7}+0.23\Psi_{5\to8}$	0.57	−0.22	−0.35	CT, $^1B_{1u}$
	40200	$0.50\Psi_{5\to7}-0.78\Psi_{6\to8}$	0.43	−0.22	−0.21	$^1B_{2u}$
	46000	$0.47\Psi_{5\to8}+0.70\Psi_{6\to9}$	0.51	−0.14	−0.37	$^1B_{1u}$, CT
	47600	$0.82\Psi_{5\to7}+0.41\Psi_{6\to8}$	0.36	0.06	−0.41	$^1E_{lux}$
m-Aminobenzoic acid	31900	$0.90\Psi_{6\to7}+0.29\Psi_{5\to8}$	0.50	−0.24	−0.26	$^1B_{1u}$, CT
	40800	$0.48\Psi_{5\to7}-0.79\Psi_{6\to8}$	0.43	−0.23	−0.20	$^1B_{2u}$
	45200	$0.83\Psi_{5\to7}+0.50\Psi_{6\to8}$	0.33	−0.05	−0.28	$^1E_{lux}$
p-Aminobenzoic acid	34900	$0.47\Psi_{5\to7}-0.84\Psi_{6\to8}$	0.41	−0.34	−0.07	$^1B_{2u}$
	37100	$0.96\Psi_{6\to7}+0.15\Psi_{5\to8}$	0.45	−0.08	−0.38	$^1B_{1u}$
	47500	$0.83\Psi_{5\to7}+0.48\Psi_{6\to8}$	0.35	−0.04	−0.31	$^1E_{lux}$

a) The coefficients of the most important configurations. $\Psi_{i\to k}$ is a configuration in which one electron is excited from ϕ_i to ϕ_k.

of *o*-aminobenzoic acid, and the third excited states of *m*- and *p*-aminobenzoic acids and *m*- and *p*-nitroanilines are composed of the $^1E_{lux}$ state of benzene and the intramolecular charge-transfer state. The former is predominant in *o*-, *m*-, and *p*-aminobenzoic acids, the latter in *m*- and *p*-nitroanilines.

The present assignment for *p*-nitroaniline is consistent with the results reported by Tanaka.[12] However, the second transition observed at about 37000 cm^{-1} in the crystalline spectrum is shifted to 34600 cm^{-1} in heptane–dioxane (9 : 1 in volume) solution.

As mentioned before, four ionic and molecular species are expected to be present in aqueous solutions of *o*-, *m*-, and *p*-aminobenzoic acids. The values of the experimental ionization constants,[15] K_1 and K_2, are listed in Table 3. The MCD and UV spectra of *o*- and *m*- aminobenzoic acids in aqueous solutions are presented in Figs. 8 and 9. As seen from Table 3, the MCD and UV spectra of aminobenzoic acids at pH 13 are due to aminobenzoate ion (IV), while the spectra at pH 0 or 1 correspond to those of protonated aminobenzoic acid (I). The solid lines in Figs. 8 and 9 express the MCD and UV spectra of *o*- and *m*-aminobenzoic acids, respectively, in acetic acid–sodium

TABLE 3. EXPERIMENTAL pK VALUES[a] FOR THE PROTON IONIZATION OF *o*-, *m*-, AND *p*-AMINOBENZOIC ACIDS

Compound	pK_1	pK_2
o-Aminobenzoic acid	2.09	4.97
m-Aminobenzoic acid	3.07	4.79
p-Aminobenzoic acid	2.43	4.85

a) $pK=-\log K$.

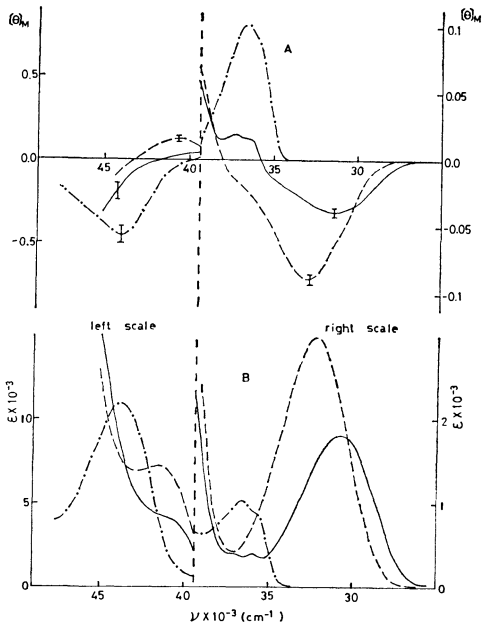

Fig. 8. MCD (A) and UV (B) spectra of *o*-aminobenzoic acid in aqueous solutions at pH 0 (—·—), pH 4.1 (——), and pH 13 (----).

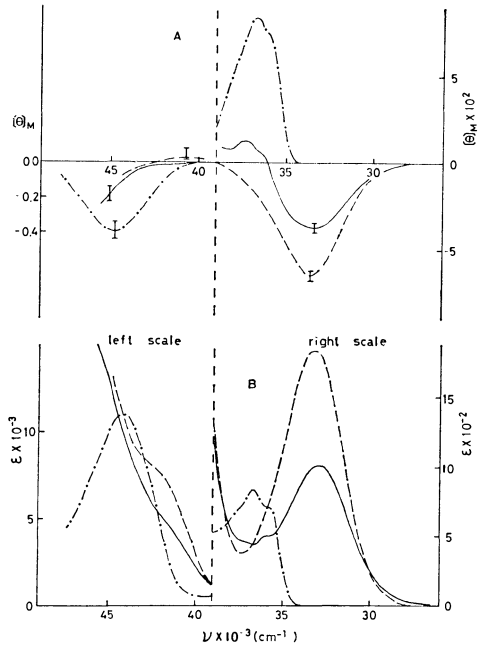

Fig. 9. MCD (A) and UV (B) spectra of *m*-aminobenzoic acid in aqueous solutions at pH 1 (—·—), pH 4.7 (——), and pH 13 (----).

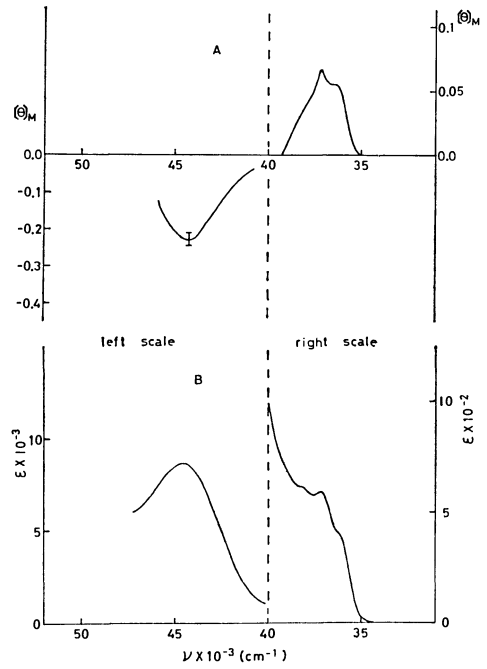

Fig. 10. MCD (A) and UV (B) spectra of benzoate ion in 0.1 M NaOH solution at room temperature.

acetate buffer solutions (pH's 4.1, 4.7), where neutral aminobenzoic acid (II), the zwitterion (III), and aminobenzoate ion (IV) are expected to coexist. Since the MCD and UV spectra of neutral aminobenzoic acid (II) and aminobenzoate ion (IV) are known and the MCD and UV spectra of the zwitterion (III) are expected to be analogous to those of benzoate ion (Fig. 10), it is possible to analyze the complicated MCD and UV spectra of *o*- and *m*-aminobenzoic acids in acetic acid–sodium acetate buffer solutions. The first positive MCD band observed in the region of 27000—36000 cm^{-1} is induced by the first $\pi \rightarrow \pi^*$ transitions of neutral aminobenzoic acid (II) and aminobenzoate ion (IV). The positive MCD band observed at about 37300 cm^{-1} is considered to be due to the first $\pi \rightarrow \pi^*$ transitions of the zwitterion (III), because of the resemblance to the MCD band of benzoate ion (Fig. 10). Thus, the electronic transitions of the zwitterion (III) of *o*- and *m*-aminobenzoic acids were detected in the MCD spectra. However, it is difficult to see from the MCD spectra whether the zwitterion (III) exists in an aqueous solution of *p*-aminobenzoic acid or not, because the MCD of neutral aminobenzoic acid (II) and aminobenzoate ion (IV) may be much stronger than that of the zwitterion (III) in *p*-aminobenzoic acid.

We conclude that the magnetic circular dichroism technique can be a useful tool for separating the overlapping absorption bands and for detecting the hidden transitions. An analysis of the MCD spectrum assisted by the PPP method allows us to elucidate the spectroscopic assignments. It is also concluded, from a detailed analysis of the MCD spectra of aminobenzoic acids in aqueous solutions, that the second positive MCD bands of *o*- and *m*-aminobenzoic acids in acetic acid–sodium acetate buffer solutions provide spectroscopic evidence for the existence of the zwitterion (III).

References

1) A. D. Buckingham and P. J. Stephens, *Ann. Rev. Phys. Chem.*, **17**, 399 (1966).
2) P. N. Schatz and A. J. McCaffery, *Quart. Rev.*, **23** 552 (1969).
3) D. Caldwell, J. M. Thorne, and H. Eyring, *Ann. Rev. Phys. Chem.*, **22**, 259 (1971).
4) P. J. Stephens, *J. Chem. Phys.*, **52**, 3489 (1970).
5) J. G. Foss and M. E. McCarville, *J. Am. Chem. Soc.*, **89**, 30 (1967).
6) D. J. Shieh, S. H. Lin, and H. Eyring, *J. Phys. Chem.*, **77**, 1031 (1973).
7) D. J. Caldwell and H. Eyring, *J. Chem. Phys.*, **58**, 1149 (1973).
8) L. Seamans and J. Linderberg, *Mol. Phys.*, **24**, 1393 (1972).
9) J. Michl and Josef Michl, *J. Am. Chem. Soc.*, **96**, 7887 (1974).
10) A. Kaito, A. Tajiri, and M. Hatano, *J. Am. Chem. Soc.*, **97**, 5059 (1975).
11) A. Kaito, A. Tajiri, and M. Hatano, *J. Am. Chem. Soc.*, **98**, 384 (1976).
12) J. Tanaka, *Bull. Chem. Soc. Jpn.*, **36**, 833 (1963).
13) H. Uchimura, A. Tajiri, and M. Hatano, *Chem. Phys. Lett.*, **19**, 513 (1973); B. Briat, D. A. Schooley, R. Records, E. Bunnenberg, C. Djerassi, and E. Vogel, *J. Am. Chem. Soc.*, **90**, 4691 (1968); W. Voelter, R. Records, E. Bunnenberg, and C. Djerassi, *ibid.*, **90**, 6163 (1968); R. E. Linder, H. Weiler-Feilchenfeld, G. Barth, E. Bunnenberg, and C. Djerassi, *Theor. Chim. Acta*, **36**, 135 (1974); J. Kolc and J. Michl, *J. Mol. Spectrosc.*, **51**, 298 (1974); V. Kratochvil, J. Kolc, and J. Michl, *ibid.*, **57**, 436 (1975).
14) H. Uchimura, A. Tajiri, and M. Hatano, *Chem. Phys. Lett.*, **34**, 34 (1975); A. Tajiri, H. Uchimura, and M. Hatano, *Chem. Lett.*, **1975**, 1021.

15) J. J. Christensen, D. P. Wrathall, R. M. Izatt, and D. O. Tolman, *J. Phys. Chem.*, **71**, 3001 (1967).
16) P. Leggate and G. E. Dunn, *Can. J. Chem.*, **43**, 1158 (1965).
17) R. Pariser and R. G. Parr, *J. Chem. Phys.*, **21**, 466, 767 (1953); J. A. Pople, *Trans. Faraday Soc.*, **49**, 1375 (1953).
18) N. Mataga and K. Nishimoto, *Z. Phys. Chem. N. F.*, **12**, 335 (1957).
19) M. Wolfsberg and L. Helmholtz, *J. Chem. Phys.*, **20**, 837 (1952).
20) P. O. Löwdin, *J. Chem. Phys.*, **18**, 365 (1950).
21) L. Seamans and A. Moscowitz, *J. Chem. Phys.*, **56**, 1099 (1972).

Reactions of Recoil ^{80}Br Activated by the (n, γ) Process with Some Gaseous Cyclanes (C_4—C_6)

Masakatsu SAEKI and Enzo TACHIKAWA

Division of Chemistry, Japan Atomic Energy Research Institute, Tokai-Mura, Ibaraki 319-11

(Received April 12, 1976)

The reactions of ^{80}Br from the (n,γ) process with cyclanes (C_4—C_6) have been systematically investigated. The primary products formed by the ^{80}Br-for-H reaction were excited and underwent at least two modes of unimolecular decomposition. One was the elimination of the H^{80}Br molecule, and the other was the cleavage of the ring, giving the corresponding bromo-olefin and olefin. The former process was important particularly in the lower-pressure end. Thus, the reaction was easily suppressed by increasing the pressure. However, the latter process showed a different feature; that is, the yields of the decomposition products stayed at an almost constant level over the whole pressure range studied. This indicates that a highly excited product decomposes preferentially through a ring-cleavage reaction. When the total organic yield from each reaction system was plotted against the carbon number of the reactant molecules, a linear correlation was obtained. After some possible consideration, it was concluded that the life of the intermediate complex might play a more important role in the reaction of ^{80}Br with cyclanes than the other factors. Some considerations about the radiolysis of the reactant molecule are also mentioned.

The primary products formed by hot atom reactions are usually excited by the kinetic energy introduced by the recoil atoms and undergo a subsequent decomposition. Studies of these decomposition processes are one of the methods which can be used to obtain information on the energetics of hot atom reactions.

In a previous paper[1] we investigated the unimolecular decomposition of excited (c-$C_3H_5{}^{80}Br$)* formed by the reaction of ^{80}Br from the (n, γ) process with cyclopropane (c-C_3H_6) and with bromocyclopropane (c-$C_3H_5{}^{80}Br$). The results showed that the median excitation energy of the primary product from the ^{80}Br-for-H reaction was higher than that from the ^{80}Br-for-Br reaction. It was also deduced that the rupture of the C–Br bond as part of the decomposition processes of the excited primary products is more important in the ^{80}Br-for-Br reaction than in the ^{80}Br-for-H reaction.

In the present work we investigated the reactions of ^{80}Br from the (n, γ) process with gaseous cyclanes of cyclobutane, cyclopentane, and cyclohexane (c-C_4H_8, c-C_5H_{10}, and c-C_6H_{12}); the stability of the ring increases in that order. The work has two prime objects. One is the determination of the relative importance of the ring-cleavage and the HBr-elimination in the decomposition of the primary products from these reactant molecules. The other is to clarify the systematics in the reactivities of cyclanes with the recoil bromine. For these purposes, the total organic yields at high pressures were carefully investigated.

Experimental

Materials. The target chemicals, c-C_4H_8, c-C_5H_{10}, and c-C_6H_{12}, were supplied by the Merck Sharp Co., the Tokyo Chem. Co., and the Nippon Rikagakuyakuhin Co. respectively. Their nominal purities are more than 99% for c-C_4H_8 and c-C_5H_{10} and more than 95% for c-C_6H_{12}. They were purified by means of an ordinary vacuum distillation method before use. The source molecules of the hot bromine atom, CF_3Br and CH_3Br, were purchased from the Matheson Co. and the Tokyo Chem. Co. The other reagents used, H_2S, O_2, Br_2, and I_2 were all of the highest purity available.

Sample Processing A quartz ampoule with a breakable seal was used as the reaction vessel. The required gases were placed in the ampoule utilizing a vacuum line. The CF_3Br was used as the source molecule for the c-C_4H_8 and c-C_5H_{10} systems, whereas CH_3Br was used for the c-C_6H_{12} system.

The JRR-4 reactor in JAERI was used as the neutron source. Samples were irradiated for 10—40 s in the T pipe, where the thermal neutron flux was 3×10^{12} n cm^{-2} s^{-1}.

Within 15 min after the end of irradiation, the irradiated samples were injected directly into a radio-gas chromatograph by the help of a vacuum line. The separation columns used were DOP column, Neopak 1A of 60/80 mesh coated with 15% dioctyl phthalate, and a silicone column, Shimalite C of 30/80 mesh coated with silicone DC 550+stearic acid. The DOP and silicone columns, both 5 m long, were used for the c-C_4H_8 and c-C_5H_{10} systems and a short DOP column, 2.8 m, for the c-C_6H_{12} system. In the operation, the temperature of the columns was raised from room temperature to 115 °C at the rate of 8 °C min^{-1}.

The products were usually identified by comparing their retention times with those of commercial bromides. When the compounds will not be commercially available, the products were identified by applying a relationship between the boiling points and the retention times previously established[1] Furthermore, the unsaturated products, such as CH_2-$CHCH_2Br$ and C_4H_7Br, were assigned on the basis of the vanishing of their radioactivities in the radiochromatogram upon the addition of inactive Br_2 to the sample after its irradiation.

The absolute yields of the products were determined by a comparative method, using Ar as the internal standard; the details of the method were described elsewhere.[1]

Results

c-C_4H_8 System. In the reactions of ^{80}Br with c-C_4H_8, we added as a scavenger O_2, H_2S, I_2, or a mixture of H_2S+O_2. The chief products were c-$C_4H_7{}^{80}Br$, $CH_2CH^{80}Br$, $CH_3{}^{80}Br$ and $C_4H_7{}^{80}Br$.[2] As minor products, $C_2H_5{}^{80}Br$, i-$C_3H_7{}^{80}Br$, n-$C_3H_7{}^{80}Br$, and others were also detected. When the scavenger was changed from the above substances to Br_2, however, the unsaturated products disappeared and some polybromo-products, such as $CH_2BrCH_2{}^{80}Br$, $CH_2{}^{80}BrBr$, and $CH^{80}BrBr_2$, became detectable.

From careful studies of the scavenger effects of O_2, H_2S, I_2, H_2S+O_2 or Br_2, it was concluded that the 2 : 3 mixture of H_2S and O_2 was the most suitable additive to suppress the thermal reaction of ^{80}Br. The scavenger of Br_2 made the unsaturated products undetectable. In the I_2 scavenging experiments, the identification of the products became difficult, because some products labelled by ^{128}I were also produced. The amount of O_2 or H_2S sufficient for the complete suppression of thermal reactions far exceeded 10 mol % of the reaction system. Thus, in the subsequent experiments, the mixture of H_2S and O_2 was used as the scavenger.

Table 1 shows the percent yields of the products at the system pressure of 600 Torr (1 Torr=133.3 Pa); the compositions of the gases are also given in the table. The products have been grouped into two different categories; one, the scavenger-insensitive group, includes $CH_2CH^{80}Br$, $C_4H_7{}^{80}Br$, i-$C_4H_9{}^{80}Br$, and c-$C_4H_7{}^{80}Br$, while the other, the scavenger-sensitive group, includes $CH_3{}^{80}Br$, $C_2H_5{}^{80}Br$, i-$C_3H_7{}^{80}Br$, and n-$C_3H_7{}^{80}Br$. The yields of the products in the latter group and that of $CH_2CH^{80}Br$ showed no clear pressure-dependence and were constant at the values shown in Table 1 within an experimental uncertainty from 151 to 798 Torr. On the contrary, the yields of all the products in the former group except $CH_2CH^{80}Br$ showed a rather significant dependence on the system pressure from 151 to 798 Torr: from 0.27 to 0.6% for $C_4H_7{}^{80}Br$, from 0.05 to 0.15% for i-$C_4H_7{}^{80}Br$, and from 1.84 to 2.42% for c-$C_4H_7{}^{80}Br$.

Due to the limitation of the vapor pressure of c-C_4H_8, the system pressure above 800 Torr was only attained by adding ethane as a pressure-builder; *e.g.*, four times as much ethane as c-C_4H_8 were added to the reaction system. Figure 1 shows the dependences of the c-$C_4H_7{}^{80}Br$ and $CH_2CH^{80}Br$ yields on the system pressure with and without a pressure-builder. In the presence of ethane, the $CH_2CH^{80}Br$ yield was already corrected for the small amount of that from ethane according to the method to be described in the next section.

Table 1. Absolute yields of products in the c-C_4H_8 system

Product	Yield (%)
$CH_2CH^{80}Br$	0.93±0.04
$C_4H_7{}^{80}Br$	0.66±0.12
i-$C_4H_9{}^{80}Br$	0.19±0.04
c-$C_4H_7{}^{80}Br$	2.24±0.03
$CH_3{}^{80}Br$	0.31±0.02
$C_2H_5{}^{80}Br$	0.09±0.01
i-$C_3H_7{}^{80}Br$	0.06±0.01
n-$C_3H_7{}^{80}Br$	0.10±0.02

Composition of gases
c-C_4H_8 : 520 Torr
CF_3Br : 10 Torr
$H_2S + O_2(2 : 3)$: 60 Torr
Ar : 10 Torr
Total pressure : 600 Torr.

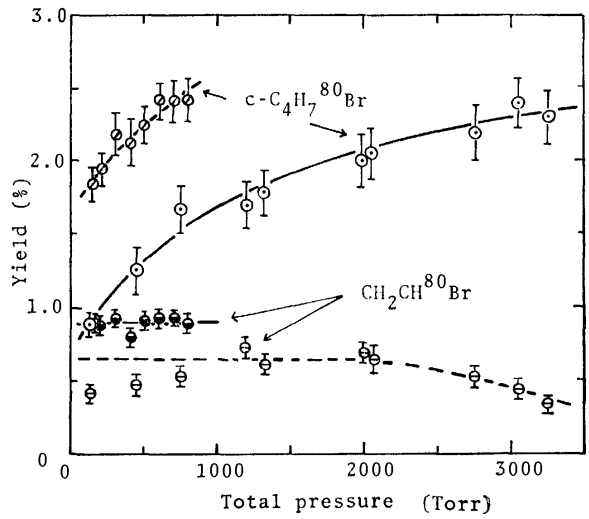

Fig. 1. Pressure-dependences of main products in c-C_4H_8 system.
In the presence of ethane; ⊙: c-$C_4H_7{}^{80}Br$, ⊖: $CH_2CH^{80}Br$.
In the absence of ethane; ∅: c-$C_4H_7{}^{80}Br$, ◒: $CH_2CH^{80}Br$.

c-C_5H_{10} System. In the c-C_5H_{10} system, the mixture of H_2S and O_2 was also used as a scavenger. The products in this system are c-$C_5H_9{}^{80}Br$, $CH_2CH^{80}Br$, $CH_2CHCH_2{}^{80}Br$, $CH_3{}^{80}Br$, and $C_4H_7{}^{80}Br$.[2] The percentage yields of these products at 400 Torr are listed in Table 2, along with the experimental conditions. Figure 2 shows the yield variations in c-$C_5H_9{}^{80}Br$, $CH_2CHCH_2{}^{80}Br$, and $CH_2CH^{80}Br$ as a function of the pressure. Ethane was also added to the reaction system as a pressure-builder in the proportion of 4 to 1. Among these products, c-$C_5H_9{}^{80}Br$ is the only product showing a pressure dependence; the yield increases significantly with the pressure at the beginning and then tends to level off.

c-C_6H_{12} System. In order for one of the main products, c-$C_6H_{11}{}^{80}Br$, to elute with a reasonable retention time, a short DOP column (2.8 m) was used for this system. Unfortunately, this column did not provide a quantitative separation of Ar and CF_3Br. Thus, the source molecule was converted from CF_3Br

Table 2. Absolute yields of products in the c-C_5H_{10} system

Product	Yield (%)
c-$C_5H_9{}^{80}Br$	0.76±0 10
$CH_2CH^{80}Br$	0.23±0.03
$CH_2CHCH_2{}^{80}Br$	0.30±0.03
$CH_3{}^{80}Br$	0.16±0.02
$C_2H_5{}^{80}Br$	0.03±0.01
$C_4H_7{}^{80}Br$	0.06±0.01

Composition of gases
c-C_5H_{10} : 300 Torr
CF_3Br : 30 Torr
$H_2S + O_2(2 : 3)$: 40 Torr
Ar : 30 Torr
Total pressure : 400 Torr.

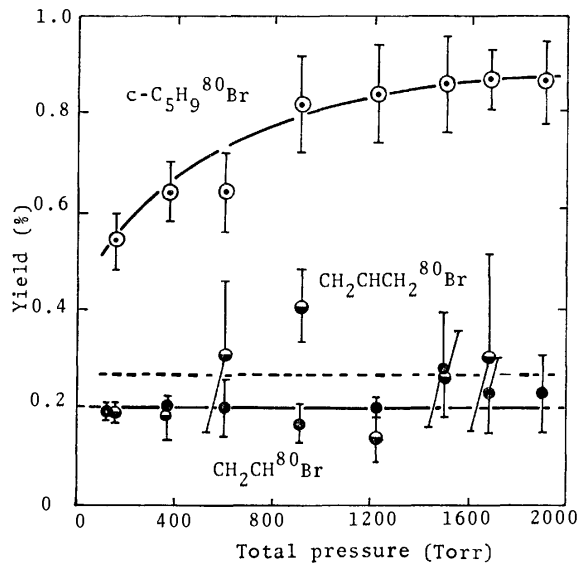

Fig. 2. Pressure-dependences of main products in *c*-C_5H_{10} system.
⊙: *c*-$C_5H_9{}^{80}Br$, ◒: $CH_2CHCH_2{}^{80}Br$, ●: $CH_2CH^{80}Br$.

to CH_3Br, on the basis of the fact that the change in the source molecule causes no significant difference in the results of the reaction of ^{80}Br from the (n, γ) process.[1]

The major products were *c*-$C_6H_{11}{}^{80}Br$, $CH_2CH^{80}Br$, and $C_4H_7{}^{80}Br$[2]; their relative yields were 1.0 : 06±0.2 : 0.6±0.2 at the system pressure of 120 Torr. Although $CH_3{}^{80}Br$ was also observed as a minor product, most of it resulted from the reaction of ^{80}Br with the source molecule. Thus, the quantitative determination of $CH_3{}^{80}Br$ from *c*-C_6H_{12} was not successful.

Discussion

Decomposition Pathways of Primary Products. When one considers the unimolecular decomposition of a primary product from a hot atom reaction, a knowledge of the decomposition mechanisms of the same compound in thermolysis and/or photolysis is very helpful. From the reported results,[3-8] the following decomposition pathways can be expected for the excited (*c*-$C_4H_7{}^{80}Br$)* and (*c*-$C_5H_9{}^{80}Br$)*:

$$(c\text{-}C_4H_7{}^{80}Br)^* \xrightarrow{S} c\text{-}C_4H_7{}^{80}Br \quad (1)$$
$$(c\text{-}C_4H_7{}^{80}Br)^* \xrightarrow{D_1} CH_2CH^{80}Br + C_2H_4 \quad (2)$$
$$(c\text{-}C_4H_7{}^{80}Br)^* \xrightarrow{D_2} H^{80}Br + C_4H_6(\diagup\!\!\diagdown) \quad (3)$$
$$(c\text{-}C_5H_9{}^{80}Br)^* \xrightarrow{S} c\text{-}C_5H_9{}^{80}Br \quad (4)$$
$$(c\text{-}C_5H_9{}^{80}Br)^* \xrightarrow{D_1} CH_2CH^{80}Br + C_2H_6 \text{ or } CH_2CHCH_2{}^{80}Br + C_2H_4 \quad (5)$$
$$(c\text{-}C_5H_9{}^{80}Br)^* \xrightarrow{D_2} H^{80}Br + c\text{-}C_5H_8 \quad (6)$$

Su *et al.* have studied the reactions of $^{80,82}Br$ from isomeric transitions with bromocyclobutane and cyclobutane.[9] However, their experimental measurements were limited to only two systems, in the gaseous phase at 800 Torr and in the liquid phase. Furthermore, they used O_2 as a scavenger and added O_2 to the reaction system in order to constitute 4 mol% of the total pressure. According to the present results, however, 4% of O_2 is not enough to reduce the non-energetic processes down to the limits of experimental uncertainty. Thus, very possibly, their results are contaminated to a significant extent by the thermal reactions.

In Fig. 1, the yield of $CH_2CH^{80}Br$ in the absence of ethane is constant within the limits of experimental uncertainties, at least up to the pressure of 800 Torr. In the presence of ethane, the $CH_2CH^{80}Br$ must be corrected for its formation from ethane. The separate experiments show that the $C_2H_5{}^{8}Br/CH_2CH^{80}Br$ ratio from ethane increases with the pressure from 6.9 at 100 Torr to 9.9 at 800 Torr. Above 800 Torr, this ratio stays constant at 9.9. Thus, the present correction is based on the assumption that these ratios are also maintained in the C_2H_6–*c*-C_4H_8 binary system. The corrected yield shows a broad maximum in the pressure range of 1000—2000 Torr. However, there is a tendency to decrease at pressures less than 1000 Torr, largely because of the uncertainty involved in the correction for the yield of $CH_2CH^{80}Br$ from ethane. Consequently, it can be considered that the yield of $CH_2CH^{80}Br$ is almost constant at pressures less than 2000 Torr, while above that point it seems to decrease slightly with the pressure.

On the other hand, the yield of *c*-$C_4H_7{}^{80}Br$ increases rapidly with an increase in the pressure at the beginning, followed by a gradual increase in the reaction systems both with and without ethane.

In the previous paper,[1] a correlation was found between the excitation energy of a primary product and the dissociation energy of a reacting bond. From the correlation, the excitation energy of the primary product formed by the ^{80}Br-for-H reaction is estimated to be around 5 eV. (The authors express the excitation energy in units of eV throughout this paper, 1 eV= 96.49 kJ mol^{-1}.) If the (*c*-$C_4H_7{}^{80}Br$)* either decomposes through Reaction 2 or stabilizes collisionally as Reaction 1, the ratio of the decomposition product and the stabilized one is calculated by applying the Kassel theory.[10] However, without any thermodynamic data for Reaction 2 available, we attempted to calculate the yield ratio using the values of A and E reported for *c*-C_4H_7Cl[3] with a value for the classical oscillators, S, of either $1/2(3N-6)$ or $2/3(3N-6)$. In these calculations, where the correct values are not used, the calculated results do not always agree quantitatively with the experimental results, but they can furnish qualitative view of the features of the decomposition-stabilization processes. The results obtained, however, are far from explaining the results shown in Fig. 1. This suggests the existence of decomposition processes other than Reaction 2.

On the thermolysis of *c*-C_4H_7Cl, Cocks and Frey reported that the activation energy of Reaction 7 was higher than that of Reaction 8:[3]

$$c\text{-}C_4H_7Cl \longrightarrow CH_2CH_2 + CH_2CHCl \quad (7)$$
$$E_a = 60.07 \pm 0.30 \text{ kcal mol}^{-1}$$
$$c\text{-}C_4H_7Cl \longrightarrow C_4H_6(\diagup\!\!\diagdown) + HCl \quad (8)$$
$$E_a = 55.24 \pm 0.19 \text{ kcal mol}^{-1}$$
$$(1 \text{ kcal mol}^{-1} = 4.184 \text{ kJ mol}^{-1})$$

They also investigated the pyrolysis of *t*-butylcyclobutane and reached the conclusion that this substrate is decomposed to ethylene and 3,3-dimethyl-1-butene.[7] Thomas *et al.* reported, in connection with thermal decomposition of methylcyclobutene, that the principal products were ethylene and propylene, and that the isomerization to 1-pentene accounted for 0.5—1.8% of the reaction.[6]

In the present case, therefore, the ring-opening reactions of the excited $(c\text{-}C_4H_7{}^{80}Br)^*$ to $C_4H_7{}^{80}Br$'s are not an important decomposition process. This consistent with the fact that the $C_4H_7{}^{80}Br$ yield has a positive dependence on the pressure. This means that the $C_4H_7{}^{80}Br$ is not a decomposition product of the excited $(c\text{-}C_4H_7{}^{80}Br)^*$, but, rather, a primary product resulting from an attack of the incident ^{80}Br on a C–C bond:

$$^{80}Br^* + c\text{-}C_4H_8 \rightarrow (C_4H_7{}^{80}Br)^*[\text{Bromobutene}] \quad (9)$$

Thus, the main decomposition process of $(c\text{-}C_4H_7{}^{80}Br)^*$ are limited in Reaction 2 or 3. No definite conclusion can be drawn as to the relative importances of these decomposition processes without adequate thermodynamic data. However, by analogy with the case of $c\text{-}C_4H_7Cl$, it is considered that the activation energy of Reaction 3 is lower than that of Reaction 2. Thus, a plausible explanation for the present results is as follows: the excited products formed by the ^{80}Br-for-H reaction with $c\text{-}C_4H_8$ decompose competitively through Reactions 2 and 3. Reaction 3 predominantly occurs with less excited primary products and is easily suppressed by an increase in the pressure. The decomposition mode of Reaction 2 giving $CH_2CH^{80}Br$ occurs with highly excited products and can only be suppressed at pressures above 2000 Torr.

As is shown in Table 2, the spectrum of the reaction products in the $c\text{-}C_5H_{10}$ system is more simple than that in the $c\text{-}C_4H_8$ system. There exists no organic product to compensate for the increase in the yield of $c\text{-}C_5H_9{}^{80}Br$ with an increase in the pressure. Thus, by analogy with the case of $c\text{-}C_4H_8$, it can be deduced, as for the decomposition processes of the excited $(c\text{-}C_5H_9{}^{80}Br)^*$, that they decompose through Reaction 5 or 6, and that Reaction 6 occurs significantly on the lower-pressure side, as can easily be understood from Fig. 2. One support for this consideration comes from the fact that the main decomposition pathway in the pyrolysis of $c\text{-}C_5H_9Br$ is Reaction 6.[4,5]

Even though the activation energy of Reaction 11 is slightly higher than that of Reaction 6,[11] the HBr-elimination-mode may still play a rather important role in the decomposition of the excited $(c\text{-}C_6H_{11}{}^{80}Br)^*$. The yields of $CH_2CH^{80}Br$ and $C_4H_7{}^{80}Br$, relative to $c\text{-}C_6H_{11}{}^{80}Br$, are high; thus, Reaction 12 must be another decomposition pathway:

$$(c\text{-}C_6H_{11}{}^{80}Br)^* \begin{cases} \xrightarrow{S} c\text{-}C_6H_{11}{}^{80}Br & (10) \\ \xrightarrow{D_1} H^{80}Br + c\text{-}C_6H_{10} & (11) \\ \xrightarrow{D_2} CH_2CH^{80}Br + C_4H_8 \text{ or } C_4H_7{}^{80}Br + C_2H_4 & (12) \end{cases}$$

The excitation energy of a primary product from a hot atom reaction spreads over an extremely wide range.[12] Thus, it can be thought that $CH_2CH^{80}Br$ in the $c\text{-}C_4H_8$ system, $CH_2CH^{80}Br$ and $CH_2CHCH_2{}^{80}Br$ in the $c\text{-}C_5H_{10}$ system, $CH_2CH^{80}Br$ and $C_4H_7{}^{80}Br$ in the $c\text{-}C_6H_{12}$ system are decomposition products from highly excited primary products. However, the greater part of the primary products is not excited enough to cleave the ring and will release $H^{80}Br$ or stabilize in collision with other molecules. However, in the present systems, no products with a negative pressure dependence were found in the pressure range studied. Thus, the experimental justification of the above consideration must rely on the measurement of $H^{80}Br$ as a function of the pressure, this has not yet suceeded.

Systematics of Total Organic Yield. It is very interesting and worth while to study the systematics in the reaction of a hot atom with various reactants in order to obtain more information about the hot atom reaction. Thus far, a number of systematic studies have been reported for the reaction of hot tritium. Rowland *et al.* have found that the yields of the tritiated alkanes and haloalkanes formed by the T-for-H reaction have a linear relationship with the NMR proton chemical shift.[13] On the other hand, Williams *et al.* have reported that the yields of CH_3T from the hot tritium abstraction of end methyl groups show no obvious effect on the electron density around the reaction site, but are correlated inversely with the $R\text{–}CH_3$ bond dissociation energy.[14]

Such discussions as have been given as examples must be based on the yield of a primary product. Unfortunately, in the present reaction system, it is rather difficult to estimate the primary yields from the ^{80}Br-for-H reactions, since not all the decomposition products can be determined experimentally, as was mentioned in the preceding section. Thus, the total organic yields found at the higher system pressure are chosen as the second-best values.

Table 3 shows the total organic yields obtained at two different system pressures, 600 and 1600 Torr, along with the experimental conditions. An excess portion of ethane which was added as a pressure-builder to the reaction system also served as a kinetic moderator to obtain identical kinetic spectra of the recoil ^{80}Br for all samples. For the $c\text{-}C_6H_{12}$ system, the experiment at 1600 Torr cannot be performed simply because the vapor pressure of $c\text{-}C_6H_{12}$ is much less than 400 Torr.

Table 3. Total organic yields at system pressures of 600 and 1600 Torr

Reactant	Total organic yield		Ratio
	600 Torr[a]	1600 Torr[b]	
$c\text{-}C_3H_6$	1.7±0.3%	2.8±0.1%	1.7±0.3
$c\text{-}C_4H_8$	1.4±0.2	2.5±0.3	1.8±0.3
$c\text{-}C_5H_{10}$	1.3±0.2	1.9±0.2	1.5±0.3
$c\text{-}C_6H_{12}$	1.0±0.1	···	···
Composition of gases	a)	b)	
Reactant	100 Torr	400 Torr	
CH_3Br	10 Torr	10 Torr	
$H_2S + O_2$ (2 : 3)	60 Torr	160 Torr	
C_2H_6	430 Torr	1030 Torr	

As may be seen in Figs. 1 and 2, at around 600 Torr the yields of the parent products are very sensitive to, and increase with, the pressure. However, the yields at the pressure of 1600 Torr are very close to the plateau values. In all cases, the ratio of the total organic yields obtained at these two different pressures stays almost constant within the limits of experimental uncertainty, as is shown in the last column of Table 3. This means that, in a qualitative sense, the excitation energies of these primary products are in a similar range. Thus, their decomposition is equally suppressed by increasing the pressure.

Consequently, the results shown in Table 3 can be compared with each other without any further adjustment. In the present case, the yields show no clear correlation with either the dissociation energy of a C–H bond[15,16] or the electron density around the hydrogen replaced.[17] On the other hand, the plots of the yields against the strain energy of the ring[18] seem to show a certain correlation; the yields decrease with the strain energy. If the total organic yield is correlated directly with the probability of the ring-opening reaction, as in Reaction 9, the most believable explanation for this results will be as follows: when the substrate is attacked by an energetic ^{80}Br, the possibility of the ring-cleavage is inversely proportional to the strain energy of the ring. Thus, a higher organic yield results from the substrate having a higher strain energy. However, it has already been confirmed that the ring-opening reaction plays a minor role in the reaction of hot atoms with cyclanes.[1,12] This is also the case in the present systems, as has already been discussed in the preceding section. Thus, all the features of the experimental results can not be interpreted only in terms of the strain of the ring.

When the total organic yields were plotted against the number of carbon atoms, a linear relationship was obtained; the yields decreased with the carbon numbers, as is shown in Fig. 3. A similar trend is also noticed in the reactions of ^{80}Br with simple alkanes;[19–24] the yields of the products resulting from the ^{80}Br-for-H reactions decrease with the carbon numbers, as is also shown in Fig. 3 as a reference. In these cases, however, the trend is not clearly seen in the total organic yields simply because, in the reactions with alkanes, the yields of the products from the ^{80}Br-for-(alkyl group) reactions constitute a greater part of the total organic yields.

There seem to exist several factors consistent with the present findings. Among them, the most conceivable ones are: 1) the elimination of $H^{80}Br$ as a decomposition process of the primary products, 2) the competition between the abstraction and substitution reactions in the primary reactions of ^{80}Br with a reactant molecule, and 3) the inherently possessed reaction probability of cyclanes toward the recoil ^{80}Br. The first factor will be ignored because of the following consideration. The elimination of $H^{80}Br$ as a decomposition process of the excited product is important only in the lower-pressure end and will be essentially suppressed at the pressure of 1600 Torr. As for the second determinant, by analogy with the reaction of recoil T,[25,26] the ^{80}Br-to-$H^{80}Br$ reaction may also be sensitive to the C–H bond strength. All the reactants

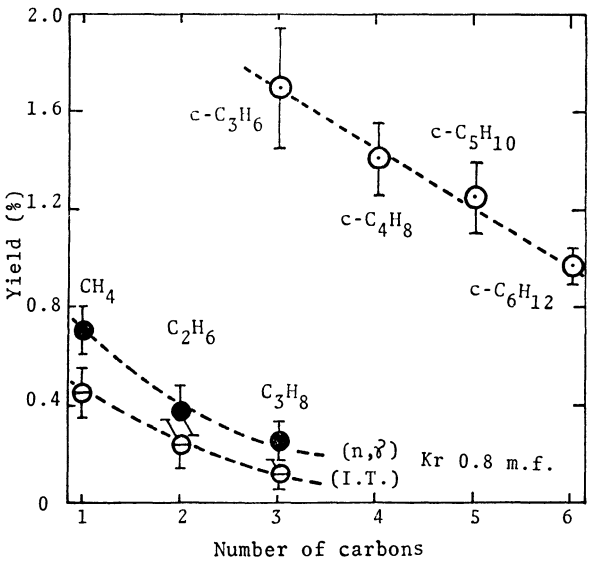

Fig. 3. Correlations between total organic yield and carbon-numbers.
⊙: Cyclane+$^{79}Br(n, \gamma)^{80}Br$, (moderator; ethane, total pressure; 600 Torr).
●: Alkane+$^{79}Br(n, \gamma)^{80}Br$, (moderator; Kr, total pressure; 700 Torr).
⊖: Alkane+$^{80m}Br(I.T.)^{80}Br$, (moderator; Kr, total pressure; 700 Torr).

chosen in the present work except *c*-C_3H_6 have a C–H bond strength in the range from 93 to 95 kcal mol^{-1}. This small variation in the bond energy is rather far from the explanation of the above correlation, suggesting the insignificance of the second factor.

Thus, with reasonably confidence, the relationship may be explained in connection with the reaction probability itself; the probability decreases with an increase in the carbon numbers. As the complexity of a molecule increases, the vibration modes available also increase. As a result, the life of a intermediate complex[27,28] will become longer, because the internal excitation energy spreads over the bonds involved. In these circumstances, the probability of the rupture of any particular bond rapidly decreases with an increase in its bond strength. In the present cases, the C–Br bond in the intermediate complex will have the weakest energy and will be broken with a high probability, ejecting the incident ^{80}Br with a reduced energy. This explanation is also consistent with the following consideration.

In the reaction of recoil T with cyclanes,[29,30] the yields of the parent products seem to stay within a certain range or seem to increase very slightly with the carbon numbers. This observation may be understood as follows: the difference in the bond energy between the C–H and C–T is very small, and the relative probability of the rupture of these bonds in the intermediate complex will hardly be influenced at all by the life of the complex.

Thus, it can be concluded that the life of the intermediate complex may play a more important role than the strain energy of the ring in the reaction of ^{80}Br with cyclanes.

Appendix

Product-Distribution and Radiolysis. As is shown in Tables 1 and 2, the numbers of the products are 8 for the *c*-C_4H_8 system and 6 for the *c*-C_5H_{10} system. In the *c*-C_6H_{12} system, this decreases to only 4. This tendency seems somewhat strange, because it is the opposite of the increase in the carbon numbers of the reacting substrate.

In the radiolysis of cyclanes, the *G* values of H_2 increase with the number of carbons. However, those of hydrocarbons, especially those resulting from the cleavage of the ring, decrease with an increase in stability of the ring.[31,23] Thus, in the present case, the variation in the number of the products from different cyclanes will be considered in connection with the stability of the reactant in radiolysis.

As was described in the chapter on "Results", the products from the *c*-C_4H_8 system were divided into two groups, scavenger-sensitive and scavenger-insensitive. The products belonging to the former group may originate from the radiolysis of the parent molecule, because they have no pressure dependence and always have low yields, particularly in highly scavenged systems.

In the experiments on *c*-C_4H_8 scavenged by Br_2, some polybromoalkanes which have a smaller carbon-skeleton than C_4 were formed. These products also resulted from the reaction of the fragments from the radiolysis. The $CH_2BrCH_2{}^{80}Br$ can be chosen as a typical example among these products. This product shows a steep scavenger curve at the beginning of the Br_2 concentration. In the system of 2% Br_2, the yield of $CH_2BrCH_2{}^{80}Br$ increased linearly with the irradiation period. This may be explained according to the following reactions initiated by the radiolysis of *c*-C_4H_8:

$$c\text{-}C_4H_8 \overset{\gamma}{\sim\!\!\sim\!\!\longrightarrow} \cdot CH_2CH_2CH_2\dot{C}H_2 \quad (13)$$

$$\cdot CH_2CH_2CH_2\dot{C}H_2 \overset{Br_2}{\longrightarrow} \cdot CH_2CH_2CH_2CH_2Br \quad (14)$$

$$\cdot CH_2CH_2CH_2CH_2Br \longrightarrow \cdot CH_2CH_2Br + C_2H_4 \quad (15)$$

$$\cdot CH_2CH_2Br \overset{Br_2}{\longrightarrow} CH_2BrCH_2Br \quad (16)$$

The butylene biradical formed by Reaction 13 may decompose to $\cdot CH_2\dot{C}H_2$ or ethylene. However, Horváth *et al.* have reported that the *G* value of C_4 products from *c*-C_4H_8 is about 2 times higher than that of C_2 products.[31] Thus, $CH_2BrCH_2{}^{80}Br$ should be chiefly formed through Reactions 13—16.

If we use Br_2 as a scavenger in the reaction with a substrate having a lower radiation-resistance, its radiolysis will, sometimes, make a hot atom reaction complex. In such cases, it is advisable to chose another reagent, such as H_2S or a mixture of H_2S and O_2, as a scavenger, because H_2S will allow the radicals from radiolysis to convert saturated hydrocarbons by abstracting the H-atom.

In the present case, a mixture of H_2S and O_2 was used as the scavenger and the irradiation length of the sample was limited as short as possible. Thus, it is certain that the contribution of radiolysis to the data dealt with in this paper is not significant.

References

1) M. Saeki and E. Tachikawa, *J. Chem. Soc., Faraday Trans. 1*, **71**, 2121 (1975).

2) According to the method described in the Experimental chapter, it was confirmed that the product, $C_4H_7{}^{80}Br$, had an unsaturated bond. Because $C_4H_7{}^{80}Br$ has many isomers, though, we cannot determine its structural formula in the present experiment. However, the product must be one of the following three compounds: *cis*-1-bromo-1-butene, 2-bromo-1-butene, and *trans*-2-bromo-2-butene, or a mixture of them, judging from the relation between the retention times of the products and their boiling points. T. E. Jordan, "Vaper Pressure of Organic Compounds," Interscience Publ., New York (1954).

3) A. T. Cocks and H. M. Frey, *J. Am. Chem. Soc.*, **91**, 7583 (1969).

4) M. N. Kale and A. Maccoll, *J. Chem. Soc.*, **1957**, 5020.

5) S. J. W. Price, R. Show, and A. F. Trotman-Dickenson, *J. Chem. Soc.*, **1956**, 3855.

6) T. F. Thomas, P. J. Conn, and D. F. Swinehart, *J. Am. Chem. Soc.*, **91**, 7611 (1969).

7) A. T. Cocks and H. M. Frey, *J. Chem. Soc., A*, **1970** 2566.

8) D. W. Vanas, N. M. Lodge, and W. D. Walters, *J. Am. Chem. Soc.*, **74**, 451 (1952).

9) Y. -Y. Su, C. Metcalfe, and H. J. Ache, *Radiochem. Radioanal. Lett.*, **18**, 349 (1974).

10) P. J. Robinson and K. A. Holbrook, "Unimolecular Reactions," Wiley-Interscience, London (1971), p. 53.

11) J. H. S. Green and A. Maccoll, *J. Chem. Soc.*, **1955**, 2449.

12) E. K. C. Lee and F. S. Rowland, *J. Am. Chem. Soc.*, **85**, 897 (1963).

13) F. S. Rowland, E. K. C. Lee, and Y. -N. Tang, *J. Phys. Chem.*, **73**, 4024 (1969).

14) J. L. Williams, S. H. Daniel, and Y. -N. Tang, *J. Phys. Chem.*, **77**, 2464 (1973).

15) J. A. Kerr, *Chem. Rev.*, **66**, 465 (1966).

16) K. C. Ferguson and E. Whittle, *Trans. Faraday Soc.*, **67**, 2618 (1971).

17) K. B. Wiberg and B. J. Nist, *J. Am. Chem. Soc.*, **83**, 1226 (1961).

18) J. D. Cox, *Tetrahedron*, **19**, 1175 (1963).

19) M. Saeki, K. Numakura, and E. Tachikawa, *Bull. Chem. Soc. Jpn.*, **45**, 1715 (1972).

20) M. Saeki and E. Tachikawa, *Radiochim. Acta*, **20**, 27 (1973).

21) K. Numakura, M. Saeki, and E. Tachikawa, *Bull. Chem. Soc. Jpn.*, **46**, 1 (1973).

22) E. Tachikawa and K. Yanai, *Radiochim. Acta*, **17**, 138 (1972).

23) K. Numakura and E. Tachikawa, *Bull. Chem. Soc. Jpn.*, **46**, 346 (1973).

24) M. Saeki and E. Tachikawa, unpublished data.

25) J. W. Root, W. Breckenridge, and F. S. Rowland, *J. Chem. Phys.*, **43**, 3694 (1965).

26) F. S. Rowland, in "MTP Inter. Rev. of Science, Phys. Chem., Series One," ed. by J. C. Polanyi, Vol. 9, Butterworths, London (1972), p. 109.

27) E. K. C. Lee and F. S. Roeland, *J. Am. Chem. Soc.*, **85**, 2907 (1963).

28) C. C. Chou and F. S. Rowland, *J. Phys. Chem.*, **75**, 1283 (1971).

29) E. Tachikawa, Ph. D. Thesis, Univ. of Calif., Irvine, 1967, p. 243.

30) D. Urch and W. Wolfgang, *J. Am. Chem. Soc.*, **83**, 2982 (1961).

31) Z. Horváth, G. Földiák, and L. Gruber, 3rd Symposium on radiation chemistry, Tihany, 1971, p. 239.

32) L. Wojnárovits and G. Földiák, 3rd Symposium on radiation chemistry, Tihany, 1971, p. 301.

Photocyclization of Diphenylmaleonitrile in the Crystalline State

Kunihiro ICHIMURA and Shoji WATANABE

Research Institute for Polymers and Textiles, Sawatari 4, Kanagawa-ku, Yokohama 221

(Received August 25, 1975)

Diphenylmaleonitrile shows polymorphism. The crystals are photochromic and afford 9,10-dicyanophenanthrene and 9,10-dihydro-9,10-dicyanophenanthrene after prolonged irradiation. The rates of photodecomposition and properties such as photochromism, absorption and fluorescence spectra depend upon the crystal form. Photochromism results from the formation of the 4a,4b-dihydrophenanthrene which is successively converted into the photoproducts.

We described the photocyclization of diarylfumaro- and maleonitrile in solution in a previous paper.[1] Since then we have observed the photochromism of the maleonitrile in the crystalline state. This prompted us to examine photochemistry in the crystalline state in connection with solution photochemistry.[2] In this paper we report on the solid state photocyclization of diphenylmaleonitrile,[3] pointing out that the photocyclization proceeds from an electronically excited state.

Results

Sargent and Timmons obtained diphenylmaleonitrile (I) for the first time as prisms of mp 134 °C in a small yield by the action of ammonia upon α-cyanobenzyl thiocyanate.[2a] We have found that I crystallizes in two forms; when I is recrystallized from cyclohexane, needle-like crystals are formed, while in contrast, when a solution of I in a mixture of dichloromethane and cyclohexane (*ca.* 1 : 1) is condensed very slowly, pale yellow prisms are deposited. The recrystallization of I from benzene–cyclohexane mixture afforded two types of crystals simultaneously. According to the differential scanning calorimetry measurement, the endothermic point of prisms appeared at 136 °C and that of needles at 137 °C due to melting point. The IR spectra of these crystals differ especially in the finger-print region. The IR spectroscopic data reported by the English authors[2a] are essentially identical with those of our prisms. Ultraviolet absorption maximum of these crystals undergoes the red shift in comparison with that in solution, prisms possessing the absorption band at a wavelength slightly higher than that of needles. The physical properties of the crystals are summarized in Table 1. The results indicate the polymorphism of I. The X-ray reflection patterns of these crystals differ a great deal, confirming the polymorphism (Fig. 1).

We found a different photochemical behavior depending on the crystal form. We happened to observe a pale red coloration of crystals when they were placed in a sunny place. The coloration was distinct when the crystals were irradiated with a mercury arc filtered through a band path filter (340—400 nm). The color tone differed with the two crystal forms. The reflection spectra of the irradiated crystals in KBr showed a difference of 20 nm in wavelength of absorption maxima between these crystals (Table 1). The first order decay time was also dependent on the crystal form. The color of the prisms faded more rapidly than that of the needles. The former had a half lifetime of 180 s at room temperature, the latter one of 700 s.

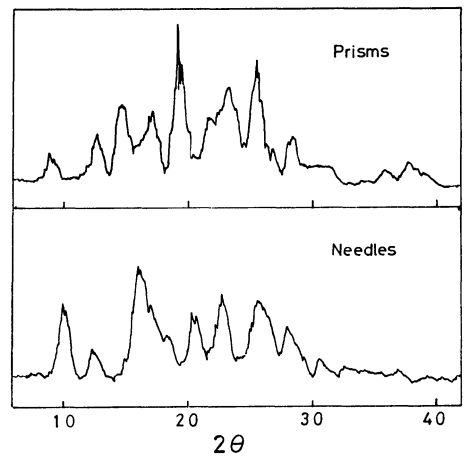

Fig. 1. X-Ray diffraction diagrams of diphenylmaleonitrile.

TABLE 1. PHYSICAL PROPERTIES OF CRYSTALS OF DIPHENYLMALEONITRILE

Appearance	Prism	Needles	Solution[1]
Mp (°C)	136.0	137.5	
Recryst. from	CH_2Cl_2–Cyclohexane	Cyclohexane	
UV spectrum; λ_{max}(nm)	286, 338	286, 336	281, 323[a]
Fluorescence (nm)	Non-fluor.	450 (25 °C) 472 (77 K)	Non-fluor.
λ_{max} of intermediate (nm)	520	500	480[b]
Half lifetime of intermediate (s)	160	700	100[b]
Photolysis	Faster	Slower	

a) In ethanol. b) In toluene.

The crystal forms also differed in fluorescence behavior; whereas the prisms were not fluorescent at all, and the exciting light produced coloration immediately, the needles were slightly fluorescent and soon turned red as the fluorescence weakened. At liquid nitrogen temperature only blue fluorescence was observed, but no red coloration of the needles. The blue fluorescence decreased sharply at −185 °C when the temperature of the crystals rose gradually.

The solid state photochemical reaction of these cystals in KBr disks was followed qualitatively by IR spectroscopy. The bands at 1308 cm^{-1} (needles) and 1301

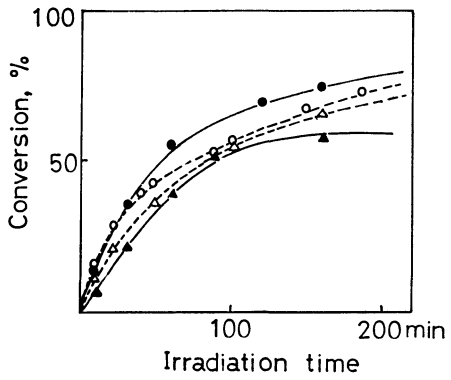

Fig. 2. Photolysis of diphenylmaleonitrile of two crystal forms dispersed in KBr. Irradiation of needles; ——▲—— with light of 300—400 nm, --△-- with light of 300—400 nm and simultaneously with light of >430 nm. Irradiation of prism; —●— with light of 300—400 nm, --○-- with light of 300—400 nm and simultaneously with light of >430 nm.

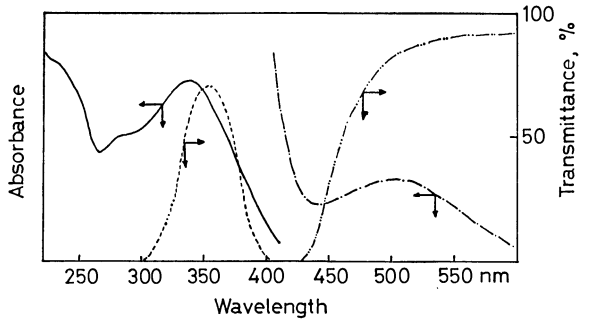

Fig. 3. Spectroscopic properties of crystalline diphenylmaleonitrile and color filters used for the photolysis. Ultraviolet spectrum of needle-like crystals in KBr disk (——), reflection spectrum of needles after irradiation with light of 300—400 nm (—·—·), Corning C. S. 7-60 filter (·····), Corning C. S. 3-72 filter (—··—··).

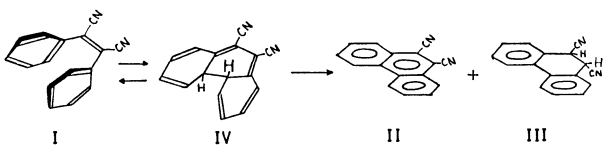

Scheme 1.

cm^{-1} (prisms) were chosen as a key band which almost disappeared after one day of irradiation with UV light from a 450 W high pressure mercury arc passed through a Corning C. S. Filter 7-60. Figure 2 shows time-conversion curves of photolysis of the two crystal forms. It is noteworthy that the rate was also affected by the crystal form; the prisms underwent photodecomposition faster than the needles. The IR spectra of these crystals after one day of irradiation were essentially identical. The characteristic bands, especially nitrile band, indicate that 9,10-dicyanophenanthrene (II) and 9,10-dihydro-9,10-dicyanophenanthrene (III) are the photoproducts.

A suspension of powdered I in water was irradiated for two days with a 100 W mercury lamp using a glass filter. The photoproducts were isolated by fractional recrystallization from methyl ethyl ketone and characterized and identified by means of IR, UV, and NMR spectra. The irradiated solid was found to consist of I, II, and III, the yields of II and III being 60% and 22%, respectively.

It is of interest to see how the excitation of the colored intermediate affects solid state photolysis. As shown in Fig. 3, the absorption maximum of the colored intermediate lies sufficiently at longer wavelength for separate excitation. The crystals dispersed in a KBr disk were simultaneously illuminated with a 450 W high pressure mercury lamp filtered with a Corning C. S. 7-60 and another 450 W lamp filtered with a Corning C. S. 3-72. The transmittances of the filteres are sketched in Fig. 3. Simultaneous irradiation resulted in very weak coloration of the crystals. However, the rate of photolysis in the early stage (within *ca.* 30%) was only slightly affected by the co-excitation; the needles underwent photodecomposition somewhat faster than in the absence of simultaneous irradiation of the colored intermediate whereas the prisms showed no effect of the co-excitation upon the rate of photolysis (Fig. 2). The IR spectra of the irradiated solids indicate that the photoproducts and the product ratio were not changed by simultaneous irradiation.

Discussion

Interest in the photocyclization of stilbenes has been focused on the nature of the intermediate and the excited state of the precursor to give phenanthrenes. Moore and co-workers proposed the 4a,4b-dihydrophenanthrene as the intermediate based on the observation of the intermediary yellow coloration (λ_{max}= 447 nm) of stilbene on UV irradiation in solution.[4] Muszkat and Fischer investigated in detail the nature of the intermediate and confirmed the hexaene system spectroscopically.[5] The excited singlet state has been recognized to play a key role in photocyclization,[6] while an alternative mechanism through a hot molecule has been proposed.[7] Evidently, the configuration of hydrogens at 4a and 4b positions of the intermediate gives a clue to whether the photocyclization proceeds *via* an electronically excited state or a higher vibrational level of the ground state. The stereochemistry of the intermediate has been discussed in connection with the rule of Woodward-Hoffmann.[5,11] However, no direct evidence for the configuration of hydrogens at 4a and 4b positions has been obtained.[8]

We have observed red coloration at λ_{max}=480 nm when diphenylfumaronitrile or maleonitrile is irradiated in certain organic solvents and ascribed this transient absorption to 9,10-dicyano-4a,4b-dihydrophenanthrene (IV).[1] It is concluded therefore that the solid state photochromism of diphenylmaleonitrile is caused by the formation and the disappearance of the colored 4a,4b-dihydrophenanthrene (IV). The solid state photocyclization could thus be interpreted to belong to the isomerization of this intermediate to III and the oxidation to II, in the same way as proposed in the solution photocyclization.[1]

It has been emphasized that the distance between

both atoms forming a covalent bond by irradiation plays a critical role to give photoproducts in the solid state.[9] Although the refined crystal structure of *cis*-stilbene derivatives is scarcely known, the result of X-ray analysis of *cis*-α-bromo-β-(2-pyridyl)styrene shows that the *ortho*-carbon of the phenyl and α-carbon of the pyridyl group are 3.42 Å apart from each other.[10] It is very likely that two phenyl groups of I are spacially arranged in a similar fashion to the case of the bromostyrene and the distance between both *ortho*-carbon atoms of two phenyl groups is sufficient to form a covalent bond in the rigid crystalline state since the critical distance which is able to form a covalent bond in the solid state photoreaction has been reported to be about 4 Å in the case of intermolecular dimerization of cinnamic acid and its related compounds.[9] From a consideration of the molecular shape in the crystalline state and the ease of solid state photocyclization to the colored intermediate of diphenylmaleonitrile, the 4a,4b-hydrogens of IV are shown to be in the *trans* configuration. It is concluded that the photocyclization of I to give IV proceeds *via* an electronically excited state. Other stilbenes, including stilbene itself, have the same hexaene system and photocyclize most probably from an electronically excited state.

The experiments of simultaneous irradiation throw light upon the subsequent reaction mechanism of the intermediate. If the process to give II and III proceeds thermally, simultaneous excitation of the colored intermediate would suppress the formation of the cyclized products (II+III), since the recovery of I from IV is photochemically allowed.[11] The results were not the case and suggest that the colored intermediate (IV) is converted either into the starting material or into the photoproducts at least partially photochemically. The formation of the 9,10-dihydrophenanthrene bearing the *trans* configuration[2b] is in line with this conclusion; the conversion of IV having *trans* hydrogens into the 9,10-dihydrophenanthrene is regarded as photochemically allowed 1,3- or 1,7-sigmatropic reaction without any considerable change of the molecular arrangement.

Although the effect of polymorphism on the photochemical behavior cannot yet be fully understood unless the refined molecular structure of both crystal forms are known, the spectroscopic data give us insight into the solid state photoreaction. The relatively large red shift of absorption maximum of the intermediate of prisms in comparison with that of needles suggests that the hexaene system of IV in prismatic crystals is more planar than that in needle-like crystals. The planar structure of IV is less favorable for stability, since two sp^3 orbitals of the intermediate force the π-electron system to be distorted. This explains the shorter half lifetime of IV in prisms.

The difference in the longest wavelength of absorption maximum between two crystal forms, though small, suggests that the molecular shape of I is dependent on the crystal form; the structure of I in prisms may be more planar than that in needles since the absorption maximum of prisms undergoes a slightly larger red shift than does that of needles. The planar structure brings about the reduction of the distance between two carbon atoms forming a covalent bond upon irradiation so that the electro-cyclization to give IV may occur more efficiently in prisms than in needles. The observation of fluorescence in needles also supports the dependence of the efficiency of photocyclization upon the crystal form. The efficiency of the cyclization to give IV in prisms could be larger than that in needles, since the prisms show no fluorescence. The dependence of the rate of photolysis upon the crystal forms therefore reflects the difference in the efficiency of photocylization to give IV.

Experimental

Measurement of Physical Properties. Infrared spectra were recorded on a Hitachi EPI-G3 type IR spectrophotometer, and UV spectra and reflection spectra of the crystals dispersed in KBr disks on a Hitachi EPS-3T spectrometer and Hitachi recording spectrophotometer type EPR-2, respectively. Fluorescence was measured with a Hitachi fluorescence spectrophotometer MPF-2A. The thermal behavior of the crystals was recorded on a Perkin-Elmer Model DSC-1B at 16 °C/min. X-Ray reflection diagrams were recorded on a Rikagaku Denki X-ray diffraction apparatus Model D-3F. Monochromatic light was obtained from JASCO CRM-FA spectro-irradiator composed of a 2 kW xenon lamp. A 450 W high pressure mercury lamp was used as the light source in other experiments.

Preparation of the Crystals of Diphenylmaleonitrile. Diphenylmaleonitrile was synthesized according to the method reported previously.[1b] The nitrile was recrystallized from cyclohexane to afford needle-like crystals which were collected and washed with cyclohexane. To a solution of the nitrile (3 g) in *ca.* 30 ml dichloromethane in an Erlenmeyer flask was added 50 ml cyclohexane, and the solution was kept to stand in the dark for a while to cultivate the prismatic crystals. The mouth of the flask was covered with a filter paper. The solvent was decanted and the crystals were treated with cyclohexane and collected by filteration. When the nitrile was recrystallized from a benzene–cyclohexane mixture, formation of two crystal forms was observed. Slower crystallization seems to favor the formation of the prisms. ν_{max} of needles (KBr); 3060, 2222, 1598, 1588, 1492, 1449, 1322, 1308, 1283, 1228, 1157, 1070, 1031, 1002, 960, 925, 862 w, 851 w, 843 w, 778, 759, 700, and 692 cm^{-1}. ν_{max} of prisms (KBr); 3060, 2222, 1596, 1587, 1499, 1445, 1321, 1301, 1280, 1221, 1180, 1160, 1070, 1027, 1000, 955, 920, 862 w, 840 w, 770, 758, and 690 cm^{-1}.

Measurement of the Colored Intermediate. KBr disks containing diphenylmaleonitrile (1 mg/150 mg) were irradiated with UV light, the reflection spectra of the colored disks being recorded at intervals. The intensity of the absorption maxima was found to decay in the first order, the half lifetime being then obtained (Table 1).

Photolysis of Diphenylmaleonitrile in KBr Disks. Diphenylmaleonitrile (0.96 mg) in KBr (150 mg) was pressed under 200 kg/cm^2, the KBr disk being held in a cell containing calcium chloride as a drying agent. Two lamp houses composed of a 450 W mercury arc were so placed that both blue (through a Corning C. S. 7-60 filter) and yellow (through a Corning C. S. 3-72 filter) beams illuminate the disk through a glass window. The IR spectra were recorded at intervals, and the amount of diphenylmaleonitrile was estimated by the decrease in intensity of the band at 1301 cm^{-1} for prisms or 1308 cm^{-1} for needles according to the calibration line. Two new peaks at 2230 and 2250 cm^{-1} due to 9,10-dihydrophenanthrene and 9,10-dicyanophenan-

threne, respectively, appear with a decrease in the nitrile band of starting material at 2222 cm^{-1}. The final spectra of both crystals were in all cases essentially identical.

Estimation of the Yields of Solid State Photoproducts. The yields of the photoproducts were estimated by UV spectroscopy as follows. The irradiation of diphenylfumaro- or maleonitrile in acidic media has been found to give 9,10-dihydro-9,10-dicyanophenanthrene as the sole product.[1] The irradiated crystals were dissolved in ethanol containing a trace amount of sulfuric acid, and the solution was illuminated with 357 nm light to convert the unreacted diphenylmaleonitrile specifically into the 9,10-dihydro derivative (III). Since I and II have absorptions above 300 nm, but not III, the difference between the spectra of solid state photoproduct above 300 nm before and after irradiation in acidic media indicates the absorbance of unreacted I. From the absorbance of the irradiated solution at 327 nm or 336 nm we obtain the quality of 9,10-dicyanophenanthrene as a solid state photoproduct. The differential spectrum was obtained by subtraction of spectrum before irradiation in acidic ethanol from that of I and III estimated as mentioned above, and was found to be essentially identical with that of II. Thus we see that the photodecomposed solid consists of only I, II, and III. The yields of II and III are found to be 60% and 22%, respectively.

The authors wish to express their thanks to Dr. H. C. Steinmetzer, University of Frankfurt am Main, for his valuable suggestions.

References

1) a) S. Watanabe and K. Ichimura, *Chem. Lett.*, **1972**, 35; b) K. Ichimura and S. Watanabe, *Bull. Chem. Soc. Jpn.*, **49**, 2224 (1976).

2) a) M. V. Sargent and C. J. Timmons, *J. Chem. Soc.*, **1964**, 2222; b) M. V. Sargent and C. J. Timmons, *ibid.*, **1964**, 5544; c) E. V. Blackburn and C. J. Timmons, *Quart. Rev., Chem. Soc.*, **23**, 482 (1969).

3) K. Ichimura and S. Watanabe, *Tetrahedron Lett.*, **1972**, 821.

4) W. H. Moore, D. D. Morgan, and F. R. Stermitz, *J. Am. Chem. Soc.*, **85**, 830 (1963).

5) K. A. Muszkat and E. Fischer, *J. Chem. Soc., B*, **1967**, 662.

6) a) F. B. Mallory, J. T. Gordon, and C. S. Wood, *J. Am. Chem. Soc.*, **85**, 828 (1963); b) R. Srinivasan and J. C. Powers, Jr., *J. Chem. Phys.*, **39**, 580 (1963).

7) H. Güsten and L. Klasinc, *Tetrahedron*, **24**, 5499 (1968).

8) T. D. Doyl, N. Filipescu, W. R. Barson, and D. Banes, *J. Am. Chem. Soc.*, **92**, 6371 (1970).

9) a) M. D. Cohen and G. M. J. Schmidt, *J. Chem. Soc.*, **1964**, 1996; b) M. D. Cohen, G. M. J. Schmidt, and F. I. Sonntag, *ibid.*, **1964**, 2000; c) G. M. J. Schmidt, *ibid.*, **1964**, 2014; d) J. Bergmann, K. Osaki, G. M. J. Schmidt, and F. I. Sonntag, *ibid.*, **1964**, 2021; e) D. Ravinovitch and G. M. J. Schmidt, *ibid.*, **1964**, 2030; f) M. Lahav and G. M. J. Schmidt, *ibid.*, **1967**, 239.

10) H. Utsumi, A. Furusaki, and I. Nitta, *Nippon Kagaku Zasshi*, **91**, 4431 (1970).

11) R. B. Woodward and R. Hoffmann, "The Conservation of Orbital Symmetry," Academic Press, New York (1970).

pH-Dependency of Photocyclization of Diarylfumaronitriles

Kunihiro ICHIMURA and Shoji WATANABE

Research Institute for Polymers and Textiles, Sawatari 4, Kanagawa-ku, Yokohama 221

(Received August 25, 1975)

The photocyclization of diarylfumaronitriles in aqueous ethanol is influenced by pH. The product ratio of 9,10-dihydro-9,10-dicyanophenanthrenes (IV) decreases with decrease in pH. Discussion is given on the acid-catalyzed isomerization of the 4a,4b-dihydrophenanthrenes to IV from results of observation of the colored intermediate.

Some stilbenes substituted by electron-withdrawing groups at the olefinic double bond give 9,10-dihydrophenanthrenes along with the phenanthrenes on UV irradiation,[1] while stilbene yields only phenanthrene but no 9,10-dihydro derivative as a photoproduct.[2-5] The product ratio of the 9,10-dihydrophenanthrenes to the phenanthrenes in the former case depends on the reaction conditions.[1] We confirmed that the yield of 9,10-dicyanophenanthrene (IIIa) undergoes a solvent effect when diphenylfumaronitrile (Ia) is irradiated in solution (Table 1). 9,10-Dihydro-9,10-dicyanophenanthrene (IVa) is formed almost exclusively in acetic acid. This indicates that the formation of dihydro derivative (IVa) is influenced specifically by the acidic nature of the solvent. This was confirmed by the sole production of IVa when Ia was irradiated in ethanol containing a trace of sulfuric acid. These observations led us to investigate the pH-dependency of the photoproduct distribution. In this paper we report the pH-dependency of several diarylfumaro- and maleonitriles (I and II) and propose a cyclization mechanism *via* 4a,4b-dihydrophenanthrenes,[6] in contrast to the free-radical mechanism proposed recently by Srinivasan and Hsu.[7]

Results

Since diarylfumaronitriles (I) are practically insoluble in water, buffered aqueous ethanol (50 w/w%) was employed as a solvent. Although all the UV absorption spectra of Ia at pH less than *ca.* 10 were identical and remained unchanged on standing in the dark, the absorbance at the longest wavelength in more alkaline solutions (*ca.* 0.1 M NaOH) decreased gradually on standing at room temperature. The electron-withdrawing group at the phenyl ring of the fumaronitrile makes the double bond so sensitive toward the alkaline medium that the absorption bands at the greatest wavelength of α-(*p*-chloro- and cyanophenyl)-α′-phenylfumaronitriles (Ib and Ic) disappear gradually even at pH *ca.* 8. The decrease of the absorbance may occur as a result of the alkali catalyzed hydration on the olefinic double bond of the fumaronitrile, as in the case of α-arylcinnamonitrile.[8] We have employed buffered solutions (pH<8) for studies on the pH-dependency of the photolysis.

In order to obtain some information on the pH effect on the photolysis of diarylfumaronitrile, aerated solutions at various pH were irradiated with light of 330 nm, and the UV spectra were recorded at intervals. Typical examples for Ia are illustrated in Fig. 1. A family of the absorption curves changed at various pH; 9,10-dihydro-9,10-dicyanophenanthrene (IVa) forms predominantly in a weakly acidic solution whereas the formation of 9,10-dicyanophenanthrene (IIIa) is observed in neutral or alkaline solutions.

It has been emphasized that diagrams of quotients of extinction differences (EDQ diagrams) can be utilized to distinguish complicated photoreactions followed UV-spectroscopically.[9] Examination of the EDQ diagrams for Ia at various pH revealed that the elementary reactions depend also on the pH of the solution; both EDQ diagrams at pH 7.0 and 5.0 are linear but that at pH 9.0 is non-linear (Fig. 1). It is therefore concluded that two elementary reactions take part in the photoreaction of Ia at pH 7.0 and 5.0, while more complex reactions occur at pH 9.0. The photolysis of the fumaronitrile (Ia) at pH less than *ca.* 7.0 thus consists of the initial photoisomerization to the maleonitrile (IIa) and the photoinduced transformation of IIa to the phenanthrenes (IIIa+IVa).[10] Similar results were obtained when α-(*p*-methoxyphenyl)-α′-phenylfumaronitrile (Id) was used. The EDQ diagram of the photoreaction of α-(*p*-cyanophenyl)-α′-phenylfumaronitrile (Ic) was found to be non-linear even at pH 7.0, while a linear EDQ diagram was obtained when the photolysis was carried out at pH 4.0.

TABLE 1. SOLVENT EFFECT ON THE YIELD OF 9,10-DICYANOPHENANTHRENE

Solv.	Yield of 9,10-dicyano-phenanthrene (%)
Cyclohexane	80
Chloroform	10—20
Toluene	70
EtOH	30
AcOH	Trace[a]
EtOH–H_2SO_4	0[b]

a) The remaining product is 9,10-dihydro-9,10-dicyanophenanthrene. b) The 9,10-dihydro compound forms exclusively.

The pH-dependency of the photocyclized product distribution was determined by the UV spectra of the photolyzed solutions at various pH where linear EDQ diagrams were obtained. The results for Ia are given in Table 2. The UV spectra of the solutions irradiated at pH less than 4 are identical with that of the dihydro compound (IVa). A family of the absorption curves for Ia intersect at 265 and 295 nm. The peaks at 326 and 339 nm due to the phenanthrene (IIIa) increase with increase in the pH of the solutions at the same ratio. It is concluded that only IIIa and IVa

are concerned in the product distribution. The product distribution from diphenylmaleonitrile was found to be practically identical with that from the fumaronitrile (Fig. 3). The absorption spectra of the irradiated solutions in alkaline medium deviated from the isosbestic points at 265 and 295 nm. This is in

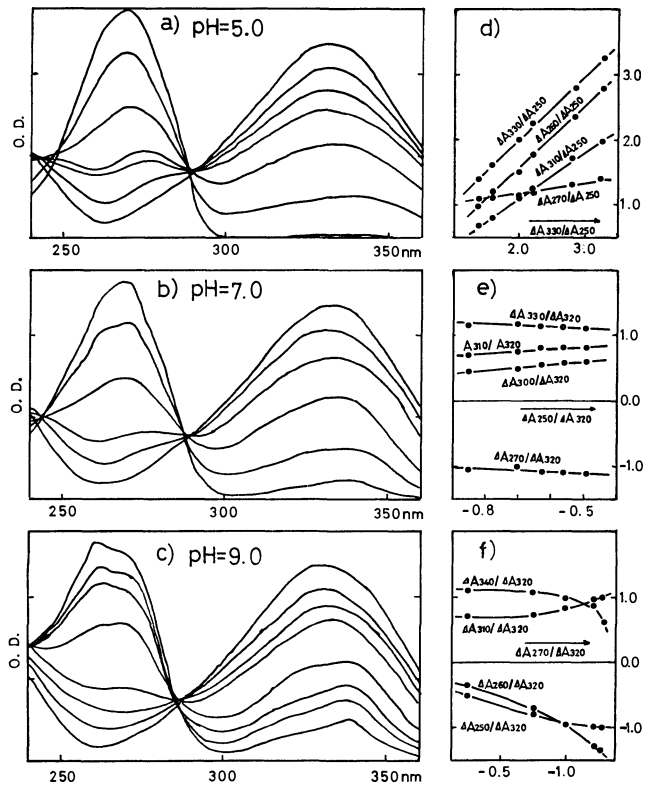

Fig. 1. The electronic absorption spectra recorded at intervals for the UV irradiation of diphenylfumaronitrile in aq. ethanol at various pH ((a): pH=5.0, (b): pH=7.0, and (c): pH=9.0) and the corresponding EDQ diagrams ((d): pH=5.0, (e): pH=7.0, and (f): pH=9.0).

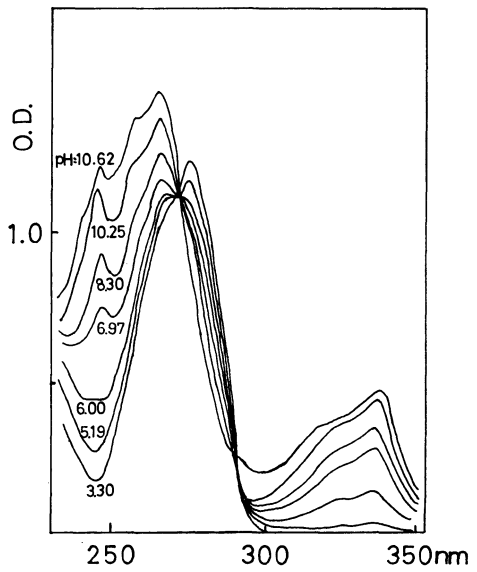

Fig. 2. The electronic absorption spectra of photoproducts from diphenylfumaronitrile irradiated in aq. ethanol at various pH.

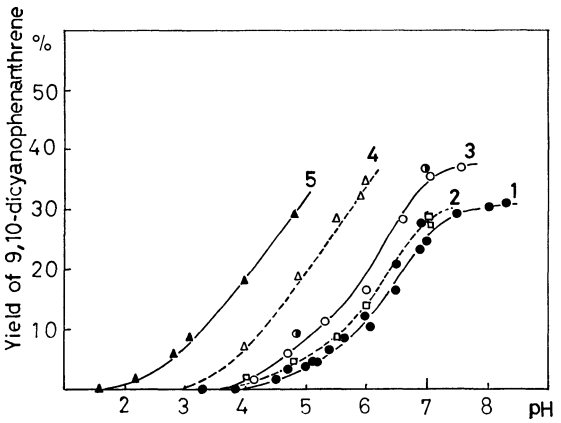

Fig. 3. pH-Dependency of the yield of 9,10-dicyanophenanthrenes; (1) 9,10-dicyanophenanthrene at 20 °C (—●—), (2) 3-methoxy-9,10-dicyanophenanthrene at 2 °C(--□--), (3) 9,10-dicyanophenanthrene at 2 °C (—○— from the fumaronitrile, —◑— from the maleonitrile), (4) 3-chloro-9,10-dicyanophenanthrene at 2 °C (--△--), (5) 3,9,10-tricyanophenanthrene at 2 °C (—▲—).

line with the anomalous photochemical behavior of this compound in alkaline region as revealed by an examination of the EDQ diagram. The other *p*-substituted diphenylfumaronitriles undergo a similar pH effect on the product distribution. The yields of the 9,10-dicyanophenanthrenes (III) at various pH were estimated by the absorbance at the longest wavelength and plotted against pH as shown in Fig. 3. The yield of phenanthrene at a given pH value increases with an increase in the electron-withdrawing power of the substituent.

As regards the effect of nitrile groups on the pH-dependency, two isomeric stilbenes, α-phenyl-β-(*p*-cyanophenyl)acrylonitrile (V) and *p,p'*-dicyanostilbene (VI), were irradiated in acidic solutions. The former underwent a pH effect similar to that of Ia, giving no 3,9-dicyanophenanthrene in acidic solutions of pH less than *ca.* 4. However, the photoreaction of the latter was not affected by the pH. The photocyclization of stilbene itself in ethanol was not influenced by addition of sulfuric acid.

We found that red coloration (λ_{max}=480 nm in toluene) occurs at room temperature on the excitation of Ia with 330 nm light in some solvents such as aromatic hydrocarbons and chloroalkanes. Although there was

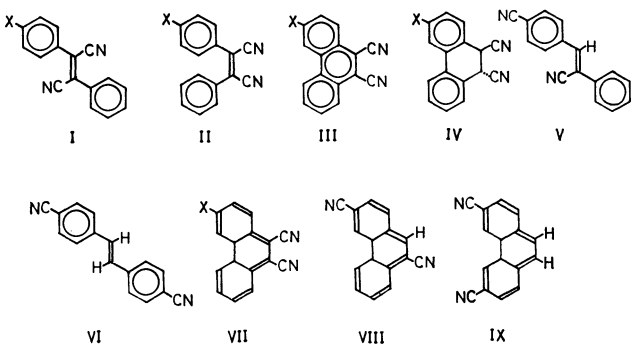

no observation of such coloration in ethanol at room temperature, the solution of Ia was found to be faintly colored at −77 °C. Bleaching of the red color was accelerated by irradiation with visible light (*ca.* 480 nm), but retarded by the lowering in temperature. The bleaching corresponds to the first order decay with a half lifetime of 100 s in toluene at room temperature.

Discussion

Stilbene photocyclizes to phenanthrene through unstable yellow colored 4a,4b-dihydrophenanthrene.[2-5,11] Sargent and Timmons have suggested that the photocyclization mechanism for Ia is similar to that of stilbene, although no experimental evidence has been presented.[1] During the course of our investigation, Srinivasan and Hsu proposed an alternative free-radical chain mechanism for this type of photocyclization.[7] They observed the incorporation of deuterium from deuterated solvents into 9,10-dihydro compounds and the dependency of quantum yield on light intensity, and concluded that the abstraction of solvent hydrogen by the excited stilbene initiates the free-radical chain reaction to afford the 9,10-dihydrophenanthrenes. The mechanism can not fully explain the pH effect of the present work.

Our observation of the transient coloration on irradiation of Ia suggests the formation of 4a,4b-dihydro-9,10-dicyanophenanthrene (VIIa) as the intermediate like that in the case of stilbene.[5] The failure to observe the intermediate (VIIa) in aqueous ethanol UV-spectroscopically may be due to the shorter half life-time. The pH-dependency of the product distribution is thus explained by the acid catalyzed isomerization of the short-lived 4a,4b-dihydrophenanthrene (VII) to the 9,10-dihydro derivative (IV) as follows: The intermediate could be protonated at the cyano group to aromatize one of the ring, followed by the further migration of proton to give IV. The exclusive formation of the 9,10-dihydrophenanthrene on irradiation of α-phenyl-β-(*p*-cyanophenyl)acrylonitrile (V) in acidic solution seems to be in line with the reaction pathway. Protonation on the cyano group at the 9-position of the 4a,4b-dihydro compound (VIII) may promote the formation of the corresponding 9,10-dihydro compound in the same way. The insensibility of the photocyclization of isomeric *p,p'*-dicyanostilbene (VI) toward acid is in line with the processes; the proton catalyzed isomerization of the 4a,4b-dihydro (IX) to the 9,10-dihydro derivative can hardly occur since proton catalyzed aromatization is unfavorable in this case.

TABLE 2. THE KINETIC PARAMETERS (see Eq. 3).

X	Temp (°C)	log (k_3/k_1)	k_2/k_1
H	20	6.5	2.8
H	2	6.0	2.4
OMe	2	6.2	2.6
Cl	2	5.2	2.3[a]
CN	2	4.2	1.7[a]

a) The values were estimated so that a straight line with a gradient −1 was obtained according to Eq. 3.

The following kinetic aspects confirm the cyclization mechanism *via* VII. As shown in Fig. 1, the 9,10-dihydrocompounds (IV) are formed even in neutral or alkaline solutions, the yield being scarcely influenced by pH at pH 7—8 (Fig. 3). The results indicate that hydroxide ion plays a minor catalytic role in the process giving the photoproducts, and that the isomerization of VII to IV involves also the process irrespective of acid.

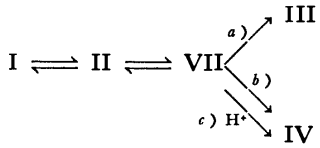

(1)

The reaction of the intermediate (VII) to give products thus consists of the following three paths as illustrated in Eq. 1 : *a*) oxidative formation of III, *b*) spontaneous isomerization to IV, and *c*) acid catalyzed isomerization to IV. We thus obtain the following equation in the region pH< 7.:

$$[D]/[P] = k_2/k_1 + k_3/k_1 \cdot [H^+] \quad (2)$$

and then

$$\log ([D]/[P] - k_2/k_1) = \log (k_3/k_1) - \mathrm{pH} \quad (3)$$

where [D] and [P] are the yields of IV and III, respectively, k_1, k_2, and k_3 corresponding to the rate constant of paths *a*, *b*, and *c*, respectively. According to Eq. 2, the ratio of the rate constants k_2/k_1 is assumed to be [D]/[P] at pH=7. The plot log ([D]/[P]−k_2/k_1) against pH gives a straight line with a gradient −1 in agreement with Eq. 3 when the estimated values for k_2/k_1 were used in the cases of Ia and Id (Fig. 4). Since the photolysis of Ib and Ic afforded non-linear EDQ diagrams even in a neutral solution, the k_2/k_1 values for these derivatives are uncertain. We have estimated them to give a straight line with a gradient −1 against pH (Table 2).

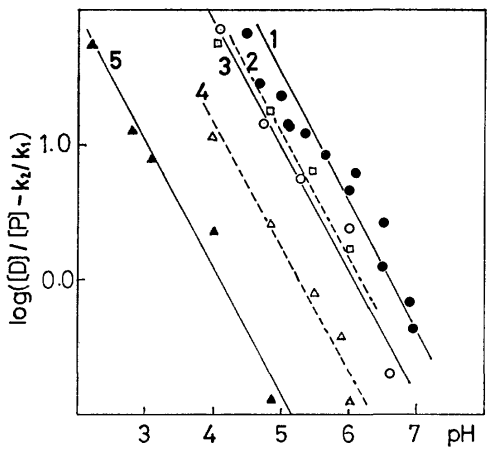

Fig. 4. pH-Dependency of photocyclization of diarylfumaronitriles; (1) diphenylfumaronitrile at 20 °C (—●—), (2) α-(*p*-anisyl)-α'-phenylfumaronitrile at 2 °C (--□--), (3) diphenylfumaronitrile at 2 °C (—○—), (4) α-(*p*-chlorophenyl)-α'-phenylfumaronitrile at 2 °C (--△--), (5) α-(*p*-cyanophenyl)-α'-phenylfumaronitrile at 2 °C (—▲—).

The spontaneous isomerization of VII to IV (path *b*) may involve an intramolecular process at least partially since the incorporation of solvent deuterium into the 9,10-dihydro compound occurs only partially.[7] From the solid state photocyclization we have concluded that VII is a *trans* isomer.[13] It is very likely that the intramolecular process occurs *via* the 1,3- or 1,7-sigmatropic shift of hydrogens of VII to afford the 9,10-dihydro derivative, which is a *trans* isomer.[1]

Experimental

All the melting points are not corrected. Ultraviolet spectra were recorded on a Hitachi EPS-3T spectrometer, and monochromatic light was obtained on a JASCO CRM-FA Spectro Irradiator consisting of a 2 kW xenon lamp.

Table 3. α,β-Diarylacrylonitrile (*p*-X-C_6H_4CH=C(CN)C_6H_4-Y-*p*)

	X	Y	Mp (°C)	Analysis (%) Calcd C	H	N	Found C	H	N
a)	H	H	88[a]	—	—	—	—	—	—
b)	Cl	H	102[b]	—	—	—	—	—	—
c)	CN	H	170	83.45	4.38	12.17	83.49	4.20	12.32
d)	OMe	H	94—95[c]	—	—	—	—	—	—
e)	CN	CN	260	79.98	3.55	16.16	79.91	3.48	16.63
f)	OMe	CN	161	78.44	4.65	10.76	78.12	4.46	10.71
g)	Me_3[d]	H	102—105	87.41	6.93	5.66	87.54	7.17	5.58

a) 88 °C.[14] b) 108 °C.[15] c) 95 °C.[16] d) 2,4,6-Trimethyl.

Table 4. α,α′-Diarylsuccinonitrile (C_6H_5(CN)CH(CN)CHC_6H_4-X-*p*)[a]

	X	Mp (°C)	Yield (%)	Analysis (%) Calcd C	H	N	Found C	H	N
a)	H	236[b]	97	—	—	—	—	—	—
b)	Cl	207—210	93	70.02	4.16	10.50	70.23	3.86	10.40
c)	CN	192	92	79.35	4.31	16.34	79.93	4.15	15.89
d)	OMe	200—202[c]	94	—	—	—	—	—	—

a) Recrystallized from acetonitrile. b) 238—239 °C.[17] c) 193 °C.[16]

Table 5. Diarylfumaronitrile (C_6H_5C(CN)=(CN)C_6H_4-X-*p*) (I)

	X	Mp (°C)	Analysis (%) Calcd C	H	N	Found C	H	N
a)	H	161[a]	—	—	—	—	—	—
b)	Cl	141—142	72.60	3.43	10.59	72.58	3.60	10.52
c)	CN	161—164	79.98	3.55	16.46	80.38	3.09	16.66
d)	OMe	142—143	78.44	4.65	10.76	78.46	4.23	10.74

a) 161 °C.[18]

Table 6. Phenanthrenes (III)

	Substituents at 3	9	10	Mp (°C)	Analysis (%) Calcd C	H	N	Found C	H	N
a)	H	CN	CN	290[a]	—	—	—	—	—	—
b)	Cl	CN	CN	240	73.15	2.69	10.69	73.57	2.29	10.55
c)	CN	CN	CN	306—307	80.60	2.79	16.60	81.10	2.68	15.97
d)	OMe	CN	CN	240—241	79.05	3.90	10.85	78.68	3.98	10.73
e)	CN	CN	H	281—282	84.21	3.51	12.28	84.77	3.52	12.25

a) 295 °C.[1]

Table 7. 9,10-Dihydrophenanthrenes (IV)

	Substituent at			Mp (°C)	Analysis (%) Calcd			Found		
	3	9	10		C	H	N	C	H	N
a)	H	CN	CN	199—204[a)]	—	—	—	—	—	—
b)	Cl	CN	CN	182—185	72.60	3.43	10.59	72.10	4.02	10.28
c)	CN	CN	CN	203—207	79.98	3.55	16.46	80.29	3.59	16.47
d)	OMe	CN	CN	154—155	78.44	4.65	10.76	77.93	3.88	10.50
e)	CN	H	CN	164—165	83.54	4.38	12.18	83.16	3.95	11.70

a) 199—204 °C.[1)]

Table 8. Ultraviolet spectra of α-phenyl-α′-(*p*-substituted phenyl)fumaronitriles (I) in 50% aqueous ethanol

	X	λ_{max} ($\varepsilon \times 10^{-4}$) nm
a)	H	215 s (1.06), 238 (0.73), 331 (1.46)
b)	Cl	222 (1.37), 237 s (0.92), 337 (1.66)
c)	CN	330 (1.72)
d)	OMe	228 (1.31), 243 s (0.92), 290 (0.34), 365 (1.65)

Solvents were distilled before use.

α,β-Diarylacrylonitriles. The preparative method for α,β-diphenylacrylonitrile was employed.[14)] The results are given in Table 3.

α,α′-Diarylsuccinonitrils. (α,α′-Diphenylsuccinonitrile as a Typical Procedure): 90 g of potassium cyanide and 65 g of ammonium chloride were dissolved in 350 ml of water. The solution was added in one portion to a warm solution of 230 g of α,β-diphenylacrylonitrile in 750 ml DMF with shaking, and the mixture was allowed to stand for 1 h. Sufficient water was added to the mixture, the precipitate was filtered, washed with water and then with alcohol and dried. The crude product 268 g, mp 230—235 °C (lit,[17)] mp 238—239 °C as *meso*-isomer), was satisfactory for further use. Results for diarylsuccinonitriles synthesized by this method are given in Table 4. The hydrocyanation of α-phenyl-β-(2,4,6-trimethylphenyl)acrylonitrile by this procedure was unsuccessful.

Diphenylfumaro- and Maleonitrile. A sodium methoxide solution prepared by dissolving 37.5 g sodium in 300 ml methanol was added dropwise under vigorous stirring to 197 g iodine and 180 g crude α,α′-diphenylsuccinonitrile in 500 ml THF. At the end of the addition the color of iodine faded with a rise of temperature of the mixture. After stirring for 1 h the solvent was evaporated, and the reaction mixture was treated with a large amount of water. The precipitated crystals were filtered, washed with water, twice with cold methanol and dried. The crude product weighed 132 g and were recrystallized from ethanol to yield 84 g crude diphenylfumaronitrile which was recrystallized once more from ethanol. Mp 159—160 °C (lit,[18)] mp 161 °C). The combined ethanol filtrates were condensed to give 25 g crude diphenylmaleonitrile of mp 112—130 °C which was repeatedly recrystallized from ethanol until the mp became constant. The maleonitrile of mp 133—134 °C (lit,[19)] mp 135 °C) weighed 16 g. α-Phenyl-α′-(*p*-substituted phenyl)-succinonitriles were oxidized in a similar manner to the procedure mentioned above. The crude products showed a wide range of mp, but the isolation of diarylmaleonitriles was not attempted. The results are summarized in Table 5. The UV spectra of diarylfumaronitriles obtained are given in Table 8.

p,p′-*Dicyanostilbene.* The compound was synthesized according to the method of Fu and Sah.[20)] Mp 277—279 °C.

9,10-Dicyanophenanthrenes. A solution of 250 mg of diarylfumaronitrile in 100 ml of dichloromethane in a Pyrex flask was irradiated in the presence of 10 mg of iodine with a 450 W high pressure mercury lamp for 8 h. After the solvent had been evaporated, the crude product was chromatographed on alumina by means of dichloromethane as an eluent. The phenanthrenes were then recrystallized from methyl ethyl ketone. The results are given in Tables 6 and 9.

9,10-Dihydro-9,10-dicyanophenanthrenes. An ethanol (100 ml) solution of 250 mg diarylfumaronitrile was irradiated in a Pyrex flask with a 450 W high pressure mercury lamp under argon stream for 14 h. After the solvent had been evaporated, the residual crystalline product was recrystallized several times from ethanol. The dihydro compounds obtained are given in Table 7. The UV data are given in Table 10.

Isolation of Diphenylmaleonitrile in Photoisomerization. Two

Table 9. Ultraviolet spectra of the phenanthrenes (III) in 50 (%) aqueous ethanol

	Substituents at			λ_{max} ($\varepsilon \times 10^{-4}$) nm
	3	9	10	
a)	H	CN	CN	238 (3.47), 252 (3.45), 261.5 (3.80), 269 s (2.75), 325 (1.26), 339 (1.59)
b)	Cl	CN	CN	219 (2.26), 243 (4.62), 253.5 (3.80), 262.5 (4.05), 274 (2.50), 332 (1.50), 343 (1.72), 383 (0.20)
c)	CN	CN	CN	215 (2.12), 248 (4.65), 260 (3.70), 333 (1.18), 344 (1.38), 370 (0.24), 390 (0.27)
d)	OMe	CN	CN	219 (2.35), 253.5 (4.58), 263 s (3.36), 284 (1.94), 352 (1.43), 362 (1.49), 380 (1.18)
e)	CN	H	CN	232 (4.42), 250 (4.64), 281 (1.01), 313 (1.50), 324 (1.48), 347 (0.19), 368 (0.17).

Table 10. Ultraviolet spectra of the 9,10-dihydrophenanthrenes (IV) in 50% aqueous ethanol

	Substituents at 3	9	10	λ_{max} ($\varepsilon \times 10^{-4}$) nm
a)	H	CN	CN	270 (1.68)
b)	Cl	CN	CN	272 (1.65)
c)	CN	CN	CN	233 (3.36), 239 (2.48), 271 (1.58)
d)	OMe	CN	CN	234 (3.02), 241 (3.26), 272 (1.63)

grams of diphenylfumaronitrile was dissolved in 150 ml 1,2-dichloroethane in a Pyrex flask and irradiated for 3 h with a mercury lamp. The solvent was evaporated to dryness, and the residue was recrystallized from ethanol to give crude starting material of mp 140—158 °C as needles. The filtrate was evaporated, the crystalline residue of mp 114—132 °C was recrystallized repeatedly from benzene-hexane to yield needle-like crystals of mp 132—134 °C. Identification was performed by mixture mp and UV absorption spectra.

Solvent Effect on the Yield of 9,10-Dicyanophenanthrene. Solutions of diphenylfumaronitrile in various solvents (5×10^{-5} M) were irradiated with 330 nm light until no more spectral change took place. The yield of 9,10-dicyanophenanthrene was calculated from the absorbance at 325 nm. The spectrum of the photoproduct in acidic solution was practically identical with that of 9,10-dihydro-9,10-dicyanophenanthrene.

Irradiation of 9,10-Dihydro-9,10-dicyanophenanthrene with Light of 270 nm. When an aerated solution of 9,10-dihydro compound in ethanol (5×10^{-5} M) was excited with 270 nm light, the absorbance at 269 nm decreased slowly with increase in the absorbance at 321 and 334 nm. The latter peaks are due to 9,10-dicyanophenanthrene.

Examination of EDQ diagrams[9] of the Photolysis of Diarylfumaronitrile at Various pH. The buffered solutions employed consist of citrate-phosphate-borate system. To a 25 ml buffer solution (0.01 M) was added *ca.* 10 ml ethanol with shaking, and then 5 ml 8×10^{-4} M ethanol solution of diarylfumaronitrile and finally ethanol in order to adjust the volume of the solution to 50 ml. A solution (4 ml) placed in a quartz cell (10×10 mm) was irradiated with 330 nm light at room temperature, and the UV spectrum was measured at intervals. The remaining sample solutions were subjected to pH measurement. Examination of EDQ diagram was carried out at pH 4.0, 5.0, 7.0, and 9.0.

Measurement of pH-Dependency of the Photoproduct Distribution. A cylindrical Pyrex cell containing 10 ml of the buffered solution was immersed in a thermostatted bath and irradiated through a quartz widnow with a 450 W mercury lamp until no more spectral change was observed. The irradiation time was *ca.* 5 min. The absorption spectra of the products at various pH showed isosbestic points. Since the prolonged irradiation caused gradual disappearance of 3,9,10-tricyanophenanthrene in aqueous ethanol, its yield was estimated by extrapolation. When buffered solutions of α-phenyl-β-(*p*-cyanophenyl)acrylonitrile (4.3×10^{-5} M) in aqueous ethanol were irradiated in a similar manner the absorption maxima at 313 and 324 nm due to 3,9-dicyanophenanthrene decreased and those at 272 and 241 nm due to 9,10-dihydro-3,9-dicyanophenanthrene increased with decrease in the pH of solutions. No isosbestic point appeared in the spectra of the irradiated solutions at various pH, the composition of the products being more complicated. No maxima due to the phenanthrene was observed at pH less than 4.

Observation of Colored Intermediate. A solution of diphenylfumaro- or maleonitrile (*ca.* 10^{-3} M) was irradiated with 320 nm light. Coloration was observed in chloroform, carbon tetrachloride, ethyl acetate, benzene, and toluene. The absorbance of the intermediate at 480 nm in toluene was recorded at intervals and found to decay following first order kinetics. The half lifetime was 100 s at room temperature.

The authors are indebted to Prof. Dr. G. Quinkert and Dr. H. C. Steinmetzer, University of Frankfurt am Main, for their valuable suggestions and discussions.

References

1) M. V. Sargent and C. J. Timmons, *J. Chem. Soc.*, **1964**, 5544.
2) F. B. Mallory, C. S. Wood, J. J. Gordon, L. C. Linquist, and M. L. Savitz, *J. Am. Chem. Soc.*, **84**, 4362 (1962).
3) W. H. Moore, D. D. Morgan, and F. R. Stermitz, *J. Am. Chem. Soc.*, **85**, 829 (1963).
4) F. B. Mallory, C. S. Wood, and J. T. Gordon, *J. Am. Chem. Soc.*, **86**, 3094 (1964).
5) K. A. Muszkat and E. Fischer, *J. Chem. Soc., B*, **1967**, 662.
6) As a preliminary report; S. Watanabe and K. Ichimura, *Chem. Lett.*, **1972**, 35.
7) R. Srinivasan and J. N. C. Hsu, *J. Am. Chem. Soc.*, **93**, 2816 (1971).
8) R. Stewart and D. J. Kroeger, *Can, J. Chem.* ,**45**, 2173 (1967).
9) G. Quinkert, *Angew. Chem.*, **84**, 1157 (1972).
10) The process of both appearance and disappearance of the intermediate (VII) in Eq. 1 can not be taken into consideration in the EDQ diagram examination, since VII was not observed UV-spectroscopically under the experimental conditions used.
11) G. S. Hammond, J. Saltiel, A. A. Lamola, N. J, Turro, J. S. Bradshaw, D. O. Cowan, R. C. Counsell, V. Vogt, and C. Dalton, *J. Am. Chem. Soc.*, **86**, 3197 (1964).
12) T. D. Doyl, N. Filipescu, W. R. Benson, and D. Banes, *J. Am. Chem. Soc.*, **92**, 6371 (1970).
13) K. Ichimura and S. Watanabe, *Tatrahedron Lett.*, **1972**, 821.
14) S. Wawzonek and E. M. Smolin, *Org. Synth.*, Coll. Vol. III, 715 (1955).
15) Beilsteins Handbuch der Organischen Chemie, Vol. 9, 693 (1926).
16) K. Brand and L. Loehr, *J. Prakt. Chem.*, **109**, 359 (1925).
17) R. B. Davis and J. A. Ward, *Org. Synth.*, Coll. Vol. IV, 392 (1963).
18) J. T. Thurston and R. L. Shriner, *J. Org. Chem.*, **2**, 183 (1937).
19) M. V. Sargent and C. J. Timmons, *J. Chem. Soc.*, **1964**, 2222.
20) S. -C. Fu and P. P. P. T. Sah, *J. Am. Chem. Soc.*, **64**, 1482 (1942).

Ring-enlargement of Methoxynaphthalenes with Dichlorocarbene to Benzotropone Derivatives

Masaru SATO, Josuke TSUNETSUGU, and Seiji EBINE

Department of Chemistry, Faculty of Science and Engineering, Saitama University, Urawa, Saitama 338

(Received December 5, 1975)

The dichlorocarbene addition to various di- and trimethoxynaphthalenes has been investigated systematically. It has been found that the carbene addition is oriented by the 1-methoxyl group to the 3,4-double bond and by the 2-methoxyl group to the 1,2-double bond of naphthalene nucleus, and that the spontaneous cyclopropane ring-opening of the intermediate carbene-adducts leads to the preferencial formation of 2,3-benzotropone over 4,5-benzotropone derivatives. The steric effects by methoxyl group seem not to be significant in either the carbene-addition or ring-opening reaction.

There are several reports on the ring-enlargement reactions of benzenoid aromatic system with dihalocarbene to seven-membered or larger ring non-benzenoid aromatic systems. For example, azulene[1] was obtained from indene, bromotropone was formed from anisole,[2] and chlorobenzotropone derivatives were prepared from methoxynaphthalenes[2,3] by ring-enlargement reactions with dihalocarbene. Recently, benzocyclooctatrienedione derivatives were synthesized by the reaction of tetramethoxynaphthalene or tetramethylpurpurogallin with dichlorocarbene.[4] A benzo[3,4]cyclobuta[1,2-*c*]tropone derivative was obtained through the ring-enlargement of methoxybiphenylene with dichlorocarbene.[5] However, scarcely no systematic investigations of dichlorocarbene addition to substituted benzenoid compounds, in contrast with that to olefinic compounds,[6] have been reported. This paper will deal with a systematic examination of the ring-enlargement of methoxynaphthalenes with dichlorocarbene and with the orientation effect of the methoxyl group on the methoxynaphthalene-dichlorocarbene addition.

Results

1,2-Dimethoxynaphthalene was treated with one equivalent amount of the dichlorocarbene source, according to Makosza's method,[7] to give three kinds of products, **1**, **2**, and **3**. The IR and NMR spectra of **1** were superimposable upon those of an authentic sample of 7-chloro-6-methoxy-2,3-benzotropone,[8] and no temperature-depression was observed on their admixture.

Compound **2** showed an NMR spectrum with two doublets at δ 6.93 and 7.51 ppm (J=12.6 Hz). The electronic spectrum of **2** was closely similar to that of 2-chloro-4,5-benzotropone.[3] These spectral data are in accordance with the structure of 2-chloro-3-methoxy-4,5-benzotropone (Fig. 1).

Compound **3** showed, in its NMR spectrum, two doublets at δ 6.62 and 7.73 ppm with a small coupling constant (J=2.0 Hz), indicating the presence of two protons in the allylic positions each other of the seven-membered ring, so suggesting that the product is identifiable as 5-chloro-7-methoxy-2,3-benzotropone. Curiously enough, **3** was not necessarily reproduced in repeated experiments. The use of a large excess of carbene source failed to improve the yield of the tropone derivatives; it resulted only in the formation of a considerable amount of an intractable substance.

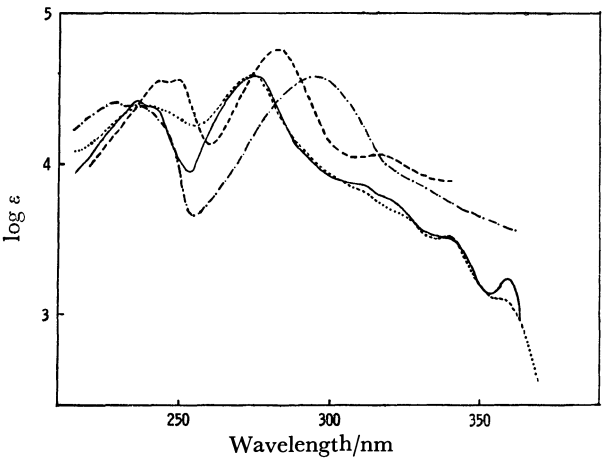

Fig. 1. The UV spectra of 4,5-benzotropones.
——: 2-Chloro-4,5-benzotropone, ·····: 2-chloro-3-methoxy-4,5-benzotropone(**2**), ----: 2-chloro-7-methoxy-4,5-benzotropone(**11**), —·—·: 2-chloro-3′-methoxy-4,5-benzotropone(**14**).

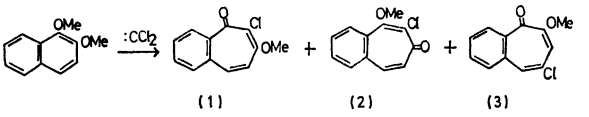

(1) (2) (3)

The reaction of 1,4-dimethoxynaphthalene with one equivalent amount of the dichlorocarbene source gave the product **4**. Its NMR spectrum showed two characteristic doublets (J=10.0 Hz), at δ 6.01 and 7.58 ppm, for H-5 and H-6, and a pair of multiplets for benzenoid 2H deshielded and benzenoid 2H not deshielded by either the carbonyl or methoxyl group. From the NMR spectra, **4** was assigned to 7-chloro-4-methoxy-2,3-benzotropone. The structure was further confirmed by conversion to the Diels-Alder adduct (**6**), whose NMR spectrum showed two olefinic doublets, at δ 6.34 and 7.08 ppm (J=9.5 Hz), indicating that **4** is unsubstituted at C-5 and C-6.

The use of three molar amounts of the dichlorocarbene source afforded an additional, thermally unstable product (**5**), which showed IR and mass spectra closely similar to those of **4**. The NMR spectrum showed two olefinic doublets (J=12.0 Hz), at δ 6.68 and 7.22 ppm. Thus, **5** was proved to be 5-chloro-4-methoxy-2,3-benzotropone.

1,3-Dimethoxynaphthalene reacted with dichloro-

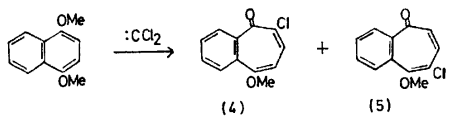

(4) (5)

carbene to give two products, **7** in an 8.0% yield and **8** in a 2.9% yield, their UV and NMR spectra were quite similar to those of 5-bromo-6-methoxy-2,3-benzotropone and 2-bromo-6-methoxy-4,5-benzotropone respectively.[9] Therefore, **7** and **8** can be said to be 5-chloro-6-methoxy-2,3-benzotropone and 2-chloro-6-methoxy-4,5-benzotropone respectively.

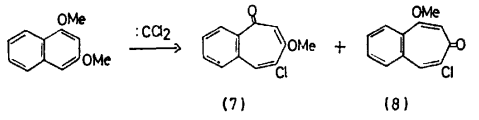

(7) (8)

Further structural evidence was obtained by the hydrolysis of **7** and **8** with concentrated hydrochloric acid in boiling ethanol to give the same product, 5-chloro-6-hydroxy-2,3-benzotropone (**9**), whose NMR spectrum showed no methoxyl proton and two olefinic protons as two singlets at δ 6.74 and 8.31 ppm, the former disappearing on the addition of deuterated water. **7** gave the Diels-Alder adduct (**10**), but **8** gave no adduct, on heating with maleic anhydride, affording an additional proof of their structures.

The reaction of 2,3-dimethoxynaphthalene with dichlorocarbene afforded a scanty yield of 7-chloro-2-methoxy-4,5-benzotropne (**11**). The structural assignment is based on the electronic (Fig. 1) and NMR spectra : methoxyl singlet at δ 4.01 ppm, two deshielded olefinic singlets at δ 7.19 and 8.32 ppm for H-3 and H-6, and a narrow multiplet at δ 7.6—7.9 ppm for four benzenoid protons.

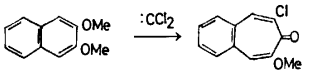

(11)

The reaction of 1,5-dimethoxynaphthalene with dichlorocarbene gave a product (**12**), in a poor yield, which was conclusively identified as 5-chloro-3'-methoxy-2,3-benzotropone by the following NMR spectrum: a doublet (J=2.0 Hz) at δ 8.27 ppm, deshielded by both methoxyl and chloro substituents, for H-4, a doublet (J=13 Hz) at δ 6.78 ppm for H-7, a doublet at δ 7.17 ppm for H-6, and an ABC-type three-proton system at δ 7.1—8.0 ppm for benzene-ring protons.

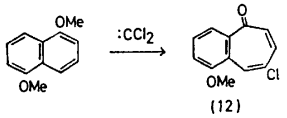

(12)

1,6-Dimethoxynapnthalene reacted with dichlorocarbene to give two products, **13** in a 9.9% yield and **14** in a 4.9% yield. The electronic spectrum of **13** was similar to that of 5-chloro-2,3-benzotropone (Fig. 2). The NMR spectrum of **13** showed an olefinic doublet (J=13.0 Hz) at δ 6.81 ppm, meaning that the

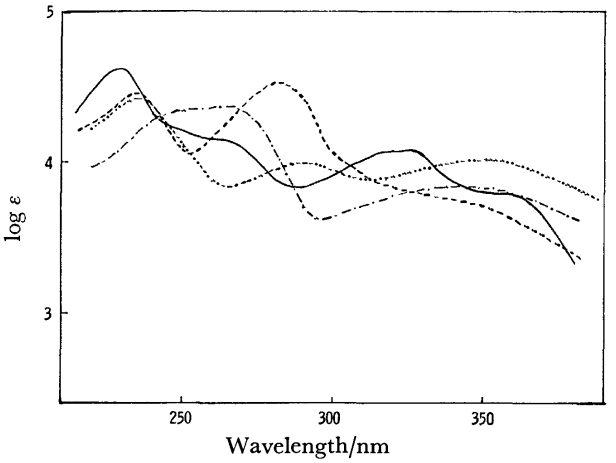

Fig. 2. The UV spectra of 2,3-benzotropones.
——: 5-Chloro-2,3-benzotropone, ·····: 5-chloro-3'-methoxy-2,3-benzotropone(**12**), ----: 5-chloro-4'-methoxy-2,3-benzotropone(**13**), —·—·: 5-chloro-6,7-dimethoxy-2,3-benzotropone(**15**).

chloro substituent is at C-5 rather than at C-7, since the chemical shift of the doublet is very similar to those of 5-chloro-2,3-benzotropone (δ 6.83 ppm) and **12** (δ 6.78 ppm). Therefore, **13** is identified as 5-chloro-4'-methoxy-2,3-benzotropone. The peri-position of the benzene ring, deshielded by the carbonyl group, appeared as a doublet (J=9.0 Hz) in the lower region (δ 8.47 ppm), indicating that the methoxyl group is situated at C-4'.

The other product (**14**) showed an NMR spectral olefinic singlet (δ 8.17 ppm) and doublet (δ 8.35 ppm, J=13.5 Hz) in a remarkably lower field; they are probably due to the anisotropy of the methoxyl group and the inductive effect of the chloro substituent. The electronic spectrum showed that **14** has a chromophore of 2-chloro-4,5-benzotropone (Fig. 1). These observations can be satisfactorily explained by assigning **14** to 2-chloro-3'-methoxy-4,5-benzotropone.

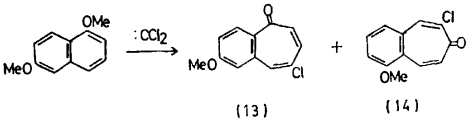

(13) (14)

1,2,3-Trimethoxynaphthalene, on treatment with dichlorocarbene, gave a sole isolable product (**15**). The electronic spectrum showed the presence of a 2,3-benzotropone structure (Fig. 2), and the NMR spectrum showed an olefinic proton signal of the seven-membered ring overlapped with benzenoid protons in a region similar to that of the H-4 of 5-chloro-2,3-benzotropone derivatives [δ 7.37 in **3** and 7.55—7.85 ppm in **7**]. Moreover, if the compound has the **16** structure, the H-4 resonance should appear in a higher field than that of 7-chloro-6-methoxy-2,3-benzotropone(**1**) (δ 7.15 ppm). This does, however, not happen. In the mass spectrum, methyl elimination preceded carbon dioxide elimination, unlike as in other benzotropone derivatives. These spectral data agree with the structure of 5-chloro-6,7-dimethoxy-2,3-benzotropone rather than with the **16** structure.

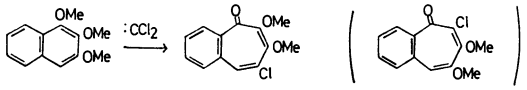

(15) (16)

1,2,4-Trimethoxynaphthalene reacted with dichlorocarbene to afford only one benzotropone derivative, in an 18% yield. The product **18** showed an NMR signal of the olefinic proton as a singlet at a fairly high field (δ 6.29 ppm) and four benzenoid protons as a pair of multiplets similar to those in 4-methoxy-2,3-benzotropones (**4** and **5**). The olefinic proton is not situated at the 6-position, since the resonance of the H-6 of 2,3-benzotropone derivatives should appear in a lower field because of the electronic effect of the carbonyl group [*e.g.*, δ 6.62 ppm in **3** and δ 7.58 ppm in **4**]. The product gave the Diels-Alder adduct (**20**) with maleic anhydride, whose NMR spectrum showed no resonance in the olefinic region, indicating that **18** has no proton at the 5- and 6-positions. Consequently, **18** proved to be 5-chloro-4,6-dimethoxy-2,3-benzotropone, excluding the **19** structure.

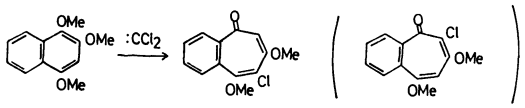

(18) (19)

The reaction of 1,2,3,4-tetramethoxynaphthalene with dichlorocarbene failed to give a difinite isolable product, but the NMR spectrum indicated the formation of a benzotropone derivative with no olefinic proton and three methoxyl proton signals, and the mass spectrum showed a molecular ion at *m/e* 280.

Discussion

It is known that two types of benzenoid aromatic compounds are susceptible to the attack of dichlorocarbene. One type includes fused-ring aromatic compounds, such as naphthalene,[10,11] phenanthrene,[10,11] and anthracene,[11,12] which have a small loss of resonance energy in the formation of the dihalocarbene adduct. The other type includes the aromatic compounds carrying an electron-donating substituent, such as methylnaphthalene[13] and methoxynaphthalenes,[2,3a,3b] in which the substituent not only facilitates the dichlorocarbene addition, but also might influence the orientation of the dichlorocarbene attack. The reaction of anisole with dibromocarbene affords 4-bromotropone,[2] and the reaction of 1-methoxynaphthalene gives 5-halo-2,3-benzotropone[3c-3e] exclusively, no other isomeric tropones being obtained.* 1,5- And 1,6-dimethoxynaphthalenes also reacted with dichlorocarbene to give exclusively 5-chloro-2,3-benzotropone derivatives **12** and **13** respectively. On the other hand, the reaction of 2-methoxynaphthalene with dihalocarbene afforded 2-halo-4,5-benzotropone. 2,3- And 1,6-dimethoxynaphthalenes reacted with dichlorocarbene to give 2-chloro-4,5-benzotropone derivatives, **11** and **14** respectively. These results suggest that dichlorocarbene adds regioselectively to the 3,4-double bond of 1-methoxynaphthalene derivatives and to the 1,2-double bond of 2-methoxynaphthalene derivatives. This selective carbene addition orientated by the methoxyl group was found to be consistent throughout the di- and trimethoxynaphthalenes (that is, the additivity of the effect from methoxyl groups was observed).

1,3-Dimethoxynaphthalene, in which both the methoxyl groups accelerate carbene addition to the 3,4-double bond, gave, as expected, the **7** and **8** products, which must have been derived *via* an intermediate 3,4-double bond adduct. 1,2,3- And 1,2,4-trimethoxynaphthalenes also gave a single product, **15** and **18** respectively. Carbene addition to 1,2,3-trimethoxynaphthalene occurs exclusively at the 3,4-double bond because of the orientation effect by the 1-methoxyl group, where the orientation to the 1,2-double bond by the 2-methoxyl group is cancelled by that to the 3,4-double bond by the 3-methoxyl group. Similarly, addition to 1,2,4-trimethoxynaphthalene takes place at the 1,2-double bond in terms of the 2-methoxyl group because the orientation effects by the 1- and 4-methoxyl groups cancel each other. 1,2-Dimethoxynaphthalene reacted with dichlorocarbene both at the 3,4-double bond, oriented by the 1-methoxyl group, to give **3** and at the 1,2-double bond, oriented by the 2-methoxyl group, to give **1** and **2** [although **3** was not necessarily reproduced in repeated experiments, as has been described above].

The ^{13}C-NMR spectra of methoxynaphthalenes[14] afford information about their ground-state electronic state, and may be expected to elucidate the regioselectivity of dichlorocarbene addition to the methoxynaphthalenes. In fact, a good correlation was observed between the orientation of carbene addition and the electron density deduced from the ^{13}C-NMR chemical shift of the 2-methoxynaphthalene derivatives. However, no such correlation was observed in 1-methoxynaphthalene or its derivatives. In 1-methoxy- and 1,3-dimethoxynaphthalene, for example, the electron density of C-4, as deduced from ^{13}C-NMR spectra, was lower than that of C-2, whereas the dichlorocarbene addition took place at the 3,4-double bond exclusively. The regiospecific addition observed in the dichlorocarbene addition to methoxynaphthalene derivatives might be explained in the following manner: the approach of dichlorocarbene to 1-methoxynaphthalene or its derivatives induces a dynamic polarization of electrons on the naphthalene nucleus by the methoxyl group and accumulates a negative charge at C-4 rather than at C-2, as in the electrophilic substitution of naphthalene derivatives, so that the electrophilic dichlorocarbene approaches asymmetrically to the 3,4-double bond from the direction of the electron-rich C-4 to form dihalocyclopropano-dihydronaphthalene intermediates.

The cyclopropane ring-opening of the intermediate carbene-adducts is largely facilitated by aromatization, leading to benzotropone derivatives, since the dichlorocarbene adduct of 1-ethoxy-3,4-dihydronaphthalene

* The reaction of 1-methoxynaphthalene with dichlorocarbene generated by Makosza's method gave 5-chloro-2,3-benzotropone exclusively in our experiment also.

was not affected even by silver(I) salt at room temperature.[15] The ring-enlargement of the intermediates led to the preferential formation of 2,3-benzotropone derivatives over 4,5-benzotropone derivatives. Thus, the intermediate adduct from 1,3-dimethoxynaphthalene with dichlorocarbene gave **7** more predominantly than **8**. A similar trend was observed in 1,2-dimethoxynaphthalene. 1,2,3- And 1,2,4-trimethoxynaphthalenes also gave only the 2,3-benzotropone derivatives, **15** and **18** respectively. Furthermore, it should be noted that the direction of the ring opening of the intermediate 1,2,3- and 1,2,4-trimethoxynaphthalene-carbene adducts to **15** and **18** respectively is comparable with that of an intermediate 1,4-dimethoxynaphthalene-carbene adduct to **5**.

Finally, the steric effect by the methoxyl group seems not to be significant in either the addition of dichlorocarbene to methoxynaphthalenes or the ring opening of the intermediate carbene adducts, because the carbene adds exclusively to the most hindered 1,2-double bond of 1,2,4-trimethoxynaphthalene and the ring opening of the adduct gives a more hindered product **18** rather than a less hindred **19**.

Experimental

Material. The 1- and 2-methoxynaphthalenes were commercially available. The 1,2-dimethoxynaphthalene was prepared by the reduction and methylation of commercially available 1,2-naphthoquinone. The 1,4-, 1,5-, 1,6-, and 2,3-dimethoxynaphthalenes were prepared by the methylation of the corresponding commercially available diols with dimethyl sulfate. The 1,3-,[16] 1,2,3-,[17] and 1,2,4-trimethoxynaphthalenes[18] were prepared according to the literature.

The *1,2,3,4-tetramethoxynaphthalene*[19] was prepared in the following manner. Dimethylisonaphthazalin[20] (3.7 g, 17 mmol) was stirred, portion by portion, into a mixture of ether (30 ml) and aqueous sodium dithionite (6.0 g in 30 ml of water). After 20 min, the mixture was transferred into a separable funnel and shaken vigorously. The ethereal layer was separated, and the aqueous layer was extracted with ether. The combined organic solution was dried over magnesium sulfate, filtered, and evaporated. The pale red residual oil was added to a solution of dimethyl sulfate (4.8 ml, 51 mmol) in ethanol (15 ml), and to this was added, drop by drop, 50% aqueous sodium hydroxide (5.1 ml) under an atmosphere of nitrogen. After it had then stood overnight, the solution was diluted with water, and the colorless needles which were thus precipitated were collected, washed with water, and dried. Yield: 3.6 g (86%); mp 49—53 °C, which rose to 52—53 °C upon chromatographic purification and recrystallization from hexane. Found: C, 67.75; H, 6.58%. Calcd for $C_{14}H_{16}O_4$: C, 67.72; H, 6.50%. NMR($CDCl_3$): δ 4.05 (s, 12H), 7.43 (q, 2H, J=3.2 Hz), and 8.09 (q, 2H, J=3.2 Hz).

Standard Procedure. Methoxynaphthalenes (0.03 mol), chloroform (3 ml, 0.037 mol), 50% aqueous sodium hydroxide (6 ml), and triethylbenzylammonium chloride (0.12 g) were placed in a 50-ml Erlenmeyer flask equipped with a potassium hydroxide tube, after which the mixture was stirred at room temperature for 15 to 16 h. The reaction mixture was then diluted with water and extracted with dichloromethane. The extract was washed with water and dried over anhydrous sodium sulfate. After the solvent had been removed, the residue was chromatographed on a silica gel column, with the elution of the benzene-ether mixture. Each fraction separated was purified by fractional chromatography or sublimation.

*7-Chloro-6-methoxy-2,3-benzotropone (**1**), 2-Chloro-3-methoxy-4,5-benzotropone (**2**), and 5-Chloro-7-methoxy-2,3-benzotropone (**3**).* 1,2-Dimethoxynaphthalene was submitted to the reaction with dichlorocarbene; after a standard work-up, the reaction mixture was chromatographed to give a dark red oil containing crystals. Rechromatography on a silica gel column and sublimation gave three crystalline products. One was 7-chloro-6-methoxy-2,3-benzotropone (**1**) (1.8%); yellow needles; mp 135—136 °C, which showed no depression on admixture with an authentic sample.[6] NMR($CDCl_3$): δ 4.05 (s, 3H), 6.85 (d, 1H, J=13.0 Hz), 7.45 (d, 1H, J=13.0 Hz), 7.5—7.9 (m, 3H), and 8.6 (m, 1H) ppm. The second (1.5%) is assigned to 2-chloro-3-methoxy-4,5-benzotropone (**2**); colorless needles; mp 95—96 °C. Found: C, 65.23; H, 4.16%. Calcd for $C_{12}H_9O_2Cl$: C, 65.31; H, 4.12%. UV(EtOH): 238 (log ε 4.39), 274.5 (4.59), 340 (3.52), and 357 nm (3.11). IR(KBr): 1641 (s), 1610 (sh), 1594(s), and 1572 (m) cm^{-1}. NMR($CDCl_3$): δ 3.95 (s, 3H), 6.93 (d, 1H, J=12.6 Hz), 7.51 (d, 1H, J=12.6 Hz), 7.65—7.85 (m, 3H), and 8.2—8.4 (m, 1H). The third product, 5-chloro-7-methoxy-2,3-benzotropone (**3**), which, curiously could not be reproduced, in repeated experiments, was eluted faster than the above two. After sublimation and recrystallization from cyclohexane, it formed nearly colorless needles; mp 100 °C. Found: C, 65.25; H, 4.05%. Calcd for $C_{12}H_9O_2Cl$: C, 65.31; H, 4.12%. UV(EtOH): 237 (log ε 4.38), 260sh (4.16), 330 (3.90), and 368 nm (3.14). IR(KBr): 1625 (s), 1610 (s), 1593 (s), and 1570 (m) cm^{-1}. NMR($CDCl_3$): δ 3.93 (s, 3H), 6.62 (d, 1H, J=2.0 Hz), 7.37 (d, 1H, J=2.0 Hz), 7.5—7.85 (m, 3H), and 8.5 (m, 1H).

*7-Chloro-4-methoxy-2,3-benzotropone (**4**) and 5-Chloro-4-methoxy-2,3-benzotropone (**5**).* The reaction of 1,4-dimethoxynaphthalene with dichlorocarbene was run using the standard procedure, and the product was chromatographed on silica gel to give two crystalline fractions. The yellow orange crystals obtained from the first elute (4.28 g, 76%) were the starting material. The second was a dark red oil which was then heated *in vacuo* to give 7-chloro-4-methoxy-2,3-benzotropone (**4**) as pale yellow crystals (0.68 g, 10.2%). Recrystallization from methanol gave an analytical sample; mp 133—133.5 °C. Found: C, 65.24; H, 4.04%. Calcd for $C_{12}H_9O_2Cl$: C, 65.31; H, 4.12%. UV(EtOH): 236.5 (log ε 4.36), 256.5 (4.24), 332 (3.81), and 382 nm (3.92). IR (KBr): 1612 (s), 1593 (s), and 1565 (s) cm^{-1}. NMR ($CDCl_3$): δ 3.97 (s, 3H), 6.01 (d, 1H, J=10.0 Hz), 7.58 (d, 1H, J=10.0 Hz), 7.6—7.9 (m, 2H), and 8.3—8.6 (m, 2H). Diels-Alder adduct with maleic anhydride (**7**): colorless crystals; mp 241—242 °C. Found: C, 60.09; H, 3.52%. Calcd for $C_{18}H_{11}O_5Cl$: C, 60.29; H, 3.48%. NMR(DMSO-d_6): δ 3.65 (s, 3H), 4.26 (d, 1H, J=10.8 Hz), 4.76 (d, 1H, J=10.8 Hz), 6.34 (d, 1H, J=9.5 Hz), 7.08 (d, 1H, J=9.5 Hz), 7.5—7.85 (m, 3H), and 7.95—8.2 (m, 1H).

The reaction with three molar amounts of the dichlorocarbene source was run and the crude product was chromatographed on silica gel to give an orange semi-solid besides the recovered substance (4.2 g, 75%). The semi-solid was recrystallized from ether to give (**4**) (0.88 g, 12.4%). The mother liguor gave an additional crop of crystals (**5**), which recrystallized from cyclohexane (0.19 g, 2.9%); mp 55.5—56.5 °C. Found: C, 65.29; H, 4.03%. Calcd for $C_{12}H_9O_2Cl$: C, 65.31; H, 4.12%. UV(EtOH): 231 (log ε 4.39), 312 (3.92), and 355 nm (3.83). IR(KBr): 1628 (s), 1608 (s), 1590 (s), 1570 (s), and 1530 (s) cm^{-1}. NMR-($CDCl_3$): δ 3.80 (s, 3H), 6.68 (d, 1H, J=12.0 Hz), 7.22 (d, 1H, J=12.0 Hz), 7.5—7.9 (m, 3H), and 8.1—8.5 (m, 2H).

*5-Chloro-6-methoxy-2,3-benzotropone (**7**) and 2-Chloro-6-methoxy-4,5-benzotropone (**8**).* The reaction of 1,3-dimethoxynaphthalene with dichlorocarbene was carried out by means of the standard procedure, and the reaction product was chromatographed on silica gel to give three fractions. The first fraction was the starting material (4.3 g, 76%). The second was recrystallized from ethanol to give 5-chloro-6-methoxy-2,3-benzotropone (**7**) (0.53 g, 8.0%); colorless needles; mp 149—151 °C. Found C, 65.10; H, 4.26%. Calcd for $C_{12}H_9O_2Cl$: C, 65.31; H, 4.12%. UV(EtOH): 252 (log ε 4.78), 261 (4.76), 270sh (4.60), 335 (4.00), and 368sh nm (3.26). IR(KBr): 1620(w), 1607(w), 1580(m), 1566(s), and 1560(s) cm^{-1}. NMR($CDCl_3$): δ 3.82 (s, 3H), 6.54 (s, 1H), 7.55—7.85 (m, 4H), and 8.55 (m, 1H). Diels-Alder adduct with maleic anhydride (**10**): colorless crystals, mp 251—253 °C. Found: C, 60.48; H, 3.47%. Calcd for $C_{16}H_{11}O_5Cl$: C, 60.29; H, 3.48%. NMR (DMSO-d_6): δ 3.68 (s, 3H), 4.0—4.45 (m, 4H), 7.5—7.8 (m, 3H), and 8.0—8.2 (m, 1H). The third was recrystallized from hexane-benzene to give 2-chloro-6-methoxy-4,5-benzotropone (**8**) (0.19 g, 2.9%); colorless crystals; mp 125—126.5 °C. Found: C, 65.14; H, 4.04%. Calcd for $C_{12}H_9O_2Cl$: C, 65.31; H, 4.12%. UV(EtOH): 256 (log ε 4.58), 263 (4.60), 273 (4.68), 288sh (4.22), and 312sh nm (3.92). IR (KBr): 1622(s), 1609(m), 1596(m), 1587(s), and 1522(m) cm^{-1}. NMR($CDCl_3$): δ 4.13 (s, 3H), 6.76 (s, 1H), 7.7—7.95 (m, 3H), 8.16 (s, 1H), and 8.55 (m, 1H).

*5-Chloro-6-hydroxy-2,3-benzotropone (**9**).* 5-Chloro-6-methoxy-2,3-benzotropone (**7**) (0.13 g, 0.6 mmol) and concentrated hydrochloric acid (1 ml) in ethanol (10 ml) were refluxed for 2.5 h. After evaporation, the residue was recrystallized from ethanol to give 5-chloro-6-hydroxy-2,3-benzotropone (**9**); colorless needles (0.10 g, 85%); mp 251 °C (dec). Found: C, 64.30; H, 3.66%. Calcd for $C_{11}H_7O_2Cl$: C, 63.94; H, 3.41%. IR(KBr): 3075—2300 (broad), 1620, 1590, 1557, and 1523 cm^{-1}. NMR (DMSO-d_6): δ 3.5 (broad, 1H), 6.74 (s, 1H), 7.8—8.1 (m, 3H), 8.31 (s, 1H), and 8.35—8.5 (m, 1H). UV(EtOH): 266 (log ε 4.48), 274.9 (4.60). 283.7 (4.54), 306 (3.72), 331 (3.78), and 350 nm (3.78).

*2-Chloro-6-methoxy-4,5-benzotropone (**8**)* (34 mg, 0.15 mmol) was similarly heated for 2 h with concentrated hydrochloric acid (0.3 ml) in ethanol (3 ml), giving the same product as described above (31 mg, 97%).

*2-Chloro-7-methoxy-4,5-benzotropone (**11**).* To a solution of 2,3-dimethoxynaphthalene (5.64 g, 0.03 mol) in chloroform (6 ml) and benzene (10 ml) were added triethylbenzylammonium chloride (0.12 g) and 40% aqueous potassium hydroxide (8 ml). After it had been stirred for 20 h at room temperature, the reaction mixture was worked-up as usual and the product was recrystallized from methanol to give 3.33 g of unchanged dimethoxynaphthalene. The filtrate was chromatographed on silica gel. The elute gave again 2.25 g of the starting material. The total recovery was 99%. The subsequent dichloromethane elute gave a yellow-brown crystalline product which, on sublimation (110 °C/2Torr) and recrystallization from methanol, afforded **11** as pale yellow needles (25 mg, 0.4%); mp 138—140 °C. The melting point was raised to 144—145 °C by repeated recrystallizations from methanol. Found: C, 65.10; H, 4.02%. Calcd for $C_{12}H_9O_2Cl$: C, 65.31; H, 4.12%. UV(EtOH): 244 (log ε 4.54), 250 (4.56), 286 (4.76), and 316 nm (4.06). IR(KBr): 1620(s), 1603sh, and 1538(w) cm^{-1}. NMR($CDCl_3$): δ 4.03 (s, 3H), 7.19 (s, 1H), 8.37 (s, 1H), and 7.6—7.9 (m, 4H).

*5-Chloro-3'-methoxy-2,3-benzotropone (**12**).* A mixture of 1,5-dimethoxynaphthalene, chloroform (twice the standard amount), 50% aqueous sodium hydroxide, and triethylbenzylammonium chloride was treated as usual. Benzene was added to the reaction mixture, and the crystals which precipitated were collected by filtration and extracted with ether by means of Soxhlet extractor, giving the starting material (2.85 g). The filtrate was evaporated and the brown residue was recrystallized from benzene to give a further amount of the starting substance (1.04 g). The mother liquor from recrystallization was charged on a silica gel-column chromatograph. The first fraction was the starting material (0.44 g), while the second was a yellow crystalline product which was rechromatographed and recrystallized to give 5-chloro-3'-methoxy-2,3-benzotropone (**12**) as yellow needles (93 mg, 1.4%); mp 123—124 °C. Found: C, 64.92; H, 4.05%. Calcd for $C_{12}H_9O_2Cl$: C, 65.31; H, 4.12%. UV(EtOH): 235 (log ε 4.42), 290 (3.99), and 348 nm (4.01). IR(KBr): 1630(w), 1586(s), and 1573(s) cm^{-1}. NMR($CDCl_3$): δ 3.99 (s, 3H), 6.78 (d, 1H, J= 13.0 Hz), 7.17 (dd, 1H, 13.0 and 2.0 Hz), 7.19 (dd, 1H, J=8.0 and 1.5 Hz), 7.63 (t, 1H, J=8.0 Hz), 8.01 (dd, 1H, J=8.0 and 1.5 Hz), and 8.27 (d, 1H, J=2.0 Hz).

*5-Chloro-4'-methoxy-2,3-benzotropone (**13**) and 2-Chloro-3'-methoxy-4,5-benzotropone (**14**).* The residue from the standard work-up in the reaction of 1,6-dimethoxynaphthalene was chromatographed on silica gel. The first elute was the recovered starting meterial (3.03 g, 55%). The second eluate (brown crystals) was rechromatographed on silica gel to give two crystalline fractions. One was recrystallized from benzene to give 5-chloro-4'-methoxy-2,3-benzotropone (**13**) as colorless leaflets (0.65 g, 9.9%); mp 144—144.5 °C. Found: C, 65.28; H, 4.03%. Calcd for $C_{12}H_9O_2Cl$: C, 65.31; H, 4.12%. UV(EtOH): 234.3 (log ε 4.26), 282 (4.53), and 340 sh nm (3.74). IR(KBr): 1624(w), 1583(s), and 1573(s) cm^{-1}. NMR($CDCl_3$): δ 3.96 (s, 3H), 6.81 (d, 1H, J=13.0 Hz), 6.9—7.5 (m, 4H), and 8.47 (d, 1H, J=9.0 Hz). The other was recrystallized from ethanol to give 2-chloro-3'-methoxy-4,5-benzotropone (**14**) as pale yellow needles (0.33 g, 4.9%); mp 198—199 °C. Found: C, 65.40; H, 4.36%. Calcd for $C_{12}H_9O_2Cl$: C, 65.31; H, 4.12%. UV(EtOH): 228 (log ε 4.41), 235 (4.40), and 294.8 nm (4.59). NMR($CDCl_3$): δ 4.02 (s, 3H), 7.16 (d, 1H, J=13.5 Hz), 8.35 (d, 1H, J=13.5 Hz), 8.17 (s, 1H), and 7.2—7.8 (m, 3H).

*5-Chloro-6,7-dimethoxy-2,3-benzotropone (**15**).* The mixture of 1,2,3-trimethoxynaphthalene (1.19 g, 5.5 mmol), chloroform (2 ml, 25 mmol), 50% aqueous sodium hydroxide (2 ml), and triethylbenzylammonium chloride (60 mg) was stirred for 16 h at room temperature. After the usual work-up, the red oily product was chromatographed on silica gel to give two fractions. The first was the recovered starting material (0.13 g, 11%). The second (yellow-orange crystals) was recrystallized from cyclohexane to give 5-chloro-6,7-dimethoxy-2,3-benzortopone (**15**) as yellow needles (0.38 g, 27.5%); mp 79—84 °C. Recrystallization from cyclohexane gave an analytical sample; mp 83.5—85 °C. Found: C, 62.62; H, 4.62%. Calcd for $C_{13}H_{11}O_3Cl$: C, 62.29; H, 4.42%. UV(EtOH): 250 sh (log ε 4.95), 265 (4.38), and 340 nm (3.83). IR(KBr): 1621(s), 1593(s), 1544(w), and 1519(m) cm^{-1}. NMR($CDCl_3$): δ 3.92 (s, 3H), 3.99 (s, 3H), 7.6—7.8 (m, 4H), and 8.4—8.6 (m, 1H). Diels-Alder adduct (**17**) with maleic anhydride: colorless crystals, mp 183—184 °C. Found: C, 58.25; H, 3.64%. Calcd for $C_{17}H_{13}O_6Cl$: C, 58.55; H, 3.76%. NMR($CDCl_3$): δ 3.73 (s, 3H), 3.85 (s, 4H), 4.05 (d, 1H, J=9.6 Hz), 4.29 (d, 1H, J=2.0 Hz), 7.4—7.7 (m, 3H), and 8.1—8.3 (m, 1H).

*5-Chloro-4,6-dimethoxy-2,3-benzotropone (**18**).* A reaction mixture obtained from the standard work-up in the

reaction of 1,2,4-trimethoxynaphthalene was chromatographed on silica gel to give the starting material (4.27 g, 81.3%), as well as 5-chloro-4,6-dimethoxy-2,3-benzotropone (**18**) as straw-colored crystals (1.15 g, 17.8%), the recrystallization of which from cyclohexane gave an analytical sample, mp 98—99 °C. Found: C, 62.47; H, 4.54%. Calcd for $C_{13}H_{11}O_3Cl$: C, 62.29; H, 4.42%. IR(KBr): 1620(s), 1590(s), 1561(s), and 1540(w) cm^{-1}. NMR($CDCl_3$): δ 3.74 (s, 3H), 3.87 (s, 3H), 6.29 (s, 1H), 7.6—7.85 (m, 2H), and 8.0—8.35 (m, 2H). Diels-Alder adduct (**20**) with maleic anhydride: colorless crystals; mp 215—216 °C. Found: C, 58.60; H, 3.80%. Calcd for $C_{17}H_{13}O_6Cl$: C, 58.55; H, 3.76%. NMR($CDCl_3$): δ 3.71 (s, 3H), 2.72 (dd, 1H, J=9.6 and 1.6 Hz), 3.94 (s, 3H), 4.22 (d, 1H, J=9.6 Hz), 4.42 (d, 1H, J=1.6 Hz), 7.4—7.7 (m, 3H), and 8.1—8.4 (m, 1H).

The authors are indebted to Professor Masamatsu Hoshino of this university for providing some of the authentic samples of benzotropone derivatives for the mixed melting point determination.

References

1) W. E. Parham and H. E. Reiff, *J. Am. Chem. Soc.*, **77**, 1177 (1955).
2) S. D. Saraf, *Can. J. Chem.*, **47**, 1169 (1969).
3) W. E. Parham, D. A. Bolon, and E. E. Schweizer, *J. Am. Chem. Soc.*, **83**, 603 (1961); b) M. K. Saxena and M. M. Bokadia, *J. Indian Chem. Soc.*, **46**, 12 (1969); c) T. Shimozawa, S, Kumakura, M. Hoshino, and S. Ebine, *Bull. Chem. Soc. Jpn.*, **44**, 586 (1971); d) S. Ebine, M. Hoshino, and T. Machiguchi, *ibid.*, **44**, 3480 (1971); e) M. V. Moncur and J. B. Grutzner, *J. Chem. Soc. Chem. Commun.*, **1972**, 667.
4) J. Tsunetsugu, M. Sato and S. Ebine, *J. Chem. Soc. Chem. Commun.*, **1973**, 363.
5) M. Sato, S. Ebine and J. Tsunetsugu, *J. Chem. Soc. Chem. Commun.*, **1974**, 846; Corrigenda, *ibid.*, **1975**, 236.
6) W. Kirme, "Carbene Chemistry," 2nd ed., Academic Press, New York and London (1971), p. 296.
7) M. Makosza and W. Warwzyniewicz, *Tetrahedron Lett.*, **1969**, 4659.
8) M. Hoshino and S. Ebine, *Bull. Chem. Soc. Jpn.*, **43**, 1781 (1970).
9) S. Ebine, M. Hoshino, and K. Takahashi, *Bull. Chem. Soc. Jpn.*, **41**, 2942 (1968).
10) F. Nerdel, J. Buddrus, W. Brodowski, J. Windhoff, and D. Klaman, *Tetrahedron Lett.*, **1968**, 1175.
11) G. Blume, T. Neumann, and P. Weyerstahl, *Ann.*, **1975**, 201.
12) R. W. Murray, *Tetrahedron Lett.*, **1960**, 27.
13) G. Blume and P. Weyerstahl, *Tetrahedron Lett.*, **1970**, 3669; *Tetrahedron*, **28**, 5281 (1972).
14) J. Tsunetsugu, M. Sato, and S. Ebine, *Analytical Instruments (Japan)*, **13**, 431 (1975).
15) M. Sato, T. Tanaka, J. Tsunetsugu, and S. Ebine, *Bull. Chem. Soc. Jpn.*, **48**, 2395 (1975).
16) R. Heck and S. Winstein, *J. Am. Chem. Soc.*, **79**, 3112 (1957).
17) A. Ueno and S. Fukushima, *Chem. Pharm. Bull.*, **14**, 129 (1966).
18) C. J. P. Spruit, *Rec. Trav. Chim. Pays-Bas*, **68**, 309 (1949).
19) Although no synthetic detail is given, see F. Serratosa and P. Sala, *Tetrahedron Lett.*, **1973**, 821.
20) L. F. Fieser, *J. Am. Chem. Soc.*, **50**, 461 (1928).

Studies on 1,2,4-Thiadiazolidine Derivatives. I. The Synthesis and Structural Determination of 2,4-Disubstituted 3,5-Disubstituted Imino-1,2,4-thiadiazolidines

Takeshi KINOSHITA, Sadao SATO, and Chihiro TAMURA

Central Research Laboratories, Sankyo Co., Ltd., Hiromachi Shinagawa-ku, Tokyo 140

(Received December 9, 1975)

The reaction of symmetrical thiourea derivatives, RNHCSNHR, with benzoyl peroxide (BPO) gave only one isomer of 2,4-disubstituted 3,5-disubstituted imino-1,2,4-thiadiazolidines, and that of nonsymmetrical thiourea derivatives, RNHCSNHR′, with BPO yielded a mixture of some of the possible isomeric derivatives. The structures of these compounds were determined by means of NMR, mass spectra, and X-ray analyses. The steric effects of peripheral groups around the thiadiazolidine ring and some reaction mechanism are discussed.

In the past years, we have studied the oxidation reactions of thiourea derivatives with benzoyl peroxide (BPO). As reported in a preliminary paper, the oxidation of 1,3-dimethylthiourea with BPO was found to afford 2,4-dimethyl-3,5-bis(methylimino)-1,2,4-thiadiazolidine (**1a**). This reaction was initially discovered in a mass spectrometer, wherein both reagents were made to react in a sample tube and we called this a mass spectrometry reaction.[1] Later on, substance **1a** was synthesized on a laboratory scale in a good yield. In 1890 Hector[2] reported the oxidation of 1,3-diphenylthiourea by use of hydrogen peroxide and assigned, without sufficient evidence, the structure **1k** (mp 136 °C) to the product of the reaction. However, IR ane UV spectral data[3] have shown that the assignment is erroneous and the structure represented by **2** is correct. This assignment has also been confirmed by an independent synthesis from 2-anilinobenzothiazole with diphenylcarbodiimide.[4]

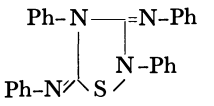

1k

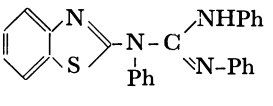

2

However, under our experimental conditions, the oxidation of 1,3-diphenylthiourea afforded 2,4-diphenyl-3,5-bis(phenylimino)-1,2,4-thiadiazolidine (**1k**, mp 51—52 °C) along with 1-benzoyl-1,3-diphenylurea. Many homologous derivatives could be synthesized under similar reaction conditions. The present paper describes these oxidation reactions and structural evidences for the related products.

Results and Discussion

Various types of thiourea derivatives have been examined as substrates for the BPO oxidation. The overall reaction may be represented in the following scheme, wherein the major by-products were benzoic acid and sulfur. The same reaction conditions were employed throughout this work, *i.e.*, the reactions were carried out by stirring the dichloromethane solution of thiourea derivatives with 1.15 equivalents of BPO for one hour at 5—10 °C. Most of the structures of the reaction products have been established by means of NMR, IR, and mass spectra and the final structural assignments of some isomers required X-ray analyses.

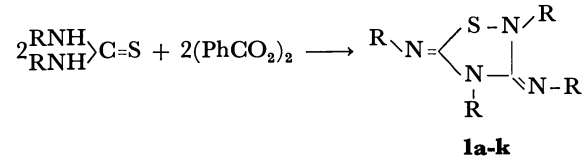

1a-k

+ $4PhCO_2H$ + $1/8\ S_8$

The first choice as the substrate for the reaction was symmetrical thiourea derivatives, RNHCSNHR, which gave 1,2,4-thiadiazolidines, **1a—k**. The fundamental reaction product of **1a** ($C_6H_{12}N_4S$, *m/e* 172) was obtained from 1,3-dimethylthiourea. The NMR spectrum showed four singlet peaks at 2.49, 3.00, 3.11, and 3.28 (δ, ppm, C_6D_6). The IR absorption at 1650 cm^{-1} and the UV spectrum, λ_{max} 229 nm (EtOH), indicate that none of the C=N bonds in this molecule are conjugated. The data including the major mass fragment ions of *m/e* 102 ($M^+ - CH_3NCNCH_3$), 73 (CH_3NCS), 70 (CH_3NCNCH_3), and 61 (CH_3NS), strongly suggest that the product **1a** should be 2,4-dimethyl-3,5-bis-(methylimino)-1,2,4-thiadiazolidine.* The formation of such a thiadiazolidine ring system has also been established by an independent X-ray analysis of an other derivative as described in a later section.

Other 1,2,4-thiadiazolidine derivatives were synthesized by similar reactions (Table 1). Boiling points of some products (**1e—i**) were difficult to measure since they easily decomposed even under reduced pressure (*ca.* 2 mmHg). The yields of **1a—k** were determined by weighing the product directly after isolation by column chromatography. The mass spectrum of one of these derivatives, **1k**, is shown Fig. 1.

Four structural isomers are possible in this series of compounds as shown in Fig. 2, but in fact only one isomer could be isolated. The three isomers, **1a′**, **1a″**, and **1a‴** might be unstable, since their molecular models are considerably sterically hindered; the methyl group at the 4-position in each structure can be but-

* There is another possibility of producing the mirror symmetrical derivative, *i.e.*,

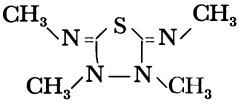

but in the NMR spectrum of **1a**, the chemical shifts of the four methyl groups have quite different values indicating that they are each situated in a different intramolecular environment. This homologue can therefore be excluded.

TABLE 1. PHYSICAL PROPERTIES AND ANALYTICAL DATA OF 1,2,4-THIADIAZOLIDINES (**1**)

Compd	R	Yield (%)	Bp °C/mmHg (Mp °C)	GLC[a] Time	GLC[a] Temp	IR[b] (cm^{-1}) C=N	Molecular[c] formula	Found (Calcd) C%	H%	N%	S%
1a	CH_3	40	88—90/2	1.42	150	1650	$C_6H_{12}N_4S$	41.78	7.06	32.45	18.68
								(41.84	7.02	32.53	18.61)
1b	CH_3CH_2	65	104—106/2.5	1.83	150	1640	$C_{10}H_{20}N_4S$	52.51	8.74	24.63	14.38
								(52.60	8.83	24.53	14.04)
1c	$CH_3CH_2CH_2$	68	126—128/2	1.83	180	1640	$C_{14}H_{28}N_4S$	59.63	9.76	19.48	11.11
								(59.11	9.92	19.70	11.27)
1d	$CH_3(CH_2)_3$	65	144—146/1.5	6.17	180	1640	$C_{18}H_{36}N_4S$	63.27	10.55	16.49	9.65
								(63.48	10.65	16.45	9.41)
1e	$CH_3(CH_2)_4$	63	oil[d]	2.33	230	1640	$C_{22}H_{44}N_4S$	66.53	11.24	14.03	8.35
								(66.61	11.18	14.12	8.08)
1f	$CH_3(CH_2)_5$	67	oil[d]	6.50	230	1640	$C_{26}H_{52}N_4S$	68.82	11.55	12.58	7.32
								(68.97	11.58	12.37	7.08)
1g	$CH_3(CH_2)_6$	72	oil[d]	3.17	270	1640	$C_{30}H_{60}N_4S$	70.66	12.00	10.94	6.40
								(70.81	11.88	11.01	6.30)
1h	$CH_3(CH_2)_7$	70	oil[d]	7.92	270	1640	$C_{34}H_{68}N_4S$	72.10	12.09	9.97	5.80
								(72.28	12.13	9.92	5.67)
1i	$EtOCH_2CH_2$	67	oil[d]	3.75	230	1640	$C_{18}H_{36}N_4O_4S$	53.58	9.01	13.75	8.02
								(53.44	8.97	13.85	7.92)
1j	$C_6H_5CH_2$	57	(81.5)	—	—	1630	$C_{30}H_{28}N_4S$	75.54	5.98	11.61	6.92
								(75.60	5.92	11.75	6.73)
1k	C_6H_5	13	(51—52)	—	—	1625	$C_{26}H_{20}N_4S$	74.31	4.75	13.28	7.69
								(74.26	4.79	13.32	7.62)

a) 2% Silicone OV-17 on Gas Chrom Q (80—100 mesh), 1 m×2 mm i. d. glass column, flow rate: 30 ml/min He, retention time in min. b) Measured in liq. film (**1a—i**) and Nujol mulls (**1j—k**). c) Molecular formula were determined by high resolution mass spectrometry. d) Decomposed at 170—200 °C (bath temp)/2—3 mmHg.

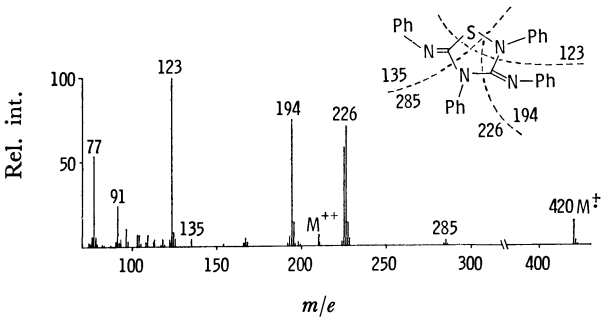

Fig. 1. Mass spectrum of **1k**.

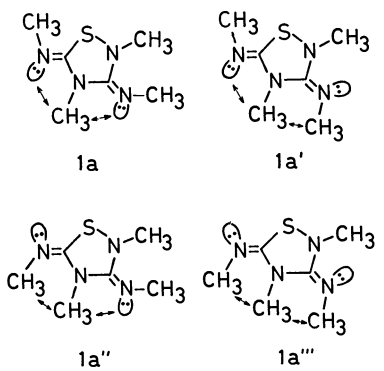

Fig. 2. Geometrical isomers of 2,4-dimethyl-3,5-bis-(methylimino)-1,2,4-thiadiazolidine.

tressed either by one or two adjacent methyl groups.[5] The lone pair electrons on the imino nitrogen atoms attached to the 3- and 5-positions might affect neighbouring substituents to a smaller extent than methyl groups. The hindrances are shown by the double headed arrows in Fig. 2.

Structurally interesting molecules could be synthesized from the nonsymmetrical thiourea derivatives ($R^1NHCSNHR^2$; R^1=aryl, R^2=alkyl). There are sixteen possible different isomeric 1,2,4-thiadiazolidine derivatives through these reactions. Even if we neglect the three labile isomers such as **1a'**, **1a''**, and **1a'''**, and the four possible isomers of each (Fig. 2), there are still four isomers, **A**, **B**, **C**, and **D** left:

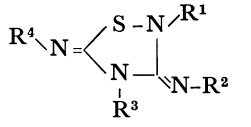

A; $R^1=R^3$=alkyl, $R^2=R^4$=aryl
B; $R^1=R^4$=aryl, $R^2=R^3$=alkyl
C; $R^1=R^4$=alkyl, $R^2=R^3$=aryl
D; $R^1=R^3$=aryl, $R^2=R^4$=alkyl

Three of these isomers could be obtained from the derivatives of 1-alkyl-3-arylthiourea. They were isolated by means of column chromatography or solubility differences in ethanol. The molecular structure of **3a** (**A**-type) was determined by X-ray analysis. The NMR spectrum of **3a** gave upfield (δ, 2.68) and down field (δ, 3.44) absorptions which were assigned to the N2 and N4 methyl groups, respectively. The assignments could be made by considering the shielding effects exerted by the diamagnetic anisotropy of the phenyl groups.

The mass spectrum of **3a** (Fig. 3) shows an ion at

m/e 226 ($C_{13}H_{10}N_2S$, MW. obsd=226.057, MW. calcd=226.056) which corresponds to the ($M^+-C_3H_6N_2$) ion. This should arise from the transannular cleavage of **3a-B** ion. Thus, the results of the mass spectrum and X-ray analysis for **3a** are apparently inconsistent. Such conflicting evidence can be explained by an intramolecular rearrangement induced by electron bombardment when the mass spectral measurement is taken.[6] Such a reaction is shown in the following scheme:

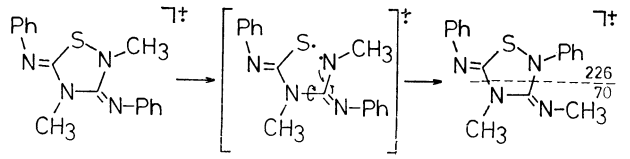

3a 3a-B

The analytical data of some **A**-type isomers are summarized in Tables 2 and 3. Their structures were established by comparison of the chemical shifts in the NMR spectra and the mass fragmentation patterns with those of **3a**.

The same reactions for thiourea derivatives containing more bulky groups at the *ortho* position in the phenyl group, such as 1-methyl-3-*o*-tolylthiourea or 1-methyl-3-(2,6-xylyl)thiourea, were carried out. These thiourea derivatives reacted with BPO to give the corresponding 1,2,4-thiadiazolidine derivatives which are sterically more hindered around the 1,2,4-thiadiazolidine ring system.

These structures were also assigned to **5** and **6** by the same procedure.

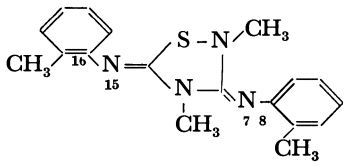

5

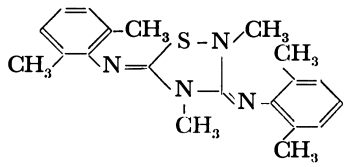

6

Table 4 shows the chemical shifts of the N2 and N4 methyl groups of **3a**, **5**, and **6**, in which the diamagnetic shift of the N2-methyl protons induced by virture of the benzene rings increases in the order of **6**>**5**>**3a**. Thus, the rotational angles about N7–C8 and N15–C16 bonds seem to parallel the increasing degree of steric hindrance.

On the other hand, it is noteworthy that 1-*t*-butyl-3-methylthiourea is oxidized to the corresponding urea and benzoic anhydride but not to a 1,2,4-thiadiazolidine derivative. In view of these results we propose the reaction mechanism as shown in Scheme 1.

TABLE 2. PHYSICAL PROPERTIES AND ANALYTICAL DATA OF 1,2,4-THIADIAZOLIDINES (**3**)

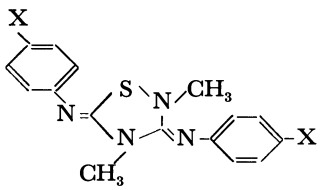

Compd	X	Yield (%)	Mp °C	NMR (δ)[a] N(2)CH_3	NMR (δ)[a] N(4)CH_3	IR[b] (cm^{-1}) C=N	Molecular[c] formula	Found (Calcd) C%	H%	N%	S%
3a	H	58	137.5	2.67	3.43	1622	$C_{16}H_{16}N_4S$	64.69	5.68	19.19	10.88
								(64.84	5.44	18.90	10.82)
3b	Me	59	136	2.67	3.41	1620	$C_{18}H_{20}N_4S$	66.71	6.23	17.08	9.91
								(66.64	6.21	17.27	9.88)
3c	OMe	64	118	2.69	3.41	1630	$C_{18}H_{20}N_4O_2S$	60.32	5.70	15.81	9.08
								(60.65	5.66	15.72	8.99)
3d	F	67	76.5	2.70	3.41	1612	$C_{16}H_{14}F_2N_4S$	57.74	4.29	16.92	9.80
								(57.82	4.25	16.86	9.65)
3e	Cl	71	126.5	2.72	3.41	1612	$C_{16}H_{14}Cl_2N_4S$	52.55	3.74	15.45	8.88
								(52.61	3.86	15.34	8.78)
3f	Br	62	128.5	2.73	3.42	1618	$C_{16}H_{14}Br_2N_4S$	42.71	3.27	12.20	7.16
								(42.31	3.11	12.34	7.06)
3g	I	53	186	2.72	3.40	1620	$C_{16}H_{14}I_2N_4S$	34.84	2.54	10.23	5.99
								(35.06	2.57	10.22	5.85)
3h	Ac	38	120.5	2.74	3.46	1612	$C_{20}H_{20}N_4O_2S$	63.18	5.23	14.77	8.44
								(63.14	5.30	14.73	8.43)
3i	NO_2	13	199.5	(2.82)	(3.50)	1616	$C_{16}H_{14}N_6O_4S$	49.94	3.75	21.71	8.43
								(49.74	3.65	21.75	8.30)

TABLE 3. PHYSICAL PROPERTIES AND ANALYTICAL DATA OF 1,2,4-THIADIAZOLIDINES (**4**)

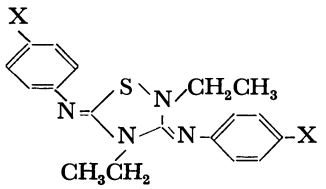

Compd	X	Yield (%)	Mp °C	NMR (δ)[a] N(2)CH_2	NMR (δ)[a] N(4)CH_2	IR[b] (cm^{-1}) C=N	Molecular[c] formula	Found (Calcd) C%	H%	N%	S%
4a	H	27	77.5	2.99	4.09	1625	$C_{18}H_{20}N_4S$	66.47	6.18	17.16	10.01
								(66.64	6.21	17.27	9.88)
4b	Me	30	93	2.98	4.06	1625	$C_{20}H_{24}N_4S$	68.48	6.76	15.63	9.11
								(68.15	6.86	15.89	9.10)
4c	OMe	31	80.5	2.98	4.05	1613	$C_{20}H_{24}N_4O_2S$	62.97	6.26	14.81	8.41
								(62.48	6.29	14.57	8.34)
4d	F	34	99	3.01	4.06	1625	$C_{18}H_{18}F_2N_4S$	59.90	4.98	15.71	8.98
								(59.98	5.03	15.54	8.90)
4e	Cl	26	117	3.03	4.06	1610	$C_{18}H_{18}Cl_2N_4S$	55.15	4.59	14.20	8.33
								(54.97	4.61	14.24	8.15)
4f	Br	49	161	3.04	4.06	1615	$C_{18}H_{18}Br_2N_4S$	45.00	3.83	11.70	6.88
								(44.83	3.76	11.62	6.65)
4g	I	49	198.5	(3.02)	(4.04)	1610	$C_{18}H_{18}I_2N_4S$	37.75	3.30	9.79	5.58
								(37.52	3.15	9.72	5.56)

a) Observed in CCl_4($CDCl_3$). b) Measured in Nujol mulls. c) Determined by high resolution mass spectrometry.

TABLE 4. PROTON CHEMICAL SHIFTS OF **3a**, **5**, AND **6** (δ, ppm)

Compd	N(2)-CH_3 CCl_4	N(2)-CH_3 C_6D_6	$\Delta^{CCl_4}_{C_6D_6}$	N(4)-CH_3 CCl_4	N(4)-CH_3 C_6D_6	$\Delta^{CCl_4}_{C_6D_6}$
3a	2.67	2.16	+0.51	3.43	3.30	+0.13
5	2.60	2.13	+0.47	3.48	3.38	+0.10
6	2.48	2.08	+0.40	3.47	3.46	+0.01

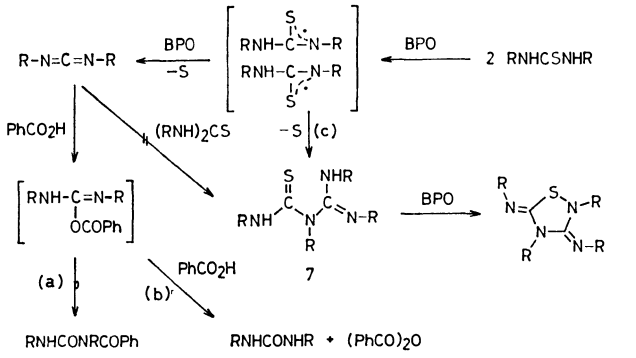

Scheme 1.

Zetzsche and his collaborators studied the reactions of carbodiimides with carboxylic acids,[7] wherein two reaction paths were reported: (a) the formation of *N*-acylureas and (b) the formation of acid anhydrides and ureas. As a general rule, aromatic carbodiimides react through route (a), but aliphatic carbodiimides give mainly acid anhydrides through route (b).[8]

Free rotation about the N-C(phenyl) bond in such a thiourea derivative as 1-methyl-3-(2,6-xylyl)thiourea may act to minimize steric hindrance when the reactants are brought closely together. However, 1-*t*-butyl-3-methylthiourea which has an even more bulky substituent may resist passing through route (c). Consequently, the latter reacts to produce a carbodiimide as a transient intermediate through route (b).

There are other reasons to support the mechanism of the formation of 1,2,4-thiadiazolidines through route (c) in Scheme 1.

1) No additional product was obtained when the mixture of 1,3-dimethylthiourea and 1,3-diisopropylcarbodiimide was brought to react in CH_2Cl_2 at room temperature for a long period. Thus the corresponding carbodiimide is not an intermediate for the formation of 1,2,4-thiadiazolidines.

2) Using a smaller amount of BPO with 1,3-diethylthiourea, the intermediate **7a** (R=Et in Scheme 1) could be isolated. Further reaction of **7a** with BPO yielded 2,4-diethyl-3,5-bis(ethylimino)-1,2,4-thiadiazolidine (**1b**). The structures of **7a** and **1b** were confirmed by their mass spectra as shown in Figs. 4 and 5,

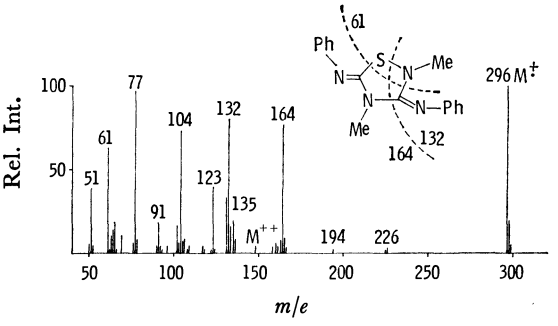

Fig. 3. Mass spectrum of **3a**.

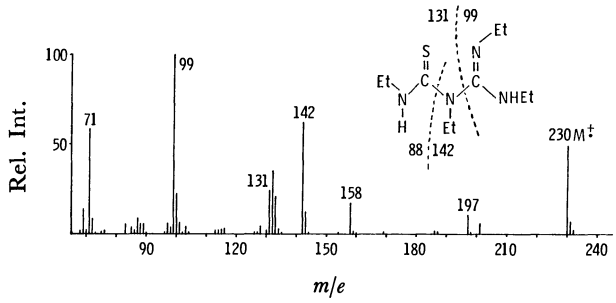

Fig. 4. Mass spectrum of **7a**.

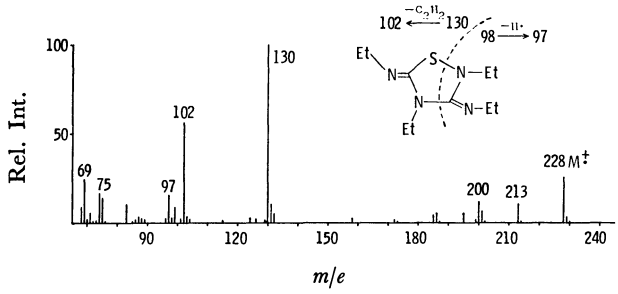

Fig. 5. Mass spectrum of **1b**.

respectively.

3) Treatment of *N*-methyl-4-morpholinethiocarboxamide(**8**) with BPO gave N^1,N^2-dimethyl-N^1-morpholinothiocarbonyl-4-morpholinecarboxamidine(**9**) which is an analog of the intermediate **7** *via* route (c). The molecular structure of **9** was determined by X-ray analysis.

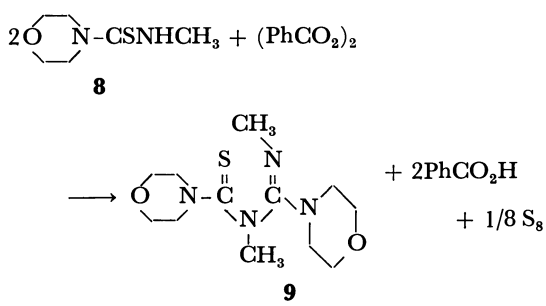

The investigation of the **B**, **C**, and **D** isomers of 1,2,4-thiadiazolidine derivatives is currently under progress.[9]

Experimental

All the melting points were measured on a Mitamura Riken micromelting point apparatus and are uncorrected. The IR spectra were obtained on a JASCO IRA-2 spectrophotometer and the UV spectra on a Cary 14 spectrophotometer. The NMR spectra were taken on a Varian A-60D spectrometer, using tetramethylsilane as an internal standard, and the mass spectra on a JEOL JMS-O1SG mass spectrometer, using a direct inlet and an ionization energy of 75 eV. The GLC analyses were carried out on a JEOL JGC-20KFP gas chromatograph equipped with a flame-ionization detector.

Materials. Commercial methyl, ethyl, *p*-nitrophenyl, phenyl isothiocyanates, benzoyl peroxide, and amines of the purest grade were used. Thiourea derivatives were prepared according to methods in literatures.[10-12]

Reaction of Symmetric Thioureas with BPO. To a solution of 1,3-dimethylthiourea (10.4 g, 0.1 mol) in dichloromethane (200 ml) was added dropwise a solution of BPO (27.8 g, 0.115 mol) in dichloromethane (200 ml) at 5—10 °C. After addition was over, the resulting slurry was stirred at the same temperature for one hour. The solution was then washed with an aqueous solution of sodium hydroxide (10 g, 0.25 mol) to remove benzoic acid.

The solvent was removed under reduced pressure and the resulting residue was chromatographed with petroleum ether–AcOEt (6 : 1) on a silica gel column to give **1a** (3.44 g). The physical properties and analytical data of **1a** are summarized in Table 1 along with the other derivatives (**1b-k**).

Reaction of Nonsymmetric Thioureas with BPO. From a dropping funnel, a solution of BPO (14 g, 0.058 mol) in CH_2Cl_2 (200 ml) was added to a solution of 1-methyl-3-phenylthiourea (8.3 g, 0.05 mol) in CH_2Cl_2 (200 ml) at 5—10 °C, and the reaction mixture was stirred at the same temperature for 1 h. Benzoic acid was removed with an aqueous solution of NaOH, and the solvent was removed under reduced pressure. The resulting residue was dissolved in cold acetone and filtered to remove the insoluble sulfur. After evaporation of the solvent, the residue was triturated with a small amount of cold ethanol and filtered to give **3a** (2.8 g). The filtrate was separated on a silica gel column using petroleum ether–AcOET (6 : 1) as an eluent to give **3a** (1.5 g). The physical properties and analytical data for the thiadiazolidine (**3a-i**, and **4a-g**) are summarized in Tables 2 and 3. Compounds **5** and **6** were obtained in a similar manner: **5** (in a 62% yield) oil. GLC: Retention Time 3.0 min, 2% Silicone OV-17 on Gas Chrom Q (80—100 mesh), 1 m×2 mm i. d. glass column, He flow rate 30 ml/min. Found: C, 66.69; H, 6.24; N, 17.22; S, 9.94%. Calcd for $C_{18}H_{20}N_4S$: C, 66.64; H, 6.21; N, 17.27; S, 9.88%. IR (Nujol): 1628 cm^{-1} (ν C=N). NMR (CCl_4): δ 2.19 (s, 3H), 2.23 (s, 3H), 2.60 (s, 3H), 3.48 (s, 3H), and 6.7—7.3 (m, 8H). **6** (in a 32% yield): mp 133.5 °C (from ethanol). Found: C, 68.23; H, 6.85; N, 15.68; S, 9.13%. Calcd for $C_{20}H_{24}N_4S$: C, 68.15; H, 6.86; N, 15.89; S, 9.10%. IR(Nujol): 1630 cm^{-1} (ν C=N). NMR (CCl_4): δ 2.12 (s, 6H), 2.48 (s, 3H), 3.47 (s, 3H), and 6.7—7.0 (m, 6H).

Reaction of 1-t-Butyl-3-methylthiourea with BPO. To a solution of 1-*t*-butyl-3-methylthiourea (0.05 mol) in CH_2Cl_2 was added a solution of BPO (0.06 mol) in CH_2Cl_2 with stirring under ice-cooling. The reaction is exothermic and started at once. After stirring for 1 h, the solvent was removed under reduced pressure and the residue was chromatographed over silica gel to give 1-*t*-butyl-3-methylurea, 1-*t*-butyl-3-benzoyl-3-methylurea and other by-products. None of 1,2,4-thiadiazolidine derivatives could be isolated under these conditions.

Isolation of the Intermediary Compound 7a. A solution of BPO (12.1 g, 0.05 mol) in CH_2Cl_2 was added dropwise to a solution of 1,3-diethylthiourea (13.2 g, 0.1 mol) in CH_2Cl_2 (200 ml) during 10 min with stirring under ice-cooling. The reaction mixture was kept at 5—10 °C for 30 min, and then washed with a solution of NaOH to remove the benzoic acid. After removal of CH_2Cl_2, the residue was separated on a silica gel column using ether as an eluent, and **7a** was isolated in a 2% yield (230 mg) along with the main product **1b**. Upon recrystallization from ether **7a** was obtained as colorless needles, mp 76.5 °C. Found: C, 52.23; H, 9.65; N, 24.28; S, 13.97%. Calcd for $C_{10}H_{22}N_4S$: C, 52.14; H, 9.63; N, 24.32; S, 13.92%. IR (Nujol): 3200, 1650, and 1560 cm^{-1}. NMR (CCl_4): δ 1.13 (t, 6H, J=7 Hz), 1.16 (t, 3H, J=7 Hz), 1.18 (t, 3H, J=7 Hz), 3.10 (q, 4H, J=7 Hz), 3.55 (q, 2H, J=7 Hz), and 3.88 (q, 2H, J=7 Hz).

Reaction of N-Methyl-4-morpholinethiocarboxamide 8 with BPO.

According to the usual procedure for the synthesis of thioureas, **8** was prepared from morpholine and methyl isothiocyanate. To a solution of **8** (3.2 g, 0.02 mol) in CH_2Cl_2 (200 ml) was added BPO (2.76 g, 0.0115 mol) portionwise at 5 °C. Separation was carried out in the same way as in the case of symmetric thioureas to give N^1,N^3-dimethyl-N^1-morpholinothiocarbonyl-4-morpholinecarboxamidine **9** (2.4 g, 84%), mp 151.5 °C (from benzene). Found: C, 50.37; H, 7.72; N, 19.50; S, 11.22%. Calcd for $C_{12}H_{22}N_4O_2S$: C, 50.32; H, 7.74; N, 19.50; S, 11.19%. IR (Nujol): 1645, 1470, 1300, and 1115 cm^{-1}. NMR (CCl_4): δ 2.94 (s, 3H), 3.22 (s, 3H), and 3.0—4.2 (m, 16H). Mass: *m/e* (rel. intensity) 286 (13, M^+), 271 (7, $M^+ - CH_3$), 253 (6, $M^+ - HS$), 200 (17, $M^+ - C_4H_8NO$), 127 (100, $M^+ - C_6H_{11}N_2OS$), 86 (12), and 83 (26).

Structure Determination by Means of X-Ray Analysis

Compounds **3a** and **9** were recrystallized from ethanol and from benzene, respectively. Intensity data of **3a** were obtained on a Rigaku four-circle automatic diffractometer with $\omega/2\theta$ scan technique up to $2\theta \leq 55°$ using Mo$K\alpha$ radiation, and those of **9** were collected from the equi-inclination Weissenberg photographs (*hk*0—*hk*6) with Cu$K\alpha$ radiation. They were corrected as regards Lorentz and polarization factors. No absorption correction was applied. Reflections of 1478 and 2439 were used for **3a** and **9**, respectively. The crystal data are given in Table 5.

3a: The structure of **3a** was solved by the symbolic addition technique. Nine atoms involving the thiadiazolidine ring system were revealed on the first E-map. Subsequent Fourier synthesis gave the position of all non-hydrogen atoms. Refinement of this structure was carried out by the block diagonal least-squares method to give the final *R*-factor of 0.082 including hydrogen atoms which are obtained from the difference map.

9: The structure of **9** was determined by the Patterson method. Several cycles of a block-diagonal least-squares refinement for all the atoms except hydrogen atoms gave the final *R*-factor of 0.133.

The fractional coordinates and anisotropic thermal parameters for **3a** and **9** are given in Tables 6 and 7, respectively, together with their standard deviations.

Table 5. Crystal data of **3a** and **9**

	3a	**9**
Formula	$C_{16}H_{16}N_4S$	$C_{12}H_{22}N_4O_2S$
M. W.	297.4	286.4
a (Å)	23.69	11.13
b	15.42	9.51
c	8.09	7.61
α (°)	90	100.8
β	90	86.1
γ	90	116.2
V (Å^3)	2955	710
Space group	Pccn	$P\bar{1}$
Z	8	2
D_{obsd} (g cm^{-3})	1.30	1.32
D_{calcd}	1.31	1.34

Lists of observed and calculated structure factors are preserved by the Chemical Society of Japan. (Document No. 7631)

Results and Discussion

3a:[13] The bond lengths and angles are given in Fig. 6. The estimated standard deviations in the bond lengths range from 0.009 to 0.016 Å; those for the bond angles range from 0.5 to 0.9°. A stereoscopic view of the molecule projected along the b-axis is shown in Fig. 7. The deviations from various least-squares planes are given in Table 8.

The S(1)–N(2) and S(1)–C(5) bond lengths of 1.731 and 1.750 Å are comparable with those found in the S(II)–Nsp^3 and S(II)–Csp^2 single bonds. The mean

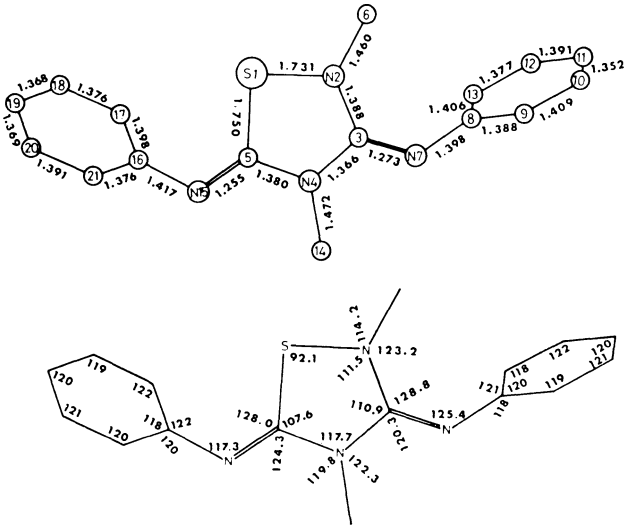

Fig. 6. Bond lengths (Å) and angles (°) of **3a**.
The mean estimated standard deviation of bond lengths is 0.011 Å, and that of bond angles is 0.7°.

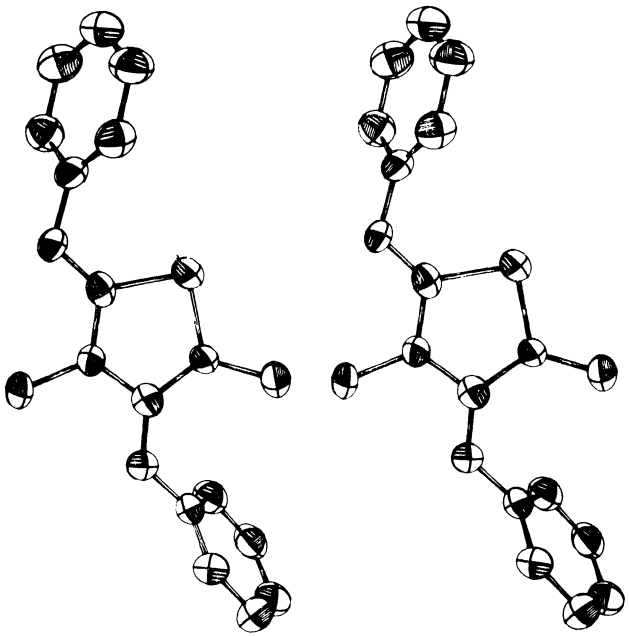

Fig. 7. Stereoscopic view down the b axis of **3a**.

TABLE 6a. FRACTIONAL COORDINATES AND ANISOTROPIC THERMAL PARAMETERS ($\times 10^4$) OF **3a**
Estimated standard deviations are given in parentheses. The anisotropic thermal parameters are in the form: $\exp[-(b_{11}h^2+b_{22}k^2+b_{33}l^2+b_{12}hk+b_{13}hl+b_{23}kl)]$.

	x	y	z	b_{11}	b_{22}	b_{33}	b_{12}	b_{13}	b_{23}
S (1)	4716(1)	1151(2)	3057(3)	12(1)	73(1)	131(3)	−2(1)	4(1)	21(2)
N (2)	5349(2)	1027(4)	4098(7)	11(1)	51(4)	108(9)	1(2)	3(3)	17(5)
C (3)	5806(3)	1218(5)	3089(10)	14(1)	45(4)	129(13)	1(2)	5(4)	−6(7)
N (4)	5634(2)	1373(4)	1505(7)	13(1)	43(4)	89(9)	−4(2)	2(3)	−8(5)
C (5)	5061(3)	1388(5)	1199(9)	15(1)	28(4)	114(12)	−2(2)	9(3)	−18(6)
C (6)	5325(3)	1262(6)	5845(10)	17(2)	68(5)	110(11)	7(3)	7(4)	3(7)
N (7)	6328(2)	1255(5)	3463(8)	12(1)	57(4)	119(11)	−1(2)	−2(3)	10(6)
C (8)	6565(3)	962(5)	4943(9)	12(1)	47(4)	109(12)	2(2)	4(3)	−12(6)
C (9)	6938(3)	1507(6)	5761(11)	14(1)	61(5)	151(14)	−3(2)	−1(4)	−10(8)
C (10)	7216(3)	1202(6)	7187(11)	18(2)	71(6)	146(15)	−1(3)	−8(4)	−21(9)
C (11)	7130(3)	385(6)	7740(11)	13(2)	80(6)	169(17)	10(3)	0(4)	4(9)
C (12)	6759(3)	−157(6)	6900(11)	16(2)	62(5)	168(16)	5(2)	12(5)	14(9)
C (13)	6479(3)	108(6)	5497(11)	15(2)	53(5)	168(15)	2(2)	4(4)	12(8)
C (14)	6035(3)	1454(6)	124(9)	17(2)	64(5)	97(12)	2(3)	5(4)	31(7)
N (15)	4846(2)	1503(4)	−202(7)	15(1)	47(4)	95(10)	−1(2)	−4(3)	23(5)
C (16)	4250(3)	1512(6)	−302(9)	15(1)	49(5)	118(13)	−1(2)	−6(4)	19(7)
C (17)	3923(3)	2154(5)	459(11)	19(2)	38(4)	162(15)	0(2)	−8(4)	−20(7)
C (18)	3346(3)	2177(6)	282(12)	17(2)	57(5)	212(19)	6(2)	−6(5)	−4(8)
C (19)	3085(4)	1563(7)	−669(12)	16(2)	72(6)	209(18)	4(3)	−8(5)	−5(9)
C (20)	3394(4)	928(6)	−1429(12)	21(2)	59(6)	213(19)	−4(3)	−15(5)	−6(9)
C (21)	3978(4)	900(6)	−1249(11)	18(2)	45(5)	176(16)	−2(2)	0(4)	−3(7)

TABLE 6b. FRACTIONAL COORDINATES ($\times 10^3$) AND ISOTROPIC THERMAL PARAMETERS OF **3a**
Estimated standard deviations are given in parentheses.

	x	y	z	Bi
H(C6a)	497(4)	60(6)	628(12)	6.0(2.7)
H(C6b)	518(4)	187(6)	604(11)	5.3(2.5)
H(C6c)	569(4)	122(6)	650(11)	5.1(2.5)
H(C9)	701(3)	219(5)	524(11)	3.7(2.2)
H(C10)	749(4)	165(5)	773(11)	4.6(2.2)
H(C11)	735(3)	19(5)	883(10)	3.1(2.1)
H(C12)	670(3)	−80(5)	742(10)	3.2(2.2)
H(C13)	739(4)	53(7)	879(13)	7.3(2.9)
H(C14a)	601(4)	216(5)	−47(11)	4.2(2.2)
H(C14b)	596(4)	99(6)	−64(11)	4.3(2.3)
H(C14c)	645(4)	137(6)	51(12)	5.3(2.3)
H(C17)	410(4)	261(7)	119(13)	5.4(2.5)
H(C18)	311(3)	266(6)	91(11)	3.9(2.9)
H(C19)	264(4)	157(5)	−70(11)	4.7(2.3)
H(C20)	321(4)	45(5)	−226(11)	4.3(2.4)
H(C21)	422(3)	43(5)	−179(11)	3.2(2.1)

value of C–N bond lengths in the thiadiazolidine ring is 1.378 Å which is compatible with those found in conjugated C–N bonds.[14] The sums of bond angles around the nitrogen atoms, N(2) and N(4), are 348.9 and 359.8° and the deviations of N(2) and N(4) from the plane consisting of the three adjacent atoms are 0.292 and 0.034 Å, respectively. The values suggest that the atomic configuration of N(4) is sp^2 hybridized, whereas the N(2) atom is sp^3 hybridized. Furthermore, there is no double bond in the thiadiazolidine ring system, only a small ring current may be expected. However, this ring system is almost planar and the maximum deviation from the mean plane is 0.035 Å. The two phenyl groups are *trans* with respect to C(3)–N(4) and the C(5)–N(4) bonds, respectively. The intramolecular non-bonded distances for N(2) ... C(8) and S(1) ... C(16) are 2.963 and 2.985 Å. The dihedral angles between the thiadiazolidine ring and these phenyl groups are 118.2 and 67.7° for planes B and C, respectively, and that between the two phenyl groups is 69.7°. The C(3)–N(7)–C(8) bond angle is 125.4° which is much greater than C(5)–N(15)–C(16) of 117.3°. This may be due to the steric hindrance between the phenyl group attached to N(7) and the

TABLE 7. FRACTIONAL COORDINATES AND ANISOTROPIC THERMAL PARAMETERS ($\times 10^4$) OF **9**

Estimated standard deviations are given in parentheses. The anisotropic thermal parameters are in the form: $\exp[-(b_{11}h^2+b_{22}k^2+b_{33}l^2+b_{12}hk+b_{13}hl+b_{23}kl)]$.

	x	y	z	b_{11}	b_{22}	b_{33}	b_{12}	b_{13}	b_{23}
S (1)	1363(2)	−1170(2)	−152(3)	82(2)	66(2)	83(4)	30(2)	−47(2)	−18(2)
C (2)	1979(6)	−729(7)	1909(9)	40(6)	30(7)	75(15)	11(5)	−7(6)	−6(7)
N (3)	2334(5)	761(6)	2939(8)	50(5)	24(6)	111(13)	27(5)	−14(6)	−5(6)
C (4)	3483(6)	1535(7)	4116(9)	52(6)	38(7)	66(15)	30(6)	−7(7)	−17(7)
N (5)	4624(6)	1569(7)	3793(9)	44(6)	83(9)	136(15)	26(6)	−1(7)	−35(9)
N (6)	2198(6)	−1769(6)	2671(8)	95(7)	18(6)	103(14)	37(6)	−19(7)	−16(7)
C (7)	2498(8)	−1613(9)	4559(11)	89(9)	41(8)	134(19)	19(7)	−23(9)	−4(9)
C (8)	1619(10)	−3138(8)	5218(13)	150(13)	32(9)	179(22)	43(9)	25(12)	5(10)
C (9)	1730(6)	−4477(6)	4134(8)	130(8)	29(6)	192(15)	43(6)	−20(8)	5(7)
C (10)	1364(10)	−4623(8)	2334(12)	150(12)	22(8)	148(21)	35(8)	−18(12)	−12(9)
C (11)	2254(9)	−3190(8)	1543(12)	120(10)	32(8)	156(20)	52(8)	−4(10)	−23(9)
C (12)	1904(8)	1827(8)	2305(12)	105(9)	60(9)	178(20)	69(8)	−43(10)	−11(10)
N (13)	3271(5)	2402(6)	5640(8)	50(5)	56(7)	84(13)	23(5)	1(6)	−30(7)
C (14)	4423(8)	3397(9)	6865(11)	69(8)	100(11)	116(19)	22(8)	−22(9)	−72(11)
C (15)	4208(10)	4811(9)	7797(13)	124(12)	58(10)	143(22)	1(9)	28(12)	−42(11)
C (16)	3011(7)	4318(6)	8784(8)	135(8)	75(8)	144(15)	42(7)	44(12)	−31(8)
C (17)	1886(10)	3386(10)	7530(14)	110(11)	100(12)	248(26)	72(10)	57(13)	−12(13)
C (18)	2005(7)	1907(8)	6573(11)	69(8)	56(9)	138(19)	30(7)	34(9)	5(9)
C (19)	4946(8)	959(11)	1999(13)	65(8)	150(15)	181(23)	44(9)	16(10)	−63(14)

TABLE 8. DEVIATIONS (Å) OF THE ATOMS FROM SEVERAL LEAST-SQUARES PLANES OF **3a**

Atom	Plane A	Atom	Plane B	Atom	Plane C
S (1)	−0.012	C (8)	0.010	C (16)	0.000
N (2)	0.029	C (9)	−0.006	C (17)	−0.002
C (3)	−0.035	C (10)	0.001	C (18)	0.003
N (4)	0.014	C (11)	0.000	C (19)	−0.002
C (5)	0.006	C (12)	0.003	C (20)	0.000
C (6)	−0.650[a)]	C (13)	−0.008	C (21)	0.000
N (7)	−0.120[a)]	C (3)	0.641[a)]	C (5)	0.893[a)]
C (14)	0.180[a)]	N (7)	−0.101[a)]	N (15)	−0.071[a)]
N (15)	0.076[a)]				

a) Not included in the calculations of the planes.

TABLE 9. INTERMOLECULAR CONTACTS WITHIN 3.7 Å OF **3a**

S (1)···C (13) (I)	3.629	C (3)···C (21) (II)	3.625
N (4)···C (21) (II)	3.629	C (5)···C (6) (III)	3.670
C (6)···N (15) (IV)	3.413	N (7)···C (10) (V)	3.601
C (8)···C (10) (V)	3.666	C (8)···C (11) (V)	3.677
C (9)···C (10) (V)	3.549	C (10)···C (14) (IV)	3.692
C (11)···C (14) (IV)	3.628	C (13)···C (20) (II)	3.671

(I)	1−x,	−y,	1−z
(II)	1−x,	−y,	−z
(III)	x,	1/2−y,	−1/2+z
(IV)	x,	y,	1+z
(V)	3/2−y,	y,	−1/2+z

C(6) atom. The intermolecular atomic distances within 3.7 Å are given in Table 9, wherein no special short interatomic distances are observed.

9: The molecular structure of **9** is shown in Fig. 8 with the bond lengths and angles. A stereoscopic drawning of the molecule is given in Fig. 9. The

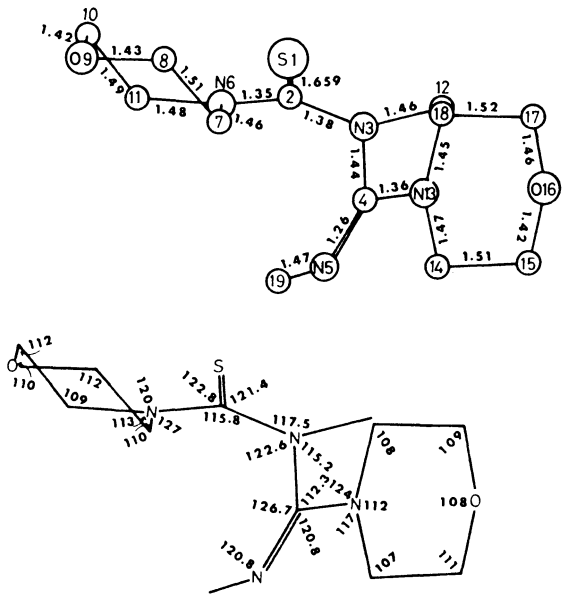

Fig. 8. Bond lengths (Å) and angles (°) of **9**.
The mean estimated standard deviation of bond lengths is 0.012 Å, and that of bond angles is 0.7°.

deviations from several least-squares planes are given in Table 10 and selected torsional angles are given in Table 11.

The sulfur atom is not bonded to N(5) and the intramolecular interatomic distance is 4.38 Å. The S=C bond length of 1.659 Å is slightly larger than the proposed value for a pure S=C bond of 1.608 Å.[15] Generally, the C–N bond distance in which the nitrogen atom is adjacent to C=X, (X=C, N, O, and S) is shorter than the usual C–Nsp^3 bond distance.[14] The values are in the range of 1.34—1.40 Å.[14] In such cases, the atomic configuration of the nitrogen atom is usually

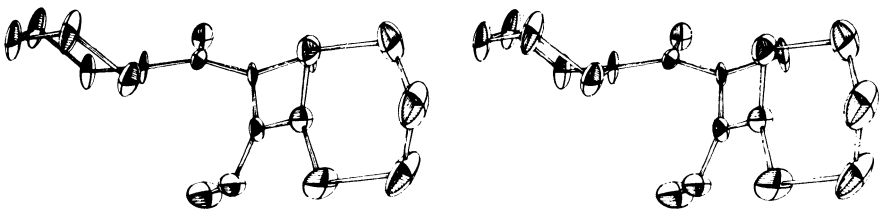

Fig. 9. Stereoscopic view down the c axis of **9**.

TABLE 10. DEVIATIONS (Å) OF THE ATOMS FROM SEVERAL LEAST-SQUARES PLANES OF **9**

Atom	Plane A	Atom	Plane B
C (14)	−0.002	C (7)	0.009
C (15)	0.002	C (8)	−0.009
C (17)	−0.002	C (10)	0.009
C (18)	0.002	C (11)	−0.009
N (13)	0.658[a)]	N (6)	0.616[a)]
O (16)	−0.707[a)]	O (9)	−0.656[a)]

a) Not included in the calculations of the planes.

TABLE 11. SELECTED TORSIONAL ANGLES (°) OF **9**

S(1)-C(2)-N(3)-C(12)	12.1	S(1)-C(2)-N(6)-C(11)	17.0
N(6)-C(2)-N(3)-C(4)	36.1	C(7)-C(2)-N(6)-N(3)	13.8
C(2)-N(3)-C(4)-N(5)	41.6	N(3)-C(4)-N(13)-C(18)	37.4
C(12)-N(3)-C(4)-N(13)	60.8	N(5)-C(4)-N(13)-C(14)	1.2

TABLE 12. INTERMOLECULAR CONTACTS WITHIN 3.7 Å OF **9**

N (5) ··· C (7) (I)	3.50	N (5) ··· C (17) (II)	3.52
C (8) ··· O (9) (III)	3.46	C (8) ··· C (10) (III)	3.66
O (9) ··· C (12) (IV)	3.61	O (9) ··· C (15) (IV)	3.63
C (10) ··· C (12) (IV)	3.68	C (10) ··· O (16) (V)	3.41
C (11) ··· O (16) (V)	3.22	C (19) ··· C (19) (VI)	3.27

(I)	1−x,	−y,	1−z
(II)	1−x,	1−y,	1−z
(III)	−x,	−1−y,	1−z
(IV)	x,	−1+y,	z
(V)	x,	−1+y,	−1+z
(VI)	1−x,	−y,	−z

in the sp^2 hybridized form due to participation with π-electrons from the neighboring double bond. In this molecule, there are three such bonds, C(2)–N(3), C(2)–N(6), and C(4)–N(13), wherein the distances are reasonable except the N(3)–C(4) distance of 1.44 Å. Lengthening of the N(3)–C(4) bond may be due to the reduction of π-bond character at this bond by twisting. The torsional angles, C(2)–N(3)–C(4)–N(5) and C(12)–N(3)–C(4)–N(13) are 41.6 and 60.8°. The dihedral angle between the mean planes consisting of C(2)–N(3)–C(12)–C(4) and N(3)–C(4)–N(13)–N(5) is 127.6°. The sums of the bond angles around nitrogen atom are 355.3, 359.9, and 353.3° for N(3), N(6), and N(13) respectively, indicating that the N(6) atom has more sp^2 character, and the other two nitrogen atoms have sp^3 character owing to the intramolecular atomic repulsion between C(12) and C(18) The interatomic distance between these atoms is 3.24 Å. A noticeably short intermolecular atomic contact is at C(19) related by a center of symmetry with a value of 3.27 Å (Table 12).

We wish to thank Mr. Hayao Shinozaki for the IR and UV spectra, Mr. Yoji Furukawa for the NMR spectra, and Mr. Kikushige Ono for the microanalyses.

References

1) T. Kinoshita and C. Tamura, *Tetrahedron Lett.*, **1969**, 4963.
2) D. S. Hector, *Ber.*, **23**, 357 (1890).
3) K. S. Suresh and C. N. R. Rao, *J. Indian Chem. Soc.*, **37**, 581 (1960).
4) V. K. Verma and K. M. Sarkar, *J. Sci. Ind. Res. (India)*, **21B**, 236 (1962).
5) M. Rieger and F. H. Westheimer, *J. Am. Chem. Soc.*, **72**, 19 (1950).
6) T. Kinoshita, S. Sato, and C. Tamura, "Abstracts of Third International Congress of Heterocyclic Chemistry," (1971), p. 531.
7) F. Zetzsche, E. Lüscher, and H. E. Meyer, *Ber.*, **71**, 1088 (1938).
8) H. G. Khorana and A. R. Todd, *J. Chem. Soc.*, **1953**, 2257.
9) T. Kinoshita, S. Sato, Y. Furukawa, and C. Tamura, *Heterocycles*, **3**, 83 (1975).
10) H. Salkowski, *Ber.*, **24**, 2724 (1891).
11) A. Skita and H. Rolfes, *Ber.*, **53**, 1247 (1920).
12) E. C. Horning, *Org. Synth.*, Coll. Vol. III, 617 (1955).
13) S. Sato, T. Kinoshita, T. Hata, and C. Tamura, *Acta Crystallogr., Sect. A*, **28**, S25 (1972); Independent analysis of this compound has appeared in C. Christophersen, T. Øttersen, K. Seff, and S. Treppendahl, *J. Am. Chem. Soc.*, **97**, 5237 (1975).
14) J. Karle and I. L. Karle, *J. Am. Chem. Soc.*, **89**, 804 (1967).
15) S. C. Abrahams, *Quart. Rev.*, **10**, 407 (1956).

Kinetics on the Carbonylation of Cyclohexene in a Methanol Solution Catalyzed by Palladium(II) Chloride–Triphenylphosphine

Hajime YOSHIDA, Nobuyuki SUGITA,* Kiyoshi KUDO,* and Yoshimasa TAKEZAKI*

Research Institute, Mitsubishi Oil Co., Ltd., Ogi-machi, Kawasaki-ku, Kawasaki 210

**Institute for Chemical Research, Kyoto University, Gokanosho, Uji 611*

(Received December 24, 1975)

Methyl cyclohexanecarboxylate was obtained in high yields by the carbonylation of cyclohexene in a methanol solution using palladium(II) chloride-triphenylphosphine as the catalyst. The effects of variables, such as initial concentration of palladium(II) chloride, pressure of carbon monoxide, and temperature, upon the rate of carbonylation were examined kinetically. A probable reaction mechanism is proposed.

The synthesis of saturated esters from olefins, carbon monoxide and alcohol according to Eq. 1, has been described[1–6] using palladium complexes as catalysts.

$$RCH{=}CH_2 + CO + R'OH \rightarrow RCH(CO_2R')CH_3 + RCH_2CH_2CO_2R' \quad (1)$$

If water is used in place of alcohol, carboxylic acids are produced.[7] Tsuji *et al.*[8,9] proposed the mechanism shown in Scheme 1 for this reaction.

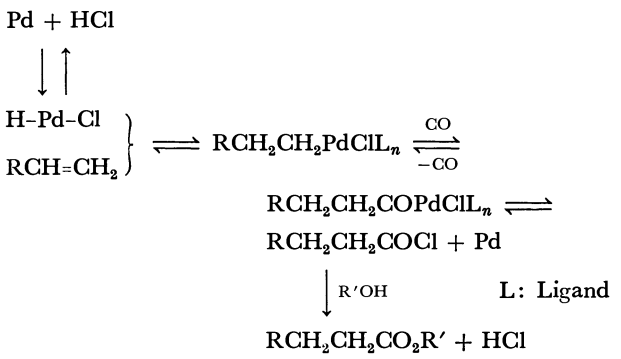

Scheme 1.

Fenton[7] considered the addition of alkoxycarbonyl or carboxyl complexes to olefins. However, very few kinetic studies have been reported on this reaction.

Methyl cyclohexanecarboxylate was obtained in high yields from cyclohexene, carbon monoxide, and methanol according to Eq. 2,

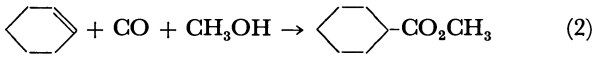

(2)

using palladium(II) chloride–triphenylphosphine as the catalyst. This paper gives the result and a discussion on the mechanism of the reaction.

Results

Preliminary Investigation. Cyclohexene was chosen as the olefin substrate since it gives no isomer. The results of carbonylation of cyclohexene under various conditions are given in Table 1. When methanol was used as the solvent, methyl cyclohexanecarboxylate was obtained in *ca.* 50% yield, a significant amount of colloidal palladium metal being found in the resulting solution. Since the palladium metal recovered was inactive for the carbonylation of cyclohexene, the low yield is attributable to the deactivation of the palladium species. In the solution containing 20% (vol.) of methanol in benzene the yield of ester increased up to 96%, no palladium metal being found during the course of reaction. Deactivation of the palladium species was negligiable.

In addition to methyl cyclohexanecarboxylate, small amounts of cyclohexyl chloride, methyl 2-chlorocyclohexanecarboxylate, and a few unidentified compounds were obtained under the conditions (Table 1). However, the sum of amounts of the remaining cyclohexene and the ester produced accounted for over 98% of the charged cyclohexene. Thus, the amounts of the by-products were neglected.

The solubility of carbon monoxide in the reaction solution was measured, the result being shown in Fig. 1. Henry's constants which were determined from the slopes of linear plots in Fig. 1 are summarized in Table 3.

The effect of stirring speed on the rate of carbonylation was examined to eliminate the effect of diffusion of carbon monoxide into the reaction solution. The yields of ester were independent of the stirring speeds

Table 1. Carbonylation of cyclohexene

Charge[a]			Conditions			Analysis		Yield[d]	MB[e]
CHE[b] (mmol)	MeOH (ml)	PhH (ml)	P_{CO} (atm)	Temp (°C)	Time (min)	CHE[b] (mmol)	MCC[c] (mmol)	(%)	(%)
19.7	20	—	54— 38	100	300	—	9.21	46.7	—
24.4	20	—	176—146	100	320	—	14.3	58.7	—
9.86	1	20	44— 40	100	180	9.19	0.54	5.5	98.7
19.7	1	20	52— 47	120	300	16.3	3.19	16.2	98.7
19.7	5	20	49— 31	100	370	3.40	16.3	82.7	99.9
49.3	10	40	50[f]	120	300	1.20	47.2	95.9	98.2

a) $PdCl_2$ (1.0 mmol) and PPh_3 (4.0 mmol) were also charged. b) Cyclohexene. c) Methyl cyclohexanecarboxylate. d) Based on the amount of initial CHE. e) Material balance = 100 × (Remaining CHE + Produced MCC)/(Initial CHE). f) The pressure was kept constant during the reaction.

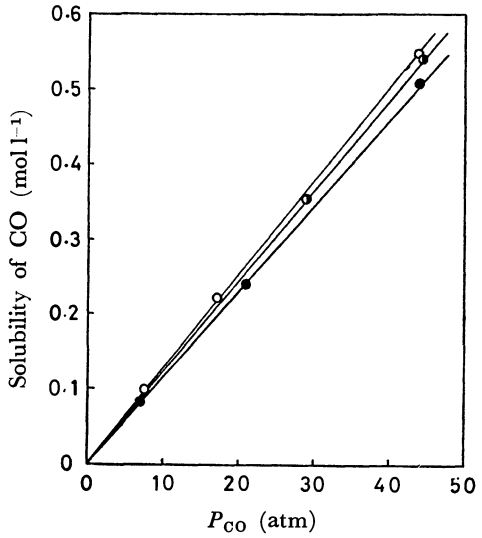

Fig. 1. Solubility of CO.
Cyclohexene 10 ml, MeOH 20 ml, PhH 80 ml, Mesitylene 10 ml. Temp: ○ 120, ◑ 110, ● 100 °C.

between 600 and 1000 rpm. Thus, all the kinetic experiments were carried out at about 750 rpm.

Kinetics. The following variables were examined kinetically: initial concentrations of palladium(II) chloride, cyclohexene, and methanol, pressure of carbon monoxide, temperature, and molar ratio of triphenylphosphine to palladium(II) chloride.

A typical time *vs.* yield curve is shown in Fig. 2. The plot of time *vs.* $X=\ln[(CHE)_0/\{(CHE)_0-(MCC)\}]$, where $(CHE)_0$ and (MCC) represent the concentrations of initial cyclohexene and ester produced, gives a straight line after the induction period of 30—60 min as shown in Fig. 3. Thus, except for the induction period of 30—60 min, the empirical formula $X=X_c(t-t_0)$ can be used, where t is reaction time and X_c and t_0 are constants characteristic of the observed straight line. All the

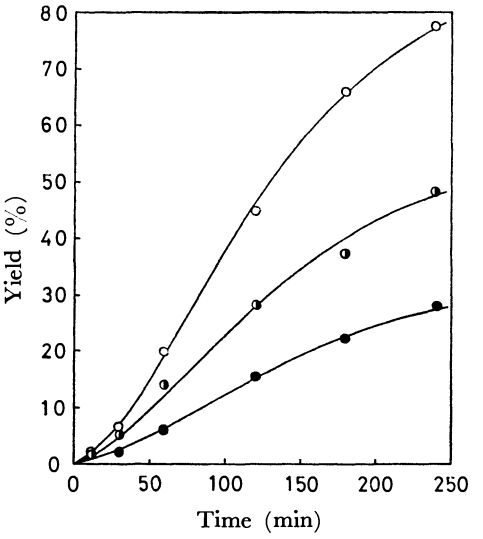

Fig. 2. Time *vs.* yield curve.
$PdCl_2$: ○ 1.66×10^{-2}, ◑ 8.38×10^{-3}, ● 4.83×10^{-3} mol l^{-1}. Other conditions were shown in Table 2. Curves were calculated according to Eq. 19.

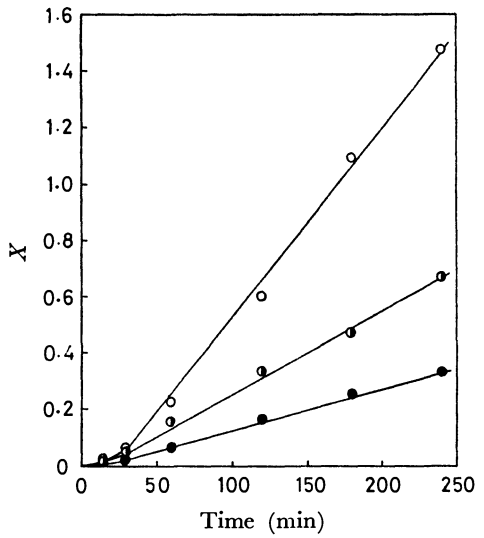

Fig. 3. Time *vs.* *X*.
Conditions were the same as those in Fig. 2.

Table 2. Kinetic data

Variables			Empirical equation $X=X_c(t-t_0)$ $X_c\times10^3$	t_0
MeOH Concn[a]	4.12	(mol l^{-1})	7.01	28
	2.07		7.02	28
$PPh_3/PdCl_2$[b]	3.01	(mol/mol)	7.11	28
	4.04		7.01	28
	7.84		6.93	27
CHE Concn[c]	0.822	(mol l^{-1})	7.01	28
	0.657		6.82	28
	0.493		6.94	28
$PdCl_2$ Concn[d]	1.66×10^{-1}	(mol l^{-1})	7.01	28
	8.38×10^{-3}		3.12	12
	4.83×10^{-3}		1.53	19
CO Press.[e] 120 °C	44.5	(atm)	7.01	28
	19.5		4.79	28
	10.5		2.98	30
108 °C	44.5		3.62	16
	21.8		2.85	17
	11.1		2.12	22
100 °C	44.5		2.68	22
	22.2		2.42	30
	11.9		2.03	35

a) $PdCl_2$ 1.70×10^{-2} mol l^{-1}, PPh_3 6.70×10^{-2} mol l^{-1}, CHE 0.822 mol l^{-1}, PhH 40—45 ml, P_{co} 44.5 atm, 120 °C, 750 rpm. b) $PdCl_2$ 1.70×10^{-2} mol l^{-1}, CHE 0.822 mol l^{-1}, MeOH 4.12 mol l^{-1}, PhH 40 ml, P_{co} 44.5 atom, 120 °C, 750 rpm. c) $PdCl_2$ 1.70×10^{-2} mol l^{-1}, PPh_3 6.70×10^{-2} mol l^{-1}, MeOH 4.12 mol l^{-1}, PhH 40—43 ml, P_{co} 44.5 atm, 120 °C, 750 rpm. d) PPh_3 6.70×10^{-2} mol l^{-1}, CHE 0.822 mol l^{-1}, MeOH 4.12 mol l^{-1}, PhH 40 ml, P_{co} 44.5 atm, 120 °C, 750 rpm. e) $PdCl_2$ 1.70×10^{-2} mol l^{-1}, PPh_3 6.70×10^{-2} mol l^{-1}, CHE 0.822 mol l^{-1}, MeOH 4.12 mol l^{-1}, 750 rpm.

kinetic results given in terms of empirical formulas are summarized in Table 2.

When the initial concentration of methanol was reduced to half, both X_c and t_0 remained unchanged,

indicating that the rate is independent of the concentration of methanol. Variation of the molar ratio of triphenylphosphine to palladium(II) chloride from 3 to 8 had no effect on either X_c or t_0, indicating that the rate is also independent of the molar ratio. A decrease in the initial concentration of cyclohexene had no effect, indicating that the rate is of first order with respect to the concentration of cyclohexene. In contrast, X_c increased as the initial concentration of palladium(II) chloride increased, while t_0 changed irregularly. An increase in the pressure of carbon monoxide caused X_c to increase, while it changed t_0 irregularly at each temperature. The rise in temperature caused an increase in X_c but hardly any in t_0.

Discussion

Reaction Mechanism. Methyl 2-chlorocyclohexanecarboxylate obtained as a by-product was reported[5] to be produced in the carbonylation of cyclohexene–palladium(II) chloride complex, (cyclohexene–$PdCl_2)_2$, in a methanol solution, but the complex, prepared by the method described by Kharasch *et al.*,[10] decomposed even at room temperature in the methanol–benzene solution, giving the precipitate of palladium metal. It thus appears to be absent under the present reaction conditions. The rapid reaction from 3 to 5, which affords methyl 2-chlorocyclohexanecarboxylate and hydride–palladium intermediate **1**, probably proceeds before the catalytic carbonylation proceeds.

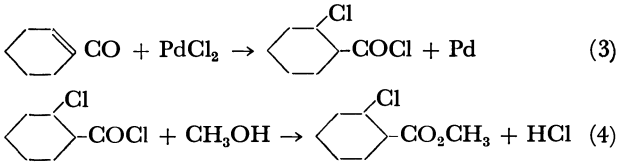

(3)

(4)

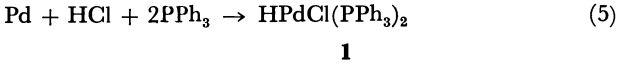

(5)

Reactions 3 and 4 have been reported[5] to proceed smoothly even at room temperature. Reaction 5 is also known[11] and complex **1** was prepared[12] from palladium(0) complex and hydrogen chloride. Insertion of the coordinated cyclohexene into the hydrogen–palladium bond in intermediate **1** would give cyclohexyl–palladium intermediate **2** (Reaction 6), which is the converted into cyclohexylcarbonyl–palladium intermediate **3** by the insertion of carbon monoxide (Reaction 7).

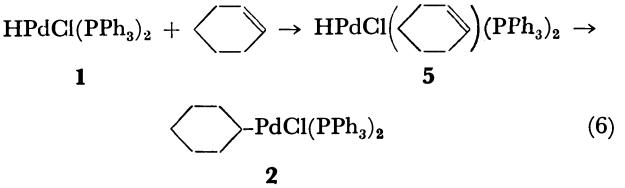

(6)

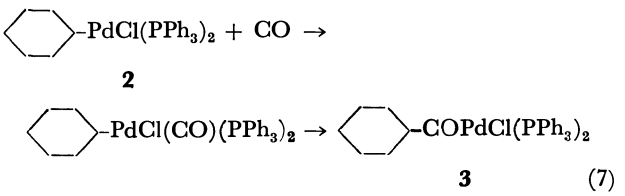

(7)

Reactions 6 and 7 have the same mechanisms as in Scheme 1. The following three mechanisms (Schemes 2, 3, and 4) can be inferred as the final process which affords methyl cyclohexanecarboxylate and regenerates the catalyst from intermediate **3**.

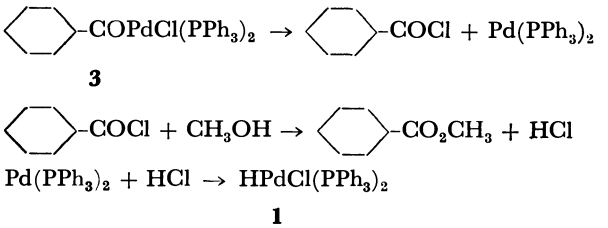

Scheme 2.

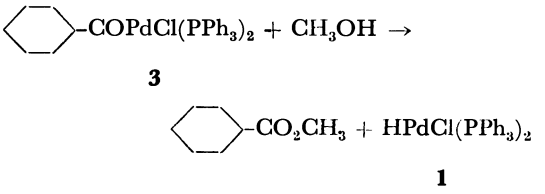

Scheme 3.

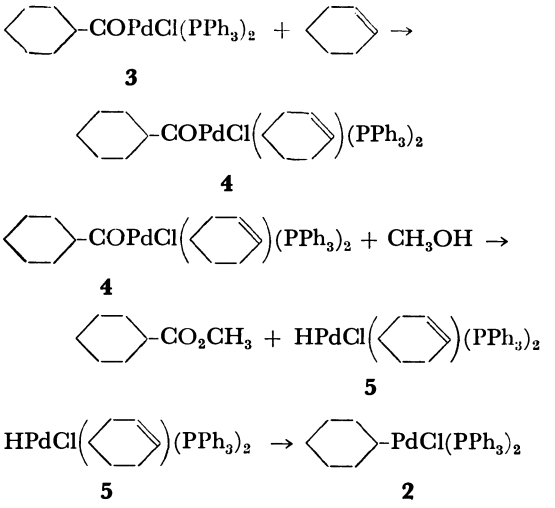

Scheme 4.

Scheme 2 is the mechanism shown in Scheme 1. Scheme 3 is deduced from the fact[13] that the alcoholysis of an acyl–palladium complex affords ester and regenerates a palladium(0) complex in the presence of a base. Scheme 4 is analogous to the mechanism of carbonylation of an allyl compound: the final product was formed by the coordination of another allyl compound.[14,15] In these three mechanisms, Scheme 4 seems to be the most probable mechanism to explain the kinetic result in which the rate of carbonylation is proportional to the concentration of cyclohexene.

Thus, the following mechanism is assumed on the basis of the reaction path described above.

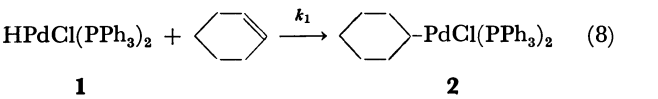

(8)

$$\mathrm{CO(Gas)} \overset{H}{\rightleftharpoons}$$

$$\mathbf{2} + \mathrm{CO(Liq.)} \overset{K_2}{\rightleftharpoons} \text{C}_6\text{H}_{11}\text{-COPdCl(PPh}_3\text{)}_2 \quad (9)$$

3

$$\mathbf{3} + \text{C}_6\text{H}_6 \xrightarrow{k_3} \text{C}_6\text{H}_{11}\text{-COPdCl(C}_6\text{H}_5\text{)(PPh}_3\text{)}_2 \quad (10)$$

4

$$\mathbf{4} + \mathrm{CH_3OH} \xrightarrow{\text{Fast}} \text{C}_6\text{H}_{11}\text{-CO}_2\text{CH}_3 + \mathbf{2} \quad (11)$$

In this mechanism, k_1 and k_3 are the rate constants of Reactions 8 and 10 respectively, and K_2 and H the equilibrium constant of Reaction 9 and Henry's constant of carbon monoxide respectively. The non-catalyzed reaction from 3 to 5, which affords intermediate **1**, is assumed to proceed rapidly. The rate of Reaction 11 is also assumed to proceed rapidly, since the rate of carbonylation was independent of the concentration of methanol.

Rate Equation. The rate equation expressing the production of methyl cyclohexanecarboxylate is derived as follows.

The material balances for palladium species and cyclohexene can be given by,

$$C_1 + C_2 + C_3 \fallingdotseq (\mathrm{PdCl_2})_0 \quad (12)$$

$$(\mathrm{CHE}) + (\mathrm{MCC}) \fallingdotseq (\mathrm{CHE})_0 \quad (13)$$

where C_n is the concentration of intermediate n, and $(\mathrm{PdCl_2})_0$ and (CHE) are the concentrations of palladium(II) chloride charged and remaining cyclohexene, respectively. The equilibrium constant K_2 can be given by,

$$K_2 = \frac{C_3}{C_2 HP} \quad (14)$$

where P is the pressure of carbon monoxide. The rate of decreasing concentration of intermediate **1** can be expressed from Reaction 8 as

$$-\frac{dC_1}{dt} = k_1 C_1(\mathrm{CHE}) \quad (15)$$

where (CHE) should be nearly equal to $(\mathrm{CHE})_0$, since Reaction 8 proceeds as an elementary process of non-catalyzed reaction before the catalytic cycle from Reaction 9 to Reaction 11 proceeds. Thus, Eq. 15 can be written as

$$C_1 = (\mathrm{PdCl_2})_0 e^{-k_1(\mathrm{CHE})_0 t} \quad (16)$$

By using Eqs. 12, 14, and 16, the rate of producing methyl cyclohexanecarboxylate is given as follows.

$$\frac{d(\mathrm{MCC})}{dt} = k_3 C_3(\mathrm{CHE})$$

$$= \frac{k_3 K_2 HP(\mathrm{PdCl_2})_0(\mathrm{CHE})}{1+K_2 HP}\{1-e^{-k_1(\mathrm{CHE})_0 t}\} \quad (17)$$

By substituting Eq. 13 into Eq. 17, the following equation is derived.

$$\ln \frac{(\mathrm{CHE})_0}{(\mathrm{CHE})_0-(\mathrm{MCC})}$$

$$= \frac{k_3 K_2 HP(\mathrm{PdCl_2})_0}{1+K_2 HP}\left\{t - \frac{1-e^{-k_1(\mathrm{CHE})_0 t}}{k_1(\mathrm{CHE})_0}\right\} \quad (18)$$

Thus, the relationship between time and the concentration of methyl cyclohexanecarboxylate is given by

$$(\mathrm{MCC}) = (\mathrm{CHE})_0(1-e^{-Z}) \quad (19)$$

where

$$Z = \frac{k_3 K_2 HP(\mathrm{PdCl_2})_0}{1+K_2 HP}\left\{t - \frac{1-e^{-k_1(\mathrm{CHE})_0 t}}{k_1(\mathrm{CHE})_0}\right\}$$

Analysis of Kinetic Data. Equation 18 is compared with the kinetic results represented by the empirical formula which gives the relationship between time and X after 30—60 min. The following correlations are obtained by comparison between Eq. 18 and the empirical formula $X=X_c(t-t_0)$.

$$X_c = \frac{k_3 K_2 HP(\mathrm{PdCl_2})_0}{1+K_2 HP} \quad (20)$$

$$t_0 = \frac{1-e^{-k_1(\mathrm{CHE})_0 t}}{k_1(\mathrm{CHE})_0} \quad (21)$$

X_c should be independent of $(\mathrm{CHE})_0$. This is actually the case (Table 2). X_c should be of the

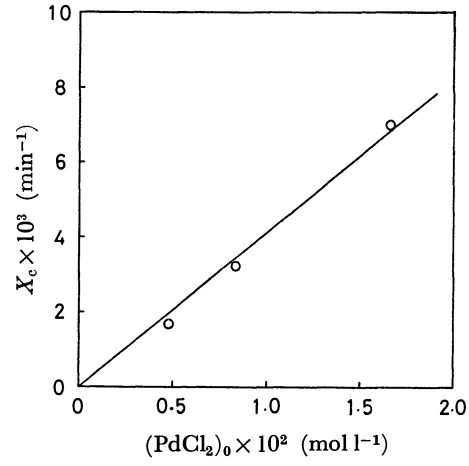

Fig. 4. Relation between $(\mathrm{PdCl_2})_0$ and X_c.
Conditions were shown in Table 2.

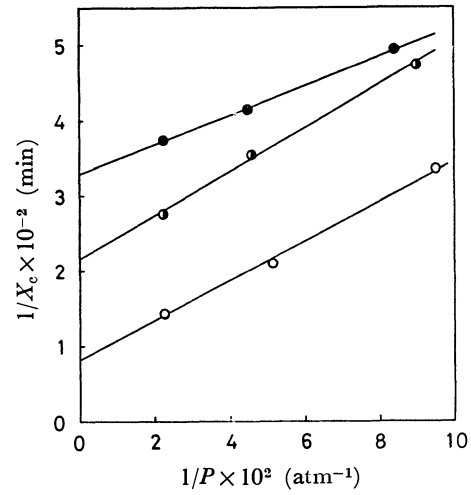

Fig. 5. Relation between $1/P$ and $1/X_c$.
Temp: ○ 120, ◑ 108, ● 100 °C.
Other conditions were shown in Table 2.

first order with respect to $(PdCl_2)_0$. The kinetic result is in line with the correlation as shown in Fig. 4. If Eq. 20 is written as Eq. 22, the reciprocal of X_c should increase linearly with increasing reciprocal of P.

$$\frac{1}{X_c} = \frac{1}{k_3K_2H(PdCl_2)_0} \cdot \frac{1}{P} + \frac{1}{k_3(PdCl_2)_0} \quad (22)$$

The kinetic result is satisfied with the correlation of Eq. 22 as shown in Fig. 5. On the other hand, the observed values of t_0 is independent of $(CHE)_0$, changing irregularly with the change in $(PdCl_2)_0$, P and temperature (Table 2). The irregularity of observed value of t_0 is related to the assumption that t_0 is constant in the empirical formula, since t_0 is in fact a function containing time as seen in Eq. 21. However, t_0 can be regarded to be constant except for the induction period of 30—60 min, since $\exp\{-k_1(CHE)_0t\}$ in Eq. 21 approaches zero with the elapse of time.

Determination of Constants. The values of k_3 and K_2H can be determined from the linear plots in Fig. 5 by means of Eq. 22. If $\exp\{-k_1(CHE)_0t\}$ is zero, Eq. 21 can be written as

$$t_0 = \frac{1}{k_1(CHE)_0} \quad (23)$$

and the value of k_1 can be estimated from the observed value of t_0. The constants obtained are summarized in Table 3. Their temperature coefficients determined from their Arrhenius plots were obtained as follows: $H=1.26$, $K_2=-18$, and $k_3=22$ kcal mol^{-1}. The value of k_1 was estimated only at 120 °C from the average of t_0 in all the data at 120 °C. From the value of k_1 obtained, $\exp\{-k_1(CHE)_0\}$ is 0.165 at 60 min when $(CHE)_0$ is 0.822 mol l^{-1}. This indicates that t_0 can be regarded to be constant at and after 60 min.

Table 3. Rate and equilibrium constants

Temp (°C)	H (mol l^{-1} atm^{-1})	K_2 (mol l^{-1})	k_1 (mol^{-1} l min^{-1})	k_3 (mol^{-1} l min^{-1})
120	1.26×10^{-2}	2.5	3.5×10^{-2}	0.75
108	1.21×10^{-2} a)	6.3		0.28
100	1.14×10^{-2}	12		0.18

a) At 110 °C.

Calculated Time-Yield Curve. Equation 18 is compared with the observed values in Fig. 2. By using the constants given in Table 3, theoretical time *vs.* yield curve was calculated by means of Eq. 19. The calculated curves (Fig. 2) are in line with the observed values including the values within 30—60 min. Other calculated curves were also consistent with the observed values over the range of the kinetic experiments at 120 °C.

The proposed mechanism sufficiently satisfies the kinetic results, but the mechanism by way of a methoxycarbonyl intermediate mentioned before does not explain them.

Experimental

Materials. Commercial palladium(II) chloride, triphenylphosphine, methyl cyclohexanecarboxylate, methyl 2-chlorocyclohexanecarboxylate, and cyclohexyl chloride were used without further purification. Cyclohexene, methanol, benzene, and mesitylene were distilled by the usual methods. Carbon monoxide was prepared by decomposing formic acid in hot sulfuric acid, *ca.* 98% purity.

Procedure. Reactions were carried out in a glass-tube placed in a stainless-steel autoclave (*ca.* 200 cm^3) equipped with a Teflon stirrer and a Teflon sampling line.

Palladium(II) chloride(0.2—1 mmol), triphenylphosphine-(3—8 mmol), cyclohexene(1—5 ml), methanol(5—10 ml), benzene(40—45 ml) and mesitylene(5 ml) were placed in the autoclave, which was then purged with nitrogen three or four times. The autoclave was heated up to 100—120 °C within 60 min and then maintained over 20 min at the desired temperature. Immediately after carbon monoxide had been pressured to 11—45 atm, stirring (600—1000 rpm) was started, this time being taken as zero time. Stirring was stopped from time to time and a sample (*ca.* 1 ml) was withdrawn through the sampling line into a trap chilled in an ice-bath within 30 s. In order to keep the pressure constant, carbon monoxide was supplied from a reservoir from time to time.

The solubility of carbon monoxide in the reaction medium was measured on the assumption that the solubility in the reaction medium is equal to that in the reaction solution without palladium(II) chloride and triphenylphosphine.

Analysis of Products. The products were identified by comparison of their retention times in gas chromatography with those of authentic samples. A PEG column (2 m, 3 mmø) with a nitrogen carrier was used at 180 °C for the determination of amounts of methyl cyclohexanecarboxylate and cyclohexene with mesitylene as an internal standard.

References

1) K. Bittler, N. v. Kutepow, and H. Ries, *Angew. Chem. Int. Ed. Engl.*, **7**, 329 (1968).
2) E. N. Frankel and F. L. Thomas, *J. Am. Oil Chem. Soc.*, **50**, 31 (1973).
3) Y. Sugi, K. Bando, and S. Shin, *Chem. Ind.*, **1975**, 397.
4) J. Tsuji, M. Morikawa, and J. Kiji, *Tetrahedron Lett.*, **1963**, 1437.
5) J. Tsuji, M. Morikawa, and J. Kiji, *J. Am. Chem. Soc.*, **86**, 4851 (1964).
6) J. Tsuji and K. Ohno, *Adv. Chem. Ser.*, **70**, 155 (1968).
7) D. M. Fenton, *J. Org. Chem.*, **38**, 3129 (1973).
8) J. Tsuji, K. Ohno, and T. Kajimoto, *Tetrahedron Lett.*, **1965**, 4565.
9) E. C. Taylor and H. Wynberg, "Advances in Organic Chemistry Methods and Results," Interscience, Vol. 6, New York (1969), p. 160.
10) M. S. Kharasch, R. C. Seyler, and F. R. Mayo, *J. Am. Chem. Soc.*, **60**, 882 (1938).
11) J. Tsuji and K. Ohno, *J. Am. Chem. Soc.*, **90**, 94 (1968).
12) K. Kudo, M. Hidai, T. Murayama, and Y. Uchida, *Chem. Commun.*, **1970**, 1701
13) J. K. Stille, L. F. Hines, R. W. Fries, P. K. Wong, D. E. James, and K. Lau, *Adv. Chem. Ser.*, **132**, 90 (1974).
14) H. Yoshida, N. Sugita, K. Kudo, and Y. Takezaki, *Nippon Kagaku Kaishi*, **1974**, 1002.
15) S. Imamura and J. Tsuji, *Tetrahedron*, **25**, 4187 (1969).

Reaction of 1-Alkylpyridinium Salts Carrying a Methyl or an Amino Group at the 2- or 4-Position with Activated Ethoxymethylene Compounds in the Presence of Alkali

Akikazu KAKEHI, Suketaka ITO, Takahisa FUNAHASHI, and Norio OGASAWARA

Department of Industrial Chemistry, Faculty of Engineering, Shinshu University, Wakasato, Nagano 380

(Received January 20, 1976)

It was found that various 1-alkyl-2-(**1a**—**d**) and 4-picolinium salts(**5a**,**b**) react smoothly with ethoxymethylene compounds(**2a**—**c**) activated by electron-withdrawing substituents in the presence of alkali to give the corresponding 1-alkyl-2-(**4a**—**i**) and 4-allylidenedihydropyridine derivatives(**6a**—**d**) in fairly good yields. 1-Methyl-2-(vinylimino)dihydropyridine(**8a**) and pyrimidine(**8b**) were obtained by the reactions of 1-methyl-2-aminopyridinium(**7a**) and pyrimidinium iodide(**7b**) with ethyl ethoxymethylenecyanoacetate(**2a**) under similar reaction conditions.

The reactions of 1-alkylpyridinium salts carrying a 2- or 4-methyl group with ethoxymethylene compounds in the presence of alkali afford the corresponding 2- or 4-allylidenedihydropyridine derivatives in fairly good yields rather than initially expected pyridinio-2-propen-1-ides.[1] The simplicity of the reaction procedure and the facile formation of allylidenedihydropyridines prompted us to extend the studies to aza-analogs, and we found that the reaction can be highly utilized for the preparation of this kind of compound.

This paper deals with the preparation of 2- or 4-allylidenedihydropyridines and the aza-analogs by the reactions of various 1-alkylpyridinium and pyrimidinium salts with activated ethoxymethylene compounds in the presence of an alkali.

Results and Discussion

*Reactions of 1-(Ethoxycarbonylmethyl)-2,6-lutidinium Bromide(**1a**) with Ethoxymethylene Compounds(**2a**—**c**).* A mixture of 1-(ethoxycarbonylmethyl)-2,6-lutidinium bromide(**1a**) and ethyl ethoxymethylenecyanoacetate(**2a**) was treated with potassium carbonate in chloroform at room temperature to give a new crystalline compound(**4a**) in 57% yield. A similar treatment of salt(**1a**) with 3-ethoxymethylenepentane-2,4-dione(**2b**) and ethyl ethoxymethyleneacetoacetate(**2c**) afforded the corresponding products(**4b**,**c**) in 47 and 55% yields, respectively.

Although the structures of the compounds(**4a**—**c**) were expected to be 2,6-lutidino-2-propen-1-ides(**3a**—**c**) by their elemental analyses and by comparison with similar reaction examples reported by Tamura *et al.*,[2]

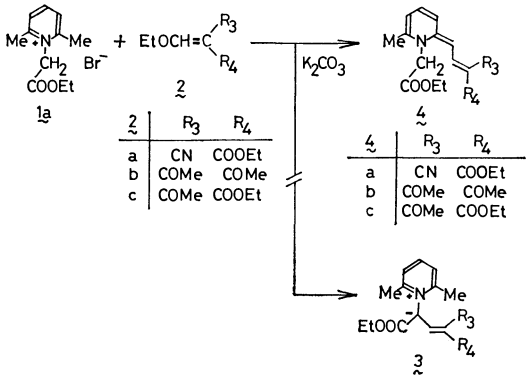

2	R_3	R_4
a	CN	COOEt
b	COMe	COMe
c	COMe	COOEt

4	R_3	R_4
a	CN	COOEt
b	COMe	COMe
c	COMe	COOEt

Scheme 1.

their spectral data were not compatible with the proposed structures: *e.g.*, the values (1735—1743 cm^{-1}) of each one carbonyl absorption in the IR spectra differ from those of the carbonyl group conjugated with carbon-carbon double bond or ylidic carbanion; the absence of one methyl group on the 2,6-lutidine ring and the presence of new olefinic AB-type protons in the NMR spectra (Table 1) show that these compounds (**4a**—**c**) are not 2,6-lutidino-2-propen-1-ides(**3a**—**c**), but the condensation products of ethoxymethylene compounds(**2a**—**c**) with a 2-methyl group on the 2,6-lutidine ring. The results are given below.

*Preparation of Other 1-Alkyl-2-(**4d**—**i**) and 4-Allylidenedihydropyridines(**6a**—**b**) and the Aza-analogs(**8a**—**b**).* From the fact that the 1-ethoxycarbonylmethyl group in the pyridinium salt(**1a**) remains intact during the course of reaction, we attempted an extension of this reaction to other 1-alkylpyridinium salts.

As expected, 1-methyl-2-picolinium(**1b**), 1-methyl-2,6-lutidinium(**1c**), and 1-allyl-2-picolinium salts(**1d**) reacted smoothly with compounds(**2a**,**b**) in the presence of potassium carbonate to yield the corresponding 2-allylidenedihydropyridine derivatives(**4d**—**i**) in over 63% yields, the reactions with 1-methyl(**5a**) and 1-allyl-4-picolinium salts(**5b**) giving similarly the corresponding 4-allylidene derivatives(**6a**—**d**) in 85, 65, 80, and 56% yields, respectively. Vinyliminodihydropyridine derivatives(**8a**, **b**) were obtained in 87 and 58% yields by the reactions of compound(**2a**) with 1-methyl-2-aminopyridinium(**7a**) and pyrimidinium iodide(**7b**). The results are given in Schemes 2, 3 and 4. On the other hand, 1-methylpyridinium and 1-methyl-3-picolinium iodides did not react with ethoxymethylene compound(**2a**) under the same conditions, nor did pyridinium salts(**1a**, **b**) react with ethyl β-ethoxyatropate and ethyl β-bromomethacrylate.

Structural elucidation of the compounds(**4d**—**i**, **6a**—**d**, and **8a**, **b**) was achieved by means of elemental analyses (Table 3) and spectroscopic investigations. The chemical shifts of skeletal protons in the NMR spectra (Table 1) of these products are as a whole similar to each other and also to those of known allylidenedihydropyridines reported recently by Acheson and Woollard.[3]

Mechanism. The reactions should be initiated by proton abstraction from the 2-, 4-methyl or 2-amino group rather than the 1-methylene group in the corresponding pyridinium(**1a**—**d**, **5a**, **b**, and **7a**) and

pyrimidinium salt(**7b**) followed by the nucleophilic addition-elimination of the resulting dihydropyridine or dihydropyrimidine intermediates(**9** and **9'**) onto the β-carbon of ethoxymethylene compounds(**2a—c**), as shown in Scheme 5. A similar mechanism was proposed by Severin and Böhme.[4] In these reactions, the presence of an appropriate removing group in ethoxymethylene compounds and high electrophilicity are necessary, since the reactions between enamines and electrophilic olefins generally afford cyclobutane derivatives,[5] and ethyl β-ethoxyatropate and ethyl β-bromomethacrylate, which are activated by only one electron-withdrawing group, did not react with pyridinium salt under basic condition. Although there are some methods for the preparation of allylidene-

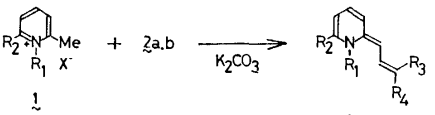

1	R_1	R_2	X
b	Me	H	I
c	Me	Me	I
d	$CH_2CH=CH_2$	H	Br

4	R_1	R_2	R_3	R_4
d	Me	H	CN	COOEt
e	Me	H	COMe	COMe
f	Me	Me	CN	COOEt
g	Me	Me	COMe	COMe
h	$CH_2CH=CH_2$	H	CN	COOEt
i	$CH_2CH=CH_2$	H	COMe	COMe

Scheme 2.

Table 1. NMR data of allylidene derivatives[6,7]

Compd No.	C-2	C-3	C-4	C-5	R_2	C-1'	C-2'	R_1[a]				R_3 and R_4[a]
4a	—	7.32 d	7.07 q	6.26 brd	2.38 s	5.37 **d**	8.07 **d**	4.67 **s**				
	$J_{3,4}=8.0$, $J_{4,5}=7.0$, $J_{1',2'}=13.0$											
4b	—	7.38 d	7.11 q	6.30 brd	2.34 s	6.84 d	7.78 d	4.70 s				2.34 s
	$J_{3,4}=8.0$, $J_{4,5}=7.0$, $J_{1',2'}=13.0$											
4c	—	7.46 d	7.05 q	6.25 brd	2.34 s	7.10 brd	8.15 brd	4.67 brs				2.40 s
	$J_{3,4}=8.0$, $J_{4,5}=7.0$, $J_{1',2'}=13.0$											
4d	—	7.0—7.4 m		6.31 brt	b)	5.38 d	7.99 d	3.54 s				
	$J=5.0$, 6.0, $J_{1',2'}=13.0$											
4e	—	7.42 drd	7.13 brt	4.31 brt	7.23 brd	6.94 d	7.75 d	3.57 s				2.34 s
	$J_{3,4}=8.0$, $J_{4,5}=6.0$, $J_{5,6}=7.0$, $J_{1',2'}=13.0$											
4f	—	7.31 d	7.10 q	6.31 brd	2.43 s	5.51 **d**	7.99 d	3.52 **s**				
	$J_{3,4}=8.0$, $J_{4,5}=7.0$, $J_{1',2'}=13.0$											
4g	—	7.60 d	7.30 q	6.52 brd	2.47 s	7.35 d	7.96 d	3.64 s				2.40 s
	$J_{3,4}=9.0$, $J_{4,5}=7.0$, $J_{1',2'}=13.0$											
4h	—	7.35 brd	7.12 brt	6.33 brt	7.22 brd	5.47 d	7.99 d	4.44 brd	5.15 drd	5.30 brd	5.75 m	
	$J_{3,4}=8.0$, $J_{4,5}=7.0$, $J_{5,6}=6.0$, $J_{1',2'}=13.0$, $J_{allyl}=5.0$, 10.0, 18.0											
4i	—	7.63 brd	7.33 brt	6.51 brt	7.42 brd	7.19 d	7.96 d	4.59 brd	5.33 brd	5.46 brd	6.00 m	2.41 s
	$J_{3,4}=8.0$, $J_{4,5}=7.0$, $J_{5,6}=6.0$, $J_{1',2'}=13.0$, $J_{allyl}=5.0$, 10.0, 17.0											
6a	6.91 d	6.82 br	—	6.36 br	6.91 d	5.56 d	7.85 d	3.51 s				
	$J_{2,3}=J_{5,6}=7.5$, $J_{1',2'}=13.0$											
6b	6.91 d	6.60 br	—	6.60 br	6.91 d	6.46 d	7.65 d	3.49 s				2.29 s
	$J_{2,3}=J_{5,6}=7.5$, $J_{1',2'}=13.0$											
6c	7.13 d	6.96 brd	—	6.47 brd	7.13 d	5.74 d	8.07 d	4.39 brd	5.31 brd	5.43 brd	5.98 m	
	$J_{2,3}=J_{5,6}=7.5$, $J_{1',2'}=13.0$, $J_{allyl}=5.0$, 10.0, 17.0											
6d	6.98 d	7.00 br	—	6.60 br	6.98 d	6.58 d	7.79 d	4.39 brd	5.23 brd	5.38 brd	5.90 m	2.36 s
	$J_{2,3}=J_{5,6}=7.5$, $J_{1',2'}=13.0$, $J_{allyl}=5.0$, 10.0, 17.0											
8a	—	7.55 brd	7.14 brt	6.62 brt	7.63 d	—	8.08 s	3.91 s				
	$J_{3,4}=9.0$, $J_{4,5}=7.5$, $J_{5,6}=6.5$											

a) The chemical shifts of protons of ethoxycarbonyl groups are δ 4.0—4.5(2H, q) and 1.0—1.5(3H, t). b) Overlapped with C-3 and C-4 proton.

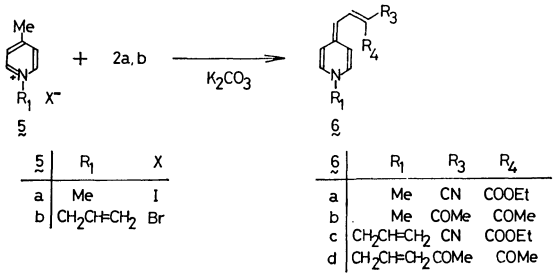

5	R_1	X
a	Me	I
b	$CH_2CH{=}CH_2$	Br

6	R_1	R_3	R_4
a	Me	CN	COOEt
b	Me	COMe	COMe
c	$CH_2CH{=}CH_2$	CN	COOEt
d	$CH_2CH{=}CH_2$	COMe	COMe

Scheme 3.

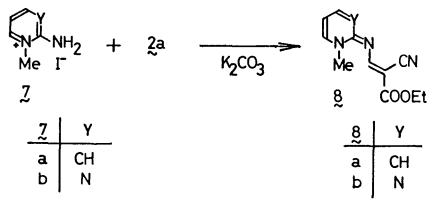

7	Y
a	CH
b	N

8	Y
a	CH
b	N

Scheme 4.

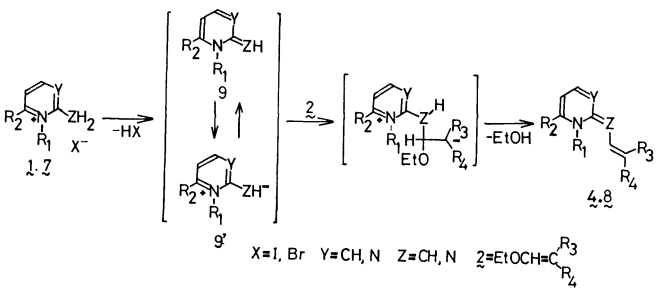

Scheme 5.

dihydropyridines, our method seems to be superior in simplicity of the reaction procedure and availability of the reactants to other methods.[3,4]

Experimental

Melting points were measured with a Yanagimoto micro-melting point apparatus and are uncorrected. Microanalyses

TABLE 2. SOME DATA AND PROPERTIES OF ALLYLIDENEDIHYDROPYRIDINES AND THEIR AZA-ANALOGS

Compd No.	Materials No.		Solvent	Yield (%)	Mp (°C)	IR (cm^{-1})			
4a	**1a**	**2a**	$CHCl_3$	57	167—170	2210	1743	1525	
4b	**1a**	**2b**	$CHCl_3$	47	110—113		1735	1510	
4c	**1a**	**2c**	$CHCl_3$	55	113—115		1740	1652	1510
4d	**1b**	**2a**	$CHCl_3$	65	143—146	2190	1519		
4e	**1b**	**2b**	$CHCl_3$	65	222(dec)		1580	1500	
4f	**1c**	**2a**	$CHCl_3$	86	149(dec)	2190	1545		
4g	**1c**	**2b**	$CHCl_3$	63	175(dec)		1515		
4h	**1d**	**2a**	EtOH	82	155—158	2185	1510		
4i	**1d**	**2b**	$CHCl_3$	67	148—151		1583	1475	
6a	**5a**	**2a**	EtOH	85	206—207	2200	1655		
6b	**5a**	**2b**	EtOH	65	186—188		1640	1570	
6c	**5b**	**2a**	$CHCl_3$	80	149—151	2195	1645		
6d	**5b**	**2b**	$CHCl_3$	56	155—158		1578	1495	
8a	**7a**	**2a**	$CHCl_3$	87	116—117	2245	1493		
8b	**7b**	**2a**	$CHCl_3$	58	223—225	2210	1681	1450	

TABLE 3. APPEARANCE AND ANALYTICAL DATA

Compd No.	Appearance	Formula	Calcd %			Found %		
			C	H	N	C	H	N
4a	Orange Needles	$C_{17}H_{20}N_2O_4$	64.54	6.37	8.86	64.29	6.19	8.69
4b	Red Needles	$C_{17}H_{21}NO_4$	67.31	6.98	4.62	67.39	6.92	4.43
4c	Red Flakes	$C_{18}H_{23}NO_5$	64.85	6.95	4.20	64.66	6.76	4.10
4d	Orange Flakes	$C_{13}H_{14}N_2O_2$	67.81	6.13	12.17	67.60	6.13	12.37
4e	Orange Needles	$C_{13}H_{15}NO_2$	71.86	6.96	6.45	71.72	7.01	6.50
4f	Orange Needles	$C_{14}H_{16}N_2O_2$	68.83	6.60	11.47	68.89	6.55	11.35
4g	Orange Needles	a)	69.97	7.55	5.83	69.93	7.40	5.78
4h	Orange Needles	$C_{15}H_{16}N_2O_2$	70.29	6.29	10.93	70.25	6.26	10.77
4i	Red Needles	$C_{15}H_{17}NO_2$	74.05	7.04	5.76	74.22	7.07	5.51
6a	Red Flakes	$C_{13}H_{14}N_2O_2$	67.81	6.13	12.17	67.81	6.09	12.17
6b	Red Needles	b)	66.36	7.28	5.95	66.25	7.41	5.99
6c	Red Flakes	$C_{15}H_{16}N_2O_2$	70.29	6.29	10.93	70.01	6.19	10.69
6d	Red Flakes	$C_{15}H_{17}NO_2$	74.05	7.04	5.76	73.79	7.02	5.63
8a	Yellow Needles	$C_{12}H_{13}N_3O_2$	62.32	5.67	18.17	62.30	5.73	18.43
8b	Orange Needles	$C_{11}H_{12}N_4O_2$	56.89	5.21	24.13	56.96	5.20	24.17

a) $C_{14}H_{17}NO_2 \cdot \frac{1}{2}H_2O$. b) $C_{13}H_{15}NO_2 \cdot H_2O$.

were carried out on a Perkin-Elmer 240 Elemental Analyzer. The NMR spectra were determined with a JEOL JNM-100 spectrometer in deuteriochloroform with tetramethylsilane as an internal standard. The chemical shifts are expressed in δ values. The IR spectra were taken with a JASCO DS-301 spectrophotometer.

*Preparation of Pyridinium (**1a—d**, **5a**, **b**, and **7a**) and Pyrimidinium Salt(**7b**).* Pyridinium salts (**1a—d** and **5a**, **b**) were prepared by the treatment of alkylating agents such as ethyl bromoacetate, methyl iodide, and allyl bromide with the corresponding pyridine derivatives without solvent, and 2-aminopyridinium(**7a**) and pyrimidinium salt(**7b**) were obtained by the reactions of 2-aminopyridine and 2-aminopyrimidine with methyl iodide in chloroform. These salts were filtered off, washed several times with ether to remove unchanged materials and used for the reactions without further purification.

*Preparation of Allylidenedihydropyridines (**4a—i** and **6a—d**) and the Aza-analogs(**8a**, **b**).* *General Procedure*: A solution of salt(2.1 mmol) and ethoxymethylene compound(2 mmol) in 50 ml of chloroform or theanol was stirred with potassium carbonate(5 g) at room temperature for 3—4 days. The reaction mixture was then filtered to remove insoluble substances and the filtrate was concentrated *in vacuo*. The residue was separated by column chromatography(alumina) using chloroform as an eluent. Recrystallization from chloroform–hexane gave yellow to red colored crystalline products.

Although the compounds(**4a—i** and **6a—d**) were formed both in chloroform or ethanol, vinyliminodihydropyridine derivatives(**8a**, **b**) were obtained only in chloroform. The latter reactions in ethanol gave only polymeric substances. Neither 1-methylpyridinium nor 1-methyl-3-picolinium iodides which have no 2- or 4-methyl group on the pyridine ring react with ethyl ethoxymethylenecyanoacetate(**2a**); pyridinium salts(**1a**, **b**) also do not react with ethyl β-ethoxyatropate or ethyl β-bromomethacrylate.

The results and some properties are summarized in Tables 1, 2, and 3.

References

1) A. Kakehi, S. Ito, T. Funahashi, and N. Ogasawara, *Chem. Lett.*, **1975**, 919.

2) a) Y. Tamura, Y. Sumida, and M. Ikeda, *J. Chem. Soc., Perkin Trans. 1*, **1973**, 2091; b) Y. Tamura, Y. Miki, Y. Sumida, and M. Ikeda, *ibid.*, **1973**, 2580.

3) R. M. Acheson and J. Woollard, *J. Chem. Soc., Perkin Trans. 1*, **1975**, 744.

4) T. Severin and H-J. Böhme, *Chem. Ber.*, **101**, 2925 (1968).

5) a) K. C. Brannock, A. Bell, R. D. Burpitt, and C. A. Kelly, *J. Org. Chem.*, **26**, 625 (1961); b) K. C. Brannock, A. Bell, R. D. Burpitt, and C. A. Kelly, *ibid.*, **29**, 801 (1964); c) I. Fleming and J. Harley-Mason, *J. Chem. Soc.*, **1964**, 2165.

6) Abbreviations of the spectral patterns are as follows: s, singlet; d, doublet; t, triplet; q, quartet; br, broad; dd, double doublets; m, multiplet.

7) The NMR spectrum of compound(**8b**) could not be taken because of its low solutility in deuteriochloroform.

The Reaction of 3,5-Dimethylisoxazole with Carbonyl Compounds

Choji KASHIMA,* Masakazu UEMORI, Yoshihiko TSUDA, and Yoshimori OMOTE*

Department of Chemistry, Tokyo Kyoiku University, Otsuka, Tokyo 112

**Department of Chemistry, University of Tsukuba, Sakura-mura, Niihari-gun, Ibaraki 300-31*

(Received January 22, 1976)

The reaction product of 3,5-dimethylisoxazole (**1**) with methyl benzoate was found to be 3-methyl-5-(benzoylmethyl)isoxazole in the presence of sodium amide in liquid ammonia. On the other hand, the reaction of **1** with ethyl acetate did not give 3-methyl-5-acetonylisoxazole under similar conditions. The latter reaction product was, however, obtained in a good yield in the presence of lithium amide in liquid ammonia. The reaction of **1** with ketones and aldehydes was proved to give 3-methyl-5-(2-hydroxyalkyl)isoxazoles regiospecifically in the presence of alkali amide. In the above reactions, further alkylation gave 3-methyl-5-(2-alkoxyalkyl)-isoxazoles in moderate yields. Compound **1** reacted with acrylaldehyde, crotonaldehyde, and cinnamaldehyde to give 1,2-addition products, 3-methyl-5-(2-hydroxyalkenyl)isoxazoles, exclusively, but methyl cinnamate and cinnamic acid gave only Michael addition products, 4-(3-methyl-5-isoxazolyl)butanoic acid derivatives.

It is well known that some aminoalkylisoxazole derivatives are antipyretic, analgesic, antitussive, anti-inflammatory, and antispasmodic drugs,[1] that some 3-alkyl-5-(alkoxymethyl)isoxazole derivatives exhibit blood-sugar-reducing activity,[2] and that some others can also be used as intermediates for the synthesis of terpenes and steroids.[3] Therefore, we were much interested in synthesizing various kinds of isoxazole derivatives. In the previous papers, we have reported the regiospecific reaction of 3,5-dimethylisoxazole (**1**) with such electrophiles as alkyl halides,[4] Schiff bases,[5] benzonitrile,[5] and ethyl cyanoformate,[6] affording 5-alkyl, 5-(2-aminoalkyl)-, 5-(2-amino-2-phenylvinyl)-3-methylisoxazoles, and diethyl (3-methyl-5-isoxazolyl)-malonate respectively. In this paper we wish to report the reaction of **1** with carbonyl compounds in the presence of alkali amide in liquid ammonia.

3,5-Dimethylisoxazole (**1**) was treated with an equimolar amount of methyl benzoate in the presence of an equimolar amount of sodium amide in liquid ammonia. 3-Methyl-5-(benzoylmethyl)isoxazole (**2**) was obtained, it was identified by a direct comparison with an authentic sample.[5] Under similar conditions, **1** was treated with ethyl acetate. However, 3-methyl-5-acetonylisoxazole (**3**) could not be detected by the GLC analysis of the reaction product. The sole product was identified with ethyl acetoacetate. This result suggested that sodium-hydrogen exchange occurred between the sodium salt (**4**) of **1** and an active methyl of ethyl acetate. From the fact that lithium-hydrogen exchange is much slower than that of sodium-hydrogen,[7] it is expected that the lithium salt (**5**) of **1** reacts ethyl acetate to give **3**. Actually, a trace of **3** was obtained when **1** was treated with ethyl acetate in the presence of butyllithium in THF. On the other hand, when lithium amide was used in liquid ammonia, **3** was obtained in a 40% yield. No isomers of **3** could be detected by the GLC and NMR analyses of the reaction product. Also, 4-pentanolide with an active methylene, reacted with **1** to give 3-methyl-5-(5-hydroxy-2-oxohexyl)isoxazole (**6**).

In the case of benzaldehyde, **1** gave 3-methyl-5-(2-hydroxy-2-phenylethyl)isoxazole (**7**) in the presence of sodium amide, its structure was confirmed by dehydration to 3-methyl-5-styrylisoxazole (**8**).[5] The similar treatment of **1** with *p*-tolualdehyde, *p*-anisaldehyde, and benzophenone gave the corresponding 2-hydroxy products, **9**, **10**, and **11**[8] respectively. In the presence of lithium amide, acetone, acetophenone, and cyclohexanone were also treated with **1** to produce the corresponding products, **12**, **13**, and **14**. However aliphatic aldehydes, such as butyraldehyde and acetaldehyde, did not still react with **1** in the presence of sodium or lithium amide in liquid ammonia.

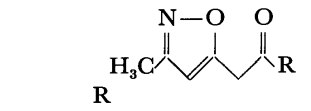

2 C_6H_5
3 CH_3
6 $CH_2CH_2CH(OH)CH_3$

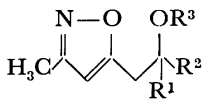

	R^1	R^2	R^3
7	C_6H_5	H	H
9	*p*-$CH_3C_6H_4$	H	H
10	*p*-$CH_3OC_6H_4$	H	H
11	C_6H_5	C_6H_5	H
12	CH_3	CH_3	H
13	C_3H_5	CH_3	H
14	$(CH_2)_5$		H
16	C_6H_5	H	CH_3
17	C_6H_5	H	CH_2CH_3
18	C_6H_5	H	$CH_2CH{=}CH_2$
19	C_6H_5	H	$CH_2C_6H_5$
20	*p*-$CH_3C_6H_4$	H	CH_3
21	*p*-$CH_3OC_6H_4$	H	CH_3
22	C_6H_5	C_6H_5	CH_3
33	*p*-$NO_2C_6H_4$	H	CH_3

Fig. 1.

The mechanism of these reactions is speculated to be as is shown in the Scheme, that is, the salt (**4** or **5**) of **1** attacks a carbonyl group, and an oxide anion (**15**) is formed. This intermediate, **15**, is neutralized with ammonium chloride to give a hydroxy derivative. If **15** is treated with alkyl halides before neutralization, alkoxy derivatives are formed. Thus, the addition of methyl iodide to the mixture of **1**, benzaldehyde, and sodium amide gave two products, namely, the expected alkoxy derivative, 3-methyl-5-(2-methoxy-2-phenyl-

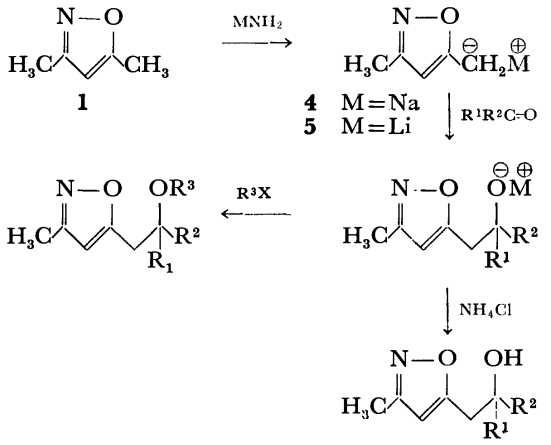

Scheme.

ethyl)isoxazole (**16**), and **7**. Also, the alkylation with ethyl bromide, allyl bromide, and benzyl bromide gave the corresponding 2-alkoxy products, **17**, **18**, and **19**. Similarly, compounds **20**, **21**, and **22** were prepared from *p*-tolualdehyde, *p*-anisaldehyde, and benzophenone respectively.

As an α,β-unsaturated carbonyl compound, chalcone was treated with **1**. Two 1 : 1 addition products were thus obtained a 1,2-addition product, 1,3-diphenyl-3-hydroxy-4-(3-methyl-5-isoxazolyl)-1-butene (**23**), and a Michael addition product, 4-(3-methyl-5-isoxazolyl)-1,3-diphenyl-1-butanone (**24**). The treatment of methyl vinyl ketone with **1** in the presence of lithium amide also gave two products, **25** and **26**. When **1** was treated with cinnamaldehyde, an 1,2-addition product, 1-(3-methyl-5-isoxazolyl)-4-phenyl-3-buten-2-ol (**27**), was obtained as well as trace amounts of a Michael addition product, 4-(3-methyl-5-isoxazolyl)-3-phenylbutanal (**28**). Similarly, **1** was treated with acrylaldehyde and crotonaldehyde to give the corresponding 1,2-addition products, **29** and **30**. On the other hand, **1** was treated with methyl cinnamate under similar conditions to give a Michael addition product **31**. 1,2-Addition products could not be detected by the IR and NMR spectral analyses of the reaction product. Furthermore, **1** was treated with an equimolar amount of cinnamic acid in the presence of two molar amounts of lithium amide to afford only a Michael addition product, 4-(3-methyl-5-isoxazolyl)-3-phenylbutanoic acid (**32**), in a poor yield. In the presence of sodium amide, the starting materials were recovered.

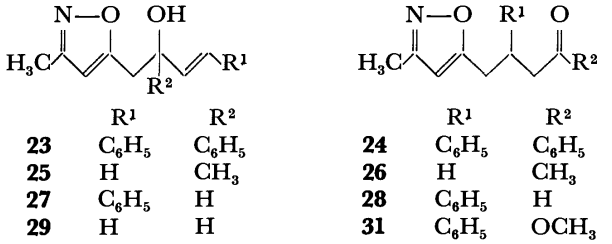

	R^1	R^2
23	C_6H_5	C_6H_5
25	H	CH_3
27	C_6H_5	H
29	H	H
30	CH_3	H

	R^1	R^2
24	C_6H_5	C_6H_5
26	H	CH_3
28	C_6H_5	H
31	C_6H_5	OCH_3
32	C_6H_5	OH

Fig. 2.

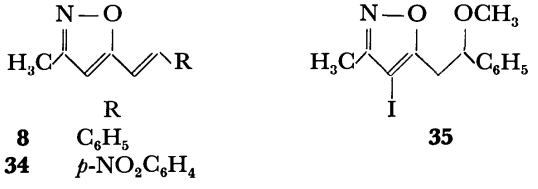

	R
8	C_6H_5
34	*p*-$NO_2C_6H_4$

35

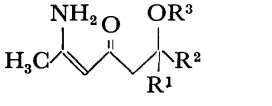

	R^1	R^2	R^3
36	C_6H_5	H	H
37	C_6H_5	H	CH_3
38	C_6H_5	C_6H_5	CH_3

Fig. 3.

Additionally, some chemical reactions of these products were examined. Under the nitration condition of **1** on the C-4 position,[9] **16** was nitrated not on the C-4 position, but on the phenyl group, to give two nitro derivatives, **33** and **34**. On the other hand, **16** was iodinated on the C-4 position of the isoxazole ring to give **35**. The hydrogenations of **7**, **16**, and **22** gave the corresponding β-aminoenones, **36**, **37**, and **38** respectively.

Experimental

All the melting points and boiling points are uncorrected. The IR spectra were recorded on a Hitachi EST-3T spectrometer, and the NMR spectra, on a Hitachi H-60 or a JEOL H-100 spectrometer. The chemical shifts are expressed in ppm, with TMS as the internal standard. The GLC analyses were performed using a Hitachi KGL-2A gas chromatograph on a 1-m column packed with Apiezon grease L.

General Procedure for the Preparation of 3-Methyl-5-(2-oxoalkyl, 2-hydroxyalkyl, and 2-hydroxyalkenyl)isoxazoles and 4-(3-Methyl-5-isoxazolyl)butanoic Acid Derivatives. To a Dry Ice cooling suspension of alkali amide (0.01 mol) in liquid ammonia (80 ml), we added, drop by drop, **1** (0.01 mol) in anhydrous ether (15 ml). After stirring for 1.5 h under a nitrogen stream, a carbonyl compound (0.01 mol) was added to the colored solution and stirring was continued for another 2 h (17 h when lithium amide was used) at −78 °C. To the reaction mixture we then added ammonium chloride (6 g), and the ammonia was removed at room temperature. The residue was decanted with dichloromethane several times. The dichloromethane solution was washed with aqueous sodium chloride and dried over anhydrous sodium sulfate. After the removal of the solvent, the residue was purified by silica gel chromatography and distillation or recrystallization. The yields and physical properties of the products are collected in Tables 1 and 3.

General Procedure for the Preparation of 3-Methyl-5-(2-alkoxyalkyl)isoxazoles. To a Dry Ice cooling suspension of sodium amide (0.01 mol) in liquid ammonia (80 ml), an anhydrous ether (15 ml) solution of **1** (0.01 mol) was added. After stirring for 1.5 h at −78 °C, a carbonyl compound (0.01 mol) was added to the colored solution and stirring was continued for another 2 h. An alkyl halide (0.01 mol) in anhydrous ether (15 ml) was then added to the mixture and stirring was continued for 2 h. The following work-up and purification were done in the manner described in *General Procedure for the Preparation of 3-Methyl-5-(2-oxoalkyl, 2-hydroxyalkyl, and 2-hydroxylalkenyl)isoxazoles and 4-(3-Methyl-5-isoxazolyl)butanoic Acid Derivatives.* The yields and the physical properties of the products are collected in Tables 2 and 3.

Dehydration of 7 to 3-Methyl-5-styrylisoxazole (8). Compound **7** (0.50 g) was added to concentrated, ice-cooled sulfuric acid (5 ml) at 0 °C. The mixture was stirred for

15 min and then poured onto crushed ice. Extractive work-up with ether and subsequent purification by recrystallization from hexane afforded **8** (24% yield), whose mp and spectral data were identical with those of an authentic sample.[5]

Nitration of ***16***. Compound **16** (0.34 g) was treated with concentrated sulfuric acid (1.84 g) and nitric acid (d=1.38, 0.22 g) in a manner similar to that in the literature.[9] Work-up and column chromatography (silical gel, chloroform) afforded **33** and **34**.

*3-Methyl-5-[(2-methoxy-2-(*p*-nitrophenyl)ethyl)]isoxazole(**33**)*. Yield, 10%, mp 93.5—950 °C (carbon tetrachloride). IR (KBr): 1611, 1516, 1349, 1104, 1009, 839 cm^{-1}, NMR ($CDCl_3$): δ 2.25 (s, 3H), 3.0—3.2 (m, 2H), 3.27 (s, 3H), 4.63 (t, 1H, J=7.2 Hz), 5.80 (s, 1H), 7.82 (ABq, 4H, J_{AB}=9.0 Hz, $\Delta\nu_{AB}$=44.7 Hz). Found: C, 59.74; H, 5.57; N, 10.67%. Calcd for $C_{13}H_{14}N_2O_4$: C, 59.53; H, 5.38; N, 10.68%.

*3-Methyl-5-(*p*-nitrostyryl)isoxazole (**34**)*. Yield, 42%, mp 175—177 °C (carbon tetrachloride). IR (KBr): 1593, 1510, 1336, 1008, 833 cm^{-1}, NMR ($CDCl_3$): δ 2.35 (s, 3H), 6.20 (s, 1H), 7.19 (ABq, 2H, J_{AB}=16.8 Hz, $\Delta\nu_{AB}$=18.0 Hz), 7.91 (ABq, 4H, J_{AB}=9.0 Hz, $\Delta\nu_{AB}$=35.5 Hz). Found: C, 62.84; H, 4.38; N, 12.09%. Calcd for $C_{12}H_{10}N_2O_3$: C, 62.60; H, 4.38; N, 12.17%.

Iodination of ***16*** *to 3-Methyl-4-iodo-5-(2-methoxy-2-phenylethyl)isoxazole (**35**)*. A mixture of **16** (0.22 g), iodine (0.12 g), and nitric acid (d=1.38, 2 drops) was stirred at 80 °C for 30 min. The resulting mixture was extracted with ether. The ether solution was washed with aqueous sodium thiosulfate and water. Work-up and column chromatography (silica gel, benzene) gave **35**. Yield, 70%, bp 156—161 °C/2 mmHg. IR (neat): 1605, 1501, 1407, 1101, 1060, 748 cm^{-1}, NMR ($CDCl_3$): δ 2.20 (s, 3H), 2.7—3.5 (m, 2H), 3.17 (s, 3H), 4.56 (dd, 1H, J=6.0, 7.2 Hz), 7.27 (s, 5H). Found: C, 45.69; H, 4.23; N, 4.25%. Calcd for $C_{13}H_{14}INO_2$: C, 45.50; H, 4.12; N, 4.08%.

Catalytic Hydrogenation of Isoxazoles ***7***, ***16***, *and* ***22***. The catalytic hydrogenation of an isoxazole (1 mmol) in ethanol (15 ml) was carried out over platinum oxide (15 mg) at room temperature, then it was filtered to remove the catalyst. The filtrate was concentrated and purified by recrystallization or distillation.

*5-Amino-1-hydroxy-1-phenyl-4-hexen-3-one (**36**)*. Yield, 70%, mp 124—126 °C (benzene-ethyl acetate). IR (KBr): 3300, 3180, 1600, 1528, 1410, 1053 cm^{-1}, NMR ($CDCl_3$): δ 1.89 (s, 3H), 2.63 (d, 2H, J=6.6 Hz), 4.8 (br. s, 1H), 4.97 (s, 1H), 5.08 (t, 1H, J=6.6 Hz), 5.5 (br. s, 1H), 7.1—7.5 (m, 5H), 9.7 (br. s, 1H). Found: C, 70.31; H, 7.28; N, 6.85%. Calcd for $C_{12}H_{15}NO_2$: C, 70.22; H, 7.37; N, 6.82%.

*5-Amino-1-methoxy-1-phenyl-4-hexen-3-one (**37**)*. Yield, 90%, bp 155—160 °C/2 mmHg. IR (neat): 3350, 3170, 1619, 1527, 1142, 1097 cm^{-1}, NMR ($CDCl_3$): δ 1.90 (s, 3H), 2.3—3.1 (m, 2H), 3.21 (s, 3H), 4.69 (dd, 1H, J=4.8, 8.4 Hz), 5.00 (s, 1H), 5.3 (br. s, 1H), 7.30 (s, 5H), 9.7 (br. s, 1H). Found: C, 71.26; H, 7.86; N, 6.14%. Calcd for $C_{13}H_{17}NO_2$: C, 71.20; H, 7.82; N, 6.39%.

*5-Amino-1,1-diphenyl-1-methoxy-4-hexen-3-one (**38**)*. Yield, 60%, mp 133—134 °C (hexane-benzene). IR (KBr): 3300, 3170, 1600, 1525, 1070, 740 cm^{-1}, NMR ($CDCl_3$): δ 1.63 (s, 3H), 3.20 (s, 3H), 3.29 (s, 2H), 4.35 (s, 1H), 4.9 (br. s, 1H), 7.1—7.5 (m, 10H), 9.6 (br. s, 1H). Found: C, 77.75; H, 7.26; N, 4.74%. Calcd for $C_{19}H_{21}NO_2$: C, 77.26; H, 7.17; N, 4.74%.

References

1) H. Kano, I. Adachi, Y. Kido, and K. Hirose, Jap. Pat. 9144, 9145 (1967); *Chem. Abstr.*, **67**, 54118w 54119x (1967).

2) J. B. Wright, U. S. Pat. 3296071 (1967); *Chem. Abstr.*, **66**, 75991v (1967).

3) a) G. Stork, S. Danishefsky, and M. Ohashi, *J. Am. Chem. Soc.*, **89**, 5459 (1967); b) G. Stork and J. E. McMurry, *ibid.*, **89**, 5463, 5464 (1967); c) K. H. Schulte-Elte, B. L. Müller, and G. Ohloff, *Helv. Chim. Acta*, **56**, 310 (1973); d) G. Saucy and J. W. Scott, Ger. Pat. 1958600, 1958646 (1970); *Chem. Abstr.*, **73**, 77236w, 77231r (1970).

4) C. Kashima, S. Tobe, N. Sugiyama, and M. Yamamoto, *Bull. Chem. Soc. Jpn.*, **46**, 310 (1973).

5) C. Kashima and Y. Tsuda, *Bull. Chem. Soc. Jpn.*, **46**, 3533 (1973).

6) C. Kashima, N. Mukai, and Y. Tsuda, *Chem. Lett.*, **1973**, 539.

7) R. J. Light and C. R. Hauser, *J. Org. Chem.*, **26**, 1716 (1961).

8) R. G. Micetich, *Can. J. Chem.*, **48**, 2006 (1970).

9) G. T. Morgan and H. Burgess, *J. Chem. Soc.*, **1921**, 697.

Solid Phase Peptide Synthesis by Oxidation-Reduction Condensation. Synthesis of Adrenocorticotropin(1—24) by Chain Elongation at the Carboxyl End on Solid Support

Hiroshi MARUYAMA, Rei MATSUEDA, Eiichi KITAZAWA, Hidekuni TAKAHAGI, and Teruaki MUKAIYAMA*

Product Development Laboratories, Sankyo Co., Ltd. Hiromachi Shinagawa-ku, Tokyo 140

**Department of Chemistry, Faculty of Science, The University of Tokyo, Bunkyo-ku, Tokyo 113*

(Received January 23, 1976)

Solid phase peptide synthesis by oxidation-reduction condensation *via* fragment condensation at the carboxyl end was established by a new monitoring method based on high pressure liquid chromatography. The merit of the method was demonstrated through the synthesis of ACTH (1—24). A resin-tetracosapeptide with quantitative amino acid ratios was easily prepared by coupling 6 fragments of 1—2, 3—7, 8—10, 11—14, 15—19, and 20—24 sequences. ACTH (1—24) with a full activity was obtained in 25% yield from the initial resin-dipeptide by hydrogen fluoride treatment and purification with carboxymethyl-cellulose chromatography.

The oxidation-reduction condensation reaction forming peptide linkage with use of triphenylphosphine (Ph_3P) and di-2-pyridyl disulfide ($(PyS)_2$) proceeds under mild conditions without basic or acidic catalysts. It has the advantage of minimizing the racemization of a carboxyl component and the side reactions of amino acids.[1] The condensation reaction has been successfully employed not only to syntheses of peptides,[2] nucleotides,[3] and coenzymes[4] but also to syntheses of various macrolides[5] *via* 2-pyridinethiol ester.[1,6] The active dehydrating agent in the reaction, phosphorane, is generated by mixing the carboxyl component with Ph_3P and $(PyS)_2$ whose melting points are 82 and 58 °C, respectively. Peptide bond formation would proceed through a cyclic transition state.[1] The high reactivity with high selectivity depends upon the stability of the intermediate of acyloxyphosphonium salt in which phosphorus atom exists largely in the pentacovalent form. This being the case, some modification is possible by changing the nature of the trivalent phosphorus compounds. As an example, the use of tris(*p*-bromophenyl)phosphite[7] in place of the triphenylphosphine increases the stability of the intermediate in polar solvents such as *N*,*N*-dimethylformamide. On the other hand, tributylphosphine decreases the stability of the intermediate which results in the decrease of selectivity in spite of the increase of reactivity.[8]

We have shown that the oxidation-reduction condensation can be successfully applied to the synthesis of LH-RH *via* fragment condensation on solid support by employing two types of chain elongation, from *C*-terminal amino acid to *N*-terminal amino acid and from *N*-terminal amino acid to *C*-terminal amino acid.[9]

The latter approach was further extended to a synthesis of ACTH(1—24).[10] This paper[11] contains a full report of the synthesis of ACTH(1—24) by a new technique to monitor the amount of amino component in solution based on high pressure liquid chromatography (HPLC). The general procedures for this approach are shown in Fig. 1.

The synthesis of ACTH(1—24) was carried out by coupling 6 fragments of 1—2, 3—7, 8—10, 11—14, 15—19, and 20—24 as shown in the following scheme.

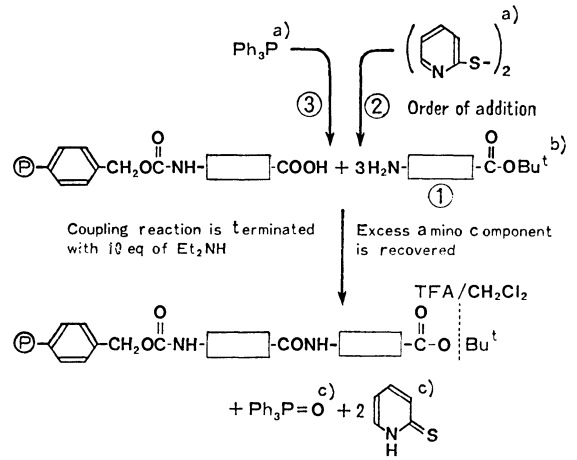

Fig. 1. General procedure for solid phase peptide synthesis by oxidation-reduction condensation.
Abbreviations, Ⓟ: copolymer of styrene-2% divinylbenzene, TFA : trifluoroacetic acid and -OBu^t : *t*-butyl ester.
a) The reagents are individually stable and safely stored but should not be mixed before addition.
b) Coupling reaction is monitored by measuring the amount of amino component in solution by means of high pressure liquid chromatography.
c) Very soluble in organic solvents and easily washed out with methylene chloride, ethanol, *etc.*

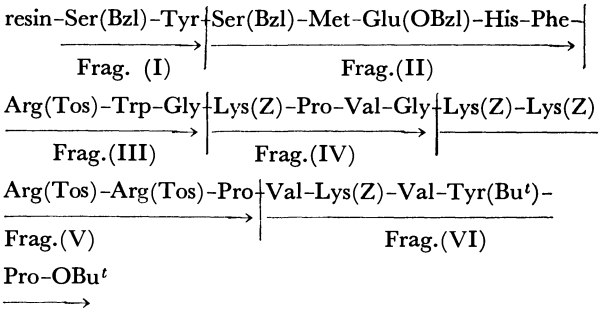

The following precautions were taken: 1) the number of amino acid residue in one fragment was chosen to be less than 5, considering the easiness of the syntheses of fragments, 2) each fragment contains a unique amino acid residue which makes it possible

to check the chain elongation by amino acid analysis, 3) each fragment has a UV absorbing moiety in order to monitor the coupling reaction by HPLC, 4) the biologically active center is included in one fragment V in order to ensure the incorporation of this fragment which could be proved by the activity. The *t*-butyl ester was selected for α-carboxyl protection since it is easily deprotected with trifluoroacetic acid. The protecting groups of side chains were benzyloxycarbonyl for ε-amino function of lysine, benzyl ester for γ-carboxyl function of glutamic acid, tosyl group for guanido function of arginine and benzyl ether for hydroxyl function of serine. In the syntheses of the fragments having these protecting groups, an α-amino protecting group must be removed without influencing the other groups. *o*-Nitrophenylsulfenyl(Nps-) protecting group was chosen for this purpose. Nps-protecting group was selectively removed under neutral conditions[10] by mixing the Nps-protected fragment with 5 fold excess each of Ph_3P and pentachlorophenol in methanol at room temperature. The pure fragment with the free amino function was quantitatively obtained by gel filtration on Sephadex LH-20 in methanol and drying *in vacuo* after evaporation of the solvent.

The syntheses of protected fragments were achieved stepwise in solution by oxidation-reduction condensation using the readily available benzyloxycarbonylamino acids except in cases of incorporation of Nps-amino acid residues which were coupled with dicyclohexylcarbodiimide (DCC) or by active ester and mixed anhydride method (M.A.) (Fig. 2). The physical properties of these intermediates are given in Table 1.

Starting with 1.5 g of 2% cross-linked resin containing 0.046 mmol of *O*-benzylseryltyrosine,[9] coupling steps of the incorporation of fragment II and III were carried out with a three-fold excess fragment and a 30 fold excess each of Ph_3P, $(PyS)_2$ and 2-pyridinethiol in methylene chloride, 6 h at −15 °C and overnight at room temperature. The steps of incorporation of fragments IV, V, and VI were carried out at room temperature in the absence of 2-pyridinethiol since carboxyl ends such as glycine and proline are free from racemization. Excess fragments were recovered in washing solvents since they did not change in the coupling reaction. They were easily purified by gel filtration on Sephadex LH-20 in methanol in 80—90% recovery yield. A successive coupling of 1 g of new resin–dipeptide with recovered fragments gave resin–tetracosapeptide with nearly quantitative amino acid ratios.

During the course of the synthesis, coupling rates were easily monitored by measuring the amount of fragment in solution by HPLC. Conditions suitable for effective separation have been found through the use of porous polymer Hitachi Gel 3010, a styrene-divinylbenzene polymer which is useful packing material for HPLC.[12]

With the use of aminated Hitachi Gel 3010,[13] eluting conditions were so chosen that the remaining fragment has a constant retention time irrespective of the fragment used for elongation, since it would not be practical to select eluting conditions in each coupling cycle with a different fragment. The problem was solved by elution with an acidic mobile phase by which each fragment was eluted always at or near the void volume separated from the other components in the coupling reaction. Taking these factors into consideration, analytical conditions were established as follows: column; aminated Hitachi Gel 3010 (5 mm i.d. × 50 cm length, Pyrex glass), mobile phase; 0.2 M hydrochloric acid, 0.1 M potassium chloride/methanol (1 : 9), flow rate; 2.0 ml/min, temperature; ambient, detector; UV (240 nm). A sample solution was prepared as follows: Add 20 μl of 0.2 M potassium hydroxide/80% methanol to 20 μl of reaction solution, and then neutralize with 20 μl of 0.2 M monopotassium citrate/80% MeOH. A definite volume (5—20 μl) of each solution was injected. For the

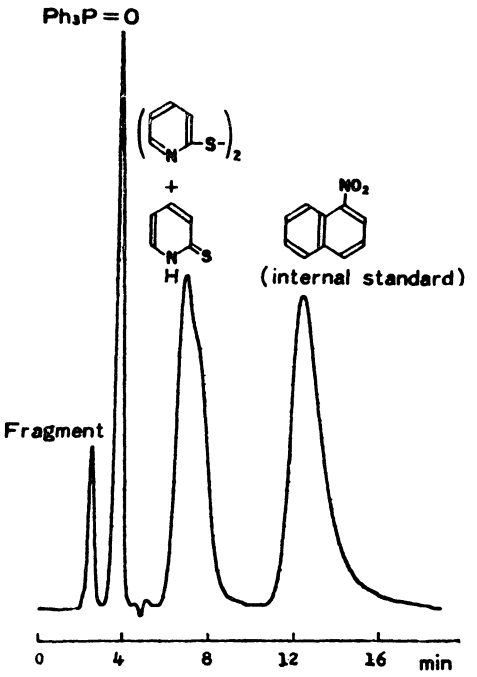

Fig. 3. A typical chromatogram by high pressure liquid chromatography.

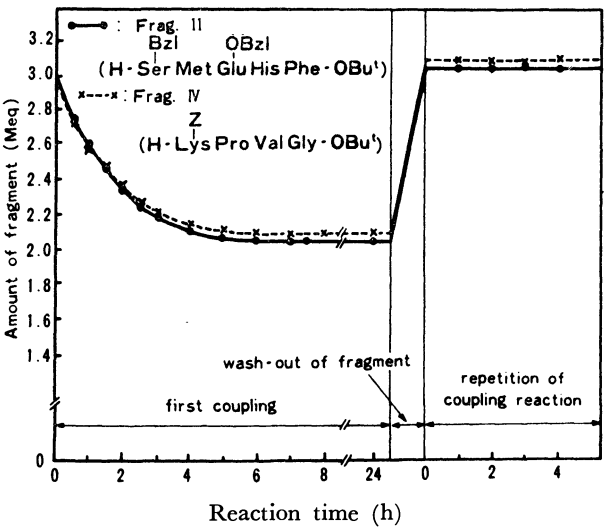

Fig. 4. Monitoring of coupling reaction by high pressure liquid chromatography.

sake of accurate determination and easy sampling, 1-nitronaphthalene was added to the reaction mixture as an internal standard. Each sample was analyzed within 15 min with an accuracy of ±1.0%.[14] A typical chromatogram is shown in Fig. 3. The remaining amino component was plotted against reaction time. Typical examples of monitoring results are shown in Fig. 4, one for the coupling of Frag. (II) and the other for that of Frag. (IV), wherein the coupling was carried out at −15 °C and room temperature, respectively. Reaction completion was principally determined by recording the time at which the curve indicates no further consumption of the fragment. Coupling was repeated until no fragment uptake was detected. It was also confirmed by determination of the amino acid ratios of the resulting peptide resin after the hydrolysis of a small portion of the resin with propionic acid–12 M hydrochloric acid (1 : 1 v/v).[15] The results at each step are given in Table 2. They indicate that fragment condensation proceeds efficiently with partial protection of side chains of amino acids.

The resin–tetracosapeptide was treated with hydrogen fluoride[16] for 30 min at 0 °C in the presence of anisole and 2-pyridinethiol. The yield of this cleavage step was 83%. The peptide was converted into acetate form and chromatographed on carboxymethyl-cellulose[17] after gel filtration on Sephadex G-25 in 1 M acetic acid. The pure ACTH(1—24)·7AcOH·$9H_2O$ which gave a single spot on thin layer chromatography and electrophoresis detected by Ehrlich, Pauly, Cl-tolidine, and ninhydrin reactions was obtained by precipitation from methanol–ethyl acetate–petroleum ether: dried *in vacuo* over phosphorus pentoxide; 41 mg, 25% yield from the initial resin–Ser(Bzl)–Tyr–OH, 43% yield from the liberated peptide from the resin. $[\alpha]_D^{20}$ −86.8° (*c* 0.5, 1% acetic acid) (lit,[18] $[\alpha]_D^{23}$ −88.6 ±2° (*c* 0.51, 1% acetic acid). Amino acid ratios after complete enzymatic digestion and acid hydrolysis[15] were in good agreement (Table 3). This shows that no detectable racemization occurred during the course of fragment condensation by oxidation-reduction process.

The ACTH activity of this purified peptide was assayed[19] by the ascorbic acid depletion test according to U.S.P. XVIII, and compared with the 2nd international standard: 96 (83—128) IU/mg identical with the value in literature.[18]

The new approach indicates that an oligopeptide as ACTH(1—24) is prepared in good yield by a simple purification procedure since the contamination of similar peptides with small difference in sequence is eliminated.

Particular merits of the method are as follows: 1) unreacted amino components can be recovered intact and recycled in the chain elongation procedure, 2) the number of protecting groups of the side chains can be reduced, 3) fragments are synthesized by the classical method from readily available Z-amino acid, 4) diacylation is avoided since excess amino components are used in solution, 5) the end peptide is homogeneous since similar contaminations are eliminated, 6) the number of acidolysis can be reduced, suitable for the acid sensitive tryptophan residue, 7) the progress and the completeness of each coupling reaction is easily analyzed by high pressure liquid chromatography.

The versatility of this approach, along with a combination of the classical synthesis in solution, promises a new possibility of facile preparation of pure peptides with long sequence, widening the extent of the usual solid phase peptide synthesis.

Experimental

All the melting points are uncorrected. Optical rotations were determined with a Perkin-Elmer Model 141 Polarimeter. Amino acid analyses were carried out on a Hitachi Amino Acid Analyzer, Model KLB-3B. High pressure liquid chromatography was performed on a Hitachi Chromatograph, Model 635 equipped with a variable UV detector. Solid phase peptide synthesis was carried out by shaking with a manual apparatus. Thin layer chromatography was

Table 2. Amino acid ratios[a] in each coupling step

	Ser	Tyr	Met	Glu	His	Phe	Arg	Gly	Lys	Pro	Val
Step I	0.97	1									
Step II	2.13	1.08	0.96	0.97	0.98	1					
Step III	2.16	1.11	0.95	0.98	0.96	1	0.97	1.01			
Step IV	2.08	1.08	0.91	1.02	0.96	1	0.99	2.01	0.99	0.96	1.02
Step V	2.11	1.06	0.92	1.01	0.98	1	2.91	2.01	2.79	1.91	0.95
Step VI	1.92	2.34	1.08	1.01	0.98	1	2.87	2.19	3.71	3.01	2.87
Theor.	(2)	(2)	(1)	(1)	(1)	(1)	(3)	(2)	(4)	(3)	(3)

a) Acid hydrolysis: propionic acid-hydrochloric acid(1 : 1 v/v), 130 °C, 2 h.

Table 3. Amino acid analyses of the synthetic ACTH (1—24)

	Ser	Tyr	Met	Glu	His	Phe	Arg	Trp	Gly	Lys	Pro	Val	Content
(I)	1.91	2.07	0.96	1	0.87	1.07	3.32	—	2.18	4.39	3.28	3.14	81%
(II)	1.78	1.98	1.02	1.15	0.98	1.10	3.41	1	1.98	4.51	2.94	3.26	78%
Theor.	(2)	(2)	(1)	(1)	(1)	(1)	(3)	(1)	(2)	(4)	(3)	(3)	

(I): Propionic acid-hydrochloric acid (1 : 1 v/v) hydrolysis, 130 °C, 2 h. (II): Digestion with trypsin and chymotrypsin (37°, 24 h) and subsequently with aminopeptidase M and prolidase (37 °C, 24 h).

carried out on precoated plates of silica gel G (E. Merck) at 5 °C.

Nps-Ser(Bzl)-Tyr(Bu^t)-OBu^t (I. Fragment I). Z-Tyr(Bu^t)-OBu^t (4.70 g, 11 mmol) was hydrogenated in 300 ml of methanol over 10% Pd/C (0.5 g) as a catalyst; the solvent was removed after filtration of the catalyst and dried *in vacuo* over phosphorus pentoxide. The residue was used as H-Tyr(Bu^t)-OBu^t. Nps-Ser(Bzl)-OH·DCHA (5.29 g, 10 mmol) was suspended in 200 ml of ethyl acetate and washed with 10% citric acid in water. Ethyl acetate layer was separated and washed with water. After drying over magnesium sulfate, ethyl acetate was evaporated and the residue was used as Nps-Ser(Bzl)-OH. Ethyl chloroformate (1.08 g, 10 mmol) was added to a stirred mixture of Nps-Ser(Bzl)-OH, *N*-methylmorpholine (1.01 g, 10 mmol) in 200 ml of tetrahydrofuran at −15 °C. After stirring for 5 min, H-Tyr(Bu^t)-OBu^t in 50 ml of tetrahydrofuran was added at −15 °C and the reaction mixture was stirred at −15 °C for 30 min and at room temperature for 5 h. After filtration of the reaction mixture, the filtrate was evaporated and dissolved in 300 ml of ethyl acetate and washed successively with 10% citric acid, water, 5% sodium bicarbonate and water. After being dried over sodium sulfate, the solvent was evaporated *in vacuo* and Nps-Ser(Bzl)-Tyr(Bu^t)-OBu^t was obtained as an oil: yield 4.42 g (69.8%), R_f 0.89 on silica gel in *n*-BuOH : AcOH : H_2O (4 : 1 : 1) and R_f 0.85 in *n*-BuOH : AcOH : H_2O; pyridine (30 : 6 : 24 : 20). Amino acid ratios (propionic acid-12 M hydrochloric acid hydrolysis)[15]: Ser, 0.98; Tyr, 1.00 Nps-protecting group of this peptide was cleaved according to the following procedure: the above dipeptide (1.74 g, 2.8 mmol) was dissolved in 100 ml of methanol and 5 fold excess each of triphenylphosphine (3.66 g, 14 mmol), pentachlorophenol (3.72 g, 14 mmol) being added and stirred at room temperature for 30 min. The mixture was condensed after filtration of the precipitate and applied to Sephadex LH-20 column (2.5×60 cm) in methanol. H-Ser(Bzl)-Tyr(Bu^t)-OBu^t was eluted in the first fraction. The peptide was dried *in vacuo* over phosphorus pentoxide after evaporation of solvent and used for an attachment to the resin.

Z-His(Z)-Pro-OBu^t (II). To a stirred mixture of Z-His(Z)-OH with one molecule of methanol (9.11 g, 20 mmol) and di-2-pyridyl disulfide (5.28 g, 24 mmol) in 100 ml of dry methylene chloride was added triphenylphosphine (6.29 g, 24 mmol) and H-Phe-OBu^t (4.43 g, 20 mmol) in 30 ml of dry methylene chloride. The mixture was stirred at room temperature overnight and washed successively with 10% citric acid, water, 5% sodium bicarbonate and water and dried over magnesium sulfate. The solvent was evaporated after addition of silica gel (100 g) and coated residue was subjected to dry column chromatography[20] on silica gel and the peptide was eluted with diethyl ether and crystallized from ethyl acetate-diethyl ether-petroleum ether: yield 10.78 g (86.0%); mp 104—105 °C; $[\alpha]_D^{20}$ 1.7° (*c* 1, methanol).

Found: C, 66.55; H, 6.13; N, 9.09%. Calcd for $C_{35}H_{38}O_7N_4 \cdot 1/2\ H_2O$: C, 66,12; H, 6.11; N, 8.82%.

Nps-Glu(OBzl)-His-Phe-OBu^t (III). Nps-Glu(OBzl)-OH·DCHA (11.74 g, 20 mmol) was converted into a free form with citric acid as in the preparation of I and used as Nps-Glu(OBzl)-OH. To a stirred mixture of Nps-Glu(OBzl)-OH, pentachlorophenol (5.32 g, 20 mmol) in 200 ml of ethyl acetate was added dicyclohexylcarbodiimide (4.12 g, 20 mmol) with ice-cooling and the mixture was stirred at 0 °C for 1 h and kept stirring overnight. The precipitated dicyclohexylurea was filtered off and the filtrate washed with 10% citric acid, water, 5% sodium bicarbonate, water and dried over sodium sulfate. The solvent was evaporated *in vacuo* and the active ester was obtained as foam and used as Nps-Glu(OBzl)-OPcp. Compound II (6.26 g, 10 mmol) was hydrogenated over 10% Pd/C as in the preparation of I and used as H-His-Phe-OBu^t. To a stirred solution of H-His-Phe-OBu^t in 200 ml of *N,N*-dimethylformamide was added 6.54 g (10 mmol) of Nps-Glu(OBzl)-OPcp and stirred at room temperature for 48 h. The solvent was removed *in vacuo* and the residue was dissolved in ethyl acetate and washed successively with 10% citric acid, water, 5% sodium bicarbonate and water. The solvent was condensed after drying over sodium sulfate and the tripeptide was obtained by precipitation with the addition of diethyl ether: yield 5.31 g (72.4%); mp 78—80 °C, $[\alpha]_D^{20}$ −18.0° (*c* 1, methanol).

Found: C, 60.69; H, 6.10; N, 11.43; S, 4.38%. Calcd for $C_{37}H_{42}N_6O_8S$: C, 60.80; H, 5.79; N, 11.50; S, 4.39%.

Nps-Met-Glu(OBzl)-His-Phe-OBu^t (IV). Nps-Met-OPcp (2.99 g, 52.8%) was obtained as foam by the same procedure as for the preparation of Nps-Glu(OBzl)-OPcp from Nps-Met-OH·DCHA (4.38 g, 10 mmol), pentachlorophenol (2.66 g, 10 mmol) and dicyclohexylcarbodiimide (2.27 g, 11 mmol). Compound III (4.0 g, 5.48 mmol) was converted into amino free form as in the preparation of H-Ser(Bzl)-Tyr(Bu^t)-OBu^t of Fragment I. To a stirred solution of this amino free peptide in 150 ml of *N,N*-dimethylformamide was added the above Nps-Met-OPcp (3.10 g, 5.48 mmol) and kept stirring at room temperature for 48 h. After working up as in the preparation of Compound III, evaporation of the solvent gave a crude peptide. This was further purified by gel filtration on Sephadex LH-20 (2.5× 60 cm) in methanol, the tetrapeptide being obtained by crystallization from ethyl acetate-petroleum ether: yield 2.98 g (62.0%); mp 160—164 °C; $[\alpha]_D^{20}$ −42.3° (*c* 1, methanol).

Nps-Ser(Bzl)-Met-Glu(OBzl)-His-Phe-OBu^t (V, Fragment II). Nps-Ser(Bzl)-OPcp was prepared by the same procedure as for Nps-Glu(OBzl)-OPcp in the preparation of III starting from Nps-Ser(Bzl)-OH·DCHA (5.30 g, 10 mmol), pentachlorophenol (2.66 g, 10 mmol) and dicyclohexylcarbodiimide (2.27 g, 11 mmol): yield 3.85 g (64.6%); mp 117—118 °C; $[\alpha]_D^{20}$ −1.85° (*c* 1, methanol).

Found: C, 44.54; H, 2.74; N, 4.87; S, 5.45; Cl ,29.35%. Calcd for $C_{22}H_{15}N_2O_5SCl_5$: C, 44.28; H, 2.53; N, 4.70; S, 5.37; Cl, 29.71%.

Compound IV (2.06 g, 2.4 mmol) was converted into amino free form as in the preparation of H-Ser(Bzl)-Tyr(Bu^t)-OBu^t of Fragment I. To a stirred solution of this amino free peptide in 100 ml of *N,N*-dimethylformamide was added the above Nps-Ser(Bzl)-OPcp (1.43 g, 2.4 mmol) and the mixture was stirred at room temperature for 48 h. After working up as in the preparation of Compound IV, crystallization from ethyl acetate-petroleum ether gave the pentapeptide: yield 1.77 g (70.8%); mp 158—160 °C; $[\alpha]_D^{20}$ −25.6° (*c* 1, methanol).

Found: C, 59.96; H, 5.89; N, 10.49; S, 6.23%. Calcd for $C_{52}H_{62}N_8O_{11}S_2$: C, 60.10; H, 6.01; N, 10.73; S, 6.17%. R_f 0.84 on silica gel in *n*-BuOH : AcOH : H_2O (4 : 1 : 1) and R_f 0.88 in *n*-BuOH : AcOH : H_2O : pyridine (36 : 6 : 20 : 24). Amino acid ratios (propionic acid-12 M hydrochloric acid (1 : 1) hydrolysis): Ser, 0.97; Met, 0.92; Glu, 1.01; His, 1.00; Phe, 0.99. Nps-protecting group of this peptide was cleaved as in the preparation of I, the resulting amino free peptide being used for the chain elongation on the resin.

Z-Trp-Gly-OBu^t (VI). To a stirred mixture of Z-Trp-OH (33.8 g, 0.1 M), H-Gly-OBu^t (14.4 g, 0.11 M) and di-2-pyridyl disulfide (25.5 g, 0.12 M) in 300 ml of

ethyl acetate was added triphenylphosphine (31.4 g, 0.12 M) with ice-cooling and stirred at room temperature for 5 h. The mixture was worked up as in the preparation of II and the peptide was crystallized from ethyl acetate-petroleum ether: yield 37.5 g (83.2%); mp 60—70 °C (lit,[21] mp 60—70 °C); $[\alpha]_D^{20}$ −20.8° (*c* 1, methanol) (lit,[21] $[\alpha]_D^{20}$ −19.6° (*c* 1, methanol)).

Z-Arg(Tos)-Trp-Gly-OBu^t (VII, Fragment III). Compound VI (9.95 g, 22 mmol) was hydrogenated over 10% Pd/C as in the preparation of I and used as H-Trp-Gly-OBu^t. To a stirred mixture of Z-Arg(Tos)-OH (9.24 g, 20 mmol), the above H-Trp-Gly-OBu^t and di-2-pyridyl disulfide (5.10 g, 24 mmol) in 300 ml of ethyl acetate was added triphenylphosphine (6.28 g, 24 mmol) with ice-cooling and stirred at room temperature for 6 h. After working up as in the preparation of II, the coated residue was subjected to dry column chromatography. On being washed with diethyl ether, the coated layer was separated and the peptide was eluted with methanol-chloroform (1 : 2 v/v). After the solvent was removed, the residue was dissolved in ethyl acetate and washed with water. After being dried over sodium sulfate, the solution was condensed and the tripeptide was obtained by precipitation with the addition of petroleum ether: yield 13.57 g (89.3%); mp 137—140 °C; $[\alpha]_D^{20}$ −24.5° (*c* 1, methanol) (lit,[21] $[\alpha]_D^{20}$ −25.1° (*c* 1, methanol)). Amino acid ratios (3 M *p*-toluenesulfonic acid hydrolysis[22]): Arg. 0.99; Trp, 0.81; Gly, 1.00. The peptide was hydrogenated over 10% Pd/C as in the preparation of H-Tyr(Bu^t)-OBu^t of Fragment I and used for chain elongation on the resin.

Z-Val-Gly-OBu^t (VIII). To a stirred mixture of Z-Val-OH (6.30 g, 25 mmol), H-Gly-OBu^t (3.60 g, 27.5 mmol) and di-2-pyridyl disulfide (6.55 g, 30 mmol) in 250 ml of benzene was added triphenylphosphine (7.90 g, 30 mmol) in 100 ml of benzene with ice-cooling and stirred at room temperature overnight and worked up as in the preparation of II, the dipeptide being obtained by crystallization from methanol-diethyl ether: yield 6.85 g (75.2%); mp 147.3 °C; $[\alpha]_D^{20}$ −27.2° (*c* 1, methanol).

Found: C, 62.42; H, 7.63; N, 7.67%. Calcd for $C_{19}H_{28}N_2O_5$: C, 62.62; H, 7.74; N, 7.69%.

Z-Pro-Val-Gly-OBu^t (IX). Compound VIII (5.10 g 14 mmol) was hydrogenated over Pd/C as in the preparation of I and used as H-Val-Gly-OBu^t. To a stirred mixture of H-Val-Gly-OBu^t, Z-Pro-OH (4.72 g, 12.9 mmol) and di-2-pyridyl disulfide (4.17 g, 18.9 mmol) in 100 ml of methylene chloride was added triphenylphosphine (4.97 g, 18.9 mmol) in 20 ml of methylene chloride with ice-cooling and stirred at room temperature overnight. The solvent was removed and the residue was dissolved in 100 ml of ethyl acetate and worked up as in the preparation of II. The peptide was crystallized from methanol-petroleum ether after being subjected to dry column chromatography with chloroform-methanol (19 : 1 v/v): yield 5.30 g (91.2%); mp 120 °C; $[\alpha]^{20}$ −90.8° (*c* 1, methanol).

Found: C, 62.57; H, 7.67; N, 8.88%. Calcd for $C_{24}H_{35}N_3O_6$: C, 62.45; H, 7.64; N, 9.10%.

Nps-Lys(Z)-Pro-Val-Gly-OBu^t (X, Fragment IV). Compound IX (1.38 g, 3.0 m mol) was hydrogenated in methanol and Nps-Lys(Z)-OH·DCHA (1.80 g, 2.93 mmol) was converted into free form as in the preparation of I. To a stirred mixture of H-Pro-Val-Gly-OBu^t, Nps-Lys(Z)-OH in 100 ml of ethyl acetate was added dicyclohexylcarbodiimide (2.0 g, 10 mmol) with ice-cooling and stirred at room temperature overnight. The dicyclohexylurea was filtered off and the filtrate was worked up as in the preparation of II. The coated residue was subjected to dry column chromatography and eluted with ethyl acetate. The solution was washed with water, dried over sodium sulfate and condensed. Addition of petroleum ether precipitates the tetrapeptide: 1.66 g (76.2%); mp 85.6 °C; $[\alpha]_D^{20}$ −101.5° (*c* 1, methanol).

Found: C, 58.25; H, 6.75; N, 11.17; S, 4.60%. Calcd for $C_{36}H_{51}N_6O_9S$: C, 58.13; H, 6.91; N, 11.30; S, 4.31%. R_f 0.87 on silica gel in *n*-BuOH : AcOH : H_2O (4 : 1 : 1) and R_f 0.89 in *n*-BuOH : AcOH : H_2O : pyridine (30 : 6 : 24 : 20). Amino acid ratios (propionic acid-12 M hydrochloric acid hydrolysis): Lys, 1.05; Pro, 0.96; Val, 0.96; Gly, 1.00. The peptide was converted into amino free form as in the preparation of fragment I and used for chain elongation on the resin.

Z-Arg(Tos)-Pro-OBu^t (XI). To a stirred mixture of Z-Arg(Tos)-OH (13.92 g, 30 mmol), H-Pro-OBu^t (5.13 g, 30 mmol) and di-2-pyridyl disulfide (6.60 g, 30 mmol) in 100 ml of methylene chloride was added triphenylphosphine (7.86 g, 30 mmol) with ice-cooling and stirred at room temperature overnight. The mixture was worked up as in the preparation of VII and the peptide was crystallized from ethyl acetate-petroleum ether: yield 13.92 g (75%); mp 114—115 °C (lit,[23] 115—118 °C); $[\alpha]_D^{25}$ −42.5° (*c* 1, methanol) (lit,[23] −42.5°).

Z-Arg(Tos)-Arg(Tos)-Pro-OBu^t (XII). Compound XI (9.30 g, 15 mmol) was hydrogenated in methanol as in the preparation of I. To a stirred mixture of H-Arg(Tos)-Pro-OBu^t, Z-Arg(Tos)-OH (6.60 g, 14 mmol) and di-2-pyridyl disulfide (3.30 g, 15 mmol) in 50 ml of methylene chloride was added triphenylphosphine (3.94 g, 15 mmol) with ice-cooling and stirred at room temperature overnight. The mixture was worked up as in the preparation of VII, the peptide being eluted with methanol on dry column chromatography. The peptide was crystallized from methanol-diethyl ether after further filtration on Sephadex LH-20 in methanol: yield 12.41 g (89%); mp 100—102 °C (lit,[23] 100—120 °C); $[\alpha]_D^{25}$ −33.3° (*c* 1, methanol) (lit,[23] −33.3°).

Nps-Lys(Z)-Arg(Tos)-Arg(Tos)-Pro-OBu^t (XIII). Compound XII (10.20 g, 11 mmol) was hydrogenated in methanol and Nps-Lys(Z)-OH·DCHA (6.14 g, 10 mmol) was converted into free form as in the preparation of I. A mixed anhydride was prepared as in the preparation of I from Nps-Lys(Z)-OH, *N*-methylmorpholine (1.01 g, 10 mmol) and ethyl chloroformate (1.08 g, 10 mmol) in 50 ml of tetrahydrofuran. To this solution was added H-Arg(Tos)-Arg(Tos)-Pro-OBu^t in 30 ml of chloroform with stirring for 1 h with ice-cooling and kept standing overnight at room temperature. The mixture was evaporated and dissolved in 100 ml of ethyl acetate and washed successively with 2 M sodium hydroxide, water, 10% citric acid and water. After drying over magnesium sulfate, the solvent was removed and the residue was subjected to Sephadex LH-20 column (2.5×60 cm) in methanol. The first fraction was pooled and the peptide was precipitated by addition of petroleum ether after condensation of methanol: yield 10.90 g (90%); mp 88—92 °C; $[\alpha]_D^{20}$ −49.1° (*c* 1, methanol).

Found: C, 54.66; H, 6.43; N, 13.88; S, 7.84%. Calcd for $C_{55}H_{74}O_{13}N_{12}S_3$: C, 54.71; H, 6.19; N, 13.92; S, 7.97%.

Nps-Lys(Z)-Lys(Z)-Arg(Tos)-Arg(Tos)-Pro-OBu^t (XIV Fragment V). Compound XIII (8.10 g, 5.5 mmol) was converted into amino free form with triphenylphosphine (7.21 g, 27.5 mmol) and pentachlorophenol (7.30 g, 27.5 mmol) in 150 ml of methanol and 150 ml of methylene chloride as in the preparation of I. The H-Lys(Z)-Arg(Tos)-Arg(Tos)-Pro-OBu^t, Nps-Lys(Z)-OH·DCHA (3.07 g, 5 mmol), *N*-methylmorpholine (0.50 g, 5 mmol) and ethyl chloroformate (0.54 g, 5 mmol) were allowed to react in 50 ml of tetrahydrofuran and 50 ml of methylene chloride and

worked up as in the preparation of XII: yield 5.30 g (74%); mp 130—135 °C; $[\alpha]_D^{20}$ −38.3° (*c* 1, methanol).

Found: C, 56.46; H, 6.58; N, 13.44; S, 6.59%. Calcd for $C_{69}H_{92}O_{16}N_{14}S_3$: C, 56.38; H, 6.32; N, 13.35; S, 6.54%. R_f 0.96 on silica gel in *n*-BuOH : AcOH : H_2O (4 : 1 : 1) and R_f 0.89 in *n*-BuOH : AcOH : H_2O : pyridine (30 : 6 : 24 : 20). Amino acid ratios (propionic acid-12 M hydrochloric acid hydrolysis): Lys, 2.00; Arg, 1.96; Pro, 0.96. Nps-protecting group of the peptide was cleaved by the same procedure as in the preparation of I and the amino free peptide was used for chain elongation on the resin.

Z-Tyr(Bu^t)-Pro-OBu^t (XV). Z-Tyr(Bu^t)-OH·DCHA (5.52 g, 10 mmol) was converted into free form as in the preparation of I. To a stirred mixture of Z-Tyr(Bu^t)-OH, H-Pro-OBu^t (1.88 g, 11 mmol) and di-2-pyridyl disulfide (2.64 g, 12 mmol) in 100 ml of ethyl acetate was added triphenylphosphine (3.14 g, 12 mmol) with ice-cooling and stirred at room temperature for 8 h. The mixture was worked up as in the preparation of II, the peptide being obtained as an oil: yield 4.60 g (87.7%).

Z-Val-Tyr(Bu^t)-Pro-OBu^t (XVI). Compound XV (4.60 g, 8.77 mmol) was hydrogenated to H-Tyr(Bu^t)-Pro-OBu^t as in the preparation of I. To a stirred mixture of Z-Val-OH (2.0 g, 8 mmol), H-Tyr(Bu^t)-Pro-OBu^t and di-2-pyridyl disulfide (2.11 g, 9.6 mmol) in 200 ml of ethyl acetate was added triphenylphosphine (2.52 g, 9.6 mmol) with ice-cooling and stirred at room temperature overnight. The mixture was worked up as in the preparation of II, the peptide being obtained by the evaporation of diethyl ether: yield 4.30 g (86.3%); mp 45—49 °C.

Nps-Lys(Z)-Val-Tyr(Bu^t)-Pro-OBu^t (XIIV). Compound XVI (4.09 g, 6.57 mmol) was hydrogenated to H-Val-Tyr(Bu^t)-Pro-OBu^t and Nps-Lys(Z)-OH·DCHA (4.07 g, 6.57 mmol) was converted into a free form. To a stirred mixture of Nps-Lys(Z)-OH and H-Val-Tyr(Bu^t)-Pro-OBu^t in 200 ml of ethyl acetate was added dicyclohexylcarbodiimide (2.71 g, 13.1 mmol) and stirred for 2 h with ice-cooling and overnight at room temperature. Dicyclohexylurea was filtered off and the filtrate was worked up as in the preparation of X. Crystallization from ethyl acetate-petroleum ether gave the tetrapeptide: yield 3.92 g (72.8%); mp 155—156 °C; $[\alpha]_D^{20}$ −56.3° (*c* 1, methanol).

Found: C, 62.13; H, 7.16; N, 9.38; S, 3.42%. Calcd for $C_{47}H_{64}N_6O_{10}S$: C, 62.37; H, 7.13; N, 9.29; S, 3.54%.

Nps-Val-Lys(Z)-Val-Tyr(Bu^t)-Pro-OBu^t (XVIII, Fragment VI). Compound XVII (2.50 g, 2.76 mmol) and Nps-Val-OH·DCHA (1.49 g, 3.32 mmol) was converted into free form as in the preparation of I. H-Lys(Z)-Val-Tyr(Bu^t)-Pro-OBu^t, Nps-Val-OH and dicyclohexylcarbodiimide (1.14 g, 5.52 mmol) were allowed to react in 100 ml of ethyl acetate and worked up as in the preparation of X. The peptide was obtained by crystallization from ethyl acetate-petroleum ether: yield 2.08 g (72.3%); mp 206—209 °C (decomp.); $[\alpha]_D^{20}$ −105.5° (*c* 1, methanol).

Found: C, 61.87; H, 7.27; N, 9.41; S, 3.11%. Calcd for $C_{52}H_{73}N_7O_{11}S \cdot 1/2H_2O$: C, 61.64; H, 7.36; N, 9.68; S, 3.16%. R_f 0.95 on silica gel in *n*-BuOH : AcOH : H_2O (4 : 1 : 1) and R_f 0.88 in *n*-BuOH : AcOH : H_2O : pyridine (30 : 6 : 24 : 20). Amino acid ratios (propionic acid -12 M hydrochloric acid hydrolysis): Lys, 0.96; Val, 1.96; Tyr, 1.00; Pro, 1.03. Nps-protecting group of this peptide was cleaved by the same procedure as in the preparation of I and was used for chain elongation on the resin.

Attachment of H-Ser(Bzl)-Tyr(Bu^t)-OBu^t to the Methylchloroformylated Resin. The methylchloroformylated resin[9] (3 g, Cl: 1.87 mmol/g) was shaken 8 h at room temperature with 1.315 g (2.8 mmol) of H-Ser(Bzl)-Tyr(Bu^t)-OBu^t, triethylamine (0.28 g, 2.80 mmol) and 30 ml of chloroform in a vessel for solid phase peptide synthesis and washed with chloroform. The unreacted peptide was recovered in washing chloroform (2.24 mmol, 83% of the theoretical value). The remaining chloroformyl groups on the resin were covered by shaking with diethylamine (4.1 g, 56.1 mmol) and 30 ml of chloroform for 8 h and washed successively with chloroform (30 ml×3), ethanol (30 ml×3), and methylene chloride (30 ml×3). The resin was washed with trifluoroacetic acid-methylene chloride (1 : 1 v/v) and *t*-butyl group was deprotected by shaking for 30 min with 30 ml of trifluoroacetic acid-methylene chloride (1 : 1 v/v). The resulting resin was washed with methylene chloride (30 ml×3), chloroform (30 ml×3), and neutralized with 30 ml of triethylamine-chloroform (1 : 10 v/v) for 10 min. The resin was washed successively with chloroform (30 ml×3), ethanol (30 ml×3), and methylene chloride and dried *in vacuo*. An aliquot of the resin was hydrolyzed in propionic acid-12 M hydrochloric acid, the peptide content being determined by amino acid analyzer to be 0.031 mmol/g of the resin.

Chain Elongation. The resin-Ser(Bzl)-Tyr-OH prepared in the above experiment (1.5 g, 0.0465 mmol of dipeptide) was placed in a vessel for solid phase peptide synthesis. The following steps were used to couple each peptide fragment: 1) washing with methylene chloride (15 ml×3), 2) addition of 3 fold excess (0.1395 mmol) of amino free peptide fragment, 30 fold excess (1.395 mmol) of di-2-pyridyl disulfide (0.307 g) and 1-nitronaphthalene (internal standard for monitoring by HPLC) in 10 ml of methylene chloride followed by shaking for 5 min, 3) addition of 30 fold excess (1.395 mmol) of triphenylphosphine (0.366 g) in 5 ml of methylene chloride followed by a reaction period, 4) washing with methylene chloride (15 ml×3), 5) washing with ethanol (15 ml×3), 6) washing with methylene chloride (15 ml×3), 7) addition of 10 fold excess (0.465 mmol) of diethylamine (0.034 g) and 30 fold excess (1.395 mmol) each of di-2-pyridyl disulfide (0.307 g) and triphenylphosphine (0.366 g) in 15 ml of methylene chloride followed by shaking for 6 h, 8) washing with methylene chloride (15 ml×3), 9) washing with ethanol (15 ml×3), 10) washing with methylene chloride (15 ml×3), 11) wash with 15 ml of trifluoroacetic acid-methylene chloride (1 : 1 v/v) containing 5% of 2-mercaptoethanol, 12) removal of butyl ester with 15 ml of trifluoroacetic acid-methylene chloride (1:1 v/v) containing 5% of 2-mercaptoethanol for 30 min, 13) washing with methylene chloride (15 ml×3), 14) washing with chloroform (15 ml×3), 15) neutralization with 15 ml of triethylamine-chloroform (1 : 10 v/v) for 10 min, 16) washing with chloroform (15 ml×3), 17) washing with ethanol (15 ml×3), 18) washing with methylene chloride (15 ml×3). The first coupling of the initial resin-Ser(Bzl)-Tyr-OH with H-Ser(Bzl)-Met-Glu(OBzl)-His-Phe-OBu^t (fragment II) and second coupling with H-Arg(Tos)-Trp-Gly-OBu^t (fragment III) were carried out at −15 °C for 6 h and overnight at room temperature in the presence of 30 eq (1.395 mmol) of 2-pyridinethiol (0.155 g). Successive coupling of H-Lys(Z)-Pro-Val-Gly-OBu^t (fragment IV), H-Lys(Z)-Lys(Z)-Arg(Tos)-Arg(Tos)-Pro-OBu^t (fragment V) and H-Val-Lys(Z)-Val-Tyr(Bu^t)-Pro-OBu^t (fragment VI) were carried out at room temperature in the absence of 2-pyridinethiol. In each coupling step, an aliquot of the resulting resin-peptide was hydrolyzed in propionic acid-12 M hydrochloric acid (1 : 1 v/v).[15] The results of amino acid analyses are given in Table 2. The unreacted fragments were recovered in washing solvents of procedures 4), 5), and 6) and the quantities of fragments were determined by amino acid analyses of the

hydrolyzate of the portion of washing solvents: Fragment II, 0.075 mmol (recovery yield 81% of the theoretical value); Fragment III, 0.081 mmol (87%); Fragment IV, 0.084 mmol (90%); Fragment V, 0.076 mmol (82%); Fragment VI, 0.085 mmol (91%). These fragments were easily isolated by means of gel filtration on Sephadex LH-20 in methanol and complete evaporation of solvent *in vacuo*. With use of these recovered fragments, peptide chain was elongated by starting with 1 g of new resin-Ser(Bzl)-Tyr-OH (0.031 mmol) according to the procedure in the above chain elongation. Coupling reaction was continued until a monitoring curve by high pressure liquid chromatography showed no consumption of the fragment (*ca.* 6—8 h); repeated until no fragment uptake was detected. Amino acid analysis of the hydrolyzate of a portion of the resulting resin-tetracosapeptide by propionic acid–12 M hydrochloric acid showed nearly quantitative coupling reaction in each step: Ser, 2.11; Tyr, 2.02; Met, 0.91; Glu, 1.01; His, 1.00; Phe 0.97; Arg, 2.79; Gly, 1.94; Lys, 3.97; Pro, 2.75; Val, 2.93.

Monitoring of Coupling Reaction by High Pressure Liquid Chromatography. With the use of aminated Hitachi Gel 3010,[13] styrene-divinylbenzene polymer, the elution conditions were so established that each fragment has a constant retention time: column, 0.5×50 cm, Pyrex glass; mobile phase, 0.2 M hydrochloric acid, 0.1 M potassium chloride-methanol (1 : 9); flow rate, 2.0 ml/min; temperature, ambient; detector, UV (240 nm). Active dehydrating agent, phosphorane, in the reaction solution should be decomposed before injection to the column, since phosphorane is eluted near the fragment. A sample solution was prepared as follows: Add 20 μl of 0.2 M potassium hydroxide-80% methanol to 20 μl of the solution and then neutralize with 20 μl of 0.2 M monopotassium citrate-80% methanol. For the sake of accurate determination and easy sampling, 1-nitronaphthalene was added to the reaction mixture as an internal standard. A definite volume (5—20 μl) of each solution was injected, each sample being analyzed within 15 min with the accuracy of ±1.0%.[14] A typical chromatogram and examples of monitoring results are shown in Figs. 3 and 4, respectively. The amount of the consumed fragment (Fig. 4) was generally smaller than the actual amount consumed in chain elongation, since the initial peak height after shaking the resin with the fragment was arbitrarily scaled as 3 meq neglecting the small amount of adsorbed fragment on the resin. This small amount of the adsorbed fragment incorporated into the peptide chain makes up the difference in the quantity consumed as shown in the graph and the required value of 1 meq.

H-Ser-Tyr-Ser-Met-Glu-His-Phe-Arg-Trp-Gly-Lys-Pro-Val-Gly-Lys-Lys-Arg-Arg-Pro-Val-Lys-Val-Tyr-Pro-OH (ACTH(1—24)). The resin-tetracosapeptide started from 1.5 g of resin-dipeptide was treated with 40 ml of dry hydrogen fluoride[16] at 0° for 30 min in the presence of 2 ml of anisole and 2-pyridinethiol[9] (0.300 g). The yield of this cleavage step was 83%. After removal of hydrogen fluoride, the residue was dried over potassium hydroxide *in vacuo*. The resin was stirred in 30 ml of trifluoroacetic acid, filtered and washed with 30 ml of trifluoroacetic acid. The combined filtrate was evaporated and the residue was dissolved in 50 ml of acetic acid and evaporated *in vacuo*. The residue was dissolved in 30 ml of water, washed with diethyl ether and passed through a Dowex 1×2 (acetate form, 2.5×10 cm) with 300 ml of water to be converted into acetate form. The solution was condensed to 20 ml and stirred at 50 °C for 12 h after addition of 1 ml of mercaptoacetic acid. The solution was evaporated *in vacuo* and subjected to gel filtration on Sephadex G-25 (2×125 cm) in 1 M acetic acid in order to separate the peptide from 2-pyridinethiol and anisole. After evaporation of the Ehrlich and Pauly positive fractions of main peak, the peptide was purified on carboxymethylcellulose column (1×55 cm) by continuous gradient elution with ammonium acetate buffer at pH 6.7[17]: 0.01 M ammonium acetate (150 ml), 0.01—0.2 M ammonium acetate (270 ml), 0.2—0.4 M ammonium acetate (600 ml), 0.4 M ammonium acetate (330 ml). The main peak in 0.2—0.4 M ammonium acetate was proceeded by a small peak in 0.01—0.2 M ammonium acetate and followed by a very small peak in 0.4 M ammonium acetate. The fractions of the main peak were condensed and purified again on carboxymethylcellulose in the same manner after gel filtration on Sephadex G-25 in 1 M acetic acid. The fractions containing a single component were pooled and condensed *in vacuo*. Desalting was achieved by gel filtration on Sephadex G-25 in 1 M acetic acid and the peptide was precipitated from methanol containing 1% of acetic acid–ethyl acetate–petroleum ether after evaporation of solvent. The pure tetracosapeptide was obtained after drying *in vacuo* for 12 h at 40 °C over phosphorus pentoxide: yield 41 mg (25.2% yield based on Ser-Tyr attached on the resin and 42.8% yield from the liberated peptide from the resin); $[\alpha]^{20}$ −86.8° (*c* 0,5. 1% acetic acid) (lit,[18] $[\alpha]_D^{22}$ −88.6° ±2° (*c* 0.51, 1% acetic acid)); UV in 0.1 M sodium hydroxide, λ_{max} 283 mμ (ε=8640) and λ_{max} 289 mμ (ε=8880) (lit,[18] λ_{max} 283 mμ (ε=8550) and λ_{max} 289 mμ (ε=8810)). Thin layer chromatography gave a single spot detected by Ehrlich, Pauly, Cl-tolidine, and ninhydrin reactions: R_f 0.28 on silica gel in *n*-BuOH : AcOH : H_2O : pyridine (30 : 6 : 24 : 20) and R_f 0 in *n*-BuOH : AcOH : H_2O (4 : 1 : 1). Paper electrophoresis with lysine as reference also gave a single ninhydrin, Pauly, Ehrlich, and Cl-tolidine positive spot: R_m 0.72 in 0.5 M formic acid–2 M acetic acid (1 : 1 v/v), 60×10 cm, 900 V, 1.5 h and R_m 0.77 in pyridine-AcOH-H_2O (10 : 0.4 : 90 v/v), 60×10 cm, 1500 V, 1 h. The peptide was characterized as heptaacetate and nonahydrate by elemental analysis. Found: C, 51.19; H, 7.05; N, 15.93; S, 0.93%. Calcd for $C_{136}H_{210}O_{31}N_{40}S \cdot 7CH_3COOH \cdot 9H_2O$: C, 51.24; H, 7.33; N, 15.94; S, 0.91%. Two mg of the peptide dissolved in 0.5 ml of Tris buffer of pH 8.5 containing 0.01 M Mg^{2+} was incubated with 50γ of trypsin (Worthington Biochemical Co., TRL 100S) and 50 γ of chymotrypsin (Worthington Biochemical Co., CDI 2LX) at 37 °C for 24 h. The solution was boiled for 15 min, cooled and then incubated with 80 γ of aminopeptidase M (Rohm & Haas) and 80 γ of prolidase (Miles Laboratories Ltd., UK8) for 48 h at 37 °C. The results of amino acid analyses of the digestion mixture and propionic acid–12 M hydrochloric acid hydrolyzate of the peptide are shown in Table 3.

Bioassay. ACTH activity of the tetracosapeptide was assayed by the ascorbic acid depletion test according to USP XVIII, and compared with the 2nd international standard. The dose response regression lines for the synthetic peptide and the standard were parallel. The activity was calculated as 96 (83—128) IU/mg, identical with the value in literature.[18]

References

1) T. Mukaiyama, R. Matsueda, and M. Suzuki, *Tetrahedron Lett.*, **1970**, 1901.

2) T. Mukaiyama, K. Goto, R. Matsueda, and M. Ueki, *Tetrahedron Lett.*, **1970**, 5293; R. Matsueda, E. Kitazawa, H. Maruyama, H. Takahagi, and T. Mukaiyama, *Chem. Lett.*, **1972**, 379; Su-Sun Wang, *J. Org. Chem.* **40**, 1235 (1975).

3) T. Mukaiyama and M. Hashimoto, *J. Am. Chem. Soc.*, **94**, 8528 (1972); M. Hashimoto and T. Mukaiyama,

Chem. Lett., **1973**, 513.
4) M. Hashimoto and T. Mukaiyama, *Chem. Lett.*, **1972**, 595.
5) E. J. Corey and K. C. Nicolaou, *J. Am. Chem. Soc.*, **96**, 5614 (1974); E. J. Corey, K. C. Nicolaou, and L. S. Melvin, Jr., *ibid.*, **97**, 653, 654 (1975).
6) T. Mukaiyama, M. Ueki, R. Matsueda, and H. Maruyama, Japanese Patent Publication No. 40054/72.
7) M. Ueki, T. Shishikura, A. Hayashida, and T. Mukaiyama, *Chem. Lett.*, **1973**, 733.
8) M. Ueki and S. Ikeda, *Chem. Lett.*, **1974**, 25.
9) R. Matsueda, H. Maruyama, E. Kitazawa, H. Takahagi, and T. Mukaiyama, *Bull. Chem. Soc. Jpn.*, **46**, 3240 (1973).
10) R. Matsueda, H. Maruyama, E. Kitazawa, H. Takahagi, and T. Mukaiyama, *J. Am. Chem. Soc.*, **97**, 2573 (1975).
11) Abbreviations recommended by the IUPAC-IUB Commission on Biochemical Nomenclature (*Pure Appl. Chem.*, **40**, 315 (1974)) are used. DCC: dicyclohexylcarbodiimide, M. A.: mixed anhydride method, PCP: pentachlorophenol, —OPcp: pentachlorophenyl ester, and DCHA: dicyclohexyl amine. Amino acid symbols denote the L-configuration.
12) H. Takahagi and S. Seno, *J. Chromatogr. Sci.*, **12**, 507 (1974).
13) We thank Dr. N. Takai of the Institute of Industrial Science, University of Tokyo, for providing us with aminated Hitachi Gel 3010.
14) The relative standard deviation of this method was 0.3—1.4% based on five replicate determination of known sample.
15) F. C. Westall, J. Scotchler, and A. B. Robinson, *J. Org. Chem.*, **37**, 3363 (1972).
16) S. Sakakibara, Y. Shimonishi, Y. Kishida, M. Okada, and H. Sugihara, *Bull. Chem. Soc. Jpn.*, **40**, 2164 (1967).
17) F. Blake, K. T. Wang, and C. H. Li, *Biochemistry*, **11**, 438 (1972).
18) R. Schwyzer and H. Kappeler, *Helv. Chim. Acta*, **46**, 1150 (1963).
19) We are indebted to Dr. J. Serizawa and Mr. T. Yoshizaki of our laboratories.
20) B. Loev and K. M. Snader, *Chem. Ind.*, **1965**, 15; 15; B. Loev and M. M. Goodman, *ibid.*, **1967**, 2026.
21) C. H. Li, B. Gorup, D. Chung, and J. Ramachandran, *J. Org. Chem.*, **28**, 178 (1963).
22) T. Y. Liu and Y. H. Chang, *J. Biol. Chem.*, **246**, 2842 (1971).
23) C. H. Li, J. Ramachandran, and D. Chung, *J. Am. Chem. Soc.*, **86**, 2711 (1964).

Studies of Sulfonyl Radicals. II.[1] Relative Reactivities of Addition Reactions of Sulfonyl Free Radicals to Vinyl Monomers

Yoshiyuki TAKAHARA, Masashi IINO, and Minoru MATSUDA

Chemical Research Institute of Non-aqueous Solutions, Tohoku University, Katahira 2-Chome, Sendai 980

(Received February 6, 1976)

Addition reactions of various vinyl monomers towards the free methanesulfonyl and arenesulfonyl radicals have been investigated. Relative reactivities of *p*-methylstyrene (M_2) to styrene (M_1) towards methane- and *para*-substituted benzenesulfonyl radicals are hardly affected by the kind of sulfonyl radical, suggesting that an unpaired electron of methanesulfonyl and arenesulfonyl radicals is localized mainly on sulfonyl groups. Relative reactivities obtained with vinyl monomers were correlated to Hammett's σ_p values with $\rho_p = -3.6$ and also to Alfrey-Price's *e* values, indicating that sulfonyl radicals are strongly electrophilic. The highest selectivity of the benzenesulfonyl radical, obtained in the comparison of the selectivity of a number of radicals in addition reactions towards three representative monomers (Table 5), also supports the above conclusion.

In previous papers concerning radical copolymerization of sulfur dioxide and styrene emphasis has been laid on two aspects of the growing sulfonyl radicals ($\sim SO_2-CH_2CH(C_6H_5)-\dot{S}O_2$ and $\sim CH_2CH(C_6H_5)-CH_2CH(C_6H_5)-\dot{S}O_2$), *viz.*, their reactivity and their relationship to the compositions of poly(styrene sulfone).[2]

In this paper we report the reactivities relative to styrene of addition reactions of various vinyl monomers towards benzenesulfonyl and other sulfonyl radicals, giving a discussion on the nature of sulfonyl radicals. The formations of sulfonyl radicals from sulfonyl iodides have been studied by many investigators.[3-5] Corrêa and Waters[3] showed that addition of sulfonyl iodide to styrene occurs with very little polymerization. They have investigated on the addition reaction of *p*-toluenesulfonyl radical to *para*- or *meta*-substituted styrenes, showing that sulfonyl radical has an electrophilic character from the values of ρ ($\rho = -0.55$ or $\rho^+ = -0.50$) in the Hammett plot.[6] Truce and his co-workers have studied addition reaction to allenes and acetylene.[4,7]

We have investigated the same type of addition reaction of various vinyl monomers such as styrene, methyl methacrylate, acrylonitrile, and 1-hexene, by using sulfonyl iodides.

Experimental

Materials. Benzene, toluene, chlorobenzene, decane, and vinyl monomers were purified in the usual way. *p*-Methylstyrene was prepared from 1-(*p*-tolyl)ethanol by $KHSO_4$ dehydration and distilled twice under reduced pressure. Vinyl monomers were stored at temperature below −20 °C after purification.

Benzene-, *p*-toluene-, *p*-chlorobenzene-, and methane-sulfonyl iodide were synthesized from the corresponding sulfonyl chlorides.[21,22] *p*-Methoxybenzenesulfonyl iodide was synthesized from anisole and chlorosulfuric acid by means of the corresponding chloride.[23] All the sulfonyl iodides except methanesulfonyl iodide were recrystallized at least twice from carbon tetrachloride and dried under reduced pressure at temperatures below −20 °C in order to prevent decomposition.

Found: C, 26.57; H, 2.05%. Calcd for $C_6H_5IO_2S$ (benzenesulfonyl iodide): C, 26.87; H, 1.87%.

Found; C, 29.88; H, 2.33%. Calcd for $C_7H_7IO_2S$ (*p*-toluenesulfonyl iodide): C, 29.79; H, 2.48%.

Found: C, 28.03; H, 2.68%. Calcd for $C_7H_7IO_3S$ (*p*-methoxybenzenesulfonyl iodide): C, 28.29; H, 2.35%.

Found: C, 23.84; H, 1.48%. Calcd for $C_6H_4ClIO_2S$ (*p*-chlorobenzenesulfonyl iodide): C, 23.82; H, 1.32%.

Competitive Addition of Styrene and p-Methylstyrene towards Benzenesulfonyl Iodide. Toluene solution containing a definite amount of styrene (0.84 to 3.22 mmol), *p*-methylstyrene (0.94 to 3.15 mmol), and benzenesulfonyl iodide (0.55 to 2.14 mmol) was placed in a Pyrex glass reaction tube covered with an aluminum foil to intercept the light. The reaction tube thus prepared was connected to a vacuum system, the solution was frozen, and then the system was degassed in the usual way at least three times. After the last freeze-pump-thaw cycle, the system was closed and disconnected from the vacuum system. The reaction tube was placed in an ice-water mixture and the reaction was initiated with daylight by removing the aluminum foil. In the dark, the reaction did not occur even after 24 h. Under our experimental conditions, benzenesulfonyl iodide charged was almost completely consumed within 30 min and the yellow reaction solution became colorless at the end of the reaction. The reaction mixture was then washed with 10% aqueous $Na_2S_2O_3$ to remove any trace of sulfonyl iodide and iodine, and the products were isolated from *ca.* 75 ml petroleum ether (bp, 40—60 °C) at −60——70 °C. After a few mg of 4-*t*-butylcatechol had been added to the petroleum ether solution to prevent polymerization, the quantities of unreacted styrene and *p*-methylstyrene were determined by GLC analysis (diethylene glycol adipate polyester column) using chlorobenzene as an internal standard. We also determined the quantities of products by NMR analysis in $CDCl_3$ using tetramethylsilane as an internal standard; relative reactivities determined by both methods were almost the same (Table 3). In the competitive addition of styrene and *p*-methylstyrene towards benzenesulfonyl iodide the ratio of the reacting monomers to initial sulfonyl iodide was nearly unity, indicating the formation of 1 : 1 adducts.

Results and Discussion

Reliability of Our Relative Rate Constants. Our first intention in this study was to confirm the fact that no reverse reaction of addition of sulfonyl radicals to vinyl monomers takes place. The free radical addition of sulfonyl iodides to olefinic double bonds has been studied extensively and the following chain mechanism is generally accepted.

$$RSO_2I \longrightarrow RSO_2\cdot + I\cdot \quad (1)$$

$$RSO_2\cdot + CH_2{=}C(R')R'' \xrightarrow{k_1} RSO_2CH_2\dot{C}(R')R'' \quad (2)$$

$$RSO_2CH_2\dot{C}(R')R'' + RSO_2I \xrightarrow{k_a}$$

$$RSO_2CH_2C(R')R''I + R\dot{S}O_2 \quad (3)$$

If we use two monomers (M_1 and M_2), then we obtain

$$\frac{\log(M_{2,0}/M_2)}{\log(M_{1,0}/M_1)} = \frac{k_2}{k_1}$$

where k_1 and k_2 are the rate constants for competitive addition reaction (Eq. 2) of M_1 (styrene) and M_2 monomer towards sulfonyl radicals, respectively, and $M_{1,0}$ (and $M_{2,0}$) and M_1 (and M_2) the initial and final concentrations, respectively, of styrene (and those of monomers which are able to compete in addition reaction with styrene).

The relative reactivities of vinyl monomers to styrene (k_2/k_1) have been determined by means of Eq. 4. If a reverse reaction of Eq. 2 occurs to a great extent, our k_2/k_1 values obtained from Eq. 4 should vary with the concentration of RSO_2I. In the competitive addition reaction of styrene and *p*-methylstyrene (M_2) towards benzenesulfonyl iodide, we have confirmed the reverse reaction does not take place, namely in Table 1 the k_2/k_1 values show no significant variation with the concentration change of benzenesulfonyl iodide. For other monomer pairs we have also checked the constancy of k_2/k_1 with varying concentrations of RSO_2I (Table 2). Skell and McNamara[8] observed in the addition of benzenesulfonyl iodide to *cis*- and *trans*-2-butene at 0°C that from either olefin, neither was isomerized during the course of reaction, indicating also the absence of the reverse reaction of Eq. 2.

Table 1. Relative reactivities (k_2/k_1) of addition reactions of *p*-methylstyrene (M_2) to styrene (M_1) towards benzenesulfonyl radical in toluene at 0 °C under various conditions[a]

$[M_1]_0$ (mol/l)	$[M_2]_0$ (mol/l)	$\frac{[M_2]_0}{[M_1]_0}$	$[PhSO_2I]_0$ (mol/l)	$\frac{k_2}{k_1}$
0.084	0.265	3.15	0.214	1.60
0.127	0.128	1.01	0.214	1.70
0.322	0.094	0.29	0.214	1.73
0.143	0.106	0.74	0.171	1.78
0.153	0.135	0.88	0.144	1.81[b]
0.127	0.128	1.01	0.105	1.63
0.124	0.121	0.98	0.104	1.66
0.124	0.121	0.98	0.104	1.69[c]
0.137	0.113	0.82	0.078	1.89
0.122	0.104	0.85	0.056	1.63
0.181	0.113	0.62	0.055	1.86

a) Reactions were initiated in daylight, unless otherwise stated. b) In the dark, reaction time; 92 h, conversion based on iodide; 67%. c) With 300 W mercury lamp, reaction time; 0.5 h.

Table 2. Relative reactivities of various pairs of M_1 and M_2 towards benzenesulfonyl radical in toluene at 0 °C

M_1	M_2	Runs[a]	k_2/k_1
Styrene	α-Methylstyrene	3	3.21±0.29[b]
	p-Methylstyrene	9	1.72±0.10
	t-Butyl methacrylate	3	0.14±0.02
	Isopropyl methacrylate	4	0.10±0.01
Methyl methacrylate	*t*-Butyl methacrylate	2	2.01±0.05
	Isopropyl methacrylate	3	1.20±0.10
Vinyl acetate	Methyl methacrylate	3	9.83±0.37
	Methyl acrylate	3	1.57±0.08
	Acrylonitrile	2	0.73±0.08
	1-Hexene	3	2.49±0.17

a) $[PhSO_2I]_0$ was varied from 0.046 to 0.302 mol/l. b) Standard deviation.

GLC analyses of the resulting solutions indicate that within experimental error, quantitative amounts of $RSO_2CH_2C(R')R''I$ were obtained in each experiment; it is strongly suggested that the polymerization process of the vinyl monomers, $RSO_2CH_2\dot{C}(R')R'' + CH_2=C(R')R'' \rightarrow RSO_2CH_2C(R')R''-CH_2\dot{C}(R')R''$, hardly occurs in accordance with the results of Corrêa and Waters.[3] Table 1 also indicates that the k_2/k_1 values are neither affected by the ratios of the concentration of styrene and *p*-methylstyrene, nor by the kind of light initiating the reactions, nor by converstion of the reaction, suggesting that our relative reactivities are reliable.

Effects of the Structure of Sulfonyl Iodides on the Relative Reactivities of p-*Methylstyrene to Styrene.* The relative rates for the addition reactions of *p*-methylstyrene to styrene towards methane- and *para*-substituted arenesulfonyl radicals are summarized in Table 3; the k_2/k_1 values of arenesulfonyl radicals are hardly affected by the kind of *para*-substituent and are almost the same as in the case of methanesulfonyl radical, suggesting that an unpaired electron of arenesulfonyl radicals is localized mainly on sulfonyl groups and that the conjugation of an unpaired electron with π-electron of phenyl rings is small since the relative rates would be affected by the stability and polarity of a radical. The results are in line with the conclusions obtained from ESR studies carried out by McMillan and Waters[9] and Davies and Roberts;[10] in spectra for the benzenesulfonyl radical, the *ortho*-hydrogen hyperfine constant [a(*o*-H)] was larger than a(*p*-H) and a relatively large value was obtained from a(*m*-H). This may be also supported by the fact that $CH_3SO_2N{=}NC_6H_5$ can

Table 3. Relative reactivities of *p*-methylstyrene to styrene towards arenesulfonyl and methanesulfonyl radicals in toluene at 0 °C

Sulfonyl radical	Runs	k_2/k_1
Cl-C$_6$H$_4$-$\dot{S}O_2$	4	1.80±0.06[a]
CH_3-C$_6$H$_4$-$\dot{S}O_2$	6	1.63±0.08 (1.53)[b]
CH_3O-C$_6$H$_4$-$\dot{S}O_2$	4	1.73±0.08 (1.78)[b]
C$_6$H$_5$-$\dot{S}O_2$	9	1.72±0.10
$CH_3\dot{S}O_2$	3	1.79±0.06

a) Standard deviation. b) Values obtained from product analyses with 60 MHz NMR.

decompose thermally into $CH_3\dot{S}O_2$ and $\dot{C}_6H_5$ at the similar rate as $C_6H_5SO_2N{=}NC_6H_5$.[11-13]

Relative Reactivities among Vinyl Monomers. Styrene, α-methylstyrene, *p*-methylstyrene, *t*-butyl methacrylate, isopropyl methacrylate, methyl methacrylate, methyl acrylate, acrylonitrile, 1-hexene, and vinyl acetate were used for competitive addition reactions. Three kinds of relative reactivities for addition of various vinyl monomers towards benzenesulfonyl radical have been determined (Table 4). Since the relative reactivities of these vinyl monomers are spread over a wide range of *ca.* 500 fold, we have used three monomers having different reactivity, styrene, methyl methacrylate, and vinyl acetate, as a reference monomer. This was found to be reasonable from the experimental results: we obtained $k_{t\text{-BuMA}}/k_{Sty}=0.138$, $k_{i\text{-PrMA}}/k_{Sty}=0.097$, $k_{t\text{-BuMA}}/k_{MMA}=2.01$, and $k_{i\text{-PrMA}}/k_{MMA}=1.20$, thus we can calculate the two k_{MMA}/k_{Sty} values from different combinations, *i.e.*, one based on *t*-BuMA and the other on *i*-PrMA. The former gave 0.069 and the latter 0.081, which agree with the value obtained from direct competitive addition reaction, $k_{MMA}/k_{Sty}=0.077$. The relative reactivity between MMA and vinyl acetate has been calculated by the analysis of NMR data.

TABLE 4. RELATIVE REACTIVITIES ON VINYL MONOMERS TOWARDS BENZENESULFONYL RADICAL IN TOLUENE AT 0 °C

Vinyl monomer	Q[a]	e[a]	σ_p[b]	k_2/k_1
α-Methylstyrene	0.98	−1.27	−0.18	3.21
p-Methylstyrene	1.27	−0.98		1.72
Styrene	1.00	−0.80	−0.01	(1.00)
t-Butyl methacrylate	1.18	−0.35		0.14
Isopropyl methacrylate	1.20	−0.15		0.10
Methyl methacrylate	0.74	0.40	0.28	0.08
Methyl acrylate	0.42	0.60	0.45	0.012
Acrylonitrile	0.60	1.20	0.66	0.006
1-Hexene	0.019	−0.28		0.02
Vinyl acetate	0.026	−0.22		0.008

a) Alfrey-Price's Q and e values, see Ref. 14. b) Hammett's *para*-substituent constants.

The relative rates based on the styrene monomer, calculated from the results in Table 2, are shown in Table 4 together with Alfrey-Price Q and e values.[14] These relative rates can be correlated with both e values and Hammett σ_p values (Fig. 1); they are divided into two groups, one (the upper line in Fig. 1) containing conjugated monomers ($Q\geq0.42$) and the other unconjugated monomers ($Q\leq0.026$). The fact that the linear relationship with a steep slope ($\rho_p=-3.6$) exists between e values (or σ_p values) and the relative rates suggests that the benzenesulfonyl radical and also other sulfonyl radicals are highly polar and electrophilic in accordance with the result of Corrêa and Waters[6] that the *p*-toluenesulfonyl radical is electrophilic.

Selectivities for addition reaction of a number of free radicals towards three representative vinyl monomers are given in Table 5. The sulfonyl radical shows the highest selectivity. This is attributable to a strong electrophilic character[20] of the benzenesulfonyl radical since the e value of monomers is an important factor for addition reactions among conjugated vinyl monomers (Fig. 1).

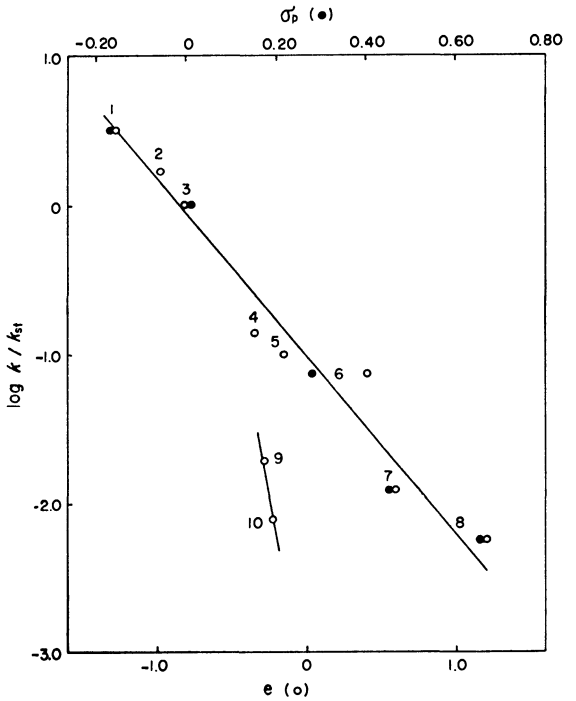

Fig. 1. Relationship between logarithmic relative reactivities and the Alfrey-Price's e (○) or the Hammett's σ_p (●) values.
1, α-Methylstyrene; 2, *p*-methylstyrene; 3, styrene (reference monomer); 4, *t*-butyl methacrylate; 5, isopropyl methacrylate; 6, methyl methacrylate; 7, methyl acrylate; 8, acrylonitrile; 9, 1-Hexene; 10, vinyl acetate.

TABLE 5. RELATIVE REACTIVIES OF RADICALS TOWARDS THREE MONOMERS

Radical	Temp (°C)	Styrene	MMA[b]	VAc[c]	Ref.
Phenyl	60	1.00	1.8	0.23	(15)
Phenyl	60	1.00	1.7	0.08	(16)
Benzoyloxy	60	1.00	0.1	0.4	(17)
Methyl	65	1.00	1.8	0.05	(18)
Polystyryl	60	1.00	1.9	0.02	(19)
Poly(AN[a])	60	1.00	0.3	0.01	(19)
Poly(MMA[b])	60	1.00	0.55	0.03	(19)
Poly(VAc[c])	60	1.00	0.33	0.01	(19)
Benzenesulfonyl	0	1.00	0.08	0.008	this work

a) Acrylonitrile. b) Methyl methacrylate. c) Vinyl acetate.

References

1) For Part I in this series, see K. Seki, M. Iino, and M. Matsuda, *Macromolecules*, **7**, 116 (1974).
2) (a) M. Matsuda and M. Iino, *Macromolecules*, **2**, 216 (1969); (b) M. Matsuda, M. Iino, T. Hirayama, and T. Miyashita, *ibid.*, **5**, 240 (1972); (c) M. Iino, K. Katagiri, and M. Matsuda, *ibid.*, **7**, 439 (1974).
3) C. M. M. da S. Corrêa and W. A. Waters, *J. Chem. Soc., C*, **1968**, 1874.
4) W. E. Truce and G. C. Wolf, *J. Org. Chem.*, **36**, 1727

(1971).
5) L. Benati, C. M. Camaggi, and G. Zanardi, *J. Chem. Soc., Perkin Trans. 1*, **1972**, 2817.
6) C. M. da S. Corrêa and W. A. Waters, *J. Chem. Soc., Perkin Trans. 2*, **1972**, 1575.
7) W. E. Truce, D. L. Heuring, and G. C. Wolf, *J. Org. Chem.*, **39**, 238 (1974).
8) R. S. Skell and J. H. McNamara, *J. Am. Chem. Soc.*, **79**, 85 (1957).
9) M. McMillan and W. A. Waters, *J. Chem. Soc., B*, **1966**, 422.
10) A. G. Davies and B. P. Roberts, *J. Chem. Soc., Perkin Trans. 2*, **1973** 626.
11) A. J. Rosenthal and C. G. Overberger, *J. Am. Chem. Soc.*, **82**, 108 (1960).
12) J. L. Kice and R. S. Gabrielsen, *J. Org. Chem.*, **35**, 1004 (1970).
13) M. Iino and M. Matsuda, unpublished data.
14) L. J. Young, "Copolymerization," ed. by G. E. Ham, Interscience, New York, N. Y. (1964), pp. 845—863.
15) W. A. Pryor and T. R. Fiske, *Trans. Faraday Soc.*, **65**, 1865 (1969).
16) J. C. Bevington and T. Ito, *Trans. Faraday Soc.*, **64**, 1329 (1968).
17) J. C. Bevington and M. Johnson, *Makromol. Chem.*, **102**, 73 (1967).
18) M. Szwarc, *J. Polym. Sci.*, **54**, 411 (1961).
19) Data cited from Table 5 in Ref. 15.
20) We have calculated the *e* value for benzenesulfonyl radical by using both the Alfrey-Price equation and line slope in Fig. 1. Thus we obtained *e* of +2.8, higher than that of acrylonitrile.
21) F. C. Whitemore and N. Thurman, *J. Am. Chem. Soc.*, **45**, 1068 (1923).
22) L. Field, F. Parsons, and R. R. Crenshaw, *J. Org. Chem.*, **29**, 918 (1964).
23) M. S. Morgan and L. H. Cretcher, *J. Am. Chem. Soc.*, **70**, 375 (1948).

Studies of Sulfonyl Radicals. III.[1] Solvent Effects on the Thermal Decomposition of Benzyl Phenylazo Sulfone

Masashi IINO, Tateo YANAGISAWA, Yozo TAKAHASHI, and Minoru MATSUDA

Chemical Research Institute of Non-aqueous Solutions, Tohoku University, Katahira 2-Chome, Sendai 980

(Received February 6, 1976)

The first-order rate constants for thermal decomposition of benzyl phenylazo sulfone (BPA, **1**) have been determined spectrophotometrically in six solvents using the free radical scavenging technique with a stable Koelsch free radical. Activation parameters in the non-polar solvents such as benzene, toluene, anisole and chlorobenzene were almost the same, but in the two polar solvents, pyridine and nitrobenzene, activation entropies decreased significantly as compared with those in the non-polar solvents. This can be explained by the solvation of the polar solvent in the transition state leading to a phenyldiazenyl and α-toluenesulfonyl radical pair.

Although well established studies of solvent effects have been reported on many ionic reactions, definite information is still lacking as to free radical reactions, because of a weak interaction between free radical and solvent.

In connection with the studies on sulfonyl radicals[1,2a] and the propagation mechanism of free radical copolymerization of sulfur dioxide and styrene,[2b-d] we became interested in solvent effects on the thermal decomposition of benzyl phenylazo sulfone (BPA, $C_6H_5CH_2SO_2$–N=N–C_6H_5), since sulfonyl radicals ($RSO_2\cdot$) have a strong electrophilic character[1,3] and an unpaired electron is localized on the sulfonyl groups.[1] Sulfonyl radicals are thus expected to behave as an electron acceptor[4] and to interact with polar or electron donating solvents. Activation parameters for the decomposition of *p*-tolyl phenylazo sulfone (TPA), which forms[6] *p*-toluenesulfonyl and phenyl radicals, are found[5] to change with solvents remarkably; in ethylbenzene $\Delta H^{\ddagger}=30.8$ kcal/mol, $\Delta S^{\ddagger}=10.7$ e.u. and in *N*,*N*-dimethylformamide $\Delta H^{\ddagger}=39.6$ kcal/mol, $\Delta S^{\ddagger}=34.4$ e.u. This is in striking contrast to the results reported on the thermal decomposition of 2,2′-azobisisobutyronitrile, *i.e.*, the maximum difference among the activation parameters determined in several solvents is found to be $\Delta\Delta H^{\ddagger}=1.78$ kcal/mol and $\Delta\Delta S^{\ddagger}=4.96$ e.u.[7]

We have determined the rate constants for BPA decomposition by using the radical scavenging technique with a stable radical, α,γ-bisdiphenylene-β-phenylallyl (Koelsch radical). The existence of radical-induced decomposition sometimes makes it difficult to determine a rate constant of unimolecular decomposition.[8] The unimolecular rate constsnt in BPA thermal decomposition, however, can be exclusively determined by the use of Koelsch radical (by capturing the radicals formed in the decomposition).[9]

Experimental

Materials. Benzyl phenylazo sulfone (BPA) was prepared by the reaction of benzene diazonium salt with sodium α-toluenesulfinate prepared[10] by treatment of α-toluenesulfonyl chloride with sodium sulfite and sodium hydrogencarbonate in water. Crude BPA was recrystallized several times from ethanol: mp 90—92 °C (dec) (lit,[9] 97—99 °C). (Found: C, 60.27; H, 4.60; N, 11.16%. Calcd for $C_{13}H_{12}N_2O_2S$: C, 59.98; H, 4.65; N, 10.76%.). The Koelsch radical was prepared according to the method of Kuhn and Neugebauer,[11] and recrystallized several times from benzene. Since Koelsch radical is known to crystallize from benzene in a 1 : 1 ratio with the solvent, the benzenated radical was pumped at 100 °C to constant weight (70 h). Found: C, 94.19; H, 5.06%. Calcd for $C_{33}H_{21}$: C, 94.93; H, 5.07%.). Galvinoxyl was prepared from 2,6-di-*t*-butylphenol.[12] Purity of this compound was given as 97.3% by a comparison of molar extinction coefficient with the reference value.[12] All the solvents were purified by distillation in the presence of Koelsch radical or DPPH just before use.

General Procedure. The rate at which BPA decomposes to give radicals scavenged by Koelsch radical was measured in the UV cell (1 cm path length). The cell, containing BPA, Koelsch radical and the solvent, was connected to a vacuum system through a stopcock, the solution being degassed by freeze-pump-thaw cycles. After the fourth freeze-pump-thaw cycle, the system was closed and disconnected from the vacuum system. The absorbance was then measured at 780 nm for Koelsch radical (shoulder) and at 769 nm for galvinoxyl (absorption maximum). The cell set in a Cary 14 UV spectrophotometer was thermostated at a definite temperature by the circulation of thermostated water into the cell holder. The temperature of the solution in the cell was determined by measuring the temperature of an identical solvent in another cell with a copper-constantan thermocouple.

Results and Discussion

Rate Constants for the Unimolecular Thermal Decomposition of BPA. The rate constants obtained by varying the concentration of BPA at 60 °C (Table 1) are considered to be of the real first-order, since each rate constant is not dependent upon the concentration of BPA. If Koelsch radical is highly effective in capturing all the radicals produced and if BPA is in large excess, a plot of time *vs.* absorbance of the Koelsch radical should follow zero-order kinetics with respect to the disappearance of Koelsch radical. A typical plot for the benzene solution is shown in Fig. 1. It follows that the first-order rate constants for the BPA decomposition can be calculated by

$$2k[\mathrm{BPA}]_0=k_0 \qquad (1)$$

where k_0 and k are the zero-order rate constant (slope of Fig. 1) for the disappearance of Koelsch radical and the first-order rate constant for the thermal decomposition of BPA (it should be noted that the first-order rate constants obtained here include the efficiency of diffusion from solvent cage).

In the case of nitrobenzene, however, a plot of time *vs.* absorbance did not give a straight line; the rate of

Table 1. First-order rate constants obtained with Koelsch radical for thermal decomposition of benzyl phenylazo sulfone in solutions at 60 °C

Solvent	$[BPA]_0 \times 10^3$ (mol/l)	$k \times 10^6$ (s^{-1})	$k_{av} \times 10^6$ (s^{-1})
Benzene	5.85	19.1	
	5.86	18.5	
	11.7	18.4	
	11.7	16.4	17.9
Benzene[a)]	5.96	19.5	
	11.7	21.0	
	23.7	18.4	19.6
Toluene	11.8	18.4	
	11.9	17.7	
	24.6	17.6	17.9
Anisole	11.8	10.3	
	17.9	11.0	
	17.9	10.3	
	23.3	9.8	
	23.8	10.8	10.4
Chlorobenzene	12.9	11.3	
	19.3	11.5	11.4
Pyridine	23.6	12.1	
	35.3	13.1	12.6
Nitrobenzene[b)]	26.6	3.13	
	32.2	3.28	
	45.6	2.62	3.01

a) Galvinoxyl used as stable free radical. b) Values obtained by extrapolating to zero concentration of Koelsch radical.

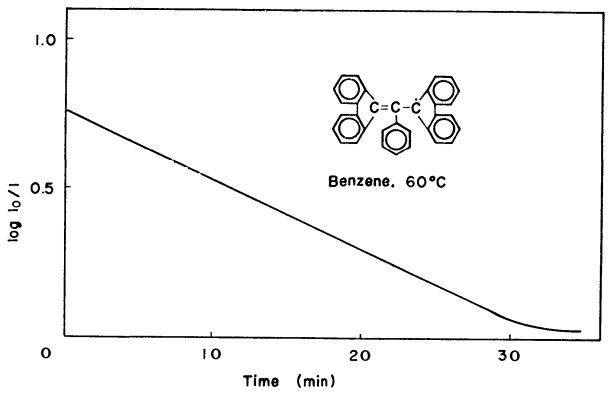

Fig. 1. Plot of absorbance at 785 nm *vs.* time for the thermal decomposition of BPA (5.83×10^{-3} mol/l) in the presence of the Koelsch radical (9.40×10^{-4} mol/l) in benzene at 60 °C.

the disappearance of Koelsch radical diminished with decreasing concentration, suggesting the occurrence of an induced decomposition by Koelsch radical in nitrobenzene. Thus, the first-order rate constant in this solvent was determined by extrapolation of the disappearance rates to zero concentration of Koelsch radical.

For BPA decomposition in benzene galvinoxyl has also been used as a stable radical (Table 1). Almost the same values of $\Delta H^{\neq}$ and $\Delta S^{\neq}$ as those in the case of Koelsch radical are obtained (Table 2), supporting the above conclusion, *viz.*, the values obtained are the real first-order rate constants. The rate constant in benzene solution using Koelsch radical (1.79×10^{-5} s^{-1} at 60 °C) is approximately the same as the value reported by Kice and Gabrielsen (1.3×10^{-5} s^{-1} at 60 °C).[9)]

Strong Solvation of Polar Solvents in the Transition State. The rate constants obtained at 45—70 °C and the activation parameters in six solvents are shown in Table 2. The activation parameters in four non-polar solvents, benzene, toluene, anisole, and chlorobenzene, are almost the same within experimental error, but those obtained in two polar solvents, pyridine and nitrobenzene, decrease as compared with the values in non-polar solvents, indicating a strong solvation of pyridine or nitrobenzene in the transition state. Since BPA decomposition reaction is endothermic (Table 2), the transition state resembles products (in this case the sulfonyl and the diazenyl radicals) more than starting material, according to Hammond postulate. The contribution of the charge transferred resonance form shown below would be a possible explanation for the polar character of the transition state, in which the polar solvents solvate.

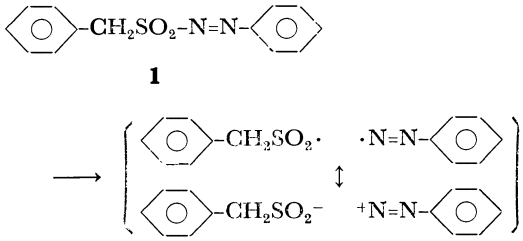

The radical pair may be stabilized by the contribution of the charge transfer between α-toluenesulfonyl radical and phenyldiazenyl radical due to the strong electron accepting nature of the former. In the thermal decomposition of alkyl arylazo sulfide (alkyl-S-N=N-Ar) the significant changes in activation parameters with solvents have been explained by the formation of ion-pair, alkyl-S^- $^+$N=N-Ar.[13)]

The isokinetic relation was plotted to give a straight line with an isokinetic temperature of 30 °C (Fig. 2, $\Delta H^{\neq}$ (34.1±2.1 kcal/mol) and $\Delta S^{\neq}$ (21.7±6.3 e.u.), obtained in the cyclohexane-benzene mixed solvent (5 : 1, vol. ratio), were also plotted).

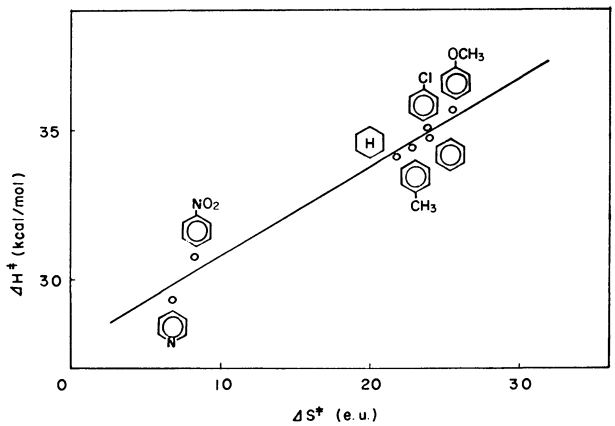

Fig. 2. Plot of isokinetic relation.

Table 2. Rate constants and activation parameters obtained with koelsch radical for thermal decomposition of benzyl phenylazo sulfone in solutions

Solvent	Runs[a]	Temp (°C)	$k_{av} \times 10^6$ (s^{-1})	$\Delta H^{\neq}$[b] (kcal/mol)	$\Delta S^{\neq}$[b] (e. u.)
Benzene	3	70.2	88.3		
	3	65.0	40.9		
	4	60.0	17.9		
	9	55.0	8.05	34.8±0.8[c]	23.9±2.3[c]
Benzene[d]	2	65.0	42.4		
	3	60.0	19.6		
	3	55.0	8.60		
	2	49.8	3.43	35.4±1.1	25.8±3.2
Toluene	3	65.0	39.5		
	3	60.0	17.9		
	3	55.0	8.13		
	3	50.0	3.47	34.4±0.1	22.7±0.4
Anisole	3	70.0	51.3		
	5	65.0	23.4		
	5	60.0	10.4		
	2	55.0	4.48	35.7±0.4	25.6±1.3
Chlorobenzene	2	70.0	55.7		
	2	65.0	25.9		
	2	60.0	11.4		
	2	55.0	5.14	35.0±0.3	23.8±1.0
Pyridine	2	60.0	12.6		
	3	55.0	6.22		
	3	50.0	2.96		
	3	45.0	1.51	29.3±1.2	6.8±3.6
Nitrobenzene	3	70.0	12.9		
	3	65.0	6.21		
	3	60.0	3.01		
	3	55.0	1.59	30.7±1.8	8.2±5.4

a) Measurements carried out with varying concentration of BPA. b) By the least-square method.
c) Standard deviation. d) Galvinoxyl used as stable free radical.

The rate constants obtained here include the efficiency in cage effect (f). A preliminary experiment gave f= 0.56 for the benzene solution at 80 °C. It seems that the change in f with the solvents gives little effect on the activation parameters.

References

1) For Part II in this series, see Y. Takahara, M. Iino, and M. Matsuda, *Bull. Chem. Soc. Jpn.*, **49**, 2268 (1976).
2) (a) K. Seki, M. Iino, and M. Matsuda, *Macromolecules*, **7**, 116 (1974); (b) M. Matsuda and M. Iino, *ibid.*, **2**, 216 (1969); (c) M. Matsuda, M. Iino, T. Hirayama, and T. Miyashita, *ibid.*, **5**, 240 (1972); (d) M. Iino, K. Katagiri, and M. Matsuda, *ibid.*, **7**, 439 (1974).
3) C. M. M. da S. Corrêa and W. A. Waters, *J. Chem. Soc., Perkin Trans. 2*, **1972**, 1575.
4) D. Booth, F. S. Dainton, and K. J. Ivin, *Trans. Faraday Soc.*, **55**, 1293 (1959).
5) M. Kobayashi, H. Minato, M. Kojima, and N. Kamigata, *Bull. Chem. Soc. Jpn.*, **44**, 2501 (1971).
6) (a) A. J. Rosenthal and C. G. Overberger, *J. Am. Chem. Soc.*, **82**, 108 (1960); (b) C. G. Overberger and A. J. Rosenthal, *ibid.*, **82**, 117 (1960).
7) R. C. Petersen, J. H. Markgraf, and S. D. Ross, *J. Am. Chem. Soc.*, **83**, 3819 (1961).
8) K. Nozaki and P. D. Bartlett, *J. Am. Chem. Soc.*, **68**, 1686 (1946).
9) J. L. Kice and R. S. Gabrielsen, *J. Org. Chem.*, **35**, 1004, 1010 (1970).
10) W. E. Truce and D. L. Heuring, *J. Org. Chem.* **39**, 245 (1974).
11) R. Kuhn and F. A. Neugebauer, *Monatsh. Chem.*, **95**, 3 (1964).
12) P. D. Bartlett and T. Funahashi, *J. Am. Chem. Soc.*, **84**, 2596 (1962).
13) J. Brokken-Zijp and H. van de Bogaert, *Tetrahedron*, **29**, 4169 (1973).

The Reaction of Organoboranes with *d*-Carvone and *l*-Perillaldehyde in the Presence of Oxygen. Evidence for a Coordination between Organoboranes and α,β-Unsaturated Carbonyl Oxygens in Their Oxygen-Induced Free Radical Reaction Process

Akira ARASE, Yuzuru MASUDA, and Akira SUZUKI*

Kitami Institute of Technology, Kitami, Hokkaido 090

**Department of Applied Chemistry, Faculty of Engineering, Hokkaido University, Sapporo 060*

(Received February 20, 1976)

Oxygen-induced 1,4-addition reactions of trialkylboranes with cyclic α,β-unsaturated carbonyl compounds were studied. Stereoselective 1,4-additions of the alkyl groups of trialkylboranes were observed in the reactions of *d*-carvone and L-perillaldehyde. Namely, it was shown that the alkyl group adds to *d*-carvone from the *trans* side with respect to isopropenyl group to give the corresponding saturated ketones. The same type of one side attack of the alkyl group to *l*-perillaldehyde was also observed. The evidence seems to strongly support the hypothesis that coordination of boron atoms of trialkylboranes to carbonyl oxygens plays an important role, even in the oxygen-induced free radical chain reaction of organoboranes with α,β-unsaturated carbonyl compounds.

It has been previously reported by us that trialkylboranes undergo rapid 1,4-addition reactions with methyl vinyl ketone[1] to give vinyloxyboranes, which undergo hydrolysis on treatment with water to form corresponding saturated ketones (Eq. 1).

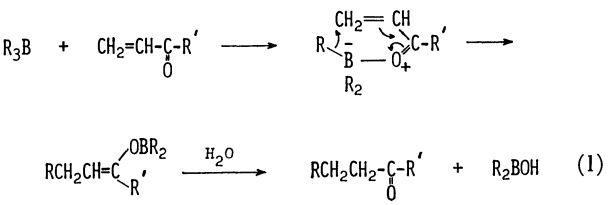

The reaction was initially considered to proceed *via* a cyclic transition state,[1] (co-ordination mechanism). The same type of reaction was shown to occur readily with other α,β-unsaturated carbonyl compounds, such as acrylaldehyde,[2] methacrylaldelyde,[3] α-bromoacrylaldelyde,[3] 2-methylcycloalkanones,[3] and isopropenyl methyl ketone.[4] However, the reaction failed when an alkyl substituent is present in the 3-position as in the cases of *trans*-crotonaldehyde and *trans*-3-penten-2-one.[4] Furthermore, it was discovered that galvinoxyl inhibits the reaction between trialkylboranes and acrylaldehyde or methyl vinyl ketone,[4] and that the reaction with 3-substituted enone systems is effectively promoted by an addition of acyl peroxide[5] or air,[6] or by photochemical means.[5] These reactions therefore were concluded to proceed by a radical chain mechanism as shown in Eq. 2.[4]

The nature of the chain propapagation step may be associated with the formation of the strong boron–oxygen bond in the vinyloxyborane, and is similar to the reaction of alkoxy radicals with trialkylboranes.[7] The failure of the reaction of 3-substituted enone systems in the absence of air or radical initiators may possibly be the result of the relatively short chain length of radical addition to these systems compared to the addition to unsubstituted systems.

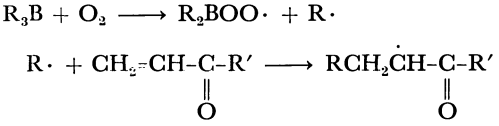

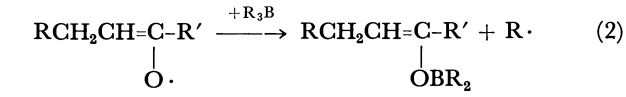

On the other hand, there are many examples which suggest that reactions of organoboranes seem to proceed *via* co-ordination mechanisms, including carbonylation reactions,[8] and reactions between organoboranes and α-halocarbanions,[9] ylids,[10] diazo compounds,[11] carbenes,[12] 2-furyllithium,[13] alkyl azides,[14] and α-azidostyrene.[15] The reaction which is considered to proceed by a coordination mechanism usually involves initial Lewis acid–Lewis base interaction between the organoborane and the substrate to form an adduct, which subsequently undergoes rearrangement with migration of an alkyl group from boron to carbon (Eq. 3).

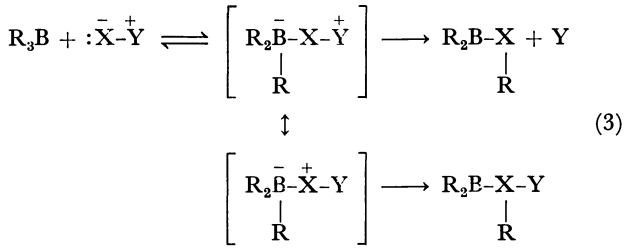

In order to know if such a Lewis acid–Lewis base interaction is involved even in the radical chain process, we conducted the reaction of trialkylboranes with *d*-carvone and *l*-perillaldehyde in the presence of oxygen.

Results and Discussion

The reaction of *d*-carvone (I) with tricyclohexylborane was carried out in aqueous tetrahydrofuran solution. During the initial stage of the reaction, a 50 mol % oxygen for tricyclohexylborane was bubbled into the solution for 1 h. Although two products, A and B, were detected by GLPC, these were not isolated by preparative GLPC or by preparative TLC. Consequently, the products, A and B, were collected as a mixture by preparative GLPC.

The elemental analysis of the mixture consisting of A and B, coincided with $C_{16}H_{26}O$. The IR spectrum

showed an absorption band at 1700 cm^{-1} due to saturated carbonyl group and the PMR spectrum in carbon tetrachloride indicated the following absorptions: 0.93 (d, J=7.0 Hz, $-CH_3$), 0.97 (d, J=7.0 Hz, $-CH_3$), 0.80—2.70 ($-CH_2-$ and $-\dot{C}H-$), 1.68 ($CH_3-\dot{C}=$), and 4.76 ($CH_2=\dot{C}-$). The mass spectra, obtained by GC-mass spectrometry, included the following peaks: *m/e* (relative intensity) 234 (29), 151 (32), 137 (100), 95 (52), 69 (32), and 55 (38) for the product A, and 234 (30), 151 (32), 137 (100), 95 (46), 69 (30), and 55 (34) for the product B. These data suggest that the products are 2-methyl-5-isopropenyl-3-cyclohexyl-1-cyclohexanones (II). The composition of the mixture was estimated by GLPC and the major product, A and the minor one, B, were 63 and 37%, respectively.

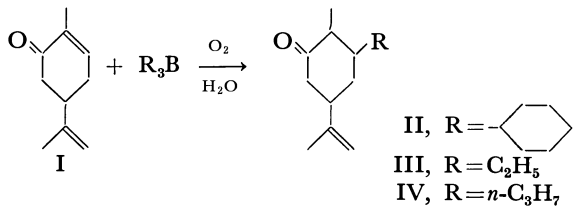

(4)

Similarly, 2-methyl-5-isopropenyl-3-ethyl-1-cyclohexanone (III) and 2-methyl-5-isopropenyl-3-propyl-1-cyclohexanone (IV) were obtained from corresponding trialkylboranes under the same reaction conditions. The results are shown in Table 1.

Table 1. Reaction of cyclic α,β-unsaturated carbonyl compounds with trialkylboranes in the presence of oxygen

α,β-Unsaturated carbonyl compound	Trialkylborane R_3B	Product	Yield,[a] %
I	Triethylborane	III	55
I	Tripropylborane	IV	60
I	Tricyclohexylborane	II	82
VII	Tricyclohexylborane	VIII	70

a) Based on the trialkylborane used.

Four stereoisomers, IIa, IIb, IIc, and IId, are considered for II. Namely, the introduction of the cyclohexyl group from the *trans* side against the isopropenyl group affords IIa or IIb, whereas the attack of the cyclohexyl group from *cis* side gives IIc or IId.

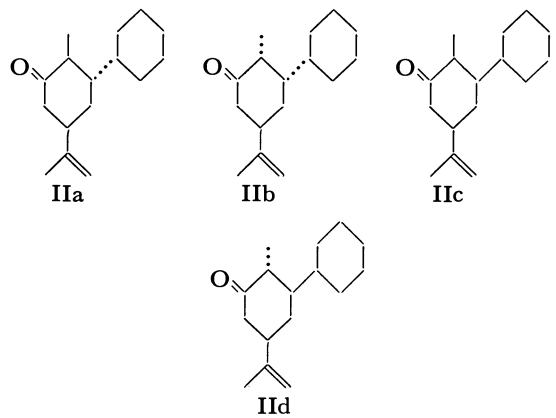

In an attempt to determine the stereochemistry, an epimerization reaction was carried out on the mixture of A and B. Thus, a mixture of A (63%) and B (37%) was treated with sodium methoxide in tetrahydrofuran at 40 °C. The reaction mixture was sampled periodically and analyzed by GLPC. The results are summarized in Table 2.

Table 2. Epimerization of IIa and IIb in the presence of sodium methoxide at 40 °C

Reaction time, h	Percent composition of IIa	and IIb	Total amount of IIa and IIb
0	63	37	100
1	72	28	100
2	74	26	99
3	74	26	100
4	74	26	99

The equilibrium distribution, 74% A to 26% B, was obtained after 2 h, and the total amount of the compounds A and B was not changed during the reaction, demonstrating that they are epimers with one another. Consequently, it was concluded that the cyclohexyl group was introduced from one side to the cyclohexenone ring of *d*-carvone.

In order to clarify whether the attack of alkyl group of organoboranes occurs *trans* or *cis* to 5-alkyl group of cyclohexenone derivatives, the reaction of 5-methyl-2-cyclohexen-1-one (V) with trimethylborane was examined as a model case of the reaction. From the experimental evidence that the reaction gave only *trans*-3,5-dimethyl-1-cyclohexanone (VI) which was identified by direct comparison of its 2,4-dinitrophenylhydrazone with that of the authentic sample prepared by House and Fischer,[16] it was decided that the methyl group of trimethylborane attacked exclusively from *trans* side to 5-methyl group (Eq. 5).

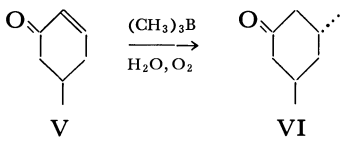

(5)

From the analogy of the above reaction and the epimerization reaction, reasonable structures for the products, A and B in the reaction of tricyclohexylborane with *d*-carvone, are assigned to IIa and IIb, respectively. These facts seem to indicate that the cyclohexyl attack occurs *trans* to isopropenyl group in *d*-carvone.

The stereoselective addition of the alkyl group of trialkylborane to 5-alkyl-2-cyclohexen-1-one derivatives mentioned above led us to examine the stereochemistry in the reaction of trialkylborane with other types of cyclic α,β-unsaturated carbonyl compounds. Thus the reaction between tricyclohexylborane and *l*-perillaldehyde (VII) was carried out under the same conditions. In the reaction, three compounds, C, D, and E were obtained. Although by preparative GLPC and by preparative TLC, the compounds C and D could not be isolated purely, the IR spectrum of the mixture consisting of 60% C and 40% D, collected by preparative

GLPC showed absorptions at 2700 and 1730 cm^{-1} due to saturated aldehyde structure. The PMR spectrum in carbon tetrachloride solution showed the following absorptions in ppm: 0.70—2.50 ($-CH_2-$ and $-\underset{|}{C}-H$); 1.73 ($CH_3-\underset{|}{C}=$); 4.71 ($CH_2=\underset{|}{C}-$); 9.70 (s, -CHO); 9.73 (S, -CHO). The mass spectra, obtained by GC-mass spectrometry, included the following peaks: m/e (relative intensity) 234 (41), 216 (12), 151 (64), 109 (100), and 83 (50) for the product C, and 234 (67), 216 (23), 151 (67), 109 (100), and 83 (99) for the product D. The elemental analysis of the mixture coincided with $C_{16}H_{26}O$. These data were all consistent with 2-cyclohexyl-4-isopropenyl-1-cyclohexanecarbaldehydes (VIIIa and VIIIb). On the other hand, the product, E, was determined from its spectroscopic data and its elemental analysis to be 2-cyclohexyl-4-isopropenyl-1-cyclohexanone (IX). Namely, it has an IR absorption peak at 1710 cm^{-1} caused by ketonic carbonyl and PMR peaks in carbon tetrachloride at 0.70—2.60 ($-CH_2-$ and $-\underset{|}{C}-H$), 1.70 ($CH_3-\underset{|}{C}=$), and 4.71 ppm ($CH_2=\underset{|}{C}-$). Addition to these data, it gave the following mass peaks: *m/e* (relative intensity) 220 (2), 138 (100), 97 (67), and 95 (46).

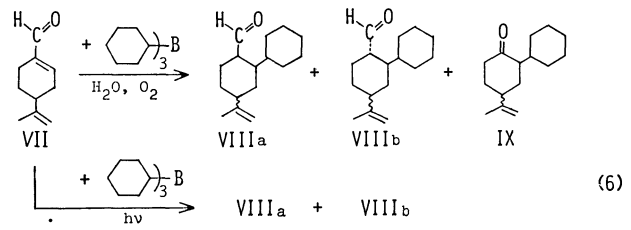

(6)

Since our efforts were mainly directed toward learning if a Lewis acid–Lewis base interaction is involved even in the radical chain process of organoborane reaction, a detailed discussion on formation of the abnormal product (IX) was not a main purpose in this paper. The reaction, however, should be considered to proceed through the following path. It is well known that alkyldioxydialkylborane is formed by air-oxidation of trialkylborane.[17]

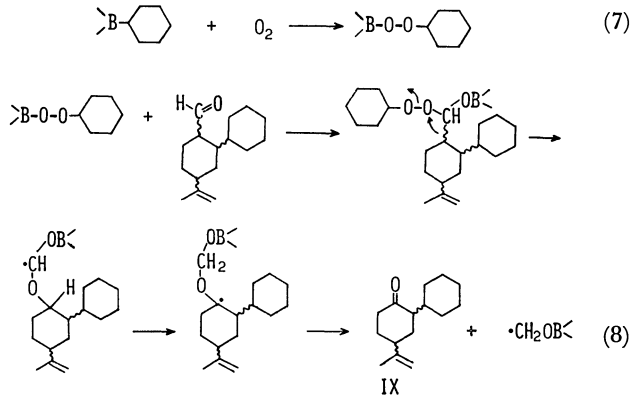

(7)

(8)

Accordingly, it appears to be possible to obtain cyclohexyldioxydicyclohexylborane from tricyclohexylborane and oxygen (Eq. 7). Such a dioxyborane reacts with *l*-perillaldehyde in a similar manner which is postulated in Baeyer-Villiger reaction as depicted in Eq. 8.[18]

If the above-mentioned mechanism is correct, the formation of such a cyclohexanone derivative (IX) should be excluded by the photochemically induced reaction[5] of tricyclohexylborane with perillaldehyde, because oxygen is not used as a radical initiator. As expected, when the reaction was carried out under UV irradiation in the absence of air, the products were shown to be VIIIa and VIIIb, and no unusual product (IX) was detected.

Table 3. Epimerization of VIIIa and VIIIb in the presence of sodium methoxide at 40 °C

Reaction time, h	Percent composition of VIIIa and VIIIb		Total amount of VIIIa and VIIIb
0	40	60	100
1	41	59	94
3.5	46	54	97
15	46	54	97

In an attempt to know the structure relationship between VIIIa and VIIIb, epimerization reaction was carried out. Thus, after a mixture of VIIIa (40%) and VIIIb (60%) was treated with sodium methoxide in tetrahydrofuran under the same reaction conditions conducted in a mixture of IIa and IIb, the reaction products were analyzed by GLPC. The results are summarized in Table 3. This evidence shows that VIIIa and VIIIb are epimers with one another, and the equilibrium ratio is 46 : 54. It is reasonable to consider that in both VIIIa and VIIIb, cyclohexyl group, the most bulky substituent on the parent cyclohexane ring, is located in the equatorial position, and that VIIIa in which the aldehyde group is in axial, is less stable than VIIIb having an aldehyde group in the equatorial position. On the other hand, it is known that protons situated in equatorial of cyclohexane ring give rise to resonances downfield from their axial counterparts.[19] In the PMR spectrum of the mixture, 40% VIIIa and 60% VIIIb, two singlet peaks due to the aldehydic protons are observed at δ=9.70 and 9.73 ppm, and their peak ratio is 2 : 3. This fact supports the structures assigned to VIIIa and VIIIb.

Although the stereochemistry of the isopropenyl group has not been fully clarified, it is considered that the cyclohexyl group of tricyclohexylborane was introduced from one side of cyclohexene ring of *l*-perillaldehyde (Eq. 9).

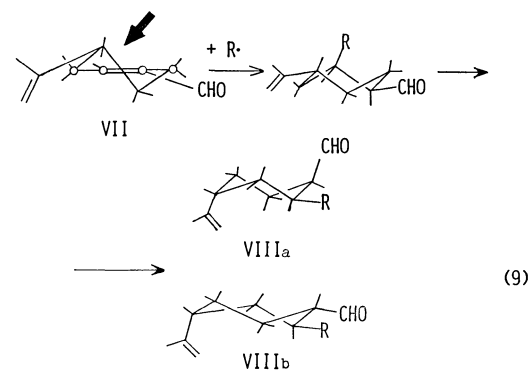

(9)

According to an analogous consideration for *d*-carvone mentioned above, it is tentatively concluded that in the products, VIIIa and VIIIb, the cyclohexyl group is located in *trans* with respect to 4-isopropenyl group (Eq. 9).

The highly stereoselective results obtained in this work seem to suggest that even when the reaction of organoboranes with α,β-unsaturated carbonyl compounds proceeds *via* a radical chain process, such a trialkylborane first approaches the carbonyl oxygen from the less hindered side of the molecule because of a Lewis acid–Lewis base intraction, and then the alkyl radical formed from the trialkylborane attacks the β-carbon from the same side of the unsaturated carbonyl derivative (Eq. 10).

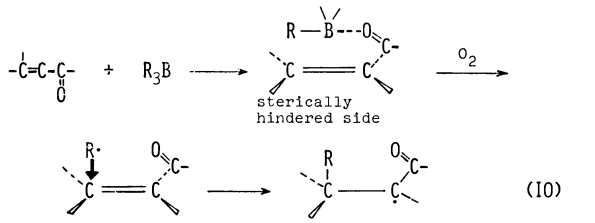

(10)

There are reports which show Lewis base–Lewis acid interactions between boron and oxygen atoms in hydroboration of olefins. For example, in the hydroboration of 7,7-dimethylnorbornene (X)[20], *endo*-attack is favored, 22% *exo*- and 78% *endo*-, while *exo*-attack is predominant in the 7,7-dimethoxy derivative (XI).[21] This result is not explained by means of steric hindrance in hydroboration, but may be rationalized in terms of a more predominant approach of borane to the methoxy side. Consequently, the present proposal is not singular.

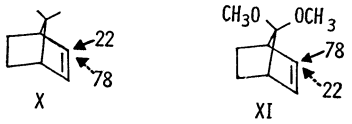

Recently, there has been an increased interest in methods for effecting 1,4-addition to α,β-unsaturated carbonyl compounds using organometallic compounds.[22–29] Although in such cases of reactions with cyclic α,β-unsaturated carbonyl compounds with substituent, mixtures containing major *trans*-1,4-addition products and minor *cis*-isomers have been reported to be obtained.[22,28,29] We did not detect corresponding *cis*-1,4-addition products in the present experiment.

Experimental

Instruments. Analytical GLPC and preparative GLPC were performed using a Hitachi Model K-53 Gaschromatograph and Varian Aerograph Model-920, respectively. PMR spectra were obtained on Hitachi Model R-20A spectrometer. Chemical shifts are reported in δ unit using TMS as the internal standard. Infra red spectra were recorded on Shimadzu 27G spectrometer. Mass spectra were obtained on Hitachi Model M-52 mass spectrometer. The light source of UV irradiation was 400W Rikosha High Pressure Mercury Lamp.

Materials. *d*-Carvone and l-perillaldehyde were distilled before use.

Reaction of Tricyclohexylborane with d-*Carvone.* Into a 25-ml round bottomed flask, equipped with a gas inlet, a septum inlet, a reflux condenser and a magnetic stirring bar, 4 mmol of tricyclohexylborane in 4 ml of THF, prepared by hydroboration of cyclohexene, under nitrogen atmosphere and 1 ml of water were charged. To the stirred solution 0.6 g (4 mmol) of *d*-carvone was added at 40 °C, and then 224 ml of air (2 mmol of oxygen) was bubbled for 1 h. After stirring for 12 h at the same temperature, the solution was saturated with sodium chloride, and the upper organic layer was analysed by GLPC. A column, packed with PEG 20 M (15%) on Diasolid M was used at 200 °C. It was indicated that the cyclohexylated products had been obtained in an 82% yield in a ratio of IIa : IIb=63 : 37. In the preparative experiment, the scale of the reaction was enlarged 10 times. After completion of the reaction, the organic layer was separated by decantation and then the lower layer was extracted with ethyl ether several times. The combined organic layer and extracts were dried over anhydrous magnesium sulfate. After removal of the solvent, the products were collected by preparative GLPC.

Anal. Found: C, 81.70; H, 11.40%. Calcd for $C_{16}H_{26}O$: C, 81.99; H, 11.18%.

Reaction of Triethylborane with d-*Carvone.* The reaction was carried out under the same conditions described above. The product, III, (yield, 55%) was collected. The IR spectrum showed an absorption at 1708 cm^{-1}. The PMR (CCl_4) spectrum showed the following absorptions: 0.80—1.05 ($-CH_3$), 1.05—2.70 ($-CH_2-$ and $-\overset{|}{C}H$), 1.72 ($CH_3-\overset{|}{C}=$), and 4.76 ($CH_2=\overset{|}{C}-$). The mass spectra (70 eV) included the following peaks: *m/e* (relative intensity) 180 (43), 151 (18), 97 (73), 95 (73), 83 (100), 69 (75), and 55 (50) for the major product, and 180 (38), 151 (8), 97 (44), 95 (64), 83 (100), 69 (56), and 55 (40) for the minor product.

Anal. Found: C, 80.10; H 11.21%. Calcd for $C_{12}H_{20}O$: C, 79.94; H, 11.18%.

Reaction of Tripropylborane with d-*Carvone.* A small scale reaction and preparative scale reaction were carried out in the same manner with that of tricyclohexylborane with *d*-carvone. The product IV (yield, 60%) was collected by GLPC. The IR spectrum showed an absorption at 1710 cm^{-1}. PMR (CCl_4) spectrum: 0.85—1.15 ($-CH_3$), 1.15—2.70 ($-CH_2-$ and $-\overset{|}{C}H$), 1.75 ($CH_3-\overset{|}{C}=$), and 4.70 ($CH_2=\overset{|}{C}-$). The mass spectra (70 eV) included the following peaks: *m/e* (relative intensity) 194 (24), 151 (14), 97 (100), 95 (56), 69 (46), and 55 (44) for the major product, and 194 (28), 151 (13), 97 (100), 95 (60), 69 (34), and 55 (48) for the minor product.

Anal. Found: C, 80.72; H, 11.63%. Calcd for $C_{13}H_{22}O$: C, 80.35; H, 11.41%.

Epimerization of IIa and IIb. The mixture (47 mg) of IIa (63%) and IIb (37%), and 0.1 ml of 0.1M-sodium methoxide in THF and diphenyl ether (internal standard for GLPC) were added into 1.9 ml of THF. The solution was stirred at 40 °C and 0.1 ml portions of the solution were periodically sampled. They were neutralized with 0.01 M-HCl, saturated with sodium chloride and then extracted with petroleum ether. The extracts were analysed by GLPC. PEG 20 M (15%) supported on Diasolid M was used as the packing materials for GLPC.

Reaction of Trimethylborane with 5-Methyl-2-cyclohexen-1-one. The reaction appratus was composed essentially of two parts. flask A and flask B. The flask A was a 100 ml-three necked flask fitted with a magnetic stirring bar, a gas inlet glass

tube, a septum inlet and an efficient condenser. Flask B was a 25 ml-flask equipped with a septum inlet and a condenser. The top of the condenser of a flask A was connected with a Tygon tube which had a syringe needle at the end. The needle was inserted into the bottom of flask B through the septum inlet.

In the flask A 1.62 g (60 mmol) of magnesium turning was placed. The entire reaction apparatus was flushed with nitrogen, and then 8.52 g (60 mmol) of methyl iodide in 20 ml of ethyl ether was added slowly to maintain a gentle reflux. After addition of methyl iodide, the mixture was stirred at 25 °C for 1 h. On the other hand, in flask B were charged 0.66 g (6 mmol) of 5-methyl-2-cyclohexen-1-one prepared by the Crossley's procedure[30] and 2 ml of THF, and the flask was cooled down to −25 °C. Then 8.5 g of boron trifluoride etherate was added dropwise to the Grignard reagent solution in flask A, and the resulting trimethylborane was introduced into flask B. A smooth dissolution of trimethylborane was observed. After generation of the trimethylborane ceased, flask A was flushed with nitrogen to sweep the remained trimethylborane in the flask into the flask B. Then the colling bath was removed, and 1 ml of water was added to the reaction mixture in B. Into the solution in flask B, 400 ml of air was bubbled slowly. After 12 h, the reaction mixture was saturated with sodium chloride, and the organic layer separated was dried over anhydrous magnesium sulfate. Thus, *trans*-3,5-dimethyl-1-cyclohexanone was isolated in a yield of 51% by GLPC at 150 °C (PEG 20 M(15%) supported on Diasolid M). 2,4-Dinitrophenylhydrazone of the ketone, recrystallized twice from ethyl alcohol, melts at 108.0—109.5 °C (literature,[16] 108.4—110 °C).

Reaction of Tricyclohexylborane with 1-Perillaldehyde. A small scale and preparative scale experiments were carried out in the same manner as described in the reaction of tricyclohexylborane with *d*-carvone. GLPC analysis (Apiezon glease L (15%) on Diasolid M at 180 °C) indicated that the products, VIII and IX, had been obtained in yields of 70% and 18%, respectively.

Anal. Found: C, 81.80; H, 11.38%. Calcd for $C_{16}H_{26}O$: C, 81.99; H, 11.18%.

Spectroscopic data of IX were as follows: IR, 1710 cm^{-1}; PMR (CCl_4), 0.70—2.60 ($-CH_2-$ and $-\overset{|}{C}H$), 1.70 ($CH_3-\overset{|}{C}=$), and 4.71 ($CH_2=\overset{|}{C}-$); mass spectrum (70 eV), m/e (relative intensity) 220 (2), 138 (100), 97 (67), and 95 (46).

Anal. Found: C, 81.80; H, 11.18%. Calcd for $C_{15}H_{24}O$: C, 81.76; H, 10.98%.

Epimerization Reaction of VIIIa and VIIIb. A reaction was carried out under the same conditions as mentioned in the epimerization of IIa and IIb.

References

1) A. Suzuki. A. Arase, H. Matsumoto, M. Itoh, H. C. Brown, M. M. Rogić, and M. W. Rathke, *J. Am. Chem. Soc.*, **89**, 5708 (1967).

2) H. C. Brown, M. M. Rogić, M. W. Rathke, and G. W. Kabalka, *J. Am. Chem. Soc.*, **89**, 5709 (1967).

3) H. C. Brown, M. M. Rogić, N. W. Rathke, and G. W. Kabalka, *J. Am. Chem. Soc.*, **90**, 4165 (1968).

4) G. W. Kabalka, H. C. Brown, A. Suzuki, S. Honma, A. Arase, and M. Itoh, *J. Am. Chem. Soc.*, **92**, 710 (1970).

5) H. C. Brown and G. W. Kabalka, *J. Am. Chem. Soc.*, **92**, 712 (1970).

6) H. C. Brown and G. W. Kabalka, *J. Am. Chem. Soc.*, **92**, 714 (1970).

7) (a) A. G. Davies and B. P. Roberts, *J. Organomet. Chem.*, **19**, P17 (1969); (b) A. G. Davies and B. P. Roberts *Chem. Commun.*, **1969**, 699. (c) A. G. Davies, D. Griller, and B. P. Roberts, *J. Chem. Soc., B*, **1971**, 1823; (d) P. J. Krusic and J. K. Kochi, *J. Am. Chem. Soc.*, **91**, 3942 (1969).

8) For example, H. C. Brown, *Acc. Chem. Res,*. **2**, 65 (1969).

9) H. C. Brown, H. Nambu, and M. M. Rogić, *J. Am. Chem. Soc.*, **91**, 6854 (1969) and references cited therein.

10) J. J. Tufariello, L. T. C. Lee, and P. Wojtkowski, *J. Am. Chem. Soc.*, **89**, 6804 (1967) and references cited therein.

11) J. Hooz and D. M. Gunn, *J. Am. Chem. Soc.*, **91**, 6195 (1969) and references cited therein.

12) A. Suzuki, S. Nozawa, N. Miyaura, and M. Itoh, *Tetrahedron Lett.*, **1969**, 2955.

13) A. Suzuki, N. Miyaura, and M. Itoh, *Tetrahedron*, **27**, 2775 (1971).

14) A. Suzuki, S. Sono, M. Itoh, H. C. Brown, M. M. Midland, *J. Am. Chem. Soc.*, **93**, 4329 (1971).

15) A. Suzuki, M. Tabata, and M. Ueda, *Tetrahedron Lett.*, **1975**, 2195.

16) H. O. House and W. F. Fischer, Jr., *J. Org. Chem.*, **33**, 949 (1968).

17) For example, see G. M. L. Cragg, "Organoboranes in Organic Synthesis," Macrel Dekker, New York (1973), p. 122.

18) (a) C. H. Hassall, *Org. React.*, **9**, 73 (1957); (b) C. J. Collins and J. F. Eastham, "The Chemistry of the Carbonyl Group," ed. by S. Patai, Interscience, New York (1966), p. 801; (c) H. S. Verter, "The Chemistry of the Carbonyl Group," ed. by J. Zabichy, Vol. 2, Interscience, New York (1970), p. 94.

19) For example, see L. M. Jackman and S. Sternhell, "Applications of Nuclear Magnetic Resonance Spectroscopy in Organic Chemistry," 2nd ed., Pergamon Press, Oxford (1969), p. 238.

20) H. C. Brown and J. H. Kawakami, *J. Am. Chem. Soc.*, **92**, 1992 (1970).

21) P. G. Gassman and J. L. Marshall, *J. Am. Chem. Soc.*, **88**, 2822 (1966).

22) H. O. House and W. F. Fischer, Jr., *J. Org. Chem.*, **33**, 949 (1968).

23) C. P. Casey and R. A. Boggs, *Tetrahedron Lett.*, **1971**, 2455.

24) R. A. Kretchmer, *J. Org. Chem.*, **37**, 2744 (1972).

25) H. O. House and M. J. Umen, *J. Am. Chem. Soc.*, **94**, 5495 (1972).

26) G. W. Kabalka and R. F. Daley, *J. Am. Chem. Soc.*, **95**, 4428 (1973).

27) C. P. Casey, D. F. Marten, and R. A. Boggs, *Tetrahedron Lett.*, **1973**, 2071.

28) R. M. Coates and L. O. Sandefur, *J. Org. Chem.*, **39**, 275 (1974).

29) E. C. Ashby and G. Heinsohn, *J. Org. Chem.*, **39**, 3297 (1974).

30) A. W. Crossley and N. Renouf, *J. Chem. Soc.*, **1915**, 602.

The Bromination and the Mercuration of Bis(dimethylglyoximato)-(styryl)pyridinecobalts(III), Styryl-type Cobaloximes

Hiraku SHINOZAKI, Minoru KUBOTA, Osamu YAGI, and Masaru TADA*

Department of Chemistry, School of Science and Engineering, Waseda University, Shinju-ku, Tokyo 160

(Received February 20, 1976)

cis and *trans-p*-Cyanostyryl(pyridine)cobaloximes (I and II) and *cis* and *trans-p*-methoxystyryl(pyridine)-cobaloximes (V and VI) were prepared by the reaction of the reduced form of cobaloxime, bis(dimethylglyoximato)-(pyridine)cobalt(I), with *cis* and *trans-p*-cyanostyryl bromides and with *cis* and *trans-p*-methoxystyryl bromides, respectively. The styryl-type cobaloximes thus obtained retained the stereochemistry, *cis* or *trans*, of the starting bromides. The bromination of these styryl-type cobaloximes (I, II, V, and VI) and of the *cis* and *trans*-styryl-(pyridine)cobaloximes (III and IV) in polar or non-polar solvents gave styryl-type bromides with the retention of configuration. The mercuration of these cobaloximes with mercury(II) acetate in DMF gave styryl-type mercurials, again retaining the original configuration.

In recent years much attention has been paid to the stereochemistry of the electrophilic substitution of alkylmetal complexes,[1] especially bis(dimethylglyoximato)-(alkyl)pyridinecobalt(III) (its conventional name, alkyl-(pyridine)cobaloxime, will be used hereafter). Little is known, however, about the stereochemistry of the electrophilic fission of vinyl-type cobalt complexes, though Johnson and Meeks[2] reported the halogenation of styryl(pyridine)cobaloxime in acetic acid and we reported the bromination and the mercuration of 1-octenyl(pyridine)cobaloxime in several solvents,[3] The halogenation of *cis* and *trans*-styryl(pyridine)cobaloxime takes place with the retention of configuration in acetic acid[2] and the bromination of *cis* and *trans*-1-octenyl-(pyridine)cobaloxime takes place with the retention and the inversion of the configuration[3] (Eq. 1).

$$\text{R-CH=CH-(Co)} \xrightarrow{Br_2} \text{R-CH=CH-Br} + \text{Br-(Co)} \quad (1)$$

We examined the steric course of the bromination and the mercuration of *para*-substituted and non-substituted styryl(pyridine)cobaloximes in varying reaction conditions to get a deeper insight into the reaction mechanism, referring to the electronic effect of the substituent on the benzene ring.

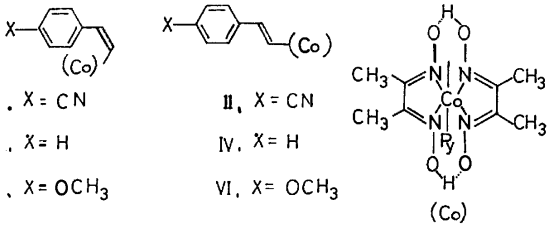

I, X = CN II, X = CN
III, X = H IV, X = H
V, X = OCH_3 VI, X = OCH_3

Syntheses of Styryl-type Cobaloximes. *cis* and *trans-p*-Cyanostyryl(pyridine)cobaloxime (I and II) were synthesized by the reaction of *p*-cyanostyryl bromides with the reduced form of pyridinecobaloxime,[4] prepared *in situ* from a dimeric bis(dimethylglyoximato)(pyridine)-cobalt(II), by a reduction using zinc powder in methanol. The similar reactions of *cis* and *trans-p*-methoxystyryl bromides were sluggish and did not give *p*-methoxystyryl(pyridine)cobaloximes (V and VI) in a reasonable yield. *p*-Methoxystyryl(pyridine)cobaloximes (V and VI), therefore, were synthesized by the action of the cobaloxime anion, bis(dimethylglyoximate)(pyridine)cobalt(I), prepared *in situ* from dimethylglyoxime, cobalt(II) chloride, pyridine, sodium hydroxide, and sodium tetrahydroborate in methanol. *cis* and *trans*-Styryl(pyridine)cobaloximes (III and IV)[5] were prepared similarly, by the reaction of *cis* and *trans*-styryl bromides with the cobaloxime anion.

The stereochemistry of the styryl-type cobaloximes is easily assigned from the coupling constants of the olefinic protons in the NMR spectra of these cobaloximes; 10 Hz, 9 Hz, and 9 Hz for I, III, and V, and 15 Hz, 15 Hz, and 14 Hz for II, IV, and VI, respectively. The steric course of the reactions of styryl bromides has been reported to be completely stereospecific with retention of configuration,[5] and the reactions with *p*-cyanostyryl bromides or *p*-methoxystyryl bromides also took the stereospecific course with retention. The rate of the displacement reaction of these bromides with cobaloxime anions is much faster at the *trans*-bromide than at its *cis*-isomer, and we needed the pure *cis para*-substituted styryl bromides for the preparations of *cis* styryl-type cobaloximes. The base treatment of *erythro*-2,3-dibromo-3-(*p*-methoxyphenyl)-propionic acid gave only *trans-p*-methoxystyryl bromide under various conditions. The base treatment of *erythro*-2,3-dibromo-3-(*p*-acetoxyphenyl)propionic acid[6] gave stereoselectively *cis-p*-acetoxystyryl bromide or its *trans*-isomer, depending upon the reaction conditions. The treatment of the dibromide with triethylamine in a non-polar solvent such as benzene gave *cis-p*-acetoxystyryl bromide exclusively. On the other hand, the treatment of the dibromide with sodium acetate in water afforded only *trans-p*-acetoxystyryl bromide. *cis-p*-Acetoxystyryl bromide was converted into *cis-p*-methoxystyryl bromide by hydrolysis of the acetoxy group followed by methylation.

Electrophilic Reaction of Styryl-type Cobaloximes. Bromination of the styryl-type cobaloximes was carried out with an equivalent amount of bromine; the reaction took place smoothly at room temperature and almost instantly in polar solvents to give the corresponding styryl-type bromides in high or quantitative yields. The compositions of the styryl bromides from each reaction are collected in Table 1. The bromination of *p*-cyanostyryl(pyridine)cobaloximes (I and II) and styryl(pyridine)cobaloximes (III and IV) in methanol gave bromides retaining the original configurational most exclusively, though the bromination of

* To whom correspondence should be addressed.

p-methoxystyryl(pyridine)cobaloximes (V and VI) gave 1,1-dibromo-2-methoxy-2-(*p*-methoxyphenyl)ethane, due to the facile methoxybromination of the resulting *p*-methoxystyryl bromides. The bromination of all six cobaloximes in dichloromethane or benzene proceeded with retention. In carbon disulfide, the reaction of *cis*-cobaloximes (I, III, or V) with an equivalent amount of bromine gave products with extensive inversion (I, 45%; III, 12%, V; 20% inversion respectively). These results were proved to be due to the isomerization of the *cis*-bromides to their *trans*-isomers under the reaction conditions from the following experimental findings. The composition of the bromides from *cis*-cobaloximes (I, III, or V) depends upon the amount of bromine used and approaches the limiting values (Fig. 1).

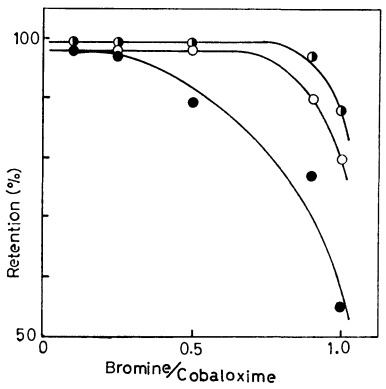

Fig. 1. Stereospecificity in the bromination of cobaloximes with varying amount of bromine.
a) ● (I), ◑ (III), ○ (V).
b) In carbon disulfide at room temperature.

These limiting values were obtained by extrapolation of the curves to an infinite amount of the bromine used, and are collected in Table 1. Brominations of the cobaloximes, therefore, are proved to proceed with retention even in carbon disulfide. This feature is in sharp contrast with the bromination of *cis* and *trans*-1-octenyl(pyridine)cobaloxime, which gives products with a preferential inversion in carbon disulfide.[3] We reexamined the bromination of 1-octenyl(pyridine)-cobaloxime with varying amounts of bromine, but no significant difference from the earlier results was observed. A temperature-effect upon the product composition was found in the case of the bromination of 1-octenyl(pyridine)cobaloxime[3] and we found that the bromination of styryl-type cobaloximes in refluxing carbon disulfide (46 °C) gave the styryl-type bromides with inversion to some extent. The compositions in Table 1 are again the limiting values from the reaction with 0.25 equivalent amount of bromine. These data show that the bromination itself takes place with a complete retention in carbon disulfide even at a higher temperature. Next, we examined the relative reactivities of the *trans*-cobaloximes (II, IV, and VI) and *trans*-1-octenyl(pyridine)cobaloxime to bromine by carrying out a competitive reaction. The relative reactivities thus obtained are 1.0 (II), 2.3 (1-octenyl(pyridine)-cobaloxime), 3.1 (IV), and 4.7 (VI); this sequence of the reactivity is accounted for by the electrophilic nature of the reaction, though a more profound difference in the reactivity, in general, can be expected for a typical electrophilic reaction of *para*-substituted styrenes.[7]

One of the possible explanations of the stereochemical consequence of the bromination is the hindered rotation of the bond between the benzylic carbon and the carbon-bearing cobaloxime moiety in an intermediate (B), which either formed in concert with the attack of bromine or formed stepwise *via* an intermediate (A) (Eq. 2). This inhibition of rotation must be due to the stereoelectronic stabilization of the benzylic cation by either a vertical stabilization,[8] originating from the conjugation between the vacant *p*-orbital and the σ-bond of carbon–cobalt, or a d-π conjugation between the vacant *p*-orbital and a filled d-orbital of the cobalt ion.[9] The rupture of the cobaloxime moiety from the cation (B) is expected to afford styryl-type bromides which retain the original configuration of the starting cobaloximes.

Dodd and Johnson[10] have described briefly, in a review article, the mercuration of the cobaloximes III and IV in acetic acid; they pointed out that inconsistent results were obtained depending on the purity of the solvent. Our mercuration of the cobaloximes (I—VI) with mercury(II) acetate in DMF, followed by the treatment with sodium chloride, gave the styryl-type mercurials. NMR analysis of the resulting mercurials dissolved in DMSO showed that the product retained the original stereochemistry of the cobaloximes. No stereochemical consequence is further altered, regardless of whether the *para*-substituent is electron

Table 1. Isomeric compositions (%) of the styryl-type bromides from bromination of styryl-type cobaloximes

Starting material	I		II		III		IV		V		VI	
Solvent \ Bromide	*cis*	*trans*	*cis*	*trans*	*cis*	*trans*	*cis*	*trans*	*cis*	*trans*	*cis*	*trans*
MeOH[a]	92	8	3	97	100	trace	trace	100	c)	c)	c)	c)
C_6H_6[a]	96	4	1	99	100	trace	trace	100	98	2	2	98
CH_2Cl_2[a]	97	3	2	98	100	trace	trace	100	96	4	6	94
CS_2[a]	98	2	3	97	100	trace	6	94	98	2	6	94
CS_2[b]	97	3	trace	100	100	trace	trace	100	98	2	trace	100

a) Reaction temperature: *ca.* 20 °C (room temperature). b) Reaction temperature: 46 °C (reflux). c) 1,1-Dibromo-2-methoxy-2-(*p*-methoxyphenyl)ethane was obtained.

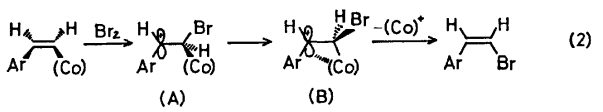

(A) (B) (2)

donating ($-OCH_3$) or electron withdrawing (-CN), and the mercuration must take the same steric course as the bromination.

In conclusion the bromination and the mercuration of *para*-substituted styryl(pyridine)cobaloximes take place with the retention of configuration to give styryl-type bromides and styrylmercury(II) chlorides in high yields; these results can be accounted for by the intervention of the benzylic cation stabilized by neighboring group participation of a cobaloxime moiety.

$$X\text{-}C_6H_4\text{-}CH{=}CH\text{-}(Co) + Hg(OAc)_2 \xrightarrow[DMF]{NaCl} X\text{-}C_6H_4\text{-}CH{=}CH\text{-}HgCl$$

Table 2. Isomeric compositions of the styryl-mercury(II) chlorides from mercuration of the styryl-type cobaloximes in DMF

Starting material	I	II	III	IV	V	VI
Yield(%)	82	49	100	84	95	49
cis(%)	97	4	100	trace	94	3
trans(%)	3	96	trace	100	6	97

Experimental

Styryl-type Bromides. *cis* and *trans*-Styryl bromide,[11,12] *cis* and *trans-p*-cyanostyryl bromides,[13] and *trans-p*-methoxystyryl bromide[14] were prepared by the reported methods. *cis-p*-Methoxystyryl bromide was prepared from *erythro*-2,3-dibromo-3-(*p*-acetoxyphenyl)propionic acid, mp 187—189 °C, which was prepared by the same procedure as that used for the prepartion of *erythro*-2,3-dibromo-3-(phenyl)propionic acid.[6]

The mixture of *erythro*-2,3-dibromo-3-(*p*-acetoxyphenyl)-propionic acid (50 g, 0.137 mol), 35 ml of triethylamine, and 250 ml of benzene was refluxed for 2 h, then the mixture was filtered to remove the triethylamine hydrobromide. The filtrate was washed successively with water, saturated aqueous $NaHCO_3$, and 2M HCl, and was dried over Na_2SO_4. The condensation of the solution gave a mixture of *cis* and *trans-p*-acetoxystyryl bromides (*cis*/*trans*=84/16) as an oil (22 g). The solution of these *p*-acetoxystyryl bromides (22 g) in ethanol (80 ml) and water (20 ml) was mixed with 4 ml of concd HCl and then refluxed for 2 h. Most of the ethanol was evaporated under reduced pressure and the aqueous solution thus obtained was extracted with benzene after the addition of more water. The benzene extract was wased with saturated aqueous $NaHCO_3$ and was dried over Na_2SO_4. Evaporation of benzene from the solution gave a light yellow solid, which was purified by passing through a silica gel column (2.5×25 cm) with hexane–ether (1 : 1) to give *p*-hydroxystyryl bromides (15.7 g). For the purification of *cis-p*-hydroxystyryl bromide, the *p*-hydroxystyryl bromides were esterified with benzoyl chloride–pyridine, and the recrystallization of the benzoates from hexane–carbon tetrachloride gave *cis-p*-benzoyloxystyryl bromide. Mp 93 °C, IR(KBr): 1730 and 700 cm^{-1}. NMR($CDCl_3$): 6.36 (1H, d, J=8 Hz) and 6.98 ppm (δ) (1H, d, J=8 Hz).

Hydrolysis of the *cis-p*-benzoyloxystyryl bromide (8.2 g) with sodium hydroxide (2.7 g) in ethanol–water (6 : 1) gave *cis-p*-hydroxystyryl bromide in quantitative yield. The methylation of the bromide by dimethyl sulfate in dry acetone in the presence of K_2CO_3 gave *cis-p*-methoxystyryl bromide (3.5 g, 71%). Bp 128—134 °C/15—16 mmHg. IR(neat): 1600, 1505, 1250, 1175, 1015, 830, and 705 cm^{-1}. NMR (CCl_4): 3.58 (3H, s), 5.96 (1H, d, J=8 Hz), 6.50 (2H, d, J=9 Hz), 6.62 (1H, d, J=8 Hz), 7.26 ppm (δ) (2H, d, J=9 Hz).

Syntheses of Styryl-type Cobaloximes. *cis* and *trans*-Styryl(pyridine)cobaloximes (III and IV) were prepared by the reaction of *cis* and *trans*-styryl bromides with the cobaloxime anion, as reported earlier.[5]

a) *cis* and *trans-p*-Cyanostyryl(pyridine)cobaloximes (I and II). To a mixture of *cis-p*-cyanostyryl bromide (2.1 g, 10 mmol) and dimeric pyridinecobaloxime, $(Co(dmgH)_2py)_2$,[4] (7.3 g, 10 mmol) in 80 ml of methanol was added under nitrogen 2.0 g of zinc powder; the mixture was stirred for 18 h at room temperature. The reaction mixture was filtered and the filtrate was condensed. The residue was dissolved in 70 ml of chloroform, and the chloroform extract was washed with water and dried over Na_2SO_4. The chloroform solution was condensed under reduced pressure and the condensate was passed through a Florisil column (2.7× 18 cm) with chloroform–ethylacetate (1 : 1) to remove impurities. Evaporation of the solvent from the eluate gave essentially pure *cis-p*-cyanostyryl(pyridine)cobaloxime (I) in the yield of 48%. Recrystallization of I from acetonitrile–benzene gave pure cobaloxime (I).

The same procedure starting with *trans-p*-cyanostyryl bromide gave *trans-p*-cyanostyryl(pyridine)cobaloxime (II) in the yield of 66%.

cis-Cobaloxime (I), mp 208—210 °C (decomp). Found: C, 53.15; H, 4.98; N, 16.92%. Calcd for $C_{22}H_{25}N_6O_4Co$: C, 53.23; H, 5.08; N, 16.93%. IR (KBr): 2230, 1600, 1560, 1440, 700, 550, 520 cm^{-1}. NMR ($CDCl_3$): 1.92 (12H, s), 5.99 (1H, d, J=10 Hz), 6.39 (1H, d, J=10 Hz), 7.06—7.86 (7H, m), 8.42—8.60 ppm (δ) (2H, m).

trans-Cobaloxime (II), mp 216—224 °C (decomp). Found: C, 53.24; H, 5.07; N, 17.10%. Calcd for $C_{22}H_{25}N_6O_4Co$: C, 53.23; H, 5.08; N, 16.93%. IR (KBr): 2230, 1605, 1565, 1450, 975, 700, 550, 520 cm^{-1}. NMR ($CDCl_3$): 2.14 (12H, s), 6.30 (1H, d, J=15 Hz), 7.40—8.00 (8H, m), 8.60—8.85 ppm (δ) (2H, m).

b) *cis* and *trans*-Methoxystyryl(pyridine)cobaloximes (V) and (VI). *cis*-Cobaloxime (V) was synthesized by the reaction of *cis-p*-methoxystyryl bromide (1.0 g, 4.7 mmol) with the cobaloxime anion prepared *in situ* from $CoCl_2 \cdot 6H_2O$ (0.95 g, 4 mmol), dimethylglyoxime (0.93 g, 8 mmol), 8 ml of 10 M-sodium hydroxide, pyridine (0.5 g), and sodium tetrahydroborate (200 mg) under nitrogen in methanol (40 ml) at 0 °C for 1 h and at room temperature for 1.5 h. The reaction mixture was extracted with benzene (50 ml× 2) after the addition of water (100 ml). The condensation of the extract after drying over Na_2SO_4 gave the residue containing *cis*-cobaloxime (V). This residue was passed through a Florisil column (2.5×20 cm) with dichloromethane and dichloromethane–ethyl acetate (2 : 1). Evaporation of the solvent from the latter fraction gave *cis*-cobaloxime (V). Recrystallization of the cobaloxime (V) from acetonitrile gave pure V in the yield of 39%.

The same procedure starting with *trans-p*-methoxystyryl bromide gave *trans-p*-methoxystyryl(pyridine)cobaloxime (VI) in the yield of 45% after recrystallization.

cis-Cobaloxime (V), mp 198—204 °C (decomp). Found: C, 52.63; H, 5.44; N, 14.00%. Calcd for $C_{22}H_{28}N_5O_5Co$:

C, 52.70; H, 5.63; N, 13.97%. IR (KBr): 1610, 1595, 1510, 1450, 1240, 850, 770, 705, 530 cm^{-1}. NMR ($CDCl_3$): 1.84 (12H, s), 3.60 (3H, s), 5.24 (1H, d, J=9 Hz), 6.10 (1H, d, J=9 Hz), 6.46 (2H, d, J=9 Hz), 6.66 (2H, d, J=9 Hz), 6.86—8.22 ppm (δ) (5H, pyridine).

trans-Cobaloxime (VI), mp 215—218 °C (decomp). Found: C, 52.49; H, 5.51; N, 14.26%. Calcd for $C_{22}H_{28}N_5O_5Co$: C, 52.70; H, 5.63; N, 13.97%. IR (KBr): 1600, 1500, 1440, 1230, 950, 830, 750, 510 cm^{-1}. NMR ($CDCl_3$): 2.00 (12H, s), 3.58 (3H, s), 5.86 (1H, d, J=14 Hz), 6.46 (2H, d, J=8 Hz), 6.59 (1H, d, J=14 Hz), 6.88 (2H, d, J=8 Hz), 7.00—8.44 ppm (δ) (5H, pyridine).

Reaction of Cobaloximes (I—VI) with Bromine. The solution of one of the cobaloximes (I—VI) (0.2 mmol) in one of the solvents (15 ml) depicted in Table 1 was treated with an equivalent amount of bromine in 1 ml of the same solvent, and the mixture was stirred for 30 min at room temperature under nitrogen. When carbon disulfide was used as a solvent, the volume of the solution was increased to 40 ml and the reaction at 46 °C was carried out by boiling the reaction mixture. The reactions with smaller equivalents of bromine were carried out in the same manner to get the limiting values listed in Table 1. After the reaction the mixture was filtered, the filtrate was condensed, and the residue was dissolved in hexane–ether (1 : 1). Passing of the solution through an alumina column (Merck II-III, 0.8×5 cm) with hexane–ether (1 : 1) gave the corresponding styryl-type bromides. The product composition was determined by a GLC analysis (2.1 m, 5%-PEG-Succinate on Chromosorb P, N_2). Identification of the bromides as *cis* and *trans*-styryl-type bromides was made by the comparison of GLC and NMR spectra of the products with those of authentic samples.

Competitive Reaction. A solution containing equal amounts (0.2 mmol) of cobaloximes II, IV, and VI was treated with 0.02 mmol of bromine and stirred for 20 min at room temperature under nitrogen. The reaction mixture was worked up as described above and the relative amounts of styryl-type bromides were determined by GLC analyses. For this purpose the relative sensitivity of the bromides in GLC analyses was determined by analyzing a mixture of the bromides with known composition. The mixture of 0.2 mmol of *trans*-styryl(pyridine)cobaloxime and *trans*-1-octenyl(pyridine)cobaloxime was subjected to the same treatment.

Mercuration of Cobaloximes (I—VI). The solution of one of the cobaloximes (I—VI, 0.2 mmol) in DMF (10 ml) was treated with 1.2 equivalents of mercuric acetate and the mixture was stirred for 30 min at room temperature. The mixture was further stirred for 10 min after addition of 2 ml of saturated aqueous solution of sodium chloride and was extracted with chloroform after further addition of water (10 ml). The extract was washed with water and dried over Na_2SO_4. Evaporation of chloroform and DMF at reduced pressure gave a styryl-type mercurial. The crude product thus obtained was passed through a silica gel column (1.0× 10 cm) with chloroform and evaporation of the solvent gave styryl-type mercury(II) chloride with retention in the yield listed in Table 2. The product composition was determined by the relative intensities of the NMR signals of the olefinic hydrogens of the product. The structure of the mercurials was confirmed by transforming these organomercury(II) chlorides into the corresponding styryl-type bromides with bromine in pyridine. *cis*-Cyanostyrylmercury(II) chloride, mp 184—185 °C. IR (KBr): 2220, 1405, 850, 540 cm^{-1}. NMR (DMSO): 6.53 (1H, d, J=12 Hz), 7.56 (1H, d, J=12 Hz), 7.95 ppm (δ) (4H, s).

trans-Cyanostyrylmercury(II) chloride, mp 232—233 °C. IR (KBr): 2230, 1500, 1170, 970, 850, 780, 550 cm^{-1}. NMR (DMSO): 6.92 (2H, s), 7.63, 7.85 ppm (δ) (4H, AB-type, J=8 Hz).

cis-Styrylmercury(II) chloride, mp 106.5—107 °C. IR (KBr): 1580, 1560, 1480, 1440, 1325, 770, 680 cm^{-1}. NMR (DMSO-d_6): 6.30 (1H, d, J=12 Hz), 7.30—7.90 ppm (δ) (6H, m).

trans-Styrylmercury(II) chloride, mp 210—211 °C. IR (KBr): 1590, 1560, 1490, 1440, 965, 720 cm^{-1}. NMR (DMSO-d_6): 6.60, 6.85 (2H, AB-type, J=18 Hz), 7.05—7.50 ppm (δ) (5H, m).

cis-Methoxystyrylmercury(II) chloride, mp 97—98 °C. IR (KBr): 1610, 1510, 1260, 1170, 830 cm^{-1}. NMR (DMSO-d_6): 3.80 (3H, s), 6.15 (1H, d, J=11 Hz), 7.20 (2H, d, J=9 Hz), 7.43 (1H, d, J=11 Hz), 7.65 ppm (δ) (2H, d, J=9 Hz).

trans-Methoxymercury(II) chloride, mp 220—222 °C. IR (KBr): 1600, 1510, 1250, 1170, 1020, 960, 830, 770 cm^{-1}. NMR (DMSO-d_6): 3.80 (3H, s), 6.50, 6.85 (2H, AB-type, J=19 Hz), 6.96 (2H, d, J=9 Hz), 7.40 ppm (δ) (2H, d, J=9 Hz).

References

1) H. Shinozaki, H. Ogawa, and M. Tada, *Bull. Chem. Soc. Jpn.*, **49**, 775 (1976) and references cited therein.

2) M. D. Johnson and B. S. Meeks, *Chem. Commun.*, **1970**, 1027.

3) M. Tada, M. Kubota, and H. Shinozaki, *Bull. Chem. Soc. Jpn.*, **49**, 1097 (1976).

4) "Inorganic Syntheses," ed. by W. L. Jolly, McGraw Hill, Vol. XI, N. Y. (1968), p. 61.

5) M. D. Johnson and B. S. Meeks, *J. Chem. Soc., B*, **1971**, 185.

6) M. Reimer, *J. Am. Chem. Soc.*, **64**, 2510 (1942).

7) J. H. Rolston and K. Yates, *J. Am. Chem. Soc.*, **91**, 1483 (1969); J. E. Dubais and A. Schwarz, *Tetrahedron Lett.*, **1964**, 2169.

8) T. G. Traylor, W. Hanstein, H. J. Berwin, N. A. Clinton, and R. S. Brown, *J. Am. Chem. Soc.*, **93**, 5715 (1971).

9) G. E. Coates, M. L. H. Green, and K. Wada, "Organometallic Compounds," Methuen, Vol. 2, London (1968), p. 215.

10) D. Dodd and M. D. Johnson, *J. Organomet. Chem.*, **52**, 77 (1973).

11) S. J. Cristol and W. P. Norris, *J. Am. Chem. Soc.*, **75**, 2645 (1953).

12) L. J. Dolby, C. Wilkins, and T. F. Frey, *J. Org. Chem.*, **31**, 1110 (1953).

13) W. Davies, B. M. Holmes, and J. F. Kefford, *J. Chem. Soc.*, **1939**, 357.

14) E. R. Trumbull, R. T. Finn, K. M. Ibne-Rasa, and C. K. Sauers, *J. Org. Chem.*, **27**, 2339 (1962).

New Cross Aldol Reactions. Titanium Tetrachloride-promoted Reactions of Silyl Enol Ethers with Carbonyl Compounds Containing A Functional Group

Kazuo BANNO

The First Research Institute, Tokushima Factory,
Otsuka Pharmaceutical Co., Ltd., Kagasuno, Kawauchi-cho Tokushima 771-01

(Received March 8, 1976)

It was found that, in the presence of titanium tetrachloride, silyl enol ethers selectively react with aldehyde or ketone function of various carbonyl compounds containing another functional group giving the corresponding cross aldols in good yields. The present cross aldol reaction was successfully applied to the synthesis of ar-turmerone, one of the volatile principles of turmeric oil.

In previous paper,[1-3] it was reported that the reactions of silyl enol ethers with various simple carbonyl compounds in the presence of titanium tetrachloride proceed under mild conditions giving the desired cross aldols in good yields. According to this procedure, it was established that cross aldols are exclusively produced in most cases and no by-products, such as the di-, poly-, and self-condensation products, and α,β-unsaturated carbonyl compounds formed in the usual base-promoted aldol condensation, are produced. Therefore, it is recognized that this reaction is one of the most useful cross aldol processes among the methods reported by House[4] *et al.* and Wittig[5] *et al.*

In the present paper, the titanium tetrachloride-promoted reaction of silyl enol ethers with a variety of carbonyl compounds containing an additional functional will be described.

In the first experiment, the reaction of ethyl pyruvate with silyl enol ether (**1**) in the presence of an equimolar amount of titanium tetrachloride was attempted at room temperature. After hydrolysis, ethyl 2-hydroxy-2,3-dimethyl-4-oxohexanoate (**2**) was obtained in an 87% yield.

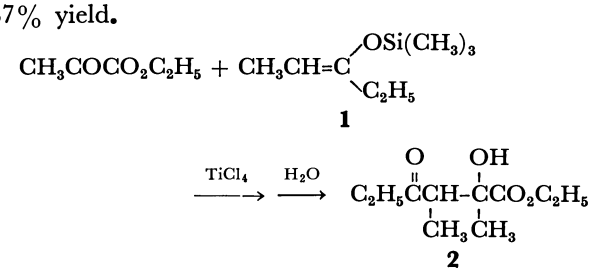

1

2

The effect of the amount of titanium tetrachloride upon the yield of **2** was investigated using the reaction of ethyl pyruvate with **1** as a model and **2** was obtained in the highest yield when an equimolar amount of titanium tetrachloride was employed.

The reactions of various silyl enol ethers with a variety of keto esters were attempted in the presence of an equimolar amount of titanium tetrachloride. These results are given in Table 1. Of these keto esters, it was found that ethyl acetoacetate did not react with silyl enol ethers under the same conditions and was recovered quantitatively.

In the next experiment, the reaction of silyl enol ethers with various dicarbonyl compounds was studied. For example, when silyl enol ether (**17**) was allowed to react with an equimolar amount of phenylglyoxal at −78 °C for 2 h, 2-hydroxy-1,3-diphenyl-1,4-pentanedione (**18**) was obtained exclusively in an 83% yield, and none of the product added to the ketone function was detected.

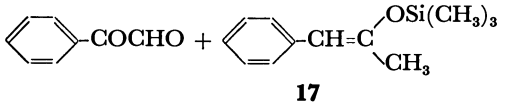

17

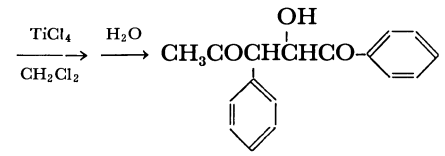

18

Unexpectedly, in the case of the reaction of 1,4-cyclohexanedione with an equimolar amount of the silyl enol ether (**10**), 1,4-bis(benzoylmethyl)-1,4-cyclohexanediol (**19**) was obtained in an 86% yield (based on **10**), and no 4-hydroxy-4-(benzoylmethyl)-1-cyclohexanone was detected by NMR and TLC analyses.

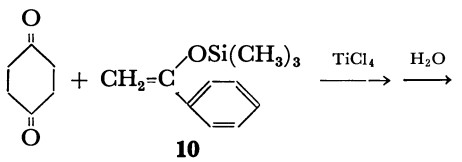

10

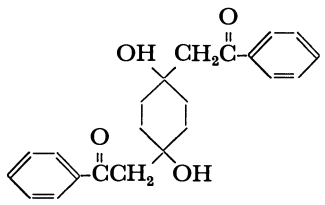

19

As described above, it should be noted that the silyl enol ether reacted only with the aldehyde function of the keto aldehyde in the presence of titanium tetrachloride at −78 °C giving the corresponding hydroxy diketone, and the silyl enol ether selectively reacted with the ketone function of the keto ester at room temperature to give the corresponding hydroxy keto ester. However, when the diketone was treated with an equimolar amount of the silyl enol ether, the latter reacted with both the ketone functions of the diketone.

Of the usual protecting groups of the carbonyl function examined,[6] it was found that only thioacetal[7] was stable and useful in the present reaction. Thus,

TABLE 1. SYNTHESIS OF HYDROXY KETO ESTERS FROM SILYL ENOL ETHERS AND KETO ESTERS

Reagents		Product	
Keto ester	Silyl enol ether	Hydroxy keto ester	Yield (%)
$CH_3COCO_2C_2H_5$	$CH_2=C(OSi(CH_3)_3)CH_3$ (**3**)	$CH_3C(=O)CH(OH)CH_2CO_2C_2H_5$, CH_3 (**4**)	55
	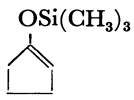 (**5**)	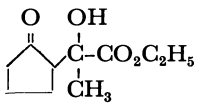 (**6**)	76
	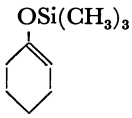 (**7**)	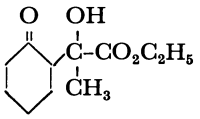 (**8**)	88
$CH_3CO-C(CH_3)(CH_3)-CO_2C_2H_5$	**7**	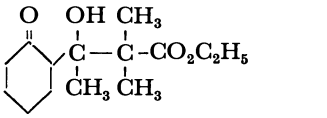 (**9**)	52
	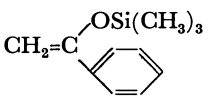 (**10**)	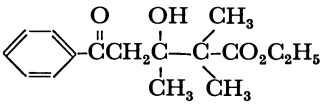 (**11**)	38
$CH_3CO(CH_2)_2CO_2C_2H_5$	**1**	$C_2H_5C(=O)CH(CH_3)-C(OH)(CH_3)-(CH_2)_2CO_2C_2H_5$ (**12**)	86
$CH_3CO(CH_2)_2CO_2C_2H_5$	**5**	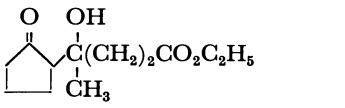 (**13**)	73
	10	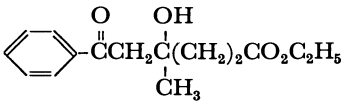 (**14**)	41
$CH_3CO(CH_2)_3CO_2CH_3$	**1**	$C_2H_5C(=O)CH(CH_3)-C(OH)(CH_3)-(CH_2)_3CO_2CH_3$ (**15**)	71
	7	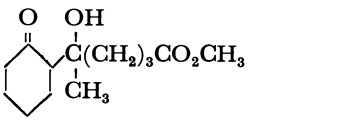 (**16**)	69

aldol formation at one of the keto groups in a diketone was performed after converting the other keto groups into its thioacetal. For example, when silyl enol ether (**3**) was allowed to react with 6,6-ethylenedithio-1-phenyl-3-heptanone in the presence of titanium tetrachloride, 7,7-ethylenedithio-4-hydroxy-4-phenethyl-2-octanone (**20**) was obtained in a 76% yield.

Next, in order to examine the influence of various functional groups on the titanium tetrachloride-promoted reaction of silyly enol ethers with carbonyl

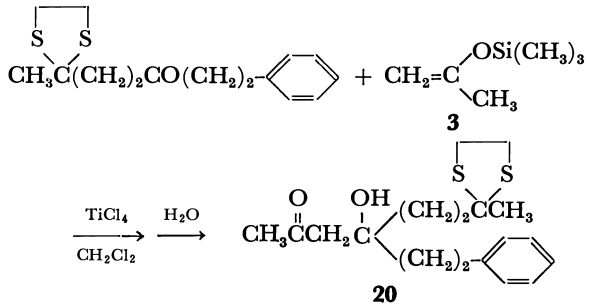

20

Table 2. Synthesis of aldols from silyl enol ethers and carbonyl compounds having a functional group

Reagents: Carbonyl compound	Reagents: Silyl enol ether	Reaction conditions: temp (°C) / time (h)	Product: Aldol	Product: Yield (%)
CCl_3CHO	**7**	−78 / 1	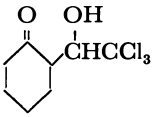 **21**	94
	10	−78 / 1	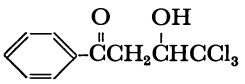 **22**	92
$CH_3CO(CH_2)_3CN$	**3**	0 / 1	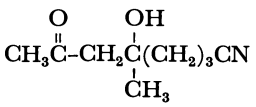 **23**	52
	5	0 / 1	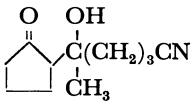 **24**	73
$CH_3COCH_2OCOCH_3$	**7**	0 / 1	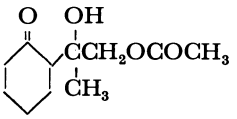 **25**	34
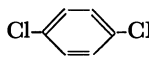	**7**	−10 / 3	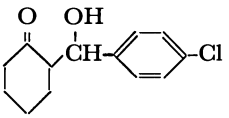 **26**	86
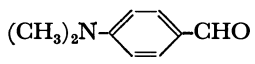	**1**	−10 / 3	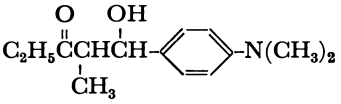 **27**	65
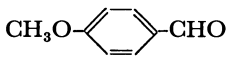	**1**	−10 / 3	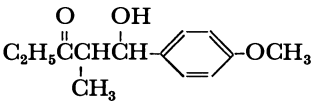 **28**	82
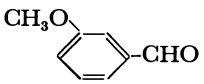	**1**	−10 / 3	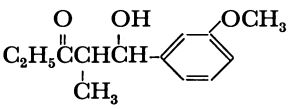 **29**	88
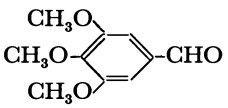	**1**	−10 / 3	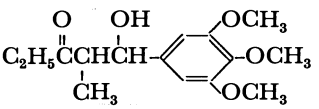 **30**	82
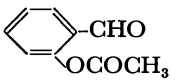	**1**	−10 / 3	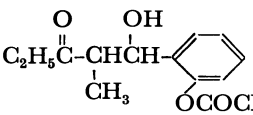 **31**	78
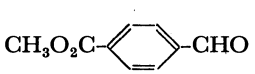	**1**	−10 / 3	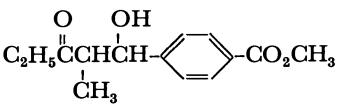 **32**	86

TABLE 2. (Continued)

Reagents: Carbonyl compound	Reagents: Silyl enol ether	Reaction conditions: temp (°C) / time (h)	Product: Aldol	Product: Yield (%)
O_2N-C$_6$H$_4$-CHO	**7**	−10 / 3	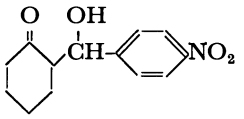 **33**	85
CH_3CO-C$_6$H$_4$-$COCH_3$	**1**	40 / 3	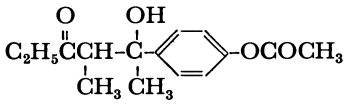 **34**	36
	10	40 / 3	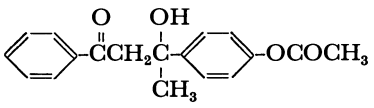 **35**	11
$C_2H_5O_2C$-C$_6$H$_4$-$COCH_3$	**1**	Room temp / 3	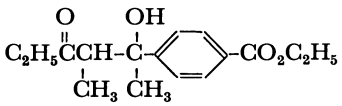 **36**	68
O_2N-C$_6$H$_4$-$COCH_3$	**10**	Room temp / 3	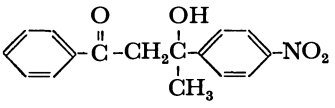 **37**	52

compounds, the reaction of silyl enol ethers with a variety of aliphatic and aromatic carbonyl compounds having, acyloxy, alkoxy, carboxy, amino, cyano, halogeno, hydroxy, and nitro substituents was investigated. The results are summarized in Table 2.

As shown is in Table 2, it is apparent that the titanium tetrachloride-promoted aldol reaction using silyl enol ethers is not influenced by groups such as acyloxy, alkoxyl, cyano, dialkylamino, halogeno, nitro, and thioacetal groups. However, in the cases of the carbonyl compounds containing active hydrogen, such as carboxyl, hydroxyl, primary amino, and secondary amino groups, no aldols were obtained and the silyl enol ethers were decomposed into the original carbonyl compounds. In these cases, it is believed that, at first, the carbonyl compound with active hydrogen reacted with titanium tetrachrloride to produce hydrogen chloride, which in turn rapidly reacted with the silyl enol ether to form the original carbonyl compound.

It was also established that the aldols were obtained by reactions of silyl enol ethers with various substituted aromatic aldehydes. In the cases of substituted aromatic ketones having an electron-attracting group, aldols were produced, but aromatic ketones having an electron-releasing group did not afford aldols for the same reaction procedure.

The utility of this new procedure was demonstrated by the synthesis of ar-turmerone,[8,9] 2-methy-6-*p*-tolyl-2-heptene-4-one, one of the volatile principles of turmeric oil.[10,11]

By dehydration of the reaction product of 4-methylacetophenone with the silyl enol ether (**3**) in the presence

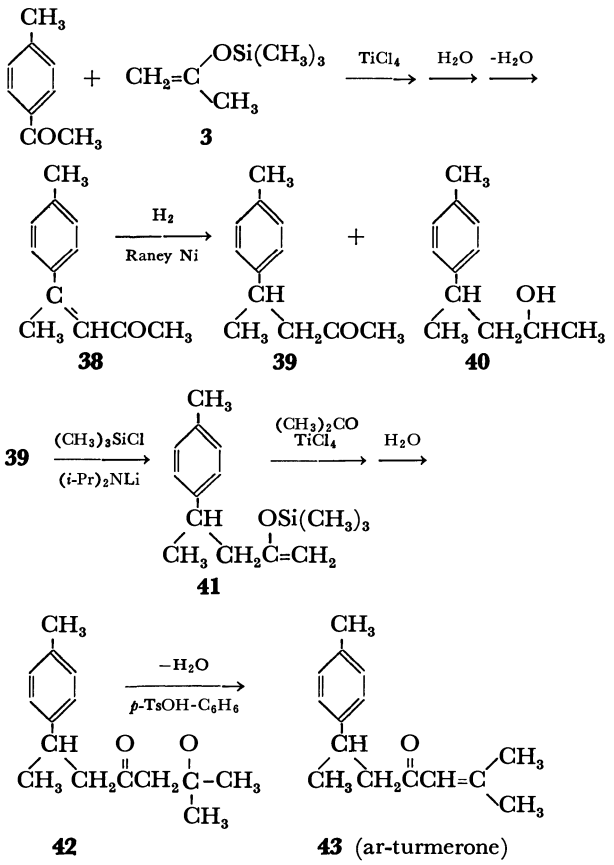

38 **39** **40** **41** **42** **43** (ar-turmerone)

of titanium tetrachloride, the α,β-unsaturated ketone (**38**) was obtained in a 53% yield, and the catalytic reduction of **38** over Raney nickel afforded the ketone

(**39**) and the alcohol (**40**) in 77% and 16% yields, respectively. The silyl enol ether (**41**), prepared from **39** according to the method of House *et al.*[12] was treated with acetone and titanium tetrachloride giving the aldol (**42**) in a 88% yield. This was dehydrated with *p*-toluenesulfonic acid–benzene to give racemic ar-turmerone (**43**) in a 92% yield. In summary, it is concluded that, in the presence of titanium tetrachloride, various silyl enol ethers react with a variety of aliphatic and aromatic carbonyl compounds containing an additional functional group, except for functional groups having active hydrogen, affording the corresponding aldols in good yields. The selective reaction forming an aldol in one of the carbonyl groups of a dialdehyde or a diketone occurs after converting the other carbonyl group into its thioacetal.

Experimental

Materials. Commercially available carbonyl compounds having the functional group, $TiCl_4$ and chlorotrimethylsilane were purified by the conventional procedures, recrystallization or distillation, before use. A commercial hexane solution of *n*-BuLi was used after standarization and commercially produced Raney nickel was thoroughly washed with methanol. 6,6-Ethylenedithio-1-phenyl-3-heptanone was prepared by the method of Araki *et al.*[13]

Methyl 6-oxohexanoate and 5-oxohexanenitril were prepared from ethyl acetoacetate and acrylonitrile according to a procedure in the literature.[14]

Trimethylsilyl enol ethers of ketones have been described in a previous paper.[3]

*Reaction of Ethyl Pyruvate with 3-Trimethylsiloxy-2-pentene (**1**)* To a dichloromethane (15 ml) solution of ethyl pyruvate (0.390 g, 3 mmol) and $TiCl_4$ (0.567 g, 3 mmol) was added a dichloromethane (30 ml) solution of silyl enol ether (**1**) (0.468 g, 3 mmol) at room temperature in an argon atmosphere, and the mixture was kept at room temperature for 3 h with stirring. After hydrolysis with cold water (30 ml), the resulting organic layer was extracted with ether (70 ml). The extract was washed with a saturated NaCl solution and dried over anhydrous Na_2SO_4. The ethereal solution was concentrated under reduced pressure. The aldol, ethyl 2-hydroxy-2,3-dimethyl-4-oxohexanoate (**2**), was obtained in an 87% (0.527 g) yield from the residue after purification by column chromatography (silica gel). The physical properties and analytic data of the product (**2**) are shown in Table. 3.

*Reaction of 6,6-Ethylenedithio-1-phenyl-3-heptanone with 2-Trimethylsiloxypropene (**3**).* As in the same procedure described above, 6,6-ethylenedithio-1-phenyl-3-heptanone (0.843 g, 3 mmol) reacted with silyl enol ether (**3**) (0.390 g, 3 mmol) in dichloromethane (40 ml) in the presence of $TiCl_4$ (0.567 g, 3 mmol) at 0 °C for 3 h. The reaction mixture was worked up as in the preparation of **2** to give a crude oil. It was purified by preparative TLC (silica gel) using dichloromethane to give 0.767 g (76%) of 7,7-ethylenedithio-4-hydroxy-4-phenethyl-2-octanone (**20**). The physical properties and analytical data of **20** are shown in Table 3.

Reaction of p-*Dimethylaminobenzaldehyde with 3-Trimethylsiloxy-2-pentene (**1**).* In a procedure similar to that described above, p-dimethylaminobenzaldehyde (0.450 g, 3 mmol) reacted with silyl enol ether (**1**) (0.474 g, 3 mmol) in dichloromethane (40 ml) in the presence of $TiCl_4$ (0.567 g, 3 mmol) at −10 °C for 3 h. The reaction mixture was quenched with aq. 5% K_2CO_3 (30 ml) at 0 °C, and the suspension was kept standing at room temperature for 10 min. After filtration, the filtrate was extracted with ether (100 ml). The organic layer was separated, dried over anhydrous Na_2SO_4 and concentrated under reduced pressure. The residue was purified by column chromatography (aluminium oxide active, neutral) to give 1-(*p*-dimethylaminophenyl)-1-hydroxyl-2-methyl-3-pentanone (**27**) in a 65% (0.458 g) yield. The physical properties and analytical data of **27** are listed in Table 3.

Reaction of p-*Acetoxyacetophenone with 1-Phenyl-1-trimethylsiloxyethylene (**10**).* A dichloromethane (10 ml) solution of 0.576 g (3 mmol) of silyl enol ether (**10**) was added dropwise into a refluxing mixture or 0.434 g (3 mmol) of *p*-acetoxyacetophenone and 0.567 g (3 mmol) of $TiCl_4$ in dichloromethane (30 ml) in an argon atmosphere within 10 min, and the reaction mixture was refluxed for 30 min. After cooling to room temperature, the reaction mixture was quenched with water (10 ml) and extracted with ether (100 ml). The resulting crude product was analyzed by chromatography on silica gel. Elution with benzene and dichloromethane (1 : 1) gave 0.098 g (11%) of 3-hydroxy-1-phenyl-3-(p-acetoxyphenyl)-1-butanone (**35**).

*Synthesis of ar-Turmerone. Preparation of 4-*p*-Tolyl-3-pentene-2-one (**38**):* A dichloromethane (40 ml) solution of 5.20 g (40 mmol) of silyl enol ether (**3**) was added to a refluxing mixture of 2.68 g (20 mmol) of *p*-methylacetophenone and 3.78 g (20 mmol) of $TiCl_4$ in dichloromethane (50 ml) in an argon atmosphere over a period of 10 min, and the reaction mixture was refluxed for 3 h. After a similar work-up, a benzene solution (50 ml) of the resulting crude was refluxed for 1 h in the presence of *p*-TsOH (0.2 g). After removal of the solvent and the unreacted starting material by distillation, **38** was isolated in a 53% (1.84 g) yield by column chromatography (silica gel) [bp 150—154 °C/25 mmHg. IR (neat): 1680, 1600 cm^{-1}. NMR (CCl_4): δ 2.20 (s, 3H), 2.37 (s, 3H), 2.50 (s, 3H), 6.45 (s, 1H), 7.0—7.7 (m, 4H)].

*Reduction of 4-*p*-Tolyl-3-pentene-2-one (**38**).* A methanol (50 ml) solution of 3.48 g (20 mmol) of **38** was treated with hydrogen for 2 h at −10 °C in the presence of commercially produced Raney nickel. About 490 ml of hydrogen was adsorbed. After filtering off the Raney nickel, the filtrate was evaporated and the residual oil was purified by column chromatography (silica gel) using dichloromethane as a developer to give 2.71 g (77%) of 4-*p*-tolyl-2-pentanone (**39**). [Found: C, 81.93; H, 9.18%. Calcd for $C_{12}H_{16}O$: C, 81,77; H, 9.15%. IR (neat): 1720 cm^{-1}. NMR (CCl_4): δ 1.25 (d, J=7 Hz, 3H), 2.01 (s, 3H), 2.38 (s, 3H), 2.68 (d, J=7 Hz, 2H), 3.0—3.5 (m, 1H), 7.15 (s, 4H)], and 0.56 g (16%) of 4-*p*-tolyl-2-pentanol (**40**) [IR (neat): 3400 cm^{-1}. NMR ($CDCl_3$): δ 1.0—1.4 (m, 6H), 1.5—2.1 (m, 2H), 2.33 (s, 3H), 2.5—4.0 (m, 2H), 7.17 (s, 4H)].

*Silylation of 4-*p*-Tolyl-2-pentanone (**39**).* A hexane solution (30.8 ml) containing 55 mmol of *n*-BuLi was mixed with 500 ml of THF. The resulting solution was cooled to −10 °C and treated with 5.5 g (55 mmol) of diisopropylamine. To this solution, 8.8 g (50 mmol) of 4-*p*-tolyl-2-pentanone (**39**) was added dropwise over a 20 min period with stirring. After stirring the mixture at the same temperature for 30 min, 6.0 g (55 mmol) of chlorotrimethylsilane was added. The reaction mixture was stirred for 30 min, diluted with 300 ml of ether, and washed rapidly with two 100 ml portions of cold aqueous 10% $KHSO_4$ and then cold aqueous 5% $NaHCO_3$. The organic layer was dried and concentrated. Fractional distillation of the residue through a spinning Teflon-band column gave fraction 1, 9.4 g (76%), bp 152—155/3.2 mmHg, containing pure 4-*p*-tolyl-2-trimethyl-

TABLE 3. PHYSICAL PROPERTIES AND ANALYTICAL DATA OF THE PRODUCTS

Product	IR (cm^{-1})	NMR (δ)	Anal. Found (%) (Calcd) C	H	N
2	[a]3505 1730 1700	[c]0.99(t, J=7 Hz, 3H), 1.20(t, J=7 Hz, 3H), 1.42(s, 1H), 1.43(d, J=7 Hz, 3H), 3.58 (b, 1H)[e]	59.13 (59.38)	8.97 (8.97)	
4	[a]3505 1735 1715	[c]1.27(t, J=7 Hz, 3H), 1.31(s, 3H), 2.12 (s, 3H), 3.57(b, 1H)[e]	54.84 (55.16)	8.40 (8.10)	
6	[a]3490 1760 1710	[c]1.29(t, J=7 Hz, 3H), 1.46(s, 3H), 1.5—2.8(m, 7H), 3.88(b, 1H)[e]	59.95 (59.98)	8.05 (8.05)	
8	[a]3505 1730 1700	[c]1.16(s, 3H), 1.23 and 1.26(t, J=7 Hz, 3/2 and 3/2H), 1.4—3.0(m, 9H), 3.16 (b, 1H)[e]	61.30 (61.66)	8.81 (8.47)	
9	[a]3500 1725 1700	[c]1.2—1.4(m, 12H), 1.5—3.0(m, 9H), 3.18(b, 1H)[e], 4.16(q, J=7 Hz, 2H)	65.21 (65.59)	9.60 (9.44)	
11	[a]3480 1715 1670	[c]1.26(t, J=7 Hz, 3H), 1.29(s, 9H), 4.30 (b, 1H)[e], 7.0—8.0(m, 5H)	68.92 (69.04)	8.01 (7.97)	
12	[a]3500 1735 1705	[c]1.02(t, J=7 Hz, 3H), 1.05(d, J=7 Hz, 3H), 1.14(s, 3H), 1.25(t, J=7 Hz, 3H), 3.35(b, 1H)[e]	— (62.58)	— (9.63)	
13	[a]3500 1770 1725	[c]1.11(s, 3H), 1.26(t, J=7 Hz, 3H), 1.5—2.5(m, 11H), 3.55(b, 1H)[e]	63.51 (63.13)	8.69 (8.83)	
14	[a]3490 1730 1670	[c]1.23(t, J=7 Hz, 3H), 1.26(s, 3H), 3.98 (b, 1H)[e], 7.4—8.1(m, 5H)	68.48 (68.16)	7.60 (7.63)	
15	[a]3505 1740 1700	[c]0.99(t, J=7 Hz, 3H), 1.04(d, J=6 Hz, 3H), 1.14(s, 3H), 3.46(b, 1H)[e], 3.61(s, 3H)	— (62.58)	— (9.63)	
16	[a]3500 1740 1700	[c]1.12 and 1.14(s, 3/2 and 3/2H), 1.3—2.6(m, 15H), 3.40(b, 1H)[e], 3.61(s, 3H)	64.31 (64.44)	9.43 (9.15)	
18	[a]3430 1720 1685	[c]2.03 and 2.08(s, 3/2 and 3/2H), 4.35 (b, 1H)[e], 7.1—8.1(m, 10H)	75.78 (76.10)	6.43 (6.01)	
19	[b]3490 1655	[d]1.5—2.1(m, 8H), 3.10(s, 4H), 4.00(s, 1H)[e], 7.4—8.1(m, 10H)	74.74 (74.97)	6.79 (6.86)	
20	[a]3480 1700	[c]1.75(s, 3H), 2.11(s, 3H), 3.30(s, 4H), 3.60(b, 1H)[e], 7.19(s, 5H)	64.12 (63.88)	7.80 (7.74)	
21	[b]3395 1695	[d]1.6—3.2(m, 9H), 3.29(d, J=5.5 Hz, 1H)[e], 4.99(d, d, J=5.5 and 2.0 Hz, 1H)	39.10 (39.13)	4.60 (4.52)	
22	[b]3440 1680	[c]3.47(d, J=5.5 Hz, 2H), 4.83(t, J=5.5 Hz, 1H), 4.92(b, 1H)[e], 7.1—8.0(m, 5H)	45.27 (44.89)	3.40 (3.39)	
23	[a]3430 2250 1720	[c]1.23(s, 3H), 2.12(s,3H), 5.39(b, 1H)[e],	63.91 (63.88)	8.75 (8.94)	8.05 (8.28)
24	[a]3500 2250 1740	[c]1.10(s, 3H), 1.3—2.9(m, 13H), 3.96(b, 1H)[e]	67.32 (67.66)	8.69 (8.78)	6.95 (7.17)
25	[a]3450 1740 1700	[c]1.13 and 1.19(s, 3/3 and 6/3H), 1.2—2.5(m, 11H), 2.03(s, 3H), 3.34 and 3.73(s, 1/3 and 2/3H)	61.18 (61.66)	8.65 (8.47)	

TABLE 3. (Continued)

Product	IR (cm^{-1})	NMR (δ)	Anal. Found (%) (Calcd) C	H	N
26	[b]3440 1695	[d]1.1—3.2(m, 9H), 3.93(d, J=2.5 Hz, 1H)[e], 4.71(d, d, J=2.5 and 8.0 Hz, 1H), 7.1—7.8(m, 4H)	65.76 (65.41)	6.06 (6.33)	
27	[a]3460 1705	[c]0.76 and 0.82(d, J=7 Hz, 3/3 and 6/3H), 2.90(s, 6H), 6.45(d,d, J=9 and 2 Hz, 2H), 7.02(d,d, J=9 and 2 Hz, 2H)	71.93 (71.45)	9.11 (9.00)	6.28 (5.95)
28	[a]3480 1710	[d]0.94(d, J=7 Hz, 3H), 1.04(t, J=7 Hz, 3H), 3.73(s, 3H), 6.97(d, J=9Hz, 2H), 7.37(d, J=9 Hz, 2H)	70.32 (70.24)	8.15 (8.16)	
29	[a]3460 1710	[c]0.83 and 0.86(d, J=7 Hz, 3/2 and 3/2H), 1.03(t, J=7 Hz, 3H), 3.77(s, 3H), 4.63 and 4.91(b, 1/2 and 1/2H)[e], 6.6—7.4(m, 4H)	70.64 (70.24)	8.07 (8.16)	
30	[a]3500 1710	[c]0.7—1.2(m, 6H), 3.76(s, 9H), 4.20(b, 1H)[e], 6.43(d, J=1.5 Hz, 2H)	63.38 (63.81)	7.92 (7.85)	
31	[a]3400 1705	[c]0.80 and 0.90(d, J= Hz, 3/2 and 3/2H), 0.94(t, J=7 Hz, 3H), 2.32(s, 3H), 3.62 (b, 1H)[e], 7.2—7.8(m, 4H)	— (67.18)	— (7.25)	
32	[a]3490 1710	[c]0.84 and 0.90(d, J=7 Hz, 3/2 and 3/2H) 0.94(t, J=7 Hz, 3H), 3.62(b, 1H)[e], 3.83(s, 3H), 7.27(d, J=8 Hz, 2H), 7.86(d, J=8 Hz, 2H)	67.17 (67.18)	7.28 (7.25)	
33	[a]3440 1700	[d]1.3—3.0(m, 9H), 4.15(d, J=4.5 Hz, 1H)[e] 5.42(d, d, J=4.5 and 7 Hz, 1H), 7.1—7.9 (m, 9H)	62.86 (62.64)	6.13 (6.07)	5.64 (5.62)
34	[a]3480 1755 1690	[c]0.81(d, J=7 Hz, 3H), 1.02(t, J=7 Hz, 3H), 1.44(s, 3H), 2.22(s, 3H), 4.10(b, 1H)[e], 6.9—7.8(m, 4H)	67.72 (68.16)	7.85 (7.63)	
35	[a]3470 1755 1670	1.56(s, 3H), 2.20(s, 3H), 4.60(b, 1H)[e], 6.8—8.0(m, 9H)	72.88 (72.46)	6.00 (6.08)	
36	[a]3500 1755 1680	[c]0.98(t, J=7 Hz, 3H), 1.04(d, J=7 Hz, 3H), 1.14(t, J=7 Hz, 3H), 1.82(s, 3H), 3.61 (b, 1H)[e], 7.27(d, J=8 Hz, 2H), 7.86(d, J=8 Hz, 2H)	— (69.44)	— (7.97)	
37	[b]3485 1670	[d]1.57(s, 3H), 3.47(d, J=17 Hz, 1H), 3.59 (d, J=17 Hz, 1H), 4.76(b, 1H)[e], 7.2—8.1(m, 9H)	67.20 (67.36)	5.33 (5.30)	4.96 (4.91)

a) Neat, b) KBr disk, c) in CCl_4, d) in $CDCl_3$, e) exchanged with D_2O.

siloxy-1-pentene (**41**) [IR (neat): 1620 cm^{-1}. NMR (CCl_4): δ 0.17 (s, 9H), 1.20 (d, J=7 Hz, 3H), 2.30 (s, 3H), 3.90 (s, 2H), 7.34 (s, 4H)] and fraction 2, 2.2 g bp 156—159 °C/3.2 mmHg, containing **41** and an unknown compound.

*Preparation of 2-Hydroxy-2-methyl-6-*p*-tolyl-4-heptanone (**42**).* To a dichioromethane (40 ml) solution of acetone (0.580 g, 10 mmol) and $TiCl_4$ (1.89 g, 10 mmol) was added a dichloromethane (10 mmol) solution of silyl enol ether (**41**) (1.24 g, 5 mmol) at 0 °C, and the reaction mixture was stirred for 1 h. After the usual work-up, the resulting crude product was analyzed by chromatography on silica gel. Elution with dichloromethane afforded 1.03 g (88%) of 2-hydroxy-2-methyl-6-*p*-tolyl-4-heptanone (**42**) [IR (neat): 3470, 1700 cm^{-1}. NMR (CCl_4): δ 1.10 (s, 6H), 1.21 (d, J=7 Hz, 3H), 2.30 (s, 3H), 2.37 (s, 2H), 2.59 (d, J=7 Hz, 2H), 3.0—3.5 (m, 1H), 3.35 (b, 1H), 7.05 (s, 4H)].

*Preparation of 2-Methyl-6-*p*-tolyl-2-heptene-4-one.* (**43**: ar-turmerone). A benzene (50 ml) solution of 2-hydroxy-2-methyl-6-*p*-tolyl-4-heptanone (**42**) (0.468 g, 2 mmol) was refluxed for 1 h in the presence of *p*-TsOH (0.2 g) with a conventional Dean Stark apparatus. After removal of the solvent, the resulting crude product was analyzed by chromatography on silica gel. Elution with benzene gave 0.420 g (97%) of 2-methyl-6-*p*-tolyl-2-heptene-4-one (**43**: ar-turmerone) [Found: C, 83.09; H, 9.35%. Calcd for $C_{15}H_{20}O$: 83.28; H, 9.32%. IR (neat): 1690, 1620 cm^{-1}. NMR (CCl_4): δ 1.23 (d, J=7 Hz, 3H), 1.80 (s, 3H), 2.30 (s, (3H), 2.56 (d, J=7 Hz, 2H), 3.0—3.5 (m, 1H), 5.93 (s, 1H), 7.06 (s, 4H)].

The author wishes to express his thanks to Professor Teruaki Mukaiyama of Tokyo University for his continuous guidance and helpful discussions. The author is also grateful to Mr. Akihiko Ostuka, vice president of Otsuka Pharmaceutical Co., Ltd., for support and encouragement throughout this work.

References

1) T. Mukaiyama, K. Narasaka, and K. Banno, *Chem. Lett.*, **1973**, 1011.
2) T. Mukaiyama, K. Banno, and K. Narasaka, *J. Am. Chem. Soc.*, **96**, 7503 (1974).
3) K. Banno and T. Mukaiyama, *Chem. Lett.*, **1975**, 741.
4) H. O. House, O. S. Crumrine, A. Y. Teranishi, and H. D. Olmstead, *J. Am. Chem. Soc.*, **95**, 3310 (1973).
5) G. Wittig and A. Hesse, *Org. Synth.*, **50**, 66 (1970).
6) Acetal, enol ether, thioenol ether, and enol acetate react with silyl enol ether or a carbonyl compound. T. Mukaiyama and M. Hayashi, *Chem. Lett.*, **1974**, 15; T. Mukaiyama, E. Kitazawa, and K. Saigo, *ibid.*, **1975**, 569; T. Mukaiyama, K. Kamio, and K. Narasaka, *ibid.*, **1974**, 565; T. Mukaiyama, T. Izawa, and K. Saigo, *ibid.*, **1974**, 323.
7) Thioacetal easily reverts to the carbonyl compound upon treatment with $CuCl_2$ and CuO in acetone. K. Narasaka, T. Sakashita, and T. Mukaiyama, *Bull. Chem. Soc. Jpn.*, **43**, 2632 (1970).
8) A. St. Pfau, *Helv. Chim. Acta*, **15**, 1482 (1932).
9) H. Rupe, G. Clar, A. St. Pfau, and P. Plattner, *Helv. Chim. Acta*, **17**, 372 (1934).
10) H. Rupe and A. Gassmann, *Helv. Chim. Acta*, **19**, 569 (1936).
11) J. Cologe and J. Chambion, *C. R. Acad. Sci.*, **222**, 557 (1946).
12) H. O. House, L. J. Czuba, and H. D. Olmstead, *J. Org. Chem.*, **34**, 2324 (1969).
13) M. Araki, S. Sakata, H. Takei, and T. Mukaiyama, *Bull. Chem. Soc. Jpn.*, **47**, 1777 (1974).
14) C. W. Yoho and R. Levine, *J. Am. Chem. Soc.*, **74**, 5597 (1952).

A Synthesis of Diosphenols[1]

Masao ŌHASHI†, Seiichi INOUE, and Kikumasa SATO*

Department of Applied Chemistry, Faculty of Engineering, Yokohama National University, Minami-ku, Yokohama 233

†*Chemical Laboratory, Seimi Chemical Co., Ltd., Chigasaki, Chigasaki-shi, Kanagawa 253*

(Received February 21, 1976)

A new synthesis of diosphenols (**1** and **2**) is described. The oxidation of 2-isopropylcyclohexanone with copper(II) chloride gave the corresponding α-diketone (**8**), which was then methylated to afford diosphenol (**1**) together with a considerable amount of isodiosphenol (**2**). In particular, pure **2** has been isolated and the characteristics of **2** are also presented.

The monoterpenoid diosphenol(*buccocamphor*)(2-hydroxy-1-*p*-menthen-3-one) (**1**) has been found in the essential oil of various *Barosma* or *Mentha* species.[2] **1** has been synthesized from many terpenoid derivatives: l-menthone,[3,4] carvomenthone,[4] piperitone,[4] and piperitone oxide [5]

Diosphenol seems to exist as a mixture of two enolate forms, **1** and **2**.

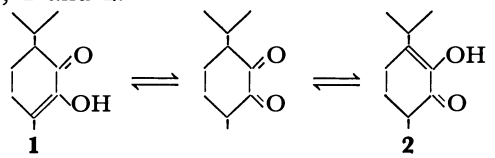

1 **2**

Recently, Shibata *et al.*[6] reexamined the method of Macbeth and Robertson[3d] and isolated the reverse enol form; isodiosphenol (3-hydroxy-3-*p*-menthen-2-one) (**2**). But the details of **2** have not yet been reported.

Now we wish to report a convenient synthesis of **1** and **2** from ethyl 1-isopropyl-2-oxocyclohexanecarboxylate (**3**)[7] which is easily obtained by the condensation of ethyl cyclohexanecarboxylate with isopropyl iodide.

When **3** was refluxed with selenium dioxide in aqueous dioxane for 35 h, 6-ethoxycarbonyl-6-isopropyl-2-hydroxy-2-cyclohexen-1-one (**4**) was obtained. Compound **4** easily reacted with morpholine and formalin in dioxane at room temperature to afford a Mannich base, which was then hydrogenolyzed with zinc powder in acetic acid to give 6-ethoxycarbonyl-6-isopropyl-2-hydroxy-3-methyl-2-cyclohexen-1-one (**5**). In order to get **1**, we examined the deethoxycarbonylization of **5**

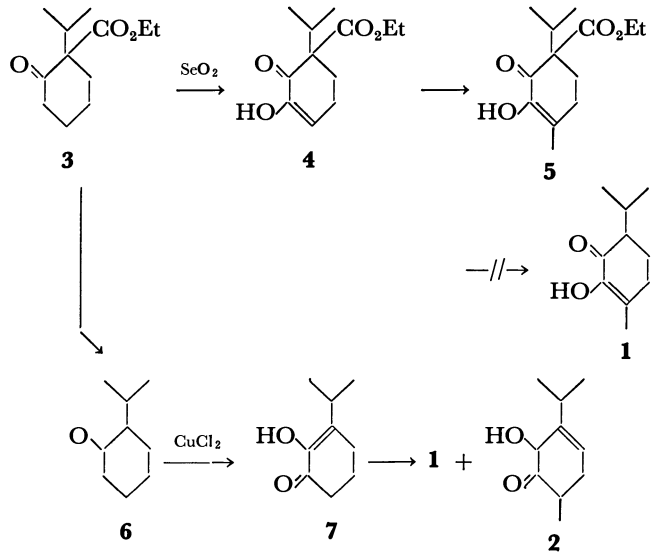

3 **4** **5** **1** **6** **7** **2**

* To whom all correspondence should be addressed.

with aqueous sulfuric acid, hydrochloric acid, or with lithium iodide dihydrate. However, in no case could **1** be obtained. The difficulty in hydrolysis of **5** is supposed to be due to the steric hindrance of the isopropyl group.[8] Then we examined the hydrolysis of **3**.

Although the attempted deethoxycarbonylization of **3** with sulfuric acid, barium hydroxide, or potassium hydroxide[9] was unfavorable, the refluxing of **3** with lithium iodide dihydrate in dimethylformamide gave 2-isopropylcyclohexanone (**6**) in excellent yield(91%).

Treatment of **6** with 4 molar amounts of copper(II) chloride in 50% acetic acid under reflux for 3 h afforded 2-hydroxy-3-isopropyl-2-cyclohexen-1-one (**7**) in moderate yield(61%). The structure of **7** was assigned on the basis of its IR, NMR, and UV spectra, and by elemental analysis. Then we examined the methylation[10] of **7** for the synthesis of **1** and **2**.

3-Alkyl-2-hydroxy-2-cycloalkenones easily reacted with morpholine and formalin in dioxane at room temperature to give corresponding bis-Mannich base.[11] Under the same conditions, compound **7** failed to react even when warmed at reflux, apparently because of the steric hindrance of the isopropyl group. However, **7** reacted with both morpholine hydrochloride and formalin in water under reflux to give the Mannich base, which was then hydrogenolyzed with zinc powder in acetic acid at 75—80 °C for 7 h, and gave a mixture of **1** and **2** in 31% yield. The ratio of the two components was **1**/**2**=62/38. Pure **1** and **2** can be isolated by crystallization or preparative GLC. The UV spectra of these two isomers in 95% ethanol slightly differ from each other: namely, **2** is bathochromic by *ca.* 1.0 nm. This result is parallel to the observations on 2-hydroxy-3-methyl-2-cyclohexen-1-one[11] and **7**. In the NMR spectra of **1** and **2**, the characteristic signals due to the methine proton in the isopropyl group and the methyl protons clearly differ from each other and are consistent with the assigned structures **1** and **2**, respectively. In mass spectra, a distinct difference between **1** and **2** is observed at *m/e* 125 (M^+—isopropyl) and 126 (association of the hydrogen shift with 125): the intensities of the two fragments are the reverse of each other. (see Experimental Section)

Finally, it should be noted that a fair amount of isodiosphenol (**2**) is formed along with **1** in the present reaction conditions and pure **2** is comparatively stable[12] at room temperature.

Experimental

All the points are uncorrected. The IR spectra were recorded with a Hitachi Model 215 spectrophotometer, and the UV spectra with a Hitachi Model EPS-3T spectro-

photometer. The NMR spactra were obtained on a JEOL Model C-60H spectrometer, with tetramethylsilane as the internal reference. The mass spectra were determined on a Hitachi RMU-6E spectrometer.

*Ethyl 1-Isopropyl-2-oxocyclohexanecarboxylate (**3**).* This substance was prepared in 74% yield according to Ref. 7.

*6-Ethoxycarbonyl-2-hydroxy-6-isopropyl-2-cyclohexen-1-one (**4**).* A mixture of **3** (8.48 g, 40 mmol), selenium dioxide (8.8 g, 80 mmol), dioxane (100 ml), and water (30 ml) was stirred for 35 h under reflux. After cooling, the deposited selenium was filtered off, the solvent was distilled, and the residue was extracted with chloroform. After drying, the extract was concentrated and the residue was distilled to give the crude product **4** (3.1 g); bp 99—130 °C/0.4 mmHg. Redistillation afforded 1.60 g (17.7%) of pure **4**; bp 99—103 °C/0.3 mmHg. IR (neat) 3420 (O–H), 1730, w. 1710, 1675 (C=O), 1620 cm^{-1} (C=C). NMR (CCl_4) δ 0.78 (3H, d, J=7.0 Hz), 0.86 (3H, d, J=7.0 Hz), 1.26 (3H, t, J=7.0 Hz), 1.6—2.7 (5H, m), 4.16 (2H, q, J=7.0 Hz), 5.60 (1H, broad s), 6.95 (1H, m); mass *m/e*; 226 (M^+), 41 (100%).

*6-Ethoxycarbonyl-2-hydroxy-6-isopropyl-3-methyl-2-cyclohexen-1-one (**5**).* To a mixture of **4** (1.30 g, 5.75 mmol), dioxane (5 ml), and morpholine (0.50 g, 5.75 mmol), formalin (0.464 g, 5.75 mmol) in dioxane (1 ml) was added at 3—4 °C and the mixture was then stirred for 20 h at room temperature. After removal of the dioxane *in vacuo*, curde Mannich base (2.0 g) was obtained. To this Mannich base, acetic acid (18 ml) and zinc powder (1.9 g) were added, and the mixture was then stirred for 7 h at 72—74 °C. After the zinc had been filtered off and the acetic acid had been removed under reduced pressure, water (10 ml) was added. After extraction with chloroform and drying with magnesium sulfate, the solvent was evaporated and the residue was chromatographed on a silica gel column. Elution with benzene–ethyl acetate (10 : 1) yielded 0.345 g (Y=25%) of **5**; which was distilled at 100—110 °C/0.3 mmHg. IR (neat) 3370 (O–H), 1740, w. 1710, 1660 (C=O), 1643 cm^{-1} (C=C); NMR (CCl_4) δ 0.75 (3H, d, J=7.0 Hz), 0.88 (3H, d, J=7.0 Hz), 1.25 (3H, t, J=7.0 Hz), 2.02 (3H, s), 2.3—3.0 (5H, m), 4.13 (2H, q, J=7.0 Hz); mass *m/e*; 240 (M^+), 41 (100%).

*2-Isopropylcyclohexanone (**6**).* To a stirred, slightly boiling solution of lithium iodide dihydrate (16.7 g, 0.099 mol) in dimethylformamide (40 ml) was added ethyl 1-isopropyl-2-oxocyclohexanecarboxylate (7.0 g, 0.033 mol) dissolved in dimethylformamide (5 ml) over a period of 5 min under nitrogen atmosphere. The mixture was then refluxed for 45 h. The resulting mixture was diluted with aqueous hydrochloric acid and extracted with ether. The extract, after washing with water and drying over magnesium sulfate, was concentrated and the residual oil was distilled to give 4.2 g (Y=91%) of **6**; bp 81—85 °C/16 mmHg (lit,[8] bp 80 °C/10 mmHg).

*2-Hydroxy-3-isopropyl-2-cyclohexen-1-one (**7**).* A mixture of **6** (1.95 g, 14 mmol), copper(II) chloride (7.53 g, 56 mmol), acetic acid (15.3 ml), and water (17.4 ml) was stirred for 3 h under reflux. After cooling, the mixture was saturated with ammonium chloride and extracted with ether. The extract was washed with aqueous ammonium chloride, dried over magnesium sulfate, and concentrated. The residual oil was distilled to give 1.30 g (Y=61%) of **7**; bp 71—73 °C/0.6 mmHg, n_D^{25}=1.4994. IR (neat) 3420 (O–H), 1665 (C=O), 1640 cm^{-1} (C=C); NMR (CCl_4) δ 1.06 (6H, d, J=7.0 Hz), 1.7—2.6 (6H, m), 3.16 (1H, heptet, J=7.0 Hz), 6.14 (1H, s); UV_{max} (95% EtOH) 275.5 nm (ε 9500). Found: C, 70.57; H, 9.24%. Calcd for $C_9H_{14}O_2$: C, 70.10; H, 9.15%. 2,4-Dinitrophenylhydrazone: mp 147—149 °C. Found: C, 54.14; H, 5.34; N, 16.77%. Calcd for $C_{15}H_{18}N_4O_5$: C, 53.89; H, 5.43; N, 16.76%.

*Methylation of **7**: 2-Hydroxy-1-*p*-menthen-3-one (**1**) and 3-Hydroxy-3-*p*-menthen-2-one (**2**).* A mixture of **7** (0.924 g, 6 mmol), morpholine (1.04 g, 12 mmol), concentrated hydrochloric acid (1.25 g, 12 mmol), water (13.8 ml), and formalin (0.973 g, 12 mmol) was stirred for 8 h under reflux. Evaporation of water *in vacuo* gave the crude Mannich base. To this Mannich base, acetic acid (18 ml) and zinc powder (3.2 g) were added, and the mixture was then stirred for 7 h at 75—80 °C. After the zinc had been filtered off and the acetic acid had been removed under reduced pressure, a small amount of water was added. After extraction with ether, washing with saturated aqueous ammonium chloride, and drying with magnesium sulfate, the solvent was evaporated and the residue (647 mg) was chromatographed on a silica gel column (elution with benzene) to give a mixture of **1** and **2** (312 mg, Y=31%, **1** : **2**=62 : 38); these give rise to 6.4 and 5.7 min retention times. (DC-200 column 3 m, 150 °C, He, 1.5 kg/cm^2). When the mixture was allowed to stand in an ice box, **1** precipitated. After filtration and recrystallization from petroleum ether, pure diosphenol (**1**) (82 mg) was obtained. Mp 82—83 °C (lit,[3d] mp 82 °C): IR (KBr) 3400 (O–H), 1665 (C=O), 1640 cm^{-1} (C=O); NMR (CCl_4) δ 0.86 (3H, d, J=7.0 Hz), 0.97 (3H, d, J=7.0 Hz), 1.80 (3H, broad s), 1.8—2.5 (6H, m), 5.99 (1H, s); UV_{max} (95% EtOH) 274 nm (ε 9600); mass *m/e* (%) 168 (M^+, 14), 126 (42), 125 (32), 43 (74), and 41 (100). The filtrate was subjected to the preparative GLC (DC-200 column 1 cm × 2 m, 150 °C, He, 150 ml/min) and pure **2** (50 mg) was obtained as a colorless oil, which boiled at 67—70 °C/0.4 mmHg, n_D^{25}=1.4925. IR (neat) 3420 (O–H), 1665 (C=O), 1640 cm^{-1} (C=C); NMR (CCl_4) δ 1.05 (3H, d, J=7.0 Hz), 1.06 (3H, d, J=7.0 Hz), 1.15 (3H, d, J=7.0 Hz), 1.6—2.5 (5H, m), 3.15 (1H, heptet, J=7.0 Hz), 6.07 (1H, broad s); UV_{max} (95% EtOH) 275 nm (ε 10000); mass *m/e* (%) 168 (M^+, 15), 126 (25), 125 (53), 43 (85), and 41 (100). Found: C, 71.80; H, 9.73%. Calcd for $C_{10}H_{16}O_2$: C, 71.39; H, 9.59%.

References

1) Presented at the 19th Annual Conference of Terpens and Essential Oils, Fukuoka, October, 1975.

2) "Rodd's Chemistry of Carbon Compounds," 2nd ed., Vol II B, Elsevier Publishing Co., Amsterdam (1968), p 202.

3) a) Y. Asahina and S. Mituhori, *J. Pharm. Soc. Jpn.*, **482**. 255 (1922); b) Y. Asahina and S. Kuwada, *ibid.*, **491**, 1 (1923); c) F. Riley, *J. Chem. Soc.*, **1932**, 1875; d) A. K. Macbeth and W. G. P. Robertson, *J. Chem. Soc.*, **1953**, 3512.

4) O. Wallach, *Ann. Chem.*, **437**, 148 (1924); **418**, 37 (1919).

5) R. H. Reitsema and V. J. Varnis, *J. Am. Chem. Soc.*, **78**, 3792 (1956).

6) H. Shibata and S. Shimizu, *Agr. Biol. Chem.*, **38**, 1741 (1974).

7) F. Nerdel, D. Frank, and H. Marschall, *Chem. Ber.*, **100**, 720 (1967).

8) K. Sato, S. Inoue, and M. Ōhashi, *Bull. Chem. Soc. Jpn.*, **47**, 2519 (1974).

9) A. Kötz and A. Michels, *Ann. Chem.*, **350**, 204 (1906).

10) Direct methylation of **7** with two equivalents of lithium diisopropylamide in tetrahydrofuran, followed by the addition of excess methyl iodide, gave a mixture of **1** and **2** in the ratio of 64 : 36 in a poor yield.

11) M. Ōhashi, T. Takahashi, S. Inoue, and K. Sato, *Bull. Chem. Soc. Jpn.*, **48**, 1892 (1975).

12) **2** can be distilled under reduced pressure below 100 °C with no decomposition.

The Abnormal Wallach Rearrangements of 4,4'-Dialkylazoxybenzenes

Ichiro SHIMAO and Shigenori MATSUMURA

Department of Industrial Chemistry, Faculty of Engineering, Toyama University, Takaoka-shi, Toyama 933

(Received February 26, 1976)

The reactions of 4,4'-dialkylazoxybenzenes (**1**) with sulfuric acid afforded 2-alkyl-5-(*p*-alkylphenylazo)phenols (**2**) and 2-alkyl-4-(*p*-alkylphenylazo)phenols (**3**) as novel rearrangement products; in certain cases 4-(*p*-alkylphenylazo)phenols (**4**) were also obtained. The ratios of these azophenols were greatly affected by the alkyl group type. In addition, the reactions gave a very small amount of 5-alkyl-2-(*p*-alkylphenylazo)phenols (**5**), which were considered as normal Wallach rearrangement products.

In 1880, Wallach and Belli[1] found that heating azoxybenzene with sulfuric acid converted it to azobenzene and 4-hydroxyazobenzene. Later, in 1900, Bamberger[2] found that a small amount of 2-hydroxyazobenzene was also formed as a by-product in the reaction. Thereafter, many mechanistic investigations about the Wallach rearrangement have been carried out.[3] But only a few studies have been reported on the Wallach rearrangement of disubstituted azoxybenzenes.[4,5]

The rearrangement reaction of *p,p'*-azoxytoluene (**1a**) with sulfuric acid has been anomalous. Bamberger[6] found that **1a** gave a substance having a melting point of 204 °C in this reaction. In 1936, Parsons and Bailar[7] reported that this reaction afforded some alkali soluble (mp 210—212 °C) and alkali insoluble materials (mp 208—210 °C) which both contained a hydroxyl group; they suggested without any sure evidence that the alkali soluble material was 3-hydroxy-4,4'-dimethylazobenzene and the alkali insoluble material was 4-methyl-4'-hydroxymethylazobenzene. Subsequently, Gore and Hughes[4] reported the isolation of a substance having the same melting point in this reaction, and they showed that the two products obtained by Parsons and Bailar[7] were identical. They also proposed, carelessly, that this substance was 2-hydroxy-4,4'-dimethylazobenzene. The result of Gore and Hughes has been widely accepted and cited.[8]

On the other hand, Cumming and Ferrier[9] reported that the irradiation of **1a** gave 5-methyl-2-(*p*-tolylazo)-phenol (**5a**) (mp 150 —151 °C). It is generally recognized that 2-hydroxyazobenzenes are exclusively obtained by the photorearrangement of azoxybenzenes. Consequently, on the basis of the substantial difference of their melting points, it appears to be extremely doubtful that the reaction of **1a** with sulfuric acid gave **5a** as the main product.

In the present investigation, we confirm the structure of the rearrangement product of **1a**, and deal with the reactions of some 4,4'-dialkylazoxybenzenes (**1**) and some other disubstituted azoxybenzenes with sulfuric acid.

Results and Discussion

The investigation of the Wallach rearrangement of disubstituted azoxybenzenes have been insufficient. Thus, in order to compare with the reaction of **1**, some examples of the normal Wallach rearrangement were carried out; the results are shown in Table 1. The unsubstituted and 3,3'-disubstituted azoxybenzenes (**6**) gave 4-hydroxyazobenzenes (**7**) as the major products and 2-hydroxyazobenzenes (**8**) as by-products, and 4,4'-dihaloazoxybenzenes (**9**) gave **8**. The azoxybenzenes were reduced to a considerable extent to yield the corresponding azobenzenes (**10**), and some resinous meterial was also found.

Table 1. Reactions of azoxybenzenes $RC_6H_4N(O)NC_6H_4R$, with sulfuric acid(85%)
(Reaction conditions: 50 °C, 30 min)

R	Yield (%)			
	6	**10**	**7**	**8**
H	45	7	42	1.6
3,3'-Me_2	29	14	43	0.8[a]
3,3'-Cl_2[b]	75		16	1.0[c]
4,4'-Cl_2[b]		58		13
4,4'-Br_2[b]		59		15

a) Mixture of **8a** and **8b**. b) 92% H_2SO_4.
c) 4-Chloro-2-(*m*-chlorophenylazo)phenol.

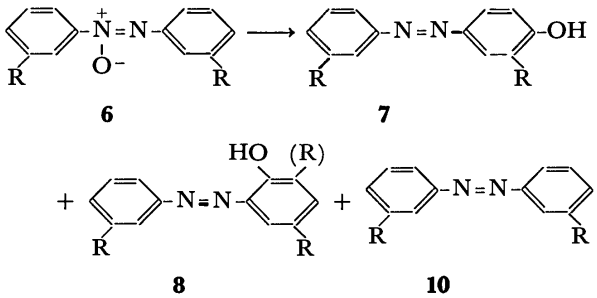

6 **7**

8 **10**

The 2-hydroxyazo compound **8** obtained from *m,m'*-azoxytoluene (**6a**) was a mixture of 4-methyl-2-(*m*-tolylazo)phenol (**8a**) and 6-methyl-2-(*m*-tolylazo)pnenol (**8b**). The ratio of **8a** to **8b** was determined by gas chromatography to be 2.5 : 1. On the other hand, the compound **8** obtained from 3,3'-dichloroazoxybenzene (**6b**) was 4-chloro-2-(*m*-chlorophenylazo)phenol.

Table 2. Reaction of 4,4'-dialkylazoxybenzenes **1** with 85% sulfuric acid (50 °C, 30 min)

	R	Yield (%)				
		1	**11**	**2**	**3**	**4**
1a	Me	3	18	21		
1b	Et	3	22	8	22	2
1c	*n*-Pr	4	25	19	4	6
1d	*i*-Pr	4	30		2	33
1e	*t*-Bu	7	33			51

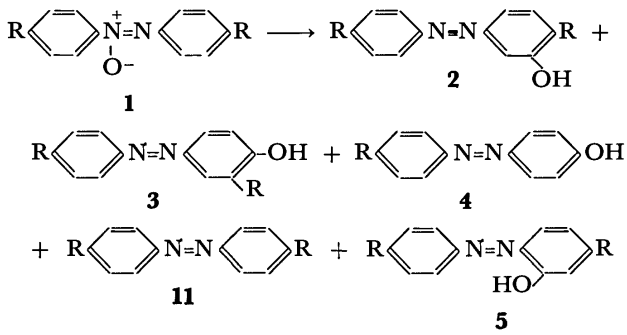

1—5, 11	R
a	Me
b	Et
c	*n*-Pr
d	*i*-Pr
e	*t*-Bu

Unlike the photorearrangement,[10] in the reaction with sulfuric acid the isomer ratios of **8** were affected by the substituents of **6**.

The compounds **1** were treated with 85% sulfuric acid at 50 °C and the reaction products were separated by column chromatography. The results are shown in Table 2.

As in the reactions of 3,3'- and 4,4'-dichloroazoxybenzenes, **1a** reacted faster than the *meta* isomer **6a**. Such results can probably be attributed to the stabilization effect of these *p*-substituents on the cationic intermediate.

The main rearrangement product of **1a** was 2-methyl-5-(*p*-tolylazo)phenol (**2a**). This compound **2a** was acetylated with acetic anhydride; then the structure of **2a** acetate was confirmed by a comparison with the sample obtained by the following synthesis:

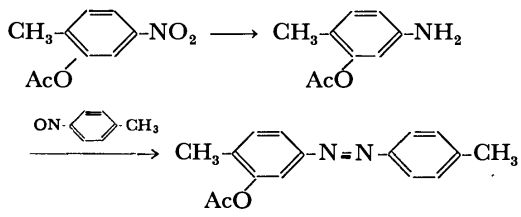

2a acetate

The melting point(211—212 °C) of **2a** was close to those[4,7] reported previously for the main product of the Wallach rearrangement of **1a**. Therefore it is evident that the conclusion of Gore and Hughes[4] is incorrect.[11] Although 5-alkyl-2-(*p*-alkylphenylazo)-phenols (**5**) appear to be the normal Wallach rearrangement products of **1**, **5a** was formed in only 0.2% yield. It is well-known that an irradiation of **1a** gives **5a**.[9,10] In order to conform the structure of **5a**, it was independently prepared by the condensation of 4-methyl-2-benzyloxyaniline and *p*-nitrosotoluene and then the debenzylation with hydrobromic acid. The gas chromatographic analysis showed that a trace amount of **5** was formed in the reaction of **1b—e**.

The 4,4'-diethylazoxybenzene (**1b**) and 4,4'-dipropylazoxybenzene (**1c**) afforded the corresponding 3-hydroxyazo compounds, **2b** and **2c**, respectively. Furthermore, **1b** and **1c** rearranged peculiarly to the 2-alkyl-4-(*p*-alkylphenylazo)phenols, **3b** and **3c**, respectively. The propyl group did not rearrange to an isopropyl group in this rearrangement.

The reactions of **1d** and **1e** yielded 4-(*p*-alkylphenylazo)phenols, **4d** and **4e**, respectively as the main products. Recently, Cox and Buncel[3] briefly communicated the formation of the same products. The rearrangement accompanied by the dealkylation was also ob-

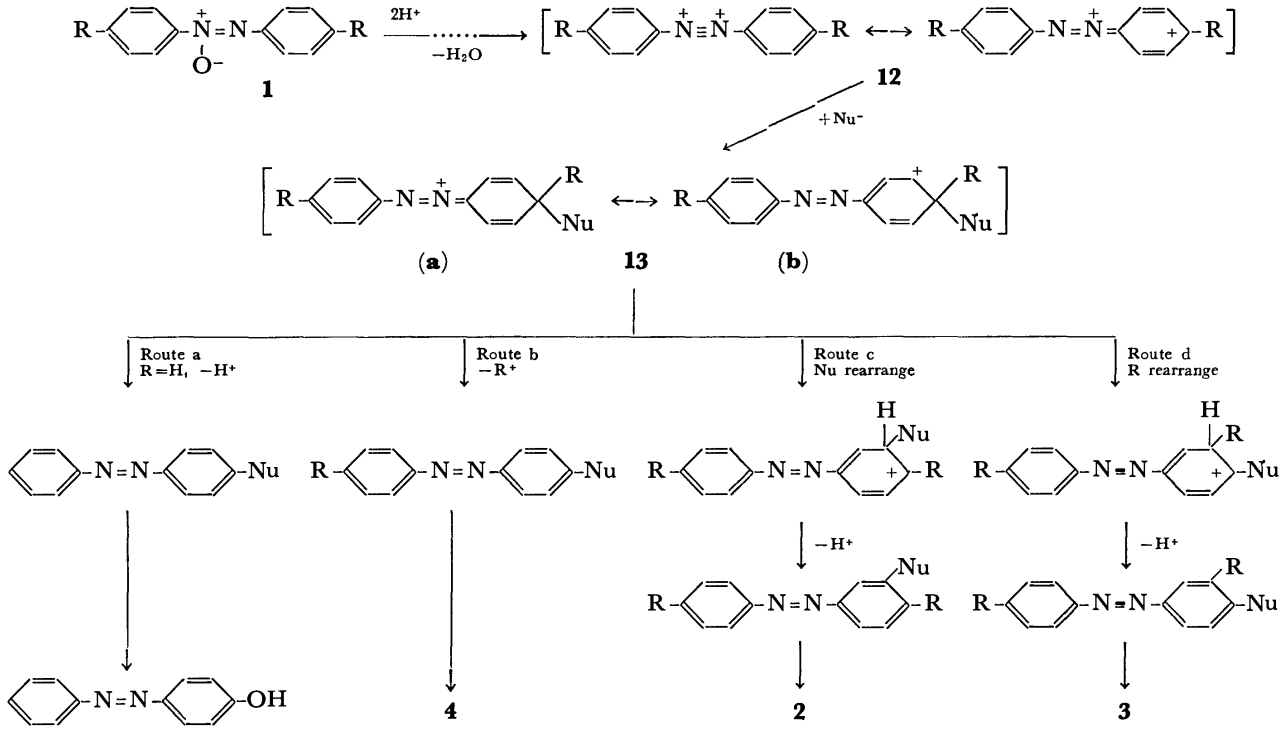

Scheme 1.

served in the reaction of **1b** and **1c**. In the reaction of **1d**, **3d** was formed as a by-product.

The mechanism shown in Scheme 1 accounts nicely for the formation of the various azophenols, except **5**: First, **1** undergoes diprotonation and then dehydration to yield the dicationic intermediate (**12**). Subsequently the nucleophile, probably HSO_4^-, attacks the dication to form the complex (**13**). When R=H, the deprotonation occurs to afford the 4-hydroxyazobenzenes (Route a). This mechanism has been proposed as a pathway of the Wallach rearrangement.[3]

On the other hand, the compounds **4** were formed by the separation of a alkyl carbonium ion from the complex **13** (Route b). When the carbonium ion is more stable, such as an isopropyl or *tert*-butyl group, the reaction proceeds preferentially by this route. In route c, the nucleophile group migrates to its *ortho* position in the complex **13** and then the deprotonation occurs to yield **2**. The compound **1a** rearranges mostly by this route. In Route d, the alkyl group migrates to its *ortho* position in **13** and then the deprotonation occurs. The compounds, **1b**, **1c**, and **1d**, which have the primary or secondary alkyl groups, rearrange by this route to form **3**.

The nucleophile attacks mostly the carbon atom attached the alkyl group. Thus the 2-hydroxyazo compounds **5** were only slightly formed. This can probably be attributed to the fact that the electron-releasing effect of the alkyl group accelerates the formation of the dicationic intermediate **12** and therefore the formation of **5** is hindered. Shemyakin and coworkers showed that the formation of 2-hydroxyazobenzenes appears to proceed by an intramolecular pathway different from that in the formation of 4-hydroxyazobenzenes.[12]

The migration of the alkyl group or the nucleophile group may be caused by the positive charge on the *ortho* carbon atom of complex **13b**. Although the methyl group does not migrate, the ethyl and propyl groups do. This is probably due to the increasing electron density on the α-carbon atom by the electron-releasing effect of the alkyl group. The secondary and tertiary alkyl groups, in which the effect of the alkyl group is larger than that of the primary alkyl group, leave as the carbonium ion (Route b). It is of interest that the reaction route is greatly affected by the type of the alkyl group. These reactions appear to be explained by the monocationic mechanism[3] proposed for the Wallach rearrangement; however, the formation of **2** and **3** may be more reasonably interpreted by the dicationic mechanism.

In analogy with the usual Wallach rearrangement, considerable amounts of azobenzenes were formed in these reactions. The formation of azobenzenes has been known for a long time; however, the mechanism is still not elucidated.[13] In addition, the reaction afforded a small amount of some unidentified products. Further work is under way to isolate and identify these products and to determine the mechanism of the formation of azobenzenes.

Experimental

The IR spectra were recorded with a JASCO IRA-1 spectrophotometer. The NMR spectra were obtained with a JEOL MH-100 spectrometer using TMS as the internal standard. The gas chromatographic analysis was carried out using a Shimadzu GC-2C apparatus on a 0.75 m×3 mm column packed with 2% Silicone OV-225. The melting points are uncorrected.

Materials. 4,4′-Dipropyl- and diisopropylazoxybenzenes (**1c** and **1d**) were prepared by the oxidation of the corresponding azo compounds. **1c** mp 63—64 °C. Found: C, 76.56; H, 7.90; N, 9.97%. Calcd for $C_{18}H_{22}N_2O$: C, 76.56; H, 7.85; N, 9.92%. **1d** mp 62—63 °C (lit,[14] 62—63 °C). The other azoxybenzenes were prepared according to the method given in the previous work.[14]

Reaction of 4,4′-Dialkylazoxybenzenes (1) with Sulfuric Acid. A solution of **1** (0.02 mol) in 85% sulfuric acid (12 ml) was heated for 30 min at 50 °C. The reaction mixture was poured into cold water, and then extracted with chloroform

Table 3. Syntheses of azophenols, **3** and **4**, R^1-C$_6$H$_4$-N=N-C$_6$H$_3$(R^2)-OH

	R^1	R^2	Yield %	Mp °C	Molecular formula	Found (Calcd) % C	H	N
3b	Et	Et	34	119—120		75.82	7.20	11.29
					$C_{16}H_{18}N_2O$	(75.56)	(7.13)	(11.02)
3c	*n*-Pr	*n*-Pr	20	56—58		76.39	8.08	9.75
					$C_{18}H_{22}N_2O$	(76.56)	(7.85)	(9.92)
3d	*i*-Pr	*i*-Pr	21	86—87		76.60	7.90	9.98
					$C_{18}H_{22}N_2O$	(76.56)	(7.85)	(9.92)
4b	Et	H	29	121—122		74.30	6.12	12.50
					$C_{14}H_{14}N_2O$	(74.31)	(6.24)	(12.38)
4c	*n*-Pr	H	18	76—77		75.04	6.67	11.43
					$C_{15}H_{16}N_2O$	(74.97)	(6.71)	(11.66)
4d	*i*-Pr	H	30	114—115		74.87	6.67	11.83
					$C_{15}H_{16}N_2O$	(74.97)	(6.71)	(11.66)
4e	*t*-Bu	H	56	127—128[a]				

a) Lit,[15] 125 °C.

or benzene. The extract was washed with water. After removal of the solvent, the residue was chromatographed on a silica gel column using benzene as a solvent. Unless otherwise noted, all the products were identified by a comparison of these mp and IR spectra with those of authentic samples.

The first fraction gave the crude **11**, contaminated by **1** and **5**, as analyzed by gas chromatography. In the reaction of **1a**, this fraction was again chromatographed on alumina using benzene as a solvent, and the residue on the column was extracted with methanol. The extract gave **5a** mp 150—151 °C (yield 0.2%).

The second fraction gave **2**, which was recrystallized from benzene. **2a** mp 211—212 °C. Found: C, 74.38; H, 5.95; N, 12.26%. Calcd for $C_{14}H_{14}N_2O$: C, 74.31; H, 6.24; N, 12.38%. **2b** mp 152.5—153 °C. Found: C, 75.35; H, 7.06; N, 11.25%. Calcd for $C_{16}H_{18}N_2O$: C, 75.56; H, 7.13; N, 11.02%. **2c** mp 126.5—127 °C. Found: C, 76.55; H, 8.01; N, 9.92%. Calcd for $C_{18}H_{22}N_2O$: C, 76.56; H, 7.85; N, 9.92%.

The azophenols, **2a**, **2b**, and **2c**, were acetylated with acetic anhydride and pyridine. The products were recrystallized from hexane. Acetate of **2a** mp 105—106 °C. Acetate of **2b** mp 78.5—80 °C. Acetate of **2c** mp 46—47 °C. Found: C, 74.27; H, 7.34; N, 8.46%. Calcd for $C_{20}H_{24}N_2O_2$: C, 74.04; H, 7.46; N, 8.64%. The mp and the IR and NMR spectra of the acetates of **2a** and **2b** were identical with those of an authentic sample prepared independently. The **2c** acetate was identified by a comparison of its IR and NMR spectra (particularly, the characteristic signals due to aryl protons) with those of the **2a** and **2b** acetates. **2c** acetate: IR (KBr): 1750 (C-O), 1220 cm^{-1} (CO-O-Ar); NMR ($CDCl_3$): δ 1.00 (t, $2CH_3$), 1.68 (m, $2CH_2$), 2.35 (s, CH_3-COO), 2.58, 2.68 (t, $2CH_2Ar$), 7.3—8.0 (m, ArH).

The third fraction gave **3**. These products were recrystallized from hexane or ethanol-water. **3b** mp 116—117 °C. **3c** mp 55—56 °C. **3d** mp 86—88 °C.

The fourth fraction gave **4**, which was recrystallized from hexane. **4b** mp 122—123 °C. **4d** mp 115—116 °C. **4e** mp 127—128 °C. Since **4c** was impure, the crude **4c** was acetylated by the usual method. After purification by column chromatography (silica gel, benzene), recrystallization from hexane afforded **4c** acetate mp 80—81 °C.

The other fractions gave a small amount of unidentified substances.

*Preparation of the Authentic Samples. (A) 2-Alkyl-4-(*p-*alkylphenylazo)phenols (3) and 4-(*p-*Alkylphenylazo)phenols (4):* These azophenols were prepared by diazocoupling of the corresponding phenols and diazonium salts. These were purified by the use of column chromatography on silica gel and recrystallization from hexane or hexane-benzene. The results are shown in Table 3.

*(B) 5-Methyl-2-(*p-*tolylazo)phenol (5a):* The azophenol **5a** was obtained by the irradiation of the ethanolic solution of **1a**, and **5a** was also prepared by the method previously reported for 6-chloro-2-(3-chlorophenylazo)phenol.[16] 4,4′-Dimethyl-2-benzyloxyazobenzene, mp 95—96 °C (yield, 20%), Found: C, 79.90; H, 6.60; N, 8.85%. Calcd for $C_{21}H_{20}N_2O$: C, 79.71; H, 6.37; N, 8.85%. The **5a** mp 151—152 °C (yield, 69%).

(C) Acetate of 2a: 3-Acetoxy-4-methylaniline was prepared by catalytic hydrogenation of 2-acetoxy-4-nitrotoluene. Mp 78—79 °C. Found: C, 65.53; H, 6.85; N, 8.63%. Calcd for $C_9H_{11}NO_2$: C, 65.44; H, 6.71; N, 8.48%.

A solution of the acetoxyaniline (0.67 g) and *p*-nitrosotoluene (0.49 g) in acetic acid was allowed to stand overnight at room temperature. The reaction mixture was poured into water, and extracted with benzene. After removal of the solvent, the extract was chromatographed on silica gel (solvent: benzene). The third fraction was recrystallized from hexane to give 3-acetoxy-4,4′-dimethylazobenzene (**2a** acetate) mp 104—105 °C. Found: C, 71.44; H, 5.79; N, 10.82%. Calcd for $C_{16}H_{16}N_2O_2$: C, 71.62; H, 6.01; N, 10.44%.

2b acetate was prepared by the same method. Mp 78—79 °C. Found: C, 72.82; H, 6.86; N, 9.38%. Calcd for $C_{18}H_{20}N_2O_2$: C, 72.95; H, 6.80; N, 9.45%.

References

1) O. Wallach and E. Belli, *Ber.*, **13**, 525 (1880).
2) E. Bamberger, *Ber.*, **33**, 3192 (1900).
3) R. A. Cox and E. Buncel, "The Chemistry of the Hydrazo, Azo and Azoxy Groups," ed. by S. Patai, John Wiley & Sons, New York (1975), p. 808, and references cited therein.
4) P. H. Gore and G. K. Hughes, *Aust. J. Sci. Res.*, **3A**, 136 (1950).
5) P. H. Gore and G. K. Hughes, *Aust. J. Sci. Res.*, **4A**, 185 (1951).
6) E. Bamberger, *Ber.*, **44**, 1967 (1911).
7) T. Parsons and J. C. Bailar, *J. Am. Chem. Soc.*, **58**, 268 (1936).
8) K. H. Schündehütte, "Houben-Weyl Methoden der Organisches Chemie," Bd X/3, (1965), p. 773.
9) W. M. Cumming and G. S. Ferrier, *J. Chem. Soc.*, **127**, 2374 (1925).
10) R. Tanikaga, *Bull. Chem. Soc. Jpn.*, **41**, 2151 (1968).
11) Cox and Buncel[3] suggested the formation of 4-methyl-4′-hydroxymethylazobenzene, as previously reported by Parsons and Bailar[7] on the basis of the reaction of hexamethylazoxybenzene (*Can. J. Chem.*, **51**, 3143 (1973)). However, this compound was not found.
12) a) M. M. Shemyakin, T. E. Agadzhanyan, V. I. Maimind, and R. V. Kudryavtsev, *Izv. Akad. Nauk SSSR, Ser. Khim*, **1963**, 1339; *Chem. Abstr.*, **59**, 12619b (1963). Although they reported the anomalous behavior of **1a**, this is probably due to the fact that the compound was not **5a** but **2a**; b) C. S. Hahn, K. W. Lee, and H. H. Jaffé, *J. Am. Chem. Soc.*, **89**, 4975 (1967).
13) B. T. Newbold, Ref., 3, p. 621.
14) I. Shimao, *Nippon Kagaku Kaishi*, **1974**, 515.
15) D. C. Colinese, D. A. Ibbitson, and C. W. Stone, *J. Chem. Soc., B*, **1971**, 570.
16) I. Shimao and H. Hashidzume, *Bull. Chem. Soc. Jpn.*, **49**, 754 (1976).

The Formation and Reaction of Carbonyl Ylide. The Copper Chelate-catalyzed Decomposition of 1-(Diazoacetyl)fluorenone in the Presence of Ethylenic and Acetylenic Compounds

Toshikazu IBATA,* Tadayuki MOTOYAMA, and Masashi HAMAGUCHI
Department of Chemistry, College of General Education, Osaka University, Toyonaka, Osaka 560
(Received March 15, 1976)

1,3-Dipolar cycloadducts were obtained by the copper chelate-catalyzed decomposition of 1-(diazoacetyl)-fluorenone in the presence of acetylenic and ethylenic dipolarophiles. The reaction proceeded *via* intermediate carbonyl ylide (**3**), which has been generated by the carbene-carbonyl reaction of **2**. The cycloaddition of **3** with ethylenic dipolarophiles was determined to proce d stereospecifically.

The thermolysis[1] and photolysis[2] of epoxides with electron-withdrawing groups, the thermolysis of 1,3,4-oxadiazolines,[3] and the reaction of carbenes with carbonyl compounds[4,5] have been known to be the general method of the formation of carbonyl ylides. In particular, the intramolecular carbene-carbonyl reaction has been recognized as one of the most convenient methods of the formation of cyclic carbonyl ylides.[5-7] For example, as the first stable five-membered cyclic carbonyl ylide, isomünchnon was obtained by the $Cu(acac)_2$ catalyzed decomposition of *N*-methyl-*N*-(diazo-*p*-nitrophenylacetyl)benzamide.[6] As a result of a continuing study of the intramolecular carbene-carbonyl reaction, we wish now to report the formation of carbonyl ylide by the copper chelate-catalyzed decomposition of 1-(diazoacetyl)fluorenone (**1**) and its cycloaddition with acetylenic and ethylenic dipolarophiles.

Results and Discussion

Cycloaddition with Acetylenic Dipolarophiles. When 1-(diazoacetyl)fluorenone (**1**) was decomposed in the presence of a 1.5 molar amount of dibenzoylacetylene and a catalytic amount of $Cu(acac)_2$ in absolute benzene at 80 °C, a cycloadduct (**4a**; $R_1=R_2=COPh$) was obtained in an 89% yield. The IR spectrum of **4a** shows a carbonyl band of cyclic ketone at 1704 cm^{-1} besides that of the benzoyl absorption at 1659 cm^{-1}, as is shown in Table 1. The methine proton, H_a, of **4a** shows a singlet at 4.22 τ which is at a field higher by 0.5 τ than those of other adducts with acetylenic dipolarophiles because of the shielding effect of the benzoyl group at the adjacent carbon. Dimethyl acetylenedicarboxylate also afforded an adduct (**4b**: $R_1=R_2=COOCH_3$) in a quantitative yield.

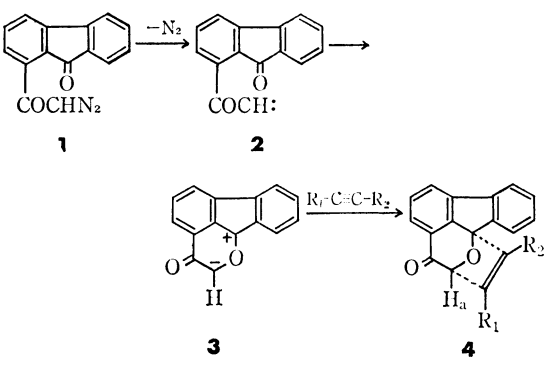

Although there are two possibilities in the direction of the cycloaddition of asymmetric acetylenes, methyl propiolate gave only one adduct (**4c**: $R_1=H$, $R_2=COOCH_3$, 80%), which exhibited a doublet methine signal of H_a at 4.78 τ and that of H_b at 2.48 τ coupled with one another ($J_{ab}=2.5$ Hz). This means that H_a and H_b are in a vicinal position and that R_2 is the methoxycarbonyl group. The NMR signal of methoxycarbonyl of **4c** at 6.51 τ is comparable to that of one OCH_3 (at 6.56 τ) of the adduct of dimethyl acetylenedicarboxylate (**4b**). Phenylacetylene yielded an adduct with a similar direction of cycloaddition (**4d**: $R_1=H$, $R_2=Ph$) in an 86% yield.

On the other hand, methyl phenylpropiolate yielded two cycloadducts, **4e** (24%) and **4f** (30%). The similarity of their IR spectra demonstrates that they are isomers different in the direction of cycloaddition. The singlet of **4e** at 6.69 τ was assigned to the methoxycarbonyl group at the R_2 position in comparison with that of **4c** (at 6.51 τ). Therefore, the singlet of **4f** at 6.30 τ was assigned to methoxycarbonyl at R_1. In general, the methoxycarbonyl group at R_2 has a methyl signal at a higher field than that of R_1 because of the

Table 1. Spectral properties of cycloadducts of 3 with acetylenic dipolarophiles

Adduct	R_1	R_2	IR (KBr, cm^{-1})		NMR ($CDCl_3$, τ)			
					H_a	H_b	$OCH_3(R_1)$	$OCH_3(R_2)$
4a	PhCO	PhCO	1704	1659	4.22(s)	—	—	—
4b	COOMe	COOMe	1707	1729	4.57(s)	—	6.23	6.55
4c	H_b	COOMe	1701	1725	4.78(d)[a]	2.48(d)[a]	—	6.51
4d	H_b	Ph	1706		4.77(d)[b]	3.15(d)[b]	—	—
4e	Ph	COOMe	1700	1710	4.40(s)	—	—	6.69
4f	COOMe	Ph	1707[c]		4.50(s)	—	6.30	—

a) $J_{ab}=2.5$ Hz. b) $J_{ab}=2.4$ Hz. c) A broad absorption was observed.

anisotropy of the fluorene ring.

Because of the contribution of a resonance formula $H-\overset{+}{C}=\overset{-}{C}-COOCH_3$ in methyl propiolate, the α-carbon with an increased electron density attacks the positively charged C_9 of the fluorene ring of carbonyl ylide (**3**) to give **4c**. In the case of phenylacetylene, π-π interaction[11] between the phenyl group and the fluorene ring regulates the direction of cycloaddtition, affording **4d**. In the addition of methyl phenylpropiolate, electronic interaction and π-π interaction compete; two products, **4e** and **4f**, are thus formed.

*Cycloaddition of **3** with Ethylenic Dipolarophiles.* Ethylenic dipolarophiles also gave cycloadducts (**5**) in high yields (Table 3). The configuration of the adducts were determined on the basis of their NMR properties. The reaction with *trans*-1,2-dibenzoylethylene gave a single adduct (**5a**), which showed doublet methine signals of H_a and H_c at 4.88 τ and 4.46 τ, and a double doublet of H_b at 5.10 τ. From the small value of the coupling constant between H_a and H_b (J_{ab}=1.6 Hz), H_a and H_b are decided to be in the *trans* configuration. The coupling constant, J_{bc}, (=4.9 Hz) also indicates that H_b and H_c are *trans*. Therefore, the structure of **5a** was determined to be as is shown in Table 2.

In general, the *cis* coupling constants of methine protons in **5** have larger values (8.0—10.6 Hz) than those of *trans* protons (1.6—6.9 Hz) in this ring system.[8-10] For example, in the two adducts of dimethyl fumarate, the minor adduct, mp 142—144 °C, was assigned to **5b**, in which H_a and H_b are *trans* (J_{ab}= 1.4 Hz) and H_b and H_c are *trans* (J_{bc}=5.6 Hz).[10] On

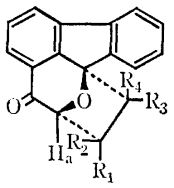

(**5**)

the contrary, in the major adduct, mp 210—213 °C, the large coupling constant of J_{ab}=8.0 Hz indicates that H_a and H_b are *cis*, while the small value of J_{bc} (=5.8 Hz) shows H_b and H_c are *trans*. An inspection of the Dreiding model of these adducts indicates that the newly formed tetrahydrofuran ring is perpendicular to the fluorene ring and that R_4 is situated under the plane of the fluorene ring. Therefore, when R_4 is the methoxycarbonyl group, the ring current of the fluorene ring causes an upper-field shift of the methyl signals, as may be seen in the NMR spectrum of **4b**.

In the reactions with asymmetric olefins, such as methyl cinnamate or methyl *p*-bromocinnamate, a single adduct was obtained; it was assigned the structure shown in Table 2 (R_1=$COOCH_3$ and R_4=Ar) on the basis of the values of the coupling constants (see Table 2) and the chemical shift of methoxycarbonyl (6.20 and 6.23 τ).

trans-Stilbene gave an adudct with a structure similar to **5a** in a 26% yield, besides a dimer(**6**) of the carbonyl ylide (70%). However, *cis*-stilbene did not form an adduct, but yielded the dimer in an 84% yield and 1-(hydroxyacetyl)fluorenone (**7**) in a 3% yield. The formation of the dimer suggests that the dipolarophilicity of *trans*-stilbene and *cis*-stilbene is lower than that of the other dipolarophiles cited above.

Styrene is much more reactive than stilbenes and affords an adduct (**5g**) which shows an H_a resonance as a double doublet coupling with both H_b and H_b' (J_{ab}=1.7 (*trans*) and $J_{ab'}$=8.5 Hz (*cis*)). Thus, R_4 is decided to be phenyl in **5g**. Methyl methacrylate gave an adduct (**5h**) in which R_3 was assigned to methoxycarbonyl, because the methoxy signal was at 6.28 τ and H_a was a double doublet. The configuration of these adducts reveals that the phenyl (or *p*-bromophenyl) group is located at the R_4 position in the adducts of phenyl-substituted ethylenic dipolarophiles, such as methyl cinnamate, methyl *p*-bromocinnamate, *trans*-stilbene, and styrene. This directing effect seems to be caused by the π-π interaction[11] between the phenyl ring of dipolarophiles and the fluorene ring of the carbonyl ylide (**3**), which might be parallel in the transition state.

When the diazo compound (**1**) was catalytically decomposed without dipolarophile, the reaction mixture turned red[12] and was then decolorized after a few ten minutes. The treatment of the reaction mixture gave, quantitatively, a white crystalline product of the head-to-tail dimer of the carbonyl ylide.[5] Since, the attempt at the isolation of the carbonyl ylide (**2**) was unsuccessful, further studies to synthesize a stable carbonyl ylide of this type are now in progress.

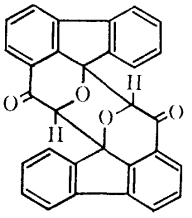

(**6**)

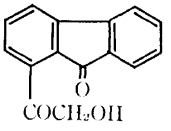

(**7**)

Experimental[13]

Materials. Fluorenone-1-carboxylic acid was prepared by the CrO_3 oxidation of fluoranthene,[14] and was treated with thionyl chloride to give the corresponding acid chloride.

*1-(Diazoacetyl)fluorenone (**1**)* was prepared by the reaction of excess diazomethane with the corresponding acid chloride according to the usual method;[15] yellow plates, mp 149—151 °C; IR(KBr), 2120 (C=N_2), 1698 (C=O), and 1600 cm^{-1} (carbonyl of diazoketone). Found: C, 72.67; H, 3.39; N, 11.35%. Calcd for $C_{15}H_8O_2N_2$: C, 72.57; H, 3.25; N, 11.29%.

Dipolarophiles. Dibenzoylacetylene,[16] dimethyl acetylenedicarboxylate,[17] methyl phenylpropiolate,[18] methyl *p*-bromocinnamate,[19] and *trans*-dibenzoylethylene[20] were prepared by the procedure described in the literature. Other crystalline dipolarophiles, such as dimethyl fumarate, methyl cinnamate, and *trans*-stilbene, were used after the purification of commercial reagents by recrystallization. Liquid dipolarophiles, methyl propiolate, phenylacetylene, styrene, and methyl methacrylate, were purified by distillation im-

Table 2. Spectral properties of cycloadducts of **3** with ethylenic dipolarophiles

Adduct	R_1	R_2	R_3	R_4	IR (KBr, cm^{-1})		NMR ($CDCl_3$, τ)[b]				OCH_3			
							H_a	H_b	H_c	$H_{b'}$	R_1	R_2	R_3	R_4
5a	PhCO	H_b	H_c	PhCO	1700	1685 1673	4.88 (d) J_{ab}=1.6 (*trans*)	5.10 (dd) J_{bc}=4.9 (*trans*)	4.46 (d)	—	—	—	—	—
5b	COOMe	H_b	H_c	COOMe	1700	1734	4.82 (d) J_{ab}=1.4 (*trans*)	6.20 (dd) J_{bc}=5.6 (*trans*)	5.83 (d)	—	6.20	—	—	6.83
5c	H_b	COOMe	COOMe	H_c	1700	1732	4.83 (d) J_{ab}=8.0 (*cis*)	5.60 (dd) J_{bc}=5.8 (*trans*)	6.30 (d)	—	—	6.53	6.31	—
5d	COOMe	H_b	H_c	Ph	1699	1735	4.77 (d) J_{ab}=1.7 (*trans*)	6.48 (dd) J_{bc}=6.9 (*trans*)	5.64 (d)	—	6.20	—	—	—
5e	COOMe	H_b	H_c	Ar[c]	1700	1736	4.78 (d) J_{ab}=1.7 (*trans*)	6.57 (dd) J_{bc}=6.8 (*trans*)	5.70 (d)	—	6.23	—	—	—
5f	Ph	H_b	H_c	Ph	1701		5.92 (d) J_{ab}=1.6 (*trans*)	6.20 (dd) J_{bc}=6.8 (*trans*)	6.00 (d)	—	—	—	—	—
5g	H_b	H_b	H_c	Ph	1687		4.97 (dd) J_{ab}=1.7 (*trans*) $J_{ab'}$=8.5 (*cis*)	6.77 (oct) J_{bc}=6.8 (*trans*) $J_{b'c}$=10.6 (*cis*)	7.68 (dd) $J_{bb'}$=13.8 (*geminal*)	5.99 (dd)	—	—	—	—
5h	H_b	H_b	COOMe	Me[a]	1702	1713	4.99 (dd) J_{ab}=1.6 (*trans*)	6.55 (dd) $J_{ab'}$=8.8 (*cis*)	— $J_{bb'}$=13.5 (*geminal*)	8.11 (dd)	—	—	6.28	—

a) 9.15 τ (s, CH_3). b) The coupling constants are shown in Hz. c) *p*-BrC_6H_4.

TABLE 3. YIELDS, MELTING POINTS, AND ANALYTICAL DATA OF CYCLOADDUCTS **4** AND **5**

Dipolarophile	Adduct	Yield	Mp (°C)	Found (%)		Calcd (%)		Molecular formula
				C	H	C	H	
PhCO-C≡C-COPh	**4a**	89	200—202	81.89	3.93	81.85	3.96	$C_{31}H_{18}O_4$
CH_3OOC-C≡C-$COOCH_3$	**4b**	100	144—146	69.60	3.95	69.61	3.89	$C_{21}H_{14}O_6$
H-C≡C-$COOCH_3$	**4c**	80	144—146	75.02	3.90	74.99	3.97	$C_{19}H_{12}O_4$
Ph-C≡C-H	**4d**	86	209—211	86.13	4.38	85.90	4.38	$C_{23}H_{14}O_2$
Ph-C≡C-$COOCH_3$	**4e**	24	208—209	80.02	4.26	78.93	4.24	$C_{25}H_{16}O_4$
	4f	30	161—163	78.85	4.32	78.93	4.24	
PhCOCH=CHCOPh (*trans*)	**5a**	92	182—184	80.79	4.43	81.56	4.42	$C_{31}H_{20}O_4$
CH_3OOCCH=CHCOOCH_3 (*trans*)	**5b**	34	142—144	69.08	4.42	69.22	4.43	$C_{21}H_{16}O_6$
	5c	54	210—213	69.15	4.41	69.22	4.43	
PhCH=CHCOOCH_3	**5d**	66	173—175	78.39	4.77	78.52	4.74	$C_{25}H_{18}O_4$
p-Br-C_6H_4CH=CHCOOCH_3 (*trans*)	**5e**	66	179—181	65.42	3.73	65.09	3.72	$C_{25}H_{17}O_4Br$
PhCH=CHPh (*trans*)	**5f**	26[a]	209—211	87.03	5.09	86.97	5.03	$C_{29}H_{20}O_2$
PhCH=CH_2	**5g**	79	211—213	84.82	4.90	85.16	4.97	$C_{23}H_{16}O_2$
CH_2=C(CH_3)$COOCH_3$	**5h**	88	184—187	74.90	5.14	74.99	5.03	$C_{20}H_{16}O_4$

a) In this reaction the dimer (**6**) was obtained in a 70% yield.

mediately before use.

*General Procedure of the Decomposition of 1-(Diazoacetyl)-fluorenone (**1**) in the Presence of Dipolarophiles.* 1-(Diazoacetyl)fluorenone (0.25 g, 1 mmol) was added, in small portions, to a benzene solution (30 ml) of a 1.5—3.0 molar amount of dipolarophile and a catalytic amount (0.02 g, 0.08 mmol) of $Cu(acac)_2$ at 80 °C. A vigorous evolution of nitrogen gas was observed immediately after the addition. The reaction mixture was separated by column chromatography on silica gel, using benzene as the eluent. The physical properties of the cycloadducts obtained are listed in Tables 1 and 2, while the yields, melting point, and results of elemental analyses are shown in Table 3.

*Formation of Dimer (**6**).* 1-(Diazoacetyl)fluorenone (0.25 g, 1 mmol) was decomposed in a benzene solution of a catalytic amount of $Cu(acac)_2$ by adding it in small portions. During the course of the addition, a vigorous evolution of nitrogen was observed and the reaction mixture turned red. After the red color has disappeared, the solvent was evaporated under reduced pressure. A white crystalline product was thus obtained in a quantitative yield; 0.22 g, mp>360 °C; IR (KBr), 1698 cm^{-1} (C=O). Found: C, 81.56; H, 3.69%. Calcd for $C_{30}H_{16}O_4$: C, 81.81; H, 3.66%.

References

1) A. Robert and B. Moisan, *J. Chem. Soc., Chem. Commun.*, **1972**, 337 and references cited therein.

2) E. F. Ullman and W. A. Henderson, Jr., *J. Am. Chem. Soc.*, **88**, 4942 (1966); K. Maruyama, S. Arakawa, and T. Otsuki, *Tetrahedron Lett.*, **1975**, 2433.

3) R. Rajagopalan and B. G. Advani, *Tetrahedron Lett.*, **1967**, 2689; W. Hoffman and H. J. Luthardt, *Chem. Ber.*, **101**, 3861 (1968).

4) M. S. Kharasch, T. Rudy, W. Nudenberg, and G. Buchi, *J. Org. Chem.*, **18**, 1030 (1953).

5) M. Takebayashi, T. Ibata, and K. Ueda, *Bull. Chem. Soc. Jpn.*, **43**, 1500 (1970); K. Ueda, T. Ibata, and M. Takebayashi, *ibid.*, **45**, 2779 (1972).

6) M. Hamaguchi and T. Ibata, *Tetrahedron Lett.*, **1974**, 4475.

7) S. Bien and A. Gillon, *Tetrahedron Lett.*, **1974**, 3073.

8) J. W. Lown and K. Matsumoto, *Can. J. Chem.*, **48**, 2215 (1970).

9) R. Huisgen, W. Scheer, G. Szeimies, and H. Hube, *Tetrahedron Lett.*, **1966**, 397.

10) In the *trans* coupling constants, *trans* J_{ab} (1.4—1.7 Hz) usually shows a smaller value than that of *trans* J_{bc} (4.9—6.9 Hz).

11) R. Huisgen, H. Hauk, R. Grashey, and H. Seidl, *Chem. Ber.*, **102**, 736 (1969).

12) The red color might be attributed to carbonyl ylide (**3**).

13) The melting points were measured by means of a Yanagimoto Micro Melting Point Apparatus and were not corrected. The IR spectra were recorded with a Hitachi IR Spectrometer Model EPI-S2, while the NMR spectra were obtained on a Varian T-60 or EM-360 instrument, using TMS as the internal standard.

14) L. F. Fieser and A. M. Seligman, *J. Am. Chem. Soc.*, **57**, 2174 (1935).

15) W. E. Bachmann and W. S. Struve, *Org. React.*, Vol. I, 50 (1942).

16) R. E. Lutz and W. R. Smithey, Jr., *J. Org. Chem.*, **16**, 51 (1951).

17) E. H. Huntress, T. E. Lesslie, and J. Bornstein, *Org. Synth.*, Coll., Vol. IV, 329 (1963).

18) T. W. Abbott, *Org. Synth.*, Coll., Vol. II, 515 (1943).

19) E. Campaigne and W. W. Meyer, *J. Org. Chem.*, **27**, 2835 (1962).

20) R. E. Lutz, *Org. Synth.*, Coll. Vol. III, 248 (1955).

The Facile Synthesis of *N*-Substituted Piperidines from Glutaraldehyde and Primary Amines with Tetracarbonylhydridoferrate

Yoshihisa WATANABE, Sang Chul SHIM, Take-aki MITSUDO,
Masakazu YAMASHITA, and Yoshinobu TAKEGAMI
Department of Hydrocarbon Chemistry, Faculty of Engineering, Kyoto University, Sakyo-ku, Kyoto 606
(Received April 10, 1976)

Ethanolic tetracarbonylhydridoferrate solution combined with glutaraldehyde is very efficient for the selective transformation of an amino group into a piperidine ring. A large variety of both aliphatic and aromatic amines react with the ferrate-glutaraldehyde at room temperature under carbon monoxide to give the corresponding *N*-alkyl- and *N*-arylpiperidines in good to excellent yields.

A large variety of methods are available for building up the piperidine ring.[1] Most of these feature the closing of the piperidine ring at the nitrogen atom. In these methods, 1,5-dihalids, 1,5-halogeno amine, 1,5-amino alcohol, 1,5-diamine, 1,3-dinitrile, pyridines, tetrahydropyran, and *N*-arylglutarimide are used as the starting materials. The major portion of the synthetic problem is the preparation of a suitable starting material. The double Mannich condensation of glutaraldehyde, amine, and acetonedicarboxylic acid provides an elegant classical synthesis of tropinone.[1b] Little attention, however, has been paid to the normal reductive amination of glutaraldehyde. Recently, sodium cyanohydroborate has been shown to be effective to be a selective reducing reagent in the preparation of *N*-heterocycles with 5- and 6-membered rings by the reductive amination of dicarbonyl compounds.[2]

The present paper will deal with the facile synthesis of a variety of *N*-alkyl- and *N*-arylpiperidines by the reductive amination of glutaraldehyde with tetracarbonylhydridoferrate as a highly selective reducing reagent; this reagent has been shown to be efficient for the reductive alkylation of amines, ketones, and indole.[3] A preliminary report of this work was published elsewhere.[3c]

Experimental

The potassium tetracarbonylhydridoferrate was prepared according to the method described in a previous paper;[4] 11—22 mmol of the ferrate was used in each run. The pentacarbonyliron, amines, aqueous glutaraldehyde (45%), and the other compounds employed were all commercial products.

Reaction Procedure. To a mixture of pentacarbonyliron (11—22 mmol), a 1 M-potassium hydroxide (33—66 mmol) solution in ethanol, and a primary amine (11—22 mmol), we added, drop by drop, 45% aqueous glutaraldehyde (11—22 mmol) for 5—10 min; the mixture was then stirred for 5—72 h at room temperature under carbon monoxide.

TABLE 1. THE PREPARATION OF *N*-SUBSTITUTED PIPERIDINES FROM GLUTARALDEHYDE AND PRIMARY AMINES USING TETRACARBONYLHYDRIDOFERRATE

Exp. No.	Amine	Reaction conditions[a]		*N*-Substitued piperidine	
		Time (h)	Carbon monoxide absorbed[b]	R[R-N $(CH_2)_5$]	Yield (%)[c]
1	Aniline	5	1.5	Phenyl	78
2	*p*-Toluidine	7.5	1.7	*p*-Tolyl	81
3	*p*-Methoxyaniline	6.5	2.1	*p*-Methoxyphenyl	79
4	*p*-Chloroaniline	7.5	1.8	*p*-Chlorophenyl	89
5	*o*-Toluidine	20	1.5	*o*-Tolyl	77
6	*o*-Methoxyaniline	18	1.6	*o*-Methoxyphenyl	82
7	*o*-Chloroaniline	72	0.4	—	—
8	1-Naphthylamine	13	1.3	1-Naphthyl	80
9	Benzylamine	5	1.6	Benzyl	90
10	α-Methylbenzylamine	5	1.5	α-Methylbenzyl	85
11	Phenethylamine	5	1.2	Phenethyl	55
12	Furfurylamine	5	1.3	Furfuryl	72
13	Cyclohexanamine	9.5	1.7	Cyclohexyl	51
14	1-Butanamine	7	1.2	Butyl	54
15	1-Hexanamine	7	1.1	Hexyl	60
16	1-Octanamine	5.5	1.1	Octyl	43
17	2-Aminoethanol	5.5	0.9	2-Hydroxyethyl	41
18	*N*,*N*-Dimethylethanediamine	5.5	1.1	2-(Dimethylamino)ethyl	47
19	Glycine methyl ester	5	1.3	$-CH_2COOCH_3$	45

a) At room temperature under carbon monoxide. Molar ratio: ferrate-glutaraldehyde-amine, 1.0 : 1.0 : 1.0.
b) Mol/mol-ferrate. c) Isolate yield. Based on the amount of the ferrate used.

The reaction was readily monitored by the GLPC analysis of the primary amine used. When all of the amine had been consumed, the reaction was stopped and the potassium carbonate formed in the reaction was filtered off. The filtrate was concentrated to 3—5 ml on a rotary evaporator and/or with a Kugelrohr apparatus, and the products were separated and purified by careful vacuum distillation, and submitted to analysis.

Analytical Procedure. The GLPC analysis was made using internal standards: a column (0.3 cm ø, 3 m) packed with 10% Versamid on Neopak 60—80 mesh. The measurements of the PMR and IR spectra were made on a JOEL Model 3H 60-NMR spectrometer and a Varian HR 220 spectrometer, and on a 215 Hitachi grating spectrometer, respectively.

Results and Discussion

N-Substituted Piperidines from Primary Amines. A large variety of primary amines were converted into the corresponding *N*-substituted piperidines in good to excellent yields with tetracarbonylhydridoferrate–glutaraldehyde under mild conditions, at room temperature and under carbon monoxide. The results are listed in Tables 1 and 2.

When aqueous glutaraldehyde (45%) is mixed with a primary amine in ethanol, an intractable condensation material is obtained after evaporating the solvents, but the ferrate–glutaraldehyde–amine system gives *N*-

Table 2. Analytical data of *N*-substituted piperidines

Exp. No.	Bp (°C)	60-PMR($CDCl_3$)[a] τ	Analyses, % Found(Calcd) C	H	N
1	99/0.2 mmHg	8.40(m, 6H), 6.92(t, 4H), 2.95(m, 5H, Ar)	81.72 (81.94)	9.29 (9.38)	8.91 (8.69)
2	56/0.7	8.40(m, 6H), 6.93(t, 4H), 7.76(s, 3H, $-CH_3$), 3.10(m, 4H, Ar)	82.08 (82.23)	10.05 (9.78)	8.04 (7.99)
3	60/3	8.35(m, 6H), 6.97(t, 4H), 6.25(s, 3H, $-OCH_3$), 3.14(s, 4H, Ar)	75.30 (75.35)	8.85 (8.95)	7.30 (7.32)
4	63/0.8	8.37(m 6H), 6.85(t, 4H), 3.00(m, 4H, Ar)	67.70 (67.52)	7.47 (7.21)	7.24 (7.16)
5	44/0.2	8.40(m, 6H), 7.20(t, 4H), 7.73(s, 3H, $-CH_3$), 3.03(m, 4H, Ar)	82.37 (82.23)	9.73 (9.78)	8.22 (7.99)
6	68/0.1	8.40(m, 6H), 7.04(t, 4H), 6.18(s, 3H, $-OCH_3$), 3.10(s, 4H, Ar)	75.63 (75.35)	9.04 (8.96)	7.45 (7.32)
8	77/0.2	8.33(m, 6H), 7.03(t, 4H), 3.33(m, 7H, Ar)	85.52 (85.26)	8.09 (8.11)	6.66 (6.63)
9	49/0.1	8.50(m, 6H), 7.66(t, 4H), 6.55(s, 2H, $-CH_2-$), 2.75(s, 5H, Ar)	81.96 (82.23)	9.96 (9.78)	8.07 (7.99)
10	50/0.4	8.60(m, 6H), 7.67(t, 4H), 8.67(d, 3H, $-CH_3$), 6.67(qu, 1H, -CH), 2.76(s, 5H, Ar)	82.23 (82.48)	10.05 (10.12)	7.25 (7.40)
11	64/0.2	8.50(m, 6H), 7.00—7.70(m, 8H), 2.83(s, 5H, Ar)	82.56 (82.48)	10.31 (10.12)	7.37 (7.40)
12	66/4	8.50(m, 6H), 7.60(t, 4H), 6.50(s, 2H, $-CH_2$), 3.82(m, 2H), 2.64(s, 1H)	72.80 (72.69)	9.22 (9.15)	8.28 (8.48)
13	42/0.3	8.50(m, 17H), 7.50(t, 4H)	—	—	—
14[b]	70/34	9.10(t, 3H), 8.50(m, 10H), 7.60(t, 6H)	74.43 (76.52)	13.57 (13.56)	9.32 (9.92)
15[b]	65/5	9.10(t, 3H), 8.60(m, 14H), 7.68(t, 6H)	76.50 (78.04)	13.24 (13.69)	7.90 (8.27)
16[b]	46/0.1	9.10(t, 3H), 8.50(m, 18H), 7.70(t, 6H)	77.45 (79.12)	13.74 (13.79)	7.05 (7.10)
17[b]	58/4	8.50(m, 6H), 7.50(m, 6H), 6.50(s, 1H, -OH), 6.40(t, 2H)	63.00 (65.07)	11.56 (11.70)	10.36 (10.84)
18	29/0.8	8.50(m, 6H), 7.73(m, 8H), 7.54(s, 6H, $-N(CH_3)_2$)	62.73 (62.20)	12.69 (12.72)	15.80 (16.07)
19	47/3	8.50(m, 6H), 7.60(t, 4H), 6.83(s, 2H), 6.30(s, 3H)	61.32 (61.12)	9.87 (9.62)	8.66 (8.91)

a) 60-PMR spectra characteristic of the piperidine ring; τ around 8.3—8.6(m, 6H, $-\overline{N-CH_2-CH_2-CH_2-CH_2-CH_2}$) and around 6.8—7.7(t, 4H, $-\overline{N-CH_2-(CH_2)_3-CH_2}$). b) Somewhat unstable to be oxidized under air with a color change.

TABLE 3. THE PREPARATION OF *N*-SUBSTITUTED PIPERIDINES FROM GLUTARALDEHYDE AND PHENYLENEDIAMINES USING TETRACARBONYLHYDRIDOFERRATE

Exp. No.	Amine	Reaction conditions[a]		Product	Yield[c] (%)
		Time(h)	Carbon monoxide absorbed[b]		
20	*o*-Phenylenediamine	9	1.7	*N*-(2-Aminophenyl)piperidine	63
21	*o*-Phenylenediamine	48	2.3	*o*-Dipiperidinobenzene	42
22	*p*-Phenylenediamine	5	1.8	*N*-(4-Aminophenyl)piperidine	73
23	*p*-Phenylenediamine	5	2.7	*p*-Dipiperidinobenzene	69

a) At room temperature under carbon monoxide. Molar ratio: ferrate-glutaradehyde-amine, 1.0 : 1.0 : 1.0 in Exps. 20 and 22, and 2.0 : 2.0 : 1.0 in Exps. 21 and 23. b) Mol/mol-ferrate. c) Isolated yield. Based on the amount of the amine used.

TABLE 4. ANALYTICAL DATA OF *N*-SUBSTITUTED PIPERIDINES FROM PHENYLENEDIAMINES

Exp. No.	Bp (°C)	60-PMR ($CDCl_3$) τ	Analyses, % Found (Calcd)		
			C	H	N
20[a]	57/0.1 mmHg	8.37(m, 6H), 7.18(t, 4H), 6.10(s, 2H, $-NH_2$), 3.23(m, 4H, Ar)	74.80 (74.96)	8.87 (9.15)	15.68 (15.89)
21	53/0.1	8.40(m, 12H), 7.03(t, 8H), 3.17(s, 4H, Ar)	78.52 (78.64)	9.66 (9.89)	12.17 (11.46)
22[a]	75/0.2	8.44(m, 6H), 7.03(t, 4H) 6.73(s, 2H, $-NH_2$), 3.17(m, 4H, Ar)	74.69 (74.96)	9.21 (9.15)	15.94 (15.89)
23	105/0.1	8.40(m, 12H), 7.00(t, 8H), 3.17(s, 4H, Ar)	78.37 (78.64)	9.77 (9.90)	11.69 (11.46)

a) IR(Neat), ν_{-NH_2} 3340 and 3440 cm^{-1}.

substituted piperidines: the ferrate acts as an efficient and highly selective reducing reagent to give the *N*-heterocycles as the only reaction products.

$$OHC(CH_2)_3CHO + RNH_2 \xrightarrow{KHFe(CO)_4} \overbrace{(CH_2)_5\,N\text{-}R}$$

The reaction proceeds smoothly with an absorption of carbon monoxide and with a color change from pale yellow brown to red.

This reaction has a great tendency to undergo a heterocyclization at the nitrogen atom of the amines, even at the ferrate–glutaraldehyde–amine molar ratio of 1.0 : 1.0 : 2.0; at this ratio *N*,*N*′-disubstituted pentanediamines are expected to be formed, but the *N*-heterocycles and the unconsumed primary amines are identified.

$$OHC(CH_2)_3CHO + 2RNH_2 \begin{cases} \xrightarrow{KHFe(CO)_4} \overbrace{(CH_2)_5\,N\text{-}R} + RNH_2 \\ \not\longrightarrow\ RNH(CH_2)_5HNR \end{cases}$$

This method can be applied to both aromatic and aliphatic amines with different functional groups. In the cases of substituted anilines, such substituents as the methyl, methoxyl, and chloro groups have almost no effect on the formation of the heterocycles when located at the *para* position, but they have some inhibitory effect when located at the *ortho* position. *o*-Methyl- and *o*-methoxyanilines require longer reaction times for completion, and from *o*-chloroaniline the corresponding piperidine could not be isolated even after a reaction time of 72 h. Such influence of the *ortho* substituents seems to be due to steric hindrance. Usual aliphatic amines, 1-butanamine and 1-octanamine, give the *N*-heterocyles, but this type of compound, simple *N*-alkylpiperidines, are somwhat unstable to be gradually oxidized under air with a color change from colorless to brown. Different aliphatic amines with such functional groups as the phenyl, hydroxyl, and carboxyl groups are also converted into the heterocycles with no difficulty. The successful results with the glycine methyl ester clearly indicate that this method can be applied to amino acids and their derivatives. This reaction seems to proceed *via* Schiff bases and immonium salts and seems to include the reduction of carbon-nitrogen double bonds.[3f]

$$OHC(CH_2)_3CHO + RNH_2 \longrightarrow \left[OHC(CH_2)_3\text{-}CH{=}N\text{-}R \longrightarrow OHC(CH_2)_4\text{-}NH\text{-}R \longrightarrow \overbrace{(CH_2)_4\,\underset{\backslash\!-\!CH^{/}}{N^+}\text{-}R} \right] \longrightarrow \overbrace{(CH_2)_5\,N\text{-}R}$$

N-Substituted Piperidines from Phenylenediamines. The results for phenylenediamines are listed in Tables 3 and 4. This reaction also proceeds readily under mild conditions. In the reaction of *o*- and *p*-phenylenediamines with the ferrate–glutaraldehyde system, two types of products, *N*-(aminophenyl)piperidines and dipiperidinobenzenes, are obtainable. The types of the products sharply depend on the ferrate–glutaraldehyde–amine molar ratio. The molar ratio of 1.0 : 1.0 : 1.0 gives the *N*-(aminophenyl)piperidines selectively.

$$C_6H_4(NH_2)_2 + OHC(CH_2)_3CHO \xrightarrow{KHFe(CO)_4} C_6H_4(NH_2)[N(CH_2)_5]$$

This results also shows that this reaction has a great tendency to undergo heterocyclization at the nitrogen atom; one of the two amino groups is selectively alkylated to the piperidine ring. The molar ratio of 2.0 : 2.0 : 1.0 gives dipiperidinobenzenes; two amino groups are derived into two piperidine rings, but *o*-phenylenediamine requires a much longer reaction time than the *p*-derivative. (Exps. 21 and 23).

The results obtained here show that this method is widely applicable for the selective transformation of the amino group into the piperidine ring.

References

1) a) A. N. Bourns, H. W. Embleton, and K. Hansuld, *Org. Synth.*, Coll. Vol. IV, 795 (1963); b) A. C. Cope, H. L. Dryden, Jr., and C. F. Howell, *ibid.*, Coll. Vol. IV, 816 (1963), and references cited therein.

2) C. F. Lane, *Synthesis*, **1975**, 135, and references cited therein.

3) a) T. Mitsudo, Y. Watanabe, M. Tanaka, K. Yamamoto, and Y. Takegami, *Bull. Chem. Soc., Jpn.*, **44**, 392 (1971); b) Y. Watanabe, M. Yamashita, T. Mitsudo, M. Tanaka, and Y. Takegami, *Tetrahedron Lett.*, **1974**, 1879; c) Y. Watanabe, T. Mitsudo, M. Yamashita, S. C. Shim, and Y. Takegami, *Chem. Lett.*, **1974**, 1265; d) Y. Watanabe, S. C. Shim, T. Mitsudo, M. Yamashita, and Y. Takegami, *ibid.*, **1975**, 699; e) Y. Watanabe, S. C. Shim, T. Mitsudo, M. Yamashita, and Y. Takegami, *ibid.*, **1975**, 955; f) Y. Watanabe, S. C. Shim. T. Mitsudo, G. Yamashita, and Y. Takegami, *Bull. Chem. Soc. Jpn.*, **49**, 1378 (1976); g) G. P. Boldrini, M. Panunzio, and A. Umani-Ronchi, *Synthesis*, 733 (1974); h) G. P. Boldrini, M. Panunzio, and A. Umani-Ronchi, *J. Chem. Soc. Chem. Commum.*, **1974**, 359; i) G. Cainelli, M. Panunzio, and A. Umani-Ronchi, *Tetrahedron Lett.*, **1973**, 2491; j) G. Cainelli, M. Panunzio, and Umani-Ronchi, *J. Chem. Soc. Parkin Trans.* 1, **1975**, 1273.

4) Y. Takegami, Y. Watanabe, H. Masada, and I. Kanaya, *Bull. Chem. Soc. Jpn.*, **40**, 1456 (1967).

Dehydroannulenes. V. Synthesis and Properties of 1,6,12,17-Tetra-*t*-butyl-2,4,13,15-tetrakisdehydro[22]annulene

Masahiko IYODA, Hideaki MIYAZAKI, and Masazumi NAKAGAWA*

Department of Chemistry, Faculty of Science, Osaka University Toyonaka, Osaka 560

(Received April 23, 1976)

The synthesis of 1,6,12,17-tetra-*t*-butyl-2,4-13,15-tetrakisdehydro[22]annulene has been performed. The tetrakisdehydro[22]annulene was found to be strongly diatropic having high conformational stability.

In view of strong diatropicity and high conformational stability of tetrasubstituted tetrakisdehydro[18]-annulene (I)[1-4] synthesis of higher analogue of I, tetrakisdehydro[22]annulene (II), seemed to be of considerable interest for the purpose gaining further insight into the aromaticity of macrocyclic $[4n+2]\pi$-electron system. The present paper is concerned with the synthesis and properties of tetra-*t*-butyltetrakis-dehydro[22]annulene (XII=II, R=*t*-Bu).[5]

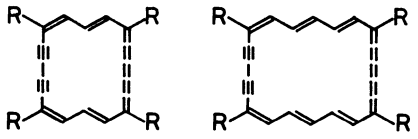

I II

3-*t*-Butyl-2-penten-4-ynal (IV) obtained from III[3] was converted into diethyl acetal (V) in the usual way. Condensation of ethyl vinyl ether[6] with V in benzene in the presence of boron trifluoride etherate yielded ethoxy acetal (VI) in a high yield. Unstable 5-*t*-butyl-2,4-heptadien-6-ynal (VII) obtained on treatment of VI with hydrogen chloride in aqueous dioxane was condensed with pinacolone to give trienyne ketone (VIII). Oxidative coupling of the trienyne ketone (VIII) with copper(II) acetate monohydrate in pyridine–methanol[7] yielded hexaendiyne diketone (IX). Bis-ethynylation of the diketone (IX) could be achieved by lithium acetylide–ethylenediamine complex[8] in tetrahydrofuran saturated with acetylene. Bis-ethynyl alcohol (X) obtained in a high yield was oxidatively coupled with copper(II) acetate in pyridine–methanol under high dilution conditions using ether as an entraining solvent to give cyclic glycol (XI). The fact that the 22-membered cyclic glycol (XI) could be obtained in 77.5% yield seems to be attributable to the molecular geometry of X favorable for intramolecular oxidative coupling.

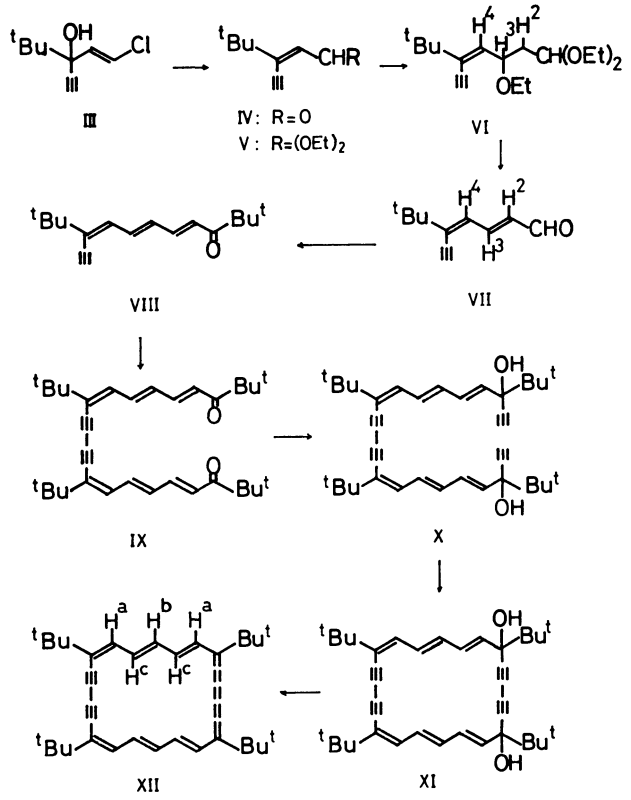

III IV: R=O V: R=(OEt)$_2$ VI VII VIII IX X XI XII

Finely powdered tin(II) chloride dehydrate was added at −60 °C under nitrogen atmosphere to a stirred solution of the cyclic glycol (XI) in ether saturated with hydrogen chloride. Resulting deep blue violet reaction mixture was worked up rapidly at a low temperature. Chromatography of the product on alumina at −20 °C followed by elution with dichloromethane–pentane gave tetra-*t*-butyltetrakisdehydro[22]-annulene (XII) as unstable dark violet crystals in a yield of 85%. The crystals of XII changed quickly to colorless solid at *ca.* 100 °C on attempted melting point determination. Full hydrogenation of XII over platinum catalyst gave tetra-*t*-butylcyclodocosane.

As illustrated in Fig. 1, XII showed closely related electronic spectrum to that of tetra-*t*-butyltetrakisde-hydro[18]annulane (I, R=*t*-Bu)[3] except for considerable bathochromic shift in XII. The NMR spectrum of XII is shown in Fig. 2. The fact that the outer protons (H^a and H^b) resonate at unusually low field and the inner protons (H^c) exhibit signals at fairly high field clearly demonstrates the induction of diamagnetic ring current indicating the aromatic nature of the tetrakisdehydro[22]annulene (XII). The fact that the NMR spectra of XII obtained at 30 °C and −40 °C exhibit no essential change (Table 1) indicates the conformational stability of the 22-membered ring with delocalized π-electron system containing formal diacetylene and hexapentaene units. The coalescence temperature of XII could not be determined owing rather rapid decomposition of XII at temperature higher than 30 °C.

The difference in chemical shifts between the signal of inner protons (τ_i) and the lowest field signal of outer protons (τ_o) can be regarded as an approximate measure of ring current. The τ_i—τ_o-value ($\Delta\tau$) for tetra-*t*-butyltetrakisdehydro[18]annulene (I, R=*t*-Bu) has

* Author to whom inquiries should be addressed.

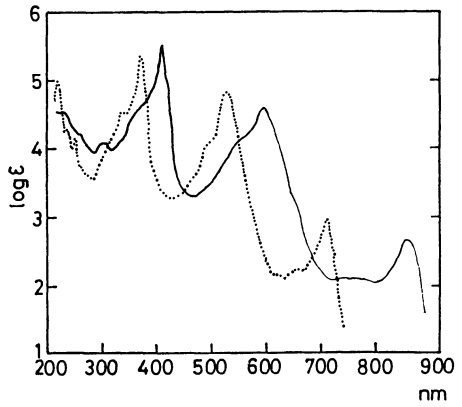

Fig. 1. Electronic spectra in THF of tetra-*t*-butyltetrakisdehydro[18]annulene (I, R=*t*-Bu) (·····) and tetra-*t*-butyltetrakisdehydro[22]annulene (XII) (——).

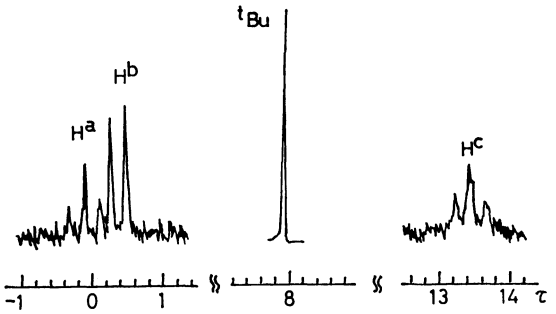

Fig. 2. NMR spectrum of tetra-*t*-butyltetrakisdehydro-[22]annulene (XII).
60 MHz, in $CDCl_3$, at 30 °C.

Table 1. NMR Parameters of tetra-*t*-butyltetrakisdehydro[22]annulene (XII), 60 MHz, $CDCl_3$

Temperature	H_b	H^a	*t*-Bu	H^c
−40 °C	−0.43 t	0.09 d	7.88 s	13.71 t
	J=13	J=13		J=13
+30 °C	−0.16 t	0.33 d	7.93 s	13.44 t
	J=13	J=13		J=13

been found to be $\Delta\tau$=14.83,[3] whereas an appreciable decrease in the value, $\Delta\tau$=13.44−(−0.16)=13.60, was observed for tetra-*t*-butyltetrakisdehydro[22]annulene (XII). The $\Delta\tau$-values for I and XII can be compared reasonably well, since these compounds have similar geometries and planarities. Therefore, the marked decrease in the $\Delta\tau$-value for XII as compared with that for I(R=*t*-Bu) can be regarded as an evidence for theoretically predicted decrease of resonance energy[9] or ring-current intensity[10] along with increase of ring size.

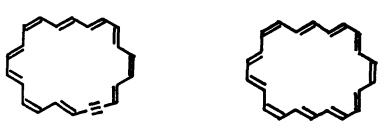

XIII XIV

It has been reported that monodehydro[22]annulene (XIII) exhibits signals of outer protons at τ1.55—3.75 and these of inner protons at τ6.55—9.30.[11] The NMR spectrum of [22]annulene (XIV) has been found to be temperature dependent indicating conformational mobility of the molecule (coalescence temperature, *ca.* 20 °C). At −90 °C, XIV showed outer proton signals at τ 0.35—0.7 and 0.9—1.5, and inner proton signals at τ 10.4—11.2.[12] A much higher diatropicity and conformational stability of XII as compared with XIII and XIV indicate that symmetrical 'acetylene-cumulene'-dehydroannulenes containing equalized acetylenic and cumulenic linkages in the cyclic system are one of the most adequate structure for the study of aromaticity of macrocyclic system.

Experimental

All melting and boiling points are not corrected. The IR spectra were measured with a Hitachi EPI-2 or EPI-G3 spectrometer, and strong; medium and weak bands were indicated by s, m and w, respectively. The UV spectra, obtained on a Hitachi EPS-3T spectrophotometer, were recorded in nm and the ε-values were given in parentheses. Shoulder was denoted by sh. The mass spectra were measured with a Hitachi RM-50 spectrometer. The NMR spectra obtained on a Varian A-60 spectrometer were given in τ-values with respect to TMS as an internal standard, and the coupling constants (J) are recorded in Hz. Silica gel (Merck, Kiesel Gel 60) or alumina (Merck, Act. II-III) was used for column chromatography, unless otherwise stated.

3-t-Butyl-2-penten-4-ynal Diethyl Acetal (V). To a mixture of slightly crude IV (63.70 g, bp 47—50 °C/400 Pa) obtained from III (88.0 g)[3] and ethyl orthoformate (160 ml) was added a solution of *p*-toluenesulfonic acid monohydrate (6.00 g, 0.968 mmol). The mixture was stirred at 30 °C for 24 h under nitrogen atmosphere, and then chilled on an ice-bath. The cooled reaction mixture was poured onto ice-water containing sodium hydrogencarbonate. The organic layer was separated and the aqueous layer was extracted with ether (100 ml×2). The combined organic layer was washed successively with sodium hydrogencarbonate and sodium chloride solutions, dried (K_2CO_3), concentrated *in vacuo*, and distilled, yielding V: 84.11 g, 78.5% based on III; bp 78–79 °C/400 Pa; MS: *m/e* 210 (M^+); IR (CCl_4): 3320 m (C≡CH), 2085 w (C≡C), 1628 w (C=C), 1200–1000 s (C–O–C) cm^{-1}; NMR (CCl_4): 4.24 (d, 1, J=7.5, olefinic), 4.78 (d, 1, J=7.5, acetal), 6.48 (m, 4, $-CH_2-$), 6.89 (s, 1, C≡CH), 8.83 (t, 6, J=7.0. CH_3), 8.83 (s, 9, *t*-Bu). Elemental analyses gave unstisfactory results presumably owing to extremely facile hydrolysis of V.

5-t-Butyl-3-ethoxy-4-hepten-6-ynal Diethyl Acetal (VI). A solution of boron trifluoride etherate (20 mg) in benzene (1 ml) was added to a solution of V (7.40 g, 0.0352 mol) in the same solvent (20 ml) at 40 °C, and then a solution of ethyl vinyl ether (2.79 g, 0.0387 mol) in the same solvent (5 ml) was slowly added. After the mixture had been kept at the same temperature for further 2 h. Finely powdered potassium carbonate was added to the cooled reaction mixture resulting in a yellow solution. The inorganic material was removed by filtration and washed with ether. The combined organic layer and washings were concentrated under reduced pressure, and distilled *in vacuo*, giving VI: 8.98 g, 90.4%; bp 110—111 °C/400 Pa; MS: *m/e* 282 (M^+); IR (CCl_4): 3320 m (C≡CH), 2070 w (C≡C), 1620 w (C=C), 1150—1050 s (C–O–C) cm^{-1}; NMR (CCl_4): 4.36 (d, 1, J=9.0, H^4), 5.42 (m, 1, H^1), 5.64 (m, 1, H^3), 6.56 (m, 6, $O-CH_2-$), 6.83 (s, 1, C≡CH), 8.30 (m, 2, H^2), 8.85

(t, 9, J=7.0, CH_3).

Found: C, 71.89; H, 10.61%. Calcd for $C_{17}H_{30}O_3$: C, 72.30; H, 10.71%.

Although VI gave rather unsatisfactory elemental analysis, it was used without further purification in the following reaction.

5-t-Butyl-2,4-heptadien-6-ynal (VII). A mixture of VI (10.00 g, 0.0354 mol), dioxane (60 ml) and 3M hydrochloric acid (50 ml) was vigorously stirred under nitrogen atmosphere at 50 °C for 3 h, and then at 40 °C for 18 h. The reaction mixture was chilled and the organic layer was separated. The aqueous layer was extracted with ether. The combined organic layer was washed successively with saturated sodium hydrogen carbonate and sodium chloride solutions, dried (Na_2SO_4), concentrated under reduced pressure, and rapidly distilled *in vacuo* under nitrogen atmosphere using short neck distilling flask to give VII: yellow liquid; 4.06 g, 70.7%; bp 60—70 °C/200 Pa; IR (CCl_4): 3300 m (C≡CH), 2810 w, 2730 w (CHO), 1687 s (C=O), 1616 s (C=C), 977 s (*trans* CH=CH) cm^{-1}; NMR (CCl_4): 0.56 (d, 1, J=7.5, CHO), 2.47 (dd, 1, J=11, 15, H^3), 3.46 (d, 1, J=11, H^4), 3.87 (dd, 1, J=7.5, 11, H^2), 8.81 (s, 9, *t*-Bu).

VII was found to be unstable changing to a red viscous liquid on standing at room-temperature for 1 h, but could be kept for several days at −20 °C under nitrogen atmosphere, and was best stored as an ether solution at 0 °C. VII gave no satisfactory elemental analyses.

Since the aldehyde (VII) decomposed partly during distillation, the reaction product was passed through a short column of alumina, and the slightly crude VII obtained on concentrating the filtrate was used without purification for further reaction.

2,4-Dinitrophenylhydrazone of VII. The crude hydrazone was obtained from VII (88 mg, 0.54 mmol), ethanol (7.4 ml), phosphoric acid (0.6 ml) and 2,4-dinitrophenylhydrazine (100 mg, 0.50 mmol), and was purified by chromatography on silica gel. Elution with petroleum ether–benzene yielded pure 2,4-dinitrophenylhydrazone: red crystals; 160 mg, 93%; mp 194.0–194.9 °C (from petroleum ether–benzene).

Found: C, 59.39; H, 5.35; N, 16.59%. Calcd for $C_{17}H_{18}N_4O_4$: C, 59.64; H, 5.30; N, 16.37%.

9-t-Butyl-2,2-dimethyl-4,6,8-undecatrien-10-yn-3-one (VIII). VI (12.2 g, 0.0433 mol) was converted into VII according to the above procedure, and the crude product dissolved in carbon tetrachloride was passed through a short column of alumina. Elution with the same solvent yielded slightly crude VII (4.91 g, light brown liquid). A solution of sodium hydroxide (2.00 g, 50.0 mmol) in ethanol (5 ml) and water (5 ml) was added under nitrogen atmosphere to a solution of the crude VII (4.91 g) and pinacolone (5.00 g, 50.0 mmol) in ethanol (60 ml) maintained at 0 °C. After being kept at 22 °C for 36 h, the reaction mixture was poured onto ice-cooled 3 M hydrochloric acid (50 ml), and extracted with ether (20 ml×3). The extract was washed successively with water and saturated sodium chloride solution, dried (Na_2SO_4), and concentrated under reduced pressure. The residue was chromatographed on alumina to give VIII: pale yellow crystals (from methanol); 3.20 g, The mother liquor of crystallization was chromatographed on silica gel, yielding further crop of VIII: 2.08 g (total yield, 5.28 g, 50.0%). An analytical specimen of VIII was obtained on further recrystallization from pentane: mp 92.5—93.5 °C; IR (CCl_4): 3300 m (C≡CH), 1678 s (C=O), 1591 s (C=C), 999 s (*trans* CH=CH) cm^{-1}; NMR (CCl_4): 2.40—3.85 (m, 5, olefinic), 6.69 (s, 1, C≡CH), 8.83 (s, 9, *t*-Bu), 8.88 (s, 9, *t*-Bu); UV (99% EtOH): λ_{max} 230 sh (5520), 239 (6670), 336 (37900) nm.

Found: C, 83.80; H, 9.97%. Calcd for $C_{17}H_{24}O$: C, 83.55; H, 9.90%.

9,14-Di-t-butyl-2,2,21,21-tetramethyl-4,6,8,14,16,18-docosahexaen-10,12-diyn-3,20-dione (IX). A solution of VIII (3.00 g, 0.0123 mol) in pyridine (15 ml) and methanol (15 ml) was added to a stirred mixture of copper(II) acetate monohydrate (15.00 g, 0.0752 mol), pyridine (50 ml) and methanol (50 ml) at 30 °C. The mixture, after being stirred for 15 h at 30—35 °C, was poured onto ice-cooled 2 M hydrochloric acid, and extracted with ether (100 ml×4). The extract was washed successively with diluted hydrochloric acid, saturated sodium hydrogencarbonate and saturated sodium chloride solutions, and dried ($MgSO_4$). Crystalline residue obtained on concentrating the extract *in vacuo* was chromatographed on alumina and eluted with benzene to give IX: yellow crystals (washed with methanol); 2.49 g, 83.3%. An analytical sample was obtained on recrystallization from methanol: yellow crystals; mp 171.5—172.5 °C; MS: *m/e* 486 (M^+), 429 (M−57); IR (CCl_4): 1678 m (C=O), 1592 s (C=C), 999s (*trans* CH=CH) cm^{-1}; NMR ($CDCl_3$): 2.40—3.81 (m, 10, olefinic), 8.78 (s, 18, *t*-Bu), 8.84 (s, 18, *t*-Bu); UV (99% EtOH): λ_{max} 246.5 (23100), 288 sh (22300), 325 sh (39800), 343 (46200), 385 (41200), 425 sh (24300) nm.

Found: C, 83.73; H, 9.41%. Calcd for $C_{34}H_{46}O_2$: C, 83.90; H, 9.53%.

9,14-Di-t-butyl-2,2,21,21-tetramethyl-3,20-diethynyl-4,6,8,14,16,18-docosahexaen-10,12-diyne-3,20-diol (X). To a stirred mixture of lithium acetylide-ethylenediamine complex[8] (3.00 g, 0.0326 mol) in THF (60 ml) saturated with acetylene was added at 30 °C a solution of IX (1.60 g, 0.00329 mol) in THF (15 ml). After being stirred for further 2 h at 30 °C under bubbling of acetylene, the reaction mixture was chilled in an ice-salt-bath, and saturated ammonium chloride solution was added dropwise at a rate to maintain the internal temperature at −5—0 °C. Then water was added to the mixture, and the organic layer was separated. The aqueous layer was extracted with ether (30 ml×3), and the extract was combined with the organic layer. The combined organic layer was washed with diluted hydrochloric acid and saturated brine, successively, dried ($MgSO_4$), and concentrated under reduced pressure. Chromatography of the residue on alumina followed by elution with benzene yielded an amorphous solid (1.71 g, 96.6%) which was washed thoroughly with pentane to give X: pale yellow crystalline powder; mp 148—150 °C; MS: *m/e* 538 (M^+), 481 (M−57), 436 (M−57—18); IR ($CHCl_3$): 3590 m (OH), 3317 m (C≡CH), 2193 w, 2106 w (C≡C), 1600 w (C=C), 995 s (*trans* CH=CH) cm^{-1}; UV (99% EtOH): λ_{max} 223.5 (29500), 262.5 (27500), 280 sh (31900), 293 (4300), 305 (49100), 327 (39300), 347 (38300), 369 (31500), 397.5 (22600) nm.

Found: C, 84.38; H, 9.34%. Calcd for $C_{38}H_{50}O_2$: C, 84.71; H, 9.35%.

1,6,12,17-Tetra-t-butyl-7,9,11,17,19,21-cyclodocosahexaen-2,4,13,15-tetrayn-1,6-diol (XI). A solution of X (1.710 g) in ether (90 ml), pyridine (90 ml) and methanol (60 ml) was added over a period of 12 h to a stirred and refluxing solution (internal temperature, 50 °C) of copper(II) acetate monohydrate (18.0 g, 0.0902 mol) in ether (180 ml), pyridine (180 ml) and methanol (40 ml) using a high-dilution apparatus. After being refluxed for further 2 h, the reaction mixture was concentrated under reduced pressure to *ca.* 200 ml, and poured onto ice-cooled 2 M hydrochloric acid (600 ml). The mixture was extracted with ether (100 ml×4), and the extract was washed successively with 2 M hydrochloric acid, saturated sodium hydrogencarbonate solution and saturated brine, dried ($MgSO_4$), and the solution was con-

centrated under reduced pressure, yielding a crystalline residue. Chromatography of the residue on alumina followed by elution with benzene gave XI (1.32 g, 77%), which was recrystallized from dichloromethane–pentane to yield pure XI: yellowish crystals, turned to dark brown soild at *ca.* 240 °C; MS: *m/e* 536 (M^+), 479 (M−57); IR (KBr-disk): 3340 m br. (OH), (988 s *trans* CH=CH) cm^{-1}; NMR ($CDCl_3$): 2.64—4.28 (m, 10, olefinic), 7.91 (br. s, 2, OH, disappeared on addition of D_2O), 8.81 (s, 18, *t*-Bu), 8.89 (s, 18, *t*-Bu); UV (99% EtOH): λ_{max} 279 sh (45400), 292 (83400), 302 (102000), 323.5 sh (12700), 360 sh (12500), 385 (17200), 409 (16200) nm.

Found: C, 84.92; H, 9.03%. Calcd for $C_{38}H_{48}O_2$: C, 85.02; H, 9.01%.

*1,6,12,17-Tetra-*t*-butyl-2,4,13,15-tetrakisdehydro[22]annulene (XII).* To a solution of XI (150 mg, 0.279 mmol) in ether saturated with hydrogen chloride (10 ml) was added under nitrogen atmosphere finely powdered tin(II) chloride dihydrate (450 mg, 1.99 mmol) at −60 °C. After being stirred for 30 min at the same temperature, resulting deep blue violet reaction mixture was mixed with ether (30 ml). The organic layer was washed successively with cold water and cold saturated sodium hydrogencarbonate solution, dried ($MgSO_4$), and concentrated under reduced pressure at a temperature below 0 °C. The dark violet residue was immediately chromatographed on alumina at −20 °C. Elution with dichloromethane–pentane (3 : 7) gave XII: 119 mg, 85%; dark violet crystals, turned to colorless solid at *ca.* 100 °C; IR (Nujol mull, measured at a low temperature): 988 (*trans* CH=CH) cm^{-1}; UV (THF): λ_{max} 222 (37000), 231 (37000), 263.5 (16000), 299 (13000), 311 (11000), 369 sh (41000), 382 (47000), 414 (35000), 552 sh (14000), 596 (46000), 732 (130), 768 (130), 858 (490) nm (*cf.*, Fig. 1); NMR: see, Table 1 and Fig. 2.

The crystals of XII decomposed rapidly on exposure to diffused daylight and air at room-temperature. Solutions of XII in pentane, ether or dichloromethane turned gradually to yellow on standing at 0 °C. TLC examination reveals that the product is a complex mixture. XII could be kept with slight decomposition at −78 °C in a diluted dichloromethane solution or crystalline state. XII gave poor elemental analysis and it would seem that the instability of XII is to blame.

Found: C, 89.92; H, 9.32%. Calcd for $C_{38}H_{46}$: C, 90.78; H, 9.22%.

Catalytic Hydrogenation of XII. A cold solution of XII (46 mg) in ethyl acetate (10 ml) was added at −20 °C to a mixture of acetic acid (20 ml) and ethyl acetate (10 ml) containing platinum catalyst (200 mg of platinum oxide was prereduced). The mixture was stirred under hydrogen atmosphere at −15——20 °C for 3 h. After the mixture had been stirred overnight at room temperature, the catalyst was removed by filtration. The filtrate was mixed with ether and washed successively with water, saturated sodium hydrogencarbonate solution and saturated brine, dried ($MgSO_4$), and the solvent was removed under reduced pressure. Yellow oily residue, which crystallized on standing, was chromatographed on alumina, and eluted with pentane to give tetra-*t*-butylcyclodocosane: 42 mg, 86%; Colorless crystals (from ethyl acetate–methanol); mp 97—101 °C; MS: *m/e* 532 (M^+), 477 (M−57), 57 (base peak); IR (CCl_4): 2940 s, 2860 s, 1476 m, 1393 w, 1365 m cm^{-1}; NMR (CCl_4): 8.32 (m, CH_2, −CH=), 9.15 (s, CH_3).

Found: C, 85.81; H, 14.36%. Calcd for $C_{38}H_{76}$: C, 85.63; H, 14.37%.

References

1) J. Ojima, T. Katakami, G. Nakaminami, and M. Nakagawa, *Tetrahedron Lett.*, **1968**, 1115; *Bull. Chem. Soc. Jpn.*, **49**, 292 (1976).

2) K. Fukui, T. Okamoto, and M. Nakagawa, *Tetrahedron Lett.*, **1971**, 3121; T. Katakami, S. Tomita, K. Fukui, and M. Nakagawa, *Chem. Lett.*, **1972**, 225; T. Katakami, K. Fukui, T. Okamoto, and M. Nakagawa, *Bull. Chem. Soc. Jpn.*, **49**, 297 (1976).

3) S. Tomita and M. Nakagawa, *Bull. Chem. Soc. Jpn.*, **49**, 302 (1976).

4) T. Nomoto, K. Fukui, and M. Nakagawa, *Tetrahedron Lett.*, **1972**, 3253; T. Nomoto, K. Fukui, and M. Nakagawa, *Bull. Chem. Soc. Jpn.*, **49**, 305 (1976).

5) For a preliminary report, see, M. Iyoda, H. Miyazaki, and M. Nakagawa, *J. Chem. Soc., Chem. Commun.*, **1972**, 431.

6) M. Müller-Cunradi and K. Pieroth, U. S. Pat., 2165962 (1936); R. Rüegg, M. Montavon, G. Ryser, G. Saucy, U. Schwieter, and O. Isler, *Helv. Chim. Acta*, **42**, 854 (1959) and the preceding papers.

7) G. Eglinton and A. R. Galbraith, *J. Chem. Soc.*, **1959**, 889.

8) D. F. Beumel, Jr. and R. F. Harris, *J. Org. Chem.*, **28**, 2775 (1963); D. F. Beumel, Jr. and R. F. Harris, *ibid.*, **29**, 1872 (1964).

9) H. C. Longuet-Higgins and L. Salem, *Proc. Roy. Soc.*, **A251**, 172 (1954); *ibid.*, **A257**, 445 (1960); C. A. Coulson and W. T. Dixon, *Tetrahedron*, **17**, 215 (1962); M. J. S. Dewar and G. J. Gleicher, *J. Am. Chem. Soc.*, **87**, 685 (1965).

10) *Inter alia*, H. P. Figeys, "Topics in Carbocyclic Chemistry," Vol. 1, ed by L. Lloyd, Logos Press, London (1969), p. 269.

11) R. M. McQuilkin and F. Sondheimer, *J. Am. Chem. Soc.*, **92**, 6341 (1970).

12) R. M. McQuilkin, B. W. Metcalf, and F. Sondheimer, *Chem. Commun.*, **1971**, 338.

Pseudohalogen Chemistry. III.[1] Orientation of Heterolytic Addition of Thiocyanogen Chloride to Some Unsymmetrical Alkenes

Robert G. Guy* and Ian Pearson
School of Natural Sciences, The Hatfield Polytechnic, P.O. Box 109, Hatfield, Hertfordshire, England
(Received January 26, 1976)

Thiocyanogen chloride reacts with various unsymmetrical alkenes, cycloalkenes, and α-arylalkenes in the presence of a radical inhibitor in acetic acid in the dark at 25 °C to yield α-chloro-β-thiocyanates, α-acetoxy-β-thiocyanates, α-hydroxy-β-thiocyanates, vinylic thiocyanates or allylic isothiocyanates in various combinations. The additions to the α-arylalkenes are regiospecific, yielding the Markownikov-orientated products, but the regiospecificity of the additions to the aliphatic alkenes depends on the structure of the alkene. The orientation of addition is discussed in terms of open carbonium ions, *e.g.* **17**, for the α-arylalkenes and cyano-sulfonium ions, *e.g.* **18**, for the aliphatic alkenes.

In Parts I[2] and II,[1] it was shown that thiocyanogen chloride, ClSCN, reacts readiiy at 25 °C with symmetrical alkenes, cycloalkenes and α-arylalkenes, *e.g.* *cis*- and *trans*-2-butene, *trans*-Δ^2-octalin, *cis*- and *trans*-stilbene, and acenaphthylene, in the presence of a radical inhibitor in acetic acid in the dark, to yield α-chloro-β-thiocyanates and α-acetoxy-β-thiocyanates. A heterolytic mechanism involving a two-step, kinetically controlled addition was postulated. For the aliphatic alkenes, the formation of a symmetrical cyanosulfonium ion, *e.g.* **1**, was proposed to account for the *trans*-stereospecific additions observed;[2] for the α-arylalkenes, the formation of an open carbonium ion, *e.g.* **2**, which exists as an ion-pair, and steric control of reaction by the thiocyanato group of the carbonium ion were proposed to account for the observed *trans*- stereoselectivity.[1]

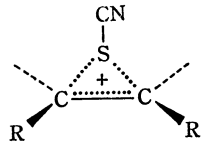

1

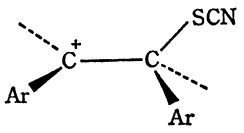

2

Here we describe the orientation of addition of thiocyanogen chloride under heterolytic conditions in acetic acid to some unsymmetrical alkenes, cycloalkenes, and α-arylalkenes.

Results

The alkenes investigated, reaction times, products, and yields are recorded in the Table 1. Constitutionally different products of the reactions were readily separated by column chromatography on silica gel, but regioisomers and stereoisomers were not completely resolved, as indicated by TLC and by IR and ^{1}H NMR spectroscopy. Structural assignments were made as before[1,2] using published IR and NMR data,[1-6] and isomer ratios were determined from the integral traces of appropriate absorption bands in the ^{1}H NMR spectra of the mixtures (see Experimental section for details).

Control experiments showed that the products listed in the Table 1 were stable under the conditions used in the reactions. No reaction occurred with *trans*-cinnamic acid, *trans*-crotonic acid, methyl *trans*-cinnamate, methyl acrylate, vinyl chloride, vinylidene chloride, trichloroethylene or vinyl bromide during 48—164 h. No isomerisation of the alkenes was observed.

Discussion

The heterolytic addition of thiocyanogen chloride, which is polarised in the manner Cl(δ−)–SCN(δ+)[7], to an unsymmetrical alkene RCH=CH_2 (R=alkyl or aryl) may yield the Markownikov-orientated adduct RCHClCH_2SCN and/or the regioisomer RCH(SCN)-CH_2Cl.

α-Arylalkenes. The data for the α-arylalkenes examined show that the addition reaction is regiospecific, yielding the Markownikov-orientated products **3**—**6** and **8** exclusively. Other data, *e.g.* the *trans*-stereoselectivity of the addition to indene (see products **4** and **5**), and the low chlorothiocyanate : acetoxythiocyanate ratios observed for the additions to styrene and indene (see Table 1) resemble those obtained for the corresponding additions to symmetrical α-arylalkenes.[1] Consequently, a similar mechanism is postulated, *i.e.* a two-step, kinetically controlled, electrophilic reaction in which the first step is the formation, as an ion-pair, of the more stable of the two possible open thiocyanato-carbonium ions, *e.g.* **17**, due to the stabilising effect of the α-aryl group. Nucleophilic attack on **17** by chloride ions or acetic acid solvent molecules, and steric control of reaction by the thiocyanato group, leads to the observed α-chloro-β-thiocyanates and α-acetoxy-β-thiocyanates which, in the case of 1,1-diphenylethylene and triphenylethylene, are readily hydrolysed to the corresponding α-hydroxy-β-thiocyanates **6** and **8** during the aqueous work-up procedure. Concomitant loss of a β-proton from **17** leads to the observed substitution products, *i.e.*, the vinyl thiocyanates **7** and **9** (*cf.* the formation of vinyl sulfides in the corresponding additions of 2,4-dinitrobenzenesulfenyl chloride to α-arylalkenes).[15] This substitution reaction becomes progressively more important as the number of stabilising aryl groups on the vinylic product increases (*cf.* the products from styrene, 1,1-diphenylethylene and triphenylethylene).

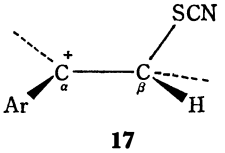

17

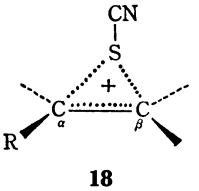

18

TABLE 1. HETEROLYTIC ADDITION OF THIOCYANOGEN CHLORIDE TO UNSYMMETRICAL ALKENES IN ACETIC ACID AT 25 °C

Alkene	Time[a] (min)	Products		Yield (%)	Cl/OAc[b]
$PhCH=CH_2$	2	$PhCHXCH_2SCN$	**3** {**a**; X=Cl / **b**; X=OAc	41 / 50	0.82
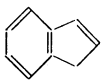	5	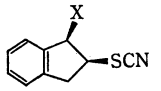	**4** {**a**; X=Cl / **b**; X=OAc	7 / 6	0.31
		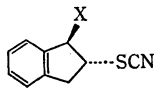	**5** {**a**; X=Cl / **b**; X=OAc	15 / 64	
$Ph_2C=CH_2$	2	$Ph_2C(OH)CH_2SCN$	**6**	77	c)
		$Ph_2C=CHSCN$	**7**	10	
$Ph_2C=CHPh$	20	$Ph_2C(OH)CH(SCN)Ph$	**8**	14	c)
		$Ph_2C=CPhSCN$	**9**	75	
$MeCH=CH_2$	10	$MeCHXCH_2Y$	**10** {**a**; X=Cl, Y=SCN / **b**; X=SCN, Y=Cl / **c**; X=OAc, Y=SCN	54 / 27 / 18	4.5
n-$BuCH=CH_2$	2	*n*-$BuCHXCH_2Y$	**11** {**a**; X=Cl, Y=SCN / **b**; X=SCN, Y=Cl / **c**; X=OAc, Y=SCN	49 / 28 / 15	5.1
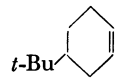	2	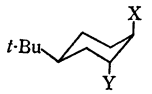	**12** {**a**; X=SCN, Y=Cl / **b**; X=Cl, Y=SCN / **c**; X=SCN, Y=OAc / **d**; X=OAc, Y=SCN	38 / 38 / 12 / 12	3.2
5α-cholest-2-ene	5	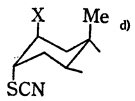	**13** {**a**; X=Cl / **b**; X=OAc	82 / 11	7.5
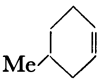	2	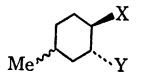	**14** {**a**; X=SCN, Y=Cl / **b**; X=Cl, Y=SCN / **c**; X=SCN, Y=OAc / **d**; X=OAc, Y=SCN	34 / 34 / 13 / 13	2.6
$Et_2C=CH_2$	2	Et_2CXCH_2SCN	**15** {**a**; X=Cl / **b**; X=OAc	23 / 43	0.54
		$MeCH(NCS)C(Et)=CH_2$	**16**	22	

a) Time for 100% reaction as indicated by titration. b) Chlorothiocyanate: acetoxythiocyanate ratio. c) Could not be determined due to hydrolysis (see text). d) Partial structure only.

Aliphatic Alkenes. The data for the aliphatic alkenes examined show that the regiospecificity of the addition reaction varies with the structure of the alkene and the nature of the nucleophile (see products **10**—**15**). Since other data, *e.g.* the stereospecific *trans*-addition to 4-*t*-butylcyclohexene, 4-methylcyclohexene, and 5α-cholest-2-ene (see products **12**—**14**), and the high chlorothiocyanate : acetoxythiocyanate ratios observed for these alkenes (see Table 1) resemble those obtained for the corresponding additions to symmetrical alkenes and cycloalkenes,[2] a similar mechanism, but with an unsymmetrical cyano-sulfonium ion intermediate, *e.g.* **18**, is postulated.

For the terminal alkenes, propene and 1-hexene, the electron-donating alkyl substituent in **18** (R= Me, *n*-Bu) allows a greater share of the positive charge to be available at C_α than at C_β, thus permitting preferential nucleophilic attack by chloride ion at C_α and formation of the Markownikov-orientated products **10a** and **11a**. Similar non-regiospecificity and isomer ratios have been observed in the corresponding additions of bromine chloride, iodine chloride, and 2,4-dinitrobenzenesulfenyl chloride.[15] The exclusive formation of the Markownikov-orientated acetoxythiocyanates **10c** and **11c** in these cases may be due to acetic acid being a weaker nucleophile than chloride ion, and thus more selective in its attack. Similar effects have been noted in additions of sulfenyl halides to alkenes.[8]

In the cases of 4-*t*-butyl- and 4-methyl-cyclohexene, the equatorial *t*-butyl and methyl groups are too remote from the reaction centre (a) to affect the ease with which the episulfonium bridge is formed on either side of the ring, and (b) to make the bridge significantly asymmetric. Consequently diaxial ring-opening, in the manner described for Δ^2-octalin and cyclohexene,[2] can occur with equal ease at C_α and C_β leading in each case to equal amounts of regioisomers (see products **12** and **14**). Similar results have been obtained in the heterolytic addition of bromine chloride to these alkenes.[9] For 5α-cholest-2-ene, steric shielding of the β-side of the molecule by the axial C_{10} methyl group leads to exclusive formation of the 2α, 3α-sulfonium ion which, on diaxial ring opening at C_2, leads to the observed 2β-chloro-3α-thiocyanate (**13a**) and 2β-acetoxy-3α-thiocyanate (**13b**). Similar regiospecificity and stereospecificity have been noted in the heterolytic addition of iodine azide[10] and iodine isocyanate[11] to this alkene.

The disubstituted terminal alkene, 2-ethylbut-1-ene,

differs from the previous alkenes in giving (a) the Markownikov-orientated adducts **15a** and **15b** exclusively (*cf.* the exclusive Markownikov addition of iodine isocyanate to 2-methylpropene)[11] and (b) the unsaturated isothiocyanate **16**. Furthermore, the chlorothiocyanate : acetoxythiocyanate ratio (see Table 1) is in the range shown by the α-arylalkenes rather than that shown by the aliphatic alkenes. It is suggested that this alkene reacts *via* the open carbonium ion **19** rather than a cyano-sulfonium ion, due to the second ethyl group conferring stability comparable to that of a single phenyl group. Concomitant proton loss from an ethyl group of the carbonium ion (*cf.* the α-arylalkenes), followed by allylic rearrangement,[12] readily accounts for the formation of the isothiocyanate **16** as shown below.

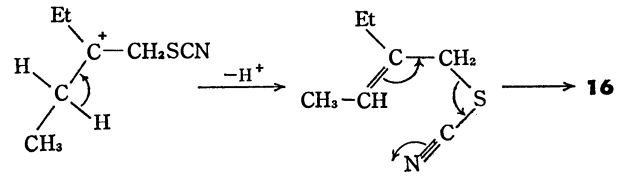

19

Reactivity of Thiocyanogen Chloride. The presence of one electron-withdrawing group deactivates the double bond sufficiently to prevent addition of thiocyanogen chloride to these alkenes. This pseudohalogen chloride is therefore comparable in reactivity to the arenesulfenyl chlorides (ArSCl), but less reactive than iodine chloride and bromine chloride.[15]

Experimental

Alkenes. 4-*t*-Butylcyclohexene (bp 64—65 °C/15 mmHg, n_D^{25} 1.4567) was prepared by dehydration of 4-*t*-butylcyclohexanol with potassium hydrogensulfate. 5α-Cholest-2-ene (mp 74—75 °C) was prepared as described.[13] The other alkenes used were commercial samples purified until their physical constants agreed with those recorded in the literature.

General Procedure. This has been described in Parts I[2] and II.[1]

Propene. Propene gave (a) a mixture of 2-chloro-1-thiocyanatopropane (**10a**) and 1-chloro-2-thiocyanatopropane (**10b**) as a colourless liquid; bp 35—37 °C/0.1 mmHg; n_D^{22} 1.5010; ν 2165(SCN)cm^{-1}; τ (in CCl_4) 5.74 (sext, *J* 6.5 Hz, CHCl), 6.08 to 6.63 (m, CHSCN and CH_2Cl), 6.75 (d, *J* 6.5 Hz, CH_2SCN), 8.30 (d, *J* 6.5 Hz, CH_3CHCl), 8.40 (d, *J* 6.5 Hz, CH_3CHSCN) (Found: C, 35.2; H, 4.7; N, 10.25%. Calcd for C_4H_6ClNS: C, 35.45; H, 4.45; N, 10.35%), and (b) 2-*acetoxy*-1-*thiocyanatopropane* (**10c**) as a colourless liquid; bp 56—57 °C/0.1 mmHg; n_D^{22} 1.4700; ν 2165(SCN), 1740 (C=O) cm^{-1}; τ (in CCl_4) 4.86 (1H, p of d, *J* 6.5 and 4.5 Hz, CHOAc), 6.87 (1H, d, *J* 4.5 Hz, one H of CH_2SCN), 6.90 (1H, d, *J* 6.5 Hz, second H of CH_2SCN), 7.93 (3H, s, $OCOCH_3$), 8.61 (3H, d, *J* 6.5 Hz, CH_3) (Found: C, 45.15; H, 5.8; N, 8.9%. $C_6H_9NO_2S$ requires C, 45.3; H, 5.7; N, 8.8%). The isomer ratio for the mixture of chlorothiocyanates was determined from the integral traces of the CHX and CH_2X (X=Cl, SCN) proton signals.

1-Hexene. 1-Hexene gave (a) a mixture of 2-chloro-1-thiocyanatohexane (**11a**) and 1-chloro-2-thiocyanatohexane (**11b**) as a colourless liquid; bp 65—67 °C/0.05 mmHg n_D^{25} 1.4891; ν 2165(SCN)cm^{-1}; τ (in $CDCl_3$) 5.84 (p, *J* 6 Hz, CHCl), 6.08 to 6.55 (m, CHSCN and CH_2Cl), 6.69 (d, *J* 6 Hz, CH_2SCN), 7.80 to 9.30 (m, C_4H_9) (Found: C, 47.6; H, 7.0; Cl, 19.85; N, 7.9%. Calcd for $C_7H_{12}ClNS$: C, 47.3; H, 6.8; Cl, 19.95; N, 7.9%), and (b) 2-*acetoxy*-1-*thiocyanatohexane* (**11c**) as a colourless liquid; bp 76 °C/0.05 mmHg; n_D^{25} 1.4684; ν 2165 (SCN), 1740 (C=O)cm^{-1}; τ (in $CDCl_3$) 4.85 (1H, q of d, *J* 6.5 and 4.5 Hz, CHOAc), 6.78 (1H, d, *J* 4.5 Hz, one H of CH_2SCN), 6.85 (1H, d, *J* 6.5 Hz, second H of CH_2SCN), 7.89 (3H, s, $OCOCH_3$), 7.95 to 9.30 (9H, m, C_4H_9) (Found: C, 53.3; H, 7.45; N, 7.3; S, 15.8%. $C_9H_{15}NO_2S$ requires C, 53.7; H, 7.5; N, 6.95; S, 15.95%). The isomer ratio for the mixture of chlorothiocyanates was determined as described for propene.

4-t-Butylcyclohexene. 4-*t*-Butylcyclohexene gave (a) a mixture of 2*ax*-chloro-1*ax*-thiocyanate-4*eq*-*t*-butylcyclohexane (**12a**) and 1*ax*-chloro-2*ax*-thiocyanato-4*eq*-*t*-butylcyclohexane (**12b**) as a pale yellow liquid; bp 78—79 °C/0.05 mmHg; n_D^{25} 1.5132; ν 2165(SCN)cm^{-1}; τ (in $CDCl_3$ at 100 MHz) 5.44 and 5.77 (each 1H, distorted q, band-width 9Hz, *J*~3 Hz, CHCl), 5.96 and 6.10 (each 1H, distorted q, band-width 9 Hz, *J*~3 Hz, CHSCN), 7.50 to 9.00 (14 H, m, CH_2 and $CHBu^t$), 9.10 (18H, s, C_3H_9) (Found: C, 57.3; H, 7.7; Cl, 15.0; N, 5.9%. Calcd for $C_{11}H_{18}ClNS$: C, 57.0; H, 7.85; Cl, 15.3; N, 6.05%), and (b) a mixture of 2*ax*-acetoxy-1*ax*-thiocyanato-4*eq*-*t*-butylcyclohexane (**12c**) and 1*ax*-acetoxy-2*ax*-thiocyanato-4*eq*-*t*-butylcyclohexane (**12d**) as a colourless liquid; bp 96 °C/0.05 mmHg n_D^{25} 1.4195; ν 2165 (SCN), 1740 (C=O)cm^{-1}; τ (in $CDCl_3$ at 100 MHz) 4.87 and 5.00 (each 1H, distorted q, band-width 10 Hz, *J*~3 Hz, CHOAc), 6.12 and 6.25 (each 1H, distorted q, band-width 10 Hz, *J*~3 Hz, CHSCN), 7.50 to 9.00 (14H, m, CH_2 and $CHBu^t$), 9.10 (18H, s, C_3H_9) (Found: C, 60.9; H, 8.25; N, 5.6; S, 12.65%. Calcd for $C_{13}H_{21}NO_2S$: C, 61.15; H, 8.3; N, 5.5; S, 12.55%). The isomer ratio for each mixture was determined from the integral traces of the CHX (X=SCN, Cl or OAc) proton signals.

5α-Cholest-2-ene. 5α-Cholest-2-ene gave (a) 2β-*chloro*-3α-*thiocyanato*-5α-*cholestane* (**13a**) as colourless needles; mp 90—92 °C after crystallization from methanol; ν 2165(SCN) cm^{-1}; τ (in $CDCl_3$ at 100 MHZ) 5.49 (1H, distorted q, band-width 9 Hz, *J*~3 Hz, CHCl) 5.95 (1H, distorted q, band-width 9 Hz, *J*~3 Hz, CHSCN), 7.50 to 9.20 (44H, m, residual H) (Found: C, 72.2; H, 10.3; N, 3.25%. $C_{28}H_{46}ClNS$ requires C, 72.45; H, 10.0; N, 3.0%), and (b) 2β-acetoxy-3α-thiocyanato-5α-cholrestane (**13b**) as colourless needles, mp 110—112 °C after crystallization from methanol, identical in physical and spectral properties with the compound described by Takeda *et al.*[4] (Found: C, 73.6; H, 10.25; N, 2.8%. Calcd for $C_{30}H_{49}NO_2S$: C, 73.9; H, 10.15; N, 2.85%).

The effect of a 3α- and a 2β-thiocyanato group on the chemical shift of a 2α- and a 3β-CHCl proton respectively was calculated using a chemical shift value of τ 5.55 for the equatorial 2α- and 3β-CHCl protons,[14] and shift values of −0.03 and −0.13 τ for the 3α- and the 2β-thiocyanato groups respectively.[5]

4-Methylcyclohexene. 4-Methylcyclohexene gave (a) a mixture of 4-methyl-*trans*-1-chloro-2-thiocyanatocyclohexane (**14b**) and 4-methyl-*trans*-2-chloro-1-thiocyanatocyclohexane (**14a**) as a colourless liquid; bp 60—62 °C/0.05 mmHg; n_D^{20} 1.5224; ν 2165(SCN)cm^{-1}; τ (in $CDCl_3$ at 100 MHz) 5.45 to 5.90 (1H, 10-line m, band-width 40 Hz, overlapping CHCl), 6.10 to 6.50 (1H, 9-line m, band-width 37 Hz, overlapping CHSCN), 7.50 to 9.10 (10 H, m, residual H) (Found: C, 50.6; H, 6.55; N, 7.35%. Calcd for $C_8H_{12}ClNS$: C, 50.65; H, 6.4; N, 7.4%), and (b) a mixture of 4-methyl-

trans-1-acetoxy-2-thiocyanatocyclohexane (**14d**) and 4-methyl-*trans*-2-acetoxy-1-thiocyanatocyclohexane (**14c**) as a colourless liquid; bp 76—78 °C/0.05 mmHg; n_D^{20} 1.4960; ν 2165(SCN), 1740 (C=O) cm^{-1}; τ (in $CDCl_3$ at 100 MHz) 4.80 to 5.30 (1H, 13-line m, band-width 44 Hz, overlapping CHOAc), 6.25 to 6.65 (1H, 14-line m, band-width 35 Hz, overlapping CHSCN), 7.50 to 9.20 (10H, m, residual H) (Found: C, 56.65; H, 7.25; N, 6.35%. Calcd for $C_{10}H_{15}NO_2S$: C, 56.35; H, 7.1; N, 6.55%). Due to overlapping, the isomer ratio for each mixture could not be determined from the integral traces of the CHX (X=SCN, Cl or OAc) proton signals; the symmetry of these signals, however, indicated that the positional isomers were present in equal amounts in both cases.

2-Ethylbut-1-ene. 2-Ethylbut-1-ene gave, in order of elution from the column, (a) *2-ethyl-3-isothiocyanatobut-1-ene* (**16**) as a colourless liquid; bp 30 °C/0.1 mmHg; n_D^{21} 1.5112; ν 3100 (=C–H), 2200 to 1980(NCS), 1640(C=C) cm^{-1}; τ (in CCl_4), 4.91 and 5.08 (each 1H, d, J 1.5 Hz, vinyl H), 5.72 (1H, q, J 7 Hz, CHNCS), 7.87 (2H, q, J 7 Hz, CH_2), 8.51 (3H, d, J 7 Hz, CH_3CHNCS), 8.87 (3H, t, J 7 Hz, CH_3CH_2) (Found: C, 59.7; H, 8.0; N, 9.55; S, 22.25%. $C_7H_{11}NS$ requires C, 59.55; H, 7.85; N, 9.9; S, 22.65%), (b) *2-chloro-2-ethyl-1-thiocyanatobutane* (**15a**) as a colourless liquid; bp 50 °C/0.1 mmHg; n_D^{21} 1.4990; ν 2165(SCN) cm^{-1}; τ (in CCl_4) 6.61 (2H, s, CH_2SCN), 8.19 (4H, q, J 7 Hz, CH_2), 8.94 (6H, t, J 7 Hz, CH_3) (Found: C, 47,3; H, 6.8; N, 7.65%. $C_7H_{12}ClNS$ requires C, 47.3; H, 6.8; N, 7.9%), and (c) *2-acetoxy-2-ethyl-1-thiocyanatobutane* (**15b**) as a colourless liquid; bp 64 °C/0.1 mmHg; n_D^{23} 1.4775; ν 2165 (SCN), 1740 (C=O) cm^{-1}; τ (in CCl_4) 6.50 (2H, s, CH_2SCN), 8.01 (3H, s, $OCOCH_3$), 8.08 (4H, q, J 7 Hz, CH_2), 9.12 (6H, t, J 7 Hz, CH_3) (Found:,C, 53.9; H, 7.25; N, 6.8%. $C_9H_{15}NO_2S$ requires C, 53.7; H, 7.5; N, 6.95%).

Styrene. Styrene gave (a) *1-chloro-1-phenyl-2-thiocyanatoethane* (**3a**) as a colourless liquid; bp 79 °C/0.05 mmHg; n_D^{23} 1.5802; ν 2165(SCN) cm^{-1}; τ (in $CDCl_3$) 2.61 (5H, s, aromatic H), 4.90 (1H, t, J 7.5 Hz, CHCl), 6.50 (2H, d, J 7.5 Hz, CH_2SCN) (Found: C, 54.7; H, 4.25; Cl, 17.65; N, 7.2; S, 16.1%. C_9H_8ClNS requires C, 54.7; H, 4.1; Cl, 17.95; N, 7.1; S, 16.15%), and (b) 1-*acetoxy*-1-*phenyl*-2-*thiocyanatoethane* (**3b**) as a colourless liquid; bp 107 °C/0.05 mmHg; n_D^{20} 1.5412; ν 2165(SCN), 1740(C=O) cm^{-1}; τ (in $CDCl_3$) 2.63 (5H, s, aromatic H), 3.96 (1H, t, J 7 Hz, CHOAc), 6.67 (2H, d, J 7 Hz, CH_2SCN), 7.85 (3H, s, $OCOCH_3$) (Found: C, 59.5; H, 5.25; N, 6.25%. $C_{11}H_{11}NO_2S$ requires C, 59.7; H, 5.0; N, 6.35%).

1-Chloro-1-phenyl-2-thiocyanatoethane (1 g) was heated under reflux with triethylamine (1 g) in toluene (25 ml) for 12 h. After cooling triethylamine hydrochloride was filtered off, and the filtrate was washed with dilute sulfuric acid and then water. Drying ($MgSO_4$) and removal of solvent gave *trans-β-thiocyanatostyrene* (0.7 g, 86%) as a colourless liquid; bp 89 °C/0.2 mmHg, n_D^{24} 1.6178; ν 2170(SCN) cm^{-1}; τ (in $CDCl_3$) 2.70 (5H, s, aromatic H), 3.06 (1H, d, J 15 Hz, *trans*-C=CHSCN), 3.60 (1H, d, J 15 Hz, *trans*-C=CHPh) (Found: C, 67.1; H, 4.25; N, 8.75%. C_9H_7NS requires C, 67.05; H, 4.4; N, 8.7%)

Indene. Indene gave (a) a mixture of *cis*- and *trans*-1-chloro-2-thiocyanatoindane (**4a** and **5a**) as a colourless liquid; bp 105—107 °C/0.05 mmHg; n_D^{27} 1.6015; ν 2165 (SCN) cm^{-1}; τ (in CCl_4) 2.50 to 3.10 (m, aromatic H) 4.63 (d, J 5.5 Hz, *cis*-CHCl), 4.73 (d, J 4.5 Hz, *trans*-CHCl), 5.65 to 6.50 (m, *cis*- and *trans*-CHSCN and one H of *trans*-CH_2), 6.65 (d, J 7.5 Hz, *cis*-CH_2), 7.00 (d of d, J 17 Hz and 5 Hz, second H of *trans*-CH_2) (Found: C, 57.4; H, 4.05; Cl, 16.5; N, 6.65%. Calcd for $C_{10}H_8ClNS$: C, 57.25; H, 3.85; Cl, 16.9; N, 6.7%), and (b) a mixture of *cis*- and *trans*-1-acetoxy-2-thiocyanatoindane (**4b** and **5b**) as a colourless liquid; bp 123—125 °C/0.05 mmHg; n_D^{25} 1.5585; ν 2165(SCN), 1740 (C=O); τ (in CCl_4) 2.60—2.90 (m, aromatic H), 3.82 (d, J 5 Hz, coincidental *cis*- and *trans*-CHOAc), 5.65 to 6.20 (m, *cis*- and *trans*-CHSCN), 6.40 (d of d, J 15.5 Hz and 7.5 Hz, one H of *trans*-CH_2): 6.60 (d, J 7 Hz, *cis*-CH_2), 7.00 (d of d, J 15.5 Hz and 6.5 Hz, second H of *trans*-CH_2), 7.96 (s, $OCOCH_3$) (Found: C, 61.45; H, 4.9; N, 6.25%. Calcd for $C_{12}H_{11}NO_2S$: C, 61.80; H, 4.75; N, 6.0%). The isomer ratio for each mixture was determined from the integral traces of the *cis*-CH_2 and the high-field *trans*-CH_2 proton signals. The *cis*- and *trans*-CHX (X=Cl, OAc) proton signals were more clearly resolved in dimethyl sulfoxide solvent [τ 4.23 (d, J 5.5 Hz, *cis*-CHCl), 4.37 (d, J 4.5 Hz, *trans*-CHCl), 3.70 (d, J 5.5 Hz, *cis*-CHOAc), 3.75 (d, J 5 Hz, *trans*-CHOAc)].

1,1-Diphenylethylene. 1,1-Diphenylethylene gave (a) 1,1-diphenyl-2-thiocyanatoethylene (**2**) as a waxy solid; ν 2165 (SCN), 1600(C=C) cm^{-1}; τ (in CCl_4) 2.40 to 2.85 (10H, m, aromatic H), 3.47 (1H, s, CHSCN). This product, on treatment with lithium aluminium hydride and then 2,4-dinitrochlorobenzene,[7] gave 1,1-*diphenyl*-2-*(2,4-dinitrophenylthio)ethylene* as yellow needles; mp 138—141 °C after crystallisation from acetic acid (Found: C, 63.1; H, 3.7; N, 7.45%. $C_{20}H_{14}N_2O_4S$ requires C, 63.5; H, 3.75; N, 7.4%), and (b) 1-*hydroxy*-1,1-*diphenyl*-2-*thiocyanatoethane* (**6**) as colourless needles; mp 99—100 °C after crystallisation from benzene–light petroleum; ν 2165 (SCN), 3350(OH) cm^{-1}; τ (in CCl_4) 2.62 (10H, s, aromatic H), 6.11 (2H, s, CH_2SCN), 7.12 (1H, s, OH); (Found: C, 70.8, H, 5.1; N, 5.5%. $C_{15}H_{13}NOS$ requires C, 70.6; H, 5.15; N, 5.5%).

Triphenylethylene. Triphenylethylene gave (a) *triphenylthiocyanatoethylene* (**9**) as colourless plates; mp 103—104 °C after crystallisation from carbon tetrachloride; ν 2165(SCN), 1530(C=C) cm^{-1}; τ (in $CDCl_3$) 2.60 to 2.98 (m, phenyl H) (Found: C, 80.5; H, 4.8; N, 4.4. $C_{21}N_{15}NS$ requires C, 80.5; H, 4.85; N, 4.45%), and (b) 1-*hydroxy*-1,1,2-*triphenyl*-2-*thiocyanatoethane* (**8**) as colourless needles; mp 165—168 °C after crystallisation from carbon tetrachloride; ν 2165(SCN), 3350(OH) cm^{-1}; τ (in $CDCl_3$) 2.65 to 3.05 (15H, m, aromatic H), 4.49 (1H, s, CHSCN), 7.04 (1H, s, OH) (Found: C, 76.5; H, 5.1, N, 4.1%. $C_{21}H_{17}NOS$ requires C, 76.1; H, 5.15; N, 4.25%).

Control Experiments. These were carried out as described in Part I.[2]

Unreactive Alkenes. *trans*-Cinnamic acid, *trans*-crotonic acid, and methyl *trans*-cinnamate were recovered quantitively from the reaction mixtures after 48—140 h, and identified by their IR spectra. Methyl acrylate, vinyl chloride, vinylidene chloride, trichloroethylene, and vinyl bromide yielded no product after 48—126 h, but were not recovered due to their loss by volatilisation during the isolation procedure.

Spectra. IR spectra were recorded with a Perkin-Elmer 237 spectrometer, and were taken for films of liquid products and for Nujol mulls of solid products. ^1H NMR spectra were recorded with Varian A60A and HA100 spectrometers, using tetramethylsilane as internal standard. In the NMR data given above, s=singlet, d=doublet t=triplet, q=quartet, p=pentet, sext=sextet, m=multiplet; band-widths are separations of outer lines.[3]

We thank Hertfordshire County Council for the award of a Research Assistantship to one of us (I.P.), and the Chemical Society for the award of a Research Grant.

References

1) Part II, R. G. Guy and I. Pearson, *J. Chem. Soc., Perkin Trans. 2*, **1973**, 1359.
2) R. G. Guy and I. Pearson, *J. Chem. Soc., Perkin Trans. 1*, **1973**, 281.
3) N. C. Franklin and H. Feltkamp, *Angew. Chem. Internat. Edn. Engl.*, **4**, 774 (1965).
4) K. Takeda, T. Komeno, J. Kawanami, S. Ishihara, H. Kadokawa, H. Tokura, and H. Itani, *Tetrahedron*, **21**, 329 (1965).
5) N. S. Bhacca and D. H. Williams, "Applications of NMR Spectroscopy in Organic Chemistry," Holden-Day, Inc., San Francisco (1964), p. 183.
6) W. E. Rosen, L. Dorfman, and M. P. Linfield, *J. Org. Chem.*, **29**, 1723 (1964).
7) A. B. Angus and R. G. R. Bacon, *J. Chem. Soc.*, **1958**, 774; R. G. R. Bacon and R. S. Irwin, *ibid.*, **1958**, 778; R. G. R. Bacon and R. G. Guy, *ibid.*, **1960**, 318: **1961**, 2428; R. G. R. Bacon, R. G. Guy, and R. S. Irwin, *ibid.*, **1961**, 2436.
8) G. M. Beverly, D. R. Hogg, and J. H. Smith, *Chem. Ind.*, **1968**, 1403; see also D. R. Hogg and J. H. Smith, *Mech. Reactions Sulfur Compounds*, **3**, 63 (1968).
9) H. J. Hageman and E. Havinga, *Rec. Trav. Chim.*, **85**, 1141 (1966).
10) A. Hassner and L. A. Levy, *J. Am. Chem. Soc.*, **87**, 4203 (1965).
11) A. Hassner, M. E. Lorber, and C. Heathcock, *J. Org. Chem.*, **32**, 540 (1967).
12) A. Fava, "The Chemistry of Organic Sulphur Compounds," Vol. 2, ed. by N. Kharasch and C. Y. Meyers, Pergamon Press, Oxford (1966), p. 73.
13) G. H. Alt and D. H. R. Barton, *J. Chem. Soc.*, **1954**, 4284.
14) E. L. Eliel and R. J. L. Martin, *J. Am. Chem. Soc.*, **90**, 689 (1968).
15) P. B. D. de la Mare and R. Bolton, "Electrophilic Additions to Unsaturated Systems," Elsevier, Amsterdam (1966), Chapt. 7 and 8; R. C. Fahey, "Topics in Stereochemistry," Vol. 3, ed. by E. L. Eliel and N. L. Allinger, Interscience, New York (1968), p. 237.

NOTES

BULLETIN OF THE CHEMICAL SOCIETY OF JAPAN, VOL. 49 (8), 2315—2316 (1976)

Reflection Spectra of Acenaphthene Crystals

Masashi TANAKA

Department of Chemistry, Faculty of Science, Nagoya University, Chikusa, Nagoya 464

(Received February 10, 1976)

Synopsis. The reflection spectra have been measured for acenaphthene crystals. The excited states of the acenaphthene molecule are similar to those of the naphthalene molecule; the lower $\pi\rightarrow\pi^*$ excited states are observed at 31100 (α), 32600 (p), 43700 (β), and 47400 (β') cm^{-1}. In the reflection spectra of the crystal, the α and β states polarized along the b axis are observed at 30900 and 41800 cm^{-1}, respectively. The p and β' states are found at 32100 and 44000 cm^{-1} in the a axis spectrum and at 31400 and 45000 cm^{-1} in the c axis spectrum.

Four lower $\pi\rightarrow\pi^*$ excited state (α, p, β, and β' bands) of the naphthalene molecule were found to be located at 32000, 34500, 45500, and 60000 cm^{-1} respectively by the study of UV spectra in solution. The α and β bands are reported to be polarized along the long molecular axis (B_{2u} symmetry) and the p and β' along the short axis (B_{1u} symmetry).

McClure[1] succeeded in obtaining the polarization direction of the first $\pi\rightarrow\pi^*$ state (α band) with the mixed crystal of naphthalene in durene. Bree[2] observed the α, p, and β' bands of acenaphthene crystal by the polarized absorption method. However, he could not find the intense β band, although the dipole-dipole approximation predicted this band would lie at 58730 and 48230 cm^{-1}, with all the intensity effectively concentrated in the higher energy component.

We have determined the band position of the β state by measuring the reflection spectra of acenaphthene crystal and have theoretically explained the difference between the observed and predicted values.

Experimental

Single crystals of acenaphthene were grown by slow evaporation from ethyl acetate solution. The crystals showed well-developed (010), (100), (101), and (111) faces. These faces were identified by a morphological examination.

Reflection spectra at normal incidence were measured over a wavelength range 650—192 nm with a reflection spectrophotometer made in our laboratory. Reflection spectra for the (010) and (100) faces are shown in Fig. 1 and the corresponding absorption spectra obtained by the Kramers-Kronig transformation[3] are shown in Fig. 2.

Results and Discussion

The acenaphthene crystal has four molecules in an orthorhombic unit cell of space group $Pcm2_1$ (C_{2v}^2)[4] in which a molecular and a crystallographic mirror plane coincide. Therefore, the B_{1u} states (p and β' bands) are polarized in the ac plane, while the B_{2u} states (α and β bands) appear only in the b polarization.

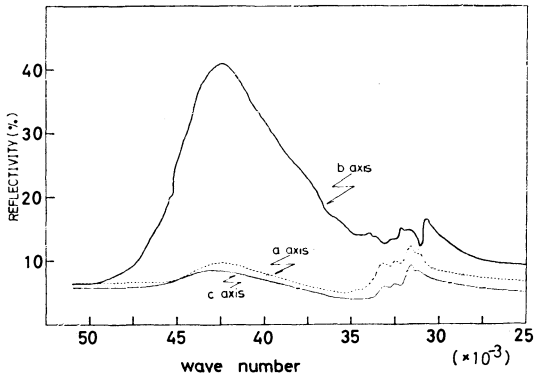

Fig. 1. The reflection spectra of the acenaphthene crystal on the ac and bc planes.

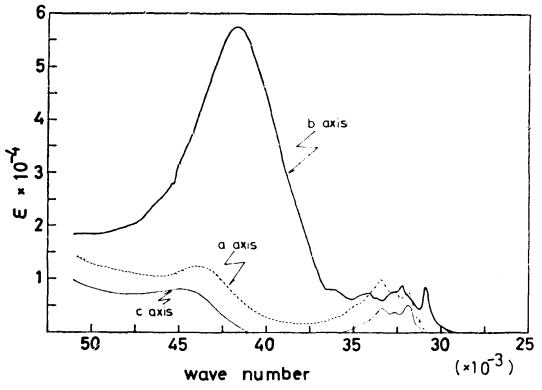

Fig. 2. The absorption spectra obtained by the Kramers-Kronig transformation of the reflection spectra of the acenaphthene crystal.

Two bands in the b axis spectrum are observed, at 30900 and 41800 cm^{-1}. The weak band at 30900 cm^{-1} corresponds to the α band at 31100 cm^{-1} in solution and is assigned to the α state of B_{2u} symmetry in the free molecule. Bree[2] observed this band at 31020 cm^{-1}. However, the intense band at 41800 cm^{-1} was not observed by Bree and can be obtained only by the reflection method. This band corresponds to the β band at 43700 cm^{-1} in solution and is assigned to the B_{2u} state of the molecule. The spectra for the ac plane has two bands. The one band in the region of 3200 cm^{-1} has a vibronic structure and the other, at about 45000 cm^{-1}, is broad; these bands correspond to the p and β' states in the free molecule, respectively. The band positions of these bands are consistent with those obtained by Bree.

In Table 1 are given the calculated exciton state energies and oscillator strengths, obtained by the CI[5]

TABLE 1. CALCULATED AND OBSERVED TRANSITION ENERGIES (E IN 1000 cm^{-1}) AND OSCILLATOR STRENGTHS (f) OF EXCITON STATES OF THE ACENAPHTHENE CRYSTAL

State			CI method[b]		RPA method I[c]		RPA method II[c]		Obsd	
			E	(f)	E	(f)	E	(f)	E	(f)
A_1	c axis	p	34.8	(0.39)	34.4	(0.31)	34.4	(0.31)	31.4	(0.10)
		p	35.9	(0)	35.2	(0)	35.2	(0)		
		β'	50.2	(0.80)	49.1	(0.52)	49.1	(0.53)	45.0	(0.4)
		β'	52.5	(0.18)	51.1	(0.10)	51.1	(0.10)		
B_1	a axis	p	34.1	(0.69)	33.6	(0.24)	33.7	(0.21)	31.2	(0.15)
		p	35.4	(0.05)	34.7	(0.25)	34.7	(0.26)		
		β'	49.4	(0.68)	48.8	(0.46)	48.9	(0.40)	44.0	(0.4)
		β'	50.6	(0.54)	49.8	(0.56)	49.9	(0.63)		
B_2	b axis	α[a]	34.1	(0)	34.0	(0)	34.0	(0)	30.9	(0.18)
		β	49.0	(6.34)	46.6	(4.39)	46.4	(4.39)	41.8	(2.0)
		β	65.2	(0)	57.0	(0)	57.0	(0)		

a) The α band in the B_2 exciton state is doublet. b) Calculation by the exciton CI method[4] when the inner zone radius is 50 Å. c) Calculations by the exciton RPA method[5] where the inner zone radii are 50 and 100 Å, respectively.

and RPA[6] methods; where the intermolecular interactions were estimated for two inner zone radii, 50 and 100 Å. The calculated values for the two inner zone radii are nearly equal; hence, convergence of the summation of intermolecular interactions has been achieved. Table 1 shows that the exciton state energies and oscillator strengths decrease more and are closer to the observed values in the RPA method than in the CI method.

The intense β band was predicted to lie at 58700 cm^{-1} by Bree, while the observed value is 41800 cm^{-1}. Using the CI and RPA methods, this band was calculated to be located at 49000 and 46600 cm^{-1}, respectively. The difference between these three calculated values can be explained by the fact that the RPA method includes the polarization effect by taking account of the double excitation, by comparison with the CI and dipole-dipole approximations. That is, the polarization effect has a strong influence on the Davydov splitting and band shift of the intense band.

The other band system (α state) at 30900 cm^{-1} is theoretically forbidden, but seems to be allowed by the mixing of higher excited states than the states taken into account in this calculation. The p band at 32000 cm^{-1} is expected to arise from a short axis transition. The calculated exciton state energies are 34400 and 35200 cm^{-1} for the A_1 exciton state and 33700 and 34700 cm^{-1} for the B_1 exciton state; these are supported by the observed values. The measured polarization ratio (f^a/f^c) is 1.5, comparable to the calculated value of 1.7. The oscillator strengths of two p states in the B_1 exciton state show different values: (0.69/0.05) in the CI method and (0.21/0.26) in the RPA method. This can be explained by the difference in the CI and RPA methods of the mixing of the nearly degenerate exciton configurations belonging to crystallographically non-equivelent sites.

References

1) D. S. McClure, *J. Chem. Phys.*, **22**, 1668 (1954); **24**, 1 (1956).
2) A. Bree, *Mol. Phys.*, **6**, 563 (1963).
3) H. J. Bowlden and J. K. Wilmskurst, *J. Opt. Soc. Am.*, **53**, 1073 (1963); D. M. Roesler, *Brit. J. Appl. Phys.*, **16**, 1119 (1965).
4) H. W. Ehrlich, *Acta Crystallogr.*, **10**, 699 (1957).
5) M. Tanaka and J. Tanaka, *Mol. Phys.*, **16**, 1 (1969).
6) M. Tanaka and J. Tanaka, *Theoret. Chim. Acta*, **30**, 81 (1973).

BULLETIN OF THE CHEMICAL SOCIETY OF JAPAN, VOL. 49(8), 2317—2318 (1976)

Dielectric Transition in a Solution of Linear Poly(vinyl acetate)

Satoru MASHIMO, Yasuo IWASA,* Akio CHIBA,* and Keniti HIGASI*

Department of Physics, Tokai University, Hiratsuka, Kanagawa 259-12

**School of Science and Engineering, Waseda University, Shinjuku-ku, Tokyo 160*

(Received March 10, 1976)

Synopsis. The dielectric constants and losses of linear poly(vinyl acetate) (PVAc) in carbon tetrachloride were measured at various temperatures and frequencies. The results provide proof that dielectric transition in solution occurs for PVAc, irrespective of its sources.

The interesting phenomenon of dielectric transition in solution was first discovered for poly(vinyl acetate) (PVAc) in toluene.[1] Later the same phenomenon was found also for PVAc in carbon tetrachloride,[2] poly(vinyl chloride) in dioxane[3] and poly(*p*-chlorostyrene) in carbon tetrachloride.[3] One interpretation[3] of this transition is that the transition indicates the change in conformation from globular chain molecules (lower temperature) to loosely coiled chain molecules (higher temperature). This new type of transition has also been discussed by several theoreticians, such as Ptitsyn *et al.*,[4] Lifshitz,[5] Edwards,[6] Domb,[7] and Saito.[8]

The purpose of this note is to clear up doubts regarding the polymer samples employed. The samples of PVAc and poly(vinyl chloride) used previously were all from commercial sources, and commercial PVAc is believed to have branched chains. A sample of linear PVAc chains was prepared for this work by the acetylation of linear poly(vinyl alcohol),[9] and its purity was checked by means of the infra-red absorption spectra. The viscosity-average molecular weight of the sample was 6.1×10^4. The carbon tetrachloride was dehydrated and distilled before use. The dielectric measurements[1-3] were carried out by the use of the apparatus described in previous reports.[2,3]

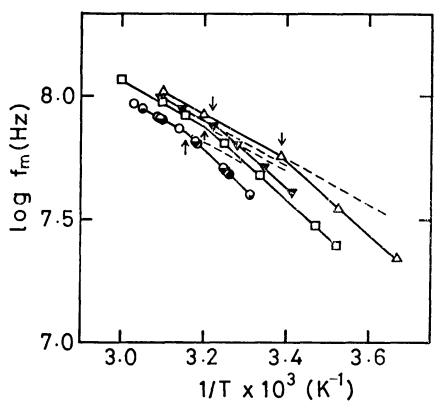

Fig. 1. Plot of $\log f_m$ against $1/T$ for PVAc in carbon tetrachloride.
△: 2.66 wt%, $\overline{M}_n=0.97\times10^4$, $\overline{M}_v=1.7\times10^4$;
▼: 1.93 wt%, $\overline{M}_n=3.0\times10^4$, $\overline{M}_v=4.3\times10^4$;
□: 2.68 wt%, linear PVAc, $\overline{M}_v=6.1\times10^4$;
●: 1.00 wt%, $\overline{M}_n=1.1\times10^5$, $\overline{M}_v=3.9\times10^5$;
○: 2.04 wt%; ◒: 3.20 wt%.

The results of the dielectric measurements are shown in Figs. 1 and 2, together with those for the commercial ones.[2,3] A dielectric transition is observed in the linear PVAc in carbon tetrachloride, too. The plot of $\log f_m$ against $1/T$ gives two straight lines. The transition temperatures (T_t) are obtained from the points at which two lines intersect. The apparent activation energy above T_t is calculated to be 4.2 kcal/mol, while it is 6.9 kcal/mol below T_t. These values

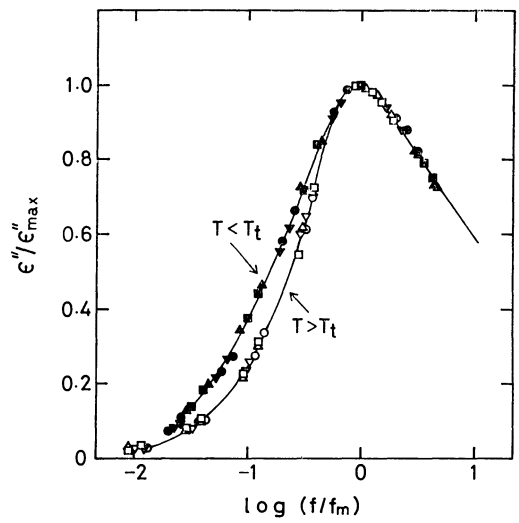

Fig. 2. Master plot of $\varepsilon''/\varepsilon''_{max}$ against $\log(f/f_m)$ for PVAc in carbon tetrachloride.
▲: 2.66 wt%, $\overline{M}_n=0.97\times10^4$, 0.0 and 13.0 °C;
△: 40.0 and 50.0 °C; ▼: 1.93 wt%, $\overline{M}_n=3.0\times10^4$, 19.7 and 25.5 °C; ▽: 44.1 and 50.3 °C; ■: 2.68 wt% linear PVAc, 11.0 and 15.0 °C; □: 50.0 and 60.0 °C; ●: 3.20 wt%, $\overline{M}_n=1.1\times10^5$, 29.0 and 35.0 °C; ○: 50.0 and 55.0 °C.

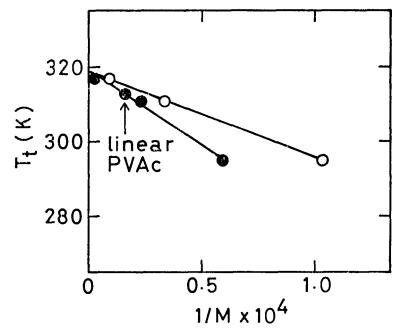

Fig. 3. Plot of T_t against the reciprocal of the molecular weight of PVAc. Open circles refer to the number-average molecular weight and closed circles the viscosity-average molecular weight.

are in complete agreement with those for the commercial PVAc. A slight change in the shape of the two loss curves at T_t is observed, and there is no difference in these curves with the sort of sample, *i.e.*, whether commercial and linear. The temperature, T_t, depends on the molecular weight of PVAc, as is shown in Fig. 3. In conclusion, the effects of the branched chains, and, possibly, of the source of the sample do not appear to play an important role in this kind of transition phenomenon.

References

1) S. Mashimo, Y. Otsubo, and K. Higasi, *Bull. Chem. Soc. Jpn.*, **43**, 3324 (1970).
2) S. Mashimo and K. Shinohara, *J. Phys. Soc. Jpn.*, **34**, 1141 (1973).
3) S. Mashimo, Y. Iwasa, A. Chiba, and K. Shinohara, *J. Phys. Soc. Jpn.*, **39**, 1529 (1975).
4) O. B. Ptitsyn, A. K. Kron, and Yu. Ye. Eizner, *J. Polym. Sci. Part C*, **16**, 3509 (1968).
5) I. M. Lifshitz, *Soviet Physics-JETP*, **28**, 280 (1969).
6) S. F. Edwards, "Critical Phenomena," ed. by M. S. Green and J. V. Sengers, Nat. Bur. Stand. Miscell. Publ. (1966), p. 225.
7) C. Domb, *Polymer*, **15**, 259 (1974).
8) N. Saito, *Repts. Progr. Polym. Phys. Jpn.*, **17**, 17 (1974).
9) W. H. McDowell and W. O. Kenyon, *J. Am. Chem. Soc.*, **62**, 415 (1940).

BULLETIN OF THE CHEMICAL SOCIETY OF JAPAN, VOL. 49 (8), 2319—2320 (1976)

Benzene Induced Shift for Some Organometallic 8-Quinolinolato Complexes: A New Criterion for the Interaction of Nitrogen with Metal

Yoshikane KAWASAKI

Department of Petroleum Chemistry, Osaka University, Yamadakami, Suita, Osaka 565

(Received March 19, 1976)

Synopsis. The benzene induced shift was measured for some organometallic 8-quinolinolato complexes. A large upfield shift (0.5—0.7 ppm) of the 2-proton of the 8-quinolinolato ligand was found in benzene when the nitrogen in the 8-quinolinolato ligand coordinated to the metal. But the shift was small (0—0.3 ppm) in the absence of nitrogen coordination.

The striking chemical shift difference of the proton resonance of molecules having polar sites caused by changing the solvent from an inert solvent such as carbon tetrachloride to benzene has been applied in many configurational studies[1-3] since the phenomenon was discovered by Bothner-By and Click[4] and Reeves and Schneider.[5] Various explanations have been put forward to interpret the phenomenon.[4,6-13] The phenomenon has been expressed by a large anisotropy of the benzene ring. Ronayne and Williams[8] have pointed out that the benzene induced shift, $\Delta=\delta'-\delta_{\text{benzene}}$ (δ' is the chemical shift of protons in inert solvents such as carbon tetrachloride, chloroform, cyclohexane, or in the pure liquid, and δ_{benzene} is the value in benzene), is positive for the protons in the neighborhood of the positively polarized sites of the molecule and negative for the protons near the negatively polarized sites. In fact, they have shown that in 4-methylpyridine, the 3-proton and the 4-methyl protons give positive Δ values and the 2-proton gives a negative Δ value. Ford and Hart[14] have shown that in tetraalkylammonium tetraalkylborates the alkyl groups of tetraalkylammonium cation give positive Δ values and the tetraalkylborate anion shows a negative Δ value.

In the present paper the benzene induced shift has been measured for some organometallic 8-quinolinolato complexes to study the coordination of the nitrogen in the 8-quinolinolato ligand to the metal.

Results and Discussion

As can be seen from Table 1, the 3- and 4-protons of the 8-quinolinolato ligand of 8-methoxyquinoline, 8-quinolinol, and all organometallic 8-quinolinolato complexes were found to show large positive Δ values. The Δ value of the 2-proton of 8-methoxyquinoline, in which the nitrogen is free from coordination or hydrogen bonding, was very small. Trimethyl(8-quinolinolato)-silane and -germane also gave rather small Δ values for the 2-proton. The value is almost the same as that of 8-quinolinol. These compounds have shown the absorption maximum at around 320 nm and, therefore, have been considered to have a non-chelated 8-quinolinolato ligand.[15] On the other hand, in the complexes with a chelated 8-quinolinolato ligand, such as trimethyl-(8-quinolinolato)tin, and in the protonated 8-methoxyquinoline, the Δ value of the 2-proton was positive and large. The amount of upfield shift is almost the same as those of the 3- and 4-portons. Other organometallic complexes with a chelated 8-quinolinolato ligand, which show the absorption maximum at about 350 nm, gave similar results. The Δ value of the 2-proton of the 8-quinolinolato ligand, therefore, may be used as a new criterion of coordination of nitrogen. The interaction of the lone pair of nitrogen in the 8-quinolinolato ligand with the metal may remove the negatively polarized charges from the nitrogen. The result leads to large positive Δ values of the 2-proton, in accordance with an empirical rule that Δ value is positive when the protons are in the neighborhood of a positively polarized site of a molecule.[7,8]

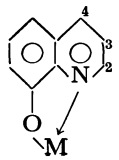

Meinema and Noltes[16] have reported that in trimethyl(8-quinolinolato)antimony chloride, the nitrogen in the 8-quinolinolato ligand does not coordinate to antimony, on the basis of the UV spectra of this complex. We[17] have, on the other hand, expected a weak interaction of nitrogen with antimony for the corresponding bromide. One of complications in these trimethyl(8-quinolinolato)antimony halides is that the UV spectra of these complexes depend on the concentration.[18] If the Δ value criterion can be applicable to these 8-quinolinolato complexes, the data in Table 1 indicate that these complexes belong to the complexes with the chelated 8-quinolinolato ligand.

In trimethyl(8-quinolinolato)antimony carboxylates, the chemical shift of the 2-proton appears at a rather low magnetic field, as compared with that of trimethyl-(8-quinolinolato)antimony halides and 8-quinolinol, although the values of the 3- and 4-protons are almost the same as other 8-quinolinolato complexes. The Δ values of the 2-proton of these trimethyl(8-quinolinolato)antimony carboxylates is small and in some cases negative. One of possible reasons for these results is that the magnetic anisotropy of the carbonyl group in the carboxylato ligand affects the intramolecular 2-proton.* In these complexes, the absorption maximum appears in the region between that of typically chelated complexes and that of non-chelated compounds.[18] Therefore, the coordination of nitrogen to antimony is probably weak, if present at all.

* The chemical shift of the 2-proton was not affected even if the concentration of these complexes was changed.

Table 1. Chemical shift in dichloromethane and benzene induced shift of some organometallic 8-quinolinolato complexes (δ value)[a]

Compound	2-H	3-H	4-H	CH_3-M	Ligand[b]	λ_{max}
8-MeQ[c]	8.77(+0.04)	7.31(+0.45)	8.02(+0.40)			297[d]
[8-MeQH]$^+$[e]	9.16(+0.71)	8.13(—)[f]	9.10(+1.02)			—[g]
8-Quinolinol[h]	8.69(+0.25)	7.37(+0.69)	8.11(+0.66)			320
$(CH_3)_3SiOx$	8.65(+0.25)	7.34(+0.69)	8.15(+0.66)	0.36(−0.11)		315[i]
$(CH_3)_3GeOx$[i]	8.68(+0.32)	7.27(+0.54)	8.00(+0.45)	0.58(−0.02)		320
$(CH_3)_3SnOx$[h]	8.53(+0.53)	7.34(+0.62)	8.17(+0.56)	0.45(−0.02)		332[j]
$(CH_3)_2Sn(Ox)NCS$[h]	8.67(+0.68)	7.58(+0.88)	8.50(+0.88)	0.97(−0.39)		361
$(C_2H_5)_2InOx$[k]	8.51(+0.58)	7.44(+0.79)	8.23(+0.71)			370
$(C_2H_5)_2TlOx$	8.42(+0.50)	7.35(+0.58)	8.14(+0.48)			380
$(CH_3)_4SbOx$	8.49(+0.48)	7.27(+0.59)	8.09(+0.43)	1.06(+0.07)		380[l]
$(CH_3)_3Sb(Ox)Cl$	8.60(+0.60)	7.34(+0.62)	8.08(+0.54)	1.91(+0.17)		353[m]
$(CH_3)_3Sb(Ox)Br$	8.69(+0.70)	7.37(+0.78)	8.17(+0.69)	2.07(+0.27)		352[m]
$(CH_3)_3Sb(Ox)O_2CCH_3$	9.06(−0.20)	7.41(+0.60)	8.20(+0.59)	1.64(+0.06)	1.96(−0.10)	340[m]
$(CH_3)_3Sb(Ox)O_2CCH(CH_3)_2$	9.10(−0.24)	7.43(+0.66)	8.19(+0.62)	1.62(+0.06)	1.14(−0.14) 2.43(−0.17)	341[m]
$(CH_3)_3Sb(Ox)O_2CH$	8.95(−0.26)	7.40(+0.65)	8.13(+0.57)	1.69(+0.16)	8.21(−0.30)	332[m]
$(CH_3)_3Sb(Ox)O_2CCH_2Cl$	9.10(−0.07)	7.46(+0.71)	8.23(+0.67)	1.62(+0.06)	4.04(+0.16)	338[m]
$(CH_3)_3Sb(Ox)O_2CCHCl_2$	9.07(+0.02)	7.46(+0.70)	8.22(+0.70)	1.72(+0.25)	5.89(−0.04)	334[m]
$(CH_3)_3Sb(Ox)O_2CCCl_3$	9.03(+0.07)	7.47(+0.76)	8.24(+0.74)	1.80(+0.33)		334[m]

a) Value in parentheses is the Δ value. b) Chemical shift of the carboxylato group. c) 8-Methoxyquinoline. d) Ref. 17. e) 8-Methoxyquinoline in 0.1 ml CF_3COOH and 0.5 ml CH_2Cl_2 or C_6H_6. f) Obscured by other signals. g) Not measured. h) Ref. 19. i) Ref. 15. j) Ref. 20. k) Ref. 21. l) Ref. 16. m) Ref. 18.

Experimental

The UV spectra were recorded on a Hitachi model 124 spectrometer with 1 mm quartz cells. The PMR measurements were made with a JEOL JNM-PS-100 spectrometer operating at 100 MHz. The chemical shift (δ) was measured relative to tetramethylsilane as the internal standard. Solvents were purified by distillation.

We wish to express our hearty thanks to Professor Rokuro Okawara for his continuous encouragement throughout this study.

References

1) P. Laszlo, *Prog. Nucl. Magn. Resonance Spectrosc.*, **3**, 231 (1967).
2) J. Ronayne and D. H. Williams, *Ann. Rev. Nucl. Magn. Resonance Spectrosc.*, **2**, 83 (1969).
3) R. Foster and C. Fyfe, *Prog. Nucl. Magn. Resonance Spectrosc.*, **4**, 1 (1969).
4) A. A. Bothner-By and R. E. Click, *J. Chem. Phys.*, **26**, 1651 (1957).
5) L. W. Reeves and W. G. Schneider, *Can. J. Chem.*, **35**, 251 (1957).
6) W. G. Schneider, *J. Phys. Chem.*, **66**, 2653 (1962).
7) J. V. Hatton and R. E. Richards, *Mol. Phys.*, **3**, 253 (1960); *ibid*, **5**, 139 (1962).
8) J. Ronayne and D. H. Williams, *J. Chem. Soc., B*, **1967**, 540.
9) Y. Kawasaki, *Mol. Phys.*, **12**, 287 (1967).
10) T. Ledaal, *Tetrahedron Lett.*, **1968**, 1683.
11) W. T. Huntress, Jr., *J. Phys. Chem.*, **73**, 103 (1969).
12) E. M. Engler and P. Laszlo, *J. Am. Chem. Soc.*, **93**, 1317 (1971).
13) K. Nikki, N. Nakagawa, and Y. Takeuchi, *Bull. Chem. Soc. Jpn.*, **48**, 2902 (1975).
14) W. T. Ford and D. J. Hart, *J. Am. Chem. Soc.*, **96**, 3261 (1974).
15) M. Wada, T. Suda, and R. Okawara, *J. Organometal. Chem.*, **65**, 335 (1974); and M. Wada, private communication.
16) H. A. Meinema, E. Rivarola, and J. G. Noltes, *J. Organometal. Chem.*, **17**, 71 (1969).
17) Y. Kawasaki, *Inorg. Nucl. Chem. Lett.*, **5**, 805 (1969).
18) Y. Kawasaki and K. Hashimoto, *J. Organometal. Chem.*, **99**, 107 (1975).
19) Y. Kawasaki, *Org. Magn. Resonance*, **2**, 165 (1970).
20) M. Wada, K. Kawakami, and R. Okawara, *J. Organometal. Chem.*, **4**, 159 (1966).
21) T. Maeda and R. Okawara, *J. Organometal. Chem.*, **39**, 87 (1972).

BULLETIN OF THE CHEMICAL SOCIETY OF JAPAN, VOL. 49 (8), 2321—2322 (1976)

Studies of the Surface of Titanium Dioxide. III. The Electrical Conduction and the Hydrogen Uptake

Toru IWAKI and Masaji MIURA

Faculty of Science, Hiroshima University, Higashisenda-machi, Hiroshima 730

(Received April 1, 1976)

Synopsis. The changes in the electrical conductance and the hydrogen uptake of titanium dioxide were examined with the introduction of hydrogen at 250—500 °C. The former was found to approach the equilibrium rapidly, compared with the latter above 350 °C.

In a previous paper,[1] it has been suggested that hydrogen atoms adsorbed on the surface of titanium dioxide, during the hydrogen reduction, form hydroxyl groups before the weight of titanium dioxide begins to decrease. Adsorbed hydrogen atoms are well known to influence the electrical conductivity remarkably.[2] In the present study, simultaneous measurements of the electrical conductance and the hydrogen uptake were performed in order to clarify the initial stage of the hydrogen reduction by comparison with the previous results.[1]

Experimental

Materials. The rutile sample was prepared by the hydrolysis of titanium tetrachloride in an aqueous medium, followed by the calcination at 600 °C for 6 h in a stream of oxygen. The surface area obtained from the nitrogen adsorption at 77 K was 11.7 $m^2 g^{-1}$. The average grain size was about 1μ.[3] Hydrogen was purified by passing it through platinum asbestos and a liquid nitrogen trap.

Procedure. The sample was placed in contact with oxygen gas at 600 °C for 30 min and then outgassed at 500 °C and 10^{-5} Torr for 3 h. Hydrogen gas was introduced at temperatures between 250 and 500 °C. A liquid nitrogen trap was installed just before the sample in order to protect it from contamination due to organic substances[4] and to condense the water vapor produced by the hydrogen reduction of the sample. The dc-electrical conductance was measured on the following two kinds of samples. One was an unpressed sample, in which four platinum electrodes were buried, while the other was pressed at 8 t cm^{-2} into a pellet, both sides of which were covered with evaporated platinum films. The hydrogen uptake and electrical conductance were measured simultaneously for the unpressed sample, the former being determined volumetrically. No appreciable hydrogen uptake of the pressed sample could be detected because of an insufficient amount of the sample and probably also because of the slow reaction rate. All experiments were carried out in a static gas system.

Results and Discussion

The electrical conductance of the unpressed sample prior to the introduction of hydrogen ranged from 10^{-9} to 10^{-8} A V^{-1} between 250 and 500 °C. The obtained activation energy is 0.35 eV, indicating that the conduction electrons are provided from the impurity levels, which are composed of oxygen vacancies produced on the surface of titanium dioxide during the activation at 500 °C.[5] Figure 1 shows the change in the electrical conductance of the unpressed sample after the introduction of hydrogen. The electrical conductance increased greatly with a rise in the temperature. The electron mobility in a rutile single crystal in the presence of hydrogen was found to be small, 0.15 $cm^2 V^{-1} s^{-1}$ at 360 °C.[6] The rate of increase in the electrical conductance at the initial stage above 350 °C obeyed the Elovich equation, which had been found to be applicable to the rate of the reduction reaction.[1] Below 350 °C it obeyed t^n partly, where t is the time and n= 0.5—0.7.

Figure 2 shows the change in the electrical con-

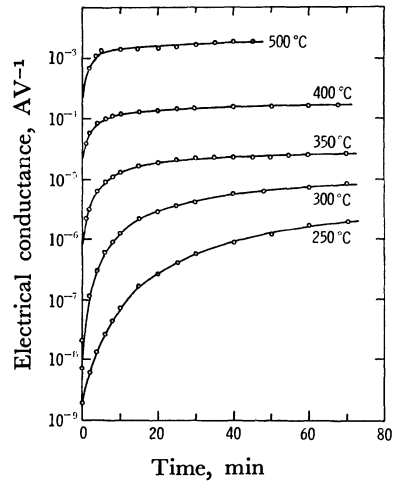

Fig. 1. Electrical conductance of the unpressed sample as a function of time after the introduction of hydrogen at 0.5 atm and several temperatures.

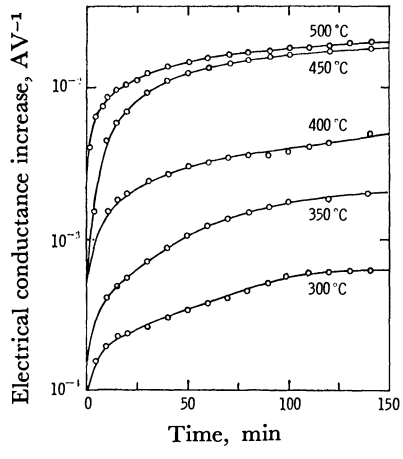

Fig. 2. Electrical conductance of the pressed sample as a function of time after the introduction of hydrogen at 0.5 atm and several temperatures.

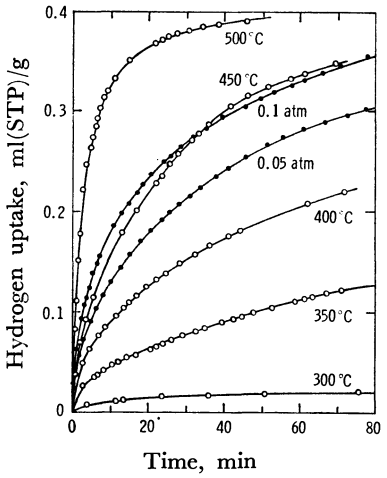

Fig. 3. Hydrogen uptake as a function of time after the introduction of hydrogen at several temperatures. The open circles indicate that the hydrogen pressure is 0.5 atm and the closed circles other hydrogen pressures at 500 °C.

ductance of the pressed sample, where the electrical conductance before the introduction of hydrogen ranged from 10^{-4} to 10^{-3} A V^{-1}. The kinetics was found to obey t^n above 350 °C, where $n=0.3$—0.6. The remarkable difference between the results in Figs. 1 and 2 may be attributable to the contacts between particles and between electrode and particles and to the mobility of the gas molecules migrating through the opening of the titanium dioxide particles.

Figure 3 shows the hydrogen uptake as a function of the time. The hydrogen uptake increased with an increase in the temperature, analogously to the electrical conductance. The rate of hydrogen uptake was found to obey the parabolic rate law. The activation energy obtained was 26 kcal mol^{-1}, indicating the chemisorption of hydrogen, followed by diffusion through the surface region into the bulk. The time required for the attainment of the equilibrium of the hydrogen uptake was short, compared with that of the weight decrease reported in the previous study.[1] The amount of the hydrogen uptake at 500 °C corresponds to a one percent surface coverage if one hydrogen atom is held to one surface oxygen atom. The differences between these findings and the previous ones may result from differences in the experimental conditions, between the static gas system and the circulating one. Nevertheless, at the initial stage, the rates of changes in both the electrical conductance and the hydrogen uptake were quite large, compared with that in the weight decrease. In the previous study, the rate-determining step in the initial stage of the hydrogen reduction was presumed to be the formation of the hydroxyl groups on the surface. The present results support the previous finding concerning the presence of adsorbed hydrogen atoms before the reduction reaction begins.

A comparison of Fig. 1 with Fig. 3 makes it clear that the electrical conductance approaches the equilibrium more rapidly than the hydrogen uptake, especially above 350 °C. The appreciable changes in both the electrical conductance and the hydrogen uptake below 350 °C are also to be noted, because the weight decrease could not be observed below 350 °C.[1] This implies that adsorbed hydrogen atoms which can not take part in the reduction reaction exist on the surface. This hydrogen may adsorb reversibly because the electrical conductance is restored to the original one by outgassing the sample after a run. Above 400 °C, the oxygen vacancies formed by the hydrogen reduction as well as the adsorbed hydrogen atoms contribute remarkably to the electrical conduction.[5]

References

1) T. Iwaki, M. Komuro, K. Hirosawa, and M. Miura, *J. Catal.*, **39**, 324 (1975).

2) G. Heiland, E. Mollow, and F. Stockman, "Solid State Physics," Vol. 8, ed. by F. Seitz and D. Turnball, Academic Press, New York, N. Y. (1959), p. 191; I. N. Pospelva and I. A. Myasumikov, *Kinet. Kataliz.*, **10**, 1097 (1969).

3) T. Iwaki, M. Komuro, S. Oda, K. Kaziwara, and M. Miura, *J. Sci. Hiroshima Univ. Ser. A*, **39**, 1 (1975).

4) T. Iwaki and M. Miura, *Bull. Chem. Soc. Jpn.*, **44**, 1754 (1971).

5) T. Iwaki, *Bull. Chem. Soc. Jpn.*, **46**, 1631 (1973).

6) M. Komuro, T. Iwaki, and M. Miura, unpublished data.

BULLETIN OF THE CHEMICAL SOCIETY OF JAPAN, VOL. 49 (8), 2323—2324 (1976)

Rapid Qualitative and Quantitative Microanalysis of Organic Substances by Means of a Glass-ring Oven Technique. III. Determination of a Trace Amount of Brucine in Strychnine Nitrate

Atsushi CHIBA

Department of Electrochemistry, Faculty of Engineering, Yokohama National University, Ohka, Minami-ku, Yokohama 233

(Received August 28, 1975)

Synopsis. A rapid and highly selective method for the microdetermination of brucine in strychnine nitrate by the ring oven technique is presented. Nitric acid was used as a developing solution and color reagent. The detection limit was 0.2 μg, and the time needed for the determination about 5 min.

The spot test and the ring oven technique, among others, have been proposed in the literature for the simple determination of an alkaloid. The trace of brucine has been adulterated by strychnine production. It was determined in various alkaloids from 10 to 15 μg by use of the ring oven technique.[1] This work deals with a new simplified procedure, in which the detection limit and the determination range have been improved.

Experimental

Apparatus. A glass ring oven[2] was used. As the bath liquid 100 ml of water was used, the analytical procedure being carried out at 90 °C.

Brucine Standard Stock Solution. Brucine (Tokyo Chemical Industry Co., Ltd.) was recrystallized from water and ethanol. After it had been dried for 48 h in a sulfuric acid desiccator, a 100-mg portion of brucine was dissolved in 100 ml of 10 vol% ethanol. This standard stock solution was diluted as required.

Color Reagent. (1.0 M) Nitric acid was used both as color reagent and as developing solution.

Filter Paper. Toyo No. 54 filter paper, diam. 55 mm, was used. The other reagents were of analytical reagent grade.

Procedure. A filter paper was set upon a ring oven maintained at 90 °C. The sample solution was dropped in the center of the filter paper. After the spot had dried, the developing solution was dropped on the same place. Brucine was removed to the ring zone with 15 μl of 1.0 M nitric acid. After the developing solution had dried, brucine was removed with 20 μl of 1.0 M nitric acid. After the developing solution had dried, the amount of brucine was determined by comparing the color intensities of all the standard rings. We used 20, 30, and 50 μl for the sample solutions. The procedure was repeated three times. The amount of brucine was obtained by averaging the values of the three measurements.

Standard Rings. A filter paper was set upon the ring oven at 90 °C. Ten microliters of the brucine standard solution containing 0.2—1.0 μg per ml was dropped in the center of the paper. After the standard solution had dried out, 15 μl of a 1.0 M nitric acid solution was dropped in the center of the paper. After this solution had dried, 20 μl of a 1.0 M nitric acid solution was then dropped. Standard ring scales containing 0.2—2.0 μg of brucine were prepared at an interval of 0.02 or 0.05 μg.

Results and Discussion

Clear rings were not formed below 90 °C. The paper sometimes burned when heating was carried out above 100 °C. Well defined rings were obtained at 90 °C. Filter paper No. 54 was found to be the best of six kinds of chromatography paper.

NO_2 gas, which gives immediate coloration, was used. Brucine was concentrated by the use of water, ammonia and hydrochloric acid. When there was not enough to concentrate in the ring zone, the concentration ring was wide and spreading.

Nitric acid was used since it can be concentrated and thus conveniently serves both as developing solution and color reagent. The ring was wide and spreading when 0.1—0.2 M nitric acid was used, but clear ring formed when 0.5—8 M nitric acid was used. Strychnine showed identical results. The ring zone often burned when nitric acid concentration exceeded 2.0 M. Thus 1.0 M solution was used. No thin and clear ring could be obtained by a single developing procedure, the error being large. A good ring could, however, be obtained by repeating the procedure twice. When the amounts of the developing solution were 15 and 20 μl, the results were better than when 10 and 10 μl, or 10 and 15 μl were used. Fifteen and 20 μl of 1.0 M

TABLE 1. EFFECT OF STRYCHNINE NITRATE ON THE DETERMINATION OF BRUCINE

Amount of brucine (μg)	Amount of strychnine nitrate(μg)	Determination error(%)
0.2	10	0
	20	0
	50	+10
	100	+20
1.0	5	0
	10	0
	20	0
	50	0
	100	+5
	200	+10
5.0	25	0
	50	0
	100	0
	250	0
	500	+5
10.0	50	0
	100	0
	200	0
	500	+5

Table 2. Determination of brucine in strychnine nitrate

Sample	Brucine detected[a)]	Concentration of brucine (μg/l g-strychnine nitrate)
A	1.5	75
B	2.0	100
C	1.0	50

a) In 100 μl.

nitric acid were used. Brucine was concentrated in the ring zone perfectly. Concentration was determined according to color intensity and width of the ring as observed under a microscope.

The ring zone was 20 mm in diameter and 0.2 mm wide, the detection limit 0.2 μg, and the determination range 0.2—20 μg. The average relative error for this technique is 5% over the whole range of concentration of brucine, 0.2—20 μg. When the developing solution dried, the concentration ring turned blood-red, then to yellow-red with the elapse of time. The coloration remained unchanged for some years.

The results are given in Table 1. When the amount of brucine is small, strychnine nitrate has little or no effect on the results. When the standard solution is added to the sample, the error becomes a little greater.

One gram of strychnine nitrate was recrystallized from water and ethanol, and mother liquor was concentrated to 5.0 ml. Brucine was determined with the use of 20, 30, and 50 μl of the mother liquor. The results are given in Table 2. Commercial strychnine nitrate contains a trace of brucine. The analytical procedure took about five minutes, the accuracy being unsatisfactory.

The sample was concentrated with 10 μl of water and its quality was determined by NO_2 gas. The method can also be applied to the analysis of medicine.

The author thanks Prof. T. Ogawa, Yokohama National University, for his suggestion.

References

1) M. B. Ćelap, T. J. Janjić, and V. D. Jevtić, *Mikrochim. Ichnoanal. Acta*, **1963**, 1042.

2) A. Chiba and T. Ogawa, *Bunseki Kagaku*, **21**, 303 (1972).

BULLETIN OF THE CHEMICAL SOCIETY OF JAPAN, VOL. 49 (8), 2325—2326 (1976)

Adduct-Formation Constants of Bis(3-trifluoroacetyl-*d*-camphorato)copper(II) with Lewis Bases

Tsunenobu SHIGEMATSU, Masakazu MATSUI, Yoshihiro SASAKI, and Matsujiro SAKURADA

Institute for Chemical Research, Kyoto University, Uji, Kyoto 611

(Received February 5, 1976)

Synopsis. The formation constants of the mono-adducts of bis(3-trifluoroacetyl-*d*-camphorato)copper(II) with the Lewis bases, such as pyridine, α-picoline, β-picoline, γ-picoline, isopropylamine, and *d*- and *l*-α-methylbenzylamine, were determined spectrophotometrically.

Some metal complexes of β-diketones react further with heterocyclic bases, amines, and phosphorate esters,[1-4] and this adduct formation reaction plays an important role in the synergistic effect for solvent extraction.[5-9]

We investigated the adduct-formation between bis-(3-trifluoroacetyl-*d*-comphorate)copper(II) and heterocyclic bases and amines, including chiral amines, because this β-diketone is chiral and bulky, and determined spectrophotometrically the formation constants.

Experimental

3-Trifluoroacetyl-*d*-camphor (Hfacam) was synthesized from ethyl trifluoroacetate and *d*-camphor using a procedure similar to that described by Hammond.[10] The copper complex, $Cu(facam)_2$, was prepared by adding an ethanol solution of the ligand to an aqueous solution of copper acetate at 60 °C. After cooling, the green crystals which precipitated were filtered off. This product was recrystallized from benzene and then sublimed three times *in vacuo* at 160 °C. (Found: C, 51.54; H, 5.14; F, 20.37%. Calcd for $C_{24}H_{28}O_4F_6Cu$: C, 51.66; H, 5.06; F, 20.43%)

The absorption spectra in benzene at 25 °C were recorded on a Hitachi 323 automatic recording spectrophotometer.

The formation constant K_1 of the mono-adduct was calculated by an equation similar to that of Rose-Drago.[11,12]

$$Cu(facam)_2 + B(\text{Lewis base}) \underset{K_1}{\rightleftharpoons} Cu(facam)_2B \qquad (1)$$

$$\frac{C_A C_B}{A-A_0} = \left[C_A + C_B - \frac{A-A_0}{\varepsilon_3-\varepsilon_1}\right]\frac{1}{\varepsilon_3-\varepsilon_1} + \frac{1}{(\varepsilon_3-\varepsilon_1)K_1} \qquad (2)$$

where A and A_0 are the absorbances at a chosen wavelength in the presence and absence of B, and C_A and C_B are the initial concentrations of $Cu(facam)_2$ and B, respectively. ε_1 and ε_3 are the extinction coefficients of $Cu(facam)_2$ and $Cu(facam)_2B$, respectively. The least-squares method was applied to obtain the best K_1 and ε_3 values.

Results and Discussion

The spectrum of $Cu(facam)_2$ in benzene (*cf.* Fig. 1-(a)) exhibited two maxima at 574 and 680 nm; it resembles those of bis(acetylacetonato)copper(II), $Cu(acac)_2$, and bis(trifluoroacetylacetonato)copper(II), $Cu(tfa)_2$, with a square-planar symmetry.[3,13] When the concentration ratio of pyridine to $Cu(facam)_2$ was in the range 0—0.6, two clear isosbestic points were present, indicating the formation of a mono-adduct. The isosbestic points vanished with increase of the pyridine concentration, and a maximum appeared at 800 nm in the pyridine solution. Moreover, the analytical results of the crystals isolated from the pyridine solution agreed with the calculated values for $Cu(facam)_2(Py)_2$. Therefore, the spectrum in the pyridine solution may be due to $Cu(facam)_2(Py)_2$. Similar spectral changes of $Cu(facam)_2$ caused by the addition of β- and γ-picolines and the analytical results of the crystals isolated from the β- and γ-picoline solutions proved the existence of the bis-adducts, $Cu(facam)_2(\beta\text{-pic})_2$ and $Cu(facam)_2(\gamma\text{-pic})_2$. With α-picoline, two isosbestic points were observed in the concentration-ratio range smaller than 1.0, suggesting a mono-adduct formation.

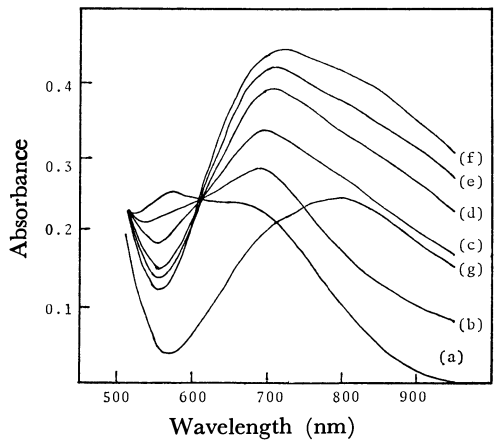

Fig. 1. Spectral change of $Cu(facam)_2$ in benzene caused by the addition of pyridine. $C_A = 4.3 \times 10^{-3}$ M, ratio of C_B/C_A; (a) 0.0; (b) 0.2; (c) 0.4; (d); 0.6; (e) 0.8; (f) 1.0; (g) pyridine.

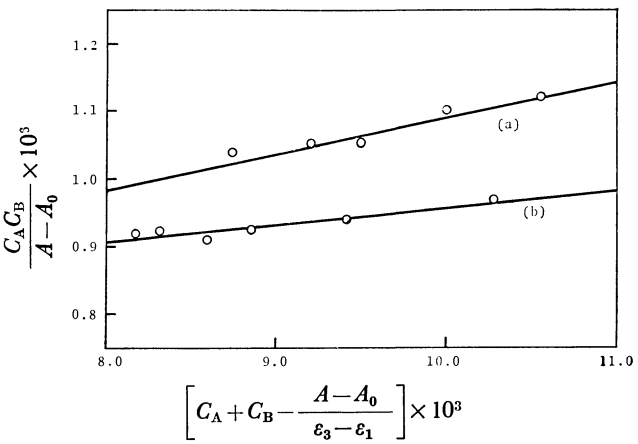

Fig. 2. Plots of $C_A C_B/(A-A_0)$ *vs.* $\left[C_A + C_B - \frac{A-A_0}{\varepsilon_3-\varepsilon_1}\right]$ for α-methylbenzylamine at 700 nm. (a) *l*-α-Methylbenzylamine, (b) *d*-α-methylbenzylamine.

Table 1. Formation constants of mono-adducts between $Cu(facam)_2$ and bases at 25±1 °C

Base	K_1 (M^{-1})
Pyridine	31.1± 4.5
α-Picoline	83.3±24.6
β-Picoline	30.9± 6.4
γ-Picoline	21.9± 5.6
Isopropylamine	26.4± 6.7
d-α-Methylbenzylamine	33.2±12.9
l-α-Methylbenzylamine	84.3±21.0

These isosbestic points vanished with the increase of the α-picoline concentration, and the spectrum in the α-picoline solution exhibited a maximum at 750 nm, with a shoulder at 850 nm. For isopropylamine, two isosbestic points at 520 and 610 nm were found in the concentration ratio range smaller than 1.0. For *d*- and *l*-α-methylbenzylamines, a dull isosbestic point at 600 nm was observed in the region smaller than 0.8, suggesting the formation of a mono-adduct.

An example of the calculation of formation constants is given in Fig. 2, and the K_1 values are summarized in Table 1. The solid lines are drawn on the basis of the calculated ε_3 and K_1 values. The agreement of the plots with the solid lines confirms the plausibility of the calculated ε_3 and K_1 values.

The comparison of the K_1 values reported in the literature[1,2,14-16] with the present data shows that the K_1 values, except that of α-picoline, increase in the order $Cu(tfa)_2 > Cu(facam)_2 > Cu(acac)_2$. This suggests that the rigid and bulky 3-trifluoroacetyl-*d*-camphor hinders the formation of the mono-adduct with bases, but that the electron-withdrawing property of the CF_3-group is still effective. The K_1 value of α-picoline is smaller than those of the other pyridine derivatives for $Cu(acac)_2$ and $Cu(tfa)_2$, whereas the relation is reversed for $Cu(facam)_2$. The K_1 values of *d*- and *l*-α-methylbenzylamine are remarkably different; this difference is difficult to explain, due to the lack of information on their mono-adducts.

References

1) D. P. Graddon and E. C. Watton, *J. Inorg. Nucl. Chem.*, **21**, 49 (1961).
2) D. P. Graddon and R. A. Schulz, *Aust. J. Chem.*, **18**, 1731 (1965).
3) C. H. Ke and N. C. Li, *J. Inorg. Nucl. Chem.*, **31**, 1383 (1969).
4) C. H. Ke and N. C. Li, *J. Inorg. Nucl. Chem.*, **28**, 2255 (1966).
5) D. Dyrssen and M. Hemnichs, *Acta Chem. Scand.*, **15**, 47 (1961).
6) H. Irving and D. N. Edgington, *J. Inorg. Nucl. Chem.*, **27**, 1359 (1965).
7) T. Shigematsu, M. Tabushi, M. Matsui, and T. Honjo, *Bull. Chem. Soc. Jpn.*, **42**, 976 (1969).
8) T. Shigematsu, T. Honjo, and M. Matsui, and M. Tabushi, *Bull. Chem. Soc. Jpn.*, **43**, 793 (1970).
9) T. Shigematsu, T. Honjo, and M. Matsui, *Bull. Chem. Soc. Jpn.*, **43**, 796 (1970).
10) K. R. Kopecky, D. Nonhebel, G. Morris, and G. S. Hammond, *J. Org. Chem.*, **27**, 1036 (1962).
11) N. J. Rose and R. S. Drago, *J. Am. Chem. Soc.*, **81**, 6138 (1959).
12) R. S. Drago, *J. Am. Chem. Soc.*, **95**, 6645 (1973).
13) R. Belford, M. Calvin, and G. C. Belford, *J. Chem. Phys.*, **26**, 1165 (1957).
14) W. R. May and M. M. Jones, *J. Inorg. Nucl. Chem.*, **25**, 507 (1963).
15) W. R. Walker and N. C. Li, *J. Inorg. Nucl. Chem.*, **27**, 2255 (1965).
16) T. Shigematsu, M. Tabushi, M. Matsui, and M. Munakata, *Bull. Chem. Soc. Jpn.*, **41**, 2656 (1968).

BULLETIN OF THE CHEMICAL SOCIETY OF JAPAN, VOL. 49 (8), 2327—2328 (1976)

Stability Constants of the Rare Earth Complexes with 2-Ethyl-2-hydroxy-3-methylbutyric Acid*

Yasuo SUZUKI and Jack E. POWELL**

Department of Industrial Chemistry, Faculty of Engineering, Meiji University, Ikuta, Tama-ku, Kawasaki 214

***Energy and Mineral Resources Research Institute and Department of Chemistry, Iowa State University, Ames, Iowa 50010, U.S.A.*

(Received March 23, 1976)

Synopsis. The stability constants of the rare-earth complexes with 2-ethyl-2-hydroxy-3-methylbutyric acid have been determined potentiometrically at 25.0 °C and at an ionic strength of 0.10, with sodium perchlorate as the supporting electrolyte.

The stability constants of the rare-earth complexes with some 2-hydroxymonocarboxylic acids have previously been determined by the authors and their coworkers.[1-3] The complexing agent employed in this study, 2-ethyl-2-hydroxy-3-methylbutyric acid, which will be abbreviated as Hehmb hereafter, was first prepared by Darzens.[4] This acid was expected to have properties similar to those of 2-hydroxyisobutyric or glycolic acids, though it has an apparently lower solubility in water. The stability constants of the rare earth-ehmb complexes were determined by pH measurements, and a comparison with those of the analogous acid complexes will be presented.

Experimental

Reagents and Apparatus. The rare-earth perchlorate solutions were prepared from the respective oxides with a purity of 99.9% or higher, supplied by the Ames Laboratory of the U. S. Atomic Energy Commission. The Hehmb used in this work was also prepared in the Ames Laboratory; it had a melting point of 75.0—75.5 °C, which agreed sufficiently well with Darzens' result, *e.g.*, 76 °C. The solubility of Hehmb in water is 8.11 g/100 g H_2O at 25.0 °C, which allows us to make a saturated solution of 0.56 mol/dm³.

A Beckman model 76 pH meter was used, with its expanded scale, throughout the work, together with Beckman 41263 glass and 39170 reference electrodes.

Procedures. The experimental procedures were similar to those used in the previous work.[3]

Results and Discussion

The acid dissociation constant of Hehmb at 25.0 °C and at an ionic strength of 0.10 with sodium perchlorate was determined to be 2.557×10^{-4}.

The ligand number, $\bar{n}$, and the free-ligand-ion concentration, $[A^-]$, were derived from the hydrogen-ion concentration previously determined and from the known stoichiometry of the solutions. Since the ligand number did not exceed 2 throughout the measurements, only the following two equilibria were considered here:

$$R^{3+} + A^- \rightleftharpoons RA^{2+}, \quad K_1 = [RA^{2+}]/[R^{3+}][A^-];$$

$$RA^{2+} + A^- \rightleftharpoons RA_2^+, \quad K_2 = [RA_2^+]/[RA^{2+}][A^-];$$

where R^{3+} denotes a trivalent rare-earth cation. The stability constants were computed on an IBM 7044 computer at the Tokai Research Establishment, Japan Atomic Energy Research Institute, Tokai-mura, Ibaraki. The computational programs used were the weighted least-squares ones originally patterned by Sullivan, *et al.*[5] and by Stagg and Powell,[1] adopted to the IBM 7044 computer. The constants thus obtained are shown in Table 1.

The stability constants of the lanthanum ehmb complexes are appreciably lower than those of the corresponding lanthanum complexes, such as 2-hydroxyisobutyrates or lactates. The increase in the constants with the descending periodic sequence down to gadolinium is far more remarkable compared with that in the case of the complexes of the analogous acids, but the subsequent increase in the constants along with the heavier rare earth elements is considerably reduced. The latter trend may be due to the steric effect of the relatively large molecules of the ligand on the cations of a smaller size. These facts indicate that Hehmb may be favorably used for separating lighter rare earths from each other.

Besides the gadolinium break, two more breaks are

Table 1. Stability constants of the rare earth complexes with 2-ethyl-2-hydroxy-3-methylbutyric acid at 25.0 °C and at $I=0.10$ ($NaClO_4$)[a]

Metal	β_1 ($=K_1$)	$\log \beta_1$	$\log \beta_2$
La	56.8	1.75	2.97
Ce	81.4	1.91	3.02
Pr	92.7	1.97	3.17
Nd	121	2.08	3.54
Pm	—	—	—
Sm	275	2.44	4.17
Eu	419	2.62	4.27
Gd	478	2.68	4.38
Tb	653	2.81	4.60
Dy	723	2.86	4.68
Ho	734	2.87	4.73
Er	886	2.95	4.81
Tm	968	2.99	4.88
Yb	1040	3.02	4.92
Lu	1070	3.03	4.86
Y	608	2.78	4.52

a) The values given in this table are subject to absolute errors of as much as ±5% in the case of K_1, and ±10% in the case of K_2. The values of K_1, however, can be compared with those for the adjacent rare earths with greater confidence.

* The work was performed at the Institute for Atomic Research and Department of Chemistry, Iowa State University, Ames, Iowa.

apparently observed: one is located between neodymium and samarium, and the other, between holmium and erbium. This result coincides with the observations of some other rare earth chelates, such as ethylenediaminetetraacetates,[6] picolinates,[7] and *N'*-methylethylenediamine-*N,N,N'*-triacetates.[8] The reason for the fine structure of the stability trend remains to be considered, together with the tetrad effect.[9,10]

The authors wish to express their gratitude to Mr. J. L. Farrell of the Institute for Atomic Research, Iowa State University, for preparing the Hehmb used in the experiment, and to Mr. T. Tsutsui of the Computational Center, Tokai Research Establishment, Japan Atomic Energy Research Institute.

References

1) W. R. Stagg and J. E. Powell, *Inorg. Chem.*, **3**, 242 (1964).
2) J. E. Powell, R. S. Kolat, and G. S. Paul, *Inorg. Chem.*, **3**, 518 (1964).
3) J. E. Powell and Y. Suzuki, *Inorg. Chem.*, **3**, 690 (1964).
4) M. G. Darzens, *C. R. Acad. Sci.*, **152**, 443 (1911).
5) J. C. Sullivan, J. Rydberg, and W. F. Miller, *Acta Chem. Scand.*, **13**, 2023 (1959).
6) E. J. Wheelwright, F. H. Spedding, and G. Schwarzenbach, *J. Am. Chem. Soc.*, **75**, 4196 (1953).
7) J. E. Powell and D. L. G. Rowlands, *Inorg. Chem.*, **5**, 819 (1966).
8) J. E. Powell, D. A. Johnson, H. R. Burkholder, and S. C. Vick, *J. Chromatogr.*, **87**, 437 (1973).
9) D. F. Peppard, G. W. Mason, and S. Lewey, *J. Inorg. Nucl. Chem.*, **31**, 2271 (1969).
10) D. F. Peppard, C. A. A. Bloomquist, E. P. Horwitz, S. Lewey, and G. W. Mason, *J. Inorg. Nucl. Chem.*, **32**, 339 (1970).

BULLETIN OF THE CHEMICAL SOCIETY OF JAPAN, VOL. 49 (8), 2329—2330 (1976)

The Polarized Crystal Spectra of *trans*(O)-$[Co(OCOCH_3)_2(en)_2]^+$ and *trans*(O)-$[Co(OCOCH_3)_2(py)_2en]^+$

Shunji NAGASAKI and Muraji SHIBATA

Department of Chemistry, Faculty of Science, Kanazawa University, Kanazawa 920

(Received March 26, 1976)

Synopsis. The polarized crystal spectra of *trans*-(O)-$[Co(OCOCH_3)_2(en)_2]Cl$ have exhibited a dichroism which can be understood by means of a vibronic D_{4h} model. On the other hand, the spectra of a new complex, *trans*(O)-$[Co(OCOCH_3)_2(py)_2en]ClO_4$, have shown a different dichroism from that in the bis(ethylenediamine) complex.

Polarized crystal spectra are useful for the assignment of the absorption bands of complexes. The spectra of various complexes of cobalt(III),[1] chromium(III),[1,2] platinum(II),[3] *etc.* have been investigated, but interest has been particularly centered on the spectra of *trans*-dihalobis(ethylenediamine)-type cobalt(III) complexes[4-6] because of the marked splitting of the first absorption band ($^1T_{1g}$ band).

In the present work we succeeded in obtaining *trans*-bis(acetato)bis(pyridine)ethylenediaminecobalt(III) perchlorate, *trans*(O)-$[Co(OCOCH_3)_2(py)_2en]ClO_4$, whose absorption spectrum in solution exhibits a marked splitting of the $^1T_{1g}$ band. The corresponding bis-(ethylenediamine) complex, *trans*(O)-$[Co(OCOCH_3)_2(en)_2]^+$, has already been reported.[7,8] Thus, in this paper the polarized crystal spectra of the two *trans*(O) complexes will be reported. The spectra were measured with a microspectrophotometer which had been constructed by the present authors.

Experimental

Measurements. The microspectrophotometer was constructed according to the literature.[9] The assembly consists of a Hitachi 323 recording spectrophotometer and a specially designed sample compartment containing a microscope. As light sources, a tungsten filament lamp and a deuterium discharge lamp were used for the visible and near-ultraviolet regions respectively. As the microscope, an Olympus POM polarising microscope was used, together with an Olympus MO 90 reflecting objective (90 X) or a Zeiss-Jena reflecting objective (40 X). The light was polarized by a quartz Rochon prism. The photomultiplier tube was a Hamamatsu TV Co., Ltd., head-on type R376.

With this apparatus the crystal spectra were measured over the frequency range from 15000 to 30000 cm^{-1} at room temperature with incident light polarized parallel ($\parallel$) and perpendicular ($\perp$) to a suitable axis. The axis was chosen under a polarizing microscope as a direction exhibiting a remarkable dichroism. Since no attempt was made to determine the thickness of the crystal, the molar extinction was not evaluated. The reliability of this apparatus was checked with the spectra of *trans*-$[CoCl_2(en)_2]Cl\cdot HCl\cdot 2H_2O$.[4,5]

Preparation of the Complex. The known complex, *trans*(O)-$[Co(OCOCH_3)_2(en)_2]^+$, was prepared as the chloride according to the method in the literature.[8] A new complex, *trans*(O)-$[Co(OCOCH_3)_2(py)_2en]ClO_4$, was prepared according to the following procedure; to an aqueous solution of *cis*-$K[Co(CO_3)_2(py)_2]\cdot 3H_2O$[10] (21.5 g, 0.05 mol) in water (100 ml), we added ethylenediamine monohydrate (3.0 g, 0.05 mol) and 3 M acetic acid (100 ml), after which the mixture was stirred at room temperature for a few days, whereby the solution became red-violet. A portion of the resulting solution was charged on a column of an ion-exchange resin (Dowex 50 WX8, Na-form), and the complexes were eluted with a 0.3 M $NaClO_4$ aqueous solution, whereupon the desired complex was eluted first, followed by *cis*-$[CoCO_3(py)_2en]^+$ and $[CoCO_3(en)_2]^+$. By repeated chromatographic separations the desired fraction was collected. After the fraction had been concentrated to a small volume, the concentrate was kept in a refrigerator to crystallize the desired complex. The recrystallization was performed from water. Yield, *ca.* 0.5 g.

Found: C, 38.80; H, 4.85; N, 11.19%. Calcd for $[Co(OCOCH_3)_2(py)_2(en)]ClO_4 = CoC_{16}H_{24}O_4N_4\cdot ClO_4$: C, 38.84; H, 4.89; N, 11.32%.

Results and Discussion

The crystal spectra of *trans*-$[CoCl_2(en)_2]Cl\cdot HCl\cdot 2H_2O$ measured with our apparatus exhibited a peak at 1600 cm^{-1} with the $\parallel$ polarization and two peaks at 16200 and 22700 cm^{-1} with the $\perp$ polarization, which agreed with the values reported in the literature: 16000 ($\parallel$), 16200 ($\perp$) and 22700 cm^{-1} ($\perp$)[4] and 15900 ($\parallel$), 16100 ($\perp$) and 23100 cm^{-1} ($\perp$).[5] These spectral data proved the usefulness of our apparatus.

Trans*(O)*-*[Co(OCOCH$_3$)$_2$(en)$_2$]Cl.* The polarized crystal spectra are shown in Fig. 1, together with the solution spectrum. The dichroism was clearly observed in the $^1T_{1g}$ band; the $\tilde{\nu}_{Ia}$ maximum is observed at 18500 cm^{-1} with both $\parallel$ and $\perp$ polarization, and the $\tilde{\nu}_{Ib}$ maximum at 23000 cm^{-1} with the $\perp$ polarization.

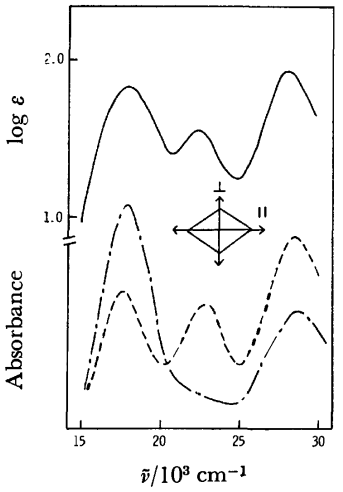

Fig. 1. Absorption spectra of *trans*(O)-$[Co(OCOCH_3)_2(en)_2]Cl$ (—— solution, ---- $\perp$, —-— $\parallel$).

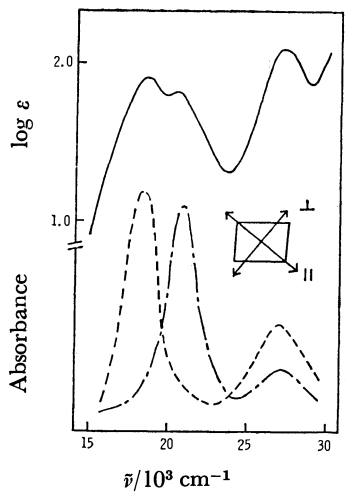

Fig. 2. Absorption spectra of *trans*(O)-[Co(OCOCH$_3$)$_2$-(py)$_2$en]ClO$_4$ (—— solution, ---- ⊥, —— ∥).

Those features are quite similar to those of the *trans*-dichloro complex. Although no crystal structure is known, the observed dichroism can be interpreted in terms of a vibronic D_{4h} model;[6] the $\tilde{\nu}_{Ia}$ is assigned to $^1E_g^a \leftarrow {}^1A_{1g}$, and the $\tilde{\nu}_{Ib}$, to $^1A_{2g} \leftarrow {}^1A_{1g}$. Concerning the second absorption band ($^1T_{2g}$ band), the maxima and intensities are different between the ∥ and ⊥ spectra. The maximum at 27600 cm^{-1} with the larger intensity may be assigned to $(^1B_{2g} + {}^1E_g^b) \leftarrow {}^1A_{1g}$, and the other maximum at 28100 cm^{-1} with the smaller intensity, to $^1E_g^b \leftarrow {}^1A_{1g}$.

trans*(O)*-[*Co(OCOCH$_3$)$_2$(py)$_2$en*]*ClO$_4$*. The solution and crystal spectra are shown in Fig. 2. This complex was identified as the *trans*(O) isomer on the basis of the splitting of the T_{1g} band. A preliminary X-ray investigation of this complex in this laboratory established that the crystal is monoclinic, with the space group C2/c, and that the O–Co–O axis makes an angle of *ca.* 45° with the crystal c axis and is on the ac plane. Thus, the ∥ polarization implies the incident light polarized along the O–Co–O axis.

In the crystal spectra, a marked dichroism is observed in the $^1T_{1g}$ band. With the ⊥ polarization, one peak is observed at 18400 and with the ∥ polarization, another peak at 21000 cm^{-1}. Those features of the dichroism differ from those of the *trans*(O)-bis(ethylenediamine) complex; hence, the vibronic D_{4h} model[6] is not applicable to the interpretation of this dichroism. Instead, a nonvibronic D_4 model may be applicable; the ⊥ band at 18400 cm^{-1} is assignable to $^1E \leftarrow {}^1A_1$, and the ∥ band at 2100 cm^{-1}, to $^1A_2 \leftarrow {}^1A_1$. As for the $^1T_{2g}$ band, the maxima and intensities are different between the ∥ and ⊥ spectra. However, the D_4 selection rule involves a forbidden $^1B_2 \leftarrow {}^1A_1$ transition.

Great thanks should be expressed to Professor Y. Kondo, Professor M. Nakahara and Dr. A. Urushiyama of Rikkyo University for their helpful guidance in the construction of the present microspectrophotometer.

References

1) S. Yamada, *Coordin. Chem. Rev.*, **2**, 83 (1967).
2) S. Yamada and R. Tsuchida, *Bull. Chem. Soc. Jpn.*, **32**, 721 (1959).
3) P. Day, A. F. Orchard, A. J. Thomson, and R. J. P. Williams, *J. Chem. Phys.*, **42**, 1973 (1965).
4) S. Yamada, A. Nakahara, Y. Shimura, and R. Tsuchida, *Bull. Chem. Soc. Jpn.*, **28**, 222 (1955).
5) R. A. D. Wentworth, *Inorg. Chem.*, **5**, 496 (1966).
6) R. Dingle, *J. Chem. Phys.*, **46**, 1 (1967).
7) M. Linhard and G. Stirn, *Z. Anorg. Allgem. Chem.*, **268**, 105 (1952).
8) K. Kuroda and P. S. Gentile, *J. Inorg. Nucl. Chem.*, **27**, 1289 (1965).
9) A. Urushiyama, Y. Ito, M. Nakahara, and Y. Kondo, *Bunko Kenkyu*, **22**, 151 (1973).
10) Y. Ida, K. Kobayashi, and M. Shibata, *Chem. Lett.*, **1974**, 423.

BULLETIN OF THE CHEMICAL SOCIETY OF JAPAN, VOL. 49 (8), 2331—2332 (1976)

The Reduction of Divalent Copper and Tetravalent Tellurium by Ascorbic Acid—Application to Copper Telluride Analysis

M. K. Joshi and Sarala Raoot

Defence Metallurgical Research Laboratory, Hyderabad, India

(Received March 26, 1975)

Synopsis. Quantitative reduction of Cu^{2+} to metal copper and Te^{4+} to metal tellurium by ascorbic acid in alkaline and acid medium respectively has been studied. Based on this a new method for easy and simultaneous determination of copper and tellurium as in copper-telluride has been developed with reproducible results.

In redox-gravimetry, ascorbic acid has been extensively employed as a metal precipitant for determining such elements as selenium,[1] silver,[2] mercury,[3] and gold.[4] In these methods, the metal ion in mineral acids is reduced to the metallic stage and weighed. Despite these applications and the versatility attained by ascorbic acid in diverse analytical methods,[5] its "reducibility" in strongly alkaline medium appears to be much less studied. And although reduction of quadrivalent selenium to metal selenium has been reported, identical observations with tellurium find a meagre mention in available literature.

Preliminary experiments revealed that when ascorbic acid was introduced separately in solutions of copper sulphate and sodium tellurite, metals copper (in strongly alkaline medium) and tellurium (in strongly acid medium) were precipitated. In NaOH solutions Cu^{2+} was reduced preferentially to metal while Te^{4+} remained in solution and a reverse phenomenon was witnessed on making the solutions acidic. Quantitative aspects of these two redox-reactions and their extension to simultaneous determination of copper and tellurium in copper telluride have been reported in this paper.

Experimental

All reagents used in these investigations were of Analytical Grade purity.

Reduction of Cu^{2+} to Metallic Copper. 2.96 g of AR copper turnings were dissolved in minimum nitric acid in a 250 ml beaker and fumed with 5 ml of sulphuric acid. The residue was dissolved in distilled water and made up to one litre. Its copper content was checked iodometrically. An aliquot portion of this solution was taken in a round bottom flask fitted with a ground glass seal condenser. 20% aqueous sodium hydroxide solution was introduced into the flask till the pale-blue gelatinous precipitate of cupric hydroxide was formed. The contents were diluted to 60—70 ml and an adequate volume of the alkali was further added to maintain its overall normality at or above 1N (a minimum volume of 60—70 ml of the reaction mixture was found to be convenient for reflux, preventing formation of a paste and facilitate observance of supernatant liquid). Crystalline ascorbic acid (a minimum of 5 to 6 times the weight of copper present in aliquot) was then added when a colloidal reddish yellow precipitate appeared almost immediately. The condenser was fitted in and the system refluxed for about 10 to 15 min on a suitable heating mantle. The reddish yellow precipitate was reduced gradually to metallic copper which settled down leaving behind a clear supernatant liquid. The system was cooled, condenser detached and the copper filtered under suction through a weighed sintered glass crucible of porosity-4. It was washed 3 to 4 times with hot 1% sodium hydroxide solution, then with hot water till free from alkali and finally with a small quantity of absolute alcohol and ether. The precipitated copper was sucked dry, heated in an air oven at 110 °C for about one hour, cooled in a desiccator and weighed to a constant weight. It was later dissolved in 1 : 1 nitric acid, diluted to about 100 ml, titrated iodometrically against 0.1 N thiosulphate solution. Results at serial nos. 1 to 7 in the table pertain to these studies. For quick routine analysis, the precipitated copper may be filtered through a Whatman 42 fitter pulp, dissolved in 1 : 1 nitric acid, washed and titrated iodometrically.

Reduction of Te^{4+} to Metallic Tellurium. 7.4 g of AR tellurium metal was dissolved in 100 ml of concentrated hydrochloric acid in a 500 ml beaker. The solution was made up to 1 liter maintaining its overall HCl normality at about 2.5 N. Tellurium content in the solution was checked gravimetrically.

A measured volume of the Te^{4+} solution was taken in a round bottom flask fitted with a ground glass seal condenser followed by an adequate volume of concentrated HCl and distilled water to achieve an overall normality at or above 2.5 N and the total volume of the reactants at 60—70 ml. Crystalline ascorbic acid (4 to 5 times the weight of tellurium in aliquot) was now added to the flask when black colloidal precipitate of tellurium was seen almost instantaneously. The system was refluxed for abour 10 min when the precipitate settles down leaving behind a clear supernatant liquid. The contents were cooled and tellurium was filtered under suction through a weighed sintered glass crucible of porosity-4. The precipitate was washed thoroughly with hot water till free from chloride ions and then with a small quantity of absolute alcohol and ether. It was sucked dry, heated in an air oven at 105 °C for about an hour, desiccated and weighed to constant weight. Results at serial nos. 8 to 14 in the table correspond to these experiments.

Separation and Estimation of Copper and Tellurium when Present Together as in Copper Telluride. Synthetic copper telluride solutions were prepared by weighing accurately electrolytic copper and high purity tellurium in weight ratios 1 : 1, 1 : 2, 2 : 1, and 2 : 3 in a 250 ml beaker and dissolving in a minimum volume of 1 : 1 nitric acid by careful heating. Excess nitric acid was removed by fuming with concentrated sulphuric acid. The residue when cooled was taken up with HCl and made up to 250 ml in a standard volumetric flask such that overall normality of HCl in the solution was maintained at about 2.5 N. In a 25 ml portion of each of these copper was first determined by ascorbic acid in alkaline medium by weighing and titration (*cf.* experimental for copper). The alkaline filtrate was transferred to a 500 ml Pyrex beaker, evaporated to 100 ml, concentrated HCl added to the prescribed normality and precipitated tellurium weighed gravimetrically (*cf.* experimental for tellurium).

Results of experiments at serial nos. 15 to 18 in the table refer to these investigations.

TABLE

Expt. No.	Copper (g)			Tellurium (g)	
	Present	Obtained gravimetrically	Obtained volumetrically	Present	Obtained gravimetrically
1	0.1773	—	0.1776	—	—
2	0.1478	0.1474	0.1474	—	—
3	0.1182	0.1180	0.1182	—	—
4	0.0739	—	0.0737	—	—
5	0.0591	0.0590	0.0591	—	—
6	0.0296	0.0294	0.0296	—	—
7	0.0148	0.0147	0.0148	—	—
8	—	—	—	0.2908	0.2895
9	—	—	—	0.1818	0.1815
10	—	—	—	0.1454	0.1452
11	—	—	—	0.0727	0.0726
12	—	—	—	0.0364	0.0363
13	—	—	—	0.0181	0.0179
14	—	—	—	0.0091	0.0092
15	0.0536	0.0535	—	0.0502	0.0501
16	0.0543	0.0542	—	0.0941	0.0939
17	0.1056	0.1055	—	0.0529	0.0528
18	0.0500	0.0497	—	0.0750	0.0746

Ratio of Cu^{2+} to Te^{4+} in experiments at serial nos. 15, 16, 17, and 18 was respectively 1:1, 1:2, 2:1, and 2:3.

Discussion

In order to study various reaction parameters, a series of experiments were carried out and it was established that the optimum conditions for a quantitative reduction of Cu^{2+} to metallic copper are, (1) 5 to 6 folds excess of ascorbic acid, (2) overall sodium hydroxide concentration at or above 1 N, (3) duration of reflux 15 to 20 min, and those for Te^{4+} to metal tellurium, (1) 4 to 5 folds excess of the acid reagent, (2) HCl concentration at or above 2.5 N and (3) time of reflux 10 to 15 min.

The close agreement between the amount of copper and tellurium taken for investigation and that obtained gravimetrically and volumetrically (for copper only) show that the accuracy is high for a fairly wide range of the metal ion concentrations, the errors being 0.2 to 0.7% for copper and 0.1 to 1.0% for tellurium. The deviations in most of the cases are on the negative side which may be attributed to the losses occuring during transfer and washing of the precipitated metals. A special feature of the present method is that both the metal ions are determined simultaneously by just altering the medium of reaction.

Studies on tellurides of silver and bismuth on identical lines and applications of the copper-ascorbic acid redox-reaction to direct determination and/or separation of copper in brasses, bronzes and aluminium alloys have shown encouraging results and will be communicated later.

Our grateful thanks are due to Dr. R. V. Tamhankar, Director, Defence Metallurgical Research Laboratory, Hyderabad for his valuable suggestion and for permission to publish this paper.

References

1) A. Kh. Batalin, *Zh. Anal. Khim.*, **15**, 507 (1960).
2) E. C. Stathis, *Anal. Chem.*, **20**, 271 (1948).
3) L. Erdey, "A Kemiai Analyzis Sulyszerinti Modezerei," Vol. II, Akademiai Kiado, Budapest (1960), p. 88.
4) E. C. Stathis and H. C. Gatos, *Ind. Eng. Chem., Anal. Ed.*, **18**, 801 (1946).
5) L. Erdey, *Chem. Anal.*, **48**, 106 (1959).

BULLETIN OF THE CHEMICAL SOCIETY OF JAPAN, VOL. 49 (8), 2333—2334 (1976)

Morpholinobenzoquinones: Synthesis and Reactions

Yoshimori OMOTE* and Toshihiko KOMATSU

Department of Chemistry, University of Tsukuba, Sakura, Niihari, Ibaraki 300-31

Department of Chemistry, Tokyo Kyoiku University, Otsuka, Bunkyo-ku, Tokyo 112

(Received January 27, 1976)

Synopsis. Two 4-morpholino-1,2-benzoquinones (5-*t*-butyl- and 5-methyl-) have been prepared by the oxidation of the corresponding catechols with silver oxide. The quinones were then condensed with *o*-phenylenediamine to give phenazines.

The oxidation of aminocatechols to the corresponding quinones has been studied by Horner,[1] Iwao[2] and Jackson,[3] but few papers on the isolation and properties of the quinones have been published. We wish now to report on the synthesis of morpholinobenzoquinones as well as on their chemical properties.

The reaction of 4-*t*-butyl-1,2-benzoquinone with morpholine gave 5-*t*-butyl-4-morpholinocatechol (**1**) in a 48% yield. The structure of **1** was confirmed on the basis of the spectroscopic data and the results of elemental analysis. Aminocatechols, such as 4-aminocatechol and 4-dimethylaminocatechol, are known to be labile to atmospheric oxygen,[1] however, **1** is stable and can be isolated as colorless crystals. The reaction of 4-methyl-1,2-benzoquinone with morpholine gave **2** in only a 7.7% yield.

The catechol **1** was oxidized with silver oxide to give 5-*t*-butyl-4-morpholino-1,2-benzoquinone (**3**). The **3** quinone was then condensed with *o*-phenylenediamine to afford a phenazine, **5**. The **6** phenazine was also obtained from the labile **4** and *o*-phenylenediamine.

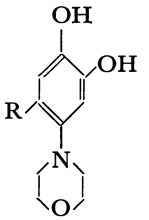

1 R=C(CH$_3$)$_3$
2 R=CH$_3$

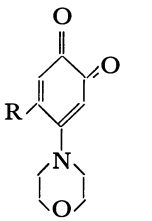

3 R=C(CH$_3$)$_3$
4 R=CH$_3$

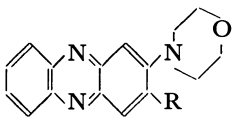

5 R=C(CH$_3$)$_3$
6 R=CH$_3$

Experimental

5-t-Butyl-4-morpholinocatechol (1). 4-*t*-Butyl-1,2-benzoquinone was prepared by the method of Pospíšil[4] from 2 g of 4-*t*-butylcatechol. Morpholine (4 ml) in tetrahydrofuran (10 ml) was slowly stirred into a solution of the quinone in terahydrofuran (30 ml) under nitrogen at 0 °C. When white precipitates appeared after stirring at room temperature, the reaction mixture was concentrated. The precipitate (1.46 g) was then recrystallized from dioxane; colorless needles, mp 240 °C (dec). UV λ_{max}^{EtOH} (ε): 220 sh (7930) and 285 (3420) nm; NMR (DMSO-d_6): δ 1.37 (s, 9H), 2.6 (m, 4H), 3.7 (m, 4H), 6.70 (s, 1H), 6.74 (s, 1H) and 8.61 (br. s, 2H, D_2O exchangeable); IR (KBr): 3500 cm^{-1} (OH). Found: C, 66.81; H, 8.64; N, 5.58%. Calcd for $C_{14}H_{21}NO_3$: 66.90; H, 8.42; N, 5.57%.

5-Methyl-4-morpholinocatechol (2). 4-Methyl-1,2-benzoquinone was prepared by the oxidation of 4-methylcatechol (2 g) with cerium(IV) sulfate.[5] Morpholine (4 ml) in methanol (20 ml) was stirred with the resulting quinone at room temperature under nitrogen. After stirring for 10 min, the mixture was concentrated and chromatographed over silica gel (eluted with benzene–ethyl acetate 4 : 1) to give 260 mg of **2** (7.7%); colorless prisms from ethyl acetate; mp 186—188 °C. UV λ_{max}^{EtOH} (ε): 263 sh (5900) and 295 (3750) nm; NMR (DMSO-d_6): δ 2.10 (s, 3H), 2.7 (m, 4H), 3.7 (m, 4H), 6.50 (s, 1H), 6.57 (s, 1H) and 8.4 (br. s, 2H, D_2O exchangeable); IR (KBr): 3450 cm^{-1} (OH).

5-t-Butyl-4-morpholino-1,2-benzoquinone (3). Silver oxide (100 mg, freshly prepared from silver nitrate) was added, in portions, to a solution of **1** (100 mg) in dry dioxane (20 ml). After the mixture had been stirred for 30 min at room temperature under argon, the resulting precipitate was removed by filtration. The filtrate was concentrated by freeze-drying to a red-orange powder (93 mg, 93%) of **3**; sublimed at 80 °C under 10^{-6} mmHg; mp 90 °C. UV $\lambda_{max}^{CHCl_3}$ (ε): 335 (2870) and 456 (2010) nm: $\lambda_{max}^{H_2O}$ (ε): 272 (10300), 330 (2200) and 510 (2870) nm; NMR ($CDCl_3$): δ 1.38 (s, 9H), 2.93 (m, 4H), 3.83 (m, 4H), 6.08 (s, 1H) and 6.39 (s, 1H); IR (KBr): 1680, 1660 and 1650 cm^{-1} (C=O). Found: C, 67.25; H, 7.74; N, 5.82%. Calcd for $C_{14}H_{19}NO_3$: C, 67.44; H, 7.68; N, 5.62%.

5-Methyl-4-morpholino-1,2-benzoquinone (4). This quinone could not be isolated, but a solution of the quinone was obtained by the treatment of the corresponding catechol, **2** with *o*-chloranil. UV λ_{max}^{EtOH} (ε): 496 (3100) nm; NMR (DMSO-d_6): δ 2.22 (d, J=1.5 Hz, 3H), 3.2 (m, 4H), 3.75 (m, 4H), 5.63 (s, 1H) and 6.25 (q, J=1.5 Hz, 1H).

2-t-Butyl-3-morpholinophenazine (5). *o*-Phenylenediamine (100 mg) in dioxane (5 ml) was added to a dioxane solution (10 ml) of **3** (100 mg); then the mixture was stirred for 20 h at room temperature under argon. After the removal of the solvent, the residue was chromatographed over silica gel to give a yellow powder (63 mg, 45%); yellow prisms from methanol; mp 140 °C. UV λ_{max}^{EtOH} (ε): 256 (117000) and 372 (14500) nm; NMR ($CDCl_3$): δ 1.63 (s, 9H), 3.00 (m, 4H), 3.94 (m, 4H) and 7.7—8.3 (m, 6H). Found: C, 75.30; H, 7.32; N, 13.23%. Calcd for $C_{20}H_{23}N_3O$: C, 74.74; H, 7.21; N, 13.07%.

2-Methyl-3-morpholinophenazine (6). To a mixture of 310 mg of 4-methylcatechol and 0.25 ml of morpholine in 20 ml of tetrahydrofuran, silver oxide (1.16 g), in portions, was added with stirring, after which the mixture was stirred for 15 further min under argon at room temperature. When the precipitate had been removed by filtration, 270 mg of *o*-phenylenediamine in tetrahydrofuran (10 ml) was dropped into the filtrate and the mixture was stirred for 20 min. After

the removal of the solvent, 16 ml of acetic anhydride containing 1 ml of pyridine was added to the residue, and the solution was warmed at 60 °C for 5 min in a water bath. When the solvent had been evaporated under reduced pressure, the resulting crystals of the acetate of *o*-phenylenediamine were removed by filtration. The filtrate was chromatographed over silica gel to give 205 mg (29.3%) of **6**; yellow prisms from methanol; mp 131—132 °C. UV λ_{max}^{EtOH} (ε): 235 (29700), 256 (45600), 382 (12100) and 410 (8670) nm; NMR ($CDCl_3$): δ 2.59 (s, 3H), 3.1 (m, 4H), 3.9 (m, 4H) and 7.5—8.3 (m, 6H). Found: C, 73.13; H, 6.17; N, 14.99%. Calcd for $C_{17}H_{17}N_3O$; C, 73.09; H, 6.13; N, 15.04%.

References

1) L. Horner and H. Lang, *Chem. Ber.*, **89**, 2768 (1956); L. Horner and K. Sturm, *Ann.*, **608**, 128 (1957).

2) J. Iwao and K. Tomino, *Yakugaku Zasshi*, **76**, 808 (1956); J. Iwao and M. Kozu, *ibid.*, **76**, 811 (1956); J. Iwao and K. Tomino, *ibid.*, **76**, 814 (1956).

3) J. Jackson and L. P. Kendel, *Biochem. J.*, **44**, 477 (1949).

4) I. Buben and J. Pospíšil, *Collect. Czech. Chem. Commun.*, **34**, 1991 (1969).

5) R. Brockhaus, *Ann.*, **712**, 214 (1968).

BULLETIN OF THE CHEMICAL SOCIETY OF JAPAN, VOL. 49 (8), 2335—2336 (1976)

Preparation of Hindered Esters from Acid Chlorides and Alcohols in the Presence of Silver Cyanide

Seiji TAKIMOTO, Junji INANAGA, Tsutomu KATSUKI, and Masaru YAMAGUCHI

Department of Chemistry, Faculty of Science, Kyushu University, Hakozaki, Higashi-ku, Fukuoka 812

(Received February 2, 1975)

Synopsis. Sterically hindered esters were prepared from the corresponding acyl chlorides and alcohols in the presence of silver cyanide. The method is superior to the conventional acyl chloride–alcohol–pyridine method as regards yield and the rapidity of reaction.

This report describes a rapid and convenient procedure for preparing sterically very crowded esters by the reaction between acyl chlorides and alcohols in the presence of silver cyanide. The results are summarized in Table 1.

The conventional acyl chloride–alcohol–pyridine method is useful for the preparation of the usual esters but it is too slow and incomplete for preparing the hindered esters. The method in which the acyl chlorides are treated with lithium alkoxides[1] and that in which the acids and alcohols are treated with trifluoroacetic anhydride[2] appear to be the most useful ones in view of the yield and the rapidity of the reaction. However, because of the strongly alkaline or acidic reaction conditions inherent to these methods, their applicability must be made with certain restrictions: in the alkoxide method, some reservation should be given to acid chlorides having α-hydrogen atoms;[1] the trifluoroacetic anhydride method is not suitable for aliphatic tertiary alcohols.[2] The present method can be applied to a wide variety of substrates with better yields. Esters of triphenylmethanol, however, can not be prepared by this method.

The reaction seems to proceed with the help of the electrophilic catalysis of silver ion though other silver salts such as silver carbonate or silver trifluoroacetate are ineffective for the ester formation. The intermediacy of the acyl cyanide as the main reaction pass might be excluded since the acyl cyanide has been reported to be less reactive to the nucleophiles than the corresponding acyl chloride.[3] Actually, in an experiment carried out with pivaloyl cyanide and 2-methyl-2-propanol in HMPA at 80 °C for 8 h, only a trace of ester could be observed. Addition of tributylamine[4] or DBU caused no acceleration in the reaction but rather retarded it.

Copper cyanide showed a similar effect but the yield of the ester was very low and the formation of a considerable amount of acid anhydride was observed.

Experimental

Silver cyanide was precipitated by mixing a potassium cyanide solution (1.95 g in 50 ml water) with a silver nitrate

TABLE 1. PERCENT YIELD OF HINDERED ESTERS

Acid chloride (0.5 mmol)	Alcohol (mmol)		Reaction conditions: Solvent (1 ml);	Temp;	Time	Ester Yield (%)[a]
Pivaloyl	2-Butanol	(0.5)	Benzene;	r. t.;	1 h	100
	2-Methyl-2-propanol	(0.6)	HMPA;	80 °C;	10 min	94
		(1.0)	Benzene;	80 °C;	30 min	100
	3-Ethyl-3-pentanol	(1.0)	HMPA;	80 °C;	10 min	57
		(1.0)	Benzene;	80 °C;	4 h	99[b]
	2,6-Dimethylphenol	(0.7)	HMPA;	80 °C;	4 h	61
		(0.5)	Benzene;	80 °C;	30 h	83[c]
2,2-Diethylbutyryl	2-Butanol	(0.5)	Benzene;	80 °C;	1 h	94
	2-Methyl-2-propanol	(1.0)	HMPA;	80 °C;	10 min	95
		(1.0)	Benzene;	80 °C;	4.5 h	90
	3-Ethyl-3-pentanol	(1.0)	HMPA;	80 °C;	30 min	75
		(1.0)	Benzene;	80 °C;	54 h	86
	2,6-Dimethylphenol	(0.5)	HMPA;	80 °C;	30 min	80
		(0.5)	Benzene;	80 °C;	75 h	90
2,4,6-Trimethylbenzoyl	2-Methyl-2-propanol	(0.5)	Benzene;	r. t.;	10 min	92
	3-Ethyl-3-pentanol	(1.0)	HMPA;	80 °C;	30 min	92
		(0.5)	Benzene;	80 °C;	3 h	82[c]
	2,6-Dimethylphenol	(0.5)	Benzene;	r. t.;	5 min	92
2-Methylpentanoyl	3-Ethyl-3-pentanol	(0.5)	Benzene;	r. t.;	3 h	95

a) Unless otherwise stated, the yields were determined by GLPC by comparison with the appropriate internal standards. b) An experiment carried out according to the trifluoroacetic anhydride method[2] gave the ester formation (13%, r. t., 1 h) but the ester gradually disappeared in eight hours. c) The yield was that of the product distilled after the work up.

Table 2. Analytical and NMR data of new esters

Ester	Found(Calcd) C%	Found(Calcd) H%	NMR, δ
2,6-Dimethylphenyl pivalate	75.74 (75.69)	8.80 (8.80)	1.42(s, 9H), 2.14(s, 6H), 7.02(s, 3H)
2-Butyl 2,2-diethylbutyrate	72.32 (71.95)	12.19 (12.08)	0.76(t, 9H, J=7.9 Hz), 0.88(t, 3H, J=9.0 Hz), 1.19(d, 3H, J=6.0 Hz), 1.35—1.90 (m, 8H), 4.80(m, 1H)
t-Butyl 2,2-diethylbutyrate	71.67 (71.95)	12.06 (12.08)	0.77(t, 9H, J=7.2 Hz), 1.34(s, 9H), 1.55(m, 6H)
3-Ethyl-3-pentyl 2,2-diethylbutyrate	74.10 (74.32)	12.50 (12.48)	0.80(t, 9H), 0.83(t, 9H), 1.36—2.10 (m, 12H)
2,6-Dimethylphenyl 2,2-diethylbutyrate	77.34 (77.37)	9.74 (9.74)	0.93(t, 9H, J=7.1 Hz), 1.89(q, 6H), 2.16(s, 6H), 7.01(s, 3H)
3-Ethyl-3-pentyl 2,4,6-trimethylbenzoate	77.55 (77.82)	9.90 (9.99)	0.91(t, 9H, J=7.0 Hz), 1.98(q, 6H, J=7.0 Hz), 2.25(s, 3H), 2.34(s, 6H), 6.81(s, 2H)
3-Ethyl-3-pentyl 2-methylpentanoate	73.01 (72.84)	12.27 (12.23)	0.83(t, 12H, J=8.0 Hz), 1.12(q, 3H, J=7.0 Hz), 1.40(m, 4H), 1.84(q, 6H, J=8.0 Hz), 2.40(m, 1H)

solution (5.1 g in 100 ml water) at room temperature, which was then washed thoroughly with water and dried for twelve hours under 2 mmHg. Of the solvents examined, benzene and HMPA gave the best results. In HMPA, the reaction completed very rapidly but the yield was slightly reduced. The NMR spectra in $CDCl_3$ were used for identification of the esters. A typical example is given below.

t-Butyl Pivalate. Pivaloyl chloride (60 mg, 0.5 mmol) was added with use of a microsyringe to a stirred mixture of silver cyanide (134 mg, 1 mmol), 2-methyl-2-propanol (44 mg, 0.6 mmol) and HMPA (1 ml) with the exclusion of moisture, the mixture being then heated at 80 °C in an oil bath. Formation of the ester was followed by GLPC by the addition of an internal standard (xylene in this case). After ten minutes the amount of ester became constant with a 94% yield. For isolation of the ester, the reaction mixture was diluted with pentane (10 ml) without addition of xylene, filtered through a celite column, washed successively with a 10% aqueous sodium hydrogencarbonate solution and water, dried with calcium sulfate, and distilled at 150 °C (bath temperature).

This work was partially supported by a Grant-in-Aid for Scientific Research from the Ministry of Education.

References

1) E. M. Kaiser and R. A. Woodruff, *J. Org. Chem.*, **35**, 1198 (1970).
2) R. C. Parish and L. M. Stock, *J. Org. Chem.*, **30**, 927 (1965).
3) J. Thesing and D. Witzel, *Angew. Chem.*, **68**, 425 (1956).
4) A. Holý and M. Souček, *Tetrahedron Lett.*, **1971**, 185.

BULLETIN OF THE CHEMICAL SOCIETY OF JAPAN, VOL. 49 (8), 2337—2338 (1976)

Pyrolysis of *S*-[2-(Phenylthio-, Phenylsulfinyl-, and Phenylsulfonyl)-ethyl]-*N*-*p*-tosylsulfilimine[1)]

Naomichi FURUKAWA, Toshifumi HATANAKA, Katsumasa HARADA, and Shigeru OAE

Department of Chemistry, The University of Tsukuba, Sakura-mura, Niihari-gun, Ibaraki 300-31

(Received February 20, 1976)

Synopsis. The β-substituent effect on the rate of Ei reaction was investigated by using *S*-[2-(phenylthio-, phenylsulfinyl-, and phenylsulfonyl)ethyl]-*N*-*p*-tosylsulfilimines. The reactivity lies in the order of β-substituents: $PhSO_2 > PhSO > PhS > Ph$. From this and the kinetic isotope effect, the rate determining step is the intramolecular β-hydrogen abstraction by the *N*-*p*-tosyl group.

In previous studies,[2)] we found that *S*-alkyl-*N*-*p*-tosylsulfilimines having a β-hydrogen atom can readily undergo pyrolysis to afford the corresponding olefins and the sulfenamide in high yields. The kinetic study revealed that the rate of the pyrolysis of *S*-1-phenyl-substitdted-*N*-*p*-tosylsulfilimine is 10^3 times faster than that of the unsubstitdted derivative. Meanwhile, the *S*-2-phenyl-substituted-derivative was found to be pyrolyzed only 2.5 times faster than the unsubstituted one. Thus, although the rates of the pyrolysis vary widely upon changing the structure of the sulfilimine, the reaction has been suggested to proceed *via* nearly an ideal concerted *cis*-elimination mechanism. In order to collect further evidence to clarify the Ei reaction and especially to examine the effect of the electron withdrawing β-substituent, *S*-[2-(phenylthio-, phenylsulfinyl-, and phenylsulfonyl)ethyl]-*N*-*p*-tosylsulfilimines were subjected to the usual pyrolysis. This paper describes the results of the kinetic study of the pyrolysis.

Results and Discussion

S-(Phenyl)ethyl-*S*-phenyl-(I), *S*-[2-(phenylthio)-ethyl]-*S*-phenyl-(II), *S*-[2-(phenylsulfinyl)ethyl]-*S*-phenyl-(III), and *S*-[2-(phenylsulfonyl)ethyl]-*S*-phenyl-(IV)-*N*-*p*-tosyl-sulfilimines were prepared in the usual manner from the corresponding sulfides with chloramine-T in methanol and subjected to the pyrolysis. The pyrolysis was carried out by heating the solution of each of these sulfilimines in chloroform. The product analyses performed by NMR spectroscopy *in situ* in $CDCl_3$, showed a mixture of the olefins and the sulfenamide.

$$\mathrm{Ph\text{-}S\text{-}CH_2CH_2X} \longrightarrow \mathrm{Ph\text{-}S\text{-}NHTs} + \mathrm{CH_2{=}CHX}$$
$$\downarrow$$
$$\mathrm{NTs}$$

(X=Ph, PhS, PhSO, $PhSO_2$)

The kinetic data were obtained by following the IR absorption of the NH band of *N*-phenylthio-*p*-toluenesulfonamide which appears at 3310 cm^{-1}. The rates of the pyrolysis were correlated well by the first order rate equation; the data are summarized in the Table together with the relative rates of other sulfilimines obtained previously.

The data in the Table indicate that the effects of the β-substituent for the pyrolysis on the reactivity lie in the following sequence: $PhSO_2 > PhSO > PhS >$ Ph. This trend corresponds to that found in the E_2 elimination reaction which we studied previously[3)] and also to that in the base-catalyzed H-D exchange.[4)]

In order to study the nature of the transition state for the Ei reaction of the sulfilimine having a strong electron withdrawing β-substituent, *S*-phenyl-*S*-[2-(phenylsulfonyl)ethyl-2,2-d_2]-*N*-*p*-tosylsulfilimine was prepared and subjected to the pyrolysis. The kinetic study indicated the isotope effect in the pyrolysis reaction, calculated as k_H/k_D, to be 4.2. This clearly indicates that the reaction is also a concerted process that involves the rate-determining intramolecular β-hydrogen abstraction by the *N*-*p*-tosyl group. This rather large value of the kinetic isotope effect, as compared to the previous values obtained for *S*-ethyl-*S*-phenyl (3.0) and *S*-(α-methylbenzyl)-*S*-phenyl-*N*-*p*-tosylsulfilimine (2.9), and the small rate-enhancement by the β-phenyl group in the pyrolysis of *S*-2-(substituted)ethyl-*N*-*p*-tosylsulfilimine, as compared to the re-

TABLE 1. THE KINETIC RESULTS OF THE PYROLYSIS OF SULFILIMINE

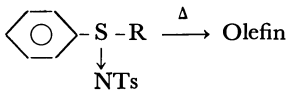

Sulfilimine R	Temp °C	k $s^{-1} \times 10^5$	Rel.[b)] rate	$\Delta H^{\neq}$ kcal/mol	$\Delta S^{\neq}$ e.u.
CH_2CH_3	80.3	1.08	1.0	26.5	−5.8
$CH_2CH_2C_6H_5$	95.2	6.28	1.5		
$CH(C_6H_5)CH_3$	31.0	16.0	10^3	20.8	−7.2
$CH_2CH_2S(O)_2C_6H_5$	60.0	34.5	4.8×10^2	20.4	−12.6
$CH_2CH_2S(O)C_6H_5$[a)]	60.0	1.12	15	26.6	−1.7
$CH_2CH_2SC_6H_5$	60.0	0.48	7	26.8	−2.4

a) In order to obtain the trend of the β-substituent, one isomer having a mp 124—127 °C was subjected to the pyrolysis. b) The relative rates are all calculated by correcting the number of available β-hydrogen atoms at 60.6 °C.

latively large acceleration by the phenyl group in the pyrolysis of *N*-ethyl-*N*-methyl-*N*-phenethylamine oxide,[5] may indicate that the transition state for the Ei reaction of *S*-(α-methylbenzyl)-*N*-*p*-tosylsulfilimine takes nearly the E_1 like process, namely S(III)–N bond cleavage is the rate-determining step, while that for the 2-phenylsulfonyl derivative corresponds to the ideal concerted Ei process, though shifting slightly to a carbanion-like state. In view of these observations in the pyrolysis of the 2-phenyl-sulfonyl derivative, the hydrogen abstraction is believed to be more important step than in the pyrolysis of the above mentioned sulfilimines. The large negative value of the activation entropy found for the 2-phenylsulfonyl compound is also in keeping with the ideal type transition state in which the large negative charge in the vicinal bulky sulfonyl group approaches the negatively charged *N*-*p*-tosyl group, thus making the transition state substantially more rigid.

Experimental

S-[*2-(Phenylthio)ethyl*]-S-*phenyl*-N-p-*tosylsulfilimine (II)*. The sulfilimine was prepared in the usual manner[6] by treating 1,2-bis(phenylthio)ethane with chloramine-T in ethanol. The yield was 84%, mp 133 °C, IR 1150, 1290 (ν_{SO_2}), 990 (ν_{SN}), NMR (δ ppm), $-CH_2CH_2-$ (s, 3.20, 4H), *p*-CH_3 (s, 2.50, 3H), Phenyl-H (m, 7.0—8.0, 14H). Found: C, 60.64; H, 4.97; N, 3.42%. Calcd for $C_{21}H_{21}S_3O_2N$: C, 60.69; H, 5.09; N, 3.37%.

S-[*2-(Phenylsulfinyl)ethyl*]-S-*phenyl*-N-p-*tosylsulfilimine (III)*. 2-(Phenylsulfinyl)ethyl phenyl sulfide (1.0 g) which was prepared from 1,2-bis(phenylthio)ethane and perbenzoic acid was dissolved in chloroform. The chloroform solution of the sulfide was treated at room temperature with chloramine-T as described above. After 30 min the solution was quenched with aqueous sodium hydroxide solution to remove *p*-toluenesulfonamide. The chloroform solution was washed with water and dried over anhyd. sodium sulfate. After the evaporation of chloroform, a solid crystalline residue was obtained in 0.7 g (70%) yield. The NMR spectra of the crude crystals indicated a broad peak at δ 2.5 ppm, suggesting that the compound (III) is a composite of two stereoisomers. The crude crystals, therefore, were separated by fractional crystallization from ethanol several times to give two different crystals; one has mp 119—120 °C, the other mp 124—127 °C. Found: C, 58.08; H, 4.79; N, 3.27%. Calcd for $C_{21}H_{21}S_3O_3N$: C, 58.44; H, 4.90; N, 3.25% (mixture).

S-[*2-(Phenylsulfonyl)ethyl*]-S-*phenyl*-N-p-*tosylsulfilimine (IV)*. A mixture of 2-(phenylthio)ethyl phenyl sulfone (2.0 g) and chloramine-T was heated in methanol solution for a few minutes in the presence of a drop of acetic acid. After the work-up, the crystalline product was isolated and recrystallized from ethanol. The yield was 1.75 g (55%) mp 87 °C. Found: C, 56.52; H, 4.74; N, 3.22%. Calcd for $C_{21}H_{21}S_3O_4N$: C, 56.35; H, 4.73; N, 3.13%.

S-[*2-(Phenylsulfonyl) ethyl*]-*2,2*-d_2-S-*phenyl*-N-p-*tosylsulfilimine*. The sulfilimine was prepared by the usual method mentinoned above from 2-(phenylthio)ethyl-2,2-d_2 phenyl sulfone, which was prepared in advance by treating the sulfone and D_2O in dioxane in the presence of sodium carbonate.

Kinetics. The kinetic study was carried out by the method reported elsewhere following the increase of the IR NH stretching band which appeared at 3310 cm^{-1}. The reaction was found to obey a good first-order kinetic equation.

Product Analysis. The olefins formed were not isolated except in the case of the phenethyl derivative. When the pyrolysis was carried out in the NMR tube until the alkyl protons of the starting sulfilimine disappeared, the NMR peaks were found to be a 1 : 1 mixture of the corresponding olefin and the sulfenamide, which corresponds to the authentic samples prepared separately.

References

1) Part V of Ei reaction.

2) S. Oae, K. Tsujihara, and N. Furukawa, *Tetrahedron Lett.*, **1970**, 2663; K. Tsujihara, N. Furukawa, and S. Oae, *Tetrahedron*, **27**, 4911 (1971); K. Tsujihara, K. Harada, N. Furukawa, and S. Oae, *ibid.*, **27**, 6101 (1971); S. Oae, K. Harada, K. Tsujihara, and N. Furukawa, *Bull. Chem. Soc. Jpn.*, **46**, 3482 (1973).

3) T. Yoshida, Y. Yano, and S. Oae, *Tetrahedron*, **27**, 5343 (1971).

4) S. Oae, W. Tagaki, and A. Ohno, *Tetrahedron*, **20**, 417 (1964).

5) A. C. Cope, M. A. Lebel, H. H. Lee, and W. E. Moore, *J. Am. Chem. Soc.*, **79**, 4720 (1957).

6) K. Tsujihara, N. Furukawa, K. Oae, and S. Oae, *Bull. Chem. Soc. Jpn.*, **42**, 2631 (1969).

BULLETIN OF THE CHEMICAL SOCIETY OF JAPAN, VOL. 49 (8), 2339—2340 (1976)

Tri(hetero)substituted Carbonium Ions. XII. A Novel Ring Expansion of 1,3-Dithiolanylium Salts into 1,3-Dithia-4-cyclohexene (1,3-Dithiine) System

Kazuhisa HIRATANI,[1] Takeshi NAKAI,* and Makoto OKAWARA

Research Laboratory of Resources Utilization, Tokyo Institute of Technology, Ookayama, Meguro-ku, Tokyo 152

(Received March 12, 1976)

Synopsis. Pyrolysis of 2-dialkylamino-4-bromomethyl-4-methyl-1,3-dithiolanylium bromides (**2**) readily prepared by bromination of the *S*-(2-methylallyl) dithiocarbamates afforded the six-membered 2-alkylimino-5-methyl-1,3-dithiines (**4**) in good yields. A reasonable mechanism for the novel ring expansion is presented.

There has been considerable interest in the ring transformations of heterocyclic systems and their synthetic applications.[2] In the preceding paper,[3] we described the pyrolysis of 2-dialkylamino-4-bromomethyl-1,3-dithiolanylium bromides (**1**) readily prepared by bromination[4] of the *S*-allyl dithiocarbamates; this affords the 2-dialkylamino-4-methyl-1,3-dithiolylium salts (**3**) with retention of the five-membered structures.

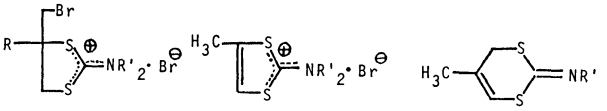

1, R=H, R′=CH_3, C_2H_5
2, R=CH_3, R′=CH_3, C_2H_5

3

4a, R′=CH_3
b, R′=C_2H_5

In this note we wish to report that pyrolysis of 2-dialkylamino-4-bromomethyl-4-methyl-1,3-dithiolanylium bromides (**2**) obtained by bromination of the *S*-(2-methylallyl) dithiocarbamates takes an entirely different course to give the six-membered 2-alkylimino-5-methyl-1,3-dithia-4-cyclohexenes (2-alkylimino-5-methyl-1,3-dithiines) (**4**). This novel ring transformation is, to our knowledge, the first example of a ring expansion of 1,3-dithiolane derivatives into 1,3-dithiine systems, although ring expansions of 1,3-dithiolane derivatives such as **5** into 2,3-dihydro-1,4-dithiine systems (**6**) are well precedented.[5]

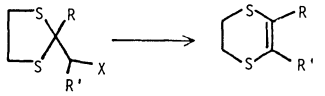

5, X=Cl, Br, OAc **6**

When the 1,3-dithiolanylium bromide **2a** (R=CH_3) was heated in bulk at the melting point (*ca.* 200 °C) for 10 min in nitrogen, **2a** was completely pyrolyzed, with the evolution of gases including methyl bromide, to afford 2-methylimino-1,3-dithiine (**4a**) and its hydrobromide salt (**4a′**) in 16% and 48% yields, respectively, along with an intractable tar. A similar pyrolysis of **2a** at 190 °C for 10 min followed by base treatment and column chromatography gave **4a** in 52%. Both **4a** and **4a′** were identified on the basis of their elemental analyses and spectroscopic properties: **4a**, IR (neat), 1592 cm^{-1} (C=N); NMR ($CDCl_3$), δ 2.05 (3H, d), 3.25 (3H, s), 3.0—3.5 (2H, m), and 6.1—6.3 (1H, m); **4a′** IR (KBr), 1580 cm^{-1} (C=N+); NMR (DMSO-d_6), δ 2.16 (3H, s), 3.33 (3H, s), 3.97 (2H, s), 6.75 (1H, s), and 7.9—9.0 (1H, br. s).

The methylimino-1,3-dithiine **4a** was allowed to react with methyl iodide to give the 2-dimethylamino-1,3-dithiinylium iodide (**7**). The UV spectrum of **7** was very similar to that of the 1,3-dithianylium salt (**8**),[6] supporting the six-membered structure for **4a**.

7 **8**, X=Br, ClO_4

A similar pyrolysis of **2b** (R′=C_2H_5) at 180—190 °C for 45 min followed by base treatment afforded the ethylimino-1,3-dithiine (**4b**) in 51% yield; **4b**, NMR (neat), δ 1.21 (3H, t), 2.04 (3H, s), 3.33 (2H, q), 3.4—3.6 (2H, m), and 6.1—6.3 (1H, m).

The tetrafluoroborate salt obtained by anion exchange of bromide **2a** with sodium tetrafluoroborate failed to undergo the ring expansion under the same conditions as in the pyrolysis of **2a** and was recovered quantitatively. This finding indicates that the thermal ring expansion is initiated by the elimination of alkyl bromide *via* the attack of the bromide anion on the *N*-alkyl carbon atoms. Therefore, the novel ring transformation is best rationalized by the following mechanism, which involves the ring expansion of the imino-1,3-dithiolane **9** formed *via* the elimination of alkyl bromide from **2**. The mechanism for the ring expansion process is analogous to the one accepted for the ring expansions[5] of **5** into **6** described above.

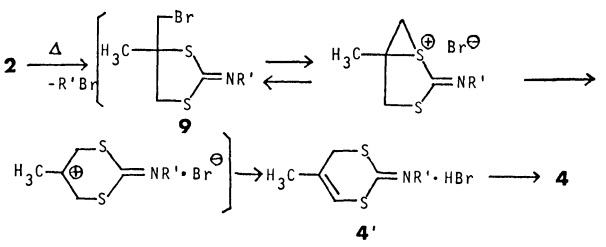

9 **4′**

Experimental

All melting points are uncorrected. NMR and IR spectra were recorded on Japan Electron Optics spectrometers

* To whom inquires should be addressed: Department of Chemical Engineering, Tokyo Institute of Technology, Meguro, Tokyo 152.

(PS-100 or MH-60) and a Hitachi EPI-S2 spectrometer, respectively.

1,3-Dithiolanylium Bromides (2) were prepared by bromination of the corresponding *S*-(2-methallyl) dithiocarbamate, following the procedures described in the previous paper[4]; **2a** ($R'=CH_3$), mp 202—204 °C; **2b** ($R'=C_2H_5$), mp 116—120 °C. Treatment of **2a** with sodium tetrafluoroborate gave the tetrafluoroborate of **2a**, mp 151—153 °C (from ethanol).

Pyrolysis of Salts 2. (*a*): When the bromide **2a** (1.36 g, 4.0 mmol) was heated at 210 °C under nitrogen, the bromide gradually melted and the evolution of gases was observed. After heating at that temperature for 10 min, the gas evolution ceased. A white solid and a yellowish oil were formed at the top side of the flask, and a dark-brown tar was left at the bottom of the flask. The white solid was collected, washed with ether, and recrystallized from acetone-ethanol to give 0.45 g (48%) of the hydrobromide of **4a** (**4a'**); mp 175—177 °C. The spectral data are described above.

Found: C, 29.72; H, 4.19; N, 5.68%. Calcd for $C_6H_{10}BrNS_2$: C, 30.00; H, 4.17; N, 5.83%.

The ethereal washings were freed from solvent to give 0.01 g (16%) of **4a** as an oily residue. The spectral data are described above.

Treatment of the hydrobromide **4a'** thus obtained with triethylamine in benzene afforded the free imine **4a** in 96% yield. Furthermore, **4a** thus obtained was allowed to react with methyl iodide in acetone to give the 1,3-dithiinylium iodide (**7**); UV (EtOH), λ_{max} 244 (sh.) and 269 nm; IR (KBr), 1570 cm^{-1} ($C{=}N^+$).

Found: C, 27.32; H, 4.02; N, 4.73%. Calcd for $C_7H_{12}INS_2$: C, 27.90; H, 3.99; N, 4.65%.

(*b*): The bromide **2a** (5.00 g, 14.9 mmol) was pyrolyzed at 190 °C for 10 min in a similar manner. After cooling, an aqueous solution of sodium carbonate was added to the residue with stirring and the resulting mixture was extracted twice with ether. The combined extracts were dried over anhydrous sodium sulfate and freed from solvent to give an oily residue. Purification of the oil by chromatography on silica gel, using chloroform as eluent, followed by distillation, gave 1.23 g (52%) of **4a**: bp 77—79 °C/0.07 mmHg.

(*c*): The bromide **2b** (3.15 g, 8.7 mmol) was pyrolyzed at 180—190 °C for 45 min. After cooling, the residue was subjected to the same work-ups as in the case of (*b*) yielding 0.76 g (51%) of **4b** as an oil. The spectral data are described above.

(*d*): The tetrafluoroborate of **2a** (0.51 g) was heated at 210 °C for 10 min. After cooling, 0.506 g (99%) of the starting salt was recovered.

References

1) Present address: Industrial Product Research Institute, Ohta-ku, Tokyo 144.

2) H. C. Van Der Plas, "Ring Transformations of Heterocyclics," Vol. 1 and 2, Academic Press, London and New York (1973).

3) T. Nakai, K. Hiratani, and M. Okawara, *Bull. Chem. Soc. Jpn.*, **49**, 827 (1976).

4) K. Hiratani, T. Nakai, and M. Okawara, *Chem. Lett.*, **1974**, 1041.

5) L. F. Fieser, C. Yuan, and T. Goto, *J. Am. Chem. Soc.*, **82**, 1996 (1960); G. Karmas, *J. Org. Chem.*, **32**, 3147 (1967); M. Tomoeda, M. Ishizaki, H. Kobayashi, S. Kanamoto, T. Koga, M. Inuzaka, and T. Furuta, *Chem. Pharm. Bull.*, **12**, 383 (1964) and *Tetrahedron*, **21**, 733 (1965); J. L. Massingill, M. G. Reinecke, and J. E. Hodgkins, *J. Org. Chem.*, **35**, 823 (1970).

6) The definite effect of the ring-size on λ_{max} for the cyclic dithiocarbamidium salts such as **8** has been fully discussed in our previous paper [T. Nakai, Y. Ueno, and M. Okawara, *Bull. Chem. Soc. Jpn.*, **43**, 3175 (1970)].

BULLETIN OF THE CHEMICAL SOCIETY OF JAPAN, VOL. 49 (8), 2341—2342 (1976)

The Photochemical Sulfenylation of Halides with Organic Disulfides

Tamotsu FUJISAWA and Hiromichi OHTA

Sagami Chemical Research Center, Nishi-Ohnuma, Sagamihara, Kanagawa 229

(Received March 29, 1976)

Synopsis. The reaction of organic disulfides with aryl radicals photochemically generated from aryl halides was investigated. Diaryl sulfides were obtained from diaryl disulfides when the radiation was provided by a low-pressure mercury lamp, while dialkyl disulfides afforded alkyl aryl sulfides whether the radiation source was a low- or a high-pressure mercury lamp.

There have been several methods reported for the formation of an aryl-sulfur linkage; in those methods, organic disulfides occupy a fairly significant position as sulfenylation reagents. The disulfide linkage is known to be cleaved by a nucleophilic[1] or electrophilic[2] attack. In addition, disulfides are good radical-trapping reagents, and the formation of an aryl-sulfur linkage by this type of reaction has been demonstrated with phenylazotriphenylmethane[3] and *N*-nitrosoacetylarylamine[4] as radical sources.

The photolysis of aryl halides is known to generate aryl radicals.[5] Halobenzenes, because of their thermal stability and availability, have more advantages as free radical sources than do azo or *N*-nitroso compounds. Thus, if disulfides can be used as scavengers of photochemically generated carbon radicals from halobenzenes, the formation of aryl-sulfur linkages would be easily achieved under milder conditions.

This reaction, however, presents a potential problem in that organic disulfides decompose on ultraviolet irradiation to give thiyl radicals.[6] In the present experiments the photochemical sulfenylatin of halobenzenes with organic disulfides was examined, and this problem was solved by the use of a large excess of halobenzenes in the presence of an aqueous solution of sodium thiosulfate.

When a solution of diphenyl disulfide in iodobenzene was irradiated in a Vycor tube with a low-pressur mercury lamp (50 W), phenyl radicals were generated and diphenyl sulfide was obtained in a 39% yield. Iodine was simultaneously formed and colored the solution deeply, thus strongly decreasing the efficiency of the photochemical reaction. Moreover, a significant part of the phenyl radicals were considered to be trapped by the iodine to regenerate the starting material instead of reacting with the disulfide. Accordingly, if the free iodine could be removed from the reaction system as soon as it is formed,[7] a better yield of diphenyl sulfide would be expected. Thus, sodium thiosulfate was used to consume iodine. A solution of diphenyl disulfide in an excess of iodobenzene and an aqueous solution of thiosulfate were stirred vigrously and irradiated with a low-pressure lamp. The yield of diphenyl sulfide was thus raised remarkably.

$$C_6H_5I + RSSR \longrightarrow RSC_6H_5 + RS\cdot + 1/2\, I_2$$

Table 1 shows the results of the sulfenylation of iodobenzene with various diaryl disulfides. Arylthio radicals partly recombine to form diaryl disulfide, which again undergoes the reaction with phenyl radicals and probably causes the yield of monosulfide to exceed the stoichiometric amount in some cases.

Compared with experiments using a low-pressure lamp, which afforded aryl phenyl sulfides in good yields, the use of a high-pressure mercury lamp (450W) resulted in a negligible yield of monosulfides, although the consumption of diaryl disulfide was large. This observation is attributable to the rapid photodecomposition of diaryl disulfide to thiyl radicals, which leads to side reactions.[8]

Dialkyl disulfides also reacted with iodobenzene to

TABLE 1. REACTION OF IODOBENZENE WITH DISULFIDES

R in disulfide	Low-pressure lamp		High-pressure lamp	
	Conversion of disulfide (%)	Yield of sulfide[a] (%)	Conversion of disulfide (%)	Yield of sulfide[a] (%)
C_6H_5	59	102	84	3
p-$CH_3C_6H_4$	72	84	73	5
p-ClC_6H_4	80	73	53	4
p-$CH_3OC_6H_4$	100	101	26	0
Me	61	117	63	90
Et	53	95	67	82
n-Pr	51	126	63	67
i-Pr	44	60	57	28
t-Bu	20	0	13	0
$PhCH_2$[b]	59	51	58	42
allyl[c]	73	34	94	31

a) Based on consumed disulfide. b) In addition to benzyl phenyl sulfide, dibenzyl sulfide was formed in a yield of 21% (low-pressuse lamp) or 13% (high-pressure lamp). c) In addition to allyl phenyl sulfide, diallyl sulfide was formed in a yield of 11% (low-pressure lamp) or 7% (high-pressure lamp).

Table 2. Reaction of aryl halides with disulfides[a)]

Ar-X (mmol)		R_2S_2 (mmol)		Solvent (ml)		Conversion of disulfide (%)	Yield of RSAr[b)] (%)
p-$CH_3C_6H_4I$	15.8	Ph_2S_2	1.77	C_6H_6	1	46	32
p-$CH_3C_6H_4I$	20.2	Et_2S_2	2.01	C_6H_6	1	44	33
C_6H_5Br	47.8	Et_2S_2	2.92	—		49	29
p-HOC_6H_4Br	23.2	*p*-$CH_3C_6H_4S-)_2$	1.53	C_6H_6	6	100	62
p-$CH_3OC_6H_4Br$	39.8	*p*-$ClC_6H_4S-)_2$	2.51	—		44	39
p-$CH_3OC_6H_4Br$	39.8	Me_2S_2	3.51	—		72	125

a) Irradiated by a low-pressure lamp (50 W). b) Based on consumed disulfide.

give alkyl phenyl sulfides on irradiation. Both low- and high-pressure lamps were effective in the formation of sulfides. An attack by a phenyl radical on the disulfide linkage rather than α-hydrogen abstruction occurred mainly, much as in the cases of thermal reactions.[3)] The yields of alkyl phenyl sulfides were influenced by steric factors. In the case of di-*t*-butyl disulfide, the consumption of the disulfide was very small and neither *t*-butyl phenyl sulfide nor *t*-butyl phenyl disulfide was obtained.

The photochemical sulfenylation by the use of disulfide was also studied with various aryl halides. The results are summarized in Table 2. The reaction effected with a low-pressure lamp afforded good yields of the expected monosulfides. *p*-Bromophenol gave diaryl sulfides by the reaction with diaryl disulfides, but the expected monosulfides could not be obtained from dialkyl disulfides.

Experimental

Reaction of Disulfides with Iodobenzene: General Procedure. Into a reaction tube (Vycor for a low-pressure lamp; Pyrex for a high-pressure lamp) were placed a disulfide (2.5 mmol), iodobenzene (5 ml), and a 1 M aqueous solution of sodium thiosulfate (5 ml). The reaction tube was degassed and sealed *in vacuo*. Irradiation was carried out with an external helical low-pressure mercury lamp (50 W) or a high-pressure mercury lamp (450 W) for 48 h with vigorous stirring. The organic layer was separated from the reaction mixture, and the aqueous layer was washed with dichloromethane. After being dried over anhydrous sodium sulfate, the combined organic layer was concentrated to exactly 10 ml. Phenyl monosulfide and recovered disulfide were identified and determined by GLPC using a standard solution of each authentic sample.

References

1) H. Burton and W. A. Davy, *J. Chem. Soc.*, **1948**, 528; A. Schonberg, A. Stephenson, H. Kaltschmidt, E. Petersen, and H. Schulten, *Ber.*, **66**, 237 (1933); T. Fujisawa, K. Hata, and T. Kojima, *Chem. Lett.*, **1973** 287.

2) B. Miller and C. -H. Han, *J. Org. Chem.*, **36**, 1513 (1971); M. D. Bentley, I. B. Douglass, and J. A. Lacadie, *J. Org. Chem.*, **37**, 333 (1972).

3) W. A. Pryor and P. K. Platt, *J. Am. Chem. Soc.*, **85**, 1496 (1963); W. A. Pryor and H. Guard, *ibid.*, **86**, 1150 (1964); W. A. Pryor and K. Smith, *ibid.*, **92**, 2731 (1970).

4) J. Degani and A. Tundo, *Ann. Chim. (Rome)*, **51**, 543 (1961).

5) R. K. Sharma and N. Kharasch, *Angew. Chem., Int. Ed. Engl.*, **7**, 36 (1968).

6) A. Parker and N. Kharasch, *Chem. Rev.*, **59**, 583 (1959); E. Block, *Quart. Rept. Sulfur Chem.*, **4**, 283 (1969).

7) D. H. Hey, D. A. Singleton, and H. Williams, *J. Chem. Soc.*, **1963**, 1958.

8) Y. Schaafsma, A. F. Bickel, and E. C. Kooyman, *Tetrahedron*, **10**, 76 (1960).

The Simulation of the ESR Spectra of the Perylene Cation on Solid Surfaces

Hisashi UEDA

National Chemical Laboratory for Industry, Mita, Meguro-ku, Tokyo 153

(Received July 2, 1975)

The simulation of the ESR spectra of the perylene cation formed on the surface of silica gel (with MoO_3), silica–alumina, and γ-alumina (with MoO_3) was studied. These oxides were pretreated in a vacuum of 10^{-5} Torr and at 300 °C, and were then brought into contact with a purified perylene solution in benzene. The main parameters which determine the shape of spectra were investigated. By comparing the experimental spectra with the simulated ones, it was concluded that unpaired electron-spin densities on the carbon atoms of the perylene cation are identical to those of the perylene cation in the H_2SO_4 solution. However, the number of γ-protons which have spin-nuclear interactions with the unpaired electron is three or less. It was found that a considerable part of the line-width is caused by g-unisotropies. If the perylene cation is bound more strongly on the surface, more g-unisotropy is observed and the half-width becomes wider. When the perylene cation is prepared in the air, O_2 and H_2O molecules coordinate to the perylene cation formed. It was found that the complex cations thus formed have different g-unisotropies and that the ESR spectrum of this cation mixture is structureless, smooth, and a continuous curve.

The perylene cation is formed when a benzene solution of perylene is added to pretreated silica gel, on which MoO_3 is supported. The pretreatment consists of heating the oxide at 300 °C and under a vacuum of 10^{-5} Torr. The ESR spectra of the perylene cations formed on those oxides which have been thus pretreated have hyperfine structures which are not found in the spectra of untreated oxides.[1-3] The present work was undertaken in order to ascertain what simulation parameters will simulate those hyperfine structures. The combinations of parameters which fit the experimental spectra well were found, and upon those parameters the probable structures of the perylene cation on oxide surfaces are discussed.

Experimental

The perylene cation is formed when a benzene solution of perylene is mixed with inorganic oxide powders which have positively charged points on their surfaces. In the present work three mixed oxides were used: (1) γ-alumina, on which 8.5% of MoO_3 was supported, (2) silica–alumina, consisting of 25% Al_2O_3 and 75% SiO_2, and (3) silica gel, on which 8.5% of MoO_3 was supported. All the oxides except the alumina sample for Fig. 4 were pretreated before mixing with a perylene solution (5 mg/ml). The pretreatment consisted of heating the mixed oxide in a Pyrex tube at 300 °C while it was evacuated to 10^{-5} Torr. After one hour the oxide was cooled and mixed with a perylene solution in benzene which had been prepared in the vacuum line. In the sample for Fig. 4 the perylene cation was prepared in the air. A benzene solution of perylene and alumina with MoO_3 were mixed and then the benzene was evaporated in the air. After the evaporation of the benzene the ESR spectra of the perylene cation (Fig. 4, solid line) were obtained. The evacuation of the sample to 10^{-5} Torr had no effect on the spectrum. After recording the spectrum, benzene was added to the sample and the ESR spectrum was taken again. Again no solvent effect was observed.

Results

In Fig. 1 the ESR spectrum of the perylene cation formed on the surface of γ-alumina (solid line) is shown. One of the simulated spectra is also shown (dotted line).

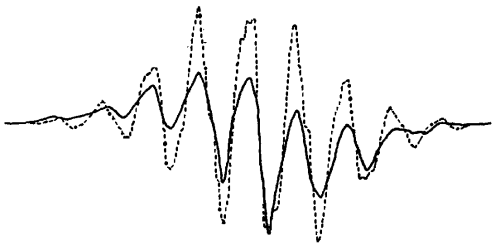

Fig. 1. ESR spectra of perylene cation on pretreated alumina (MoO_3) surfaces. The dotted curve is a simulated spectrum.

The parameters used for the simulation spectrum were $a_\alpha=4.10$, $a_\beta=3.10$, and $a_\gamma=0.46$ G, which are common through Figs. 1—5.[4,5] In the case of Fig. 1, $NA=4$, $NB=4$, $NC=3$, and $W=1.84$ G were used. NC and W could not be decided separately. $NC=3$ was selected in connection with Fig. 3, after which $W=1.84$ G was adopted.

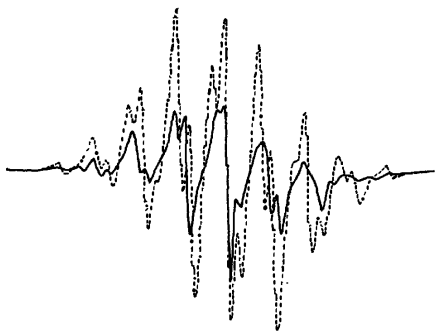

Fig. 2. ESR spectra of perylene cation on pretreated silica–alumina surfaces. The dotted curve is a simulated spectrum.

In Fig. 2 the ESR spectrum of the perylene cation formed on the surface of silica–alumina (solid line) is shown. One of the simulated spectra is also shown (dotted line). The parameters used for Fig. 2 were $NA=4$, $NB=4$, $NC=0$, and $W=2.98$ G. The further splitting of the 9-line spectrum is caused by $a_\alpha-a_\beta=1.0$ G. The line widths of the 9-line (or 18-line)

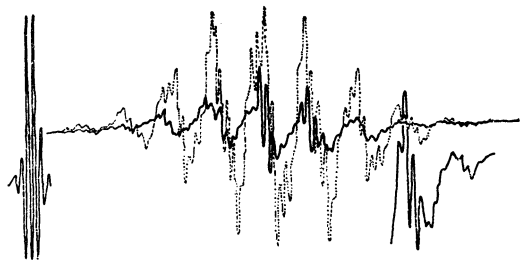

Fig. 3. ESR spectra of perylene cation on pretreated silica gel (MoO_3) surfaces. The dotted curve is a simulated spectrum.

spectrum of Fig. 2 are determined by both NC and W. Therefore, $NC=0$ and $W=2.98$ G should not be accepted with their face values.

In Fig. 3 the ESR spectrum of the perylene cation formed on the surface of silica gel (solid line) is shown. One of the simulated spectra is also shown (dotted line). The parameters used for Fig. 3 were $NA=4$, $NB=4$, $NC=3$, and $W=1.33$ G. The total number of the hyperfine lines to be obtained theoretically is $(NA+1)$-$(NB+1)(NC+1)=100$. The central part of the second derivative curve of the experimentally obtained spectrum is shown to the left of the first derivative curves. In the second derivative curve, the variations in the curvatures of the spectral line are more intensified than the first derivative curve. An important point found in the experimental spectrum is that the total number of hyperfine lines is an even number. The two equally strong, most intense lines in the center of the spectrum typically demonstrate this fact. In the case of Fig. 3, therefore, $NC=3$ is an essential parameter. Considering this fact, $NC=3$ was used in the simulation of Fig. 1. In order to see the less intense hyperfine lines, a part of the 10-times-amplified spectrum is shown to the right of the figure.

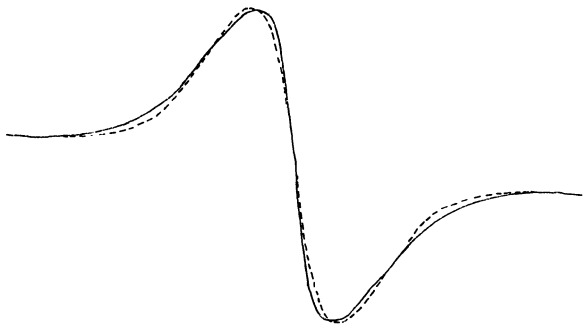

Fig. 4. ESR spectra of perylene cation prepared in the air. The dotted curve is a simulated spectrum which was calculated by assuming a half width of 8.20 G.

In Fig. 4 the ESR spectrum of the perylene cation which was prepared in the air on the alumina surface (solid line) is shown. As a mathematical problem, $NA=4$, $NB=4$, and $W=8.20$ G give a satisfactorily simulated spectrum (dotted line). However, $W=8.20$ G, considering $a_\alpha=4.10$ G, is too large to interpret. Therefore, some other simulations must be tried. For this reason the spectra in Fig. 5 were calculated.

In Fig. 5 three simulated spectra, 5A, 5B, and 5C,

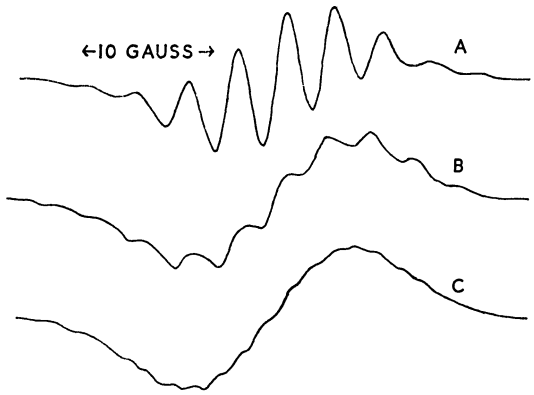

Fig. 5. The simulated ESR spectra for the perylene cation prepared in the air. A: Single g-factor with line width of 1.0 G. B: A spectrum obtained by averaging the spectrum A by a set of unisotropic g-factors. C: A spectrum obtained by averaging two of B-type spectrum different g-tensors.

are shown. The 5A spectrum was obtained by $a_\alpha=a_\beta=3.60$ G (a g-unisotropy of 1.0 G or $\delta g=0.0006$ is included in these values), $NA=4$, $NB=4$, and $W=1.82$ G. This is similar to the one in Fig. 1. On the base of 5A, the 5B spectrum was calculated assuming g-unisotropy. The unisotropic principal values of g, $g_1(2.0009)$, $g_2(2.0030)$, and $g_3(2.0051)$ were assumed. In 1800 directions uniformly distributed in the three-dimensional space, the g-factors were computed from those three principal values. The 1800 spectra obtained by these g-factors were then averaged. The 5B spectrum thus obtained shows that the assumption of only one set of unisotropic g-factors is not enough to get a smooth simulation curve in Fig. 4. If two perylene cations with different principal values of the g-factor are assumed, a smoother curve, 5C, is obtained. In the 5C spectrum, $g_{11}(2.0009)$, $g_{12}(2.0030)$, $g_{13}(2.0051)$, and $g_{21}(2.0019)$, $g_{22}(2.0040)$, and $g_{23}(2.0061)$ were assumed. In practice, the 5B′ spectrum was computed from g_{21}, g_{22}, and g_{23} in the same way as that for 5B. The 5B and 5B′ spectra were then averaged.

Discussion

The Unpaired Electron-spin-density Distribution in the Perylene Cation. One of the γ-protons of the perylene cation on the silica gel surface, as is shown by the simulation in Fig. 3, does not have a hyperfine interaction with the unpaired electron. If one of the γ-protons is removed from the perylene molecule, and if the cation becomes a $C_{20}H_{11}\cdot$ radical, the molecular symmetry changes and the a_α and a_β values should change from 4.10 G and 3.10 G respectively. In the present simulations, $a_\alpha=4.10$ and $a_\beta=3.10$ G gave satisfactory results. This suggests that the migration of the proton was not so large as to cause a great change in the π-electron orbital.

The Factors Affecting the Linewidth. There are three main sources which contribute to the magnitude of the half-width, W: (1) the magnetic dipole-dipole interactions, (2) the unaveraged unisotropic hyperfine splitting

caused by the restricted motions of the cation, and (3) the unisotropy in the *g*-factor.

The contribution of (1) is estimated from the linewidth of Fig. 3 to be about 0.2 G. The contribution from (2) will be about 2 G because it will be about 50% of a_α (4.10 G). The contribution from (3) apparently becomes quite large in some cases. In Fig. 5, if two of the principal values differ from the third value +0.0021 and −0.0021 respectively, the half-width becomes so wide that the entire spectrum looks continuous. A half-width of 8.2 G can give a simulated spectrum which resembles the experimentally obtained spectrum.

The Different States of the Perylene Cation on Three Oxides.

Silica Gel: If a completely degassed and dehydrated sample is used, the half-width can be reduced to 0.2 G and the detailed structure of the spectrum can be observed. The motions of the perylene cation are quite free in this case, and as a result the unisotropy in the *g*-factor is considerably reduced.

Silica–Alumina: In Fig. 2, $NC=0$ and $W=2.98$ G were used as simulation parameters. In the W value the width caused by $NC=3$ and $a_\gamma=0.46$ G may be hidden. The reason why a_γ is not observed is the unisotropy in the *g*-factor. If unisotropy of 0.0003 in the principal values of the *g*-factor is assumed, the resulting linewidth is 0.46 G. Therefore, a_γ becomes invisible. On silica–alumina surfaces, the motions of the perylene cation are more restricted than those on silica gel. However, the linewidth caused by the unisotropy of the *g*-factor is not so large as to submerge the 1.0 G difference between a_γ and a_β.

γ-Alumina: *In the Presence of Air and Humidity.* The perylene cation prepared in the presence of air and humidity gives the ESR spectrum shown in Fig. 4. If we assume two different states of the perylene cation, which have differently unisotropic *g*-factors, a spectrum like Fig. 5C may be obtained. This holds true if, for example, we assume (P^+O_2), a perylene cation to which O_2 is weakly bonded, and (P^+OH_2), a perylene cation to which H_2O is weakly bonded. If (P^+O_2) has the *g*-factor of (g_{11}, g_{12}, g_{13}) and (P^+OH_2) has the *g*-factor of (g_{21}, g_{22}, g_{23}) used for Fig. 5C, and if there is an equal mixture of those two species, a spectrum just like Fig. 5C is observed. It will also be possible to use alternate species, such as P^+O (an atomic oxygen is adsorbed by the cation) or P^+O_2-1 and P^+O_2-2 (two differently coordinated oxygen molecules to a perylene cation) as well as P^+O_2 and P^+OH_2. It remains for future study to determine which of them are really present.

γ-Alumina: *Cation Formation in a Vacuum.* When a perylene solution is mixed with calcined alumina with MoO_3 in a vacuum line, the effects of O_2 and H_2O will be mostly removed from the spectrum. However, even after repeating the pretreatment several times, the ESR spectrum of the perylene cation cannot be resolved any more than that in Fig. 1. The reason for this is that the motions of the perylene cation are more restricted than those on silica–alumina. If the motion of the cation is more restricted, the unisotropy of the hyperfine structure can be observed more; also, the unisotropy of the *g*-factor will be observed still more. For these reasons, the half-width value, 1.84 G, for Fig. 1 includes the width due to the *g*-factor unisotropy. Seeing that, in the case of silica–alumina, $a_\alpha-a_\beta=1.0$ G was detected in the experimental spectrum, while in the case of alumina it was almost unobservable, the half-width due to the *g*-unisotropy is 1.0 G. This corresponds to a *g*-unisotropy of 0.0006.

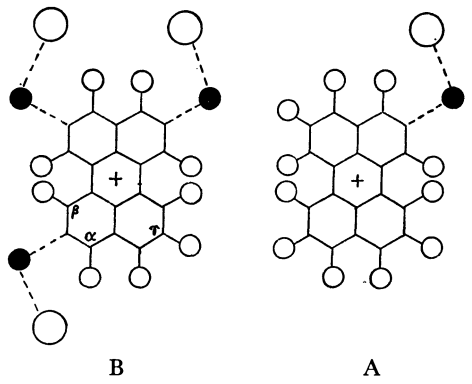

Fig. 6. Perylene cation on oxide surfaces. A: Fixed at one point and has relatively free motions. The cation on silica gel surface. B: Fixed at several points, and has restricted motions. The cation formed in the air on alumina surface. A large circle signifies an oxygen atom (anion) and a small filled circle signifies a fixed proton.

Conclusion. An oxygen atom, an oxygen ion, or molecules containing oxygen will bond weakly to the perylene cation, formed and stabilized on an oxide surface. The unpaired electron of the perylene cation migrates slightly to the atomic or molecular orbital of oxygen. The spin-orbit coupling in the oxygen orbitals affects the energy level of the unpaired electron and causes the *g*-factor to become slightly more unisotropic. The unisotropy of the *g*-tensor is averaged by the motion of the perylene cation allowed on the surface. The degree of averaging depends on the oxide carriers used. The pictures shown in Fig. 6 illustrate some aspects of the perylene cation formed on oxide surfaces.

References

1) H. Ueda, *J. Chem. Phys.*, **62**, 3362 (1975).
2) H. Ueda, *Nippon Kagaku Kaishi*, **1975**, 422.
3) H. Ueda, *Can. J. Chem.*, **46**, 891 (1968); *Bull. Chem. Soc. Jpn.*, **43**, 319 (1970); **47**, 1338 (1974); H, Ueda and N. Todo, *Can. J. Chem.*, **51**, 885 (1973).
4) J. P. Colpa and J. R. Bolton, *Mol. Phys.*, **6**, 273 (1963).
5) J. R. Bolton and G. K. Fraenkel, *J. Chem. Phys.*, **40**, 3307 (1964).

Rotational Isomerism and Intermolecular Interaction in the Liquid Phase

Tsunetake FUJIYAMA and Masao KAKIMOTO*

Department of Chemistry, Faculty of Science, Tokyo Metropolitan University, Setagaya, Tokyo 158
**Department of Chemistry, Faculty of Science, The University of Tokyo, Hongo, Tokyo 114*

(Received September 2, 1975)

The Raman intensities of some fundamental lines of 1,2-dichloroethane and 1,2-dibromoethane and related molecules with internal rotation axes were observed at various temperatures. The observed relative intensities were corrected for some systematic errors expected in the intensity measurement. The importance of a local-field effect was emphasized. The van't Hoff plot of the observed intensity ratios of the *trans* and *gauche* isomers showed the existence of strong intermolecular interactions in the liquid phase. The intermolecular interaction energy in the liquid phase was theoretically estimated from both the macroscopic and microscopic points of view. The usefulness of a dipole-dipole interaction model was emphasized.

Rotational isomerism has been one of the major subjects in the field of physical chemistry. Many investigations have been concerned with the determination of the energy difference between rotational isomers, ΔE. In doing so, one uses the van't Hoff relation and plots the logarithms of the intensity ratio of the vibration spectra of two isomers against $1/T$, where T is the absolute temperature, and thus obtains ΔE from the slope of the plot. This method may be reasonable for the study of ΔE in the gas phase. In the case of a liquid, however, ΔE may be dependent on the temperature because of the existence of intermolecular interactions.

The present report will be concerned with the accurate measurement of the relative intensities of the Raman lines corresponding to the rotational isomers and with the determination of the interaction terms which mainly contribute to ΔE. In order to estimate the interaction energy from the microscopic point of view, it is necessary to know the relative population of the rotational isomers coexisting in the liquid phase. Detailed discussions will also be given for some experimental problems in determining relative populations from the observed Raman intensities.

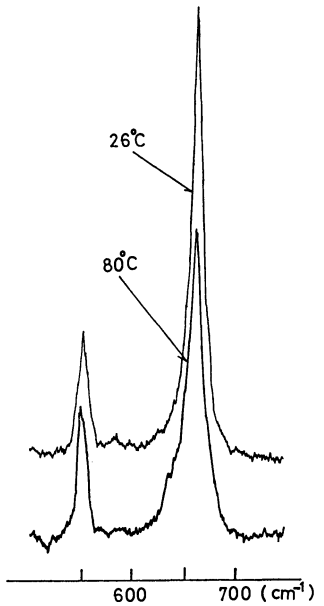

Fig. 1. Raman spectra of 1,2-dibromoethane in the region of 700—500 cm^{-1}.

Experimental

The samples used in the present work were commercial products. After fractional distillation, the purity was checked by gas chromatography.

The Raman spectra were recorded using a laser Raman spectrometer designed and constructed by the authors.[1] The instrument is composed of a He–Ne gas laser source (NEC, GLC 108, 50 mW), a Spex 1401 double monochromator, a HTV R-376 photomultiplier (S-20 response), a handmade lock-in amplifier (375 cps modulation), and a recorder. The linearity of the whole electronic system has been carefully tested. From the standard errors estimated by a linear fitting of the final output voltage against the light energy, the linearity of the whole system was claimed to be better than 1% of the full scale as long as the full scale output voltage was within 10—0.3 V[1]. Special attention was paid to the stability of the laser source.

The stability of the laser output during the spectral measurement was observed by monitoring the light energy which penetrated through the 100% reflectance mirror of the laser cavity. When the output power of the laser source drifted more than 1% during the intensity measurements, the data observed were completely discarded.

The high-temperature cell used for the measurement has been described previously.[2] The accuracy of the observed temperature is within ± 1 °C.

The 754 and 654 cm^{-1} lines of 1,2-dichloroethane were used for the relative intensity measurements. These two lines correspond to the C–Cl stretching vibrations of the *trans* and *gauche* isomers respectively. As for 1,2-dibromoethane, the, 660 cm^{-1} (of *trans*) and the 551 cm^{-1} (of *gauche*) lines were used. Those four lines have scattering cross sections large enough for their relative intensities to be observed with a high accuracy. Relative intensity measurements were repeated eight times at each temperature, the reproducibility of the observed integrated intensities was more than 99%. A typical trace of the observed spectra of 1,2-dibromoethane is illustrated in Fig. 1, which may demonstrate the actual S/N ratio of the observation. The relative intensity areas were determined by a weight method. The averaged value of the eight intensity data was taken as the observed Raman intensity. The maximum deviation of the observed intensity from the averaged value was less than 2%.

Results and Discussion

Correction of the Intensity Data for Systematic Errors. In a previous report, the apparent intensity change due to the temperature has been throughly discussed for typical liquid systems, where the importance of a local-field effect and a density effect have been emphasized.[2] According to the conclusion of the report, an appropriate factor or local-field correction for Raman scattering, L, may be expressed as:

$$L = \frac{(n^2+2)^4}{81}, \tag{1}$$

if the variation in the refractive index over the frequency range of the Raman shift can be ignored. The refractive indices for different temperatures may be estimated from the empirical Eykman equation:

$$\frac{n^2-1}{n+0.4} = \frac{d}{M} \times C, \tag{2}$$

where C is a constant characteristic for a molecule; M the molecular weight, and d, the density.[3] The density, d, as a function of temperature may be found in the International Critical Tables.[4]

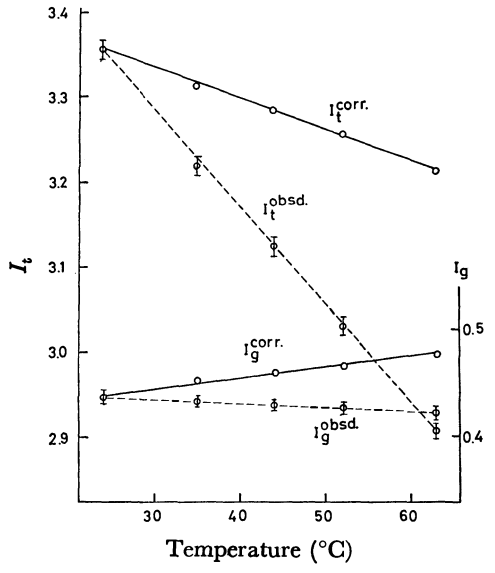

Fig. 2. Raman intensity changes due to temperature for 1,2-dibromoethane.
Observed value; ·····, corrected value; ——.

The observed relative intensities were corrected for the above two factors. The importance and the validity of those corrections are most obvious for 1,2-dibromoethane. In Fig. 2, the observed (denoted as I^{obsd}) and corrected (denoted as I^{corr}) intensities are plotted against the temperature in arbitrary units. It may be seen from the figure that both I_t^{obsd} (of the *trans* isomer) and I_g^{obsd} (of the *gauche* isomer) decrease in magnitude as the temperature increases. If the scattering cross section of the *trans* and *gauche* bands do not change in magnitude within the temperature range of the present experiment, this result is obviously strange because the *trans* and *gauche* isomers are in a thermal equilibrium. After being corrected for the effects of the density and a local-field, however, I_t^{corr} decreases in magnitude as the temperature increases, while I_g^{corr} increases in magnitude within the same temperature range.

Determination of the Relative Population of Rotational Isomers. If we know a scattering cross section of individual Raman lines, the relative population of rotational isomers can be determined from the observed intensity data. Haltman *et al.*[5] have discussed this problem in the case of an infrared absorption and proposed this relation:

$$\frac{A_1}{\alpha_1} + \frac{A_2}{\alpha_2} = C_T, \tag{3}$$

if components 1 and 2 are in thermal equilibrium. In Eq. 3, C_T is the total concentration of components 1 and 2; A, the band area, and α, the absorption coefficient. A similar relation holds for the case of a Raman scattering;

$$\frac{I_t^{obsd}}{\Omega_t} + \frac{I_g^{obsd}}{\Omega_g} = C, \tag{4}$$

or

$$I_g^{obsd} = -(\Omega_g/\Omega_t)I_t^{obsd} + \Omega_g C \tag{4'}$$

where Ω is an absolute scattering cross section, and C, a constant determined by the experimental conditions. By plotting I_g^{obsd} against I_t^{obsd} at series of temperatures, a straight line with a slope of $-(\Omega_g/\Omega_t)$ is generated as long as the scattering cross sections, Ω_g and Ω_t, are constant over the temperature range. As was emphasized in the preceding section, however, the correction of the intensity data for the systematic errors is a pivotal point for the determination of (Ω_g/Ω_t) by the use of Eq. 4.[6] Therefore, Eq. 4 should be modified to:

$$\frac{I_t^{corr}}{\Omega_t} + \frac{I_g^{corr}}{\Omega_g} = C. \tag{5}$$

The same intensity correction is also important in the case of infrared absorption, because the observed band area, A, should be corrected for the same types of systematic errors.[7,8]

Figure 3 shows the plotting of I_g^{corr} against I_t^{corr} at a series of temperatures for 1,2-dibromoethane. As is to be expected from Eq. 5, the plot gives a straight

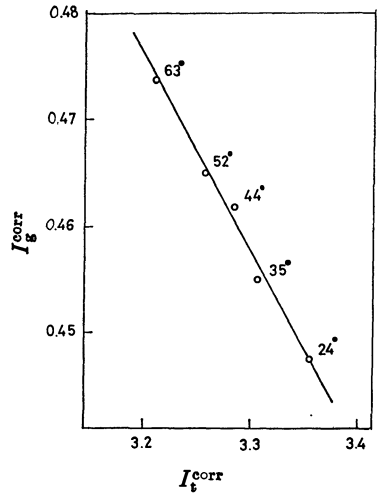

Fig. 3. $I_g^{corr} - I_t^{corr}$ plot for 1,2-dibromoethane.

line with a slope of $-(\Omega_g/\Omega_t)=-0.18$ for 1,2-dibromoethane. The number ratio of the *trans* and *gauche* isomers can, then, be calculated from this relation:

$$\frac{n_t}{n_g}=\frac{I_t^{corr}}{I_g^{corr}}\frac{\Omega_g}{\Omega_t}. \tag{6}$$

In the case of 1,2-dichloroethane, the $I_g^{corr}-I_t^{corr}$ plot was not successful, because the temperature dependence of the relative intensities of the *trans* and *gauche* bands was very small.

van't Hoff Plot and Energy Difference between Rotational Isomers. It has been widely accepted that the energy difference between the *trans* and *gauche* isomers, $\Delta E=E_g-E_t$, can be obtained by the use of the van't Hoff relation:

$$\ln\left(\frac{n_t}{n_g}\right)=A^\circ+\left(\frac{\Delta E}{kT}\right) \tag{7}$$

where A° is a constant; k, the Boltzmann constant, and T, the absolute temperature. Equation 7 claims that a straight line relation should hold between $\ln(n_t/n_g)$ and $(1/T)$. Actually, the observed $\ln(n_t/n_g)$ is plotted against $(1/T)$ in Fig. 4. We see from the figure that a

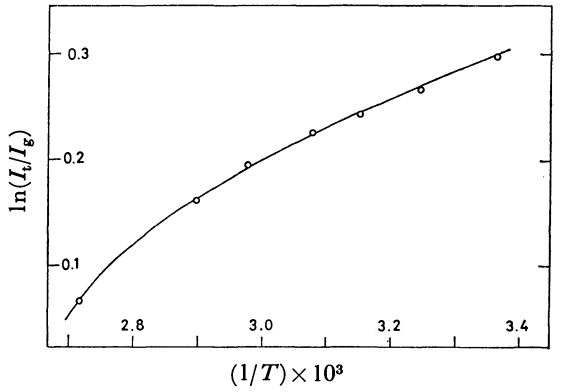

Fig. 4. Relation between $\ln(n_t/n_g)$ and $(1/T)$ for 1,2-dibromoethane.

straight line relation does not hold for the present results. This probably means that ΔE depends on the temperature in the case of liquid 1,2-dibromoethane. The effects of the entropy changes due to the temperature are included in the constant term, A°, of Eq. 7. These effects are ascertained to be negligible in the present discussion if we take into account the frequency changes in the torsional vibrations due to the temperature, and if we assume that the molecular structure is independent of the temperature within the temperature range of the present experiment. It is important to add that the absolute scattering cross sections of the *trans* and *gauche* bands are verified to be independent of the temperature from the plotting of Fig. 3.

From the $\ln(n_t/n_g)$ against $(1/T)$ plot, the ΔE values of 650—900 cal/mol are obtained according to the temperature range under consideration. If we fit the observed points to a linear function, the value of 750 cal/mol is obtained for ΔE of liquid 1,2-dibromoethane. Similar anomalous behavior for van't Hoff plot has been observed for the molecules whose *gauche* forms have large dipole moments, such as 1,2-dichloroethane and 1,1,2,2-tetrabromoethane. In the case of

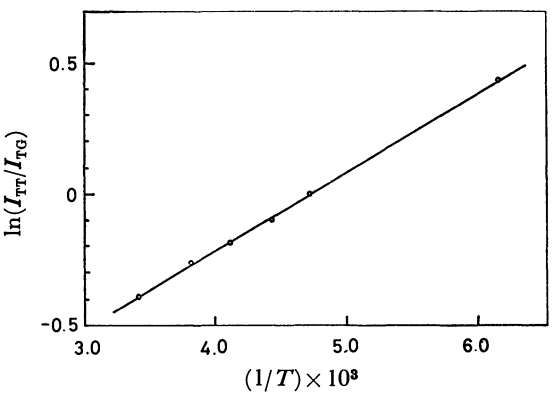

Fig. 5. van't Hoff plot for the TT- and TG-bands of pentane.

non-polar molecules, on the other hand, beautiful straight lines have been obtained for the van't Hoff plot. A typical example observed for the TT- and TG-form bands of pentane is illustrated in Fig. 5.[9] These results indicate that ΔE is dependent on the temperature and that the temperature dependency may arise from intermolecular interactions related with a dipole moment. As the *trans* isomer has no dipole moment, only the interaction between the *gauche* isomers will be considered.

Taking into account the intermolecular interactions expected in the liquid phase, we may rewrite Eq. 7 as:

$$\ln\left(\frac{n_t}{n_g}\right)=A^\circ+\left(\frac{\Delta E^\circ}{kT}\right)+\left(\frac{H}{kT}\right) \tag{8}$$

where H represents the stabilization energy of the *gauche* isomer due to the intermolecular interaction of the dipole type, and where ΔE° menas the intrinsic energy difference between rotational isomers or the energy difference in the rotational isomers when they are well isolated from other molecules. In other words, ΔE° is to be compared with the energy difference observed in the gas phase. If an interaction term, H/kT, be estimated, the $\ln(n_t/n_g)$ values for the gas phase can be estimated from those observed in the liquid phase:

$$\ln\left(\frac{n_t}{n_g}\right)_{gas}=\ln\left(\frac{n_t}{n_g}\right)_{liquid}-\left(\frac{H}{kT}\right) \tag{9}$$

Estimation of the Interaction Energy: Macroscopic. The simplest way of estimating the interaction energy, H, has been proposed by Watanabe.[10] The idea is based upon the reaction field of Onsager in a dilectric field.[11]

If we consider the dielectric field of Onsager, and consider a small cavity with a radius, a, in a continuous medium of the dielectric constant, ε, a dipole moment, μ, at the center of this cavity should cause dielectric polarization in the continuous medium. The polarization in turn exerts a field, F, upon the original dipole:

$$F=\frac{2(\varepsilon-1)}{2\varepsilon+1}\frac{\mu}{a^3} \tag{10}$$

In the present case, the *gauche* isomer can be represented by the sphere, because the *trans* isomer has no dipole moment. The *gauche* isomer in the liquid phase will then possess an excess of electrostatic energy by an amount of:

$$H = \frac{(\varepsilon-1)}{2\varepsilon+1}\frac{\mu_g}{a^3} \tag{11}$$

as compared with that of the free molecule, where, in the present case, μ_g, is the permanent dipole moment of the *gauche* isomer. The corresponding energy change in the *trans* isomer with no dipole moment is negligible. By introducing the observed μ_g, and ε values of Morino *et al.*[12] into Eq. 11, the (H/kT) values were obtained. Then the expected values of $\ln(n_t/n_g)_{gas}$ were calculated by the use of Eq. 9. The results are given in the last column of Table 1 and are illustrated on Fig. 6 (denoted as the Onsager Field). Obviously, the calculated points of $\ln(n_t/n_g)$ for different temperatures fall on a straight line, from which the $\Delta E°$ value expected for the gas phase is calculated to be 1.6 kcal/mol and the $\ln(n_t/n_g)$ value, to be 1.53 at 20 °C. The experimental $\Delta E°$ values observed by the dielectric constant measurement,[13] and the vibration spectra[14–16] are 1.4—1.78 kcal/mol. These values agree well with the calculated value of 1.6 kcal/mol. The logarithmic relative population, $\ln(n_t/n_g)$, as observed by a gas-phase electron-diffraction method, has been reported to be 1.38—1.7 at 20 °C.[17] The agreements between the expected and observed values are quite satisfactory; this indicates the validity of the way of estimating the interaction term, H, on a macroscopic base.

Table 1. Observed and calculated $\ln(n_t/n_g)$-values at various temperatures

(I) Dipole-dipole interaction, (II) dipole-dipole interaction+dipole-induced dipole interaction, (III) reaction field of Onsager.

Temperature (°C)	Observed (Liquid)	Calculated (I)	(II)	(III)
24	0.300	0.755	0.951	1.534
35	0.269	0.690	0.878	1.444
44	0.245	0.640	0.822	1.372
52	0.232	0.603	0.779	1.318
63	0.199	0.544	0.713	1.233
72	0.164	0.490[a]	0.654[a]	1.157[a]
97	0.071	0.362[a]	0.522[a]	1.018[a]

a) Density as a function of the temperature is not given in these temperature ranges (see Ref. 4).

Estimation of the Interaction Energy: Microscopic. The preceding discussion has been based upon a macroscopic point of view. As the macroscopic estimation of H was quite successful, it is of much importance to calculate the interaction term, H, on a microscopic base, also.

Consider the environments to be built up of gas-like molecules dispersed in a vacuum to give the actual density of the liquid phase, instead of looking on them as continuous dielectrics. Only the interactions between the *gauche* isomers are considered in the estimation of H, because the *gauche* isomer has a large dipole moment. Then, H is expressed as:[18,19]

$$H = H_1 + H_2 \tag{12}$$

where

$$H_1 = -\frac{4\pi^2}{27}\frac{\mu_g^4}{kT}\left(\frac{\rho}{W_m}\right)^2\frac{N_a^2}{1+(n_t/n_g)} \tag{12a}$$

$$H_2 = -\frac{4\pi^2}{27}\alpha m^2\left(\frac{\rho}{W_m}\right)^2 N_a^2 \tag{12b}$$

and

$$m = \frac{\mu_g}{1-\frac{4\pi^2}{27}\left(\frac{\rho}{W_m}\right)N_a^2\alpha\left[\frac{\mu_g^2}{kT}\frac{1}{1+(n_t/n_g)}+\alpha\right]} \tag{12c}$$

In Eqs. 12, μ_g is a dipole moment of the *gauche* isomer; ρ, the density; W_m, the molecular weight; α, the averaged polarizability of a *trans-gauche* mixture; N_a, Avogadro's number, and k, the Boltzmann constant. H_1 corresponds to the dipole-dipole interaction between the *gauche* isomers, and H_2, the dipole-induced dipole interaction. By introducing the observed values of μ_g,[12] ρ, and α[20] into Eqs. 12, we obtained the expected values, $\ln(n_t/n_g)$, by the use of Eq. 9. The results are summarized in Table 1 and are illustrated in Fig. 6. The results show that the value of 1.2 kcal/mol is obtained for $\Delta E°$ if we consider only the dipole-dipole interaction in the estimation of H (see Fig. 6, denoted as Dipole-Dipole). If we add the dipole-induced dipole interaction term, the value of 1.4 kcal/mol, is obtained for $\Delta E°$ (see Fig. 6, denoted as Dipole-Induced Dipole). As the observed $\Delta E°$'s are 1.4—1.78 kcal/mol, the agreement between the calculated and observed values seems satisfactory. On the other hand, Table 1 and Fig. 6 show that the agreement between the calculated and observed $\ln(n_t/n_g)$'s is less satisfactory than that obtained by the preceding macroscopic estimation.

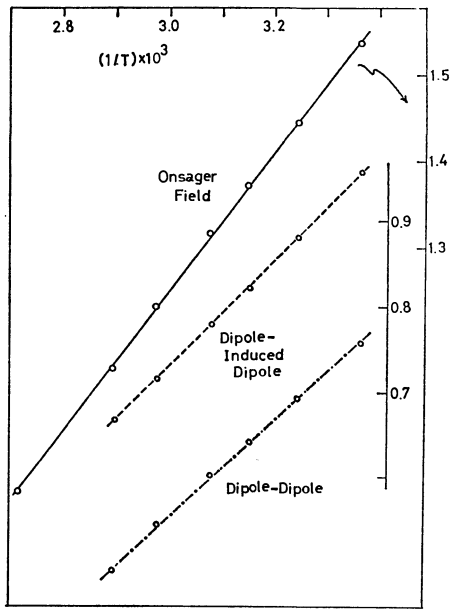

Fig. 6. Expected values for $\ln(n_t/n_g)_{gas}$ for 1,2-dibromoethane (as for the notations, see the text).

The present theoretical approach to estimating the interaction term, H, is based upon an extremely simple model. As has been described in a reference,[19] we first estimated the total interaction energy using a dipole interaction model, and then we averaged it over all possible orientations and distances of the interacting pair. In the averaging process, we assumed a distribution function of the simple Boltzmann type, and we truncated the Taylor expansion of the distribution

function at the first-order term with respect to $(1/T)$. These treatments are certainly over-simplified. The numerical results, however, suggest the possibility of estimating the thermodynamic quantities of the liquid phase by such a purely microscopic approach. Attention must be paid to the fact that the interaction term obtained by the present calculation is expressed in terms of purely molecular quantities, such as a dipole moment and polarizability, instead of a dielectric constans, a very macroscopic quantity, although the polarizability and the molecular radius are *practically* calculated from such macroscopic quantities as the refractive index and the density.

The authors are indebted to all the members of the Shimanouchi Laboratory of The University of Tokyo and to Professor Takehiko Shimanouchi for their helpful correspondence about this work.

References

1) T. Fujiyama and M. Tasumi, *Bunko Kenkyu*, **20**, 28 (1971).

2) T. Fujiyama, *Bull. Chem. Soc. Jpn.*, **46**, 87 (1973).

3) Weissberger *et al.*, "Organic Solvents," Technique of Organic Chemistry, Interscience Publishers, Inc., Vol. VII, New York (1955).

4) "International Critical Tables," Vol. III, McGraw-Hill, New York (1928).

5) K. O. Hartman, G. L. Carlson, W. G. Fately, and R. E. Witowski, *Spectrochim. Acta, Part A*, **24**, 157 (1968).

6) Actually, a plot of $I_g^{obsd.}$ (the 551 cm^{-1} line) against $I_t^{obsd.}$ (the 660 cm^{-1} line) gives a straight line, but with a *negative* value for (Ω_g/Ω_t) for 1,2-dibromoethane.

7) S. R. Polo and M. K. Wilson, *J. Chem. Phys.*, **23**, 2376 (1955).

8) T. Fujiyama and B. L. Crawford, Jr., *J. Phys. Chem.*, **72**, 2174 (1968).

9) T. Fujiyama and M. Tasumi, unpublished.

10) I. Watanabe, S. Mizushima, Y. Morino, *Sci. Pap. Inst. Phys. Chem. Research, Tokyo*, **40**, 425 (1943): S. Mizushima and H. Okazaki, *J. Am. Chem. Soc.*, **71**, 3411 (1949).

11) L. Onsager, *J. Am. Chem. Soc.*, **58**, 1486 (1936).

12) I. Watanabe, I. Miyagawa, and Y. Morino, *Rept. Radiation Chem. Res. Inst. Tokyo Univ.*, **3**, 25 (1947).

13) I. Watanabe, S. Mizushima, and Y. Morino, *Sci. Pap. Inst. Phys. Chem. Res. Tokyo*, **39**, 401 (1942) (Dielectric Constant, 1.4 kcal/mol).

14) T. Shimanouchi, H. Tsuruta, and S. Mizushima, *Sci. Pap. Inst. Phys. Chem. Res. Tokyo*, **45**, 51 (1944) (I. R., 1.45 kcal/mol).

15) H.J. Bernstein, *J. Chem. Phys.*, **18**, 897 (1950) (I. R., 1.77 kcal/mol).

16) Y. A. Pentin and J. M. Tatevskii, *Dokl. Akad. Nauk SSSR*, **108**, 290 (1956) (1.78 kcal/mol).

17) J. Brunvoll, Thesis submitted to University of Oslo (1962); K. Kveseth and O. Bastiansen, Private communication (1973). The present authors are indebted to Dr. Kveseth and Professor Bastiansen for their helpful correspondence about this problem.

18) M. Kakimoto and T. Fujiyama, *Bull. Chem. Soc. Jpn.*, **48**, 2258 (1975).

19) M. Kakimoto and T. Fujiyama, *Bull. Chem. Soc. Jpn.*, **48**, 3003 (1975).

20) The α vatue was estimated from the refractive index values through the Lorentz-Lorenz relation. As the refractive index is known only for an equilibrium mixture of the two isomers, we could not distinguish the polarizabilities of the two isomers.

Heterogeneous Catalysis in Liquid-Phase Oxidation of Olefin. I. Activity of Vanadium System Catalysts for Oxidation of Cyclohexene

Katsuomi TAKEHIRA and Toshio ISHIKAWA

National Chemical Laboratory for Industry, Mita, Meguro-ku, Tokyo 153

(Received October 27, 1975)

The catalytic activities of various binary oxides containing vanadium for the liquid-phase oxidation of cyclohexene have been studied, in comparison with those of one component oxides and soluble metal acetylacetonates. The reaction was carried out at 60 °C in benzene solvent. The distribution of reaction products suggests the occurrence of autoxidation and epoxidation when vanadium system catalysts are used. Among the binary catalysts, V–Cr and V–Mo systems showed relatively high specific activities, especially high activity being obtained by the former systems calcined at a low temperature. It seems that cyclohexene oxide is formed mainly by two successive catalytic processes, *i.e.*, the formation of cyclohexenyl hydroperoxide by autoxidation and the selective oxidation of cyclohexene with the hydroperoxide. The machanism of epoxidation was confirmed by the reaction of cyclohexene with *t*-butyl hydroperoxide in the presence of V–Cr catalyst.

Studies have been carried out in the field of liquid-phase oxidation of olefins with insoluble catalysts containing transition metals. Cyclohexene was often used as a model reactant.[1,2] Meyer *et al.*[1] showed the heterogeneous-homogeneous character of the reaction with MnO_2 and CoO as catalysts. Gould and Rads[2] studied the distribution of reaction products and suggested that the atomic number and oxidation state of transition metal in the catalyst are important in determining the course of the reaction. However, these studies are almost restricted to the activity of one component metal oxide, scarcely any attempts to test the catalytic activity of binary oxide system being made.

V_2O_5 was found to be comparatively active for the liquid-phase oxidation of acrylaldehyde.[3] It has been frequently used as a catalyst for vapor-phase oxidation of some hydrocarbons, many investigations being published about the high activity obtained by combining V_2O_5 and another oxide. The high activity is thought to be caused by the formation of different structures from those of original oxides.[4] A similar phenomenon is expected also in a liquid-phase oxidation. Vanadium-chromium binary oxide shows higher activity than the individual one component oxide in the liquid-phase oxidation of acrylaldehyde.[5] The catalytic activity of the binary oxide was discussed in connection with its structure, and the active species in this catalyst was thought to be phase Y which is a chromium isopolyvanadate.

On the other hand, soluble metal complexes of vanadium, as well as those of molybdenum or tungsten, catalyze the selective epoxidation of olefin with organic hydroperoxide.[6] The oxidation of cyclohexene with binary oxide catalyst containing vanadium seems to be of interest in view of the epoxidation. For the purpose of studying the effects of addition of second component to vanadium pentoxide, various binary oxides containing vanadium were prepared, and their catalytic activities for the oxidation of cyclohexene have been examined in comparison with those of one component oxides and soluble metal acetylacetonates. These results are reported in this paper.

Experimental

Catalysts. Metal acetylacetonates [$Me(acac)_n$], *i.e.*, $VO(acac)_2$, $Cr(acac)_3$, $Mn(acac)_2$, $Mn(acac)_3$, $Fe(acac)_3$, $Co(acac)_2$, $Co(acac)_3$, $Ni(acac)_2$, $Cu(acac)_2$, $Zn(acac)_2$, and $MoO_2(acac)_2$ (Tokyo Chemical Industry Co.) were used.

One component metal oxides were prepared as follows. Cr_2O_3, Mn_2O_3, Fe_2O_3, CoO, NiO, CuO, ZnO, and Bi_2O_3 were prepared by calcination of the corresponding metal hydroxides at 450 °C for 6 h in air. The hydroxide was precipitated by addition of dilute aqueous ammonia to an aqueous solution of the corresponding metal nitrate, followed by separation from the solution by filtration, sufficient washing with water, and drying at 100 °C for one day. V_2O_5 was prepared by calcining V_2O_5 hydrate precipitated by addition of concentrated nitric acid to a warm aqueous solution of NH_4VO_3 and the subsequent washing, and drying mentioned above. MoO_3 and WO_3 were similarly prepared by calcining $H_2MoO_4 \cdot H_2O$ and H_2WO_4, respectively.

In order to study the effects of addition of second component (C_{II}) to V_2O_5, 20 kinds of binary system oxides, *i.e.*, V–Li (1/1),* V–Na (1/1), V–K (1/1), V–Mg (1/1), V–Ca (1/1), V–Sr (1/1), V–Ba (1/1), V–Cr (1/0.4), V–Mn (1/0.4), V–Fe (1/0.4), V–Co (1/0.4), V–Ni (1/0.4), V–Cu (1/0.4) V–Zn (1/0.4), V–Mo (1/0.2), V–W (1/0.2), V–B (1/0.4), V–P (1/0.4), V–Sb (1/0.4), and V–Bi (1/0.4), were prepared in the following way. A mixture of V_2O_5 hydrate and raw material of second component; hydroxide of alkali or alkaline earth metal, nitrate of Cr, Mn, Fe, Co, Ni, Cu, Zn, or Bi, $H_2MoO_4 \cdot H_2O$, H_2WO_4, H_3BO_3, H_3PO_4, or Sb_2O_5, was kneaded with a small amount of water at 80 °C for 6 h.** The resulting paste was dried at 100 °C for one day, and calcined at 400 °C for 3 h in the air. Since V–Cr and V–Mo systems showed high specific activities, both systems were calcined at 600 and 800 °C in order to study the effects of calcination temperature. For the purpose of indicating the calcination temperature, catalysts are denoted by $V\text{–}C_{II(400)}$, $V\text{–}C_{II(600)}$, and $V\text{–}C_{II(800)}$, respectively.

In all cases, a particle size of metal oxide used as catalyst was smaller than 100 mesh.

Apparatus and Procedure of Reaction. The oxidation reaction was carried out at 60 °C and under 1 atm of oxygen using a gas-sealed system with an oxygen recycling unit (Fig. 1). Catalyst and benzene as a solvent were put into the reactor. Cyclohexene (20.0 ml, prepurified by passing over activated alumina to eliminate hydroperoxide) was then added, and the stirring of the reaction mixture and bubbling of oxygen (flow

* The fractional number in parentheses is the atomic ratio of V/C_{II}.

** A three component system, V–S–K (1/1/2), was also made from a mixture of V_2O_5 hydrate and K_2SO_4.

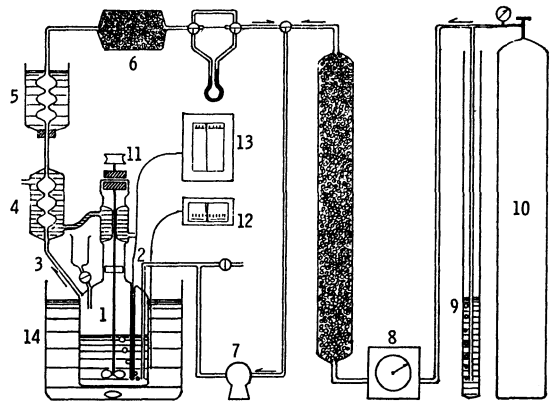

Fig. 1. Reaction apparatus.
1: Reactor, 2: gas inlet, 3: gas outlet, 4: water-cooled condenser, 5: ice–water-cooled condenser, 6: carbon dioxide-elimination tube, 7: gas-recycling pump, 8: gas meter, 9: pressure controller, 10: O_2 tank, 11: magnetic stirrer, 12: reaction temperature controller, 13: reaction temperature recorder, 14: glycerol bath.

rate; 200 ml/min) into it were started. The effluent gas mixture flowing out from the reactor was passed through the condensers and the carbon dioxide-elimination tube, and was recycled by the pump into the reactor. In order to keep the inside pressure at one atm, oxygen was supplied through a gas meter.

In order to clarify the mechanism of epoxidation the reaction of cyclohexene with *t*-butyl hydroperoxide was carried out in benzene under 1 atm of dry nitrogen using a 20 ml of glass flask. The reactor was placed on a shaker so that the catalyst was uniformly suspended.

Analyses of Reaction Products and Catalysts. The oxidation products were assayed as follows. Cyclohexenyl hydroperoxide was determined by the iodometric method described by Wagner *et al.*[7] The remaining components were determined by gas chromatography using a column of PEG 6000 after treating the sample with a sufficient amount of triphenylphosphine so as to reduce quantitatively the hydroperoxide into alcohol.[2] Solvent of benzene was used as an internal standard. Cyclohexene (unconverted), cyclohexene oxide, cyclohexenone, and cyclohexenol were determined. In the case of the reaction with *t*-butyl hydroperoxide, the unreacted hydroperoxide and cyclohexene oxide formed were determined by the iodometric method and gas chromatography, respectively.

The catalysts were analyzed by the following methods. The surface area was determined by the BET method using nitrogen. Powder-type X-ray diffraction pattern was obtained with a diffractometer of Geigerflex D-3F type (Rigaku Denki Co.) with Cu$K\alpha$ radiation. Infrared spectrum was recorded with a JASCO-DS 403 G grating spectrophotometer with samples prepared in the form of KBr pressed discs.

Results and Discussions

When an olefin is oxidized by radical chain mechanism, the peroxy radical formed has two reactivities, hydrogen abstraction from olefin and addition to olefin. It was experimentally found that both contributions change a great deal with the structure of olefin.[8,9] According to the result of cyclohexene oxidation by Mayo *et al.*,[8] the main part of the autoxidation products is cyclohexenyl hydroperoxide, and the amount of cyclohexene oxide is very small, indicating that hydrogen abstruction proceeds mainly. It might be concluded that cyclohexene oxide is scarcely formed in the radical chain reaction. Experiments with use of a radical initiator also gave similar results. As an example, by the 4 h reaction in benzene solvent with a thermal initiator of azobisisobutyronitrile (AIBN) (10^{-2} mol/l), 90.4% of cyclohexenyl hydroperoxide, 3.2% of cyclohexene oxide, 2.5% of cyclohexenone, and 3.9% of cyclohexenol were formed.***

However, it was reported that relatively large amount of cyclohexene oxide was formed in the case of using some transition metal catalysts. Gould and Rado[2] carried out the oxidation of neat cyclohexene using soluble acetylacetonates or insoluble oxides of various transition metals as a catalyst at 70 °C under the oxygen pressure of 6.5 atm. A relatively high yield of cyclohexene oxide was obtained with molybdenum or vanadium compound catalyst, such as $Mo_2(acac)_2$, VO-

TABLE 1. REACTION RESULTS WITH $Me(acac)_n$ CATALYST[a]

Cat.	Conv. (%)	Yield (%)		Select. (%)		Rate ($\times 10^6$mol/l s)		Ind. Per. (min)	React. time (min)
		Oxide	HPO	Oxide	HPO	R_{max}	R_{end}[b]		
$VO(acac)_2$	—	—	—	—	—	—	—	—	240
$Cr(acac)_3$	—	—	—	—	—	—	—	—	240
$Mn(acac)_2$	5.40	0.23	3.88	4.3	71.9	43.8	8.6	145	265
$Mn(acac)_3$	6.10	0.21	3.33	3.4	54.6	80.5	15.6	5	114
$Fe(acac)_3$	0.78	0.07	0.64	9.0	81.9	6.3	6.3	222	300
$Co(acac)_2$	7.10	0.22	4.52	3.1	63.7	79.0	11.7	32	100
$Co(acac)_3$	2.60	0.13	1.97	5.0	75.8	8.6	6.3	74	240
$Ni(acac)_2$	2.30	0.08	1.96	3.5	85.2	6.3	6.3	53	240
$Cu(acac)_2$	2.30	0.08	1.77	3.5	77.0	13.3	10.2	94	180
$Zn(acac)_2$	—	—	—	—	—	—	—	—	240
$MoO_2(acac)_2$	—	—	—	—	—	—	—	—	240

a) 20 ml of cyclohexene, 50 ml of benzene and 7×10 ml of metal acetylacetonate were used. The reaction temperature was 60 °C. The O_2 pressure was 1 atm. b) The rate of oxygen absorption just before the cessation of the reaction.

*** Each of these values was calculated based on converted cyclohexene, showing selectivity.

TABLE 2. REACTION RESULTS WITH ONE COMPONENT METAL OXIDE CATALYST[a)]

Cat.	Conv. (%)	Yield (%)		Select. (%)		Rate ($\times 10^6$mol/l s)		Ind. Per. (min)	React. time (min)
		Oxide	HPO	Oxide	HPO	R_{max}	R_{end}		
V_2O_5	1.56	0.36	0.61	23.1	39.1	3.1	2.4	120	300
Cr_2O_3	2.00	0.10	1.58	5.0	79.0	5.5	4.7	150	240
Mn_2O_3	4.95	0.18	3.96	3.6	80.0	13.3	7.8	19	240
Fe_2O_3	0.74	0.03	0.63	4.1	85.3	1.6	1.6	212	240
CoO	2.60	0.08	1.94	3.1	74.6	4.7	3.9	93	240
NiO	—	—	—	—	—	—	—	—	240
CuO	—	—	trace	—	—	—	—	—	240
ZnO	—	—	—	—	—	—	—	—	240
MoO_3	—	trace	trace	—	—	—	—	—	240
WO_3	—	—	—	—	—	—	—	—	240
Bi_2O_3	—	—	—	—	—	—	—	—	240

a) 20 ml of cyclohexene, 50 ml of benzene and 50 mg of metal oxide were used. The reaction temperature was 60 °C. The O_2 pressure was 1 atm.

$(acac)_2$, MoO_3 or V_2O_5. Therefore, in the present work, the activity of one component metal catalyst was first of all studied. The following results were obtained by use of acetylacetonates and oxides of several metals as catalysts.

Activities of One Component Metal Catalysts. The results with metal acetylacetonate catalysts are given in Table 1. Cobalt and manganese also show high activity. The activity depends on the oxidation states or coordination numbers. In the reaction with $Co(acac)_2$ catalyst, a rapid absorption of oxygen was observed after the color of reaction solution turned from pink to green, suggesting the formation of cobaltic ion. The induction period was shortened by the addition of *t*-butyl hydroperoxide, the oxygen absorption being also accompanied by a similar change of color. Hydroperoxide seemes to be decomposed by way of its coordination to cobalt. Then, the chain reaction starts. In contrast, $Co(acac)_3$ shows relatively low activity which may be ascribed to the larger stability of the six-coordinated octahedral structure.[10)] A long induction period and a low activity observed with $Mn(acac)_2$ indicate that manganous ion inhibited, as reported by Gould and Rado[2)] the autoxidation of cyclohexene by reacting with cyclohexenyl peroxy radical. $Cr(acac)_3$ was reported to have activity in the oxidation of neat cyclohexene.[2)] However, it showed no oxygen absorption in the present work. The deactivation observed especially with $Co(acac)_2$ and $Mn(acac)_3$ seems to result from the formation of the metal oxides or basic chelate. This is supported by the fact that precipitates formed during the course of reaction.

The results of the reactions with several matal oxides catalysts are given in Table 2. Mn_2O_3 shows the highest activity. In spite of the inactivity of chromium and vanadium in the chelate form, their oxides showed activity. Meyer *et al.*[1)] reported that chromium(III) oxides seem to initiate the reaction only by the decomposition of hydroperoxide, while cyclohexene itself may be the initiating agent in the reaction activated by cobalt and manganese oxides. In the present study, the long induction period observed in the reaction with chromium(III) oxide may be due to the accumulation of the hydroperoxide. Manganese oxide exhibiting a considerably short induction period is thought to initiate the reaction without decomposing the hydroperoxide.

Concerning the reaction products, the following results were obtained. The main product with the active catalysts was cyclohexenyl hydroperoxide, the amount of cyclohexene oxide being very small. The selectivity of the hydroperoxide was lower with manganese and cobalt catalysts than with the other catalysts except V_2O_5. This is thought to be caused by the formation of cyclohexenol and cyclohexenone accompanied by the radical decomposition of hydroperoxide. Contrary to the results obtained by Gould and Rado,[2)] MoO_3, $MoO_2(acac)_2$, and $VO(acac)_2$ gave no epoxide. Fairly high selectivity of the epoxide was attained only with V_2O_5. The other catalysts showed low values of selectivity which are near those obtained by using the thermal initiator AIBN.

Details of the Reaction with V_2O_5. In order to clarify the oxidation with V_2O_5 and compare the results with that with other catalysts, several reactions were carried out. The distributions of products in the reactions are given in Table 3. V_2O_5 showed a higher selectivity of cyclohexene oxide than the other catalysts. The high selectivity does not seem to be explained by the radical chain mechanism. The epoxidation with V_2O_5 seems to proceed either by the oxygen activation

TABLE 3. DISTRIBUTION OF OXIDATION PRODUCTS[a)]

Cat.	Conv. (%)	Select. (%)				React. time (min)
		HPO	ONE	OL	Oxide	
$Co(acac)_2$	12.31	61.7	15.7	18.8	2.7	240
$Mn(acac)_3$	10.72	61.6	12.3	15.5	2.5	240
Mn_2O_3	6.69	69.5	8.5	10.9	2.4	240
Cr_2O_3	4.17	77.3	6.7	8.3	2.4	240
V_2O_5	1.81	34.1	4.1	24.5	20.7	240
$V\text{-}Cr_{(400)}$	5.73	40.3	10.6	27.3	23.4	300
V-Mn	2.58	33.8	9.8	29.8	20.1	300

a) 50 ml of cyclohexene and 50 ml of benzene were used with metal acetylacetonate of 10^{-1} mol or metal oxide of 100 mg. The reaction temperature was 60 °C. The O_2 pressure was 1 atm.

mechanism or the hydroperoxide intermediate mechanism. The former can be shown by

$$\text{Cat.} + O_2 \longrightarrow (\text{Cat.}\text{-}O_2) \quad (1)$$

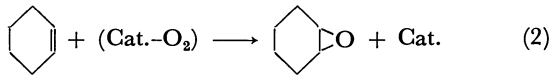

(2)

and the latter by

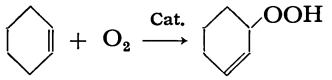

(3)

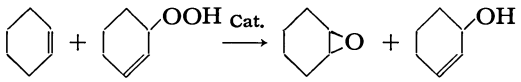

(4)

Reaction 3 proceeds by a radical chain mechanism.

Various studies have been carried out on the formation and reactivity of adsorbed oxygen species on the surface of metal oxides in the field of vapor-phase oxidation. Yoshida *et al.*[11] considered that O_2^-, an adsorbed oxygen species on partially reduced V_2O_5–SiO_2 catalyst, oxidizes propylene at room temperature by a mechanism involving the intermediate of epoxide structure. In the present study, the reduced vanadium species existed also in V_2O_5 catalyst,† and the oxygen activation mechanism is therefore possible. However, in spite of this argument in favor of the oxygen activation process, the fairly large amount of hydroperoxide in the products suggests the availability of another mechanism involving the radical chain reaction 3. The hydroperoxide intermediate mechanism is also supported by the presence of a large amount of cyclohexenol.

In the reactions with cobalt and manganese catalysts, the main products were cyclohexenyl hydroperoxide, cyclohexenol, and cyclohexenone, and the formation of cyclohexene oxide was very small. Such distribution of products may be explained by an acceleration of the radical chain reaction due to the Haber-Weiss mechanism. The distribution of oxidation products with Cr_2O_3 was similar to that with cobalt and manganese catalysts. Cr_2O_3 seems to accelerate the radical chain reaction by decomposing the hydroperoxide.

Reaction Results with Binary Oxide Catalysts. V_2O_5 catalyzes the epoxidation of cyclohexene. The activity of V_2O_5 catalyst increases in acrylaldehyde oxidation when it is modified with another metal oxide, Cr_2O_3, resulting in change of catalyst structure.[5] Similar phenomena concerning the catalyst for vapor-phase oxidation have been reported.[4] The catalytic activities of various binary oxides containing vanadium were tested also in the liquid-phase oxidation of cyclohexene.

Oxygen absorption was observed for several binary oxides. The results are given in Table 4. Concerning the maximum rate of oxygen absorption (R_{max}), the activity of the catalysts can be put in the order $\text{V–Cr}_{(400)} \gg \text{V–Cr}_{(600)} \gg \text{V–Mn} > \text{V–P} > \text{V–Fe} \simeq \text{V–Bi} \simeq \text{V–Mo}_{(800)}$, the other systems showing extremely low activity. The V–Cr system in particular showed high activity. This binary system showed higher activity when calcined at lower temperature, which coincides with results observed in the study of acrylaldehyde oxidation.[5] The activity of the V–Mo system, in contrast, appeared only when calcined at 800 °C. With respect to the formation of cyclohexene oxide, most of these binary systems showed comparatively higher ability than the one component metal oxides (Table 2) or metal acetylacetonates (Table 1).

Structure and Activity of V–Cr and V–Mo Systems. In the liquid-phase oxidation with insoluble metal oxide catalysts, the reaction proceeds by a heterogeneous initiation mechanism on the surface of catalysts.[1] The specific surface area (S_s) of the catalyst having relatively high activity was measured and is given in Table 5, together with the specific activity (R_{max}/S), *i.e.*, the maximum rate of oxygen absorption per unit surface area of the catalyst. The V–Cr system calcined at a low temperature also showed higher values in specific activity.

According to the results of X-ray diffraction analysis (Fig. 2), $\text{V–Cr}_{(400)}$ and $\text{V–Cr}_{(600)}$ showed diffraction

Table 4. Reaction results with binary oxide catalyst[a]

Cat.	Conv. (%)	Yield (%)		Select. (%)		Rate ($\times 10^6$mol/l s)		Ind. Per. (min)	React. time (min)
		Oxide	HPO	Oxide	HPO	R_{max}	R_{end}		
$\text{V–Cr}_{(400)}$	8.52	1.90	3.44	22.3	40.4	25.8	20.6	91	300
$\text{V–Cr}_{(600)}$	3.92	0.98	1.38	25.0	35.2	14.9	14.9	165	330
$\text{V–Cr}_{(800)}$	1.29	0.27	0.34	20.9	26.4	2.3	2.3	200	270
V–Mn	4.39	0.86	1.99	19.6	45.3	4.7	4.7	103	270
V–Fe	3.33	0.56	1.27	16.8	38.2	3.1	3.1	133	270
V–Ni	1.88	0.33	0.74	17.6	39.1	1.6	1.6	194	270
$\text{V–Mo}_{(800)}$	1.76	0.57	0.12	32.4	6.8	3.1	1.6	108	270
V–W	0.53	0.11	0.29	20.8	54.7	0.8	0.8	247	270
V–P	1.39	0.59	0.31	42.4	22.3	3.9	3.9	110	270
V–Sb	1.44	0.65	0.21	45.2	14.6	2.4	2.4	198	270
V–Bi	3.23	0.62	0.39	19.2	12.1	3.1	2.4	100	270

a) 20 ml of cyclohexene, 50 ml of benzene, and 50 mg of binary oxide were used. The reaction temperature was 60 °C. The O_2 pressure was 1 atm. No oxidation occurred for a period of 300 min with the binary oxides (not contained in this Table), *i.e.*, V–alkali metal, V–alkaline earth metal, V–Co, C–Cu, V–Zn, $\text{V–Mo}_{(400)}$, and $\text{V–Mo}_{(600)}$ catalysts.

† The existence of the V^{4+} ions was suggested by ESR measurement.

Table 5. Surface area and specific activity of binary oxide catalyst

Cat.	S_s (m^2/g)	R_{max}/S ($\times 10^6$mol/l s m^2-cat.)
$V\text{-}Cr_{(400)}$	7.3	62.5
$V\text{-}Cr_{(600)}$	8.0	36.0
$V\text{-}Cr_{(800)}$	2.5	16.4
V-Mn	11.5	9.4
V-Fe	23.4	3.1
$V\text{-}Mo_{(400)}$	1.1	—
$V\text{-}Mo_{(600)}$	1.4	—
$V\text{-}Mo_{(800)}$	1.3	53.2
V-P	4.0	20.3
V-Bi	3.5	18.8
V_2O_5	5.2	10.9

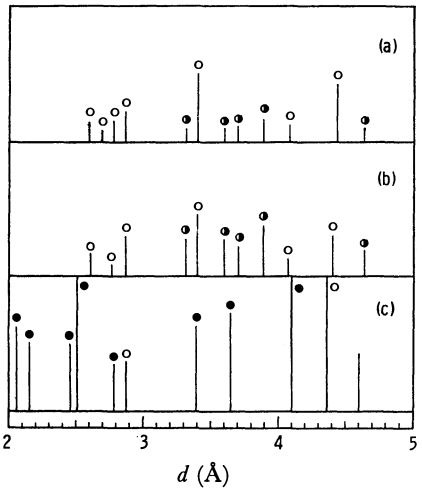

Fig. 2. X-Ray diffraction patterns of V–Cr system catalysts.
(a) $V\text{-}Cr_{(400)}$, (b) $V\text{-}Cr_{(600)}$, (c) $V\text{-}Cr_{(800)}$,
○: V_2O_5, ◑: phase Y, ●: $CrVO_4$.

lines of V_2O_5 and phase Y which was reported to be a chromium isopolyvanadate.[5] However, $V\text{-}Cr_{(800)}$ showed no lines of phase Y but gave the lines of V_2O_5 and chromium orthovanadate ($CrVO_4$). While $V\text{-}Cr_{(800)}$ showed the line of d=4.38 Å which is thought to be of the plane (001) in pure V_2O_5, the lines observed with $V\text{-}Cr_{(400)}$ and $V\text{-}Cr_{(600)}$ gave the values 4.43 and 4.41 Å, respectively. This indicates that the c-axis of V_2O_5 crystal was elongated in $V\text{-}Cr_{(400)}$ and $V\text{-}Cr_{(600)}$, suggesting the formation of interfacial solid solution.†† The diffraction peaks of phase Y were slightly stronger in the pattern of $V\text{-}Cr_{(600)}$ than in that of $V\text{-}Cr_{(400)}$, while the line width of the peaks was broader in the latter. Thus, it seems that the crystallinity of phase Y is lower in the catalyst calcined at lower temperature. In the IR spectra, the absorption bands of phase Y[5] were observed in both $V\text{-}Cr_{(400)}$ and $V\text{-}Cr_{(600)}$, especially sharply in the latter catalyst. However, $V\text{-}Cr_{(800)}$ showed no such absorption bands. Thus, phase Y and the solid solution were observed in the active V–Cr binary catalysts. Phase Y is mainly formed in the catalysts prepared from NH_4VO_3 and $Cr(NO_3)_3\cdot 9H_2O$.[5] On the other hand, the catalysts in the present work were prepared from V_2O_5 hydrate and $Cr(NO_3)_3\cdot 9H_2O$. In spite of the difference in the preparative method, the formation of phase Y was observed in both cases.

The specific activity of $V\text{-}Mo_{(800)}$ came next to that of $V\text{-}Cr_{(400)}$. However, $V\text{-}Mo_{(400)}$ and $V\text{-}Mo_{(600)}$ were inactive. Concerning the catalytic activity of the V–Mo system, studies have been carried out in the field of vapor-phase oxidation, and the relationship between the activity and the structure of this system was studied in detail. The activity of this system was explained either by the formation of solid solution of MoO_3 in V_2O_5,[4] or by the formation of chemical compounds.[13] Two types of compound, *i.e.*, $Mo_6V_9O_{40}$ and $Mo_4V_6O_{25}$, were formed in the catalyst used for the oxidation of benzene to maleic anhydride. The X-ray diffraction patterns of $V\text{-}Mo_{(400)}$ and $V\text{-}Mo_{(800)}$ are shown in

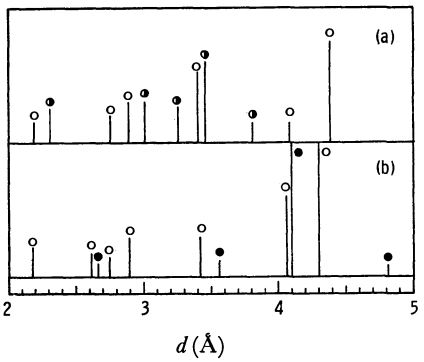

Fig. 3. X-Ray diffraction patterns of V–Mo system catalysts.*
(a): $V\text{-}Mo_{(400)}$, (b): $V\text{-}Mo_{(800)}$.
○: V_2O_5, ◑: MoO_3, ●: $Mo_6V_9O_{40}$.
* The pattern of $V\text{-}Mo_{(600)}$ was similar to of $V\text{-}Mo_{(400)}$.

Fig. 3. $V\text{-}Mo_{(400)}$ gave only the diffraction lines of V_2O_5 and MoO_3. However, in the IR spectra of $V\text{-}Mo_{(400)}$ and $V\text{-}Mo_{(600)}$, two weak absorption bands were observed at 955 and 1035 cm^{-1} together with the bands of V_2O_5 and MoO_3, suggesting the formation of some amorphous structure. On the other hand, $V\text{-}Mo_{(800)}$ showed several new lines together with the lines of V_2O_5, and the d-spacings of the new peaks were in fair agreement with the values of $Mo_6V_9O_{40}$. The diffraction data also indicate formation of solid solution. The d-spacing value of the strongest line of V_2O_5, *i.e.*, d=4.38 Å (001) in pure V_2O_5 and observed in $V\text{-}Mo_{(400)}$, was found at d=4.30 Å in $V\text{-}Mo_{(800)}$. Consequently, the lattice dimension of c-axis is shortened. According to the results of IR analysis of $V\text{-}Mo_{(800)}$, the absorption band assigned to the stretching vibration of V=O double bond was slightly displaced toward lower frequency from 1020 cm^{-1} of pure V_2O_5, broadening considerably. The results agree fairly well with those obtained by Yoshida.[4] Thus, a solid solution of MoO_3 in V_2O_5, belonging to a substitutional type, is formed in $V\text{-}Mo_{(800)}$. $V\text{-}Mo_{(400)}$ or $V\text{-}Mo_{(600)}$ is

†† It was confirmed that the interfacial solid solution is formed in the binary system. It was observed by Kurina *et al.*[12] that the solid solution is also formed in the binary oxide prepared from NH_4VO_3 and $Cr(NO_3)_3\cdot 9H_2O$. However, the existence of phase Y was not reported.

considered to be a simple mixture of V_2O_5, MoO_3 and the amorphous structure, and V–$Mo_{(800)}$ to consist of the solid solution and $Mo_6V_9O_{40}$. $Mo_6V_9O_{40}$ contains a reduced vanadium species, V^{4+}, the amount of which is one-ninth of the total vanadium.[13] The reduced vanadium species is also included in the solid solution.[4] V–$Mo_{(400)}$ and V–$Mo_{(600)}$ are inactive††† in spite of the existence of V_2O_5. Since MoO_3 initiates no oxidation, the activity of V–$Mo_{(800)}$ may be due to the reduced species. This V^{4+} ion was also considered to be contained in both Y and the solid solution observed in the V–Cr system. However, this system also contains a chromium species which is considered to be active for the decomposition of hydroperoxide in the form of Cr_2O_3. Thus, though the increase of activity caused by the addition of both chromium and molybdenum oxides seems to be correlated with change of catalyst structure, detailed discussions on this problem are necessary.

Details of the Activity of V–Cr System. The V–Cr system was found to be fairly active for cyclohexene oxidation, especially for the oxidation. In order to elucidate the mechanism of the reaction, the distribution of products in the reaction with V–$Cr_{(400)}$ was studied. The results are shown in Table 3 together with those of the V–Mn catalyst.

Both V–$Cr_{(400)}$ and V–Mn gave a product distribution similar to that with V_2O_5, fairly high selectivity of cyclohexene oxide being obtained. The epoxidation, therefore, is thought to proceed mainly by the hydroperoxide intermediate mechanism in the same way as in the reaction with V_2O_5. On the other hand, the hydroperoxide may be formed by radical chain reaction. The binary system catalysts might have two types of active site, one effective for the radical chain reaction and the other for the epoxidation with the hydroperoxide. Arzoumanian *et al.*[14] reported that the high selectivity of epoxide is obtained in the cyclohexene oxidation with soluble metallic catalyst system, and that this catalyst system is made up of two types of active component; a complex of Rh or Ir effective for the autoxidation, and that of Mo or V for the selective epoxidation. In the present study, it can be presumed that the two types of active site coexist on the surface of catalyst active for epoxidation.

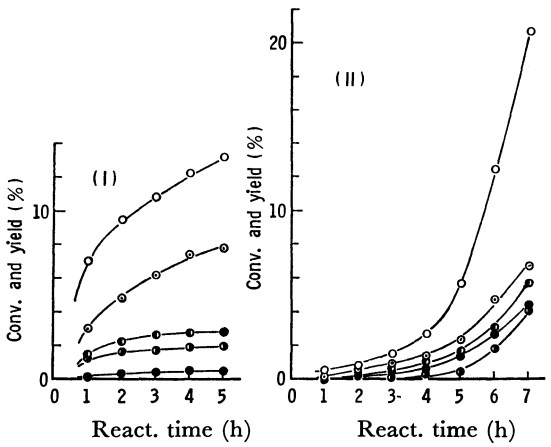

Fig. 4. Product distribution of the cyclohexene oxidation with $Co(acac)_2$ (I) and V–$Cr_{(400)}$ (II).
Reaction temperature: 60 °C, concentration of catalyst: 10^{-3} mol/l ($Co(acac)_2$), 1 g/l (V–$Cr_{(400)}$).
P_{O_2}: 1 atm
○: Conversion of cyclohexene,
⊙: yield of cyclohexenyl hydroperoxide,
◑: yield of cyclohexenone,
◐: yield of cyclohexenol,
●: yield of cyclohexene oxide.

††† This inactivity may be due to the amorphous structure.

Table 6. Epoxidation of cyclohexene with *t*-butyl hydroperoxide[a]

Cat.	Conv. of hydroperoxide (%)	Yield of epoxide (%)
$MoO_2(acac)_2$[c]	64.3	72.6
$VO(acac)_2$[c]	33.5	38.4
$Co(acac)_2$[c]	53.1	5.6
V–$Cr_{(400)}$[d]	26.3	35.6

a) Concentrations of cyclohexene and *t*-butyl hydroperoxide were 0.45 and 0.41 mol/l, respectively. Solvent was benzene, and the reaction temperature was 60 °C. b) Based on reacted hydroperoxide. c) Concentration of catalyst was 10^{-3} mol/l, and reaction time was 2 h. d) Concentration of catalyst was 5 g/l, and reaction time was 3 h.

$Co(acac)_2$ shows high activity at the beginning of the reaction, its activity being lowered with reaction time (Fig. 4). This seems to be due to the change of chelate into the insoluble state. Concerning the distribution of products, cyclohexeneyl hydroperoxide continued to be the main component throughout the reaction time, the amount of cyclohexene oxide remaining very small. Cyclohexene oxide is considered to be formed by the addition mechanism in radical chain reactions as recognized with AIBN. Thus, a typical autoxidation proceeds in the reaction with $Co(acac)_2$ catalyst. In contrast, the activity of V–$Cr_{(400)}$ was low at the biginning of the reaction but increased rapidly with reaction time. That is, the lowering of activity was not observed with this binary oxide. The selectivity of cyclohexenyl hydroperoxide was not so high as in the reaction with $Co(acac)_2$. The amount of both cyclohexene oxide and cyclohexenol was larger than that of cyclohexenone resulting from the decomposition of cyclohexenyl hydroperoxide. In order to clarify the mechanism of epoxidation, several reactions of cyclohexene with *t*-butyl hydroperoxide were carried out in the presence of catalyst (Table 6). $MoO_2(acac)_2$ shows high activity for epoxidation with hydroperoxide.[6] A small amount of epoxide observed in the case with $Co(acac)_2$ seems to be found by the reaction of cyclohexene with *t*-butyl peroxyradical. The yield of epoxide obtained with V–$Cr_{(400)}$ is similar to that with $VO(acac)_2$, suggesting that epoxidation by the hydroperoxide intermediate mechanism proceeds together with the radical decomposition of hydroperoxide. The successive catalytic processes concerning the formation of the epoxide (Eqs. 3 and 4) are supported; the first one consists of the hydroperoxide formation as in a typical autoxidation process, and the second, a selective olefin oxidation wherein the hydroperoxide acts as the oxidizing agent.

References

1) C. Meyer, G. Clement, and J.C. Balaceanu, *Proc. Int. Congr. Catal.*, 3rd, 1964, **1**, 184 (1965).
2) E. S. Gould and M. Rado, *J. Catal.*, **13**, 238 (1969).
3) K. Takehira, T. Nishimura, M. Araki, T. Hayakawa, and T. Ishikawa, *Yuki Gosei Kagaku Kyokai Shi*, **29**, 586 (1971).
4) S. Yoshida, *Shokubai*, **10**, 90 (1968) and references cited therein.
5) K. Takehira, T. Nishimura, M. Araki, T. Hayakawa, and T. Ishikawa, *Nippon Kagaku Kaishi*, **1974**, 652.
6) M. N. Sheng and J. G. Zajacek, *J. Org. Chem.*, **35**, 1839 (1970).
7) C. D. Wagner, R. H. Smith, and E. D. Peters, *Anal. Chem.*, **19**, 976 (1947).
8) D. E. Van Sickle, F. R. Mayo, and R. M. Arluck, *J. Am. Chem. Soc.*, **87**, 4824 (1965).
9) D. E. Van Sickle, F. R. Mayo, R. M. Arluck, and M. G, Syz, *J. Am. Chem. Soc.*, **89**, 967 (1967).
10) G. M. Bulgakova, I. P. Skibida, and Z. K. Maizus, *Kinet. Catal.*, **12**, 61 (1971).
11) S. Yoshida, T. Matsuzaki, T. Kashiwazaki, K. Mori, and K. Tarama, *Bull. Chem. Soc. Jpn.*, **47**, 1564 (1974) and references cited therein.
12) L. N. Kurina, O. N. Ediseeva, V. F. Anufrienko, S. T. Chistanova, N.M. Simkin, and V. A. Zozulya, *Kinet. Katal.*, **11**, 614 (1970); V. A. Anufrienko, S. T. Chistanova, and L. N. Kurina, *ibid.*, **11**, 1079 (1970).
13) R. H. Munch and E. D. Pierron, *J. Catal.*, **3**, 406 (1964).
14) H. Arzoumanian, A. Blanc, U. Hartig, and J. Metzger, *Tetrahedron Lett.*, **1974**, 1011.

Electronic Spectra and Electronic Structure of TCNQ Complexes

Jiro TANAKA, Masashi TANAKA, Takashi KAWAI, Teruhiro TAKABE, and Osamu MAKI
Department of Chemistry, Faculty of Science, Nagoya University, Nagoya 464
(Received December 11, 1975)

Electronic spectra of several TCNQ complexes have been measured with single crystals by the transmission method. The assignment of electronic transitions are presented based on the electronic structure of the crystals. The molecular viewpoint is stressed in a theoretical treatment. The spectra are interpreted in terms of the charge transfer between TCNQ species and the local transitions of TCNQ and the donor molecules. It is shown that the electronic structure of the crystal may be deduced from the spectral analysis. The magnetic and electric properties of several conducting TCNQ complexes are discussed by this model with the wavefunctions determined by a theoretical calculation and the analysis of the spectral results.

Electronic absorption spectra of TCNQ complexes have been investigated for single crystals and powdered samples by many people. Although there have been many comprehensive papers and reviews on the structural, electronic and magnetic properties of these crystals,[1-5] but the interesting electronic processes of these complexes are still not satisfactorily explained in a comprehensive way.

Recently the study on optical spectra becomes more important, because the remarkable electronic properties of high conductive TCNQ salts may be elucidated by the analysis of their electronic spectra. In the present paper we will discuss the single crystal electronic absorption spectra of several TCNQ complexes, together with the discussions of the electronic structures and the intermolecular interactions. The interpretation of the electronic spectra is presented and the magnetic and electric properties are studied with the model calculation. The aim of this paper is to give an unified view on different aspects of physical properties based on the chemical constitution and electronic structure of the crystals. We try to find a reasonable concept of the characteristic properties of organic conductors from structural points of view, hoping that this analysis will be a useful guide for the design and synthesis of new conducting organic materials. It will be shown that the electronic spectrum may give a useful diagonosis on the electronic structure of TCNQ complexes.

Experimental

The materials were prepared by the methods of Melby *et al.*[6] and Melby.[7] Very thin crystals were prepared by recrystallization from dry acetonitrile and their absorption spectra were measured by the microspectrophotometer designed in this laboratory. The thickness of the crystals used for the transmission measurement was less than a few micron, but it was difficult to measure the thickness very accurately.

The spectrophotometer consists of a light source, a monochromator of Carl Zeiss M4Q and a detector with a PbS photocell and a HTV 446 photomultiplier tube. An Olympus microscope was used with Carl Zeiss Ultrafluar objectives of 32 and 100 magnifing power. The lenses are achromatic for 700—230 nm, but it is not guaranteed for the near infrared region, therefore we have used possibly large crystals to avoid the effect of aberration. A quartz polarizer of Rochon type was used to obtain a polarized light. The crystalline axis and the indices of the developed planes were checked and confirmed by taking X-ray photographs with crystals which were large enough for the X-ray experiment. Sometimes very thin crystals were prepared by recrystallization on a quartz slide glass, and the crystalline habit was checked by the polarizing microscope and compared with the large one determined by the X-ray method.

Crystalline Structure and Electronic Configuration of TCNQ Complexes

The crystals of TCNQ complexes can be classified into two groups, in one group the donor and TCNQ make a stacking pair (D^+A^-), while in the other group TCNQ makes the column by itself ($A\cdot A\cdot A\cdot \cdots$) and the donor forms their own column or take their own positions.[3] In this study we concentrate on the latter type of crystals which is more interesting than the ordinary DA complex. The complexes forming TCNQ columns show variable ratio of the donor to TCNQ; there is a variety of type of (D: A) ratio as 1: 1, 1: 2, 2: 3, and 2: 4. For complexes having TCNQ more than 1: 1 mole ratio, neutral TCNQ molecules are involved. The names and abbreviations of typical donors or cations are shown in Fig. 1.

The X-ray crystal structure analysis on these complexes revealed that there are a little but significant difference of the bond length between the neutral, negative and a half-ionized TCNQ species. Actually the crystallographic results show that these differently

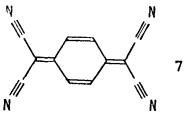

7,7,8,8-Tetracyanoquinodimethane — TCNQ

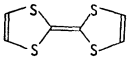

Tetrathiafulvalene — TTF

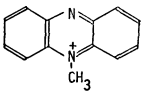

N-Methylphenazinium cation — $(NMP)^+$

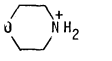

Morpholinium cation — $(Mor)^+$

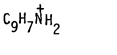

Quinolinium cation — Q^+

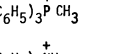

Methyltriphenylphosphonium cation — $(MTPP)^+$

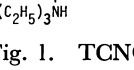

Triethylammonium cation — $(TEA)^+$

Fig. 1. TCNQ and several donor molecules.

harged species are situated on different sites in the crystal.

In crystals such as $Q(TCNQ)_2$,[8] $TMPD(TCNQ)_2$,[9] and $Ac(TCNQ)_2$[10] the structure of all TCNQ is equivalent, which may imply that the negative charges may be completely delocalized all over the TCNQ columns. However, from a view of strong electron correlation effect between electrons on the same and the nearest neighbour molecules, it seems more reasonable that extra electrons may reside in alternate site to relieve the repulsion. In this case both the negative and the neutral TCNQ coexist, however, it was difficult to discern which is the anion or the neutral species, and the X-ray scattering method will give only an average structure of the charged and neutral molecules. Therefore a most plausible electron configuration of the 1 : 2 type crystal is that the excess electrons are localized on alternate TCNQ site and the neutral TCNQ is sandwiched between anions, and such a locally ordered structure may fluctuate, and a superposition of two alternative structures will give an apparently equivalent crystal structure. We may call this type of electron configuration as an alternant type.

An apparent chemical constitution of the complex does not necessarily mean an equivalence of the electronic structure, for instance, recent X-ray analyses of TTF–TCNQ[11–13] show that the bond lengths for TCNQ in this complex are close to a half-charged anion. This is in harmony with recent experiments on ESCA and IR studies of TTF–TCNQ.[14,15] These studies give evidences of incomplete charge transfer from TTF to TCNQ that the crystal is considered to contain both $(TCNQ)^0$ and $(TCNQ)^-$. For this reason, it may be more plausible that this crystal has an alternant type structure as its basic configuration rather than that all TTF and TCNQ are singly ionized. Further consideration will be given in later sections.

In crystals with 2: 4 or 2: 3 donor to TCNQ ratio, electrons are thought to be localized on particular paired sites, hence, we may call this type of configuration as an island type.[16,17]

In crystal in which all TCNQ have a negative charge, the TCNQ column forms either a linear chain or a dimeric pair, and the phase transition was observed to change the linear form to the dimeric form at low temperature.[18,19]

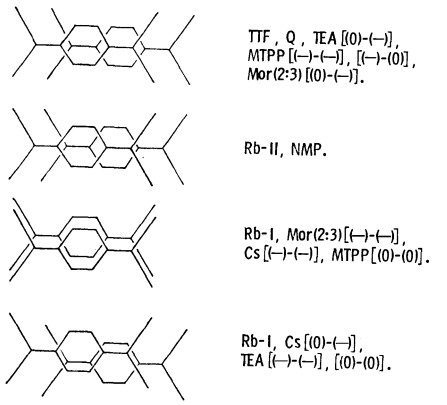

Fig. 3. Nearest neighbour overlap of TCNQ molecules.

In Fig. 2 different types of electron configuration of TCNQ column are schematically classified. The most important type from a view of good electric conduction may be an alternant type and an island type. In the following we will discuss the electron interaction between TCNQ molecules in the crystal by these basic electron configurations. The types of the interactions are the dimer type, the island type and the alternant type. For the linear chain structure, the interaction must be considered to obey the crystal symmetry of the one-dimensional lattice, however, the TCNQ complex we have treated in this paper has a dimeric structure rather than a linear chain structure, therefore our theoretical treatment may be limited to the coupled molecular model. The extension to include the exciton interaction between different cells may not be difficult, but the excited state of CT character may be easily trapped because of their large polarization effect, and empirically the magnitude of the exciton type interaction will be not so significant for such CT complexes, therefore the exciton treatment is not developed in this study.

The mode of overlapping of TCNQ molecules is shown in Fig. 3, and a tendency may be seen that a pair made of neutral and charged TCNQ takes a similar conformation, in which a direct overlap is avoided by displacing one molecule to the other.[3] A pair made of both charged TCNQ species takes several different conformations, but it shows a tendency of larger overlap than the former type.

Donors	Ratios of Donor to Acceptor	Electron Configurations	Types of Interactions
Rb,K,Li,Mor	1:1	···· / / (/ /) / / ····	Dimer Type
TTF,NMP	1:1	···· / / (/ / /) / / ····	Alternant Type
Q,Ac,TMPD	1:2		
Cs,Mor	2:3	···· / / (/ / /) / / ····	Island Type
TEA,MTPP	2:4	···· / / (/ / / /) / / ····	

Fig. 2. Electronic configurations of TCNQ columns and types of interactions.

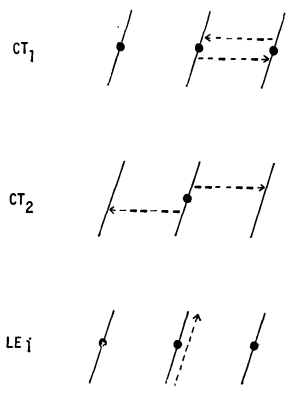

Fig. 4. Basic excited configurations in TCNQ columns.

Theoretical Analysis of Electronic Spectra

The electronic spectra of TCNQ anion in solution was studied by Boyd and Phillips[20] and the molecular orbital calculation was carried out by Lowitz.[21] For the TCNQ complex crystals, Iida[22] has pointed out that there are three types of transitions in the visible and near infrared region. The basic excited configurations are shown in Fig. 4. The LE excited level means locally excited level of TCNQ anion and we denote the lowest one of this kind as LE_1 and the second one by LE_2, and so on. The CT_1 level is the charge transfer between the TCNQ anions and the CT_2 level is the charge transfer from the anion to the neutral TCNQ. In actual crystals, these levels interact to each other, and complicated spectral patterns are observed. In the following we attempt to analyse the spectral features of the complex by calculating the intermolecular interaction between the levels of different TCNQ molecules with the modified Hubbard Hamiltonian,[23,1] which is further modified by our own recipe.

The wavefunction of the system may be described by an antisymmetrized product of the molecular orbitals of the constituent TCNQs. The Hamiltonian of the system may be given by

$$H=\sum_{pi}\sum_{qj}\sum_{\sigma}\langle\phi_{pi}|-\frac{\hbar^2}{2m}\Delta_\mu+\sum_{s\alpha}V(R_{s\alpha}-r_\mu)|\phi_{qj}\rangle a^+_{pi\sigma}a_{qj\sigma}+\frac{1}{2}\sum_{pi}\sum_{qj}\sum_{rk}\sum_{sl}\sum_{\sigma\sigma'}(\phi_{pi}\phi_{sl}|\phi_{qj}\phi_{rk})a^+_{pi\sigma}a^+_{qj\sigma'}a_{rk\sigma'}a_{sl\sigma} \quad (1)$$

where ϕ_{pi} and ϕ_{qj} denote the i-th and the j-th molecular orbitals of the p and q molecules and σ indicates spin functions. The Coulomb repulsion integral is written with a notation that

$$(\phi_{pi}\phi_{sl}|\phi_{qj}\phi_{rk})=\int\phi^*_{pi}(\mu)\phi_{sl}(\mu)\frac{e^2}{r_{\mu\nu}}\phi^*_{qj}(\nu)\phi_{rk}(\nu)dv_\mu dv_\nu. \quad (2)$$

In this calculation we restrict our attention to the higher MO of TCNQ, m and m-1, where the singly occupied highest MO in $TCNQ^-$ is written by m and the doubly occupied second highest MO by m-1.

The intermolecular interaction between p and q molecules is considered only for the nearest neighbours, and we retain the interactions which are first order to the electron overlap. Then the Hamiltonian is given by

$$H=\sum_{p,q}\sum_{i,j=m-1}^{m}\sum_{\sigma}t^{pq}_{ij}a^+_{pi\sigma}a_{qj\sigma}+\sum_{p}U^{pp}_{mm}n_{pm\alpha}n_{pm\beta}+\sum_{p,q}\sum_{\sigma\sigma'}U^{pq}_{mm}n_{pm\sigma}n_{qm\sigma'}+\sum_{p,q}\sum_{\sigma\sigma'}D_{pq}a^+_{pm\sigma}a^+_{qm-1\sigma'}a_{qm\sigma'}a_{qm\sigma} \quad (3)$$

where

$$t^{pq}_{ij}=\langle\phi_{pi}|-\frac{\hbar^2}{2m}\Delta_\mu+\sum_{s\alpha}V(R_{s\alpha}-r)|\phi_{qj}\rangle \quad (4)$$

$$U^{pp}_{mm}=(\phi_{pm}\phi_{pm}|\phi_{pm}\phi_{pm}) \quad (5)$$

$$U^{pq}_{mm}=(\phi_{pm}\phi_{pm}|\phi_{qm}\phi_{qm}) \quad (6)$$

and

$$D_{pq}=(\phi_{pm}\phi_{qm}|\phi_{qm-1}\phi_{qm}). \quad (7)$$

Here V is the neutral core potential and we evaluate the transfer integral t^{pq}_{ij} by the extended Hückel method as

$$t^{pq}_{ij}=KWS^{pq}_{ij} \quad (8)$$

where W is the orbital energy of TCNQ, and we have used the value given by the photoemission experiment of -7.5 eV[14,24] and K is set equal to 1.2. Actually this choice is rather empirical as in the extended Hückel method where K is taken in the range of 1.0—2.0. We have also attempted to evaluate each term in the integral, namely the kinetic energy and the neutral core potential energy of the electron moving between p and q molecules, and they are found to be proportional to the overlap integral S^{pq}. The transfer integral t was also shown to be proportional to the overlap integral and it was nearly the same order of magnitude with the value estimated by Eq. 4. In the latter sections it will be seen that this choice is reasonable from a view of consistency of the spectral and magnetic properties of various complexes. In the actual calculation we have used the molecular orbital of Lowitz[21] for $TCNQ^-$ and the four term SCF-AO of Clementi *et al.*[25] The calculated overlap and transfer integrals are listed in Table 1.

The Coulomb repulsion energy U^{pp}_{mm} and U^{pq}_{mm} are those for the electrons on the same and the nearest neighbour sites, and they were calculated for a typical arrangement of the crystal by using Nishimoto-Mataga potential and the results are

$$U^{pp}_{mm}=3.95\text{ eV} \text{ and } U^{pq}_{mm}=2.29\text{ eV}.$$

The former value is the same with the value given by Hiroma, Kuroda and Akamatu.[26] The difference between these two terms is 1.66 eV, but the spectral analysis shows that it may be about 1.5 eV, therefore we estimate the screening effect of the electronic polarization[27] as being a factor of 0.9, and newly define the spectroscopic U value as

$$U=\eta(U^{pp}_{mm}-U^{pq}_{mm})=1.5\text{ eV} \quad (9)$$

where η=0.9. It appears that the η value is not so different for various crystals and it seems unlikely that η is very small and U is reduced to a great extent by the polarization of large conjugated molecules.

The Coulomb energy difference between the CT_2 and the ground configurations, which is important in the island type and the alternant type systems, may be written as U', where U' will be approximately given by

$$U'=U^{pq}_{mm}-U^{pq+1}_{mm}. \quad (10)$$

The numerical estimate of this small difference of energy may be a difficult problem, because it will require an accurate calculation including the Madelung energy of the crystal for two different configurations. Actually it may be either positive or negative values depending on the structure of the complex and it will give a measure of either the island or the alternant type configuration is stable in the ground state. Here we have empirically estimated the energy values from spectroscopic results to fit the calculated energy levels with the observed spectra, instead of evaluating this term by the calculation.

The last term D^{pq} means the interaction energy between the LE_1 and CT_1 configurations, and it is approximately estimated by the dipole-dipole interaction of the two transition dipoles. The size of the transition moment of the LE_1 band was estimated with the experimental data of solution spectra as 1.46 Å. The transition length for the CT_1 band was approximated as

Table 1. Molecular integrals of TCNQ complexes

		p q	i j	S_{ij}^{pq}	t_{ij}^{pq}(eV)	D_{pq}(eV)
Rb-I	1:1	(−)—(−)′	m $m-1$	0.0051	−0.0459	−0.3243
			m m	0.0348	−0.3132	
		(−)—(−)″	m $m-1$	0.0072	−0.0648	−0.0651
			m m	0.0109	−0.0981	
Rb-II	1:1	(−)—(−)′	m $m-1$	0.0100	−0.0900	−0.0860
			m m	0.0083	−0.0747	
K	1:1	(−)—(−)′	m $m-1$	0.0025	−0.0225	
			m m	0.0301	−0.2709	
		(−)—(−)″	m $m-1$	0.0054	−0.0486	
			m m	0.0143	−0.1287	
Na	1:1	(−)—(−)′	m $m-1$	0.0027	−0.0243	
			m m	0.0298	−0.2682	
		(−)—(−)″	m $m-1$	0.0057	−0.0513	
			m m	0.0165	−0.1485	
Mor	1:1	(−)—(−)′	m $m-1$	0.0021	−0.0189	
			m m	0.0394	−0.3546	
TMB	1:1	(−)—(−)′	m $m-1$	0.0128	−0.1152	
			m m	0.0200	−0.1800	
TMA	2:3	(−)—(−)′	m $m-1$	0.0029	−0.0261	
			m m	0.0393	−0.3537	
Q	1:2	(0)—(−)	m $m-1$	0.0124	−0.1116	−0.1871
			m m	0.0153	−0.1377	
Ac	1:2	(0)—(−)	m $m-1$	0.0110	−0.0990	−0.0701
			m m	0.0067	−0.0603	
TMPD	1:2	(0)—(−)	m $m-1$	0.0147	−0.1323	−0.0125
			m m	0.0146	−0.1314	
		(−)—(0)′	m $m-1$	0.0121	−0.1089	−0.0131
			m m	0.0150	−0.1350	
TTF	1:1	(0)—(−)	m $m-1$	0.0108	−0.0972	−0.1945
			m m	0.0153	−0.1377	
NMP	1:1	(0)—(−)	m $m-1$	0.0005	−0.0045	−0.1340
			m m	0.0121	−0.1089	
Cs	2:3	(0)—(−)	m $m-1$	0.0120	−0.1080	−0.1161
			m m	0.0137	−0.1233	
		(−)—(−)′	m $m-1$	0.0011	−0.0099	−0.2568
			m m	0.0303	−0.2727	
Mor	2:3	(0)—(−)	m $m-1$	0.0091	−0.0819	−0.1268
			m m	0.0156	−0.1404	
		(−)—(−)′	m $m-1$	0.0002	−0.0018	−0.2868
			m m	0.0353	−0.3177	
MTPP	2:4	(0)—(−)	m $m-1$	0.0133	−0.1197	−0.1450
			m m	0.0184	−0.1656	
		(−)—(−)′	m $m-1$	0.0097	−0.0873	−0.1442
			m m	0.0183	−0.1647	
TEA	2:4	(0)—(−)	m $m-1$	0.0145	−0.1305	−0.1008
			m m	0.0164	−0.1476	
		(−)—(−)′	m $m-1$	0.0145	−0.1305	−0.0178
			m m	0.0127	−0.1143	
Bpy[a)]	2:4	(−)—(−)′	m $m-1$	0.0157	−0.1413	
			m m	0.0154	−0.1386	

a) (N,N'-Dibenzyl-4,4′-bipyridylium)$_2$ (TCNQ).

S_{mm}^{pq} R^{pq} and its center was placed in the midpoint of the two TCNQ molecules.

The energy level of the LE_1 is also important in spectral analysis, and it was estimated from the solution's spectral data as 1.5 eV and we denote it as Δ in the following formula. The calculation for the crystal was carried out with the model system, in which a possibly small unit to consider the interaction was selected. We have illustrated in Fig. 2 the unit by brackets and a translation unit by the square mark on the top.

For the dimer type system the configuration interaction between the ground, CT_1 and LE_1 levels must be considered. An approximate energy level scheme and wavefunctions obtained by the perturbational calculation are shown in Fig. 5. Numerical values of energy levels are calculated by diagonalizing the secular deter-

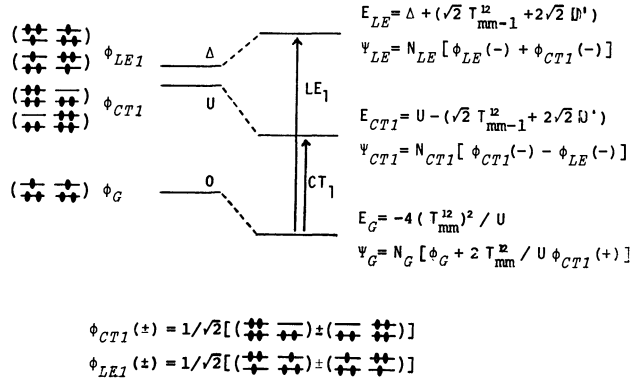

Fig. 5. Energy levels of a dimer type interaction. Actually the diagonal energy of CT_1 and LE_1 is nearly the same, namely $\Delta=U$.

minant for the symmetrical and the antisymmetrical states. The secular equations are

$$\begin{vmatrix} 0 & 2t^{12}_{m.m} & 0 & \mathrm{G} \\ & U & \sqrt{2}\,t^{12}_{m.m-1} & \mathrm{CT_1}^{(+)} \\ & & \Delta & \mathrm{LE_1}^{(+)} \\ U & \sqrt{2}\,(t^{12}_{m.m-1}+2D^{12}) & & \mathrm{CT_1}^{(-)} \\ & \Delta & & \mathrm{LE_1}^{(-)} \end{vmatrix} \quad (11)$$

where the off-diagonal energy values were estimated by the procedures mentioned above. The calculation was carried out for Rb(TCNQ)–I crystal, which has a dimer type configuration.[28] Also this model was applied for TMTTF (bis-tetramethylene-tetrathiafulvalene) because it may form dimer type crystal. The results of calculation are tabulated in Table 2 with with the observed spectral data. It is found that the agreements are fairly well for these crystals.

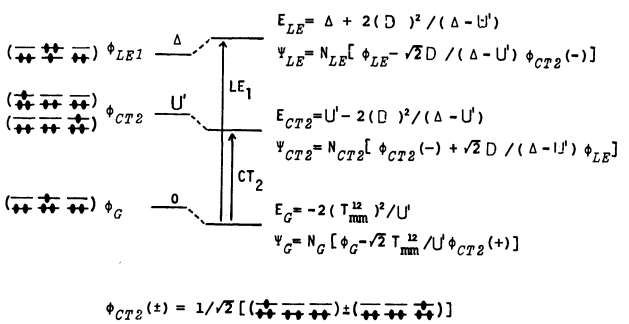

Fig. 6. Energy levels of an alternant type interaction.

For the dimer system the singlet ground state is stabilized to the triplet state, because the coupling of two neighbouring spins by the CT interaction is allowed for only the singlet state. The comparison of the calculated S–T separation energy with the magnetic susceptibility data will be given in the later section.

For the alternant system, the ground, the CT_2 and the LE_1 configurations were considered. An approximate solution by the perturbational treatment is illustrated in Fig. 6. The CT_2 level is not so close to the LE_1 level that the mixing between these configurations is not so significant. The secular determinants are as follows.

$$\begin{vmatrix} 0 & \sqrt{2}\,t^{12}_{mm} & \mathrm{G} \\ & U' & \mathrm{CT_2}^{(+)} \\ U' & -\sqrt{2}\,D^{12} & \mathrm{CT_2}^{(-)} \\ & \Delta & \mathrm{LE_1}^{(-)} \end{vmatrix} \quad (12)$$

TABLE 2. ELECTRONIC ABSORPTION BANDS OF SEVERAL TCNQ COMPLEXES
Comparison of observed and calculated values.

		CT_2				CT_1				LE_1			
	Type	ΔE[a] Obsd (Calcd)	Intensity Calcd $f(\perp)$	Intensity Calcd $f(\parallel)$	Intensity Obsd ratio $(\perp/\parallel)$	ΔE[a] Obsd (Calcd)	Intensity Calcd $f(\perp)$	Intensity Calcd $f(\parallel)$	Intensity Obsd ratio $(\perp/\parallel)$	ΔE[a] Obsd (Calcd)	Intensity Calcd $f(\perp)$	Intensity Calcd $f(\parallel)$	Intensity Obsd ratio $(\perp/\parallel)$
Rb(TCNQ)–I	D					8.5 (8.5)	0.22	0.42	≈0.5	17.5 (19.8)	0.52	0.11	≈1.6
$Q(TCNQ)_2$	A	5.5 (6.1)	0	0.21	0					12.0 (13.1)	0	0.09	≈0
TTF(TCNQ)	A	3.0 (3.0)	0	0.28	0					12.0 (13.3)	0	0.08	0
TMTF(TCNQ)	D					≈4.0 (3.6)	0	0.18	0	18.0 (21.3)	0	0.08	0
NMP(TCNQ) (triclinic)	A	5.5 (5.5)	0.01	0.15	≈0					12.5 (12.7)	0.23	0.11	≈1.5
$Cs_2(TCNQ)_3$	I	6.0 (5.8)	0.002	0.18	0	11.0 (10.8)	0.08	0.52	0.1	17.7 (17.2)	0.13	0.08	3.5
$Mor_2(TCNQ)_3$	I	6.0 (6.4)	0.002	0.22	0	11.5 (11.5)	0.08	0.66	0.04	17.5 (17.9)	0.13	0.16	5.0
$(MTPP)_2(TCNQ)_4$	I	≈4.0 (4.0)	0.003	0.34	≈0	11.0 (11.1)	0.21	0.20	0.4	17.7 (15.9)	0.33	0.01	4.3
$(TEA)_2(TCNQ)_4$	I	≈4.0 (4.0)	0.001	0.27	0	11.0 (10.6)	0.13	0.11	0.5	17.7 (15.4)	0.19	0.001	3.6

a) ΔE in 10^3 cm^{-1}.

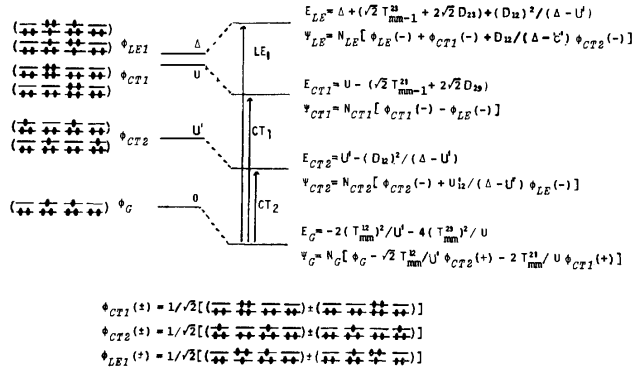

Fig. 7. Energy levels of an island type interaction. The diagonal energies are nearly the same for CT_1 and LE_1 states, namely $\Delta = U$.

The results of numerical calculation are shown for Q, TTF and the triclinic form of NMP–TCNQ crystals. The discussion on the calculated and the experimental results will be given for each crystals in the next section.

For the alternant system the spin correlation between the neighbouring sites can not be expected to be large, because the pairing scheme by the CT interaction between the nearest neighbour sites is not conceivable.

The island type system involves both the CT_1 and the CT_2 configurations and the calculation was carried out including these and LE_1 configurations. An approximate energy level scheme is given in Fig. 7. The numerical calculation was carried out with the secular equations given below.

$$\begin{vmatrix} 0 & \sqrt{2}\,t_{mm}^{12} & 2t_{mm}^{23} & 0 & \\ & U' & 0 & -D^{12} & \\ & & U & \sqrt{2}\,t_{m.m-1}^{23} & \\ & & & \Delta & \end{vmatrix} \begin{matrix} G \\ CT_2^{(+)} \\ CT_1^{(+)} \\ LE_1^{(+)} \end{matrix} \qquad (13)$$

$$\begin{vmatrix} U' & 0 & -D^{12} & \\ & U & \sqrt{2}\,(t_{m.m-1}^{23}+2D^{23}) & \\ & & \Delta & \end{vmatrix} \begin{matrix} CT_2^{(-)} \\ CT_1^{(-)} \\ LE_1^{(-)} \end{matrix}$$

The results of calculations are shown in Table 2 for Cs, Mor, TEA, and MTPP–(TCNQ) complexes. Here the oscillator strengths of the electronic transitions are estimated for each transitions with reference to the stacking axis of TCNQ columns and they are given by *f*-numbers parallel and perpendicular to the stacking axis. It is found that the mixing of the CT_1 level with the LE_1 level gives significant changes of the polarization character guessed by the oriented gas model. The comparison of the calculated results with the experimental results will be given in the later section.

All calculations were performed at the Computation Center of Nagoya University.

Interpretation of Crystalline Spectra

Rb(TCNQ)–I. The crystalline structure of Rb(TCNQ)–I was analyzed by Hoekstra, Spoelder and Vos[28] and the crystals have monoclinic symmetry with the space group $P2_1/c$. The projection of molecules onto the developed crystalline plane is shown in Fig. 8, where the TCNQ ions form rows along the a-axis and

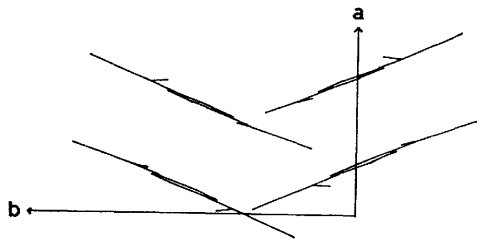

Fig. 8. Projection of Rb(TCNQ)–I onto the developed (001) plane.

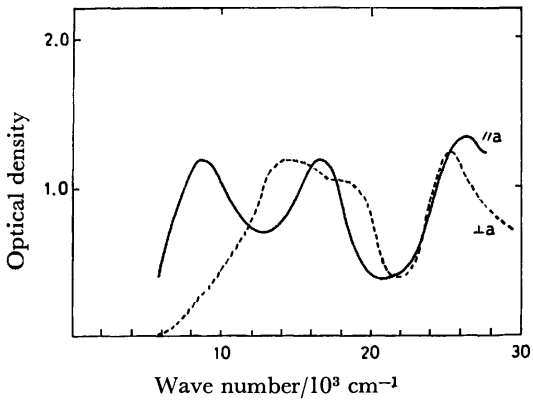

Fig. 9. Polarized absorption spectra on the (001) plane of a single crystal of Rb(TCNQ)–I.
——: a axis, ·····: b axis.

the interplanar distances show alternation of 3.159 Å and 3.484 Å, which implies that dimeric pairs are formed in the crystals. The crystalline absorption spectra were measured along the a- and b-axes of the (001) plane, and are shown in Fig. 9. The lowest energy transition is regarded as the CT_1 transition, and its energy and the polarization ratio are in fairly good agreement with the calculated results. The LE_1 band of $(TCNQ)^-$ shifts to the higher energy region by 3000—4000 cm^{-1}, and it seems that the blue shift of the LE_1 band is a characteristic of the dimer type electron configuration of TCNQ complex crystals. The calculated results of the energy and the polarization ratio of the LE_1 band are not in perfect, but in farily good agreement with the observed tendency of the spectra. The blue sflift of the LE_1 band is interpreted as the mixing of the CT_1 and the LE_1 levels. The third transition at 26000 cm^{-1} region may be reasonably assigned to the second band of $(TCNQ)^-$, namely the LE_2 band, because the second band of $(TCNQ)^-$ in acetonitrile solution appears at 24000 cm^{-1}.

The peaks of main absorption bands are in reasonable agreement with the powder spectra given by Sakai *et al.*[29] and Oohashi and Sakata,[30] and the polarized spectra presented here give an evidence of the CT character of the lowest energy transition.

Q(TCNQ)₂. The crystalline structure of Q-$(TCNQ)_2$ was analyzed by Kobayashi, Marumo and Saito[8] and the projection of molecules onto the developed (100) plane is shown in Fig. 10. The structure is disordered as regard to the orientation of quinolinium ions. The crystalline absorption spectra were measured with the (100) plane with the light polarized

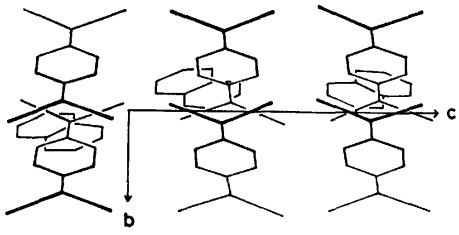

Fig. 10. Projection of $Q(TCNQ)_2$ onto the developed (100) plane.

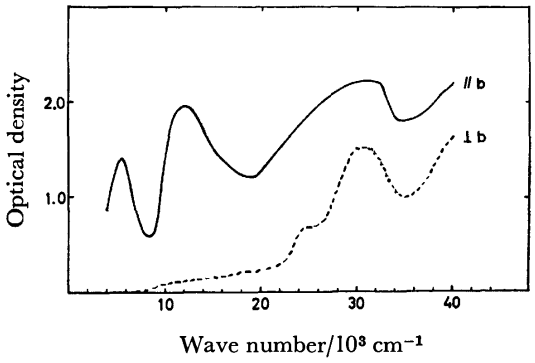

Fig. 11. Polarized absorption spectra on the (100) plane of a single crystal of $Q(TCNQ)_2$.
——: b axis, ……: c axis.

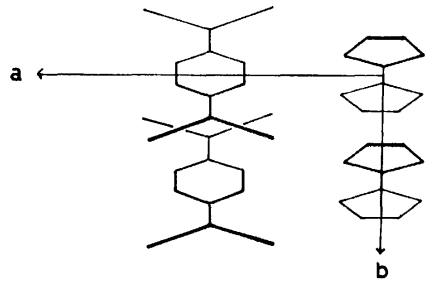

Fig. 12. Projection of (TTF) (TCNQ) onto the developed (001) plane.

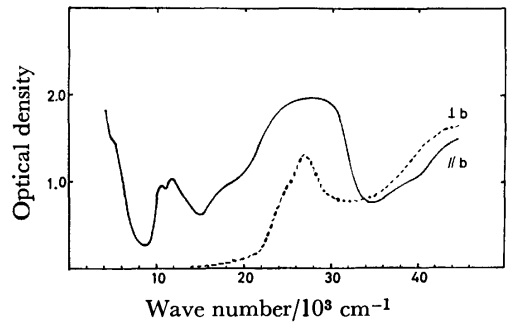

Fig. 13. Polarized absorption spectra on the (001) plane of a single crystal of (TTF) (TCNQ).
——: b axis, ……: a axis.

parallel to the b- and c-axis and the spectra are shown in Fig. 11. The spectra are typical of the alternant type structure that the CT_2 transition is at the lowest energy region and the LE_1 band is not shifted to the higher energy region. Namely the CT_2 band is observed at about 5500 cm^{-1} and the LE_1 band is found at 12000 cm^{-1}. The LE_1 band is not shifted because the mixing of the CT_2 and the LE_1 levels is not so significant, for the diagonal energy values of the CT_2 level is much less than that of the LE_1 level. The energy of the CT_2 level is certainly smaller than that of the CT_1 level and we have estimated the U' value for this crystal at 0.8 eV, which is much smaller than the U value of 1.5 eV of the dimer system. The results of calculation are shown in Table 2 and it is seen that the observed and calculated results are in fairly good agreement. It will mean that the assumed alternant model is reasonable to interpret the electronic spectra of this crystal.

The absorption bands at above 26000 cm^{-1} region along the b-axis may be due to the LE_2 state and the first excited state of neutral TCNQ molecule and the band found at 31000 cm^{-1} may be ascribed to the local transition of the quinolinium cation. The appearance of the LE_1 band at lower energy region at about 12000 cm^{-1} implies that the electronic configuration of TCNQ column is an alternant type. This criterion may be used for the analysis of the spectra of other TCNQ complex crystals.

TTF(TCNQ). The crystal of TTF(TCNQ) is the best conducting organic complex hitherto known[4,31-34] and the optical spectra have been intensively investigated by several groups.[35-37] The present result provides a polarization measurement in the near infrared and visible region by the transmission measurement, therefore it may be interesting to compare the result with the former investigations by other methods.

The crystalline structure of the complex was analyzed by Kistenmacher, Phillips and Cowan[11] at room temperature and by Blessing and Coppens[12] at low temperature. The projection of molecules onto the (001) plane is shown in Fig. 12. Both TCNQ and TTF form independent segregated columns along the b-axis. The CT transition will be particularly polarized along this axis, and actually it is found that the absorption edge of the CT band is observed along the b-axis (Fig. 13). The maximum of this band could not be found by the transmission method, because it was in the out of the range of the present spectrophotometric system.

The peak of this transition was observed by Torrance *et al.*[37] with a powdered sample at 3000 cm^{-1}, while Jacobsen, Tarner, Garito and Heeger[36] measured the reflectivity of the single crystal from 4000 cm^{-1} down to 50 cm^{-1} and found that the maximum of conductivity lies at 1300 cm^{-1}. We also measured the single crystal reflectivity from 35000 cm^{-1} to 4000 cm^{-1}, and confirmed the result of Grant *et al.*,[35] and by combining this result with the infrared data of Jacobsen *et al.* we calculated the absorption maximum by Kramers-Kronig transformation to be at 3000 cm^{-1}.[38] The peak of absorption is located at 3000 cm^{-1}, therefore the character of this transition is assigned as the CT_2 type by the analogy with the spectra of other complexes. The CT band is observed at the lowest energy region and the LE_1 band is appeared at 12000 cm^{-1} without any blue-shift, hence the electron configuration of TTF(TCNQ) will be an alternant type, or at least an alternant type mixed with an island type. The mixing of an island type with an alternant type is an

important feature of the present crystal, and anyhow it implies that an electron transfer from TTF to TCNQ is incomplete.

The theoretical calculation of the energy level is carried out by the alternant model with the U' value of 0.35 eV and the result is in satisfactory agreement with the observed energy, the intensity and the polarization ratio of both the CT_2 and LE_1 bands. In spite of this, the spectral feature of this complex is very close to other island type crystals, therefore the basic electron configuration may involve an island type. Then, in addition to the CT_2 band, the CT_1 and LE_1 bands will be mixed, but this type of mixing could not be confirmed distinctly in the present spectra. Namely, the band at 18000 cm^{-1} region along the b-axis may be a shifted LE_1 band mixed with the CT_1 band in the island model, however, the TTF cation may absorb in this region along this direction, because it has own absorption bands at 18000, 23000, 29000, and 40000 cm^{-1}.[39] A recent unpublished result by Torrance and coworkers[40] gave absorption bands in TTF-$Br_{0.76}$ at 5000, 13000, and 18000 cm^{-1}, but the intensities were smaller than that of TCNQ anion. Therefore the band appearing at 18000 cm^{-1} along the b-axis is reasonably considered to be a mixed CT_1 and LE_1 bands. Thus the spectral results support a strong mixing of the alternant and the island type.

In addition to this, the broad absorption bands around 24000—30000 cm^{-1} region are ascribed to the negative and neutral TCNQ species, because the maximum of these absorptions are expected at 24000 and 25000 cm^{-1}, respectively. These are another reasons to assign the electron configuration of this crystal to the mixed alternant and island types.

Following the theoretical calculation the ground state is represented by $0.91\ \varphi_A + 0.41\ \varphi_I$, where the starting set is a pure alternant configuration, and it means that the electron configuration is 83% of the alternant and 17% of the island type. Then extra neutral vacant sites are produced adjacent to the island site, and if these sites were filled by further electrons from the donor molecule, then the amount of charge transfer will be 0.585. For this population, the ground state is written as 50% of the alternant and 50% of the island configurations, which is in perfect agreement with the spectral properties discussed above.

There are several evidences[12-15] that an electron transfer from TTF to TCNQ is not complete, and the present results give another evidences that both TCNQ and TTF columns are partially ionized and the excess charges may delocalize or fluctuate within or between columns. This view may give an important clue to the understanding of this particular complex.

Of course, other interpretations on the spectral propeties of TTF(TCNQ) have been presented by the metallic band model[4,36,41] or the polaron theory,[42] but our approach is based on a molecular model, which may give wide correlations with other TCNQ complexes.

TMTF(TCNQ). Ueno, *et al.*[43] have synthesized bi(4,5-tetramethylene-1,3-dithiol-2-ylidene), (TMTF), which is an analogue of TTF, and prepared its complex with TCNQ and kindly gifted us the crystals. We have

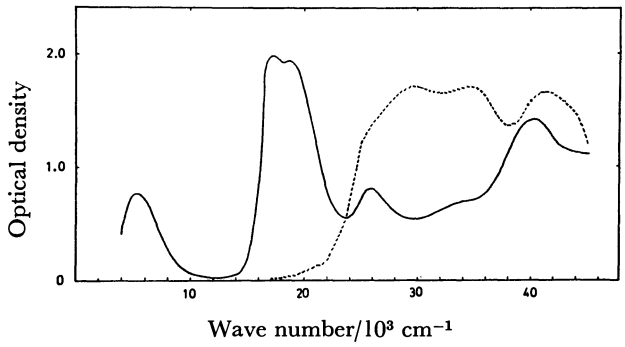

Fig. 14. Polarized absorption spectra on the (010) plane of a single crystal of (TMTF) (TCNQ).
——: a axis, ·····: c axis.

measured and compared the spectral property with that of TTF(TCNQ). The crystalline data of TMTF-(TCNQ) was examined and it was found that the crystal is triclinic and the lattice constants are $a=7.07$, $b=13.39$ and $c=6.91$ Å and $\alpha=70.9$, $\beta=105.0$ and $\gamma=93.0°$. The crystalline absorption spectra were measured along the a- and c-axis, and the CT band was found along the a-axis with a maximum at 5500 cm^{-1} (Fig. 14). The LE_1 band was also found along the a-axis with a maximum at 17400—19500 cm^{-1}. Although the crystalline structure of the complex is not yet determined, the structure of the crystal may be supposed that the stacking axis of $(TCNQ)^-$ is along the a-axis. The appearance of the LE_1 band at higher energy region indicates that the interaction between the CT_1 level and the LE_1 level in the dimer or in the linear chain structure may be very strong in this crystal. Actually the calculated values of transition energies for the dimeric system of TTF(TCNQ) are very close to the experimental values found for TMTF(TCNQ) (Table 2). From these analysis it is supposed that the electronic structure of TCNQ in this crystal will be all negatively charged with a dimeric or a linear chain structure. However, another possibility that the crystal may have a D^+A^- type structure may remain because the crystal structure is not yet determined.

NMP(TCNQ). Two crystalline forms of NMP-(TCNQ) have been reported[44] and the crystalline structure analysis have been carried out only for the good conducting triclinic system by Fritchie[45] and recently by Kobayashi.[46] It has been shown that columns of both TCNQ and NMP develop parallel to the a-axis in the triclinic crystal.

Both the monoclinic and the triclinic crystals were prepared from the same acetonitrile solution, and they were distinguished by the color on transmission or reflection. Their developed faces were confirmed by taking the X-ray photographs and they were (001) plane for the triclinic and (100) plane for the monoclinic crystals. The projection of molecules onto the (001) plane of the triclinic crystal is shown in Fig. 15. Following the crystal structure analysis, it has been presumed that the crystal contains only $(TCNQ)^-$ and $(NMP)^+$ species, but the explanation on the magnetic susceptibility of this crystal[2,47] may be difficult by a fully charged and stacked model. Soos has suggested a model that TCNQ column may contain some neutral

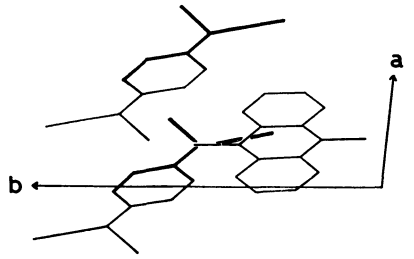

Fig. 15. Projection of triclinic (NMP) (TCNQ) onto the developed (001) plane.

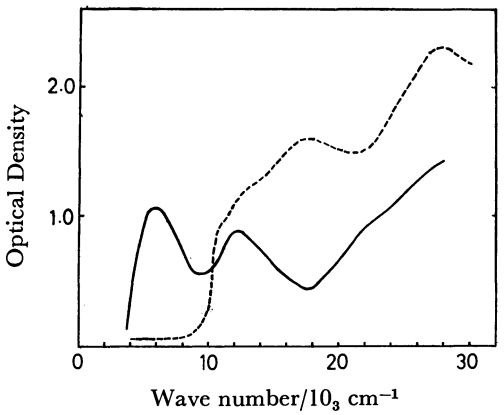

Fig. 16. Polarized absorption spectra on the (001) plane of a single crystal of triclinic (NMP)(TCNQ).
——: a axis, ·····: b axis.

species to explain several physical properties.

The spectra measured with the triclinic crystal for the (001) plane are shown in Fig. 16, and it is easily found that the CT band appears solely along the a-axis at 5500 cm^{-1}, and the LE_1 band is observed at about 12000 cm^{-1}. This result is a typical pattern of an alternant electron configuration, namely excess electrons exist on alternate TCNQ sites. It may mean that an electron transfer from $(TCNQ)^-$ to $(NMP)^+$ may occur at almost every alternate TCNQ sites. By this transfer a half of $(NMP)^+$ ions will become neutral radicals, and the absorption band at 17000 cm^{-1} region may be assigned as due to the neutral radicals, since Sakata and Nagakura[48] have found the absorption in this region with neutral radicals. It seems that NMP radicals also take alternate configurations, since if the radicals are paired another strong band should appear at 13000 cm^{-1} region, but it is not clearly found in the spectra.

The result of theoretical calculation by the alternant model with the U' value of 0.7 eV is in good agreement with the spectra of the triclinic crystal. The CT band appearing at 5500 cm^{-1} is interpreted on this basis as a CT_2 band. The dichroic intensity ratio for the CT_2 and LE_1 bands are satisfactorily explained, and the broad bands appearing at 12000 cm^{-1} region along the a- and b-axis are assigned to the LE_1 band. The absorption bands around 26000—28000 cm^{-1} region are assigned as the superposed TCNQ neutral and ionic species. A recent reflectivity measurement of this crystal provides an evidence of the presence of neutral TCNQ species.[38]

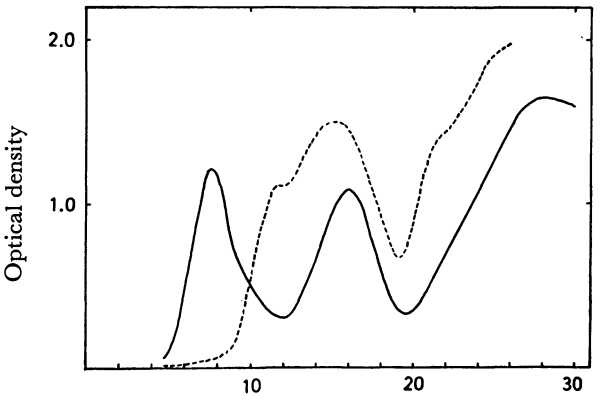

Fig. 17. Polarized absorption spectra on the (100) plane of a single crystal of monoclinic (NMP) (TCNQ).
——: b axis, ·····: a axis.

The crystalline absorption spectra of the monoclinic form were measured with the (100) plane, and the CT band was found at higher energy than for the triclinic crystal (Fig. 17). The LE_1 band is blue shifted. Although the crystalline structure of this form has not yet been published,[44] but it is suggested to be composed of D^+A^- stacks. Then the spectral result is explained in such a way that the lowest energy transition is a CT between $(TCNQ)^-$ and $(NMP)^+$, and the bands at 12000 and 16000 cm^{-1} are the LE bands of $(TCNQ)^-$ and $(NMP)^+$, respectively. A nearly diamagnetic behaviour of this crystal[44] will be also consistent with the D^+A^- model of this crystal.

Thus the variation of the physical properties of the triclinic and the monoclinic NMP(TCNQ) is reasonably explained by the change of the electron configuration of the crystals.

$Cs_2(TCNQ)_3$. The crystalline structure was determined by Fritchie and Arthur.[16] It belongs to a monoclinic system of the space group $P2_1/c$. One of the TCNQ in the unit cell is situated on the center of symmetry and is considered as neutral, and other two non-centric TCNQ are analyzed to have negative charges. The localization of the charge is also confirmed by the photoemission spectroscopy.[49] The projection of molecules onto the developed crystalline plane is shown in Fig. 18. The TCNQ column elongates along the b-axis with interplanar spacings of 3.22 Å for adjacent charged molecules. In Fig. 3 the overlap for charged species is shown to be larger than for the mixed species.[3] Since the center of TCNQ molecules are lined along the b-axis, the CT bands may be observed particularly along the b-axis, if the mixing of the CT and LE_1 levels is not significant. Also the long-axis of TCNQ is inclined 45° to the b-axis, therefore the LE type bands are expected to give the dichroic intensity ratio of 1 : 1 for the b- and a-axis.

The crystalline absorption spectra have been measured before by Hiroma *et al.*,[26] but we have measured again to extend into near infrared and the spectra with the (001) plane are shown in Fig. 19. Two CT bands found at 6000 and 11000 cm^{-1} mainly along the b-axis. The lower energy band is considered as the CT_2 type

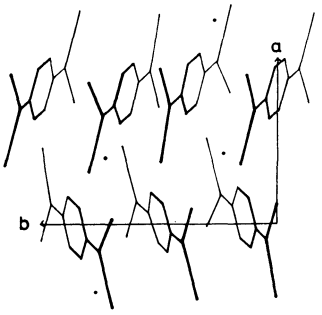

Fig. 18. Projection of $Cs_2(TCNQ)_3$ into the developed (001) plane.

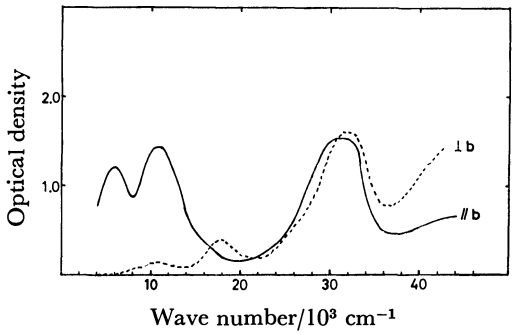

Fig. 19. Polarized absorption spectra on the (001) plane of a single crystal of $Cs_2(TCNQ)_3$.
——: b axis, ……: a axis.

between the neutral and charged TCNQ molecules, and the higher energy one is the CT_1 band mixed to some extent with the LE_1 band. The mixing between these two transitions is verified by a theoretical calculation. The blue shift of the LE_1 band is as much as 5000 cm^{-1}, and the change of the intensity is very remarkable, and these characteristics are reasonably explained by the interaction of the CT_1 and LE_1 levels. The deviation of the observed intensity ratio (3.5) from the oriented gas model (1.0) is also accounted for by this calculation as the effect of the mixing of the CT_1 and LE_1 levels. The observed dichroic ratio for the LE_2 band (1.06) is in good agreement with the oriented gas model (1.0) because the LE_2 level is not significantly influenced by other levels except that the band is blue shifted by 2000 cm^{-1}.

The characteristic of the island type electron configuration is exemplified with these spectra that both the CT_2 and CT_1 bands are observed along the stacking axis of TCNQ columns; the LE_1 band is blue shifted and the dichroic intensity ratio are changed from the oriented gas model by the interaction of the CT_1 and LE_1 levels.

(Mor)$_2$(TCNQ)$_3$. The crystal structure of (morpholinium)$_2$(TCNQ)$_3$ was determined by Sundaresan and Wallwork[50]; the crystals are monoclinic, belonging to the space group $P2_1/c$. Two of three TCNQ species in the unit cell are negatively charged, while the other TCNQ is neutral. The overlapping of the charged molecules and the charged and neutral molecules are shown in Fig. 3, and the patterns are similar to other systems having the same charge distributions.[3]

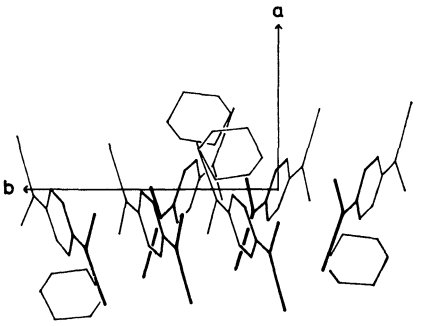

Fig. 20. Projection of $(Mor)_2(TCNQ)_3$ onto the developed plane.

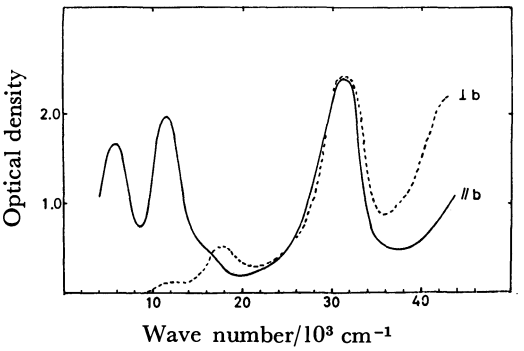

Fig. 21. Polarized absorption spectra on the (001) plane of a single crystal of $(Mor)_2(TCNQ)_3$.
——: b axis, ……: a axis.

The crystalline absorption spectra were measured with the (001) plane and the projection of molecules onto this plane is shown in Fig. 20. The column of TCNQ elongates along the b-axis, and the long-axis of TCNQ molecule is inclined to the b-axis by 45°. The spectra are shown in Fig. 21 and two CT bands are clearly observed along the b-axis with maximum at 6000 and 11500 cm^{-1}. The band at 6000 cm^{-1} is assigned to the CT_2 band, the band at 11500 cm^{-1} is the CT_1 mixed with the LE_1 band. The LE_1 band is found at 17500 cm^{-1}; it is blue shifted as much as 5000 cm^{-1}. The dichroic intensity ratio of the LE_1 band is also changed from the oriented gas model of 1.0 to 3.0. On the other hand the LE_2 band shows the same intensity for the b- and a-axis in accordance with the oriented gas model.

The observed energies and the polarization characteristics are well explained by a theoretical calculation with an island model, and it is very interesting that a gross feature of the spectra is very close to the spectra of $Cs_2(TCNQ)_3$ in spite of a great difference in chemical nature of the cationic group. It will mean that the crystalline spectra reflect the electron configuration of the crystal.

(TEA)$_2$(TCNQ)$_4$. The crystal structure of triethylammonium TCNQ complex was determined by Kobayashi, Ohashi, Marumo and Saito;[17] the crystal is triclinic with space group $P\bar{1}$, and four TCNQ molecules form a repeating unit in the column. Two of four TCNQ molecules in the centrosymmetric inside pair are considered to have negative charges and two

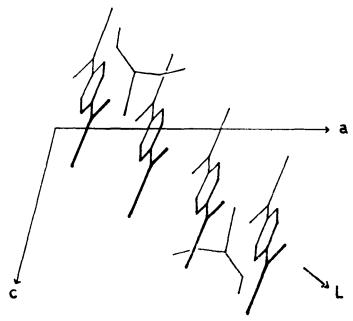

Fig. 22. Projection of $(TEA)_2(TCNQ)_4$ onto the developed (010) plane.

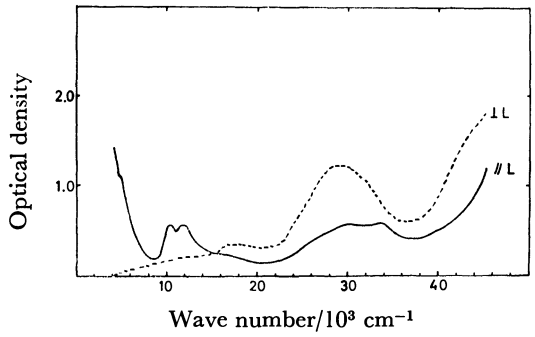

Fig. 23. Polarized absorption spectra on the (010) plane of a single crystal of $(TEA)_2(TCNQ)_4$
——: Parallel to the stacking axis, L,
……: perpendicular to the stacking axis.

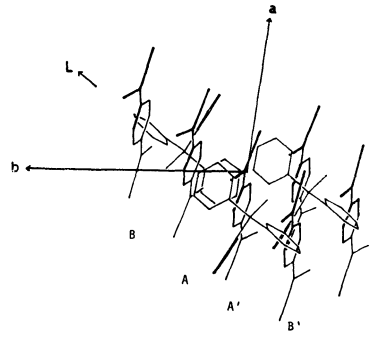

Fig. 24. Projection of $(MTPP)_2(TCNQ)_4$ onto the developed (001) plane.

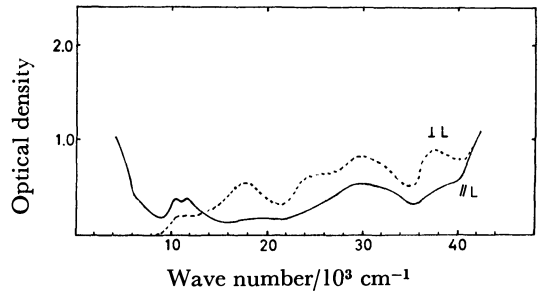

Fig. 25. Polarized absorption spectra on the (001) plane of a single crystal of $(MTPP)_2(TCNQ)_4$.
——: Parallel to the stacking axis, L,
……: perpendicular to the stacking axis.

outer TCNQ molecules are thought to be neutral. Thus the structure is typical of an island type configuration. The stacking axis of TCNQ column makes about 40° to the a-axis in the (010) projection, and the long-axis of the TCNQ molecule makes 50° to the stacking axis (Fig. 22). On this projection the LE_1 and LE_2 bands are expected to give a dichroic intensity ratio of 1.4 with the stacking axis ($I_\perp/I_{//}$).

The crystalline absorption spectra measured with the (010) plane in the direction parallel and perpendicular to the stacking-axis are shown in Fig. 23. Along the stacking axis prominent absorptions are found at around 4000 and at 11000 cm^{-1}, and two bands are observed at 17700 and 29000 cm^{-1}. Although the maximum of the lowest energy band is not found, but it is unambiguously assigned to the CT_2 band because of its polarization, and the next band at 11000 cm^{-1} is a transition to the coupled LE_1 and CT_1 states. Another coupled transition of the CT_1 and LE_1 states is found at 17700 cm^{-1}. The energy levels, the intensities and the dichroic ratio of these transitions are well explained by the theoretical calculation as a consequence of the mxing of the LE_1 and CT_1 levels. The distribution of intensities between these two bands and the change of the dichroic ratio suggests that the mixing is very efficient between these two levels. The pattern of the spectra may be typical of 2: 4 type island electron configuration, in which negatively charged TCNQ species are surrounded by neutral TCNQ molecules. The CT_2 band may have lower energy than that of 2: 3 type system, because the electron correlation between the neighbour sites is much reduced by a presence of the extra neutral TCNQ molecule. The absorption bands at 28000—30000 cm^{-1} are assigned to the LE_2 bands of $(TCNQ)^-$ and $(TCNQ)_2$, and the dichroic ratio is about 2.0, which is in fairly good agreement with the oriented gas ratio.

$(MTPP)_2(TCNQ)_4$. The crystalline structure of methyltriphenylphosphonium TCNQ was determined by McPhail, Semeniuk and Chesnut,[51] and by Konno and Saito.[52] The crystal belongs to a triclinic system with the space group of $P\bar{1}$. The tetrad structure was found for TCNQ column, but the standard deviation for the bond distances are larger than the difference of bond distances of $(TCNQ)^0$ and $(TCNQ)^-$. The crystalline absorption spectra were measured with the (001) plane, and the projection of molecules onto this plane is shown in Fig. 24. The stacking axis of TCNQ makes about 45° to the b-axis on this projection, and the long-axis of the TCNQ molecule is inclined about 50° to the stacking axis of TCNQ column.

The spectra shown in Fig. 25 are very close to that of $(TEA)_2(TCNQ)_4$, therefore it seems more probable that the electrons are localized within two TCNQ molecules rather than that they delocalize over the column. The lowest energy absorption was found around 4000 cm^{-1} region along the stacking axis, and it is assigned to the CT_2 band. Two prominent peaks were observed at 11000 and 17700 cm^{-1} region and these are regarded as the transitions to the mixed LE_1 and CT_1 states. The observed energy values and the dichroic intensity ratios are well accounted for by the theoretical calculation based on the island model. The LE_2 band appears at 25000 and 30000 cm^{-1} region, and this

splitting will imply that the TCNQ species exist as negative and neutral ones in the crystal.

The spectral similarity between $(TEA)_2$- and $(MTPP)_2(TCNQ)_4$ is very striking that a similar electron configuration of TCNQ column is supposed for these chemically different crystals. Among four TCNQ molecules labelled by A, A', B and B' in Fig. 24,[51] the spectral, magnetic and a slight variation of bond length support that electrons may be localized on A and A' sites, but the mode of overlapping may not be in favour of this assignment.

Energy Separation of the Triplet and Singlet States

The magnetic susceptibilities of TCNQ complexes have been measured for various crystals by many people, and experimental data of the energy separations for the triplet and singlet states have been accumulated.[1,5] The singlet state of the coupled TCNQ dimers will be stabilized by the CT interaction as compared to the triplet state, because the CT interaction could not be expected for the triplet state because of Pauli principle.[52] Following the perturbational calculation given in the previous section, the singlet state of the dimer will be stabilized to the triplet state approximately by

$$J = \frac{4t_{mm}^2}{U} \tag{14}$$

where U is the spectroscopic electron correlation energy, and t_{mm} is the transfer integral between the half-filled highest occupied orbitals. Although there may be a slight change of U values depending on the crystalline structure and the electron configuration, but we may take it as a constant value of 1.5 eV. The J values are calculated by Eq. 14 for several complexes which have TCNQ pairs and the results are shown in Table 3. The experimental J values are estimated by the temperature dependence of the magnetic susceptibility. It is seen that the agreement between the experimental and the calculated J values is reasonably good in spite of a simple model used for the calculation. Although the structure of the alkaline salts of TCNQ are not dimeric in a rigorous sense,[5] as in their low temperature phase another neighbour site is found close to the dimer pair.[18,19] In spite of this the magnitude of the second transfer integral t_2 is one third of the dimer pair, so we have ignored this effect in this treatment.

Table 3. Calculated and observed magnetic J values

	J-values (eV)		Reference	
	Calcd	Obsd	Magnetic data	Crystal structure
Rb-I	0.27	0.28	56	28
Na	0.19	0.16	57	18
K	0.19	0.25	56	19
Mor (1:1)	0.34	0.36	58	63
TMA	0.33	>0.2	59	64
TMB[a]	0.11	0.20	56	65
Mor (2:3)	0.27	0.31	58	50
Cs (2:3)	0.19	0.16	60	16
TEA (2:4)	0.032	0.034	61	16
MTPP (2:4)	0.068	0.065	61	51
BPY (2:4)	0.05	0.05—0.072	62	66
TTF (>60°K)	b)	b)	53, 54	11, 12

a) (1,2,3-Trimethylbenzimidazolium)-(TCNQ).
b) See text.

For the alternant type crystal the stabilization by the charge transfer effect may be small since the CT interaction can not be expected as the first order effect. In fact very small J values were found NMP, Q and Ac–TCNQ complexes.[2] These results may be well explained by the model that these crystals have the alternant electron configuration, and the CT type stabilization may not occur significantly.

The susceptibility of the TTF–TCNQ crystal behaves differently from other good conducting crystals; it shows a distinct temperature dependence even in the metallic state.[53,54] In view of an importance of accurate susceptibility data[53] for the analysis of the electronic structure of the crystal, we have attempted to fit the calculated susceptibility by our model with the observed one, although there remain several parameters which may be checked by other methods. The susceptibility will be particularly dependent on the number of active spins, therefore the number of electron transfer may be guessed by this work.

The calculation of transfer integrals in and between the TTF and TCNQ chains were carried out by Berlinsky *et al.*,[24] and by using their values we may estimate the CT interaction between the chains as being negligible and that within the TTF chain is 0.007 or 0.086 eV depending on either sulphur 3p or 3d orbitals being used. For the TCNQ chain, we have used our own integral values, and the S–T separation is estimated as 0.052 eV. In order to simplify the calculation, the dimeric state in TTF chain is also assumed to have the same activation energy of 0.052 eV. Then the spins on the TCNQ and TTF chains are divided into the island and alternant type and the number of the transferred electron and their distributions are adjusted to fit the calculated curve with the observed one. The susceptibility was calculated by using the dimer model for the island system and Heisenberg model[55] for the alternant system. The best fits were obtained by using the following set of parameters: Case 1. TCNQ chain, alternant 0.25 (J=0.024 eV), island 0.335 (J=0.052 eV); TTF chain, alternant 0.17 (J=0.008 eV), island 0.415 (J=0.052 eV), the number of electron transfer is 0.585; Case 2. TCNQ chain, alternant 0.48 (J=0.021 eV), island 0.11 (J=0.052 eV); TTF chain, alternant 0.10 (J=0.010 eV), island 0.49 (J=0.052 eV), the number of electron transfer is 0.59. By these parameters the observed curve was reproduced with the error less than 10%.

We have completely ignored the interaction between the spins on the island and alternant system within the chain, and actually the interaction of these clusters may not be simple enough to allow such a simple treatment. The ratio of the alternant and the island system were not exactly the same in TCNQ chain by both parameters, but it is roughly in agreement with the analysis presented in the previous section. Moreover the number of charge transfer is in good agreement with the X-ray

result of Coppens (0.48—0.60).[13] The number of charge transfer may vary with temperature, but such a consideration was not included in this calculation.

Electrical Conductivity and Electronic Structure

Variety of TCNQ complexes may be classified into several groups from the electrical conductivity[2,67]; (a) the low conductive group which are nearly insulating or semiconducting with high activation energies, (b) the intermediate case which are semiconducting with small activation energies, and (c) the good conducting ones which behave like metal.

Alkaline salts of 1:1 composition, which may form the dimer type crystals, and several island type crystals which have localized electrons belong to class (a).[67] Following the one-electron band theory[5] the high resistivity will be explained by the band gap produced by the Peierls transition at low temperatures.

According to Ovchinikov,[68] the band gap in the one-dimensional Hubbard model is given by $U-4t$, and we may compare the observed activation energies of various crystals with the estimated activation energies given by

$$\Delta E = \frac{1}{2}(U-4t) \tag{15}$$

Here t values are given in Table 1 and we take an average of two nearest neighbour values and the results of the calculation are tabulated in Table 4. The agreement between the calculated and the experimental values is not so bad for these crystals. From a view of the Mott theory[69] on the metal to insulator transition, we may compare $4t$ values for several crystals with U values. It gives $U>4t$ for most crystals, therefore the metallic state will not be easily realized. The smallest U' values is 0.35 eV of TTF(TCNQ), therefore the small U' is apparently in favour of the metallic state, but still the inter- and intra-site Coulomb energies are by no means negligible. The transfer integrals are in the range of 0.35—0.10 eV, and it is larger for the dimer type configuration than the alternant or the island type, but U is larger again for the dimer type.

Suezaki[70] has calculated the conductivity of TCNQ complexes by the Hubbard Hamiltonian, and has proposed a formula that

$$\sigma = \sigma_0 e^{-\Delta E/kT}$$

$$\sigma_0 = \frac{1}{12\pi}\frac{e^2 n\delta^2}{\hbar}\frac{t}{U} \tag{16}$$

where δ is the vector connecting between two TCNQ molecules. We have evaluated by using our t and U values for $(TEA)_2(TCNQ)_4$, and σ_0 is estimated as

Table 4. Activation energies for semiconductivity

	ΔE(eV) Calcd	ΔE(eV) Obsd	References
Na	0.33	0.33	67
K	0.35	0.35	67
Rb-I	0.35	0.49	82
Rb-II	0.60	0.17	82

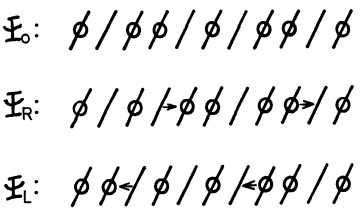

Fig. 26. Basic electron configurations of TTF(TCNQ). The top row represents the ground state without field (Ψ_0). The middle row shows an electron flowed into the right (Ψ_R), and the bottom row exhibits a flow into the opposite direct on (Ψ_L).

$8\,\Omega^{-1}\,cm^{-1}$ for the b-axis, which is a reasonable fit as compared to the observed value of $4\,\Omega^{-1}\,cm^{-1}$.[67] However, the same formula applied to $(MTPP)_2(TCNQ)_4$ and $Cs_2(TCNQ)_3$[67] gives the results which are two or three orders of magnitudes larger than the experimental values. For $Q(TCNQ)_2$ the calculated one is one or two orders of magnitudes smaller than the observed values,[67,71] therefore this formula may be limited for explaining the electrical properties of these complexes.

All good conducting TCNQ complexes like Q, NMP, Ac and TTF(TCNQ) have alternant electron configuration as a basic unit; in addition, they have a common characteristic that the cation groups are stacked to form their own columns. It seems certain that the cation stack also plays an important role in the conduction mechanism. For example, the TTF column may be even more conductive than TCNQ column,[54] however, not all TTF complexes show good conductivity,[72] therefore the correlation of motion of electrons and holes on both chains may be very significant. Bloch *et al.*[73] discussed this point from a band theory, and suggested that the overlapping of the energy levels of the donor and the acceptor bands is important. A partial electron transfer from the donor to acceptor column may be realized by such a band scheme.

We have tried to estimate the conductivity based on our model of TTF(TCNQ). The basic electron configuration of TCNQ column in this particular crystal is written by an admixture of an island and an alternant type as is explained in the previous section. The ground state wavefunction for the column will be given by

$$\psi_0 = a\varphi_A + b\varphi_I \tag{17}$$

and the basic electron configurations are depicted in Fig. 26. The coefficients a and b may be estimated from the spectral and structural analyses as mentioned before.

By applying the electric field $\boldsymbol{E}$, one of the electron in the island cluster may flow into the right or the left sites and the newly produced states are described as Ψ_R and Ψ_L. The difference of population of these two states are statistically estimated by the Boltzmann distribution as

$$\omega(\boldsymbol{E}) = \frac{e^{e\boldsymbol{r}_0\cdot\boldsymbol{E}/kT} - e^{-e\boldsymbol{r}_0\cdot\boldsymbol{E}/kT}}{e^{e\boldsymbol{r}_0\cdot\boldsymbol{E}/kT} + e^{-e\boldsymbol{r}_0\cdot\boldsymbol{E}/kT}} = \frac{e\boldsymbol{r}_0\cdot\boldsymbol{E}}{kT} \tag{18}$$

where $\boldsymbol{r}_0$ is the distance between the center of two TCNQs. Here we have assumed that the positive charges on the cation site are fixed.

The crystalline structure analysis on TTF(TCNQ) showed that the lattice spacing is uniform for one unit translation, and it implies that electrons and holes are delocalized over more than several lattice sites but not fixed at particular sites without any activation energy at high temperature phase.

The probability of electron transfer between the island and alternant sites may be evaluated by the Fermi golden rule assuming that the transition is isoenergetic. Namely the transition rates are given by

$$W_R = \frac{2\pi}{\hbar}|\langle\psi_R|H|\psi_0\rangle|^2\rho_R(\varepsilon, \boldsymbol{E}) \tag{19}$$

or

$$W_L = \frac{2\pi}{\hbar}|\langle\psi_L|H|\psi_0\rangle|^2\rho_L(\varepsilon, \boldsymbol{E})$$

where $\rho(\varepsilon, \boldsymbol{E})$ is the state density under the field, which is approximated by the reciprocal of the band width $2t$ multiplied by the field factor, and $\rho_R(\varepsilon, \boldsymbol{E})$ and $\rho_L(\varepsilon, \boldsymbol{E})$ are differently populated when the field is applied, say into the right direction, as

$$\rho_R(\varepsilon, \boldsymbol{E}) - \rho_L(\varepsilon, \boldsymbol{E}) = \omega(\boldsymbol{E})/2t \tag{20}$$

The fluctuation time of electron, τ_R and τ_L, are related to these probabilities as $\tau_R = 1/W_R$ and $\tau_L = 1/W_L$. The flow of electron along the applied field will be given by

$$\begin{aligned} \boldsymbol{J}_R &= er_0\left(\frac{1}{\tau_R} - \frac{1}{\tau_L}\right) \\ &= \frac{\pi}{\hbar}t\cdot er_0\cdot\omega(\boldsymbol{E}) \end{aligned} \tag{21}$$

where t is the transfer integral evaluated in the previous section. The conductivity σ per unit length is given by $\boldsymbol{J}/\boldsymbol{E}$ multiplied by n, the number of mobile electron along the chain in an unit volume, as

$$\sigma = \frac{\pi}{\hbar}t\cdot(er_0)^2\frac{n}{kT} \tag{22}$$

and the numerical value is easily evaluated as 2950 Ω^{-1}cm^{-1} for the case of equal mixing of the island and the alternant configurations with an electron transfer of 0.585 from TTF to TCNQ, and it is 1231 Ω^{-1} cm^{-1} for an electron transfer of 0.50 at 300 K. The observed values are in the range of 500—1000 Ω^{-1} cm^{-1} according to Cohen, Coleman, Garito and Heeger.[32] The temperature dependence of the conductivity is T^{-1} by Eq. 22, however, Groff, Suna and Merrifield[34] reported $T^{-2.3}$ behaviour in this crystal. If the number of electron transfer or back transfer from TTF to TCNQ has T^{-1} dependence, then n in Eq. 22 may also shows T^{-1} dependence, and the observed tendency may be qualitatively explained.

Here we have localized the cation charges on particular sites, but it may fluctuate also, and this fluctuation will be essential for good conductivity as mentioned before. If we suppose that a similar electron configuration exists for the cation column and count the contribution of both chain independently, the value of conductivity may be approximately doubled and the expected maximum value at 58 K may be 3×10^4 Ω^{-1}cm^{-1}. The ideally coherent motion of electron in both chains may be involved in the giant conduction[31] particularly observed in this crystal. As another example, a recent measurement of the highest organic conductivity at room temperature by Bloch, Cowan, Bechgaard, Pyle, Banks and Poehler[74] on (HMTSF)(TCNQ) showed the value as large as 1391 to 2178 Ω^{-1} cm^{-1}, which are nearly the same magnitude with the maximum value of the above mentioned mechanism.

For other alternant type crystals like NMP and Q(TCNQ), the mixing of the island configuration is smaller than for TTF(TCNQ), and a similar calculation is carried out by assuming that the electron transfer occurs at the island site and its population is determined from the spectral analysis. The results are as follows; NMP(TCNQ), $\sigma_{calcd}=220$ Ω^{-1} cm^{-1}, $\sigma_{obsd}=180$[2]—200[47] Ω^{-1} cm^{-1}; Q(TCNQ), $\sigma_{calcd}=410$ Ω^{-1} cm^{-1}, $\sigma_{obsd}=100$[67]—70[71] Ω^{-1} cm^{-1}. These results are in fairly good agreement to each other.

As regard to the giant conductivity of TTF(TCNQ) at low temperature, Anderson, Lee, and Saitoh[75] have presented a view that the activation energy may be the coupling energy of Josephson junction. Interestingly, these authors and Lee, Rice, and Anderson [76,77] thought that the Peierls transition occurs already at room temperature. Our viewpoint on this system is that the longer period than the short period of normal lattice is already mixed in at room temperature, and an apparent lattice constant may represent the averaged period, hence our view may involve the same content as Anderson *et al.*[75-77] With TTF(TCNQ) the diffuse X-ray lines were observed by Denoyer, Comes, Garito, and Heeger[78] and Kagoshima, Anzai, Kajinuma, and Ishiguro[79] even at room temperature which indicated that the longer period than the normal lattice might be mixed. Although these authors explained it by the Kohn anomaly in the one-dimensional metallic lattice, but we may explain it by a partial mixing of the island type structure, which may have nearly triple lattice period.

Next we may try to estimate the polarizability and hence the dielectric constant in the static field for the mixed alternant and island type crystals. The polarizability α and the dielectric constant ε of the TCNQ chain may be given by

$$\alpha = \bar{m}(\boldsymbol{E})/\boldsymbol{E} = \langle\psi_R|er|\psi_R\rangle\omega(\boldsymbol{E})/\boldsymbol{E}$$

and

$$\simeq b^2\frac{(er_0)^2}{kT}$$

$$\varepsilon = 1 + 4\pi N\alpha \tag{23}$$

where Nb^2 is the number of active site in an unit volume of the crystal. The calculated results are $\varepsilon=3400$ for TTF(TCNQ) and $\varepsilon=330$ for NMP(TCNQ) at 4.2 K. The observed values are $\varepsilon=(3.2\pm0.7)\times10^3$ for TTF(TCNQ)[80] and $\varepsilon=350\pm50$[81] for NMP(TCNQ). The agreement between the observed and calculated results is quite satisfactory in spite of our simple model used for the calculation. Although our calculation on TTF(TCNQ) is based on the structure determined at room temperature, but we believe that the basic electronic structure is the same even at 4.2 K. In the low temperature phase below 54 K, the correlation of electronic motion may be lost within and between chains, presumably because a 3D regularity inhibits a labile electron motion as in other island type crystals.

Finally we must comment on the design of good conducting organic molecules. First of all good conducting TCNQ complexes which we have studied have an alternant electron configuration as the basic unit and the admixture of an island type configuration increases the conductivity significantly. In this respect a perfectly charged chain is not suitable, and a column with some vacancies will be essential.

A good overlap between TCNQ molecules will be, undoubtedly, very important in the intermolecular interaction, but the size of the transfer integral is limited as large as 0.15 eV between $TCNQ^0$ and $TCNQ^-$. Hence a small U' value for the alternant system may be significant to increase the mixing of the island type, and it may drop even to nearly zero value for some particular crystals by the balance of Coulomb forces within and between columns. The good overlap and the formation of the one-dimensional column of the donor (cation) group is also a necessary condition, because our experience shows that all good conducting crystals have both TCNQ and cation columns. It will imply that a nice balance of charges and a coherent motion of electrons and holes will be possible or facilitated by the interaction between two columns through the variable electron transfer mechanism and a correlation of Coulombic interaction. Anyway the fluctuation of the charges in the chain and the fractional charge transfer between the donor and the acceptor columns are most important for the good conductivity. It necessarily imposes a critical condition for the donor and the acceptor molecules to have a peculiar character that their radicals must be stable enough to form a complex chain with their parent molecules. It means that excess charges must be shared between several molecules, and this condition is actually satisfied in TCNQ complexes as well as TTF complexes.[81]

In concluding this paper the importance of the optical studies of these complexes must be emphasized, particularly in the infrared region, because it will give fundamental information of the electronic structure of these crystals. Although our treatment is concentrated on the molecular approach, but the physical parameters found in this study will be useful even for the band theoretical investigations.

The authors are grateful to Professors Makoto Okawara and Dwaine O. Cowan for the kind gifts of TTF(TCNQ) crystals, and to Dr. Jerry B. Torrance for kind information and comment. They also thank to Professor Yoshihiko Saito for many crystallograpflic information, and to Drs. Motomichi Inoue and Hitosi Sumi for helpful discussions. One of the authors (J. T.) thanks to Professors Takehiko Shimanouchi and Takeo Yamamoto of the University of Tokyo for the use of the Tool-IR system of the Computation Center of the University of Tokyo.

References

1) Z. Soos, *Ann. Rev. Phys. Chem.*, **25**, 121 (1974).
2) I. F. Shchegolev, *Phys. Status Solidi A*, **12**, 4 (1972).
3) F. H. Herbstein, *Perspect. Struct. Chem.*, **4**, 166, ed. by J. D. Dunitz and J. A. Ibers, John Wiley (1971).
4) A. J. Heeger and A. F. Garito, "Low Dimensional Cooperative Phenomena," ed. by H. J. Keller, Plenum Press, New York (1975), p. 89.
5) J. Kommandeur, "Low Dimensional Cooperative Phenomena," ed. by H. J. Keller, Plenum Press, New York (1975), p. 65; J. G. Vegter, J. Kommandeur, and P. A Fedders, *Phys. Rev.* **B7**, 2929 (1973); J. G. Veger, P. I. Kuindersma, and J. Kommandeur, "Conduction in low-mobility materials," Taylor and Francis, (1971): J. G. Vegter and J. Kommandeur, *Mol. Cryst. Liq. Cryst.* **30**, 11 (1975).
6) L.R. Melby, R. J. Harder, W. R. Hertler, W. Mahler, R. E. Benson, and W. E. Mochel, *J. Am. Chem. Soc.*, **84**, 3374 (1962).
7) L. R. Melby, *Can. J. Chem.*, **43**, 1448 (1965).
8) H. Kobayashi, F. Marumo, and Y. Saito, *Acta Crystallogr.* **B27**, 373 (1971).
9) A. W. Hanson, *Acta Crystallogr.*, **B24**, 768 (1968).
10) H. Kobayashi, *Bull. Chem. Soc. Jpn.*, **47**, 1346 (1974).
11) T. J. Kistenmacher, T. E. Phillips, and D. O. Cowan, *Acta Crystallogr.* **B30**, 763 (1974).
12) R. H. Blessing and P. Coppens, *Solid State Comm.*, **15**, 215 (1974).
13) P. Coppens, *Phys. Rev. Lett.*, **35**, 98 (1975).
14) W.D. Grobman, R. A. Pollak, E. E. Eastman, E. T. Mass, Jr., and B. A. Scott, *Phys. Rev. Lett.*, **32**, 534 (1974).
15) W. T. Wozniak, G. Depasquali, M. V. Klein, R. L. Sweany, and T. L. Brown, *Chem. Phys. Lett.*, **33**, 33 (1975).
16) C. J. Fritchie, Jr. and P. Arthur Jr., *Acta Crystallogr.*, **21**, 139 (1966).
17) H. Kobayashi, Y. Ohashi, F. Marumo, and Y. Saito, *Acta Crystallogr.*, **B26**, 459 (1970).
18) M. Konno and Y. Saito, *Acta Crystallogr.*, **B30**, 1294 (1974); *ibid.*, **B31**, 2007 (1975).
19) M. Konno and Y. Saito, *Acta Crystallor.*, to be published.
20) R. H. Boyd and W. D. Phillips. *J. Chem. Phys.* **43**, 2927 (1965).
21) D.A. Lowitz, *J. Chem. Phys.*, **46**, 4698 (1967).
22) Y. Iida, *Bull. Chem. Soc. Jpn.*, **42**, 71, 673 (1969).
23) J. Hubbard, *Proc. R. Soc., Ser. A*, **276**, 238 (1963); **281**, 401 (1964); **285**, 542 (1965).
24) A. J. Berlinsky, J. F. Coleman, and L. Weiler, *Solid State Commun.* **15**, 795 (1974).
25) E. Clementi, C. C. J. Roothaan, and M. Yoshimine, *Phys. Rev.*, **127**, 1618 (1962).
26) S. Hiroma, H. Kuroda, and H. Akamatu, *Bull. Chem. Soc. Jpn.*, **44**, 9 (1971).
27) O. H. LeBlanc, Jr., *J. Chem. Phys.* **42**, 4307 (1965).
28) A. Hoekstra, T. Spoelder, and A. Vos, *Acta Crystallogr.*, **B28**, 14 (1972).
29) N. Sakai, I. Shirotani, and S. Minomura, *Bull. Chem. Soc. Jpn.*, **45**, 3314 (1972).
30) Y. Ohashi and T. Sakata, *Bull. Chem. Soc. Jpn.*, **46**, 3330 (1973).
31) L. B. Coleman, M. J. Cohen, D. J. Sandman, F. G. Yamagishi, A. F. Garito, and A. J. Heeger, *Solid State Commun.* **12**, 1125 (1973).
32) M. J. Cohen, L. B. Coleman, A. F. Garito, and A. J. Heeger, *Phys. Rev.*, **B10**, 1298 (1974).
33) J. Ferraris, D. O. Cowan, V. Walatka, Jr., and J. H. Perlstein, *J. Am. Chem. Soc.*, **95**, 348 (1973).
34) R. P. Groff, A. Suna, and R. E. Merrifield, *Phys. Rev. Lett.*, **33**, 418 (1974).
35) P. M. Grant, R. L. Greene, G. C. Wrighton, and G. Castro, *Phys. Rev. Lett.*, **31**, 1311 (1973).
36) C. S. Jacobsen, D. B. Tanner, A. F. Garito, and A. J. Heeger, *Phys. Rev. Lett.*, **33**, 1559 (1974); D. B. Tanner, C.S. Jacobsen, A. F. Garito, and A. J. Heeger, *Phys. Rev.*, **B13**, 3381 (1976).

37) J. B. Torrance, B. A. Scott, and F. B. Kaufman, *Solid State Commun.* **17**, 1369 (1975).
38) M. Tanaka, J. Tanaka, C. Tanaka, and H. Anzai, unpublished results.
39) F. Wudl, G. M. Smith, and E. G. Hutnagel, *Chem. Commun.* **1970**, 1453.
40) J. B. Torrance, private communication.
41) A. A. Bright, A. F. Garito, and A. J. Heeger, *Solid State Commun.*, **13**, 943 (1973); *Phys. Rev.*, **B10**, 1328 (1974); D. B. Tanner, C. S. Jacobsen A. F. Garito, and A. J. Heeger, *Phys. Rev. Lett.*, **32**, 1301 (1974).
42) H. Hinkelmann and H. G. Reik, *Solid State Commun.*, **16**, 567 (1975).
43) Y. Ueno, Y. Masuyama, and M. Okawara, *Chem. Lett.* **1975**, 603; Y. Ueno and M. Okawara, *ibid.*, **1975**, 1135.
44) L. B. Coleman, S. K. Khanna, A. F. Garito, A. J. Heeger, and B. Morosin, *Phys. Lett.*, **42A**, 15 (1972); the structure of a monoclinic form was briefly reported by B. Morosin, *Phys. Lett.*, **53A**, 455 (1975).
45) C. J. Fritchie, Jr., *Acta Crystallogr.*, **20**, 892 (1966).
46) H. Kobayashi, *Bull. Chem. Soc. Jpn.*, **48**, 1373 (1975).
47) A. J. Epstein, S. Etemad, A. F. Garito, and A. J. Heeger, *Phys. Rev.*, **B5**, 952 (1972).
48) T. Sakata and S. Nagakura, *Bull. Chem. Soc. Jpn.*, **42**, 1497 (1969).
49) B. H. Schechtman, S. F. Lin, and W. E. Spicer, *Phys. Rev. Lett.*, **34**, 667 (1975).
50) T. Sundaresan and S.C. Wallwork, *Acta Crystallogr.*, **B28**, 491 (1972).
51) A. T. McPhail, G. M. Semeniuk, and D.B. Chesnut, *J. Chem. Soc., A*, **1971**, 2174; M. Konno and Y. Saito, *Acta Crystallogr.*, **B29**, 2815 (1973).
52) J. Tanaka, M. Inoue, M. Mizuno, and K. Horai, *Bull. Chem. Soc. Jpn.*, **43**, 1998 (1970).
53) J. C. Scott, A. F. Garito, and A. J. Heeger, *Phys. Rev.*, **B10**, 3131 (1974).
54) Y. Tomkiwicz, B. A. Scott, L. J. Tao, and R. S. Title, *Phys. Rev. Lett.*, **32**, 1363 (1974); J. E. Gulley and J. F. Weiher, *ibid.*, **34**, 1061 (1975).
55) J. C. Bonner and M. E. Fisher, *Phys. Rev.*, **135**, A640 (1964).
56) T. Hibma, P. Dupuis, and J. Kommandeur, *Chem. Phys. Lett.*, **15**, 17 (1972).
57) R. M. Vlasova, I. A. Smirnov, L. S. Sochava, and A. I. Skerle, *Fiz. Tverd. Tela*, **10**, 2990 (1968).
58) J. C. Bailey and D. B. Chesnut, *J. Chem. Phys.*, **51**, 5118 (1969).
59) R. G. Kepler, *J. Chem. Phys.*, **39**, 3528 (1963).
60) D. B. Chesnut and P. Arthur, Jr., *J. Chem. Phys.*, **36**, 2969 (1962).
61) D. B. Chesnut and W. D. Phillips, *J. Chem. Phys.*, **35**, 1002 (1961).
62) L. Shields, *J. Chem. Soc., Faraday Trans. 2*, **70**, 1372 (1974). A value of 0.072 eV will be reported by G. J. Ashwell, D. D. Eley, I. Diaconu, M. R. Willis, and J. Woodward; a private communication of M. R. Willis.
63) T. Sundaresan and S. C. Wallwork, *Acta Crystallogr.*, **B28**, 3507 (1972).
64) H. Kobayashi, T. Danno, and Y. Saito, *Acta Crystallogr.*, **B29**, 2693 (1973).
65) D. Chasseau, J. Ganltier, C. Hauw, and M. Schvoerer, *C. R. Acad. Sci., Paris, Ser. C*, **275**, 1491 (1972).
66) T. Sundaresan and S. C. Wallwork, *Acta Crystallogr.*, **B28**, 2474 (1972).
67) W. J. Siemons, P. E. Bierstedt, and R. G. Kepler, *J. Chem. Phys.*, **39**, 3523 (1963).
68) A. A. Ovchinikov, *Sov. Phys. JETP*, **30**, 1160 (1970).
69) N. F. Mott, *Adv. Phys.*, **13**, 325 (1964).
70) Y. Suezaki, *J. Phys. Soc. Jpn.*, **34**, 89 (1973).
71) L. I. Buravov, D. N. Fedutin, and I. F. Shchegolev, *Sov. Phys. JETP*, **32**, 612 (1971).
72) R. C. Wheland and J. L. Gillson, to be published.
73) A. N. Bloch, D. O. Cowan, and T. O. Pohler, "Energy and Charge Transfer in Organic Semiconductor," ed. by K. Masuda and M. Silver, Plenum Press (1974).
74) A. N. Bloch, D. O. Cowan, K. Bechgaard, R. E. Ryle, R. H. Banks, and T. O. Poehler, *Phys Rev. Lett*, **34**, 1561 (1975).
75) P. W. Anderson, P. A. Lee, and M. Saitoh, *Solid State Commun.*, **13**, 595 (1973).
76) P. A. Lee, T. M. Rice, and P. W. Anderson, *Phys. Rev. Lett.*, **31**, 462 (1973).
77) P. A. Lee, T. M. Rice, and P. W. Anderson, *Solid State Commun.*, **14**, 703 (1974).
78) F. Denoyer, F. Comes, A. F. Garito, and A. J. Heeger, *Phys. Rev. Lett.*, **35**, 445 (1975).
79) S. Kagoshima, H. Anzai, K. Kajinuma, and T. Ishiguro, *J. Phys. Soc. Jpn.*, **39**, 1143 (1975).
80) S. K. Khanna, A. F. Garito, A. J. Heeger, and R. C. Jaklevic, *Solid State Commun.*, **16**, 667 (1975); S. K. Khanna, E. Ehrenfreund, A. F. Garito, and A. J. Heeger, *Phys. Rev.*, **B10**, 2205 (1974).
81) F. Wudl, E. E. Schafer, W. M. Walsh, Jr., L. W. Rupp, F. J. DiSalvo, J. V. Waszczak, M. L. Kaplan, and G. A. Thomas, to be published.

Heat of Ion Exchange Reaction as Determined by Means of Flow Micro-Calorimetry. I. Cation Exchange in Aqueous System

Tetsuo MORIMOTO, Hiromitu NAONO,† Kuniji NŌSO,* and Yasumasa SHIGETOMI*

Department of Chemistry, Faculty of Science, Okayama University, Tsushima, Okayama 700
**Department of Chemistry, Okayama College of Science, Ridai-cho, Okayama 700*

(Received January 5, 1976)

The applicability of flow micro-calorimetry to the measurement of ion exchange heat was investigated by use of H-form resin of Dowex 50W×4 having a low degree of cross-linking. It was found that: accurate measurement of ion exchange heat can be performed by means of flow micro-calorimetry; the data obtained include additional heat effects such as heats of invasion and dilution; the effects can be exactly analyzed experimentally and eliminated for calibrating the data of pure ion exchange heat. The ion exchange heat thus obtained for the H-form resin and alkali metal ions was found to agree with the results obtained by means of heat of immersion measurements.

A number of fundamental studies have been carried out on ion exchange phenomena as regards the origin of selectivity of ion exchangers.[1-3] Combining the calorimetric data and the selectivity coefficients on ion exchange phenomena, Cruickshank and Meares,[4] Myers and Boyd,[5] and Boyd *et al.*[6] developed the thermodynamics of ion exchange reactions and attempted to elucidate the exchange phenomena in terms of the properties of ions and the structure of resins. In order to measure the ion exchange heat, they adopted the same calorimetric technique as that used for the measurement of immersion heat. The heat of ion exchange reaction can be measured step by step over the whole range of loading on one kind of ion.

A report has been given on flow micro-calorimetry[7] for the measurement of heat of adsorption from solution, which makes it possible to measure sensitively a small amount of heat evolved in a solid-liquid system.

The present paper deals with the applicability of flow micro-calorimetry to the measurement of ion exchange heat of alkali metal ions with H^+ ions, by use of a cation exchange resin, Dowex 50 W×4, made of poly(styrene sulfonate) and having relatively homogeneous sites for the exchange of alkali metal ions.

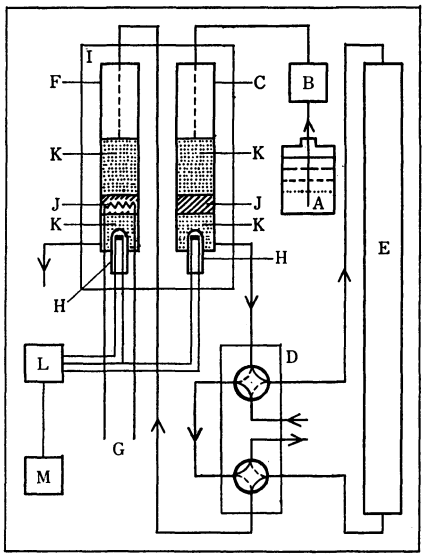

Fig. 1. Flow micro-calorimeter for the heat of ion exchange reaction. A, Reservoir for water; B, constant flow pump; C, reference column; D, exchange valves; E, reservoir for solution; F, detection column; G, calibration heater; H, thermistor; I, metal thermostat; J, ion exchange resin; K, glass beads; L, amplifier; M, recorder.

Experimental

Materials. Poly(styrene sulfonate) type resin, Dowex 50W×4 was used as a cation exchanger. The resin was washed with dilute hydrochloric acid until the well-defined H-form was ensured, followed by washing with distilled water. The total exchange capacity of the resin thus treated was 4.35 meq/g for alkali metal ions. Alkali metal chlorides of guaranteed grade were employed for the preparation of electrolyte solutions.

Ion Exchange Calorimetry. The apparatus was essentially the same as that used for the measurement of heat of adsorption from solution.[7] Figure 1 shows a diagram of the flow micro-calorimeter. The main part of this apparatus consists of a liquid column chromatograph, JLC-2A (Japan Electron Optics Laboratory Co., Ltd.). The resin (0.1 ml in apparent volume) was sandwiched by glass beads (65—100 mesh) and placed in a bed in the same position as that of both detection and reference columns. A coiled platinum resistance wire of 0.1 mm in diameter and 25 cm in length was embedded in the sample bed of the detection column, used for the calibration of the heat evolved by ion-exchanging. Change in temperature caused by ion exchange reaction or passage of electrical current through the platinum wire was detected with a thermistor connected by copper leads to a Wheatstone bridge, another arm of which was constructed by a similar thermistor placed in the reference column so that the calorimeter operates as a type of twin calorimeter. All the reacting solutions or water were forced to flow through the sample bed with a constant rate, 0.36 ml/min, by use of a constant flow pump.

The procedure for ion exchange calorimetry was carried out as follows. After the attainment of thermal equilibrium, the H-form resin set in the columns was washed with distilled water by passing through with the flow pump, until a constant base line was attained. Then, a certain amount of electrical energy was supplied to the platinum heater, the temperature rise being recorded. The calibration measurements were repeated by supplying various amounts of electrical energy. Next, the flowing liquid was converted from water into an electrolyte solution by means of exchange valves (Fig. 1). The heat

† Present address: Department of Chemistry, Faculty of Science, Kwansei Gakuin University, Uegahara, Nishinomiya, Hyogo 662.

liberated by the exchange of alkali metal ions with H^+ ions in the resin was recorded. All the measurements of ion exchange heat were carried out at 30 °C and within a reproducibility of ±5%. The amount of ions which underwent exchange was determined by titrating the eluted solution with a standard 0.01 M NaOH solution.

Results and Discussion

Figure 2 shows the peaks corresponding to the heats generated when various amounts of electrical energy were supplied under a flow rate, 0.36 ml/min, of water. Here, the rate of heat generation was 0.076 J/min. The relation between the peak area (Fig. 2) and the electrical energy supplied is shown in Fig. 3. We see that the peak area is proportional to the electrical energy supplied, and that the straight line passes the origin of the co-ordinates. A preliminary test[7] showed that the slope of the calibration curves does not depend upon the rate of heat generation, but varies with the flow rate of liquid. Thus, the flow rate of liquid was kept constant during the course of the experiment.

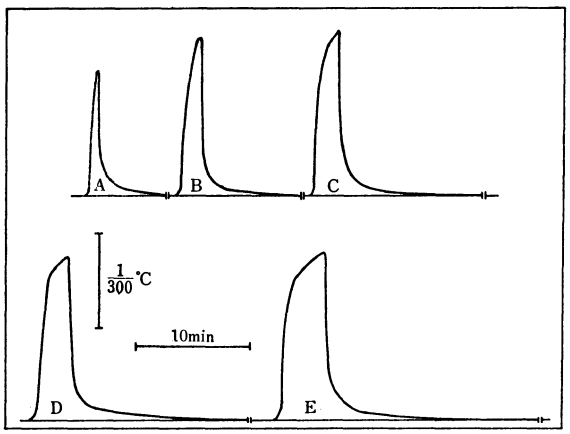

Fig. 2. Calibration peaks at 30 °C.
Peaks, A, B, C, D, and E were obtained by supplying electrical energy of 0.1515, 0.3063, 0.4690, 0.6188, and 0.7653 J respectively.

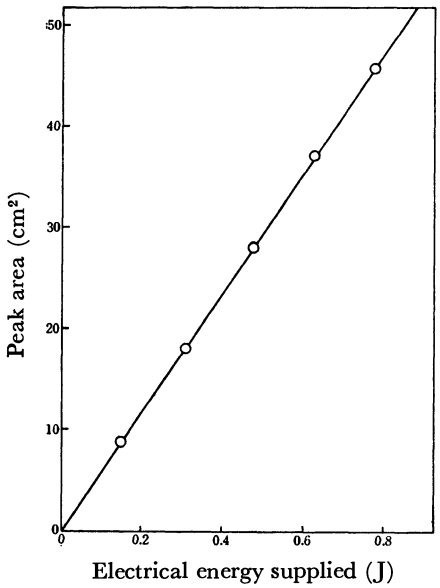

Fig. 3. Relation between peak area and electrical energy supplied.

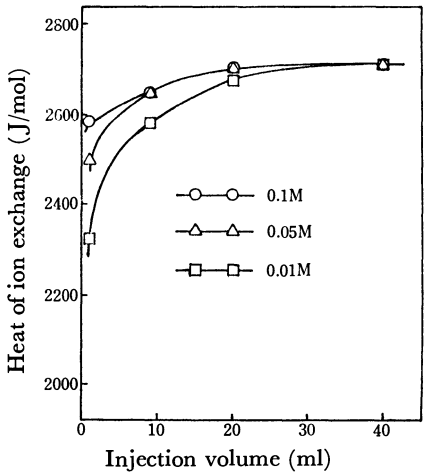

Fig. 4. Dependence of heat of ion exchange (Na^+) upon injection volume.

Figure 4 shows the molar heat of ion exchange (J/mol) as a function of the injected volume of 0.05 M solution to a constant amount (0.1 ml) of the resin. The heat evolution due to ion exchange reaction increases with increasing amount of solution injected and reaches a constant value when the volume of injected solution exceeds 10 ml. Such a slight heat evolution at the initial stage of injection may be due to partial exchange of ions at a slightly greater distance from the position of thermistor as compared to the cases where the volume of injected solution exceeds 10 ml. Thus, the measurement on the molar heats of ion exchange reaction was carried out by injecting 40 ml solution.

Figure 5 shows a few peaks obtained when the flowing liquids were exchanged successively by means of the exchange valves in the order: water, electrolyte solution, water. Preliminary tests showed that the higher the concentration of the solution and the greater the atomic weight of the ions injected, the steeper the peaks, whereas the peak area, obtained on a given alkali ion species are the same irrespective of the concentration of the solution. The peaks were obtained by injecting 40 ml of 0.05 M solution of Li^+, Na^+, and K^+ ions, and 60 ml of 0.035 M solution of Rb^+ and Cs^+ ions, respectively. The results show that the exchange reaction of alkali metal ions with H^+ ions in the H-form resin is exothermic except for the case of Li^+ ions. A small endothermic peak appeared after the flowing liquid was changed from an electrolyte solution to water except for the case of Li^+ ions.

Concerning these phenomena, the following experiment was carried out. The H-form resin set in the detection column of the calorimeter was converted to the Na-form by flowing a sufficient amount of NaCl solution, washed with water completely, and subjected to the injection of 40 ml of 0.05 M NaCl solution. When washing with water and injection of NaCl solution were repeated, the same recording was obtained as shown in each underlying curve in Fig. 5. The results show that a pair of small peaks appear, exothermic at the initial

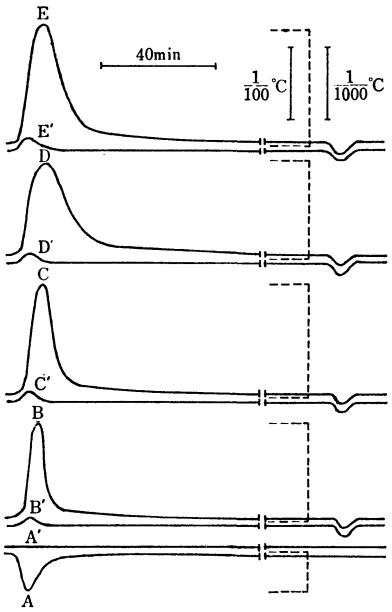

Fig. 5. Heat of ion exchange reaction of alkali metal ions with H^+ ions in resin. A, Li^+; B, Na^+; C, K^+; D, Rb^+; E, Cs^+. Curves A′, B′, C′, D′, and E′ (sensitivity 1/1000 °C) show the heat generation when a solution was injected to the resin containing the same cation species. Peaks directed upward mean "exothermic" and directed downward "endothermic".

stage just after the injection of a solution, and endothermic at the initial stage of washing, except for the case of Li^+-loading, where a nearly straight line appears. The areas of both peaks appearing in a curve are almost the same, being also lose to the area of endothemic peaks appearing at the latter part of the corresponding main run. The heat evolution which took place was too small to be detected. However, it appeared when the concentration was high, the sign being the same as that of heat of ion exchange reaction. The same phenomenon was also found when a solution of H^+ ions was injected into the H-form resin, the sign of heat generation being the same as that in the case of Li^+ ions. It is not easy to find the cause of the occurrence of such small peaks. The ion exchange reaction might be accompanied by a weak interaction of ions in solution with the field of exchanging sites such as invasion or adsorption which may involve hydration and dehydration of ions concerned. We could infer that the small endothermic peaks appearing in the process of washing with water are due to physical interaction such as desorption of ions from the network of resin. The main peak of exchange reaction might be determined by exchange reaction and physical interaction. In order to obtain the energy of pure exchange reaction, we should subtract the contribution of the weak interaction from the total heat effects.

In the present system, the boundaries between water and electrolyte solution would be formed every time the exchange valves are operated, moving in the detection column through the position of the temperature sensing element. Since the diffusion of ions or dilution of the solution would gradually take place near the boundaries during the course of liquid flow, a small amount of heat generation can be expected when a moving boundary layer passes through the position of the thermistor. In order to test the heat generation by dilution, the layer of resin was replaced by glass beads which are considered not to act upon neutral alkali chloride solution. The exchange operation of the valves was carried out as before. No visible peaks appeared when the concentration of the solution was 0.05 M.

Table 1. Ion exchange heat of alkali metal ions with Dowex 50WX4, H-form cation exchange resin

Metal ion	Quantity exchanged (meq)	Heat evolved (J)	Ion exchange heat (J/mol)
Li^+	0.1558	−0.196	−1260 (−920.5)
Na^+	0.1549	0.432	2790 (3598.2)
K^+	0.1589	0.730	4590 (5313.7)
Rb^+	0.1546	0.815	5270 (—)
Cs^+	0.1524	0.876	5750 (6192.3)

Ion exchange heats in parenthesis were calculated from those by Boyd *et al.*,[6] which were obtained by exchanging any alkali metal ions for Na^+ ions in Na-form Dowex 50 WX4.

The molar heat of ion exchange of alkali metal ions with H^+ ions in the H-form resin was obtained by calibrating the heat of invasion. The results are listed in Table 1 together with those reported by Boyd *et al.*[6] The molar heats agree with those obtained by the other method. The ion exchange heat depends strongly upon the extent of ion loading particularly in highly cross-linked resin. In the latter case, the heat of ion exchange is high at the initial loading of ions, decreases gradually with increasing loading of ions and sharply near 60—80 % loading. On the other hand, the exchanger, Dowex 50 W×4, is of relatively low extent of cross-linking, representing only a small dependence of the exchange heat upon ion loading. This makes us convince the coincidence of two kinds of data on ion exchange heat, *i.e.* of differential heats reported by Boyd *et al.* and intergral heats.

References

1) R. L. Gustafson and J. A. Lirio, *J. Phys. Chem.*, **72**, 1502 (1968).
2) K. E. Becker, S. Lindenbaum, and G. E. Boyd, *J. Phys. Chem.*, **70**, 3834 (1966).
3) G. E. Boyd and A. Schwarz, *J. Phys. Chem.*, **71**, 1355 (1967).
4) E. H. Cruickshank and P. Meares, *Trans. Faraday Soc.*, **53**, 1289 (1957).
5) G. E. Myers and G. E. Boyd, *J. Phys. Chem.*, **60**, 521 (1956).
6) G. E. Boyd, F. Vaslow, and S. Lindenbaum, *J. Phys. Chem.*, **68**, 590 (1964).
7) T. Morimoto and H. Naono, *Bull. Chem. Soc. Jpn.*, **45**, 700 (1972).

Electronic Configuration Analysis of Molecular Deformations

Takashi OKADA, Shigeru NAGASE, Kizashi YAMAGUCHI, and Takayuki FUENO
Department of Chemistry, Faculty of Engineering Science, Osaka University, Toyonaka, Osaka 560
(Received January 20, 1976)

A procedure is described which enables to trace the variations of electronic configuration of molecular systems undergoing structural deformation. The mapping operator proposed by Trindle is used to derive a reference set of molecular orbitals which is suitable to the analysis of the wave functions for deformed molecules. The method has been applied to the twisting of ethylene as well as the electrocyclic reactions of butadiene. The results corroborate Bader's symmetry requirement for the electronic excitations accompanying nuclear displacements.

The method of configuration analysis[1] has made it possible to disclose the electronic-structural features of a transient molecular system in comparison with a pertinent reference system. In this method, any configuration Ψ_σ^P of a given system P is expressed as a linear combination of configurations Ψ_λ^Q which are constructed of the molecular orbitals (MO) for the reference system Q:

$$\Psi_\sigma^P = \sum_\lambda l_{\sigma\lambda}\Psi_\lambda^Q \quad (1)$$

The coefficients $l_{\sigma\lambda}$ are evaluated through calculations of appropriate minor determinants of the matrix $\boldsymbol{B}$ such that

$$\boldsymbol{\phi}^P = \boldsymbol{\phi}^Q\boldsymbol{B} \quad (2)$$

where the row vactor $\boldsymbol{\phi}$ represents a set of orthonormal MO's for each system. The matrix $\boldsymbol{B}$ can be expressed as

$$\boldsymbol{B} = (\boldsymbol{C}^Q)^\dagger\boldsymbol{C}^P \quad (3)$$

where $\boldsymbol{C}^P$ and $\boldsymbol{C}^Q$ denote the relevant LCAO matrices for $\boldsymbol{\phi}^P$ and $\boldsymbol{\phi}^Q$, respectively.

The foregoing procedure may be applied to the interpretations of nuclear displacement processes such as molecular vibrations and chemical reactions. However, the method as it stands is based on the assumption that the AO basis set $\boldsymbol{\chi}$ has the same implication for both systems P and Q. Consider two equivalent wave functions expressed in different coordinate systems. These functions can be identified with each other by means of configuration analysis, only if the two coordinate systems are superposed by translation alone. That is to say, the invariance for the rotation of coordinate systems does not hold in this method of configuration analysis. Therefore, there appears a difficulty in its applications to the processes accompanied by molecular deformations. In such cases, different meanings must be given to the AO basis sets $\boldsymbol{\chi}^P$ and $\boldsymbol{\chi}^Q$, on which the MO's ϕ_i^P and ϕ_i^Q are to be based, respectively.

To cope with the situation delineated above, it is advantageous to introduce the mapping procedure which has been proposed by Trindle.[2-4] By making use of the mapping operator which projects the MO's ϕ_i^Q defined in the $\boldsymbol{\chi}^Q$ space onto the $\boldsymbol{\chi}^P$ space, we obtain a set of mapped orbitals ϕ_i^R:

$$\boldsymbol{\phi}^R = \boldsymbol{\phi}^Q\boldsymbol{R} \quad (4)$$

where $\boldsymbol{R}$ is the mapping operator in the matrix representation. Use of the mapped orbitals as reference orbitals renders the configuration analysis meaningful.[5] Thus, the configurations mixed in this way correspond only to the charge reorganization during the nuclear displacement. The weight of the ground configuration so calculated for the ground electronic state is equivalent to the state overlap which Trindle defined in his mapping analysis as a criterion of the orbital-symmetry allowedness of thermal reactions.[2]

It should be noted that an analogous multi-configurational representation has been proposed by Trindle and Collins in their energy-based mapping analysis.[4] Practically, however, their method could hardly be applied to problems involving a large number of configurations. There one would inevitably encounter with too numerous degrees of freedom to determine simultaneously the mapping operator and the configurational mixing coefficients with confidence.

Applications and Discussion

To illustrate the use of the present method we here apply it to two processes, the twisting of ethylene and the ring-closure of butadiene to cyclobutene. The molecular geometries were all taken from the literature.[6] Use was made of the CNDO/2 wave functions[7] in a single-determinant approximation. The mapping operators were obtained by the original overlap-based formalism.[2]

(A) Twisting of Ethylene. We have examined the wave function of a twisted ethylene molecule, for which the dihedral angle between the two CH_2 planes is assumed to be 45°. The SCF MO's calculated for the planar ethylene were projected onto the AO basis set of the twisted ethylene. The mapped orbitals $\boldsymbol{\phi}^R$ thus obtained are used as the reference orbitals in the configuration analysis. Given in Table 1 are the absolute values of the configurational coefficients which are larger than 0.01. Each excited singlet configuration is designated by the pair of occupied and unoccupied MO's which are specified according to the irreducible representations of the D_{2h} point group. The symmetries of configurations are indicated in the second column.

As Table 1 shows, the coefficients for the excited configurations are relatively small, indicating that the

Table 1. Absolute values of the configurational coefficients for the twisting of ethylene[a]

Configuration	Symmetry	Coefficient
Ground	A_g	0.998
$1b_{1u} \rightarrow 2b_{1g}^*$	A_u	0.039
$1b_{2u} \rightarrow 1b_{2g}^*$	A_u	0.039
$1b_{1g} \rightarrow 2b_{1g}^*$	A_g	0.010

a) At the twisting angle of 45°.

charge distribution in ethylene suffers relaxation only slightly if the nuclear motion takes place. The effect of charge redistribution on the height of rotational barrier is, therefore, expected to be small.

More important in Table 1 is the trend that, aside from the totally symmetric excited configuration, the ground configuration mixes only with those configurations of the A_u symmetry. The twisting motion of ethylene also possesses the A_u symmetry. Thus, the excited configurations to be mixed, if slightly, with the ground configuration upon nuclear displacement have the same symmetry as the normal coordinate which is responsible for the displacement. The results are in agreement with the generalization first put forth by Bader.[8]

(B) Ring-closure of Butadiene. Two stereochemical courses, conrotatory and disrotatory, are investigated. Since butadiene (*s-cis*) possesses the C_{2v} symmetry, the corresponding representations will be used throughout this section. Thus, the conrotatory and disrotatory reaction modes may be characterized by the A_2 and B_2 representations, respectively. Two intermediate structures I and II as well as the product structure F have been examined for each reaction. The distance between the terminal carbon atoms was assumed to change linearly with the CH_2 rotation angles θ in the course of reaction. The structures I and II correspond to $\theta=50$ and 80°, respectively.

The results of calculations are shown in Tables 2 and 3, where the absolute values of the coefficients for dominantly contributing configurations only are listed. It can be seen here also that Bader's rule is fulfilled. That is, except for the A_1 configurations, only the excited configurations having the A_2 and B_2 symmetries are mixed with the ground configuration in the conrotatory(A_2) and disrotatory(B_2) reactions, respectively.

Comparison of Table 2 with Table 3 shows that the two stereochemical courses have quite contrasting features. Thus, in the conrotatory reaction (Table 2) the configurational coefficients change continuously throughout, whereas in the disrotatory reaction mode (Table 3) there is no composite configuration at all

TABLE 2. ABSOLUTE VALUES OF THE CONFIGURATIONAL COEFFICIENTS FOR THE CONROTATORY RING-CLOSURE OF BUTADIENE

Configuration	Symmetry	Coefficient[a]		
		I	II	F
Gound	A_1	0.904	0.441	0.374
$1b_2\rightarrow 2b_2^*$	A_1	0.205	0.396	0.380
$1a_2\rightarrow 2a_2^*$	A_1	0.155	0.352	0.364
$1b_2\rightarrow 6b_1^*$	A_2	0.127	0.122	0.094
$3b_1\rightarrow 2b_2^*$	A_2	0.127	0.133	0.093
$1a_2\rightarrow 6a_1^*$	A_2	0.087	0.114	0.092
$(1b_2, 1a_2)\rightarrow(2b_2^*, 2a_2^*)$	A_1	0.035	0.317	0.370
$(1b_2, 1b_2)\rightarrow(2b_2^*, 2b_2^*)$	A_1	0.023	0.178	0.193
$(1a_2, 1a_2)\rightarrow(2a_2^*, 2a_2^*)$	A_1	0.013	0.141	0.177
$(1b_2, 1a_2)\rightarrow(2b_2^*, 6a_1^*)$	A_2	0.020	0.102	0.093
$(1b_2, 1a_2)\rightarrow(2a_2^*, 6b_1^*)$	A_2	0.022	0.097	0.091
$(3b_1, 1a_2)\rightarrow(2b_2^*, 2a_2^*)$	A_2	0.022	0.106	0.090

a) I, intermediate I for which $\theta=50°$; II, intermediate II for which $\theta=80°$; F, product (cyclobutene).

TABLE 3. ABSOLUTE VALUES OF THE CONFIGURATIONAL COEFFICIENTS FOR THE DISROTATORY RING-CLOSURE OF BUTADIENE

Configuration	Symmetry	Coefficient[a]		
		I	II	P
Ground	A_1	0.975	—	—
$5a_1\rightarrow 2b_2^*$	B_2	0.099	—	—
$3a_1\rightarrow 2b_2^*$	B_2	0.092	—	—
$3b_1\rightarrow 6b_1^*$	A_1	0.067	—	—
$2a_1\rightarrow 2b_2^*$	B_2	0.065	—	—
$1a_2\rightarrow 9b_1^*$	B_2	0.053	—	—
$(1a_2, 1a_2)\rightarrow(2b_2^*, 2b_2^*)$	A_1	—	0.796	0.838
$(1a_2, 1a_2)\rightarrow(2b_2^*, 9a_1^*)$	B_2	—	0.015	0.265
$(1a_2, 1a_2)\rightarrow(2b_2^*, 6a_1^*)$	B_2	—	0.300	0.238
$(4b_1, 1a_2)\rightarrow(2b_2^*, 2b_2^*)$	B_2	—	0.102	0.131
$(3b_1, 1a_2)\rightarrow(2b_2^*, 2b_2^*)$	B_2	—	0.325	0.126
$(1a_2, 1a_2)\rightarrow(2b_2^*, 8a_1^*)$	B_2	—	0.099	0.090

a) I, intermediate I for which $\theta=50°$; II, intermediate II for which $\theta=80°$; P, product (cyclobutene).

that is common to structures I and II. In the former reaction, therefore, the nuclear motion is accompanied by a smooth development in relaxation in charge distribution, thus rendering the molecular deformation energetically favorable. The discontinuity of the configurational mixing in the latter reaction is obviously due to the interchange between the highest occupied and lowest unoccupied MO's in the course of reaction, a characteristic which inheres in orbital-symmetry forbidden reactions.

As can be seen from Tables 2 and 3, the mixing of the excited A_1 configurations is especially small in the disrotatory reaction. In this reaction, therefore, the electronic relaxation due to the approach of the terminal CH_2 groups, which should be characterized as a motion with the A_1 symmetry, must be by far less efficient than in the conrotatory reaction. This may be taken as an indication that the steric course of ring closure is governed by the ease of the approaching motion of the two CH_2 groups rather than the ease of thier rotational motions. The interpretation is compatible with the potential energy surfaces calculated by van der Lugt and Oosterhoff[10] for the two steric courses of reaction.

References

1) H. Baba, S. Suzuki, and T. Takemura, *J. Chem. Phys.*, **50**, 2078 (1969).
2) C. Trindle, *J. Am. Chem. Soc.*, **92**, 3251 (1970).
3) C. Trindle, *Theor. Chim. Acta*, **18**, 261 (1970).
4) C. Trindle and F. S. Collins, *Int. J. Quantum Chem.*, **5**, 195 (1971).
5) S. Nagase, K. Takatsuka, and T. Fueno, *J. Am. Chem. Soc.*, **98**, 3838 (1976).
6) A. D. Mitchell, Ed., "Table of Interatomic Distances and Configuration in Molecules and Ions," The Chemical Society, London (1958).
7) J. A. Pople and D. L. Beveridge, "Approximate Molecular Orbital Theory," McGraw-Hill (1970).
8) R. F. W. Bader, *Mol. Phys.*, **3**, 137 (1960).
9) R. B. Woodward and R. Hoffmann, "The Conservation of Orbital Symmetry," Academic Press, New York (1970).
10) W. Th. A. M. van der Lugt and L. J. Oosterhoff, *J. Am. Chem. Soc.*, **91**, 6042 (1969).

The Thermodynamics of Nonstoichiometric $Pr_{1-y}Gd_yO_{1.5+\delta}$

Kazuhiro ENDO,** Shigeru YAMAUCHI, Kazuo FUEKI,* and Takashi MUKAIBO

Department of Industrial Chemistry, Faculty of Engineering, The University of Tokyo, Hongo, Bunkyo-ku, Tokyo 113

**Department of Synthetic Chemistry, Faculty of Engineering, The University of Tokyo, Hongo, Bunkyo-ku, Tokyo 113*

(Received February 2, 1976)

In order to contribute to the study of the thermodynamics of point defects in ionic crystals, the nonstoichiometry, δ, of $Pr_{1-y}Gd_yO_{1.5+\delta}$ ($y=0$, 0.1, 0.2, and 0.4) with a wide nonstoichiometric composition range was measured as a function of the oxygen partial pressure. Assuming that excess oxygen ions preferentially occupy Z-sites of the bixbyite structure and that the Pr^{3+} and Pr^{4+} ions are distributed on cationic sites at random, the equilibrium constant, K, was calculated for

$$2Pr^{4+} + O_z^{2-} = 2Pr^{3+} + V_z + \frac{1}{2}O_2$$

It was found that $\ln K$ changes with δ in the relation;

$$\ln K = A + B\delta + C\delta^2$$

The parabolic dependence of $\ln K$ on δ is interpreted in terms of the changes in the energy of the defect formation and in the interaction energy between defects with the volume.

As transport phenomena in solids are closely related to point defects, the elucidation of a transport mechanism necessitates detailed studies of its defects. Since the pioneering works by Wagner and Schottky,[1] many studies have been made of point defects and nonstoichiomitry in ionic crystals. In early thermodynamic treatments the ideal solution approximation was employed to deal with point defects.[2] Although the approximation was experimentally proved to be applicable to many cases, some difficulties arose in the interpretation of the thermodynamic and transport properties of ionic crystals, which have wide nonstoichiometric composition ranges.[3] Several models, *e.g.*, the blocking model,[4-7] the microdomain model,[8,9] and the cluster model,[10-14] have been proposed for picturing the structure of point defects in such nonstoichiometric crystals. However, scarcely no experimental verification of these models has been undertaken.

In order to elucidate the relation between the defect structure and the thermodynamic or transport properties of nonstoichiometric oxides, the present authors have carried out a series of studies of the $Pr_{1-y}Gd_yO_{1.5+\delta}$ system.

There are several phases between $PrO_{1.5}$ and $PrO_{2.0}$.[15,16] At high temperatures, $PrO_{1.5}$ takes the hexagonal structure (A-type) called the θ-phase, whereas it takes the cubic structure (C-type) at low temperatures. The fluorite structure oxide, $PrO_{2+\delta}$, is called the α-phase. Between the fluorite structure oxide and the C-type one, there are several phases, such as the ι and β phases. Above 900 °C, a relatively wide nonstoichiometric phase called the σ-phase appears. The structure of the σ-phase is substantially the bixbyite one, which is regarded as a distorted fluorite structure regularly lacking one fourth of its anions. Anionic vacant sites are characteristic of the bixbyite structure and were named "Z-sites" by Anderson.[17] Hyde *et al.*[15] have pointed out that excess anions in the bixbyite structure oxide may occupy the Z-sites. The preferential occupancy of the Z-sites by excess oxygen ions in a bixbyite structure was experimentally verified from the relationship between the lattice parameter of Y_2O_3 doped with ZrO_2 and its density.[18] It was also previously shown by the present authors[19] that the X-ray peak intensity due to the superstructure of $Pr_{1-y}Gd_yO_{1.5+\delta}$ decreases with the increase in δ.

The present work aims to contribute to the thermodynamics of nonstoichiometric solids containing high-concentration-point defects, using σ-phase solid solutions of $Pr_{1-y}Gd_yO_{1.5+\delta}$ as samples.

Experimental

Praseodymium oxide and gadolinium oxide of a 99.99% purity, supplied by the Shin-etsu Chemical Company, were used as the starting materials. These oxides were dissolved in G. R. grade nitric acid, and the two solutions were mixed in the desired proportions. The mixed solution was then added to a solution of G. R. grade oxalic acid to obtain the coprecipitate of praseodymium gadolinium oxalate, which was then converted into an oxide solid solution, $Pr_{1-y}Gd_yO_{1.5+\delta}$, by calcination, followed by heating at 1550 °C for homogenization.

About 1.5 g of the oxide sample was weighed in a quartz basket, suspended from a Cahn RG Electrobalance with a quartz fibre and placed in a reaction tube heated by an electric furnance. The oxygen partial pressure in the tube was controlled by gas mixtures of argon and oxygen. The circulation of the gas mixtures was carried out by means of an electromagnetic piston pump. The nonstoichiometry was determined gravimetrically, assuming that the $Pr_{1-y}Gd_yO_{1.5+\delta}$ solid solutions were stoichiometric in a pure CO atmosphere.

Results and Discussion

Figures 1 to 4 give the nonstoichiometry δ of σ-phase oxide, $Pr_{1-y}Gd_yO_{1.5+\delta}$, as a function of the oxygen partial pressure and the temperature. As may be seen in these figures, the stability region of the σ-phase extends upon the formation of solid solutions between praseodymium oxide and gadolinium oxide. If point defects in the nonstoichiometric σ-phase oxide tend to form a local or long-range ordering, the stability region of the σ-phase will be narrowed by the addition of gadolinium oxide to praseodymium oxide, because the ordering is

** Present address, Electrotechnical Laboratory, Tanashi, Tokyo 188

prevented by the formation of a solid solution. The results of the present work, therefore, suggest that point defects in the σ-phase oxide are distributed at random. The dependence of the electronic conductivity on δ was well interpreted in terms of the random distribution of Pr^{3+} and Pr^{4+} in the $Pr_{1-y}Gd_yO_{1.5+\delta}$ solid solution.[20]

Accordingly, the equilibrium between σ-phase oxide and oxygen can be expressed by;

$$2Pr^{4+} + O_z^{2-} = 2Pr^{3+} + V_z + \frac{1}{2}O_2 \qquad (1)$$

where O_z^{2-} denotes oxygen ions occupying the Z-site

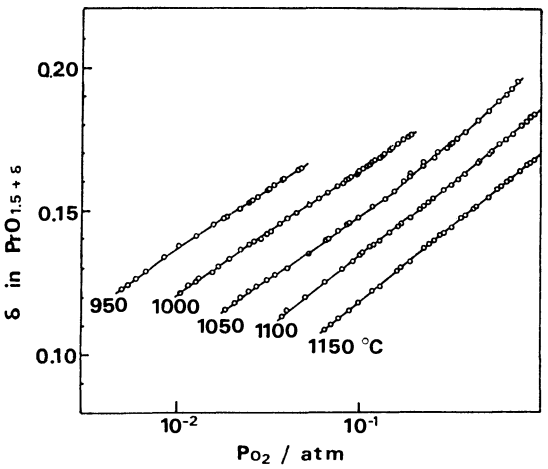

Fig. 1. The dependence of δ on P_{O_2} for $PrO_{1.5+\delta}$.

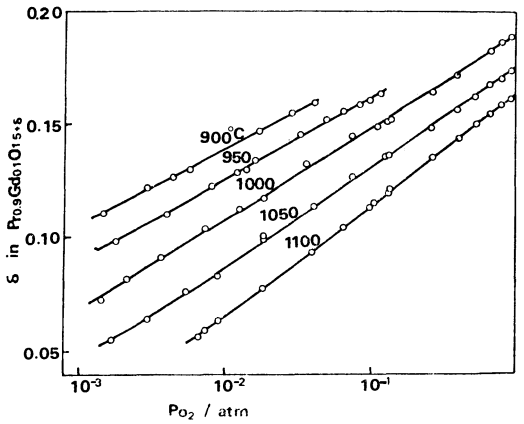

Fig. 2. The dependence of δ on P_{O_2} for $Pr_{0.9}Gd_{0.1}O_{1.5+\delta}$.

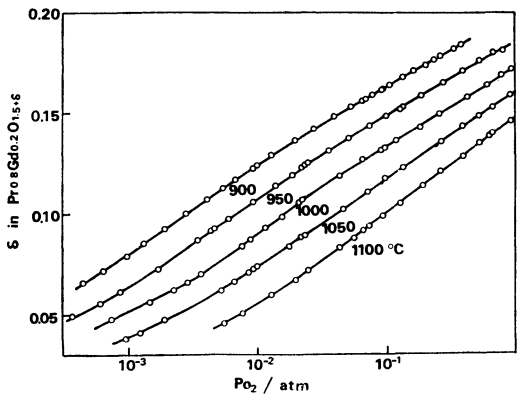

Fig. 3. The dependence of δ on P_{O_2} for $Pr_{0.8}Gd_{0.2}O_{1.5+\delta}$.

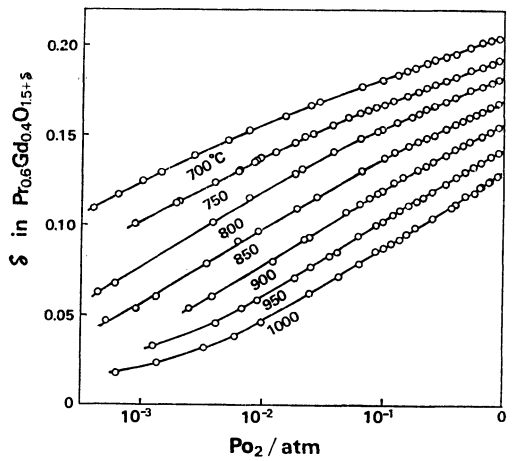

Fig. 4. The dependence of δ on P_{O_2} for $Pr_{0.6}Gd_{0.4}O_{1.5+\delta}$.

and where V_z represents the vacant Z-site. The mass action law for (1) is;

$$K = \frac{[Pr^{3+}]^2[V_z]P_{O_2}^{1/2}}{[Pr^{4+}]^2[O_z^{2-}]} = \frac{(0.5-\delta)(1-y-2\delta)^2P_{O_2}^{1/2}}{4\delta^3}. \qquad (2)$$

If the interaction between defects is extremely weak, the value of K should be constant, as is shown by Eq. 2. It may be seen, however, that $\ln K$ is not constant, but parabolically changes with the increase in δ.

In order to examine whether or not the relation between $\ln K$ and δ is well expressed by;

$$\ln K = A + B\delta + C\delta^2 \qquad (3)$$

the values of A, B, and C were determined by the least-squares method. The solid lines in Fig. 5 represent the least-squares curves, which are in good coincidence with the open circles.

The dependence of $\ln K$ on δ indicates that the energy required for the formation of point defects is a function of the concentration of oxygen ions occupying Z-sites.

The dependence of $\ln K$ on δ might be interpreted by other models, *e.g.*, a model wherein $V_O^{\cdot}$, $V_O^{\cdot\cdot}$, V_{Pr}'', and V_{Pr}''' vacancies are taken into consideration; the blocking model, wherein defects of the same kind do not occupy two neighboring sites, or the Bragg-Williams approximation, wherein the bixbyite structure is regarded as an ordered phase consisting of an O_I sublattice and an O_z sublattice. However, the results of calculation did not agree with the observed ones.

A similar dependence of $\ln K$ on δ, given in Fig. 5 and Eq. 3, has been reported for a few hydride systems.[21,22] As to the other oxide systems, preliminary experiments by the present authors have shown that the $TbO_{1.5+\delta}$ of the bixbyite structure and the $CeO_{2-\delta}$ of the fluorite structure have wide nonstoichiometric composition ranges and that $\ln K$ changes parabolically with δ.

Harashima *et al*[21] have interpreted the dependence of the composition of hydrides on the hydrogen pressure, assuming that the energy of the formation of defects and the interaction energy between defects depends on the molar volume of the crystal. Below, Harashima's treatment will be extended to the present system in

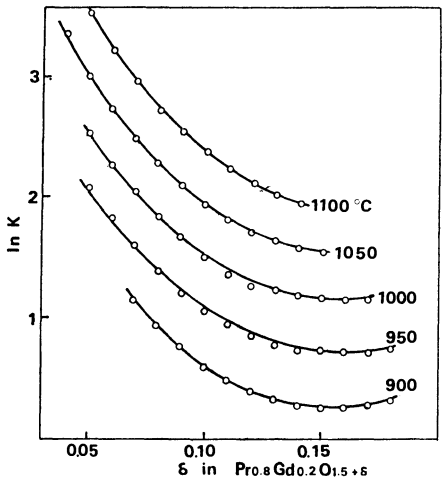

Fig. 5. The dependence of ln K on δ for $Pr_{0.8}Gd_{0.2}O_{1.5+\delta}$.

order to interpret the relation between ln$K$ and δ.

Let us denote the number of cationic sites in $Pr_{1-y}Gd_yO_{1.5+\delta}$ of the bixbyite structure by $2N$, the number of total praseodymium ions by $2N(1-y)$, and the number of Z-sites by N. Assuming the random distribution of O_z^{2-} ions on Z-sites and that of Pr^{3+} and Pr^{4+} ions on cationic sites, we obtain the following expression for the Gibbs free energy of a crystal;

$$G(N_z) = G_0(T) + H(N_z) - kT\ln\left\{\frac{N!}{N_z!(N-N_z)!}\times\frac{[2N(1-y)]!}{(2N_z)![2N(1-y)-2N_z]!}\right\} \quad (4)$$

where N_z is the number of O_z^{2-} ions, $G_0(T)$ is the Gibbs free energy at a constant T for the stoichiometric oxide ($\delta=0$, $N_z=0$), and $H(N_z)$ is the difference in enthalpy between the nonstoichiometric oxide (δ, N_z) and the stoichiometric oxide.

N_z is independent of the content of Gd^{3+} ions, y; therefore, the contribution of Gd^{3+} ions to the Gibbs free energy is included in $G_0(T)$. By differentiating Eq. 4 with N_z and replacing $N_z/2N$ by δ, one obtains;

$$\ln[\lambda_{O_2}]^{1/2} = \ln\left[\frac{4\delta^3}{(0.5-\delta)(1-y-2\delta)^2}\right] + \frac{\partial H(\delta)/\partial\delta}{2NkT} \quad (5)$$

where λ_{O_2} is the absolute activity of the oxygen molecule. The relation between the absolute activity and the oxygen partial pressure is;

$$\ln[\lambda_{O_2}] = \ln P_{O_2} - \frac{\chi_{O_2}}{kT} + \frac{\Psi}{N_0kT} \quad (6)$$

where χ_{O_2} is the dissociation energy of the molecular oxygen, Ψ is the free energy function $(G_T^\circ - H_0^\circ)/T$, and N_0 is Avogadro's number. From Eqs. 2, 5, and 6, we obtain:

$$\ln K = \frac{1}{kT}\left[\frac{1}{2N}\cdot\frac{\partial H(\delta)}{\partial\delta} + \frac{\chi_{O_2}}{2}\right] - \frac{\Psi}{2N_0k} \quad (7)$$

In Eq. 7, χ_{O_2} is constant and Ψ is independent of δ. If ε is the energy required for introducing an atomic oxygen into the bixbyite lattice to form an O_z^{2-} ion and two Pr^{4+} ions converted from Pr^{3+} ions, ω is the interaction energy between two adjacent O_z^{2-} ions, and z is the number of neighboring sites of an O_z^{2-} ion, the enthalpy changes, $H(N_z)$ and $H(\delta)$, are expressed by;

$$H(N_z) = -N_z\varepsilon - \frac{z}{2}N_z\left(\frac{N_z}{2N}\right)\omega \quad (8)$$

$$H(\delta) = -2N(\varepsilon\delta + z\omega\delta^2) \quad (9)$$

When ε and ω are constant, these equations give the enthalpy changes for the regular solution.

According to Harashima, ε and ω change with the volume of the crystal, V;

$$\varepsilon = \varepsilon_0 + \left(\frac{\partial\varepsilon}{\partial V}\right)(V-V_0) \quad (10)$$

$$\omega = \omega_0 + \left(\frac{\partial\omega}{\partial V}\right)(V-V_0) \quad (11)$$

where ε_0, ω_0, and V_0 represent ε, ω, and V respectively at $\delta=0$. The insertion of Eqs. 10 and 11 into Eq. 9 yields;

$$H(\delta) = -2N\left\{\delta\left[\varepsilon_0 + \left(\frac{\partial\varepsilon}{\partial V}\right)(V-V_0)\right] + z\delta^2\left[\omega_0 + \left(\frac{\partial\omega}{\partial V}\right)(V-V_0)\right]\right\} \quad (12)$$

Since the volume of a crystal can be determined by the condition $(\partial G/\partial V)_T=0$, it follows from Eqs. 4 and 9 that;

$$\left(\frac{\partial G}{\partial V}\right)_{T,\delta} = \left(\frac{\partial G_0}{\partial V}\right)_T - 2N\delta\left(\frac{\partial\varepsilon}{\partial V}\right)_{T,\delta} - 2Nz\delta^2\left(\frac{\partial\omega}{\partial V}\right)_{T,\delta} = 0 \quad (13)$$

Taylor's expansion of $(\partial G_0/\partial V)_T$ at V_0 gives;

$$\left(\frac{\partial G_0}{\partial V}\right)_{T,\delta} \fallingdotseq \left(\frac{\partial G_0}{\partial V}\right)_{T,V_0} + \left(\frac{\partial^2 G_0}{\partial V^2}\right)_{T,V_0}(V-V_0) \fallingdotseq -\left(\frac{\partial P}{\partial V}\right)_{V_0}(V-V_0)$$

Therefore,

$$\left(\frac{\partial G_0}{\partial V}\right)_T = \frac{V-V_0}{\kappa V_0} \quad (14)$$

where κ is the compressibility. From Eqs. 13 and 14, we obtain:

$$V - V_0 = 2N\kappa V_0\left[\delta\left(\frac{\partial\varepsilon}{\partial V}\right) + z\delta^2\left(\frac{\partial\omega}{\partial V}\right)\right] \quad (15)$$

By inserting Eq. 15 into Eq. 12 and omitting the term of δ^4, one obtains;

$$H(\delta) = -2N\left\{\varepsilon_0\delta + \left[z\omega_0 + 2N\kappa V_0\left(\frac{\partial\varepsilon}{\partial V}\right)^2\right]\delta^2 + 4N\kappa V_0 z\left(\frac{\partial\varepsilon}{\partial V}\right)\left(\frac{\partial\omega}{\partial V}\right)\delta^3\right\}$$

By putting v as the molecular volume and replacing V by $2Nv$, one obtains;

$$H(\delta) = -2N\left\{\varepsilon_0\delta + \left[z\omega_0 + \kappa v_0\left(\frac{\partial\varepsilon}{\partial v}\right)^2\right]\delta^2 + 2\kappa z v_0\left(\frac{\partial\varepsilon}{\partial v}\right)\left(\frac{\partial\omega}{\partial v}\right)\delta^3\right\} \quad (16)$$

where v_0 is the value of v at $\delta=0$. From Eqs. 7 and 16, one obtains;

$$\ln K = -\frac{1}{kT}\left\{\varepsilon_0 + 2\left[z\omega_0 + \kappa v_0\left(\frac{\partial\varepsilon}{\partial v}\right)^2\right]\delta + 6z\kappa v_0\left(\frac{\partial\varepsilon}{\partial v}\right)\left(\frac{\partial\omega}{\partial v}\right)\delta^2 - \frac{\chi_{O_2}}{2}\right\} - \frac{\Psi}{2N_0k} \quad (17)$$

By a comparison of Eq. 17 with Eq. 3, one obtains;

$$A = -\frac{1}{kT}\left(\varepsilon_0 - \frac{\chi_{O_2}}{2}\right) - \frac{\Psi}{2N_0k} \quad (18)$$

$$B = -\frac{2}{kT}\left[z\omega_0 + \kappa v_0\left(\frac{\partial\varepsilon}{\partial v}\right)^2\right] \quad (19)$$

$$C = -\frac{6z\kappa v_0}{kT}\left(\frac{\partial\varepsilon}{\partial v}\right)\left(\frac{\partial\omega}{\partial v}\right) \quad (20)$$

As may be seen in Eqs. 18, 19, and 20, A, B, and C depend on the temperature. Therefore, the values of ε_0, RTB and RTC were calculated for various temperatures and averaged, instead of the values of A, B, and C. Those values are expected to be less dependent on the temperature. The results are summarized in Table 1.

Table 1. Estimated energy parameter for $Pr_{1-y}Gd_yO_{1.5+\delta}$[a]

y	ε_0 kcal mol^{-1}	RTB kcal mol^{-1}	RTC kcal mol^{-1}	$\partial\varepsilon/\partial v$ cm^{-3}	$\partial\omega/\partial v$ kcal cm^{-3}	ω_0 kcal mol^{-1}
0.0	87.2 (±0.7)	−45 (±10)	110 (±25)	−0.95	1.2	5.9
0.1	85.9 (±2)	−60 (±25)	180 (±30)	−0.95	1.9	8.4
0.2	83.1 (±0.4)	−92 (± 3)	290 (± 5)	−0.96	3.1	14
0.4	81.4 (±1.4)	−94 (± 9)	310 (±50)	−0.96	3.4	14

a) The values in parentheses are the standard deviations.

The values of χ_{O_2} and Ψ were taken from the JANAF Thermochemical Tables.[23] Since ε_0 is the energy required for introducing one atomic oxygen into a crystal to form one O_z^{2-} ion and two Pr^{4+} ions converted from Pr^{3+} ions, it is expected to be independent of the gadolinium content. As may be seen in Table 1, ε_0 is nearly independent of the temperature and the gadolinium content as expected.

The values of RTB and RTC are much scattered and depend on y and the temperature. These results may be attributed to the temperature dependence of κ, $(\partial\varepsilon/\partial v)$, and $(\partial\omega/\partial v)$. Because of the lack of compressibility data available for the calculation, it is difficult to calculate accurate values of B and C, but a rough estimation is possible.

Provided that the second term of the right hand side of Eq. 15 can be omitted, one obtains;

$$\frac{\partial\varepsilon}{\partial v} \fallingdotseq \frac{V - V_0}{\kappa V_0\delta} \quad (21)$$

From the compressibility data of Sm_2O_3 and Gd_2O_3,[24] the reciprocal of the compressibility of σ-phase $PrO_{1.5+\delta}$, $(1/\kappa)$, is estimated as 2×10^{11} dyn cm^{-2}. The $(V-V_0)/V_0\delta$ ratio can be calculated from the lattice parameter of $Pr_{1-y}Gd_yO_{1.5+\delta}$.

If $Pr_{1-y}Gd_yO_{1.5+\delta}$ is regarded as an solid solution consisting of $(1-y-2\delta)$ mol of $PrO_{1.5}$, 2δ mol of PrO_2, and y mol of $GdO_{1.5}$, Vegard's law holds, as is shown in Fig. 6, and the lattice parameter of $Pr_{1-y}Gd_yO_{1.5+\delta}$ is represented by;

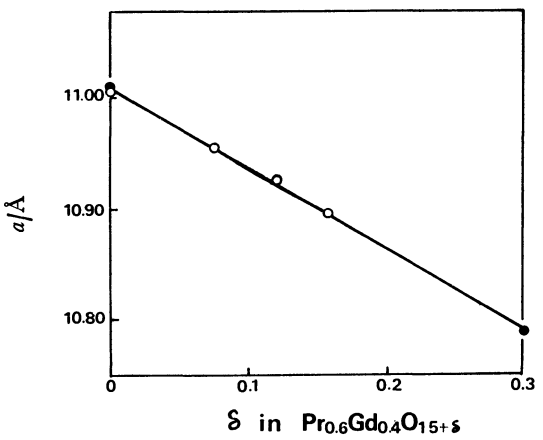

Fig. 6. The relationship between a and δ in $Pr_{0.6}Gd_{0.4}O_{1.5+\delta}$.
○: Observed, ●: calculated.

$$a = (1-y-2\delta)a_{PrO_{1.5}} + 2\delta a_{PrO_2} + y a_{GdO_{1.5}}$$

Therefore,

$$\frac{V - V_0}{V_0\delta} = \frac{a^3 - a_0^3}{\delta a_0^3} \fallingdotseq \frac{(da^3/d\delta)}{a_0^3} = \frac{6(a_{PrO_2} - a_{PrO_{1.5}})}{a_0} \quad (22)$$

The values of $(\partial\varepsilon/\partial v)$ calculated by means of Eqs. 21 and 22, and the values of ω_0 and $(\partial\omega/\partial v)$ calculated with the help of Eqs. 19 and 20 and $(\partial\varepsilon/\partial v)$ are listed in Table 1. Since the lattice parameter of $Pr_{1-y}Gd_yO_{1.5+\delta}$ decreases with an increase in y, ω_0 will be increased as y increases. Because of the lack of accuracy of κ, the values of $(\partial\varepsilon/\partial v)$ and $(\partial\omega/\partial v)$ are less accurate than those of ω_0.

Conclusion

In order to effect a thermodynamic study of bixbyite-type oxides, the nonstoichiometry δ in $Pr_{1-y}Gd_yO_{1.5+\delta}$ was determined as a function of the oxygen partial pressure. It was found that the nonstoichiometric region is extended upon the addition of gadolinium oxide and that, when $y=0.4$, δ can be increased until more than half of the praseodymium ions become tetravalent. The equilibrium between oxygen and nonstoichiometric oxide was calculated based on the random distribution of excess oxygen ions on Z-sites and of Pr^{3+} and Pr^{4+} ions on cationic sites. The parabolic dependence of $\ln K$ on δ was found.

Assuming that the energy of defect formation and the interaction energy between defects change with the molar volume of oxide, the dependence of $\ln K$ on δ was interpreted.

References

1) C. Wagner and W. Schottky, *Z. Phys. Chem.*, **B11**, 163 (1930).
2) F. A. Kröger, "The Chemistry of Imperfect Crystals," North-Holland, Amsterdam (1964).

3) L. Eyring and M. O'Keefe, "The Chemistry of Extended Defects in Non-Metallic Solids," North-Holland, Amsterdam (1970).
4) P. Kofstand and A. Z. Hed, *J. Am. Ceram. Soc.*, **50**, 681 (1967).
5) P. Kofstand and A. Z. Hed, *J. Electrochem. Soc.*, **115**, 102 (1968).
6) M. S. Seltzer and A. Z. Hed, *J. Electrochem. Soc.*, **117**, 303 (1970).
7) P. L. Land, *J. Phys. Chem. Solids*, **34**, 1839 (1973).
8) S. M. Ariya and M. P. Morozova, *J. Gen. Chem. USSR*, **28**, 2647 (1957).
9) J. S. Anderson, *Bull. Soc. Chem. Fr.*, **1969**, 2203.
10) B. T. M. Willis, *Nature*, **197B**, 755 (1963).
11) B. T. M. Willis, "The Chemistry of Extended Defects in Non-Metallic Solids," North-Holland, Amsterdam (1970). p. 272.
12) W. L. Roth, *Acta Crystallogr.*, **13**, 140 (1960).
13) F. Koch and J. B. Cohen, *Acta Crystallogr.*, **B25**, 275 (1969).
14) A. K. Cheetham, B. E. F. Fender, and R. I. Taylov, *J. Phys. Chem.*, **4**, 2160 (1971).
15) B. G. Hyde, D. J. M. Bevan, and L. Eyring, *Phil. Trans. R. Soc., (London)*, **259A**, 583 (1966).
16) L. Eyring, "High Temperature Oxides II," ed. by L. Eyring, Academic Press, New York (1970), p. 41.
17) J. S. Anderson, "Modern Aspects of Solid State Chemistry," ed. by C. N. R. Rao, Plenum Press, New York - London (1970), p. 78.
18) R. J. Bratton, *J. Am. Ceram. Soc.*, **52**, 213 (1969).
19) K. Endo, S. Yamauchi, K. Fueki, and T. Mukaibo, *Bull. Chem. Soc. Jpn.*, **49**, 1191 (1976).
20) K. Endo, S. Yamauchi, K. Fueki and T. Mukaibo, *J. Solid State Chem.*, to be published.
21) A. Harashima, T. Tanaka, and K. Sakaoku, *J. Phys. Soc. Jpn.*, **3**, 208 (1948).
22) D. P. Schumacher, *J. Chem. Phys.*, **40**, 153 (1964).
23) JANAF Thermochemical Tables, NSRDS-NBS 37, Office of Standard Reference Data, National Bureau of Standards, Washington, D. C. (1971).
24) C. E. Curtis and J. R. Johnson, *J. Am. Ceram. Soc.*, **40**, 15 (1957).

Photochemistry of Cyclobutanes. I. Photolysis of Naphthalene *peri*-Fused Cyclobutanes in Rigid Media. Photocleavage from an Upper Triplet State

Koichi HONDA, Akira YABE, and Hideaki TANAKA

National Chemical Laboratory for Industry, Nishiyawata, Hiratsuka-shi, Kanagawa 254

(Received February 12, 1976)

The photocleavage reaction of naphthalene *peri*-fused cyclobutanes (I—IV) in rigid media is found to proceed from one (or several) of the upper triplet states. Nearly planar cyclobutanes (I—III), which were photocleaved in fluid solutions to yield acenaphthylene and 1,2-ethylenedicarboxylic acid derivatives, afford 1,8-naphthalenediacrylic acid derivatives in addition to the above products by irradiation in rigid media. Twisted cyclobutane (IV), which is considerably stable to irradiation in fluid solutions, was also photocleaved in rigid media to give dimethyl 1,8-naphthalenediacrylate. An NMR study shows that the formation of these diacrylic acid derivatives from I—IV in rigid media is considerably stereospecific. The yield ratio of diacrylic acid derivatives to acenaphthylene formed in the photolysis of I—III is independent of the viscosity of the solvents, *i.e.*, of the matrix rigidity, but depends on other properties of the rigid solvents. A concerted mechanism is proposed for the photocleavage reaction of I—IV in rigid media in order to explain the photochemistry different from that in fluid solutions.

There are two possible modes for the photocleavage of four-membered rings of cyclobutane compounds. In the case of cyclobutanes formed from the photocycloaddition of two olefins, one mode of cleavage corresponds to the photoreverse reaction and another leads to the formation of new olefins, if the two modes are not equivalent. However, the photolysis of cyclobutane derivatives frequently shows cleavage-mode selectivity in spite of the energetic possibility of both cleavage modes. It is important to find the factors determining this selectivity. One of the factors must be the steric strain of the cyclobutane ring caused by the interaction of substituent groups. This is supported by the fact that highly-twisted strain-free cyclobutanes are remarkably stable to irradiation.

The present authors studied the photolysis of some naphthalene *peri*-fused cyclobutanes (I—IV) to elucidate the factors influencing the cleavage mode. In fluid solutions, the photocleavage of I—III having nearly planar cyclobutane rings takes place from S_1 and T_1, affording only one mode of cleavage products, acenaphthylene and 1,2-ethylenedicarboxylic acid derivatives, but twisted strain-free cyclobutane IV is not photocleaved. In contrast, the irradiation of I—III in rigid media results in two possible modes of cleavage, giving 1,8-naphthalenediacrylic acid derivatives (the valence isomers of I—III) in addition to the photocleavage products observed in fluid solutions. Moreover, IV, for which two photocleavage modes are equivalent, is also photolyzed in rigid media to yield a diacrylate.

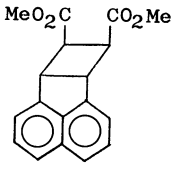

I

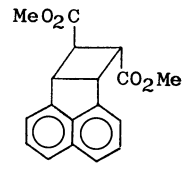

II

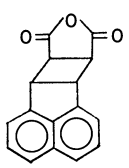

III

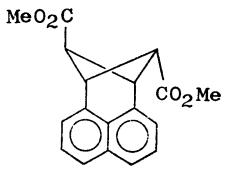

IV

In the present paper, the present authors report that the photocleavage reaction of I—IV in rigid glassy matrices proceeds from higher triplet state(s) by a concerted mechanism, and that this causes a photochemical reaction different from that in fluid solutions.

Experimental

Cyclobutanes I—IV were prepared by a method described elesewhere.[1] All the compounds were purified by repeated recrystallization and the purity was checked by GLC. Low-temperature photolysis was performed in EPA (5: 5: 2) prepared by mixing diethyl ether, isopentane and ethanol, in MP by mixing 3-methylpentane and isopentane, and in glycerol. The solvents except for glycerol were used after purification using alumina column chromatography. A spectrally-pure grade glycerol was used without further purification.

Electronic absorption spectra were obtained using a Shimadzu D-40R spectrometer, emission spectra using a Hitachi MPF-2 spectrometer, and NMR spectra using a Hitachi R-24A instrument.

Two different cell-Dewar arrangements (the cell was immersed in a Dewar containing a coolant) were used. One arrangement consisted of a small cylindrical quartz cell (with a 10-mm pathlength and a 10-mm diameter) and a quartz Dewar equipped with two large flat windows (parallel each other, 20 mm in diameter). This arrangement was used in order to achieve complete photochemical conversion of all sample in the cell. The completely converted samples were used to study the photochemical reaction of the photoproducts. The other arrangement consisted of a cubic quartz cell (with a 10-mm pathlength) and a quartz Dewar equipped with three flat windows (two are parallel and one is at right angles to the other two, 10 mm in diameter). This arrangement was used for following photochemical changes simultaneously using absorption and emission spectroscopy. Generally, liquid nitrogen was used as the coolant, and Dry Ice–ethanol or ice water–sodium chloride was used for glycerol solvent.

A 500-W high-pressure mercury arc lamp with quartz optics (Ushio-501C), a water heat filter (with a 10-mm pathlength), and Toshiba glass filters UV D25 and UV 29 (transparent between 270 and 400 nm) were used for ordinary irradiation. A neutral filter (50% transparency) was added to the lamp system for changing the light intensity. Simultaneous irradiation with two light beams was obtained using the following

light sources: a 10-W low pressure mercury lamp with the Toshiba UV D25 filter (to cut out the 185 nm radiation) for excitation, and the 500-W mercury arc system with Toshiba glass filters VV 40 and UV 39 (transparent between 370 and 470 nm) for long-wavelength light irradiation.

The concentration of samples for photochemistry and spectroscopy was usually about 10^{-4} M. Almost all experiments were performed in an aerated system, since the photochemical reactions were confirmed to be unaffected by air after a comparison between aerated and degassed samples.

An immersion photoreactor consisting of a quartz reaction vessel (doughnut type with a 10-mm pathlength and a 250-ml volume), a quartz Dewar jacket, a quartz jacket for lamp cooling (using circulating water) and a 100-W high-pressure mercury arc lamp was used for the preparative work. The reactor was the most satisfactory one of the several reactors tested. Solutions of I—IV (50 mg in 500 ml EPA) were divided into two 250-ml portions and each was irradiated in the reactor. Irradiation and thawing was repeated to achieve as large a degree of conversion as possible. After the irradiation of each portion for a total of 3 h, the solutions were added and the solvent was evaporated off under reduced pressure. NMR spectra of the residue were obtained without further isolation and the formation of 1,8-naphthalenediacrylic acid derivatives were confirmed, but isolation of the products by preparative GLC was unsuccessful.

Results

Identification of the Products. The photochemical reaction of cyclobutanes I—IV in an EPA rigid glassy matrix at liquid nitrogen temperature was followed using UV spectroscopy; the cyclobutane bands gradually disappeared while the bands of the products grew at longer wavelengths. The starting and the fully-converted spectra of I are shown in Fig. 1, as an example of the spectral changes of the cylobutanes. The photochemical reactions of I—III in fluid solutions were cleavage into acenaphthylene and 1,2-ethylenedicarboxylic acid derivatives,[2] and IV was found to be rather stable to irradiation in fluid solutions.[3] The frozen-state spectrum of acenaphthylene obtained by the photolysis of I in an EPA solution at room temperature under otherwise similar conditions is also shown in Fig. 1. A comparison of the final spectra resulting from the photolysis of I in rigid and fluid states of EPA solutions (Fig. 1) suggests the formation of acenaphthylene and unidentified product(s) resulting in a broad band at about 340—350 nm in EPA at 77 K under the irradiation of I in an EPA matrix. The spectral changes of II and III were similar to that of I, and the final spectra were a superposition of the spectra of acenaphthylene and unidentified products. The irradiation of IV in the rigid matrix also caused spectral changes and gave product(s) having a broad band at about 340 nm, but no acenaphthylene was formed. The conversion efficiency of the highly-twisted cyclobutane, IV, was lower than that of the nearly planar cyclobutanes, I—III.

The unidentified products characteristic of the rigid-state photolysis of I—IV, P_I—P_{IV}, respectively, were identified to be 1,8-naphthalenediacrylic acid derivatives which were formed by the photocleavage of the cyclobutane rings of I—IV, on the basis of their photochemical behavior and absorption, fluorescence and NMR spectra.

Photochemical Behavior of P_I—P_{IV}: The products from the photolysis of I—IV in an EPA glassy matrix did not undergo any more photochemical reactions in the matrix due to selective irradiation. However, after the matrix was melted by warming to room temperature, P_I—P_{IV} reacted easily under the same irradiation to give products whose spectra closely resembled those of the starting cyclobutanes I—IV. Since the irradiation of these products from P_I—P_{IV} at room temperature no

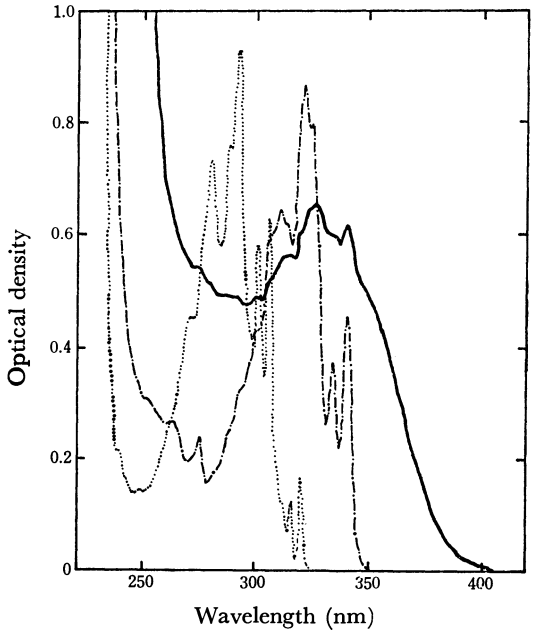

Fig. 1. Absorption spectrum of I in EPA at 77K (···); after irradiation at 77K (—); after irradiation at room temperature and frozen at 77K, *i.e.*, spectrum of produced acenaphthylene (-·-·-).

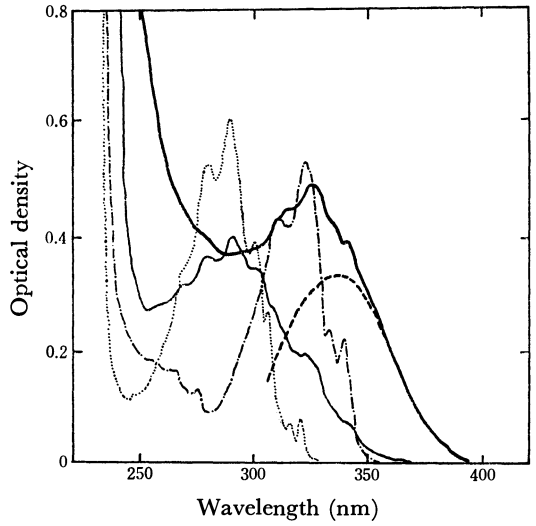

Fig. 2. Absorption spectrum of I in EPA at room temperature (···); after irradiation at 77K and warmed up to room temperature (—); after irradiation at wavelengths longer than 330 nm (—). The operations were sequential.
Absorption spectrum of acenaphthylene (see caption to Fig. 1) (-·-·-) and net absorption spectrum of P_I derived from the spectral separation (---).

longer gave acenaphthylene as did I—III,[4] most of them are considered to be twisted cyclobutanes like IV, if they are indeed cyclobutanes. Acenaphthylene coexisting with P_I—P_{III} remained almost unchanged throughout these photochemical procedures. Thus, the net absorption spectra of P_I—P_{III} could be respectively obtained as the differences between the superposed spectra and that of the remaining acenaphthylene. The spectral change of P_I and its net absorption spectrum obtained in these procedures are shown in Fig. 2. The net spectra of P_I—P_{III} and the spectrum of P_{IV} resemble each other and their maximum peaks occur at about 330—340 nm in EPA solutions at room temperature.

The net absorption spectra and the photochemical behavior of P_I—P_{IV} agreed well with those of 1,8-naphthalenediacrylic acid derivatives, which was expected from our previous study of the photochemistry of dimethyl 1,8-naphthalenediacrylate (V).[1] The irradiation of V in fluid solutions gave predominantly intramolecular head-to-tail adducts (the main product is IV), while V is photochemically unreactive in rigid matrices. The photochemistry of 1,8-naphthalenediacrylic anhydride (VI) was not studied but was inferred to be almost the same as that of V except for the formation of larger amounts of head-to-head adducts like III due to the fixed structure of VI. This was consistent with the photochemical behavior observed with respect to P_{III}.[4]

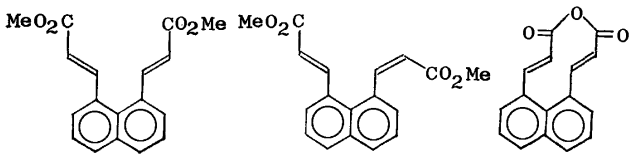

trans, trans V *trans, cis* V VI

Fluorescence Spectra of P_I—P_{IV}: Absorption and fluorescence spectral changes of I—IV due to irradiation in EPA at 77 K were observed simultaneously. The fluorescence was measured using 290, 340, or 365 nm radiation for excitation. The fluorescence of both the starting cyclobutanes and the products were observed using 290 nm light for excitation, while using 340 or 365 nm light, only product fluorescence was observed. Intense fluorescence bands due to the products from I—IV appeared and increased with irradiation time in parallel with the growth of the absorption bands of the products, while the intensity of the fluorescence of I—IV decreased at the same time. Since acenaphthylene does not fluoresce,[5] the observed fluorescence of the products was attributed to P_I—P_{IV} even in the case of I—III. The excitation spectra of the fluorescence of the products from I—IV agreed well with the absorption spectra of P_I—P_{IV}, respectively.

The shape and the position of the fluorescence spectra of P_I—P_{IV} agree well with those of V and probably VI, as is shown in Fig. 3. No phosphorescence of P_I—P_{IV} was observed and the intensity of the fluorescence was lowered remarkably upon melting the matrix. This is in accord with the observation with respect to V (non-phosphorescent, with a fluorescence quantum yield in

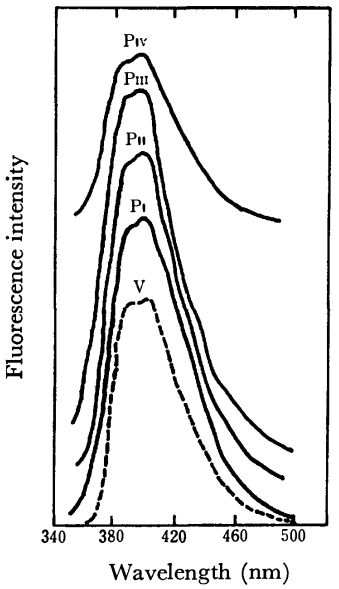

Fig. 3. Fluorescence spectra of P_I—P_{IV} observed after 1 min-irradiation of I—IV in EPA at 77K respectively, and that of *trans, trans* V in EPA matrix (excited with 340 nm light).

EPA of *ca.* 0.9 at 77 K and *ca.* 0.03 at room temperature).[1] These emission spectral observations also suggest that P_I—P_{IV} are 1,8-naphthalenediacrylic acid derivatives.

NMR Spectra of P_I—P_{IV}: Preparatory work on the photolysis of I—IV in EPA at 77 K was performed in order to confirm the formation of the diacrylic acid derivatives. Since the isolation of P_I—P_{IV} from the reaction mixtures by means of preparative GLC was unsuccessful because of the thermal high-reactivity of these substances, an attempt was made to detect them by means of proton NMR spectroscopy. The formation of the dialkenes could be confirmed clearly, since their NMR peaks (of vinyl and/or methyl protons) are not interrupted by the peaks of compounds coexisting with them.[6]

The NMR spectrum of P_I agreed with that of authentic *trans, trans* V, while those of P_{II} and P_{IV} were identical with each other and agreed with that of authentic *trans, cis* V.[7] The spectrum of P_{III} was

TABLE 1. NMR SPECTRAL DATA OF P_I—P_{IV}

Compound	NMR ($CDCl_3$) δ ppm	Assignment
P_I	3.80 (s, *trans* methyl H) 6.29, 8.37 (pair of d, J=15.6 Hz, *trans* vinyl H) 7.2—7.8 (m, aromatic H)	dimethyl *trans, trans*-1,8-naphthalenediacrylate, (*trans, trans* V)
P_{II}, P_{IV}	3.80 (s, *trans* methyl H) 3.59 (s, *cis* methyl H) 6.29, 8.37 (pair of d, J=15.6 Hz, *trans* vinyl H) 6.16 (d, J=12.6 Hz, *cis* vinyl H)[a] 7.2—7.8 (m, aromatic H)	dimethyl *trans, cis*-1,8-naphthalenediacrylate, (*trans, cis* V)
P_{III}	6.16, 8.01 (pair of d, J=15.6 Hz, *trans* vinyl H) 7.2—7.8 (m, aromatic H)	*anti*-1,8-naphthalenediacrylic anhydride, (VI)

a) Another doublet peak is expected to be hidden in the peaks for aromatic protons.

considered to be reasonable for that of VI, although the authentic spectrum of this substance could not be obtained.[8] The observed NMR spectral data of P_I—P_{IV} and their assignments are shown in Table 1. The NMR study suggests that the formation of diacrylic acid derivatives from I—IV in rigid matrices is stereospecific to within the sensitivity of the NMR spectrometer.[6]

Product Yield. The yield of the photocleavage products upon the photolysis of I—IV in an EPA rigid matrix was estimated on the basis of the UV spectra resulting from irradiation to the point of complete conversion. In the case of I—III, the spectral separation of two olefinic products was effected by the photochemical procedures described above. The amount of the products was calculated from the intensity of their spectra using ε at λ_{max}: 4900 (340 nm) for acenaphthylene, 17400 (335 nm) for *trans, trans* V and VI, and 13000 (332 nm) for *trans, cis* V.[9] The quantum yields for the photocleavage of I—IV in rigid matrices were remarkably small and actually zero, since prolonged irradiation with monochromatic light (290 or 313 nm light from the 500 W Hg lamp) which is strong enough for reactions at room temperature scarcely caused any reaction in EPA at 77 K. Thus, the relative disappearance rates of the starting cyclobutanes for irradiation with strong filtered light were determined spectrally in order to compare their photochemical reactivity. The product yield and relative disappearance rate are summarized in Table 2. The total yield of the photocleavage products is much smaller than 100% with respect to all the cyclobutanes studied, and reactions other than photocleavage reach about 60% of the total reactions, as is shown in Table 2.

Table 2. Product yields in the photolysis of I—IV in EPA at 77 K

Compound	R[a]	Product yield (%)		
		Acenaphthylene	1,8-Naphthalenedialkene	Others
I	1.0	13	28	59
II	2.0	44	12	44
III	2.3	20	20	60
IV	0.5	—	43	57

a) Relative disappearance rate.

Fluorescence and Phosphorescence of I—IV. Remarkably intense fluorescence and fairly intense phosphorescence were observed for I—IV in rigid media. The fluorescence and phosphorescence spectra of I—IV in EPA solutions at 77 K were similar to those of naphthalene except that the former was located at a wavelength about 10 nm longer than the latter. The quantum yields for fluorescence and phosphorescence were determined using naphthalene as a standard (ϕ_f=0.55, ϕ_p=0.10 in EPA at 77 K).[10] Phosphorescence lifetimes were also measured by the usual method. The results, summarized in Table 3, show that the cyclobutanes have almost the same emission spectral characteristics as naphthalene, and possess considerably long phosphorescence lifetimes.

Contribution of Upper Triplet State(s). Photocleavage into 1,8-naphthalenedialkenes proceeds only in those instances in which solvents are changed into rigid glasses and the long-lived phosphorescence of the cyclobutanes is observed. This was confirmed using glycerol as a solvent at several reaction temperatures (0 to −80 °C) where the solvent was convertible from a cooled viscous fluid into a rigid glass. Thus, it is suggested that the actual substrates of the photochemical reaction in rigid media are the lowest triplets of the cyclobutanes and the reaction proceeds from upper triplet states which are populated when the metastable triplet absorbs another photon of sufficient energy. In order to verify this, two standard experiments were performed with respect to the cyclobutanes in EPA at 77 K.

Table 3. Quantum yields for fluorescence and phosphorescence, and the phosphorescence lifetime of I—IV in EPA at 77 K[a]

Compound	φ_f	φ_p	τ_p(s)
I	0.58	0.05	2.54
II	0.61	0.07	2.47
III	0.46	0.05	2.40
IV	0.13	0.10	2.54

a) φ_f, φ_p, and τ_p denote the quantum yields for fluorescence (excited with 290 nm light) and phosphorescence (excited with 313 nm light), and the phosphorescence lifetime derived from the decay at the 490 nm and 520 nm peaks, respectively. Naphthalene (φ_f=0.55, φ_p=0.10 in EPA at 77 K)[10] was used as a standard.

Table 4. Dependence of the primary rate of formation of photocleavage products on the light intensity

Rate (full intensity)/Rate (50% intensity)

Compound	Acenaphthylene	1,8-Naphthalenedialkene
I	4.0	3.9
II	3.8	3.9
III	4.0	4.0
IV	—	4.0

(1) The dependence of the primary rate of formation of the photocleavage products on the light intensity was determined. When the intensity of the incident light was decreased to one half using the neutral filter of 50% transparency, the rate was decreased to about a fourth with respect to the formation of both acenaphthylene and dialkenes. The ratio of the rate at full intensity to that at a one-half intensity is shown in Table 4. The fact that the rate is approximately proportional to the square of the light intensity suggests that almost all the photocleavage products are formed by a two-photon mechanism.

(2) The effect of simultaneous irradiation with strong long-wavelength light on the product forming rate was measured. The rate due to a weak source of 254 nm light increased seven- to eight-fold when the samples were irradiated simultaneously with intense light (370—470 nm) which itself had no effect on the cyclobutanes.[11] The effective wavelengths of the second beam

corresponded to those at which the intense bands of the triplet-triplet absorption spectra of naphthalene and alkylnaphthalenes are located.[12] In the case of I—III, the product ratio of acenaphthylene and 1,8-dialkenylnaphthalene was almost independent of irradiation with the long-wavelength light. These results also show that the photocleavage reaction of I—IV in rigid matrices proceeds from upper triplet state(s) formed by the subsequent absorption of two photons.

Table 5. Solvent effect on the photocleavage of I

Solvent	Viscosity (p)[13]	Cleavage ratio (A : N)[a]
EPA (5:5:2)[b]	$\approx 10^5$	31 : 69
Glycerol[c]	$\approx 10^{12}$	85 : 15
IP-3MP (97:3)[b]	8.9×10^5	66 : 34
IP-3MP (50:50)[b]	5.9×10^8	62 : 38
IP-3MP (0:100)[b]	9.4×10^{11}	69 : 31

a) A=acenaphthylene, N=dimethyl 1,8-naphthalenediacrylate. b) At 77 K (liq. nitrogen). c) At 196 K (Dry Ice–ethanol).

Solvent Effect. In order to examine the effect of the solvents used as matrices on the cleavage mode of the cyclobutanes I—III, the photocleavage of I was studied in some rigid solvents. The yield ratio of the acenaphthylene and *trans, trans* V formed from I according to the two photocleavage modes is shown in Table 5. The ratios are nearly equal to within the experimental errors for the hydrocarbon solvents IP-3-MP, which have remarkably different viscosity but are otherwise similar in nature,[13] while the ratio varies for solvents of different nature. Thus, the ratio of the two modes of cleavage is found to be independent of solvent viscosity, *i.e.*, the rigidity of the matrix, but is found to depend on some other solvent characteristics.

Discussion

Reaction from the Upper Triplet State(s). The photocleavage reaction of I—IV in rigid matrices is found to proceed from the upper triplet state(s) formed by the subsequent absorption of two photons. Since the photoexciting moiety of the cyclobutane compounds is the naphthalene ring, the cleavage is expected to occur in one (or several) of the upper triplet states of the naphthalene chromophore. The triplet state energies (10^3 cm^{-1}) of naphthalene itself, and probably of I—IV, are as follows: T_1=21.3, T_2=30.8, T_3=38.7, T_4=45.5, T_5=58.9, and T_6=63.7.[14] The T_1-T_4 and T_1-T_6 absorption transitions have remarkably large extinction coefficients (33000 and 55000, respectively), but only the former transition is possible energetically under the present conditions. Furthermore, the energy of the T_1-T_4 transition is in accord with the second-photon energy which is effective in causing the reaction. Thus, the photocleavage reaction may be occuring in any of the states T_2-T_4 of the cyclobutanes.

The contribution of the upper triplet state(s) has been reported by Kolc and Michl[15] for a photochemical study of the ring-opening of naphthalene-fused cyclobutenes into the pleiadene family in rigid matrices. Furthermore, it was found that the *cis* dimer of acenaphthylene is also photocleaved to acenaphthylene from the upper triplet state(s) in rigid matrices.[16] It seems to be noteworthy that the long-lived T_1 state of naphthalene chromophore acts as a second-photon receiver in all the reactions described above.

The photochemical reactions of I—III in fluid media take place from the S_1 and T_1 states rather efficiently at room temperature, whereas the reactions of I—IV in rigid matrices occur almost exclusively from the upper triplet state(s). This shows that the S_1 and T_1 states of I—III become unreactive in rigid matrices, although those of IV are inactive even in fluid solutions. In other words, thanks to the unreactivity of the S_1 and T_1 states and the long lifetime of the T_1 state, the reaction from the upper triplet becomes noticeable in rigid matrices. The difference of the reactivities in fluid and in rigid media suggests that the reaction from the S_1 and T_1 states requires some activation energy. The activation energy of I—III may be so small that the reaction can proceed in fluid solutions. Since the reaction from the S_1 and T_1 states is stopped in rigid matrices, the S_1 and T_1 states of I—III should dissipate most of their energy as emission (and as heat). In fact, the fluorescence yields for I—III in EPA matrices at 77 K are about two times larger than those at room temperature, although the yield of IV does not change so much.

Side Reactions. In fluid media, reactions other than photocleavage are unimportant in I—III and IV is stable under the usual conditions, while in rigid media, side reactions become about 60% of the total photochemical reactions (Table 2). Therefore, most of the side reactions in rigid media seem to be related to the upper triplet states. However, photoionization and photosensitized solvent decomposition are excluded from the side reactions because these high-energy processes are energetically impossible in such low upper triplet states as T_2-T_4. Moreover, secondary photolysis of the primary olefinic products is also excluded, since the products are considerably stable to irradiation in rigid matrices. Hence, the side reactions are expected to be fragmentations of I—IV in upper triplet states except for the cleavage of the cyclobutane ring.

In view of the fact that absorption bands based on the naphthalene rings of I—IV disappear almost completely, but that no long-wavelength bands other than those due to the cleavage products appear, the destruction of the naphthalene rings seems to be involved in the side reactions, though the details are not known. In fact, naphthalene itself undergoes photolysis under similar conditions, and its spectrum is gradually changed to an ambiguous one having bands at shorter wavelengths.

Reaction Mechanism. The primary products in fluid solutions show that the photocleavage proceeds preferentially through biradical intermediates (VII).[2] Nonformation of naphthalenedialkenes demonstrates that biradicals (VIII), which are expected to lead, at least partly, to the dialkenes even in rigid media,[17] are energetically unfavorable intermediates.[18] If the reaction in the upper triplet states proceeds by a biradical mechanism, the predominant formation of acenaphth-

ylene must hold for the photolysis in rigid glassy matrices. The occurence of two modes of cleavage in rigid matrices must be explained in terms of a change in the reaction mechanism. The difference in the photochemistries in fluid solutions and in rigid matrices is attributable to the difference in the reaction mechanism for the S_1 and T_1 states and that for the upper triplet states. Therefore, a concerted mechanism is proposed for the photocleavage reactions of I—III in rigid media.

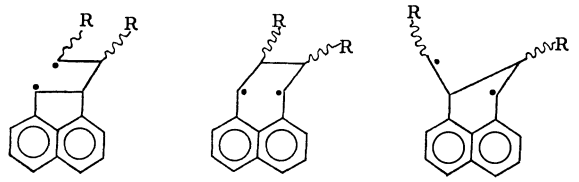

VII VIII IX

R=CO_2Me or 2R=$(CO)_2O$ R=CO_2Me

In contrast to I—III, IV is inactive in the S_1 and T_1 states. The cleavage of its strain-free cyclobutane ring may require much a higher energy than in the cases of I—III. For the upper triplet states, the energetic requirement is satisfied and the cleavage can proceed. It is also supposed that a concerted mechanisms for the reaction of IV in rigid media, without rationalization by the MO theory, from an analogy with naphthalene-fused cyclobutene compounds which are inert in the S_1 and T_1 states and reactive in upper triplet states.[15]

A concerted mechanism for the cleavage reactions for I—IV in rigid matrices is supported by the stereospecific formation of naphthalenedialkenes. If the formation is through the biradical VIII (in the case of I—III) or IX (in the case of IV), geometrical isomers of the diolefinic products must be observed except for the case of II, since the inversion of the cycloheptane ring of VIII and the cyclohexane ring of IX is possible even in rigid media. In fact, Pagni *et al.*[17] reported that biradicals of the IX type are highly flexible and ring inversion occurs easily in an ethanol matrix at liquid nitrogen temperature.

The ineffectiveness of matrix rigidity on the yield ratio of the two photocleavage products from I and probably from II and III (Table 5) also supports the concerted cleavage mechanism. If the reaction is nonconcerted, biradicals VII and VIII must be affected differently by solvent rigidity when they change their geometries at the product forming stage, and consequentely, the ratio must vary with matrix rigidity. The dependence of the yield ratio on the solvent may be explained in terms of a solvent-induced shift of the relative positions of the crossing points of the potential curves for the upper triplet cyclobutanes and of those for some excited states of the olefinic products.

Substituent and Structual Effects. A comparison of the photolysis of isomers I and II shows that II always gives a greater amount of acenaphthylene and has a higher reactivity than I (Table 2). In a glycerol matrix, II gives only acenaphthylene. This is obviously due to the higher ring strain of II caused by the interaction of the naphthalene ring with the substituent at its *cis* position. Kaupp[19] has reported in a study of the photocleavage of some phenyl-substituted cyclobutanes that the cleavage of the *cis*-disubstituted bond is particularly favored due to the relief of a large part of the steric strain in the cyclobutane ring. The relative reactivity (Table 2) shows that IV is less reactive than I—III even in reactions from the upper triplet states in spite of its higher phosphorescence yield.

Therefore, ring strain is an important factor for determining the cleavage mode and the reactivity even in reactions from the upper triplet states.

The authors are grateful to Mr. Kazuhiro Kashiwagi for his assistance during the experiments.

References

1) K. Honda, A. Yabe, and H. Tanaka, *Bull. Chem. Soc. Jpn.*, **48**, 2062 (1975).

2) In the cases of I and II, small amounts of isomerization products (I→II, II→I) were found in the course of the photochemical reactions in fluid solutions, but the final products after complete irradiation were acenaphthylene, dimethyl maleate and dimethyl fumarate. The formation of the isomers of cyclobutane and ethylenedicarboxylate suggests that the photocleavage reactions of I, II, and probably III proceed by a biradical mechanism in fluid solutions.

3) Prolonged intense irradiation of IV in fluid solutions caused some reactions other than the cleavage of the cyclobutane ring.

4) In the case of products from P_{III}, a small amount of acenaphthylene was formed by irradiation. This suggests that a small amount of III was involved in the products from P_{III}.

5) R. Livingston and K. S. Wei, *J. Phys. Chem.*, **71**, 541 (1967); A. Bree, C. Y. Fan, and R. A. Kydd, *Spectrochim. Acta, Part A*, **25**, 1375 (1969). Although the fluorescence spectrum of acenaphthylene in hexane at 77 K determined by a photographic method has been reported (V. I. Mikhailenko and P. A. Teplyakov, *Opt. Spectrosk.*, **22**, 48 (1967); *Opt. Spectrosc.*, **22**, 24 (1967)), we could not detect the fluorescence.

6) In the cases of I—III, 1,2-ethylenedicarboxylic acid derivatives must be formed as one of photocleavage products, but they produced almost no NMR peaks. These derivatives may have been removed by a solvent during evaporation under reduced pressure. Thus, their stereochemistries (in the cases of I and II) are unknown.

7) The NMR spectrum of *trans, cis* V was measured without isolation in the course of the photoisomerization of *trans, trans* V.[1]

8) The synthesis of VI from 1,8-naphthalenediacrylic acid by the usual methods was unsuccessful.

9) The molar extinction coefficient of VI was assumed to be nearly equal to that of *trans, trans* V. The coefficient of *trans, cis* V was assumed to be three quarters of that of *trans. trans* V, since the value for a *cis* acrylic group has about one half of that for a *trans* group in the usual aromatic acrylic acid derivatives.

10) R. S. Becker, "Theory and Interpretation of Fluorescence and Phosphorescence," Wiley Interscience (1969), p.118.

11) When an intense light source (*e.g.*, 500-W mercuty arc with UV 29 filter) was used for exciting a sample, the effect of the second light was negligibly small.

12) Y. H. Meyer, R. Astier, and J. M. Leclercq, *J. Chem. Phys.*, **56**, 801 (1972).

13) W. G. Herkstroeter, "Creation and Detection of the Excited State," Vol. I, Part A, Marcel Dekker (1971), p. 43.

14) J. B. Birks, "Organic Molecular Photophysics," Vol. 1,

John Wiley and Sons (1973), p. 25.

15) J. Michl and J. Kolc, *J. Am. Chem. Soc.*, **92**, 4148 (1970); J. Kolc and J. Michl, *ibid.*, **95**, 7391 (1973).

16) Unpublished results; the *trans* dimer of acenaphthylene is decomposed into acenaphthylene exclusively from S_1 and/or T_1.

17) R. M. Pagni, C. R. Watson, Jr., J. E. Bloor, and J.R. Dodd, *J. Am. Chem. Soc.*, **96**, 4064 (1974); C. R. Watson, Jr., R. M. Pagni, J. R. Dodd, and J. E. Bloor, *ibid.*, **98**, 2551 (1976).

18) Other possible biradical intermediates for the dialkenes are less favorable than IX, since they are not stabilized by benzylic resonance and their formation requires scission of the C–C bond of the four-membered ring far from the naphthalene ring, the exciting chromophore.

19) G. Kaupp, *Angew. Chem. Int. Ed. Engl.*, **13**, 817 (1974).

Hydrogen Bonding Systems Containing Hydrogen Fluoride. III.* Infrared Frequency Shifts and CNDO/2 Calculations on HF-Carbonyl Compound Complexes

Mitsunori TSUDA, Hidekazu TOUHARA, Koichiro NAKANISHI,** and Nobuatsu WATANABE

Department of Industrial Chemistry, Faculty of Engineering, Kyoto University, Kyoto 606

(Received February 14, 1976)

CNDO/2 calculations were carried out for the hydrogen bonded complexes between hydrogen fluoride (HF) and a series of organic compounds having a carbonyl group as a proton acceptor. Infrared spectral measurements were also made to obtain the frequency shifts of H–F stretching vibration, $\Delta\nu_{HF}$, for the same complexes in dilute carbon tetrachloride solution. Optimum geometry was obtained on the assumption of planar complex. For all the carbonyl compounds used, the interatomic angles, $\angle$C–O···H, were 120°—123° for the most stable conformation. The changes in the distance between H atom and F atom, ΔR_{HF}, were in good correlation with $\Delta\nu_{HF}$ obtained from IR spectra. Calculated hydrogen bond energies were also in good correlation with $\Delta\nu_{HF}$, though their absolute values were somewhat larger than those derived from experimental observations. This indicates that the CNDO/2 calculations give relatively correct enthalpy values for the hydrogen bond complexes of a given donor with a series of molecules having a common acceptor group. Other correlations of $\Delta\nu_{HF}$ with properties expected to change with the hydrogen bond formation were also confirmed. These include the energies of each bond obtained by the partitioning of the total energy and the force constant of H–F bond. The electron population on the oxygen atom and other atoms participating in the hydrogen bond formation, the charge transfer, ionization potentials and dipole moment enhancements were also calculated and discussed in terms of the measure of hydrogen bond strength.

One of the unique physico-chemical properties of hydrogen fluoride (HF) is a strong tendency to form the hydrogen bonding complexes with various organic molecules. It has been recognized experimentally that the frequency shift of H–F stretching mode due to hydrogen bond formation, $\Delta\nu_{HF}$, and the hydrogen bond energy, ΔH, are unusually larger than the corresponding quantities for any other hydrogen bonding systems.[1-4] On the other hand, HF has a simple geometrical structure and its electronic structure is also relatively simple. To date, many molecular orbital calculations for HF hydrogen bonding systems have been carried out by both non-empirical and semi-empirical methods.[5,6] The results of these calculations give theoretical insight into the nature of hydrogen bonding interactions of HF. However, reliable experimental evidence is often missing and no attempt has been made to compare the well-established experimental data with the calculated results for a series of hydrogen bond complexes consisting of a fixed proton donor (HF) and various proton acceptors.

In the present study, a series of organic compounds which have a carbonyl group were chosen as proton acceptor and the nature of their HF complexes was examined. Reasons for our choice of acceptors are: since the carbonyl group is found in organic molecules such as ketones, aldehydes and amides, their proton accepting ability is distributed over a wide range, making it possible for us to deal with molecules having largely differing pK_a values; the geometry of carbonyl compounds is usually simple and well-defined. The following carbonyl compounds were chosen: formaldehyde, acetaldehyde, propionaldehyde, butyraldehyde, acetone, methyl ethyl ketone, methyl propyl-ketone and *N*,*N*′-dimethylformamide (DMF). CNDO/2 calculations were carried out on the hydrogen bonded structure of HF. Optimized geometry and the corresponding hydrogen bond energy were obtained. The values of $\Delta\nu_{HF}$ were also determined for the same acceptors in dilute carbon tetrachloride solution by the method described previously.[4]

Experimental

The experimental procedures and apparatus used to obtain infrared frequency shift were the same as those reported previously.[3,4] The solubility of aldehydes in CCl_4 was so small that determination of equilibrium constant of complex formation was impossible. Only the $\Delta\nu_{HF}$ could be determined (Table 1).

Method of Calculation

The CNDO/2 calculations were carried out by means of the original parameterization of Pople, Segel and Santry.[7,8] Throughout the calculations, the standard geometries were used and kept constant for all the proton acceptor monomers, and the geometry of proton donor (HF) was fully optimized with respect to the total energy. Figure 1 shows the specifications of geometry for hydrogen bonding complexes.

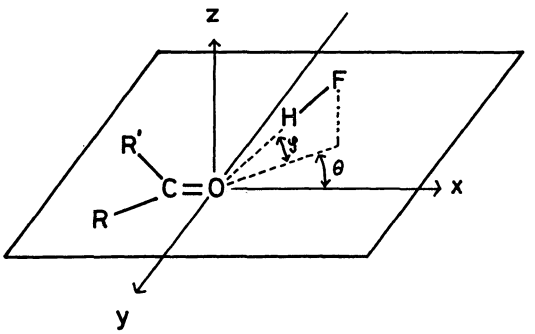

Fig. 1. Geometry specifications for HF carbonyl compound complexes.

* Part II: Ref. 4.

** To whom correspondence should be addressed.

Table 1. Calculated optimum geometries and energies, and experimental infrared frequency shift for HF–carbonyl compound complexes

Acceptor	Formal-dehyde	Acetal-dehyde	Propioal-dehyde	Butyral-dehyde	Acetone	Methyl ethyl ketone	Methyl propyl ketone	*N,N*-Di-methyl-formamide	HF (mono-mer)
Calculated Optimum Geometries									
R(F–O) (Å)	2.434	2.416	2.416	2.416	2.403	2.402	2.403	2.392	
R(H–F) (Å)	1.021	1.024	1.024	1.024	1.027	1.027	1.027	1.030	1.000
ΔR(H–F) (Å)	0.021	0.024	0.024	0.024	0.027	0.027	0.027	0.030	0
	57°	57°	57°	57°	60°	59°	59°	60°	
Calculated Optimum Energies									
ΔE (kcal/mol)	−14.48	−16.53	−16.58	−16.61	−18.44	−18.43	−18.46	−20.73	
ΔE_{corr} (kcal/mol)	−5.4	−6.1	−6.1	−6.2	−6.8	−6.8	−6.8	−7.7	
					(−6.9)[a]			(−7.6)[a]	
E_{HF} (eV)	−19.13	−18.95	−18.95	−18.94	−18.77	−18.77	−18.78	−18.62	−20.42
ΔE_{HF} (eV)	1.30	1.48	1.48	1.48	1.65	1.65	1.65	1.80	0
E^R_{HF} (eV)	−18.79	−18.57	−18.56	−18.56	−18.35	−18.35	−18.35	−18.15	−20.33
ΔE^R_{HF} (eV)	1.54	1.76	1.77	1.77	1.98	1.98	1.98	2.18	
K(H–F) (mdyn/Å)	17.20	16.90	16.70	16.76	16.42	16.37	16.34	16.17	19.12[b]
Experimental Data									
ν_{HF} (cm^{-1})	3468	3410	3399	3404	3298	3320	3302	3151	3961[c]
$\Delta\nu_{HF}$ (cm^{-1})	493	551	562	557	663	640	658	810	

a) Ref. 4. b) J. A. Pople and D. L. Beveridge, in "Approximate Molecular Orbital Theory," McGraw-Hill Book Company, New York (1970). c) H. Hyman and J. J. Katz, in "Non-Aqueous Solvent System," ed. by T. C. Waddington, Academic Press, New York, N. Y. (1965), Chap. 2.

The optimum geometries and corresponding total energies were obtained by the following procedure.

(1) The HF molecule is first placed on the x-axis in xy-plane. As shown in Fig. 1, the xy-plane is one of the planes of symmetry for the acceptor molecule and the x-axis is the extension line of C=O bond of the acceptor molecule. The distance between fluorine and oxygen atoms, R(F–O), was optimized with respect to the total energy.

(2) On the xy-plane, angular orientation of the HF molecule with respect to C=O bond was optimized by rotating the HF molecule around the origin toward the smaller alkyl group of acceptor molecule by an angle θ.

(3) Keeping R(F–O) and θ constant, the atomic distance R(H–F) is optimized.

(4) Finally R(F–O) is again optimized by keeping R(H–F) and θ constant.

The above procedures seem to be sufficient for obtaining optimum geometries, since the values obtained remain unchanged even when both R(H–F) and θ were again optimized in the same manner. The following comment is given as regards the calculated optimum geometry and energy for each HF complex. The angle ϕ (Fig. 1) was assumed to be zero. For HF–formaldehyde complex, a CNDO/2 calculation has been reported by Schuster.[9] Both θ and ϕ were optimized in his calculation. However, as pointed out by Morokuma[10] and by Kollman and Allen,[5] the angular dependence of hydrogen bond energy was estimated to be very small in CNDO/2 and other empirical calculations, which is in contrast with the results of more refined *ab initio* calculations for the same complex. Optimization with respect to ϕ in the CNDO/2 calculations may not be justified. The structure of hydrogen bonding complex can well be described by means of a general hybridization model.[11,12] Since there should be a trigonal hybrid orbital on the oxygen atom of carbonyl group in the molecular plane, the assumption that $\phi=0$ may be sufficiently reasonable.

According to Schuster's calculation, the hydrogen bond energy, ΔE, for HF–formaldehyde complex is insensitive to ϕ. Our calculated ΔE value was −14.48 kcal/mol for HF–formaldehyde complex. This is almost comparable with those of Schuster[9] for the case that $\phi=0$, a minor discrepancy being due to the difference in the geometry used for formaldehyde monomer.

Results and Discussion

Geometry of HF Hydrogen Bonding Complexes. The optimum geometries calculated for the complexes between HF and a series of carbonyl compounds are summarized in Table 1. The optimum values of θ are 57—60° for all the complexes studied. This is consistent with the general hybridization model for the hydrogen bonds. Since there is a trigonal hybridization on the

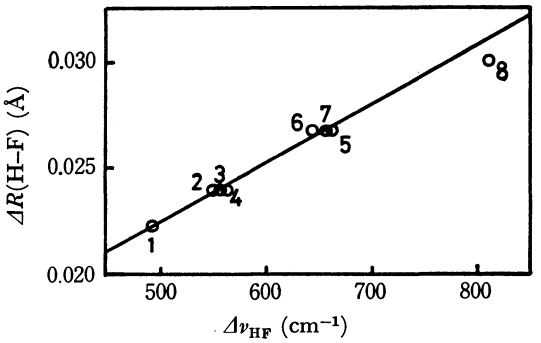

Fig. 2. Plots of ΔR(H–F) *vs.* $\Delta\nu_{HF}$;
1, formaldehyde; 2, acetaldehyde; 3, propionaldehyde; 4, butyraldehyde; 5, acetone; 6, methyl ethyl ketone; 7, methyl propyl ketone; 8, *N,N*-dimethylformamide.

oxygen atom of the carbonyl group, the values of θ seem to meet our expectation. It is interesting to examine the possible correlation between the change in atomic distances accompanied by hydrogen bond formation and the infrared frequency shift. As shown in Fig. 2, the change in H–F distance, ΔR(H–F), was found to increase linearly with $\Delta\nu_{HF}$.

Hydrogen Bonding Energy and the Badger-Bauer Relationship. The hydrogen bonding energy ΔE we obtained are given in Table 1. The partitioning of total molecular energy was also carried out, the results and the force constants of H–F bond also being summarized in Table 1.

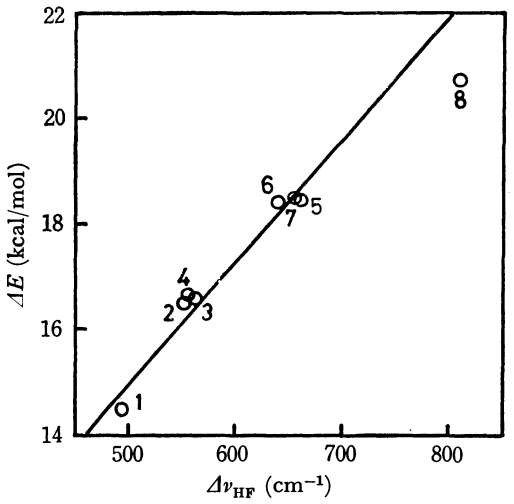

Fig. 3. Plots of ΔE *vs.* $\Delta\nu_{HF}$. The number of points is the same as that in Fig. 2.

Badger-Bauer Relationship: A linear correlation, called the Badger-Bauer relationship, is known to exist between the hydrogen bond energy and the frequency shift.[13–16] A linear correlation could also be recognized between the calculated hydrogen bond energy ΔE and experimental frequency shift, $\Delta\nu_{HF}$, except for the case of HF–DMF complex (Fig. 3). The results indicate that relative values of ΔE can be reasonably estimated from the present calculations for HF–aldehyde and HF–ketone complexes. The deviation for HF–DMF complex will not be due to the fact that the relative value for this complex is unjustifiable.

This will be confirmed from the following discussion. The ΔE values for HF–acetone and HF–DMF complexes were calculated to be -18.44 and -20.73 kcal/mol, respectively (Table 1), while the enthalpy of complex formation values, ΔH, for the above two in carbon tetrachloride solution have been estimated to be -6.9 and -7.6 kcal/mol, respectively, from infrared spectroscopic measurement.[4] However, the ratio, $\Delta E/\Delta H$, for HF–acetone complex agrees fairly well with that for HF–DMF complex within experimental error.[17] This indicates that the relative value of ΔE for HF–DMF complex is also as reasonable as those for other complexes. The discrepancy found for HF–DMF complex may be due to the fact that the nature of the hydrogen bond differs from the other since DMF monomer has a conjugated system and its highest occupied orbital is not σ- but π-orbital. The anomaly for HF–DMF complex was observed in all the correlations tested.

It is recognized that semi-empirical calculations such as CNDO/2 overestimate the hydrogen bond energy.[5] The discrepancy between ΔE and ΔH is seriously large, even when the difference between experimental environment and the assumption in theoretical calculation is taken into considerations. However, since the calculated ΔE values are relatively valid, we may define a corrected ΔE value which is normalized so as to satisfy the experimental ΔH values both for HF–acetone and HF–DMF complexes. These normalized energy values (denoted by ΔE_{corr}) are also given in Table 1.

Semi-empirical methods such as CNDO/2 calculation involve optional parameters and the problem of which parameterization is the most suitable for representing such delicate interactions as the hydrogen bond remains.[18] However, the present calculations for the hydrogen bond complexes between a fixed proton donor and a series of proton acceptors with a fixed functional group should provide fairly reasonable (relative) values of hydrogen bond energy probably because of the compensation of various factors concerning parameterization. It is concluded that the present treatment is useful for estimating the hydrogen bond energy which cannot be obtained due to experimental difficulty (*e.g.*, in the case of HF–aldehyde complexes).

Partitioning of Total Energy: The total molecular energy E may be decomposed into one and two center terms;[7]

$$E = \sum_{A} E_A + \sum_{A}\sum_{B} E_{AB} \qquad (1)$$

The two center term, E_{AB}, can be interpreted as a measure of the strength of A–B bond and written as[19]

$$E_{AB} = E^R_{AB} + E^V_{AB} + E^J_{AB} + E^K_{AB} + E^N_{AB}. \qquad (2)$$

The leading term of the RHS of Eq. 2, E^R_{AB}, represents the contribution of resonance integral to E_{AB}[20] and is given by[19]

$$E^R_{AB} = 2\sum_{\mu\in A}\sum_{\nu\in B} P_{\mu\nu}\beta_{\mu\nu}S_{\mu\nu}. \qquad (3)$$

An analysis of E^R_{AB} is equivalent to a population analysis in which the individual terms are weighted with an energy factor $\beta_{\mu\nu}$. The amounts of change in E_{AB} and E^R_{AB} for H–F bond,

$$\Delta E_{HF} = E_{HF}(\text{monomer}) - E_{HF}(\text{complex}) \qquad (4)$$

$$\Delta E^R_{HF} = E^R_{HF}(\text{monomer}) - E^R_{HF}(\text{complex}) \qquad (5)$$

were expected to be more directly correlated with $\Delta\nu_{HF}$. As shown in Fig. 4, both ΔE_{HF} and ΔE^R_{HF} are in good correlation with $\Delta\nu_{HF}$ values.

Force Constant of H–F Bonds: The force constant K(H–F) of H–F bond can be approximately evaluated from the second derivative of the total energy with respect to H–F distance at an equilibrium geometry (Table 1). It decreases with an increase in the strength of hydrogen bond. A linear correlation holds with ν_{HF} (Fig. 5).

Electron Populations and Charge Transfer. The electron populations on the atoms participating in the formation of hydrogen bond or the charge transfer due to the hydrogen bond formation may be utilized as a measure of hydrogen bond strength. The electron

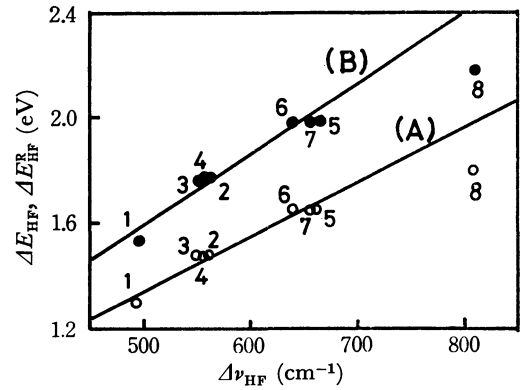

Fig. 4. (A) Plots of ΔE_{HF} *vs.* $\Delta\nu_{HF}$; (B) plots of ΔE^{R}_{HF} *vs.* $\Delta\nu_{HF}$. The number of points is the same as that in Fig. 2.

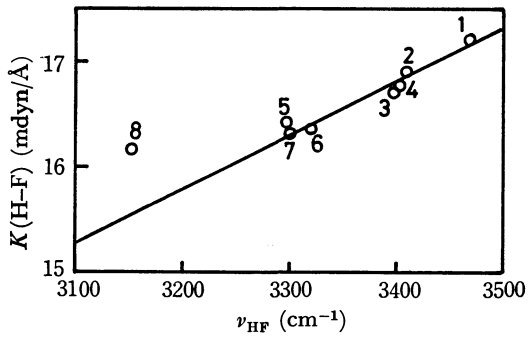

Fig. 5. Plots of K(H—F) *vs.* ν_{HF}. The number of points is the same as that in Fig. 2.

populations on F, H, O and C atoms for monomers and complexes and the amount of charge transfer from the proton acceptors to the proton donor, ΔQ, are summarized (in Table 2).

Correlations with Hydrogen Bond Energy: Del Bene[11,21] pointed out from the results of *ab initio* calculations that the net electron population on the proton accepting sites (atoms) is a good measure of the hydrogen bond strength. In accordance with this suggestion, the electron population on the oxygen atoms of proton acceptor and ΔQ are plotted against ΔE_{corr}. Good linear correlations have been obtained except for the HF–DMF complex (Fig. 6).

Electron Population on Oxygen Atom: Although the above correlations are successful, more detailed analysis on the electron population on the oxygen atom will give

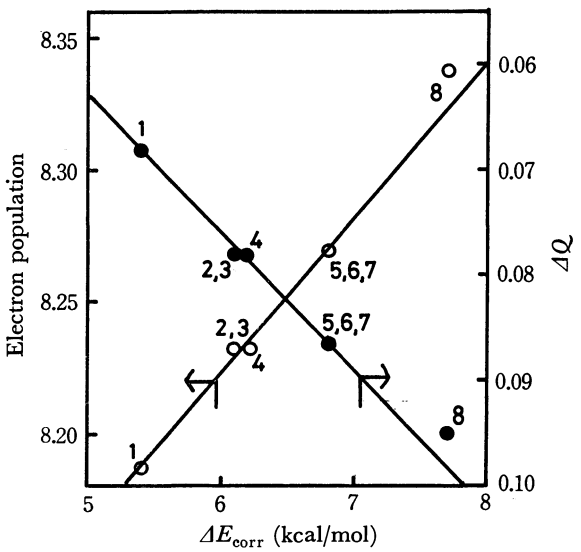

Fig. 6. Plots of electron population on O atom of proton acceptor monomer and the amount of charge transfer by hydrogen bond against ΔE_{corr}. The number of points is the same as that in Fig. 2.

further insight into the nature of the present hydrogen bond systems. First, let us examine the changes in the electron populations on each atom participating F–H···O=C hydrogen bond. The following changes were observed on the electron populations when the hydrogen bonding complex was formed (Table 2): For all the complexes studied, there were an increase in the electron population on the fluorine atom and a decrease in the electron population both on the hydrogen and carbon atoms. On the other hand, a decrease in the electron population on the oxygen atom was observed only for the cases of HF–DMF and HF–formaldehyde complexes. This led us to calculate the contributions of σ- and π-electrons to the total electron population. Table 3 shows, as an example, the amounts of change in the electron populations on the O and C atoms for HF–formaldehyde and HF–acetaldehyde complexes. It is seen that there is a decrease in the σ-electron population and an increase in the π-electron population for each complex, and that the sign of the change in total electron population depends on the relative magnitude of both contributions.

It is thus concluded that, for all the complexes other than HF–formaldehyde and HF–DMF, there are some

Table 2. Electron populations on F, H, O, and C atoms and the amounts of charge transfer ΔQ for HF hydrogen bonding complexes

Acceptor	F	H	O (monomer)	O (complex)	C (monomer)	C (complex)	ΔQ
HF (monomer)	9.2262	0.7738					
Formaldehyde	9.3226	0.7456	8.1868	8.1848	5.7905	5.7590	0.0682
Acetaldehyde	9.3377	0.7400	8.2316	8.2333	5.7605	5.7257	0.0777
Propionaldehyde	9.3381	0.7398	8.2314	8.2340	5.7649	5.7305	0.0779
Butyraldehyde	9.3383	0.7397	8.2320	8.2349	5.7684	5.7341	0.0780
Acetone	9.3518	0.7348	8.2695	8.2751	5.7417	5.7066	0.0866
Methyl ethyl ketone	9.3520	0.7347	8.2690	8.2754	5.7468	5.7121	0.0867
Methyl propyl ketone	9.3518	0.7347	8.2695	8.2761	5.7504	5.7158	0.0865
N,*N*-Dimethylformamide	9.3647	0.7302	8.3389	8.3379	5.6535	5.6252	0.0949

Table 3. Electron population changes on carbon and oxygen atoms of carbonyl group for HF–formaldehyde and HF–acetaldehyde complexes

Atom	Formaldehyde		Acetaldehyde	
	O	C	O	C
$2P_\pi$	+0.0512	−0.0512	+0.0635	−0.0554
$2S_\sigma$	−0.0209	+0.0055	−0.0232	+0.0059
$2P_\sigma$	−0.0323	+0.0142	−0.0386	+0.0146
σ-Total	−0.0532	+0.0197	−0.0618	+0.0206
Total	−0.0020	−0.0315	+0.0017	−0.0348

more transfers of π-electrons from methyl-, ethyl-, or propyl group into carbonyl group by the hyperconjugation effect which is accompanied by hydrogen bond formation. The increase in the electron population on the oxygen atom for these complexes should be due to the fact that the increase in the π-electron population by this effect exceeds the decrease in the σ-electron population. The lack of hyperconjugation effect in the HF–formaldehyde and HF–DMF complexes might be responsible for the decrease in the total electron population on the oxygen atom.

Ionization Potential and Dipole Moment Enhancement. The proton accepting abilities of the carbonyl group have been discussed in detail by Cook.[22] It is of interest to calculate the energy, $E_{C=O}$, of the carbonyl group for monomer and complex and the first ionization potential (IP) and to examine possible correlations of the frequency of the C=O stretching vibration, $\nu_{C=O}$, with them. The results of calculation for $E_{C=O}$ and IP are given in Table 4. We see that the calculated $E_{C=O}$ values are parallel with the $\nu_{C=O}$ values given by Cook.[22] A similar parallelism can be confirmed for any pairs from ΔE_{corr}, $\Delta\nu_{HF}$, and $\Delta E_{C=O}$ (the change in the amount of $E_{C=O}$ by the hydrogen bond formation).

IP as a Measure of Hydrogen Bond Strength: The calculated IP values for proton acceptor monomers are compared with those obtained experimentally in Fig. 7.[22,23] A satisfactory correspondence holds between them, though the calculated values are always somewhat larger than the observed ones (DMF is an exception). Cook has pointed out that there is a linear relationship between IP and $\nu_{C=O}$ and the latter can be used as a measure of the hydrogen bond strength. The $\nu_{C=O}$ will exhibit a shift due to the hydrogen bond formation and can also be used as a measure of hydrogen bond strength, though the shift, $\Delta\nu_{C=O}$, could not be detected for HF-complexes.[24] Careful examination of the IP values (Table 4) leads to the conclusion that they cannot always be used as a measure of hydrogen bond strength. The values for $\Delta\nu_{HF}$, $\nu_{C=O}$, $E_{C=O}$, and ΔE_{corr} are almost constant for three aldehydes except formaldehyde and for three ketones, whereas the values of both observed and calculated IP decrease continuously from acetaldehyde to methyl propyl ketone.

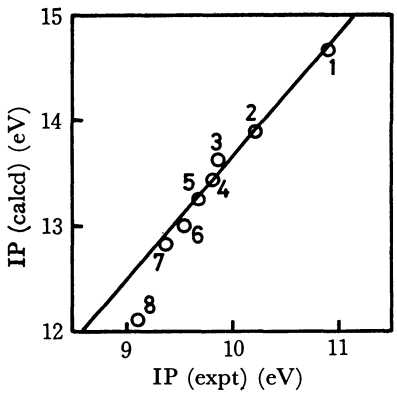

Fig. 7. Plots of calculated ionization potential *vs.* experimental ionization potential for all acceptor monomers. The number of points is the same as that in Fig. 2.

The failure of correlation may be interpreted as follows. The first ionization potential of proton acceptor monomer depends on the properties of the highest occupied orbital. This is considered to be a measure of the charge transfer and/or of the proton accepting ability. However, since various kinds of interactions other than the charge transfer (*e.g.*, electrostatic, dispersion, and repulsive) may contribute to the hydrogen bond energy, one cannot always discuss the strength of hydrogen bond in terms of the facility of charge transfer and accordingly the first ionization potential. It is important to evaluate how much the ionization potential of proton acceptor monomer reflects the properties of electrons available for hydrogen bonding.[21,11]

Anomaly in HF–DMF Complex: For all the acceptor monomers except DMF, the highest occupied orbitals are σ-orbital. It consists almost exclusively of the lone pair orbital. In contrast, the highest occupied orbital of DMF monomer is π-orbital. Since the highest

Table 4. Energy of carbonyl group, ionization potential and dipole moment enhancement for HF hydrogen bond complexes

Acceptor	$\nu_{C=O}$ (cm^{-1}) (Monomer)	$E_{C=O}$ (eV)		$\Delta E_{C=O}$ (eV)	IP (eV)		$\Delta\mu$(D)
		(Monomer)	(Complex)		(Expt)	(Calcd)	
Formaldehyde		−45.54	−45.13	0.39	10.90[b]	14.68	1.05
Acetaldehyde	1733[a]	−44.26	−43.78	0.48	10.21[a]	13.90	1.34
Propionaldehyde	1738[a]	−44.29	−43.81	0.48	9.86[a]	13.64	1.36
Butyraldehyde	1729[a]	−44.29	−43.81	0.48	9.81[a]	13.45	1.39
Acetone	1717[a]	−43.11	−42.53	0.58	9.69[a]	13.25	1.41
Methyl ethyl ketone	1722[a]	−43.15	−42.56	0.59	9.54[a]	13.01	1.43
Methyl propyl ketone	1717[a]	−43.14	−42.55	0.59	9.39[a]	12.84	1.46
N,*N*-Dimethylformamide	1684[a]	−43.37	−42.46	0.91	9.11[a]	12.12	1.73

a) Ref. 22. b) Ref. 23.

occupied orbital would take the main part in hydrogen bond, calculations on HF–DMF complex were performed for two models, a π-hydrogen bond model in which the HF molecule approaches perpendicular to the molecular plane of acceptor molecule, and a σ-hydrogen bond model which is the same as that for other complexes. The π-hydrogen bond model was found to have less hydrogen bond energy than the σ-hydrogen bond model. Similar results have been recognized in the *ab initio* calculations on HF–HCN and HF–formaldehyde hydrogen bonds.[11,25] This was ascribed to the fact that the energy of electrons in π-orbital is considered to be more favorable for the charge transfer in hydrogen bond than that in σ-orbital. However, the σ-orbital has a higher electron density on the site of hydrogen bonding and accordingly has a higher probability of interaction with proton donor than the π-orbital. Thus the electrons in the σ-orbital seem to give greater contribution to hydrogen bonding. This may explain the anomaly of HF–DMF complex.

Dipole Moment Enhancement: It is well-known for typical hydrogen bonding that the dipole moment of hydrogen bond complex becomes larger than the sum of the dipole moments of its components.[26] The calculated values for the increase in dipole moment $\Delta\mu$ are given in Table 4. No correlations were recognized between $\Delta\mu$ and ΔE_{corr}. For the HF–aldehyde complexes, with HF–formaldehyde as an exception, the $\Delta\mu$ values increase in the order, acetaldehyde$<$ propionaldehyde$<$butyraldehyde, while the ΔE_{corr} values remain almost constant. The $\Delta\mu$ can be divided into two contributions, one due to induced dipole moment, $\Delta\mu_{ind}$, and the other to charge transfer, $\Delta\mu_{ct}$.[26] Since the $\Delta\mu_{ct}$ for these HF–aldehyde complexes would be almost the same, the behavior of overall $\Delta\mu$ can be interpreted as the increase of contributions of $\Delta\mu_{ind}$ in the order given above.

In conclusion, the present CNDO/2 calculations could give, though semi-quantitative, a fairly good description of the properties of HF hydrogen bond complexes. Correlations with experimental $\Delta\nu_{HF}$ would serve to overcome the lack of energetic information due to experimental difficulties. Success and failure of correlations with the quantities used as a measure of hydrogen bond strength may furnish further insight to the understanding of HF hydrogen bonds.

The authors thank Dr. Shigeo Yoneda for his kind guidance and suggestions. They are also grateful for permission to use the facilities at the Computer Center of Kyoto University.

References

1) D. N. Schepkin, *Opt. Spectrosk.*, **19**, 709 (1965).
2) D. N. Schepkin, *Teor. Eksp. Khim.*, **2**, 276 (1966).
3) H. Touhara, H. Shimoda, K. Nakanishi, and N. Watanabe, *J. Phys. Chem.*, **75**, 2222 (1971).
4) M. Tsuda, H. Touhara, K. Nakanishi, and N. Watanabe, *J. Phys. Chem.*, **80**, 362 (1976).
5) P. A. Kollman and L. C. Allen, *Chem. Rev.*, **72**, 282 (1972) and earlier papers cited therein.
6) More recent works since that given in Ref. 5 are too numerous to list in full. The following is by no means complete. (a) A. Johansson, P. A. Kollman, and S. Rothenberg, *Theor. Chim. Acta*, **29**, 167 (1973); (b) P. A. Kollman, A. Johansson, and S. Rothenberg, *Chem. Phys. Let.*, **24**, 199 (1974); (c) L. A. Curtiss and J. A. Pople, *J. Mol. Spectrosc.*, **48**, 413 (1973); (d) G. H. F. Diercksen, W. von Niessen, and W. P. Kraener, *Theor. Chim. Acta*, **31**, 205 (1973); (e) W. von Niessen, *Theor. Chim. Acta*, **31**, 297 (1973): (f) see also Refs. 11 and 25.
7) J. A. Pople, D. P. Santry, and G. A. Segal, *J. Chem. Phys.*, **43**, S129 (1965).
8) J. A. Pople and G. A. Segal, *J. Chem. Phys.*, **43**, S136 (1965).
9) P. Schuster, *Theor. Chim. Acta*, **19**, 212 (1970).
10) K. Morokuma, *J. Chem. Phys.*, **55**, 1236 (1971).
11) J. E. Del Bene and F. T. Marchese, *J. Chem. Phys.*, **58**, 926 (1973).
12) J. E. Del Bene, *J. Chem. Phys.*, **58**, 3139 (1973).
13) R. M. Badger and S. H. Bauer, *J. Chem. Phys.*, **5**, 839 (1937).
14) R. M. Badger, *J. Chem. Phys.*, **8**, 288 (1940).
15) G. C. Pimentel and A. L. McClellan, "The Hydrogen Bond," Freeman, San Francisco, Calif. (1960).
16) S. N. Vinogradov and R. H. Linnell, "Hydrogen Bonding," Van Nostrand Reinhold, New York, N. Y. (1971).
17) The experimental values for ΔH may be somewhat underestimated because of specific and non-specific solvations of carbon tetrachloride for HF and acceptor molecules, but the effect on the ratio is negligible.
18) It is not clear, however, whether any improvement on the parameterization can remove the defect of semi-empirical methods in their application to hydrogen bonds.
19) H. Fischer and H. Kollmar, *Theor. Chim. Acta*, **16**, 163 (1970).
20) For other terms, see Ref. 19.
21) J. E. Del Bene, *J. Chem. Phys.*, **57**, 1899 (1972).
22) D. Cook, *J. Am. Chem. Soc.*, **80**, 49 (1958).
23) F. I. Vilesov, *Dokl. Akad. Nauk SSSR*, **132**, 1332 (1960).
24) In the present infrared measurement, the concentration of proton acceptor was kept much greater than that of HF in order to carry out measurements under the experimental conditions by which only 1 : 1 complex exists. Hence we could not determine accurately the shift of $\nu_{C=O}$ due to hydrogen bond formation, since the excess proton acceptor monomer band interfered with it.
25) J. E. Del Bene, *Chem. Phys. Lett.*, **24**, 203 (1974).
26) H. Ratajczak and W. J. Orville-Thomas, *J. Chem. Phys.*, **58**, 911 (1973).

An INDO-MO Study of the Conformations and Electronic Structures of $HCHOH^+$, CH_3CHOH^+, $(CH_3)_2COH^+$, $HCO_2H_2^+$, $CH_3CO_2H_2^+$, and $CH_3OH_2^+$

Katsutoshi OHKUBO, Toshiaki YOSHIDA, and Katsumi TOMIYOSHI

Department of Synthetic Chemistry, Faculty of Engineering, Kumamoto University, Kurokami, Kumamoto 860

(Received February 14, 1976)

INDO-SCF calculations were performed on several protonated compounds, $HCHOH^+$ CH_3CHOH^+, $(CH_3)_2COH^+$, $HCO_2H_2^+$, $CH_3CO_2H_2^+$, and $CH_3OH_2^+$, and also on the corresponding parent molecules in order to investigate their conformations and electronic structures. Geometric optimization resulted in reasonable conformations as compared with the previous *ab initio* calculations and in sufficient magnitudes of the energy differences between the rotational isomers in comparison with the NMR observations. The change in the electronic structures of the parent molecules due to protonation is also discussed by paying attention to the polarization caused by electron delocalization, hybridization at the proton-bound oxygen atom, the protonation energy, and the ionization potentials.

Protonated weak bases formed quantitatively in low-temperature "magic acid" solutions have hitherto received considerable attention, because such cations are important as intermediates in acid-catalyzed hydrolysis reactions and in the determination of Brønsted base strengths. Concerning the structures of tautomers or rotational isomers of the protonated species, Olah *et al.*[1] have extensively studied the low-temperature NMR spectra of these substances.

However, the structures of protonated aldehydes, ketones, acids, and alcohols, which were investigated in the present work, have been the object of only limited investigations as regards their molecular orbital treatments. Only protonated formaldehyde, acetaldehyde, and formic acid have been studied in detail in a few *ab initio* calculations. The geometric optimization of CH_3CHOH^+ and $HCO_2H_2^+$ by Ros[2] with small Gaussian basis set (32/2) brought about an incorrect relative stability of their rotational isomers, and large Gaussian basis set (73/3) calculations performed by Csizmadia *et al.*[3,4] improved the discrepancy of this relative stability on the base of results obtained under geometric assumptions.

Recently, the present authors have undertaken a semi-empirical INDO-MO study of several protonated compounds with particular attention being paid to their optimized conformations, electronic structures, and the magnitude of the energy difference between tautomers or rotational isomers. The present INDO calculations with sufficient geometric optimization were almost successfully carried out so that the above subjects may be discussed without any need to consider the solvent effect on the protonated species in super-acid solutions.

Method of Calculation

The semi-empirical calculations of HCHO, CH_3CHO, $(CH_3)_2CO$, HCO_2H, CH_3CO_2H, CH_3OH, and their protonated species (unstable alkoxy-protonated species were neglected in the protonated acids) were carried out using the INDO-SCF method[5] which is considered to be reliable for bond angles, but less so for bond lengths.[6]

The bond lengths and angles which are to be optimized are shown in Fig. 1 in which most of the fixed lengths and angles were taken from the standard tables,[7] except for those of HCHO and CH_3CHO (which were taken from Ref. 2). The optimization of geometric parameters was carried out by means of a repeated SCF-procedure. This was performed first on the bond lengths for fixed bond angles, then in turn on the angles until the most

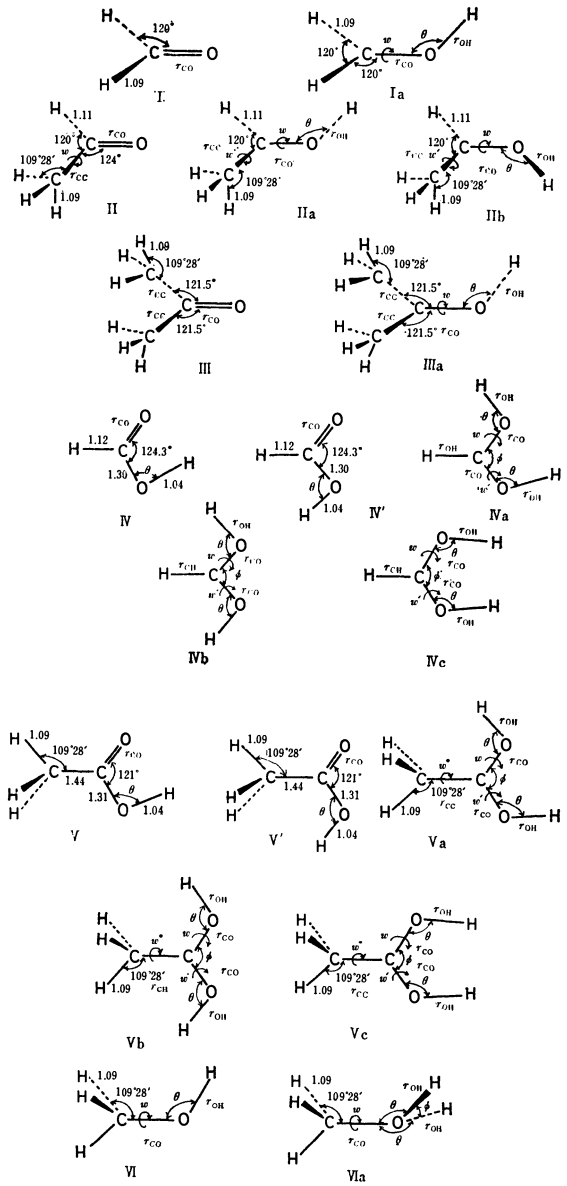

Fig. 1. Geometric parameters for parent molecules and protonated species.

stable conformations had identical bond lengths and angles, and finally the optimized geometries were recalculated by changing all their bond lengths and angles by the amounts of ± 0.02 Å and $\pm 2°$, respectively, as a check on the reliability of the optimization results. In the cases of $HCO_2H_2^+$ and $CH_3CO_2H_2^+$, the optimized r_{CO}, r_{OH}, and r_{HC} (or r_{CC}) values in the energetically most stable *cis-trans* isomer (IVa or Va in Fig. 1) were commonly used for the other unstable isomers.

Results and Discussion

Optimized Conformations. Let us first examine the optimized conformations of the parent molecules before discussing those of the protonated species. The bond length of the C=O bond was calculated to be slightly longer than the experimental value by 0.02—0.04 Å for all the molecules, except CH_3OH, with an overestimation of the θ values for the acids to the extent of *ca.* 4°, while the value (1.36 Å) for CH_3OH was shorter by 0.074 Å than the experimental value (1.434 Å[8]) with $r_{OH}=1.04$ Å (expt.[8])$=0.937$ Å) and $\theta=107°$ (expt.[8])$=105°56'$). Some parent molecules such as CH_3OH and HCHO have already been calculated by the INDO method without any geometric assumptions,[5] but the geometric assumptions used here did not show as serious defects in comparison with the complete optimization results,[5] so that the protonated species may be treated under same geometric assumptions as the parent molecules.

In regard to the rotations of the CH_3 group about the C–C bond (CH_3CHO) and about the C–O bond (CH_3OH), the rotational barriers obtained from the energy difference between the most stable staggered conformations (SII and SVI) and the most unstable eclipsed conformers (EII and EVI) were estimated to be 0.35 kcal/mol (expt.[9])$=1.16$ kcal/mol) for CH_3-CHO and 0.83 kcal/mol (expt.[8])$=1.07$ kcal/mol; *ab initio*[10])$=1.59$ kcal/mol) for CH_3OH (see Fig. 2). The INDO calculations resulted in smaller rotational barriers than those obtained from the experimental results, probably because the approximations involved in the INDO method neglect multiple-center (more than two-center) repulsion integrals.

Concerning two possible isomers of HCO_2H and CH_3CO_2H (Fig. 1), the *trans* forms (IV and V) of both the acids, which have smaller bond angles (θ) than the *cis* form by 1° were found to be more stable by 1.69

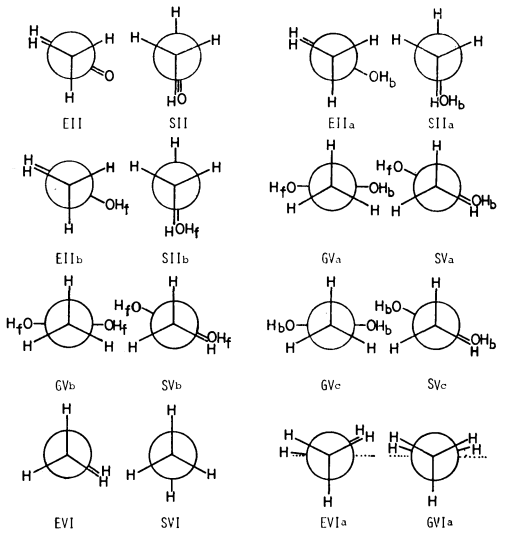

Fig. 2. Energetically most stable and unstable conformations of the protonated species during the CH_3 rotation around the C–C or C–O bond. (The subscripts of b and f mean the back and the front respectively.)

TABLE 1. OPTIMIZED VALUES FOR THE GEOMETRIC PARAMETERS

Species	$r_{C=O}$	r_{CO}	r_{OH}	r_{CC}	θ	ϕ	ω	ω'	ω''	r_{HC}
I	1.25(1.21)									
Ia		1.28(1.27)	1.05(0.985)		121°(120°)		90°(90°)			
II	1.26(1.22)			1.44(1.50)						
IIa		1.29(1.27)	1.04(0.985)	1.41(1.50)	119°(121°)		0°(0°)	0°(0°)		
IIb		1.29(1.27)	1.04(0.985)	1.42(1.50)	119°(118.5°)		0°(0°)	0°(0°)		
III	1.27(1.24)			1.45(1.55)						
IIIa		1.31	1.04	1.43	118°					
IV	1.26(1.25)				112°(107.8°)					
IV′	1.26(1.25)				113°(118°)					
IVa		1.30(1.31)	1.04(0.98)		118°(118°)[a]	118°(124°)	0°(0°)	0°(0°)		1.12(1.09)
IVb		1.30(1.31)	1.04(0.98)		118°(118°)	114°(124°)	0°(0°)	0°(0°)		1.12(1.09)
IVc		1.30(1.31)	1.04(0.98)		120°(121°)	125°(124°)	0°(0°)	0°(0°)		1.12(1.09)
V	1.27(1.25)				112°(107.8°)					
V′	1.27(1.25)				113°(107.8°)					
Va		1.31	1.04	1.44	117°	113°	0°	0°	0°	
Vb		1.31	1.04	1.44	118°	109°	0°	0°	0°	
Vc		1.31	1.04	1.44	119°	120°	0°	0°	0°	
VI		1.36(1.434)	1.04(0.937)		107°(105°56′)		0°			
VIa		1.39	1.04		121°	65°	0°			

Bond lengths are in Å units. Values in parentheses are experimental,[7] optimized[2] (underlined), and assumed values[2] (doubly underlined). a) 116° has been given for the other C–O–H angle.

kcal/mol for HCO_2H or by 5.33 kcal/mol for CH_3CO_2H than the other forms. The experimentally determined energy difference between *trans* (IV) and *cis* (IV') HCO_2H (IV is more stable than IV'), 2.0 kcal/mol, is well reflected in the computed value of 1.63 kcal/mol, even though previous *ab initio* calculations of IV and IV' gave overestimated energy differences of 8.1 kcal/mol (for (32/2) basis sets)[2] and 9.46 kcal/mol (for (73/3) basis sets).[3] The energy difference (1.69 kcal/mol) between IV and IV' of $H_aC(=O_a)OH_b$ can be roughly explained using the Coulomb attraction or repulsion energy estimated from $0.5292Q_AQ_B/r_{AB}$ (Q_A and Q_B=formal charges of A and B atoms; r_{AB}=nuclear distance between A and B). As a result, the difference in the Coulomb attractions (IV—IV'=3.34 kcal/mol for the O_a–H_b and −1.29 kcal/mol for the negatively charged H_a-positively charged H_b attractions) makes IV more stable than IV' by 2.05 kcal/mol. The energy difference between V and V' for $CH_3C(=O_a)OH_a$ was also explained similarly by the O_a–H_a attraction and the CH_3–H_a repulsion. It is noteworthy here that, in the *trans* isomers of both the acids, hydrogen bonding cannot be expected between the O_a and H_b (or H_a) atoms (overlap populations were negative).

Now, let us focus on the optimized conformations of the protonated species (Table 1). Protonation on the oxygen atom resulted the C–O bond length being increased by 0.03—0.04 Å with respect to the r_{CO} of the parent molecule. The magnitude of the C–O bond stretching was in good agreement with that expected from *ab initio* calculations of $HCO_2H_2^+$ and $CH_3CO_2H_2^+$,[2] but the r_{OH} value of 1.04 Å given consistently for all the protonated species except $HCHOH^+$ (r_{OH}=1.05 Å) appears to be considerably overestimated in comparison with r_{OH}=0.985 Å of $HCO_2H_2^+$ calculated by Ros.[2]

In regard to the bond angles, the C–O–H bond angle (θ) fell in the range from 117° (Va) to 121° (VIa), and those of Ia and Va, b, c, were found to be almost identical for both the INDO and *ab initio*[2] calculation results. Interestingly, the O–C–O bond angles (ϕ) which were assumed to be 124°[2] or 120°[3] in the previous *ab initio* calculations are different for the three isomers of the protonated acids. They increased systematically for a decrease in the distance between the two hydrogen atoms of the O–H bonds, that is, with increasing H–H repulsion. However, the magnitude of the change in the ϕ value (11°) appears to be too large, nevertheless the INDO calculation tends to underestimate the electron-electron repulsions.[5,11]

Here, we will discuss the CH_3 rotation about the C–C bond for the two isomers of CH_3CHOH^+ and the three isomers of $CH_3CO_2H_2^+$ and about the C–O bond for $CH_3OH_2^+$. As can be seen from Fig. 2, the staggered (SIIa, SIIb, SVa, SVb, and SVc) and gauche-like (GVIa) conformations having minimum H–H repulsions or maximum H–O attractions were found to be the most stable, while the eclipsed (EIIa, EIIb, and EVIa) structures possessing maximum H–H repulsion and the gauche structures (GVa, GVb, and GVc) having minimum H–O attraction were the most unstable. The rotational barriers falling in the range of 0.005—0.48 kcal/mol indicate free CH_3 rotations in the above protonated species except for *trans*-CH_3CHOH^+ (barrier=0.86 kcal/mol). Therefore, the CH_3 rotation, especially that in $CH_3CO_2H_2^+$, does not appear to play an important role in the determination of the relative stability of the protonated isomers.

Charge Densities, Protonation Energies, Dipole Moments, and Ionization Potentials. The change in the electron distributions for protonation will be discussed first by noticing the charge densities of the parent molecules and the energetically most stable protonated conformers

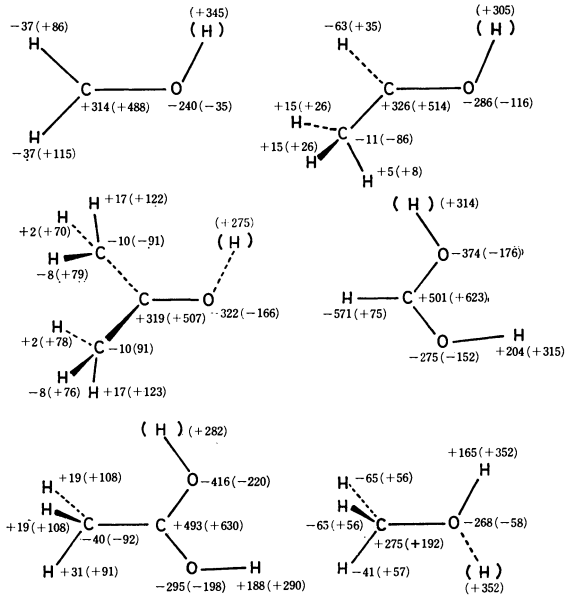

Fig. 3. Change in the charge distribution on the protonation. (Values in parentheses are those of the most stable protonated conformers, and all the values are in units of 10^{-3} electrons.)

(Fig. 3). Ros[2] has already pointed out on the basis of the results of his *ab initio* calculation that there is a general shift (polarization) of electrons from the terminal carbon-bound hydrogens (but not from the proton-bound oxygen) towards the incoming proton. This trend was also observed from the change in the charge distributions estimated by the present INDO calculations. The computed charge distributions appear reliable in view of the fact that the computed dipole moments of the parent molecules (those of the protonated species are unknown) are in satisfactory agreement with the experimental values.[12–16]

The protonation also brought about a change in the electronic properties of the parent molecule, especially in the bond between the carbon and the proton-bound oxygen. The protonation decreased the overlap population of the above C–O bond by from 7.9% (HCHO) to 12.4% (CH_3CO_2H). The decrease in the π-type overlap population (16.8% for HCHO–35.5% for CH_3CO_2H) was found to be more marked than for the σ-type (5.0% for CH_3CHO–6.8% for CH_3CO_2H). The remarkable change in the π-conjugation of the C–O bond on the protonation is ascribed not only to the stretching of the C–O bond but also to the change in the hybridization at the proton-bound oxygen atom,

TABLE 2. ELECTRONIC PROPERTIES OF THE PARENT AND PROTONATED SPECIES

Species	Dipole moment/eV		*PA*/kcal mol^{-1}		*IP*/eV		Overlap population of C–O		
	Calcd	Obsd	Calcd	Obsd	Calcd	Obsd	π	σ	Total
I	2.10	2.27[a]	227	166[f]	13.92	10.87[f]	0.198	0.701	0.899
Ia	3.13				26.21		0.165	0.664	0.829
II	2.86	2.72[a]	308	183[f]	13.26	10.28[f]	0.185	0.679	0.864
IIa	7.62				23.57		0.137	0.645	0.782
IIb	4.65				24.24		0.139	0.644	0.783
III	2.26	2.90[b]	328	202[g]	12.79	9.92[h]	0.174	0.655	0.829
IIIa	3.18				22.42		0.118	0.618	0.736
IV	1.68	1.42[c]	310	175[g]	13.63	11.05[i]	0.173	0.692	0.865
IV′	4.36				13.49		0.173	0.693	0.866
IVa	2.46				24.94		0.118	0.643	0.761
							(0.120)	(0.647)	(0.767)
IVb	2.47				24.65		0.119	0.647	0.766
IVc	4.70				25.08		0.119	0.647	0.766
V	1.80	1.50[d]	334	188[g]	12.87	10.35[i]	0.162	0.668	0.830
V′	4.89				12.73		0.162	0.668	0.830
Va	2.44				23.86		0.105	0.623	0.728
							(0.106)	(0.627)	(0.733)
Vb	3.95				23.35		0.105	0.634	0.739
Vc	2.74				24.15		0.105	0.627	0.732
VI	1.75	1.83[e]	273	180[g]	14.30	10.85[i]	0.036	0.601	0.637
VIa	6.39				24.57		0.021	0.562	0.583

Values in parentheses are those for the *trans* C–O bond with respect to the H–C bond. a) Ref. 12. b) Ref. 13. c) Ref. 14. d) Ref. 15. e) Ref. 16. f) Ref. 18. g) Ref. 19. h) Ref. 20. i) Ref. 21.

because the magnitude of the decrease in the π-type overlap population for a simple expansion of the C–O bond length without the incoming proton is markedly different from that for protonation. For example, the simple stretching of r_{CO} in HCHO from 1.25 Å (the optimized r_{CO} for HCHO) to 1.28 Å (the r_{CO} for $HCHOH^+$) decreased the π overlap population from 0.198 to 0.187, while protonation decreased it from 0.198 to 0.165. This trend can also be recognized in the other species, even in CH_3OH which has a pseudo π-conjugation at the C–O bond (π bond-orders=0.223 in CH_3OH and 0.139 in $CH_3OH_2^+$). The change in the hybridization at the oxygen atom upon protonation results in a protonation energy (proton affinity), because hybridization of the oxygen lone-pairs (defined by the %s or %p character) correlates linearly with the proton affinity (PA).[17] In this sense, the incoming proton predominantly interacts not only with the highest-occupied (HO), nonbonding oxygen-lone-pair-orbital expanding perpendicularly to the C–O bond axis, but also with the oxygen lone-pair orbital conjugating with the carbon pi-orbital at the lower MO (next to the HOMO). In this respect, the order of the computed *PA* values which correspond consistently to one half of the magnitude of the observed results[18,19] was well reflected in that of the observed *PA* values (Table 2). Protonation at the oxygen atom also decreased the electron density predominantly on the HO oxygen-lone-pair orbital and lowered the ionization potential (*IP*) of the parent molecule. As can be seen from Table 2, the IP values of the parent molecules became markedly large due to the protonation, and the computed *IP* values, IP_{calcd}, were found to be systematically overestimated in comparison with the observed *IP* values,[20,21] IP_{obsd}, ($IP_{obsd}/IP_{calcd}\approx 0.8$).

Relative Stability between the Rotational Isomers. In CH_3CHOH^+, $HCO_2H_2^+$, and $CH_3CO_2H_2^+$, two keto-protonated isomers have been proposed for each species as the result of NMR spectroscopic investigations:[1] IIa and IIb, IVa and IVb, and Va and Vb in Fig. 1. The relative stabilities determined using the present INDO calculations, the previous *ab initio* computations,[2–4] and by the NMR spectra[1] are summarized in Fig. 4. In regard to the energy difference (1.85 kcal/mol) between IIa and IIb, the present INDO result is in good agreement with the experimental value (about 1 kcal/mol) and with the *ab initio* calculations for large Gaussian basis sets[3] (1.15 kcal/mol), although small basis sets of Gaussian exponents (32/2)[2] failed in the estimation of the relative stability between IIa and IIb (IIa was computed to be less stable than IIb). The Coulomb repulsion of H_a–H_b in $CH_3CH_aOH_b^+$ (1.55 and 2.41 kcal/mol for IIa and IIb, respectively) and of CH_3–H_b (6.29 and 6.98 kcal/mol for IIa and IIb, respectively) makes the *cis* isomer (IIa) more favorable energetically than the other isomer (IIb) by 1.55 kcal/mol, a value which roughly corresponds to the energy difference between IIa and IIb. A remark should be made about the H_a–H_b repulsion: a value (2.41 kcal/mol for IIb) larger than this value (1.55 kcal/mol for IIa) was given by the larger positive charge of H_a (0.074) in IIb ($Q_{H_b}=+0.303$; $r_{H_a-H_a}=2.976$ Å) as compared with that of H_a (0.035) in IIa ($Q_{H_b}=+0.305$; $r_{H_a-H_a}=2.284$ Å). In this respect, the energy contribution terms listed in Table 3 indicate that IIa has smaller nuclear repulsions and larger one-electron attractions than IIb.

The relative stabilities of the protonated isomers of $HCO_2H_2^+$, IVa>IVb>IVc, was in agreement with the

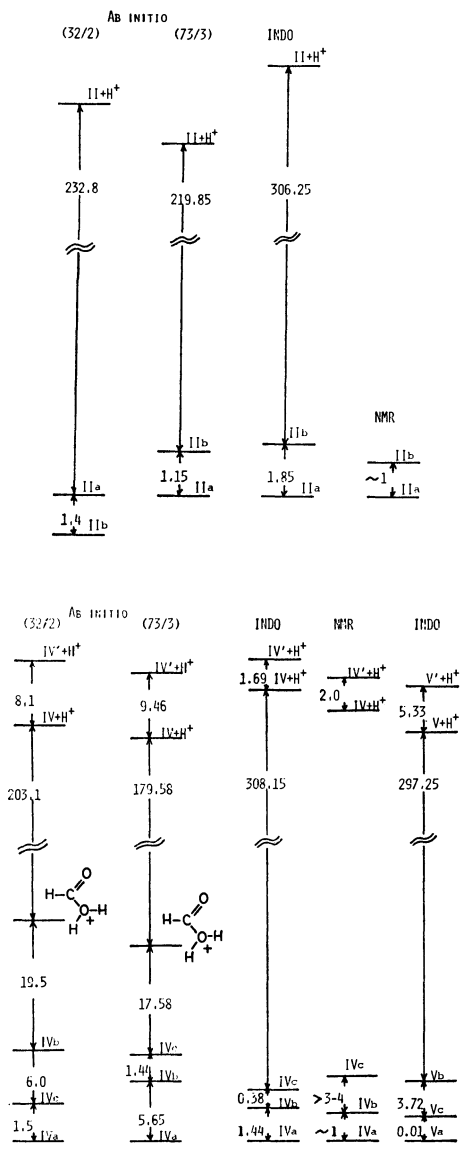

Fig. 4. Energy difference between the protonated isomers. (Values are in units of kcal/mol.)

Table 3. Energy contribution terms for parent and protonated species

Species	Total energy a.u.	One-electron energy a.u.	Inter-electronic repulsion a.u.	Nuclear repulsion a.u.
II	−34.1955	−130.4510	57.0996	39.1559
IIa	−34.6863	−137.3585	58.2054	39.1559
IIb	−34.6833	−135.9006	56.5944	44.6223
IV	−43.3811	−148.0520	65.7870	38.8839
IV′	−43.3784	−147.4676	65.4633	38.6259
IVa	−43.8749	−152.4360	64.4880	44.0731
IVb	−43.8726	−152.2294	64.3953	43.9615
IVc	−43.8720	−152.1936	64.3338	43.9878
V	−51.8375	−217.5575	97.8508	67.8691
V′	−51.8290	−217.5589	97.8074	67.9225
Va	-52.3699_2	−222.7850	96.4307	73.9844
Vc	-52.3699_0	−222.5534	96.3056	73.8779
Vb	−52.3640	−222.6517	96.3570	73.9307

NMR results[1] and with the results of the *ab initio* calculation obtained by Csizmadia *et al.*[3] (Ros's data: IVa>IVc>IVb). Although the energy difference (1.44 kcal/mol) between IVa and IVb corresponds approximately to that (about 1 kcal/mol) of the NMR results, the difference (0.38 kcal/mol) between IVb and IVc is too small for comparison with the experiment (3—4 kcal/mol).[1] This may be attributable to an underestimation of the electron-electron repulsions. As can be seen from Table 3, the small repulsion terms, especially the electron repulsions, which favor IVc and IVb rather than IVa, were overcome by the one-electron energy term, and the relative stabilities follow the order: IVa>IVb>IVc.

Concerning the isomers of $CH_3CO_2H_2^+$, a discrepancy between the order of relative stabilities calculated by the INDO calculations (Va>Vc>Vb) and that found from the NMR spectra (Va>Vb≫Vc)[1] was observed. This discrepancy may also be ascribed to an underestimation of the electron repulsion in view of the fact that the electron repulsion, in addition to the nuclear repulsion, makes Vc most favorable, even though a reasonable order (Va>Vb>Vc) can be obtained from the attraction term. It should be stressed here that the *cis-trans* conformers (IVa and Va) in both the acids were not stabilized by the hydrogen bonding between the *cis*-oxygen and the *trans*-hydrogen atoms because the appreciable long distances between the two atoms (about 2.40 Å in IVa and about 3.31 Å in Va) brought about negative overlap populations (−0.0008 for IVa and −0.0002 for Va), even though the effect of the hydrogen bonding has been demonstrated on the basis of the IR spectroscopic investigation of protonated carboxylic acids.[22]

At any rate, the present INDO calculations of the protonated isomers brought about sufficient results for the determination of their relative stabilities in contrast with the previous *ab initio* calculation results.[2-4]

The calculations were carried out on a FACOM 230-75 computer at the Data Processing Center of Kyushu University.

References

1) G. A. Olah, A. M. White, and D. H. O'Brien, *Chem. Rev.*, **70**, 561 (1970), and references therein.
2) P. Ros, *J. Chem. Phys.*, **49**, 4902 (1968).
3) A. C. Hopkinson, K. Yates, and I. G. Csizmadia, *J. Chem. Phys.*, **52**, 1784 (1970).
4) A. C. Hopkinson and I. G. Csizmadia, *Can. J. Chem.*, **52**, 546 (1974).
5) J. A. Pople and D. L. Beveridge, "Approximate Molecular Orbital Theory," McGraw-Hill, New York, N. Y. (1970).
6) M. D. Newton, W. A. Lathan, W. J. Hehre, and J. A. Pople, *J. Chem. Phys.*, **52**, 4064 (1970).
7) L. E. Sutton, Ed., "Interatomic Distances," Chem. Soc., London, Special Publication No. 11 (1958), and No. 18 (1965).
8) E. V. Ivash and D. M. Dennison, *J. Chem. Phys.*, **21**, 1804 (1953).
9) R. W. Kilb, C. C. Lin, and E. B. Wilson, Jr., *J. Chem. Phys.*, **26**, 1695 (1957).

10) L. Pederson and K. Morokuma, *J. Chem. Phys.*, **46**, 3941 (1967).
11) H. Fisher, H. Kollmar, and H. O. Smith, *Tetrahedron Lett.*, **1968**, 5821.
12) I. Omura, K. Higashi, and H. Baba, *Bull. Chem. Soc. Jpn.*, **29**, 504 (1956).
13) C. H. Townes and A. L. Shawlow, "Microwave Spectroscopy," McGraw-Hill, New York, N. Y. (1955).
14) H. Kim, R. Keller, and W. D. Gwinn, *J. Chem. Phys.*, **37**, 2748 (1962).
15) J. O. Jenkins and J. W. Smith, *J. Chem. Soc., B*, **1970**, 1538.
16) D. A. Ibbitson and L. F. Moore, *J. Chem. Soc., B*, **1967**, 80.
17) K. Ohkubo, K. Tsuchihashi, T. Yoshida, and M. Okada, *Bull. Chem. Soc. Jpn.* **49**, 480 (1976).
18) J. L. Beauchamp and R. C. Dunbar, *J. Am. Chem. Soc.*, **92**, 1477 (1970).
19) J. Long and B. Munson, *J. Am. Chem. Soc.*, **95**, 2427 (1973).
20) J. D. Morrison and A. J. C. Nicholson, *J. Chem. Phys.*, **20**, 1021 (1952).
21) K. Watanabe, *J. Chem. Phys.*, **26**, 542 (1957).
22) C. J. Clemett, *Chem. Commun.*, **1970**, 211.

Thermal Decomposition of Dimethyl Ether in the Presence of Nitrogen Oxide

Kohji TADASA,* Naomi IMAI, Tetsuo INABA, and Yutaka KUBOKAWA**
Faculty of Liberal Arts and Sciences, University of Osaka Prefecture, Sakai, Osaka 591
(Received March 19, 1976)

The effect of NO addition on the thermal decomposition of CH_3OCH_3 has been studied at 500 °C. The rate of pyrolysis decreases markedly when the amount of NO is small, but increases linearly with increase in amount. Acceleration of pyrolysis was studied. Major reaction products are CH_4, CH_2O, CO, H_2O, and N_2, the minor ones being H_2, N_2O, and C_2H_6. The quantities of all the products were determined under different conditions except CH_2O and H_2O. It was found that the rate of formation is nearly of first order with respect to both NO and CH_3OCH_3. A reaction scheme is proposed. It is suggested that the rate of decomposition is nearly equal to that of the second order reaction $NO+CH_3OCH_3 \rightarrow HNO+CH_3OCH_2$.

The thermal decompositions of lower hydrocarbons, aldehydes, ketones, ethers *etc.* proceed *via* free radical chain reactions in the gas phase. Nitrogen oxide has been used as an effective inhibitor for these free-radical reactions, since it combines readily with free radicals. Nitrogen oxide, however, reacts easily with the molecules of these organic compounds, forming free radicals. Thus, the two effects of nitrogen oxide, inhibitive and accelerative, make the reaction mechanism very complicated.

When nitrogen oxide is added in a free-radical thermal decomposition of an organic substance, the rate of the reaction first decreases and then increases with the amount of addition, giving rise to a minimum rate. The minimum rate is not sufficiently small as compared with the uninhibited rate to suggest that the free-radical reaction is completely surpressed, even at the minimum rate, owing to the accelerating action of nitrogen oxide. In the case of dimethyl ether, however, the minimum rate is very small as compared with the uninhibited rate, and the inhibitive and the accelerative parts are distinctly separated in the nitrogen oxide pressure-rate curve. Thus, dimethyl ether is thought to be suitable for the study of the effects of nitrogen oxide on pyrolysis.

Investigations[1–3] has been carried out on the nitrogen oxide inhibited pyrolysis of dimethyl ether mainly following the total pressure change. We have measured the quantities of the reaction products under different conditions and derived a reaction scheme.

Experimental

Commercial dimethyl ether and nitrogen oxide were purified by repeated bulb-to-bulb distillation.

The reaction was studied at 500 °C in a conventional static system. The products of the pyrolysis were separated by means of cold traps and a Toepler pump, and analyzed quantitatively by gas chromatography. The apparatus, techniques of separation and analysis are similar to those described previously.[4]

Results

All the runs were carried out at 500 °C. The quantitative analyses were made for CH_4, CO, N_2, N_2O, H_2, and C_2H_6, among the products of pyrolysis. CH_2O and H_2O were formed in large amounts, but these were not determined because of inaccuracy of the measurements.

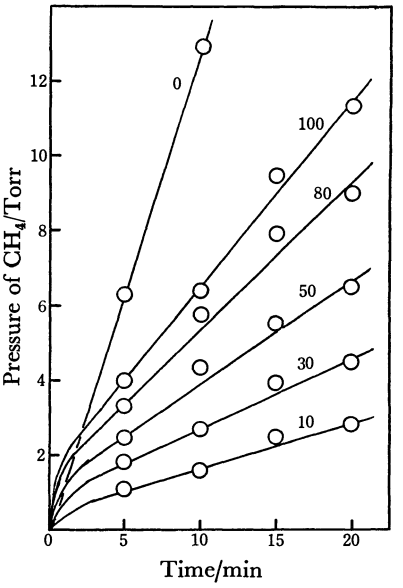

Fig. 1(a).

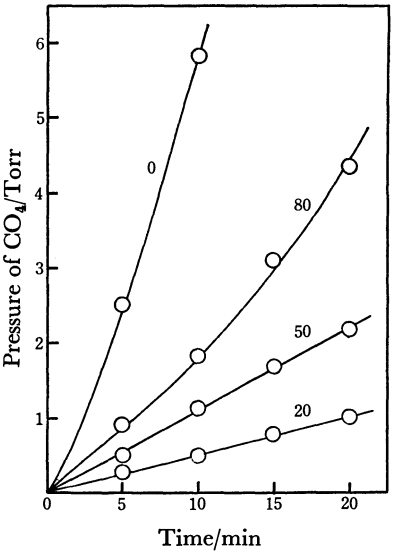

Fig. 1(b).

* Present address: Department of Agricultural Chemistry, College of Agriculture, Shinshu University, Ina, Nagano 396.
** Present address: Department of Applied Chemistry, College of Engineering, University of Osaka Prefecture, Sakai, Osaka 591.

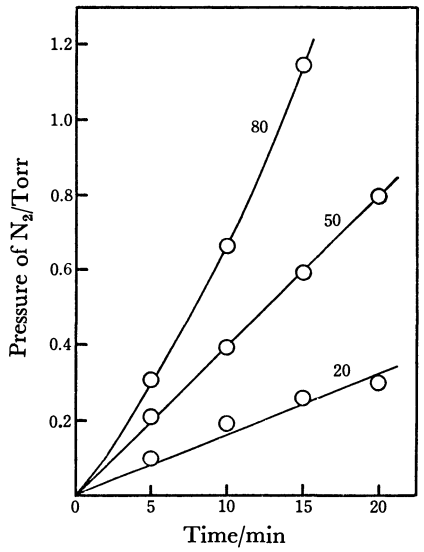

Fig. 1(c).

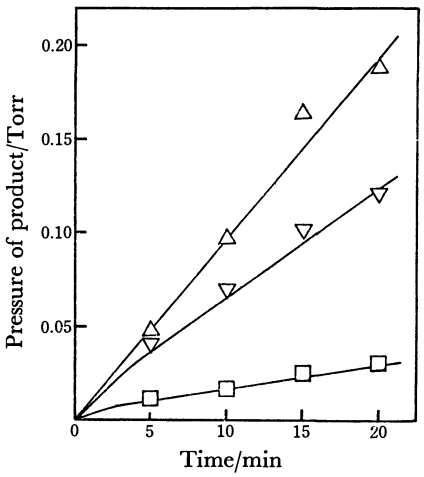

Fig. 1(d).

Fig. 1. Yields of products in the pyrolysis of 100 Torr CH_3OCH_3 and various NO pressures (in Torr) at 500 °C.
(a) CH_4, (b) CO, (c) N_2, (d) △: H_2, ▽: N_2O, □: C_2H_6 (×10).
P_{NO}=50 Torr.

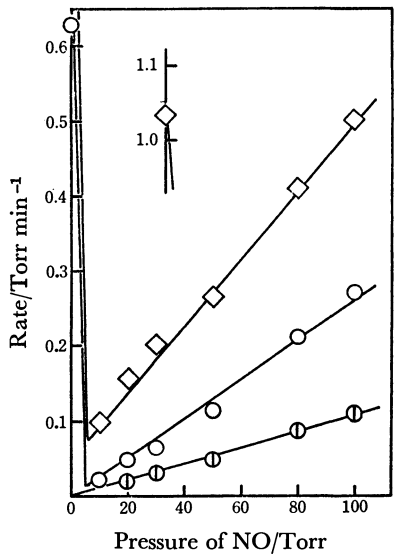

Fig. 2(a).

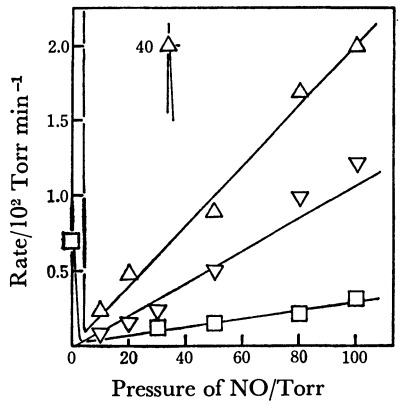

Fig. 2(b).

Fig. 2. Plot of rate of formation *vs.* NO pressure for the pyrol sis of 100 Torr CH_3OCH_3 at 500 °C.
(a) ◇: CH_4, ○: CO, ⓘ: N_2,
(b) △: H_2, ▽: N_2O, □: C_2H_6 (×10).

No CH_3OH was observed in detectable amount, although it is an important pyrolysis product of CH_2O.

The yields of the products were determined at different times during the course of uninhibited and inhibited pyrolyses. Some results are shown in Fig. 1. For most products the yields increase linearly with time from the beginning of the reaction. The rate of CH_4 formation, however, is higher in the initial period of the pyrolysis than after 5 min, as is often the case in pyrolysis. The rate of CH_4 formation was obtained from intercept of the slope in the yield-time plot.

The dependence of the rate of product formation on the pressure of NO added to the reaction mixture is shown in Fig. 2 for the pyrolysis of CH_3OCH_3 at 100 Torr pressure and 500 °C. In the uninhibited pyrolysis, the rates of formation are 1.04, 0.63, and 0.40 Torr min^{-1} for CH_4, CO, and H_2 respectively, addition of 10 Torr of NO reducing them to 0.095 (9% of uninhibited rate), 0.015 (2%), and 0.0025 (0.6%), respectively. The addition of an increased amount of NO causes a linear increase in the rates of formation of all products analyzed. The extrapolated straight lines pass through the origin except for CH_4 which has a small intercept on the vertical axis.

Figure 3 shows the relation between the rates of product formation and the CH_3OCH_3 pressure in the pyrolysis with 50 Torr of NO. The plots show linearity except for CH_4, for which the plot gives a curve slightly concave downwards.

Discussion

The thermal decomposition of CH_3OCH_3 has been established by a number of workers to proceed by a free-radical chain process, which is as follows.[5-7]

$$CH_3 + CH_3OCH_3 \longrightarrow CH_4 + CH_3OCH_2$$
$$CH_3OCH_2 \longrightarrow CH_2O + CH_3$$

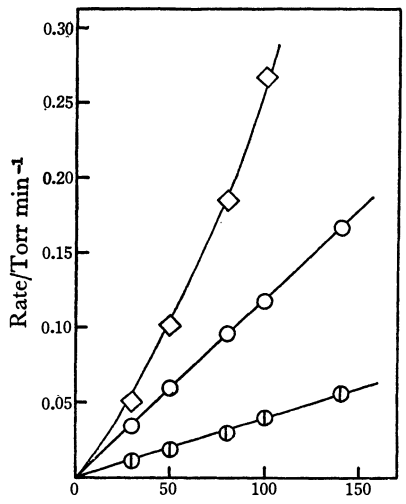

Fig. 3(a).

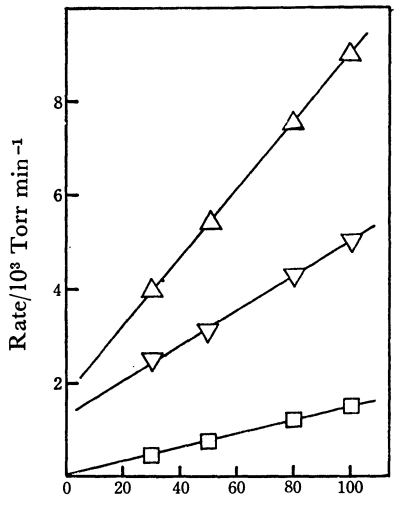

Fig. 3(b).

Fig. 3. Plot of rate of formation *vs.* CH_3OCH_3 pressure for the pyrolysis of 50 Torr NO at 500 °C.
(a) ◇: CH_4, ○: CO, ⓘ: N_2,
(b) △: H_2, ▽: N_2O, □: C_2H_6 (×10).

It has been established that CH_2O once produced also undergoes free-radical chain decomposition.[6,8]

$$CH_3 + CH_2O \longrightarrow CH_4 + CHO$$
$$H + CH_2O \longrightarrow H_2 + CHO$$
$$CHO + M \longrightarrow CO + H + M$$

Thus CH_3OCH_3 decomposes by two stoichiometric steps:

$$CH_3OCH_3 \longrightarrow CH_4 + CH_2O \quad (I)$$
$$CH_2O \longrightarrow CO + H_2 \quad (II)$$

Accordingly the rates of CO and H_2 formation increase with time in the early period. In Fig. 1(b) (NO=0 Torr) a concave curve is shown for the CO yield.

In the pyrolysis with NO, however, the CO yield increases linearly with time, suggesting that CO is not a secondary product. Stoichiometric relation (II) does not hold in the inhibited pyrolysis, since the H_2 yield is much smaller than that of CO.

In this work, the major products analyzed are CH_4, CO, and N_2, the N_2 yield being about half that of CO. The same ratio of CO and N_2 is also observed in the CH_2O–NO pyrolysis, where the following stoichimetry holds approximately.

$$CH_2O + NO \longrightarrow CO + H_2O + (1/2)N_2$$

A similar ratio of CO and N_2 found in the CH_3OCH_3–NO pyrolysis seems to suggest that they are formed by processes similar to the CH_2O–NO pyrolysis. By the addition of NO, CH_3OCH_3 seems to decompose according to two stoichiometric relations:

$$CH_3OCH_3 \longrightarrow CH_4 + CH_2O \quad (I)$$
$$CH_3OCH_3 + NO \longrightarrow CH_4 + CO + H_2O + (1/2)N_2 \quad (II)$$

Thus the following relation is expected to hold between the rates of product formation.

$$R_{CH_2O} = R_{CH_4} - R_{CO}$$
$$R_{H_2O} = R_{CO} = 2R_{N_2}$$

McKenney *et al.*[3] studied the NO inhibited pyrolysis of CH_3OCH_3 over the temperature range 500—600 °C and proposed a reaction mechanism, which indicates that NO inhibits the reaction by

$$CH_3 + NO \rightleftharpoons CH_3NO \rightleftharpoons CH_2NOH \longrightarrow \text{products}$$

and

$$CH_3 + CH_2NOH \longrightarrow CH_3CH_2\text{–}NOH \longrightarrow C_2H_6 + NO$$

while it accelerates the reaction by

$$NO + CH_3OCH_3 \longrightarrow HNO + CH_3OCH_2$$

According to their scheme, CH_3 and H, the latter being formed by the decomposition of HNO,

$$HNO + M \longrightarrow H + NO + M$$

take part in the chain decomposition of CH_3OCH_3, even when a sufficient amount of NO is added. According to their argument, R_{CH_4} is expressed by

$$R_{CH_4} \propto [CH_3OCH_3]^{3/2}$$

being independent of [NO]. R_{H_2} should be equal to a half of the NO accelerated part of the rate of CH_3OCH_3 decomposition. Their prediction concerning R_{CH_4} and R_{H_2} is not consistent with the results we obtained at 500 °C.

The results we obtained show kinetics and stoichiometry which lead to the following scheme.

$$NO + CH_3OCH_3 \longrightarrow HNO + CH_3OCH_2 \quad (1)$$
$$NO + CH_3OCH_2 \longrightarrow HNO + CH_3 + CHO \quad (2)$$
$$NO + CH_3OCH_2 \longrightarrow CH_3NO + CH_2O \quad (3)$$
$$NO + CH_3 \longrightarrow CH_3NO \quad (4)$$
$$NO + CHO \longrightarrow HNO + CO \quad (5)$$
$$CH_3NO + HNO \longrightarrow CH_4 + NO + NO \quad (6)$$
$$HNO + HNO \longrightarrow OH + OH + N_2 \quad (7)$$
$$OH + HNO \longrightarrow H_2O + NO \quad (8)$$
$$CH_3OCH_3 + M \longrightarrow CH_3 + CH_3O + M \quad (9)$$
$$NO + CH_3O \longrightarrow HNO + CH_2O \quad (10)$$

In contrast to that of McKenny *et al.*, the scheme indicates that HNO and CH_3NO do not decompose, but they react with each other or react with radicals, *i.e.*, Eqs. 6—8.

The above reaction Schemes (1—10) give the following relations with regard to the reaction rates.

$$R_{CH_4} = R_6 = R_1 + R_9 = k_1[NO][CH_3OCH_3] + k_9[CH_3OCH_3][M] \quad (i)$$

$$R_2 = \{k_2/(k_2+k_3)\}R_1$$

$$R_3 = \{k_3/(k_2+k_3)\}R_1$$

$$R_5 = R_2 = 2R_7 = R_8$$

$$R_{CO} = R_5,\ R_{N_2} = R_7,\ R_{H_2O} = R_8$$

hence

$$R_{CO} = R_{H_2O} = 2R_{N_2} = \{k_1k_2/(k_2+k_3)\}[NO][CH_3OCH_3] \quad (ii)$$

$$R_{CH_2O} = R_3 + R_{10} = R_3 + R_9 = \{k_1k_3/(k_2+k_3)\}[NO][CH_3OCH_3] + k_9[CH_3OCH_3][M] \quad (iii)$$

The experimental results satisfy the reaction orders in Eqs. i, ii, and iii. In Eq. i the first term represents the rate of the reaction between NO and CH_3OCH_3 (1), and the second one represents that of the initiating step in the thermal chain decomposition of CH_3OCH_3 alone (9). This might be due to the fact that the second term is very small compared with the first term in Eq. i, the CH_4 line intersects the Y axis just above the origin in Fig. 2(a), and the CH_4-curve is slightly concave in Fig. 3(a). The reaction orders of the CO and N_2 formation in Eq. ii are satisfied by the results in Figs. 2(a) and 3(a). Eqs. i, ii, and iii give the relation

$$R_{CH_2O} = R_{CH_4} - R_{CO}$$

which is also supported by the results.

The following reactions are proposed for the formation of minor products H_2, N_2O, and C_2H_6.

$$HNO + HNO \longrightarrow H_2 + NO + NO \quad (11)$$

$$HNO + HNO \longrightarrow H_2O + N_2O \quad (12)$$

$$CH_3NO + CH_3NO \longrightarrow C_2H_6 + NO + NO \quad (13)$$

When the rates of Eqs. 11, 12, and 13 are much smaller than those of Eqs. 6, 7, and 8, the following rate equations result from Schemes 1—13.

$$R_{H_2} = R_{11} = (k_{11}/k_7)R_7 = (k_{11}/2k_7)R_2 = \{k_1k_2k_{11}/2k_7(k_2+k_3)\}[NO][CH_3OCH_3]$$

$$R_{N_2O} = R_{12} = (k_{12}/k_7)R_7 = (k_{12}/2k_7)R_2 = \{k_1k_2k_{12}/2k_7(k_2+k_3)\}[NO][CH_3OCH_3]$$

$$R_{C_2H_6} = \{2k_1(k_2+k_3)k_7k_{13}/k_2k_6^2\}[NO][CH_3OCH_3]$$

These rate equations coincide with the reaction orders found experimentally (Fig. 2(b) and Fig. 3(b)). Since Eqs. 11, 12, and 13 are much slower than Eqs. 1—8, the addition of Eqs. 11, 12, and 13 to Schemes 1—10 does not cause any serious change in the rate equations (Eqs. i, ii, and iii).

The following ratios of the rate constants are obtained from the results.

$$k_2/k_3 = 1.5$$

$$k_{11}/k_7 = 0.017$$

and

$$k_{12}/k_7 = 0.011$$

It is well-known that HNO reacts with itself by Eq. 12,[9] but Eq. 7 has been suggested to take place more quickly at about 500 °C.[4,10] Both reactions (Eqs. 7 and 11) involve the internal rearrangement of $(HNO)_2$, while, in Reactions 6, 8, 11, and 13, HNO or CH_3NO release H or CH_3 when they react with each other or react with radicals. Reactions of the latter type have been proposed by Szabó.[11]

In the reaction schemes proposed above, radicals, CH_3OCH_2, CHO, and CH_3O are attached by NO before they decompose. Even if these radicals decompose first and then the fragment radicals or atoms combine with NO, the above rate equation does not change. As an example, replacement of Eq. 5 by the following two steps

$$CHO + M \longrightarrow CO + H + M$$

and

$$H + NO + M \longrightarrow HNO + M$$

does not alter the rate of the CO formation (Eq. iii).

NO undergoes disproportionation to N_2 and NO_2 in the presence of free radicals, according to the following mechanism.[12]

$$NO + R \longrightarrow RNO$$

$$RNO + 2NO \longrightarrow RNO(NO)_2 \longrightarrow RN_2ONO_2 \longrightarrow R + N_2 + NO_3$$

$$NO_3 + NO \longrightarrow NO_2 + NO_2$$

The reactions do not seem to be important since they cannot explain the reaction order of N_2 formation. No NO_2 was observed amongst the pyrolysis products.

References

1) L. A. K. Staveley and C. N. Hinshelwood, F. R. S., *Proc. R. Soc. London, Ser. A*, **159**, 192 (1937); M. J. Molera, J. A. G. Dominguez, and E. G. Olea, *An. Quim.*, **69**, 445 (1973).

2) N. Imai and O. Toyama, *Bull. Chem. Soc. Jpn.*, **35**, 860 (1962).

3) D. J. Mckenney, B. W. Wojciechowski, and K. J. Laidler, *Can. J. Chem.*, **41**, 1993 (1963).

4) K. Tadasa, N. Imai, and T. Inaba, *Bull. Chem. Soc. Jpn.*, **47**, 548 (1974).

5) F. O. Rice and K. F. Herzfeld, *J. Am. Chem. Soc.*, **56**, 284 (1934); J. A. Leemakers, *ibid.*, **56**, 1899 (1934).

6) S. W. Benson, *J. Chem. Phys.*, **25**, 27 (1956); S. W. Benson and D. V. S. Jain, *ibid.*, **31**, 1008 (1959).

7) D. J. McKenney and K. J. Laidler, *Can. J. Chem.*, **41**, 1984 (1963).

8) S. Kodama, Y. Takezaki, and R. Fujie, *Nippon Kagaku Zasshi*, **72**, 892 (1951).

9) R. Atkinson and R. J. Cvetanović, *Can. J. Chem.*, **51**, 370 (1973).

10) K. Tadasa, N. Imai, and T. Inaba, *Bull. Chem. Soc. Jpn.*, **47**, 2979 (1974).

11) Z. G. Szabó, *Nature*, **170**, 246 (1952); Z. G. Szabó, P. Huhn, and A. Bergh, *Adv. Catal.*, **9**, 343 (1957); Z. G. Szabó and F. Márta, *J. Am. Chem. Soc.*, **83**, 768 (1961).

12) M. I. Christie, *Proc. R. Soc. London, Ser. A*, **249**, 248, 258 (1959); E. J. Burrel, *J. Phys. Chem.*, **66**, 401 (1962); M. I. Chrie and M. A. Voisey, *Trans. Faraday Soc.*, **65**, 408 (1969); M. I. Christie and J. M. Edwards, *J. Chem. Soc., A*, **1969**, 1134.

Solid-state Properties of Evaporated Methyl Viologen

Kentaro MURANO, Yusuke KAMURA,* and Hiroo INOKUCHI**
The Institute for Solid State Physics, The University of Tokyo, Roppongi, Minato-ku, Tokyo 106
(Received March 22, 1976)

The methyl viologen film evaporated at about 250 °C has a violet color, and its electronic absorption spectrum resembles that of the enzymatically reduced methyl viologen. The evaporated film becomes colorless upon the introduction of air. By means of the photoemission spectroscopical method, a very low ionization potential, 3.6 eV, was obtained for the evaporated methyl viologen film. The character of the evaporated methyl viologen is a free-radical one, and its specific resistivity is very low as compared with other organic radicals.

Methyl viologen (abbreviated as MV hereafter) was found to be a good oxidation-reduction indicator by Michaelis and Hill in 1933.[1] This compound has been widely used in the research field of biochemistry, for the oxidation-reduction reaction is conducted by the transfer of one electron and its redox potential is independent of the hydrogen-ion concentration of the solution. For example, the enzymatic reduction of MV in the presence of hydrogenase is as follows:

$$1/2H_2 + MV^{2+} \xrightarrow{\text{hydrogenase}} H^+ + MV^+$$

where MV^{2+} and MV^+ represent oxidized and reduced methyl viologen respectively; the structures of the reduced and oxidized MV are shown below.

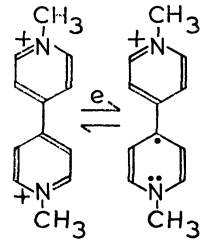

Oxidized-MV Reduced-MV

MV could be evaporated *in vacuo* at about 250 °C. The color of the evaporated film was violet, and the electronic spectrum resembled that of the enzymatically reduced MV. This evaporated film will be denoted as "reduc-MV." When the evaporated film was exposed to air, the violet color of the film vanished and the electronic spectrum changed to that of the oxidized MV (denoted as "oxi-MV").

In order to ascertain the reduc-MV, we measured the solid-state properties of these two species of MV, reduc-MV and oxi-MV. The vacuum ultraviolet photoemission spectrum of the reduc-MV, which is stable only in a vacuum, and that of the oxi-MV were observed, and the difference in the ionization potentials (*IP*) of the two species, as estimated from their photoemission spectra, is discussed.

Moreover, in order to understand the electron transport in the organic radical, the electrical conductivity of these MV films was observed.

* Present address: Hatano Research Institute, F. D. S. C., Ochiai, Hatano 257.

** Present address: Institute for Molecular Science, Okazaki 444.

Experimental

The electronic absorption spectrum of the 'oxidized MV' in an aqueous solution and that of the enzymatically 'reduced MV,' which was reduced by a hydrogen gas in the presence of hydrogenase, were obtained by an ordinary method. The film was obtained on a quartz plate by evaporation at about 250 °C under a vacuum of 10^{-4} Torr. The absorption spectra of the evaporated film and that exposed to air were measured.

The measurements of the vacuum ultraviolet-photoemission spectroscopy were carried out using a vacuum ultraviolet monochromator combined with a hydrogen-discharge lamp. The photoemission measurement was done by the ac modulated retarding potential method described earlier,[2] but with a little modification of the collector-cell housing. The energy distribution curves (EDCs) of the reduc-MV and oxi-MV were thus obtained. The spectral dependence of the quantum yield (SDQY) was also found for oxi-MV. These measurements were carried out at about 3×10^{-6} Torr because the reduc-MV was easily changed to the oxi-MV under a low vacuum.

The electrical conductivity of these species was measured at 8×10^{-7} Torr in a high-vacuum bell-jar system by the two-probe method. The aluminum metal for the electrodes and the MV were successively evaporated on a clean quartz substrate as a surface-type arrangement; the details of the experimental procedure have been reported in a previous paper.[3]

In order to introduce a dry oxygen gas into the bell-jar, oxygen gas from a commercial cylinder was flowed to the bell-jar *via* a molecular sieve trap cooled with liquid nitrogen, and the change in the conductivity was examined. To observe the temperature dependence of the conductivity, the sample was heated by an outside-mantle heater.

Results and Discussion

Electronic Absorption Spectra. Figure 1 shows the electronic absorption spectra. The spectrum of the

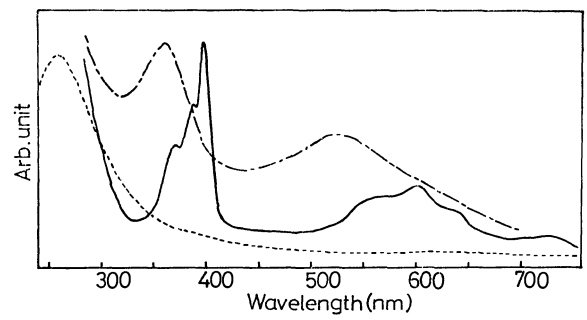

Fig. 1. The electronic spectra of MV.
---: Oxidized MV, —: enzymatically reduced MV (in aqueous solution), -·-: reduc-MV (in solid state).

oxidized MV reveals the absorbance maximum at 260 nm. The spectrum of enzymatically reduced MV has its vibrational structures at 367, 384, and 394 nm and another peak at 605 nm. The electronic spectrum of the reduced MV was investigated by Michaelis and Hill.[1] They proposed that the one excess electron belongs to the reduced form and is shared by the two nitrogen atoms, and that the blue color is explained by their resonance.

On the other hand, the spectrum of the evaporated film of MV shows the absorbance maxima at 358 and 520 nm. This spectrum resembles that of the enzymatically reduced MV, and the energy differences between the 358 nm peak of the film and 394 nm peak of the reduced MV, and also between the former's 520 nm and the later's 605 nm peak, are about 8700 cm^{-1}. When the evaporated film of MV was exposed to air, the violet color of the film disappeared and the spectrum coincided with that of the oxidized MV.

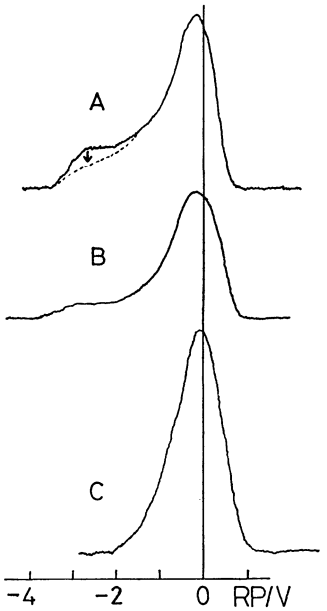

Fig. 2. The EDCs of reduc- and oxi-MV as a function of incident photon energy. A, B; reduc-MV. C; oxi-MV. Incident photon energy. A; 7.75 eV. B; 8.16 eV. C; 7.75 eV. ↓ shows the change of EDC from reduc-MV to oxi-MV.

Vacuum Ultraviolet Photoemission Spectroscopy. The EDCs of the photoelectron emitted by vacuum ultraviolet-light radiation are shown in Fig. 2. The EDCs of the reduc-MV produced by the incident-light energies of 7.75 and 8.16 eV are the two upper curves, while that of the oxi-MV irradiated by a photon energy of 7.75 eV is the bottom curve. A low-energy stationary peak was observed in all spectra, while a shoulder was obviously observed in the two upper spectra.

The values of the stopping voltage, V_0, and the saturation voltage, V_s, of the retarding potential for photoemission are obtained from the EDCs; they are listed in Table 1. The *IP* was calculated from V_0 and V_s by means of the following equation;

$$IP = h\nu - e(V_s - V_0)$$

Table 1. The incident photon energy, V_0, V_s, and the *IP* of the reduc- and oxi-MV

	EDC				$Y^{1/3}$
	$h\nu$(eV)	V_0(V)	V_s(V)	*IP*(eV)	*IP*(eV)
Reduc-MV	7.75	−3.5	0.7	3.6	
	8.16	−3.8	0.7	3.7	
Oxi-MV	7.75	−2.1	0.9	4.8	4.8—4.9

The calculated ionization potentials are also listed in Table 1. The stopping voltage of the oxi-MV was low compared with that of the reduc-MV, and the energy difference between them reached more than 1 eV.

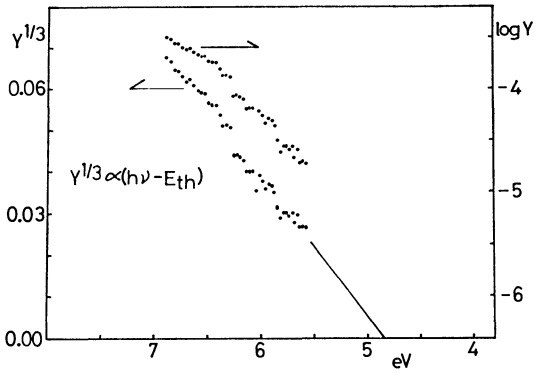

Fig. 3. The SDQY plots and cube root plots of the photoemission yield for oxi-MV.

Figure 3 shows SDQY near the threshold-energy region. Considering the experimental error, the small ripples of the plots are meaningless. The quantum yield decreased gradually with a decrease in the photon energy. The quantum yield in organic crystals and charge-transfer complexes near the threshold energy is subject to the conventional power law:

$$Y^{1/3} \propto (h\nu - E_{th})$$

where E_{th} is the threshold energy.[4]

The threshold energy value of 4.8—4.9 eV was obtained for oxi-MV from the above equation. This value was nearly equal to the *IP* calculated from the EDC of the oxi-MV. The threshold energy of the reduc-MV was not obtained accurately, because the photoemission is sensitive to surface conditions. The EDC of the reduc-MV changed gradually to that of the oxi-MV, as is shown by ↓ in Fig. 2. The phenomenon results because the surface of the reduc-MV gradually changes to the oxi-MV.

From Table 1, the difference of *IP* between the reduc- and oxi-MV can be seen to be more than 1 eV. This finding is consistent with the concept that the reduced form has one excess electron, which may occupy the lowest vacant molecular orbital of the oxi-MV.

The *IP* of the reduc-MV is very low compared with those of other organic substances. Only the organic dyes, crystal violet and malachite green have comparably low *IP* values.[5] Crystal violet and malachite green have a dimethyl amino group, which is constructed of four-valencies nitrogen atoms. The resonance may be

expected to occur over the whole molecule, and this resonance reduces the value of *IP*. Taking into account the low *IP* of the substance containing the dimethyl amino group measured by Nakato *et al.*, we consider that the same behavior can be expected in the reduc-MV.[6]

Electrical Conductivity. From the voltage dependence of the electrical conductivity for the two species of MV, there exists an ohmic contact. The electrical conductivity was held to be constant during the long observation period; also, the observation was carried out under a high vacuum, 8×10^{-7} Torr, so the predominant contribution to the conductivity is electronic, not ionic.

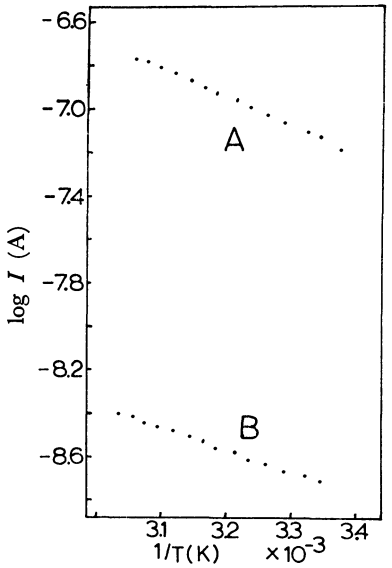

Fig. 4. The temperature dependence of the electrical current of the reduc- and oxi-MV. A; reduc-MV. B; oxi-MV.

The temperature dependence of the electrical conductivity is shown in Fig. 4. From the plot of log I *vs.* $1/T$, the activation energies of 0.2_6 and 0.2_0 eV were obtained for the reduc-MV and oxi-MV respectively by means of the following equation;

$$\sigma = \sigma_0 \exp(-\Delta E/kT)$$

where σ is the electrical conductivity; ΔE, the apparent activation energy, k, the Boltzmann constant, and T, the absolute temperature. The activation energy and the electrical current are summarized in Table 2. The difference in the activation energies of the reduc- and oxi-MV is so small that it is meaningless.

The specific resistance of the reduc-MV was estimated to be 10^5—10^6 Ωcm, for the thickness of the sample was estimated to be 10^3—10^4 Å. This value, 10^5—10^6 Ωcm, is extraordinary small compared with those of the polycyclic aromatics, polymer and organic dyes; it is in the range of the inorganic semiconductors.

Table 2. The electrical current of some species of MV[a]

State	T(°C)	ΔE(eV)	I(A)
Reduc-MV	17	0.26	1.5×10^{-13}
	17		6.3×10^{-8}
	28		7.7×10^{-8}
	54		1.7×10^{-7}
Reduc-MV+O_2	23		4.7×10^{-8}
	15		4.3×10^{-8}
Reduc-MV+O_2+H_2O	17		2.5×10^{-6}
Oxi-MV	17	0.20	2.2×10^{-9}
	54		3.8×10^{-9}

a) Applied voltage: 20V.

The color of the reduc-MV did not change upon the introduction of water-free oxygen, while the electrical conductivity decreased a little. The high conductivity of the reduc-MV was not, therefore, attributed to the oxygen. The electrical conductivity increased extraordinarily when the reduc-MV was exposed to the atmosphere, and the maximum current reached 2.5×10^{-6} A. In this procedure, the color of the reduc-MV vanished, so the coexistence of oxygen and water is shown to be necessary for the change from reduc-MV to oxi-MV. When the oxygen and water were excluded to measure the conductivity of oxi-MV, the oxi-MV was less conductive than reduc-MV. The reduc-MV exists as a radical, so it is reasonable to ascertain its high conduction by its having excess electrons.

The authors wish to express their gratitude to Yoshio Kohno for his operation of the high-vacuum electrical-conductivity-measurement system and Dr. Tomohiko Hirooka for his helpful discussions.

References

1) L. Michaelis and E. S. Hill, *J. Gen. Physiol.*, **16**, 859 (1933); L. Michaelis and E. S. Hill, *J. Am. Chem. Soc.*, **55**, 1481 (1933).

2) T. Hirooka, K. Tanaka, K. Kuchitsu, M. Fujihira, H. Inokuchi, and Y. Harada, *Chem. Phys. Lett.*, **18**, 390 (1973).

3) Y. Maruyama and H. Inokuchi, *Bull. Chem. Soc. Jpn.*, **39**, 1418 (1966).

4) T. Hirooka, M. Kochi, J. Aihara, H. Inokuchi, and Y. Harada, *Bull. Chem. Soc. Jpn.*, **42**, 1481 (1969).

5) F. Gutmann and L. E. Lyons, Ed,. "Organic Semiconductors," John Wiley and Sons (1967), p. 694.

6) Y. Nakato, M. Ozaki, A. Egawa, and H. Tsubomura, *Chem. Phys. Lett.*, **9**, 615 (1971); Y. Nakato, M. Ozaki, and H. Tsubomura, *Bull. Chem. Soc. Jpn.*, **45**, 1299 (1972).

The Pressure and Temperature Dependences of the Second Virial Coefficients and the Chain Dimensions of Polydimethylsiloxane Solutions

Kenji KUBOTA, Kenji KUBO, and Kazuyoshi OGINO

Department of Pure and Applied Sciences, College of General Education, The University of Tokyo, Komaba, Meguro-ku, Tokyo 153

(Received April 8, 1976)

A new light-scattering optical cell was designed in order to perform light-scattering measurements at various temperatures and under pressures up to 400 kg/cm^2. The second virial coefficients and the radii of gyration were determined at high polymer dilutions for polydimethylsiloxane in cyclohexyl bromide at 27.0, 36.5, 47.2, and 56.2 °C, in benzene and toluene at 27.0 °C, and in chlorobenzene at 30.0 °C. The method employed to determine the dimensions of the polymer is described. By a series of measurements of polydimethylsiloxane solutions, it is shown that the second virial coefficients, the radii of gyration, and the fundamental thermodynamic properties of the solutions depend on the pressure. The correlation between values of A_2 and $\langle S^2 \rangle^{1/2}$ shows that pressure influences these quantities through its effect on the polymer-solvent interaction parameter, χ or z. The values of the relative partial molar excess volume were calculated directly from the data. The obtained data were compared with the excluded volume theories and the corresponding state theories; the agreement was fair.

The most important thermodynamic variables of the systems are the composition, the temperature, and the pressure. For polymer solutions, a very extensive literature exists on the dependence of the chemical potential upon the composition and the temperature, but the pressure was generally held constant. Solution theories have traditionally emphasized an energetic difference in the chemical nature and intermolecular force. However, recent works[1-3] in polymer solution thermodynamics have shown the importance of a difference in free volume, or in degrees of thermal expansion and isothermal compressibility, between the polymer and the solvent.

By mixing the polymer and the solvent, the free volumes change towards an intermediate value characteristic of the mixture. These changes contribute strongly to the thermodynamic functions of the mixture: ΔH_M, ΔS_M, ΔG_M as well as ΔV_M. In particular, the free volume contribution to the interaction parameter, χ, is remarkable. Accordingly, a large difference in the free volume between the polymer and the solvent will influence the χ parameter strongly. This accounts for the existence of the lower critical solution temperature.[4]

The application of pressure will cause a change in the difference in the free volume through the difference of the compressibility between the polymer and the solvent and the corresponding effect on the χ parameter. Then, the effect of the pressure is remarkable. It is evident that the pressure effect on $\langle S^2 \rangle$ and A_2 should be large. The pressure dependence of the critical solution temperature is negative near the upper critical solution temperature in the case of a negative value of ΔV_M. This predicts that the Flory temperature will decrease with the pressure. The solvent becomes better for the polymer with an increase in the pressure, and A_2 and $\langle S^2 \rangle$ should increase. Besides, the pressure dependence of the lower critical solution, where the free volume contribution is dominant, is particularly large.

Accordingly, a complete knowledge of the systems requires a knowledge of the effect of the pressure,[5] and the pressure should be included as an available independent variable.

Schulz and Lechner[5-7] studied the effect of the pressure on light scattering for polystyrene solutions. They measured up to 800 atm. The results are in semiquantitative agreement with a theoretical treatment of the pressure effects. An interesting change in the A_2 of polystyrene in *trans*-decalin with the pressure was observed.

Gaeckle and Patterson[8] studied the second virial coefficients and the radii of the gyration of polyisobutylene in 2-methylbutane and polystyrene in 2-butanone up to 110 atm. They showed that the corresponding state theories are good representations of the pressure effects.

McDonald and Claesson[9] examined the light-scattering properties of various pure solvents and the second virial coefficients of polystyrene in 4-methyl-2-pentanone up to 5000 atm. The polymer solution showed a limiting behavior above 2000 atm in terms of the magnitude of both the second virial coefficient and the radius of gyration.

In this work, polydimethylsiloxane in cyclohexyl bromide (theta solvant), benzene, toluene, and chlorobenzene (good solvents) were examined, using a modified Shimadzu light scattering photometer (PG-21) and a high-pressure optical cell which had been designed for this work. Polydimethylsiloxane was chosen since it has a very large thermal expansion coefficient and isothermal compressibility compared with other polymers.

Thermodynamic Considerations

Pressure and Temperature Dependence of A_2. At low concentrations the following equation is valid:

$$-\Delta\mu_1/RT = cV_1/M + A_2c^2V_1 \quad (1)$$

Here, V_1 is the molar volume of the pure solvent at the experimental temperature and pressure and c is the usual concentration, *i.e.*, the weight of the polymer per volume of the solution. The second virial coefficient is related to the excess chemical potential of the solvent:

$$A_2 = -\Delta\mu_1^E/RTc^2V_1 \quad (2)$$

According to the Gibbs-Helmholtz equation, the excess chemical potential of the solvent is split into an enthalpy term, $\Delta\bar{H}_1$, and an entropy term, $\Delta\bar{S}_1^E$. Thus, two corresponding terms are obtained for the second virial coefficient:

$$A_2 = A_{2,H} + A_{2,S} \quad (3)$$

$$A_{2,H} = -\Delta\bar{H}_1/RTc^2V_1 \quad (4)$$

$$A_{2,S} = \Delta\bar{S}_1^E/Rc^2V_1 \quad (5)$$

Then, from the temperature dependence of A_2 at a constant pressure and weight fraction, the values of $A_{2,H}$ and $A_{2,S}$ can be calculated:

$$A_{2,H} = \alpha TA_2 - T(\partial A_2/\partial T)_P \quad (6)$$

$$A_{2,S} = A_2(1-\alpha T) + T(\partial A_2/\partial T)_P \quad (7)$$

By combining Eqs. 4 and 5 with Eqs. 6 and 7, we obtain:

$$\Delta\bar{H}_1/RT = c^2V_1T((\partial A_2/\partial T)_P - \alpha A_2) \quad (8)$$

$$\Delta\bar{S}_1^E/R = c^2V_1((1-\alpha T)A_2 + T(\partial A_2/\partial T)_P) \quad (9)$$

On the other hand, from the pressure dependence of A_2 at a constant temperature and weight fraction, the relative partical molar excess volume is obtained:

$$\Delta\bar{V}_1/V_1 = c^2RT(-(\partial A_2/\partial P)_T - \beta A_2) \quad (10)$$

Here, α and β are the thermal expansion coefficient and the isothermal compressibility of the solvent respectively.

Excluded Volume Effects and the χ Parameter. Equations 8 and 10 give $\Delta\bar{H}_1$ and $\Delta\bar{V}_1$ in the dilute region where the solution is nonuniform according to the excluded volume effect. These values cannot be directly compared with the usual heat and volume measurements made at higher concentrations where the polymer molecules interpenetrate and the solution is uniform. Consequently, in order to estimate the free energy parameter, χ, from the value of A_2 obtained from the light-scattering measurements, the evaluation of the excluded volume effect is necessary.

According to the dilute solution theories, the nonuniformity of the solution gives rise to the penetrating function, $\Phi(z)$, in the expression of A_2:[10]

$$A_2 = 4\pi^{3/2}N_A\langle S^2\rangle^{3/2}\Phi(z)/M^2 = 4\pi^{3/2}N_A\langle S^2\rangle^{3/2}zh(z)/M^2 \quad (11)$$

$$z = (1/4\pi)^{3/2}(v_{2,sp}^2/N_AV_1)M^2(1-2\chi)/\langle S^2\rangle_0^{3/2} \quad (12)$$

Here z is the excluded volume parameter, while $v_{2,sp}$ and $\langle S^2\rangle_0^{1/2}$ are the specific volume of the polymer and the unperturbed mean-square radius of the gyration of the polymer.

Direct thermodynamic measurements of the heats and volumes of mixing leading to the values of $\Delta\bar{V}_1$ and $\Delta\bar{H}_1$ have been made between 20—80% of a polymer in general. If the values of A_2 of dilute polymer solutions were available for use in finding the chemical potential of the solvent for high concentrations, the values of $\Delta\bar{V}_1$ and $\Delta\bar{H}_1$ could be predicted from Eqs. 8 and 10.[8,11] In comparison with the Flory-Huggins equation, the theoretical expression of A_2 at a sufficiently high concentration is written as follows:

$$A_2^c = v_{2,sp}^2(1/2-\chi)/V_1 \quad (13)$$

In this equation, the excluded volume effect function $h(z)$ is absent. Therefore, A_2^c, the second virial coefficient at a high concentration, can be obtained from the experimental values of a dilute solution through division by $h(z)$:

$$A_2^c = A_2/h(z) \quad (14)$$

Moreover, $h(z)$ can be evaluated from $\langle S^2\rangle$ using excluded volume effect theories, and then A_2^c or χ can be estimated. Transforming the concentration into volume fraction, we obtain:

$$\phi_2 = cv_{2,sp} \quad (15)$$

A change in the volume on mixing, ΔV_M, is symmetrical in the volume fractions of the components, *i.e.*:

$$\Delta V_M/V = D\phi_1\phi_2 \quad (16)$$

By differentiating Eq. 16 with the number of the solvent, we obtain:

$$\Delta\bar{V}_1/V_1 = D\phi_2^2 \quad (17)$$

Consequently, from Eqs. 10 and 17 we obtain:

$$D = (RT/v_{2,sp}^2)(-(\partial A_2^c/\partial P)_T - \beta A_2^c) \quad (18)$$

On the other hand, by combining Eqs. 13 and 14 we obtain:

$$\chi_{1,H} = -T(\partial\chi/\partial T)_P = T(\partial(V_1TA_2^c/v_{2,sp}^2)/\partial T)_P = (V_1T/v_{2,sp}^2)((\partial A_2^c/\partial T)_P - \alpha A_2^c) \quad (19)$$

Thus, the pressure dependence of the parameters can be obtained from the second virial coefficients for dilute solutions.

Experimental

Materials. The polydimethylsiloxane is from the Shinetsu Chemical Co., with 50×10^4 CS and 10×10^4 CS. The M_V values of these polymers are 14.6×10^4 (1) and 10.6×10^4 (2) respectively.[12] The polydimethylsiloxane (PDMS)-(1) was fractionated by means of the fractional solution method into 13 fractions, using benzene (good solvent) and methanol (poor solvent). The 12th fraction (1F12) of $M_W=57.8\times10^4$ ($M_W/M_N<1.02$) was used in this work. The PDMS-(2) was fractionated in the same way into 8 fractions, and the 3rd fraction (2F3) of $M_W=7.30\times10^4$ was used. All the solvents (cyclohexyl bromide, benzene, toluene, and chlorobenzene) were reagent-grade and were further purified before use.

Apparatus. A high pressure optical cell was constructed. The cell, of a cylindrical form, was made of brass (Fig. 1). The windows were made of quartz (12 mm×5 mm) and were

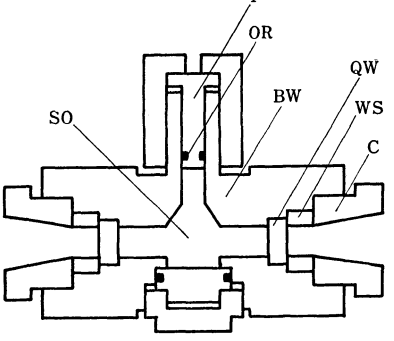

Fig. 1. High pressure optical cell (side view): (P) piston; (B) body; (CP) cap; (OR) O-ring gasket; (QW) quartz window; (WS) window spacer; (SO) solution.

tightened using the conventional unsupported area technique.[13] The capacity of the cell was *ca.* 5 cm³. All the O-rings were of Teflon, were stored in pure solvents for about 1 month prior to use, and were cleaned with an ultrasonic cleaner before measurement. The dimensions of the cell were designed so that the cell could be used for the Shimadzu light-scattering photometer (PG-21) without any modification. The pressure was generated by compressing the polymer solu tions directly. The pressure was determined by a solid-front pressure gauge (Heise Bourdon Gauge).

Procedure. The polymer solution was made up to approximately the required concentration and was cleared of dust by ultracentrifugation. The optical cell was connected to the pressure tube (1/16″ o.d. and 0.5 mm i.d.) and heated to the required temperature, and the solution was compressed to the required pressure. About one hour was necessary for the solution to become homogeneous and for the pressure gradient to be got rid of before measurements. The concentration of the solution was determined by weighing the solution and the polymer after measurements. The scattered light intensity was measured at the angle of 90°.

Determination of the Optical Constant, K, *at High Pressures.* In order to determine the absolute scattered intensity, a relative method was employed. The intensity of the solution was measured under the same conditions as those of the solvent.

The radius of the gyration of the polymer is determined by measurements of the wavelength dependence or the scattering-angle dependence or disymmetry of the scattered intensity. In this work, the following method was employed in order to determine $P(90)$, the value of the scattering function at the angle of 90°. It is assumed that the molecular weight of the polymer is constant as a function of the pressure; that is, no aggregation or decomposition happens.

According to Debye,[14] the following equation in terms of the Rayleigh ratio is yielded:

$$Kc/R_{90} = 1/MP(90) + 2A_2c \tag{20}$$

As this relation is still valid at high pressure,

$$K^*c/R_{90} = 1/MP(90) + 2A_2c \tag{21}$$

where $K^*=Kf$. K is the optical constant at 0 kg/cm². The factor, f, which indicates the change in K with the pressure has a magnitude less than unity.

Substitution and rearrangement give:

$$Kc/R_{90} = 1/MP(90)f + 2A_2c/f \tag{22}$$

Here, the direct measurable quantities as a function of the pressure are R_{90} and c. Plotting Kc/R_{90} *vs.* c gives an intercept value which is $1/MP(90)f$ and a slope of $2A_2/f$. In the case of $\langle S^2\rangle^{1/2} \ll \lambda$, $P(90)$ is unity, and as the optical constant, K, does not vary with the molecular weight of the polymer, by measuring the scattered intensity of the solution of the polymer with the radius of gyration, which is much smaller than the wavelength of the light, f is determined from the intercept value to be as is expressed in Eq. 23:

$$Kc/R_{90} = 1/Mf + 2A_2c/f \tag{23}$$

Using this value of f, $P(90)$ can be determined from the intercept and A_2 can be determined from the slope obtained from Eq. 22. With this value of $P(90)$, $\langle S^2\rangle$ is determined. PDMS (2F3) is used in order to determine f. The radius of the gyration of 2F3 is obtained by extrapolating the data given by Schulz and Haug;[15] it gives *ca.* 60Å for $\langle S^2\rangle_0^{1/2}$. This is much smaller than the wavelength of the light, and the assumption $P(90)=1$ is reasonable.

Results

The absolute Rayleigh ratio of cyclohexyl bromide as a function of the pressure is shown in Fig. 2 as an example, while the f-factor of PDMS in cyclohexyl bromide are shown in Fig. 3. The Rayleigh ratio decreases linearly with the pressure. This can be intuitively expected, for an increase in the pressure tends to produce a more ordered state.[9] The magnitude of the decrease is variable, depending on the solvents. The changes in the Rayleigh ratio of the solvents, $(\partial \ln R_{90}^{\circ}/\partial P)_T$, are 2.76×10^{-4}, 3.81×10^{-4}, 3.38×10^{-4}, and 1.01×10^{-4} l/kg cm^{-2} for cyclohexyl bromide, benzene, toluene, and chlorobenzene respectively. It seems that there is a correlation between the magnitude of compressibility and that of the decrease in the Rayleigh ratio for the solvents.

The values of A_2 obtained for each solvent are summarized in Table 1. The values of A_2 are shown in Figs. 4 and 5 as a function of the pressure for PDMS (1F12) and of $\langle S^2\rangle^{1/2}$ in Fig. 6 as a function of the temperature under various pressures for 1F12 in cyclohexyl bromide. These values under 0 kg/cm² agree well with the results obtained by Schulz and Haug.[15] The unperturbed dimensions of the polymer were

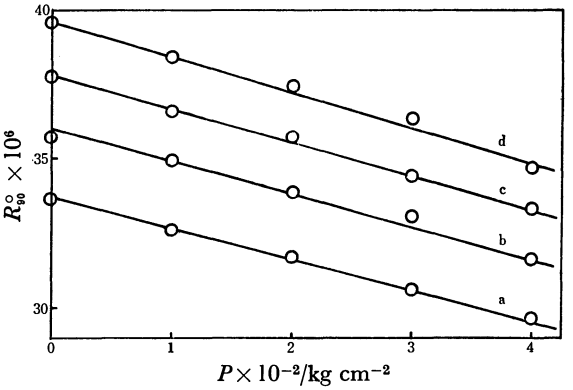

Fig. 2. Absolute Rayleigh ratio of cyclohexyl bromide as a function of pressure at 27.0 °C (a), 36.5 °C (b), 47.2 °C (c), and 56.2 °C (d).

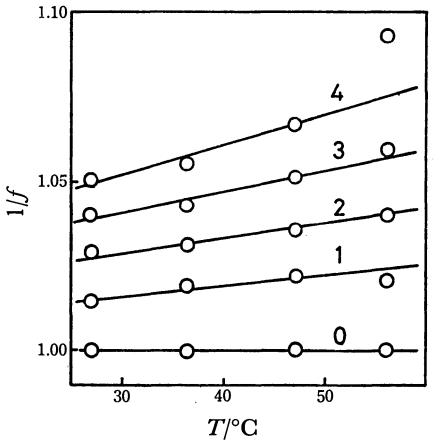

Fig. 3. f-Factor for PDMS in cyclohexyl bromide as a function of temperature unde 0(0), 100(1), 200(2), 300(3), and 400(4) kg/cm².

Table 1. Second virial coefficients of polydimethylsiloxane solutions

Pressure (kg/cm_2)	$A_2 \times 10^5$ cm^3 mol/g^2			
	Cyclohexyl bromide			
	27.0 °C	36.5 °C	47.2 °C	56.2 °C
0	−0.158	3.62	6.57	9.54
100	0.258	4.37	7.39	10.0
200	0.538	5.04	7.94	10.4
300	0.782	5.48	8.20	10.7
400	0.995	5.76	8.52	11.1
	Benzene	Toluene	Chlorobenzene	
	27.0 °C	27.0 °C	30.0 °C	
0	29.5	45.0	10.4	
100	30.2	44.6	11.0	
200	30.2	46.3	11.6	
300	30.3	46.7	12.1	
400	30.0	46.7	12.5	

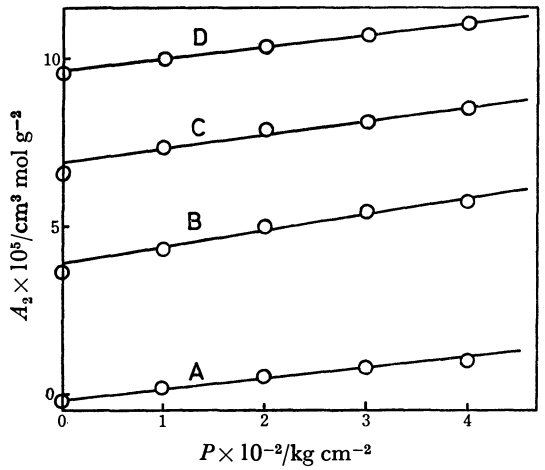

Fig. 4. The second virial coefficient, A_2, as a function of pressure for PDMS (1F12) in cyclohexyl bromide at 27.0 °C (A), 36.5 °C (B), 47.2 °C, and 56.2 °C (D).

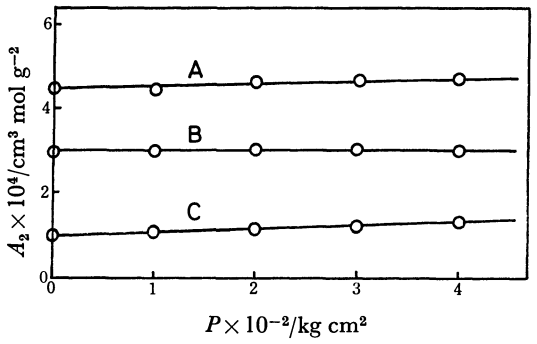

Fig. 5. The second virial coefficient, A_2, as a function of pressure for PDMS (1F12) in toluene at 27.0 °C (A), in benzene at 27.0 °C (B), and in chlorobenzene at 30.0 °C (C).

determined by reading off the $<S^2>^{1/2}$ *vs.* temperature plot at the temperature of $A_2=0$. In Fig. 7, the θ-temperatures for various pressures determined in this way are shown. θ-Temperature decreases with the pressure and decreases more slowly as the pressure

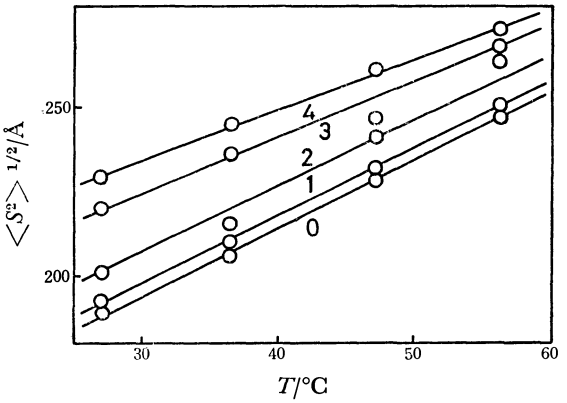

Fig. 6. The radius of gyration, $<S^2>^{1/2}$, as a function of temperature for PDMS (1F12) in cyclohexyl bromide under 0(0), 100(1), 200(2), 300(3), and 400(4) kg/cm^2.

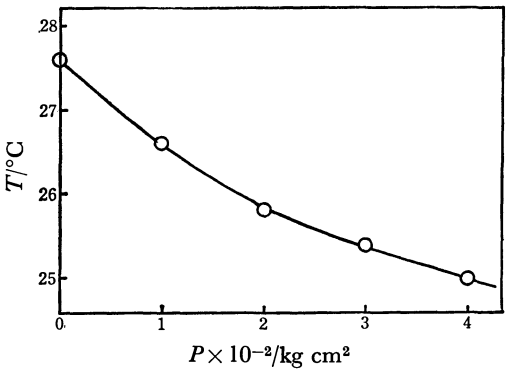

Fig. 7. θ-Temperature as a function of pressure for PDMS in cyclohexyl bromide.

increases. θ-Temperature seems to have a tendency to reach a limiting value at high pressures. Both A_2 and $<S^2>^{1/2}$ increases with the pressure, in accord with negative values of ΔV_m. The change in $<S^2>^{1/2}$ with the pressure is more rapid than that of A_2. The dimension increases about 20% under 400 kg/cm^2. Accordingly, the effect of the pressure makes the solvent better for the polymer.

Using Eqs. 6 and 7, A_2 can be separated into $A_{2,H}$ and $A_{2,S}$. These values are summarized in Table 2. At θ-temperature $-A_{2,H}$ and $A_{2,S}$ (these cancel each other out) increase considerably with the pressure and the solvent becomes more endothermal. At higher temperatures, however, $-A_{2,H}$ decreases with the pressure and the solvent becomes less endothermal. From this fact and from the fact that A_2 increases with the pressure, it is evident that the contribution of the entropy term is larger than the enthalpy term.

In polar solvents, cyclohexyl bromide and chlorobenzene, the extent of the change in A_2 with the pressure is larger than in good solvents, benzene and toluene. In particular, A_2 in benzene seems to be independent of the pressure.

From the pressure dependence of A_2 and Eq. 10, the values of the relative partial molar excess volume were obtained; they are tabulated in Table 3. It is evident from this table that the volume contracts on mixing for all solvents.

TABLE 2. $A_{2,H}$ AND $A_{2,S}$ OF PDMS IN CYCLOHEXYL BROMIDE

Pressure (kg/cm²)	$A_{2,H}\times10^3$ cm³ mol/g²				$A_{2,S}\times10^3$ cm³ mol/g²			
	θ-point	35 °C	45 °C	55 °C	θ-point	35 °C	45 °C	55 °C
0	−1.26	−1.05	−0.859	−0.779	1.26	1.08	0.924	0.871
100	−1.34	−1.10	−0.851	−0.679	1.34	1.14	0.920	0.775
200	−1.43	−1.16	−0.824	−0.642	1.43	1.20	0.897	0.742
200	−1.45	−1.17	−0.838	−0.627	1.45	1.21	0.906	0.732
400	−1.52	−1.20	−0.818	−0.600	1.52	1.25	0.899	0.709

TABLE 3. RELATIVE PARTIAL MOLAR EXCESS VOLUMES OF SOLVENTS IN PDMS SOLUTIONS

$\Delta\bar{V}_1\times10^6$ cm³/mol (c=0.01 g/cm³)

Cyclohexyl bromide

27.0 °C	36.5 °C	47.2 °C	56.2 °C
−14.1	−15.2	−16.3	−16.4

Benzene	Toluene	Chlorobenzene
27.0 °C	27.0 °C	30.0 °C
−6.28	−21.5	−16.5

Discussion

Absolute Rayleigh Ratio of the Solvents. The values in Fig. 2 are the absolute Rayleigh ratios of the solvents obtained in the manner described above. The experimental values of this ratio were reproducible within the limit of experimental error. The isotropic Rayleigh ratio is defined as follows:[16]

$$R_{iso} = (2\pi^2/\lambda_0^4)kT(\tilde{n}(\partial\tilde{n}/\partial P))^2/\beta \quad (24)$$

By experiments, the total Rayleigh ratio is measured. Since a statistical independence is assumed for the assorted fluctuation phenomena,

$$R_{total} = R_{iso} + R_{aniso} \quad (25)$$

The anisotropic component of the Rayleigh ratio is defined using the degree of depolarization, ρ_u, and R_{total} is written as follows:

$$R_{total} = R_{iso}(6+6\rho_u)/(6-7\rho_u) \quad (26)$$

According to McDonald and Claesson,[9] R_{aniso} is nearly independent of the pressure. The change in R_{total} with the pressure is determined by the contribution of the R_{iso} term in Eq. 25; therefore, the degree of depolarization increases with the pressure, and the contribution of R_{aniso} to R_{total} increases. This means that the refractive index of the solvent increases with the pressure, but the $(\partial\tilde{n}/\partial P)_T$ term decreases more rapidly with the pressure. Since the anisotropic characteristics are related to the structural properties of the liquids, a further examination is warranted. The refractive index of benzene under high pressures is available,[17] and the calculation of the depolarization can be done. The pressure dependence of the Rayleigh ratio of benzene was examined by McDonald and Claesson.[9] Their results are in good agreement with the above.

The Pressure Dependence of the θ-Temperature. In the PDMS+cyclohexyl bromide solution, the θ-temperature decreases with the pressure. At the θ-temperature, A_2 becomes zero and $d\theta/dP$ is expressed by the following equation:

$$d\theta/dP = -(\partial A_2/\partial P)_T/(\partial A_2/\partial T)_P \quad (27)$$

From the values of A_2 tabulated in Table 1, $(\partial A_2/\partial T)_P$ and $(\partial A_2/\partial P)_T$ are obtained. Under 0 kg/cm² the θ-temperature is 27.6 °C. The value of $(\partial A_2/\partial T)_P$ at 27.6 °C and under 0 kg/cm² is 4.72×10^{-6}, while that of $(\partial A_2/\partial P)_T$ is 4.5×10^{-8}, which gives $d\theta/dP=-0.95\times10^{-2}$ deg/kg cm^{-2}. The value of the corresponding $d\theta/dP$ obtained from the experiments (Fig. 7) is -0.96×10^{-2} deg/kg cm^{-2}. These values are consistent.

The pressure coefficient of a critical solution temperature is given by the relation:[18]

$$dT_c/dP = T(\partial\Delta\bar{V}_1/\partial\phi_2)_c/(\partial\Delta\bar{H}_1/\partial\phi_2)_c \quad (28)$$

In the vicinity of the upper critical solution temperature, the process of mixing is endothermal, and $(\partial\Delta\bar{H}_1/\partial\phi_2)_c$ must be negative. A negative value of the volume change on mixing is obtained (see Table 3), so $(\partial\Delta\bar{V}_1/\partial\phi_2)_c$ is positive. Consequently, dT_c/dP must be negative. This is in good agreement with the negative value of $d\theta/dP$. The pressure coefficient of the upper critical solution temperature of PDMS in cyclohexyl bromide must be small, of the order of 10^{-2}. According to Gaeckle and Patterson,[8] the pressure dependence of A_2 in the vicinity of the lower critical solution temperature, polyisobutylene in 2-methylbutane, is very large, and $(\partial A_2/\partial P)_T$ is 2.2×10^{-6} cm³ mol g^{-2} bar^{-1}. The dT_c/dP of the lower critical solution temperature is 0.44 deg/bar, in contrast to PDMS in cyclohexyl bromide. This behavior is due to the difference in the pressure contribution. At the lower critical solution temperature, the free volume contribution is dominant and the pressure dependence is large. At the upper critical solution temperature, polystyrene in cyclohexane,[19] dT_c/dP is in the order of 10^{-3} and changes in sign depending on the molecular weight. These are reflected in the extent of $(\partial A_2/\partial P)_T$.

Pressure and Temperature Dependence of $\langle S^2\rangle_0$. The values of $\langle S^2\rangle^{1/2}$ at the θ-temperature give the unperturbed chain dimensions of the polymer. The radius of gyration is related to the coil expansion coefficient, α:

$$\langle S^2\rangle = \langle S^2\rangle_0\alpha^2 \quad (29)$$

The coil expansion coefficient, α, is changed through pressure and temperature. For PDMS in cyclohexyl bromide at different temperatures and pressures, the α's were plotted against the corresponding values of A_2, as is shown in Fig. 8. A single curve was obtained. This shows that the effect of the pressure on the chain dimension is not at all different from that of the temperature and that $\langle S^2\rangle_0$ is a function of the pressure. According to Schulz and Lechner,[5-7] the radius of gyration changes with the pressure, although A_2 remains

nearly constant, and the unperturbed dimensions are influenced by the pressure. Moreover, if the pressure dependence of the unperturbed dimension is not included in the estimation of α, the plot of α against A_2 does not give a single curve.[8] Therefore, it must be concluded that $\langle S^2\rangle_0$ is influenced by the pressure.

For the same value of A_2 under various pressures, $\langle S^2\rangle^{1/2}$ for PDMS in cyclohexyl bromide increases with the pressure. This indicates that the unperturbed dimension is an increasing function of the pressure. The unperturbed chain dimension, $\langle S^2\rangle_0^{1/2}$, was determined by interpolating the θ-temperature in the $\langle S^2\rangle^{1/2}$ plot against the temperature under various pressures, as is shown in Fig. 6. These values were 191, 193, 200, 216, and 227 Å for 0, 100, 200, 300, and 400 kg/cm^2 respectively. The increase in the dimensions with the pressure reaches *ca.* 20% at 400 kg/cm^2. On the other hand, the temperature dependence of the unperturved chain dimension $(\partial \ln\langle R^2\rangle_0/\partial T)_P$ of PDMS is 0.75×10^{-3} l/deg. Since θ-temperature decreases with the pressure, the increase in the unperturbed chain dimension is directly due to the pressure. As Gaeckle and Patterson have shown, this result indicates the pressure effect of the solvent packing on the population of conformations or rotational isomers of polymer. It is usually believed that the solvent has little effect on the unperturbed dimensions of a polymer, but in the present case it should not be disregarded. Even a small effect of solvent packing on the rotational isomer equilibrium would have important consequences in the polymer solution thermodynamics. In the case of PDMS, this effect is large. PDMS has, as an irregular form, pendant CH_3 groups spaced by comparatively long Si–O and Si–C bonds. The irregularity in the cross section of the chain will make the effect of the solvent packing large.[20]

These results show that α should be determined considering the pressure effect on the unperturbed chain dimension and that the excluded volume effect should be examined by including the pressure effect as well as the temperature.

Pressure and Temperature Dependence of A_2 *and* $\langle S^2\rangle$. The excluded volume effect was examined at different temperatures and pressures using Eq. 11 and the corresponding value of A_2 given in Table 1, while the values of $zh(z)$ were calculated for PDMS in cyclohexyl bromide. Figure 8 shows the relation between α and $zh(z)$; it may be seen that the points for different temperatures and pressures do approximately fall on a single curve, as expected from the theory. This is not changed even by the effects of polydispersity on the values of A_2 and $\langle S^2\rangle^{1/2}$, as has examined by Gaeckle and Patterson.[8]

A number of closed expressions for the expansion factor, α, of the polymer relating to A_2 or z are also presented. In the usual treatment, the penetrating function, Φ, is plotted against α. In this work, however, in order to estimate A_2^c or χ, α was plotted against $zh(z)$. This plot makes clear the tendency of the change in α. The abscissa in Fig. 8, $zh(z)$, was obtained from the Krigbaum-Carpenter-Kaneko-Roig (KCKR) theory[21] with three values of the ρ-parameter: 0, 0.4, and 1. The ρ-parameter depends on the ratio of the

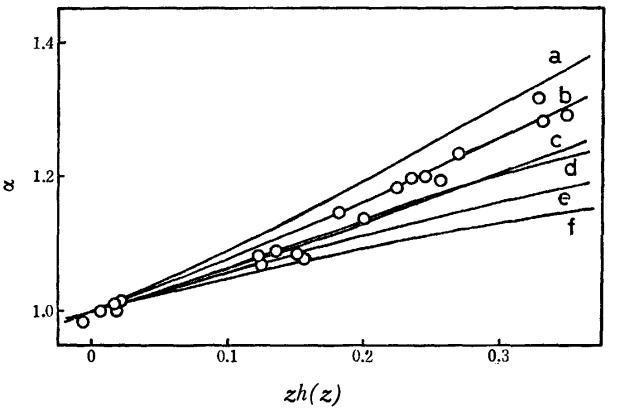

Fig. 8. The coil expansion factor, α, for PDMS (1F12) in cyclohexyl bromide at various temperatures and pressures. Curves a, b, and c are given by the Fixman-Stockmayer expression for α, Eq. 30, and the KCKR theory for A_2 with ρ equal to 0, 0.4, and 1, respectively. Curves d, e, and f are given by the Flory-Stockmayer modification, Eq. 31, and the KCKR theory for A_2 with ρ equal to 0, 0.4, and 1, respectively. The abscissa, $zh(z)$, is proportional to A_2.

total number of intramolecular contacts to the number of long-range contacts. The evaluation of z from α was obtained by using the Fixman-Stockmayer expression[22] and the Flory-Stockmayer modification[23]:

$$\alpha^3 - 1 = 2z \tag{30}$$

$$\alpha^5 - \alpha^3 = 1.276z \tag{31}$$

The resulting six curves of α against $zh(z)$ are shown in Fig. 8. It is noticeable that $zh(z)$ is equal to $\alpha^3\Phi$. The experimental data are well expressed by Eq. 30 and $\rho=0.4$.

The penetrating function, Φ, was also examined. Five conjugate closed expressions were compared with the experimental data. These were the Flory[24]-Flory, Krigbaum, Orofino:[25] Flory, Stockmayer modification[23]-Flory, Krigbaum, Orofino modification;[23] Fixman[22]-Kurata;[26] Yamakawa-Tanaka;[27] and Casassa[28] equations. The experimental points were in better agreement with the Casassa equation than the others. The Casassa equation corresponds to the KCKR theory with the ρ-parameter equal to 0. These results show that pressure effect on the excluded volume effect is quite similar to the temperature effect.

Relative Partial Molar Excess Volumes and Heats of the Solvent. In order to evaluate the volumes and heats of dilution, Eqs. 8 and 10 were used. In Table 2, $A_{2,H}$ and $A_{2,S}$ are shown, while in Table 3, the $\Delta\bar{V}_1$ values are tabulated.

For all the solvents the $\Delta\bar{V}_1$ values were negative, and the absolute value of $\Delta\bar{V}_1$ for cyclohexyl bromide decreases with the temperature. Throughout the pressure range of the experiment, $(\partial A_2/\partial P)_T$ was nearly constant, and the pressure dependence of $\Delta\bar{V}_1$ was not remarkable. However, according to McDonald and Claesson,[9] A_2 reaches a limiting value at a high pressure. Consequently, $(\partial A_2/\partial P)_T$ becomes zero and the volume of dilution at a high pressure is directly related to the limiting value of A_2. Their results show that the change in the volume on mixing at a high pressure decreases and

reaches a limiting value.

The value of $\Delta\tilde{V}_1$ varies depending on the solvent. However, the values for the polar solvents, cyclohexyl bromide and chlorobenzene, are very similar. The value of $\Delta\tilde{V}_1$ for cyclohexyl bromide depends mainly on $(\partial A_2/\partial P)_T$. On the contrary, those of the good solvents, benzene, toluene, and chlorobenzene, depend mainly on the term of βA_2 in Eq. 10. This is because the value of A_2 is about ten times larger than that for the θ-solvent. In the case of polyisobutylene in 2-methylbutane, $(\partial A_2/\partial P)_T$ term is much larger than βA_2 term. For θ-solvent the $(\partial A_2/\partial P)_T$ term is dominant over $\Delta\tilde{V}_1$.

In comparing $A_{2,S}$ with $A_{2,H}$, the contribution of $A_{2,S}$ is larger to A_2 and the pressure effect is effectively reflected in the entropy term.

The KCKR theory was used to obtain the $h(z)$ function in order to furnish values of A_2^c for use in Eqs. 18 and 19. In this theory, the values of the ρ-parameter equal to 0, 0.2, and 1 give results corresponding to the well-known Casassa,[28] Kurata-Yamakawa,[26] and Flory-Krigbaum[29] theories respectively. In accordance with the KCKR[21] and Gaeckle and Patterson,[8] and from a comparison with the experimental results shown in Fig. 8, an intermediate value of 0.4 was used for the ρ-parameter in evaluating $h(z)$. Then the $h(z)$ function was calculated from the KCKR theory, and A_2^c was obtained from the values of A_2 in a dilute solution. From Eq. 13 the χ-parameter was obtained. The χ-parameter decreases with the temperature and the pressure.

The values of D at the temperature of 27.0, 36.5, 47.2, and 56.2 °C for PDMS in cyclohexyl bromide in Eq. 18 were obtained; they were -1.08×10^{-3}, -1.26×10^{-3}, -1.00×10^{-3}, and -0.878×10^{-3} respectively.

From the change in A_2 at zero pressure, values of the enthalpic parameter, κ, were obtained for PDMS cyclohexyl bromide. They were 0.197 at 27.0 °C and 0.178 at 56.2 °C. The corresponding values of the entropic parameter, ψ, were 0.196 at 27.0 °C and 0.194 at 56.2 °C.

Comparison of the Pressure Dependence of A_2 *with the Predictions of Newer Theories.* The second virial coefficient is related to the polymer-solvent interaction parameter, χ, through Eqs. 11 and 12. The pressure dependence of χ can be predicted using a newer theory of polymer solution. The following equations were used to predict the pressure dependence of χ and that of A_2^c in the concentrated range of the polymer solution:

$$\chi_1/c_1 = -\tilde{U}_1\nu^2/\tilde{T}_1 + (1/2)\tilde{C}_{p,1}(\tau+\pi\tilde{P}_1\tilde{V}_1^2/(\tilde{P}_1\tilde{V}_1^2+1))^2 \quad (32)$$

$$\chi_1 = (P_1^*V_1^*/\tilde{V}_1RT)(A^2\alpha T/2+Y) - V_1^*Q/R(s_1/s_2)^2 \quad (33)$$

$$\chi_1/c_1 = (1/\tilde{V}_1\tilde{T}_1)(1-(P_2^*/P_1^*)^{1/2}(\tilde{V}_1/\tilde{V}_2))^2 + \delta \quad (34)$$

Equations 32, 33, and 34 are given by the Patterson theory, the Flory theory, and the solubility parameter theory respectively.

Here $\tilde{U}_1$ and $\tilde{C}_{P,1}$ are the reduced configurational energy and the heat capacity of the pure solvent. $\tilde{P}_1$, $\tilde{V}_1$, and $\tilde{T}_1$ are the reduced pressure, the volume, and the temperature of the solvent. P_1^*, V_1^*, and T_1^* are the characteristic pressure, volume, and temperature of the solvent. A and Y are defined as follows;

$$A = (1-T_1^*/T_2^*)(P_2^*/P_1^*) - (s_2/s_1)(X_{12}/P_1^*) \quad (35)$$

$$Y = (X_{12}/P_1^*)(s_2/s_1)^2 \quad (36)$$

The Flory theory essentially predicts these quantities, using a van der Waals model of the liquid state and a partition function similar to the Hirschfelder-Eyring cell partition function.[30] Then,

$$\tilde{U}_1 = -\tilde{V}_1^{-1} \quad (37)$$

$$\tilde{C}_{p,1}^{-1} = (1-(2/3)\tilde{V}_1^{-1/3}) - 2(1-\tilde{V}_1^{1/3})/(\tilde{P}_1\tilde{V}_1^2+1) \quad (38)$$

The τ-parameter is related to the difference between the thermal expansion coefficient of the solvent and the polymer, and is defined by:

$$\tau = 1 - T_1^*/T_2^* \quad (39)$$

The ν^2-parameter is related to the difference in cohesive energy and size between the solvent and the polymer segment. The π-parameter is similarly related to the difference between the reduction parameter, P^*, of the components and is defined by:

$$\pi = P_1^*/P_2^* - 1 \quad (40)$$

c_1 is the number of external degrees of freedom of the solvent molecule. This is calculated from the relation:

$$c_1 = P_1^*V_1^*/RT_1^* \quad (41)$$

In the Flory theory, the X_{12} parameter measures the interchange energy on the formation of contacts between the solvent and the polymer, Q is analogously defined to represent the entropy arising from the interchange of neighboring molecules, and s_1 and s_2 denote the number of surface sites for segments of the respective species.

In treating the thermodynamics of the PDMS solutions, the τ, π, and c_1 parameters were determined from Eqs. 39, 40, and 41. Moreover, ν^2, X_{12}, Q, and δ were decided to fit with the zero pressure data of A_2.

The pressure dependence of A_2 was predicted from Eqs. 32, 33, and 34 using the parameters decided as above. The evaluation of A_2 from χ was done by means of the KCKR theory.

The values of $(\partial A_2/\partial P)_T$ predicted by Eq. 34 were all overestimated. Equation 34 was obtained by combining the solubility parameter theory with the corresponding state theory. In the solubility parameter theory, the Berthelot relation is assumed for the energy of the (1—2) contacts relative to the (1—1) and (2—2) contacts. Also, the parameter δ expresses the correction of entropy. In PDMS solution, the contribution of the entropy is unusually large. Consequently, the error from δ may be large. Besides, as Flory has described,[31] the Berthelot relation is not a good assumption for the polymer solutions.

For cyclohexyl bromide and chlorobenzene solutions, the values of A_2 predicted by Eqs. 32 and 33 were underestimated. Also, the negative values of $(\partial A_2/\partial P)_T$ were obtained. The reason for this is that these solvents are both polar solvents, and that the configurational energy is not expressed in the form of $1/V$ which was assumed by Flory[2] for liquids. Especially, for chlorobenzene $(\partial U/\partial V)_T$ is an increasing function of the volume at a constant temperature.[32] Therefore, the equation of state defined by Flory is not in conformity with the polar solvents.

For benzene and toluene, the curves of A_2 predicted by Eq. 32 are a little underestimated compared with the experimental results. The fitted ν^2 parameter is small, corresponding to $X_{12}=4.54$ and 3.72 cal/cm^3 respectively, as obtained from the relation of $X_{12}=\nu^2 P_1^*$. The slopes predicted from Eq. 32 are -4.0×10^{-8} and -1.0×10^{-8} cm^3 mol g^{-2}/kg cm^{-2} at 27.0 °C for benzene and toluene. The predicted values of χ at 27.0 °C under zero pressure are in good agreement with the results reported by Kuwahara.[33] They are 0.48 for benzene and 0.46 for toluene at 25.0 °C; on the other hand, in this experiment 0.47 and 0.44 were found respectively.

The $c_1\nu^2$ term in Eq. 32 increases with the pressure, and the interchange energy contribution increases. However, the $\tilde{C}_{P,1}$ term decreases with the pressure, and the effect of the pressure on the free volume or the equation of state term makes the polymer more soluble to the solvent. This suggests the significance of the contribution of the free volume. Indeed, the $\chi_{1,H}$ term predicted from Eq. 32 decreases with the pressure. In the Patterson theory, the Q term in the Flory theory is neglected. For PDMS solutions the contribution of the Q term to χ is usually large;[34] consequently, the entropy term of χ in the Patterson theory was overestimated and $(\partial A_2/\partial P)_T$ was underestimated. However, this behavior of $\chi_{1,H}$ is in agreement with the behavior of $A_{2,H}$ of the cyclohexyl bromide solution at higher temperatures.

For benzene the curve of A_2 predicted from Eq. 33 was also examined. The $(\partial A_2/\partial P)_T$ predicted from Eq. 33 using values of X_{12} and Q parameter equal to 5.26 cal/cm^3 and -0.01 cal/cm^3 deg obtained by Flory and Shih[34] was underestimated and negative. The predicted value of $(\partial A_2/\partial P)_T$ was -2.5×10^{-8} cm^3 mol g^{-2}/kg cm^{-2} at 27.0 °C. $\chi_{1,H}$ which is given by the $\chi_{1,H}=-T(\partial\chi/\partial T)$ relation; χ is defined by Eq. 33 and decreases with the pressure. Also, the free volume term of χ in Eq. 33 decreases with pressure. However, for a benzene solution the free volume term or the equation of state term contribution to the free energy predicted from Eq. 33 is unusually small and the interchange energy contribution is large. PDMS has an extremely large thermal expansion coefficient and isothermal compressibility compared to the other polymers, for example, polystyrene; it corresponds to the small values of P^* and T^*. Consequently, the A parameter (Eq. 35) is small. Because of this, the contribution of X_{12} to χ is dominant.

For polyisobutylene in 2-methylbutane, which gives a θ-temperature associated with the lower critical solution temperature of 45 °C, the free volume contribution is dominant and the $(\partial A_2/\partial P)_T$ predicted from Eq. 32 is positive and large. Its value is 2.2×10^{-6} and 3.4×10^{-6} cm^3 mol g^{-2}/kg cm^{-2} at 24 and 57 °C respectively. These values are in good agreement with the results of Gaeckle and Patterson.[8] This means that the pressure effect is well explained when the free volume contribution is dominant. In the vicinity of the upper critical solution temperature, the energy contribution is predominant over the free volume contribution, and the energy contribution predicted from the corresponding state theory is overestimated.

This discrepancy in the PDMS solution may be related to the discrepancy of the excess volume predicted from the corresponding state theory against the experiment.[34] Especially the estimation of the excess volume of mixing is important in considering the pressure effect. The behavior of A_2 for polystyrene in *trans*-decalin is related to the volume change on mixing.[19] At a high pressure A_2 shows a limiting behavior and the excess volume depends on the pressure. However, the corresponding state theory gives a qualitative prediction of the pressure contribution.

The authors thank the Ministry of Education in Japan for a Grant-in-Aid.

References

1) I. Prigogine, "The Molecular Theory of Solutions," North Holland Publishing Co., Amsterdam (1957).
2) P. J. Flory, *Discuss. Faraday Soc.*, **49**, 7 (1970).
3) D. Patterson and G. Delmas, *Trans. Faraday Soc.*, **65**, 708 (1969).
4) D. Patterson, *Macromolecules*, **2**, 672 (1969).
5) G. V. Schulz and M. Lechner, *J. Polym. Sci., Part A-2*, **8**, 1885 (1970).
6) M. Lechner and G. V. Schulz, *Eur. Polym. J.*, **6**, 945 (1970).
7) G. V. Schulz and M. Lechner, in "Light Scattering from Polymer Solutions," M. B. Huglin, Ed., Academic Press, New York, N. Y. (1971).
8) D. Gaeckle and D. Patterson, *Macromolecules*, **5**, 136 (1972).
9) C. J. McDonald and S. Claesson, *Chemica Scripta*, **4**, 155 (1973).
10) M. Kurata and W. H. Stockmayer, *Fortschr. Hochpolym. Forsch.*, **3**, 196 (1963).
11) K. Kubo and K. Ogino, *Bull. Chem. Soc. Jpn.*, **44**, 997 (1971).
12) Shin-Etsu technical data, T6-4.
13) P. W. Bridgman, "Physics of High Pressure," Bell and Sons, London (1949).
14) P. Debye, *J. Appl. Phys.*, **15**, 338 (1944).
15) G. V. Schulz and A. Haug, *Z. Phys. Chem. Neue Folge.*, **34**, 328 (1962).
16) C. I. Carr, Jr. and B. H. Zimm, *J. Chem. Phys.*, **18**, 1616 (1950).
17) F. E. Gibson and J. F. Kincaid, *J. Am. Chem. Soc.*, **60**, 511 (1938).
18) I. Prigogine and R. Defay, "Chemical Thermodynamics," Longmans, Green and Co., London (1954).
19) S. Saeki, N. Kuwahara, M. Nakata, and M. Kaneko, *Polymer*, **16**, 445 (1975).
20) Hsiang Shih and P. J. Flory, *Macromolecules*, **5**, 758 (1972).
21) W. R. Krigbaum, D. K. Carpenter, M. Kaneko, and A. Roig, *J. Chem. Phys.*, **33**, 921 (1960).
22) M. Fixman, *J. Chem. Phys.*, **23**, 1656 (1955).
23) W. H. Stockmayer, *Makromol. Chem.*, **35**, 54 (1960).
24) P. J. Flory, *J. Chem. Phys.*, **17**, 303 (1949).
25) T. A. Orofino and P. J. Flory, *J. Chem. Phys.*, **26**, 1067 (1957).
26) M. Kurata, M. Fukatsu, H. Sotobayashi, and H. Yamakawa, *J. Chem. Phys.*, **41**, 139 (1964).
27) H. Yamakawa, *J. Chem. Phys.*, **48**, 2103 (1968).
28) E. F. Casassa and H. Markovitz, *J. Chem. Phys.*, **29**, 493 (1958).
29) P. J. Flory and W. R. Krigbaum, *J. Chem. Phys.*, **18**,

1086 (1950).
30) H. Eyring and J. O. Hirschfelder, *J. Phys. Chem.*, **41**, 249 (1937).
31) A. Abe and P. J. Flory, *J. Am. Chem. Soc.*, **87**, 1838 (1965).
32) R. E. Gibson and O.H. Loeffler, *J. Am. Chem. Soc.*, **61**, 2515 (1939).
33) N. Kuwahara, *J. Polym. Sci., A*, **1**, 2395 (1963).
34) P. J. Flory and Hsiang Shih, *Macromolecules*, **5**, 761 (1972).

Flotation of MnO_4^- and Fe^{3+} Ions by the Combined Use of Sodium Silicate and Cationic Surfactant

Isao TAKAYANAGI,* Koichi KOBAYASHI,** Keiko HACHISUKA, and Tsunetaka SASAKI***

Department of Chemistry, Faculty of Science, Tokyo Metropolitan University, Setagaya, Tokyo 158

(Received April 16, 1976)

The removals of MnO_4^- and Fe^{3+} ions from an aqueous solution by the combined use of silicate ions(SiO_3^{2-}) and a cationic surfactant, hexadecyltrimethylammonium chloride (HTAC), were studied by means of ion flotation techniques. The effect of variables such as pH, the surfactant concentration, and the order of addition of the reagents on the floatability of the ions were studied. More than 98 and 97% of the MnO_4^- and Fe^{3+} ions, respectively, could be floated under the optimum conditions. The optimum composition of SiO_3^{2-} and HTAC was found to be about 0.9 in mole fraction of SiO_3^{2-} for both systems. It was also found that the order of the addition of the reagents markedly affects the floatability. Further, a schematic model of flotation was proposed, taking account of the compositions of the sublate. MnO_4^- and Fe^{3+} ion flotations differed from each other in that MnO_4^- ions combine with SiO_3^{2-} ions through the double layer of HTAC molecules, which are subsequently coagulated and floated by HTAC, while Fe^{3+} ions or polynuclear Fe^{3+} ions combine directly with SiO_3^{2-} ions, which are subsequently coagulated and floated by HTAC.

Ion flotation has been employed for the removal of inorganic anions and cations from an aqueous solution. The process involves the formation of a surface-active complex by the addition of surface-active ions opposite in charge to the ions to be separated. The complex is then floated by means of gas bubbles introduced into the solution. Various studies have been made of the reagents available for flotation and of the mechanism of flotation.[1] Among the possible processes of ion flotation, the use of a surfactant with or without a polyelectrolyte has been confirmed to be effective for the flotation of anions, cations, and particles.[2] Goto and Izumi have reported the removal of heavy metal ions from an aqueous solution by using polyethylenepolyamine.[3] Cu^{2+}, Cd^{2+}, and Co^{2+} ions have been more effectively removed from an aqueous solution by the combined use of macromolecular or polymer anions, such as bentonite, and cationic surfactants than by the simple use of an anionic surfactant.[4,5] So far, no application of ion flotation has been made to the removal of cations and anions from an aqueous solution by the combined use of silicate ions and a cationic surfactant, which also belongs to this category.

The present study is intended to establish the feasibility of ion flotation for the removal of anions and cations such as Fe^{3+} and MnO_4^- ions from an aqueous solution by the combined use of silicate ions and a cationic surfactant, hexadecyltrimethylammonium chloride (HTAC).

Experimental

Materials. The concentrated solution of about 2×10^{-3} mol/l permanganate solution was prepared by dissolving extra-pure grade potassium permanganate into triply distilled water; the solution was stocked in a dark room. The concentration of permanganate ions was determined by the usual method of titrating with a standard solution of sodium oxalate.

The iron(III) chloride used was of analytical reagent grade $FeCl_3\cdot6H_2O$, and was purified before use by recrystallization. A stock solution of 7.45×10^{-3} mol/l concentration was prepared by dissolving iron(III) chloride in triply distilled water, with the addition of a small amount of sulfuric acid to make the solution of pH 1.4. The concentration of Fe^{3+} ions was determined with an atomic absorption spectrometer (Techtron Pty., Ltd., Model-AA-100), using an aqueous solution of Mohr's salt of known concentration as a standard.

The cationic surfactant used was of pure grade hexadecyltrimethylammonium chloride (HTAC) supplied by the Kao Soap Co., Ltd.; its aqueous solution was prepared by dissolving HTAC in triply distilled water. The solution was employed after diluting just before use. The solution of silicate ions (SiO_3^{2-}) was prepared by dissolving reagent grade water glass in triply distilled water. The sodium hydroxide used for controlling pH was of extra-pure reagent grade, and was purified by precipitation from its saturated solution.

All other chemicals were of analytical reagent grade unless otherwise specified and were used without further purification.

Procedure. *MnO_4^- Ion Flotation*: In a test tube 1.65 cm in inner diameter and 16.5 cm in length, 10 ml of water, a given amount of potassium permanganate solution, and varying amounts of HTAC and sodium silicate solutions were introduced; the volume was filled with water to a total of 12 ml. The test tube of the sample solution was allowed to stand for 2 min and was slowly and repeatedly turned upside down. Then the precipitates formed with MnO_4^- were shaken for 10 s by hand and were floated with minute bubbles. After 5 min, the underlying liquid was taken out of the test tube and was centrifuged to remove the remaining precipitates. The concentration of permanganate ions in the solution was determined by a colorimeter (Bausch and Lomb, Spectronic 20) at 720 nm.

The floatability (%) of MnO_4^- ions was given by

$$F = \frac{C_i - C_f}{C_i} \times 100\%$$

where C_i and C_f denote the initial and final concentrations of MnO_4^- ions, respectively.

The concentration of HTAC and SiO_3^{2-} in the solution was determined as follows.

HTAC Concentration: Five ml of the solution without the precipitate was taken in a flask and mixed with 0.1 ml of Bromophenol Blue solution as a color indicator (a mixture of

* Present address: Shiseido Co., Ltd., 1-38-10, Kyojima, Sumida-ku, Tokyo 131.

** Address all correspondence to the present address: Laboratory of Chemistry, Musashi Institute of Technology, 1-28-1 Tamatsutsumi, Setagaya, Tokyo 158.

*** Present address: Department of Chemistry, Faculty of Science, Tokai University, Hiratsuka, Kanagawa 259-12.

0.08% Bromophenol Blue, 62.5% acetic acid, 10.25% Na_2SO_4, and 27.17% water). The solution was titrated with sodium octadecylsulfate solution in a water bath at 60 °C.[6] The amount of HTAC in the sublate was calculated from the difference in the amount of HTAC in the solution before and after the precipitate formation.

SiO_3^{2-} Concentration: The concentration of SiO_3^{2-} was colorimetrically determined by the color developed by the addition of ammonium molybdate.[7] The absorbance was measured at 830 nm and the amount of SiO_3^{2-} in the sublate was calculated similarly to that of HTAC mentioned above. In some cases, the amount of SiO_3^{2-} in the sublate could not be determined as a difference owing to its small content. In such a case the sublate was removed and washed with distilled water, subjected to combustion in a platinum crucibles, fused with anhydrous sodium carbonate, and dissolved in triply distilled water. The solution was adjusted to pH 2 with sulfuric acid, and the amount of SiO_3^{2-} in the solution was determined by the colorimetry.

Fe^{3+} Ion Flotation. The varying amounts of Fe^{3+}, HTAC, and SiO_3^{2-} solutions and a small amount of sodium hydroxide solution were introduced into a graduated test tube 1.0 cm in inner diameter and 17 cm in length. The total volume of the solution was increased with water to 10 ml. The solution was treated in the same manner as in the case of the MnO_4^- ion flotation. After the flotation, about 5 ml of the underlying solution was taken out of the test tube for the measurements of the pH, concentration of HTAC, SiO_3^{2-}, and Fe^{3+}, from which the floatability of Fe^{3+} and the composition of the sublate were calculated. The floatability of the Fe^{3+} ions was calculated similarly to that of MnO_4^-.

The measurements of the flotation were carried out at room temperature, about 25 °C.

Results and Discussion

MnO_4^- Ion Flotation. Figure 1 shows the floatability of MnO_4^- as a function of total molar concentration of Na_2SiO_3+HTAC and mole fraction of Na_2SiO_3 in the mixture at pH 11. The area circumscribed by the curve shows the optimum region of MnO_4^- flotation, where more than 85% of MnO_4^- is floated. The triangles show the systems of less than 85% floatability, while the circles and squares indicate the systems with floatabilities of 90 and 98%, respectively. As may be seen in Fig. 1, the mole fractions of SiO_3^{2-} in the sample solution fall in a narrow range from 0.86 to 0.94 in the region of optimum flotation. In the upper region neighboring this optimum region (system No. 6 for instance), the flotation is not so efficient, although the permanganate ions coagulate completely. In the region of excess HTAC, the solution becomes turbid and the floatability decreases. Table 1 lists the floatability (F), and the solution and sublate compositions of the representative systems No. 1, 2, and 3 in the optimum flotation region in Fig. 1. Among these systems, a maximum floatability of 98% was obtained for the No. 2 system. From Table 1, the mole ratios of SiO_3^{2-} to HTAC of the sublates are seen to be about 2 for the three systems, while the mole ratios of HTAC to MnO_4^- are about 15.9, 7.52, and 2.47 for systems No. 1, 2, and 3 respectively, these decrease with decreasing amount of the total concentration of SiO_3^{2-}+HTAC.

Table 1. Floatability of MnO_4^-, and solution and sublate compositions of the MnO_4^-–SiO_3^{2-}–HTAC system

No.	F (%)	MnO_4^- (10^{-4} mol/l)[a]	HTAC (10^{-4} mol/l)	SiO_3^{2-} (10^{-4} mol/l)
1	85	1.91 (1.61)	26.3 (25.6)	200 (50.0)
2	98	2.01 (1.98)	15.7 (14.9)	137 (28.3)
3	91	2.08 (1.89)	4.92 (4.67)	54.0 (10.5)

( ) Indicates sublate compositions.
a) Mole number of each component in the sublate produced in 1 l solution.

In agreement with these data, some models of the sublate structure are proposed for these systems, as shown in Fig. 2.† In these models the double molecules bridging HTAC between MnO_4^- and SiO_3^{2-} are

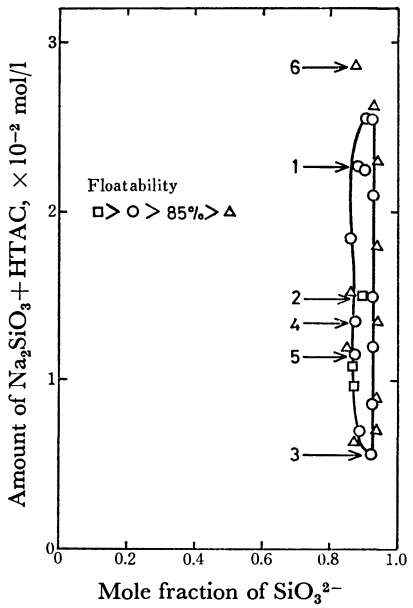

Fig. 1. Diagram of MnO_4^- ion flotation by SiO_3^{2-} and HTAC.

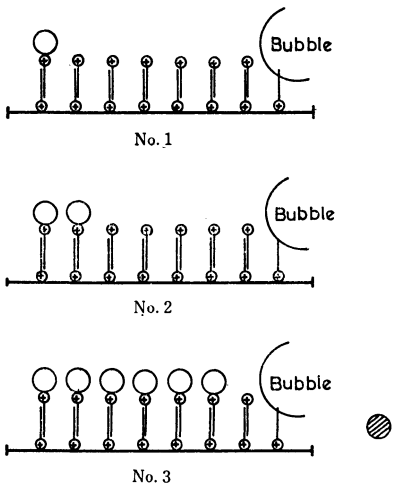

Fig. 2. A schematic drawing of sublate structure of MnO_4^-–SiO_3^{2-}–HTAC precipitate. ⊢⊣: $(SiO_3^{2-})_n$, ○: combined MnO_4^-, ◍: free MnO_4^-, ⊕—: HTAC.

† An exact agreement of the composition was not attempted, for the sake of simplicity.

indicated. HTAC also acts to float the sublates by attracting them to bubbles.

Now, in model No. 1, most MnO_4^- ions combine with silicate ions in the manner indicated in Fig. 2, but the excess positive charge due to the double molecular HTAC ions not combined with MnO_4^- increases the hydrophilicity and decreases the floatability. On the other hand, in model No. 3, nearly the full attachment of MnO_4^- ions is in equilibrium with some free MnO_4^- ions not attached to the silicate back-bone which does not float. Thus, the floatability of MnO_4^- again decreases. Therefore, a maximum of floatability is expected to appear somewhere between the two systems. System No. 2 may be considered to be such a system.

Table 2. Floatability of MnO_4^- and order of addition of reagents

No.	F(%)	
	HTAC+SiO_3^{2-}	SiO_3^{2-}+HTAC
2	98	90
4	96	91
5	91.6	88

The effect of order of the addition of reagents on the floatability of MnO_4^- was also investigated. The results are shown in Table 2. As seen, the addition of SiO_3^{2-} to systems No. 2, 4, and 5 followed by HTAC shows less floatability than the addition of the reagents in the reverse order. This effect may be explained by the fact that HTAC combines mainly with SiO_3^{2-}, as is evidenced by the white precipitate of hexadecyltrimethylammonium silicate which forms, to which MnO_4^- attaches only weakly. Thus the floatability decreases in the fomer case, while in the latter case HTAC combines with both MnO_4^- and SiO_3^{2-}, enabling MnO_4^- to float by the double molecular bridge of HTAC.

Since in the case of MnO_4^- flotation we attempted merely to confirm the possibility of flotation of the anion by the polymer and surfactant addition, the pH of the solution (about 11) was not varied to study its effect on floatability.

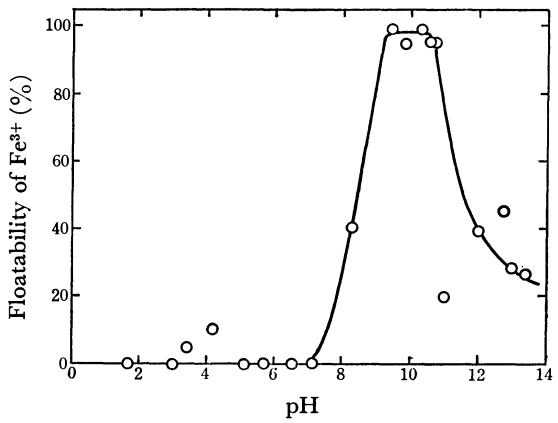

Fig. 3. Floatability *vs.* pH for Fe^{3+}–SiO_3^{2-}–HTAC system. Fe^{3+}: 7.45×10^{-5} mol/l, SiO_3^{2-}: 1.56×10^{-2} mol/l, HTAC: 2.02×10^{-3} mol/l.

Fe^{3+} Ion Flotation. In the case of Fe^{3+} ion flotation, as in the previous study,[8] the dissolved state of Fe^{3+} ions influencing the floatability was largely affected by the change in the pH, different from the case of MnO_4^-. Figure 3 shows the effect of the pH on the floatability for the Fe^{3+}–SiO_3^{2-}–HTAC system. As shown in Fig. 3, the floatability increases sharply at about pH 7 and reaches a maximum at a pH value from 9.4 to 10.7, showing an F of 97%. In the case of Fe^{3+} ion flotation by silicate ions and cationic surfactant, the Fe^{3+} ions directly combine with SiO_3^{2-}, which also combines with HTAC. At a pH value lower than 7, the floatability is practically zero for the Fe^{3+}–SiO_3^{2-}–HTAC system, presumably due to the strong adsorption of H^+ on the silicate back-bone with the exclusion of the adsorption of both Fe^{3+} and HTAC ions. In the case of Fe^{3+} ion flotation by an anionic surfactant alone and by bentonite and a cationic surfactant, the rise in floatability is seen at about pH 3 and above, as has been reported by Rubin and Johnson.[2,10] In the case of Fe^{3+} ion flotation, the iron polynuclear species forms at a certain pH, as has been reported by E. Matijevic *et al.*,[9] and then is floated by SiO_3^{2-} ions and HTAC.

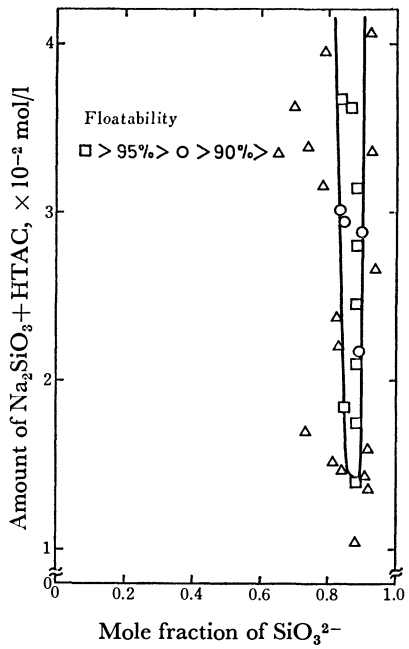

Fig. 4. Diagram of Fe^{3+} ion flotation by SiO_3^{2-} and HTAC.

Figure 4 shows the floatability diagram for Fe^{3+} at pH 9.4—10.7, similar to Fig. 1. The optimum region of Fe^{3+} ion flotation was observed in mole fractions of SiO_3^{2-} ranging from 0.85 to 0.90 and above the total concentration of 14.1×10^{-3} mol/l. In the region outside the optimum condition, the solution became turbid. In this solution the coagulation did not occur when the fraction of SiO_3^{2-} was smaller, while for a larger mole fraction of SiO_3^{2-}, it did occur, though the coagulate formed did not float. The diagram of Fig. 4 is quite similar to the case of MnO_4^-. Table 3 shows the optimum floatability and the compositions in mole of Fe^{3+}-sublate produced in 1 l solution, together with

Table 3. Sublate composition of the MnO_4^-–SiO_3^{2-}–HTAC and Fe^{3+}–SiO_3^{2-}–HTAC systems

F (%)	MnO_4^- (10^{-4} mol/l)[a)]	Fe^{3+} (10^{-4} mol/l)	HTAC (10^{-3} mol/l)	SiO_3^{2-} (10^{-3} mol/l)
97.7		0.728	1.624	8.50
98.0	1.980		1.487	2.83

a) The same as mentioned in Table 1.

those of the MnO_4^--sublate. It is seen that the SiO_3^{2-}/HTAC ratios in the sublate at optimum floatability are about 5 for the Fe^{3+}–SiO_3^{2-}–HTAC system, as shown in Table 3, while the ratio is 2 for the MnO_4^-–SiO_3^{2-}–HTAC system. This difference can be expected, since in the former system Fe^{3+} ions combine directly with SiO_3^{2-} ions, while in the latter system cationic surfactant molecules act as bridges between MnO_4^- ions and SiO_3^{2-} ions. Figure 5 shows such a difference in the structures of the MnO_4^-–SiO_3^{2-}–HTAC and Fe^{3+}–SiO_3^{2-}–HTAC systems.

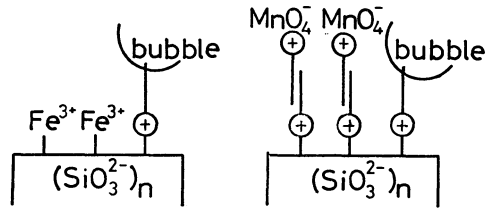

Fig. 5. Comparison of sublate structures of MnO_4^-–SiO_3^{2-}–HTAC and Fe^{3+}–SiO_3^{2-}–HTAC precipitates.

The flotation of Fe^{3+} ions was also carried out at higher Fe^{3+} concentrations near the optimum pH conditions. Thus, the effect of the order of addition of reagents upon the floatability could also be studied. The results are shown in Figs. 6, 7, and 8. As may be seen in Fig. 6, hardly any difference in the order of addition of regaents appears at the Fe^{3+} ion concentration of 6.68×10^{-5} mol/l, and the maximum floatability of 98% was obtained under the optimum conditions. In the more concentrated solution of 3.15×10^{-3} mol/l

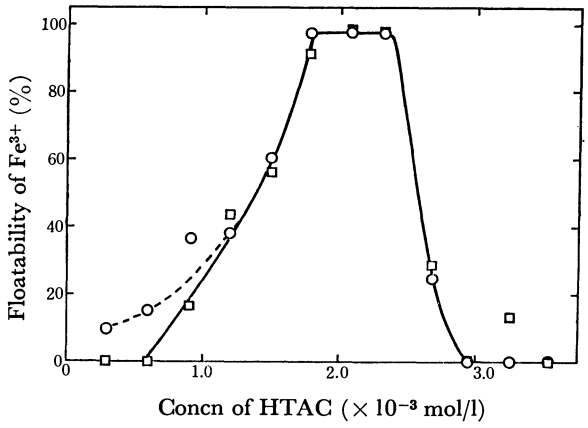

Fig. 6. Floatability *vs.* concn of HTAC for Fe^{3+}–SiO_3^{2-}–HTAC system. Fe^{3+}: 6.68×10^{-5} mol/l, SiO_3^{2-}: 1.58×10^{-2} mol/l, pH: 10.35.
—: Addition of Fe^{3+}, SiO_3^{2-}, OH^-, and HTAC in this order.
---: Addition of Fe^{3+}, OH^-, SiO_3^{2-}, and HTAC in this order.

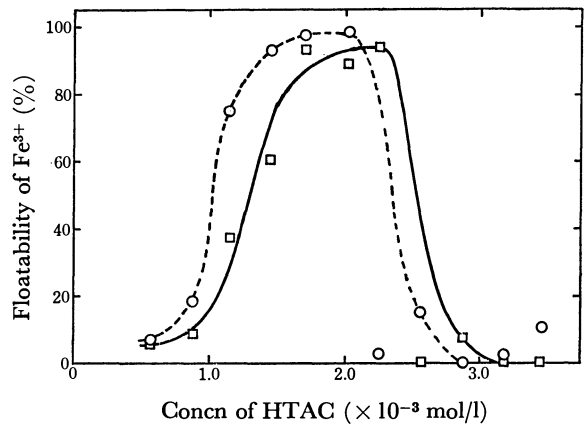

Fig. 7. Floatability *vs.* concn of HTAC for Fe^{3+}–SiO_3^{2-}–HTAC system. Fe^{3+}: 3.15×10^{-3} mol/l, SiO_3^{2-}: 1.56×10^{-2} mol/l, pH: 9.85.
—: Addition of Fe^{3+}, SiO_3^{2-}, OH^-, and HTAC in this order.
---: Addition of Fe^{3+}, OH^-, SiO_3^{2-}, and HTAC in this order.

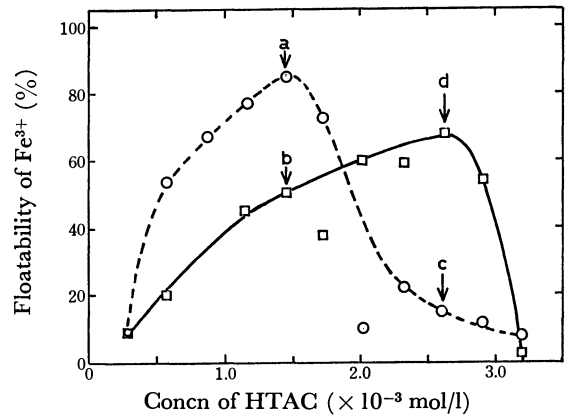

Fig. 8. Floatability *vs.* concn of HTAC for Fe^{3+}–SiO_3^{2-}–HTAC system. Fe^{3+}: 6.99×10^{-3} mol/l, SiO_3^{2-}: 1.56×10^{-2} mol/l, pH: 9.60.
—: Addition of Fe^{3+}, SiO_3^{2-}, OH^-, and HTAC in this order.
---: Addition of Fe^{3+}, OH^-, SiO_3^{2-}, and HTAC in this order.

(Fig. 7), the difference in the order of addition of reagents slightly appears. Here, in the case of the addition in the order of Fe^{3+}, OH^-, SiO_3^{2-}, and HTAC, the optimum floatability of F=98% was obtained at the HTAC concentration of 2.0×10^{-3} mol/l, while in the case of the addition in the order of Fe^{3+}, SiO_3^{2-}, OH^-, and HTAC, the optimum floatability of F=94% was obtained at the HTAC concentration of 2.0×10^{-3} mol/l. The position of peaks are the same as that of Fig. 6, but the floatability is seen to decrease slightly with the increase of Fe^{3+} ions. On further increase of Fe^{3+} ions to 6.99×10^{-3} mol/l, the floatability showed a maximum of F=85.5% at the HTAC concentration of 1.4×10^{-3} mol/l for the addition in the order of Fe^{3+}, OH^-, SiO_3^{2-}, and HTAC, while a far smaller maximum of F=67.5% was obtained at the HTAC concentration of 2.61×10^{-3} mol/l for the addition in the order of Fe^{3+}, SiO_3^{2-}, OH^-, and HTAC.

The above difference may be due to the difference in structure of the sublate formed. In order to investigate the compositions of the sublate at points *a*, *b*, *c*, and *d* in Fig. 8 and to elucidate the mechanism of flotation, the compositions of each sublate and the total precipitate were determined. These results are shown in Table 4. In the case of the addition in the order of Fe^{3+}, OH^-, SiO_3^{2-}, and HTAC, the polynuclear Fe^{3+} ions may form and combine with SiO_3^{2-}, resulting in coagulation and flotation. This may explain the effective flotation of Fe^{3+} with a smaller amount of cationic surfactant. On the other hand, each Fe^{3+} ion combines directly with a SiO_3^{2-} ion in the case of the addition in the order of Fe^{3+}, SiO_3^{2-}, OH^-, and HTAC. In this case, a larger amount of cationic surfactant is required at optimum floatability, as shown in Fig. 8. From these considerations together with the compositions given in Table 4, schematic structures of the sublate for the Fe^{3+}–SiO_3^{2-}–HTAC system have been presented in Fig. 9. As can be seen, in the case of system *a* the polynuclear Fe^{3+} ion forms, attaches to SiO_3^{2-}, and is effectively floated by HTAC, while in the case of system

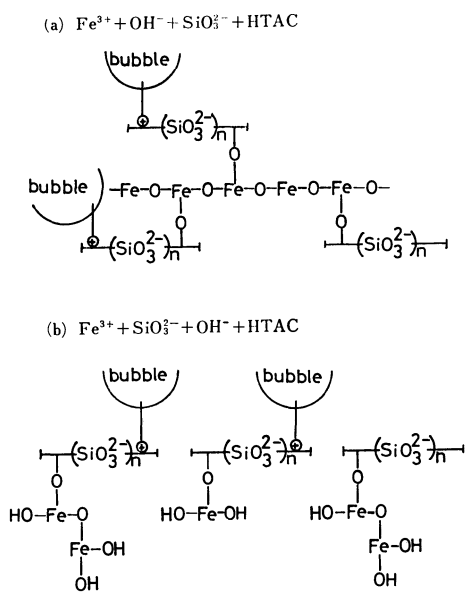

Fig. 9. Difference of sublate (precipitate) structure due to the difference of order of SiO_3^{2-} and HTAC addition.

Table 4. Sublate and precipitate compositions as affected by the order of SiO_3^{2-} and HTAC addition

No.	F (%)	Fe^{3+} (10^{-3} mol/l)[a]	HTAC (10^{-3} mol/l)	SiO_3^{2-} (10^{-3} mol/l)
a	85.6	6.89(5.98)	1.48(1.48)	13.2(12.2)
b	50.6	6.93(3.54)	1.48(1.48)	13.9(11.6)
c	15.6	6.94(1.09)	2.60(2.60)	12.8(9.60)
d	67.5	6.92(4.72)	2.60(2.60)	13.7(12.0)

( ) Indicates sublate compositions.
a) The same as mentioned in Table 1.

b, each Fe^{3+} ion combines rather directly with SiO_3^{2-} and is floated by HTAC, showing lower *F* values. In Fig. 9, the models are presented so that the numbers of moles of HTAC, Fe^{3+}, and SiO_3^{2-} in the precipitate are equal for the systems *a* and *b*. At higher concentrations of HTAC, it is evident from Fig. 9 that the increase of the composition of HTAC in the sublate *a* does not affect the wettability of the sublate (system *c*), while the increase of HTAC in the sublate *b* increases the floatability by the increase of the attachments of HTAC to the SiO_3^{2-}–Fe^{3+} complex having no HTAC (system *d*).

References

1) R. Lemlich, "Adsorptive Bubble Separation Techniques," Academic Press, New York and London (1972); F. Sebba, "Ion Flotation," Elsevier, Amsterdam, London, and New York (1962).
2) T. Sasaki, *Nippon Kogyo Kaishi*, **85**, 610 (1969).
3) T. Goto and M. Izumi, *Nippon Kagaku Kaishi*, **1974**, 1315.
4) K. Kobayashi, *Bull. Chem. Soc. Jpn.*, **48**, 1180 (1975).
5) K. Kobayashi, *Bull. Chem. Soc. Jpn.*, **48**, 1745, 1750 (1975).
6) M. J. Rosen and H. A. Goldsmith, "Systematic Analysis of Surface-Active Agents," Vol. XII, Interscience (1960), p. 69.
7) E. B. Sandell, "Colorimetric Determination of Traces of Metals," 3rd ed., Interscience Pub., New York (1959).
8) Unpublished data.
9) E. Matijevic and G. E. Janauer, *J. Colloid Interface Sci.*, **21**, 197 (1966).
10) A. J. Rubin and J. D. Johnson, *Anal. Chem.*, **39**, 298 (1967).

Equilibrium Dialysis Studies of the DNA-Acridine Complexes

Yukio KUBOTA, Yoshio EGUCHI, Kazumasa HASHIMOTO, Masaaki WAKITA, Yumi HONDA, and Yasuo FUJISAKI

Department of Chemistry, Yamaguchi University, Yamaguchi 753

(Received April 19, 1976)

The strong binding of acridine dyes with DNA was studied by means of equilibrium dialysis. Ten acridine derivatives were used to elucidate the effect of the dye structure on the nature of strong binding. In the strong binding, up to one dye molecule per 4—6 nucleotides was bound with the change of free energy in 5—9 kcal mol^{-1}. The introduction of bulky groups to the 10 or 3,6-positions of the acridine ring led to a marked decrease in both the association constant and the maximum number of binding sites per DNA phosphate. These findings suggest that, when a dye molecule is intercalated, the dye is located in such a way that the bulky groups attached to the acridine ring produce some steric hindrance to the binding.

The binding of acridine dyes to DNA has been extensively studied because of their biological activity and the general interest for the binding interaction of a macromolecule with small molecules.[1,2] It is generally believed that at least two types of binding processes are involved: weak and strong binding processes.[3] The weakly bound dye molecules are thought to be outside the double helix and stacked along the phosphate backbone.[4,5] Lerman[6,7] proposed the intercalation model for the strong binding, in which the dye molecules are inserted in a sandwich-like way between adjacent base pairs of DNA by the extension and the local unwinding of the helix. Though the general features of the model are widely accepted,[1,2] the exact location of the strongly bound dye molecules is not yet known. One of approaches to elucidate the possible location of the intercalating dye is a systematic investigation of the effects of the dye structure on the binding nature.

In the present study, the nature of strong binding was examined by means of equilibrium dialysis, using five 3,6-diaminoacridines and five 10-alkylderivatives of acridine orange. The aims of this study are: (1) to determine the thermodynamic parameters for the strong binding, (2) to reveal the effects of the dye structure on these parameters, and (3) to obtain some information on the location of the intercalative acridine dyes.

Experimental

Materials. Calf thymus DNA was purchased from Worthington Biochemical Corporation. The concentration of DNA was calculated from the absorbance at 260 nm, using the molar extinction coefficient per nucleotide residue (ε= 6600 M^{-1} cm^{-1}).[8]

Acridine orange and proflavine were obtained from Chroma and British Drug Houses, respectively. 3,6-Bis(methylamino)-acridine (Ac[NHMe]$_2$), 3,6-bis(ethylamino)acridine (Ac[NHEt]$_2$), and 3,6-bis(diethylamino)acridine (Ac[NEt_2]$_2$) were the same as previously reported.[9] 10-Alkylderivatives of acridine orange (R=methyl, propyl, pentyl, isopropyl, and benzyl) were prepared according to the method of Miethke and Zanker;[10] these are hereafter abbreviated as AO-methyl, AO-propyl, AO-pentyl, AO-isopropyl, and AO-benzyl. These dyes were purified by repeating crystallization and chromatography. Any trace of impurity was not detected by thin-layer chromatography on silica gel for each dye.

Methods. All dialysis experiments were made at ionic strengths of 0.01 and 0.11; these conditions were such that the Donnan effect could be neglected.

Both DNA and dye were dissolved in 0.005 M phosphate buffer (pH 6.9) and ionic strength was controlled by addition of NaCl solution. The DNA solutions (5 cm^3) were sealed in dialysis bags prepared from constant length (9 cm) of cellulose tubing (1.5 cm in diameter; Visking Co.) which had been cleaned by being boiled in 1% sodium hydrogencarbonate. These bags were immersed in 50 cm^3 brown flasks containing 30 cm^3 of dye solutions; the flasks had been coated with silicone to reduce the adsorption of dye. The initial dye concentrations ranged from 8×10^{-6} to 1.5×10^{-5} M except for Ac-[NEt_2]$_2$, AO-isopropyl and AO-benzyl at ionic strength of 0.11 ($(4—7)\times10^{-5}$ M). The flasks were mechanically rocked for 60 h in a thermostat.

For the determination of equilibrium dye concentration, both outer and inner solutions were analyzed because of the large adsorption of dye on the dialysis bag. The concentration of free dye (C_f) was determined from the absorbance of the outer solution at an appropriate wavelength for each system. Inner solutions were analyzed spectrophotometrically after dissociation of the DNA–dye complexes with an equal volume of 0.2 M LiCl in methanol.[11] Then the concentration of the bound dye was taken as a difference between the dye concentration of the inner solution and that of the outer solution.

All spectrophotometric measurements were made with a Shimadzu QV-50 spectrophotometer using the expanded scale whenever necessary.

For a single binding process to equivalent and independent binding sites, the following equation can be derived:[12]

$$r/C_f = K(n-r) \tag{1}$$

where r is the number of bound dye molecules per DNA phosphate, K is the association constant between a dye molecule and a binding site, and n is the maximum number of binding sites per DNA phosphate. By rearranging Eq. 1 one can obtain:

$$1/C_f = K(n/r-1). \tag{2}$$

Accordingly, a plot of $1/C_f$ against $1/r$ should give a straight line crossing the axes at $1/r=n$ and $1/C_f=-K$. If m independent binding processes are present, Eq. 2 holds for each binding and therefore one can obtain:

$$1/C_f = \sum_{i=1}^{m} K_i(n_i/r_i-1) \tag{3}$$

Then the plot of $1/C_f$ against $1/r$ cannot be linear.

Results and Discussion

Typical plots of $1/C_f$ against $1/r$ at various temperatures are shown in Figs. 1 and 2. A linear relationship

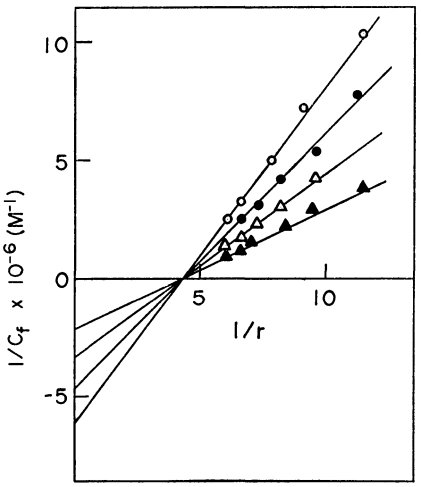

Fig. 1. Plots of $1/C_f$ against $1/r$ for the DNA–Ac[NHEt]$_2$ system at ionic strength of 0.01.
(○) 25 °C, (●) 31 °C, (△) 38 °C, (▲) 45 °C.

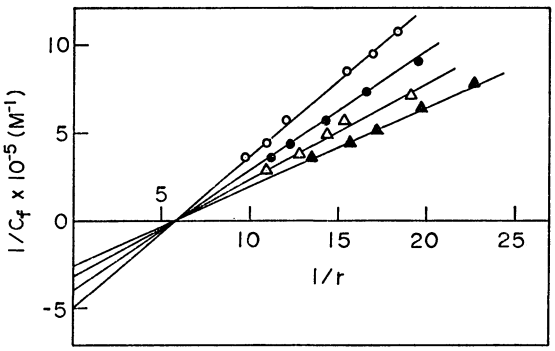

Fig. 2. Plots of $1/C_f$ against $1/r$ for the DNA–Ac[NEt$_2$]$_2$ system at ionic strength of 0.01.
(○) 25 °C, (●) 31 °C, (△) 38 °C, (▲) 45 °C.

between $1/C_f$ and $1/r$ was pretty good. From such plots, both K and n were determined by extrapolating the linear portion to $1/C_f$ and $1/r$ axes, respectively. As can be seen in Figs. 1 and 2, the K values are dependent on the temperature, while the n values seem to be constant within the experimental errors in the temperature ranges examined. In general, the $1/C_f$ *vs.* $1/r$ curves deviated from the linearity at low $1/r$ values ($r>0.2$); presumably due to the weak binding process.[4,5] Armstrong *et al.* proposed that, at low ionic strength, a binding of dye dimers takes place at high r values by binding of a second dye molecule to those already intercalated.[11] To avoid complications for the analysis of data,[11,13] we restrained our study to the range of strong binding ($r<0.15$) at relatively high ionic strengths.

Thermodynamic parameters, the change of free energy ($\Delta G°$), enthalpy ($\Delta H°$) and entropy ($\Delta S°$) were calculated using the following equations.

$$\Delta G° = -RT\ln K \quad (4)$$

$$\Delta H° = -Rd\ln K/d(1/T) \quad (5)$$

$$\Delta S° = (\Delta H° - \Delta G°)/T \quad (6)$$

A plot of log K against $1/T$ for each system gave a straight line in the temperature ranges examined (25—45 °C).

Table 1. Thermodynamic parameters at 25 °C

Dye	Ionic strength	n	$k\times10^{-5}$ (M^{-1})	$-\Delta G°$ (kcal mol^{-1})	$-\Delta H°$ (kcal mol^{-1})	$\Delta S°$ (cal deg^{-1} mol^{-1})
Proflavine	0.01	0.22	48	9.1	8.5	2.0
	0.11	0.20	3.1	7.5	8.7	−4.0
Ac[NHMe]$_2$	0.01	0.24	61	9.3	9.0	1.0
	0.11	0.22	6.7	7.9	8.7	−2.7
Ac[NHEt]$_2$	0.01	0.23	60	9.2	8.8	1.3
	0.11	0.21	3.9	7.6	8.8	−4.0
Ac[NEt$_2$]$_2$	0.01	0.17	4.9	7.8	5.2	8.7
	0.11	0.15	0.17	5.8	5.3	1.7
Acridine orange	0.01	0.22	55	9.2	8.8	1.3
	0.11	0.20	2.6	7.4	8.6	−4.0
AO-methyl	0.01	0.23	51	9.2	9.0	1.0
	0.11	0.21	4.4	7.7	9.2	−5.0
AO-propyl	0.01	0.23	54	9.2	8.5	2.3
	0.11	0.20	3.4	7.5	8.8	−4.4
AO-pentyl	0.01	0.24	53	9.2	8.5	2.3
	0.11	0.20	3.7	7.6	8.6	−3.4
AO-isopropyl	0.01	0.17	15.6	8.4	6.5	6.4
	0.11	0.17	0.61	6.5	6.2	1.0
AO-benzyl	0.01	0.18	18.4	8.5	6.9	5.4
	0.11	0.18	0.63	6.5	6.5	0

The thermodynamic parameters calculated from the data of equilibrium dialysis are listed in Table 1. These results show that the thermodynamic parameters depend on the dye structure and can be summarized as follows. (1) The n values for all acridine dyes do not exceed 0.25 ($0.15<n<0.25$); this is consistent with the findings reported earlier.[13–16] (2) The value of the association constant for all 3,6-diaminoacridines, except Ac[NEt$_2$]$_2$, are of the same order of magnitude. The K and $\Delta G°$ values for the DNA–proflavine and DNA–acridine orange complexes are in good agreement with the values in the literatures.[14,15,17] (3) The thermodynamic parameters for AO-methyl, AO-propyl and AO-pentyl are almost the same as those for acridine orange. (4) The K and n values for AO-isopropyl, AO-benzyl and Ac[NEt$_2$]$_2$ are much smaller than those for the other dyes. A marked increase in the $\Delta S°$ value is observed for these dyes when compared to the $\Delta S°$ value for the other dyes. The results imply that the bulky substituents of these dyes may exert some steric effect on the binding.

Due to the presence of bulky substituents such as diethylamino and isopropyl on the acridine ring, the original intercalation model of Lerman[6,7] may be modified.[18,19] According to the model proposed by Pritchard *et al.*,[18] the positively charged nitrogen of the acridine ring associates closely with the negatively charged oxygen of the phosphate group. Therefore, it can be predicted that any substituent on the ring nitrogen strongly affects the binding. However, the results of AO-methyl, AO-propyl and AO-pentyl show no dependence on the length of the alkyl chains attached to the ring nitrogen (Table 1). On the other hand, the results of AO-isopropyl, AO-benzyl and Ac[NEt$_2$]$_2$

indicate that the introduction of the bulky groups to the 10- or 3,6-positions of the acridine ring leads to a remarkable decrease in the K and n values. Further, the smaller K value for $Ac[NEt_2]_2$ in comparison with those for AO-isopropyl and AO-benzyl (Table 1) suggests that the bulky groups attached to the 3,6-positions have more pronounced effect on the binding than the bulky groups on the ring nitrogen do. In agreement with the findings of Löber and Achtert,[20] our results may be interpreted to show that the 10-position is not so important for the strong binding and that the acridine dyes examined in this study are intercalated in such a way that the 3,6-diamino groups are directed towards the DNA phosphate groups or very close to them. In such a location, the bulky substituents at the 3,6-positions would show significant steric effect. Even in such a location, however, it is expected that the bulky groups such as isopropyl and benzyl on the ring nitrogen still produce some steric hindrance to the binding. Therefore, such bulky groups may lie in the groove of the DNA helix so as to minimize the steric hindrance. In an attempt to elucidate further the effect of the dye structure on the strong binding, flow polarized fluorescence and viscosity studies are currently in progress.

The authors are indebted to Dr. Mitsuo Zama for his valuable advice for the method of equilibrium dialysis.

References

1) A. R. Peacocke, "Acridines," ed. by R. M. Acheson, Interscience Publishers, New York (1973), p. 723.
2) E. R. Lochmann and A. Micheler, "Physico-Chemical Properties of Nucleic Acids," Vol. 1, ed. by J. Duchesne, Interscience Publishers, New York (1973), p. 223.
3) A. R. Peacocke and J. N. H. Skerrett, *Trans. Faraday Soc.*, **52**, 261 (1956).
4) D. F. Bradley and M. K. Wolf, *Proc. Natl. Acad. Sci. U. S.*, **45**, 944 (1959).
5) A. L. Stone and D. F. Bradley, *J. Am. Chem. Soc.*, **83**, 3627 (1961).
6) L. S. Lerman, *J. Mol. Biol.*, **3**, 18 (1961).
7) L. S. Lerman, *Proc. Natl. Acad. Sci. U. S.*, **49**, 94 (1963).
8) H. R. Mahler, B. Kline, and B. D. Mehrotra, *J. Mol. Biol.*, **9**, 801 (1964).
9) Y. Kubota, *Bull. Chem. Soc. Jpn.*, **46**, 2630 (1973).
10) E. Miethke and V. Zanker, *Z. Phys. Chem. Frankfurt*, **18**, 375 (1958).
11) R. W. Armstrong, T. Kurucsev, and U. P. Strauss, *J. Am. Chem. Soc.*, **92**, 3174 (1970).
12) G. Scatchard, *Ann. N. Y. Acad. Sci.*, **51**, 660 (1949).
13) D. M. Crothers, *Biopolymers*, **6**, 575 (1968).
14) N. F. Ellerton and I. Isenberg, *Biopolymers*, **8**, 767 (1969).
15) S. Ichimura, M. Zama, H. Fujita, and T. Ito, *Biochim. Biophys. Acta*, **190**, 116 (1969).
16) W. Bauer and J. Vinograd, *J. Mol. Biol.*, **47**, 419 (1970).
17) J. Chambron, M. Daune, and Ch. Sadron, *Biochim. Biophys. Acta*, **123**, 306 (1966).
18) N. J. Pritchard, A. Blake, and A. R. Peacocke, *Nature*, **212**, 1360 (1966).
19) A. Blake and A. R. Peacocke, *Biopolymers*, **6**, 1225 (1968).
20) G. Löber and G. Achtert, *Biopolymers*, **8**, 595 (1969).

Studies of Iron(II) Complexes with Several Schiff Bases: New Examples of $^5T_2$-$^1A_1$ Equilibrium

Yonezo MAEDA, Yoshimasa TAKASHIMA, and Yuzo NISHIDA

Department of Chemistry, Faculty of Science, Kyushu University, Hakozaki, Higashiku, Fukuoka 812

(Received September 2, 1975)

Iron complexes with the Schiff bases of quinolinecarbaldehyde and pyridinecarbaldehyde were prepared. Mössbauer spectra and magnetic susceptibilities of the compounds, $Fe(pipa)_2(NCS)_2$, $Fe(pa)_2(NCS)_2$, $Fe(pot)_2(NCS)_2 \cdot 1/2CHCl_3$, $Fe(ppt)_2(NCS)_2$, $Fe(ppca)_2(NCS)_2$, and $Fe(ppa)_2(NCS)_2$ were studied in the temperature range between 298 and 27 K. It was found that these complexes showed an incomplete $^5T_2$-$^1A_1$ transition in the solid. The compound $Fe(poca)_2(NCS)_2$ also showed a similar phenomenon. The observations of the behavior of the various complexes indicated that the magnetic changeover from spin-paired to spin-free would be closely associated with a modification of the crystal lattice. The $FeL'Cl_2$(L': the Schiff bases of quinolinecarbaldehyde) were found to have distorted tetrahedral structures.

The spectral study of a substantial series of complexes derived from the Schiff bases of 2-pyridinecarbaldehyde has already been completed.[1] The iron(II) complexes of *N*-(2-pyridylmethylene)methylamine exhibit quite similar magnetic and spectroscopic behavior to that of the iron(II) complexes of 2,2'-bipyridine and 1,10-phenanthroline. A series of iron(II) complexes with the Schiff bases of quinolinecarbaldehyde and pyridinecarbaldehyde were prepared. The spectroscopic and magnetic properties of some compounds possessing anomalous magnetic properties are reported in this work. From a structural point of view, the iron complexes with the Schiff bases of quinolinecarbaldehyde and pyridinecarbaldehyde are well correlated with those of 2,2'-bipyridine and aliphatic α,α'-diimine, *i.e.*, they all contain –N=C–C=N group which directly participates in the co-ordination. As may readily be seen in the figure, however, the Schiff bases of pyridinecarbaldehyde(a) and quinolinecarbaldehyde(b) are in an intermediate state between 2,2'-bipyridine(c), and α,α'-diimine(d) compounds with respect to the conjugated double bond.

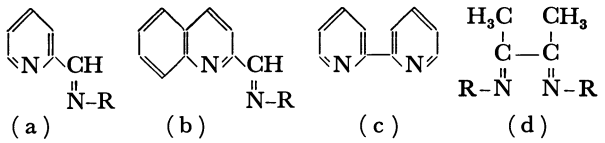

(a) (b) (c) (d)

It has been observed that certain iron(II) complexes of 2,2'-bipyridine,[2] 1,10-phenanthroline,[3] and 2-(aminomethyl)pyridine[4] have magnetic moments which are dependent on temperature. It was suggested that the intermediate magnetic moment might be due to a thermal equilibrium between the high- and low-spin states. Recently iron(II) compounds which exhibit an incomplete $^5T_2$-$^1A_1$ transition have been reported.[5]

Experimental

Materials. Quinoline derivatives were prepared from 2-quinolinecarbaldehyde and aromatic or aliphatic amines. The preparation of the 2-quinolinecarbaldehyde was accomplished by reduction of ω,ω-dibromoquinaldine with silver nitrate.[6] 2-Pyridinecarbaldehyde was purchased from the Ishizu Pharmaceutical Co., Ltd. The ligand abbreviations used in this work are, qa for *N*-(2-quinolylmethylene)aniline, qipa for *N*-(2-quinolylmethylene)isopropylamine, qot for *N*-(2-quinolylmethylene)-*o*-toluidine, qpt for *N*-(2-quinolylmethylene)-*p*-toluidine, qea for *N*-(2-quinolylmethylene)ethylamine, qba for *N*-(2-quinolylmethylene)benzylamine, pa for *N*-(2-pyridylmethylene)aniline, pipa for *N*-(2-pyridylmethylene)isopropylamine, pot for *N*-(2-pyridylmethylene)-*o*-toluidine, ppt for *N*-(2-pyridylmethylene)-*p*-toluidine, ppna for *N*-(2-pyridylmethylene)-*p*-nitroaniline, ppca for *N*-(2-pyridylmethylene)-*p*-chloroaniline, poca for *N*-(2-pyridylmethylene)-*o*-chloroaniline, ppa for *N*-(2-pyridylmethylene)-*p*-anisidine, pba for *N*-(2-pyridylmethylene)benzylamine and ph for 2-pyridinecarbaldehyde hydrazone.

Preparations of the Complexes. The complexes were prepared by mixing iron(II) salts and the Schiff bases in an ethanolic solution.

The crystals were collected and recrystallized from water, acetone or chloroform. To avoid any possible oxidation, the procedures were carried out in a nitrogen atmosphere, using air-free ethanol. The complexes are generally stable to oxidation in the solid state. The complexes, however, were stored in a nitrogen atmosphere. The complexes prepared are listed in Table 1 together with analytical and magnetic data. Microanalyses were carried out at the Elemental Analysis Center of Kyushu University.

Measurements. Mössbauer effect measurements were made with a spectrometer described elsewhere.[7] Cobalt-57 diffused into palladium foil was used as the source. The isomer shifts, δ_N, were measured relative to the center of the spectrum of sodium nitroprusside which was used as velocity calibration. The absorbers used are very thin of approximately 0.067 mg of ^{57}Fe per cm^2 so that the saturation effect becomes negligible. The transmitted counts were stored at the rate of 60000—600000 counts per channel over a period of 18—50 h to minimize the statistical error. Magnetic susceptibilities between 77 and 295 K were measured on the polycrystalline samples by the Faraday method, while magnetic susceptibilities at 295 K were measured by the Gouy method. $HgCo(NCS)_4$ was used as the calibration substance.

Diamagnetic corrections were made for the ligands and anions. The effective magnetic moment, μ_{eff}, was obtained from the relation $\mu_{eff}=2.83\sqrt{\chi_m T}$, where χ_m is the molar susceptibility after applying diamagnetic corrections.

Reflectance and infrared spectra were obtained with apparatus described elsewhere.[8]

The conductivities of the complexes in one of solutions of acetone, chloroform and water, were measured using a Yanagimoto bridge and a cell which had been previously calibrated with aqueous KCl solutions.

TABLE 1. ANALYTICAL AND MAGNETIC DATA

Complexes	Found (%)			Calcd (%)			μ_{eff}(BM.) at 295K
	C	H	N	C	H	N	
$Fe(qa)Cl_2$	53.03	3.32	7.68	53.48	3.34	7.80	5.06
$Fe(qipa)Cl_2$	48.00	4.30	8.52	48.00	4.31	8.62	5.12
$Fe(qot)Cl_2$	54.70	3.89	7.44	54.69	3.75	7.51	5.11
$Fe(qpt)Cl_2$	54.87	3.71	7.39	54.69	3.75	7.51	5.17
$Fe(qea)_2(NCS)_2$	57.21	4.41	15.23	57.79	4.45	15.56	5.48
$Fe(qba)_2(NCS)_2$	64.92	12.56	4.30	65.07	12.65	4.22	5.52
$Fe(qea)_2Cl_2 \cdot 1/2H_2O$	56.75	5.05	10.60	57.14	4.96	11.11	5.39
$Fe(qba)_2Cl_2 \cdot 1/2H_2O$	64.38	4.71	8.61	64.97	4.62	8.92	5.30
$Fe(pa)_2Cl_2$	58.42	4.29	11.24	58.66	4.07	11.41	5.13
$Fe(pipa)_2(NCS)_2$	51.37	5.28	18.03	51.29	5.13	17.95	4.33
$Fe(pa)_2(NCS)_2$	58.27	3.81	15.81	58.22	3.73	15.67	5.30
$Fe(pot)_2(NCS)_2 \cdot 1/2CHCl_3$	55.08	4.12	13.13	54.84	3.93	13.47	5.32
$Fe(ppt)_2(NCS)_2$	58.76	4.20	14.77	59.59	4.26	14.90	5.15
$Fe(ppna)_2(NCS)_2$	50.00	3.22	17.33	49.85	2.88	17.89	5.41
$Fe(ppca)_2(NCS)_2$	51.44	3.17	13.62	51.66	2.98	13.91	5.45
$Fe(poca)_2(NCS)_2$	51.24	3.48	14.03	51.66	2.98	13.91	5.48
$Fe(ppa)_2(NCS)_2$	56.05	3.97	13.92	56.19	4.01	14.05	5.17
$Fe(pba)_3(NCS)_2 \cdot H_2O$	63.27	5.52	14.50	63.24	4.88	14.40	1.13
$Fe(ph)_3(NCS)_2$	44.56	4.01	28.73	44.86	3.93	28.79	0.85

TABLE 2. CONDUCTIVITY DATA OF SOME IRON COMPLEXES (10^{-3}M)

Complexes	Λ_m (mho cm^{-2} mol^{-1})	Solvent[1)]
$Fe(pa)_2Cl_2$	22.0	A
$Fe(pa)_2(NCS)_2$	4.3	A
$Fe(pot)_2(NCS)_2 \cdot 1/2CHCl_3$	0.1	A
$Fe(ppt)_2(NCS)_2$	0.1	A
$Fe(pba)_3(NCS)_2 \cdot H_2O$	149.0	W
$Fe(ph)_3(NCS)_2$	150.3	W
$Fe(poca)_2(NCS)_2$	0	C
$Fe(ppca)_2(NCS)_2$	0	C
C $Fe(ppa)_2(NCS)_2$	0	C

The measurements were performed at 25 °C. Abbreviations: A: acetone, C: chloroform, W: water.

Results and Discussion

All the complexes prepared are listed in Table 1. The results obtained by elemental analysis agreed well with the calculated values. The effective magnetic moments at 295 K are also listed in the Table 1.

Conductivities. The molar conductivities of these complexes described in Table 2 exhibit a pattern consistent with their proposed structures. The iron complexes $Fe(pa)_2Cl_2$, $Fe(pa)_2(NCS)_2$, $Fe(pot)_2(NCS)_2 \cdot 1/2CHCl_3$, $Fe(ppt)_2(NCS)_2$, $Fe(poca)_2(NCS)_2$, $Fe(ppca)_2(NCS)_2$, and $Fe(ppa)_2(NCS)_2$ were non-electrolytic in acetone or chloroform. The molar conductivities of a water solution of $Fe(pba)_3(NCS)_2 \cdot H_2O$ and $Fe(ph)_3(NCS)_2$ show that the compounds behave as uni-bivalent electrolytes. The conductivities of some of these compounds are not listed in Table 2, because they could not be determined owing to their low solubility in organic solvents.

Mössbauer Spectra. For an $Fe^{2+}(d^6)$ system, a separate Mössbauer transition could be observed for the high and low-spin states. The time of change from one spin state to the other must therefore be longer than 1×10^{-7} s, the lifetime of the ^{57}Fe excited state. The ^{57}Fe Mössbauer data obtained are given in Tables 3 and 4. The Mössbauer spectra of compounds $Fe(pipa)_2(NCS)_2$, $Fe(pa)_2(NCS)_2$, $Fe(pot)_2(NCS)_2 \cdot 1/2CHCl_3$, $Fe(ppt)_2(NCS)_2$, $Fe(ppa)_2(NCS)_2$, and $Fe(ppca)_2(NCS)_2$ at a variety of temperatures are shown in Figs. 1—6.

The values of the isomer shift and quadrupole splitting of $Fe(pa)_2(NCS)_2$ at 298 K would appear to fall in the region of those characteristic of a high-spin six-coordinated iron(II) compound. The spectrum changes to that of a low-spin iron(II) compound at 27 K, partly leaving the high-spin doublet. This result coincides well with the magnetic susceptibility data which are at intermediate values between those of high-spin and low-spin iron(II) compounds.

On the other hand, the spectrum of $Fe(pipa)_2(NCS)_2$ measured at 298 K consists of superimposed lines that are assigned to high-spin and low-spin iron(II) compounds, respectively. The spectrum changes to the spectrum characteristic of a low-spin iron(II) compound at 196 K, *i.e.*, a small isomer shift and a small quadrupole splitting are observed. The Mössbauer spectra of $Fe(pa)_2Cl_2$, $Fe(pba)_3(NCS)_2 \cdot H_2O$, and $Fe(ph)_3(NCS)_2$, which contain similar ligands, were measured for a comparison of the Mössbauer parameter. The spectrum of $Fe(ppna)_2(NCS)_2$ was also measured at 83 K and iron was found to be in the high-spin state.

In view of the strong electron acceptability of the nitro group, one would expect that the nitrogen atom of imine accepts appreciable electrons providing a strong bond with the iron atom.[9)] This expectation, however, was found to be unreasonable as can be seen from the data given in Table 3, *i.e.*, $Fe(ppna)_2(NCS)_2$ is in a high-spin state at 83 K. The differences in the field strengths were not observed for pa, and ppt. The fraction ΔS_L in Table 4 shows the ratio of the absorption

TABLE 3. INFRARED FREQUENCIES AND REFLECTANCE SPECTRAL AND MÖSSBAUER SPECTRAL DATA

Complexes	Vibrational data (cm^{-1})	Reflectance data (cm^{-1})	Mössbauer data (mm/s) at 298 K		at 83 K	
			δ_N	ΔE	δ_N	ΔE
$Fe(qipa)Cl_2$	355[b,s] 320[b,m]	25600[m] 18500[m] 17100[s]	1.11	2.78	1.21	2.86
$Fe(qa)Cl_2$	355[b,s] 325[b,m]	23100[w,sh] 17300[s] 16500[s]	1.13	2.82	1.13	2.80
$Fe(qot)Cl_2$	355[b,s] 319[b,m]	25600[sh] 23500[sh] 18100[w] 16700[m]	1.08	2.59	1.13	2.67
$Fe(qpt)Cl_2$	358[b,s] 353[b,m] 327[b,m]	24600[sh] 23300[sh] 18200[w] 16800[m] 15900[sh]	1.04	2.68	1.16	2.82
$Fe(qea)_2(NCS)_2$	2045[c] 2060[c]	15400[s,br] 8700[sh]	1.28	1.86	1.43	2.70
$Fe(qba)_2(NCS)_2$	2045[c] 2058[c]	14900[s,br]	1.26	1.62	1.43	2.45
$Fe(qea)_2Cl_2 \cdot 1/2H_2O$		15300[s,br]	1.29	2.27	1.42	2.78
$Fe(qba)_2Cl_2 \cdot 1/2H_2O$		15300[s,br]	1.29	1.69	1.40	2.46
$Fe(pa)_2Cl_2$	257[b] 233[b]	26000[m] 15200[s,br]	1.20	2.96	1.33	3.32
$Fe(pba)_3(NCS)_2 \cdot H_2O$	2042[c] 2060[c]	25400[m] 19600[sh] 17500[s]	0.52	0.33	(d)	
$Fe(ph)_3(NCS)_2$	2040[c] 2060[c]	27400[m] 22200[sh] 19200[s]	0.55	0.33	(d)	
$Fe(pipa)_2(NCS)_2$[a]	2050[c] 2057[c] 2100[c]	25000[m] 19200[sh] 16300[s,br]				
$Fe(pa)_2(NCS)_2$[a]	2046[c] 2070[c] 2100[c,sh]	24400[sh] 17500[sh] 15700[s,br]				
$Fe(pot)_2(NCS)_2 \cdot 1/2CHCl_3$[a]	2030[c] 2060[c] 2100[c,sh]	22000[m] 16800[sh] 15000[s,br]				
$Fe(ppt)_2(NCS)_2$[a]	2038[c] 2055[c]	20400[w] 16400[sh] 14600[s,br]				
$Fe(ppna)_2(NCS)_2$	2030[c] 2055[c]	26000[m] 15400[s,br]	(e)		1.32	3.05
$Fe(ppca)_2(NCS)_2$[a]	2030[c] 2045[c]	26000[s] 15600[s,br] 9520[s]				
$Fe(poca)_2(NCS)_2$[a]	2048[c]	29000[s] 18000[sh] 16300[s,br] 9100[s]				
$Fe(ppa)_2(NCS)_2$[a]	2050[c]	24000[m] 17000[sh] 15200[s,bs]				

Abbreviations: (a) Mössbauer parameters for these compounds are summarized in Table 4. (b) Vibration of Fe–Cl. (c) Vibration of NCS. (d) These parameters were not measured. (e) These parameters were not observable. (s) strong, (m) middle, (w) weak, (sh) shoulder, (br) broad.

TABLE 4. MÖSSBAUER PARAMETERS FOR IRON COMPLEXES HAVING SPIN EQUILIBRIUM

Complexes	High-spin state (mm/s) at 298 K		at 83 K		Low-spin state (mm/s) at 298 K		at 83 K		ΔS_L
	δ_N	ΔE	δ_N	ΔE	δ_N	ΔE	δ_N	ΔE	
$Fe(pipa)_2(NCS)_2$	1.22	1.85	a		0.58	0.54	0.63	0.46	1.00
$Fe(ppa)_2(NCS)_2$	1.29	2.51	1.27	3.09	a		0.66	0.63	0.74
$Fe(ppt)_2(NCS)_2$	1.26	2.65	1.29	3.06	a		0.67	0.68	0.34
$Fe(pa)_2(NCS)_2$	1.22	2.47	1.34	3.09	a		0.66	0.70	0.35
$Fe(ppca)_2(NCS)_2$	1.24	2.41	1.30	3.09	a		0.67	0.72	0.33
$Fe(pot)_2(NCS)_2 \cdot 1/2CHCl_3$	1.28	2.50	1.30	2.93	a		0.62	0.64	0.35
$Fe(poca)_2(NCS)_2$	1.25	2.22	1.33	2.88	a		0.59	0.51	0.15

Abbreviation: (a) These absorptions could not be observed.

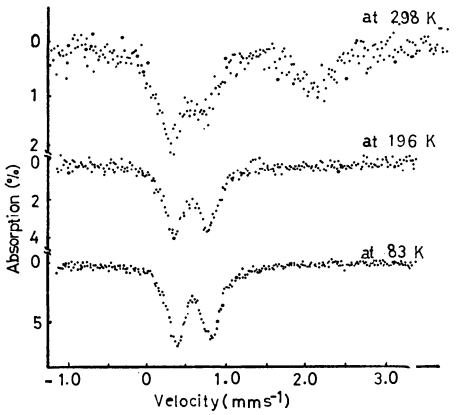

Fig. 1. Mössbauer spectra of $Fe(pipa)_2(NCS)_2$ at a variety of temperatures.

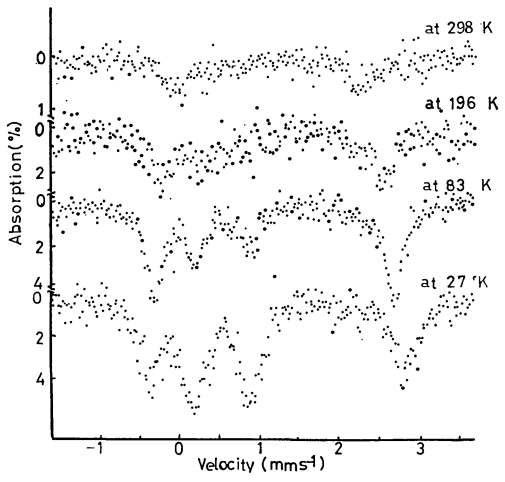

Fig. 2. Mössbauer spectra of $Fe(pa)_2(NCS)_2$ at a variety of temperatures.

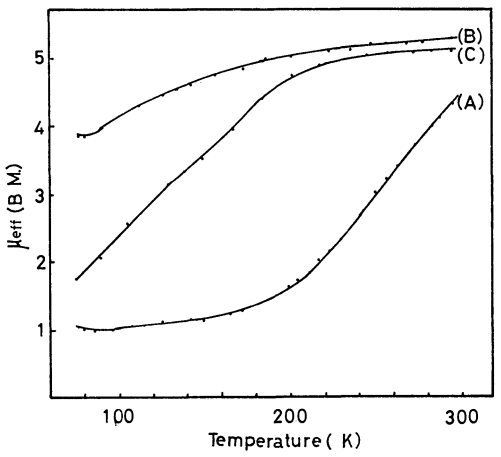

Fig. 7. Variation of the magnetic moment μ_{eff} with temperature for (A) $Fe(pipa)_2(NCS)_2$, (B) $Fe(pa)_2(NCS)_2$, and (C) $Fe(ppa)_2(NCS)_2$.

appropriate to the temperature-insensitive paramagnetism usually found for low-spin iron(II) compounds. It is concluded, therefore, that at 83 K the ground state is in the $^1A_1$ state and that this is the state populated almost exclusively. An interpretation of the magnetic data in terms of an antiferromagnetic-type exchange interaction between neighboring iron atoms is unrealistic since no reasonable fit of the curves for χ_A could be obtained for any value of the exchange coefficient J and since the Mössbauer spectra show that the population of one of the two sites increases with a decrease in temperature. On the other hand, the Mössbauer spectra of the compounds $Fe(pa)_2(NCS)_2$, $Fe(pot)_2(NCS)_2 \cdot 1/2CHCl_3$, and $Fe(ppa)_2(NCS)_2$ show that both high and low-spin states are populated at 27 K and that the transition is incomplete at 27 K (13 K for the last complex). To account for the magnetism of the cross-over compounds theoretically by applying the van Vleck approach[12] is not a good method for this system since such an attempt for systems having spin-paired and spin-free equilibria has failed.[13] For the $^1A_1$-$^5T_2$ equilibrium, the equilibrium constant K_{eq} is given by $K_{eq}=(\mu_o^2-\mu_L^2)/(\mu_H^2-\mu_o^2)$, where μ_H and μ_L are the magnetic moments of the high-spin and low-spin isomers, respectively. Plots of ln K_{eq} *vs.* $1/T$ for $Fe(pipa)_2(NCS)_2$ and $Fe(pa)_2(NCS)_2$ are given in Fig. 8. This calculation for $Fe(pa)_2(NCS)_2$ is based on the assumption that the magnetism of the high-spin state follows a normal Curie-Weiss law, $\chi_m^{corr}=3.7\times10^{-6}/(T+20)$, only over the temperature range from 250 to 300 K. Although using the limited range of temperatures available may introduce considerable uncertainties in the Weiss and Curie constants, the above equation was applied to the lower temperature and μ_H was calculated from this equation. μ_L was taken as 0.8 BM to take into account the temperature-insensitive paramagnetism. For $Fe(pipa)_2(NCS)_2$, the same equation was applied.

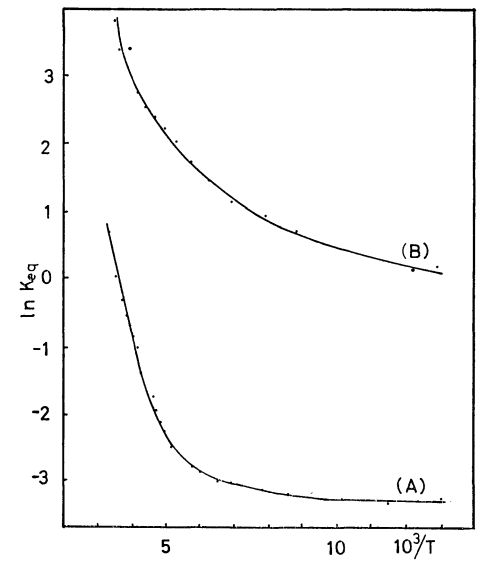

Fig. 8. Curves of ln K_{eq} against $1/T$ for (A) $Fe(pipa)_2(NCS)_2$ and (B) $Fe(pa)_2(NCS)_2$.

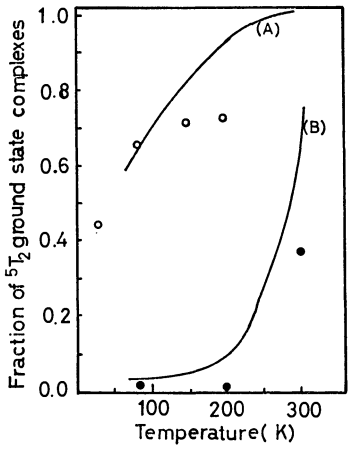

Fig. 9. Plots of the ratio of $^5T_2$ ground state complexes derived from magnetism of $Fe(pa)_2(NCS)_2$(A) and $Fe(pipa)_2(NCS)_2$(B) with temperature, and the ratio of the spectral area of the iron of high-spin state to the total area of the Mössbauer spectra of A(shown by white circle) and B(shown by black circle) at a variety of temperatures.

The fractions of the $^5T_2$ ground state complexes, n_H, derived from the magnetism of $Fe(pa)_2(NCS)_2$ and $Fe(pipa)_2(NCS)_2$, are plotted *vs.* T in Fig. 9. The ratio of the absorption area of the high-spin state to the total absorption area, ΔS_H, is also shown for various temperatures in Fig. 9. The Mössbauer spectra of $Fe(pa)_2(NCS)_2$ was also measured at 148 K using the melting point of propanol. For $Fe(pa)_2(NCS)_2$, $n_L=0.37$ was derived from the magnetic data at 83 K. On the other hand, $\Delta S_L=0.35$ was calculated from the Mössbauer absorption area under the assumption that the Debye-Waller factors, f_H and f_L, were equal. For $Fe(ppt)_2(NCS)_2$, $n_L=0.37$ and $\Delta S_L=0.34$ are calculated from the magnetic data and the Mössbauer data, respectively. It is assumed that the Debye-Waller factors, f_H and f_L, are almost equal at 83 K. Fig. 9, however, shows that at temperatures higher than 80 K, ΔS_H is less than n_H. This fact can be accounted for by the differences in the Debye-Waller factors, f_H and f_L, at higher temperatures, that is, f_H is less than f_L. The above differences would result from modifications of the crystal lattice or changes in the bond length between the central metal atom and coordinated atoms.

In the case of *N*-(2-pyridylmethylene)aniline derivatives, the fraction changed to the $^1A_1$ state at 83 K decreases in the order: ppa>pa≈ppt≈ppca>ppna. This would also be expressed by the order, $-OCH_3$> $-H\approx-CH_3\approx-Cl>-NO_2$, with respect to the substitutional group. The electron acceptor strength would be expected to increase in the order, $-OCH_3<-CH_3<$ $-H<-Cl<-NO_2$, on the basis of the sigma constant of the Hammett rule. This would seem to explain the fact that the higher electron acceptability of the functional group of the C-4 position brings about decreasing coordinating ability of the N atom in aniline.

The ΔH derived for the magnetic changes of $Fe(pipa)_2(NCS)_2$ remains constant at 3.94 kcal/mol (1380 cm^{-1}) over the temperature range of 224—273 K and is constant at 0.13 kcal/mol (45.5 cm^{-1}) between 87 and 151 K. Between 151 and 224 K ΔH changes continuously. The marked variations of ΔH of the compounds suggest a temperature dependence of the heat capacity of the compounds. Accordingly, it is conceivable that slight modifications of the crystal lattice occur in these compounds.

Electronic Spectra. The reflectance spectra of the iron complexes between 28000 and 4000 cm^{-1} were measured at 298 K. The positions of the absorption maxima are listed in Table 3. The spectra of octahedral iron(II) complexes usually show only comparatively weak bands due to the d-d transitions.[14] The $^5T_{2g}$-$^5E_{2g}$ transition band due to the high-spin form of the complexes which occurs at about 9000—12000 cm^{-1} was not observed, because of very strong charge-transfer bands. The d-d transitions for $Fe(qipa)Cl_2$ and the other substances were also not observed for the same reason, although tetrahedral iron(II) complexes are known to show usually strong band at about 5000 cm^{-1}.

Infrared Spectra. The infrared spectra of iron complexes were studied in the range between 4000 and 200 cm^{-1} at 298 K. Two strong Fe–Cl bands are observed for $Fe(qa)Cl_2$, $Fe(qipa)Cl_2$, $Fe(qot)Cl_2$ and $Fe(qpt)Cl_2$ in accordance with the IR data of $Fe(quinoline)_2Cl_2$[15] which has a tetrahedral structure. It might be assumed from this result that these complexes having $FeLCl_2$-type compositions possess a tetrahedral structure.

For N-bonded thiocyanate, the following absorption ranges are proposed:[16] ν_1 2040—2080, ν_2 465—480, and ν_3 780—860 cm^{-1}. Inspection of Table 3 indicates that in the $^5T_{2g}$ state all the thiocyanates are N-bonded. For $Fe(pipa)_2(NCS)_2$, there is another band at 2100 cm^{-1} at room temperature, which aries from the C–N stretching mode bonded to the iron atom of the $^1A_1$ state,[3] because both the high- and low-spin states are observed in $Fe(pipa)_2(NCS)_2$ at 298 K, as obtained from the Mössbauer spectra and magnetic propoerties. The splitting of the C–N stretching mode is revealed for the $^5T_2$ ground state of some of the complexes by a slight indentation of the main peak. This splitting could be considered to be a *cis*-configuration of the compound.[3] The compounds, $Fe(ppa)_2(NCS)_2$ and $Fe(poca)_2(NCS)_2$, show a sharp absorption for C–N stretching at about 2050 cm^{-1}. The compound, $Fe(pipa)_2(NCS)_2$, shows a very small splitting for C–N stretching at 2050 and 2057 cm^{-1}. This may support for the interpretation of a *trans*-configuration for the compound.

References

1) P. Krumholz, *J. Am. Chem. Soc.*, **75**, 2163 (1953); P. Krumholz, *Inorg. Chem.*, **4**, 609 (1965); M. A. Robinson, J. D. Curry, and D. H. Busch, *Inorg. Chem.*, **2**, 1178 (1963).
2) E. König and G. Ritter, *Phys. Lett.*, **43A**, 488 (1973).
3) E. König and K. Madeja, *Inorg. Chem.*, **6**, 48 (1967); Goodwin and R. N. Sylva, *Aust. J. Chem.*, **21**, 83 (1968).
4) G. A. Renovitch and W. A. Baker, Jr., *J. Am. Chem. Soc.*, **89**, 6377 (1967).
5) E. König, G. Ritter, and H. A. Goodwin, *Chem. Phys.*, **5**, 211 (1974).
6) D. L. Hammick, *J. Chem. Soc., A*, **1926**, 1303.
7) Y. Takashima and Y. Maeda *J. Inorg. Nucl. Chem.*, **31**, 1337 (1969).
8) Y. Maeda, Y. Sasaki, and Y. Takashima, *Inorg. Chim. Acta*, **13**, 141 (1975).
9) H. H. Jaffé, *Chem. Rev.*, **53**, 191 (1953).
10) R. E. Watson and A. J. Freeman, *Phys. Rev.*, **120**, 1125 (1960).
11) J. H. Nelson, L. C. Nathan, and R. O. Ragsdale, *Inorg. Chem.*, **7**, 1840 (1968).
12) J. H. Van Vleck, "The Theory of Electronic and Magnetic Susceptibilities," Oxford University Press, Oxford (1932), p. 181.
13) A. H. Ewald, R. L. Martin, I. G. Ross, and A. H. White, *Proc. R. Soc. London, Ser. A*, **280**, 235 (1964).
14) G. Winter, *Aust. J. Chem.*, **21**, 2859 (1968).
15) C. D. Burbridge and D. M. L. Goodgame, *J. Chem. Soc., A*, **1968**, 1074.
16) R. H. Toeniskoetter and S. Solomon, *Inorg. Chem.*, **7**, 617 (1968); P. C. H. Mitchell and R. J. P. Williams, *J. Chem. Soc., A*, **1960**, 1912; J, Lewis, R. S. Nyholm, and P. W. Smith, *ibid.*, **1961**, 4590.

The Kinetics of the Reaction between the Chromium(III) Ion and the Ethylenediamine-*N,N,N',N'*-tetraacetate Ion in the Presence of Hydrogen Peroxide

Katsumi YAMAMOTO and Kousaburo OHASHI

Department of Chemistry, Faculty of Science, Ibaraki University, Mito 310

(Received September 3, 1975)

The rate of the reaction between chromium(III) ion and ethylenediamine-*N,N,N',N'*-tetraacetate was found to be accelerated upon the addition of a large excess of hydrogen peroxide. Under such a condition the rate of $Cr^{III}(edta)(H_2O)^-$ formation shows a first-order dependence on the concentrations of hydrogen peroxide and chromium(III) ions, but is independent of the concentration of EDTA. The rate of $Cr^{III}(edta)(H_2O)^-$ formation catalyzed by the hydrogen peroxide increases with an increase in the pH and decreases with an increase in the acetate ion concentration. The kinetic study suggested that the initiation of the reaction takes place as follows: $Cr(III)+H_2O_2 \longrightarrow Cr(IV)+OH\cdot+OH^-$ The reaction mechanism of the hydrogen-peroxide catalysis is discussed in terms of the formation of the chromium(IV)- and /or the chronium(V)-EDTA complex in the course of the reaction. It was found that monohydroxochromium(III) is much more reactive than the chromium (III) ion toward hydrogen peroxide.

Though the reactivities of trivalent and sexavalent chromium ions with EDTA are very small at room temperature, Pribil *et al.*[1] and the present authors[2,3] have observed that $Cr^{III}(edta)(H_2O)^-$ was formed instantaneously when the chromium(VI) ion was reduced by reagents such as ascorbic acid in the presence of EDTA. This reaction was utilized for the spectrophotometric determination of the concentrations of reducing agents.[2,3]

Though the chemical properties of chromium(II), chromium(III), and chromium(VI) ions have been extensively investigated, those of chromium(IV) and chromium(V) ions are little known.[4]

Recently, Beck and Durham[5] investigated semiquantitatively the reduction of the chromium(VI) ion by hydrazine in the presence of EDTA; they suggested that chromium(IV)- and chromium(V)-EDTA complexes[6] act as intermediates in the course of the redox reaction.

The present authors found that the chromium(III) ion easily reacted with EDTA in the presence of hydrogen peroxide, as in the case of the reduction of the chromium(VI) ion by reducing agents in the presence of EDTA.

In this connection, a kinetic study of the formation of $Cr^{III}(edta)(H_2O)^-$ in the presence of hydrogen peroxide was carried out.

Experimental

Materials. A solution of chromium(III) perchlorate was prepared by the reduction of sodium dichromate in perchloric acid with hydrogen peroxide. The concentration of the chromium(III) ion was determined by the following procedure. A solution of the chromium(III) ion was heated with an excess of EDTA at 90 °C and pH 3.90 for 50 min. The concentration of the chromium(III) ion was calculated from the known molar extinction coefficient of $Cr^{III}(edta)(H_2O)^-$ at 550 nm. The stock solution of EDTA was standardized using calcium ions. The concentration of the reagent-grade hydrogen peroxide was determined by titration with a standard potassium permanganate solution. The pH and ionic strength of the reaction mixture were adjusted by the addition of an acetate buffer solution and sodium perchlorate respectively.

All the other chemicals were of a reagent grade.

Measurement of the Reaction Rate. To a chromium(III) ion solution in an Erlenmeyer flask we successively added the acetate buffer solution, the EDTA solution, and the hydrogen peroxide solution. Then this complete solution was transferred into a quartz spectrophotometer cell with a light path 1 cm in length. The temperature of the optical cells was controlled to 25±0.1 °C by circulating water through the cell holder. The kinetic measurements were carried out by recording the change in absorbance at 550 nm as a function of the time using a Hitachi EPS-3 type spectrophotometer. In every experiment hydrogen peroxide was present in a large excess relative to the concentrations of the chromium(III) ion and EDTA. The initial pH of the reaction solution was measured immediately after the initiation of the reaction with a Hitachi-Horiba F-5 pH meter. The variation in pH during the reaction was within 0.02 pH unit.

Results and Discussion

Reaction of the Chromium(III) Ion with EDTA in the Absence of Hydrogen Peroxide. The kinetics of the reaction of the chromium(III) ion with EDTA was studied by Hamm.[7] He found that the rate of the formation of $Cr^{III}(edta)(H_2O)^-$ did not depend upon the concentration of EDTA, and that it was very sensitive to the pH of the reaction mixture. Schwarzenbach and Biedermann[8] showed that one water molecule is contained in the first coordination sphere of the chromium(III)-EDTA complex. Moreover Ogino *et al.*[9,10] reported that the chromium(III)-EDTA complex was present as $Cr^{III}(edta)(H_2O)^-$ in the pH range from 3.6 to 5.3.

The dependence of the EDTA concentration on the formation rate was also examined in this work. The rate constant very slightly decreased with an increase in the EDTA concentration. The formation rate is independent of the acetate ion in the concentration range from 0.40 M to 0.05 M. Table 1 shows the first-order rate constants for the reaction between the chromium(III) ion and EDTA which were obtained in this work.

Reaction of the Chromium(III) Ion with EDTA in the Presence of Hydrogen Peroxide. The change in the absorption spectra of the chromium(III) ion solution

TABLE 1. CONDITIONAL RATE CONSTANTS k_{obsd} OF THE FORMATION OF $Cr^{III}(edta)(H_2O)^-$ AT 25 °C AND I=0.35 ($NaClO_4$)

pH	$[CH_3COO^-]$ M	k_{obsd} [a] $M^{-1}s^{-1}$	k [b] s^{-1}
3.30	0.05	2.3×10^{-5}	
	0.10	1.5×10^{-5}	8.3×10^{-6}
	0.20	1.2×10^{-5}	
	0.35	1.1×10^{-5}	
3.52	0.05	3.6×10^{-5}	
	0.10	2.3×10^{-5}	1.4×10^{-5}
	0.20	1.9×10^{-5}	
	0.35	1.6×10^{-5}	
3.70	0.05	5.2×10^{-5}	
	0.10	3.3×10^{-5}	2.1×10^{-5}
	0.20	2.5×10^{-5}	
	0.35	2.0×10^{-5}	
4.00	0.05	1.1×10^{-4}	
	0.10	7.2×10^{-5}	3.8×10^{-5}
	0.20	5.1×10^{-5}	
	0.35	4.3×10^{-5}	
4.50	0.05	3.7×10^{-4}	
	0.10	2.1×10^{-4}	1.0×10^{-4}
	0.20	1.3×10^{-4}	
	0.35	9.1×10^{-5}	

a) The rate constants of the reaction between the chromium(III) ion and EDTA in the presence of hydrogen peroxide. b) The rate constants of th reaction between the chromium(III) ion and EDTA in the absence of hydrogen peroxide.

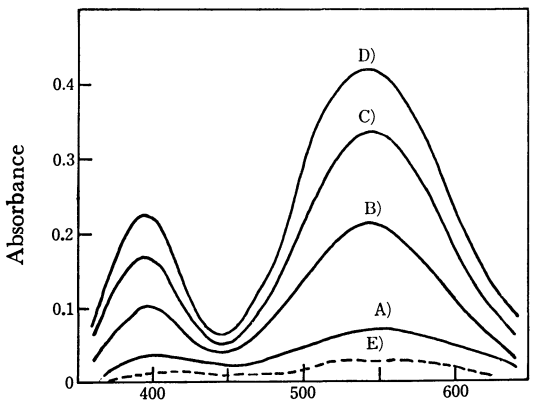

Fig. 1. The absorption spectral change of chromium (III) ion solution in the presence of EDTA upon the addition of hydrogen peroxide. $[Cr^{3+}]=5.47\times10^{-3}$ M, $[EDTA]=6.40\times10^{-3}$ M, $[H_2O_2]=4.18$ M, pH 4.10, $[CH_3COO^-]=0.10$ M, I=0.35, 25 °C.
A) 4 min, B) 15 min, C) 28 min, D) 45 min, E) 45 min (absence of H_2O_2) after the initiation of the reaction.

in the presence of EDTA upon the addition of a large excess of hydrogen peroxide is shown in Fig. 1. The change in the absorption spectra suggests that the reaction product of the chromium(III) ion is $Cr^{III}(edta)(H_2O)^-$. Curve E (45 min after the initiation of the reaction) in Fig. 1 is the absorption spectrum obtained in the absence of hydrogen peroxide. The rate of the formation of $Cr^{III}(edta)(H_2O)^-$ in the presence of

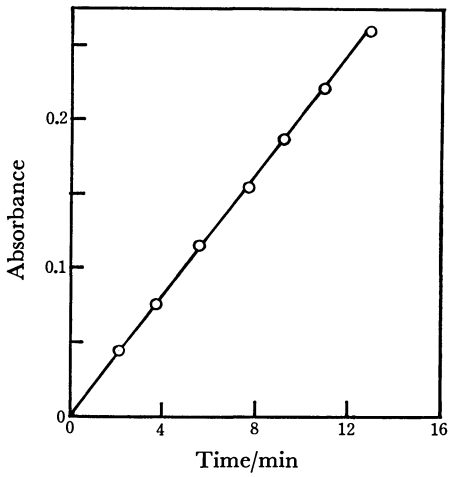

Fig. 2. Typical kinetic runs of the reaction between chromium(III) ion and EDTA in the presence of hydrogen peroxide.
$[EDTA]=2.00\times10^{-2}$ M, $[H_2O_2]=5.05$ M, $[Cr^{3+}]=7.13\times10^{-3}$ M, $[CH_3COO^-]=0.10$ M, pH 3.82, I=0.35, 25 °C, 550 nm.

hydrogen peroxide was found to be much larger than that in the absence of hydrogen peroxide.

The plot of the absorbance at 550 nm *vs.* the time were linear for at least 15% of the whole reaction (Fig. 2). Therefore, the zeroth-order rate constants of the formation of $Cr^{III}(edta)(H_2O)^-$ were determined from the initial slope of the absorbance *vs.* the time plots.

The formation rate of $Cr^{III}(edta)(H_2O)^-$ is independent of the order of the addition of the hydrogen peroxide and EDTA solutions to the chromium(III) solution.

Dependence of the Chromium(III)-ion and Hydrogen-peroxide Concentrations on the Formation Rate of $Cr^{III}(edta)(H_2O)^-$. The dependence of the concentration of the chromium(III) ion on the rate of the formation of $Cr^{III}(edta)(H_2O)^-$ was examined in the presence of a large excess of hydrogen peroxide at pH 3.82 and

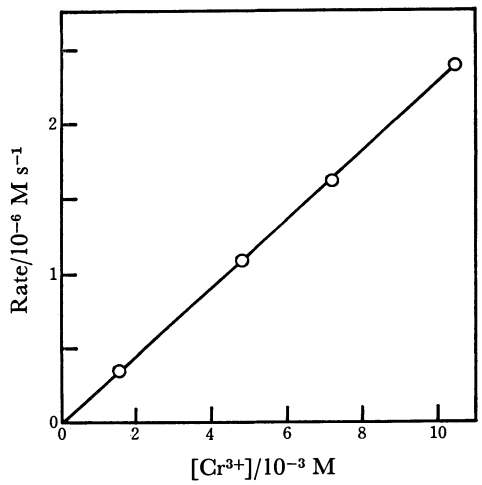

Fig. 3. The relation between the rate for the formation of $Cr^{III}(edta)(H_2O)^-$ and the concentration of chromium(III) ion.
$[EDTA]=2.00\times10^{-2}$ M, $[H_2O_2]=5.05$ M, pH 3.82, $[CH_3COO^-]=0.10$ M, I=0.35, 25 °C.

25 °C. As is shown in Fig. 3, the linear relationship between the chromium(III)-ion concentration and the formation rate indicates that the reaction rate has a first-order dependence with respect to the concentration of the chromium(III) ion. It was also found that the formation rate has a first-order dependence on the hydrogen peroxide in the concentration range 1.5 M to 5.0 M at a given pH and at a given acetate ion concentration.

Dependence of EDTA. The formation rate is independent of the EDTA concentration, as is shown in Fig. 4.

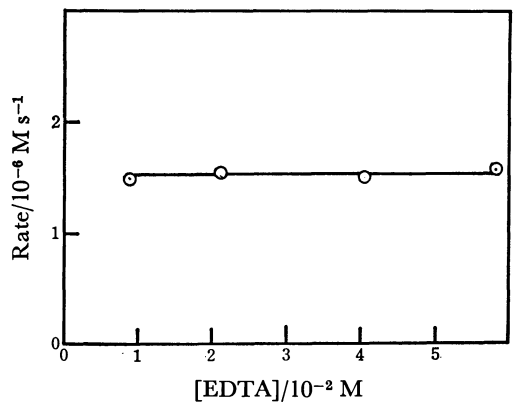

Fig. 4. The relation between the rate for the formation of $Cr^{III}(edta)(H_2O)^-$ and the concentration of hydrogen peroxide.
$[Cr^{3+}]=7.13\times10^{-3}$ M, $[EDTA]=2.00\times10^{-2}$ M, pH 3.82, $[CH_3COO^-]=0.10$ M, $I=0.35$, 25 °C.

The rate law for the hydrogen peroxide-catalyzed formation of $Cr^{III}(edta)(H_2O)^-$ is represented by Eq. 1:

$$\frac{d[Cr^{III}(edta)(H_2O)^-]}{dt} = k_{obsd}[Cr(III)][H_2O_2] \quad (1)$$

where k_{obsd} represents the observed second-order rate constant under the given conditions.

Effects of the pH and the Acetate Ion on the Formation Rate of $Cr^{III}(edta)(H_2O)^-$. The formation rate of $Cr^{III}(edta)(H_2O)^-$ in the presence of hydrogen peroxide was found to increase with an increase in the pH in the pH range from 3.30 to 4.50. It was also found that the formation rate decreases with an increase in the acetate-ion concentration. The observed second-order rate constants under various experimental conditions are listed in Table 1. These data clearly indicate a linear relationship between k_{obsd} and reciprocal concentration of the acetate ions, with an intercept at any given pH. Thus, the conditional second-order rate constant may be expressed by Eq. 2:

$$k_{obsd} = k'_{obsd} + \frac{k''_{obsd}}{[CH_3COO^-]} \quad (2)$$

The conditional rate constants, k'_{obsd} and k''_{obsd}, at the given pH are listed in Table 2.

The initiation of the reaction must take place by means of Reaction 3:

$$Cr(III) + H_2O_2 \xrightarrow{slow} Cr(IV) + OH\cdot + OH^- \quad (3)$$

For the subsequent reactions after Reaction 3 the following reaction paths are possible:

$$Cr(III) + OH\cdot \xrightarrow{fast} Cr(IV) + OH^- \quad (4)$$

the rapid complex formation step of the chromium(IV)–EDTA complex,

$$Cr(IV) + EDTA \xrightarrow{fast} Cr(IV)\text{–}EDTA \quad (5)$$

and the reduction of the chromium(IV)–EDTA complex by chromium(III) ion and/or hydrogen peroxide.

$$Cr(IV)\text{–}EDTA + Cr(III) \xrightarrow{fast} Cr^{III}(edta)(H_2O)^- + Cr(IV) \quad (6)$$

$$Cr(IV)\text{–}EDTA + \frac{1}{2}H_2O_2 \xrightarrow{fast} Cr^{III}(edta)(H_2O)^- + \frac{1}{4}O_2 + \frac{1}{2}H_2O \quad (7)$$

The possibility of the formation of chromium(V) and chromium(V)–EDTA can not be excluded. Therefore, Eqs. 8—11 may be added to Eqs. 4—7:

$$Cr(IV) + OH\cdot \xrightarrow{fast} Cr(V) + OH^- \quad (8)$$

$$Cr(V) + EDTA \xrightarrow{fast} Cr(V)\text{–}EDTA \quad (9)$$

$$Cr(V)\text{–}EDTA + Cr(III) \xrightarrow{fast} Cr(IV)\text{–}EDTA + Cr(IV) \quad (10)$$

$$Cr(V)\text{–}EDTA + \frac{1}{2}H_2O_2 \xrightarrow{fast} Cr(IV)\text{–}EDTA + \frac{1}{4}O_2 + \frac{1}{2}H_2O \quad (11)$$

No evolution of oxygen gas was observed up to about one half-life. Therefore, the possibility of Reactions 7 and 11 may be very small.

The predominant species of EDTA at pH 3.30 are H_2edta^{2-} (78%) and H_3edta^- (22%), while those at pH 4.50 are H_2edta^{2-} (97%) and $Hedta^{3-}$ (3%). Such a variation in species of EDTA does not affect the formation rate of $Cr^{III}(edta)(H_2O)^-$ in the presence of hydrogen peroxide, since the rate is independent of the EDTA concentration.

Although no detailed explanation of the effect of the acetate ion can be given, the interaction of the acetate ion with the chromium(III) ion through the formation of the hydrogen bond[11] may be one of the reasons for the retardation of the rate.

The chromium(III) ion was appreciably hydrolyzed to the monohydroxochromium(III) ion ($CrOH^{2+}$) under the present experimental conditions. Reaction 3 can be rewritten as Reaction 12:

Table 2. Conditional rate constants, k'_{obsd} and k''_{obsd} of the formation of $Cr^{III}(edta)(H_2O)^-$ at 25 °C and $I=0.35$ ($NaClO_4$)

pH	k'_{obsd} $M^{-1}\,s^{-1}$	k''_{obsd} s^{-1}
3.30	8.9×10^{-6}	6.3×10^{-7}
3.52	1.4×10^{-5}	1.5×10^{-6}
3.70	1.6×10^{-5}	2.0×10^{-6}
4.00	3.0×10^{-5}	4.0×10^{-6}
4.50	5.0×10^{-5}	1.4×10^{-5}

$$\left\{\begin{array}{c} Cr^{3+} \\ K \Big\| H^{+} \\ CrOH^{2+} \end{array}\right\} + H_2O_2 \longrightarrow Cr(IV) + OH\cdot + OH^- \quad (12)$$

Assuming the hydrolysis of the chromium(III) ion, the rate constant, k'_{obsd}, is represented by Eq. 13:

$$k'_{obsd} = \frac{k[H^+]+k_{OH}K}{[H^+]+K} \quad (13)$$

where $K(K=[CrOH^{2+}][H^+]/[Cr^{3+}])$ is the first hydrolysis constant of the chromium(III) ion and where k and k_{OH} are the second-order rate constants for the reactions involving a chromium(III) ion and a monohydroxochromium(III) ion respectively. If $k_{OH}K \gg k[H^+]$ is assumed, the reciprocal of k'_{obsd} is expressed as:

$$\frac{1}{k'_{obsd}} = \frac{[H^+]}{k_{OH}K} + \frac{1}{k_{OH}} \quad (14)$$

A plot of $1/k'_{obsd}$ *vs.* $[H^+]$ shows a linear relationship. The values of k_{OH} and K are 6.2×10^{-5} M^{-1} s^{-1} and 8.3×10^{-5} M respectively at 25 °C and $I=0.35$. The value of K has been determined to be 1.3×10^{-4} M at 15 °C.[12] The slightly smaller value of K obtained in this work compared with that in the literature may be brought about by the differences in the experimental conditions and method.

The fact that the monohydroxochromium(III) ion is much more reactive than the chromium(III) ion toward hydrogen peroxide is very similar to the observation regarding the relative reactivity of the monohydroxomanganese(III) ion and the manganese(III) ion toward $N_2H_5^+$,[13] and to that of the monohydroxocerium(IV) ion and the cerium(IV) ion toward $N_2H_5^+$.[13] The H-atom transfer mechanism was proposed for the reaction between the monohydroxocerium(IV) ion and $N_2H_5^+$.[14]

Though there is no reason for supposing that the mechanism for the reaction of the monohydroxochromium(III) ion with hydrogen peroxide is the H-atom transfer, the possibility of this mechanism can not necessarily be excluded.

Ogard and Taube[15] suggested that the chromium(IV) ion is very labile for the substitution on the basis of the kinetics of the dissociation reaction of $Cr(Cl)(H_2O)_5^{2+}$ in the presence of an oxidizing agent.

The occurrence of the hydrogen peroxide-catalyzed reaction found in this work must be ascribed to the substitution lability of chromium(IV) or chromium(V), and the large oxidizing power and stability constant of chromium(IV)–EDTA or chromium(V)–EDTA.

The authors wish to express their thanks to Mr. Shigehira Iida for his assistance in this work.

References

1) R. Pribil, V. Simon, and J. Dolezal, *Chem. Listy*, **46**, 88 (1952).
2) K. Yamamoto and K. Ohashi, *Bunseki Kagaku*, **19**, 120 (1970).
3) K. Yamamoto, K. Ohashi, and A. Onuma, *Bunseki Kagaku*, **20**, 57 (1971).
4) The quinquevalent chromium compound is known by the synthesis of $Ba_3(CrO_4)_2$; N. Matsuura and M. Nishikawa, "Inorganic Chemistry," II, Morikita Book Co., Tokyo (1973), p. 147.
5) M. T. Beck and D. A. Durham, *J. Inorg. Nucl. Chem.*, **32**, 1971 (1970).
6) The structures of Cr(IV)–EDTA and Cr(V)–EDTA complexes are uncertain.[5]
7) R. E. Hamm, *J. Am. Chem. Soc.*, **75**, 5670 (1953).
8) G. Schwarzenbach and W. Biedermann, *Helv. Chim. Acta*, **31**, 459 (1948).
9) The equilibrium constant ($K=[Cr^{III}(edta)(CH_3COO)^{2-}]/[Cr^{III}(edta)(H_2O)^-][CH_3COO^-]$) for the reaction between the acetate ion and $Cr^{III}(edta)(H_2O)^-$ is 0.61 M^{-1} at 25 °C.[10]
10) H. Ogino, T. Watanabe, and N. Tanaka, *Inorg. Chem.*, **14**, 2093 (1975).
11) R. E. Hamm, R. L. Johnson, R. H. Perkins, and R. E. Davis, *J. Am. Chem. Soc.*, **80**, 4469 (1958).
12) F. Basolo and R. G. Pearson, "Mechanism of Inorganic Reactions—A Study of Metal Complexes in Solution," John Wiley & Sons, Inc. (1958), p. 32.
13) G. Davies and K. Kustin, *J. Phys. Chem.*, **73**, 2248 (1969).
14) J. I. Morrow and G. W. Sheeres, *Inorg. Chem.*, **11**, 2606 (1972).
15) A. E. Orgard and H. Taube, *J. Phys. Chem.*, **62**, 357 (1958).

The Neutron Activation Analysis of Mercury in Soil

Souichi NAKANO,* Jukichi HONBOH, and Noriake URABE

Department of Synthetic Chemistry, Faculty of Engineering, Kumamoto University, Kurokami, Kumamoto 860

(Received October 22, 1975)

A radiochemical neutron activation procedure has been designed for the determination of mercury in soils. After the irradiation of 100 mg of soil it was decomposed with a hydrofluoric and perchloric acid mixture in a platinum crucible, and the mercury was separated radiochemically by solvent extraction from sulfuric acid·potassium iodide media into toluene, followed by precipitation as a sulfide. The radioactivity of ^{197}Hg was measured by using a Ge(Li) detector. The chemical yield, as determined by atomic absorption spectrophotometry, was high enough, and the precision was satisfactory. The detection limit is estimated to be 1—2 ppb [$(1—2)\times 10^{-10}$ g] by this method. The above procedure was applied to the determination of mercury in soils sampled in the Kumamoto and Minamata districts and in between.

The mercury contamination of soil has no less serious an influence on man and his ecosystem than do those of foodstuff, air, and water, so its detailed investigation should be pushed forward. Neutron activation analyses for mercury in various materials have been reported by a number of workers;[1] however, such analyses for mercury in soil have been few.[2]

An important step to improve the accuracy and detection limits in the activation analysis of mercury in matrices consists of radiochemical separation. Various methods have been used for separation by many investigators,—for instance, distillation or evaporation,[3-7] solvent extraction,[8,9] isotopic exchange,[5] anion exchange,[10-14] precipitation,[2,14-16] deposition,[15,17] and adsorption.[6] The present authors investigated a solvent extraction method of mercury with toluene from sulfuric acid·potassium iodide-treated samples to achieve a complete, satisfactory separation.[18] The procedure was studied in order to determine whether or not it was satisfactory in precision and detection limits. In addition, it was relatively simple and quick. The atomic absorption method was used for the determination of the chemical yield as an auxiliary means.

Because of the volatile nature of mercury and its compounds, the problem of mercury loss from a heated matrix is important; in this study it was checked by means of an atomic absorption method.

The activities of either ^{197}Hg or ^{203}Hg have generally been used for the determination. Because of the more convenient half-life, cross section, and target abundance of ^{197}Hg than ^{203}Hg (64 h, 3.1×10^3 b, 0.146% and 47 d, 4.9 b, 29.8% respectively),[19] the γ-ray of ^{197}Hg and the X-rays of ^{197}Au were measured by the present procedure.

After the method mentioned above had been established, the contents of mercury in 11 soil samples from Kumamoto and Minamata and in between were determined and discussed.

Experimental

Irradiation Facilities, Instruments, and Reagents. The samples and standards were irradiated in the S-Pipe of the JRR-4 Reactor at the Japan Atomic Energy Research Institute. The thermal neutron flux was 2×10^{13} n cm^{-2} s^{-1}. The activities were measured with a 41.5 cm^3 Ge(Li) detector (ORTEC) coupled to a 4096-channel pulse-height analyzer (Toshiba USC-1 model 10). A Perkin-Elmer model 303 atomic absorption spectrophotometer equipped with a recorder readout was used. The reagents used were of the JIS special grade from Wako Pure Chemical, unless otherwise mentioned. Doubly distilled water was used for the pre-irradiation procedure.

Procedure. Sample Preparation and Irradiation: All of the soil samples were taken from 30 cm deep, dried in the atmosphere at room temperature, ground in an agate mortar, and finally passed through a JIS 125 sieve. Into a quartz vial (5 mm$\phi\times$4 cm), 100 mg of a soil sample was placed. A standard consisted of 5.0×10^{-7} g of mercury (in the form of mercury (II) acetate in 0.1 M acetic acid), which was transferred to a quartz vial with a micropipet and absorbed onto 100 mg of silica powder (from E. Merck, Germany). All the vials were sealed with an oxygen-city gas torch. The above procedure was performed in a dustless room throughout, and the mortar, the quartz vials, and the glassware were washed with *aqua regia* and water prior to use. A standard and five samples were packed together in a polyethylene capsule; this unit was irradiated for 5 h and then left for 24 h in order to permit the short-lived nuclides to decay.

Decomposition and Radiochemical Separation: The main components of the soil seemed to be mineral granules and humus, to which mercury as a contaminant seemed to adhere *via* natural water beside that involved in the soil in nature. In any case, it was necessary to decompose the components completely for the following extraction procedure.

Irradiated vials were washed with 6 M nitric acid, water, and acetone before opening. The contents were then thoroughly transferred to a 20 ml platinum crucible. Onto the matrix 1.00 mg of mercury (in the form of mercury(II) chloride in 0.1 M hydrochloric acid) was added as a carrier. With 2 ml of 46% hydrofluoric acid and 1.5 ml of 60% perchloric acid, the sample was decomposed at 160 ± 5 °C for 45 min in an oil bath. Then 1 ml of a saturated boric acid solution was pipetted into the crucible, and the mixture was heated again for 5 min. The decomposed sample solution was transferred to a 50 ml volumetric flask, and subsequently diluted with 15 ml of 20 M sulfuric acid, 1 ml of a 5.0×10^{-2} M potassium iodide solution, and water to make 6.0 M sulfuric acid and a 1.0×10^{-3} M potassium iodide solution. The mixture was transferred to a 100 ml separatory funnel. With 10 ml of toluene added, it was shaken for 3 min by means of a mechanical shaker and then allowed to stand. After the aqueous phase had been discarded, the organic phase was washed with a 50 ml portion of the aqueous 6.0 M sulfuric acid and a 1.0×10^{-3} M potassium iodide solution. A 1 ml aliquot of the organic phase was taken for atomic absorption spectrometry in order to ascertain the recovery. With 50 ml of a 200 μg/ml mercury

* Present address: Radioisotopic Laboratory, Kumamoto University Medical School, Honjoh, Kumamoto 860.

solution (in the form of mercury(II) chloride in 0.1 M hydrochloric acid), radioactive mercury was stripped from the remaining phase, precipitated with hydrogen sulfide, and filtered by means of suction on 25 mmϕ filter paper (Toyo Roshi No. 5C).

A standard sample was processed in a manner similar to that used for soil samples.

γ-Ray Spectrometry: The filter paper with the precipitates was heat-sealed in a polyethylene sheet, and its radioactivity was measured with a Ge(Li) detector for 1000 s. For quantitations, conventional peak integration and background subtraction were applied to the 68.8 keV X-ray from ^{197}Au, and to the composite peak of the 77.6 keV γ-ray of ^{197}Hg and 78.0 keV X-ray from ^{197}Au.

Results and Discussion

The Determination of Mercury Retention after Decomposition. To determine mercury retention after decomposition process, 1 ml of a mercury(II) chloride solution (10.0 mg Hg/ml), 2 ml of 46% hydrofluoric acid, and 1.5 ml of 60% perchloric acid were added to 100 mg of soil in a 20 ml platinum crucible. Covered, it was heated in an oil bath at an appropriate temperature until the contents appeared to be transparent; then the contents were cooled to room temperature and diluted to 50 ml in a volumetric flask with water. The mercury concentration was subsequently measured by atomic absorption spectrometry.

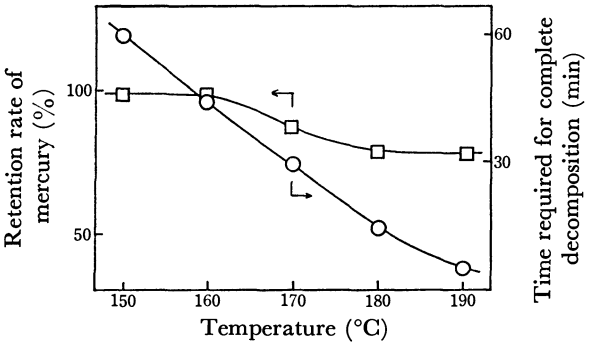

Fig. 1. Retention rate of mercury after complete decomposition of soil in a platinum crucible and the time required for *vs.* temperature. The initial contents: 100 mg of soil, 10.0 mg of mercury in the form of mercury(II) chloride, 2 ml of 46% hydrofluoric acid, and 1.5 ml of 60% perchloric acid. Determined with an atomic absorption method.

As is shown in Fig. 1, the retention rate of mercury (in the form of mercury(II) chloride) after the complete decomposition of the soil was 98% up to 160 °C and dropped toward higher temperatures, and the time required for complete decomposition became approximately 15 min shorter with each 10 °C elevation in temperature. This indicates that the optimum conditions for complete decomposition without loss were at 160 °C for 45 min.

The Determination of Extraction Curve of Mercury(II). The extractability of mercury(II) was examined as follows. To a 10 ml graduated test tube with a ground stopper, 0.5 ml of a mercury(II) chloride solution (1.00 mg Hg/ml) and appropriate volumes of 20 M sulfuric acid and either a 5.0×10^{-3} M or a 5.0×10^{-1} M potassium iodide solution were added. The contents were diluted to the 5 ml mark with water. With 5 ml of toluene added, the tube was dipped in a water bath at 20 °C for 15 min, shaken vigorously by hand for 3 min, and then allowed to stand. Each phase was then separated, centrifuged, and submitted to atomic absorption measurement.

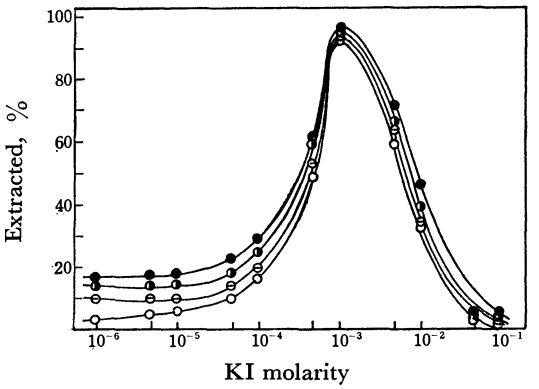

Fig. 2. Extraction curves of mercury into toluene as functions of potassium iodide and sulfuric acid concentrations. The initial mercury concentration: 100 μg/ml in the form of mercury(II) chloride in aqueous phase. Temperature: 20 °C. Determined with an atomic absorption method. ●: 8.0, ◑: 6.0, ⊖: 4.0, ○: 2.0 M sulfuric acid.

The extraction curves of mercury in Fig. 2 indicate that the maximum extraction was obtained at approximately 1×10^{-3} M potassium iodide. This concentration is somewhat higher than that reported by Byrne and Gorenc.[18] The differences in initial mercury concentration and temperature between the present method and that in the literature are 100 μg/ml, and 20 °C, and 1 μg/ml, and 25 °C, respectively.

Examples of the γ-spectra during and after the radiochemical separation procedure are given in Figs. 3 and 4 respectively. Figure 3 shows a typical spectrum of the extracted toluene phase, while Fig. 4 shows one of the final mercury sulfide precipitate. Both spectra indicate typical photopeaks of 68.8 keV (^{197}Au X-ray),

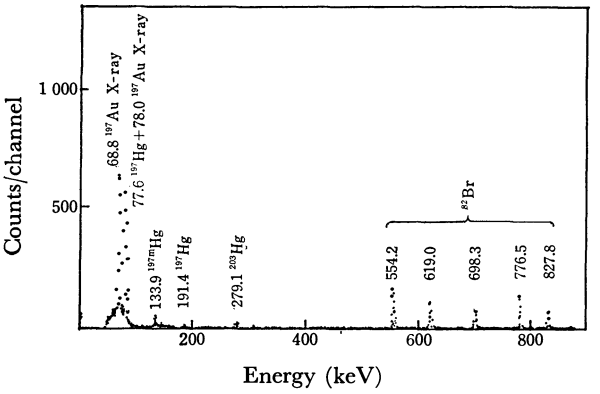

Fig. 3. An example of γ-ray spectrum of the toluene extract. Thermal neutron flux: 2×10^{13} n cm^{-2} s^{-1}, Time of irradiation: 5 h, Time of decay: 30 h, Counting time: 1000 s. Measured with a Ge(Li) detector.

TABLE 1. MERCURY CONTENTS IN SOILS COLLECTED AT 11 SPOTS BETWEEN KUMAMOTO AND MINAMATA CITIES

Spot No.	1	2	3	4	5	6	7	8	9	10	11
Mercury found (ppm)	1.87	1.01	0.74	0.84	1.03	1.32	1.25	10.3	4.9	0.36	6.6

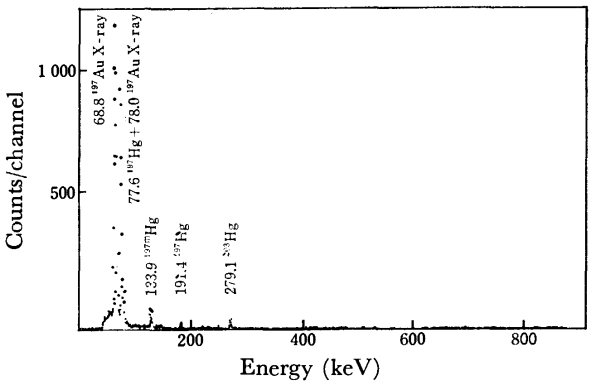

Fig. 4. An example of γ-ray spectrum of the final mercury sulfide precipitate. Time of decay: 32 h. Other conditions were the same as in Fig. 3.

77.6 keV (^{197}Hg)+, 78.0 keV (^{197}Au X-ray), and others emitted by radioactive mercuries.[20] The probable spectral overlaps of these photopeaks with those emitted by ^{169}Yb (63.5 keV), ^{182}Ta (67.7 keV), ^{153}Sm (69.6 keV), and ^{187}W (71.9 keV) were considered, but they gave no problem in this work because no others emitted by any nuclide could be detected in the spectra. In Fig. 3 there exist photopeaks emitted by ^{82}Br, which might be extracted in an oxidized form. The peak heights of radioactive mercury in Fig. 4 were about twice those in Fig. 3 as a result of the improvement in the self-shielding and geometry.

The amount of mercury in the soil was calculated by means of the following equation;

Mercury contents in soil (ppm)

$$= 5.0\times10^{2}\times\frac{1}{W_x}\cdot\frac{C_x\varepsilon_s}{C_s\varepsilon_x}\exp\{1.08\times10^{-2}\times(t_x-t_s)\}$$

where W_x is the weight of irradiated soil (mg),

C_x and C_s are the counts/1000 s of a sample and a standard respectively,

ε_x and ε_s are the absorbances of a sample and a standard with atomic absorption respectively, and

t_x and t_s are the elapsed times after the irradiation of a sample and a standard respectively (h).

The procedure described above was applied to the determination of the mercury contents in the soil sample of Spot No. 7 in Table 1, with irradiation in a capsule. The average mercury concentration, based on five replicate analyses, was 1.25 ppm, with a relative standard deviation of 3.7%. The precision was thus satisfactory. The recovery averaged 82%. The detection limit (twice the square root of the background counts under the peak of interest) is estimated at 1—2 ppb [$(1—2)\times10^{-10}$ g in 100 mg of a sample] by this method.

Furthermore, the proposed procedure was applied to the determinations of the mercury contents in 11 soil samples, which were collected on March 3, 1975, along National Route 3 between Kumamoto and Minamata cities. Duplicate analyses were made on each of the samples except for Spot No. 7; the results are summarized in Table 1. All of the procedure after irradiation was done in two days by two persons. The average of 11 determinations was 2.7 ppm, extremely high compared to those in the literature.[2] The results show that the contamination of soil with mercury has spread all over the area.

This study has been supported by a Grant-in-Aid for the Co-utilization Program of the Japan Atomic Energy Research Institute from the Ministry of Education. The authors wish to thank Mr. Takemi Takano of The University of Tokyo for his valuable technical suggestions, and Mr. Kazutoshi Mori and Mr. Yukuo Shudo of this university for their assistance during the investigation.

References

1) G. J. Lutz, R. J. Boreni, R. S. Maddock, and W. W. Meinke, "NBS Technical Note 467 Activation Analysis: A Bibliography through 1971," U.S. Department of Commerce, N.B.S., Washington D.C. (1972).
2) J. Wimmer and E. Haunold, *Bodenkultur*, **24**, 25 (1973).
3) H. L. Rook, T. E. Gills, and P. D. LaFleur, *Anal. Chem.*, **44**, 1114 (1972).
4) H. Ruf and H. Rohde, *Z. Anal. Chem.*, **263**, 116 (1973).
5) R. Schelenz and J. F. Diehl, *Z. Anal. Chem.*, **265**, 93 (1973).
6) H. A. van der Sloot and H. A. Das, *Anal. Chim. Acta*, **70**, 439 (1974).
7) J. Rosenberg and S. Salmela, *Radiochem. Radioanal. Lett.*, **21**, 23 (1975).
8) H. Bader and E. Hedrich, *Lebensm. -Wiss. Technol.*, **5**, 178 (1972).
9) R. A. Nadkarni and B. C. Haldar, *J. Radioanal. Chem.*, **10**, 181 (1972).
10) H. Seitner, W. Kiesl, F. Kluger, and F. Hecht, *J. Radioanal. Chem.*, **7**, 235 (1971).
11) F. Montoloy, M. Heurtebise, and J. Lubkowitz, *J. Radioanal. Chem.*, **11**, 167 (1972).
12) K. Ishida, S. Kawamura, and M. Izawa, *Anal. Chim. Acta*, **50**, 351 (1970).
13) D. E. Becknell, R. H. Marsh, and W. Allie, Jr., *Anal. Chem.*, **43**, 1230 (1971).
14) J. T. Tanner, M. H. Friedman, D. H. Lincoln, L. A. Ford, and M. Jaffee, *Science*, **177**, 1102 (1972).
15) K. K. S. Pillay, C. C. Thomas, Jr., J. A. Sondel, and C. M. Hyche, *Anal. Chem.*, **43**, 1419 (1971).
16) A. Hirose, I. Horiuchi, and D. Ishii, *Anal. Chim. Acta*, **75**, 41 (1975).
17) J. I. Kim and H. Stärk, *Radiochim. Acta*, **13**, 213 (1970).
18) A. R. Byrne and D. Gorenc, *Anal. Chim. Acta*, **59**, 81 (1972).
19) I. M. H. Pagden, G. J. Pearson, and J. M. Bewers, *J. Radioanal. Chem.*, **8**, 127 (1971).
20) C. E. Crouthamel, F. Adams, and R. Dams, "Applied Gamma-Ray Spectrometry," 2nd ed., Pergamon Press, Oxford (1970), p. 639.

The Kinetic Study of the Oxidation Reaction of the Tris(2,2′-bipyridine)-cobalt(II) Ion and the Ethylenediamine-*N,N,N′,N′*-tetraacetato-cobaltate(II) Ion by the Peroxodisulfate Ion

Kousaburo OHASHI, Morito MATSUZAWA, Eichi HAMANO, and Katsumi YAMAMOTO

Department of Chemistry, Faculty of Science, Ibaraki University, Mito 310

(Received November 26, 1975)

The kinetics of the oxidation of Co^{II}–EDTA and $Co^{II}(bpy)_3^{2+}$ by the peroxodisulfate ion ($S_2O_8^{2-}$) in acidic media have been studied spectrophotometrically; EDTA and bpy represent ethylenediamine-*N,N,N′,N′*-tetraacetic acid and 2,2′-bipyridine respectively. The stoichiometry of the reactions of Co^{II}–EDTA with the peroxodisulfate ion was $2Co^{II}\text{–EDTA}+S_2O_8^{2-}=2Co^{III}(edta)^-+2SO_4^{2-}$. The rate for the oxidation of Co^{II}–EDTA by the peroxodisulfate ion is independent of the concentration of Co^{II}–EDTA, but first-order dependent with respect to the peroxodisulfate-ion concentration. The rate law is $d[Co^{III}(edta)^-]/dt=2k[S_2O_8^{2-}]$. The rate-determining step must be the decomposition of $S_2O_8^{2-}$ into $2SO_4^{\cdot-}$. The first-order rate constant, the activation enthalpy, and the activation entropy are 5.5×10^{-8} s^{-1}, 24 kcal mol^{-1}, and -12 eu respectively at pH 3.60, 25 °C, and $I=0.50$ ($NaClO_4$). Two moles of $Co^{II}(bpy)_3^{2+}$ are oxidized by one mole of the peroxodisulfate ion. For the oxidation of $Co^{II}(bpy)_3^{2+}$, the following reaction path and rate law were proposed:

$$Co^{II}(bpy)_3^{2+}+S_3O_8^{2-}\overset{K_e}{\rightleftharpoons}[Co^{II}(bpy)_3^{2+}\cdot S_2O_8^{2-}]\overset{k}{\longrightarrow}Co^{III}(bpy)_3^{3+}+SO_4^{2-}+SO_4^{\cdot-}$$

$$Co^{II}(bpy)_3^{2+}+SO_4^{\cdot-}\overset{\text{fast}}{\longrightarrow}Co^{III}(bpy)_3^{3+}+SO_4^{2-}$$

$$\frac{d[Co^{III}(bpy)_3^{3+}]}{dt}=\left\{\frac{2k\cdot K_e}{1+K_e[S_2O_8^{2-}]}\right\}[S_2O_8^{2-}][Co^{II}(bpy)_3^{2+}]_T$$

At pH 3.60, 25 °C, and $I=0.50$ (Na_2SO_4), the rate constant, k, and the equilibrium constant, K_e, are 0.53 s^{-1} and 5.6 M^{-1} respectively. The difference in the rate law and mechanism between Co^{II}–EDTA and Co^{II}–$(bpy)_3^{2+}$ may come from the difference in charge on the cobalt(II) complexes.

A large number of investigations have been done in the field of the oxidation of metal ions,[1–3] metal complexes,[4–6] and various organic compounds[7,8] by the peroxodisulfate ion. The rate for the oxidation reactions of positively charged metal complexes such as $Fe^{II}(bpy)_3^{2+}$ [4] and $Os^{II}(bpy)_3^{2+}$ [6] by the peroxodisulfate ion is first-order dependent on the concentrations of the peroxodisulfate ion and also the metal complex. These have, however, been few of the oxidation reaction of the negatively charged metal complex by the peroxodisulfate ion. Recently, studies of the kinetics of the oxidation reaction of Co^{II}–EDTA using various oxidizing agents, for example, $Fe^{III}(CN)_6^{3-}$,[9,10] $Fe^{III}(bpy)_3^{3+}$,[11] $Fe^{III}(phen)_3^{3+}$,[11] and Mn^{III}–EDTA[11] have been carried out. Previously, the present authors have reported the kinetics of the oxidation reaction of the nitrilopolyacetate–cobalt(II) ion by chromic acid ($HCrO_4^-$) in acidic media, and suggested that the oxidation reaction proceeds through an inner-sphere mechanism.[12]

The present kinetic study of the oxidation reactions of Co^{II}–EDTA and $Co^{II}(bpy)_3^{2+}$ with the peroxodisulfate ion was carried out spectrophotometrically in order to obtain information on the behavior of the negatively and positively charged cobalt(II) complexes toward the oxidant.

Experimental

Materials. The Co^{II}–EDTA solution was prepared by adding an equivalent amount of an Na_2H_2edta solution to a cobalt(II) solution. For the preparation of the $Co^{II}(bpy)_3^{2+}$ solution, the concentration of 2,2′-bipyridine was kept at ten times that of the cobalt(II) ion.

Standard solutions of potassium peroxodisulfate were prepared by dissolving known quantities of the reagent into redistilled water. The peroxodisulfate ion solution was prepared just before use to avoid any decomposition. The adjustment of the pH of the solution was made by adding the acetate buffer solution. The ionic strengths of the solutions of Co^{II}–EDTA and $Co^{II}(bpy)_3^{2+}$ were adjusted to 0.50 by the addition of sodium perchlorate and sodium sulfate respectively.

All the other chemicals were of a reagent grade.

Measurement of the Reaction Rate. The solutions of potassium peroxodisulfate, the acetate buffer, and Co^{II}–EDTA were thermostated at a desired temperature. In each experiment, portions of these solutions were pipeted into a flask, the peroxodisulfate being added last to the solution containing Co^{II}–EDTA, and the time was counted from its addition. A portion of the solution was transferred into a 1 cm cell placed in a thermostated cell compartment of a Hitachi Model EPS-3-type spectrophotometer. The variation in the absorbance of the solution was measured at 540 nm.

The kinetic-measurements for $Co^{II}(bpy)_3^{2+}$ were performed at 420 nm by the stopped-flow technique using a Hitachi EPS-1-type rapid-scan spectrophotometer. The solution of $Co^{II}(bpy)_3^{2+}$ and the peroxodisulfate ion was thermostated at 25 °C before the initiation of the reaction.

All the kinetic experiments were carried out under the condition of a large excess of the peroxodisulfate-ion concentration with respect to the Co^{II}–EDTA and $Co^{II}(bpy)_3^{2+}$ concentration.

Results and Discussion

The Oxidation Reaction of Co^{II}–EDTA with $S_2O_8^{2-}$. Figure 1 shows the absorption spectral change of the Co^{II}–EDTA[13] solution upon the addition of a large excess of the peroxodisulfate ion under the conditions of pH 3.60 and 50 °C. The oxidation product, $Co^{III}(edta)^-$ was characterized spectrophotometrically. The stoichiometry for the oxidation of Co^{II}–EDTA by the

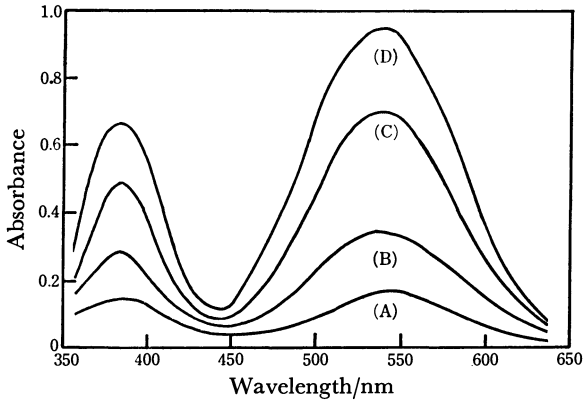

Fig. 1. Absorption spectral change of the Co^{II}–EDTA solution with the addition of peroxodisulfate ion solution at pH 3.60, 50 °C, and I=0.50 ($NaClO_4$).
(A) 2.0 h, (B) 4.5 h, (C) 10.0 h, (D) 13.5 h after the addition of peroxodisulfate ion.
[Co^{II}–EDTA]=3.08×10^{-3} M, [$S_2O_8^{2-}$]=3.68×10^{-2} M.

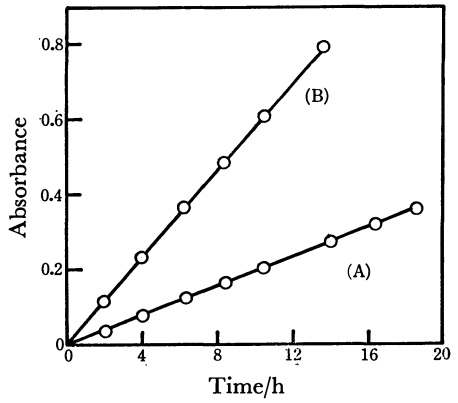

Fig. 2. Typical kinetic runs of the reaction between Co^{II}–EDTA and peroxodisulfate ion at 540 nm, pH 3.60, 40 °C, and I=0.50 ($NaClO_4$).
[Co^{II}–EDTA]=3.08×10^{-3} M.
(A) [$S_2O_8^{2-}$]=8.65×10^{-3} M, (B) [$S_2O_8^{2-}$]=2.89×10^{-2} M.

peroxodisulfate ion was confirmed spectrophotometrically as follows:

$$2Co^{II}\text{–EDTA} + S_2O_8^{2-} = 2Co^{III}(edta)^- + 2SO_4^{2-}$$

The plots of the absorbance *vs.* the time show a straight line for 80% of the whole reaction (Fig. 2). This behavior of the change in the absorbance with the time indicates that the oxidation rate is zero-order with respect to the Co^{II}–EDTA concentration. The kinetic data are shown in Table 1.

Table 1. Kinetic data for the oxidation of Co^{II}–EDTA by the peroxodisulfate ion

Concentration of Co^{II}–EDTA (10^{-3}M)	Rate[a] (10^{-6} M s^{-1})
2.0	1.2
4.0	1.2
5.0	1.2
7.4	1.3
10.0	1.2

a) [$S_2O_8^{2-}$]=8.65×10^{-2} M, pH 3.60, 50 °C, I=0.50.

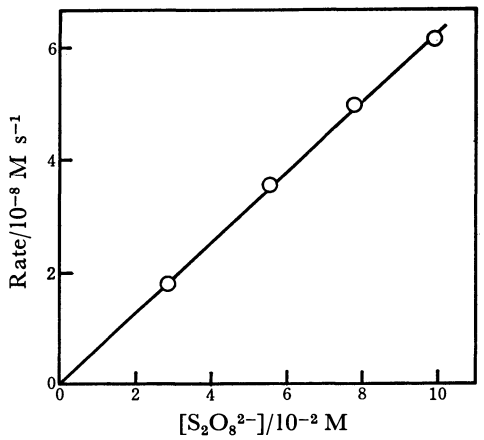

Fig. 3. Plot of the apparent rate for the peroxodisulfate oxidation of Co^{II}–EDTA *vs.* [$S_2O_8^{2-}$] at pH 3.60, 40 °C, and I=0.50 ($NaClO_4$).
[Co^{II}–EDTA]=3.02×10^{-3} M.

In order to determine the effect of the peroxodisulfate-ion concentration on the rate, the reaction was carried out at four different initial concentrations of the peroxodisulfate ion. As is shown in Fig. 3, the plot of the apparent rate *vs.* the peroxodisulfate-ion concentration shows a straight line (Fig. 3). The rate law for the oxidation reaction of Co^{II}–EDTA with the peroxodisulfate ion is represented by Eq. 1:

$$\frac{d[Co^{III}(edta)^-]}{dt} = 2k[S_2O_8^{2-}] \quad (1)$$

where k is the first-order rate constant at a given pH value. The determination of the rate constants was performed in the temperature range from 50 °C to 75 °C. The rate constant at 25 °C was obtained by the extrapolation of the Arrhenius plots. The values of the rate constant at 25 °C and 75 °C, and of the activation enthalpy and entropy, are summarized in Table 2.

The effect of the pH on the oxidation rate was investigated in the pH range from 3.50 to 5.36. Table 3

Table 2. The rate constants, equilibrium constant, and activation parameters for the peroxodisulfate oxidation of Co^{II}–EDTA and $Co^{II}(bpy)_3^{2+}$

Complex ion	Rate constant (s^{-1})	K_e (M^{-1})	ΔH^* (kcal mol^{-1})	ΔS^* (eu)
Co^{II}–EDTA	5.5×10^{-8} [a]	—	24	−12
	2.3×10^{-5} [b]			
$Co^{II}(bpy)_3^{2+}$	0.53[c]	5.6	—	—

a) pH 3.60, 25 °C, I=0.50. b) pH 3.60, 75 °C, I=0.50. c) pH 3.60, 25 °C, I=0.50.

Table 3. The rate constants for the peroxodisulfate oxidation of Co^{II}–EDTA at various pHs

pH	Rate constant[a] (s^{-1})
3.50	1.1×10^{-6}
4.10	1.0×10^{-6}
5.36	9.8×10^{-7}

a) at 50 °C and I=0.50.

shows the first-order rate constant at various pH values. The rate constant increases with a decrease in the pH value, but the variation in the rate constant is negligibly small.

The rate-determining step in the oxidation reaction of Co^{II}–EDTA with the peroxodisulfate ion must be homolytic fission into two sulfate radicals, since the oxidation rate is first-order with respect to the peroxodisulfate-ion concentration and is independent of the Co^{II}–EDTA concentration. The path for the oxidation of Co^{II}–EDTA may be represented by Eqs. 2 and 3:

$$S_2O_8^{2-} \xrightarrow{\text{slow}} 2SO_4^{\cdot-} \quad (2)$$

$$Co^{II}\text{–EDTA} + SO_4^{\cdot-} \xrightarrow{\text{fast}} Co^{III}(edta)^- + SO_4^{2-} \quad (3)$$

Kolthoff and Miller[15] investigated the kinetics of the decomposition reaction of the peroxodisulfate ion in an acidic solution. They demonstrated that the rate law for the decomposition reaction was of the form:

$$-d[S_2O_8^{2-}]/dt = k_1[S_2O_8^{2-}] + k_2[S_2O_8^{2-}][H^+]$$

and that the contribution of the second term could be neglected above pH 2.0.

The values of the rate constant and the activation parameters of the peroxodisulfate-ion oxidation of Co^{II}–EDTA are different from those of the auto-decomposition reaction.[15] No detailed explanations of the differences in the effect of the hydrogen ion, the rate constant, and the activation parameters between the peroxodisulfate-ion oxidation reaction of Co^{II}–EDTA and the auto-decomposition reaction of the peroxodisulfate ion can be given.

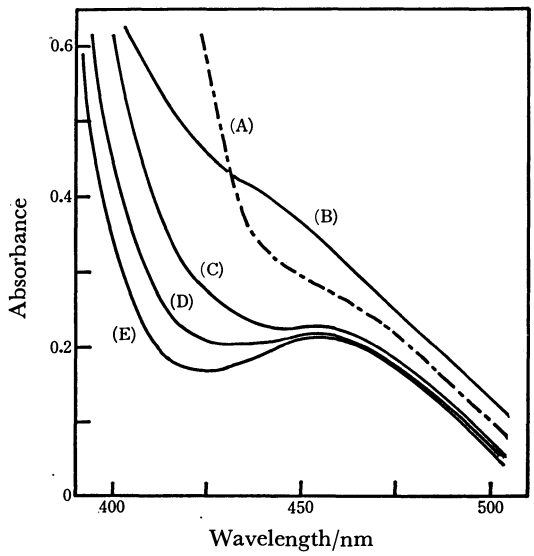

Fig. 4. Absorption spectra of the species related to the reaction of $Co^{II}(bpy)_3^{2+}$ with peroxodisulfate ion.
(A) Spectrum of $Co^{II}(bpy)_3^{2+}$ solution in the pH range from 3.10 to 6.50.
(B) Spectrum obtained for the reaction of $Co^{II}(bpy)_3^{2+}$ with peroxodisulfate ion at pH 6.50 after the completion of the reaction.
(C) Spectrum obtained for the reaction of $Co^{II}(bpy)_3^{2+}$ with peroxodisulfate ion at pH 5.50 after the completion of the reaction.
(D) Spectrum obtained for the reaction of $Co^{II}(bpy)_3^{2+}$ with peroxodisulfate ion at pH 4.03 after the completion of the reaction.
(E) Spectrum obtained for the reaction of $Co^{II}(bpy)_3^{2+}$ with peroxodisulfate ion in the pH range from 3.10 to 3.60 after the completion of the reaction.
$[Co^{II}(bpy)_3^{2+}]=3.00\times10^{-3}$ M, $[S_2O_8^{2-}]=3.00\times10^{-2}$ M.

The Oxidation of $Co^{II}(bpy)_3^{2+}$ by $S_2O_8^{2-}$. Figure 4 shows the change in the absorption spectra with the pH of the solution, which was obtained for the reaction of $Co^{II}(bpy)_3^{2+}$ with the peroxodisulfate ion. Curve E, which was obtained in the pH range from 3.10 to 3.60, coincides with the absorption spectrum of $Co^{III}(bpy)_3^{3+}$. However, the absorption spectra of the products obtained above pH 3.60 do not coincide with that of $Co^{III}(bpy)_3^{3+}$. Consequently, the kinetic measurements of the oxidation reaction were carried out at pH 3.60. The oxidation product obtained above pH 3.60 was not characterized.

The stoichiometry for the reaction of $Co^{II}(bpy)_3^{2+}$ with the peroxodisulfate ion was examined spectrophotometrically. If two moles of $Co^{II}(bpy)_3^{2+}$ are oxidized by one mol of the peroxodisulfate ion under an excess of the $Co^{II}(bpy)_3^{2+}$ concentration with respect to the peroxodisulfate-ion concentration, the absorbance (D) at a given wavelength after the completion of the reaction is shown by Eq. 4:

$$D = \varepsilon_{Co^{II}(bpy)_3^{2+}}([Co^{II}(bpy)_3^{2+}]-2[S_2O_8^{2-}]) + 2\varepsilon_{Co^{III}(bpy)_3^{3+}}[S_2O_8^{2-}] \quad (4)$$

where $\varepsilon_{Co^{III}(bpy)_3^{3+}}$ and $\varepsilon_{Co^{II}(bpy)_3^{2+}}$ denote the molar extinction coefficients of $Co^{III}(bpy)_3^{3+}$ and $Co^{II}(bpy)_3^{2+}$ respectively. At 420 nm, $\varepsilon_{Co^{III}(bpy)_3^{3+}}$ and $\varepsilon_{Co^{II}(bpy)_3^{2+}}$ are 61.0 and 157.0 respectively. At $[Co^{II}(bpy)_3^{2+}]=4.50\times10^{-3}$ M, Eq. 4 can be rewritten as Eq. 5:

$$D = 0.707 - 192[S_2O_8^{2-}] \quad (5)$$

Figure 5 shows the plots of the absorbance *vs.* $[S_2O_8^{2-}]$ at pH 3.60. The values of the intercept and slope are 0.702 and −188 respectively. This result illustrates that the overall reaction can be represented as follows:

$$2Co^{II}(bpy)_3^{2+} + S_2O_8^{2-} = 2Co^{III}(bpy)_3^{3+} + 2SO_4^{2-}$$

The plots of log (A_t-A_∞) *vs.* the time show a straight

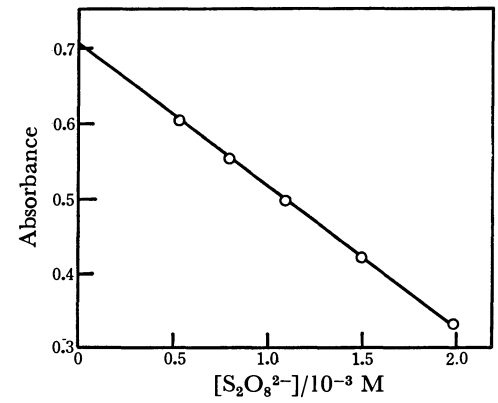

Fig. 5. Plot of the absorbance *vs.* $[S_2O_8^{2-}]$ for the reaction of $Co^{II}(bpy)_3^{2+}$ with peroxodisulfate ion. The measurements of absorbance were made at pH 3.60, 25 °C, and 420 nm.
$[Co^{II}(bpy)_3^{2+}]=4.50\times10^{-3}$ M.

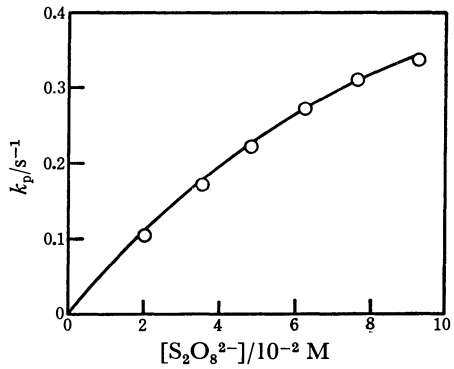

Fig. 6. Plot of the pseudo-first-order rate constant *vs.* $[S_2O_8^{2-}]$ at pH 3.60, 25 °C, and I=0.50 (Na_2SO_4). $[Co^{II}(bpy)_3^{2+}]=3.00\times10^{-3}$ M.

line for at least 80% of the whole reaction, where A_t is the absorbance at time t and A_∞, the absorbance after all the $Co^{II}(bpy)_3^{2+}$ has been oxidized to $Co^{III}(bpy)_3^{3+}$. This indicates that the rate of the oxidation of $Co^{II}(bpy)_3^{2+}$ by the peroxodisulfate ion is first-order-dependent on the concentration of $Co^{II}(bpy)_3^{2+}$. As is shown in Fig. 6, the relation between the apparent pseudo-first-order rate constants, k_p, which were evaluated from the slope of the log (A_t-A_∞) *vs.* time plots, and the concentrations of the peroxodisulfate ion is not linear. This result seems to be compatible with the existence of a pre-equilibrium between the $Co^{II}(bpy)_3^{2+}$ and $S_2O_8^{2-}$ to form an ion-pair, which then undergoes decomposition to give $Co^{III}(bpy)_3^{3+}$ and the sulfate radical ion. The reaction paths may be represented as follows:

$$Co^{II}(bpy)_3^{2+} + S_2O_8^{2-} \overset{K_e}{\rightleftharpoons} [Co^{II}(bpy)_3^{2+}\cdot S_2O_8^{2-}]$$
$$\overset{k}{\longrightarrow} Co^{III}(bpy)_3^{3+} + SO_4^{\cdot-} + SO_4^{2-} \quad (6)$$

followed by

$$Co^{II}(bpy)_3^{2+} + SO_4^{\cdot-} \overset{\text{fast}}{\longrightarrow} Co^{III}(bpy)_3^{3+} + SO_4^{2-} \quad (7)$$

No effect of the pH on the rate of the oxidation could be found in the pH range from 3.1 to 3.6. The ion-pair formation between metal complexes and the peroxodisulfate ion has been reported on the basis of the kinetic data of the oxidation reaction.[16] Furthermore, for the oxidation of $Fe^{II}(bpy)_3^{2+}$ by the peroxodisulfate ion, ion-pair formation as an intermediate was postulated.[11] The rate law for the peroxodisulfate oxidation of $Co^{II}(bpy)_3^{2+}$ is represented by Eq. 8:

$$\frac{d[Co^{III}(bpy)_3^{3+}]}{dt} = \left\{\frac{2k\cdot K_e}{1+K_e[S_2O_8^{2-}]}\right\}[S_2O_8^{2-}][Co^{II}(bpy)_3^{2+}]_T \quad (8)$$

where k and K_e are the first-order rate constant and the equilibrium constant ($K_e=[Co^{II}(bpy)_3^{2+}\cdot S_2O_8^{2-}]/[Co^{II}(bpy)_3^{2+}][S_2O_8^{2-}]$) for Reaction 6 respectively, and where $[Co^{II}(bpy)_3^{2+}]_T$ is the total concentration of the tris(2,2'-bipyridine)cobalt(II) ion. The reciprocal of the observed second-order rate constant is shown by Eq. 9:

$$\frac{1}{k_{obsd}} = \frac{1}{2k\cdot K_e} + \frac{1}{2k}[S_2O_8^{2-}] \quad (9)$$

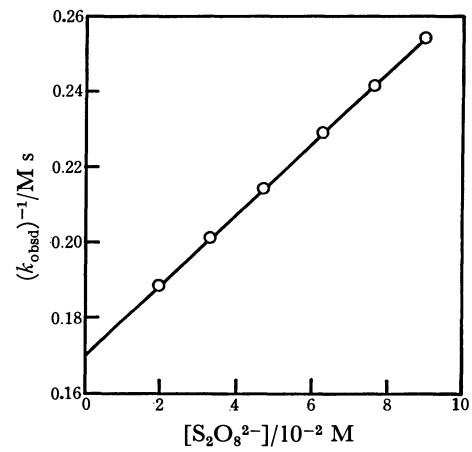

Fig. 7. Plot of the inverse of the observed second-order rate constant *vs.* $[S_2O_8^{2-}]$ at pH 3.60, 25 °C, and I= 0.50 (Na_2SO_4). $[Co^{II}(bpy)_3^{2+}]=3.00\times10^{-3}$ M.

The plot of $1/k_{obsd}$ *vs.* $[S_2O_8^{2-}]$ shows a straight line (Fig. 7). The linear plot is consistent with the occurrence of the reaction of 6 and 7. The values of k and K_e are listed in Table 2.

It seems likely that the oxidation reaction of $Co^{II}(bpy)_3^{2+}$ with the peroxodisulfate ion would proceed through an outer-sphere mechanism, since the oxidation product is $Co^{III}(bpy)_3^{3+}$.

The standard oxidation-reduction potentials for the $Co^{II}(bpy)_3^{2+}$–$Co^{III}(bpy)_3^{3+}$ couple and the $Co^{II}(edta)^{2-}$–$Co^{III}(edta)^-$ couple are 0.37 V[17] and −0.37 V[18] respectively. With regard to the standard oxidation-reduction potential, the rate for the oxidation of $Co^{II}(bpy)_3^{2+}$ by the peroxodisulfate ion is expected to be smaller than that for the oxidation of Co^{II}–EDTA by the peroxodisulfate ion. As is shown in Table 2, however, reactivity of $Co^{II}(bpy)_3^{2+}$ against the peroxodisulfate ion was found to be much larger than that of Co^{II}–EDTA. The differences in reactivity and in rate law between $Co^{II}(bpy)_3^{2+}$ and Co^{II}–EDTA may come from the difference in the charge on the cobalt(II) complexes.

References

1) Y. K. Gupta and D. D. Misra, *Bull. Chem. Soc. Jpn.*, **32**, 1306 (1959).
2) D. M. Yost, *J. Am. Chem. Soc.*, **48**, 152 (1926).
3) D. M. Yost and W. H. Clausen, *J. Am. Chem. Soc.*, **53**, 3349 (1931).
4) S. Raman and C. H. Brubaker, Jr., *J. Inorg. Nucl. Chem.*, **31**, 1091 (1969).
5) R. W. Chlebek and N. W. Lister, *Can. J. Chem.*, **45**, 2411 (1967).
6) D. H. Irvine, *J. Chem. Soc.*, **1958**, 2166.
7) Y. K. Gupta and S. J. Ghosh, *J. Inorg. Nucl. Chem.*, **11**, 320 (1957).
8) D. L. Ball, *Dissert. Abstr.*, **16**, 2300 (1959).
9) D. H. Huchital and R. G. Hodges, *Inorg. Chem.*, **12**, 998, 1004 (1973).
10) H. Ogino, M. Takahashi, and N. Tanaka, *Bull. Chem. Soc. Jpn.*, **47**, 1426 (1974).
11) R. G. Wilkins and R. E. Yelin, *J. Am. Chem. Soc.*, **92**, 1191 (1970).

12) K. Ohashi, A. Onuma, K. Yamamoto, and Y. Kurimura, *Nippon Kagaku Zasshi*, **92**, 51 (1971).
13) The equilibrium constant ($K=[Co^{II}(Hedta)(H_2O)^-]/[Co^{II}(edta)^{2-}][H^+]$) is $10^{3.1}$ M^{-1} at 20 °C and $I=0.10$.[14] Co^{II}–EDTA complex exists as $Co^{II}(Hedta)(H_2O)^-$ and $Co^{II}(edta)^{2-}$ in the pH range from 3.50 to 5.36. The formula of Co^{II}–EDTA used in this paper represents the mixture of $Co^{II}(edta)^{2-}$ and $Co^{II}(Hedta)(H_2O)^-$.
14) G. Anderegg, *Helv. Chim. Acta*, **47**, 1801 (1964).
15) I. M. Kolthoff and I. K. Miller, *J. Am. Chem. Soc.*, **73**, 3055 (1951).
16) H. Galiba, L. J. Csanyi, and Z. G. Sozabo, *Z. Anorg. Allg. Chem.*, **287**, 169 (1956).
17) E. Paglia and C. Sironi, *Gazz. Ckim. Ital.*, **81**, 1125 (1957).
18) Y. A. Im and D. H. Busch, *J. Am. Chem. Soc.*, **83**, 3357 (1961); The IUPAC sign convention is used.

Halogenation and Nitration of Some Mixed Ligand Acetylacetonatocobalt(III) Complexes

Kashiro KURODA, Kouzou YOSHITANI,* Kazufumi KUNIGITA,**
Yukiko KAMIIBA, and Kiyokatsu WATANABE
Department of Chemistry, Faculty of Science, Ehime University, Matsuyama, Ehime 790
(Received December 2, 1975)

In six kinds of mixed ligand acetylacetonatocobalt(III) complexes ($(NH_3)_4$-, $(en)_2$-, α-trien-, β-trien-, *fac(N)*-*i*-dtma-, and *mer(N)*-*i*-dtma-complexes†), the methine hydrogen of the coordinated acetylacetonate ion has been substituted with chlorine, bromine, and iodine, and in five of them excepting the *mer(N)*-*i*-dtma complex, it has been substituted with a nitro group. The halogenated and the nitrated complexes were isolated and identified by means of electronic absorption spectra and NMR spectra. The effects of the substitutions on the properties and the characteristics of the substitution reactions are described and discussed.

Collman and his collaborators have investigated extensively various electrophilic substitutions, such as halogenation, nitration, and acetylation at the central methine of the ligand in acetylacetonatometal complexes.[1] *N*-Halogenosuccinimides have been found to be excellent reagents for halogenation,[2] and a mixture of copper(II) nitrate and acetic anhydride for nitration.[3] However, the complexes they studied are mostly tris(acetylacetonato)metal(III) or bis(acetylacetonato)-metal(II), which are neutral and soluble in organic solvents. Only a few papers have reported that mixed ligand acetylacetonatometal complexes were substituted at the methine by electrophiles.[4] It has also been reported that the acetylacetonatobis(ethylenediamine)-cobalt(III) ion, $[Co(acac)(en)_2]^{2+}$, is not brominated even under forced conditions.[5] The present authors have recently succeeded in the bromination of *fac(N)*- and *mer(N)*-[Co(acac)(*i*-dtma)]ClO_4† with *N*-bromosuccinimide in a ethanol(50%)–water mixture.[6] Therefore, it was thought worthwhile to further examine these substitutions, using the other kinds of mixed ligand acetylacetonatocobalt(III) complexes, especially those with high positive charges. As a result, the halogenation and the nitration were accomplished without difficulty in several kinds of the cationic complexes. This report deals with the preparation and characterization of the substituted complexes and a preliminary consideration of the substitution mechanism.

Experimental

Materials, Analysis, Apparatus, and Measurements. All the chemicals used were of the reagent grade and were used without further purification. The carbon, hydrogen, and nitrogen in the synthesized complexes were analyzed by the Analytical Center of the Institute for Chemical Research of Kyoto University. The visible and ultraviolet absorption spectra were measured in aqueous solution with a Hitachi EPS-3T Recording Spectrophotometer. The optical rotations were counted with a JASCO DIP-180 Polarimeter at 589 and 405 nm. The proton NMR spectra were recorded with a Japan Electron Optics JNM-100 Spectrometer (100 MHz), using deuterium oxide as the solvent and *t*-butanol as the internal reference. The temperature of the probe was maintained at 22±1 °C.

Chlorination, Bromination, and Iodination. The halogenations were carried out using *N*-halogenosuccinimides in methanol(50%)–water or acetone(50%)–water mixtures at *ca.* 50 °C. Since the procedures of the halogenation for each acetylacetonato complex were quite similar, only a representative case will be described below.

A solution of $[Co(acac)(en)_2](ClO_4)_2$[7] (2.4 g) in 15 ml of water was mixed with a solution of *N*-chlorosuccinimide (0.8 g) in 15 ml of acetone. The mixture was stirred at *ca.* 50 °C for 30 min, and was then concentrated to *ca.* 10 ml at that temperature. A red precipitate resulted upon the addition of 1 ml of 6 M $HClO_4$ with cooling. The precipitate was recrystallized with 10 ml of warm water and the addition of a few drops of 6 M $HClO_4$. The product was washed with ethanol and ether. Yield, 1.5 g.

Nitration. The nitration was carried out in a manner similar to Collman's method for the nitration of $[Co(acac)_3]$.[8] Again, since the procedures for each complex were quite similar, only a representative case will be described.

Finely divided copper(II) nitrate trihydrate (0.7 g) was mixed into 60 ml of acetic anhydride at 0 °C and the mixture was stirred for 15 min. Into the mixture was added 1.2 g of $[Co(acac)(en)_2](ClO_4)_2$. The mixture was stirred at 0 °C for 1 h and then at room temperature for another hour. The bluish product thus obtained was poured into an ice(90 g)–water (90 g) mixture. The double liquid mixture was stirred until it became homogeneous and reddish brown (*ca.* 1 h). The solution was then concentrated to *ca.* 15 ml in a rotary evaporator below 60 °C. A brown-red precipitate resulted upon the addition of 1 ml of 6 M $HClO_4$ followed by cooling. It was recrystallized with 10 ml of warm water and the addition of a few drops of 6M $HClO_4$. The product was washed with ethanol and ether. Yield, 0.6 g.

Six kinds of mixed ligand acetylacetonatocobalt(III) complexes ($[Co(acac)(NH_3)_4](ClO_4)_2$,[7] $[Co(acac)(en)_2](ClO_4)_2$, α-$[Co(acac)(trien)](ClO_4)_2$,[7] β-$[Co(acac)(trien)]Br_2$,[7] *fac(N)*-[Co(acac)(*i*-dtma)]ClO_4,[6] and *mer(N)*-[Co(acac)(*i*-dtma)]ClO_4[6]) were attempted for their chlorination, bromination, iodination, and nitration in manners similar to that described above, and all but the nitration of *mer(N)*-[Co-

* Present address: Department of Chemistry, Faculty of Science, Hiroshima University, Higashisenda-machi, Hiroshima 730.

** Present address: Department of Chemistry, Faculty of Science, Kobe University, Nada-ku, Kobe 657.

† The following abbreviations are used in this article: en, ethylenediamine; trien, triethylenetetramine; *i*-dtma, bis(2-aminoethyl)aminoacetate ion (4-diethylenetriaminemonoacetate ion); acac, acetylacetonate ion (2,4-pentanedionate ion); Clacac, chloroacetylacetonate ion (3-chloro-2,4-pentanedionate ion); Bracac, bromoacetylacetonate ion; Iacac, iodoacetylacetonate ion; O_2Nacac, nitroacetylacetonate ion.

TABLE 1. RESULTS OF ELEMENTAL ANALYSIS OF THE COMPLEXES

Complex	Composition	F.W.	Found (%)			Calcd (%)		
			C	H	N	C	H	N
$[Co(Clacac)(NH_3)_4](ClO_4)_2$	$CoC_5H_{18}O_{10}N_4Cl_3$	459.51	12.88	4.28	12.14	13.07	3.95	12.19
$[Co(Bracac)(NH_3)_4](ClO_4)_2$	$CoC_5H_{18}O_{10}N_4Cl_2Br$	503.96	11.91	3.77	11.11	11.92	3.60	11.12
$[Co(Iacac)(NH_3)_4](ClO_4)_2\cdot H_2O$	$CoC_5H_{20}O_{11}N_4Cl_2I$	568.98	10.61	3.97	9.97	10.55	3.54	9.85
$[Co(O_2Nacac)(NH_3)_4](ClO_4)_2$	$CoC_5H_{18}O_{12}N_5Cl_2$	470.07	12.96	4.15	14.96	12.78	3.86	14.90
$[Co(Clacac)(en)_2](ClO_4)_2$	$CoC_9H_{22}O_{10}N_4Cl_3$	511.59	21.02	4.56	10.87	21.13	4.34	10.95
$[Co(Bracac)(en)_2](ClO_4)_2$	$CoC_9H_{22}O_{10}N_4Cl_2Br$	556.04	19.82	4.15	10.29	19.44	3.99	10.08
$[Co(Iacac)(en)_2](ClO_4)_2$	$CoC_9H_{22}O_{10}N_4Cl_2I$	603.04	17.76	3.79	9.18	17.93	3.68	9.29
$[Co(O_2Nacac)(en)_2](ClO_4)_2\cdot H_2O$	$CoC_9H_{24}O_{13}N_5Cl_2$	540.16	20.02	4.57	12.95	20.01	4.48	12.97
α-$[Co(Clacac)(trien)](ClO_4)_2$	$CoC_{11}H_{24}O_{10}N_4Cl_3$	537.63	24.32	4.41	10.27	24.57	4.50	10.42
α-$[Co(Bracac)(trien)](ClO_4)_2$	$CoC_{11}H_{24}O_{10}N_4Cl_2Br$	582.08	22.92	4.28	9.69	22.70	4.16	9.63
α-$[Co(Iacac)(trien)](ClO_4)_2$	$CoC_{11}H_{24}O_{10}N_4Cl_2I$	629.08	20.79	3.93	8.77	21.00	3.85	8.91
α-$[Co(O_2Nacac)(trien)](ClO_4)_2$	$CoC_{11}H_{24}O_{12}N_5Cl_2$	548.18	24.10	4.45	12.81	24.10	4.41	12.78
β-$[Co(Clacac)(trien)](ClO_4)_2\cdot H_2O$	$CoC_{11}H_{26}O_{11}N_4Cl_3$	555.64	23.39	4.77	9.95	23.78	4.71	10.08
β-$[Co(Bracac)(trien)](ClO_4)_2$	$CoC_{11}H_{24}O_{10}N_4Cl_2Br$	582.08	22.74	4.21	9.62	22.70	4.16	9.63
β-$[Co(Iacac)(trien)](ClO_4)_2$	$CoC_{11}H_{24}O_{10}N_4Cl_2I$	629.08	20.92	3.96	8.87	21.00	3.85	8.91
β-$[Co(O_2Nacac)(trien)](ClO_4)_2\cdot H_2O$	$CoC_{11}H_{26}O_{13}N_5Cl_2$	566.19	23.34	4.48	12.38	23.33	4.63	12.37
fac(*N*)-$[Co(Clacac)(i\text{-dtma})]ClO_4$	$CoC_{11}H_{20}O_8N_3Cl_2$	452.14	28.98	4.52	9.29	29.22	4.46	9.29
fac(*N*)-$[Co(Iacac)(i\text{-dtma})]ClO_4$	$CoC_{11}H_{20}O_8N_3ClI$	543.59	24.31	3.72	7.74	24.30	3.71	7.73
fac(*N*)-$[Co(O_2Nacac)(i\text{-dtma})]ClO_4$	$CoC_{11}H_{20}O_{10}N_4Cl$	462.69	28.55	4.54	11.85	28.56	4.36	12.11
mer(*N*)-$[Co(Clacac)(i\text{-dtma})]ClO_4$	$CoC_{11}H_{20}O_8N_3Cl_2$	452.14	28.99	4.57	9.28	29.22	4.46	9.29
mer(*N*)-$[Co(Iacac)(i\text{-dtma})]ClO_4$	$CoC_{11}H_{20}O_8N_3ClI$	543.59	24.15	3.71	7.72	24.30	3.71	7.73

(acac)(*i*-dtma)]ClO_4 were successful. The single unsuccessful attempt at nitration was due to the insolubility of the complex in the nitration reagent. The results of the elemental analysis of the complexes obtained are shown in Table 1. (The results for the brominated species of *i*-dtma complexes have previously been reported.[6])

Preparation of $(+)_{589}$-$[Co(acac)(en)_2](ClO_4)_2$ *and Its Halogenation.* A diastereoisomer of the bis(ethylenediamine) complex, $(+)_{589}$-$[Co(acac)(en)_2][(+)_{589}$-$AsOC_4H_4O_6]_2$, was prepared by the standard method.[9] One gram of the diastereoisomer was suspended in 45 ml of ethanol and 5 ml of aqueous 2 M $NaClO_4$ was added. The mixture was stirred at *ca.* 45 °C until the solid phase changed to white (*ca.* 30 min). After the solid ($(+)_{589}$-$AsOC_4H_4O_6Na$) was removed by filtration, the orange-red filtrate was concentrated to *ca.* 10 ml, whereupon an additional white precipitate resulted, which was then removed. The filtrate was then placed overnight in a refrigerator, and the red crystals thus formed were collected and washed with ethanol and ether. Yield, 0.5 g. $[\alpha]_{589}=+478°$, $[\alpha]_{405}=-2475°$. The specific rotation was not changed by recrystallization.

The halogenation of the optical isomer was carried out in the same manner as that for the inactive complex. $[\alpha]_{589}=+506°$, $[\alpha]_{405}=-2600°$ for the chlorinated complex, $[\alpha]_{589}=+473°$, $[\alpha]_{405}=-2440°$ for the brominated complex, and $[\alpha]_{589}=+460°$, $[\alpha]_{405}=-2395°$ for the iodinated complex.

Results and Discussion

Absorption Spectra. The absorption spectra of $[Co(acac)(en)_2](ClO_4)_2$ and its halogenated and nitrated species, as well as those of $[Co(acac)_3]$ and $[Co(Xacac)_3]$ (X=Cl, Br, I, NO_2) are shown in Figs. 1 and 2. The spectra of the other set of complexes with the same ammine or amine ligand have patterns quite similar to those of the set of bis(ethylenediamine) complexes, some of which have been presented elsewhere.[6,7,10] The numerical values of the absorption maxima are summarized in Table 2.

Since the halogenation and nitration of $[Co(acac)_3]$ have been well-established, the spectral variations observed between the spectrum of $[Co(acac)_3]$ and those of $[Co(Xacac)_3]$ may be adopted as an indication of the substitutions at the methine of the ligand. Thus, as may be seen in Fig. 1 and Table 2, the wave numbers

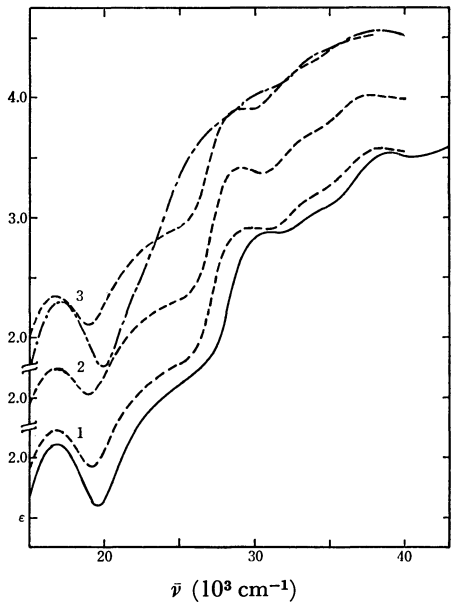

Fig. 1. Absorption spectra of $[Co(acac)_3]$ and its halogenated and nitrated species.
—: $[Co(acac)_3]$ ---1: $[Co(Clacac)_3]$
-·-: $[Co(O_2Nacac)_3]$ ---2: $[Co(Bracac)_3]$
---3: $[Co(Iacac)_3]$

Table 2. Absorption maxima of acetylacetonatocobalt(iii) complexes and their halogenated and nitrated species

	I		Sp	
	$\bar{\nu}(10^3 cm^{-1})$	(ε)	$\bar{\nu}(10^3 cm^{-1})$	(ε)
$[Co(acac)(NH_3)_4](ClO_4)_2$	19.70	(92.0)	30.91	(4500)
$[Co(Clacac)(NH_3)_4](ClO_4)_2$	19.70	(111.4)	29.41	(4660)
$[Co(Bracac)(NH_3)_4](ClO_4)_2$	19.70	(113.6)	29.41	(4440)
$[Co(Iacac)(NH_3)_4](ClO_4)_2$	19.70	(119.6)	28.94	(3760)
$[Co(O_2Nacac)(NH_3)_4](ClO_4)_2$	20.10	(93.6)	*ca.* 31	(*ca.* 4100)
$[Co(acac)(en)_2](ClO_4)_2$	20.04	(139.4)	30.72	(4200)
$[Co(Clacac)(en)_2](ClO_4)_2$	20.04	(163.2)	29.16	(4200)
$[Co(Bracac)(en)_2](ClO_4)_2$	20.04	(164.8)	29.16	(3960)
$[Co(Iacac)(en)_2](ClO_4)_2$	20.04	(171.2)	28.86	(3560)
$[Co(O_2Nacac)(en)_2](ClO_4)_2$	20.49	(140.6)	*ca.* 31	(*ca.* 3900)
α-$[Co(acac)(trien)](ClO_4)_2$	20.20	(151.8)	30.77	(4240)
α-$[Co(Clacac)(trien)](ClO_4)_2$	20.20	(171.4)	29.24	(4220)
α-$[Co(Bracac)(trien)](ClO_4)_2$	20.20	(173.6)	29.20	(3900)
α-$[Co(Iacac)(trien)](ClO_4)_2$	20.20	(180.4)	28.86	(3480)
α-$[Co(O_2Nacac)(trien)](ClO_4)_2$	20.62	(152.8)	*ca.* 31	(*ca.* 3800)
β-$[Co(acac)(trien)]Br_2$	19.92	(206.6)	30.63	(3800)
β-$[Co(Clacac)(trien)](ClO_4)_2$	19.92	(223.2)	29.11	(3800)
β-$[Co(Bracac)(trien)](ClO_4)_2$	19.92	(233.6)	29.07	(3640)
β-$[Co(Iacac)(trien)](ClO_4)_2$	19.92	(237.6)	28.82	(3320)
β-$[Co(O_2Nacac)(trien)](ClO_4)_2$	20.41	(227.2)	*ca.* 31	(*ca.* 3800)
fac(*N*)-$[Co(acac)(i\text{-dtma})]ClO_4$	18.98	(170.0)	30.72	(4120)
fac(*N*)-$[Co(Clacac)(i\text{-dtma})]ClO_4$	19.01	(182.0)	29.24	(4020)
fac(*N*)-$[Co(Bracac)(i\text{-dtma})]ClO_4$	19.01	(184.8)	29.20	(3800)
fac(*N*)-$[Co(Iacac)(i\text{-dtma})]ClO_4$	19.05	(188.8)	28.90	(3520)
fac(*N*)-$[Co(O_2Nacac)(i\text{-dtma})]ClO_4$	19.46	(185.8)	*ca.* 31	(*ca.* 3800)
mer(*N*)-$[Co(acac)(i\text{-dtma})]ClO_4$	19.84	(157.6)	30.58	(4160)
mer(*N*)-$[Co(Clacac)(i\text{-dtma})]ClO_4$	19.92	(176.6)	28.94	(4160)
mer(*N*)-$[Co(Bracac)(i\text{-dtma})]ClO_4$	19.92	(178.6)	28.90	(3980)
mer(*N*)-$[Co(Iacac)(i\text{-dtma})]ClO_4$	19.92	(184.8)	28.65	(3600)

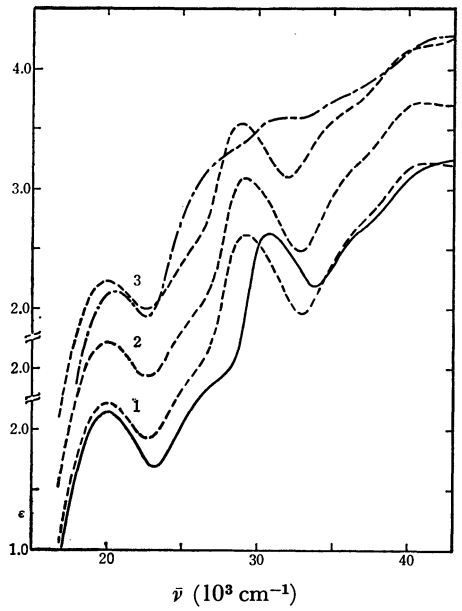

Fig. 2. Absorption spectra of $[Co(acac)(en)_2](ClO_4)_2$ and its halogenated and nitrated species.
—: $[Co(acac)(en)_2](ClO_4)_2$
-·-: $[Co(O_2Nacac)(en)_2](ClO_4)_2$
---1: $[Co(Clacac)(en)_2](ClO_4)_2$
---2: $[Co(Bracac)(en)_2](ClO_4)_2$
---3: $[Co(Iacac)(en)_2](ClO_4)_2$

of the first bands of $[Co(Xacac)_3]$ (X=Cl, Br, I) are nearly equal to that of $[Co(acac)_3]$, whereas the intensities of the formers are rather higher than that of the latter. The specific band arising around 30×10^3 cm^{-1} (which has been attributed to the transition of an electron from the metal t_{2g} to the ligand π^* orbitals[11]) shifts to lower wave numbers with nearly equal intensity upon halogenation. These spectral movements are observable, with a slightly modified and rather pronounced feature, between the spectra of each group containing an acetylacetonato complex and its halogenated species, as may be seen in the figure and the table.

The spectral shift of $[Co(O_2Nacac)_3]$ from $[Co(acac)_3]$ may be summarized as follows. First, the first band shifts to a higher wave number with an increase in the band intensity. Second, the specific band expands with a considerable deformation of the band feature, and no clear maximum is observable. This expansion and deformation probably comes from an overlap of the absorption of the nitro group (*ca.* 27×10^3 cm^{-1}) onto the $\pi^*\leftarrow t_{2g}$ band. These spectral variations are also observable in each spectrum of the nitrated complexes, although the increase in intensity of the first band is very small in a few cases.

Thus, the absorption spectra, together with the results of the elemental analysis and NMR spectra described

below, indicate that all the acetylacetonato complexes studied have been substituted by halogens and all but *mer*(*N*)-[Co(acac)(*i*-dtma)]ClO_4 by a nitro group at the methine of the ligand. The spectral relationships for the complexes can be summarized as follows:

(1) with respect to the first bands,

$$\bar{\nu}_{acac} \simeq \bar{\nu}_{Clacac} \simeq \bar{\nu}_{Bracac} \simeq \bar{\nu}_{Iacac} \text{ and } \bar{\nu}_{acac} < \bar{\nu}_{O_2Nacac}$$

$$\varepsilon_{acac} < \varepsilon_{Clacac} < \varepsilon_{Bracac} < \varepsilon_{Iacac} \text{ and } \varepsilon_{acac} \leqslant \varepsilon_{O_2Nacac}$$

(2) with respect to the specific bands,

$$\bar{\nu}_{acac} > \bar{\nu}_{Clacac} \simeq \bar{\nu}_{Bracac} > \bar{\nu}_{Iacac}$$

$$\varepsilon_{acac} \simeq \varepsilon_{Clacac} > \varepsilon_{Bracac} > \varepsilon_{Iacac}$$

NMR Spectra. The proton NMR spectra were measured to further verify the substitutions at the methine of the ligand. The resonances of the methine protons observed around 4.5 ppm in the spectra of the unsubstituted complexes disappeared completely in those of the substituted complexes, supporting our identification. As an illustration, a set of representative spectra is shown in Fig. 3.

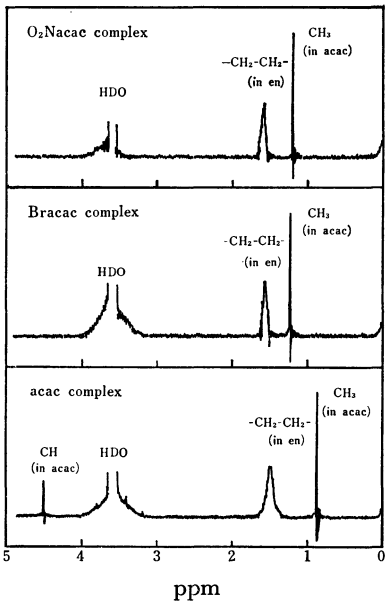

Fig. 3. NMR spectra of $[Co(acac)(en)_2](ClO_4)_2$ and its brominated and nitrated species.

Preparation. Acetylacetonatobis(ethylenediamine)-cobalt(III) is usually obtained as an iodide salt owing to its ease of isolation.[9] Bromination of the iodide salt was also attempted using *N*-bromosuccinimide. However, a redox reaction appeared to occur simultaneously, and the reaction product was too complicated to isolate the brominated species. The perchlorate salt is more soluble in water than the iodide, and is very soluble in methanol, ethanol, and acetone, especially when it is wet. Therefore, the perchlorate is a little difficult to handle in its preparation. However, this property is rather suitable for the substitutions, and no trouble was found in this regard. The property was also utilized to convert $(+)_{589}$-$[Co(acac)(en)_2][(+)_{589}$-$AsOC_4H_4O_6]_2$ into $(+)_{589}$-$[Co(acac)(en)_2](ClO_4)_2$. The lack of success in the bromination of $[Co(acac)(en)_2]^{2+}$ by Collman *et al.*,[5] although the detail of their procedure is not available, is assumed to be due simply to an unsuitable counter anion. A more or less similar situation was experienced for the other acetylacetonato complexes, and since β-$[Co(acac)(trien)](ClO_4)_2$ is especially soluble in the organic solvents, the bromide salt, which is a little easier to handle in isolation, was used as the starting substance.

The halogenated and nitrated species, in general, are less soluble in water and have better crystallizability than their parent complex. Thus, in the cases of the halogenations, the substituted complex sometimes appears as crystals during the reaction.

Characteristics of the Substitution Reactions. Because of the very similar behavior of the chelated acetylacetonate ion to that of the aromatic hydrocarbons, it is widely accepted that these substitution reactions are ionic rather than radical processes. It has therefore been argued[4a] on this assumption that, because of the electrostatic interaction between the substrates and the electrophiles, cationic acetylacetonatometal complexes are more resistant to substitutions at the methine than neutral and anionic complexes. However, our results indicate that this is not necessarily true, since the substituted complexes were obtained easily and without distinct differences in yields by similar procedures for substrates which were unipositive and dipositive. A quantitative comparison of the rate of chlorination also indicated that the charge of the complex was not a dominant factor in the substitution,[10] and rather the degree of distortion from the regular octahedron structure appeared to be more influential since the dipositive β-trien complex was the most reactive. The following is a possible explanation for this minor effect of the net charge of the complex upon the reactions.

According to the Pauling electroneutrality principle, the net charge of a complex ion is distributed among the atoms which exist on the surface of the ion. Thus, the methine hydrogen must be more positive, as the net

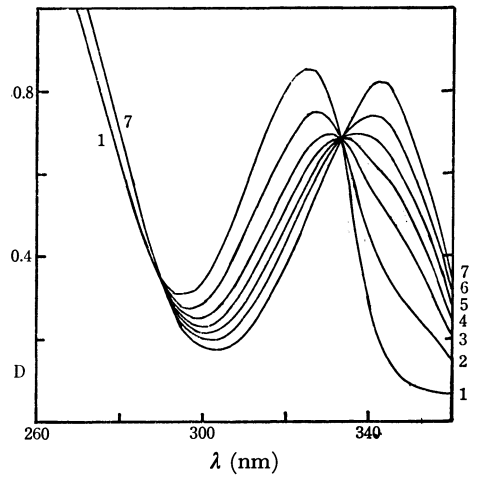

Fig. 4. A change of the absorption curve of $[Co(acac)(en)_2]^{2+}$ in the presence of *N*-chlorosuccinimide.
Condition: [Comp]$=2\times10^{-4}$ M, [NCS]$=3\times10^{-4}$ M, [$HClO_4$]$=2\times10^{-3}$ M, Temp=40 °C.
1: 0 min (the reactant complex without NCS), 2: after 10 min, 3: after 25 min, 4: after 40 min, 5: after 60 min, 6: after 100 min, 7: after ∞ min and the resultant complex.

Table 3. Rate constants, k, for the chlorination of $[Co(acac)(en)_2]^{2+}$ by *N*-chlorosuccinimide

No.	[Complex] $\times 10^{-4}$M	[NCS] $\times 10^{-4}$M	[$HClO_4$] $\times 10^{-3}$ M	[Other Substances]	Temp °C	x_{40} %	k $\times 10^2$ mol^{-1} min^{-1}
1	2	3	2	0	35	57.2	1.01[b]
2	2	3	2	0	40	65.3	1.36[b]
3	2	3	2	0	45	74.4	1.97[c]
4	2	3	4	0	40	66.1	1.41[b]
5	2	3	2	[$NaClO_4$]=1$\times 10^{-2}$M	40	65.9	1.42[b]
6	2	3	2	[C_2H_5OH]=50%	40	55.5	0.98[b]
7	2	6	2	0	40	90.7	1.35[c]
8	2[a]	3	2	0	40	65.1	1.36[b]
9	2[a]	0	2	0	40	no change in rotation and absorption	
10	2[a]	3	2	0	40	change in rotation: $-0.247° \rightarrow -0.280°$ at 405 nm	
11	2	2	2	0	40	48.0	x_∞ (%)=80.8

a) An optical active isomer was used. b) The average value calculated from x_{10}, x_{25}, x_{40}, x_{60}, and x_{100}. c) The average value calculated from x_{10}, x_{25}, x_{40}, and x_{60}.

charge of the complex ion increases. This means that the methine carbon in the more positive ion is possibly the more negative and is the more reactive with the electrophilic reagents. It may be considered that the increase in reactivity compensates the effect of the electrostatic repulsion between the complex cation and the electrophile.

In order to examine the above consideration and to clarify the reaction pathway, some kinetic measurements were carried out on the chlorination of $[Co(acac)(en)_2]^{2+}$. A spectral change is illustrated in Fig. 4 and the concentrations of the complex during the reaction were obtained from the optical densities at 343 nm. The result of the measurements is summarized in Table 3.

In order to obtain the rate constant, it was at first assumed that the reaction was of the second order and obeyed the quation,

$$k = \frac{2.303}{(b-a)} \frac{1}{t} \log \frac{a(b-x)}{b(a-x)}$$

where a and b are the initial concentrations of the reactant complex and *N*-chlorosuccinimide (NCS), respectively. However, the values of k calculated at different times in a run are not in agreement, but decrease as the time increases. Since the isosbestic points at 290 and 333 nm were strictly maintained during the reaction, it is certain that the only reaction of the reactant complex was the chlorination. Therefore, the cause of the decrease in k with time must reside in a reaction of NCS, which consumes NCS without chlorinating the complex. This assumption was confirmed by an equimolar experiment (No. 11), in which x_∞ was not 100%, but 80.8%. Thus, the kinetic equation can be assumed to be

$$\frac{dx}{dt} = k(a-x)(b-(1+c')x) = k(a-x)(b-cx)$$

and

$$k = \frac{2.303}{(b-ac)} \frac{1}{t} \log \frac{a(b-cx)}{b(a-x)}$$

where c can be estimated from the equimolar experiment as

$$\frac{19.2}{80.8} = \frac{c'}{1} \qquad c = 1 + c' = 1.238$$

With this approximation, the values of k in a run agree to within 3% of each other and the values thus obtained are tabulated in the table.

Several characteristics can be pointed out from the table.

(1) Without NCS, the reactant complex, involving the optical active complex, is stable under the conditions of these experiments. (No. 9).

(2) The rate in the ethanol(50%)–water mixture is considerably smaller than those in aqueous solutions. (No. 6).

(3) An increase in the concentration of $HClO_4$, as well as of $NaClO_4$, hardly accelerates the velocity. (Nos. 4, 5).

(4) The optically active isomer reacts with the same velocity as the inactive complex, as expected. (No. 8).

(5) The optical rotation increases with the evolution of the reaction, and α_∞ is identical with the value calculated from the rotation of the isolated active $[Co(Clacac)(en)_2](ClO_4)_2$. (No. 10).

The kinetic equation and these characteristics of the reaction may, as a whole, indicate that the reaction proceeds with a direct attack of NCS molecule onto the substrate, for which no bond rupture between the metal and the ligands is involved as an activation process. It is also supposed that the dipolar water molecules surrounding the reactants have sufficient power to activate the reactant ions and molecules.

References

1) J. P. Collman, "Transition Metal Chemistry," ed. by R. L. Carlin, Marcel Dekker, Inc., Vol. 2, New York (1966), pp. 35—45, and the references cited therein.

2) R. W. Kluiber, *J. Am. Chem. Soc.*, **82**, 4839 (1960); J. P. Collman, R. A. Moss, H. Maltz, and C. C. Heindel, *ibid.*, **83**, 531 (1961).

3) J. P. Collman, R. L. Marshall, W. L. Young (III), and S. D. Goldby, *Inorg. Chem.*, **1**, 704 (1962).

4) (a) Y. Fujii, E. Kyuno, and R. Tsuchiya, *Bull. Chem.*

Soc. Jpn., **42**, 1301 (1969); (b) Y. Fujii, *ibid.*, **43**, 1722 (1970); (c) S. Kaizaki, J. Hidaka, and Y. Shimura, *Inorg. Chem.*, **12**, 135 (1973).

5) Ref. 1, p. 44.

6) K. Kuroda, Y. Mori, H. Matsunaga, K. Kunigita, and K. Watanabe, *Bull. Chem. Soc. Jpn.*, **48**, 234 (1975).

7) K. Yoshitani, K. Kunigita, K. Watanabe, and K. Kuroda, *Chem. Lett.*, **1975**, 573.

8) J. P. Collman and W. L. Young(III), *Inorg. Synth.*, Vol. VII, pp. 205—207.

9) I. K. Reid and A. M. Sargeson, *Inorg. Synth.*, Vol. IX, pp. 167—169.

10) K. Kuroda and Y. Kamiiba, *Chem. Lett.*, **1975**, 1027.

11) I. Hanazaki, F. Hanazaki, and S. Nagakura, *J. Chem. Phys.*, **50**, 265 (1969).

Studies on Pulse Polarography. IV. Normal Pulse Polarographic Behavior of Fe(II) in an Unbuffered Medium and Catalytic Wave for Fe(II)-Chlorate System

Sadayuki HIMENO

Department of Chemistry, College of General Education, Kobe University, Nada-ku, Kobe 657

(Received January 26, 1976)

The normal pulse polarogram of Fe(II) showed a double-wave behavior in an unbuffered solution containing iodate. The results of pulse polarographic and cyclic voltammetric studies indicate that colloidal $Fe(OH)_2$ formed by the reaction between aqua-Fe(II) and OH^- arising from the iodate reduction is responsible for the second wave. A catalytic wave was observed in the presence of chlorate in Tast polarography. The catalytic wave which appears to be a polarographic maximum, has an abnormal form, in which the current increases at every second or third drop because of the depletion of colloidal $Fe(OH)_2$ around the electrode. The catalytic current is due to the reaction of chlorate with colloidal $Fe(OH)_2$ formed in the vicinity of the electrode.

Pulse polarography developed for differentiating the faradaic and charging currents has a better sensitivity as compared with DC polarography and is suitable for trace analysis. In normal pulse polarography, successively increasing potential pulses are applied to the electrode, one pulse per drop with DME, from the initial (resting) potential, which is generally chosen in the potential region where no faradaic process occurs. A current-voltage curve in normal pulse polarography is quite similar to that obtained by current-sampled DC (Tast) polarography.

It has been established that dissolved oxygen is reducible at DME so that high concentration of OH^- is generated at the electrode surface in neutral, unbuffered solution. In the course of the pulse polarographic study of iron-group metals in an unbuffered solution containing dissolved oxygen, it was observed that colloidal $Ni(OH)_2$ generated around the electrode gives an unusual peak on the normal pulse polarogram.[1]

During the investigation of normal pulse polarographic behavior of Fe(II) in an unbuffered solution, it was found that in the presence of colloidal $Fe(OH)_2$, chlorate gives the current enhancement due to the catalytic process, the nature of which was quite analogous to the nitrate system.[2] Iodate was used in the case of Fe(II) since dissolved oxygen shows a marked trend to oxidize Fe(II) to Fe(III).

In order to explain the nature of chlorate catalytic wave observed on Fe(II) reduction wave in an unbuffered medium containing dissolved oxygen, Ruvinskii *et al.* postulated a catalytic reaction with participation of Fe(0) hydroxo complex deposited on the electrode surface.[3] They assumed a catalytic regeneration of Fe(II) hydroxo complex in order to explain a large increase of current.

This paper describes the normal pulse polarographic behavior of Fe(II) in unbuffered solutions containing iodate and also the characteristics of the catalytic current induced by colloidal $Fe(OH)_2$ because their mechanism is not consistent with the results obtained. The mechanism of the process is presented.

Apparatus and Reagents

Apparatus. Polarographic measurements were carried out with a Princeton Applied Research Polarographic Analyzer, Model 174 in conjunction with the Linear Sweep Module Accessory, Model 174/51. This module, which synchronizes the potential scan with DME, permits the scan to start after pre-selected interval during the growth of a drop and to be completed within the lifetime the of drop. The drop time was controlled using a Mechanical Drop Timer, Model 172-A. Polarograms were recorded on a Riken Denshi X-Y Recorder, Model D-8C. The capillary employed had a $m^{2/3} \cdot t^{1/6}$ of 1.45 $mg^{2/3}\,s^{-1/2}$ in 0.1 M KNO_3 solution in an open circuit. One mercury drop was used for HMDE and a fresh drop was suspended from the tip of a mercury plated platinum wire for each measurement unless otherwise stated. The pH of the solution was measured with a Toa Denpa pH Meter, Model HM-8. An external saturated calomel electrode (SCE) was used as a reference electrode. Nitrogen was used to remove dissolved oxygen from the solution. The cell was immersed in water bath maintained at 25 ± 0.1 °C.

Reagents. All chemicals were of reagent grade and were used without further purification. Water used for preparation of the solutions was de-ionized on an ion-exchange resin bed and then distilled twice with a quartz apparatus.

Results

Normal Pulse Polarographic Behavior of Fe(II) in Unbuffered Solutions Containing Iodate. A typical normal pulse polarogram of 0.6 mM Fe(II) in 0.1 M KCl containing iodate (pH 5.1) is shown in Fig. 1. The reduction of iodate under these conditions proceeds as follows.[4]

$$IO_3^- + 3H_2O + 6e = I^- + 6OH^- \quad (E_{1/2} = -1.1\ V)$$

When the initial potential was set at -0.70 V, more anodic than the reduction potential of iodate, the normal pulse polarogram of Fe(II) consisted of only one wave with half-wave potential of -1.41 V. However, when the initial potential was chosen in the potential region where the reduction of iodate took place, the polarogram of Fe(II) had two waves. The second wave, which had a peak at the potential of -1.58 V disappeared completely by buffering the solution, indicating that the wave was due to the effect of OH^- arising from the reduction of iodate.

The relationship between the wave heights and pH of the solution is given in Fig. 2. Only a single-step reduction wave was obtained below pH 3.8 since no local high pH values occurred at the electrode. On increasing pH, the peak height of the second wave

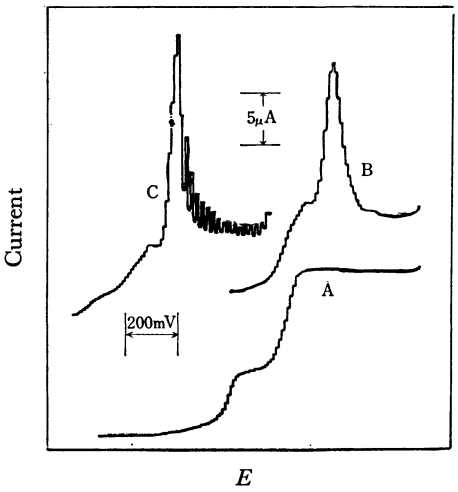

Fig. 1. Normal pulse polarograms of 0.6 mM Fe(II) in 0.1 M KCl (pH 5.1).
Iodate concentration (mM); A) 0.1, $E_i = -0.70$ V. B) 0.1, with violent agitation of capillary. $E_i = -1.20$ V. C) 0.2, with mild agitation of capillary. $E_i = -1.20$ V.
Drop time; 2 s.

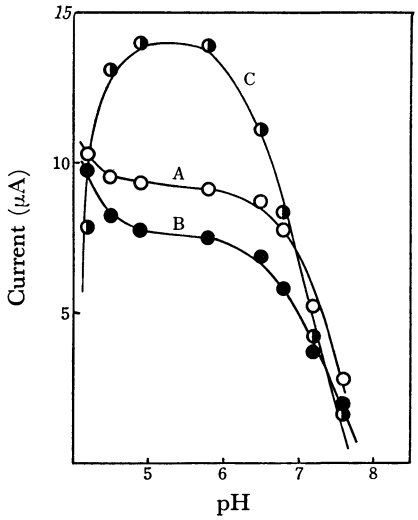

Fig. 2. Effect of pH on pulse polarographic wave of 1.0 mM Fe(II) in 0.1 M KCl containing 0.1 mM iodate.
A) 1st wave, $E_i = -0.70$ V. B) 1st wave, $E_i = -1.20$ V. C) 2nd wave, $E_i = -1.20$ V.
Drop time; 1 s.

increased and reached its limiting value in the pH range 4.8—6.0. The second wave decreased in height above pH 7.0 because of the precipitation of $Fe(OH)_2$ ($K_{sp} = 10^{-15}$).[5] The first wave obtained when the initial potential was set at −0.70 V was always greater than that obtained at −1.20 V and decreased gradually with increasing pH in the whole pH range studied. This indicates that the concentration of aqua-Fe(II) decreases around the electrode due to hydrolysis at the initial potential.

Figure 3 shows the wave heights as a function of Fe(II) concentration. It was found that the first wave increases almost linearly with Fe(II) concentration up

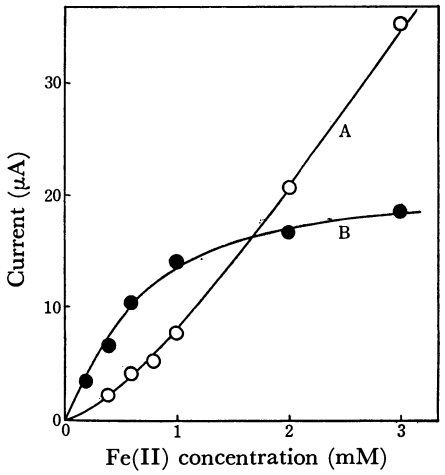

Fig. 3. Pulse polarographic currents as a function of Fe(II) concentration in 0.1 M KCl (pH 5.0) containing 0.1 mM iodate.
A) 1st wave. B) 2nd wave.
$E_i = -1.20$ V, Drop time; 2 s.

to 3 mM but starts asymptotically from the origin, while the relation between the second wave and Fe(II) concentration is not linear.

With a given Fe(II) concentration, the peak current of the second wave increased almost linearly with iodate concentration up to approximately 0.25 mM. Above this concentration, the second wave went through a maximum and then decreased as shown in Fig. 4, while the first wave decreased gradually on increasing iodate concentration.

From the results, it can be assumed that the first wave corresponds to the reduction of aqua-Fe(II) and the second to that of $Fe(OH)_2$ formed chemically between aqua-Fe(II) and OH^- in the vicinity of the electrode at the initial potential. It was also found that the peak height of the second wave decreases with increase in

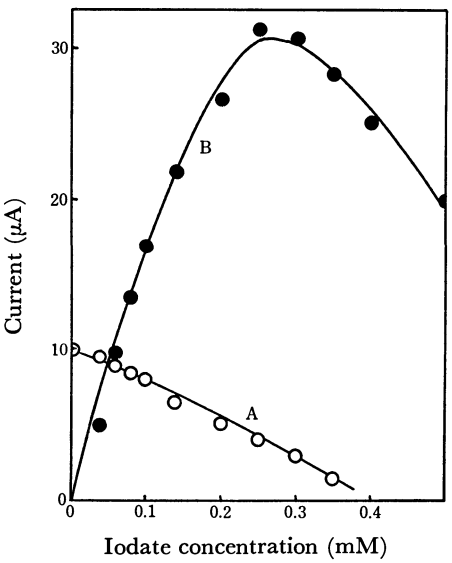

Fig. 4. Effect of iodate concentration on pulse polarographic wave of 1.0 mM Fe(II) in 0.1 M KCl (pH 5.5).
A) 1st wave. B) 2nd wave.
$E_i = -1.20$ V, Drop time; 1 s.

the concentration of the supporting electrolyte. This can be explained by the assumption that the coagulation of colloidal $Fe(OH)_2$ occurs and $Fe(OH)_2$ in the flocculated state can no longer be reduced. It can be confirmed by the fact that colloidal $Ni(OH)_2$ shows a similar behavior, its solubility being almost the same order as that of $Fe(OH)_2$.[1)]

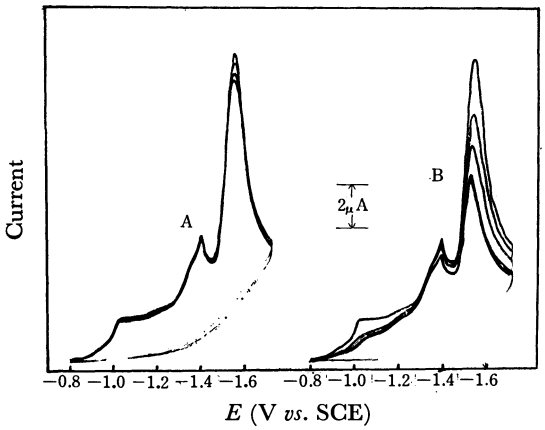

Fig. 5. Linear sweep voltammograms of 0.4 mM Fe(II) in 0.1 M KCl (pH 5.0) containing 0.08 mM iodate at DME.
A) With violent agitation of capillary. B) With mild agitation of capillary.
Pre-selected time; 1 s, Scan rate; 200 mV/s.

A periodical alternation of high and low currents appeared at every second drop with mild agitation of capillary (Fig. 1). The unusual phenomenon was also investigated by means of linear sweep voltammetry at DME. The current-voltage curve exhibited the same two peaks with peak potentials, −1.40 and −1.55 V, respectively as observed in normal pulse polarography (Fig. 5). On increasing iodate concentration, the first wave decreased with an increase of the second one. This might be ascribed to the reduction of colloidal $Fe(OH)_2$ formed in the vicinity of the electrode. Reproducible current-voltage curves were obtained in the multiple cathodic scans either when the capillary was agitated violently or when the solution was stirred with a magnetic stirrer. However, with mild agitation of the capillary, the second peak decreased gradually in the multiple scans. The results suggest that the reproducible production of colloidal $Fe(OH)_2$ at every drop cannot be obtained in a quiet solution.

In order to clarify the nature of Fe(II)–OH^- system, a number of cyclic voltammetric studies have been carried out with the use of HMDE. Table 1 gives the relationship between scan rates and peak currents of 0.4 mM Fe(II) in 0.1 M KCl containing 0.1 mM iodate. The value of $i_p/v^{1/2}$ is practically constant for the first wave, indicating that the process was diffusion controlled. However, the peak current of the second wave shows an abnormal current increase at greater scan rates.

Chlorate Catalytic Wave in Tast Polarography. Fe(II) in unbuffered solutions catalyzes the reduction of chlorate in Tast polarography (Fig. 6). This catalytic wave did not yield a limiting current but showed a

Table 1. Relationship between scan rate (v) and peak current of 0.4 mM Fe(II) in 0.1 M KCl

v (mV/s)	$v^{1/2}$	i_1[a)] (μA)	$i_1/v^{1/2}$	i_2[b)] (μA)	$i_2/v^{1/2}$
10	3.16	2.60	0.82	1.61	0.51
20	4.47	3.60	0.81	3.83	0.86
50	7.07	5.45	0.77	9.23	1.31
100	10.0	8.33	0.83	14.5	1.45
200	14.1	10.89	0.77	23.23	1.64

a) 1st wave without iodate. b) 2nd wave with 0.1 mM iodate.

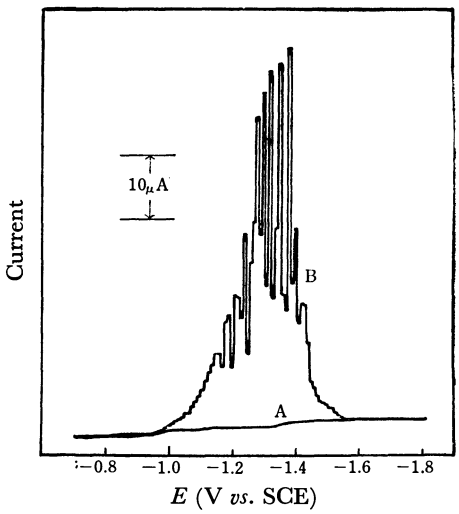

Fig. 6. Tast polarograms.
A) 0.4 mM Fe(II) in 0.1 M KCl (pH 5.0) containing 0.1 mM iodate. B) Solution (A) with 40 mM chlorate.
Drop time; 1 s.

maximum (peak) on the rising portion of Fe(II) reduction wave. The average peak current obtained in DC polarography was practically independent of the height of the mercury reservoir. Its temperature coefficient was +4.9% per degree, indicating that the current was kinetically controlled.

The relationship between the catalytic currents and chlorate concentration with 0.4 mM Fe(II) in 0.1 M KCl at different concentrations of iodate is shown in Fig. 7.

The catalytic wave could be obtained in the pH range 4.1—6.5, the range agreeing closely with that at which the second wave was obtained in normal pulse polarography (Fig. 2).

The catalytic wave decreased with an increase in the concentration of the supporting electrolyte and disappeared on buffering the solution.

Figure 8 shows the effect of iodate concentration on the catalytic wave. At the same Fe(II) and chlorate concentrations, the catalytic wave first increased and then decreased gradually when the iodate concentration was increased beyond 0.25 mM. This effect is in line with the observation made on varying iodate concentration in normal pulse polarography (Fig. 4).

The current-time curves of an individual drop at various potentials for the catalytic wave were recorded. The instantaneous i-t curves show the current increase at every second or third drop. However, the current

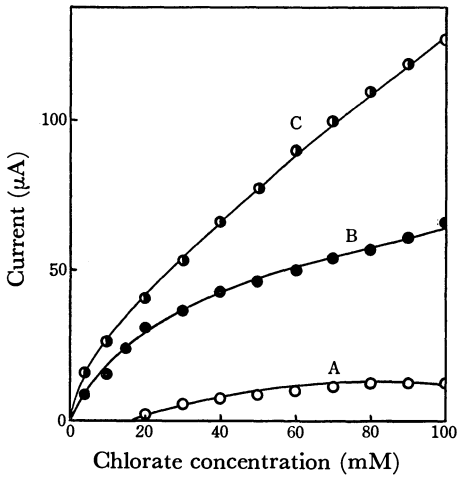

Fig. 7. Catalytic currents as a function of chlorate concentration in the solution 0.4 mM Fe(II) in 0.1 M KCl (pH 5.3).
Iodate concentration (mM); A) 0, B) 0.04, C) 0.2.
Drop time; 1 s.

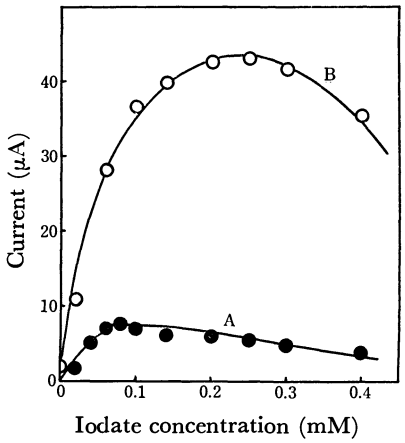

Fig. 8. Effect of iodate concentration on chlorate catalytic currents in the solution 0.4 mM Fe(II) in 0.1 M KCl (pH 5.5).
Chlorate concentration (mM); A) 2.0, B) 20.
Drop time; 1 s.

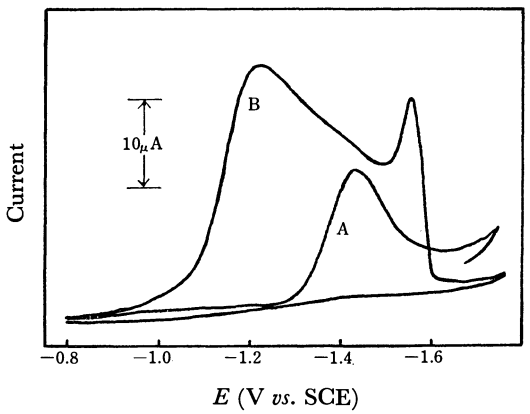

Fig. 9. Cyclic voltammograms.
A) 0.4 mM Fe(II) in 0.1 M KCl (pH 5.0) containing 1 mM chlorate. B) Solution (A) with 0.05 mM iodate.
Scan rate; 100 mV/s.

increased at every drop when the solution was stirred. This anomalous behavior is quite similar to recent observations on the nitrate system.[2)]

Cyclic voltammetric investigations with HMDE were carried out in order to investigate more precisely the role of $Fe(OH)_2$ in the reduction of chlorate. Figure 9 shows the current-voltage curve (B) recorded in the solution 0.4 mM Fe(II) in 0.1 M KCl containing 1 mM chlorate and 0.25 mM iodate. The curve shows two peaks with peak potentials, −1.22 and −1.56 V, respectively. The first wave is ascribed to the catalytic wave, probably involving the discharge of aqua-Fe(II), the second one being responsible for the reduction of colloidal $Fe(OH)_2$. When the cathodic potential scan was carried out up to −1.4 V (more positive than the second wave), the catalytic wave continued to increase in height in the multiple cathodic scans. However, when colloidal $Fe(OH)_2$ was electroreduced in the first scan, the catalytic wave could no longer be observed in the following scans. Similarly, in the absence of iodate, the curve corresponded to the reduction of aqua-Fe(II) (curve (A) in Fig. 9). This indicates that if iron exists as colloidal $Fe(OH)_2$ around the electrode, the catalytic reaction can take place.

The heights of the peaks obtained after the initial electrolysis at various potentials are shown in Fig. 10. When the initial electrolysis was carried out at a potential between −1.05 and −1.35 V for 0.4 mM Fe(II) in 0.1 M KCl containing 1 mM chlorate, the current-voltage curve was found to be almost the same as the one obtained in the presence of both iodate and chlorate (curve (B), Fig. 9). Similar experiments were carried out for 0.4 mM Fe(II) in 0.1 M KCl containing 0.04 mM iodate. The results are also shown in Fig. 10. We see that the first wave (the reduction wave of

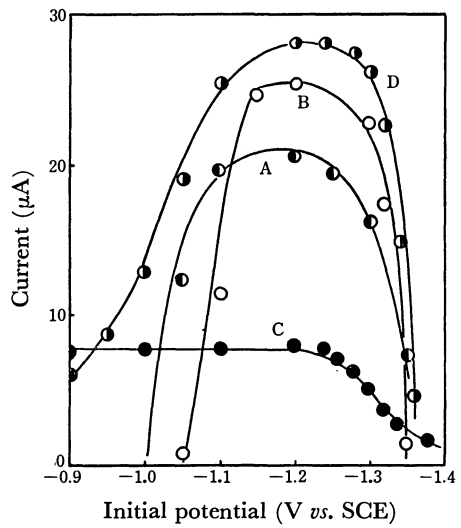

Fig. 10. Relationship between the initial potential and peak currents of 0.4 mM Fe(II) in 0.1 M KCl containing.
1 mM chlorate; A) 1st wave, $E_p = -1.22$ V. B) 2nd wave, $E_p = -1.56$ V.
0.04 mM iodate; C) 1st wave, $E_p = -1.42$ V. D) 2nd wave, $E_p = -1.56$ V.
Initial electrolysis time; 30 s. Scan rate; 200 mV/s.

aqua-Fe(II)) decreases in the potential region between −1.25 V and −1.40 V, since aqua-Fe(II) is partly reduced directly to Fe(0) at the initial potential and the concentration of aqua-Fe(II) diminishes around the electrode. The second wave (the reduction wave of colloidal $Fe(OH)_2$) then appears after the initial electrolysis at potentials more positive than the reduction potential of aqua-Fe(II).

Discussion

On the basis of pulse polarographic and cyclic voltammetric experiments, we can assume that the main product of the reaction between aqua-Fe(II) and OH^- produced around the electrode is colloidal $Fe(OH)_2$, which is responsible for the second wave. This assumption is also supported by the thermodynamic data that the formal potentials of Fe(II)/Fe(0) and $Fe(OH)_2$/Fe(0) are equal to −0.44 and −0.88 V, respectively.[5]

It has been established that the initial adsorption of the depolarizer produces an unusual peak on the normal pulse polarogram.[6–9] Wopschall and Shain have also stated that a significant increase in the current function at faster scan rates is an indication of the presence of weak adsorption in cyclic voltammetry with HMDE.[10] Thus, from the shape of the normal pulse polarogram and the results in Table 1, we can conclude that colloidal $Fe(OH)_2$ is adsorbed weakly on the electrode surface at the initial potential. This is in line with the work of Dahms, who reported the presence of adsorption of $Fe(OH)_2$ on DME by means of galvanostatic charging curves.[11]

From the fact that the peak currents of the second wave are about 30 μA in both normal pulse polarography (Fig. 4) and cyclic voltammetry (Fig. 10), the second wave might be ascribed to the discharge of both adsorbed $Fe(OH)_2$ and colloidal $Fe(OH)_2$ in the neighborhood of the electrode but not to the discharge of adsorbed $Fe(OH)_2$ only.

Ruvinskii *et al.*[3] postulated that the current enhancement with chlorate is due to the chemical reaction between chlorate and Fe(0) hydroxo complex formed on the electrode surface by the reduction of Fe(II) hydroxo complex and the current drop is due to the decomposition (amalgamation) of Fe(0) hydroxo complex deposited on the electrode surface.

$$\mathrm{Fe(II)(OH)}_x \xrightarrow{2e} \mathrm{Fe(0)(OH)}_x \longrightarrow \mathrm{Fe(Hg)} + x\mathrm{OH}^- \qquad (x = 1, 2, \text{ and } 3)$$

$$\uparrow\!\!_____\!\!\downarrow \; \mathrm{ClO_3^-}$$

However, this seems to be improbable since no catalytic wave can be observed when colloidal $Fe(OH)_2$ is electroreduced (Fig. 9). It can be seen in Fig. 10 that colloidal $Fe(OH)_2$ can no longer be produced at the plateau potentials of Fe(II) reduction wave (more negative than −1.4 V) because of the direct reduction of aqua-Fe(II) to Fe(0). The potential coincides with that at which the catalytic current drops abruptly to the reduction current of Fe(II). This indicates that participation of Fe(0) hydroxo complex in the catalytic process is negligible and the nature of the catalytic process is related to the chemical reaction of colloidal $Fe(OH)_2$ with chlorate.

The mechanism for the catalytic effect might be as follows: Chlorate is chemically reduced by colloidal $Fe(OH)_2$ formed in the vicinity of the electrode; the unstable Fe(III) hydroxo complex is then reduced at the cathode, resulting in a catalytic reduction current.

Cyclic voltammetric studies with HMDE (Fig. 10) show that the catalytic wave also appears in the absence of iodate when the initial electrolysis is carried out in the potential region between −1.05 and −1.35 V. It is impossible to explain completely the occurrence of the catalytic wave under these conditions. However, this is probably because a trace of colloidal $Fe(OH)_2$ exists around the electrode. It should be noted that the second wave, whose peak potential is identical to that of the reduction of colloidal $Fe(OH)_2$ can also be observed (curve (B), Fig. 10). This suggests that OH^- is liberated in the vicinity of the electrode by the reduction of chlorate, although the reduction product of chlorate cannot be detected. This is easily realized by the fact that no second wave appears when the electrolysis is carried out in a buffered solution (pH 5.5). Since the amount of OH^- produced in this way is directly related to the formation of colloidal $Fe(OH)_2$, the process may acquire an autocatalytic character.

It can be seen that the amount of colloidal $Fe(OH)_2$ formed at every drop is not reproducible in a quiet solution (Figs. 1(C) and 5). If stirring of the solution is insufficient after detachment of the individual mercury drops, accumulation of aqua-Fe(II) in the close neighborhood of the electrode cannot be made constant at every drop. The anomalous *i-t* curves obtained for the catalytic wave may be explained in this way.

The author wishes to thank Professor Atsuyoshi Saito for his valuable advice and for helpful discussions throughout this investigation.

References

1) A. Saito and S. Himeno, *Nippon Kagaku Kaishi*, **1975**, 1751.
2) A. Saito and S. Himeno, *Chem. Lett.*, **1975**, 1001.
3) O. E. Ruvinskii, Ya. I. Tur'yan, A. K. Neverova, and T. N. Lobova, *Zh. Anal. Khim.*, **30**, 624 (1975).
4) J. Heyrovsky and J. Kuta, "Principles of Polarography," Academic Press, New York (1965), p. 242.
5) W. M. Latimer, "Oxidation Potentials," Prentice-Hall, Inc., New York (1952), p. 220.
6) G. C. Barker and J. A. Bolzan, *Z. Anal. Chem.*, **216**, 15 (1965).
7) R. Guidelli, *J. Electroanal. Chem.*, **18**, 5 (1968).
8) W. H. Reinmuth and K. Balasubramanian, *J. Electroanal. Chem.*, **38**, 79 (1972).
9) A. Saito and S. Himeno, *Nippon Kagaku Kaishi*, **1974**, 2340.
10) R. H. Wopschall and I. Shain, *Anal. Chem.*, **39**, 1514 (1967).
11) H. Dahms, *J. Electroanal. Chem.*, **8**, 5 (1964).

A Light Scattering Study of the Hydrolytic Behavior of Zirconium(IV) and Niobium(V) in a Hydrochloric Acid Solution

Yoshinobu SHIOKAWA, Akiko SATO, and Shin SUZUKI

The Research Institute for Iron, Steel and Other Metals, Tohoku University, Katahira 2-chome, Sendai 980

(Received February 28, 1976)

The hydrolytic behavior of zirconium(IV) and niobium(V) in a hydrochloric acid solution was studied using light scattering measurements. It is found that the species of zirconium(IV) have a degree of polymerization of 3 and a charge per monomer unit of 1.5 in a 1.5 M hydrochloric acid solution with $[Cl^-]=1.7$ M. Also, it was found that for a chloride ion concentration of 11 M, the species of niobium(V) are monomeric in 8—11 M hydrochloric acid and colloidal below 8 M. The effect of standing time of the hydrochloric acid solution of niobium(V) was also investigated.

The nature of hydrolysis and polymerization of metal ions in aqueous solutions has been clarified by Sillén and his co-workers.[1] They have employed accurate potentiometric measurements for a wide range of concentrations of reacting species and for a controlled, relatively high ionic strength. Alekseeva *et al.*[2] have studied potentiometrically the hydrolytic polymerization of zirconium(IV) and hafnium(IV) in perchloric acid solutions at pH 0.3—1.5. However, the state of the metal ions, which are highly hydrolyzable and have a strong tendency to precipitate, has been investigated in strong acid solutions. At high acidities, direct potentiometric measurements of hydrogen ions set free in the hydrolytic process are not possible. Norén[3] has employed an indirect technique using a fluoride membrane electrode in his investigation of the hydrolysis of zirconium(IV) and hafnium(IV).

However, interesting aspects of these metals in aqueous solutions have been also observed in other than potentiometric measurements. Yagodin *et al.*[4] pointed out that a part of the zirconium(IV) is in a form which can not extracted by tributyl phosphate (TBP), and that the amount of non-extractable substance corresponds to the amount of zirconium which could not be determined by the usual method using pyrocatechol violet. They also observed that in nitric acid solutions of zirconium there were two types of hydrolytic species, one being complexes with mobile equilibrium and the other stable ones without equilibrium. Suzuki and Inoue[5] have studied the stability of protactinium(V) in a perchloric acid solution employing thenoyl trifluoroacetone(TTA)–benzene extraction, ion exchange, filtration, and synergism of diisobutyl carbinol on the TTA–benzene extraction. It was observed that the method of preparation and concentration of protactinium both affected the behavior of the protactinium in a perchloric acid solution, a part of the protactinium being in a form which was not adsorbed by a cation exchange resin, and that the protactinium species extracted in the TTA–benzene solution were not stable. Mitsugashira[6] has also found that, in a perchloric acid solution of protactinium(V), non-extractable species were present in a di(2-ethylhexyl)phosphoric acid–benzene extraction study.

Therefore, in aqueous solutions of metal ions which are highly hydrolyzable and have a strong tendency to precipitate, species with irreversible processes are often present. Thus it is attractive to follow an approach from a view different from equilibrium analysis such as solvent extraction. It is also interesting to compare the results of this approach with that of equilibrium analysis. In the present work, the states of zirconium(IV) and niobium(V) in hydrochloric acid solutions were studied by means of Rayleigh light scattering measurements. These measurements are basically independent of equilibrium analysis such as solvent extraction. Therefore, this is a sensitive method for weighing the species in solution, and can therefore provide observations of the polynuclear complexes formed by the hydrolytic process.

Experimental

The zirconium obtained as $ZrOCl_2 \cdot 8H_2O$ was recrystallized from concentrated hydrochloric acid. The salt was dissolved in the hydrochloric acid and finally the acidity of the zirconium solution was adjusted to 1.5 M and the chloride ion concentration to 1.7 M with sodium chloride.

A hydrochloric acid solution of niobium was prepared as follows. Niobium(V) oxide was fused with potassium bisulfate in the ratio of 1 gram of the oxide to 10 grams of the bisulfate. This melt was cooled and dissolved in a warm 4%-ammonium oxalate solution. The resulting solution was filtered and alkalized with 10% ammonia with vigorous stirring. The precipitate thus obtained was separated by centrifugation and washed with dilute hydrochloric acid solutions. This precipitate was dissolved in concentrated hydrochloric acid. Hydrogen chloride was passed through the resulting solution for several hours, initially at room temperature and finally in an ice bath. The solution was then diluted drop by drop with vigorous stirring to the desired concentration with respect to the hydrochloric acid using a hydrochloric acid solution of suitable concentration. The chloride ion concentration was adjusted to 11.0 M with lithium chloride, which was synthesized from lithium carbonate and hydrochloric acid.

The amount of zirconium was determined by EDTA utilizing back titration with copper(II) and niobium gravimetrically as an oxide, igniting niobium hydroxide precipitated by tannin. The acidity of the solution was determined by titration with a standard sodium hydroxide solution.

Light scattering measurements were made using a 4 cm semioctagonal or square cell at 436 nm with a Shimadzu PG-21 light scattering photometer modified in order to increase the sensitivity. The photometer was calibrated using benzene, so as to obtain 47.5×10^{-6} cm^{-1} for the total Rayleigh ratio. This benzene was washed with concentrated sulfuric acid, passed through an activated aluminium oxide column, and then carefully distilled prior to use. Measurements of the

redistilled water gave reasonable values for the Rayleigh ratio $(2.70—2.90)\times10^{-6}$ cm^{-1}.

Refractive index increments were determined at 436 nm and at 25 °C using a Shimadzu DR-3 photoelectric differential refractometer calibrated with sodium chloride solutions.

Each sample was filtered through a Millipore MF filter having a pore diameter of 0.22 μm or a Fluorinert filter having a pore diameter of 0.2 μm, directly into cell, which had been previously rendered dust free. This clean solution was subjected to light scattering and then the refractive index increment was measured. During these procedures, the acidity of the solution remained unchanged.

Results

In a previous paper,[7] the present authors pointed out that the cross-term including the concentration scattering and density scattering, suggested by Bullough, does not need to be taken into account. Therefore, the relation between the Rayleigh ratio and the degree of polymerization, derived by Tobias and Tyree,[8] is valid. The weight-average degree of polymerization N is associated with the excess Rayleigh ratio R^* due to the zirconium or niobium species by

$$\frac{1}{N}=\frac{H\phi\psi^2 m}{R^*}-\frac{z^2 m}{2(m_3+m_5)} \qquad (1)$$

$$H=2000\pi^2n^2/\lambda^4N_A$$

where ϕ is the volume fraction of water, N_A Avogadro's number, n the refractive index of the solution, and λ the wave length of the light. The symbols m, z, and ψ denote the molarity, the absolute value of the charge, and the differential refractive index of the monomeric zirconium or niobium, respectively. The definition of ψ is

$$\psi=\left(\frac{\partial n}{\partial m}\right)-\frac{zm_3}{2(m_3+m_5)}\left(\frac{\partial n}{\partial m_3}\right)-\frac{zm_5}{2(m_3+m_5)}\left(\frac{\partial n}{\partial m_5}\right) \qquad (2)$$

where m_3 and m_5 are the concentrations of the acid and of the supporting electrolyte, respectively. Attention should be paid to the excess Rayleigh ratio expressed as a function of the degree of polymerization and charge.

Zirconium(IV). The influence of the zirconium concentration on the total Rayleigh ratio was investigated for a 1.5 M hydrochloric acid solution with $[Cl^-]=1.7$ M, as is shown in Fig. 1. The Rayleigh ratio, obtained for a 1.5 M hydrochloric acid solution with $[Cl^-]=1.7$ M, was subtracted from the total Rayleigh ratio of the zirconium solution to give the excess Rayleigh ratio due to zirconium species. The excess Rayleigh ratio is also shown in Fig. 1. The results are reproducibile to within a few percent.

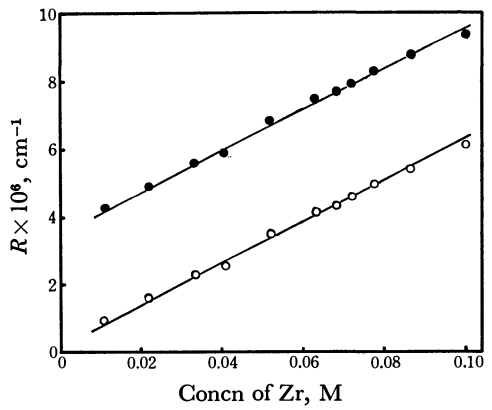

Fig. 1. Dependence of Rayleigh ratio on Zr concentration: ●, total Rayleigh ratio; ○, excess Rayleigh ratio.

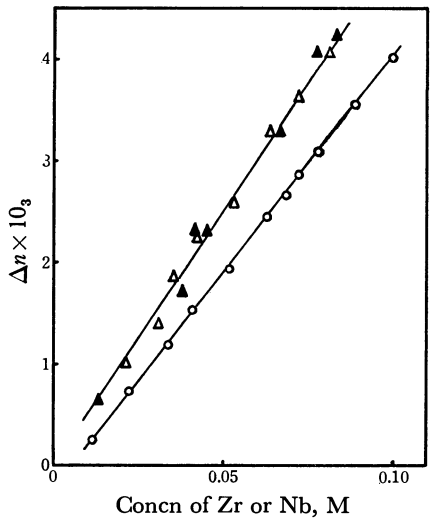

Fig. 2. Refractive index increment of Zr or Nb in HCl solutions: ○, Zr in 1.5 M HCl+0.2 M NaCl; △, Nb in 11 M HCl; ▲, Nb in 8.0 M HCl+3.0 M LiCl.

The refractive index increments of zirconium solutions were determined, as is shown in Fig. 2, where Δn is the difference of the refractive indices between the zirconium solution and a 1.5 M hydrochloric acid solution with $[Cl^-]=1.7$ M. The value found from the slope for $\partial n/\partial m$ is 4.02×10^{-2} l/M. The refractive index increments for hydrochloric acid solutions were also determined, as is shown in Fig. 3. In this figure, Δn is the difference in the refractive indices between a hydro-

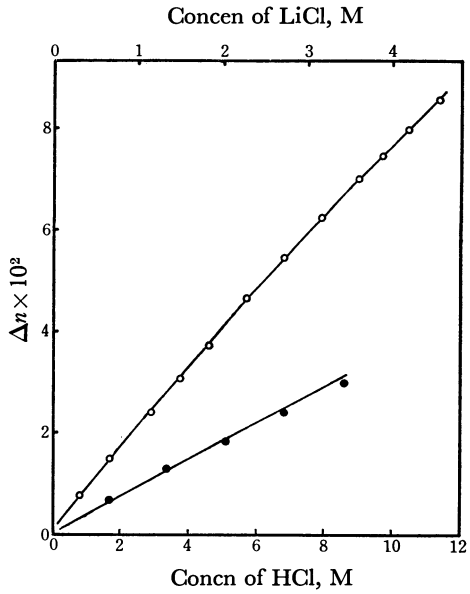

Fig. 3. Refractive index increment of HCl and LiCl solutions: ○, HCl; ●, LiCl.

chloric acid solution and redistilled water and is expressed as

$$\Delta n = -1.03\times10^{-4}m_3^2 + 8.77\times10^{-3}m_3 + 1.68\times10^{-4}. \quad (3)$$

The refractive index increments of sodium chloride solutions were taken from Ref. 9. The value found for $\partial n/\partial m_3$ is 8.46×10^{-3} l/M and that for $\partial n/\partial m_5$ is 1.01×10^{-2} l/M. The volume fraction of water in zirconium solutions was taken to be approximately that of a 1.7 M hydrochloric acid solution and was calculated from the density of the hydrochloric acid solution at 20 °C. The value found is 0.967.

The procedure[8] for applying Eq. 1 is to consider the charge z to be a parameter. A plot of the degree of polymerization, N, *vs.* the zirconium concentration, m, is made for the various values assumed for z. The value of z for which N is independent of m is the correct value for the charge, and the corresponding value of N yields the proper degree of polymerization. Figure 4 indicates that the weight-average degree of polymerization is 3 and that the average charge per zirconium atom is 1.5.

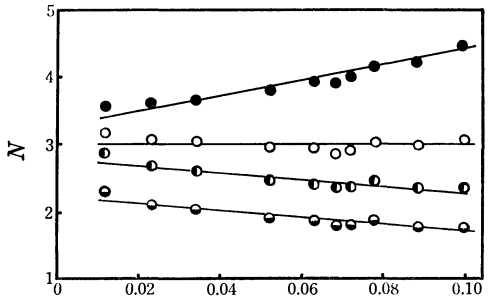

Fig. 4. Plot of the degree of polymerization *vs.* concentration of Zr with the charge as a parameter: ◒, $z=0$; ◐, $z=1$; ○, $z=1.5$; ●, $z=2$.

Niobium(V). The effect of the hydrochloric acid concentration of the niobium solutions on the excess Rayleigh ratio was examined at niobium concentrations of 0.05 M. As is shown in Fig. 5, no appreciable change could be found in the range of acidity from 8 to 11 M, whereas below 8 M a rapid increase is observed.

The effect of the niobium concentration on the total Rayleigh ratio was investigated in two series of experiments. One is for the 11 M hydrochloric acid solution of niobium and the other is for the 8 M solution. The

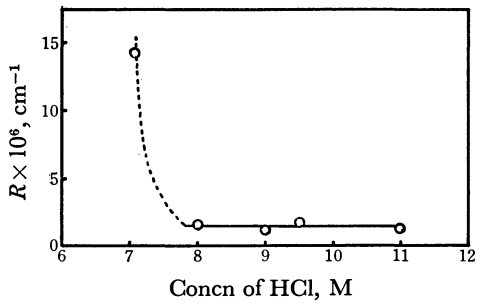

Fig. 5. Dependence of excess Rayleigh ratio on HCl concentration; [Nb(V)]=0.05 M; [Cl⁻]=11 M.

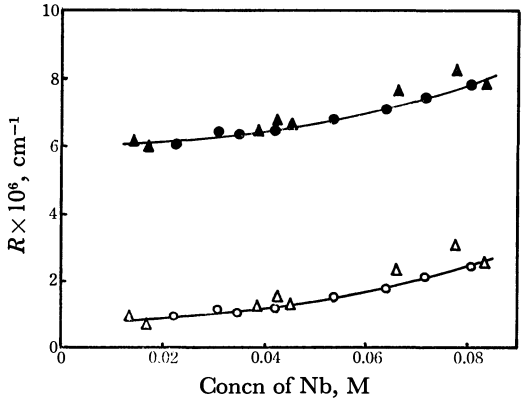

Fig. 6. Dependence of Rayleigh ratio on Nb concentration: ●, total Rayleigh ratio of Nb in 11 M HCl; ○, excess Rayleigh ratio of Nb in 11 M HCl; ▲, total Rayleigh ratio of Nb in 8.0 M HCl+3.0 M LiCl; △, excess Rayleigh ratio of Nb in 8.0 M HCl+3.0 M LiCl.

reproducibilities of these experiments were poor and thus the total Rayleigh ratio shown in Fig. 6 is approximately equal to the mean value of the measured ratio. The Rayleigh ratio obtained for the 11 M hydrochloric acid solution, or the 8 M solution with [Cl⁻]=11 M, was subtracted from the total Rayleigh ratio for a niobium solution in order to obtain the excess Rayleigh ratio due to the niobium species.

The refractive index increments of the niobium were determined in two series of experiments, as is shown in Fig. 2, where Δn is the difference in the refractive index between the niobium solutions and an 11 M hydrochloric acid solution or an 8 M solution with [Cl⁻] =11 M. The value found for $\partial n/\partial m$ is 5.18×10^{-2} l/M for both experiments. The refractive index increments of lithium chloride solutions were also determined, as is shown in Fig. 3. The value found for $\partial n/\partial m_5$ is 8.62×10^{-3} l/M and the values for $\partial n/\partial m_3$ were calculated using Eq. 3. The volume fraction were calculated from the density of the hydrochloric acid and lithium chloride solutions at 20 °C. For the 11 and 8 M series, the value found are 0.755 and 0.766, respectively.

Figure 7 shows the plots of the degree of polymerization *vs.* the concentration of niobium with the charge as a parameter in 11 and 8 M hydrochloric acid solutions

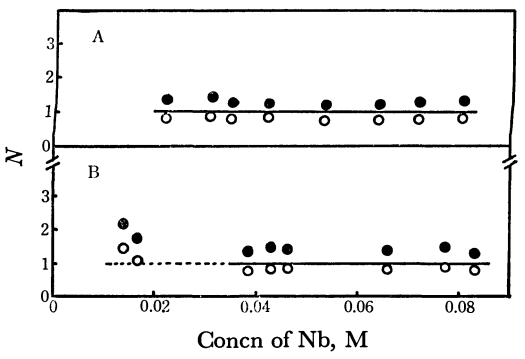

Fig. 7. Plots of the degree of polymerization *vs.* concentration of Nb with the charge as a parameter: ○, $z=0$; ●, $z=3$.
Series A, Nb in 11 M HCl.
Series B, Nb in 8.0 M HCl+3.0 M LiCl.

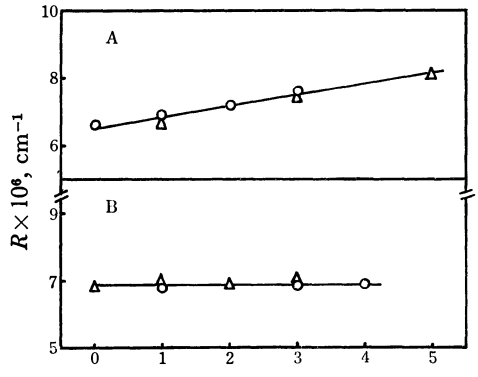

Fig. 8. The effect of standing time on the total Rayleigh ratio of Nb solutions.
Series A, Nb in 8.0 M HCl+3.0 M LiCl: ○, 0.0396 M Nb; △, 0.0430 M Nb.
Series B, Nb in 9.5 M HCl+1.5 M LiCl: ○, 0.0381 M Nb; △, 0.0409 M Nb.

of niobium. There is little difference in the degree of polymerization between the plots for $z=0$ and those for $z=3$. Considering both the poor reproducibility for the total Rayleigh ratios and the impossiblity of a species carrying four or five charges per niobium atom in the solution, we may estimate the degree of polymerization to be unity for the two series. However, it is not all possible to estimate the charge.

The relation between the total Rayleigh ratio of a niobium solution and the standing time after preparation was examined for 8 and 9.5 M hydrochloric acid solutions, as is shown in Fig. 8. At an acidity of 8 M, the total Rayleigh ratio changes appreciably, but it does not change at 9.5 M over several days. Also, the effect of a longer standing time on 8 M hydrochloric acid solutions was examined. However, no reproducible results could be obtained. In these solutions, thehydrolytic precipitation was observed within about ten days after the preparation, and thus, the poorly reproducible results may be related to the precipitation.

Discussion

Zirconium(IV). Assuming species to have constant charge, the weight-average degree of polymerization was found to be 3 and the charge per zirconium atom to be 1.5 in a 1.5 M hydrochloric acid solution. This result is qualitatively consistent with that obtained by ultracentrifugation[10] and with that obtained by spectrophotometry.[11]

From TTA–benzene extraction and spectrophotometric measurements, Zielen and Connick[12] found polynuclear complexes of $Zr_3(OH)_4^{8+}$ and $Zr_4(OH)_8^{8+}$, and also evaluated their hydrolytic constants, as is shown in a footnote to Fig. 9. In this footnote, additional data[13] for the formation of mononuclear complexes are listed. Using these constants, the distribution of these complexes at a hydrogen ion concentration of 1.5 M was calculated, as is shown in Fig. 9a, and as was the weight-average degree of polymerization and the charge per zirconium atom, which is shown in Fig. 9b. These

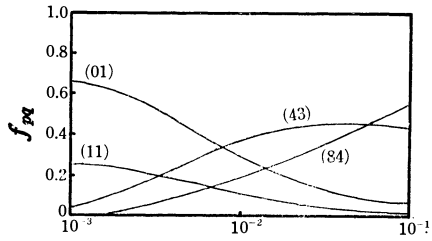

Fig. 9(a).

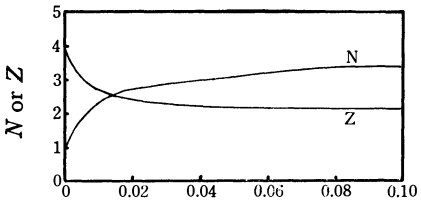

Fig. 9(b).

Fig. 9. Distribution f_{pq}, degree of polymerization N, and charge per one atom Z of Zr solution at $[H^+]=1.5$ M, which are calculated by hydrolytic constants, $\log\beta_{11}=-0.22$, $\log\beta_{21}=-0.84$, $\log\beta_{31}=-1.88$, $\log\beta_{41}=-3.05$, $\log\beta_{43}=5.39$, and $\log\beta_{84}=8.24$. In the (pq) p and q denote the composition of complex $Zr_q(OH)_p^{4q-p}$ and f_{pq}, N, and Z are defined as follow: $f_{pq}=q[Zr_q(OH)_p^{4q-p}]/[Zr]_{tot}$, $N=\sum_{p,q} q f_{pq}$, and $Z=\sum_{p,q}(4-p/q)f_{pq}$

results for a 1.7 M chloride solution are assumed to be valid, though these constants were evaluated with respect to a 2 M perchlorate solution. No appreciable error should be introduced, at least in the degree of polymerization, from this assumption, since Babko and Gridchina[14] have found that the degree of polymerization is the same in perchloric, hydrochloric and nitric acid solutions using a dialysis method. The degree of polymerization and the charge shown in Fig. 9b are consistent with the present results, except for a slight discrepancy of the charge. This discrepancy may be explained by experimental errors and/or by the diminishing charge for the coordination of chloride ions in the present chloride solutions.

The agreement between the results obtained by the solvent extraction and spectrophotometric method and that by the light scattering method is interesting from two point of view. One is concerned with the assumptions used in the experimental method and the other with the existence of species with irreversible processes. Now, the experimental methods based on different principles, such as solvent extraction and light scattering, were conducted under individual and separate assumptions. This agreement suggests that these assumptions are appropriate, at least in this case. However, in a zirconium solution there are often species with irreversible processes, as mentioned before. Thus, this agreement suggests that these species only slightly contribute to the behavior of these solutions.

Niobium(V). A hydrochloric acid solution of niobium is less stable than a solution of zirconium. Hydrolytic precipitation appears even in 10 M hydro-

chloric acid solutions with a niobium concentration of 0.01—0.1 M within a few hours after the preparation. However, maintaining the chloride ion concentration at 11 M, as is shown in Fig. 5, the precipitation does not appear for an 8 M hydrochloric acid solution of niobium. Below hydrochloric acid concentrations of 8 M, the rapid increase of excess Rayleigh ratio must be related to the formation of hydrolytic colloidal particles. The constancy of the excess Rayleigh ratio for acidities of 8—11 M suggests that monomeric species are predominant. These species may be forms of $Nb(OH)_m$-Cl_n^{5-m-n}, as has been suggested by Kanzelmeyer *et al.*[15]

It is interesting to note that a species in an 8 M hydrochloric acid solution of niobium is transformed into a colloidal particle for a 7 M solution. This transformation suggests that the intermediate polymer of niobium is unstable or that it can exist only in a narrow range of hydrochloric acid concentrations. This phenomenon is extremely different from the case of a zirconium solution, in which the polymer can exist stably over a wide range of concentrations. On the other hand, some investigations have indicated the existence of a niobium polymer.[16-18] This discrepancy may be explained by the different conditions of solutions and/or of the preparations of the solutions.

As is shown in Fig. 8, a standing effect is perceived for an 8 M hydrochloric acid solution of niobium but no effect was found for a 9.5 M solution a few days after the preparation of solution. This effect on the Rayleigh ratio must be associated with an increase in the degree of polymerization, because the Rayleigh ratio depends only slightly on the charge. The difference in the standing effect between 8 and 9.5 M solutions suggests that some species which are present in the 8 M solution and are hardly present in the 9.5 M solution, may be related to the polymerization process.

References

1) A. E. Martell, "Coordination Chemistry," Vol. 1, von Nostrand, New York (1971), p. 491.
2) I. I. Alekseeva, I. I. Nemzer, and L. I. Yuranova, *Zh. Neorg. Khim.*, **20**, 92 (1975).
3) B. Norén, *Acta Chem. Scand.*, **27**, 1369 (1973).
4) G. A. Yagodin, A. M. Chekmarev, and V. G. Kazak, *Zh. Neorg. Khim.*, **15**, 1284 (1970); G. A. Yagodin, V. G. Kazak, and V. V. Tarasov, *ibid.*, **17**, 2399 (1972); G. A. Yagodin, E. G. Teterin, and V. G. Kazak, *ibid.*, **17**, 3026 (1972); G. A. Yagodin and V. G. Kazak, *ibid.*, **18**, 107 (1973).
5) S. Suzuki and Y. Inoue, *Bull. Chem. Soc. Jpn.*, **39**, 1705 (1966); S. Suzuki and Y. Inoue, *ibid.*, **42**, 1916 (1969); S. Suzuki and Y. Inoue, *ibid.*, **42**, 2523 (1969).
6) T. Mitsugashira, *Bull. Chem. Soc. Jpn.*, **44**, 1305 (1971).
7) Y. Shiokawa and S. Suzuki, *Bull. Chem. Soc. Jpn.*, **48**, 171 (1975).
8) R. S. Tobias and S. Y. Tyree, Jr., *J. Am. Chem. Soc.*, **81**, 6385 (1959).
9) M. B. Huglin, "Light Scattering from Polymer Solutions," Academic Press, New York (1972), p. 181.
10) J. S. Johnson and K. A. Kraus, *J. Am. Chem. Soc.*, **78**, 3937 (1956).
11) S. Tribalat and L. Schriver, *C. R. Acad. Sci., Ser. C*, **274**, 849 (1972).
12) A. J. Zielen and R. E. Connick, *J. Am. Chem. Soc.*, **78**, 5785 (1956).
13) L. G. Sillén and A. E. Martell, "Stability Constants," Spec. Publ. No. 17, The Chemical Society, London (1964), p. 45.
14) A. K. Babko and G. I. Gridchina, *Zh. Neorg. Khim.*, **6**, 1326 (1961).
15) J. H. Kanzelmeyer, J. Ryan, and H. Freund, *J. Am. Chem. Soc.*, **78**, 3020 (1956).
16) G. I. Gridchina, *Zh. Neorg. Khim.*, **8**, 634 (1963).
17) G. I. Gridchina, *Zh. Neorg. Khim.*, **11**, 299 (1966).
18) N. N. Kuznetsova, *Zh. Anal. Khim.*, **23**, 1485 (1968).

The Syntheses and Properties of Bis(3-hydroxy-2-methyl-4-pyronato) Complexes of Bivalent Metal Ions

Hideyoshi MORITA, Shigeru SHIMOMURA, and Shinichi KAWAGUCHI*

Faculty of Pharmaceutical Sciences, Tokushima University, Shomachi, Tokushima 770

**Department of Chemistry, Faculty of Science, Osaka City University, Sumiyoshiku, Osaka 558*

(Received March 13, 1976)

Bis(3-hydroxy-2-methyl-4-pyronato) complexes of cobalt(II), nickel(II), copper(II), and zinc(II) have been prepared: $CoL_2(OH_2)_2$, $NiL_2(OH_2)_2$, CuL_2, and $[ZnL_2(OH_2)_2]\cdot 1/2H_2O$. The 2,2′-bipyridine-(bpy) and 1,10-phenanthroline(phen) adducts of these complexes were also synthesized: CoL_2(bpy), CoL_2(phen), NiL_2(bpy), ZnL_2(bpy), and ZnL_2(phen). Based on the magnetic, spectral, and thermogravimetric data, the structures of these complexes are proposed: all of the cobalt(II), nickel(II), and zinc(II) complexes are octahedral, and CuL_2 is square planar. The NMR spectra of the zinc(II) complexes are discussed.

3-Hydroxy-2-methyl-4-pyrone occurs naturally is also obtained by the alkaline hydrolysis of streptmycin salts.[1] The pyrone has a caramel-like odor, and is used as a spice in bread and cakes. However, the compound is not harmless, the oral lethal dose (LD_{50}) for rats being 1.48 g/kg.[2] On the other hand, Nickell and Gordon reported on a stimulatory effect of this pyrone on plant growth, and suggested that the effect might be brought about by its metal chelate since methoxylation of the hydroxyl group of pyrone renders it inactive.[3] Thus a detailed study of the metal complexes of the pyrone is desirable.

The stability constants have been determined for a number of metal complexes of this pyrone.[4] Several tervalent metal complexes were isolated,[5,6] but no example of the mixed ligand complex containing another base has been reported.

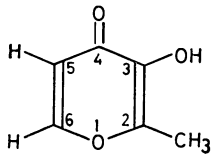

Fig. 1. 3-Hydroxy-2-methyl-4-pyrone.

This paper reports on the syntheses and structural studies of the bivalent metal complexes of 3-hydroxy-2-methyl-4-pyrone (HL, Fig. 1) and their 2,2′-bipyridine and 1,10-phenanthroline adducts.

Experimental

Syntheses of Complexes. Bis(3-hydroxy-2-methyl-4-pyronato)diaquacobalt(II), $CoL_2(OH_2)_2$: A 20 ml portion of 1 M NaOH solution was added to *ca.* 100 ml of warm aqueous ethanol (1:1 by volume) containing 2.54 g (0.02 mol) of 3-hydroxy-2-methyl-4-pyrone and 2.39 g (0.01 mol) of cobalt(II) chloride hexahydrate. The mixture was stirred for *ca.* 30 minutes and then kept standing overnight in a refrigerator. A dull yellow precipitate was obtained by filtration, washed with water and ethanol successively, and air dried. Yield: *ca.* 2.5 g, 72%.

The corresponding nickel(II), copper(II), and zinc(II) complexes, $NiL_2(OH_2)_2$, CuL_2, and $[ZnL_2(OH_2)_2]\cdot 1/2H_2O$, were also prepared by the same method in 81, 80, and 78% Yields, respectively.

Bis(3-hydroxy-2-methyl-4-pyronato)bipyridinecobalt(II), CoL_2(bpy): A mixture containing 1.72 g (0.005 mol) of $CoL_2(OH_2)_2$ and 0.78 g (0.005 mol) of 2,2′-bipyridine in 200 ml of acetone was stirred for *ca.* 5 h and then filtered and washed with acetone. The crude complex was recrystallized from hot acetone and air dried. Yield: *ca.* 2.0 g, 86%.

In a similar fashion, NiL_2(bpy), ZnL_2(bpy), CoL_2(phen) and ZnL_2(phen) were obtained in 60, 85, 86, and 85% yields, respectively.

Analyses and Measurements. Metal contents in these complexes were determined by atomic absorption. The results of elemental analysis are shown in Table 1 together with some properties. The visible and ultraviolet absorption and reflection spectra were obtained with Hitachi EPS-3 and Shimadzu MPS-5000 recording spectrophotometers. The infrared spectra (4000—400 cm^{-1}) were obtained with a Hitachi EPI-G2 infrared spectrophotometer by the KBr disk method, and those in the 700—200 cm^{-1} region with a Jasco DS-701G infrared spectrophotometer by the CsI disk method. The magnetic susceptibility was determined at room temperature by the Faraday method with an automatically recording magnetic balance (Shimadzu Seisakusho Co., Ltd.). Mercury(II) tetraisothiocyanatocobaltate(II) was used as a reference

TABLE 1. COLOR AND ANALYTICAL DATA OF THE ISOLATED COMPLEXES

Complex	Color	Found (Calcd), %					Magnetic moment
		C	H	N	M	H_2O	B.M. (K)
$CoL_2(OH_2)_2$	dull yellow	41.44(41.76)	4.52(4.09)		16.93(17.03)	10.1(10.44)	4.74(303)
CoL_2(bpy)	orange	56.19(56.79)	3.97(3.90)	6.22(6.02)			4.56(297)
CoL_2(phen)	reddish orange	58.34(58.91)	3.75(3.71)	5.73(5.72)			4.59(297)
$NiL_2(OH_2)_2$	yellow green	41.55(41.78)	4.39(4.09)		17.29(17.02)	9.9(10.45)	3.21(303)
NiL_2(bpy)	green	56.13(56.81)	4.04(3.90)	6.30(6.02)			3.13(297)
CuL_2	pale green	45.57(45.94)	3.35(3.21)		19.63(20.25)		1.84(297)
$[ZnL_2(OH_2)_2]\cdot 1/2H_2O$	white	39.97(39.94)	4.48(4.19)		18.07(18.13)	11.1(12.49)	
ZnL_2(bpy)	pale yellow	55.72(56.01)	3.92(3.85)	5.93(5.94)	14.08(13.86)		
ZnL_2(phen)	pale yellow	57.85(58.14)	3.62(3.66)	5.64(5.65)	13.15(13.19)		

Table 2. Characteristic IR bands (cm^{-1}) of the isolated complexes

Assignment	ν(C=O)	ν(C=C)	ν(M–O)	Base
HL	1650s	1620vs, 1560s		
$CoL_2(OH_2)_2$	1600s	1570vs, 1500s	466s, 273s	
CoL_2(bpy)	1599vs	1570vs, 1507s	452s, 243s	1022w, 779m, 739w, 422s
CoL_2(phen)	1599vs	1569vs, 1508s	450s, 240s	1419m, 869m, 730m, 423m, 286m
$NiL_2(OH_2)_2$	1598s	1574vs, 1499s	470s, 284s	
NiL_2(bpy)	1598vs	1572vs, 1510s	457m, 272s	1027w, 769m, 740w, 423m
CuL_2	1613vs	1579vs, 1506s	395m, 235s	
$[ZnL_2(OH_2)_2]\cdot 1/2H_2O$	1608s	1576vs, 1508s	472m, 243s	
ZnL_2(bpy)	1602vs	1573vs, 1509s	457m, 230s	1022w, 780m, 740w, 417m
ZnL_2(phen)	1600vs	1572vs, 1510s	457m, 230s	1419m, 870m, 727m, 422m, 286m

substance. Diamagnetic corrections were calculated from Pascal's constants. Thermogravimetric curves were obtained with a Rigaku Denki 8002 H/D differential thermobalance at a heating rate of 3 °C/min in the air. The NMR spectra were measured in $(CD_3)_2SO$ at 100 MHz with a JNM-PS-100 spectrometer (Japan Electron Optics Lab. Co., Ltd.) using tetramethylsilane as an internal reference.

Results and Discussion

Infrared Spectra and Thermogravimetric Data. The characteristic IR bands of the metal complexes of 3-hydroxy-2-methyl-4-pyrone and their base adducts summerized are in Table 2. They were assigned in reference to the literature.[7-11] The frequencies of the C=O and C=C stretching vibrations in all these complexes are smaller by *ca.* 50 cm^{-1} than those in the free ligand. This suggests that the 3-hydroxy-2-methyl-4-pyronate ion is coordinated to the metal ion through both oxygen atoms of the carbonyl and hydroxyl groups, and that the delocalization of the olefinic and carbonyl electrons of the 3-hydroxy-2-methyl-4-pyronate ion takes place.[12]

The OH stretching bands of $CoL_2(OH_2)_2$, $NiL_2(OH_2)_2$ and $[ZnL_2(OH_2)_2]\cdot 1/2H_2O$ are shown in Fig. 2. The OH stretching bands of cobalt(II) and nickel(II) complexes are observed at *ca.* 3420 cm^{-1}, both being sharp. In contrast the zinc(II) complex exhibits a very broad band at 3480 cm^{-1}, which might be composed of the OH stretching bands of both the coordinated and lattice water. Thermogravimetric analysis of the three complexes shows that the zinc(II) complex begins to liberate water at around 80 °C, and the nickel(II) and cobalt(II) complexes at around 115 and 105 °C, respectively. The difference in the temperature of water liberation suggests that the zinc(II) complex may contain lattice water, although the thermogravimetric analysis can not discriminate the coordinated and lattice water.

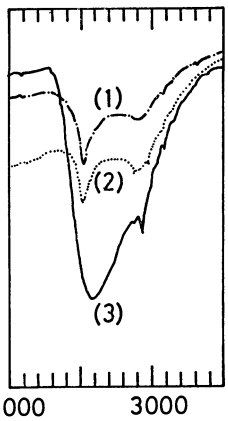

Fig. 2. The IR spectra of: (1) $CoL_2(OH_2)_2$; (2) $NiL_2(OH_2)_2$; and (3) $[ZnL_2(OH_2)_2]\cdot 1/2H_2O$.

The IR spectra of adducts containing heterocyclic diamine (phen or bpy) consist of bands due to the 3-hydroxy-2-methyl-4-pyronate ligand and those of the coordinated diamine. The bands in the 1700—1500 cm^{-1} region are little affected by the coordination of the diamine, no new bands being observed in this region. Thus the bands around 1600 and 1570 cm^{-1} are assigned mainly to the C=O and C=C stretching vibrations, respectively, of the 3-hydroxy-2-methyl-4-pyronate ligand. The coordination of phen to the metal ion is evidenced by the new bands at around 1420, 865, and 725 cm^{-1},[9,10] and the coordination of bpy is also revealed by the shift and split of the characteristic band (751 cm^{-1}) of the free ligand into two bands around 780 and

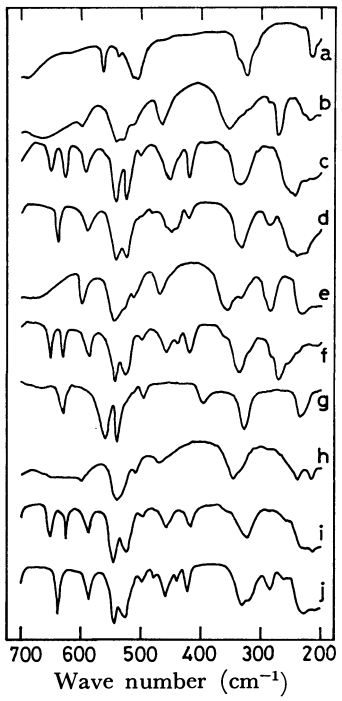

Fig. 3. The far-IR spectra of: (a) HL; (b) $CoL_2(OH_2)_2$; (c) CoL_2(bpy); (d) CoL_2(phen); (e) $NiL_2(OH_2)_2$; (f) NiL_2(bpy); (g) CuL_2; (h) $[ZnL_2(OH_2)_2]\cdot 1/2H_2O$; (i) ZnL_2(bpy); and (j) ZnL_2(phen).

740 cm^{-1},[10,11] and by the appearance of a new band at around 1020 cm^{-1}.[10,11]

The far-IR spectra in the 700—200 cm^{-1} region of the present complexes are shown in Fig. 3. They are assigned tentatively as listed in Table 2 in reference to literature.[8] In the case of adducts containing heterocyclic diamine, the bands assigned to the metal-oxygen stretching are shifted towards the lower-frequency side (around 455 cm^{-1}), the new bands attributable to bpy or phen appearing at *ca.* 420 cm^{-1}. The above shift may be caused by the weakening of the metal-oxygen bond due to the coordination of diamine.

Electronic Spectra and Magnetic Data. Both the absorption (in ethanol) and reflection spectra of the 3-hydroxy-2-methyl-4-pyronate complexes are shown in Figs. 4 and 5, their magnetic moments being listed in Table 1. In the 20000—7000 cm^{-1} region, $CoL_2(OH_2)_2$, CoL_2(bpy) and CoL_2(phen) show absorption bands at *ca.* 18000(sh) (ε=41.8), 8600 (ε=2.6), and 7570 (ε=3.1) cm^{-1}, at *ca.* 19000(sh) (ε=67.2) and 9200 (ε=5.9)

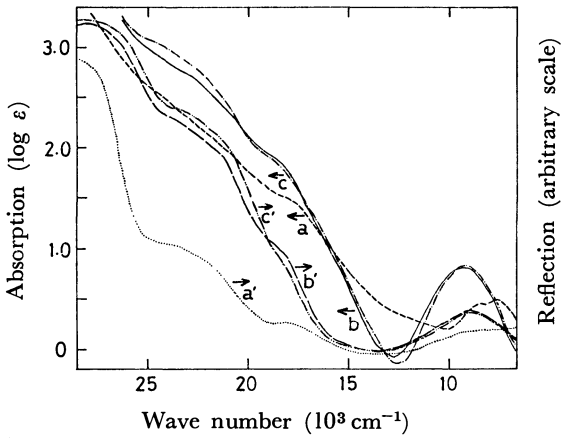

Fig. 4. The absorption and reflection spectra of: (a) and (a'), $CoL_2(OH_2)_2$; (b) and (b'), CoL_2(bpy); (c) and (c'), CoL_2(phen).

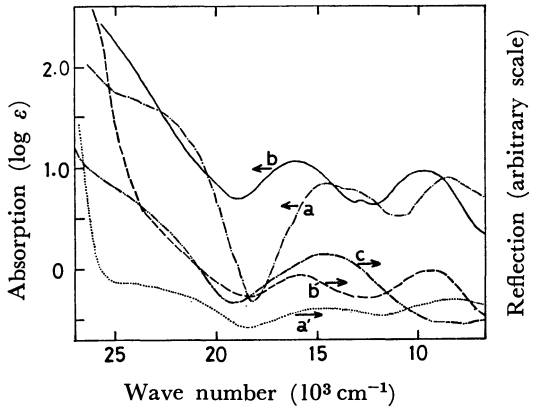

Fig. 5. The absorption and reflection spectra of: (a) and (a'), $NiL_2(OH_2)_2$; (b) and (b'), NiL_2(bpy); (c), CuL_2.

cm^{-1}, and at *ca.* 19200(sh) (ε=65.6) and 9100 (ε=6.1) cm^{-1}, respectively. The reflection spectra of these complexes are similar to the corresponding absorption spectra in solution. The results reveal that all these cobalt(II) complexes are octahedral in the two phases, although the magnetic moments of CoL_2(bpy) and CoL_2(phen) are a little lower than the value usually observed for the octahedral cobalt(II) complexes.[13]

The absorption spectra of $NiL_2(OH_2)_2$ and NiL_2(bpy) in the 20000—7000 cm^{-1} region exhibit bands at 14500 (ε=5.5), 13000 (ε=4.6), and 8500 (ε=7.0), and at 16100 (ε=11.9), 12900 (ε=2.6), and 8800 (ε=7.3) cm^{-1}, respectively. The reflection spectra of these complexes are also similar to the corresponding absorption spectra. The spectra and the observed magnetic moments of $NiL_2(OH_2)_2$ (3.21 B. M.) and NiL_2(bpy) (3.13 B. M.) suggest that both of the nickel(II) complexes are octahedral.

The observed magnetic moment (1.84 B. M.) of CuL_2 is normal, indicating that there is no copper-copper interaction. The reflection spectrum of this copper(II)

Table 3. NMR spectra of the zinc(II) complexes in dimethyl sulfoxide solution (δ, ppm)

Complex	HL	Base
	CH_3 5 6	
	2.22 6.30 7.99	
	($J_{5,6}$=5.1)	
$[ZnL_2(OH_2)_2]\cdot 1/2H_2O$	2.32 6.52 8.11	
	($J_{5,6}$=4.8)	
		bpy
		3 and 3' 4 and 4' 5 and 5' 6 and 6'
		8.44 7.95 7.45 8.74
		($J_{3,4}$=8.0, $J_{3,5}$=1.2, $J_{3,6}$=1.0,
		$J_{4,5}$=7.6, $J_{4,6}$=1.7, $J_{5,6}$=4.9)
ZnL_2(bpy)	2.28 6.39 8.02	8.49 8.05 7.55 8.70
	($J_{5,6}$=5.2)	($J_{3,4}$=8.0, $J_{3,5}$=1.3, $J_{3,6}$=0.8,
		$J_{4,5}$=7.7, $J_{4,6}$=1.7, $J_{5,6}$=4.9)
		phen
		2 and 9 3 and 8 4 and 7 5 and 6
		9.17 7.78 8.51 8.00
		($J_{2,3}$=4.5, $J_{2,4}$=1.5, $J_{3,4}$=8.3)
ZnL_2(phen)	2.26 6.26 7.91	8.92 7.93 8.72 8.10
	($J_{5,6}$=5.2)	($J_{2,3}$=4.4, $J_{2,4}$=—, $J_{3,4}$=8.4)

Coupling constants, J, have the unit of Hz.

complex in the 20000—8000 cm^{-1} region shows only one symmetrical d-d band at 14700 cm^{-1}. Troporone and 3-hydroxy-2-methyl-4-pyrone are very similar ligands, both coordinating to a metal ion through oxygen atoms of the hydroxy and carbonyl groups to form a five-membered chelate ring. The absorption spectrum of Cu(troporonato)$_2$ exibits a weak band at 14700 cm^{-1} ($\varepsilon \approx 100$).[14] This complex has the O_4-tetracoordinate planar structure around the copper ion, although the plane including the copper and oxygen atoms makes an angle of 4.9° with the plane of the seven membered ring.[15] The close resemblance of the reflection spectrum of CuL_2 to the absorption spectrum of Cu(troporonato)$_2$ strongly suggests the O_4-tetracoordinate planar structure for CuL_2 in solid.

NMR Spectra of Zn(II) Complexes. The NMR spectra of $[ZnL_2(OH_2)_2]\cdot 1/2H_2O$, ZnL_2(bpy), and ZnL_2(phen) in dimethyl sulfoxide solutions are shown in Table 3. The assingments are based on integration of the peak area in comparison with the NMR spectra of InL_3,[6] 2,2′-bipyridine,[16] and 1,10-phenanthroline and its metal complexes.[17]

In the spectrum of $[ZnL_2(OH_2)_2]\cdot 1/2H_2O$, the resonance peak at 8.81 ppm due to the OH proton of free HL is lost, the resonance peaks of protons 5 and 6 and methyl protons of this ligand being shifted downfield by 0.22, 0.12, and 0.10 ppm, respectively, due to chelation to zinc(II) ion.

In the case of ZnL_2(bpy), the downfield shifts of the protons 5, 6 and methyl protons of the pyronate ligand are much smaller, *i.e.* 0.09, 0.03 and 0.06 ppm, respectively, than those in $[ZnL_2(OH_2)_2]\cdot 1/2H_2O$. Signals of the protons 5 and 6 of this ligand in ZnL_2(phen) are shifted upfield by 0.04 and 0.08 ppm, respectively, while the peak for the methyl protons is shifted down field by 0.04 ppm. This might be caused by a decrease in the electron donation from the chelating oxygen atoms to the metal because of the coligation of bpy or phen to the zinc(II) ion, or by the magnetic anisotropy effect of the ring current of these diamines.

The resonance peaks of the protons 6 and 6′ of bpy in ZnL_2(bpy), and the protons 2 and 9 of phen in ZnL_2(phen) are shifted upfield by 0.04 and 0.25 ppm, respectively, than those of free diamines. Miller and Prince reported that an upfield shift for the 2 and 9 ring protons of phen in the tris-1,10-phenanthroline complexes of Co(III), Fe(II), Ru(II), and Zn(II) and the tetrakis-1,10-phenanthroline complexes of Ca(II) and Mg(II) is probably due to a metal-nonbonded hydrogen interaction.[17] In the present case of ZnL_2(phen), the upfield shift of the 2 and 9 protons of phen may also be due to a similar effect.

The authors are grateful to Dr. Shunji Utsuno of Shizuoka University for his mesurement of the reflcetion spectra.

References

1) J. R. Schenck and M. A. Spielman, *J. Am. Chem. Soc.*, **67**, 2279 (1945).
2) H. Horiguchi, "Kogai Shokuhin," Sankyo Shuppan K. K., Tokyo (1974), p. 169.
3) L. G. Nickell and P. N. Gordon, *Agr. Biol. Chem.*, **27**, 65 (1963).
4) L. G. Sillen and A. E. Martell, "Stability Constants of Metal-Ion Complexes," Special Publication No. 17, The Chemical Society, London (1964), p. 473.
5) H. Morita, Y. Hayashi, S. Shimomura, and S. Kawaguchi, *Chem. Lett.*, **1975**, 339.
6) D. G. Tuck and M. K. Yang, *J. Chem. Soc., A*, **1971**, 3100.
7) K. Yamada, *Bull. Chem. Soc. Jpn.*, **35**, 1323 (1962).
8) B. Hutchinson, J. Takemoto, and K. Nakamoto, *J. Am. Chem. Soc.*, **92**, 3335 (1970); K. Nakamoto, C. Udovich, and J. Takemoto, *ibid.*, **92**, 3973 (1970).
9) A. A. Schilt and R. C. Taylor, *J. Inorg. Nucl. Chem.*, **9**, 211 (1959).
10) R. G. Inskeep, *J. Inorg. Nucl. Chem.*, **24**, 763 (1962).
11) S. P. Sinha, *Spectrochim. Acta*, **20**, 879 (1964).
12) Y. Murakami and K. Mera, *Bull. Chem. Soc. Jpn.*, **39**, 369 (1966).
13) R. L. Carlin, "Transition Metal Chemistry," Marcel Dekker, Vol. 1, New York (1965), p. 1.
14) S. Antosik, N. M. D. Brown, A. A. McConnell, and A. L. Porte, *J. Chem. Soc., A*, **1969**, 545.
15) W. M. Macintyre, J. M. Robertson, and R. F. Zahrobsky, *Proc. R. Soc. London, A*, **289**, 161 (1965).
16) S. Castellano, H. Gunter, and S. Ebersole, *J. Phys. Chem.*, **69**, 4166 (1965).
17) J. D. Miller and R. H. Prince, *J. Chem. Soc.*, **1965**, 3185.

Equilibria of Complex Formation in Aqueous Solution between Lead(II) and Thallium(I) Ions, and Cyclic and Linear Polyethers

Mutsuo KODAMA[1] and Eiichi KIMURA*

Department of Chemistry, College of General Education, Hirosaki University, Bunkyo, Hirosaki 036
**Institute of Pharmaceutical Sciences, Hiroshima University School of Medicine, Kasumi, Hiroshima 734*

(Received March 19, 1976)

log K, ΔH and ΔS values were polarographically determined for the interaction in aqueous solution of Pb^{2+} and Tl^{+} ions with a cyclic polyether, 1,4,7,10,13,16-hexaoxacyclooctadecane(18-crown-6), and a linear polyether, tetraethylene glycol dimethyl ether(tetraglyme). The stability constant of a 1:1 Pb^{2+} complex with the macrocyclic ligand is four figures higher than that with the linear ligand. This macrocyclic effect is explained in terms of entropy.

The stability of a complex between a given cyclic polyether and a cation is dependent on the cation diameter, as illustrated by a case in which the preference of 18-membered cyclic hexaether **1** and **2** (2.6—3.2 Å macrocycle hole cavity) for divalent metal ions decreases in the order; $Pb^{2+}(2.4)>Ba^{2+}(2.7)>Sr^{2+}(2.3)>Hg^{2+}(2.2)>Ca^{2+}(2.0$ Å).[2] The size selectivity is determined by several effects such as electrostatic attraction between metal ion and ligand, ligand conformational change, changes in total particle number, dehydration of the metal ion and ligand, or hydration of the metal-ligand complex. In the thermodynamic study on the 1:1 complexes of **1** and **2** with divalent metal ions, Izatt *et al.* showed that the complexation with Sr^{2+} is more favorable entropically but less so enthalpically than with Ba^{2+}.[3] This suggests that the dominant effects in determining size selectivity are the endothermic removal of water from the hydration sheath with an accompanying gain in entropy, both of which are known more pronounced for the more strongly hydrated Sr^{2+} ion.[4] However, for the complex formation with Pb^{2+} ion which stands linking between Sr^{2+} and Ba^{2+} in terms of ionic diameter, no thermodynamic functions have been reported as yet.

A macrocyclic effect of $\approx 10^4$-fold stability enhancement was found between K^{+}(2.7 Å) complex of an open-chain hexaether, **3**, and those of the macrocyclic analogs such as **1** or **2**.[5] It was postulated that entropic forces work against complete envelopment of the cation by the non-cyclic polyether. However, recent studies on the macrocyclic tetramine system[6-8] disclosed the fact that thermodynamic parameter ΔH often plays more important role in the macrocyclic effect which is linked to ligand solvation effects.[9]

In order to investigate the complexing properties and a major source of the macrocyclic effect, the present polarographic study was undertaken on the interaction of Pb^{2+} with 1,4,7,10,13,16-hexaoxacyclooctadecane-

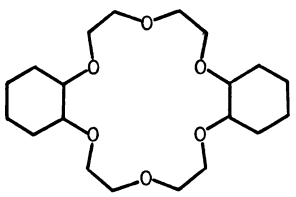

Dicyclohexyl-18-crown-6
1. isomer A **2.** isomer B

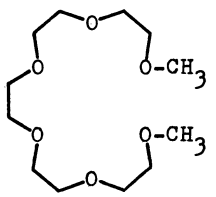

3. Pentaglyme

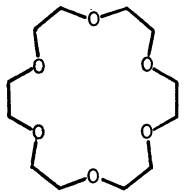

4. 18-Crown-6

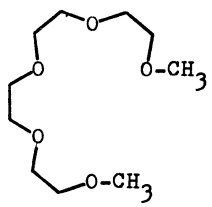

5. Tetraglyme

(18-crown-6), **4**, and tetraethylene glycol dimethyl ether (tetraglyme), **5**, in aqueous solution. Stability constant K, ΔH and ΔS values have also been determined for Tl^{+} complex formation with **4**. The studies constitute a part of our investigations into the macrocyclic effects.[8,10,11] Similar studies have been reported on the metal ion complexes containing analogous ligands, $H_{3-n}(CH_2CH_2OCH_2CH_2OCH_2CH_2)_nNH_{3-n}$, **6**.[12-15]

Experimental

Reagents. A standard solution of thallium(I) perchlorate was prepared by dissolving pure thallium metal in a reagent grade perchloric acid. A standard lead(II) nitrate solution was prepared by dissolving pure lead(II) nitrate crystals in redistilled water. Tetraethylammonium perchlorate(TEAP) was prepared by the method given by Fujinaga, Izutsu and Takaoka,[16] and purified by recrystallization from water. 18-Crown-6, **4**, (Aldrich Chemical Company, Inc.) was recrystallized from acetonitrile. The ionic strength of the sample solutions was adjusted to 0.10 by adding an appropriate amount of TEAP. The other reagents were of analytical reagent grade and were used without further purification.

Apparatus and Experimental Procedures. The d.c. current-voltage curves were obtained by using a manual polarograph similar to that of Kolthoff and Lingane[17] or a Yanagimoto P-8 pen-recording polarograph. For all the measurements, we used a dropping mercury electrode with an m value of 0.915 mg/s and a drop time, t_d, of 5.00 s in an air-free 0.10 M $NaClO_4$ solution at the mercury height of 65 cm, with an open circuit. A saturated calomel electrode (SCE) with a large area was used as a reference electrode. All the free ligands we used gave no reduction wave. In order to prevent the precipitation of metal ions as hydroxides, the pH of the sample solutions were adjusted to 2.00 by adding $HClO_4$. The oxygen dissolved in the sample solution was removed by bubbling pure nitrogen gas through the solution.

Results

Polarographic Behavior of Pb^{2+} and Tl^{+} in Solutions Containing 4. Crown ligand **4** lowered the surface tension at the interface of a mercury-electrolyte solution, changing the electrocapillary curve considerably in the potential range from −0.30 to −1.40 V *vs.* SCE (Fig. 1).

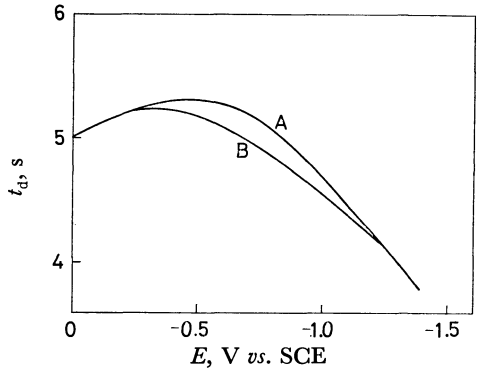

Fig. 1. Electrocapillary curves (A) without and (B) with **4** of 2.50×10^{-3} M at I=0.10 M (TEAP), pH=2.00.

The lowering was found to be independent of the solution pH and the nature of supporting electrolyte. Although no tensammetric wave was observed, the depression of the electrocapillary curve may be indicative of an adsorption of **4** at the mercury electrode surface. This was supported by the effect of the adsorbed **4** on the d.c. polarogram of cadmium(II) ion (Fig. 2). However, **4** had no depressing effect on the d.c. polarographic behavior of Pb^{2+} and Tl^{+} even at concentration above 50×10^{-3} M.

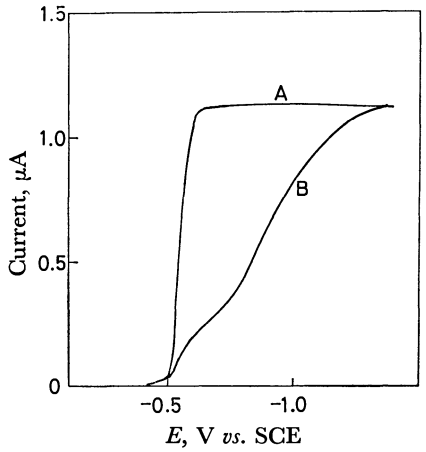

Fig. 2. Polarograms of Cd^{2+} (A) wthout and (B) with **4** of 21.8×10^{-3} M. I=0.10 M (TEAP) and pH=2.00.

The lead and thallium ions invariably gave single well-defined waves under the present experimental conditions. The plots of $\log(i/(i_1-i))$ *vs.* d.c. potential, E, gave straight lines with reciprocal slopes of −31—−32 mV and −58——61 mV for Pb^{2+} and Tl^{+}, respectively. Their limiting currents (i_1) were exactly proportional to their bulk concentrations and to the square root of the effective pressure on the dropping mercury electrode. Thus, the two electron reduction of Pb^{2+} and one electron reduction of Tl^{+} in the presence of **4** were polarographically defined to be reversible. The half-wave potential, $E_{1/2}$, and i_1 underwent little pH effect within the range 1.0—3.0. Complexation was demonstrated by the negative shift of $E_{1/2}$, $\Delta E_{1/2}$, upon increasing the ligand concentration, [**4**]. The slope in

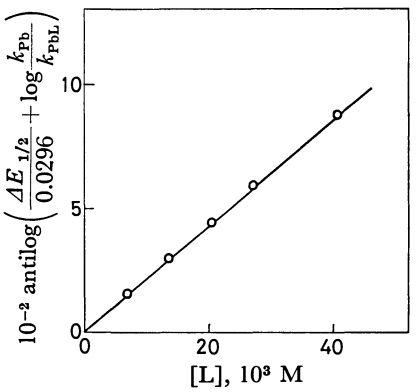

Fig. 3. Determination of the stability constant for Pb^{2+}-**4** complex. A plot of antilog $(\Delta E_{1/2}/0.0296+\log(k_{Pb}/k_{PbL}))$ *vs.* [**4**]. $[Pb^{2+}]=0.25\times10^{-3}$ M, I=0.10 M, pH=2.00, 25 °C.

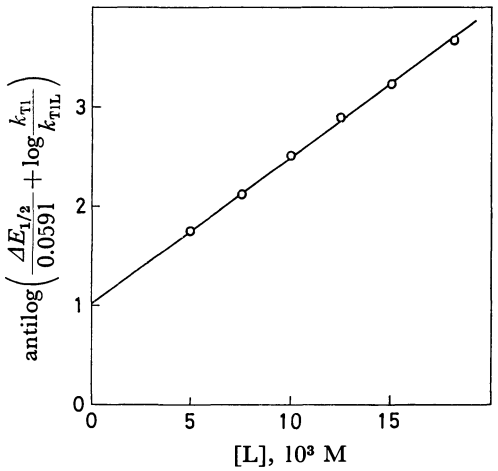

Fig. 4. Determination of the stability constant for Tl^{+}-**4** complex. A plot of antilog$(\Delta E_{1/2}/0.0591+\log(k_{Tl}/k_{TlL}))$ *vs.* [**4**]. $[Tl^{+}]=0.25\times10^{-3}$ M, I=0.10 M, pH=2.00, 25 °C.

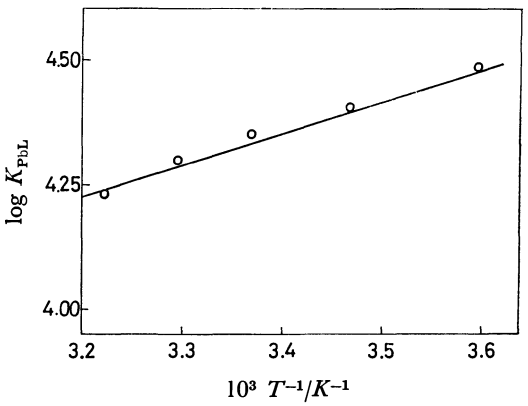

Fig. 5. Temperature dependence of the stability constant of Pb^{2+}-**4** complex.

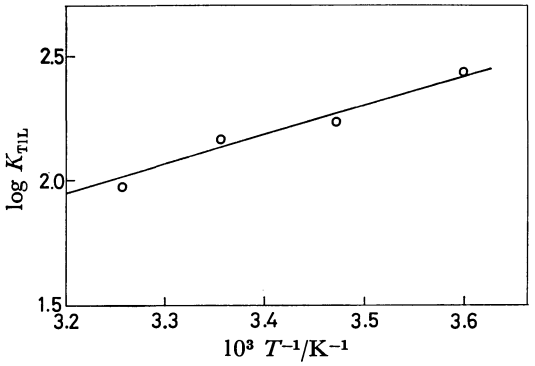

Fig. 6. Temperature dependence of the stability constant of Tl^{+}–**4** complex.

the linear relation between antilog($n\Delta E_{1/2}/0.0591 + \log(k_M/k_{ML})$) and [**4**] immediately allowed the estimation of the 1 : 1 complex stability constant for both metal ions, where logarithm of the diffusion current constant ratio, k_M/k_{ML}, was 0.06 for Pb^{2+} and 0.04 for Tl^{+} system (Figs. 3 and 4). Stability constants, K_{PbL} and K_{TlL}, were measured at various temperatures (5—35 °C) to estimate thermodynamic functions (Figs. 5 and 6). The results are summarized in Table 1.

Table 1. Stability constants (I=0.10 M. 25 °C) and thermodynamic functions

Complex	log K [a]	$-\Delta H$ [a] kcal mol^{-1}	ΔS [a] cal K^{-1} mol^{-1}
Pb^{2+}–(18-Crown-6)	4.4±0.1	3.1±0.2	9.7±1
Tl^{+}–(18-Crown-6)	2.2±0.1	5.4±0.3	−8.3±1
Pb^{2+}–Tetraglyme	0.5±0.1 (log β_1)	3.2±0.2	−8.3±1
Pb^{2+}–(Tetraglyme)$_2$	1.6±0.1 (log β_2)	6.4±0.3	−14.3±2

a) Uncertainties are the standard deviations.

Polarographic Behavior of Lead(II) in Tetraglyme **5** *Solution.* The solution containing Pb^{2+}, **5**, and 0.1 M TEAP also gave a reversible polarographic wave. As in the case of the cyclic ligand system, the increase in the concentration of **5**, [**5**], caused a negative shift of $E_{1/2}$. However, a plot of [antilog($\Delta E_{1/2}/0.0296 + \log(k_{Pb}/k_{PbL}) - 1$]/[**5**] instead of antilog($\Delta E_{1/2}/0.0296 + \log(k_{Pb}/k_{PbL})$) *vs.* [**5**] gave a straight line with an intercept of finite value (Fig. 7). The electrode reaction mechanism is thus written as

$$PbL^{2+} \rightleftharpoons Pb^{2+} + 2e^- + Hg \rightleftharpoons Pb(Hg)$$
$$\Big\Updownarrow$$
$$PbL_2^{2+}$$

and the shift of the half-wave potential is expressed in the form

$$\Delta E_{1/2} = 0.0296 \log (1 + K_{PbL}[5] + K_{PbL}K^*_{PbL_2}[5]^2) + 0.0296 \log \frac{k_{PbL}}{k_{Pb}}$$

where K_{PbL} and $K^*_{PbL_2}$ denote the first and second successive formation constants, respectively, of lead(II)-tetraglyme complex. From the intercept and slope of

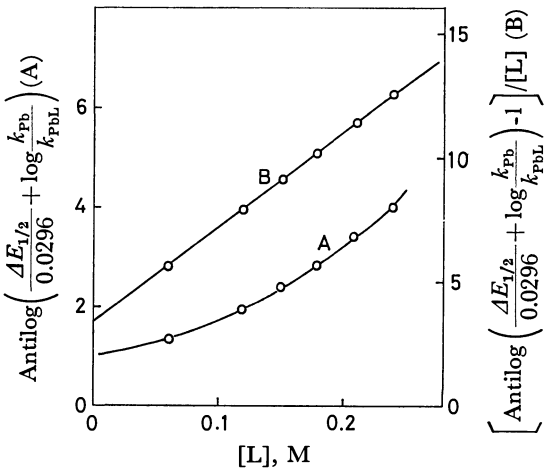

Fig. 7. Determination of the stability constants for Pb^{2+}–**5** complexes. Plots of [antilog($\Delta E_{1/2}/0.0296 + \log(k_{Pb}/k_{PbL})$) − 1]/[**5**] and antilog ($\Delta E_{1/2}/0.0296 + \log(k_{Pb}/k_{PbL})$) *vs.* [**5**]. [$Pb^{2+}$]=0.40×10^{-3} M, I=0.10 M, pH=2.00, 25 °C.

the above linear relation, $K_{PbL}(\beta_1)$ and $K_{PbL}K^*_{PbL_2}(\beta_2)$ values were determined. They were also measured at various temperatures (10—35 °C) in order to determine the thermodynamic parameters (Table 1 and Fig. 8). The polarography of Tl^{+} ion in the tetraglyme solution was also studied. However, little evidence indicating the complex formation was obtained.

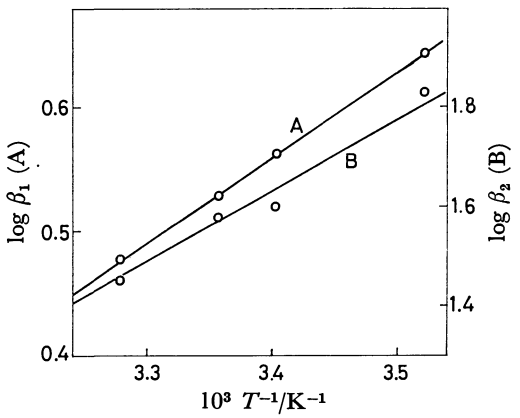

Fig. 8. Temperature dependence of stability constants for 1 : 1 (β_1) and 1 : 2 (β_2) Pb^{2+} -**5** complexes.

Discussion

Crown ether undergoes adsorption to the mercury electrode surface to block the electrochemical reactions of Cd^{2+}, but not of Pb^{2+} or Tl^{+}. This might be relevant in some way to the selective ion transport phenomena across cell membranes. The metal ions such as Pb^{2+} or Tl^{+} may pass through the artificial membrane of the 18-crown-6 in complex forms possibly by repeating dissociation and complexation before reaching the electrode surface. On the other hand, Cd^{2+} ion shows the low permeability probably because of its low affinity for **4**. We observed that the presence of **4** similarly hindered the reduction of transition metal ions like

Cu^{2+}, which is known to be incapable of forming stable complexes with **4**.[2b]

The agreement of the stability constant of $10^{4.4}$ for the 1:1 Pb^{2+}–**4** complex with those for Pb^{2+}–**1** or –**2** (log K 4—5) determined by Christensen *et al.*[2a] is noteworthy in view of the difference in side groups as well as in the methods. A comparison of the present Pb^{2+} data with those of the alkali earth metal ion[3] discloses a remarkable entropic effect contributing to the Pb^{2+} complex stability. The special affinity of the bicylic polyoxadiaza ligand, **6** (n=3), for Pb^{2+} over Ba^{2+} or Sr^{2+} is similarly accounted for by the greater entropic contribution.[12] Considering the fact that the dehydration of Pb^{2+} ion causes the least entropic increase among the three divalent metal ions,[4] the major contribution to the large positive ΔS value upon the Pb^{2+} complex formation might result from other sources.

The measurement for a linear polyoxy ligand, **5**, was conducted in the identical conditions. No complication took place as in the case of **4**. It was found that **5** forms a 1:1 and a 2:1 complex with Pb^{2+} in aqueous solution. The second successive stability constant ($K^*_{PbL_2}$) is greater than the first one. The large enthalpic gain due to small expenditure of energy for the dehydration of Pb^{2+}–**5** (1:1) complex outweighs the loss of entropy, making an overall free energy change for the additional ligation feasible.

Comparison of stability constants of 1:1 complexes for the linear (though short of one oxygen atom) and cyclic ligands allows the estimation of the macrocyclic effect of *ca.* 10^4-fold that is entirely accounted for by the favorable entropy contribution. The *macrocyclic effect* in the present case can be regarded as a synonym to *chelate effect.*

Thallium(I) ion forms with **4** a 1:1 complex having the stability constant of $10^{2.2}$ at I=0.10 and 25 °C. The high exothermicity exceeds the unfavorable entropy change. Unlike Pb^{2+} or smaller metal ions, Tl^+ is too large (2.8 Å diameter) to fit the macrocyclic cavity and has to lie above the plane of the six oxygen atoms, in analogy to Rb^+(2.9 Å).[18,19] Hence, the desolvation, a major factor contributing to positive entropy change upon complexation in some metal ions would not be sufficient for the ligand substitution of Tl^+_{aq}.

References

1) To whom correspondence should be addressed.
2) For reviews, see a) J. J. Christensen, D. J. Eatough, and R. M. Izatt, *Chem. Rev.*, **74**, 351 (1974); b) C. J. Pederson and H. K. Frensdorff, *Angew. Chem. Int. Ed.*, **11**, 16 (1972); c) D. Midgly, *Chem. Soc. Rev.*, **1975**, 549.
3) R. M. Izatt, D. P. Nelson, J. H. Rytting, B. L. Haymore, and J. J. Christensen, *J. Am. Chem. Soc.*, **93**, 1619 (1971).
4) D. L. Wright, J. H. Holloway, and C. N. Reiley, *Anal. Chem.*, **37**, 884 (1965).
5) H. K. Fresdorff, *J. Am. Chem. Soc.*, **93**, 600 (1971).
6) F. P. Hinz and D. W. Margerum, *J. Am. Chem. Soc.*, **96**, 4993 (1974).
7) F. P. Hinz and D. W. Margerum, *Inorg. Chem.*, **13**, 2941 (1974).
8) M. Kodama and E. Kimura, *J. Chem. Soc., Chem. Commun.*, **1975**, 891.
9) G. F. Smith and D. W. Margerum, *J. Chem. Soc., Chem. Commun.*, **1975**, 807.
10) M. Kodama and E. Kimura, *J. Chem. Soc., Chem. Commun.*, **1975**, 326.
11) M. Kodama and E. Kimura, *J. Chem. Soc., Dalton*, **1976**, 116.
12) G. Anderegg, *Helv. Chim. Acta*, **58**, 1218 (1975).
13) J. M. Lehn and J. P. Sauvage, *Chem. Commun.*, **1971**, 440.
14) J. M. Lehn and J. P. Sauvage, *J. Am. Chem. Soc.*, **97**, 6700 (1975).
15) V. M. Loyola, R. G. Wilkins, and R. Pizer, *J. Am. Chem. Soc.*, **97**, 7382 (1975).
16) T. Fujinaga, K. Izutsu, and K. Takaoka, *J. Electroanal. Chem.*, **12**, 203 (1966).
17) I. M. Kolthoff and J. J. Lingane, "Polarography," Vol. 1, Interscience Publishers, New York (1952), p. 297.
18) D. Bright and M. R. Truter, *Nature*, **225**, 176 (1970).
19) D. Bright and M. R. Truter, *J. Chem. Soc., B*, **1970**, 1544.

Binuclear Metal Complexes. XV.[1] Copper(II) and Nickel(II) Complexes of Binucleating Ligands Derived From 3-Formylsalicylic Acid and Diamines[2]

Mitsunori TANAKA, Michiyo KITAOKA, Hisashi OKAWA,*,** and Sigeo KIDA*

Faculty of Education, Kagawa University, Takamatsu, Kagawa 760

**Department of Chemistry, Faculty of Science, Kyushu University, Hakozaki, Higashi-ku, Fukuoka 812*

(Received March 29, 1976)

Copper(II) and nickel(II) complexes of the 3-formylsalicylic acid–diamine Schiff bases, H_4fsaen, H_4fsapn, H_4fsatn, H_4fsaph, and H_4fsach, where en, pn, tn, ph, and ch denote ethylenediamine, propylenediamine, trimethylenediamine, *o*-phenylenediamine, and 1,2-cyclohexanediamine respectively, have been obtained and characterized. Binuclear copper(II) complexes, Cu_2(fsaen)·$2H_2O$, Cu_2(fsapn)·$2H_2O$, Cu_2(fsatn)·$2H_2O$, Cu_2(fsaph)·H_2O, and Cu_2(fsach)·$2H_2O$, show a strong antiferromagnetic spin-exchange interaction between metal ions, $-2J$ values being more than 555 cm^{-1}. It was revealed that Ni_2(fsaen)·$3H_2O$, Ni_2(fsapn)·$3H_2O$, Ni_2(fsaph)·$5H_2O$, and Ni_2(fsach)·$3H_2O$ are novel binuclear complexes composed of one paramagnetic and one diamagnetic nickel(II) ions. On the other hand, Ni_2(fsatn)·$5H_2O$ is a binuclear complex of paramagnetic nickel(II) ions. Its magnetism obeys the Curie-Weiss law in the range from liquid nitrogen temperature to room temperature with the Weiss constant of −40 K.

In the previous papers of this series,[3,4] we have reported that 3-formylsalicylic acid and its Schiff bases with alkyl amines form binuclear copper(II) and nickel(II) complexes. In those complexes the phenolic oxygen operates as a bridging group, and the carboxylate oxygen and the formyl oxygen or imino nitrogen coordinate to metal ion. It is supposed that two organic moieties are constructed *trans* to each other (Fig. 1).

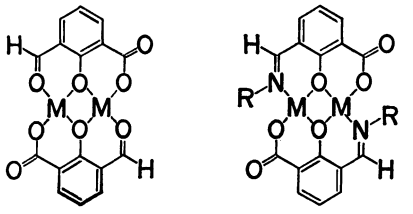

Fig. 1.

The Schiff bases derived from 3-formylsalicylic acid and diamines would form binuclear complexes bridged by the phenolic oxygens. One of the purposes of this study is synthesizing binuclear copper(II) complexes with these Schiff bases and investigating the spin-spin exchange interaction between copper(II) ions.

Geometrical requirement of the ligands results in the formation of a *cis*-configuration complex with respect to the imino nitrogens and the carboxylate oxygens. Therefore, the "inside" coordination site has N_2O_2-coordinating atoms, while the "outside" coordination site has O_4-coordinating atoms. Since there is a considerable difference in the ligand field strength between the "inside" and "outside" coordination spheres, the present ligands might form a binuclear nickel(II) complex composed of one paramagnetic and one diamagnetic metal ions. Synthesis of the binuclear nickel(II) complex of a novel spin-state is another purpose of this study.

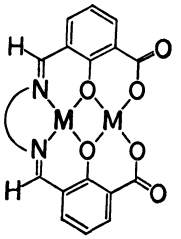

Fig. 2.

The 3-formylsalicylic acid–diamine Schiff bases utilized in this study are as follows: H_4 fsaen (Schiff base with ethylenediamine), H_4fsapn (propylenediamine), H_4fsatn (trimethylenediamine), H_4fsaph (*o*-phenylenediamine), and H_4fsach (1,2-cyclohexanediamine). The binuclear copper(II) and nickel(II) complexes with these ligands were synthesized and characterized on the basis of elemental analyses, infrared spectra, visible spectra, and magnetic measurements. The binuclear complexes are abbreviated as Cu_2(fsaen), Ni_2(fsapn), and so on. The mononuclear complexes, M(H_2fsaen)·$1/2H_2O$ and M(H_2fsapn)·$1/2H_2O$ (M=Cu(II) and Ni(II)), were also isolated and characterized.

Experimental

Syntheses. 3-Formylsalicylic acid was prepared after the method of Duff and Bills.[5] The synthetic procedures of the complexes are the same in principle. Syntheses of Cu(H_2fsaen)·$1/2H_2O$, Cu_2(fsaen)·$2H_2O$, and Ni_2(fsaen)·$3H_2O$ are represented.

Cu_2(H_2fsaen)·$1/2H_2O$. 3-Formylsalicylic acid (136 mg) was dissolved in an aqueous solution (30 ml) of sodium carbonate (55 mg), and then ethylenediamine (30 mg) was added. To this hot solution was added an aqueous solution (10 ml) of copper(II) acetate monohydrate (100 mg). Soon purple needles separated. After the reaction mixture was warmed at 60°C for a while, the product was isolated, washed with hot water and dried under reduced pressure.

Cu_2(fsaen)·$2H_2O$. An aqueous solution (30 ml) containing 3-formylsalicylic acid (136 mg), ethylenediamine (30 mg) and sodium carbonate (55 mg) was warmed at *ca.* 60°C

** To whom correspondence may be addressed.

TABLE 1. ELEMENTAL ANALYSES OF COMPLEXES

Complex[a]	Found (%)				Calcd (%)			
	C	H	N	M	C	H	N	M
$Cu(H_2fsaen)\cdot 1/2H_2O$	50.85	3.38	6.65	14.92	50.65	3.54	6.56	14.89
$Cu(H_2fsapn)\cdot 1/2H_2O$	52.00	3.67	6.37	14.71	51.76	3.89	6.35	14.41
$Ni(H_2fsaen)\cdot 1/2H_2O$	51.45	3.52	6.89	13.57	51.22	3.58	6.64	13.91
$Ni(H_2fsapn)\cdot 1/2H_2O$	52.18	4.36	6.22	13.11	52.33	3.98	6.42	13.46
$Cu_2(fsaen)\cdot 2H_2O$	41.28	3.07	5.15	24.60	41.95	3.13	5.44	24.66
$Cu_2(fsapn)\cdot 2H_2O$	42.80	3.43	5.28	24.33	43.10	3.43	5.29	24.00
$Cu_2(fsatn)\cdot 2H_2O$	42.86	3.45	5.29	23.92	43.10	3.43	5.29	24.00
$Cu_2(fsaph)\cdot H_2O$	48.90	2.45	5.32	24.68	48.45	2.59	5.13	23.30
$Cu_2(fsach)\cdot 2H_2O$	46.54	3.72	4.56	21.94	46.40	3.89	4.92	22.32
$Ni_2(fsaen)\cdot 3H_2O$	40.98	3.34	5.26	22.15	41.28	3.46	5.35	22.42
$Ni_2(fsapn)\cdot 3H_2O$	42.48	3.81	5.12	22.08	42.44	3.75	5.21	21.83
$Ni_2(fsatn)\cdot 5H_2O$	39.37	4.01	4.83	20.26	39.77	4.22	4.88	20.32
$Ni_2(fsaph)\cdot 5H_2O$	43.17	3.79	4.45	19.01	43.48	3.65	4.61	19.32
$Ni_2(fsach)\cdot 3H_2O$	45.35	4.33	4.66	20.68	45.72	4.19	4.85	20.32

a) $fsaen^{4-}=C_{18}H_{12}N_2O_6$, $fsapn^{4-}=fsatn^{4-}=C_{19}H_{14}N_2O_6$, $fsaph^{4-}=C_{22}H_{10}N_2O_6$, and $fsach^{4-}=C_{22}H_{18}N_2O_6$.

and to this mixture was added an aqueous solution (15 ml) of copper(II) acetate monohydrate (200 mg). This was heated at 60°C for 30 min and yellowish brown prisms which separated were collected, washed with hot water and dried under reduced pressure.

$Ni_2(fsaen)\cdot 3H_2O$. To a warm aqueous solution (30 ml) of 3-formylsalicylic acid (136 mg), ethylenediamine (30 mg) and sodium carbonate (55 mg), an aqueous solution (15 ml) of nickel(II) acetate tetrahydrate (250 mg) was added. The mixture was maintained at this temperature for 1 h. Red prisms which separated were collected, thoroughly washed with hot water, and dried under reduced pressure.

Elemental analyses of the mononuclear and binuclear metal complexes are given in Table 1.

Measurements. Infrared spectra were measured with a Hitachi 215 grating infrared spectrometer on a KBr disk. Reflectance spectra were recorded with a Shimadzu multipurpose spectrophotometer Model MPS-5000. Magnetic susceptibilities were measured by the Faraday method from liquid nitrogen temperature to room temperature. Diamagnetic correction was done using the Pascal constants.[6] Effective magnetic moment was calculated by the equation, $\mu_{eff}=2.828\sqrt{(\chi_A-N\alpha)T}$. The temperature-independent paramagnetism, $N\alpha$, for a paramagnetic nickel(II) ion is estimated at 193×10^{-6} e.m.u./mol.[7]

Results and Discussion

Mononuclear Complexes. Color and physical properties for the mononuclear complexes are tabulated in Table 2. The infrared absorption bands at 1725—1705 and at 1645—1635 cm^{-1} are tentatively assigned to the

TABLE 2. COLOR, SPECTRAL DATA, AND MAGNETIC MOMENTS OF MONONUCLEAR COMPLEXES

Complex	Color	Infrared (cm^{-1})		Visible (cm^{-1})	μ_{eff} (T(K)) (B.M.)
		C=O	C=N		
$Cu(H_2fsaen)\cdot 1/2H_2O$	purple	1705	1645	18100	1.85 (294.3)
$Cu(H_2fsapn)\cdot 1/2H_2O$	purple	1705	1645	18200	1.84 (292.9)
$Ni(H_2fsaen)\cdot 1/2H_2O$	yellow	1725	1635	18500	diamag.
$Ni(H_2fsapn)\cdot 1/2H_2O$	orange	1720	1635	18600	diamag.

C=O stretching vibration of free carboxyl group and the coordinated azomethin group respectively. The ligand field band for $Cu(H_2fsaen)\cdot 1/2H_2O$ and for $Cu(H_2fsapn)\cdot 1/2H_2O$ well corresponds to the band for *N,N'*-disalicylideneethylenediaminatocopper(II)[8-10] and for *N, N'*-disalicylidenepropylenediaminatocopper(II)[10,11] respectively. The room temperature magnetic moment for $Cu(H_2fsaen)\cdot 1/2H_2O$ and for $Cu(H_2fsapn)\cdot 1/2H_2O$ also is substantially equal to 1.84 B.M.[12] for *N,N'*-disalicylideneethylenediaminatocopper(II) and 1.81 B.M.[12] for *N,N'*-disalicylidenepropylenediaminatocopper(II) respectively. These facts imply that each of the present complexes has a similar structure to the corresponding *N,N'*-disalicylidenealkylenediaminatocopper-(II) complex.

It is clear that $Ni(H_2fsaen)\cdot 1/2H_2O$ and $Ni(H_2fsapn)\cdot$

TABLE 3. COLOR, SPECTRAL DATA AND MAGNETIC MOMENTS OF BINUCLEAR COPPER(II) COMPLEXES

Complex	Color	Infrared (cm^{-1})		Visible (cm^{-1})		$\mu_{eff}(T(K))$ (B.M.)
		C=O	C=N			
$Cu_2(fsaen)\cdot 2H_2O$	yellowish brown	1565	1640	13400	18200	0.76(295.4)
$Cu_2(fsapn)\cdot 2H_2O$	yellowish brown	1560	1630	13000	18000	0.85(299.0)
$Cu_2(fsatn)\cdot 2H_2O$	blue	1580	1630	14600	17500	0.68(295.4)
$Cu_2(fsaph)\cdot H_2O$	brown	1550	1620	15000	18000	0.89(296.7)
$Cu_2(fsach)\cdot 2H_2O$	yellowish brown	1560	1635	15100	17400	1.03(298.4)

$1/2H_2O$ have a planar configuration, since they are diamagnetic and their reflectance spectra possess only one ligand field band around 18500 cm^{-1}, which corresponds to the band for *N,N'*-disalicylideneethylenediaminatonickel(II)[10] and *N,N'*-disalicylidenepropylenediaminatonickel(II).[10]

Binuclear Copper(II) Complexes. In Table 3 color, infrared and visible absorption bands, and effective magnetic moments for the binuclear copper(II) complexes are given. No absorption band was found in the region 1750—1650 cm^{-1}. Instead a broad and strong band was found around 1550—1580 cm^{-1}. In general the $\nu_{C=O}$ mode of carboxyl shifts to lower frequency by coordination.[13] In the case of binuclear complexes of 3-formylsalicylic acid[3] and its Schiff bases,[4] the C=O stretching vibration was found around 1550 cm^{-1}. Therefore it seems reasonable to assign the band at 1580—1550 cm^{-1} to the coordinated carboxylate group.

The reflectance spectra of the complexes show two bands in the visible region. The second (higher energy) band for $Cu_2(fsaen)\cdot 2H_2O$ and for $Cu_2(fsapn)\cdot 2H_2O$ is well in accordance with the band for $Cu(H_2fsaen)\cdot 1/2H_2O$ and for $Cu(H_2fsapn)\cdot 1/2H_2O$, respectively. The position of the second band for $Cu_2(fsaph)\cdot H_2O$ is practically equal to that of the band (17900 cm^{-1}) for *N, N'*-disalicylidene-*o*-phenylenediaminatocopper(II).[10,12] Therefore, the second band was tentatively assigned to the "inside" copper(II) (CuN_2O_2-chromophor). The band at 17500 cm^{-1} for $Cu_2(fsatn)\cdot 2H_2O$ is considerably higher in energy compared with 16600 cm^{-1} [10] for *N,N'*-disalicylidenetrimethylenediaminatocopper(II). Sinn *et al.*[12,14] have found that dichloro[*N,N'*-disalicylidenetrimethylenediaminatocopper(II)]copper(II) and dichloro[*N, N'*-disalicylidenetrimethylenediaminatocopper(II)]zinc(II) have a d-d band at 17100 cm^{-1}. This fact implies that the coplanarity of the plane in *N,N'*-disalicylidenetrimethylenediaminatocopper(II) is enhanced on forming a binuclear complex bridged by the phenolic oxygen.[12,14] Therefore the band at 17500 cm^{-1} of $Cu_2(fsatn)\cdot 2H_2O$ is attributed to the $[CuN_2O_2]$-chromophor. On the other hand, the first (lower energy) band is tentatively assigned to the "outside" copper(II) ion. It is not clear if a water molecule coordinates to the "outside" copper from an apical direction.

Sub-normal magnetic moments of the complexes at room temperature suggest a partial spin-pairing between copper(II) ions. The magnetic susceptibility was measured at various temperatures (77.4—300 K). The results are shown in Fig. 3. The magnetisms were well interpreted in terms of the Bleaney-Bowers equation,[15]

$$\chi_A = \frac{Ng^2\beta^2}{3kT}\left[1+\frac{1}{3}\exp(-2J/kT)\right]^{-1} + N\alpha,$$

where J is the exchange integral, k the Boltzmann constant, N the Avogadro number, β the Bohr magneton, and g the Lande *g*-factor. The magnetic parameters, $-2J$, g, and $N\alpha$, obtained from the best fit of the experimental values to the theoretical values are given in Table 4.

It is well known[12,14,16,17] that the copper(II) complexes with the tetradentate Schiff bases of salicylaldehyde form binuclear copper(II) complexes bridged by the phenolic oxygens when treated with copper(II) chloride or copper(II) bromide. The magnetic properties of these complexes have been elucidated by Sinn *et al.*,[16] and the $-2J$ values, the energy separation between the singlet and triplet states, are evaluated at 98—472 cm^{-1}. It is apparent that the present complexes exhibit a stronger antiferromagnetic spin-exchange interaction compared with dihalogeno[*N,N'*-disalicylidenealkylenediaminatocopper(II)]copper(II) complexes. In these complexes it seems that the steric hindrance between the halogen and the hydrogen attached to the 3-position (next to the phenolic oxygen) of the aromatic ring is sufficiently large to deform the (X=halogen) plane to a pseudotetrahedral geometry.[16,18] In fact it was demonstrated from X-ray analysis[19] that the "outside" configuration of dichloro-[*N, N'*-disalicylideneethylenediaminatocopper(II)]copper(II) is pseudotetrahedral. On the other hand, no steric hindrance is expected in our complexes, since the carboxyl group attached to the 3-position of the salicylaldehyde moiety takes part in coordination. Thus

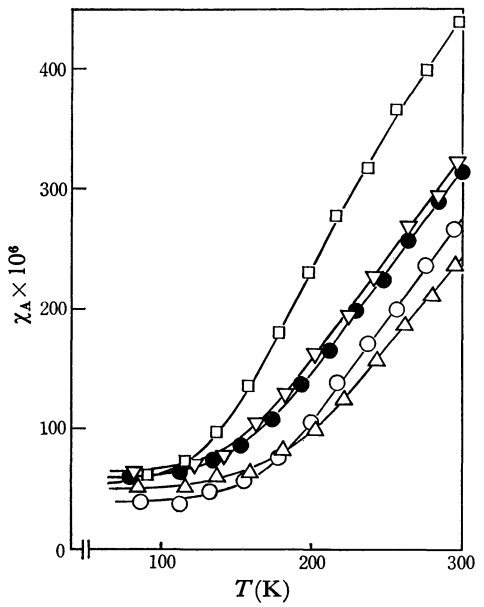

Fig. 3. Temperature variation of magnetic susceptibility of (○)$Cu_2(fsaen)\cdot 2H_2O$, (●)$Cu_2(fsapn)\cdot 2H_2O$, (△)$Cu_2(fsatn)\cdot 2H_2O$, (▽)$Cu_2(fsaph)\cdot H_2O$, and (□)$Cu_2(fsach)\cdot 2H_2O$.

Table 4. Magnetic parameters, $-2J$, g, and $N\alpha$, for binuclear copper(II) complexes

Complex	$-2J$ (cm^{-1})	g	$N\alpha\times 10^6$ (c.g.s./mol)
$Cu_2(fsaen)\cdot 2H_2O$	660	2.20	40
$Cu_2(fsapn)\cdot 2H_2O$	655	2.20	60
$Cu_2(fsatn)\cdot 2H_2O$	720	2.20	50
$Cu_2(fsaph)\cdot H_2O$	650	2.20	65
$Cu_2(fsach)\cdot 2H_2O$	555	2.20	55

TABLE 5. COLOR, SPECTRAL DATA, AND MAGNETIC MOMENTS OF BINUCLEAR NICKEL(II) COMPLEXES

Complex	Color	Infrared (cm^{-1}) C=O	C=N	Visible (cm^{-1})			$\mu_{eff}(T(K))^{a)}$ (B.M.)
$Ni_2(fsaen)\cdot 3H_2O$	red	1555	1623	9400	16000	18300	2.17(295.3) [3.14]
$Ni_2(fsapn)\cdot 3H_2O$	orange	1555	1625	9600	15000	18700	2.27(299.0) [3.23]
$Ni_2(fsatn)\cdot 5H_2O$	blue	1560	1635	8200 14500	9700 17100	12400	3.36(298.3)
$Ni_2(fsaph)\cdot 5H_2O$	reddish orange	1550	1620	9500	15500	18500	2.33(296.6) [3.28]
$Ni_2(fsach)\cdot 3H_2O$	orange	1555	1625	9100	14800	18500	2.25(294.8) [3.21]

a) Magnetic moment per nickel(II) ion. The value in a bracket is calculated on the assumption that one of nickel(II) ions is diamagnetic.

the configuration of the "outside" copper $\begin{pmatrix} O & O \\ & Cu \\ O & O \end{pmatrix}$ is substantially planar and two tetragonal planes of the "inside" and "outside" copper(II) ions form a coplane. Thereby the spin exchange between the metal ions may be efficiently caused by a super-exchange mechanism through the oxygen P_π-orbitals.[20]

Binuclear Nickel(II) Complexes. The infrared spectra of the binuclear nickel(II) complexes are similar to those of the corresponding copper(II) complexes. Each reflectance spectrum of $Ni_2(fsaen)\cdot 3H_2O$, $Ni_2(fsapn)\cdot 3H_2O$, $Ni_2(fsaph)\cdot 5H_2O$, and $Ni_2(fsach)\cdot 3H_2O$ has three d-d bands in visible region. The band around 18500 cm^{-1} seems to correspond to the band for the mononuclear nickel(II) complexes. The bands around 9500 and 15500 cm^{-1} imply that these complexes contain a nickel(II) of octahedral configuration. Accordingly, the coordination of water from apical positions was supposed for the "outside" nickel. The bands around 9500 and 15500 cm^{-1} were assigned to the $^3T_{2g}\leftarrow{}^3A_{2g}$ and $^3T_{1g}\leftarrow{}^3A_{2g}$ transitions respectively. Since the 10 Dq for hexaaquonickel(II) is estimated at 8500 cm^{-1},[21] the ligand field in the present complexes is stronger than H_2O.

The magnetic moments calculated per one nickel(II) ion are much lower than the spin-only value 2.83 B.M. This may be explained by (a) antiferromagnetic spin-pairing between paramagnetic nickel(II) ions or (b) formation of binuclear complex containing one paramagnetic and one diamagnetic nickel(II) ions. The visible spectra of the complexes seem to support the latter possibility. In order to obtain further evidence magnetic susceptibility was measured at various temperatures. In Fig. 4, $1/(\chi_A - N\alpha)$ is plotted against temperature. As is seen in Fig. 4 the magnetisms of the complexes are well interpreted in terms of the Curie-Weiss law ($\chi_A = C/(T-\theta)$). It should be noted that the Weiss constants are very small (at best 4 K). The phenolic oxygen-briged binuclear nickel(II) complexes so far reported obey the Curie-Weiss law in the range from liquid nitrogen temperature to room temperature with a relatively large Weiss constant more than 30 K.[3,4,22,23] Accordingly it is concluded that $Ni_2(fsaen)\cdot 3H_2O$, $Ni_2(fsapn)\cdot 3H_2O$, $Ni_2(fsaph)\cdot 5H_2O$, and

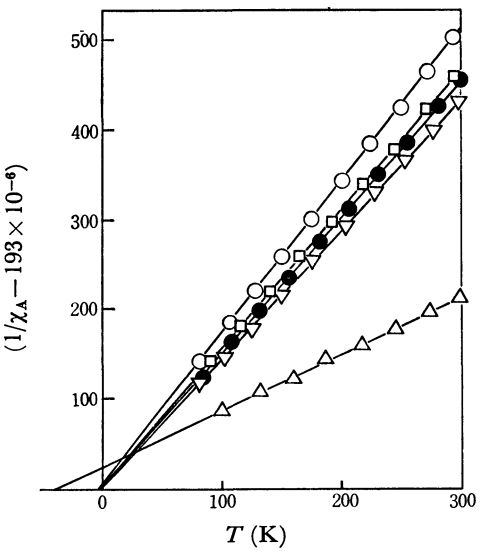

Fig 4. Plots of inverse susceptibilities as a function of temperature for (○)$Ni_2(fsaen)\cdot 3H_2O$, (●)$Ni_2(fsapn)\cdot 3H_2O$, (△)$Ni(fsatn)\cdot 5H_2O$, (▽)$Ni_2(fsaph)\cdot 5H_2O$, and (□)$Ni_2(fsach)\cdot 3H_2O$ per a nickel atom.

$Ni_2(fsach)\cdot 3H_2O$ are novel complexes composed of one paramagnetic and one diamagnetic nickel(II) ions. Thus, magnetic moments per binuclear units were calculated to give 3.14—3.28 B.M., which are quite common to a nickel(II) in an octahedral environment.

Paramagnetic-diamagnetic binuclear nickel(II) complexes are rare.[22] The success in synthesizing paramagnetic-diamagnetic binuclear nickel(II) complexes with the present ligands is obviously cocerned with a considerable difference in the ligand field strength between the "inside" and "outside" coordination sites. The coordinatively selective property of the ligands also leads to the formation of the copper(II)-paramagnetic nickel(II) complex (CuNi(fsaen))[24] and other hetero-metal binuclear complexes.[25] The Schiff bases derived from 1,3,5-triketones and diamines,[26-29] which are similar in coordinating mode to our ligands, should form paramagnetic-diamagnetic binuclear nickel(II) complexes.

The color and the visible spectrum of $Ni_2(fsatn)\cdot$

$5H_2O$ are markedly different from other nickel(II) complexes. It is known that *N,N'*-disalicylidenetrimethylenediaminatonickel(II) maintains a planar structure.[10,30] However its d-d band is fairly low in energy, demonstrating a weaker ligand field of the ligand with a 6-6-6 condensed ring system compared with the tetradentate salicylaldehyde-Schiff bases with a 6-5-6 condensed ring system. The binuclear nickel(II) complex of the macrocycle obtained from 2-hydroxy-5-methylisophthalaldehyde and 1,3-propanediamine (nickel(II) ions are bridged by the phenolic oxygens) is known to have a high-spin state, where the nickel is coordinated with chloride ion in the apical position.[23] From this fact it is likely that the "inside" ligand field strength of H_4fsatn decreases to allow the fifth (and the sixth) coordination from an apical position when the phenolic oxygen operates as a bridge. The room temperature magnetic moment of Ni_2(fsatn)·$5H_2O$ is 3.36 B.M. per one nickel(II) ion. The magnetic moment decreases with lowering of temperature to 2.97 B.M. at 87.5 K. The $1/(\chi_A - N\alpha)$ plots against temperature obey the Curie-Weiss law with the large Weiss constant −40 K. This value is quite comparable to those (−35—−41 K) found for the binuclear nickel(II) complexes of 3-formylsalicylic acid–monoamine Schiff bases.[4] Thus it is evident that Ni_2(fsatn)·$5H_2O$ is a binuclear complex composed of two paramagnetic nickel(II) ions.

The authors are grateful to the Ministry of Education for a Scientific Research Grant-in-Aid.

References

1) Part XIV: M. Tanaka, H. Okawa, R. Miyashita, and S. Kida, *Chem. Lett.*, **1974**, 1401.
2) Presented at the Meeting of Chugoku-Shikoku and Kyushu Branches of Chem. Soc. of Japan, Tottori, November, 1975.
3) M. Tanaka, H. Okawa, I. Hanaoka, and S. Kida, *Chem. Lett.*, **1974**, 71.
4) M. Tanaka, H. Okawa, T. Tamura, and S. Kida, *Bull. Chem. Soc. Jpn.*, **47**, 1669 (1974).
5) J. C. Duff and E. J. Bills, *J. Chem. Soc.*, **1932**, 1987.
6) Earnshaw, "Introduction to Magnetochemistry," Academic Press, London (1968), pp. 5, 6.
7) C. J. Ballhausen, "Introduction to Ligand Field Theory," McGraw-Hill, Inc. (1962), p. 142.
8) S. M. Grawford, *Spectrochim. Acta*, **19**, 255 (1963).
9) R. Belford and T. Piper, *Mol. Phys.*, **5**, 251 (1962).
10) R. H. Holm, *J. Am. Chem. Soc.*, **82**, 5632 (1960).
11) R. S. Dawning and F. L. Urbach, *J. Am. Chem. Soc.*, **91**, 5977 (1969).
12) S. J. Gruber, C. M. Harris, and E. Sinn, *J. Inorg. Nucl. Chem.*, **30**, 1805 (1968).
13) K. Nakamoto, "Infrared Spectra of Inorganic and Coordination Compounds," 2nd ed., John-Wiley & Sons, Inc. (1970), p. 232.
14) S. J. Gruber, C. M. Harris, and E. Sinn, *Inorg. Nucl. Chem. Lett.*, **4**, 107 (1968).
15) B. Bleaney and K. D. Bowers, *Proc. R. Soc. London, Ser. A*, **214**, 451 (1952).
16) S. J. Gruber, C. M. Harris, and E. Sinn, *Inorg. Chem.*, **7**, 268 (1968); *J. Inorg. Nucl. Chem.*, **30**, 1805 (1968).
17) M. Kato, Y. Muto, H. B. Janassen, K. Imai, and T. Tokii, *Bull. Chem. Soc. Jpn.*, **43**, 1066 (1970).
18) C. M. Harris, H. R. H. Patil, and E. Sinn, *Inorg. Chem.*, **6**, 1102 (1967).
19) C. A. Bear, J. M. Waters, and T. N. Waters, *Chem. Commun.*, **1971**, 703.
20) S. Kida, Y. Nishida, and M. Sakamoto, *Bull. Chem. Soc. Jpn.*, **46**, 2428 (1973).
21) C. K. Jørgensen, *Acta Chem. Scand.*, **9**, 1362 (1955); **10**, 887 (1956).
22) H. Okawa, T. Tokii, Y. Muto, and S. Kida, *Bull. Chem. Soc. Jpn.*, **46**, 2464 (1973).
23) N. F. Pilkington and R. Robson, *Aust. J. Chem.*, **23**, 2225 (1970).
24) H. Okawa, M. Tanaka, and S. Kida, *Chem. Lett.*, **1974**, 987.
25) H. Okawa, Y. Nishida, M. Tanaka, and S. Kida, Presented at the 24th Symposium of Coordination Chemistry, Kanazawa, October, 1974.
26) F. Sagara, K. Kobayashi, and K. Ueno, *Bull. Chem. Soc. Jpn.*, **45**, 900 (1972).
27) R. L. Lintvedt, L. L. Borer, D. P. Murtha, J. M. Kuszaj, and M. D. Glick, *J. Am. Chem. Soc.*, **97**, 2925 (1975).
28) B. Tomlonovic, R. L. Hough, M. D. Glick, and R. L. Lintvedt, *J. Am. Chem. Soc.*, **97**, 2925 (1975).
29) D. E. Fenton and S. E. Gayda, *Inorg. Chim. Acta*, **14**, L11 (1975).
30) W. C. Hoyt and G. W. Everett, Jr., *Inorg. Chem.*, **8**, 2013 (1969).

The Mechanism of the Hydrolysis of Condensed Phosphates. IV. The Hydrolysis of Pyro-, Tripoly-, Trimeta-, and Tetrametaphosphates in Aqueous Organic Solvents

Makoto WATANABE, Shoji SATO, and Hajime SAITO*

Department of Industrial Chemistry, Chubu Institute of Technology, Matsumoto-cho, Kasugai-shi, Aichi 487
**Department of Applied Chemistry, Faculty of Engineering, Nagoya University, Chigusa-ku, Nagoya 464*

(Received April 15, 1976)

The hydrolysis of sodium pyro-, tripoly-, trimeta-, and tetrametaphosphates was run in water, aqueous ethanol, aqueous glycerol, aqueous acetonitrile, aqueous dimethyl sulfoxide, and aqueous tetrahydrofuran at various pH values and temperatures. The initial concentration of the phosphates was 0.025 mol/l. The hydrolysis of the poly- and metaphosphates followed first-order kinetics with respect to the concentration of the phosphate, under all conditions studied. The hydrolysis of sodium pyro- and tripolyphosphates was an acid-catalyzed reaction and that of sodium trimeta- and tetrametaphosphates was an acid- and base-catalyzed reaction. In acidic solutions, the rate of hydrolysis of the poly- and metaphosphates in water was slower than that in any aqueous organic solution. It is concluded that the nucleophilicity of the water molecule in the aqueous organic solutions may increase on account of the interaction of the water molecule with the organic molecules. The hydrolysis of sodium pyro-, tripoly-, trimeta-, and tetrametaphosphates in acidic solutions is considered to be of the S_N2 type, because the overall-reaction rate is highly dependent on the nucleophilicity of the water molecule. The solvent effect on the rate of hydrolysis of sodium tripolyphosphate in basic solutions was the same as that in acidic solutions and hence the mechanism of the hydrolysis of sodium tripolyphosphate in basic solutions may be the same as that in acidic solutions. The rate of hydrolysis of sodium trimeta- and tetrametaphosphates in a basic water solvent was much faster than that in basic aqueous ethanol and basic aqueous dimethyl sulfoxide and was largely slower than that in basic aqueous glycerol. Consequently, the mechanism of the hydrolysis of sodium trimeta- and tetrametaphosphates in basic solutions seems to differ from that in acidic solutions. The acceleration of the rate of hydrolysis of the metaphosphates by the organic molecules depends significantly upon the activation energy. The activation energy of the hydrolysis of sodium pyro-, tripoly-, trimeta-, and tetrametaphosphates was 17—34 kcal/mol in the pH range of 1.0—12.2 and increased with an increase in the pH value of the phosphate solution in water and aqueous ethyl alcohol solvents.

The tetrahedral phosphorus atom of organic compounds having a P=O bond is sensitive for nucleophilic attack.[1] Wieker and Thilo proposed the same mechanism for the hydrolysis of long-chain polyphosphate by examining the catalytic effect of metal cations on the hydrolytic polyphosphate degradation.[2] In previous papers by the authors,[3,4] the solvent effect on the rate of hydrolysis of sodium pyro-, tripoly-, trimeta-, and tetrametaphosphates was examined by running the hydrolysis in water, aqueous dioxane, aqueous formic acid, and aqueous acetic acid. According to the results, the hydrolysis of sodium pyro- and tripolyphosphates at any pH value and that of sodium trimeta- and tetrametaphosphates in acidic solutions were considered to be S_N2 reactions. The types of solvents used in our previous experiments were not numerous. Therefore, in the present paper, the solvent effect on the rate of hydrolysis of sodium pyro-, tripoly-, trimeta-, and tetrametaphosphates is examined by using aqueous ethanol, aqueous glycerol, aqueous acetonitrile, aqueous dimethyl sulfoxide, and aqueous tetrahydrofuran as solvents. Ethanol and glycerol are protic solvents and acetonitrile, dimethyl sulfoxide, and tetrahydrofuran are dipolar aprotic solvents. The hydrogen atom of the OH-group contained in the first group can form a hydrogen bond with the oxygen atom of a water molecule and the oxygen or the nitrogen atom present in the second group can form a hydrogen bond with the hydrogen atom of a water molecule.

Experimental

Materials and Procedure. All the materials except sodium tripoly-, trimeta-, and tetrametaphosphates were of a commercial grade. Sodium tripoly-, trimeta-, and tetrametaphosphates were produced by the method described in Refs. 5 and 6. The solvents used in this experiment and their dielectric constants are listed in Table 1. The dielectric constants were measured by using an Ando Denki TR-1C VHF material characteristics test assembly. The initial concentration of sodium pyro-, tripoly-, trimeta-, and tetrametaphosphates was 0.025 mol/l. This concentration is suitable for analysis. pH control of the phosphate solutions was made by the same method as that described in previous papers by the authors by using nitric acid and aqueous tetramethyl ammonium hydroxide.[3,4] The pH adjustment was made to within ± 0.1 unit of the desired pH value. The pH change of

TABLE 1. SOLVENTS USED FOR THE HYDROLYSIS OF PYRO-, TRIPOLY-, TRIMETA-, AND TETRAMETAPHOSPHATES AND THEIR DIELECTRIC CONSTANTS

Solvent	Dielectric constant	Symbol
Water		S_1
25 vol% aqueous ethanol	63	S_2
20 vol% aqueous ethanol	65	S_3
35 vol% aqueous glycerol	64	S_4
30 vol% aqueous acetonitrile	69	S_5
25 vol% aqueous dimethyl sulfoxide	73	S_6
20 vol% aqueous dimethyl sulfoxide	73	S_7
25 vol% aqueous tetrahydrofuran	59	S_8
20 vol% aqueous tetrahydrofuran	65	S_9

the phosphate solution of the S_5 solvent in basic media with the elapse of reaction time was very large and it was difficult to maintain the pH of the solution to within ± 0.1 unit of the desired pH value. Therefore, the hydrolysis of the phosphates in the S_5 solvent was not run in basic media. The reaction temperature was maintained at 30, 50, or 70 ± 0.05 °C by using a thermostat. The separation and determination of the phosphate species in the sample solution were carried out by using the same method as described in previous papers.[3,4] However, the separation of the hydrolysis products of trimeta- and tetrametaphosphates for all alkaline solutions was not good, and hence, after the basic sample solutions were acidified with nitric acid, the acidified solutions were spotted on filter papers. For the hydrolysis of sodium trimeta- and tetrametaphosphates in the S_4 solvent, 1 ml of a saturated aqueous sodium chloride solution was added to 10 ml of the sample solution and then the separation of the phosphate species in the solution was carried out by using one-dimensional paper chromatography. Since the boiling point of tetrahydrofuran is 65 °C, the hydrolysis of the phosphates in the S_8 and S_9 solvents was not run at 70 °C.

Results and Discussion

Order of the Reactions and the pH Dependence of the Reaction Rates. The hydrolysis of sodium pyro-, tripoly-, trimeta-, and tetrametaphosphates obeyed first-order kinetics with respect to the concentration of the phosphate under the conditions studied. The rate constants of the hydrolysis of the phosphates are listed in Tables 2—5. In all the solvents used in this experiment, the rate of hydrolysis of the short-chain polyphosphates (pyro- and tripolyphosphates) decreases with an increase in the pH of the solution and this tendency is the same as that found in previous experiments.[3,7] Since the hydrolytic degradation of pyrophosphate is very slow in a basic solution and the measurement of the rate of hydrolysis of pyrophosphate in basic media is difficult, only the hydrolysis of tripolyphosphate was run in basic solutions. As Tables 2 and 3 show, the hydrolysis of the short-chain polyphosphates is an acid-catalyzed reaction in all solvents. In the case of the hydrolysis of the small-ring metaphosphates (trimeta- and tetrametaphosphates), the rate of hydrolysis of the small-ring metaphosphates decreases in acidic solutions and increases in basic solutions with an increase in the pH value for all solvents.[8] Therefore, the hydrolysis of

Table 2. Rate constants (min^{-1}) for the hydrolysis of pyrophosphate

pH	Solvent[a]	Reaction temp (°C) 30	50	70
1.0	S_1	8.50×10^{-5}	7.40×10^{-4}	4.70×10^{-3}
	S_2	1.42×10^{-4}	9.19×10^{-4}	5.27×10^{-3}
	S_4	1.03×10^{-4}	7.90×10^{-4}	4.79×10^{-3}
	S_5	1.02×10^{-4}	7.70×10^{-4}	4.70×10^{-3}
	S_6	2.68×10^{-4}	1.62×10^{-3}	7.82×10^{-3}
	S_8	1.61×10^{-4}	1.09×10^{-3}	
2.0	S_1	7.89×10^{-6}	1.30×10^{-4}	1.55×10^{-3}
	S_2	1.03×10^{-5}	1.54×10^{-4}	1.62×10^{-3}
	S_4	7.92×10^{-6}	1.33×10^{-4}	1.57×10^{-3}
	S_5	8.94×10^{-6}	1.38×10^{-4}	1.58×10^{-3}
	S_6	1.93×10^{-5}	2.47×10^{-4}	2.24×10^{-3}
	S_8	1.09×10^{-5}	1.60×10^{-4}	

a) For the solvents, refer to Table 1.

Table 3. Rate constants (min^{-1}) for the hydrolysis of tripolyphosphate

pH	Solvent[a]	Reaction temp (°C) 30	50	70
1.0	S_1	7.48×10^{-4}	5.38×10^{-3}	2.94×10^{-2}
	S_3	9.03×10^{-4}	6.30×10^{-3}	3.64×10^{-2}
	S_4	7.98×10^{-4}	5.48×10^{-3}	3.07×10^{-2}
	S_5	8.05×10^{-4}	5.60×10^{-3}	2.97×10^{-2}
	S_7	1.55×10^{-3}	9.89×10^{-3}	4.80×10^{-2}
	S_9	9.30×10^{-4}	6.60×10^{-3}	
2.0	S_1	8.70×10^{-5}	8.29×10^{-4}	6.10×10^{-3}
	S_3	1.05×10^{-4}	9.81×10^{-4}	7.04×10^{-3}
	S_4	8.99×10^{-5}	8.53×10^{-4}	6.30×10^{-3}
	S_5	9.41×10^{-5}	8.80×10^{-4}	6.34×10^{-3}
	S_7	1.84×10^{-4}	1.57×10^{-3}	1.02×10^{-2}
	S_9	1.18×10^{-4}	1.05×10^{-3}	
8.0	S_1		9.82×10^{-6}	
	S_3		1.19×10^{-5}	
	S_4		1.17×10^{-5}	
	S_5		1.09×10^{-5}	
	S_7		1.46×10^{-5}	
	S_9		1.23×10^{-5}	
10.0	S_1		3.31×10^{-6}	
	S_3		3.91×10^{-6}	
	S_4		3.61×10^{-6}	
	S_5		3.52×10^{-6}	
	S_7		5.73×10^{-6}	
	S_9		4.00×10^{-6}	

a) For the solvents, refer to Table 1.

Table 4. Rate constants (min^{-1}) for the hydrolysis of trimetaphosphate

pH	Solvent[a]	Reaction temp (°C) 30	50	70
1.0	S_1	1.35×10^{-3}	1.13×10^{-2}	7.50×10^{-2}
	S_2	1.62×10^{-3}	1.38×10^{-2}	8.95×10^{-2}
	S_4	1.49×10^{-3}	1.25×10^{-2}	8.11×10^{-2}
	S_5	1.40×10^{-3}	1.20×10^{-2}	7.80×10^{-2}
	S_6	2.58×10^{-3}	2.07×10^{-2}	1.30×10^{-1}
	S_8	1.82×10^{-3}	1.52×10^{-2}	
2.0	S_1	6.28×19^{-5}	5.89×10^{-4}	4.37×10^{-3}
	S_2	8.20×10^{-5}	7.71×10^{-4}	5.64×10^{-3}
	S_4	7.35×10^{-5}	6.92×10^{-4}	5.07×10^{-3}
	S_5	6.95×10^{-5}	6.52×10^{-4}	4.85×10^{-3}
	S_6	1.30×10^{-4}	1.16×10^{-3}	8.55×10^{-3}
	S_8	8.89×10^{-5}	8.13×10^{-4}	
11.5	S_1	7.86×10^{-6}	1.31×10^{-4}	1.60×10^{-3}
	S_2	2.16×10^{-6}	4.53×10^{-5}	6.69×10^{-4}
	S_4	4.86×10^{-5}	6.30×10^{-4}	6.17×10^{-3}
	S_6	8.12×10^{-7}	1.97×10^{-5}	3.28×10^{-4}
12.2	S_1	5.72×10^{-5}	9.61×10^{-4}	1.17×10^{-2}
	S_2	1.90×10^{-5}	4.07×10^{-4}	6.19×10^{-3}
	S_4	2.47×10^{-4}	2.62×10^{-3}	2.44×10^{-2}
	S_6	1.18×10^{-5}	2.64×10^{-4}	4.15×10^{-3}

a) For the solvents, refer to Table 1.

Table 5. Rate constants (min^{-1}) for the hydrolysis of tetrametaphosphate

pH	Solvent[a]	Reaction temp (°C) 30	50	70
1.0	S_1	1.42×10^{-4}	1.54×10^{-3}	1.28×10^{-2}
	S_2	1.86×10^{-4}	1.98×10^{-3}	1.58×10^{-2}
	S_4	1.58×10^{-4}	1.69×10^{-3}	1.40×10^{-2}
	S_5	1.61×10^{-4}	1.70×10^{-3}	1.44×10^{-2}
	S_6	3.20×10^{-4}	3.16×10^{-3}	2.46×10^{-2}
	S_8	2.61×10^{-4}	2.73×10^{-3}	
2.0	S_1	1.00×10^{-5}	1.29×10^{-4}	1.21×10^{-3}
	S_2	1.63×10^{-5}	1.81×10^{-4}	1.51×10^{-3}
	S_4	1.27×10^{-5}	1.49×10^{-4}	1.27×10^{-3}
	S_5	1.22×10^{-5}	1.43×10^{-4}	1.29×10^{-3}
	S_6	3.07×10^{-5}	3.22×10^{-4}	2.53×10^{-3}
	S_8	1.80×10^{-5}	1.91×10^{-4}	
12.2	S_1	1.17×10^{-6}	3.33×10^{-5}	6.51×10^{-4}
	S_2	6.00×10^{-7}	1.73×10^{-5}	3.35×10^{-4}
	S_4	3.17×10^{-6}	6.13×10^{-5}	8.30×10^{-4}
	S_6	4.01×10^{-7}	1.25×10^{-5}	2.62×10^{-4}

a) For the solvents, refer to Table 1.

small-ring metaphosphates is an acid- and base-catalyzed reaction in all solvents, and this is also in good agreement with the results obtained for previous experiments.[4,7] In the course of the hydrolysis of sodium tetrametaphosphate in the acidic S_1–S_8 solvents and the basic S_2 and S_5–S_8 solvents, trimetaphosphate was detected on a paper chromatogram and the quantity of the trimetaphosphate was too small for an accurate determination. Otani, Miura, and Doi have reported that trimetaphosphate was detected as the intermediate of the hydrolytic degradation of tetrapolyphosphate in an acidic aqueous solution.[9] Tetrametaphosphate is hydrolyzed to tetrapolyphosphate in the first step of hydrolytic degradation,[10] and hence, the trimetaphosphate detected in this experiment from the hydrolysis of sodium tetrametaphosphate may be produced by the hydrolysis of the tetrapolyphosphate which is produced by the hydrolysis of tetrametaphosphate. Accordingly, it can be said that there is little difference in the hydrolytic processes for tetrametaphosphate in either the S_1 and S_4 solvents or in the S_2, S_5, S_6, and S_8 solvents. In order to obtain information concerning the mechanism of the hydrolysis of sodium pyro-, tripoly-, trimeta-, and tetrametaphosphates, the activation energy and log A

Table 6. Activation energies, ΔE_A (kcal/mol) and log A (A: frequency factor) for the hydrolysis of sodium pyrophosphate

Solvent[a]	pH=1.0 ΔE_A	log A	pH=2.0 ΔE_A	log A
S_1	20.8	10.9	27.3	14.6
S_2	19.1	9.9	26.0	13.8
S_4	19.7	10.2	27.3	14.6
S_5	19.6	10.1	27.0	14.4
S_6	17.2	8.8	24.4	12.9
S_8	18.6	9.6	26.2	13.9

a) For the solvents, refer to Table 1.

Table 7. Activation energies, ΔE_A (kcal/mol) and log A (A: frequency factor) for the hydrolysis of sodium tripolyphosphate

Solvent[a]	pH=1.0 ΔE_A	log A	pH=2.0 ΔE_A	log A
S_1	19.1	10.7	22.5	12.1
S_3	18.9	10.5	21.8	11.7
S_4	19.0	10.6	21.9	11.7
S_5	18.8	10.5	21.7	11.6
S_7	17.4	9.8	20.7	11.2
S_9	19.1	10.7	21.3	11.4

a) For the solvents, refer to Table 1.

Table 8. Activation energies, ΔE_A (kcal/mol) and log A (A: frequency factor) for the hydrolysis of sodium trimetaphosphate

Solvent[a]	pH=1.0 ΔE_A	log A	pH=2.0 ΔE_A	log A	pH=11.5 ΔE_A	log A	pH=12.2 ΔE_A	log A
S_1	20.7	12.1	21.8	11.6	27.4	14.7	27.5	15.6
S_2	20.8	12.2	21.8	11.7	29.6	15.7	29.9	16.8
S_4	20.7	12.1	21.8	11.6	25.0	13.7	23.4	13.2
S_5	20.8	12.2	21.8	11.6				
S_6	20.3	12.0	21.5	11.6	31.0	16.3	30.3	16.9
S_8	20.7	12.2	21.6	11.5				

a) For the solvents, refer to Table 1.

Table 9. Activation energies, ΔE_A (kcal/mol) and log A(A: frequency factor) for the hydrolysis of sodium tetrametaphosphate

Solvent[a]	pH=1.0 ΔE_A	log A	pH=2.0 ΔE_A	log A	pH=12.2 ΔE_A	log A
S_1	23.2	12.9	24.8	12.9	32.6	17.6
S_2	23.0	12.8	23.4	12.1	32.7	17.4
S_4	23.1	12.9	23.9	12.3	28.8	15.3
S_5	23.1	12.8	24.0	12.4		
S_6	22.4	12.6	22.8	12.0	33.5	17.8
S_8	22.9	12.9	23.0	11.8		

a) For the solvents, refer to Table 1.

(A: frequency factor) of the hydrolysis of the phosphates were calculated by means of an Arrhenius plot and are listed in Tables 6—9. Since the activation energy and log A for the hydrolysis of sodium pyro- and tripolyphosphates in acidic solutions increase with an increase in the pH value, the decrease of the rate of hydrolysis for both the short-chain polyphosphates with increasing pH value depends highly upon the activation energy in all acidic solutions studied. The activation energy of the hydrolysis of sodium trimeta- and tetrametaphosphates increases with an increase in the pH value in all acidic solutions, while log A of the hydrolysis of both the small-ring metaphosphates decreases with an increase in the pH value. The decrease in the rate of hydrolysis with increasing pH value, therefore, depends upon both the activation energy and the frequency factor in all the acidic solutions studied. For basic solutions, the increase in the rate of hydrolysis of sodium trimetaphosphate with an increase in the pH value in

the S_1 and S_2 solvents is highly dependent upon an entropy term, while those in the S_4 and S_6 solvents depend on an energy term and on energy and entropy terms, respectively.

Difference in the Stability of the Hydrolysis of Phosphates. According to the results shown in Tables 2—5, sodium pyrophosphate is more stable against hydrolytic degradation than sodium tripolyphosphate and sodium trimetaphosphate much more subject to hydrolytic scission than is sodium tetrametaphosphate. It can be seen by comparing the results in Tables 6 and 8 with those in Tables 7 and 9, respectively, that the stability of sodium pyrophosphate against hydrolytic scission depends upon an energy term or upon both energy and entropy terms, while the stability of sodium tetrametaphosphate depends entirely on an energy term under the conditions studied. The stability of chain phosphate against hydrolytic degradation decreases, in general, with the chain length of the phosphate,[7] and it can reasonably be accepted that the longer the chain of the phosphate, the greater the probability of hydrolytic scission of a P–O–P linkage. This explanation can not be applied to the stability of small-ring metaphosphates because the chain length of tetrametaphosphate is longer than that of trimetaphosphate. The stability of tetrametaphosphate against hydrolysis is explained by Van Wazer as follows: a tetrametaphosphate ring exhibits a greater number of possible atomic configurations and modes of internal motion than does a trimetaphosphate ion, so that the latter is essentially more rigid and hence more subject to scission.[7] According to Griffith and Rutt,[11] a trimetaphosphate ion has D_{3h} symmetry (planar form) and a tetrametaphosphate ion has C_{2h} symmetry (chair form) in an aqueous solution. The former may be more rigid than the latter. By quantum-chemical consideration, the stability of a system generally proceeds with an increase in the number of obtainable states of the system. The discussion given above and the kinetic data obtained in this experiment seem to support Wazer's explanation of the stability of tetrametaphosphate against hydrolytic scission.

The Solvent Effect on the Rate of Hydrolysis. As is shown in Tables 2—5, in acidic media, the rate of hydrolysis of sodium pyro-, tripoly-, trimeta-, and tetrametaphosphates in pure water is slower than that in the ethanol–water, glycerol–water, acetonitrile–water, dimethyl sulfoxide–water, and tetrahydrofuran–water solvents at the same pH values and reaction temperatures. The solvent effect of ethanol, glycerol, and acetonitrile on the rate of hydrolysis of short-chain and small-ring phosphates in acidic media is a small, while that of dimethyl sulfoxide and tetrahydrofuran in acidic media is very marked. The rate of hydrolysis of sodium pyro-, tripoly-, trimeta-, and tetrametaphosphates in aqueous dimethyl sulfoxide and aqueous tetrahydrofuran is about 1.5—3.0 and 1.3—2.0 times faster, respectively, than that in pure water. In organic reactions, the effect of the dielectric constant of a solvent on a reactant has been discussed extensively.[12] The relation between the rate constant for the hydrolysis of the phosphates and the dielectric constant of the sample solutions is not parallel and is complex. The present authors have discussed the solvent effect on the rate of hydrolysis of sodium pyro-, tripoly-, trimeta-, and tetrametaphosphates by dioxane, formic acid, and acetic acid in previous papers.[3,4] Depending upon the same consideration of the previous papers, the solvent effect in this experiment can reasonably be explained in terms of the difference in the nucleophilicity of the water molecule in each solution as follows. (1) In the case of protic solvents, ethanol and glycerol can interact with a water molecule and hence the hydrogen bond between water molecules may be broken and a hydrogen bond may then be established between the hydrogen atom of the OH group of the protic organic molecules and the oxygen atom of a water molecule. The hydrogen bond between the protic organic molecules and a water molecule may be weaker than that between water molecules, because the polarity of a water molecule is larger than that of ethanol and glycerol molecules. Therefore, the nucleophilicity of the water molecule in aqueous ethanol and aqueous glycerol is larger than that in pure water. The nucleophilic attack by the water molecule of aqueous ethanol and aqueous glycerol on the phosphorus atom of the phosphates may be more favorable energetically than that in pure water. (2) The oxygen atom of dimethyl sulfoxide and tetrahydrofuran and the nitrogen atom of acetonitrile can form a hydrogen bond with the hydrogen atom of a water molecule, and hence the hydrogen bond between water molecules is broken. Accordingly, the nucleophilicity of the water molecule in the aqueous organic solvents may be larger than that in pure water and the nucleophilic attack of the water molecule in aqueous dimethyl sulfoxide, aqueous tetrahydrofuran, and aqueous acetonitrile may also be more favorable energetically than that in pure water. From the results listed in Tables 6—9, it can be said that the acceleration of the rate for short-chain and small-ring phosphates by the organic solvents in acidic media depends mainly upon the activation energy. This appears to support considerations (1) and (2) above. According to the above discussion, since the overall-reaction rates of the hydrolysis of sodium pyro-, tripoly-, trimeta-, and tetrametaphosphates in acidic media are highly dependent upon the nucleophilicity of the water molecule and the hydrolysis of the phosphates is an acid-catalyzed reaction, one can describe a series of elementary reactions for the hydrolysis of the poly- and metaphosphates as follows:

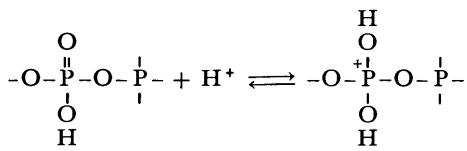

(1)

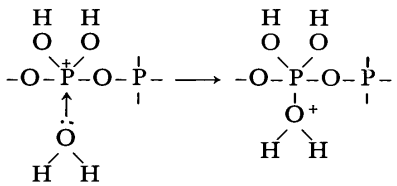

(2)

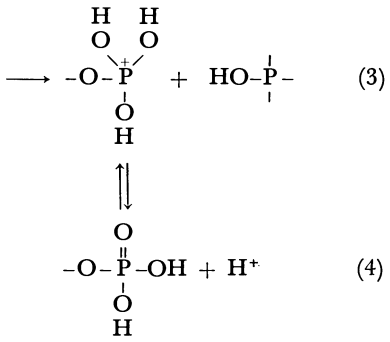

(3)

(4)

The phosphate ion on the right-hand side of reaction (1) may more readily accept the nucleophilic attack of a water molecule than the phosphate on the left-hand side of reaction (1). The rate-determining step for the hydrolysis of the poly- and metaphosphates in an acidic solution may be the second step because the overall-reaction rate is highly dependent upon the nucleophilicity of the water molecule, as mentioned above. Therefore, the hydrolysis of sodium pyro-, tripoly-, trimeta-, and tetrametaphosphates in acidic solutions may be of the S_N2 type. This conclusion is in good agreement with that of the reaction mechanism of organic phosphorus(V) compounds having P=O bonds[1] and that of the hydrolytic mechanism of long-chain polyphosphates proposed by Wieker and Thilo.[2]

In basic solutions, as is shown in Table 3, the solvent effect on the rate of hydrolysis of sodium tripolyphosphates is the same as that in acidic solutions, and the hydrolysis of the polyphosphate in basic solutions may also be of the S_N2 type. The kinetic data in Tables 4 and 5 show that the solvent effect on the rate of hydrolysis of sodium trimeta- and tetrametaphosphates in basic solutions is much different from that in acidic solutions. The rate of hydrolysis of both metaphosphates in pure water is much faster than that in the S_2 and S_6 solvents and is much slower than that in the S_4 solvent. From the results in Tables 8 and 9, the acceleration or the retardation of the rate of hydrolysis of both metaphosphates in the basic S_2, S_4, and S_6 solvents in comparison with the rate of hydrolysis in the basic S_1 solvent depends upon an energy term. This tendency is almost the same as that obtained in a previous paper by the authors.[4] The hydrolytic reaction mechanism for sodium trimeta- and tetrametaphosphates in basic solutions is not the same as that in acidic solutions. It can be concluded that there are other elementary reactions affecting the overall-reaction rate of the hydrolysis of sodium trimeta- and tetrametaphosphates in basic solutions, other than the nucleophilic attack of a water molecule on the phosphorus atom of the phosphates.

References

1) A. J. Kirby and S. G. Warren, "The Organic Chemistry of Phosphorus," Elsevier, New York (1967), p. 274.
2) W. Wieker and E. Thilo, *Z. Anorg. Allg. Chem.*, **313**, 296 (1961).
3) M. Watanabe, *Bull. Chem. Soc. Jpn.*, **47**, 2048 (1974).
4) M. Watanabe, S. Sato, and H. Saito, *Bull. Chem. Soc. Jpn.*, **48**, 4593 (1975).
5) L. F. Audrieth, *Inorg. Synth.*, Vol. III, (1950), pp. 101, 104.
6) R. N. Bell, L. F. Audrieth, and O. F. Hill, *Ind. Eng. Chem.*, **44**, 568 (1952).
7) J. R. Van Wazer, "Phosphorus and Its Compounds," Interscience Publishers, New York (1958), pp. 452, 679, and the references therein.
8) The rate constant for the hydrolysis of sodium tetrametaphosphate at pH 11.5 is not listed in Table 5. The rate of hydrolysis of tetrametaphosphate at pH 11.5 is much slower than that at pH 12.2 (see Ref. 4).
9) T. Otani, M. Miura, and T. Doi, *Kogyo Kagaku Zasshi*, **66**, 593 (1963).
10) J. Crowther and A. E. R. Westman, *Can. J. Chem.*, **34**, 969 (1956).
11) W. P. Griffith and K. J. Rutt, *J. Chem. Soc., A*, **1968**, 2331.
12) K. Okamoto, "Kyukaku Chikan Hanno S_N2 Hanno," Tokyo Kagaku Dojin, Tokyo (1969), p. 202.

Successive Spectrophotometric Determination of Palladium and Platinum

Kingo MIZUNO and Giroku MIYATANI*

Department of Chemistry, Faculty of Liberal Arts, Iron and Steel Technical College, Nishikoya, Amagasaki-shi, Hyogo 661

**Department of Metallurgy, Faculty of Engineering, Kansai University, Senriyama, Suita-shi, Osaka 565*

(Received April 17, 1976)

The absorbance of the water soluble red complex of palladium(II) and 4-(2-pyridylazo)resorcinol (PAR) was measured at 513 nm. Concd hydrochloric acid and tin(II) chloride were added to an aliquot of the red solution, and both the palladium complex and the excess of PAR were decolorized by the reduction of the azo radical of PAR. The absorbance of the platinum complex with tin(II) chloride was measured at 403 nm.

The photometric determination of many metals by using 4-(2-pyridylazo)resorcinol (PAR) has been described. It is known that palladium(II) reacts with PAR to form four kinds of stable 1 : 1 chelates. One of them is green at pH below 4 and the others are red at pH above 4.[1] We found that the water soluble red complex at pH 10.3—11 had an absorption maximum at about 520 nm in 0.01 M EDTA.[2] By the use of the EDTA–NaOH solution, not only a masking of many diverse ions but also a buffer action at 10.5 has been achieved, and 30 times of platinum(IV) was scarcely interfered in the determination of palladium.

The tin(II) chloride method is widely used for the spectrophotometric determination of micro amounts of platinum.[3] But in the presence of palladium it gives a positive error in the determination of platinum, so that the regions available to this method are limited.

It has been known that many azo compounds are easily reduced with tin(II) chloride in concentrated hydrochloric acid.[4,5] We found that PAR and its palladium complex were also reduced and almost completely decolorized. This reductive reaction was combined with the determination of platinum; the spectrophotometric determination of Pd-PAR complex was carried out at 513 nm and then the determination of platinum at 403 nm. By using this procedure the successive determination of palladium and platinum became possible.

Experimental

Apparatus. A Hitachi double beam spectrophotometer model 200-20 with 1 cm cuvettes, a Hitachi recorder model QPD53, and a Hitachi-Horiba pH meter model H-5 were used.

Reagents. A standard palladium stock solution was made by dissolving 500 mg of metal in aqua regia and evaporating to dryness on a water bath After evaporating to dryness three times with hydrochloric acids, the residue was dissolved with 0.1 M hydrochloric acid and made up to 500 ml with 0.1 M hydrochloric acid. This solution was standardized gravimetrically by the dimethylglyoxime method. The palladium test solution was prepared by diluting 5 ml of stock solution and 4.5 ml of 1 M hydrochloric acid and diluted to 500 ml with water. This test solution contained 9.86 μg of palladium per ml.

A standard platinum solution was made by dissolving 100 mg of pure platinum in a few ml of aqua regia and evaporating to dryness; then 5 ml of concd hydrochloric acid and 0.1 g of sodium chloride were added and the solution evaporated to dryness. The residue was dissolved in 20 ml of 6 M hydrochloric acid and the solution was diluted to exactly 1 l. This standard solution contained 100 μg of platinum per ml.

A 0.1% PAR solution was prepared by dissolving 0.25 g of PAR (free acid form, Dojin Pharmaceutical Laboratories, Kumamoto, Japan) to 2 ml of 1 M sodium hydroxide solution, and diluting to 250 ml with water. This solution was stored in a polyethylene bottle.

An EDTA buffer solution having a pH of 10.5 was prepared by adding 100 ml of 1 M sodium hydroxide to about 200 ml of EDTA aqueous solution in which was dissolved 18.6 g of EDTA (di-sodium salt) and diluting to 500 ml with water.

The tin(II) chloride solution was made by dissolving 115 g of $SnCl_2 \cdot 2H_2O$ in 170 ml of warm concd hydrochloric acid and diluting to 500 ml with water. A stick of pure tin was placed in the bottle to keep the solution in the reduced state.

All the other chemicals used were of reagent grade.

Recommended Procedure. To the sample solution containing 0—100 μg palladium and 0—300 μg platinum, 5 ml of 0.1 M EDTA buffer solution (pH 10.5) and 0.5 ml of 0.1% PAR solution were added (if needed, the pH ought to be adjusted to 10.3—10.5 by 0.1 M sodium hydroxide). Then the solution was warmed in a water bath at 80 °C for 10 min and was cooled. The solution was diluted to 50 ml with water to determine its absorbance at 513 nm. A blank was run through the whole procedure, using water.

To a 25 ml residual solution of determined palladium contents, 7 ml of concd hydrochloric acid was added and stirred, followed by the addition of 10 ml of tin(II) chloride solution. The solution was diluted to 50 ml with water to determine its absorbance at 403 nm.

The authentic absorbance of platinum was provided by substracting 0.001 for each 10 μg palladium from its observed absorbance. By these procedures palladium and platinum were successively determined.

Results and Discussion

Measurements of Absorption Spectra. Figure 1 shows the absorption spectra of PAR and Pd-PAR. In the previous paper[2] measurements were carried out at 520 nm. However, as it turned out that the absorption maximum of Pd-PAR complex was at 513 nm, in this study measurements were carried out at this wavelength at pH 10.3—10.5. Under these conditions the molar extinction coefficient was 2.6×10^4 and the sensitivity which gave the absorbance of 0.001 was 0.0041 μg-Pd^{2+}/cm^2. To the beaker containing 49.3 μg palladium, 5 ml of 0.1 M EDTA buffer solution and 0.5 ml of 0.1% PAR solution were added. The solution was heated at 80 °C for 10 min and cooled, then 7 ml of concd hydrochloric acid was added to it. In addition,

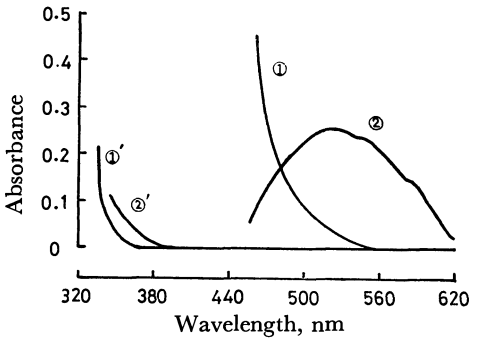

Fig. 1. Absorption curves of PAR, Pd-PAR and their decolorized.
①PAR (0.5 mg/50 ml), ② Pd-PAR (Pd: 49.3 μg/50 ml), ①′ and ②′ signify the solutions being reduced corresponding to ① and ②.

Table 1. Determination of palladium and platinum in synthetic mixtures

Absorbance of PAR complex[a]			Absorbance of tin(II) chloride complex			
Pd(II) added (μg)	Pt(IV) added (μg)	Absorbance at 513 nm	Pd taken (μg)	Pt taken (μg)	Absorbance at 403 nm	Correction value
0	100	0.002	0	50	0.040	
0	200	0.004	0	100	0.080	
0	300	0.003	0	150	0.120	
9.86	0	0.049	4.93	0	0.001	
29.6	0	0.147	14.8	0	0.001	
49.3	0	0.245	24.65	0	0.001	
9.86	100	0.050	4.93	50	0.041	0.040
9.86	200	0.049	4.93	100	0.082	0.081
9.86	300	0.049	4.93	150	0.122	0.121
29.6	100	0.147	14.8	50	0.041	0.038
29.6	200	0.148	14.8	100	0.084	0.081
29.6	300	0.146	14.8	150	0.123	0.120
49.3	100	0.244	24.65	50	0.045	0.040
49.3	200	0.244	24.65	100	0.085	0.080
49.3	300	0.245	24.65	150	0.125	0.120

a) Total volume 50 ml, PAR 0.5 mg/50 ml.

when one drop of tin(II) chloride was added, the solution of Pd-PAR complex changed from green to colorless. As the tin(II) chloride content increased, PAR and its palladium complex were reduced and almost completely decolorized. In Fig. 1, ① and ② are the absorption curves of PAR and Pd-PAR respectively, and ①′ and ②′ are the blanks of ① and ② respectively. ①′ and ②′ have no absorption at 403 nm, which is the wavelength for platinum. For determining the platinum contents, the sensitivity of this procedure was not different from Sandell's procedure.

The Successive Determination of Palladium and Platinum. The results shown in Table 1 were obtained from the analysis of some known synthetic mixtures containing 0—49.3 μg palladium and 0—300 μg platinum. In the case of no platinum, palladium gave an absorbance as if the absorbance of platinum were 0.001. In the presence of palladium, the absorbance of platinum increased 0.001 for each 10 μg palladium (5 μg palladium in determining platinum contents). By these corrections of the absorbance of platinum, a good linear relationship was found between the platinum content and its absorbance.

The Successive Determination of Other Metals and Platinum. As the photometric determination of many metals can be carried out by using PAR,[6] other metals and platinum can be determined in succession. In place of PAR the heterocyclic azo dyestuffs will be able to be used.

The authors wish to thank Dr. Eiichi Ibuki, Professor in the Kyoto College of Pharmacy, for his advice on this work. They also thank Dr. Hiromu Imai, Professor in Kansai University, and Dr. Takeshige Oyama, Professor in the Iron and Steel Technical College, for their ardent encouragement.

References

1) H. Hoshino, R. Yamashita, T. Yotsuyanagi, and K. Aomura, *Nippon Kagaku Kaishi*, **1974**, 495.
2) K. Mizuno, A. Uwano, and G. Miyatani, *Bunseki Kagaku*, **25**, 113 (1976).
3) E. B. Sandell, "Colorimetric Determination of Traces of Metals," 3rd ed., Interscience (1959), p. 726.
4) G. Hilgetag and A. Martini, "Preparative Organic Chemistry" 4th ed., John Wiley and Sons (1972), p. 568.
5) S. Umesawa, "Yuki Kagaku II," New ed., Maruzen, Tokyo (1962), p. 165.
6) R. G. Anderson and G. Nickless, *Analyst*, **92**, 207 (1967).

Kinetics of Ligand Substitution Reaction of Some Aminopolyacetatonickel(II) Complexes with Reference to Activation Parameters

Shigenobu FUNAHASHI and Motoharu TANAKA*

Laboratory of Analytical Chemistry, Faculty of Science, Nagoya University, Chikusa-ku, Nagoya 464

(Received May 13, 1976)

The substitution reactions of some Ni(II)–L complexes (L: ethylenediamine-*N,N'*-diacetate, edda^{2-}; nitrilotriacetate, nta^{3-}; iminodiacetate, ida^{2-}) with 4-(2-pyridylazo)resorcinol (H_2par) have been studied spectrophotometrically at I=0.10. Rate constant k (mol dm^{-3}, s) at 25 °C, activation enthalpy ΔH^{*}/kJ mol^{-1} and activation entropy ΔS^{*}/J K^{-1} mol^{-1} are respectively: 1.7×10^{3}, 58.5 and 12.5 for k[Ni^{2+}][Hpar^{-}]; 4.0×10^{2}, 51.8 and −22 for k[Ni(nta)$^{-}$][Hpar^{-}]; 1.0×10^{3}, 41.8 and −46 for k[Ni(edda)][Hpar^{-}]; 2.7×10^{-4}, 109 and 30 for k[(par)-Ni(edda)$^{2-}$]; 5.1×10^{-3}, 88 and 17 for k[(par)Ni(Hedda)$^{-}$]; 1.7×10^{3}, 122 and 226 for k[Ni(ida)][Hpar^{-}]. In terms of activation parameters some discussions are made on the effect of coordinated ligands on the lability of leaving ligands and pre-equilibrium involving partial dissociation of leaving ligands.

Extensive investigations[1] have indicated that the ligand substitution reaction of metal chelates with multidentate ligands proceeds through an intermediate in which a central metal ion is bonded with both leaving and entering ligands and that the cleavage of the bond between the metal and leaving ligand is the rate-determining step. We have previously reported the kinetics and mechanism of ligand substitution reactions of Ni(II)–NTA and Ni(II)–EDDA complexes with PAR at 25 °C[2]**. We have pointed out on the basis of values of rate constants that the effect of ligands already present in a complex on the ease of replacement of the leaving ligand is closely related to the electron-donating properties of the ligands.[2,3] It seems worthwhile to consider the labilization of the leaving ligands by the bound ligand in terms of activation parameters.

Experimental

Preparation of all reagents except IDA, instrumentation and experimental procedure for measuring equilibria and reaction rates are the same as described previously.[2] Reagent grade IDA, obtained from Dojin-do Chemical Co., Japan, was recrystallized twice from distilled water.

Results

Ligand Substitution Reaction of the Ni(II)–EDDA Complex with PAR. The ligand substitution reaction of the ethylenediamine-*N,N'*-diacetatonickel(II) complex with 4-(2-pyridylazo)resorcinol at 17.1, 20.3, and 23.2 °C has been measured by the same method as described previously.[2] The mechanism proposed for the reaction is as follows:[2]

$$\mathrm{Ni(edda)} + \mathrm{Hpar^-} \xrightarrow{k_1} \mathrm{(par)Ni(edda)'} + \mathrm{H^+} \quad (1)$$

$$\mathrm{(par)Ni(edda)^{2-}} \xrightarrow{k_2} \mathrm{Ni(par)} + \mathrm{edda'} \quad (2)$$

$$\mathrm{(par)Ni(edda)^{2-}} + \mathrm{H^+} \rightleftharpoons \mathrm{(par)Ni(Hedda)^-} \quad K^{\mathrm{H}}_{\mathrm{(par)Ni(Hedda)}}$$

$$\mathrm{(par)Ni(Hedda)^-} \xrightarrow{k_{2,\mathrm{H}}} \mathrm{Ni(par)} + \mathrm{edda'}$$

$$\mathrm{Ni(par)} \xrightarrow[\text{fast}]{+\mathrm{Hpar^-}} \mathrm{Ni(par)_2^{2-}} \quad (2)$$

The rate constants and formation constants of the protonated complex at various temperatures, and the values of activation parameters are given in Table 1.

Ligand Substitution Reaction of the Ni(II)–NTA Complex with PAR. The ligand substitution reaction of the nitrilotriacetatonickel(II) complex with 4-(2-pyridylazo)resorcinol at 20.2 and 15.4 °C has been followed as described previously.[2] The reaction proceeds as follows:[2]

$$\mathrm{Ni(nta)^-} + \mathrm{Hpar^-} \underset{k_{-1}}{\overset{k_1}{\rightleftharpoons}} \mathrm{(par)Ni(nta)^{3-}} + \mathrm{H^+} \quad (3)$$

$$\mathrm{(par)Ni(nta)^{3-}} \xrightarrow{k_2} \mathrm{Ni(par)} + \mathrm{nta'}$$

$$\mathrm{Ni(par)} \xrightarrow[\text{fast}]{+\mathrm{Hpar}} \mathrm{Ni(par)_2^{2-}} \quad (4)$$

Rate constants at various temperatures and activation

Table 1. Rate constants for ligand substitution of Ni(II)–EDDA with PAR, activation parameters and stability constants of the protonated complex

Reaction temp/°C	k_1 / mol^{-1} dm^3 s^{-1}	k_2/s^{-1}	$k_{2,\mathrm{H}}$/s^{-1}	$K^{\mathrm{H}}_{\mathrm{(par)Ni(Hedda)}}$/mol^{-1} dm^3	
17.1	6.1×10^{2}	8.0×10^{-5}	2.1×10^{-3}	$10^{8.06\pm0.10}$	
20.3	7.5×10^{2}	1.3×10^{-4}	2.6×10^{-3}	$10^{8.04\pm0.10}$	
23.2	9.0×10^{2}				
25.0[a]	1.0×10^{3}	2.7×10^{-4}	5.1×10^{-3}	$10^{8.02\pm0.10}$	
ΔH^{*}/kJ mol^{-1}	41.8±1.5	109±10	88±15	ΔH/kJ mol^{-1}	0±10
ΔS^{*}/J K^{-1} mol^{-1}	−46±5	30±30	17±30	ΔS/J K^{-1} mol^{-1}	154±30

a) Ref. 2.

* To whom correspondence should be addressed.

** Ligand abbreviations are: EDDA (H_2edda) for ethylenediamine-*N N'*-diacetic acid; NTA (H_3nta) for nitrilotriacetic acid; IDA (H_2ida) for iminodiacetic acid; PAR (H_2par) for 4-(2-pyridylazo)resorcinol.

TABLE 2. RATE CONSTANTS FOR LIGAND SUBSTITUTION OF Ni(II)–NTA WITH PAR AND ACTIVATION PARAMETERS

Reaction temp/°C	k_1 / mol^{-1} dm^3 s^{-1}	$k_1 k_2/k_{-1}$ / s^{-1}
15.4	1.94×10^{2}	2.56×10^{-6}
20.2	2.74×10^{2}	4.08×10^{-6}
25.0[a)]	4.00×10^{2}	5.26×10^{-6}
$\Delta H^{\ddagger}$/kJ mol^{-1}	51.8 ± 2.5	
$\Delta S^{\ddagger}$/J K^{-1} mol^{-1}	-22 ± 5	

a) Ref. 2.

parameters are summarized in Table 2.

Ligand Substitution Reaction of the Ni(II)–IDA Complex with PAR. We have studied the ligand substitution reaction of the bis(iminodiacetato)nickel(II) complex with PAR:

$$\text{Ni(II)–IDA} + \text{PAR} \rightleftharpoons \text{Ni(II)–PAR} + \text{IDA} \quad (5)$$

Under the present experimental conditions, the Ni(II)–IDA and Ni(II)–PAR complexes are the 1 : 2 complexes *i.e.* $Ni(ida)_2^{2-}$ and $Ni(par)_2^{2-}$, respectively. The dominant species of PAR is the monoionic species $Hpar^-$. Reaction (5) is so much favored to the right that the reaction of the Ni(II)–IDA complex with PAR goes to completion. The overall ligand substitution reaction is described as

$$Ni(ida)_2^{2-} + 2Hpar^- \longrightarrow Ni(par)_2^{2-} + 2ida' \quad (6)$$

where ida' represents IDA not combined to nickel. The initial rates were analyzed. The reaction was found to be of first-order with respect to $Ni(ida)_2^{2-}$ and $Hpar^-$. Some conditional second-order rate constants are summarized in Table 3.

TABLE 3. CONDITIONAL RATE CONSTANTS FOR REACTION OF THE Ni(II)–IDA COMPLEX WITH PAR I=0.10 ($NaClO_4$)

C_{IDA} / mol dm^{-3}	log [H$^+$] / mol dm^{-3}	k_0 / mol^{-1} dm^3 s^{-1}	$\alpha_{ida(H)}/\{K^{ida}_{Ni(ida)_2}(C_{IDA}-2C_{Ni})\}$
		30.0±0.1 °C[a)]	
5.60×10^{-4}	8.631	36.0	7.94×10^{-3}
1.12×10^{-3}	8.407	28.4	6.03×10^{-3}
5.60×10^{-4}	8.908	23.5	5.01×10^{-3}
5.60×10^{-4}	9.15	18.0	3.55×10^{-3}
		25.0±0.1 °C[b)]	
1.12×10^{-3}	8.628	9.50	4.17×10^{-3}
1.12×10^{-3}	9.062	5.17	1.95×10^{-3}
1.12×10^{-3}	8.926	7.43	2.46×10^{-3}
1.12×10^{-3}	8.163	22.0	1.07×10^{-2}
5.60×10^{-4}	8.851	12.6	5.62×10^{-3}
		19.3±0.1 °C[a)]	
5.60×10^{-4}	8.203	13.0	2.29×10^{-2}
5.60×10^{-4}	8.656	6.50	8.91×10^{-3}
5.60×10^{-4}	8.909	5.60	5.62×10^{-3}
5.60×10^{-4}	9.148	4.05	3.72×10^{-3}
1.12×10^{-3}	7.736	16.9	3.16×10^{-2}
1.12×10^{-3}	8.988	2.92	2.34×10^{-3}
		14.1±0.2 °C[a)]	
5.60×10^{-4}	8.248	8.29	2.29×10^{-2}
5.60×10^{-4}	8.701	4.05	8.71×10^{-3}
5.60×10^{-4}	8.977	3.2	5.13×10^{-3}
5.60×10^{-4}	9.169	2.7	3.63×10^{-3}
5.60×10^{-4}	9.209	2.7	3.47×10^{-3}
5.60×10^{-4}	8.453	6.7	1.48×10^{-2}

a) $C_{Ni}=1.02\times10^{-5}$, $C_{PAR}=1.00\times10^{-4}$ mol dm^{-3}.
b) $C_{Ni}=5.09\times10^{-6}$, $C_{PAR}=5.00\times10^{-5}$ mol dm^{-3}.

The dependence of IDA concentration on the conditional rate constant points to predissociation of IDA in $Ni(ida)_2^{2-}$ because the values of the rate constant decrease with increasing concentration of IDA and $-\log[H^+]$. We assume the following reaction scheme:

$$Ni(ida)_2^{2-} \rightleftharpoons Ni(ida) + ida' \quad (7)$$

$$Ni(ida) + Hpar^- \xrightarrow{k_2} Ni(par) \xrightarrow[fast]{+Hpar^-} Ni(par)_2^{2-} \quad (8)$$

Then the rate equation of the formation of $Ni(par)_2^{2-}$ is given by

$$\text{Rate} = k_2[Ni(ida)][Hpar^-]$$

$$= k_2\frac{\alpha_{ida(H)}}{K^{ida}_{Ni(ida)_2}(C_{IDA}-2C_{Ni})}[Ni(ida)_2^{2-}][Hpar^-] \quad (9)$$

where C_{IDA} and C_{Ni} are the total concentrations of IDA and nickel ion, respectively, and $\alpha_{ida(H)}=1+K^{H}_{Hida}[H^+]+K^{H}_{Hida}K^{H}_{H_2ida}[H^+]^2$.* The conditional rate constants are plotted against the values of $\alpha_{ida(H)}/\{K^{ida}_{Ni(ida)_2}(C_{IDA}-2C_{Ni})\}$ in Fig. 1. The non-zero intercept in the plot indicates another reaction path not involving predissociation of IDA in $Ni(ida)_2^{2-}$. The reaction, therefore, proceeds through two parallel reaction paths for which the following rate equation can be deduced:

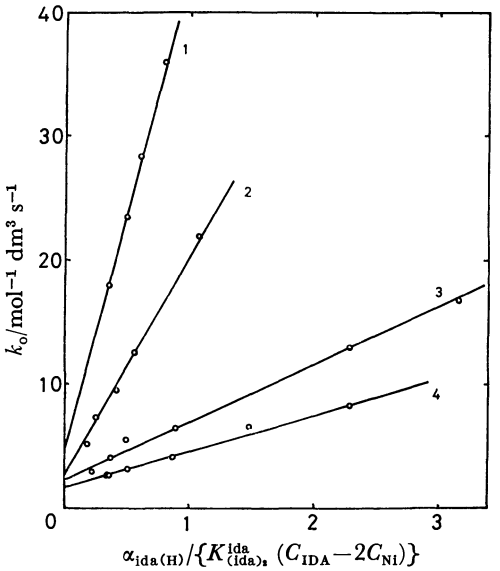

Fig. 1. Dependence of k_0 on the function $\alpha_{ida(H)}/\{K^{ida}_{Ni(ida)_2}(C_{IDA}-2C_{Ni})\}$.
Reaction temp/°C, 1: 30.0; 2: 25.0; 3: 19.3; 4: 14.1.

* $K^{ida}_{Ni(ida)_2}=[Ni(ida)_2^{2-}]/\{[Ni(ida)][ida^{2-}]\}$, $K^{H}_{Hida}=[Hida^-]/\{[ida^{2-}][H^+]\}$, $K^{H}_{H_2ida}=[H_2ida]/\{[Hida^-][H^+]\}$. The values for these stability constants at a given temperature are available (G. Anderegg *Helv. Chim. Acta*, **47**, 1801 (1964)).

$$\frac{d[Ni(par)_2^{2-}]}{dt} = k_1[Ni(ida)_2^{2-}][Hpar^-] + k_2[Ni(ida)][Hpar^-] = \left\{k_1 + \frac{k_2\alpha_{ida(H)}}{K^{ida}_{Ni(ida)_2}(C_{IDA}-2C_{Ni})}\right\} \times [Ni(ida)_2^{2-}][Hpar^-] \quad (10)$$

Thus the observed second-order rate constant k_0 is equal to $k_1+k_2\alpha_{ida(H)}/\{K^{ida}_{Ni(ida)_2}(C_{IDA}-2C_{Ni})\}$. Rate constants at various temperatures are tabulated in Table 4.

Table 4. Rate constants for ligand substitution of Ni(II)–IDA with PAR and activation parameters

Reaction temp/°C	k_1 / mol^{-1} dm^3 s^{-1}	k_2 / mol^{-1} dm^3 s^{-1}
14.1	≈1.6	2.9×10^2
19.3	≈2.1	4.8×10^2
25.0	≈3.0	1.7×10^3
30.0	≈4.5	3.8×10^3
ΔH^*/kJ mol^{-1}		122±15
ΔS^*/J K^{-1} mol^{-1}		226±50

Activation parameters for k_2 are 121±15 kJ mol^{-1} for the activation enthalpy and 226±50 J K^{-1} mol^{-1} for the activation entropy. Activation parameters for k_1 are not evaluated because of uncertainty.

Table 5. Thermodynamic parameters for nickel complexes

Ligand	N_xO_y	ΔH/kJ mol^{-1}	ΔS/J K^{-1} mol^{-1}	log K (25 °C)	Ref.
NH_3	N_1	−17	−2	2.83	c
Acetate	O_1	0	8	0.41	d
en	N_2	−38.7	14	7.49	e
Oxalate	O_2	1.3	1.0×10^2	5.16	f
Glycinate	N_1O_1	−18.3	56	6.13	g
IDA	N_1O_2	−21.1	84	8.07	h
MIDA[a]	N_1O_2	−20	1.0×10^2	8.67	i
NTA	N_1O_3	−10.6	1.8×10^2	11.49	j
EDDA	N_2O_2	−41.8	1.2×10^2	13.65	k
HEDTA[b]	N_2O_3	−43.1	1.9×10^2	17.1	l
EDTA	N_2O_4	−36	2.4×10^2	18.7	l

a) Methyliminodiacetic acid. b) *N'*-(2-Hydroxyethyl)-ethylenediamine-*N,N,N'*-triacetic acid. c) K.B. Yatsimirskii and P.M. Milyukov, *Zh. Fiz. Khim.*, **31**, 843 (1957). d) Calculated from the data (N. Tanaka and K. Kato, *Bull. Chem. Soc. Jpn.*, **32**, 516 (1959)). e) F. Holmes and D. R. Williams, *J. Chem. Soc., A*, **1967**, 1702. f) A. McAuley and G. H. Nancollas, *J. Chem. Soc.*, **1961**, 2215. g) R.M. Izatt, H.D. Johnson, and J. J. Christensen, *J. Chem. Soc., Dalton Trans.*, **1972**, 1152. h) G. Anderegg, *Helv. Chim. Acta*, **47**, 1801 (1964). i) G. Anderegg, *Helv. Chim. Acta*, **48**, 1718 (1965). j) J.A. Hull, R.H. Davies, and L. A. K. Staveley, *J. Chem. Soc.*, **1964**, 5422. k) G. Degischer and G. H. Nancollas, *Inorg. Chem.*, **9**, 1259 (1970). l) D.L. Wright, J.H. Holloway, and C.N. Reilley, *Anal. Chem.*, **37**, 884 (1965).

Discussion

In order to estimate thermodynamic parameters for pre-equilibrium of partial dissociation preceding the rate-determining steps in substitution, we need to consider thermodynamic parameters for some nickel complexes.

Thermodynamic parameters for some nickel complexes are given in Table 5 where the data are presented in the order of numbers of available coordination sites; N_xO_y represents a ligand having x nitrogen atoms and y oxygen atoms for coordination. The data in Table 5 illustrate a striking difference between ΔH and ΔS values for nitrogen and oxygen donors. The Ni(edda) complex is formed with exothermic enthalpy similar to that of the $Ni(en)^{2+}$ complex and the stability constant of the former is larger than that of the latter due to the contribution of positive entropy for chelation of carboxylates. The ΔH values for nitrogen coordination are appreciably more exothermic and constitute the major portion of ΔH. The contribution of nickel–carboxylate bonds to the total ΔH values is very small (see values for acetate and oxalate in Table 5). Interactions with carboxylate groups, being of a more electrostatic character, would be expected to have only a small and probably endothermic effect. It is possible to estimate approximate values for the contribution made by each nickel–nitrogen bond and each nickel–oxygen bond by assuming additivity. We can deduce the ΔH and ΔS values per coordinated nitrogen atom to be about 20 kJ mol^{-1} and about 0 J K^{-1} mol^{-1}, respectively, and per coordinated oxygen atom which forms a chelate ring, about 0 kJ mol^{-1} and 40—60 J K^{-1} mol^{-1}, respectively.

Results in the present study are summarized in Table 6. The rate-determining step of reactions A, B, and C (Table 6) is the dissociation of a water molecule coordinated to nickel(II). We have previously pointed

Table 6. Activation parameters for reactions of some nickel(II) complexes

Reaction (Equation number in the text)	Rate equation	Reaction product	Rate constant at 25 °C k(mol dm^{-3}, s)	ΔH^*/kJ mol^{-1}	ΔS^*/J K^{-1} mol^{-1}
A[a]	$k[Ni^{2+}][Hpar^-]$	$Ni(par)_2^{2-}$	1.7×10^3	58.5± 2.5	12.5± 5
B (Eq. 3)	$k[Ni(nta)^-][Hpar^-]$	(par)Ni(nta)	4.0×10^2	51.8± 2.5	−22 ± 5
C (Eq. 1)	k[Ni(edda)][Hpar$^-$]	(par)Ni(edda)$'$	1.0×10^3	41.8± 1.5	−46 ± 5
D (Eq. 2)	$k[(par)Ni(edda)^{2-}]$	$Ni(par)_2^{2-}$	2.7×10^{-4}	109 ±10	30 ±30
E (Eq. 2)	$k[(par)Ni(Hedda)^-]$	$Ni(par)_2^{2-}$	5.1×10^{-3}	88 ±15	17 ±30
F (Eq. 8)	$k[Ni(ida)][Hpar^-]$	$Ni(par)_2^{2-}$	1.7×10^3	122 ±15	226 ±50

a) Ref. 3. (The values of k at 20.0 and 15.4 °C are 1.25×10^3 and 8.43×10^2 mol^{-1} dm^3 s^{-1}, respectively.)

out that there should be the dissociation of one donor oxygen atom of the coordinated ligand in the Ni–NTA and Ni–EDDA complexes before the incoming ligand (PAR) can gain a coordination foothold.[2] The $\Delta S^{\neq}$ value for reactions B and C which is more negative than that for reaction A is attributable to the dissociation of a carboxylate at the pre-equilibrium step. On the other hand, as the contribution of such dissociation of carboxylate to $\Delta H^{\neq}$ may be regarded as about 0 kJ mol^{-1} (*vide supra*), the decrease in $\Delta H^{\neq}$ in going from reaction A to B and C supports the view that the labilization of the remaining water molecules by the bound ligands is closely related to the electron-donating properties of the latter ligands: when a ligand coordinated to the central metal ion donates electrons to the central metal to a greater extent, the bond of the central metal with the remaining coordinated water molecules will be weakened and more easily broken.

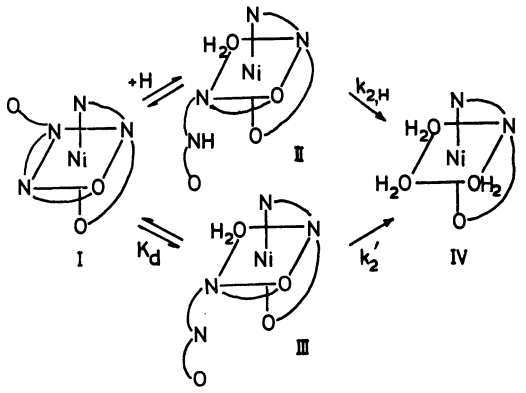

Fig. 2. Proposed reaction mechanism for the dissociation of the intermediate. EDDA and PAR are symbolized as O–N–N–O and N–N–O, respectively. Charges are omitted.

In our previous paper,[2] it was pointed out that judging from the stability constants of EDDA[4]: $[Hedda^-]/\{[edda^{2-}][H^+]\}=10^{9.57}$ and $[H_2edda]/\{[Hedda^-][H^+]\}=10^{6.48}$, the proton in the protonated complex (II in Fig. 2) should be attached to a nitrogen atom in the EDDA which is the most basic. In this work, we determined the values of the stability constants of the protonated complex at 17.1 and 20.3 °C which are the same as the value at 25.0 °C within an experimental error (Table 1). This indicates that the enthalpy for reaction I→II in Fig. 2 is zero kJ mol^{-1}. All the enthalpies for the protonation of nitrogen atoms in MIDA, NTA, and EDDA are approximately −30 kJ mol^{-1}.[5] Taking into account the fact that the contribution of nickel–carboxylate bonds to the total enthalpy values is rather small, the enthalpy for detaching a nitrogen atom in the (par)Ni(edda)$^{2-}$ complex seems to be about 30 kJ mol^{-1}. In reaction I→II in Fig. 2, the endothermic enthalpy for detaching a nitrogen–nickel bond is compensated by the exothermic enthalpy for binding a proton to a nitrogen atom, and so the net enthalpy change for reaction I→II may be nearly zero kJ mol^{-1}.

It may be of interest to examine the difference in rates between reactions D and E from kinetic and mechanistic point of view. The difference in activation parameters for k_2 (reaction D in Table 6) and $k_{2,H}$ (reaction E in Table 6) is explained on the basis of the equilibria preceding rate-determining steps. If we accept a possible mechanism given in Fig. 2, k_2 is given as follows

$$k_2 = K_d k_2'$$

where K_d is the equilibrium constant between I and III and k_2' is a rate constant for the rate-determining step (III→IV). The first Ni–N bond rupture (I→III) would require an energy corresponding to $\Delta H \approx 20$ kJ mol^{-1} and $\Delta S \approx 0$ J K^{-1} mol^{-1}. This is consistent with our experimental data of the activation parameters for $k_{2,H}$ (II→IV) and k_2' (III→IV) within error limits.

In the substitution of the Ni(II)–IDA complex with PAR, the formation of a mixed-ligand intermediate involving both IDA and PAR could not be observed. However, by analogy with the EDDA and NTA systems, it seems reasonable to speculate that the reaction for the IDA system also proceeds through an intermediate with both leaving and entering ligands. Then the k_2 process in Eq. 10 corresponds to an overall reaction involving formation of the mixed-ligand intermediate and dissociation of the leaving ligand IDA from the intermediate. The large activation enthalpy for reaction F in Table 6 is close to the sum of the activation enthalpies for reactions B (or C) and E: the intermediate is not so stable. The large enthaly of activation for reaction F is largely offset by an exceptionally large entropy of activation. But sufficient information is not available to explain such a remarkably positive entropy of activation.

References

1) R. G. Wilkins, "The Study of Kinetics and Mechanism of Reactions of Transition Metal Complexes," Allyn and Bacon, Inc., Boston (1974), p. 217.
2) S. Funahashi and M. Tanaka, *Inorg. Chem.*, **9**, 2092 (1970).
3) S. Funahashi and M. Tanaka, *Inorg. Chem.*, **8**, 2159 (1969).
4) L. C. Thompson, *J. Inorg. Nucl. Chem.*, **24**, 1083 (1962).
5) S. Yamada, J. Nagase, S. Funahashi, and M. Tanaka, *J. Inorg. Nucl. Chem.*, **38**, 617 (1976).

Studies on Leuckart-Wallach Reaction Paths

Keiichi Ito, Hitoshi Oba, and Minoru Sekiya
Shizuoka College of Pharmacy, Oshika, Shizuoka 422
(Received March 17, 1975)

The Leuckart-Wallach reaction paths were investigated by means of catalytic reduction in the Leuckart-Wallach reaction system and on the basis of analogous formic acid reductions. It was determined that, in the early stage of the Leuckart-Wallach reaction, ammonia, amine and also formamide undergo addition reactions to carbonyl compounds. The addition of formamide catalyzed by formic acid plays a significant role only for the more reactive substrates such as benzaldehyde. The behaviors of plausible intermediates for the formic acid reduction are discussed on the basis of the data of similar formic acid reductions.

The Leuckart-Wallach reaction is well known[1-4] as a process for the reductive amination of aldehydes and ketones. Many workers have been involved in experiments designed to elucidate the mechanism of the reaction. Some have commented on the ammonia- or the amine-addition mechanism of the carbonyl condensation stage and others on the formamide-addition mechanism. Furthermore, the mechanism of the second stage, reduction, is still in dispute. The present work involving catalytic reduction of the Leuckart-Wallach reaction system relating to formic acid reduction bears significantly upon the understanding of the reaction path.

Results and Discussion

Process of the Leuckart-Wallach Reaction. A number of reagents such as ammonium formate, ammonium formate–formic acid, formamide–formic acid, and formamide–ammonium formate have been used[1] for reactions with carbonyl compounds. The overall reactions with respect to the formation of *N*-formyl primary amine can be illustrated by the equations shown in Scheme 1. The formations of *N*-formyl secondary amine and tertiary amine can be similarly formulated by replacing the ammonium formate and formamide with their *N*-alkyl analogs. The carbon dioxide formation in these reactions is indicative of the participation of formic acid as the reducing agent. Several workers have conducted the reduction of carbonyl compounds with formamide alone, although no convincing determination has been made of its reducing capacity. In these cases, the actual reducing agent may be ammonium

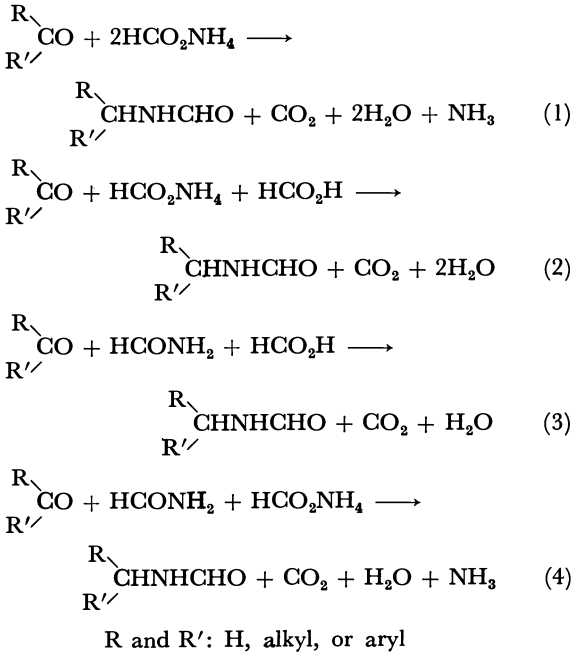

R and R′: H, alkyl, or aryl

Scheme 1.

formate which can plausibly be derived from formamide by hydrolysis with water produced in the reaction mixture. In our trials of the reactions of benzaldehyde and cyclohexanone with formamide[5] (Table 1) almost no carbon dioxide was detected during the course of the reaction, which proceeded only at higher temperatures and required a much longer period. This diminishes the possibility of reduction with ammonium formate generated from formamide. In the reaction of benzal-

Table 1. The Leuckart-Wallach reactions[a] of benzaldehyde and cyclohexanone

Run No.	Substrate	Reagent	Reaction temp (°C)	Reaction time (h)	Yield (%) of the product[b]			
					RNHCHO	R_2NCHO	R_3N	Total
1	C_6H_5CHO	$HCONH_2$	165—170	10.0	55	11	2	68[c]
2		HCO_2H–$HCONH_2$	100—105	7.7	30	8	23	61[d]
3		HCO_2NH_4	120—125	4.7	24	10	42	76
4		$HCONH_2$	165—170	10.0	32	30	0	62
5		HCO_2H–$HCONH_2$	110—115	6.8	30	43	0	73
6		HCO_2NH_4	100—110	4.5	21	62	0	83

a) Carried out using C_6H_5CHO (0.1 mol) and $C_6H_{10}O$ (0.2 mol) with 10-fold amounts of the reagent, $HCONH_2$, HCO_2NH_4, and $HCONH_2$ added with HCO_2H (1.5 molar equiv. to the substrate). b) Yield is based on the product isolated. R = $C_6H_5CH_2$– and C_6H_{11}–. c) Amaron was obtained as a by-product. d) *N*,*N*′-Benzylidenebisformamide was obtained as a by-product.

dehyde with formamide amaron (2,3,5,6-tetraphenylpyrazine), in addition to the amine products, was isolated. In previous papers by the present authors the formations of amaron and lophine (2,4,5-triphenylimidazole) in the reactions of *N,N'* benzylidenebisformamide[6] and *N*-benzylideneaniline[7] with formamide are well documented and were interpreted as clues to support the idea of self oxidation-reduction reactions. In view of these papers, it is then suggested that the reaction of benzaldehyde with formamide alone appears to proceed similarly to the self oxidation-reduction course. From this abnormality of the reduction course, the reaction with formamide alone may be distinguished from others involving formic acid reduction. Accordingly, the decription hesreafter is chiefly concerned with the reactions involving formic acid reduction.

Although the Leuckart-Wallach reaction involves many elementary steps, the path of the reaction can be divided into two important stages, the formation of the C–N bond and the formic acid reduction to amine.

The Initial Condensation Stage. Two arguments have been postulated for the initial stage of the Leuckart-Wallach reaction, the addition of ammonia or amines[8–12] and the addition of formamide[12–18] to carbonyl compounds. As long as ammonium formate undergoes dehydration to formamide at the reaction temperature, the participation of ammonium formate as formamide in the reaction is possible. Conversely, the participation of formamide as ammonium formate is possible when the hydrolysis of formamide occurs with water formed in the reaction mixture. Therefore, the interconversion[1] between ammonium formate and formamide allows the participation of these two species in every fashion of the Leuckart-Wallach reaction in Scheme 1. It has been a problem to determine whether the actual participating species is ammonium formate or formamide.

Using benzaldehyde and cyclohexanone as carbonyl compounds, preliminary experiments were undertaken on the typical reactions with formamide, formic acid–formamide, and ammonium formate (Table 1). The difficulty in defining the behaviors of the reagents comes from the dual roles played by the reagents in both the initial C–N bond formation and the succeeding reduction. In order to understand how the reagents react initially with the carbonyl compounds, it is desirable, if possible, to eliminate the succeeding reduction by the same reagents.

Experiments for this purpose were carried out on the catalytic reductions of the carbonyl compounds in the presence of the Leuckart-Wallach reagents below the temperature (100 °C) at which the reagents affect the carbon dioxide formation. In this manner, formic acid reduction is eliminated and replaced by catalytic reduction. Using a palladium-on-charcoal catalyst, high-pressure hydrogenation of the Leuckart-Wallach reaction system occurred with benzaldehyde under standardized conditions at 90—100 °C.

The affinities of formamide and *N*-benzylformamide for benzaldehyde can be realized from the results of

Table 2.[a] Catalytic reduction[b] of benzaldehyde in the Leuckart-Wallach reaction system

Run No.	Additive[c]	Reaction time (min)	Yield (%) of the product[d]					
			ROH	RNHCHO	R_2NH	R_2NCHO	R_3N	Total
a. In the system involving formamides								
1	$HCONH_2$(1.0)	120	96	0	—	0	0	96
2	$HCONH_2$(1.0) HCO_2H(0.5)	160	13	28	—	20	31	92
3	RNHCHO(1.0) HCO_2H(0.5)	80	96	97[e]	—	2	trace	98
4	$HCONH_2$(1.0) HCO_2H(0.5) B_2O_3(1.0)	120	62	20	—	9	6	97
5	$HCONH_2$(1.0) HCO_2H(0.5) H_2O(1.0)	70	38	0	—	2	52	92
b. In the system involving formates of ammonia and amines								
6	Ammonium carbonate(1.0)	30	0	0	58	—	35	94
7	HCO_2NH_4(1.0)	60	18	0	—	5	72	95
8	HCO_2NH_4(1.0) HCO_2H(0.5)	40	17	0	—	5	74	96
9	RNH_2(1.0)	15	0	0	94	—	trace	94
10	RNH_2(1.0) HCO_2H(0.5)	15	0	0	50	19	29	98
11	R_2NH(1.0)	40	25	0	24[e]	—	68	93
12	R_2NH(1.0) HCO_2H(0.5)	30	19	0	—	20	73	92

a) R = $C_6H_5CH_2$– b) Hydrogenation condition—catalyst, 10% Pd–C, 1 g; initial hydrogen pressure, 80 kg/cm² (room temp); reaction temp, 90—100 °C. c) Molar equivalents of the additives to benzaldehyde (0.1 mol) used are given in parenthesis. d) Yield of the product isolated is calculated from the starting benzaldehyde. e) Recovery.

runs 1, 2, and 3 in Table 2, although the reduction of unreacted benzaldehyde to benzyl alcohol is shown. Formamide itself was shown to be inert to benzaldehyde. On the other hand, in the presence of formic acid, formamide led to the formation of not only *N*-benzylformamide but also *N,N*-dibenzylformamide and tribenzylamine. Under the same conditions, *N*-benzylformamide affected the formation of only a small amount of *N,N*-dibenzylformamide. In consideration of the appreciable formation of *N,N*-dibenzylformamide and tribenzylamine in run 2 it was then required to know whether water, which was formed in the reaction mixture, participates in the product formation, since water hydrolyzes formamide into another reactive ammonium formate. Runs 4 and 5 in Table 2 carried out in the presence of a desiccant, boron trioxide, and of water, respectively, offered clear information on the effect of water on the reaction. In the former, the addition of boron trioxide considerably reduced the yields of *N,N*-dibenzylformamide and tribenzylamine relative to *N*-benzylformamide, whereas, in the latter, the addition of water considerably increased the yield of tribenzylamine without the formation of *N*-benzylformamide. The result of run 5 closely resembles that of run 8 carried out using ammonium formate in place of the formamide of run 2. In view of the above facts, the water added can be understood to affect an increase in the participation of ammonium formate and the desiccant to affect an increase in the participation of formamide. In such a reaction in the presence of formic acid, the interaction between formamide and benzaldehyde is actually recognized to occur, although the participation of ammonium formate also occurs. Formic acid as an additive can then be regarded as an acid catalyst for the reaction between formamide and benzaldehyde.

Next, an examination by the same hydrogenation procedure was attempted in order to observe the behavior of ammonium formate with benzaldehyde. The catalytic reductions of benzaldehyde in the presence of ammonium formate and of ammonia (ammonium carbonate was used) resulted in the formation of tribenzylamine and dibenzylamine, in free and *N*-formylated forms, in the yields given in Table 2. It is inferred that dibenzylamine is derived from the initially formed benzylamine, and tribenzylamine stepwise through dibenzylamine. This was demonstrated by carrying out the reduction in the presence of benzylamine and of dibenzylamine, where the effect of the additional presence of formic acid was also checked, as can be seen for runs 9, 11, 10, and 12 in Table 2. From the above results, it was found that in the ammonium formate medium under the hydrogenation conditions, the carbonyl addition of the amine species proceeds stepwise leading to benzylamine, dibenzylamine and finally tribenzylamine. The reaction was shifted to the formation favorable to tribenzylamine when formic acid was present.

Following the same catalytic reduction procedure, an examination was then made using cyclohexanone. Formamide was, however, inert with cyclohexanone in the hydrogenation system, probably owing to the low

Table 3.[a] Catalytic reduction[b] of cyclohexanone in the Leuckart-Wallach reaction system

Run No.	Additive[c]	Reaction time (min)	Yield (%) of the product[d]			
			ROH	RNH_2	R_2NH	Total
1	$HCONH_2$(1.0)	—	—	—	—	0
2	$HCONH_2$(1.0) HCO_2H(0.5)	—	—	—	—	0
3	Ammonium carbonate(1.0)	210	1	15	82	98
4	HCO_2NH_4(1.0)	210	0	6	93	99
5	RNH_2(1.0)	180	5	3[e]	92	97
6	RNH_2(1.0) HCO_2H(0.5)	180	trace	2[e]	92	92

a) R=⟨H⟩–. b) Hydrogenation condition—catalyst, 10% Pd–C, 6 g; initial hydrogen pressure, 80 kg/cm² (room temp); reaction temp, 55—60 °C. c) Molar equivalents of the additives to the cyclohexanone (0.2 mol) used are given in parenthesis. d) Yield of the product isolated is calculated from the starting cyclohexanone. e) Recovery.

temperature (60 °C) which restricts the carbon dioxide formation. As can be seen in Table 3, ammonia and ammonium formate lead to the formation of cyclohexylamine and, more favorably, dicyclohexylamine. Cyclohexylamine, even in the presence of formic acid, was shown to greatly effect the formation of dicyclohexylamine in the same hydrogenation system. No formation of tricyclohexylamine from cyclohexanone was observed even for hydrogenation in the presence of dicyclohex l-amine. The lack of any tricyclohexylamine formation throughout the above runs may be due to a steric hindrance.

The Formic Acid Reduction Stage. After an understanding of the behaviors of formamide and ammonium

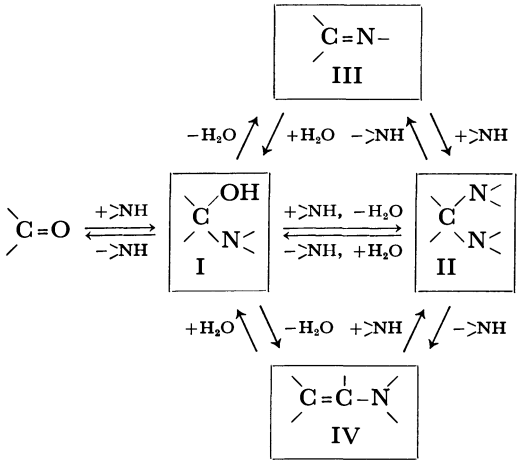

Relation to the reagent

a. In the case of >NH=ammonia and amines
NH_3 and $-NH_2$ ⟶ I, II, III
>NH ⟶ I, II, IV (with >CHCO–)

b. In the case of >NH=$HCONH_2$ and HCONH–
$HCONH_2$ ⟶ I, II, III
HCONH– ⟶ I

Scheme 2.

formate toward carbonyl compounds, the formic acid reduction stage in the Leuckart-Wallach reaction encounters a problem. Plausible intermediates resulting from the addition and condensation reactions of ammonia (from ammonium formate) and of formamide with the carbonyl compounds can be described as in Scheme 2. In the Leuckart-Wallach reaction, how these intermediates participate in the formic acid reduction is a subject to be studied in relation to their catalytic reductions.

For Ammonia or Amine Condensation Intermediates: Both the formic acid and the catalytic reductions of Schiff's bases[7,19] of type III and enamine[20] of type IV in Scheme 2 are well documented to result in the reduction of their C=N and C=C double bonds, respectively. In previous work,[11,21-24] several available analogs of types I and II such as 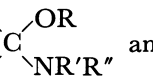 and 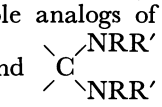 (R, R', and R''≠H) have been known to undergo reductive fission of one of the two bonds to the hetero-atom to give a tertiary amine by formic acid reduction, as well as catalytic reduction, as is shown in the following schemes:

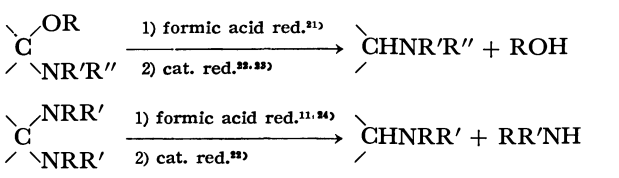

Since in these reported reduction, reductive fission has been realized to occur directly, the intermediates of types I and II 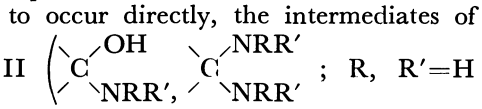 ; R, R'=H or alkyl) seem to undergo reductive fission without dehydration and deamination, respectively.

Thus, any type of intermediate shown in Scheme 2 can produce the same amine products upon reduction with formic acid, as well as upon catalytic reduction.

For Formamide Condensation Intermediates: Plausible condensation intermediates from formamide may be assumed to be of types I, II and III in Scheme 2. Previous papers appear to draw some insight relative to the formic acid and catalytic reductions of types I and II. There have been reported the catalytic reduction of 4-oxazolidinones and tetrahydro-4H-1,3-oxazin-4-ones,[25] the formic acid reduction of 3-aryl-3-hydroxyphthalimidines[26] and the catalytic[27] and the formic acid reductions[6] of *N,N'*-benzylidenebisamides. These substrates are regarded as analogs of types I and II. The reductions affect the reductive fissions, as is shown by the dotted lines in the following schemes, resulting in *N*-acylated amines. The patterns of these reactions

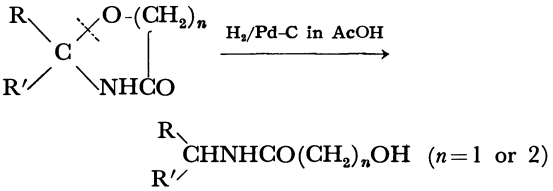

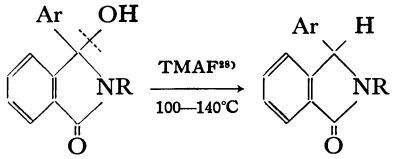

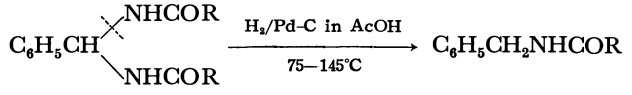

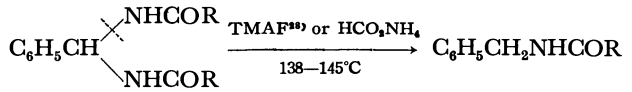

may not be in conflict in receiving types I and II as plausible intermediates.

In order to obtain further information about an intermediate of type I, an examination was directed to the synthesis of *N*-(α-hydroxybenzyl)amide and its formic acid reduction. The synthesis was successfully performed by the hydrolysis of *N*-(α-piperidinobenzyl)-benzamide with aqueous acetic acid. The formic acid reduction of *N*-(α-hydroxybenzyl)benzamide with TMAF[28] proceeded at 95—100 °C, while carbon dioxide was detected in a short period. Although most of the material was converted into benzaldehyde and benzamide, benzylamine was obtained even in a low yield (about 3%) through hydrolysis. Neverthless, it may be possible for the benzaldehyde reaction that *N*-(α-hydroxybenzyl)formamide exists in a certain equilibrium for the conventional use of a large excess of formamide. Type I is therefore referred to as a plausible intermediate in the reaction with formamide.

Comprehensive Aspect of the Leuckart-Wallach Reaction. In spite of the confusion in the previous arguments for the Leuckart-Wallach reaction, the present work in the catalytic reduction system has demonstrated both the ammonia- or amine-addition and the formamide-addition to the carbonyl compound in the initial stage. The latter was shown to be favorable for rather reactive carbonyl compounds such as benzaldehyde, while the presence of formic acid was necessary. *N*-Alkylformamide was nearly inert with the carbonyl compounds as demonstrated by the interaction of benzaldehyde with *N*-benzylformamide. The behaviors of plausible intermediates for formic acid reduction in the Leuckart-Wallach reaction are described in relation to their catalytic reduction which proceeded in a similar fashion giving the same amine products. Since mutual conversion between the intermediates are possible, it appears difficult to decide the actual intermediate undergoing the formic acid reduction for each of the various carbonyl compounds. In opposition to previously reported statements, clear accounts for the features of the Leuckart-Wallach reaction can be drawn from our results. In the formic acid reductions, the formamide-condensation intermediates are reduced to *N*-formyl primary amine, while the ammonia- or amine-condensation intermediates are reduced to primary, secondary and tertiary amines, the former two undergoing successive *N*-formylation or reacting competitively with the carbonyl compound. Ammonium formate as a reacting species therefore reacts to produce tertiary

amine and/or *N*-formyl secondary amine rather than *N*-formyl primary amine, particularly under conditions accelerating the carbonyl addition (the presence of formic acid is effective), whereas formamide reacts in favor of the production of *N*-formyl primary amine. The reaction with formamide as given by Eq. 3, however, involves a considerable participation of ammonium formate generated from formamide by the hydrolysis with water formed in the reaction mixture. In conformity with the above features several papers dealing with the behaviors of the Leuckart-Wallach reagents for the preparative purpose of yielding *N*-formyl primary amine have reported that a mixture of formamide and formic acid or ammonium formate is more efficient in several cases[9,13,16,29] rather than the use of ammonium formate alone. The predominant formation of *N*-formyl primary amine by the increase in the formamide participation is brought on by the reaction with formamide alone, but in this case the reduction is suggested to be caused through self oxidation-reduction of the carbonyl compound rather than by formic acid.

Experimental

Reaction of Benzaldehyde with Formamide, Formic Acid–Formamide and Ammonium Formate (Table 1). The reactions of benzaldehyde were carried out by heating with constant stirring of the reagents, *i.e.*, freshly distilled formamide (run 1), formic acid-formamide (run 2) and dried ammonium formate (run 3). The starting amounts and the reaction temperatures are listed in Table 1. In runs 2 and 3 considerable CO_2 evolution was observed, whereas in the run with formamide almost none was detected even at the high temperature given. The products were concentrated by distilling off the excess of the reagents under reduced pressure in runs 1 and 2, whereas in run 3 this was accomplished by benzene extraction since the reaction mixture solidified. In run 2, *N,N'*-benzylidenebisformamide, mp 148—149 °C [lit,[30] mp 149—150 °C], was isolated in a 24% yield from the residue as a benzene insoluble material. The concentrates were subjected to fractional distillation under reduced pressure to give two fractions, bp 134—136 °C/0.3 mmHg and bp 164—166 °C/0.3 mmHg, leaving a resinous residue only in run 1. The first solid fraction was identified as *N*-benzylformamide, mp 57—59 °C. The second fraction was shown to be composed of tribenzylamine and *N,N*-dibenzylformamide. Their separation was accomplished by passing dry HCl through the benzene solution, resulting in the precipitation of tribenzylamine hydrochloride, mp 226—228 °C. After filtration, the filtrate was freed of HCl by treating with aqueous $NaHCO_3$, dried over $MgSO_4$ and concentrated to leave crystals which were identified as *N,N*-dibenzylformamide, mp 49—50 °C. The foregoing distillation residue obtained in run 1 was chromatographed through silica gel using $CHCl_3$ as an eluent. From earlier fractions 1.5 g of amaron was obtained, mp 245—246 °C [lit,[30] mp 246—247 °C].

All the products obtained above were identified by comparison of their IR spectra with those of authentic specimens and by the mixed melting point test. Their yields are shown in Table 1.

Reactions of Cyclohexanone with Formamide, Formic Acid–Formamide and Ammonium Formate (Table 1). The reactions of cyclohexanone were carried out in a way similar to those of benzaldehyde under the conditions listed in Table 1. In the course of the reactions, considerable CO_2 was detected when formic acid–formamide and ammonium formate were used. The reaction solutions were concentrated under reduced pressure to remove excess amounts of the reagents. In every run, the resulting residue was distilled into two fractions, bp 123—125 °C/4 mmHg and bp 150—154 °C/4 mmHg, leaving a resinous residue only in the run with formamide (run 4). The former fraction was shown to be *N*-cyclohexylformamide [Found: C, 66.36; H, 10.36; N, 10.71%. Calcd for $C_7H_{13}NO$: C, 66.10; H, 10.30; N, 11.01%] and the latter *N,N*-dicyclohexylformamide, mp 53—56 °C [Found: C, 74.65; H, 10.98; N, 6.71%. Calcd for $C_{13}H_{23}NO$: C, 74.59; H, 11.08; N, 6.69%]. Their yields are recorded in Table 1.

Catalytic Reductions of Benzaldehyde in the Leuckart-Wallach Reaction System (Table 2). In the presence of the reagents indicated in Table 2, the high-pressure hydrogenation of benzaldehyde was carried out over a Pd–C catalyst under the conditions given in Table 2. The reductions were accomplished by constant shaking at 90—100 °C, for which a preliminary test showed no formation of CO_2, and were continued until the pressure drop nearly ceased. After filtration of the autoclave contents, the filtrates were concentrated, whereupon benzyl alcohol was distilled together with formamide. With the addition of water to the distillates followed by distillation, benzyl alcohol alone was steam-distilled and isolated by saturation of the resulting distillate with K_2CO_3 and then by extraction with benzene. The above concentration residues were subjected to distillation under reduced pressure. In runs 5, 7, 8, and 12, where *N,N*-dibenzylformamide and tribenzylamine were present in the residue, this product was distilled as a mixture at bp 142—160 °C/0.2 mmHg. Their separation was accomplished by the same procedure as described in the first section. In addition to *N,N*-dibenzylformamide and tribenzylamine, *N*-benzylformamide was present in the residue in runs 2, 3, and 4, and free dibenzylamine in that of run 10. For these runs all the *N*-benzylformamide and dibenzylamine were distilled separately from the other two products at bp 125—129 °C/0.2 mmHg and bp 122—127 °C/1 mmHg, respectively. In runs 6, 9, and 11, where the residue was composed of dibenzylamine and tribenzylamine, these products were simply separated as two distillates, bp 122—127 °C/1 mmHg and bp 165—171 °C/1 mmHg, respectively. All the products were identified by comparison of their IR spectra with those of authentic specimens and by mixed melting point tests. Their yields are recorded in Table 2.

Catalytic Reductions of Cyclohexanone in the Leuckart-Wallach Reaction System (Table 3). As indicated in Table 3, the high-pressure hydrogenations of cyclohexanone were carried out in the presence of the Leuckart-Wallach reagents over a Pd–C catalyst. The reduction temperature was maintained at 55—60 °C, a temperature for which formic acid reduction was not effective. After filtration of the autoclave contents, the filtrates combined with methanolic rinsings were concentrated, whereupon volatile cyclohexylamine was distilled together with MeOH. Acidification of the distillates with aqueous HCl followed by concentration gave cyclohexylamine hydrochloride. In run 4, the concentration residue was wholly solidified as crystals, while in run 6 only partly so, and the crystals were identified to be dicyclohexylammonium formate, needles from acetone–MeOH, mp 161—162 °C [lit,[15] mp 166—167 °C]. Found: C, 68.75; H, 11.08; N, 6.23%. Calcd for $C_{13}H_{25}NO_2$: C, 68.68; H, 11.08; N, 6.16%. Mixtures composed of cyclohexanol and dicyclohexylamine were obtained as the filtrate in run 6 and as the concentration residue in runs 3 and 5. The two components of these mixtures were separated by distillation under reduced pressure. During the distillation, dicyclohexylamine and cyclohexanol partly formed a crystalline sublimate, which was identified as

the adduct, $(C_6H_5)_2NH\cdot C_6H_5OH$, mp 51—54 °C [lit,[31] mp 47—48 °C]. Found: C, 76.14; H, 12.37; N, 5.02%. Calcd for $C_{18}H_{35}NO$: C, 76.80; H, 12.53; N, 4.98%. The yields of the products are recorded in Table 3.

Preparation of N-(α-Hydroxybenzyl)benzamide and its Formic Acid Reduction. A suspension of 2.9 g of powdered *N*-(α-piperidinobenzyl)benzamide[32] in 42 ml of 3% AcOH was heated at 85 °C for 10—15 min with vigorous stirring and then immediately cooled. The suspended precipitates were collected by filtration, washed with a small amount of cold water and quickly dried. Recrystallization from dry $CHCl_3$ gave needles of *N*-(α-hydroxybenzyl)benzamide, mp 100—102 °C. Yield, 0.8 g (35%). IR ν_{max} (KBr) 3265, 1640, 1520, and 1032 cm^{-1}. Found: C, 74.29; H, 5.78; N, 6.17%. Calcd for $C_{14}H_{13}NO_2$: C, 73.99; H, 5.77; N, 6.16%.

A mixture of 4.6 g of *N*-(α-hydroxybenzyl)benzamide and 28 g of TMAF[28] was heated with stirring at 95—100 °C for about 40 min, after which the CO_2 detected was negligible. The reaction solution was concentrated under reduced pressure, whereupon benzaldehyde was distilled off together with the excess TMAF. Basification of the distillate with KOH and extraction with benzene gave benzaldehyde in a 95% yield. In order to detect *N*-benzylbenzamide in the residue, which was mostly composed of benzamide, a hydrolyzed solution of the residue with 50% ethanolic KOH was subjected to GLC using a column packed with Carbowax 20 M on 20% KOH-Chromosorb W. The benzylamine was detected in a 3% yield.

The authors wish to thank Mr. K. Narita and the other members of the Analysis Center of this college for the elemental analyses.

References

1) M. L. Moore, *Org. React.* Vol. V, 301 (1949).
2) O. H. Wheeler, "The Chemistry of the Carbonyl Group," ed. by S. Patai, Interscience Publishers, New York, N. Y. (1966), p. 530.
3) C. A. Buehler and D. E. Pearson, "Survey of Organic Syntheses," Wiley-Interscience, New York, N. Y. (1970), p. 427.
4) H. W. Gibson, *Chem. Rev.*, **69**, 679, 687 (1969).
5) Note its hygroscopic property, because available formamide often contains a small amount of ammonium formate.
6) M. Sekiya, Y. Harada, and K. Tanaka, *Chem. Pharm. Bull. (Tokyo)*, **15**, 833 (1967).
7) M. Sekiya, K. Ito, A. Hara, and J. Suzuki, *Chem. Pharm. Bull. (Tokyo)*, **15**, 802 (1967).
8) O. Wallach, *Ann. Chem.*, **343**, 54 (1905).
9) F. S. Crossley and M. L. Moore, *J. Org. Chem.*, **9**, 529 (1944).
10) E. R. Alexander and R. B. Wildman, *J. Am. Chem. Soc.*, **70**, 1187 (1948).
11) E. Staple and E. C. Wagner, *J. Org. Chem.*, **14**, 559 (1949).
12) W. H. Davies and M. A. T. Rogers, *J. Chem. Soc.*, **1944**, 126.
13) J. Doeuvre and J. L. Courtois, *Bull. Soc. Chim. Fr.*, **11**, 545 (1944).
14) V. J. Webers and W. F. Bruce, *J. Am. Chem. Soc.*, **70**, 1422 (1948).
15) P. Mastalgi, M. Metayer, and G. de Bievre-Gallin, *Bull. Soc. Chim. Fr.*, **1948**, 662; M. Metayer, *ibid.*, **1948**, 1097.
16) C. B. Pollard and D. C. Young, *J. Org. Chem.*, **16**, 661 (1951).
17) M. Mousseron, R. Jacquier, and R. Zagdoun, *Bull. Soc. Chim. Fr.*, **1952**, 197; M. Mousseron, R. Jacquier, and R. Zagdoun, *ibid.*, **1953**, 974.
18) A. F. Rekasheva and G. P. Miklukhin, *Zh. Obshch. Khim.*, **26**, 2155 (1956).
19) R. Boltzly and O. Kauder, *J. Org. Chem.*, **16**, 173 (1951); K. Mori, H. Sugiyama, and M. Sekiya, *Chem. Pharm. Bull. (Tokyo)*, **19**, 1722 (1971).
20) P. L. deBenneville and J. H. Macartney, *J. Am. Chem. Soc.*, **72**, 3073 (1950); G. Opitz and W. Merz, *Ann. Chem.*, **652**, 163 (1962).
21) K. Ito, H. Oba, and M. Sekiya, *Chem. Pharm. Bull. (Tokyo)*, **20**, 2112 (1972).
22) N. Sakura, K. Ito, and M. Sekiya, *Chem. Pharm. Bull. (Tokyo)*, **20**, 1156 (1972).
23) M. Senkus, *J. Am. Chem. Soc.*, **67**, 1515 (1945).
24) H. T. Clarke, H. B. Gillespie, and S. Z. Weisshaus, *J. Am. Chem. Soc.*, **55**, 4571 (1933); A. Lukasiewicz, *Tetrahedron*, **19**, 1789 (1963).
25) K. Ito and M. Sekiya, *Chem. Pharm. Bull. (Tokyo)*, **20**, 1762 (1972).
26) M. Sekiya and Y. Terao, *Chem. Pharm. Bull. (Tokyo)*, **20**, 2128 (1972).
27) M. Sekiya and M. Tomie, *Chem. Pharm. Bull. (Tokyo)*, **15**, 238 (1967).
28) The distillable liquid formate, bp 91—93 °C/18 mmHg, composed of formic acid and trimethylamine; L. F. Fieser and M. Fieser, "Reagents for Organic Synthesis," Vol. 1, John Wiley & Sons, Inc., New York, N. Y. (1967), p. 1231; M. Sekiya, *Yuki Gosei Kagaku Kyokaishi*, **34**, 67 (1976); K. Narita and M. Sekiya, *Chem. Pharm. Bull. (Tokyo)*, in press.
29) A. W. Ingersoll, J. H. Brown, C. K. Kim, W. D. Beauchamp, and G. Jennings, *J. Am. Chem. Soc.*, **58**, 1808 (1936).
30) K. Bülow, *Chem. Ber.*, **26**, 1972 (1893).
31) C. F. Winaus, *J. Am. Chem. Soc.*, **61**, 3591 (1939).
32) M. Sekiya and H. Sakai, *Chem. Pharm. Bull. (Tokyo)*, **17**, 32 (1969).

Preparation and Reactions of 4-Alkoxy-2,2-bis(trifluoromethyl)-thietanes and 5-Alkoxy-3,3-bis(trifluoromethyl)dithiolanes

Tomoya KITAZUME, Toru OTAKA, Ryutaro TAKEI, and Nobuo ISHIKAWA

Department of Chemical Technology, Tokyo Institute of Technology, Ookayama, Meguro-ku, Tokyo 152

(Received December 27, 1975)

4-Alkoxy-2,2-bis(trifluoromethyl)thietanes, **3** (R=Me and Et), were prepared by the reactions of 2,2,4,4-tetrakis(trifluoromethyl)-1,3-dithietane with alkyl vinyl ethers in a KF–DMF system. A bimolecular condensation product, bis[4,4-bis(trifluoromethyl)thietan-2-yl]ether, **5**, was obtained by the treatment of **3** with concentrated sulfuric acid. On the other hand, when treated with sulfur in DMF in the presence of diethylamine, **3** gave 5-alkoxy-3,3-bis(trifluoromethyl)-1,2-dithiolanes, **8**, in rather good yields. Several reactions of these thietanes and 1,2-dithiolanes, including those with butyllithium, were examined.

In our previous paper, it has been reported that hexafluorothioacetone (**2**) is liberated gently from its dimer, 2,2,4,4-tetrakis(trifluoromethyl)-1,3-dithietane (**1**), in a potassium fluoride–*N*,*N*-dimethylformamide system.[1] Since the dimer is a stable liquid which can be prepared from hexafluoropropene and sulfur directly, the compound seemed to be a useful starting material for the hexafluorothioacetone derivatives. Thus, the earlier studies have been continued, and we now wish to report on the preparation of cycloadducts of hexafluorothioacetone liberated from **1**, with alkyl vinyl ethers and on several reactions of the cycloadducts, 4-alkoxy-2,2-bis(trifluoromethyl)thietanes, and its sulfurized dithiolane derivatives, 5-alkoxy-3,3-bis-(trifluoromethyl)-1,2-dithiolanes.

Results and Discussion

Preparation of 4-Alkoxy-2,2-bis(trifluoromethyl)thietanes (3). The cycloadduct of hexafluorothioacetone with ethyl vinyl ether, 3- or 4-ethoxy-2,2-bis(trifluoromethyl)-thietane, has been reported, though the structure has not been proved conclusively.[2] By the reaction of 2,2,4,4-tetrakis(trifluoromethyl)-1,3-dithietane (**1**) with ethyl vinyl ether in the presence of potassium fluoride in *N*,*N*-dimethylformamide, we obtained the same adduct in a good yield. On the basis of its mass spectrum, the structure was established as to be 4-ethoxy-2,2-bis-(trifluoromethyl)thietane (**3**, R=Et). That is, fragment peaks corresponding to $(CF_3)_2C$–CH_2^+ (*m/e* 164) and EtO–CH=S^+ (*m/e* 90), which resulted from the cleavage of the 4-ethoxythietane ring, as well as to the M^+ 254 molecular ion, were observed. However, the fragment peak corresponding to EtO–CH=$C^+(CF_3)_2$ (*m/e* 208), which should have resulted from another isomer, the 3-ethoxy compound, was not observed. When methyl vinyl ether was used in the above reaction, a similar 4-methoxy compound, **3** (R=Me), was obtained.

Thus, in this heterolytic cycloaddition, hexafluorothioacetone behaved as being normally polarized, *e.g.*, into a negative sulfur atom and a positive carbon atom, although a few examples have appeared in the literature in which hexafluorothioacetone reacts as if the thiocarbonyl group is polarized in the "reverse" direction.[3,4]

Reactions of 4-Alkoxy-2,2-bis(trifluoromethyl)thietanes. As cyclic monothioacetals, 4-alkoxy-2,2-bis(trifluoromethyl)thietanes were presumed to be susceptible to the attack of an acid or a base.

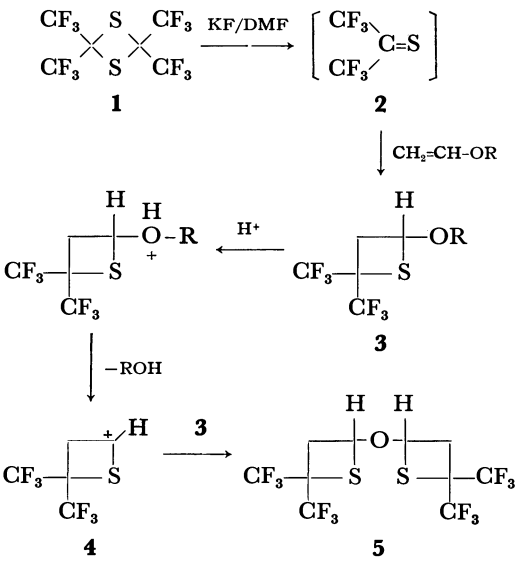

1 **2** **3** **4** **5**

When a solution of the thietane **3** (R=Et) in concentrated sulfuric acid was kept at room temperature for several hours, a bimolecular condensation product was obtained. The structure of this compound was established from its spectral analysis as to be bis[4,4-bis(trifluoromethyl)thietan-2-yl]ether (**5**). In the IR spectrum, no absorption band due to either a OH or SH group was observed. In the ^{19}F NMR spectrum, only one multiplet signal due to CF_3 groups appeared, while in the ^1H NMR spectrum, two signals due to two unequivalent CH_2 protons and one triplet signal due to the CH proton were observed in the appropriate positions. In the mass spectrum, two fragment peaks, *m/e* 209 (base peak) and *m/e* 225, as well as the parent peak, M^+ 434, appeared; they resulted from the cleavage of the ether linkage.

The pathway of the formation of **5** was presumed to be as is shown above. Protonation on the oxygen atom of **3**, followed by the loss of alcohol, gives a carbonium ion, **4**, which is stabilized by the adjacent sulfur atom. This carbonium ion finally attacks another molecule of **3** to give **5**. In order to confirm the formation of the cation, **4**, we carried out the following reactions.

In the presence of sulfuric acid, the ethoxythietane **3** (R=Et) was allowed to react with a large excess of methanol at room temperature. As reaction products, we thus obtained methoxythietane, **3** (R=Me), and

4,4,4-trifluoro-3-mercapto-3-(trifluoromethyl)butyraldehyde dimethyl acetal **6**, in yields of 17 and 30% respectively. The structure of **6** was elucidated from the spectral data. An absorption band due to SH appeared at 2550 cm^{-1} in its IR spectrum, and four signals due to the CH, OCH_3, SH, and CH_2 protons appeared appropriately in its NMR spectrum.

In this reaction, it was presumed that **3** (R=Me) was formed by an alkoxyl exchange *via* the carbonium ion, **4**, whereas **6** was formed by the further nucleophilic attack of a methanol molecule on **3**, which resulted in a cleavage of the thietane ring.

When the reaction mixture was treated with 2,4-dinitrophenylhydrazine and aqueous sulfuric acid, 2,4-dinitrophenylhydrazone of **6** was obtained in a 63% yield. This hydrazone, **7**, was also provided in a good yield (76%) directly from **3** (R=Et and Me) by treatment with 2,4-dinitrophenylhydrazine. These results mean that the cyclic monothioacetal **3**, as well as the dimethyl acetal **6**, behaved equivalently to an aldehyde, as had been expected.

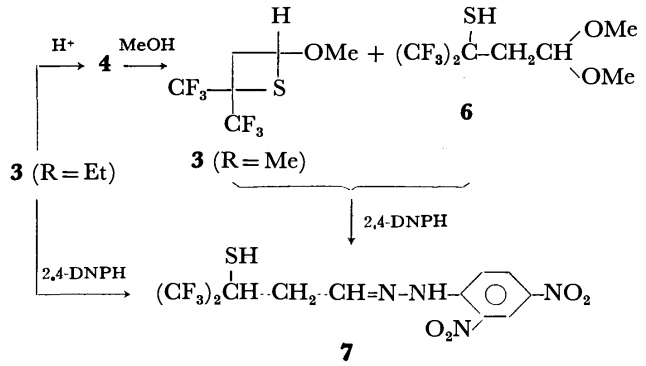

When the ethoxythietane (**3**, R=Et) in a polar solvent was treated with diethylamine or potassium hydroxide at room temperature, 5-ethoxy-3,3-bis(trifluoromethyl)-1,2-dithiolane (**8**) was obtained as the main product. This base-catalyzed disproportionation seems to occur because the five-membered ring of 1,2-dithiolane is thermodynamically more stable than the four-membered ring of thietane.

Preparation of 5-Alkoxy-3,3-bis(trifluoromethyl)-1,2-dithiolanes. An example of the ring-expansion reaction of thietanes into 1,2-dithiolanes involving heating with sulfur has been reported.[5] This direct sulfurization was, however, applied in vain in the preparation of **8** from **3**. In the presence of a base such as diethylamine, however, the thietane, **3**, reacted with sulfur in *N,N*-dimethylformamide, and the 1,2-dithiolane **8** was obtained in a rather good yield:

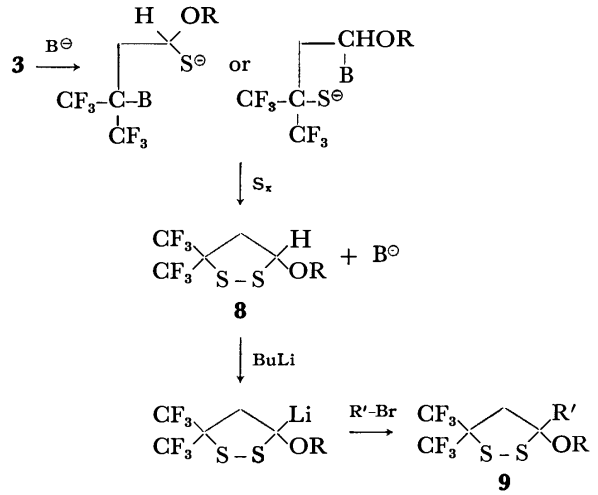

The structure of this 1,2-dithiolane derivative, **8**, was evident from its ^{19}F NMR and mass spectra. The two trifluoromethyl groups of the dithiolane were nuclear-magnetically unequivalent, while those of the thietane compound, **3**, were equivalent, as has been described before. We assumed that, while the five-membered ring is not co-planar,[6] the four-membered ring is nearly co-planar or that its frequency between axial and equatorial vibrations is so quick that the NMR at room temperature is not distinguishable.

The Alkylation of Thietane, 3, and Dithiolane, 8. Because of the adjacent sulfur atom, the carbon atom of the 4-position of the thietane, **3**, and of the 5-position of the dithiolane, **8**, had been expected to be lithiated to give a carbanionic intermediate.

The five-membered 1,2-dithiolane compound, **8**, was easily lithiated with butyllithium in a hexane–tetrahydrofuran solution, and the resulting lithio compound reacted with alkyl bromides to give their 5-alkyl derivatives, **9** (Table 1).

In contrast with the above-mentioned results, the four-membered thietane compound, **3**, gave ring-opened monothioacetal, 4-alkoxy-4-butylthio-1,1-difluoro-2-(trifluoromethyl)-1-butene, **11**, by the similar reaction. The structure of this compound, **11** (R=Et), was also evident from its spectral data. In the IR spectrum, the presence of the C=C double bond was revealed by the absorption at 1748 cm^{-1}. In the ^{19}F NMR spectrum, three signals due to the CF_2=C–CF_3 group appeared. In the ^1H NMR, two noticeable signals due to methine and methylene groups appeared, in addition to those due to butyl and ethyl groups.

Table 1. Preparation of the dithiolane **9**

R	R'	Yield (%)	Bp (°C/mmHg)	^{19}F NMR CF_3		J (Hz)	F Anal (%) Found	Calcd
Me	$CH_2CO_2CH_3$	45	147—150/4	−11.2 q	−11.6 q	10.2	33.3	33.1
Me	$CH_2(CH_2)_3CH_3$	59	120—122/3	−10.3 q	−11.8 q	11.8	33.5	33.3
Et	$CH_2CO_2CH_3$	62	155—156/3	−10.5 q	−11.2 q	9.0	31.6	31.8
Et	$CH_2(CH_2)_3CH_3$	79	125—127/3	−10.3 q	−12.0 q	9.4	32.0	32.0

a) Measured in neat. The values are given in δ ppm from ext. CF_3CO_2H.

TABLE 2. PREPARATION OF THE MONOTHIOACETAL

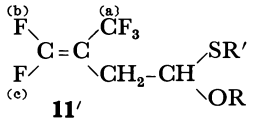

11′

Product R	Product R′	Reactant	Reac. Temp (°C)	Yield (%)	Bp (°C/mmHg)	^{19}F NMR ppm[a] a	b	c	^{19}F NMR J (Hz) J_{ab}	J_{bc}	J_{ca}	F Anal (%) Found	Calcd
Me	*n*-Bu	*n*-BuLi	−60	59	87—90/27	−16.7	−1.0	2.3	20.7	16.9	10.5	34.3	34.1
		n-BuMgBr	r.t.	56									
Me	Ph	PhMgBr	r.t.	63	103—105/20	−17.3	−2.0	1.3	19.3	15.6	10.1	32.2	31.9
Et	*n*-Bu	*n*-BuLi	−60	53	94—95/19	−16.8	−0.7	2.6	19.7	18.3	9.9	32.3	32.5
		n-BuMgBr	r.t.	60									
Et	Ph	PhMgBr	r.t.	67	130—132/27	−17.4	−1.6	1.6	20.1	15.3	10.1	30.7	30.4
Et	Et	EtMgI	r.t.	37	86—90/17	−17.5	−1.8	0.7	19.5	16.8	9.8	36.1	36.0

a) See footnote a) of Table 1.

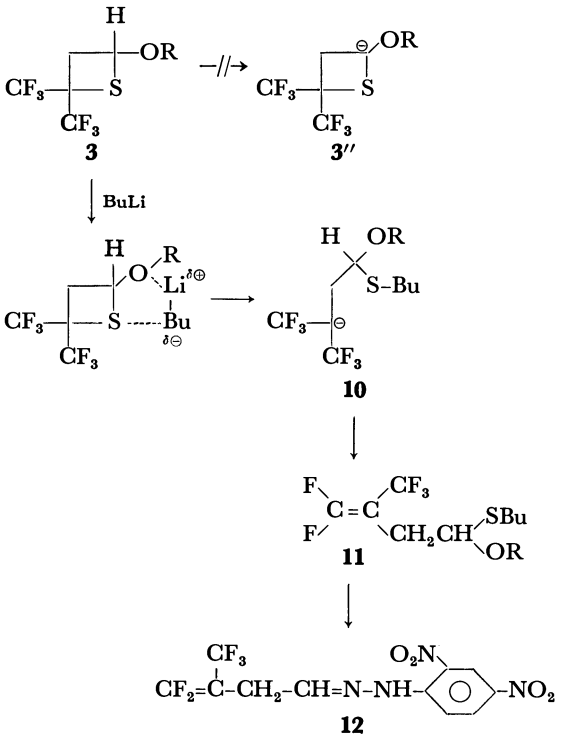

3 3″ 10 11 12

The reaction mechanism was presumed to be as is shown above. Thus, the thietane, **3**, did not give the expected carbanion, **3″**; instead the sulfur atom was attacked by the butyl anion. This must be ascribed to the low stability of the **3″** carbanion, which is too much strained to have a *p*-orbital occupied by two electrons at the 3-carbon atom. The attack of the butyl anion on the sulfur atom might have been promoted by the co-ordination of alkoxy oxygen on lithium, as is shown in the scheme. The reaction was terminated by the liberation of a fluoride ion from one of the trifluoromethyl groups, giving the α-olefin, (**11**).

In order to obtain a range of compounds of this type, we also carried out the reaction of alkoxythietanes (**3**) with Grignard reagents. The corresponding monothioacetals (**11′**) were obtained in good yields (Table 2).

Further, these nomothioacetals yielded a hydrazone, **12**, by a reaction with 2,4-dinitrophenylhydrazine, thus behaving like acetals,[4] as had been expected.

Experimental

4-Ethoxy-2,2-bis(trifluoromethyl)thietane (3, R=Et). A mixture of 2,2,4,4-tetrakis(trifluoromethyl)-1,3-dithietane (36.4 g, 0.1 mol), ethyl vinyl ether (14.4 g, 0.2 mol), potassium fluoride (5.8 g, 0.1 mol) and *N,N*-dimethylformamide (70 ml) was stirred for 24 h at room temperature. The whole was poured into water, and the separated oily material was extracted with diethyl ether. The extract was dried over magnesium sulfate, and the solvent was removed. The residue was then subjected to vacuum distillation, giving **3** (R=Et) (18.3 g) (bp 78—80 °C/70 mmHg (lit,[2] bp 43 °C/10 mmHg)) in a 72% yield.

Found: F, 44.4%. Calcd for $C_7H_8F_6OS$: F, 44.9%. ^{19}F NMR*: δ −3.1 (s). MS: M$^+$ 254, *m/e* 164 ($(CF_3)_2C$–CH_2), *m/e* 90 (EtO–CH=S), *m/e* 145 (CF_2=C(CF_3)CH_2).

4-Methoxy-2,2-bis(trifluoromethyl)thietane (3, R=Me). (bp 145—148 °C/760 mmHg) was obtained in a 68% yield by using methyl vinyl ether instead of ethyl vinyl ether in the above procedure.

Found: F, 47.7%. Calcd for $C_6H_6F_6OS$: F, 47.5%. ^{19}F NMR: δ −3.0 (s).

Bis[4,4-bis(trifluoromethyl)thietan-2-yl] Ether (5). Alkoxythietane **3** (R=Et or Me) (0.04 mol) was dissolved in concd sulfuric acid (10 ml), after which the solution was allowed to stand for 1 h at room temperature. The reaction mixture was then poured into ice water and worked up as has been described above. The crude product solidified upon being stored in an ice-box; it was recrystallized from petroleum ether to give **5**, mp 91—92 °C. Yield: 76% from **3** (R=Et) and 82% from **3** (R=Me).

Found: C, 27.5; H, 1.13; F, 52.4%. Calcd for $C_{10}H_6F_{12}OS_2$: C, 27.7; H, 1.39; F, 52.2%. ^{19}F NMR (in CCl_4): δ 6.5 (m). ^{1}H NMR ($CDCl_3$): τ 6.95 and 7.28 (d of d each, $C\underline{H}_2$, J_{gem}=15.0 Hz), 4.55 (t, $C\underline{H}$, J_{vic}=9.0 Hz). MS: M$^+$ 434, *m/e* 225 ($C_5H_3F_6SO$), *m/e* 209 ($C_5H_3F_6S$).

Reaction of 3 (R=Et) with Methanolic Sulfuric Acid. A mixture of **3** (R=Et, 10.16 g, 0.04 mol), concd sulfuric acid (8 ml), and methanol (40 ml) was stirred for 11 days at room

* All the ^{19}F NMR chemical shifts throughout this article are given in δ ppm from external trifluoroacetic acid. They were measured in neat unless the solvent is indicated.

temperature. The reaction mixture was then poured into water, and a separated oily material was extracted with diethyl ether. Two products, 4-methoxy-2,2-bis(trifluoromethyl)-thietane (**3**, R=Me) and 4,4,4-trifluoro-3-mercapto-3-(trifluoromethyl)butyraldehyde dimethyl acetal, **6**, were separated from each other by means of gas chromatography. The yields, 17% for **3** (R=Me) and 30% for **6**, were determined by GLC, using nitrobenzene as the internal standard.

Thiol **6**: Found: F, 41.7%. Calcd for $C_7H_{10}F_6O_2S$: F, 41.9%. IR: 2550 (S–H), 1070, 1050 (C–O–C) cm^{-1}. ^{19}F NMR: δ −5.6 (s). ^1H NMR τ 5.45 ($CH_2C\underline{H}$, t, J=5.5 Hz), 6.80 ($2\times OC\underline{H}_3$, s), 6.89 ($S\underline{H}$, s), 7.80 ($C\underline{H}_2CH$, d).

4,4,4-Trifluoro-3-mercapto-3-(trifluoromethyl) butyraldehyde 2,4-Dinitrophenylhydrazone (**7**). 2,4-Dinitrophenylhydrazine (2.18 g, 0.011 mol) was dissolved in a mixture of ethanol (47 ml), water (14 ml), and concd sulfuric acid (10 ml). Ethoxythietane **3** (R=Et, 2.54 g, 0.01 mol) was added to this solution, and the whole was stirred for 24 h at room temperature. The precipitated product was collected by filtration and recrystallized from benzene to give the 2,4-dinitrophenylhydrazone; mp 131—132 °C (3.08 g, 76%).

Found: C, 32.4; H, 1.42; N, 13.8; F, 28.0%. Calcd for $C_{11}H_8F_6N_4O_4S$: C, 32.5; H, 1.47; N, 13.8; F, 28.1%. IR: 3305 (NH), 2570 (SH), 1615 (C=N), 1510, 1340 (NO_2) cm^{-1}. ^{19}F NMR ($CHCl_3$): δ −6.5 (s).

5-Alkoxy-3,3-bis(trifluoromethyl)-1,2-dithiolane (**8**). *a) By the Disproportionation of* **3**: Ethoxythietane **3** (R=Et, 5.08 g, 0.02 mol) was dissolved in *N,N*-dimethylformamide (15 ml), and then diethylamine (1.63 g, 0.02 mol) was added to this solution. The whole was stirred for 72 h at room temperature. The reaction mixture was worked up as usual, giving 5-ethoxy-3,3-bis(trifluoromethyl)-1,2-dithiolane (**8**, R=Et) (bp 73—75 °C/11 mmHg, 1.57 g) in a yield of 55%. In the potassium hydroxide–methanol system, the same product was obtained in a 55% yield.

Found: C, 29.5; H, 2.67; F, 39.6%. Calcd for $C_7H_8F_6OS_2$: C, 29.4; H, 2.82; F, 39.8%. ^{19}F NMR: δ −6.4 (q), −8.6 (q). J_{F-F}=10.4 Hz.

No other identifiable products were separated from the distillation residue.

b) By the Sulfurization of **3**: A mixture of ethoxy thietane (**3**, R=Et) (20.3 g, 0.08 mol), sulfur (3.07 g, 0.09 mol), diethylamine (2.92 g, 0.04 mol), and dimethylformamide (50 ml) was refluxed for 1 h. The reaction mixture was then poured into water, and the separated oily material was extracted with diethyl ether. The usual work-up gave the dithiolane (**8**, R=Et) (13.0 g) in a yield of 57%.

When methoxythietane (**3**, R=Me) was sulfurized in a similar way, methoxy dithiolane (**8**, R=Me) (bp 103—105 °C/50 mmHg) was obtained in a 46% yield.

Found: F, 42.1%. Calcd for $C_6H_6F_6OS_2$: F, 41.9%. ^{19}F NMR: δ −6.5 (q), −7.5 (q). J_{F-F}=10.2 Hz.

4-Alkoxy-4-alkyl(or phenyl)thio-1,1-difluoro-2-(trifluoromethyl)-1-butene (**11′**). *a) Reaction of Alkoxythietane* **3** *and Butyllithium*: A hexane solution of butyllithium (1.71 N, 13 ml, 0.022 mol) was stirred into a solution of ethoxythietane (**3**, R=Et) (5.08 g, 0.02 mol) in dry tetrahydrofuran (50 ml) with the temperature kept at −50—−60 °C. After 2 h of stirring at −60 °C, the reaction mixture was poured into water and worked up as usual. Vacuum distillation gave a 1-butene compound, **11** (R=Et) (3.10 g, 53%); bp 94—95 °C/19 mmHg.

Found: F, 32.3%. Calcd for $C_{11}H_{17}F_5OS$: F, 32.5%. IR: 1748 (C=C) cm^{-1}. ^1H NMR: τ 5.60 (t, $CH_2C\underline{H}<$), 6.1—6.9 (m, $S-CH_2C\underline{H}_2C\underline{H}_2$), 7.3—7.7 (m, $OC\underline{H}_2$), 8.3—8.7 (m, $SC\underline{H}_2$) 8.85 (t, $OCH_2C\underline{H}_3$), 8.98 (t, $S(CH_2)_3C\underline{H}_3$). ^{19}F NMR: (Table 2). MS: M^+ (not observed), *m/e* 203 (M^+−SBu), *m/e* 147 (EtO–CH–SBu).

The reaction with methoxythietane **3** (R=Me) gave a similar product, **11** (R=Me), in a 59% yield (Table 2).

b) Reaction of Alkoxythietane **3** *with a Grignard Reagent.* Intoa solution of a Grignard reagent prepared from phenyl bromide (6.91 g, 0.044 mol), magnesium (1.15 g, 0.04 mol), and dry tetrahydrofuran (30 ml), 4-ethoxy-2,2-bis(trifluoromethyl)-thietane **3** (R=Et) (10.16 g, 0.04 mol) was added in the course of 30 min at room temperature. After 3 h of stirring at that temperature, the reaction mixture was worked up as usual. The distillation of the crude product gave an oil, **11′** (R=Et, R′=Ph) (8.23 g, 67%); bp 130—132 °C/27 mmHg.

Found: F, 30.7%. Calcd for $C_{13}H_{13}F_5OS$: F, 30.4%. ^1H NMR: τ 2.5—2.9 (m, Ar$\underline{H}$), 5.37 (t, $CH_2C\underline{H}<$), 5.9—6.9 (d of q, $C\underline{H}_2CH_3$), 7.38 (d, $C\underline{H}_2CH<$), 8.80 (t, $CH_2C\underline{H}_3$). ^{19}F NMR: (Table 2).

Similar reactions with other Grignard reagents were also carried out (Table 2).

4,4-Difluoro-3-(trifluoromethyl)-3-butanal 2,4-Dinitrophenylhydrazone (**12**). Into a solution of 2,4-dinitrophenylhydrazine (2.18 g, 0.011 mol) in ethanol (47 ml), **11′** (R=Et, R′=Bu) (2.92 g, 0.01 mol) and dilute sulfuric acid (concd H_2SO_4 10 ml and H_2O 14 ml) were added. The whole was stirred for 24 h at room temperature, and then worked up as usual. The crude product was recrystallized from acetone to give 2,4-dinitrophenylhydrazone (3.40 g, 96%); mp 120—120.5 °C.

Found: C, 37.4; H, 1.97; N, 16.1; F, 26.9%. Calcd for $C_{11}H_7N_4O_4F_5$: C, 37.3; H, 1.99; N, 15.8; F, 26.8%. IR: 3280 (N–H), 1755 (C=C), 1505, 1365 (NO_2) cm^{-1}. ^{19}F NMR: δ −16.7 (d of d, CF_3), −1.67 (q of d, CF_2), 2.00 (d of q, CF_2).

References

1) T. Kitazume and N. Ishikawa, *Bull. Chem. Soc. Jpn.*, **46**, 3285 (1973).
2) W. J. Middleton, *J. Org. Chem.*, **30**, 1395 (1965).
3) W. J. Middleton and W. H Sharkey, *J. Org. Chem.*, **30**, 1384 (1965).
4) Z. Zubovics and N. Ishikawa, *J. Fluorine Chem.*, **8**, 43 (1976).
5) S. Yurugi, H. Yonemoto, T. Fushimi, and M. Numata, *Yakugaku Zasshi*, **80**, 1691 (1961).
6) (a) O. Foss and O. Tjomsland, *Acta Chem. Scand.*, **11**, 1426 (1957); (b) G. Bergson and L. Schotte, *ibid.*, **12**, 367 (1958).

Photolysis of Organic Azides. II.[1] The Photolysis of 2,2′-Diazidobiphenyl in Rigid Matrices at Low Temperatures

Akira YABE and Koichi HONDA

National Chemical Laboratory for Industry, Nishiyawata, Hiratsuka, Kanagawa 254

(Received January 14, 1976)

The direct, triplet-sensitized, and low-temperature photolyses of 2,2′-diazidobiphenyl have been studied. The direct irradiation afforded 4-azidocarbazole, and the triplet sensitization resulted in the predominant formation of the azo dimer, accompanied by a low yield of benzo[*c*]cinnoline. The photolysis in a rigid matrix at 77 K afforded benzo[*c*]cinnoline quantitatively. The mechanism for its preferential formation in low-temperature matrix photolysis is discussed, and we propose a biphotonic process involving a dinitrene *via* a mononitrene.

The photolysis of 2-azidobiphenyl has received considerable attention in recent years. It has been well established by Swenton and his co-workers[2] that the direct photolysis results in the predominant formation of carbazole and that the triplet sensitization leads to the predominant formation of the azo dimer (2,2′-diphenylazobenzene). In connection with studies of 2-azidobiphenyl, it became of interest to examine the photolytic reaction of 2,2′-diazidobiphenyl (I) and to determine whether the intramolecular azo compound benzo[*c*]cinnoline (II) is given by the triplet-sensitized photolysis.

In our preliminary study[1] of the photolysis of I, we found that, although the sensitized photolysis fell short of our expectations, the low-temperature photolysis in a rigid matrix led to the quantitative formation of II, suppressing other competitive reactions. The preferential intramolecular-azo-bond formation of vicinal diazido compounds under these conditions may provide a useful method for the preparation of cyclo-azo compounds. In this paper, the direct and sensitized photolyses of I and 2,2′-diazido-6,6′-dimethylbiphenyl (VII) at room temperature are examined by comparison with those of 2-azidobiphenyl. Moreover, the low-temperature photolyses in rigid matrices are studied, and we propose a mechanistic scheme involving a dinitrene, which accounts for the exclusive formation of II, on the basis of the absorption spectra at 77 K.

Results

Direct Irradiation of I. It has previously been reported[3] that the direct irradiation of I in heptane affords 4-azidocarbazole (III) in a 50% yield, together with trace amounts of II. We reinvestigated it briefly for a mechanistic study in connection with the sensitized and low-temperature photolyses. In addition to III (55—65%) as the major product, II and the bimolecular product IV were identified in trace amounts (<1%) (Table 1). In the case of I, the photochemical reaction is not simple compared with the photolysis of 2-azidobiphenyl because III and IV still have one more reactive azido group. With the increase in the irradiation time, most of the photoproducts become intractable polymeric materials. Hence, the yields of these compounds (also VI, which will be described later) are subject to experimental indefiniteness. Therefore, the following product yields were determined in an earlier stage which could be analyzed. Unless otherwise stated, the product analysis was carried out within about 20% of conversion at most. Among the final products, the azo dimer (V) of III was not detected, although the irradiation of isolated III seemed to afford the azo dimer, which was characterized by an absorption spectrum with a broad peak between 350 and 400 nm. The yield of III is rather insensitive to solvents, as is shown in Table 2.

Table 1. Products from the irradiation of I

Reactants	Solvent	Temperature	Products
I(4×10^{-4} M)[a]	Hexane	Room temp	III (65%), II & VI (trace)
I(10^{-2} M)[a]	Hexane	Room temp	III (55%), II & VI (trace)
I(10^{-2} M), Acetophenone (1.8 M)[b]	Benzene	Room temp	VI (45%), II (<5%), IV (trace)
I(10^{-2} M), Benzophenone (0.5 M)[b]	Benzene	Room temp	VI (40%), II (<5%), IV (trace)
I(6×10^{-4} M)[a]	EPA	77 K	II (98%)
I(6×10^{-4} M)[a]	3MP	77 K	II (98%)
I(5×10^{-4} M)[a]	Glycerol	201 K	II (55%), III (10%)

a) Irradiation with a 6W low-pressure mercury lamp. b) Irradiation with a 100W high-pressure mercury lamp through a filter solution of 0.13 wt% naphthalene in ethyl alcohol.

Table 2. Effect of solvents on the direct irradiation of I[a]

Solvent	Yield of III
Hexane	50—55%
Ether	48—54%
Benzene	45—52%
2-Propanol	46—52%

a) 10^{-2} M solution of I; irradiation with a 6W low-pressure mercury lamp through a UV-D25 filter.

Sensitized Photolysis of I. In connection with the photolysis of 2-azidobiphenyl, where the triplet sensitizer led to the predominant formation of the azo compound, we could expect that triplet sensitizers would increase the yield of II in the photolysis of I. With this expectation, we used acetophenone and benzophenone, which are good triplet sensitizers in the case of 2-azidobiphenyl. Both sensitizations afforded the intermolecular azo compound (VI), instead of the expected II, as the major

product, although the yield of II increased relatively (<*ca.* 5%) (Table 1).

Low-temperature Photolysis of I in a Rigid Matrix. Photolyses of azido compounds at low temperatures in rigid matrices have been studied with considerable attention from the spectroscopic point of view of the nitrenes resulting from them. It is well-known that the irradiations of many aromatic azides in organic matrices at the temperature of liquid nitrogen afforded indefinitely stable intermediate nitrenes.[4] However, no study of the low-temperature photolysis of vicinal diazido compounds has been reported. It is thus of interest to examine whether both mononitrenes and dinitrenes are trapped or converted to some final products under these conditions.

We found that the intramolecular azo compound II was formed effectively with a short irradiation of I in a rigid matrix at low temperatures. The irradiation of I in EPA (5:5:2), 3-methylpentane (3 MP), or methylcyclohexane–isopentane (1:3) at 77 K resulted in an almost quantitative formation of II. The photolysis of I in a glycerol matrix at −72 °C gave 55% of II and about 10% of III. At 77 K the dependence of the yield of II on the solvents was not observed, and there were no reactions with solvents.

Photolysis of VII. In order to study the steric effects on the reactivity of the vicinal two azido groups, the photolysis of VII was briefly examined. The first attempt at the pyrolysis and photolysis of VII by Coffin and Robbins[5] resulted in amorphous materials which could not be characterized. Our attempts to obtain the intramolecular azo compound (1,10-dimethylbenzo[*c*]-cinnoline: VIII) by the triplet-sensitized photolysis of a 10^{-3} M solution of VII in benzene with acetophenone or benzophenone gave only unidentified polymeric materials, like the direct irradiation. However, the irradiation of a 5×10^{-4} M solution of VII in EPA at 77 K afforded expected VIII in a 60% yield.

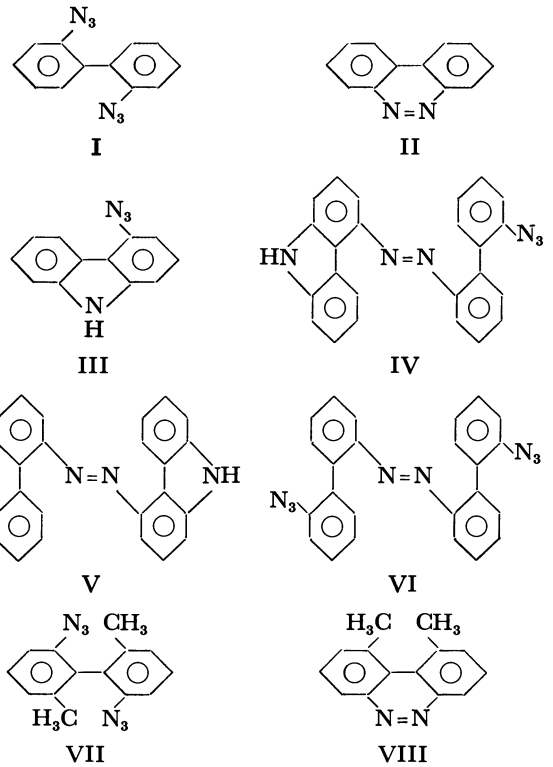

Discussion

The results of the photolysis at room temperature indicate that the reaction mechanism is rather similar to that for 2-azidobiphenyl. The direct irradiation led exclusively to the inserted compound (III) in the *o'*-position of biphenyl, and the azo compound formation is almost negligible. The lower yield of III, compared with the yield of carbazole in the case of 2-azidobiphenyl, must be due to some subsequent reactions by one more azido group, resulting in polymeric materials. Also, the triplet sensitization was similar to that of 2-azidobiphenyl. The predominant formation of the intermolecular azo compound rather than the intramolecular one could be explained in terms of a structural factor of *o,o'*-disubstituted biphenyls. Although it is difficult to deduce exactly the structure of the excited triplet I, which is presumed to be the precursor for the azo bond formation,[6] the two azido groups must be situated in positions which are far apart from each other, as is shown in Ia. In view of the spectroscopic study of

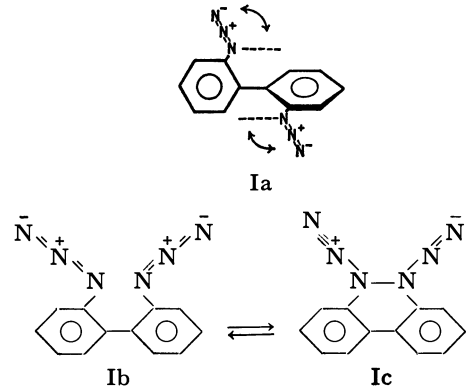

hindered biphenyl compounds, the twisting about the central (1,1')bond (the angle θ between the two benzene rings) seemed to be similar to that of 2,2'-dimethylbiphenyl ($\theta=70°$), since the effective radius of an azido group is 2.04 Å,[7] compared to 2.0 Å of a methyl group. Moreover, the close similarity of the absorption spectra of 2-azidobiphenyl, I, and VII indicates that such interaction between two "vicinal" azido groups, as represented by the structures of Ib and Ic, is negligible. Thus, the bulky two azido groups are partly free to rotate about the C–N bond at room temperature, as is shown in Ia, and they must prefer the intermolecular one.

The photolysis of I in a rigid matrix at 77 K gave a clear-cut product different from that obtained at room temperature. There is no doubt that the matrix rigidity suppresses a bimolecular reaction. The intramolecular insertion in the *o'*-position, however, could be a possible reaction like the carbazole formation by the irradiation of 2-azidobiphenyl in a rigid matrix at 77 K.[8a] In what follows, we wish to discuss the low-temperature photolysis. The possible mechanisms leading to II from I may be depicted as follows.

Path A involves the azido-azido intramolecular-interacting structure Ic; Path B, the attack on an

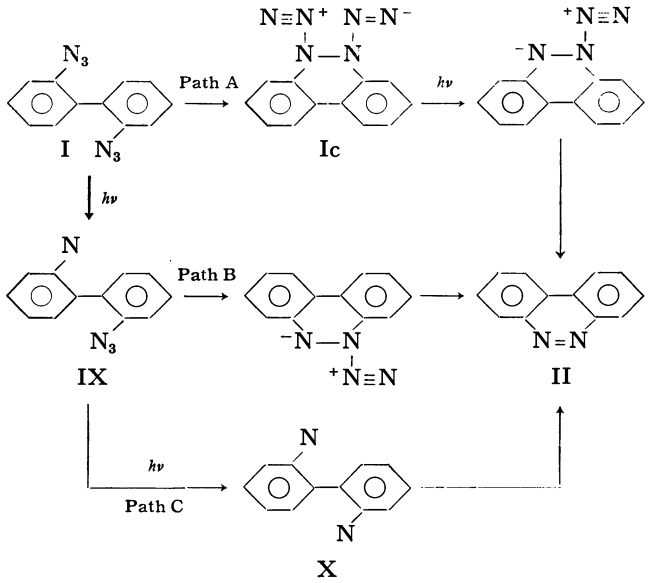

intramolecular azido group by the nitreno group (IX); and Path C, the intramolecular recombination of the nitreno groups (2,2′-dinitrenobiphenyl: X) *via* IX. Although the Ic structure in Path A was excluded in the case of photolysis at room temperature, it must be considered a little possible in low-temperature photolysis because the rotation about the C–N bond may be locked in the plane of the ring at 77 K.[8b] If the two azido groups are locked in a rather non-hindered state, the activation energy for the rotation of benzene rings must be lowered to only a few kcal/mol. However, the observed absorption spectrum at 77 K does not shift from that at room temperature. Therefore, the twisting about the central (1,1′) bond seems to be similar to that at room temperature. Thus, Path A may be ruled out, although the mechanisms involving Ic in an excited state still remain as possibilities.

Both Paths B and C involve 2-azido-2′-nitrenobiphenyl (IX) as an intermediate, whereas Path A does not require a discrete intermediate. It seemed first that II was produced directly without being trapped as the nitrene or dinitrene intermediate upon the direct irradiation of I. However, the results from the absorption spectra which are followed with a faint irradiation indicate at least a two-step process (Fig. 1). The absorption peaks of I at 232 and 252 nm decreased slightly upon a faint irradiation. Then, with the increase in irradiation the strong peaks belonging to II appeared rapidly in the same region. When the cell which was immersed in liquid nitrogen was taken up outside at room temperature after a faint irradiation at 77 K, and after this procedure had been repeated over and over again, III was obtained, whereas it was never detected after complete irradiation at 77 K within the limits of our analytical method. These results indicate that IX is trapped as an intermediate in the initial stage of photolysis. In Fig. 1, the decrease in absorbance at about 250 nm after a faint irradiation means that only a small fraction of I is converted to IX in preference to the formation of II. The extinction coefficient of II (33000 at 250 nm) is larger than that (18400 at 252 nm) of I; consequently, that of IX near

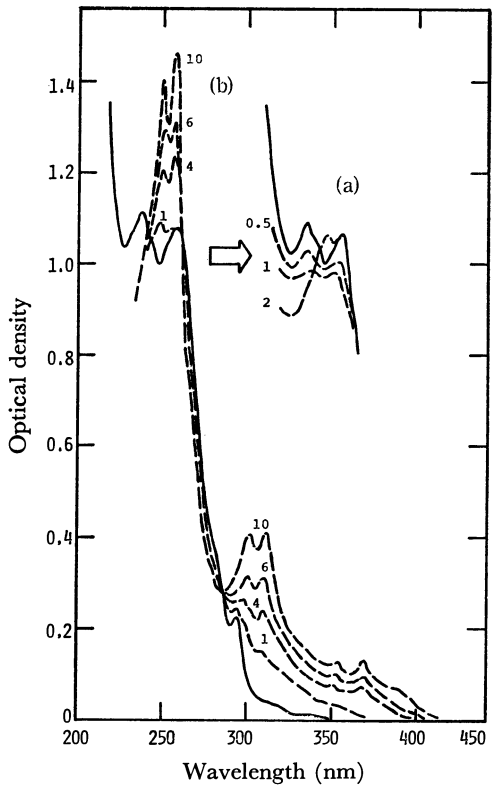

Fig. 1. Absorption spectra of I in EPA at 77 K, —: before irradiation, ---: (a) in the region at ɒ50 nm after irradiation through the 1/2 slit, (b) after irradiation through the open slit. Numbers refer to irradiation time in minutes.

250 nm is estimated to be less than that of I. When the cell with the decrease in absorbance at 250 nm was kept in the dark at 77 K, the absorbance increased very slightly (about 2—3%) for periods as long as 4 h. Although this increase in absorbance may indicate the formation of II from IX along Path B, the rate is almost negligible compared with that of the formation upon further irradiation.

Another clue to elucidating whether the mechanism is Path B or C is the dependence of the formation rate of the final product, II, on the incident-light intensity. Path C is a biphotonic process, whereas Path B is monophotonic. The yields of II *vs.* the irradiation time

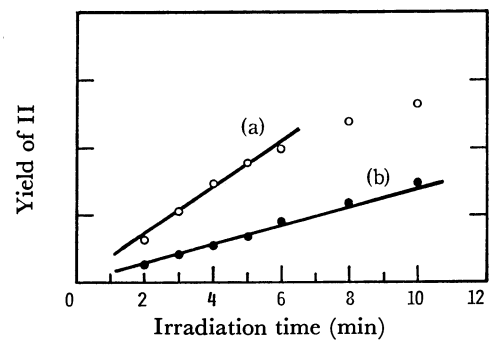

Fig. 2. Dependence of the formation rate of II from I in EPA at 77 K on the light intensity, (a) ○: I_0, (b) ●: $I_0/2$. The ratio of the formation rate is 1: 1/3.4, which is calculated from the slopes of (a) and (b).

were plotted in each case of light intensity, I_0 and $I_0/2$ (Fig. 2). The observed ratio for the formation rate of II is 1 : 1/3.4. Since the extinction coefficient of the product (II) at 253.7 nm is high, and since the diffusion rate in a glassy matrix at 77 K is remarkably low, the actual rate in the case of I_0 is deduced to be additional. Hence, the ratio must approach further to 1/4, which is a theoretical value if it is a biphotonic process.

Thus, it may be concluded that the mechanism for the formation of II in low-temperature matrix photolysis involves the dinitrene (X) *via* the mononitrene (IX). This conclusion is supported by the following observation; the formation of II is due both to the low temperature and to the rigidity of matrices. When the irradiation of I in an isopentane–methylcyclohexane (3: 1) matrix, which formed II quantitatively at 77 K, was carried out in a slightly softened matrix at a slightly increased temperature (about 90 K), the yield of II decreased remarkably, presumably to below 10% (the small amounts of the photoproduct prevented accurate yield data). At the temperature of methanol–solid carbon dioxide (−72 °C), the photolysis gave 55% of III, as at room temperature. At the same temperature, on the contrary, the irradiation in a glycerol matrix with high viscosity (about 10^{13} Poise[9]) gave III in a 55% yield, together with about 10% of II, although the yield of II decreased considerably compared with that in a rigid matrix at 77 K. These results agree with the observations in trapping aromatic nitrenes. Reiser and his co-workers[8b] have found that many aromatic nitrenes are indefinitely stable in a rigid matrix at 77 K, and that a small increase in the temperature (from 77 to 90 K) sufficient to soften slightly the matrix invariably causes the nitrenes to disappear. When 2-azidobiphenyl was irradiated in a glycerol matrix at −72 °C, 2-nitrenobiphenyl could no longer be trapped and carbazole was formed directly. At this temperature the formation of carbazole from 2-nitrenobiphenyl proceeded thermally with no photon, although the conversion of trapped 2-nitrenobiphenyl into carbazole at 77 K was a less efficient photolytic process. This activation energy was estimated to be 8 kcal/mol[8b] or 11.46 kcal/mol.[6] This must also be roughly the case for I. In the stage in which IX is generated, the insertion reaction leading to III must be competitive with the decomposition of the second azido group. Although the latter is still efficient, even at low temperatures, the former, which is an activated process, must be highly affected by the reaction temperature. That is, the formation of III from IX, which is a facile thermal reaction at room temperature or even at −72 °C, is greatly suppressed in a rigid matrix at 77 K. Thus, generated IX survives and is converted into the dinitrene (X) upon further irradiation. Although the quantum yield (Φ_2) for the decomposition of the second azido group could not be determined, we can presume it to be as follows. The quantum yields for the decomposition of I and VII at room temperature are 0.44 and 0.42 respectively, and these must be very similar to the quantum yields (Φ_1) for the decomposition of the first azido group at low temperatures. If it is assumed that the ratio of Φ_2/Φ_1 lies between 2.2 and 3.0, which was found for several *p*,*p*′-diazido compounds,[8c] then Φ_2 is estimated to be between 0.8 and 1.0. According to Reiser and his co-workers,[8a] in the case of 2-azidobiphenyl, the quantum yield of carbazole formation which is 0.44 at 25 °C lowers greatly to 0.01—0.02 in a rigid matrix at 77 K. In our cases, it is suggested that the insertion must become negligible compared with the highly efficient decomposition.

In general, the dinitrenes resulting from vicinal[10] and geminal[11] diazides have not been trapped even in a rigid matrix at low temperatures (higher than 77 K). The process to II from X must be fast. Thus, the formation of II from I (and of VIII from VII) may be regarded as a consecutive first-order reaction as follows:

$$\mathrm{I} \xrightarrow[k_1]{h\nu} \mathrm{IX} \xrightarrow[k_2]{h\nu} (\mathrm{X}) \xrightarrow[\text{fast}]{} \mathrm{II}$$

The kinetics in the photolysis of the dimethyl derivatives (VII) was obtained conveniently because the absorption peak belonging to the mononitrene was not seriously interfered with that of the final product (VIII). In Fig. 3, the absorption peaks at 308 and 330 nm belong to the intermediate mononitrene and the final product 1,10-dimethylbenzo[*c*]cinnoline (VIII) respectively. On the basis of these spectral data and the independent analysis of the decomposed diazide, the concentration-time relationship shown in Fig. 4 was obtained. Although we withhold all stoichiometric discussion because the plots for the mononitrene may have a fairly large experimental error, there is no doubt that the relationship between these three curves indicates $k_2 > k_1$ at least.

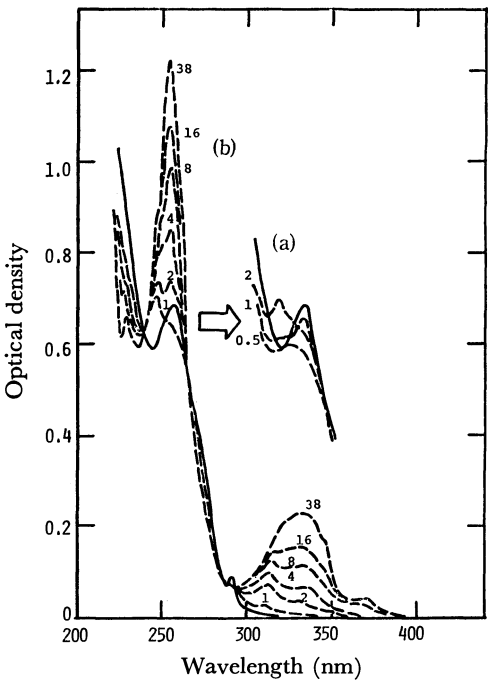

Fig. 3. Absorption spectra of VII in EPA at 77 K, —: before irradiation, ---: (a) in the region at 250 nm after irradiation through the 1/2 slit, (b) after irradiation through the open slit. Numbers refer to irradiation time in minutes.

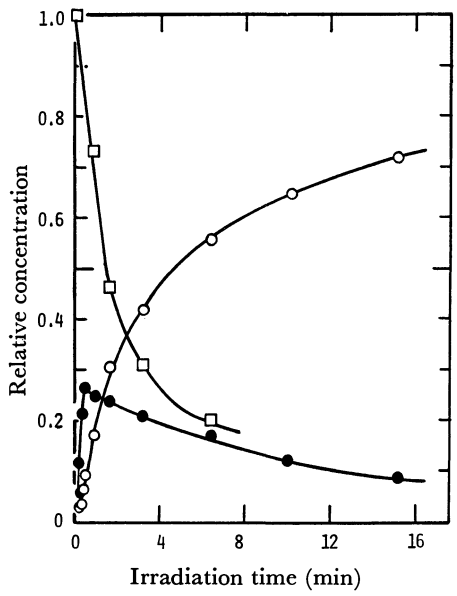

Fig. 4. Kinetics of the photolysis of VII in EPA at 77 K; □: diazide (VII), ●: nitrenoazide, ○: VIII.

Experimental

All the melting points are uncorrected. IR and UV spectra were recorded on JASCO Model IR-S and Shimadzu Model D-40R spectrophotometers respectively. NMR spectra were recorded on a Hitachi Model R-24A spectrometer at 60 MHz using TMS as an internal standard. Mass spectra were recorded on a Hitachi Model RMU-6M spectrometer. The microanalyses were performed at the Institute of Physical and Chemical Research.

Materials. *2,2'-Diazidobiphenyl (I)* was prepared from 2,2'-diaminobiphenyl by Procedure A of Smith and Brown.[12] The crude material was purified by column chromatography on silica gel and was recrystallized twice from ether–hexane; mp 70—71 °C. IR (KBr): 2180, 2120 (N_3) cm^{-1}. UV (Ether): $\lambda_{max}(\varepsilon)$ 252 (18400), 232 (19000) nm. MS: *m/e* 236 (M^+), 208 (M^+-N_2), 180 (M^+-2N_2). Found: C, 60.81; H, 3.51; N, 36.80%. Calcd for $C_{12}H_8N_6$: C, 61.01; H, 3.41; N, 35.57%.

2,2'-Diazido-6,6'-dimethylbiphenyl (VII) was prepared by the method of Coffin and Robbins.[5] After purification by silica gel column chromatography,it was recrystallized from ethanol; mp 58—59 °C (lit, 56—57 °C[5]). IR(KBr): 3100—2950, 2250 and 2160 (N_3) cm^{-1}. UV (Hexane): 288sh (2500), 254 (19900) nm. NMR ($CDCl_3$): δ 7.5—6.8 (m, 6H), 1.95 (s, 6H). MS: *m/e* 264 (M^+), 236 (M^+-N_2), 208 (M^+-2N_2).

The solvents used in the spectroscopic study and in low-temperature photolysis were dried over sodium wire or a molecular sieve and finally passed through a column of alumina.

Irradiation of Azides. The light source for spectroscopic studies was an Ushio USH-500D 500W high-pressure mercury lamp equipped with a Nikon G-250 monochromator. Irradiations for spectroscopic studies of low-temperature photolysis were carried out with a cell which had been immersed in liquid nitrogen or solid carbon dioxide–ethanol contained in a quartz Dewar vessel equipped with optical windows on opposite sides. Irradiations on preparative scale at room temperature were carried out under nitrogen with a conventional immersion well-type reactor equipped with an Ushio UM-102 100W high-pressure mercury lamp. In a low-temperature photolysis, a cylindrical cell immersed in coolants was irradiated with the low-pressure mercury lamp protected with a transparent quartz Dewar vessel.

Product Analysis. The separation and the yield determination of the photoproducts were carried out with a preparative layer chromatograph (Merck Silicagel 60 F_{254}) and a Hitachi high-speed liquid chromatograph Model 634, followed by UV analysis. The identity of II was confirmed by comparison with an authentic sample. The other products were identified on the basis of the following microanalyses and spectral data.

4-Azidocarbazole (III): mp 118—120 °C. IR (KBr): 3480 (NH), 2170 (N_3) cm^{-1}. UV (Ether): 343 (4020), 328 (3500), 301 (7300), 292 (7300), 250 (23000) nm. MS: *m/e* 208 (M^+), 180 (M^+-N_2). Found: C, 68.99; H, 4.22; N, 26.48%. Calcd for $C_{12}H_8N_4$: C, 69.22; H, 3.87; N, 26.91%.

4-(2'-Azido-2-biphenylylazo)carbazole (IV): mp 122—124 °C. IR (KBr): 3480 (NH), 2170 (N_3) cm^{-1}. UV (Ether): 435 (9900), 306 (9700), 250 (35300) nm. MS: *m/e* 388 (M^+), 360 (M^+-N_2).

2,2'-Bis(o-azidophenyl)azobenzene (VI): mp 144—146 °C. IR (KBr): 2180, 2160 (N_3) cm^{-1}. UV (Ether): 460 (250), 325 (8200) nm. MS: *m/e* 416 (M^+), 388 (M^+-N_2), 360 (M^+-2N_2). Found: C, 69.02; H, 4.14; N, 26.04%. Calcd for $C_{24}H_{16}N_8$: C, 69.22; H, 3.87; N, 26.91%.

1,10-Dimethylbenzo[c]*cinnoline (VIII)*: mp 110—111 °C (lit, 96 °C[5]). IR (KBr): 3080—3000, 1595, 1572, 1460, 1442, 1420, 1385, 1335 cm^{-1}. UV (MeOH): 331 (8900), 252 (36000) nm. NMR ($CDCl_3$): δ 8.7—7.1 (m, 6H), 2.55 (s, 6H). MS: *m/e* 208 (M^+), 180 (M^+-N_2), 179.

References

1) Part 1: A. Yabe and K. Honda, *Tetrahedron Lett.*, **1975**, 1079.

2) (a) J. S. Swenton, *Tetrahedron Lett.*, **1968**, 3421; (b) J. S. Swenton, T. J. Ikeler, and B. H. Williams, *Chem. Commun.*, **1969**, 1263; (c) J. S. Swenton, T. J. Ikeler, and B. H. Williams, *J. Am. Chem. Soc.*, **92**, 3103 (1970).

3) J. H. Boyer and G. J. Mikol, *Chem. Commun.*, **1969**, 734.

4) R. S. Berry, "Nitrenes," ed. by W. Lwowski, Interscience Publishers, New York, N. Y. (1970), p. 34.

5) B. Coffin and R. F. Robbins, *J. Chem. Soc.*, **1965**, 1252.

6) P. A. Lehman and R. S. Berry, *J. Am. Chem. Soc.*, **95**, 8614 (1973).

7) A. Treinin, "The Chemistry of the Azido Group," ed. by S. Patai, Interscience Publishers, New York, N. Y. (1971), p. 3.

8) (a) A. Reiser, H. M. Wagner, and G. Bowes, *Tetrahedron Lett.*, **1966**, 2635; (b) A. Reiser, G. Bowes, and R. J. Horne, *Trans. Faraday Soc.*, **62**, 3162 (1966); (c) A. Reiser, H. M. Wagner, R. Marley, and G. Bowes, *ibid.*, **63**, 2403 (1967); (d) A. Reiser and R. Marley, *ibid.*, **64**, 1806 (1968); (e) A. Reiser, F. W. Willilets, G. C. Terry, V. Williams, and R. Marley, *ibid.*, **64**, 3265 (1968).

9) W. G. Herkstroeten, "Creation and Detection of the Excited State," ed. by A. A. Lamola, Marcel Dekker, New York, N. Y. (1971), p. 43.

10) Our unpublished results. Presented in part at the 32-nd meeting of the Chemical Society of Japan, April 1975, Tokyo (3A16).

11) L. Barash, E. Wasserman, and W. A. Yager, *J. Am. Chem. Soc.*, **89**, 3931 (1967).

12) P. A. S. Smith and B. B. Brown, *J. Am. Chem. Soc.*, **73**, 2435, 2438 (1951).

Reaction of Alkyl Halides with Mercury(II) Salts in Tetrahydrofuran. A Facile Preparation of 4-Alkoxybutyl Acetates and Chlorides

Nanao WATANABE, Sakae UEMURA,* and Masaya OKANO*,**

Koei Chemical Co., Ltd., Joto-ku, Osaka 536

**Institute for Chemical Research, Kyoto University, Uji, Kyoto 611*

(Received December 12, 1975)

The reaction of primary and secondary alkyl iodides and bromides with $Hg(OAc)_2$ and $HgCl_2$ in tetrahydrofuran (THF) affords the THF-incorporated compounds (**1**), $RO(CH_2)_4X$ [X=OAc and Cl, respectively], in good yields. When $HgBr_2$ and aqueous or alcoholic $Hg(ClO_4)_2$ were used as mercury(II) salts, the yields of **1**(X=Br, OH, and OR') were low. Similar treatment with HgI_2 gave scarcely any **1**. A reaction scheme which involves *O*-alkyltetrahydrofuranium ion as the intermediate is proposed for the formation of **1**.

Reactions of alkyl halides with mercury(II) salts are of current interest.[1-5] In a previous paper[5] we showed that primary and secondary alkyl halides react with $Hg(SCN)_2$ in THF to give the THF-incorporated compounds, $R[O(CH_2)_4]_nNCS(-SCN)$ ($n=1$, 2), the reaction proceeding through *O*-alkyltetrahydrofuranium ion intermediate. During the course of application of this reaction to various other mercury(II) salts we found that the reaction using mercury(II) acetate and chloride gives $RO(CH_2)_4X$ (X=OAc and Cl) in good yields. Although the direct replacement of the halogen atom in alkyl halides by the carboxyl moiety of mercury(II) salts of carboxylic acids in THF or other organic solvents has been reported,[2] no description is given on the formation of such a THF-incorporated compound. In the present paper we describe the results of the reaction with various mercury(II) salts and discuss its reaction scheme.

Results and Discussion

Reaction with $Hg(OAc)_2$ or $HgCl_2$. The reaction was carried out by stirring alkyl iodides or bromides and mercury(II) salts in THF at refluxing temperature for several hours. The products were the THF-incorporated compounds (**1**) and the expected substitution products (**2**) (Scheme 1). From primary and secondary alkyl iodides or bromides, **1** ($n=1$) was mainly obtained, while alkyl bromides having strong S_N1 characteristics such as *t*-butyl and α-methylbenzyl bromides reacted to give only **2**. Typical results are summarized in Table 1. Predominant formation of **1** ($n=1$) with small amounts of **1** ($n=2$) was characteristic especially in the case of $Hg(OAc)_2$, in contrast to the reaction with $Hg(SCN)_2$ where both **1** ($n=1$) and **1** ($n=2$) were formed as main products.[5] Alkyl chlorides scarcely reacted under the conditions shown in Table 1.

$$RX + HgZ_2 + THF \longrightarrow \underset{\mathbf{1}\ (n=1,\ 2)}{R[O(CH_2)_4]_nZ} + \underset{\mathbf{2}}{RZ} \quad (1)$$

Reaction with $HgBr_2$, HgI_2, or $Hg(ClO_4)_2$. The reaction with $HgBr_2$ or HgI_2 under similar conditions to those described above gave mainly high-boiling substances which seemed to be **1** ($n\geq 2$). As an example, from the reaction of ethyl iodide with $HgBr_2$ for 2 h, **1** ($n=1$) was obtained in 26% yield together with large amounts of high-boiling substances. When the reaction was continued for an additional 4 h, the yield of **1** ($n=1$) decreased to 10%. In the case of HgI_2, **1** ($n=1$) was obtained only in a very low yield, high-boiling substances being mainly formed even under milder reaction conditions. All the starting alkyl halide was consumed in all the cases. On the other hand, the reaction with $Hg(ClO_4)_2$ in THF containing water or an alcohol afforded **1** ($n=1$) and **2** where Z=OH or OR' in good yields, only small amounts of high-boiling substances being formed in this case (see Experimental).

Reaction Scheme. Because of the similarity of the products to those in the reaction with $Hg(SCN)_2$,[5] the reaction seems to proceed through a scheme involving an oxonium ion intermediate as has been proposed in the case of $Hg(SCN)_2$ (Scheme 2). If no considerable competing attacks on this intermediate cation by another THF molecule and by some other nucleophiles

Table 1. Reaction of RX with $Hg(OAc)_2$ or $HgCl_2$ in THF

(A) With $Hg(OAc)_2$[a]

RX	React temp (°C)	React time (h)	Yields (%)[b] **1** ($n=1$)	**1** ($n=2$)	**2**
EtI	70—75	7	68	5	22
n-PrI	70—75	7	66	—[c]	30
i-PrI	70—75	5	50	3	35
i-PrBr	60—65	8	45	—	29
n-BuI	70—75	7	68	3	29
s-BuBr	70—75	8	37	—	29
CH_2=$CHCH_2Br$	70—75	2.5	62	8	17
$PhCH_2Br$	65—68	7	40[d]	—	42[d]
t-BuBr	70—72	4	0	0	45[d]
PhCH(Me)Br	45—48	2	0	0	90[d]

(B) With $HgCl_2$[a]

RX	React temp (°C)	React time (h)	Yields (%)[b] **1** ($n=1$)	**1** ($n=2$)	**2**
EtI	70—75	6	68	14	—[c]
i-PrI	70—75	7	68	2	—
n-BuI	70—75	7	70	9	8
CH_2=$CHCH_2Br$	70—75	2	56	8	21
$PhCH_2Br$	60—65	1	19[d]	—	67[d]

a) RX, 20 mmol. HgZ_2, 20 mmol. THF, 15 ml. b) Determined by GLC. c) Not determined. d) Isolated yield.

** To whom correspondence should be addressed.

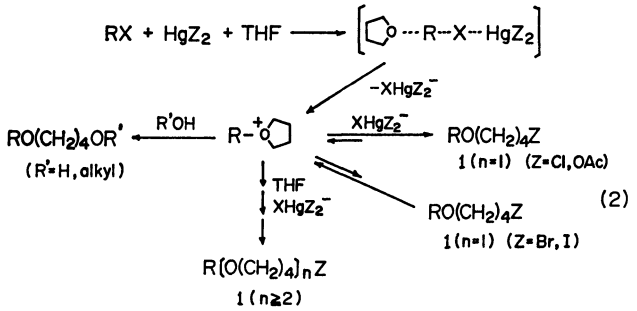

such as water or an alcohol take place, almost exclusive formation of $RO(CH_2)_4Z$ or $RO(CH_2)_4X$ by the S_N2-like attack of $XHgZ_2^-$ where X=I or Br and Z=Cl, OAc, Br, or I should be expected. Here, in the cases of Z=Cl, OAc, and Br a favorable attack by Z can occur to give only $RO(CH_2)_4Z$ because the affinity of I to Hg^{2+} is much greater than that of Cl, OAc, and Br to it by considering HSAB principle[6] (Hg^{2+} is a soft acid; Cl^- and OAc^- are hard bases, Br^- is a borderline base, and I^- is a soft base). In view of the fact that the yields of **1** ($n=1$) were low and considerable amounts of high-boiling substances were formed in the cases of Z=Br and I, the stability of the products, **1** ($n=1$), under the reaction conditions should also be taken into consideration. We have observed in these cases that a longer reaction time resulted in the formation of high-boiling substances which are probably composed of many THF molecule inserted compounds, **1** ($n>2$). It has been found that the reaction of $RO(CH_2)_4Br$ with $Hg(SCN)_2$ proceeds rapidly to give $RO(CH_2)_4NCS$ and $RO(CH_2)_4$-SCN *via* *O*-alkyltetrahydrofuranium ion.[5] This indicates that the reverse reaction from **1** ($n=1$) to the oxonium ion occurs in the presence of a mercury(II) salt, its extent depending a great deal on the kind of Z. The ease of departure of the leaving groups (Z) in S_N1 reaction is known to decrease in this order: I>Br>OAc>OH,OR.[7]

Table 2. Reaction of $EtO(CH_2)_mBr$ with HgZ_2 in n-Bu_2O[a]

m	Z	React temp (°C)	React time (h)	EtO-$(CH_2)_m$Z Yield (%)[b]	EtO-$(CH_2)_m$Br Recovered (%)[b]
2	Cl	70—75	8	0	99
3	Cl	70—75	8	0	92
4	Cl	70—75	8	89	trace
4	OAc	65—70	2	13	80
4	OAc	70—78	7	81	15
5	Cl	70—78	8	7	61

a) $EtO(CH_2)_m$ Br, 10 mmol. HgZ_2, 10 mmol. n-Bu_2O, 8 ml. b) Determined by GLC.

In order to confirm the above explanation, the reaction of $EtO(CH_2)_mBr$ ($m=2$—5) with $HgCl_2$ or $Hg(OAc)_2$ was carried out with n-Bu_2O as a solvent. The results are given in Table 2. As expected, when $m=4$ thermodynamically more stable $EtO(CH_2)_4Cl$ or $EtO(CH_2)_4OAc$ was obtained in a good yield, while no reaction occurred when $m=2$ and 3 in accordance with a similar result by Winstein *et al.*[8] We also confirmed that the reaction of $EtO(CH_2)_4Cl$ with $HgBr_2$ in n-Bu_2O gave no $EtO(CH_2)_4Br$ under the conditions shown in Table 2 and that of $EtO(CH_2)_4Br$ with HgI_2 in THF gave readily a lot of high-boiling substances.

Experimental

GLC analyses were carried out on a Yanagimoto G800-T and a Shimadzu 5APTF apparatus using DEGS (1m), PEG 6000 (2 and 3m), and EGSS-X (1m) columns (carrier gas, H_2 and N_2 respectively). The NMR spectra were recorded with Varian EM-360 and JEOL MH-100 spectrometers in $CDCl_3$, using TMS as an internal standard. The IR and Mass spectra were taken with Hitachi EPI-S2 and JEOL JMS-01SG spectrometers, respectively.

Materials. All the organic substances, including the solvents, were used after distillation, while commercial inorganic salts were used without further purification. ω-Ethoxyalkyl bromides, $EtO(CH_2)_mBr$, were prepared by the reported method.[9] Authentic samples of **1** ($n=1$, Z=OAc) were prepared by the acetylation of 4-alkoxybutanol synthesized[9] from 1,4-butandiol, sodium, and alkyl bromide. Authentic samples of **1** ($n=1$, Z=Cl) were prepared by the reported method; thus $PhCH_2O(CH_2)_4Cl$ was prepared from benzyl chloride, THF, and $ZnCl_2$,[10] and n-$BuO(CH_2)_4Cl$ from n-$BuO(CH_2)_4OH$ and $SOCl_2$.[11] Commercial authentic samples of **2** were used.

Reaction of Alkyl Halides with $Hg(OAc)_2$ or $HgCl_2$ in THF (Table 1). The following example shows a typical procedure. To a suspension of $Hg(OAc)_2$ (12.8 g, 40 mmol) in THF (30 ml) was added n-PrI (6.8 g, 40 mmol) at 70—75 °C and the resulting homogeneous solution was kept for 7 h under stirring. After being cooled down to room temperature, Et_2O (300 ml) was added and the precipitated inorganic salt was filtered off. The filtrate was washed several times with aqueous KI in order to remove a small amount of dissolved mercury (II) salt and then dried over $MgSO_4$. Distillation gave two fractions, D_1 (propyl acetate, 0.58 g, bp 50—75 °C) and D_2 (4-propoxybutyl acetate, 3.53 g, bp 101—104 °C/20 mmHg), and left 0.2 g of residue.

The boiling points (°C/mmHg) of **1** ($n=1$, Z=OAc) are as follows: R=Et, 90—91/24 (lit,[12] 192—193/756); R=*i*-Pr, 93—95/20; R=*n*-Bu, 118—120/25; R=*s*-Bu, 105—108/24; R=allyl, 104—106/24; R=benzyl, 112—115/2. Those of **1** ($n=1$, Z=Cl) are as follows; R=Et, 56—57/19 (lit,[13] 142/760); R=*i*-Pr, 71—73/25; R=*n*-Bu, 94—95/22 (lit,[11] 84/13); R=allyl, 90—92/35; R=benzyl, 102—104/1 (lit,[10] 137—140/12). **1** ($n=2$ Z=OAc), R=Et, 120—122/2. **1** ($n=2$, Z=Cl), R=Et, 120—125/7; R=*i*-Pr, 88—90/1; R=*n*-Bu, 127—128/4. NMR, IR, and mass spectra of all compounds support the structures. Although some of **1** ($n=2$) could not be isolated in a pure state, the retention time in GLC and NMR spectra supports each structure.

Reaction of n-BuI with Aqueous $Hg(ClO_4)_2$ in THF. Red mercury(II) oxide (4.4 g, 20 mmol) was added to a mixture of THF (15 ml) and 60% $HClO_4$ (6.8 g, 40 mmol), and the mixture was gently heated on a water bath (40—60 °C) under stirring until almost all the mercury(II) salt has dissolved (10—20 min). After being cooled down to room temperature, 4 ml of water and 3.7 g (20 mmol) of n-BuI were added to the mixture which was then stirred at 40 °C for 4 h. The products were then analyzed directly by GLC by use of internal standards: n-BuOH, 0.76 g (10.3 mmol), 51% yield: n-$BuO(CH_2)_4$-OH, 0.90 g (6.2 mmol), 31%; n-$BuO(CH_2)_4O$-n-Bu, 0.36 g (1.8 mmol), 9%. An authentic sample of n-$BuO(CH_2)_4O$-n-Bu was prepared from n-$BuO(CH_2)_4Br$, n-BuOH, and sodium; bp 138—139 °C/40 mmHg (lit,[14] 234—236 °C/760 mm-

Hg). Distillation left only a small amount of residue (<0.05 g).

Reaction of n-*BuI with Alcoholic* $Hg(ClO_4)_2$ *in THF.* To a mercury(II) perchlorate (20 mmol) solution of THF prepared by the same method as described above was added 15 g of *n*-BuOH and 3.7 g (20 mmol) of *n*-BuI. The mixture was then stirred at 40 °C for 4 h. After being cooled down to room temperature, Et_2O (200 ml) was added and the precipitated inogranic salt was filtered off. The filtrate was washed with aq. KI and dried. After evaporation of ether, the products in residue were analyzed by GLC by using some internal standards: *n*-Bu_2O, 1.23 g (9.5 mmol), 47%; *n*-$BuO(CH_2)_4O$-*n*-Bu, 0.96 g (4.8 mmol), 24%; *n*-$BuO(CH_2)_4OH$, 0.23 g (1.6 mmol), 8%. Distillation left only a small amount of residue (<0.05 g).

Reaction of $EtO(CH_2)_mBr$ *with* $HgCl_2$ *or* $Hg(OAc)_2$ *in* n-Bu_2O. *(Table 2).* A typical procedure is given in the following. To a suspension of $HgCl_2$ (2.8 g, 10 mmol) in *n*-Bu_2O (8 ml) was added $EtO(CH_2)_5Br$ (1.95 g, 10 mmol) at 70—75 °C and the resulting mixture was kept for 8 h under stirring. After being cooled down to room temperature, the mixture was filtered from the solid part and the filtrate was analyzed by GLC: recovered $EtO(CH_2)_5Br$, 1.19 g (6.1 mmol), 61%; $EtO(CH_2)_5Cl$, 0.11 g (0.7 mmol), 7%. An authentic sample of $EtO(CH_2)_5Cl$ was prepared by action of $SOCl_2$ on $EtO(CH_2)_5OH$ in pyridine; bp 88 °C/43 mmHg (lit,[13] 72 °C/17 mmHg).

References

1) N. Watanabe, M. Okano, and S. Uemura, *Bull. Chem. Soc. Jpn.*, **47**, 2745 (1974).
2) R. C. Larock, *J. Org. Chem.*, **39**, 3721 (1974).
3) A. McKillop and M. E. Ford, *Tetrahedron*, **30**, 2467 (1974).
4) J. S. Filippo, Jr. and L. J. Romano, *J. Org. Chem.*, **40**, 782 (1975).
5) N. Watanabe, S. Uemura, and M. Okano, *Bull. Chem. Soc. Jpn.*, **48**, 3205 (1975).
6) R. G. Pearson, *Chem. Brit.*, **3**, 103 (1967).
7) E. S. Gould, "Mechanism and Structure in Organic Chemistry," Holt, Rinehart and Winston Inc., New York, N. Y. (1959), p. 261.
8) S. Winstein, E. Allred, R. Heck, and R. Glick, *Tetrahedron*, **3**, 1 (1958).
9) L. I. Smith and J. A. Sprung, *J. Am. Chem. Soc.*, **65**, 1276 (1943).
10) G. G. Munoz and R. Madronero, *Chem. Ber.*, **95**, 2184 (1962).
11) P. Rempp, *Bull. Soc. Chim. Fr.*, **1957**, 844.
12) A. Dewael, *Bull. Soc. Chim. Belges*, **35**, 302 (1926).
13) P. M. Frearson and E. S. Stern, *J. Chem. Soc.*, **1958**, 3064.
14) T. P. Hobin, *Polymer*, **6**, 407 (1965).

The Photolysis and Thermolysis of 3-(Diphenylhydroxymethyl)-4-(diphenylmethylene)-2-cyclobuten-1-one and Its 2-Bromo Derivative[1)]

Fumio Toda and Eishiro Todo

Department of Industrial Chemistry, Faculty of Engineering, Ehime University, Matsuyama 790

(Received January 20, 1976)

The photolysis of the title methyleneccyclobutenone (**1**) and 2-bromomethylenecyclobutanone (**9**) in MeOH afforded 4,4-diphenyl-3-(2,2-diphenylvinyl)-2-buten-4-olide (**5**) and 3,3,5-triphenyl-1,3-dihydronaphtho[1,2-*c*]-furan-2-one (**11**) respectively. The photolysis of **1** and **9** in benzene, however, afforded 4,4-diphenyl-3-(diphenylvinylidene)-4-butanolide (**2**), and bromo-derivative of **5** (**8**) and **11** respectively. The thermolysis of **1** and **9** in *o*-xylene afforded **2** and 2-bromo derivative of **5**(**10**) respectively. The mechanisms of these reactions were discussed. The solvent effect on the photolysis of **1** and **9** was also discussed.

The photochemical conversion of cyclobutenedione into the bisketene intermediate *via* a Norrish Type I reaction is well established.[2,3)] In order to compare the photolysis of methylenecyclobutenone with that of cyclobutenedione, we studied the photolysis of the title compounds (**1** and **9**) in benzene and MeOH; we found that all the reactions afford products which are probably derived from alleneketene intermediates (**3** and **12**) initially formed by Norrish Type I reactions of **1** and **9** respectively. It was also found that the thermolysis of **1** and **9** probably proceeds *via* the alleneketene intermediates, **3** and **12** respectively.

The irradiation of **1** in benzene for 1 h afforded 4,4-diphenyl-3-(diphenylvinylidene)-4-butanolide (**2**) in an 82% yield. The formation of **2** can be explained in terms of intramolecular esterification involving the alleneketene (**3**) as an intermediate produced by the α-cleavage of **1**. Such an easy lactonization has been demonstrated in the photochemical conversion of 3,4-bis (diphenylhydroxymethyl) cyclobut-3-ene-1,2-dione into 4,4,8,8-tetraphenyl-3,7-dioxabicyclo[3.3.0]octane-2,6-dione.[3)]

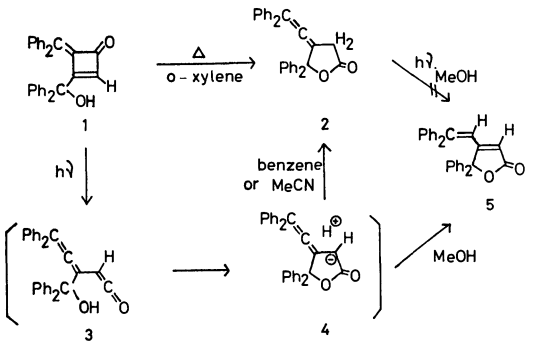

Scheme 1.

In contrast with the photolysis of **1** in benzene, the photolysis of **1** in MeOH afforded 4,4-diphenyl-3-(2,2-diphenylvinyl)-2-buten-4-olide (**5**) in a 35% yield as the sole isolable product. This reaction would also proceed *via* **3**. It seems that the type of reaction product depends on whether the solvent used is polar or nonpolar. It is clear, however, that **5** was not derived from **2**, because the irradiation of **2** in MeOH did not give **5**, and **2** was recovered unchanged. Nevertheless, a polar solvent is not always sufficient for the formation of **5** in the photolysis of **1**; the photolysis of **1** in MeCN afforded **2**, but not **5**. The formation of **5** can be interpreted by assuming the ion pair (**4**) as an intermediate; it would easily be protonated in MeOH on its allene carbon.

The heating of **1** in *o*-xylene under reflux for 5 h afforded **2** in a 75% yield. This reaction would also proceed *via* the **3** initially formed by the thermal α-cleavage of **1**.

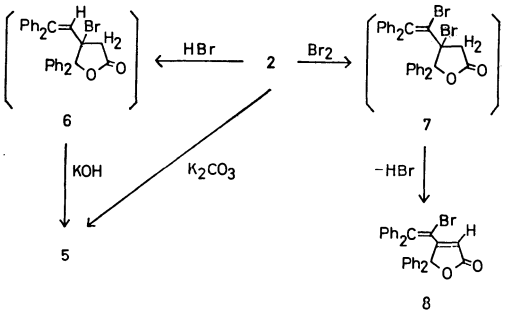

Scheme 2.

The prototropic rearrangement of **2** into **5** occurred easily when **2** was treated with K_2CO_3 in MeOH. The conversion of **2** into **5** was also performed by the treatment of **2** with HBr, followed with KOH. The dehydrobromination of the Br_2-addition product of **2** (**7**) afforded the bromo-derivative of **5** (**8**).

The photolysis and thermolysis of the 2-bromo derivative of **1** (**9**) gave slightly different results from

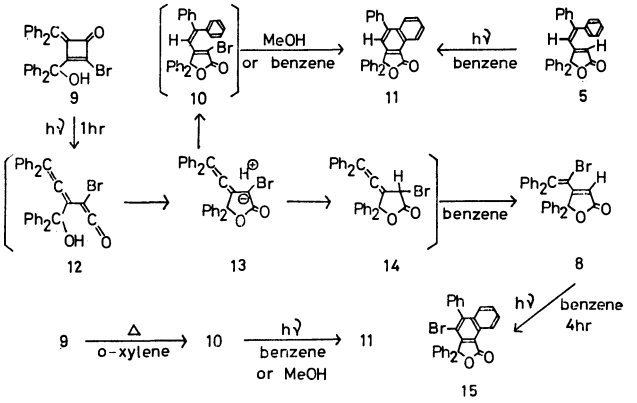

Scheme 3.

those of **1**. The thermolysis of **9** under the same conditions as those used for **1** afforded the 3-bromo derivative of **5** (**10**) in a 46% yield. The photolysis of **9** in benzene under the same conditions as those used for **1** afforded **8** and 3,3,5-triphenyl-1,3-dihydronaphtho[1,2-*c*]furan-2-one (**11**) in 25 and 27% yields respectively, whereas the photolysis in MeOH afforded **11** in a 20% yield as the sole isolable product. All these reactions can be interpreted by assuming the ion pair (**13**) to be the intermediate which was produced by the intramolecular esterification of the alleneketene intermediate (**12**) initially formed by the α-cleavage of **9** similar to the case of **1**. The ion pair (**13**) would be more stabilized by an inductive effect of Br than would **4**.

In the thermolysis of **9**, **10** would be derived directly from **13**, but not from **14**; the latter probably affords **8**, because the average bond energy of C–H (99) is larger than that of C–Br (68 kcal/mol). The thermal stability of **2** supports this.

The formation of **8** and **11** in the photolysis of **9** in benzene can be interpreted by assuming **14** and **10** as intermediates; *i.e.*, the process involves the rearrangement of Br of **14** and an electrocyclic reaction, followed by the dehydrobromination of **10** to afford **8** and **11** respectively. Evidence for the intermediacy of **10** was obtained by the photolysis of **10** in benzene and MeOH, which affords **11** in 84 and 57% yields respectively. In a similar manner, the prolonged photolysis of **5** and **8** in benzene afforded **11** and its 4-bromo derivative (**15**) respectively. These reactions are similar to the photochemical conversion of stilbene into phenanthrene.[4,5] The exclusive formation of **11** in the photolysis of **9** in MeOH can be interpreted in the way employed for the interpretation of the solvent effect on the photolysis of **1**; *i.e.*, **13** would easily be protonated in MeOH on its allene carbon.

Experimental

All the melting points are uncorrected. The photolysis was carried out at room temperature under a nitrogen atmosphere, using light from a 100-W high-pressure mercury lamp (Riko Kagaku Sangyo Co.), filtered through Pyrex glass. The IR, UV, and NMR spectra were measured in Nujol mull, $CHCl_3$, and $CDCl_3$ respectively, unless otherwise stated. The mass spectra were measured with an ionization energy of 75 eV.

*Photolysis of **1** in Benzene.* A solution of **1**[6] (0.6 g) in benzene (150 ml) was irradiated for 1 h. The crude crystals left after the evaporation of the solvent were recrystallized from MeOH to afford **2** as colorless needles; 0.49 g (82%); mp 112—113 °C. IR: 1790 (C=O), 1400 (CH_2), and 1205 cm^{-1} (lactone); λ_{max}: 270 nm (ε, 14500); NMR: 2.2—3.3 (m, Ph, 20H) and 6.35 τ (s, CH_2, 2H); MS: *m/e* (rel intensity) 414 (M^+, 72), 386 (M^+-CO, 17), and 204 (386−Ph_2CO, 100).

Found: C, 86.77; H, 5.31%. Calcd for $C_{30}H_{22}O_2$: C, 86.93; H, 5.35%.

*Photolysis of **1** in MeOH.* A solution of **1** (0.4 g) in MeOH (150 ml) was irradiated for 6 h. The oily material left after the evaporation of the solvent was dissolved in CCl_4, after which the solution was chromatographed on Al_2O_3. The crude crystals obtained from the fraction eluted with benzene were recrystallized from MeOH to afford **5** as pale yellow prisms; 0.14 g (35%); mp 148—150 °C. IR: 1755 (C=O), 1625 (C=C), and 1220 and 1180 cm^{-1} (lactone); λ_{max}: 327 nm (ε, 19100); NMR: 2.3—3.2 (m, Ph, 20H), 3.35 (s, =CH, 1H), and 4.85 τ (s, =CH, 1H); MS *m/e* (rel intensity): 414 (M^+, 7), 370 (M^+-CO_2, 84), 232 (M^+-Ph_2CO, 21), and 204 (232−CO, 100).

Found: C, 86.81; H, 5.15%. Calcd for $C_{30}H_{22}O_2$: C, 86.93; H, 5.35%.

*Thermolysis of **1** in o-Xylene.* A solution of **1** (0.071 g) in *o*-xylene (10 ml) was heated under reflux in a nitrogen atmosphere for 5 h. The crude crystals left after the evaporation of the solvent were recrystallized to afford **2**; 0.053 g (75%).

*Conversion of **2** into **5**.* *a*) When a mixture of **2** (0.056 g), K_2CO_3 (0.1 g) and MeOH (20 ml) was heated under reflux for 1 h, **5** was obtained after recrystallization from MeOH; 0.045 g (81%). *b*) Into a solution of **2** (0.097 g) in $CHCl_3$ (10 ml), HBr was bubbled for 10 min. The oily material left after the evaporation of the solvent was dissolved in 0.5% KOH–MeOH (20 ml), after which the solution was heated under reflux for 1 h. The recrystallization from MeOH of the crude crystals obtained by the dilution of the reaction mixture with water afforded **5**, 0.05 g (52%).

*Preparation of **8**.* To a solution of **2** (0.092 g) in $CHCl_3$ (10 ml), Br_2 (0.05 g) was added. The oily material left after the evaporation of the solvent crystallized when treated with AcOEt (1 ml).

The recrystallization of the crude crystals from AcOEt afforded **8** as pale yellow prisms; 0.054 g (42%); mp 217—218 °C. IR: 1760 (C=O), 1605 (C=C), and 1265 and 1210 cm^{-1} (lactone); λ_{max}^{EtOH}: 248 (31600), 318 (6300), and 332 nm (ε, 5600); NMR: 2.3—3.2 (m, Ph, 18H), 3.6—3.8 (m, Ph, 2H), and 4.18 τ (s, =CH, 1H); MS *m/e* (rel intensity): 494 and 492 (M^+, each 16), 450 and 448 (M^+-CO_2, each 28), 413 (M^+—Br, 20), 369 (413−CO_2, 24), 292 (369—Ph, 28), 231 (413—Ph_2CO, 96), and 203 (231—CO, 100).

Found: C, 72.85; H, 4.16%. Calcd for $C_{30}H_{21}O_2Br$: C, 73.02; H, 4.25%.

*Thermolysis of **9** in o-Xylene.* A solution of **9** (0.318 g) in *o*-xylene (10 ml) was heated under reflux in a nitrogen atmosphere for 5 h. The crude crystals left after the evaporation of the solvent were recrystallized from AcOEt to afford **10** as pale yellow leaflets; 0.147 g (46%); mp 217—218 °C. IR: 1760 (C=O), 1610 (C=C), and 1230 cm^{-1} (lactone); λ_{max}^{EtOH}: 238 (17700) and 328 nm (ε, 13400); NMR: 2.0—3.0 (m, Ph, 18H), 3.3—3.6 (m, Ph, 2H), and 3.73 τ (s, =CH, 1H).

Found: C, 73.10; H, 4.18%. Calcd for $C_{30}H_{21}O_2Br$; C, 73.02; H, 4.25%.

*Photolysis of **9** in Benzene.* A solution of **9** (0.43 g) in benzene (150 ml) was irradiated for 1 h. The crude product left after the evaporation of the solvent was recrystallized from MeOH–$CHCl_3$ (1: 1) (10 ml) to afford **8**; 0.108 g (25%). The evaporation of the solvent of the mother liquor left after the separation of **8** gave crude crystals, which were then recrystallized from MeOH–acetone to afford **11** as colorless prisms; 0.097 g (27%); mp 157—158 °C. IR 1750 (C=O) and 1180 and 1130 cm^{-1} (lactone); λ_{max}: 250 (31700) and 314 nm (ε, 9900).

NMR: 1.7—2.8 τ (m, Aromatic); MS *m/e* (rel intensity): 412 (M^+, 75), 368 (M^+-CO_2, 27), 335 (M^+—Ph, 73), and 307 (335−CO, 100).

Found: C, 87.31; H, 4.75%. Calcd for $C_{30}H_{20}O_2$: C, 87.35; H, 4.89%.

*Photolysis of **9** in MeOH.* A solution of **9** (0.4 g) in MeOH (150 ml) was irradiated for 1 h. The crude crystals left after the evaporation of the solvent were recrystallized from MeOH–acetone to afford **11**: 0.082 g (25%).

*Photolysis of **10** in Benzene and MeOH.* A solution of **10** (0.102 g) in benzene (150 ml) was irradiated for 2 h. The crude crystals left after the evaporation of the solvent were

recrystallized from MeOH–acetone to afford **11**; 0.072 g (84 %). When a solution of **10** (0.05 g) in MeOH (150 ml) was irradiated for 2 h, and then worked up as above, 0.024 g (57%) of **11** was obtained.

*Photolysis of **5** in Benzene.* A solution of **5** (0.167 g) in benzene (150 ml) was irradiated for 3 h. The recrystallization from MeOH–acetone of the crude crystals left after the evaporation of the solvent afforded **11**; 0.13 g (76%).

*Photolysis of **8** in Benzene.* A solution of **8** (0.1 g) in benzene (150 ml) was irradiated for 4 h. The crude crystals left after the evaporation of the solvent were recrystallized from MeOH–$CHCl_3$ to afford **15** as colorless needles; 0.06 g (60%); mp 276—279 °C. IR: 1765 (C=O) and 1200 and 1140 cm^{-1} (lactone); λ_{max}: 320 (10000) and 332 nm (ε, 8800); NMR: 1.8—2.8 τ (m, Aromatic); MS *m/e* (rel intensity): 492 and 490 (M^+, each 58), 448 and 446 (M^+-CO_2, each 20), 411 (M^+—Br, 14), 367 (411—CO_2, 100), and 290 (367—Ph, 58).

Found: C, 73.42; H, 3.71%. Calcd for $C_{30}H_{19}O_2Br$: C, 73.31; H, 3.87%.

References

1) A part of this paper has previously been briefly reported; F. Toda and E. Todo, *Chem. Lett.*, **1974**, 1279.

2) O. L. Chapman, C. L. McIntosh, and L. L. Barber, *Chem. Commun.*, **1971**, 1162.

3) F. Toda and E. Todo, *Bull. Chem. Soc. Jpn.*, **48**, 583 (1975).

4) R. E. Buckles, *J. Am. Chem. Soc.*, **77**, 1040 (1955).

5) For the photochemical conversion of stilbene into phenanthrene, it has been reported that oxygen acts as a reagent of the dehydrogenation of the dihydrophenanthrene initially formed by the electrocyclic reacti n of stilbene; F. B. Mallory, C. S. Wood, J. T. Gordon, L. C. Lindquist, and M. L. Savitz, *J. Am. Chem. Soc.*, **84**, 4361 (1962). Therefore, in the photochemical conversions of **5** and **8** into **11** and **15** respectively, the oxygen which contaminates the nitrogen atmosphere seems to act as a reagent of dehydrogenation.

6) F. Toda and K. Akagi, *Tetrahedron Lett.*, **1970**, 5289.

Aminosugars. XXV. Synthesis of Benzyl 2-Acetamido-2-amino-2,3,4-trideoxy-α-D-*arabino*-hexopyranoside[1]

Juji YOSHIMURA, Masaharu IWAKAWA, and Yoshio OGURA

Laboratory of Chemistry for Natural Products, Faculty of Science, Tokyo Institute of Technology, Meguro-ku, Tokyo 152

(Received January 24, 1976)

As the attempted substitution of methyl 4-deoxy-2,3-di-*O*-mesyl-6-*O*-trityl-α-D-*xylo*-hexopyranoside with sodium azide gave the unsaturated compound: methyl 2,3,4-trideoxy-6-*O*-trityl-α-D-*glycero*-hex-2-enopyranoside (**4**), benzyl 2-acetamido-4,6-*O*-benzylidene-2-deoxy-α-D-mannopyranoside was used as the starting material, which was converted into benzyl 2-acetamido-2-deoxy-3-*O*-mesyl-6-*O*-trityl-α-D-mannopyranoside (**10**). For the deoxygenation of C-4 position, chlorination of **10** with sulfuryl chloride gave unexpectedly benzyl 3′-*O*-mesyl-6′-*O*-trityl-α-D-talopyranosid [2′,3′,4′; 4,5,6]-2-methyl-4,5-dihydro-6*H*-oxazine, due to the anchimeric effect of the C_2-axial acetamido group. However, previous change of the conformation of **10** by the substitution of C_3-mesyl group with azido group gave successfully the corresponding chloro derivative (**13**). Reduction of **13** with tributyltin hydride gave the corresponding 3,4-epimino derivative (**14**), due to participation of initially hydrogenated azido group, but, catalytic hydrogenation of **14** gave the title compound as the main product.

L-Tuberactidine: α-(4-hydroxyl-2-imino-hexahydro-6(*R*)-pyrimidinyl)-(*S*)-glycine,[2] was found as the unique component of a peptide antibiotic, tuberactinomycin A.[3] In order to synthesize L-tuberactidine by utilization of sugars for the two asymmetric configurations, the title compound was synthesized as the key intermediate. This paper describes the synthesis and a few anchimeric effects of neighbouring groups in aminosugars found in the course of the study.

Results and Discussion

For the synthesis of a 2,3-diamino-2,3,4-trideoxy-hexose derivative from a neutral sugar, deoxygenation of *C*-4 position and introduction of amino groups into *C*-2 and *C*-3 positions are necessary. Concerning the title compound, Guthrie *et al.*[4] synthesized methyl 3-amino-2-azido-4,6-*O*-benzylidene-2,3-dideoxy-α-D-altropyranoside by ring opening of the corresponding 2,3-epimino derivative with azide anion, which was obtained from D-glucose *via* ten-step conversions. This compound has the same configuration as the title compound, excepting the presence of C_4-hydroxyl group, but the C_4-deoxygenation after introduction of C_3-amino group was considered to be a rather difficult problem. On the other hand, it is known that some reagents such as potassium ethylxanthate,[5] sodium iodide and zinc dust,[6] trimethyl phosphite,[5] and others[7] apt to give unsaturated sugars from the corresponding vicinal disulfonates, while sodium azide gave mainly direct displacement products.[8] Consequently, we have firstly tried a one-step introduction of 2,3-diamino groups into a 4-deoxy sugar.

Partial hydrolysis of methyl 4,6-*O*-benzylidene-2,3-di-*O*-mesyl-α-D-glucopyranoside[5,9] with 70% acetic acid at 90—95 °C gave methyl 2,3-di-*O*-mesyl-α-D-glucopyranoside (**1**) in 98% yield. Tritylation of **1** gave the corresponding 6-*O*-trityl derivative, which was then chlorinated with sulfuryl chloride[10] to give the corresponding 4-chloro-4-deoxy derivative (**2**) in 88% yield. Hydrogenation of **2** with tributyltin hydride gave the desired 4-deoxy derivative (**3**) quantitatively. However, reaction of **3** with sodium azide in *N*,*N*-dimethylformamide for 20 h at refluxing temperature gave the corresponding 2,3-unsaturated compound (**4**) and starting material as main products in 15% and 38% yields, respectively. Although other three minor products were not examined and the reaction mechanism is also ambiguous, this fact indicates that the unsaturation is preferential in this reaction, and that the deoxygenation of *C*-4 position does not make any advantages for the vicinal diazide formation. The structure of **4** was supported by the long range couplings of the allylic system ($J_{1,3}$=2.0, $J_{2,4}$=1.0) in the PMR spectrum (Table 1).

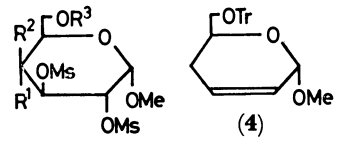

(**4**)

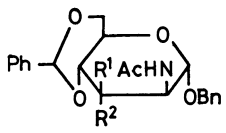

(**1**) R^1=OH, R^2=R^3=H
(**2**) R^1=H, R^2=Cl, R^3=Trityl
(**3**) R^1=R^2=H, R^3=Trityl

(**5**) R^1=OH, R^2=H
(**6**) R^1=OMs R^2=H
(**7**) R^1=H, R^2=N_3

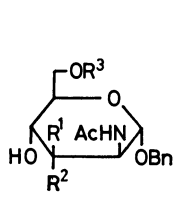

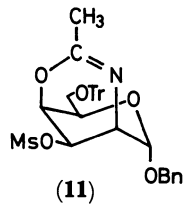

(**11**)

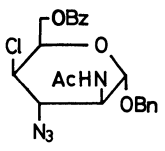

(**13**)

(**8**) R^1=R^3=H, R^2=NH_2
(**9**) R^1=R^3=H, R^2=NH-C(=NH)NH_2
(**10**) R^1=OMs, R^2=H, R^3=Trityl
(**12**) R^1=H, R^2=N_3, R^3=Bz

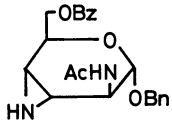

(**14**)

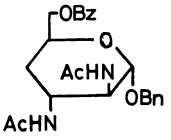

(**15**)

Because more simple and fewer steps are desired for synthesis of optically active none-carbohydrate compounds, benzyl 2-acetamido-4,6-*O*-benzylidene-2-deoxy-α-D-mannopyranoside (**5**)[11] was used as the starting

TABLE 1. PMR PARAMETERS OF RING PROTONS OF COMPOUNDS **4**, **7**, **11**, **12**, AND **13**

Compound	H_1	H_2	H_3	H_4	H_5	H_6	$H_{6'}$	Other protons
4	4.89(broad s) $J_{1,2}$=*ca.* 2.0 $J_{1,3}$=*ca.* 1.5	5.76(m) $J_{2,3}$=10.0 $J_{2,4}$=1.0	5.97(m) $J_{3,4}$=3.0 $J_{3,4'}$=4.5	2.0—1.83(m) $J_{4,5}+J_{4',5}$= 14.8	4.12(sex) $J_{5,6}$=6.0	3.25(q) $J_{5,6}$=4.2	3.07(q) $J_{6,6'}$= 10.0	7.6—7.18 (Ph) 3.47(OMe)
7[a]	4.65(broad s) $J_{1,2}$=<0.5	4.35(q) $J_{2,3}$=3.0	4.09(t) $J_{3,4}$=3.5	3.88(q) $J_{4,5}$=9.0	*ca.* 4.28(m) $J_{5,6}$=6.9	4.24(q) $J_{5,6}=J_{6,6}$=10.0	3.67(t)	7.55—7.22(Ph), 5.57 (methine), 1.97(NAc), 4.70 and4.55(ABq; J=12.0)
11	4.84(d) $J_{1,2}$=2.0	*ca.* 3.77(m)	5.15(t) $J_{2,3}=J_{3,4}$=2.1	*ca.* 4.63(m)	3.86(broad t) $J_{4,5}$=2.1	3.27(d) $J_{5,6}$=7.2		7.55—7.18(Ph); 4.50 and 4.63(CH_2); ABq, J=12.0, 2.96(OMs), 1.87(CMe)
12[a]	4.72(d) $J_{1,2}$=<1.0	*ca.* 4.4(m) $J_{2,3}=J_{3,4}$=*ca.* 3.3	4.10(t)	3.85(q) $J_{4,5}$=11.0	*ca.* 4.22(m)	*ca.* 4.5(broad d)		8.10—7.20(Ph) 1.93(NAc)
13	4.88(t) $J_{1,2}=J_{1,3}$ =1.0	4.30(m) $J_{2,3}$=2.8	4.0(broad s) $J_{3,4}=J_{4,5}$=3.5	4.14(t)	4.69(m) $J_{5,6}$=3.0	4.52(q) $J_{5,6'}$ =5.0	4.38(q) $J_{6,6'}$ =10.0	8.10—7.25(Ph); 6.36 (NH; J=9.0), 1.98 (NAc), 4.75 and 4.54 (CH_2; ABq, J=12.0)

a) NH proton was deuterated.

material in the next experiments. Mesylation of **5** in pyridine gave the corresponding 3-*O*-mesylate (**6**) in a good yield, which was then transformed into 3-azido-3-deoxy derivative (**7**) of D-*altro* type. Hydrogenation of **7** gave the corresponding 3-amino-3-deoxy-derivative (**8**), which was then converted into 3-guanidino-3-deoxy derivative (**9**) by fusion with sodium cyanamide.[12]

For the deoxygenation of *C*-4 position, 4,6-*O*-benzylidene group of **6** was hydrolyzed and then tritylated to give benzyl 2-acetamido-2-deoxy-3-*O*-mesyl-6-*O*-trityl-α-D-mannopyranoside (**10**) in 62% yield. Chlorination of **10** in pyridine with sulfuryl chloride gave a product (**11**) in 80.5% yield, which contains no chlorine atom, and the analytical values consisted with that of monodehydrated product of **10**. Besides, the appearance of H_3 signal as a triplet (J=2.1 Hz) having no long range coupling and the absence of NH proton signal in the PMR spectrum of **11** indicates the normal *C1* conformation and the formation of intramolecular oxazin ring by the participation of axial 2-acetamido group. Consequently, **11** was characterized to be benzyl 3'-*O*-mesyl-6'-*O*-trityl-α-D-talopyranosid[2',3',4';4,5,6]-2-methyl-5,6-dihydro-4H-oxazine. Because the 4-*O*-chlorosulfonyl group formed in the initial step of the chlorination is a good leaving group, the participation of axial acetamido group to the β-carbon observed above will be very reasonable, and a similar participation was recently reported by Meyer zu Reckendorf *et al.*[13] Several attempts to open the oxazine-ring of **11** gave unsuccessful results.

To avoid the participation of the axial acetamido group, conformational change of the lactol ring is

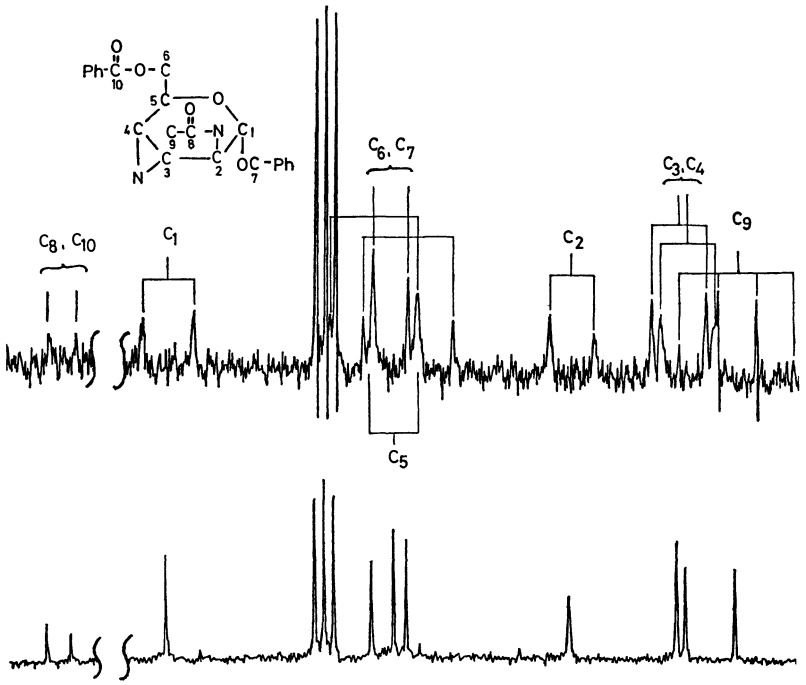

Fig. 1. CMR spectrum of compound **14**.

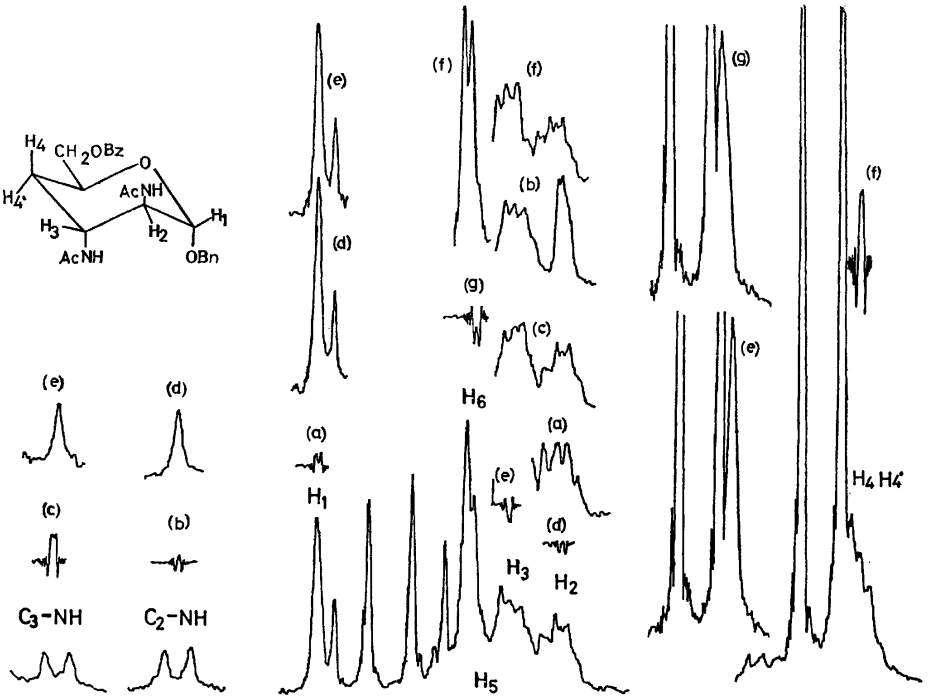

Fig. 2. The proof of the structure of **16** with the decoupling technique.

desirable. So, **7** was partially hydrolyzed, and then partially benzoylated to give benzyl 2-acetamido-3-azido-6-*O*-benzoyl-2-deoxy-α-D-altropyranoside (**12**) in 80% yield. The chlorination of **12** gave the corresponding 4-chloro-4-deoxy derivative (**13**) in 70.5% yield as expected. The coupling constants of ring protons of **12** are very similar to that of **7** (Table 1), indicating the *C1* conformation of **12**. However, it is characteristic that the $J_{1,2}$ values of them are smaller than that of **11** having a typical *C1* conformation, due to the flattening of the pyranose-ring. This tendency of D-*altro*-configuration of **7** and **12** is stronger than that of D-*manno*-configuration of **6** ($J_{1,2}$=1.5) and **10** ($J_{1,2}$=1.0). Consequently, it is deduced that a slight deformation of the conformation in **12** prevented the anchimeric contribution of C_2-acetamido group. It is also noteworthy that **13** has still *C1* conformation, nevertheless, the pyranose-ring has four axial substituents. It seems likely to be due to the dipolar repulsions between four electronegative substituents (Cl, N_3, NHAc, and OBn).

Hydrogenation of chlorine atom of **13** with tributyltin hydride proceeded smoothly together with that of the azido group. The structure of the product (**14**) could not be confirmed to be either the corresponding 3-amino or 3,4-epimino derivative by usual methods, but CMR spectrum (Fig. 1) indicated the presence of only two methylene carbons. Consequently, the structure was determined to be benzyl 2-acetamido-6-*O*-benzoyl-3,4-epimino-2,3,4-trideoxy-α-D-altropyranoside. This conclusion suggests that the hydrogenation of azido group was faster than that of the chlorine atom. Hydrogenation of **14** in the presence of Raney nickel gave fortunately the desired 3-amino-3,4-dideoxy derivative as main product, which was then converted into 3-acetamido derivative (**15**) in 60% yield. The configuration of **15** was completely proved by the double resonance technique in the PMR spectrum (Fig. 2). By irradiation of H_1 and two NH protons (a, b, c), multiplets at *δ ca.* 4.15 and 4.30 were assigned to H_2 and another ring proton (H_3) of the position of the acetamido group, respectively, and the reverse irradiation (d, e) indicated that only the latter is vicinal to the ring methylene protons at *δ ca.* 1.84, showing the sharpening of them. These facts indicate that the deoxygenated position should be *C*-4. Moreover, the conclusion was confirmed by the irradiation of ring-methylene protons (f) and a ring proton (H_5) other than two acetamido positions (g).

Experimental

All melting points were determined with Yanaco micro melting point apparatus and not corrected. The solutions were evaporated under reduced pressure at a bath temperature not exceeding 50 °C. The IR spectra were measured in KBr discs with a Hitachi EPI-GS spectrometer. The PMR spectra were obtained at 100 MHz with a JEOL 4H-100 spectrometer in deuteriochloroform, using TMS as an internal reference. Specific rotations were measured in a 0.5-dm tube with a Carl Zeiss SEP-AL polarimeter in chloroform unless otherwise stated. Chemical shifts and coupling constants were recorded in *δ* and Hz units, and IR frequencies in cm^{-1}.

Methyl 2,3-Di-O-mesyl-α-D-glucopyranoside (*1*). A suspension of methyl 4,6-*O*-benzylidene-2,3-di-*O*-mesyl-α-D-glucopyranoside (7 g, 16 mmol) in 70% acetic acid (100 ml) was heated at 90—95 °C for 4 h under monitering with TLC until the starting material has disappeared, and then evaporated to give white powder which was crystallized from ethanol. Yield, 5.5 g (98%), mp 148—149 °C; $[\alpha]_D^{22}$+84.2° (*c* 1.0, acetone).

Found: C, 31.07; H, 5.15; S, 17.83%. Calcd for $C_9H_{18}O_{10}S_2$: C, 30.85; H, 5.18; S, 18.30%.

Methyl 4-Chloro-4-deoxy-2,3-di-O-mesyl-6-O-trityl-α-D-galactopyranoside (*2*). A solution of **1** (1 g, 2.9 mmol) and trityl chloride (1 g, 3.6 mmol) in pyridine (30 ml) was kept at room temperature, and then poured into ice-water to give the corresponding 6-*O*-trityl derivative in 86% (1.5 g) yield (mp 155—

156 °C after recrystallization from benzene). To an ice-cooled solution of 6-*O*-trityl derivative (1.5 g, 2.5 mmol) in pyridine was added dropwise sulfuryl chloride (0.27 ml, 3.3 mmol) with stirring, and then poured into ice–water after standing overnight at room temperature. The resulting solution was extracted with chloroform, and the extract was treated in a usual manner to give a sirup (1.36 g, 88%) which was crystallized and recrystallized from methanol. Mp 130—131 °C, $[\alpha]_D^{23}$ +53.0° (*c* 1.0).

Found: C, 55.04; H, 5.11; S, 10.21%. Calcd for $C_{28}H_{31}O_9S_2Cl$; C, 55.02; H, 5.11; S, 10.49%.

*Methyl 4-Deoxy-2,3-di-*O*-mesyl-6-*O*-trityl-α-*D*-*xylo*-hexopyranoside* (**3**). A solution of **2** (200 mg, 0.33 mmol), tributyltin hydride (0.5 ml) and a catalytic amount of 2,2′-azobisisobutyronitrile in toluene (8 ml) was heated at 80—90 °C for 20 h under argon atmosphere, and then evaporated to give crystals quantitatively, which were recrystallized from ethanol. Mp 187—188 °C; $[\alpha]_D^{23}$ +59.5° (*c* 1.0).

Found: C, 58.51; H, 5.90; S, 11.05%. Calcd for $C_{28}H_{32}O_9S_2$: C, 58.31; H, 5.59; S, 11.12%.

*Methyl 2,3,4-Trideoxy-6-*O*-trityl-α-*D*-glycero-hex-2-enopyranoside* (**4**). A suspension of **3** (1.0 g, 1.7 mmol) and sodium azide (680 mg, 10 mmol) in DMF (30 ml) was refluxed for 20 hr, poured into water, and the resulting solution was extracted with ether. The ether layer was washed with saturated sodium chloride, dried with sodium sulfate, and then evaporated to give a sirup which showed five spots on TLC (benzene:ethyl acetate=95:5). The starting material (R_f= 0.20; 380 mg, 38%) and 5 (R_f=0.58; 100 mg, 15%) were isolated as main products on a sillica gel column (benzene). $[\alpha]_D^{22}$ −22.6° (*c* 1.0); IR: 1660 (C=C).

Found: C, 80.14; H, 6.90%. Calcd for $C_{26}H_{26}O_3$: C, 80.80; H, 6.78%.

*Benzyl 2-Acetamido-4,6-*O*-benzylidene-2-deoxy-3-*O*-mesyl-α-*D*-mannopyranoside* (**6**). To an ice-cooled solution of benzyl 2-acetamido-4,6-*O*-benzylidene-D-deoxy-α-D-mannopyranoside (200 mg, 0.5 mmol) in pyridine (2 ml) was added dropwise methanesulfonyl chloride (150 mg, 1.3 mmol) with stirring. The resulting solution was kept at room temperature for 4 h, Poured into ice–water, and the crystals (230 mg, 96%) deposited were recrystallized from ethanol. Mp 167—168 °C; $[\alpha]_D^{23}$+114.5° (*c* 1.5); IR: 3280 (NH), 1650 and 1535 (amide), 1370 (sulfonate).

Found: C, 57.90; H, 5.74; N, 3.08%. Calcd for $C_{23}H_{27}O_8SN$: C, 57.85; H, 5.70; N, 2.93%.

*Benzyl 2-Acetamido-3-azido-4,6-*O*-benzylidene-2,3-dideoxy-α-D-altropyranoside* (**7**). A solution of **6** (1.0 g, 2.1 mmol) and lithium azide (1.0 g, 143 mmol) in HMPA (50 ml) was heated at 150—157 °C overnight, poured into cold sodium chloride solution, and then extracted with ether. The extracts were washed with 5% sodium chloride, dried, and evaporated to give a sirup (740 mg, 83%) which was crystallized and recrystallized from ethanol. Mp 160 °C; $[\alpha]_D^{23}$ +70.8° (*c* 1.2); IR: 3280 (NH), 2100 (N_3), 1650 and 1535 (amide).

Found: C, 62.39; H, 5.75; N, 13.34%. Calcd for $C_{22}H_{24}N_4O_5$: C, 62.25; H, 5.70; N, 13.20%.

*Benzyl 2-Acetamido-3-amino-4,6-*O*-benzylidene-2,3-dideoxy-α-D-altropyranoside* (**8**). A suspension of **7** (740 mg 1.7 mmol) and Raney nickel (2.3 g) in ethanol (80 ml) was hydrogenated in an autoclave under a hydrogen pressure of 80—100 kg/cm² at room temperature overnight, and then filtered. Evaporation of the filtrate gave crystals (600 mg, 88%) which were recrystallized from ethanol. Mp 236—238 °C; $[\alpha]_D^{19}$ +82.0° (*c* 1.02); IR: 3160—3350 (NH), 1660 and 1560 (amide).

Found: C, 66.25; H, 6.69; N, 6.92%. Calcd for $C_{22}H_{26}N_2O_5$: C, 66.31; H, 6.58; N, 7.03%.

Benzyl 2-Acetamido-2,3-dideoxy-3-guanidino-α-D-altropyranoside (**9**). To a solution of **8** (0.45 g, 1.13 mmol) in aqueous ethanol containing equimolar hydrochloric acid was added cyanamide (72 mg, 1.7 mmol), then the temperature of the mixture was raised to 130 °C in an oil-bath during 1 h, and the mixture was kept at the temperature for 30 min. The glassy reaction mixture was dissolved in aqueous ethanol, treated with IRA-410 (OH form, 5 ml) overnight, and then filtered, The filtrate was heated at 90—100 °C for 6 h together with acetic acid (70%, 40 ml), evaporated, and then absorbed on an Amberlite CG-50 column (20 ml). The column was eluated. in turn with water (200 ml), aqueous ammonia (2.8%, 200 ml), water (200 ml) and then 0.5 M hydrochloric acid. The last effluent of pH 6—8 was evaporated, and the residue was extracted with ethanol. The ethanol extract was treated with IRA-410 (OH^- form, 20 ml) overnight, and the filtrate was evaporated to give a colourless glassy solid (200 mg, 50%) which is positive in the Sakaguchi reaction. $[\alpha]_D^{23}$ +58.7° (*c* 1.07, water).

Found: C, 49.63; H, 6.91; N, 14.85%. Calcd for $C_{16}H_{24}N_4O_5\cdot 2H_2O$; C, 49.47; H, 7.27; N, 14.43%.

*Benzyl 2-Acetamido-2-deoxy-3-*O*-mesyl-6-*O*-trityl-α-*D*-mannopyranoside* (**10**). A suspension of **6** (3.07 g, 6.4 mmol) in 70 % acetic acid (100 ml) was heated at 60—70 °C for 6 h, and after evaporation of the solvent, the residue was washed with petroleum ether. A solution of the dried residue and trityl hloride (2.6 g, 9.3 mmol) in pyridine (50 ml) was kept at room temperature overnight, and evaporated. The residue was purified on a silica gel column (benzene: ethyl acetate=4: 1) to give crystals (2.52 g, 62%). Mp 179—180 °C; $[\alpha]_D^{22}$ +37.4° (*c* 1.0, acetone); IR: 3350 (NH), 1650 and 1520 (amide).

Found: C, 65.92; H, 5.93; N, 2.04; S. 5.12%. Calcd for $C_{35}H_{37}NO_8S$: C, 66.54; H, 5.90; N, 2.22; S, 5.08%.

*Benzyl 3′-*O*-Mesyl-6′-*O*-trityl-α-*D*-talopyranosid[2′,3′,4′; 4,5,6]-2-methyl-5,6-dihydro-4*H*-oxazine* (**11**). To an ice-cooled solution of **10** (1.0 g, 1.6 mmol) in pyridine (50 ml) was added dropwise sulfuryl chloride (0.16 ml, 2.0 mmol), and the mixture was evaporated, after standing overnight in a refrigerator. The residue was dissolved in chloroform, and the solution was washed in turn with cold 2 M hydrochloric acid, saturated sodium hydrogen carbonate and sodium chloride, dried, and then removal of the solvent gave a sirup (1.04 g, 80.5%) which was crystallized from ethanol. Mp 129—130 °C; $[\alpha]_D^{24}$ +18.1° (*c* 1.0); IR: 1660 (C=N), 1360 (sulfonic ester).

Found: C, 68.44; H, 5.72; N, 2.29; S, 5.29%. Calcd for $C_{35}H_{35}O_7S$: C, 68.49; H, 5.74; N, 2.28; S, 5.23%.

*Benzyl 2-Acetamido-3-azido-6-*O*-benzoyl-2,3-dideoxy-α-D-altropyranoside* (**12**). A suspension of **7** (3.5 g, 8.3 mmol) in 70% acetic acid (50 ml) was heated at 60—70 °C for 5 hr, the resulting solution was evaporated, and then the residue was washed with petroleum ether. To a chilled solution of the dried residue in pyridine (50 ml) was added dropwise benzoyl chloride (1.1 ml, 9.5 mmol), the mixture was kept at room temperature overnight, poured into cold saturated sodium hydrogen carbonate, and then extracted with chloroform. Treatment of the extract in a usual manner gave a sirup (3.0 g, 80%) which was purified on a silica gel column (ethyl acetate). $[\alpha]_D^{23}$ +51.7° (*c* 1.0); IR: 3300 (NH, OH), 2100 (N_3), 1720 (ester), 1650 and 1540 (amide).

Found: C, 59.43; H, 5.58; N, 12.30%. Calcd for $C_{22}H_{24}O_6N_4$: C, 59.99; H, 5.49; N, 12.72%.

*Benzyl 2-Acetamido-3-azido-6-*O*-benzoyl-4-chloro-2,3,4-trideoxy-α-D-idopyranoside* (**13**). To an ice-cooled solution of **12** (1.5 g, 3.4 mmol) in pyridine (30 ml) was added dropwise sulfuryl chloride (0.32 ml, 4.0 mmol), the mixture was kept overnight in a refrigerator, and the solvent was evaporated. The residue was dissolved in chloroform, and the solution was washed in turn with cold 2 M hydrochloric acid, saturated

sodium bicarbonate, saturated sodium chloride, dried, and evaporation of the solvent afforded crystals (1.1 g, 70.5%) which was recrystallized from ethanol. Mp 175 °C; $[\alpha]_D^{23}$ +79.8 °C (*c* 1.0); IR: 3250 (NH), 2100 (N_3); 1720 (ester), 1650 and 1550 (amide).

Found: C, 57.39; H, 5.07; N, 12.18%. Calcd for $C_{22}H_{23}O_5N_4Cl$: C, 57.39; H, 5.05; N, 12.21%.

Benzyl 2-Acetamido-6-O-benzoyl-2,3,4-trideoxy-3,4-epimino-α-D-altropyranoside (**14**). A solution of **13** (250 mg, 5.4 mmol) tributyltinhydride (3.0 ml) and catalytic amount of 2,2′-azobisisobutylonitrile in toluene was heated at 80—90 °C for 3 days under argon atmosphere, and crystals deposited at room temperature were filtered and recrystallized from toluene. Mp 142—143 °C; $[\alpha]_D^{22}$ +32.2° (*c* 1.0); IR: 3200—3300 (NH), 1710 (ester); 1660 and 1530 (amide and epimino); CNR (ppm): Ac (22.96), C_3 and C_4 (29.39, 30.53), C_2 (44.70), CH_2 (66.09, 70.71), C_5 (67.78), C_1 (97.78), C=O (165.89, 169.06).

Found: C, 66.09; H, 6.21; N, 6.93%. Calcd for $C_{22}H_{26}O_5N_2$: C, 66.31; H, 6.58; N, 7.03%.

Benzyl 2,3-Diacetamido-6-O-benzoyl-2,3,4-trideoxy-α-D-arabino-hexopyranoside (**15**). A suspension of **14** (200 mg, 0.5 mmol) and Raney nickel (2 g) in ethanol (10 ml) was hydrogenated in an autoclave at room temperature for 2 days, filtered, and the filterate was evaporated to give a sirup. The sirup in pyridine was acetylated with acetic anhydride at room temperature overnight, and the reaction mixture was poured into ice-water to give crystals which were recrystallized from ethanol–hexane. Yield, 130 mg (60%); Mp 214—215 °C; $[\alpha]_D^{22}$ −4.0° (*c* 0.5); IR: 3200—3300 (NH), 1720 (ester), 1660, 1640, 1560, and 1550 (amide).

Found: C, 64.12; H, 6.50; N, 6.09%. Calcd for $C_{23}H_{28}O_6N_2$: C, 64.47; H, 6.59; N, 6.54%.

The authors are indebted to Dr. K. Ajisaka and Mr. H. Matsumoto for NMR measurements, and members of the Laboratory of Organic Analysis for microanalyses.

References

1) Part XXIV, *Nippon Kagaku Kaishi*, **1975**, 1958.
2) T. Wakamiya, T. Shiba, T. Kaneko, H. Sakakibara, T. Noda, and T. Take, *Bull. Chem. Soc. Jpn.*, **46**, 949 (1973).
3) A. Nagata, T. Ando, R. Izumi, H. Sakakibara, T. Take, K. Hayano, and J. Abe, *J. Antibiot.*, **21**, 681 (1968); R. Izumi, T. Noda, T. Ando, T. Take, and A. Nagata, *ibid.*, **25**, 201 (1972). cf. T. Wakamiya and T. Shiba, *Bull. Chem. Soc. Jpn.*, **48**, 2502 (1975).
4) R. D. Guthrie and D. Murphy, *J. Chem. Soc.*, **1965**, 3828.
5) E. Albano, D. Horton, and T. Tsuchiya, *Carbohyd. Res.*, **2**, 349 (1966).
6) R. S. Tipson and A. Cohen, *Carbohyd. Res.*, **1**, 338 (1965).
7) R. J. Ferrier., *Adv. Carbohyd. Res.*, **24**, 199 (1969).
8) J. Kovar, V. Dienstbierova, and J. Jary, *Collect. Czech. Chem. Commun.*, **32**, 2498 (1967).
9) J. Honeyman and J. W. W. Morgan, *J. Chem. Soc.*, **1955**, 3660.
10) H. Arita, N. Ueda, and Y. Matsushima, *Bull. Chem. Soc. Jpn.*, **45**, 567 (1972).
11) J. Yoshimura, H. Sakai, N. Oda, and H. Hashimoto, *Bull. Chem. Soc. Jpn.*, **45**, 2027 (1972).
12) J. Yoshimura, T. Sekiya, and Y. Ogura, *Bull. Chem. Soc. Jpn.*, **47**, 1219 (1974).
13) W. Meyer zu Reckendorf, U. Kamprath-Scholz, E. Bischof, and N. Wassiliadou-Micheli, *Chem. Ber.*, **108**, 3397 (1975).

Aminosugars. XXVI. Synthesis of Amido-bonded Disaccharides Containing Hexosaminuronic Acids[1]

Juji YOSHIMURA, Hiroaki ANDO, Tadahide SATO, Shigeru TSUCHIDA,* and Hironobu HASHIMOTO

Laboratory of Chemistry for Natural Products, Faculty of Science, Tokyo Institute of Technology, Meguro-ku, Tokyo 152

(Received February 7, 1976)

Synthesis and properties of amido-bonded disaccharides containing hexosaminuronic acids are described. The amino group of D-gluco- and D-mannosamine derivatives was acylated with D-gluco- and D-mannosaminuronic acid derivatives by the dicyclohexylcarbodiimide method, and the protecting groups of a few products were removed. Some of them showed the additive patterns of components in their PMR spectra.

2-Acetamido-2-deoxy-D-glucuronic acid[2-4] and -D-mannuronic acid[5] have been found as a component of several bacterial cell-walls. These hexosaminuronic acids also arouse interest in their polyfunctional character. For examples, several antibiotics such as blasticidine S,[6] gougerotin,[7] and polyoxin C[8] include an amido bond between a certain hexosaminuronic acid and a peptide. Although amido-bonded disaccharides have not been found in nature up to date, we synthesized some of them containing usual aminosugars and uronic acids, and analyzed their PMR spectra as the additive pattern of component sugars in a previous paper.[9]

In this paper, similar disaccharides between hexosaminuronic acids and aminosugars were synthesized, and their properties were examined.

Results and Discussion

In this study, benzyl 2-amino-2-deoxy-α-D-glucopyranoside (**1**),[10] benzyl 2-amino-4,6-*O*-benzylidene-2-deoxy-α-D-mannopyranoside (**2**)[11] and its de-*O*-benzylidenated derivative (**3**)[9] were used as aminosugars, and benzyl 2-acetamido- (**4**)[12] and 2-benzyloxycarbonylamido-2-deoxy-α-D-glucopyranosiduronic acid (**5**)[13] benzyl 2-acetamido-2-deoxy-α-D-mannopyranosiduronic acid (**6**)[11] as hexosaminuronic acids.

Condensation of **1** and **4** or **5** in pyridine by the dicyclohexylcarbodiimide (DCC) method for five days gave precipitates of a mixture of the product and dicyclohexylurea (DCU), from which benzyl 2-(benzyl 2-acetamido- (**7**) or 2-benzyloxycarbonylamino-2-deoxy-α-D-glucopyranosiduronyl) amino-2-deoxy-α-D-glucopyranoside (**8**) was obtained by fractional crystallization both in 71% yield. These compounds having the D-*gluco*-type unit are not so soluble even in water and alcohols, and have higher melting points compared with that including the D-*manno*-type unit. The structure of **7** was confirmed by the conversion into the corresponding penta-*O*-acetate (**9**). Similar condensation of **1** and **6**, and separation of the product and DCU by a silica gel column chromatography gave benzyl 2-(benzyl 2-acetamido-2-deoxy-α-D-mannopyranosiduronyl)amino-2-deoxy-α-D-glucopyranoside (**10**) in 64% yield. Acetylation of **10** gave the corresponding penta-*O*-acetate (**11**) in 80% yield.

In the case of **2** and **4**, and also **3** and **6**, the corresponding disaccharides were separated in a pure state only as the tri-*O*-acetate (**13**) and penta-*O*-acetate (**15**), respectively. Treatment of **13** in ethanol with a tiny amount of metallic sodium gave benzyl 2-(benzyl

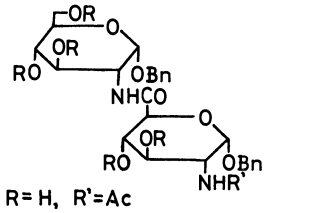

7 R=H, R'=Ac
8 R=H, R'=benzyloxycarbonyl
9 R=R'=Ac

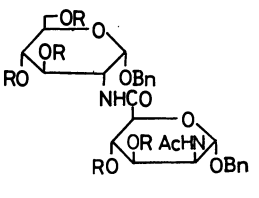

10 R=H
11 R=Ac

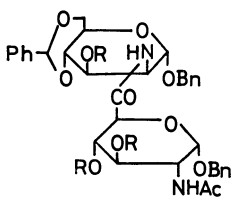

12 R=H
13 R=Ac

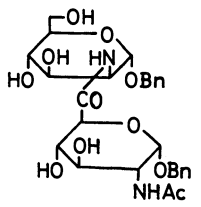

14

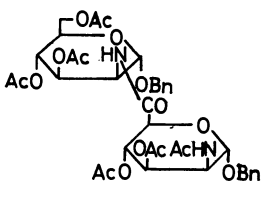

15

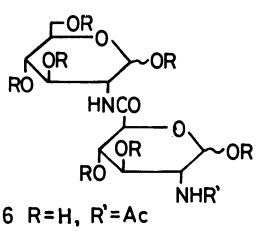

16 R=H, R'=Ac
17 R=H, R'=H·HCl
18 R=R'=Ac

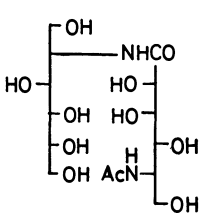

19

* Present address: Arai High School, Koizumo Arai-shi 944.

Table 1. The additivity of NMR signals in amido-bonded disaccharides observed in partial ring-protons[a,b]

	H_1	H_2	H_3	H_4
9	5.07; d, $J_{1,2}$=3.6		5.75; t, $J_{3,4}$= 9.9	5.52; t, $J_{4,5}$= 9.2
	5.32; d, $J_{1,2}$=3.6			
	(5.17; d, $J_{1,2}$=3.4)	(*ca.* 4.81)	(5.73; t, $J_{3,4}$= 9.8)	(5.34; t, $J_{4,5}$= 9.2)
	[5.27; d, $J_{1,2}$=3.6]	[*ca.* 4.93]	[5.82; t, $J_{3,4}$=12.0]	[5.72; t, $J_{4,5}$= 9.0]
15	4.79; d, $J_{1,2}$=*ca.* 1.5	$J_{2,3}$=4.0	5.34; q, $J_{3,4}$=10.0	5.14; t, $J_{4,5}$=*ca.* 10.0
	4.88; d, $J_{1,2}$=*ca.* 1.0			
	(4.80; d, $J_{1,2}$=*ca.* 1.0	(4.62; q, $J_{2,3}$=4.5)	(5.34; q, $J_{3,4}$=10.0)	(5.12; t, $J_{4,5}$= 9.3)[9]
	[4.93; d, $J_{1,2}$=2.0]	[4.70; $J_{2,3}$=4.5]	[5.40; q, $J_{3,4}$=10.0]	[5.25; q, $J_{4,5}$=10.0][11]
18	6.13; d, $J_{1,2}$=3.8	*ca.* 4.45; m	5.28; t, $J_{3,4}$= 9.8	5.13; t, $J_{4,5}$= 8.5
	(6.13; d, $J_{1,2}$=3.6)	(*ca.* 4.48; m)	(5.20; t, $J_{3,4}$= 9.8)	(5.16; t, $J_{4,5}$= 9.0)

a) NMR data (chemical shift, splitting and coupling constant) in parentheses and brackets show those of component *O*-acetylated aminosugar and uronic acid moiety, respectively. b) Compound **9** and its component sugars were measured in pyridine-d_5 and others in chloroform-d_1.

2-acetamido-2-deoxy-α-D-glucopyranosiduronyl)amino-4,6-*O*-benzylidene-2-deoxy-α-D-mannopyranoside (**12**). Partial hydrolysis of **12** with 60% acetic acid gave the corresponding de-*O*-benzylidenated product (**14**).

On the other hand, hydrogenation of **7** and **8** in the presence of palladium–charcoal gave the corresponding free sugars (**16** and **17**) having fairly high melting points in 80 and 66% yields, respectively. Further hydrogenation of **16** with excess sodium borohydride gave quantitatively the corresponding crystalline alditol (**19**). Acetylation of **16** in pyridine with acetic anhydride unexpectedly gave the unchanged materials, but acid-catalyzed acetylation with perchloric acid–acetic anhydride gave successfully the corresponding hepta-*O*-acetate (**18**). The glycosidic configurations of **18** were determined to be α, α from the coupling constants, $J_{1,2}$=3.8 Hz (Fig. 1) and specific rotation ($[\alpha]_D^{23}$ +115°). For the synthesis of amido-bonded trisaccharides, condensation of **17** with **5** by the DCC method was tried several times, but only unsuccessful results were obtained, partly due to the insolubility of **17**.

As was pointed out in the previous paper, PMR spectra of amido-bonded sugars were supposed to show the additive patterns of the component monosaccharides.

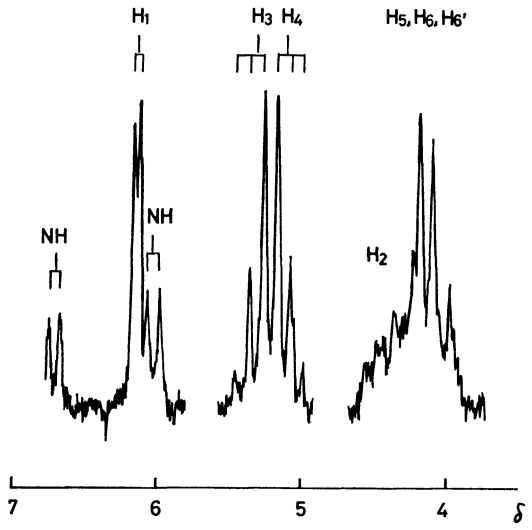

Fig. 1. Ring-proton signals in the NMR spectrum of **18** (in $CDCl_3$ at 100 MHz).

However, the analysis of spectra of pyranose-pyranose type compounds mentioned above were rather difficult due to superimposed signals. The simplest signal pattern in the spectrum of **18** indicated that H_1, H_3, and H_4 protons in both pyranose-rings are almost in the same magnetic circumstance. As was shown in Table 1, the similar additivity was scarcely observed in the spectra of **9** and **15** having the same configuration in both pyranose-rings.

Experimental

The melting points were determined on a sulfuric acid bath and uncorrected. Optical rotations were measured in a 0.5-dm tube with a Carl Zeiss photoelectric polarimeter. NMR spectra were recorded at 100 MHz with a JNM-4H-100 spectrometer. IR spectra were recorded with a Hitachi Model EPI-G2 spectrophotometer. Chemical shifts and coupling constants were recorded in δ and Hz units and IR frequencies in cm^{-1}.

Benzyl 2-(Benzyl 2-acetamido-2-deoxy-α-D-glucopyranosiduronyl)-amino-2-deoxy-α-D-glucopyranoside (**7**). To a solution of benzyl 2-amino-2-deoxy-α-D-glucopyranoside (**1**) hydrochloride(14.0 g, 45.8 mmol) and benzyl 2-acetamido-2-deoxy-α-D-glucopyranosiduronic acid (**4**) (15.0 g, 46.1 mmol) in dry pyridine (140 ml) containing triethylamine (4.6 g, 46 mmol) was added DCC (10 g, 50 mmol), and the resulting solution was stirred at room temperature for 5 days. The gelatinous materials deposited were filtered. The amorphous solid obtained by addition of acetic acid (5%, 10 ml) to the above filtrate was also gathered. Both solids were dissolved in DMF and insoluble DCU was filtered off. The residues obtained by evaporation of the filtrate were crystallized twice from methanol–pyridine. Yield, 18.8 g (71%); mp 283—284 °C (decomp); $[\alpha]_D^{23}$ +156° (*c* 1.0, DMF); IR: 1650 and 1550 (amide) cm^{-1}.

Found: C, 57.96; H, 6.20; N, 4.81%. Calcd for $C_{28}H_{36}N_2O_{11}$: C, 58.32; H, 6.29; N, 4.86%.

Acetylation of **7** by the usual manner, and crystallization of the product from ethanol gave the corresponding penta-*O*-acetate (**9**) in 80% yield. Mp 201—202 °C; $[\alpha]_D^{23}$ +66° (*c* 1.0, pyridine); IR: 1745 (ester), 1685, 1660, 1525 (amide) cm^{-1}.

Found: C, 57.73; H, 5.79; N, 3.52%. Calcd for $C_{38}H_{46}N_2O_{16}$: C, 58.01; H, 5.89; N, 3.56%.

Benzyl 2-(Benzyl 2-benzyloxycarbonylamino-2-deoxy-α-D-glucopyranosiduronyl)amino-2-deoxy-α-D-glucopyranoside (**8**). Condensation of hydrochloride of **1** (11 g, 36 mmol) and benzyl 2-

benzyloxycarbonylamino-2-deoxy-α-D-glucopyranosiduronic acid (**5**) (15 g, 36 mmol) in a similar manner as **7**, and recrystallization of the product from pyridine–methanol gave **8** in 71 % (17 g) yield. Mp 272—272.5 °C (decomp); $[\alpha]_D^{23}$ +170° (*c* 1.0, pyridine); IR: 1650, 1525 (amide) cm^{-1}.

Found: C, 60.85; H, 6.02; N, 4.29%. Calcd for $C_{34}H_{40}N_2O_{11}$: C, 61.07; H, 6.03; N, 4.19%.

Benzyl 2-(Benzyl 2-acetamido-2-deoxy-α-D-mannopyranosiduronyl)-amino-2-deoxy-α-D-glucopyranoside (**10**). A solution of hydrochloride of **1** (2.2 g, 7.2 mmol), benzyl 2-acetamido-2-deoxy-α-D-mannopyranosiduronic acid (**6**) (2.4 g, 7.3 mmol) and DCC (1.5 g, 7.3 mmol) in pyridine (6 ml) and triethylamine (1.2 ml) was stirred for 5 days at room temperature, and DCU deposited was filtered off. Evaporation of the filtrate gave a syrup which was fractionally separated on a silica gel column (benzene–methanol=10 : 1) to give the crystalline product which was recrystallized three times from ethanol. Yield, 2.7 g (65%), mp 223—223.5 °C; $[\alpha]_D^{23}$ +142° (*c* 0.57, pyridine), IR: 1655, 1555, 1520 (amide) cm^{-1}.

Found: C, 58.21; H, 6.24; N, 5.07%. Calcd for $C_{28}H_{36}N_2O_{11}$: C, 58.32; H, 6.29; N, 4.86%.

Base-catalyzed acetylation of **10** in a usual manner gave the corresponding penta-*O*-acetate (**11**) in 80% yield, which was purified from ethanol–petroleum ether. Amorphous white solid sintered at 85 °C and melted at 124—125 °C. $[\alpha]_D^{23}$ +54° (*c* 0.92, pyridine); IR: 1740 (ester), 1680, 1510 (amide) cm^{-1}.

Found: C, 57.84; H, 5.95; N, 3.43%. Calcd for $C_{38}H_{46}N_2O_{16}$: C, 58.01; H, 5.89; N, 3.56%.

Benzyl 2-(Benzyl 2-acetamido-3,4-di-O-acetyl-2-deoxy-α-D-glucopyranosiduronyl)amino-3-O-acetyl-4,6-O-benzylidene-2-deoxy-α-D-mannopyranoside (**13**). A solution of benzyl 2-amino-4,6-*O*-benzylidene-2-deoxy-α-D-mannopyranoside (**2**) (1.5 g, 4.2 mmol), **4** (1.4 g, 4.3 mmol), and DCC (1.0 g, 4.85 mmol) in pyridine (20 ml) was stirred for 3 days at room temperature, filtered, and then the filtrate was evaporated to give a syrup (2.6 g). To a solution of this syrup in pyridine (4 ml) was added acetic anhydride (1.5 g), and after 2 h, the reaction mixture was poured into ice–water. The solid mass deposited was collected, dried, and then recrystallized from large amount of ethanol to give **13** in 69% yield. Mp 252—253 °C; $[\alpha]_D^{23}$ +90.5° (*c* 1.1, pyridine); IR: 1680, 1560 (amide) cm^{-1}.

Found: C, 62.01; H, 5.65; N, 3.76%. Calcd for $C_{41}H_{46}N_2O_{14}$: C, 62.27; H, 5.86; N, 3.54%.

De-*O*-acetylation of **13** (2.0 g, 2.5 mmol) in absolute ethanol (600 ml) with a trace amount of metallic sodium gave a syrup which was crystallized from methanol to give **12** in 72% (1.2 g) yield. Mp 153—155 °C; $[\alpha]_D^{23}$ +97.8° (*c* 0.64, pyridine); IR: 1650, 1525 (amide) cm^{-1}.

Found: C, 63.01; H, 6.22; N, 4.35%. Calcd for $C_{35}H_{40}N_2O_{11}$: C, 63.24; H, 6.07; N, 4.21%.

Benzyl 2-(Benzyl 2-acetamido-2-deoxy-α-D-glucopyranosiduronyl)-amino-2-deoxy-α-D-mannopyranoside (**14**). A solution of **12** (0.50 g, 0.75 mmol) in 60% acetic acid (20 ml) was heated for 1 h at 80 °C, and then evaporated to give a hard syrup which was crystallized from methanol. Yield, 0.33 g (76%); mp 138—140 °C; $[\alpha]_D^{23}$ +107° (*c* 0.19, DMF); IR: 1680, 1560 (amide) cm^{-1}.

Found: C, 58.01; H, 6.42; N, 4.76%. Calcd for $C_{28}H_{36}N_2O_{11}$: C, 58.32; H, 6.29; N, 4.86%.

Benzyl 2-(benzyl 2-acetamido-3,4-di-O-acetyl-2-deoxy-α-D-mannopyranosiduronyl)amino-3,4,6-tri-O-acetyl-2-deoxy-α-D-mannopyranoside (**15**). Benzyl 2-amino-2-deoxy-α-D-mannopyranoside (**3**) (0.37 g, 1.2 mmol) and **6** (0.40 g, 1.2 mmol) were condensed in a similar manner as above, and the syrupy product was acetylated to give syrupy penta-*O*-acetate (1.0 g) which was purified on a silica gel column (benzene–methanol= 10: 1). Yield, 0.71 g (75%); $[\alpha]_D^{23}$ +72.8° (*c* 0.60, pyridine); IR, 1750 (ester), 1680, 1670, and 1545 (amide) cm^{-1}.

Found: C, 57.72; H, 5.81; N, 3.32%. Calcd for $C_{38}H_{46}N_2O_{16}$: C, 58.01; H, 5.89; N, 3.58%.

2-(2-Acetamido-2-deoxy-D-glucopyranuronyl)amino-2-deoxy-D-glucopyranose (**16**). A suspension of **7** (5.0 g, 8.7 mmol) in methanol (100 ml) adjusted to pH 2 with hydrochloric acid was hydrogenated in the presence of palladium–charcoal (10%, 10 g), and then filtered. Concentration of the filtrate gave no products, but, extraction of the filtered mass several times with hot water gave white solid which was recrystallized from hot water. Yield, 2.8 g (80%); mp 261—262 °C (decomp); IR: 1650, 1620, 1570, and 1540 (amide) cm^{-1}.

Found: C, 42.25; H, 6.31; N, 7.23%. Calcd for $C_{14}H_{24}N_2O_{11}$: C, 42.42; H, 6.10; N, 7.07%.

2-(2-Amino-2-deoxy-D-glucopyranuronyl)amino-2-deoxy-D-glucopyranose Hydrochloride (**17**). A suspension of **8** (12.0 g, 17.9 mmol) in water containing equimolar amount of hydrochloric acid was hydrogenated in the presence of palladium–charcoal (10%, 10 g), filtered, and then evaporated to give a white mass which was recrystallized from water–ethanol. Yield 4.6 g (66 %); mp 230—231 °C (decomp); $[\alpha]_D^{23}$ +80° +62.4° (*c* 1.0, H_2O, 72 h); IR: 1640, 1510 (amide), 1560 ($NH_2 \cdot HCl$) cm^{-1}.

Found C, 36.40; H, 6.01; N, 6.79; Cl, 9.09%. Calcd for $C_{12}H_{22}N_2O_{10} \cdot HCl$: C, 36.88; H, 5.93; N, 7.17; Cl, 9.07%.

2-(2-Acetamido-1,3,4-tri-O-acetyl-2-deoxy-α-D-glucopyranuronyl)amino-1,3,4,6-tetra-O-acetyl-2-deoxy-α-D-glucopyranose (**18**). To an ice-cooled suspension of **16** (0.60 g, 1.5 mmol) in acetic anhydride (15 ml) was added several drops of perchloric acid under stirring, and the resulting solution was kept at room temperature for 30 min, poured into ice–water, and then extracted with chloroform. The extract was washed successively with water, aqueous sodium hydrogencarbonate and water, dried and then evaporated to give crystals which were recrystallized from ethanol. Yield, 0.63 g (60%); mp 190—191 °C $[\alpha]_D^{23}$ +115° (*c* 1.0, $CHCl_3$).

Found: C, 48.92; H, 5.69; N, 4.06%. Calcd for $C_{28}H_{38}N_2O_{18}$: C, 48.70; H, 5.55; N, 4.06%.

2-(5-Acetamido-5-deoxy-L-gulonyl)amino-2-deoxy-D-glucitol (**19**). To an aqueous solution of **16** (0.30 g, 0.76 mmol) was added portionwise sodium borohydride (0.10 g, 3 mmol) with stirring, the resulting solution was stirred at room temperature for 2 h, and then neutralized with Amberlite 120 (H^+ form). The neutral solution was evaporated, and a methanol solution of the residue was evaporated repeatedly to remove boric acid. The product thus obtained was crystallized from methanol–ether. Yield 0.30 g (99%); mp 83—84 °C; $[\alpha]_D^{23}$ −21° (*c* 1.0, H_2O); IR, 1660, 1640, and 1550 (amide).

Found: C, 41.59; H, 7.06; N, 6.87%. Calcd for $C_{14}H_{28}N_2O_{11}$: C, 42.00; H, 7.05; N, 7.00%.

The authors are indebted to the members of the Laboratory of Organic Analysis for microanalysis and to Mr. H. Matsumoto for NMR measurements.

References

1) Part XXV, J. Yoshimura, M. Iwakawa, and Y. Ogura *Bull. Chem. Soc. Jpn.*, **49**, 2506 (1976).
2) W. R. Clark and J. Mclaughlin, *J. Biol. Chem.*, **230**, 81 (1958).
3) A. R. Williamson and S. Zamenhof, *J. Biol. Chem.*, **238**, 2255 (1963).
4) S. Hanessian and T. H. Haskell, *J. Biol. Chem.*, **239**, 2758 (1964).
5) S. Hase and Y. Matsushima, *J. Biochem.*, **69**, 559 (1971).
6) S. Takeuchi and H. Yonehara, *J. Antibiot. (Tokyo)*, **11**, 1 (1958).

7) T. Kanzaki and A. Miyake, *J. Antibiot. (Tokyo)*, **15**, 93 (1962).
8) K. Isono and S. Suzuki, *Tetrahedron Lett.*, **203** (1968).
9) J. Yoshimura, Y. Motoki, M. Ikeda, N. Oda, and H. Hashimoto, *Nippon Kagaku Kaishi*, **1975**, 1958.
10) J. Yoshimura, K. Fujimori, Y. Sugiyama, and H. Ando., *Bull. Chem. Soc. Jpn.*, **44**, 3131 (1971).
11) J. Yoshimura, H. Sakai, N. Oda, H. Hashimoto, *Bull. Chem. Soc. Jpn.*, **45**, 2027 (1972).
12) J. Yoshimura, T. Sato, and H. Ando, *Bull. Chem. Soc. Jpn.*, **42**, 2352 (1965).
13) H. Weidmann and H. K. Zimmerman, *Ann. Chem.*, **639**, 198 (1961); K. Heyns and H. Paulsen, *Chem. Ber.*, **88**, 188 (1955).
14) J. Yoshimura, H. Hashimoto, and H. Ando, *Carbohyd. Res.*, **4**, 435 (1967); **5**, 82 (1967).
15) H. Weidmann and H. K. Zimmerman, *Ann. Chem.*, **684**, 226 (1965).

Synthesis of 2,7-Di-*t*-butyl-4,5,9,10-tetraphenyltricyclo[6.2.0.0^{3,6}]deca-1,3(6),4,7,9-pentaene. A Benzo[1,2: 4,5]dicyclobutene[1]

Fumio TODA and Yutaka TAKAHARA

Department of Industrial Chemistry, Faculty of Engineering, Ehime University, Matsuyama 790

(Received March 29, 1976)

The title compound (**15**) which has two cyclobutadienes fused to a benzene ring, was synthesized by heating *dl*- (**7**), *meso*-3,8-di-*t*-butyl-1,5,6,10-tetraphenyldeca-3,4,6,7-tetraene-1,9-diyne (**8**), or *E,Z*-3,4-bis(1-*t*-butyl-3-phenyl-2-propynylidene)-1,2-diphenyl-1-cyclobutene (**12**).

Benzocyclobutene has been an interesting subject in relating to antiaromatic cyclobutadiene,[2] and some derivatives of benzocyclobutadiene have been isolated.[3-5] It is, however, much more interesting to fuse an additional cyclobutadiene further to the benzene ring of benzocyclobutadiene, because the resulting carbocycle which has two antiaromatic cyclobutadienes is formally a 10π electrons system. As the first example of this carbocycle, the title compound (**15**) was prepared according to the following routes.

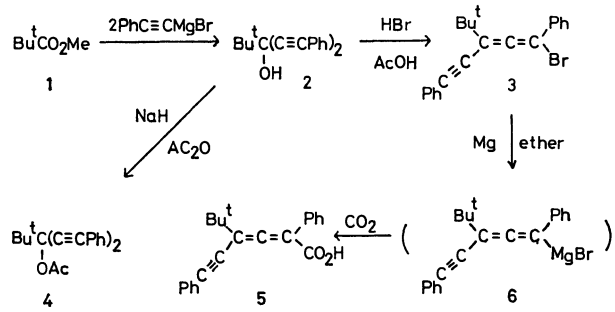

3-*t*-Butyl-1,5-diphenylpenta-1,4-diyn-3-ol (**2**) was prepared by the reaction of methyl pivalate (**1**) with two molar amounts of phenylethynylmagnesium bromide. The treatment of **2** with hydrobromic acid and acetic anhydride afforded 1-bromo-3-*t*-butyl-1,5-diphenylpenta-1,2-dien-4-yne (**3**) and the acetate of **2** (**4**), respectively. The reaction of **3** with magnesium in ether resulted in an ethereal solution of the Grignard reagent (**6**), which on treatment with carbon dioxide afforded 1-carboxy derivative (**5**).

Both the treatments of **3** and **4** with CuCl in *N,N*-dimethylformamide (DMF) according to the previously-reported procedure,[6] afforded *dl*- (**7**)[7] and *meso*-3,8-di-*t*-butyl-1,5,6,10-tetraphenyldeca-3,4,6,7-tetraene-1,9-diyne (**8**), and 3,6-di-*t*-butyl-1,5,8-triphenyl-6-phenylethynylocta-3,4-diene-1,7-diyne (**9**)[7] in the yields summarized in Table 1. The treatment of an ethereal solution of **6** with CuCl also gave **7**, **8**, and **9** in the yields shown in Table 1.

In order to characterize the structure of **9**, the following reactions were carried out. The oxidation of **9** with potassium permanganate afforded 3,6-di-*t*-butyl-1,5,8-triphenyl-6-phenylethynylocta-3,4-diene-7-yne-1,3-dione (**10**). An evidence for the α-diketone structure of **10** was obtained by its sodium borohydride reduction into 3,6-di-*t*-butyl-1,5,8-triphenyl-6-phenylethynylocta-3,4-dien-7-yne-1,2-diol (**11**) which shows NMR signals of two vicinal methine protons. Furthermore, the fact that the stretching frequencies of allene of **10** (1930 cm^{-1}) are lower than those of **11** (1940 cm^{-1}), supported the structure of **10** in which a conjugation between the α-diketone and allene moieties is possible.

The *meso* structure of **8** was elucidated on the basis of its thermal conversion into *E,Z*-3,4-bis(1-*t*-butyl-3 phenyl-2-propynylidene)-1,2-diphenyl-1-cyclobutene (**12**). The *E,Z*-structure of **12** was determined by means of its NMR spectrum which shows two *t*-butyl signals. The *E,Z*-structure of **12** was further confirmed by its oxidation with potassium permanganate which affords thermally stable *E,Z*-4,5-dibenzoyl-3,6-di-*tert*-butyl-1,8-diphenylocta-3,5-diene-1,7-diyne (**13**).

Because it has been well established that thermal 2+2 cyclization of diallene proceeds by conrotatory manner,[8,9] the diallene (**8**) which affords *E,Z*-dimethylene-cyclobutene (**12**) by heating should be *meso*-form. Finally, the another diallene (**7**) would be *dl*-form.

Table 1. Yields (%) of **7**, **8**, and **9**

	7	**8**	**9**
3 $\xrightarrow[\text{DMF}]{\text{CuCl}}$	11	11	54
4 $\xrightarrow[\text{DMF}]{\text{CuCl}}$	19	16	41
6 $\xrightarrow[\text{ether}]{\text{CuCl}}$	13	13	69

Heating of **7** in benzene under reflux in nitrogen atmosphere for 30 min gave the title compound (**15**) as greenish blue needles in almost quantitative yield. The UV spectrum of **15** showed the absorption bands at 394 and 643 nm. These bands at longer wavelength region are typical for benzocyclobutene derivatives.[3,4] In the mass spectrum, **15** showed a divalent ion peak at *m/e* 271. The thermal conversion of **7** into **15** presumably proceeds *via* the *E,E*-isomer of **12** (**14**) which was initially formed by a conrotatory cyclization of **7**. In the cyclization of **7**, formation of the *Z,Z*-isomer of **14** would be prohibited because of a steric repulsion between the two *t*-butyl groups. The formation of **15** by a thermal cycloaddition between the two acetylene moieties of **14** is reasonable because such cycloaddition of acetylenes has been reported.[3] Nevertheless, such the cycloaddition reaction which forms two cyclobutadienes and one benzene ring at a time has not been reported, even though this reaction is probably not a

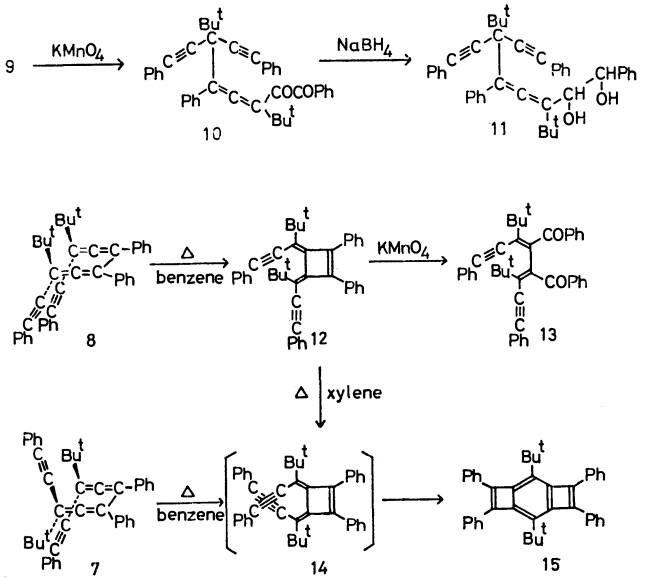

concerted one.

The heating of **8** in *o*-xylene under reflux also afforded **15** in almost quantitative yield. This reaction probably proceeds *via* **12** and **14** successively, because the same treatment of **12** which was prepared from **8** gave **15**. Nevertheless, **12** was inert to the thermal reaction in benzene. This result shows that the conversion of the *E,Z*-geometry of **12** into the *E,E*-one can be performed in boiling *o*-xylene but not in boiling benzene.

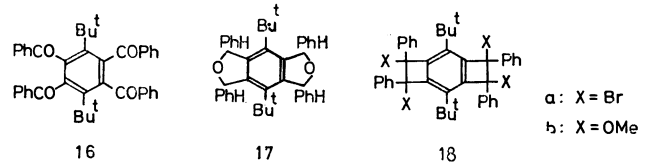

In solution, **15** was immediately oxidized but in the crystalline state it was fairly stable and turned gradually into 2,3,5,6-tetrabenzoyl-1,4-di-*t*-butylbenzene (**16**). The treatment of **16** with sodium borohydride followed by hydrogen bromide afforded 1,7-dioxa-4,10-di-*t*-butyl-2,6,8,12-tetraphenyltricyclo[7.3.0.0^{3,11}]dodeca-3,5(9),10-triene (**17**) in almost quantitative yield. The addition of bromine to **15** afforded 4,5,9,10-tetrabromo-2,7-di-*t*-butyl-4,5,9,10-tetraphenyltricyclo[6.3.0.0^{3,6}]deca-1,3(6),7-triene (**18a**), which on treatment with methanol gave the tetramethoxy derivative (**18b**).

Experimental

All the melting points are uncorrected. The IR, UV, and NMR spectra were measured in Nujol mull, $CHCl_3$, and $CDCl_3$, respectively, unless otherwise stated. The mass spectra were measured with an ionization energy of 75 eV.

Synthesis of **2**. To an ethereal solution of ethylmagnesium bromide prepared from Mg (50 g), ethyl bromide (220 g), and ether (1 l), was added a solution of phenylacetylene (208 g) in ether (1 l) under stirring during the period of 1 h. This solution was stirred for further 2 h, and then heated under reflux for 1 h. Into this solution, was added a solution of methyl pivalate (113 g) in ether (500 ml) during the period of 1 h. The reaction mixture was heated under reflux for 2 h, decomposed with dil HCl, and then extracted with ether. The ethereal solution was washed with water and dried over anhydrous Na_2SO_4. The crude crystals left after the evaporation of the solvent were recrystallized from hexane to afford **2** as colorless needles; 196 g (71%); mp 59 °C. IR: 3540 (OH) and 2210 cm^{-1} (C≡C); NMR: 2.3—2.7 (m, Ph, 10H), 7.36 (s, OH, 1H), and 8.72 τ (s, Bu^t, 9H).

Found: C, 87.23; H, 6.75%. Calcd for $C_{21}H_{20}O$: C, 87.46; H, 6.99%.

Synthesis of **3** *and* **5**. To an ice-cooling solution of **2** (144 g) in acetic acid (140 ml), was added concd HBr (72 ml). The reaction mixture was stirred for 1 h under ice-cooling, decomposed with water, and then extracted with petroleum ether. The organic solution was washed with aqueous $NaHCO_3$ and water successively, and dried over anhydrous Na_2SO_4. The evaporation of the solvent afforded **3** as colorless oil; 160 g (91 %), which was used without further purification for all the following synthesis. IR (liquid): 1940 cm^{-1} (C=C=C).

A mixture of **3** (15 g), Mg (1 g), and ether (200 ml) was stirred under N_2 atmosphere for 1 hr, and then heated under reflux for 0.5 h. Into the ethereal solution, CO_2 was bubbled for 2 h. The reaction mixture was decomposed with dil HCl and extracted with ether. The ethereal solution was washed with water and dried over anhydrous Na_2SO_4. The crude crystals left after the evaporation of the solvent were recrystallized from petroleum ether–CCl_4 (10: 1) to afford **5** as colorless needles; 10.1 g (74%); mp 150—152 °C. IR: 1930 (C=C=C) and 1700 cm^{-1} (C=O); λ_{max} 274 nm (ε, 31600); NMR: −1.0 (s, CO_2H, 1H), 2.3—2.8 (m, Ph, 10H), and 8.80 τ (s, Bu^t, 9H).

Found: C, 83.46; H, 6.35%. Calcd for $C_{22}H_{20}O_2$: 83.51; H, 6.37%.

Synthesis of **4**. A mixture of **2** (5 g), NaH (0.44 g), and benzene (25 ml) was kept to stand at room temperature for 1 h. Into this solution, Ac_2O (1.8 g) was added, and the mixture was heated under reflux for 15 min. The crude crystals left after the evaporation of the solvent were recrystallized from hexane to afford **4** as colorless needles; 5.2 g (91%); mp 105 °C. IR: 2210 (C≡C) and 1740 cm^{-1} (C=O); λ_{max}: 254 (35300) and 279 nm (ε, 1440); NMR: 2.2—2.8 (m, Ph, 10H), 7.87 (s, Me, 3H), and 8.70 τ (s, Bu^t, 9H).

Found: C, 83.76; H, 6.57%. Calcd for $C_{23}H_{22}O_2$: C, 83.60; H, 6.71%.

Synthesis of **7**,**8**, *and* **9**. *Procedure A)*. A solution of **2** (253 g) and CuCl (130 g) in DMF (630 ml) was kept to stand at room temperature for 12 h. The crude crystals formed were filtered, washed with MeOH, and dried. The crude crystals were dissolved in acetone (300 ml). The crystals formed after th acetone solution was kept to stand for 5 h were recrystallized from AcOEt to afford **7** as colorless needles; 21.5 g (11%). This compound turned into **15** immediately when melted at 145 °C, and melted again at 296—297 °C. This melting point was measured in N_2 atmosphere[7]. IR ($CHCl_3$): 2200 (C≡C) and 1940 cm^{-1} (C=C=C); λ_{max}: 275 (52900) and 297 nm (ε, 41000); NMR: 2.1—2.8 (m, Ph, 20H) and 8.79 τ (s, Bu^t, 18H); MS *m/e*: 542 (M^+).

Found: C, 92.75; H, 6.78%. Calcd. for $C_{42}H_{38}$: C, 92.94; H, 7.06%.

The crystals formed after the acetone mother liquor was kept to stand for further 5 h were recrystallized from acetone to afford **9** as colorless prisms; 104.4 g (54%); mp 149—151 °C. IR ($CHCl_3$): 2200 (C≡C) and 1940 cm^{-1} (C=C=C); λ_{max}: 280 (30,900) and 297 nm (ε, 26600); NMR: 2.1—2.8 (m, Ph, 20H) and 8.69 and 8.83 τ (each s, Bu^t, 9H); MS *m/e*: 542 (M^+).

Found: C, 92.97; H, 6.81%. Calcd for $C_{42}H_{38}$: C, 92.94; H, 7.06%.

The DMF solution left after the separation of **7** and **9** was decomposed with water and extracted with ether. The ethereal solution was washed with water and dried over anhydrous Na_2SO_4. The crude crystals left after the evaporation of the solvent were recrystallized from acetone to afford **8** as colorless

prisms; 21.1 g (11%); mp 123—124 °C. IR ($CHCl_3$): 2200 (C≡C) and 1940 cm^{-1} (C=C=C); λ_{max}: 276 (59000) and 316 sh nm (ε, 28700); NMR: 2.4—3.7 (m, Ph, 20H) and 8.79 τ (s, Bu^t, 18H); MS *m/e*: 542 (M^+).

Found: C, 92.81; H, 6.84%. Calcd for $C_{42}H_{38}$: C, 92.94; H, 7.06%.

Procedure B). A solution of **4** (50 g) and CuCl (25 g) in DMF (120 ml) was heated at 50 °C for 6 h, and then kept to stand for 12 h. The treatment of the reaction mixture by the same procedure as that used in *Procedure A*, afforded **7** (8.1 g, 19%), **8** (6.8 g, 16%), and **9** (17.5 g, 41%).

Procedure C). To an ethereal solution of **6** prepared from **2** (15 g), Mg (1 g), and ether (200 ml), was added CuCl (7.5 g) under stirring at room temperature during the period of 1 h. The reaction mixture was decomposed with dil HCl and extracted with ether. Fractional recrystallization of the crude crystals left after the evaporation of the solvent by the same procedure as that used in *Procedure A*, afforded **7** (1.5 g, 13%), **8** (1.5 g, 13%), and **9** (8 g, 69%).

*Oxidation of **9** with $KMnO_4$.* A solution of **9** (1 g) and $KMnO_4$ (3 g) in acetone (30 ml) was heated under reflux for 6 h. After excess $KMnO_4$ was decomposed with EtOH, MnO_2 formed was filtered off. The crude crystals left after the evaporation of the solvent were recrystallized from AcOEt–MeOH (1: 1) to afford **10** as colorless prisms; 0.74 g (70%); mp 120—121 °C. IR: 1930 (C=C=C) and 1670 cm^{-1} (C=O); λ_{max}: 255 nm (ε, 53400): NMR: 2.1—2.9 (m, Ph, 20H), and 8.75 and 9.10 τ (s, Bu^t, 9H). Ms *m/e*: 578(M^+).

Found: C,87.54; H, 6.38%. Calcd for $C_{42}H_{38}O_2$: C, 87.77; H, 6.66%.

The reduction of **10** (0.5 g) with $NaBH_4$ (0.5 g) in MeOH–THF (1: 1) (20 ml) afforded, **11** as colorless needles after recrystallization from MeOH; 0.41 g (82%); mp 160—161 °C. IR: 3530 (OH), 1940 (C=C=C), and 1020 cm^{-1} (C–O); λ_{max}: 250 (35000) and 257 nm (ε, 35000); NMR: 2.0—2.9 (m, Ph, 20H), 5.10 and 5.80 (d, J=9 Hz, CH, 1H), 6.60 (s, OH, 2H), and 8.80 τ (s, Bu^t, 18H); MS *m/e*: 578 (M^+).

Found: C, 86.88; H, 7.22%. Calcd for $C_{42}H_{42}O_2$: C, 87.16; H, 7.31%.

*Synthesis of **12**.* A solution of **8** (1 g) in benzene (20 ml) was heated under reflux for 2 h. The crude crystals left after the evaporation of the solvent were recrystallized from acetone to afford **12** as pale yellow needles; 0.98 g (98%); mp 161—162 °C. IR: 2200 cm^{-1} (C≡C); λ_{max}: 318 nm (ε, 40600); NMR: 2.3—3.0 (m, Ph, 20H), and 8.47 and 8.90 τ (s, Bu^t, 9H); MS *m/e*: 542 (M^+).

Found: C, 92.72; H, 6.87%. Calcd for $C_{42}H_{38}$: C, 92.94; H, 7.06%.

*Oxidation of **12**.* A solution of **12** (1 g) and $KMnO_4$ (3 g) in acetone (30 ml) was heated under reflux for 2 h. The reaction mixture was treated by the same procedure as that used for the oxidation of **9** afforded **13** as colorless prisms; 0.86 g (81%); mp 129—130 °C. IR: 2160 (C≡C) and 1640 cm^{-1} (C=O); λ_{max} 270 nm (ε, 40900); NMR: 2.4—4.0 (m, Ph, 20H), and 8.50 and 8.80 τ (s, Bu^t, 9H); MS *m/e*: 574 (M^+).

Found: C, 87.54; H, 6.39%. Calcd for $C_{42}H_{38}O_2$: C, 87.77; H, 6.66%.

*Synthesis of **15**.* When a solution of **7** (2 g) in benzene (15 ml) was heated under reflux in N_2 for 1 h, greenish blue needles were formed. Filtration of the crystals under N_2 atmosphere afforded **15**; 1.96 g (98%); mp 296—297 °C. λ_{max}: 394 and 643 nm; NMR: 2.65 (s, Ph, 20H) and 8.88 τ (s, Bu^t, 18H); MS *m/e* (relative intensity): 543 (M^++1, 53), 542 (M^+, 100), 271.5 ($(M+1)^{2+}$, 12), and 271 (M^{2+}, 23). Since **15** was sensitive to oxygen, its melting point, UV, and NMR spectra were measured in N_2 atmosphere, and its correct molecular coefficient in the UV spectrum could not be obtained.

Found: C, 92.85; H, 6.99%. Calcd for $C_{42}H_{38}$: C, 92.94; H, 7.06%.

When **8** and **12** were heated in *o*-xylene under reflux in N_2 for 1 h, **15** was obtained in 97 and 98% yield, respectively.

*Oxidation of **15** into **16**.* When powdered **15** (1 g) was allowed to keep in the air at room temperature for 1 day, **16** was obtained, after recrystallization from acetone, as yellow prisms; 1.06 g (95%); mp 246—247 °C. IR: 1660 and 1640 cm^{-1} (C=O); λ_{max}: 300 (29000), 330 sh (19800), and 350 sh nm (ε, 9400); NMR: 2.5—2.9 (m, Ph, 20H) and 9.20 τ (s, Bu^t, 18H); MS *m/e*: 606 (M^+).

Found: C, 83.06; H, 6.15%. Calcd for $C_{42}H_{38}O_4$: C, 83.14; H, 6.31%.

*Conversion of **16** into **17**.* A mixture of **16** (0.1 g), sodium borohydride (0.6 g), MeOH (15 ml), and tetrahydrofuran (5 ml) was kept to stand at room temperature for 1 h. The reaction mixture was decomposed with water, and then extracted with ether. The ethereal solution was washed with water, and dried over anhydrous Na_2SO_4. The evaporation of the solvent left crude crystals (IR: 3400 and 1070 cm^{-1} (OH)), which were dissolved in $CHCl_3$ (5 ml). Through this solution, HBr was bubbled for 10 min at room temperature. The crude crystals left after the evaporation of the solvent were recrystallized from MeOH to afford **17** as colorless needles; 0.09 g (94%); mp 173—175 °C. IR: 1075 cm^{-1} (ether); λ_{max}: 297 nm (ε, 22600) NMR: 2.5—3.1 (m, Ph, 20H), 7.06 (s, CH, 4H), and 9.32 τ (s, Bu^t, 18H); MS *m/e*: 578 (M^+).

Found: C, 86.88; H, 7.09%. Calcd for $C_{42}H_{42}O_2$: C, 87.16; H, 7.31%.

*Formation of **18a** and **18b**.* To a solution of Br_2 (1.8 g) in $CHCl_3$ (10 ml), was added **15** (2.7 g) under N_2 atmosphere. The colorless prisms formed were filtered, washed with $CHCl_3$ to result in **18a**, 3.87 g (90%); mp>300 °C. λ_{max}: 305 nm (ε, 5800).

Heating of a mixture of **18a** (1.7 g) and MeOH (20 ml) under reflux for 1 h afforded **18b**, after recrystallization from AcOEt, 1.06 g (82%); mp 271—273 °C. IR: 1100 cm^{-1} (ether); λ_{max}: 273 (3700) and 284 nm (ε, 2500); NMR: 2.65 (s, Ph, 20H), 7.20 (s, OMe, 12H), and 8.85 τ (s, Bu^t, 18H); MS *m/e*: 666 (M^+).

Found: C, 82.78; H, 7.48%. Calcd for $C_{46}H_{50}O_4$: C, 82.84; H, 7.56%.

References

1) A preliminary communication has been reported: F. Toda and M. Ohi, *J. Chem. Soc., Chem. Commun.*, **1975**, 506.

2) M. P. Cava and M. J. Mitchell, "Cyclobutadiene and Related Compounds," Academic Press, New York and London (1967), pp. 181—218.

3) H. Straub, *Angew. Chem.*, **86**, 412 (1974).

4) F. Toda and N. Dan, *J. Chem Soc., Chem. Commun.*, **1976**, 30.

5) Very recently, the IR and UV spectra of benzocyclobutene itself have been recorded: O. L. Chapman, C. C. Chang, and N. R. Rosenquist, *J. Am. Chem. Soc.*, **98**, 261 (1976).

6) F. Toda and Y. Takehira, *J. Chem. Soc., Chem. Commun.*, **1975**, 174.

7) In the preliminary communication,[1] we have incorrectly reported that the structures of **7** and **9** are *E,E*- (**14**) and *E,Z*-3,4-bis(1-*t*-butyl-3-phenyl-2-propynylidene)-1,2-diphenyl-1-cyclobutene (**12**), respectively. However, the structures of **7** and **9** should be corrected to read as those depicted in this report. We have also reported[1] that **7** melts at 243—245 °C. However, the data should be corrected to read as those described in this paper (measured in N_2 atmosphere), because the previously-reported data are those obtained by the measurement in the air.

8) R. B. Woodward and R. Hoffmann, *J. Am. Chem. Soc.*, **87**, 395 (1965).

9) K. Kleveland and L. Skattebøl, *J. Chem Soc., Chem. Commun.*, **1973**, 432.

A New Type of Induced Decomposition. II.[1] Decomposition of Phenylpropioloyl Peroxide and *t*-Butyl Phenylperoxypropiolate in Solution

Nobuyuki MURAMOTO, Tameichi OCHIAI, Masayuki YOSHIDA, and Osamu SIMAMURA

Department of Chemistry, Faculty of Science, Tokyo University, Hongo, Tokyo 113

(Received March 8, 1976)

Decomposition of phenylpropioloyl peroxide and *t*-butyl phenylperoxypropiolate in cumene, toluene, and cyclohexane was investigated. Product analysis and kinetic study together with the findings that radicals separately generated caused the decomposition of these peroxides demonstrate of a new type of induced decomposition involving radical attack on the triple bond of these peroxides and subsequent β-scission.

Although the chemistry of carbon radicals such as alkyl, vinyl, and phenyl radicals are well documented, much less attention has hitherto been focussed on the ethynyl radical R–C≡C·, in which it is expected the sp hybrid nature of the orbital carrying an odd electron may impart any special characteristics to the behaviour of this type of radicals. One fruitful method for generation of ethynyl radicals is the photolysis of ethynyl iodides.[2,3] An alternative approach to ethynyl radicals should be provided by homolysis of appropriate acetylenic peroxides. Thus we have studied the decomposition in solution of phenylpropioloyl peroxide and *t*-butyl phenylperoxypropiolate with the expectation that it would generate the phenylethynyl radicals. However, there did not appear to be strong indication of the generation of free phenylethynyl radicals, but evidence for a new type of induced decomposition was afforded as preliminarily reported elsewhere.[1] The present paper gives a detailed account of the study of this type of induced decomposition.

Results and Discussion

Phenylpropioloyl peroxide (I) and *t*-butyl phenylperoxypropiolate (II) were allowed to decompose in cumene, toluene, and cyclohexane at 80° and 110°C under a nitrogen atmosphere, and the products were examined (see Tables 1 and 2). Operation of a homolytic mechanism in the decomposition of these compounds is demonstrated by the formation of bicumyl and α-methylstyrene in cumene and of bibenzyl in toluene, all arising from radicals derived from the solvents. Moreover, the formation of acetone and *t*-butyl alcohol in the decomposition of the peroxy-ester (II) is characteristic of the intervention of the *t*-butoxyl radical. The peroxide (I) and the peroxy-ester (II) gave relatively small amounts of carbon dioxide and higher yield of the parent acid compared with common diacyl peroxides and *t*-butyl peroxyacetate. This fact may suggest that the phenylpropioloyloxyl radical if generated by homolysis from these peroxides may tend to abstract a hydrogen atom from a solvent molecule rather than to undergo fission to give carbon dioxide and a phenylethynyl radical. If the carbon dioxide had come solely from the phenylpropioloyloxyl radical, the phenylethynyl radical must have been generated in the corresponding amount, which in turn would have given rise to phenylacetylene by abstraction of a hydrogen atom from a hydrogen donor in the surroundings. Since the phenylethynyl radical is expected to abstract a hydrogen atom readily because of the large heat of formation of an sp C–H bond,[4] the very low yield of phenylacetylene actually found seems to indicate that this radical could have hardly been formed in these decompositions. Thus, the carbon dioxide actually found must have been evolved from some sourses other than the phenylpropioloyloxyl radical. In this connection, the formation of 1,3-diphenylpropyne in toluene and (phenylethynyl)cyclohexane in cyclohexane is of interest, since the combination of a radical derived from a solvent molecule and a

Table 1. Products from decomposition of phenylpropioloyl peroxide at 80 °C[a]

Products[b]	Solvent		
	Toluene	Cumene	Cyclohexane
CO_2	0.54	0.15	0.66
$PhC{\equiv}CCO_2H$	0.89	1.50	0.48
$PhC{\equiv}CCH_2Ph$	0.17		
$PhC{\equiv}CC_6H_{11}$			0.56
$[PhC(CH_3)_2]_2$		0.03	
$PhC(CH_3){=}CH_2$		0.44	
$PhCH_2CH_2Ph$	0.05		

a) 3.20 mmol in 20 ml of solvent. b) In mol per mol of peroxide.

Table 2. Products from decomposition of *t*-butyl phenylperoxypropiolate at 110 °C

Solvent	Toluene	Cumene	Cyclohexane[a]	Cyclohexane[b]
Peroxy-ester, mmol	2.65	2.92	0.82	8.88
Solvent, ml	15.0	15.0	7.0	100.0
Products[c]				
CO_2	0.675	0.377		
$PhC{\equiv}CCO_2H$	0.268	0.442	0.199	0.12
$PhC{\equiv}CH$	0.011	0.003	nil	
$PhC{\equiv}CCH_2Ph$	0.385			
$PhC{\equiv}C{-}C_6H_{11}$			0.668	0.62
$(PhC(CH_3)_2)_2$		0.353		
$Ph(CH_3)C{=}CH_2$		0.366		
$PhCH_2CH_2Ph$	0.023			
t-BuOH	0.585	0.623	0.970	
Me_2CO	0.106	0.158	trace	

a) At 80 °C. b) Photolysis at room temperature. c) Mol per mol of peroxide.

phenylethynyl radical scarcely formed is improbable. These experimental results taken as a whole point to a decomposition pattern different from what is expected from simple homolysis at the peroxidic linkage, and an induced decomposition was suspected. This view is supported by a kinetic study of the decomposition. Kinetic runs were carried out in toluene under a nitrogen atmosphere and followed by iodometric titration. The peroxy-ester (II) disappeared apparently with first order kinetics, but change in the initial concentration of the peroxy-ester from 0.0085 M to 0.12 M resulted in a 1.3-fold increase in the rate of decomposition (Table 3), a fact indicative of the co-operation of an induced pathway. The decomposition of the peroxide (I) in toluene at 70° did not obey a first-order rate law, but approximately a 3/2-order rate law, $-d[p]/dt=k[p]^{3/2}$, where [P] is the concentration of the peroxide (I), the plot of $[P]^{-1/2}$ against time giving a more satisfactory straight line. The observed 3/2-order rate constants, k, are listed in Table 4. They varied with the initial concentration of the peroxide, and their plots against the inverse square root of the initial concentration of the peroxide (I), $[P_0]^{-1/2}$, gave a straight line, which is represented by $k=k_i+k_1[P_0]^{-1/2}$. Thus, the rate of decomposition is approximately expressed by

$$-d[P]/dt = k_1[P] + k_i[P]^{3/2},$$

where k_1 and k_i were found to be 5.9×10^{-5} s^{-1} and 1.6×10^{-3} s^{-1} M$^{-1/2}$, respectively. The presence of a 3/2-order term together with the finding that the rate of decomposition is significantly diminished by traces of oxygen present in the reacting system supports the concurrence of an induced path.[5] Thus the following Reaction sequence 1—5, in which SH stands for a solvent molecule, may represent important pathways for the decomposition of the peroxide (I).

Table 3. Rate constants for thermal decomposition of *t*-butyl phenylperoxypropiolate in toluene at 110 °C

Initial concn, M	$k\times10^5$ s^{-1}
0.0085	2.15, 2.09
0.120	2.60, 2.79

Table 4. Observed 3/2-order rate constants, k, for phenylpropioloyl peroxide in toluene at 70 °C

Initial concn, M	$k\times10^{-3}$ s^{-1} M$^{-1/2}$
0.01	2.00, 2.32
0.05	1.89, 1.95
0.10	1.78, 1.64

$$(PhC{\equiv}CCO_2)_2 \xrightarrow{k_1} 2PhC{\equiv}CCO_2\cdot \quad (1)$$
(I)

$$PhC{\equiv}CCO_2\cdot + SH \xrightarrow{k_2} PhC{\equiv}CCO_2H + S\cdot \quad (2)$$

$$S\cdot + (I) \xrightarrow{k_3} PhC(\cdot){=}C(-S)CO_2{-}O_2CC{\equiv}CPh \quad (3)$$

$$PhC(\cdot){=}C(-S)CO_2{-}O_2CC{\equiv}CPh \xrightarrow{k_4} PhC{\equiv}C{-}S + CO_2 + PhC{\equiv}CCO_2\cdot \quad (4)$$

$$2S\cdot \xrightarrow{k_5} S{-}S \quad (5)$$

A similar sequence of reactions will readily be written down for the peroxy-ester (II). Decomposition of the peroxide (I) produces phenylpropioloyloxyl radicals, which abstract a hydrogen from solvents. The newly formed solvent radical S· adds to the triple bond of the peroxide (I) to give vinylic radicals, which would then decompose into an acetylenic compound, a phenylpropioloyloxyl radical, and a molecule of carbon dioxide. Evidently the large heat of formation of carbon dioxide facilitates such a β-scission reaction. The major products of the decomposition are readily explained by reference to this reaction sequence. The absence of 1,3-diphenyl-3,3-dimethylpropyne from the decomposition in cumene is probably due to the circumstances that the α,α-dimethylbenzyl radical is very sluggish in the addition reaction to the triple bond because of its resonance stabilization and bulkiness. The rate law of the decomposition which includes a 3/2 power term[6] is also readily derived by the usual stationary state approximation with the reasonable assumption of Reaction 4 being much more rapid than Reaction 3.

The incursion of an induced path of decomposition is further supported by the following experiments, in which radicals separately generated caused the decomposition of the peroxides at relatively low temperatures, at which they cannot otherwise undergo appreciable decomposition. The peroxide (I) or the peroxy-ester (II) was heated in toluene at 35 °C for 15 h under a nitrogen atmosphere in the presence of di-*t*-butyl diperoxyoxalate, which is known to decompose readily at low temperatures generating *t*-butoxyl radicals.[7] A considerable part of the peroxides decomposed and the characteristic product was 1,3-diphenylpropyne in each case (Table 5). Control experiments showed that these peroxides did not undergo homolytic fission to a measurable extent in the absence of the diperoxyoxalate under otherwise similar conditions. Evidently *t*-butoxyl radicals, generated from the diperoxyoxalate, abstracted

Table 5. Decomposition of phenylpropioloyl peroxide and *t*-butyl phenylperoxypropiolate in the presence of di-*t*-butyl diperoxyoxalate at 35 °C for 15 h under nitrogen

	Phenyl-propioloyl peroxide	*t*-Butyl phenylperoxy-propiolate
Peroxide taken, mmol[a]	1.34	2.40
Peroxide decomposed, mmol	1.26	0.94
$(t\text{-BuOOCO})_2$, mmol	1.76	2.43
Products, mmol		
CO_2	4.56	5.44
$PhC{\equiv}CCH_2Ph$	0.54 (0.43)[b]	0.48 (0.51)[b]
$PhCH_2CH_2Ph$	0.72	1.87

a) In 8 ml of toluene. b) Mol per mol of peroxide decomposed.

a hydrogen atom from toluene to give a benzyl radical, and this radical immediately attacked the triple bond in the acetylenic peroxides finally to afford 1,3-diphenylpropyne.

N-Nitrosoacetanilide, a generator of phenyl radicals,[8] also brought about the decomposition of the peroxy-ester (II) at room temperature, 1,2-diphenylacetylene being produced (Table 6).

Table 6. Decomposition of *t*-butyl phenylperoxypropiolate induced by the phenyl radical at room temperature for 16 h under nitrogen

Solvent	Hexane	Acetone
$PhN(NO)COCH_3$, mmol	2.44	2.45
Peroxide taken, mmol[a]	1.75	1.88
Peroxide decomposed, mmol	0.46	1.00
Products, mmol		
CO_2	0.371	0.836
PhC≡CPh	0.0578 (0.127)[b]	0.259 (0.259)[b]

a) In 8 ml of solvent. b) Mol per mol of peroxide decomposed.

A toluene solution of acetyl peroxide and *di-t*-butyl diperoxyoxalate was kept at 35 °C under a nitrogen atmosphere for 15 h and iodometric titration showed that the acetyl peroxide remained undecomposed, whereas the diperoxyoxalate is believed to have decomposed completely under such reaction conditions.[7] Under similar experimental conditions, benzoyl peroxide did not decompose at all, either (Table 7). Obviously the benzyl radical does not displace the carboxyl group of the peroxides which have no α,β-unsaturated bond.

Table 7. Behaviour of benzoyl and acetyl peroxide in the presence of decomposing di-*t*-butyl diperoxyoxalate in toluene at 35 °C under nitrogen

	$(PhCOO)_2$	$(CH_3COO)_2$
Peroxide taken, mmol[a]	1.88	1.92
Remaining Peroxide, mmol	1.86	1.99
$(t\text{-BuOOCO})_2$, mmol	1.64	2.69
Time, h	18	15

a) In 8 ml of toluene at 35 °C, under nitrogen.

These results strongly support the addition-elimination mechanism shown in Reactions 3 and 4 for the induced decomposition of the peroxide (I). Similar addition-elimination mechanisms had been postulated in radical induced reaction of methyl propenyl ketone,[9] crotonaldehyde,[10] and phenyl azide[11] at rather high temperatures. Since the discovery of the induced decomposition of benzoyl peroxide by Bartlett and Nozaki,[5] numerous studies[12] have been made, but the present mechanism is unique in that radicals attack the site of unsaturation exclusively.

Experimental

Materials. Toluene, cumene, cyclohexane, and hexane were washed successively with concentrated sulphuric acid and water, dried with calcium chloride, and distilled over sodium, and middle fractions were used. Acetone was purified by distillation after drying with potassium carbonate. Benzoyl peroxide was purified by dissolving in dichloromethane and precipitating with methanol. *t*-Butyl hydroperoxide was purified by distillation, bp 32 °C/12 mmHg.

Product Analysis by Vapour-phase Chromatography. VPC analyses were carried out on a Perkin Elmer Vapor Fractometer Model 154-D using helium as a carrier gas and the following stainless steel columns: 1) a 4 m column packed with polyethylene glycol (15%) at 120° for analysis of acetone, *t*-butyl alcohol, phenylacetylene, and 2-phenylpropene; 2) a 0.4 m column packed with silicone grease SE 30 (15%) at 193°C for analysis of cyclohexylphenylacetylene; 3) a 1 m column packed with silicone grease SE 30 (15%) at 199 °C for analysis of bibenzyl, 1,3-diphenylpropyne, and 2,3-dimethyl-2,3-diphenylbutane. Commercial products were used for comparison of common compounds, but authentic samples of 1,3-diphenylpropyne[13] and cyclohexylphenylacetylene[14] were prepared according to the directions described in the literature.

Phenylpropioloyl Peroxide. Sodium peroxide (2.0 g) was added to a solution of phenylpropioloyl chloride[15] (5.0 g) in ether (50 ml) at −5 °C. The mixture was stirred for 10 min, and then a little water was added dropwise, the temperature being kept at 0—−5 °C. After a vigorous reaction subsided, a further 5 ml of water was added and the mixture was allowed to warm to room temperature. The ether layer was separated and the aqueous layer was extracted with three 10 ml portions of ether. The combined ether solution was washed with 5% sodium carbonate solution and then with water, dried with sodium sulphate and concentrated under reduced pressure. The residue was washed with cold methanol and dissolved in a small amount of dichlomethane. Precipitation by addition of a large quantity of cold methanol gave 3.8 g of crystals, mp 94.1—94.2 °C (Found: C, 73.54; H, 3.32%. Calcd for $C_{18}H_{10}O$: C, 74.48; H, 3.47%. Purity, 99.8% by iodometric titration[16]).

t-Butyl Peroxyphenylpropiolate. Phenylpropioloyl chloride[15] (5.03 g) and 10 ml of water containing 2.09 g of potassium hydroxide were added simultaneously over a period of 40 min to a stirred solution of 2.91 g of *t*-butyl hydroperoxide in 20 ml of water. The temperature was maintained at 8—10 °C during the addition. The reaction mixture was stirred overnight at room temperature. The organic layer was separated and washed successively with 10% aqueous sodium carbonate and saturated sodium chloride solution. The viscous oil obtained (8.3 g, 68%) was dissolved in ether and the solution dried with anhydrous sodium sulphate. Crystallization from ether at −78 °C gave a pure specimen (Found: C, 71.74; H, 6.36%. Calcd for $C_{13}H_{14}O_3$: C, 71.54; H, 6.47%. Purity, 99% by iodometric titration[16]).

Decomposition of Phenylpropioloyl Peroxide and t-Butyl Phenylperoxypropiolate in Solutions. A typical run was as follows. A solution of the peroxide (3.20 mmol) in 20 ml of solvent was placed in a two-necked reaction flask equipped with a gas inlet-tube and a reflux condenser which was connected to a trap cooled with solid carbon dioxide–acetone. The other end of the trap was attached to a tube containing Ascarite–magnesium perchlorate. Nitrogen gas was passed through the solution for a while to remove dissolved oxygen. The flask was placed in a bath kept at 80 °C and the peroxide was allowed to decompose completely, a slow stream of nitrogen being passed through the solution. The reaction mixture was diluted to 25.0 ml with the same solvent. A ten millilitre aliquot of the solution was extracted with 5% aqueous sodium carbonate solution. The extract was acidified with hydrochloric acid and the phenylpropiolic acid liberated was extracted with ether and

weighed. The residual solution was washed with 5% aqueous sodium carbonate solution and examined by VPC. The products were identified by comparing their retention times with those of authentic samples. Carbon dioxide was absorbed in an Ascarite–magnesium perchlorate tube and the tube weighed.

Decomposition of Phenylpropioloyl Peroxide and t-*Butyl Phenylperoxypropiolate in the Presence of Di-*t*-butyl Diperoxyoxalate.* A typical run was as follows. A solution of the phenylperoxypropiolate (2.40 mmol) in 8.0 ml of toluene was placed in a two-necked reaction flask equipped with a gas inlet-tube and a reflux condenser which was connected to a trap cooled with acetone and solid carbon dioxide. The other end of the trap was attached to a tube containing Ascarite–magnesium perchlorate. Nitrogen was bubbled through the solution vigorously for a while to remove dissolved oxygen, and di-*t*-butyl diperoxyoxalate[7] (2.43 mmol) was added to the solution. The flask was placed in a constant-temperature bath kept at 35 °C and the peroxy-ester were allowed to decompose, a very slow stream of nitrogen being passed through the reaction mixture. After 15 h (5 half-life period of *t*-butyl diperoxyoxalate), the reaction mixture was diluted to 10.0 ml with toluene in a measuring flask. A 1.0 ml portion of this solution was pipetted out for determination of undecomposed peroxy-ester by iodometry.[16] The remainder of the solution was treated with 10% sodium carbonate solution, and the aqueous layer was separated, acidified with hydrochloric acid and extracted with ether. The ether was removed under reduced pressure and the acidic residue was weighed. The organic layer was treated with 5 ml of acetic acid containing a very small quantity of iron(III) chloride and 1 g of sodium iodide, and the mixture was allowed to stand for 20 min at room temperature in order to decompose the remaining peroxypropiolate; the liberated iodine was reduced with sodium thiosulphate solution, and the organic layer was washed with 10% aqueous sodium carbonate, dried with anhydrous sodium sulphate, and analyzed by VPC. Carbon dioxide was absorbed in an Ascarite–magnesium perchlorate tube and the tube weighed.

*Reaction of Acetyl Peroxide or Benzoyl Peroxide in the Presence of Decomposing Di-*t*-butyl Diperoxyoxalate in Toluene.* A solution of acetyl peroxide (1.92 mmol) and di-*t*-butyl diperoxyoxalate (2.69 mmol) in 8.0 ml of toluene was kept at 35 °C for 15 h under a nitrogen atmosphere. The reaction mixture was diluted to 10.0 ml with toluene. Three 1.0 ml portions of the mixture were taken to determine undecomposed acetyl peroxide by iodometric titration.[16]

Experiments with benzoyl peroxide were carried out similarly.

Decomposition of t-*Butyl Phenylperoxypropiolate in the Presence of* N-*Nitrosoacetanilide.* A typical run was as follows. A solution of the peroxypropiolate (1.75 mmol) and *N*-nitrosoacetanilide (2.44 mmol) prepared according to Grieve and Hey's procedure[8] in 8 ml of hexane was allowed to decompose for 16 h at room temperature under a nitrogen atmosphere. The reaction mixture was diluted to 10 ml with hexane and a 1.0 ml portion of the mixture was withdrawn to determine the undecomposed peroxy-ester by iodometric titration.[16] The remaining solution was treated with sodium iodide (1 g) and 10 ml of acid acetic solution of iron(III) chloride (0.002%). (In the case of acetone solution, the solvent was removed under reduced pressure, and replaced by 10 ml of chloroform. The chloroform solution was then treated with sodium iodide in a way similar to the above.) The mixture was allowed to stand for 15 min, and the liberated iodine was reduced with aqueous thiosulphate solution. The aqueous layer was separated and extracted with benzene. The extracts were combined with the organic layer, washed successively with a 10% sodium carbonate solution and a satruated sodium chloride solution, and dried with anhydrous sodium sulphate. After removal of most of the solvent, the residue was diluted to 2.0 ml with benzene and analyzed by VPC.

Kinetics Measurements. The decomposition of the peroxide (I) or the peroxy-ester (II) was followed by iodometric titration according to Swern's method.[16] In a reaction vessel fitted with a gas inlet-tube and a reflux condenser was placed 50 ml of purified toluene. The vessel was heated in a thermostatted oil bath, and nitrogen was bubbled through the solution for more than two hours. The peroxide (I) of the peroxy-ester (II) was then added to the solution, and allowed to decompose, a slow stream of nitrogen being passed. Aliquots were withdrawn periodically, quenched by chilling to −78 °C, treated with NaI–$CHCl_3$–AcOH (containing 0.002% $FeCl_3$-$6H_2O$), and titrated with a standard sodium thiosulphate solution.

References

1) Part I of this series: N. Muramoto, T. Ochiai, O. Simamura, and M. Yoshida, *Chem. Commun.*, **1968**, 717.

2) N. Kharasch and L. Göthlich, *Angew. Chem.*, **74**, 651 (1962).

3) G. Martelli, P. Spagnolo, and M. Tiecco, *J. Chem. Soc., B*, 1413 (1970); G. Martelli, P. Spagnolo, and M. Tiecco, *Chem. Commun.*, **1969**, 282.

4) J. A. Kerr, *Chem. Revs.*, **66**, 465 (1966).

5) K. Nozaki and P. D. Bartlett, *J. Am. Chem. Soc.*, **68**, 1686 (1946).

6) C. G. Swain, W. H. Stockmayer, and J. T. Clarke, *J. Am. Chem. Soc.*, **72**, 5426 (1950).

7) P. D. Barlett, E. P. Benzing, and R. E. Pincock, *J. Am. Chem. Soc.*, **82**, 1762 (1960).

8) W. S. M. Grieve and D. H. Hey, *J. Chem. Soc.*, **1934**, 1797.

9) J. N. Pitts, Jr., R. S. Tolberg, and T. W. Martin, *J. Am. Chem. Soc.*, **76**, 2843 (1954).

10) E. R. Allen and J. N. Pitts, Jr., *J. Phys. Chem.*, **70**, 1691 (1966).

11) J. E. Leffler and H. H. Gibson, Jr., *J. Am. Chem. Soc.*, **90**, 4117 (1968).

12) For a review see: T. Suehiro, *Yuki Gosei Kagaku Kyokai Shi*, **27**, 701 (1969).

13) J. R. Johnson, T. L. Jacobs, and A. M. Schwartz, *J. Am. Chem. Soc.*, **60**, 1885 (1938).

14) H. K. Black, D. H. S. Horn, and B. C. L. Weedon, *J. Chem. Soc.*, **1954**, 1704.

15) S. Ruhemann and R. W. Merriman, *J. Chem. Soc.*, **87**, 1389 (1905).

16) L. S. Silbert and D. Swern, *Anal. Chem.*, **30**, 385 (1958).

17) J. R. Slagle and H. J. Shine, *J. Org. Chem.*, **24**, 107 (1959).

A New Type of Induced Decomposition. III.[1] Induced Decomposition of Cinnamoyl Peroxide, *t*-Butyl Peroxycinnamate and *t*-Butyl 2,3-Diphenylperoxypropionate in Solution

Tameichi Ochiai, Yoshitsugu Usuda, Masayuki Yoshida, and Osamu Simamura
Department of Chemistry, Faculty of Science, Tokyo University, Hongo, Tokyo 113
(Received March 8, 1976)

Phenyl and benzyl radicals were found to induce decomposition of cinnamoyl peroxide or *t*-butylperoxycinnamate to give stilbene and 1,3-diphenylpropene, respectively. Similarly, *t*-butoxyl radicals caused *t*-butyl 2,3-diphenylperoxypropionate to decompose affording stilbene. A mechanism is proposed which involves a radical attack on a substrate peroxide producing a radical carrying an odd electron on the carbon atom β to the carboxyl group and its subsequent collapse to final products by way of β-scission.

In previous papers we showed that phenylpropioloyl peroxide and *t*-butyl phenylperoxypropiolate decompose *via* a new type of induced path involving a radical attack on the triple bond of the peroxides and a subsequent β-scission.[1] We now extended the study to cinnamoyl peroxide[2] and *t*-butyl peroxycinnamate,[3] and *t*-butyl 2,3-diphenylperoxypropionate.

Results and Discussion

trans-Cinnamoyl peroxide or *t*-butyl peroxycinnamate was heated in toluene at 35 °C for 15 h under a nitrogen atmosphere in the presence of di-*t*-butyl diperoxyoxalate, a generator of *t*-butoxyl radicals.[4] Significant part of these peroxides, which are both stable at this temperature in the absence of decomposing di-*t*-butyl diperoxyoxalate, was decomposed, the characteristic product being 1,3-diphenylpropene (see Table 1), which resulted from the reaction with benzyl radicals generated by the action of *t*-butoxyl radicals on toluene.

Similarly phenyl radicals, generated from *N*-nitrosoacetanilide,[5] caused the decomposition of *cis*- and *trans*-cinnamoyl peroxides and *t*-butyl peroxycinnamate to give stilbene (Table 2).

These results are satisfactorily explained by assuming the following reaction sequence (1)—(2) in keeping with the reaction sequence with the acetylenic peroxide set forth in previous papers.[1] Benzyl or phenyl radicals add to the double bond of the peroxides (I and II) to give intermediate radicals (III), which then decompose into 1,3-diphenylpropene or stilbene (Reactions 1 and 2).

Table 1. Decomposition of *trans*-cinnamoyl peroxide and *t*-butyl peroxycinnamate in the presence of di-*t*-butyl diperoxyoxalate at 35 °C for 15 h under nitrogen[a]

	Cinnamoyl peroxide	*t*-Butyl peroxycinnamate
Peroxide taken, mmol	1.39	2.49
Peroxide decomposed, mmol	1.15	1.63
$(t\text{-BuOOCO})_2$, mmol	2.15	2.77
Products, mmol		
CO_2	5.16	7.04
$PhCH{=}CHCH_2Ph$	0.63 (0.55)[b]	1.45 (0.89)[b]
$PhCH_2CH_2Ph$	0.73	0.40

a) In 8 ml of toluene. b) Yields in mol per mol of peroxide decomposed.

$$PhCH{=}CHCO_2X + R\cdot \longrightarrow Ph\dot{C}H\text{-}CHRCO_2X \quad (1)$$

I: X = PhCH=CHCO$_2$ II: X = *t*-BuO — III

$$Ph\dot{C}H\text{-}CHRCO_2X \longrightarrow PhCH{=}CHR + CO_2 + X\cdot \quad (2)$$

$$R\cdot + PhCH{=}CHCO_2X \longrightarrow PhCH{=}\overset{\displaystyle CO_2X}{\overset{|}{C}}\text{-}H \quad (3)$$

$$\longrightarrow PhCH{=}CHR + CO_2 + X\cdot$$

R· = $PhCH_2\cdot$ or Ph·

Table 2. Decomposition of *cis*- and *trans*-cinnamoyl peroxides and *t*-butyl peroxycinnamate induced by phenyl radicals at room temperature under nitrogen

	cis-Cinnamoyl peroxide		*trans*-Cinnamoyl peroxide		*t*-Butyl peroxycinnamate	
Peroxide taken, mmol	1.28	0.162	1.33	1.31	2.05	1.97
PhN(NO)Ac, mmol	1.92	1.19	2.39	6.20	2.90	2.75
Solvent (ml)	PhH (8)	PhCl (4)	PhCl (8)	PhCl (8)	Hexane (8)	Me_2CO (8)
Time, h	20	50	47	47	16	16
Peroxide decomposed, mmol	0.78	0.162	0.63	0.97	0.94	1.06
Products,[a] mmol						
cis-Stilbene	0.008 (0.01)	nil	nil	nil	nil	nil
trans-Stilbene	0.34 (0.43)	0.032 (0.20)	0.069 (0.11)	0.22 (0.23)	0.41 (0.44)	0.19 (0.18)
CO_2					0.51	1.14

a) Yields in moles per mole of peroxides decomposed are given in parentheses.

A possible alternative mechanism may be a direct bimolecular homolytic displacement reaction, in which benzyl or phenyl radicals directly displace the CO_2X group on the α-carbon atom of *t*-butyl peroxycinnamate (II) or cinnamoyl peroxide (I) (Reaction 3). This mechanism, however, can safely be ruled out because both *cis*- and *trans*-cinnamoyl peroxides afforded with phenyl radicals a considerable amount of *trans*-stilbene together with traces of the *cis*-isomer (Table 2). *cis*- and *trans*-Cinnamoyl peroxides would have given stilbene in different isomer rations, if the direct displacement by phenyl radicals had taken place.

In the foregoing scheme, the decomposition of *t*-butyl peroxycinnamate induced by the phenyl radical involves the 2-(*t*-butylperioxycarbonyl)-1,2-diphenylethyl radical (III) (reaction 2), which then decomposes into stilbene, carbon dioxide, and the *t*-butoxyl radical. The same intermediate radical (III) may be generated by abstraction of a β-hydrogen atom from *t*-butyl 2,3-diphenylperoxypropionate (IV), which, accordingly, is expected to undergo a similar type of induced decomposition.

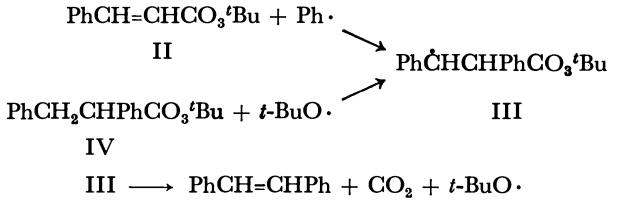

Table 3. Decomposition of *t*-butyl 2,3-diphenylperoxypropionate in the presence of di-*t*-butyl diperoxyoxalate[a)]

Peroxypropionate taken, mmol	0.300	0.299
(*t*-BuOOCO)$_2$, mmol	none	0.302
Peroxypropionate decomposed, mmol	0.0615 (20.5)[b)]	0.0936 (31.3)
Products, mmol		
$(PhCH_2)_2$	0.0018 (0.6)	0.0021 (0.7)
$PhCH_2CH(Ph)O^tBu$	0.0072 (2.4)	0.0062 (2.1)
PhCH=CHPh	0.0121 (4.0)	0.0348 (11.6)

a) The peroxypropionate was decomposed in 3.0 ml of chlorobenzene in degassed ampoules at 35 °C for 12 h. b) Yields in percent based upon the starting peroxypropionate are given in parentheses. Yields given are the averages of results from three in dependent decompositions.

This expectation proved to be true in the following experiments. *t*-Butyl 2,3-diphenylperoxypropionate was heated in chlorobenzene at 35 °C for 12 h in the presence or absence of di-*t*-butyl diperoxyoxalate as radical generator (Table 3). The presence of the diperoxyoxalate increased the decomposition of the peroxypropionate (IV) to 31.3%, while the decomposition took place only to an extent of 20.5% in its absence. The diperoxyoxalate increased the yield of stilbene from 4.0% to 11.6%, but did not affect the yields of bibenzyl 0.6%) and *t*-butyl 1,2-diphenylethyl ether (2%). *t*-Butyl 2,3-diphenylperoxypropionate belongs to a class of peroxy-esters such as *t*-butyl 2-phenylperoxyacetate and 2-methyl-2-phenylperoxypropionate which are rather labile even at relatively low temperature.[3)] It is highly probable, therefore, that the initial homolysis takes place generating a 1,2-diphenylethyl and a *t*-butoxyl radical and a molecule of carbon dioxide in a cage of solvent. Among the products identified, *t*-butyl 1,2-diphenylethyl ether is obviously a cage combination product between a 1,2-diphenylethyl and a *t*-butoxyl radical, since its yield was not changed when more *t*-butoxyl radicals were produced by adding di-*t*-butyl diperoxyoxalate. Bibenzyl was probably formed by disproportionation of 1,2-diphenylethyl radical together with the corresponding amount of stilbene. The stilbene formed in excess of this amount must have been provided by the action of the *t*-butoxyl radical on the starting peroxypropionate, abstraction of a hydrogen atom giving the intermediate radical (III) postulated above and this radical in turn decomposing to give stilbene. In the presence of di-*t*-butyl diperoxyoxalate, the concentration of *t*-butoxyl radicals available in solution will be increased resulting in efficient abstraction of a hydrogen atom, and the amount of stilbene is thus increased.

Experimental

Materials. Chlorobenzene, toluene, and hexane were washed with concentrated sulphuric acid and then with water, dried with calcium chloride, and distilled, and middle fractions were used. *trans*- and *cis*-Cinnamoyl peroxides,[2)] *t*-butyl peroxycinnamate,[3)] di-*t*-butyl diperoxyoxalate,[4)] and *N*-nitrosoacetanilide[5)] were prepared by the published procedures.

t-Butyl 2, 3-Diphenylperoxypropionate. 2, 3-Diphenylpropionic acid, prepared by the published procedure,[6)] mp 87.5—88.0 °C (lit,[6)] mp 88—89 °C), was heated with thionyl chloride under reflux for 7 h and the resulting 2,3-diphenylpropionyl chloride was distilled under reduced pressure, bp 132—134 °C/1.5 mmHg. A solution of this chloride (4.83 g) in 20 ml of anhydrous pentane was added slowly (1.3 h) to a stirred solution of 2.77 g of *t*-butyl hydroperoxide in 2.42 g of pyridine and 60 ml of anhydrous pentane cooled in an ice–water bath. The reaction mixture was allowed to warm to room temperature and stirred for 2 h. A small amount of water was added, followed by pentane until all the precipitate was dissolved. The organic layer was washed with 10% aqueous sodium carbonate, dried over anhydrous sodium sulphate, and cooled in a bath of acetone and solid carbon dioxide, to give a crystaline precipitate, which was filtered off and recrystallized from pentane several times. The yield was 3 g (51%), mp 74.5—76.1 °C (Found: C, 76.48; H, 7.37%. Calcd for $C_{19}H_{22}O_3$: C, 76.48; H, 7.43%. Purity, 100.8% by iodometric titration[7)]); IR (Nujol) 1775 cm^{-1} ($\nu_{C=O}$); NMR ($CDCl_3$) τ 8.95 (s, 9H, *t*-Bu), 6.0—7.2 (m, 3H, CH_2CH), 2.81 (broad s, 5H, phenyl), and 2.70 (broad s, 5H, phenyl).

Decomposition of trans*-Cinnamoyl Peroxide and* t*-Butyl Peroxycinnamate in the Presence of Di-*t*-butyl Diperoxyoxalates.* A typical run was as follows. A solution of the peroxide (1.39 mmol) in 8 ml of toluene was placed in a two-necked reaction flask equipped with a gas inlet tube and a reflux condenser which was connected to a trap cooled with acetone and solid carbon dioxide. The other end of the trap was attached to a tube containing Ascarite–magnesium perchlorate. Nitrogen was bubbled through the solution vigorously for a while to remove dissolved oxygen, and di-*t*-butyl diperoxyoxalate (2.15 mmol) was added to the solution. The flask was placed in a bath kept at 35 °C and the peroxides were allowed to decompose, a very slow stream of nitrogen being passed

through the solution during the course of the reaction. After 15 h (5 half-life periods of di-*t*-butyl diperoxyoxalate[4]), the reaction mixture was diluted to 10.0 ml with toluene. A 1.0 ml portion of this solution was pipetted out to analyze for undecomposed peroxy-ester by iodometric titration.[7] The remainder of the solution was treated with 10% sodium carbonate solution. The aqueous layer was separated, acidified with hydrochloric acid and extracted with ether. The ether was removed under reduced pressure and the acidic residue was weighed. The organic layer was treated with 5 ml of acetic acid containing very small quantity of iron(III) chloride and 1 g of sodium iodide, and the mixture was allowed to stand for 20 min at room temperature in order to decompose the remaining peroxide. The iodine liberated was reduced with sodium thiosulphate solution. The organic layer was washed with 10% aqueous sodium carbonate solution, dried over anhydrous sodium sulphate, and analyzed by VPC (Table I).

Decompositions of cis- *and* trans-*Cinnamoyl Peroxides and* t-*Butyl Peroxycinnamate in the Presence of* N-*Nitrosoacetanilide.* A typical run was as follows. A solution of the peroxy-ester (II, 2.05 mmol) and *N*-nitrosoacetanilide (2.90 mmol) in 8 ml of hexane was allowed to decompose for 16 h at room temperature under a nitrogen atmosphere. The reaction mixture was diluted to 10 ml with hexane and a 1.0 ml portion of the mixture was taken to determine undecomposed peroxy-ester by iodometric titration.[7] The remaining solution was treated and analyzed in the same way as described above (Table 2).

Decomposition of t-*Butyl 2,3-Diphenylperoxypropionate in Chlorobenzene.* A solution (3 ml) of the 2,3-diphenylperoxypropionate in chlorobenzene (0.10 M) was degassed (three freeze-thaw cycles) and allowed to decompose in a bath kept at 35 °C for 12 h. One millilitre aliquot of the reaction mixture was dissolved in 10 ml of chloroform. A small piece of solid carbon dioxide, 0.5 g of sodium iodide, and a little Iron(III) chloride solution in glacial acetic acid (*ca.* 0.002%) were added successively. The resulting mixture was kept at about 60 °C under nitrogen for 15 min and the iodine liberated was titrated with standard sodium thiosulphate solution(0.0316M). The aqueous layer was extracted with chloroform. The extracts were combined with the organic layer, washed with 10% aqueous sodium carbonate, and dried over anhydrous sodium sulphate. The solution was concentrated to 5.0 ml by distillation through a helix-packed column, a weighed amount of diphenylmethane was added as an internal standard, and the whole was subjected to VPC analysis (Table 3).

Decomposition of t-*Butyl 2,3-Diphenylperoxypropionate in the Presence of Di-*t*-butyl Diperoxyoxalate in Chlorobenzene.* A solution (3 ml) of the 2,3-diphenylperoxypropionate (0.1 M) and diperoxyoxalate (0.1 M) in chlorobenzene was degassed and heated at 35 °C for 12 h. The reaction mixture was treated and analyzed in the same way as described above (Table 3).

Product Analysis. Analysis of the products was carried out by vapor phase chromatography on a Hitachi Gas Chromatograph Model K-53 FID or a Perkin Elmer Vapor Fractometer Model 154-D. Most of the products were identified by comparing their VPC retention times on Apiezon grease L (5%) at 190 °C or SE 30 (15%) at 199 °C with those of commercial samples. Stilbene was further identified by comparing its UV spectrum with that of an authentic sample. Carbon dioxide was absorbed on Ascarite–magnesium perchlorate and weighed. *t*-Butyl 1,2-diphenylethyl ether was isolated from the reaction mixture by preparative thin layer chromatography and was identified by elemental analysis and IR and NMR spectra (Found: C, 84.70; H, 8.50%. Calcd for $C_{18}H_{22}O$: C, 84.99; H, 8.72%), IR (neat) 1200 cm^{-1} characteristic of *t*-BuO;[8] NMR (CCl_4) τ 9.12 (s, 9H, *t*-Bu), 7.30 (d, 2H, J=6.1 Hz, CH_2), 2.95 (broad s, 5H, phenyl).

References

1) Part I of this series: N. Muramoto, T. Ochiai, O. Simamura, and M. Yoshida, *Chem. Commun.*, **1968**, 717; Part II: N. Muramoto, T. Ochiai, O. Simamura, and M. Yoshida, *Bull. Chem. Soc. Jpn.*, **49**, 2518 (1976).

2) O. Simamura, K. Tokumaru, and H. Yui, *Tetrahedron Lett.*, 5141 (1966).

3) P. D. Bartlett and R. R. Hiatt, *J. Am. Chem. Soc.*, **80**, 1398 (1958).

4) P. D. Bartlett, E. P. Benzing, and R. E. Pincock, *J. Am. Chem. Soc.*, **82**, 1762 (1960).

5) W. S. M. Grieve and D. H. Hey, *J. Chem. Soc.*, **1934**, 1797.

6) C. R. Hauser and W. R. Dunnavant *Org. Synth.* **40**, 38 (1960).

7) L. S. Silbert and D. Swern, *Anal. Chem.*, **30**, 385 (1958).

8) H A. Ory, *Anal. Chem.* **32**, 509 (1960).

The Decomposition of *t*-Butyl *erythro*- and *threo*-2,3-Diphenylperoxybutyrate in Solution. The Product Analysis and the Cage Effect

Tameichi OCHIAI, Masayuki YOSHIDA, and Osamu SIMAMURA
Department of Chemistry, Faculty of Science, Tokyo University, Hongo, Tokyo 113

(Received March 8, 1976)

Decomposition of *t*-butyl *erythro*- and *threo*-2,3-diphenylperoxybutyrate was examined in solution at 60 °C; there was no indication of induced decomposition taking place as is the case with *t*-butyl 2,3-diphenylperoxypropionate. Various hydrocarbons resulting from the reaction of the 1,2-diphenylpropyl radical in a variety of ways were identified in the product, and *t*-butyl 1,2-diphenylpropyl ether was found to be formed as cage recombination product in the *threo*/*erythro* isomeric ratio which depended on the stereochemistry of the starting peroxybutyrate.

In a previous paper[1] we have demonstrated that *t*-butyl 2,3-diphenylperoxypropionate undergoes decomposition involving a pathway induced by radicals and gives stilbene as product characteristic of this pathway.

$$PhCH_2CHPhCO_3{}^tBu \longrightarrow PhCH_2CHPh\cdot + CO_2 + t\text{-}BuO\cdot \quad (1)$$

$$PhCH_2CHPhCO_3{}^tBu + t\text{-}BuO\cdot \longrightarrow PhC\dot{H}CHPhCO_3{}^tBu + t\text{-}BuOH \quad (2)$$

$$PhC\dot{H}CHPhCO_3{}^tBu \longrightarrow PhCH{=}CHPh + CO_2 + t\text{-}BuO\cdot \quad (3)$$

In order to study the stereochemistry of a β-scission reaction of the type shown in reaction 3, we examined the decomposition of *t*-butyl *erythro*- and *threo*-2,3-diphenylperoxybutyrate (I) in the expectation that they might afford α-methylstilbene (Reaction 6) in different *cis* to *trans* ratios, thus giving some clue to elucidation of the stereochemical course.

$$MePhCHCHPhCO_3{}^tBu \longrightarrow MePhCHCHPh\cdot + CO_2 + t\text{-}BuO\cdot \quad (4)$$

$$MePhCHCHPhCO_3{}^tBu + t\text{-}BuO\cdot \longrightarrow MePhC\dot{C}HPhCO_3{}^tBu + t\text{-}BuOH \quad (5)$$

$$MePhC\dot{C}HPhCO_3{}^tBu \longrightarrow MePhC{=}CHPh + CO_2 + t\text{-}BuO\cdot \quad (6)$$

Results and Discussion

t-Butyl *erythro*-2,3-diphenylperoxybutyrate, mp 96.5—98 °C (dec), and the *threo*-isomer, mp 56.5—57 °C (dec), were prepared from the corresponding acid chloriods and *t*-butyl hydroperoxide according to the usual method and decomposed in chlorobenzene and toluene at 60 °C. The results are summarized in Table 1.

The yield of α-methylstilbene, a product expected from the induced decomposition (Reactions 5 and 6) was relatively low, and the *cis-trans* ratios did not differ appreciably. The decomposition of *t*-butyl *erythro*-2,3-diphenylperoxybutyrate in chlorobenzene was not accelerated in the presence of di-*t*-butyl diperoxyoxalate, a generator of the *t*-butoxyl radical,[2] contrary to the case with *t*-butyl 2,3-diphenylperoxypropionate,[1] and furthermore, kinetic measurements showed that the peroxybutyrate decomposes according to a strict first order rate law without any indication of induced decomposition ($k=6.29\times10^{-5}$ s^{-1} at 60 °C in toluene);[3] accordingly, it may safely be said that with the diphenylperoxybutyrate the hydrogen abstraction of the type shown in Eq. 5 is operative only to a very limited extent, if at all. Thus, the purpose of examining the stereochemistry of Reaction 6 envisaged in the beginning was defeated.

TABLE 1. PRODUCTS FROM DECOMPOSITION OF *erythro*- AND *threo*-2,3-DIPHENYLPEROXYBUTYRATE[a]

Peroxybutyrate / Solvent	*erythro* PhCl	*threo* PhCl	*erythro* $PhCH_3$	*threo* $PhCH_3$
Products[b]				
1,2-Diphenylpropane	7.1	8.2	1.6	1.3
dl-2,3-Diphenylbutane	1.0	1.2		
meso-2,3-Diphenylbutane	1.0	1.2		
cis-α-Methylstilbene	1.6	2.3	2.4	2.5
trans-α-Methylstilbene	1.8	2.4	1.7	0.7
erythro-Ether (II)	6.3	2.9	4.7	2.4
threo-Ether (II)	5.5	8.7	4.5	6.9
1,2,3-Triphenylbutane			39	25
Bibenzyl			7.3	8.1

a) The peroxybutyrate (0.30 mmol) in 3.0 ml of solvent was decomposed at 60 °C for 36 h in degassed and sealed ampoules. b) Yields in per cent based upon the starting peroxybutyrate are estimated by VPC and average values from two independent decompositions are given.

The precursor of 1,2-diphenylpropane, one of the major products is obviously the 1,2-diphenylpropyl radical produced in Reaction 4. It either abstracts a hydrogen atom from some hydrogen donors including acetone formed from the *t*-butoxyl radical or disproportionates giving 1,2-diphenylpropane and α-methylstilbene. The fact that the yield of 1,2-diphenylpropane is much lower in toluene than in chlorobenzene is explained by the combination reaction of the 1,2-diphenylpropyl radical with the benzyl radical generated from toluene by hydrogen abstraction by the *t*-butoxyl radical furnished by Reaction 4, giving 1,2,3-triphenylbutane. Thus, Table 1 shows that the 1,2-diphenylpropyl group is better accounted for in the decomposition in toluene than in chlorobenzene. In the absence of the benzyl radical much of the 1,2-diphenylpropyl radical certainly combined with itself to give the dimeric product, which it was not attempted to detect in the present analysis.

2,3-Diphenylbutanes were formed in chlorobenzene solvent in the same *dl*/*meso* ratio of 1.0 from both diastereomeric peroxybutyrates, whereas in toluene none of the butanes was produced at all. Obviously, the butanes are formed by combination of the free 1,2-

diphenylpropyl with the methyl radical generated by decomposition of the *t*-butoxyl radical outside the solvent cage; in toluene the concentration of the methyl radical is too low to give the butanes since the methyl radical or the *t*-butoxyl radical for that matter reacts efficiently with toluene by abstruction of hydrogen.

t-Butyl 1,2-diphenylpropyl ether (II) was isolated by preparative thin-layer chromatography on silica gel, and the structure was established on the basis of the NMR and IR spectra and analytical data. The NMR spectrum showed the ether isolated to be a mixture of the diastereomers. Thus, one set of signals consisting of a sharp singlet at τ 9.15 (9H) and two doublets at τ 8.94 (3H) and 5.56 (1H) corresponding to *t*-butyl, methyl, and methine protons, respectively, is assigned to the *erythro*-diastereomer, and the other set of signals at τ 9.03 (singlet 9H), 8.70 (doublet 3H), and 5.48 (doublet 1H) quite similar in appearance to those of the first set and all shifted to lower field regions is assigned to the *threo*-isomer, because of the fact that *t*-butyl *erythro*-2,3-diphenylperoxybutyrate and *erythro*-2,3-diphenylbutyric acid show the proton signals due to *t*-butyl and methyl groups all at higher field regions than the corresponding peaks shown by the *threo*-peroxybutyrate and *threo*-acid.

A similar ether, namely *t*-butyl 1,2-diphenylethyl ether, is formed in the thermolysis of *t*-butyl 2,3-diphenylperoxypropionate in chlorobenzene, and this has been shown to be the cage recombination product between the *t*-butoxyl and the 1,2-diphenylethyl radical.[1] *t*-Butyl 1,2-diphenylpropyl ether was therefore thought, by analogy, also to be a cage product, and experiments with scavenger confirmed this view. Thus, the amount and isomer ratio of the ether produced did not change appreciably (Table 2) in the presence of 4-oxo-2,2,6,6-tetramethylpiperidine-1-oxyl,[4] which is known to capture radicals generated in the autoxidation of diphenylmethane very efficiently, that is, almost at the same rate as molecular oxygen does.[5]

Table 2. *t*-Butyl 1,2-diphenylpropyl ether from decomposition of *t*-butyl *erythro*-2,3-diphenylperoxybutyrate in toluene in the presence of 4-oxo-2,2,6,6-tetramethylpiperidine-1-oxyl[a]

Nitroxyl, M	*t*-Butyl Ether	
	erythro + *threo*[b]	*threo*/*erythro*
0.00	9.2	0.96
0.14	8.8	0.92
0.40	8.7	0.89
0.80	8.3	0.89

a) The peroxybutyrate (0.10 M) was decomposed at 60 °C for 36 h in degassed and sealed ampoules. b) Yields in per cent based upon the starting peroxybutyrate.

The formation of 1,2,3-triphenylbutane (25—39%) in the decomposition in toluene shows that 1,2-diphenylpropyl radicals from the peroxybutyrate combined outside the solvent cage with free benzyl radicals generated from toluene by hydrogen abstraction by the *t*-butoxyl radical, while absence of even traces of benzyl *t*-butyl ether from the product indicates that all *t*-butoxyl radicals have been consumed before they combine with benzyl radicals; accordingly, the *t*-butoxyl radical does not have any chance to react with free 1,2-diphenylpropyl radicals to yield *t*-butyl 1,2-diphenylpropyl ether outside the cage.

A change in solvent from toluene to chlorobenzene caused a slight increase in the yield of the *t*-butyl ether (II); this effect may be attributed to solvent viscosity effect (chlorobenzene, 0.51 cP; toluene, 0.39 cP at 60 °C).[6]

All these observations considered above support that almost all of the *t*-butyl ether (II) is formed in the solvent cage.

Obviously, the *threo* to *erythro* ratio in which *t*-butyl 1,2-diphenylpropyl ether (II) was produced depends on the stereochemistry of the starting peroxybutyrate (I). The decomposition of the isomeric peroxybutyrates, with special regard to the cage effect, may be formulated as shown in the annexed scheme, in which the solvent cage is denoted by brackets. These peroxybutyrates undergo most likely a two-bond scission[7] giving rise to a 1,2-diphenylpropyl and a *t*-butoxyl radical and carbon dioxide, the last of which is omitted from the scheme for the sake of simplicity. It is assumed that, at the moment of generation, a radical pair (III) of 1,2-diphenylpropyl and *t*-butoxyl as a whole retains the stereochemistry of the parent peroxybutyrate and that the stereoisomeric radical pairs interconvert in the cage with rate constants k_r and k_r'. Thus, the diffusion of radicals from the cage with rate constant k_d results in the formation of out-of-cage products and the recombination of radicals give isomeric *t*-butyl 1,2-diphenylpropyl ethers $II_{erythro}$ and II_{threo} with rate constants k_c and k_c', respectively. The usual steady state treatment of this reaction scheme using the yields of the respective ethers in toluene gives the relative values of the reaction constants as follows: $k_c=1$, as standard; $k_c'=1.1$; $k_d=10$; $k_r=21$; $k_r'=12$.

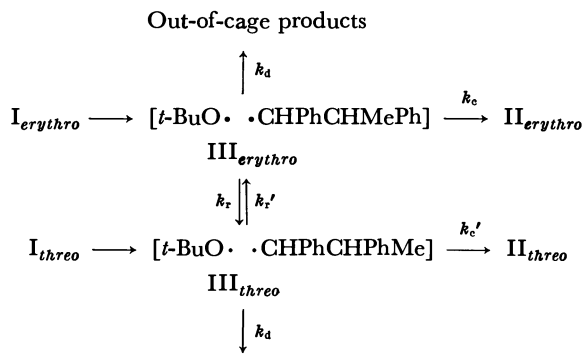

Although it is natural to suppose that the radical pair in the cage (III) consisting of a 1,2-diphenylpropyl and a *t*-butoxyl radical resembles the parent peroxybutyrate in stereochemistry and, therefore, that such structures as shown below are probable for the diastereomeric radical pairs in the cage, further discussion in terms of steric effects of substituents would seem

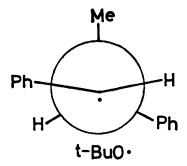

$III_{erythro}$

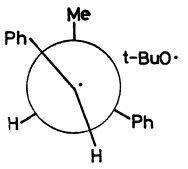

III_{threo}

meaningless, because, in the first place, such steric effects are not known accurately enough and secondly, the difference between the interconversion rates $k_r=21$ and $k_r'=12$ corresponds to an energy difference between the two conformations of only 370 cal/mol at 60 °C.

Greene and his coworkers studied the cage effect in the thermolysis of *S*-(+)-*t*-butyl 2-phenylperoxypropionate using butanethiol as a scavenger and determined the relative rates of the processes occurring in the cage.[8]

We attempted experiments with 1-propanethiol as possible scavenger in the decomposition of *t*-butyl *erythro*-2,3-diphenylperoxybutyrate in toluene at 60 °C, but copious precipitation of 2,3-diphenylbutyric acid took place, which was not observed in the absence of the thiol. The acid was evidently produced by the direct bimolecular reaction of the thiol and the peroxybutyrate, since the normal mode of the decomposition of the peroxybutyrate is thought to be a two-bond scission expelling a molecule of carbon dioxide.[7] In view of this finding the use of thiols seems to be inadequate for scavenging experiments.

Experimental

Materials. Di-*t*-butyl diperoxyoxalate,[2] 4-oxo-2,2,6,6-tetramethylpiperidine-1-oxyl,[4] 2,3-diphenylbutane,[9] benzyl *t*-butyl ether,[10] and *trans*-[11] and *cis*-α-methylstilbene[12] were prepared by published procedures.

The following compounds were also prepared for comparison with reaction products in VPC analysis.

erythro-*1,2,3-Triphenylbutane.* *erythro*-1,2,3-Triphenyl-1-butanone[13] (2.0 g) was hydrogenated in 60 ml of ethanol containing 10 drops of concentrated hydrochloric acid over 290 mg of 10% palladium on carbon catalyst at room temperature under atmospheric pressure. The catalyst and the solvent were removed, and the product was chromatographed on silica gel using benzene as eluent and recrystallized from ethanol to give 0.6 g (31%) of *erythro*-1,2,3-triphenylbutane (Found: C, 92.60; H, 7.72%. Calcd for $C_{22}H_{22}$: C, 92.26; H, 7.74%), mp 88.0—88.5 °C; *m/e* 286 (M^+); NMR ($CDCl_3$) τ 9.0 (d, 3H, J= 6.0 Hz, CH_3), 7.7—6.8 (m, 4H, $-CH\dot{C}H\dot{C}H_2-$), and 3.5—2.6 (m, 15H, phenyls).

1,2-Diphenylpropane. *trans*-α-Methylstilbene (1.7 g) in 50 ml of ethanol was hydrogenated over 10% palladium on carbon (91 mg) under atmospheric pressure at room temperature. Hydrogenation was stopped when the hydrogen uptake corresponded to one mole of hydrogen per mole of the compound. Removal of the catalyst and solvent left a colourless liquid, which was gas-chromatographically pure, yield 1.5 g (88%).

t-*Butyl* erythro-*2,3-Diphenylperoxybutyrate.* *erythro*-2,3-Diphenylbutyric acid[14] was allowed to react with thionyl chloride at room temperature for 7 h. The resulting *erythro*-2,3-diphenylbutyryl chloride (1.77 g), without further purification, was added to a stirred solution of 1.0 g of *t*-butyl hydroperoxide in 0.9 g of pyridine and 60 ml of pentane cooled in an ice–water bath. The addition required 15 min and stirring was continued for four more hours. Cold 10% aqueous sulphuric acid was added, and the product was extracted with ether. The ethereal layer was washed with cold 10% aqueous sodium carbonate solution and then with water, and dried with anhydrous sodium sulphate at 0 °C. After removal of the solvent under reduced pressure, the residue was recrystallized from ether to give 1.4 g (67%) of *t*-butyl *erythro*-2,3-diphenylperoxybutyrate (Found: C, 77.04; H, 7.90%. Calcd for $C_{20}H_{24}O_3$: C, 76.89; H, 7.94 %. Purity, 99% by iodometric titration[15]), mp 96.5—98.0 °C (dec); IR (Nujol) 1760 cm^{-1} ($\nu_{C=O}$); NMR ($CDCl_3$) τ 9.08 (s, 9H, *t*-Bu), 8.99 (d, J=5.9 Hz, 3H, CH_3), 6.8—6.1 (m, 2H, $-C\dot{H}C\dot{H}-$), and 3.0—2.4 (m, 10H, phenyls).

t-*Butyl* threo-*2,3-Diphenylperoxybutyrate.* *threo-2,3*-Diphenylbutyronitrile (mp 31.5—32.5 °C; lit,[14] mp 35—36 °C), prepared from benzyl cyanide and α-chloroethylbenzene according to the procedure of Hauser and Brasen[14] with the modification that the anion derived from benzyl cyanide and sodium amide was added to α-chloroethylbenzene, was hydrolyzed by heating in a mixture of 50% aqueous sulfuric acid and glacial acetic acid under reflux for 80 h. The resulting crude *threo*-acid was dissolved in acetone and the solution allowed to evaporate slowly to dryness at room temperature until a mixture of crystalline *threo*- and *erythro*-2,3-diphenylbutyric acids formed. Well developed larger crystals of the *threo*-acid were sorted out manually, mp 135.3—136.0 °C (lit,[14] mp 130—133 °C). The *threo*-acid (3.0 g) was treated with thionyl chloride at room temperature for 20 h. The resulting acid chloride, without purification, was dissolved in 25 ml of anhydrous pentane, and the solution added very slowly (40 min) to a solution of *t*-butyl hydroperoxide (1.56 g) and pyridine (1.17 g) in 25 ml of anhydrous pentane cooled in an ice–water bath. The reaction mixture was stirred for 2 h at 2 °C, while a pasty mass formed. Ice–water (20 ml) was added to the reaction mixture and the organic layer was washed successively with 10% sulphuric acid, water, 10% sodium carbonate, and water, and dried with anhydrous sodium sulphate at 0 °C overnight. The dried solution was chilled in a Dry Ice bath, and the crystals which separated were filtered off and recrystallized from pentane–dichloromethane (1: 1) to give 1.5 g (37%) of *t*-butyl *threo*-2,3-diphenylperoxybutyrate (Found: C, 77.01; H, 7.53%. Calcd for $C_{20}H_{24}O_3$: C, 76.89; H, 7.74%. Purity, 98% by iodometric titration[15]), mp 56.5—57.0 °C (dec); IR (Nujol) 1760 cm^{-1} ($\nu_{C=O}$); NMR ($CDCl_3$) τ 8.80 (s, 9H, *t*-Bu), 8.59 (d, 3H, J=5.9 Hz, CH_3), 6.8—6.1 (m, 2H, $-C\dot{H}C\dot{H}-$), and 3.2—2.7 (m, 10H, phenyls).

Decomposition of t-*Butyl* erythro- *or* threo-2,3-*Diphenylperoxybutyrate in Solution.* A solution of either peroxybutyrate in chlorobenzene (3.0 ml, 0.100 M) was placed in an ampoule, degassed (three freeze-thaw cycles), and, the ampoule having been sealed, allowed to decompose in a constant-temperature bath at 60 °C for 36 h. A weighed amount of diphenylmethane was then added as an internal standard to the reaction mixture and it was subjected to VPC (Hitachi Gas Chromatograph Model K-53 FID). The following three columns were used: a 2 m column packed with Apiezon L grease (5%) to analyze for *meso*- and *dl*-2,3-diphenylbutanes, *t*-butyl 1,2-diphenylpropyl ether, and *trans*-α-methylstilbene at 190 °C; a 2 m column packed with Ucon oil LB-550-X (5%) plus a 1 m column packed with Silicone grease (5%) to analyze for *cis*-α-methylstilbene and 1,2-diphenylpropane at 175 °C; and a 300 ft. capillary column coated with Apiezone L grease to separate *erythro*- and *threo*-*t*-butyl 1,2-diphenylpropyl ethers.

The decomposition in toluene was carried out in a similar manner as described above.

Decomposition of the *erythro*-peroxybutyrate in the presence of 4-oxo-2,2,6,6-tetramethylpiperidine-1-oxyl was similarly

carried out in toluene (Table 2).

Decomposition of t-*Butyl* erythro-*2,3-Diphenylperoxybutyrate in Chlorobenzene in the Presence of Di-*t*-butyl Diperoxyoxalate.* A solution of *t*-butyl *erythro*-2,3-diphenylperoxybutyrate (1.02 mmol) and di-*t*-butyl diperoxyoxalate (1.45 mmol) in chlorobenzene (3.0 ml) was heated at 35 °C for 14.5 h under a nitrogen atmosphere, and the remaining peroxybutyrate was determined by iodometric titration[15] (0.75 mmol, 74% of the peroxybutyrate used). A control experiment without di-*t*-butyl diperoxyoxalate showed the same result, demonstrating that the peroxyoxalate caused no induced decomposition.

Separation and Purification of t-*Butyl 1,2-Diphenylpropyl Ether and 1,2,3-Triphenylbutane.* *t*-Butyl *erythro*-2,3-diphenylperoxybutyrate (1.2 g) in 50 ml of toluene was heated at 61 °C for 70 h under nitrogen. After removal of most of the solvent by distillation under atmospheric pressure, the mixture was distilled under reduced pressure (0.1—0.5 mmHg), while the temperature of the heating bath was maintained below 160 °C. The distillate was subjected to purification by thin-layer chromatography on silica gel using chloroform–petroleum ether (1: 1) as eluent. A band of R_f 0.6 was extracted with diethyl ether, the extract condensed, and the residue purified by trap-to-trap distillation to give *t*-butyl 1,2-diphenylpropyl ether (Found: C, 85.11; H, 8.91%. Calcd for $C_{19}H_{24}O$: C, 85.02; H, 9.01 %), IR (neat) 1195 cm^{-1} characteristic of *t*-BuO.[16]

The residue from the vacuum distillation was chromatographed on silica gel. The faster-moving component was purified by molecular distillation to give an oil, which was gas chromatographically pure, *m/e* 286 (M^+) (Found: C, 92.56; H, 8.01%. Calcd for $C_{22}H_{22}$: C, 92.26; H, 7.74%). Comparison of its IR and NMR spectra with those of authentic *erythro*-1,2,3-triphenylbutane led to the conclusion that the oil was a mixture of *erythro*- and *threo*-1,2,3-triphenylbutanes in equal amounts.

Kinetics of Decomposition of t-*Butyl erythro-2,3-Diphenylperoxybutyrate.* A solution of the peroxybutyrate (*ca.* 0.1 M) in toluene was decomposed in sealed tubes at 60 °C. The tubes were removed from the bath at intervals and chilled at −78 °C to quench the reaction. The peroxybutyrate was determined by titration according to Swern's method,[15] and plots of the logarithms of the concentration of the peroxybutyrate *vs.* time gave a straight line up to 85% decomposition.

References

1) T. Ochiai, Y. Usuda, M. Yoshida, and O. Simamura, *Bull. Chem. Soc. Jpn.*, **49**, 2522 (1976).
2) P. D. Bartlett, E. P. Benzing, and R. E. Pincock, *J. Am. Chem. Soc.*, **82**, 1762 (1960).
3) *t*-Butyl 2-phenylperoxypropionate decomposes in cumene at 60 °C in a similar rate ($k=8.38$ and $8.49\times10^{-5}s^{-1}$).[8]
4) R. Brière, H. Lemaire, and A. Rassat, *Bull. Soc. Chim. Fr.*, **1965**, 3273.
5) M. S. Khloplyankina, A. L. Buchachenko, M. B. Neiman, and A. G. Vasil'eva, *Kinet. Katal.*, **6**, 394 (1965); *Chem. Abstr.*, **63**, 9775 h (1965).
6) T. Titani, *Bull. Chem. Soc. Jpn.*, **2**, 95 (1927); J. Timmermans and F. Martin, *J. Chim. Phys.*, **23**, 747 (1926).
7) P. D. Bartlett and R. R. Hiatt, *J. Am. Chem. Soc.*, **80**, 1398 (1958).
8) J. P. Engstrom and F. D. Greene, *J. Org. Chem.*, **37**, 968 (1972).
9) J. B. Conant and A. H. Blatt, *J. Am. Chem. Soc.*, **50**, 551 (1928).
10) P. T. Lansbury and V. A. Pattison, *J. Org. Chem.*, **27**, 1933 (1962).
11) C. F. Koelsch and R. V. White, *J. Org. Chem.*, **6**, 602 (1941).
12) D. J. Cram and F. A. A. Elehafez, *J. Am. Chem. Soc.*, **74**, 5828 (1952).
13) H. E. Zimmerman and W. H. Chang, *J. Am. Chem. Soc.*, **81**, 3634 (1959).
14) W. R. Brasen and C. R. Hauser, *J. Am. Chem. Soc.*, **79**, 395 (1957); C, R. Hauser, D. Lednicer, and W. R. Brasen, *ibid.*, **80**, 4345 (1958); C. R. Hauser and W. R. Brasen, *ibid.*, **78**, 494 (1956).
15) L. S. Silbert and D. Swern, *Anal. Chem.*, **30**, 385 (1958).
16) H. A. Ory, *Anal. Chem.*, **32**, 509 (1960).

Synthesis and Properties of Organocobalt(III)octaethylporphyrins

Hisanobu OGOSHI, Ei-ichi WATANABE, Norihisa KOKETSU, and Zen-ichi YOSHIDA
Department of Synthetic Chemitry, Kyoto University, Kyoto 606
(Received March 15, 1976)

The syntheses of alkylcobalt(III)octaethylporphyrins(OEP) *via* nucleophilic attack of the Co(I) complex to unsaturated compounds are reported. Olefins with an electron-withdrawing group and acetylenes react with Co(I)(OEP), whereas olefins with an electron-donating group such as propylene and cyclohexene are unreactive. A novel ring cleavage of cyclopropyl methy ketone initiated by Co(I)(OEP) affords alkylCo(III)(OEP). The reduction of cobalt(II) *N*-methyloctaethylporphyrin acetate results in intramolecular methyl migration from nitrogen to the central cobalt atom. Five-coordination has been established for the organocobalt(III)(OEP) complexes on the basis of their analytical, infrared and NMR data. Some anomalous behavior of the proton signals of the α-carbon atom in their NMR spectra has been discussed in terms of quadrupolar relaxation and electronegativity of the cobalt ion.

The potential nucleophilicity of the d^8 metal ion in a macrocyclic square planar ligand is of particular interest because of its chemical relevance to vitamin B_{12s}[1] and homogeneous catalysts.[2] For example, cobalt(I)[1a,c,f,g] and rhodium(I)[3] ions, bound to a wide variety of square planar ligands, undergo nucleophilic substitution with alkyl halides and addition to olefins and acetylenes, to generate trivalent metal complexes, accompanied by the formation of metal–carbon bonds.

In earlier studies[4] on the rhodium(I)octaethylporphyrin[Rh(I)(OEP)] as a model system of vitamin B_{12}, we have noted novel carbon–carbon cleavage reactions of a number of substituted cyclopropanes and strained polycyclics such as quadricyclene, bicyclobutane, and their derivatives, yielding stable organorhodium(III) complexes. Clarke and his co-workers[5] first reported the synthesis of alkylcobalt(III)etioporphyrin-II by the reaction of Co(I)porphyrin with alkyl halides. The reaction with unsaturated compounds, however, has not been reported previously. We have now examined the generality of these reactions for cobalt(I)octaethylporphyrin. The present work describes the addition to olefins and acetylenes, the ring cleavages of three membered ring compounds, and ring cleavage reaction of cyclopropyl methyl ketone. The novel methyl migration in cobalt(II) *N*-methyloctaethylporphyrin is also reported.[6]

Results and Discussion

Nucleophilic Substitution. A variety of methods to generate cobalt(I) complex as precursor for higher valent cobalt complexes with unsaturated equatorial ligand have been exploited.[1f,g] In this study, the reduction of Co(II)porphyrin was performed by the method used for the generation of Co(I)tetraphenylporphyrin[Co(I)(TPP)][7] and Co(I)etioporphyrin-II [Co(I)(etio)].[5] The NMR spectrum of pyridine-d_5 solution of Co(I)(OEP) thus obtained showed signals at τ 1.03 (s, =CH–), 6.90 (q, $-CH_2-$), and 8.40 (t, $-CH_3$). The chemical shifts are shifted to higher field than those observed for the Co(III)(OEP) complexes, apparently indicating the existence of the low-spin diamagnetic cobalt(I) complex. Attempts to reduce bromopyridinecobalt(III)octaethylporphyrin with sodium borohydride in ethanol to Co(I)(OEP) failed, and only resulted in quantitative formation of Co(II)(OEP). Reduction of Co(II)(OEP) with borohydride in THF was also unsuccessful.

The reaction of Co(I)(OEP) with alkyl halides gave alkyl Co(III)(OEP) in moderate yields. Treatment of Co(I)(OEP) with methyl iodide, ethyl iodide, ethyl 2-bromopropionate, and 2-bromoethylamine yielded the corresponding organocobalt(III)porphyrins (**1**, **2**, **3**, and **4**). The products from benzyl bromide and tertiary alkyl halides were not isolable because of their thermal instability and/or susceptibility to light. Clarks and co-workers[5] have previously assigned a hexacoordinate structure for the alkyl Co(III)(ethio) complex. They proposed a water molecule as the sixth ligand based on the single sharp hydroxy stretching band at 3670 cm^{-1}. No IR absorption due to coordinated water, however, was observed for the OEP complexes, **1**—**4**. In the NMR no signal associated with water protons was detected in $CDCl_3$. These facts together with analytical data led us to conclude that all the alkyl-Co(III)(OEP) complexes are pentacoordinate. Diamagnetic character of these complexes is evidently shown by the positions of chemical shifts and sharp signals of the peripheral ethyl and methene protons. In general, a pentacoordinate structure is a most unusual geometry for the trivalent state of cobalt.[8,9] However a few examples of the isolation of stable pentacoordinate complexes are known for the cobalt(III) complexes of bae.*[10] Furthermore, it has been argued that a strongly electron-donating ligand would be expected to more easily form a pentacoordinate alkylcobalt(III) complexes in the order bae*>salen*>$(dmg)_2$*>[(do)(doH)pn].*[11]

trans-β-Bromostyrene reacted readily with Co(I)-(OEP), with complete retention of configuration, to yield exclusively the *trans*-styrylcobalt(III)complex, (**5**). Similarly complete retention of configuration has been reported in the reaction of cobaloxime(I) with *trans*-β-bromostyrene.[12]

Reaction with Olefins and Acetylenes. Addition of the olefins substituted with an electron-withdrawing group to a tetrahydrofuran solution of Co(I)(OEP),

* Abbreviations used: bae, *N,N'*-ethylenebis(acetylacetoneiminato); salen, *N,N'*-ethylenebis(salicylideneiminato); dmg, dimethylglyoximato; [(do)(doH)pn], 1,3-bis-(biacetylmonoximeimide)propane.

Table 1. Microanalysis of Co(III)(OEP) complexes

Compound	Formula	C(%) Found	C(%) Calcd	H(%) Found	H(%) Calcd	N(%) Found	N(%) Calcd
(1)	$C_{37}H_{47}N_4Co$	72.76	73.24	7.83	7.80	9.31	9.23
(2)	$C_{38}H_{49}N_4Co$	72.45	73.52	7.74	7.96	8.84	9.03
(3)	$C_{41}H_{53}N_4O_2Co$	71.08	69.62	7.72	7.71	8.04	8.09
(4)	$C_{38}H_{50}N_5Co$	68.77	71.67	7.50	7.86	11.00	11.00
(5)	$C_{44}H_{51}N_4Co$	76.00	76.08	7.43	7.40	8.18	8.06
(6)	$C_{39}H_{48}N_5Co$	72.24	72.50	7.65	7.48	10.81	10.84
(7)	$C_{38}H_{47}N_4Co$	72.81	73.64	7.89	7.80	8.94	9.04
(8) [a] (9) [a]	$C_{44}H_{51}N_4Co$	75.80	76.08	7.34	7.40	8.20	8.06
(14)	$C_{38}H_{49}N_4OCo$	71.75	71.67	7.55	7.76	8.80	8.80
(15)	$C_{41}H_{53}N_4OCo$	72.59	72.76	7.84	7.89	8.67	8.28
(16) [b]	$C_{37}H_{46}N_4ClCo$	68.96	68.98	7.46	7.56	8.69	8.94
(17)	$C_{39}H_{50}N_4O_2Co$	69.90	70.35	7.63	7.53	8.40	8.46

a) A mixture of (**8**) and (**9**). b) Analysis of Cl; Calcd: 5.95%. Found: 5.53%.

followed by treatment with a portion of aqueous alkali (0.1 N) gave exclusively β-substituted alkylcobalt(III)-porphyrins, (**6**) and **3**, in moderate yield (Eq. 1). It was clearly proved by the NMR signals due to the

$$[Co(I)(OEP)]^- \xrightarrow[2.\ H_2O\text{-}NaOH]{1.\ CH_2{=}CHX} Co(III)(OEP)\cdot CH_2CH_2X \quad (1)$$

X: CN, (**6**); CO_2Et, (**3**)

axially coordinated alkyl protons that the bond formation had taken place at the β carbon atom (*vide infra*). This is also supported by the fact that the product obtained from ethyl acrylate was identical with an authentic sample of 2-(ethoxycarbonyl)ethylcobalt(III)(OEP) (**3**). In marked contrast to the olefins with an electron-withdrawing substituent, the reaction with propylene and cyclohexene resulted in spontaneous formation of divalent cobalt complex before addition of aqueous alkaline solution. As has been proposed in the reaction of cobaloxime(I) and other Co(I) complexes with olefins,[1f,g] it seems that the reaction species is not a hydrido complex (**13**) but rather a complex anion (**12**). However, the presence of **13** cannot be completely excluded under the present conditions since a small amount of the α-styryl complex (**9**) was formed in the reaction with phenylacetylene as described below.

$$[Co(I)(OEP)]^- + HC{\equiv}CPh \xrightarrow{H_2O(D_2O)} H\!\!\diagup\!\!\diagdown\!\!Ph \quad Co(III)(OEP) \quad (2)$$

(**12**) → (**8**)

(**12**) $\xrightarrow{H_2O(D_2O)}$ D\!\!\diagup\!\!\diagdown\!\!Ph, Co(III)(OEP) (**10**)

$$[Co(III)(OEP)H(D)] \longrightarrow Ph\!\!\diagup\!\!\diagdown\!\!H \quad Co(III)(OEP) \quad (3)$$

(**13**) → (**9**)

(**13**) → Ph\!\!\diagup\!\!\diagdown\!\!D, Co(III)(OEP) (**11**)

Introduction of acetylene gas into the THF solution

Table 2. Visible spectra and characteristic infrared spectra of cobalt OEP complexes

λ_{max} (nm) (log ε_{max}) in $CHCl_3$

	I	II	III	IR bands (cm^{-1}) [c]	Assignment
$[Co(I)(OEP)]^-$	396 [a]	520 [a]	548 [a]		
(1)	393 (5.34)	519 (4.02)	552 (4.37)		
(2)	392 (5.30)	520 (4.00)	551 (4.37)		
(3)	392 (5.27)	517 (4.02)	551 (4.41)	1750	ν(C=O)
(4)	388 (5.28)	524 (4.01)	554 (4.43)	3250, 3305	ν(N-H)
(5)	393 (5.38)	524 (4.02)	556 (4.44)	1490, 1558, 1585, 3050, 720	Phenyl vibrations
(6)	391 (5.25)	519 (4.02)	552 (4.45)	2225	ν(C≡N)
(7)	392 (5.40)	520 (4.01)	554 (4.45)	1568	ν(C=C)
(8) (9)	394 [b]	525 [b]	556 [b]	1590, 1600, 1610, 3050, 3300, 698	Phenyl vibrations
(14)	392 (5.31)	520 (4.01)	552 (4.43)	3570	ν(O-H)
(15)	392 (5.24)	520 (3.96)	552 (4.43)	1720	ν(C=O)
(16)	392 (5.30)	524 (3.97)	554 (4.36)	695	ν(C-Cl)
(17)	428 (4.80)	542 (3.78)	588 (3.92)	1615	ν(C=O)

a) Measured in THF. b) A 3: 1 mixture of (**8**) and (**9**). c) Measured in a KBr disk.

TABLE 3. ^{1}H NMR SPECTRA (100 MHz) OF ORGANOCOBALT(III)OEP COMPLEXES IN $CDCl_3$ (τ value)

	Assignment						
	Equatorial ligand			Axial ligand			
	$=CH_2-$	$-CH_2-$	$-CH_3$	H_a	H_b	H_c	H_d
(**12**)	1.03(s, 4H)[a]	6.90(q, 16H)[a]	8.40(t, 24H)[a]				
(**1**)	−0.08(s, 4H)	6.00(q, 16H)	8.12(t, 24H)	15.20(brs, 3H)[b] 15.30(s, 3H)[b,c]			
(**16**)	−0.39(s, 4H)	5.73(q, 16H)	7.90(t, 24H)	12.03(brs, 2H) 12.53(s, 2H)[c]			
(**2**)	0.00(s, 4H)	6.00(q, 16H)	8.11(t, 24H)	14.08(br) 14.38(q, 2H)[c]	15.47(t, 3H) 15.23(t, 3H)[c]		
(**3**)	−0.01(s, 4H)	5.98(q, 8H) 6.02(q, 8H)	8.13(t, 24H)	12.71—16.72(br) 14.34(m, AA′BB′, 4H)[c]	14.22(br)	7.11(q, 2H)	9.64(t, 3H)
(**6**)	−0.07(s, 4H)	5.98 5.99 (dq, 16H)	8.12(t, 24H)	14.28 (br, 4H)			
(**14**)[h]	−0.05(s, 4H)	5.99 6.01 (dq, 16H)	8.14(t, 24H)	14.36(br)	13.08(t, 2H)		
(**4**)[e]	−0.03(s, 4H)	5.86(q, 16H)	8.14(t, 24H)	16.17(br)	12.75(br)		
(**15**)	0.02(s, 4H)	6.02(q, 16H)	8.15(t, 24H)	14.37(br, 2H) 14.70(m, 4H)[c]	15.00(qu, 2H)	10.90(t, 2H) 10.70(t, 2H)[c]	9.38(s, 3H) 9.50(s, 3H)[c]
(**7**)	−0.09(s, 4H)	5.97(q, 8H) 6.00(q, 8H)	8.13(t, 24H)	10.81(brm, 1H) J_{ab}=4.0, J_{bc}=4.0, J_{ac}=13.0 Hz	10.26(t, 1H)	12.00(q, 1H)	
(**8**)[d]	0.17 (s)	6.03(q) 6.05(q)	8.14(t)	9.94(br) J_{ab}=4.0 Hz	11.30(d)	6.10(m)[f]	3.50(m)[g]
(**9**)[d]	−0.05(s)	6.00(dq)	8.14(t)	10.85(d)	12.67(d)	7.73(m)[f]	4.33(m)[g]
(**5**)	−0.11(s, 4H)	5.98(q, 8H) 6.00(q, 8H)	8.12(t, 24H)	10.12(brd, 1H) J_{ab}=12 Hz	11.00(d, 1H)	5.10(m, 2H)[f]	3.79(m, 3H)[g]

Abbreviations used: s, singlet; d, doublet; t, triplet; q, quartet; qu, quintet; m, multiplet; br, broad.
(**1**), $-C(H_a)_3$; (**2**), $-C(H_a)_2C(H_b)_3$; (**3**), $-C(H_a)_2C(H_b)_2CO_2C(H_c)_2C(H_d)_3$; (**4**), $-C(H_a)_2C(H_b)_2NH_2$; (**5**), $-C(H_a)=C(H_b)Ph$; (**6**), $-C(H_a)_2C(H_b)_2CN$; (**7**), $C(H_a)=C\begin{matrix}(H_b)\\(H_c)\end{matrix}$; (**8**), $-C(H_a)=C(H_b)Ph$; (**9**), $CPh=C\begin{matrix}(H_a)\\(H_b)\end{matrix}$; (**14**), $-C(H_a)_2C(H_b)_2OH$; (**15**), $-C(H_a)_2C(H_b)_2COC(H_d)_3$.
a) Measured in pyridine-d_5. b) Measured at 220 MHz. c) Measured in the presence of pyridine. d) A 3: 1 mixture; for details, see Discussion. e) NH: not detected. f) Phenyl, *o*-H. g) Phenyl, *m*-H and *p*-H. h) OH: not detected.

of Co(I)(OEP) gave vinylcobalt(III)(OEP) (**7**) isolated in 19% yield. Phenylacetylene readily reacted with the Co(I)(OEP) and the product (29% yield based on the NMR spectrum) was found to be a mixture of *cis*-β-styryl (**8**) and α-styrylCo(III)(OEP) (**9**). They were not separable by chromatography.

The ratio of isomers **8** and **9** was determined as 3: 1 by intensity ratio of the *meso*-proton chemical shifts at τ 0.17 and −0.05. As demonstrated in Table 3, full assignments of the NMR signals were accomplished by comparing the spectra of complexes **8** and **9**, with that of the *trans*-conformer **5** and that for mixture of partially deuterated styryl complexes (**10**) and (**11**) prepared from deuteration experiments. Assignments were also confirmed with the aid of the spectra for the corresponding *cis*- and *trans*-β-styryl rhodium(III)(OEP) complexes.[4] The relatively small vicinal coupling constant (4.0 Hz) compared to that observed for **5** (J_{trans}=12.0 Hz) rationalizes the stereochemistry of *cis*-conformer **8**. The α-styryl complex **9** has been also confirmed by the β-carbon proton signals at τ 10.85 and 12.76 with the coupling constant of 1.5 Hz due to geminal protons. Furthermore, inspection of molecular models suggests that anisotropic shielding of a phenyl group in the *cis*-conformer **8** causes high field shifts of the *meso*-positions and in turn the phenyl group would experience the ring current of the porphyrin ring. Thus the higher field peak at τ 0.17 is assigned to the *meso*-protons of **8**. The chemical shifts of the phenyl protons appear at a higher magnetic field than those of the *trans*-conformer **5**.

For cobaloxime(I), it has been reported that a mixture of α-styryl and *cis*-β-styryl complexes is formed in a mildly alkaline solution.[12,13] The formation of an α-styryl complex may arise from a hydridocobalt(III) complex (**13**) as has been discussed for the cobaloximes.[12-15] The reaction yields for the acetylenic compounds are considerably lower due to the generation of Co(II)(OEP) during chromatography. In contrast, the reactions of cobaloxime and Rh(OEP) with acetylenic compounds give quantitative formation of the vinylmetal complexes.[4,12-15] It is of interest to note that the Co(I) complex of the water soluble porphyrin catalyzes only the reduction of acetylene[16] whereas we have obtained the vinylcobalt(III) complex **7**. Thus, low yields may be in part ascribed to the homolytic decomposition of the carbon–cobalt(III) bond to Co(II)(OEP) and a radical species.

Reaction with Three Membered Ring Compounds. Co(I)(OEP) reacted readily with ethylene oxide and ethyleneimine to yield 2-hydroxyethyl- and 2-aminoethylcobalt(III)(OEP), **14** and **4**, respectively. The cleavage of the C–X bond was confirmed by the IR and NMR spectra. For example, **14** shows a sharp hydroxy stretching vibration at 3570 cm^{-1} and NMR

$$[Co(I)(OEP)]^- + \triangle^{X} \xrightarrow{H_2O} Co(III)(OEP)\cdot CH_2CH_2XH \quad (4)$$

X: O, (**14**); NH, **4**

signals at τ 14.36 and 13.08, assigned to α-and β-carbon protons of the axially coordinated alkyl group respectively. Likewise reaction of ethyleneimine gave the 2-aminoethyl analogue, identical with the product obtained from β-bromoethyl amine. The analytical values of the product are somewhat poor, presumably due to its low stability in the crystalline state. However, the infrared spectrum shows clear bands at 3250, 3305 cm^{-1}, characteristic of the N–H stretching vibration of the primary amino group.[17] In the NMR spectrum two signals assignable to the α- and β-methylene protons are observed at τ 16.17 and 12.75, respectively. These spectral data support the proposed structure **4**.

As described in the introduction, Rh(I)(OEP) cleaves cyclopropanes with an electron-withdrawing substituent to form the Rh–C bond at the γ-position with respect to form the Rh–C bond at the γ-position with respect to the substituent.[4] This fact is surprising since the cyclo-

$$[M(I)(OEP)]^- + X\text{-}\overset{2}{\underset{1}{\triangle}}\overset{}{\underset{3}{}} \xrightarrow{H_2O} M(III)(OEP)\cdot {}^{\alpha}CH_2{}^{\beta}CH_2{}^{\gamma}CH_2X \quad (5)$$

M=Rh: X=CH_3CO, CO_2Et
M=Co: X=CH_3CO, (**15**)

propane ring is considered to be stable towards the nucleophilic attack, and in general cleavage of cyclopropane ring by nucleophiles proceeds under severe conditions.[18] At room temperature, treatment of $[Co(I)(OEP)]^-$ with cyclopropyl methyl ketone gave readily 4-oxopentyl-cobalt(III)(OEP) (**15**). The ring fission along the 1, 2 bond was verified by the NMR spectrum which showed a broad signal at τ 14.37, a multiplet at 15.00 and a triplet at 10.90, assignable to α-, β-, and γ-carbon protons, respectively. A sharp singlet due to the terminal methyl group was observed at τ 9.38. However, no product was obtained for cyanocyclopropane but reaction with ethyl cyclopropanecarboxylate gave a small amount of product which showed a sharp carbonyl stretching absorption at 1720 cm^{-1}. In both cases, chloromethylcobalt(III)(OEP) (**16**) was isolated as a major product by the competitive substitution with the solvent methylene chloride. This result indicates that the reaction with cyclopropyl derivatives to form a σ bond is relatively slow and the unreacted Co(I) complex anion still remained in the reaction mixture.

In rhodium octaethylporphyrin the *endo*-configuration has been established for the product obtained from nortricyclanone.[19] It has thus been suggested that cleavage of the cyclopropyl ring by a rhodium(I) anion follows a S_N2 mechanism, *e.g.*, the reaction does not proceed *via* a π-type complex formed between the cyclopropane and the complex anion but rather *via* an intermediate carbanion stabilized by an electron-withdrawing substituent (Scheme 1). The observed activation by an acyl group may imply a similar mechanism.

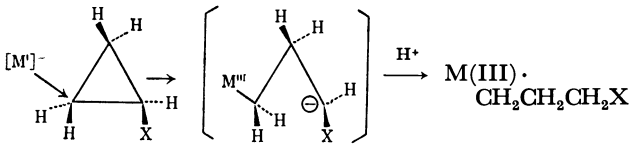

Scheme 1.

Weber and Schrauzer have reported that rhodoxime(I) is less nucleophilic than cobaloxime(I) in the substitution with alkyl halides.[20] Marked difference in the reactivity between Co(I)(OEP) and Rh(I)(OEP), however, may arise from the difference in stability of the various oxidation states. For metalloporphyrins, the cobalt ion is able to exist in the various oxidation states such as Co(I), Co(II) and Co(III).

Intramolecular Methyl Migration to Cobalt Atom. Reduction of Co(II) *N*-methyloctaethylporphyrin acetate $[Co(II)(N\text{-MeOEP})]^+OAc^-$ (**17**) with sodium borohydride proceeded to completion in thirty minutes at room temperature. The expected monovalent complex (**18**) was not obtained, but the trivalent cobalt-methyl derivative **1**, generated in 58% yield.

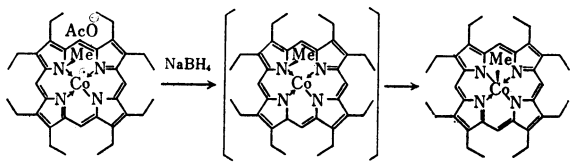

17 **18** **1**

In contrast with the complicated visible spectra of *N*-alkyl metalloporphyrin,[21] the generated complex showed a characteristic spectrum of metalloporphyrins.[22] Conclusive evidence for the cobalt–methyl bond was provided by the NMR spectrum which is identical with that observed for **1**. The complex is also identical with the protuct obtained by the substitution of pyridinebromocobalt(III)(OEP)[21] with methyl lithium. Grigg and co-workers[23] have reported that alkyl groups in Ni(II) and Pd(II) *N*-alkyl corroles migrate thermally from the pyrrolic nitrogen to the β-carbon atom of the pyrrolic ring. Perhaps the methyl migration proceeds through nucleophilic attack of the Co(I) ion, which may be assisted by the release of strain in the porphyrin ring coordination.

Previously we observed the migration of an alkyl group from nitrogen to the central metal atom for the dirhodium(I) complex of *N*-alkyl OEP (**19**) concomitant with the oxidation of the monovalent state of the metal, yielding alkylmetal(III) σ-complexes.[4] The present study suggests that the alkyl migration in the complex **19** proceeds *via* an intermediate analogous to

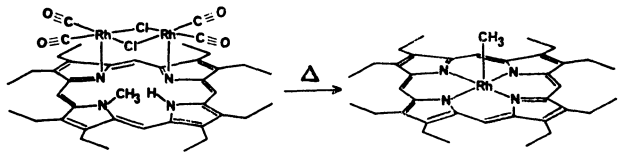

19 1

the postulated monovalent metal complex **18**. The present alkyl migration can be considered to be an intramolecular oxidative addition through the C–N bond to the Co(I) ion.

^1H NMR Spectra. Table 3 lists the NMR spectra of the alkylcobalt(III) complexes. Structures are proposed on the basis of the proton chemical shifts of the axially coordinating alkyl groups. These protons experience the influence of the ring current of the porphyrin macrocycle. The chemical shifts for the methyl and ethyl complexes **1** and **2** are quite similar to those observed for the corresponding aquoalkylcobalt(III) complexes of etioporphyrin II.[6] The hydrogens of the carbon directly attached to the cobalt atom (denoted as H_a in Table 3) appear at lower field as compared with those for other corresponding alkyl metalloporphyrins. For example, methyl hydrogens in the complex **1** resonate at τ 15.20, whereas the chemical shifts of the methyl hydrogens in Rh(OEP)·CH_3·H_2O[4] and Ge(porphin)$(CH_3)_2$[24] appear at 16.47 and 17.98, respectively. The hydrogens in the alkyl group for Rh(OEP)·R·H_2O, and Ge(porphin)(R_2) appear in the expected order C_α–H_2>C_β–H_2>C_γ–H_2……. In contrast, the methyl protons in the ethyl complex **2** resonate at lower magnetic field than those of the methylene protons. This lower field shift of the C_α-hydrogen can be explained if we assume that the cobalt(III) ion in the organocobalt porphyrin is more electronegative than those of other metals. This explanation seems to be reasonable since the geminal coupling constant in the vinyl complex **7** is relatively large (J_{gem}=4.0 Hz) as compared with those (<1 Hz) for other vinyl metal complexes.[4,12,13] In general, a large geminal coupling constant is associated with a high electronegativity of the substituent of the vinyl derivatives.[25]

Figure 1 shows representative spectra of Co(III)(OEP)R in the high field region in $CDCl_3$. Anomalous line broadening has been observed for the proton signals of α-carbon atom. The broadening is common to all the complexes. The rest of the signals of the axial alkyl group are all normal, indicating the absence of dimer-formation in solution as reported for cobaloximes.[26] Clarke and his co-workers have ascribed similar line broadenings for the C_α-hydrogens in etioporphyrin II to the poorly resolved nuclear spin-spin coupling between ^{59}Co–^{1}H.[6] If this is true, it seems rather surprising since the naturally occurring cobalt (100%, ^{59}Co) has a large electric quadrupole moment, Q= 0.5×10^{-24} cm^2 [27] and hence spin-spin coupling between protons and a nucleus is normally not observed in solution due to rapid spin-relaxation of the quadrupolar nucleus.[28] Accordingly, spin coupling between protons and cobalt has never been observed for either the pentacoordinate[29] or hexacoordinate alkyl cobalt σ

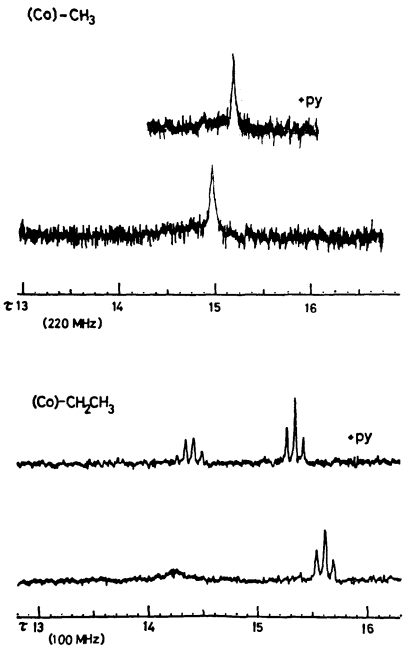

Fig. 1. NMR spectra of **1** and **2** in the high field region (measured in $CDCl_3$).

complexes hitherto reported. As is shown in Fig. 1, the signal shape was appreciably sharpened to give well resolved hyperfine structure when an excess amount of pyridine was added. Consequently, the expected quartet of the methylene group at τ 14.38 could definitely be identified for the ethyl cobalt(III)(OEP) **2**. Concomitantly, signal due to C_α-hydrogens was shifted to higher field by 0.4—0.5 ppm while slight shift to lower field was observed for the signal due to C_β-hydrogens. These observations lead us to postulate that the broadened line shape of the C_α-hydrogens is due to partially relaxed cobalt–proton coupling caused by quadrupolar relaxation. Similar phenomena have been observed for tricarbonyl(η-cycloheptatrienyl)vanadium(I)[30] and the mechanism is well understood.[28] The rate of relaxation depends on the strength of the coupling between the quadrupole moment and fluctuating electric field gradients at quadrupolar nucleus.[28] The electric field gradient at the cobalt atom in the pentacoordinate porphyrin complex might be weak; in consequence, despite a relatively large value of Q, the quadrupole coupling constant might be small enough to observe ^{1}H–^{59}Co spin-spin coupling. Coordination of pyridine would cause an increase in the covalency of the cobalt(III)–carbon bond and in turn the field gradient becomes so strong as to yield complete decoupling in the present system. It would be of great use to elucidate the mechanism of the line broadening in respect of the controversial problems related to the nature of Co–carbon bonds in vitamin B_{12}.[31–33]

Figure 2 shows the spectra of Co(OEP)·$CH_2CH_2CO_2Et$ **3** and Co(OEP)·$CH_2CH_2CH_2COCH_3$ **15** in the high field region. Again signals due to the C_α-hydrogens are broad and overlapped by a less resolved peak due to C_β-hydrogens. In the presence of pyridine, **3** shows a sharp multiplet at τ 14.34, typical of AA'BB' pattern,[34] for the protons (C_α–H and C_β–H) while **15** showed a

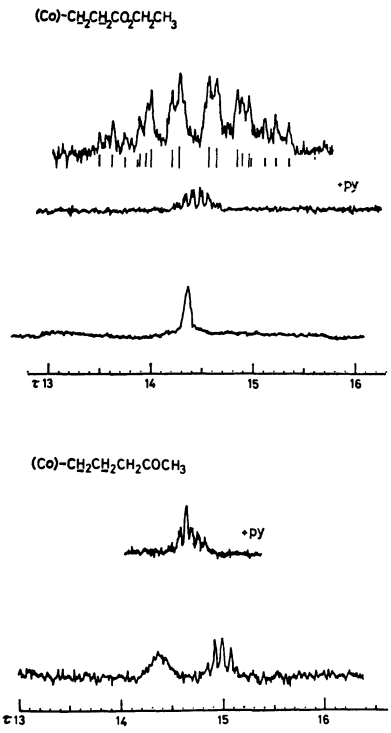

Fig. 2. 100 MHz NMR spectra of **3** and **15** in the high field region (measured in $CDCl_3$).

multiplet at ≈14.70 associated with C_α- and C_β-protons. The AA'BB' type splitting may arise from the exclusive presence of a rotational conformer as reported in 1,2-disubstituted ethane.[34,35]

Of the organocobalt(III)(OEP) complexes some, **3,5—9**, show double quartets due to the methylene protons of the peripheral ethyl groups of porphyrin, even though the difference in chemical shifts between the two quartets is quite small. Axial ligation of some unsaturated organic group forms a different magnetic anisotropic effect above and below the macrocyclic plane (diastereotopism).[36] The ratio of intensity for the two quartets is almost unity. Therefore, four of the methylene groups and the rest of four methylenes experience the different magnetic anisotropy due to the five coordinated metalloporphyrin. Free rotation of peripheral ethyl groups around the bond between the CH_2 and porphyrin carbon atom seems to be restricted to some extent due to the crowding of the ethyl groups.

Experimental

Spectral Measurements. Visible spectra (340—700 nm) were obtained in chloroform using a Hitachi EPS-3T spectrophotometer, and infrared spectra (4000—400 cm^{-1}) were determined in a KBr disk with a Hitachi-G3 spectrophotometer. NMR spectra were taken on Varian HA-100 and HR-220 spectrophotometers. All NMR spectra except for Co(I)(OEP) were recorded with deuteriochloroform as solvent and tetramethylsilane as internal standard. Pyridine was dried and distilled prior to use.

Reaction of Co(I)(OEP) with Organic Halides. A General Procedure: Co(II)(OEP) (100 mg) and sodium amalgam (2%, 3.0 g) were placed in a two necked flask (50 ml). The center neck was connected to a high vaccum tap and another neck was connected *via* a high vaccum tap to a 25 ml flask. Dry tetrahydrofuran (30 ml) was introduced to the flask and the solution was deareated by a repeated freeze-thaw method, and then stirred magnetically overnight. The color of the solution changed from reddish purple to lustrous orange-red. After the solution was transfered through a glass filter to the 25 ml flask, an excess of degassed alkyl halide (methyl iodide, ethyl iodide, ethyl 2-bromopropionate, *trans*-β-bromostyrene, or 2-bromoethylamine) was added, and then the solution was stirred for 10 min in the absence of light. The color of the solution changed to dark red. Methylene chloride (15 ml) was added to the reaction mixture and the solution was then

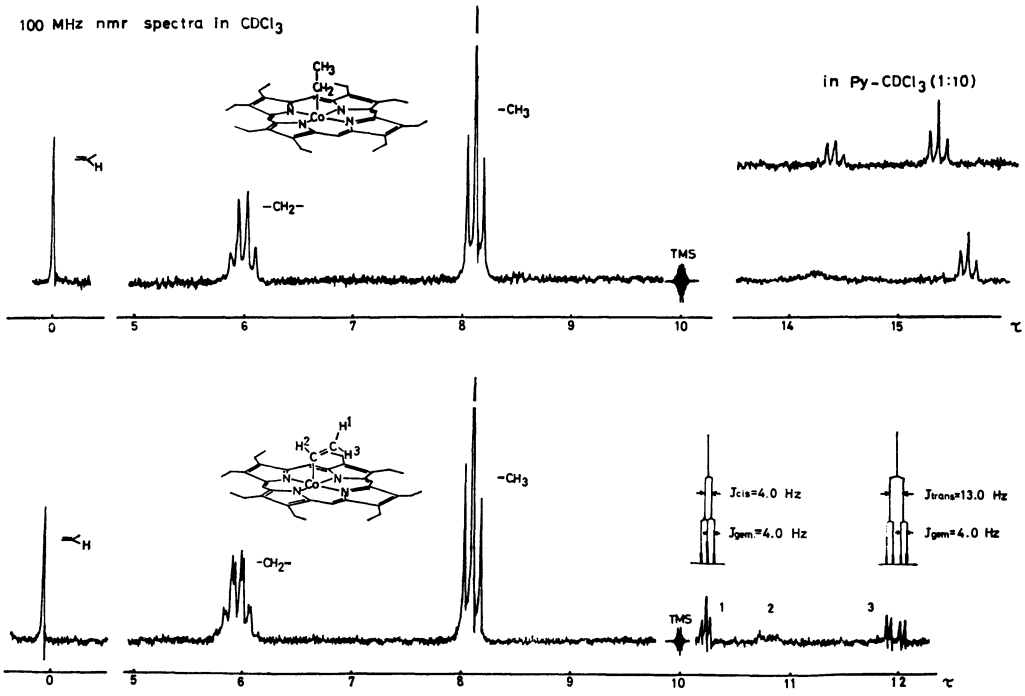

Fig. 3. 100 MHz NMR spectra of **2** and **7** measured in $CDCl_3$.

poured into 200 ml of cold water. The organic layer was separated, successively washed with water (200 ml × 3), and dried over Na_2SO_4. The solvent was removed at room temperature under reduced pressure and the residue was chromatographed on thin layer silica gel with benzene–methylene chloride (Merck, 60 PF_{254}, 20×20×0.1 cm^{-1}). The reddish orange zone was separated and extracted with methylene chloride. The solvent was removed and recrystallization of the residue afforded alkylcobalt(III)(OEP).

Co(OEP)·CH_3: This was eluted with methylene chloride–petroleum ether (1:3). Recrystallization from methylene chloride–petroleum ether afforded purple prisms (67 mg, 65%).

Co(OEP)·CH_2CH_5: This was eluted with methylene chloride–petroleum ether (1:5). Recrystallization from methylene chloride–petroleum ether afforded purple crystals (63 mg, 60%).

Co(OEP)·$CH_2CH_2CO_2Et$: Elution was carried out with methylene chloride–hexane (1:3). Recrystallization from methylene chloride–acetone gave purple crystals (50 mg, (42.7%).

trans-*Co(OEP)·CH=CHPh*: Eluent: methylene chloride–petroleum ether (1:3). Recrystallization from methylene chloride–petroleum ether afforded purple crystals (67 mg, 57%).

Co(OEP)·$CH_2CH_2NH_2$: β-Bromoethyl amine was prepared prior to use by treating its hydrogen chloride salt with an equimolar amount of triethylamine. The purification procedure is the same as that described above except that the organic layer was washed with diluted hydrobromic acid (200 ml×5). Elution was carried out with methylene chloride–methanol (10:1). Recrystallization from methylene chroride–petroleum ether afforded dark purple crystals (43 mg, 40%).

Reaction of Co(I)(OEP) with Olefins, Acetylenes and Three Membered Ring Compounds. A General Procedure: An excess molar amount of the substrate was added to (acrylonitrile, ethyl acrylate, phenylacetylene, ethylene imine or cyclopropyl methyl ketone) or bubbled into (acetylene and ethylene oxide) the THF solution of Co(I)(OEP) prepared from 100 mg of Co(II)(OEP) as described above. The reaction mixture was stirred for 15 min and then a portion of 0.5 M NaOH was poured into the reaction vessel. Stirring was continued until the solution turned dark red (10—30 min). The succeeding procedures for separation and purification of the products are identical with those described in the reaction with alkyl halides.

Co(OEP)·CH_2CH_2CN: Eluted with methylene chloride–petroleum ether (1:3). Recrystallization from methylene chloride–petroleum ether affords purple crystals (50 mg, 44%).

Co(OEP)·$CH_2CH_2CO_2Et$: The products are identical with those prepared from ethyl 2-bromopropionate as described above (35 mg, 30%).

Co(OEP)·$CH=CH_2$: Thin layer chromatography of the reaction mixture on silica gel indicated that Co(II)(OEP) was formed together with alkyl cobalt complexes. Highly insoluble Co(II)(OEP) was removed by filtration before the separation by TLC was carried out. Recrystallization from methylene chloride–petroleum ether yielded vinyl cobalt(III)(OEP) (18 mg, 19%).

cis-*Co(OEP)·CH=CHPh and Co(OEP)·PhC=CH_2*: Monitoring reaction procedure by means of TLC showed that Co(II)(OEP) had generated during the reaction together with vinyl complexes. Elution was carried out with methylene chloride–hexane (1:5). Recrystallization from methylene chloride–acetone gave a mixture of *cis*-Co(OEP)·CH=CHPh and Co(OEP)·PhC=CH_2 (3:1) (34 mg, 29%). The deuteration experiment was carried out according to the general procedures described above except an addition of deuterium oxide solution of NaOD in place of aqueous NaOH solution.

Co(OEP)·CH_2CH_2OH: Eluent chloroform–hexane (1:2). Recrystallization from chloroform–hexane gave purple crystals (72 mg, 67%).

Co(OEP)·$CH_2CH_2NH_2$: The products are identical with those obtained in the reaction of Co(I)(OEP) with 2-bromoethylamine (35 mg, 33%).

Co(OEP)·$CH_2CH_2CH_2COCH_3$: Elution was carried out with methylene chloride–petroleum ether (1:3). Recrystallization from methylene chloride–petroleum ether gave 50 mg of deep purple crystals (44%).

Reaction with Carboethoxycyclopropane. The method used is entirely analogous to that described in the reaction with cyclopropyl methyl ketone. The main zone separated from TLC gave chloromethyl derivative, Co(OEP)·CH_2Cl. Recrystallization from methylene chloride–acetone gave 87 mg of deep purple crystals (79.8%). A minor zone gave an alkyl derivative (2 mg) with carbonyl stretching band at 1720 cm^{-1}.

Reaction with Cyanocyclopropane. The reaction mixture was stirred for 30 min. Co(OEP)CH_2Cl was obtained (31 mg, 37.5%).

Analytical data for the alkylcobalt(III)(OEP) complexes are given in Table 1. Visible and characteristic infrared data are listed in Table 2 and NMR data in Table 3. All reactions and manipulations involving cobalt(I) complexes were performed entirely under an atmosphere of purified argon. A 2% sodium amalgam was prepared by addition of mercury to the melted sodium metal in toluene. All procedures involving alkylcobalt(III) complexes were carried out in the dark whenever possible.

Intramolecular Methyl Migration. *N*-methyloctaethylporphyrinatocobalt(II) acetate [Co(*N*-MeOEP)]$^+OAc^-$ was prepared by a usual method[22] from Co(II) acetate and *N*-methyloctaethylporphyrin.[37] 80 mg of *N*-methyloctaethylporphyrinatocobalt(II) acetate was dissolved in THF and air was purged by argon. 10 mg of $NaBH_4$ in aqueous sodium hydroxide solution (0.5 M 0.5 ml) was added to the solution and the reaction mixture was stirred for 35 min. The color of the solution changed from dark green to dark red. Ten ml of methylene chloride was added to the solution and washed with water, and dried over Na_2SO_4 and evaporated. The resulting residue was chromatographed on silica gel (TLC 20×20×0.1 cm) with methylene chloride–petroleum ether (1:3). Recrystallization from methylene chloride–petroleum ether afforded deep purple crystals (42 mg, 57.6%).

Reaction of Co(III)(OEP)Br·py with Methyllithium. To 100 mg of pyridinobromocobalt(III)octaethylporphyrin[21] dissolved in anhydrous dimethoxyethane was added an equimolar amount of methyllithium prepared from methyl iodide and lithium metal under nitrogen. The reaction was monitored by TLC (silica gel). After the reaction was completed, the reaction mixture was poured into 200 ml of water, washed with water several times and dried over Na_2SO_4. The succeeding procedures are identical with those described above. Recrystallization from methylene chloride–petroleum ether afforded Co(OEP)–CH_3 (72 mg, 55%).

This work was partially supported by a Grant-in-Aid for Scientific Research from the Ministry of Education, Japan (No. 911503).

References

1) (a) G. N. Schrauzer, *Acc. Chem. Res.*, **1**, 97 (1968); (b) H. A. O. Hill, J. M. Pratt, and R. J. P. Williams, *Chem. Britain*, **5**, 156 (1969); (c) G. N. Schrauzer, "Bioinorganic

Chemistry," R. Dessey, J. Dillard, and L. Tayler, ed., Am. Chem. Soc., W. D. (1971), Chapter 1; (d) J. M. Pratt, "The Inorganic Chemistry of Vitamin B_{12}," Academic Press, New York (1972); (e) H. A. O. Hill, "Inorganic Biochemistry," Vol. 2, G. L. Eichhorn ed., Elsevier, Amsterdam (1973), Chapter 30; (f) J. M. Pratt and P. J. Craig, *Adv. Organometal. Chem.*, **11**, 331 (1971); (g) D. Dodd and M. D. Johnson, *Organometal. Chem. Rev.*, **52**, 1 (1973).

2) (a) J. Halpern, *Acc. Chem. Res.*, **3**, 386 (1970); (b) G. N. Schrauzer, Ed., "Transition Metals in Homogeneous Catalysis," Marcel Dekker, New York (1971); (c) B. R. James, "Homogeneous Hydrogenation," John Wiley & Sons, New York (1973).

3) J. H. Weber and G. N. Schrauzer, *J. Am. Chem. Soc.*, **92**, 726 (1970); J. P. Collman, D. W. Murphy, and G. Dolcetti, *ibid.*, **95**, 2687 (1973); J. P. Collman and M. R. MacLaury, *ibid.*, **96**, 3019 (1974).

4) H. Ogoshi, T. Omura, and Z. Yoshida, *J. Am. Chem. Soc.*, **95**, 1666 (1973); H. Ogoshi, J. Setsune, T. Omura, and Z. Yoshida, *ibid.*, **97**, 6461 (1975).

5) D. A. Clarke, R. Grigg, and A. W. Johnson, *Chem. Commun.*, **1966**, 208; D. A. Clarke, D. Dolphin, R. Grigg, A. W. Johnson, and H. A. Pinnock, *J. Chem. Soc.*, **1968**, 881.

6) Preliminary communication, H. Ogoshi, E. Watanabe, N. Koketzu, and Z. Yoshida, *J. Chem. Soc., Chem. Commun.*, **1974**, 943.

7) H. W. Whitlock, Jr. and B. K. Bower, *Tetrahedron Lett.*, **1965**, 4827.

8) F. A. Cotton and G. Wilkinson, F. R. S., "Advanced Inorganic Chemistry," 2nd ed., Interscience Publishers, New York (1966), p. 873.

9) F. Basolo and R. G. Pearson, "Mechanisms of Inorganic Reactions," 2nd ed., John Wiley & Sons, New York (1967), p. 147.

10) G. Costa, G. Mestroni, G. Tauzher, and L. Stefani, *J. Organometal. Chem.*, **6**, 181 (1966); G. Costa, G. Mestroni, and L. Stefani, *ibid.*, **7**, 493 (1967); C. Floriani, M. Puppis, and F. Calderazzo, *ibid.*, **12**, 209 (1968); G. Costa and G. Mestroni, *ibid.*, **11**, 325 (1968).

11) A. Bigotto, G. Costa, G. Mestroni, G. Pelliger, A. Puxeddu, E. Reisenhofer, L. Stefani, and G. Tauzher, *Inorg. Chim. Acta*, **4**, 41 (1970).

12) M. D. Johnson and B. S. Meeks, *J. Chem. Soc., B*, **1971**, 185.

13) M. Nguyen, K. N. -V. -Duong, and A. Gaudemer, *J. Organometal. Chem.*, **25**, 231 (1970).

14) G. N. Schrauzer and J. Kohnle, *Chem. Ber.*, **97**, 3056 (1964).

15) G. N. Schrauzer and R. J. Windgassen, *J. Am. Chem. Soc.*, **89**, 1999 (1967).

16) E. B. Fleischer and M. Krishnamurthy, *J. Am. Chem. Soc.*, **94**, 1382 (1972). TPPS: *meso*-tetra(*p*-sulfonatophenyl)-porphin.

17) K. Nakanishi, "IR Absorption Spectroscopy," Nankodo, Tokyo (1960).

18) E. W. Yankee, F. D. Badea, N. E. Howe, and D. J. Cram, *J. Am. Chem. Soc.*, **95**, 4210 (1973); E. W. Yankee, B. Spencer, N. E. Howe, and D. J. Cram, *ibid.*, **95**, 4220 (1973), and cited prior work.

19) H. Ogoshi, J. Setsune, and Z. Yoshida, *J. Chem. Soc., Chem. Comm.*, **1975**, 572.

20) J. H. Weber and G. N. Schrauzer, *J. Am. Chem. Soc.*, **92**, 726 (1970).

21) R. Grigg, G. Shelton, and A. Sweeney, *J. Chem. Soc., Perkin Trans. 1*, **1972**, 1789.

22) J. E. Falk, "Porphyrins and Metalloporphyrins," Elsevier, Amsterdam (1964).

23) R. Grigg, A. W. Johnson, and G. Shelton, *Justus Liebigs Ann. Chem.*, **746**, 32 (1971); M. J. Broadhurst, R. Grigg, G. Shelton, and A. W. Johnson, *Chem. Commun.*, **1970**, 231.

24) J. E. Maskasky and M. E. Kenney, *J. Am. Chem. Soc.*, **95**, 1443 (1973).

25) L. M. Jackman and S. Stemhell, "Applications of Nuclear Magnetic Resonance Spectroscopy in Organic Chemistry," 2nd ed., Pergamon Press, Braunshweig (1969), p. 277.

26) L. M. Ludwick and T. L. Brown, *J. Am. Chem. Soc.*, **91**, 5188 (1969); A. W. Herlinger and T. L. Brown, *ibid.*, **94**, 388 (1972).

27) Japan Chem. Soc., Ed., "Handbook on Chemistry," Maruzen Co., Ltd., Tokyo (1966), p. 1177.

28) J. A. Pople, *Discuss. Faraday Soc.*, **43**, 192 (1967); R. A. Dwek and R. E. Richards, *ibid.*, **43**, 196 (1967); R. H. Holm and E. H. Abbott, *Coordination Chem.*, **1**, 264 (1971).

29) H. A. O. Hill, K. G. Mrallee, G. Bellinger, G. Mestroni, and G. Costa, *J. Organometal, Chem.*, **11**, 167 (1968).

30) G. M. Whitesides and H. L. Mitchell, *J. Am. Chem. Soc.*, **91**, 2245 (1969).

31) M. W. Penley, D. G. Brown, and J. M. Wood, *Biochem.*, **9**, 4302 (1973).

32) T. E. Needham, N. A. Matwiyoff, T. E. Walker, and H. P. C. Hogenkamp, *J. Am. Chem. Soc.*, **95**, 5019 (1973).

33) K. G. Caulton, *J. Am. Chem. Soc.*, **95**, 4076 (1973); K. L. Brown, D. Chernoff, D. J. Keljo, and R. G. Kallen, *ibid.*, **94**, 6697 (1972); J. D. Brodie, *Proc. Nat. Acad. Sci, USA*, **62**, 461 (1969); H. P. C. Hogenkamp and S. Holms, *Biochem.*, **9**, 1886 (1970); R. L. Courtright, R. S. Drago, J. A. Nusz, and M. S. Nozari, *Inorg. Chem.*, **12**, 2809 (1973); R. J. Guschl and T. L. Brown, *ibid.*, **12**, 2815 (1973); R. A. Larossa and T. L. Brown, *J. Am. Chem. Soc.*, **96**, 2072 (1974).

34) R. J. Abraham, "The analysis of High Resolution NMR Spectra," Elsevier, Amsterdam (1971), Chapter 4; H. Günter, *Angew. Chem.*, **84**, 907 (1972).

35) R. C. Hirst and D. M. Grant, *J. Chem. Phys.*, **40**, 1909 (1964).

36) R. J. Abraham and K. M. Smith, *Tetrahedron Lett.*, **1971**, 3335.

37) W. E. McWen, *J. Am. Chem. Soc.*, **68**, 711 (1946).

CIDNP Investigation of Aminyl Radicals Formed by Thermolysis of Triazenes[1)]

Klaus ALBERT, Karl-Michael DANGEL, and Anton RIEKER*
Department of Organic Chemistry, University of Tübingen, D-74 Tübingen, Auf der Morgenstelle, G.F.R.
Hiizu IWAMURA,* and Yuzo IMAHASHI
Department of Chemistry, Faculty of Science, The University of Tokyo, Hongo, Bunkyo-ku, Tokyo 113
(Received March 19, 1976)

Thermolysis of asymmetric triazenes Ar–N=N–NH–R **1** produces anilines Ar–NH_2 **2**, hydrocarbons R–H **3**, and *N*-alkylated anilines Ar–NH–R **4** as the main reaction products. ^{1}H-and ^{13}C-CIDNP experiments show polarization of nuclei in Ar–NH_2, Ar–NH–R, R–H and some additional products (especially ring alkylated anilines). These observations are in agreement with the formation of an intermediate radical pair [Ar–NH··R] which must have been formed *via* homolysis of the tautomeric form ArNH–N=N–R **1′**. Temperature-dependent ^{13}C-NMR spectra show a rapid equilibrium between **1** and **1′** at room temperature and above, the tautomeric form **1** being predominant. From the CIDNP spectra the signs of the ^{1}H and ^{13}C hyperfine couplings of aminyl radicals Ar–NH· and alkyl radicals R· have been determined.

Recently an important role of free radicals in the reactions of onium compounds with nucleophiles was pointed out.[1,2)] Electron transfer from nucleophiles to onium ions should initially lead to the primary radical pair I, Scheme 1, from which cage and escape products and/or secondary cages II might be formed. Alternatively, a direct ionic recombination of both components could occur to form a homopolar bond which consecutively would homolyse into the same radical pairs.

As a mechanistic model of one of these reactions, namely, the reaction of aryldiazonium salts with strongly nucleophilic amines or amide anions,[3)] we have examined the thermolysis of 1-aryl-3-alkyltriazenes **1** in various solvents at 125—135 °C.

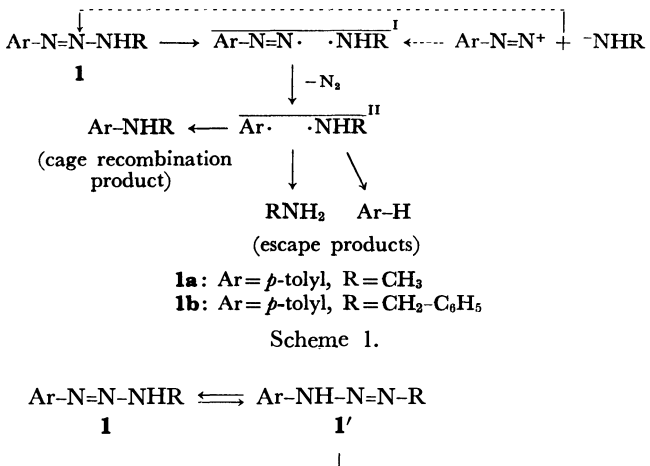

Scheme 1.

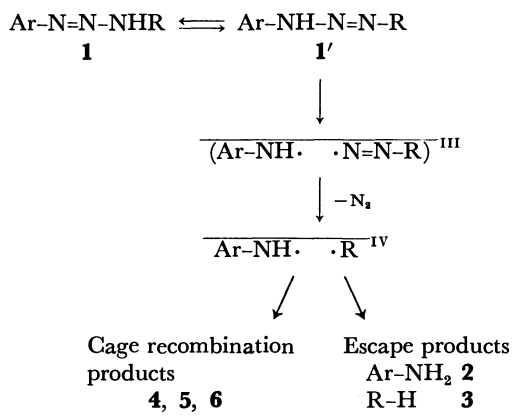

Scheme 2.

Contrary to the expectation (derived from the structure of triazenes **1**) that arenes ArH and amines R–NH_2 as escape products and *N*-alkylaniline derivatives as the cage recombination products would be formed predominantly in hydrogen-donating solvents as shown in Scheme 1, anilines Ar–NH_2 **2** have been found as the main products indicating the preferential formation of arylaminyl (anilino) radicals in these reactions. Therefore we wish to propose Scheme 2 as revealed by the ^{1}H- and ^{13}C-CIDNP investigations and by the product analysis of the thermal decomposition of the triazenes.

Experimental

The triazenes **1** were synthesized in analogy with the preparation of 1-phenyl-3-methyltriazene[4)] or purchased from Willow Brook Labs. Inc., Waukesha, Wisc., USA. The samples were crystallized from petroleum ether before use. The authentic sampeles for the reaction products are commercially available except *N*-methyl-*p*-toluidine **4a**, *N*-benzyl-*p*-toluidine **4b** and 2-benzyl-4-methylaniline **5b**. These were prepared according to the literature.[5,6)]

The ^{1}H-NMR spectra were obtained on a Hitachi R-20 B (60 MHz) spectrometer and a Bruker HFX-90 (90 MHz) spectrometer (δ ppm from TMS). In typical CIDNP experiments, solutions of 38 mg of triazene in 0.4 ml of solvent (Hitachi) or 70 mg in 1 ml of solvent (Bruker) were heated in the spectrometer probe. CIDNP spectra were registered at 130 °C by a continuous wave scan of 600 Hz/200 s on both instruments. For the Bruker instrument an internal deuterium lock made of DMSO-d_6 was sealed in a 2 mm capillary and placed concentrically in a sample tube of 5 mm o.d., using a perforated vortex plug to allow for gas escape.

The ^{13}C-NMR spectra were obtained at 25.15 MHz on a JEOL PS 100 PFT spectrometer and at 22.628 MHz on the Bruker HFX-90 instrument. The internal deuterium lock described above was used with both instruments. The diameter of the capillary was raised to 4 mm and to 5 mm as a consequence of the 8 mm o.d. (JEOL) and 10 mm o.d. (Bruker) sample tubes. Further conditions for the JEOL instrument: a radiofrequency 45° pulse of 11 μs was applied with a repetition time of 1.0 s over the spectrum width of 6.25 KHz. Accumulation of the FID signals was started at 30 s after insertion of a sample solution (185 mg of **1b** in 1 ml of a solvent, for

* To whom correspondence should be addressed.

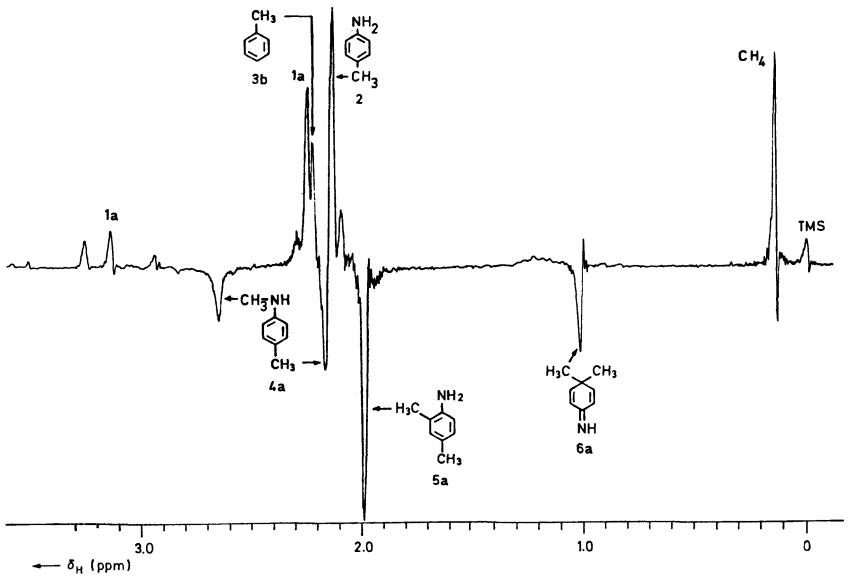

Fig. 1. ^{1}H-CIDNP spectrum (90 MHz) obtained on a solution of 3-methyl-1-*p*-tolyltriazene **1a** in *o*-dichlorobenzene decomposing at 130 °C.

TABLE 1. ^{1}H-CIDNP (δ ppm FROM INTERNAL TMS) IN THE THERMOLYSIS OF **1a** IN 1,1,2,2-TETRACHLOROETHANE (TCE), *trans*-DECALIN (DC), AND 1,2-DICHLOROBENZENE (DCB)

TCE[a]	DC	DCB	Assignment	No. of compound	CIDNP
0.20	0.18	0.13	CH_4	**3a**	strong A
1.18	—	1.01	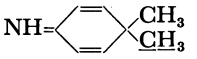	**6a**	E
2.12	2.04	1.98	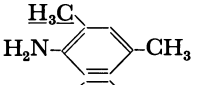	**5a**	strong E
2.22	2.16	2.13	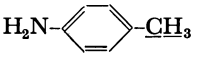	**2**	weak A
2.38	—	2.15	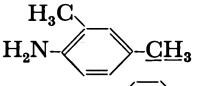	**5a**	weak E[b]
2.38	—	2.15	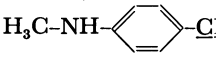	**4a**	weak E[b]
2.79	2.76	2.64	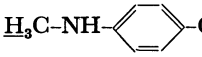	**4a**	E
2.98	—	—	CH_3Cl	**7**	short-lived E
6.41	6.28[c]	—	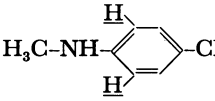	**4a**	A[b,d]
6.54	6.42[c]	—			A[b,d]
6.41	6.28[e]	—	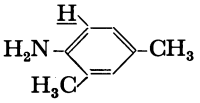	**5a**	A[b,d]
6.54	6.42[e]	—			A[b,d]
6.47	6.32	—	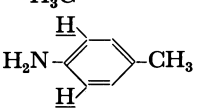	**2**	E
6.59	6.46	—			E
6.86	6.75	—	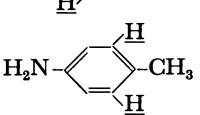	**2**	A
6.99	6.88	—			A
2.30	2.27	2.24	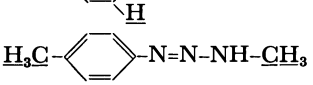	**1a**	no
3.21	3.19	3.14			no

a) No additional weak emission signals at δ 0.88 and 1.00 in TCE can be assigned. b) Due to the overlap of shift values of **4a** and **5a**, discrimination is not possible. c) Shifts of authentic sample taken at 37 °C with Varian A 60: 6.24, 6.38 ppm. d) No CIDNP observed in TCE. e) Shifts of authentic sample taken at 37 °C with Varian A 60: 6.23, 6.37 ppm.

example) into the preheated NMR probe and was continued until the sum of 300 was obtained. Further condition for the Bruker instrument: *ca.* 300 mg of triazene **1a** in 2 ml of solvent was decomposed. The probe was preheated at 80 °C and accumulation started 40 s after the temperature had reached 130 °C. A 10 μs pulse was applied 1024 times with a repetition time of 0.4 s over the spectrum width of 5.0 KHz. In each case the sample temperature was controlled as usual by preheated nitrogen flow and thermostatted by a heat-sensor in an effluent gas stream.

Unless otherwise stated, the assignment of both the ^{1}H- and ^{13}C-CIDNP signals was made by careful comparison of chemical shifts with those of the authentic samples under the same experimental conditions. This was effectively done by adding small amounts of the authentic sample to the reacion mixture-right before and after recording the CIDNP spectra and observing the corresponding increase in absorption intensity of the signals in question. Product analyses were performed by vapor phase chromatography on Shimadzu GC-4A and on Perkin Elmer F-7 instruments in the usual manner using authentic samples for comparison. The amount of nitrogen-plus methane evolved was determined volumetrically by means of a thermostatted azotometer.

Results and Discussion

a) ^{1}H-CIDNP Results. All the results are summarized in Tables 1 and 2. The aliphatic region

Table 2. ^{1}H-CIDNP (δ ppm from internal TMS) in the thermolysis of **1b** in 1,1,2,2-tetrachloroethane (TCE), *trans*-decalin (DC) and 1,2-dichlorobenzene (DCB)

TCE	DC	DCB	Assignment	No. of compound	CIDNP
1.21		1.09		**6b**	weak E
2.20	2.16	2.12	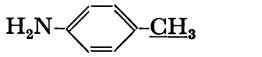	**2**	strong A
2.18		2.19	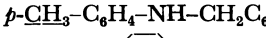	**4b**	weak E[b]
2.21		2.19	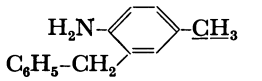	**5b**	weak E[b]
2.28		2.22		**3b**	A
2.77	2.69	2.65	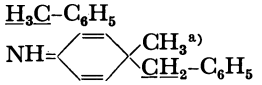	**6b**	E
2.94	2.88	2.87	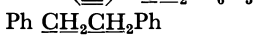	**8**	A
3.84	3.80	3.78	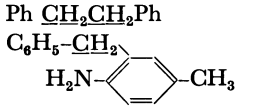	**5b**	strong E
4.25	4.16	4.20	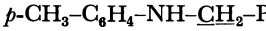	**4b**	weak broad E
4.55				**9**	very weak E
6.46	6.32		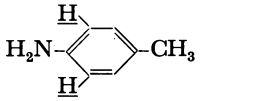	**2**	E
6.59	6.46				E
6.85	6.74		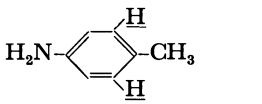	**2**	A
7.00	6.88				
	6.35		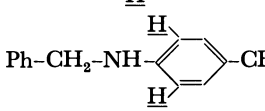	**4b**	A[b]
	6.48				A[b]
6.47	6.34		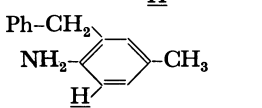	**5b**	[b]
6.60	6.47				
	6.79		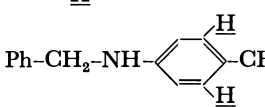	**4b**	[b]
	6.95				
7.18	7.12		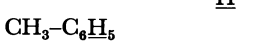	**3b**	later E
7.21			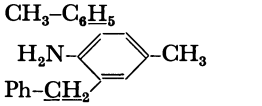	**5b**	E
7.23			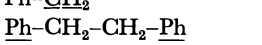	**8**	A
7.34	7.21		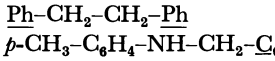	**4b**	E
2.39	2.25	2.34	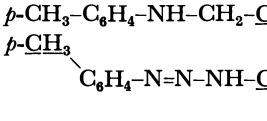		no
4.89	4.67	4.82		**1b**	no
7.36					no

a) Assignment tentative. b) Due to overlap, assignment of the anilino part CIDNP signals to **4b** or **5b** is impossible.

of a typical ^{1}H-CIDNP spectrum of the thermolysis of **1a** in *o-dichlorobenzene* at 130 °C is reproduced in Fig. 1. At this temperature the intensity of the *N*-methyl and aromatic methyl singlets at δ 3.14 and 2.24, respectively, due to **1a** decreases with a half-life of 2—3 min. A strongly polarized absorption due to methane is noted at δ 0.13 throughout a 10—12 min period of the reaction. There are several emission singlets in the methyl region of the spectrum. The one at δ 1.01 is tentatively assigned to the methyl protons of 4,4-dimethyl-cyclohexa-2,5-dien-1-imine **6a**.[7,8] The strongest emission at δ 1.98 corresponds to the *ortho*-methyl group of 2,4-dimethylaniline **5a**. Both the aromatic methyl and *N*-methyl protons of *N*-methyl-*p*-toluidine **4a** cause weak emission signals at δ 2.15 and 2.64, respectively. The signal of the aromatic *p*-methyl protons of **5a**, also for which emission is predicted, coincides with that of **4a**. At δ 2.13 the methyl signal of *p*-toluidine **2** itself is observed in weakly enhanced absorption. Some toluene has also been formed as can be seen from the signal at δ 2.22.

The thermal decomposition of the triazene **1a** in 1,1,2,2-tetrachloroethane and in *trans*-decalin supplements the above CIDNP experiments. In *1,1,2,2-tetrachloroethane* a short-lived emission at δ 2.98 is considered to be due to methyl chloride **7** formed in 12% yield (vapor phase chromatography) specifically in this solvent. In the aromatic region, the high-field part of the AA'BB' pattern is emissive while the low-field half is slightly enhanced during the first 5 min period of the reaction. Although the AA'BB' multiplet due to the aromatic ring protons of *p*-toluidine and its *N*-methyl derivative **4a** is quite similar under these conditions and also the doublet of H-6 of 2,4-dimethylaniline **5a** is found at the same shift values as H-2,6 of **4a**, we might conclude that the CIDNP effect is derived from the main reaction product *p*-toluidine. At a later stage of the reaction (8—15 min) we note a new emission singlet at the chemical shift corresponding to the aromatic protons of toluene. At the end of the reaction (30 min after the start) in 1,1,2,2-tetrachloroethane, the signals at δ 1.18, 2.12, and 7.18 are barely detected as absorptions, suggesting the formation of only a small amount of imine **6a**, aniline **5a**, and toluene, respectively (*vide infra*).

In *trans-decalin* the high-field half of the AA'BB' pattern shows emission for *p*-toluidine and enhanced absorption for **4a**/**5a**. The latter two, of course, cannot be distinguished.

The ^{1}H-CIDNP experiments with 1-*p*-tolyl-3-benzyltriazene **1b** (Ar=*p*-$CH_3C_6H_4$, R=CH_2Ph; Table 2) in principle support our results obtained from thermolysis of **1a**. Therefore, they are not discussed in detail. It should be mentioned, however, that toluene **3b** is formed mainly *via* the benzyl radical and that bibenzyl **8** also shows CIDNP.

b) ^{13}C-CIDNP Results. A nearly full interpretation of the polarized signals during thermolysis of **1a** has been successfully achieved and is given in Table 3. As shown in Fig. 2 (decalin solution), the aliphatic region is not very informative since most of the aromatic *C*-methyl signals coincide and are compensated due to alternating polarizations. Thus it depends on small changes of the reaction conditions, whether the signal at δ 20.6—20.7 ppm is in weak absorption or emission.

The CIDNP pattern of the aliphatic region of **1a** in *o*-dichlorobenzene is shown in Fig. 3 with a clear-cut emission mode of the 20.6 ppm line. The low CIDNP intensity of the aromatic *C*-methyl signals might be due to short spin-lattice relaxation times of these carbon atoms as a result of spin rotation mechanisms available for the methyl groups. On the other hand, those methyl groups originating from the methyl radical of the radical pair III (Scheme 2) show reasonable enhancement factors. This is true for the *N*-methyl carbon of **4a** and for the 2-methyl group of **5a**, which are clearly detected as being in enhanced absorption in or close to the region of the solvent signals. Consequently, lower ^{13}C-hyperfine coupling constants a_i of the aromatic methyl carbon atoms in arylaminyl radicals with

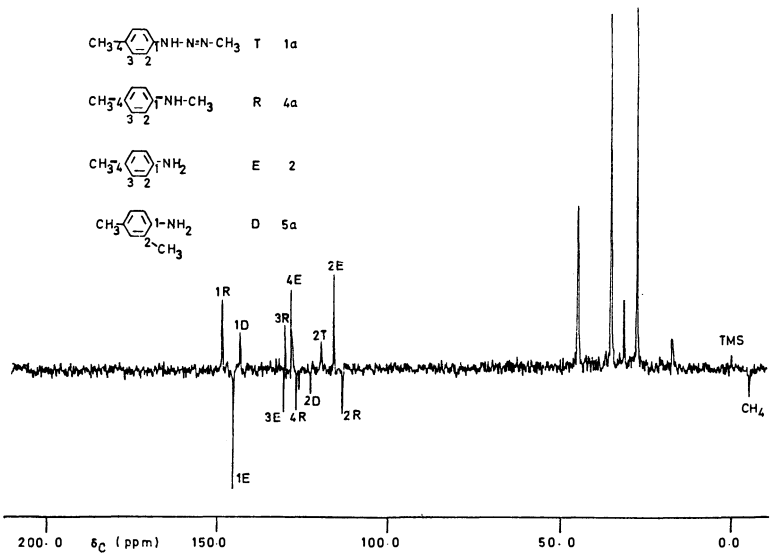

Fig. 2. ^{13}C-CIDNP spectrum (22.628 MHz, PFT) obtained on a solution of **1a** in *trans*-decalin.

TABLE 3. ^{13}C-CIDNP[a] IN THERMOLYSIS OF **1a** AT 135 °C

TCE		DC		DCB		Assignment		CIDNP
A[b]	B[b]	A[b]	B[b]	A[b]	B[b]			
−4.0	−4.9	−4.6	−5.1	−3.5	−4.9	CH_4	(**3a**)	E
17.7	16.9	16.9	16.9	17.2	16 9	2-CH_3	(**5a**)	A
20.4	20.7	20.7	20.6	20.4	20.7	4-CH_3	(**4a**)	vwA[c]
20.6	20.7	20.7	20.6	20.6	20.7	4-CH_3	(**2**)	vwE[c]
21.8		21.4		21.4		CH_3	(**3b**)	
28.7	27.9	—	—	—	—	CH_3Cl	(**7**)	wA
31.0	31.0	31.1	31.1	30.0	30.9	*N*-CH_3	(**4a**)	A
39.5	36.8	—	—	—	—			wE
112.5	113.0	113.0	113.2	111.7	113.0	C-2	(**4a**)	E
116.0	115.6	115.8	115.7	115.3	115.6	C-2	(**2**)	sA
	119.2		119.3		119.5	C-2	(**1a**)	
123.2	122.5	122.4	122.4	122.6	122.4	C-2	(**5a**)	E
125.6	125.4	125.8	125.6	125.5	—	C-4	(**3b**)	wE
126.2	126.5	126.2	126.5	125.0	126.2	C-4	(**4a**)	E
128.2	127.5	127.6	127.5	127.9	127.4	C-4	(**2**)	A
128.7	128.5	128.4		129.1		C-3	(**3b**)	
129.2		—	—	—	—			A
129.6	129.5	128.6		129.3		C-2	(**3b**)	
129.7	129.5	130.0	129.6	129.0	129.5	C-3	(**4a**) (**1a**)	wA
130.5	130.0	130.4	129.9		130.0	C-3	(**2**)	wE
	134.7				134.7	C-4	(**1a**)	
138.2		137.7		137.6		C-1	(**3b**)	
140.7	139.9	—	—	—	—			A
142.8	142.1	142.5	142.5	142.6	142.4	C-1	(**5a**)	A
144.7	144.0	144.8	144.6	144.7	144.5	C-1	(**2**)	sE
					146.7	C-1	(**1a**)	
147.1	147.3	147.9	147.8	146.7	147.6	C-1	(**4a**)	A

a) Shifts are given in δ ppm from internal TMS; TCE=1,1,2,2-tetrachloroethane, DC=*trans*-decalin, DCB=1,2-dichlorobenzene; w=weak, vw=very weak, s=strong. b) *A*: 25.15 MHz spectra; *B*: 22.628 MHz spectra. c) The signal at 20.6—20.7 ppm is due to the overlap of the 4-methyl signals of **2** and **4a**. Thus it depends on small variations of the reaction conditions (solvent, temperature, concentration) whether it appears in weak emission or weak enhanced absorption.

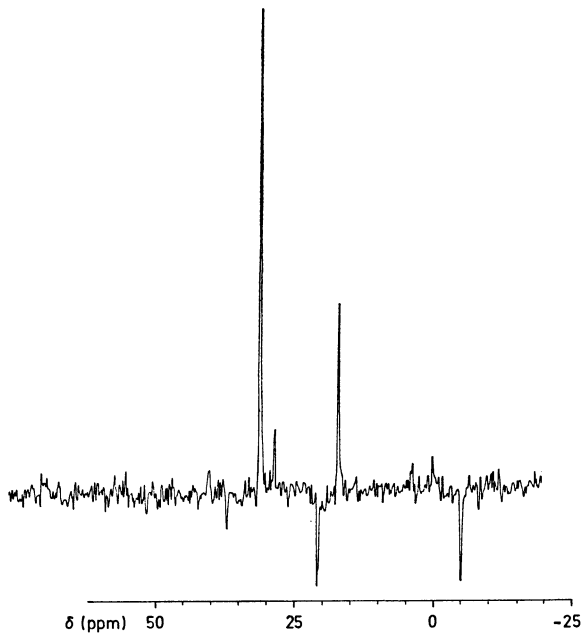

Fig. 3. The ^{13}C PFT CIDNP pattern of the aliphatic region of a reacting solution of **1a** in *o*-dichlorobenzene.

respect to a_{CH_3} seem to be mostly responsible for the low intensity.

The methane resonance at δ—5 is found in emission. In the case of ^{1}H–^{13}C coupled spectra the methane signal appears as a quintet (J_{H-C}=125 Hz) showing a relatively large Δg effect (superimposed multiplet and net effect) which seems to be reasonable (*vide infra*).

In the aromatic region the spectrum is more complicated. All the observed resonances can, however, be assigned to compounds **2**, **4a**, and **5a**, already determined by ^{1}H-CIDNP as recombination and escape products. The signs of polarization at C-1, C-2, C-3, and C-4 for *p*-toluidine **2** are E, A, E, and A, respectively. The positionally alternating signs are inversed in *N*-methyl-*p*-toluidine **4a**. In striking contrast to the methyl carbons, we note that, while the aromatic C-1 and C-4 are the weakest in the thermally equilibrated spectra because of the lack of the nuclear Overhauser effect under wide-band proton decoupling, these carbons show strongest polarization (see Table 3). The greater T_1 values for these quaternary carbons are considered mainly to be responsible for the apparent increase in enhancement. The enhancement factors of the ^{13}C-signals of toluene **3b** are small; the effect cannot always be reproduced. ^{13}C-signals of **6a** could not be

Table 4. ^{13}C-CIDNP[a] in the thermolysis of **1b**

TCE	DC	Assignment	CIDNP
20.4	20.7	CH_3 (**2**, **4b**, **5b**)	vwA
21.4	21.4	CH_3 (**3b**)	vwE
25.3	—		wE
37.2	37.8	CH_2 (**5b**)	A
49.8	49.8	N-CH_2 (**4b**)	A
113.7	114.0	C-2 (**4b**)	E
116.0	115.9	C-2 (**2**)	sA
117.2	—		A
121.7	119.5	C-2 (**1b**)	
126.0	125.8	C-4 (**3b**)	E
127.0	127.3	C-5 and C-4′ (**5b**)	wA
127.6	127.1	C-4 (**4b**) and (**5b**)	E
128.0	127.6	C-4′ (**4b**)[b] and C-4 (**2**)	A
128.4	127.9	C-4 (**2**)	sA
129.0	128.7	C-2′ or C-3 (**3b**)	A
129.4	128.9	C-3 (**3b**)	A
129.8	129.5	C-2 (**3b**)	E
130.5	130.1	C-3 (**2**)	E
131.0		C-3 or C-2′ (**4b**)[b]	A
137.6	137.7		E
	137.9	C-1 (**3b**)	A
140.8	140.9	C-1′ (**4b**)[b]	sE
—	142.2		A
142.7	143.1	C-1 (**5b**)	A
144.7	144.8	C-1 (**2**)	sE
147.0	147.0	C-1 (**4b**)	sA
155.3	—		E

a) Shifts are given in δ_{ppm} from internal TMS; resonance frequency 25.15 MHz; TCE=1,1,2,2-tetrachloroethane, DC=*trans*-decalin; w=weak, vw=very weak, s=strong. b) Numbering of the *N*-benzyl ring: N-CH_2- 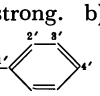

detected, which is not unreasonable due to the small amount of **6a** present and to the unknown line positions.

The ^{13}C-CIDNP results obtained on **1b** (Table 4, Fig. 4) support our findings with **1a**, although the spectrum is more complicated, since R in Scheme 2 is now $CH_2C_6H_5$. The signals of **6b** could not be assigned so far.

c) Product Analyses. A typical thermolysis of a 0.33—0.39 M solution of **1a** in decalin at 130 °C gives the following products as revealed by VPC analyses: *p*-toluidine (**2**), 38%; *N*-methyl-*p*-toluidine (**4a**), 11%; toluene (**3b**), 4%; 2,4-dimethylaniline (**5a**), 5%. The intensities of further peaks in VPC are not greater than 0.9%. Therefore, the cyclohexadienimine **6a** is formed in yields <1%. An experiment performed in 1,2-dichlorobenzene as solvent (0.33 M) showed the following product analysis: **2**, 40%; **4a**, 13%; **3b**, 2%; **5a**, 7%. Ditolylamine and bitolyl derivatives were difficult to determine by VPC; bibenzyl was not detected.

p-Azotoluene could be isolated by preparative thin-layer chromatography in 3—4% yield (thermolysis in 1,2-dichlorobenzene). Methane was determined volumetrically together with nitrogen evolved. Provided that 96—97% of the theoretical amount[9a] of nitrogen is formed, the yield of methane can be calculated to be about 44—45% (in decalin) and 11—12% (in 1,2-dichlorobenzene).

d) Mechanistic Implications. Chemical Aspects: While the thermal decomposition of 1,3-diaryltriazenes has been thoroughly reported,[10] little is known on the mechanism of similar reactions of 3-alkyl-1-aryltriazenes,[11] aside from kinetic measurements and a study of gaseous products.[9b] All the results of our present work appear to be well interpreted in terms of Scheme 2; the tautomeric form **1′** decomposes to give *p*-tolylaminyl-methyldiazenyl radical pair. Elimination of nitrogen molecule from the latter component of the pair should be very facile ($\geq 10^7$—10^9 s^{-1}) and leads to *p*-tolylaminyl-alkyl radical pair IV $\overline{p\text{-}CH_3\text{-}C_6H_4\text{-}NH\cdot}$ $\cdot\overline{R}$. There are three positions available for the *p*-tolylaminyl radical to cage-recombine with the alkyl radical as shown in Scheme 3 by the canonical structure of the former. The first one should lead direct to *N*-alkyl-*p*-toluidine **4**. The other two are expected to

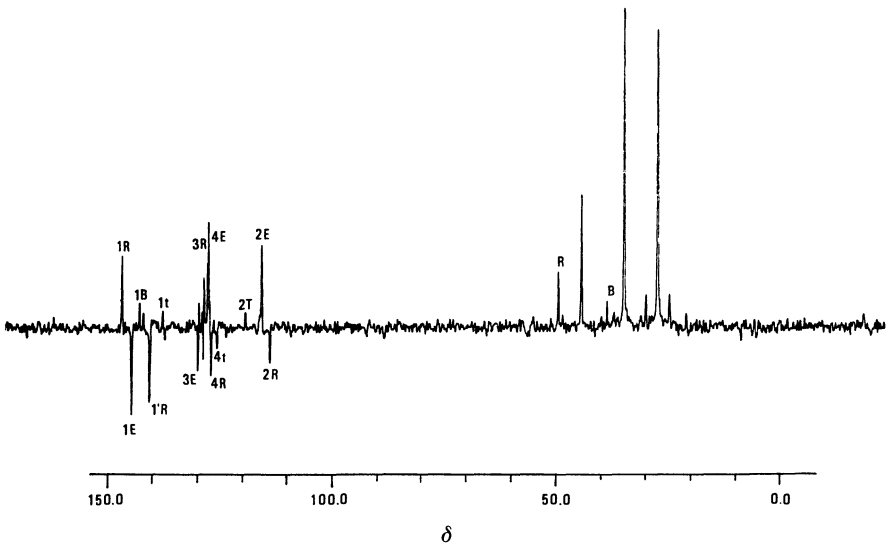

Fig. 4. ^{13}C-CIDNP spectrum (25.15 MHz PFT) of a decomposing solution of 3-benzyl-1-*p*-tolyltriazene **1b** in decalin at 125 °C.

give the corresponding cyclohexadienimines **6** and **10**. The 2-alkyl-4-methyl derivative out of these two appears to be susceptible to 1,3-prototropy under the experimental conditions to form 2-alkyl-4-methylaniline **5** as the final product. This 1,3-prototropy must be much faster than the relaxation time (spin-lattice) of the protons.[12] Thus the memory of polarization in pair IV is transferred to the rearranged **5**, while the steady-state concentration of **10** is considered too low to be detected by NMR even if intensities of their signals might be enhanced by CIDNP.

p-Tolyl-alkylaminyl radical pair II $\overline{p\text{-}CH_3\text{-}C_6H_4\cdot \cdot NHR}$ in Scheme 1 cannot explain the formation of

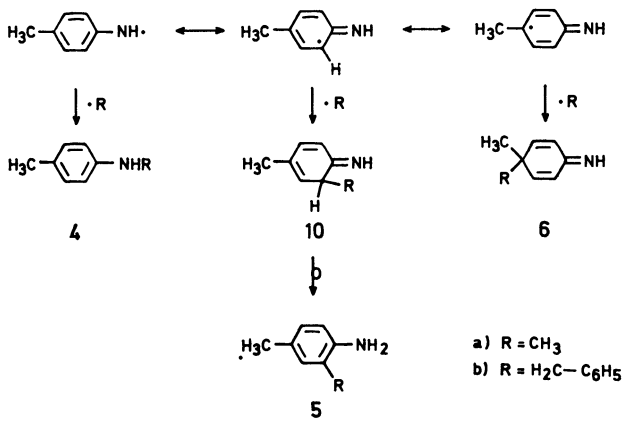

Scheme 3.

these two recombination products (**5** and **10**). The predominant formation of *p*-toluidine **2** instead of toluene in thermolysis of **1a** as one of the escape products is also consistent with Scheme 2. Our mechanistic interpretation that **1** decomposes *via* its tautomeric 1-alkyl-3-aryltriazene form **1'** is further supported by the thermal stability of 1-*p*-tolyl-3,3-dimethyltriazene which decomposes only at 245—250 °C[3] in contrast to 120—130 °C of **1**. The formation of a more stable arylaminyl radical as compared to methylaminyl radical is considered to be a driving force of the reaction going by way of **1'**. The thermochemically calculated N–H bond dissociation energies of aniline and methylamine are 92.3 and 97.8 (105.0 observed) kcal/mol,[13] respectively, supporting the above explanation.

The formation of toluene in 2—5% yield (as compared to 36—38% of *p*-toluidine **2** in thermolysis of **1a**) might indicate the small contribution of Scheme 1 to these reactions; toluene could then be formed by escape of *p*-tolyl radicals from the cage II $\overline{p\text{-}CH_3\text{-}C_6H_4\cdot \cdot NHCH_3}$ followed by abstraction of the hydrogen atom from solvents. On the other hand, we have precedents for the formation of arenes either by the following induced decomposition reaction of triazenes[14a]

$$Ar\text{-}N{=}N\text{-}NRR' + Et_3Sn\cdot \longrightarrow Ar\cdot + N_2 + Et_3Sn\text{-}NRR'$$

$$Ar\cdot + Et_3SnH \longrightarrow Ar\text{-}H + Et_3Sn\cdot$$

or by the thermolysis[14] of a pentaza-1,4-diene[Ar–N=N–N(CH_3)–N=N–Ar] which could be formed under the reaction conditions.

Discussion on CIDNP: According to the theory of S-T_0 transitions in the radical pair models of CIDNP,[15] the sign of polarization is given by $\mu\cdot a_i\cdot \Delta g\cdot \varepsilon$, where Δg is the difference in the *g* factors in the radical pair, a_i is the hyperfine coupling constant of ^1H and ^{13}C of interest, μ is minus for singlet precursors and plus for triplet and random phase reactions, and ε is taken as

Table 5. Isotropic hyperfine coupling constants; signs as determined by CIDNP

Radical	Nucleus	*a*-Values [G] Experimental	Calculated	Signs determined by CIDNP
$CH_3\cdot$	H	23.0[17]	(−)23.0[a]	−
	C	38.3[18]	(+)38.5[a]	+
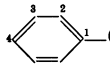	H-2	5.13[21]	− 6.31[22]	−[b]
	H-3	1.77[21]	+ 3.55[22]	
	H-4	6.17[21]	− 5.54[22]	
	H-5	16.34[21]	− 16.72[22]	−
	C-1	14.45[23]	− 12.33[22]	−
	C-2		+ 11.64[22]	+[c]
	C-3		− 8.52[22]	−
	C-4		+ 10.42[22]	+
	C-5	24.45[23]	+ 32.30[22]	+
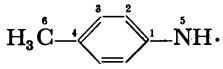	H-2	6.0[d]	− 5.43[d]	−
	H-3	2.1[d]	+ 3.09[d]	+
	H-5	14.0[d]	− 20.46[d]	
	H-6		+ 5.2[e]	+
	C-1			−
	C-2			+
	C-3			−
	C-4			+
	C-6			+

a) Calculated values taken from Ref. 18, signs taken from Ref. 15. b) Average of H-2, H-3, H-4, the signals of which coincide. c) CIDNP signals coincide with those of other C-atoms. d) The values of the unsubstituted phenylaminyl radical taken from Ref. 17. e) Estimated from $\rho^{\pi}_{C-4}=0.179$ in Ref. 17.

plus for cage recombination and minus for escape products. In $\overline{p\text{-}CH_3C_6H_4NH\cdot\cdot R}$ the arylaminyl radical has a larger g value (*ca.* 2.0030[16,17]) than the alkyl counterpart $R\cdot$ ($g_{CH_3}=2.0026$,[18] $g_{CH_2-H_5C_6}=2.0025$[17]). The pertaining hyperfine coupling constants available from literature ESR data and/or estimated from calculations are summarized in Table 5.

The sings for $\cdot CH_3$, and $H_3CC_6H_4NH\cdot$ (thermolysis of **1a**) derived from CIDNP correspond nicely to the calculated ones (Table 5), thus providing an experimental proof for the sign of hfs which can otherwise be difficult to determine experimentally.[19] To the best of our knowledge, the sings and values of a_i for *p*-tolylaminyl itself do not appear to have been determined by other methods.[20]

The observed proton enhanced absorption and carbon emission for *methane* are due to opposite a_i sign (negative for hydrogen and positive for carbon) in the methyl radical. When CIDNP signal is emission in *p*-toluidine **2**, the corresponding nucleus in *N*-methyl-*p*-toluidine **4a** shows a signal of enhanced absorption. The contrasting sign inversion of polarization is interpreted in terms of recombination *vs.* escape products: different sign in ε. The positional sign alternation clearly demonstrated in C-1 through C-4 of **2** and **4a** corresponds to sign alternation in the hyperfine coupling as shown in Table 5.

While *N*-methyl-*p*-toluidine **4a**, 2,4-dimethylaniline **5a** and 4,4-dimethylcyclohexa-2,5-dien-1-imine **6a** which are considered to be derived from the same cage are formed in a ratio of about 1 : 0.5 : 0.08, the observed relative intensities of their proton emission signals due to the entering methyl group are 1 : 9.3 : 2.6. This means that the enhancement factor for the *N*-methyl group of *N*-methyl-*p*-toluidine should be unduly small. The trend may be ascribed to smaller T_1 value of these protons due to quadrupole relaxation by the nitrogen atom.

The toluene formed from **1a** shows clear-cut CIDNP (emission) only of C-4. This would be compatible with Scheme 1, since only C-1 (this position is C-4 in toluene) of *p*-tolyl has a large (positive) a_i value.[24] A weak enhanced absorption, sometimes observed for the methyl protons, may be also explained by a *p*-tolyl σ-radical ($a_{CH_3}=2.4$ G[25]). The *delayed emission* for the aromatic protons of toluene in 1,1,2,2-tetrachloroethane (TCE) may be considered as being derived from a secondary decomposition reaction of the intermediately formed azo compounds, *e.g.* $p\text{-}CH_3C_6H_4\text{–}N{=}N\text{–}X$ in which X will be a fragment or some combination of TCE employed as a solvent. The polarized methyl chloride observed in TCE must also emanate from a secondary pair, since simple chlorine abstraction by polarized methyl radicals escaped from pair IV should result in the opposite CIDNP sign.

The hyperfine signs derived from the CIDNP observed in the thermolysis of **1b** again support Scheme 2 with respect to *p*-tolylaminyl and benzyl radicals (Table 5). Only an effective sign of averaged hyperfine coupling can be obtained on the ring protons of the benzyl radical since these protons show singlets in the products, **4b**, **5b**, and **8**. There is a deviation, however, for the aromatic protons of the later-appearing toluene. Applying the Kaptein rules, one would expect from the observed emission an average plus sign for the a_i values of H-2, H-3, H-4 of benzyl. However, according to the MO calculations (Table 5) and the observations on **4b**, **5b**, and **8**, the overall sign should be negative. A

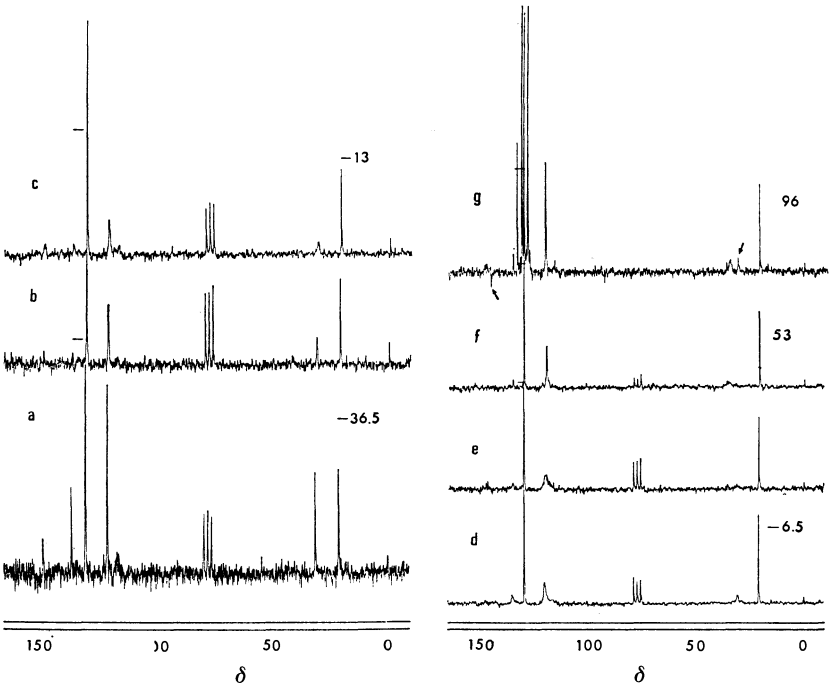

Fig. 5. ^{13}C-NMR spectra (20.1 MHz) of 3-methyl-1-*p*-tolyltriazene **1a** in $CDCl_3$ at various temperatures: (a)—(f) in $CDCl_3$ and (g) in *o*-dichlorobenzene.
The arrows in (g) show CIDNP signals already coming out.

reasonable explanation stems from the fact that the above mentioned effect can be observed only in TCE. Obviously in this solvent some of the reaction products (*e.g.* **3b**) can be formed *via* different pathways (see also discussion of methyl chloride formation in thermolysis of **1a** in TCE). In the reaction path *via* pair IV (R= CH_2Ph) especially the nuclei in the recombination products **4b** and **5b** and in bibenzyl **8** are polarized, whereas in some other reaction (not involving the benzyl radical) the ring protons of the later-formed toluene are polarized preferentially. One candidate for a radical component in such a pair would be the *p*-tolyl radical (ring proton hfs signs expected to be >0; ring carbon hfs signs the same as in the benzyl radical).[24]

e) Tautomerism in ***1a*** The occurrence of tautomerism in **1a** assumed to account for the chemical product formation and CIDNP in the thermolysis of this compound has been independently confirmed by IR-[26] and ^{1}H-NMR[27] spectroscopy. An additional support has been obtained in this work by the temperature dependent ^{13}C-NMR spectra. As shown in Fig. 5, all the ^{13}C signals (due to **1a**) are sharp at −36.5 °C in $CDCl_3$ and consistent with structure **1a**, namely, 1-*p*-tolyl-3-methyltriazene. The singlets due to *N*-CH_3, C-1, C-2, and C-4 start to broaden at about −25 °C. This broadening is so effective that *N*-methyl and C-1 carbons cannot be seen at 2—53 °C. Only the singlet at δ 129.4 due to C-3 remains constant in its peak height. The *N*-methyl signal becomes again observable at temperatures only higher than 60 °C. The position is, however, shifted to the lower field by 3.9 ppm, indicating the enhanced rate of prototropy and increase in the population of tautomeric 1-methyl-3-*p*-tolyltriazene structure **1a'** at higher temperatures. Closer inspection of the spectrum at −36.5° (Fig. 5) reveals that there is an additional weak singlet at δ 54.0 which could be due to *N*-methyl carbon of **1a'**. In the case of the signal of C-2 (120.0 ppm) we note at −36.5 °C a "satellite" of very low intensity on the highfield side (115.6 ppm) which might be attributed to C-2 of **1a'**. At about 2 °C the two signals coalesce and at 53 °C we observe the fast exchange singlet at 119.1 ppm.

f) CIDNP, its Advantages and Limitation in Mechanistic Studies. ^{1}H- and ^{13}C-CIDNP investigations have shown that triazenes **1** may thermolyse *via* the tautomeric form **1'** and that radical pairs like IV can be intermediates, thus qualitatively proving the conclusions drawn from chemical product analysis. It is even possible to give the hfs signs of carbon and hydrogen atoms of *p*-tolyl-aminyl unambiguously, although no ESR spectrum of this radical has been measured.

New reaction paths, hitherto not taken into account,[9] *e.g.* formation of **5** and **6**, were discovered. One of these compounds, **6**, still resists chemical isolation and separate preparation untill the present day. On the other hand, the CIDNP technique of a level employed in this study does not necessarily give quantitative account of the decomposition of all the triazene molecules. The chemical product analyses of the thermolysis of **1a** show a large excess of "escape" products, **2** and **3a**, over the "recombination" products **4a**, **5a**, **6a**. The formation of methane **3a** (0.33 M solution of **1a**) depends a great deal on the solvent used: 46% (in decalin) and 12% (in tetrachloroethane). This effect has also been found for other 3-alkyl-1-aryltriazenes in solvents of the corresponding hydrogen donating ability.[9b] The amount of *p*-toluidine **2** does not differ much in decalin and tetrachloroethane. This indicates that a part of the reaction might proceed *via* ionic pathways induced by traces of water or acid present in the system.[27,28]

We would like to add that, whereas it is difficult to interpret our CIDNP data in terms of pair III only, we were not able to disclose the positive role of the methyldiazenyl radical in Scheme 2. If there is an internal return to **1'** by recombination, it is usually the case in which CIDNP is detected in the starting material as exemplified by the photolysis of phenylazocumene.[29] Our failure to detect CIDNP in the starting material may be due to a shorter life-time of the methyldiazenyl as opposed to the phenyldiazenyl radicals. Either prototropic tautomerism in the starting materials (*vide supra*) or quadrupole relaxation due to the nitrogen atoms could also be responsible for making the possible CIDNP effect in **1** obscure.[30]

We wish to thank the Japan Society for the Promotion of Science and Deutscher Akademischer Austauschdienst for the awards of visiting professorship to A. R. (1973 in Tokyo) and to H. I. (1974 in Tübingen), respectively. The cooperative research reported here was made possible through grants from the Ministry of Education, Science and Culture of Japan and from Founds der Chemischen Industrie.

References

1) CIDNP. IV. For part III of the series see: S. Berger, S. Hauff, P. Niederer, and A. Rieker, *Tetrahedron Lett.*, **1972**, 2581. See also: H. Iwamura, Y. Imahashi, K. Kushida, K. Aoki, and S. Satoh, *Bull. Chem. Soc. Jpn.*, **49**, 1690 (1976).

2) H. Zollinger, *Acc. Chem. Res.*, **6**, 335 (1975); A. Rieker, P. Niederer, and D. Leibfritz, *Tetrahedron Lett.*, **1969**, 2487; A. Rieker, *Ind. Chim. Belg.*, **36**, 1078 (1971); A. Rieker, P. Niederer, and H. B. Stegmann, *Tetrahedron Lett.*, **1971**, 3873.

3) A. Rieker, P. Niederer, and K. -M. Dangel, *Chem. Ber.*, **109**, in press (1976).

4) O. Dimroth, *Ber.*, **38**, 2328 (1905).

5) E. Bamberger and P. Wulz, *Ber.*, **24**, 2077 (1891).

6) R. E. Davies, H. T. Openshaw, F. S. Spring, R. H. Stanley, and A. R. Todd, *J. Chem. Soc.*, **1948**, 295.

7) The chemical shift values of the corresponding methyl protons are δ 1.15 and 1.28 in structurally analogous 1-methylene-4,4-dimethylcyclohexa-2,5-diene [*cf.* H. E. Zimmerman, P. Hackett, D. F. Juers, J. M. McCall, and B. Schröder, *J. Am. Chem. Soc.*, **93**, 3653 (1971)] and 4,4-dimethylcyclohexa-2,5-dienone (this study), respectively.

8) Formulae and numbers of compounds are given in Table 1.

9) a) In the thermolysis of 1-phenyl-3-methyltriazene in cumene at 120 °C, 97.5% of N_2 was evolved; see: B. A. Dolgoplosk, B. L. Erusalimskiĭ, V. A. Krol, and L. M. Romanov, *Zh. Obshch.*, **24**, 1775 (1954); *Chem. Abstr.*, **49**, 12339c (1955); b) A. Cserhegyi, G. Szent-Györgyi, and O. Dobis, *Magy. Kém. Foly.*, **77**, 607 (1971).

10) F. Heusler, *Justus Liebigs Ann. Chem.*, **260**, 227 (1890);

G. T. Morgan and L. P. Walls, *J. Chem. Soc.*, **1930**, 1502; H. Fischer, *Z. Naturforsch., Teil A*, **23**, 2109 (1968); E. Lippmaa, T. Saluvere, T. Pehk, and A. Olivson, *Org. Magn. Reson.*, **5**, 339, 429 (1973).

11) S. V. Rykov and A. V. Kessenikh, Paper presented at the International Symposium on Chemically Induced Dynamic Polarisation of Nuclei and Electrons, Tallinn, Estonia USSR, August 13—16, 1972.

12) For the fast rearrangement of 2,4-cyclohexadien-1-imines into *o*-semidines, see: P. Welzel, C. Dietz, and G. Eckhardt, *Chem. Ber.*, **108**, 3550 (1975).

13) J. D. Cox and G. Pilcher, "Thermochemistry of Organic and Organometallic Compounds," Academic Press, London (1970).

14) a) J. Hollaender, W. P. Neumann, and G. Alester, *Chem. Ber.*, **105**, 1540 (1972); b) H. Minato and M. Oku, *Bull. Chem. Soc. Jpn.*, **38**, 1529 (1965).

15) A. R. Lepley and G. L. Closs, "Chemically Induced Magnetic Polarization," John Wiley & Sons, New York, London, Sydney, Toronto (1973).

16) R. V. Lloyd and D. E. Wood, *Mol. Phys.*, **20**, 735 (1971).

17) R. V. Lloyd and D. E. Wood, *J. Am. Chem. Soc.*, **96**, 659 (1974).

18) R. W. Fessenden, *J. Phys. Chem.*, **71**, 74 (1967).

19) From a standard ESR measurement, only absolute values of isotropic hfs are determined. Recently a contact shift measurement in high-resolution NMR has been shown to give signs of hfs experimentally: I. Morishima, T. Yonezawa, and K. Goto, *J. Am. Chem. Soc.*, **92**, 6651 (1970).

20) For a review on aminyls, see: W. C. Danen and F. A. Neugebauer, *Angew. Chem.*, **87**, 823 (1975); *Angew. Chem. Int. Ed.*, **14**, 783 (1975).

21) P. Neta and R. H. Schuler, *J. Phys. Chem.*, **77**, 1368 (1973).

22) E. Gey, *Z. Chem.*, **14**, 279 (1974).

23) A. M. Ihrig, P. R. Jones, Il Nam Jung, R. V. Lloyd, J. L. Marshall, and D. E. Wood, *J. Am. Chem. Soc.*, **97**, 4477 (1975).

24) R. J. Hayward and B. R. Henry, *Chem. Phys. Lett.*, **20**, 394 (1973).

25) F. Barigelletti, G. Poggi, and A. Breccia, *J. Chem. Soc., Faraday Trans. 2*, **70**, 1198 (1974).

26) D. Hadži and J. Jan, *Spectroscopy Lett.*, **1**, 139 (1968).

27) N. S. Isaacs and E. Rannala, *J. Chem. Soc., Perkin Trans. 2*, **1974**, 899.

28) V. Ya. Andakushkin, B. A. Dolgoplosk, and I. I. Radchenko, *Zh. Obshch. Khim.*, **26**, 2972 (1956); *Chem. Abstr.*, **51**, 8674a (1957); M. Kawanishi, I. Otani, and H. Nozaki, *Tetrahedron Lett.*, **1968**, 5575; E. H. White, H. Maskill, D. J. Woodcock, and M. A. Schroeder, *ibid.*, **1969**, 1713; V. Zverina, M. Remes, J. Divis, J. Marhold, and M. Matrka, *Coll. Czech. Chem. Comm.*, **38**, 251 (1973); R. Kreher and K. Goph, *Z. Naturforsch.*, **31B**, 217 (1976).

29) N. A. Porter, L. J. Marnett, C. H. Lochmuller, G. L. Closs, and M. Shobataki, *J. Am. Chem. Soc.*, **94**, 3664 (1972).

30) In the case of phenylazosulfide decomposition, no CIDNP is observed in spite of the possible occurrence of internal recombination of the geminate radical pair (J. Brokken-Zijp and H. van de Bogaert, *Tetrahedron Lett.*, **1974**, 249.

Multifunctional Hydrolytic Catalyses. V. The Reaction of *o*-Substituted Benzohydroxamic Acids and *p*-Nitrophenyl Acetate[1]

Toyoki KUNITAKE, Yoshio OKAHATA, Reiko ANDO, and Sumio HIROTSU

Department of Organic Synthesis, Faculty of Engineering, Kyushu University, Fukuoka 812

(Received March 22, 1976)

Salicylohydroxamic acid(SHA), *N*-methylsalicylohydroxamic acid(MSHA), and *N*-methylphthalohydroxamic acid(MPHA) were prepared and their acylation reactions with *p*-nitrophenyl acetate were studied in aqueous ethanol at 30 °C. Both the acidity and nucleophilicity of the hydroxamic acid group were affected by the functional *ortho*-substituents(–OH, –COOH). In particular, the undissociated hydroxamic acid group in the MPHA monoanion possessed nucleophilic reactivity. This was brought forth by the general base assistance of the adjacent carboxylate group, as confirmed by the presence of the solvent isotope effect of $k^H/k^D=2.5$. Only the hydroxamate anion acted as the nucleophile in all other cases.

At the active site of serine proteases, the nucleophilic reactivity of the seryl hydroxyl group is enhanced by hydrogen bonding with the aspartic carboxylate *via* the histidyl imidazolyl group.[2] We prepared several catalytic compounds which possess the hydroxamate and imidazole functions as model serine proteases, and employed them for the hydrolysis of phenyl esters.[3-5] In these systems, acylation by phenyl esters occurs at the hydroxamate site without assistance of the neighboring imidazolyl groups. The latter function is involved only in the deacylation process.

The juxtaposition of two functional groups at the hydrogen-bonding distance would be advantageous for realization of the simultaneous involvement of these functional groups in a single reaction step. The two functional groups at the *ortho* position of the benzene ring can form intramolecular hydrogen bonding as in salicylic acid and phthalic acid. It should be interesting to prepare benzohydroxamic acid derivatives with *ortho*-substituents having hydrogen-bonding capacity and to investigate their catalytic behavior, in connection with the multifunctional character of the acylation process of serine proteases.

The *o*-substituted benzohydroxamic acids employed in this study are salicylohydroxamic acid (SHA), *N*-methylsalicylohydroxamic acid (MSHA), and *N*-methylphthalohydroxamic acid (MPHA). The nucleophilic reactivity of these compounds was compared with those of unsubstituted counterparts, benzohydroxamic acid (BHA) and *N*-methylbenzohydroxamic acid (MBHA).

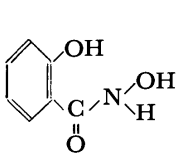

SHA

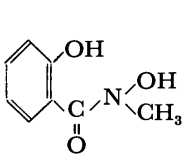

MSHA

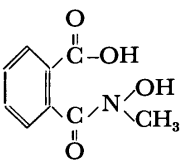

MPHA

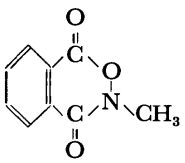

MPHA anhydride

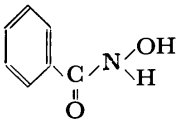

BHA

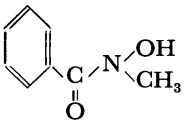

MBHA

Experimental

Materials. *p*-Nitrophenyl acetate was prepared by acylation of *p*-nitrophenol with acetic anhydride and recrystallized from cyclohexane, mp 78 °C (lit,[6] mp 81—82°C).

Salicylohydroxamic acid was prepared from salicyloyl chloride (bp 62 °C/12 mmHg) and hydroxylamine. The crude product was purified in the form of the copper chelate and then recrystallized from water, mp 161—162 °C (lit,[7] mp 169 °C).

N-Methylsalicylohydroxamic acid was similarly prepared in chloroform in the presence of triethylamine from salicyloyl chloride and *N*-methylhydroxylamine. The crude product was purified in the form of the copper chelate, and then recrystallized from water, mp 133—135 °C(lit,[7] mp 136 °C).

N-Methylphthalohydroxamic acid anhydride was synthesized as follows: 14 g (0.1 mol) of phthalic anhydride, 18 g (0.21 mol) of *N*-methylhydroxylamine hydrochloride and 23 g (0.25 mol) of triethylamine were dissolved in 300 ml of dry DMF and heated for 30 min at 100 °C. Then solvent was removed *in vacuo* and the residual oil was extracted with hot cyclohexane. Colorless flakes separated upon cooling, mp 120 °C. Yield, 40—60%. Found: C, 61.10; H, 3.98; N, 8.01%. Calcd for $C_9H_7NO_3$: C, 61.02, H, 3.98; N, 7.91%.

Determination of pK_a. The pK_a values for the hydroxyl and hydroxamic acid groups were determined by the potentiometric titration and the UV spectrophotometric titration at 0.1 M KCl, 30 °C in 28.9 v/v% EtOH–H_2O.

The pK_a value of the hydroxamic acid group of SHA was determined by the potentiometric titration of 0.01 M SHA with 0.1 M NaOH, using Eq. 1.

$$pK_a = pH + \log\frac{1-\alpha}{\alpha} \quad (1)$$

where α is the degree of dissociation. The pK_a value of the hydroxyl group in SHA was determined by UV spectrophotometric titration at 330 nm, using Eq. 2.

$$pK_a = pH + \log\frac{OD_I - OD}{OD - OD_M} \quad (2)$$

where OD_M and OD_I are absorbances at 330 nm of the undissociated and dissociated phenolic hydroxyl groups, respectively, and OD is the absorbance (330 nm) at a given pH. OD_I was obtained by extrapolation of OD values at pH 10—12[5,8] and OD_M was obtained at pH 9: $OD_I=0.516$ and $OD_M=0.290$.

The two pK_a values for MSHA were similarly determined using OD_I (330 nm)=0.506 and OD_M (330 nm)=0.480.

The pK_a of the hydroxamic acid group of MPHA was determined by the potentiometric titration (Eq. 1). The

pK_a of the carboxylic acid group could not be determined by the conventional procedure, because MPHA was readily hydrolyzed to phthalic acid at pH<6. The $pK_{a,HA}$ of MPHA in the deuterated solvent was determined by potentiometric titration in 28.9 v/v% EtOD-D_2O at 30 °C, μ=0.1 with 0.1 M KOH in D_2O: $pK^D_{a,HA}$=9.80±0.15. The pD values were taken as the pH meter readings plus 0.40 at 30 °C.[9]

Rate Measurements. The reaction of PNPA with hydroxamic acids was carried out in the presence of large excesses of the latter, and the formation of *p*-nitrophenolate anion was followed at 401 nm. The reactions obeyed the pseudo-first-order kinetics. The rate constant k_{total} was determined from absorbances of *p*-nitrophenolate at time *t*, OD_t, and at the infinite time, OD_∞. When the reaction was slower, k_{total} was obtained from Guggenheim plots[10] of up to 2—3 half-lives. The apparent second-order rate constant of acylation, $k_{a,obsd}$ was calculated from the rate constants of total and spontaneous hydrolyses.

$$k_{a,obsd} = \frac{k_{total} - k_{spont}}{[HA]_T} \quad (3)$$

where $[HA]_T$ is the total concentration of hydroxamic acids. The hydrolysis condition is 28.9 v/v% EtOH-H_2O, 30 °C, μ=0.1 (KCl) and pH 6.5—9.5. Phosphate, Tris, and Barbital buffers were used.

The reaction of MPHA and PNPA in the deuterated medium was studied at 30 °C, μ=0.1 (KCl), pD 7.1—9.2 in 28.9 v/v% EtOD-D_2O. The buffer solution was prepared from sufficiently dried Tris and commercial 30% DCl in D_2O.

Instruments. Electronic spectra were obtained with a Hitachi 124 UV-visible spectrophotometer equipped with a thermostated cell compartment. A Toa digital pH meter (Model HM-15A) was employed for the pH measurement, and a Toa pH stat system was used for the potentiometric titration. The reaction rates were calculated using a programmable desk calculator Compet 364P. The least-squares method was used wherever possible. The correlation coefficient was better than 0.99 unless stated otherwise.

Results

pK_a Values. The pK_a value of the hydroxamic acid group is considerably influenced by the *ortho*-substituent, as summarized in Table 1. The $pK_{a,HA}$ value of SHA, 7.90, is lower than that of benzohydroxamic acid by 1.45 pK_a units. This is attributable to the stabilization of the monoanionic species SHA^- by the intramolecular hydrogen bonding, as already considered in order to explain the pK_a difference between the carboxyl groups of salicylic acid and benzoic acid ($pK_{a,COOH}$=2.98 and 4.21 respectively, in water, 25 °C)[11] The $pK_{a,OH}$ value of SHA, 10.3, is close to those of phenol and *m*-hydroxybenzoic acid (9.95 and 9.74, respectively, in water, 25 °C),[12] in spite of electrostatic repulsion of the neighboring hydroxamate anion. This may be explained by the stabilization of the dianionic species due to hydrogen bonding. In accord with this view, $pK_{a,OH}$(=12.7) for MSHA which cannot form hydrogen bonding is much higher and is close to that of salicylic acid ($pK_{a,OH}$=13.0[13] in

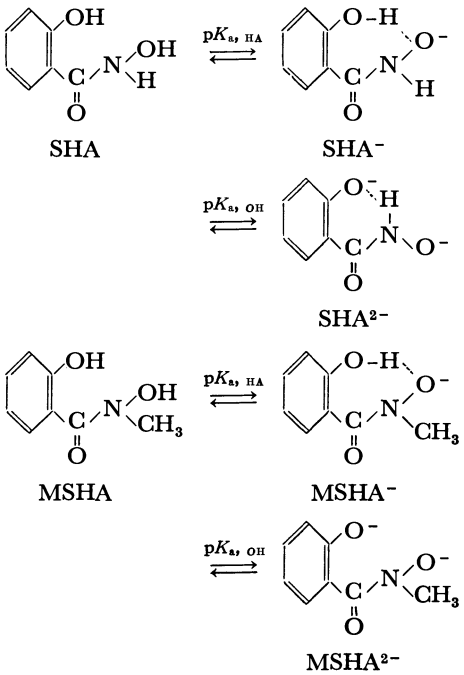

(4) (5)

Table 1. Acid dissociation constants and rate constants of acylation[a]

Benzohydroxamic acid	Substituent[b]	pK_a[c]	k_a $M^{-1}s^{-1}$
BHA[d]	R=H, X=H	HA: 9.35 (PT)	50.0
SHA	R=H, X=OH	HA: 7.90±0.07 (PT); OH: 10.3 ±0.1 (UV)	k_A-= 4.85; $k_{A^{2-}}$=60
MBHA	R=CH_3, X=H	HA: 8.59[e]	16[f]
MSHA	R=CH_3, X=OH	HA: 6.70±0.09 (PT); OH: 12.7 ±0.3 (UV)	0.080
MPHA	R=CH_3, X=COOH	HA: 9.50±0.07 (PT)[g]; COOH: <4	k_{HA}= 0.22; k_A-=10.8

a) 28.9 v/v% EtOH-H_2O, 30 °C, μ=0.1 (KCl). b) 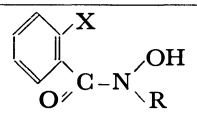 c) HA; hydroxamic acid group. OH; phenol group. COOH; carboxylic acid group. PT; pK_a determined by potentiometric titration. UV; pK_a determined by UV spectrophotometric titration. d) from Ref. 5 e) from Ref. 14. f) Condition: 25 °C, 12 v/v% EtOH-H_2O, μ=0.08. Estimated from the data of Ref. 16. g) $pK^D_{a,HA}$ μ=9.80±0.15 in 28.9 v/v% EtOD-D_2O, 30 °C, μ=0.1 (KCl).

water, 25 °C). The lower $pK_{a,HA}$ value of MSHA relative to that of MBHA (6.70 and 8.59,[14] respectively) again suggest the hydrogen-bonding stabilization of the monoanionic species.

The higher $pK_{a,HA}$ value of MPHA relative to that of MBHA (9.50 and 8.60, respectively) may be caused by stabilization of the monoanionic species by the intramolecular hydrogen bonding or by the electrostatic repulsion in the dianionic species.

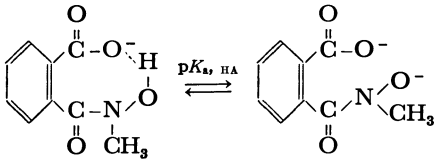

(6)

Hydrolysis of MPHA Anhydride. MPHA anhydride is readily converted to the ring-opened derivative, MPHA, in acidic and alkaline solutions. Furthermore, MPHA is easily hydrolyzed to phthalic acid at pH<*ca.* 6 due to the general acid catalysis of the neighboring carboxyl group. This hydrolysis is complete in less than 3 h at pH 4.5, 30 °C. The MPHA anhydride shows an absorption maximum at 294 nm (ε=2520) in CH_3CN. The ring-opened product gives ε=230 at 294 nm, pH 8.57. The absorbance difference at 294 nm was used to follow the ring opening reaction, and the apparent first-order rate constant was calculated from the ordinary first-order plot. The experiments carried out at four concentrations of MPHA anhydride (1.0, 2.0, 3.0, and 4.0×10^{-4} M) gave the following rate constant: $k_{obsd}=(1.89\pm0.04)\times10^{-2}$ s^{-1} in 1.4 v/v% CH_3CN–H_2O, 30 °C, μ=0.1 (KCl), pH 8.57, 0.1 M Tris buffer.

Reaction of PNPA with o-Substituted Benzohydroxamic Acids. The reactions of PNPA (10^{-4} M) with *o*-substituted benzohydroxamic acids (10^{-2}—5×10^{-4} M) were carried out in 28.9 v/v% EtOH–H_2O in the pH range of 6.5 to 9.5.

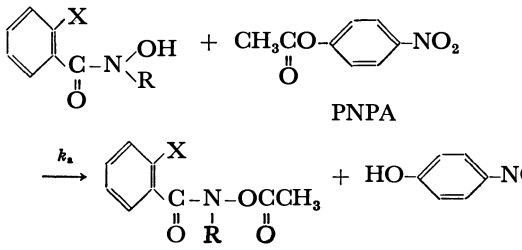

(7)

The apparent second-order rate constant $k_{a,obsd}$ was calculated according to Eq. 3. The pH-rate profiles are given in Fig. 1. If the hydroxamate anion is the only nucleophile, the profile is composed of an ascending limb (slope=1) and a plateau. However, this is not the case for most of the *o*-substituted benzohydroxamic acids. These anormal behavior is more clearly seen in the plot of $k_{a,obsd}$ against α_{HA} (degree of dissociation of hydroxamic acid) given in Figs. 2 and 3.

In Fig. 2, the plots for BHA give a straight line which passes the origin. This indicates that the hydroxamate anion acts as the nucleophile, as have been shown for a variety of simple hydroxamic acids.[15–18] On the other hand, the plots for SHA give a linear relation up to

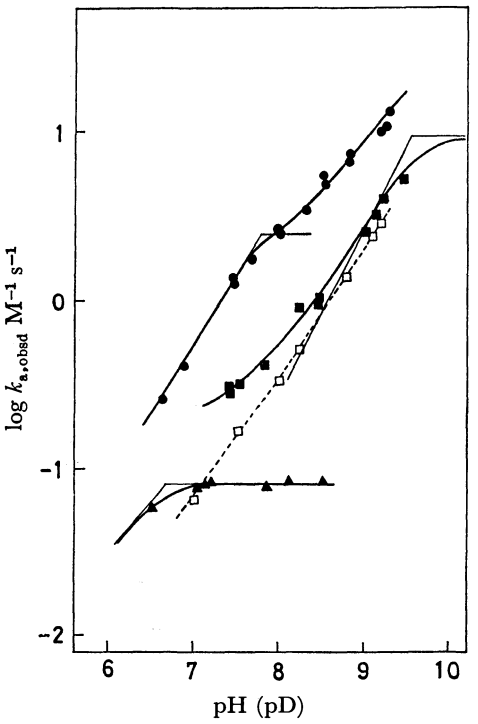

Fig. 1. pH-rate profile of the reaction of PNPA with *o*-substituted benzohydroxamic acids. Reaction Condition; 30 °C, μ=0.1 (KCl) in 28.9 v/v% EtOH–H_2O ●; SHA, ■; MPHA, ▲; MSHA in 28.9 v/v% EtOD–D_2O □; MPHA.

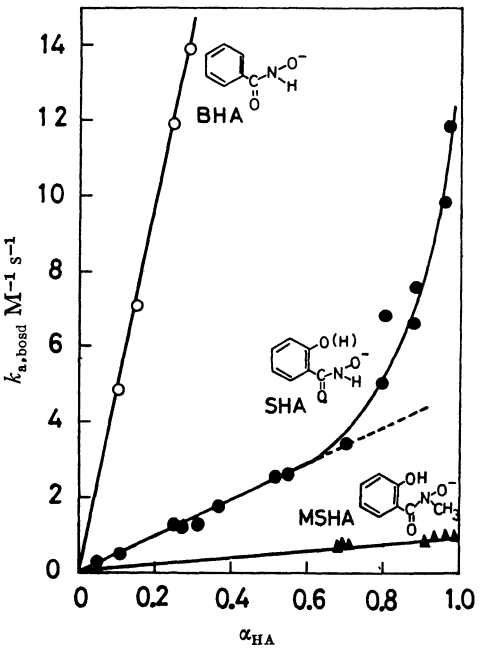

Fig. 2. Reaction of PNPA with some hydroxamic acids. Reaction condition: 28.9 v/v% EtOH–H_2O, 30 °C, μ=0.1 (KCl), 0.15 M Barbital buffer.

$\alpha_{HA}\approx0.5$, and then show a steep rise. The slope of the steeper portion is close to that of BHA.

SHA can exist in three forms: neutral, monoanionic and dianionic species (Eq. 4). Since the linear portion of the $k_{a,obsd}$–α_{HA} relation passes the origin, the neutral species cannot be reactive, and the apparent

rate constant will be composed of the monoanionic and dianionic terms as follows:

$$k_{a,obsd} = k_{A^-}\left[\frac{\alpha_{HA}(1-\alpha_{OH})}{1-\alpha_{OH}(1-\alpha_{HA})}\right] + k_{A^{2-}}\left[\frac{\alpha_{HA}\cdot\alpha_{OH}}{1-\alpha_{OH}(1-\alpha_{HA})}\right] \quad (8)$$

where k_{A^-} and $k_{A^{2-}}$ are second-order rate constants for the monoanionic and dianionic species, respectively. α_{HA} and α_{OH} are degrees of dissociation of the hydroxamic acid and phenol groups, respectively.

The solid curve for SHA was calculated from Eq. 8 using pK_a values of Table 1 and by assuming appropriate k_{A^-} and $k_{A^{2-}}$ values. The best fit with the experimental data was obtained for $k_{A^-}=4.85\ M^{-1}\ s^{-1}$ and $k_{A^{2-}}=60\ M^{-1}\ s^{-1}$.

A similar situation may as well exist for MSHA. However, the $k_{a,obsd}-\alpha_{HA}$ relation for this hydroxamic acid is simple as shown in Fig. 1. This is explained by the fact that $pK_{a,OH}$ of MSHA is rather high (12.7) and that the dianionic form is virtually nonexistent in the pH range employed (pH 6.5—8.5). The k_{A^-} value calculated from the slope is $0.080\ M^{-1}\ s^{-1}$.

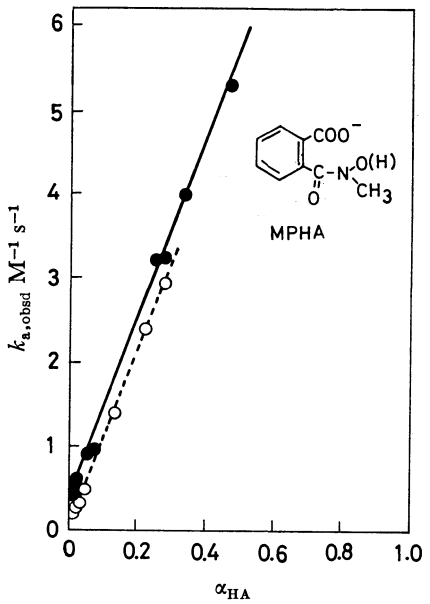

Fig. 3. Reaction of PNPA with MPHA. Reaction condition; 30 °C, μ=0.1 (KCl)
●; 28.9 v/v% EtOH–H_2O, 0.15 M Tris
○; 28.9 v/v% EtOD–D_2O, 0.1 M Tris

Figure 3 gives $k_{a,obsd}-\alpha_{HA}$ relations for MPHA in undeuterated and deuterated media. Two linear relations are obtained with different intercepts. The fact that positive intercepts were observed suggests that the undissociated hydroxamic acid possesses nucleophilic reactivity. Since the concentration of the neutral MPHA species is negligible based on the estimated $pK_{a,COOH}$ value (see Table 1), the apparent rate constant is given by

$$k_{a,obsd} = k_{A^-}\cdot\alpha_{HA} + k_{HA}(1-\alpha_{HA}) \quad (9)$$

where k_{A^-} and k_{HA} are second-order rate constants for $MPHA^{2-}$ and $MPHA^-$ species, respectively (Eq. 6).

The k_{A^-} and k_{HA} values were calculated using the slopes and intercepts of the linear relations, and the deuterium solvent kinetic isotope effects were calculated as listed in Table 2.

Table 2. Deuterium solvent isotope effects in the reaction of PNPA with MPHA[a]

	Solvent: 28.9 v/v% EtOH–H_2O	Solvent: 28.9 v/v% EtOD–D_2O	k^H/k^D
k_{A^-}[b]	$10.8\ M^{-1}\ s^{-1}$	$10.6\ M^{-1}\ s^{-1}$	1.0
k_{HA}[b]	$0.22\ M^{-1}\ s^{-1}$	$0.088\ M^{-1}\ s^{-1}$	2.5

a) 30 °C, μ=0.1 (KCl), 0.1 M Tris buffer b) Calculated from Eq. 9.

Discussion

Acyl Transfer to Undissociated Hydroxamic Acid. The kinetic data summarized in Table 2 indicate that the monoanionic species of phthalohydroxamic acid, $MPHA^-$, possess nucleophilic reactivity toward PNPA. The following monoanionic species cannot be kinetically distinguished.

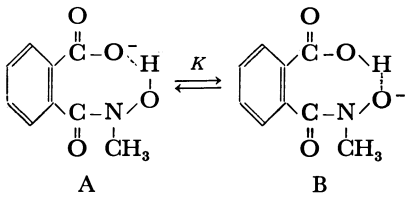

(10)

The reaction rates for species A and B are given, respectively, by

$$v_A = k_A[A][PNPA] \quad (11)$$

$$v_B = k_B[B][PNPA] = k_BK[A][PNPA] \quad (12)$$

where k_A and k_B are second-order rate constants for the respective species and K is the equilibrium constant.

pK_a of *N*-methylbenzohydroxamic acid is 4—5 pK_a units higher than that of benzoic acid,[12] and a similar pK_a difference may be expected for the first ionizations of the two functional groups of MPHA. Then, K is estimated to be 10^{-4}—10^{-5}. If species B is solely responsible for the observed rate constant ($k_{HA}=0.22\ M^{-1}\ s^{-1}$), k_B must be as large as 2000—20000 $M^{-1}\ s^{-1}$. This value is too large for a nonmicellar hydroxamate anion.[19] Furthermore, if species B is the effective nucleophile, the observed isotope effect must arise from the general acid catalysis of the neighboring carboxylic acid. This is unlikely for a substrate with good leaving group (PNPA).

These arguments now establish species A as the effective nucleophile. The carboxylate-catalyzed cleavage of PNPA in unlikely, since its second-order rate constant is estimated to be *ca.* $10^{-6}\ M^{-1}\ s^{-1}$.[21] Therefore, the observed reactivity is explained as the nucleophilic attack of the undissociated hydroxamic acid assisted by the general base catalysis of the *ortho*-carboxylate group (**1**).

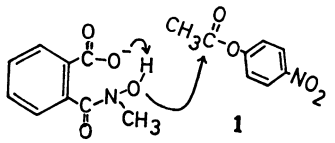

1

The solvent isotope effect observed ($k^{H}_{HA}/k^{D}_{HA}=2.5$, Table 2) is consistent with this mechanism. Although the observed isotope effect is by itself consistent with the direct general base catalysis of the carboxylate anion and buffer bases, this mechanism cannot explain the observed rate constant. The magnitude of this isotope effect is similar to that ($k^{H}/k^{D}=2.28$) found by Kirby and Lloyd for the general base catalysis of the neighboring carboxylate group in the hydrolysis of 2-carboxyphenyl 4-hydroxybutyrate (**2**).[22]

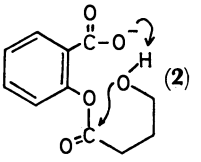
(2)

The solvent isotope effect was not observed for the reaction of the dianionic species, $MPHA^{2-}$, in agreement with the simple nucleophilic mechanism for the hydroxamate anion.

To our knowledge, the above mechanism (**1**) is the first example of the *intermolecular*, concerted nucleophilic attack on the ester carbonyl group. The reaction of simple hydroxamate anions with phenyl esters have been investigated extensively.[15-18] In all these cases, it was confirmed that only the anionic species were effective nucleophiles. This was also the case with bifunctional catalysts which contain hydroxamic acid and imidazole group[3,4,5,23,24] Apparently, the presence of the intramolecular hydrogen bonding as inferred from the pK_a data must render the concerted action more feasible.

Acyl Transfer to Hydroxamate Anion. It should be interesting to see how the *ortho*-substituent affects the reactivity of the hydroxamate anion. This question may be discussed in terms of the Brønsted relation. The Brønsted relation has been shown to hold true for several classes of hydroxamic acids.[15,17,26]

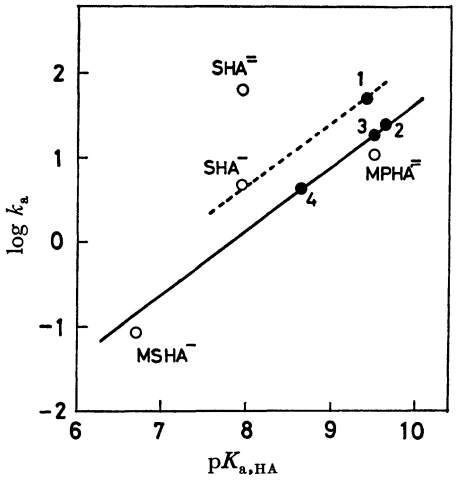

Fig. 4. Brønsted plots for the reaction of hydroxamic acids with PNPA.
Reaction condition; 30 °C, 28.9 v/v% EtOH–H_2O, μ=0.1 (KCl).
1; BHA, 2; *N*-phenylisobutyrohydroxamic acid, 3; *N*-benzylbenzohydroxamic acid, 4; *N*-methyl-α-naphthohydroxamic acid.

The solid line in Fig. 4 is obtained for several *N*-substituted hydroxamic acids with no additional functional groups and is given by

$$\log k_a = 0.68pK_a - 4.8 \quad (13)$$

The slope is the same as that reported by Hershfield and Bender[26] for some other *N*-substituted hydroxamic acids under a somewhat different condition. The plots for two *N*-methylhydroxamate anions, $MPHA^{2-}$ and $MSHA^{-}$, are located very close to this relation. The broken line is a tentative Brønsted relation for *N*-unsubstituted hydroxamic acids obtained by using the plot for BHA and the slope (0.72) found by Dessolin *et al.* for a series of *N*-unsubstituted hydroxamic acids under a different condition.[17] The plot for SHA^{-} agrees with this relation. This indicates that lowering of the nucleophilicity of SHA^{-} ($k_{A^-}=4.85\ M^{-1}\ s^{-1}$) relative to that of BHA ($k_{A^-}=50\ M^{-1}\ s^{-1}$) is accompained by the corresponding decrease in pK_a. Thus, the hydrogen bonding of the hydroxamate anion with the *ortho* hydroxyl group brought forth decreases of both of nucleophilicity and basicity.

In contrast, the plot for the dianionic form SHA^{2-} is considerably deviated: $k_{A^{2-}}$ is larger than expected from $pK_{a,HA}$. This may be explained as follows: (1) the nucleophilicity of the hydroxamate anion in SHA^{2-} is intrinsically greater than that of SHA^{-} or (2) the phenolate anion in SHA^{2-} is directly involved in the reaction besides the hydroxamate anion. The second-order rate constant of the reaction of PNPA and a phenoxide anion of $pK_a \approx 10$ has been estimated to be $0.97\ M^{-1}\ s^{-1}$ under a comparable condition.[21] This value is too small compared with the $k_{A^{2-}}$ value observed, and, consequently, the phenoxide anion cannot act as a nucleophile to any significant extent. Therefore, the increased reactivity is attributed to the increased nucleophilicity of the hydroxamate anion, which was probably caused by activation due to hydrogen bonding with the neighboring phenoxide anion (see Eq. 4).

Turnover of MPHA. MPHA is readily obtained as the cyclic anhydride. If the acyl hydroxamate intermediate is quickly converted to the cyclic compound with expulsion of the acetate ion, the catalytic cycle would be completed as below.

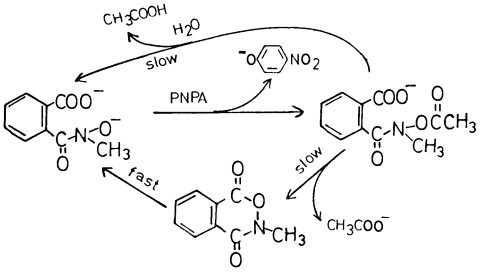

The first-order rate constant of the ring-opening step is $1.89\times10^{-2}\ s^{-1}$ at pH 8.57, and the apparent rate of acylation of MPHA is $(0.86—1.8)\times10^{-4}\ s^{-1}$ with PNPA of $(0.9—1.9)\times10^{-4}$ M under similar conditions. Therefore, the cyclic intermediate, if formed, would be readily converted to the reactive catalyst, and the ring opening process could not be rate-determining in the catalytic cycle.

However, the turnover of MPHA was not clearly observed when it was reacted with excess PNPA. This means that the deacylation step was negligibly slow. It was expected that the deacetylation rate would be enhanced by facile cyclization or by the general base catalysis of the *ortho*-carboxylate group. Unfortunately, both of these processes were proved to be insignificant. Attempted preparation of the acetyl derivative was not successful, and the separate determination of the rate of deacylation was impossible.

References

1) Contribution No. 355 from this department. Presented in part at the 30th annual meeting of the Chemical Society of Japan, Osaka, April 1974.

2) D. M. Blow, J. J. Birktoft, and B. S. Hartley, *Nature*, **221**, 337 (1969).

3) T. Kunitake and Y. Okahata, *Chem. Lett.*, **1974**, 1057; *Macromolecules*, **9**, 15 (1976).

4) T. Kunitake and Y. Okahata, *Bioorg. Chem.*, **4**, 136 (1975).

5) T. Kunitake and S. Horie, *Bull. Chem. Soc. Jpn.*, **48**, 1304 (1975).

6) I. Heilbron and H. M. Bunbury, "Dictionary of Organic Compounds," Oxford Univ. Press., New York, N.Y. (1953).

7) N. N. Ghosh, A. Mukherjee, and A. Bhattacharyya, *J. Indian Chem. Soc.*, **48**, 637 (1971).

8) A. Albert and E. P. Serjeant, "Ionization Constants of Acids and Bases. A Laboratory Manual," Methuen & Co., (1962), Chapt. 4.

9) R. Lummy, E. L. Smith, and R. R. Glantz, *J. Am. Chem. Soc.*, **73**, 4330 (1951).

10) E. A. Guggenheim, *Phil. Mag.*, **2**, 538 (1926).

11) J. F. J. Dippy, *Chem. Rev.*, **25**, 151 (1939).

12) S. G. Vanderberg, G. Henrich, and J. M. Vundennbelt, *Anal. Chem.*, **25**, 726 (1954).

13) R. Kuhn and A. Wassermann, *Helv. Chim. Acta*, **11**, 1 (1928).

14) G. M. Steinberg and R. Swidler, *J. Org. Chem.*, **30**, 2362 (1965).

15) T. Kunitake, Y. Okahata, and R. Ando, *Bull. Chem. Soc. Jpn.*, **47**, 1509 (1974).

16) M. Dessolin and M. Laloi-Diard, *Bull. Soc. Chim. Fr.*, **1971**, 2946.

17) M. Dessolin, M. Laloi-Diard, and M. Vilkas, *Bull. Soc. Chim. Fr.*, **1970**, 2573.

17) M. Dessolin, M. Laloi-Diard, and M. Vilkas, *Bull. Soc. Chim. Fr.*, **1970**, 2573.

18) W. B. Gruhn and M. L. Bender, *J. Am. Chem. Soc.*, **91**, 5883 (1969).

19) Large rate enhancements were found in micellar hydroxamate anions.[20]

20) *e.g.*, T. Kunitake, S. Shinkai, and Y. Okahata, *Bull. Chem. Soc. Jpn.*, **49**, 540 (1976).

21) W. P. Jencks and J. Carriuolo, *J. Am. Chem. Soc.*, **82**, 1778 (1960).

22) A. J. Kirby and G. H. Lloyd, *J. Chem. Soc., Perkin Trans. 2*, **1974**, 637.

23) T. Kunitake, Y. Okahata, and T. Tahara, *Bioorg. Chem.*, in press.

24) The only exception appears to be a copolymer of *N*-methylacrylohydroxamic acid and 4-vinylimidazole which was found very recently to perform the concerted nucleophilic attack.[25]

25) T. Kunitake and Y. Okahata, *J. Am. Chem. Soc.*, in press.

26) R. Hershfield and M. L. Bender, *J. Am. Chem. Soc.*, **94**, 1376 (1972).

Reactions of Dihydridotetrakis(triphenylphosphine)ruthenium(II) with Olefins and Isolation of New Ruthenium-Olefin Complexes

Sanshiro KOMIYA and Akio YAMAMOTO

Contribution from Research Laboratory of Resources Utilization, Tokyo Institute of Technology, Ookayama, Meguro-ku, Tokyo 152

(Received March 24, 1976)

Dihydridotetrakis(triphenylphosphine)ruthenium(II), $RuH_2(PPh_3)_4$, reacts with olefins (ethylene, propylene, styrene and butadiene) to give olefin-coordinated complexes of the type, $Ru(olefin)(PPh_3)_3$ and equimolar amounts of their hydrogenation products per mol of the dihydride complex. The olefin coordinated with ruthenium can be exchanged with other olefins. Olefin-coordinated complexes easily react with molecular hydrogen to afford tetrahydridotris(triphenylphosphine)ruthenium, $RuH_4(PPh_3)_3$, releasing alkane at room temperature. Under hydrogen atmosphere, catalytic hydrogenation of the olefins smoothly takes place with $RuH_2(PPh_3)_4$. (Ethylene)tris(triphenylphosphine)ruthenium(0) reacts with methyl iodide to give propylene and a trace of bu a-dien.e along with methane, ethylene, and small amounts of ethane and butenes. The formation of propylene suggests that oxidative addition involving cleavage of the C–H bond of ethylene to ruthenium giving a hydrido-vinyl complex may be taking place. Reactions of $Ru(C_2H_4)(PPh_3)_3$ with methyl-d_3 iodide and ethyl iodide, and of $Ru(C_3H_6)(PPh_3)_3$ with methyl iodide were examined to test the generality of this type of reaction. The reaction of $Ru(C_2H_4)(PPh_3)_3$ with CD_3I released CD_4 and CD_2H_2 together with CD_3H suggesting the involvement of α-hydrogen abstraction.

Recent progress in organo-transition metal chemistry has contributed to better understanding of the reaction mechanisms in various olefin catalysis with transition metals and their compounds. Study of properties of transition metal dihydride complexes[1] or transition metal complexes, which form dihydride complexes on reaction with molecular hydrogen,[2] has shed light on the detailed mechanism how an olefin coordinates to the transition metal hydride and is inserted between the metal-to-hydrogen bond. Dihydridotetrakis(triphenylphosphine)ruthenium(II),[3] **1**, has been found to serve as a particularly illustrative model compound of olefin catalyses, since it is itself catalytically active in hydrogenation, isomerization,[4] polymerization[5] and isotopic hydrogen exchange[6] of olefins, and on the other hand it gives many olefin-coordinated complexes on reactions with various olefins. We describe here characterization and properties of these olefin-coordinated complexes (ethylene, propylene, styrene and butadiene complexes) and the mechanism of formation of the olefin complexes from **1**. We have previously found that a seemingly simple olefin-coordinated complex with an apparent composition of Ru(alkyl methacrylate)$(PPh_3)_3$ was in fact a hydrido–propenyl type complex $RuH\{CH=C(CH_3)C(O)OR\}(PPh_3)_3$ which was formed by oxidative addition involving cleavage of C–H bond adjacent to the double bond.[7] Examination of the properties of the present olefin-complexes also revealed some features which may be best accounted for by assuming the contribution of a hydrido-vinyl type structure.

Results and Discussion

*Reactions of $RuH_2(PPh_3)_4$ **1** with Olefins.* The dihydridoruthenium complex **1** reacts with very electronegative olefins such as tetracyanoethylene and maleic anhydride to give stable olefin complexes[3] and initiates the polymerization of less electronegative vinyl compounds such as acrylonitrile, methacrylonitrile, acrylaldehyde and methyl acrylate.[5] Olefins such as ethylene, propylene, styrene and butadiene, on the other hand, react with **1** to give their hydrogenated products and ruthenium complexes containing these olefins.

$$\underset{\mathbf{1}}{RuH_2(PPh_3)_4} + \diagdown C{=}C \diagup \longrightarrow$$

$$Ru(olefin)(PPh_3)_3 + PPh_3 + \diagdown C{-}C \diagup \quad (H \text{ on } \diagup,\ H \text{ on } \diagdown)$$

2, olefin = ethylene
3, olefin = propylene
4, olefin = styrene
5, olefin = butadiene

These olefin-complexes **2**—**5** are thermally labile than complexes containing very electronegative olefins but can be isolated under appropriate conditions. Table 1 summarizes the analytical data, yields, NMR data and physical properties of the isolated complexes.

The reactions of ethylene, propylene and styrene with **1** proceed smoothly at room temperature to form quantitatively 1 equiv. of ethane, propane and ethylbenzene, respectively. The hydrogenation product of butadiene with **1** consisted of 1-butene and small amounts of *cis*- and *trans*-2-butene, the latters may be formed by isomerization of 1-butene catalyzed by **1**.[4] The molar ratio of the sum of the *cis*- and *trans*-2-butene to 1-butene decreased with increase in the amount of butadiene used in the reaction. The result also suggests that the isomerization of 1-butene was catalyzed by the remaining dihydride complex **1** and not by the butadiene-complex.

In the presence of a large excess of butadiene, **1** afforded an extremely soluble complex which could not be completely characterized but appears to contain two butadiene molecules coordinated with ruthenium.

Characterization of the Olefin-coordinated Complexes. The isolated complexes were characterized by means of elemental analysis, IR and NMR spectroscopy and chemical reactions.

None of the isolated olefin-complexes showed an IR

TABLE 1. ANALYTICAL AND NMR DATA AND PHYSICAL PROPERTIES OF OLEFIN COMPLEXES

	Complex[a]	Analysis (Found) C %	H %	Color Dec. pt. (°C)	Yield	^{1}H-NMR[b]	^{31}P-NMR[f]
2	$Ru(E)(PPh_3)_3$	73.8 (73.4)	5.5 (5.4)	White 150—155	49%	1.5—2.5 (br, $C_2\underline{H}_4$)[c]	
3	$Ru(P)(PPh_3)_3$	74.9 (73.6)	5.1 (5.5)	White 170	—		
4	$Ru(St)(PPh_3)_3$	76.0 (75.1)	5.4 (5.4)	Red purple —	—	7.51 (br, $=C\underline{H}_2$)[d] 5.79 (br, $=C\underline{H}-$)	
5	$Ru(BD)(PPh_3)_3$	74.4 (74.0)	6.2 (5.4)	Greenish yellow 185	37%	−0.05 (br, H_a)[c,e] 1.49 (br, H_b)[c,e] 4.91 (br, H_c)[c,e]	58.7 (t, P_1)[g] 50.5 (d, P_2)[g]

a) Abbreviation: E, ethylene; P, Propylene; St, styrene; BD, butadiene. b) δ Value in ppm downfield from TMS positive; t, triplet; d, doublet; br, broad unresolvable signal. c) Solvent: benzene-d_6. d) Solvent: styrene. e) See text for the designation. f) Chemical shifts in ppm downfield positive from external PPh_3 g) $J_{P_1-P_2}=12$ Hz, see text for designation of P_1 and P_2.

band ascribable to ν(Ru–H). Unambiguous assignment of the ν(C=C) band of the coordinated olefin was not feasible because the shift of the weak ν(C=C) band to lower frequency on coordination of the olefin to ruthenium makes it overlap with other strong bands due to triphenylphosphine.

a) Ethylene- and Propylene-coordinated Complexes: On iodolysis in benzene solution at room temperature complex **2** released one equiv. of ethylene, whereas thermolysis and acidolysis of **2** liberated ethane in addition to ethylene. The reaction product of **2** with acetic acid gave the known hydrido acetate complex $RuH(OAc)(PPh_3)_3$.[8] The formation of ethane in the acidolysis and thermolysis may be caused by intervention of an ethylruthenium complex formed by *ortho*-metallation of one of the triphenylphosphine ligands in **2** by presence of equilibria such as:

$$(C_2H_4)Ru(PPh_3)_3 \rightleftharpoons \mathbf{2}$$

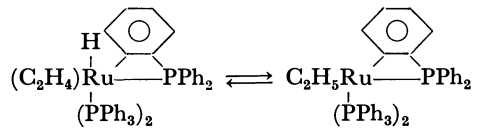

A low activity of the ethylene complex **2** in comparison to the high activity of the dihydride complex **1** for polymerization of vinyl compounds may be also due to the presence of the above equilibria. In contrast with **2**, the propylene-coordinated complex **3** released only small amounts of propylene on iodolysis, thermolysis and acidolysis.

The NMR spectrum of **2** in benzene showed a broad band at δ 1.5—2.5 which may be due to the coordinated ethylene. In the presence of added ethylene both peaks of the coordinated and uncoordinated ethylene were observed and they showed broadening on raising the temperature suggesting an exchange reaction taking place between the coordinated and uncoordinated ethylene. Further support for the exchange was obtained by studying the exchange reaction of C_2D_4 with **2**.[4,6]

b) Styrene-coordinated Complex 4: The styrene-coordinated complex **4** can be obtained as a purple solid which can be crystallized from toluene containing styrene. In the absence of free styrene, complex **4** is unstable and readily decomposed in many solvents. Addition of a large excess of toluene to **4** caused the separation of a yellow precipitate which was identified as $RuH_2(PPh_3)_4$ on the basis of its elemental analysis and IR spectrum showing a ν(Ru–H) band at 2080 cm^{-1}. The decomposition of **4** in toluene released ethylbenzene and strene in a molar ratio of *ca.* 3: 1. The combined molar amount of ethylbenzene and styrene was equivalent to **4**. When **4** was decomposed in tetrachloroethylene, which carries no hydrogen to be abstracted, the molar ratio of ethylbenzene to styrene sharply decreased to 1: 9. The fact indicates that the solvent was the major hydrogen source in decomposition of **4** in toluene. The generation of the small amount of ethylbenzene in the decomposition of **4** in tetrachloroethylene may be ascribed to hydrogen abstraction from the triphenylphosphine ligands. The decomposition product in tetrachloroethylene had a composition close to $Ru(C_2Cl_4)(PPh_3)_3$. The molar ratio of ethylbenzene to styrene generated in the decomposition of **4** in various solvents depended on the solvents used; *e,g.*, in pyridine the ratio was 1:3. No gas was released on iodolysis of **4**.

Because of the instability of **4** in solvents other than styrene itself, the NMR spectrum of **1** was observed in styrene. In addition to the signals of ethylbenzene, two broad peaks at δ 7.51 and 5.79 were observed in a ratio of 1: 2. By comparison of the peak intensities of these peaks with the resonances of ethylbenzene, 1 equiv. of which was confirmed to be formed by an independent method using gas chromatography, these broad peaks are assigned to vinyl protons of styrene coordinated to ruthenium in a 1: 1 molar ratio.

c) Butadiene-coordinated Complex 5: The ^{1}H-NMR spectrum of **5** in benzene shows three peaks of an equal intensity at δ −0.05, 1.49, and 4.91 ppm. These signals may be due to protons H_a, H_b, and H_c of butadiene coordinated with ruthenium as illustrated by a model below to represent one of the possible structures for this complex:

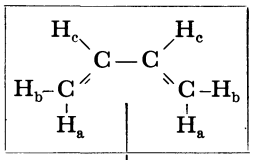

P_2—Ru—P_2

P_1

5 $P_1=P_2=PPh_3$

Keim reported the preparation of a butadiene-coordinated rhodium complex having a composition of $Rh(C_4H_6)(PPh_3)(Ph_2PC_6H_4)$ which shows three peaks of equal intensity at δ 0.4, 2.3, and 4.9 ppm and assigned these peaks in a similar manner to the present case.[9]

The proton decoupled ^{31}P-NMR spectrum of **5** shows an AX_2 type spectrum at 58.7 (triplet) and 50.5 ppm (doublet) downfield from reference PPh_3 in a ratio of 1 : 2. The spectrum is consistent with the above structure having two equivalent and one non-equivalent triphenylphosphine ligands.

Reactions of the Olefin-complexes with Hydrogen. Contact of a benzene solution of $Ru(olefin)(PPh_3)_3$ with molecular hydrogen at room temperature converts the coordinated olefin into its hydrogenated product and gives the known tetrahydridotris(triphenylphosphine)-ruthenium.[10] The reaction probably proceeds through an unstable intermediate $RuH_2(olefin)(PPh_3)_3$ from which alkane may be produced.

$$Ru(olefin)(PPh_3)_3 + H_2 \longrightarrow RuH_2(olefin)(PPh_3)_3$$
$$\downarrow$$
$$Ru(PPh_3)_3 + \text{alkane}$$
$$\downarrow +2H_2$$
$$RuH_4(PPh_3)_3$$

Olefin Exchange Reactions. The olefin coordinated with ruthenium in the isolated complexes **2**—**5** can be readily displaced by another olefin. Scheme 1 summarizes the typical exchange reactions. Ethylene in **2** may be readily displaced by styrene with liberation of ethylene and ethane, and styrene in **4** by ethylene with release of styrene and ethylbenzene. Methacrylonitrile displaces ethylene in **2** and styrene in **4** to give a methacrylonitrile-coordinated complex with a ν(C≡N) band at 2180 cm^{-1} which is shifted to lower frequency by *ca.* 40 cm^{-1} from the ν(C≡N) band of free methacrylonitrile, the shift indicating a coordination through the olefinic double bond to ruthenium.[11] The ^{1}H-NMR spectrum of the methacrylonitrile-complex having broad peaks of the vinylic protons of the coordinated methacrylonitrile at δ 5.3 and 4.9 ppm, which are shifted to higher field than the resonances of free methacrylonitrile, also suggests the π-type coordination. Purification of the complex by recrystallization has failed.

In contrast to the reaction of vinyl acetate with **1** which causes the C–O bond cleavage of vinyl acetate to give ethylene and $RuH(OAc)(PPh_3)_3$[12] the reaction of vinyl acetate with **2** gave a vinyl acetate–ruthenium complex with a ν(C=O) band at 1736 cm^{-1}. The structure of the complex has not been fully characterized.

As reported separately, the reaction of ethyl methacrylate with **2** or **4** gave a new oxidative addition product **6**, which has a five-membered ring as shown in Scheme 1.[7] Reaction of ethylene with **6** partially converted **6** to **2**.

Evidence for Oxidative Addition of Olefins to Ruthenium Affording Hydrido-vinylic Complexes. The bonding between an olefin and a transition metal in an olefin-coordinated complex is generally elucidated in terms of Dewar-Chatt-Duncanson model[13] and there are ample examples[14] in which the side-on type π-coordination of the olefin to the metal has been established by X-ray structural determination.[15] However, we recently encountered a case that a seemingly simple olefin complex between between alkyl methacrylate and ruthenium turned out to have a σ-vinylic-hydrido structure, $RuH(CH{=}C(CH_3)COOR)(PPh_3)_3$, **6**. This complex appeared first as a simple olefin complex on the basis of characterization technique we routinely employ. For example, thermolysis, iodolysis and acidolysis of the complex liberated the alkyl methacrylate. However the treatment with methyl iodide released the methyl substituted product of the alkyl methacrylate at the β-position, *i.e.*, $CH_3CH{=}C(CH_3)(COOR)$. This result

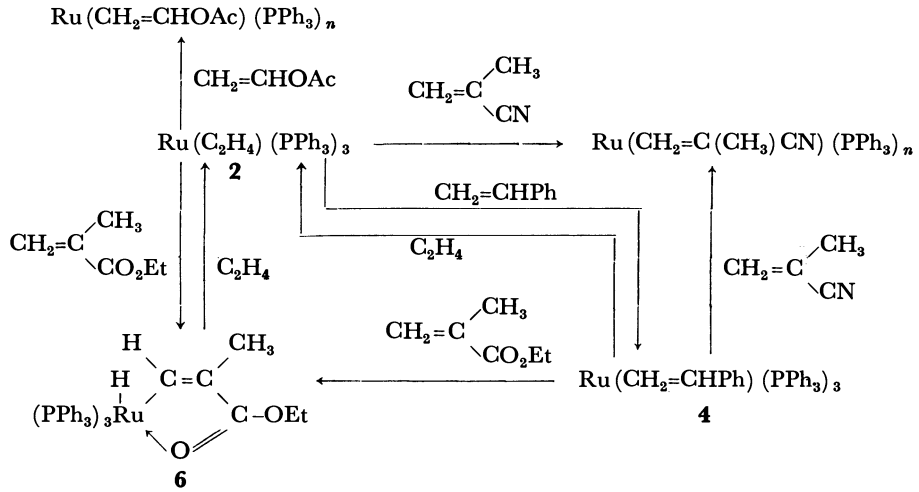

Scheme 1. Exchange reactions between olefin-coordinated complexes.

Table 2. Reactions of olefin complexes with alkyl halides

Olefin complex	RX	Temp (°C)	Compositions of gases evolved[b]									
			CH_4[a]	C_2H_4	C_2H_6	C_3H_6	C_3H_8	C_4H_6	Δ^1-C_4H_8	Δ^2-C_4H_8 *cis*	2-C_4H_8 *trans*	C_4H_{10}
$Ru(C_2H_4)(PPh_3)_3$ **2**	MeI	−30		100	0	t	0	0	tt	0	0	0
	MeI	rt	86	82	7	9	0	tt	tt	2	tt	0
	MeI	65	79	81	7	12	0	t	t	t	tt	0
	EtI	rt	0	80	t	0	0	tt	10	tt	tt	10
$Ru(C_3H_6)(PPh_3)_3$ **3**	MeI	65		t	t	58	6	11	21	1	3	0

a) Percentage of gas evolved per mol of olefin complex. b) Compositions of the gases other than methane in percentage. The symbols t and tt mean that very small amounts of the gases were detected; t, <0.5%; tt, 0.05%.

together with the IR and NMR spectral analysis led us to the conclusion that the methacrylate-coordinated complex has the hydrido-vinylic structure, which has prompted us to reexamine the olefin-coordinated complexes reported here to see if the seemingly olefin-coordinated complexes actually have hydrido-σ-vinyl structures or if a tautomeric equilibrium such as shown below may exist:

$$(PPh_3)_3Ru\cdots\overset{CH_2}{\underset{CH_2}{\|}} \rightleftharpoons (PPh_3)_3Ru\begin{matrix}\diagup CH{=}CH_2\\ \diagdown H\end{matrix}$$

Neither NMR nor IR spectra of **2** showed any sign of the hydridovinyl structure and chemical reactions of **2**, such as thermolysis, iodolysis, and acidolysis provide no information to support the presence of the hydrido-vinyl species. However, experimental results in favor of the involvement of the hydrido-vinylic species were obtained from the analysis of the reaction products of **2** and **3** with alkyl halides. Table 2 shows the compositions of gases evolved on reactions of **2** and **3** with methyl and ethyl iodides. The composition of the evolved gas on treatment of **2** with methyl iodide varied depending on the reaction temperature. At −30° the gas evolved consisted predominantly of ethylene and traces of propylene and 1-butene. Upon raising the reaction temperature the content of propylene in the evolved gas significantly increased. The similar reaction of **2** with ethyl iodide produced a considerable amount of 1-butene. Noteworthy here is the formation of butadiene although in a minute amount. Scheme 2 shows the reaction paths and olefins expected to be produced, provided that the oxidative addition of methyl iodide to the suspected vinyl-hydrido species should take place.

Formation of methane and ethane in the reaction of methyl iodide with **2** may be accounted for by assuming reductive elimination of the methyl and hydrido ligands and intermolecular coupling of the methyl ligands in the assumed reaction intermediate **8a** which may be formed by oxidative addition of methyl iodide to the hydrido-vinylic intermediate **7** in Scheme 2. Ethylene may arise directly by liberation of the coordinated ethylene from **2** and/or by reductive elimination of the ethyl and hydrido ligands in **8a**. The formation of propylene may be accounted for by reductive elimination of the methyl and vinyl ligands in **8a**. Butadiene may also arise by intermolecular coupling of the two vinyl groups in **8a**. If the assumption of the presence of the vinyl-hydrido species **7** should be valid, the fact that the amount of propylene increases at the

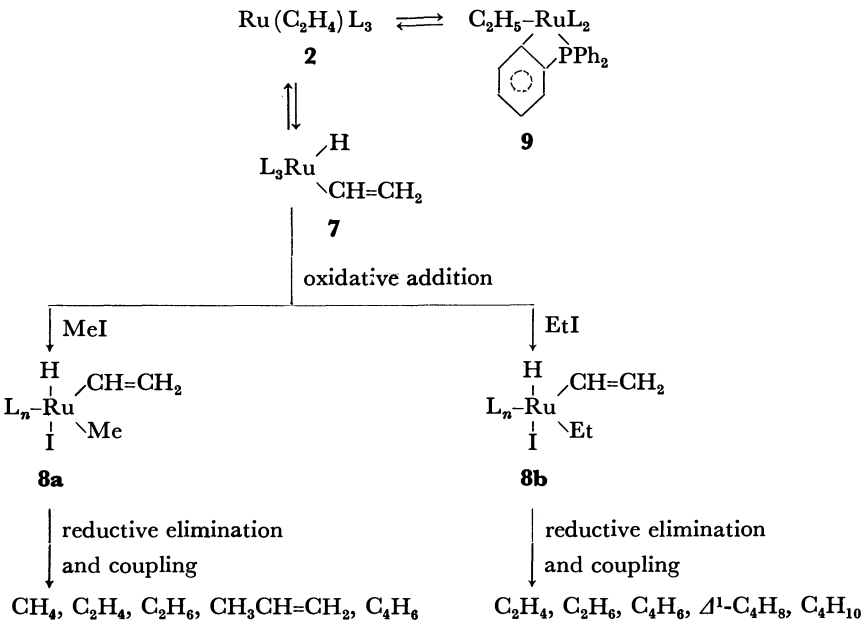

Scheme 2.

expense of ethylene as temperature rises may indicate the shift of the equilibrium between **2** and **7** to the side of **7**. The reaction path **2**→**7**→**8a**, on the other hand, does not account for the formation of butenes in the reaction of **2** with methyl iodide, and it seems necessary to invoke the intervention of the previously discussed ethylruthenium species *(vide supra)* which might produce butene by cross-coupling with the vinyl complex **8a**. The presence of the ethylruthenium species such as **9** in Scheme 2 has previously been suggested on the basis of experiments using deuterated compounds.[6,16]

Similar arguments may be advanced to account for the reaction products of **2** with ethyl bromide by assuming an intermediate **8b** in Scheme 2. 1-Butene formed in the reaction of **2** with ethyl iodide may be produced by reductive elimination of the ethyl and vinyl groups and butane by an intermolecular coupling of the ethyl groups in **8b**.

In order to obtain further information on the reaction of the olefin complex with alkyl halide, the reaction products of **2** with methyl-d_3 iodide were examined. The gas evolved on reaction of **2** with CD_3I at 65 °C was fractionated by GLC and analyzed by mass spectrometry. The result of the product analysis revealed another unexpected aspect of the reaction as shown in experimental section. The formation of CD_4 may be explained by deuterium abstraction from CD_3I or by α-elimination process. The former possibility does not reconcile with the formation of polydeuterated butenes C_4D_8, C_4D_7H and others. Therefore we propose that α-elimination is involved here as shown below.

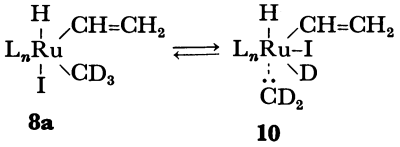

8a **10**

We have previously presented evidence for such α-elimination reaction in the decomposition of a methyl–iron complex.[17] Formation of CD_3H, C_2H_4, C_2H_3D, C_2D_6, and $C_3H_3D_3$ can be elucidated by assuming the species **8a** and **10** shown above. The formation of polydeuterated butenes may be accounted for by H–D exchange in the ethyl group in species **9** and in the vinyl group in species **10** and cross-coupling of the ethyl and vinyl groups.

In order to examine the generality of this type of reaction the reaction products of other ethylene-complexes, $Fe(C_2H_4)(diphos)_2$[18] and $Pd(C_2H_4)(PPh_3)_2$,[19] with methyl iodide were examined. Ethylene and methane were the main products and only traces of propylene and butenes were detected.

Table 2 also includes the reaction products of $Ru(C_3H_6)(PPh_3)_3$ **3** with methyl iodide at 65 °C. In addition to propylene and propane considerable amounts of butadiene and butenes accompanied by traces of ethylene and ethane were produced. The pattern of the product distribution is noticeably different from that of the reaction of **2** and alkyl halide, and it is required to invoke another type of a reaction intermediate as shown below.

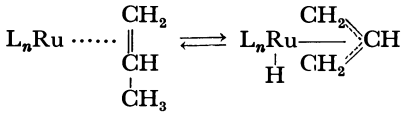

The predominant formation of 1-butene and its isomerization products may be accounted for by postulating the involvement of the π-allyl-hydrido species. The formation of butadiene requests α-elimination of the methyl group to produce a hydrido-carbene species, which may combine with the π-allyl group. The formation of π-allyl-hydrido species from a π-propylene complex has a precedent in a nickel complex prepared by Bönneman *et al.*,[20] and we have also observed hydrogen abstraction from the methyl group in the alkyl methacrylate complex **6**.[7]

The formation of propylene and butenes from **2** and methyl and ethyl iodides may be alternatively explained by postulating the insertion of ethylene into the Ru–CH_3 or Ru–C_2H_5 bond formed by oxidative addition of the alkyl halides to **2**, followed by β-elimination to produce propylene and butenes leaving a ruthenium hydride. However, the bulk of evidence presented here is difficult to explain without assuming the hydrogen abstraction from the coordinated olefins.

The results we reported here indicates the quite complicated nature of the olefin complexes when they are subjected to various reactions. The behavior of the olefin complexes has implications in the mechanisms of ethylene polymerization by Phillips process using chromium oxide,[21] and palladium-promoted substitution reactions of olefins.[22]

Experimental

General. All the reactions were carried out under nitrogen atmosphere or in a vacuum. Solvents and olefins were purified by usual methods and stored under nitrogen before use. Liquid olefins were introduced by trap-to-trap distillation in a vacuum into the reaction vessel containing the dihydrido-ruthenium complex, **1**. Gaseous olefins were bubbled into or brought in contact with the solution of the dihydrido complex.

Analysis of gases was carried out by mass spectrometry and gas chromatography. Non-condensable gas at liquid nitrogen temperature was collected using a Toepler pump, by which the volume of the gas was measured. Analysis of the hydrogenated products in the reaction of olefins with the ruthenium complexes were carried out by gas chromatography using Shimadzu-3BT Gas Chromatograph after collecting the liquid by trap-to-trap method. IR and NMR spectra were measured with a Hitachi-EPI-G3 spectrometer and a JEOL-100 MHz spectrometer. Complex **1** was prepared by the method reported previously.[3]

(Ethylene)tris(triphenylphosphine)ruthenium, **2**. Complex **1** (798 mg, 0.693 mmol) in benzene was brought in contact with ethylene (3.73 mmol) for a day at room temperature. The color of the solution changed from yellow to red brown accompanied by evolution of ethane which was 110% per mol of complex **1**. By concentration of or on addition of hexane to the solution, white crystals were obtained which were washed several times with hexane and dried in a vacuum. Bubbling ethylene into the 20 ml toluene suspension of complex **1** (4.0 g, 3.5 mmol) at room temperature turned the color of the solution to red in an hour and off-white crystals precipi-

tated in a few hours. (Yield: 49%).

Reaction of 2 with Iodine. Complex **2** (0.1569 g, 0.171 mmol) in benzene readily reacted with excess iodine liberating only ethylene (3.96 ml, 0.177 mmol) which was 103% of the calculated value, at room temperature.

Thermal Decomposition, Acidolysis and Oxidation of Complex 2. By thermal decomposition of complex **2** up to 200 °C ethylene and ethane (the molar ratio was 1: 0.6 and total amount was 56% for complex **2**) were evolved. By the reaction of complex **2** (0.16 mmol) with sulfuric acid (10 ml), ethylene and ethane (the molar ratio was 1: 1 and total amount was 0.058 mmol, 36%) were evolved. Oxidation of **2** by dry oxygen liberated ethylene.

Reaction of 2 with Methyl Iodide. Methyl iodide (1 ml) was introduced to complex **2** (245 mg, 0.267 mmol) by trap-to-trap distillation. The colorless mixture turned rapidly to black accompanied by evolution of a gas mixture at room temperature. The contents of C_1, C_2, C_3, C_4 olefins and alkanes evolved at −30 °C, room temperature and 65 °C are listed in Table 2.

Reaction of 2 with Methyl-d_3 Iodide. Methyl-d_3 iodide (0.5 ml) reacted with complex **2** to liberate various gases at 65 °C. The content of the isotopic mixture of the gaseous hydrocarbons formed was analyzed by mass spectrometry after separating the components by gas chromatography. The product consisted of the following compositions.

Methane: CD_4, 65%; CD_3H, 35%, the other, trace. Ethylene: C_2H_4, 79%, C_2H_3D, 21%; the other, trace. Ethane: C_2D_6, main; the other, trace. Propylene: $C_3H_3D_3$, main; the other, trace. Butene: the whole range of butenes from C_4D_8 to C_4H_8 were detected.

Reaction of Complex 2 with Ethyl Iodide. Excess ethyl iodide was introduced to complex **2** to release ethylene, butane and 1-butene, and small amounts of ethane, and *cis*- and *trans*-2-butene at room temperature. (see Table 2).

Reaction of Complex 2 with Ethyl Methacrylate. Ethyl methacrylate (2 ml) was introduced to complex **2** (106 mg, 0.108 mmol) by trap-to-trap distillation. Ethylene (20 ml) was evolved and yellow crystals were obtained after the reaction mixture was stirred for a day at room temperature. The yellow complex was identified as $RuH(CH{=}C(CH_3)COOEt)(PPh_3)_3$ on the basis of its IR spectrum; ν(Ru–H), 1960 cm^{-1}; ν(C=O), 1580 cm^{-1}. In the case of the reaction of **2** with *cis*-β-ethyl methacrylate-d_1 (isotopic purity, 72%), deuterated ethylene (C_2H_4, 52%; C_2H_3D, 39%; $C_2H_2D_2$, 9%) was evolved but the resulted complex was scarcely deuterated. Deuteriums in ethyl methacrylate recovered after the reaction were found to be distributed in vinyl and methyl positions (isotopic purity, 9%).

Reaction of Complex 2 with Styrene. Styrene (2 ml) was introduced to complex **2** (155 mg, 0.192 mmol) by trap-to-trap distillation. The initial partly heterogeneous solution gradually changed to a reddish purple homogeneous solution liberating ethylene (4.23 ml, 0.189 mmol) in a day at room temperature. Although the resultant complex was not purified sufficiently because of its instability toward solvents, it is considered to be a styrene-coordinated complex $Ru(St)(PPh_3)_3$ by comparison of its color and stability with the styrene complex prepared from **1** and styrene.

Reaction of 2 with Acetic Acid. Acetic acid (0.5 ml) in benzene (2.5 ml) was introduced to complex **2** (191 mg, 0.209 mmol) by trap-to-trap distillation. The colorless heterogeneous mixture thus formed changed to a yellow homogeneous solution liberating ethylene and ethane in a molar ratio of 2: 1 (total amount of the gas was 0.167 mmol) at room temperature in a few hours. The yellow precipitate was obtained by concentrating the homogeneous solution and was identified as $RuH(OAc)(PPh_3)_3$ by comparison of its IR spectrum with that of an authentic sample. ($\nu(OCO)_{asym}$, 1530 cm^{-1}; $\nu(OCO)_{sym}$, 1450 cm^{-1}).

Reaction of 2 with Methacrylonitrile. Methacrylonitrile (2.0 ml) was introduced to complex **2** (482 mg, 0.527 mmol) by trap-to-trap distillation. A yellow homogeneous solution was obtained accompanied by evolution of ethylene (0.392 mmol) in a day at room temperature. Excess methacrylonitrile was evaporated completely to give a yellow oily product. From its extract with hexane a yellow solid was obtained. The IR spectrum of the yellow solid showed a $\nu(C{\equiv}N)$ band at 2180 cm^{-1} and its NMR spectrum in C_6D_6 showed signals attributable to coordinated methacrylonitrile through the double bond. (δ $C{=}CH_2$, 5.3 and 4.9 ppm; CH_3, 1.3 ppm) and some other unidentified small peaks in a range 1—3 ppm. The resultant complex is tentatively assigned as Ru(methacrylonitrile)-$(PPh_3)_3$.

(Propylene)tris(triphenylphosphine)ruthenium, 3. Propylene (147 ml) was brought in contact with complex **1** (533 mg, 0.463 mmol) in toluene (15 ml) in a sealed system for 2 days at room temperature. Propane (11.4 ml, 110% per complex **1**) was liberated. By adding hexane to the toluene solution a pale brown precipitate was obtained which was washed with hexane and dried in a vacuum. Thermolysis at *ca.* 170 °C and acidolysis by sulfuric acid liberated a small amount of propylene. (5%).

Reaction of 3 with Methyl Iodide. Excess methyl iodide (2 ml) was introduced to complex **3** (*ca.* 100 mg) by trap-to-trap distillation at room temperature and methane, propylene and 1-butene were liberated. Small amounts of *cis*- and *trans*-2-butene, butadiene and propane were also detected.

(Styrene)tris(triphenylphosphine)ruthenium, 4. Styrene (3.12 g) was introduced to complex **1** (1.20 mmol) to give a homogeneous purple solution at room temperature in a day. No polymer was obtained from the solution. The solution was evaporated in a vacuum line and ethylbenzene (1.13 mmol) which corresponds to 94% equivalent of complex **1** was detected in the volatile matter. Red crystals were obtained on crystallization from the mixture of styrene and toluene. When complex **4** was dissolved in excess toluene, styrene and ethylbenzene in a molar ratio of 67: 33 were released. From the solution yellow crystals of $RuH_2(PPh_3)_4$ were recovered. (Found: C, 74.9; H, 5.2%. Calcd for $C_{72}H_{62}P_4Ru$: C, 75.1; H, 5.4%.) ν(Ru–H), 2080 cm^{-1} (KBr disk). Complex **4** decomposed also in pyridine to produce a yellow precipitate, apparently $RuH_2(PPh_3)_4$. In pyridine, styrene and ethylbenzene in a molar ratio of 26: 74 were evolved. Complex **4** reacted with tetrachloroethylene to afford a brown complex $Ru(C_2Cl_4)(PPh_3)_3$ releasing styrene and ethylbenzene in a molar ratio of 89: 11. The brown complex was washed several times with hexane and dried in a vacuum. (Found: C, 63.8; H, 4.5%. Calcd for $C_{56}H_{45}Cl_4Ru$: C, 63.7; H, 4.3%.)

Reaction of Complex 4 with Ethylene. Ethylene (300 ml) was brought in contact with complex **4** (*ca.* 300 mg) which was frozen in benzene (5 ml) at −196 °C. Temperature of the reaction mixture was raised up to room temperature immediately. A brown homogeneous solution was obtained in 1 h. In the solution styrene and ethylbenzene were detected in a molar ratio of 1: 1. The benzene solution was evaporated to dryness by freeze-drying method to give a pale yellow solid which was tentatively assigned to $Ru(C_2H_4)(PPh_3)_3$ based on the result of thermolysis giving ethylene and ethane in a molar ratio of 2: 1 and no styrene.

Reaction of Complex 4 with Ethyl Methacrylate. Ethyl methacrylate (2 ml) was introduced to complex **4** (*ca.* 300 mg) by trap-to-trap distillation. The color of the solution changed to yellow in an hour and yellow crystals were obtained with

release of styrene. The yellow crystals were identified as $RuH(CH{=}C(CH_3)COOEt)(PPh_3)_3$ by IR spectroscopy. ν(Ru–H), 1960 cm^{-1}; ν(C=O) 1580 cm^{-1}.

Reaction of Complex 4 with Dry Deuterium Chloride. Dry deuterium chloride was introduced to complex **4** (*ca.* 300 mg) in C_6D_6 by trap-to-trap distillation. After 1 day a red purple precipitate was obtained. All the volatile matter was collected and examined by NMR spectroscopy. Deuterated styrene in which vinyl protons were deuterated by 20% were detected.

Reaction of Complex 4 with Methacrylonitrile. Excess methacrylonitrile reacted with complex **4** at room temperature giving the same compound as the complex obtained from the reaction of complex **2** with methacrylonitrile.

Reaction of Complex 4 with Acrylonitrile. Acrylonitrile (5.0 ml) was introduced to complex **4** (*ca.* 100 mg) by trap-to-trap distillation. Slow polymerization of acrylonitrile took place at room temperature. Yield 1.26 g (31%).

Reaction of Complex 4 with Carbon Dioxide. Carbon dioxide was bubbled into a mixture of toluene and styrene containing the styrene complex for a day at room temperature to give a brown solution. By adding hexane to the brown solution, a brown precipitate was obtained and was washed several times with hexane and dried in a vacuum. The IR spectrum of the brown precipitate shows new bands at 1932 (w), 1660 (m), 1635 (s), 1505 (m), and 600 (s) cm^{-1}. Thermolysis of the brown precipitate (82 mg) liberated carbon dioxide (1.47 ml, 0.0656 mmol). dec 120 °C.

Reaction of Complex 4 with Hydrogen. Hydrogen was bubbled into the styrene solution of complex **4** for a week at room temperature to give a yellow precipitate. Styrene was found to be completely converted to ethylbenzene and $RuH_2(PPh_3)_4$ was obtained. ν(Ru–H), 2080 cm^{-1}.

(Butadiene)tris(triphenylphosphine)ruthenium, ***5***. Butadiene (2.22 mmol) was brought in contact with complex **1** (1.30 g, 1.13 mmol) in benzene (10 ml) in a sealed system for a day at room temperature to give greenish yellow crystals releasing butenes. In the gas phase 1-butene, *trans*-2-butene and *cis*-2-butene (the molar ratio of 75: 18: 7) were formed and no butadiene was detected. Greenish yellow crystals were recrystallized from benzene or toluene as yellowish green needles which were washed several times with hexane and dried in a vacuum. Thermolysis of the resulted crystals gave *ca.* 5% of 1-butene and acidolysis gave no gas.

A large excess of butadiene (9.59 mmol) reacted with complex **1** (1.86 g, 1.62 mmol) to give an oily product and 1-butene with a small amount of *trans*- and *cis*-2-butene. The oily product could not be characterized because of the difficulty of purification, but the NMR spectrum of the oily product showed signals attributable to the coordinated butadiene (−0.75, 2.00, and 4.54 ppm down field from TMS) and triphenylphosphine. As the amount of butadiene absorbed in the reaction was *ca.* 2.7—3.8 mmol, two butadiene molecules appear to be coordinated to ruthenium.

Reaction of Complex 2 and 5 with Hydrogen. Hydrogen (300 ml) was brought in contact with a benzene suspension (*ca.* 5 ml) of **2** (*ca.* 200 mg) giving a yellow brown homogeneous solution at room temperature. Only ethane was detected in the gas phase. After 1 day white needles were formed, which were identified as $RuH_4(PPh_3)_3$ on the basis of IR analysis and its reaction with PPh_3 affording hydrogen and $RuH_2(PPh_3)_4$. Complex **5** in benzene also reacted with hydrogen at room temperature similarly giving $RuH_4(PPh_3)_3$ and butane. ν(Ru–H), 1940 cm^{-1}.

References

1) A. P. Ginsberg, *Transition Metal Chem.*, **1**, 111 (1965); M. L. H. Green and D. J. Jones, *Adv. Inorg. Chem. Radiochem.*, **7**, 115 (1965); E. L. Muetterties, "Transition Metal Hydrides," Vol. I, Marcel Dekker, New York (1971); B. L. Shaw, "Inorganic Hydrides," Robert Maxwell, London (1967); H. D. Kaesz and R. B. Saillant, *Chem. Rev.*, **72**, 231 (1972).

2) For example: J. A. Osborn, F. H. Jardine, J. F. Young, and G. Wilkinson, *J. Chem. Soc., A*, **1966**, 1711; L. Vaska and R. E. Rhodes, *J. Am. Chem. Soc.*, **87**, 4970 (1965); and other references listed in the above reviews, 1).

3) T. Ito, S. Kitazume, A. Yamamoto, and S. Ikeda, *J. Am. Chem. Soc.*, **92**, 3011 (1970); J. J. Levison and S. D. Robinson, *J. Chem. Soc., A*, **1970**, 2947.

4) S. Komiya and A. Yamamoto, submitted to *J. Molecul. Cat.*, 1976.

5) S. Komiya, A. Yamamoto, and S. Ikeda, *Bull. Chem. Soc. Jpn.*, **48**, 101 (1975).

6) S. Komiya, A. Yamamoto, and S. Ikeda, *J. Organometal. Chem.*, **42**, C65 (1972).

7) S. Komiya and A. Yamamoto, *Chem. Lett.*, **1975**, 475; S. Komiya, T. Ito, and A. Yamamoto, J. Cowie, and J. Ibers, *J. Am. Chem. Soc.*, **98**, 3874 (1976).

8) D. Rose, J. D. Gilbert, R. P. Richardson, and G. Wilkinson, *J. Chem. Soc., A*, **1969**, 2610; S. D. Robinson and M. F. Uttley, *J. Chem. Soc., Chem. Commun.*, **1972**, 1047; *J. Chem. Soc., A*, **1973**, 1912.

9) W. Keim, *J. Organometal. Chem.*, **16**, 191 (1969).

10) W. H. Knoth, *J. Am. Chem. Soc.*, **94**, 104 (1972).

11) B. L. Ross, J. G. Grasselli, W. M. Ritchey, and H. H. Kaesz, *Inorg. Chem.*, **2**, 1023 (1963); M. F. Farona and F. R. Tompkin, *Spectrochim. Acta*, **A**, **24**, 788 (1968).

12) S. Komiya and A. Yamamoto, *J. Chem. Soc., Chem. Comm.*, **1974**, 523; *J. Organometal. Chem.*, **87**, 333 (1975).

13) M. J. S. Dewar, *Bull. Soc. Chim. Fr.*, C79 (1951); J. Chatt and L. A. Duncanson, *J. Chem. Soc.*, **1953**, 2939.

14) M. Herberhold, "Metal π-Complexes," Vol, I, II, Elsevier Publ. Comp., Amsterdam, London, New York (1972).

15) For example, C. D. Cook, C. H. Koo, S. C. Nyburg, and M. T. Shiomi, *Chem. Commun.*, **1967**, 426; J. A. Wunderlich and D. P. Mellor, *Acta Crystallogr.*, **7**, 130 (1954); *ibid.*, **8**, 57 (1955).

16) R. A. Schunn, *Inorg. Chem.*, **9**, 2567 (1970).

17) T. Ikariya and A. Yamamoto, *J. Chem. Soc., Chem. Commun.*, **1974**, 720.

18) G. Hata, H. Kondo, and A. Miyake, *J. Am. Chem. Soc.*, **90**, 2278 (1968).

19) R. Van der Linde and R. O. de Jongh, *Chem. Commun.*, **1971**, 563.

20) H. Bönnemann, *Angew. Chem.*, **82**, 699 (1970); *Angew. Chem., Int. Ed. Engl.*, **9**, 736 (1970).

21) For example, F. I. Karol, G. L. Karapinka, C. Wu, A. W. Dow, R. N. Johnson, and W. L. Carrick, *J. Polym. Sci., Part A-1*, **10**, 2621 (1972).

22) J. M. Davidson and C. Triggs, *J. Chem. Soc., A*, **1968**, 1324, 1331; Y. Fujiwara, I. Moritani, S. Danno, R. Asano, and S. Teranishi, *J. Am. Chem. Soc.*, **91**, 7166 (1969); R. F. Heck, *ibid.*, **90**, 5518, 5526; 5531; 5535; 5542 (1968); *ibid.*, **91**, 6707 (1969).

Studies of Carbenium Ion on Unsaturated Carbon. II.[1] Exclusive Formation of Benzofurans *via* Vinyl Cations in the Solvolytic Reactions of 1-Aryl-2,2-bis(*o*-methoxyphenyl)vinyl Halides

Takaaki SONODA, Shinjiro KOBAYASHI, and Hiroshi TANIGUCHI

Department of Applied Chemistry, Faculty of Engineering, Kyushu University, Hakozaki, Fukuoka 812

(Received March 27, 1976)

The reactions of 1-aryl-2,2-bis(*o*-methoxyphenyl)vinyl halides (**4**)—(**7**) in 80% aqueous ethanol (80% EtOH), acetic acid (AcOH), or 70% aqueous *N*,*N*-dimethylformamide gave benzofurans (**8**)—(**10**), respectively. The kinetic results *i.e.*, 1) first-order reaction rates, 2) large α-substituent effect ($\rho = -4.12$ against σ^+), 3) large leaving group effect ($k_{Br}/k_{Cl} = 85$ in 80% EtOH and 28 in AcOH) and 4) the solvent effect ($m = 0.53$), are consistent with the formation of the intermediate vinyl cations (**3**) which are captured exclusively by the β-*o*-methoxyl group. In the reaction of vinyl bromide (**7**), the formation of 7—9% of benzofuran (**11**) results from the β-*o*-methoxyphenyl migration in the vinyl cation (**17**) followed by cyclization. The exclusive intramolecular cyclization of the vinyl cations is discussed in terms of the proximity effect of the β-*o*-methoxyl group.

Extensive studies on solvolysis of vinyl derivatives in the last decade have definitely substantiated the vinyl cations as the reactive intermediates.[2] In these reactions, the products are generally those compounds derived from the nucleophilic attack of solvents or nucleophiles on the intermediate vinyl cations. Acetylenic compounds are obtained if β-hydrogens are present in the vinyl substrates. The same kinds of compounds are also formed by the rearrangement of vinyl cations.[3] Moreover, there are several examples

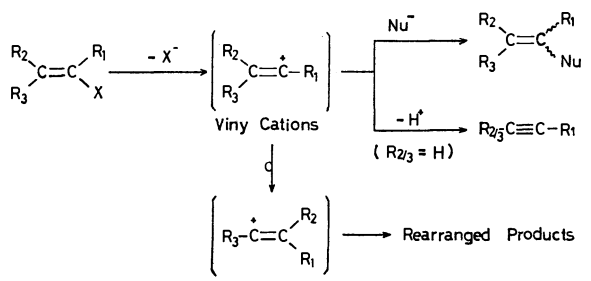

of the participation of neighboring groups, such as β-sulfur atom,[4] ω-double bond,[5] or ω-triple bond,[6] which resulted in the formation of cyclized compounds. However, the selectivity of the cyclization is not high since the external nucleophilic attack to vinyl cations competes with the cyclization.

We found that in solvolytic conditions 1-aryl-2,2-bis(*o*-methoxyphenyl)vinyl halides (**1**) underwent a new type of internal cyclization to benzofurans (**2**) *via* vinyl cation intermediates (**3**). The most remarkable feature

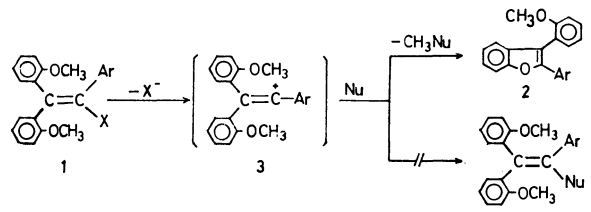

of these reactions is that the formation of benzofurans occurs exclusively and that no other product is obtained by an external nucleophilic attack to the vinyl cations even in the presence of strong nucleophiles.

This paper describes the results of kinetics in relation to α-substituent group, solvent, and leaving group effects aimed at confirming the intermediacy of the vinyl cations (**3**) in the reaction of **1**.

Results

Products. Vinyl halides (**4**)—(**7**) were prepared by bromination or chlorination of the corresponding ethylenes, which is similar to the method used for the preparation of the 2-*p*-methoxyphenylvinyl derivatives.[7]

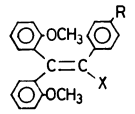

4 R=OCH_3, X=Br
5 R=OCH_3, X=Cl
6 R=CH_3, X=Br
7 R=H, X=Br

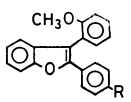

8 R=OCH_3
9 R=CH_3
10 R=H

The reaction of 2,2-bis(*o*-methoxyphenyl)-1-(*p*-methoxyphenyl)vinyl bromide (**4**) in 80% EtOH at 120 °C for 4 h in the presence of excess sodium hydroxide (NaOH) gave 2-(*p*-methoxyphenyl)-3-(*o*-methoxyphenyl)benzofuran (**8**); this was isolated and its structure was determined by microanalysis and by comparing its characteristic UV spectrum with other benzofuran derivatives. The NMR spectrum of the crude product was identical with that of the isolated **8**, which indicates the exclusive formation of **8**. The reactions of **4** in other solvent systems *i.e.*, AcOH and 70% aqueous *N*,*N*-dimethylformamide, always gave **8** in essentially quantitative yields. The selective formation of **8** was not affected by strong nucleophiles. In the presence of sodium azide, the reaction of **4** in 80% EtOH at 120 °C for 6 h also gave **8** as a sole product. The reaction of **4** in 80% EtOH at 120 °C for 4 h in the presence of 1.5 and 3 equivalents of sodium *p*-toluenethiolate afforded **8** exclusively, with 47 and 74% yields of methyl *p*-tolyl sulfide, respectively, which were derived from the capture of methyl moieties by the nucleophile *p*-toluenethiolate ions. A similar result, leading to a quantitative formation of **8**, was obtained in the reaction of the corresponding vinyl chloride (**5**) in basic 80% EtOH at 160 °C for 25 h.

The reaction of 2,2-bis(*o*-methoxyphenyl)-1-*p*-tolylvinyl bromide (**6**) in basic 80% EtOH at 160 °C for 43 h

gave 3-(*o*-methoxyphenyl)-2-*p*-tolylbenzofuran (**9**) as the sole product.

In contrast to 1-(*p*-methoxyphenyl)- and 1-*p*-tolylvinyl derivatives (**4**) and (**6**), the reaction of 1-phenylvinyl derivative (**7**) was much more sluggish; two different products were obtained. The NMR spectrum of the reaction of 2,2-bis(*o*-methoxyphenyl)-1-phenylvinyl bromide (**7**) in basic 80% EtOH at 160 °C for 204 h (95% reaction) showed two kinds of methoxyl singlets (at δ 3.45 and 3.34 in CCl_4) which were different from the methoxyl signals of the starting vinyl bromide (**7**). Integration of the two different methoxyl signals showed two products to be present in the ratio of 93: 7. The major one of these products was isolated as the picrate (mp 108—109 °C). Microanalysis of the picrate and the UV spectrum of the major product regenerated by alumina chromatography (see Table 1) showed the major one as a benzofuran derivative of $C_{21}H_{16}O_2$ (**10**). Attempts to isolate the minor product from the filtrate of the picrate (the major/minor ratio of 74/26) by formation of the picrate, by crystallization, and by thin-layer chromatography (silica gel) failed. However the high-pressure liquid chromatogram (alumina, hexane) of the filtrate showed two peaks and their UV spectra were measured by the stop-flow scanning method. As shown in Table 1, the UV spectrum of the major peak of the chromatogram showed λ_{max} at 306 nm, which was identical with that of the isolated major product (**10**). The minor peak, whose UV spectrum showed λ_{max} at 320 nm, was then assigned to the minor product (**11**). By consideration of the NMR and IR spectra of the reaction mixture and the UV spectrum of the minor product, the minor one has only one methoxyl group and can not be a product such as a ketone or ethyl vinyl ether which may be derived from external nucleophilic attack,[7] it was assigned as the isomeric benzofuran of the major one. The structures of isomeric **10** and **11** were determined as follows.

As shown in Table 1 benzofurans with 2-methoxyphenyl groups (**8**, **12**, and **13**) have higher λ_{max} than the benzofurans with 2-phenyl groups (**14** and **15**), or the benzofuran with 2-tolyl group (**9**). On the basis of this trend of chromophores, the major product (**10**) whose UV spectrum shows a lower λ_{max} (306 nm) than the minor one (320 nm) is assigned to a 2-phenyl-substituted benzofuran entity and then the minor one to a 2-methoxyphenyl-substituted benzofuran. Consequently, it is concluded that the major product (**10**) in the reaction of **7** is 3-(*o*-methoxyphenyl)-2-phenylbenzofuran and the minor one (**11**) is 2-(*o*-methoxyphenyl)-3-phenylbenzofuran.

The reactions of **7** in basic 50% EtOH at 160 °C for

Table 1. Ultraviolet spectra of 2-aryl- and 2,3-diarylbenzofurans in cyclohexane

Compound	λ_{max} (nm)		
12[a]	325 (20600),	310 (33500),	303 (30600)
	270 (22000),	280 (15900),	247 (47000)
13[a]	327 (33400),	312 (33800),	298 (19100)
	290 (18200),	278 (14600),	234 (12100)
14[b]	316 (24000),	304 (32400),	296 (25700)
	290 (24000),	232 (10700),	226 (10700)
8	316 (27500),	250 (17400)	
9	307 (24800),	238 (17200)	
10	305 (21400),	240 (17700)	
	306 (—)[c]	248 (—)[c]	
11	320 (—)[c]	263 (—)[c]	
15[a]	305 (22900),	237 (22200)	

a) H. Taniguchi, unpublished results. b) Taken from Ref. 23. c) Measured by stop-flow scanning method of high-pressure liquid chromatography in hexane.

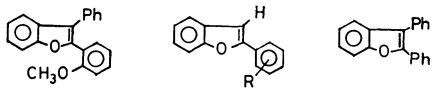

11 **12** R=OCH_3-*p* **15**
13 R=OCH_3-*o*
14 R=H

Table 2. Kinetics of solvolysis of triarylvinyl halides in aqueous ethanol

Compd	M×10⁵	NaOH M×10⁵	Solvent	Temp (°C)	$k\times10^4$ (s^{-1})	Method[a]
4	4700	10000	80% EtOH	120	2.52 ±0.04	t
	4700	40000	80% EtOH	120	2.22 ±0.03	t
	239	400	80% EtOH	120	2.44 ±0.03	u
	8.8	10.0	80% EtOH	120	2.46 ±0.03	u
	4700	10000	80% EtOH	130	5.47 ±0.07	t
	239	400	80% EtOH	130	5.71 ±0.13	u
	8.7	10.0	80% EtOH	130	5.11 ±0.03	u
	239	400	80% EtOH	140	13.92 ±0.23	u
	239	400	80% EtOH	150	24.12 ±0.44	u
				160	43.0[b]	
	148	300	70% EtOH	120	4.80 ±0.06[c]	u
	151	300	90% EtOH	120	0.98 ±0.04[c]	
5	3.52	16.0	80% EtOH	140	0.160±0.001	u
	3.64	80.0	80% EtOH	140	0.168±0.001	u
6	3.28	80.0	80% EtOH	160	0.617±0.006	u
7	635	1250	80% EtOH	160	0.026±0.001	n

a) t, titration method, u, UV method, n, NMR method. b) Extrapolated from data at lower temperature. c) Rates are averages of duplicate determinations.

26 h (96% reaction), and in AcOH with excess silver acetate at 118 °C for 21 h (100% reaction) also gave these isomeric benzofurans in similar product ratios (the **10**/**11** ratios of 93/7 and 91/9, respectively).

Kinetics. Reaction rates of vinyl halides (**4**)—(**7**) in aqueous EtOH with NaOH and in AcOH with NaOAc were measured by titration of the formed bromide ions (titration method), and by measuring the UV spectra of the reaction mixtures (UV method). Since the results from the titration method were identical with those from the UV method within experimental errors, most of the measurements were made by the UV method. The reaction rates of **7** in 80% EtOH and of **5** in AcOH were followed by NMR spectroscopy (NMR method) as the reaction rates of these reactions were very sluggish.

The kinetic results in aqueous EtOH are summarized in Table 2. All the runs followed accurately the first-order kinetic law. The rate constants were not affected by the concentrations of the substrates and the added base(NaOH). Solvent polar effects were studied with **4** in 70, 80, and 90% EtOH. A plot of log k for **4** *vs.* Grunwald-Winstein's Y value[8] is linear and the m value is 0.53 at 120 °C. The reactivity ratio of (**4**) 1650: (**6**) 24: (**7**) 1 suggests a large α-substituent effect. The Hammett plot of log k against σ^+ [9] gave $\rho=-4.12$ (correlation coefficient $r=0.999$) in 80% EtOH at 160 °C. The bromide (**4**)/chloride (**5**) reactivity ratio in 80% EtOH at 140 °C is 85. Activation parameters for solvolysis of **4** in 80% EtOH are $\Delta H^{\neq}=26.8\pm0.4$ kcal/mol and $\Delta S^{\neq}=-7\pm1$ e.u. (120 °C).

Solvolysis rates of **4** and **5** in AcOH are shown in Table 3. The reactions obeyed good first-order kinetics up to 80% conversion. The bromide (**4**)/chloride (**5**) reactivity ratio in AcOH at 140 °C is 27.8.

TABLE 3. KINETICS OF SOLVOLYSIS OF 2,2-BIS-(*o*-METHOXYPHENYL)-1-(*p*-METHOXYPHENYL)VINYL BROMIDE (**4**) AND CHLORIDE (**5**) IN ACETIC ACID

Compd	$M\times10^5$	NaOAc $M\times10^5$	Temp. (°C)	$k\times10^4$ (s^{-1})	Method[a]
4	988	1278	120	0.54±0.01	u
	3.58	8.90	120	0.58±0.01[b]	u
	3.30	7.76	140	3.33±0.06	u
5	934	1864	140	0.12±0.01	n

a) u, UV method; n, NMR method. b) Rate is an average of duplicate determinations.

Discussion

Evidence for the Vinyl Cation Intermediates. Several possible mechanisms for the exclusive intramolecular cyclization of 1-aryl-2,2-bis(*o*-methoxyphenyl)vinyl halides are shown in Scheme 1.

Path A *via* vinyl cation intermediates can be supported by the following criteria. The solvolysis rates fit first-order rate plots and do not depend on the base concentrations. The large α-substituent effect ($\rho=-4.12$ against σ^+) suggests the formation of a cation center on the α-carbon in the transition state. The solvent polar effect ($m=0.53$ at 120 °C) also indicates the cationic intermediate. Moreover, in addition to the electrophilic catalysis by the silver ions, the large leaving group effect ($k_{Br}/k_{Cl}=85$ in 80% EtOH and 27.8 in AcOH) suggests a heterolytic C–X bond fission in the rate-determining step. These reactivity ratios which depend on solvent,[7,10] α-substituent,[10,11] and leaving group[7,12,13] effects are similar to those of the solvolysis of vinyl halides for which the intermediacy of vinyl cations has been established.

On the other hand, the possibilities of paths B–D, which may compete with the S_N1 mechanism in the solvolysis of vinyl derivatives,[2] can be ruled out as follows. Path B involves an external nucleophilic attack on the double bond followed by displacement of the halogen by the β-*o*-methoxyl oxygen with elimination of the nucleophile. This pathway is unlikely in 80% EtOH or AcOH since the rate constants do not depend on the base concentrations. The nucleophilic addition-elimination mechanism was observed in the solvolysis of 9-(α-haloarylidene)fluorenes in 80% EtOH with strong nucleophiles,[14] but the kinetic behavior of the fluorenyl systems are very different from those of our systems. Path C is a rate-determining electrophilic addition (protonation) followed by a methoxyl oxygen attack with elimination of the hydrogen halide.[15,16] If path C could operate in our systems, the electrophilic addition should be faster in AcOH than in 80% EtOH. However, the solvolysis rates of **4** and **7** in 80% EtOH were faster than in AcOH ($k_{80\%\ EtOH}/k_{AcOH}$ of 4.4 for **4** at 120 °C and of 1.4 for **5** at 140 °C). Moreover, the

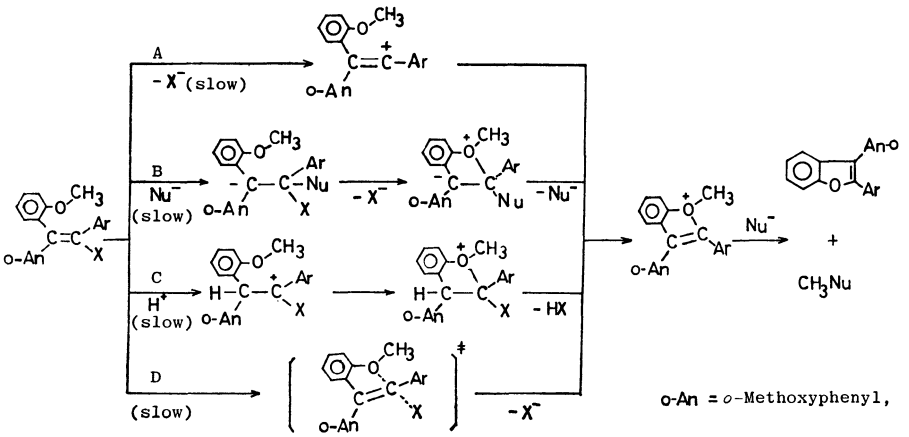

Scheme 1. Possible reaction paths for cyclization reaction.

effect of the leaving groups for the electrophilic addition-elimination route suggests the reactivity order: $k_{Cl} > k_{Br}$,[13] which is contrary to our systems. The exclusive cyclization to benzofurans and the lack of incorporation of the external nucleophiles suggest path D, which involves a one-step direct intramolecular S_N2-type attack of the β-*o*-methoxyl oxygen on the α-carbon with synchronous elimination of the halogen. However, such direct displacements at vinyl carbons are energetically unfavorable,[17] and have so far not been observed in vinyl systems. In path D, it could be expected that the solvolysis of 2-*o*-methoxyphenyl-substituted vinyl halides should be faster than that of the corresponding 2-*p*-methoxyphenyl-substituted vinyl derivatives in which the anchimeric acceleration by the β-methoxyl group is inherently impossible to operate. In practice, however, the solvolysis of 1,2,2-tris(*p*-methoxyphenyl)vinyl bromide (**16**)[7] is faster than that of **4** (k(**16**)/k(**4**) ratio of 1.7 in 80% EtOH at 120 °C and of 1.1 in AcOH at 120 °C). This result argues against the possibility of the anchimeric acceleration by the neighboring β-*o*-methoxyl group.

Cyclization vs. *2-o-Methoxyphenyl Migration.* As in the case of saturated carbenium ions, the rearrangement of the reactive vinyl cations to more stable cations is a characteristic feature of vinyl cation intermediates. In vinyl cations two types of rearrangements are known: to the double bond[18] (Eq. 1) and across the double bond[3,19] (Eq. 2).

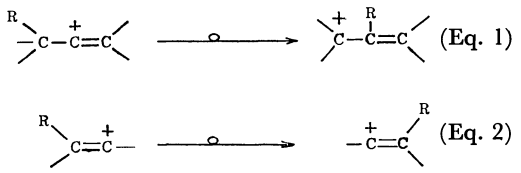

Solvolysis of **7** gave small amounts of **11** (7, 7, and 9% in 50% EtOH, 80% EtOH, and AcOH with AgOAc, respectively) in addition to the normal cyclization product (**10**). Benzofuran (**11**) resulted from the 2-*o*-methoxyphenyl migration in the vinyl cation (**17**) to the more stable vinyl cation (**18**). The rearranged vinyl cation (**18**) is also exclusively attacked by the β-*o*-methoxyl oxygen. These results indicate that the nucleophilic attacks to the vinyl cation (**17**) are in the following ordering: internal nucleophilic attack (cyclization)>2-*o*-methoxyphenyl group participation (migration)≫external nucleophilic attack.

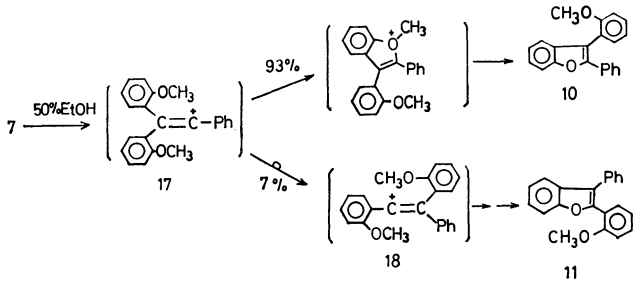

In conclusion, it is a remarkable feature of the solvolytic reactions of 1-aryl-2,2-bis(*o*-methoxyphenyl)-vinyl halides (**1**) that exclusive cyclization to benzofurans (**2**) occurs in preference to the external nucleophilic attack to the vinyl cations (**3**) even in the presence of the strong nucleophiles. The origin of this exclusive cyclization can be discussed as follows. There exists a large steric hindrance between the aryl groups in **1**, because the substituents attached to the unsaturated carbons are held in the plane of the molecule. Vinyl cations (**3**) have the sp-hybridized structure and the α-aryl rings of the vinyl cations come to be perpendicular to the molecular plane in order to allow the π-orbital of the α-aryl groups to overlap well with the vacant *p*-orbital of the vinyl cations.[2] While some of the *cis* α-aryl and β-*o*-methoxyphenyl steric interaction is relieved in the sp-hybridized vinyl cations, the approach of the external nucleophiles to the cation center is still retarded because of the steric and electronic repulsions between the β-substituents and the approaching nucleophiles.[13,20] Moreover, even if such an external nucleophilic attack had occurred, the resulted vinyl derivatives (**19**) should be still sterically hindered. On the other hand, the intramolecular attack of the β-*o*-methoxy oxygen atoms upon the vinyl cations is entropically favorable since the β-*o*-methoxyl groups are located in suitable positions to attack the vacant *p*-orbital of the vinyl cations (**3**) and the resulted oxonium ions (**20**) are stabilized by the relief of the steric repulsion presented in the starting materials.[21] It seems likely that the proximity effect of the β-*o*-methoxyl group, in addition to the stability of the resulting product, is the driving force of the exclusive cyclization.

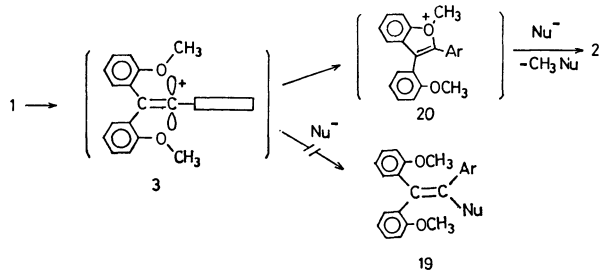

Experimental

All melting points are uncorrected. NMR spectra were taken on a JEOL JNM-MH-60 spectrometer. All mass spectra were obtained with a JEOL JMS-07 spectrometer. UV spectra were recorded with HITACHI 124, Shimadzu UV-200S, and UV-202S spectrometers. All IR spectra were obtained with a Shimadzu IR-400 spectrometer. Aqueous ethanolic mixtures were prepared according to Grob.[10] Acetic acid was prepared by refluxing glacial acetic acid with 1% acetic anhydride and then fractionally distilling. Sodium acetate solutions were prepared by disolving analytical sodium carbonate in acetic acid. *N,N*-Dimethylformamide (DMF) was dried over phosphorus pentoxide overnight and the fraction boiling at 78—79.5 °C (28—30 mm) was collected and stored over molecular sieves. 70% aqueous DMF was obtained according to Kaufman.[11]

Preparation of Vinyl Halides. Vinyl halides were prepared by appropriate modifications of the methods used for the preparation of 2-*p*-methoxyphenyl-substituted vinyl halides.[7] Spectral data of the vinyl halides are given in Table 4.

2,2-Bis(o-methoxyphenyl)-1-(p-methoxyphenyl)vinyl Bromide (4). *1,1-Bis(o-methoxyphenyl)-2-(p-methoxyphenyl)ethanol*: A solution of *o*-methoxyphenylmagnesium bromide was prepared in the usual manner from magnesium (2.43 g, 0.1

mol), *o*-bromoanisole (18.71 g, 0.1 mol), and ether (80 ml). As soon as the metal reacted, ethyl *p*-methoxyphenylacetate (9.71 g, 0.05 mol) in ether (40 ml) was added and the reaction mixture was heated under reflux for 20 min and allowed to stand overnight. The aqueous solution was extracted twice with CH_2Cl_2 and the combined extracts and the ether layer were washed with water, dried over Na_2SO_4, and evaporated to dryness. The solid obtained (10.75 g, 59%) was recrystallized three times (CH_2Cl_2–EtOH) and gave white needles, mp 164—169 °C, of 1,1-bis(*o*-methoxyphenyl)-2-(*p*-methoxyphenyl)ethanol. IR(Nujol): 3500 cm^{-1} (OH). NMR ($CDCl_3$, δ): 3.44 (d-s, 6H, OCH_3), 3.66 (d-s, 5H, OCH_3 and CH_2), 4.83 (s, OH), 6.45—7.45 (m, 12H, arom.). Found: C, 75.54; H, 6.73%. Calcd for $C_{23}H_{24}O_4$: C, 75.80; H, 6.69%.

2,2-Bis(o-methoxyphenyl)-1-(p-methoxyphenyl)ethylene: Phosphoric acid (85%, 8 ml) was added to 1,1-bis(*o*-methoxyphenyl)-2-(*p*-methoxyphenyl)ethanol (7.3 g, 20.1 mmol) and the mixture was kept at 100 °C for 3 h with stirring. The cooled mixture was washed four times with water by decantation and the residual oil was dissolved in CH_2Cl_2 and dried over Na_2SO_4. After solvent removal, recrystallization from CH_2Cl_2–EtOH (1:4) gave 2,2-bis(*o*-methoxyphenyl)-1-(*p*-methoxyphenyl)ethylene, mp 99.5—100.5 °C (6.57 g, 95%). NMR ($CDCl_3$, δ): 3.50 (s, OCH_3), 3.61 (s, OCH_3), 3.70 (s, OCH_3), 6.52—7.25 (m, 13H, =CH– and arom.). UV: λ_{max} (cyclohexane); 285 nm (ε 19200) and 208 (37000).

2,2-Bis(o-methoxyphenyl)-1-(p-methoxyphenyl)vinyl Bromide (4): 1. To 1,1-bis(*o*-methoxyphenyl)-2-(*p*-methoxyphenyl)-ethanol (6.06 g, 0.017 mol) in AcOH (24 ml), bromine (2.75 g, 0.017 mol) was added and the mixture was kept for 30 min with stirring. The mixture was poured into water and extracted with ether. The ether extract was washed with saturated $NaHCO_3$ solution and water, and dried over Na_2SO_4. After solvent removal, the residual oil was chromatographed over neutral alumina. The solvent removal from the benzene fraction gave the solid (2.33 g, 33%). Recrystallization (benzene–EtOH 1:1) afforded white needles, mp 126.5—128 °C, of 2,2-bis(*o*-methoxyphenyl)-1-(*p*-methoxyphenyl)vinyl-bromide (**4**). Found: C, 65.20; H, 5.05%. Calcd for $C_{23}H_{21}O_3Br$: C, 64.95; H, 4.98%.

2. *N*-Bromosuccinimide (1.8 g, 10 mmol) and benzoyl peroxide (50 mg) were added to 2,2-bis(*o*-methoxyphenyl)-1-(*p*-methoxyphenyl)ethylene (3.5 g, 10 mmol) in CCl_4 (50 ml). The mixture was refluxed for 1 h with irradiation with a photographic reflector spot lamp. After cooling to 0 °C, the succinimide was filtered and the filtrate washed with water, dilute NaOH solution, and water again. After solvent removal, recrystallization (CH_2Cl_2–EtOH 1:1) gave **4** (4.52 g, 71%), mp 128—130 °C.

2,2-Bis(o-methoxyphenyl)-1-(p-methoxyphenyl)vinyl Chloride (5). To 2,2-bis(*o*-methoxyphenyl)-1-(*p*-methoxyphenyl)-ethylene (2.79 g, 8.05 mmol) in CCl_4 (20 ml), chlorine (0.6 g, 8.475 mmol) was added over the period of 120 min. After the solution was stirred for an additional 90 min, the solvent was evaporated and a white solid (2.68 g, 87%) precipitated. Recrystallization (CH_2Cl_2–EtOH) gave 2,2-bis(*o*-methoxyphenyl)-1-(*p*-methoxyphenyl)vinyl chloride (**5**), mp 112—113 °C. Found: C, 72.38; H, 5.63%. Calcd for $C_{23}H_{21}O_3Cl$: C, 72.53; H, 5.56%.

2,2-Bis(o-methoxyphenyl)-1-p-tolylvinyl Bromide (6). *1,1-Bis(o-methoxyphenyl)-2-p-tolylethanol*: To *o*-methoxyphenylmagnesium bromide (23.8 g, 0.112 mol) in ether (100 ml), dry benzene (40 ml) and then ethyl *p*-tolylacetate (10.0 g, 0.056 mol) in dry benzene (44 ml) were added, and the solution was allowed to stand overnight. After the solution was refluxed for 20 min, 2M-HCl (90 ml) was added and the reaction mixture was extracted with CH_2Cl_2. Work-up of the reaction mixture gave the solid. Recrystallization (CH_2Cl_2–EtOH 1:2) gave 1,1-bis(*o*-methoxyphenyl)-2-*p*-tolylethanol (15.11 g, 77.5%), mp 168—169 °C. NMR($CDCl_3$, δ): 2.20 (s, CH_3), 3.42 (d-s, 6H, OCH_3), 3.68 (s, CH_2), 4.84 (s, OH), 6.65—7.50 (m, 12H, arom.). IR(Nujol): 3570 cm^{-1} (OH). Found: C, 79.03; H, 6.98%. Calcd for $C_{23}H_{24}O_3$: C, 79.28; H, 6.94%.

2,2-Bis(o-methoxyphenyl)-1-p-tolylethylene: 1,1-bis(*o*-methoxyphenyl)-2-*p*-tolylethanol (10.0 g, 0.028 mol) was treated with phosphoric acid (85%, 15 ml) at 100 °C for 3 h. Work-up of the reaction mixture gave 2,2-bis(*o*-methoxyphenyl)-1-*p*-tolylethylene (8.69 g, 92%), mp 87.2—88.8 °C (EtOH). NMR (CCl_4, δ): 2.20 (s, CH_3), 3.43 (s, OCH_3), 3.56 (s, OCH_3), 6.55—7.20 (m, 13H, =CH– and arom.). UV: λ_{max} (cyclohexane); 283 nm (ε 17800), 220 (26900). Found: C, 83.58; H, 6.82%. Calcd for $C_{23}H_{22}O_2$: C, 83.60; H, 6.71%.

2,2-Bis(o-methoxyphenyl-1-p-tolylvinyl Bromide (6): Bromine (0.97 g, 6.05 mmol) in CCl_4 (10 ml) was added slowly to 2,2-bis(*o*-methoxyphenyl)-1-*p*-tolylethylene (2.0 g, 6.09 mmol) in CCl_4 (15 ml) while cooling, with stirring which continued for an additional 30 min. Solvent removal gave the solid and recrystallization (CH_2Cl_2–EtOH 1:5) gave white needles, mp 123—124 °C, of 2,2-bis(*o*-methoxyphenyl)-1-*p*-tolylvinyl bromide (**6**) (3.25 g, 87.5%). Found: C, 67.17; H, 5.33%. Calcd for $C_{23}H_{21}O_2Br$: C, 67.49; H, 5.17%.

2,2-Bis(p-methoxyphenyl)-1-phenylvinyl Bromide (7). *1,1-Bis(o-methoxyphenyl)-2-phenylethanol*: To *o*-methoxyphenylmagnesium bromide(*o*-bromoanisole, 22.47 g, 0.12 mol, magnesium, 2.67 g, 0.11 mol) in ether (100 ml), ethyl phenylacetate (8.2 g, 0.05 mol) in dry benzene (70 ml) was added slowly and heated under reflux for 4 h. On cooling, 2M-HCl (70 ml) was added and a work-up of the reaction mixture similar to that of 1,1-bis(*o*-methoxyphenyl)-2-(*p*-methoxyphenyl)-ethanol gave the precipitate (10.23 g, 61%). Recrystallization (CH_2Cl_2–EtOH) gave 1,1-bis(*o*-methoxyphenyl)-2-phenylethanol, mp 154 °C. NMR ($CDCl_3$, δ): 3.43 (d-s, 6H, OCH_3), 3.72 (s, CH_2), 4.83 (broad s, OH), 6.64—7.46 (m, 13H, arom.). IR (Nujol): 3560 cm^{-1} (OH). Found: C, 78.92; H, 6.63%. Calcd for $C_{22}H_{22}O_3$: C, 79.01; H, 6.63%.

2,2-Bis(o-methoxyphenyl)-1-phenylethylene: 1,1-Bis(*o*-methoxyphenyl)-2-phenylethanol (5.0 g, 0.015 mol) was treated with phosphoric acid (11 ml) at 100 °C for 3 h. Work-up of the reaction mixture gave 2,2-bis(*o*-methoxyphenyl)-1-phenylethylene (4.59 g, 97%), mp 91—92 °C. NMR (CCl_4, δ): 3.41 (s, OCH_3), 3.57 (s, OCH_3), 6.55—7.15 (m, 14H, =CH– and arom.). UV: λ_{max} (cyclohexane) 284 nm (ε 16000), 250 (12500). Found: C, 83.24; H, 6.40%. Calcd for $C_{22}H_{20}O_2$: C, 83.51; H, 6.37%.

2,2-Bis(o-methoxyphenyl)-1-phenylvinyl Bromide (7): 2,2-bis(*o*-methoxyphenyl)-1-phenylethylene (3.50 g, 0.01 mol) was treated with *N*-bromosuccinimide (2.00 g, 0.012 mol) and benzoyl peroxide (50 mg) in CCl_4 (70 ml) in a manner similar to that used preparation of **4**. The solid obtained (3.87 g, 89%) was recrystallized (CH_2Cl_2–EtOH 2:5) to give white needles, mp 142—143 °C, of 2,2-bis(*o*-methoxyphenyl)-1-phenylvinyl bromide (**7**). Found: C, 66.85; H, 4.85%. Calcd for $C_{22}H_{19}O_2Br$: C, 66.84; H, 4.84%.

Reaction of 2,2-Bis(o-methoxyphenyl)-1-(p-methoxyphenyl)vinyl Bromide (4). Reaction in 80% EtOH: Vinyl bromide (**4**) (70 mg, 0.164 mmol) in 80% EtOH (20 ml) containing NaOH (0.5 mmol) was kept in a sealed ampoule at 120 °C for 8 h. The solvent was removed and ether was added, then the inorganic salt was removed, dried over Na_2SO_4, and the ether was evaporated to give 3-(*o*-methoxyphenyl)-2-(*p*-methoxyphenyl)benzofuran (**8**) exclusively. The NMR spectrum and the thin-layer chromatogram of the crude product showed no

chromophor; its structure was assigned to 3-(*o*-methoxyphenyl)-2-phenylbenzofuran (**10**), as discussed in Table 1. Attempts to isolate the minor product from the filtrate of the picrate by TLC or by formation of the picrate failed. The high-pressure liquid chromatogram of the filtrate (by Shimadzu 840 instrument; column, Varian-Aerograph Micro Pack AL-10 2.2$\phi \times$0.25 m; eluent, hexane; flow rate, 0.4 ml/min) showed two separated peaks and their UV spectra were recorded by the stop-flow method, as shown in Table 1. The assignment of these peaks was previously discussed.

Kinetics. *Titration Method*: Kinetic runs were achieved according to a method similar to Rappoport's.[7] Titration of the bromide ions against standard silver nitrate using Eosin or Uranin indicators (Fajans method) showed ambiguous end-points of titration, so this method was abandoned. Titrimetri-rate constants were determined by the Volhald method as follows. The reaction mixtures in ten to fifteen sealed ampoules, each of which was quenched at appropriate times, were diluted with water ten times. A weighted quantity of the standard silver nitrate was added to each solution. After addition of concd nitric acid (2 ml), nitrobenzene (3—5 ml), and iron alum solution (2 ml), back-titration by the standard 0.01 M potassium thiocyanate gave a sharp end-point.

UV Method: The reaction mixtures of UV concentration in ten to fifteen ampoules were quenched at appropriate intervals and the change in the absorbance (at 300—310 nm) of the reaction mixture was followed by an UV spectrometer. In some runs, concd reaction mixtures were diluted to UV concentration and their UV spectra were measured.

NMR Method: Five to six sealed ampoules, each of which contained vinyl halides (50 mg) in 80% EtOH or AcOH with buffers, were quenched at appropriate times. After work-up of the reaction mixtures, rate constants were obtained by following the relative NMR intensities of the different methoxyl peaks of vinyl halides and benzofurans.

All rate constants are calculated by the least-squares method.

References

1) Part I; S. Kobayashi, M. Shinya, T. Nakano, and H. Taniguchi, *Nippon Kagaku Zasshi*, **92**, 322 (1971).

2) Reviews for solvolysis of vinyl derivatives. a) M. Hanack, *Acc. Chem. Res.*, **3**, 209 (1970); b) G. Modena and U. Tonellato, *Adv. Phys. Org. Chem.*, **9**, 185 (1971); c) P. J. Stang, *Prog. Phys. Org. Chem.*, **10**, 205 (1973); d) L. R. Subramanian and M. Hanack, *J. Chem. Educ.*, **52**, 80 (1975).

3) a) M. A. Imhoff, R. H. Summerville, P. v. R. Schleyer, A. G. Martinez, M. Hanack, T. E. Dueber, and P. J. Stang, *J. Am. Chem. Soc.*, **92**, 3802 (1970); b) G. Modena and U. Tonellato, *J. Chem. Soc.*, **1971**, 381; c) G. Cappozzi, G. Melloni, and G. Modena, *ibid., C*, **1971**, 3018; d) P. J. Stang and T. E. Dueber, *J. Am. Chem. Soc.*, **95**, 2683, 2686 (1973); e) Z. Rappoport and Y. Houminer, *J. Chem. Soc., Perkin Trans. 2*, **1973**, 1506; f) K. P. Jäckel and M. Hanack, *Tetrahedron Lett.*, **1974**, 1637.

4) a) G. Modena, U. Tonellato, and F. Naso, *Chem, Commun.*, **1968**, 1363; b) G. Modena and U. Tonellato, *ibid.*, **1968**, 1676. For a recent report of their series of studies, see P. Bassi and U. Tonellato, *J. Chem. Soc., Perkin Trans. 1*, **1973**, 669.

5) R. G. Bergman and T. C. Clarke, *J. Am. Chem. Soc.*, **96**, 7934 (1974).

6) M. J. Chandy and M. Hanack, *Tetrahedron Lett.*, **1975**, 4515.

7) Z. Rappoport and A. Gal, *J. Am. Chem. Soc.*, **91**, 5246 (1969).

8) A. H. Fainberg and S. Winstein, *J. Am. Chem. Soc.*, **78**, 2770 (1956).

9) H. C. Brown and Y. Okamoto, *J. Am. Chem. Soc.*, **80**, 4979 (1958).

10) C. A. Grob and C. Cseh, *Helv. Chim. Acta*, **47**, 194 (1964).

11) L. L. Miller and D. A. Kaufman, *J. Am. Chem. Soc.*, **90**, 7282 (1968).

12) Z. Rappoport and Y. Apeloig, *Tetrahedron Lett.*, **1970**, 3233.

13) Z. Rappoport and Y. Apeloig, *J. Am. Chem. Soc.*, **97**, 821, 836 (1975).

14) Z. Rappoport and A. Gal, *J. Org. Chem.*, **37**, 1174 (1972).

15) P. E. Peterson and J. M. Indelicato, *J. Am. Chem. Soc.* **90**, 6515 (1968).

16) Z. Rappoport, T. Bässler, and M. Hanack, *J. Am. Chem. Soc.*, **92**, 4985 (1970).

17) D. R. Kelsey and R. G. Bergman, *J. Am. Chem. Soc.*, **93**, 1953 (1971).

18) a) W. D. Pfeifer, C. A. Bahn, P. v. R. Schleyer, S. Bocher. C. E. Harding, K. Hummel. M. Hanack, and P. J. Stang, *ibid.*, **93**, 1513 (1971); b) D. R. Kelsey and R. G. Bergman, *ibid.*, **93**, 1941 (1971); c) K. P. Jäckel and M. Hanack, *Tetrahedron Lett.*, **1975**, 4295.

19) A. G. Martinez, M. Hanack, P. H. Summervelli, P. v. R. Schleyer, and P. J. Stang, *Angew. Chem. Int. Ed. Engl.*, **9**, 302 (1970).

20) Z. Rappoport and T. Kaspi, *J. Chem. Soc., Perkin Trans. 2*, **1972**, 1102.

21) The aromatic stabilization by cyclization may be ruled out as a driving force of exclusive cyclization. For 1,2-bis(*p*-methoxyphenyl)-2-(*o*-dimethylaminophenyl)vinyl bromide also afforded an exclusive cyclization to *N*-methyl-2,3-bis(*p*-methoxyphenyl)indole in basic 80% EtOH and the intermediate onium ion, *N,N*-dimethylindolium ion, was isolated as its perchlorate, in which the aromatic stabilization by the five-membered ring can not exist. H. Taniguchi, *J. Chem. Soc., Chem. Commun.*, in press.

22) K. Auers and F. Arndt, *Ber.*, **42**, 540 (1909).

23) A. S. Angeloni, F. Delmoro, and M. Tramontini, *Ann. Chim. (Roma)*, **53**, 1751 (1963).

Organic Photochemical Reactions. XXIV. Photocycloaddition of Propanal to 1,3-Cyclohexadiene[1]

Kensuke SHIMA,* Tadatoshi KUBOTA,[2] and Hiroshi SAKURAI

*Department of Industrial Chemistry, Faculty of Engineering, Miyazaki University, Miyazaki 880
Institute of Scientific and Industrial Research, Osaka University, Suita, Osaka 565

(Received March 29, 1976)

The photocycloaddition of propanal to 1,3-cyclohexadiene leads to oxetanes, as well as to the dimers of 1,3-cyclohexadiene. A mechanism of oxetane formation is proposed in which singlet excited propanal attacks a ground-state 1,3-cyclohexadiene to give a singlet complex with a charge-transfer character. The complex either decays to the ground-state reactants or reacts to give oxetanes. Quantum yield measurements and kinetic analysis show a rate constant of 4×10^9 $M^{-1}s^{-1}$ for singlet complex formation from propanal and 1,3-cyclohexadiene in benzene. The quenching data of propanal fluorescence support such a mechanism.

The photocycloaddition of carbonyl compounds with olefins to form oxetanes is a topic of recent preparative and mechanistic interest.[3,4] Although a few cases are now known for which ketone singlets attack the olefins,[4c,4d,4e,4f] ketone triplets are generally thought to be the chemically active species in oxetane formation.[3] For electron-rich olefins the reaction is usually believed to involve an electrophilic attack[5] by the oxygen atom of the n,π^* state of the ketone on the olefin. For electron-deficient olefins, the reaction is considered to involve a nucleophilic attack by the electron-rich π^* orbital of the n,π^* singlet state of the ketone.[4d,4e,5] Recently, it has been suggested that an exciplex which leads to oxetane formation is formed between excited carbonyl compounds and olefins.[5,6] However, the reaction of excited carbonyl compounds with conjugated dienes has been little studied.[7] Conjugated dienes have frequently been used as quenchers of the triplet excited state of ketones because of their relatively low triplet energies.[8] However, in the case of benzophenone, the n,π^* triplet state can still undergo photoaddition to conjugated dienes to form oxetanes, in inefficient competition with triplet energy transfer.[7e]

Recently there has been interest in the interaction of acetone with conjugated dienes, studied both by the observation of the fluorescence quenching of singlet acetone[9] and by the isolation of oxetane products.[7b,7d,7f,7h,10] However, few attempts have been made to analyze the products[3g] and mechanism of photoaddition of alkanals such as propanal whose intersystem crossing rate constant seems to be as small as that of acetone.[11] In view of these facts, the photoreaction of propanal with 1,3-cyclohexadiene was investigated. We wish to report our results on the products and mechanism of the interaction of propanal with conjugated dienes;[12] it is interesting to compare our results with those of acetone.[7h]

Results and Discussion

Reaction Products. Irradiation of propanal in the presence of 1,3-cyclohexadiene resulted in the formation of oxetane I and II in good yield. Dimers of 1,3-cyclohexadiene were also formed as minor products. The products assigned the oxetane structures were 1:1 adducts of propanal with the diene, and the IR spectra showed the absence of any carbonyl or hydroxyl group. Instead, each compound showed a strong band in the region 1000—900 cm^{-1}, which is the reported absorption region of the oxetane ring.[13] Oxetanes exhibited two signals near δ 4.7 and one signal near δ 3.0. The former absorptions were assigned to the ring protons α to the ring oxygen, while the higher field absorption was assigned to the ring hydrogen β to the ring oxygen. These are consistent with the reported absorption ranges.[3e,14] The stereochemical assignments for I and II were made on the basis of their vicinal H–H coupling constants in oxetanes. $J_{a,b}$ in the *cis*-isomer II is larger than that in the *trans*-isomer I and as large as $J_{b,c}$ in I and II. These are consistent with the reported observations.[15] The alternative orientation III of cycloaddition was ruled out by the fact that decoupling experiments showed the presence of the coupling between olefinic protons and H_b.

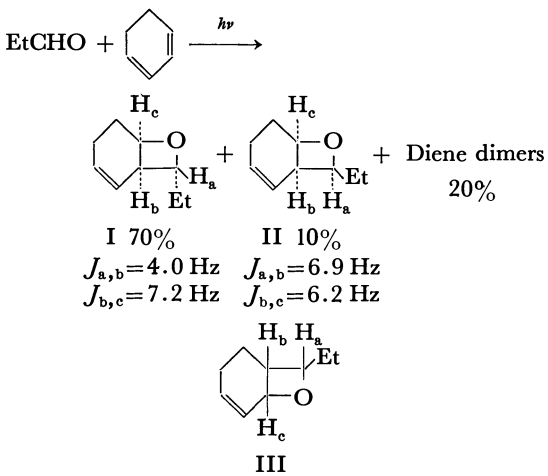

III

Mechanism. In these investigations, the irradiation of propanal with 1,3-cyclohexadiene was conducted in a Pyrex apparatus. Under these conditions, only propanal is excited to its n,π^* singlet state. The UV spectra showed no evidence for a ground-state complex of propanal with the diene. Formation of the diene dimers is thought to proceed *via* the attack of a triplet diene on another ground-state diene molecule.[16] Alkanals and alkanones are believed to have triplet energies of $\approx$80 kcal/mol,[17–19] and after efficient diffusion-controlled transfer[20] of triplet energy (E_T) to the diene (E_T=54 kcal/mol),[21] efficient formation of diene dimers is expected; therefore, the formation of

oxetanes in good yield is mechanistically interesting.

The following routes are possible for oxetane formation: (i) triplet propanal attacks the diene directly to produce the oxetane; (ii) the triplet diene which is produced by energy transfer from triplet propanal attacks ground-state propanal;[7c] or (iii) excited singlet propanal attacks the diene.

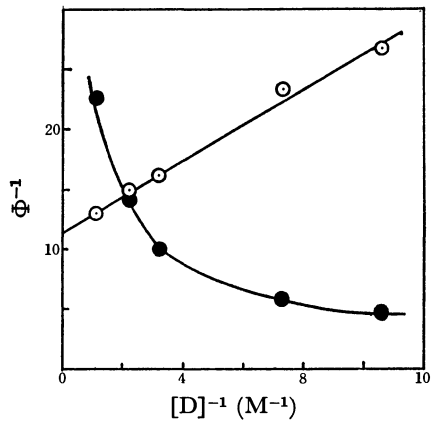

Fig. 1. Dependence of the reciprocal of the quantum yield for products formation on the reciprocal of 1,3-cyclohexadiene concentration; ○, oxetanes; ●, dimers. Slope=1.6 M, Intercept=11.6.

Figure 1 shows plots of the quantum yields for the formation of oxetanes and the diene dimers as a function of 1,3-cyclohexadiene concentration. The dimers decrease as the concentration of 1,3-cyclohexadiene increases. On the other hand, plots for oxetanes are linear up to high concentrations of 1,3-cyclohexadiene. This indicates that different precursors exist for the formation of oxetanes and dimers. It is well known that dimers are formed *via* diene triplets.[16] Therefore, if oxetanes were formed by route (i) or (ii), dimers would have to increase with the concentration of 1,3-cyclohexadiene. This is incompatible with the results. Route (ii) is also ruled out by the fact that oxetanes are hardly obtained under conditions such as those under which triplet dienes are exclusively formed (phenanthrene-sensitized experiments). Therefore, route (iii) is thought to be the mechanism of this reaction. Furthermore, the following evidence indicates that oxetane formation results from the attack of singlet propanal on the diene: (a) the fluorescence of propanal is quenched by addition of 1,3-cyclohexadiene (Fig. 2); and (b) the yield of diene dimers decreases by *ca.* 20% in the presence of air, while that of oxetanes is unchanged. The quantum yield for oxetane formation is much lower than unity even at very high diene concentrations, implying that the reaction of propanal singlet with 1,3-cyclohexadiene is inefficient. The mechanism suggested in the following Scheme is conceivable. The observed inefficiency in formation of oxetanes can be accounted for by formation of an intermediate, C, which can collapse to oxetanes or to propanal and 1,3-cyclohexadiene.

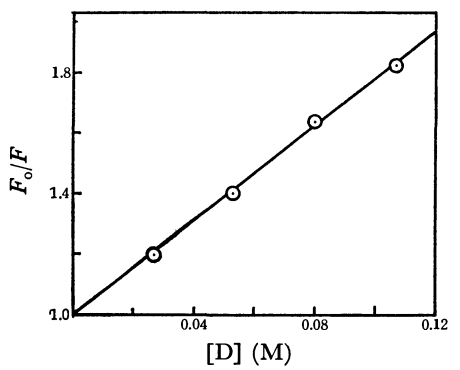

Fig. 2. Stern-Volmer plot for the fluorescence quenching of propanal by 1,3-cyclohexadiene.

$$P \xrightarrow{h\nu} {}^1P$$
$$^1P \xrightarrow{k_1} P + h\nu'$$
$$^1P \xrightarrow{k_2} P$$
$$^1P \xrightarrow{k_3} {}^3P$$
$$^1P + D \xrightarrow{k_4} C$$
$$C \xrightarrow{k_5} P + D$$
$$C \xrightarrow{k_6} \text{Oxetanes}$$
$$^3P + D \xrightarrow{k_7} {}^3D + P$$
$$^3D + D \xrightarrow{k_8} \text{Diene dimers}$$
$$^3D \xrightarrow{k_9} D$$
$$^3P \xrightarrow{k_{10}} P$$

^1P: singlet propanal ^3P: triplet propanal
^3D: triplet 1,3-cyclohexadiene C: singlet complex

Steady-state treatment of the species ^1P, ^3P, ^3D, and C leads to the expressions

$$\frac{1}{\Phi_{ox}} = \frac{k_5+k_6}{k_6} + \frac{(k_1+k_2+k_3)(k_5+k_6)}{k_4k_6}[D]^{-1} \quad (1)$$

$$\Phi_d = \frac{k_3k_7k_8[D]^2}{(k_1+k_2+k_3+k_4[D])(k_7[D]+k_{10})(k_8[D]+k_9)} \quad (2)$$

where Φ_{ox} and Φ_d are the quantum yields for the formation of oxetanes and dimers, respectively. The behavior predicted by Eq. 1 is observed experimentally, as shown in Fig. 1.

The rate of quenching of triplet propanal by 1,3-cyclohexadiene, k_7, is thought to be diffusion-controlled (in benzene, 5×10^9 M^{-1} s^{-1}).[20] Therefore, if the rate of radiationless decay of the propanal triplet, k_{10}, is assumed to be $\approx 10^6$ s^{-1},[22] at concentrations of diene greater than 0.1 M, $k_{10} \ll k_7[D]$ and Eq. 2 becomes Eq. 3.

$$\Phi_d = \frac{k_3k_8[D]}{(k_1+k_2+k_3+k_4[D])(k_8[D]+k_9)} \quad (3)$$

Rearranging Eq. 3 gives Eq. 4.

$$\frac{1}{\left(1+\frac{k_9}{k_8}[D]^{-1}\right)\Phi_d} = \frac{k_1+k_2+k_3}{k_3}\left(1+\frac{k_4}{k_1+k_2+k_3}[D]\right) \quad (4)$$

Figure 3 is a plot of $\Phi_d^{-1}(1+k_9/k_8[D])^{-1}$ against [D], where k_9/k_8 is calculated from the data of Hammond and coworkers[23] to be 0.03. Equation 4 explains the

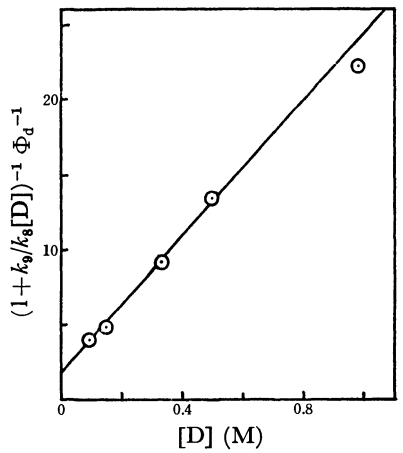

Fig. 3. Plot of $(1+k_9/k_8[D])^{-1}\,\Phi_d^{-1}$ against [D].

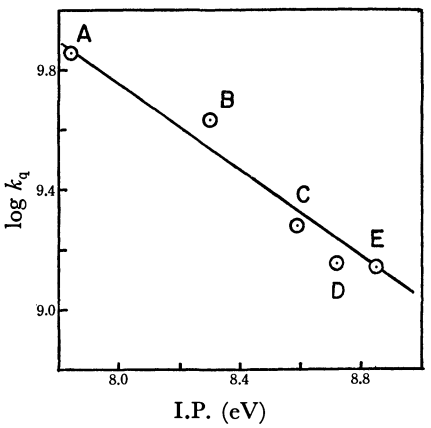

Fig. 4. Correlation of quenching rate constants for propanal with diene ionization potentials.

behavior of the dimerization of 1,3-cyclohexadiene qualitatively.

A Stern-Volmer treatment of the fluorescence quenching (Fig. 2) using Eq. 5 yields a slope of 7.8 M^{-1}.

$$\frac{F_0}{F} = 1 + \frac{k_4[D]}{k_1+k_2+k_3} \qquad (5)$$

F_0: propanal fluorescence intensity in the absence of 1,3-cyclohexadiene

F: propanal fluorescence intensity in the presence of 1,3-cyclohexadiene

The slope and intercept of the Stern-Volmer analysis for oxetane formation with the diene (Fig. 1) show the following:

$$\frac{\text{intercept}}{\text{slope}} = \frac{k_4}{k_1+k_2+k_3} = 7.3M^{-1}$$

This is in good agreement with the value of $k_4/(k_1+k_2+k_3)$ obtained from the quenching of fluorescence of propanal by 1,3-cyclohexadiene, 7.8 M^{-1} (Eq. 5). These results indicate that the fluorescence quenching and oxetane formation by the diene proceed *via* the same intermediate and offer some experimental support to the kinetic Scheme proposed above.

The fluorescence of propanal was also quenched by other conjugated dienes (Table 1). The singlet excitation energy of 1,3-butadiene has been suggested to lie at 112 kcal/mol or somewhat higher[24] and that of 1,3-cyclohexadiene is unlikely to be very different. The lowest excited singlet level of propanal is expected to be a few kilocalories per mole below that of acetone (84 kcal/mol), since the absorption spectrum of propanal is red-shifted by ≈10 nm from that of acetone.[25] Therefore, such quenching is unlikely to proceed by physical energy transfer. It is noteworthy that the rate constants for quenching by 2,5-dimethyl-2,4-hexadiene and 1,3-cyclohexadiene are essentially equal to that for diffusion in the solvent, benzene. In Fig. 4 the function log k_q is plotted against ionization potentials of several 1,3-dienes. The linear behavior indicates that charge transfer interaction contributes to stabilization of this quenching process.[26] The efficient endothermic quenching and linear relationship between log k_q and ionization potentials suggest that the complex mentioned previously is an exciplex involving the interaction between the highest filled orbital of the conjugated diene and the half-vacant n-orbital of propanal.[5a] The simple Hückel MO calculations[27] suggest that the wave-function coefficient of the highest filled orbital of the conjugated diene is largest at the p-orbital of either end. Therefore, an attack by the non-bonding oxygen electron on either end of the diene generates a more stable exciplex. The stability of this exciplex seems to determine the regioselectivity of oxetane formation.

Table 1 shows that rate constants for quenching of propanal n,π^* singlet state by dienes are 5—20 times greater than rate constants for quenching of acetone n,π^* singlet state. These results are consistent with the data suggested by Dalton *et al.*[28] The greater reactivity of propanal n,π^* singlet state toward dienes will probably be a steric effect, *i.e.*, that interaction of the highest filled orbital of conjugated dienes with the electrophilic oxygen *n* orbital in the plane of the carbonyl is less sterically hindered in aldehydes than in ketones, as

Table 1. Diene ionization potentials and rate constants for fluorescence quenching of propanal by conjugated dienes

Diene	$k_q\tau$,M^{-1} a)	k_q,$M^{-1}\,s^{-1}$ b)	I.P.,c) eV
2,5-Dimethyl-2,4-hexadiene (A)	13 (2.07)	7.2×10^9	7.84
1,3-Cyclohexadiene (B)	7.8(1.45)	4.3×10^9	8.30
1,3-Pentadiene (C)	3.5(0.17)	1.9×10^9	8.59
2,3-Dimethyl-1,3-butadiene (D)	2.6(0.19)	1.4×10^9	8.72
Isoprene (E)	2.5(0.13)	1.4×10^9	8.85

a) $k_q=k_4$: quenching rate constants. The values in parentheses are those for acetone.[7h,9b] b) Calculated from the data of Turro *et al.*, Ref. 9c. τ (the lifetime of singlet propanal) is estimated to be 1.8 ns. c) See Ref. 26.

suggested by Dalton *et al.*[11b]

Experimental

General. IR spectra were obtained on a Hitachi EPI-S2 spectrophotometer. UV spectra were obtained on a Hitachi 124 spectrophotometer. Fluorescence spectra were obtained on a Hitachi MPF-2A spectrofluorometer. NMR spectra were taken on a Hitachi Perkin-Elmer R-20 spectrometer. VPC were performed on a Shimadzu GC-3AF. A 2 m 25% PEG 6000 on a Chromosorb W column was used for analysis of the products.

Materials. Benzene was treated with concentrated sulfuric acid, washed with water, and finally purified by distillation over sodium. 1,3-Cyclohexadiene was prepared as described by Marvel and Hartzell.[29] 2,3-Dimethyl-1,3-butadiene was prepared by the method of Allen and Bell.[30] Propanal, 1,3-pentadiene, isoprene, and 2,5-dimethyl-2,4-hexadiene were obtained commercially, and were purified by distillation before use.

Irradiation of Propanal and 1,3-Cyclohexadiene. In a Pyrex vessel, a mixture of propanal (14.5 g, 0.25 mol) and 1,3-cyclohexadiene (20 g, 0.25 mol) was irradiated for 55 h with a 350 W high-pressure mercury lamp. After removal of the reactants, the remaining liquid was distilled under reduced pressure to give a liquid (5.9 g, bp 73—105 °C/18 mmHg), leaving a viscous liquid (1 g). VPC (PEG 6000, 130 °C) of the distillate showed oxetane I (70%), II (10%), and 1,3-cyclohexadiene dimers (20%). 1,3-Cyclohexadiene dimers were identified by a comparison of their VPC retention times (PEG 6000 and DNP) with those of authentic samples.[16] Oxetane I and II were isolated by preparative VPC on a 2 m 25% PEG 6000 column at 125 °C.

Oxetane I was collected as a colorless oil: bp 70—71 °C/18 mmHg; IR 1650 (C=C) and 982 cm^{-1} (oxetane ring); NMR (CCl_4) δ 0.90 (t, J=6.5 Hz, 3H, methyl), 1,1—2.5 (m, 6H, methylene), 2.76 (*ca.* q, 1H, H_b), 3.89 (td, J=4.0 and 6.0 Hz, 1H, H_a), 4.88 (dt, J=3.0 and 7.2 Hz, 1H, H_c), and 5.83 (m, 2H, olefinic). Found: C, 78.23; H, 10.40%; mol wt, (cryoscopic in benzene), 144. Calcd for $C_9H_{14}O$: C, 78.21; H, 10.21%; mol wt, 138.

Oxetane II was collected as a colorless oil: IR 1650 (C=C) and 983 cm^{-1} (oxetane ring); NMR (CCl_4) δ 0.73 (t, J=7.1 Hz, 3H, methyl), 1.0—2.5 (m, 6H, methylene), 3.10 (q, J=6 Hz, 1H, H_b), 4.63 (q, J=6.9 Hz, 1H, H_a), 4.90 (dt, J=2.5 and 6.3 Hz, 1H, H_c), and 5.83 (m, 2H, olefinic). Found: C, 78.00; H, 10.29%. Calcd for $C_9H_{14}O$: C, 78.21; H, 10.21%.

Quantum Yields. Benzene solutions (4 ml) containing 0.11 M propanal and 0.1—1 M 1,3-cyclohexadiene were degassed and sealed in 10 ml o.d. quartz tubes which had been attached to Pyrex tubes *via* graded seals. The sample tubes were then irradiated on a merry-go-round apparatus at room temperature, using a 350 W high pressure mercury lamp and a filter solution with a path length of about 1 cm containing 5 g potassium hydrogen phthalate made up to 1 l with distilled water (>310 nm). Photolysis was carried out to 10% or less conversion (irradiation time, 30 min); the conversion was linear out to 80 min. Actinometers (propanal–2-methyl-2-butene system)[4b] were photolyzed simultaneously. The solutions were analyzed on VPC (PEG 6000, 125 °C), using tetralin as the internal standard.

Sensitization with Phenanthrene. A benzene solution containing 0.12 M propanal, 0.13 M 1,3-cyclohexadiene, and 0.02 M phenanthrene was degassed, sealed, and irradiated for 20 min through a filter solution containing 15 g naphthalene made up to 1 l with hexane (>320 nm). The formation of oxetanes was only <1% of diene dimers, according to VPC, though it was expected to be 20% of diene dimers at such a diene concentration. The formation of a small amount of oxetanes was considered to be due to the directly excited propanal.

Fluorescence Quenching. A propanal solution, 0.2 M, was prepared in benzene. A known volume of the propanal solution was pipetted into a quartz fluorescence cell and the fluorescence was observed using an excitation wavelength of 320 nm. Aliquots of dienes were added to the solution by means of a micro syringe while monitoring the decrease in fluorescence intensity at 420 nm.

Quenching with Oxygen. Two samples were prepared. Each contained 4.0 ml of a benzene solution of 0.13 M propanal and 0.052 M 1,3-cyclohexadiene. One was degassed and sealed. Both samples were irradiated for 45 min with a 350 W high pressure mercury lamp through a potassium hydrogen phthalate cut-off filter (>310 nm). The yield of diene dimers in the non-degassed sample was less than that in the degassed sample by *ca.* 20%, but that of oxetanes was unchanged in both samples, according to VPC (PEG 6000, 125 °C).

References

1) Part XXIII, C. Pac, H. Sakurai, K. Shima, and Y. Ogata, *Bull. Chem. Soc. Jpn.*, **48**, 277 (1975). A preliminary communication of the present paper appeared: T. Kubota, K. Shima, S. Toki, and H. Sakurai, *Chem. Commun*, **1969**, 1462.

2) Present address: The Shionogi Research Laboratory, Shionogi & Co., Ltd., Fukushima-ku, Osaka.

3) Reviews: a) L. L. Muller and J. Hamer, "1,2-Cycloaddition Reactions," Interscience, New York (1967), p. 111; b) D. R. Arnold, *Advan. Photochem.*, **6**, 301 (1968).

4) a) S. Toki and H. Sakurai, *Bull. Chem. Soc. Jpn.*, **40**, 2885 (1967); b) H. Sakurai, K. Shima, and S. Toki, *Nippon Kagaku Zasshi*, **89**, 537 (1968); c) N. J. Turro and P. A. Wriede, *J. Am. Chem. Soc.*, **92**, 320 (1970); d) J. C. Dalton, P. A. Wriede, and N. J. Turro, *ibid.*, **92**, 1318 (1970); e) J. A. Barltrop and H. A. J. Carless, *ibid.*, **94**, 1951 (1972); f) L. A. Singer, G. A. Davis, and V. P. Muralidharan, *ibid.*, **91**, 897 (1969); g) N. C. Yang and W. Eisenhardt, *ibid.*, **93**, 1277 (1971).

5) a) N. J. Turro, J. C. Dalton, K. Dawes, G. Farrington, R. Hautala, D. Morton, M. Niemczyk, and N. Schore, *Acc. Chem. Res.*, **5**, 92 (1972); b) P. J. Wagner, *ibid.*, **4**, 168 (1971).

6) I. E. Kochevar and P. J. Wagner, *J. Am. Chem. Soc.*, **94**, 3859 (1972).

7) a) J. A. Barltrop and B. Hesp, *J. Chem. Soc.*, **1965**, 5182; b) E. H. Gold and D. Ginsburg, *Angew. Chem.*, **78**, 207 (1966); c) J. Saltiel, R. M. Coates, and W. G. Dauben, *J. Am. Chem. Soc.*, **88**, 2745 (1966); d) J. A. Barltrop and H. A. J. Carless, *Chem. Commun.*, **1970**, 1637; e) J. A. Barltrop and H. A. J. Carless, *J. Am. Chem. Soc.*, **93**, 4794 (1971); f) P. Dowd, A. A. Gold, and K. Sachdev, *ibid.*, **92**, 5724, 5725 (1970); P. Dowd, G. Senqupta, and K. Sachdev, *ibid.*, **92**, 5727 (1970); g) D. Bryce-Smith, A. Gilbert, and M. G. Johnson, *J. Chem. Soc., C*, **1967**, 383; h) J. A. Barltrop and H. A. J. Carless, *J. Am. Chem. Soc.*, **94**, 8761 (1972).

8) See, for example, P. J. Wagner and G. S. Hammond, *Advan. Photochem.*, **5**, 21 (1968).

9) a) F. S. Wettack, G. D. Renkes, M. G. Rockley, N. J. Turro, and J. C. Dalton, *J. Am. Chem. Soc.*, **92**, 1793 (1970); b) N. C. Yang, M. H. Hui, and S. A. Bellard, *ibid.*, **93**, 4056 (1971); c) R. R. Hautala and N. J. Turro, *ibid.*, **93**, 5595 (1971).

10) K. Shima, Y. Sakai, and H. Sakurai, *Bull. Chem. Soc. Jpn.*, **44**, 215 (1971).

11) a) A. A. Lamola and N. J. Turro, "Energy Transfer and Organic Photochemistry," Wiley-Interscience, New York (1969), p. 193; b) J. C. Dalton, M. W. Geiger, and J. J. Snyder, *J. Am. Chem. Soc.*, **98**, 398 (1976).
12) For a preliminary account of this work, see Ref. 1.
13) G. M. Barrow and S. Searles, *J. Am. Chem. Soc.*, **75**, 1175 (1953).
14) D. R. Arnold, R. L. Hinman, and A. H. Glick, *Tetrahedron Lett.*, **1964**, 1425.
15) a) N. J. Turro and P. A. Wriede, *J. Org. Chem.*, **34**, 3562 (1969); b) J. J. Beerboom and M. S. von Wittenau, *ibid.*, **30**, 1231 (1965).
16) D. Valentine, N. J. Turro, and G. S. Hammond, *J. Am. Chem. Soc.*, **86**, 5202 (1964).
17) J. C. Dalton and N. J. Turro, *Ann. Rev. Phys., Chem.*, **21**, 499 (1970).
18) See Ref. 11a, pp. 193, 194.
19) E. K. C. Lee, M. W. Schmidt, R. G. Shortridge, Jr., and G. A. Haninger, Jr., *J. Phys. Chem.*, **73**, 1805 (1969).
20) See Ref. 11a, pp. 44, 50.
21) See Ref. 11a, pp. 102, 105.
22) The rate of radiationless decay of the acetone triplet is estimated to be $\approx 10^6$ s^{-1}.[17,18]
23) a) L. M. Stephenson, D. G. Whitten, G. F. Vesley, and G. S. Hammond, *J. Am. Chem. Soc.*, **88**, 3665 (1966); b) L. M. Stephenson and G. S. Hammond, *Pure Appl. Chem.*, **16**, 125 (1968).
24) R. Srinivasan, *Advan. Photochem.*, **4**, 113 (1966).
25) J. G. Calvert and J. N. Pitts, Jr., "Photochemistry," Wiley, New York (1966), pp. 369, 377.
26) D. A. Labianca, G. N. Taylor, and G. S. Hammond, *J. Am. Chem. Soc.*, **94**, 3679 (1972).
27) R. Daudel, R. Lefebvre, and C. Moser, "Quantum Chemistry," Interscience, New York (1959), p. 59.
28) They reported that rate constants for triethylamine quenching of alkanal n,π^* singlet states are 5—10 times greater than rate constants for triethylamine quenching of analogous alkanone n,π^* singlet states.
29) C. S. Marvel and G. E. Hartzell, *J. Am. Chem. Soc.*, **81**, 448 (1959).
30) C. F. H. Allen and A. Bell, *Org. Synth.*, Coll. Vol. III, 312 (1955).

Photolyses of Ethyl Azidoformate in Cyclic Ethers

Noboru TORIMOTO, Tadao SHINGAKI,* and Toshikazu NAGAI*
Science Education Institute of Osaka Prefecture, Sumiyoshi-ku, Osaka 558
**College of General Education, Osaka University, Toyonaka, Osaka 560*
(Received April 2, 1976)

Ethoxycarbonyl nitrene, generated by the photolysis of ethyl azidoformate (I), were inserted preferentially into the α C–H bonds of cyclic ethers. The α C–H bonds of cyclic ethers were much more reactive than the corresponding C–H bonds of hydrocarbons for the insertion of the nitrene. In addition, the reactions in cyclic ethers with an alkyl group at the α-position gave unsaturated alkoxyurethanes *via* a cleavage of the ring C–O bond. It was found that the nitrene insertion into the α C–H bonds of *cis*- and *trans*-2,5-dimethyltetrahydrofurans proceeded non-stereospecifically, while the insertion into the C–H bonds of hydrocarbons proceeded stereospecifically. The formation of the alkoxyurethanes can be explained by a mechanism in which an O–N ylide is included as an intermediate of the nitrene reaction; the non-stereospecific insertion of the nitrene give support to this mechanism.

The relative reactivities for the insertion of nitrenes toward C–H bonds have been reported for primary: secondary:tertiary,[1,2] exo:endo, bridge:bridgehead,[3,4] and axial: equatorial[5] C–H bonds, and in those earlier experiments hydrocarbons have been employed as the substrates. In the reaction of ethoxycarbonyl nitrene, which was generated by the photolysis of ethyl azidoformate, with cyclic ethers, was found that the α C–H bonds showed unusually large reactivities compared with the corresponding C–H bonds of hydrocarbons in the insertion of the nitrene, and observed that cyclic ethers with an α-methyl (or ethyl) group gave unsaturated alkoxyurethanes as a result of the ring C–O bond cleavage. According to Nozaki's report, ethoxycarbonyl nitrene is inserted into the α C–H bonds of five- and six-membered cyclic ethers[6] and into the α-methylene C–H bonds of cyclohexanone ethylene acetal; this is, in a radical sense, a hydrogen abstraction-recombination process.[7] On the other hand, the nitrene insertion into the cyclohexane ring C–H bonds of the acetal was explained in terms of the intermediacy of the oxygen-imine or the direct attack of the singlet nitrene on the C–H bonds. In the present paper, we wish to report that the reaction of the nitrene with cyclic ethers includes an O–N ylide (oxygen-imine) as an intermediate and that the nitrene insertion into the α C–H bonds of the ethers proceeds by means of a mechanism different from that advanced in the insertion into the hydrocarbon C–H bonds.[8]

Results and Discussion

Photolyses of Ethyl Azidoformate in Cyclic Ethers. Ethyl azidoformate (I) in cyclic ether (III) was irradiated by the light (mainly 2537 Å) of a low-pressure mercury arc at 0 °C with stirring under an atmosphere of nitrogen. The insertion products (IV) of ethoxycarbonyl nitrene (II) into the C–H bonds of the cyclic ethers, except for the three- and four-membered cyclic ethers, were obtained accompanied by the hydrogen abstraction product, urethane (VI), and small amounts (0.5—2%) of diethyl hydrazoformate (VII). In addition, the reactions of I with α-alkyl cyclic ethers gave unsaturated alkoxyurethanes (V). No insertion products into the ring C–H bonds were recognized in the reactions with the three- and four-membered cyclic

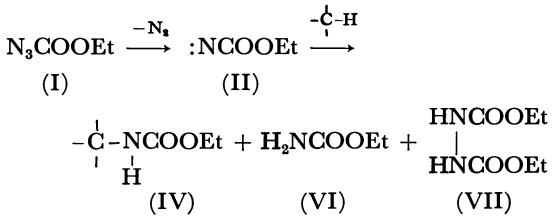

ethers. In the reactions with the five- and six-membered cyclic ethers, the insertion took place preferentially at the ring C–H bonds of the α-position. The yields of the products mentioned above are listed in Table 1.

The reaction in 2-methyltetrahydrofuran, which bears a tertiary hydrogen atom, gave an increased yield of urethanes (VI) compared with the reactions in tetrahydrofuran and in tetrahydropyran. This can be understood in terms of hydrogen abstraction by the triplet nitrene.[9] The reactions with the small ring ethers gave comparatively low yields of VI. It seems that some of the triplet nitrene and/or some of the amido radical, HNCOOEt, has been consumed in the ring-opening polymerization of the small-ring ethers employed.

Relative Reactivities. As has been mentioned above, the α C–H bonds of the cyclic ethers are more reactive than the others for the nitrene insertion; the reactivities of the α C–H bonds are greatly enhanced. Therefore, in order to compare the insertion reactivities of the C–H bonds of the cyclic ethers with those of cyclohexane, the photolysis of I was carried out in a mixture of equimolar amounts of a cyclic ether and cyclohexane. The product distributions and the relative reactivities are summarized in Table 2. These relative reactivities are displayed in Fig. 1, where they are compared with

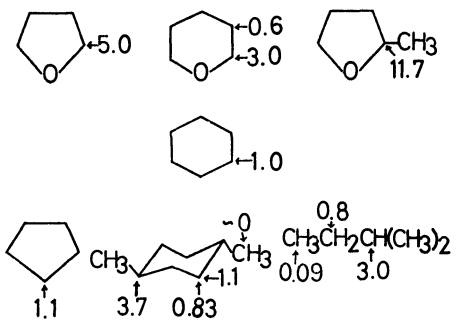

Fig. 1. Relative reactivit.es of various C–H bonds.

TABLE 1. PHOTOLYSES OF I IN CYCLIC ETHERS

Ether (III)	Product (%)[a]		
	Insertion (IV)	Ring-opening (V)	Abstraction (VI)
(a) 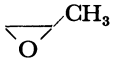		(a) CH_2=$CHCH_2ONHR$[b] 21	12
(b) 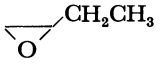		(b) CH_3CH=$CHCH_2ONHR$ 13	10
(c)		ND[c]	9
(d) 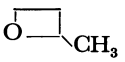		(d) CH_2=$CHCH_2CH_2ONHR$ 28	23
(e)	(e) 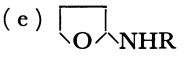 25		21
(f) 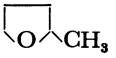	(f) 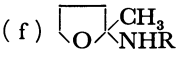 12	(f) CH_2=$CHCH_2CH_2CH_2ONHR$ 7	34
(g)	(g_1) 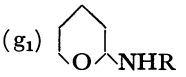 25		16
	(g_2) 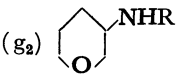 5		

a) Calculated on the basis of the azide used. b) R: COOEt. c) ND: not detected.

TABLE 2. PHOTOLYSIS OF I IN A MIXTURE OF A CYCLIC ETHER AND CYCLOHEXANE

Product (%)[a]				
Insertion (IV)		Cyclohexyl-urethane	Type of C–H bond	Relative reactivity[b]
(e)	18.1	10.8	2° (Ring-α)	5.0(±0.1)[c]
(f)	6.9	7.0	3° (Ring-α)	11.7(±1.1)
(g_1)	13.3	13.5	2° (Ring-α)	3.0(±0.2)
(g_2)	2.6		2° (Ring-β)	0.6(±0.1)

a) Calculated on the basis of the azide used. b) Relative reactivities: per C–H bond of cyclohexane. c) The relative errors appear in parentheses.

those of some hydrocarbons,[10] obtained in experiments carried out under the same conditions as the present work.

The relative reactivities of primary, secondary, and tertiary C–H bonds of the cyclic hydrocarbons toward ethoxycarbonyl nitrene are as follows: $1° \ll 2° < 3°$; these values are about the same as those of the corresponding C–H bonds of the acylic hydrocarbons. On the other hand, it was found that the α C–H bonds of the cyclic ethers were much more reactive than the corresponding C–H bonds of hydrocarbons in the nitrene insertion. Such unusual reactivities suggest that the insertion in question must proceed by a mechanism other than that proposed in the reaction with hydrocarbons.[3,8,11] Therefore, the reaction of I with cyclic ethers was studied from the stereochemical point of view as one approach to the problem.

Stereochemistry of the Insertion Reaction. Ethyl azidoformate (I) was irradiated in *cis*- and *trans*-2,5-dimethyltetrahydrofurans (IIIh and IIIi). Two insertion products (stereoisomers) into the α C–H bonds and the abstraction product were well separated from the reaction mixture by the use of gas chromatography. The IR and NMR spectral data of neither of these stereoisomers, however, led to a decision between the two alternative conformations because of the extreme similarity of their IR and NMR spectra. Methyl azidoformate (VII) was then employed instead of I, since the structures of the insertion product into IIIh were more simple than those formed in the reaction of I. The reaction of VII gave two insertion products (stereoisomers, XI and XII) and an abstraction product (methyl carbamate) in yields of 19% and 53% respectively. A comparison between the reactions of VII and I showed that the interrelationships of the yields, the VPC retention times, and the IR and NMR spectra between XI and XII were very similar to those between IVh_1 and IVh_2. Such information may lead to the consideration that the conformations of XI and XII correspond to those of IVh_1 and IVh_2 respectively. The NMR spectrum of a mixture of the insertion products, XI and XII, is shown in Fig. 2-i. Each of the peaks in Fig. 2 was due to XI or XII, judging from a comparison of the peak areas. After a shift reagent, $Eu(fod)_3$, had been added to the solution, the NMR spectrum was measured (Fig. 2-ii). The singlet peak (XIIb) of the 2-methyl protons of XII was shifted to a field lower than that (XIb) of XI. Their peaks were far separated by the further addition of the shift reagent (Fig. 2-iii), while the induced downfield shift for the NH proton

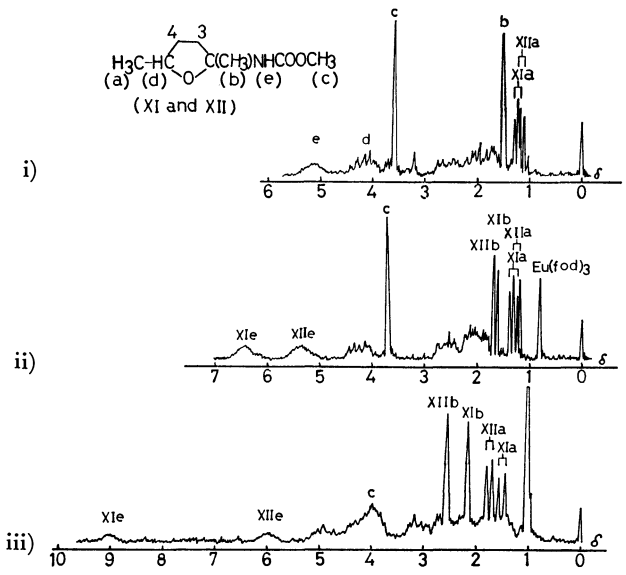

Fig. 2. NMR spectra of a mixture of XI and XII in ratio of 45: 55.
i) A 0.2 ml of CCl_4 contains 20 mg of a mixture of XI and XII.
ii) The solution contains 3 mg of $Eu(fod)_3$.
iii) The solution contains 9 mg of $Eu(fod)_3$.

(XIIe) of XII was smaller than that (XIe) of XI. The addition of the shift reagent caused a downfield shift of XII larger than that of XI also with regard to the two doublet peaks (XIIa and XIa) of the 5-methyl protons. These findings can be explained as follows: the bulky shift reagent approaches the ethereal oxygen atom through an opening in the crowded environment of two methyl and one NHR groups. The *cis*-isomer (with regard to two methyl groups), one of the stereoisomers, coordinates to the shift reagent at the side on which the NHR group in the isomer is located, thus giving XIII. The other, the *trans*-isomer, coordinates to the shift reagent at the opposite side of the NH group, thus giving XIV.

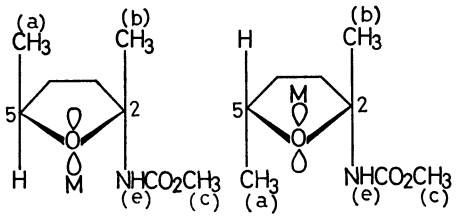

The singlet peak of the 2-methyl protons of XIV should then be shifted to a field lower than that of XIII. The peaks of XI and XII in Fig. 2 were thus assigned to the protons of XIII and XIV respectively. The difference between the induced shifts of the XIa and XIIa peaks, in spite of the relationship between the 5-methyl group and the shift reagent being the same at both XIII and XIV, shows that XIV might be formed more rapidly than XIII. That is, a coordination equilibrium in the *trans*-isomer lies further toward XIV compared with an equilibrium in the *cis*-isomer. The great downfield shift of the XIe peak compared with that of the XIIe peak means that the difference in the distances between the shift reagent and the NH proton affects the shift more strongly than that in the concentrations of the adducts (XIII and XIV).

In the case of I, one insertion product, IVh_1, has the same conformation as XI, while the other, IVh_2, has the same conformation as XII since XI and XII correspond to IVh_1 and IVh_2 respectively, as has been described above. Table 3 shows the product yields in the reactions of I.

The coordination compound between the shift reagent and the NH or the $COOCH_3$ group is not formed. If the coordination compound between the shift reagent and the NH group were formed, the peak (XIIe) of the NH proton must be shifted downfield as well as the XIe peak. If the coordination compound between the shift reagent and the $COOCH_3$ group were formed, the induced downfield shifts for the ester methyl protons (Peak c) must have larger magnitudes than those for the 2-methyl protons(Peak b)(Fig. 2-i—ii).

It may be concluded that the insertion reactions of the nitrene (II) into α C–H bonds of the cyclic ethers proceed non-stereospecifically, in contrast to the stereospecific insertion of II into the C–H bonds of hydrocarbons.[3,8,11]

The nitrene (II) is able to coordinate, by means of its nitrogen atom, to an ethereal oxygen atom as the nitrene does to the sulfur atoms of thioethers[12,13] and sulfoxides[13,14] to give the nitrogen-sulfur ylides. Therefore, the reaction of the nitrene with ethers is initiated by an electrophilic attack of the nitrene on the ethereal

Table 3. Photolyses of I in *cis*- and *trans*-2,5-dimethyltetrahydrofurans

Ether (III)	Product (%)[a]			
	Insertion (IV)		Ring-opening (V)	Abstraction (VI)
	IVh_1	IVh_2	(h) $CH_2=CH(CH_2)_2CHONHR$[b] (R = CH_3)	
(h) R_1[d]: H, R_2: CH_3	8	13	ND[e]	54
(i) R_1: CH_3, R_2: H	8	11	12	53
Mixture of h and i[e]	11	15	8	34

a) b) c) See Table 1, footnotes. d) 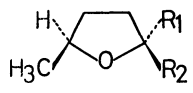 e) A mixture of h and i in a ratio of 45:55 was used.

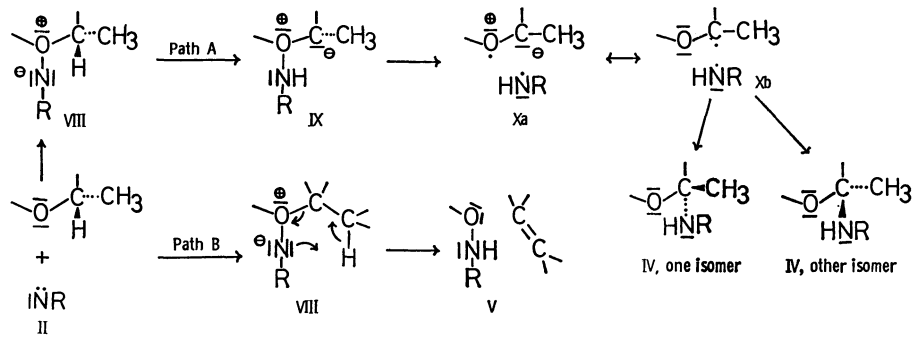

Scheme 1.
R: COOEt
Path A Insertion into α C–H bond
Path B Cleavage of ring C–O bond

oxygen atom to give an O–N ylide (oxygen-imine intermediate, Scheme 1).

The ylide (VIII) abstracts a proton from the α C–H bond to give IX, followed by the homolytic cleavage of the O–N bond to give a radical species (X). The radical, ṄHR, combines with the α-carbon radical to give IV (Path A). On the other hand, VIII leads to V *via* hydrogen abstraction from the α-methyl or α-methylene group and the cleavage of the C–O bond in a concerted pericyclic manner (Path B).

The non-stereospecific insertion by ethoxycarbonyl nitrene into C–H bonds of cyclic ethers does not exclude a hydrogen abstraction-recombination mechanism.

The triplet nitrene is able to abstract a hydrogen atom from the α-position of ethers, giving an amido radical and XI, whose recombination leads to the insertion products (IV isomers).

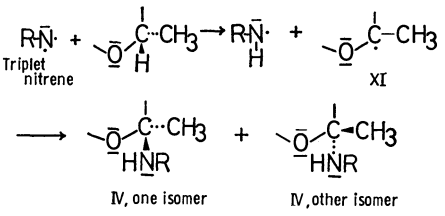

Scheme 2.

The mechanism of Scheme 2 has been ruled out for the nitrene insertion into C–H bonds of hydrocarbons.[8,11] The XI radical, however, is stabilized by the adjacent oxygen atom in comparison with a hydrocarbon radical. Consequently, IV may be formed by the radical recombination.

In the isomerization from the O–N ylide (VIII) to the insertion product (IV), the distance between the nitrogen atom and one C–H bond, to which the nitrene would be inserted, seems to be an important factor. In the case of tetrahydropyran, the insertion product (IVg_1) into the α C–H bond, which is located nearly at the nitrogen atom of the ylide, is derived from the ylide intermediate. On the other hand, the insertion product (IVg_2) into the β C–H bond is formed by the one-step mechanism[8] proposed in the reaction of nitrene with hydrocarbons, since the β C–H bond is too far from the ylide nitrogen atom. These two distinct mechanisms can explain the difference between the reactivities of the α and β C–H bonds shown in Table 2.

Experimental

The IR spectra were recorded on a Hitachi EP-S photometer and a Nippon Bunko (JASCO) Model IR-E photometer, while the NMR spectra were taken on Hitachi R-20 and Hitachi R-24 instruments, using tetramethylsilane as the internal standard. Gas chromatography (VPC) was done on Shimadzu GC-2C and Nippon Denshi (JEOL) JGC 20K units, employing as absorbents: A, 20% Ucon Oil 5 HB 2000 on Celite (60—80 mesh); B, 10% polyethylene glycol succinate on Neopak 1A (60—80 mesh). The products were separated by VPC, and the structures of the products were determined by means of elemental analyses and by measurements of the IR and NMR spectra. The quantitative analyses of the products by VPC and test for the stability of each product during VPC analysis have been described in a previous paper.[15]

Materials. The ethyl azidoformate (I) was prepared by the method of Lwowski and Mattingly.[16] The methyl azidoformate (VII) was prepared from methyl chloroformate and sodium azide in the manner used for the preparation of ethyl azidoformate; bp 24 °C/40 mmHg; yield, 83%. All the cyclic ethers, except for oxetanes (IIIc and IIId), dichloromethane, and cyclohexane were used after the commercial reagents had been purified according to the published directions.[17] The oxetane was prepared by the ring closure of 3-chloropropyl acetate,[18] which had been obtained by the chlorination of 1,3-propanediol[19] followed by the acetylation.[20] The 2-methyloxetane was prepared in a way similar to the synthesis of oxetane. The introduction of dry hydrogen chloride into 500 g (5.6 mol) of 1,3-butanediol gave 314 g (3 mol) of the chlorohydrin;[21] bp 63—65 °C/11 mmHg; yield, 54%. A reaction of the chlorohydrin (314 g) and acetic acid (240 g, 4 mol) gave 260 g (1.7 mol) of the ester;[22] bp 70—74 °C/13 mmHg; yield, 57%. The ester (260 g) was cyclized by potassium hydroxide into 42 g (0.6 mol) of 2-methyloxetane; bp 60 °C,[23-25] yield; 35%. NMR (CCl_4, τ): 4.8—5.4 (CH, m), 5.5 (ring γ-CH_2, m), 7.0—8.0 (ring β-CH_2, m), 8.65 (CH_3, d). The cyclohexylurethane was prepared from cyclohexylamine and ethyl chloroformate.[16] The data of mp, IR, and NMR were in good agreement with those reported in the literature. The *cis*-2,5-dimethyltetrahydrofuran (IIIh) (bp 90 °C (lit, 90—91 °C)) was prepared by the ring closure of *dl*-2,5-hexanediol[26] (*dl*-diol), which had itself been obtained by the separation of a mixture of *dl*- and *meso*-diols.[27] The *trans*-2,5-dimethyltetrahydrofuran (IIIi), bp 93 °C (lit, 92—

94 °C) was also prepared from *meso*-diol separated from the mixture. Their IR and NMR spectra were in good agreement with those reported in the literature.[28] In the same manner, a mixture of *cis*- and *trans*-2,5-dimethyltetrahydrofurans was prepared by the ring closure of a mixture of *dl*- and *meso*-diols; bp 92—94 °C; yield, 86%. No photochemical isomerization between *cis*- and *trans*-2,5-dimethyltetrahydrofurans was observed under the conditions of these experiments.

Photolyses of I in Cyclic Ethers. A solution of 5.0 g (0.043 mol) of ethyl azidoformate in 0.5 mol of a cyclic ether was irradiated, with stirring and cooling at 0 °C, by a low-pressure mercury lamp (internal-irradiation type) until the evolution of nitrogen was not observed. The nitrogen evolved then gave almost the theoretical amount based on the azide used. The excess substrate was removed by distillation at 25—75 °C under 25—30 mmHg pressure. The residue was analyzed by VPC on Columns A and B. Urethane (VI) had IR and NMR spectra and a VPC retention time identical with those of authentic VI, and a mixed melting point with the authentic sample was undepressed. Ethyl hydrazoformate (VII) was obtained in the yields of 0.02—0.08 g from every experiment; mp 132 °C,[29] IR (Nujol, cm^{-1}): 3240 (NH), 1754 and 1693 (C=O), 1260 (C–O). NMR ($CDCl_3$, τ): 3.24 (NH, 2H, s), 5.80 (CH_2, 4H, q), 8.73 (CH_3, 6H, t). Found: C, 40.96; H, 6.73; N, 15.98%. Calcd for $C_6H_{12}O_4N_2$: C, 40.90; H, 6.87; N, 15.90%. The spectral data of IR and NMR, and elemental analyses of unsaturated *N*-alkoxyurethanes (V) are presented in Table 4.

(a) In Propylene Oxide (IIIa), 1,2-Epoxybutane (IIIb), and 2-Methyloxetane (IIId): *N*-Allyloxyurethane (Va, 1.3 g), *N*-2-

Table 4. NMR and IR data, and analyses of V

V	NMR (τ) in CCl_4	IR (neat, cm^{-1}) NH	IR (neat, cm^{-1}) C=O	IR (neat, cm^{-1}) C–O	Formula		Analyses C%	Analyses H%	Analyses N%
(Va)[31]	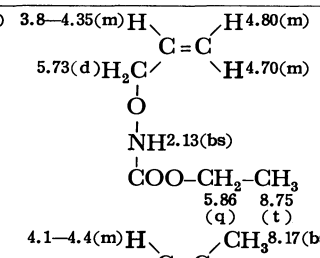	3250	1718	1260	$C_6H_{11}O_3N$	Found	50.03	7.29	9.60
						Calcd	49.64	7.64	9.65
(Vb)	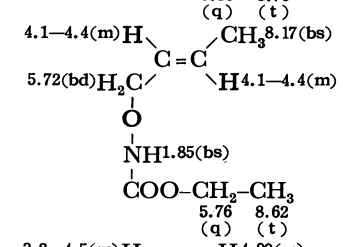	3260	1720	1266	$C_7H_{13}O_3N$	Found	52.56	8.20	8.95
						Calcd	52.81	8.23	8.80
(Vd)	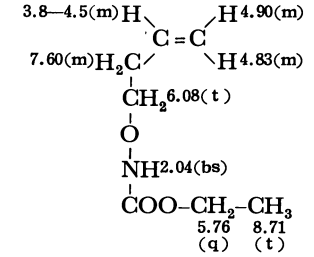	3260	1716	1262	$C_7H_{13}O_3N$	Found	53.05	8.39	8.38
						Calcd	52.81	8.23	8.80
(Vf)	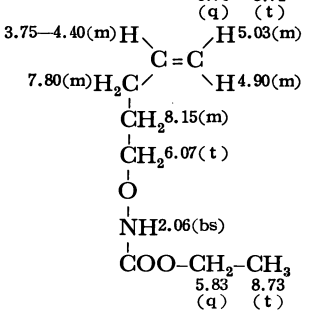	3260	1720	1260	$C_8H_{15}O_3N$	Found	55.14	8.99	8.10
						Calcd	55.47	8.73	8.09
(Vh)	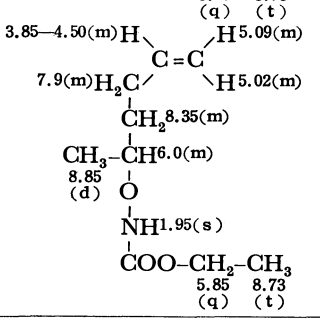	3230	1720	1260	$C_9H_{17}O_3N$	Found	57.72	9.42	7.39
						Calcd	57.73	9.15	7.48

butenyloxyurethane (Vb, 0.9 g), and *N*-3-butenyloxyurethane (Vd, 1.9 g) were isolated.

(b) In Tetrahydrofuran (IIIe): Ethyl 2-tetrahydrofurylcarbamate (IVe, 1.7 g) was isolated. IVe: IR (neat, cm^{-1}): 3300 (NH), 1705 (C=O), 1260 (C–O). NMR (CCl_4, τ): 4.00 (NH, bs), 4.4—4.8 (ring-CH, m), 5.94 (ester-CH_2, q), 6.0—6.5 (ring δ-CH_2, m), 7.7—8.5 (ring β- and γ-CH_2, 4H, m), 8.83 (ester-CH_3, t).[30] Found: C, 52.63; H, 8.45; N, 8.70%. Calcd for $C_7H_{13}O_3N$: C, 52.81; H, 8.23; N, 8.80%.

(c) In 2-Methyltetrahydrofuran (IIIf): Ethyl 2-methyl-2-tetrahydrofurylcarbamate (IVf, 0.29 g) and *N*-4-pentenyloxyurethane (Vf, 0.52 g) were isolated. IVf: IR (neat, cm^{-1}): 3310 (NH), 1760 (C=O), 1258(C–O). NMR (CCl_4, τ): 4.50 (NH, bs), 5.6-6.2 (ring δ-CH_2, m), 5.87 (ester-CH_2, q), 7.5—8.5 (ring β- and γ-CH_2, 4H, m), 8.76 (ester-CH_3, t), 8.80 (α-CH_3, s). Found: C, 55.03; H, 9.04; N, 8.21%. Calcd for $C_8H_{15}O_3N$: C, 55.47; H, 8.73; N, 8.09%.

(d) In Tetrahydropyran (IIIg): Ethyl 2-tetrahydropyranylcarbamate (IVg_1, 1.9 g) and ethyl 3-tetrahydropyranylcarbamate (IVg_2, 0.37 g) were isolated. IVg_1: IR (neat, cm^{-1}): 3300 (NH), 1710 (C=O), 1250 (C–O). NMR (CCl_4, τ): 4.00 (NH, bs), 5.16 (C_2-methine, 1H, bt), 5.86 (ester-CH_2, q), 6.0—6.6 (C_6-methylene, 2H, m), 8.0—8.9 (C_3-, C_4-, and C_5-methylene, 6H, m), 8.76 (ester-CH_3, t).[30] Found: C, 55.01; H, 9.15; N, 8.06%. Calcd for $C_8H_{15}O_3N$: C, 55.47; H, 8.73; N, 8.09%. IVg_2: IR (neat, cm^{-1}): 3300 (NH), 1700 (C=O), 1250 (C–O). NMR (CCl_4, τ): 4.65 (NH, bs), 5.88 (ester-CH_2, q), 6.0—6.6 (C_2- and C_6-methylene, 4H, m), 6.7—6.9 (C_3-methine, m), 8.0—8.9 (C_4- and C_5-methylene, 4H, m), 8.77 (ester-CH_3, t). Found: C, 54.92; H, 9.16; N, 8.19%. Calcd for $C_8H_{15}O_3N$: C, 55.47; H, 8.73; N, 8.09%.

(e) In cis-2,5-Dimethyltetrahydrofuran (IIIh): Ethyl *cis*-2,5-dimethyl-2-tetrahydrofurylcarbamate (IVh_1, 0.64 g) and ethyl *trans*-2,5-dimethyl-2-tetrahydrofurylcarbamate (IVh_2, 1.0 g) were isolated. IVh_1: IR (neat, cm^{-1}): 3300 (NH), 1710 (C=O), 1265 (C–O). NMR (CCl_4, τ): 5.25 (NH, bs), 6.00 (ester-CH_2, q), 5.55—6.25 (ring α-CH, m), 7.22—8.42 (ring β- and γ-CH_2, 4H, m), 8.50 (δ-CH_3, s), 8.75 (α-CH_3, d), 8.85 (ester-CH_3, t). Found: C, 57.50; H, 9.27; N, 7.60%. Calcd for $C_9H_{17}O_3N$: C, 57.73; H, 9.15; N, 7.48%. IVh_2: IR (neat, cm^{-1}): 3290 (NH), 1705 (C=O), 1260 (C–O). NMR (CCl_4, τ): 5.05 (NH, bs), 6.00 (ester-CH_2, q), 5.5—6.2 (ring α-CH, m), 7.22—8.38 (ring β- and γ-CH_2, 4H, m), 8.50 (δ-CH_3, s), 8.85 (α-CH_3, d), 8.77 (ester-CH_3, t). Found: C, 57.57; H, 9.10; N, 7.56%. Calcd for $C_9H_{17}O_3N$: C, 57.73; H, 9.15; N, 7.48%.

(f) In trans-*2,5-Dimethyltetrahydrofuran (IIIi)*: IVh_1 (0.64 g), IVh_2 (0.88 g), and *N*-(1-methyl-4-pentenyloxy)urethane (Vh, 0.96 g) were isolated.

(g) In a Mixture of IIIh and IIIi: IVh_1 (0.88 g), IVh_2 (1.2 g), and Vh (0.64 g) were isolated.

Photolysis of Methyl Azidoformate. A solution of 4.4 g (0.043 mol) of methyl azidoformate in 0.5 mol of *cis*-2,5-dimethyltetrahydrofuran (IIIh) was irradiated in the same manner as in the case of ethyl azidoformate. Methyl *cis*-2,5-dimethyl-2-tetrahydrofurylcarbamate (IVj_1), methyl *trans*-2,5-dimethyl-2-tetrahydrofurylcarbamate (IVj_2), and methyl carbamate were thus isolated in the yields of 0.52 g, 0.90 g, and 1.7 g respectively. IVj_1: IR (neat, cm^{-1}): 3290 (NH), 1710 (C=O), 1265 (C–O). NMR (CCl_4, τ): 4.90 (NH, bs), 5.55—6.12 (ring α-CH, m), 6.42 (ester-CH_3, s), 7.20—8.60 (ring β- and γ-CH_2, 4H, m), 8.51 (δ-CH_3, s), 8.74 (α-CH_3, d). Found: C, 55.52; H, 8.66; N, 8.10%. Calcd for $C_8H_{15}O_3N$: C, 55.47; H, 8.73; N, 8.09%. IVj_2: IR (neat, cm^{-1}): 3300 (NH), 1715 (C=O), 1270 (C–O). NMR (CCl_4, τ): 4.90 (NH, bs), 5.55—6.12 (ring α-CH, m), 6.42 (ester-CH_3, s), 7.20—8.60 (ring β- and γ-CH_2, m), 8.51 (δ-CH_3, s), 8.83 (α-CH_3, d). Found: C, 55.58; H, 8.66; N, 8.18%. Calcd for $C_8H_{15}O_3N$: C, 55.47; H, 8.73; N, 8.09%. Methyl carbamate was identified by comparing its VPC retention time and IR and NMR spectra with those of the authentic sample. No photochemical mutual isomerization between *cis* and *trans* isomers of the insertion products was observed under the conditions of these experiments.

Photolysis of I in a Mixture of a Cyclic Ether and Cyclohexane. A solution of I (5.0 g, 0.043 mol) in III (0.25 mol) and a cyclohexane (21 g, 0.25 mol) mixture was irradiated internally as has been described above. The excess of the substrate was removed by distillation, and the residue was analyzed by VPC. The *N*-cyclohexylurethane was identified by comparison with the authentic sample. The yields of the insertion products and urethane are displayed in Table 2.

The authors are particularly indebted to Dr. Hisao Arakawa for his help in the preparation of this paper and for his many useful suggestion for its improvement.

References

1) M. F. Slooan, T. J. Prosser, N. R. Newburg, and D. S. Breslow, *Tetrahedron Lett.*, **1964**, 2945; D. S. Breslow, T. J. Prosser, A. F. Marcantonio, and C. A. Genge, *J. Am. Chem. Soc.*, **89**, 2384 (1967).

2) W. Lwowski and T. J. Maricich, *J. Am. Chem. Soc.*, **86**, 3164 (1964); **87**, 3630 (1965).

3) D. S. Breslow, E. I. Edward, R. Leonè, and P. von R. Sc leyer, *J. Am. Chem. Soc.*, **90**, 7097 (1968).

4) J. Meinwald and D. H. Aue, *Tetrahedron Lett.*, **1967**, 2317.

5) T. Shingaki, M. Inagaki, N. Torimoto, and M. Takebayashi, *Chem. Lett.*, **1972**, 155.

6) H. Nozaki, S. Fujita, H. Takaya, and R. Noyori, *Tetrahedron*, **23**, 45 (1967).

7) T. Hiyama, S. Fujita, and H. Nozaki, *Bull. Chem. Soc. Jpn.*, **45**, 3500 (1972).

8) W. Lwowski, "Carbonylnitrenes," in "Nitrenes," ed. by W. Lwowski, Interscience Publishers, New York (1970), p. 185, and references quoted therein.

9) J. S. McConaghy, Jr. and W. Lwowski, *J. Am. Chem. Soc.*, **89**, 4450 (1967).

10) Presented in part at the 24th Annual Meeting of the Chemical Society of Japan, Osaka, Japan, April (1971); Abstract, Vol. 3, p. 1133.

11) W. Lwowski, *Angew. Chem.*, **79**, 922 (1967); *Angew. Chem. Int. Ed. Engl.*, **6**, 897 (1967)

12) W. Ando, N. Ogino, and T. Migita, *Bull. Chem. Soc. Jpn.*, **44**, 2278 (1971).

13) L. Horner and A. Christmann, *Chem. Ber.*, **96**, 388 (1963).

14) L. Horner, G. Bauer, and J. Dorges, *Chem. Ber.*, **98**, 2631 (1965); P. Robson and P. H. R. Speakman, *J. Chem. Soc., B.*, **1968**, 463.

15) T. Shingaki, M. Inagaki, M. Takebayashi, and W. Lwowski, *Bull. Chem. Soc. Jpn.*, **45**, 3567 (1972).

16) W. Lwowski and T. W. Mattingly, *J. Am. Chem. Soc.*, **87**, 1974 (1965).

17) J. A. Riddic and W. B. Gunger, "Organic Solvents," in "Techniques of Chemistry," Vol. VII, ed. by A. Weissberger, Wiley-Interscience, New York, N. Y. (1970).

18) C. R. Noller, *Org. Synth.*, Coll. Vol. III, 835, (1955).

19) C. S. Marvel and H. O. Calvery, *Org. Synth.*, Coll. Vol. I, 533 (1956).

20) C. F. H. Allen and F. W. Spangler, *Org. Synth.*, Coll. Vol. III, 203 (1955).

21) The chlorohydrin obtained by this method is composed of two isomers, 3-chloro-1-butanol and 4-chloro-2-butanol.[23] The former has a bp of 74 °C/16 mmHg, while the later has a bp of 61 °C/10 mmHg or 67 °C/20 mmHg.[24]

22) 3-Chlorobutyl acetate: bp 74—76 °C/14 mmHg.[23] 3-chloro-1-methylpropyl acetate: bp 70 °C/16 mmHg.[23,24]

23) S. Searles, Jr., K. A. Pollart, and F. Block, *J. Am. Chem. Soc.*, **79**, 952 (1957).

24) F. Sondheimer and R. B. Woodward, *J. Am. Chem. Soc.*, **75**, 5438 (1953).

25) N. G. Gaylord, J. H. Crowdle, W. A. Himmler, and H. J. Pepe, *J. Am. Chem. Soc.*, **76**, 59 (1954).

26) D. D. Reynolds and W. O. Kenyon, *J. Am. Chem. Soc.*, **72**, 1955 (1950).

27) R. M. Dadson and Victor C. Nelson, *J. Org. Chem.*, **33**, 3966 (1968).

28) M. Lj. Mihailović, R. I. Mamuzić, Lj. Žigić-Mamujić, T. Bošnjak, and Ž. Čekovic, *Tetrahedron*, **23**, 215 (1967).

29) N. Rabjohn, *Org. Synth.*, Coll. Vol. III, 375 (1955).

30) The NMR spectra of IVe and IVg_1 were in good agreement with those in Ref. 6.

31) These data were identical with those of the product obtained by the nitrene insertion into the O–H bond when I was photolyzed in allyl alcohol, T. Shingaki, M. Inagaki, N. Torimoto, and M. Takebayashi, Symposium of Organic Free Radical reactions, Nagoya, October (1971), Abstract, p. 9.

Dehydroaunulenes. VI. Synthesis and Properties of 1,6,12,17-Tetraphenyl-2,4,13,15-tetrakisdehydro[22]annulene

Shuzo AKIYAMA, Tateo NOMOTO, Masahiko IYODA, and Masazumi NAKAGAWA*

Department of Chemistry, Faculty of Science, Osaka University, Toyonaka, Osaka 560

(Received April 23, 1976)

1,6,12,17-Tetraphenyl-2,4,13,15-tetrakisdehydro[22]annulene has been synthesized. The sparlingly soluble tetrakisdehydro[22]annulene was found to be conformationally stable and strongly diatropic.

As reported in previous papers of this series, interesting difference has been observed between the properties of tetra-*t*-butyl-[1] and tetraphenyltetrakisdehydro[18]annulenes.[2] The successful synthesis of tetra-*t*-butyltetrakisdehydro[22]annulene (VIII)[3] prompted us to synthesize tetraphenyltetrakisdehydro[22]annulene (VI) with the purpose to compare their properties.

The aldol condensation of 5-phenyl-2,4-heptadien-6-ynal (I)[4] with acetophenone gave II in a high yield. Oxidative coupling of II with copper(II) acetate in pyridine–methanol yielded diketone (III) as red crystals in an almost quantitative yield. Bis-ethynylation of III could be achieved by lithium acetylide–ethylenediamine complex.[5] Bis-ethynyl alcohol (IV) obtained as yellow fine crystals was oxidatively coupled under high dilution conditions to yield cyclic glycol (V) which could be separated into diastereomers. It was found that V forms containing 1 mol of ethyl acetate as a solvent of crystallization. Formation of similar adducts has been observed in some acyclic[6] and cyclic acetylene glycols.[7]

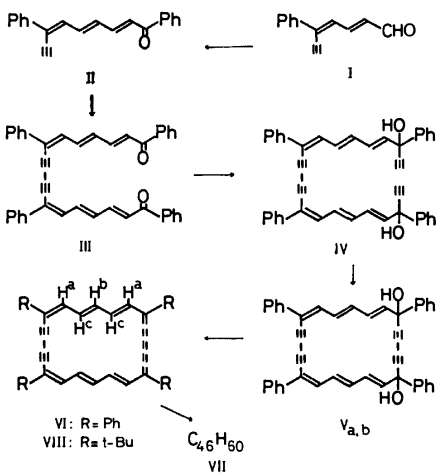

Scheme 1.

A solution of V in dichloromethane was mixed at −15 °C with a solution of tin(II) chloride dihydrate in concentrated hydrochloric acid. Tetrakisdehydro[22]-annulene (VI) was obtained as unstable and sparlingly soluble black violet crystals. Full hydrogenation of VI over platinum catalyst yielded a mixture of stereoisomers of a saturated hydrocarbon, tetraphenylcyclodocosane (VII). The tetrakisdehydro[22]annulene (VI) forms air sensitive CT-complex with 2,4,7-trinitrofluorenone.

Electronic spectrum of VI consists of three main absorption bands showing characteristic feature of [4*n*+2]annulenes as illustrated in Fig. 1. The spectrum of VI was found to be closely related with that of tetra-*t*-butyltetrakisdehydro[22]annulene (VIII)[3] although VI showed remarkable bathochromic shift.

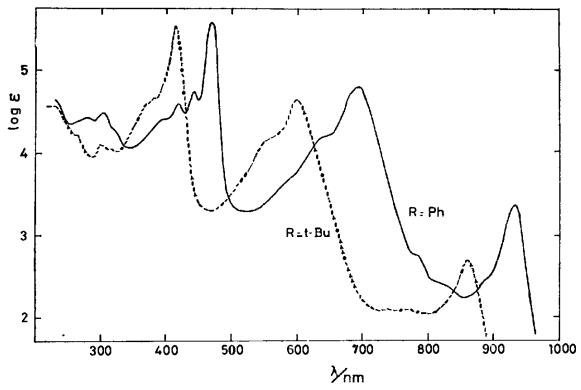

Fig. 1. Electronic spectra of tetra-*t*-butyltetrakisdehydro[22]annulene (VIII) (···) and tetraphenyltetrakisdehydro[22]annulene (VI) (—) in THF.

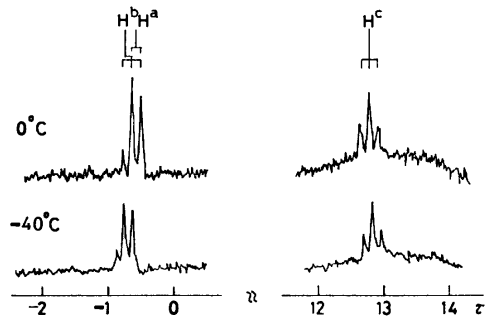

Fig. 2. 100 MH ^{1}H FT-NMR spectra of tetraphenyltetrakisdehydro[22]annulene (VI) in THF-d_8.

The ^{1}H FT-NMR spectra of VI indicate clearly that the tetrakisdehydro[22]annulene (VI) is strongly diatropic showing outer proton signals at a low-field and those of inner protons at fairly high-field (Fig. 2). The NMR parameters of VI are summarized in Table 1 together with those of VIII for comparison. The NMR spectra were essentially temperature independent indicating high conformational stability of the tetrakisdehydro[22]-annulene ring. Appreciable down-field shift for both of the inner and outer proton signals of VI as compared with those of VIII seems to be attributable to deshielding effect of ring current of phenyl groups. Inversely, down-field shift of *ortho*-protons in phenyl groups reflects deshielding effect of diamagnetic ring current induced in the 22-membered ring.

* Author to whom correspondence should be addressed.

Table 1. 100 MHz H^1 FT-NMR parameters of VI (in THF-d_8) and VIII (in $CDCl_3$) τ-Values, J in Hz.

	VI		VIII
	−40 °C	0 °C	−40 °C
H^b	−0.79 t	−0.62 t	−0.43 t
	J=14	J=14	J=13
H^a	−0.72 d	−0.55 d	0.09 d
	J=14	J=14	J=13
o-H of Ph	0.93 d	1.04 d	
	J=8	J=8	
m,p-H of Ph	2—2.5m	2—2.5m	
H^c	12.80 t	12.76 t	13.71 t
	J=14	J=14	J=13

It was found that VI is less stable and less soluble than the tetra-*t*-butyl analogue (VIII). Remarkable bathochromic shift of electronic spectrum of VI as compared with that of VIII indicates that phenyl groups exert larger electronic perturbation on the dehydroannulene system than *t*-butyl groups. These facts are the further support for the suitable nature of *t*-butyl group as substituent[1] in the study of aromaticity of dehydroannulene system.

Experimental

All melting and boiling points are not corrected. The IR spectra were obtained on a Hitachi EPI-2 or EPI-3G spectrometer. The electronic spectra, measured with a Hitachi-EPS-3T spectrophotometer, were recorded in nm and the ε-values were given in parentheses. Shoulder was denoted by sh. The mass spectra were obtained on a Hitachi RM-50 spectrometer. The ^1H NMR spectra obtained on a Varian XL-100 spectrometer were given in τ-values with respect to TMS as an internal standard, and the coupling constants (J) are recorded in Hz. Silica gel (Merck, Kiesel Gel 60) or alumina (Merck, Act. II—III) was used for column chromatography, unless otherwise stated.

1,7-Diphenyl-2,4,6-nonatrien-8-yn-1-one (II). A solution of sodium hydroxide (0.26 g, 6.6 mmol) in 50% aqueous ethanol (4 ml) was added to a stirred and ice-cooled mixture of I (1.20 g, 6.6 mmol), acetophenone (0.79 g, 6.6 mmol) and ethanol (15 ml). After the mixture had been stirred for 2 h, yellow crystals deposited were collected and washed successively with water, methanol and water to give fairly pure II: mp 92—95 °C; IR (CCl_4): 3300 (C≡CH), 1600 (C=C), 1015, 1000 (*trans* CH=CH) cm^{-1}; NMR (CCl_4): 6.38 (s, 1, C≡CH), 2.52 (m, 15, olefinic and aromatic).

Found: C, 88.49; H, 5.72%. Calcd for $C_{21}H_{16}O$: C, 88.70; H, 5.67%.

1,7,12,18-Tetraphenyl-2,4,6,12,14,16-octadecahexaen-8,10-diyn-1,18-dione (III). A solution of II (7.00 g, 0.025 mol) in pyridine (70 ml) and methanol (70 ml) was added over 30 min period to a solution of copper(II) acetate monohydrate (14.5 g) in pyridine (70 ml) and methanol (70 ml) at room-temperature. After being stirred for 3 h, reddish orange crystals deposited were collected and washed with water and methanol. Slightly crude III (mp 210—214 °C, 6.92 g, 99%) was dissolved in benzene and passed through a short column of alumina. Concentration of the filtrate under reduced pressure yielded pure III: red crystals; mp 213—216 °C; IR (KBr-disk): 1640 (C=O), 1590, 1580, 1565 (C=C and aromatic), 1010, 1000 (*trans* CH=CH) cm^{-1}.

Found: C, 88.98; H, 5.29%. Calcd for $C_{42}H_{30}O_2$: C, 89.05; H, 5.30%.

3,9,14,20-Tetraphenyl-4,6,8,14,16,18-docosahexaen-1,10,12,21-tetrayn-3,30-diol (IV). Lithium acetylide–ethylenediamine complex[5] (6.5 g, 0.07 mol) was added to THF (100 ml) saturated with acetylene. A solution of II (1.00 g, 1.77 mmol) in the same solvent (500 ml) was added to the mixture over 2 h-period under slow bubbling of acetylene, and saturated ammonium chloride solution (30 ml) was added to the reaction mixture under cooling in an ice-salt-bath. The aqueous layer was extracted with ether, and the extract was combined with the organic layer. The combined organic layer was washed successively with saturated ammonium chloride and sodium chloride solutions, and dried ($MgSO_4$). Brown crystalline powder obtained on concentration of the organic layer was dissolved in benzene and chromatographed on alumina (20 g). Elution with ether–benzene (1:9—2:8) yielded acyclic glycol, IV: yellow crystalline solid (attempts to recrystallize this material were failed); mp 84—86 °C; 0.69 g, 63%; NMR (CCl_4): 7.65 (s, 1, OH), 7.28 (s, 1, C≡CH), 4.23—3.03 (m, 5, olefinic), 2.78 (m, 6, *m,p*-H of phenyl), 2.48 (m, 4, *o*-H of phenyl).

Found: C, 88.84; H, 5.78%. Calcd for $C_{46}H_{34}O_2$: C, 89.29; H, 5.54%.

1,6,12,17-Tetraphenyl-8,9,11,17,19,21-cyclodocosahexaen-2,4,13,-15-tetrayn-1,6-diol (V). To a stirred and refluxing solution of copper(II) acetate monohydrate (2.5 g) in pyridine (200 ml), ether (200 ml) and methanol (100 ml) was added a solution of IV (0.95 g, 1.54 mmol) in pyridine (115 ml), ether (115 ml) and methanol (50 ml) over 7.5 h-period using a high dilution apparatus. After being refluxed for further 30 min, the reaction mixture was stirred overnight at a room-temperature. The mixture was concentrated to 1/2 volume under reduced pressure, and the concentrate was extracted with ether (300 ml). The extract was washed successively with chilled water, diluted hydrochloric acid and brine, and dried (Na_2SO_4). Evaporation of the solvent under reduced pressure gave crude cyclic glycol, V (brown crystalline powder). The oxidative coupling was repeated 3 times under the same reaction conditions using the same quantity of materials. Crude (total 2.33 g, 83%), thus obtained, was dissolved in benzene (20 ml). Crystals deposited on standing the benzene solution were collected and washed with benzene–hexane to give one diastereomer of the cyclic glycol, V_a (yellow tiny cubes, 0.52 g, 18%). Recrystallization of the crystals from ethyl acetate yielded V_a containing 1 mol of the solvent: mp *ca.* 200 °C (dec); IR (KBr-disk): 3700—3100 (OH), 2190 (C≡C), 1715 (C=O), 990 (*trans* CH=CH) cm^{-1}; UV (THF): λ_{max} 254.5 (29700), 262 (29800), 280 (17200), 348 (107000), 394 (13500), 416 (17500), 441 (16800) nm; NMR (acetone-d_6): 2.0—4.1 (m, 30, olefinic and aromatic), 4.45 (s, 2, OH), 5.95 (q, 2, CH_2), 8.03 (s, 3, CH_3CO), 8.79 (t, 3, CH_3).

Found: C, 85.29; H, 5.74%. Calcd for $C_{46}H_{32}O_2 \cdot CH_3COOC_2H_5$: C, 85.20; H, 5.72%.

The mother liquor obtained on filtrating the crude V_a was chromatographed on alumina (100 g). The other diastereomer of the cyclic glycol, V_b (light brown crystalline powder, 0.68 g, 24%) was obtained on elution with ether–benzene (4:6), which was recrystallized from benzene–hexane to give pure V_b: yellow needles; mp *ca.* 200 °C (dec); IR (KBr-disk): 3700—3100 (OH), 2190 (C≡C), 990 (*trans* CH=CH) cm^{-1}; UV(THF): λ_{max} 254.5 (27000), 262 (26300), 280 (14900), 348 (98600), 394 (12400), 416 (15900), 441 (15400) nm; NMR (acetone-d_6): 2.0—4.1 (m, 30, olefinic and aromatic), 4.42 (s, 2, OH).

Found: C, 89.57; H, 5.58%. Calcd for $C_{46}H_{32}O_2$: C,

89.34; H, 5.65%.

1,6,12,17-Tetraphenyl-2,4,13,15-tetrakisdehydro[22]annulene (VI). A solution of tin(II) chloride dihydrate (0.1 g, 4 mmol) in concentrated hydrochloric acid (2 ml) was added in one portion to a stirred and chilled (−15 °C) solution of V_b (10 mg, 0.016 mmol) in dichloromethane (80 ml). After 3 min, ice-water was added to the reaction mixture. Resulting dark green organic layer was washed successively with cold water, diluted sodium hydrogen carbonate solution and cold water, and dried (K_2CO_3). The organic layer was passed through a short column of alumina (5 g). Evaporation of the solvent under reduced pressure at low temperature yielded VI: unstable deep violet fine crystals; 8.5 mg, 90%; UV (THF): λ_{max} 290 (25800), 305.5 (29600), 400 (24200), 419 (38200), 442 (54700), 469 (363000), 682 (59500), 942 (2300) nm; NMR: see, Table 1 and Fig. 2.

Owing to unstable nature of VI, elemental analyses gave unsatisfactory results.

V_a containing 1 mol of ethyl acetate also gave VI in a high yield under the same reaction conditions.

CT-Complex of VI with 2,4,7-Trinitrofluorenone. A solution of VI in cold dichloromethane was mixed with a large excess of a solution of 2,4,7-trinitrofluorenone in the same solvent. Dark green fine needles were obtained on standing the mixture at 0 °C for 1 h. Elemental analyses gave no definite results, presumably owing to the sensitivity of the complex to atmospheric oxygen.

Catalytic Hydrogenation of VI. V_b (0.30 g, 0.049 mmol) was converted into VI according to the above procedure. Freshly obtained VI in THF (5 ml) was added to ethyl acetate (100 ml) containing platinum oxide catalyst (0.10 g), and the mixture was vigorously stirred under hydrogen atmosphere at −15 °C for 5 h. Resulting colorless solution was concentrated under reduced pressure to give colorless crystalline material (0.025 g, 84% based on V_b), which was dissolved in hexane and passed through a short column of alumina (Woelm, W200). Crystals obtained on concentration of the filtrate under reduced pressure were recrystallized from pentane–hexane to give VII: colorless rods; mp 108—117 °C; NMR (CD_2Cl_2): 2.6—3.0 (m, 20, aromatic), 7.3—7.6 (m, 4, CH), 8.1—9.0 (m, 36, CH_2).

Found: C, 89.88; H, 9.84%, M^+ 612. Calcd for $C_{46}H_{60}$: C, 90.13; H, 9.87%, Mol. wt, 612.

References

1) T. Katakami, S. Tomita, K. Fukui, and M. Nakagawa, *Chem. Lett.*, **1972**, 225; S. Tomita and M. Nakagawa, *Bull. Chem. Soc. Jpn.*, **49**, 302 (1976).

2) K. Fukui, T. Okamoto, and M. Nakagawa, *Tetrahedron Lett.*, **1971**, 3121; T. Katakami, K. Fukui, T. Okamoto, and M. Nakagawa, *Bull. Chem. Soc. Jpn.*, **49**, 297 (1976).

3) M. Iyoda, H. Miyazaki, and M. Nakagawa, *J. Chem. Soc., Chem. Commun.*, **1972**, 431; M. Iyoda, H. Miyazaki, and M. Nakagawa, *Bull. Chem. Soc. Jpn.*, **49**, 2306 (1976).

4) R. Muneyuki, M. Morimoto, H. Tanaka, T. Katakami M. Iyoda, and M. Nakagawa, *Bull. Chem. Soc. Jpn.*, **46**, 2565 (1973).

5) D. F. Beumel, Jr. and R. F. Harris, *J. Org. Chem.*, **28**, 2775 (1963); *ibid.*, **29**, 1872 (1964).

6) F. Toda and K. Akagi, *Tetrahedron Lett.*, **1968**, 3695.

7) J. Ojima, T. Katakami, G. Nakaminami, and M. Nakagawa, *Bull. Chem. Soc. Jpn.*, **49**, 292 (1976).

The Reaction of Arylthallium(III) Compounds with Metal Nitrite. Synthesis of Nitroarenes.[1]

Sakae UEMURA,* Akio TOSHIMITSU, and Masaya OKANO
Institute for Chemical Research, Kyoto University, Uji, Kyoto 611

(Received April 23, 1976)

Arylthallium(III) compounds react smoothly with various metal nitrites such as $NaNO_2$, KNO_2, and $AgNO_2$ in trifluoroacetic acid to give nitroarenes in good yields. It has been clarified that the reaction proceeds through substitution of thallium moiety by nitroso group at the (*ipso*) position where thallium was attached previously to aromatic ring to give nitrosoarenes, followed by their oxidation to nitroarenes.

Recently Davies and Thomas reported a facile nitrodethallation of arylthallium(III) compounds by nitrogen dioxide which can be used for selective introduction of a nitro group into aromatic substrates.[2] In the course of our studies on the substitution of thallium moiety in arylthallium(III) compounds by halogen or pseudohalogen[3] we found that a similar nitrodethallation also occurred readily by use of metal nitrite through a different reaction scheme from that by nitrogen dioxide. This reaction may be useful as an alternative method for selective nitration of arenes.

Results and Discussion

When a mixture of *p*-tolylthallium(III) compound (**1**, R^1=Me, R^2=R^3=H) and sodium nitrite was stirred in trifluoroacetic acid at room temperature for 3 h, *p*-nitrotoluene (**2**, R^1=Me, R^2=R^3=H) was obtained almost quantitatively (Scheme 1). No formation of *m*- and *o*-

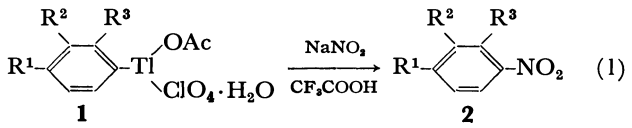

(1)

nitrotoluene shows that the replacement of thallium moiety by NO_2 occurred at the position where thallium was attached previously to aromatic ring. The reaction also took place in other organic acids such as chloroacetic acid and acetic acid, but it was slower and the yield of *p*-nitrotoluene was lower than that in trifluoroacetic acid, a side-product sometimes being formed. Almost no reaction occurred in organic solvents such as pyridine, dioxane, DMF, and acetonitrile even at refluxing temperature in which halogeno- and pseudohalogenodethallation proceeded smoothly.[3] It was found that the yield of *p*-nitrotoluene is affected by concentrations of both **1** and $NaNO_2$ in trifluoroacetic acid, lower concentration being preferable for higher yield of *p*-nitrotoluene. Other metal nitrites such as $AgNO_2$ and KNO_2 were also effective for this reaction. Typical results are summarized in Table 1.

Application of the reaction to other **1** such as *o*- and *m*-xylyl- and *p*-anisylthallium(III) compounds also afforded readily almost quantitative yield of **2**. In the case of phenyl- and chlorophenylthallium(III) compounds, however, the yield of **2** was low and considerable amounts of nitrosoarene and resinous products were formed. When potassium dichromate was added in

Table 2. Results of nitrodethallation of **1**[a]

1 R^1	R^2	R^3	(mmol)	$NaNO_2$ (mmol)	CF_3CO_2H (ml)	**2** Yield (%)[b]
Me	H	H	2	6	15	97
Me	Me	H	2	6	15	99
Me	H	Me	2	6	15	100
MeO	H	H	2	6	15	92[c]
H	H	H	1	3	15	25[d]
H	H	H	1	3	15	60[e]
H Cl	H	Cl[f] H	2	6	15	16[f,g]
H Cl	H	Cl[f] H	1	2	15	51[e,f]

a) At 25 °C for 3 h. b) Based on **1**. c) At 25 °C for 10 min. d) PhNO 27%. e) $K_2Cr_2O_7$ (1 mmol) was added. f) *o*:*p*=20:80. g) ClC_6H_4NO 11%.

Table 1. Effects of solvent, concentration of reactants, and metal nitrite in nitrodethallation of **1** (R^1=Me, R^2=R^3=H)

1 (R^1=Me, R^2=R^3=H) (mmol)	MNO_2 (mmol)	Solvent (ml)	Temp (°C)	Time (h)	**2** (R^1=Me, R^2=R^3=H) Yield (%)[a]
2	$NaNO_2$ 6	CF_3CO_2H 15	25	3	97
2	$NaNO_2$ 12	CF_3CO_2H 15	25	3	51
4	$NaNO_2$ 12	CF_3CO_2H 15	25	3	76
5	$NaNO_2$ 15	$ClCH_2CO_2H$ 25	100	10	54
5	$NaNO_2$ 15	CH_3CO_2H 25	25	5	0
5	$NaNO_2$ 15	CH_3CO_2H 25	100	5	55[b]
2	$AgNO_2$ 6	CF_3CO_2H 15	25	3	87
2	KNO_2 6	CF_3CO_2H 15	25	3	89

a) Based on **1**. b) Other product; *p*-tolyl acetate 9%.

* To whom correspondence should be addressed.

these reaction systems, the yield of **2** increased, no nitrosoarene being detected. The results are given in Table 2. The nitrodethallation procedure is applicable even without the isolation of intermediate arylthallium-(III) compounds. As an example, nitroarenes could be obtained (*in situ* nitrodethallation) when the reaction was carried out at 25 °C for 3 h by adding sodium nitrite to trifluoroacetic acid solution of arylthallium-(III) compound prepared by the method[4] of McKillop *et al.* The yields and isomer ratios of some nitroarenes are as follows ($K_2Cr_2O_7$ was also added in the case of halobenzene): toluene (87%, *o*: *m*: *p*=13: 1: 86), *t*-butylbenzene (92%, *o*: *m*: *p*=2: 6: 92), *o*-xylene (90%, 3-: 4-=7: 93), *m*-xylene (100%, only 4-), mesitylene (27%), biphenyl (mononitro- 47%, dinitro-53%), chlorobenzene (50%, *o*: *p*=19: 81) and bromobenzene (34%, *o*: *p*=19: 81). These isomer ratios should reflect those of intermediate arylthallium(III) compounds.

Metal nitrite reacts with various organic and inorganic acids to give nitrous acid (HNO_2). This gives NO^+ or N_2O_3 in acidic media, the latter being known as a carrier of nitrosyl ion (Scheme 2).[5a,b]

$$\begin{aligned} &NaNO_2 + CF_3COOH \rightleftarrows \\ &\qquad HNO_2 + CF_3CO_2Na \\ &2HNO_2 \rightleftarrows N_2O_3 + H_2O \\ &HNO_2 + H^+ \rightleftarrows NO^+ + H_2O \end{aligned} \quad (2)$$

The presence of nitrosyl ion in trifluoroacetic acid has been shown by cryoscopic experiments and spectral data.[6] From these facts and the reported data for electrophilic nitrosodethallation of arylthallium(III) compounds with nitrosyl chloride (NOCl),[7] nitrosoarenes should be expected as the intermediates in our case. In fact, nitrosoarenes were detected in the reaction products in the cases of phenyl- and chlorophenylthallium(III) compounds. For the sake of clarification we investigated the reaction products and their yields in the nitrodethallation of **1** (R^1=Me, R^2=R^3=H). It was found that when the reaction is stopped in a very short time, *p*-nitrosotoluene (**3**) is mainly formed together with a small amount of *p*-nitrotoluene (Scheme 3). The yield of each product

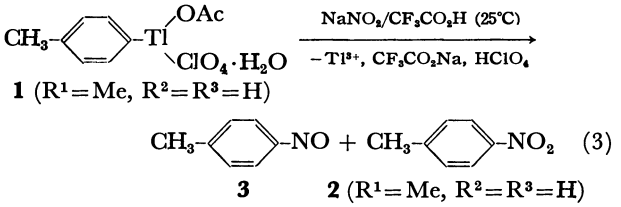

1 (R^1=Me, R^2=R^3=H)

3 **2** (R^1=Me, R^2=R^3=H) (3)

is plotted against reaction time in Fig. 1. It is seen that the reaction is consecutive involving the conversion of **3** into **2** (R^1=Me, R^2=R^3=H). In order to know how **3** can be converted into **2** (R^1=Me, R^2=R^3=H), the oxidation of **3** prepared separately by the reported method[8] to **2** (R^1=Me, R^2=R^3=H) was examined under various conditions (Table 3). The oxidation of **3** to **2** (R^1=Me, R^2=R^3=H) was rather slow in trifluoroacetic acid containing sodium nitrite, but the addition of thallium(III) salt and perchloric acid, both of which are expected to be formed in the reaction shown in Scheme 3, enhanced the rate remarkably.

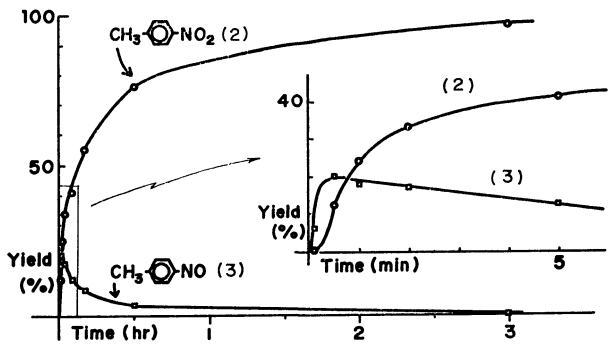

Fig. 1. Effect of reaction time on product and yield in the reaction of Scheme 3. Reaction conditions; **1** 2 mmol, $NaNO_2$ 6 mmol, CF_3CO_2H 15 ml, at 25 °C.

When **1** (R^1=MeO, R^2=R^3=H) was used as an additive, a very good yield of **2** (R^1=MeO, R^2=R^3=H) was obtained, **3** being partly oxidized to **2** (R^1=Me, R^2=R^3=H). This result shows that **1** and/or some species derived from **1** has a strong oxidizing ability and also that the oxidation of *p*-nitrosoanisole to the corresponding nitro compound is faster than that of **3**.

The yield of **2** from **1** (R^1=R^2=R^3=H and R^1 or R^3=Cl or H, R^2=H) was low, while the addition of $K_2Cr_2O_7$ increased it. When the reaction was stopped in a short time in the cases without $K_2Cr_2O_7$, the main product was nitrosoarene. As an example, from **1** (R^1=R^2=R^3=H) nitrosobenzene was obtained in 37% and 51% yield for 2 min and 10 min reaction, respectively, together with a small amount of nitrobenzene (<1.3%), and from **1** (R^1 or R^3=Cl or H, R^2=H) only chloronitrosobenzene was obtained in 14% yield for 2 min reaction (under the conditions shown in Fig. 1). At first glance it seems that the addition of $K_2Cr_2O_7$ helps the oxidation of nitroso compounds. However, it was clarified that the oxidation of nitrosobenzene to nitrobenzene was slow and a lot of nitrosobenzene was lost to unidentified compounds under various conditions (Table 3) or even in the presence of $K_2Cr_2O_7$ (See

Table 3. Results of the oxidation of *p*-nitrosotoluene to *p*-nitrotoluene[a]

3 (mmol)	$NaNO_2$ (mmol)	Additive (mmol)	Time (min)	**2** (R^1=Me, R^2=R^3=H) Yield (%)
2	6	—	10	0.4
2	6	—	180	90
2	6	$Tl(OAc)_3$ 2	10	25
2	6	70% $HClO_4$ 2	10	50
2	6	$Tl(OAc)_3$ 2, 70% $HClO_4$ 2	10	96
2	6	**1** (R^1=MeO, R^2=R^3=H) 2	10	48[b]

a) CF_3CO_2H 15 ml, at 25 °C. b) *p*-$MeOC_6H_4NO_2$ (89%) was also formed.

Experimental). Therefore the reason for effectiveness of the potassium salt in these cases seems to be attributed to other factors, *i.e.*, oxidation of C–Tl bond by $K_2Cr_2O_7$ followed by NO_2^- attack, a similar scheme having been proposed in the cases of arylpalladium(II) compounds,[9]

In order to confirm the mechanistic difference of nitrodethallation by metal nitrite from that by nitrogen dioxide,[2] nitrodethallation of **1** (R^1=Me, R^2=R^3=H) with nitrogen dioxide was carried out in trifluoroacetic acid at 25 °C, the reaction being stopped after 2 min. Only *p*-nitrotoluene was detected as the product (54% yield), no *p*-nitrosotoluene being formed (Compare with Fig. 1).

From the results it can be concluded that nitrodethallation of **1** with metal nitrite proceeds through electrophilic substitution of thallium moiety by NO^+ to give nitroso compounds followed by facile oxidation to nitro compounds (Scheme 4).

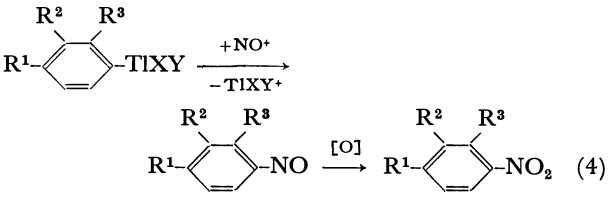

(4)

Experimental

GLC analyses were carried out on a Shimadzu 5APTF apparatus using PEG 6000 (25%)-Chromosorb W (1 m) and Apiezon L (30%)-Celite (1 m) columns (N_2 as a carrier gas).

Materials. Arylthallium(III) acetate perchlorate monohydrate[10] and bistrifluoroacetates[4] were prepared by reported methods. Commercial sodium nitrite was used without further purification. Nitrogen dioxide was prepared by the method of Brook.[11] Commercial organic solvents and substances of guaranteed grade were used. All the nitro compounds and nitrosobenzene were available either commercially or from previous studies in our laboratory. *p*-Nitrosotoluene was synthesized by the reduction of *p*-nitrotoluene to *p*-tolylhydroxylamine followed by oxidation using sodium dichromate.[8]

Reaction of 1 with Sodium Nitrite in Trifluoroacetic Acid (Tables 1 and 2). The following shows a typical experimental procedure. To a white suspension of **1** (R^1=Me, R^2=R^3=H) (0.94 g, 2 mmol) in trifluoroacetic acid (15 ml) was added solid sodium nitrite (0.41 g, 6 mmol) at 25 °C in one portion. The color of the mixture immediately turned dark-brown. The mixture was stirred at 25 °C for 3 h, during which period evolution of a small amount of brown fume was observed. The resulting yellow heterogeneous mixture was poured into water (100 ml) and the products were extracted with benzene. The extract was washed with aq. $NaHCO_3$ and dried over $MgSO_4$. The solvent was removed at atmospheric pressure. GLC analysis of the residue showed the presence of **2** (R^1=Me, R^2=R^3=H) (1.94 mmol, 97%) as the sole product.

When the reaction was stopped in a short time (10 s—0.5 h), variable amount of **3** was detected in GLC together with **2** (R^1=Me, R^2=R^3=H) (See Fig. 1).

Reaction of 1 (R^1=Me, R^2=R^3=H) with Nitrogen Dioxide in Trifluoroacetic Acid. To a solution of nitrogen dioxide[11] (1.5 ml, 50 mmol) in trifluoroacetic acid (15 ml) was added solid **1** (R^1=Me, R^2=R^3=H) (0.94 g, 2 mmol) at 25 °C in one portion and the resulting mixture was stirred for 2 min followed by addition of 100 ml of water to stop the reaction. After the usual work-up procedure, GLC analysis of the organic residue showed the presence of **2** (R^1=Me, R^2=R^3=H) (1.1 mmol, 54%) and none of **3**.

Oxidation of p-*Nitrosotoluene (3) to* p-*Nitrotoluene [2 (R^1=Me, R^2=R^3=H)] (Table 3).* To a stirred solution of $Tl(OAc)_3$ (0.76 g, 2 mmol) and 70% $HClO_4$ (0.29 g, 2 mmol) in trifluoroacetic acid (15 ml) was added solid sodium nitrite (0.41 g, 6 mmol) at 25 °C to give a brown suspension. To this suspension was added **3** (2.39 g, 2 mmol) and the solution was stirred for 10 min. After the usual work-up procedure, GLC analysis of the organic residue showed the presence of **2** (R^1=Me, R^2=R^3=H) (1.94 mmol) and unreacted **3** (0.06 mmol). This indicates that 96% of **3** was oxidized.

Oxidation of Nitrosobenzene to Nitrobenzene [2 R^1=R^2=R^3=H)]. To a green solution of nitrosobenzene (0.10 g, 1 mmol) in trifluoroacetic acid (15 ml) were added solid sodium nitrite (0.14 g, 2 mmol) and $Tl(OAc)_3$ (0.38 g, 1 mmol) in one portion and the resulting dark brown mixture was stirred at 25 °C for 3 h. Water (*ca.* 100 ml) was then added to give a dark brown tarry compound which was filtered. The filtrate was extracted with benzene. GLC analysis of the benzene extract showed the presence of nitrobenzene (0.11 mmol) and nitrosobenzene (0.13 mmol), indicating that 11% of the starting material was oxidized to nitrobenzene, 13% of it was recovered unreacted, and 76% of it was transformed to unidentified compounds. When a similar treatment was carried out with the addition of $K_2Cr_2O_7$ (0.29 g, 1 mmol), 16% of the starting material was oxidized to nitrobenzene and 18% of it was recovered unreacted.

References

1) Presented at the 33rd Annual Meeting of the Chemical Society of Japan, Fukuoka, October, 1975.
2) B. Davies and C. B. Thomas, *J. Chem. Soc., Perkin Trans. 1*, **1975**, 65.
3) a) S. Uemura, Y. Ikeda, and K. Ichikawa, *Tetrahedron*, **28**, 3025 (1972); b) S. Uemura, Y. Ikeda, and K. Ichikawa, *Tetrahedron*, **28**, 5499 (1972); c) S. Uemura, S. Uchida, M. Okano, and K. Ichikawa, *Bull. Chem. Soc. Jpn.*, **46**, 3254 (1973); d) S. Uemura, A. Toshimitsu, M. Okano, and K. Ichikawa, *Bull. Chem. Soc. Jpn.*, **48**, 1925 (1975).
4) A. McKillop, J. D. Hunt, M. J. Zelesko, J. S. Fowler, E. C. Taylor, G. McGillivray, and F. Kienzle, *J. Am. Chem. Soc.*, **93**, 4841 (1971).
5) a) F. A. Cotton and G. Wilkinson, "Advanced Inorganic Chemistry," 3rd ed., Interscience, New York, N. Y. (1972), p. 360; b) J. March, "Advanced Organic Chemistry: Reactions, Mechanisms, and Structure," McGraw-Hill, New York, N. Y. (1968), p. 485.
6) U. A. Spitzer and R. Stewart, *J. Org. Chem.*, **39**, 3936 (1974).
7) E. C. Taylor, R. H. Danforth, and A. McKillop, *J. Org. Chem.*, **38**, 2088 (1973).
8) H. Wieland and A. Roseeu, *Ber.*, **48**, 1119 (1915).
9) P. M. Henry, *J. Org. Chem.*, **36**, 1886 (1971).
10) K. Ichikawa, S. Uemura, T. Nakano, and E. Uegaki, *Bull. Chem. Soc. Jpn.*, **44**, 545 (1971).
11) A. G. Brook, *J. Chem. Soc.*, **1952**, 5040.

Synthesis of 3,4-Di-*O*-acetyl-6-azido-2,6-dideoxy-2-(2′,4′-dinitroanilino)-α-D-glucopyranosyl Chloride

Seiichiro OGAWA, Hitoshi FUJIMORI, and Tetsuo SUAMI

Department of Applied Chemistry, Faculty of Engineering, Keio University, Hiyoshi, Yokohama 223

(Received April 28, 1976)

The title compound has been prepared as an intermediate for the chemical synthesis of glycosides of 2,6-diamino sugar.

In the present communication, we should like to report a preparation of the title compound which is a useful intermediate for the chemical synthesis of α-glycosides of 2,6-diamino sugar.

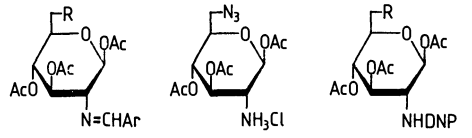

1 R = OTs
2 R = N_3

3

4 R = N_3
5 R = NHDNP

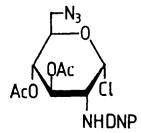

6

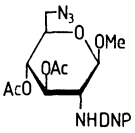

7

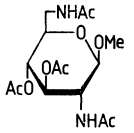

8

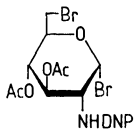

9

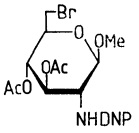

10

Treatment of 1,3,4-tri-*O*-acetyl-2-deoxy-2-(*p*-methoxybenzylideneamino)-6-*O*-tosyl-β-D-glucopyranose (**1**)[1] with sodium azide in *N,N*-dimethylformamide at 80—90 °C for 3 h resulted in displacement of the tosyloxy group with an azide ion to give the 6-azido compound (**2**) in 75% yield. Hydrolysis of **2** with hydrochloric acid gave a crystalline 1,3,4-tri-*O*-acetyl-2-amino-6-azido-2,6-dideoxy-β-D-glucopyranose hydrochloride (**3**) in 73% yield. Treatment of **3** with 2,4-dinitrofluorobenzene in an alkaline solution gave 1,3,4-tri-*O*-acetyl-6-azido-2,6-dideoxy-2-(2′,4′-dinitroanilino)-β-D-glucopyranose (**4**) in 74% yield, whose structure was confirmed by converting it into 1,3,4-tri-*O*-acetyl-2,6-dideoxy-bis(2′,4′-dinitroanilino)-β-D-glucopyranose (**5**).[2] Attempt to prepare α-glycosyl bromide of this azido sugar was not successful, because partial replacement of the azido group by a bromine ion was accompanied when **4** was treated with a common brominating reagent. Thus bromination of **4** with hydrobromic acid in acetic acid resulted in the formation of 3,4-di-*O*-acetyl-6-bromo-2,6-dideoxy-2-(2′,4′-dinitroanilino)-α-D-glucopyranosyl bromide (**9**) in 85% yield. Compound **9** reacted with an excess of methanol in the presence of silver carbonate in dioxane to give methyl 3,4-di-*O*-acetyl-6-bromo-2,6-dideoxy-2-(2′,4′-dinitroanilino)-β-D-glucopyranoside (**10**) in 53% yield.

Chlorination of **4** was effected by treatment with hydrogen chloride in ether at 0 °C and gave 3,4-di-*O*-acetyl-6-azido-2,6-dideoxy-2-(2′,4′-dinitroanilino)-α-D-glucopyranosyl chloride (**6**) in 68% yield as a relatively stable crystalline substance. Methanolysis of **6** in the presence of silver carbonate gave methyl β-glucopyranoside (**7**) in 44% yield, which was further converted into methyl 2,6-diacetamido-3,4-di-*O*-acetyl-2,6-dideoxy-β-D-glucopyranoside (**8**) by the usual method.

Experimental[3]

1,3,4-Tri-O-acetyl-2-deoxy-2-(p-methoxybenzylideneamino)-6-O-tosyl-β-D-glucopyranose (1). This compound was prepared from 2-deoxy-2-*p*-methoxybenzylideneamino-D-glucopyranose by the method of Morel.[1] Mp 203—204 °C, $[\alpha]_D^{20}$ +103° (*c* 2, chloroform) [lit,[1] mp 203—204 °C, $[\alpha]_D^{20}$ +99.3° (*c* 2, chloroform)].

1,3,4-Tri-O-acetyl-6-azido-2,6-dideoxy-2-(p-methoxybenzylideneamino)-β-D-glucopyranose (2). A mixture of **1** (12 g), sodium azide (12 g), and *N,N*-dimethylformamide (300 ml) was heated at 80—90 °C under stirring for 3 h. The reaction mixture was evaporated and the residue was extracted with chloroform (200 ml). The extract was washed with water, dried over anhydrous sodium sulfate, and evaporated to give a syrup, which was recrystallized from ethanol to give 7.4 g (75%) of **2**, mp 123.5—124 °C, $[\alpha]_D^{25}$ +127° (*c* 2, chloroform). PMR ($CDCl_3$): δ 1.90 (s, 3), 2.03 (s, 3), 2.06 (s, 3) (OAc), 3.33—3.63 (m, 2, CH_2N_3), 3.87 (s, 3, OMe), 5.15 (t, 1, $J_{3,4}=J_{4,5}=9$ Hz, H-4), 5.50 (t, 1, $J_{2,3}=9$ Hz, H-3), 6.00 (d, 1, $J_{1,2}=9$ Hz, H-1), 6.97 (d, 2), 7.71 (d, 2) (ABq, aromatic ring proton), 8.22 (s, 1, N=CHAr).

Found: C, 53.70; H, 5.33; N, 12.21%. Calcd for $C_{20}H_{24}N_4O_8$: C, 53.59; H, 5.40; N, 12.50%.

1,3,4-Tri-O-acetyl-2-amino-6-azido-2,6-dideoxy-β-D-glucopyranose Hydrochloride (3). To a warm solution of **2** (1.33 g) in acetone (5 ml) was added dropwise 5 M aq. hydrochloric acid (2 ml) under vigorous agitation. The white solid precipitated immediately. After the reaction mixture had been set aside at room temperature for several hours, the product was collected by filtration, washed with ether, and recrystallized from methanol to give 0.69 g (73%) of **3**, mp 147—154 °C (dec), $[\alpha]_D^{25}$ +55.8° (*c* 1, H_2O), $[\alpha]_D^{24}$ +43° (*c* 0.5, methanol).

Found: C, 39.46; H, 5.16; N, 15.10; Cl, 9.46%. Calcd for $C_{12}H_{18}N_4O_7 \cdot HCl$: C, 39.30; H, 5.22; N, 15.28; Cl, 9.67%.

1,3,4-Tri-O-acetyl-6-azido-2,6-dideoxy-2-(2′,4′-dinitroanilino)-β-D-glucopyranose (4). To a stirred mixture of **3** (1.6 g) and sodium hydrogen carbonate (0.9 g) in 50% aq. acetone (12 ml) was added 2,4-dinitrofluorobenzene (0.9 g), and the mixture was allowed to stand at room temperature overnight. Then the mixture was evaporated to dryness and the residue was extracted with ethyl acetate. The extracts were evaporated to give a syrup, which was recrystallized from ethanol to give 1.6 g (74%) of **4**, mp 115.5—116 °C, $[\alpha]_D^{20}$ +108° (*c* 1, chloroform), $[\alpha]_D^{25}$ +102° (*c* 1, acetone). PMR ($CDCl_3$): δ

1.95 (s, 3), 2.03 (s, 3), 2.11 (s, 3) (OAc), 3.45—3.60 (m, 2, C$\underline{H}_2$N$_3$), 5.29 (t, 1, $J_{3,4}=J_{4,5}=9.5$ Hz, H-4), 5.67 (t, 1, $J_{2,3}=9.5$ Hz, H-3), 6.12 (d, 1, $J_{1,2}=8.5$ Hz, H-1).

Found: C, 44.03; H, 4.17; N, 16.89%. Calcd for $C_{18}H_{20}N_6O_{11}$: C, 43.55; H, 4.06; N, 16.93%.

1,3,4-Tri-O-acetyl-2,6-dideoxy-2,6-bis(2′,4′-dinitroanilino)-β-D-glucopyranose (5). A solution of **3** (0.4 g) in methanol containing 6 M hydrochloric acid (0.2 ml) was hydrogenated in the presence of 10% palladium on carbon for 5 h at room temperature (the initial hydrogen pressure of 3.4 kg/cm^2). The catalyst was removed by filtration and the filtrate was evaporated to give a crude diamine dihydrochloride. This was directly treated with 2,4-dinitrofluorobenzene (1 g) in ethanol (4 ml) and acetone (16 ml) in the presence of sodium hydrogen carbonate (1 g) for 2 days at room temperature. The reaction mixture was evaporated and the residue was extracted with chloroform. The crude product was chromatographed on silica gel (16 g) with 3: 1 benzene–ethyl acetate as the eluant to give 0.24 g (35%) of **5**, after recrystallization from chloroform–ethanol, mp 280—281 °C, $[\alpha]_D^{15}$ +111° (*c* 1, acetone). PMR (DMSO-d_6): δ 1.87 (s, 3), 1.94 (s, 3), 2.13 (s, 3) (OAc), 4.74 (td, 1, $J_{1,2}=8.5$ Hz, $J_{2,3}=9$ Hz, $J_{2,NH}=3$ Hz, H-2), 5.17 (t, 1, $J_{3,4}=9$ Hz, H-4), 5.90 (t, 1, H-3), 6.30 (d, 1 H-1).

Found: C, 45.53; H, 4.19; N, 13.06%. Calcd for $C_{24}H_{24}N_6O_{15}$: C, 45.28; H, 3.80; N, 13.21%.

3,4-Di-O-acetyl-6-azido-2,6-dideoxy-2-(2′,4′-dinitroanilino)-α-D-glucopyranosyl Chloride (6). Dry hydrogen chloride was introduced into a solution of **4** (6 g) in dry ether (100 ml) at 0 °C until saturation was completed. The solution was allowed to stand at room temperature for 20 h. The resulting crystals were collected by filtration to give 4 g (68%) of **6**, mp 164—166 °C (dec). Recrystallization from chloroform–ether gave an analytically pure sample, mp 170 °C (dec), $[\alpha]_D^{25}$ +167° (*c* 1, chloroform). PMR (DMSO-d_6): δ 6.90 (d, 1, $J_{1,2}=3$ Hz, H-1).

Found: C, 40.37; H, 3.62; N, 17.37; Cl, 7.64%. Calcd for $C_{16}H_{17}N_6O_9Cl$: C, 40.63; H, 3.62; N, 17.77; Cl, 7.50%.

Methyl 3,4-Di-O-acetyl-6-azido-2,6-dideoxy-2-(2′,4′-dinitroanilino)-β-D-glucopyrauoside (7). A mixture of **6** (1 g), silver carbonate (5 g), and Drierite (14 g) in dioxane (40 ml) and methanol (40 ml) was stirred at room temperature in the dark for a week. An insoluble matter was removed by filtration and the filtrate was evaporated to give a syrup, which was chromatographed on silica gel (40 g) with 40: 3 benzene–ethyl acetate as the eluant. The fractions containing a main component were evaporated and the residue was recrystallized from chloroform–ethanol to give 0.43 g (44%) of **7**, mp 170.5—171 °C, $[\alpha]_D^{25}$ +61.3° (*c* 1, chloroform). PMR (CDCl$_3$): δ 1.96 (s, 3), 2.11 (s, 3) (OAc), 3.58 (s, 3, OMe), 4.71 (d, 1, $J_{1,2}=8$ Hz, H-1), 5.17 (t, 1, $J_{3,4}=J_{4,5}=9$ Hz, H-4), 5.52 (t, 1, $J_{2,3}=9$ Hz, H-3).

Found: C, 43.40; H, 4.30; N, 17.96%. Calcd for $C_{17}H_{20}N_6O_{10}$: C, 43.59; H, 4.30; N, 17.94%.

Methyl 2,6-Diacetamido-3,4-di-O-acetyl-2,6-dideoxy-β-D-glucopyranoside (8). Compound **7** (0.38 g) was treated with methanolic ammonia (16 ml) at room temperature overnight. At this time, the mixture became a clear solution and TLC indicated the formation of a single product. Then Dowex 1×2 (OH$^-$) was added to the solution and the mixture was stirred until all the product was consumed. The resin was removed by filtration and the filtrate was evaporated to give a syrup, which was hydrogenated in water in the presence of platinum oxide (30 mg) at room temperature overnight. The product was then treated with acetic anhydride (5 ml) in pyridine (5 ml) at room temperature overnight. The crude product was recrystallized from ethyl acetate to give 0.12 g (41%) of **8**, mp 208—210 °C, $[\alpha]_D^{25}$ −39° (*c* 1, acetone). PMR (DMSO-d_6): δ 1.80 (s, 3), 1.85 (s, 3), 1.93 (s, 3), 2.00 (s, 3) (Ac), 4.57 (d, 1, $J_{1,2}=9$ Hz, H-1), 4.80 (t, 1, $J_{3,4}=J_{4,5}=10$ Hz, H-4), 5.17 (t, 1, $J_{2,3}=10$ Hz, H-3).

Found: C, 49.72; H, 6.57; N, 7.76%. Calcd for $C_{15}H_{24}N_8O_{12}$: C, 49.99; H, 6.71; N, 7.77%.

Hydrolysis of **8** with 6 M hydrochloric acid at 100 °C for 2 h gave 2,6-diamino-2,6-dideoxy-D-glucopyranose dihydrochloride, which was identified with an authentic specimen derived by hydrolysis of antibiotic neamine.

Methyl 3,4-Di-O-acetyl-6-bromo-2,6-dideoxy-2-(2′,4′-dinitroanilino)-β-D-glucopyranoside (10). To a solution of **4** (2 g) in methylene chloride (10 ml) was added acetic acid (30 ml), saturated with hydrobromic acid under stirring at −20—−15 °C, and the reaction mixture was allowed to stand at the same temperature for 2 h. The mixture was poured into ice–water and extracted with chloroform. The extracts were washed with aq. sodium hydrogen carbonate and water, dried over anhydrous sodium sulfate, and evaporated to give a syrup, which was crystallized from chloroform–petroleum ether to give 1.9 g (85%) of 3,4-di-*O*-acetyl-6-bromo-2,6-dideoxy-2-(2′,4′-dinitroanilino)-α-D-glucopyranosyl bromide (**9**), mp 146—150 °C (dec). This compound did not give satisfactory analytical data (Found: C, 35.36; H, 3.25; N, 8.12%).

Compound **9** (1 g) was treated in the presence of silver carbonate (9 g) in methanol (25 ml) and dioxane (25 ml) under stirring at room temperature overnight. An insoluble matter was removed by filtration and the filtrate was evaporated to give a syrup, which was chromatographed on silica gel (40 g) with 10: 1 benzene–ethyl acetate as the eluant to give 0.41 g (53%) of **10**, mp 183—186 °C, $[\alpha]_D^{20}$ +46.2° (*c* 0.5, chloroform). PMR (DMSO-d_6): δ 1.77 (s, 3), 2.09 (s, 3) (OAc), 3.57 (s, 3, OMe), 4.17 (broad septet, 1, $J_{1,2}=6.5$ Hz, $J_{2,3}=7.5$ Hz, $J_{2,NH}=3$ Hz, H-2), 5.27 (d, 1, H-1), 9.03 (d, 1, N$\underline{H}$).

Found: C, 40.03; H, 3.92; N, 8.18; Br, 15.75%. Calcd for $C_{17}H_{20}N_3O_{10}Br$: C, 40.32; H, 3.98; N, 8.29; Br, 15.79%.

References

1) Ch. J. Morel, *Helv. Chim. Acta*, **61**, 1501 (1958).

2) An α-anomer reported by Meyer zu Reckendorf and his coworkers has physical constants very close to those of **5**, but, in the PMR spectrum, a signal due to the anomeric proton appeared at δ 6.10 as a doublet having 3-Hz spacing, clearly differentiating it from **5**. W. Meyer zu Reckendorf, L. Rolf, and N. Wassiliadou-Micheli, *Carbohydr. Res.*, **45**, 307 (1975).

3) Melting points were determined in capillaries in a liquid bath and are uncorrected. Solutions were evaporated under diminished pressure at 40—50 °C. PMR spectra were measured at 60 MHz on a Varian A-60D spectrometer in chloroform-*d* (CDCl$_3$) or dimethyl-d_6 sulfoxide (DMSO-d_6)with reference to tetramethylsilane as an internal standard and the peak positions are given in δ-values. Values given for coupling constants are of first-order. Elemental analyses were performed by Mr. Saburo Nakada, to whom our thanks are due.

Reaction of Carboxylic Acids with Dioxygen Complexes: A Mechanistic Aspect of the Reaction[1]

Shigeaki MUTO and Yoshio KAMIYA

Department of Reaction Chemistry, Faculty of Engineering, The University of Tokyo, Hongo, Tokyo 113

(Received May 1, 1976)

The reaction of carboxylic acids with dioxygen complexes $MO_2(PPh_3)_2$(M=Pt, Pd) at low temperature gives rise to the selective formation of H_2O_2 and the corresponding dicarboxylato complexes characterized by their physical properties. It is suggested that the reaction can be influenced by either the capability of reactant for coordination to metal center or the stability of resulting metal complex. An equimolar addition of $CH_2ClCOOH$ to the dioxygen complexes in the presence of triphenylmethyl bromide at *ca.* −70 °C gives triphenylmethyl hydroperoxide and the corresponding monocarboxylato complexes in good yields, indicating that the reaction of organic acids with $MO_2(PPh_3)_2$ proceeds by stepwise mechanism.

Recently a study on the reaction of metal dioxygen complexes with a variety of organic compounds has received considerable attention. In general, the coordinated molecular oxygen to a metal complex is considered to be peroxidic on the basis of increased O–O bond length.[2] Benzoyl chloride and triphenylmethyl bromide (TPMB) react with $NiO_2(t\text{-BuNC})_2$ to give the corresponding peroxides.[3] Although Vaska[4] and Wilke *et al.*[5] also mentioned the formation of H_2O_2 upon protonation of $IrO_2Cl(CO)(PPh_3)_2$ and $NiO_2(PPh_3)_2$, respectively, the determination of reaction products and the elucidation of protonation mechanism still remain unclarified. In order to elucidate the reaction mechanism, the reaction of some carboxylic acids and phenols with square planar dioxygen complexes $MO_2(PPh_3)_2$ (M=Pt, Pd) was investigated.

In this work, we wish to report that the reaction of organic acids with $MO_2(PPh_3)_2$ results in the selective formation of H_2O_2 and the corresponding dicarboxylato complexes, and that the reaction proceeds by stepwise mechanism. The reaction of *o*- and *p*-substituted phenols was investigated in detail.

Experimental

Melting points were determined on a Yazawa hot-stage apparatus and uncorrected. Chloroacetic acid, triphenylphosphine(PPh_3), and TPMB were purified by recrystallization from ethanol or benzene. All the dioxygen complexes were prepared according to the procedure in literature.[6] The IR spectra were recorded as Nujol mulls on a Nippon Bunko IR-G spectrophotometer(4000—400 cm^{-1}), calibrated with polystyrene film. The NMR spectra were obtained on a JEOL Model JMN-4H-100 spectrometer in $CDCl_3$ solution containing tetramethylsilane as an internal standard. H_2O_2 and triphenylmethyl hydroperoxide obtained by equimolar addition of $CH_2ClCOOH$ to the dioxygen complexes in the presence of TPMB were analyzed by the conventional iodometric method.

General Procedure. The reactions were carried out in CH_2Cl_2 solution in the air or under a nitrogen atmosphere at 0 °C. The total volume was 4 ml for CH_3COOH(4.37 M) and 2 ml for $CH_2ClCOOH$(1.00 M). The concentration of $MO_2(PPh_3)_2$ was in the range $4.23\times10^{-3}-8.83\times10^{-2}$ M. The peroxide formed during the course of reaction was transferred in a vacuum(*ca.* 10^{-2}Torr) and then titrated by iodometry. The transfer efficiency was *ca.* 98 percent. The peroxide transfered could be considered principally to be H_2O_2 since the amount of the peroxide drastically decreased when treated with catalase.

Preparation of Dicarboxylato Complexes. *$Pt(OCOCH_2Cl)_2(PPh_3)_2$*: To a CH_2Cl_2 solution (20 ml) of $PtO_2(PPh_3)_2 1.5C_6H_6$(0.186 g, 0.214 mmol) was added excess $CH_2ClCOOH$(0.189 g, 2.00 mmol) under N_2 at 0 °C. Immediately the yellow solution turned colorless. The solution was stirred for 1 h at room temperature. Removal of the solvent *in vacuo* left a white residue which was recrystallized from ethanol to yield a white solid(0.134 g, 88.2% based on the dioxygen complex used). The solid was identified as $Pt(OCOCH_2Cl)_2(PPh_3)_2$ on the basis of its physical properties(Table 3).

$Pd(OCOCH_2Cl)_2(PPh_3)_2$: A similar treatment of $PdO_2(PPh_3)_2$(0.183 g, 0.235 mmol) with $CH_2ClCOOH$(0.189 g, 2.00 mmol) afforded a yellow solid of $Pd(OCOCH_2Cl)_2(PPh_3)_2$ (0.127 g, 87.7%) which was recrystallized from hexane–ethanol (1: 1 by volume). Physical properties for the yellow solid are also given in Table 3.

Preparation of Monocarboxylato Complexes. *$Pt(OCOCH_2Cl)Br(PPh_3)_2$*: To a CH_2Cl_2 solution(50 ml) of $PtO_2(PPh_3)_2 1.5C_6H_6$(0.869 g, 1.00 mmol) was added equimolar $CH_2ClCOOH$(0.107 g, 1.13 mmol) under N_2 at the temperature of ethanol–Dry Ice. After the resulting orange solution was stirred for 5 min, TPMB(0.329 g, 1.02 mmol) was slowly added. The reaction mixture was stirred another 3 h at the same temperature. The orange solution was allowed to stand overnight in a refrigerator. The reaction mixture containing an appreciable amount of white precipitated was distilled *in vacuo* at room temperature to give 0.841 g(yield 94.2%) of the monocarboxylate, white solid, along with colorless crystals which were chromatographed on alumina(about 300 mesh, deactivated with 1 ml of H_2O/100 g of alumina) and eluted with diethyl ether. The colorless crystals were identified as triphenylmethyl hydroperoxide from the data of its elemental analysis(Found: C, 82.89, H, 5.81%. Calcd for $C_{19}H_{16}O_2$: C, 82.57; H, 5.81%), mp (83—84 °C, lit,[7] 81—82 °C), IR, and chemical reactions. The hydroperoxide exhibited intense IR absorption at 3490 cm^{-1} characteristic of hydroperoxy moiety which shifted at higher frequency (3540 cm^{-1}) when treated with excess PPh_3, indicating that the peroxide was reduced to the corresponding alcohol. The yield of triphenylmethyl hydroperoxide was 0.230 g (83.5% based on the dioxygen complex used).

$Pd(OCOCH_2Cl)Br(PPh_3)_2$: A similar treatment of $PdO_2(PPh_3)_2$(0.789 g, 1.00 mmol) with TPMB(0.291 g, 0.990 mmol) in the presence of $CH_2ClCOOH$(0.107 g, 1.13 mmol) gave a yellow solid of $Pd(OCOCH_2Cl)Br(PPh_3)_2$(0.582 g, 81.4%) and triphenylmethyl hydroperoxide(0.291 g, 50.6% based on TPMB used) which was also purified by the chromatographic method under the same conditions, using benzene–diethyl ether as an eluent. As a by-product, a similar yellow solid was isolated from the residue insoluble in CH_2Cl_2. The solid was

Table 1. Formation of H_2O_2 by the reaction of organic acids with dioxygen complexes in CH_2Cl_2 at 0 °C

Dioxygen complex	$\times 10^5$ mol	Acid	Atmosphere	H_2O_2[a] ($\times 10^5$ mol)	Yield[b] (%)
$PtO_2(PPh_3)_2$	1.69	CH_3COOH	Air	1.18	70.9
	1.69	$CH_2ClCOOH$	N_2	1.30	76.9
	8.40	$CH_2ClCOOH$	Air	5.58	66.4
	5.74	$CH_2ClCOOH$	N_2	3.01	52.4
	5.74	$CH_2ClCOOH$	N_2	0.99[c]	17.2
$PdO_2(PPh_3)_2$[d]	11.28	CH_3COOH	N_2	7.57	67.1
	11.12	$CH_2ClCOOH$	N_2	8.37	75.3
	17.66	$CH_2ClCOOH$	N_2	13.11	74.2
	7.18	$CH_2ClCOOH$	N_2	5.60	76.6
	7.18	$CH_2ClCOOH$	N_2	0.02[c]	0.24
$IrO_2Cl(CO)(PPh_3)_2$	3.71	$CH_2ClCOOH$	Air	trace	—
$RuO_2(OH)(NO)(PPh_3)_2$	4.44	$CH_2ClCOOH$	Air	0.10	2.16

a) Titrated by iodometry after 1 h. b) The yields were calculated on the basis of the dioxygen complexes used. c) Treated with catalyse prior to titration. d) Reaction temperature was 2 °C.

characterized as $PdBr_2(PPh_3)_2$ by analysis (Found: C, 54.46; H, 3.87; Br, 20.18%. Calcd for $C_{36}H_{30}Br_2P_2Pd$: C, 54.46; H, 3.83; Br, 20.21%). The IR spectrum was identical with that of an authentic sample prepared by other routes.

Results and Discussion

Reaction of Carboxylic Acids with $MO_2(PPh_3)_2$. The experimental results on the reaction of CH_3COOH or $CH_2ClCOOH$ with $MO_2(PPh_3)_2$ (M=Pt, Pd) are given in Table 1. $MO_2(PPh_3)_2$ reacted with the organic acids in the air or under a nitrogen atmosphere to give H_2O_2 in 52—77% yield (based on the dioxygen complexes used). The high yields of H_2O_2 under N_2 strongly indicate that H_2O_2 is derived from the coordinated molecular oxygen of $MO_2(PPh_3)_2$. The fact that the yields of H_2O_2 under air are less than those under N_2 suggests that the reaction proceeds stoichiometrically. Formation of H_2O_2 was scarcely recognized in the reaction of $IrO_2Cl(CO)(PPh_3)_2$ and $RuO_2(OH)(NO)(PPh_3)_2$ with $CH_2ClCOOH$.

Table 2. Effect of pK_a on the yields of H_2O_2 at 0 °C[a]

Acid (1.00 M)	pK_a (at 25 °C)	H_2O_2 Yield (%) $PtO_2(PPh_3)_2$	H_2O_2 Yield (%) $PdO_2(PPh_3)_2$[b]
Chloroacetic acid	2.86	66.4	75.3
Benzoic acid	4.21	18.9	32.7
Acetic acid	4.76	76.9[c]	53.5
p-Nitrophenol	7.15		7.1
p-Acetylphenol	≈8	8.6	
Phenol	9.99		8.9
Hydroquinone[d]	9.91[e]	5.3	
Catechol[d]	9.45	85.1	33.6
Catechol[d]	9.45	1.2[f]	trace
3,5-Di-*t*-butyl-catechol[d]	≈9	66.5	32.0
o-Aminophenol[d]		83.2	36.5
Indene	21	—[g]	—[g]

a) All the reactions were carried out under N_2 for 1 h. b) Reaction temperature was 2 °C. c) [CH_3COOH] was 4.73 M. d) Concentration of phenols was 8.25×10^{-2} M. e) pK_a value at 20 °C. f) Treated with catalase prior to iodometry. g) No peroxide was detected by iodometry.

The effect of pK_a(H^+) of the organic acids on the yield of H_2O_2 was also investigated. The yield of H_2O_2 seems to be roughly correlated with the pK_a of substrates (Table 2). Namely the formation of H_2O_2 shows an upward trend with the decreased pK_a value. However, the yield in the presence of bonzoic acid (pK_a= 4.21) was much less than that in CH_3COOH (pK_a= 4.76). *o*-Substituted phenols reacted with **1a** under the same conditions to provide H_2O_2 in 83—85% yield, suggesting that the reaction is fairly influenced by either the capability of substrates for coordination to the metal center or the stability of the resulting metal complex. Namely, the reason why *o*-substituted phenols are more preferred is that their dianions are good ligands. From these results, the following reaction seems to take place.

$$\underset{\textbf{1a}; M=Pt \quad \textbf{1b}; M=Pd}{MO_2(PPh_3)_2} + 2RCOOH \longrightarrow M(OCOR)_2(PPh_3)_2 + H_2O_2 \qquad (1)$$

3a; M=Pt, R=CH_2Cl
3b; M=Pd, R=CH_2Cl
3c; M=Pt, R=CH_3
3d; M=Pt, R=C_6H_5

The analytical data for dicarboxylato complexes **3a** and **3b** obtained in the reaction of $MO_2(PPh_3)_2$ with $CH_2ClCOOH$ and recrystallized from ethanol are given in Table 3. The infrared spectra of **3a** and **3b** are similar to each other. Whereas **1a** and **1b** showed intense absorption due to oxygen-oxygen stretching, respectively, at 821 and 869 cm^{-1}, there were no strong bands in the 900—800 cm^{-1} region for the carboxylates. No band was observed in the region of the spectra near 2200 cm^{-1} which can be attributed to a metal-hydrogen stretching.[8] The complexes exhibited absorptions at 1644—1624 and 1099 cm^{-1} characteristic of a metal-carboxylate and coordinated PPh_3, respectively. The large shift of the ν(C=O) bands of **3a** and **3b** to lower frequency from that of the corresponding free acid

Table 3. Analytical data of the carboxylates

Complex	Mp (°C)	Formula	Analysis (%) Calcd (Found) C	H	Cl	Br	IR(in CH_2Cl_2), cm^{-1}
3a	252—254(dec)	$C_{40}H_{34}O_4Cl_2P_2Pt$	52.48 (52.40)	3.72 (4.02)	7.76 (7.86)		1624m, 1604m, and 1099s
3b	152—157(dec)	$C_{40}H_{34}O_4Cl_2P_2Pd$	58.73 (58.02)	4.16 (4.87)	8.69 (8.65)		1644s, 1608m, and 1099s
4a[a)]	267—269(dec)	$C_{41}H_{38}O_2BrClP_2Pt$	52.81 (52.72)	3.79 (3.83)	3.81 (3.69)	8.57 (8.83)	1662s, 1603w, 1607sh, and 1097s
4b[a)]	145—154(dec)	$C_{41}H_{38}O_2BrClP_2Pd$	58.38 (58.19)	4.19 (4.40)	4.21 (3.92)	9.47 (11.01)	1660sh, 1646w, 1606s, and 1098s

a) Calcd as $M(OCOCH_2Cl)Br(PPh_3)_2 \cdot 0.5C_6H_6$. w; weak, m; medium, s; strong, sh; shoulder.

seems to be due to the interaction between the carbonyl moiety and the central metal. These dicarboxylato complexes gave elemental analyses (Table 3) consistent with the proposed structures, respectively. The NMR spectra also indicates that the complexes could be characterized as $M(OCOCH_2Cl)_2(PPh_3)_2$. Similarly it was confirmed that **3c** and **3d** had characteristic absorptions at 1565 and 1617 cm^{-1}, respectively, attributable to the ν(C=O) of coordinated carboxylates.

Mechanistic Aspect of the Reaction. When **1a** and **1b** were treated with double molar quantity of $CH_2ClCOOH$ at *ca.* −70 °C, characteristic color changes of the solution were observed. The CH_2Cl_2 solution of **1a** gradually turned orange from yellow and then became colorless. In a similar manner, **1b** changed from light blue to wine red, and then to yellow. The IR spectra of **1a** and **1b** treated with exactly equimolar $CH_2ClCOOH$ to the complexes at *ca.* −70 °C were taken in CH_2Cl_2 solution at ambient temperature. Although the spectra were very similar to those of the corresponding dicarboxylates, an other new strong band was observed at *ca.* 3380 cm^{-1} which might be attributed to an oxygen-hydrogen stretching. No band due to the ν(C=O) of free acid was, of course, observed in the region of the spectra near 1700 cm^{-1}. Treatment of **1a** with CH_3COOD under the same conditions also gave an IR spectrum having the characteristic new band at *ca.* 2500 cm^{-1} which might be assigned to the ν(O–D). The results suggest that the reaction of $CH_2ClCOOH$ with $MO_2(PPh_3)_2$ proceeds by stepwise mechanism as shown below:

$$MO_2(PPh_3)_2 \xrightarrow{CH_2ClCOOH} M(OOH)(OCOCH_2Cl)(PPh_3)_2$$
2a; M=Pt
2b; M=Pd

$$\xrightarrow{CH_2ClCOOH} M(OCOCH_2Cl)_2(PPh_3)_2 + H_2O_2 \quad (2)$$
3a; M=Pt
3b; M=Pd

The reaction of a metal hydride with gaseous oxygen gives a metal hydroperoxide as a reactive intermediate.[9] In our complexes, isolation of **2a** and **2b** from the reaction mixtures was unsuccessful because of their thermal labilities. **2b** in particular was unstable in solution and decomposed to give palladium metal when allowed to stand for several minutes at room temperature. In order to elucidate the reaction mechanism, we attempt to prepare triphenylmethyl hydroperoxide by the successive equimolar addition of $CH_2ClCOOH$ and TPMB to $MO_2(PPh_3)_2$ at −70 °C as shown in the following.

$$MO_2(PPh_3)_2 \xrightarrow[\text{in } CH_2Cl_2]{CH_2ClCOOH} M(OOH)(OCOCH_2Cl)(PPh_3)_2$$
$$\xrightarrow{TPMB} M(OCOCH_2Cl)Br(PPh_3)_2 + Ph_3COOH \quad (3)$$

In the reaction of **1a** and **1b**, the hydroperoxide was obtained in 83.5 and 50.7% yields, respectively. In the absence of the complexes no peroxidation of TPMB with gaseous oxygen took place at all. The lower yield in **1b** seems to be due to a smaller stability of **2b**.

Analytical data for the monocarboxylates are given in Table 3. The IR spectra of **4a** and **4b** were close to those of the corresponding dicarboxylates. The NMR spectra of **4a** and **4b**, taken in $CDCl_3$ solution, exhibited singlet peaks at δ 3.31 and 3.39 ppm, respectively, which were easily assignable to their methylene protons. The identification of hydroperoxide was performed by its physical properties and chemical reactions (see Experimental).

The results strongly suggest that the reaction of $MO_2(PPh_3)_2$ with carboxylic acids proceeds by stepwise mechanism (2).

The authors would like to thank Dr. E. Niki, the University of Tokyo, for his valuable discussions.

References

1) A part of this paper was presented at the 32 th Annual Meeting of the Chemical Society of Japan, Tokyo, April 1975; *Chem. Lett.*, **1975**, 809

2) (a) S. J. LaPlaca and J. A. Ibers. *J. Am. Chem. Soc.*, **94** 1144 (1972); (b) J. A. McGinnety, R. J. Doedens, and J. A. Ibers, *Inorg. Chem.*, **6**, 2243 (1967); (c) T. Kashiwagi, N. Kasai, N. Yasuoka, M. Kakudo, S. Takahashi, and N. Hagihara, *Chem. Commun.*, **1969**, 743.

3) Sei Otsuka, A. Nakamura, Y. Tatsuno, and M. Miki, *J. Am. Chem. Soc.*, **94**, 3761 (1972).

4) L. Vaska, *Science*, **140**, 809 (1963).

5) G. Wilke, H. Schott, and P. Heimbach, *Angew. Chem. Int. Ed. Engl.*, **6**, 92 (1967).

6) (a) L. Malatesta and M. Angoletta, *J. Chem. Soc.*, **1957**, 1186; (b) L. Malatesta and C. Cariello, *ibid.*, **1958**, 2323; (c) S. Takahashi, K. Sonogashira, and N. Hagihara, *Nippon Kagaku Zasshi*, **87**, 610 (1966).

7) R. Criegee and H. Dietrich, *Ann.*, **560**, 135 (1948).

8) J. C. Bailar, Jr. and H. Itatani, *Inorg. Chem.* **4**, 1618 (1965).

9) K. R. Grundy, K. R. Laing, and W. R. Roper, *Chem. Commun.*, **1970**, 1500.

Syntheses of Some Alkoxy-, Dialkoxy-, and Alkoxyamino-sulfonium Ions and Their *O*-Methylene and *N*-Methylene PMR Chemical Shifts

Hiroshi MINATO,* Kei YAMAGUCHI, Kentaro OKUMA, and Michio KOBAYASHI

Department of Chemistry, Tokyo Metropolitan University, Fukazawa, Setagaya, Tokyo 158

(Received March 24, 1976)

Alkylation of sulfenates proved to be a good method for synthesis of alkoxysulfonium ion not obtainable by alkylation of sulfoxides. Dialkoxy- and alkoxyamino-sulfonium ions were prepared by alkylation of sulfinates and sulfinamides. Ethoxy- and methoxymorpholinophenylsulfonium tetraphenylborates were obtained as high-melting crystals, which almost quantitatively alkylated amines at room temperature. PMR spectra of $RR'\overset{\oplus}{S}$–OCH_AH_BR'' and $RR'\overset{\oplus}{S}$–$N(R'')CH_AH_BR'''$ were determined, and the relationship between $\delta_A-\delta_B$ and (R,R') were examined.

Sulfonium ions containing hetero atom substituents are interesting compounds, and some of them have been investigated in our laboratoris.[1-3] The two hydrogens of *O*-methylene and *N*-methylene groups in alkoxy- and amino-sulfonium ions are expected to be magnetically non-equivalent if the other two substituents on the sulfonium sulfur atom are different. It seems to be of interest to determine the PMR spectra of $RR'\overset{\oplus}{S}$–OCH_AH_BR'' and $RR'\overset{\oplus}{S}$–$N(R'')CH_AH_BR'''$ and to study the relationship between $\delta_A-\delta_B$ and (R,R'). Some new alkoxy-, dialkoxy-, and alkoxyamino-sulfonium ions were synthesized, and their PMR spectra were examined.

Results and Discussion

Alkoxysulfonium ions were prepared by two different methods. The first method used was alkylation of sulfoxides.[4,5] Ethoxysulfonium trifluoromethanesulfonates (triflates) **1a—c** were prepared by ethylation of the corresponding sulfoxides with ethyl triflate in CD_3NO_2. Alkoxysulfonium salts have been studied by various groups, but few papers described ethoxysulfonium salts.[6-8] In these papers, PMR data were not shown.

$$\underset{\underset{\downarrow}{O}}{R\text{–}S\text{–}R'} + CF_3SO_3Et \longrightarrow \underset{\underset{O\text{–}Et}{|}}{R\text{–}\overset{\oplus}{S}\text{–}R'}\ CF_3SO_3^{\ominus}$$

1 {**a**: R=Me, R'=*p*-Tol; **b**: R=$PhCH_2$, R'=Ph; **c**: R=Et, R'=Bu

Since neopentylation of sulfoxides is not possible, neopentyloxysulfonium ions cannot be prepared from sulfoxides. Although alkylation of sulfenates has not been described in the literature, it is expected to be a possible method for producing alkoxysulfonium salts. Hogg and Robertson[9] treated sodium arenesulfenate with a 10-fold excess of FSO_3Me in 30% aq. dioxane, but a methoxysulfonium ion was not formed. When an equimolar mixture of neopentyl benzenesulfenate and methyl triflate in nitromethane was allowed to stand for 10 min at 34 °C, its PMR spectrum showed that the sulfenate was quantitatively converted to methylphenylneopentyloxysulfonium triflate **1d**. Thus, alkylation of a sulfinate appears to be a good method for producing an alkoxysulfonium ion.

$$Ph\text{–}S\text{–}O\text{–}CH_2CMe_3 + CF_3SO_3Me \longrightarrow Ph\text{–}\overset{\oplus}{S}(Me)\text{–}OCH_2CMe_3\ CF_3SO_3^{\ominus}$$

1d

Compared with **1a—c**, the neopentyloxysulfonium salt **1d** is less stable. When a nitromethane solution of **1d** was allowed to stand at 34 °C, about 10% decomposed in 2 days. When a nitromethane solution of **1d** was evaporated and the residue was treated with an acetone solution of $NaBPh_4$, the corresponding anion-exchanged salt was not obtained, and decomposition products were found. When a CD_3NO_2 solution of **1d** was heated at 75 °C for 18 h, it completely decomposed, and neopentyl alcohol was one of the main product. Apparently a *neopentyloxy*arylalkylsulfonium ion is unstable. Among dialkoxyarylsulfonium ions (**3**) (discussed later), methoxy*neopentyloxy*-*p*-tolylsulfonium triflate (**3a**) and methoxy*benzyloxy*-*p*-tolylsulfonium triflate (**3b**) are found to decompose in solution whereas dimethoxy-*p*-tolylsulfonium triflate (**3c**) is stable in solution.

Dialkoxysulfonium ions were synthesized by alkylation of sulfinates.[1] From alkyl ethanesulfinates and alkyl triflate dialkoxyethylsulfonium triflates **2a—c** were prepared.

$$\underset{\underset{\downarrow}{O}}{Et\text{–}S\text{–}OR} + CF_3SO_3R' \xrightarrow{CD_3NO_2} \underset{\underset{O\text{–}R'}{|}}{Et\text{–}\overset{\oplus}{S}\text{–}OR}\ CF_3SO_3^{\ominus}$$

2 {**a**: R=CH_2CMe_3, R'=Et; **b**: R=CH_2CMe_3, R'=Me; **c**: R=Et, R'=Me

PMR spectra showed that sulfinates were completely converted to dialkoxysulfonium ions.

When benzyl and neopentyl *p*-toluenesulfinates were treated with methyl triflate, the solution became viscous suggesting the occurrence of polymerization, and the corresponding dialkoxysulfonium ions **3a** and **3b** were not obtained. In the case of methyl *p*-toluenesulfinate, the corresponding dimethoxy-*p*-tolylsulfonium salt **3c** was successfully prepared in solution.[1] It is worth

$$\underset{\underset{\downarrow}{O}}{p\text{-Tol–S–OR}} + CF_3SO_3Me \xrightarrow{CD_3NO_2} \underset{\underset{O\text{–}Me}{|}}{p\text{-Tol–}\overset{\oplus}{S}\text{–OR}}\ CF_3SO_3^{\ominus}$$

3 {**a**: R=CH_2Ph; **b**: R=CH_2Me_3; **c**: R=Me

noting that alkoxyneopentyloxyethylsulfonium ions are stable in solution, whereas methoxyneopentyloxy-*p*-tolylsulfonium ion is unstable in solution.

Alkoxyaminosulfonium salts were prepared by alkylation of sulfinamides.[2]

$$\underset{\underset{O}{\downarrow}}{Ar\text{-}S\text{-}NRR'} + CF_3SO_3R'' \xrightarrow{CD_3NO_2} Ar\text{-}\overset{\oplus}{S}(\underset{O\text{-}R''}{\downarrow})\text{-}NRR'\ CF_3SO_3^{\ominus}$$

4 { **a**: Ar=*p*-Tol, R=Ph, R′=Me, R″=Me; **b**: Ar=*p*-Tol, R, R′=$-(CH_2)_4-$, R″=Et; **c**: Ar=Ph, R, R′=$-CH_2CH_2OCH_2CH_2-$, R″=Et; **d**: Ar=Ph, R, R′=$-CH_2CH_2OCH_2CH_2-$, R″=Me

When *N*-phenyl-*N*-methyl-*p*-tolylsulfinamide was treated with methyl triflate in CD_3NO_2 at −20 °C, decomposition took place and the corresponding sulfonium salt **4a** was not found. This apparent instability of a methoxy-*N*-phenylaminosulfonium ion may be related with the low electron density on the nitrogen atom due to the resonance with the phenyl ring. Methoxypyrrolidino-*p*-tolylsulfonium triflate (**4b**) was stable so long as it was kept in solution but decomposed upon evaporation of the solvent. This decomposition may be related with the greater nucleophilicity of the dialkylamino nitrogen atom which attack the alkoxy alkyl group of **4b** itself (pyrrolidinium salts were found to be products of decomposition). The pK_a of morpholine (8.36)[10] is between that of *N*-methylaniline (4.85)[10] and that of pyrrolidine (11.27),[10] and it appeared that alkoxymorpholinosulfonium salts may be stable enough for isolation as solids, since the electron-density on the morpholine nitrogen is not too great nor too small.

When *N*-benzenesulfinylmorpholine was mixed with an equimolar amount of CF_3SO_3R'' (R″=Et or Me) in CD_3NO_2 at room temperature, **4c** or **4d** was formed, which was isolated as stable solids and converted into high-melting crystals by exchanging its anion with $NaBPh_4$.

The reaction of ethoxymorpholinophenylsulfonium tetraphenylborate with pyridine or triethylamine gave ethylated amine (91—95%) and the original sulfinamide (94—98%).

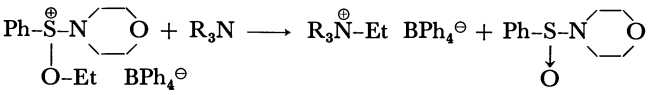

This is in quite a contrast with the reaction of methyl-*p*-tolylmethoxysulfonium ion with nucleophiles which yielded a mixture of various products.[5] If optically-active **4** is prepared (either by resolution of diastereomers with optically-active anions or by alkylation of optically-active sulfinamides derivable from optically-active sulfinates,[11] it can be used as asymmetric alkylating agents, and optically-active sulfinamides can be recovered which can be used again by alkylating it with alkyl triflate. Among various sulfonium salts, **4** is the best alkylating agent.

The PMR spectra of these sulfonium ions were determined, and their *O*-methylene and *N*-methylene chemical shifts are compared in Table 1. Magnetic non-equivalence of methylene protons in sulfinates (RSO_2CH_2R')[12] and sulfinamides ($RSONR'CH_2R''$)[13,14] has been described in the literature, but that in alkoxy-, dialkoxy-, and alkoxyamino-sulfonium ions is described here for the first time.

The relationship between $\delta_A-\delta_B$ and R,R′ in $RR'\overset{\oplus}{S}\text{-}OCH_AH_BR''$ and $RR'\overset{\oplus}{S}\text{-}N(R'')CH_AH_BR''$ are summarized in Table 2. The pairs of R and R′ always giving rise to different δ_A and δ_B are 1) aryl and alkyl, 2) aryl and alkoxy, and 3) aryl and $-O^{\ominus}$, and those giving rise to equal δ_A and δ_B are 1) aryl and alkylamino, and 2) aryl and benzyl.

The non-equivalence of the methylene protons shown in Table 1 is due to the difference in the magnetic environments caused by the chiral sulfur atom.[15] Although N–$\overset{\oplus}{S}$ and O–$\overset{\oplus}{S}$ bonds may have some partial

Table 1. Comparison of O-CH_2 and N-CH_2 ^{1}H-NMR absorptions in $RR''\overset{\oplus}{S}\text{-}OCH_2R''$ and $RR'\overset{\oplus}{S}\text{-}N(R'')CH_2R'''$

	Ph-S(→O)-CH_AH_B-Me	Bu-S(→O)-CH_AH_B-Me	p-Tol-S(→O)-CH_AH_B-Me	Ph-S(→O)-N⟨morpholine⟩	Et-S(→O)(→O)-CH_AH_B-Me	Et-S(→O)-O-CH_AH_B-Me	Et-S(→O)-O-CH_2CMe_3	Tol-S(→O)-CH_AH_B-Me	Tol-S(→O)-O-CH_AH_B-Me
$(\delta_A+\delta_B)/2$ (ppm)	4.33(q)	4.36(q)	4.57(q)	4.55(q)	3.94(q)	4.66(q)	4.68(q)	4.16-4.48(m)	3.36-4.32(m)
$\delta_A-\delta_B$ (ppm)	0	0	0	0	≒0	≒0	≒0	>0	>0
J_{AB} (Hz)	0	0	0	0	≒0	≒0	≒0	>0	>0
Solvent	CD_3NO_2	CD_3NO_2	CD_3NO_2	$(CD_3)_2CO$	CD_3NO_2	CD_3NO_2	CD_3NO_2	CD_3NO_2	neat

	Et-S(→O)(→O)-O-CH_AH_B-CMe_3	Et-S(→O)-O-CH_AH_B-CMe_3	Et-S(→O)-O-CH_2CMe_3	Ph-S(→O)-CH_AH_B-CMe_3	Tol-S(→O)(→O)-CH_AH_B-CMe_3	Ph-S(→O)-N⟨morpholine⟩	Ph-S(→O)-N⟨morpholine⟩	Tol-S(→O)-O-N⟨morpholine⟩	Tol-S(→O)-O-N⟨morpholine⟩	Me-S(→O)-O-N(Et)-CH_AH_B-Me
	3.90(q)	4.26(q)	4.29(q)	3.92(q)	3.36(q)	3.20-3.50(m)	2.16-3.32(m)	3.10-3.90(m)	2.57-3.41(m)	(m)[a]
	0.067	0.067	0.065	0.23	0.40	>0	>0	>0	>0	0.35[a]
	9.4	8.8	9.0	9.1	9.1	>0	>0	>0	>0	10[a]
	CCl_4	CD_3NO_2	CD_3NO_2	CD_3NO_2	CD_3NO_2	$(CD_3)_2CO$	$(CD_3)_2CO$	CD_3NO_2	CD_3NO_2	$CDCl_3$

(a) The data by R. M. Moriarty, *J. Org. Chem.* **30**, 600 (1965): Chemical shifts are not described.

(s, 3, $C\underline{H}_3C_6H_4$–), 3.10—3.90 (m, 4, $-C\underline{H}_2N$), 4.57 (q, 2, $-OCH_2$–), 7.32—7.80 (q, 4, $-C_6H_4$–).

Ethoxymorpholinophenylsulfonium Tetraphenylborate. After a mixture of *N*-benzenesulfinylmorpholine (7.6 mmol), ethyl triflate (7.6 mmol) and nitromethane (20 ml) was allowed to stand overnight at room temperature, the solvent was evaporated. The residue was dissolved in a small amount of acetone, and sodium tetraphenylborate (7.6 mmol) was added. Ether was added till the solution became turbid, and in 1 h white crystals were formed; yield, 4.2 g (99%), mp 143 °C. Found: C, 77.57; H, 6.96; N, 2.53%. Calcd for $C_{36}H_{38}O_2$-NB: C, 77.27; H, 6.84; N, 2.50%. PMR (CD_3COCD_3), $\delta=1.49$ (t, 3, CH_3), 3.20—3.50 (m, 4, $-CH_2N$–), 3.50—3.80 (m, 4, $-CH_2C\underline{H}_2O$–), 4.55 (q, 2, $CH_3C\underline{H}_2O$–), 6.60—8.00 (m, 5, Ph–).

Methoxymorpholinophenylsulfonium tetraphenylborate was prepared in a similar manner. Yield, 94%; mp 139 °C. Found: C, 78.68; H, 7.06; N, 2.71%. Calcd for $C_{35}H_{36}O_2$-NB: C, 77.06; H, 6.65; N, 2.57%. PMR(CD_3COCD_3), $\delta=3.38$—3.71 (m, 4, $-CH_2N$), 3.71—4.05 (m, 4, $-CH_2O$), 4.37 (s, 3, CH_3O–), 6.75—8.12 (m, 5, Ph).

Reaction between Ethoxymorpholinophenylsulfonium Tetraphenylborate and Amines. An equimolar mixture of the reactants in CD_3COCD_3 was allowed to stand for 2.5 h at 34 °C, and its PMR spectrum showed the completion of the reaction. Ether was added, and the precipitates formed were filtered. The filtrate was concentrated, and the sulfinamide obtained was dissolved in CCl_4 and its amount was determined by PMR with tetrachloroethane as the internal standard. From triethylamine, $Et_4\overset{\oplus}{N}B\overset{\ominus}{Ph_4}$ (94.8%) and *N*-benzenesulfinylmorpholine (94.3%) were obtained. From pyridine, $C_5H_5\overset{\oplus}{N}$–Et $B\overset{\ominus}{Ph_4}$ (91.0%) and *N*-benzenesulfinylmorpholine (98.2%) were obtained.

References

1) H. Minato, K. Yamaguchi, and M. Kobayashi, *Chem. Lett.*, **1975**, 307.

2) H. Minato, K. Yamaguchi, and M. Kobayashi, *Chem. Lett.*, **1975**, 991.

3) H. Minato, K. Okuma, and M. Kobayashi, *J. Chem. Soc., Chem. Commun.*, **1975**, 868.

4) M. G. Ahmed, R. W. Alder, G. H. James, M. L. Sinnott, and M. C. Whiting, *Chem. Commun.*, **1968**, 1533.

5) K. Tsumori, H. Minato, and M. Kobayashi, *Bull. Chem. Soc. Jpn.*, **46**, 3503 (1973).

6) R. Annanziata, M. Cinquini, and S. Colonna, *J. Chem. Soc., Perkin Trans. 1*, **1973**, 1231.

7) K. K. Anderson, *J. Org. Chem.*, **35**, 706 (1970).

8) C. R. Johnson and D. McCants, Jr., *J. Am. Chem. Soc.*, **87**, 5404 (1965); C. R. Johnson, C. C. Bacon, and W. D. Kingsbury, *Tetrahedron Lett.*, **1972**, 501.

9) D. R. Hogg and A. Robertson, *Tetrahedron Lett.*, **1974**, 3783.

10) M. Kotake, Ed., "Constants of Organic Compounds," Asakura Publishing Co., Tokyo (1963), p. 584.

11) A. Nudelman and D. J. Cram, *J. Am. Chem. Soc.*, **90**, 3869 (1968).

12) J. W. Wilt and W. J. Wagner, *Chem. Ind.*, **1964**, 1389.

13) M. Raban, *Chem. Commun.*, **1967**, 1017.

14) R. M. Mcriar y, *J. Org. Chem.*, **30**, 600 (1965).

15) L. M. Jackman, "Applications of Nuclear Magnetic Resonance Spectroscopy in Organic Chemistry," The Macmillan Co., New York (1959), pp. 99—103.

16) D. G. Farnum and G. Mehta, *J. Am. Chem. Soc.*, **89**, 2970 (1967); *ibid.*, **91**, 3256 (1969).

17) E. G. Miller, D. R. Rayner, H. T. Thomas, and K. Mislow, *J. Am. Chem. Soc.*, **90**, 4861 (1968).

18) S. Kobayashi, H. Danda, and T. Saegusa, *Bull. Chem. Soc. Jpn.*, **46**, 3214 (1973); R. L. Hansen, *J. Org. Chem.*, **30**, 4322 (1965).

19) S. Kobayashi, H. Danda, and T. Saegusa, *Bull. Chem. Soc. Jpn.*, **47**, 2699 (1974).

20) F. A. L. Anet, R. D. Trepka, and D. J. Cram, *J. Am. Chem. Soc.*, **89**, 357 (1967); J. Jacobs and K. Mislow, *ibid.*, 5288 (1967).

21) Y. Miyaji, H. Minato, and M. Kobayashi, *Bull. Chem. Soc. Jpn.*, **44**, 862 (1971).

constants (hfsc) in the former signal is close to that of hfsc's of arylcyclohexadienyl duryl nitroxides among the newly prepared nitroxides.[4] These findings as well as the observations that the former signal was replaced by that of Xa lead us to assign the former signal to the deuterated benzoyloxycyclohexadienyl duryl nitroxide (IXa) (Scheme 3).

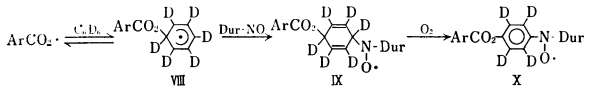

VIII IX X

a : Ar=C_6H_5 b : Ar=4-$CH_3C_6H_4$
c : Ar=4-$CH_3OC_6H_4$ d : Ar=4-ClC_6H_4
e : Ar=4-$NO_2C_6H_4$

Scheme 3.

Contrary to the case in benzene-d_6, benzoyloxycyclohexadienyl duryl nitroxide (II) was not detected at all in the decomposition of BPO in benzene. Undoubtedly II is oxidized easily by traces of oxygen, while the oxidation of IXa proceeds slowly on account of the deuterium isotope effects.

The decomposition of bis(4-methylbenzoyl) peroxide (Me–BPO) in benzene-d_6 at 45 °C in the presence of nitrosodurene resulted in the formation of one stable paramagnetic species, the deuterated duryl 4-methylbenzoyloxycyclohexadienyl nitroxide (IXb, a_N=13.3 and $a_{\beta-D}$=1.4 gauss), which was then oxidized to a dehydrogenated nitroxide (Xb, a_N=9.8 gauss) on exposure to air. In the decomposition of Me–BPO at 50 °C, however, duryl 4-methylphenyl nitroxide (VIb)[4] was detected in addition to IXb. Bis(4-methoxybenzoyl) peroxide (MeO–BPO) gave a similar nitroxide (IXc, a_N=13.1 and $a_{\beta-D}$=1.5 gauss) at 45 °C and a mixture of IXc and its dehydrogenated nitroxide (Xc, a_N=9.7 gauss) at 50 °C, but none of a spin adduct of 4-methoxyphenyl radicals (VIc) was obtained. The air oxidation of IXc led to the formation of Xc. The alternative assignment of IXb and IXc to arylcyclohexadienyl duryl nitroxides (XIb and XIc, respectively) can be ruled out on the basis of the facts[4] that 4-methyl- and 4-methoxyphenylazotriphenylmethane (Me–PAT and MeO–PAT, respectively) do not yield any amounts of XIb and XIc, but afford the aryl duryl nitroxides, VIb and VIc, respectively. Thus, even if 4-methyl- and 4-methoxyphenyl radicals were generated in the decomposition of Me–BPO and MeO–BPO, respectively, the nitroxides, XIb and XIc, would not be formed at all.

When bis(4-chlorobenzoyl) and bis(4-nitrobenzoyl) peroxide (Cl–BPO and NO_2–BPO, respectively) were decomposed in the presence of nitrosodurene at 45 °C in benzene-d_6, the ESR signals (a_N=13.3 and $a_{\beta-D}$=1.5 gauss from Cl–BPO, and a_N=13.4 and $a_{\beta-D}$=1.6 gauss from NO_2–BPO) similar to those of IXb and IXc were observed and then replaced by other signals (a_N=9.6 gauss from both Cl–BPO and NO_2–BPO) by the air oxidation. The initially observed signals are similar in the shape and the magnitude of a_N to, but different in the magnitude of $a_{\beta-D}$ from, those of the spin adducts, XId (a_N=13.5 and $a_{\beta-D}$=2.1 gauss) and XIe (a_N=13.6 and $a_{\beta-D}$=2.0 gauss), formed from 4-chloro- and 4-nitrophenylazotriphenylmethane in benzene-d_6, respectively.[4] Although Cl–BPO and NO_2–BPO might produce XId and XIe through 4-chloro- and 4-nitrophenyl radicals, respectively, it can be assumed that the nitroxide radicals, IXd, Xd, IXe, and Xe, are also formed in the present cases by analogy with the behavior of the other peroxides.

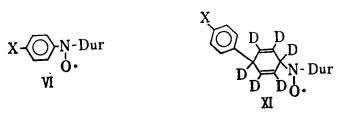

VI XI

a : X=H b : X=CH_3
c : X=CH_3O d : X=Cl
e : X=NO_2

Finally, it is interesting to note that the spin adduct of 4-methylphenyl radicals (VIb) was detected in the decomposition of Me–BPO at 50 °C, whereas none such was observed in the decomposition of MeO–BPO at the same temperature. This finding might reflect the higher activation energy required for the decarboxylation of 4-methoxybenzoxyl radicals than for that of 4-methylbenzoxyl radicals.[7]

Experimental

Nitrosodurene,[5] substituted dibenzoyl peroxides,[8] and 4-iodophenyl benzoate[9] were prepared according to the methods described in the literatures.

Decomposition of the peroxides was carried out as follows: a solution of nitrosodurene (5 mM) and a peroxide (10 mM) in benzene or benzene-d_6 was purged with argon for 2 min in an ESR tube prior to decomposition in order to remove dissolved oxygen and was heated at the specified temperature for 5 min. The ESR spectra were recorded on a JEOL JES-ME-lX spectrometer. Photolysis of 4-iodophenyl benzoate(VII) was carried out by irradiation of the solution (nitrosodurene, 5 mM and VII, 10 mM in carbon tetrachloride) in a Pyrex tube directly in the cavity by means of a 400 W high pressure mercury arc lamp.

References

1) T. Nakata, K. Tokumaru, and O. Simamura, *Tetrahedron Lett.*, **1967** 3303 *Bull. Chem. Soc. Jpn.*, **43**, 3315 (1970); J. Saltiel and H. C. Curtis, Jr., *J. Am. Chem. Soc.*, **93**, 2056 (1971).

2) J. Bargon, *J. Am. Chem. Soc.*, **93**, 4630 (1971).

3) P. G. Cookson, A. G. Davies, and B. P. Roberts, *J. Chem. Soc., Chem. Commun.*, **1976**, 289.

4) T. Suehiro, M. Kamimori, K. Tokumaru, and M. Yoshida, *Chem. Lett.*, **1976**, 531.

5) S. Terabe and R. Konaka, *J. Chem. Soc., Perkin Trans. 2*, **1973**, 1252.

6) A 1,4-disubstituted structure was tentatively assigned to the spin adducts although 1,2- and/or 1,4-disubstituted isomers might be formed, which are undistinguishable by ESR spectrum.

7) T. Suehiro and M. Ishida, *Bull. Chem. Soc. Jpn.*, **44**, 1692 (1971).

8) C. G. Swain, W. H. Stockmayer, and J. T. Clark, *J. Am. Chem. Soc.*, **72**, 5426 (1950).

9) C. Willgerodt and G. Wiegand, *Ber.*, **42**, 3763 (1909).

The Photochemical Reaction of 2-Alkoxy-1,4-naphthoquinones with Olefins. III.[1] The Re-examination of the Structures of the Photo-addition Compounds and the Reaction Mechanism

Tetsuo OTSUKI

Department of Chemistry, Faculty of Science, Kyoto University, Kyoto 606

(Received February 26, 1976)

In the photochemical reaction of 2-alkoxy-1,4-naphthoquinones with a variety of olefins, two types of photo-addition compounds are found to be produced: the cyclobutane-ring compounds and the oxetanol-ring compounds. Although the present author has assigned the structure of a tetrahydropyran-ring compound to one of the photo-addition compounds primarily on the basis of the analyses of the spectral data, the previously proposed structures should be corrected to an oxetanol-ring compound on the basis of the chemical reactivities. Although some cyclobutane-ring compounds were stable enough to be isolated as final reaction products, the other cyclobutane-ring compounds, though once produced, were too unstable to undergo the subsequent photochemical reaction to give oxetanol-ring compounds on further irradiation. The stability of the cyclobutane-ring compounds was dependent on both the substituents of the olefins and the wavelength of the light. The origin of the stability and the reaction mechanism were investigated.

A variety of compounds characterized by their stimulating physiological activity have been synthesized by means of the photochemistry of quinones.[2] Thus, the photochemical reactions of quinones with olefins have attracted several workers.[3-8] Although 1,4-naphthoquinone has been known to yield photo-addition compounds with olefins, the yields are, in general, low, partly because the photo-reduction of 1,4-naphthoquinone proceeds competitively to form such photo-reduction compounds as 1,4-naphthoquinhydrones or 1,4-naphthalenediol. These complicated features originate partly from the higher oxidation potential of 1,4-naphthoquinone.[9,10]

2-Alkoxy-1,4-naphthoquinones, on the other hand, have lower oxidation potentials than that of 1,4-naphthoquinone;[9,10] hence, the photo-addition products of 2-alkoxy-1,4-naphthoquinones with olefins could be isolated in fairly good yields as a result of a smooth reaction, while there were no photo-reduction products such as quinhydrones or 1,4-diol. The photo-addition compounds obtained in the reaction mentioned above could be classified into two types. Although the present author has assigned the structure of 10-hydroxy-3,4,4a,5-tetrahydro-1*H*-naphtho[2,3-*c*]pyran-5-one derivatives, **1**, to one of the photo-addition compounds[1] primarily on the basis of the analyses of the spectral data, every attempt to derive **1** to 1,4-naphthoquinone derivatives or 1,4-naphthalenediol derivatives *via* keto-enol change, has proven unsuccessful. Thus, in this report the previously proposed structure, **1**, will be revised to the structure, **2**, that of the oxetanol derivatives. The chemical evidences preferring the structure **2** to **1** will be presented. In addition, the course of the reaction was much influenced by both the substituents of the olefins and the wavelength of the light. The mechanism of the reaction, as well as the factors determining these photo-addition products, was investigated.

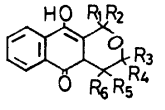

1

Results and Discussion

The 2-alkoxy-1,4-naphthoquinones examined here are 2-methoxy-, 2-ethoxy-, 2-isopropoxy-, and 2-allyloxy-1,4-naphthoquinones. The olefins selected in this work are 1-hexene, 1-heptene, 1-octene, 1-nonene, 1-decene, cyclohexene, cyclooctene, 1,5-cyclooctadiene, 2-bicyclo[2.2.1]heptene, 2,5-bicyclo[2.2.1]heptadiene, styrene, indene, α-methylstyrene, 1,1-diphenylethylene, and 1,1-di-*p*-tolylethylene.

A benzene solution of a mixture of a 2-alkoxy-1,4-naphthoquinone and an olefin was subjected to irradiation by a high-pressure Hg arc lamp with and/or without the application of a filter, A or B. The transmission characteristics of the filters, A and B, are shown in Table 1. Neither the precipitation of 2-alkoxy-1,4-naphthoquinhydrones nor any coloration was observed during the course of the reaction, even when olefin had active hydrogen atoms, such as 1-hexene; that is, the reaction proceeded smoothly. This is one of the extremely different features of 2-alkoxy-1,4-naphthoquinones compared with 1,4-naphthoquinone itself. The structures of these photo-addition compounds, which were obtained in fairly good yields in every case examined here, proved to be classifiable into two types, **2** and **3**, depending on both the substituents of the olefins and the wavelength of the light.

Table 1. Transmission characteristics of the filter

	0% Transmission (nm)	50% Transmission (nm)	90% Transmission (nm)
Filter A	360	390	450
Filter B	390	420	470

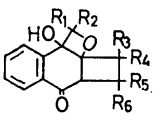

2

(or the structure 1)

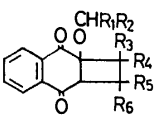

3

When 2-alkoxy-1,4-naphthoquinones and olefins, with the exceptions of 1,1-diphenylethylene and 1,1-di-

p-tolylethylene, were subjected to photochemical reactions under irradiation with no filter, the photo-addition products proved to have, in general, the structure, **2**. On irradiation with use of a filter (A or B), however, these olefins yielded another type of photo-addition compound, **3**. Under the conditions with and/or without a filter, on the other hand, 1,1-diphenylethylene or 1,1-di-*p*-tolylethylene was found to give exclusively the photo-addition compound, **3**. First, the determination of the structures of the photo-addition products will be described.

The Re-examination of the Structure of the Photo-addition Compounds, 2: The re-examination of the structure of the photo-addition compounds, **2**, will be illustrated by referring to the photo-product obtained in the reaction of 2-methoxy-1,4-naphthoquinone with styrene, a typical example. A benzene solution (20 ml) of 2-methoxy-1,4-naphthoquinone (1 mmol) and styrene (2 mmol) was subjected to irradiation by a high-pressure Hg arc lamp (300 W) without a filter until the quinone was completely consumed. The quantum efficiency of the photochemical reaction for the disappearance of 2-methoxy-1,4-naphthoquinone in its reaction with styrene was estimated to be 0.18 (with the filter, A). After the usual work-up of the reaction mixture, white needles were obtained as the main reaction product in a 69% yield. The elemental analysis and the molecular weight determined by mass spectrometry reveal that the photo-addition compound was composed of one molecule of 2-methoxy-1,4-naphthoquinone and one molecule of styrene. The photo-addition compound contained both a hydroxyl group and a carbonyl group, judging from the inspection of the IR and UV spectra. In the ^{1}H-NMR spectrum (Fig. 1), the signal corresponding to H_c disappeared after the treatment of the chloroform solution with D_2O. The nuclear spin-spin interactions among H_a, H_b, H_d, and H_e were confirmed by the spin decoupling technique. When 2-methoxy-d_3-1,4-naphthoquinone was subjected to the same photochemical reaction, the ^{1}H-NMR signals corresponding to H_f and H_g (Fig. 1) disappeared. On the other hand, the ^{1}H-NMR signal corresponding to H_d disappeared completely when 2-methoxy-1,4-naphthoquinone-3-*d* was used in the reaction. These results indicate that the protons, denoted by H_d, H_f, and H_g, of the photo-addition compound originated from the 2-methoxy-1,4-naphthoquinone moiety. Taking into consideration either of the two structures, **4** or **5**, one can reasonably explain the spectral data of the photo-addition compound. Of these, **4** was characterized by an oxetanol ring as well as a cyclobutane ring. A similar structure was once suggested by Anett[11] for the reaction product obtained by the photochemical reaction of 2-methoxy-1,4-naphthoquinone with vinyl acetate and by Ellis and Jones[12] for the photo-dimerization product of 2-methoxy-1,4-naphthoquinone. On the other hand, **5**, characterized by a tetrahydropyran ring and previously proposed by the present author,[1] should be converted to 1,4-naphthoquinone derivatives or 1,4-naphthalenediol derivatives *via* a keto-enol change. Every attempt to do so, how-

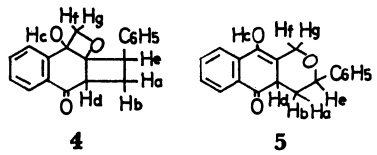

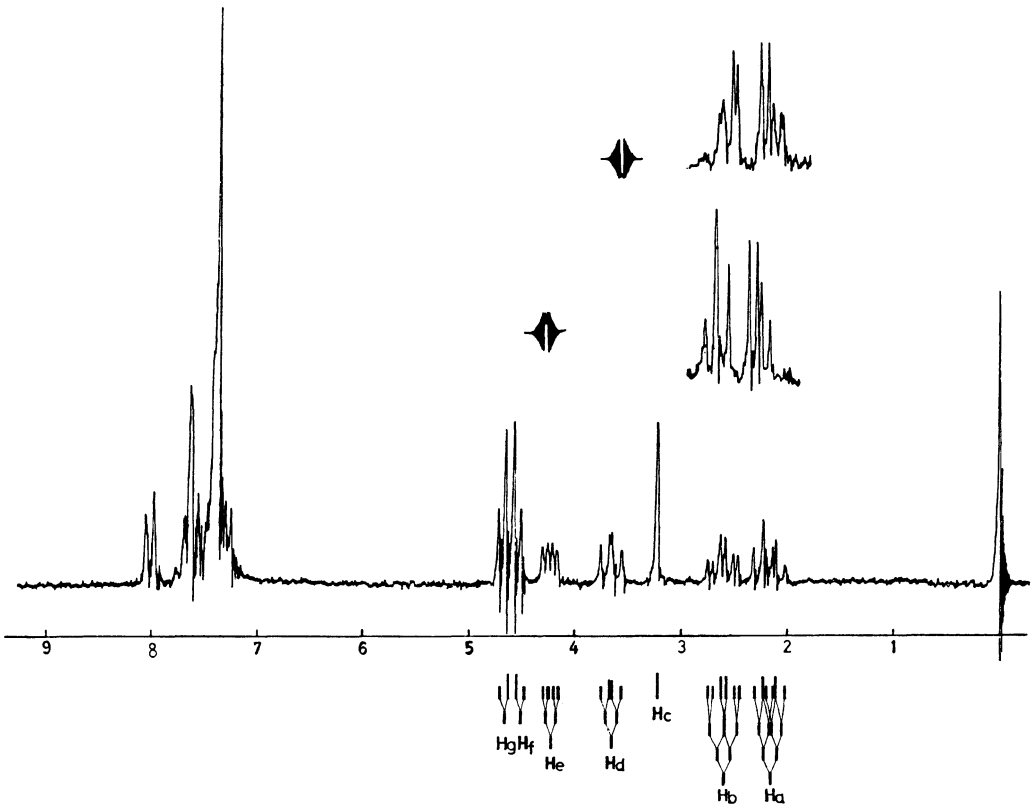

Fig. 1. ^{1}H-NMR spectrum of the photo-addition compound.

ever, had no success. When the photo-addition compound was acetylated with acetic anhydride for 3 h, a mono-acetylated product, **6**, was obtained (yield: 83%).[13]

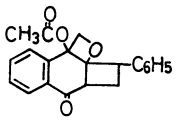

6

The Acid-catalyzed Decomposition of the Photo-addition Compound: After the treatment of the photo-addition compound with hydrochloric acid or sulfuric acid in a chloroform solution at room temperature, a mixture of two products, **7a** and **7b**, was isolated in a 60% yield. **7a** and **7b** have the same molecular weight, suggesting that a formaldehyde unit is released during the treatment. By the photochemical reaction of 1,4-naphthoquinone with styrene we obtained, in actual, the same mixture of **7a** and **7b**, although the relative ratio of the two compounds was not compatible. The 1,4-diacetoxynaphthalene derivative, **8**, was isolated as the sole reaction product when **7a**, as well as **7b**, was treated by sodium acetate–acetic anhydride under reflux conditions. These results confirmed that **7a** and **7b** are isomeric with each other.[14]

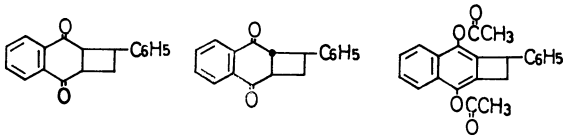

7a **7b** **8**

The Bromination of the Photo-addition Compound: The bromination of the photo-addition compound with bromine in a chloroform solution at room temperature gave a mixture of two compounds, **9** (54%) and **10** (32%). Since **10** was revealed to have a hydroxyl group through the inspection of the IR spectrum, the acetylation of **10** was performed and an acetyl derivative, **11**, was isolated. **9** and **11** were also obtained through the bromination of the acetyl derivative of the photo-addition compound, **6**, in 50 and 36% yields respectively. The structure of **9** was further confirmed by the isolation of **9** as one of the reaction products from the bromination reaction of **7b**.

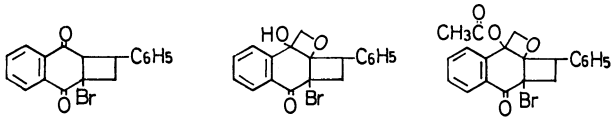

9 **10** **11**

The Clemmensen Reduction of the Photo-addition Compound: Three reaction products, **12**, **13**, and **14**, were isolated from the reaction mixture of the Clemmensen reduction of the photo-addition compound in 17, 7, and 12% yields respectively. **12** was revealed to be the derivative of 1-methylnaphthalene through the isolation of 1-methylnaphthalene as the thermal decomposition product of **12**. The coloration of **14** to deep yellow by ferric sulfate in ethanol suggested the existence of the phenolic hydroxyl group; this is confirmed by the fact that the acetylation of **14** with sodium acetate–acetic anhydride yielded an acetyl derivative, **15**. Moreover, the possibility of 1,4-naphthalenediol derivatives could be excluded since the oxidation of **14** by silver oxide in ether failed to yield 1,4-naphthoquinone derivatives.

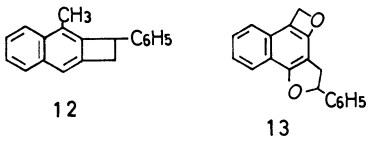

12 **13**

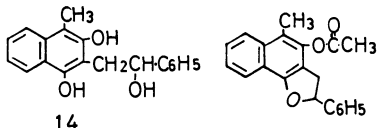

14 **15**

The ^{13}C-NMR Spectrum of the Photo-addition Compound: The ^{13}C-NMR spectrum of the photo-addition compound was measured in a solution of chloroform (the chemical shifts were calibrated from TMS as the internal standard): δ; 26.63, 43.44, 49.63, 70.62, 82.33, 90.95, 126.92, 127.05, 127.41, 128.26, 129.17, 130.26, 134.93, 137.60, 143.43, and 197.24 ppm. These data suggest that the photo-addition compound contains six different kinds of sp^3-carbon atoms as its constituents.

From the results described above, it can be deduced that the photo-addition compound should have the structure, **4**, characterized by an oxetanol ring as well as a cyclobutane ring. Here, the present author would like to correct the previously proposed structure, **5**, for the photo-addition compound.

A similar type of photo-addition compound, **2**, obtained in the photochemical reaction of 2-alkoxy-1,4-naphthoquinone with olefins is tabulated in Table 2.

The Structure of the Photo-addition Compounds, **3**: As a typical example, the photochemical reaction of 2-methoxy-1,4-naphthoquinone with 1,1-diphenylethylene will be described. A benzene solution (20 ml) of 2-methoxy-1,4-naphthoquinone (1 mmol) and 1,1-diphenylethylene (2 mmol) was subjected to irradiation by high-pressure Hg arc lamp (300 W) without a filter. After the complete consumption of the quinone, white crystals were isolated as a sole reaction product in a 63% yield. The elemental analysis and the mass data require that the photo-addition compound is composed of one molecule each of 2-methoxy-1,4-naphthoquinone and 1,1-diphenylethylene. The IR and UV spectra show the existence of the carbonyl group, but not the hydroxyl group. The ^1H-NMR spectrum was compatible with the structure, **3a**. The assignment of the ^1H-NMR signals was concreted by the reaction using 2-methoxy-d_3-1,4-naphthoquinone as the starting material. Upon being heated in carbon tetrachloride, the photo-addition compound, **3a**, decomposed again to give 2-methoxy-1,4-naphthoquinone and 1,1-diphenylethylene quantitatively. The half-life of **3a** was estimated to be about 92 min at 75±1 °C.

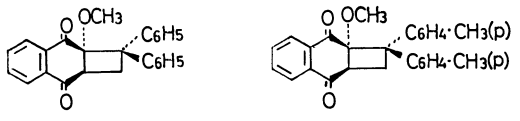

3a **3b**

Table 2. The photo-addition compounds obtained in the reaction of 2-alkoxy-1,4-naphthoquinones with olefins

2-Alkoxy-1,4-naphthoquinone	Olefin	Yields of the Photo-addition Compounds[a]	
		2	**3**
2-Methoxy-1,4-naphthoquinone	1-Hexene	25% (**2a**)	
2-Methoxy-1,4-naphthoquinone	1-Heptene	50 (**2b**)	
2-Methoxy-1,4-naphthoquinone	1-Octene	67 (**2c**)	40%[b] (**3e**)
2-Methoxy-1,4-naphthoquinone	1-Nonene	48 (**2d**)	
2-Methoxy-1,4-naphthoquinone	1-Decene	45 (**2e**)	
2-Methoxy-1,4-naphthoquinone	Cyclohexene	39 (**2f**)	
2-Methoxy-1,4-naphthoquinone	Cyclooctene	74 (**2g**)	
2-Methoxy-1,4-naphthoquinone	1,5-Cyclooctadiene	29 (**2h**)	
2-Methoxy-1,4-naphthoquinone	2-Bicyclo[2.2.1]heptene	50 (**2i**)	
2-Methoxy-1,4-naphthoquinone	2,5-Bicyclo[2.2.1]heptadiene	35 (**2j**)	
2-Methoxy-1,4-naphthoquinone	Indene	73 (**2k**)	
2-Methoxy-1,4-naphthoquinone	Styrene	69 (**2l**=**4**)	50[c] (**3d**)
2-Methoxy-1,4-naphthoquinone	α-Methylstyrene	9 (**2m**)	69[d] (**3c**)
2-Methoxy-1,4-naphthoquinone	1,1-Diphenylethylene		63 (**3a**)
2-Methoxy-1,4-naphthoquinone	1,1-Di-*p*-tolylethylene		71 (**3b**)
2-Ethoxy-1,4-naphthoquinone	Styrene	60 (**2n**)	
2-Ethoxy-1,4-naphthoquinone	1,1-Diphenylethylene		60 (**3f**)
2-Isopropoxy-1,4-naphthoquinone	Styrene	7.1 (**2o**)	41 (**3g**)[e]
2-Allyloxy-1,4-naphthoquinone	Styrene	27 (**2p**)	

a) The yields were calculated on the basis of the quinones consumed in the photochemical reaction without a filter, unless otherwise mentioned. b) The yield was calculated after 90% of the quinone has been consumed in the photochemical reaction with the filter A. c) The yield was calculated after 89% of the quinone has been consumed in the photochemical reaction with the filter A. d) The yield was calculated for a mixture of two isomers, **3c**-I and **3c**-II. e) In a previous report, 2,2-dimethyl-3-phenyl-3,4,4a,-5,10,10a-hexahydro-2*H*-naphtho[2,3-*b*]pyran-5,10-dione was suggested as the probable structure of **3g**. However, **3g** was deduced to have a cyclobutane ring because the IR and UV spectra of **3g** have characteristics similar to those of **3d**, and as the product of ether cleavage of **3g** we obtained 1-hydroxy-8-phenyl-3,4-benzobicyclo[4.2.0]oct-3-ene-2,5-dione; IR(liq. film); 3400(OH), 1670 cm^{-1} (C=O). ^{1}H-NMR($CDCl_3$); δ: 2.30—3.00(2H, C-7 CH_2, m), 2.80 (1H, OH, s), 3.38 (1H, C-6 CH, dd, J=4.0, 8.0 Hz), 3.92 (1H, C-8 CH, dd, J=2.0, 8.0 Hz), 7.10—8.20 ppm (9H, aromatic-H, m).

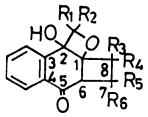

2

	R_1	R_2	R_3	R_4	R_5	R_6
2a	H	H	C_4H_9(*n*)	H	H	H
2b	H	H	C_5H_{11}(*n*)	H	H	H
2c	H	H	C_6H_{13}(*n*)	H	H	H
2d	H	H	C_7H_{15}(*n*)	H	H	H
2e	H	H	C_8H_{17}(*n*)	H	H	H
2f	H	H	H	$-(CH_2)_4-$		H
2g	H	H	H	$-(CH_2)_6-$		H
2h	H	H	H	$-(CH_2)_2$ $(CH_2)_2-$ $CH=CH$		H
2i	H	H	H	$-CH-CH_2-CH-$ $(CH_2)_2$		H
2j	H	H	H	$-CH-CH_2-CH-$ $CH=CH$		H
2k	H	H	H	$-C_6H_4CH_2$(*o*)$-$		H
2l	H	H	C_6H_5	H	H	H
2m	H	H	C_6H_5	CH_3	H	H
2n	CH_3	H	C_6H_5	H	H	H
2o	CH_3	CH_3	C_6H_5	H	H	H
2p	$CH=CH_2$	H	C_6H_5	H	H	H

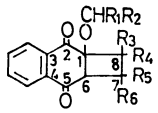

3

	R_1	R_2	R_3	R_4	R_5	R_6
3a	H	H	C_6H_5	C_6H_5	H	H
3b	H	H	$C_6H_4\cdot CH_3$(*p*)	$C_6H_4\cdot CH_3$(*p*)	H	H
3c	H	H	C_6H_5	CH_3	H	H
3d	H	H	C_6H_5	H	H	H
3e	H	H	C_6H_{13}(*n*)	H	H	H
3f	CH_3	H	C_6H_5	C_6H_5	H	H
3g	CH_3	CH_3	C_6H_5	H	H	H

The Structure of the Photo-addition Compounds and Its Relation to the Substituents of Olefins and the Wavelength of Irradiation: With 1,1-diphenylethylene or 1,1-di-*p*-tolylethylene, 2-alkoxy-1,4-naphthoquinone was found to yield exclusively the photo-addition compound, **3a** or **3b**, characterized by a cyclobutane ring, independent of the wavelength of irradiation. On the other hand, in the photochemical reaction of 2-alkoxy-1,4-naphthoquinone with olefins other than 1,1-diphenylethylene and 1,1-di-*p*-tolylethylene, both of the two different types of photo-addition compounds, **2** and **3**, were obtained, depending on whether the irradiation was with or without a filter (Table 2).

In the photochemical reaction of the quinone with α-methylstyrene, the photo-addition compound, **3c**, was the main reaction product (69% yield); the photo-addition compound, **2m**, was obtained as a minor reaction product (9% yield) on irradiation without a filter. In contrast with the case of α-methylstyrene without a filter, the photo-addition compound, **2l** or **2c**, characterized by an oxetanol ring as well as a cyclobutane ring, could be isolated as a stable product in the reaction of the quinone with another olefin, such as styrene or 1-octene, but none of any cyclobutane-ring compound, such as **3d** or **3e**, could be obtained after the consumption of the quinone had been completed (Fig. 2). By cutting the light of a shorter wavelength with a filter (A or B), one could obtain, however, a cyclobutane-ring compound, **3d** or **3e**, as well as an oxetanol-ring compound, **2l** or **2c**, even in a reaction with styrene or with 1-octene (Fig. 3). The results obtained above indicate that the cyclobutane-ring compounds, once produced, undergo further reaction upon irradiation at a shorter wavelength to the oxetanol-ring compounds, depending on their stabilities. Thus, the tendency of the susceptibility to further reactions is as follows: adduct from 1,1-diphenylethylene or its derivatives < adduct from α-methylstyrene < adduct from the other olefins, such as styrene or 1-octene. The source of the stability of the adduct, **3**, to the light will be discussed in the following sections.

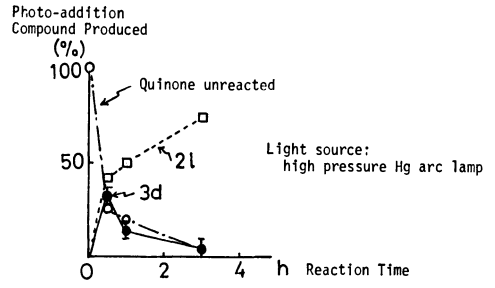

Fig. 2. Photochemical reaction of 2-methoxy-1,4-naphthoquinone with styrene.

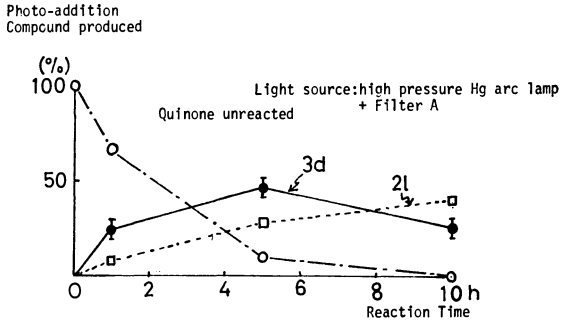

Fig. 3. Photochemical reaction of 2-methoxy-1,4-naphthoquinone with styrene.

The Stability of the Photo-addition Compounds, 3, in Relation to the Substituents of Olefins: The absorption characteristics of the photo-addition compounds, **3**, are summarized in Table 3. In the UV spectrum of **3a** dissolved in carbon tetrachloride or acetonitrile, a new shoulder at a longer wavelength [365 nm(CCl_4), 361 nm(CH_3CN)] appeared which could not be observed in **3d** or **3e**. This absorption can be compared in its wavelength and absorption coefficient [UV_{max} (CH_3CN): 340 nm (ε: 597)] to the charge-transfer band observed in [2,2]paracyclophanequinone.[15] This suggests that the intramolecular interactions exist in the photo-addition compound, **3a**.

Table 3. The absorption characteristics of the photo-addition compounds **3**

Photo-addition compounds	Solvents	Absorption characteristics nm (ε)
3a	CCl_4	303(2.0×10^3), 312(1.9×10^3), 352(1.7×10^2), 365(1.5×10^2)
	CH_3CN	303(1.9×10^3), 312(1.7×10^3), 349(1.5×10^2), 361(1.4×10^2)
3d	CCl_4	301(2.8×10^3), 310(2.6×10^3), 343(4.5×10^2)
	CH_3CN	301(2.6×10^3), 301(2.4×10^3), 339(4.5×10^2)
3e	CCl_4	300(1.4×10^3), 309(1.3×10^3), 352(1.6×10^2)
	CH_3CN	300(1.5×10^3), 308(1.4×10^3), 349(1.7×10^2)

These intramolecular interactions could be understood further by an inspection of the ^{1}H-NMR data. That is, the ring protons of phenyl groups in the compound, **3a**, show complicated ^{1}H-NMR signals which otherwise show broad singlet-like ^{1}H-NMR signals such as those in 1,1-diphenylethylene as a starting olefin. The intramolecular interactions are demonstrated more clearly by the ^{1}H-NMR spectrum of **3b** in carbon tetrachloride, which exhibits the existence of two different kinds of *p*-tolyl groups. That is, two different kinds of methyl protons appeared at δ=2.06 and 2.28 ppm, and two different sets of a multiplet of four protons appeared as an AB-quartet pattern which is characteristic of a para-substituted benzene ring. One of these AB-quartets possessed δ-values of 6.75 and 7.01 ppm (J=10.0 Hz), and the other, those of 7.01 and 7.27 ppm (J=8.0 Hz). The methyl protons of 1,1-di-*p*-tolylethylene as a starting olefin, on the other hand, appeared at δ=2.36 ppm and an AB-quartet of the aromatic protons possesses δ-values of 7.01 and 7.15 ppm (J=8.0 Hz). A comparison of these ^{1}H-NMR data with those of the starting olefins shows that the chemical shifts of the protons belonging to one of the *p*-tolyl groups move to higher field in the photo-addition compound, **3b**. Presumably these shifts to a higher field originate from the anisotropy of the aromatic rings as well as the carbonyl

groups of the quinone moiety in the compound, **3b**. In fact, an inspection of the molecular model reveals that the quinone moiety and one of the *p*-tolyl groups of the olefin moiety are in close proximity.

These results presented above suggest the existence of intramolecular interactions through π-electrons in the cyclobutane type of the photo-addition compounds, **3**, derived from 2-methoxy-1,4-naphthoquinone and 1,1-diphenylethylene or its derivatives.

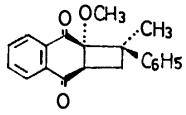

3c-I

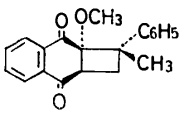

3c-II

In the photochemical reaction of 2-methoxy-1,4-naphthoquinone with α-methylstyrene, the adduct obtained was confirmed to be a mixture of **3c**-I and **3c**-II from an inspection of the ^{1}H-NMR spectra. Because of the non-symmetrical nature of α-methylstyrene, the possible formation of two isomers is explicable; *i.e.*, one is an isomer which has intramolecular interactions between the quinone moiety and the phenyl group of the olefin moiety through π-electrons, **3c**-I, while the other is an isomer which has no interactions, **3c**-II. On irradiation by a high-pressure Hg arc lamp without a filter, the ratio of the isomer contents, **3c**-I/II, was estimated to be 1.0/1.5, as determined by the integration of the ^{1}H-NMR signals. The ratio, **3c**-I/II, was found to be dependent on the wavelength of the light source used (Table 4). The relative ratio of the isomers, **3c**-I/II, is

Table 4. The ratio of the isomer contents, **3c**-I/II, in the photochemical reaction of 2-methoxy-1,4-naphthoquinone with α-methylstyrene[a)]

Filter used[b)]	**3c**-I	**3c**-II
None	1.0	1.5
Filter A	1.0	3.9
Filter B	1.0	5.1

a) The ratio was estimated on the basis of the integration of the ^{1}H-NMR signals of the mixture. b) The light source used was a high-pressure Hg arc lamp.

increased as the relative transmittance at the shorter wavelength is increased by changing the filters. Moreover, on irradiating a benzene solution of a mixture of the two isomers in a Pyrex glass tube by means of a high-pressure Hg arc lamp without a filter, **3c**-II was found to decompose selectively. These results indicate that the isomer, **3c**-I, is more stable than **3c**-II. That is, the cyclobutane ring in the photo-addition compound, **3**, is deduced to be stabilized by intramolecular interactions through π-electrons. The energy relaxation mode *via* the intramolecular interactions might play a considerably important role in the photo-addition compound, **3**, although the sterical requirements exerted by the substitutents of the olefin moiety should also be taken into consideration at the same time for the H-abstraction by excited carbonyl groups in **3**.[16)]

From the results tabulated in Table 4 one can observe that the amount of the isomer, **3c**-II, always surpassed that of **3c**-I. The formation of **3c**-I is less favored, presumably because of the sterical requirements, though the isomer, **3c**-I, once formed, may be more stable than **3c**-II on further irradiation. These sterical requirements might play a more important role in the selective formation of a cyclobutane-ring compound in the case of styrene or 1-octene than in α-methylstyrene. Only one of the possible isomers, **3d** or **3e**, could be obtained, but neither **3d'** nor **3e'**, when styrene or 1-octene and 2-methoxy-1,4-naphthoquinone were submitted to irradiation with a filter. The cyclobutane-ring compound, **3d** or **3e**, was confirmed to have no intramolecular interactions by an inspection of the UV and ^{1}H-NMR spectra.

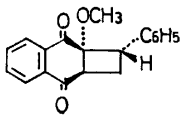

3d

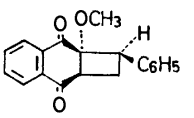

3d'

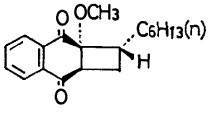

3e

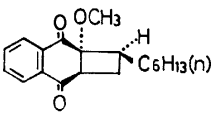

3e'

The Reversibility of the Formation of the Cyclobutane-ring Compounds, 3: On further irradiation without a filter, the cyclobutane-ring compound, **3a**, slowly photo-decomposed to give 2-methoxy-1,4-naphthoquinone and 1,1-diphenylethylene. Moreover, when, under the same conditions, the photochemical decomposition of the compound, **3a**, was investigated in the presence of an excess of styrene, the sole reaction product isolated was determined to be **21**; the same product as that derived from the photochemical reaction of 2-methoxy-1,4-naphthoquinone with styrene without a filter. On the other hand, since the cyclobutane-ring compound, **3d**, quantitatively photo-rearranged to the compound, **21**,[17)] a similar photochemical reaction of **3d** was examined in the presence of an excess of 1,1-diphenylethylene; then the compound, **3a**, was isolated as well as **21**. These results are illustrated in Scheme 1. The results presented can all be explained assuming that the formation of a cyclobutane-ring compound is reversible on irradiation.

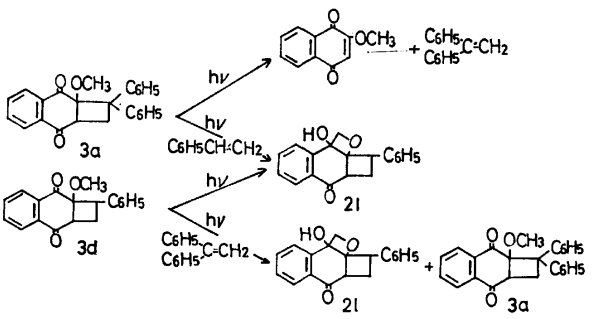

Scheme 1.

The Reaction Scheme. In the photochemical reaction of 2-alkoxy-1,4-naphthoquinones with olefins, the first stage of the reaction should be the formation of cyclobutane-ring compounds, **3**, from the photo-excited

quinones and olefins. Severals of the cyclobutane-ring compounds derived from such olefins as 1,1-diphenylethylene, 1,1-di-*p*-tolylethylene and α-methylstyrene are stabilized by intramolecular interactions through π-electrons as well as by sterical requirements for the intramolecular H-abstraction by an excited carbonyl group.[16] In another case, the cyclobutane-ring compounds are rather unstable upon further irradiation to undergo the subsequent photochemical reaction *via* intramolecular H-abstraction by a carbonyl group to yield the oxetanol-ring compounds, **2**, which are themselves stable upon further irradiation. The extent of the reversible reaction to the starting quinone and the olefin (Route (a)) is considerable for the diradical, **16**, derived from **3a**, **3b**, **3c**, or **3f**, presumably because of the lower dissociation energy of the bond connecting the quinone with olefin moieties. The bonding between the quinone and olefin moieties of the diradical, **16**,

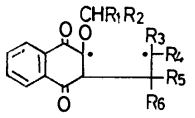

16

could be weakened by the aryl (or methyl) substitutents of the olefin moiety. Thus, although the cyclobutane-ring compounds, **3a**, **3b**, **3c**, or **3f**, can be relatively stabilized as a result of the intramolecular interactions through π-electrons, the decomposition to the quinone and the olefin might be predominant and no further photochemical reaction to the oxetanol-ring compounds, **2**, could proceed when the cyclobutane-ring compounds, **3**, were irradiated by light of a shorter wavelength.

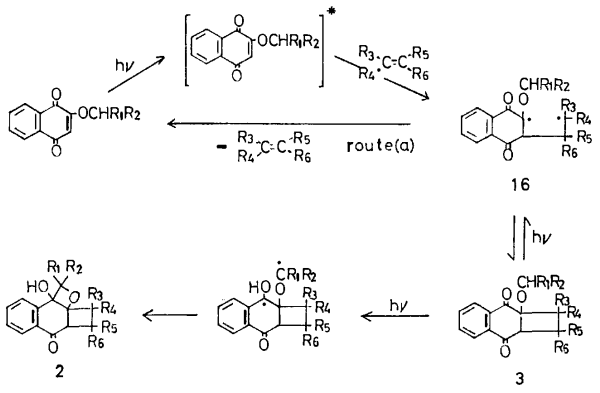

Scheme 2.

The possible reaction mechanism is summarized in Scheme 2.

Experimental

Starting Materials. *Quinones*: The 2-alkoxy-1,4-naphthoquinones were prepared by the etherification of 2-hydroxy-1,4-naphthoquinone with an appropriate alcohol in the presence of concd sulfuric acid or the boron trifluoride–ether complex, according to the literature; 2-methoxy-1,4-naphthoquinone: mp 178.0—180.5 °C,[18] 2-ethoxy-1,4-naphthoquinone: mp 118.0—119.0 °C,[19] 2-isopropoxy-1,4-naphthoquinone: mp 111.5—112.0 °C,[20] and 2-allyloxy-1,4-naphthoquinone: mp 98.0—100.0 °C.[20]

Olefins: 1,1-Di-*p*-tolylethylene was synthesized by the Grignard reaction of *p*-tolylmagnesium bromide and ethyl acetate; then the 1,1-di-*p*-tolylethanol thus produced was subjected to dehydration with 20% sulfuric acid; mp 61.0 °C.[21] The other olefins examined here were commercially available and were purified by distillation before use.

General Procedures. 2-Alkoxy-1,4-naphthoquinone (1 mmol) and olefin (2 mmol) were dissolved in benzene (20 ml) and irradiated in a glass tube by means of a high-pressure Hg arc lamp (300 W) through a 5-cm-thick water layer. After the 2-alkoxy-1,4-naphthoquinone had been completely consumed, the benzene was distilled off under reduced pressure. The reaction mixture was purified by chromatography on silica gel and then further purified by recrystallization from an appropriate solvent.

Identification of the Photo-addition Compounds. *8-Butyl-2-hydroxy-3,4-benzo-1,2-epoxymethanobicyclo[4.2.0]oct-3-en-5-one (**2a**)*; colorless oil (yield, 25%). Mass; *m/e*=272 (M^+). IR (liq. film); 3480 (OH), 2920, 2840 (CH), 1680 cm^{-1} (C=O). ^{1}H-NMR (CCl_4): δ; 0.96 (3H, CH_3, br t), 1.40 (6H, aliphatic-H, br m), 1.65-1.90 (2H, C-7 CH_2, m), 2.84 (1H, C-8 CH, m), 3.28 (1H, C-6 CH, t, *J*=10.0 Hz), 3.80 (1H, OH, s), 4.34, 4.56 (2H, C-10 CH_2, AB-q *J*=6.0 Hz), 7.24—7.92 ppm (4H, aromatic-H, m).

*8-Pentyl-2-hydroxy-3,4-benzo-1,2-epoxymethanobicyclo[4.2.0]oct-3-en-5-one (**2b**)*; white needles from hexane (yield, 50%). Mp 80.0—81.0 °C. Mass; *m/e*=286 (M^+). Found: C, 75.78; H, 8.05%. Calcd for $C_{18}H_{22}O_3$: C, 75.49; H, 7.74%. IR (KBr disk); 3360 (OH), 2920, 2840 (CH), 1670 cm^{-1} (C=O). ^{1}H-NMR (CCl_4); δ: 0.92 (3H, CH_3, br t), 1.36 (8H, aliphatic-H, m), 1.64—1.90 (2H, C-7 CH_2, m), 2.92 (1H, C-8 CH, m,) 3.28 (1H, C-6 CH, t, *J*=10.0 Hz), 3.92 (1H, OH, s), 4.34, 4.56 (2H, C-10 CH_2, AB-q, J=6.0 Hz), 7.22—7.96 ppm (4H, aromatic-H, m).

*8-Hexyl-2-hydroxy-3,4-benzo-1,2-epoxymethanobicyclo[4.2.0]oct-3-en-5-one (**2c**)*; white needles from hexane(yield, 67%); mp 101.0—101.5 °C. Mass; *m/e*=300(M^+). Found: C, 76.21; H, 8.32%. Calcd for $C_{19}H_{24}O_3$: C, 75.97; H, 8.05%. IR (KBr disk); 3320 (OH), 2920, 2840(CH), 1680 cm^{-1} (C=O). ^{1}H-NMR (CCl_4); δ: 0.92 (3H, CH_3, br t), 1.36 (10H, aliphatic-H, m), 1.64—1.90 (2H, C-7 CH_2, m), 2.92 (1H, C-8 CH, m), 3.30 (1H, C-6 CH, t, *J*=10.0 Hz), 3.50 (1H, OH, s), 4.38, 4.58 (2H, C-10 CH_2, AB-q, *J*=6.0 Hz), 7.28—7.96 ppm (4H, aromatic-H, m).

*8-Heptyl-2-hydroxy-3,4-benzo-1,2-epoxymethanobicyclo[4.2.0]oct-3-en-5-one (**2d**)*; white needles from benzene–hexane (yield, 48%); mp 84.0—85.0 °C. Mass; *m/e*=314 (M^+). IR (KBr disk); 3340 (OH), 2940, 2860 (CH), 1680 cm^{-1} (C=O). ^{1}H-NMR ($CDCl_3$); δ: 0.88 (3H, CH_3, br t), 1.10—1.92 (14H, aliphatic-H, m), 2.80 (1H, OH, s), 2.84 (1H, C-8 CH, m), 3.40 (1H, C-6 CH, t, *J*=8.0 Hz), 4.44, 4.62 (2H, C-10 CH_2, AB-q, *J*=8.0 Hz), 7.28—8.00 ppm (4H, aromatic-H, m).

*8-Octyl-2-hydroxy-3,4-benzo-1,2-epoxymethanobicyclo[4.2.0]oct-3-en-5-one(**2e**)*; white needles from petroleum ether (yield, 45 %); mp 110.0—111.0 °C. Mass; *m/e*=328 (M^+). IR (KBr disk); 3340 (OH), 2940, 2860 (CH), 1680 cm^{-1} (C=O). ^{1}H-NMR ($CDCl_3$); δ: 0.90 (3H, CH_3, t), 1.10—2.00 (16H, aliphatic-H, m), 2.80 (1H, OH, s), 2.82 (1H, C-8 CH, m), 3.46 (1H, C-6 CH, t, *J*=8.0 Hz), 4.56, 4.64(2H, C-10 CH_2, AB-q, *J*=8.0 Hz), 7.30—8.04 ppm (4H, aromatic-H, m).

*2-Hydroxy-7,8-tetramethylene-3,4-benzo-1,2-epoxymethanobicyclo-[4.2.0]oct-3-en-5-one(**2f**)*; colorless oil (yield, 39%). Mass; *m/e*=270 (M^+). IR (liq. film); 3350 (OH), 2920, 2840 (CH), 1660 cm^{-1} (C=O). ^{1}H-NMR ($CDCl_3$); δ: 0.80—3.25 (10H, aliphatic-H, m), 3.42 (1H, C-6 CH, d, *J*=8.0 Hz), 4.48, 4.64 (2H, C-10 CH_2, AB-q, *J*=6.0 Hz), 4.80 (1H, OH, s), 7.24—8.10 ppm (4H, aromatic-H, m).

*7,8-Hexamethylene-2-hydroxy-3,4-benzo-1,2-epoxymethanobicyclo[4.2.0]oct-3-en-5-one(**2g**)*; white needles (yield, 74%); mp 191.0—198.0 °C (decomp). Mass; *m/e*=298 (M^+). IR (KBr disk); 3360 (OH), 2920, 2840 (CH), 1660 cm^{-1} (C=O). ^{1}H-NMR ($CDCl_3$); δ: 0.90—3.00 (14H, aliphatic-H, m), 3.04 (1H, C-6 CH, d, J=8.0 Hz), 4.52, 4.64 (2H, C-10 CH_2, AB-q, J=6.0 Hz), 4.72 (1H, OH, s), 7.36—8.12 ppm (4H, aromatic-H, m).

*7,8-(3-Hexenylene)-2-hydroxy-3,4-benzo-1,2-epoxymethanobicyclo[4.2.0]oct-3-ene-5-one(**2h**)*; white crystals (yield, 29%); mp 184.0—186.0 °C (decomp). Mass; *m/e*=296 (M^+). IR (KBr disk); 3320(OH), 3000, 2910, 2840 (CH), 1670 cm^{-1} (C=O). ^{1}H-NMR ($CDCl_3$); δ: 1.00—2.80 (11H, aliphatic-H and OH, m), 3.16 (1H, C-6 CH, d, J=10.0 Hz), 4.68 (2H, C-10 CH_2, br s), 5.52 (2H, C-3′ and C-4′ CH′ s, br d), 7.28—7.96 ppm (4H, aromatic-H, m).

*2-Hydroxy-7,8[2′,3′]bicyclo[2.2.1]heptano-3,4-benzo-1,2-epoxymethanobicyclo[4.2.0]oct-3-en-5-one(**2i**)*; white crystals from chloroform (yield, 50%); mp 214.0—217.0 °C. Mass; *m/e*=282 (M^+). Found: C, 76.49; H, 6.63%. Calcd for $C_{18}H_{18}O_3$: C, 75.56; H, 6.44%. IR (KBr disk); 3420 (OH), 2960, 2930, 2880 (CH), 1670 cm^{-1} (C=O). ^{1}H-NMR ($CDCl_3$); δ: 1.04—2.16 (7H, aliphatic-H, m), 2.42 (2H, aliphatic-H, m), 2.82 (1H, OH, s), 2.90 (2H, aliphatic-H, m), 4.56, 4.72 (2H, C-10 CH_2, AB-q, J=6.0 Hz), 7.24—7.92 ppm (4H, aromatic-H, m).

*2-Hydroxy-7,8[2′,3′]bicyclo[2.2.1]hept-5′-eno-3,4-benzo-1,2-epoxymethanobicyclo[4.2.0]oct-3-en-5-one(**2j**)*; white crystals from chloroform (yield, 35%); mp 199.0—201.0 °C. IR (KBr disk); 3380 (OH), 2960, 2880 (CH), 1665 cm^{-1} (C=O). ^{1}H-NMR ($CDCl_3$); δ: 1.22 (3H, aliphatic-H, m), 2.76 (2H, aliphatic-H, m), 2.60 (1H, OH, s), 3.06 (2H, aliphatic-H, m), 4.64, 4.78 (2H, C-10 CH_2, AB-q, J=6.0 Hz), 6.04 (2H, C-5′ and C-6′ CH′ s, m), 7.24—7.96 ppm (4H, aromatic-H, m).

*2-Hydroxy-indeno[2′,3′-7,8]-3,4-benzo-1,2-epoxymethanobicyclo[4.2.0]oct-3-en-5-one(**2k**)*; white needles from benzene–petroleum ether (yield, 73%); mp 225.0—227.0 °C (decomp). Mass; *m/e*=304 (M^+). Found: C, 79.22; H, 5.28%. Calcd for $C_{20}H_{16}O_3$: C, 78.93; H, 5.30%. IR (KBr disk); 3320 (OH), 2920 (CH), 1675 cm^{-1} (C=O). ^{1}H-NMR ($CDCl_3$); δ: 2.04 (1H, OH, s), 2.64 (1H, C-7 CH, m), 3.04 (2H, C-1′ CH_2, dd, J=6.0, 10.0 Hz), 3.19 (1H, C-6 CH, m), 4.42(1H, C-8 CH, m), 4.48, 4.76 (2H, C-10 CH_2, AB-q, J=6.0 Hz), 7.10—8.00 ppm (8H, aromatic-H, m).

*2-Hydroxy-8-phenyl-3,4-benzo-1,2-epoxymethanobicyclo[4.2.0]oct-3-en-5-one(**21=4**)*; white needles from benzene (yield, 69%); mp 164.0—164.5 °C. Mass; *m/e* 292 (M^+). Found: C, 78.03; H, 5.45%. Calcd for $C_{19}H_{16}O_3$: C, 78.08; H, 5.52%. IR (KBr disk); 3250 (OH), 2940 (CH), 1675 cm^{-1} (C=O). UV_{max} ($CHCl_3$); 290 nm (ε: 3.0×10^3). ^{1}H-NMR ($CDCl_3$); δ: 2.16 (1H, C-7 CH, m), 2.58 (1H, C-7 CH, m), 3.22 (1H, OH, s), 3.62 (1H, C-6 CH, dd, J=8.0, 12.0 Hz), 4.18 (1H, C-8 CH, dd, J=6.0, 10.0 Hz), 4.56, 4.64 (2H, C-10 CH_2, AB-q, J=6.0 Hz), 7.24—8.10 ppm (9H, aromatic-H, m). ^{13}C-NMR ($CDCl_3$); δ: 26.63 (t, C-7), 43.44 (d, C-8), 49.63(d, C-6), 70.62 (s, C-1), 82.33 (t, C-10), 90.95 (s, C-2), 126.92 (aromatic-C), 127.05 (aromatic-C), 127.41 (aromatic-C), 128.26 (aromatic-C), 128.56 (aromatic-C), 129.17 (aromatic-C), 130.26 (aromatic-C), 134.93 (aromatic-C), 137.60 (aromatic-C), 143.43 (aromatic-C), 197.24 ppm (s, C-5) (chemical shifts were calibrated from TMS as an internal standard).

*2-Hydroxy-8-methyl-8-phenyl-3,4-benzo-1,2-epoxymethanobicyclo[4.2.0]oct-3-en-5-one(**2m**)*; white needles from benzene (yield, 9%); mp 201.0—204.0 °C. Found: C, 78.23; H, 5.88%. Calcd for $C_{20}H_{18}O_3$: C, 78.41; H, 5.92%. IR (KBr disk); 3400 (OH), 2950 (CH), 1680 cm^{-1} (C=O). ^{1}H-NMR ($CDCl_3$); δ: 1.52 (3H, CH_3, s), 2.34 (1H, C-7 CH, dd, J=6.0, 10.0 Hz), 2.44 (1H, OH, s), 3.08 (1H, C-7 CH, t, J=10.0 Hz), 3.40 (1H, C-6 CH, dd, J=6.0, 10.0 Hz), 4.62, 4.70 (2H, C-10 CH_2, AB-q, J=8.0 Hz), 7.14—8.00 ppm (9H, aromatic-H, m).

*2-Hydroxy-10-methyl-8-phenyl-3,4-benzo-1,2-epoxymethanobicyclo[4.2.0]oct-3-en-5-one(**2n**)*; white needles from benzene (yield, 60%); mp 168.0—169.0 °C. Found: C, 78.83; H, 5.73%. Calcd for $C_{20}H_{18}O_3$: C, 78.41, H, 5.92%. IR (KBr disk); 3280 (OH), 2980 (CH), 1680 cm^{-1} (C=O). ^{1}H-NMR ($CDCl_3$); δ: 1.16 (3H, CH_3, d, J=6.0 Hz), 2.16 (1H, C-7 CH, m), 2.58 (1H, C-7 CH, m), 2.94 (1H, OH, s), 3.62 (1H, C-6 CH, dd, J=8.0, 12.0 Hz), 4.18 (1H, C-8 CH, dd, J=8.0, 12.0 Hz), 4.70 (1H, C-10 CH, q, J=6.0 Hz), 7.22—8.10 ppm (9H, aromatic-H, m).

*10,10-Dimethyl-2-hydroxy-8-phenyl-3,4-benzo-1,2-epoxymethanobicyclo[4.2.0]oct-3-en-5-one(**2o**)*; white needles from benzene (yield, 7.1%); mp 117.0—118.0 °C. Mass; *m/e*=320 (M^+). Found: C, 78.55; H, 6.22%. Calcd for $C_{21}H_{20}O_3$: C, 78.72; H, 6.29%. IR (KBr disk); 3320 (OH), 2990, 2920 (CH), 1680 cm^{-1} (C=O). ^{1}H-NMR ($CDCl_3$); δ: 0.92 (3H, CH_3, s), 1.46 (3H, CH_3, s), 2.16 (1H, C-7 CH, m), 2.58 (1H, C-7 CH, m), 2.92 (1H, OH, s), 3.62 (1H, C-6 CH, dd, J=8.0, 12.0 Hz), 4.18 (1H, C-8 CH, dd, J=6.0, 10.0 Hz), 7.20—8.16 ppm (9H, aromatic-H, m).

*2-Hydroxy-8-phenyl-10-vinyl-3,4-benzo-1,2-epoxymethanobicyclo[4.2.0]oct-3-en-5-one(**2p**)*; white needles from benzene (yield, 27%); mp 139.0—140.0 °C. Mass; *m/e*=318 (M^+). IR (KBr disk); 3280 (OH), 3060, 3020, 2880 (CH), 1680 cm^{-1} (C=O). ^{1}H-NMR ($CDCl_3$); δ: 2.16 (1H, C-7 CH, m), 2.58 (1H, C-7 CH, m), 3.00 (1H, OH, s), 3.80 (1H, C-6 CH, dd, 8.0, 10.0 Hz), 4.12 (1H, C-8 CH, dd, J=6.0, 10.0 Hz), 5.04—6.16 (4H, vinyl-H and C-10 CH, m), 7.22—8.19 ppm (9H, aromatic-H, m).

*8,8-Diphenyl-1-methoxy-3,4-benzobicyclo[4.2.0]oct-3-ene-2,5-dione(**3a**)*; white crystals (yield, 63%); mp 112.0—113.0 °C. Mass; *m/e*=188 (2-methoxy-1,4-naphthoquinone rest), 180 (1,1-diphenylethylene rest). Found: C, 81.47; H, 5.39%. Calcd for $C_{25}H_{20}O_3$: C, 81.50; H, 5.47%. IR (KBr disk); 1680 cm^{-1} (C=O). ^{1}H-NMR (CCl_4); δ: 3.24 (3H, OCH_3, s), 3.40 (3H, C-6 CH and C-7 CH_2, m), 6.70—7.90 ppm (14H, aromatic-H, m). UV_{max} (CCl_4); 303 nm (ε: 2.0×10^3), 312 (1.9×10^2), 352 (1.7×10^2), 365 (1.5×10^2), UV_{max} (CH_3CN); 303 nm (ε: 1.9×10^3), 312 (1.7×10^3), 349 (1.5×10^2), 361 (1.4×10^2).

*8,8-Di-p-tolyl-1-methoxy-3,4-benzobicyclo[4.2.0]oct-3-ene-2,5-dione(**3b**)*; colorless oil (yield, 71%). Mass; *m/e*=208 (1,1-di-*p*-tolylethylene rest), 188 (2-methoxy-1,4-naphthoquinone rest). IR (KBr disk); 1680 cm^{-1} (C=O). ^{1}H-NMR (CCl_4); δ: 2.06 (3H, CH_3, s), 2.28 (3H, CH_3, s), 3.20 (3H, OCH_3, s), 3.16—3.52 (3H, C-6 CH and C-7 CH_2, m), 6.75, 7.01 (4H, aromatic-H, AB-q, J=10.0 Hz), 7.01, 7.27 (4H, aromatic-H, AB-q, J=8.0 Hz), 7.40—7.92 ppm (4H, aromatic-H, m).

*1-Methoxy-8-methyl-8-phenyl-3,4-benzobicyclo[4.2.0]oct-3-ene-2,5-dione(**3c**)*; white crystals (yield, 69%). Mass; *m/e*=306 (M^+). Found: C, 78.27; H. 5.50%. Calcd for $C_{20}H_{18}O_3$: C, 78.41; H, 5.92%. IR (KBr disk); 1685 cm^{-1} (C=O). **3c**-I; ^{1}H-NMR (CCl_4); δ: 1.60 (3H, CH_3, s), 2.44 (2H, C-7 CH_2,d, J=10.0 Hz), 3.20 (3H, OCH_3, s), 3.60 (1H, C-6 CH, t, J=10.0 Hz), 6.90—7.97 ppm (9H, aromatic-H, m). **3c**-II; ^{1}H-NMR (CCl_4); δ: 1.16 (3H, CH_3, s), 2.16 (2H, C-7 CH_2, m), 3.05 (3H, OCH_3, s), 3.40 (1H, C-6 CH, m), 7.14 (5H, aromatic-H, br s), 7.60—8.20 ppm (4H, aromatic-H, m).

*1-Methoxy-8-phenyl-3,4-benzobicyclo[4.2.0]oct-3-ene-2,5-dione(**3d**)*; white crystals (yield, 50% after 89% of quinone was consumed on irradiation with the filter A.); mp 142.5—144.0 °C. Mass; *m/e*=292 (M^+). Found: C, 77.79; H, 5.43%. Calcd for $C_{19}H_{16}O_3$: C, 78.06; H, 5.52%. IR (KBr disk); 1680 cm^{-1} (C=O). ^{1}H-NMR ($CDCl_3$); δ: 2.52, 3.08 (2H, C-7

Reactions of Aroylhydrazones. II.[1] Oxidative Cyclization of Benzil Bis(aroylhydrazones) to Substituted 1,2,3-Triazoles

Mohammed A. E. SHABAN*† and Mahmoud A. M. NASSR
Chemistry Department, Faculty of Science, Alexandria University, Alexandria, Egypt
(Received September 16, 1975)

Benzil bis(aroylhydrazones) were oxidized with iodine and yellow mercury(II) oxide to 1-(1-α-aroyloxyarylideneamino)-4,5-diphenyl-1,2,3-triazoles. The structure of the prepared compounds was determined by studying their chemical and spectral properties.

Bis(aroylhydrazones) of 1,2-dicarbonyl compounds have been known to undergo oxidation to give different products[2-5] depending upon the parent 1,2-dicarbonyl compound[2,5] and the oxidizing agent used.[2,6] Oxidation of these compounds with alkaline potassium hexacyanoferrate(III) or iodine and yellow mercuric oxide was first reported by Stolle[6] to give products which ascribed, at that time, 1,2,3,4-dihydrotetrazine structures.[6,8] However, the structure of the oxidation products was reassigned to be substituted 1-amino-1,2,3-triazoles on the basis of their infrared,[2] nuclear magnetic resonance,[2] and X-ray analyses.[9]

Continuing our studies on the reactions of hydrazones,[4,5,10-12] we report now the preparation and oxidative cyclization, with iodine and yellow mercuric oxide, of benzil bis(aroylhydrazones) (**1**) to 1-(α-aroyloxyarylideneamino) - 4,5 - diphenyl - 1,2,3 - triazoles (**6**) with emphasis on their spectral and some of their chemical properties.

Results and Discussion

Benzil bis(aroylhydrazones) **1** were prepared in 70—85% yield by condensing benzil with two equivalents of the required aroylhydrazine in ethanol. The infrared spectra of the bis-hydrazones showed the amide I bands of the aroylhydrazone residues at 1680—1670 cm^{-1} in addition to strong C=N absorption at 1650 cm^{-1} and NH bands at 3250—3200 cm^{-1}. Unlike benzil bis(arylhydrazones) which are orange to brown in color, the bis(aroylhydrazones) are colorless. This is attributed to the different types of tautomerism exhibited by these compounds. Thus, whereas the bis(arylhydrazones) were shown to exhibit arylhydrazono-arylazo tautomerism,[13] benzil bis(aroylhydrazones) exhibit a keto-enol tautomerism (**1**⇌**2**) as evidenced by giving pale yellow colors with sodium methoxide, greenish brown colors with neutral ferric chloride solution, as well as by forming stable cupric complexes.[14] Preliminary studies indicated that the stability of these complexes is due to the formation of tetradentate ligands (**3**) similar to those of osulose bis-(thiosemicarbazones).[15,16] The NMR spectrum of benzil bis(benzoylhydrazone) (**1a**) showed the four phenyl groups as a twenty-proton multiplet at δ 7.53 and the two hydrazono protons as a two-proton singlet at δ 12.85.

Oxidation of the bis-hydrazones **1** with iodine and yellow mercuric oxide in absolute ether afforded crystalline products having two hydrogens less than the parent bis-hydrazone and have no amide or NH absorptions in their infrared spectra. The oxidation products, however, showed strong ester absorption at 1760—1740 cm^{-1} in addition to the C=N absorption at 1640 cm^{-1}. The NMR spectrum of the oxidation product of benzil bis(benzoylhydrazone) revealed the absence of the two hydrazono protons of the parent compound and showed only a twenty-proton multiplet (four phenyl groups) at δ 7.50. The oxidation products were thus assigned the structure of 1-(α-aroyloxyarylideneamino)-4,5-diphenyl-1,2,3-triazoles (**6**). This assignment is in agreement with our[1,4,5] as well as with others[2,3,9] findings. The oxidation products are formed (see Scheme 1) first by abstraction of the two hydrazono hydrogens of **1** to give the bis(aroylazoene) (**4**) which cyclizes to the triazole derivative (**5**) followed by migration of the acylonium ion detached from N-2 of the triazole ring to the nucleophilic oxygen of the polarized acylamino group on N-1 to give **6**.

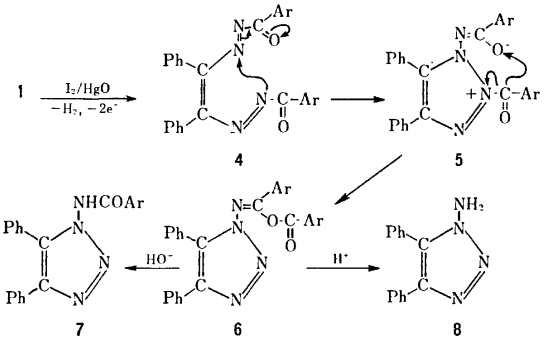

Scheme 1.

Compatible with the assigned structure **6**, is the splitting of their enol ester groups on alkali hydrolysis with methanolic ammonia at room temperature yielding the expected 1-aroylamino-4,5,-diphenyl-1,2,3-triazoles (**7**) and one equivalent of the corresponding benzoic acid. Infrared spectra of **7** revealed the absence of the ester absorption bands of their precursors with concomitant absorption at 1700—1660 (amide I) and 3250—3200 cm (NH) due to the newly formed amide function. Acid hydrolysis, with aqueous hydrochloric acid, of **6** or **7** split off two or one equivalent respectively of the corresponding benzoic acid and gave one and the same product from the differently substituted **6** and **7** namely: 1-amino-4,5-diphenyl-1,2,3-triazole (**8**).

* Present address: Laboratory for Carbohydrate Research, Harvard Medical School at Masaschusetts General Hospital, Boston, Massachusetts 02114, U.S.A.
† To whom inquiries should be addressed.

TABLE 1.

Compound	Mp °C	Yield %	Found % C	Found % H	Found % N	Formula	Calcd % C	Calcd % H	Calcd % N	IR: ν_{max}^{KBr} C=N	IR: ν_{max}^{KBr} CONH	IR: ν_{max}^{KBr} NH
*Benzil bis(aroylhydrazones) (**1**)*												
1a	207[17]	75	75.2	4.9	12.3	$C_{28}H_{22}N_4O_2$	75.3	5.0	12.5	1650	1670	3200
1b	180	70	75.5	5.2	12.2	$C_{30}H_{26}N_4O_2$	75.9	5.5	11.8	1650	1670	3200
1c	195	80	75.6	5.3	11.4	$C_{30}H_{26}N_4O_2$	75.9	5.5	11.8	1650	1680	3250
1d	220	75	70.9	5.3	10.9	$C_{30}H_{26}N_4O_4$	71.1	5.2	11.1	1650	1670	3250
1e	240	75	64.6	4.1	10.7	$C_{28}H_{20}Cl_2N_4O_2$	64.2	3.9	10.7	1650	1680	3250
1f	275	85	64.4	4.1	10.6	$C_{28}H_{20}Cl_2N_4O_2$	64.2	3.9	10.7	1650	1680	3250
*1-(α-Aroyloxyarylideneamino)-4,5-diphenyl-1,2,3-triazoles (**6**)*												
6a	190[2]	40	75.4	4.4	12.7	$C_{28}H_{20}N_4O_2$	75.7	4.5	12.6	1640	1760	
6b	260	35	76.3	4.9	12.0	$C_{30}H_{24}N_4O_2$	76.3	5.1	11.9	1640	1750	
6c	170	40	76.6	5.0	11.6	$C_{30}H_{24}N_4O_2$	76.3	5.1	11.9	1640	1750	
6d	180	40	71.1	4.6	11.2	$C_{30}H_{24}N_4O_4$	71.4	4.8	11.1	1640	1740	
6e	240	45	65.3	3.5	10.6	$C_{28}H_{18}Cl_2N_4O_2$	65.5	3.5	10.9	1640	1750	
6f	192	50	65.3	3.5	10.6	$C_{28}H_{18}Cl_2N_4O_2$	65.5	3.5	10.9	1640	1750	
*1-Aroylamino-4,5-diphenyl-1,2,3-triazoles (**7**)*												
7a	266	70	73.9	5.0	16.3	$C_{21}H_{16}N_4O$	74.1	4.7	16.5		1670	3200
7b	265	60	74.4	4.8	15.4	$C_{22}H_{18}N_4O$	74.6	5.1	15.8		1675	3200
7c	245	70	74.7	4.7	15.4	$C_{22}H_{18}N_4O$	74.6	5.1	15.8		1700	3250
7d	185	70	71.7	4.6	15.3	$C_{22}H_{18}N_4O_2$	71.3	4.9	15.3		1665	3350
7f	225	80	69.3	4.5	15.6	$C_{21}H_{15}ClN_4O$	69.2	4.1	15.4		1665	3350

Thermal rearrangement of 1-(α-benzoyloxybenzylideneamino)-4,5-diphenyl-1,2,3-triazole (**6a**), by heating above its melting point, gave 1-dibenzoylamino-4,5-diphenyl-1,2,3-triazole (**9**) through the 1,3-acyl migration of the enol benzoate group. The infrared spectrum of **9** showed only CON absorption band at 1720 cm^{-1} and no ester or NH absorptions. Compound **9** was also obtained when **8** was benzoylated with benzoyl chloride in pyridine. Conversely, **9** was converted to **8** on hydrolysis with aqueous hydrochloric acid. It was interesting to find out that both **6a** and **9** gave exactly the same mass spectrometric fragmentation pattern (see Scheme 2). This is probably due to the thermal isomerization of **6a** to **9** on the probe of the mass spectrometer before it undergoes fragmentation. Thus, both compounds showed the molecular ion peak (M^+) at *m/e* 444 in addition to the fragments at *m/e* 416 (M^+-N_2), *m/e* 311[$M^+-(N_2+PhCO)$]. The latter ion loses an *N*-benzoyl radical to give the diphenylaziridinium ion at *m/e* 192 which successively loses a nitrogen atom to give the diphenylacetylene ion at *m/e* 178 and a phenyl radical to give the phenylacetylene ion at *m/e* 101.

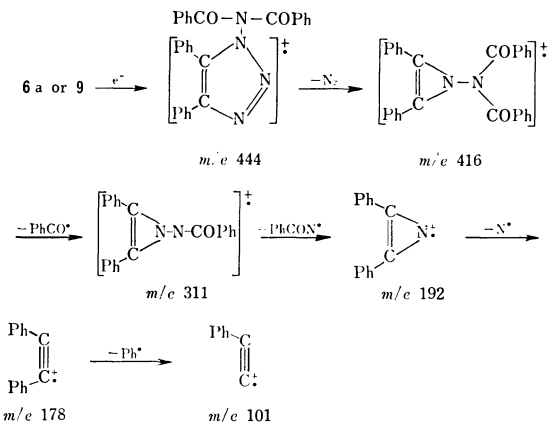

Scheme 2.

Refluxing of either **6a**, **7a**, or **8** with acetic anhydride gave 1-acetamido-4,5-diphenyl-1,2,3-triazole (**10**).

Experimental

Melting points were determined on a Kofler block and are uncorrected. Infrared spectra were recorded, for potassium bromide discs, with a Unicam SP 200 spectrophotometer. Nuclear magnetic resonance spectra were recorded at 60 MHz with a Varian T-60 spectrophotometer and with deuteriodimethylsulfoxide as a solvent containing 1% tetramethylsilane as internal standard. Mass spectral analyses were performed on a Varian M-66 spectrometer. Homogeneity of the prepared compounds were checked by thin layer chromatography on Silica Gel G plates, and the spots were detected by spraying with 20% (v/v) sulfuric acid, followed by heating on a hot plate for a few minutes.

*Benzil Bis(aroylhydrazone) (**1a—1f**; Table 1).* A solution of benzil (1 g) in ethanol (30 ml) was treated with the solution of the required aroylhydrazine (2 equivalents) in ethanol (20 ml) and a few drops of glacial acetic acid, and the mixture was heated on a water bath for 45 min. The mixture was kept at room temperature for an overnight, and the bishydrazone which separated was filtered and crystallized from 1 : 1 mixture of methanol-benzene. The bis-hydrazones are soluble in methanol and ethanol and are insoluble in hexanes.

*1-(α-Aroyloxyarylideneamino)-4,5-diphenyl-1,2,3-triazoles (**6a—6f**; Table 1).* A suspension of benzil bis(aroylhydrazone)

(1 g) in absolute ether (150 ml) was treated with yellow mercuric oxide (2 g), magnesium oxide (0.2 g) and iodine (2 g) for 96 h at room temperature. The suspension was filtered, and the inorganic residue was washed with chloroform (3 × 100 ml), and the filtrate and washings were combined and successively extracted with potassium iodide and sodium thiosulfate solutions and then with water and dried (sodium sulfate). Evaporation of the solvents gave the products which were crystallized from methanol.

*1-Aroylamino-4,5-diphenyl-1,2,3-triazoles (**7a**—**7f**; Table 1).* A solution of 1-(α-aroyloxyarylideneamino)-4,5-diphenyl-1,2,3-triazole (1 g) in methanol (200 ml) was treated with 20% ammonium hydroxide solution (20 ml) for 24 h at room temperature. The mixture was evaporated under reduced pressure, and the residue was triturated with water and filtered. The products were crystallized from methanol (see Table 1). Acidification of the filtrate gave one equivalent of the corresponding substitute benzoic acid.

*1-Amino-4,5-diphenyl-1,2,3-triazole (**8**).* Hydrolysis of compounds **6a**—**6e** or **7a**—**7f** (1 g) was carried out by heating under reflux, with concentrated hydrochloric acid (20 ml) for 24 h after which the reaction mixture was cooled, diluted with ether (200 ml), and the ethereal layer was washed with a saturated solution of sodium hydrogencarbonate and water and then dried (sodium sulfate). Evaporation of the solvent gave **8** (72—81% yield) which crystallized from benzene in plates, mp 136 °C. IR: ν_{max}^{KBr} 3300 cm^{-1} (NH). Found: C, 71.3; H, 5.0; N, 23.5%. Calcd for $C_{14}H_{12}N_4$: C, 71.2; H, 5.1; N, 23.7%. Acidification of the washings gave the corresponding substituted benzoic acid (two equivalents from **6** and one equivalent from **7**).

*1-Dibenzoylamino-4,5-diphenyl-1,2,3-triazole (**9**). (A) From **6a**:* Compound **6a** (0.5 g) was heated at 190 °C in an oil bath for 2 h and then left to cool. The solidified mass was triturated with methanol and filtrered. Crystallization from methanol gave **9** (0.4 g) as plates, mp 155—156 °C. IR: ν_{max}^{KBr} 1720 cm^{-1} (CON). Found: C, 75.5; H, 4.4; N, 12.7%. Calcd for $C_{28}H_{20}N_4O_2$: C, 75.7; H, 4.5; N, 12.6%.

*(B) From **8**:* A solution of **8** (0.5 g) in dry pyridine (5 ml) was treated with benzoyl chloride (2 ml) for 48 h at room temperature. The mixture was poured into ice-water, and the product, which separated, was filtered off and washed with water. Crystallization from methanol gave **9** (0.5 g) as plates, mp 155—157 °C. IR: ν_{max}^{KBr} 1720 cm^{-1} (CON). Found: C, 75.6; H, 4.5; N, 12.8%. Calcd for $C_{28}H_{20}N_4O_2$: C, 75.7; H, 4.5; N, 12.6%.

*1-Acetamido-4,5-diphenyl-1,2,3-triazole (**10**). (A) From **6a**:* Compound **6a** (0.5 g) in acetic anhydride (15 ml) was heated under refluxed for 2 h after which it was poured onto ice and left until the excess acetic anhydride hydrolyzed. The product was filtered, washed with water, and crystallized from methanol to give **10** (0.2 g) as plates, mp 178—180 °C. IR: ν_{max} 3300 (NH), 1670 cm^{-1} (COHN). Found: C, 69.3; H, 5.3; N, 20.0%. Calcd for $C_{16}H_{14}N_4O$: C, 69.1; H, 5.1; N, 20.1%.

*(B) From **7a**:* Compound **7a** (0.5 g) was treated in the same way as described above to give **10** (0.3 g), mp 178—180 °C. Found: C, 68.9; H, 5.1; N, 20.0%.

*(C) From **8**:* Compound **8** was refluxed with acetic anhydride as described above to give **10** in 80% yield having the same properties as mentioned.

References

1) Part 1: M. A. E. Shaban, M. A. M. Nassr, and M. A. M. Moustafa, *J. Heterocycl. Chem.*, **12**, 1295 (1975).
2) D. Y. Curtin and N. Y. Alexandrou, *Tetrahedron*, **19**, 1697 (1963).
3) D. Y. Curtin and N. Y. Alexandrou, *Tetrahedron*, **22**, 1309 (1966).
4) H. El Khadem and M. Shaban, *J. Chem. Soc., C*, **1967**, 519.
5) H. El Khadem, M. Shaban, and M. Nassr, *J. Chem. Soc., C*, **1969**, 1416.
6) R. Stolle, *Ber.*, **59**, 1743 (1926).
7) H. von Pechmann and W. Bauer, *Ber.*, **33**, 644 (1900).
8) H. von Pechmann and W. Bauer, *Ber.*, **42**, 659 (1909).
9) H. Bauer, A. J. Boulton, W. Fedeli, A. R. Katritzky, A. Majid-Hamid, F. Mazza, and A. Vaciago, *J. Chem. Soc., Perkin Trans. 2*, **1972**, 662.
10) H. El Khadem, M. Shaban, and M. Nassr, *Carbohydr. Res.*, **23**, 103 (1972).
11) H. El Khadem, M. Nassr, and M. Shaban. *J. Chem. Soc., C*, **1968** 1465.
12) H. El Khadem, M. Shaban, and M. Nassr. *J. Chem. Soc., C*, **1970** 2167.
13) A. J. Fatiadi and H. S. Isbell, *Carbohydr. Res.*, **5**, 302 (1967).
14) M. A. E. Shaban and M. A. Nassr, to be published.
15) G. Henseke and M. Winter, *Chem. Ber.*, **89**, 956 (1956).
16) F. H. H. Carlsson, A. J. Charlson, and E. C. Watton, *Carbohydr. Res.*, **36**, 359 (1974).
17) G. Struve, *J. Prakt. Chem.*, **50**, 295 (1984).

Studies in Heterocyclics. VI.[1] Synthesis of Thiazolo-Benzo-Triazepines

M. P. MAHAJAN,* S. M. SONDHI, and N. K. RALHAN**
Department of Chemistry, Punjabi University, Patiala 147002, India

(Received October 21, 1975)

2-Imino-3-(*o*-aminoaryl)-4-thiazolines (II) gave thiazolo-benzo-triazepines(I) on condensation with various aliphatic carboxylic acids. Both *N*-acyl(III) and *N,N'*-diacyl derivatives(IV) were isolated, and the mono-acyl derivatives(III) were also cyclized to thiazolo-benzo-triazepines.

In continuation of our study on the synthesis of bridgehead seven membered heterocyclic systems, we report herewith the synthesis of a new ring system, *i.e.*, thiazolo[2,3-*d*][1,3,5]benzo-triazepines. Thiazolo-benzo-triazepines (Ia—d; Table 2) have been synthesized according to Scheme 1.

2-Imino-3-(*o*-aminoaryl)-4-thiazolines(II) were synthesized according to the scheme described earlier.[2] The stochiometric quantities of II and requisite carboxylic acid when refluxed in toluene gave thiazolo-benzo-triazepines(I) in one step. In a number of attempts to achieve the synthesis of I by refluxing II and excess carboxylic acids (RCOOH; R=H, CH_3, C_2H_5) in the presence of acetic anhydride, the diacyl derivatives (IV; Table 1) were formed. The characteristic features of IR spectra of these diacyl derivatives are the presence of >NH and >C=O at 3330 and 1635 cm^{-1} in IV ($R_1=R_2=R=H$); at 3270 and 1660 cm^{-1} in IV ($R_1=R_2=H$; $R=CH_3$); at 3350 and 1665 cm^{-1} in IV ($R_1=R_2=H$; $R=C_2H_5$). The structure of IV ($R_1=R_2=H$, $R=CH_3$) was also supported by its NMR spectrum (100 MHz; $CDCl_3$) which shows a singlet at δ 2.14 (3H; CH_3–C(=O)–NH); a singlet at δ 2.30 (3H, CH_3–C(=O)–N=), one H amidic proton at δ 8.60 and aromatic multiplet at δ 6.71—7.96 for C_6H_5–C=CH– and –NH–(C$_6$H$_4$)–N=. These diacyl drivatives did not give I as suggested by Kanaoka *et al.*[3]

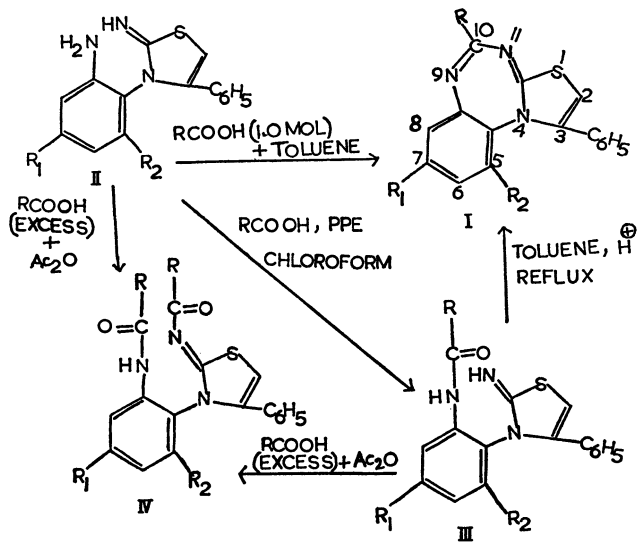

(a) $R_1=H$, $R_2=H$, $R=H$, CH_3, C_2H_5
(b) $R_1=CH_3$, $R_2=H$, $R=H$, CH_3, C_2H_5
(c) $R_1=OCH_3$, $R_2=H$, $R=H$, CH_3, C_2H_5
(d) $R_1=H$, $R_2=CH_3$, $R=H$, CH_3, C_2H_5

Scheme 1.

When stoichiometric quantitaties of the carboxylic acid and II along with polyphosphate ester (PPE) in chloroform were refluxed, only mono acyl derivatives (III) were obtained. The IR spectrum of III ($R_1=R_2=H$; $R=CH_3$) showed the characteristics >C=NH; >C=O vibrations at 3260 and 1650 cm^{-1}, respectively. The NMR spectrum (100 MHz; $CDCl_3$) also gave a singlet at δ 2.15 (3H; CH_3CO); a multiplet between δ 6.2—7.92 (10H; C_6H_5–C=CH– and –N–C_6H_4–N–); and a singlet at δ 6.50 (1H; >C=NH). These monoacyl derivatives are cyclized to I on refluxing in toluene. Moreover III are acylated to IV on heating with excess of carboxylic acids and acetic anhydride.

Experimental

The melting points are uncorrected. Microanalysis was carried out by the Microanalytical Service, CSIRO, Australia. IR spectra were run in KBr wafers on a Perkin-Elmer Infracord-137 spectrophotometer, and NMR spectra were recorded on a Varian HA-100 spectrometer.

2-Acylimino-3-(o-acylamino-substituted phenyl)-4-phenyl-4-thiazolines (IV). 3-(*o*-Aminophenyl)-2-imino-4-phenyl-4-thiazoline (2.67 g; 0.01 mol), acetic acid (10 ml) and acetic anhydride (10 ml) were heated under reflux for 3 h. The clear solution thus obtained was evaporated to dryness under reduced pressure and the solid so obtained was recrystallized from ethanol to afford IV ($R_1=R_2=R=CH_3$).

All the other derivatives using formic acid and propionic acid (IVa—d) were prepared following a procedure similar to that described above. Yield, mp, and microanalytical data are reported in Table 1.

3-(o-Acetamidophenyl)-2-imino-4-phenyl-4-thiazoline (III); ($R_1=R_2=H$, $R=CH_3$). 3-(*o*-Aminophenyl)-2-imino-4-phenyl-4-thiazoline (0.534 g; 0.002 mol), acetic acid (0.12 g; 0.002 mol); polyphosphate ester (3.0 g) and chloroform (20 ml) were heated under reflux for 2 h. The solvent was removed under reduced pressure and the residue was treated with aqueous sodium hydrogencarbonate. The solid obtained was filtered, washed with water, air dried and recrystallized from THF/Pet. ether (bp 80—100 °C); yield 0.43 g. (70%), mp 153 °C (Found: C, 65.98; H, 4.64; N, 13.45%. Calcd for $C_{17}H_{15}N_3SO$: C, 66.02; H, 4.85; N, 13.59%).

2-Acetylimino-3-(o-acetamidophenyl)-4-phenyl-4-thiazoline (IVa)

* Present address: Department of Chemistry, I.I.T. Kanpur.
** To whom corresponce should be addressed.

Table 1. Physical constants of IV

Sr. No.	Substituents			Yield %	Mp °C	Found %				Calcd %			
	R	R_1	R_2			C	H	N	S	C	H	N	S
IVa	H	H	H	77	203	63.11	4.02	13.20	—	63.15	4.02	13.00	—
	CH_3	H	H	80	223	64.66	5.00	11.70	—	64.95	4.84	11.96	—
	C_2H_5	H	H	80	213	66.09	5.40	11.01	—	66.49	5.54	11.08	—
IVb	H	CH_3	H	70	191	—	—	12.26	9.31	—	—	12.46	9.49
	CH_3	CH_3	H	82	220	65.59	5.35	11.35	—	65.75	5.20	11.50	—
	C_2H_5	CH_3	H	84	215	—	—	—	8.38	—	—	—	8.14
IVc	H	OCH_3	H	72	184	61.30	4.19	11.68	—	61.18	4.24	11.90	—
	CH_3	OCH_3	H	80	212	—	—	—	8.41	—	—	—	8.39
	C_2H_5	OCH_3	H	76	206	—	—	10.09	—	—	—	10.26	—
IVd	H	H	CH_3	76	205	64.23	4.36	12.28	—	64.09	4.45	12.46	—
	CH_3	H	CH_3	78	228	65.99	5.31	11.31	—	65.75	5.20	11.50	—
	C_2H_5	H	CH_3	75	232	—	—	10.82	8.30	—	—	10.68	8.14

All the compounds (IVa—d) were crystallized from ethanol.

Table 2. Physical constants of I

Sr. No.	Substituents			Yield %	Mp °C	Found %			Calcd %		
	R	R_1	R_2			C	H	N	C	H	N
Ia	H	H	H	73	245	59.65	3.87	14.84	59.31	3.97	15.16
	CH_3	H	H	74	241	70.25	4.32	14.03	70.10	4.47	14.43
	C_2H_5	H	H	80	238	70.64	4.63	13.55	70.81	4.91	13.77
Ib	H	CH_3	H	65	236	70.01	4.26	14.31	70.00	4.46	14.43
	CH_3	CH_3	H	68	234	70.76	4.72	13.56	70.81	4.91	13.77
	C_2H_5	CH_3	H	72	230	71.51	5.23	13.25	71.47	5.32	13.16
Ic	H	OCH_3	H	60	214	66.25	4.35	13.71	66.46	4.23	13.68
	CH_3	OCH_3	H	58	216	67.17	4.52	13.10	67.28	4.67	13.08
	C_2H_5	OCH_3	H	76	212	68.10	5.10	12.32	68.05	5.07	12.53
Id	H	H	CH_3	62	176	70.20	4.25	14.32	70.10	4.46	14.43
	CH_3	H	CH_3	62	175	70.75	4.80	13.87	70.81	4.91	13.71
	C_2H_5	H	CH_3	68	172	71.36	5.31	13.21	71.47	5.32	13.16

All the compounds (Ia—d) were crystallized from toluene.

from 3-(o-Acetamidophenyl)-2-imino-4-phenyl-4-thiazoline (IIIa). 3-(*o*-Acetamidophenyl)-2-imino-4-phenyl-4-thiazoline (IIIa) (0.618 g; 0.002 mol), acetic acid (10 ml) and acetic anhydride (10 ml) were heated under reflux for 2 h. The solution obtained was evaporated to dryness under reduced pressure and the solid residue obtained was recrystallized from ethanol, mp 223 °C, yield 0.500 g. (70%) (Found: C, 64.62; H, 5.13; N, 11.66%. Calcd for $C_{19}H_{17}N_3SO_2$: C, 64.95; H, 4.84; N, 11.96%).

The identity of the compound was confirmed by undepressed mixture mp with the authentic sample obtained by the alternative route described above.

3-Phenyl-(10-substituted)-thiazolo[2,3-d][1,5,3]benzotriazepines (**Ia—d**). *(i) III to I*: 3-(*o*-Acetamidophenyl)-2-imino-4-phenyl-4-thiazoline (0.618 g; 0.002 mol) was refluxed in toluene (20 ml) with a drop of acetic acid for 3 h. The solvent was removed under reduced pressure and the solid residue obtained was recrystallized from toluene to afford I ($R_1=R_2=H$, $R=CH_3$). Yield 0.35 g (60%), mp 241 °C (Found C, 70.30; H, 4.52; N, 14.31%. Calcd for $C_{17}H_{13}N_3S$: C, 70.10, H, 4.47; N, 14.43%).

(ii) II to I: 3-(*o*-Aminophenyl)-2-imino-4-phenyl-4-thiazoline (0.543 g; 0.002 mol), acetic acid (0.12 g; 0.002 mol) were refluxed in toluene (20 ml) for 3 h. After removal of the solvent under reduced pressure, the solid obtained was recrystallized from toluene to afford I ($R_1=R_2=H$; $R=CH_3$), yield 0.42 g (74%); mp 241 °C.

I ($R_1=R_2=H$; $R=CH_3$) obtained from routes (i) and (ii) was identical since its mixed mp was underpressed and superimposable IR spectra were obtained.

All the other derivatives of (Ia—d) were prepared by means of method (ii). The yield, mp and microanalytical data are reported in Table 2.

Salient features of IR spectrum of I ($R_1=R_2=H$; $R=CH_3$) are the absence of original bands at 3260 and 1650 cm^{-1} due to >C=NH and >C=O functions and the presence of >C=N vibrations at 1610 cm^{-1}. Other derivatives of Ia ($R_1=R_2=R=H$) and ($R_1=R_2=H$; $R=C_2H_5$) also show the absence of >C=O and >N-H bands. NMR spectra of Ia ($R_1=R_2=H$; $R=H$) and ($R_1=R_2=H$; $R=CH_3$) show the absence of protons due to amino acid >C=NH functions.

References

1) Part V: M. P. Mahajan, S. M. Sondhi, and N. K. Ralhan, *Bull. Chem. Soc. Jpn.*, **49**, 2651 (1976).

2) S. K. Vasudeva, M. P. Mahajan, and N. K. Ralhan, *Ind. J. Chem.*, **11**, 1204 (1973).

3) Y. Kanaoka, T. Homada, and O. Yonemitsu, *Chem. Pharm. Bull.*, **18**, 587 (1970).

Molecular Rearrangements. VII. *N*-Alkylarylamines (III). Thermal Rearrangement of Secondary Arylamines

A. M. Osman, M.Z.A. Badr,* and A. E. Abdel-Rahman

Chemistry Department, Faculty of Science, Assiut University, Assiut, Egypt, A.R.E.

(Received January 6, 1976)

Heating of *N*-benzyl-*o*- and *p*-toluidines resulted in migration of the benzyl group to the corresponding toluidine nucleus. The pyrolysis of *N*-benzyl-*o*-toluidine produced ammonia, toluene, bibenzyl, *trans*-stilbene, *o*-toluidine together with 4-amino-3-methyldiphenylmethane and 2,3-diphenyl-7-methylindole. *N*-benzyl-*p*-toluidine resulted into the same neutral products together with ammonia, *p*-toluidine, 2,3-diphenyl-5-methylindole together with 2,7-dimethyl-9-phenylacridine. Using phenol or quinoline as solvents, the normal rearranged products were accompanied with 2- and 4-benzylphenols and 2- and 4-benzylquinolines. It was concluded that the pyrolysis of the secondary amines proceeds through their homolytic fission to benzyl and the corresponding toluidino free radicals. Homolysis of some primary products was also observed.

The present paper describes a thermal rearrangement of *N*-benzyl-*o*- and -*p*-toluidines, involding a homolytic fission of the alkyl–*N*-bond. *N*-Benzyl-*o*-toluidine changed on heating in nitrogen atmosphere at about 333 °C to give ammonia, toluene, bibenzyl, *trans*-stilbene, *o*-toluidine, 4-amino-3-methyldiphenylmethane, and 2,3-diphenyl-7-methylindole.

Similarly, *N*-benzyl-*p*-toluidine, under similar conditions at 315 °C, underwent pyrolysis to afford the same neutral products, ammonia, *p*-toluidine, 2,3-diphenyl-5-methylindole and 2,7-dimethyl-9-phenylacridine.

Heating each of *N*-benzyl-*o*- and -*p*-toluidine at its boiling point for several days, gave about the same products but in lower yields, together with some benzaldehyde.

The general feature of this pyrolytic process appears to occur through a mechanism differing in nature from that induced by Lewis acid catalysis.[1]

The formation of toluene, bibenzyl, together with the corresponding toluidines and isomeric diphenylmethylindoles strongly suggests a free radical mechanism.

The homolytic character for the thermal pyrolysis of *N*-alkylarylamines was further confirmed through its study in high boiling solvents and the use of scavengers under nitrogen atmosphere. In phenol, the normal products of the amines rearrangements were obtained together with 2- and 4-benzylphenols. However, in anisole, which underwent preceding pyrolysis, *o*- and *p*-cresols were produced together with phenol, *o*- and *p*-benzylphenols.

The thermal rearrangement of each of *N*-benzyl-*o*- and *p*-toluidines in quinoline gave the normal rearrangement products together with 2- and 4-benzylquinolines, as summarized in Table 1.

Coupling of benzyl radical (I) and toluidino radicals (II) produced the least stericaly hindered isomer, 3-methyl-4-aminodiphenylmethane, from *N*-benzyl-*o*-toluidine. However, from *N*-benzyl-*p*-toluidine, 2-amino-5-methyldiphenylmethane was not separated but most favorably consumed, after its preliminary production, into the formation of 2,7-dimethyl-9-phenylacridine as final product according to the following scheme.

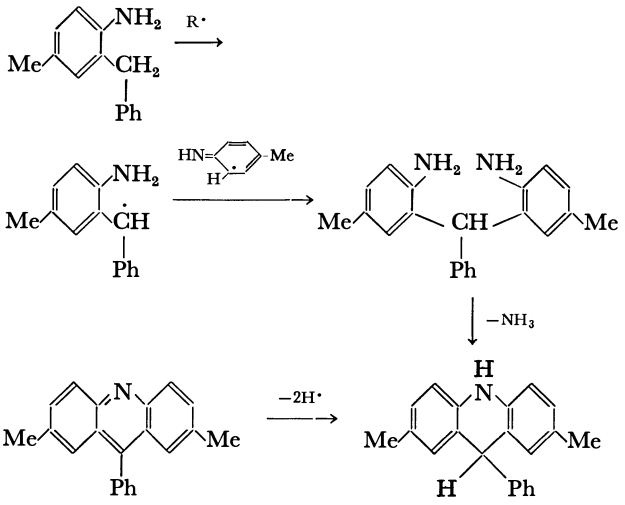

Heating *o*- or *p*-toluidine alone in a sealed tube at about 315—330 °C for 12 days had resulted in the formation of ammonia.

Consequently, ammonia was assumed to be partially formed through intermediate formation of amino free radical[2] and tolyl radical as observed in isomeric toluidines pyrolysis under the rearrangement conditions.

The formation of both isomeric 2,3-diphenyl-7-methylindole (III) and 2,3-diphenyl-5-methylindole (IV) can be explained according to the following scheme:

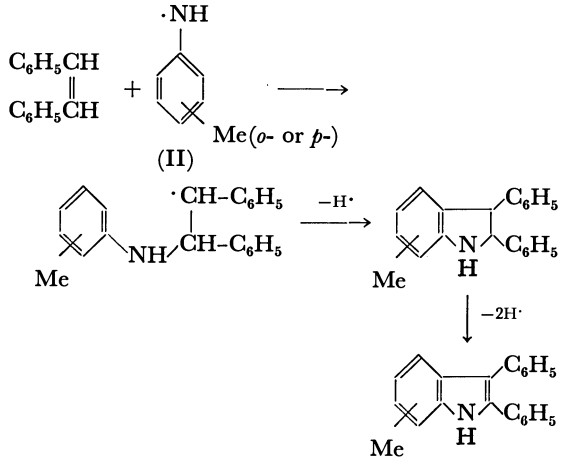

III and IV

* To whom correspondance should be addressed.

Table 1. Products of pyrolysis of *N*-benzyl-*o*- and *p*-toluidines

Exp. No.	Condition: Solvent (g)	Condition: Temp (°C)	Condition: Time (day)	Amine (g): Isomer	Amine (g): Used	Amine (g): Consumed	Products (g): Ammonia	Toluene 110—112°C	Bibenzyl 118—125°C/5 mmHg	Stilbene	Toluidine 72—77°C/5 mmHg	Benzyltoluidine 155—158°C/4 mmHg	Diphenylmethylindole 205—210°C/4 mmHg	Benzyl derivative
1		Reflux	46[e,i]	*o*-	40	28	Exist	0.08	0.2	Trace	5[b]	1.2[h]	1.5[t]	—
			15[e,ii]	*p*-	40	23	Exist	0.1	0.2	Trace	5[d]	—[m,i]	6.0[g]	—
2		330	12	*o*-	40	34	Exist	7.3	0.5	Trace	10[c]	1.1[h]	—	—
		315	12	*p*-	40	31	Exist	3.5	1.7	Trace	5.2[d]	—[m,ii]	1.0[g]	—
3[b]	Phenol (11)	330	12	*o*-	40	37	Exist	3.2	0.5	Trace	8[c]	1.3[h]	0.7[k]	3.1[l,i]
		315	12	*p*-	40	32	Exist	3.0	0.4	Trace	7[d]	—[m,iii]	3.0[g]	1.5[l,ii]
4[b]	Anisole(11)	330	12	*o*-	40	36	Exist	6.3	0.3	Trace	9[c]	4.0[h]	0.5[k]	—[l,i]
		315	12	*p*-	40	34	—[j]	3.5	0.1	Trace	6[d]	—[m,iv]	1.7[g]	—[l,ii]
5[b]	Quinoline(15)	330	12	*o*-	40	37	Exist	8.3	0.3	Trace	8[c]	1.8[h]	0.3[k]	1.5[n,i]
		315	12	*p*-	40	38	Exist	3.2	0.2	Trace	7[d]	—[m,v]	1.1	2.7[n,ii]

a) Benzyl derivative of solvent used. b) In nitrogen atmosphere. c) *o*-Toluidine. d) *p*-Toluidine. e) Benzaldehyde was separated and identified. (i) 0.7 g. (ii) 0.5 g. f) 2,3-Dimethyl-7-methylindole. g) 2,3-Diphenyl-5-methylindole. h) 4-Amino-3-methyldiphenylmethane. (i) Identified by paper chromatography as mixture of benzylphenols and by GLC analysis, (i) in ratio of (76.3%) *o*- and (23.7%) *p*-isomers; (ii) in ratio of (89.5%) *o*- and (10.5%) *p*-isomers. (j) Methylamine collected as hydrochloride salt. k) Colorless plates, mp 181—182 °C, IR spectrum showed an absorption at 3450 cm^{-1} (NH), not farther identified. l) Identified as phenols mixture, (i) yield (2.3 g.) in ratio of (67.3%) phenol and (32.7%) cresols, in ratio of *o*-cresol (95.7%) and *p*-cresol (4.3%), (ii) yield (1.1 g.) in ratio of (65.7%) phenol and (34.3%) cresols, in ratio of *o*-cresol (83.1%) and *p*-cresol (16.9%), together with benzylphenols (1.1 g) in ratio of (94.8%) *o*- and (5.2%) *p*-isomers. m) 2,7-Dimethyl-9-phenyl-acridine, collected at bp 230—240 °C/mmHg; M^+ *m/e* 283, (Found: C, 88.9; H, 6.2; N, 4.9%. Calcd for $C_{21}H_{17}N$: C, 89; H, 6; N, 5%) (i) 2.1 g, (ii) 0.7 g, (iii) 0.5 g, (iv) 1 g, (v) 0.2 g. n) Identified by TLC as mixture of 2- and 4-benzylquinolines and by GLC analysis to be (i) in ratio of (44%) 2- and (56%) 4-isomer, (ii) in ratio of (42%) 2- and (58%) 4-isomers.

trans-Stilbene could be resulted by radical abstraction of the methylene hydrogens from bibenzyl.

In anisole separation of *o*- and *p*-benzylphenols instead of benzylanisoles during amines rearrangement insures that anisole had rearranged under such conditions prior to substitution step by benzyl radical.

Migration of the methyl group of anisole was assumed to go through an intramolecular route, which was confirmed by absence of any other methyl derivative, together with the separation of higher yields of *o*-cresol. However, formation of *p*-cresol partially through an intermolecular migration of the methyl group within a solvent cage[3] could not be excluded.

Similarly, methylamine was expected to be formed intermolecularly, from *p*-toluidino radical and the methyl radical from anisole, through *N*-methyl-*p*-toluidine as preliminary product, which undergoes pyrolysis homolytically[4] into *p*-tolyl radical and methylamino radicals, the latter of which gives methylamine. However, methylamine formation was not observed in *N*-benzyl-*o*-toluidine pyrolysis with anisole.

Thermal rearrangement of either of *N*-benzyl-*o*- and -*p*-toluidines in quinoline gave the normal rearrangement products together with 2- and 4-benzylquinolines in a ratio similar to that obtained in the pyrolysis of benzyl naphthyl ethers[5] or *N*-benzyl-*N*-methylaniline[2] with quinoline as solvent, justifying the similarity in nature of all such types of rearrangements.

Experimental

Analysis. IR spectra were measured with a Pye-Unicam IR spectrophotometer, Model SP 200 g. The UV absorptions were carried out by a Pye-Unicam UV spectrophotometer, Model SP 8000. GLC analysis was carried out by a Pye-Unicam gas chromatograph, "series 104" dual flame ionization detector, temperature programed, Model 24. The column used was 20% SE 30 on chromosorb W (35—80 mesh). Thin layer chromatographic analysis of benzylquinolines was carried out on silica gel (25—40 mesh) using hexane–ethyl acetate (3:7 by vol.); paper chromatographic analysis of benzylphenols was carried out using C. Schleicher and Schull paper No. 2816, using 1-butanol–water–ethanol mixture (5:5:1.7 by volume) as eluent. Mass spectral measurements were recorded on both, varian MAT CH-4, and AEI MS-9 mass spectrometers at 70 eV.

Pyrolysis of Each of N-*Benzyl*-o- *and* -p-*toluidines.* Heating each of *N*-benzyl-*o*-toluidine for 10 days at 320 °C and *N*-benzyl-*p*-toluidine for 10 days at 310 °C in sealed tubes, not resulted in their pyrolysis. However, heating each of the secondary amines at elevated temperatures and for the periods as specified in Table 1, either alone or with phenol, anisole or quinoline in nitrogen atmosphere and the reaction products were distilled first under atmospheric pressure where ammonia was evolved and trapped as its hydrochloride, and toluene collected. The higher boiling products were separated into neutral and amine fractions by treatment with

concd HCl and extraction with ether.

Phenolic products were separated by means of Claisen's solution. The results are summarized in Table 1.

Preparation of Reference Compounds.

N-*Benzyl*-o-*toluidine*[6]: Bp 158—160 °C/5 mmHg; mp 56—57 °C.

N-*Benzyl*-p-*toluidine*[7]: Bp 160—162 °C/4 mmHg; n_D^{30}: 1.5985.

2-*Benzylphenol*[8]: Bp 170—180 °C/15 mmHg; phenylurethane derivative, mp 117 °C.

4-*Benzylphenol*[9]: Bp 170—180 °C/14 mmHg; mp 84 °C; benzoate, mp 87 °C.

2-*Benzylquinoline*[10]: Bp 235—240 °C/19 mmHg; picrate, mp 156—157 °C.

4-*Benzylquinoline*[11]. Bp 230 °C/17 mmHg; picrate, mp 178—179 °C.

trans-*Stilbene*[12]. Mp 123—124 °C.

Bibenzyl[13]. Mp 52—53 °C; 4,4′-dinitro derivative, mp 180 °C.

2,3-*Diphenyl*-5-*methylindole*[14]. Mp 153—154 °C.

2,3-*Diphenyl*-7-*methylindole*[15]. Mp 128—129 °C.

4-*Amino*-3-*methyl*-*diphenylmethane*[16]: Bp 160—162 °C, mp 63—64 °C; picrate, mp 181—182 °C, benzyl derivative, mp 135—136 °C.

2,7-*Dimethyl*-9-*acridine*[17]: Mp 171—172 °C; picrate, mp 267—268 °C.

References

1) A. W. Hofman and C. A. Martius, *Ber.*, **4**, 742 (1871); J. Reilly and W. J. Hickinbottom, *J. Chem. Soc.*, **117**, 103 (1920); A. Micheel, *Ber*,. **14**, 2105, (1881); *J. Chem. Soc.*, **42**, 787 (1920); W. J. Hickinbottom, *J. Chem. Soc.*, **117**, 103 (1920); A. Micheel, *Ber.*, **14**, 2105 (1881); *J. Chem. Soc.*, **42**, 787 (1920); W. J. Hickinbottom, *J. Chem. Soc.*, **1934**, 1700.

2) N. J. Freswell and B. G. Gowenlock, "Advances in Free Radical Chemistry," ed. by G. H. Williams, Vol. II, Academic Press, London (1967), pp. 1—5.

3) Y. Ogata and K. Takagi, *J. Org. Chem.*, **35**, 1644, (1970).

4) M. Z. A. Badr and M. M. Aly, *Can. J. Chem.*, **52**, 293 (1974).

5) M. Z. A. Badr and M. M. Aly, *Tetrahedron*, **28**, 3401 (1972); M. Z. A. Badr and H. A. H. El-Sherief, *Can. J. Chem.*, **50**, 259 (1972).

6) a) C. Courtot and P. Petitcolas, *Bull. Soc. Chim. Fr.*, **39**, 452 (1925); b) H. Law, *J. Chem. Soc.*, **101**, 158 (1912).

7) R. E. Davies, H. T. O. Penshaw, F. S. Spring, and A. R. Todd, *J. Chem. Soc.*, **1948**, 295.

8) F. M. Elkobaisi and W. J. Hickinbottom, *J. Chem. Soc.*, **1959**, 1873.

9) R. C. Huston, *J. Am. Chem. Soc.*, **46**, 2775 (1924).

10) H. Decker and R. Poschorr, *Ber.*, **39**, 3400 (1904).

11) I. P. Rabe and R. Pasternack, *Ber.*, **46**, 1026 (1913).

12) D. A. Baffard and W. M. Dehn, *J. Am. Chem. Soc.*, **54**, 3969 (1932).

13) S. Cannizzaro and A. Rossi, *Ann.*, **121**. 251 (1862).

14) R. Japp, T. Murray, *Ber.* **26**, 2039 (1893).

15) R. Japp, T. Murray, *Ber.*, **26**, 2641 (1893).

16) F. D. Chattaway and W. H. Lewis, *J. Chem. Soc.*, **85**, 590 (1904).

17) J. M. Birehell and D. H. Thorpe, *J. Chem. Soc.*, **1968**, 2900.

The Preparation of Tetramethylphthalic Anhydride[1)]

Koji CHIBA, Eiji ENDO, Tokio SAKAMOTO, Eiji SATO, Ryoichi FUKUHARA, and Toshiko KOBAYASHI

Department of Applied Chemistry, Faculty of Engineering, Yamagata University, Yonezawa-shi, Yamagata 992

(Received April 23, 1976)

The alkaline hydrolysis of bis(nitromethyl)prehnitene (**1**) with aqueous sodium hydroxide gave almost quantitatively disodium tetramethylphthalate (**11**). Under milder conditions the sodium salts of tetramethylphthalimide (**8**), *N*-hydroxytetramethylphthalimide (**10**), and 2-hydroxy-3-hydroxyimino-4,5,6,7-tetramethylphthalimide (**9**) were formed, probably as intermediate products of the above reaction. But, pentamethylphenylnitromethane (**14**) and bis(nitromethyl)isodurene (**15**) were not hydrolyzed in an aqueous base. From the above results, it is recognized that the sodium nitronate from **1** is unstable in a different way from general nitronates such as the sodium salt of **14** or **15**. It appears that the instability of **1** arises from the two adjacent nitromethyl groups on the benzene ring.

Phthalic anhydride is used chiefly in the manufacture of alkyd resins, plasticizers, dyes, and pigments. Also, tetrachlorophthalic anhydride is commercially available in heat-stable alkyd resins, dye intermediates, *etc.* Similarly, if polymethylphthalic anhydride could be easily prepared, it would have many uses. But phthalic anhydride is a very unreactive compound with respect to alkylation. Also, tetramethylphthalic anhydride (**13**) or acid is hard to obtain from hexamethylbenzene by the selective oxidation.[2)]

We have previously reported that bis(nitromethyl)-prehnitene (**1**) was obtained by the nitration of hexamethylbenzene with benzoyl nitrate by Willstätter's method.[3,4)] In the present paper, the reaction of **1** with an aqueous base was studied, and a useful procedure for preparing **13** was found.

Hitherto, many studies of the acid hydrolysis of nitroalkanes have been reported. For example, the acid hydrolysis of a salt of a primary or secondary nitroalkane affords an aldehyde or a ketone, respectively, and nitrous oxide (Nef reaction).[5,6)] Closely related to the Nef reaction is the hydrolysis of free primary nitroalkanes with concentrated mineral acid to the corresponding carboxylic acids and hydroxylamine salts.[7)] It is considered that the above reactions of nitroalkanes require an initial acid-catalyzed isomerization to nitronic acid.[8)] But no reports of the alkaline hydrolysis of a salt of a nitroalkane or free nitroalkane seem to have been made.

Results and Discussion

1 was treated with 5% sodium hydroxide at 75 or 100 °C. By addition of silver nitrate solution to the resulting solution, the products were isolated as their silver salts, which were treated with methyl iodide. From the methylated reaction mixture, *N*-methyltetramethylphthalimide (**8'**), 2-methoxy-3-methoxyimino-4,5,6,7-tetramethylphthalimidine (**9'**), *N*-methoxytetramethylphthalimide (**10'**), and dimethyl tetramethylphthalate (**11'**) were isolated by column chromatography. Further, from the reaction mixture in an early stage a trace of methyl 2-cyano-3,4,5,6-tetramethylbenzoate (**12'**) was also isolated.

The reaction was followed by measuring the yields of these products. The results are given in Table 1. Under milder conditions **8'**, **9'**, and **10'** were obtained (Expt. No. 1). But, on continued warming, they rapidly decreased, whereas **11'** increased. Finally, an almost quantitative yield of **11'** was obtained.

TABLE 1. REACTION OF BIS(NITROMETHYL)PREHNITENE WITH AN AQUEOUS SODIUM HYDROXIDE

Expt. No.	Conditions		Yields (mol %)[a)]				
	Temp (°C)	Time (min)	**8'**	**9'**	**10'**	**11'**	Unknowns (wt %)
1	75	10	14	2	13	49	8
2	100	15	2	—	15	64	10
3	100	30	—	—	10	77	—
4	100	5 h	—	—	—	97	—

a) The yields were determined by GLC after the products were methylated by warming their silver salts in methyl iodide.

On the other hand, after **1** was treated with 5% sodium hydroxide at 100 °C for 9.5 h, the acidification of the hydrozate with diluted hydrochloric acid gave almost quantitatively tetramethylphthalic anhydride (**13**). The filtrate reduced Fehling's solution. This fact suggested that the hydroxylamine salt was produced, but further investigations were not carried out. Also, when **1** was treated with 10% sodium hydroxide, almost similar results were obtained. But, when pentamethylphenylnitromethane (**14**) or bis(nitromethyl)isodurene (**15**) was treated with 5% sodium hydroxide at 100 °C for 10 h, the acidification of the resulting solution with hydrochloric acid gave unreacted **14** or **15** only. Moreover, upon treatment with 35% hydrochloric acid at 100 °C for 5 h in a sealed tube, **1** was recovered unchanged.

From the above results, it is recognized that the sodium nitronate (**2**) from **1** is unstable in a different way from general nitronates such as the sodium salt of **14** or **15**, and so the conversion of **1** to the phthalate (**11**) does not require the initial isomerization to the free nitronic acid. It appears that the instability of **1** arises from the two adjacent nitromethyl groups on the benzene ring.

A plausible reaction path is shown in the following scheme. But there is no evidence pertaining to the mechanism of conversion of nitronate to hydroxamate.

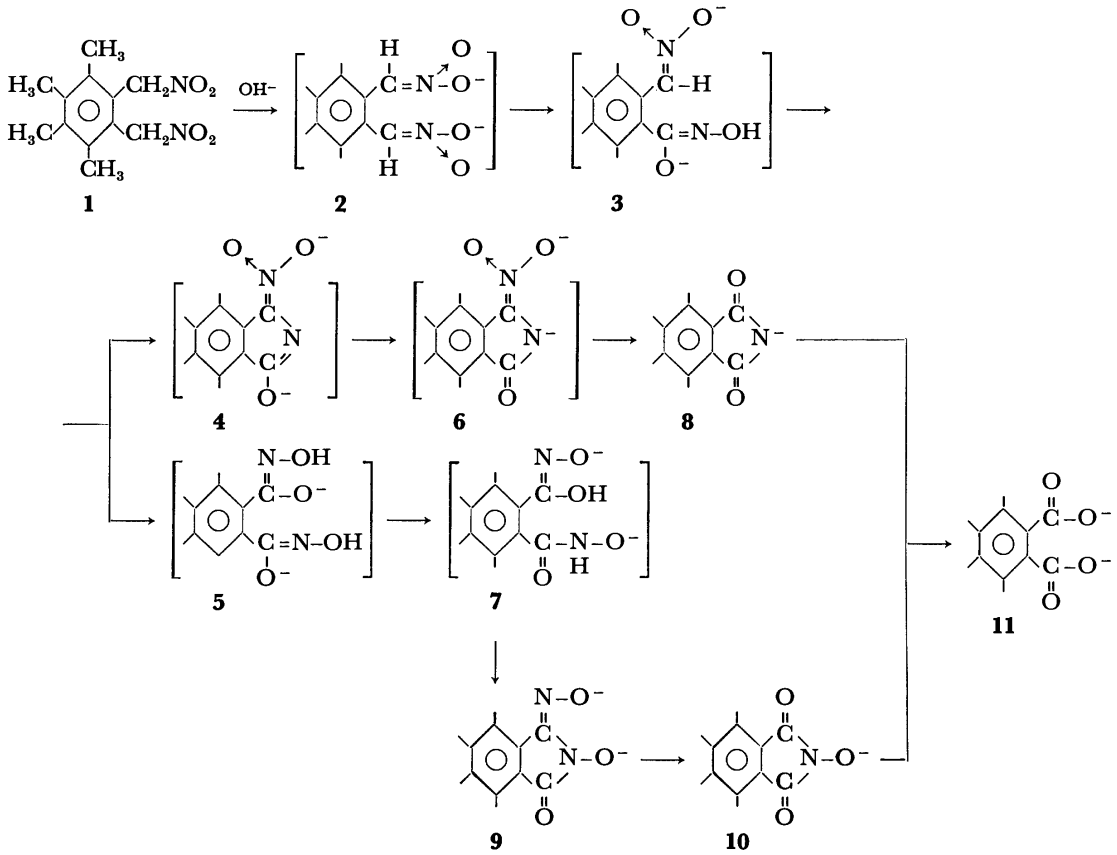

Scheme 1.

Disodium tetramethylphthalate (**11**) is easily converted to **13** by acidification, probably since the steric repulsion of four methyl groups on the benzene ring facilitates the cyclization between two carboxyl groups. The phthalic acid could not be isolated. Similarly, the hydroxamate **3** or **7** would be easily converted to the cyclized product **4** or **9**, respectively, which is finally hydrolyzed to produce **11**. But it is not clear which is chosen more preferentially as an intermediate, sodium tetramethylphthalimide (**8**) or sodium *N*-hydroxytetramethylphthalimide (**10**).

Experimental

Analyses. All melting points are uncorrected. IR spectra were recorded by means of a Hitachi EPI-S2 spectrometer, while NMR spectra were obtained by a Hitachi R-22 NMR spectrometer at 90 MHz, using tetramethylsilane as an internal standard. The GLC analyses were carried out on a Hitachi 063 apparatus, using Silicone DC 550 (25%)-Celite 545 (4 mm×1 m) columns (Temp: 215 °C; Carrier gas: H_2 40 ml/min).

Materials. **1**, **14**, and **15** were obtained by the nitration of hexamethylbenzene with acetyl nitrate according to the following method.

Fuming nitric acid (30 g, d=1.5) was added over a period of 0.5 h to vigorously stirred acetic anhydride (150 ml), keeping the temperature between 15 and 20 °C by the use of an ice bath. The resulting solution was added to a solution of hexamethylbenzene (14.0 g) in carbon tetrachloride (150 ml), and stirred at about 5 °C for 2 h. The reaction mixture was poured into water (450 ml). The organic layer was separated and washed with dilute sodium carbonate and then with water. Concentration and cooling of the solution yielded a white crystalline solid. Its chromatography (7.2 g) on silica gel gave **14** (0.2 g, mp 85—87 °C; lit,[10] 86—88 °C) from the light petroleum eluates; **1** (6.5 g, mp 139—140 °C; lit,[3] 139 °C) and **15** (0.2 g) from the benzene elutes. **1** and **4** were identified by comparison of these IR and NMR spectra with those of authentic samples. The structure of **15** was deduced from elemental analysis and spectral data.

15: colorless needles, mp 146—147 °C. Found: C, 56.83; H, 6.57; N, 10.96%. Calcd for $C_{12}H_{16}N_2O_4$: C, 57.13; H, 6.39; N, 11.10%. IR (KBr, cm^{-1}): 1542 and 1386 ($-NO_2$). NMR ($CDCl_3$, δ ppm): 2.29 (s, Ar–CH_3, 3H), and 5.75 (s, –C-H_2–, 4H).

General Procedures. **1** (0.100 g) was treated with 5% sodium hydroxide (15 ml) at 75 or 100 °C in a sealed tube. The resulting solution was cooled to room temperature, and treated with a large excess of silver nitrate solution (4.0 g/20 ml). After cooling, the precipitate was collected by filtration, dried, and refluxed with methyl iodide (1 g) in benzene (50 ml) for 6 h. An insoluble material was filtered off, and the filtrate was evaporated to dryness under reduced pressure.

Isolation of the Products. The following example shows a typical experimental procedure (Expt. No. 1, Table 1).

The residue (0.1 g) obtained by the evaporation of the above filtrate was chromatographed on a column (1×12 cm) of alumina (10 g, 200—300 mesh) and eluted successively with petroleum ether (50 ml), petroleum ether–benzene (1: 1, 100 ml), benzene (50 ml), benzene–diethyl ether (1: 1, 100 ml), diethyl ether (50 ml), and diethyl ether–methanol (100 ml). Each fraction was evaporated, and the residue was recrystallized from methanol to afford the following products successively: *N*-methyltetramethylphthalimide (**8'**), dimethyl tetrameth-

ylphthalate (**11′**), 2-methoxy-3-methoxyimino-4,5,6,7-tetramethylphthalimidine (**9′**), and *N*-methoxytetramethylphthalimide (**10′**). **8′**, mp 180—181 °C, was identified by comparison with the IR and NMR spectra of an authentic sample.[9] The structures of **9′**, **10′**, and **11′** were deduced from their elemental analyses and spectral data.

9′: colorless prisms, mp 156—158 °C. Found: C, 64.61; H, 7.06; N, 10.73%. Calcd for $C_{14}H_{18}N_2O_3$: C, 64.10; H, 6.92; N, 10.68%. IR (KBr, cm^{-1}): 1725 (C=N), 1637 (C=N), 1265, 1146, 1121, 1037, 994, and 932 (C–N, C–O or N–O). NMR ($CDCl_3$, δ ppm): 2.15 (d, Ar–CH_3, 6H), 2.50 (d, Ar–CH_3, 6H), and 4.04 (d, O–CH_3, 6H).

10′: colorless needles, mp 203—204 °C. Found: C, 67.15; H, 6.32; N, 6.18%, mol wt (Rast), 236. Calcd for $C_{13}H_{15}NO_3$: C, 66.93; H, 6.48; N, 6.01%; mol wt, 223. IR (KBr, cm^{-1}): 1760, 1719 (C=O), 1254, 1146, 1102, 998, and 905 (C–N, C–O, or N–O). NMR ($CDCl_3$, δ ppm): 2.24 (s, Ar–CH_3, 6H), 2.56 (s, Ar–CH_3, 6H), and 4.00 (s, O–CH_3, 3H).

11′: colorless plates, mp 127.5—128.5 °C. Found: C, 66.95; H, 7.33%. Calcd for $C_{14}H_{18}O_4$: C, 67.10; H, 7.25%. IR (KBr, cm^{-1}): 1724 (C=O), 1233, and 1162 (C–O–C). NMR ($CDCl_3$, δ ppm): 2.25 (Ar–CH_3, 6H), 2.35 (Ar–CH_3, 6H), and 3.85 (–OCH_3, 6H).

Further, from the reaction mixture in an early stage (Expt. No. 1) a trace of **12′**, mp 75—76 °C, was also isolated; it was identified by comparing its retention time in GLC and its IR spectrum with those of an authentic sample.[9]

The progress of the reactions was followed by GLC. The results are shown in Table 1. The yields of products were caculated by assuming that the ratio of the peak areas was identical with the weight ratio of the products. Here, the peak of **8′** overlapped with that of **11′**, and so, if necessary, the ratio of **8′** to **11′** was derived from the result of the column chromatography.

*Preparation of Tetramethylphthalic Anhydride (**13**).* To 5% sodium hydroxide (50 ml), **1** (1.00 g) was added, and the mixture was stirred at 100 °C for 9.5 h. The reaction mixture was cooled to room temperature, and acidified by the addition of 2M hydrochloric acid. The resulting white precipitate was collected by filtration, dried (0.77 g, 95 mol % as **13**), and recrystallized from benzene: colorless needles, mp 238—239 °C. Found: C, 70.70; H, 5.81%; mol wt (Rast), 200. Calcd for $C_{12}H_{12}O_3$: C, 70.61; H, 5.88%; mol wt, 204. IR (KBr, cm^{-1}): 1834, 1767 (C=O), 1200, and 910 (C–O). NMR ($CDCl_3$, δ ppm): 2.3 (Ar–CH_3, 6H) and 2.6 (Ar–CH_3, 6H).

Further, **13** (0.4 g) was dissolved in 2 M sodium hydroxide (30 ml), and the solution was treated with excess silver nitrate solution. The resulting precipitate was collected by filtration, dried, and refluxed with excess methyl iodide (1.5 ml) in benzene (30 ml) for 4 h. After filtration of the insoluble materials, the filtrate was evaporated, and the residue was recrystallized from methanol to afford **11′** (0.3 g) as colorless plates.

The authors would like to express their thanks to Professor Shunroku Kanno of Yamagata University for his advice, and to Professor Tadashi Yamaguchi of Tohoku University and Professor Shigeru Hayama of Yamagata University for the elemental analyses.

References

1) Studies on the Oxidation of Hexamethylbenzene. Part III; Part II: K. Chiba and S. Tomura, *Nippon Kagaku Kaishi*, **1973**, 2188.
2) K. Chiba, S. Tomura, and Y. Mizuno, *Nippon Kagaku Kaishi*, **1973**, 1959.
3) R. Willstätter and H. Kubli, *Ber.*, **42**, 4163 (1909).
4) K. Chiba and E. Sato, *Nippon Kagaku Kaishi*, **1973**, 1249.
5) J. U. Nef, *Ann.*, **308**, 264 (1899).
6) W. E. Noland, *Chem. Rev.*, **55**, 137 (1955).
7) S. B. Lippincott, *Ind. Eng. Chem.*, **31**, 118 (1939).
8) H. Feuer, "The Chemistry of the Nitro and Nitroso Groups," Part 1, Interscience, New York (1969), p. 349.
9) K. Chiba, E. Endo, and K. Yamaka, *Bull. Chem. Soc. Jpn.*, **48**, 743 (1975).
10) H. Suzuki, *Bull. Chem. Soc. Jpn.*, **43**, 879 (1960).

NOTES

BULLETIN OF THE CHEMICAL SOCIETY OF JAPAN, VOL. 49 (9), 2617—2618 (1976)

Solvation of Metal Acetylacetonate in Organic Solvents

Fumio KAWAIZUMI, Norifumi MATSUMIYA, and Yutaka MIYAHARA

Department of Chemical Engineering, Faculty of Engineering, Nagoya University, Chikusa-ku, Nagoya 464

(Received February 6, 1976)

Synopsis. The velocities of ultrasonic waves in solutions of metal acetylacetonate in organic solvents were measured with an ultrasonic interferometer operating at 4MHz at 5 and 15 °C. The solvation behavior was marked in the [Mg(acac)$_2$]-methanol system. The results are compared with those of such different methods as IR and NMR spectroscopies.

The behavior of metal acetylacetonates in organic solvents has been the subject of considerable interest in various areas. Many of the experimental results of the metal acetylacetonates in solution have been interpreted on the basis of the hydrogen-bonding between the complexes and the solvent, or of the hydration/solvation of the complexes.[1-4] For example, Yamamoto *et al.* have related the heat of solution of cobalt(III) acetylacetonate in alcohols and in water to solvation phenomena of the solute.

In relation to our previous study of the hydration of cobalt and iron complexes in aqueous media,[5] metal acetylacetonates attract our attention because of the following facts; they are large complexes without electric charge and the acetylacetones coordinated to the central metal atom sterically hinder the approach of the solvent molecules. The lack of electric charge and the steric hindrance are the unfavorable factors for electrostrictive solvation.

The present study deals with the determination of the degree of solvation of such acetylacetonates as [Be(acac)$_2$], [Mg(acac)$_2$], and [Co(acac)$_3$] in various organic solvents. The same study in aqueous solutions will also be necessary, but is impossible owing to the insufficient solubility of the complexes. The degree of solvation was determined from the adiabatic compressibilities of the solutions. It should be kept in mind that in the present method the term "solvation" means the existence of a certain incompressible region in the solution, while the bulk solvents in solution are assumed to be compressible.

All of the metal acetylacetonates are those commercially available and were used without further purification, except for [Be(acac)$_2$], which was purified once from a solution in acetone. The organic solvents used were acetone, acetylacetone, benzene, methanol, and chloroform. The first three solvents were purified by distillation after suitable treatments. Methanol and chloroform were of guaranteed and spectral grades, respectively.

The adiabatic compressibilities of the solutions were obtained by measurement of the ultrasonic velocities using an ultrasonic interferometer operating at 4 MHz. Details of the experimental apparatus and the method of determination of the solvation number are essentially the same as before.[5,6] Preliminary experiments revealed that as expected, [Co(acac)$_3$] is not solvated in benzene at 30 °C. Measurements were therefore carried out at 15 and 5 °C. But the experiments at 5 °C were very limited by the low solubilities of the metal acetylacetonates at this temperature.

The results are summarized in Table 1, where K_m is the (relative) partial molar compression of the solute and the subscript zero refers to infinite dilution. For $K_m > 0$, K_m becomes the molar solvation volume (cm^3/mol). For $K_m < 0$, it signifies the non-existence of an incompressible region in the solution and in this case, the values of K_m represent the quantities related to the compressibility of the solute in solution.[7] In the present paper, however, the cases of negative values of K_{m0} will be excluded from the discussion below.

TABLE 1. K_{m0} (ml/mol) FOR THE METAL ACETYLACETONATES

		[Be(acac)$_2$]	[Co(acac)$_3$]	[Mg(acac)$_2$]
5 °C	CH_3OH	10	35	102
	CH_3COCH_3	(−66)	—	—
	$CHCl_3$	(−113)	(−199)	—
15 °C	CH_3OH	(−11)	0	53
	CH_3COCH_3	(−17)	0	—
	$CHCl_3$	(−154)	(−160)	—
	$CH_3COCH_2COCH_3$	(−143)	(−96)	—
	C_6H_6	(−122)	−126)	—

Table 1 shows that only methanol can solvate with metal acetylacetonates and that solvation to [Mg(acac)$_2$] is more marked than to [Be(acac)$_2$] and [Co(acac)$_3$]. The solvation numbers calculated from the posivite values of K_{m0} are shown in Table 2.

TABLE 2. SOLVATION NUMBER IN METHANOL (mol/mol)

	[Be(acac)$_2$]	[Co(acac)$_3$]	[Mg(acac)$_2$]
5 °C	0.2	0.8	2.6
15 °C	N.S.	N.S.	1.3

N.S.: non-solvated

The results for the solutions in benzene are reasonable, since benzene can hardly solvate under ordinary conditions.

The present results in methanol and in chloroform are compared with those given by the different methods. The IR spectra obtained by Davis and Fackler,[2] using deuteriochloroform ($CDCl_3$) in carbon tetrachloride and methanol in carbon tetrachloride as the solvents, give an indication that no or very weak hydrogen-bonding occurred with the tetrahedral bis metal ketoenolate complexes, like [Be(acac)$_2$], that stronger hydrogen-

bonding to the planar bis complexes occurred and that for tris complexes the interaction occurred with both deuteriochloroform and methanol. In addition, from NMR techniques, the hydrogen-bonding interaction of $[Co(acac)_3]$ and $[Cr(acac)_3]$ with the solvent in the mixture of chloroform and carbon tetrachloride was observed.[3] The vapor pressure measurement showed that the rareearth acetylacetonates form disolvate with methanol but not with chloroform.[8]

For the solvent methanol, all of these results, together with the present work, agree with one another, whereas some disagreements exist for $[Co(acac)_3]$ and the solvent chloroform. These disagreements arise partially from the fact that the hydrogen-bonding interactions detected by IR and NMR spectroscopies are not always strong enough to correspond to the formation of an incompressible region in the solution or of the solvate in solid form.

The solvation numbers for $[Mg(acac)_2]$ given in Table 2 suggest that the solvated methanol occupies the two vacant sites on the opposite side of the planar structure of the complex. According to the model of Davis and Fackler,[2] chloroform and methanol can form hydrogen-bonding to the oxygen atoms of the chelate in bis metal β-ketoenolate, but the present work does not give any direct information of the position of the solvated methanol.

References

1) P. D. Hopkins and B. E. Douglas, *Inorg. Chem.*, **3**, 357 (1964).
2) T. S. Davis and J. P. Fackler, Jr., *Inorg. Chem.*, **5**, 242 (1966).
3) L. S. Frankel, C. H. Langford, and T. S. Stengle, *J. Phys. Chem.*, **74**, 1376 (1970).
4) T. Tarumoto and Y. Yamamoto, *Chem. Lett.*, **1973**, 7.
5) F. Kawaizumi and Y. Miyahara, *Bull. Chem. Soc. Jpn.*, **44**, 1979 (1971) and the references cited therein.
6) F. Kawaizumi, H. Nomura, and Y. Miyahara, *Nippon Kagaku Zasshi*, **87**, 939 (1966).
7) H. Nomura and Y. Miyahara, *J. Appl. Polym. Sci.*, **8**, 1643 (1964).
8) G. W. Pope, J. F. Steinbach, and W. F. Wagner, *J. Inorg. Nucl. Chem.*, **20**, 304 (1961).

BULLETIN OF THE CHEMICAL SOCIETY OF JAPAN, VOL. 49 (9), 2619—2620 (1976)

Hartree-Fock-Slater Calculations of the ESCA Chemical Shifts for Transition Metal Atoms

Kazuyuki TATSUMI and Takayuki FUENO

Department of Chemistry, Faculty of Engineering Science, Osaka University, Toyonaka, Osaka 560

(Received February 26, 1976)

Synopsis. Hartree-Fock-Slater calculations have been carried out for inner-shell orbitals of some transition metal atoms (Ni, Rh, and Pt), and the core ionization energies computed by the transition state approximation. It is found that the ionization energy shifts do not conform to the conventional charge-potential approximation; the electron populations in individual valence d and s orbitals need to be considered separately.

Recent developments in X-ray photoelectron spectroscopy (ESCA) have supplied a great amount of information on core-electron binding energies in atoms and molecules. The changes in the core-electron ionization potentials of an atom in given molecules relative to an appropriate standard are designated as chemical shifts. Siegbahn *et al.*[1] proposed that the shifts in ionization potential ΔE_i^A for core orbital i of atom A are related to the corresponding changes in atomic charge ΔQ_A by

$$\Delta E_i^A = k_i^A \Delta Q_A + \Delta V_A \qquad (1)$$

where k_i^A is an adjustable parameter and the term ΔV_A denotes the change in the Coulomb potential at A due to the other atoms in the molecule. Implicit in Eq. 1 is the assumption that the core binding energy is a function of the initial state of the molecule; the reorganization energy upon ionization is assumed to be independent of the identity of atoms as long as they are in similar bonding environments. The charge-potential formula (1) has been applied extensively to series of compounds comprising first and second row atoms.[2] However, extention of the treatment to transition metal compounds is still lacking because of the great complexity of their bonding properties.

In the present article, we will deal with the core ionization potential shifts of transition metal atoms (Ni, Rh, and Pt) as well as some light atoms (C, N, and F) as the functions of atomic charge. The Hartree-Fock-Slater calculations have been carried out for these isolated atoms using the numerical technique. The transition state model[3] was employed to compute the energy difference between the ground state and an ionized state. The results justify the conventional charge-potential approximation for the case of light atoms but decisively indicate its breakdown for the transition metal atoms.

Method

The radial part of the Hartree-Fock wave equation for electrons in a free atom or ion has been solved numerically by Slater's X_α method.[4] A general procedure for numerical integrations as outlined by Pratt[5] was followed. The "exchange scaling parameter" α was chosen so that the statistical X_α total energy equals the configuration-averaged Hartree-Fock energy.[6]

In obtaining the ionization energies, we have invoked the concept of the "transition state," a hypothetical state of an atom or a molecule in which it is assumed that half an electron has been removed from the orbital in question.[4] The ionization energy E_i associated with the ith orbital is thus the negative of the ith one-electron orbital energy ε_i in the transition state.

Results and Discussion

The core ionization potentials of various atoms were calculated by varying the fractional occupation number of valence orbitals. We here direct our attention to the shifts ΔE_i of ionization potentials, taking the values for neutral atoms as standard ($Q=0$).

Figure 1 shows the shifts ΔE_{2p} of the core 2p orbital for a nickel atom with variations in the "valence-orbital net charges" Q(3d) and Q(4s). The charges were varied in the range between -0.3 and 0.9 of an electron, where the configuration of a neutral nickel atom is assumed to be $(\text{core})^{10}(3s)^2(3p)^6(3d)^8(4s)^2$. We see that ΔE_{2p} increases monotonically with increasing Q(3d)and Q(4s). Both plots appear to be slightly concave upward but may essentially be regarded as linear.

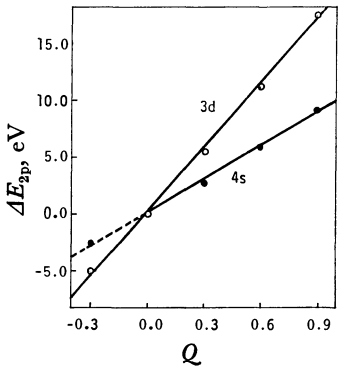

Fig. 1. Plots of the 2p-electron ionization energy shifts ΔE_{2p} of a nickel atom against the 3d as well as 4s orbital net charge.

The slopes for the two linear plots given in Fig. 1 differ clearly from each other. The slopes obtained by the least-squares treatments of the calculated data were $k_{2p}(3d)=18.76$ eV/e and $k_{2p}(4s)=9.84$ eV/e. The results suggest that, for a nickel atom, the effects of the 3d and 4s electron populations on the E_{2p} would have to be considered separately.

Some core-orbital k_i values obtained as above for the C, N, and F atoms as well as the Ni, Rh, and Pt atoms are summarized in Table 1. Two points are noteworthy with these k_i values. First, the shifts of E_{1s} for the light atoms do not depend on the origin of the charge; $k_{1s}(2s)$ is nearly equal to $k_{1s}(2p)$ for each atom. In other words,

Table 1. Exchange scaling parameters α and the calculated k_i values for atoms (eV/e)

Atom(core)[a]	α	Valence orbital	k_i	k_i(CNDO)[b]
C (1s)	0.75928	2s	16.46	21.9
		2p	16.53	
N (1s)	0.75197	2s	18.35	21.5
		2p	18.65	
F (1s)	0.73732	2s	21.96	27.6
		2p	21.81	
Ni (2p)	0.70896	3d	18.76	
		4s	9.84	
Rh (3d)	0.70217	4d	12.52	
		5s	8.21	
Pt (4f)	0.69306	5d	11.90	
		6s	8.10	

a) The orbitals denoted in parentheses show the core orbitals i from which an electron is removed upon ionization. b) Ref. 7.

the binding energy is little influenced by the difference in hybridization of valence orbitals.

Second, the k_i values calculated for the 2p, 3d, and 4s core orbitals of the Ni, Rh, and Pt atoms, respectively, all differ appreciably between the influencing d and s valence orbitals. Thus, the d orbital population exerts an apparently greater influence on the core binding energy of an inner-shell electron than does the valence s orbital population. In discussing the ESCA chemical shifts of transition metal atoms, therefore, we should look into the electron populations in individual d and s valence orbitals separately.

In Table 1 the values of k_{1s}[7] for the C, N, and F atoms in molecules obtained by fitting the observed 1s-electron chemical shifts to the CNDO/2 atomic charges are also listed. The k_{1s} (CNDO) values are uniformly greater than the Hartree-Fock-Slater k_{1s} values calculated. This may be attributed in part to the contraction of valence orbitals in molecules as a result of the accumulation of electronic charge in the bonding region.[8] The contraction should render the core orbitals in molecules more sensitive to the density of a valence electron than in isolated molecules.

Despite these numerical disagreements, the results of the present treatment of atoms lend support to the adequacy of the conventional charge-potential approximation for first-row atoms in molecules. The view that the k_{1s} values are quite different for the influencing 2s and 2p electrons[9] is thus unjustifiable. The better correlation of the two-parameter theory[9] to the shifts as compared with the conventional single-parameter treatment[1,7] is perhaps an artefact arising from the limited accuracy of the CNDO formalism itself. By contrast, it will be essential to resort to a multi-parameter treatment in interpreting the core-electron chemical shifts for transition metal atoms present in metal complexes.

References

1) K. Siegbahn, C. Nordling, A. Fahlman, R. Nordberg, K. Hamrin, J. Hedman, G. Johansson, T. Bergmark, S. -E. Karlsson, I. Lindgren, and B. Lindberg, "ESCA Atomic, Molecular and Solid State Structure Studied by Meams of Electron Spectroscopy," Uppsala, Almqvist and Wiksells (1967).

2) a) D. T. Clark, D. B. Adams, and D. Kilcast, *Chem. Phys. Lett.*, **13**, 439 (1972); *J. Chem. Soc., Faraday Trans. 2*, **1972**, 1819; b) D. W. Davis and D. A. Shirley, *J. Chem. Phys.*, **56**, 671 (1972); *Chem. Phys. Lett.*, **15**, 185 (1972); c) J. C. Carver, R. C. Gray, and D. M. Hercules, *J. Am. Chem. Soc.*, **96**, 6851 (1974).

3) J. C. Slater, *Adv. Quantum Chem.*, **6**, 1 (1972).

4) J. C. Slater, *Phys. Rev.*, **81**, 385 (1951).

5) G. W. Pratt, Jr., *Phys. Rev.*, **88**, 1217 (1952).

6) K. Schwarz, *Phys. Rev.*, **B5**, 2466 (1972); *Theor. Chim. Acta (Berl.)*, **34**, 225 (1974).

7) K. Siegbahn, C. Nordling, G. Johansson, J. Hedman, P. F. Hedén, K. Hamrin, U. Gelius, T. Bergmark, L. O. Werme, R. Manne, and Y. Baer, "ESCA Applied to Free Molecules," North-Holland, Amsterdam (1969).

8) M. J. Feinberg and K. Ruedenberg, *J. Chem. Phys.*, **54**, 1495 (1971).

9) F. O. Ellison and L. L. Larcom, *Chem. Phys. Lett.*, **10**, 580 (1971).

BULLETIN OF THE CHEMICAL SOCIETY OF JAPAN, VOL. 49 (9), 2621—2622 (1976)

Fouling Mechanism in Liquid Phase Oxidation of Carbon Monoxide Catalyzed by Palladium(II) Salts in Acetic Acid Solvents

Toshinobu IMANAKA, Tetsuo MATSUMOTO, Toshio KIMURA, Katsumi SAKURAI, and Shiichiro TERANISHI

Department of Chemical Engineering, Faculty of Engineering Science, Osaka University, Toyonaka, Osaka 560

(Received March 6, 1976)

Synopsis. The fouling mechanism during catalytic activity in the liquid phase oxidation of carbon monoxide has been investigated using catalytic acetic acid solutions containing palladium(II) salts and lithium nitrate as oxidants. The fouling phenomenon becomes understandable upon the recognition that the active palladium catalysts react with the nitrite ion formed during the oxidation reaction to produce inactive-stable complexes.

The liquid phase oxidations of carbon monoxide have been investigated as an extension of the Wacker process[1-4] in water and several reactions catalyzed by palladium salts have also been studied using acetic acid as a solvent.[5-8] Many of these studies were done with respect to the steady state reactions, but only a few have been made on the fouling process during the reaction. The present authors have previously investigated the mechanism of the CO-oxidation reaction using palladium salts in acetic acid solvents[9] and it was shown that the catalytic activity in $Pd(NO_3)_2$ and $Pd(OAc)_2$ systems decrease more rapidly than in the $PdCl_2$ system.

In the present work, the fouling mechanism of the CO-oxidation reaction was studied kinetically using a stirred reactor. It can be considered that the NO_2^- produced by reduction in the catalytic solutions during the reaction reacts with palladium complexes to give inactive-stable complexes.

Experimental

The palladium chloride solutions used were prepared by refluxing palladium chloride(II) and lithium chloride in acetic acid solvents dehydrated by phosphorus pentoxide. These solutions, which were 100 ml in volume, were diluted with 400 ml of dehydrated acetic acid after the addition of lithium nitrate. The catalytic solutions of $Pd(NO_3)_2$ and $Pd(OAc)_2$ were prepared by adding lithium nitrate to the solution of $Pd(NO_3)_2$ or $Pd(OAc)_2$ dissolved in dehydrated acetic acid (100 ml). Carbon monoxide and carbon dioxide were prepared by dehydrating with calcium chloride. Air, oxygen, and nitrogen gases used were dried over silicagel after removing a small amount of carbon dioxide and water with concd sulfuric acid and rod-like sodium hydroxide. The materials used for the preparation of these mixtures were those commercially available. The amount of NO_2^- was determined by measuring the absorbance of light (530 nm) emitted using Griess (G.R.) reagent.

The reactor,[3,4] which was made of glass with a 75 mm inside diameter and a height of 145 mm, was used for bubbling the mixtures of gases with a downward glass filter. The stirrer had a two bladed impeller at a position 40 mm from the bottom of the reactor and the reactions were carried out at 30 °C. The reaction mixtures of the gasses were analyzed by gas chromatography after condensation of acetic acid.

Results and Discussion

In the $Pd(OAc)_2$ system with the highest catalytic activity, the relation between the reaction rate in the steady state and the feed rate or the stirring rate was investigated using the reactor described above. It was shown that the mass transfer rates were unchanged for feed rates of 10—20 cm^3/s and for a stirring rate of 900 rpm., therefore, under these conditions, the rate-determining step is the chemical-reaction processes. Accordingly, all the experiments were carried out under the conditions of $F \geq 10$ cm^3/s and $N=900$ rpm. In the case of $PdCl_2$ or $Pd(NO_3)_2$ systems, it was confirmed that the rate-determining step was the chemical-reaction processes under these conditions.

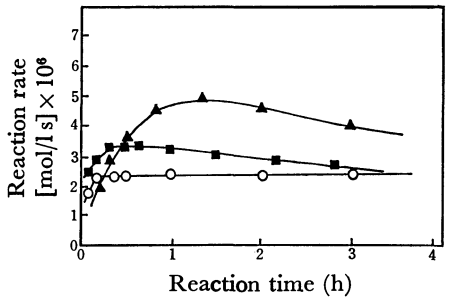

Fig. 1. The dependence of the reaction rate on the reaction time.
○: $PdCl_2$ C_{pd}: 3.59×10^{-4} (mol/l), ■: $Pd(NO_3)_2$ C_{pd}: 2.00×10^{-4} (mol/l), ▲: $Pd(OAc)_2$ C_{pd}: 2.00×10^{-4} (mol/l). C_{co}: 3.30×10^{-4} (mol/l), C_{NO_3} 0.290 (mol/l).

The oxidation rates of carbon monoxide catalyzed by palladium salts are shown in Fig. 1. In the case of palladium chloride, the oxidation rate became linear with time after about 10 min and remained constant for several hours. However, the activity decreased gradually after a long reaction period and the color of the solutions varied from an initial brown to yellow at the end. In the cases of $Pd(NO_3)_2$ and $Pd(OAc)_2$ catalysts, the reaction rate reached a maximum after several minutes and its activity decreased gradually without any precipitate. This reaction rate is of first order with respect to the concentration of the palladium salts, and therefore, the overall rate expression can be represented by

$$r = r_\infty \exp(-k_d t),$$

where r_∞ represents the steady state reaction rate and k_d the rate constant of the fouling reaction. The logarithm of the rates for constant concentration of palladium *versus* reaction time in the $Pd(NO_3)_2$ system for the

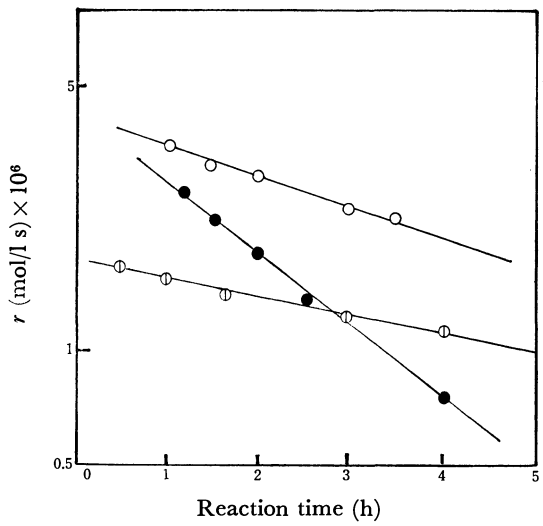

Fig. 2. The dependence of activity of $Pd(NO_3)_2$ catalyst on the reaction time.

	[$LiNO_3$]	CO%	O_2%	N_2%	[NO_2^-]
◫	0.232 [M]	6	18.8	75.2	8800 [μg-N/l]
○	0.928 [M]	15	17.0	68.0	17800 [μg-N/l]
●	1.16 [M]	6	0	94.0	34300 [flg-N/l]

$C_{pd}=0.995—1.02\times10^{-4}$ (mol/l).

various concentrations of lithium nitrate and the various feed streams are linear, as is shown in Fig. 2, and the fouling rate constants were calculated from the slopes. The fouling rate constants increase with decreasing oxygen content in the feed streams and with increasing concentration of NO_2^- formed by the reduction of NO_3^-. In Fig. 3, the logarithm of k_d is plotted against the logarithm of the concentration of NO_2^- formed during the oxidation reaction under the various catalytic solutions and feed streams of carbon monoxide. The values of k_d in the $Pd(NO_3)_2$ system are greater than those in the $Pd(OAc)_2$ system, as is shown in Fig. 3 and were much greater than those ($k_d=0$) in the $PdCl_2$ system under similar conditions. The best fit to the data are seen to be straight lines with slopes of one, which corresponds to a first order reaction in the case of the $Pd(NO_3)_2$ system and of 3.3, in the $Pd(OAc)_2$ system. These results show that the fouling process in the case of the $Pd(NO_3)_2$ catalyst is associated with the concentration of NO_2^- equivalent to $Pd(NO_3)_2$ and in the case of the $Pd(OAc)_2$ catalyst, two moles of NO_2^- to one mole of $Pd(OAc)_2$.

It is well known that NO_2^- in solutions reacts with acetic acid to produce NO_3^- and NO, as is shown by:

$$HOAc + NO_2^- \longrightarrow OAc^- + HNO_2 \quad (2)$$

$$3HNO_2 \longrightarrow H_3O^+ + NO_3^- + 2NO \quad (3)$$

Tamura and Yasui[8] have reported that NO resulting from formula (3) does not form a stable palladium nitrosyl complex. No precipitate is produced with OAc^- formed by in formula (2) and the catalytic activity does not change with the addition of 10% of water in the solution. The fouling rate constants are independent of the concentrations of palladium salts, $LiNO_3$ and

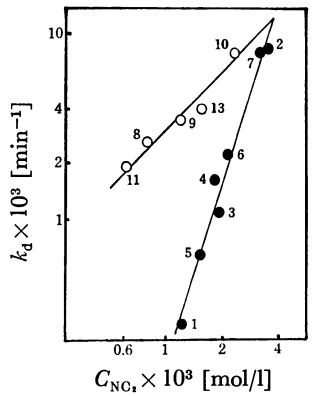

Fig. 3. The dependence of the rate constant of decay on the nitrite ion concentration.
○: $Pd(NO_3)_2$, ●: $Pd(OAc)_2$.

Catalysts		$C_{pd}\times10^4$ (mol/l)	$C_{NO_2}\times10^1$ (mol/l)	CO%	
	1	1.79	7.25	5	95 (O_2)
	2	1.19	10.0	25	75 (N_2)
	3	1.57	10.0	10	90 (air)
$Pd(OAc)_2$	4	3.18	7.25	10	90 (O_2)
	5	7.34	5.80	4	96 (air)
	6	3.43	7.25	10	90 (N_2)
	7	1.90	10.0	20	80 (N_2)
	8	1.00	2.32	10	90 (air)
	9	1.01	9.28	15	85 (air)
	10	1.02	11.6	6	94 (N_2)
$Pd(NO_3)_2$	11	1.01	2.32	6	94 (air)
	12	0.995	2.32	20	80 (N_2)
	13	1.01	4.64	20	80 (N_2)

carbon monoxide, but do depend on the concentration of NO_2^- in the solutions.

It can be concluded that the fouling process causes the formation of inactive-stable palladium nitro complexes by the NO_2^- formed during the CO-oxidation reaction, and its fouling reaction rate decreases according to the following sequence:

$$Pd(NO_3)_3 > Pd(OAc)_2 \gg PdCl_2.$$

References

1) T. Imanaka, H. Mizuno, S. Matsumoto, and S. Teranishi, *Nippon Kagaku Kaishi*, **1976**, 25.
2) A. B. Fasman, W. A. Kolodov, and A. W. Sokolbskii, *Dokl. Akad. Nauk. SSSR*, **155**, 484 (1964).
3) T. Imanaka, S. Matsumoto, S. Wakimura, and S. Teranishi, *Kogyo Kagaku Zasshi*, **74**, 1071 (1971).
4) T. Imanaka, S. Matsumoto, S. Wakimura, and S. Teranishi, *Kogyo Kagaku Zasshi*, **74**, 222 (1971).
5) G. D. Shier, *Am. Chem. Soc., Div. Petrol. Chem., Prepr.*, **14**, B123 (1969).
6) S. Uemura, Y. Ikeda, and K. Ichikawa, *Chem. Commun*, **1971**, 390.
7) P. M. Henry and G. A. Ward, *J. Am. Chem. Soc.*, **93**. 1494 (1971).
8) M. Tamura and T. Yasui, *Kogyo Kagaku Zasshi*, **72**, 575 (1969).
9) T. Imanaka, T. Matsumoto, K. Sakurai, and S. Teranishi, *Nippon Kagaku Kaishi*, to be published.

BULLETIN OF THE CHEMICAL SOCIETY OF JAPAN, VOL. 49 (9), 2623—2624 (1976)

Photochemistry in the Adsorbed Layer. VII. Steric Hindrance in the Type II Cleavage of Adsorbed Alkyl Ketones

Masakazu ANPO and Yutaka KUBOKAWA

Department of Applied Chemistry, College of Engineering, University of Osaka Prefecture, Mozu-Umemachi, Sakai, Osaka 591

(Received March 16, 1976)

Synopsis. The type I selectivity in the photolysis of adsorbed alkyl ketones is larger for 3-methyl-2-pentanone than for 2-pentanone. Such behavior can be explained by the concept that the type II cleavage is more hindered for the former owing to a steric hindrance arising from the presence of a solid surface.

Recently we have investigated the spectra and photochemistry of alkyl ketones adsorbed on porous Vycor glass and found the general characteristics of the photochemistry in the adsorbed layer.[1-6] The change in the photochemical reactivity caused by adsorption has been discussed mainly from the electronic aspects. It seems likely that such a change in the photochemical reactivity is attributed in part to the steric effect arising from the presence of a solid surface. An example of this steric effect has been found in the type II cleavage of adsorbed alkyl ketones. The results are described in the present paper.

Experimental

Materials. 3-Methyl-2-pentanone (Tokyo Kasei Kogyo Co., Ltd.) was purified by preparatory chromatography and then vacuum distilled bulb-to-bulb. Analysis by vapor phase chromatography equipped with flame ionization detection showed no impurity. Porous Vycor glass (Corning, No. 7930) was used as an adsorbent.

Apparatus and Procedure. Details of the apparatus and procedures were described previously.[1-6] A conventional vacuum system was used in conjuction with a special quartz cell capable of studying the spectra and photolysis in the adsorbed layer. The specimen of porous Vycor glass which had been heated in oxygen to remove carbonaceous impurities was introduced into the cell and degassed at 500 °C for 7 h. Photolysis was carried out using an ultra high pressure mercury lamp without filter, after ketone molecule had been adsorbed on the specimen. Analysis was carried out by vapor phase chromatography using a 3 m column of porapak Q for hydrocarbons and a 2 m column of molecular sieve 5A for the noncondensable gases.

Results and Discussion

The results of the photolysis of adsorbed 3-methyl-2-pentanone (3-M-2-P) at room temperature are given in Table 1, and those of its photolysis in the gas phase in Table 2. In the gas phase photolysis the rate of ethylene formation is three times higher than that of radical product formation. Such behavior is in agreement with that reported by other workers,[7] who showed that the type II reaction is predominant in the gas phase (below 30 °C) and in solution. Comparison of Tables 1 and 2 show that the rate of radical product formation in the adsorbed layer is much higher than that of ethylene formation. Results of the photolysis of adsorbed 2-pentanone (2-P)[1,6] are given in Table 1. It is seen that the type I selectivity is higher in the adsorbed layer than in the gas phase, its extent being much larger for 3-M-2-P than for 2-P. Furthermore, the marked increase observed in going from 2-P to 3-M-2-P arises mainly from the decrease in the rate of ethylene formation. Such a high type I selectivity in the adsorbed layer was attributed to suppression of the recombination of the radical pairs as well as increased probability of α-cleavage, leading to the increase in the rate of radical product formation.[6] However, it is difficult to explain the marked higher type I selectivity of 3-M-2-P as compared to that of 2-P.

In order to obtain information on the nature of the excited states in the photolysis, the effect of added nitrogen oxide on ethylene formation from adsorbed 3-M-2-P has been investigated in a similar manner to that described previously.[1] The maximum reduction of ethylene formation by added nitrogen oxide, *i.e.*, the formation of ethylene from the triplet excited state, was about 47%, almost the same as the corresponding value observed

TABLE 1. RESULTS OF THE PHOTOLYSIS OF ADSORBED ALKYL KETONES AT 25 °C [a]

	Amount adsorbed[b] 10^{-6} mol/g	Yield of type II 10^{-3} ml/5 min	Yield of[c] type I 10^{-3} ml/5 min	Selectivity (type I/II)
3-Methyl-2-pentanone	5.36	0.21	1.07	5.1
	21.40	0.48	2.21	4.6
	42.80	0.65	2.59	4.0
2-Pentanone[d]	4.28	0.72	0.65	0.89
	22.00	1.92	1.24	0.65

a) The molar extinction coefficient at the wavelength of maximum absorption, ε for 3-methyl-2-pentanone was 1.45 times larger than that for 2-pentanone in the adsorbed layer. This ratio hardly changed with increasing amount of the ketone adsorbed.[2] b) The amount adsorbed of 4.47×10^{-6} mol/g corresponds to $\theta=0.005$ using 25 A^2 as the area that occupied by each molecule. As the amount adsorbed decreases, a marked increase in the type I selectivity as well as in the overall efficiency of the photolysis occurs (Table 2). Such a behavior would be attributed to a heterogeneity of the surface, *i.e.*, the presence of special active sites.[6] c) The amounts of minor products such as methane, propane, butene, and hexane did not exceed 15% of the amount of butane, indicating that the rate of the type I reaction is approximately equal to the rate of butane formation. d) M. Anpo and Y. Kubokawa, *Bull. Chem. Soc. Jpn.*, **48**, 3085 (1975).

Table 2. Results of the photolysis of gaseous 3-methyl-2-pentanone at 30 °C

Relative Yield	CH_4	C_2H_6	C_2H_4	C_3H_8	C_3H_6	C_4H_{10}	C_4H_8	C_5H_{12}	C_6H_{14}
	1.45	1.90	100.0	0.65	4.30	16.6	1.56	5.70	8.20

3-Methyl-2-pentanone pressure, 18.0±0.5 Torr. Irradiation time, 15 min. Selectivity was identified as $(\phi_{C_3}+\phi_{C_4}+\phi_{C_5}+\phi_{C_6})/(\phi_{C_2H_4})$.

with 2-P. There was no marked difference in the lifetimes of the triplet states of 2-P and 3-M-2-P determined from the Stern-Volmer plots for ethylene quenching with nitrogen oxide. This suggests that there is no difference in the nature on the excited states in the adsorbed layer photolysis between both ketones.

The type II reaction proceeds *via* 1,4-biradical intermediate formed by the intramolecular hydrogen abstraction.[8] A favorable conformation would be necessary for such γ-hydrogen abstraction to take place. A six-membered transition state has been proposed for this reaction. On a solid surface the rapid tumbling motion of molecules would be hindered, formation of such a six-membered transition state being disturbed. The steric hindrance would be expected to be more significant for 3-M-2-P than for 2-P owing to the presence of a bulky methyl group instead of a hydrogen. Thus, the marked lower rate of ethylene formation observed with the former as compared to the latter is explicable. Such steric requirements for the type II cleavage have been proposed by Turro and Weiss[9] who found a marked difference in the photochemical behavior of *cis* and *trans*-2-propyl-4-*t*-butylcyclohexanones in cyclohexane solution.

References

1) Y. Kubokawa and M. Anpo, *J. Phys. Chem.*, **78**, 2442 (1974).
2) M. Anpo and Y. Kubokawa, *J. Phys. Chem.*, **78**, 2446 (1974).
3) M. Anpo, S. Hirohashi, and Y. Kubokawa, *Bull. Chem. Soc. Jpn.*, **48**, 985 (1975).
4) Y. Kubokawa and M. Anpo, *J. Phys. Chem.*, **79**, 2225 (1975).
5) M. Anpo, T. Wada, and Y. Kubokawa, *Bull. Chem. Soc. Jpn.*, **48**, 2663 (1975).
6) M. Anpo and Y. Kubokawa, *Bull. Chem. Soc. Jpn.*, **48**, 3085 (1975).
7) P. J. Wagner and G. S. Hammond, *J. Am. Chem. Soc.*, **87**, 4009 (1965); F. S. Wettack and W. A. Noyes, Jr., *ibid.*, **90**, 3901 (1968).
8) N. C. Yang, S. P. Elliott, and B. Kim, *J. Am. Chem. Soc.*, **91**, 7551 (1969); N. J. Turro, J. C. Dalton, K. Dawes, G. Farrington, R. Hautala, D. Morton, M. Niemczyk, and N. Schore, *Acc. Chem. Res.*, **5**, 92 (1972), and references therein.
9) N. J. Turro and D. S. Weiss, *J. Am. Chem. Soc.*, **90**, 2185 (1968).

BULLETIN OF THE CHEMICAL SOCIETY OF JAPAN, VOL. 49 (9), 2625—2626 (1976)

Molar Volume Equations of Several Molten Binary Systems

Junichi MOCHINAGA, Kazuo IGARASHI, Hideo KURODA, and Hironori IWASAKI

Department of Synthetic Chemistry, Faculty of Engineering, Chiba University, Yayoi-cho, Chiba 280

(Received April 12, 1976)

Synopsis. The molar volumes of YCl_3–KCl, YCl_3–NaCl, YCl_3–$CaCl_2$, $PrCl_3$–KCl, $PrCl_3$–NaCl, $PrCl_3$–$CaCl_2$, $NdCl_3$–KCl, $NdCl_3$–NaCl, and $NdCl_3$–$CaCl_2$ systems in molten state were measured. The results are represented by empirical equations as functions of both temperature and composition. The calculations were carried out by using the methods of least squares and Powell's procedure.

It is important to know the molar volumes of molten salts, since they are used for the calculation of molar values in thermodynamics. The molar volume equation has been customarily expressed as a function of temperature for a fixed mole fraction. If empirical equations for the molar volumes of molten mixture systems are obtained as functions of temperature and mole fraction, they are convinient for the estimation of molar volumes at any temperature and composition over the measured range. Since the molar volume is given as a linear function of temperature, the empirical equation is given as follows.

$$V_m = \sum_0^n a_n x^n + \left(\sum_0^n b_n x^n\right) T$$

where V_m is the averaged molar volume of the molten mixture system in cm^3/mol, a_n and b_n the parameters, x the mole fraction of rare-earth chlorides, and T the temperature in K. The parameters were calculated by the method of least squares, and Powell's method.[1,2] The latter is considered to be effective for finding the minimum value of function containing several variables. The molar volumes calculated from the resulting empirical equations are in agreement with the observed values within 2%.

Experimental

Materials. Rare-earth chlorides were prepared by a procedure similar to that reported.[3] KCl, NaCl, and $CaCl_2$ were dried by heating at a temperature 50 °C below their melting points *in vacuo*.

Measurement. The dilatometer method was used. The volume of the dilatometer, which was made of transparent silica, was determined by use of distilled water at room temperature since the thermal expansion coefficient of quartz is much smaller than that of molten salts. The meniscus of melt in the dilatometer was read with a cathetometer.

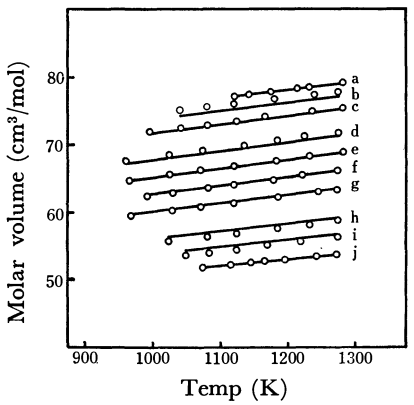

Fig. 1. Molar volumes of YCl_3–$CaCl_2$ system in molten state; ○: observed values, —: calculated values by empirical equation (n=2), a: mole fraction of YCl_3 1.0, b: 0.929, c: 0.849, d: 0.700, e: 0.599, f: 0.500, g: 0.398, h: 0.221, i: 0.125, j: 0 ($CaCl_2$: 1.0).

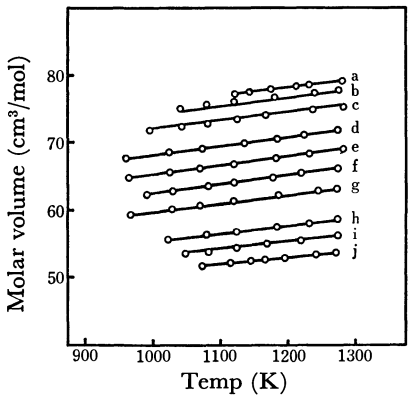

Fig. 2. Molar volumes of YCl_3–$CaCl_2$ system in molten state; ○: observed values, —: calculated values by empirical equation (n=3), a: mole fraction of YCl_3 1.0, b: 0.929, c: 0.849, d: 0.700, e: 0.599, f: 0.500, g: 0.398, h: 0.221, i: 0.125, j: 0 ($CaCl_2$: 1.0).

TABLE 1. PARAMETERS OF EMPIRICAL EQUATIONS FOR MOLTEN BINARY SYSTEMS (n=3)

System	a_0 (×10)	a_1 (×10)	a_2 (×10)	a_3 (×10)	b_0 (×10^{-2})	b_1 (×10^{-2})	b_2 (×10^{-2})	b_3 (×10^{-2})
YCl_3–KCl	2.5133	8.4872	−13.0034	8.1121	2.2033	−4.6025	10.6857	−6.8596
YCl_3–NaCl	2.1124	4.9782	−3.1680	2.1865	1.5030	−0.9367	2.7031	−1.8426
YCl_3–$CaCl_2$	4.1616	0.2464	3.2924	−1.3030	0.9483	1.2902	−1.1699	0.1151
$PrCl_3$–KCl	2.5547	7.3695	−10.3620	5.1980	2.1675	−3.1106	7.4261	−3.9764
$PrCl_3$–NaCl	2.1124	3.0262	2.3676	−2.7460	1.5030	0.5474	−1.7208	2.1769
$PrCl_3$–$CaCl_2$	4.0348	1.9796	−1.5171	0.2628	1.0851	1.5488	−2.4048	2.2774
$NdCl_3$–KCl	2.5547	4.1783	−3.2497	1.9470	2.1675	−0.8841	1.9325	−1.3067
$NdCl_3$–NaCl	2.1124	3.1752	0.6594	−0.5344	1.5030	0.6079	−0.8599	0.6721
$NdCl_3$–$CaCl_2$	4.0348	−0.0979	3.4814	−1.9880	1.0851	2.5231	−4.3237	2.6247

Results and Discussion

Comparisons between the observed molar volumes and the values for the molten YCl_3–$CaCl_2$ system obtained by means of empirical equations are given in Figs. 1 and 2 for $n=2$ and $n=3$, respectively. Fitting of the resulting equation for the observed molar volumes is better in the case of $n=3$ than that of $n=2$. The molar volumes of the respective pure component salts in molten state can be obtained from the values at $x=0$ or $x=1$. The parameters for these molten binary systems are given in Table 1. All the excess molar volumes calculated by means of the equations are small. The intersections between experimental curves and additivity lines in the molar volume isotherms were observed except for $PrCl_3$–KCl and $NdCl_3$–KCl systems.

Calculations were carried out with the computers in the University of Tokyo and Chiba University.

References

1) M. J. D. Powell, *Computer J.*, **7**, 155 (1964).
2) M. J. D. Powell, *Computer J.*, **5**, 147 (1962).
3) J. Mochinaga, and K. Irisawa, *Bull. Chem. Soc. Jpn.*, **47**, 364 (1974).

BULLETIN OF THE CHEMICAL SOCIETY OF JAPAN, VOL. 49 (9), 2627—2628 (1976)

A Theoretical Analysis of Rotational Isomerism; CNDO/2 Calculations of *i*-PrSMe, *i*-PrSEt, *i*-Pr-S-*n*-Pr, and $(i\text{-Pr})_2S$[1]

Masaru OHSAKU,* Norihisa BINGO, Kanzo EIDA, and Hiromu MURATA

Department of Chemistry, Faculty of Science, Hiroshima University, Higashisenda-machi, Hiroshima 730

(Received April 12, 1976)

Synopsis. CNDO/2 calculations of *i*-PrSMe, *i*-PrSEt, *i*-Pr-S-*n*-Pr, and $(i\text{-Pr})_2S$ gave the stable conformations of these molecules and the optimized angles of ϕ(CSC) of the first three molecules considered.

Conformational analyses of *i*-PrSMe, *i*-PrSEt, *i*-Pr-S-*n*-Pr, and $(i\text{-Pr})_2S$ have been performed extensively on the basis of vibrational spectra and normal coordinate treatment.[2-4] However, for these molecules no theoretical conformational analysis has yet been performed. In the present study in order to test the previous experimental results, the present authors investigated the conformational analyses of these molecules by the CNDO/2 method.[5]

The molecular parameters used for the computations are as follows: r(C–H)=1.09 Å, r(C–S)=1.81 Å, r(C–C)=1.54 Å—ϕ(CSC)=99° or the optimized values for *i*-PrSMe, *i*-PrSEt, *i*-Pr-S-*n*-Pr, and ϕ(CSC)=99, 104, or 109° for $(i\text{-Pr})_2S$—and the other angles were assumed to be tetrahedral. The dihedral angles were 180 and 60° for the *trans* (T) and *gauche* (G) forms, respectively.

With *i*-PrSMe, a local minimum appeared at a rotational angle of *ca.* 60 °. That is, the calculations show that the G (C_1) form is more stable than the T (C_s) form. The present result agrees well with the observed.[2]

For *i*-PrSEt, the stability was assumed to be in the order: GT>GG>TT.[4] In this molecule, conformations are taken into consideration around bonds 1 and 2, H–C(–C)–S–CH_2–CH_3. The CNDO/2 calculations indicate the stability: GT>TT>GG>TG. The most stable form, GT, is well reproduced by the calculations. However, the stabilities for the TT and GG forms are in reverse order of those observed.[4] For the IR study, the most unstable form, TG, is excluded from consideration, since the repulsions between methyl groups in the ethyl and isopropyl groups may be too great.[4] This is explained qualitatively by the present calculations.

For *i*-Pr-S-*n*-Pr, conformations were taken into consideration around bonds 1, 2, and 3, H–C(–C)–S–CH_2–CH_2–CH_3, and from the calculations it was found that the forms which have the T conformation about bond 2 are more stable than those of the G conformation. This agrees well with the experimental result that GTT is the most stable form,[4] although the present calculations show that the energy minimum form is GTG. As has been noted previously,[6] the conformation around the

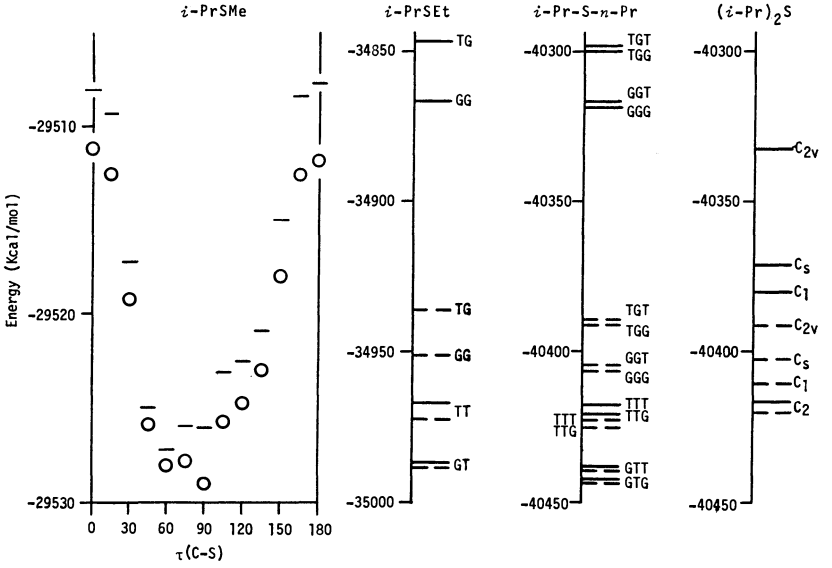

Fig. 1. Total energy as a function of internal rotation angle—original parameters.[5]
i-PrSMe: — ϕ(CSC)=99°, ○ ϕ(CSC)=105°.
i-PrSEt: — ϕ(CSC)=99°, -- ϕ(CSC)=105.6°.
i-Pr-S-*n*-Pr: — ϕ(CSC)=99°, -- ϕ(CSC)=105.9°.
$(i\text{-Pr})_2S$: ϕ(CSC)=99°; C_2=−40413, C_1=−40303, C_s=−40295, C_{2v}=−40183 (kcal/mol), — ϕ(CSC)=104°, -- ϕ(CSC)=109°.

* To whom all correspondence should be addressed.

C–S bond is very difficult to determine from only the vibrational spectra and the normal coordinate treatment. Therefore, the CNDO/2 method is available to determine the conformation around the C–S bond for these molecules.

Four conformations can be assumed for $(i\text{-Pr})_2S$: C_2, C_s, C_1, and C_{2v}. It appears that the conformational energy is due mainly to the interactions between methyl groups of the isopropyl groups on both sides. In connection with these interactions, the stability can be predicted to be in the order: $C_2>C_s>C_1>C_{2v}$. The vibrational spectra confirm this order.[4] The CNDO/2 calculations give the result, $C_2>C_1>C_s>C_{2v}$, and the stability between the C_1 and C_s forms is reversed. However, the most stable and unstable forms are well reproduced by the calculations.

The CSC angle was then optimized without changing the other structural parameters assuming the G, GT, and GTT forms for *i*-PrSMe, *i*-PrSEt, and *i*-Pr–S–*n*-Pr, respectively. The angles obtained are 105, 105.6, and 105.9° for *i*-PrSMe, *i*-PrSEt, and *i*-Pr–S–*n*-Pr, respectively. The angles become larger with increasing weight of the normal alkyl group. These angles are rather large in comparison with the 98°52′ of MeSMe[7] and rather close to the 103.9° for MeSEt.[8] Therefore, these angles appear to be reasonably optimized. The results of the calculations using the optimized angles are also considered. The tendency is nearly the same as in the case of $\phi(\text{CSC})=99°$. For $(i\text{-Pr})_2S$, the optimization of angle ϕ(CSC) was not carried out. The total energy decreases with increasing angle from 99° to 109°. Therefore, it is predicted that the angle is larger in this molecule than in other molecules treated.

All of the calculations were also carried out using $K_d=0.492$ instead of 0.75 and others original values,[5] where K_d is the constant of the off-diagonal core matrix elements in relation to third-row elements. As a result, the order of the stability scarcely varied from the case of $K_d=0.75$, but the energy difference between the rotational isomers was slightly refined, *e.g.*, the energy difference between the T and G forms of *i*-PrSMe is postulated to be *ca.* 1—1.5 kcal/mol from the IR study.[2]

Recently, the appropriateness of CNDO/2 studies of molecular conformations has been discussed for some molecules involving third-row elements.[9,10] Generally, the CNDO/2 calculation gives larger energy differences between the rotational isomers than observation. However, this method reproduces energy minimum conformations and some angles fairly well. The CNDO/2 calculation, therefore, is useful as one of the methods of analyzing experimental results, such as the normal coordinate treatment.

The authors wish to thank Dr. Kimihiko Hirao of the Shiga University of Medical Science for his helpful advice. All calculations were performed at the Computing Center of Hiroshima University.

References

1) Presented in part at the 34th Annual Meeting of the Chemical Society of Japan, Hiratsuka, April, 1976.
2) M. Ohsaku, Y. Shiro, and H. Murata, *Bull. Chem. Soc. Jpn.*, **45**, 3480 (1972).
3) D. W. Scott and M. Z. El-Sabban, *J. Mol. Spectrosc.*, **30**, 317 (1969).
4) M. Ohsaku, H. Murata, and Y. Shiro, *Spectrochim. Acta*, to be published.
5) J. A. Pople and D. L. Beveridge, "Approximate Molecular Orbital Theory," McGraw-Hill, New York, N. Y. (1970).
6) M. Ohsaku, *Bull. Chem. Soc. Jpn.*, **48**, 1037 (1975).
7) L. Pierce and M. Hayashi, *J. Chem. Phys.*, **35**, 479 (1961).
8) K. Oyanagi, T. Fukuyama, and K. Kuchitsu, Preprints of the 32nd Annual Meeting of the Chemical Society of Japan, Vol. 1, (1975), p. 112.
9) A. Veillard, *Chem. Phys. Lett.*, **33**, 15 (1975).
10) Th. Weller, D. Klöpper, and H. -J. Köhler, *Chem. Phys. Lett.*, **36**, 475 (1975).

BULLETIN OF THE CHEMICAL SOCIETY OF JAPAN, VOL. 49 (9), 2629—2630 (1976)

Solvent Extraction Equilibria of Acids. IV. Tetrachloroferric Acid in a Hexane Containing Trioctylphosphine Oxide-Aqueous Chloride Solution System

Tatsuya SEKINE, Yoshiyuki ZENIYA, and Masaru NIITSU*

Department of Chemistry, Science University of Tokyo, Kagurazaka, Shinjuku-ku, Tokyo 162
**Faculty of Pharmaceutical Sciences, Josai University, Sakado, Saitama 350-02*

(Received October 7, 1975)

Synopsis. From the distribution ratio of iron(III) between hexane containing trioctylphosphine oxide (TOPO) and a 4 mol dm^{-3} aqueous (H, Na)Cl solution, the extraction constants for the two complexes, $K_{ex_1}=[FeCl_3(TOPO)_2]_{org}[Fe^{3+}]^{-1}[Cl^-]^{-3}[TOPO]_{org}^{-2}$ and $K_{ex_4}=[HFeCl_4(TOPO)_2]_{org}[Fe^{3+}]^{-1}[H^+]^{-1}[Cl^-]^{-4}[TOPO]_{org}^{-2}$, were determined to be $10^{4.5}$ and $10^{4.3}$, respectively. The extractability of tetrachloroferric acid are discussed by comparing the K_{ex} value with that for perchloric acid.

Solvent extraction of iron(III) from hydrochloric acid with oxygen-containing solvents, such as diethyl ether, is one of the oldest applications of this method to metal ions[1,2] and, as reviewed by Diamond and Tuck[3] and Marcus and Kertes,[4] the extracted species is recognized to be tetrachloroferric acid, $HFeCl_4$. In the present work, this extraction was reinvestigated using hexane containing a small amount of trioctylphosphine oxide (TOPO) as the organic phase and the equilibria in the system are discussed.

Experimental and Statistical

The experiments and the analysis of the data were performed in a similar manner to other studies in this series.[5-7] The stock iron(III) solution was prepared by dissolving ferric chloride in hydrochloric acid. All the procedures were performed in a room with the temperature thermostatically controlled at 25±0.3 °C. A portion of hexane containing TOPO and the same volume of an aqueous 4 mol dm^{-3} (H, Na)Cl solution containing 1×10^{-3} mol dm^{-3} iron(III) were placed in a stoppered glass tube, stirred vigorously for 15 min and centrifuged. The iron(III) content in the organic phase was determined from the optical absorption at 425 nm after it was colored by β-isopropyltropolone[8,9] and that in the aqueous phase was determined from the absorption at 480 nm after it was colored by thiocyanate.[10]

All the species in the organic phase are denoted by the subscript "org" and those in the aqueous phase by the lack of any subscript. The stability constants for iron(III) complexes in the aqueous phase are:

$$\beta_n = [FeCl_n^{3-n}][Fe^{3+}]^{-1}[Cl^-]^{-n} \quad (1)$$

As will be seen below, the extraction constants for the trichloride and tetrachloride complexes of iron(III) can be written as:

$$K_{ex_1} = [FeCl_3(TOPO)_2]_{org}[Fe^{3+}]^{-1}[Cl^-]^{-3}[TOPO]_{org}^{-2} \quad (2)$$

and

$$K_{ex_4} = [HFeCl_4(TOPO)_2]_{org}[Fe^{3+}]^{-1}[H^+]^{-1}\times[Cl^-]^{-4}[TOPO]_{org}^{-2} \quad (3)$$

The distribution ratio of iron(III) under the present conditions can be written as:

$$D = [Fe(III)]_{org,total}[Fe(III)]_{total}^{-1}$$
$$= ([FeCl_3(TOPO)_2]_{org}+[HFeCl_4(TOPO)_2]_{org})\times([Fe^{3+}]+[FeCl^{2+}]+[FeCl_2^+])^{-1} \quad (4)$$

By substituting Eqs. 1 through 3 into 4, we can write:

$$D = \{[TOPO]_{org}^2(K_{ex_1}[Cl^-]^3+K_{ex_4}[H^+][Cl^-]^4)\}\times(1+\beta_1[Cl^-]+\beta_2[Cl^-]^2)^{-1} \quad (5)$$

and thus,

$$\log\{D(1+\beta_1[Cl^-]+\beta_2[Cl^-]^2)[Cl^-]^{-3}[TOPO]_{org}^{-2}\} = \log(K_{ex_1}+K_{ex_4}[H^+][Cl^-]) \quad (6)$$

The values of these extraction constants can be obtained by a curve-fitting method using the following standard curve:[12]

$$Y = \log(1+v), \quad X = \log v \quad (7)$$

Results and Discussion

The slope of the log D *vs.* log $[TOPO]_{org}$ plot was +2 for hydrogen-ion concentrations of the 4 mol dm^{-3} chloride solution of either 1×10^{-2} or 1 mol dm^{-3}. The extraction of iron(III) in 4 mol dm^{-3} chloride solutions increased with an increase in the hydrogen-ion concentration. Figure 1 shows the log D *vs.* log [H$^+$] plot.

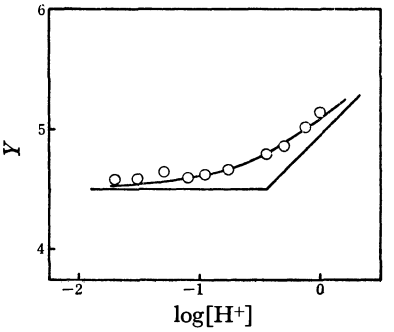

Fig. 1. Increase in the distribution ratio of Fe(III) as a function of the hydrogen-ion concentration. Org. phase: hexane initially containing 3×10^{-3} mol dm^{-3} TOPO. Aq. phase: 4 mol dm^{-3} (H, Na)Cl. The ordinate is $Y=\log\{D(1+\beta_1[Cl^-]+\beta_2[Cl^-]^2)[Cl^-]^{-3}\times[TOPO]_{org}^{-2}\}$. The solid curve is obtained by introducing the extraction constants K_{ex_1} and K_{ex_4} into Eq. 6.

From the dependence of D on the hydrogen-ion and TOPO concentrations described above, the extracted species are assumed to be mainly $FeCl_3(TOPO)_2$ and $HFeCl_4(TOPO)_2$ in the lowest and highest hydrogenion concentration regions, respectively. Using the stability constants previously obtained in 4 mol dm^{-3} aqueous Na(Cl, ClO_4) medium[11] ($\beta=10^{0.88}$ and $\beta_2=10^{0.80}$,

those of the higher complexes being negligibly small) and by correcting for the free TOPO concentration due to the extraction of hydrochloric acid, the data were analyzed by the curve-fitting method. The constants in Eqs. 2 and 3 were determined to be $K_{ex_1}=10^{4.5}$ and $K_{ex_2}=10^{4.3}$, respectively. The solid curve in Fig. 1 was calculated by introducing these constants into Eq. 6.

The extraction of iron(III) chloride with TOPO has been reported previously,[11,13-15] but the equilibria involved have not been discussed in detail.

The dissociation of $HFeCl_4$, a very strong acid which is comparable to perchloric acid,[3,4] should be negligible in hexane containing a small amount of TOPO as in the case of perchloric acid already discussed,[5] and therefore, Eqs. 2—6 can be applied for the present data. On the other hand, the dissociation of this acid should be taken into account in various polar organic solvents saturated in water. This may be one of the reasons why the extraction constant in Eq. 3 has never been reported in previous reports on iron(III) chloride extraction.

The solvation number of $HFeCl_4$ has also been found to be two with respect to tributylphosphate (TBP).[16] The IR absorption of TBP in benzene due to the stretching vibration of the phosphoryl group has been systematically studied.[17] It was found[17] that the shift of the TBP absorption band to lower frequencies upon extracting iron(III) from 6 mol dm^{-3} hydrochloric acid was similar to that which occurred with the TBP solvating nitrates of lanthanoides. Thus it should be reasonable to assume that since the central metal ion should be coordinated to TBP in the extracted iron(III) complex of that report, the TOPO molecules in the present study should be bound to $HFeCl_4$ through a coordination bond, but not to the proton through a hydrogen-bond.

In previous work,[11] neither the $FeCl_3$ nor the $FeCl_4^-$ complex was detected in 4 mol dm^{-3} aqueous chloride solutions to within the limit of experimental error and thus the determination of the following extraction constant was not possible from the present data:

$$K_{ex}(\text{acid}) = [HX(TOPO)_2]_{org}[H^+]^{-1}[X^-]^{-1}[TOPO]_{org}^{-2} \quad (8)$$

However, on assuming that β_4 is smaller than 10^{-1}, the lower limit of the constant in Eq. 8 for the tetrachloroferric acid (X^- is $FeCl_4^-$) was estimated to be $K_{ex}(HFeCl_4)>10^{5.3}$, which is more than ten times the value for perchloric acid (X^- is ClO_4^-) in the 4 mol dm^{-3} ionic medium with TOPO in hexane[9] ($K_{ex}(HClO_4)=10^{4.16}$). Since perchloric acid is known to be one of the most extractable inorganic acids using solvating type extractants,[3-5] one possible explanation for the high extractability of this complex acid may be given as follows: the TOPO molecules are coordinated to the central iron(III) in the complex. However, further information is necessary before a final conclusion can be drawn.

The authors are very grateful to Dr. Akira Yamasaki of the Electrocommunications University, Tokyo, for valuable discussions concerning this work.

References

1) M. Hanroit, *Bull. Soc. Chim. Fr.*, **7**, 171 (1892).
2) J. W. Rothe, *Chem. News.*, **66**, 182 (1892).
3) R. M. Diamond and D. G. Tuck, *Prog. Inorg. Chem.*, **2**, 109 (1960).
4) Y. Marcus and A. S. Kertes, "Ion Exchange and Solvent Extraction of Metal Complexes," Wiley-Interscience, New York (1969), p. 575.
5) T. Sekine and M. Niitsu, *J. Inorg. Nucl. Chem.*, **37**, 1054 (1975).
6) M. Niitsu and T. Sekine, *J. Inorg. Nucl. Chem.*, **38**, 1053 (1976).
7) M. Niitsu and T. Sekine, *J. Inorg. Nucl. Chem.*, **38**, 1057 (1976).
8) D. Dyrssen, *Trans. Royal Inst. Technolog. Stockholm, No.* **188** (1962).
9) T. Sekine, H. Honda, and Y. Zeniya, *J. Inorg. Nucl. Chem.*, **38**, 1347 (1975).
10) E. B. Sandell, "Colorimetric Determination of Traces of Metals" Interscience, New York (1959) p. 522.
11) T. Sekine and T. Tetsuka, *Bull. Chem. Soc. Jpn.*, **45**, 1620 (1972).
12) T. Sekine and D. Dyrssen, *J. Inorg. Nucl. Chem.*, **26**, 1727 (1964).
13) J. O. Hibbits, W. F. Davis, and M. R. Menke, *Talanta*, **4**, 61 (1960).
14) J. O. Hibbits, W. F. Davis, and M. R. Menke, *Talanta*, **8**, 164 (1961).
15) T. Ishimori and E. Nakamura, "Data of Inorganic Solvent Extraction" Res. Rept. Jpn. At. Energy Res. Inst., JAERI-**1047** (1963).
16) T. Ishimori, K. Watanabe, and T. Fujino, *Nippon Genshiryoku Gakkai Shi*, **3**, 19 (1961).
17) N. Saito and A. Yamasaki, *Bull. Chem. Soc. Jpn.*, **36**, 1055 (1963).

BULLETIN OF THE CHEMICAL SOCIETY OF JAPAN, VOL. 49 (9), 2631—2632 (1976)

Circular Dichroism of Nickel(II) and Copper(II) Complexes with Optically Active Diamines Containing a Pyrrolidinyl Group

Tasuku MURAKAMI, Sadao KITAGAWA, and Masahiro HATANO

Chemical Research Institute of Non-Aqueous Solutions, Tohoku University, Katahira, Sendai 980

(Received March 27, 1976)

Synopsis. Nickel(II) and copper(II) complexes of diamines containing a (*S*)-pyrrolidinyl group were prepared and their absorption and CD spectra were measured.

Chelating agents with (*S*)-pyrrolidine ring(s) form stereospecific metal complexes, since the nitrogen atom within the pyrrolidine ring coordinates only with the *S*-configuration.[1,2] As an example, *fac*(*N*)-*Λ*-[Ni(L-prolinate)$_3$]$^-$ was predominantly isolated from an aqueous solution containing nickel(II) carbonate and L-proline.[1] In this note, we wish to report the circular dichroism (CD) of nickel(II) and copper(II) complexes with optically active diamines containing a pyrrolidinyl group.

Experimental

From L-proline, the two optically active diamines, (*S*)-2-(aminomethyl)pyrrolidine (abbreviated to amp) and (*S*)-2-(*N*-methylaminomethyl)pyrrolidine (mamp), were prepared *via* their amides by the usual method.[3] Tris(amp)nickel (II) perchlorate was obtained from 1: 3 mixing of nickel(II) perchlorate

and amp in an aqueous solution. Found: C, 32.43; H, 6.59; N, 14.76%. Calcd for [Ni($C_{15}H_{36}N_6$)] (ClO_4)$_2$: C, 32.28; H, 6.50; N, 15.06%. The absorption and CD spectra of the tris(amp) complex were measured in methanol. For the yellow bis-type complexes of amp and mamp, which have a square planar structure, the spectral measurements were carried out as follows. Difinite amounts of nickel(II) perchlorate and each diamine were mixed in a 1: 2 ratio in an aqueous solution. The blue solution was evaporated and dried in vacuo at 50 °C to give a yellow solid. The solid was dissolved in a difinite amount of nitromethane and the spectra were measured. No absorption band originating from an octahedral species was detected in the spectra obtained in this way.

The copper(II) complex of amp was prepared by 1: 2 mixing of copper(II) nitrate and amp and that of mamp by mixing of copper(II) perchlorate and mamp in an aqueous solution. Found for the bis(amp) complex: C, 30.67; H, 6.35; N, 14.31 %. Calcd for [Cu($C_{10}H_{24}N_4$)] (NO_3)$_2$: C, 30.97; H, 6.24; N, 14.45%. Found for the bis(mamp) complex: C, 38.11; H, 7.62; N, 14.53%. Calcd for [Cu($C_{12}H_{28}O_4$)] (ClO_4)$_2$: C, 38.26; H, 7.49; N, 14.87%.

Results and Discussion

In general, the tris((*S*)-diamine) cobalt(III) complex prefers a *Λ*-configuration of *lel*-form(*Λ*-*δδδ*) to a *Δ*-configuration of *ob*-form.[4] A similar situation was assumed in some tris(diamine)nickel(II) complexes.[5,6] The tris complex of amp, which has an asymmetric carbon atom with an *S*-configuration, is also expected to adopt predominantly a *Λ*-configuration.

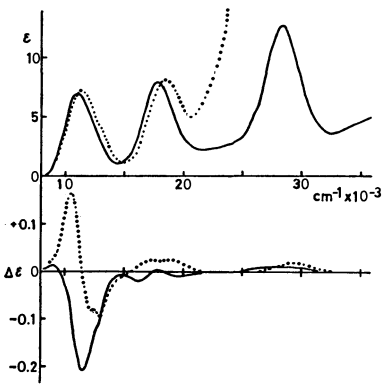

Fig. 1. Absorption and CD spectra of [Ni(amp)$_3$]$^{2+}$ (—) and [Ni((*S*)-3-phenyl-1,2-propanediamine)$_3$]$^{2+}$ (···) in methanol.

Figure 1 shows the absorption and CD spectra of tris(amp)nickel(II) together with those of tris((*S*)-3-phenyl-1,2-propanediamine) complex. The tris(amp) complex exhibits a large negative CD band at the higher wavenumber side and a small positive band at the lower wavenumber side within the region of the first absorption band ($^3A_{2g}\rightarrow{}^3T_{2g}$), which is only one magnetically allowed transition of the three spin-allowed d-d transitions. The CD pattern, a positive component at lower wavenumber and a negative at higher wavenumber, indicates that the complex adopts a *Λ*-configuration as expected.[5,6]

The CD spectra of most of the tris((*S*)-diamine)nickel-(II) complexes have a large positive component and a small negative one at the lower and higher wavenumber sides, respectively, in the region of the first absorption band (Fig. 1; Refs. 5 and 6). In the CD curve of the tris (amp) complex, however, the CD magnitudes of the two components are opposite. This is attributable to

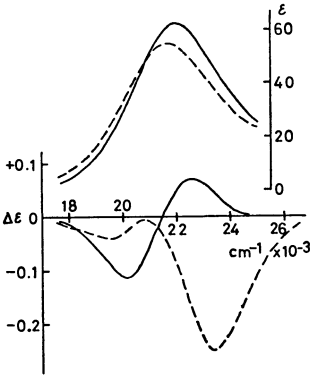

Fig. 2. Absorption and CD spectra of [Ni(amp)$_2$]$^{2+}$ (—) and [Ni(mamp)$_2$] (---) in nitromethane.

the asymmetric nitrogen atom with the *S*-configuration in the pyrrolidine ring. Such a CD curve has also been obtained in the case of tris(L-prolinato)nickel(II).[1]

The absorption and CD spectra of the bis-type yellow complexes of amp and mamp are shown in Fig. 2. The bis(amp) complex exhibits two CD bands, negative at 20200 cm^{-1} and positive at 22500 cm^{-1}. These two bands probably correspond to the two magnetically allowed d-d transitions (d_{xz}, $d_{yz} \rightarrow d_{x^2-y^2}$, $d_{xy} \rightarrow d_{x^2-y^2}$) of a square planar-type nickel(II) complex. In general, the bis-type yellow complex of *S*-diamine exhibits only one negative CD band at about 22000 cm^{-1} in nitromethane.[7,8] Thus, the appearance of the positive CD band in the bis(amp) complex is due to the asymmetric nitrogen atom in the pyrrolidine ring.

On the other hand, the bis(mamp) complex exhibits only negative CD (Fig. 2). This suggests that another asymmetric nitrogen atom of the methyl-substituted amino group in mamp plays the opposite role in CD sign to the asymmetric nitrogen atom in the pyrrolidine ring. Thus the nitrogen atom of the methylsubstituted amino group in the bis(mamp) complex is expected to have an *R*-configuration.

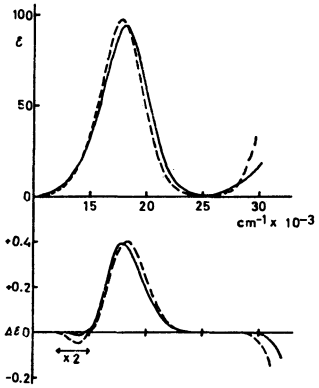

Fig. 3. Absorption and CD spectra of $[Cu(amp)_2]^{2+}$ (—) and $[Cu(mamp)_2]^{2+}$ (---) in water.

Figure 3 shows the absorption and CD spectra of the copper(II) complexes of amp and mamp in aqueous solutions. These two complexes exhibits very similar CD curves which have a main positive CD band at *ca.* 18000 cm^{-1} and a weak negative band at *ca.* 14000 cm^{-1}. Results showing that in some bis(diamine)copper(II) complexes the *N*-substitution of diamine greatly affects the CD spectra have been reported by Morita and Yoshikawa.[9] In the case of mamp, however, the substituted methyl group does not seem to be significant for the CD spectrum of the copper(II) complex. Thus, the *N*-substituted methyl group of mamp may have a different effect on the optical activity of the copper(II) complex from that of the nickel(II) complex.

References

1) J. Hidaka and Y. Shimura, *Bull. Chem. Soc. Jpn.*, **43**, 2999 (1970).
2) S. Kitagawa, T. Murakami, and M. Hatano, *Inorg. Chem.*, **14**, 2347 (1975).
3) M. Saburi, Y. Tsujito, and S. Yoshikawa, *Inorg. Chem.*, **9**, 1476 (1970).
4) E. J. Corey and J. C. Bailar, Jr., *J. Am. Chem. Soc.*, **81**, 2620 (1959).
5) F. Woldbye, "Studies over Optisk Aktivitet," Polyteknisk Forlag, Copenhagen (1969).
6) R. S. Treptow, *Inorg. Chem.*, **7**, 1229 (1968).
7) B. Bosnich, J. H. Dunlop, and R. D. Gillard, *Chem. Commun.*, **1965**, 274.
8) S. Arakawa, T. Nozawa, and M. Hatano, *Bull. Chem. Soc. Jpn.*, **47**, 2643 (1974).
9) M. Morita and S. Yoshikawa, *J. Chem. Soc., Chem. Commun.*, **1972**, 578.

BULLETIN OF THE CHEMICAL SOCIETY OF JAPAN, VOL. 49 (9), 2633—2634 (1976)

Reaction Process between Cobalt Tungstate and Chlorine

Hisao NISHIHARA, Ryoko MATSUZAKI, and Yuzo SAEKI

Research Laboratory of Resources Utilization, Tokyo Institute of Technology, Ookayama, Meguro-ku, Tokyo 152

(Received May 8, 1976)

Synopsis. The reaction between $CoWO_4$ and chlorine proceeds above about 585 °C to form WO_2Cl_2 and $CoCl_2$. In the presence of carbon, the reaction proceeds above about 345 °C to form $CoCl_2$ and WO_3, the WO_3 subsequently reacts with chlorine to form WO_2Cl_2 and $WOCl_4$.

The development of the chlorine process for the recovery of tungsten and cobalt from the sludge generated in the electrochemical grinding of WC-Co cemented carbide is important for the future. The sludge consists of 69% $CoWO_4$, 20% Na_2WO_4, 10% WC, and 1% C. In order to obtain chlorides of tungsten and cobalt from the sludge by selective chlorination, it is necessary to clarify the chlorination processes of the constituents of the sludge.

Concerning the reaction between $CoWO_4$ and chlorine, no information is presently available. In this report, the reaction processes between $CoWO_4$ and chlorine, and between $CoWO_4$ and chlorine in the presence of carbon are examined.

The sample of $CoWO_4$ used was prepared by adding an aqueous $Co(NO_3)_2 \cdot 6H_2O$ solution to an aqueous $Na_2WO_4 \cdot 2H_2O$ solution.[1] Both the salts used were guaranteed reagents. The resulting precipitate was washed with water, air-dried, and dehydrated at 400 °C. The sample obtained was confirmed to be $CoWO_4$[2] by X-ray analysis.

The weight change on the heating of 0.3 g of $CoWO_4$ placed in a quartz crucible in a dry chlorine stream was examined using a thermal balance with a quartz helix. The chlorine flow-rate was maintained at 50 ml/min. and a heating rate of 2.5 °C/min was employed. The sensitivity of the quartz helix was about 0.13 mg/0.01 mm. The results are shown in Fig. 1 (curve (a)).

The TG curve shows that the reaction between $CoWO_4$ and chlorine proceeds above about 585 °C.

The product formed by the chlorination of $CoWO_4$ was examined by heating 6 g of $CoWO_4$ in a quartz boat at a specified temperature and at a chlorine flow-rate of 350 ml/min for 1 h. The products obtained were examined by X-ray analysis[3] using Ni-filtered Cu radiation.

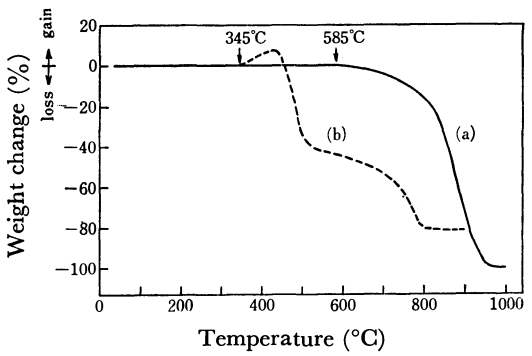

Fig. 1. TG curves of $CoWO_4$ (a), and a mixture of $CoWO_4$ and C(b) in a chlorine stream.

The volatile products obtained by the chlorination of $CoWO_4$ at 600—800 °C were WO_2Cl_2 and $CoCl_2$. No chlorination product was observed in the boat placed in the heating zone. From these experimental results, it was found that the reaction between $CoWO_4$ and chlorine proceeds above about 585 °C to form WO_2Cl_2 and $CoCl_2$.

The chlorination process of metal oxides was affected by the existence of carbon.[4,5] Thus, the effect of the existence of carbon on the reaction between $CoWO_4$ and chlorine was examined. The sample of carbon used was prepared by the pyrolysis of guaranteed reagent grape sugar.

The TG curve of a mixture of $CoWO_4$ and carbon ($CoWO_4$: C=1 : 8 by molar ratio) on heating in a chlorine stream is shown in Fig. 1 (curve (b)).

It is observed that the sample weight increased above about 345 °C, then decreased above about 430 °C, and reached a constant value above about 850 °C. The residue in the crucible, after heating the sample up to 900 °C, was carbon.

The products formed by chlorinating $CoWO_4$ in the presence of carbon at a specified temperature for 0.5 h were examined by X-ray analysis.[2,3,6] The results are shown in Table 1. The weight percentages of the chlorides in the volatile product obtained outside the heating zone were calculated from chemical analysis.[7] The values are shown in parenthesis in Table 1.

Table 1. Chlorination products of a mixture of $CoWO_4$ and C

Temp (°C)	In the boat	Outside the heating zone
380	$CoWO_4$, WO_3, $CoCl_2$	WO_2Cl_2
500	$CoWO_4$, $CoCl_2$	WO_2Cl_2 (>99.9%)
		$WOCl_4$ (<0.1%)
600	$CoWO_4$, $CoCl_2$	$WOCl_2$ (>99.9%)
		$WOCl_4$ (<0.1%)
		$CoCl_2$ (<0.1%)
700	$CoCl_2$	WO_2Cl_2 (95%)
		$WOCl_4$ (2%)
		$CoCl_2$ (3%)
800	$CoCl_2$	WO_2Cl_2 (53%)
		$WOCl_4$ (23%)
		$CoCl_2$ (24%)

At 380 °C, WO_3 and $CoCl_2$ were formed in the boat, and WO_2Cl_2 was obtained outside the heating zone. Above 500 °C, no WO_3 was observed in the boat. Considering the fact that the reaction between WO_3 and chlorine in the presence of carbon begins at about 330 °C and proceeds markedly above about 400 °C to form

volatile WO_2Cl_2 and $WOCl_4$,[4] it appears to be probable that above 500 °C, the WO_3 formed by the chlorination of $CoWO_4$ subsequently reacts with chlorine to form volatile WO_2Cl_2 and $WOCl_4$. Above 600 °C, $CoCl_2$ was obtained outside the heating zone, as well as in the boat. It may be considered that since the vapor pressure of $CoCl_2$ became appreciable above 600 °C,[8] the $CoCl_2$ formed by the chlorination of $CoWO_4$ vaporized and condensed outside the heating zone. Also, the ratio of $WOCl_4$ to WO_2Cl_2 in the volatile product increased with an increase in the reaction temperature. This fact was considered to support the above-mentioned estimate that WO_2Cl_2 and $WOCl_4$ were formed by the chlorination of the WO_3 formed by the chlorination of $CoWO_4$.[4] Furthermore, the weight gain observed at temperatures from 345 to 430 °C in Fig. 1 (curve (b)) was found to be due to the formation of non-volatile WO_3 and $CoCl_2$ by the chlorination of $CoWO_4$.

From these experimental results, the reaction between $CoWO_4$ and chlorine in the presence of carbon proceeds above about 345 °C to form $CoCl_2$ and WO_3, the WO_3 subsequently reacts with chlorine to form WO_2Cl_2 and $WOCl_4$.

In the absence of carbon, the reaction between $CoWO_4$ and chlorine proceeds above about 585 °C to form $CoCl_2$ and WO_2Cl_2, as described above. Considering the fact that the chlorination of WO_3 begins at about 680 °C to form WO_2Cl_2,[4] it appears probable that the WO_2Cl_2 was directly formed by the chlorination of $CoWO_4$ without passing through WO_3.

The authors wish to thank the Ministry of Education for research funds.

References

1) I. K. Taimni and I. S. Ahuya, *Anal. Chim. Acta*, **21**, 3 (1959).
2) ASTM card, 15—867.
3) O. Jarchow, F. Schröder, and H. Schulz, *Z. Anorg. Allgem. Chem.*, **363**, 58 (1968); ASTM card, 15—381.
4) Y. Saeki, T. Takuma, and K. Funaki, *Kogyo Kagaku Zasshi*, **73**, 1093 (1970).
5) Y. Saeki, T. Ōno, and R. Matsuzaki, *Kogyo Kagaku Zasshi*, **74**, 828 (1971).
6) H. Hess and H. Hartung, *Z. Anorg. Allgem. Chem.*, **344**, 157 (1966); ASTM card, 5—363.
7) Y. Saeki, A. Kato, and R. Matsuzaki, *Chem. Lett.*, **1975**, 935.
8) H. Schäfer and K. Krehl, *Z. Anorg. Allgem. Chem.*, **268**, 25 (1952); H, Schäfer, *Z. Anorg. Allgem. Chem.*, **278**, 300 (1955).

BULLETIN OF THE CHEMICAL SOCIETY OF JAPAN, VOL. 49 (9), 2635—2636 (1976)

Cobalt(II) and Nickel(II) Complexes with Schiff Bases Obtained from Salicylaldehyde Derivatives and *N*-(2-Aminoethyl)-piperazine[1)]

Hiro KUMA and Shoichiro YAMADA

Institute of Chemistry, College of General Education, Osaka University, Toyonaka, Osaka 560

(Received June 3, 1976)

Synopsis. Cobalt(II) and nickel(II) complexes have been synthesized with Schiff bases derived from ring-substituted salicylaldehydes and *N*-(2-aminoethyl)-piperazine. Bis-(Schiff base)-metal(II complexes have been isolated. All of them have an octahedral structure, in which the Schiff bases are terdentate. The results are compared with those for complexes of related ligands.

It was reported previously that ligands of the type Ia formed bis(Schiff base)-complexes with cobalt(II) and nickel(II), the structure of which was planar, tetrahedral, octahedral or penta-coordinate, depending upon X as well as upon the metal ion.[2,3)] Ligands of the type Ib, abbreviated as X-salen-pip, contain another nitrogen atom in the heterocyclic ring and might function as a quadridentate ligand. It seems interesting to explore such a possibility, and at the same time to examine if there is any significant electronic effect of the introduced NH group on the donor strength of the β nitrogen atom in the same ligand.

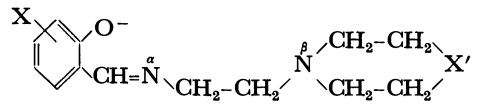

I

(a) X′=CH_2, (b) X′=NH

In the present work, cobalt(II) and nickel(II) complexes with ligands of the type Ib were synthesized and the structure was examined mainly on the basis of spectral and magnetic data. The results were discussed in comparison with those for the corresponding complexes with ligands Ia.

Experimental

Materials. The nickel(II) complexes were prepared by the following method. A solution of nickel(II) chloride hexahydrate (0.01 mol) in ethanol (50 ml) was added to a solution of X-salicylaldehyde (0.022 mol) and *N*-(2-aminoethyl)-piperazine (0.022 mol) at 60 °C. To the resulting solution was added a solution of sodium carbonate in a small amount of water or potassium ethoxide (0.008 mol) in ethanol, and the mixture was stirred at 60 °C for about 3 h. After cooling the precipitate was collected and recrystallized from pyridine or methanol to yield olive-green microcrystals. These nickel(II) complexes are soluble in hot pyridine, slightly soluble in methanol, and insoluble in benzene and chloroform.

The cobalt(II) complexes were prepared in orange microcrystals by a method similar to that for the corresponding nickel (II) complexes. Recrystallization was carried out from pyridine. They are soluble in hot pyridine and almost insoluble in the common organic solvents.

Analytical data of the complexes prepared in the present work are shown in Table 1.

Measurements. Electronic absorption spectra were measured on a Shimadzu MPS-50L spectrophotometer. Magnetic measurements were carried out at room temperature by the Gouy method using $CoHg(SCN)_4$ as a calibrant.

Results and Discussion

Cobalt(II) complexes of the type Co(X-salen-pip)$_2$ were obtained in the present work, X being 5-Cl, 5-Br, and 5-NO_2. These complexes in the solid state show very similar spectra, which have one d-d band at about 10500 cm^{-1} (Table 2). The band maximum is comparatively close to those of the corresponding cobalt(II) complexes of ligands Ia, which were concluded to be octahedral.[3)] The octahedral structure, therefore, is assigned to the present cobalt(II) complexes. In these complexes the ligands are considered to function as a terdentate ligand. In view of the results of the previous studies, it seems most likely that the β nitrogen atom, in addition to the phenolic oxygen and the imine nitrogen atom, is coordinated to the cobalt(II) ion.

These cobalt(II) complexes are of a high-spin type, the values of the magnetic moments at room temperature being 4.6 to 4.8 BM. These values, particularly the lowest value (4.6 BM) for the complex with X=5-NO_2, may appear to be too low for the expected stereochemistry. A similar phenomenon was reported for

TABLE 1. ANALYTICAL DATA OF METAL COMPLEXES OF THE TYPE M(X-salen-pip)$_2$·nH_2O

M(II)	X	n	Calcd, %			Found, %			μ[a)]
			C	H	N	C	H	N	
Co	5-Cl	0.5	51.92	5.87	13.96	51.66	5.69	13.99	4.8
	5-Br	1	44.65	5.19	12.02	44.80	4.92	12.16	4.7
	5-NO_2	1	49.44	5.75	17.75	49.49	5.31	17.52	4.6
Ni	H	0	59.67	6.93	16.06	59.48	6.88	15.92	3.2
	5-Cl	0	52.73	5.79	14.19	52.19	5.74	14.04	3.2
	5-Br	1	44.66	5.19	12.02	44.84	4.88	12.05	3.1
	5-NO_2	0	50.91	5.59	13.70	51.13	5.58	13.74	3.0

a) μ: BM at room temperature.

Table 2. Main d-d absorption band maxima of $M(X\text{-salen-pip})_2 \cdot nH_2O$ in Nujol mulls

M(II)	X	n	ν, kK
Ni	H	0	10.5, 17.5
	5-Cl	0	10.5, 17.5
	5-Br	1	10.5, 17.6
	5-NO_2	0	10.7, 17.5
Co	5-Cl	0.5	10.3
	5-Br	1	10.2
	5-NO_2	1	10.3

octahedral cobalt(II) complexes with ligands of the type Ia and was ascribed to a partial oxidation of the solid.[3]

Nickel(II) complexes of the type $Ni(X\text{-salen-pip})_2$ were obtained in the present work. Since they are only slightly soluble in appropriate solvents, Nujol mull spectra have been measured. The d-d band maxima are shown in Table 2. These complexes exhibit spectra, which are typical of the octahedral nickel(II) complex. The d-d bands at about 10.1—10.4 kK may be assigned to a transition $^3T_{2g} \leftarrow {}^3A_{2g}$ in the scheme of the O_h ligand field symmetry. No absorption bands appear in the lower frequency region, where the five-coordinate and the tetrahedral species are expected to absorb.

They are paramagnetic with magnetic moments of 3.0 to 3.3 BM at room temperature. It is, therefore, presumed that these nickel(II) complexes may have an octahedral structure.

Thus the ligands in these complexes are found to function as a terdentate ligand with the β nitrogen atom bound to the nickel(II) ion. This result differs from that reported previously for ligands of the type Ia. All the nickel(II) complexes of the ligands Ia are diamagnetic and planar in the solid state.[3] The difference in this respect between the ligands Ia and Ib may be ascribed to the electronic factor, since the steric condition is very similar for the ligands of the two types. It is rather surprising that such an apparently slight difference in the ligands gives rise to a remarkable difference in the structure of their nickel(II) complexes.

References

1) Presented, in part, at the 25th National Symposium on Coordination Chemistry, Tokyo, October, 1975.

2) L. Sacconi, P. Nannelli, and U. Campigli, *Inorg. Chem.*, **4**, 818 (1965).

3) L. Sacconi, P. Nannelli, N. Nardi, and U. Campigli, *Inorg. Chem.*, **4**, 943 (1965); L. Sacconi, M. Ciampolini, and G. Speroni, *Inorg. Chem.*, **4**, 1116 (1965).

BULLETIN OF THE CHEMICAL SOCIETY OF JAPAN, VOL. 49 (9), 2637—2638 (1976)

Gamma-Rays Treatment of Odorous Compound in Water

Setsuko IRIE, Norio KATO, and Shosaku KINOSHITA
Radiation Center of Osaka Prefecture, Sakai, Osaka 593

(Received October 28, 1975)

Synopsis. γ-Rays treatment of earthy odors in public water supplies due to the metabolites in Lake Biwa was studied. The odorous compound was isolated from the metabolites and was identified to be geosmin by the use of gas chromatograph-mass spectrometer. The effect of additives and competition reaction with *p*-nitroso-*N*,*N*-dimethylaniline revealed that geosmin is decomposed effectively by hydroxyl radical produced by the radiolysis of water.

Recently, mustry and earthy odors in public water supplies have become a serious social problem.[1,2] Although attempts have been carried out to remove the odors, no satisfactory method has been developed. Activated carbon can remove some of the odors, but it is expensive and the adoption of this method is restricted to water plants of large municipalities. Chlorine has proved to be useful for removing the odors, but it intensifies some odors, particularly the musty-earthy odor of bluegreens. In comparison with these methods, treatment by ionizing radiation is more promising since the radiolysis product of water is known to effectively decompose trace constituents present in dilute solution[3-8] and chemical application of radiation sources is expected to become advantageous with the increase in the use of atomic energy, through it is expensive at present.

Experimental

Separation and Identification of Odorous Metabolites of Actinomyces Biwako-C Strain. Biwako-C strain was obtained from the Murano purification plant. It was inoculated on Romano agar medium.[9] The medium was incubated with a spore suspension prepared from a slant agar medium of the organism, and the culture flasks were incubated at 28 °C for 8 days with shaking. The shaken cultures (10 liters) thus obtained were distilled and the distillate was extracted with methylene chloride. After being dried, the methylene chloride solution was carefully evaporated, giving a small amount of earthy-smelling oil.

Gas chromatography (GC) was carried out on a 20% SE-30 column (glass tube 2 m×3 mm i.d., on 60—80 mesh chromosorb W) with a Shimadzu gas chromatograph (Model GC-5A). Temperature was raised from 100 to 220 °C at 5 °C/min. Nitrogen (40 ml/min) was used as a carrier gas. Gas-mass spectrum (GC-MS) was measured with a Shimadzu gas chromatograph-mass spectrometer (Model LKB 9000). A column of 3% SE-30 (glass tube 2 m×3 mm i.d., on 60—80 mesh chromosorb W) was used for the measurement. Temperatures of the column and ion source were 150 and 230 °C, respectively.

Irradiation Procedures and Analysis. All chemical reagents were of analytical grade. Aqueous solutions were bubbled with Argon for 40 min. prior to irradiation. Oxygen and nitrous oxide were added to the solution by bubbling for 40 min. Irradiation was carried out with ^{60}Co γ-rays (10000 Ci) at room temperature. The extracts were concentrated in a water bath (30 °C) and then analyzed on a gas chromatograph. After γ-irradiation the odor compound was extracted with methylene chloride from the aqueous solution and was analyzed quantitatively with a gas chromatograph with use of bibenzyl as an internal standard. Threshold odor tests (TO test)[10] following the standard method were carried out in order to confirm the removal of the odors and to compare this treatment with other methods.

Results and Discussion

Identification of the Odor Substances. Biwako-C strain produces a strong earthy odor on liquid cultures with Romano agar medium. The odor metabolite was isolated from the culture as follows. It was distilled at 100°C and the distillate was extracted with dichloromethane. The solution was then evaporated carefully under a slightly reduced pressure. After the evaporation of dichloromethane, a scarcely volatile and oily substance with a strong earthy odor was obtained. In order to identify the isolated odor substance, we measured its gas chromatograph spectra with use of the temperature raising attachment. The spectrum has several peaks except those due to solvent, the peak at the retention time of 17 min. being the main one. The retention time is the same as that of geosmin(I).[11] The spectrum

(I)

of geosmin is measured under the same conditions as for the odor substance. The result suggests that the odor substance is ascribed to geosmin. For the sake of confirmation the mass spectrum of the compound was measured with a gas chromatograph-mass spectrometer and compared with that of geosmin. The parent peak is *m/e* 182 and the highest one *m/e* 112. The mass pattern is similar to that of geosmin. These results unambiguously indicate that the odor substance produced by Biwako-C strain, which is found in the raw water of public water supplies, can be identified as geosmin. Geosmin is thus the origin of the objectionable odor of the public water supplies.

The Effect of γ-Irradiation. In order to examine the effect of γ-irradiation for the removal of the odors we adopted a model system-water solutions containing a given concentration of synthesized geosmin. Table 1 gives the values of threshold odor (TO) treated by γ-irradiation of the odorous water with various doses as well as those treated with activated carbon. It is seen that the initial concentration of odor substances, 100, 200, and 400, decreases. The values were determined by the Standard Method for Water Quality. γ-irradiation to a total dose as low as 8.5×10^2 rads is enough to reduce the TO value of the water to the value obtained by carbon treatment (concentration of 50 ppm) for 30

Table 1. Threshold odor reduction of artificially produced odorous water upon exposure to γ-irradiation

Sample	Threshold Odor[a]					
	Original	Activated Carbon		γ-Irradiation (total dose)[b]		
		10 ppm	50 ppm	8.5×10^2 rads	2.5×10^3 rads	8.3×10^3 rads
A	100[c]	40	10	18	10	5
B	200	61	14	20	10	5
C	400	91	30	22	10	5

a) Threshold odor was determined by the Standard Method for Water Quality. b) Dose rates are 5.1×10^3 rad/h, 1.5×10^4 rad/h, 5.0×10^4 rad/h. c) Concentration of geosmin is 1 ppb.

min. The result suggests that γ-irradiation is effective for the reduction of the odor.

Mechanism of the Reduction of the Odor. Although the real system of water supply is not so simple as the model system we adopted, a study of the decomposition process of the synthesized geosmin in distilled water is indispensable to reveal the fundamental mechanism of the reduction of the odor. Figure 1 shows the destruction of geosmin in water by γ-irradiation with various doses. The concentration of geosmin was determined by gas chromatography with the use of bibenzyl as an internal standard. 1 mg geosmin in 1 liter water undergoes almost completely decomposition giving a value less than the least detectable one by γ-irradiation to a total dose of 5.0×10^4 rads with a dose rate of 3.0×10^4 rad/h. The dependence of the rate of destruction on the dose rate is shown in Fig. 2. The slope is 0.62. The value suggests that destruction is caused by the intermediates, which disappear by second order reaction, probably by radicals. In order to confirm this radical mechanism, the effect of additives is examined. Addition of ethanol (0.02 M), a good hydroxyl radical scavenger, decreases the G-value, though the addition of N_2O, which is a hydrated electron scavenger, increases it. The results indicate that the destruction of geosmin is caused by radicals, especially by hydroxyl radical produced by the radiolysis of water.

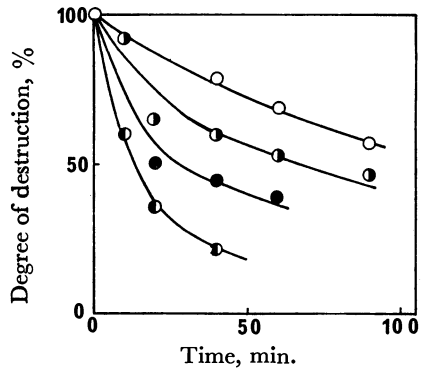

Fig. 1. Destruction of a 1 mg/l geosmin solution. Dose rates are
(○) 2.6×10^3 rad/h, (◑) 5.0×10^3 rad/h, (●) 1.1×10^4 rad/h, (◐) 3.0×10^4 rad/h.

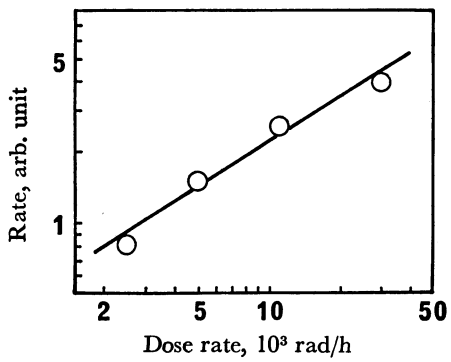

Fig. 2. Dependence of the rate of destruction on the dose rate.

The rate constant of the reaction of OH radicals with geosmin, which is considered to be the primary step for removal of the odors, is determined by competition kinetics using *p*-nitroso-*N*,*N*-dimethylaniline[12] as follows.

$$\mathrm{OH} + \mathrm{PNDA} \xrightarrow{k_1} \text{Product}$$

$$\mathrm{OH} + \text{geosmin} \xrightarrow{k_2} \text{Product}$$

where PNDA is *p*-nitroso-*N*,*N*-dimethylaniline. The decrease of PNDA determined by absorption spectra at 440 nm is expressed by

$$\frac{1}{G(-\mathrm{PNDA})} = \frac{1}{G(\mathrm{OH})}\left\{1+\frac{k_2(\text{geosmin})}{k_1(\mathrm{PNDA})}\right\}$$

The relation between $1/G(-\mathrm{PNDA})$ and (geosmin)/(PNDA) is linear. From the slope the k_2 value of 6.5×10^9 $M^{-1}s^{-1}$ is obtained with use of the k_1 value of 1.1×10^{11} $M^{-1}s^{-1}$.[13] The k value is slightly higher than that of ethanol and phenol. The high k value also confirms the fact that the odor is easily decomposed by γ-irradiation.

References

1) Report of the AWWA Committee on Tastes and Odors *J. Am. Water Works Assn.*, **62**, 59 (1970).
2) T. Kikuchi, T. Mimura, Y. Itoh, Y. Moriwaki, K. Negoro, Y. Masada, and T. Inoue, *Chem. Pharm. Bull.*, **21**, 2339 (1973).
3) C. J. Touhill, E. C. Martin, M. P. Fujihara, D. E. Olesen, J. E. Stein, and G. McDonnel, *J. Water Pollut. Control. Fed.*, **41**, 44 (1969).
4) D. S. Ballantine, *Isotop. Radiat. Technol.*, **8**, 415 (1971).
5) D. M. J. Compton, *Isotop. Radiat. Technol.*, **8**, 453 (1971).
6) N. Suzuki, T. Nagai, H. Hotta, and M. Washino, *Bull. Chem. Soc. Jpn.*, **48**, 2158 (1975). *Int J. Appl. Radiat. Isotopes*, **26**, 726 (1975).
7) A. H. Vajdic, *J. Am. Water Works Assn.*, **6**, 459 (1971).
8) M. Gerrard, *Isotop. Radiat. Technol.*, **8**, 429 (1971).
9) A. H. Romano, and R. S. Safferman, *J. Am. Water Works Assn.*, **55**, 169 (1963).
10) "Standard Method for Water Quality," p. 126 (1970), Japan Water Works Association.
11) N. N. Gerber, *Tetrahedron Lett.*, **1968**, 2971.
12) I. Kraljic, and C. N. Trumbore, *J. Am. Chem. Soc.*, **87**, 2547 (1965).
13) R. L. Willson, C. L. Greenstock, G. E. Adams, R. Wageman, and L. M. Dorfman, *Int. J. Radiat. Phys. Chem.*, **3**, 211 (1971).

BULLETIN OF THE CHEMICAL SOCIETY OF JAPAN, VOL. 49 (9), 2639—2640 (1976)

Preparation of 2,3,4,6-Tetra-*O*-benzyl-D-mannose

Shinkiti KOTO, Naohiko MORISHIMA, Yoko MIYATA, and Shonosuke ZEN

School of Pharmaceutical Sciences, Kitasato University, Shirokane, Minato-ku, Tokyo 108

(Received February 27, 1976)

Synopsis. 2,3,4,6-Tetra-*O*-benzyl-D-mannopyranose was prepared from methyl α-D-mannopyranoside. Improved preparations of 2,3,4,6-tetra-*O*-benzyl-α-D-glucopyranose and -galactopyranose are described.

Since Schmidt, *et al.*[1] announced the preparation of a useful synthetic intermediate, 2,3,4,6-tetra-*O*-benzyl-α-D-glucopyranose, many compounds of this type have been synthesized on various occasions.[2-4] In relation to our search for a systematic synthesis of oligosaccharide,[5,6] this note describes a preparation of 2,3,4,6-tetra-*O*-benzyl-D-mannopyranose (II) from methyl α-D-mannopyranoside. The syrupy compound II is, to the authors' knowledge, a new derivative of D-mannose and was characterized as a crystalline *p*-nitrobenzoate (α-anomer, III).

The following points are worthy of notice. The entire process of preparing the tetra-*O*-benzyl derivative of common hexoses from their corresponding methyl glycosides was significantly improved, in comparison with previous procedures.[1,3,4,7,8]

The use of a large excess of benzyl chloride, the ratio to methyl glycoside being as large as 25: 1 (v/w), in the presence of sodium hydride prevents the reaction from a sudden, violent initiation.[9] Examination of the reaction mixture indicated that the benzylation was essentially finished when the mixture recovered its fluidity with the change of color. The benzylation with use of powdered potassium hydroxide with[2] or without[1] a diluent such as *p*-dioxane was not so practical, because even after much longer heating with occasional additions of fresh potassium hydroxide the reaction was not always complete. It should also be noted that even short unnecessary heating in the hydrolysis step brought about a considerable loss of the desired products.[10]

Experimental

General. Melting points were determined by a Yanagimoto Micro Melting Point apparatus. Optical rotations were measured by a DIP-180 (Japan Spectroscopic) in a jacketed 1-dm cell. PMR was recorded by a Varian S-60-T Spectrometer. TLC was carried out over silica gel No. 7731 (Merck) with coloration by charring with sprayed aqueous sulfuric acid (10%). The column chromatography was done over silica gel (Kanto Kagaku) with irrigation of a mixed solvent system of benzene and 2-butanone.

Methyl α-D-mannopyranoside (Sigma), methyl α-D-glucopyranoside (Tokyo Kasei), and methyl β-D-galactopyranoside (Sigma) were well powdered and stored over phosphorus pentoxide. Sodium hydride (*ca.* 50% in oil, Wako) and benzyl chloride (Koso) were used without any purification.

2,3,4,6-Tetra-O-benzyl-D-mannopyranose (II). A mixture of methyl α-D-mannopyranoside (5 g), sodium hydride (8.5 g, with the oil), and benzyl chloride (125 ml) in a 500-ml round bottomed flask was heated at 125—130 °C (bath temperature) with vigorous stirring (preferably by a magnetic mixer) for 70—90 min under anhydrous conditions. During the course of the reaction, as mentioned earlier,[7] a gray reaction mixture first stiffened with evolution of hydrogen gas and much heat,[11] and then it turned into a yellow thin slurry. After removal of the insoluble material, the solution was concentrated by a water-pump over a boiling water bath to give a yellow syrup (21—25 g), which contained the dispersion oil.

A portion of this syrup (1.0 g) was purified over a column of silica gel to give pure methyl 2,3,4,6-tetra-*O*-benzyl-α-D-mannopyranoside (I), 0.55 g (95%), $bp_{0.01}$ 240—245 °C, $[\alpha]_D^{20}$ +27° (*c* 1, $CHCl_3$), $\delta_H^{CDCl_3}$ (ppm, TMS): 3.31 (3H, singlet, O–C$\underline{H}_3$), 7.30 (15H, singlet, C$_6\underline{H}_5$–), 7.20 (5H, singlet, C$_6\underline{H}_5$–).

Found: C, 75.89; H, 6.92%. Calcd for $C_{35}H_{38}O_6$: C, 75.79; H, 6.91%.

Hydrogenolysis of I (25 mg) over palladium black in methanol at room temperature under 50 psi for 8 h gave crystals (3.7 mg), mp 186—188 °C, which did not depress the melting point of the authentic specimen and showed an IR spectrum (KBr) identical with that of the authentic sample of methyl α-D-mannopyranoside.

The entire syrup mentioned above was immediately heated with a mixture of acetic acid (250 ml) and aqueous sulfuric acid (3M, 30 ml) at 80—85 °C (inside temperature) with good stirring for 30 min. The mixture was diluted with cold water (300 ml) and benzene (300 ml). After washing the organic layer by aqueous sodium hydrogencarbonate and then by water, it was concentrated to give a syrup, which was chromatographed to afford a homogeneous syrup of II, 8.5—10 g (60—72%). Washing this material with cold hexane gave an analytical sample, $[\alpha]_D^{20}$ +11° (*c* 0.9, $CHCl_3$).

Found: C, 75.12; H, 6.67%. Calcd for $C_{34}H_{36}O_6$: C, 75.53; H, 6.71%.

Refluxing II (33 mg) in methanol (0.8 ml) containing methanesulfonic acid (3 μl) for 26 h, followed by chromatography, afforded a homogeneous syrup (21 mg, 61%), which showed an identical PMR spectrum in $CDCl_3$ with that of the above-mentioned I.

2,3,4,6-Tetra-O-benzyl-1-O-p-nitrobenzoyl-α-D-mannopyranose (III). II (0.2 g) was treated with *p*-nitrobenzoyl chloride (0.1 g) in pyridine (1 ml) overnight. The mixture was processed as usual and was chromatographed to give a homogeneous syrup of III as a faster-moving product which was crystallized by diisopropyl ether. Recrystallization from this solvent furnished an analytical sample, 0.12 g (50%), mp 106.5—107 °C, $[\alpha]_D^{20}$ +59° (*c* 0.8, $CHCl_3$), ν_{max}^{KBr} (cm^{-1}): 1730 (carbonyl), 1535, 1355 (nitro), $\delta_H^{CDCl_3}$ (ppm, TMS): 6.46 (1H, a doublet, J=2 Hz), H-1 (equatorial); 7.2—7.4 (20H), C$_6\underline{H}_5$–; a multiplet centered at 8.13 (4H), –C$_6\underline{H}_4$–.

Found: C, 71.58; H, 5.85; N, 1.87%. Calcd for $C_{41}H_{39}NO_9$: C, 71.39; H, 5.70; N, 2.03%.

The β-anomer of III was obtained as a slower-moving syrupy product, which was further washed with cold hexane, $[\alpha]_D^{20}$ −11° (*c* 0.5, $CHCl_3$), $\delta_H^{CDCl_3}$ (ppm TMS): 5.57 (1H, a doublet, J=2 Hz), H-1 (axial); 7.2—7.4 (20 H), C$_6\underline{H}_5$–; a quasi-singlet at 8.15, –C$_6\underline{H}_4$–.

Found: C, 71.07; H, 5.81; N, 1.97%. Calcd for $C_{41}H_{39}NO_9$: C, 71.39; H, 5.70; N, 2.03%.

2,3,4,6-Tetra-O-benzyl-α-D-glucopyranose. The hydrol-

ysis step was carried out at 80—85 °C for 30 min by employing a mixture of acetic acid (250 ml) and aqueous hydrochloric acid (6M, 35 ml) for a syrupy benzylation product (*ca.* 25 g) obtained from 5 g of methyl α-D-glucopyranoside. The hydrolyzate was diluted with cold water (300 ml) and hexane (50 ml) with stirring. Crude crystals (7.5—8 g) were recrystallized from hot ethyl acetate (100 ml) to give a pure material, 4.5—5 g (32—36%), mp 149—149.5 °C, $[\alpha]_D^{20}$ +48° (*c* 1, dioxane). [Lit,[1] mp 148 °C, $[\alpha]_D^{25}$ +48.3° (*c* 3, dioxane)]. (Found: C, 75.59; H, 6.78%).

2,3,4,6-Tetra-O-*benzyl*-α-D-*galactopyranose.* The crude oily benzylation product (*ca.* 25 g) obtained from 5 g of methyl β-D-galactopyranoside gave methyl 2,3,4,6-tetra-*O*-benzyl-β-D-galactopyranoside as crystals, 11.4 g (80%), mp 82—83 °C. [Lit,[4] 80—81 °C].

This galactoside (10 g) was hydrolyzed by heating at 80—85 °C for 20 min with a mixture of acetic acid (100 ml) and aqueous sulfuric acid (3M, 12 ml). The mixture was processed in the same manner as II and chromatographed to give a syrup. This was crystallized from cyclohexane containing little diisopropyl ether to give a practically pure product, 5.4 g (54%), mp 63—66 °C, $[\alpha]_D^{20}$ +74° (*c* 0.8, benzene). [Lit,[5] mp 66—68 °C, $[\alpha]_D^{20}$ +77° (*c* 2.3, benzene)]. (Found: C, 75.02; H, 6.62%).

References

1) O. T. Schmidt, T. Auer, and H. Schmadel, *Chem. Ber.*, **93**, 556 (1960).

2) R. Barker and H. G. Fletcher, jr., *J. Org. Chem.*, **26**, 4605 (1961); S. Tejima and H. G. Fletcher, Jr., *i. id.*, **28**, 2999 (1963); C. P. J. Glaudemans and H. G. Fletcher, J ., *ibid.*, **28**, 3004 (1963); N. Pravdic and D. Keglevic, *Tetrahedron*, **21**, 1987 (1965); R. Harrison and H. G. Fletcher, Jr., *J. Org. Chem.*, **30**, 2317 (1965); T. Ueno, N. Kurihara, S. Hashimoto, and M. Nakajima, *Agr. Biol. Chem.*, **31**, 1346 (1967); S. Koto, T. Tsumura, Y. Kato, and S. Umezawa, *Bull. Chem. Soc. Jpn.*, **41**, 2765 (1968); A. Hasegawa, N. Kurihara, D. Nishimura, and M. Nakajima, *Agr. Biol. Chem.*, **32**, 1123 (1968); R. K. Ness, H. W. Diehl, and H. G. Fletcher, Jr., *Carbohydrate Res.*, **13**, 23 (1970); M. Dejter-Juszynski and H. M Flowers, *ibid.*, **18**, 219 (1971); Y. Nishimura, T. Tsuchiya, and S. Umezawa, *Bull. Chem. Soc. Jpn.*, **44**, 2521 (1971); S. Umezawa, Y. Nishimura, H. Hineno, K. Watanabe, S. Koike, T. Tsuchiya, and H. Umezawa *ibid.*, **45**, 2847 (1972); H. Umezawa, T. Tsuchiya, R. Muto, and S. Umezawa, *ibid.*, **45**, 2842 (1972); S. Koto, Y. Takebe, and S. Zen, *ibid.*, **45**, 291 (1972); Y. Takagi, T. Tsuchiya, and S. Umezawa, *ibid.*, **46**, 1261 (1973); S. Koto, N. Kawakatsu, and S. Zen, *ibid.*, **46**, 876 (1973); F. Micheel, O.-E. Brodde, and K. Reinking, *Justus Liebigs Ann. Chem.*, **1974**, 124; J. M. J. Flechet and H. H. Baer, *Carbohyd. Res.*, **42**, 369 (1975).

3) P. W. Austin, F. E. Hardy, J. G. Buchanan, and J. Baddiley, *J. Chem. Soc.*, **1964**, 2128.

4) P. W. Austin, F. E. Hardy, J. G. Buchanan, and J. Baddiley, *J. Chem. Soc.*, **1965**, 1419.

5) S. Koto, Y. Hamada, and S. Zen, *Chem. Lett.*, **1975**, 587.

6) S. Koto, N. Morishima, and S. Zen, *Chem. Lett.*, **1976**, 61.

7) M. E. Tate and C. T. Bishop, *Can. J. Chem.*, **41**, 1801 (1963).

8) H. H. Baer, J. M. J. Flechet, and U. Williams, *Can. J. Chem.*, **52**, 3337 (1974).

9) Diminution of the ratio even to 20: 1 often allowed the reaction to run out of control.

10) For example, the yield of tetra-*O*-benzylglucose was less than 7% after heating at 80—85 °C for 50 min.

11) This violent reaction usually continued for about 10 min.

BULLETIN OF THE CHEMICAL SOCIETY OF JAPAN, VOL. 49 (9), 2641—2642 (1976)

A New Type of Induced Decomposition. IV.[1] Pyrolysis of *t*-Butyl Peroxy-3-butenoate in the Gas Phase

Tameichi OCHIAI, Masayuki YOSHIDA, and Osamu SIMAMURA

Department of Chemistry, Faculty of Science, Tokyo University, Hongo, Tokyo 113

(Received March 8, 1976)

Synopsis. *t*-Butyl peroxy-3-butenoate decomposes in the gas phase at 115 °C to give carbon dioxide, 1-butene, acetone, 1,5-hexadiene, methane, and ethane. Experiments with iodine, an efficient radical scavenger, indicate the operation of induced decomposition. The mechanism of the formation of 1-butene and 1,5-hexadiene is discussed in terms of a new type of induced decomposition.

In previous communications[1] we reported that *t*-butyl peroxy-esters derived from α,β-unsaturated carboxylic acids undergo a new type of induced decomposition and proposed a mechanism, in which radicals (S·) derived from solvent (SH) by hydrogen-abstraction add to the unsaturated bond of a peroxide to give an intermediate radical (I) carrying an odd electron on the carbon atom β to the carboxyl group and this radical subsequently undergoes β-scission to afford an olefin, a molecule of carbon dioxide, and a *t*-butoxyl radical (Reactions 1 and 2 in the following scheme).

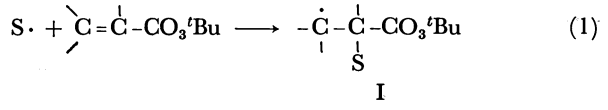

(1)

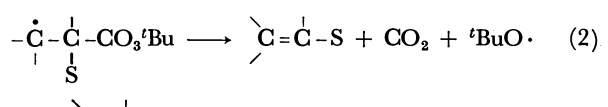

(2)

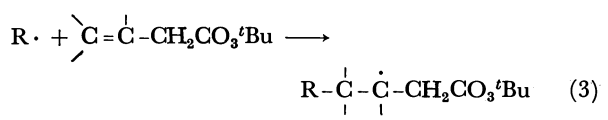

(3)

SH=solvent

Radicals similar to structure I can also be generated by addition of a radical to the γ-position of β,γ-unsaturated peroxy-esters (Reaction 3), which therefore may undergo β-scission in a way similar to Reaction 2. With the view of examining such a possibility the decomposition of *t*-butyl peroxy-3-butenoate was studied.

Results and Discussion

The results of the decomposition of *t*-butyl peroxy-3-butenoate (II) in the gas phase at 115 °C are summarized in Table 1. The major products identified by VPC were carbon dioxide, 1-butene, 1,5-hexadiene, acetone, methane, and ethane, and are readily explained by assuming the following series of reactions.[2] Acetone and ethane result from Reactions 5 and 6. Methane arises from methyl radicals by hydrogen-abstraction from some hydrogen donating species in the system (Reaction 7).

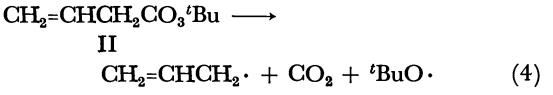

(4)

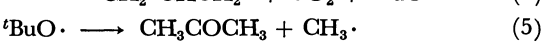

(5)

(6)

(7)

SH=hydrogen donor

TABLE 1. PRODUCTS FROM PYROLYSIS OF *t*-BUTYL PEROXY-3-BUTENOATE AT 115 °C FOR 3 h

	Run 1	Run 2
Peroxybutenoate, mmol	0.585	0.519
Products, mmol		
Carbon dioxide	0.599 (1.02) [a]	0.512 (0.986)
1-Butene	0.160 (0.274)	0.138 (0.266)
Acetone	0.444 (0.759)	0.389 (0.749)
1,5-Hexadiene	0.136 (0.232)	0.120 (0.231)
Methane	0.054 (0.093)	0.053 (0.101)
Ethane	0.083 (0.144)	0.067 (0.129)

a) Yields in mol per 1 mol of the peroxybutenoate are given in parentheses.

The formation of 1-butene and 1,5-hexadiene is satisfactorily explained, as is anticipated in the introduction, thus:

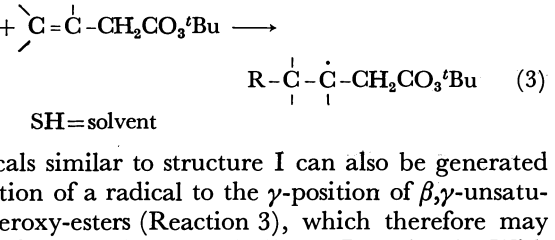

(8)

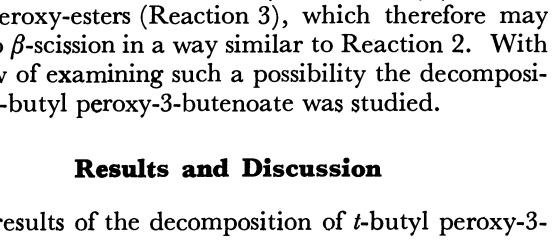

(9)

The addition of a methyl radical to the peroxy-3-butenoate gives 1-(*t*-butylperoxycarbonylmethyl)propyl radical, which then decomposes into 1-butene, a molecule of carbon dioxide, and a *t*-butoxyl radical (Reaction 8). 1,5-Hexadiene is given through a similar addition-elimination mechanism (Reaction 9).

An alternative mechanism for the formation of 1-butene and 1,5-hexadiene is the combination of the allyl and methyl radical (Reactions 10 and 11):

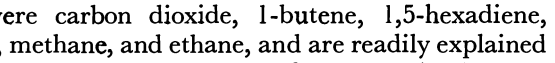

(10)

(11)

The exclusive operation of this mechanism, which does not involve any induced path, is ruled out by the experiments summarized in Table 2. The peroxy-3-butenoate was heated in the presence of iodine, an effective radical scavenger, or nitrogen, inert molecules towards radicals, at 115 °C for 1.0 h, and the amount of carbon dioxide evolved was measured. Since the peroxy-3-butenoate affords carbon dioxide quantitatively (Table 1), the amount of carbon dioxide obtained corresponds to that

Table 2. Decomposition of *t*-butyl peroxy-3-butenoate in the presence of iodine or of nitrogen[a)]

Run	Peroxy-butenoate mmol	I_2 mmol	N_2 mmol	CO_2 mmol produced
1	0.281	nil	0.897	0.244 (0.868) [b)]
2	0.286	nil	0.854	0.246 (0.860)
3	0.300	nil	0.890	0.261 (0.870)
4	0.289	0.168	nil	0.179 (0.620)
5	0.277	0.601	nil	0.034 (0.12)
6	0.294	0.564	nil	0.073 (0.25)
7	0.287	0.618	nil	0.056 (0.20)

a) At 115 °C, for 1.0 h, in the gas phase. b) Yields in mol per 1 mol of peroxide are given in parentheses.

of the peroxy-3-butenoate decomposed. Under the above conditions 87% of the starting peroxy-3-butenoate underwent the decomposition in the presence of 0.9 mmol of nitrogen, while only 62% of the peroxy-3-butenoate was decomposed in the presence of 0.17 mmol of iodine, and the extent decomposition further decreased with increasing iodine concentration. These findings indicate that iodine scavenges efficiently the free radicals which otherwise will cause induced decomposition of the peroxy-3-butenoate and thus support the operation of an induced pathway for the formation of 1-butene and 1,5-hexadiene.

Experimental

t-Butyl Peroxy-3-butenoate. 3-Butenoic acid[3)] (4.7 g), bp 69.0—70.0 °C/12 mmHg, was heated under reflux for 30 min with 1.2 molar equivalents of thionyl chloride, and the resulting 3-butenoyl chloride (3 g) was distilled, bp 95—96 °C. A solution of this chloride (1.68 g) in 8 ml of anhydrous pentane was added to a stirred solution of *t*-butyl hydroperoxide (bp 32 °C/12 mmHg, 1.91 g) and pyridine (1.36 g) in anhydrous pentane (7 ml) at −20——25 °C over a period of 1.3 h. The resulting mixture was allowed to warm to 0 °C, the supernatant solution decanted into a vessel containing ice–water, the remaining pyridinium chloride washed twice with pentane, and the washings added to the ice–water. The organic layer was separated, washed successively with 4 ml of 5% sulfuric acid, 4 ml of 10% aqueous sodium carbonate, and water. and dried with anhydrous sodium sulphate. After removal of pentane under reduced pressure, the oily residue was distilled to give 1.5 g (59%) of *t*-butyl peroxy-3-butenoate, bp 16 °C/2 mmHg (Found: C, 60.60; H, 9.04%. Calcd for $C_8H_{14}O_3$: C, 60.74; H, 8.92%. Purity, 96% by iodometric titration[4)]), IR (neat) 1645 ($\nu_{C=C}$) and 1785 cm^{-1} ($\nu_{C=O}$).

Pyrolysis of t-*Butyl Peroxy-3-butenoate.* A typical run was as follows. *t*-Butyl peroxy-3-butenoate (0.58 mmol) was placed in a glass vessel (730 ml), which was then degassed (three freeze-thaw cycles), sealed and immersed in an oil bath maintained at 115 °C, and the peroxy-ester was allowed to decompose in the gas phase for 3 h. After cooling to room temperature, the vessel was attached to a vacuum system, and the products were transferred to a sampling tube for VPC analysis.

Analyses were carried out with a Perkin Elmer Vapor Fractometer Model 154-D by using helium as carrier gas and the following stainless steel column: 1) A 2m column packed with Silica gel, Type 15 at 51 °C for analysis for methane, ethane, and carbon dioxide; 2) a 2m column packed with dimethylsulfolane at 60 °C for analysis for 1-butene, 1,5-hexadiene and acetone. For authentic materials for comparison commercial products were used except 1,5-hexadiene, which was prepared according to a published procedure.[5)]

References

1) Part I: N. Muramoto, T. Ochiai, O. Simamura, and M. Yoshida, *Chem. Commun.*, **1968**, 717; Part II: *Bull. Chem. Soc. Jpn.*, **49**, 2518 (1976); Part III: T. Ochiai, Y. Usuda, M. Yoshida, and O. Simamura, *ibid.*, **49**, 2522 (1976).

2) The peroxybutenoate is thought to undergo a synchronous two-bond scission since the allyl radical is relatively stable [P. D. Bartlett and R. R. Hiatt, *J. Am. Chem. Soc.*, **80**, 1398 (1958)].

3) E. Rietz, *Org. Synth.*, Coll. Vol. III, 851 (1955).

4) L. S. Silbert and D. Swern, *Anal. Chem.*, **30**, 385 (1958).

5) A. Turk and H. Chanan, *Org. Synth.*, Coll. Vol. III, 121 (1955).

BULLETIN OF THE CHEMICAL SOCIETY OF JAPAN, VOL. 49 (9), 2643—2644 (1976)

Reduction of α,β-Unsaturated Nitrile to Saturated Nitrile with Sodium Borohydride

Fumio TODA and Mutsushi KANNO

Department of Industrial Chemistry, Faculty of Engineering, Ehime University, Matsuyama 790

(Received April 1, 1976)

Synopsis. α,β-Unsaturated nitrile (**1**) was easily reduced to saturated nitrile (**2**) with sodium borohydride. Phenyl- (**7a**) and 2-phenanthryl-cyanoacetylene (**7b**) were also reduced with sodium borohydride to the saturated nitriles, **8a** and **8b**, respectively.

The reduction of α,β-unsaturated nitrile (**1**) to saturated nitrile (**2**) can be achieved in poor yield by photochemical,[1] electrochemical,[2] and catalytic hydrogenation.[3] Profitt *et al.*[4] reported that magnesium in methanol is a good reagent for the reduction of **1** to **2**. On the other hand, we have found that sodium borohydride ($NaBH_4$) is effective for the reduction and that $NaBH_4$ is useful for the reduction of conjugated cyanoalkyne (**7**) to cyanoalkane (**8**).

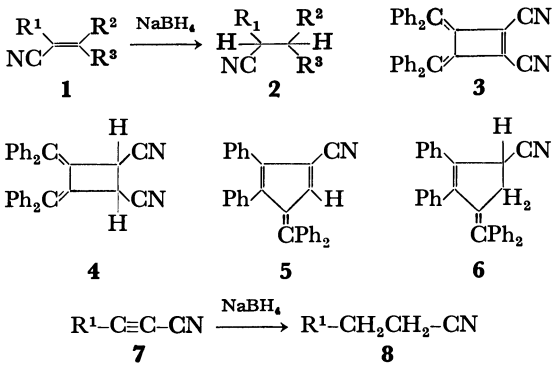

Scheme 1.

Treatment of conjugated cyanoalkanes (**1a—h**) with $NaBH_4$ afforded the reduction products (**2a—c** and **2f**) in the yields summarized in Table 1. In the cases of **1e**, **1g**, and **1h**, however, the reduction of their double bonds was accompanied by the substitution with hydrogen of the nitro and methoxyl groups which had been bound to olefinic carbon. The substitution of nitro group with hydrogen is in contrast with the $NaBH_4$ reduction of nitroolefin to nitroalkane.[6] The cyclic cyanoalkenes, 1,2-dicyano-3,4-bis(diphenylmethylene)-1-cyclobutene (**3**) and 2-cyano-3,4,6,6-tetraphenylfulvene (**5**), were also easily reduced with $NaBH_4$ to their dihydro derivatives, **4** (85) and **6** (90%), respectively. On the contrary, the catalytic reduction of **3** on Raney-Ni afforded **4** only in 20% yield.

Since the $NaBH_4$ reduction product of **3** (**4**) was identical with the catalytic reduction product of **3**, **4** would have a *cis*-form, and the former reduction seems to proceed stereospecifically. Nevertheless, since the *rac*-form[7] of **2b** isomerized into the *meso*-form (**2b**) under the reduction conditions, it is not clear whether the steric course of the $NaBH_4$ reduction is stereospecific or not.

Table 1. Yields, melting points and NMR spectral data of the $NaBH_4$ reduction products (**2**, **4**, **6**, and **8**)

	Reactant R¹	R²	R³	Product	Yield (%)	Mp (°C)	τ_{CH} (ppm)
1a	Ph	CN	H	**2a**[5]	56	67— 68 (lit,[5] 67—68)	—
1b	Ph	CN	Ph	**2b**[7]	92	235 (lit,[7] 238)	4.80 (s)
1c	Ph	H	Ph	**2c**[8]	82	51— 52 (lit,[8] 52)	6.00 (1H, t, J=7 Hz) 6.90 (2H, d, J=7 Hz)
1d	Ph	Ph	H	**2c**	100	51— 52 (lit,[8] 52)	6.00 (1H, t, J=7 Hz) 6.90 (2H, d, J=7 Hz)
1e	Ph	NO_2	Ph	**2c**	92	51— 52 (lit,[8] 52)	6.00 (1H, t, J=7 Hz) 6.90 (2H, d, J=7 Hz)
1f	*p*-NO_2-C_6H_4–	H	Ph	**2f**	66	92— 93	5.75 (1H, t, J=7 Hz) 6.75 (2H, d, J=7 Hz)
1g	*p*-NO_2-C_6H_4–	NO_2	Ph	**2f**	92	92— 93	5.75 (1H, t, J=7 Hz) 6.75 (2H, d, J=7 Hz)
1h	*p*-NO_2-C_6H_4–	OMe	Ph	**2f**	75	92— 93	5.75 (1H, t, J=7 Hz) 6.75 (2H, d, J=7 Hz)
7a	Ph	—	—	**8a**[8]	70[a]	oil	—
7b	2-$C_{14}H_9$–	—	—	**8b**	78	118—120	6.95 (2H, t, J=6 Hz) 7.25 (2H, t, J=6 Hz)
3	—	—	—	**4**	85	231—232	5.63 (s)
5	—	—	—	**6**	90	196—198	4.65 (1H, t, J=6 Hz) 6.52 (2H, d, J=6 Hz)

a) The yield was calculated on the basis of the crude oil.

The $NaBH_4$ reduction was also useful for conjugated cyanoalkyne. The treatment of phenyl- (**7a**) and 2-phenanthrylcyanoacetylene (**7b**) with $NaBH_4$ afforded the tetrahydro derivatives, **8a** and **8b**, respectively (Table 1).

Experimental

All the melting points are uncorrected. The NMR spectra were measured in $CDCl_3$.

General Procedure of the $NaBH_4$ Reduction. To a stirred solution of conjugated cyanoalkene or cyanoalkyne (0.2 g) in 99% EtOH (20 ml) was added $NaBH_4$ by portions until gas evolution ceased (*ca.* 0.1 g) at room temperature. All the reactions were slightly exothermic and ceased within 1 h. The crude crystals formed by the decomposition of the reaction mixture with water were filtered and then recrystallized. When oily material was formed at the decomposition, it was taken up in ether. The ethereal solution was washed with water and dried over anhydrous Na_2SO_4. The crude crystals remaining after the evaporation of the solvent were recrystallized. O fthe reduction products, **2a**—**c** and **8a** were characterized by the comparison of their infrared spectra and/or melting points with those of authentic samples. All the new reduction products (**2f**, **4**, **6**, and **8b**) were characterized on the basis of their NMR spectra (Table 1) and elemental analyses. The analytical data are as follows:

2f) Found: C, 71.28; H, 3.97%. Calcd for $C_{15}H_{12}O_2N_2$: C, 71.41; H, 4.80%.

4) Found: C, 88.17; H, 5.02%. Calcd for $C_{32}H_{22}N_2$: C, 88.45; H, 5.10%.

6) Found: C, 90.58; H, 5.49%. Calcd for $C_{31}H_{23}N$: C, 90.92; H, 5.66%.

8b) Found: C, 88.21; H, 5.45%. Calcd for $C_{17}H_{13}N$: C, 88.28; H, 5.67%.

References

1) M. Pereyre, G. Colin, and J. Valade, *Tetrahedron Lett.*, **1967**, 4805.

2) A. P. Tomilov and V. A. Kimov, *Electrokhimiya*, **3**, 232 (1967); *Chem. Abstr.*, **66**, 121521s (1967).

3) D. V. Sokolskii and L. V. Volkova, *Izv. Akad. Nauk Kaz. SSR., Ser. Khim.*, **14**, 69 (1964); *Chem. Abstr.*, **62**, 3933f (1965).

4) J. A. Profitt, D. S. Watt, and E. J. Corey, *J. Org. Chem.*, **40**, 127 (1975).

5) A. Cobb, *J. Am. Chem. Soc.*, **45**, 604 (1923).

6) A. Hassner and C. Heathcock, *J. Org. Chem.*, **29**, 1350 (1964).

7) W. G. Kofron and C. R. Hauser, *J. Org. Chem.*, **35**, 2089 (1970).

8) C. J. Pouchert, "The Aldrich Library of Infrared Spectra," Aldrich Chemical Co., Inc., New York (1970), p. 816.

BULLETIN OF THE CHEMICAL SOCIETY OF JAPAN, VOL. 49 (9), 2645—2646 (1976)

Photochemical Conversion of Methoxyketene Intermediate into Methyl Ester in the Photolysis of 2-Methoxy-3-diphenylmethyl-4-diphenylmethylene-2-cyclobuten-1-one

Fumio Toda, Yozo Todo, and Eishiro Todo

Department of Industrial Chemistry, Faculty of Engineering, Ehime University, Matsuyama 790

(Received April 12, 1976)

Synopsis. The photolysis of methylenecyclobutenone in the presence of benzophenone or oxygen affords the one carbon diminished product, methyl 4,4-diphenyl-2-diphenylmethyl-2,3-butadienoate. The reaction pathway is discussed.

Nozaki and his collaborators reported that the photochemical conversion of diphenylketene into benzophenone under nitrogen atmosphere in a higher yield than 50% is puzzling.[1] We found that the photolysis of methylenecyclobutenone (**1**) in the presence of benzophenone or oxygen affords the one carbon diminished product, methyl 4,4-diphenyl-2-diphenylmethyl-2,3-butadienoate (**5**), and that the reaction can well be rationalized by means of the cycloaddition reaction of the methoxyketene intermediate (**2**) initially produced by the α-cleavage of **1**, with benzophenone or oxygen.

The irradiation of a solution of **1** and benzophenone in benzene under nitrogen atmosphere for 5 h afforded **5** in 31% yield. The structure of **5** was elucidated on the basis of its reaction with bromine which affords 3-bromo-4,4-diphenyl-2-diphenylmethyl-2-buten-4-olide (**6**). Base-catalyzed hydrolysis of **5** afforded the corresponding acid (**7**). The formation of **5** can be interpreted by assuming the cycloaddition product (**3**) of **2** and benzophenone as an intermediate. The intermediacy of **2** is undoubted, since the photochemical α-cleavage of methylenecyclobutenone to alleneketene has been established.[2] The ring cleavage of **3** can give **5** and diphenylketene, the latter being converted into benzophenone in the same manner as reported.[1]

The photolysis of **1** in benzene under oxygen atmosphere also afforded **5** in 10% yield. This can be interpreted by assuming **4** as an intermediate, decarboxylation of which affords **5**. Since neither benzophenone nor oxygen is necessary for the photochemical α-cleavage of methylenecyclobutenone,[2] benzophenone and oxygen would only be used for the formation of **3** and **4**, respectively. In their absence, the photolysis of **1** in benzene did not give **5**, **1** being recovered unchanged. This shows that the photochemical α-cleavage of **1** to **2** is reversible.

Experimental

All the melting points are uncorrected. Photolysis was carried out at room temperature, with light from a 400-W high-pressure mercury lamp (Riko Kagaku Sangyo Co.), filtered through Pyrex glass. The IR, UV, and NMR spectra were measured in Nujol mull, $CHCl_3$, and $CDCl_3$, respectively. The mass spetrum was measured with an ionization energy of 75 eV.

*Photolysis of **1** in the Presence of Benzophenone.* A solution of **1** (0.1 g) and benzophenone (0.07 g) in benzene (250 ml) was irradiated under nitrogen atmosphere for 8 h. The crude crystals remaining after evaporation of the solvent were recrystallized from MeOH to afford **5** as colorless prisms; 0.03 g (31%); mp 135—136 °C. IR: 1940 (C=C=C), 1720 (C=O), and 1240 cm^{-1} (ester); λ_{max}: 252 nm (ε, 18800); NMR: 2.5—3.4 (m, Ph, 20H), 4.57 (s, CH, 1H), and 6.34τ (s, Me, 3H); MS *m/e* (rel intensity): 416 (M^+, 25), 385 (M^+—OMe, 56), 357 (385—CO, 66), and 167 ($Ph_2\overset{+}{C}H$, 100).

Found: C, 86.37; H, 5.73%. Calcd for $C_{30}H_{24}O_2$: C, 86.51; H, 5.81%.

*Photolysis of **1** under Oxygen Atmosphere.* A solution of **1** (0.1 g) in benzene (250 ml) was irradiated under oxygen atmosphere for 15 h. The crude crystals remaining after evaporation of the solvent were recrystallized from MeOH to afford **5**; 0.01 g (10%).

*Conversion of **5** into **6**.* Bromine (0.03 g) was added at room temperature to a solution of **5** (0.1 g) in $CHCl_3$ (10 ml). The crude crystals remaining after evaporation of the solvent were recrystallized from AcOEt to afford **6** as colorless prisms; 0.1 g (86%); mp 150 °C. IR: 1760 (C=O), 1630 (C=C), and

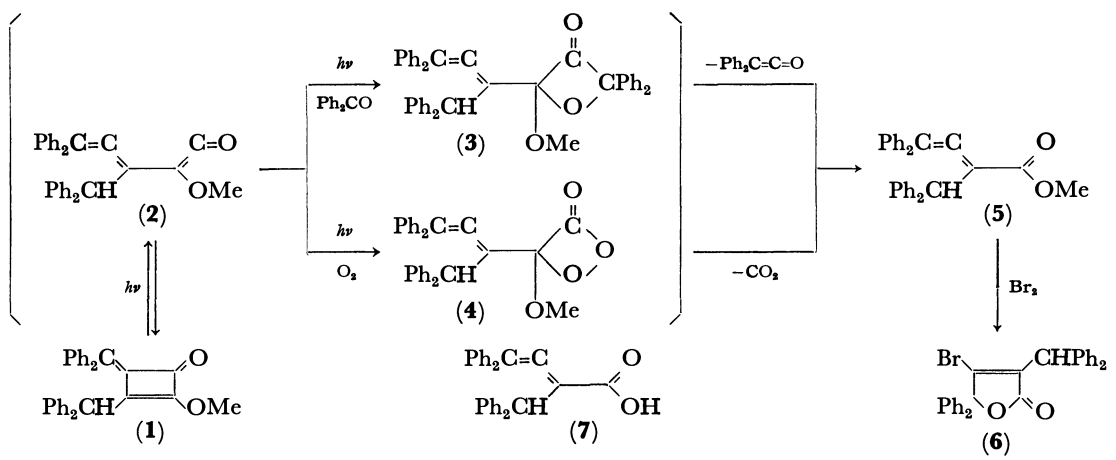

1140 cm^{-1} (lactone); λ_{max}: 245 nm (ε, 9600); NMR: 2.4—2.8 (m, Ph, 20H) and 4.38τ (s, CH, 1H).

Found: C, 72.42; H, 4.41%. Calcd for $C_{29}H_{21}O_2Br$: C, 72.35; H, 4.40%.

Hydrolysis of ***5***. A solution of **5** (0.1 g) in 5% KOH–MeOH (20 ml) was heated under reflux for 5 h. The crude crystals formed after the decomposition of the reaction mixture with water were recrystallized from hexane–CH_2Cl_2 to afford **7** as colorless needles; 0.09 g (93%); mp 185—186 °C. IR: 2620 (CO_2H), 1940 (C=C=C), and 1670 cm^{-1} (C=O); λ_{max}: 243 (19200) and 253 nm (ε, 19200); NMR: −1.33 (s, CO_2H, 1H), 2.6—3.1 (m, Ph, 20H), and 4.61 τ (s, CH, 1H).

Found: C, 86.49; H, 5.42%. Calcd for $C_{29}H_{22}O_2$: C, 86.54; H, 5.51%.

References

1) H. Nozaki, M. Nakano, and K. Kondo, *Tetrahedron*, **22**, 477 (1966).

2) F. Toda and E. Todo, *Chem. Lett.*, **1974**, 1279.

BULLETIN OF THE CHEMICAL SOCIETY OF JAPAN, VOL. 49 (9), 2647—2648 (1976)

Photochemical Reduction of 2,3-Dihydro-2,3-methano-1,4-naphthoquinones with Xanthene

Kazuhiro MARUYAMA and Soji TANIOKA

Department of Chemistry, Faculty of Science, Kyoto University, Kyoto 606

(Received April 14, 1976)

Synopsis. Photochemical reduction of 2,3-dihydro-2-methyl-2,3-methano-1,4-naphthoquinone (**1a**) and 2,3-dihydro-2,3-dimethyl-2,3-methano-1,4-naphthoquinone (**1b**) with xanthene was investigated. 6,7,8,9-Tetrahydrobenzocycloheptene-5,9-dione derivatives and stereochemical isomers of the so-called "1,2-adducts" of xanthene to carbonyl groups were isolated as the reaction products. CIDNP technique was applied for the examination of the course of the reactions.

The titled compounds have two vicinal carbonyl groups connected with cyclopropane ring in the molecule, and their photochemical behavior is quite interesting compared with those of 1,4-naphthoquinone and of 1,4-naphthoquinone 2,3-epoxide. Their relative photochemical reactivities for hydrogen abstraction from xanthene are in the following order: 2-methyl-1,4-naphthoquinone > 2,3-dihydro-2-methyl-2,3-methano-1,4-naphthoquinone > 1,4-naphthoquinone 2,3-epoxide.[1] In this work photochemical reaction of **1a** and **1b** with xanthene was investigated in detail.

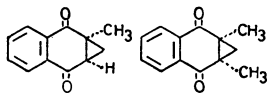

(**1a**) (**1b**)

Experimental

Irradiation of a benzene solution of **1a-b** and xanthene (1:2, M/M) for six hours at a room temperature gave four major products in the respective yields given in the following schemes. The yields of products are mean values of several runs. The products, **2a**; mp 145—146 °C, IR (KBr); $\nu_{C=O}$=1670, ν_{OH}=3400 cm^{-1}, and **3a**; mp 216—218 °C, IR (KBr); $\nu_{C=O}$=1655, ν_{OH}=3400 cm^{-1}, are both 1:1 adduct of **1a** and xanthene[2], and are in the relation of configurational isomers each other, which are confirmed by elemental analysis and spectroscopy along with the chromic acid oxidation of them to give rise to the same products; *i.e.*, **1a** and xanthone. Reduction product (mp 162—164 °C) of **2a** with sodium borohydride revealed that the attaching position of xanthene moiety was at C_4, because the hydrogen atom thus introduced (bonded to C_1) coupled with no other protons. Reduction of **3a** under identical condition afforded the corresponding secondary alcohol (mp 170—172 °C), which led to the same conclusion.

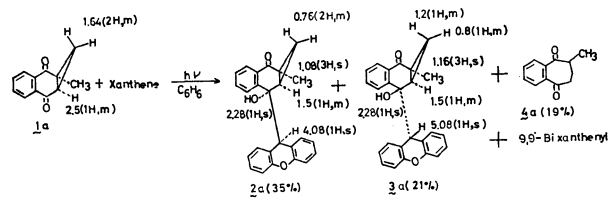

Scheme 1.

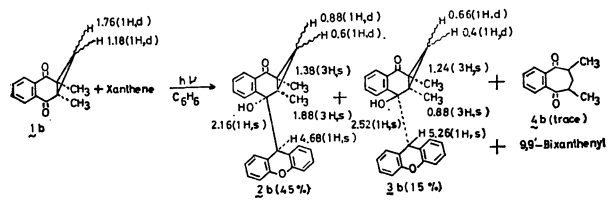

Scheme 2.

Assignment of the configuration of **2a** and **3a** rests on their PMR spectra. Outstanding differences of **2a** and **3a** in their PMR spectra are, at first, the chemical shifts of benzene ring protons; in **2a**, ring protons spread into the region of δ: 5.6—7.5 ppm, but in **3a** into δ: 6.8—8.0 ppm (for comparing, in **1a**, in the region of δ: 7.5—8.0 ppm), which is indicative that in **2a**, there are magnetically stronger interactions among three benzene rings than those in **3a**[3]. The other supports for the configutation of **2a** and **3a** are the followings. The methylene protons (*endo*- and *exo*-H) of **2a** give a coincided multiplet, centred at δ: 0.76 (2H) ppm, and the methine proton of xanthenyl moiety appears at δ: 4.08 (1H, s) ppm. On the contrary, in **3a** the methylene protons appear as two separated multiplets, δ: 1.2 (*endo*-H, 1H, m) and δ: 0.80 (*exo*-H, 1H, m) ppm and the methine proton of xanthenyl moiety gives a singlet at δ: 5.08 (1H, s) ppm. The *endo*- and *exo*-H were assigned by referring the works reported[4a,4b], *i.e.*, in **2a**, coupling constants of protons in cyclopropane moiety are J_{trans}: 5.5 Hz, J_{cis}: 7.5 Hz, J_{gem}: 5.5 Hz, and those in **3a** are J_{trans}: 6.3 Hz, J_{cis}: 8.4 Hz J_{gem}: 5.6 Hz.

Such a situation is essentially same for configurational isomers, **2b** and **3b**, but in these cases the methylene protons of **2b** and **3b** appear as two separated doublets (their *endo*- or *exo*-configurations are remained to be decided). Chemical shifts of representative protons are described in Scheme-1 and Scheme 2.

The structure of the third product, **4a** (mp 30 °C), was determined by comparison with the authentic sample prepared by Zn-CH_3COOH reduction of **1a**[5]. The other product in the

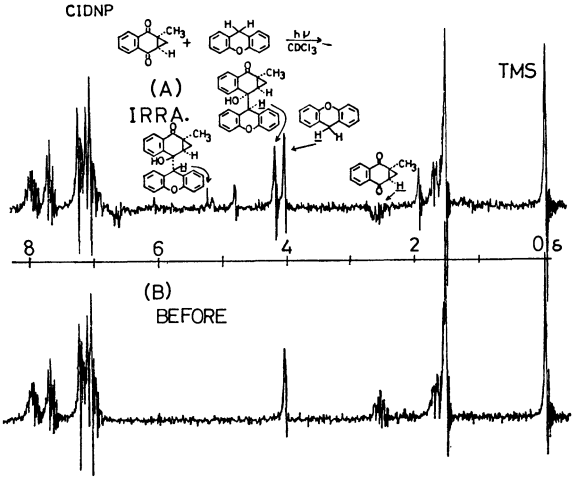

Fig. 1. Examination of the reaction of **1a** with xanthene by means of CIDNP technique.

reaction of **1a** and xanthene was 9,9′-bixanthenyl, which was identified by comparison (mixed melting point, chromatographic, spectroscopic, and chemical behaviors) with authentic sample.

The structure of **4b** (mp 97—98 °C), produced in trace, was determined by comparison with the authentic sample, which was prepared by reduction of **1b**.

Examination of the reaction by means of CIDNP revealed some insight of the reaction course. Methine proton of xanthenyl moiety of 1,2-adducts showed absorption polarization (see Fig. 1). The phenomenon leads to the conclusion that 1,2-adduct of **1a** (or **1b**) and xanthene is mostly produced via direct recombination of the original triplet radical pair composed of **5** and xanthenyl radical[6].

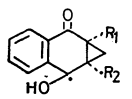

5a : $R_1=CH_3$, $R_2=H$
5b : $R_1=CH_3$, $R_2=CH_3$

5

Emission polarization of methine proton of methano-naphthoquinone moiety is another remark indicating the re-production of **1a** from **5a**.

References

1) The relative reactivity was estimated by following the remained amount of xanthene in the reacting mixture after one hour reaction at a room temperature (carbonyl compound: xanthene=0.075/0.15, M/M).

2) Elemental analyses of **2a**, **3a**, **2b**, and **3b** and integrations of their PMR signals reveal that these products are composed of 1 : 1 ratio of **1a** or **1b** with xanthene.

3) From the inspection of the molecular models the assignments of the structures are straightforward.

4) a) W. Rundel and P. Kastner, *Justus Liebigs Ann. Chem.*, **737**. 87 (1970); b) J. Heller, A. Yogev and A. S. Dreiding, *Helv. Chim. Acta*, **55**, 1003 (1972).

5) T. Asano, S. Imai, K. Okawa and T. Hanafusa, *Nippon Kagaku Zasshi*, **92**, 532 (1971).

6) K. Maruyama, T. Otsuki, and Y. Naruta, *Bull. Chem. Soc. Jpn.*, **49**, 791 (1976) and references cited therein.

BULLETIN OF THE CHEMICAL SOCIETY OF JAPAN, VOL. 49 (9), 2649—2650 (1976)

Syntheses of 4-(4-Hydroxy-2,6-dimethylphenyl)-1,2-butanediol and 4-(4-Hydroxy-2,6-dimethylphenyl)-2-butanol.

Kenji UNEYAMA, Hironori SAKUMOTO, and Sigeru TORII*

Department of Industrial Chemistry, School of Engineering, Okayama University, Okayama, 700

(Received May 4, 1976)

Synopsis. 4-(4-Hydroxy-2,6-dimethylphenyl)-1,2-butanediol (**3**) and 4-(4-hydroxy-2,6-dimethylphenyl)-2-butanol (**4**) as precursors for a theaspirone synthesis have been synthesized starting from 3,5-dimethylphenyl methyl ether.

One of the synthetic approach toward theaspirone[1] (**1**) has been focused on how to prepare efficiently the key intermediate, 3,5,5-trimethyl-4-(3-hydroxybutyl)-4-hydroxy-2-cyclohexenone which undergoes acid promoted cyclization leading to **1**. A promising approach would be an electrochemical cyclization of the phenol derivatives **3** and **4** leading to cyclohexadienones **2**, since 3-(4-hydroxyphenyl)propanoic acid,[2] hydroquinone bis(2-hydroxyethyl) ether,[3] and 2,4,6-tri-*t*-butylphenol[4] have been known to suffer anodic oxidation affording 1-oxa-spiro[4,5]deca-6,9-diene-2,8-dione, 8-(2-hydroxyethoxy)-8-methoxy-1,4-dioxaspiro[4,5]deca-6,9-diene, and 2,4,6-tri-*t*-butyl-4-methoxy-2,5-cyclohexadienone, respectively.

Thus, our attention has been paid to the syntheses of 4-(4-hydroxy-2,6-dimethylphenyl)-1,2-butanediol (**3**) and 4-(4-hydroxy-2,6-dimethylphenyl)-2-butanol (**4**) as starting compounds for the electrolytic cyclization.

The Clemmensen reduction of 3-(2,6-dimethyl-4-methoxybenzoyl)propanoic acid (**5**) and subsequent methylation with diazomethane afforded **6b** in 90% yield. The alcohol **7** obtained by the reduction of **6b** with lithium aluminum hydride was converted into the corresponding xanthate in quantitative yield. The thermal decomposition of the xanthate[5] took place instantaneously at the temperature range between 300—360 °C affording the olefin **8** in 73% yield. Oxidation of **8** with potassium permanganate at −45—−40 °C gave the diol **9** in 57% yield along with 19% of the starting material.

Treatment of **9** with boron tribromide[6] in anhydrous dichloromethane at −70 °C furnished the triol **3** in 69% yield without suffering bromination of aliphatic hydroxy groups on C_1 and C_2. The inertness of the vicinal hydroxyl groups toward the bromination reagent would be due to the formation of the stable chelated complex as illustrated in **10**.[7] In fact, the action of boron tribromide to the alcohol **18** induced the formation of the bromides **19** and **20** preferentially. In order to affect the efficient formation of the phenolic alcohol **4**, lithium metal reduction of the benzyl ether **17** in liquid ammonia was performed.

The cleavage of the methoxyl group of **6a** with boron tribromide followed by methylation with diazomethane provided the phenol ester **11b**. Benzylation of **11b** in DMF was accomplished in 84% yield. The subsequent reduction of **12** to **13** with lithium aluminum hydride and the transformation of **13** to the corresponding xanthate were performed similarly in 88% yield from **12**. The thermolysis of the xanthate took place at 350 °C affording the desired olefin **14** and the phenolic olefin **15** in 40% and 18%, respectively. The higher temperature on the thermolysis and the prolonged heating of the products facilitated the cleavage of the benzyl group.

Ozonolysis of **14** followed by reduction of the ozonide yielded the aldehyde **16** in 74%. Grignard reaction of **16** with methyl magnesium iodide afforded the alcohol **17** in 86%. Finally, reductive scission of the benzyl group of **17** with lithium in liquid ammonia provided the diol **4** in 76%.

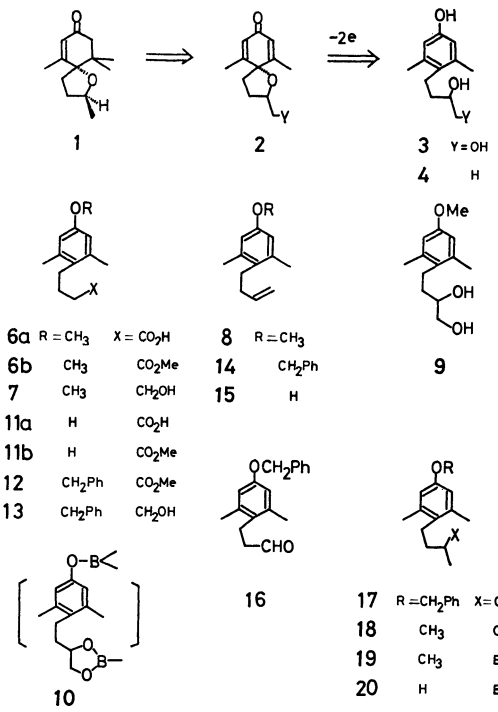

Experimental

The NMR and IR spectra were determined with Hitachi R-24 and Hitachi WPI-S2, respectively.

3-(2,6-Dimethyl-4-methoxybenzoyl)propanoic Acid (5). Friedel-Crafts reaction of 1 g of 3,5-dimethylanisole and 0.82 g of succinic anhydride with 2.2 g of aluminum chloride in 6 ml of nitrobenzene and 0.5 ml of CS_2 at −10—−5 °C for 9 h gave 1.58 g (85%) of **5** as colorless crystals, mp 102—102.5 °C: IR (Nujol) 3300—2350 (CO_2H), 1713 (CO_2H), 1696 (C=O) cm^{-1}; NMR ($CDCl_3$) δ 9.35 (br. s, 1H, CO_2H), 6.59 (br. s, 1H, ArH), 6.53 (br. s, 1H, ArH), 3.75 (s, 3H, CH_3O), 3.29—2.53 (m, 4H, CH_2), 2.29 (s, 3H, CH_3), 2.16 (s, 3H, CH_3). Found: C, 66.33; H, 6.99%. Calcd for $C_{13}H_{16}O_4$: C, 66.09; H, 6.83%.

4-(2,6-Dimethyl-4-methoxyphenyl)butanoic Acid (6a). Clemmensen reduction of 3.88 g of **5** gave 3.66 g (90%) of **6** as colorless crystals, mp 96.5—97 °C (benzene–hexane): IR (Nujol) 3350—2350, 1699 (CO_2H) cm^{-1}; NMR ($CDCl_3$) δ

10.05 (br. s, 1H, CO_2H), 6.58 (br. s, 1H, ArH), 6.53 (br. s, 1H, ArH), 3.75 (s, 3H, CH_3O), 2.87—2.11 (m, 4H, CH_2Ar, CH_2CO), 2.27 (br. s, 6H, CH_3) 2.11—1.61 (m, 2H, CH_2). Found: C, 70.14; H, 7.93%. Calcd for $C_{13}H_{18}O_3$: C, 70.24; H, 8.16%.

4-(2,6-Dimethyl-4-methoxyphenyl)-1-butanol (7). Reduction of the methyl ester **6b** was performed with $LiAlH_4$ in ether affording **7** as a colorless oil in 98% yield: IR (neat) 3350 (OH) cm^{-1}; NMR ($CDCl_3$) δ 6.58 (br. s, 1H, ArH), 6.54 (br. s, 1H, ArH), 3.76 (s, 3H, CH_3O), 3.65 (t, J=6.0 Hz, 2H, CH_2O), 2.63 (t, J=7.2 Hz, 2H, CH_2Ar), 2.26 (br. s, 6H, CH_3), 1.75 (br. s, 1H, OH), 1.81—1.16 (m, 4H, CH_2). Found: C, 74.76; H, 9.97%. Calcd for $C_{13}H_{20}O_2$; C, 74.96: H, 9.68%.

4-(2,6-Dimethyl-4-methoxyphenyl)-1-butene (8). The xanthate of **7** was prepared in 98% yield as described previously.[5] The decomposition of 3.496 g of the xanthate took place at 360 °C to form a fumy vapor which was collected in a receiver to give 2.2 g of a yellow oil, whose chromatography over alumina (hexane–CH_2Cl_2 20:1) gave 1.624 g (73%) of **8** as a colorless oil; IR (neat) 1640 (C=C) cm^{-1}; NMR ($CDCl_3$) δ 6.58 (br. s, 1H, ArH), 6.54 (br. s, 1H, ArH), 6.30—4.82 (m, 3H, CH_2=CH), 3.77 (s, 3H, CH_3O), 2.93—2.53 (m, 2H, CH_2Ar), 2.53—1.93 (m, 2H, CH_2), 2.28 (br. s, 6H, CH_3). Found: C, 81.87; H, 9.82%. Calcd for $C_{13}H_{18}O$: C, 82.06; H, 9.53%.

4-(2,6-Dimethyl-4-methoxyphenyl)-1,2-butanediol (9). Into a stirred solution of 0.2 g of **8** in 3 ml of EtOH was added dropwise aq $KMnO_4$ (0.16 g of $KMnO_4$, 0.12 g of $MgSO_4$, 4 ml of H_2O) at −45—−40 °C in 20 min. After stirring at the temperature for additional 2 h and warming to room temperature, the mixture was decantated and the precipitate was rinced with hot water. The combined organic layer was concentrated and extracted with AcOEt to yield 0.135 g of **9** as a colorless oil after chromatographed over silica gel (AcOEt–CH_2Cl_2 1:1): IR (neat) 3367 (OH) cm^{-1}; NMR (CCl_4) δ 6.41 (br. s, 1H, ArH), 6.35 (br. s, 1H, ArH), 4.02 (br. s, 2H, OH), 3.69 (s, 3H, CH_3O), 3.80—3.20 (m, 3H, CH_2O, CHO), 2.64 (t, J=7.8 Hz, 2H, CH_2Ar), 2.18 (br, s, 6H, CH_3) 1.84—1.01 (m, 2H, CH_2). Found: C, 69.34; H, 9.13%. Calcd for $C_{13}H_{20}O_3$: C, 69.61; H, 8.99%.

4-(2,6-Dimethyl-4-hydroxyphenyl)-1,2-butanediol (3). Into a stirred solution of 96 mg of **9** in 2 ml of dry CH_2Cl_2, was added dropwise cautiously 429 mg of BBr_3 at −70 °C under nitrogen. After stirring at −70 °C for 1 h and then at 0 °C for 30 min, the mixture was quenched with 2 ml of saturated $NaHCO_3$ followed by saturated Na_2CO_3. The organic layer was extracted with AcOEt, dried (Na_2SO_4), and concentrated *in vacuo*. The residue was chromatographed over silica gel (AcOEt–CH_2Cl_2 1:1) to yield 62 mg (69%) of **3** as a white solid, mp 107—108 °C (benzene); IR (Nujol) 3345 (OH) cm^{-1}; NMR ($CDCl_3$) δ 8.18—7.18 (br. s, 1H, OH), 6.62 (br. s, 2H, ArH), 4.91—2.96 (m, 5H, OH, OH, CH_2O, CHO), 2.96—2.54, (m, 2H, CH_2Ar), 2.24 (s, 3H, CH_3), 2.20 (s, 3H, CH_3), 1.94—1.28 (m, 2H, CH_2). Found: C, 68.54; H, 8.91%. Calcd for $C_{12}H_{18}O_3$: C, 68.55; H, 8.63%.

4-(2,6-Dimethyl-4-hydroxyphenyl)butanoic Acid (11a). In a similar manner, reaction of 0.5 g of **6a** with 0.43 ml of BBr_3 gave 0.45 g (97%) of **11a** as colorless crystals, mp 127.5—128.5 °C (benzene–AcOEt); IR (Nujol) 3504 (OH), 3400—2400, 1688 (CO_2H) cm^{-1}; NMR ($CDCl_3$) δ 7.66 (br. s, 2H, OH, CO_2H), 6.53 (br. s, 1H, ArH), 6.45 (br. s, 1H, ArH), 2.95—2.23 (m, 4H, CH_2Ar, CH_2CO), 2.25 (s, 3H, CH_3), 2.22 (s, 3H, CH_3), 2.23—1.62 (m, 2H, CH_2). Found: C, 68.94; H, 7.94%. Calcd for $C_{12}H_{16}O_3$: C, 69.21; H, 7.74%.

Methyl 4-(2,6-dimethyl-4-benzyloxyphenyl)butanoate (12). *O*-Benzylation of **11b** gave **12** as a colorless oil: IR (neat) 1735 (CO_2Me) cm^{-1}; NMR ($CDCl_3$) δ 7.34 (br. s, 5H, Ph), 6.57 (br. s, 2H, ArH), 4.97 (br. s, 2H, CH_2O), 3.55 (s, 3H, CH_3O), 2.89—2.14 (m, 4H, CH_2Ar, CH_2CO), 2.25 (br. s, 6H, CH_3), 2.14—1.59 (m, 2H, CH_2). Found: C, 76.77; H, 8.03%. Calcd for $C_{20}H_{24}O_3$: C, 76.89; H, 7.74%.

4-(2,6-Dimethyl-4-benzyloxyphenyl)butanol (13). Reduction of **12** with $LiAlH_4$ in ether was performed in an usual manner affording **13** as a colorless oil; IR (neat) 3320 (OH) cm^{-1}; NMR ($CDCl_3$) δ 7.24 (br. s, 5H, Ph), 6.51 (br. s, 2H, ArH), 4.83 (s, 2H, CH_2O), 3.46 (t, J=6.0 Hz, 2H, CH_2O), 2.92 (br. s, 1H, OH), 2.64 (t, J=6.6 Hz, 2H, CH_2), 2.19 (s, 6H, CH_3), 1.71—1.28 (m, 4H, CH_2). Found: C, 80.09; H, 8.79%. Calcd for $C_{19}H_{24}O_2$: C, 80.24: H, 8.51%.

4-(2,6-Dimethyl-4-benzyloxyphenyl)-1-butene (14) and 3,5-Dimethyl-4-(3-butenyl)phenol (15). The thermolysis of the xanthate of **13** was performed similarly as described[5] affording **14** (40%) and **15** (18%) as colorless oils: **14** IR (neat) 1636 (C=C) cm^{-1}; NMR ($CDCl_3$) δ 7.30 (br. s, 5H, Ph), 6.54 (br. s, 2H, ArH), 6.32—4.74 (m, 3H, CH_2=CH), 4.95 (s, 2H, CH_2O), 2.98—2.53 (m, 2H, CH_2Ar), 2.53—1.90 (m, 2H, CH_2), 2.24 (s, 6H, CH_3). Found: C, 85.60; H, 8.61%. Calcd for $C_{19}H_{22}O$: C, 85.67; H, 8.32%. **15** IR (neat) 3400 (OH), 1636 (C=C) cm^{-1}; NMR ($CDCl_3$) δ 6.54 (br. s, 1H, ArH), 6.40 (br. s, 1H, ArH), 6.24—4.75 (m, 3H, CH_2=CH), 4.63 (br. s, 1H, OH), 2.96—2.45 (m, 2H, CH_2Ar), 2.45—1.94 (m, 2H, CH_2), 2.25 (s, 3H, CH_3), 2.21 (s, 3H, CH_3). Found: C, 82.01; H, 9.34%. Calcd for $C_{12}H_{16}O$: C, 81.77; H, 9.15%.

3-(2,6-Dimethyl-4-benzyloxyphenyl)propanal (16). Ozonolysis of **14** was carried out as usually to give **16** (74%) as a colorless oil: IR (neat) 1721 (CHO) cm^{-1}; NMR ($CDCl_3$) δ 9.66 (t, J=1.8 Hz, 1H, CHO), 7.31 (br. s, 5H, Ph), 6.56 (br. s, 2H, ArH), 4.99 (s, 2H, CH_2O), 3.18—2.79 (m, 2H, CH_2Ar), 2.79—2.15 (m, 2H, CH_2), 2.27 (s, 6H, CH_3). Found: C, 80.41; H, 7.80%. Calcd for $C_{18}H_{20}O_2$: C, 80.56; H, 7.51%.

4-(2,6-Dimethyl-4-benzyloxyphenyl)-2-butanol (17). The alcohol **17** was prepared in 86% yield by Grignard reaction of **16** with MeMgI: IR (neat) 3360 (OH) cm^{-1}; NMR ($CDCl_3$) δ 7.31 (br. s, 5H, Ph), 6.57 (br. s, 2H, ArH), 4.94 (s, 2H, CH_2O), 3.65 (m, 1H, CH), 2.96—2.40 (m, 2H, CH_2Ar), 2.45 (br. s, 1H, OH), 2.26 (s, 6H, CH_3), 2.02—1.30 (m, 2H, CH_2), 1.09 (d, J=6.0 Hz, 3H, CH_3). Found: C, 80.00; H, 8.67%. Calcd for $C_{19}H_{24}O_2$: C, 80.24; H, 8.51%.

4-(2,6-Dimethyl-4-hydroxyphenyl)-2-butanol (4). Treatment of 62 mg of **17** with 13 mg of Li metal in 0.2 ml of dry THF and 5 ml of liquid ammonia at −50 °C for 4 h and an usual work-up provided 32 mg (76%) of **4** as a colorless oil: IR (neat) 3300 (OH) cm^{-1}; NMR (CCl_4) δ 8.24—4.54 (br. m, 2H, OH), 6.42 (br. s, 2H, ArH), 3.66 (m, 1H, CH), 3.08—2.34 (m, 2H, CH_2Ar), 2.19 (s, 3H, CH_3), 2.15 (s, 3H, CH_3), 1.94—1.34 (m, 2H, CH_2), 1.15 (d, J=6.6 Hz, 3H, CH_3) Found: C, 73.90; H, 9.42%. Calcd for $C_{12}H_{18}O_2$: C, 74.19; H, 9.34%.

References

1) (a) G. Weiss, M. Koreeda, and K. Nakanishi, *J. Chem. Soc., Chem. Commun.*, **1973**, 565; (b) J. N. Marx, *Tetrahedron*, **31**, 1251 (1975) and references cited therin.

2) (a) H. Iwasaki, L. A. Cohen, and B. Witkop, *J. Am. Chem. Soc.*, **85**, 3701 (1963); (b) A. I. Scott, P. A. Dodson, F. McCapra, and M. B. Meyers, *ibid.*, **85**, 3702 (1963).

3) P. Margaretha and P. Tissot, *Helv. Chim. Acta*, **58**, 933 (1975).

4) A. Ronlan and V. D. Parker, *J. Chem. Soc., C*, **1971**, 3214.

5) S. Torii, K. Uneyama, and M. Isihara, *J. Org. Chem.*, **39**, 3645 (1974).

6) F. L. Benton and T. E. Dillon, *J. Am. Chem. Soc.*, **64**, 1128 (1942).

7) W. Schafer and B. Franck, *Chem. Ber.*, **99**, 160 (1966).

BULLETIN OF THE CHEMICAL SOCIETY OF JAPAN, VOL. 49 (9), 2651—2652 (1976)

Studies on Heterocyclics. V.[1] Synthesis of Thiazolotriazepines

M. P. MAHAJAN,* S. M. SONDHI, and N. K. RALHAN**

Department of Chemistry, Punjabi University, Patiala 147002, India

(Received September 23, 1975)

Synopsis. The possible psychosedative, bridgehead thiazolo[2,3-*c*]-1,2,4-triazepines have been synthesized by the condensation of 2-hydrazinothiazoles with β-chloropropionyl chloride.

Recent trends in the synthesis of pharmacologically active compounds, *viz.* thiazolodiazepines[2-4] and oxazolodiazepines,[5] prompted us to carry out the synthesis of thiazolo[2,3-*c*]-1,2,4-triazepines, a new ring system (Scheme 1).

It was anticipated that the most direct route to 2*H*,3*H*,4*H*,5*H*-7-phenylthiazolo[2,3-*c*]-1,2,4-triazepine (VI; R=H) and its derivatives would be from 2-hydrazino-4-arylthiazoles (I)[6] *via* the intermediate V. The method used for the synthesis of thiazolo [2,3-*c*]-1,2,4-triazepines (VI) was analoguos to that used by Fozard and Jones[7] for the synthesis of 2-oxo-2,3,4,5-tetrahydro-1*H*-pyrimido [1,2-*a*] [1,3] diazepinium bromide.

The reaction of I with β-chloro propionyl chloride (II) may give either of the two heterocycles IV[8] and VI. The structure IV can be excluded from the consideration that monoacylation and carbamoylation always occur on the exocyclic amino group[9-14] in α-amino-*N*-heterocyclic compounds. Chloroacyl chloride has been shown to undergo reaction with amines selectively[15,16] with the carbonyl group forming an amide bond leaving V as the only possible intermediate.

Thus $-NH_2$ of hydrazine which is most basic[17] (*i.e.* the strongest nucleophile) will attack at the carbon of the carbonyl which is most electrophilic, resulting in the formation of the intermediate V (Table 1). The IR spectrum of V (R=H) shows characteristic –NH– and >C=O vibrations at 3350 and 1690 cm^{-1}. V is then cyclised in the presence of dry pyridine to VI. The IR spectrum of (VI, R=H) shows bands at 3360 (–NH–); and 1665 (>C=O) cm^{-1}. NMR spectrum (VI: R=Br) taken in $CDCl_3$ (100 MHz) shows a singlet at δ 2.02 (2H) due to $N-CH_2-$ and another singlet at δ 1.8 (2H) due to $-CH_2-\overset{O}{\overset{\|}{C}}-$ and aromatic multiplet at δ 6.8—7.7 (5H) due to $Br-C_6H_4-\overset{|}{C}=CH-$.

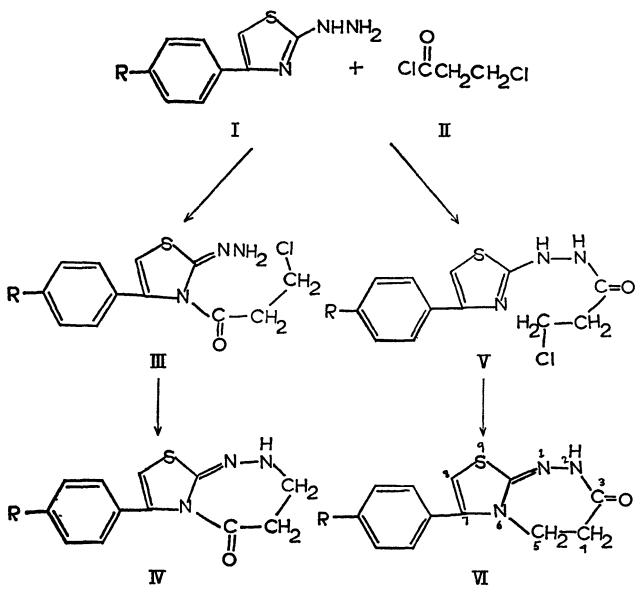

Scheme 1.

Experimental

The melting points are uncorrected. Microanalysis was carried out by the Mciroanalytical Service., CSIRO, Australia. IR spectra were obtained in KBr wafers on a Perkin-Elmer Infracord-137 spectrophotometer, and NMR spectra were recorded on a Varian HA-100 spectrometer.

2-Hydrazino-4-(substituted phenyl)thiazoles (I). 2-Chloro-4-phenylthiazole[6] (3.92 g, 0.02 mol), pyridine (2 ml), hydrazine hydrate (5 ml), and ethanol (20 ml) were taken in a flask. The reaction mixture was heated under reflux for 2 h and the solvent was removed under reduced pressure. The residue was poured into cracked ice and the solid thus obtained was crystallized from ethanol or benzene; yield 3.2 g (84%); mp 162 °C. Found: C, 56.64; H, 4.79; N, 22.25%; while: $C_9H_9N_3S$ requires: C, 56.54; H, 4.71; N, 21.99%. NMR spectrum (100 MHz; $CDCl_3$) shows aromatic protons as multiplet at δ 6.8—7.9 and the $-NHNH_2$ protons at δ 2.5—3.5.

The other 2-hydrazino-4-(substituted phenyl)thiazoles were prepared in an analoguos manner.

2-(3-Chloropropionylhydrazino)-4-(p-substituted phenyl)thiazoles (V). 2-Hydrazino-4-phenylthiazole (1.91 g, 0.01 mol) dissolved in tetrahydrofuran (15 ml) was added with stirring over a period of 15 minutes to an ice cooled β-chloropropionyl chloride (10 ml). The solid separated in the reaction mixture and excess of β-chloropropionyl chloride was decomposed with crushed ice, filtered, washed with cold water, and crystallized from ethanol. Yield, mp, solvent of crystallization, and microanalytical data are given in Table 1.

The other 2-(3-Chloropropionylhydrazino)-4-(*p*-substituted phenyl)thiazoles were prepared in a similar way.

2H,3H,4H,5H-7-(p-substituted phenyl)thiazolo[2,3-c]-1,2,4-triazepine-3-ones (VI). 2-(3-Chloropropionylhydrazino)-4-phenylthiazole (1.0 g) was dissolved in dry pyridine (10 ml) and left to stand at room temperature for 30 minutes. The reaction mixture was diluted with water and the solid obtained was crystallized from ethanol.

The other 2*H*,3*H*,4*H*,5*H*-7-(*p*-substituted phenyl)thiazolo [2,3-*c*]-1,2,4-triazepine-3-ones were prepared in a similar way. Yield, mp, solvent of crystallization and microanalytical data are given in Table 2.

* Present address: Department of Chemistry, I. I. T., Kanpur.

** To whom correspondence should be addressed.

Table 1. Physical constants of V

Sr. No.	Substituents	Yield %	Mp °C	Molecular formula	Elemental analysis Found % C	H	N	S	Calcd % C	H	N	S
Va	H	71	212	$C_{12}H_{12}N_3OSCl$	51.14	4.48	14.81	11.38	51.24	4.27	14.94	11.38
Vb	CH_3	70	219	$C_{13}H_{14}N_3OSCl$	—	—	14.13	10.67	—	—	14.23	10.84
Vc	OCH_3	68	209	$C_{13}H_{14}N_3O_2SCl$	—	—	13.26	10.20	—	—	13.50	10.28
Vd	Br	75	222	$C_{12}H_{11}N_3OSClBr$	—	—	11.70	8.91	—	—	11.36	8.88
Ve	Cl	72	218	$C_{12}H_{11}N_3OSCl_2$	—	—	13.24	10.05	—	—	13.33	10.15
Vf	C_2H_5	65	226	$C_{14}H_{16}N_3OSCl$	—	—	13.51	10.50	—	—	13.59	10.52

All the compounds (Va—f) were crystallized from ethanol.

Table 2. Physical constants of VI

Sr. No.	Substituents	Yield %	Mp °C	Molecular formula	Elemental analysis Found % C	H	N	S	Calcd % C	H	N	S
VIa	H	75	173	$C_{12}H_{11}N_3OS$	58.43	4.51	17.12	13.06	58.77	4.48	17.14	13.06
VIb	CH_3	70	149	$C_{13}H_{13}N_3OS$	—	—	16.10	12.40	—	—	16.21	12.35
VIc	OCH_3	72	146	$C_{13}H_{13}N_3O_2S$	—	—	14.98	11.41	—	—	15.27	11.63
VId	Br	68	170	$C_{12}H_{10}N_3OSBr$	—	—	13.26	9.71	—	—	12.96	9.87
VIe	Cl	73	155	$C_{12}H_{10}N_3OSCl$	—	—	14.69	11.10	—	—	14.53	11.07
VIf	C_2H_5	62	162	$C_{14}H_{15}N_3OS$	—	—	15.21	11.45	—	—	15.38	11.72

All the compounds (VIa—f) were crystallized from ethanol.

References

1) Part IV, M. P. Mahajan, S. M. Sondhi, and N. K. Ralhan, *Aust. J. Chem.*, (Communicated).

2) E. F. Elslager, J. R. Mclean, S. C. Perricone, D. Potoczak, H. Veloso, D. F. Worth, and R. H. Whealock, *J. Med. Chem.*, **14**, 397 (1968).

3) E. F. Eslager, D. F. Worth, N. F. Haley, and S. C. Perricone, *J. Heterocycl. Chem.*, **5**, 609 (1968).

4) E. F. Elslager, D. F. Worth, and S. C. Perricone, *J. Heterocycl. Chem.*, **6**, 491 (1969).

5) T. Miyadera, A. Terada, M. Fukunaga, Y. Kawano, T. Kamioka, C. Tamura, H. Takagi, and R. Tachikawa, *J. Med. Chem.*, **14**, 520 (1971).

6) D. S. Bariana, H. S. Sachdeva, and K. S. Narang, *J. Org. Chem.*, **23**, 427 (1955).

7) A. Fozard and G. Jones, *J. Chem. Soc.*, **1964**, 2763.

8) Mrs. T. R. Vakula and V. R. Srinivasen, *Ind. J. Chem.*, **9**, 901 (1971).

9) M. Tisler and B. Stanovnik, *Adv. Heterocycl. Chem.*, **9**, 211 (1968).

10) A. Schoberi and K. H. Magosch, *Justus Liebigs Ann. Chem.*, **74**, 742 (1971).

11) F. Kroknke, B. Kickhofer, and C. Thoma, *Chem. Ber.*, **88**, 1117 (1956).

12) F. Kurzer, *Adv. Heterocycl. Chem.*, **5**, 168 (1955).

13) J. Sandstorm, *Adv. Heterocycl. Chem.*, **9**, 181 (1968).

14) A. H. Land, *Chem. Heterocycl. Compounds*, **5**, 595 (1957).

15) C. R. Greco and J. F. Warchol, *J. Org. Chem.*, **36**, 604 (1971).

16) K. Pilgram and R. D. Skiles, *J. Org. Chem.*, **38**, 1575 (1973).

17) C. Bulow, *Ber.*, **42**, 2599; 3555; 4429; (1909).

The Heat of Solution and Solvation Number of Lithium Salts in Water–Alcohol Mixtures

Michio MASHIMA, Takao TAKASE, Shinroku FUKUDA, and Norio BABA

Faculty of Engineering, Niigata University, Gakko-cho, Nagaoka-shi 940

(Received June 6, 1975)

The solvation numbers of LiCl and LiI, and of KI for comparison, in water–MeOH mixtures and water–*i*-PrOH mixtures were determined at an infinite dilution at 25 °C from the adiabatic compressibility. The heats of solution of these salts were also determined. In general, with an increase in the concentration of alcohol the solvation number increases initially to reach a maximum at 10—30 mol% alcohol, then it decreases to a minimum and increases again from about 75 mol% alcohol. The maximum solvation numbers of the salts determined are as follows: LiCl 11.2 mol/mol at 30 mol% MeOH; LiCl 11.5 mol/mol at 15 mol% *i*-PrOH; LiI 8.2 mol/mol at 12 mol% *i*-PrOH and KI 14.0 mol/mol at 10 mol% *i*-PrOH. The larger the cation, the larger the solvation number. Also, the composition of the solvant where the salt containing larger ions has a maximum solvation number has a lower concentration of alcohol. The maximum solvation number of LiI containing a larger anion is smaller than that of LiCl because an iodide ion has a much larger structure-breaking effect than a chloride ion. By the way, there seems to be difference in the structure of the mixed solvent before and after the maximum solvation number.

The heats of solution and the hydration numbers of the cobalt(III) complexes and simple salts at an infinite dilution at 25 °C have been reported.[1] In this experiment the solvation numbers of lithium chloride, lithium iodide, and potassium iodide for comparison, which are soluble in alcohol, in water–methyl alcohol (subsequently designated MeOH), and water–isopropyl alcohol (subsequently designated *i*-PrOH) mixtures, were determined at an infinite dilution at 25 °C from the adiabatic compressibility. The heats of solution of lithium chloride and lithium iodide at an infinite dilution were also determined. Moreover, the A and B coefficients of the viscosity in the Jones-Dole expression[2] of lithium chloride in water–MeOH mixtures were determined.

Experimental

Determination of Heat of Solution. The heats of solution were determined with a twin-type conduction micro calorimeter with copper-constantan thermocouples, a commercial model (CM-502) of Ōyōdenki Kenkyujo. This apparatus, wrapped in a polyethylene sheet, was put in a thermostat regulated at 25±0.01 °C. This was connected with a d. c. voltage amplifier (a commercial model PM-17A) and a recorder (a commercial model EPR-10A of Tōa Electronics, Ltd.). The heat of solution was calculated from the area drawn by the recorder. The cells for dissolving salts are made of stainless steel. The solid sample was thrown into a cell containing 40 ml of the solvent by means of the attached device. Known amounts of heat occurred in the cell with liquid paraffin when a heater was used; these amounts were then used for obtaining the comparative area, from which the heats of solution of salts were calculated. The quantity of heat which was actually measured is less than, or equals, one figure. Figure 1 shows the heats of solution of lithium chloride in the 12.9 mol% MeOH–water mixture and in the 83.5 mol% *i*-PrOH–water mixture, and that of lithium iodide in water. The heat of solution at an infinite dilution was obtained by the extrapolation of the concentration to zero because the heat of solution per mol of electrolytes decreased linearly with a decrease in the concentration in this case.

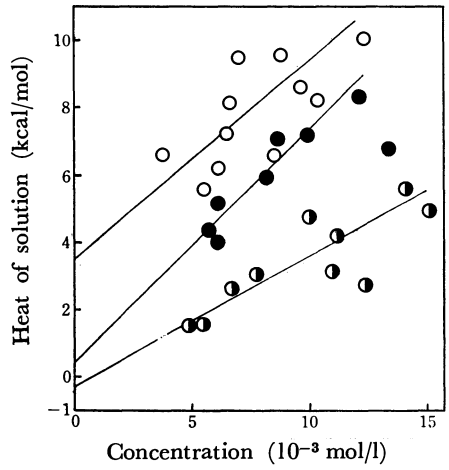

Fig. 1. Relationship between the concentration and the heat of solution (25 °C).
○: LiCl (12.9 mol% MeOH), ●: LiCl (83.5 mol% *i*-PrOH), ◑: LiI (water).

Determination of Solvation Number. The solvation number at an infinite dilution, determined from the adiabatic compressibility[3,4] was obtained by measuring the velocity of sound in the solution by means of an ultrasonic interferometer which had been placed in a thermostat maintained at 25±0.01 °C. The frequency used was 1 MHz. This apparatus was a commercial model (UAC-1-2A) of Chōonpa Kōgyō. Purified water for a solvent was boiled and used immediately after cooling. The solvation number was determined from the (relative) differential specific compressibility; that is,

$$K_{x0} = \lim_{x\to 0}[(d-x)/d_1-(K/K_1)]/x$$

where d and d_1 are the densities of the solution and the solvent, and where x is the concentration of the solution. It was assumed that the composition of the sheath of solvation was the same as that of the solvent.

B-*Coefficient of Viscosity.* The kinematic viscosity of the solution was measured with a kinematic viscosimeter of the Cannon-Fenske type, while the viscosity of the solution was obtained by the multiplication of the kinematic viscosity by its density. The density was measured with a Gay-Lussac-type pycnometer with a capacity of 10 ml. The A and B coefficients of viscosity of the solution in the Jones-Dole expression[2] were calculated from the viscosity of the solution;

$$\eta = \eta_0(1+A\sqrt{c}+Bc)$$

where η_0 is the viscosity of the solvent, c is the molarity, and both A and B are the characteristic constants on the solute.

Table 1. Heats of solution in water and hydration numbers of lithium salts at an infinite dilution (25°C)

Salt	Hydration number		Heat of solution		Hydration number of Li^+	Heat of solution of Li^+
	(mol/mol)	(10^{-4} g/ml)[a]	(kcal/mol)	(10^{-3} mol/l)[a]	(mol/g-ion)[b]	(kcal/g-ion)[b]
LiCl	4.7	3—15	+1.6	6—15	2.7	+2.8
$LiNO_3$	7.0	2—10	+0.3	5—22	2.7	+2.8
LiI	7.1	1—11	−0.3	5—15	4.4	

Hydration number (mol/g-ion)[1] Cl^- 2.0, NO_3^- 4.3, I^- 2.7. Heat of solution (kcal/g-ion)[1] Cl^- −1.2, NO_3^- −2.5. a) The determined range of concentration of the solution. b) Values obtained by subtracting that of an anion from that of a salt.

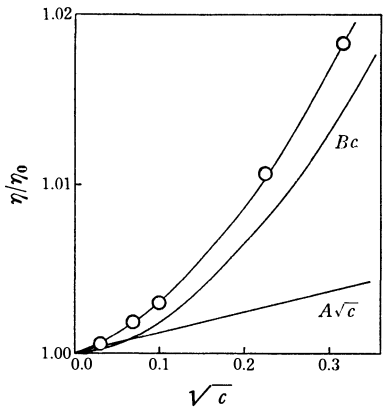

Fig. 2. Relationship between the relative viscosity and the square root of molarity of aqueous solution of lithium chloride (25 °C).

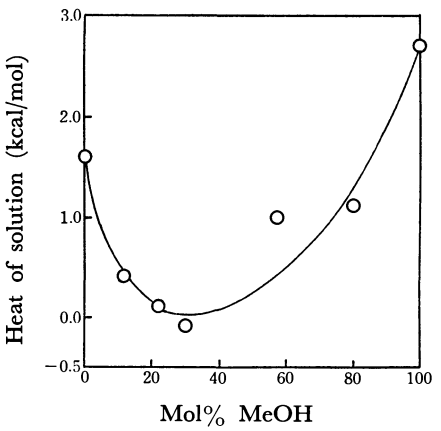

Fig. 3. Heat of solution of lithium chloride in water–MeOH mixture at infinite dilution (25 °C).

Figure 2 shows the relationship between the relative viscosity and the square root of the molarity of an aqueous solution of lithium chloride, drawn to obtain the *A* and *B* coefficients of the viscosity.

Determination of Electric Conductivity. The electric conductivity was measured with an electric conductivity outfit, a commercial model MY-7 of the Yanagimoto Mfg. Co., Ltd. The electrodes were made of platinum gild with platinum black. The equivalent electric conductivity was determined by measuring the resistance of the solution and by extrapolating the concentration to zero because the equivalent electric conductivity of strong electrolytes changed linearly against the square root of the concentration. The cell for measuring the resistance of the solution was put in a thermostat regulated at 25 °C.

Samples. The samples such as lithium salts which are of a guaranteed or extra pure grade were used without further purification. The alcohol was dried with an aluminum amalgam or dehydrated copper sulfate and distilled before use.

Results and Discussion

Table 1 shows the heats of solution in water and the hydration numbers of three kinds of lithium salts at an infinite dilution at 25 °C. The heat of solution in water and the solvation number of a lithium ion were obtained by subtracting those of a negative ion from those of lithium salts, because the additive property held on both the heats of solution in water and the hydration numbers of a nitrate ion and a chloride ion of the simple salts.[1] The hydration number of a lithium ion obtained from that of chloride was, consequently, consistent with that obtained from nitrate, *i.e.*, 2.7 mol/g-ion. Similarly, the heat of solution of a lithium ion was +2.8 kcal/g-ion. However the hydration number of a lithium ion, obtained from the others, did not agree with that obtained from the others, *i.e.*, 4.4 mol/g-ion.

The heats of solution of lithium chloride in water–MeOH mixtures at an infinite dilution at 25 °C are shown in Fig. 3. The heat of solution decreases initially with an increase in the concentration of MeOH to a minimum value at about 30 mol% MeOH, but thereafter it increases. A similar tendency in this system had been reported by Slansky.[5] The heat of mixing per mol of water and MeOH has a maximum value at about 30 mol% MeOH.[6] The viscosity,[7] the velocity of sound,[8] and the refractive index[9] of the mixture have also maxima at almost the same

Table 2. Heats of solution and solvation numbers of lithium chloride and lithium iodide in water, MeOH, and *i*-PrOH respectively (25 °C)

Salt	Solvent	Heat of solution (kcal/mol)	Solvation number (mol/mol)	Heat of solution: Solvation number (kcal/mol)
LiCl	Water	+1.6	4.7	+0.34
	MeOH	+2.7	7.7	+0.35
	i-PrOH	+4.4	10.3	+0.43
LiI	Water	−0.3	7.1	−0.04
	i-PrOH	+3.4	2.5	+1.36

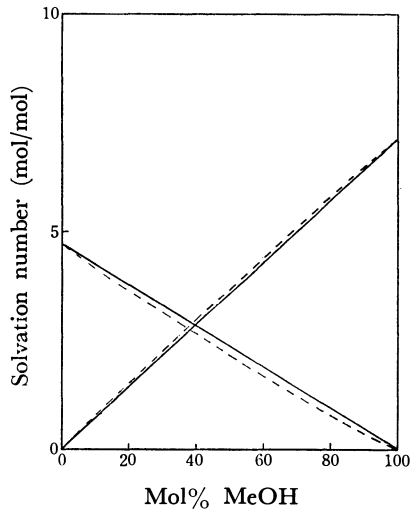

Fig. 4. Relationship between the composition of the sheath of solvation and that of the solvent.
----: Calculated value.

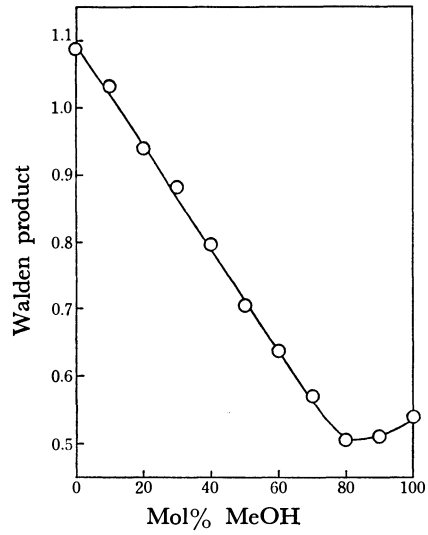

Fig. 5. Walden product of lithium chloride in water–MeOH mixtures at infinite dilution (25 °C).

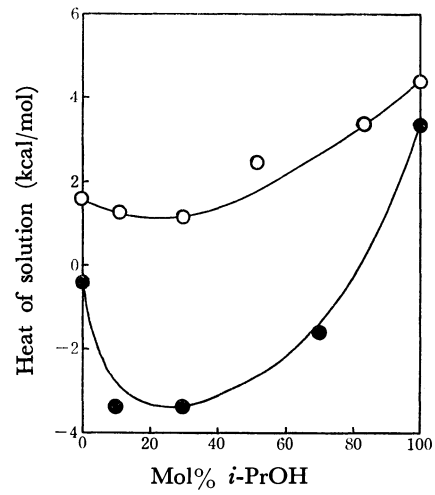

Fig. 6. Heats of solution of lithium chloride and lithium iodide in water–*i*-PrOH mixture at infinite dilution (25 °C).
○: LiCl, ●: LiI.

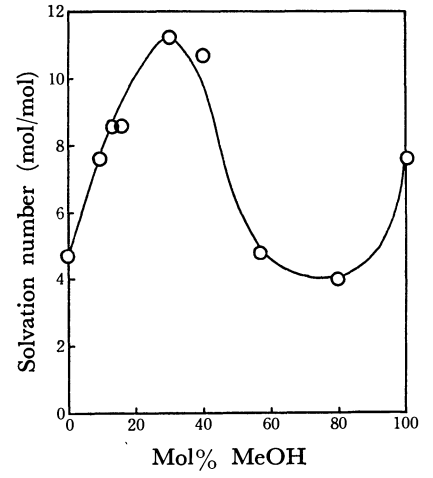

Fig. 7. Solvation number of lithium chloride in water–MeOH mixture at infinite dilution (25 °C).

compositions. The heats of solution and solvation numbers of lithium chloride and lithium iodide in water, MeOH, and *i*-PrOH at an infinite dilution at 25 °C are indicated in Table 2. The composition of the sheath of solvation was calculated from the heat of solution per mol of hydrated water or solvated MeOH (Table 2) so that the calculated value of the heat of solution was consistent with the actually determined value (shown in Fig. 3), assuming that the solvation number increases linearly against the concentration of MeOH. Consequently, the composition of the sheath of solvation was little different from that of the solvent, shown by the dotted lines in Fig. 4. Figure 5 shows the Walden products[10] of lithium chloride in water–MeOH mixtures at an infinite dilution at 25 °C. It may be seen in Fig. 5 that the Walden product decreases almost linearly, without having a constant value, in the water-rich region. From these results it seems reasonable to assume that lithium chloride does not solvate selectively water or MeOH in water–MeOH mixtures.[11]

Figure 6 shows the heats of solution of lithium chloride and lithium iodide in water–*i*-PrOH mixtures at an infinite dilution at 25 °C. The heat of solution has a minimum value at 15—20 mol% *i*-PrOH. The heat of mixing[6] and the velocity of sound[8] of the mixture have maxima at almost the same concentration of *i*-PrOH, much like water–MeOH mixtures.

Figure 7 shows the solvation number of lithium chloride in water–MeOH mixtures at an infinite dilution at 25 °C, determined from the adiabatic compressibility. The composition of the sheath of solvation was assumed to be identical with that of the solvent in this case, according to the estimation described above. The solvation number of lithium chloride in water–MeOH mixtures increases with an increase in the MeOH content up to a maximum at about 30 mol% MeOH, thereafter it decreases to a minimum at about 75 mol% MeOH, and then increases again. Thus, the solvation number is probably strongly influenced by the structure of the solvent, that it has a maximum seems to be attributable to a difference in

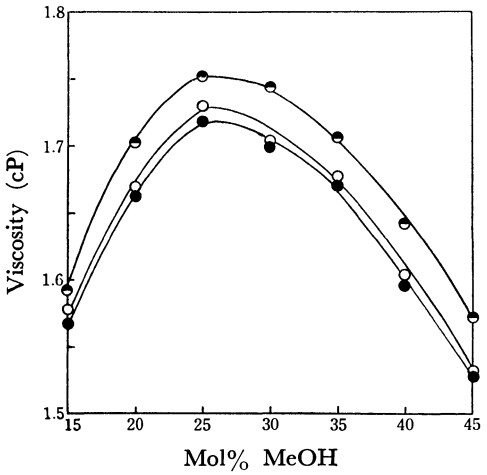

Fig. 8. Viscosity of water–MeOH mixtures containing lithium chloride at 25 °C.
◓: LiCl 0.1 mol/l, ○: LiCl 0.01 mol/l, ●: LiCl 0.001 mol/l.

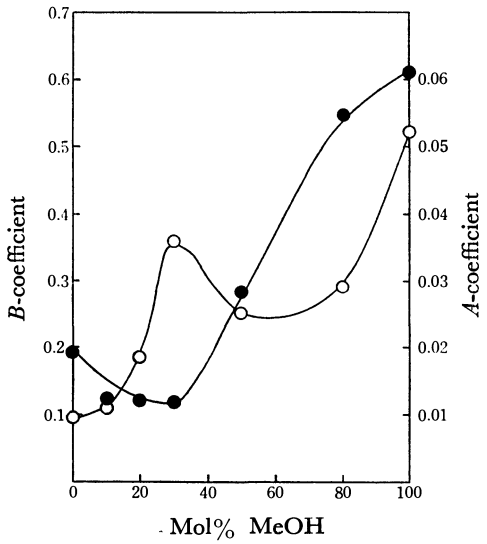

Fig. 9. *A* and *B*-coefficient of viscosity of lithium chloride in water–MeOH mixture (25 °C).
○: *A*-coefficient of viscosity,
●: *B*-coefficient of viscosity.

the structure of the solvent before and after the maximum solvation number, much like water–ethanol systems.[12–15] Many physicochemical properties of water–MeOH mixtures have maxima in a water-rich region. For example, the viscosity of the solution has a maximum at about 25 mol% MeOH, as is shown in Fig. 8. The maximum solvation number of lithium chloride in water–MeOH mixtures is 11.2 mol/mol at about 30 mol% MeOH.

In view of the values of the hydration number previously determined by the present authors,[1] the larger a cation is, the larger the hydration number. Also, the larger the electric charge of the cation, the smaller the hydration number. This result is the reverse of the concept universally believed. The ionic hydration numbers obtained by the authors were $Li^+=2.7$, $K^+=8.4$. The hydration number of the lithium ion was smaller than the literature data, *e.g.*,

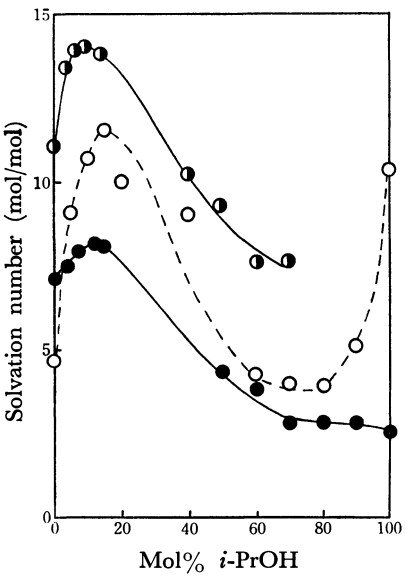

Fig. 10. Solvation numbers of lithium chloride, lithium iodide and potassium iodide in water–*i*-PrOH mixture at infinite dilution (25 °C).
○: LiCl, ●: LiI, ◑: KI.

$Li^+=4.0$,[16] while that of the potassium ion was larger than $K^+=3.5$.[16] Hence, the solvation number determined from the velocity of sound in the solution appears to contain the region in which the molecules around the ion are fixed (A-region) and a part of the outer region (B-region) of the Frank and Wen model for the sheath of solvation.[17,18]

The *A* and *B* coefficients of the viscosity of lithium chloride in water–MeOH mixtures were determined in an effect to investigate the interaction between the solute ion and the solvent in the mixtures at an infinite dilution at 25 °C. These values are plotted against the MeOH content in Fig. 9. The *A* coefficient has a maximum and the *B* coefficient has a minimum at about 30 mol% MeOH, where the solvation number is at its maximum. Consequently, it is considered that the coulombic force between the solute ions is at the maximum, and that the interaction between the solute ion and the solvent is at the minimum, at this composition.[19,20] In a water-rich region, the sheath of solvation determined by this method can be considered to increase with an increment in the MeOH content, because the distance between the solute ion and the solvent increases, as may be seen from the *B* coefficient of viscosity. As a result, the solvation number increases with an increase in the MeOH content when the degree of the increment in the thickness of the sheath of solvation is not very large. Accordingly, when the solvation number determined by this method is at the maximum, the interaction between the ion and the solvent is at the minimum because the distance between them is greatest at that composition, and the heat of solution of the salt is at the minimum, too. The Walden products of lithium chloride in water–MeOH mixtures, as may be seen in Fig. 5, show that the apparent average size of the cation and the anion solvated increases with an increase in the MeOH content in the water-rich region, it has

no constant value in that region. However, the solvation number of *t*-butyl chloride in water–ethanol mixtures has a minimum, determined by Arnett and his co-workers.[12,13] This may be related to the fact that the Walden product of lithium chloride in water–ethanol mixtures has nearly a constant value from 0 to 25 wt% ethanol,[21] despite the effect of the size of the solute.

The solvation numbers of lithium chloride, lithium iodide, and potassium iodide in water–*i*-PrOH mixtures at an infinite dilution at 25 °C are shown in Fig. 10. The experiment on potassium iodide could not be carried out, though, in a solvent more than about 70 mol% *i*-PrOH because the salt was little soluble in the solvent. The maximum solvation numbers of the salts determined are as follows: lithium chloride, 11.5 mol/mol at 15 mol% *i*-PrOH; lithium iodide, 8.2 mol/mol at 12 mol% *i*-PrOH; and potassium iodide, 14.0 mol/mol at 10 mol% *i*-PrOH.

Comparing the solvation number of lithium iodide with that of potassium iodide, both values have roughly the same tendency with regard to the MeOH content, and potassium iodide, which has a larger cation, has a larger solvation number than lithium iodide at all the compositions. Therefore, a potassium ion seems to have an apparent larger sheath of solvation than a lithium ion. On the other hand, the apparent sheath of solvation of a lithium ion appears to be smaller and to be composed of the A region for the most part, because the ion is solvated strongly, much as in pure MeOH.[22,23]

Next, the effect of the solvent on the solvation number will be discussed. As may be seen in Figs. 7 and 10, the maximum solvation number of lithium chloride in a water–*i*-PrOH mixture is larger than that in water–MeOH mixtures, and the composition of the solvent where lithium chloride has the maximum value in water–*i*-PrOH mixtures exists in a lower concentration of alcohol than that in water–MeOH mixtures. This is probably because the apparent sheath of solvation of the salt increases in size for *i*-PrOH molecules which are larger than MeOH molecules.

Comparing the solvation number of lithium chloride with that of lithium iodide, lithium iodide, which has a larger anion, has a larger hydration number than lithium chloride, much as in the case of cations. However, lithium iodide has a smaller solvation number than lithium chloride from about 3 mol% *i*-PrOH, and the maximum solvation number of lithium iodide is smaller than that of lithium chloride. The reason for this is that: the B region of the sheath of solvation of an iodide ion is extremely large because it has a much larger structure-breaking effect than a chloride ion.[24] As a result, the A region and a part of the B region of the ion are determined as the sheath of solvation, resulting in its having a smaller solvation number than a chloride ion.

In the range of high *i*-PrOH concentrations, the solvation number of lithium iodide does not increase, unlike as in the case of lithium chloride. This tendency is presumably due to the same effect of an iodide ion.

References

1) M. Mashima, K. Sakai, W. Takamura, and T. Takase, *Nippon Kagaku Kaishi*, **1974**, 1024; M. Mashima, H. Usami, S. Suzuki, and T. Takase *ibid.*, **1975**, 963.

2) G. Jones and M. Dole, *J. Am. Chem. Soc.*, **51**, 2950 (1929).

3) H. Shiio, *J. Am. Chem. Soc.*, **80**, 70 (1958).

4) F. Kawaizumi, H. Nomura, and Y. Miyahara, *Nippon Kagaku Zasshi*, **87**, 939 (1966).

5) C. Slansky, *J. Am. Chem. Soc.*, **62**, 2430 (1940).

6) T. Katayama, *Kagaku Kogaku*, **26**, 361 (1962).

7) G. Tamman and M. E. Pillsbury, *Z. Anorg. Chem.*, **172**, 243 (1928).

8) B. Jacobson, *Arkiv for Kemi*, **2**, 177 (1950).

9) K. Y. Chu and A. R. Thompson, *J. Chem. Eng. Data*, **7**, 358 (1962).

10) P. Walden, H. Ulich, and G. Busch, *Z. Phys. Chem.*, **123**, 429 (1926).

11) R. W. Gurney, "Ionic Processes in Solution," Dover Publications Inc., New York (1953), p. 69.

12) E. M. Arnett, W. G. Bentrude, J. J. Burke, and P. M. Duggleby, *J. Am. Chem. Soc.*, **87**, 1541 (1965).

13) E. M. Arnett, and D. R. Mckelvey, *J. Am. Chem. Soc.*, **88**, 2548 (1966).

14) F. Hibbert, F. A. Long, and F. A. Water, *J. Am. Chem. Soc.*, **91**, 2381 (1969).

15) I. Lee and J. B. Hyne, *Can. J. Chem.*, **46**, 2339 (1968).

16) J. O'M. Bockris and P. P. S. Saluja, *J. Phys. Chem.*, **76**, 2140 (1972).

17) H. S. Frank and M. W. Evans, *J. Chem. Phys.*, **13**, 507 (1945).

18) H. S. Frank and W. Y. Wen, *Discuss. Faraday Soc.*, **24**, 133 (1957).

19) R. H Stokes and R. H. Mills, "Viscosity of Electrolytes and Related Properties," Pergamon Press Inc., New York (1965).

20) M. Kaminsky, *Discuss. Faraday Soc.*, **24**, 171 (1957).

21) G. Wada, *Nippon Kagaku Zasshi*, **77**, 391 (1956).

22) A. R. Gordon, J. A. Davies, and R. L. Kay, *J. Chem. Phys.*, **19**, 749 (1951).

23) A. R. Gordon, R. E. Jervis, D. R. Muir, and J. P. Butler, *J. Am. Chem. Soc.*, **75**, 2855 (1953).

24) O. D. Bonner and C. F. Jumper, *Infrared Phys.*, **13**, 233 (1973).

Apparatus for Thermal Analytic Microscopy and Its Application to Cholesteryl Nonanoate*

Kazuko Sasaki KUNIHISA and Seiichi HAGIWARA**

National Chemical Laboratory for Industry, Honmachi, Shibuya-ku, Tokyo 151

***Tokyo Rikoh Company, Kitamachi, Hoya-shi, Tokyo 188*

(Received June 30, 1975)

The phase transitions of cholesteryl nonanoate were studied by means of a newly constructed apparatus for thermal analytic microscopy incorporating a thermoelement. It was possible to determine the heat of mesophase transitions more accurately. The transition values of cholesteryl nonanoate on cooling were obtained with the same accuracy as those on heating. The heat of the smectic-solid transition was obtained by slow cooling, which suppressed the supercooling. The vortices caused by cholesteric spherulites, which are similar to those of cholesteryl octanoate, change to circular arrangements of batonnets in the smectic phase. Color changes were observed at the cholesteric-smectic transition in extremely thick specimens. The relations between texture, color, and heat at the cholesteric-smectic transition of cholesteryl nonanoate are discussed.

On the basis of the results of previous works,[1,2] a new apparatus was constructed for thermal analytic microscopy and applied to a study of the phase transitions of cholesteryl nonanoate.

Apparatus

The apparatus is shown in Fig. 1.

Sample Cells. The sample cells are similar to those used previously (Fig. 2)[2] the microscopic cell being equivalent to the thermal ones. The body is made of stainless steel (0.5 mm thick) except for the center part. The cover and the center of the body are made of Pyrex glass. Two kinds of covers have been prepared. One is slightly smaller than the inner diameter of the body easily drops onto the center glass part. It is employed for thin layer (10—20 μ) samples. The other exactly fits the edge inside the top of the body (Fig. 2). It produces an extremely thick layer (300—350 μ) for the study of the characteristic colors at transformation, independent of the retardation color caused by the thin anisotropic layer.

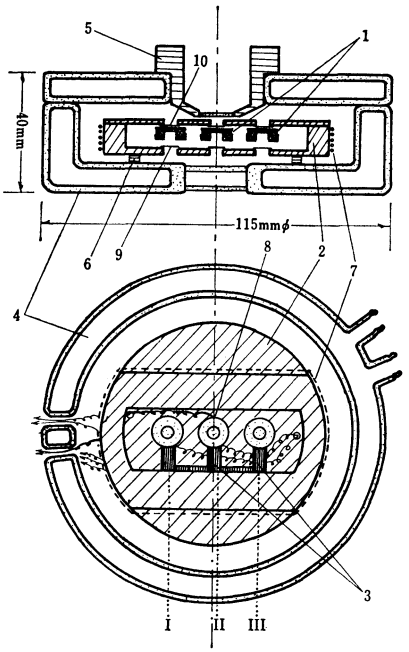

Fig. 1. Apparatus. 1: Sample cell; 2: copper block; 3: thermoelement; 4: jacket; 5: Teflon adapter for microscope; 6: Teflon support; 7: heater; 8: thermocouple for temperature measurement; 9 and 10: glass plates.

Copper Block. A disk-like copper block with a high heat capacity, part of which had been cut off, is used. It has a cover (1.5 mm thick) for maintaining a homogeneous temperature distribution in the interior of the block. A part of the block is cut off to make the thermal conditions as close as possible to those of the three cells.

Connection between Thermoelements. Since a thermoelement is a synthetic material made of several kinds of semiconductor compounds, the thermoelectric power is to some extent dependent on the properties of each thermoelement, and the contact potential differences arisen from the junctions between thermoelements and the block are not identical. Therefore, when the copper block has an inhomogeneous temperature distribution, the differences between each contact potential difference increase. In order to eliminate the potential disturbances, all the thermoelements are connected with the same thermoelement material (Fig. 1).

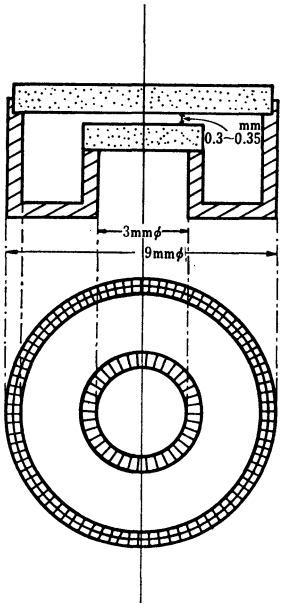

Fig. 2. Sample cells made of glass and stainless steel.

* Presented at the 32nd National Meeting of the Chemical Society of Japan, Tokyo, April, 1975.

Table 1. Transition values for cholesteryl myristate

		Cryst.-Sm.		Sm.-Ch.		Ch.-Iso.	
		T °C	Q cal/g	T °C	Q cal/g	T °C	Q cal/g
Heating	this work	70.6	18.9	78.4	0.55	83.5	0.37
	previous work[1]	70.6	18.2	78.4	0.5	83.5	0.3
Cooling	this work	50—67	17.4	78.4	0.64	83.6	0.52
	previous work[1]	52—67	16.3	78.5	0.6	83.5	0.5

Jacket. Water is circulated in the glass jacket. Teflon is utilized partly to buffer the heat effect caused by the aproach of the microscope. Three small Teflon pieces are used to place the copper block in the interior of the jacket.

The block heater, the thermocouples for temperature measurement and monitoring, and the sample cell holders are of the same materials as in the previous apparatus.[1]

Results

Calibration by Stearic Acid. By using the heat of the fusion of stearic acid[3] the performance of the apparatus was examined. At the heating or cooling rate of 0.63 °C/min the following items were checked: (1) the sensitivities of the thermoelements, I, II, and III (Fig. 1); (2) the dependence of the heat effect on the sensitivity range of an amplifier, and (3) the dependence of the heat effect on the sample weight.

Comparison of the Apparatus with the Previous One. The peak area for the heat of fusion of stearic acid was found to be 40% greater than that of the previous work.[1] This indicates that the connection of thermoelements is effective in improving the sensitivity of the apparatus. In addition, the base lines of the thermograms were greatly stabilized. The apparatus in the preceding work showed good base lines only with slow heating or cooling.

Calibration by Cholesteryl Myristate. The transition values of cholesteryl myristate were estimated by a comparison with those of the previous work [1] The results on heating or cooling at the rate of 0.63 °C/min are given in Table 1. The apparatus can determine the heat of mesophase transition to one more significant figure than that of the previous results.[1] The heats of two mesophase transitions on cooling were found to be considerably larger than those on heating. The heat of the crystallization of stearic acid is 2% larger than that of fusion. Thus, the thermoelectric effect of the thermoelements shows a hysteresis. A small peak area, such as the mesophase-mesophase transition, depends greatly on the way of drawing a base line under the peak. The difference between the values on cooling and heating, however, amounts to more than 20% of the heat of the mesophase transition. It is much larger than 2% in the case of stearic acid.

Simultaneous Observation in Microscopy and DTA. Figure 3 shows the thermograms and the temperature curves*** of stearic acid with notations of the microscopic changes. Point 'i' indicates the initiation of melting or crystallization, and 'f', the finish of the microscopic change. The temperature 'f' agrees with the starting point of the plateau (69 °C) on the temperature curve. The peak of fusion, 'p', agrees with the end point of the plateau. The temperature for both the complete view change in the microscopy and

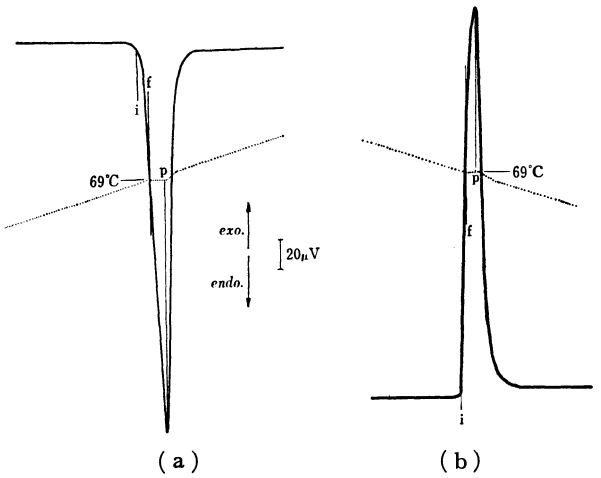

(a) (b)

Fig. 3. DTA and temperature curves of stearic acid on heating(a) and cooling(b), with notations denoting microscopic change. Sample weight, 11.91 mg; scanning rate, 0.63 °C/min; amp. range, ±250 μV; chart speed, 240 mm/h. Full line: DTA; dotted line: temperature of sample. i: Initiation of melting or crystallization in the microscopic view. f: Finish of the change in the same view as 'i.' p: Peak point of the DTA curve.

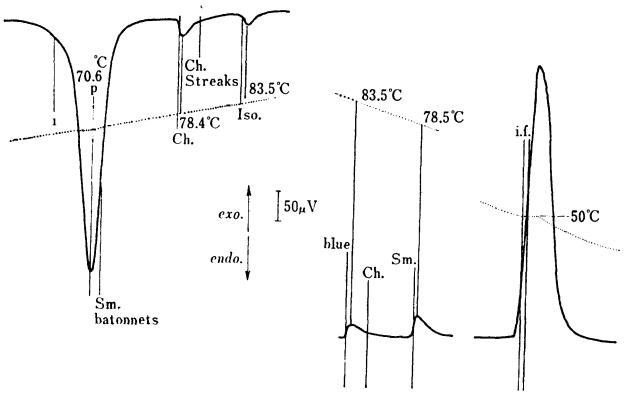

(a) (b)

Fig. 4. DTA and temperature curves of cholesteryl myristate with notations denoting the microscopic change on heating(a) and cooling(b). Sample weight, 66.22 mg; rate, 0.63 °C/min; amp. range, ±500 μV; chart speed, 240 mm/h.

*** The temperature was measured by a thermocouple soldered to the copper cell holder of the center cell.

TABLE 2. TRANSITION VALUES FOR CHOLESTERYL NONANOATE.

Scanning rate and reference	Heating				Cooling					
	Solid-Ch.		Ch.-Iso.		Iso.-Ch.		Ch.-Sm.		Sm.-Solid	
°C/min	T °C	Q cal/g	T °C	Q cal/g	T °C	Q cal/g	T °C	Q cal/g	T °C	Q cal/g
0.6—2.5	77.8	10.6	92.0	0.24	92.0	0.27	72.5	0.19	43—30	10.3
Ref. 5	80.8	10.2	93.0	0.22	86	0.23	66	0.11	super-cooling	
Ref. 6	77.8	11.4	91.7	0.25	—	—	74.6	0.14	—	—

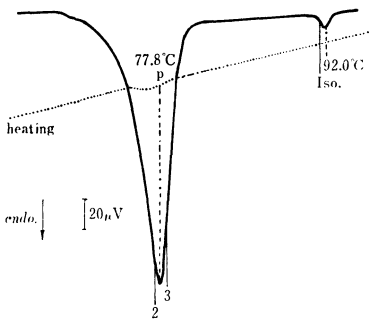

Fig. 5. DTA and temperature curves of cholesteryl nonanoate on heating, with the number of Photos. 2 and 3. Sample weight, 88.53 mg; rate, 0.63 °C/min; samp. range, ±250 μV; chart speed, 240 mm/h.

the peak on the thermogram is equal to 69 °C, the temperature of the fusion of stearic acid.

Figure 4 shows the curves of cholesteryl myristate, with notations denoting the appearance of typical textures. The isotropic-cholesteric transition peak on cooling agrees with the appearance of the homeotropic blue color, but not with that of the cholesteric focal conic texture. According to Gray, both the homeotropic and the focal conic textures belong to the same phase.[4]

The agreement between microscopic and DTA observations has thus been established.

Phase Transitions of Cholesteryl Nonanoate. Thermal Data of Cholesteryl Nonanoate: The sample was purified as in the previous work.[1] Table 2 gives the transition values of cholesteryl nonanoate. The heat of crystallization was measured by slow cooling, which helped to suppress the supercooling.[5] The heat of the isotropic-cholesteric transition on cooling is somewhat

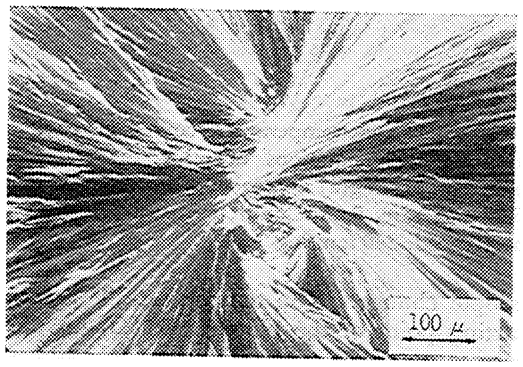

Photo. 1. Spherulitic center of a solid of cholesteryl nonanoate crystallized from the melt.

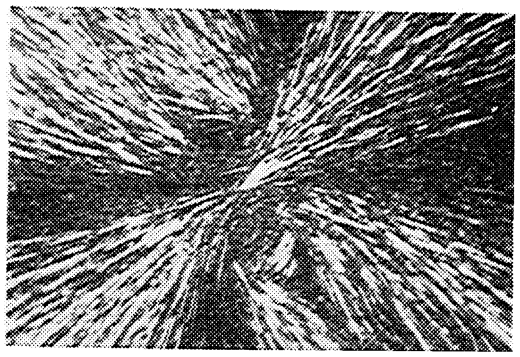

Photo. 2. Melting state around the peak point of the transition to the cholesteric phase.

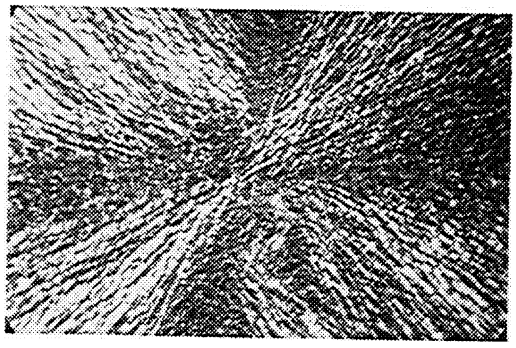

Photo. 3. Cholesteric texture just after the peak.

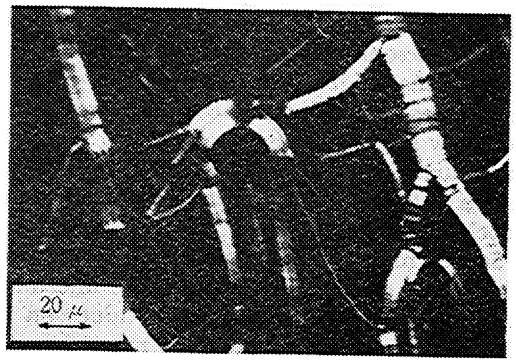

Photo. 4. Oily streaks of the cholesteric phase of cholesteryl nonanoate.

larger than that on heating, as was found for cholesteryl myristate.

Microscopic observation and DTA: Figure 5 shows the curves on heating (0.63 °C/min), along with the numbers of the photographs. Photograph 1 shows the center of a solid phase radially grown from the smectic phase, taken at room temperature. Photo. 2 shows a transient

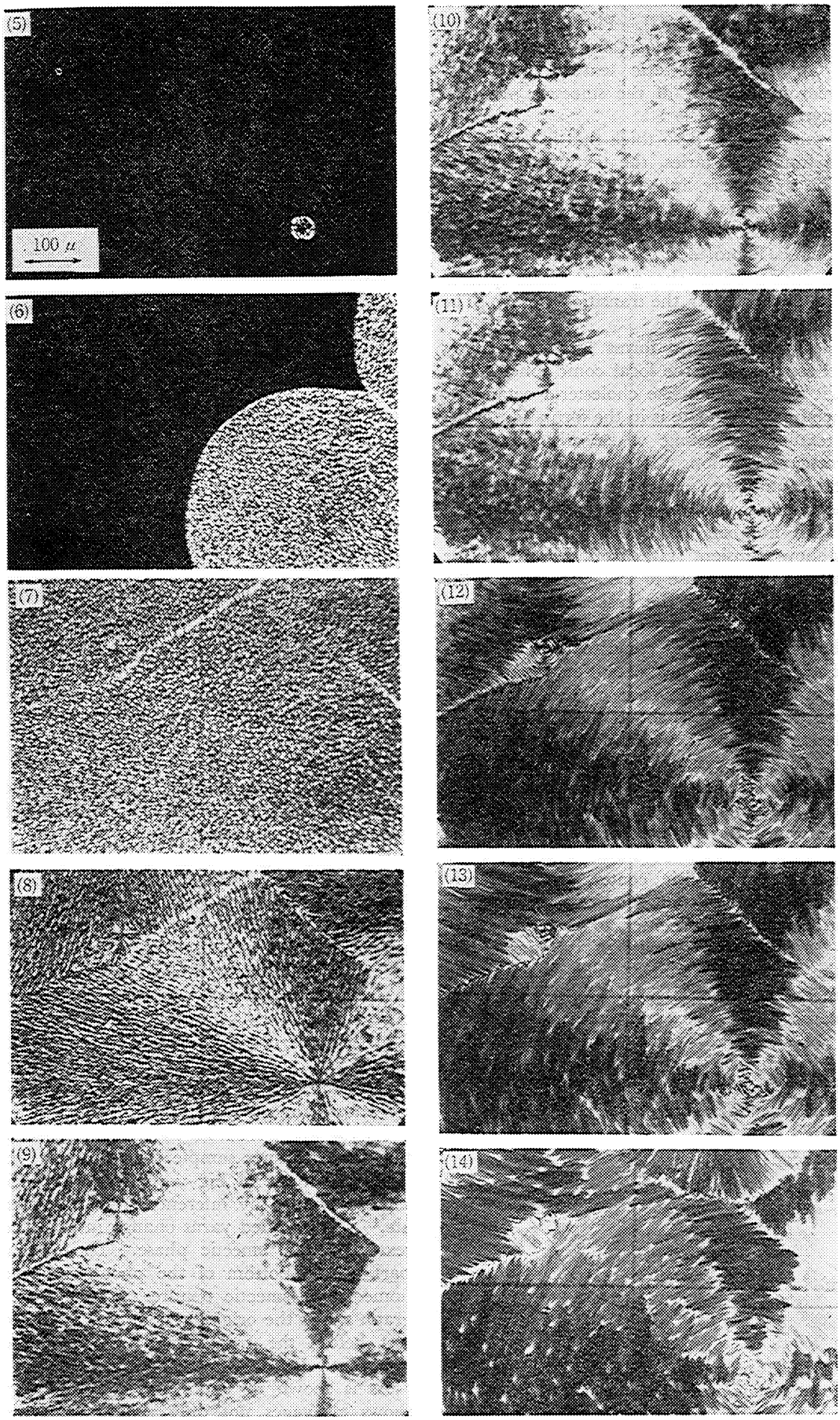

Photos. 5—14. The microscopic views from the occurrence of the spherulite of cholesteric texture to the appearance of the solid phase in cholesteryl nonanoate on cooling. 5: 84.3 °C; 6: 82.3 °C; 7: 79.5 °C; 8: 73.8 °C; 9: 73.5 °C, 10: 73.2 °C; 11: 72.7 °C; 12: 72.6 °C; 13: 72.2 °C; 14: 43 °C.

state to the mesophase (77.6 °C). Photo. 3 shows the cholesteric phase at 78.3 °C, just after the transition peak (77.8 °C). Th cholesteric texture closely resembles a microscopic view of the smectric phase in cholesteryl myristate.

When the sample layer is so thick that it behaves as a liquid free from boundaries, the texture shows oily streaks.[7] The streaks are linked to each other or are branched and separated by isotropic parts, which become clear as the cholesteric-isotropic transition point approaches (Photo. 4). The streak marked by the light and dark portions changes into small spherulites arranged linearly near the transition point. The spherulite is optically negative.

Cholesteryl nonanoate also forms large spherulites like spherical assemblies of the focal conic spherules in the cholesteric phase, much like cholesteryl octanoate. The difference from octanoate is in the formation of the basket-like texture, consisting of smectic batonnets, after the vortex formation. The smectic texture is extremely stable until the solid phase appears. Figure 6 shows the thermogram on cooling (0.63 °C/min), along with the numbers of Photos. 5—14. These photographs show transient states from the spherulitic growth of the cholesteric phase to the appearance of the solid phase, passing through the basket-like texture of the smectic phase. Photos. 5—7 show the spherulitic growth of the cholesteric focal conic texture, much as in the case of octanoate. No heat evolution accompanies the growth, much as in the case of the cholesteric phase of myristate. Photo. 8 shows the occurrance of a radial ordering at 73.8 °C, which corresponds to the starting point of the peak of the cholesteric-smectic transition. Photo. 9 indicates an ordering in the direction vertical to the radial one. The spherulitic center at the right bottom in the photograph looks like a fylfot or an Airy's spiral. Photo. 10 shows a very speedy vortex around the spherulitic center, which clearly indicates the occurrence of some kind of association on spherical surfaces from the center to the boundary. Photos. 11—13 show the growth of the basket-like texture of the smectic batonnets. The peak of the cholesteric-smectic transition is 72.5 °C ('p' in Fig. 6). The microscopic phenomena are almost finished by 'p'. Photo. 14 shows a fan-like solid phase, which appears in the right top portion in the photograph. The 'f' in Fig. 6 corresponds to the point where the solid covers the smectic texture.

In transmitted light, the visible light intensities increase with the thickness of the sample layer. A thick sample shows, at first, a light blue color with the peak of isotropic-cholesteric transition before the generation of the cloudy cholesteric phase. The color variation during the cholesteric-smectic transition is: first light yellow, then strong yellow, orange, red and finally deep blue. The colors become mixed with the variation Red and other colors remain in the microscopic view when the final blue appears. The arrows in Fig. 6 show the ranges of color appearance. The 'n' in the figure means "no color." The view at 'n' is only a dim light as the result of mixing all the colors. The color variation is similar to that in the case of taking an analyser off. The vortex in Photo. 10 is accompanied by so speedy a color variation that observation cannot follow it.

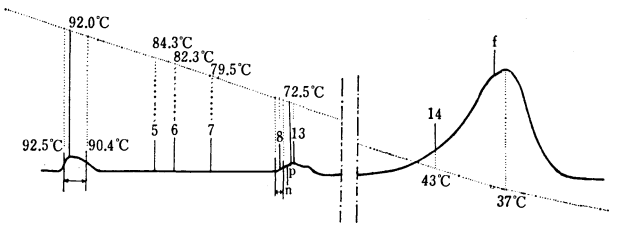

Fig. 6. DTA and temperature curves of cholesteryl nonanoate on cooling, with the number of Photos. 5—14. The experimental conditions are the same as in Fig. 5. The arrows show the ranges of color appearance.

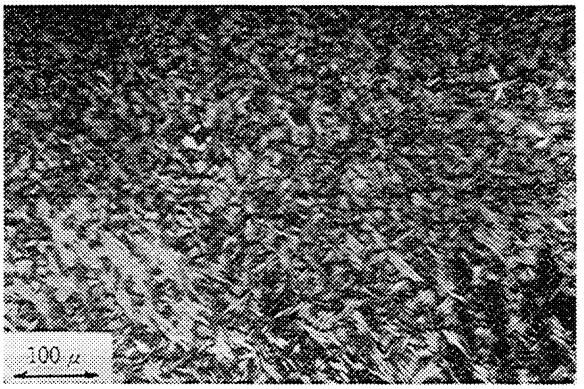

Photo. 15. Cholesteric-smectic transition state of cholesteryl nonanoate in a thin specimen.

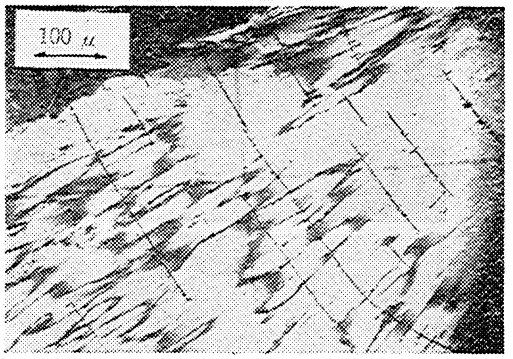

Photo. 16. Cleavages of thin solid film of cholesteryl nonanoate.

Photograph 15 shows the cholesteric-smectic transition for a thinner sample than that of Photo. 5—14. The coils made of big yarns in Photo. 15 suggest a smectic texture by inference from cholesteryl octanoate.[1] The coiled yarns change into the homeotropic texture of the smectic phase. The optically extinct part at the bottom of the photograph indicates the homeotropic smectic texture. The top of the photograph shows the original cholesteric focal conic texture just before the transformation. The selective color light scattering does not appear in this case.

As is shown in Photo. 16, a radially grown solid shows cleavages not only radially but also circumferencially. Solidification on a free surface gives dendritic crystals similar to cholesteryl octanoate.

Discussion

Relation between the Light Scattering in Transmission and in Reflection. A thin, anisotropic specimen generally looks colored under crossed polars because of its own retardation. The thickness most sensitive to retardation is in the range of less than 100 μ. In this work, color observation was carried out for extremely thick samples of more than 300 μ. Therefore, the color observed at the transformation is independent of the thickness. In transmitted light, the visible light intensity increases much more for a thick specimen than for a thin one, making a good contrast to the case of reflected light.[8] In a specimen thicker than 300 μ the molecules in a mesophase may be oriented randomly as a whole, since numbers of molecules restricted by boundary are negligible. Therefore, a theory based on the homeotropical model seems not to be applicable. If the mesophase, however, consists of a crystal structure with a higher order, such as the spherical symmetry of spherulite, the optical axis may naturally be normal to the glass boundary.

The color variation number reflected light was observed using a Mettler fusion-point apparatus. The colors from blue to red were observed in the range of 74—72 °C. Except for the red color, the selective reflection color and the color obtained by our apparatus are complementary. Ennulat[8] studied the selective light reflection of several cholesteryl esters with a monochromator; he found that the wavelengths from 470 nm to 590 nm showed, in the temperature range of 76.78—76.12 °C, the respective intensity maxima with regard to nonanoate. The characteristic colors of this work correspond to the complementary colors of those observed at Ennulat, but the temperature does not agree with his result, although the temperature range 0.7 °C found by us is almost the same as his result (0.66 °C).

Mechanism of the Occurrence of the Vortex. A large spherulite in the cholesteric phase consists of small spherulites with a focal conic texture. In other words, the spherulite has a double structure. An ordinary cholesteric focal conic texture changes into the randomly coiled yarns of the smectic phase, but not into the vortex (Photo. 15). Only an ordered structure of spherical symmetry makes a vortex at the cholesteric-smectic transition. Before being transformed into a vortex, a spherulite seems to be almost solidified by the development of the radial order. In Photo. 9 the isotropic part disappears except for the isogyres of the spherulites. If the same order develops further, the stress force may be accumulated in the system, which will thus be destroyed, and the substance will start to flow as a fluid. In the field of spherical symmetry, the center may be regarded as a singular point similar to a source in hydrodynamics. Consequently, a vortex will come from every spherulite. This inference is just one of many possibilities. A more essential mechanism of vortex formation may be related to the transformation from an optically negative phase to an optically positive phase. A color-light scattering accompanied by a vortex may also be related to some antisymmetric force, such as a twist force caused by the transformation.

Relation between Optical and Thermal Phenomena. It was observed that the microscopic changes in both the fusion and the crystallization of stearic acid agreed with the starting points of the peaks (Fig. 3), suggesting that an optical change precedes the corresponding thermal change. Similar relations were also observed for all the transitions of cholesteryl myristate and nonanoate except for the fusion. The peaks of their fusion show loose curves because of a premelting effect, which makes the starting points of the peaks less clear.

We wish to express our thanks to Dr. Yorihiro Satomi of National Chemical Laboratory for Industry for his guidance regarding the employment of the Mettler fusion-point apparatus.

References

1) K. S. Kunihisa and S. Hagiwara, *Bull. Chem. Soc. Jpn.*, **49**, 1204 (1976).
2) K. S. Kunihisa and T. Shinoda, *Bull. Chem. Soc. Jpn.*, **48**, 3506 (1975).
3) P. E. Slade, Jr. and L. T. Jenkins, "Thermal Characterization Techniques," Marcel Dekker, New York (1970); K. S. Markley, "Fats and Oils," 2nd ed. Part 4, Fatty Acids, Interscience Publishers, (1967).
4) G. W. Gray, "Molecular Structure and the Properties of Liquid Crystals," Academic Press, London and New York (1962).
5) E. M. Barrall II, R. S. Porter, and J. F. Johnson, *J. Phys. Chem.*, **71**, 1224 (1967).
6) G. J. Davis, R. S. Porter, and E. M. Barrall II, *Mol. Cryst. Liq. Cryst.*, **10**, 1 (1970); *ibid.*, **11**, 319 (1970).
7) G Friedel, *Ann. Phys., Paris*, (9) **18**, 273 (1922).
8) R. D. Ennulat, *Mol. Cryst. Liq. Cryst.*, **13**, 337 (1971).

An Application of $H_{0,max}$ for Estimating the Catalytic Action of Solid Acids and Bases in the Isopropylation of *m*-Cresol

Tohr YAMANAKA

Central Research Laboratory of Takasago Perfumery Co., Ltd., Kamata, Ohta-ku, Tokyo 144

(Received January 12, 1976)

A method of estimating the acid-base property of the active sites in terms of the correlation between the catalytic activities of various solids and their $H_{0,max}$ values is presented. The $H_{0,max}$ denotes an H_0 value of the strongest acidic sites and/or conjugate acids of the strongest basic sites. The types of catalytic actions over oxides, hydroxides, a sulfide, sulfates, phosphates, tungstates, and multi-component solid acids in the liquid-phase isopropylation of *m*-cresol without a solvent were classified into three groups: *via* a carbonium ion, *via* a carbanion, and concerted actions. The selectivity for the ortho-isopropylation over every catalyst increased with the increase of $H_{0,max}$, and this effect of $H_{0,max}$ was explained by the orientation of the adsorbed *m*-cresol on the catalyst surface.

It has been well known that a catalytic action changes continuously with the variation in the acid-base property of catalysts.[1,2] A quantitative description of the property with a universal parameter is required for reaction analysis, catalyst design, and developemtnt.[1] In liquid-phase reactions, the p*H* and acidity functions (*e.g.*, H_0 and H_- defined by Hammett *et al.*) have often been used as the parameters of homogeneous catalysts.[2] The electronegativities of metal ions[1] and effective negative charges on combined oxygens[1] have sometimes been used as the parameters of solid catalysts, but they are insensitive to the surface structure.[3]

As a measure of the acidic property of solid acid catalysts, "the highest acid strength" on the H_0 scale has been used in correlations with the catalytic activity and the selectivity for estimating catalytic actions.[4] Recently, the present authors reported a new titration method[5] of the acid-base strength distribution on the common H_0 scale, where the H_0 of the basic sites denotes the ability of proton donation of the conjugate acids. On the acid-base strength distributions of various solids, an H_0 value (termed $H_{0,max}$) which indicates the H_0 value of the strongest acidic sites and/or the strongest basic sites was found. The $H_{0,max}$ of acidic sites has essentially the same value as the highest H_0 value. The acidic sites of $H_0 \geq H_{0,max}$ and the basic sites of $H_0 \leq H_{0,max}$ coexisted on the same solid surface where both sites were measured. Therefore, the role of $H_{0,max}$ as a parameter indicating a basic property as well as an acidic property on a common H_0 scale is noticeable.

On the other hand, the author and others[6] have been studying the development of solid catalysts in the liquid-phase isopropylation of *m*-cresol (I) with propylene, in order to prepare thymol (II), an important starting material for menthol. The isopropylation involved the multiple formation of the nuclear-substituted products and their ethers. It could not be estimated, on the basis of the literature,[7] whether and how the catalytic activity and the selectivity for the *ortho*-isopropylation of the OH group in I varied with the surface properties of the catalysts. In the vapor phase,[8] a few kinds of solids were investigated, but the results did not provide a guide for the catalyst development.

In this paper, $H_{0,max}$ will be presented as a useful parameter for estimating the acid-base property of the active sites and the catalytic actions over a solid acid, base, and acid-base bifunctional catalysts.

An Approach to Estimate Catalytic Actions

The catalytic activities of solid acid-base catalysts were schematically correlated with their $H_{0,max}$ values as is illustrated in Fig. 1 in the following semiquantitative approach. In the R+R'H→R″ reaction, where the order of the acid strength of the reactants is R'H> R and where the order of base strength is R>R'H, the catalytic action is expected to involve the formation of one or two activated species, *i.e.*, a carbonium ion (RH^+), a carbanion (R'^-), or coordination complexes (R_p and $R'H_p$) which are formed by acidic (A) and/or basic site (B).[9] R_p and $R'H_p$ represent

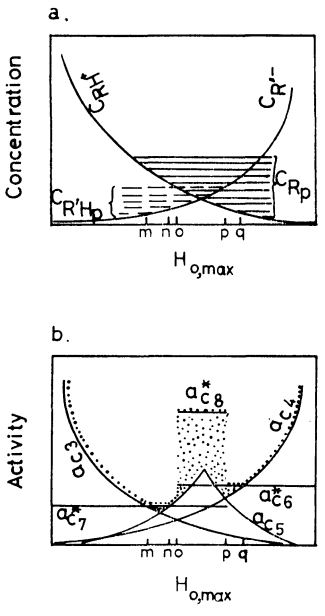

Fig. 1. An illustration for the concentration of activated species (C) and catalytic activities (a_c) *vs.* $H_{0,max}$. a^*_c denotes the maximum value of a_c when $H_{0,A}=H_{0,max}$ and/or $H_{0,B}=H_{0,max}$. The numerical subscribed to an a_c denotes the elementary step *via* which the reaction is catalyzed. The dotted curves and regions represent the overall a_c value to be observed.

a kind of activated complex, $\{B^{+\delta}\rightarrow R^{-\delta}\cdots H^{+}\cdots A'^{-}\}$ and $\{B\cdots H^{+}\cdots R'^{+\delta-1}\rightarrow A^{-\delta}\}$. H'A denotes an acidic site (A) of the Brønsted type.

When the reaction proceeds *via* RH^+ and/or R'^-, the strongest sites on the catalyst surface will be most effective in activating each reactant. At a low coverage of acidic and/or basic sites, the H_0 value of the strongest acidic or basic sites, $H_{0,max}$, will affect the catalytic action more strongly than the site amounts of various strengths.

Then ratios of an activated ionic specie to reactant in an equilibrium may be expressed as:[2c]

$$\log (C_{RH^+}/C_R) = \alpha - H_{0,max};$$
$$\alpha = pK_{RH^+} - \log (f_Z f_{RH^+}/f_{ZH^+} f_R) \quad (1)$$
$$\log (C_{R'^-}/C_{R'H}) = H_{0,max} - \beta;$$
$$\beta = pK_{R'H} - \log (f_Z f_{R'H}/f_{ZH^+} f_{R'^-}) \quad (2)$$

where C, f, and K denote a concentration, an activity coefficient, and an ion dissociation constant defined by the suffix, and where $H_{0,max}$ corresponds to the strongest ability of the proton donation of acidic sites or that of the conjugate acids of basic sites to Z.[5,10] Z represents the indicator base for the titration. C_R and $C_{R'H}$ are regarded as the concentrations of R and R'H in a phase in contact with the surface of physically adsorbed on the surface. The correlation between C_{RH^+} or $C_{R'^-}$ and $H_{0,max}$ in a given reaction medium is illustrated in Fig. 1-a.

In a concerted action, proton or electron transfer between a reactant and active sites will be partial or imperfect. The strength of the individual action of active sites will go in parallel with their acid or base strengths.[3] Therefore, the strongest acidic or basic sites and the basic or acidic sites adjacent to them will be most effective in activating each reactant. It can be postulated as the first approximation that the functions of the strengths of active sites against (C_{R_p}/C_R) or $(C_{R'H_p}/C_{R'H})$ are expressed by $\{(\alpha'-H_{0,max})+(H_{0,B}-\beta')\}$, $\{(\alpha'-H_{0,A})+(H_{0,max}-\beta')\}$, $\{(\alpha''-H_{0,max})+(H_{0,B}-\beta'')\}$, and $\{(\alpha''-H_{0,A})+(H_{0,max}-\beta'')\}$, analogously to Eqs. 1 and 2. Here, $H_{0,A}$ and $H_{0,B}$ denote the H_0 value of the acidic or basic sites which are adjacent to the strongest basic or acidic sites respectively. That is, the arrangement of sites with various H_0 values plays an important role, as does the $H_{0,max}$ value.[9] Provided that α', β', α'', and β'' are independent of $H_{0,max}$, C_{R_p} and $C_{R'H_p}$ are functions of $(H_{0,B}-H_{0,max})$ or $(H_{0,max}-H_{0,A})$. Because of $H_{0,B}\leq H_{0,max}$ and $H_{0,A}\geq H_{0,max}$, C_{R_p} and $C_{R'H_p}$ have their maximum values, independent of $H_{0,max}$, when $H_{0,B}=H_{0,max}$ and $H_{0,A}=H_{0,max}$. This corresponds to the case when the extreme surface where the acidic sites and the basic sites having $H_0=H_{0,max}$ are adjacent to each other. In Fig. 1-a, C_{R_p} and $C_{R'H_p}$ are illustrated as horizontal curves, which vary with the arrangement of sites. Here, the formation of R_p or $R'H_p$ can be expected only when C_{R_p} or $C_{R'H_p}$ is greater than C_{RH^+} or $C_{R'^-}$ respectively.

The activated species over active sites will participate in the following elementary steps:

$$RH^+ + R'H \ (3); \quad R + R'^- \ (4); \quad RH^+ + R'^- \ (5);$$
$$R_p + R'H \ (6); \quad R + R'H_p \ (7); \quad R_p + R'H_p \ (8)$$

In the steps involving a single activated specie (Eqs. 3, 4, 6, and 7), the rates are proportional to the concentration of the corresponding specie. In the steps involving two activated species (Eqs. 5 and 8), the rates are not always proportional to their concentrations, but depend predominantly on the second power of the minor activated specie. The catalytic activities (a_c's) of solids *via* each elementary step involving the formation of activated species in Fig. 1-a are illustrated in Fig. 1-b. Among Steps (3) to (8), the catalytic action of a solid with an $H_{0,max}$ value involves the step which contributes to the highest a_c value. Then, the overall a_c throughout the $H_{0,max}$ values illustrated by the dotted curve and the dotted regions in Fig. 1-b. The overall a_c means the a_c value observed experimentally.

The shape of the overall a_c curve and region depends on the acid-base properties and structures of the reactants concerned; especially, C_{R_p} or $C_{R'H_p}$ will increase if the reactant possesses a functional group which accepts the push-pull action of the active sites.[9] It may be remarked that the bump and fall of the overall a_c curve reflects well the change in the predominant catalytic action at $H_{0,max}=m$, n, or o, and at p or q on the abscissa. Therefore, the acid-base properties of the active sites and their catalytic actions can be estimated in terms of the correlation between a_c and $H_{0,max}$ over various catalysts ranging widely in $H_{0,max}$ values.

The correlations in Fig. 1 are similar to those in a homogeneous catalyst system,[2a] but somewhat different because of the effects of the "surface heterogeneity"[11] and the reduced freedom of an adsorbent, so that it reacts only with another species in its vicinity.

Results and Discussion

The formulae of the products and *m*-cresol (I) are shown in Fig. 2. The H_0 values of the strongest acidic sites ($\{H_{0,max}\}_A$) and the conjugate acids of the strongest basic sites ($\{H_{0,max}\}_B$) of catalysts and the compositions of the reaction mixtures are summarized in Table 1. Here, the catalysts are identified by the numerals used in the Experimental section. The values of $\{H_{0,max}\}_A$ and $\{H_{0,max}\}_B$ were the same when both of them were obtained. The $\{H_{0,max}\}_B$ values of CaO, $Ca(OH)_2$, and MgO were all greater than 6.8, although they could not be determined exactly because of the formation of a precipitate during basicity measurements.[5] Both $\{H_{0,max}\}_A$ and $\{H_{0,max}\}_B$ will be used below as the $H_{0,max}$ value of a catalyst. γ-Al_2O_3 is sometimes regarded as acidic,[8] but no acidity of $H_0\leq 6.8$ was observed on γ-Al_2O_3 in this study. Some of the reaction mixture contained resin, but the resin content was not more than 5 mol% at the conversion of I=90 mol% and so was ignored in this study. CaO gave *ortho*-isopropylated products exclusively.[6]

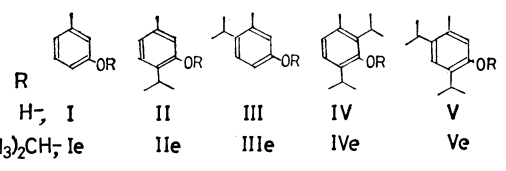

Fig. 2. Formulae of *m*-cresol (I) and the products.

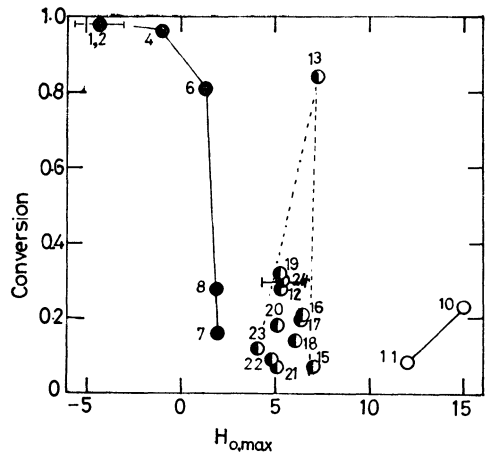

Fig. 3. Correlation between conversion and $H_{0,max}$ in the isopropylation at 300 °C for 4 h.
●: $H_{0,max} \leq 2$, ◐: $4 \leq H_{0,max} < 8$, ○: $H_{0,max} > 10$.

Apparent a_c vs. $H_{0,max}$ Plots and Catalytic Actions. An apparent a_c was obtained as a total conversion of I (mole fraction) at a constant time and temperature. In Fig. 3, the conversions are plotted against the $H_{0,max}$ values in the −5.6—+15 range. *m*-Cresol is a stronger acid ($pK_a \fallingdotseq 10$) than propylene ($pK_a \fallingdotseq 35$[12]). Therefore, catalytic actions *via* the isopropyl cation, the *m*-toluenide anion, or coordinated species of I and/or propylene were expected. The curves through the apparent a_c's in Fig. 3 indicate a bump-and-fall profile similar to the overall a_c curve in Fig. 1. The catalysts may be classified into three groups in terms of the $H_{0,max}$ value: ≤2 (Group 1), 4—8 (Group 2), and ≥10 (Group 3).

In Fig. 3, the a_c in Group 1 increases monotonously with the decrease in $H_{0,max}$ values. The catalytic action corresponds to Eq. 3, and can be explained by Scheme A.[8,13] The isopropyl cation must be formed by the acidic sites of $H_0 \leq 2$. A'^- is more strongly basic than the original basic sites on the surface; the H_0 of the original basic sites is less than $H_{0,max}$. Provided that the reaction occurs on a solid surface, the adsorption of I on A'^- is probable.

The a_c in Group 3 is regarded as increasing monotonously with $H_{0,max}$. This corresponds to Eq. 4. Therefore, the catalytic action must proceed *via* the carbanion, as is shown in Scheme B. Over the basic sites of $H_0 \geq 10$, the abstraction of a proton from the OH group of I occurs easily in Step 1. Hence, *m*-toluenide anions are formed.

In Fig. 3, the plots of Group 2 are raised to various heights above the extension from the conversion-$H_{0,max}$ curves of Groups 1 and 3. The a_c's of Group 2 correspond to a_{c5}, a_{c6}, a_{c7}, or a_{c8}, and the catalytic action of Eq. 5, 6, 7, or 8 is estimated. Provided that *m*-cresol and/or propylene can accept a concerted action, the variations among the a_c's of Group 2 can be explained in terms of their dependence on the arrangement of sites on the surface. This arrangement will be most suitable for concerted actions over γ-Al_2O_3 (No. 13), while it will be most inadequate over the catalysts plotted at the bottom in Group 2 (21, 22, and 15). The most effective catalytic action on the overall a_c of catalysts corresponds to Eq. 8.

On the solid surfaces in Group 2, acidic and basic sites of moderate strength coexist. Compared with Group 1 or 3, the acidic sites in Group 2 are too weak to protonate propylene or to abstract a proton from the OH group of I. Therefore, concerted actions may be postulated as Scheme C. On the surface of a metal oxide, I will be adsorbed by leaving a proton on an oxygen anion (B) and by forming a *m*-tolyloxide with the adjacent metal ion (A). This corresponds to the adsorption model of phenol on MgO[14] and may be comparable to the phenoxide formation on γ-Al_2O_3.[15] It should be noted that the smaller the H_0 of conjugate acidic sites (BH^+), the more easily isopropyl cations are formed. In Scheme C, it is assumed that isopropyl cations are formed by the proton from the OH group of I. As supporting evidence, isopropyl *m*-tolyl ether (I_e) was not isopropylated over CaO under the same conditions as in the isopropylation of I.

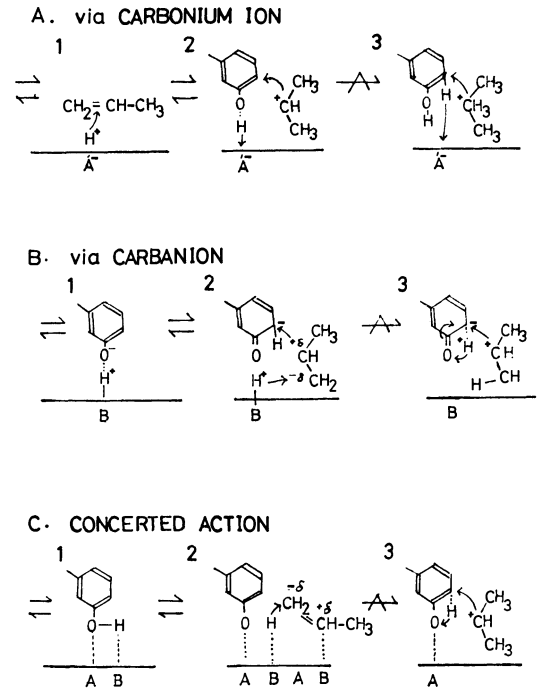

Effects of $H_{0,max}$ on the Selectivity. In order to compare it with the *para*-isopropylation, the selectivity for the *ortho*-isopropylation (ϕ) was defined as follows:

$$\phi = \frac{\text{total } \textit{ortho}\text{-isopropylated products}}{\text{total isopropylated products except } I_e}$$

where one-half of the *ortho-para*-isopropylated products (V and V_e) were considered the ortho-isopropylated products.

In Fig. 4, the ϕ's are plotted against the $H_{0,max}$ values by using the data at the conversion of $I \geq 0.2$. At a conversion of less than 0.2, the trace of the para-isopropylated products could not be detected with sufficient accuracy. ϕ increases roughly with the $H_{0,max}$ values. An increase in $H_{0,max}$ means an increase in the strength of the basic sites and a decrease in the strength of the acidic sites. Therefore, it can be interpreted in terms of the orientation of I adsorbed on the surface. The electrostatic repulsion between

TABLE 1. $\{H_{0,max}\}_A$, $\{H_{0,max}\}_B$, AND COMPOSITION OF REACTION MIXTURES

Catalyst			Composition[a] (mol%)						
No.	$\{H_{0,max}\}_A$	$\{H_{0,max}\}_B$	I	II	III	IV	V	I_e	II_e
1	−5.6∼−3	—	2.3	16.7	15.0	5.7	23.2	—	21.8
2	−5.6∼−3	—	2.5	18.0	10.8	2.8	34.1	—	18.3
4	−1.0	—	4.5	25.6	4.2	10.5	50.7	—	4.5
6	1.3	—	19.2	43.5	—	6.7	16.6	1.6	1.8
7	2.0	2.0	84.5	12.6	—	—	—	2.9	—
8	2.0	2.0	71.8	14.9	4.8	1.5	—	7.0	—
10	—	15	76.8	21.1	—	—	—	2.1	—
11	—	12	91.7	8.3	—	—	—	—	—
12	5.3	5.3	71.9	18.5	—	2.3	—	7.3	—
13	—	7.2	16.3	62.6	3.8	9.4	—	1.2	3.2
15	—	7	92.7	7.3	—	—	—	—	—
16	6.4	6.4	78.6	13.3	—	1.4	—	6.7	—
17	6.3	6.3	80.6	13.8	—	—	—	3.4	—
18	6.0	6.0	86.5	9.6	—	—	—	3.9	—
19	5.2	5.2	67.8	20.7	2.7	3.8	—	2.7	2.4
20	5.2	5.2	82.4	11.8	—	—	—	5.8	—
21	5.0	5.0	93.1	6.9	—	—	—	—	—
22	4.8	4.8	90.6	9.4	—	—	—	—	—
23	4.0	4.0	86.6	13.4	—	—	—	—	—
24	4∼6.8	4∼6.8	70.2	16.5	—	2.4	—	5.2	4.4
25	—	>6.8	29.0	55.5	—	15.5	—	—	—
26	—	>6.8	92.9	7.1	—	—	—	—	—
27	—	>6.8	91.5	8.5	—	—	—	—	—

a) The compositions of the ethers other than I_e and II_e were as follows: Catalyst No. 1; IV_e, 9.9, V_e, 5.4, No. 2; IV_e, 6.6, V_e, 6.9, No. 6; III_e, 10.4, No. 13; IV_e, 3.5, No. 17; III_e, 2.2, No. 24; III_e, 1.5; the others were not detected.

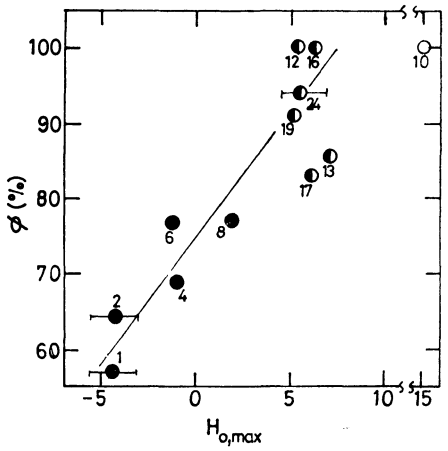

Fig. 4. Correlation between ϕ and $H_{0,max}$ at the same reaction condition to Fig. 3. Catalysts are characterized by the same marks as used in Fig. 3.

π-electrons of the benzene ring of I and the surface will increase with an increase in the base strength (the ability of electron donation) of the surface, that is, with an increase in the $H_{0,max}$ value. The distance of the *para*-position is further from the surface than the *ortho*-position. Consequently, ϕ increases with $H_{0,max}$. The same interpretation has been presented in the methylation of phenol with methanol, for the *ortho*-selectivities over solid acids are lower than those over solid bases,[14,16] even though the interpretation in the literature is merely qualitative.

The $H_{0,max}$ may, therefore, be considered a parameter to represent the surface acid-base property quantitatively. Apart from catalytic actions, $H_{0,max}$ as a surface property of solid will be discussed elsewhere.[17]

Experimental

Catalysts. The following commercial available solids were ground and sieved to prepare a powder of 100—200 mesh. Oxides: WO_3 (6), Sb_2O_3 (7), BaO (10), γ-Al_2O_3 (13, Nikki Chemicals Co., Ltd.), ZnO (16), Bi_2O_3 (17), B_2O_3 (20), TiO_2 (22), ThO_2 (24), CaO (25), and MgO (27). Hydroxides: $Ba(OH)_2$ (15) and $Ca(OH)_2$ (26). A sulfide: ZnS (12). Sulfates: $Al_2(SO_4)_3$ (4) and $NiSO_4 \cdot 7H_2O$ (8). Phosphates: $AlPO_4$ (18) and $Zn_3(PO_4)_2 \cdot 4H_2O$ (19). Tungstates: $Na_2WO_4 \cdot 2H_2O$ (11), $CaWO_4$ (21) and $MgWO_4$ (23). Others: Silica-Alumina-L (1, Nikki Chemicals Co., Ltd.) and Japanese acid clay (2, Wako Pure Chemicals Ind., Ltd.). The numerals in parentheses indicate the corresponding solids. The solids without proviso were of a guaranteed reagent grade. Prior to grinding, $NiSO_4 \cdot 7H_2O$ and CaO were calcined at 300 °C for 4 h in a dry N_2 stream. The solids were stored in glass bottles in the same way as were the commercial reagent used in this study. No particular caution was taken to exclude the adsorption of a trace of moisture in the atmosphere.

Acid-Base Strength Distribution and $H_{0,max}$. A new titration method[5] was used for the determination of acid-base strength distributions of the solids, which expressed in the distribution curves. The values of $\{H_{0,max}\}_A$ and

$\{H_{0,max}\}_B$ were obtained as the H_0 value at the intersection of the acid or base strength distribution curve and the abscissa indicating acidity=0 or basicity=0 respectively.[17] The $\{H_{0,max}\}_A$ value was obtained when it was less than 6.8. The $\{H_{0,max}\}_B$ value was obtained when it was greater than 1.5.

Isopropylation and Analysis of Reaction Products. Desired amounts of I (of a guaranteed reagent grade) and of a catalyst were weighed into an autoclave of a 100-ml capacity equipped with a magnetic stirrer and with gas inlet-outlet pipes. Displacing the air with dry N_2 gas, the apparatus was cooled to −60 °C. The liquid propylene was measured volumetrically as it passed into the autoclave through one of the pipes. The initial mole ratio of propylene to I was 3.0. The amount of the catalyst was 15 wt% against I. The apparatus was heated at 300 °C for 4 h and then cooled to room temperature. After the unreacted propylene had been released, the reaction mixture was dissolved with ether. The ether solution was washed with water, dried over Na_2SO_4, and concentrated. Then the reaction mixture was analyzed by means of a gas chromatograph, using a Kotaki Model GU-21A apparatus on a 2 m×5 mm ϕ column packed with 20 wt% of silicone oil (D.C. 200) on Celite-545 (60—80 mesh). The column temperature was 165 °C, and He gas was used as the carrier at 1.2 kg/cm^2. Isopropyl benzoate was used as the internal standard. Some of the reaction mixture was fractionated into components by means of a modified fractional gas chromatograph, and each of them was identified by means of its infrared absorption spectrum in a Nujol mull.

The measurement of the acid-base strength distribution and that of the isopropylation were done at the same time.

The author wishes to thank Mr. Fumio Nakata for his helpful assistance in the experiments, and also the Takasago Perfumery Co., Ltd., for its permission to publish this article.

References

1) T. Seiyama and I. Mochida, *Kagaku Sosetsu*, No. 3, p. 131 (1973).

2) *e.g.*, a) M. Kilpatrick, *Adv. in Catal.*, **6**, 241, Academic Press, New York (1954); b) R. P. Bell, *ibid.*, **4**, 151, (1952); c) F. A. Long and M. A. Paul, *Chem. Rev.*, **57**, 935 (1957).

3) a) K. Tanaka and A. Ozaki, *J. Catal.*, **8**, 1 (1967); b) M. Misono, Y. Saito, and Y. Yoneda, *ibid.*, **9**, 135 (1967); c) I. Mochida, A. Kato, and T. Seiyama, *ibid.*, **22**, 23 (1971).

4) M. Misono, Y. Saito, and Y. Yoneda, *J. Catal.*, **10**, 88 (1968).

5) T. Yamanaka and K. Tanabe, *J. Phys. Chem.*, **79**, 2409 (1975).

6) T. Yamanaka, F. Nakata, and A. Komatsu, Japan Patent 70-15491; *Chem. Abstr.*, **73**, 55808 g (1970).

7) a) S. H. Patkinson and B. S. Friedman, "Friedel Crafts and Related Reactions," Vol. 2, Part 1, ed. by G. A. Olah, Interscience Publishers, New York (1964), p. 75; b) W. Hahn, U.S. Parent 3290389 (1963); *Chem. Abstr.*, **57**, 13683 h (1962).

8) a) M. Nitta, K. Yamaguchi, and K. Aomura, *Bull. Chem. Soc. Jpn.*, **47**, 2897 (1974); b) *ibid.*, **47**, 2360 (1974).

9) K. Tanabe, "Solid Acid and Bases," Kodansha, Tokyo, Academic Press, New York, London (1967).

10) H. A. Benesi, *J, Am. Chem. Soc.*, **78**, 5490 (1956).

11) K. J. Laidler, "Catalysis," Vol. 1, ed. by P. H. Emmett, Reinhold, New York (1954), p. 75.

12) C. C. Chang and R. J. Kokes, *J. Catal.*, **38**, 491 (1975).

13) P. 3 of Ref. 7a.

14) T. Nishizaki and K. Tanabe, *Shokubai*, **15**, 94 (1973), (33th Symp. Catalysis, Preprint of Papers).

15) D. R. Taylor and K. H. Ludlum, *J. Phys. Chem.*, **76**, 2882 (1972).

16) K. Tanabe, *Shokubai*, **17**, 72 (1975).

17) T. Yamanaka and K. Tanabe, *J. Phys. Chem.*, **80**, July (1976), in press ("A Representative Parameter, $H_{0,max}$ of Acid-base Strength on Solid Metal-Oxygen Compounds").

Catalytic Properties of Metal Sulfates Supported on γ-Al_2O_3 in the Liquid-Phase Isopropylation of *m*-Cresol with Propylene

Tohr YAMANAKA

Central Research Laboratory of Takasago Perfumery Co., Ltd., Kamata, Ohta-ku, Tokyo 144

(Received May 1, 1976)

γ-Al_2O_3 was impregnated with various metal sulfates, calcined, and used as catalysts in the liquid-phase isopropylation of *m*-cresol at 250—300 °C, with the propylene pressure in the range from 15 to 79 kg/cm². The catalytic activities of the sulfates were in the order: $Al_2(SO_4)_3 > ZnSO_4 \approx NiSO_4 > FeSO_4 > CuSO_4 > Li_2SO_4 \approx$ none $\approx CaSO_4 > Na_2SO_4$. The order of the selectivity ϕ for *ortho*-isopropylation over *para*-isopropylation was opposite to that of the catalytic activity. $FeSO_4/Al_2O_3$ catalysts resulted in the best ϕ value and fairly high activity, which were independent of the calcination temperature over the range of 300—500 °C. The formation of Brønsted acidic sites with $1 \leq H_0 \leq 3$ as catalytically-active sites was estimated for the $FeSO_4/Al_2O_3$ and $ZnSO_4/Al_2O_3$ catalysts.

In the past few years,[1] the present authors have studied the use of solid catalysts in the liquid-phase isopropylation of *m*-cresol (I) with propylene (IV) for the preparation of thymol (II), which is an important starting material for menthol. Solid acids, such as silica–alumina and $Al_2(SO_4)_3$, showed high catalytic activity, but the selectivity for *ortho*-isopropylation (ϕ) was not high enough to suppress the formation of 4-isopropyl-5-methylphenol (III) to within the industrial requirements. On the other hand, γ-Al_2O_3 and solid bases such as CaO showed high ϕ values, but were of insufficient catalytic activity.[1b] When some metal sulfates were supported on γ-Al_2O_3, the resultant solids were found to catalyze the reaction with high efficiency and a high ϕ value.[1a] Yet, little has been studied of their catalytic actions. Later, some interesting results were presented on the catalytic activity of supported metal sulfates (on γ-Al_2O_3 and SiO_2) in the vapor phase isopropylation of I with IV.[2a] In this case, the distribution of products other than thymol was different from that in the liquid-phase isopropylation, and therefore, these results are not helpful in the estimation of the catalytic action in the liquid phase.

In this paper, the catalytic properties of various metal sulfates supported on γ-Al_2O_3 are reported for liquid-phase isopropylation, and compared with the recent investigations on the properties of supported sulfates.[2-6]

Experimental

Preparative Procedure of the Catalysts (A). The desired amount of a metal sulfate was dissolved in distilled water, and 75 g of γ-Al_2O_3 (Nikki Chemicals Co., Ltd.; BET surface area: 205 m²/g) of 100—200 mesh was added to the solution. Na_2SO_4, $Li_2SO_4 \cdot H_2O$, $CaSO_4 \cdot 1/2H_2O$, $ZnSO_4 \cdot H_2O$, $CuSO_4$, $Al_2(SO_4)_3$, $FeSO_4 \cdot 7H_2O$, and $NiSO_4 \cdot 7H_2O$ of guaranteed reagent grade were used. The weight of the dissolved sulfate in the anhydrous state was 25 g. After standing for 15—16 h, the impregnated solid was filtered, and washed with 200 ml of distilled water 3 times. The resultant solid was evaporated to dryness on a water bath, and calcined at 500 °C for 4 h. No particular attention was paid to exclude traces of moistures.

Preparative Procedure of the Catalysts (B). Before filtration in the above procedure, the suspension of the impregnated solid in the sulfate solution was concentrated, evaporated to dryness and calcined. In this case, the impregnated amount of the sulfate was expressed in wt% based on the weight of the dissolved sulfate in the anhydrous state against the resultant catalyst.

Surface Acidity of the Catalysts. The acid-base strength distribution of the catalysts were measured by a titration method.[7]

Analysis of $FeSO_4/Al_2O_3$ Catalysts. 0.5 g of the catalyst was dissolved in 25 ml of H_3PO_4 and 10 ml of 33 wt% H_2SO_4 by heating in a CO_2 stream. The iron(II) content was determined by titrating the solution with $KMnO_4$ at room temperature.[8a]

The iron(II) in an extract of the catalyst with dil. HCl was oxidized into iron(III) by HNO_3.[9] The total iron content was determined by titration in the presence of a Variamine Blue B Base which was used as an indicator.[10]

The SO_4^{2-} content in the HCl extract was determined based on the amount of $BaSO_4$ precipitate which had been separated using an ordinary procedure.[8b]

Reaction Procedure (A). The isopropylation of I with IV was carried out in the liquid phase without solvents in an autoclave of 100 ml volume. The IV pressure (P) was maintained constant with the incremental addition of IV. The amount of catalyst (W) was 15 wt% with respect to the initial amount of I.

Reaction Procedure (B). The liquid-phase isopropylation of I was also carried out without the incremental addition of IV. The initial mole ratio IV/I was 3.0. W was 5 or 15 wt% with respect to the initial amount of I.

Products Analysis. After the desired reaction period, the autoclave was cooled rapidly to room temperature in a cold water stream. After the unreacted IV had been released, the reaction mixture was dissolved in ether. The ether solution was washed with water, dried over Na_2SO_4 and concentrated.

Then the reaction mixture was analyzed using gas chromatography, with a Kotaki Model GU-21A on a 2 m × 5 mmϕ column packed with 20 wt% of silicone oil (D.C. 200) on Celite-545 (60—80 mesh). The column temperature was 165 °C, and He was used as the carrier at 1.2 kg/cm². Some of the reaction mixture were fractionated into components by a modified fractional gas chromatograph, and each component was identified by the IR absorption spectrum in a Nujol mull.

Results and Discussion

The products of the isopropylation were thymol (II; main product), 4-isopropyl-5-methylphenol (III), 2,6-diisopropyl-5-methylphenol, 2,4-diisopropyl-5-methyl-

TABLE 1. EFFECTS OF THE IMPREGNATED AMOUNT OF SULFATES[a]

Impregnated amount (wt%)	$ZnSO_4/Al_2O_3$[b]				$FeSO_4/Al_2O_3$[c]	
	θ (min)	x (mol%)	ϕ (mol%)	Acidity of $1 \leq H_0 \leq 3$ (meq/g)	x (mol%)	ϕ (mol%)
0	240	11	100	0		
0.5				0		
5					15	100
10					66	86
20	20	83	79	0.8	87	78
30					74	79
40	50	79	74	0.07	29	100
80	100	81	74	0.04		
100					11	100

a) Catalysts were prepared using Procedue B; calcined at 300 °C for 4 h. b) Reaction Procedure B was employed at 250 °C. c) Reaction Procedure A was employed at 260 °C for 20 min.

TABLE 2. EFFECTS OF SULFATES ON CATALYTIC PROPERTIES

Catalyst	Reaction procedure[c]	t (°C)	θ (min)	x (mol%)	ϕ (mol%)	S
$Al_2(SO_4)_3/Al_2O_3$[b]	B	250	1	96	72	4.53
$ZnSO_4/Al_2O_3$[b]	B	250	8	83	79	4.53
$NiSO_4/Al_2O_3$[b]	B	250	12	84	76	4.30
$FeSO_4/Al_2O_3$[b]	B	260	20	87	78	4.31[d]
$CuSO_4/Al_2O_3$[b]	B	300	10	97	76	4.47
$CaSO_4/Al_2O_3$[b]	B	300	240	73	93	3.93
Li_2SO_4/Al_2O_3[b]	B	300	240	81	89	2.89
Na_2SO_4/Al_2O_3[b]	B	300	240	28	100	2.84
$Al_2(SO_4)_3/Al_2O_3$[a]	A	260	10	95	81	4.53
$ZnSO_4/Al_2O_3$[a]	A	260	10	94	87	4.53
$NiSO_4/Al_2O_3$[a]	A	260	10	94	85	4.30
$FeSO_4/Al_2O_3$[a]	A	260	10	67	93	4.31[d]
$FeSO_4/Al_2O_3$[a]	A	260	30	94	94	4.31[d]
$CuSO_4/Al_2O_3$[a]	A	260	10	5	100	4.47
γ-Al_2O_3	B	300	240	84	86	3.74
γ-Al_2O_3	B	250	240	11	100	3.74

a) Impregnated using Procedure A; calcined in N_2 at 500 °C for 4 h. b) Impregnated with a sulfate of 20 wt% using Procedure B; calcined in air at 300 °C for 4 h. c) P was 25 kg/cm² using Procedure A. Following Procedure B, $P_{at\ \theta=0}$ was 65 kg/cm² at 250 °C and 79 kg/cm² at 300 °C. d) The S value of $Fe_2(SO_4)_3$ was 4.49.

phenol, a small amount of isopropyl *m*-tolyl ether (I_e), and also a small amount of the isopropyl ethers of the products. No 6-isopropyl-5-methylphenol, 3-isopropyl-5-methylphenol, or isothymol were found as products. The kinds and distributions of the by-products are obviously different from those resulting from vapor-phase isopropylation.[2]

The catalytic properties of the supported catalysts are presented in Tables 1 and 2, where t, P, θ, x, ϕ, and S respectively denote the reaction temperature, pressure of IV, reaction time, conversion of I, selectivity for *ortho*-isopropylation, and electronegativity of the sulfate supported or of Al_2O_3. ϕ was defined as the ratio, $100 \times$ {total *ortho*-isopropylated products}/{total isopropylated products excepting I_e}. The catalytic activities were compared to each other in terms of x, θ, or t. The impregnated amount of a sulfate due to Procedure A was estimated to be less than 10 wt%. The amount of $FeSO_4$ impregnated using Procedure A varied from 3 to 8 wt%, which was determined from the Fe content of the $FeSO_4/Al_2O_3$ catalysts in a series of preparative runs. The values of S were calculated on a relative compactness scale in terms of the Sanderson method.[11]

Catalytic Activity. From Table 1, the activities of catalysts prepared by Procedure B appear to have maximum values for an impregnated amount of *ca.* 20 wt%. It can be deduced from Table 2 that the effect of the sulfate on the activity of the catalysts follows the order: $Al_2(SO_4)_3 > ZnSO_4 \approx NiSO_4 > FeSO_4 > CuSO_4 > Li_2SO_4 \approx$ none $\approx CaSO_4 > Na_2SO_4$.
It is noted that this order holds for both catalysts prepared following Procedure B with 20 wt%-impregnation, as well as those following Procedure A.

Moreover, this is consistent with the order of activities of catalysts supported with various sulfates and calcined at arbitrary temperatures in reaction involving the protonation of olefins, namely, $Al_2(SO_4)_3 > NiSO_4 > BeSO_4 > Li_2SO_4 >$ none over SiO_2 and $Al_2(SO_4)_3 > BeSO_4 > NiSO_4 > MgSO_4 >$ none $> Li_2SO_4 \approx Na_2SO_4$ over γ-Al_2O_3 in the vapor-phase isopropylation of *m*-cresol with propylene,[2a] $MnSO_4 > ZnSO_4 > Cr_2(SO_4)_3 >$

$CuSO_4$>none over silica–alumina in the vapor-phase ethylation of benzene with ethylene,[5] and $Al_2(SO_4)_3$>$ZnSO_4$>$MnSO_4$>K_2SO_4 over silica gel in the vapor-phase hydration of propylene.[4]

Whereas the catalytic activities of unsupported sulfates are sensitive to the preparative conditions such as the calcination temperature,[12] it will be remarked that these orders are almost the same. In these studies, catalytic actions are estimated to involve the protonation of propylene or ethylene,[3-5] and the sulfates are estimated to affect the catalytic activities as a source of acidic sites of the Brønsted type.[2-5] It follows that the relative catalytic activity of the supported catalyst depends on the intrinsic properties of the sulfates.[6] The electronegativity S represents the power of individual atoms in a molecule to attract electrons. Therefore, the acid strength of the molecule can be expressed, to a first approximation, by the value of S: the greater S, the stronger the electron accepting power.[11] Table 2 shows that the order of the activities of supported catalysts or γ-Al_2O_3 is much the same as the order of the S values. The catalytic activity of the supported catalyst appears to depend predominantly on the acid strength of the sulfate.

It will be deduced from Table 2 that only sulfates having the S values greater than that of γ-Al_2O_3 are effective in improving the catalytic activity of γ-Al_2O_3 by the support.

Selectivity. In Table 2, the order of selectivities ϕ is just the opposite to that of the activities, namely, the greater the S of the sulfate, the lower the ϕ of the supported catalyst. The ϕ of a catalyst does not vary with x or θ. This is interpreted as follows.

Phenols have been known to be adsorbed *via* their OH groups, on basic sites of a catalyst.[2,13] No acidic site with $H_0 \leq 6.8$ but basic sites whose conjugate acids had H_0 values less than 7 were observed on γ-Al_2O_3 used as the carrier.[7] Over the supported catalysts, *m*-cresol (I) was adsorbed either on the basic sites of γ-Al_2O_3 when they are exposed, or on the basic sites of the supported sulfate when the sulfate covered the entire surface of γ-Al_2O_3. (Even if the surface possesses strong acidic sites, the coexistence of weak basic sites is reasonable.[14]) Isopropylation occurs between the isopropyl cations formed on the Brønsted acidic sites[5] and the I adsorbed on the basic sites.[2] When the vicinity of the basic sites is strongly acidic, the aromatic ring of I orients itself coplanar to the surface because of the interaction between π-electrons and the surface. On the other hand, when the vicinity of the basic sites is basic, the aromatic ring is tilted upward such that the para position is farther from the surface than the ortho position because of the electrostatic repulsion between the π-electrons and the surface.[13,15] Then, the attack of the isopropyl cation from the surface to the para position is retarded by means of resistance to the transfer of the cation or by means of reduced entropy change. Thus, ϕ increases for a decrease in the acid strength in the vicinity of the basic sites according to a similar scheme as has often been remarked for selectivity in the alkylation of phenols.[15]

Because the acid strength of the surface is predominantly affected by the acid strength of the sulfate,[3] the order of ϕ can be interpreted from the above discussion. In confirmation, the present author found that the apparent activation energy about the rate constant (first order with respect to I) in the formation of 4-isopropyl-5-methylphenol was lower by *ca.* 16 kcal/mol than the formation of thymol. In addition, the higher ϕ value of the catalysts prepared following Procedure A than those prepared by Procedure B in Table 2 are interpreted as being due to the basicity of the exposed γ-Al_2O_3.

It was pointed out by Nitta *et al.*[2a] that the selectivity of thymol formation did not depend on the kind of sulfate supported on γ-Al_2O_3 in the vapor phase isopropylation of I. It should be noted that their definition of the selectivity is quite different from ϕ in the present report and does not indicate the effect of the relative reactivities at the *ortho* and *para* positions.

$FeSO_4/Al_2O_3$ Catalyst. From Table 2, the catalyst impregnated with $FeSO_4$ (labelled the "$FeSO_4$/Al_2O_3 catalyst") will be distinguished from other catalysts in respect of its excellent ϕ value and fairly high catalytic activity, The selectivity of thymol over the catalyst was as high as 74—86 mol% of the total products in the reactions presented in Table 2 and in Fig 3. When heated in the atmosphere, hydrated $FeSO_4$ is known to convert into $Fe_2(SO_4)_3$, $(Fe_2O_3)_n \cdot (SO_3)_m$ (basic iron sulfates), or Fe_2O_3.[15] Most of the Fe was found to be Fe(III) and the ratio, {SO_3 and/or SO_4^{-2}}/Fe(III), was found to be 0.8—1.1 upon analysis of the catalyst prepared by Procedure A. The necessity of SO_3 or SO_4^{2-} for the catalytic action was supported by the fact that a catalyst impregnated with $Fe(OH)_3$ instead of $FeSO_4$ was virtually inactive. Consequently, the $Fe_2O_3 \cdot (SO_3)_2$ or $\{Fe_2(SO_4)_3\}_2 \cdot Fe_2O_3$ was postulated to arise from the $FeSO_4$ participating in the catalytic action.

The catalytic activity and the selectivity ϕ were not affected by the calcination temperature to within 300—500 °C, as is shown in Fig. 1. These insensitivities satisfy the industrial requirements of stable catalytic

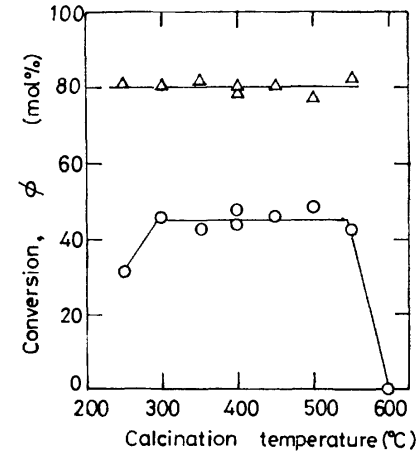

Fig. 1. Effects of calcination temperature on activity and ϕ of $FeSO_4/Al_2O_3$ catalysts prepared by Procedure B. γ-Al_2O_3 were impregnated with $FeSO_4$ by 25 wt% and calcined in air for 4 h. ○: Conversion, △: ϕ. Reaction Procedure B was employed at 260 °C, for 20 min, with W=5 wt%.

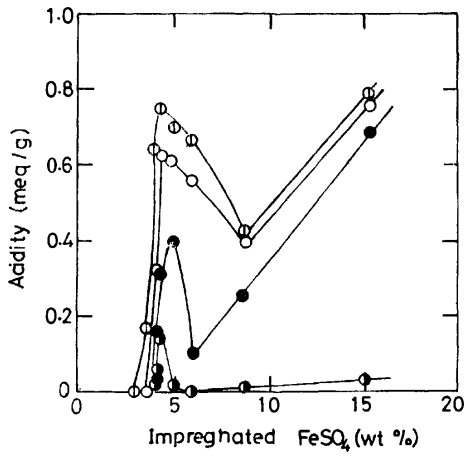

Fig. 2. Acidities of $FeSO_4/Al_2O_3$ catalysts prepared by Procedure A. ⊕, $H_0 \leq 4$; ○, $H_0 \leq 3.3$; ●, $H_0 \leq 1.5$; ◑, $H_0 \leq -3$.

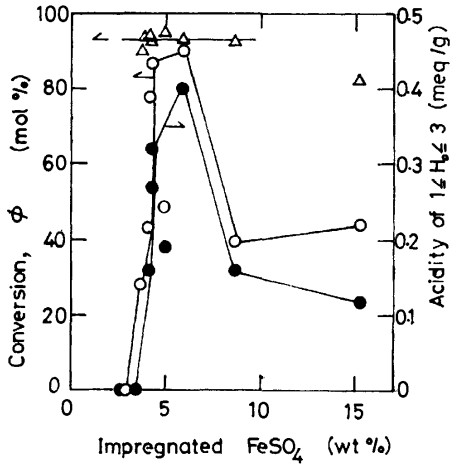

Fig. 3. Effects of impregnated amount on catalytic activity, ϕ, and the acidity of $1 \leq H_0 \leq 3$ over $FeSO_4/Al_2O_3$ catalyst prepared by Procedure A. Reaction Procedure A was employed at 260 °C, for 15 min, with $P = 15$ kg/cm^2. ○: Conversion, △: ϕ, ●: acidity of $1 \leq H_0 \leq 3$.

properties. It has been remarked that the acidic properties of metal sulfates are sensitive to the calcination temperature, and especially the strongest acidic sites on the surface can exist only for a particular calcination temperature with sufficient care being taken to exclude traces of moisture.[2-4,6] Therefore, catalytic activity greatly depends on the calcination temperature when the strongest acidic sites prevail in the catalytic action.[6]

Figure 1 suggests that the active acidic sites on $FeSO_4/Al_2O_3$ are not so strong. The acidities of the catalysts over various H_0 ranges are shown in Fig. 2. The catalyst impregnated with 15 wt% $FeSO_4$, presented in Figs. 2 and 3, was prepared following Procedure A without the washing process. In Fig. 3, the catalytic activity and the acidity for $1 \leq H_0 \leq 3$ indicate correlations exactly in parallel to the impregnated amount and have maximum values for an impregnated amount of about 6 wt%. (The acidities for $1 \leq H_0 \leq 3$ were determined from acid-strength distribution curves correlating the acidities, shown in Fig. 2, the H_0 values.) Then, acidic sites with $1 \leq H_0 \leq 3$ are postulated to be active in the present reaction and to arise most efficiently from $FeSO_4$ at an impregnated amount of about 6 wt%. The strength of the acidic sites will be affected by the interaction between γ-Al_2O_3 and the species arising from $FeSO_4$.

Provided that the acidic sites of a particular H_0 range arise from a particular surface structure, sites on γ-Al_2O_3, where $FeSO_4$ is adsorbed by impregnation and are converted into acidic sites with $1 \leq H_0 \leq 3$, are considered to be filled to an impregnated amount of about 6 wt%. Above this value, the surface of the γ-Al_2O_3 will be occupied by $FeSO_4$ in a scheme different from lower impregnated amounts, which reduces the exposed γ-Al_2O_3 on the surface in the vicinity of the individual adsorbed $FeSO_4$, where efficiency of the $FeSO_4$ for acidic sites, with $1 \leq H_0 \leq 3$ is lowered and instead the efficiency for acidic sites of other types is increased. The catalytic action of acidic sites with $1 \leq H_0 \leq 3$ are interpreted by their arrangement toward the basic sites of γ-Al_2O_3 in the most suitable structure so that isopropyl cations easily attack the adsorbed I. The constant high ϕ value for impregnated amounts less than 9 wt% in Fig. 3 is supported by the basic property of the exposed γ-Al_2O_3 in the vicinity of the acidic sites. While the lower ϕ value at an impregnated amount of about 15 wt% implies a higher coverage of γ-Al_2O_3.

If acidic sites with $1 \leq H_0 \leq 3$ protonate propylene as do the acidic sites over the supported sulfate catalysts,[2-4] they are Brønsted acidic sites.

It is suggested from Table 1 that the active acidic sites on the $ZnSO_4/Al_2O_3$ catalyst are of $1 \leq H_0 \leq 3$. Though, it cannot be deduced that strength of the active sites on the other catalysts in this study are the same, the stronger H_0 range of the sites may not be in contradiction when the sulfate of the stronger acidity, such as $Al_2(SO_4)_3$, is supported.

The author wishes to thank Nikki Chemicals Co., Ltd., for its support in the experimental analysis of the solids. In addition, he thanks Mr. Fumio Nakata for his helpful assistance in the experiments and also the Takasago Perfumery Co., Ltd., for its permission to publish this article.

References

1) a) T. Yamanaka, F. Nakata, and A. Komatsu, Japan Patent SHO 46-3053; *Chem. Abstr.*, **74**, 125150 h (1971); Brit. Patent, 1212597 (1970); Fr. Patent, 1599373 (1970); b) *ibid.*, Japan Patent SHO 45-14591; *Chem. Abstr.*, **73**, 55808 g (1970).

2) a) M. Nitta, K. Yamaguchi, and K. Aomura, *Bull. Chem. Soc. Jpn.*, **47**, 2897 (1974); b) *ibid.*, **47**, 2360 (1974).

3) K. Tarama, S. Teranishi, K. Hattori, and T. Ishibashi, *Shokubai*, **4**, 69 (1962).

4) a) Y. Ogino, *Shokubai*, **4**, 73 (1962); b) *ibid.*, **3**, 191 (1961).

5) Y. Fukui, H. Takaoka, J. Ishii, K. Hirai, and T. Takahashi, *Bull. Chem. Soc. Jpn.*, **40**, 446 (1967).

6) K. Tanabe, "Solid Acids and Bases," Kodansha, Tokyo, Academic Press, New York, London (1970).
7) T. Yamanaka and K. Tanabe, *J. Phys. Chem.*, **79**, 2409 (1975).
8) a) I. M. Kolthoff, P. J. Elving, and E. B. Sandwell, "Treatise on Analytical Chemistry," 2, Part II, Interscience Publishers, New York, London (1961), p. 274; b) *ibid.*, 7, Part II (1961), p. 59.
9) T. Katsura, "Zikken Kagaku Koza," Maruzen, Vol. 15, Tokyo (1957), p. 270.
10) K. Ueno, "Chelate Titration Method," (in Japanese), Nankodo (1961), p. 259.
11) R. T. Sanderson, Translation into Japanese of "Inorganic Chemistry," (Reinhold, New York (1967)), Hirokawa, Tokyo (1971).
12) T. Takeshita, R. Ohnishi, and K. Tanabe, *Catal. Rev.* **8** (1), 29 (1973).
13) D. R. Taylor and K. H. Ludlum, *J. Phys. Chem.*, **76**, 2882 (1972).
14) M. Misono, *Shokubai*, **15**, 9 (1973).
15) K. Tanabe, *Shokubai*, **17**, 72 (1975).
16) a) T. Kawaguchi and S. Hasegawa, *Kogyo Kagaku Zasshi*, **73**, 88 (1970); b) T. Kawaguchi and S. Hasegawa, *Nippon Kagaku Zasshi*, **91**, 1038 (1970).

Conductance of Some High Valence Type Electrolytes in Mixed Solvents. I. Conductance of Tris(1,10-phenanthroline)iron(II) Sulfate and Chloride in Water–Methanol Mixtures at 25 °C*

Eiji KUBOTA and Masatoki YOKOI

Department of Chemistry, Faculty of Science, Shinshu University, Asahi, Matsumoto 390

(Received February 2, 1976)

The conductance of tris(1,10-phenanthroline)iron(II) sulfate, $Fe(phen)_3SO_4$, and chloride, $Fe(phen)_3Cl_2$, has been measured in water–methanol mixed solvent at 25 °C. The data of the sulfate could be explained by means of the Fuoss-Onsager equation (1957) and the Fuoss-Onsager-Skinner equation (1965) on the assumption that the salt is completely dissociated in the entire composition range of the solvent system. Application of the Fuoss-Hsia equation which contains a $c^{3/2}$ term gave association constants increasing from a value of $K_A=40$ in water to $K_A=3900$ in methanol. The $\log K_A$ *vs.* $1/D$ plot is in good agreement with ion association theoreies. The limiting equivalent conductance of $Fe(phen)_3^{2+}$ ion was estimated to be 34.3 in water and 62.3 in methanol.

The behavior of 1 : 1 electrolyte in various solvents has been investigated extensively by conductance measurements.[1] The extended Fuoss-Onsager theory[2] was applied satisfactorily to the analysis of the data, ion association being studied in low dielectric constant media. On the other hand, the investigation of the high valence type electrolyte solutions was often restricted to aqueous solutions because of the limited solubility of the electrolytes in organic solvents. *m*-Benzenedisulfonates of bivalent metals were studied in methanol[3] and some aqueous organic mixture solvents.[4] Tris(1,10-phenanthroline)iron(II) ion is a large bivalent cation, the salts having sufficient solubility in methanol. Thus conductance measurements of the salts in water–methanol mixtures were undertaken for the purpose of studying the change in ion association equilibrium with the variation of the composition of the solvent mixture.

Experimental

Materials. $Fe(phen)_3SO_4$ was prepared by adding a little excess amount of GR 1,10-phenanthroline to the aqueous iron(II) sulfate solution.[5] The solution was concentrated at below 60 °C and the sulfate was precipitated by addition of acetone. The precipitate was dissolved again in water, the procedure being repeated several times. The precipitate was finally crystallized from water and dried at room temperature.

$Fe(phen)_3Cl_2$ was prepared by adding sodium chloride to the aqueous solution of the sulfate and recrystallized from water.[5]

The water content of the sulfate and chloride dried in a dessicator containing silica gel or calcium chloride was not stoichiometric. The number of the water of crystallization was usually less than five. The total cation concentration of each stock solution ($\approx 10^{-2}$ M) was analyzed with Dowex 50-X2 ion exchange resin. The purity of the samples was further checked by spectrophotometry.

Solvents. Methanol was purified by distillation over the activated magnesium and aluminum amalgam.[6] It was then redistilled, the middle fraction being collected. The specific conductivity was less than 8×10^{-8} ohm^{-1} cm^{-1}. Conductivity water was obtained by passing distilled water through a mixed bed ion exchange resin. The specific conductivity was less than 3×10^{-7} ohm^{-1} cm^{-1}.

Apparatus and Measurement. A Jones-type bridge was used for the conductance measurement, alternative current of 3—10 kHz being applied to the bridge. The standard resistors had a precision of ±0.02% and the bridge showed a reproducibility of ±0.005%. Two flask type cells of cell constants of 0.14520 and 0.23322 cm^{-1} were used. The solutions were prepared by adding a certain quantity of the stock solution from a weighing burette to the solvent placed in the cell. Resistance values were obtained by extrapolation to infinite frequency. The temperature of the liquid paraffin bath was controlled to 25.000±0.005 °C. The viscosity B coefficients of $Fe(phen)_3SO_4$ in water and 100% methanol were measured with calibrated Cannon-Fenske type viscometers.

Results and Discussion

The observed conductance values are given in Tables 1 and 2 for the sulfate and the chloride, respectively.

The conductance data of the sulfate were analyzed first by the Fuoss-Onsager (1957)[2] and Fuoss-Onsager-Skinner (1965)[7] equations for symmetrical electrolytes. The form of the former equation for unassociated electrolytes[8] is

$$\Lambda = \Lambda_0 - Sc^{1/2} + Ec\log c + Jc \qquad (1)$$

where Λ_0 is the equivalent conductance at infinite dilution, c is the molar concentration, S is the Onsager slope. Coefficients S, E and J are dependent on temperature, dielectric constant D, viscosity η of the solvent, and Λ_0. J is also a function of ion size parameter $\mathring{a}$.

The conductance equation for associated electrolytes is

$$\Lambda = \Lambda_0 - Sc^{1/2}\gamma^{1/2} + Ec\gamma\log c\gamma + Jc\gamma - K_A c\gamma\Lambda f_\pm^2 \qquad (2)$$

where K_A is the association constant, $f_\pm$ is the mean activity coefficient, and γ is the degree of dissociation. The $f_\pm$'s were calculated by the extended Debye-Hückel theory[9] with the same ion size parameter $\mathring{a}$ as that in J.

In the case of electrolytes containing large ions, the Jc term is replaced by $(J-B\Lambda_0)c$, where B is the viscosity B coefficient of the electrolyte in the solution.

* Presented in part at the 21th Conference on Coordination Chemistry of Chemical Society of Japan, Nagoya, October, 1971; also at the 27th Anual Meeting of the Chemical Society of Japan, Nagoya, October, 1972.

Table 1. Equivalent conductances and concentrations of $Fe(phen)_3SO_4$ in water-methanol at 25 °C[a,b]

10^4c	Λ	10^4c	Λ	10^4c	Λ
0% Methanol $D=78.30$ $10^3\eta=8.903$		20% Methanol $D=69.95$ $10^3\eta=14.00$		40% Methanol $D=60.93$ $10^3\eta=15.93$	
1.7449	108.28	3.3222	69.113	3.3426	55.332
2.1891	107.64	3.9045	68.631	4.2818	54.618
2.1982	107.26	4.4100	68.288	4.8797	54.198
2.3916	107.13	5.2756	67.700	5.6334	53.773
3.0204	106.32	6.1300	67.198	7.3160	52.850
3.1801	106.05	7.1049	66.720	8.6318	52.230
4.7348	104.51	9.2170	65.751	9.7974	51.822
4.8243	104.50	10.890	65.061	11.795	51.140
6.7251	102.98	12.911	64.420	13.935	50.501
8.1661	102.04	15.104	63.725	15.929	49.984
8.7436	101.66	19.911	62.656		
11.171	100.45				
11.634	100.15				
12.946	99.606				
13.912	99.149				
16.024	98.300				
16.620	98.087				
60% Methanol $D=51.61$ $10^3\eta=14.03$		80% Methanol $D=42.58$ $10^3\eta=10.06$		100% Methanol $D=32.70$ $10^3\eta=5.445$	
3.0998	54.141	2.0453	61.211	2.0213	71.307
3.7259	53.418	3.0450	58.903	2.3577	69.390
4.4924	52.696	4.7475	55.848	3.3124	65.096
5.1893	52.105	5.3592	55.001	3.9301	62.855
6.1165	51.437	5.6976	54.561	5.3710	58.883
7.3333	50.600	7.0787	52.980	6.8495	55.832
8.9194	49.698	7.9637	52.102	8.5750	53.106
10.746	48.843	8.9017	51.302	9.0710	52.365
12.215	48.201	11.377	49.601	10.335	50.845
13.603	47.735			11.601	49.418

a) c, in M dm^{-3}; Λ, in ohm^{-1} cm^2 equiv.$^{-1}$. b) D, dielectric constant; η, viscosity(poise), Ref. 29.

The form of the equation (1965) for unassociated electrolytes is

$$\Lambda = \Lambda_0 - Sc^{1/2} + E'c\log(6E_1'c) + Lc \quad (3)$$

and for associated electrolytes

$$\Lambda = \Lambda_0 - Sc^{1/2}\gamma^{1/2} + E'c\gamma\log(6E_1'c\gamma) + Lc\gamma - K_Ac\gamma\Lambda f_\pm^2 \quad (4)$$

where L is a parameter depending on $\mathring{a}$.

Analysis was carried out according to the method of Fuoss[8] and Kay[10] applying both 1957 and 1965 theories to the observed $c-\Lambda$ data.

The conductance data of the chloride, 2 : 1 type unsymmetrical electrolyte, were analyzed using the Fuoss-Edelson technique,[11] based on the Onsager limiting theory. The second association to form the nonconducting species as $MA^+ + A^- \rightleftharpoons MA_2$ was assumed to be negligible, only the equilibrium $M^{2+} + A^- \rightleftharpoons MA^+$ being considered. It was also assumed that $\lambda_{MA^+} = 1/2\lambda_{M^{2+}}$. The Debye-Hückel limiting theory[12] was used for the calculation of the activity coefficient f_{2+}. Λ_0 and K_A are the adjustable parameters. They were determined finally by extrapolation.

Table 2. Equivalent conductances and concentrations of $Fe(phen)_3Cl_2$ in water-methanol at 25 °C[a]

10^4c	Λ	10^4c	Λ	10^4c	Λ
0% Methanol $D=78.30$ $10^3\eta=8.903$		20% Methanol $D=69.95$ $10^3\eta=14.00$		40% Methanol $D=60.93$ $10^3\eta=15.93$	
1.5694	108.21	1.5820	71.010	2.2729	56.786
2.0332	107.96	2.3041	70.612	3.1029	56.365
2.2691	107.54	2.9353	70.249	4.0519	55.967
3.5838	106.81	5.2676	69.318	5.6200	55.480
5.4804	105.76	8.4920	68.399	7.6521	54.977
8.0381	104.98	11.152	67.816	10.651	54.311
9.1204	104.43	14.083	67.262	14.526	53.599
12.451	103.40			20.635	52.739
60% Methanol $D=51.61$ $10^3\eta=14.03$		80% Methanol $D=42.58$ $10^3\eta=10.06$		100% Methanol $D=32.70$ $10^3\eta=5.445$	
2.4275	56.100	1.6605	67.381	1.4743	108.23
2.8863	55.768	3.3682	65.500	2.5915	107.26
3.3092	55.539	5.5051	63.863	3.7608	106.50
4.3059	55.108	6.1547	63.522	5.1994	105.71
4.8409	54.846	6.9758	63.078	6.9131	104.90
7.9237	53.773	9.4788	61.820	9.7950	103.74
11.493	52.867	12.216	60.810	12.386	102.83
16.637	51.708				

a) Table 1, a) and b).

All the calculations were performed on FACOM 230-60, HITAC 8800/8700, and HITAC 10-II remote batch system computers[13] using the program in FORTRAN IV.[14]

The data of $Fe(phen)_3SO_4$ were fitted with both Eqs. 1 and 3 of complete dissociation over the entire range of the solvent composition. However, application of Eq. 2 or 4 for an associated electrolyte gave negative K_A values. The values of Λ_0 and $\mathring{a}$ ($\mathring{a}_J$ from Eq. 1 and $\mathring{a}_L$ from Eq. 3) obtained are summarized in Table 3, which also includes the values of $\sigma\Lambda$, the standard deviation, calculated by means of the expression

$$\sigma\Lambda = \left[\frac{\sum(\Lambda_{exp.}-\Lambda_{calcd})^2}{(N-3)}\right]^{1/2} \quad (5)$$

where N is the number of experimental points.

The $\mathring{a}_J$'s and $\mathring{a}_L$'s are about 7.0 Å. There seems to be no systematic change of the value with solvent composition. The viscosity correction was examined for the data of water and 100% methanol. The calculated parameters are also given in Table 3. The correction gave no noticeable change in the parameter values.

The ionic conductance data of $Fe(phen)_3Cl_2$ were analyzed by the Fuoss-Edelson technique and the Λ_0 and K_A values obtained are given in Table 4.

The conductance data of the sulfate could be inter-

TABLE 3A. CONDUCTANCE PARAMETERS FOR $Fe(phen)_3SO_4$ IN WATER-METHANOL AT 25 °C, CALCULATED FROM FUOSS-ONSAGER EQUATION[a]

Solvents (wt%)	Λ_0	$\mathring{a}_J$	$\sigma\Lambda$	N
0	114.58±0.06	7.06±0.08	0.14	17
0[b]	114.55±0.06	7.30±0.08	0.14	17
20	75.74±0.07	6.81±0.08	0.11	11
40	61.99±0.06	6.95±0.08	0.08	10
60	62.65±0.08	6.91±0.07	0.10	10
80	72.64±0.06	6.66±0.03	0.08	9
100	96.05±0.35	6.78±0.07	0.50	10
100[b]	96.05±0.35	6.84±0.07	0.50	10

TABLE 3B. CONDUCTANCE PARAMETERS FOR $Fe(phen)_3SO_4$ IN WATER-METHANOL AT 25 °C, CALCULATED FROM FUOSS-ONSAGER, SKINNER EQUATION[a]

Solvents (wt%)	Λ_0	$\mathring{a}_L$	$\sigma\Lambda$	N
0	114.58±0.07	7.06±0.08	0.14	17
20	75.73±0.07	6.81±0.09	0.11	11
40	61.98±0.07	6.95±0.08	0.09	10
60	62.65±0.09	6.90±0.07	0.11	10
80	72.63±0.07	6.66±0.04	0.08	9
100	96.00±0.42	6.79±0.07	0.50	10

a) Λ_0, limiting conductance (ohm^{-1} cm^2 equiv.$^{-1}$); $\mathring{a}_J$, $\mathring{a}_L$, ion size parameter (Å); $\sigma\Lambda$, standard deviation of N, experimental points. b) With viscosity corrections; $B=1.9_3$ (0%); $B=3.7_8$ (100% Methanol).

TABLE 4. CONDUCTANCE PARAMETERS FOR $Fe(phen)_3Cl_2$ IN WATER-METHANOL AT 25 °C, CALCULATED FROM FUOSS-EDELSON TECHNIQUE[a]

Solvents (wt%)	Λ_0	λ_0^-	λ_0^+	K_A	$\sigma\Lambda$	N
0	110.61	76.35[b]	34.26	6	0.07	8
20	72.73			6	0.02	7
40	58.70			3	0.02	8
60	58.70			5	0.01	8
80	70.82			19	0.09	7
100	114.63	52.38[c]	62.25	—	0.43	8

a) K_A, ion association constant (M^{-1} dm^3); $\lambda_0^{\pm}$, limiting ionic conductance (ohm^{-1} cm^2 equiv.$^{-1}$). b) Ref. 27. c) Ref. 28.

preted by means of the conductance equation of complete dissociation in a solvent of a high methanol content. The association constants of *m*-benzenedisulfonates of vibalent metals were reported to be of the order of 10^4 in methanol at 25°C.[3,4] The ion association theories of Bjerrum,[15] Fuoss[16] and Yokoyama-Yamatera[17] predict fairly large values of association constant for 2 : 2 electrolyte in methanol. It seems to be difficult to explain why $Fe(phen)_3SO_4$ is completely dissociated in a low dielectric constant solvent such as aqueous methanol even though it contains a large ion.

The Fuoss-Onsager equation has been frequently used to represent the conductance of a hypothetical completely dissociated electrolyte. Within the last few years use of a more complete conductance equation according to Fuoss and Hsia[18] in the form of Fernandez-Prini,[19]

$$\Lambda = \Lambda_0 - Sc^{1/2} + Ec\log c + J_1c - J_2c^{3/2} \quad (6)$$

has been discussed in a number of publications.[20] Coefficient J_2 is also a function of $\mathring{a}$. The combination of equations,

$$K_A = (1-\gamma)/(c\gamma^2 f_\pm^2)$$

and

$$\Lambda = \gamma(\Lambda_0 - Sc^{1/2}\gamma^{1/2} + Ec\gamma\log c\gamma + J_1c\gamma - J_2c^{3/2}\gamma^{3/2}) \quad (7)$$

yields the following expression for associated electrolytes:

$$\Lambda = \Lambda_0 - Sc^{1/2}\gamma^{1/2} + Ec\gamma\log c\gamma + J_1c\gamma - J_2c^{3/2}\gamma^{3/2} - K_Ac\gamma\Lambda f_\pm^2 \quad (8)$$

where $f_\pm$ is calculated by Eq. 9[9] following the extended Debye-Hückel theory:

$$-\log f_\pm = \frac{Ac^{1/2}\gamma^{1/2}}{(1+B\mathring{a}c^{1/2}\gamma^{1/2})} \quad (9)$$

where A and B depend upon the solvent properties.[21]

The coefficients J_1 and J_2 in Eqs. 6 and 8 are

$$J_1 = \sigma_1\Lambda_0 + \sigma_2;\quad J_2 = \sigma_3\Lambda_0 + \sigma_4 \quad (10)$$

where

$$\sigma_1 = \frac{(\kappa\mathring{a}b)^2}{24c}\left[1.8147 + 2\ln\frac{\kappa\mathring{a}}{c^{1/2}} + \frac{2(2b^2+2b-1)}{b^3}\right] \quad (10a)$$

$$\sigma_2 = \alpha\beta + \frac{\beta\kappa\mathring{a}}{c^{1/2}} - \frac{\beta\kappa\mathring{a}b}{16c^{1/2}}\left[1.5337 + \frac{4}{3b} + 2\ln\frac{\kappa\mathring{a}}{c^{1/2}}\right] \quad (10b)$$

$$\sigma_3 = \frac{b^2(\kappa\mathring{a})^3}{24c^{3/2}}\left[0.6094 + \frac{4.4748}{b} + \frac{3.8284}{b^2}\right] \quad (10c)$$

$$\sigma_4 = \frac{\beta(\kappa\mathring{a}b)^2}{24c}\left[\frac{2(2b^2+2b-1)}{b^3} - 1.9384\right] + \frac{\alpha\beta\kappa\mathring{a}}{c^{1/2}} + \frac{\beta(\kappa\mathring{a})^2}{c} - \frac{\beta b(k\mathring{a})^2}{16c}\left[1.5405 + \frac{2.2761}{b}\right] - \frac{\beta^2\kappa\mathring{a}b}{16c^{1/2}\Lambda_0}\left[\frac{4}{3b} - 2.2194\right] \quad (10d)$$

In Eqs. 10a—10d, α and β are the relaxation and the electrophoretic coefficients, respectively, and b is Bjerrum's parameter given by $b=Z^2e^2/(\mathring{a}DkT)$.[22]

Application of Eq. 8 was examined for the data of sulfate for the entire solvent composition range. Yokoyama and Yamatera applied the Fuoss-Hsia equation to our conductance data[24] of the sulfate in water and reported $K_A=36$.[23]

Starting with preliminary values for Λ_0 and $\mathring{a}$ obtained from the Fuoss-Onsager equation, the corresponding parameters appearing in Eq. 8 were calculated by numerical computations.[14] The program,[13] operating essentially according to the method of Kay,[10] involved successive approximation of γ until $|\gamma_i-\gamma_{i-1}|\leqq 1\times10^{-6}$ and iterative determinations of Λ_0, K_A, and $\mathring{a}$ by solving equations of the form

$$\Delta\Lambda = \frac{\partial\Lambda}{\partial\Lambda_0}\Delta\Lambda_0 + \frac{\partial\Lambda}{\partial K_A}\Delta K_A + \frac{\partial\Lambda}{\partial\mathring{a}}\Delta\mathring{a} \quad (11)$$

for each experimental point. The calculations were discontinued when $\Delta\mathring{a}\leqq 1\times10^{-13}$ and finally the $\sigma\Lambda$ value was calculated by Eq. 5.

TABLE 5. CONDUCTANCE PARAMETERS FOR $Fe(phen)_3SO_4$ IN WATER-METHANOL AT 25 °C, CALCULATED FROM FUOSS-HSIA EQUATION IN THE FORM FERNANDEZ-PRINI[a)]

Solvents (wt%)	q	Λ_0	$\mathring{a}_{J_2}$	K_A	$\sigma\Lambda$	N
0	14.3	114.33±0.10	12.9±0.5	35± 5	0.09	17
0[b)]	14.3	114.33±0.10	12.8±0.5	34± 5	0.09	17
20	16.0	75.44±0.07	13.2±0.3	61± 4	0.04	11
40	18.4	61.78±0.07	14.8±0.2	120± 6	0.02	10
60	21.7	62.22±0.11	17.4±0.2	282±12	0.03	10
80	26.3	74.40±0.28	19.8±0.4	868±39	0.09	9
100	34.3	105.97±0.36	25.4±0.1	3939±63	0.08	10
100[b)]	34.3	105.90±0.37	25.4±0.1	3905±64	0.08	10

a) q, Bjerrum's distance (Å). b) With viscosity corrections; $B=1.9_3$ (0%); $B=3.7_8$ (100% Methanol).

Different combinations of the values for Λ_0, K_A, and $\mathring{a}$ may provide almost equally good fits of the conductance equation to the experimental data. In order to investigate the dependence of $\sigma\Lambda$ on $\mathring{a}$ calculations were repeated for a series of ionic separation $\mathring{a}$ between 5 and 30 Å with 0.05 Å increments.

The results are summarized in Table 5. The viscosity correction was examined for the data of water and 100% methanol. The correction made little effect on the parameter values as in the case of analysis by Eq. 1 or 3. The association was observed in the whole range of solvent composition. The $\sigma\Lambda$'s are slightly improved as compared with the values in Table 3. The Λ_0's are very close to those of Table 3 in the solvent of low methanol content, but larger than that obtained from the assumption of complete dissociation in pure methanol. The $\mathring{a}$ values change with the solvent composition, increasing from 12.9 Å in water to 25.5 Å in methanol. The variation of $\mathring{a}$ is parallel to that of the Bjerrum's critical distance q given by $q=Z^2e^2/(2DkT)$,[22)] which varies from 14.3 Å to 34.3 Å (Table 5). The results might be regarded to be in close accordance with the results of Justice[25)] and other authors,[26)] who set $\mathring{a}=q$ in the analysis of 1 : 1 type slightly associated electrolytes.

Log K_A is plotted against reciprocal of dielectric constant in Fig. 1. The ionic crystal radius sum of the complex sulfate is estimated to be about 10 Å. The K_A values are calculated from the ion association theories of Bjerrum, Fuoss and Yokoyama-Yamatera for contact distance of 10 Å and are also plotted in Fig. 1. The observed points start under the line of Yokoyama-Yamatera theory and cross the line, but they are all in the range between the prediction of the Bjerrum and Fuoss theories. The application of Fuoss-Hsia equation[18)] to the analysis of the present data seems to be more satisfactory, the results being consistent with the prediction of the ion association theories.

The limiting ionic conductance of the complex ion in water was estimated from the Λ_0 values by substructing $\lambda_{Cl^-}=76.35$[27)] for the chloride or $\lambda_{SO_4^{2-}}=80.0$[27)] for the sulfate. These values coincide with 34.3. In methanol, the ionic conductance of the complex ion is estimated from the Λ_0 of the chloride as 62.3 ($\lambda_{Cl^-}=52.4$[28)]). The ratio of λ^+ of the complex ion in water to that in methanol is close to the ratio for tetraethylammonium ion whose λ^+ is 32.6 in water[27)] and 60.5 in methanol.[28)] This resemblance would be due to a similar charge to radius ratio of both ions. The limiting ionic conductance of sulfate ion in methanol is about 44 if we use $\lambda^+=62.3$ from the Λ_0 in Table 5. The value should be further checked by the measurements of conductance and transference number for other sulfates in methanol.

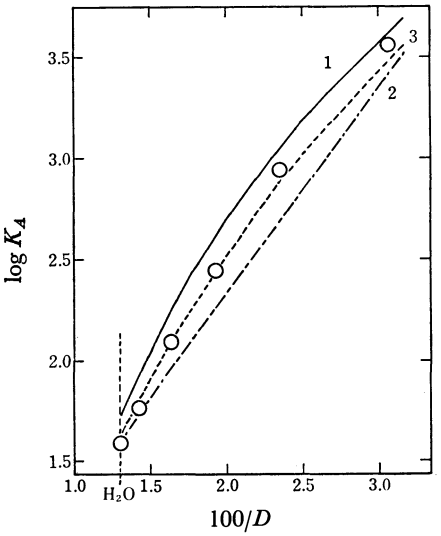

Fig. 1. Plots of log K_A *vs.* $1/D$.
○, Present work at 25 °C. Curves 1, 2, and 3 are theoretical curves due to Bjerrum (——), Fuoss (– – –) and Yokoyama-Yamtera's (– · – · –) theories with $\mathring{a}=10$ Å.

The authors wish to thank the staff of the Nagoya University Computation Center, Tokyo University Computation Center and Shinshu University Remote Batch Computation Center for the use of computers.

References

1) a) G. J. Janz and R. P. T. Tomkins, "Nonaqueous Electrolytes Handbook," Vol. 1, Academic Press, New York-London (1972), p. 145, 1063; *ibid.*, Vol. 2 (1973), p. 800; b) R. Fernandez-Prini, "Physical Chemistry of Organic Solvent Systems," ed. by A. K. Convington and T. Dickinson, Prenum Press, London-New York (1973), p. 588; c) A. D'Aprano and R. M. Fuoss, *J. Solution Chem.*, **3**, 45 (1974); *ibid.*, **4**, 91 (1975); *ibid.*, **4**, 175 (1975); d) L. Broadwater and R. L. Kay, *ibid.*, **4**, 745 (1975).

2) a) R. M. Fuoss and L. Onsager, *J. Phys. Chem.*, **61**, 668 (1957); b) R. M. Fuoss and Accascina, "Electrolytic Conductance," Interscience Publishers, New York, N. Y. (1959), Chap. VIII—XVII.
3) R. Lovas, G. Macri and S. Petrucci, *J. Am. Chem. Soc.*, **92**, 6502 (1970).
4) a) E. Kubota, M. Yokoi, and S. Shikata, *Nippon Kagaku Zasshi*, **85**, 89 (1964); b) M. Yokoi and E. Kubota, *ibid.*, **86**, 894 (1965); c) H. Tsubota and G. Atkinson, *J. Phys. Chem.*, **71**, 1131 (1967).
5) a) F. Blau, *Monatsh.*, **19**, 669 (1898); b) P. Pfeiffer and Fr. Tappermann, *Z. Anorg. Chem.*, **215**, 273 (1933).
6) a) H. Lund and J. Bjerrum, *Ber.*, **64**, 210 (1931); b) A. A. Maryott, *J. Am. Chem. Soc.*, **63**, 3079 (1941); c) H. Hartley and H. R. Raikes, *J. Chem. Soc.*, **1925**, 524.
7) R. M. Fuoss, L. Onsager, and J. F. Skinner, *J. Phys. Chem.*, **69**, 2581 (1965).
8) a) R. M. Fuoss, *J. Am. Chem. Soc.*, **81**, 2659 (1959); b) Ref. 2b, Chap. XV—XVII.
9) R. A. Robinson and R. H. Stokes, "Electrolyte Solutions," Butterworths, London (1965), p. 229.
10) R. L. Kay, *J. Am. Chem. Soc.*, **82**, 2099 (1960).
11) R. M. Fuoss and D. Edelson, *J. Am. Chem. Soc.*, **73**, 269 (1951).
12) Ref. 9, p. 230.
13) FACOM 230-60, Nagoya University Computation Center; HITAC 8800/8700, Tokyo University Computation Center; HITAC 10-II remote batch system, connected to Tokyo University Computation Center.
14) Registered to Nagoya University Computation Center's libraries.
15) a) N. Bjerrum, *Kgl. Danske Videnskab. Selskab.*, **7**, No. 9 (1926); b) S. Petrucci, "Ionic Interactions," Vol 1, Academic Press, New York-London, (1971), p. 121.
16) a) R. M. Fuoss, *J. Am. Chem. Soc.*, **80**, 5059 (1958); b) Ref. 15b, p. 132.
17) a) H. Yokoyama and Yamatera, *Chem. Lett.*, **1973**, 337; b) H. Yokoyama and Yamatera, *Bull. Chem. Soc. Jpn.*, **48**, 1770 (1975).
18) a) R. M. Fuoss and K. L. Hsia, *Proc. Natl. Acad. Sci. U.S.*, **57**, 1550 (1966); *ibid*,. **58**, 1818 (1967); b) K. L. Hsia and R. M. Fuoss, *J. Am. Chem. Soc.*, **90**, 3055 (1968).
19) R. Fernandez-Prini, *Trans.Faraday Soc.*, **65**, 3311 (1969).
20) a) D. F. Evans and D. Gardam, *J. Phys. Chem.*, **72**, 3281 (1968); b) A. D'Aprano and R. M. Fuoss, *ibid.*, **72**, 4723 (1968); c) Y. C. Chiu and R. M. Fuoss, *ibid.*, **72**, 4123 (1968); d) R. Fernandez-Prini, *Trans. Faraday Soc.*, **64**, 2146 (1968); e) E. Baumgartner, M. Busch, and R. Fernandez-Prini, *J. Phys. Chem.*, **74**, 1821 (1970); f) A. D'Aprano, *ibid.*, **75**, 3290 (1971); g) E. M. Hanna, A. D. Pethybrige, and E. J. Prue, *Electrochim. Acta*, **16**, 677 (1971); *J. Phys. Chem.*, **75**, 291 (1971); *J. Solution Chem.*, **3**, 563 (1974); h) M. L. Jansen and H. L. Yeager, *J. Phys. Chem.*, **77**, 3089 (1973); *ibid.*, **78**, 1380 (1974); i) P. Beronius, *Acta Chem. Scand.*, **A28**, 77 (1974); *ibid.*, **A29** (1975); j) C. F. Mattina and R. M. Fuoss, *J. Phys. Chem.*, **79**, 1604 (1975); k) Ref. 1b, p. 525; l) Ref. 26b, 26c, 26d).
21) Ref. 9, p. 230.
22) Ref. 15.
23) H. Yokoyama and H. Yamatera, *Bull. Chem. Soc. Jpn.*, **48**, 2708 (1975).
24) Presented in part at the 21th Conference on Coordination Chemical Society of Japan, Nagoya, October. 1971.
25) a) J. C. Justice. *J. Chim. Phys. Physicochim. Biol.*, **65**, 353 (1968); J. C. Justice, R. Bury, and C. Treiner, *ibid.*, **65**, 1780, (1968); J. C. Justice. *ibid.*, **66**, 1193 (1969); C. Treiner and J. C. Justice, *ibid.*, **68**, 56 (1971); b) J. C. Justice, *Electrochem. Acta*, **16**, 701 (1971).
26) a) M. A. Matesich, J. A. Nadas, and D. F. Evans, *J. Phys. Chem.*, **74**, 4568 (1970); D. F. Evans, J. A. Nadas, and M. A. Matesich, *ibid.*, **75**, 1708 (1971); M. A. Matesich, J. Knoefel, H. Feldman, and D. F. Evans, *ibid.*, **77**, 363 (1973); b) C. DeRossi, B. Sesta, M. Battistini, and S. Petrucci, *J. Am. Chem. Soc.*, **94**, 2961 (1972); c) J. Barthel, J. C. Justice, and R. Wachter, *Z. Phys. Chem.*, **84**, 100 (1973); d) E. Reard and J. C. Justice, *J. Solution Chem.*, **3**, 633 (1974).
27) Ref. 9, pp. 463, 465.
28) M. Spiro, Ref. 1b, p. 673.
29) R. G. Bates and R. A. Robinson, "Chemical Physics of Ionic Solutions," ed. by B. E. Conway and R. G. Barradas, Wiley, N. Y. (1966), p. 211.

The Dual Fluorescence Nature of Some *N*-Monosubstituted Salicylamides

Michio KONDO

Central Research Laboratories, Sankyo Co., Ltd., Hiromachi 1-2-58, Shinagawa-ku, Tokyo 140

(Received March 10, 1976)

Dual fluorescence from *N*-methylsalicylamide (**1**) in alcoholic solutions was observed under excitation by 280 nm light, and was ascribed to two different molecular species: one with and the other without intramolecular proton transfer in the lowest excited singlet state. Some related compounds having two identical chromophores showed similar dual emission spectra with weak emission bands at shorter wavelengths. This fact was explained as being due to the intramolecular energy transfer between the two chromophores in the excited state. From the temperature dependence of the intensity ratio of the two emission bands for these compounds, the difference between the activation energies for the two emissive states was estimated.

In general, fluorescence of an aromatic molecule occurs only from the lowest excited singlet state and therefore, consists of a single band.[1] However, there are a few exceptional cases in which a molecular system having only one chromophore exhibits dual fluorescence: in the cases of (i) exciplex formation (ii) acid-base equilibrium in the excited state which greatly differs from that in the ground state, and (iii) anomalous dual emission in the case of *p*-dimethylaminobenzonitrile in polar solvents.[2,3]

In this paper, the author reports that *N*-methylsalicylamide (**1**) and some related derivatives show dual fluorescence in alcoholic solvents and single fluorescence in other solvents. The origin of this dual fluorescence and its behavior, especially a possible intramolecular energy transfer for the conversion of the emitting state, are discussed.

Experimental

N-Methylsalicylamide (**1**, mp 88 °C) and *N*-benzylsalicylamide (**2**, mp 134 °C) were prepared by the reaction of methyl salicylate with aqueous methylamine in methanol and with benzylamine, respectively. *N,N'*-disalicyloylethylenediamine (**3**, mp 182 °C), -trimethylenediamine (**4**, mp 180 °C), and -hexamethylenediamine (**5**, mp 141 °C) were prepared from methyl salicylate and appropriate diamines. The products were purified by recrystallization from ethanol.

Absorption and fluorescence spectra were recorded on a Hitachi Model 356 spectrophotometer and a Hitachi Model MPF-2 fluorescence spectrophotometer, respectively.

Temperature-dependent studies of the fluorescence spectra were carried out in a quartz dewar in which the temperature can be controlled to whitin ±0.2 °C around room temperature during the period necessary for recording a fluorescence spectrum.

A slit width corresponding to a wavelength of 8 nm was chosen for both the incident and emitted light.

Results

In Table 1 are shown the peak positions of the absorption and emission bands of **1** in various solvents. The first absorption band lies at about 300 nm and is slightly blue shifted for an increase in the solvent polarity.

The fluorescence emissions of **1** in all solvents examined were very strong. This indicates that the lowest excited singlet state is a π-π^* state. The emission band with a large Stokes' shift can be explained as emission by an intramolecular proton transfer from the phenolic OH to the carbonyl group. This is accomplished through thermal relaxation from the Frank-Condon state, as Weller has proposed for methyl salicylate.[4] This explanation seems to be reasonable because it is well known that phenolic hydroxyl has an increased acidity and the carbonyl group has increased basicity in the excited singlet state.[5]

Another point of interest in Table 1 is that a new emission band with about one half of the intensity of the longer wavelength band, appears at about 338 nm when an ethanol solution of **1** is irradiated by 280 nm light (Fig. 1). (Hereafter, the emission band at about

TABLE 1. PEAK POSITIONS OF ABSORPTION AND EMISSION SPECTRA OF *N*-METHYLSALICYLAMIDE IN VARIOUS ORGANIC SOLVENTS

Solvent	Absorption		Emission	
	λ_{max}(nm)	ε_{max}	λ_{ex}: 280 nm	320 nm
Cyclohexane	306	5050	440	441
1,2-Dichloroethane	304	4850	440	440
Ethyl ether	305	5100	432	433
Dioxane	304	5000	434	434
Ethyl acetate	304	4850	433	432
Acetonitrile	303	4550	431	432
Ethanol	301	4350	423	423
			338	

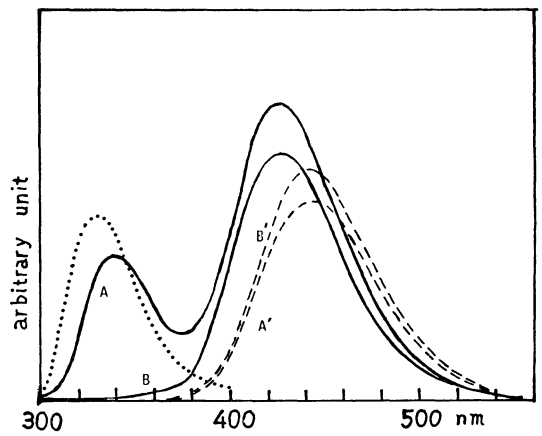

Fig. 1. Emission spectra of *N*-methylsalicylamide in ethanol (——) and in cyclohexane (----), irradiated by 280 nm (A and A') and 320 nm (B and B') light and of *N*-methyl-*o*-methoxybenzamide in ethanol (·····) irradiated by 280 nm light.

Table 2. Emission spectrum of *N*-methylsalicylamide in various alcohols

Solvent		Excitation: 280 nm			320 nm	
		λ_F(max)	I[a)]	I_B/I_R	λ_F(max)	I[a)]
Methanol	B-band	338 nm	375	0.95	419	335
	R	420	395			
Ethanol	B	338	380	0.52	423	593
	R	423	725			
1-Propanol	B	336	410	0.48	424	715
	R	424	850			
2-Propanol	B	336	415	0.47	424	770
	R	424	890			
1-Butanol	B	336	380	0.42	424	840
	R	424	895			
Ethylene glycol	B	341	452	1.00	422	387
	R	421	452			

a) Intensity in arbitrary units.

Table 3. Ratios of the intensities of the B-band to the R-band for several salicylamides in methanol under irradiation by 280 nm light at room temperature

Compound	Concn[a)]	Absorption		Emission (280 nm excitation)				
		λ_{max}	ε_{max}	B-band	I_B[b)]	R-band	I_R[b)]	I_B/I_R
1	4.7	300	4400	338	385	420	349	0.93
2	4.9	301	4500	341	308	422	354	0.87
3	4.5	302	8700	338	85	427	592	0.14
4	4.2	302	8900	339	85	426	695	0.12
5	4.3	301	8700	339	140	423	860	0.16

a) $\times 10^{-5}$ M. b) Intensity in arbitrary units.

338 nm is referred to as the B-band and that at about 425 nm is the R-band). Weller has observed a weak emission band around 350 nm for methyl salicylate in methylcyclohexane, together with another strong emission band at about 442 nm, but he failed to observe the corresponding emission band at shorter wavelengths for a methanol solution of methyl salicylate. The light source he used, a high-pressure mercury arc, Q-81, together with a filter system UG-11 and aqueous potassium chromate, produced almost zero intensity at wavelengths below 300 nm. This may be the reason why he missed the emission band at shorter wavelengths.

In Table 2 are displayed the relative intensity of the two emission bands of **1** in several alcohols. The intensity of the B-band is independent of the solvent, but that of the R-band distinctly increases upon changing the solvent from methanol to butanol. In ethylene glycol, the intensities of both bands are comparable to those in methanol. The ratio, I_B/I_R, is largest in methanol and ethylene glycol.

In Table 3 are summarized the ratios, I_B/I_R, of several related compounds in methanol solutions subject to 280 nm irradiation. These solutions were of about the same concentration. The molar extinction coefficients for the compounds **3**, **4**, and **5** are about twice those for **1** and **2**, reflecting the presence of the two identical chromophores in each molecule. On the other hand, the values of I_B/I_R are about 0.9 for **1** and **2**, while they are about 0.1—0.2 for **3**, **4**, and **5**. The intensities of the R-band of **3**, **4**, and **5** are clearly much larger than those of **1** and **2**, whereas those of the B-bands are much smaller for **3**, **4**, and **5** than for **1** and **2**. These observations suggest that some intramolecular interactions between the two chromophores are operative in photophysical processes in the excited state.

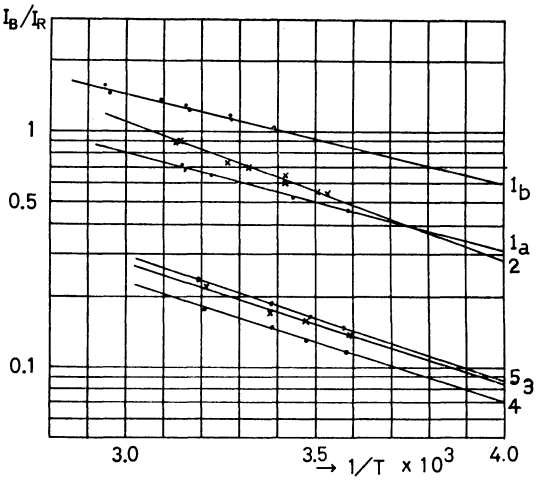

Fig. 2. Temperature variation of the intensity ratio, I_B/I_R.

The ratio, I_B/I_R, shows a temperature dependence. Plotting the quantity log (I_B/I_R) against $1/T$ for several systems resulted in good linear relationships, as is shown in Figure 2. These lines are well expressed by the following equation:

$$\log (I_B/I_R) = A - \frac{\Delta E^*}{2.303RT} \quad (1)$$

In Table 4 are given the ΔE^* values obtained from the slopes of these lines. They are about 2.0 kcal/mol with some divergence.

Table 4. Energy difference (ΔE^*) between two activation energies for the two emissive states

Compound	Solvent	ΔE^*(kcal/mol)
1a	Ethanol	1.76
b	Ethylene glycol	1.67
2	Ethanol	2.72
3	Methanol	2.39
4	Methanol	2.38
5	Methanol	2.41

Discussion

The Origin of the B-band. Irradiation of **1** in alcoholic solutions by 280 nm light yielded two emission bands at about 338 nm (B-band) and 425 nm (R-band). The R-band can be interpreted as emission from the lowest excited singlet state, which is characterized by intramolecular proton transfer.

As mentioned in the introduction, there are some examples showing dual emission bands under special conditions. In the case of **1**, for example, negligible concentration effects may rule out the excimer mechanism as the origin of the B-band. The emission bands from the cation, the neutral molecule, and the anion of salicylamide are located at 383, 435, and 417 nm, respectively.[6] Therefore, the B-band cannot be ascribed to ionic species in the excited state. Recently, Rotkiewicz *et al.*[3] have found new spectroscopic evidence which casts some doubt on the previous interpretation of the anomalous luminescence of *p-N,N*-dimethylaminobenzonitrile and they assigned the two emission bands to two excited species differing in polarity and in the orientation of the $-N(CH_3)_2$ group. This interpretation, however, also does not seem to be applicable to the present case.

Zadorozhnji observed two emission bands for salicylic acid and methyl salicylate but a single luminescent band for salicylamide.[7] He explained the two emission bands as transitions from the two extreme distances in the same vibrational level in the excited state to the same branch of the ground state potential curve, provided that the energy of the intramolecular hydrogen bond in the excited state is considerably higher than that in the ground state. However, this does not seem to explain the excitation-wavelength dependence of the occurrence of the B-band.

The excitation spectrum obtained by monitoring the R-band or the B-band of **1** in ethanol (1.06×10^{-5} M) has a peak at 310 or 299 nm, respectively (no correction was made for, *e.g.*, the energy distribution of the xenon lamp light source). The energy difference between these two wavelengths is 3.38 kcal/mol. The fact that the two excitation spectra were different for the two emission bands, seems to suggest the coexistence of two molecular species in the ground state. With regards to this point it has been reported from parachor measurements that salicylamide exists in an intramolecularly hydrogen bonded form in acetone, ethyl acetate, and dioxane, but this intramolecular hydrogen bond is disrupted in ethanol.[8] However, the peak position and the half width of the first absorption band of **1** in ethanol differ little from those in cyclohexane, indicating that the intramolecular hydrogen bond of **1** survives in ethanol solutions.

The relative intensity of the two emission bands showed a rather marked temperature dependence, while the absorption spectrum of **1** in ethanol, for example, showed a negligible temperature dependence over the range from 10 to 40 °C. Therefore, it is difficult to ascribe the B-band to the molecular species having no intramolecular hydrogen bond in the ground state.

Taking into consideration that the two emission bands were observed only for alcoholic solutions irradiated by 280 nm light, it is assumed that the proton exchanges between alcohol molecules and the solute molecules in the excited state play an important role in the appearance of the B-band. The B-band may originate from a molecular species having no intramolecular hydrogen bonds in the excited state, because the fluorescence band of *N*-methyl-*o*-methoxybenzamide in ethanol, which was measured for comparison, was found to be at about 330 nm, very close to the B-band in question (Fig. 1). The solute molecules excited by 280 nm light reach higher vibrational levels in the excited states. Then some molecules change conformation into species without the intramolecular hydrogen bond through intermolecular interactions with protic solvents, returning to the ground state with the resulting B-band emission. Although water is considered to be more active in proton exchange, the B-band was not observed for aqueous solutions of **1**, although a single broad emission band was observed at about 417 nm, which is ascribed to an anionic species.

Intramolecular Energy Transfer. The ratio, $I_B/I_R=0.14$ for compounds with two identical chromophores in the molecule is in sharp contrast to the values of about 0.9 for **1** and **2**. In the present case, the mean intermolecular distance of about 55 nm estimated from the sample concentration (*ca.* 5×10^{-5} M) is too great for intermolecular energy transfer *via* the exciton mechanism.[9] Furthermore, the fact that the ratios, I_B/I_R, are independent of the number of methylene groups joining the two identical chromophores conflicts with the results of the fluorescence study on a number of diphenylalkanes, where excimer fluorescences were found for diphenylpropane derivatives only.[10] Therefore, it is very likely that some intramolecular interactions are operative between the two chromophores in **3**, **4**, and **5** in the excited state.

Under irradiation by ordinary light sources, it is generally accepted that no chromophoric molecule could be brought to states for which two chromophores in the same molecule are excited by the simultaneous absorption of two photons. In other words, in an excited molecule, one chromophore has to be in the excited state while the other is in the ground state.

Since the B-band of the excited chromophore partially overlaps with the absorption band of the chromophore in the ground state, which is intramolecularly hydrogen bonded, the energy transfer between two chromophores in the same molecule may occur efficiently. The R-band, on the other hand, does not undergo this kind of energy transfer, resulting in relatively weak B-bands for compounds **3**, **4**, and **5**.

Temperature Dependence of the Ratio, I_B/I_R. Considering molecules excited by 280 nm light, some molecules break the intramolecular hydrogen bond resulting in the B-state which can emit B-band fluorescence, while other molecules undergo intramolecular proton transfer yielding the R-state which is responsible for the R-band. For simplicity, it is assumed that back processes may be neglected. Under these conditions, the relative intensity, I_B/I_R, is given by

$$I_B/I_R = \frac{k_f^B/(k_f^B+k_d^B)}{k_f^R/(k_f^R+k_d^R)} \cdot \frac{k^B}{k^R} \quad (2)$$

where the k values are the rate constants for the elementary processes represented in Scheme 1.

$S_0 + h\nu \rightarrow S^*$		absorption	(a)
$S^* \rightarrow S_1$		vibrational relaxation	(b)
$S_1 \rightarrow S_1^R$	k^R	intramolecular proton transfer	(c)
$S_1 \rightarrow S_1^B$	k^B	changing conformation into the B-state	(d)
$S_1^R \rightarrow S_0^R + h\nu^R$	k_f^R	R-band emission	(e)
$S_1^B \rightarrow S_0^B + h\nu^B$	k_f^B	B-band emission	(f)
$S_1^R \rightarrow S_0^R$	k_d^R	internal conversion	(g)
$S_1^B \rightarrow S_0^B$	k_d^B	internal conversion	(h)

Scheme 1.

Assuming the Arrhenius equations for elementary processes (c) and (d), that $k^R=A^R\exp(-E^R/RT)$ and $k^B=A^B\exp(-E^B/RT)$, and that the other processes are temperature independent, can be rewritten as

$$I_B/I_R = K\exp(-\Delta E^*/RT) \quad (3)$$

where $K=\{k_f^B(k_f^R+k_d^R)/k_f^R(k_f^B+k_d^B)\}(A^B/A^R)$ and $\Delta E^*=E^B-E^R$.

Weller has estimated the E^R value to be less than 2.6 kcal/mol for salicylic acid.[4] From this value and the ΔE^* values in Table 4, the E^B value was evaluated to be about 4.5 kcal/mol. This value seems to be reasonable for the activation energy of intramolecular hydrogen bond disruption. Recently, Shizuka *et al.* obtained a similar value for the rapid radiationless decay process of 2,4-bis-(dimethylamino)-6-(2-hydroxy-5-methyphenyl)-*s*-triazine, though the details of the process were not determined.[11]

References

1) M. Kasha, *Discuss. Faraday Soc.*, **9**, 14 (1950).
2) E. Lippert, W. Luder, and H. Boos, "Advances in Molecular Spectroscopy," Pergamon Press, London (1962), p. 443.
3) K. Rotkiewicz, K. H. Grellmann, and I. R. Grabowski, *Chem. Phys. Lett.*, **19**, 315 (1973).
4) A. Weller, *Z. Elektrochem.*, **60**, 1144 (1956).
5) A. Weller, *Z. Phys. Chem. N.F.*, **3**, 238 (1955).
6) S. G. Schulman, P. J. Kovi, and J. F. Young, *J. Pharm. Sci.*, **62**, 1197 (1973).
7) V. R. Shastry and W. V. Rhagwat, Vikram, *J. Vikram Univ.*, **7**, 33 (1963); *Cf.* CA **64**, 11886h (1966).
8) B. A. Zadorozhnji, *Zh. Prikl. Spektrosk.*, **5**, 349 (1966); *Cf.* CA **66**, 60510p (1967).
9) Th. Foerster and K. Kasper, *Z. Phys. Chem, N.F.*, **1**, 275 (1954); B. Stevens, *Adv. Photochem.*, **8**, 161 (1971).
10) F. Hirayama, *J. Chem. Phys.*, **42**, 3163 (1965).
11) H. Shizuka, K. Matsui, T. Okamura, and I. Tanaka, *J. Phys. Chem.*, **79**, 2731 (1975).

The Solubilities and Kraft Points of Fatty Acid Soaps of Odd Carbon Numbers

Keizo OGINO and Yukinori ICHIKAWA

Faculty of Science and Technology, Science University of Tokyo, Noda, Chiba 278

(Received March 12, 1976)

The solubilities of sodium soaps of odd carbon-number fatty acids were measured at various temperatures and the Kraft points[1] of the soaps were determined from the phase diagrams showing the temperature dependence of equilibria among monomers, micelles, and hydrated solid. It was found that the Kraft points were related with the carbon numbers of the fatty acids in a zig-zag curve.

The solubility of sodium soaps of fatty acids at room temperature usually decreases with increasing alkyl chain length. The only soaps that do not require elevation of temperature for dissolution are sodium oleate (sodium *cis*-9-octadecanoate) and some soaps of the less saturated fatty acids. The solubilities of most sodium soaps containing long alkyl chains in water at room temperature are lower than those of unsaturated fatty acid soaps. Many reports have been presented on the solubility of sodium soaps, but they are concerned with the fatty acid soaps of even carbon numbers originating from natural fatty oils.[2-6]

Recently, the advance of organic synthesis makes the fatty acids of odd carbon numbers readily available for technical uses. For the current industrial activity, it is necessary to investigate the properties of sodium soaps of odd carbon-number fatty acids. Thus the solubilities in water and the Kraft points have been determined for the sodium soaps of fatty acids of odd carbon numbers in this study.

Experimental

Materials. The sodium soaps of pentanoic (C_5), heptanoic (C_7), nonanoic (C_9), undecanoic (C_{11}), tridecanoic (C_{13}), and pentadecanoic (C_{15}) acids were prepared by neutralizing these acids with ethanolic sodium hydroxide. These soaps were purified by recrystallization and stored in a dessicator at room temperature. The fatty acids were supplied from Ajinomoto Co., Ltd.; their properties have been listed in a previous work.[7]

Determinations of Solubility. The solubility was determined in 200×15 mm Pyrex test-tubes in which 40 ml of water and a sufficient amount of a sodium soap were mixed so as to precipitate the solid phase. The equilibrium was ascertained by the approach in two directions, from the unsaturated and from the supersaturated states. The tubes were stoppered and thermostatted within ±0.02 °C for 24 h. The solution was permitted to stand until the suspended crystals settled. The crystals were filtered by a small glass filter fastened to the inlet of a 25 ml pippet. During the transfer of the solution from the test tube to a weighing bottle through the pippet, the weighing bottle was kept cold in an ice-bath and covered to prevent loss of water vapor. Then the bottle containing the solution was heated to evaporate the water and the residual soap was dried in vacuum at 60 °C for 24 h. The content of the weighing bottle was weighed before and after the evaporation and drying. The dried soap was stored in a dessicator at room temperature before use. The solubility was calculated as the weight of soap (grams) dissolved in 100 g of water.

Determination of CMC. CMC was determined by measuring the specific conductivity of a soap solution at various temperatures. The specific conductivity was measured with a Conduct Meter Model CH-IDB of the Toa Electric Wave Co., Ltd.

Results and Discussion

The solubilities of sodium salts of pentanoic, heptanoic, nonanoic, undecanoic, tridecanoic, and pentadecanoic acids obtained from the experiments are given in Table 1.

The solubilities presented in weight percent have been plotted in Fig. 1. The plots showing the solubilities of sodium pentanoate and heptanoate are presented at the upper right corner in Fig. 1. From the results, it is clear that these two alkyl soaps dissolve appreciably at room temperature. The Kraft points for these soaps were not determined because these soaps freeze at −5 °C. It should be noticed that the melting points of pentanoic and heptanoic acids are −34.5 and −10.5 °C respectively, which are far lower than the freezing points of the corresponding soaps.

On the other hand, the solubilities of all the soaps of the larger carbon numbers are small at room temperature, and increase as a linear function of the temperature until the concentrations reach the critical values. When either the concentration or the temperature goes beyond this critical threshold, the ionic soap species in a monomolecularly dispersed state seem to undergo some kind of aggregation, accompanied by an enormous increase in the solubility. This is a well-defined critical micelle concentration (CMC). That is, the maximum solubility of the monomer ions or molecules appears at CMC; if this saturation point is exceeded, a new phase, the micelles, appears. This point can be clearly detected when the maximum solubility (presented in molarity) is plotted against $1/T$, as shown in Fig. 2.

In Table 2 the critical concentration C_K have been given with the corresponding temperatures.

In order to determine the Kraft point, the critical micelle concentration (CMC) was measured at different temperatures. For the determination of CMC, the electric conductivity method was applied, though many other methods might be applicable.[8-11]

Figure 3 shows the specific conductivity, κ, of aqueous solutions of sodium pentadecanoate at various concentrations at 55 and 65 °C. As shown in Fig. 3, the relations of the specific conductivity with the concentration slightly bend at certain concentrations of the soap solution, that is, at the CMC.

Shinoda *et al.* have mentioned that the Kraft point can be compared to the phase diagram of the ice–water system. In solutions of soaps, the concentration

Table 1. Solubilities of the sodium soaps of odd fatty acids

Temp °C	g/100 g-H_2O	Volume normality (mol/l)	Temp °C	g/100 g-H_2O	Volume normality (mol/l)	Temp °C	g/100 g-H_2O	Volume normality (mol/l)	Temp °C	g/100 g-H_2O	Volume normality (mol/l)
		Sodium pentanoate C_5				24.00	1.65	79.1×10^{-3}	7.00	0.41	19.6×10^{-3}
6.00	15.98	12.88	2.01	8.00	6.45	23.00	1.25	79.0×10^{-3}	5.00	0.26	12.7×10^{-3}
5.02	13.81	11.13	0.00	5.99	4.83	22.00	1.20	57.7×10^{-3}	3.02	0.13	12.7×10^{-3}
4.00	12.00	9.67	−1.01	4.69	3.78	20.00	0.77	46.6×10^{-3}			
3.00	9.30	7.50	−2.00	4.00	3.25			Sodium tridecanoate C_{13}			
		Sodium heptanoate C_7				45.00	1.298	54.92×10^{-3}	35.00	0.258	10.92×10^{-3}
5.02	12.70	8.34	0.00	5.50	3.62	43.00	0.796	33.70×10^{-3}	35.00	0.229	9.70×10^{-3}
4.00	10.75	7.07	−1.01	3.50	2.40	42.01	0.649	27.49×10^{-3}	30.00	0.200	8.50×10^{-3}
3.00	9.00	5.91	−2.00	3.40	2.32	40.00	0.441	18.69×10^{-3}	25.01	0.185	7.85×10^{-3}
2.01	5.85	3.84				39.01	0.390	16.52×10^{-3}	23.00	0.166	7.04×10^{-3}
		Sodium nonanoate C_9				38.00	0.339	14.37×10^{-3}	20.00	0.126	5.33×10^{-3}
14.00	7.05	391.3×10^{-3}	9.02	1.16	64.6×10^{-3}	35.98	0.246	10.44×10^{-3}	15.00	0.124	5.25×10^{-3}
12.99	4.46	258.7×10^{-3}	8.00	1.12	62.1×10^{-3}			Sodium pentadecanoate C_{15}			
12.01	3.86	214.2×10^{-3}	7.00	1.06	58.9×10^{-3}	57.00	1.230	46.59×10^{-3}	40.00	0.068	2.59×10^{-3}
11.00	1.90	105.6×10^{-3}	6.01	0.99	55.0×10^{-3}	55.01	0.487	18.41×10^{-3}	38.00	0.067	2.53×10^{-3}
10.50	1.59	88.5×10^{-3}	5.00	0.93	51.7×10^{-3}	54.02	0.469	17.73×10^{-3}	35.98	0.064	2.44×10^{-3}
10.00	1.21	66.9×10^{-3}	4.00	0.94	52.1×10^{-3}	53.01	0.418	15.80×10^{-3}	35.00	0.062	2.33×10^{-3}
9.50	1.17	65.2×10^{-3}				52.00	0.126	4.77×10^{-3}	33.00	0.060	2.27×10^{-3}
		Sodium undecanoate C_{11}				50.00	0.116	4.38×10^{-3}	30.01	0.059	2.22×10^{-3}
28.00	7.53	245.9×10^{-3}	19.00	0.72	34.6×10^{-3}	47.02	0.110	4.16×10^{-3}	25.01	0.058	2.20×10^{-3}
27.00	3.27	156.8×10^{-3}	18.04	0.69	32.6×10^{-3}	45.00	0.086	3.25×10^{-3}	23.00	0.056	2.10×10^{-3}
26.01	2.29	109.9×10^{-3}	15.00	0.63	30.2×10^{-3}	42.01	0.069	2.63×10^{-3}	20.00	0.052	1.98×10^{-3}
25.01	2.25	107.8×10^{-3}	10.00	0.51	24.8×10^{-3}						

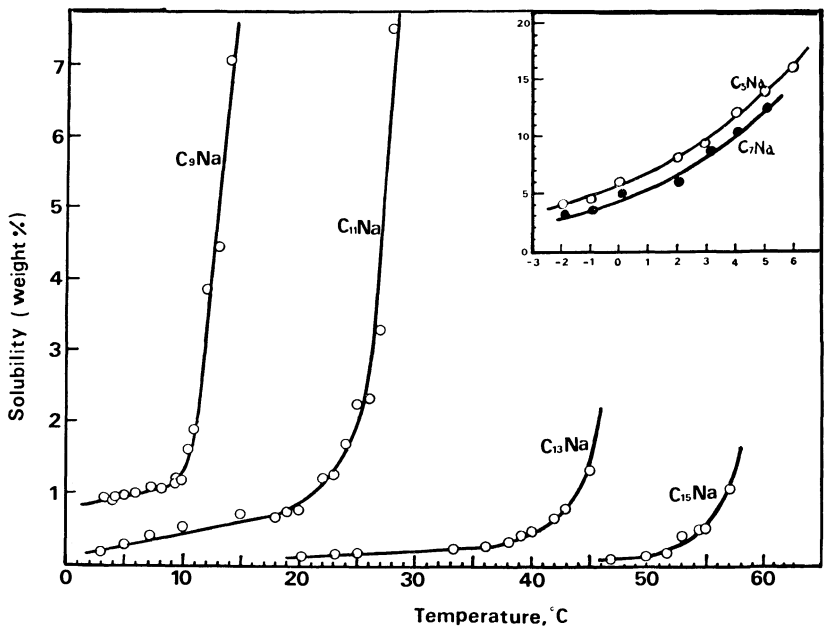

Fig. 1. Solubilities of soaps of the fatty acids with odd carbon numbers.

of monomeric soap molecules plays a role similar to the vapor pressure in the vapor–liquid equilibrium of a one-component system.[12,13] According to Shinoda's analogy, we depicted the phase diagram in the vicinity of the Kraft point of sodium pentadecanoate as shown in Fig. 4.

The Kraft point here can be interpreted as the point at which the solid hydrated soap and the micelles are in equilibrium with the monomers: in terms of the phase rule for three phase systems composed of two components, the equilibrium among the three phase (hydrated solid⇄monomers⇄micelles) is univariant, so that at a given pressure the point is fixed. The concept of the Kraft point as a freezing point of the micelles is also supported by Shinoda.

Hydrolysis is the main source of error in studies of

Table 2. Critical concentrations of sodium soaps

Sodium soap	Temperature °C	Critical concentration $C_k \times 10^3$ (mol/l)
C_5	—	—
C_7	—	—
C_9	10.5	63.91
C_{11}	26.2	40.12
C_{13}	39.8	11.70
C_{15}	52.8	4.05

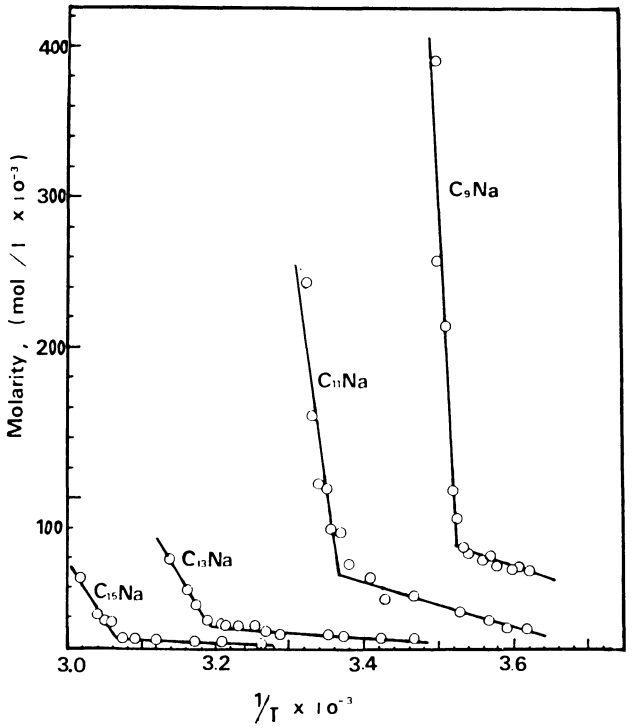

Fig. 2. Solubilities of soaps of the fatty acids with odd carbon numbers showing breaks in the curves for higher alkyl soaps.

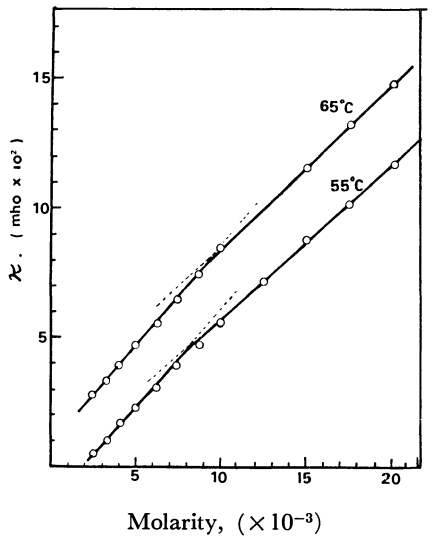

Fig. 3. Specific conductivity-concentration curves for sodium pentadecanoate.

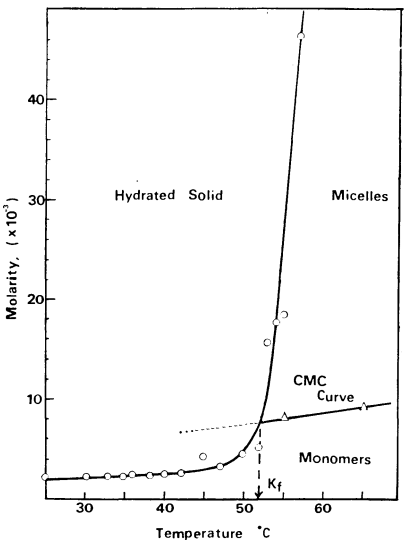

Fig. 4. Phase diagram in the vicinity of the Kraft point of sodium pentadecanoate.

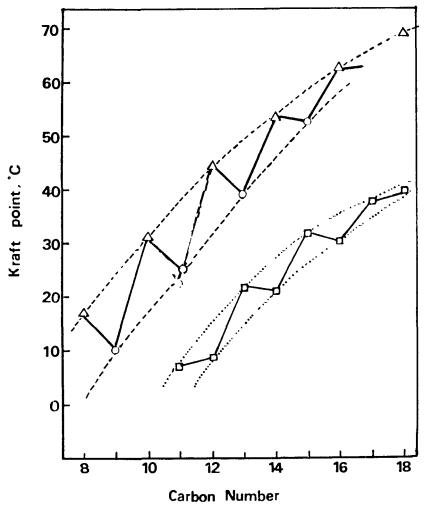

Fig. 5. Kraft points of sodium soaps.
△ ○: Sodium soaps, □: sodium alkylsulfates.

soap solutions. Therefore, in most of the works performed on the solubilities of soaps, alkaline solutions have been used as the solvent in place of pure water to prevent hydrolysis. In this work, we used distilled water free from carbon dioxide as the solvent, thus minimizing the effect of hydrolysis. From the results, the measurements of the Kraft points seemed to be little influenced by the hydrolysis product, fatty acid.

Similar results were also obtained for the soaps of the other fatty acids, and it was found that the Kraft points agree closely with the melting points of the corresponding fatty acids. When one plots the Kraft points of soaps of saturated fatty acids against the number of carbon atoms, a zig-zag curve (high at even carbon numbers and low at odd) is obtained, as shown in Fig. 5. Here the Kraft points of soaps of even carbon number are cited from McBain's report.[14] Figure 5 shows also the Kraft points of sodium normal alkylsulfates.[15]

In a previous work, we studied the melting behavior of binary and ternary mixtures of odd carbon-number fatty acids. Those results would be useful for the determination of the Kraft points of commercial soaps consisting of mixed soaps of various fatty acids.

References

1) M. Demarcq, Inds. Corps. gras., **2**, 341, 370 (1946), **3**, 13 (1947), through Abs. Tech. Press No. 786, 369 (1947).
2) J. W. McBain and W. J. Elford, *J. Chem. Soc.*, **129**, 421 (1926).
3) J. W. McBain and M. C. Field, *J. Phys. Chem.*, **30**, 1545 (1926).
4) J. W. McBain and W. W. Lee, *Oil and Soap* **20**, 17 (1943).
5) R. D. Vold, *J. Am. Chem. Soc.*, **63**, 2920 (1941).
6) R. D. Vold and M. J. Vold, *J. Phys. Chem.*, **49**, 36 (1945).
7) K. Ogino and M. Okamoto, *Yukagaku*, **24**, 474 (1975).
8) H. V. Tartar and K. A. Wright, *J. Am. Chem. Soc.*, **61**, 539 (1939).
9) J. W. McBain "Solution of Soaps and Detergents as Colloidal Electrolytes," in Alexanders Colloid Chem. Vol 5, p. 144 (1944).
10) H. B. Klevens, *J. Phys. Chem.*, **52**, 130 (1948).
11) M. E. L. McBain and E. Hutchinson, "Solubilization," Academic Press, New York (1955).
12) K. Shinoda and T. Soda, *J. Phys. Chem.*, **67**, 2072 (1963).
13) K. Shinoda and E. Hutchinson, *J. Phys. Chem.*, **66**, 577 (1962).
14) J. W. McBain and W. C. Sierichs, *J. Am. Oil Chem. Soc.*, **35**, 221 (1948).
15) H. Lange and M. J. Schwuger, *Kolloid Z. Z. Polym.*, **233**, 145 (1968).

Characteristics of Coordination Compounds of Calcein Blue for a Tunable Organic Liquid Laser

Totaro IMASAKA, Teiichiro OGAWA, and Nobuhiko ISHIBASHI
Faculty of Engineering, Kyushu University, Hakozaki, Fukuoka 812
(Received April 3, 1976)

The lasing and spectroscopic properties of coordination compounds of Calcein Blue with aluminium, calcium, strontium, and barium in water and in a water–ethanol mixture were investigated. The chelate formation improved the lasing properties of Calcein Blue, since the fluorescence quantum yield was increased by the formation of rigid rings in the molecule, and the lasing wavelength could be modified by the metal ion. By using these coordination compounds, tunable laser emissions were observed in the spectral range of 400—478 nm with a low threshold excitation intensity. The threshold excitation intensities excited by the nitrogen laser, the pulse width of which was very short (2.5 ns), were formulated by means of the spectral parameters for such molecules as its Stokes shift was large and its singlet-singlet absorption could be ignored. The calculated values obtained by this formula agreed well with the experimental values in water.

The organic liquid laser has proved itself to be an effective tool for the spectroscopy of atoms and molecules because of its intense power, its narrow bandwidth, and the tunability of its wavelength. Up to this time the organic dyes and scintillators, the fluorescence quantum efficiencies of which are high, have been used as laser materials. The properties of dyes have been improved to obtain a high conversion efficiency, a wide tuning range, a high solubility especially in water, and a high stability. The rigid ring formation of an amide group of coumarin reduces the energy transfer to the vibrational and rotational states and improves the quantum efficiency of the dye.[1] The tuning range is expanded by broadening the fluorescence spectrum in the presence of acidic exciplexes and a neutral form of 4-methylumbelliferone.[2,3] The gain of the organic liquid laser is, however, generally small probably because of its wide fluorescence spectrum. The surfactant increases the solubility of the laser material in water and reduces the thermal fluctuation of the refractive index of the dye solution in the case of a continuous oscillation of the dye laser.[1] The chemical stability of dyes is increased by the trifluoromethylation of the methyl group of 7-diethylamino-4-methylumbelliferone.[4] Nevertheless, there is a need for a laser material with a higher conversion efficiency, a wider tuning range, a higher solubility in water, and a higher chemical stability, especially in the ultraviolet region.

The gain spectroscopy and the threshold analysis provide useful information on the lasing property and the improvement of the laser material. The gain spectroscopy of 4-methylumbelliferone[3] and the threshold analysis of rhodamine B and 6G[5,6] have been carried out previously. However, the threshold analysis under a short-pulse excitation has not been carried out in detail.

The laser action of the coordination compound with a sufficiently high quantum efficiency is expected if there is no particular quenching by the metal ion. Two kinds of organic chelate lasers have hitherto been reported. One of them is europium benzoylacetonate,[7] the first organic laser: its laser emission is due to the emission from a metal ion and its spectral range is very narrow. The other one is the metal phthalocyanine,[8,9] the first organic liquid laser: its spectral property can not be modified reversibly, for example by varying the pH of the solution, and it behaves as an organic dye, as it is usually called.

The laser action of Calcein Blue(4-methylumbelliferone-methyleneiminodiacetic acid) has been reported previously, and the effect of oxygen in the solution has been investigated.[10] On the other hand, Calcein Blue is well-known as a metalfluorechromic indicator in the complexometric determination of zirconium,[11] gallium,[12] and some alkali earth metals.[13]

In the previous letter, we have reported that the coordination compounds of Calcein Blue with aluminium, calcium, strontium, and barium can give laser emission and that the spectral properties of the coordination compound can be modified by changing the metal ions or by varying the pH of the solution.[14] In the present study, a further investigation of the spectral properties and laser characteristics of the coordination compounds of Calcein Blue and the threshold analysis of these lasers has been carried out for the purpose of finding excellent laser materials.

Experimental

Apparatus (Lasers). An experimental arrangement to obtain laser emission is shown in Fig. 1. The exciting source used is a nitrogen laser, which is similar to that described by Basting *et al*,[15] and by Maeda and Miyazoe.[16] It has a 30 cm tube and two 8 nF capacitors made of polyester films and aluminium foils. The output power is 700 kW at 20 kV input, and the pulse width is 2.5 ns (measured by

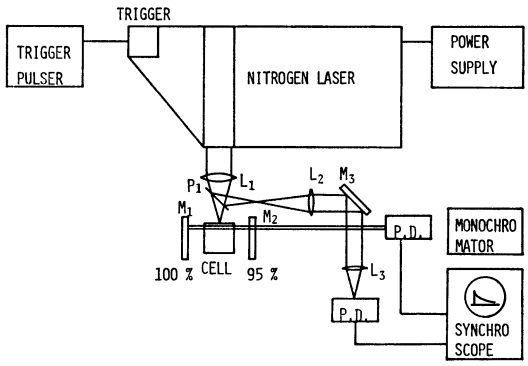

Fig. 1. Experimental arrangement.

a Tektronix 519 oscilloscope). The intense peak power and the short pulse width of the nitrogen laser are suitable for the excitation of an organic liquid laser and for the threshold analysis.

The ultraviolet output of a pulsed nitrogen laser is focused by a spherical lens L_1(f=10 cm) on the surface of the solution of the laser material in a square quartz cell (1×1×5 cm). The cavity of the liquid laser consists of two dielectric coated mirrors with reflectivities of 100 percent (M_1) and 95 percent (M_2), respectively. In the case of tuning the laser oscillation the mirror with 100 percent reflectivity was replaced by a grating (Hitachi Ltd. 3×3 cm, 500 nm blaze, 600 groove/mm) and the square quartz cell was replaced by a quartz cell with nonparallel sides. The laser oscillation of the coordination compound was detected by means of a photocell and was confirmed by observing the coherent radiation. The spectra of the laser emission were photographed by means of an Adam Hilger prism monochromator, and the wavelength was calibrated by a low-pressure mercury lamp. A part of nitrogen laser emission was taken out by a quartz plate (P_1) and was detected by a photodiode (NEC LSD 39A; bandwidth 1 GHz). The signal was integrated by a capacitor (C=3000 pF, R=200 kΩ, and the peak intensity was measured by means of a synchroscope (Iwatsu SS5157).

Apparatus (Fluorescence and Absorption Spectra). The fluorescence spectrum was measured by means of a Hitachi MPF 4 fluorescence spectrophotometer; its spectral response was calibrated by using a rhodamine B cell. The fluorescence spectrum of a concentrated solution was measured in the similar configuration of a quantum counter system using a triangle cell, in which the incident light irradiated the hypotenuse surface of the sample and the fluorescence was measured at a right angle to the incident radiation. The dependence of the fluorescence intensity (peak value) on the concentration of 4-methylumbelliferone was measured by this method. The fluorescence intensity is independent of its concentration above 10^{-4} mol/l. This shows that the excitation light is absorbed completely and that the emission intensity is dependent only on its quantum efficiency, not on its absorbance. The true emission spectrum normalized by the quantum efficiency and the quantum efficiency of the concentrated solution can be measured directly without diluting the solution. It is necessary to use a concentrated solution, since the properties in the concentrated solution may differ from those in the dilute solution because of the difference in the degree of aggregation which may occur in high concentrations. Some deviation from the true fluorescence spectrum due to the self-absorption may occur; however, it is small for 4-methylumbelliferone, Calcein Blue, and its complexes, since the superposition of the fluorescence and absorption spectra is very small (below 1 percent).

The absorption spectra were measured in a split-beam method by using a Hitachi 356 two wavelength/double-beam spectrophotometer.

Reagents. The 4-methylumbelliferone (Tokyo Kasei) was recrystallized twice from water and ethanol to obtain transparent crystals. The Calcein Blue (Dojindo Lab.) was used without purification. The calcium chloride (guaranteed grade; Kishida Chemical Co.), strontium chloride (guaranteed grade; Kishida Chemical Co.), barium chloride (guaranteed grade; Ishizu Pharmaceutical Co.), and aluminium ammonium sulfate (guaranteed grade; Wako Pure Chemical Ind.) were used without purification.

Procedure. A 2.5×10^{-3} mol/l solution of Calcein Blue was prepared by dissolving 0.0803 gram of Calcein Blue and by diluting the solution to 100 ml with freshly distilled water, and adjusted to below pH 4 by adding a buffer solution of sodium acetate. A 10^{-3} mol/l sample solution was prepared by adding the following solutions to a 25 ml volumetric flask in turn; 10 ml of 2.5×10^{-3} mol/l Calcein Blue, a few ml of a 2.5×10^{-3} mol/l metal ion solution (10 ml was used for the formation of the 1 : 1 complex), a solution of sodium acetate, ammonia, or sodium hydroxide to adjust the pH from 4 to 13, and distilled water. The coagulation of aluminium ions or the precipitation of calcium, strontium, and barium hydroxides and carbonates, which disturb the laser action by the scattering of the laser beam, can be reduced by this procedure.

Results

Spectral Properties of Calcein Blue. Calcein Blue has a methyleneiminodiacetic acid group on the 8 position of 4-methylumbelliferone and exhibits three forms(denoted by (1), (2), and (3)) at the respective pH regions, as is shown in Fig. 2. The UV absorption

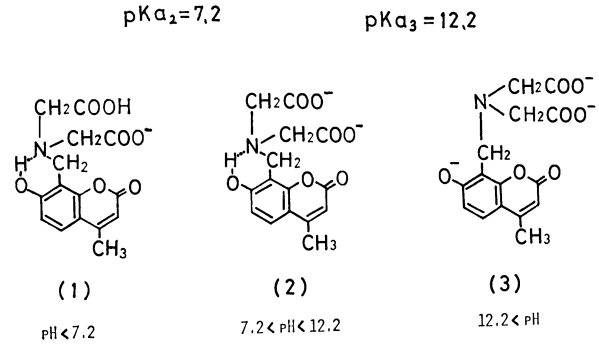

Fig. 2. Structure of Calcein Blue.
The form (1) has two ionizable hydrogen atoms (below pH 7.2). The form (2) has one ionizable hydrogen atom (pH 7.2—12.2). The form (3) has no ionizable hydrogen atom (above pH 12.2).

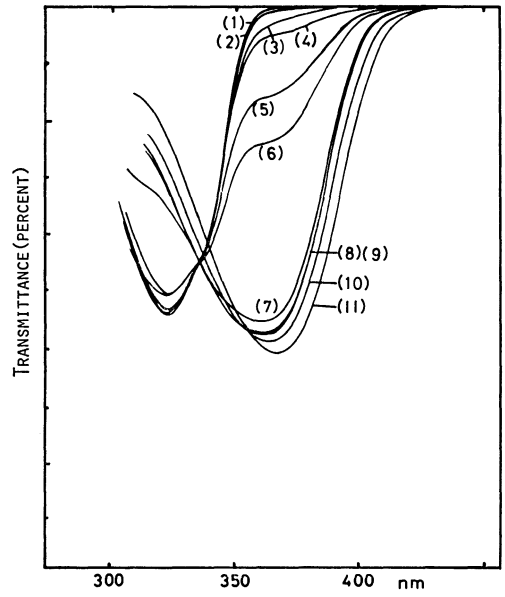

Fig. 3. Absorption spectra of Calcein Blue at various pH.
pH: (1) 3.3 (2) 4.4 (3) 5.1 (4) 6.0 (5) 6.6 (6) 6.8 (7) 8.6 (8) 9.6 (9) 10.2 (10) 11.7 (11) 12.8 concentration: 2.5×10^{-5} mol/l.

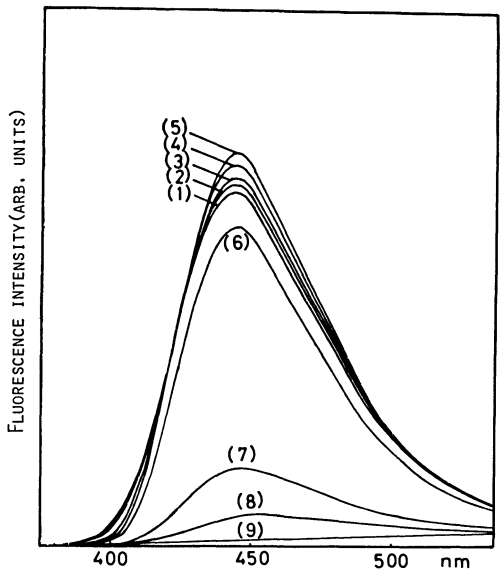

Fig. 4. Fluorescence spectra of Calcein Blue at various pH.
pH: (1) 3.3 (2) 4.2 (3) 5.1 (4) 7.6 (5) 9.5 (6) 11.5 (7) 12.7 (8) 13.4 (9) blank. Concentration: 10^{-3} mol/l, $\lambda_{ex}=337$ nm.

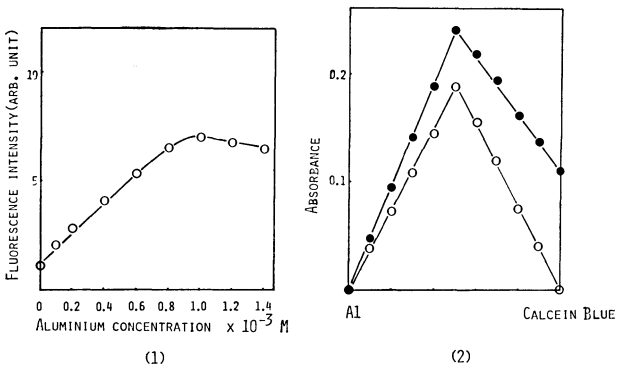

Fig. 5. Composition of aluminium Calcein Blue.
(1) Mole ratio plot of the fluorescence intensity. Concentration of Calcein Blue: 10^{-3} mol/l, $\lambda_{ex}=337$ nm, $\lambda_{em}=410$ nm, pH=5.0.
(2) Continuous variation plot of absorbance. (●): Experimental values, (○): the absorbance of the coordination compound, which is obtained by substructing the absorption of Calcein Blue from the experimental value, concentration of the mixture: 4.0×10^{-4} mol/l, pH=5.0, $\lambda_{abs}=350$ nm.

and fluorescence spectra were measured at various pH values and are shown in Figs. 3 and 4. The existence of three forms of Calcein Blue is confirmed since two isosbestic points are observed at 335 and 354 nm in the UV spectra. As the form of Calcein Blue changes from (1) to (2), the maximum of the absorption band shifts to longer wavelengths: however, the extinction coefficient at 337 nm (the lasing wavelength of the nitrogen laser) does not vary. The wavelength of the maximum emission does not move, and the intensity increases gradually. The small variation in the fluorescence quantum efficiency may be due to the small deformation in the structure by the dissociation of the

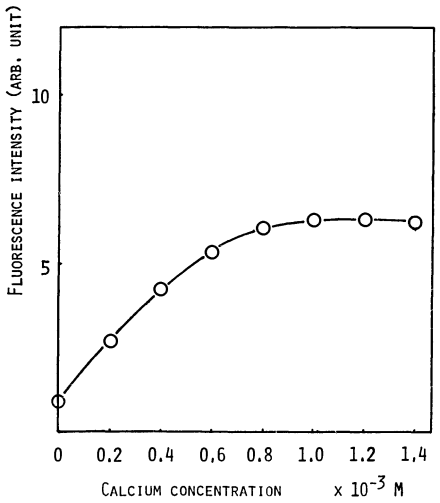

Fig. 6. Composition of calcium Calcein Blue.
Mole ratio plot of the fluorescence intensity. Concentration of Calcein Blue: 10^{-3} mol/l, $\lambda_{ex}=337$ nm, $\lambda_{em}=450$ nm.

hydrogen ion (Fig. 2 (1), (2)). As the form changes from (2) to (3), the extinction coefficient at 337 nm gradually decreases, while the fluorescence intensity decreases steeply. Calcein Blue in the form (3) is non-fluorescent, since the side chain, the methyleneiminodiacetic acid group, becomes flexible by the breakage of the hydrogen bond.[17]

The dependences of the molar extinction coefficient of Calcein Blue at 370 nm and that of the fluorescence intensity at 446 nm on the pH were measured; the acid dissociation constants of pK_a2 and pK_a3 were determined to be about 7.2 and 12.2 respectively.

Composition of Coordination Compound. The color change in the solution of Calcein Blue from blue to violet upon the addition of aluminium ions implies the formation of a coordination compound. The dependence of the fluorescence intensity of the aluminium Calcein Blue on the aluminium concentration was measured in order to determine the composition of the complex; the mole ratio plot is shown in Fig. 5 (1). The figure indicates that a 1 : 1 binary complex of aluminium Calcein Blue is formed at pH 5, since the fluorescence intensity increases as the concentration of the aluminium increases up to an equimolar composition. The gradual decrease in the aluminium excess region may be due to the light scattering by aluminium hydroxide formed in the solution. The absorbance of aluminium Calcein Blue was also measured; the continuous variation plot is shown in Fig. 5 (2). The maximum absorbance was obtained at the equimolar concentration, and the formation of a 1 : 1 binary complex was confirmed.

The dependence of the fluorescence intensity of calcium Calcein Blue on the calcium concentration is shown in Fig. 6. The fluorescence intensity is constant above the equimolar concentration. Accordingly, the metal ion was mixed in a 1 : 1 proportion to the ligand molecule for the preparation of the coordination compound.

Spectral Properties of Aluminium Calcein Blue. The

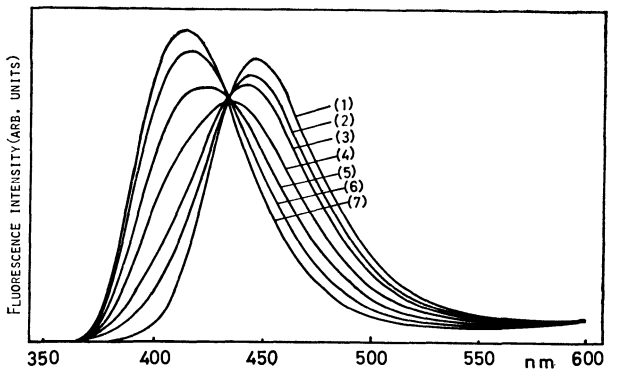

Fig. 7. Fluorescence spectra of aluminium Calcein Blue at various aluminium concentration at pH 6.0. Concentration of Calcein Blue: 10^{-3} mol/l, $\lambda_{ex}=$ 337 nm, concentration of aluminium (mol/l): (1) 0 (2) 0.1×10^{-3} (3) 0.2×10^{-3} (4) 0.4×10^{-3} (5) 0.6×10^{-3} (6) 0.8×10^{-3} (7) 1.0×10^{-3}.

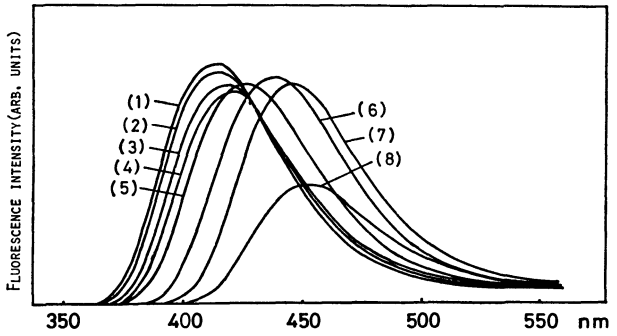

Fig. 8. Fluorescence spectra of aluminium Calcein Blue at various pH. Concentration of aluminium Calcein Blue: 10^{-3} mol/l, pH: (1) 5.0 (2) 6.0 (3) 7.1 (4) 7.9 (5) 9.0 (6) 10.0 (7) 11.0 (8) 12.0, $\lambda_{ex}=$ 337 nm.

fluorescence spectra of the coordination compound of aluminium Calcein Blue at various aluminium concentrations are shown in Fig. 7. The contribution of the coordination compound in the fluorescence spectrum increases as the aluminium concentration increases, as is indicated by the shift of the band to shorter wavelengths. The emission intensity of the coordination compound is stronger than that of the ligand molecule. The iso-emissive point shows that no side reaction takes place.

The effect of the pH on the fluorescence spectrum and the molar extinction coefficient at 370 nm of aluminium Calcein Blue (1 : 1 mixture) are shown in Figs. 8 and 9. The fluorescence spectrum shifts to longer wavelengths as the pH increases, since the complex dissociates to an ion and a ligand in this pH region. The coordination compound of aluminium Calcein Blue is formed predominantly below pH 5, and the equilibrium shifts to the dissociation and the release of a proton occur simultaneously, since the fluorescence spectra show no iso-emissive point.

It is well known that the quantum efficiency of the dyes and the complexes increases in a hydrophobic solvent since the interaction between the solute and the solvent decreases. The laser action is expected to

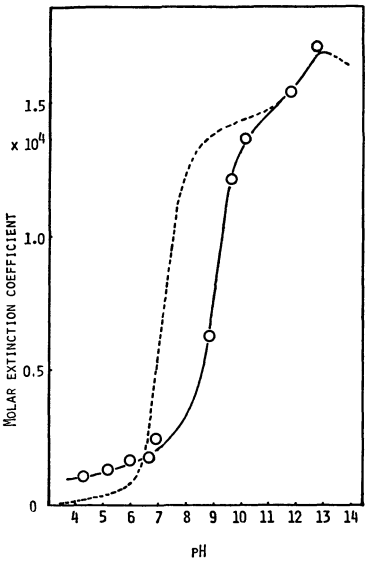

Fig. 9. Molar extinction coefficient at 370 nm at various pH. Solid curve: aluminium Calcein Blue, broken curve: Calcein Blue.

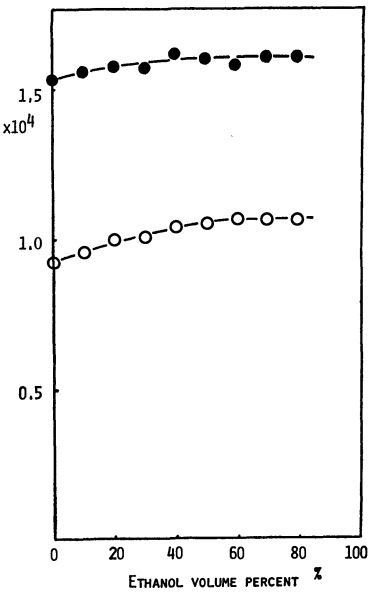

Fig. 10. Fluorescence intensity (○: arbitrary units) and molar extinction coefficient (●) of aluminium Calcein Blue in water-ethanol mixture. $\lambda_{ex}=337$ nm, $\lambda_{em}=446$ nm, $\lambda_{abs}=337$ nm.

be obtained in a ethanol–water mixture under a low excitation intensity. The dependences of the molar extinction coefficient and the fluorescence intensity of aluminium Calcein Blue on the volume percentage of ethanol in water were measured; they are shown in Fig. 10. Although the absorption and the fluorescence spectra do not shift, the extinction coefficient and the fluorescence intensity increase gradually as the ethanol volume percent increases. The quantum efficiency of the aluminium complex does not increase much, since it is already high and near unity in water. The small variation in the spectra indicates that the form and the composition of the coordination compound in

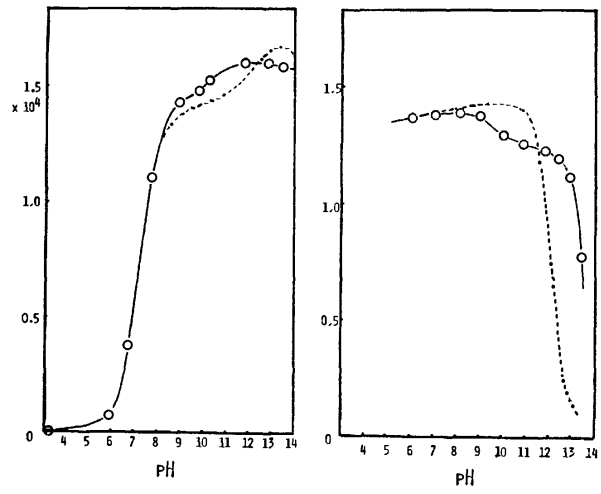

Fig. 11. Molar extinction coefficient (left) and fluorescence intensity (right: arbitrary units) at various pH. Solid curve: barium Calcein Blue, broken curve: Calcein Blue, $\lambda_{abs}=337$ nm, $\lambda_{ex}=337$ n,, $\lambda_{em}=446$ nm.

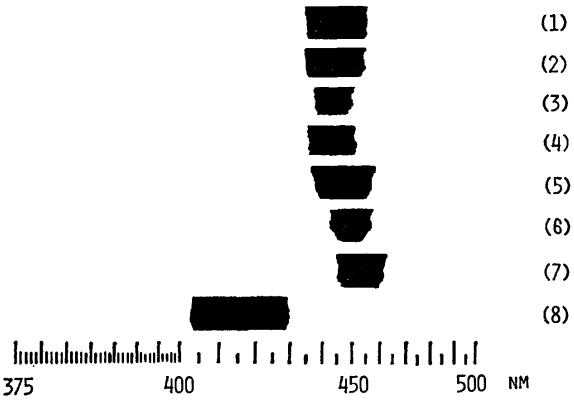

Fig. 12. Laser spectra of Calcein Blue and the complexes.
(1) Calcein Blue (pH 5) (2) Ca Calcein Blue (pH 5) (3) Sr Calcein Blue (pH 5) (4) Ba Calcein Blue (pH 5) (5) Ca Calcein Blue (pH 12) (6) Sr Calcein Blue (pH 12) (7) Ba Calcein Blue (pH 12) (8) Al Calcein Blue (pH 5).

an ethanol–water mixture are identical to those in water.

Spectral Properties of Barium and Calcium Calcein Blue. Barium and calcium Calcein Blue have intense fluorescences at about pH 9 and 13.[13] The dependences of the molar extinction coefficient at 370 nm and the fluorescence intensity at 446 nm of barium Calcein Blue on the pH were measured in detail (*cf.* Fig. 11), in order to clarify the variation in the composition of the coordination compound. The coordination compound of barium Calcein Blue is formed in the region above pH 8, and it has an intense fluorescence even at pH 13. The structure of barium Calcein Blue in the pH 8—13.5 region is proposed to be the form in which a phenolic hydrogen is substituted by an alkali earth metal ion and the free side chain is bound by the metal ion.[13] In this structure the barium ion may not be surrounded by the other oxygen atom, since the barium

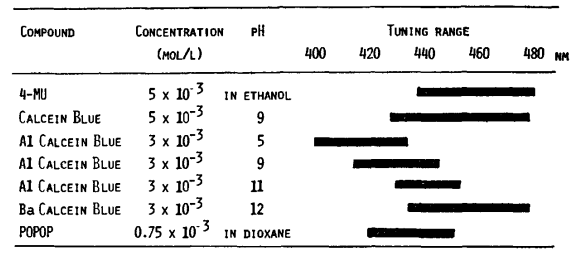

Fig. 13. Tuning ranges of lasers of dyes and coordination compounds.

ion is doubly charged and the quantum yield is not so high as that of aluminium Calcein Blue.

Lasing Wavelength. The laser spectra of Calcein Blue and the coordination compounds are shown in Fig. 12. The laser action of Calcein Blue is observed at around 446 nm at pH 5, but not at pH 12. The coordination compounds of Calcein Blue with calcium, strontium, and barium lase at around 450, 452, and 454 nm respectively at pH 12. It is noteworthy that the coordination compound with an alkali earth metal ion lases at longer wavelengths as the atomic weight of the metal ion increases. The stability constant and the electrostatic force by the metal ion decrease as the atomic weight and the ion radius increase, and the perturbation of the calcium ion to the ligand molecule is expected to be stronger than that of barium. The red shift in the heavier atom complex might be due to the steric effect.

Calcein Blue forms a coordination compound with an aluminium ion at around pH 5, and it lases at around 418 nm; the wavelength is shorter than that of Calcein Blue.

Tuning Range. The tuning ranges (the wavelength ranges in which the narrow-band oscillation is possible) of the coordination compound lasers are shown in Fig. 13, where 4-methylumbelliferone and 1,4-bis(5-phenyloxazol-2-yl)benzene(POPOP) are included for the sake of comparison. Tunable laser emission from 436 nm to 480 nm was observed from the solution of Calcein Blue (pH 9). The tuning range of the aluminium Calcein Blue complex is 400—435 nm at pH 5 and it is longer in the wavelength at a higher pH value. The barium complex lases in the range of 435—478 nm, as in the case of 4-methylumbelliferone. In this way the laser action of the coordination compound of Calcein Blue can be observed in the range from near ultraviolet (400 nm) to blue green (478 nm) with a low threshold excitation intensity by changing the metal ion and by varying the pH. The full width at the half maximum of the laser emission was a few nanometer, which would be due to the short pulse width of the nitrogen laser (2.5 ns) and to the lack of the resolution of the grating. The dioxane solution of the POPOP shows superradiation (amplified spontaneous emission) in a solution more concentrated than 10^{-3} mol/l, and the tunable laser action was not observed at 10^{-3} mol/l.

Discussion

Threshold Analysis. The threshold equation of

the laser action represents a relation between all the parameters affecting lasing; critical inversion, emission wavelength, losses, dye concentration, and extinction coefficient. The gain, α, of the organic liquid laser is written as[3]:

$$\alpha = \sum_i [\sigma_{emi} N_i^* - \sigma_{si} N_i - k_i] - d \quad (1)$$

The summation in the equation shows the sum on such different species as the ligand and the coordination compound. In this equation, σ_{emi} is the emission cross section; σ_{si}, the singlet-singlet absorption cross section at the wavelength of the laser emission, and N_i and N_i^* the population in the ground and the excited states. The first term of this equation is the amplifying term due to the fluorescence; the second term is the loss term due to the singlet-singlet absorption at the lasing wavelength, and the third term, k_i, is the loss term due to the triplet-triplet absorption. The last term, d, represents the loss of the resonating cavity. The third term can be neglected because the pulse width of the excitation source of the nitrogen laser is short (2.5 ns) enough to be able to ignore the absorption from the triplet state.

The gain, α, can be set at zero under the threshold condition, thus,

$$\sum_i [\sigma_{emi} N_i^* - \sigma_{si} N_i] - d = 0. \quad (2)$$

When there are only two species, such as a ligand and a complex, the weight-averages ($\bar{\sigma}_{em}$ and $\bar{\sigma}_s$) are substituted;

$$\bar{\sigma}_{em} N^* - \bar{\sigma}_s N - d = 0. \quad (3)$$

Then, the critical inversion, N^*/N, at the threshold is written as follows;

$$\left[\frac{N^*}{N}\right]_{threshold} = \frac{\bar{\sigma}_s + d/N}{\bar{\sigma}_{em}}. \quad (4)$$

The rate of the formation of N^* by the excitation is represented by:

$$\frac{dN^*}{dt} = \bar{\sigma}' I(t) N - \left(\frac{1}{\tau}\right) N^* \quad (5)$$

where $I(t)$ is the intensity of the excitation source; $\bar{\sigma}'$, the absorption cross section at the wavelength of the nitrogen laser, and τ, the lifetime of fluorescence. This differential equation gives the critical inversion, N^*/N, approximately as follows:

$$\frac{N^*}{N} \simeq \tau \bar{\sigma}' I(t). \quad (6)$$

From Eqs. 4 and 6, we obtain:

$$I_{threshold} \simeq \frac{\bar{\sigma}_s + d/N}{\tau \bar{\sigma}' \bar{\sigma}_{em}}. \quad (7)$$

The absorption cross section, $\bar{\sigma}_s$, at the lasing wavelength is small in the case of a coumarin compound, such as Calcein Blue and its complexes, because the Stokes shifts of these compounds are large and the superposition of the fluorescence and absorption spectra is rather small, and thus $\bar{\sigma}_s$ can be neglected. When $\bar{\sigma}_{em}$ ($=\lambda^4 E/8\pi c\eta^2\tau$) is substituted,[3] Eq. 7 becomes:

$$I_{threshold} \simeq \frac{8\pi c\eta^2 d}{N\bar{\sigma}'\lambda^4 E} \propto \frac{\eta^2 d}{n\bar{\varepsilon}\lambda^4 E}. \quad (8)$$

In this equation, E is the fluorescence intensity normalized by its quantum efficiency; η the refractive index; $\bar{\varepsilon}$, the weight-average of the molar extinction coefficient at the wavelength of the nitrogen laser, and λ the wavelength of the maximum fluorescence intensity. The observed value of the extinction coefficient can be used for $\bar{\varepsilon}$ in the equation. The population in the ground state can be set at the total concentration, n.[18]

The equation can clarify the characteristics of a laser material with a large Stokes shift. The threshold excitation intensity of a given compound can be calculated, and the usefulness of that compound as a laser material can be estimated by the use of spectral parameters. This threshold excitation equation shows the λ^4 term in the denominator requires a higher excitation intensity in the shorter wavelength region; thus, the laser material should be more efficient in this region.

Experimental Evidence for Eq. 8. The dependence of the threshold excitation intensity of the laser emission of 4-methylumbelliferone on the concentration was measured, as it is a typical coumarin compound. The linear relation of n *vs.* $1/I$ was obtained; it proves that the main loss is not the absorption of the laser material, but the loss in the laser cavity. Eq. 8 is thus confirmed.

Laser Emission of Calcein Blue. The threshold excitation intensity of Calcein Blue was calculated from the data of the absorption (Fig. 3) and fluorescence (Fig. 4) spectra; it is represented by the broken line in Fig. 14. The experimental results are also plotted in this figure. The threshold excitation intensity gradually decreases up to pH 11 as the percentage of the form (2) increases. Calcein Blue is non-fluorescent and does not lase above pH 12. The experimental values of the threshold excitation intensity agree well with the calculated ones; Eq. 8 is thus proved to be useful. The wavelength of the laser emission of Calcein Blue is 446 nm and is independent of the pH as in the case of the fluorescence spectrum.

Laser Emission of Aluminium Calcein Blue. The

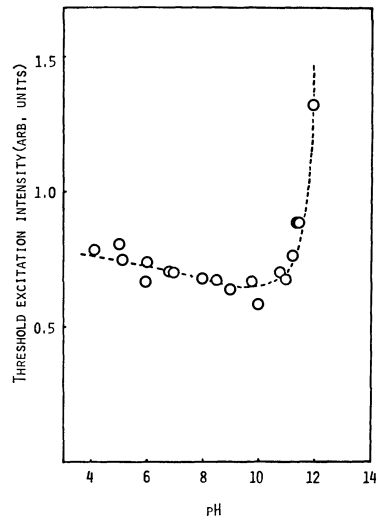

Fig. 14. Dependence of the threshold excitation intensity of Calcein Blue (arbitrary units, ----: calculated value, ○: experimental values) on pH.

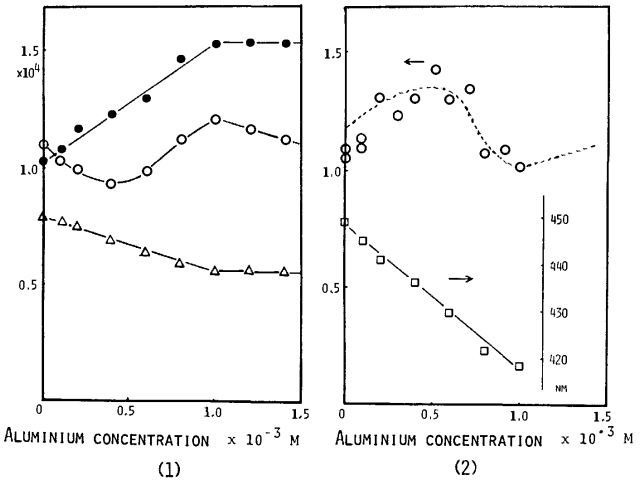

Fig. 15. (1) Dependences of the molar extinction coefficient $\bar{\varepsilon}$(●), the fluorescence intensity E(○: arbitrary units), and λ^4 (△: arbitrary units) of aluminium Calcein Blue on the aluminium concentration. (2) Dependences of the threshold excitation intensity (arbitrary units, ---: calculated value, ○: experimental values) and lasing wavelength (□) of aluminium Calcein Blue on the aluminium concentration. Concentration of Calcein Blue: 10^{-3} mol/l.

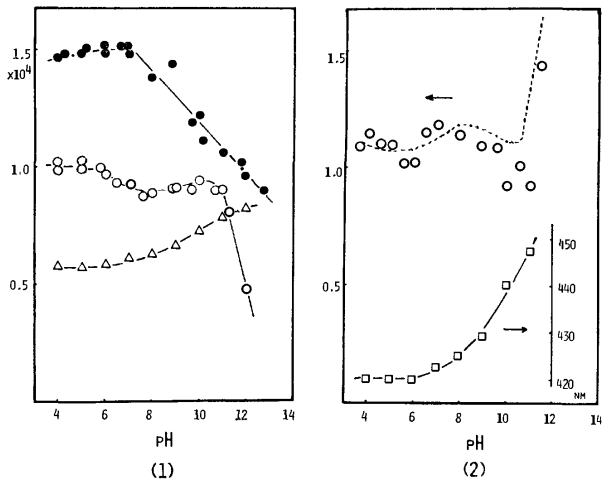

Fig. 16. (1) Dependences of the molar extinction coefficient $\bar{\varepsilon}$(●), the fluorescence intensity E(○: arbitrary units), and λ^4 (△: arbitrary units) of aluminium Calcein Blue on pH. (2) Dependences of the threshold excitation intensity (arbitrary units, ---: calculated value, ○: experimental values) and lasing wavelength (□) of aluminium Calcein Blue on pH. Concentration of aluminium Calcein Blue (1 : 1 mixture): 10^{-3} mol/l.

dependence of the fluorescence intensity, E, the molar extinction coefficient at 337 nm, $\bar{\varepsilon}$, and λ^4 on the aluminium concentration in the Calcein Blue solution are shown in Fig. 15(1). The threshold excitation intensity of the aluminium-Calcein Blue mixture is calculated from the spectroscopic parameters and is shown in Fig. 15(2), along with the experimental values. The increase in $\bar{\varepsilon}$ upon the increase in the aluminium concentration compensates for the decrease in λ^4, and the threshold excitation intensity does not vary much. The calculated value agrees with the experimental value, and it is confirmed that the laser action of the coordination compound is not quenched by the metal ion. However, it is impossible to observe the laser action when a molar excess of aluminium is added in the Calcein Blue solution. This may be due to the scattering effect of aluminium hydroxide; it is known that aluminium hydroxide is formed in the region of pH 4.5—10, then the excess aluminium coagulates and disturbs the laser action more severely than it does the fluorescence.

The lasing wavelength of the aluminium-Calcein Blue mixture gradually shifts to shorter wavelengths as in the case of the fluorescence spectrum, as is shown in Fig. 15(2). In this way the lasing wavelength of this mixture can be modified by varying the aluminium concentration in the Calcein Blue solution.

The data of the fluorescence intensity E, the extinction coefficient $\bar{\varepsilon}$, and λ^4 at various pH values are shown in Fig. 16(1). From these spectroscopic parameters, the threshold excitation intensity of aluminium Calcein Blue was calculated; it is shown in Fig. 16(2). Both the experimental and the calculated values have two minima, and they are consistent. The minimum at pH 11 is due to the dissociation to a ligand and an ion. Above pH 12 the laser action was not observed,

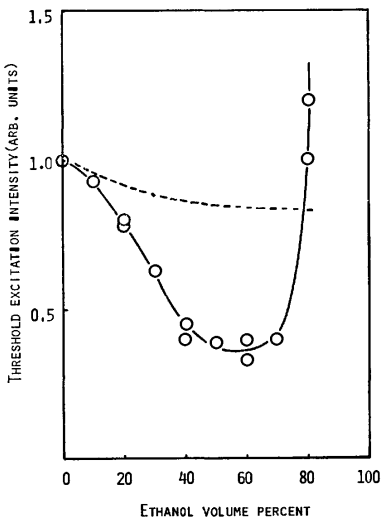

Fig. 17. Dependence of the threshold excitation intensity (arbitrary units) of aluminium Calcein Blue (10^{-3} mol/l) on the ethanol percent in the solvent (water). Solid curve: experimental values, broken curve: calculated value.

as in the case of Calcein Blue itself.

The wavelength of the laser emission of aluminium Calcein Blue is dependent on the pH. In order to modify the wavelength of the laser emission, it will be better to vary the pH than to vary the aluminium concentration, because the pH can be varied easily, for example, by adding a little acid or sodium hydroxide.

The threshold excitation intensity at various volume percentages of ethanol in the solvent was also calculated; the results are shown along with the experimental values in Fig. 17. Both the experimental and the calculated values decrease with an increase in the ethanol per-

Table 1. Characteristics of lasers of coordination compounds

Material	pH	λ_{las} (nm)	Threshold[a]	Fluorescence intensity (E)[a]	$\lambda_{fl}^{4}E$	ε[b]
C. B.	5	446	11	98	92	1.0
C. B.	12	—	no lasing	52	53	0.9
Al C. B.	5	418	11	104	75	1.5
Al C. B.	12	—	no lasing	54	54	0.9
Ca C. B.	5	446	11	96	90	—
Ca C. B.	12	450	12	98	95	—
Sr C. B.	5	446	11	96	90	—
Sr C. B.	12	452	13	96	95	—
Ba C. B.	5	446	11	96	90	1.0
Ba C. B.	12	454	13	94	95	0.9
4 MU	10	453	10	100	100	1.6
POPOP	d)	423	4	89	68	3.7
Al C. B.	e)	418	4	122	88	1.5

Concentration: 10^{-3} mol/l. a) Relative value for 4 MU. b) ε: molar extinction coefficient($\times 10^4$). c) C. B.: Calcein Blue. d) solvent: dioxane. e) solvent: 60 percent ethanol in water.

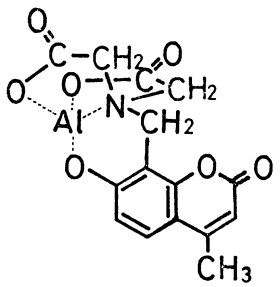

Fig. 18. The suggested structure of aluminium Calcein Blue. The aluminium ion is surrounded by a phenolic oxygen atom, two calboxylic oxygen atoms, and a nitrogen atom of iminodiacetic acid; however, the figure does not specify the number of the hydrogen atom attached to oxygen atoms and the coordination number of the aluminium atom.

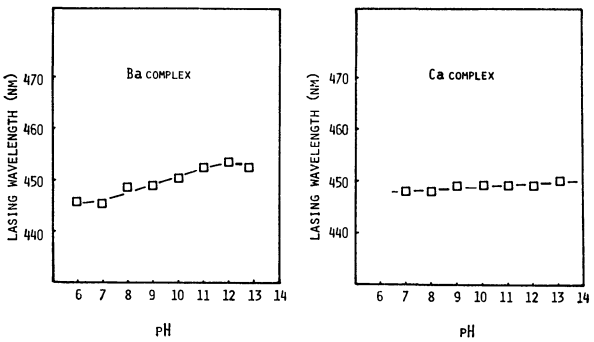

Fig. 19. Dependences of the lasing wavelength of calcium Calcein Blue (10^{-3} mol/l) and barium Calcein Blue (10^{-3} mol/l) on pH.

centage, as had been expected; however, the experimental value decreases more rapidly than does the calculated one. The variation in the refractive index in the mixture is small ($n_{D\ water}=1.3330$, $n_{D\ ethanol}=1.3618$) and can not induce the discrepancy. It may be due to the variation in the refractive index of the solution by heating by the irradiation of the nitrogen laser. However, the effect may not be large enough to induce such a large discrepancy. The steep increase in the threshold excitation intensity above 80 percent is due to the insolubility of the aluminium complex and to the light scattering in an ethanol–water mixture.

It has been reported that the lasing wavelength of 4-methylumbelliferone is modified in a water–ethanol mixture by an exciplex formation. In the case of an aluminium complex, the spectrum and the lasing wavelength in a water–ethanol mixture are close to those in water.

The structure of the aluminium Calcein Blue complex is suggested to be as is indicated in Fig. 18, since (1) the results of the continuous variation and mole ratio plots indicate the formation of a 1 : 1 complex between aluminium and Calcein Blue, (2) aluminium Calcein Blue should have a more rigid structure than Calcein Blue, as its quantum efficiency is larger than that of Calcein Blue, and (3) the phenolic oxygen coordinates with the aluminium ion since the phenolic electron does not take part in the resonance of the π electrons in the molecule, as the fluorescence spectrum does not shift to longer wavelengths. In this structure the aluminium ion is surrounded not only by a nitrogen atom but also by one phenolic and two carboxylic oxygen atoms, and binds the side chains. The structure of aluminium Calcein Blue is more rigid than that of Calcein Blue, in which neither of the side chains (CH_2COO^-) is bound.[17] The formation of such rigid rings in the molecule increases the quantum yield of the material and reduces the threshold excitation intensity.

Laser Emission of Barium and Calcium Calcein Blue. The threshold excitation intensity of the alkali earth complex was calculated. Though the calcium complex lased up to pH 13.5, as had been expected from the calculated value, no quantitative comparison was carried out since the complex decomposed rapidly in high pH solution.

The effects of pH on the lasing wavelengths of barium and calcium Calcein Blue are shown in Fig. 19. The lasing wavelength of the barium complex can be modi-

fied by increasing the pH; however, that of calcium Calcein Blue can be modified only a little.

Laser Emission of Zirconium Calcein Blue. It has been reported that a zirconium ion is able to form a coordination compound with Calcein Blue at pH 5.[11] However, the laser action of this compound was not observed, since the intensity of the fluorescence was not strong and the light scattering by zirconium hydroxide disturbed the laser action at the concentration of 10^{-3} mol/l.

Laser Characteristics of Coordination Compounds. The characteristics of the lasers of the coordination compounds of Calcein Blue and dyes at 10^{-3} mol/l are listed in Table 1. Aluminium Calcein Blue at pH 12 and barium, strontium, and calcium Calcein Blue at pH 5 were identical to Calcein Blue in the threshold, in the wavelength, and in the intensity of the fluorescence band. This may indicate that no coordination compound is formed. The aluminium complex at pH 5 has the most intense fluorescence, and it is an excellent lasing material. The contribution of λ^4, however, does not induce the reduction of the threshold excitation intensity, since the laser emission occurs in the near UV region. Barium, strontium, and calcium complexes at pH 12 have relatively high thresholds compared with Calcein Blue and 4-methylumbelliferone. Though the fluorescence intensity of the POPOP is rather small, the threshold excitation intensity is relatively low, probably because of the large molar extinction coefficient and the solvent effect. The aluminium complex is considered to be superior to POPOP as a laser material, because of (1) the smaller intramolecular loss, since the quantum efficiency is larger (this would be significant for long-pulse excitation), (2) the better tuning capability (the laser action of POPOP is superradiation at 10^{-3} mol/l), (3) the variation in the lasing wavelength by the chelate reaction, and (4) the higher solubility in water. Furthermore, the threshold excitation intensity of an aluminium complex can be reduced by dissolving it in a water–ethanol mixture as low as that of POPOP at the same concentration.

Aluminium Calcein Blue lases in a month from preparation, and it is stable enough for practical use. However, the complex with the alkali earth metal ion in a high pH solution (above pH 13) decomposes in several hours. Calcein Blue can be easily recovered as precipitates from the complex solution by making the solution acidic.

Conclusion

The threshold excitation intensity of the organic liquid laser under a short-pulse excitation can be calculated by means of a simple equation by using its spectral parameters, such as the wavelength of the fluorescence emission at the maximum intensity, the fluorescence intensity, the concentration, and the molar extinction coefficient. The equation has been applied to the coordination compounds of Calcein Blue and found to be useful for the estimation of the lasing capability of a new material.

The coordination compounds of Calcein Blue have interesting characteristics as laser material; the lasing wavelength is easily modified by the complex formation and dissociation reactions, they are soluble in water, and their threshold values are low enough for practical use, since the quantum yield is near unity as a result of the ring formation. The complex with aluminium lases very efficiently at a shorter wavelength than any other efficiently-lasing coumarin derivatives and is stable enough for practical use. Thus, the coordination compound is proved to be a useful laser material.

The authors wish to thank Professors Yasushi Miyazoe and Mitsuo Maeda for their guidance in the construction of the nitrogen laser and for their advice in the measurement of the laser emission. We also wish to thank Mr. Kenyu Kina for his advice in the measurement of the fluorescence and absorption spectra and for his discussions. The authors are also thankful to Dr. Koichi Yamada and Dr. Kazuo Yugi (Toray Industries, Inc.) for supplying a roll of polyester film for the capacitor of the nitrogen laser.

References

1) S. A. Tuccio, K. H. Drexhage, and G. A. Reynolds, *Opt. Commun.*, **7**, 248 (1973).
2) C. V. Shank and A. Dienes, *Appl. Phys. Lett.*, **16**, 405 (1970).
3) A. Dienes, C. V. Shank, and R. L. Kohn, *IEEE J. Quantum Electron.*, QE-**9**, 833 (1973).
4) E. J. Schimitschek, J. A. Trias, M. Taylor, and J. E. Celto, *IEEE J. Quantum Electron.*, QE-**9**, 781 (1973).
5) F. P. Schäfer, B. B. Snavely, C. V. Shank, E. P. Ippen, K. H. Drexhage, and T. W. Hänsch, "Topics in Applied Physics," Vol. 1, ed. by F. P. Schäfer, Springer-Verlag Berlin Heidelberg N. Y. (1973), p. 91.
6) O. G. Peterson, J. P. Webb, and W. C. McColgin, *J. Appl. Phys.*, **42**, 1917 (1971).
7) A. Lempicki and H. Samelson, *Phys. Lett.*, **4**, 133 (1963).
8) P. P. Sorokin and J. R. Lankard, *IBM J. Res. Dev.*, **10**, 162 (1966).
9) B. I. Stepanov, A. N. Rubinov, and V. A. Mostovnikov, *JETP Lett.*, **5**, 117 (1967).
10) J. B. Marling, D. W. Gregg, and S. T. Thomas, *IEEE J. Quantum Electron.*, QE-**6**, 570 (1970).
11) R. V. Hems, G. F. Kirkbright, and T. S. West, *Anal. Chem.*, **42**, 784 (1970).
12) H. N. Elsheimer, *Talanta*, **14**, 97 (1967).
13) J. H. Eggers, *Talanta*, **4**, 38 (1960).
14) N. Ishibashi, T. Imasaka, T. Ogawa, M. Maeda, and Y. Miyazoe, *Chem. Lett.*, **1974**, 1315.
15) D. Basting, F. P. Shäfer, and B. Steyer, *Opt-electron.*, **4**, 43 (1972).
16) M. Maeda and Y. Miyazoe, *Jpn. J. Appl. Phys.*, **13**, 827 (1974).
17) T. L. Har and T. S. West, *Anal. Chem.*, **43**, 136 (1971).
18) C. V. Shank, A. Dienes, and W. T. Silfvast, *Appl. Phys. Lett.*, **17**, 307 (1970).

The Crystal and Molecular Structure of an Anti-inflammatory Agent, 1-(Cyclopropylmethyl)-4-phenyl-6-methoxy-2(1*H*)-quinazolinone(SL-573)

Michio KIMURA, Toshiyuki HIROHASHI, and Hisao YAMAMOTO

Institute for Biological Science, Sumitomo Chemical Co., Ltd., Takatsukasa, Takarazuka, Hyogo 665

(Received April 9, 1976)

The crystal structure of the title compound (SL-573), crystallized from an ethyl acetate solution, has been determined by the single-crystal X-ray diffraction method. The crystals are monoclinic, with the space group $P2_1/a$, and these cell constants: $a=17.395(11)$, $b=8.371(5)$, $c=10.871(7)$ Å, $\beta=99°56(4)'$, and $Z=4$. The intensities were measured visually from equi-inclination integrated Weissenberg photographs taken with Cu $K\alpha$ radiation. The structure was solved by the symbolic addition method. The final R factor was 0.119 for 3284 reflections. The molecules are placed in pairs around the centers of symmetry and are linked by van der Waals' distances less than 3.94 Å. The dihedral angle between the quinazoline and phenyl ring planes was found to be 42.8°.

Recently several reports have been published on the syntheses and pharmacology of various quinazolines with marked anti-inflammatory activities.[1-3] Of these, 1-(cyclopropylmethyl)-4-phenyl-6-methoxy-2(1*H*)-quinazolinone(SL-573) has been reported to exhibit not only remarkably anti-inflammatory and analgesic activities in acute inflammation, but also effectiveness in adjuvant-induced chronic inflammation with a low toxicity, especially a minimum gastrointestinal lesion in animal tests.[1] In order to elucidate its pharmacological activities in terms of the molecular conformation, the title compound has now been studied by the X-ray diffraction method.

Experimental

Crystals suitable for X-ray analysis were grown from an ethyl acetate solution. They were rectangular prisms elongated along the b-axis. The unit-cell dimensions were determined from Weissenberg photographs calibrated with NaCl powder patterns superposed on them. The density was measured by flotation in an aqueous solution of KI. The crystal data are listed in Table 1. Crystal specimens with dimensions of $0.527\times0.466\times0.303$ and $0.507\times0.327\times0.547$ mm were selected for data collection around the a and b axes respectively. Weissenberg photographs for the layers of 0kl-12kl and h0l-h6l were taken with nickel-filtered Cu $K\alpha$ radiation. The intensities of 3284 independent reflections were estimated visually. The intensities were corrected for Lorentz and polarization factors, but no corrections were applied for the absorption and the spot shapes. The absolute scale and overall temperature factors ($B=3.81$ Å^2) were determined by Wilson's plot.[4]

Solution and Refinement of the Structure

The symbolic addition procedure[5] was used to solve the structure. Normalized structure factors, $|E_h|$, were calculated, and a set of Σ_2 relationships was tabulated. A starting set of three origin-defining reflections and three reflections assigned symbols are shown in Table 2. Each of these reflections had a high $|E_h|$ value and a large number of Σ_2 interactions. The signs or symbols of 252 reflections out of 473 with $|E_h|\geqslant1.4$

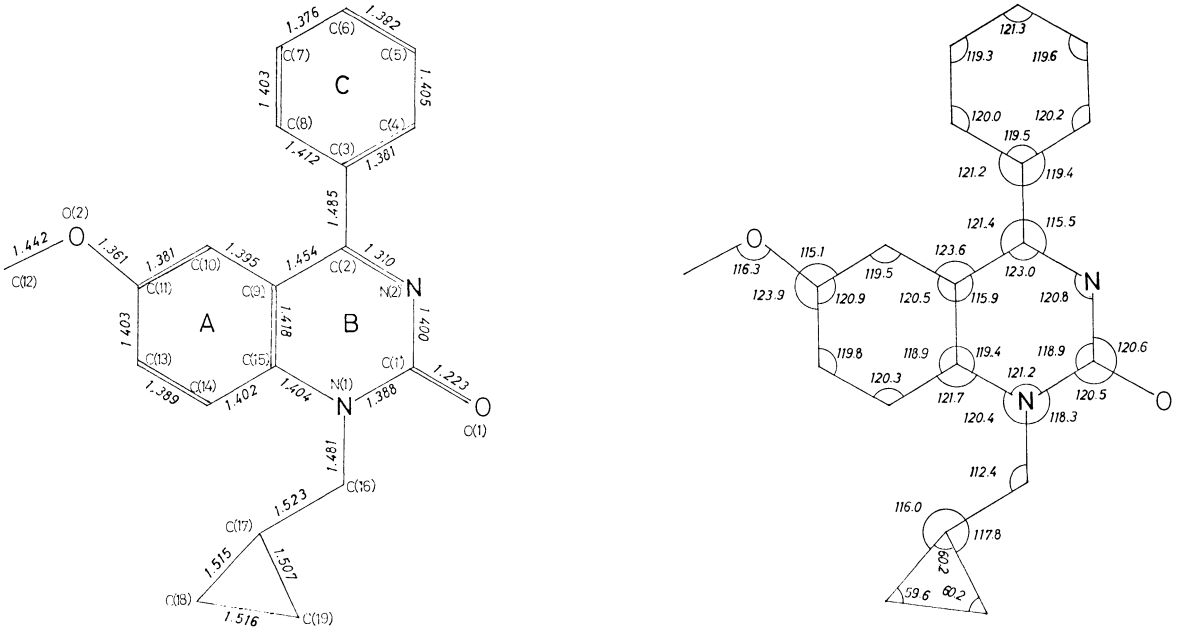

(a) (b)

Fig. 1. (a) Bond distances (l/Å) of the molecule and numbering system. (b) Bond angles (φ/°) of the molecule.

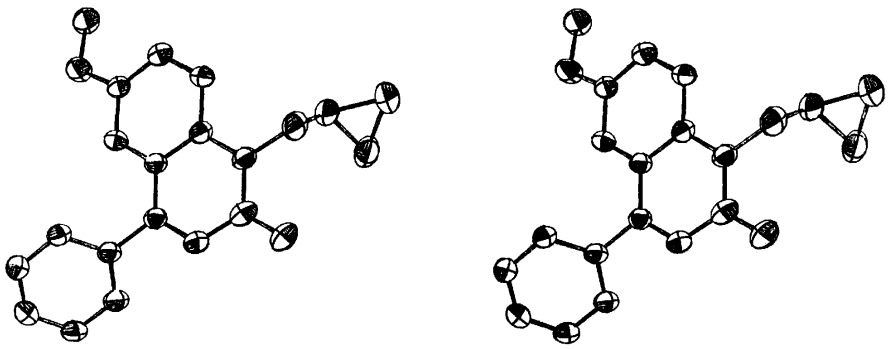

Fig. 2. A stereoview of the molecular structure of SL-573. The thermal ellipsoids are drawn at the 50% probability level. This drawing (0.765 inch/Å) was prepared using the computer program ORTEP (C. K. Johnson, 1965).

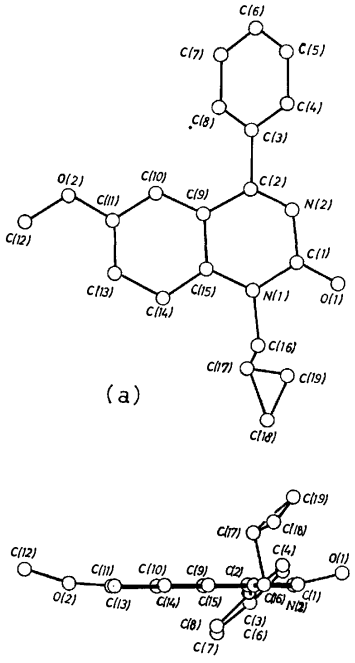

Fig. 3. The molecule viewed (a) normal to the quinazoline ring plane, (b) along the quinazoline ring plane from C(2)–C(3) direction.

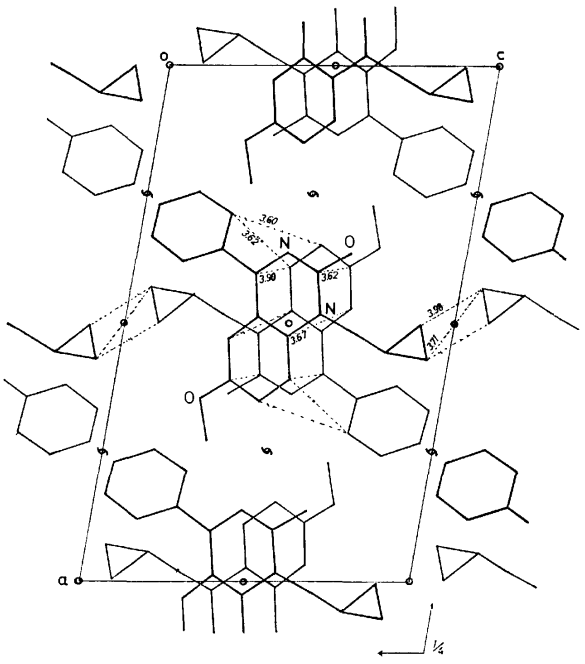

Fig. 4. Projection of the structure along the b axis.

Table 1. Crystal data

Crystal system	monoclinic
Systematic absence	$h0l$ with odd l, $0k0$ with odd k
Space group	$P2_1/a$
a	17.395±0.011 Å
b	8.371±0.005
c	10.871±0.007
β	99°34′±4′
V	1561.0 Å^3
Z	4
D_c	1.304 g/cm^3
D_m	1.307 g/cm^3

Table 2. Initial Set

H	$\|E_h\|$	Sign or symbol
$32\bar{9}$	4.26	+
433	2.67	+
$26\bar{5}$	4.67	+
12, 7, 0	4.75	a
11, 3, 3	4.05	b
$24\bar{8}$	4.03	c

were determined by Σ_2 relationships. The symbols had two possibilities, $a=b=c=(+)$ or $a=b=(-)$ and $c=(+)$. Three-dimentional E-maps were computed with each of these phase combinations. The positions of 19 non-hydrogen atoms were obtained from the E-map based on the latter combination, $a=b=(-)$ and $c=(+)$. The remaining four atoms were revealed on a subsequent Fourier map. The R value, $\Sigma||F_o|-|F_c||/\Sigma|F_o|$, at this stage was 0.411 for all 23 non-

TABLE 3. FINAL ATOMIC PARAMETERS ($\times 10^4$), WITH THEIR STANDARD DEVIATIONS IN PARENTHESES

(a) Fractional atomic coordinates and anisotropic temperature factors[a] for non-hydrogen atoms.

Atom	x	y	z	B_{11}	B_{22}	B_{33}	B_{12}	B_{13}	B_{23}
C(1)	4013(3)	8201(6)	5682(5)	25(2)	133(8)	89(5)	12(6)	35(5)	5(10)
C(2)	4032(2)	6865(6)	3780(4)	19(1)	113(7)	63(4)	3(5)	9(4)	25(8)
C(3)	3562(2)	6239(6)	2614(5)	17(1)	134(8)	69(4)	2(5)	7(4)	20(9)
C(4)	2887(3)	5397(7)	2676(5)	20(2)	173(9)	78(5)	−5(6)	12(4)	43(11)
C(5)	2448(3)	4750(8)	1588(6)	23(2)	236(12)	87(5)	−54(8)	8(5)	28(13)
C(6)	2702(3)	4945(8)	457(5)	28(2)	256(13)	69(5)	−28(8)	−3(5)	2(13)
C(7)	3351(3)	5844(8)	360(5)	26(2)	229(12)	66(4)	−14(7)	13(4)	32(12)
C(8)	3798(3)	6474(7)	1445(5)	20(2)	179(9)	71(4)	17(6)	15(4)	40(11)
C(9)	4878(2)	6755(6)	4008(4)	18(1)	112(7)	60(4)	−1(5)	9(4)	16(8)
C(10)	5305(2)	5920(6)	3239(5)	18(1)	125(7)	67(4)	7(5)	0(4)	3(9)
C(11)	6110(2)	5966(6)	3487(5)	19(2)	143(8)	65(4)	13(6)	14(4)	−10(9)
C(12)	7288(3)	4789(10)	3079(6)	20(2)	291(14)	96(6)	57(8)	18(5)	−58(15)
C(13)	6503(3)	6838(7)	4503(5)	21(2)	156(9)	79(5)	0(6)	20(4)	−17(10)
C(14)	6081(3)	7616(6)	5302(5)	19(1)	145(8)	73(4)	−16(6)	10(4)	−34(10)
C(15)	5264(2)	7568(6)	5080(5)	21(2)	111(7)	66(4)	−5(5)	20(4)	5(8)
C(16)	5209(3)	9142(6)	7023(5)	33(2)	110(7)	82(5)	11(6)	31(5)	−51(10)
C(17)	5544(3)	7986(7)	8056(5)	30(2)	151(9)	75(5)	−21(7)	26(5)	−49(10)
C(18)	5690(3)	8666(8)	9366(6)	44(3)	247(13)	76(5)	−44(10)	14(6)	−96(14)
C(19)	5028(3)	7497(8)	8976(6)	47(3)	190(11)	73(5)	−18(9)	43(6)	−16(12)
N(1)	4820(2)	8307(5)	5887(4)	21(1)	119(6)	73(4)	−5(5)	26(3)	−21(8)
N(2)	3634(2)	7517(6)	4570(4)	20(1)	156(7)	74(4)	8(5)	17(3)	−2(8)
O(1)	3638(2)	8732(6)	6448(4)	30(1)	238(9)	99(4)	24(6)	45(4)	−79(10)
O(2)	6474(2)	5142(5)	2671(4)	19(1)	229(8)	89(4)	45(5)	5(3)	−90(9)

a) The anisotropic temperature factors are expressed in this form:
$$\exp[-(B_{11}h^2+B_{22}k^2+B_{33}l^2+2B_{12}hk+2B_{13}hl+2B_{23}kl)].$$

(b) Atomic coordinates ($\times 10^4$) for hydrogen atoms.

Atom	x	y	z	B(Å^2)	Atom	x	y	z	B(Å^2)
H(1)	2690	5240	3577	3.97	H(10)	5673	9883	6787	4.01
H(2)	1908	4112	1634	4.53	H(11)	5063	6293	9363	4.93
H(3)	2382	4363	−378	4.57	H(12)	4428	7864	8859	4.93
H(4)	3518	6052	−552	4.49	H(13)	6199	8350	10022	5.35
H(5)	4330	7163	1388	3.94	H(14)	5565	9922	9518	5.35
H(6)	5004	5240	2441	3.37	H(15)	5881	7330	7480	4.02
H(7)	7140	6889	4669	3.88	H(16)	6700	4600	2600	4.73
H(8)	6385	8272	6108	3.66	H(17)	7400	4400	2600	4.73
H(9)	4793	9919	7361	4.01	H(18)	7400	4200	4000	4.73

hydrogen atoms. The refinement of the structure was carried out by the block-diagonal least-squares method until the R value reached 0.152. A difference Fourier map using all the reflections indicated the positions of all 18 hydrogen atoms. In further refinement, however, the hydrogen atom coordinates calculated from geometrical considerations were used and were not refined. All the hydrogen atoms were given the same isotropic temperature factors as those of the atoms to which they are attached. The final R value was 0.119 for all the observed reflections. The final atomic parameters are shown in Table 3. The atomic scattering factors were taken from the "Internatioal Tables for X-ray Crystallography".[6] A list of the observed and calculated structure factors is kept by the office of the Chemical Society of Japan, (Document No. 7628).

All the calculations were carried out on the IBM 370 computer at the Computer Center of the Sumitomo Chemical Co., Ltd., using UNICS programs[7] revised for IBM 370 by Michio Kimura, one of the present authors.

Results and Discussion

The bond distances and angles are shown in Fig. 1. The mean estimated standard deviations of the bond distances and angles for the non-hydrogen atoms were 0.011 Å and 0.7° respectively. The averages of the aromatic C–C bond distances and C–C–C angles in the benzene ring C are 1.393 Å and 120.0° respectively. The six-membered ring, A, has a mean C–C bond distance of 1.393 Å and a mean C–C–C angle of 120.0°. These values are quite reasonable. The C(1)–N(1) bond distance of 1.388 Å is similar to those observed in other heterocyclic rings, for instance, dihydrothymidine[8], dihydrouracil[9]; and 5-methyluridine[10].

Table 4. Equations of least-squares planes in the $AX+BY+CZ+D=0$[a] form

The displacements (l/Å) of atoms from the planes are given in square brackets.

Plane I: Rings A and B

$-0.0925X-0.8447Y+0.5272Z+3.2259=0$

[C(1) 0.088, C(2) −0.077, C(3) −0.238, C(9) −0.003, C(10) 0.071, C(11) 0.054, C(12) 0.458, C(13) −0.035, C(14) −0.053, C(15) −0.017, C(16) 0.011, N(1) 0.002, N(2) −0.015, O(1) 0.218, O(2) 0.102]

Plane II: Rings C and C(2)

$0.5178X-0.8460Y+0.1271Z+1.0888=0$

[C(2) 0.021, C(3) −0.009, C(4) −0.019, C(5) −0.002, C(6) 0.040, C(7) −0.016, C(8) −0.013, C(9) 0.871, N(2) −0.766]

Plane III: Rings A, C(2), and N(1)

$-0.1024X-0.8359Y+0.5393Z+3.2109=0$

[C(1) 0.148, C(2) −0.055, C(3) −0.230, C(9) 0.007, C(10) 0.056, C(11) 0.029, C(13) −0.045, C(14) −0.038, C(15) 0.009, C(16) 0.077, N(1) 0.052, N(2) 0.031, O(2) 0.054]

The dihedral angles between Planes I and II, and Planes II and III, are 42.80° and 43.72° respectively.

a) X, Y, and Z are orthogonal coordinates in Å related to the crystal axes by:

$$\begin{bmatrix} X \\ Y \\ Z \end{bmatrix} = \begin{bmatrix} 1 & 0 & \cos\beta \\ 0 & 1 & 0 \\ 0 & 0 & \sin\beta \end{bmatrix} \begin{bmatrix} a \\ b \\ c \end{bmatrix}$$

Table 5. Intermolecular distances (<4Å)

	Distance		Distance
C(15)···C(10)[i]	3.67 Å	C(2)···C(14)[i]	3.90 Å
C(14)···C(2)[i]	3.90	C(13)···C(2)[i]	3.81
C(14)···C(4)[i]	3.62	C(13)···C(4)[i]	3.60
C(1)···C(11)[i]	3.62	C(4)···C(14)[i]	3.62
C(2)···C(13)[i]	3.81	C(14)···C(3)[i]	3.93
C(9)···C(9)[i]	3.63	C(1)···C(10)[i]	3.77
C(10)···C(1)[i]	3.77	C(2)···C(11)[i]	3.84
C(10)···C(9)[i]	3.79	C(9)···C(10)[i]	3.79
C(11)···C(1)[i]	3.62	C(11)···C(2)[i]	3.84
C(12)···C(1)[i]	3.77	C(4)···C(13)[i]	3.60
C(15)···C(9)[i]	3.77	C(19)···C(18)[ii]	3.98
C(1)···C(12)[i]	3.77	C(18)···C(18)[ii]	3.71
C(3)···C(14)[i]	3.93		

Symmetry code	Symmetry operation		
none	x	y	z
i	$1-x$	$1-y$	$1-z$
ii	$1-x$	$2-y$	$2-z$

The O(1)–C(1) bond distance of 1.223 Å are comparable with the value of 1.211 Å for 10-methylisoalloxazine hydrobromide dihydrate[11] and that of 1.213 Å for 3-phenyl-2,4-(1*H*,3*H*)-quinazolinedione.[13] The molecular conformation and thermal ellipsoids are illustrated by a stereoview in Fig. 2. Interest in the conformation of SL-573 is probably centered on the geometry of the linkage [C(2)–C(3) bond] between the phenyl group and the quinazoline ring. The

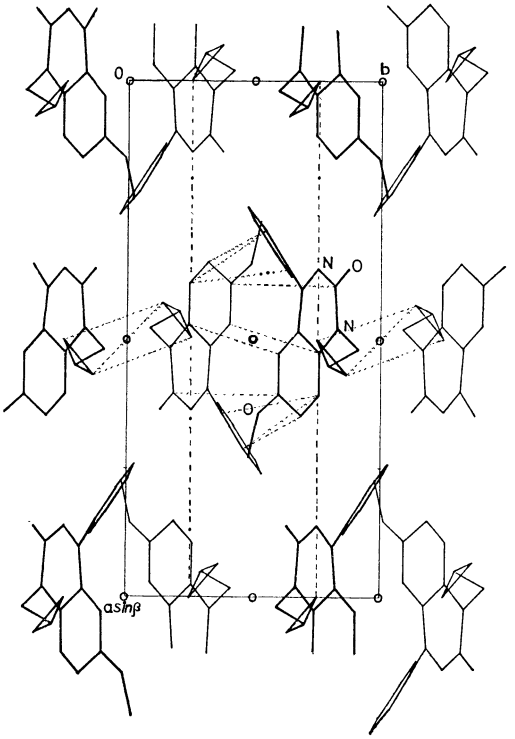

Fig. 5. Projection of the structure along the c axis.

quinazoline ring is very nearly planar, and the phenyl ring is planar within the limits of accuracy. The least-squares planes and the deviations of atoms from these planes are given in Table 4. The O(2) and C(16) atoms are on the quinazoline ring plane, and the O(1) and C(12) atoms deviate from the plane, as is shown in Fig. 3. The C(2)–C(3) bond length is 1.485 Å, close to the value of 1.477 Å proposed by Dewar and Schmeising[12], for the C_{sp^2}–C_{sp^2} single bond. This fact suggests that π-bonding is absent in the C(2)–C(3) bond. The steric repulsion caused by the hydrogens prevents the phenyl plane from being coplanar with the quinazoline ring; the dihedral angle between the phenyl and quinazoline planes is 42.8°. An inspection of the intermolecular distances (Table 5) indicates that the packing of the molecules is very efficient. The molecular arrangement in the crystal viewed along the b and c axes is illustrated in Figs. 4 and 5. The molecules are placed in pairs around the centers of symmetry and form tightly packed columns of molecules in the b axis direction. All the intermolecular contacts correspond to the van der Waals interaction. The shortest intermolecular distance is 3.60 Å, while the others are almost all within 3.94 Å.

References

1) H. Yamamoto, C. Saito, S. Inaba, H. Awata, M. Yamamoto, Y. Sakai, and T. Komatsu, *Arzneim-Forsch.*, **22**, 1958 (1972).

2) T. Komatsu, H. Awata, Y. Sakai, T. Inukai, M. Yamamoto, S. Inaba, and H. Yamamoto, *Arzneim-Forsch.*, **23**, 1266 (1973).

3) K. Sozo, *Kagaku to Kogyo (Tokyo)*, **27**, 307 (1975).

4) A. J. C. Wilson, *Nature*, **50**, 151 (1942).

5) I. L. Karle and J. Karle, *Acta Crystallogr.*, **16** 969 (1963), **21**, 894 (1966).
6) "International Tables for X-ray Crystallography," Vol. III Kynoch Press, Birmingham (1962) pp. 202—203.
7) T. Sakurai *et al.*, Universal Crystallographic Computation Program System (I), (II), published by The Crystallographic Society of Japan 1967.
8) J. Konnert, I. L. Karle and J. Karle, *Acta Crystallogr.* **B26**, 770 (1970).
9) D. C. Rohrev and M. Sundaralingam, *Acta Crystallogr.* **B26**, 546 (1970).
10) D. J. Hunt and E. Subramanian, *Acta Crystallogr.*, **B25**, 2144 (1969).
11) B. L. Trus and C. T. Fritchie, *Acta Crystallogr.*, **B25**, 1911 (1969).
12) M. J. S. Dewar and H. N. Schmeising, *Tetrahedron*, **5**, 166 (1959).
13) Y. Kitano, M. Kashiwagi, and Y. Kinoshita, *Acta Crystallogr.*, **B28**, 1223 (1972).

Studies of the Removal of Dye Ions by Adsorbing Particle Flotation

Koichi KOBAYASHI, Nobuhiro WATABE, and Tsunetaka SASAKI

Department of Chemistry, Faculty of Science, Tokyo Metropolitan University, Setagaya, Tokyo 158

(Received April 19, 1976)

The removal of an anionic dye, Scarlet Red, a zwitterionic dye, Congo Red, and a cationic dye, Crystal Violet, from aqueous solutions was studied by the method of adsorbing particle flotation, using bentonite and benzylhexadecyldimethylammonium chloride as flotation agents. More than 99% of the Crystal Violet and Scarlet Red and 96% of the Congo Red could be floated under optimum conditions. It was found that a larger amount of a cationic surfactant was required for the flotation with an increase in the anionic nature of the dye ions, although the flotation was efficient irrespective of the ionic nature of dyes used. From this fact, the flotations of anionic and cationic dyes were confirmed to differ from each other in that the cationic-dye ions are floated by a direct exchange adsorption on bentonite, while the anionic-dye ions are floated by the adsorption on bentonite through the bimolecular layer of the cationic surfactant. The flotation efficiency of a dye ion, particularly of zwitterionic dye, was confirmed to depend on the pH.

A limited number of studies have been reported of the flotation of dye ions.[1-4] Karger *et al.* examined in detail the solvent sublation process for the removal of two dyes, Methyl Orange and Rhodamine B, using hexadecyltrimethylammonium bromide as the collector and 2-octanol as the immiscible organic liquid layer.[5-7] We ourselves have previously reported that Cu^{2+},Cd^{2+}, and Co^{2+} ions were effectively removed from an aqueous solution by adsorbing particle flotation,[8-10] which is considered to be an effective method of flotation. The process is defined as the removal of the dissolved materials by the flotation of the particle-like bentonite upon which the ions to be removed is adsorbed. So far, however, no application of the adsorbing particle flotation has been made to the removal of dye ions from an aqueous solution. Dye ions are especially suited to the study of flotation since they include various types of ions—namely anions, cations, and zwitterions—and they can be easily detected visually or assayed by colorimetry.

The present paper will describe the applicability of adsorbing particle flotation for the removal of dye ions, such as anionic Scarlet Red, zwitterionic Congo Red, and cationic Crystal Violet, from their aqueous solutions. Here, the effects of the gas-flow time, the pH, the amount of bentonite, the amount of the cationic surfactant, and the nature of the dye ions on the flotation efficiency have been studied.

Experimental

Materials. The benzylhexadecyldimethylammonium chloride (BHDAC) was obtained from the Nippon Oils and Fats Co., Ltd., and was purified by recrystallization from acetone. The bentonite powder(Bt) used as an ion exchanger was obtained from the Wako Pure Chemical Co., Ltd.; the fraction passing through a 350-mesh sieve was collected and dried under reduced pressure. The dyes used included cationic Crystal Violet(CV), anionic Scarlet Red(SR), and zwitterionic Congo Red(CR). These dyes were purified by recrystallization from ethanol and ether. A stock solution of the dye ions of a 1×10^{-4} mol/l concentration was prepared by dissolving these dyes in triply distilled water.

Apparatus and Procedure. The apparatus used for the flotation measurements was the same as has been described in a previous paper.[2] The sample solution of flotation was prepared by introducing 1 ml of a stock solution of the dye ions, and given amounts of Bt and BHDAC into a 10-ml measuring flask, adjusting the pH to a desired value, and diluting the solution to 10 ml with water. Nitrogen gas humidified with water vapor and controlled to a constant rate of gas-flow was bubbled through a glass filter (No. 4) into a flotation cell containing about 10 ml of the sample solution. After the flotation, the underlying liquid was taken out of the flotation cell for the determination of the dye-ion and Bt contents.

For the determination of the dye-ion concentration, the light absorption were measured for the dye ions and the calibration curves were prepared at their maximal absorption wavelengths (500 nm for CR, 580 nm for CV, and 500 nm for SR). The initial concentration of each dye ion of the sample solution was determined by using these calibration curves before the Bt addition. However, the dye-ion concentration after the flotation cannot be determined similarly since the measurement is hindered by the presence of the Bt-particle, which also reduces the light intensity by scattering. The concentration of the dye ions of such a solution was estimated by assuming that the absorbance at the maximal absorption wavelength is the sum of the absorbances of the dye ions and the scattering by Bt, while the absorbance at the minimal absorption wavelength is considered to be mainly due to the scattering by Bt. Then, the calibration curves of Bt without the dyes at the maximal and minimal absorption wavelengths were drawn. The amount of Bt in the sample was determined from the absorbance at the minimal absorption wavelength by applying the calibration curve of Bt at the minimal absorption wavelength; the contribution of the absorbance due to Bt at the maximal wavelength was estimated by applying the calibration curve of Bt at the maximal absorption wavelength. The absorbance due to dye ions alone was obtained by subtracting this contribution from the total absorbance by the sample solution at the maximal absorption wavelength. The concentration of dye ions was determined by using the calibration curve for the dye ions at the maximal absorption wavelength.

The flotation efficiency of the dye ions or Bt is conventionally expressed by:

$$F = \frac{C_i - C_f}{C_i} \times 100\%$$

where C_i and C_f are the initial and final concentrations respectively of the dye ions or Bt.

Results and Discussion

Gas-Flow Time, Amount of Bt, and Flotation Efficiency. First, we studied the effects of the amount of added Bt and the gas-flow time on the flotation efficiency for

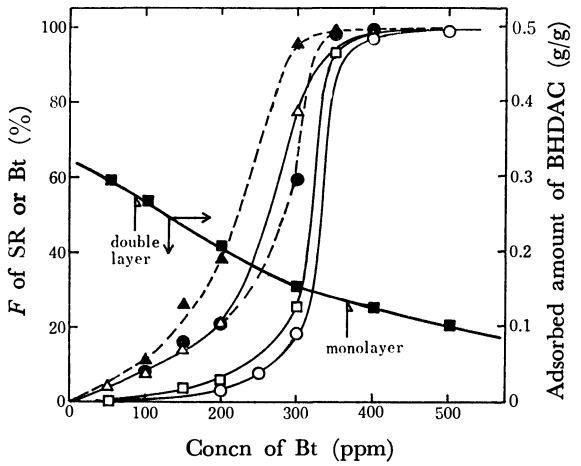

Fig. 1. Effect of gas-flow time on flotation efficiency.
SR: 1×10^{-5} mol/l, BHDAC: 50 ppm, gas-flow rate: 5 ml/min, pH: 5.4—5.9, gas-flow time (○, ●: 2 min, □: 5 min, △, ▲: 15 min), ——: F of SR, ----: F of Bt, ■: adsorbed amount of BHDAC.

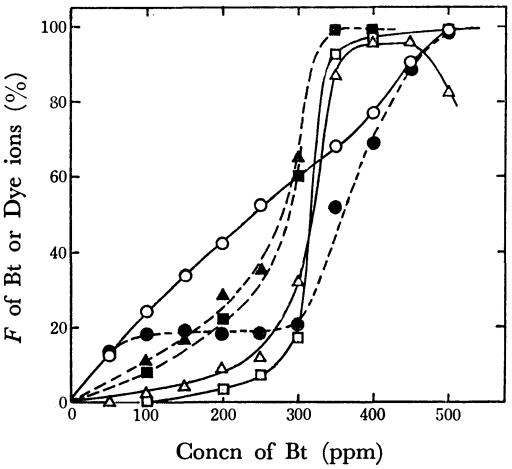

Fig. 2. Effect of ionic nature of dye on flotation efficiency.
Dye ions: 1×10^{-5} mol/l, BHDAC: 50 ppm, gas-flow rate: 5 ml/min, gas-flow time: 2 min, ——: F of dye ions (○: CV, △: CR, □: SR), ----: F of Bt (●: CV, ▲: CR, ■: SR).

the SR–BHDAC–Bt system, keeping the amount of BHDAC and the gas-flow rate constant. The results are shown in Fig. 1. As may be seen in the figure, flotation efficiencies of SR and Bt increase with the increases in the gas-flow time and in the amount of Bt added. The curves sharply rise in the vicinity of 300 ppm Bt, and nearly 100% flotation efficiencies of SR and Bt are obtained at 400 ppm Bt. In the region of Bt content below 400 ppm, the flotation efficiency of SR is lower than that of Bt. This may suggest the presence of free SR being adsorbed neither on Bt nor on an aqueous surface. Since SR alone and the SR–BHDAC complex are not easy to float, as will be shown later (Fig. 8), the coincidence of the SR and Bt curves near 100% flotation at about 400 ppm may indicate the complete adsorption of SR on Bt. Further, the amount of adsorption of BHDAC on Bt, though not directly measured, was presumed from the adsorption isotherm on Bt of hexadecyltrimethylammonium chloride,[11] which has a molecular structure similar to that of BHDAC. The solid squares in Fig. 1 indicate the amount of the adsorption of BHDAC on Bt on such an assumption. Here, the arrows indicate a monolayer and a bimolecular layer adsorption of BHDAC, as estimated from the base-exchange capacity of Bt.[11] As may be seen in the figure, the flotation efficiency of Bt decreases from 100% to a very low value in the concentration region from the monolayer to the bimolecular layer adsorption. This behavior is similar to those reported in a previous paper.[11] Since an F value of 100% was obtained at the gas-flow time of 2 min and above, all the subsequent experiments were carried out under the conditions of 50 ppm BHDAC, 0 to 500 ppm Bt, 1×10^{-5} mol/l dye, pH 5.4 to 5.9, a gas-flow time of 2 min, and a gas-flow rate of 5 ml/min.

Ionic Nature of Dyes and Flotation Efficiency. In order to study the effect of the ionic nature on the flotation efficiency, the flotation experiments were carried out for CR and CV by varying the amount of added Bt under the same conditions as for SR. The results for the flotation efficiency of dye ions and Bt are illustrated by the solid and broken lines respectively in Fig. 2, together with the experimental results for SR shown in Fig. 1. The flotation efficiencies of the dye ions and Bt increase for all the dye–Bt–BHDAC systems with an increase in the amount of added Bt. Here, zwitterionic CR behaves as an anion under experimental condition of a pH value between 5 and 6 since it has an isoelectric point of about 3. Therefore, the F curves for CR–BHDAC–Bt and SR–BHDAC–Bt systems are similar in their behavior: the F curve of the dye ions is lower than that of Bt, and beyond 400 ppm of Bt addition, F increases to 95—97% for both Bt and dye flotation efficiencies. In the case of cationic CV, however, the flotation efficiency of Bt exhibits a low plateau in the region of a small Bt addition: it then increases sharply near the 300 ppm Bt addition, and rise to nearly 100% in the vicinity of 500 ppm Bt. In the case of CV flotation, the flotation efficiency of the dye ions is higher than that of Bt over the whole region of Bt added, while the flotation efficiency of the dye ions is lower than that of Bt in the cases of CR and SR. These discrepancies indicate the existence of free dye ions not adsorbed on Bt; in the case of CV the free ions are adsorbed directly on bubbles and are floated, while CR and SR are not adsorbed and are not floated: this adsorption effect is dominant in the region of smaller amounts of Bt addition and lower F values, where there is not much Bt available for CV adsorption. Further, the possibility that CR and SR combine with BHDAC and float is considered. However, such a possibility can not be practically expected considering the flotation data for various anionic dyes by several cationic surfactants[12] and also the results shown in Fig. 8.

The effects of the anionic and cationic dyes on the flotation efficiency of Bt were further studied in detail in relation to the system without any added dye. The results are shown in Fig. 3. As may be seen in the figure, the flotation curves of Bt for the anionic dye–

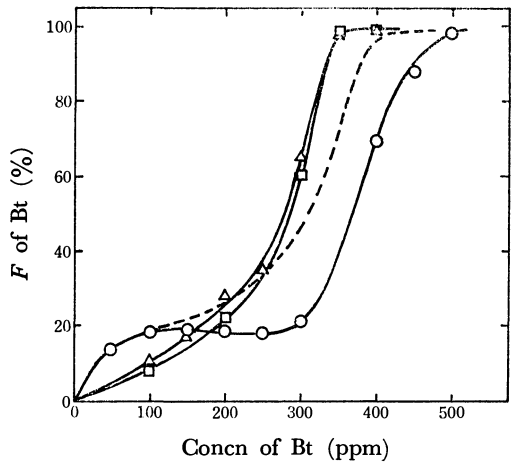

Fig. 3. Effect of dye ions on flotation efficiency of Bt. Dye ions: 1×10^{-5} mol/l, BHDAC: 50 ppm, gas-flow rate: 5 ml/min, gas-flow time: 2 min, ——: F of Bt (○: CV, □: SR, △: CR), ----: F of Bt for system of no added dyes.

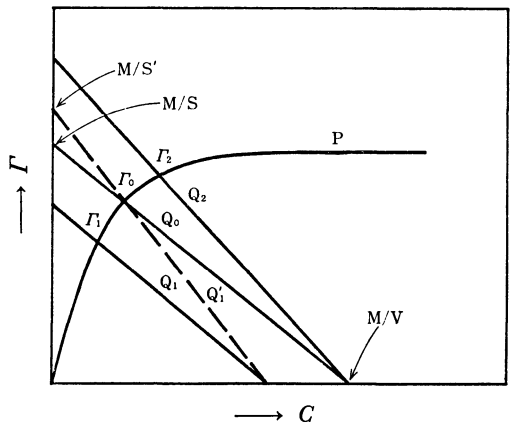

Fig. 4. Relation between amount of adsorption and equilibrium concentration of BHDAC.

BHDAC–Bt and cationic dye–BHDAC–Bt systems shift left and right, respectively, to the curve of the BHDAC–Bt system. These phenomena can be explained from the amount of BHDAC adsorption as follows.

The amount of adsorption of BHDAC on Bt, Γ, can be calculated from the adsorption isotherm;

$$\Gamma = f(C) \tag{1}$$

and

$$S\Gamma + VC = M \tag{2}$$

where V is the volume of solution; C and M, the equilibrium concentration and the total amount of BHDAC respectively, and S, the total amount of Bt added to the system. According to these equations, the value of Γ is graphically obtained to be as is shown in Fig. 4. In this figure, the P and Q lines express Eqs. 1 and 2 respectively, while the point of intersection, Γ, gives the amount of adsorption for a given S, V, and M. Since the intercept of Eq. 2 on the ordinate is M/S, and since that of the abscissa is M/V, Γ is a function of M/S and M/V for a given Eq. 1, that is, for the BHDAC–Bt system. If the straight line, Q_0, expresses

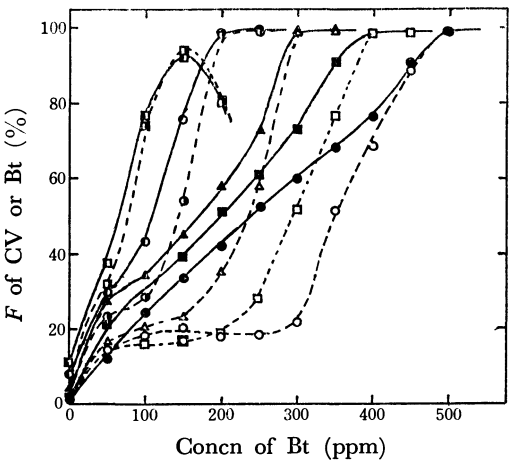

Fig. 5. Effect of BHDAC on flotation efficiency. CV: 1×10^{-5} mol/l, BHDAC (◨, ◧: 10 ppm, ◐, ◑: 20 ppm, △, ▲: 30 ppm, □, ■: 40 ppm, ○, ●: 50 ppm), pH: 5.3—5.9, gas-flow rate: 5 ml/min, gas-flow time: 2 min, ——: F of CV, ----: F of Bt.

Eq. 2 for the system without a dye, the Γ_0 value in Fig. 4 is the amount of adsorption for this system. Now, the amount of effective BHDAC, M, decreases when SR or CR are added because the dye combines with it. Thus, Eq. 2 for the SR system moves from Q_0 to Q_1, and the point of intersection, Γ_1, shifts towards a smaller value. To restore Γ_1 to the original value, Γ_0, for the system without a dye, the value of S should be decreased to S' so as to increase the M/S ,as is shown by the broken line, Q'_1. This means that the same F value can be obtained by a smaller addition of Bt to the SR and CR systems as compared with the system without a dye: this results in a shift of the SR and CR curves in Fig. 3 to the left. In the case of the CV–BHDAC–Bt system, the effective S available for BHDAC adsorption decreases because some of the adsorption sites of Bt are occupied by cationic CV. The decrease in S increases the M/S value, Eq. 2 moves from Q_0 to Q_2 and the Γ_0 value increases to Γ_2. This results in an opposite effect to that in the case of SR and shifts the F curve of CV to the right of that for the system without a dye.

Concentration of BHDAC and Flotation Efficiency. Figure 5 shows the flotation efficiencies of CV and Bt as a function of the amount of Bt for various concentrations of BHDAC. As may be seen in the figure for a given concentration of BHDAC, at a relatively small amount of Bt addition, the F for CV flotation is larger than that for Bt, while both values are close or agree and become 100% at larger amounts of Bt addition, regardless of the concentration of BHDAC. In the case of an BHDAC addition of 10 ppm, however, the flotation efficiency of Bt and CV shows a maximum less than 100% at 150 ppm Bt. This means that the amount of BHDAC adsorbed decreases below the minimum amount of BHDAC adsorption necessary for 100% flotation.

In Fig. 5, the weight ratio of BHDAC/Bt may be observed to be constant to about 1/10 at the shoulder of $F\simeq100\%$, regardless of the amount of BHDAC added. According to the adsorption isotherm of

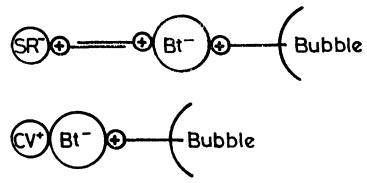

Fig. 6. Comparison of sublate structure of SR–Bt–BHDAC and CV–Bt–BHDAC systems. ⊕——: BHDAC.

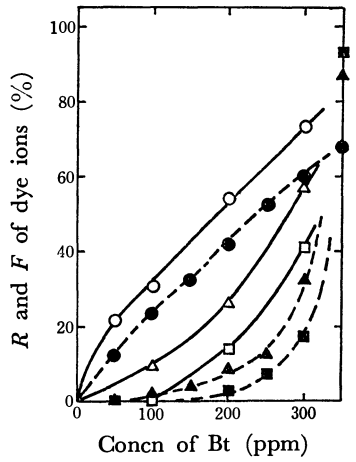

Fig. 7. Effect of dye ions on percent removal of dye ion. Dye ion: 1×10^{-5} mol/l, BHDAC: 50 ppm, gas-flow rate: 5 ml/min, gas-flow time: 2 min, ——: R of dye ions (○: CV, □: CR, △: SR), ----: F of dye ions (●: CV, ■: CR, ▲: SR).

BHDAC on Bt (Fig. 4) this means the constancy of M/S and that Γ is independent of M/V. This can be realized only when the adsorption isotherm (Eq. 1) shows an initial rise very close to the ordinate and exhibits a distinct shoulder, as has previously been reported.[11] Further, since, in this condition, the dyes and Bt nearly completely float, the above BHDAC/Bt ratio is nearly equal to the composition of the BHDAC–Bt sublate. Thus, when we compare the SR system of 50 ppm BHDAC and 400 ppm Bt in Fig. 1 with the CV system of 40 ppm BHDAC and 400 ppm Bt in Fig. 5, both of them showing a nearly 100% flotation efficiency of the Bt and dye ions, a larger amount of surfactant is required for the sublate of SR than for that of CV. Some tentative models for such systems are shown schematically in Fig. 6. The situation is quite similar to the case of Fe^{3+} and MnO_4^- flotation previously reported.[13]

Centrifuging. For systems in which the F values of Bt and dye ions are nearly 100%, as is shown in Figs. 1 and 2, the dye ions are considered to be completely adsorbed on Bt and subsequently floated by BHDAC. However, when the F value is less than 100% and when the curves for dye and Bt do not coincide, some dye ions are considered not to be combined with Bt. To confirm such details, the underlying liquid of the system after flotation carried out under the conditions of Fig. 2 was centrifuged for 20 min at 4000 rpm. In Fig. 7, the total percentage of the removal (R) of dye ions centrifuged and floated, namely,

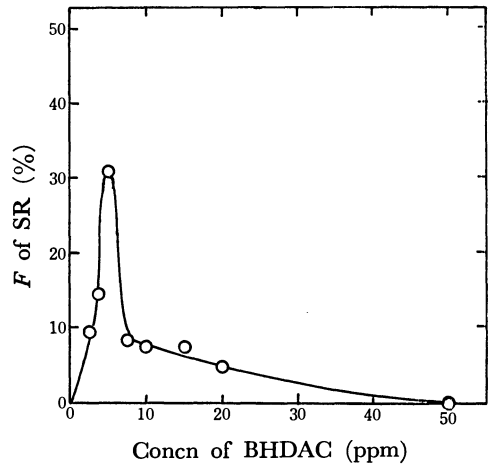

Fig. 8. Flotation efficiency of SR *vs.* BHDAC concentration for SR–BHDAC system. SR: 1×10^{-5} mol/l, gas-flow rate: 5 ml/min, gas-flow time: 2 min.

the percentage obtained by subtracting the percentage of dye ions remaining after centrifugation from 100%, is plotted against the amount of added Bt as solid lines. The dye flotation curves of Fig. 2 are also drawn for comparison. As may be seen, the total removal curves of CV, SR, and CR are located above the flotation curve. The difference in the ordinate between the two curves gives the amount of dyes combined with Bt and retained in the solution. In Fig. 7, the total percentage of the removal of CV is read as 22% for the system of 50 ppm Bt, where the total percentage of the removal of Bt is found to be 100%. From these data, together with the 14% flotation efficiencies of both Bt and CV at 50 ppm Bt addition (Fig. 2), the following equations are obtained:

$$F_0 + F_1 = 14, \quad F_0 + F_1 + S_1 = 22,$$

$$S_1/F_1 = (100-14)/14, \quad S_0 + S_1 + F_0 + F_1 = 100$$

where F_0 is the flotation efficiency of CV ions adsorbed directly on bubbles; F_1, the percentage of CV ions adsorbed on Bt and floated; S_0, the percentage of free CV ions remaining in the solution, and S_1, the percentage of CV ions adsorbed on Bt and remaining in the solution. From the above equations, F_0, F_1, S_0, and S_1 are calculated to be 12.7%, 1.3%, 78.0%, and 8.0%. Thus, we can confirm the amounts of the dye ions in various states in the solution and in the sublate, although this is an instance of rather incomplete flotation, as judged from the position on the curve in Fig. 7.

Flotation of the SR–BHDAC System. Figure 8 shows the flotation efficiency curve for the SR–BHDAC system without Bt. A sharp but small rise in flotation efficiency is seen in the relatively low concentration region. This result shows that the possible formation of the SR–BHDAC complex, if any, does not contribute appreciably to the SR flotation efficiency.[13] Rather, it decreases the free SR ion and hinders the adsorbing flotation, as has been mentioned above. The experiment also confirms that the addition of Bt is essential for a high flotation efficiency, with the possible sublate structure shown in Fig. 6.

Effect of the pH on the Flotation Efficiency. The

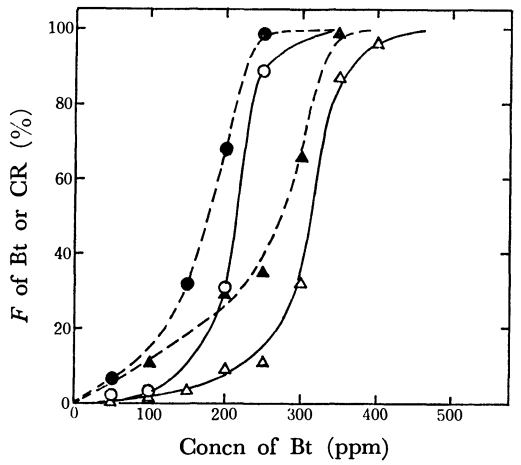

Fig. 9. Effect of pH on flotation efficiencies of CR and Bt. CR: 1×10^{-5} mol/l, BHDAC: 50 ppm, gas-flow rate: 5 ml/min, gas-flow time: 2 min, ——: *F* of CR (○: pH 2, △: pH 5—6), ----: *F* of Bt (●: pH 2, ▲: pH 5—6).

effect of the pH on the ion flotation is usually considered to be important. Figure 9 shows the effect of the pH on the flotation efficiency of the CR and Bt of the CR–BHDAC–Bt system. Here, we used CR as a dye since it is sensitive to the pH because of its zwitterionic nature. The measurements were made at pH 2 and 5, adjusted by the addition of hydrochloric acid. Since the isoelectric point of CR is near 3, CR ions are considered to be in the cationic and anionic forms respectively at the respective pHs. It may be expected, therefore, that the *F* curve of Bt shifts right at pH 2 and left at pH 5 to the *F* curve of Bt without dye addition, as is shown in Fig. 3. The result obtained at pH 5 is in accord with the expectation, while the result at pH 2 is contrary to what is expected: the *F* curve of Bt markedly shifts even left to that of the SR shown in Fig. 2. This can be explained by saying that, since the H^+ ion concentration at pH 2 is markedly higher than that of the BHDAC ion (10^{-5} mol/l), the adsorption of the BHDAC cation on Bt is hindered by hydrogen-ion adsorption; the effect is equal to the reduction of the BHDAC concentration as far as the amount of adsorption is concerned. Thus, the shift of the *F* curve for CR at pH 2 is in the same direction as that for SR, as shown in Fig. 3. Here, as the concentration of the hydrogen ion is much larger than that of the SR ions in Fig. 2, the shift for CR is expected to be far greater than that for SR.

Table 1. The optimum conditions of dye-ion flotation

Dye	CV^+	$CR^\pm$	SR^-
Dye concn. (mol/l)	1×10^{-5}	1×10^{-5}	1×10^{-5}
Surfactant concn. (ppm)	15	50	50
Bt concn. (ppm)	150	400	350
Surfactant/Bt	1/10	1/8	1/7
Gas-flow time (min)	2	2	2
Gas-flow rate (ml/min)	5	5	5
F of dye (%)	98	96	98
Volume of liquid taken (ml)	10	10	10

Optimum Condition of Flotation. The optimum conditions of dye-ion flotation obtained in this study are tabulated in Table 1. In Table 1, the BHDAC/Bt ratio expresses the composition of the solution, which also represents the composition of the sublate for the reasons mentioned already. This table confirms that a larger amount of cationic surfactant is required for the flotation with an increase in the anionic nature of the dye ions; this is in accord with the results obtained for Fe^{3+} and MnO_4^- ion flotation.[12]

References

1) J. J. Bikerman, "Foams," Rheinhold Pub. Co., New York, N. Y. (1953), p. 178.
2) F. Sebba, "Ion Flotation," Elsevier Pub., London and New York (1962), pp. 120—122.
3) R. Lemlich, "Adsorptive Bubble Separation Techniques," Academic Press, New York and London (1972), pp. 145—156.
4) N. Aoki and T. Sasaki, *Bull. Chem. Soc. Jpn.*, **39**, 939 (1966).
5) A. B. Caragay and B. L. Karger, *Anal. Chem.*, **38**, 652 (1966).
6) B. L. Karger, A. B. Caragay, and S. B. Lee, *Separ. Sci.*, **2**, 39 (1967).
7) B. L. Karger, T. A. Pinfold, and S. E. Palmer, *Separ. Sci.*, **5**, 603 (1970).
8) K. Kobayashi, *Bull. Chem. Soc. Jpn.*, **48**, 1180 (1975).
9) K. Kobayashi, *Bull. Chem. Soc. Jpn.*, **48**, 1750 (1975).
10) K. Kobayashi, H. Sato, K. Kachi, M. Nakamura, and T. Sasaki, *Bull. Chem. Soc. Jpn.*, **48**, 3533 (1975).
11) T. Inakazu, K. Kobayashi, and T. Sasaki, *Bull. Chem. Soc. Jpn.*, **48**, 3008 (1975).
12) I. Takayanagi, K. Kobayashi, K. Hachisuka, and T. Sasaki, *Bull. Chem. Soc. Jpn.*, **48**, 2419 (1976).
13) E. Fukada, K. Kobayashi, and T. Sasaki, *Bull. Chem. Soc. Jpn.*, to be published.

Temperature-independent Delayed Fluorescence of Benzo[*f*]quinoline in Biphenyl Host: A New Interpretation of Delayed Fluorescence Behavior around 77 K

Yoshihumi KUSUMOTO,* Yasuhiko GONDO, and Yoshiya KANDA

Department of Chemistry, Faculty of Science, Kyushu University, Hakozaki, Higashi-ku, Fukuoka 812

(Received April 28, 1976)

The delayed fluorescence observed in the mixed crystals of benzo[*f*]quinoline in biphenyl host has been found to be independent of temperature in the low temperature region from 90 K down to liquid helium temperature, and subtraction of this temperature-independent contribution from the observed total delayed fluorescence intensity above 90 K has given straight-line fits of the log I_{DF}/I_P^2 *vs.* $1/T$ plots, that is, a single activation energy has been obtained over the whole temperature range studied, instead of two different ones as usually assumed. Such a correction has also been given to a new attempt of log I_{DF} *vs.* $1/T$ plots successfully. Moreover, the decay behavior of the delayed luminescence has been studied over the wide temperature and concentration range. It has been concluded that the decay behavior of the temperature-independent delayed fluorescence may mainly be responsible for the nonexponential decay of the delayed fluorescence around 77 K.

Since the delayed fluorescence (DF) was first observed in 1958,[1] a number of studies have been made in a variety of liquid solutions,[2] in rigid glassy solutions,[3] in vapor phases[4] and in so-called "pure" crystals[5] as well as mixed crystals.[6–12] Early investigations in the mixed crystal systems were carried out at temperatures higher than 77 K by many investigators, particularly by Hirota *et al.*[8] and McGlynn and his co-workers,[13] and it has been concluded that the guest triplet excitation migration is a thermally activated process and occurs through the host triplet exciton band. In addition, the kinetic model for the delayed luminescence (phosphorescence and delayed fluorescence) has been proposed and substantiated except for the DF behavior in the vicinity of 77 K, that has been a deadlock encountered in the usual kinetic model and some interpretations have been made thereupon.[8b,13] Under such circumstances, we have investigated the temperature and concentration dependence of DF of benzo[*f*]quinoline in biphenyl host crystals, the temperatures and the concentrations extending over a wide range of 4.2—230 K and 10^{-2}—10^{-4} mol/mol, respectively.

We observed the temperature-independent delayed fluorescence (TIDF) in the low temperature region where the nature of DF had never been satisfactorily understood. Similar TIDF had been noticed by several investigators,[8b,14–16] but the significance of TIDF has never been explored. In this paper, we will discuss the significance of this TIDF for the usual temperature-dependent model. Some of these results have been presented previously as brief reports.[17,18]

Experimental

Chemicals and Samples. The chemicals used were obtained from Tokyo Kasei Kogyo Co., Ltd. Biphenyl was recrystallized twice from ethanol, and was further purified by repeated zone refining over 200 passes. Benzo[*f*]quinoline was subjected to the same chemical treatment as described previously,[19] and was finally zone refined with 250 passes. The polycrystalline samples used were prepared from the melts between two fused-silica plates mounted in a brass or a copper block holder, as will be mentioned later on.

Apparatus. The emission spectra were recorded with a photoelectric recording system which was essentially composed of a Bausch & Lomb 500-mm grating monochromator equipped with an RCA 1P28 photomultiplier, a DC preamplifier incorporating a Teledyne Philbrick operational amplifier model 1009, and a Hitachi recorder model QPD-54. The lifetimes of the delayed luminescence were measured with an Iwasaki SS-5004 synchroscope at appropriate wavelengths. A Becquerel-type rotating-disk phosphoroscope was used to exclude normal fluorescence. Excitation radiation was obtained from a 1-kW high-pressure mercury arc lamp, model Orc-CH-612. The excitation light beam was passed through a selective filter combination.

A Dewar cryostat system has been devised to keep the temperature nearly constant during observation. The brass and copper block holders were used for the regions above and below 77 K, respectively. The equipment was constructed according to Nakamura *et al.*[20] The temperature was raised by natural evaporation of the liquid helium or liquid nitrogen, as the case may be. The rate of evaporation was so slow that we were able to monitor constantly the temperatures of the sample crystals and the intensities of luminescence.

The temperatures higher than 77 K were measured by means of a calibrated copper-constantan thermocouple in contact with a fused-silica plate, and by a Yokogawa microammeter type MPs. The temperatures lower than 77 K were measured with a calibrated 1/8-W, 51-Ω Allen-Bradley carbon resistor which was attached to a portion of the copper block holder close enough to the sample to ensure good thermal contact. The resistance was measured with a hand-made DC Wheatstone bridge incorporating a Yokogawa electronic galvanometer type 2707 and a Yokogawa decade resistance box type RV-61.

Results

Observations at 77 K. Figure 1 shows a comparison of the delayed and normal fluorescence of a polycrystalline sample of biphenyl doped with benzo[*f*]quinoline. The normal and the delayed fluorescence spectrum are in good agreement with each other, confirming that the observed DF is genuine. We have already confirmed that the guest-delayed luminescence is genuine in a previous paper.[21]

We examined the temperature and concentration

* Present Address: Chemical Institute, College of Liberal Arts, Kagoshima University, Korimoto, Kagoshima 890

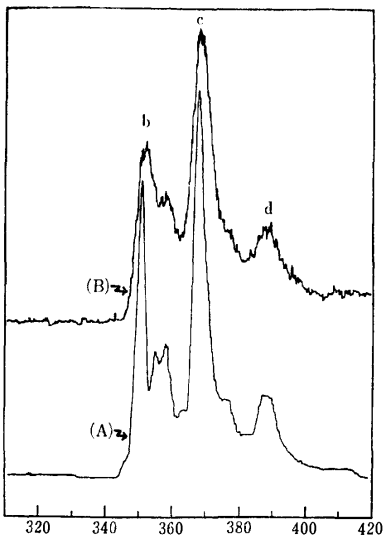

Fig. 1. Comparison of (A) normal and (B) delayed fluorescence of benzo[*f*]quinoline in biphenyl host at 77 K. Concn: 1.0×10^{-3} mol/mol. Slit width: (A) 1.0 mm (corresponding to 1.6 nm), (B) 2.5 mm (4.0 nm).

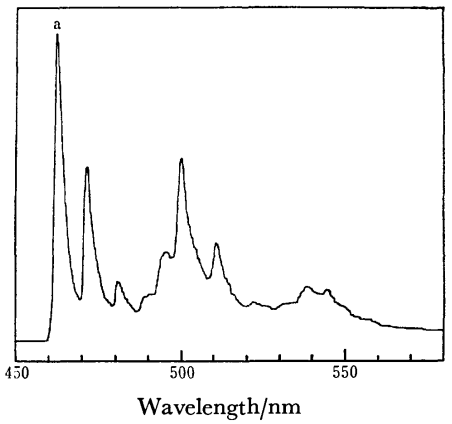

Fig. 2. Phosphorescence spectrum of benzo[*f*]quinoline in biphenyl host at 77 K. Concn: 1.0×10^{-3} mol/mol.

dependence in the delayed luminescence in respect of several bands a, b, c and d shown in Figs. 1 and 2.

Temperature Dependence of Intensity. Results in the Temperature Region above 77 K: General features of the temperature dependence of the delayed luminescence intensity were almost identical with those of Hirota and Hutchison,[8a] Hirota,[8] and Misra and McGlynn.[10] The temperature dependences of the delayed luminescence at a guest concentration of 1.2×10^{-2} mol/mol are shown in Fig. 3 as a typical example; results obtained at more dilute concentrations (10^{-3} and 10^{-4} mol/mol) were essentially the same. It can be inferred from Fig. 3 that the DF intensity seems to become constant in the lower temperature region. This was confirmed experimentally as will be described later.

Results in the 4.2—77 K Temperature Range: The temperature dependences of the delayed luminescence intensity at various guest concentrations are shown in

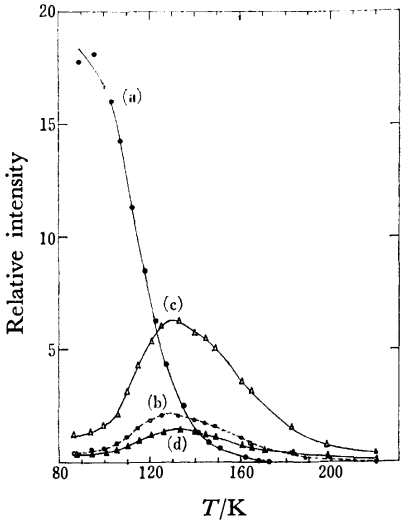

Fig. 3. Temperature dependence of the delayed luminescence of benzo[*f*]quinoline in biphenyl host in the temperature region above 77 K. Concn: 1.2×10^{-2} mol/mol. (a): Phosphorescence intensity observed at 464 nm, *i.e.*, the 0,0-band shown in Fig. 2; (b), (c), and (d): delayed fluorescence intensities observed at the corresponding bands shown in Fig. 1. No correction was made for the spectral response of the apparatus.

Figs. 4a, 4b, and 4c. At a concentration of 1.2×10^{-2} mol/mol (Fig. 4a), the DF intensity was essentially independent of temperature in the range of 25—77 K, while at lower temperatures it was dependent on temperature and reached a sharp maximum around 10 K. Similar behavior was also observed at a guest concentration of 1.25×10^{-3} mol/mol (see Fig. 4b). However, the maxima around 13 K were fairly lower than those in Fig. 4a. At a more dilute concentration of 1.0×10^{-4} mol/mol, the DF intensity remained constant over a wider range (4.2—77 K), without any appreciable maximum around 10 K (see Fig. 4c). This is quite different from the behavior of the other two cases as shown in Figs. 4a and 4b. By application of an empirical relation of Misra and McGlynn,[10] $T_{max}=0.06\,\Delta E/k$, to the maximum around 10 K, an activation energy of the order of 100 cm^{-1} was predicted. This shallow depth and the disappearance of the maximum around 10 K in the concentration as low as 10^{-4} mol/mol lead to a conclusion that the pertinent trap is of the so-called X-trap. In this connection, it may be noted that the mixed crystals studied in the temperature range of 4.2—77 K are sufficiently pure in the sense that this shallow depth is smaller by a factor of 10 than the depth involved in the thermal activation process to be discussed later on, and hence the presence of this shallow trap does not give any influence on the later discussion.

The phosphorescence intensity appeared to be independent of temperature at lower temperatures, while at higher temperatures it fell off with an increase in temperature, in every case shown in Figs. 4a, 4b, and 4c.

Decay Behavior. Results in the Temperature Region above 77 K: The decay behavior of the delayed lumines-

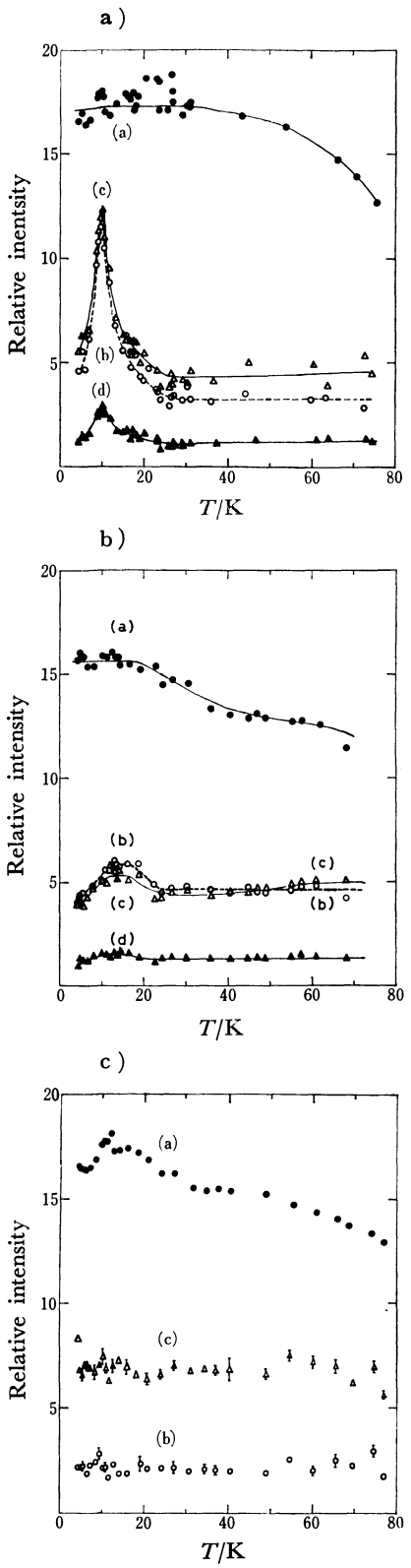

Fig. 4. Temperature dependence of the delayed luminescence of benzo[*f*]quinoline in biphenyl host in the 4.2—77 K temperature range. For the notation (a), (b), (c), and (d), see the figure caption to Fig. 3. Concn: a) 1.2×10^{-2}, b) 1.25×10^{-3}, c) 1.0×10^{-4} mol/mol. Magnification of the delayed fluorescence intensity to the phosphorescence intensity: a) × 10, b) × 20, c) × 25. No correction was made for the spectral response of the apparatus.

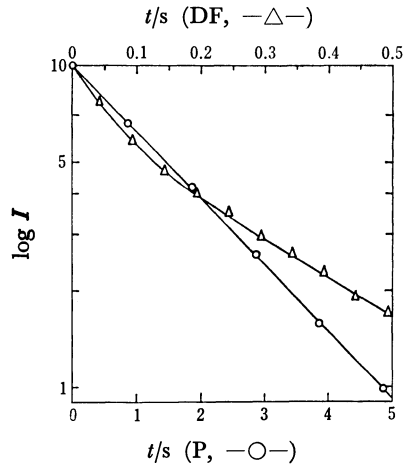

Fig. 5. Phosphorescence (P) and delayed fluorescence (DF) decays of benzo[*f*]quinoline in biphenyl host at 31 K. Concn: 1.2×10^{-2} mol/mol. The upper scale is for the plots of DF decay, and the lower scale for the plots of P decay. The initial intensities are obtained by extrapolation and arbitrarily normalized to 10.

cence at temperatures above 77 K is essentially in agreement with those observed by Hirota and Hutchison[8a] and Hirota.[8] The decay of the phosphorescence was observed to be exponential up to about 100 K and became nonexponential at higher temperatures. The decay of DF was nonexponential in a short time decay region even around 77 K, while it was exponential in a long time decay region. Such an apparently exponential decay behavior only in the long time region was also observed for the overall nonexponential decay of the phosphorescence.

Results in the 4.2—77 K Temperature Range: The decay characteristics of the delayed luminescence observed in the temperature range of 4.2—77 K were investigated for the concentration range of 10^{-2}—10^{-4} mol/mol. The phosphorescence decays were exponential in this temperature range, whereas the DF decays were generally nonexponential in the same temperature range. A typical decay behavior of the delayed luminescence observed for a concentration of 1.2×10^{-2} mol/mol at 31 K is shown in Fig. 5. At long times, however, the DF decay became exponential. As for DF, therefore, we will confine our discussion hereafter to the exponential decay region, that is, the long time decay region. In Fig. 6 is shown the temperature dependence of the delayed luminescence lifetimes measured at the concentration of 1.2×10^{-2} mol/mol. The phosphorescence lifetimes at the temperatures above about 100 K were obtained only in the long time decay region, whereas those below about 100 K were obtained in the whole decay region due to the exponential decay behavior of the phosphorescence. The point observed at the so-called characteristic temperature,[8b,22] where deviation from exponential decay behavior of the phosphorescence begins to appear, is marked with an arrow in Fig. 6. The temperature dependences of the decay behavior observed at the more dilute concentrations of 1.25×10^{-3} and 1.0×10^{-4} mol/mol were similar to that at the higher concentration just mentioned above. As

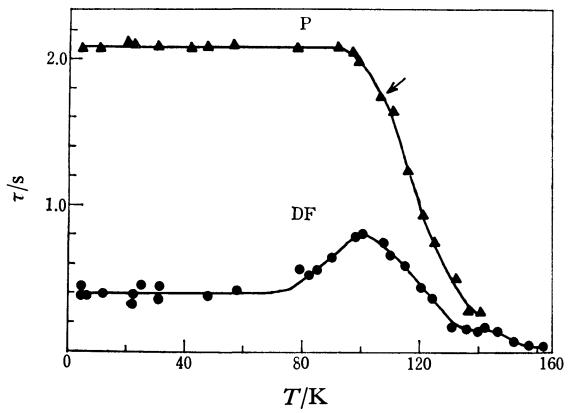

Fig. 6. Temperature dependence of the P and DF lifetimes of benzo[*f*]quinoline in biphenyl host. Concn: 1.2×10^{-2} mol/mol. The arrow refers to the characteristic temperature.

shown in Fig. 6, the decay behavior of the DF and phosphorescence remains constant at least in the temperature range of 4.2—70 K. The mean lifetimes obtained in this temperature range are 2.09 and 0.39 s for the phosphorescence and DF decays, respectively.

Discussion

Kinetics. Since the kinetic model used here has been discussed in detail by many authors,[3a,6a,8,10–12,22] we will briefly summarize the usual temperature-dependent kinetic model for the convenience of discussion. The rate processes with the relevant rate constants are identified in Table 1.[11b] The rate equations for the singlet and triplet guest populations are given by

$$\frac{d[S_{1G}]}{dt} = R_0 - (K_1+k_2)[S_{1G}] + K_4[T_{1G}]^2 \quad (1)$$

$$\frac{d[T_{1G}]}{dt} = \frac{k_2R_0}{K_1+k_2} - K_3[T_{1G}] - k_6[T_{1G}]^2 \quad (2)$$

where

$$k_6 = K_4(2K_1+k_2)/(K_1+k_2) + K_5 \quad (3)$$

From straightforward manipulation of Eqs. 1 and 2, the expressions for the steady-state intensities and the decays of phosphorescence (P) and DF are given by

$$I_P = k_3{*}k_3[(4K+1)^{1/2}-1]/2k_6 \quad (4)$$

$$I_{DF} = k_1{*}K_4K_3^2[(4K+1)^{1/2}-1]^2/[4k_6^2(K_1+k_2)] \quad (5)$$

$$I/I_P = (1-A)/[\exp(K_3t)-A] \quad (6)$$

$$I/I_{DF} = (1-A)^2/[\exp(K_3t)-A]^2 \quad (7)$$

where

$$K = k_2k_6R_0/(K_1+k_2)K_3^2 = A/(1-A)^2 \quad (8)$$

$$A = \frac{k_6[T_{1G}]_0}{K_3+k_6[T_{1G}]_0} = \frac{(1+4K)^{1/2}-1}{(1+4K)^{1/2}+1} \quad (9)$$

From Eqs. 4 and 5, one obtains

$$I_{DF}/I_P^2 = k_1{*}K_4/[(K_1+k_2)k_3{*}^2] \quad (10)$$

The temperature dependences of the quantities K_4, K_5, k_6, and K are given as

$$K_4,\ K_5,\ k_6,\ K \propto \exp(-\Delta E/kT) \quad (11)$$

where ΔE is the energy separation between the host and guest triplet states, and k Boltzmann's constant. With these expressions for the quantities K_4, K_5, k_6, and K, one may predict the temperature dependences of the delayed luminescence intensities and decays, assuming all the other rate constants to be independent of these quantities.[11] In the temperature-dependent triplet-triplet annihilation kinetics described above, it is assumed that there is no significant temperature-independent long range direct interaction between guest triplet states.[11b] It will be shown, however, that such an assumption does not necessarily hold, at least phenomenologically, in the vicinity of 77 K and below.[17,18] Since the kinetic model used here is the temperature-dependent one, the DF intensity (I_{DF}) in Eqs. 4 and 10 should duly be temperature-dependent. Since our experiment revealed the presence of the temperature-independent portion in I_{DF} (I_{TIDF}), the above-described expressions should be applied only for $[(I_{DF})_{total}-I_{TIDF}]$, where $(I_{DF})_{total}$ is the observed total I_{DF}.

Table 1. Definition of the rate processes involved in the triplet-triplet annihilation

	Process[a]	Rate constant	Remarks[b]
(0)	$S_{0H}\rightarrow S_{1G}$	R_0	Over-all rate constant
(1)	$S_{1G}\rightarrow S_{0G}+h\nu$	$k_1{*}$	Radiative
(1′)	$S_{1G}\rightarrow S_{0G}$	k_1	Nonradiative } $K_1\equiv k_1+k_1{*}$
(2)	$S_{1G}\rightarrow T_{1G}$	k_2	Intersystem crossing
(3)	$T_{1G}\rightarrow S_{0G}+h\nu$	$k_3{*}$	Radiative
(3′)	$T_{1G}\rightarrow S_{0G}$	k_3	Nonradiative } $K_3\equiv k_3+k_3{*}$
(4)	$T_{1G}+T_{1G}\rightarrow S_{1G}+S_{0G}$	K_4	Triplet-triplet annihilation producing excited singlet state of guest
(5)	$T_{1G}+T_{1G}\rightarrow T_{1G}+S_{0G}$	K_5	Bimolecular triplet quenching

a) S_0: Ground singlet state; S_1: lowest excited singlet state; T_1: lowest excited triplet state; G: guest; H: host. b) For detail, see text.

Significance of TIDF in Evaluation of Activation Energy. As shown in Figs. 3 and 4, I_P observed in the lower temperature region was dependent on temperature, contrary to the prediction from the kinetic model. The origin of this temperature dependence of I_P in the lower temperature region is not clear at present, although some explanations have been offered.[14,15] From expressions (4), (5), and (10), and relations (11) on the temperature dependence, one can obtain the following three Arrhenius plots:[11]

(1) In the higher temperature region, log I_P *vs.* $1/T$ (plot (1))
(2) in the lower temperature region, log I_{DF} *vs.* $1/T$ (plot (2))
(3) in the whole temperature region, log I_{DF}/I_P^2 *vs.* $1/T$ (plot (3))

Accordingly, we can obtain the activation energy ΔE from the above three plots. Plot (2) has for the first time been attempted by us. Figure 7 shows that the plot of log $[(I_{DF})_{total}-I_{TIDF}]$ *vs.* $1/T$ instead of log $(I_{DF})_{total}$ *vs.* $1/T$ gives a good straight-line fit for plot (2). The straight-line fit of log I_P *vs.* $1/T$ plot in the higher temperature region as predicted from plot

Table 2. Activation energies[a] and ratios $(I_{DF})_c/(I_{DF})_m$

Guest concn (mol/mol)	Band[c]	T_{max}/K[d]	ΔE (cm^{-1})[b] From T_{max}[e]	$\log I_{DF}/I_P^2$ vs. $1/T$ Uncorrected[f]	$\log I_{DF}/I_P^2$ vs. $1/T$ Corrected[f]	$\log I_{DF}$ vs. $1/T$ Corrected[g]	$\log I_P$ vs. $1/T$	$\frac{(I_{DF})_c}{(I_{DF})_m}$[h]
1.2×10^{-2}	b	129	1495	1630	1700	1470	1810	0.2
	c	130	1507	1640	1680	—	—	0.2
	d	132	1530	—	—	—	—	0.25
1.25×10^{-3}	b	125	1450	1950	1900	1440	1850	0.07
	c	124	1437	1920	1900	—	—	0.06
	d	124.5	1443	—	—	—	—	0.07
1.0×10^{-4}	b	129	1495	2000	2080	1550	1840	0.07
	c	128	1484	2090	2160	—	—	0.08
	d	128.5	1489	—	—	—	—	0.06

a) See Ref. 23. b) Activation energy calculated from the temperature dependence of the delayed luminescence. See text. c) See Fig. 1. d) T_{max} is the temperature at which maximum intensity of DF occurs. e) Calculated from an empirical relation, $T_{max}=0.06\,\Delta E/k$. See Ref. 10. f) See text. g) Only the corrected plot gives a good fit to a straight line. See text. h) $(I_{DF})_c$ denotes the DF intensity at 85 K, where I_{DF} approximately equals the temperature-independent contribution, *i.e.*, I_{TIDF}. $(I_{DF})_m$ refers to T_{max}.

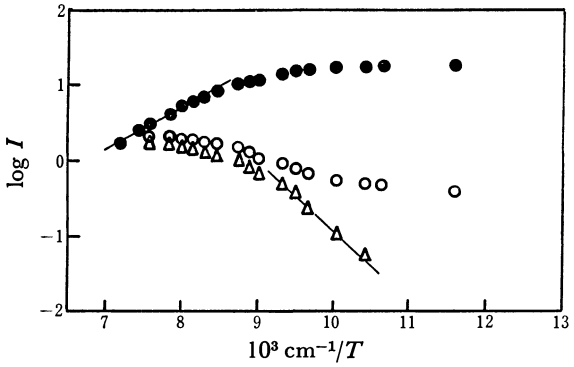

Fig. 7. Plots of $\log (I_{DF})_{total}$ (○), $\log [(I_{DF})_{total}-I_{TIDF}]$ (△), and $\log I_P$ (●) *vs.* $1/T$ with I_{DF} at band b shown in Fig. 1. Concn: 1.2×10^{-2} mol/mol.

(1) is also shown in Fig. 7. The thermal activation energies thus obtained are listed in Table 2. According to Misra and McGlynn,[10] plot (3) gave a good fit to a straight line in the high temperature region, whereas the deviation therefrom was observed in the low temperature region, showing a much smaller slope in the latter temperature region. They have suggested on the basis of the smaller activation energy obtained from this smaller slope that DF observed in the vicinity of 77 K may well be due to the annihilation involving thermal depopulation of defect states. However, DF around 77 K was independent of temperature in our cases as shown in Fig. 4. Moreover, as mentioned above, I_{DF} was independent of temperature in a wide range below 90 K. Therefore, such an analysis as given by Misra and McGlynn should be re-examined taking into account of this TIDF.[17] As Fig. 8 shows, subtraction of the temperature-independent contribution gave straight-line fits of the semilog plots over the whole temperature region studied. The thermal activation energies thus obtained are also listed in Table 2 in the column "corrected," while the corresponding "uncorrected" values

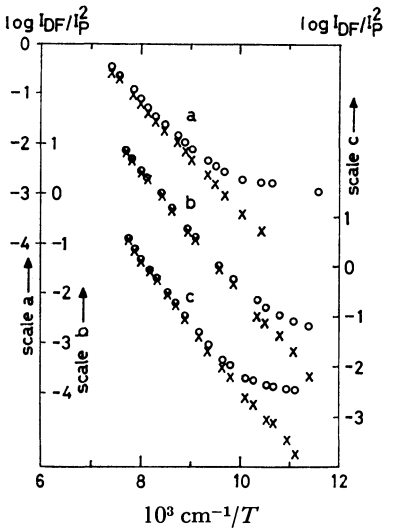

Fig. 8. Plots of $\log (I_{DF})_{total}/I_P^2$ (○) and $\log [(I_{DF})_{total}-I_{TIDF}]/I_P^2$ (×) *vs.* $1/T$ with I_{DF} at band b. Concn: a) 1.2×10^{-2}, b) 1.25×10^{-3}, c) 1.0×10^{-4} mol/mol.

are listed in the neighboring column. The activation energies obtained from the semilog plots, as seen in Table 2, are comparable with the corresponding spectroscopic value[23] of 1465 cm^{-1}, in particular for those obtained from plot (2). The activation energies obtained from plot (3) seem to be dependent on concentration. This may be due to the presence of the trap giving rise to another very weak delayed fluorescence observed at very low concentrations and high temperatures.[24] In order to check the "concentration effect" of the activation energies obtained from plot (3), an exhaustive purification of biphenyl host crystals has been made by repeated zone refining and taking the non-emissive portions of the specimen. The semilog plots for the trap-free benzo[*f*]quinoline–biphenyl mixed crystals are shown in Figs. 9 and 10, and the activation energies evaluated from the corrected plots are listed in Table 3. The validity of the

TABLE 3. ACTIVATION ENERGIES AND RATIOS $(I_{DF})_c/(I_{DF})_m$ OBTAINED FROM THE TRAP-FREE MIXED CRYSTALS[a)]

Guest concn (mol/mol)	Band	ΔE (cm^{-1})				$\frac{(I_{DF})_c}{(I_{DF})_m}$[b)]
		$\log I_{DF}/I_P^2$ *vs.* $1/T$		$\log I_{DF}$ *vs.* $1/T$	$\log I_P$ *vs.* $1/T$	
		Uncorrected	Corrected	Corrected		
1.0×10^{-2}	c	1580	1530	1540	1550	0.12
1.0×10^{-3}	c	1590	1560	1210	1820	0.04

a) Refer to footnotes to Table 2.
b) The other values of the ratio are 0.06 and 0.05 for bands b and d at the guest concentration of 1.0×10^{-3} mol/mol respectively, and 0.17 for band b at the guest concentration of 1.0×10^{-2} mol/mol.

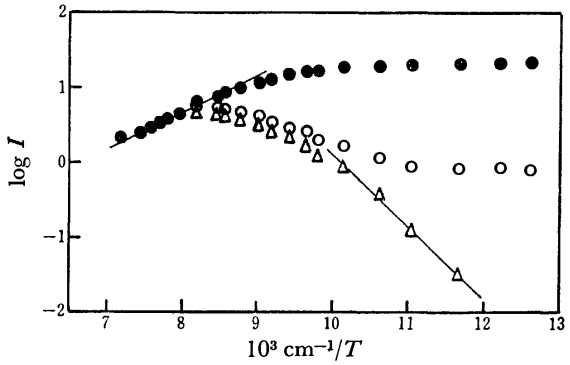

Fig. 9. The same plots as shown in Fig. 7 with I_{DF} at band c, using the trap-free benzo[*f*]quinoline-biphenyl mixed crystals. Concn: 1.0×10^{-2} mol/mol.

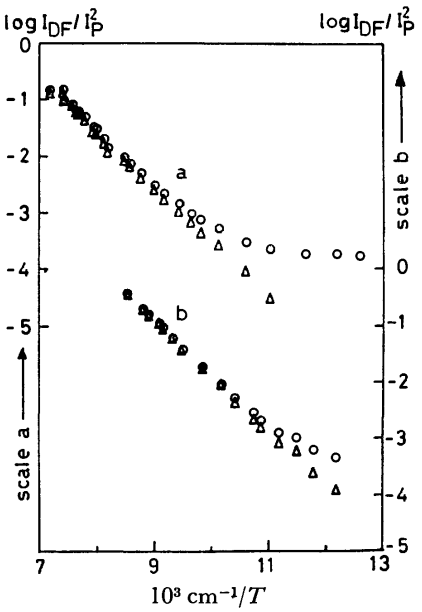

Fig. 10. Plots of $\log(I_{DF})_{total}/I_P^2$ (○) and $\log[(I_{DF})_{total}-I_{TIDF}]/I_P^2$ (△) *vs.* $1/T$ with I_{DF} at band c, using the trap-free benzo[*f*]quinoline-biphenyl mixed crystals. Concn: a) 1.0×10^{-2}, b) 1.0×10^{-3} mol/mol.

correction emphasized above is evident. Moreover, the activation energies obtained from plot (3) at two different concentrations are in accordance with each other within the experimental error. Therefore, it may be concluded that the thermal activation energy is in principle independent of concentration.

For comparison, we have also applied this type of correction to plot (3) of the experimental results on the phenanthrene–biphenyl system published by Misra and McGlynn,[10)] obtaining a straight line that covers the whole temperature range studied. Accordingly, above-described suggestion made by McGlynn *et al.*[10,11b,13)] on DF in the low temperature region, in particular in the vicinity of 77 K, is hardly convincible.

In Table 2 are also collected the values of T_{max}, the temperature at which maximum intensity of DF occurs, and the host-guest triplet separations ΔE deduced from T_{max} through the empirical relation.[10)] The values of T_{max} seem to be in agreement with one another within the experimental error, and hence so seem the corresponding values of ΔE.

A New Interpretation of Decay Behavior around 77 K. The experimental results on the decay behavior are in good agreement with the kinetic model except for the unusual decay behavior of DF around 77 K. The decay deviates considerably from the exponential behavior in the lower temperature region, where the exponential decay would be expected from the usual temperature-dependent model. This peculiarity in the DF decay around 77 K has already been pointed out by Hirota[8b)] and Misra and McGlynn.[10)] Hirota[8b)] reported that the DF decays in the vicinity of 77 K were independent of temperature. On the other hand, Misra and McGlynn[10)] suggested on the nonexponential decays of DF around 77 K that some kinds of traps, probably imperfections in the host-crystal lattice, might be responsible for this decay behavior. Incidentally, Misra[15)] found the temperature-independent decays in the temperature range 6—77 K for the phenanthrene–biphenyl and naphthalene–biphenyl mixed crystal systems. As can be seen in Figs. 5 and 6, the TIDF decay behavior remains constant at temperatures below about 70 K and is still nonexponential in this temperature range. Here, it should be noted that the existence of this temperature-independent delayed-luminescence decay observed over a wide range of temperature is compatible with Hirota's observation of the temperature-independent decay in a smaller range of temperature. Thus, it may be concluded that the unusual decay behavior of DF around 77 K may be due to the presence of TIDF portion. In other words, if no TIDF existed practically, the decay law of DF in the vicinity of 77 K would be exponential, as have been observed experimentally in some mixed crystals.[10,22)] The phosphorescence decay that is exponential even in the vicinity of 77 K, is not affected at all by the nonexponential decay behavior of TIDF, as can be understood through the fact that DF around 77 K is much weaker than the phospho-

rescence.

Nature of TIDF. We evaluated the intensity ratio of DF at 85 K and at T_{max}, I_{DF} (85 K)/$I_{DF}(T_{max})$, since I_{DF} at 85 K equals approximately to its temperature-independent contribution. This ratio gives an approximate value for the fraction of all triplets which decay *via* a second-order mechanism, namely triplet-triplet annihilation, in the temperature-independent range.[14,15] The ratios thus obtained with different guest concentrations are also listed in the last columns of Tables 2 and 3. It may be noted that these ratios seem to depend on the guest concentration. Particularly, the ratios at the concentration of the order of 10^{-2} mol/mol are larger than those at the other lower concentrations. This concentration effect is definitely beyond the experimental error. Since average distances between guests in the biphenyl host crystals are 15.3, 32.9, and 71.2 Å in the concentrations of 10^{-2}, 10^{-3}, and 10^{-4} mol/mol respectively according to Chandrasekhar's expression,[25] the direct triplet-triplet annihilation between guests hardly seems to be operative except for the case of the concentration of 10^{-2} mol/mol. At the high concentration of 10^{-2} mol/mol, the triplet-triplet annihilation due to exchange interaction might be responsible for the existence of TIDF in connection with the relatively higher values of the ratios described above. The fact that we observed TIDF at the low guest concentration of 10^{-4} mol/mol seems to suggest that it may be significant to study the problem of the distribution of guest molecules in mixed crystals.[26]

In the hope to decide whether such an opportune overlap of the T-T absorption and T-S emission as occuring in benzo[*f*]quinoline is responsible for the existence of TIDF,[3b] we have undertaken a similar study with naphthalene as guest in place of benzo[*f*]-quinoline, since this kind of overlap does not take place with this guest. We also observed TIDF and obtained a value of 0.012 for the ratio described above at the concentration of 10^{-2} mol/mol.[27] Thus, the above-mentioned overlap of T-T and T-S transitions is not necessarily required for the occurrence of TIDF.

In conclusion, on the sound basis of the observation of TIDF, we show a new way in which we refrain from invoking traps arbitrarily. The experimental results presented above, however, are not enough to elucidate the nature of TIDF. Further detailed experiments are required to clarify this question fully. Detailed results of this study will be given in Ref. 28.

References

1) H. Sponer, Y. Kanda, and L. A. Blackwell, *J. Chem. Phys.*, **29**, 721 (1958); N. W. Blake and D. S. McClure, *ibid.*, **29**, 722 (1958).

2) C. A. Parker, "Advances in Photochemistry," Vol. 2, ed. by W. A. Noyes, Jr., G. S. Hammond, and J. N. Pitts, Jr., Interscience Publishers, Inc., New York, N. Y. (1964), p. 305; C. A. Parker, "The Triplet State," ed. by A. B. Zahlan, Cambridge University Press, London (1967), p. 354.

3) (a) T. Azumi and S. P. McGlynn, *J. Chem. Phys.*, **39**, 1186 (1963); (b) R. E. Kellogg, *ibid.*, **41**, 3046 (1964).

4) A. B. Zahlan, S. Z. Weisz, R. C. Jarnagin, and M. Silver, *J. Chem. Phys.*, **42**, 4244 (1965); B. Stevens, M. S. Walker, and E. Hutton, "The Triplet State" in Ref. 2, p. 239; G. L. Powel, *J. Chem. Phys.*, **47**, 95 (1967); G. F. Finger and A. B. Zahlan, *ibid.*, **50**, 25 (1969).

5) R. G. Kepler, J. C. Caris, P. Avakian, and E. Abramson, *Phys. Rev. Lett.*, **10**, 400 (1963); W. L. Peticolas, J. Goldsborough, K. E. Rieckhoff, *ibid.*, **10**, 43 (1963); R. A. Keller, *J. Chem. Phys.*, **42**, 4050 (1965).

6) (a) H. Sternlicht, G. C. Nieman, and G. W. Robinson, *J. Chem. Phys.*, **38**, 1326 (1963); (b) G. C. Nieman and G. W. Robinson, *ibid.*, **37**, 2150 (1962); (c) M. A. El-Sayed, M. T. Wauk, and G. W. Robinson, *Mol. Phys.*, **5**, 205 (1962).

7) M. Zander, *Z. Electrochem.*, **68**, 301 (1964).

8) (a) N. Hirota and C. A. Hutchison, Jr., *J. Chem. Phys.*, **42**, 2869 (1965); (b) N. Hirota, *ibid.*, **43**, 3354 (1965).

9) L. Azarraga, T. N. Misra, and S. P. McGlynn, *J. Chem. Phys.*, **42**, 3720 (1965).

10) T. N. Misra and S. P. McGlynn, *J. Chem. Phys.*, **44**, 3816 (1966).

11) (a) M. Kinoshita and S. P. McGlynn, *Mol. Cryst.*, **3**, 163 (1967); (b) M. Kinoshita and S. P. McGlynn, *ibid.*, **4**, 231 (1968).

12) S. P. McGlynn, T. N. Misra, and E. F. McCoy, International Symposium on Luminescence, Munich, 1965, ed. by H. Kallmann and N. Riehl, Karl Thiemig, Munich, Germany (1966), p. 98.

13) S. P. McGlynn, M. Kinoshita, M. McCarville, B. N. Srinivasan, and J. W. Rabalais, *Photochem. Photobiol.*, **8**, 349 (1968). Papers of McGlynn and his co-workers on delayed luminescence are listed in this article.

14) G. F. Hatch and G. C. Nieman, *J. Chem. Phys.*, **48**, 4116 (1968).

15) T. N. Misra, *J. Chem. Phys.*, **58**, 1235 (1973).

16) M. Yagi, S. Nagakura, and H. Hayashi, *Chem. Phys. Lett.*, **18**, 272 (1973).

17) Y. Kusumoto, Y. Gondo, and Y. Kanda, *Chem. Lett.*, **1974**, 81.

18) Y. Kusumoto, Y. Gondo, and Y. Kanda, Preprint of the 7th Molecular Crystal Symposium, Nikko, Japan (1975), A-27, p. 79.

19) Y. Kanda and R. Shimada, *Spectrochim. Acta*, **15**, 211 (1959).

20) N. Nakamura and H. Chihara, *J. Phys. Soc. Jpn.*, **22**, 201 (1967).

21) Y. Kusumoto, T. Edamura, Y. Gondo, and Y. Kanda, *Mem. Fac. Sci., Kyushu Univ., Ser. C*, **7**, 165 (1970).

22) M. Kinoshita, T. N. Misra, and S. P. McGlynn, *J. Chem. Phys.*, **45**, 817 (1966).

23) The spectroscopic energy gap of host triplet-guest triplet state is 1465 cm^{-1} for the benzo[*f*]quinoline-biphenyl system, which is obtained by adopting a value of 23010 cm^{-1} for the triplet state of biphenyl.[8] Incidentally, a preliminary study of the X-trap phosphorescence of biphenyl crystal locates the crystal lowest triplet state around 23150 cm^{-1}, a much more favorable value (S. Wada, Y. Gondo, and Y. Kanda, unpublished results).

24) With lower concentrations and higher temperatures, we detected the very weak trap-delayed fluorescence as well as a trap-fluorescence in a shorter wavelength region than that of the guest emission. It should be particularly emphasized that the trap emission became weaker by a more extensive purification of the host biphenyl crystal. For further details, see Ref. 28.

25) C. Chandrasekhar, *Rev. Mod. Phys.*, **15**, 1 (1943).

26) M. Schwoerer and H. C. Wolf, *Mol. Cryst.*, **3**, 177 (1967).

27) Y. Kusumoto, Y. Gondo, and Y. Kanda, unpublished results.

28) Y. Kusumoto, thesis to be sumbitted to Kyushu University.

Composition and Some Physical Properties of Complex TCNQ Anion Radical Salts Containing Quinolinium, *N*-Methylquinolinium, and their Isomeric Cations

Yoshio MATSUNAGA and Tomio TANAKA*

Department of Chemistry, Faculty of Science, Hokkaido University, Sapporo 060

(Received June 11, 1976)

Complex TCNQ anion radical salts containing quinolinium, isoquinolinium, and their methyl derivatives were prepared. Quinolinium and cations having molecular envelopes of 2-methylnaphthalene form 1 : 2 salts, whereas isoquinolinium and cations having molecular envelopes of 1-methylnaphthalene give 2 : 3 salts. Only *N*-methylquinolinium forms salts containing the solvent of crystallization. The room temperature resistivities of the polycrystalline compactions are in the range from 0.5 to 3.9 ohm cm, and the Seebeck coefficients are in the range from -41 to -54 μV/deg for the 1 : 2 salts and in the range from -12 to -23 μV/deg for the 2 : 3 salts. The diffuse reflection spectra of all the salts are similar to each other. A splitting of the band in the 10×10^3 cm^{-1} region was observed only for the 1 : 2 salts. In the total reflectance spectra, the salts show Drude-like edges in the region from 6×10^3 to 8×10^3 cm^{-1}.

The complex anion radical salt quinolinium(TCNQ)$_2$ is one of the most highly conducting organic materials.[1,2] The resistivity value at room temperature of the pressed polycrystalline sample has been reported to be 0.25 ohm cm, and that of single crystals along the needle axis 0.01 ohm cm. The minimum resistivity has been observed for single crystals at 223 K by Walatka and Perlstein and at 240 K by Buravov *et al.*[3,4] According to the crystal structure analysis made by Kobayashi *et al.*, the cation adopts either of the alternative orientations with equal probability.[5] The composition appears to depend upon small variations introduced in the cation. The *N*-methylquinolinium cation has been shown to form a 2 : 3 salt and its isomer, the quinaldinium cation, a 1 : 2 salt.[6] Moreover, the former salt has been reported by Flandrois *et al.* to contain approximately one mole of acetonitrile per mole of the salt and by Murakami and Yoshimura two moles of the same solvent per mole of the salt.[7–9] It is of interest to examine more fully complex salts with isomeric cations. Accordingly, the authors set out to study the composition and some physical properties of the isoquinolinium salt and methyl-substituted quinolinium and isoquinolinium salts.

Experimental

Materials. Quinoline, isoquinoline, quinaldine, lepidine, and 6-methyl-, 7-methyl-, and 8-methyl-quinolines were commercially obtained, and used without further purification. The onium iodides were prepared by the usual reactions with hydroiodic acid or methyl iodide. The complex TCNQ salts were crystallized when onium iodide and TCNQ separately dissolved in hot acetonitrile were mixed. They were purified by recrystallization from the same solvent. The compositions were determined by the microanalysis of carbon, hydrogen, and nitrogen, and were checked by the ratio of the optical density at 400 nm to that at 842 nm. This quantity has been reported to be about 1.2 for the 2 : 3 salts and from 1.7 to 2.0 for the 1 : 2 salts.[10]

Measurements. The electrical resistivities and thermoelectric motive force of polycrystalline compactions were measured as a function of the temperature by methods similar to those described elsewhere.[11] The diffuse reflectance of samples diluted with sodium chloride was measured by means of a Beckman DK 2A spectroreflectometer in the range from 325 to 2500 nm. The reference was pure sodium chloride. The spectrum was then plotted using the Kubelka-Munk function. The total reflectance of the compactions was also recorded on the same instrument in the range from 700 to 2700 nm employing a polished copper plate as a reference.

Results and Discussion

Composition. Six new complex TCNQ anion radical salts are listed in Table 1. The results of microanalysis are consistent with their 2 : 3 or 1 : 2 composition, but the ratio of the optical density at 400 nm to that at 842 nm tends to be larger than the above-mentioned figures. For example, Buvet *et al.* obtained 2.00, 1.20, and 1.85 for the quinolinium, *N*-methylquinolinium, and quinaldinium salts respectively.[10] The present values are respectively 2.18, 1.34, and 2.15. Especially, the values found for the 7-methyl- and 8-methylquinolinium salts are much larger than expected. Although the quinolinium cation has been known to form a 1 : 2 salt, the isomer, the isoquinolinium cation, was found to form a 2 : 3 salt. Thus, the distribution of a positive charge in the cationic nucleus appears to be the most important factor determining the composition in this pair of TCNQ salts. The methyl-substituted cations are classified into two groups on the basis of the composition of the resulting TCNQ salts. One group consists of *N*-methylquinolinium, lepidinium, and 8-methylquinolinium, which give 2 : 3 salts. The other includes quinaldinium, *N*-methylisoquinolinium, 6-methylquinolinium, and 7-methylquinolinium. They form 1 : 2 salts. This classification cannot be correlated with the position of the nitrogen atom in the nuclei, but can be correlated with the position of the methyl group. The cations in the first group have molecular envelopes of 1-methylnaphthalene, and those in the second group envelopes of 2-methylnaphthalene. This finding is in sharp contrast with the result found for quinolinium and isoquinolinium cations and also with the report on aminoquinolinium cations by Libera and Bretschneider.[12] All the TCNQ salts containing 2-amino-, 3-amino-,

* Present address: Mitsui Toatsu Chemicals, Inc., Totsuka, Yokohama.

Table 1. Compositions of TCNQ anion radical salts

Cation		Analysis (%) C	H	N	D_{400}/D_{842}
Isoquinolinium	Found	74.69	3.10	22.34	1.44
	Calcd for 2 : 3	74.47	3.01	22.52	
Lepidinium	Found	74.66	3.49	21.42	1.32
	Calcd for 2 : 3	74.65	3.58	21.77	
8-Methylquinolinium	Found	75.04	3.43	21.75	2.28
	Calcd for 2 : 3	74.65	3.58	21.77	
N-Methylisoquinolinium	Found	73.98	3.17	22.82	2.35
	Calcd for 1 : 2	73.90	3.28	22.81	
6-Methylquinolinium	Found	74.01	3.18	22.86	2.21
	Calcd for 1 : 2	73.90	3.28	22.81	
7-Methylquinolinium	Found	73.40	3.04	23.15	2.85
	Calcd for 1 : 2	73.90	3.28	22.81	

4-amino-, and 5-aminoquinolinium cations were reported to be of 1 : 2 composition. Since the amino group is a little smaller than the methyl group, the latter may be a substituent of such critical size that the molecular envelope dominates the charge distribution in the determination of the composition of complex TCNQ salts.

The *N*-methylquinolinium salt, to which a 1 : 2 composition was originally assigned by Melby *et al.* on the basis of microanalysis,[1] has been shown to be actually of 2 : 3 composition on the basis of the optical density ratio at 400 and 842 nm.[6,10] Differential-scanning calorimetric examinations indicated the presence of an endothermic change above 90 °C assignable to the loss of the solvent of crystallization reported by Flandrois *et al.* and also by Murakami and Yoshimura.[8,9] The enthalpy change observed in this work is in the range from 10 to 15 kcal/mol depending upon the preparations. These values are intermediate between those reported by the above-mentioned two groups: about 5 kcal/mol and 19.1 kcal/mol. Our preparations showed weight losses of about 8.5 percent by heating at 120 °C, indicating the presence of two moles of acetonitrile per mole of the 2 : 3 salt (calculated value: 8.35%). The results of microanalysis before and after the weight loss are in good agreement with the proposed compositions (see Table 2). It may be added that the calculated values for the 2 : 3 salt containing this amount of the solvent are very close to those for the originally assumed 1 : 2 salt, namely, C, 73.90, H, 3.28, and N, 22.81%. This conclusion agrees with that of Murakami and Yoshimura except for the ratio of the cation to the TCNQ, which they suggested to be 1 : 1.6.[9,13] The salt crystallized from acetone showed a weight loss of 9.8 percent by heating. This amount corresponds to 1.7 moles of acetone per mole of the 2 : 3 salt. Employing the less volatile ethyl methyl ketone as the solvent, the salt with a better defined composition could be isolated. The composition is consistent with a 2 : 3 salt containing one mole of the solvent. The observed weight loss by heating, about 7.7%, agrees fairly well with the calculated one, 7.41%. The microanalytical results after heating again agree with a 2 : 3 composition. Contrary to the case of acetonitrile, the loss of these ketones by heating could not be detected by differential-scanning calorimetry. However, the process is well demonstrated by a drastic change of the electrical resistivity as is described in the next section. The last salt in Table 2 was crystallized from boiling ethyl acetate and found to be free from the solvent and to be of 2 : 3 composition. Finally, it must be emphasized that in all the *N*-methylquinolinium salts prepared here the ratio of the cation to the TCNQ is stoichiometric: that is 2 : 3.

Table 2. Composition of *N*-methylquinolinium TCNQ salts

Solvent		Analysis (%) C	H	N
Acetonitrile	Found	73.61	3.79	22.90
	Calcd for 2 : 3 with $2CH_3CN$	73.30	3.90	22.80
Acetonitrile[a]	Found	75.09	3.44	21.98
	Calcd for 2 : 3	74.65	3.58	21.77
Ethyl methyl ketone	Found	73.99	4.13	19.86
	Calcd for 2 : 3 with C_4H_8O	74.05	4.14	20.15
Ethyl methyl ketone[a]	Found	74.70	3.49	21.34
	Calcd for 2 : 3	74.65	3.58	21.77
Ethyl acetate	Found	74.62	3.57	21.22
	Calcd for 2 : 3	74.65	3.58	21.77

a) After the loss of the solvent of crystallization.

Electrical Properties. The electrical resistivities, activation energies for semiconduction, and Seebeck coefficients at 20 °C for polycrystalline compactions are listed in Table 3. The present resistivity values are in the range from 0.5 to 3.9 ohm cm and the activation energies from 0.03 to 0.09 eV. The lowest values for these two quantities were observed with the quinolinium and isoquinolinium salts. As the single crystals of the former salt are known to exhibit a resistivity minimum below room temperature, these values may be considered to arise mostly from contact between the crystals. Therefore, they may be near the limiting values obtainable with compactions of high-conductivity TCNQ salts. The Seebeck coefficients are almost constant or become slightly more negative at the higher temperatures in the measured range (see curve a in Fig. 2). Its

Table 3. Electrical properties of compactions of complex TCNQ salts

Cation	Resistivity at 20 °C (ohm cm)	Activation energy at 20 °C (eV)	Seebeck coeff. at 20 °C (μV/deg)
Quinolinium	0.5	0.03	−41
Isoquinolinium	0.5	0.03	−12
N-Methylquinolinium (with $2CH_3CN$)	3.5	0.24	−23
N-Methylquinolinium (with C_4H_8O)	3.9	0.04	−22
Lepidinium	1.7	0.05	−12
8-Methylquinolinium	1.6	0.06	−21
Quinaldinium	1.2	0.04	−45
N-Methyl-isoquinolinium	0.5	0.09	−47
6-Methylquinolinium	1.9	0.05	−54
7-Methylquinolinium	3.2	0.07	−49

magnitude appears to be largely determined by the composition, namely, the 2 : 3 salts give values from −12 to −23 μV/deg and the 1 : 2 salts values from −41 to −54 μV/deg. Similar behavior has been reported to be characteristic of high conductivity TCNQ salts.[4] Buravov *et al.* have examined the Seebeck coefficient of the quinolinium (1 : 2), acridinium (1 : 2), and 3,3′-diethylthiazolino-2,2′-carbocyaninium (1 : 2) salts and found that the values are nearly independent of temperature above 100 or 150 K and that they are practically the same for all three. The average value they obtained is −60 μV/deg. According to their theory, the coefficient is a function of the composition, however, the relation is so complicated that their equation has been solved only for the 1 : 2 salts. In the high temperature limit, the coefficient S for the 1 : 2 salts can be approximated by $S=-(k/|e|)\ln 2=-59.8$ μV/deg, which is in excellent agreement with their experimental results but not with the present values. Recently, Beni *et al.* have obtained the same theoretical value for the 1 : 2 salts employing an equation derived in connection with the strong coupling Hubbard model.[14] Their equation for the high temperature saturation thermoelectric power is

$$S = -\frac{k}{|e|}\ln 2(1-\rho)/\rho,$$

where ρ is the carrier concentration defined by the ratio of the number of carriers to the number of sites. If we take $\rho=1/2$, the equation yields $S=-59.8$ μV/deg. Conversely, ρ may be estimated to be 0.52—0.55 assuming tentatively the room temperature values as the saturation values and employing the above equation as novel way of determining the amount of charge following a proposal made by Beni *et al.* Similarly, values from 0.60 to 0.62 may be obtained for the 2 : 3 salt. On the other hand, the equation yields $S=0$ for $\rho=2/3$.

The *N*-methylquinolinium salt crystallized from acetonitrile has been reported to show a large irreversible increase in the resistivity by the loss of the solvent of crystallization.[13] In our measurements, the activation energy for semiconduction was temperature-dependent and was about 0.24 eV at 20 °C. The resistivity remained at about 3 ohm cm between 30 and 50 °C, then increased gradually above 50 °C and sharply above 55 °C. The value at 103 °C was about 4300 ohm cm. After this heating process, the room temperature resistivity became about 8000 ohm cm. On the other hand, compaction made after the loss of the solvent of crystallization showed a resistivity of about 2600 ohm cm and an activation energy of 0.25 eV at 20 °C. These values are close to those reported by Murakami and Yoshimura, about 2000 ohm cm and 0.3 eV, and are essentially the same as those given by the solvent-free salt crystallized from ethyl acetate (see curve c in Fig. 1).

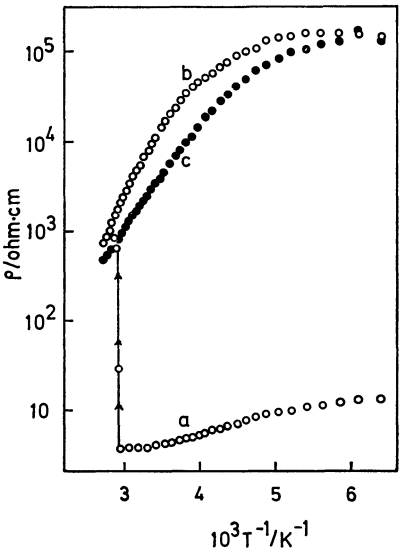

Fig. 1. Electrical resistivities of *N*-methyl quinolinium-TCNQ (2 : 3) salts, (a) with ethyl methyl ketone of crystallization, (b) after the loss of ethyl methyl ketone, and (c) the solvent-free salt crystallized from ethyl acetate.

The results of measurements made on the salt crystallized from ethyl methyl ketone are shown in Fig. 1. The resistivity change occurred over a rather narrow temperature range. The irreversible increase began at 63 °C and ended at 84 °C. The resistivity value at the latter temperature was about 1000 ohm cm and that at room temperature after the loss of the solvent about 10000 ohm cm. Thus, curve b and the corresponding curve observed with the salt crystallized from acetonitrile are in close resemblance with each other. The behavior of the salt crystallized from acetone was very similar to that mentioned above. However, an abrupt increase in the resistivity was observed in a slightly lower temperature range. The increase began at 50 °C and ended at 65 °C, reflecting the volatility of the solvent.

The drastic change in the Seebeck coefficient by the loss of the solvent of crystallization is illustrated in Fig. 2 for the salt crystallized from acetonitrile. The coefficient becomes more negative and markedly temperature dependent by the loss of acetonitrile (see curve b). A minimum value of −0.4 mV/deg is located near 240 K. Above this temperature, the slope defined by $dS/d(1/T)$ is as large as −0.26 V. The same slope

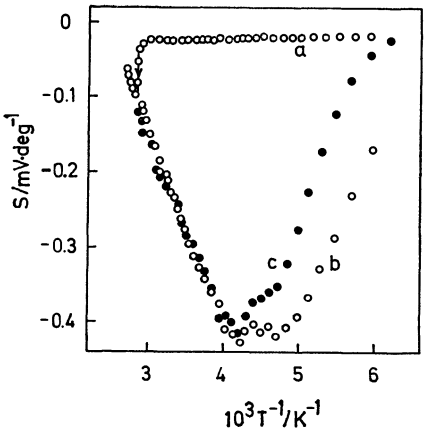

Fig. 2. Seebeck coefficients of *N*-methylquinolinium-TCNQ (2 : 3) salts, (a) with acetonitrile of crystallization, (b) after the loss of acetonitrile, and (c) the solvent-free salt crystallized from ethyl acetate.

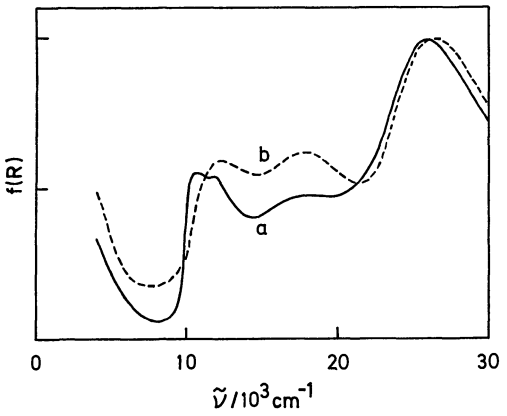

Fig. 3. Diffuse reflection spectra, (a) quinolinium-TCNQ (1 : 2) salt and (b) isoquinolinium-TCNQ (2 : 3) salt.

could be observed with the solvent-free salt crystallized from boiling ethyl acetate (see curve c). However, the agreement between these two below 240 K is merely qualitative.

Optical Properties. The visible and near infrared absorption spectra of complex TCNQ anion radical salts both of intermediate- and high-conductivity are known to resemble each other and to consist of four bands, the maxima of which are approximately located at $<4\times10^3$, 10×10^3, 17×10^3, and 27×10^3 cm^{-1}.[15-17] On the basis of polarized normal-incidence reflection of the methyltriphenylphosphonium salt, the assignment of these bands has been made by Oohashi and Sakata. The band in the near infrared region arises from the charge-transfer interaction between the $TCNQ^-$ anion radical and the neutral molecule and the second one from the charge-transfer interaction between the anions. The latter two bands have been attributed to locally-excited transitions in the anion radical and/or the neutral molecule. Among the TCNQ salts studied here, the following five were examined for diffuse reflection spectra by Iida some years ago: the quinolinium, *N*-methylquinolinium, *N*-methylisoquinolinium, quinaldinium, and lepidinium salts. A splitting of the

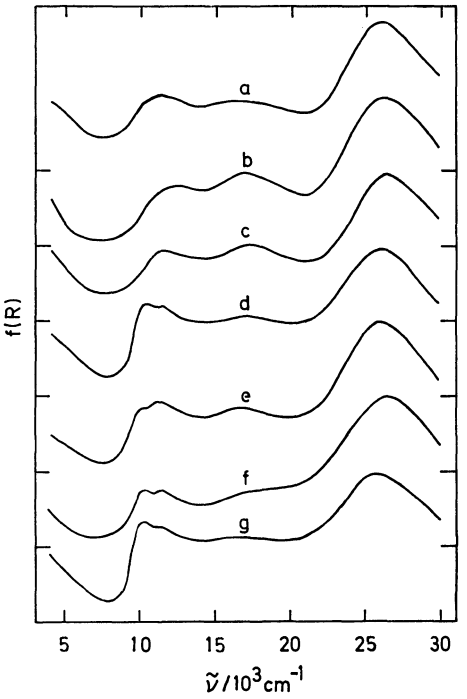

Fig. 4. Diffuse reflection spectra of the complex TCNQ anion radical salts containing (a) *N*-methylquinolinium (solvent-free), (b) lepidinium, (c) 8-methylquinolinium, (d) quinaldinium, (e) 6-methylquinolinium, (f) 7-methylquinolinium, and (g) *N*-methylisoquinolinium.

band around 10×10^3 cm^{-1} was noted in the case of *N*-methylquinolinium and *N*-methylisoquinolinium salts. Assuming a 1 : 2 composition for these five, Iida has noted that the splitting becomes appreciable with an increase of the electrical resistivity. As a matter of fact, such splitting has been commonly observed in the intermediate- and high-conductivity 1 : 2 salts.[15,16] However, the present work clarifies that the five salts studied by Iida are not of the same composition. The measurements on the present five 1 : 2 and four 2 : 3 salts revealed that the spectral pattern is essentially determined by the composition. The difference caused by the composition may be best exemplified by a comparison of the spectrum of the quinolinium salt with that of the isoquinolinium salt exhibiting almost the same electrical resistivity. As is shown in Fig. 3, the quinolinium salt shows a doublet in the 10×10^3 cm^{-1} region. The maxima of the sharp peaks are located at 10.5×10^3 and 11.0×10^3 cm^{-1}. Both previous workers noted only one maximum for this 1 : 2 salt. The location of the former peak agrees well with that recorded by Iida and that of the latter with the value reported by Oohashi and Sakata. On the other hand, a broad single band appears at 12.3×10^3 cm^{-1} in the isoquinolinium salt. The spectra of the complex salts containing methylated cations are presented in Fig. 4. Again, the 1 : 2 salts are generally distinct from the 2 : 3 salts. A splitting of the band in the 10×10^3 cm^{-1} region can be clearly observed in all the 1 : 2 salts but not in the 2 : 3 salts. It must be noted, however, a shoulder around 10×10^3 cm^{-1} is present in the spectrum of the solvent-free *N*-methylquinolinium salt, the only intermediate-conductivity salt examined in the present

work.

Polarized reflectance spectra have been measured on single crystals of $Cs_2(TCNQ)_3$ by Vlasova and Gutman.[18] This complex salt has a resistivity of the order of 10^4 ohm cm at room temperature and has been classified into intermediate-conductivity salts by Siemons *et al.*[2] The reflectance for light polarized parallel to the needle axis rises from a minimum of about 2 percent at 14.5×10^3 cm^{-1} to a value of about 17 percent at 10×10^3 cm^{-1}. They have considered such a rapid decrease of the reflectance to such a low value to be typical of the plasma edge observed with metals and semiconductors and have estimated the plasma frequency for this salt to be 2.8×10^{15} s^{-1}. The spectral behavior of an organic metal, tetrathiofulvalene–tetracyanoquinodimethane (TTF–TCNQ), with a resistivity of the order of 10^{-3} ohm cm along the needle axis has been examined similarly by Bright *et al.* and also by Grant *et al.*[19-21] The change in the reflectance for light polarized parallel to the conducting axis is much more pronounced than that reported for $Cs_2(TCNQ)_3$, less than 1 percent at 7×10^3 cm^{-1} and 34 percent at 5×10^3 cm^{-1} according to the former group. The plasma frequency has been estimated to be 1.80×10^{15} and 2.1×10^{15} s^{-1} and the electronic relaxation time, 2.83×10^{-15} and 2.3×10^{-15} s by Bright *et al.* and by Grant *et al.*, respectively. The conductivity calculated on the basis of these optical data is in good agreement with the measured d.c. conductivity. Bright *et al.* have extended their measurements to 0.8×10^3 cm^{-1} employing a polycrystalline compaction. In this case, the measured reflectance is an average over all crystalline orientations in the solid. Therefore, the component parallel to the conducting axis must be extracted by subtracting the reflectance due to the transverse directions and by correcting the resultant value for $\overline{\cos^2\theta}$. The perpendicular reflectance was assumed constant in the infrared region and equal to the minimum value at the plasma edge. Although, among the salts studied above, only the quinolinium salt is known to show metallic behavior at room temperature, the authors included the measurements of the total reflectance spectra of polycrystalline compactions to find out what kind of optical data one can obtain for these complex TCNQ salts and whether metallic salts can be distinguished from nonmetallic ones by such data.

The spectra for light polarized parallel to the conducting axis were derived from the data on polycrystalline compactions following the procedure proposed by Bright *et al.* In Fig. 5, the Drude-like edges observed with the quinolinium and isoquinolinium salts are presented. The reflectance of the former salt shows a minimum centered at 6.8×10^3 cm^{-1} and rises to a value of 13 percent at 5×10^3 cm^{-1}. There are weak peaks located at 9.9×10^3 and 11.3×10^3 cm^{-1} which may correspond to the absorption bands around 10×10^3 cm^{-1} (see Fig. 3). The curve of the latter salt is shifted slightly to the high-energy side. The minimum is located at 7.5×10^3 cm^{-1} and the value at 5×10^3 cm^{-1} is about 27 percent. In the 10×10^3 cm^{-1} region, a broad band centered at 10.6×10^3 cm^{-1} appears with a shoulder around 9×10^3 cm^{-1}. One assumes that the

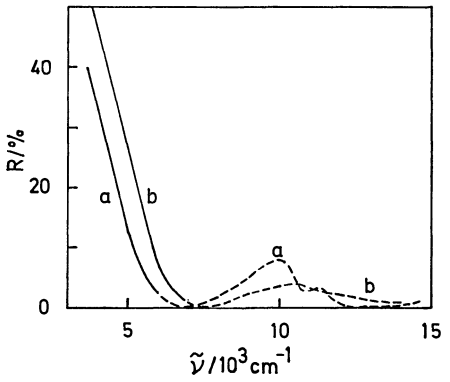

Fig. 5. Reflectance spectra for light polarized parallel to the conducting axis derived from polycrystalline measurements, (a) quinolinium-TCNQ (1 : 2) salt and (b) isoquinolinium-TCNQ (2 : 3) salt.

dielectric constant ε is a function of frequency ω and is given by

$$\varepsilon = \varepsilon_0 - \frac{\omega_p^2}{\omega^2 + i\omega/\tau}$$

where ε_0 is the frequency-independent background dielectric constant, ω_p is the plasma frequency, and τ is the electronic relaxation time. The reflectance R is given in terms of the real and imaginary parts of the dielectric constant $\varepsilon = n^2(1-i\kappa)^2$ by the well-known Drude formula

$$R = \frac{n^2(1+\kappa^2)+1-2n}{n^2(1+\kappa^2)+1+2n}$$

The best fit was obtained with $\varepsilon_0=2.18$, $\omega_p=2.31\times10^{15}$ s^{-1}, and $\tau=1.73\times10^{-15}$ s for the quinolinium salt and with $\varepsilon_0=2.36$, $\omega_p=2.62\times10^{15}$ s^{-1}, and $\tau=1.91\times10^{-15}$ s for the isoquinolinium salt. The solid curves in Fig. 5 are parts of the reflectance fitted to the above expression. In the vicinity of the minimum, the fits cannot be good because of the approximations employed. If the conventional expression relating the plasma frequency and the d.c. conductivity for metals, $\sigma = \omega_p^2\tau/4\pi$, is assumed using the above values for ω_p and τ, one obtains an estimate of 817 ohm^{-1} cm^{-1}, which markedly higher than the experimental value

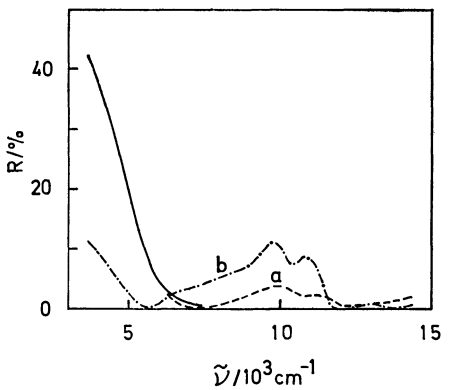

Fig. 6. Reflectance spectra for light polarized parallel to the conducting axis derived from polycrystalline measurements, (a) *N*-methylquinolinium-TCNQ salt with acetonitrile of crystallization and (b) the same salt after the loss of the solvent.

Table 4. Optical data for TCNQ anion radical salts

Cation (Composition)	ε_0	ω_p (10^{15} s^{-1})	τ (10^{-15} s)	σ (ohm^{-1} cm^{-1})
Quinolinium (1 : 2)	2.18	2.31	1.73	817
Isoquinolinium (2 : 3)	2.36	2.62	1.91	1160
N-Methylquinolinium (2 : 3) with $2CH_3CN$	1.89	2.27	1.68	766
Lepidinium (2 : 3)	2.45	2.66	1.53	958
8-Methylquinolinium (2 : 3)	1.78	1.98	1.39	482
Quinaldinium (1 : 2)	1.75	1.87	1.41	436
N-Methylisoquinolinium (1 : 2)	2.05	2.09	1.69	653
6-Methylquinolinium (1 : 2)	1.77	1.75	1.72	466
7-Methylquinolinium (1 : 2)	1.74	1.79	1.38	391
N-Methylphenazinium (1 : 1)	1.51	1.99	0.96	336
Acridinium (1 : 2)	1.85	1.93	1.55	511

reported by Walatka and Perlstein of 100 ohm^{-1} cm^{-1}.[3]

The change in the spectrum of the *N*-methylquinolinium salt with the loss of the acetonitrile of crystallization is sharp as is shown in Fig. 6. The reflectance at 5×10^3 cm^{-1} decreases from 20 percent to 2.5 percent and the minimum shifts from 7.5×10^3 cm^{-1} to 5.2×10^3 cm^{-1}. The latter change is in the direction opposite to that one might expect from a comparison between $Cs_2(TCNQ)_3$ and TTF–TCNQ. Furthermore, the peaks around 10×10^3 cm^{-1} are intensified by a factor of three, and additional peaks appear in the range from 6×10^3 to 9×10^3 cm^{-1}. Thus, an increase by a factor of one thousand in the electrical resistivity is reflected by a significant change in the spectrum. Therefore, it is rather surprising to see in the other high-conductivity salts that the reflectance in the near-infrared region varies considerably by from 4 percent in the 7-methylquinolinium salt to 22 percent in the lepidinium salt at 5×10^3 cm^{-1}. The minima are scattered in the range from 6×10^3 to 8×10^3 cm^{-1}. The estimates of the background dielectric constant, plasma frequency, relaxation time, and conductivity are listed in Table 4. The *N*-methylphenazinium and acridinium salts included in the table are known to be as conducting as the quinolinium salt and to show resistivity minima below room temperature.[4,22] It may be noted that the estimated d.c. conductivity for the former salt is in good agreement with the value observed by Coleman *et al.*, 380 ohm^{-1} cm^{-1}.[22] Such an agreement is probably fortuitous. The experimental conductivity may depend considerably upon the crystals. The value reported by Coleman *et al.* is more than twice that obtained by Shchegolev *et al.*[23] The latter group has reported a conductivity of about 70 ohm^{-1} cm^{-1} along the direction of the TCNQ column of the acridinium salt.[4] Therefore, it appears to be difficult to judge whether the conductivity estimated from the optical data is in agreement with the experimental value or not. The remarkable feature of the data in Table 4 is the relative insensitivity of the estimated conductivity to the materials. Moreover, there appears to be no correlation with the resistivity observed for polycrystalline compactions. As has been pointed out by Grant *et al.*, the observed Drude-like edge may be of other than simple metallic origin.[20]

The authors wish to express their thanks to Dr. Jun-ichi Aihara for his help in the estimation of the optical data.

References

1) L. R. Melby, R. J. Harder, W. R. Hertler, W. Mahler' R. E. Benson, and W. E. Mochel, *J. Am. Chem. Soc.*, **84**, 3374 (1962).
2) W. J. Siemons, P. E. Bierstedt, and R. G. Kepler, *J. Chem. Phys.*, **39**, 3523 (1963).
3) V. Walatka, Jr. and J. H. Perlstein, *Mol. Cryst. Liq. Cryst.*, **15**, 269 (1971).
4) L. I. Buravov, D. N. Fedutin, and I. F. Shchegolev, *Soviet Phys. JETP*, **32**, 612 (1971).
5) H. Kobayashi, F. Marumo, and Y. Saito, *Acta Crystallogr.*, **B 27**, 373 (1971).
6) P. Dupuis and J. Néel, *C. R. Acad. Sci. Paris, Sér. C*, **265**, 688 (1967).
7) S. Flandrois, P. Libert, and P. Dupuis, *Sci. Papers Inst. Org. Phys. Chem., Wroclaw Tech. Univ.*, No. 7 269 (1974).
8) S. Flandrois, P. Libert, and P. Dupuis, *Phys. Stat. Sol.*, (*a*) **28**, 411 (1975).
9) M. Murakami and S. Yoshimura, *Bull. Chem. Soc. Jpn.*, **48**, 157 (1975).
10) R. Buvet, P. Dupuis, J. Néel, and J. Perichon, *Bull. Soc. Chim. Fr.*, **1969**, 3991.
11) K. Kan and Y. Matsunaga, *Bull. Chem. Soc. Jpn.*, **45**, 2096 (1972).
12) L. Libera and H. Bretschneider, *Z. Chem.*, **13**, 383 (1973).
13) M. Murakami and S. Yoshimura, *J. Phys. Soc. Jpn.*, **38**, 488 (1975).
14) G. Beni, J. F. Kwak, and P. M. Chaikin, *Solid State Commun.*, **17**, 1549 (1975).
15) Y. Iida, *Bull. Chem. Soc. Jpn.*, **42**, 637 (1969).
16) Y. Oohashi and T. Sakata, *Bull. Chem. Soc. Jpn.*, **48**, 1725 (1975).
17) J. B. Torrance, B. A. Scott, and F. B. Kaufman, *Solid State Commun.*, **17**, 1369 (1975).
18) R. M. Vlasova and A. I. Gutman, *Soviet Phys. Solid State*, **13**, 2356 (1972).
19) A. A. Bright, A. F. Garito, and A. J. Heeger, *Solid State Commun.*, **13**, 943 (1973).
20) P. M. Grant, R. L. Greene, G. C. Wrighton, and G. Castro, *Phys. Rev. Lett.*, **31**, 1311 (1973).
21) A. A. Bright. A. F. Garito. and A. J. Heeger, *Phys. Rev. B*, **10**, 1328 (1974).
22) L. B. Coleman. J. A. Cohen. A. F. Garito. and A. J. Heeger, *Phys. Rev. B*, **7**, 2122 (1973).
23) I. F. Shchegolev, L. I. Buravov, A. V. Zvarykina, and R. B. Lyubovskii, *Soviet Phys. JETP Lett.*, **8**, 218 (1968).

Concentration Fluctuation and the Light-scattering Spectrum

Kenji IWASAKI, Masami TANAKA, and Tsunetake FUJIYAMA

Department of Chemistry, Faculty of Science, Tokyo Metropolitan University, Setagaya-ku, Tokyo 158

(Received April 13, 1976)

Light-scattering spectra were observed for binary solutions of carbon disulfide–chloroform at various concentrations. The relation between the Rayleigh-line intensity and the concentration fluctuation was derived. Using the proposed relation and the observed Rayleigh intensity, the concentration dependence of the concentration fluctuation was then determined. The results suggest that chloroform and carbon disulfide molecules have a tendency to get together in the binary solution.

Local fluctuation in the concentration is considered to afford information which is useful to understand the state of mixing from a molecular point of view. On the basis of this belief, we have planned a series of analyses of the temperature and concentration dependence of the concentration fluctuation in solutions. This, the first report of the series, will concern itself mainly with the determination of the concentration fluctuation through the observation of light-scattering spectra.

A light-scattering spectrum consists of a Rayleigh line, a pair of Brillouin lines, and a Rayleigh wing. Since the concentration fluctuation contributes to only the Rayleigh line, we can determine the concentration fluctuation from the Rayleigh intensity in a binary solution. We will derive an equation which relates the Rayleigh intensity of a light-scattering spectrum with the concentration fluctuation. Then the concentration dependence of the concentration fluctuation will actually be observed for the carbon disulfide–chloroform system through Rayleigh-intensity measurements. We chose the carbon disulfide–chloroform system because the concentration fluctuation of the system has been discussed previously on the basis of a band-width measurement of the infrared absorption spectra.[1]

Experimental

The light-scattering spectrometer used in the present study was designed and constructed in our laboratory.[2] Figure 1 shows the schematic layout of the spectrometer. The instrument is composed of a He-Ne gas laser source (NEC, GLG108, 50 mW), a Fabry-Perot interferometer, a lock-in amplifier (NF, LI573), and an X-Y recorder. The spacer between the interferometer etalons has a thickness of 6 mm, giving a free spectral range of 0.82 cm^{-1} and an overall instrumental half-width of about 0.042 cm^{-1}. The interferometer was pressure-scanned by evacuating the box enclosing the etalons and by allowing air to leak into the box slowly. The samples used in this experiment were commercially available reagents: carbon disulfide without further purification and chloroform purified by a column chromatography on alumina. The binary solutions of carbon disulfide and chloroform were made dust-free by the use of a Millipore-filter FG with a pore size of 0.2 μm. The test of a solution being dust-free can be done in principle by comparing the observed Rayleigh intensity with the true Rayleigh intensity of dust-free samples. As the true Rayleigh intensity is unknown, however, the dust-free test was done by comparing the observed Rayleigh intensity with the best data among the many Rayleigh intensities reported so far. In the case of the light-scattering spectrum, the L–P ratio, defined by $I_C/2I_B$, is the measure of being dust-free, because the Rayleigh intensity, I_C, is strongly influenced by the existence of dust, while the Brillouin intensity, I_B, is hardly influenced at all by the existence of dust. The observed L–P ratios are summarized in Table 1. It may be seen from the table that the present data agree well with those measured by Cummins *et al.*[3] The reason why our values are slightly larger than Cummins' is the difference in the methods by which the spectral components are separated. Because Cummins verified the dust-free state for water, whose L–P ratio is nearly zero, it seems that our optical purification and experimental techniques can realize a nearly dust-free state. Though a dust-free checking method like this is applicable only for pure liquids on which many intensity data are reported, we believe that mixture samples can be purified by the same method as that applied for pure liquids. The preparation (filtration and injection of a sample into a cell) of the sample was repeated five times or more, and the best value was chosen as the measured value. The refractive index of the sample was measured by means of a Shimadzu-Bausch Lomb Abbe refractometer 3L. The composition derivative of the refractive index at the mole fraction, x, was estimated from the difference between refractive indices measured at $x\pm0.05$. All the measurements were performed at the temperature of 20 ± 0.5 °C.

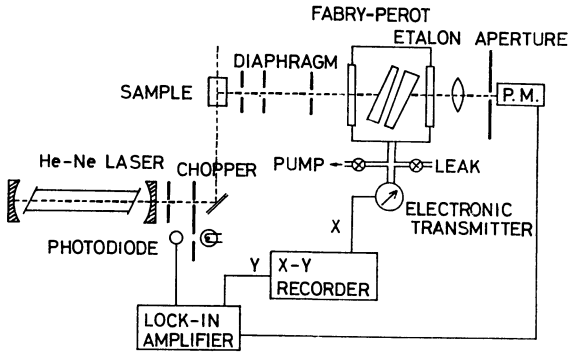

Fig. 1. Schematic layout of light scattering spectrometer.

Results and Discussion

Reduction of Rayleigh Intensity to Concentration Fluctuation. Miller presented an equation which relates the Rayleigh intensity of the light-scattering spectrum with the composition derivative of the chemical potential.[4] Following his theory, we derive an equation which directly relates the Rayleigh intensity of the light-scattering spectrum to the concentration fluctuation. Imagine a small-volume element which contains a constant number of moles, n_1, of one component in a binary solution at a constant temperature and

Table 1. Observed intensities for pure liquids

Liquid	Rayleigh intensity[a]		L-P ratio		Rayleigh wing intensity
	Obsd (24.5 °C)	Calcd	Present (24.5 °C)	Reference[b] (20.0 °C)	
Carbon disulfide	2.00	2.45	0.78	0.71	very strong
Benzene	1.31	1.02	0.93	0.84	medium
Chloroform	1.00	1.00	0.69	—	weak
Diethyl ether	0.82	0.80	0.41	0.35	very weak
Hexane	0.69	0.65	0.36	0.35	very weak
Acetone	0.60	0.57	0.48	0.44	weak
Ethanol	0.43	0.27	0.34	0.23	very weak

a) Relative values, the intensity of chloroform being chosen as a standard.
b) See Ref. 3.

pressure. If we consider the dielectric constant, ε, as a function of the entropy, S, the pressure, P, and the number of moles, n_2, of the other component, the mean-square fluctuation in the dielectric constant, $\langle(\Delta\varepsilon)^2\rangle$, is expressed by:

$$\begin{aligned}\langle(\Delta\varepsilon)^2\rangle = {} & (\partial\varepsilon/\partial P)^2_{S,n_2}\langle(\Delta P)^2\rangle + (\partial\varepsilon/\partial S)^2_{P,n_2}\langle(\Delta S)^2\rangle \\ & + 2(\partial\varepsilon/\partial S)_{P,n_2}(\partial\varepsilon/\partial n_2)_{S,P}\langle\Delta S\Delta n_2\rangle \\ & + (\partial\varepsilon/\partial n_2)^2_{S,P}\langle(\Delta n_2)^2\rangle \qquad (1)\end{aligned}$$

because $\langle\Delta S\Delta P\rangle=\langle\Delta P\Delta n_2\rangle=0$. Of the four terms on the right-hand side of Eq. 1, the first term contributes to a Brillouin intensity, while the remaining three terms contribute to a Rayleigh intensity. Thus, we can express Eq. 1 as:

$$\langle(\Delta\varepsilon)^2\rangle = \langle(\Delta\varepsilon_B)^2\rangle + \langle(\Delta\varepsilon_R)^2\rangle \qquad (2)$$

where

$$\langle(\varepsilon_B)^2\rangle = (\partial\varepsilon/\partial P)^2_{S,n_2}\langle(\Delta P)^2\rangle \qquad (3)$$

and

$$\begin{aligned}\langle(\Delta\varepsilon_R)^2\rangle = {} & (\partial\varepsilon/\partial S)^2_{P,n_2}\langle(\Delta S)^2\rangle \\ & + 2(\partial\varepsilon/\partial S)_{P,n_2}(\partial\varepsilon/\partial n_2)_{S,P}\langle\Delta S\Delta n_2\rangle \\ & + (\partial\varepsilon/\partial n_2)^2_{S,P}\langle(\Delta n_2)^2\rangle \qquad (4)\end{aligned}$$

In these expressions, the $\langle\Delta S\Delta n_2\rangle$ term cannot be calculated from any observable quantities. Therefore, we express ε as a function of the temperature, T, the pressure, P, and the number of moles, n_2, of the other component. We thus obtain:

$$\begin{aligned}\langle(\Delta\varepsilon)^2\rangle = {} & (\partial\varepsilon/\partial T)^2_{P,n_2}\langle(\Delta T)^2\rangle + 2(\partial\varepsilon/\partial T)_{P,n_2} \\ & \times (\partial\varepsilon/\partial P)_{T,n_2}\langle\Delta T\Delta P\rangle \\ & + (\partial\varepsilon/\partial P)^2_{T,n_2}\langle(\Delta P)^2\rangle + 2(\partial\varepsilon/\partial P)_{T,n_2} \\ & \times (\partial\varepsilon/\partial n_2)_{T,P}\langle\Delta P\Delta n_2\rangle \\ & + (\partial\varepsilon/\partial n_2)^2_{T,P}\langle(\Delta n_2)^2\rangle + 2(\partial\varepsilon/\partial T)_{P,n_2} \\ & \times (\partial\varepsilon/\partial n_2)_{T,P}\langle\Delta T\Delta n_2\rangle \qquad (5)\end{aligned}$$

instead of Eq. 1. Combining Eqs. 2, 3, and 5, we obtain the expression for $\langle(\Delta\varepsilon_R)^2\rangle$. In this expression, all the necessary terms can be calculated from the observable quantities. The mean square fluctuations[5] of Eqs. 3 and 5 are calculated to be:

$$\left.\begin{aligned}&\langle(\Delta T)^2\rangle = kT^2/C_V, \quad \langle\Delta T\Delta P\rangle = kT^2\alpha/\beta_T C_V \\ &\langle(\Delta P)^2\rangle = kT/V\beta_S, \quad \langle\Delta T\Delta n_2\rangle = \langle\Delta P\Delta n_2\rangle = 0\end{aligned}\right\} \qquad (6)$$

where k is the Boltzmann constant; C_V, the heat capacity at a constant volume; α, the thermal expansivity; β_T, the isothermal compressibility, and β_S, the adiabatic compressibility. Combining Eqs. 2, 3, 5, and 6, we get:

$$\langle(\Delta\varepsilon_R)^2\rangle = \frac{kT^2}{C_P}\left(\frac{\partial\varepsilon}{\partial T}\right)^2_{P,n_2} + \left(\frac{\partial\varepsilon}{\partial n_2}\right)^2_{T,P}\langle(\Delta n_2)^2\rangle \qquad (7)$$

where C_P is the isobar heat capacity. The first term of Eq. 7 is related to entropy fluctuation by:

$$\begin{aligned}\left(\frac{\partial\varepsilon}{\partial S}\right)^2_{P,n_2}\langle(\Delta S)^2\rangle &= \left(\frac{\partial\varepsilon}{\partial T}\right)^2_{P,n_2}\left(\frac{\partial T}{\partial S}\right)^2_{P,n_2}\langle(\Delta S)^2\rangle \\ &= \left(\frac{\partial\varepsilon}{\partial T}\right)^2_{P,n_2}\left(\frac{T}{C_P}\right)^2 kC_P \\ &= \frac{kT^2}{C_P}\left(\frac{\partial\varepsilon}{\partial T}\right)^2_{P,n_2} \qquad (8)\end{aligned}$$

The second term of Eq. 7, on the other hand, is the mean-square fluctuation of n_2 in a small volume containing a constant n_1. Therefore, Eq. 7 can be rewritten symbolically as:

$$\langle(\Delta\varepsilon_R)^2\rangle = \begin{pmatrix}\text{entropy fluctua-}\\\text{tion term}\end{pmatrix} + \begin{pmatrix}\text{concentration fluctua-}\\\text{tion term}\end{pmatrix} \qquad (9)$$

Thus, we could express the concentration fluctuation, $\langle(\Delta n_2)^2\rangle$, in terms of $\langle(\Delta\varepsilon_R)^2\rangle$ and $\langle(\Delta S)^2\rangle$. It is important to emphasize that a small-volume element is chosen because it contains a constant number of moles, n_1. If the incident light, whose electric vector is polarized perpendicular to the scattering plane, passes through the fluctuation volume, V^*, in which mean mole number of one component, n_1, is confined, the intensity of light scattered perpendicularly to the incident light is given in terms of the Rayleigh ratio:

$$R_{90} = (\pi^2/\lambda_i^4)V^*\langle(\Delta\varepsilon)^2\rangle \qquad (10)$$

where λ_i is the wavelength of the incident light. By combining Eqs. 7 and 10, the Rayleigh ratio for a Rayleigh line is expressed as:

$$\begin{aligned}(R_{90})_R = (\pi^2/\lambda_i^4)\Bigg\{ & \frac{kT^2V^*}{C_P}\left(\frac{\partial\varepsilon}{\partial T}\right)^2_{P,n_2} \\ & + \left(\frac{\partial\varepsilon}{\partial n_2}\right)^2_{T,P} V^*\langle(\Delta n_2)^2\rangle\Bigg\} \qquad (11)\end{aligned}$$

Now, we introduce three relations:

$$d\varepsilon = 2\,n\,dn$$

$$dx_2 = dn_2 x_1/(n_1+n_2)$$

$$C_P/V^* = C_{Pg}\cdot M/V^* = C_{Pg}\rho$$

where n is a refractive index; x_1 and x_2, the mole fractions of the 1 and 2 components; C_{Pg}, the isobar heat capacity per gram; ρ, the density, and M, the weight of V^*. Substituting these relations into Eq. 11, we find:

$$(R_{90})_R = (\pi^2/\lambda_1^4)\frac{4kn^2T^2}{C_{Pg}\rho}\left(\frac{\partial n}{\partial T}\right)^2_{P,x_2} + (\pi^2/\lambda_1^4)4n^2\left(\frac{\partial n}{\partial x_2}\right)^2_{T,P} V^*\langle(\Delta x_2)^2\rangle \quad (12)$$

Since the first term of Eq. 12 arises from the entropy fluctuation, the Rayleigh ratio for entropy fluctuation is expressed as:

$$(R_{90})_S = (\pi^2/\lambda_1^4)\frac{4kn^2T^2}{C_{Pg}\rho}\left(\frac{\partial n}{\partial T}\right)^2_{P,x_2} \quad (13)$$

Combine Eqs. 12 and 13, an equation which directly relates the observed Rayleigh intensity with the concentration fluctuation is obtained:

$$V^*\langle(\Delta x_2)\rangle = (\lambda_1^4/\pi^2)\frac{1}{4n^2(\partial n/\partial x_2)^2_{T,P}}\{(R_{90})_R-(R_{90})_S\} \quad (14)$$

From Eq. 14 we can determine $V^*\langle(\Delta x_2)^2\rangle$ experimentally, observing $(R_{90})_R$ and estimating $(R_{90})_S$ by the use of Eq. 13. The concentration fluctuation can be determined in the form of $V^*\langle(\Delta x_2)^2\rangle$ from the observation of the light-scattering spectrum. We cannot, however, determine the concentration fluctuation in the form of $\langle(\Delta x_2)^2\rangle$ from the light-scattering spectrum. We will call this $V^*\langle(\Delta x_2)^2\rangle$ the "fluctuation ability" hereafter.

Light-scattering Spectra. The observed spectra for the chloroform–carbon disulfide system are given in Fig. 2. It may be seen from the figure that the intensity of a Rayleigh line increases remarkably on passing from pure liquids to binary solutions. The intensity change in the Brillouin lines, on the other hand, is small in comparison with that of a Rayleigh line. The background intensity due to a Rayleigh wing is largest for pure carbon disulfide and smallest for pure chloroform.

Determination of the Rayleigh Ratio. The procedure for separating a Rayleigh line from Brillouin lines and from a Rayleigh wing is illustrated in Fig. 3. A Rayleigh wing is assumed to be almost flat along a frequency axis. The outer halves of the Brillouin lines are assumed to be equal to the non-overlapping line shapes. Thus, the intensity of a Rayleigh line was determined by eliminating the areas corresponding to the Rayleigh wing and the Brillouin lines.

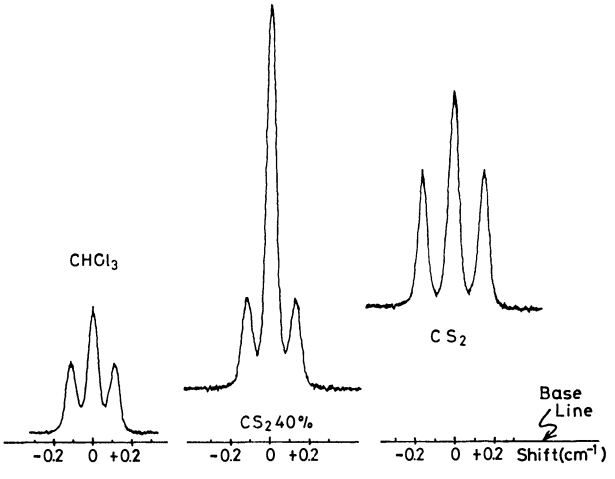

Fig. 2. Observed spectra for chloroform–carbon disulfide system.

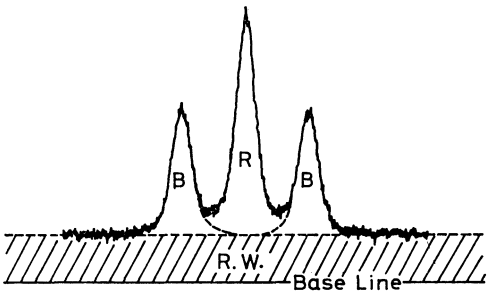

Fig. 3. Separation of Rayleigh line from light scattering spectra (schematic). R: Rayleigh line, B: Brillouin line, R.W.: Rayleigh wing.

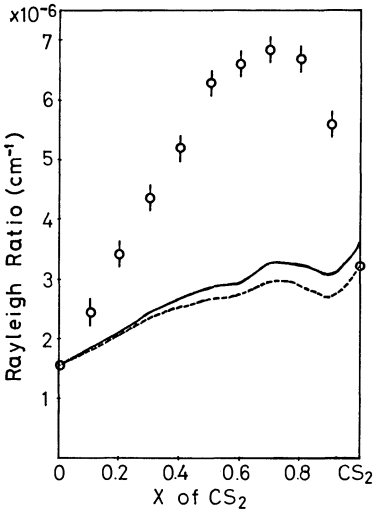

Fig. 4. Concentration dependence of Rayleigh intensity of chloroform–carbon disulfide system. The open circles correspond to $(R_{90})_R$, the solid line $(R_{90})_S$ and the broken line $(R_{90})_S{}^*$. Errors are indicated by the vertical lines.

The reliability of the observed Rayleigh ratios was checked by the use of Eq. 13. The observed Rayleigh ratios and the calculated Rayleigh ratios by Eq. 13 are compared in Table 1.

Since the observed Rayleigh intensities are relative values, we have to express the observed relative intensities, I_R, in terms of the Rayleigh ratios. We first calculate $(R_{90})_S$ for pure chloroform by the use of Eq. 13. We call this $(R_{90})_S{}^{CHCl_3}$. Then, the Rayleigh ratio for binary mixtures, $(R_{90})_R$, is calculated to be:

$$(R_{90})_R = I_R \times \frac{(R_{90})_S^{CHCl_3}}{I_R^{CHCl_3}} \quad (15)$$

where $I_R{}^{CHCl_3}$ is a relative Rayleigh intensity for pure chloroform.[6] The calculated Rayleigh ratios are plotted by open circules in Fig. 4.

Determination of the Concentration Fluctuation. The theoretical values of $(R_{90})_S$ at each mole fraction were

Table 2. Observed rayleigh ratios for a rayleigh line and rayleigh ratios for entropy fluctuation in chloroform–carbon disulfide system

Mole fraction of CS_2	$(R_{90})_R$ (cm^{-1}) (20±0.5 °C)	$(R_{90})_S$ (cm^{-1}) (20 °C)	K	$(R_{90})_S^*$ (cm^{-1})
	$\times 10^{-6}$	$\times 10^{-6}$		$\times 10^{-6}$
0	1.55±0.06	1.55	1	1.55
0.105	2.43	1.82	0.987	1.80
0.203	3.42	2.11	0.975	2.05
0.301	4.34	2.42	0.963	2.33
0.398	5.20	2.65	0.951	2.52
0.495	6.31±0.24	2.83	0.939	2.66
0.599	6.61	2.90	0.926	2.69
0.693	6.86	3.24	0.914	2.96
0.799	6.71	3.21	0.901	2.90
0.898	5.59	3.04	0.889	2.70
1.000	3.18±0.05	3.63	0.876	3.18

calculated by substituting the observed values of λ_i, n, T, ρ, $(\partial n/\partial T)_{P,x_2}$, and the C_{Pg} values from the table[7] into Eq. 13 (see Table 2). The observed $(R_{90})_S$ for pure carbon disulfide was slightly different from that calculated from Eq. 13. This disagreement may be ascribed to the separation of a Rayleigh line from the light-scattering spectra. For the observation of the concentration fluctuation, however, the essential quantity is not $(R_{90})_S$ but $\{(R_{90})_R-(R_{90})_S\}$, that is, in intensity increment due to the concentration fluctuation. Therefore, the calculated $(R_{90})_S$ was corrected by means of a suitable parameter to:

$$(R_{90})_S^* = K \times (R_{90})_S$$

where K was chosen so that the calculated $(R_{90})_S$ for pure carbon disulfide was equal to the observed one. The K value for each concentration was thought to change continuously[8] from 1 to 0.876, the latter value of which is the correction factor for pure carbon disulfide (see the 4th column Table 2).

Using the Rayleigh ratios, $(R_{90})_R$, and the Rayleigh ratios for entropy fluctuations, $(R_{90})_S$, the fluctuation ability, $V^*\langle(\Delta x_2)^2\rangle$, was calculated from Eq. 14 at each concentration.

The reliability of the concentration fluctuations observed from Rayleigh intensities in the light-scattering spectra were examined with respect to two main factors:

1) the accuracy of the measured relative Rayleigh intensity, and

2) the observation of $(\partial n/\partial x)_{T,P}$.

The procedure of sampling is most important. As has been described in the previous paragraph, the samples were prepared so as to be almost dust-free. However, there was still a little doubt about the possibility of realizing a dust-free situation for all the samples observed. Therefore, we prepared a sample more than five times for one observation and took the best value as the observed value. We repeated the above procedure four times. The maximum deviation of the observed value from the averaged value was considered to be the error expected for the observed value (see the vertical lines of Fig. 4). The value of $(\partial n/\partial x)_{T,P}$ at the mole fraction x was obtained from the difference between the refractive indices at x±0.05. The precision of the refractive indices observed by means of an Abbe refractometer is about ±0.0001. As the determination of the concentration is precise enough, the precision of $(\partial n/\partial x)_{T,P}$ is about ±0.002. Taking into account the above two factors, the precision for the observed $V^*\langle(\Delta x_2)^2\rangle$ values is estimated to be about $\pm 0.174\times 10^{-23}$ cm^{-1} (see the vertical line of Fig. 5).

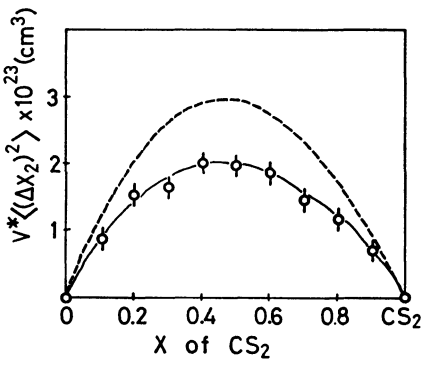

Fig. 5. Concentration dependence of concentration fluctuation for chloroform–carbon disulfide system. The open circules correspond to concentration fluctuation observed for chloroform–carbon disulfide system. The broken line shows concentration fluctuation expected for the ideal binary solution. Errors are indicated by the vertical lines.

Concentration Fluctuation. The concentration dependence of the concentration fluctuation observed for the chloroform–carbon disulfide system is shown in Fig. 5. Consider first the concentration fluctuation expected for the ideal binary solution, whose components are mixed with each other without intermolecular interaction. When a mixture of the 1 and 2 components behaves as a mixture of two simple particles, the chemical potential of the 2 component, μ_2, is given by:

$$\mu_2 = \mu_2^\circ + kT\ln x_2 \qquad (16)$$

where μ_2° is the standard chemical potential. If the chemical potential is known, the fluctuation ability is calculated to be:

$$N\langle(\Delta x_2)^2\rangle = \frac{kTx_1}{(\partial\mu_2/\partial x_2)_{T,P}} \qquad (17)$$

TABLE 3. EVALUATION OF FLUCTUATION ABILITIES FOR CHLOROFORM-CARBON DISULFIDE SYSTEM

Mole fraction of CS_2	$\{(R_{90})_R-(R_{90})_S^*\}$ (cm^{-1})	n_D^{20}	$(\partial n/\partial x_2)_{T,P}$ (20 °C)	$V^*\langle(\Delta x_2)^2\rangle$ (cm^3)
0	0 $\times10^{-6}$	1.4452	—	— $\times10^{-23}$
0.105	0.63	1.4474	0.117	0.89
0.203	1.37	1.4700	0.130	1.52
0.301	2.01	1.4830	0.150	1.65
0.398	2.68	1.4984	0.156	1.99
0.495	3.66	1.5143	0.181	1.98
0.599	3.92	1.5346	0.190	1.87
0.693	3.90	1.5525	0.212	1.47
0.799	3.82	1.5756	0.232	1.16
0.898	2.89	1.6000	0.254	0.71
1.000	0	1.6280	—	—

where N is the mean number of particles in V^*. Notice that the fluctuation ability is expressed in terms of N and $\langle(\Delta x_2)^2\rangle$ instead of V^* and $\langle(\Delta x_2)^2\rangle$. By combining Eqs. 16 and 17, we get:

$$N\langle(\Delta x_2)^2\rangle = x_2(1-x_2) \tag{18}$$

or

$$V^*\langle(\Delta x_2)^2\rangle = \frac{x_2(1-x_2)}{\rho_n} \tag{19}$$

where ρ_n is the number density and where $N=\rho_n V^*$. The broken line of Fig. 5 shows the fluctuation ability of a binary solution as predicted by Eq. 19. It may be seen from the figure that the observed fluctuation ability of the chloroform–carbon disulfide system is smaller than the prediction of Eq. 19 throughout all the mole fractions. This result suggests that there is a tendency inherent to the chloroform–carbon disulfide system which keeps the macroscopic concentration constant, even in a small volume. If we consider mixing from a microscopic point of view, the concept of concentration fluctuation corresponds to the variation in the concentration due to the thermal motion of molecules within a small volume. When there is no intermolecular interaction, the thermal motion of component molecules can be regarded as completely random. Therefore, the concentration fluctuation can be predicted by means of Eq. 18 or 19. Actually, however, the observed concentration dependence of the concentration fluctuation is different from that of Eq. 18 or 19, which indicates that the thermal motion of the component molecules is not random. This is probably to be ascribed to intermolecular interactions between the molecules of the same and/or different species. Instead of studying the nature of the intermolecular interactions directly, we introduce the concept of the association of molecules. If molecules of the same species have a tendency to get together in a binary solution, the concentration fluctuation takes a larger value than that of an ideal solution. In this case, a few molecules move in close association, therefore, the local concentration change due to thermal motion is much larger than that for the thermal motion of a single molecule. When molecules of different species have a tendency to get together, on the other hand, the concentration fluctuation takes a smaller value than that of an ideal solution. In this case, a complex molecule which is formed from molecules of different species behaves as a single molecule; therefore, the exchange of molecules between the inside and the outside of the small volume in question due to thermal motion brings about a much smaller concentration change inside the volume. The present results obtained for chloroform–carbon disulfide system suggest, therefore, that there is an inherent tendency in chloroform–carbon disulfide system which keeps the macroscopic concentration constant, even in a small volume. A more quantitative analysis of this problem will be made in the next report.

References

1) T. Fujiyama, M. Kakimoto, and T. Suzuki, *Bull. Chem. Soc. Jpn.*, **49**, 606 (1976); The $V^*\langle(\Delta x_2)^2\rangle$ values of the present report are slightly different from those reported in Ref. 1. Readers are invited to have more confidence in the present values.

2) K. Iwasaki, M. Tanaka, and T. Fujiyama, *Bunko Kenkyu*, **25**, 134 (1976).

3) H. Z. Cummins and R. W. Gammon, *J. Chem. Phys.*, **44**, 2785 (1966).

4) G. A. Miller, *J. Phys. Chem.*, **71**, 2305 (1967).

5) L. D. Landau and E. M. Lifshitz, "Statistical Physics," Pergamon Press, London (1958).

6) Table 1 shows that the ratio of the observed and calculated Rayleigh intensities is quite different from unity in carbon disulfide and in benzene, and almost unity for the other solvents. This singular phenomenon in carbon disulfide is considered to be due to the analytical process of separating the Rayleigh wing and the Rayleigh line. Therefore, chloroform was chosen as the intensity standard in the case of the binary solution of chloroform-carbon disulfide.

7) "International Critical Tables," McGraw-Hill, New York (1926).

8) The parameter, K, was introduced so as to correct the deviation between the observed and calculated intensities originating from the entropy fluctuation in carbon disulfide (see the first and second columns of Table 1). As the deviation is most obvious in carbon disulfide, it can also be expected in binary solutions of carbon disulfide and other solvents. In the case of a binary solution of carbon disulfide and chloroform, the effect is considered to be proportional to the concentration of carbon disulfide.

The Concentration Dependence of the Raman Intensity in Binary Mixtures and the Determination of Polarizability and Hyperpolarizability Derivative Tensors

Jun KOIKE, Tetsuo SUZUKI, and Tsunetake FUJIYAMA

Department of Chemistry, Faculty of Science, Tokyo Metropolitan University, Setagaya-ku, Tokyo 158

(Received May 1, 1976)

Raman intensities were observed at various concentrations. The observed lines were: the ν_8 line of CH_3CN (in CCl_4 and CH_3I), the ν_3 line of CH_3I (in CCl_4), and the ν_2 line of $CHCl_3$ (in CCl_4). Even after the elimination of the local-field effect, the Raman intensities showed concentration dependencies. The observed solvent effects were explained quantitatively by the use of the dipole interaction model. The polarizability and hyperpolarizability derivatives were determined for the ν_8 fundamental of CH_3CN. The criteria for the internal standard method were discussed quantitatively.

In the preceding report,[1] the solvent effects on the absolute infrared intensities have been discussed quantitatively from the viewpoint of dipole-dipole interaction. It has been shown that the interaction of the dipole-dipole type is a quite reasonable model in explaining the spectroscopic information observed in various binary solutions. It has also been shown in the report that the polarizability derivatives can be determined by observing the solvent effects on the infrared-absorption intensities.

The present report will concern itself with the observation of the Raman intensities of acetonitrile, methyl iodide, chloroform, and carbon tetrachloride in their binary mixtures. Our interest lies in:

1) the possibility of determining the magnitude of polarizability and hyperpolarizability derivatives through the observation of the solvent effects on Raman intensities, and

2) the examination of the criteria for the internal-standard method, which is widely used for the representation of Raman intensities.

Experimental

The spectrometer used for the present work was designed and constructed by the authors. The instrument is composed of a He-Ne gas laser source (NEC, GLG-108, 50 mW), a JSG-125 grating monochromator (JEOL), a HTV R-376 photomultiplier (S-20 response), a handmade lock-in amplifier (375 cps modulation), and a recorder.

The linearity of the whole system with respect to an intensity axis was carefully checked. First the output current of the photomultiplier was plotted against the light energy. The linearity was perfect for the output voltage of 20 V with $R_p=1$ MΩ. Then, the linearity of the amplifier was tested by using attenuators (0.1—120 db for each 0.1 db). Finally, the linearity of the whole system was checked by plotting the final recorder output voltage against the light energy which passes through the entrance slit of the monochromator. The light energy was attenuated by using neutral filters (Kenko, ND). From the standard errors estimated from the linear fitting, the linearity of the whole system was ascertained to be better than 1% of the full scale as long as the output voltage was less than 10 V.

Special attention was paid to the output power of the laser source. The stability of the laser output during the individual spectral measurements was observed by monitoring the light energy which penetrated through the 100-percent reflectance mirror of the laser cavity. When the power of the laser source drifted more than 1 percent during the measurements, the data observed were completely discarded.

All the chemicals were commercial products of a spectroscopic grade. The carbon tetrachloride and methyl iodide were purified by fractional distillation just before the spectral measurement. The chloroform was purified by column chromatography on alumina. The acetonitrile was used without further purification.

The Raman spectra were observed for; the ν_1 band of carbon tetrachloride, the ν_2 band of chloroform, the ν_8 band of acetonitrile, and the ν_3 band of methyl iodide in the binary solutions of $CHCl_3$–CCl_4, CH_3CN–CCl_4, CH_3I–CCl_4, and CH_3CN–CH_3I. All the spectra were recorded at the temperature of 22±1 °C. The band areas were determined by the weight method. The observations were repeated eight times for each concentration. The deviations of the observed band areas from the averaged values were less than 3 percent. The reproducibility of the observed peak frequency was within ±2 cm^{-1}, and no peak frequency shift due to the different concentrations was observed. All the bands observed had intensities strong enough for us to obtain accurate intensity data by the use of our instrument.

Results and Discussion

Concentration Dependence of Relative Intensity. Consider the observation of the relative intensities of two Raman lines arising from two components of a binary solution. The quantities related to the two Raman lines will be distinguished by the suffixes a and b. The observed intensity, I, is proportional to the molar concentration, c_m, the scattering cross section per molecules, Ω, and the corresponding factor for the internal field effect[2]; *i.e.*,

$$I_a = C \cdot c_{ma} \Omega_a \frac{1}{n_s} \left[\frac{n_a^2+2}{(n_a/n_s)^2+2} \right]^4 \quad (1)$$

$$I_b = C \cdot c_{mb} \Omega_b \frac{1}{n_s} \left[\frac{n_b^2+2}{(n_b/n_s)^2} \right]^4 \quad (2)$$

where C is a constant and where n_a, n_b, and n_s are, respectively, the refractive indices of the a component, the b component, and the mixture of the a and b components. It can immediately be concluded from these equations that:

$$\frac{\Omega_a}{\Omega_b} = \frac{I_a}{I_b} \frac{c_{mb}}{c_{ma}} \left[\frac{n_b^2+2}{n_a^2+2} \frac{(n_a/n_s)^2+2}{(n_b/n_s)^2+2} \right]^4 \quad (3)$$

Thus, we can obtain the ratio, Ω_a/Ω_b, of the scattering cross sections from the observed intensity ratio, I_a/I_b,

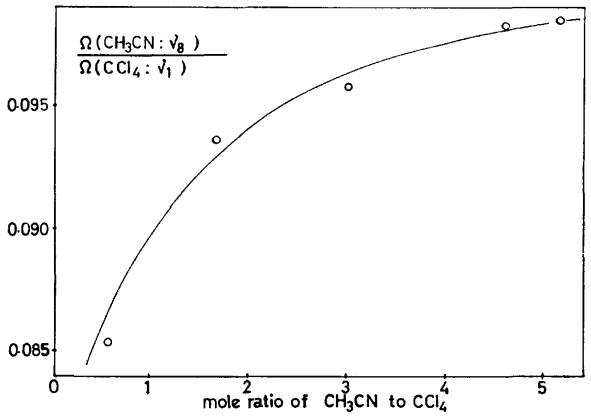

Fig. 1. Concentration dependence of $\Omega(CH_3CN;\ \nu_8)/\Omega(CCl_4;\ \nu_1)$.

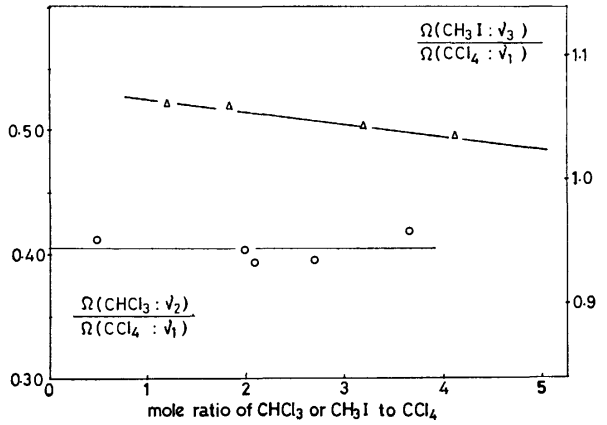

Fig. 2. Concentration dependence of $\Omega(CHCl_3;\ \nu_2)/\Omega(CCl_4;\ \nu_1)$ (circle) and $\Omega(CH_3I;\ \nu_3)/\Omega(CCl_4;\ \nu_1)$ (triangle).

because c_{ma}/c_{mb} is known from the experimental conditions and because the refractive indices can be measured by the use of a refractometer.

Figure 1 shows the ratio of the scattering cross section of the ν_8 band of acetonitrile, $\Omega(CH_3CN;\ \nu_8)$, and that of the ν_1 band of carbon tetrachloride, $\Omega(CCl_4;\ \nu_1)$, observed at several concentrations. It may be seen from the figure that the $\Omega(CH_3CN;\ \nu_8)/\Omega(CCl_4;\ \nu_1)$ ratio decreases as the concentration of acetonitrile decreases. Thus, $\Omega(CH_3CN;\ \nu_8)$ and/or $\Omega(CCl_4;\ \nu_1)$ vary with the change in concentration.

Figure 2 shows the $\Omega(CHCl_3;\ \nu_2)/\Omega(CCl_4;\ \nu_1)$ and $\Omega(CH_3I;\ \nu_3)/\Omega(CCl_4;\ \nu_1)$ ratios observed for the $CHCl_3$–CCl_4 and CH_3I–CCl_4 systems respectively at various concentrations. Obviously, the ratios are not dependent on the concentration. These results probably suggest that $\Omega(CHCl_3;\ \nu_2)$, $\Omega(CH_3I;\ \nu_3)$, and $\Omega(CCl_4;\ \nu_1)$ do not depend on the concentration. Therefore, the concentration dependency of $\Omega(CH_3CN;\ \nu_8)/\Omega(CCl_4;\ \nu_1)$ of Fig. 1 can be ascribed to the concentration dependency of $\Omega(CH_3CN;\ \nu_8)$.

Figure 3 shows the $\Omega(CH_3CN;\ \nu_8)/\Omega(CH_3I;\ \nu_3)$ ratio observed for the CH_3CN–CH_3I system at various concentrations. It may be seen from the figure that the $\Omega(CH_3CN;\ \nu_8)/\Omega(CH_3I;\ \nu_3)$ ratio increases as the concentration of acetonitrile increases. The magnitude of

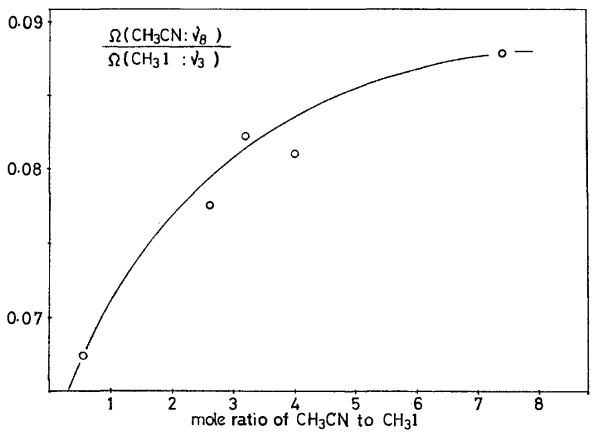

Fig. 3. Concentration dependence of $\Omega(CH_3CN;\ \nu_8)/\Omega(CH_3I;\ \nu_3)$.

the relative cross-section change due to the concentration is as large as that observed for the CH_3CN–CCl_4 system, which may indicate that the concentration dependence is to be ascribed mostly to the physical property of acetonitrile. In the following discussion, therefore, we will focus our attention on the role of a large dipole moment of acetonitrile.

Hyperpolarizability and Dipole Field. It is known that a scattering cross-section is proportional to the square of a transition polarizability, $\boldsymbol{\alpha}_1$,

$$\Omega \propto (\boldsymbol{\alpha}_1)^2 \tag{4}$$

and:

$$(\boldsymbol{\alpha}_1) = (\partial\boldsymbol{\alpha}/\partial Q)\langle I|Q|F\rangle$$

where $\boldsymbol{\alpha}_1$ is a transition polarizability tensor, Q is a normal coordinate, and $\langle I \mid Q \mid F\rangle$ is a matrix element corresponding to the transition between vibrational levels I and F. An i,j-element of a transition polarizability tensor of a molecule changes its magnitide when surrounding molecules produce an electric field, $\langle \boldsymbol{F}_0\rangle_{av}$, on the position of the molecule. As is illustrated in Appendix I, an i,j-element of a transition polarizability under the influence of $\langle \boldsymbol{F}_0\rangle_{av}$ is expressed by the following equation:

$$(\alpha_1)_{ij} = (\alpha_1^0)_{ij} + (\beta_1^0)_{ijk}\langle \boldsymbol{F}_{0k}\rangle_{av} \tag{5}$$

where $(\alpha_1^0)_{ij}$ is an i,j-element of a transition polarizability tensor of an isolated molecule, $(\beta_1^0)_{ijk}$ is an element of a transition hyperpolarizability tensor, and $\langle \boldsymbol{F}_{0k}\rangle_{av}$ is a k-component of $\langle \boldsymbol{F}_0\rangle_{av}$ (see Appendix I).

There are many types of intermolecular interactions which produce electric fields at the position of a given molecule in liquids or solutions. The simplest and most important of these is the interaction of a dipole-dipole type. A molecule with a dipole moment affects the orientational distribution of surrounding molecules through dipole-dipole or dipole-induced dipole interactions. This results in the appearance of a non-zero averaged electric field at the position of the central dipole. For a binary solution, this averaged electric field, $\langle \boldsymbol{F}_{0k}\rangle_{av}$, has been calculated to be[3];

$$\langle \boldsymbol{F}_{0k}\rangle_{av} = \frac{4\pi^2}{27}N_a^2\mu\left[\left(\frac{\mu^2}{kT}+\alpha\right)\frac{\rho}{W_m}c_m + \left(\frac{\mu_s^2}{kT}+\alpha_s\right)\frac{8}{A}c_{ms}\right] \tag{6}$$

with

$$A=\left[\left(\frac{W_m}{\rho}\right)^{1/3}+\left(\frac{W_{ms}}{\rho_s}\right)^{1/3}\right]^3,$$

where μ is a permanent dipole moment, α, the polarizability; c_m, the molar concentration: ρ, the density; W_m, the molecular weight; T, the temperature; k, the Boltzmann constant, and N_a, the Avogadro number. The symbols suffixed by "s" correspond to the solvent molecule.

Symmetry considerations of $(\alpha_1^0)_{ij}$ and $(\beta_1^0)_{ijk}$ are described in Appendix II. Using the results obtained in Appendix II, together with the discussion of Appendix III, we obtain the expression of $\Omega(CH_3CN;\nu_8)/\Omega(CCl_4;\nu_1)$ in temrs of $(\alpha_1^0)_{ij}$, $(\beta_1^0)_{ijk}$, and $\langle F_{0k}\rangle_{av}$ as:

$$\frac{\Omega(CH_3CN;\nu_8)}{\Omega(CCl_4;\nu_1)}=\left(\frac{14}{15}\right)\frac{1}{Q_1(\alpha_1^0)^2}[B+A\langle F_{0z}\rangle_{av}], \quad (7)$$

with

$$A=2[Q_8(\alpha_1^0)_{xy}Q_8(\beta_1^0)_{xyz}+Q_8(\alpha_1^0)_{yz}Q_8(\beta_1^0)_{yzz}]$$

and

$$B=Q_8(\alpha_1^0)_{xy}^2+Q_8(\alpha_1^0)_{yz}^2,$$

where $Q(\alpha_1^0)_{ij}$ is the i,j-element of the transition polarizability tensor which is related with the normal coordinate Q, and where $\langle F_{0z}\rangle_{av}$ is the electric field produced at an acetonitrile molecule in the direction of the molecular axis. No electric field is produced at a carbon tetrachloride molecule, because it has no permanent dipole moment.

Determination of Transition Polarizability and Transition Hyperpolarizability. Equation 7 predicts that a linear relation will hold between $\Omega(CH_3CN;\nu_8)/\Omega(CCl_4;\nu_1)$ and $\langle F_{0z}\rangle_{av}$ if the dipole interaction model is reasonable. Figure 4 shows the relation between the observed $\Omega(CH_3CN;\nu_8)/\Omega(CCl_4;\nu_1)$ and the calculated $\langle F_{0z}\rangle_{av}$ values. In the calculation of $\langle F_{0z}\rangle_{av}$, the permanent dipole moment of acetonitrile was taken to be 3.92 D.[4] Obviously, a linear relation holds between the relative cross-section and the electric dipole field. From the slope, A^*, and the intercept, B^*, of the line, we can determine the corresponding terms of Eq. 7. From the results of Fig. 4, A^* and B^* are given the values of 7.18×10^3 (dyn^{-1} esu) and 0.0776 respectively.

According to the preceding report,[1] the magnitude of $Q_8(\alpha_1^0)_{yz}$ has been observed to be 0.0204 (Å^3) from the measurement of the infrared absorption intensity for the ν_8 fundamental band of acetonitrile in a carbon tetrachloride solution. The $Q_1(\alpha_1^0)$ value of carbon tetrachloride, on the other hand, can be determined by the absolute intensity measurement of the ν_1 fundamental line. Kato *et al.* have reported the $|Q_1(\alpha_1^0)|^2$ value to be 1.99×10^{-50} (cm^6).[7] Thus, we can obtain the following values and relations for the ν_8 line of methyl cyanide:

$$Q_8(\alpha_1^0)_{xy}=0.0352\ (Å^3),$$
$$Q_8(\alpha_1^0)_{yz}=0.0204\ (Å^3),$$

and:

$$|3.52Q_8(\beta_1^0)_{xyz}|+|2.04Q_8(\beta_1^0)|=7.654\times10^{-8}(Å^6\ \text{dyn}^{-1}\ \text{esu}) \quad (8)$$

As is illustrated in Appendix II, all the necessary transition polarizabilities for an e-type fundamental of C_{3v} symmetry are $Q(\alpha_1^0)_{yz}$ and $Q(\alpha_1^0)_{xy}$. That is to say, the scattering polarizability tensor can be completely determined by observing the solvent effects on the infrared absorption and the Raman spectra. In the case of the infrared absorption spectra, only $Q(\alpha_1^0)_{yz}$ is obtained through this relation:

$$\Gamma_c\propto\left(\frac{\partial\mu_y^0}{\partial Q_8}\right)^2+2\left(\frac{\partial\mu_y^0}{\partial Q_8}\right)Q_8(\alpha_1^0)_{yz}\langle F_{0z}\rangle_{av}$$

where Γ_c is an absolute absorption intensity observed in a solution and $(\partial\mu_y^0/\partial Q_8)$ is a dipole moment derivative which can be determined by observing the absolute infrared absorption intensity of the ν_8 fundamental in the gas phase. The sign of the product, $(\partial\mu_y^0/\partial Q_8)Q_8(\alpha_1^0)_{yz}$, can be determined from the solvent effect data; therefore, the sign of $Q_8(\alpha_1^0)_{yz}$ can be definitely determined if the sign of $(\partial\mu_y^0/\partial Q_8)$ is known. In the case of the Raman spectra, on the other hand, the sum, $Q(\alpha_1^0)_{yz}^2+Q(\alpha_1^0)_{xz}^2$, can be obtained. Thus, the signs of $Q(\alpha_1^0)$'s are ambiguous; that is, only an absolute value, $|Q(\alpha_1^0)|$, is obtained by this method.

The ν_3 Line of Methyl Iodide. For an a_1-type line of C_{3v} symmetry, the relation corresponding to Eq. 7 is obtained. As an example, the ν_3 fundamental line of methyl iodide in a carbon tetrachloride solution is expressed as:

$$\frac{\Omega(CH_3I;\nu_3)}{\Omega(CCl_4;\nu_1)}=\left(\frac{1}{15}\right)\frac{1}{Q_1(\alpha_1^0)^2}(B+A\langle F_{0z}\rangle_{av}) \quad (9)$$

with:

$$A=18Q_3(\alpha_1^0)_{xx}Q_3(\beta_1^0)_{xxz}+8Q_3(\alpha_1^0)_{zz}Q_3(\beta_1^0)_{zzz}+2Q_3(\alpha_1^0)_{xx}Q_3(\beta_1^0)_{zzz}+2Q_3(\alpha_1^0)Q_3(\beta_1^0)_{xxz}$$

and:

$$B=9Q_3(\alpha_1^0)_{xx}^2+2Q_3(\alpha_1^0)_{xx}Q_3(\alpha_1^0)_{zz}+4Q_3(\alpha_1^0)_{zz}^2$$

Although the observed data of Fig. 2 for CH_3I–CCl_4 system are not accurate enough, we tried to determine the necessary transition polarizability and transition hyperpolarizability for the ν_3 line of methyl iodide. From the plotting of $\Omega(CH_3I;\nu_3)/\Omega(CCl_4;\nu_1)$ against $\langle F_{0z}\rangle_{av}$, the slope, A^*, and the intercept, B^*, were obtained to be:

$$A^*=-0.0309\times10^{-4}\ \text{dyn}^{-1}\ \text{esu},$$

and:

$$B^*=1.104$$

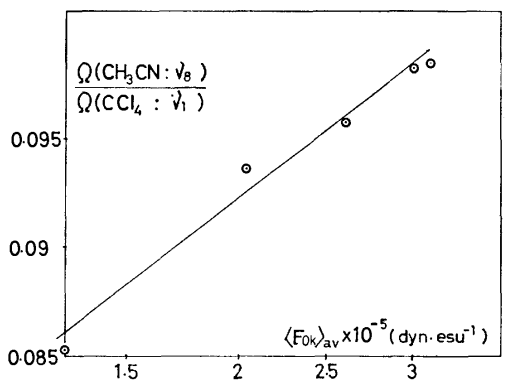

Fig. 4. Plotting of $\Omega(CH_3CN:\nu_8)/\Omega(CCl_4;\nu_1)$ against $\langle F_{oz}\rangle_{av}$.

TABLE 1. $\langle F_{0z}\rangle_{av}$ VALUES CALCULATED FOR $CHCl_3$, CH_3I, AND CH_3CN IN CCl_4 SOLUTIONS

Mole ratio of $CHCl_3$	$\langle F_{0z}\rangle_{av}$ ($\times 10^{-3}$ dyn esu)	Mole ratio of CH_3I	$\langle F_{0z}\rangle_{av}$ ($\times 10^{-4}$ dyn esu)	Mole ratio of CH_3CN	$\langle F_{0z}\rangle_{av}$ ($\times 10^{-5}$ dyn esu)
0.492	1.007	0.550	0.892	0.540	0.741
1.026	1.498	1.214	1.294	1.679	1.474
1.981	1.966	1.840	1.529	2.990	1.889
2.095	2.004	3.202	1.827	4.580	2.013
2.688	2.165	4.124	1.947	5.217	2.231
3.648	2.341				
$\mu_{CHCl_3}=1.05$ D (Ref. 6)		$\mu_{CH_3I}=1.65$ D (Ref. 5)		$\mu_{CH_3CN}=3.92$ D (Ref. 4)	

Using these values and the previous data[1]; ${}^{Q_3}(\alpha_1^0)_{zz}=-1.13\times10^{-25}$ (cm^3), we can obtain the following values and relations;

$${}^{Q_3}(\alpha_1^0)_{xx} = -1.164\times10^{-25} \text{ or } 1.888\times10^{-25}\ cm^3$$

and:

$$18{}^{Q_3}(\alpha_1^0)_{xx}{}^{Q_3}(\beta_1^0)_{xxz} + 8{}^{Q_3}(\alpha_1^0)_{zz}{}^{Q_3}(\beta_1^0)_{zzz} + 2{}^{Q_3}(\alpha_1^0)_{xx}{}^{Q_3}(\beta_1^0)_{zzz} + 2{}^{Q_3}(\alpha_1^0)_{zz}{}^{Q_3}(\beta_1^0)_{xxz} = -9.224\times10^{-51}\ cm^6\ dyn^{-1}\ esu. \quad (10)$$

The A^* and B^* values for the ν_3 line of methyl iodide can be determined in another way. By combining Eqs. 7 and 9, $\Omega(CH_3CN;\nu_8)/\Omega(CH_3I;\nu_3)$ can be expressed as:

$$\frac{\Omega(CH_3CN;\nu_8)}{\Omega(CH_3I;\nu_3)} = \frac{\Omega(CH_3CN;\nu_8)}{\Omega(CCl_4;\nu_1)} \Big/ \frac{\Omega(CH_3I;\nu_3)}{\Omega(CCl_4;\nu_1)} = \frac{(B^*_{CH_3CN}+\langle F_{0z}\rangle_{av}A^*_{CH_3CN})}{(B^*_{CH_3I}+\langle F_{0z}\rangle_{av}A^*_{CH_3I})} \quad (11)$$

As we have the observed $\Omega(CH_3CN;\nu_8)/\Omega(CH_3I;\nu_3)$ values of Fig. 3, and the $B^*_{CH_3CN}$ and $A^*_{CH_3CN}$ values, we can calculate the $A^*_{CH_3I}$ and $B^*_{CH_3I}$ values for the ν_3 line of methyl iodide in the carbon tetrachloride solution as:

$$A^* = -0.0305\times10^{-4}\ dyn^{-1}\ esu$$

and:

$$B^* = 1.528.$$

These values are not very different from those obtained in the previous way.

Criteria for the Internal Standard Method. The present results afford some useful information about the reliability of a so-called internal standard method for the determination of relative Raman intensities which are mutually comparable. The concentration dependency of a relative intensity of a Raman line arises from the existence of the concentration-dependent term, $A^*\langle F_{0z}\rangle_{av}$, of Eq. 7 or 9.

We have very little knowledge about the magnitude of A^*. Therefore, we first compare the magnitudes of $\langle F_{0z}\rangle_{av}$ of chloroform, methyl iodide, and acetonitrile in carbon tetrachloride solutions. Table 1 shows the $\langle F_{0z}\rangle_{av}$ values of chloroform, methyl iodide, and acetonitrile calculated for carbon tetrachloride solutions. It may be seen from the table that the orders of $\langle F_{0z}\rangle_{av}$ are 10^3 for chloroform, 10^4 for methyl iodide, and 10^5 for acetonitrile, in units of dyn esu^{-1}. The difference arises, of course, from the difference in the magnitude of the dipole moments. The dipole moment of acetonitrile is 3.92 D[4], while those of methyl iodide and chloroform are 1.65 D[5] and 1.05 D[6] respectively. These facts are definitely reflected in the observed Raman intensity changes due to the concentration, as is shown in Figs. 1 and 2. Thus, we can conclude that the concentration dependence of a Raman intensity is more distinct for a molecule with a larger dipole moment.

If A^* is large, on the other hand, the concentration dependence of Raman intensity may be large enough to be observed even though $\langle F_{0z}\rangle_{av}$ is small. It has been shown that $A^*\approx0.07\times10^{-5}$ dyn^{-1} esu and $A^*\approx-0.03\times10^{-4}$ dyn^{-1} esu for the ν_8 of acetonitrile and ν_3 of methyl iodide respectively. The corresponding $\langle F_{0z}\rangle_{av}$ values are, respectively, $\approx10^5$ dyn esu^{-1} and $\approx10^4$ dyn esu^{-1}; the result is that the products, $A^*\times\langle F_{0z}\rangle_{av}$, have almost the same magnitudes. In the former case, the main factor which makes the concentration dependence observable is $\langle F_{0z}\rangle_{av}$, while in the latter it is the magnitude of A^*. Detailed discussions of the magnitude of A^* from the viewpoint of the transition polarizability and transition hyperpolarizability are quite difficult at this stage, because A^* is a rather complicated function of the transition polarizability and the transition hyperpolarizability (see Eq. 7 or 9). As there have been reported quite a few number of values for ${}^{Q}(\alpha_1^0)$ and ${}^{Q}(\beta_1^0)$ with their definite signs, except the ${}^{Q}(\alpha_1^0)\approx10^{-26}$ cm^3 and ${}^{Q}(\beta_1^0)\approx10^{-32}$ $cm^3\ dyn^{-1}$ esu, we can only conclude that the concentration dependence might be observed even for a molecule with a much smaller dipole moment. Incidentally, the plus and minus signs of A^* correspond to the increase and decrease in scattering cross sections with the increase in the concentration (see Figs. 1 and 2).

Appendix I. Definition of an Apparent Transition Polarizability Derivative

The energy, U, of a molecule in an electric field, $\boldsymbol{F}$, is expressed as a function of $\boldsymbol{F}$:

$$U = U(\boldsymbol{F}) \quad (A1)$$

The Maclaurin expansion of Eq. A1 yields:

$$U = U(0) - \sum\mu_i^0F_i - \frac{1}{2!}\sum_{ij}\alpha_{ij}^0F_iF_j - \frac{1}{3!}\sum_{ijk}\beta_{ijk}^0F_iF_jF_k - \cdots \quad (A2)$$

and:

$$\mu_i^0 = -(\partial U/\partial F_i)_0$$
$$\alpha_{ij}^0 = -(\partial^2 U/\partial F_i \partial F_j)_0$$
$$\beta_{ijk}^0 = -(\partial^3 U/\partial F_i \partial F_j \partial F_k)_0$$

The coefficients, μ_i^0, α_{ij}^0, and β_{ijk}^0 are independent of $\boldsymbol{F}$. They are called, respectively, a permanent dipole moment, a polarizability, and a hyperpolarizability.

Put a molecule which has a permanent dipole moment, $\boldsymbol{\mu}$, polarizability, $\boldsymbol{\alpha}^0$, and hyperpolarizability, $\boldsymbol{\beta}^0$, in an electric field, $\boldsymbol{F}$. Then the total dipole moment, $\boldsymbol{m}$, of the molecule is:

$$\boldsymbol{m} = \boldsymbol{\mu}^0 + \boldsymbol{p} \tag{A3}$$

where $\boldsymbol{p}$ is an dipole moment induced by the electric field, $\boldsymbol{F}$:

$$\boldsymbol{p} = \boldsymbol{\alpha}^0 \cdot \boldsymbol{F} + \frac{1}{2}\boldsymbol{\beta}^0 : \boldsymbol{FF} \tag{A4}$$

In the present problem, $\boldsymbol{F}$ is composed of two different electric fields. One is an electric field, $\boldsymbol{F}_1$, of radiating light, while the other is an electric field, $\boldsymbol{F}_m$, produced by molecules in a condensed phase. Thus, an induced moment, $\boldsymbol{p}$, is expressed as:

$$\boldsymbol{p} = \boldsymbol{p}_1 + \boldsymbol{p}_m,$$

where $\boldsymbol{p}_1$ is a dipole moment induced by $\boldsymbol{F}_1$ and $\boldsymbol{p}_m$ is that induced by $\boldsymbol{F}_m$. Therefore, the induced moment, $\boldsymbol{p}_1$, is:

$$\begin{aligned}\boldsymbol{p}_1 &= \boldsymbol{p} - \boldsymbol{p}_m \\ &= \left[\boldsymbol{\alpha}^0 \cdot (\boldsymbol{F}_1 + \boldsymbol{F}_m) + \frac{1}{2}\boldsymbol{\beta}^0 : (\boldsymbol{F}_1 + \boldsymbol{F}_m)(\boldsymbol{F}_1 + \boldsymbol{F}_m)\right] \\ &\quad - \left[\boldsymbol{\alpha}^0 \cdot \boldsymbol{F}_m + \frac{1}{2}\boldsymbol{\beta}^0 : \boldsymbol{F}_m \boldsymbol{F}_m\right] \\ &= \boldsymbol{\alpha}^0 \cdot \boldsymbol{F}_1 + \boldsymbol{\beta}^0 : \boldsymbol{F}_m \boldsymbol{F}_1 + \frac{1}{2}\boldsymbol{\beta}^0 : \boldsymbol{F}_1 \boldsymbol{F}_1\end{aligned} \tag{A5}$$

In the present work, the last term of Eq. A5 may be neglected, because $\boldsymbol{F}_1$ is small. Thus,

$$\begin{aligned}\boldsymbol{p}_1 &= \boldsymbol{\alpha}^0 \cdot \boldsymbol{F}_1 + \boldsymbol{\beta}^0 : \boldsymbol{F}_m \boldsymbol{F}_1 \\ &= [\boldsymbol{\alpha}^0 + \boldsymbol{\beta}^0 \cdot \boldsymbol{F}_m] \cdot \boldsymbol{F}_1\end{aligned} \tag{A6}$$

Here, we define "an apparent polarizability" as:

$$\boldsymbol{\alpha} = \boldsymbol{\alpha}^0 + \boldsymbol{\beta}^0 \cdot \boldsymbol{F}_m \tag{A7}$$

Then the induced moment is expressed in this form:

$$\boldsymbol{p}_1 = \boldsymbol{\alpha} \cdot \boldsymbol{F}_1$$

which formally coincides with usual expression for an induced moment. Therefore, an i,j-element of α becomes:

$$\alpha_{ij} = \alpha_{ij}^0 + \sum_k \beta_{ijk}^0 F_{mk} \tag{A8}$$

where F_{mk} is a k-component of $\boldsymbol{F}_m$.

In order to obtain an explicit expression for a Raman scattering cross-section, it is necessary to rewrite Eq. A8 in terms of transition polarizability and transition hyperpolarizability derivatives, which are defined as:

$$^Q(\alpha_1^0)_{ij} = (\alpha_1^0)_{ij}\langle I|Q|F\rangle$$
$$(\alpha_1^0)_{ij} = (\partial \alpha_{ij}^0/\partial Q)_0,$$

and:

$$^Q(\beta_1^0)_{ijk} = (\beta_1^0)_{ijk}\langle I|Q|F\rangle$$
$$(\beta_1^0)_{ijk} = (\partial \beta_{ijk}^0/\partial Q)_0, \tag{A9}$$

where Q is a normal coordinate. Differentiating Eq. A8 with respect to Q, we rewrite Eq. A8 as:

$$^Q(\alpha_1)_{ij} = {}^Q(\alpha_1^0)_{ij} + \sum_k {}^Q(\beta_1^0)_{ijk} F_{mk} + \sum_k \beta_{ijk}^0 (\partial F_{mk}/\partial U)_0 \tag{A10}$$

As $\boldsymbol{F}$ is almost independent of the molecular vibration, we finally obtain:

$$^Q(\alpha_1)_{ij} = {}^Q(\alpha_1^0)_{ij} + \sum_k {}^Q(\beta_1^0)_{ijk} F_{mk} \tag{A11}$$

In the present work, F_{mk} will be replaced by $\langle \boldsymbol{F}_{0k} \rangle_{av}$. It is important to add that the k direction should be parallel to the molecular axis under consideration, because the averaged dipole field has a non-zero value only in the direction of the dipole moment. Thus, Eq. A11 can be rewritten as:

$$^Q(\alpha_1)_{ij} = {}^Q(\alpha_1^0)_{ij} + {}^Q(\beta_1^0)_{ijk}\langle \boldsymbol{F}_{0z} \rangle_{av}$$

where the molecular axis being chosen is the z-axis.

Appendix II. Symmetry Properties of α and β

The molecules studied in the present study belong to the point groups of C_{3v} and T_d. Thus, we will confine our discussion to C_{3v} and T_d symmetries.

a) Polarizability. If a molecule is in an equilibrium position, the polarizability is invariant with respect to the operations, S, of the symmetry group of the molecule:

$$S(\alpha_{ij}^0) = \alpha_{ij}^0 \tag{A12}$$

Eq. A12 requires that some polarizability components, α_{ij}^0, vanish. As an example, let us consider a rotation about the z-axis by an angle of φ. The corresponding symmetry operation, S, is expressed as:

$$S\begin{pmatrix}\alpha_{xx}^0\\ \alpha_{yy}^0\\ \alpha_{xy}^0\\ \alpha_{xz}^0\\ \alpha_{yz}^0\\ \alpha_{zz}^0\end{pmatrix} = \begin{pmatrix} a^2 & b^2 & 2ab & 0 & 0 & 0\\ b^2 & a^2 & -2ab & 0 & 0 & 0\\ -ab & ab & a^2-b^2 & 0 & 0 & 0\\ 0 & 0 & 0 & a & b & 0\\ 0 & 0 & 0 & -b & a & 0\\ 0 & 0 & 0 & 0 & 0 & 1\end{pmatrix}\begin{pmatrix}\alpha_{xx}^0\\ \alpha_{yy}^0\\ \alpha_{xy}^0\\ \alpha_{xz}^0\\ \alpha_{yz}^0\\ \alpha_{zz}^0\end{pmatrix} \tag{A13}$$

where $a=\cos\varphi$ and $b=\sin\varphi$. From Eqs. A12 and A13,

$$a^2\alpha_{xx}^0 + b^2\alpha_{yy}^0 + 2ab\alpha_{xy}^0 = \alpha_{xx}^0$$

and similar relations for other symmetry operation. Thus, for C_{3v} symmetry, these relations;

$$\alpha_{xx}^0 = \alpha_{yy}^0 \neq \alpha_{zz}^0$$

and

$$\alpha_{xy}^0 = \alpha_{xz}^0 = \alpha_{yz}^0 \tag{A14}$$

are obtained. Eq. A14 shows that the polarizability tensor has only the diagonal elements and that the polarizability ellipsoid will become a rotation ellipsoid about the z-axis. These are the results obtained for a molecule in an equilibrium position.

For the displacements of nuclei due to vibration, the symmetry of the molecule is destroyed except when the vibrational mode is totally symmetric. Consider a molecule whose nuclei deviate from their equilibrium position according to a particular normal mode. There are two ways of applying symmetry operations, S, for the molecule. One is to apply the symmetry operations to the polarizability directly, while the other is to apply the symmetry operations to the normal coordinate. The results obtained by these two methods should be the same. Thus,

$$S\alpha_{ij}^0(Q_1, Q_2, \ldots\ldots, Q_n) = \alpha_{ij}^0(S_0Q_1, S_0Q_2, \ldots\ldots, S_0Q_n) \tag{A15}$$

where the symmetry operations are distinguished as S_0 and S, simply because $\boldsymbol{\alpha}$ is a tensor quantity, while Q_i is a vector quantity. In order to calculate the right-hand side of Eq. A15, we have to know the transformation property of a normal coordinate due to the symmetry operation.

Consider a molecule with C_{3v} symmetry like acetonitrile. The normal coordinates, Q_s and $Q_{s'}$, are transformed by the C_3 operation thus:

$$Q_s \xrightarrow{C_3} -\frac{1}{2}Q_s - \frac{\sqrt{3}}{2}Q_{s'}$$

and: (A16)

$$Q_{s'} \xrightarrow{C_3} \frac{\sqrt{3}}{2}Q_s - \frac{1}{2}Q_{s'}$$

The polarizability is expressed in terms of normal coordinates:

$$\alpha^0_{ij} = (\alpha^0_{ij})_0 + \sum_k (\partial\alpha^0_{ij}/\partial Q_k)Q_k \tag{A17}$$

By combining Eqs. A16 and A17, we obtain this relation for α^0_{xx}:

$$\frac{\partial(\alpha^0_{xx})}{\partial(C_3Q_s)} = -\frac{1}{2}\left(\frac{\partial\alpha^0_{xx}}{\partial Q_s}\right)+\frac{\sqrt{3}}{2}\left(\frac{\partial\alpha^0_{xx}}{\partial Q_{s'}}\right)$$
$$= -Q_s(\alpha^0_1)_{xx}/2 + \sqrt{3}Q_{s'}(\alpha^0_1)_{xx}/2 \tag{A18}$$

From Eq. A13, on the other hand,

$$\frac{\partial(C_3\alpha^0_{xx})}{\partial Q_s} = \frac{1}{4}\left(\frac{\partial\alpha^0_{xx}}{\partial Q_s}\right)+\frac{3}{4}\left(\frac{\partial\alpha^0_{yy}}{\partial Q_s}\right)-\frac{\sqrt{3}}{2}\left(\frac{\partial\alpha^0_{xy}}{\partial Q_s}\right)$$
$$= Q_{s'}(\alpha^0_1)_{xx}/4 + 3Q_s(\alpha^0_1)_{yy}/4 - \sqrt{3}Q_s(\alpha^0_1)_{xy}/2 \tag{A19}$$

By equating Eqs. A18 and A19, we obtain this relation:

$$\frac{3}{4}(Q_s(\alpha^0_1)_{xx} + Q_s(\alpha^0_1)_{yy})$$
$$= \frac{\sqrt{3}}{2}(Q_{s'}(\alpha^0_1)_{xx} + Q_s(\alpha^0_1)_{xy}) \tag{A20}$$

Similar but different relations are obtained for other polarizability derivatives and for other normal coordinates by applying the C_3 and σ_v operations. The transformation relations:

$$Q_s \xrightarrow{\sigma_v} -Q_s$$
$$Q_{s'} \xrightarrow{\sigma_v} Q_{s'} \tag{A21}$$

are used for the σ_v operation. From these results, the following relations between the polarizability derivatives or transition polarizability derivatives are obtained:

$$Q_s(\alpha^0_1)_{xx} = Q_s(\alpha^0_1)_{yy} = Q_s(\alpha^0_1)_{zz} = Q_{s'}(\alpha^0_1)_{zz} = 0$$
$$Q_{s'}(\alpha^0_1)_{xy} = Q_{s'}(\alpha^0_1)_{yz} = Q_s(\alpha^0_1)_{xz} = 0$$
$$Q_s(\alpha^0_1)_{xy} = Q_{s'}(\alpha^0_1)_{yy} = -Q_{s'}(\alpha^0_1)_{xx}$$
$$Q_s(\alpha^0_1)_{yz} = Q_{s'}(\alpha^0_1)_{xz} \tag{A22}$$

b) Hyperpolarizability. Generally, a hyperpolarizability tensor has ten independent elements because of its symmetry property. These elements are related to each other in accordance with the molecular symmetry. The procedure of finding the relations between the hyperpolarizability derivatives is exactly the same as that discussed in a). For example, consider a rotation about the z-aixs by an angle of φ. The matrix representation for S corresponding to Eq. A13 is:

$$S\begin{pmatrix}\beta^0_{xxx}\\ \beta^0_{yyy}\\ \beta^0_{xxy}\\ \beta^0_{xyy}\\ \beta^0_{xxz}\\ \beta^0_{yyz}\\ \beta^0_{xyz}\\ \beta^0_{xzz}\\ \beta^0_{yzz}\\ \beta^0_{zzz}\end{pmatrix} = \begin{pmatrix} a^3 & b^3 & 3a^2b & 3ab^2 & 0 & 0 & 0 & 0 & 0 & 0\\ -b^3 & a^3 & 3ab^2 & -3a^2b & 0 & 0 & 0 & 0 & 0 & 0\\ -a^2b & ab^2 & a^3-2ab^2 & 2a^2b-b^3 & 0 & 0 & 0 & 0 & 0 & 0\\ ab^2 & a^2b & b^3-2a^2b & a^3-2ab^2 & 0 & 0 & 0 & 0 & 0 & 0\\ 0 & 0 & 0 & 0 & a^2 & b^2 & 2ab & 0 & 0 & 0\\ 0 & 0 & 0 & 0 & b^2 & a^2 & -2ab & 0 & 0 & 0\\ 0 & 0 & 0 & 0 & -ab & ab & a^2-b^2 & 0 & 0 & 0\\ 0 & 0 & 0 & 0 & 0 & 0 & 0 & a & b & 0\\ 0 & 0 & 0 & 0 & 0 & 0 & 0 & -b & a & 0\\ 0 & 0 & 0 & 0 & 0 & 0 & 0 & 0 & 0 & 1\end{pmatrix} \times \begin{pmatrix}\beta^0_{xxx}\\ \beta^0_{yyy}\\ \beta^0_{xxy}\\ \beta^0_{xyy}\\ \beta^0_{xxz}\\ \beta^0_{yyz}\\ \beta^0_{xyz}\\ \beta^0_{xzz}\\ \beta^0_{yzz}\\ \beta^0_{zzz}\end{pmatrix} \tag{A23}$$

where $a=\cos\varphi$ and $b=\sin\varphi$. As is shown in Appendix I, the elements on which at least one z is subscribed are important in the present work. In other words, only the submatrix of Eq. A23 enclosed in the square of the dotted line is important for the present discussion. It is necessary, therefore, to know the symmetry property of the submatrix. A comparison of Eqs. A13 and A23 shows that the submatrix is exactly the same as that of Eq. A13.

The transformation of β with respect to a normal coordinate is the same as that described in a), as β_{ijk} is expressed as:

$$\beta^0_{ijk} = (\beta^0_{ijk})_0 + \sum_l \left(\frac{\partial\beta^0_{ijk}}{\partial Q}\right)Q_l \tag{A24}$$

Thus, we ascertain the relations between the hyperpolarizability derivatives or transition hyperpolarizabilities by direct analogy with Eq. A22:

$$Q_s(\beta^0_1)_{xxz} = Q_s(\beta^0_1)_{yyz} = Q_s(\beta^0_1)_{zzz} = Q_{s'}(\beta^0_1)_{zzz} = 0$$
$$Q_{s'}(\beta^0_1)_{xyz} = Q_{s'}(\beta^0_1)_{yzz} = Q_s(\beta^0_1)_{xzz} = 0$$
$$Q_s(\beta^0_1)_{xyz} = Q_{s'}(\beta^0_1)_{yyz} = -Q_{s'}(\beta^0_1)_{xxz}$$
$$Q_s(\beta^0_1)_{yzz} = Q_{s'}(\beta^0_1)_{xzz} \tag{A25}$$

Appendix III. Reduction to a Scattering Cross-section

In order to calculate a scattering cross-section, it is necessary to know the actual geometric conditions of the Raman spectral measurement. In the present work, the observed Raman intensities are expressed as:

$$\Omega \propto ((\alpha_1)^2_{YZ} + (\alpha_1)^2_{ZZ}) \tag{A26}$$

where X, Y, and Z are the spece-fixed Cartesian coordinates. The relations between the polarizability tensors expressed in the molecular-fixed Cartesian coordinates and the space-fixed Cartesian coordinates are:

$$\alpha^2_{YZ} = \frac{1}{15}\sum_i \alpha^2_{ii} - \frac{1}{15}\sum_{i<j}\alpha_{ii}\alpha_{jj} + \frac{1}{5}\sum_{i<j}\alpha^2_{ij}$$
$$\alpha^2_{ZZ} = \frac{1}{5}\sum_i \alpha^2_{ii} + \frac{2}{15}\sum_{i<j}\alpha_{ii}\alpha_{jj} + \frac{4}{15}\sum_{i<j}\alpha^2_{ij} \tag{A27}$$

Eqs. A26 and A27, together with Eq. A22, give the cross section, $\Omega(e)$, for the e-type line of a molecule with C_{3v}

symmetry:

$$\Omega(e) \propto \frac{14}{15}({}^{Q}(\alpha_1)^2_{xy} + {}^{Q}(\alpha_1)^2_{yz}) \quad \text{(A28)}$$

In the case of the a_1-type line of C_{3v} symmetry, the relations corresponding to Eq. A22 are:

$$\begin{aligned} &{}^{Q}(\alpha_i^0)_{xx} = {}^{Q}(\alpha_i^0)_{yy},\ {}^{Q}(\alpha_i^0)_{zz}, \\ &{}^{Q}(\alpha_i^0)_{xy} = {}^{Q}(\alpha_i^0)_{yz} = {}^{Q}(\alpha_i^0)_{zx} = 0 \end{aligned} \quad \text{(A29)}$$

Therefore, the cross section, $\Omega(a_1)$, for the a_1-type line of a molecule with C_{3v} symmetry is expressed as:

$$\begin{aligned} \Omega(\alpha_1) \propto 3{}^{Q}(\alpha_1)^2_{xx}/5 + 2{}^{Q}(\alpha_1)_{xx}{}^{Q}(\alpha_1)_{zz}/15 \\ + 4{}^{Q}(\alpha_1)^2_{zz}/15 \end{aligned} \quad \text{(A30)}$$

By inserting Eq. A11 into Eq. A28 or A30, and by neglecting the terms corresponding to $\langle \boldsymbol{F}_{0k} \rangle^2_{av}$, we can express the Raman scattering cross-section in terms of α_1, β_1, and $\langle \boldsymbol{F}_{0k} \rangle_{av}$.

References

1) M. Kakimoto and T. Fujiyama, *Bull. Chem. Soc. Jpn.*, **48**, 2258 (1975).

2) M. Kakimoto and T. Fujiyama, *Bull. Chem. Soc. Jpn.*, **48**, 3003 (1975).

3) G. Eckhardt and W. G. Wagner, *J. Mol. Spectrosc.*, **19**, 407 (1966); G. Fini, P. Mirone, and P. Patella, *J. Mol. Spectrosc.*, **28**, 144 (1968); P. Mirone, *Chem. Phys. Lett.*, **4**, 323 (1969); G. Fini, M. G. Giorgini, and P. Mirone, *Gaz. Chim. Ital.*, **102**, 288 (1972); T. Fujiyama, *Bull. Chem. Soc. Jpn*, **46**, 87 (1973).

4) S. N. Ghosh, R. Trambarulo, and W. Gordy, *Phys. Rev.*, **87**, 172 (1952); *J. Chem. Phys.*, **21**, 308 (1953).

5) R. G. Shulman, B. P. Dailey, and C. H. Townes, *Phys. Rev.*, **78**, 145 (1950).

6) C. P. Smyth and S. O. Morgan, *J. Am. Chem. Soc.*, **50**, 1547 (1928).

7) Y. Kato, Thesis submitted to The University of Tokyo (1969).

Analysis of the Effect of Added Electrolyte on the Micellar Catalysis

Keishiro SHIRAHAMA

Department of Chemistry, Faculty of Science and Engineering, Saga University, Saga 840

(Received February 19, 1976)

The effect of added electrolyte on micelle-catalyzed reaction was analyzed. The log [L.S] *vs.* log (total counter ion concentration) plot gives a straight line, where [L.S] is a limiting slope on a rate-surfactant concentration plot at an infinitely dilute micellar concentration. The slope is related to the number and the magnitude of the Coulombic term that may be included in the concentration effect of reactants, and in the intrinsic micellar effect, or the relative stabilization of a transition state in the presence of micelles. The above treatment was applied to (1) the hydrolysis of trimethyl orthobenzoate in sodium dodecyl sulfate solution, (2) the fading reaction of Crystal Violet in hexadecyltrimethylammonium bromide (CTABr) solution, and (3) the nucleophilic substitution reaction of 2,4-dinitrofluorobenzene in CTABr solution. It was found that the concentration effect is predominant in (1), while the relative stabilization of the transition state occurs in (2) and (3) in addition to the concentration effect.

A marked inhibition takes place in many systems on addition of an electrolyte to a micelle-catalyzed reaction. The interpretation of experimental results seems to be qualitative since most experiments were performed at a constant surfactant concentration with varying concentration of added electrolyte.[1-6] The constant surfactant concentration with various amounts of the added electrolyte is not considered to be at a corresponding state. As an example, cmc decreases with an increase in the added electrolyte concentration leading to the increase in micellar concentration.

In a previous paper,[7] a formula was derived for a micelle-catalyzed reaction based upon a microheterogeneous reaction. This was found to be useful for describing the mode of such as rate-surfactant concentration profile, inhibition of a micellar catalysis by an added electrolyte, and an activation energy, taking the hydrolysis of trimethyl orthobenzoate (MOB) in sodium dodecyl sulfate (SDS) solution as a model system.

This communication shows the obtained data to be in line with the derived equations, analysis of the effect of the added electrolyte on the micellar catalysis being made. The selected systems are: (1) MOB–SDS–NaCl system which has been examined by using the published data,[4] (2) Crystal Violet (CV)–Hexadecylammonium bromide (CTABr)–NaBr system,[8,9] and (3) 2,4-dinitrofluorobenzene (DNFB)–CTABr–NaBr system.[5]

Theoretical

The following equation was derived for a chemical reaction of the type, A+B→P, in a micellar solution.[7]

$$k_2 = (\phi_{es}K_AK_Bf+1)k_b/(\phi_mK_A+1) \quad (1)$$

where k_2 is the second-order reaction rate constant in a micellar solution, and k_b that in the bulk, K_A and K_B are the distribution coefficients of reactants A and B between the micellar and bulk phases, respectively, ϕ_m and ϕ_{es} are the volume fractions of the micelles and the effective surface reaction-layer around a micelle, respectively, and $f=\exp(-\Delta G^*/RT)$ represents an intrinsic micellar effect, where $\Delta G^*=G_m^*-G_b^*$, G_m^*, and G_b^*, being the activation free energies in the presence and absence of micelles, respectively. At a very low concentration with respect to micelles, under which assumption Eq. 1 was derived, the volume fractions are represented by $\phi_m=\alpha_m[M]$ and $\phi_{es}=\alpha_{es}[M]$, where α_i is the molar volume of region i, and [M] the micellar concentration, both quantities being on the monomer concentration basis. We get the following equation from Eq. 1.

$$[L.S] = \lim_{[M]\to 0} d(k_2/k_b)/d[M] = \alpha_{es}K_AK_Bf - \alpha_mK_A \fallingdotseq \alpha_{es}K_AK_Bf \quad (2)$$

where [L.S.] denotes the limiting slope of a rate-surfactant concentration profile. The last approximation in Eq. 2 is fairly good for most cases of efficient micellar catalysis. The electrical surface potential of a micelle, ψ_0 is written as a function of the total counter ion concentration, C_t:[10]

$$\psi_0 = -(kT/z_ie)\ln C_t + \text{constant} \quad (3)$$

where k is the Boltzmann constant, T absolute temperature, and z_ie the electric charge of reactant i. If the electrostatic term is included, *e.g.*, in K_B, it should be of the form, $K_B=K_0\exp(-z_Be\psi_0/kT)$, where K_0 is a nonelectrostatic part of the distribution coefficient. The f-factor also may contain a $z_ie\psi_0$ term if the relative stabilization of the transition state is electrostatically caused by the surface potential. In this case, z_i is the number of charge of the transition state taken relative to that of the reactant state, in the rate-determining step. Taking logarithm of Eqs. 2 and 3, and rearranging, we have

$$\ln [L.S] = -\nu \ln C_t + \text{constant} \quad (4)$$

where $\nu=\sum_i[-z_ie\psi_0/|e\psi_0|]$ is the algebraic sum of the number of surface potential terms possibly contained in K_A, K_B and/or in f-terms. If $z_ie\psi_0<0$, K_A and K_B concentrate ionic reactant A and B, respectively, around micelles, and f-term accelerates the reaction, and *vice versa*. The dependence of α_{es} on c_t is neglibigly small. Although Eq. 1 was derived for a reaction system consisting of a buffered reaction partner (H^+ or OH^- for most cases), it is easily extended to a system in which no buffered reactant is included:

$$k_2 = (\phi_{es}K_AK_Bf+1)k_b/(\phi_mK_A+1)(\phi_{es}K_B+1) \quad (5)$$

which is similar to an equation derived by Yatsimirski *et al.*,[6] and leads to the following formula.

$$[L.S] = \lim_{[M]\to 0} d(k_2/k_b)/d[M] = \alpha_{es}K_AK_Bf - \alpha_mK_A - \alpha_{es}K_B \fallingdotseq \alpha_{es}K_AK_Bf \quad (6)$$

The last approximation again holds for efficient micelle-catalyzed reactions. Thus the present treatment does not depend on whether a reaction partner is buffered or not.

Experimental

Most of the experimental techniques were taken from previous works;[4,5,8,9] only the modifications and specifications will be mentioned.

Materials. The synthesis and purification of MOB was the same as in literatures,[4,11] its purity being checked by NMR and UV spectroscopies. DNFB (Tokyo Chemical Ind. Co., Ltd.) was distilled under reduced pressure. CV (C.I. Basic Violet 3) of reagent grade (Wako Pure Chemical Ind. Ltd.) was used. The SDS was the same sample as used previously.[12] CTABr (Tokyo Chemical Ind. Ltd.) was recrystallized once from carbon tetrachloride, and three times from acetone-ethanol mixture (15 : 2 in volume). The cmc's at 25 °C are 8.2 mM for the SDS, and 0.95 mM for the CTABr, which are in good agreement with the authentic values.[13]

Procedures. The reaction was followed with a spectrophotometer (Hitachi model 139) equipped with a pen recorder. The temperature of the cell chamber was kept constant by circulating water from a thermostat. Into 1 ml of a solution containing the surfactant and electrolyte which had been equilibrated in a cuvette, was added 1 ml of a substrate solution with a pipette, and the reaction mixture was quickly stirred with a tiny plastic rod. The substrate solution and the pipette were equilibrated in a thermostat.

Results and Discussion

MOB–SDS System. The second-order rate constants of the MOB hydrolysis at 25 °C with pH 5.40 (0.01 M sodium acetate buffer) are shown in Fig. 1 as a function of SDS concentration, where the multiphasic feature of the profile is partly seen. The initial gradual rise followed by a linear portion would be due to a large substrate-micelle concentration ratio, not assumed explicitly in Eq. 1. Thus the linear portion was taken as a [L.S], since a constant amount of substrate per micelle (probably one substrate molecule per micelle) may be partitioned there. The slope of the linear portion becomes smaller on addition of NaCl. In Fig. 2, log[L.S] is plotted against log C_t in accordance with Eq. 4, where the relation, C_t=cmc+ the buffer concentration + the added electrolyte concentration, is assumed. A slope of $\nu=0.98\fallingdotseq 1$ was obtained. This is identical with the one[7] evaluated by analyzing the data of Dunlap and Cordes.[4] It should be noted that a slope at relatively concentrated region of NaCl (>0.1 M) was used in the previous analysis,[7] because the micellar concentration remains nearly constant at 0.01 M SDS with an increase in NaCl concentration. On the other hand, a slope at relatively low region of the added salt concentration (0—0.03 M) was employed in the present work. The conclusion is naturally the same: $\nu\fallingdotseq 1$ is caused by the concentration effect of proton around micelles, or $K_B=K_0\exp(-z_B e\psi_0/kT)$ with $z_B=1$. The electrostatic stabilization of the transition state is not so important, since the oxonium, a reactant of the rate-determing step, is stabilized to the same degree as the carbonium ion at the transition state, resulting in no relative stabilization, which is contrary to the conclusion of Dunlap and Cordes.[4]

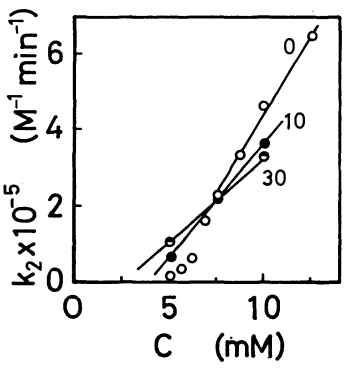

Fig. 1. The second-order rate constant of MOB-SDS system (25 °C, pH 5.40). The numbers in the figure represent the amount of added NaCl in mmol/l. The rate constant at SDS concentration=4 mmol/l in 10 mmol/l NaCl solution coincides with that in 30 m mol/l NaCl solution.

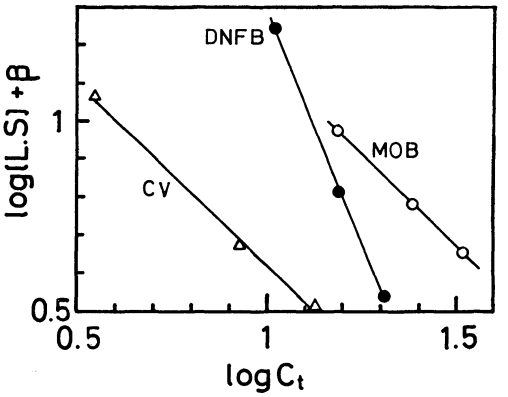

Fig. 2. log[L.S] *vs.* log C_t, C_t in mmol/l.

CV–CTABr System. The fading reaction of Crystal Violet was carried out in 3 mM NaOH solution at 30 °C. The pseudo-first-order rate constants are shown in Fig. 3 as a function of CTABr concentration with various amount of added NaBr. The added electrolyte suppresses the reaction rates at all CTABr concentrations studied. The linear portion was too small to determine the [L.S] directly, because of a strong saturating tendency as compared with those of MOB–SDS and DNFB–CTABr systems. The [L.S] was determined by graphical differentiation. The log[L.S] *vs.* log C_t plot in Fig. 2 gives $\nu=0.94\fallingdotseq 1$, which may be brought about by a little complicated mechanism: the carbonium dye is charged similarly to CTABr micelles, and the same charge yields $\exp(-|e\psi_0|/kT)$ term in K_A, which is, however, cancelled out by $\exp(+|e\psi_0|/kT)$ term contained in K_B, or the OH^- concentration effect. The resultant effect would be zero unless there is a relative stabilization by the micellar charge. It seems that the relative stabilization of the transition state is affected by the fact that the reactant dye is similarly charged to micelles and therefore destabilized, while the transition state is

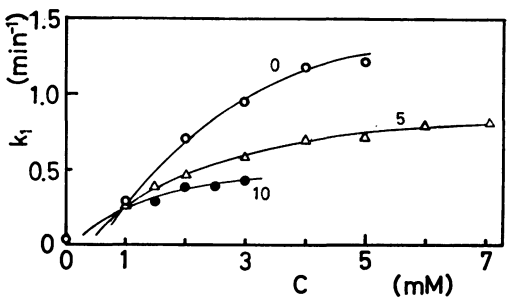

Fig. 3. The pseudo-first-order rate constant of CV–CTABr system (30 °C, 3 mmol/l NaOH). The numbers in the figure refers to the amount of added NaBr in mmol/l.

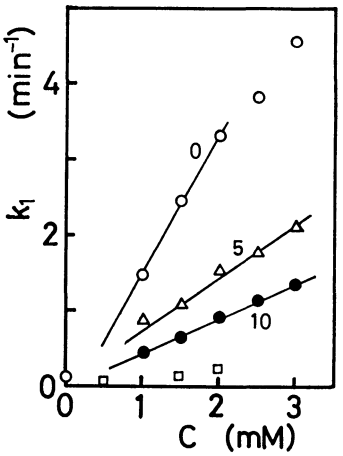

Fig. 4. The pseudo-first-order rate constant of DNFB–CTABr system (25 °C, 10 mmol/l). The numbers in the figure refers to the amount of added NaBr in mmol/l. The squares are the results of Bunton and Robinson.[5]

presumed to be an uncharged alcohol which has little sensitivity to the electrostatic potential. This conclusion is in line with that of Albrizzio *et al.* who stated "one expects less electrostatic destabilization for the zwitterion transition state than for the cation ground state by the cationic micellar surface," stressing the importance of the electrostatic contribution.[8b] The effect of the added electrolyte is offset in the concentration effects between K_A and K_B. The experimentally observed dependence ($\nu \fallingdotseq 1$) should be ascribed to the relative stabilization of the transition state, *viz.*, the f-term contains $\exp(+|z_i e\phi_0|/kT)$ term.

DNFB–CTABr System. The pseudo-first-order rate constants of the nucleophilic substitution reaction of DNFB in the presence of 10 mM NaOH at 25 °C are shown in Fig. 4, as a function of CTABr concentration, where the results under the same conditions as those reported by Bunton and Robinson are also added.[5] The rate they observed remains low even above the cmc (*ca.* 0.6 mM in 10 mM NaOH at 25 °C), while ours increases steeply near the cmc. A similar difference was also reported by Blandamer and Reid.[15] The [L.S] was easily taken owing to the marked efficiency in the micellar catalysis. The slope (Fig. 2)

Table 1. Analysis of the electrostatic contribution to the micellar catalysis

System	$-z_i e\phi_0/\lvert e\phi_0\rvert$			ν_{th}	ν_{ob}
	K_A	K_B	f		
MOB-SDS	0	1	0	1	0.98
CV-CTABr	−1	1	1	1	0.94
DNFB-CTABr	0	1	1	2	2.4

gives $\nu=2.4$, which is unexpectedly large, but can be interpreted as follows. In addition to a term included in K_B, or the OH^- concentration effect, there must be a contribution from the f-term. The Meisenheimer complex[3,14] which is presumably at the transition state may have a negative charge giving rise to the stabilization of the activated anion by the micellar surface potential. Bunton and Robinson ascribed the strong catalysis to the incorporation of DNFB in micelles which give hydroxide ions electrostatically favorable environment to attack the organic substrate,[5] but they did not make any further analysis. It is not clear whether the residual contribution $\nu-2=0.4$ comes from the dipole-field interaction or for some other reason. The reaction between DNFB and aniline in CTABr solution is scarcely sensitive to the added electrolyte.[3] No electrostatic term is included in either K_A, K_B, or in the f-term, since the two reactants as well as the Meisenheimer complex are neutral in this case leading to the result $\nu=0$.

Remarks. The present treatment is useful in clarifying the nature of micellar catalyses, especially as regards the electrostatic effect. The results are summarized in Table 1. A tacit assumption underlying Eqs. 1 and 5 is that the micellar structure does not change much on addition of electrolytes. This assumption might not hold, but the micellar structure would not change so much, since the concentration of added electrolyte is deliberately limited as little as 0.05 M in the present work.

The author thanks Dr. Y. Moroi, Kyushu University, for his interest and discussion.

References

1) P. Heitmann, *Eur. J. Biochem.*, **5**, 305 (1968).
2) L. R. Romsted and E. H. Cordes, *J. Am. Chem. Soc.*, **90**, 4406 (1968).
3) C. A. Bunton and L. Robinson, *J. Am. Chem. Soc.*, **92**, 351 (1970).
4) R. B. Dunlap and E. H. Cordes *J. Am. Chem. Soc.*, **90**, 4395 (1968).
5) C. A. Bunton and L. Robinson, *J. Org. Chem.*, **34**, 780 (1969).
6) A. K. Yatsimirski, K. Martinek, and I. V. Berezin, *Tetrahedron*, **27**, 2855 (1971).
7) K. Shirahama, *Bull. Chem. Soc. Jpn.*, **48**, 2673 (1975).
8) a) J. Baumrucker, M. Calzadilla, and E. H. Cordes, in "Reaction Kinetics in Micelles," Plenum Press, New York (1973), p 47; b) J Albrizzio, J. Archila, T. Rudolfo, and E. H. Cordes, *J. Org. Chem.*, **37**, 871 (1972).
9) E. F. Duynstee and E. Grunwald, *J. Am. Chem. Soc.*, **81**, 4540, 4542 (1959).

10) J. T. Davies and E. K. Rideal, "Interfacial Phenomena," Academic Press, New York, N.Y. (1961), p. 146.
11) S. M. McElvain and J. T. Venerable *J. Am. Chem. Soc.*, **72**, 1661 (1950).
12) K. Shirahama and T. Kashiwabara, *J. Colloid Interface Sci.*, **36**, 65 (1971).
13) P. Mukerjee and K. J. Mysels, "Critical Micelle Concentrations of Aqueous Surfactant Systems," U.S. Government Printing Office, Washington D.C. (1971).
14) L. M. Casillio, E. J. Fendler, and J. H. Fendler, *J. Chem. Soc., B*, **1971**, 1377.
15) M. J. Blandamer and D. J. Reid, *J. Chem. Soc., Faraday Trans. 1*, **71**, 2156 (1975).

A Study of *trans* Influence in Methylmercury(II) Compounds by Means of Vibrational Analysis

Noriko IWASAKI

Faculty of Engineering, Kumamoto University, Kurokami, Kumamoto 860

(Received January 10, 1976)

Force constants K(Hg–C) were evaluated for a series of methylmercury compounds: CH_3HgX (X=CH_3, F, Cl, Br, I, CN, SCN, $As(CH_3)_3$, SCH_3, $SHgCH_3$, and $S(HgCH_3)_2$). It was found that K(Hg–C) increases in the following order of X: $S(HgCH_3)_2(1.86) < I(2.27) < SCH_3(2.33) = CH_3(2.330) < As(CH_3)_3(2.37) \leq Br(2.37_7) \leq SHgCH_3(2.38) \leq Cl(2.38_2) < SCN(2.39) < F(2.55) < CN(2.61$ md/Å). This order coincides, except for the cases of CN and $As(CH_3)_3$, with the order of increase in the first ionization potential of X for X=I, SCH_3, CH_3, Br, Cl, and F. Since this effect of X upon K(Hg–C) is regarded as a vibrational *trans* influence, this order was compared with that of the coupling constants in NMR, $J(^{199}Hg-^{13}C)$ and $J(^{199}Hg-^{1}H)$, and with the order of the bond-dissociation energy of CH_3HgX into $\cdot CH_3$ and $\cdot HgX$.

A number of organomercuric compounds with the general formula of R–Hg–X have been reported, where R represents an alkyl or aryl group, and X, an inorganic or organic ligand. It is well known that the Hg–C bonding in those compounds is stable and essentially covalent in nature, but it is considerably affected by the ligand, X. Since the C–Hg–X bonding is linear, this effect may be regarded as the "*trans* influence" of the X upon the C–Hg bond. This has been investigated extensively by various methods. For instance, Hatton *et al.*[1] studied the variation in $^{199}Hg-^{1}H$ geminal coupling constants by varying the ligand, X. Henneike[2] calculated the $^{199}Hg-^{13}C$ and $^{199}Hg-^{1}H$ coupling constants by the extended Hückel MO method. Charnley and Skinner[3] evaluated the Hg–C bond-dissociation energies from thermodynamic measurements in the gas phase. The frequencies of the Hg–C stretching vibration and even some force constants, K(Hg–C), have been reported.[4–19] These values, however, have rather limited significance for the discussion of the *trans* influence of methylmercury compounds because, as is well known, the vibrational frequency is not proportional to the force constant, and the available data on force constants, K(Hg–C), were not calculated by the same principle, *e.g.*, using the same valence field and the same assumption of dynamic units in a molecule. Therefore, in the present study, force constants K(Hg–C) were evaluated for a series of methylmercury compounds (CH_3HgX (X=CH_3, F, Cl, Br, I, CN, SCN, $As(CH_3)_3$, SCH_3, $SHgCH_3$, and $S(HgCH_3)_2$) in order to elucidate the *trans* influence of the X upon the Hg–C bond. The numerical data

TABLE 1. BOND LENGTHS(Å) AND BOND ANGLES[a] USED FOR THE CALCULATIONS

$(CH_3)_2Hg$	r(Hg-C)=2.094[22,b]	
CH_3HgF	r(Hg-C)=2.06[23,c]	r(Hg-F)=1.93[d]
CH_3HgCl	r(Hg-C)=2.061[24,b]	r(Hg-Cl)=2.282[24,b]
CH_3HgBr	r(Hg-C)=2.074[24,b]	r(Hg-Br)=2.406[24,b]
CH_3HgI	r(Hg-C)=2.087[25,b]	r(Hg-I)=2.528[25,b]
CH_3HgCN	r(Hg-C)=2.082[26,e,f]	r(Hg-CN)=2.051[26,e,f]
	r(C-N)=1.141[26,e,f]	θ(Hg-C-N)=180[26,e,f]
CH_3HgSCN	r(Hg-C)=2.06[23]	r(Hg-S)=2.50[27]
	r(S-C)=1.58[16]	r(C-N)=1.21[16]
	θ(Hg-S-C)=120[16]	θ(S-C-N)=180[16]
$CH_3HgAs(CH_3)_3^+$	r(Hg-C)=2.06[23]	r(Hg-As)=2.11[g]
	r(As-C)=1.948[29,e,h]	θ(Hg-As-C)=112.8[29,e,h]
CH_3HgSCH_3	r(Hg-C)=2.094[22,b]	r(Hg-S)=2.36[30,e]
	r(S-C)=1.70[30,e]	θ(Hg-S-C)=111[30,e]
$(CH_3Hg)_2S$	r(Hg-C)=2.094[22,b]	r(Hg-S)=2.47[31,i]
	θ(Hg-S-Hg)=105[31,i]	
$(CH_3Hg)_3S^+$	r(Hg-C)=2.09[22,b]	r(Hg-S)=2.47[31,i]
	θ(Hg-S-Hg)=117, 111, and 105[j]	

a) All the θ(C–Hg–X) that are 180° are omitted in this table. b) By microwave. c) Estimated from the tendency for r(Hg–C) to decrease with X=I, Br, and Cl. d) Calculated by r(Hg–X)$-r_c$(X)$+r_c$(F), where X=Cl, Br, and I, and where r_c denotes Pauling's covalent radius. e) By X-ray diffraction. f) By neutron diffraction. g) The r(Hg–As) was calculated by r_c(As)$+r_i(Hg^{2+})-0.18$, assuming that the ionic radius (1.10 Å)[28] of Hg^{2+} in HgX_4^{2-} may be transferred to CH_3HgX molecules and that r_c(As)$+r_i(Hg^{2+})$ may be corrected by −0.18 Å, which is the difference between the observed $r(Pt^{2+}-As)$[29] and the sum of r_c(As)$+r_c(Pt^{2+})$, where r_i denotes the ionic radius. h) Transferred from $Pt_2Cl_4[As(CH_3)_3]_2$, and θ(Hg–As–C) is the mean value of the three angles. i) Calculated based on measurements of the dipole moments of $(CH_3Hg)_2S$, $(C_2H_5Hg)_2S$, and $CH_3HgSHgC_2H_5$. j) The vibrational analyses were carried out for the various assumed θ(Hg–S–Hg)'s under the C_{3v} symmetry.

Table 4. The K(Hg-C), ν(Hg-C), ionization potentials (IP), coupling constants ($J(^{199}Hg-^{1}H)$), and bond-dissociation energies (D) of CH_3HgX complexes

X	K(Hg-C) md/Å	ν(Hg-C) cm^{-1}	IP[32] eV	$J(^{199}Hg-^{1}H)$[1] Hz	D[3,a] kcal/mol
F	2.55	561	17.42	—	—
CN	2.61	565	14.1	176	—
SCN	2.39	540	—	208	—
Cl	2.38_2	539	13.01	215.8	63.8±2.9
Br	2.37_7	538	11.84	212	61.3±2.8
$S(HgCH_3)_2$	1.86	538 529	—	—	—
I	2.27	526	10.45	200	58.5±3.1
$SHgCH_3$	2.38	530 525	—	156.6	—
CH_3	2.330	550 515	9.95	100.6	51.5±2
SCH_3	2.33	533	9.84[b]	—	—
$As(CH_3)_3$	2·37	537	8.3	180	—

a) $CH_3HgX \rightarrow \cdot CH_3 + \cdot HgX$ in the gas phase at 20 °C. b) Transferred from the IP of CH_3SH.

on the IR and Raman spectra used for the calculations were taken from the literature[4-19] except for $X=SCH_3$, $SHgCH_3$ and $S(HgCH_3)_2$, the data of which are obtained in this work. Some features of these IR and Raman spectra reduced from the assignments are described.

Experimental

The numerical data of the IR and Raman spectra used for the present calculations were taken from the literature[4-19] except for the following three samples, which were prepared according to the literature[20,21] and well confirmed by measurements of the mp and by elemental analysis of mercury:

CH_3HgSCH_3: mp 25 °C (lit,[20] 25 °C).

$(CH_3Hg)_2S$: mp 145 °C (lit,[20] 145 °C). Found: Hg, 85.6%. Calcd: Hg, 86.6%.

$(CH_3Hg)_3SClO_4$: mp 144 °C (lit,[21] 143 °C). Found: Hg, 77.63%. Calcd: Hg, 77.31%.

The infrared spectra of CH_3HgSCH_3, $(CH_3Hg)_2S$ and $(CH_3Hg)_3SClO_4$ were recorded with KBr disks from 300 to 4000 cm^{-1} and with Nujol mulls on polyethylene sheet from 30 to 600 cm^{-1} at 23 °C. The infrared spectra of $(CH_3Hg)_2S$ and $(CH_3Hg)_3SClO_4$ were recorded from 200 to 600 cm^{-1} with polyethylene matrices at 77 K. The instruments used were a JASCO-403G grating IR spectrometer and a HITACHI FIS-3 grating far-IR spectrometer. The Raman spectra of $(CH_3Hg)_3SClO_4$ were recorded in the powder state and in a saturated aqueous solution (about 15 wt%) with a JEOL JRS-O2AS and a JRS-S1 Raman spectrometer equipped with an Ar^+-ion laser as a source.

Calculations

The vibrational analysis was carried out using the Urey-Bradley field. The methyl group was treated as a dynamic unit. The bond lengths and bond angles used for the calculations are listed in Table 1 along with the references.

Results and Discussion

The IR and Raman spectra of CH_3HgSCH_3 have previously been reported.[18,19] The IR spectrum of $(CH_3Hg)_2S$ has been reported only in the NaCl region,[20] and so the IR spectrum in a region lower than 650 cm^{-1} was measured in this study. Its Raman spectrum could not be recorded, because $(CH_3Hg)_2S$ decomposed into HgS within one minute after exposure to the Ar^+-ion laser beam. The spectra and their assignments will be reported in a separate paper. Here the description will be limited to some tendencies reduced from the assignments of the bands for CH_3HgSCH_3, $(CH_3Hg)_2S$, and $(CH_3Hg)_3SClO_4$: a) the asymmetric deformation, the symmetric deformation, and the rocking vibrations of the methyl group appear at 1404, 1177, and 768 cm^{-1} respectively, when the methyl group is attached to the mercury atom, and at 1431, 1310—1284, and 955 cm^{-1} when it is attached to the sulfur atom; b) the Hg–C stretching vibration of CH_3–Hg is found at 515—565 cm^{-1}; c) the Hg–S stretching bands of $(CH_3Hg)_2S$ split into four under the influence of the lattice field, though there should be two; therefore the values of (354+334)/2 and (310+291)/2 cm^{-1} are used for the calculations as the antisymmetric and symmetric Hg–S stretching frequencies respectively.

As may be seen in Table 2, a satisfactory agreement between the calculated and experimentally observed frequencies is obtained. The force constants are summarized in Table 3. Arranging the X of CH_3HgX in an increasing order of K(Hg–C), a vibrational *trans* influence series is obtained, where the numerical values of K(Hg–C) are written in parentheses in md/Å units: $S(HgCH_3)_2(1.86) < I(2.27) < SCH_3(2.33) = CH_3(2.330) < As(CH_3)_3(2.37) < Br(2.37_7) \leq SHgCH_3(2.38) \leq Cl(2.38_2) < SCN(2.39) < F(2.55) < CN(2.61)$.

On the other hand, the K(Hg–C) of CH_3HgX in the generalized valence field increase in the following order of X: I(2.290 md/Å)[12] < Cl(2.42)[9] < Br(2.48)[10] according to Meić[9,10,12] and Randić,[9,10] or I(2.50 md/Å) < Br(2.60) < CN(2.78) according to Goggin and Woodward.[13] Since not only the values of K(Hg–C) but also the order of X thus depend upon the types of the potential function, the recalculation in this work is regarded as significant for the investigation of

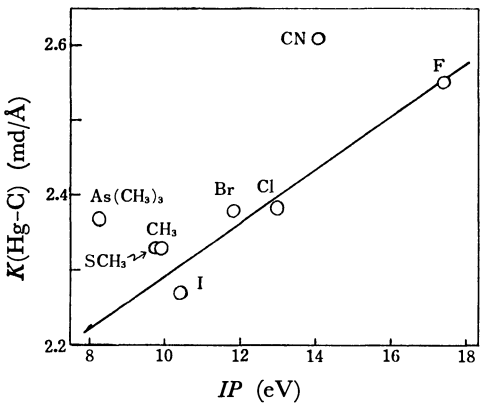

Fig. 1. Relation between K(Hg–C) and the ionization potentials of X.

the *trans* influence.

Let us now discuss the factor which will determine the K(Hg–C). As may be seen in Fig. 1, a linear relationship is found between K(Hg–C) and the first ionization potential, *IP*, of X for this series, except in the cases of X=CN and $As(CH_3)_3$, whose K(Hg–C) values are considerably larger than those to be expected from the linearity. The increase in K(Hg–C) with the increase in the first ionization potential of X can be explained in terms of the inductive effect of X through the σ path. On the other hand, the deviation in the linearity may be ascribed to the π-back donation from the mercury to the arsine group.

Some previously reported data may be referred to in order compare them with the presented vibrational *trans*-influence order (Table 4). The order of K(Hg–C) is considerably different from that of $J(^{199}Hg\text{–}CH_3)$[1,2]: $CH_3 < SHgCH_3 < CN < As(CH_3)_3 < I < SCN < Br < Cl$. Particularly, cyanide changes its position extremely between K(Hg–C) and $J(^{199}Hg\text{–}CH_3)$. The K(Hg–C) increases parallel to the increase in the bond-dissociation energy.[3] It is worthwhile to refer the present results to the well-known *trans*-effect series established in Pt(II) complexes, where CN<I<Br<Cl.[33] Thus, the presently obtained *trans*-influence series for methylmercury compounds is unique in the position of CN.

The author is gratefull to Professor Sigeo Kida of Kyushu University for his valuable discussions. The numerical calculations were carried out with the FACOM 230-25 computer system of Kumamoto University and with the FACOM 230-60 computer system of Kyushu University.

References

1) J. V. Hatton and W. G. Schneider, and W. Siebrand, *J. Chem. Phys.*, **39**, 1330 (1963).
2) H. F. Henneike, *J. Am. Chem. Soc.*, **94**, 5945 (1972).
3) T. Charnley and H. A. Skinner, *J. Chem. Soc.*, **1951**, 1921.
4) H. S. Gutowsky, *J. Chem. Phys.*, **17**, 128 (1949).
5) A. M. W. Bakke, *J. Mol. Spectrosc.*, **41**, 1 (1972).
6) D. Breitinger, A. Zober, and M. Neubauer, *J. Organomet. Chem.*, **30**, C49 (1971).
7) J. H. S. Green, *Spectrochim. Acta*, **24A**, 863 (1968).
8) Z. Meić and M. Randić, *J. Mol. Spectrosc.*, **39**, 39 (1971).
9) Z. Meić and M. Randić, *J. Chem. Soc. Faraday Trans. 2*, **68**, 444 (1972).
10) Z. Meić and M. Randić, *Trans. Faraday Soc.*, **64**, 1438 (1968).
11) Z. Meić, *Croat. Chem. Acta*, **41**, 179 (1969).
12) Z. Meić, *J. Mol. Struct.*, **23**, 131 (1974).
13) P. L. Goggin and L. A. Woodward, *Trans. Faraday Soc.*, **62**, 1423 (1966).
14) J. R. Hall and J. C. Mills, *J. Organomet. Chem.*, **6**, 444 (1966).
15) R. P. J. Cooney and J. R. Hall, *Aust. J. Chem.*, **22**, 2117 (1969).
16) J. Relf and R. P. Cooney, *J. Organomet. Chem.*, **39**, 75 (1972).
17) P. L. Goggin, R. J. Goodfellow, S. R. Haddock, and (in part) J. G. Eary, *J. Chem. Soc. Dalton*, **1972**, 647.
18) R. A. Nyquist and J. R. Mann, *Spectrochim. Acta*, **28A**, 511 (1972).
19) N. Iwasaki, J. Tomooka, and K. Toyoda, *Bull. Chem. Soc. Jpn.*, **47**, 1323 (1974).
20) J. H. Clarke and L. A. Woodward, *Spectrochim. Acta*, **23A**, 2077 (1967).
21) T. Kondo, *Yakugaku Zasshi*, **84**, 137 (1963).
22) E. S. Rao, B. P. Stoicheff, and R. Turner, *Can. J. Phys.*, **38**, 1516 (1960).
23) A. F. Wells, "Structural Inorganic Chemistry," Oxford Univ. Press (1962), p. 892.
24) W. Gordy and J. Scheridan, *J. Chem. Phys.*, **22**, 92 (1954).
25) C. Feige and H. Hartmann, *Z. Naturforsch.*, **22a**, 1286 (1967).
26) J. C. Mills, H. S. Preston, and C. H. L. Kennard, *J. Organomet. Chem.*, **14**, 33 (1968).
27) a) D. Gredenić, *Quart. Rev.*, **19**, 303 (1965); b) "Tables of Interatomic Distances and Configuration in Molecules," Chem. Soc. Spec. Publ., No. 11 (1958) and No. 18.
28) R. D. Shannon, C. T. Prewitt, *Acta Crystallogr.*, **B25**, 925 (1969).
29) S. F. Watkins, *J. Chem. Soc., A*, **1970**, 168.
30) D. C. Bradley and N. R. Kuncher, *J. Chem. Phys.*, **40**, 2258 (1964).
31) a) M. Kesler, *Croat. Chem. Acta*, **34**, 123 (1962); b) M. Kesler, *ibid.*, **36**, 165 (1964).
32) V. I. Vedeneyev, L. V. Gurvich, V. N. Kondrat'yev, V. A. Medvedev, and Ye, L. Frankevich, "Bond Energies, Ionization Potentials and Electron Affinities," Edward Arnold, London (1966), Table 11.
33) F. Basolo and R. Johnson, "Coordination Chemistry," W. A. Benjamin, New York (1964).

Preparation and Geometrical Isomers of Cobalt(III) Complexes with Tridentate O–S–O Ligand Thiodiacetate or 3,3′-Thiodipropionate

Kan KANAMORI, Tokiko SUDANI, and Kiyoyasu KAWAI

Faculty of Literature and Science, Toyama University, Gofuku, Toyama 930

(Received March 31, 1976)

cis(S)-fac- and *trans(S)-fac-*Isomers of bis(thiodiacetato)cobaltate(III), *trans(O)-mer-*, *s-cis(O)-fac-*, and *u-cis(O)-fac-*isomers of (thiodiacetato)(diethylenetriamine)cobalt(III) and *trans(O)-mer-*isomer of (3,3′-thiodipropionato)(diethylenetriamine)cobalt(III) were prepared. Their geometrical configurations were assigned on the basis of their absorption and PMR spectra. The stereochemistry of the Co(III) complex with a tridentate ligand thiodiacetate is similar to that of the Co(III) complex with iminodiacetate.

Metal complexes with amino carboxylates containing the sulfide group have been recognized as regards their biochemical importance.[1] However, only a few studies have been carried out on stereochemistry of cobalt(III) complexes with sulfide ligands.[2] Thiodiacetic acid we chose is a simple ligand of typical linear type which contains one sulfide group. The framework of the coordinated ligand around Co(III) ion is similar to that of iminodiacetate ligand O–N–O.

In this paper,[3] the preparation and separation of isomers of bis(thiodiacetato)cobaltate(III), (thiodiacetato)(diethylenetriamine)cobalt(III) and (3,3′-thiodipropionato)(diethylenetriamine)cobalt(III) are reported. The stereochemistry of the complexes is discussed in relation to that of the ida Co(III) complexes.[4,5]

Experimental

Preparation of cis(S)- *and* trans(S)-*Hydrogen Bis(thiodiacetato)-cobaltate(III)* : $H[Co(tda)_2]\cdot nH_2O$

(1) cis(S)-$H[Co(tda)_2]\cdot 3H_2O$ *(Green Isomer)*: To a suspension containing 3.0 g (0.02 mol) of thiodiacetic acid in 30 dm³ of water was added 1.1 g (0.01 mol) of freshly prepared $Co(OH)_3$.[6] The mixture was stirred at room temperature for about an hour. The reaction mixture was filtered in order to remove a small amount of insoluble material. 20 dm³ of ethanol was added to the filtrate. The green complex deposited was filtered and washed with ethanol and ether. The crude complex was recrystallized from as little water as possible by adding a small amount of ethanol. Found: C, 23.00; H, 3.22; S, 15.08%. Calcd for $H[CoC_8H_8O_8S_2]\cdot 3H_2O$: C, 23.42; H, 3.69; S, 15.63%.

(2) trans(S)-$H[Co(tda)_2]\cdot 6H_2O$ *(Violet Isomer)*: The reaction mixture obtained by the same method as in (1) was stirred at about 80 °C for half an hour. The resulting mixture was filtered in order to remove a fairly large amount of insoluble material. The violet filtrate was cooled to room temperature. A small amount of violet precipitate appeared. Recrystallization of the complex was unsuccessful because of its instability in water. Found: C, 20.48; H, 4.31; S, 14.11%. Calcd for $H[CoC_8H_8O_8S_2]\cdot 6H_2O$: C, 20.69; H, 4.57; S, 13.81%.

(3) Preparation and Separation of the Isomers of $[Co(tda)(dien)]^+$: A mixture containing 5.0 g (0.019 mol) of $[CoCl_3(dien)]$,[7] 4.2 g (0.028 mol) of thiodiacetic acid and 1.6 g (0.028 mol) of potassium hydroide in 50 dm³ of water was heated at *ca.* 50 °C and stirred for about an hour. The resulting mixture was filtered in order to remove a small amount of insoluble material. The red filtrate was poured into a column (30 mm × 450 mm) containing strong-acid cation exchange resin (Dowex 50 W × 8 200—400 mesh, hydrogen form). After the column had been swept with water, the adsorbed band was eluted with 0.15 M sodium perchlorate at a rate of *ca.* 2.5 dm³/min. Three colored bands, red (I), pinkish red (II), and pink (III) were eluted one after the other. Each eluate was concentrated to dryness in a vacuum evaporator. The resulting isomers contaminated with a large amount of sodium perchlorate were washed with ethanol. Each isomer obtained was dissolved in as little water as possible to recrystallize. The pure complex was obtained by adding ethanol to the solution. The yield of isomer (I) was less than those of other two. Found for isomer (I): C, 22.88; H, 4.31; N, 10.52%. Found for isomer (II): C, 22.93; H, 4.33; N, 10.21%. Found for isomer (III): C, 22.89; H, 4.55; N, 10.38%. Calcd for $[CoC_8H_{17}N_3O_4S]ClO_4\cdot 0.5H_2O$: C, 22.95; H, 4.34; N, 10.04%.

(4) Preparation of $[Co(tdp)(dien)]ClO_4\cdot H_2O$: The complex was prepared by the same method as in (3) except for the use of 3,3′-thiodipropionic acid instead of thiodiacetic acid. Only one violet band was eluted. Found: C, 26.13; H, 5.21; N, 9.38%. Calcd for $[CoC_{10}H_{21}N_3O_4S]ClO_4\cdot H_2O$: C, 26.35; H, 5.10; N, 9.22%.

Measurement. Electronic absorption spectra were measured with a Hitachi 124 spectrophotometer. PMR spectra were recorded on a JEOL MH-60 spectrometer. Deuterium oxide was used as a solvent with *t*-butyl alcohol (TBA) as an internal standard.

Results and Discussion

Three geometrical isomers, one meridional(*mer*) and two facial(*fac*) with respect to the coordination of O–S–O ligand thiodiacetate, are expected for bis(thiodiacetato)cobaltate(III) complex (Fig. 1). However, only two isomers were isolated. The electronic absorption spectra of the isomers obtained are shown in Fig. 2 and their data are given in Table 1. The charge transfer band due to the coordinated sulfide of bis(L-methioninato)Co(III) complex is situated at the lower energy side for *trans(S)*-isomer in comparison with *cis(S)*-isomer.[2] We see from Fig. 2 and Table 1 that the sulfide charge transfer band of the green isomer is situated at the energy side (*ca.* 32×10^3 cm^{-1}) higher

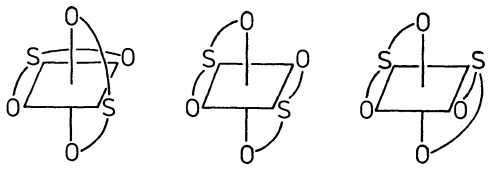

trans(S)-mer *trans(S)-fac* *cis(S)-fac*

Fig. 1. The geometrical isomers of $[Co(tda)_2]^-$.

TABLE 1. ABSORPTION DATA OF $[Co(tda)_2]^-$, $[Co(tda)(dien)]^+$, AND $[Co(tdp)(dien)]^+$ a)

	First band $\nu_{max}(\log \varepsilon_{max})$	Second band $\nu_{max}(\log \varepsilon_{max})$	Sulfide C.T. $\nu_{max}(\log \varepsilon_{max})$	Other bands $\nu_{max}(\log \varepsilon_{max})$
trans(S)-fac-$[Co(tda)_2]^-$ violet isomer	18.0 (2.06)	——	29.5 (3.75)	*ca.* 21 (1.6) 38.5 (3.98)
cis(S)-fac-$[Co(tda)_2]^-$ green isomer	16.9 (2.18)	*ca.* 24 (2.3)	*ca.* 32 (3.8)	39.5 (4.02)
trans(O)-mer-$[Co(tda)(dien)]^+$ isomer I	19.4 (1.95)	*ca.* 28 (2.3)	*ca.* 35 (3.7)	43.9 (4.26)
s-cis(O)-fac-$[Co(tda)(dien)]^+$ isomer II	19.9 (1.96)	*ca.* 29 (2.2)	*ca.* 35 (3.9)	44.6 (4.21)
u-cis(O)-fac-$[Co(tda)(dien)]^+$ isomer III	19.3 (2.05)	28.2 (2.39)	*ca.* 35 (3.8)	42.7 (4.25)
trans(O)-mer-$[Co(tdp)(dien)]^+$	18.2 (2.08) *ca.* 21 (1.7)	26.6 (2.39)	*ca.* 36 (3.7)	39.8 (3.72)

a) The frequencies are given in $10^3\ cm^{-1}$.

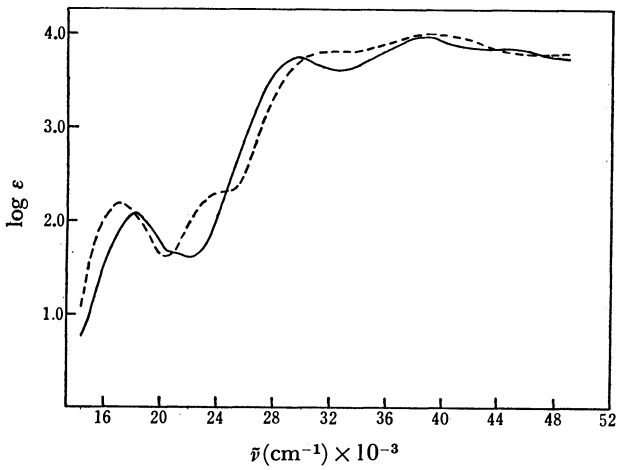

Fig. 2. Absorption (AB) curves of $[Co(tda)_2]^-$ ions in water: *trans(S)-fac*-$[Co(tda)_2]^-$; violet isomer (——), *cis(S)-fac*-$[Co(tda)_2]^-$; green isomer (----).

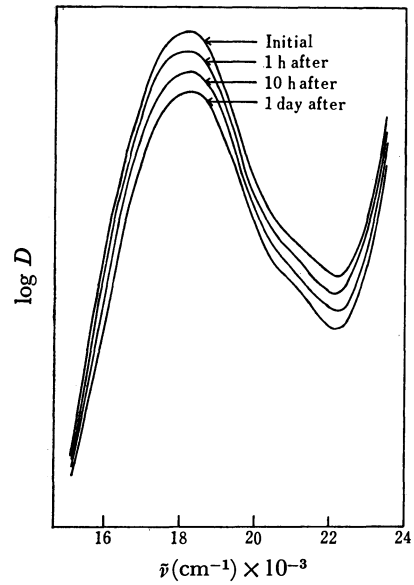

Fig. 3. Time dependence of absorption intensity of *trans(S)-fac*-$[Co(tda)_2]^-$ in water.

than that of the violet one (*ca.* $30 \times 10^3\ cm^{-1}$). This indicates that the former has *cis(S)* configuration and the latter *trans(S)* one. This assignment is supported by the semiempirical consideration for the pattern of the first absorption band.[8] Namely, *cis(S)*-isomer might be expected to show a sharp band in the lower energy side and *trans(S)*-isomer a broad one in the higher energy side. This is realized as shown in Fig. 2. Considering the framework of the coordinated ligands, iminodiacetate (ida) and tda, $[Co(tda)_2]^-$ is similar to $[Co(ida)_2]^-$ though the ligand field strength due to tda is slightly less than that of ida. In the case of ida Co-(III) complex, the *mer*-isomer has not been obtained except for the mixed complex $[Co(ida)(dien)]^+$.[5] This suggests that the *trans(S)*-isomer isolated in the present work is a *fac* coordinated one rather than a *mer* one.

The *trans(S)*-isomer shows an interesting shoulder at *ca.* $21 \times 10^3\ cm^{-1}$ (Fig. 2), which is independent of the degradation product or the isomerization of the complex, since its absorption intensity diminishes regularly with that of the main absorption peak at *ca.* $18 \times 10^3\ cm^{-1}$ (Fig. 3).

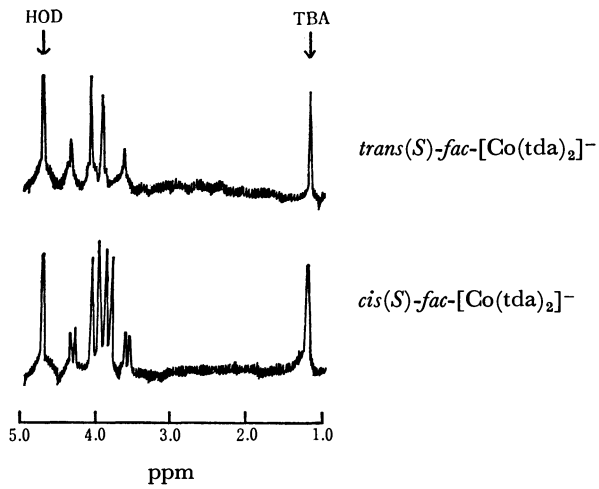

Fig. 4. Proton magnetic resonance spectra (60 MHz) of the two isomers of $[Co(tda)_2]^-$.

TABLE 2. CHEMICAL SHIFTS[a] AND COUPLING CONSTANTS[b] FOR THE AB PROTONS OF $[Co(tda)_2]^-$ AND $[Co(tda)(dien)]^+$

	$[Co(tda)_2]^-$		$[Co(tda)(dien)]^+$	
	trans(S)-fac violet isomer	*cis(S)-fac* green isomer	*s-cis(O)-fac* isomer II	*u-cis(O)-fac* isomer III
AB pattern	4.134	4.067	4.037	4.178
		3.988		4.083
	3.667	3.616	3.613	3.619
		3.530		
J_{AB} (Hz)	17	18	17	16

a) Values are ppm downfield from TBA at $\delta = 1.234$ ppm (wrt DSS at 0).
b) Mean values in Hz; signs were not determined.

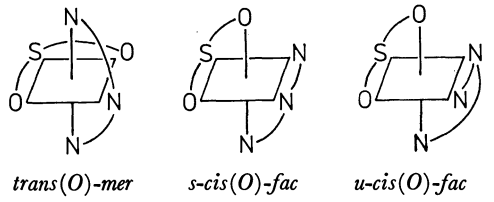

Fig. 5. The geometrical isomers of $[Co(tda)(dien)]^+$.

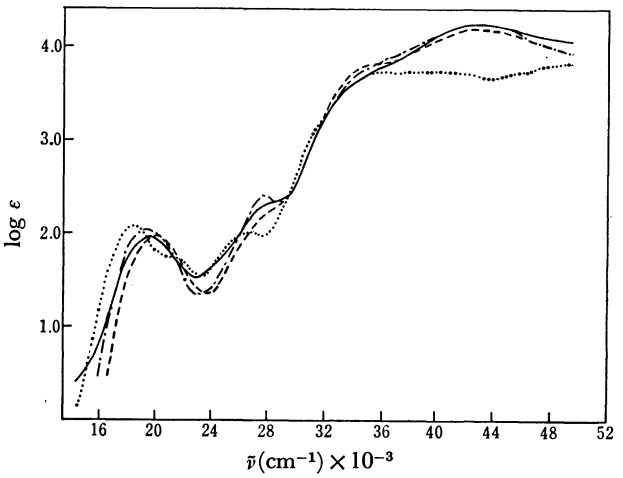

Fig. 6. Absorption (AB) curves of $[Co(tda)(dien)]^+$ isomers and $[Co(tda)(dien)]^+$ in water : *trans(O)-mer*-$[Co(tda)(dien)]^+$; isomer I(——), *s-cis(O)-fac*-[Co(dta)-(dien)]$^+$; isomer II (----), *u-cis(O)-fac*-[Co(tda)-(dien)]$^+$; isomer III (— — —), *trans(O)-mer*-[Co(tdp)-(dien)]$^+$ (·····).

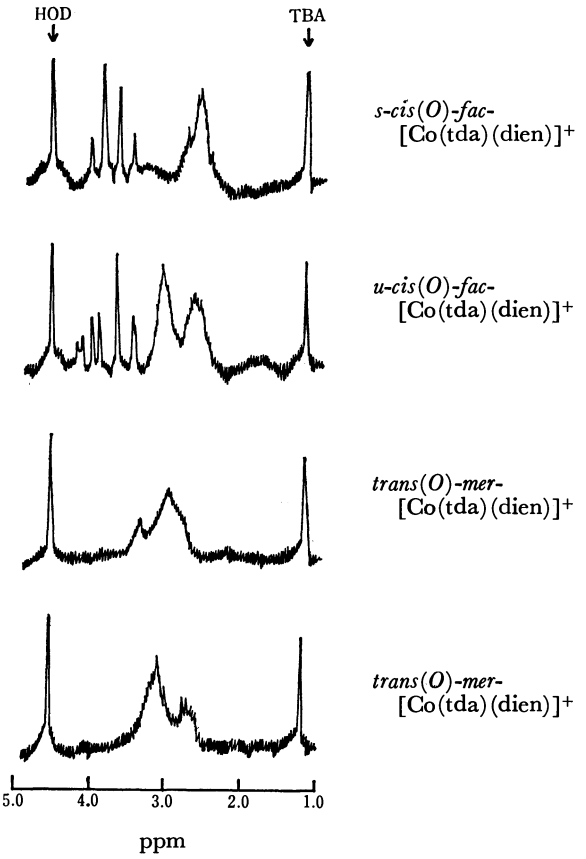

Fig. 7. Proton magnetic resonance spectra (60 MHz) of the three isomers of $[Co(tda)(dien)]^+$ and the one isomer of $[Co(tdp)(dien)]^+$.

The PMR spectra of *cis(S)*- and *trans(S)*-$[Co(tda)_2]^-$ are shown in Fig. 4 and their data in Table 2. Since the *trans(S)*-isomer has a plane of symmetry (Fig. 1), two pairs of methylene protons in the coordinated tda are fixed in the same chemical environment. The *trans(S)*-isomer is thus expected to exhibit one AB quartet due to two spin-coupled protons. On the other hand, the *cis(S)*-isomer is C_1 symmetry and two AB quartets are expected. As seen in Fig. 4, the *trans-(S)*-isomer assigned from the absorption spectral consideration exhibits one AB quartet, whereas the *cis(S)*-isomer shows two AB quartets.

In order to confirm the assignment of geometrical isomers of $[Co(tda)_2]^-$, the mixed type complex $[Co(tda)-(dien)]^+$ was synthesized. Three geometrcial isomers *trans(O)-mer*, *s-cis(O)-fac*, and *u-cis(O)-fac** are expected (Fig. 5). Three isomers were isolated by ion-exchange column chromatographic method (see Experimental). The electronic absorption spectra of the three isomers of $[Co(tda)(dien)]^+$ are shown in Fig. 6. From the splitting pattern of the first absorption band,[8] the isomer first eluted is assigned to *trans(O)*-type which only *mer* coordination is possible. Thus, it is considered that the remaining two isomers are *cis(O)-fac*-type. This designation coincides with that on the basis of the column chromatographic elution order,[9] *viz.*,

* The prefix *s* denotes symmetrical arrangement and prefix *u* unsymmetrical arrangement.

the *trans(O)-mer*-isomer which has low dipole moment is eluted earlier than the two *cis(O)*-isomers.

In order to assign the remaining two *cis(O)*-isomers, their PMR spectra were recorded (Fig. 7 and Table 2). The plane of symmetry in *s-cis(O)-fac*-[Co(tda)(dien)]$^+$ gives rise to only one AB pattern as in the case of *trans-(S)-fac*-[Co(tda)$_2$]$^-$. On the other hand, *u-cis(O)-fac*-[Co(tda)(dien)]$^+$ has no plane of symmetry. The two pairs of methylene protons of the tda ligand should differ in the chemical environment (Fig. 5). In Fig. 7, the PMR spectrum of isomer II shows only one AB quartet and that of isomer III exhibits the split at the lower field component of the corresponding AB quartet. It is unknown in the present that the high field component does not split. This consideration leads isomer II to *s-cis(O)-fac*-[Co(tda)(dien)]$^+$ and isomer III to *u-cis(O)-fac*-[Co(tda)(dien)]$^+$. On the basis of this assignment, the column chromatographic elution order for the three isomers becomes *trans(O)-mer*, *s-cis(O)-fac* and *u-cis(O)-fac*. The order is similar to that for the isomers of analogous complex, [Co(ida)-(dien)]$^+$.[5] The PMR spectrum of *trans(O)-mer*-[Co-(tda)(dien)]$^+$ provided little information on the structure of the isomer because of its low solubility in D_2O.

The coordination mode of ida is regulated in [Co-(ida)(dien)]$^+$ by the dominant coordination of dien.[5] The present results are similar to the case of ida Co(III) complex. Of the three isomers of [Co(tda)$_2$]$^-$ complex, *viz.*, the two *fac*-isomers except for *mer*-type were obtained and the three isomers containing *mer*(tda)-type were obtained for [Co(tda)(dien)]$^+$ complex.

The above conclusion can be confirmed by the attempt to isolate the isomers of [Co(tdp)(dien)]$^+$. Molecular model examination suggests that in expansion from the five-membered chelate ring to the six-membered ring, the *fac* coordination of O–S–O ligand strains more than the *mer* one. Only one isomer was obtained for [Co(tdp)(dien)]$^+$ complex. The absorption spectral measurement indicates that the isomer obtained is *mer*(tdp)-form (Fig. 6). The broad splitting of the first absorption band is more remarkable for *trans(O)-mer*-[Co(tdp)(dien)]$^+$ than for *trans(O)-mer*-[Co(tda)(dien)]$^+$. This may arise from the weakness of the ligand field strength due to the change from the five-membered chelate ring to the six-membered ring.

The PMR spectrum of *trans(O)-mer*-[Co(tdp)(dien)]$^+$ where ABCD or AA'BB' pattern can be expected is apparently similar in chemical shifts to that of *trans(O)-mer*-[Co(tda)(dien)]$^+$, but the assignment in detail is difficult. The results indicate that the only one isomer for [Co(tdp)(dien)]$^+$ is *trans(O)-mer*-form and that the molecular model consideration is reasonable.

In conclusion, the stereochemistry of Co(III) complex with tda is similar to that of ida Co(III) complex in both case of the bis type[4] and the mixed one.[5] The tda ligands in *trans(S)*-[Co(tda)$_2$]$^-$ is facially coordinated as in the case of *trans(N)*-[Co(ida)$_2$]$^-$.

References

1) C. A. McAuliffe, J. V. Quagliano, and L. M. Vallarino, *Inorg. Chem.*, **5**, 1996 (1966); S. E. Livingstone and J. D. Nolan, *ibid.*, **7**, 1447 (1968); C. A. McAuliffe, *ibid.*, **12**, 1699 (1973).

2) J. H. Worrell and D. H. Busch, *Inorg. Chem.*, **8**, 1563 (1969); J. Hidaka, S. Yamada, and Y. Shimura, *Chem. Lett.*, **1974**, 1478.

3) The following abbreviations are used for the ligands; "ida" for an iminodiacetate ion, "tda" thiodiacetate ion, "tdp" 3,3'-thiodipropionate ion and "dien" diethylenetriamine.

4) J. Hidaka, Y. Shimura, and R. Tsuchida, *Bull. Chem. Soc. Jpn.*, **35**, 567 (1962).

5) J. I. Legg and D. W. Cooke, *Inorg. Chem.*, **5**, 594 (1966).

6) H. Ley and H. Winkler, *Ber.*, **42**, 3900 (1909); **45**, 375 (1912).

7) *Inorg. Synth.*, **7**, 207 (1963).

8) H. Yamatera, *Bull. Chem. Soc. Jpn.*, **31**, 95 (1958).

9) G. V. Kauffman, R. P. Pinnel, and L. T. Takahashi, *Inorg. Chem.*, **1**, 544 (1962).

A Kinetic Study of the Chromium(II) Reduction of Several (Amino acid)pentaamminecobalt(III) Complexes

Hiroshi OGINO, Keiichi TSUKAHARA, and Nobuyuki TANAKA

Department of Chemistry, Faculty of Science, Tohoku University, Aoba, Aramaki, Sendai 980

(Received April 30, 1976)

A kinetic study of the chromium(II) reduction of (O-bonded amino acid)pentaamminecobalt(III) complexes has been carried out in acid solutions. The second-order rate constants in $M^{-1}\,s^{-1}$ (1 M = 1 mol dm^{-3}) at 25 °C and I = 1.0 M ($NaClO_4$) for α-alanine, phenylalanine, α-aminoisobutyric acid, β-alanine, β-aminobutyric acid, γ-aminobutyric acid, and ε-aminohexanoic acid complexes are 1.8×10^{-2}, 1.5×10^{-2}, 2.4×10^{-3}, 7.5×10^{-2}, 5.0×10^{-2}, 1.22×10^{-1}, and 1.49×10^{-1} respectively. The values of ΔH^{*} lie in the range of 6.4—7.7 kcal mol^{-1} (1 cal = 4.184 J), and those of ΔS^{*}, in the range of −42—−37 cal $K^{-1}\,mol^{-1}$, except for the α-aminoisobutyric acid complex, the ΔH^{*} and ΔS^{*} values of which are 11.4 kcal mol^{-1} and −32 cal $K^{-1}\,mol^{-1}$ respectively. The role of the amino acid ligands in the inner-sphere electron-transfer reactions is discussed.

The chromium(II) reduction of a number of carboxylatopentaamminecobalt(III) complexes has been known to proceed predominantly through an inner-sphere mechanism.[1,2] In these reactions, the steric crowding of the alkyl groups influences the electron-transfer rate significantly. The chromium(II) reduction of the pentaammineglycinecobalt(III) complex has also been investigated by several researchers[3-5] and found to proceed predominantly through an inner-sphere mechanism. The reduction rate of this complex was found to be smaller than that of the acetatopentaamminecobalt(III) complex. This fact was interpreted in terms of the difference in the positive charge on the complexes.

In this work, the rate of the chromium(II) redution of a number of (O-bonded amino acid)pentaamminecobalt(III) complexes was measured in acid solutions in order to reveal the factors which control the electron-transfer reaction rate. The abbreviations used in this work are as follows: amino acid=amH, $^{-}O_2CCH_2NH_3^{+}$ (glycine)=glyH, $^{-}O_2CCH(CH_3)NH_3^{+}$ (α-alanine)=alaH, $^{-}O_2C(CH_2)_2NH_3^{+}$ (β-alanine)=balaH, $^{-}O_2CCH(CH_2C_6H_5)NH_3^{+}$ (phenylalanine)=pheH, $^{-}O_2CCH_2CH(CH_3)NH_3^{+}$ (β-aminobutyric acid)=babH, $^{-}O_2CC(CH_3)_2NH_3^{+}$ (α-aminoisobutyric acid)=aibH, $^{-}O_2C(CH_2)_3NH_3^{+}$ (γ-aminobutyric acid)=gabH, and $^{-}O_2C(CH_2)_5NH_3^{+}$ (ε-aminohexanoic acid)=ahH.

Experimental

Reagents. (O-bonded amino acid)pentaamminecobalt(III) complexes were prepared as perchlorates by the method reported previously.[6,7] The $[Co(babH)(NH_3)_5](ClO_4)_3$ and $[Co(ahH)(NH_3)_5](ClO_4)_3$ complexes were purified by the use of an SP-Sephadex C-25 column. Each amino acid complex adsorbed on the column moved faster than aquapentaamminecobalt(III) ions with an 0.3 M $NaClO_4$ solution at pH 3 (1 M = 1 mol dm^{-3}). Table 1 gives the analytical data of the complexes used in this work.

All the solutions used for the measurements were prepared from redistilled water. A solution of hexaaquachromium(III) perchlorate was prepared from sodium dichromate as has been reported previously.[8] A chromium(II) perchlorate solution was prepared by the reduction of the hexaaquachromium(III) perchlorate with a zinc amalgam in a nitrogen atmosphere. The hydrogen-ion concentration of the chromium(II) solution was determined by a method reported previously.[9,10] A sodium perchlorate solution was prepared by neutralizing a primary standard sodium carbonate solution with perchloric acid.

Product Analyses. The products of the reactions of Cr^{2+} ions with $Co(alaH)(NH_3)_5^{3+}$ and $Co(aibH)(NH_3)_5^{3+}$ ions were examined. After the reaction had been quenched by the introduction of air into the system, the solution was cooled and passed through an SP-Sephadex C-25 column chilled below 5 °C with a water-jacket. The colored species were adsorbed on the column in four bands: pink, bluish violet, red, and green from the bottom to the top of the column. The pink species was eluted with an 0.1 M $HClO_4$–0.1 M $NaClO_4$ solution and was identified as Co^{2+} ions. The bluish violet species was eluted with an 0.1 M $HClO_4$–0.3 M $NaClO_4$ solution and was found to be chromium(III) species. The visible spectrum of the species was similar to $Cr(H_2O)_6^{3+}$, but not identical. Therefore, the species was considered to be $Cr(amH)(H_2O)_5^{3+}$ or a mixture of $Cr(amH)(H_2O)_5^{3+}$ and $Cr(H_2O)_6^{3+}$. The red species was eluted with an 0.1 M $HClO_4$–0.3 M $NaClO_4$ solution and identified as

Table 1. Analytical data of the cobalt(III) complexes used in this work

Compound	Calcd (%)			Found (%)		
	C	H	N	C	H	N
$[Co(O_2CCH_2NH_3)(NH_3)_5](ClO_4)_3$	4.49	4.14	15.69	4.37	4.36	15.75
$[Co(O_2CCH(CH_3)NH_3)(NH_3)_5](ClO_4)_3$	6.78	4.18	15.81	6.77	4.39	15.93
$[Co(O_2CC(CH_3)_2NH_3)(NH_3)_5](ClO_4)_3$	8.80	4.44	15.41	8.60	4.59	15.14
$[Co(O_2C(CH_2)_2NH_3)(NH_3)_5](ClO_4)_3$	6.78	4.18	15.81	6.46	4.31	15.80
$[Co(O_2C(CH_2)_3NH_3)(NH_3)_5](ClO_4)_3$	8.80	4.44	15.41	9.08	4.62	15.23
$[Co(O_2C(CH_2)_5NH_3)(NH_3)_5](ClO_4)_3\cdot 2H_2O$	11.82	5.30	13.79	12.36	5.03	13.32
$[Co(O_2CCH(CH_2C_6H_5)NH_3)(NH_3)_5](ClO_4)_3\cdot H_2O$	17.27	4.52	13.43	17.63	4.61	13.37
$[Co(O_2CCH_2CH(CH_3)NH_3)(NH_3)_5](ClO_4)_3$	8.80	4.44	15.41	8.82	4.62	15.20

$Co(amH)(NH_3)_5^{3+}$. The green species was eluted with an 0.1 M $HClO_4$–0.9 M $NaClO_4$ solution and identified as $(H_2O)_4Cr(OH)_2Cr(H_2O)_4^{4+}$, which was considered to have been derived by the air oxidation of Cr^{2+} ions.[11,12]

The chromium content was determined spectrophotometrically in the form of CrO_4^{2-} after oxidation with an alkaline hydrogen peroxide solution. The cobalt(II) content was determined spectrophotometrically as $Co(NCS)_4^{2-}$ in 50% acetone. The cobalt(III) complexes were reduced to cobalt(II) with a zinc amalgam and then subjected to the determination of the cobalt(II) as $Co(NCS)_4^{2-}$. From the results of the product analyses, it was confirmed that 1 mol of Cr^{2+} is consumed per mole of the $Co(alaH)(NH_3)_5^{3+}$ or $Co(balaH)(NH_3)_5^{3+}$ complex.

The amounts of amH and Co^{2+} released by the Cr^{2+} reduction were determined for the reactions of $Co(alaH)(NH_3)_5^{3+}$ and $Co(aibH)(NH_3)_5^{3+}$. The following procedures were employed: the reaction mixture was poured into an SP-Sephadex column. The solution which was passed through the column was reserved. The effluent was collected until the Co^{2+} band almost reached the bottom of the column by eluting with a cold 0.1 M $HClO_4$–0.1 M $NaClO_4$ solution. The solution reserved and the effluent were then combined and alkalified with NaOH. The solution was heated on a boiling-water bath for half an hour to expel the ammonia and then acidified with $HClO_4$. The alaH content of the solution was determined spectrophotometrically with ninhydrin, as has been reported by Yemm and Cocking.[13] The aibH content was determined by pH titration under nitrogen with a standard NaOH solution. The pH values were measured with a Hitachi-Horiba F-5 pH meter.

Kinetic Measurments. Solutions containing a cobalt(III) complex, $NaClO_4$ and $HClO_4$ were added to an optical cell, which was then sealed with a serum cap. After the solution has been purged with nitrogen gas for 15 min, the reaction was initiated by the addition of a Cr^{2+} solution with a syringe. The change in the absorbance with the time was followed at 500 nm with a Hitachi EPS-3 spectrophotometer. The ionic strength of the solution was adjusted to 1.0 M throughout the work, unless otherwise stated. The temperature was controlled by circulating water through the cell holder. The temperature was kept constant within 0.1 °C at each desired temperature.

Results

Determination of the Rate Constants of the Electron-transfer Reactions. The spectral changes observed during the reaction of Cr^{2+} with the pentaamminecobalt(III) complex of balaH, gabH, ahH, or babH gave three isosbestic points within the range of 340—600 nm. The electron-transfer reactions of Cr^{2+} with the $Co(amH)(NH_3)_5^{3+}$ complexes are considered to proceed predominantly through an inner-sphere mechanism; this is on the basis of the earlier observation of the reaction of $Co(glyH)(NH_3)_5^{3+}$:[5]

$$Cr^{2+} + Co(amH)(NH_3)_5^{3+} + 5H^+ \rightarrow Cr(amH)(H_2O)_5^{3+} + Co^{2+} + 5NH_4^+ \quad (1)$$

The rate of the reaction of Cr^{2+} with the pentaamminecobalt(III) complex ligating alaH, pheH, or aibH was smaller than that of the complex ligating balaH, gabH, ahH, or babH, and in the cases of the former complexes the isosbestic points collapsed with the time, as is shown in Fig. 1. This may be attributed to the occurrence of the Cr^{2+}-catalyzed aquation of $Cr(amH)(H_2O)_5^{3+}$:

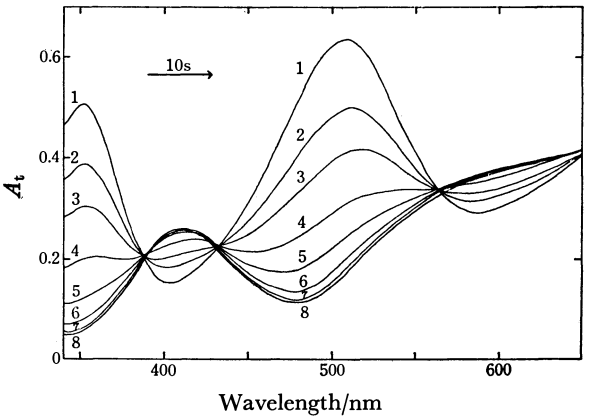

Fig. 1. The spectral changes during the reaction of Cr^{2+} with $Co(alaH)(NH_3)_5^{3+}$ at $[Cr^{2+}]_0=0.100$ M, $[Co(III)]_0=9.59\times10^{-3}$ M, $[H^+]=0.100$ M, 35 °C, and $I=1.0$ M ($NaClO_4$): 1, 20 s; 2, 2 min 20 s; 3, 4 min 20 s; 4, 8 min 20 s; 5, 13 min 20 s; 6, 20 min 20 s; 7, 29 min 20 s; 8, 39 min 20 s after the reaction. Times given are for start of scan at 340 nm.

$$Cr(amH)(H_2O)_5^{3+} + Cr^{2+} \rightarrow Cr^{2+} + amH + Cr(H_2O)_6^{3+} \quad (2)$$

If Reaction 1 obeys this rate equation:

$$-\frac{d[Co(III)]}{dt} = k[Co(III)][Cr^{2+}] \quad (3)$$

Equation 4 can be derived thus:

$$\log\frac{\varepsilon_{Co(III)}l([Cr^{2+}]_0-[Co(III)]_0)-\varepsilon_{Cr(III)}l[Cr^{2+}]_0+A_t}{A_t-A_\infty} = \frac{[Cr^{2+}]_0-[Co(III)]_0}{2.303}kt + \log\frac{[Cr^{2+}]_0}{[Co(III)]_0} \quad (4)$$

where $[Cr^{2+}]_0$ and $[Co(III)]_0$ indicate the initial concentrations of Cr^{2+} and $Co(amH)(NH_3)_5^{3+}$ respectively. A_t and A_∞ denote the absorbances at time t and infinity respectively. The symbols, $\varepsilon_{Co(III)}$ and $\varepsilon_{Cr(III)}$, are the molar absorption coefficients of $Co(amH)(NH_3)_5^{3+}$ and $Cr(amH)(H_2O)_5^{3+}$ at 500 nm respectively, and l denotes the optical path length. The plots of the left-hand side of Eq. 4 *vs.* t for each system expect that of the aibH complex gave a linear relation for at least three half-lives. The second-order rate constant, k, was determined from the slope of this straight line. In these calculations, the values of $\varepsilon_{Cr(III)}$ were estimated from the values of A_∞. Equation 4 held even in the reactions for the alaH and pheH complexes. This may be because of the following reasons: (a) Reaction 2 is much slower than 1. (b) The ε value of $Cr(amH)(H_2O)_5^{3+}$ is quite similar to that of $Cr(H_2O)_6^{3+}$ at the wavelegth used for the measurements (500 nm). (c) The $\varepsilon_{Cr(III)}$ value is much smaller than the $\varepsilon_{Co(III)}$ value at 500 nm. In the reaction of Cr^{2+} with $Co(aibH)(NH_3)_5^{3+}$, however, the accurate determination of the values of A_∞ was difficult due to the considerable contribution of Reaction 2 to Reaction 1. Therefore, the method of Guggenheim[14] was employed.

Kinetic measurements were carried out under various concentrations of Cr^{2+} (0.05—0.1 M), $Co(amH)$-

Table 2. Rate constans of the reaction of Cr^{2+} with $Co(amH)(NH_3)_5^{3+}$

amH	Temp/°C	$10^2\ k^{a)}/M^{-1}\,s^{-1}$
alaH	25.0	1.8±0.1
	34.5	2.6±0.1
	40.5	3.4±0.1
	45.0	4.0±0.1
aibH	25.0	0.24±0.01
	34.5	0.43±0.02
	40.0	0.63±0.01
	44.8	0.82±0.01
balaH	24.8	7.5±0.3
	30.0	9.5±0.1
	35.0	11.7±0.1
	39.8	14.0±0.1
gabH	25.3	12.2±0.2
	34.7	18.5±0.7
	43.8	24.3±0.1
ahH	25.3	14.9±0.2
	35.5	23.5±0.3
	44.7	34.7±0.3
babH	25.0	5.0±0.1
	35.5	7.7±0.2
	44.7	11.8±0.3
pheH	25.0	1.5±0.1
	35.0	2.2±0.1
	44.0	3.5±0.1

a) Each value is the average of two to eleven determinations. The uncertainty is the average deviation.

$(NH_3)_5^{3+}$ (5×10^{-3}—1×10^{-2} M), and hydrogen ions (0.1—0.5 M). The second-order rate constants (k) were found to be independent of the concentration of the hydrogen ions. The rate constants at various temperatures are given in Table 2, and the kinetic parameters, in Table 3, along with the data obtained by other researchers.

Cr^{2+}-catalyzed Aquation of $Cr(amH)(H_2O)_5^{3+}$. The analytical results for Co^{2+} and amH released by the Cr^{2+} reduction are summarized in Table 4, which shows that the amount of amH is always smaller than that of Co^{2+} and that it increases with the reaction time. These findings support the consideration that the mechanism of the electron-transfer reactions is predominantly of the inner-sphere type[16] and indicate that the prolonged contact of $Cr(amH)(H_2O)_5^{3+}$ with Cr^{2+} causes Reaction 2 to a considerable extent. If the reaction between Cr^{2+} and $Co(aibH)(NH_3)_5^{3+}$ proceeds exclusively through an inner-sphere mechanism, the rate constant of the Cr^{2+}-catalyzed aquation of $Cr(aibH)(H_2O)_5^{3+}$ is estimated from the data given in Table 4 to be approximately $7\times10^{-5}\ M^{-1}\,s^{-1}$.

Discussion

The data given in Table 3 show the following facts: (a) The substitution of methyl groups or a benzyl group for α hydrogens of glyH causes a decrease in the rate of the electron-transfer reaction (compare the k values of glyH, alaH, aibH, and pheH complexes). (b) The rate of the electron-transfer reaction increases with the increase in the number of methylene groups between carboxylate and ammonium groups in amH (compare the k values of glyH, balaH, gabH, and ahH complexes). (c) The ΔH^* values as well as the ΔS^* values of all the complexes except the aibH complex are quite similar to each other.

It has been shown that cobalt(III) ammine complexes ligating alkyl carboxylate ligands were reduced by Cr^{2+} at carbonyl oxygen atoms.[17-19] Fact (a) indicates that the substitution of bulky groups for α hydrogens of glyH hinders the C=O attacking by Cr^{2+}. It is known that the rates of the reduction of *N*-methyl-substituted glycinepentaamminecobalt(III) ions by Cr^{2+} decrease with the increase in the number of the *N*-methyl groups.[5] The data given in Table 3 indicate that the alkyl substitution on the methylene group in glyH hinders the C=O attack more seriously than that on the ammonium nitrogen does. This result can be understood when the steric crowding around the C=O group is considered.

The steric crowding around the C=O group in $Co(O_2C(CH_2)_nNH_3)(NH_3)_5^{3+}$ may increase as the number of methylene groups between carboxyl and ammonium groups increases; hence, the rate of the electron-transfer reactions would decrease with the increase in the number of methylene groups. However, Fact (b) is opposed to this expectation. The discrepancy may be understood by considering electrostatic repulsions between the ammonium group, the cobalt(III) center, and the attacking Cr^{2+} ion. The positively charged ammonium group will tend to be separated from the positively charged cobalt(III) center due to the electrostatic repulsion. Therfore, the charge separation between the ammonium group and the cobalt(III) center becomes larger as the methylenic chain of the amH becomes longer. The approach of the positively charged Cr^{2+} ion to the C=O moiety becomes easier as the number of methylene groups of the amH increases. Balahura and Jordan made it clear that the conformation of the coordinated formate ion in $Co(O_2CH)(NH_3)_5^{2+}$ is of Form I (R=H).[19]

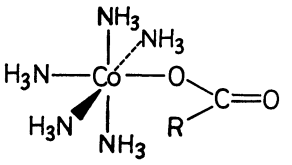

I

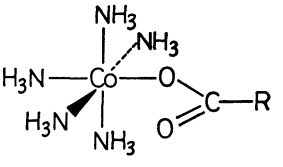

II

For other cases such as with the acetato complex, they claimed that Form II would be greatly favored by steric consideration. For the conformation of the amH in $Co(amH)(NH_3)_5^{3+}$, Form II would be favored over Form I. When this conformational situation and the electrostatic repulsion between the ammonium group and the cobalt(III) center are considered, molecular models indicate that the $-(CH_2)_nNH_3^+$ group takes a severely restricted orientation and that the steric crowding around the C=O group is slightly altered

Table 3. Kinetic data for the reaction of Cr^{2+} with $Co(amH)(NH_3)_5^{3+}$

amH (pK_a)[a]	k / $M^{-1}s^{-1}$	$\Delta H^{\neq}$[d] / kcal mol^{-1}	$\Delta S^{\neq}$[d] / cal K^{-1} mol^{-1}	Ref.
$\bar{O}OCCH_2\overset{+}{N}H_3$	0.064[b]	7.7±0.2	−38±1	5
(2.35)	0.064[c]			This work
$\bar{O}OC(CH_2)_2\overset{+}{N}H_3$	0.075[c]	7.4±0.6	−39±2	This work
(3.55)				
$\bar{O}OC(CH_2)_3\overset{+}{N}H_3$	0.122[c]	9.9	−30	4
(4.03)	0.122[c]	6.4±0.3	−41±1	This work
$\bar{O}OC(CH_2)_5\overset{+}{N}H_3$	0.15[c]	7.7±0.1	−37±1	This work
(4.43)				
$\bar{O}OCCH_2\overset{+}{N}H_2(CH_3)$	0.044[b]	8.0±0.2	−38±1	5
(2.35)				
$\bar{O}OCCH_2\overset{+}{N}H(CH_3)_2$	0.038[b]	7.5±0.2	−40±1	5
(2.15)				
$\bar{O}OCCH_2\overset{+}{N}(CH_3)_3$	0.016[b]	7.7±0.2	−41±1	5
(1.84)				
$\bar{O}OCCH_2CH(CH_3)\overset{+}{N}H_3$	0.050[c]	7.3±0.1	−40±1	This work
(3.55)				
$\bar{O}OCCH(CH_3)\overset{+}{N}H_3$	0.049[c]	8.0±0.3	−37±1	15
(2.34)	0.018[c]	7.4±0.1	−42±1	This work
$\bar{O}OCCH(CH_2C_6H_5)\overset{+}{N}H_3$	0.015[c]	7.5±0.2	−42±1	This work
(2.20)				
$\bar{O}OCC(CH_3)_2\overset{+}{N}H_3$	0.0024[c]	11.4±0.2	−32±1	This work
(2.36)				

a) 25 °C and I=0 M. The K_a value is defined for this equilibrium: $amH_2^+ \rightleftharpoons amH + H^+$. The data for pK_a are taken from A. E. Martell and L. G. Sillén, "Stability Constants, Supplement No. 1," The Chemical Society, London (1971). b) 25 °C and I=1.0 M ($LiClO_4$). c) 25 °C and I=1.0 M ($NaClO_4$). d) The uncertainty is the standard deviation from the least-squares fit for the activation parameters. The computations were carried out on a NEAC-2200 Model 700 at the Computer Center at Tohoku University. 1 cal=4.184 J.

Table 4. The analytical results for Co^{2+} and amH released by the reaction of Cr^{2+} with $Co(amH)(NH_3)_5^{3+}$

Complex	The initial concentrations of the reactants		Reaction time/min	The concentrations of the products		Product ratio
	$[Cr^{2+}]_0\times10^3$/M	$[Co(III)]_0\times10^3$/M		$[Co^{2+}]\times10^3$/M	$[amH]\times10^3$/M	$\frac{[amH]}{[Co^{2+}]}$
$Co(aibH)(NH_3)_5^{3+}$ [a]	103	21.3	90	11.9±0.6	3.0±0.2	0.25±0.03
	103	30.0	90	18.6±0.9	3.5±0.3	0.19±0.03
	103	29.6	180	20.3±1.0	8.6±0.4	0.42±0.04
$Co(alaH)(NH_3)_5^{3+}$ [b]	100	9.87	5	6.19±0.31	<0.25	<0.04
	100	9.59	50	10.0±0.5	2.5±0.2	0.25±0.03

a) At 25 °C, I=0.7 M ($NaClO_4$), and $[H^+]$=0.090 M. b) At 35 °C, I=1.0 M ($NaClO_4$), and $[H^+]$=0.10 M.

by the increase in the methylenic chain length. It should also be noted that the variation in the pK_a values of amH may influence the rate constants. The pK_a values of the amH are given in Table 3. The rate constants of the pentaamminecobalt(III) complexes ligating sarcosine, balaH, gabH, and ahH increase with the increase in the pK_a values. Molecular models indicate that the steric crowding around the C=O groups of these complexes is comparable with respect to the attack on the C=O groups by Cr^{2+}. The increase in pK_a values may cause the increase in the electron density of the carboxylate group, which, in turn, may make the attack of the carboxylate position by Cr^{2+} easier.

The similarity in the activation parameters among all the complexes studied except the aibH complex indicates that the reactions take place by the same mechanism. Although the $\Delta H^{\neq}$ and $\Delta S^{\neq}$ values of the aibH complex are larger than those of the other complexes by 4—5 kcal mol^{-1} and 5—10 cal K^{-1} mol^{-1} respectively, the product analyses indicated that the mechanism for the aibH complex was predominantly

$(NH_3)_5CoOOCCH_3^{2+}$ 0.35[a]	
$(NH_3)_5CoOOCCH_2CH_3^{2+}$ 0.14[b]	$(NH_3)_5CoOOCCH_2NH_3^{3+}$ 0.064[d]
$(NH_3)_5CoOOC(CH_2)_2CH_3^{2+}$ 0.08[c]	$(NH_3)_5CoOOC(CH_2)_2NH_3^{3+}$ 0.075[e]
	$(NH_3)_5CoOOC(CH_2)_3NH_3^{3+}$ 0.122[e]
	$(NH_3)_5CoOOC(CH_2)_5NH_3^{3+}$ 0.15[e]

Scheme 1. Comparison of the second-order rate constants (in $M^{-1}\,s^{-1}$) of the reactions of Cr^{2+} with $Co(O_2C(CH_2)_nCH_3)(NH_3)_5^{2+}$ and $Co(O_2C(CH_2)_n-NH_3)(NH_3)_5^{3+}$ at 25 °C and $I=1$ M, unless otherwise indicated.
a) Ref. 2 and M. B. Barrett, J. H. Swinehart, and H. Taube, *Inorg. Chem.*, **10**, 1983 (1971). b) E. S. Gould, *J. Am. Chem. Soc.*, **88**, 2983 (1966); at 25 °C and $I=1.5$ M. c) H. Taube, *J. Am. Chem. Soc.*, **77**, 4481 (1955). d) Ref. 5. e) This work.

of an inner-sphere type.

The second-order rate constant of the reactions of Cr^{2+} with some pentaamminecobalt(III) complexes ligating $^-O_2C(CH_2)_nCH_3$ and $^-O_2C(CH_2)_nNH_3^+$ ligands are compared in Scheme 1. The rate of the carboxylato complexes decreases with the increase in the methylenic chain length. This trend is in contrast with that observed for the amH complexes. Although the positive charge of the butyrato complex is less than those of the amH complexes, the rate of the former complex is smaller than those of $Co(gabH)(NH_3)_5^{3+}$ and $Co(ahH)(NH_3)_5^{3+}$. As has been mentioned above, the $-(CH_2)_nNH_3^+$ group takes a severely restricted orientation and the ammonium group is located apart from the C=O moiety. On the other hand, the alkyl group, which is electrically neutral, is able to wander about in the vicinity of the C=O moiety in the same complex ion. Therefore, the alkyl group may hinder increasingly the attack on the C=O group by Cr^{2+} with the increase in the methylenic chain length.

References

1) H. Taube, "Mechanisms of Inorganic Reactions," Adv. Chem. Ser., Am. Chem. Soc. publ. No. 49 (1965), p. 107.
2) H. Taube and E. S. Gould, *Acc. Chem. Res.*, **2**, 321 (1969).
3) K. D. Kopple and G. F. Svatos, *J. Am. Chem. Soc.*, **82**, 3227 (1960).
4) R. T. M. Fraser, *Inorg. Chem.*, **3**, 1561 (1964).
5) H. Holwerda, E. Deutsch, and H. Taube, *Inorg. Chem.*, **11**, 1965 (1972).
6) J. Fujita, T. Yasui, and Y. Shimura, *Bull. Chem. Soc. Jpn.*, **38**, 654 (1965).
7) Some of the complexes were kindly provided by Professor Kazuko Ogino, College of Medical Sciences, Tohoku University.
8) H. Ogino and N. Tanaka, *Bull. Chem. Soc. Jpn.*, **41**, 1622 (1968).
9) E. L. King and J. A. Neptune, *J. Am. Chem. Soc.*, **77**, 3186 (1955).
10) K. D. Kopple and R. R. Miller, *Inorg. Chem.*, **2**, 1204 (1963).
11) M. Ardon and R. A. Plane, *J. Am. Chem. Soc.*, **81**, 3197 (1959).
12) R. W. Kolaczkowski and R. A. Plane, *Inorg. Chem.*, **3**, 322 (1964).
13) E. W. Yemm and E. C. Cocking, *Analyst*, **80**, 209 (1955).
14) E. A. Guggenheim, *Phil. Mag.*, [7] **2**, 538 (1926).
15) R. Bembi and W. U. Malik, *J. Inorg. Nucl. Chem.*, **37**, 570 (1975).
16) The data given in Table 4 reveal that at least 80% of the electron-transfer reaction between Cr^{2+} and $Co(aibH)-(NH_3)_5^{3+}$ proceeds through an inner-sphere path.
17) K. L. Scott and A. G. Sykes, *J. Chem. Soc., Dalton*, **1972**, 1832.
18) S. A. Stritar and H. Taube, *Inorg. Chem.*, **8**, 2281 (1969).
19) R. J. Balahura and R. B. Jordan, *Inorg. Chem.*, **12**, 1438 (1973).

Crystal Structure and Magnetic Properties of Hydrothermally Synthesized Barium Ferrite, $Ba_4Fe_9O_{20}H_6$*

Katsuki KITAHAMA and Ryôiti KIRIYAMA

The Institute of Scientific and Industrial Research, Osaka University, Yamadakami, Suita, Osaka 565

(Received May 4, 1976)

A new barium ferrite, $Ba_4Fe_9O_{20}H_6$, has been synthesized by a hydrothermal technique. This crystallizes in a monoclinic system with $a=10.263(5)$, $b=5.986(3)$, $c=14.559(6)$ Å, $\beta=95.20(3)°$, $Z=2$, space group C2/m. The structure was determined by Patterson and Fourier methods from three-dimensional X-ray counter data and refined by block-diagonal least-squares calculations to $R=0.098$ for 1128 reflections. The structure consists of condensed layers of ferrite anions, $Fe(OH)_6^{3-}$ clusters, and Ba^{2+} cations; it has the character of a crystal growth from aqueous solutions. The presence of Fe^{2+} was confirmed; such ions are located in the condensed ferrite layer. Consequently, the true formula should be written as $Ba_4[Fe^{III}(OH)_6][Fe^{II}Fe_7^{III}O_{14}]$. This crystal is ferrimagnetic below the Nèel point of 515 K. The magnetic moment was estimated to be about 10 μ_B per formula unit at 0 K.

The BaO–Fe_2O_3 and BaO–Fe_2O_3–MeO systems have been studied by many workers because of their great importance as useful magnetic materials. Most of them have been synthesized by firing or flux methods at temperatures higher than 700 °C.[1,2] Hydrothermal syntheses of these substances seem worthwhile, not only for the manufacture of magnetic materials but for the reaction chemistry with respect to the amphoteric behavior of Fe^{3+} ions in aqueous solutions. Of these, barium monoferrite, $BaFe_2O_4$, has an interesting structure characterized by wide-open cavities.[3] In the early stage of hydrothermal studies, our aim was to ascertain whether Ba^{2+} cations leach through the channels of this structure, as is often observed in zeolites, or not. Such hydrothermal treatments and growth of new barium ferrites, however, revealed that the reaction proceeds through dissolution of the starting material. By processing $Ba(OH)_2$ and Fe_2O_3 under hydrothermal conditions, four kinds of barium ferrite were obtained: these are $Ba_4Fe_9O_{20}H_6$, $Ba_8Fe_{13}O_{30}H_6$,[4] and two modifications of $BaFe_4O_7$.[5,6] Successive X-ray studies showed that their crystal structures certainly reflect some characteristics of the crystal growth from aqueous solutions. This paper is concerned with the crystal structure and magnetic properties of $Ba_4Fe_9O_{20}H_6$. This substance was designated Phase II among the hydrothermal products and was considered to have the structure of a modified Y ferrite in a previous paper.[7]

Experimental

Preparation. Barium hydroxide octahydrate (0.63 g), and α-Fe_2O_3 (0.32 g), both of which were commercial guaranteed reagent grade, and 5 ml of distilled water were charged in a platinum capsule with a lid. The capsule was inserted into a Morey bomb sealed with a copper gasket. The contents were heated at a rate of 4 °C min^{-1} up to 300 °C, kept at this temperature for 5 days, and then quenched into ice water. The pressure inside the bomb during the reaction was roughly estimated as 150 bar from a filling ratio-temperature diagram given by Kennedy.[8] Partial reduction of Fe^{3+} to Fe^{2+} may be caused by hydrogen, probably resulting from corrosion of the stainless steel vessel by water. In fact, for a shorter reaction period of one or two days, where the reduction was not enough, the product was contaminated with a hexagonal phase ($P6_3/m$) of $BaFe_4O_7$. The crystalline product was filtered and then washed with distilled water. The obtained crystals were platy hexagons in shape and were strongly magnetic, so they could be easily separated by use of a hand magnet.

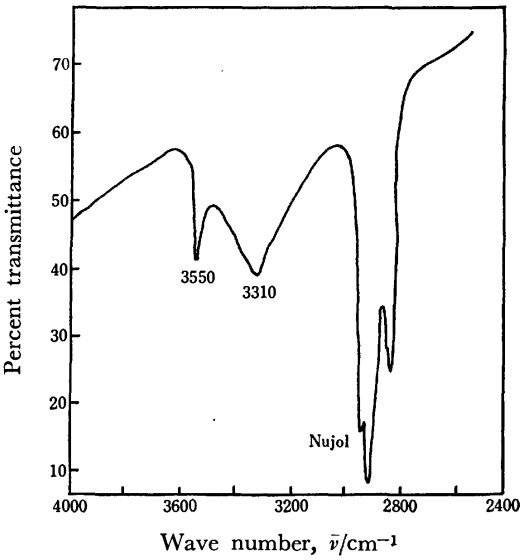

Fig. 1. Infrared spectra of $Ba_4Fe_9O_{20}H_6$.

Chemical Composition. The molar ratio of Ba/Fe was determined as 4 : 8.89 from an ordinary gravimetry measurement and as 4 : 8.80 by a fluorescent X-ray analysis; these values agree within their experimental errors. The presence of OH groups was evidenced by IR spectroscopy. As shown in Fig. 1, the two OH stretching bands occurred at about 3550 and 3310 cm^{-1}, whereas no peak were observed in the region 1500—1800 cm^{-1}. The weight loss corresponding to $3H_2O$ was found at about 695 K by means of TG analysis; from this the amount of H could be determined. The presence of ferrous ions was detected from the color test of $K_3Fe(CN)_6$ in an aqueous solution. Although its amount was roughly estimated from iodometry, the exact content was successfully determined by referring to the number of peaks assigned to oxygen atoms in the electron density maps described below.

X-Ray Data Collections. The crystals synthesized hydrothermally were dark red transparent hexagonal plates; almost all crystals were twins or aggregates grown epitaxially. A

* Thesis submitted by one of the authors(K.K.) to Osaka University in partial fulfillment of the requirements for the degree of Doctor of Science.

Table 1. Crystal data for $Ba_4Fe_9O_{20}H_6$

Space group C2/m	$\rho_{obsd}=5.06$ g cm^{-3}
$a=10.263(5)$ Å	$\rho_{calcd}=5.137$
$b=5.986(3)$	$F(000)=1248$ e cell^{-1}
$c=14.559(6)$	F. W. $=1377.98$ g mol^{-1}
$\beta=95.20(3)°$	$V=890.72$ Å^3
$Z=2$	$\mu_{MoK\alpha}=158.9$ cm^{-1}

single crystal happened to be found with the shape of an irregular hexagonal plate with dimensions of $0.08\times0.04\times0.015$ mm^3; this crystal was used for the present X-ray study. Weissenberg and precession photographs indicated the crystal to be monoclinic, with a space group either C2, Cm, or C2/m; the last group was confirmed by solution of the structure (the systematic absences: hkl, $h+k$ odd). The same crystal was mounted on a Rigaku four-circle diffractometer with its c-axis along the ϕ-axis of the goniostat. The lattice parameters were determined from the setting angles of the same diffractometer, using Mo$K\alpha_1$ radiation. The results are listed in Table 1 together with other crystal data. Intensity data were collected by use of zirconium-filtered Mo$K\alpha$ radiation, with a 2θ-ω scan mode. The scan speed was 1°min^{-1} in 2θ and background intensities were measured for 10 s at both ends of the scan. In total, 1128 independent reflections with $\sin\theta/\lambda$ less than 0.65 Å^{-1} were measured. The reference reflections that were monitored periodically showed no significant intensity fluctuations during the collection of intensity data. For reflections having scan counts below the background levels, the intensity values were taken as 0.0. No corrections were made for absorption or extinction.

Magnetization. Magnetic properties were measured by means of a Faraday method on a Naruse electro-mechanical balance equipped with an automated recording device. The values of magnetization were calibrated by using powdered nickel (99.999%).

Mössbauer Spectroscopy. The measurement was made on a Hitachi AA40 Mössbauer spectrometer with a ^{57}Co(Pd) source moving against a specimen in a constant acceleration mode. An iron foil was used for the calibration of velocity.

Structure Determination and Refinement

Three-dimensional Patterson maps showed peaks only on the planes at $y=0$, 1/2, and at about $y=1/4$, and suggested the presence of mirror planes perpendicular to the b-axis. Because these peaks were comparable in height, owing to the periodical stacking of oxygens, Patterson maps were calculated again with reflections of $\sin\theta/\lambda>0.4$ Å^{-1} and with a sharpening factor of $B=2.0$ Å^2. (Of the 1128 reflections, 280 were eliminated from this calculation; the sum of $|F_0|$ of these 280 reflections amounts to 50% of the $\Sigma|F_0|$ of the total reflections.) Such a modification of the Patterson function resolved the diffuse peaks and was helpful in solving the structure. Thus the positions of Ba and Fe were easily determined. All positions of oxygen atoms were found on successive three-dimensional electron density maps phased with Ba and Fe atoms. Although a full-matrix least-squares refinement was started from these atomic positions in the isotropic mode, the structure did not converge below $R=0.15$. Therefore, the block-diagonal least-squares refinement was performed, varing the individual isotropic thermal parameters, an overall temperature factor, and a scale factor. At the stage of $R=0.118$, anisotropic thermal parameters were introduced for Ba an Fe atoms. Difference Fourier maps computed at this stage showed no ripple higher than 2.0 e Å^{-1}. After four further cycles of refinement, R dropped to 0.098. No atomic parameters shifted by more than one fourth of their associated standard deviations in the final cycle. The scattering factors for Ba^{2+}, Fe^{3+} (applied for all Fe), and O^- were taken from *International Tables for X-Ray Crystallography, Vol. IV.*[9] The quantity minimized during the least-squares procedure was $\Sigma w(|F_o|-|F_c|)^2$, all weights being unity. All computations were performed on the NEAC 2200/700 computer of this university, using local modifications of RSSFR-5, RSFLS, HBLS V, and RSDA-4 in the UNICS program system,[10] and the stereoscopic drawing program ORTEP written by Johnson.[11] The observed and calculated structure factors are compared in Table 2. The final positional thermal parameters are given in Table 3.

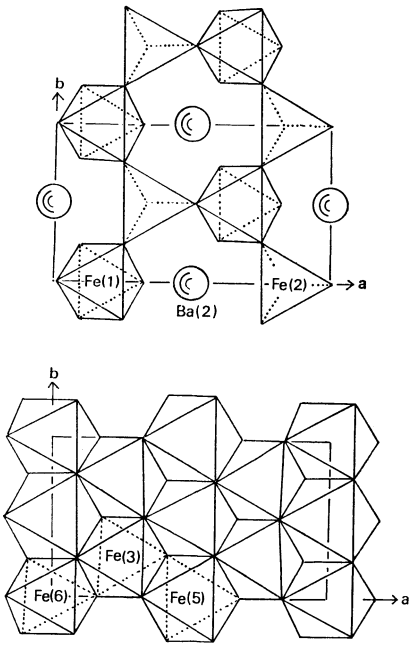

Fig. 2. Two kinds of slices in the condensed ferrite layer viewed along the c* direction. Above: one of the outer slices of the triple layer ($z\approx0.19$). Below: a middle sheet of the triple layer.

Results and Discussion

Crystal Structure. The structure consists of eminent triple layers of oxygen coordination polyhedra around Fe atoms parallel to the (001) plane, and Fe$(OH)_6^{3-}$ anion clusters and Ba^{2+} cations both intervening between triple layers. Of the nine Fe atoms in the chemical formula, seven atoms are coordinated octahedrally by oxygen atoms while the other two are surrounded tetrahedrally. The triple layer is composed of two kinds of slices: that is, one type is sandwiched between the others. As shown in Fig. 2, each

TABLE 2. OBSERVED AND CALCULATED STRUCTURE FACTORS ($\times 1/2$) FOR $Ba_4Fe_9O_{20}H_6$

H	FO	FC
K = 0 L = 0		
2	30	29
4	10	15
6	115	117
8	105	97
10	42	46
12	0	4
K = 0 L = 1		
-12	82	83
-10	56	56
-8	63	60
-6	47	51
-4	164	180
-2	44	47
0	45	43
2	69	72
4	68	70
6	108	114
8	74	71
10	11	9
12	22	21
K = 0 L = 2		
-12	157	154
-10	0	4
-8	28	26
-6	76	79
-4	38	32
-2	83	94
0	19	19
2	21	30
4	88	90
6	112	111
8	129	140
10	20	16
12	11	8
K = 0 L = 3		
-12	32	32
-10	16	19
-8	30	23
-6	186	183
-4	53	43
-2	34	46
0	56	60
2	100	106
4	107	129
6	51	61
8	58	60
10	0	0
12	132	129
K = 0 L = 4		
-12	9	7
-10	0	12
-8	29	24
-6	52	43
-4	213	245
-2	0	17
0	121	142
2	130	151
4	123	138
6	61	66
8	129	134
10	28	25
12	23	18
K = 0 L = 5		
-12	25	21
-10	34	25
-8	144	137
-6	69	70
-4	74	83
-2	0	6
0	236	272
2	18	14
4	53	57
6	61	66
8	11	8
10	91	94
12	14	17
K = 0 L = 6		
-12	117	100
-10	108	92
-8	31	22
-6	49	54
-4	182	206
-2	0	7
0	87	82
2	33	32
4	82	91
6	81	85
8	24	21
10	32	36
12	13	5
K = 0 L = 7		
-12	78	58
-10	48	47
-8	9	12
-6	32	29
-4	64	64
-2	139	139
0	6	5
2	42	39
4	17	19
6	82	77
8	95	96
10	16	16
K = 0 L = 8		
-12	40	32
-10	0	9
-8	54	52
-6	121	119
-4	37	44
-2	120	125
0	15	8
2	43	37
4	247	253
6	67	68
8	32	33
10	32	33
K = 0 L = 9		
-12	10	8
-10	57	48
-8	59	53
-6	5	0
-4	105	104
-2	0	3
0	91	90
2	114	110
4	38	40
6	11	11
8	68	65
10	25	27
K = 0 L = 10		
-10	13	13
-8	178	170
-6	60	59
-4	37	37
-2	44	45
0	139	140
2	21	13
4	19	14
6	48	52
8	17	14
10	67	71
K = 0 L = 11		
-10	58	54
-8	33	29
-6	13	10
-4	71	71
-2	97	93
0	34	35
2	26	27
4	18	21
6	96	90
8	0	8
10	45	41
K = 0 L = 12		
-10	31	33
-8	17	10
-6	29	26
-4	44	38
-2	71	71
0	126	117
2	21	17
4	55	50
6	14	21
8	66	65
K = 0 L = 13		
-10	0	1
-8	18	12
-6	93	85
-4	33	29
-2	96	89
0	31	18
2	44	41
4	143	136
6	21	19
8	0	7
K = 0 L = 14		
-8	73	67
-6	71	65
-4	53	50
-2	23	23
0	107	103
2	77	77
4	12	8
6	14	12
8	75	81
K = 0 L = 15		
-8	84	75
-6	10	13
-4	0	8
-2	12	16
0	18	31
2	65	55
4	28	30
K = 0 L = 16		
-8	74	67
-6	0	10
-4	98	92
-2	85	77
0	3	3
2	47	38
4	18	9
6	30	39
K = 0 L = 18		
-4	74	67
-2	68	69
0	15	33
2	0	5
4	74	67
-2	68	69
0	15	13
2	0	5
K = 1 L = 0		
1	9	14
3	224	232
5	39	36
7	47	47
9	30	29
11	25	24
13	46	47
K = 1 L = 1		
-13	28	33
-11	7	11
-9	39	40
-7	57	60
-5	37	34
-3	16	14
-1	18	7
1	45	42
3	114	113
5	88	83
7	8	9
9	105	106
11	86	77
13	0	9
K = 1 L = 2		
-13	16	14
-11	13	13
-9	109	105
-7	8	18
-5	64	58
-3	5	8
-1	5	3
1	114	98
3	118	117
5	38	47
7	32	32
9	81	74
11	52	58
K = 1 L = 3		
-13	0	1
-11	3	8
-9	123	122
-7	74	68
-5	20	26
-3	188	195
-1	140	122
1	59	61
3	44	42
5	58	62
7	22	30
9	88	90
11	0	4
K = 1 L = 4		
-13	35	32
-11	48	43
-9	42	34
-7	30	28
-5	24	20
-3	15	2
-1	143	141
1	30	33
3	57	68
5	111	126
7	41	44
9	30	26
11	20	13
K = 1 L = 5		
-13	33	25
-11	48	45
-9	0	0
-7	25	25
-5	41	48
-3	126	140
-1	32	28
1	39	31
3	136	149
5	41	46
7	97	107
9	0	9
11	28	29
K = 1 L = 6		
-11	18	9
-9	63	64
-7	104	103
-5	17	22
-3	19	22
-1	55	54
1	3	4
3	94	95
5	54	56
7	36	37
9	75	78
11	53	57
K = 1 L = 7		
-11	24	22
-9	45	43
-7	72	74
-5	96	100
-3	17	5
-1	103	95
1	121	105
3	71	69
5	16	13
7	26	26
9	39	38
11	45	49
K = 1 L = 8		
-11	21	25
-9	81	84
-7	27	23
-5	54	55
-3	116	114
-1	43	36
1	162	150
3	6	1
5	9	12
7	94	96
9	83	85
11	0	0
K = 1 L = 9		
-11	28	25
-9	10	15
-7	16	15
-5	8	6
-3	12	16
-1	89	82
1	16	8
3	19	19
5	87	90
7	31	31
9	27	26
K = 1 L = 10		
-11	82	76
-9	0	1
-7	17	19
-5	92	92
-3	80	78
-1	12	1
1	5	6
3	88	86
5	40	40
7	86	87
9	26	27
K = 1 L = 11		
-11	20	28
-9	20	20
-7	55	55
-5	90	88
-3	45	43
-1	26	24
1	102	90
3	112	111
5	39	38
7	15	8
9	66	67
K = 1 L = 12		
-9	13	12
-7	49	50
-5	49	48
-3	23	17
-1	69	64
1	38	34
3	39	32
5	14	6
7	15	13
9	26	24
K = 1 L = 13		
-9	64	66
-7	18	16
-5	26	19
-3	77	74
-1	25	27
1	128	110
3	25	19
5	29	28
7	76	75
K = 1 L = 14		
-9	43	34
-7	12	12
-5	45	38
-3	73	68
-1	51	49
1	13	3
3	30	28
5	61	69
7	44	41
K = 1 L = 15		
-7	0	5
-5	53	51
-3	20	13
-1	49	38
1	31	23
3	0	5
5	54	56
K = 1 L = 16		
-7	36	35
-5	80	72
-3	27	27
-1	46	48
1	66	65
3	50	56
5	38	26
K = 1 L = 17		
-5	29	38
-3	13	2
-1	46	54
1	19	19
3	48	42
K = 1 L = 18		
-3	10	11
-1	16	19
1	65	85
K = 2 L = 0		
0	266	262
2	140	123
4	23	18
6	209	216
8	31	24
10	30	34
12	36	32
K = 2 L = 1		
-12	27	31
-10	108	108
-8	0	2
-6	136	137
-4	52	50
-2	146	131
0	52	44
2	13	4
4	24	18
6	63	62
8	99	93
10	0	10
12	54	53
K = 2 L = 2		
-12	98	92
-10	32	21
-8	13	9
-6	173	172
-4	12	7
-2	145	126
0	98	80
2	125	112
4	62	55
6	65	59
8	39	49
10	48	46
12	14	16
K = 2 L = 3		
-10	21	14
-8	38	40
-6	61	64
-4	60	64
-6	145	144
-4	109	100
-2	93	100
0	151	122
2	19	4
4	26	33
6	129	140
8	11	11
10	45	43
12	83	84
K = 2 L = 4		
-12	32	34
-10	19	21
-8	41	38
-6	43	48
-4	79	85
-2	49	56
0	39	26
2	327	323
4	85	92
6	51	56
8	51	52
10	65	67
12	13	11
K = 2 L = 5		
-12	54	50
-10	37	39
-8	61	63
-6	118	126
-4	20	22
-2	97	111
0	207	177
2	43	43
4	98	99
6	89	97
8	22	27
10	64	67
12	31	35
K = 2 L = 6		
-12	59	53
-10	158	148
-8	7	1
-6	76	85
-4	73	88
-2	28	30
0	58	41
2	49	49
4	13	15
6	77	79
8	58	62
10	87	95
K = 2 L = 7		
-10	0	15
-8	53	54
-6	41	45
-4	81	90
-2	61	59
0	77	64
2	26	22
4	61	57
6	0	7
8	33	35
10	63	63
K = 2 L = 8		
-12	47	45
-10	32	38
-8	0	9
-6	83	90
-4	51	54
-2	206	230
0	62	48
2	46	43
4	118	120
6	102	107
8	8	10
10	83	81
K = 2 L = 9		
-10	18	11
-8	12	20
-6	54	66
-4	38	45
-2	84	83
0	18	9
2	156	147
4	0	3
6	26	24
8	34	37
10	0	2
K = 2 L = 10		
-8	95	103
-6	58	58
-4	68	74
-2	0	6
0	114	119
2	124	108
4	21	15
6	72	72
8	93	95
10	29	36
K = 2 L = 11		
-10	62	60
-8	56	58
-6	30	32
-4	47	49
-2	58	56
0	104	94
2	24	22
4	24	27
6	30	33
8	52	52
K = 2 L = 12		
-8	38	40
-6	61	64
-4	60	64
-2	17	11
0	35	25
2	14	15
4	0	4
6	95	90
8	38	36
K = 2 L = 13		
-8	24	24
-6	0	15
-4	13	25
-2	121	123
0	46	39
2	12	9
4	107	103
6	48	46
8	26	31
K = 2 L = 14		
-8	25	23
-6	104	110
-4	34	33
-2	46	47
0	47	44
2	93	92
4	17	15
6	32	30
K = 2 L = 15		
-6	14	16
-4	33	28
-2	25	33
0	0	0
2	16	5
4	64	65
6	41	39
K = 2 L = 16		
-6	37	36
-4	51	52
-2	45	49
0	51	55
2	99	93
4	6	15
K = 2 L = 17		
-4	46	52
-2	8	1
0	31	29
2	9	8
K = 2 L = 18		
-2	61	77
0	9	5
K = 3 L = 0		
1	11	15
3	200	195
5	35	24
7	41	41
9	30	23
11	28	25
K = 3 L = 1		
-9	39	39
-7	55	53
-5	30	24
-3	0	10
-1	9	9
1	38	33
3	106	99
5	92	83
7	9	7
9	92	93
11	72	70
K = 3 L = 2		
-11	19	13
-9	98	94
-7	16	22
-5	54	51
-3	12	5
-1	0	0
1	97	83
3	125	106
5	38	38
7	36	31
9	68	64
11	51	53
K = 3 L = 3		
-11	6	6
-9	114	113
-7	73	65
-5	15	17
-3	163	155
-1	111	97
1	50	51
3	53	44
5	56	51
7	27	32
9	80	85
11	0	3
K = 3 L = 4		
-11	41	39
-9	44	37
-7	21	25
-5	25	19
-3	0	5
-1	121	117
1	27	26
3	61	57
5	108	108
7	44	44
9	24	23
11	20	13
K = 3 L = 5		
-11	49	43
-9	8	4
-7	25	23
-5	47	50
-3	119	126
-1	25	21
1	47	39
3	137	126
5	35	38
7	88	91
9	0	6
11	22	31
K = 3 L = 6		
-11	7	11
-9	55	58
-7	92	92
-5	0	14
-3	123	111
-1	39	40
1	15	8
3	95	86
5	51	48
7	31	31
9	66	72
11	53	55
K = 3 L = 7		
-11	21	23
-9	40	36
-7	62	66
-5	79	86
-3	15	11
-1	94	92
1	114	94
3	63	60
5	0	3
7	26	23
9	38	38
K = 3 L = 8		
-11	11	24
-9	76	80
-7	23	17
-5	43	45
-3	97	100
-1	37	36
1	149	131
3	12	2
5	7	9
7	86	88
9	72	75
K = 3 L = 9		
-11	20	23
-9	20	15
-7	0	8
-5	0	2
-3	0	12
-1	68	70
1	8	8
3	24	24
5	80	82
7	32	30
9	25	27
K = 3 L = 10		
-9	4	4
-7	19	19
-5	77	83
-3	62	66
-1	0	0
1	0	4
3	81	77
5	41	36
7	80	83
9	27	24
K = 3 L = 11		
-9	0	9
-7	26	21
-5	53	56
-3	6	9
-1	26	21
1	43	54
3	42	39
5	6	8
7	74	77
9	0	5
K = 3 L = 12		
-11	0	5
-9	68	70
-7	8	8
-5	0	12
-3	0	2
-1	8	5
1	11	15
3	32	30
5	35	24
7	9	7
9	92	93
11	72	70
K = 3 L = 13		
-9	59	61
-7	7	14
-5	15	14
-3	65	70
-1	22	20
1	111	103
3	0	15
5	28	29
7	69	69
K = 3 L = 14		
-7	8	14
-5	27	34
-3	60	63
-1	44	47
1	11	3
3	16	23
5	63	63
K = 3 L = 15		
-7	8	6
-5	42	44
-3	18	10
-1	37	34
1	20	19
3	11	9
5	51	53
K = 3 L = 16		
-5	70	69
0	82	72
2	95	87
4	32	32
6	0	8
8	56	56
K = 3 L = 17		
-3	13	0
-1	35	48
1	0	20
K = 4 L = 0		
0	339	344
2	31	19
4	20	21
6	95	91
8	78	74
10	36	43
K = 4 L = 1		
-10	48	48
-8	55	51
-6	38	41
-4	129	121
-2	26	23
0	42	25
2	56	51
4	64	55
6	96	96
8	59	57
10	8	11
K = 4 L = 2		
-10	0	5
-8	21	22
-6	62	58
-4	27	24
-2	81	77
0	0	4
2	15	13
4	56	50
6	102	90
8	104	107
10	12	11
K = 4 L = 3		
-10	19	18
-8	16	19
-6	152	147
-4	45	32
-2	20	29
0	61	43
2	92	74
4	96	97
6	47	49
8	51	46
10	15	1
K = 4 L = 4		
-10	16	13
-8	19	18
-6	35	32
-4	163	161
-2	14	9
0	110	99
2	130	116
4	112	102
6	48	50
8	106	106
10	25	19
K = 4 L = 5		
-10	25	19
-8	112	111
-6	53	56
-4	56	55
-2	10	11
0	228	195
2	22	18
4	44	38
6	51	50
8	14	4
10	72	82
K = 4 L = 6		
-10	84	77
-8	24	21
-6	37	41
-4	135	144
-2	10	6
0	54	39
2	29	26
4	65	62
6	74	77
8	21	19
10	29	30
K = 4 L = 7		
-10	39	41
-8	0	11
-6	14	17
-4	43	49
-2	96	106
0	8	2
2	44	36
4	8	8
6	63	60
8	77	79
K = 4 L = 8		
-10	14	10
-8	41	39
-6	93	100
-4	22	28
-2	84	93
0	8	5
2	37	26
4	193	192
6	50	54
8	32	30
K = 4 L = 9		
-10	45	41
-8	41	42
-6	0	1
-4	72	83
-2	12	4
0	82	72
2	32	32
4	32	32
6	0	8
8	56	56
K = 4 L = 10		
-8	130	140
-6	42	46
-4	31	33
-2	29	36
0	123	111
2	22	18
4	19	14
6	41	40
8	23	12
K = 4 L = 11		
-8	22	23
-6	11	8
-4	54	59
-2	71	80
0	31	31
2	26	23
4	13	13
6	69	77
K = 4 L = 12		
-8	22	5
-6	19	18
-4	27	32
-2	52	57
0	100	87
2	21	17
4	45	41
6	17	19
K = 4 L = 13		
-6	65	71
-4	28	25
-2	65	72
0	0	13
2	35	32
4	122	117
K = 4 L = 14		
-6	51	54
-4	44	43
-2	23	19
0	89	85
2	64	61
4	0	5
K = 4 L = 15		
-4	17	8
-2	6	11
0	24	26
2	51	47
K = 4 L = 16		
-2	58	69
0	0	1
K = 5 L = 0		
1	11	11
3	153	149
5	36	27
7	28	36
9	20	20
K = 5 L = 1		
-9	31	34
-7	49	51
-5	36	29
-3	16	9
-1	5	8
1	31	24
3	76	76
5	65	58
7	11	0
9	81	86
K = 5 L = 2		
-9	85	79
-7	0	14
-5	46	45
-3	0	0
-1	8	11
1	79	72
3	88	80
5	25	28
7	26	26
9	64	59
K = 5 L = 3		
-9	93	95
-7	55	48
-5	11	14
-3	142	138
-1	93	79
1	38	39
3	21	17
5	45	40
7	20	22
9	67	70
K = 5 L = 4		
-9	29	25
-7	3	16
-5	21	16
-3	13	3
-1	95	95
1	31	27
3	45	47
5	96	90
7	34	30
9	29	22
K = 5 L = 5		
-9	3	4
-7	17	14
-5	30	39
-3	92	95
-1	15	18
1	18	13
3	105	100
5	34	35
7	81	85
9	12	5
K = 5 L = 6		
-9	54	52
-7	80	75
-5	19	19
-3	12	9
-1	33	31
1	14	7
3	77	72
5	49	40
7	19	22
K = 5 L = 7		
-9	37	34
-7	52	61
-5	66	77
-3	18	18
-1	60	63
1	83	76
3	57	49
5	8	12
7	15	19
K = 5 L = 8		
-9	68	67
-7	22	24
-5	36	37
-3	74	83
-1	24	23
1	110	104
3	0	0
5	17	7
7	69	73
K = 5 L = 9		
-7	17	14
-5	0	4
-3	15	19
-1	61	65
1	12	2
3	0	12
5	65	66
7	15	23
K = 5 L = 10		
-7	11	15
-5	57	71
-3	52	60
-1	9	2
1	13	9
3	63	60
5	33	34
K = 5 L = 11		
-7	35	39
-5	60	66
-3	25	32
-1	16	17
1	74	73
3	83	86
5	28	31
K = 5 L = 12		
-5	25	36
-3	14	9
-1	43	50
1	27	29
3	29	23
K = 5 L = 13		
-5	21	17
-3	44	55
-1	21	20
1	89	84
3	0	14
K = 5 L = 14		
-3	45	52
-1	32	36
1	0	2
K = 6 L = 0		
0	155	156
2	77	66
4	18	12
6	135	131
8	21	13
K = 6 L = 1		
-8	14	5
-6	84	86
-4	33	34
-2	76	74
0	26

TABLE 3. FINAL POSITIONAL PARAMETERS ($\times 10^4$) AND THERMAL PARAMETERS ($Å^2 \times 10^2$)[a]

	x/a	y/b	z/c	B_{11} or B	B_{22}	B_{33}	B_{12}	B_{13}	B_{23}
Ba(1)	1445(2)	0	4138(2)	86(6)	59(6)	69(6)	0	−17(5)	0
Ba(2)	5295(2)	0	2189(2)	68(6)	12(6)	210(8)	0	−1(5)	0
Fe(1)	1926(4)	0	1755(4)	55(14)	22(13)	36(13)	0	−7(11)	0
Fe(2)	8595(4)	0	2068(4)	50(13)	18(13)	53(14)	0	−15(11)	0
Fe(3)	2500	2500	0	59(13)	15(13)	53(13)	−10(11)	−2(10)	9(11)
Fe(4)	5000	0	5000	63(20)	50(20)	30(19)	0	−1(15)	0
Fe(5)	5000	0	0	180(28)	109(26)	205(29)	0	−4(23)	0
Fe(6)	0	0	0	21(18)	31(19)	36(19)	0	−3(14)	0
O(1)	970(13)	2341(15)	761(13)	74(21)					
O(2)	2805(14)	2401(16)	2461(14)	108(24)					
O(3)	3906(15)	2429(17)	4346(14)	119(24)					
O(4)	3338(19)	0	765(19)	64(30)					
O(5)	386(18)	0	2438(18)	36(28)					
O(6)	3808(22)	0	6019(22)	117(36)					
O(7)	8447(20)	0	743(20)	70(31)					

a) Estimated standard deviations are given in parentheses. The anisotropic thermal factors are of the form $T=\exp\left[-\frac{1}{4}(h^2a^{*2}B_{11}+\cdots+2klb^*c^*B_{23})\right]$.

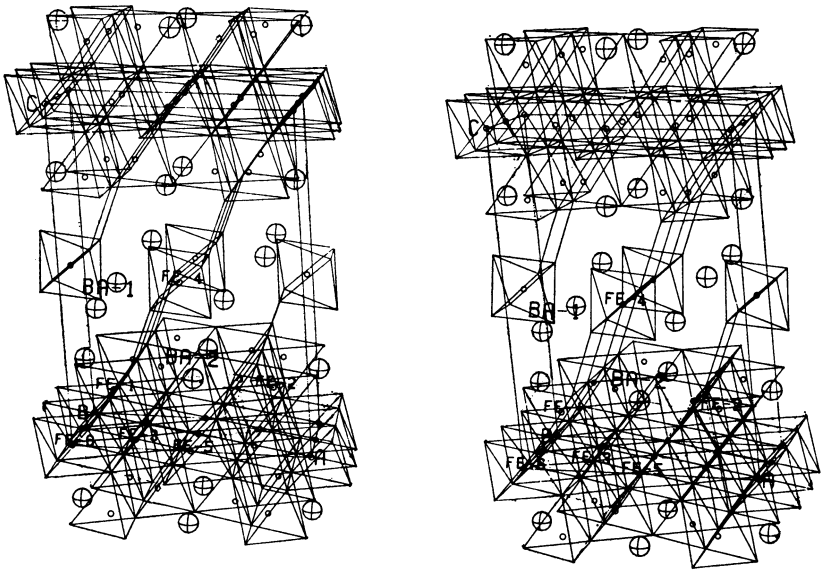

Fig. 3. Stereoscopic drawing of the crystal structure of $Ba_4Fe_9O_{20}H_6$.

$Fe(OH)_6^{3-}$ cluster between these layers. Interatomic distances are summarized in Table 4.

Ba(1) and Ba(2) are surrounded respectively by nine and ten oxygen atoms at distances ranging from 2.61 to 3.02 Å. It is noticeable that each Ba is close to one oxygen atom, with a separation of less than 2.70 Å. Similar situations occur in $BaFe_2O_4$ obtained by firing,[3] in $Ba_2[Al_2(OH)_{10}]$[12], and $Ba_3[Al_2(OH)_{12}]$,[13] both grown from aqueous solutions, and in $Ba(OH)_2 \cdot 8H_2O$.[14] On the other hand, in hexagonal barium ferrites,[15] such a close contact of Ba to O is not found, but their structures are close-packed build-ups of O and Ba: for example, in $Ba_2Zn_2Fe_{12}O_{22}$ (ofen referred to as Y ferrite), Ba is surrounded by twelve oxygens at distances between 2.95 and 3.26 Å.[16]

The coordination octahedron around Fe(4) consists of four equivalent oxygen atoms [O(3)] in equatorial positions and two O(6) atoms in axial positions. This octahedron is much more regular than the other Fe octahedra and does not share any vertices, edges, or faces with the adjacent polyhedra. These findings strongly suggest that all vertices of the octahedron around Fe(4) are occupied by OH groups. The equatorial oxygen O(3) in the cluster is close to O(2) in the triple layer, at a distance of 2.872 Å, and forms a weak hydrogen bond, while the axial oxygen O(6) does not participate in any hydrogen bond. This hydrogen-bonding scheme is quite consistent with the IR spectrum described above. Each of the four equivalent hydrogen bonds is shown in the stereoscopic drawings of Fig. 3, together with the $Fe(OH)_6^{3-}$ clusters, Ba^{2+} ions, and triple layers of condensed ferrite anions.

One would expect the Fe–O distances to provide a powerful assistance for establishing the position of Fe

TABLE 4. INTERATOMIC DISTANCES (l/Å)

(a) Ba-O distances		
Ba(1)-O(5)	2.611(25)	*once*
-O(3^{iv})	2.741(18)	*twice*
-O(3)	2.906(14)	*twice*
-O(6^{iv})	3.011(3)	*twice*
-O(3^{v})	3.065(15)	*twice*
Ba(2)-O(6^{vi})	2.687(31)	*once*
-O(4)	2.753(23)	*once*
-O(1^{i})	2.756(16)	*twice*
-O(2)	2.989(14)	*twice*
-O(2^{i})	3.005(13)	*twice*
-O(5^{i})	3.015(3)	*twice*
(b) Fe-O distances		
Fe(1) octahedron		
Fe(1)-O(2)	1.941(14)	*twice*
-O(5)	1.942(23)	*once*
-O(4)	2.134(26)	*once*
-O(1)	2.183(16)	*twice*
Fe(2) tetrahedron		
Fe(2)-O(2^{i})	1.868(13)	*twice*
-(5^{ii})O	1.868(19)	*once*
-O(7)	1.921(30)	*once*
Fe(3) octahedron		
Fe(3)-O(1)	2.004(16)	*twice*
-O(4)	2.011(16)	*twice*
-O(7^{iii})	2.041(17)	*twice*
Fe(4) octahedron		
Fe(4)-O(6)	2.007(30)	*twice*
-O(3)	2.022(14)	*4 times*
Fe(5) octahedron		
Fe(5)-O(4)	2.120(23)	*twice*
-O(1^{i})	2.134(14)	*4 times*
Fe(6) octahedron		
Fe(6)-O(1)	1.996(12)	*4 times*
-O(7^{iii})	2.006(25)	*twice*
(c) Me-Me distances (l<4.0 Å)		
Ba(1)-Fe(1)	3.548(7)	*once*
-Fe(4^{v})	3.615(2)	*twice*
-Fe(4)	3.749(3)	*once*
Ba(2)-Fe(5)	3.174(4)	*once*
-Fe(2)	3.407(5)	*once*
-Fe(1)	3.458(5)	*once*
-Fe(2^{ix})	3.461(5)	*twice*
-Fe(1^{i})	3.514(3)	*twice*
Fe(1)-Fe(3)	3.064(5)	*twice*
-Fe(6)	3.085(5)	*once*
-Ba(2)	3.458(5)	*once*
Fe(2^{v})	3.458(3)	*twice*
Fe(2^{vii})	3.490(6)	*once*
-Ba(2^{ix})	3.514(5)	*twice*
-Ba(1)	3.548(7)	*once*
Fe(2)-Ba(2)	3.407(5)	*once*
-Fe(6^{ii})	3.454(6)	*once*
-Fe(3^{iii})	3.457(5)	*twice*
-Fe(1^{i})	3.458(3)	*twice*
-Ba(2^{i})	3.461(5)	*twice*
-Fe(1^{ii})	3.490(6)	*once*
Fe(3)-Fe(5)	2.970(1)	*twice*
-Fe(6)	2.970(1)	*twice*
-Fe(3^{x})	2.993(2)	*twice*
-Fe(1)	3.064(5)	*twice*
-Fe(2^{iii})	3.457(5)	*twice*
Fe(4)-Ba(1^{i})	3.615(2)	*4 times*
-Ba(1)	3.749(3)	*twice*
Fe(5)-Fe(3)	2.790(1)	*4 times*
-Fe(6^{i})	2.993(2)	*twice*
-Ba(2)	3.174(3)	*twice*
Fe(6)-Fe(3)	2.970(1)	*4 times*
-Fe(5^{ix})	2.993(2)	*twice*
-Fe(1)	3.085(5)	*twice*
-Fe(2^{iii})	3.454(6)	*twice*

(d) A hydrogen bond

O(3)-O(2) 2.873(27)

symmetry code			
none	x,	y,	z,
i	$\frac{1}{2}+x$,	$-\frac{1}{2}+y$,	z,
ii	$1+x$,	y,	z,
iii	$1-x$,	$-y$,	$-z$,
iv	$\frac{1}{2}-x$,	$\frac{1}{2}-y$,	$1-z$,
v	$-\frac{1}{2}+x$,	$-\frac{1}{2}+y$,	z,
vi	$1-x$,	$-y$,	$1-z$,
vii	$-1+x$,	y,	z,
viii	$-x$,	$-y$,	$1-z$,
ix	$-\frac{1}{2}+x$,	$\frac{1}{2}+y$,	z,
x	x,	$-y$,	z,

with oxidation number two. All Fe–O distances in the tetrahedron (mean 1.88 Å) and octahedra (mean 2.01 Å) other than those concerning Fe(1) and Fe(5) are nearly equal to those of Fe with oxidation number three, as reported in the literature.[17] On the other hand, distances of Fe–O concerning Fe(5) are significantly larger (2.12—2.13 Å), in fair agreement with typical values for Fe with oxidation number two. Hence, the position of Fe with oxidation number two could be confirmed to be in the middle slice of the triple layer. As a consequence, the formula should be written $Ba_4[Fe^{III}(OH)_6][Fe^{II}Fe_7^{III}O_{14}]$. This finding suggests that Ba^{2+} ions, $[Fe(OH)_6]^{3-}$ ions, and some condensed ferrite anions with sheet-like structures exist generally in the hydrothermal medium.

The Fe–O distances around Fe(1) vary from 1.941 to 2.183 Å. In this octahedron, O–O distances of the shared edges in the basal plane are shorter than those of the unshared edges in the top plane which faces toward the outside of the triple layer. The Fe(1) is displaced toward the outside of the triple layer, so that Fe(1) is closer to the three oxygens of the shared vertices (1.942 and twice 1.941 Å) than to those of the shared edges (2.134 and twice 2.183 Å). Such a variety of Fe–O distances was also found in α-Fe_2O_3[18] and in two modifications of $BaFe_4O_7$.[5] In the former case, where two FeO_6 octahedra are stacked by sharing their faces, the distortion was explained in terms of a

large electronic interaction between two Fe across the shared plane. The repulsion between Fe^{3+} and Ba^{2+} might cause an additional distortion in the structure of both modifications of $BaFe_4O_7$. In the present case, however, the distances of Fe(1)–O can not be understood only by such local interactions. This suggests that the three Fe(1)–O bonds concerning the oxygen atoms shared by FeO_4 tetrahedra are more covalent than the other three.

Polymerization of ferrite anions has been discussed by many workers.[19–21] On the basis of the structure of $Ba_4[Fe(OH)_6][Fe_8O_{14}]$ determined just above, we suppose three stages of condensation of ferrite anions, such as the following: (1) The free hydroxo-complex anion, $[Fe(OH)_6]^{3-}$, found in solution is enclosed into nuclei of the lattice together with Ba^{2+} cations. (2) The condensation of the hydroxo-complex anions proceeds with accompanying dehydration, and the FeO_6 octahedra necessarily share their vertices or edges with each other. (3) During such a condensation process, a part of the FeO_6 octahedra are allowed to convert into FeO_4 tetrahedra, as evidenced by the Fe(2) tetrahedra kept back in the crystal lattice. If all FeO_6 octahedra transform to FeO_4 tetrahedra sharing their vertices, then the resulting framework of condensed ferrites would become tetrahedral chains or a two- or three-dimensional network analogous to silicates, aluminosilicates, and aluminates. Such a situation is encountered in barium monoferrite, $BaFe_2O_4$, obtained by firing. We have recently found another example of a three-dimensional framework of FeO_4 tetrahedra in $Ba_8Fe_{13}O_{30}H_6$[5] synthesized by a hydrothermal reaction.

Magnetic Properties. The easy axis of magnetization was examined by a combined use of an optical microscope and a hand permanent magnet. Batches of samples were classified into two groups because of their quite remarkably different magnetizations; the easy magnetization axes of one batch of samples lay on the basal plane of the hexagonal plates, while those of the other batch were directed toward the outside of the plane. The single crystal used for this X-ray study was obtained from the former; its easy magnetization axis pointed in the a-direction. The latter batch of crystals emerged less frequently. These distinct groups of samples showed somewhat different Mössbauer spectra; these are compared in Fig. 4. Such a difference can not be explained in terms of a preferred orientation of the sample grains. It is therefore probable that two modifications would occur, owing to only slight differences in either the contents or the locations of Fe atoms with oxidation number two. Although the Mössbauer spectra are quite complicated, a tentative assignment was made for three Fe species by assuming that the oxidation numbers of all Fe are three and that their isomer shifts are in the range of $0.0<\delta<0.7$ mm s^{-1} (referred to Fe foil). Considering the numbers of equivalent positions and the coordination number of oxygens, we assigned the three Fe species to Fe(2), Fe(1), and Fe(3) in the increasing order of δ. The Mössbauer parameters thus obtained are given in Table 5.

The magnetic measurement was made only for crystals

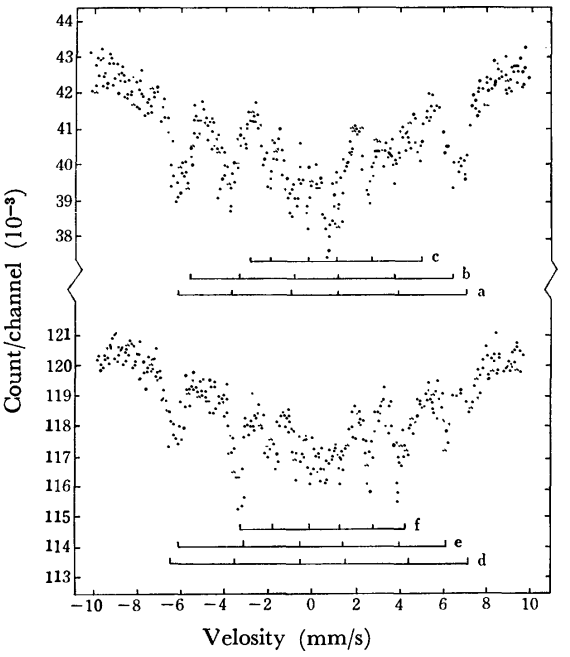

Fig. 4. Mössbauer spectra of $Ba_4Fe_9O_{20}H_6$.
Above: crystals with easy magnetization axes directed toward out of the (001) plane. Below: crystals with easy magnetization axes lying the (001) plane.

TABLE 5. MÖSSBAUER PARAMETERS OF $Ba_4Fe_9O_{20}H_6$

Spectra (in Fig. 4)	Isomer shift[a] ε/mm s^{-1}	Quadrupole splitting δ/mm s^{-1}	Inner field H_{int}/kG[b]
a	0.37	−0.16	413
b	0.31	−0.11	380
c	0.09	−0.33	346
d	0.21	0.06	425
e	0.23	0.11	383
f	0.30	0.10	313

a) with respect to the centroid of the spectrum of iron foil at 293 K. b) $1G=10^{-4}$ T.

with easy axes parallel to the (001) plane. The variation of magnetization against field strength was measured from 900 to 12000 G at room temperature. The value stayed constant at 13.80 ± 0.05 emu g^{-1} above 2000 G and saturation was considered to be reached. Figure 5 shows the temperature dependence of magnetization from 77 to 573 K measured at 4000 G, together with the Néel point, $T_N=515$ K. This plot is far from a Langevin curve, indicating complicated mechanisms of magnetic interaction. An extrapolation of this curve gives a magnetic moment of about $10\,\mu_B$ per formula corresponding to just two Fe^{3+} ions. If the magnetic moments are simply ordered parallel and antiparallel below T_N, then a space group of P2/m with the same cell dimensions or doubling of the unit sell in volume would be required for the magnetic unit cell.

Twining. Twinning of this crystal would be expected to occur in various ways, owing to the pseudo-hexagonal symmetry possessed by the triple layer of the condensed ferrite anion in the structure (the axial

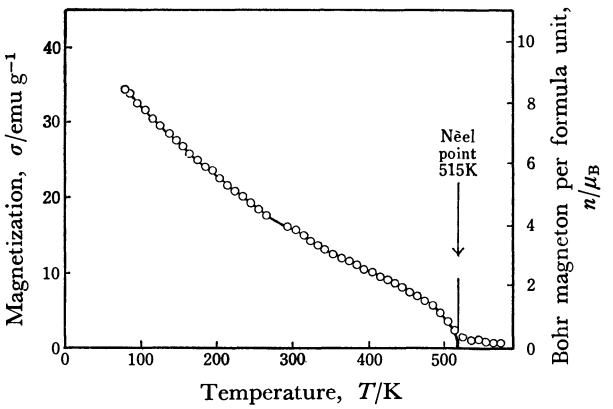

Fig. 5. Variation of magnetization at 4000 G with temperature.

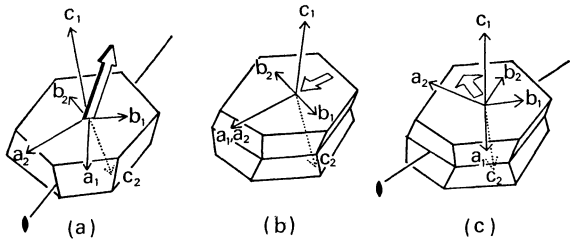

Fig. 6. Three twin laws of $Ba_4Fe_9O_{20}H_6$.
(a) [110] axial twinning. (b) Twin and composition plane (001). (c) [130] axial twinning. Directions of easy magnetization axes are shown by open arrows. Twin axes are shown by diad axes in (a) and (c).

ratio of a/b is 1.714). In fact three kinds of twin laws were confirmed by X-ray techniques, and the direction of the easy magnetization axis for each twinned specimen was determined by use of a permanent magnet. Relative orientations of individual crystals, which were determined by Weissenberg and precession photographs, are shown in Fig. 6 together with the direction of easy magnetization. The first kind is the [110] axial twinning; here the easy direction is perpendicular to the twin axis, but it leans at an angle of about 30° from the normal of the (001) plane (Fig. 6a). The second is not axial, and the (001) plane corresponds to the twin and composition plane (Fig. 6b). In this case, the a-axes of both individuals are coincident and the easy magnetization axis is parallel to this direction. The third twinning is [130] axial twinning, in which the easy magnetization axis is perpendicular to the twin axis and lies on the (001) plane (Fig. 6c). It is plausible that twinning repeats during the crystal growth according to these laws. Many sorts of polysynthetic twins were found very often under an optical microscope. In addition, the latter two kinds of twins appeared as a mixture in a batch, while the first appeared in a different batch. The direction of easy magnetization can not be explained solely on the basis of a vector sum of individual contributions. This finding also suggests the occurrence of two or more modifications in this compound.

The authors thank Dr. Masayasu Tokonami of this Institute for his assistance in the X-ray intensity data collection. The authors also thank Dr. Hideko Kiriyama of this Institute for her helpful criticisms of the manuscript.

References

1) Y. Goto and T. Takada, *J. Am. Ceram. Soc.*, **43**, 150 (1960); S. Mori, *ibid.*, **49**, 600 (1966).
2) J. Smit and H. P. J. Wijn, "Ferrites," International ed., Tokyo Electrical Enginnering Press, Tokyo (1965), p. 117.
3) H. Mitsuda, S. Mori, and C. Okazaki, *Acta Crystallogr.*, **B27**, 1263 (1971).
4) K. Kitahama and R. Kiriyama, *Acta Crystallogr.*, **A28**, S62 (1972).
5) S. Okamoto, S. I. Okamoto, and T. Ito, *Acta Crystallogr.*, **B29**, 832 (1973).
6) S. Okamoto, H. Sekizawa, and S. I. Okamoto, *J. Phys. Chem. Solids*, **36**, 591 (1975).
7) R. Kiriyama, T. Tsai, and K. Kitahama, *Ferrites*: Proc. Intern. Conf. 1970, Japan, p. 171, Univ. Tokyo Press (1971).
8) G. C. Kennedy, *Am. J. Sci.*, **248**, 540 (1950); **255**, 724 (1957).
9) "International Tables for X-Ray Crystallography," Vol. IV, Kynoch Press, Birmingham (1974), pp. 71—98 and 148—150.
10) T. Sakurai, Ed., "UNICS Program System," Crystallographic Society of Japan (1967).
11) C. K. Johnson, ORTEP. Oak Ridge National Laboratory Report ORNL-3794 (1965).
12) A. H. Moinuddin Ahmed and L. S. Dent Glasser, *Acta Crystallogr.*, **B26**, 867 (1970).
13) A. H. Moinuddin Ahmed and L. S. Dent Glasser, *Acta Crystallogr.*, **B25**, 2169 (1969).
14) H. Manohar and S. Ramaseshan, *Z. Kristallogr., Kristallgeom., Kristallphys., Kristallchem.*, **119**, 357 (1964).
15) P. B. Braun, *Philips Research Repts.*, **12**, 491 (1957).
16) W. D. Townes and J. H. Fang, *Z. Kristallogr., Kristallgeom., Kristallphys,. Kristallchem.*, **131**, 196 (1970).
17) R. D. Shannon and C. T. Prewitt, *Acta Crystallogr.*, **B25**, 925 (1969).
18) R. L. Blake, R. E. Hessevick, T. Zoltai, and L. W. Finger, *Am. Mineral.*, **51**, 123 (1966).
19) K. Inouye, *Kagaku to Kogyo*, **27**, 571 (1974).
20) H. Schuger, C. Walling, R. B. Jones, and H. B. Gray, *J. Am. Chem. Soc.*, **1967**, 3712.
21) K. M. Towe and W. F. Bradley, *J. Colloid Interface Sci.*, **24**, 384 (1967).

A Mössbauer Study of Graphite Intercalated with Iron(III) Chloride and Aluminum Chloride

Takeshi TOMINAGA, Takuhiko SAKAI, and Tomohiko KIMURA

Department of Chemistry, Faculty of Science, The University of Tokyo, Bunkyo-ku, Tokyo 113

(Received June 2, 1976)

The Mössbauer spectra of graphite–$FeCl_3$ and graphite-$FeCl_3$–$AlCl_3$ compounds with varying $FeCl_3/AlCl_3$ ratios were measured. At 298 K, the isomer shift of the Fe^{3+} peak of $FeCl_3$ intercalated in the graphite–$FeCl_3$ compounds was larger than that of pure anhydrous $FeCl_3$, and two sets of Fe^{2+} quadrupole doublets appeared in the spectra of the graphite-$FeCl_3$–$AlCl_3$ compounds with $FeCl_3/AlCl_3$ ratios of approximately one or less. These results may be accounted for in terms of the transfer of graphite π-electrons to intercalated $FeCl_3$.

In 1967 one of the present authors (T.T.) investigated the Mössbauer spectra of the graphite–$FeCl_3$ intercalation compounds with a view to obtaining a clue as to the nature of the bonding in such systems.[1] The isomer shift of the intercalated iron(III) chloride was found to be larger than that of pure anhydrous iron(III) chloride, indicating the possibility of the transfer of graphite π-electrons to the intercalated molecules. Similar results have been reported thereafter from several groups of workers for the Mössbauer spectra of graphite intercalated with iron chloride, or iron chloride and aluminum chloride.[2-9] In contrast to the previous report[3] that the spectra of the graphite–$FeCl_3$–$AlCl_3$ compounds were essentially the same as those of the graphite–$FeCl_3$ compound, we have recently observed the presence of quadrupole doublets of Fe^{2+} in the Mössbauer spectra of the graphite–$FeCl_3$–$AlCl_3$ compounds with $FeCl_3/AlCl_3$ ratios of about one or less.[9]

The object of the present article is to report the detailed results of the Mössbauer spectroscopic study on the graphite–$FeCl_3$–$AlCl_3$ compounds with varying $FeCl_3/AlCl_3$ ratio so as to elucidate the chemical states of iron chloride intercalated in such systems.

Experimental

Materials. A pulverized natural graphite (Spectroscopic Powder) purchased from Union Carbide Corp. was used for preparation of the intercalation compounds. The graphite–$FeCl_3$ compounds were obtained by procedures similar to those described in the literature.[10] Mixtures of weighed quantities of graphite and anhydrous iron(III) chloride were heated in sealed glass tubes between 230 and 350 °C. The products were freed from unreacted iron chloride by washing with hot 2 M HCl and then dried at 110 °C. The products were analyzed for their metal content by decomposition to oxides. The chlorine content was determined by neutron activation analysis. The analytical results of the intercalation compounds obtained under various heating conditions are summarized in Table 1.

The graphite–$FeCl_3$–$AlCl_3$ compounds were prepared by methods essentially similar to those reported in the literature.[11,12] Mixtures of graphite with anhydrous iron(III) chloride and aluminum chloride were heated in sealed glass tubes at temperatures between 210 and 300 °C, and excess metal chlorides were removed by washing with hot 2 M HCl. The analytical results of the products prepared under various conditions are also summarized in Table 1.

Mössbauer Spectroscopy. The Mössbauer spectra of the intercalation compounds were measured at 298 and 80 K by using a Hitachi AA-40 or a Shimadzu MEG-1A Mössbauer spectrometer with a ^{57}Co source diffused into copper foil. The isomer shifts are given as related to the centroid of the spectrum of iron foil at 298 K. The errors in isomer shifts and quadrupole splittings are generally of the order of 0.02—0.03 mm/s, except for the spectra subjected to larger uncertainties because of weak absorption intensities or the complexity of overlapping peaks.

Results and Discussion

Graphite–$FeCl_3$ Compounds. As a typical example of the graphite–$FeCl_3$ compounds, Mössbauer spectra of $C_{10}FeCl_3$ (compound II with 55.8 % $FeCl_3$) at 298 and 80 K are illustrated in Figs. 1a and 2a respectively. The spectrum at 298 K consists of a single absorption peak of Fe^{3+} with an isomer shift of 0.50 mm/s, which is obviously larger than that of pure anhydrous iron(III) chloride, $FeCl_3$ (δ=0.42 mm/s). This observation is in agreement with the results obtained previously,[1-8] and may indicate that the graphite π-electrons are transferred to the d-orbitals of iron in all iron(III) chloride molecules rather than in one quarter of the intercalated molecules as postulated by Dzurus and Hennig.[12,13] Such an electron transfer mechanism may be further confirmed by the reverse effect observed in boron nitride–$FeCl_3$ compounds:[14] the isomer shift of $FeCl_3$ intercalated in boron nitride was lower than that of pure anhydrous $FeCl_3$, revealing that an electron transfer from $FeCl_3$ to boron nitride layers probably takes place in the system. However, the isomer shift of $C_{10}FeCl_3$ at 80 K (0.54 mm/s) is very close to that of pure anhydrous $FeCl_3$ (0.52 mm/s). Hence, it is probable that the electron transfer from graphite to $FeCl_3$ is considerably attenuated at low temperatures.

The Mössbauer spectra of all the graphite–$FeCl_3$ preparations appear to be essentially similar; the isomer shift does not change significantly with the $FeCl_3$ content or with the heating temperature (Table 2). It is worth mentioning that only a very weak component of an Fe^{2+} doublet was observed in the spectrum of C_9FeCl_3 prepared by heating at 350 °C (compound III), whereas no iron(II) state was detected in the spectrum of $C_{10}FeCl_3$ reheated at 300 °C *in vacuo* (compound IV). On heating $C_{10}FeCl_3$ at 400 °C in vacuum or air, two sets of Fe^{2+} doublets arose in the spectrum, indicating the formation of $FeCl_2$ by decomposition.

Graphite–$FeCl_3$–$AlCl_3$ Compounds. The Mössbauer spectra of typical graphite–$FeCl_3$–$AlCl_3$ compounds at 298 and 80 K are represented in Figs. 1 and 2 respective-

Table 1. Analyses of the intercalation compounds prepared in this work

Compound	Heating conditions	Analytical (%)			$FeCl_3/AlCl_3$[a]	Cl/(Fe+Al)[a]
		C	$FeCl_3$	$AlCl_3$		
Graphite-$FeCl_3$ compounds:						
I	230 °C, 4 h	56.6	43.4	—	—	3.01±0.05
II	250 °C, 4 h	44.2	55.8	—	—	3.05±0.07
III	350 °C, 4 h	39.6	60.4	—	—	
IV	II reheated 300 °C, 4 h	50.8	49.2	—	—	
Graphite-$FeCl_3$-$AlCl_3$ compounds:						
V	270 °C, 4 h	40.9	48.5	10.6	4	
VI	210 °C, 4 h	41.9	38.0	20.1	1.5	
VII	210 °C, 4 h	42.1	34.4	23.5	1.2	
VIII	220 °C, 4 h	64.2	20.1	15.7	1.0	
IX	300 °C, 6 h	61.7	14.3	24.0	0.5	
X	300 °C, 24 h	73.1	6.8	20.1	0.3	2.93±0.07
XI	230 °C, 4 h	82.6	4.9	12.5	0.3	2.99±0.02

a) Molar or atomic ratio.

Table 2. Mössbauer parameters of the intercalation compounds prepared in this work[a]

Compound	Temperature (K)	Fe^{2+}				Fe^{3+}
		Inner doublet		Outer doublet		
		δ	ΔE_Q	δ	ΔE_Q	δ
		(mm/s)				
Graphite-$FeCl_3$ compounds:						
I	298	—	—	—	—	0.49
II	298	—	—	—	—	0.50
	80	—	—	—	—	0.54
III	298	—	—	—	—	0.50
IV	298	—	—	—	—	0.49
Graphite-$FeCl_3$-$AlCl_3$ compounds:						
V	298	—	—	—	—	0.50
VI	298	—	—	—	—	0.46
VII	298	—	—	—	—	0.47
VIII	298	1.11	0.86	(1.09)	(1.76)	0.45
	80	1.23	1.05	(1.24)	(2.10)	0.52
IX	298	1.08	0.72	1.06	1.61	(0.45)
	80	1.25	0.97	1.23	2.09	(0.50)
X	298	1.05	0.78	1.12	1.49	(0.45)
	80	1.20	1.03	1.21	2.05	(0.50)
XI	80	1.18	0.96	1.19	1.91	(0.52)

a) Parameters given in parentheses involve rather large uncertainties (±0.05 mm/s) due to the weak absorption intensities of overlapping peaks.

ly. The Mössbauer spectra at 298 K of the graphite–$FeCl_3$–$AlCl_3$ compounds with $FeCl_3/AlCl_3$ ratios of 4—1.2 (compounds V to VII) were essentially similar to those of the graphite–$FeCl_3$ compounds composed of an Fe^{3+} singlet alone (Figs. 1b and 1c.) As the $FeCl_3/AlCl_3$ ratio was decreased to one, however, a weak Fe^{2+} quadrupole doublet appeared in addition to the Fe^{3+} peak (compound VIII, Fig. 1d). In the spectra of the compounds with $FeCl_3/AlCl_3$ ratios of 0.5 and 0.3 (compounds IX and X), a second Fe^{2+} doublet arose outside of the initial doublet, and the intensities of both doublets exceeded that of the Fe^{3+} peak (Figs. 1e and 1f). Hence we may presume that iron chloride molecules intercalated in the graphite–$FeCl_3$–$AlCl_3$ compounds with $FeCl_3/AlCl_3$ ratios of 0.3—0.5 exist predominantly in high-spin iron(II) states.

The Mössbauer spectra at 80 K of the intercalation compounds with $FeCl_3/AlCl_3$ ratios of 1—0.3 (compounds VIII to XI) similarly show the presence of the Fe^{2+} doublets. However, the Fe^{2+}/Fe^{3+} area ratio at 80 K becomes considerably smaller than that at 298 K; thus the percentage of the Fe^{2+} fraction tends to decrease with the decrease in temperature. Although the origin of such temperature dependence of the Fe^{2+}/Fe^{3+} area ratio cannot yet be explained without ambiguities, it is likely that the transfer of graphite π-electrons to

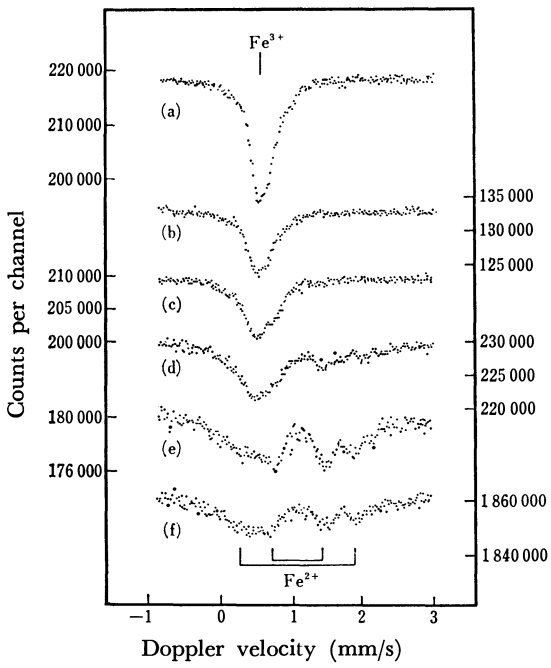

Fig. 1. Mössbauer spectra at 298 K of (a) graphite–$FeCl_3$ intercalation compound, and (b)—(f) graphite–$FeCl_3$–$AlCl_3$ intercalation compounds: (a) compound II, (b) compound V, (c) compound VI, (d) compound VIII, (e) compound IX, (f) compound X.

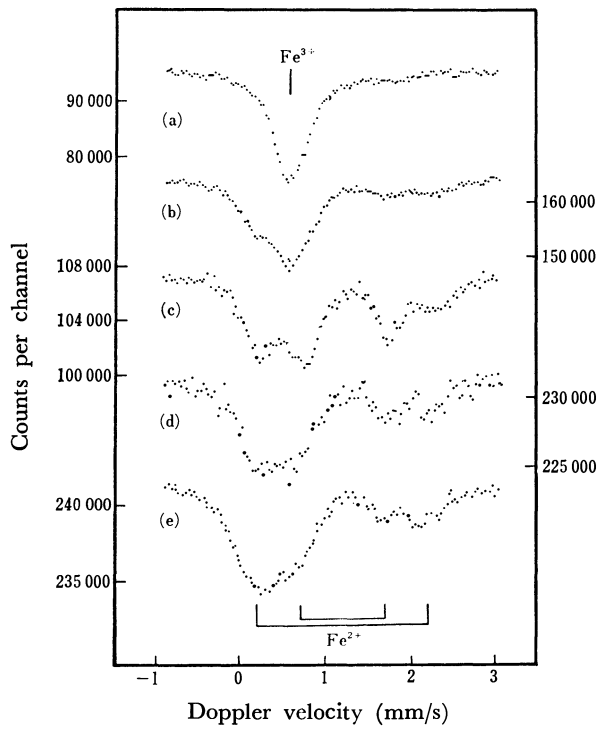

Fig. 2. Mössbauer spectra at 80 K of (a) graphite–$FeCl_3$ intercalation compound, and (b)—(e) graphite–$FeCl_3$–$AlCl_3$ intercalation compounds: (a) compound II, (b) compound VIII, (c) compound IX, (d) compound X, (e) compound XI.

$FeCl_3$ may be attenuated at low temperatures, as has been observed with the graphite–$FeCl_3$ compounds; the other possibilities, such as an effect due to the difference in temperature dependence of the recoilless fractions of Fe^{2+} and Fe^{3+} species,[15] or any irreversible change in structure over the above temperature range,[16] may be ruled out.

As shown in Table 2, two sets of quadrupole doublets with nearly equal isomer shifts arise in the Mössbauer spectra of the graphite–$FeCl_3$–$AlCl_3$ compounds with $FeCl_3/AlCl_3$ ratios of 1—0.3. This is indicative of the presence of two kinds of Fe^{2+} ion sites, one of which (corresponding to the inner doublet) may not differ appreciably from the Fe^{2+} site in pure anhydrous $FeCl_2$ because their Mössbauer parameters are alike. Moreover, it is worthwhile mentioning that the Mössbauer parameters of the Fe^{2+} doublets of the graphite–$FeCl_3$–$AlCl_3$ compounds are generally similar to those of the Fe^{2+} peaks of the graphite–$FeCl_2$ compounds obtainable by reduction of the graphite–$FeCl_3$ compounds.[4,6-8] The origin of the two Fe^{2+} sites in the graphite–$FeCl_2$ compounds has been ascribed to dissimilar distortions from a regular octahedron of chlorine in the $FeCl_2$ structure.[8]

The appearance of the Fe^{2+} doublets in the graphite–$FeCl_3$–$AlCl_3$ compounds with small $FeCl_3/AlCl_3$ ratios may be tentatively accounted for as follows.[17] If the $AlCl_3$ concentration in the metal halide layer is small, a graphite π-electron donated to an Fe^{3+} ion may be shared among several neighboring Fe^{3+} ions through a rapid exchange process, and eventually will increase the isomer shift of the Fe^{3+} single peak. As the $AlCl_3$ concentration exceeds the $FeCl_3$ concentration ($FeCl_3/AlCl_3 \leq 1$), the donated electron may be localized on one Fe^{3+} ion to produce Fe^{2+}, since the iron ion is surrounded with Al^{3+} ions which are not electron acceptors, and no direct exchange of an electron between Fe^{3+} ions is probable. Accordingly, this may give evidence that a species of the type $C_n^+Cl^-$-$FeCl_2 \cdot 3AlCl_3$ is formed by the transfer of graphite π-electrons in the compounds with $FeCl_3/AlCl_3$ ratios of about 0.3, as postulated by Dzurus and Hennig.[12]

The present authors wish to express their thanks to Professor Nobufusa Saito, of the University of Tokyo, for his encouragement and support.

References

1) N. Saito, T. Tominaga, M. Takeda, Y. Ohe, F. Ambe, and H. Sano, *Proc. 7th Jpn. Conf. Radioisotopes*, **1967**, 231.
2) B. V. Liengme, M. W. Bartlett, J. G. Hooley, and J. R. Sams, *Phys. Lett.*, **A25**, 127 (1967).
3) A. G. Freeman, *Chem. Commun.*, **1968**, 193.
4) J. G. Hooley, M. W. Bartlett, B. V. Liengme, and J. Sams, *Carbon*, **6**, 681 (1968).
5) F. D. Grigutsch, D. Hohlwein, and A. Knappwost, *Z. Phys. Chem. (Frankfurt am Main)*, **65**, 322 (1969).
6) V. G. Jadhao, R. M. Singru, G. M. Joshi, K. P. R. Pisharody, and C. N. R. Rao, *Z. Phys. Chem. (Frankfurt am Main)*, **92**, 139 (1974).
7) M. J. Tricker, E. L. Evans, P. Cadman, N. C. Davies, and B. Bach, *Carbon*, **12**, 499 (1974).
8) K. Ohashi and I. Tsujikawa, *J. Phys. Soc. Jpn*, **36**, 422 (1974); *ibid.*, **37**, 63 (1974).
9) T. Tominaga, T. Sakai, and T. Kimura, *Chem. Lett.*,

1974, 853.

10) W. Rüdorff and H. Schulz, *Z. Anorg. Allgem. Chem.*, **245**, 121 (1940).

11) R. C. Croft, *J. Appl. Chem.*, **2**, 557 (1952).

12) M. L. Dzurus and G. R. Hennig, *J. Am. Chem. Soc.*, **79**, 1051 (1957).

13) Dzurus and Hennig[12] postulated the presence of species of the type $C_n^+Cl^-FeCl_2 \cdot 3FeCl_3$ in the graphite–$FeCl_3$ compounds on the basis of electrical measurements.

14) A. G. Freeman, *J. Chem. Soc., A*, **1969**, 1307.

15) The Fe^{2+}/Fe^{3+} area ratios measured at 298 and 80 K for a mixture of pure anhydrous $FeCl_2$ and $FeCl_3$ were nearly equal, within about 10% uncertainty. The layer structures of pure anhydrous iron chlorides may be essentially retained in the intercalation compounds where they are sandwiched between graphite layers.

16) The spectrum at 298 K was reproducible even after the compound had been cooled to 80 K and then warmed up to room temperature again.

17) We may exclude the possibility of the formation of $FeCl_2$ by decomposition under the conditions employed in this work. In fact, the observed Cl/(Fe+Al) ratios (Table 1) were close to 3, while the ratio should be as low as 2.76 if $FeCl_3$ was completely decomposed to $FeCl_2$ in the compounds with $FeCl_3/AlCl_3$ ratio of about 0.3.

Solvent Effects on the ESR Spectra of Copper(II) Complexes. A Consideration of the Donicity of Water and Methanol

Tateaki OGATA, Tadashi FUJISAWA, Nobuyuki TANAKA,* and Hiroshi YOKOI**

Department of Environmental Chemistry, Yamagata Technical College, Yonezawa 992

**Department of Chemistry, Faculty of Science, Tohoku University, Sendai 980*

***Chemical Research Institute of Non-aqueous Solutions, Tohoku University, Sendai 980*

(Received June 7, 1976)

Solvent effects on the ESR spectra of bis(2,6-dimethyl-3,5-heptanedionato)copper(II) ([Cu(dibm)$_2$]) and a similar copper(II) complex were investigated in some detail. A clear relationship between the ESR parameters and the donicity of the solvents was confirmed, and this is discussed with the intention of investigating the donicities of water and methanol. The donor number for water in an aqueous solution was estimated to be about 30 from a precise analysis of the ESR spectra of [Cu(dibm)$_2$] in water-methanol mixtures.

The concept of donicity has become increasingly important in the chemistry of non-aqueous solvents, but the donicities of some protic solvents such as water and alcohol still remain open to investigation.[1,2] Solvent effects on various properties of metal complexes have been studied widely for the purpose of determining the donicity of the solvents. Gutmann has found a relationship between the donicity or donor number (DN) of a solvent and the visible absorption band of bis(acetylacetonato)oxovanadium(IV) dissolved in the solvent.[2] Adato and Eliezer[3] have investigated solvent effects on the ESR spectra of bis(acetylacetonato)-copper(II) in connection with the DN of the solvents, but there seems to be some uncertainty in their data, as is described below. In addition, they did not refer at all to the DN of water or methanol.

The purpose of the work reported here is to re-investigate the relationship between the ESR parameters and the DN of solvents, using some stable planar copper(II) complexes which are soluble in many solvents, and to attempt to estimate the DN of water and methanol.

Experimental

Bis(2,6-dimethyl-3,5-heptanedionato)copper(II) (hereafter abbreviated to [Cu(dibm)$_2$]) and bis(*N*-salicylidenepropylaminato)copper(II)([Cu(*N*-Pr-sal)$_2$]) were prepared and purified by the usual method.[4,5] For the ligand of the former complex, 2,6-dimethyl-3,5-heptanedione, which was purchased from the Eastman Kodak Company, was used.

Acetonitrile, propylene carbonate, *N*,*N*-dimethylformamide, and dimethyl sulfoxide were purified according to the methods in the literature.[6-8] The other solvents were purified by the usual method.[9]

ESR spectra of the complexes in solutions (about 10 mM) were measured with a Hitachi 771 X-band ESR spectrometer at 77 K. Mixtures of toluene and the other solvents at various molar fractions were used as solvents.

Results and Discussion

The Relationship between the ESR Parameters and the DN of Solvents. As the first step in this study, it is absolutely necessary to obtain well-defined ESR spectra, and this could be achieved by using mixtures of toluene and the other solvents. Several typical ESR spectra of [Cu(dibm)$_2$] in various solvents at 77 K are shown in Fig. 1. All the spectral line shapes observed in this work were of axial or nearly axial symmetry,[10] and, in addition, the line-widths were rather narrow. Hence, the $g_{//}$ and $|A_{//}|$ values can be accurately determined from these spectra.

The $g_{//}$ and $|A_{//}|$ values of planar copper(II) complexes respectively increase and decrease to a significant extent as the axial ligand field is strengthened by apical coordination of the solvent molecules. Therefore, these values, as well as $g_{\perp}$, are good parameters for use in the investigation of the donicity of the solvents. The data obtained from the work reported here are given in Table 1, together with the DN and dipole moments (μ) of the solvents, where the DN of toluene was assumed to be approximately zero. Table 1 clearly indicates that $g_{//}$ and $|A_{//}|$ do not correlate with μ, but with DN. A correlation between $g_{//}$ and DN is shown in Fig. 2; the $g_{//}$ value increases with DN, and the order of the solvents is the same as that previously reported with regard to DN.[1] This result, therefore, suggests that the $g_{//}$ value can be used to estimate the DN. Similar results were obtained for [Cu(*N*-Pr-sal)$_2$]; for example, its $g_{//}$ values were 2.225 in pure toluene(T), 2.245 in T–DMF and 2.260 in

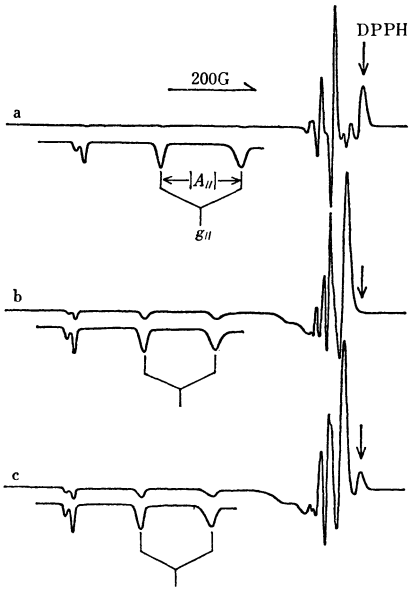

Fig. 1. ESR spectra of [Cu(dibm)$_2$] in pure T (a), T-MeOH (b) and T-DMSO (c).

TABLE 1. ESR DATA IN VARIOUS SOLVENTS

Solvent	$g_{//}$[a]	$\frac{\lvert A_{//}\rvert^{a)}}{10^{-4}\ cm^{-1}}$	DN	$\frac{\mu}{10^{-18}\ cm\ esu}$
Toluene (T)	2.251	193	0	0.37
Nitromethane (NM)	2.254	198	2.7	3.54
Nitroethane (NE)	2.259	195	—	3.60
1-Nitropropane (NP)	2.265	190	—	3.59
Acetonitrile (AN)	2.282	181	14.1	3.37
Propylene carbonate (PC)	2.277	185	15.1	5.2
Acetone (AC)	2.284	179	17.0	2.27
Water (W)	2.297[b]	178[b]	18.0	1.8
Methanol (MeOH)	2.290 2.289[c] 2.288[d] 2.291[e]	175 176[c] 175[d] 177[e]	19.1	1.66
Tetrahydrofuran (THF)	2.284	181	20.0	1.68
N,*N*-Dimethylformamide (DMF)	2.293	174	26.6	3.86
Dimethyl sulfoxide (DMSO)	2.294	175	29.8	3.9
Pyridine (Py)	2.297	168	33.1	2.20

a) These values were obtained in solvents of various toluene molar fractions at 77 K. No dependency of the data on the molar fraction was found. b) Obtained in an MeOH-water mixture. c) Obtained in an MeOH-NP mixture. d) Obtained in an MeOH-PC mixture. e) Obtained in a pure MeOH.

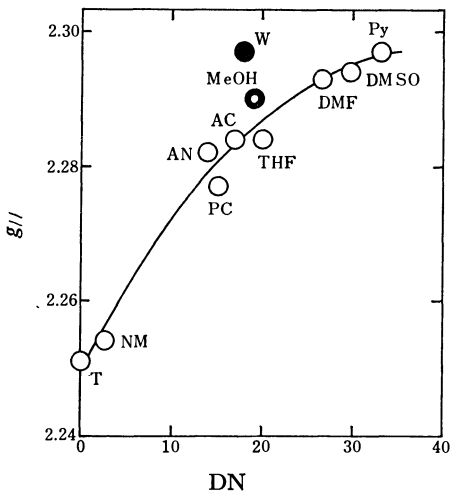

Fig. 2. The relationship between $g_{//}$ value and DN.

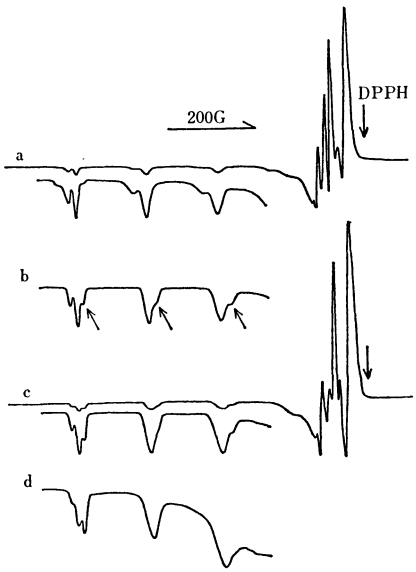

Fig. 3. ESR sepctra of [Cu(dibm)$_2$] in MeOH-water mixture at MeOH molar fractions of 0.31 (a), 0.57 (b), 0.80 (c), and 1.00 (d). The arrows are the absorption line due to MeOH adduct.

T-DMSO. Its $|A_{//}|$ values also decreased for an increase in DN.

Hence, the authors comment on the data of Adato and Eliezer.[3] First, when DMSO, DMF and other solvents were used, the resulting ESR spectra were all broad and not well-defined, and from these spectra it was not possible to obtain data similar to those in Ref. 3. Some of the data in Ref. 3 could be reproduced using solvents without purification. Accordingly, a great deal of this data is considered to be due to bis(acetylacetonato)copper(II) which interacts with impurities in the solvents. Second, it is theoretically reasonable to discuss the $g_\perp$ value of a planar copper(II) complex from the point of view of solvent effects as has been done in the case of the visible absorption spectra of bis(acetylacetonato)oxovanadium(IV).[11] Generally speaking, however, it is not easy to determine accurately the $g_\perp$ values of copper(II) complexes in solution.[12] Adato and Eliezer applied an approximate method to estimate $g_\perp$ from the equation, $g_0 = (1/3)(g_{//}+2g_\perp)$, using the experimentally-determined g values in two different states (g_0 for a fluid solution and $g_{//}$ for a rigid or glassy solution). It must be noted, however, that this method is likely to introduce some uncertainty into the results, because the solvent effects are not always the same for the two different states,[13] and because some complexes exist in solution as two or more configurationally different species in equilibrium.[14] In order to discuss solvent effects as rigorously as possible, therefore, the authors use only the $g_{//}$ and $|A_{//}|$ values determined in solutions at 77 K throughout this report.

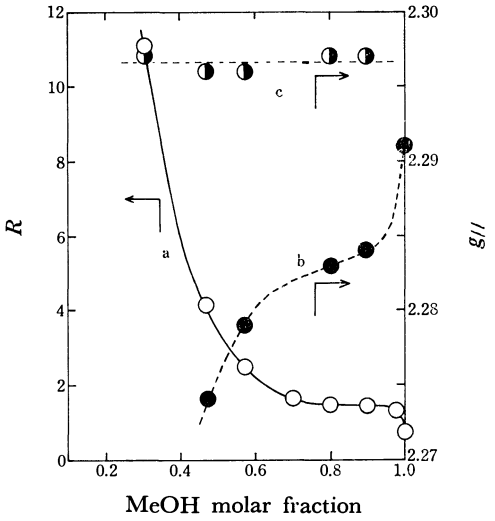

Fig. 4. Plots of R (a) and the $g_{//}$ values of MeOH (b) and water (c) adducts against the molar fraction of MeOH in MeOH–water mixtures.

Donicity of Water and Methanol. As shown in Table 1, the $g_{//}$ values were almost the same in the solvent systems T–MeOH, NP–MeOH and pure MeOH. Furthermore, the $g_{//}$ value in the T–MeOH system did not change with the MeOH molar fraction. This fact indicates that the stereochemical and electronic structures of the MeOH adduct do not depend on environmental changes. Using this $g_{//}$ value and the relationship between DN and $g_{//}$ shown as a solid line in Fig. 2, the DN of MeOH can be estimated to be larger than 19.1 (the generally accepted value[15]), but smaller than 33.8 (the value estimated by Gutmann from the data of Selbin[2]).

On the other hand, the ESR behavior in the water–MeOH system was entirely different. Several ESR spectra in water–MeOH mixtures at different MeOH molar fractions are shown in Fig. 3. The ratios (R) of the water adduct to the MeOH adduct in the ESR absorption intensity, which are nearly proportional to the ratios of their concentrations,[16] were plotted against the MeOH molar fraction, as shown in Fig. 4. Although Fig. 4 indicates that there is a correlation between R and the MeOH molar fraction, its implications appear to be complicated; they should be considered from the standpoint of the preferential solvation of water in this solvent system.

The fact that the $g_{//}$ value of the MeOH adduct in the water–MeOH system varies remarkably with the MeOH molar fraction means that the effects of water in the methanolic solution are significant even at low concentrations. The tendency of the $g_{//}$ value to decrease with an increase in water concentration indicates that the bonding between the complex and the MeOH molecules in the adduct becomes weak, although no definite explanation for this can be offered at the present time. On the other hand, the $g_{//}$ value of the water adduct is constant, as is seen in Fig. 4. This means that water and methanol as solvents have almost the same structural and electronic effects on this water adduct. Using this $g_{//}$ value and the relationship given by a solid line in Fig. 2, the DN of water could be estimated to be about 30, which coincides with the value previously reported by Gutman.[1]

The authors wish to thank Professor Taro Isobe for his encouragement and discussion during the course of this study.

References

1) U. Mayer and V. Gutmann, *Structure and Bonding*, **12**, 113 (1972).
2) V. Gutmann, "Coordination Chemistry in Non-aqueous Solutions," Springer-Verlag (1968).
3) I. Adato and I. Eliezer, *J. Chem. Phys.*, **54**, 1472 (1971).
4) D. P. Graddon and E. C. Watton, *J. Inorg. Nucl. Chem.*, **21**, 49 (1961).
5) P. Pfeiffer and H. Glaser, *J. Prakt. Chem.*, **153**, 265 (1939).
6) J. F. Coetzee, *Pure Appl. Chem.*, **13**, 492 (1966).
7) N. Tanaka and K. Harada, to be published.
8) N. Tanaka and T. Ogata, to be published.
9) J. A. Riddick and W. B. Bunger, "Techniques of Chemistry, Vol. II, Organic Solvents," 3rd ed., Wiley-Interscience, New York (1972).
10) T. Vänngård and R. Aasa, Proc. Ist. Int. Conf., "Paramagnetic Resonance," Jerusalem, 1962, Academic Press, New York (1963), p. 509.
11) J. Selbin and T. R. Ortoland, *J. Inorg. Nucl. Chem.*, **26**, 37 (1964).
12) There have been few papers on the precise computer-simulation analysis of the glassy-solution ESR spectra of copper(II) complexes with well-resolved hyperfine structures. The fact that most copper(II) complexes are of "approximately" axial symmetry in the ligand field makes the precise analysis of their ESR spectra difficult; R. Nieman and D. Kivelson, *J. Chem. Phys.*, **35**, 156 (1961); A. D. Toy, S. H. H. Chaston, J. R. Pilbrow, and T. D. Smith, *Inorg. Chem.*, **10**, 2219 (1971); H. Yokoi, unpublished results.
13) It is observed that many copper(II) complexes in solutions are different in color for the two states.
14) H. Yokoi, M. Sai, and T. Isobe, *Bull. Chem. Soc. Jpn.*, **45**, 1100 (1972).
15) G. Olofsson, *Acta Chem. Scand.*, **22**, 1352 (1968).
16) H. Yokoi, M. Otagiri, and T. Isobe, *Bull. Chem. Soc. Jpn.*, **44**, 2402 (1971).

Preparation of Some Alkylthallium(III) Dichlorides and Their Reactions with Potassium and Copper Halides

Sakae UEMURA,* Akio TOSHIMITSU, and Masaya OKANO
Institute for Chemical Research, Kyoto University, Uji, Kyoto 611

(Received July 24, 1975)

A simple synthesis is given for the stable monoalkylthallium(III) dichloride, $C_6H_5CH(OR)CH_2TlCl_2$ (**1**) from the corresponding diacetate (**2**) and potassium chloride in methanol or acetonitrile. **1**(R=Me) reacts slowly with potassium and copper(I) halides to give mainly α-methoxystyrene and $C_6H_5CH(OMe)CH_2X$ (X=Cl, Br, I), respectively. It is concluded that **1**(R=Me) is less susceptible than **2**(R=Me) to S_N1, S_N2, and S_Ni reactions.

In contrast to the readily prepared monoarylthallium(III) dihalides, monoalkylthallium(III) dihalides are unstable[1,2] and their successful isolation has so far been limited to pyridiomethylthallium(III) dichloride[3] and neopentylthallium(III) dihalide.[4] We report herewith on the preparation of 2-alkoxy-2-phenylethylthallium(III) dichlorides and their behavior towards metal halides in various solvents.

Results and Discussion

Preparation of 2-Alkoxy-2-phenylethylthallium(III) Dichloride (1). It was found that the reaction shown below proceeds at the refluxing temperature of the solvent (Table 1).

$$\underset{\text{OR}}{\overset{|}{\text{PhCHCH}_2\text{Tl(OAc)}_2}} \xrightarrow[\text{MeOH or MeCN}]{\text{KCl}} \underset{\text{OR}}{\overset{|}{\text{PhCHCH}_2\text{TlCl}_2}} \quad (1)$$

2 **1**

(R=Me, Et, *n*-Pr, *i*-Pr)

Isolation of **1** was carried out by evaporating the filtrate under reduced pressure and also by adding water to the filtrate. The former procedure gave a colorless tarry residue soluble in organic solvents such as methanol, DMSO and pyridine. The NMR spectrum of the residue showed the presence of monoalkylthallium(III) species other than **2** and dialkylthallium(III) species from several coupling constants J_{Tl-H} (Table 2). The latter procedure gave a white amorphous solid, sparingly soluble in almost all solvents, together with 10—15% of phenylacetaldehyde. Recrystallization of the solid from a large volume of acetonitrile gave **1** (Table 1). The difference in solubility of the tarry residue and **1** may be due to the difference in the mode of association.

It has been reported that the reaction of methyl thallium(III) diacetate with aqueous sodium chloride gives methyl chloride instead of the corresponding dichloride. The difference in behavior of methylthallium(III) diacetate and **2** to chloride ion can be ascribed to their difference in susceptibility to S_N2 reaction. Since **2** has a bulky $C_6H_5CH(OR)$-group on the carbon which bears Tl moiety, it seems that the attack of chloride anion from the rear to expel $Tl(OAc)_2$ is hindered profoundly. We therefore attempted to isolate a similar compound by the reaction of KCl with 2-methoxy-2-methyl-2-phenylethylthallium(III) diacetate (**2'**)[5] which has more bulky substituent than **2**. However, even in the reaction in MeCN at room temperature for 1 h, neither the corresponding alkylthallium(III) dichloride nor alkyl chloride was obtained, benzyl methyl ketone being produced instead in 83% yield. The ketone was also obtained in 85—95% yield with use of KBr, KI, or even KOAc in place of KCl, while almost all of **2'** was recovered (only 6% yield of ketone) under similar conditions without potassium salt. The results suggest that potassium cation prompts the decomposition of **2'** to a thallium(I) salt and an alkyl cation, the latter giving the ketone after phenyl migration (Scheme 2). The reason why phenyl migration is more prominent in the reaction of **2'** than in that of **2** might be explained by the difference in the steric crowding in **2'** and **2**. The thermal instability of **2'** as compared to **2** has been observed in many cases.[6]

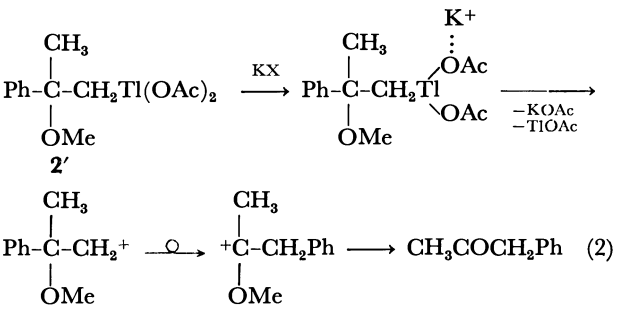

Comparison of Reactivities of 1(R=Me) and 2(R=Me) under Various Conditions (Table 3). First, the stability of **1**(R=Me) was checked by heating **1**(R=Me) in acetonitrile, 1,4-dioxane, and methanol for 5 h for comparison with that of **2**(R=Me). In acetonitrile and methanol almost no decomposition occurred. In 1,4-dioxane the total yields of the decomposition products were only 20% as shown in Scheme 3, while **2**(R=Me) gave 40—80% yield of the decomposition products under the same conditions. The fact that **3**(X=Cl) and **5** were scarcely obtained suggests both S_Ni and S_N1 type reactions of **1** to be very slow. Second, in the reaction with potassium halide only a low yield of **3** was obtained, showing that S_N2 displacement of thallium moiety in **1** by halide anions is very slow. A considerable amount of α-methoxystyrene(**4**) was obtained in methanol especially in the reaction with KI or KBr, while **4** was not produced from **2** under the same conditions.[5] We confirmed that **3**(X=I or Br) is not the precursor of **4** under the reaction conditions. Although the details of this dehydrothallation reaction giving **4** are not yet

* To whom all correspondence should be addressed.

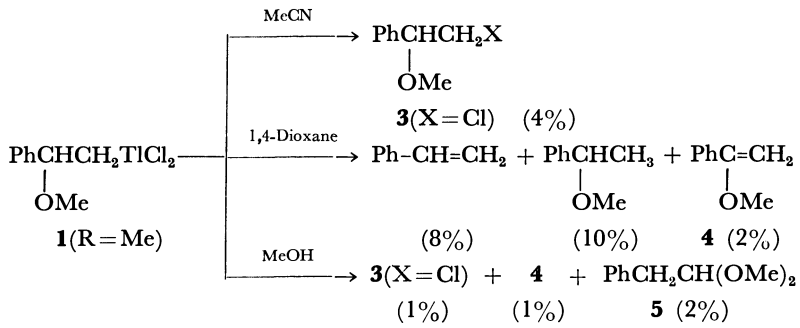

(3)

clear, such reaction is not common in organothallium compounds. So far it has been proposed only in the allylic oxidation of cyclohexene by $Tl(OAc)_3$ to explain the formation of 2-cyclohexenyl acetate.[7] The reaction of **1**(R=Me) with copper(I) salt was carried out. The yield of **3** was low except in the case of copper(I) bromide. Almost no reaction occurred with copper(I) cyanide and thiocyanate in contrast to the case of **2**(R=Me) from which **3** was obtained in a good yield by use of many kinds of copper(I) salts.[5] This also shows that **1**(R=Me) is less reactive than **2**(R=Me).

From all results on reactivities of **1** described above it can be concluded that **1** is less susceptible to S_N1, S_N2, and S_Ni reactions than **2**.

Experimental

The IR spectra were taken with Hitachi EPI-S2 and Perkin-Elmer 521 spectrometers in paraffin mull and KBr disks. The far-infrared spectra (400—30 cm^{-1}) were taken with a Hitachi FIS-3 spectrometer in paraffin mull or liquid film. The NMR spectra were recorded with Varian A-60 and EM-360 and JEOL MH-100 spectrometers in suitable solvents, using TMS as an internal standard. GLC analyses were carried out on a Shimadzu 5APTF apparatus, using Apiezon L(30%)-Celite(1 m) and PEG 6000(25%)-Chromosorb W (3 m) columns (N_2 as the carrier gas).

Materials. All the organic materials except **2**[5] and **2'**[5] were purified by distillation before use, while commercial inorganic materials were used without further purification.

Table 1. Preparation and properties of 2-alkoxy-2-phenylethylthallium(III) dichloride (**1**)

2 (mmol) R		KCl (mmol)	Solvent[a] (ml)		Yield[b] (%)	**1**[c] Mp (dec.) (°C)	Found (Calcd) C	H	Tl
Me	5	20	MeCN	25	33	146—147	26.4(26.3)	2.7(2.7)	49.1(49.8)
Me	3	6	MeOH	15	24				
Et	3	12	MeOH	15	45	89—91	28.3(28.3)	3.2(3.1)	48.4(48.1)
Et	3	12	MeCN	15	22				
n-Pr	3	12	MeOH	15	43	105—107	30.9(30.0)	3.7(3.5)	47.3(46.6)
i-Pr	3	12	MeOH	15	32	78—79	30.5(30.0)	3.4(3.5)	47.7(46.6)

a) The reaction was carried out at refluxing temperature for 1 h. In the case of R=*i*-Pr, for 0.5 h. b) Crude product, based on the amount of **2**. c) Recrystallized from a large amount of acetonitrile.

Table 2. J_{Tl-H} (in Hz) and δ (in ppm) of some organothallium(III) compounds

Compound	Solvent	J_{Tl-H_B} (δ_B)	J_{Tl-H_C} (δ_C)	J_{Tl-H_A} (δ_A)
OEt Ph-$CH_ACH_BH_CTlCl_2$[a,b] **1**(R=Et)	d_6-DMSO	757 (2.56)	917 (2.62)	630 (4.65)
	CD_3OD	755 (2.86)	932 (2.93)	671 (4.74)
OEt Ph-$CH_ACH_BH_CTl(OAc)_2$[c] **2**(R=Et)	d_6-DMSO	780 (2.67)	934 (2.88)	701 (4.52)
	CD_3OD	780 (2.93)	937 (3.06)	741 (4.69)
	$CDCl_3$[d]	768 (3.08)	921 (3.11)	737 (4.82)
OMe $(Ph-CH_ACH_BH_C)_2TlCl$[c]	$CDCl_3$	274 (2.50)	486 (2.69)	325—345 (4.85—4.95)

a) In the form of a colorless tarry residue. b) Similar J values were obtained in the cases of **1**(R=Me, *n*-Pr, and *i*-Pr). c) White amorphous solid, prepared by the method given in Ref. 5. d) Reported in Ref. 5.

Table 3. Reaction[a] of 1(R=Me) (1 mmol) with KX and CuX

KX or CuX (2 mmol)	Solvent (10 ml)	Products (yield,[b] %)		
		3	4	5
—	MeOH	1	1	2
—	MeCN	4	0	—
KCl	MeOH	1[c]	1	2
KCl	MeCN	4[c]	0	—
KBr	MeOH	7[d]	24	2
KBr	MeCN	6[d]	0	—
KI	MeOH	8[e]	44	0
KI	MeCN	11[e]	9	—
CuCl	MeCN	19[c]	0	—
CuBr	MeCN	51[f]	0	—
CuI	MeCN	20[g]	0	—

a) At reflux for 5 h. b) Based on the amount of **1**. c) X=Cl. d) X=Br. e) X=I. f) X=Br (43%) and X=Cl (8%). g) X=I (19%) and X=Cl (1%).

*Preparation of 2-Methoxy-2-phenylethylthallium(III) Dichloride (**1**, R=Me).* A white heterogeneous mixture of **2**(R=Me) (2.29 g, 5 mmol) and potassium chloride (2.38 g, 20 mmol) in acetonitrile (25 ml) was stirred under reflux** for 1 h (Table 1). The white precipitate (1.8 g) composed of a mixture of TlCl and KCl was filtered off. The filtrate was evaporated at 20 Torr leaving a colorless tarry residue (*ca.* 2.5 g), a part of which being used for NMR measurement. For isolation, 150 ml of ice-water was added to the filtrate, and a white voluminous solid formed was filtered and washed three times with small portions of ether (0.67 g, 33% yield). Recrystallization from 300 ml of acetonitrile afforded 0.43 g of a white amorphous solid (21% yield) of **1**(R=Me); mp 146—147 °C (dec.). IR; 1454 (m), 1100 (s), 765 (s), 700 (s), 640 (m), 420 (s), and 405 (sh) cm^{-1} (weak absorptions are not shown). The spectrum clearly shows the absence of absorptions due to ν_{CO_2} characteristic of **2**(R=Me)[5] and also that of strong absorptions at 162 and 100 cm^{-1} which bis(2-methoxy-2-phenylethyl)thallium(III) chloride has. The IR spectrum of the latter compound is as follows: 1450 (s), 1093 (s), 761 (s), 698 (s), 640 (m), 569 (m), 274 (m), 233 (m), 162 (s), and 100 (s) cm^{-1}.

** At room temperature the reaction was incomplete even after 5 h, the separation of **1**(R=Me) from the unreacted **2**(R=Me) being difficult.

GLC analysis of the organic layer after the usual work-up of the filtrate revealed the presence of 1.17 mmol of phenylacetaldehyde (23% yield), 0.09 mmol of methyl α-methylbenzyl ether (1.6%), and trace amounts of unidentified compounds.

*Preparation of **1**(R=Et, n-Pr, i-Pr, n-Bu, and i-Bu).* In the case of **1**(R=Et, *n*-Pr, and *i*-Pr), the white solid (*ca.* 1—1.5 g) obtained by the method described above was washed three times with methanol (10 ml×3) to remove water and some organic products, leaving crude **1**. Each compound (Table 1) was obtained by washing the crude product with 20 ml of MeOH and by evaporating the methanol washing. We could also isolate crude **1**(R=*n*-Bu and *i*-Bu) as a white solid by a similar treatment in 30—50% yield, but the analysis was unsatisfactory.

*Reaction of **1**(R=Me) with KI.* To a white suspension of **1**(R=Me) (0.82 g, 2 mmol) in methanol was added 0.67 g (4 mmol) of KI and the resulting yellow heterogeneous mixture was stirred under reflux for 5 h. After being cooled down to room temperature the mixture was filtered from the yellow precipitate(0.55 g; a mixture of **1**, KI, and thallous salts) and water(100 ml) was added to the filtrate which was extracted with benzene. GLC analysis of a part of the extract revealed the presence of α-methoxystyrene (**4**) (44%), **3**(X=I) (8%), styrene (5%), and methyl α-methylbenzyl ether (5%) (butyrophenone as an internal standard). Distillation gave 30 mg of almost pure **4**(bp 58—60 °C/22 Torr). The NMR and IR spectra and retention time in GLC of **4** was identical with those of an authentic sample prepared by the reported method.[8]

References

1) H. Kurosawa and R. Okawara, *J. Organomet. Chem.*, **10**, 211 (1967).
2) A. G. Lee, "The Chemistry of Thallium," Elsevier, Amsterdam (1971), pp. 213—215; A. G. Lee, "Organometallic Reactions," Vol. 5, ed. by E.I. Becker and M. Tsutsui, Willey-Interscience, New York, N. Y. (1975), pp. 58—60.
3) R. G. Coombes, M. D. Johnson, and D. Vamplew, *J. Chem. Soc., A*, **1968**, 2297.
4) M. D. Johnson, *Chem. Commun.*, **1970**, 1037.
5) S. Uemura, K. Zushi, A. Tabata, A. Toshimitsu, and M. Okano, *Bull. Chem. Soc. Jpn.*, **47**, 920 (1974).
6) S. Uemura, K. Zushi, and M. Okano, unpublished data.
7) J. B. Lee and M. J. Price, *Tetrahedron*, **20**, 1017 (1964).
8) D. B. Killian, G. F. Hennion, and J. A. Nieuwland, *J. Am. Chem. Soc.*, **57**, 544 (1935).

Oxidation of Acetaldehyde Catalyzed by Cobalt(II) Tetraphenylporphyrin

Meguru TEZUKA, Osamu SEKIGUCHI, Yasukazu OHKATSU, and Tetuo OSA

Department of Synthetic Chemistry, Faculty of Engineering, University of Tokyo, Hongo, Bunkyo-ku, Tokyo 113

(Received August 7, 1975)

Cobalt(II) tetraphenylporphyrins catalyzed the autoxidation of acetaldehyde giving peracetic acid quantitatively. The *p*-substituents of phenyl groups of tetraphenylporphyrin influenced the catalytic activity, cobalt(II) tetra(*p*-methylphenyl)porphyrin being remarkably active. The effect of the base added into the reaction system was such that an appropriate quantity of the base gave rise to a maximum rate of oxidation. The rate equation was determined experimentally. From the results of kinetics and ESR study, it was concluded that an oxygen molecule activated through the electron transfer from a cobalt(II) ion abstracted the hydrogen of acetaldehyde to initiate the autoxidation.

So far, a number of studies have been made with regard to various porphyrins, especially from the viewpoint of a model compound of oxygen carrier in living system such as hemoglobin.[1]

On the other hand, as the model of heterogeneous catalysts, the thermostable and easily accessible tetraphenylporphyrins of phthalocyanines have been investigated,[2] since the compounds, where every metal ion is surrounded by the same ligand, are convenient for catalytic research of the metal ion. Cobalt(II) tetraphenylporphyryin (CoTPP) is well known to take up an oxygen molecule reversibly.[3] However, the reactivity of coordinated oxygen has been scarcely investigated. In the case of metal phthalocyanine or polyphthalocyanine, the low-valent metal ion activates oxygen molecule to catalyzed the autoxidation of cumene, acetaldehyde, and so on.[4] Therefore, it is expected that metal porphyrin behaves similarly because of the analogy of the structure of both compounds.

We have confirmed that an oxygen molecule activated to the superoxide through the electron transfer from CoTPP abstracts the hydrogen of acetaldehyde to initiate the auoxidation. The effect of the *p*-substituents of phenyl rings (Fig. 1) was examined and cobalt(II) tetra(*p*-methylphenyl)porphyrin [Co-(*p*-CH_3)-TPP] was found to be remarkably active. The effect of the base added into the reaction system was explained in terms of porphyrin-base complex from the ESR study.

Experimental

Synthesis of Catalysts. Tetraphenylporphyrin (H_2TPP) was prepared according to the method by Falk.[5] Pyrrole (0.8 mol) and benzaldehyde(0.8 mol) were refluxed in 3 l of propionic acid for one-half hour under nitrogen atmosphere. On being left to stand, H_2TPP was precipitated. The crystals were filtered, washed several times with methanol and then with hot water, and dried; yield, approximately 20%.

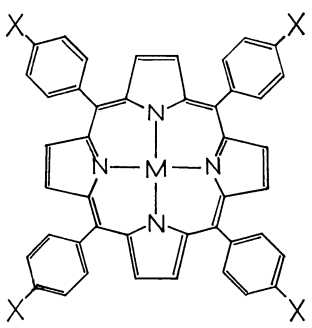

Fig. 1. Metal tetra(*p*-substituted phenyl)porphyrin.

Cobalt(II) tetraphenylporphyrin (CoTPP) was prepared according to the method by Rothemund and Menotti.[6] Five hundred mg of H_2TPP was refluxed in 50 ml of chloroform and 50 ml of glacial acetic acid saturated with cobalt(II) acetate for two hours, then 100 ml of methanol being added. The crude CoTPP precipitated on cooling was filtered, washed several times with methanol, and dried; yield, approximately 80%. The crude CoTPP prepared above was repeatedly treated with cobalt(II) acetate by a similar method except for the use of the CoTPP in place of H_2TPP to complete the complexation. The product was then subjected to the Soxhlet extraction with methanol, the unreacted materials being removed. Cobalt(II) tetra(*p*-methylphenyl)porphyrin [Co(*p*-CH_3)TPP], tetra(*p*-methoxyphenyl)prophyrin [Co(*p*-OCH_3)TPP], and tetra(*p*-chlorophenyl)porphyrin [Co(*p*-Cl)TPP] were also synthesized by the method described above from *p*-tolualdehyde, *p*-anisaldehyde, and *p*-chlorobenzaldehyde, respectively, in place of benzaldehyde as the starting material. The reagents used in the synthesis of catalysts had been purified by the ordinary methods.

Oxidation of Acetaldehyde. The oxidation of acetaldehyde was carried out in ethyl acetate at 10 °C using a closed oxygen-circulating system, similar to that described previously.[7] The reaction was started by the addition of a certain amount of acetaldehyde to the solution. The amount of oxygen absorbed during the course of the reaction was pursued by means of a gas burrete. Acetaldehyde was distilled under nitrogen atmosphere just before use. Ethyl acetate was purified by distillation. Pyridine and *N,N*-dimethylformamide as additive were also distilled under reduced pressure.

Analysis. All the peroxides in the liquid phase were estimated by an iodometric titration designed to determine the separate concentrations of hydrogen peroxide, peracetic acid and other peroxides.[8] Hydrogen peroxide was first estimated by charging 1 to 2 ml of an accurately weighed sample into an Erlenmeyer flask containing 150 ml of 5% sulfuric acid and sufficient cracked ice; the temperature of the mixed solution was maintained at 0 to 5 °C; titration was carried out with 0.1 N ceric sulfate until the salmon color of the ferroin indicator disappeared. The concentration of hydroperoxide in the feedstock of the solution obtained after oxidation was below 3×10^{-3} wt% in every experiment. To the resulting mixture was added 10 ml of a 10% potassium iodide solution, and the iodine liberated was titrated with 0.1 N sodium thiosulfate. Peracetic acid was thus estimated. The solution was then for 5 to 10 min, and the liberated iodine was titrated with sodium thiosulfate. The active oxygen in various peroxides other than hydrogen peroxide and peracetic

Table 1. Oxidation of acetaldehyde by Co(*p*-CH_3)TPP catalyst

Concn of acetaldehyde (M)	Concn of catalyst (mM)	Concn of oxygen (mM)	$-d[O_2]/dt$ ($\times 10^4$ M s^{-1})	k[a] ($\times 10^2$ $M^{-3/2}$ s^{-1})	R_i[b] ($\times 10^7$ M s^{-1})	Chain-length[c]
0.50	5.0	11.5	0.81	2.9	2.0	400
1.00	5.0	11.5	2.20	2.8	3.7	590
1.25	5.0	11.5	3.30	3.0	5.4	620
1.00	0.8	11.5	0.75	2.4	0.44	1700
1.00	1.4	11.5	1.1	2.7	0.95	1200
1.00	2.0	11.5	1.5	3.0	1.8	870
1.00	4.0	11.5	2.1	3.0	3.4	620
1.00	10	11.5	3.0	2.7	6.9	430
1.00	5.0	4.6	1.1	2.3	0.95	1200
1.00	5.0	7.5	1.8	3.0 (Av. 2.8)	2.5	720

In ethyl acetate at 10 °C. a) Calcd according to Eq. 3. b) Calcd according to Eq. 8. c) Calcd according to $(-d[O_2]/dt)/R_i$.

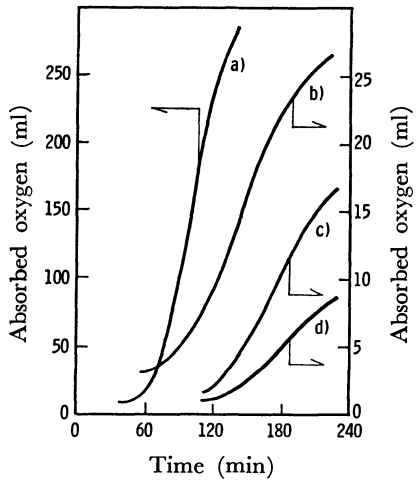

Fig. 2. Oxidation of acetaldehyde by cobaltous tetra-(*p*-substituted phenyl)porphyrin catalysts in ethyl acetate at 10 °C.
Acetaldehyde (0.5 M). Catalysts (5 mM). X: a) $-CH_3$, b) $-OCH_3$, c) -Cl, d) -H.

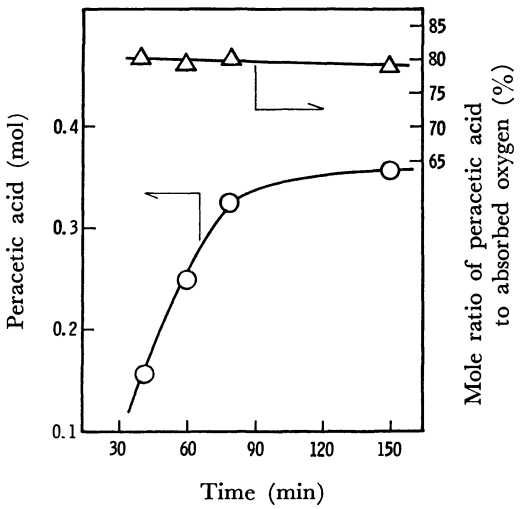

Fig. 3. Peracetic acid produced in oxidation of acetaldehyde by Co(*p*-CH_3)TPP catalyst in ethyl acetate at 10 °C.
Acetaldehyde (1.0 M). Catalyst (5 mM).

acid was thus estimated. From preliminary experiments, the titration was confirmed to be suitable. Peracetic acid could be completely analyzed at 0 to 5 °C, and any other peroxides which might be formed during the reaction were titrated in the last titration step. Neither separate quantification of acetaldehyde monoperacetate (AMP nor analysis of acids which might be formed) was made.

ESR Study. The ESR spectra of a solution of Co(*p*-CH_3)TPP in ethyl acetate were recorded at −196 °C with a JEOL Model JES-PE-IX spectrometer. The solution was prepared by the complete removal of dissolved oxygen according to the usual freeze-pump-thaw method. Oxygen or air was subsequently introduced little by little, when necessary, to get signals of the activated oxygen. The spectra were also measured in the presence of pyridine as an additive. The *g*-factors and coupling constants of the spectra were determined in comparison with those of Mn^{2+} marker.

Results and Discussion

In the absence of a catalyst, acetaldehyde was not oxidized within three hours at 10 °C. However, as shown in Fig. 2, the presence of CoTPP caused the absorption fairly soon, indicating the occurrence of the autoxidation of acetaldehyde. The *p*-substituents attached to the phenyl groups of porphyrin ring influenced the catalytic activity, the *p*-methyl group in particular making the corresponding porphyrin remarkably active. The activity of Co(*p*-CH_3)TPP was ten times as much as that of the other porphyrins. The order of activity was $-CH_3 \gg -CHO_3 > -Cl > -H$. This does not correspond to that of oxidation potentials of *p*-substituted porphyrins obtained by a cyclic voltammetric method.[9] This shows that the effect of the *p*-substituent cannot be explained only from the viewpoint of the electron-donating or attracting property of the substituent.

In the autoxidation, peracetic acid was obtained selectively and accumulated as the reaction proceeded. Hydrogen peroxide or any other peroxides could not be detected by titration (see Experimental). The mole ratio of peracetic acid formed to oxygen molecule absorbed remained constant *ca.* 0.8 in the course of the oxidation (Fig. 3). This suggests that Co(*p*-CH_3)-TPP has no ability to decompose peracetic acid sub-

stantially under the reaction conditions, in contrast to the fact that general transition metal salts and complexes can decompose peroxides heterolytically:

$$ROOH + M^{(n+1)+} \longrightarrow ROO\cdot + M^{n+} + H^{+} \quad (1)$$

$$ROOH + M^{n+} \longrightarrow RO\cdot + M^{(n+1)+} + OH^{-} \quad (2)$$

This also indicates that the initiation of autoxidation does not involve the formation of free radicals by the decomposition of peracetic acid.

The catalytic effect of Co(p-CH_3)TPP is deduced by kinetic consideration. The rate equation was (Table 1):

$$-d[O_2]/dt = k[CH_3CHO]^{1.5}[O_2]^{0.5}[Co(p\text{-}CH_3)TPP]^{0.5} \quad (3)$$

in which k was obtained as 2.8×10^{-2} $l^{3/2}$ $mol^{-3/2}$ s^{-1} over the range of concentration of acetaldehyde (0.5 to 1.25 M) and Co(p-CH_3)TPP (0.8 to 10 mM) and the partial pressure of oxygen (0.4 to 1.0atm) in the oxidation system.

For autoxidation under the conditions of fairly long chain-length and sufficient partial pressure of oxygen,

$$RH \longrightarrow R\cdot \qquad R_i \quad (4)$$

$$R\cdot + O_2 \longrightarrow RO_2\cdot \quad (5)$$

$$RO_2\cdot + RH \xrightarrow{k_p} ROOH + R\cdot \quad (6)$$

$$2RO_2 \xrightarrow{k_t} \text{non-radicals} \quad (7)$$

the rate equation is

$$-d[O_2]/dt = k_p k_t^{-1/2}[RH]R_i^{1/2} \quad (8)$$

in which RH, R_i, k_p, and k_t, represent acetaldehyde, the initiation rate, the propagation rate constant and the termination rate constant, respectively.[10]

Comparison of Eq. 3 with Eq. 8 leads to Eq. 9 as the expression of the initiation rate:

$$R_i = k_i[CH_3CHO][O_2][Co(p\text{-}CH_3)TPP] \quad (9)$$

where k_i denotes $k^2k_p^{-2}k_t$. As regards acetaldehyde, the constant k_p at 10 °C is approximately calculated to 3.6×10^3 l mol^{-1} s^{-1} from k_p at 0 °C (2.7×10^3 l mol^{-1} s^{-1})[11] and the activation energy of k_p (4.2 kcal/mol), which is assumed to be equal to that of n-decanal.[12] The constant k_t may be 1.04×10^8 l mol^{-1} s^{-1} which is reported for the value of k_t at 0 °C of acetaldehyde,[11] since the value can be considered to be almost independent on the temperature. Therefore, $k_pk_t^{-1/2}$ for acetaldehyde can be calculated to be 0.36 $l^{1/2}$ $mol^{-1/2}$ $s^{-1/2}$ at 0 °C. As the concentration of oxygen dissolved in ethyl acetate at 10 °C and at atmospheric pressure is 1.15×10^{-2} mol l^{-1},[13] the constant k_i is calculated to be approximately 0.6×10^{-2} l^2 mol^{-2} s^{-1}. This value is slightly smaller than that of Fe or Fe, Co polyphthalocyanine catalyst but much smaller than that of Fe, Cu polyphthalocyanine catalyst.[14] We see from Table 1 that the chain of the autoxidation is long enough to satisfy Eq. 8.

Equation 9 suggests that the initiation mechanism can be described as follows:

$$Co^{2+}(p\text{-}CH_3)TPP + O_2 \rightleftharpoons [Co^{3+}(p\text{-}CH_3)TPP]\cdots O_2^{-} \quad (10)$$

$$[Co^{3+}(p\text{-}CH_3)TPP]\cdots O_2^{-} + CH_3CHO \longrightarrow [Co^{3+}(p\text{-}CH_3)TPP]\cdots O_2H^{-} + CH_2\dot{C}O \quad (11)$$

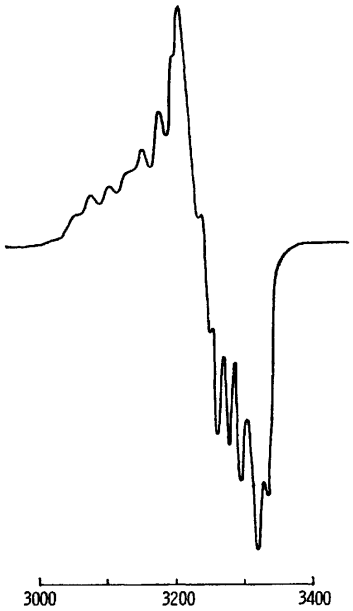

Fig. 4. ESR spectrum of Co(p-CH_3)TTP in ethyl acetate containing oxygen (*ca.* 0.02 atm.) at −196 °C. ν=9.262 GHz, field in gauss.

An evidence of the activation of oxygen molecule, namely, the formation of superoxide through the electron transfer, might be given by ESR study. In the absence of oxygen, Co(p-CH_3)TPP in ethyl acetate gave a complex pattern of lines at −196 °C. This could be attributed to the overlapping spectra of Co(p-CH_3)-TPP in ethyl acetate glass and the polycrystals due to the segregation of Co(p-CH_3)TPP.[15] After the contact with oxygen, a new type of singal appeared in addition to the original spectrum (Fig. 4). The new signal of the hyperfine splittings due to cobalt(II) was attributed to the superoxide formed through the electron transfer from the d_{z^2} orbital of cobalt to $2p\pi^*$ orbital of oxgen molecule according to the investigations relating to porphyrin–oxygen complex.[15-19] The electro-generated superoxide ion gave a similar spectrum except that it did not display the hyperfine lines.[20-22] These results seem to support firmly the step expressed in Eq. 10.

After the completion of the oxidation, the catalyst was recovered almost quantitatively and could be used with the same activity in the subsequent experiment as in the previous run. This suggests the regeneration of the catalyst as follows.

$$[Co^{3+}(p\text{-}CH_3)TPP]\cdots O_2H^{-} \longrightarrow Co^{2+}(p\text{-}CH_3)TPP + HO_2\cdot \quad (12)$$

The hydroperoxy radical can also abstract the hydrogen atom from acetaldehyde to initiate the oxidation forming hydrogen peroxide.

$$HO_2\cdot + CH_3CHO \longrightarrow CH_3\dot{C}O + H_2O_2 \quad (13)$$

Although no hydrogen peroxide could be detected by titration throughout this study, the step 13 may be another initiation reaction step in the autoxidation. In either case, it is concluded that an oxygen molecule activated by Co(p-CH_3)TPP can abstract the hydrogen of acetaldehyde. The hydroperoxy radical, in addition

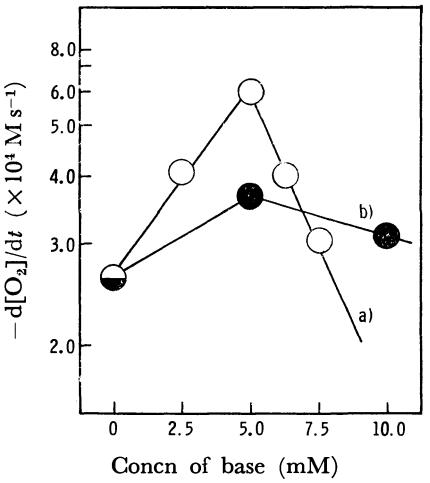

Fig. 5. Effect of base on oxidation of acetaldehyde by Co(*p*-CH_3)TPP catalyst in ethyl acetate at 10 °C. Acetaldehyde (1.0 M). Catalyst (5 mM). Base: a) pyridine, b) *N*,*N*-dimethylformamide.

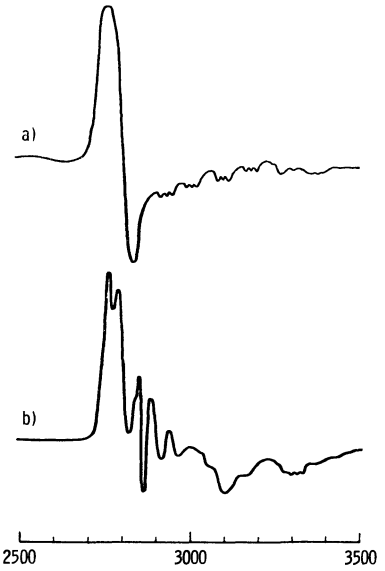

Fig. 6. ESR spectrum of Co(*p*-CH_3)TPP in ethyl acetate containing pyridine [a) 0.1, b) 5.0 vol %] at −196 °C. *ν*: a) 9.250, b) 9.238 GHz, field in gauss.

to reaction 13, may react with other free radicals to become inert compounds.

$$HO_2\cdot + R\dot{C}O \longrightarrow RCOO_2H \quad (14)$$

$$HO_2\cdot + RCOO_2\cdot \longrightarrow RCOO_2H + O_2 \quad (15)$$

Addition of a base such as pyridine or *N*,*N*-dimethylformamide into the reaction system influenced the rate of oxidation (Fig. 5). The rate increased with the addition of pyridine, becoming maximum at 5×10^{-3}M concentration. The maximum rate was about 2.5 times of that in the absence of the base. In contrast, further addition caused a decrease in the rate. A similar phenomenon was observed also with regard to *N*,*N*-dimethylformamide, although it was not so prominent as in the case of pyridine. A similar effect of the base was found in the study of polyphthalocyanine catalyst.

The effect of the base was also examined by ESR study. Figure 6 shows the spectra of Co(*p*-CH_3)TPP in ethyl acetate containing pyridine. At low concentration of pyridine (0.1 vol%), a spectrum was obtained which displayed superhyperfine splittings due to the interaction with one nitrogen (Fig. 6a). This indicates that the species present at this concentration of pyridine is a 1 : 1 complex, where pyridine coordinates to the cobalt(II) ion as a fifth ligand. The result given in Fig. 6b was obtained for higher concentration of pyridine (5 vol%). Although the spectrum lacks superhyperfine lines, it would be reasonably ascribed to a 2 : 1 pyridine–Co(*p*-CH_3)TPP complex, where pyridine occupies both the fifth and sixth coordination sites, as discussed in detail by Walker[15,17,19] in his study on Co(*p*-OCH_3)TPP–amine complex on toluene glass. After contact with oxygen, a spectrum similar to that in Fig. 4 was also obtained in the presence of pyridine, the amount of which was approximately such an amount as to produce the 1:1 complex. This may be attributed to the complex of Co(*p*-CH_3)TPP with one pyridine and one oxygen molecule as the fifth and sixth ligands, respectively. Therefore, from the result of ESR study, the effect of the base on the rate of oxidation (Fig. 5) could be explained by the concept that an appropriate amount of base would coordinate to the central cobalt(II) ion of the planar porphyrin molecule as a fifth ligand, facilitating the electron transfer from the cobalt(II) ion to the oxygen molecule as the sixth ligand. However, the excess base prevents the oxygen molecule from the coordination sites. The effect of the excess base, especially pyridine, is partly ascribed to the deactivation of the peroxy radical, namely the chain-carrier of autoxidation by the complex formation,[23] resulting in a decrease in the rate of oxidation.

From the results described above it would be most accepted that the catalyst activates an oxygen molecule to superoxide, which abstracts the labile hydrogen from acetaldehyde to initiate autoxidation.

We would like to express our thanks to Prof. Taiseki Kunugi for his valuable advice and discussion.

References

1) W. Lautsch, W. Broser, and H. Gnichtel, *Angew. Chem.*, **66**, 123 (1954); *J. Polymer. Sci.*, **17**, 479 (1955); W. Lautsch, B. Wiemer, D. Zschenderlein, H. J. Kreage, W. Bandel, D. Gunther, G. Schultz, and H. Gnichtel, *Kolloid-z*, **161**, 36 (1958); J. H. Wang and W. S. Briniger, *Proc. Natl. Acad. Sci. U.S.*, **46**, 958 (1960).

2) J. Manassen and A. Bar Ilan, *J. Catal.*, **17**, 86 (1970); A Wolberg and J. Manassen, *J. Am. Chem. Soc.*, **92**, 2982 (1970).

3) K. Yamamoto and T. Kwan, *J. Catal.*, **18**, 354 (1970).

4) H. Hock and H. Kropf, *J. Prakt. Chem.*, **9**, 193 (1959); T. Hara, Y. Ohkatsu, and T. Osa, *Chem. Lett.*, **1973**, 103, 953; Y. Kamiya, *Tetrahedron Lett.*, **1968**, 4965.

5) J. E. Falk, "Porphyrins and Metalloporphyrins," Elsevier, Amsterdam (1964).

6) P. Rothemund and A. R. Menotti, *J. Am. Chem. Soc.*, **70**, 1808 (1948).

7) A. Misono, T. Osa, Y. Ohkatsu, and M. Takeda, *Kogyo Kagaku Zasshi*, **69**, 2129 (1966).

8) F. P. Greenspan, *Anal. Chem.*, **20**, 1061 (1948).
9) M. Tezuka, Y. Ohkatsu, and T. Osa, *Bull. Chem. Soc. Jpn.*, **49**, 1435 (1976).
10) N. M. Emanuel, E. T. Denisov, and Z. K. Maizus, "Liquid-Phase Oxidation of Hydrocarbons," Pleunum Press, New York (1967).
11) G. E. Zaikov, J. A. Howard, and K. U. Ingold, *Can. J. Chem.*, **47**, 3017 (1969).
12) H. R. Cooper and H. W. Melville, *J. Chem. Soc.*, **1951**, 1984.
13) Chem. Soc. Jpn., Ed., "Kagaku Binran," 2 nd ed., Maruzen, Tokyo (1975).
14) To be contributed.
15) F. A. Walker, *J. Am. Chem. Soc.*, **92**, 4235 (1970).
16) D. V. Stynes, H. C. Stynes, J. A. Ibers, and B. R. James, *J. Am. Chem. Soc.*, **95**, 1142 (1973).
17) F. A. Walker, *J. Am. Chem. Soc.*, **95**, 1150 (1973).
18) B. B. Wayland, J. V. Minkiewicz, and M. E. Abd-Elmageed, *J. Am. Chem. Soc.*, **96**, 2795 (1974).
19) F. A. Walker, *J. Am. Chem. Soc.*, **95**, 1154 (1973).
20) D. L. Maricle and W. G. Hodgson, *Anal. Chem.*, **37**, 1562 (1965).
21) M. E. Peover and B. S. White, *Electrochim. Acta*, **11**, 1061 (1966).
22) M. Tezuka, Y. Ohkatsu, and T. Osa, *Bull. Chem. Soc. Jpn.*, **48**, 1471 (1975).
23) J. R. Thomas, *J. Am. Chem. Soc.*, **85**, 591 (1963).

Studies on the Tautomerism of 2-Anilinopyridine and Related Heterocycles

Yoshiyuki TAKAHASHI, Soichi OTSUKA, Hideyuki MASUDA, Minoru HIROTA,*
Yoshio ITO,† and Yoshiki HAMADA†

Department of Applied Chemistry, Faculty of Engineering, Yokohama National University, Minami-ku, Yokohama 233
†Department of Pharmacy, Meijo University, Yagoto-Urayama, Tempaku-ku, Nagoya 468

(Received September 19, 1975)

2-(*N*-Methylanilino) and 1-methyl-2-phenylimino derivatives of pyridine and quinoline were prepared as models for the amino and the imino tautomers of 2-anilino-pyridine and -quinoline. The ultraviolet, infrared and NMR spectra of these compounds were compared with those of the model compounds. The spectral data show that the amino tautomers are by far preferred in various solvents. The pK_a measurement on 1-methyl-2-phenylimino-1,2-dihydropyridine allows the assumption of the tautomeric equilibrium constant.

Tautomerism of aminopyridines has long been studied by several investigators, and earlier researches, mostly by chemical means, was summarized by Angyal *et al.*[1] 2-Aminopyridine is proved to exist as amino- (**1a**) by comparing its ultraviolet spectrum with those of 1-methyl-2-pyridoneimine and 2-dimethylaminopyridine,[2] and M. J. Cook *et al.*[3] have determined the tautomeric equilibrium constant between **1a** and **1b**.

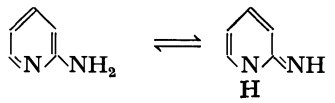

(**1a**) (**1b**)

The infrared spectroscopic studies affirmed the above conclusion,[4,5] and the dipole moment[6] and mass spectrometric[7,8] investigations were also carried out. Molecular orbital calculations[9] have predicted that the amino tautomer is more stable than the imino one.

As to anilinopyrines Cook *et al.* have recently discussed their tautomeric behavior on the basis of the ultraviolet spectra.[10] On the other hand, Bell[11] and Rud'ko[12] measured the infrared spectra of a series of substituted 2-anilinopyridines and assumed the existence of the imino tautomers. The present authors have investigated on the splittings of the N–H stretching absorptions of 2-anilino-pyridines and -lepidines, and assigned them to the rotational isomers.[13] The possibility of the tautomeric equilibrium is rejected on the basis of the fact that 3-carboline, which can exist as tautomers but not as rotational isomers, show only a single symmetric N–H stretching band. The present report deals with the tautomerism of 2-anilinopyridine and related heterocycles by means of ultraviolet, proton magnetic resonance and molecular orbital theoretical approaches, and excludes the presence of the considerable amounts of the imino tautomers.

Experimental

Preparation of Materials. 2-Anilinopyridine and Its Methyl Derivatives: 2-Anilinopyridine (**2**) and 2-(*N*-methylanilino)-pyridine (**3**) are known substances, and prepared by the condensation of 2-chloropyridine with aniline or *N*-methylaniline according to the procedures reported previously.

1-Methyl-2-phenylimino-1,2-dihydropyridine (1-methylpyridone phenylimine) (**4**), the model of the imino tautomer, was prepared by the following procedure. In a sealed tube, 11.4 g of 2-chloropyridine and 28.4 g of methyl iodide were heated for 3 h at 130 °C to produce 2-iodo-1-methylpyridinium iodide. The product of this methylation procedure depends on the reaction temperature, and 2-chloro-1-methylpyridinium iodide is obtained when the reaction is run at room temperature for 24 h. The 2-chloro and 2-iodo methiodides were identified by the different chemical shifts (δ: 4.40 and 4.48, respectively) of *N*-methyl protons. The iodo-methiodide thus obtained was condensed with aniline by heating it with an excess of aniline for 1 h at 100 °C. The crude 1-methyl-2-anilinopyridinium iodide was recrystallized from chloroform. Brownish yellow needles with mp 175—178 °C (decomp.). Yield: 55%. The same iodide was obtained by reacting 2-anilinopyridine with methyl iodide.

The elimination of hydrogen iodide to produce the anhydrobase (**4**) was accomplished by reacting freshly prepared silver oxide. The crude anhydrobase was obtained almost quantitatively and then it was extracted with cyclohexane and recrystallized from hexane. Yellow prisms with mp 70.5 °C. Found: C, 78.50; H, 6.61; N, 15.31%. Calcd for $C_{12}H_{12}N_2$: C, 78.23; N, 6.57; N, 15.20%. MS, *m/e* 184 (parent peak).

2-Anilino-4-methylquinoline[16] *and Its Methyl Derivatives*: 2-(*N*-methylanilino)-4-methylquinoline (**6**) is a hitherto unknown substance and prepared by a similar procedure with 2-anilino-4-methylquinoline. A mixture containing 5.3 g of 2-chloro-4-methyl-quinoline, 3.9 g of *N*-methylaniline, 4.3 g of anhydrous potassium carbonate and a few drops of pyridine was heated for 4 h at 140 °C. The reaction mixture was digested with 50 ml of 30% aqueous K_2CO_3 solution. Then, the product was extracted with chloroform and distilled under reduced pressure. Recrystallization from hexane gave yellow prisms. Yield; 58% mp, 81 °C. Found: C, 81.95; H, 6.51; N, 11.52%. Calcd for $C_{17}H_{16}N_2$: C, 82.22;, H, 6.49; N, 11.28%. 1,4-Dimethyl-2-phenylimino-1,2-dihydroquinoline (1-methyl-2-lepidone phenylimine) (**7**) was prepared similarly to 1-methyl-2-phenylimino-1,2-dihydropyridine. The final product was recrystallized from hexane to give yellow prisms. Overall yield from 2-chloro-4-methylquinoline is 9.2%. Mp, 112 °C. Found: C, 82.43; H, 6.63; N, 11.35%. Calcd for $C_{17}H_{16}N_2$: C, 82.22; H, 6.49; N, 11.28%. MS, *m/e* 248 (parent peak).

Measurements of the Spectra. Ultraviolet spectra were measured with a Hitachi EPS-3T recording spectrophotometer in various solvents. The solvents were purified in the following way. Chloroform and carbon tetrachloride were carefully distilled immediately before use, and water was distilled at least twice. The others were commercially available spectrograde ones. NMR spectra were measured with a JEOL JNM C60-H high resolution spectrometer and,

* To whom correspondence should be addressed.

Table 1. The ultraviolet spectra

Compound	Solvent	λ_{max} (nm)	ε_{max} (cm mol l^{-1})	Compound	Solvent	λ_{max} (nm)	ε_{max} (cm mol l^{-1})
2-Anilinopyridine (**2**)	C_6H_{12}	300—310 sh	7000		CH_3OH	320	7500
		275	18600			260	8500
	CH_3CN	305—310 sh	7500		H_2O	318	10200
		273	21100			250	7900
	CH_3OH	310—315 sh	7000	2-Anilino-4-methyl-quinoline (**5**)	C_6H_{14}	360	9400
		273	19700			345	10600
2-(*N*-Methyl-anilino)pyridine (**3**)	C_6H_{12}	293	10900		$CHCl_3$	355	9600
		243	11200			347 sh	9300
	CH_3CN	310—315	6500		CH_3OH	355	8300
		285	9300			349	8700
		240	9200	2-(*N*-Methyl-anilino)-4-methyl-quinoline (**6**)	C_6H_{14}	358 sh	8200
	CH_3OH	310	5900			346	9200
		282	8000		$CHCl_3$	360 sh	8000
		241	9000			350	8600
1-Methyl-2-pyridone phenylimine (**4**)	C_6H_{12}	373	4100		CH_3OH	356 sh	6900
		280	11900			347	7300
	CCl_4	374	4200	1,4-Dimethyl-2-phenylimino-1,2-dihydro-quinoline (**7**)	C_6H_{14}	383	8900
		283	11800		CCl_4	383	7800
	CH_3CN	366	4800		$CHCl_3$	378	9400
		285	11300		CH_3OH	370	10700
	$CHCl_3$	366	5900				
		288	13500				
	$HCO(CH_3)_2$	370	5500				
		288	12800				

sh: shoulder.

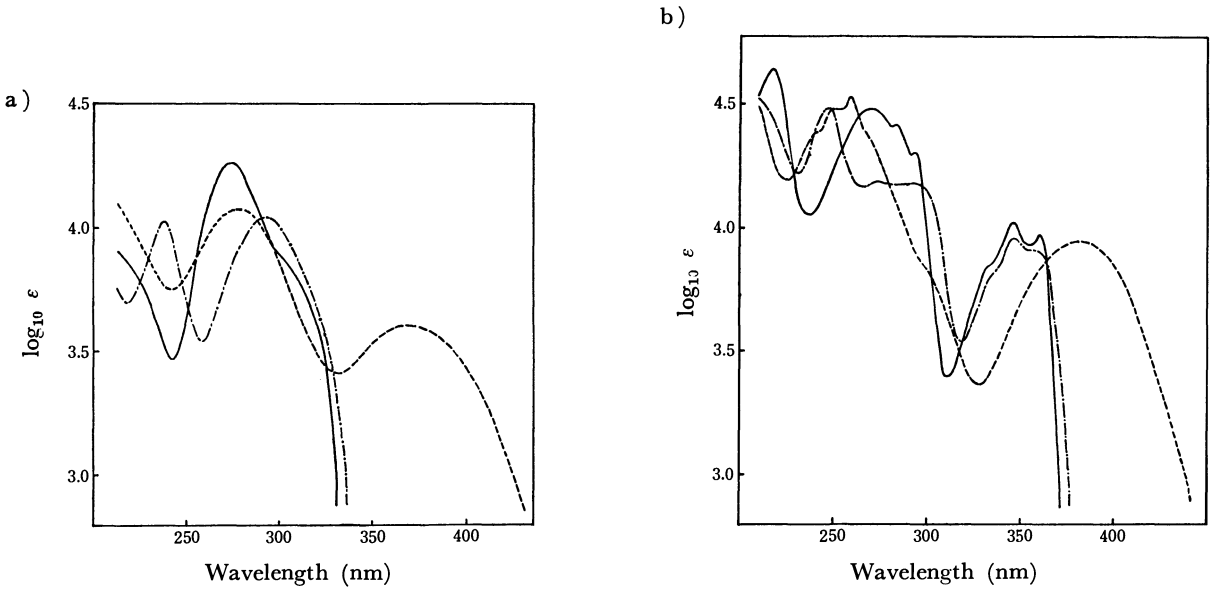

Fig. 1. The ultraviolet spectra of a) 2-anilinopyridine (**2**) [——] and its *N*-methyl derivatives (**3**) [—·—] and (**4**) [——]; b) 2-anilino-4-methylquinoline (**5**) [——] and its *N*-methyl derivatives (**6**) [—·—] and (**7**) [——].

when necessary, $Eu(fod)_3$ was used to separate the overlapping signals. Infrared spectra were obtained by employing a Hitachi Model 225 grating infrared spectrometer. Besides the usual 4000—400 cm^{-1} region spectra in potassium bromide pellets, the 1700—1600 cm^{-1} region ($\nu_{C=N}$ region) spectra were measured in various solvents of a wide range of polarity, including both protic and aprotic ones. Mass spectra were determined with a Hitachi RMU-6L mass spectrometer.

Results and Discussion

Ultraviolet Spectra and MO Calculations. The ultraviolet absorption maxima of 2-anilinopyridine, 2-anilino-4-methylquinone and their *N*-methyl derivatives are given in Table 1 and some typical spectra of them are illustrated in Fig. 1. As recognized at a glance of Fig. 1, the spectra of 2-anilinopyridine and

TABLE 2. THE RESULTS OF MO CALCULATIONS[25]

a) Total π-Electronic and Transition Energies.

Compound			Amino-form	Imino-form
2-Anilino-pyridine	E_π	HMO(β_0)	20.0374	19.9436
		PPP(eV)	−625.8672	−624.5931
	ΔE[a]	HMO($-\beta_0$)	1.4958	1.0243
		PPP(eV)	4.9228	4.3306
			(251.8 nm)	(286.3 nm)
2-Anilino-quinoline	E_π	HMO(β_0)	25.7376	25.7350
		PPP(eV)	−886.7434	−886.0459
	ΔE[a]	HMO($-\beta_0$)	1.1756	0.9080
		PPP(eV)	4.5632	3.9081
			(271.7 nm)	(317.2 nm)

b) Bond Orders.

Bond	2-Anilinopyridine		2-Anilinoquinoline	
	Amino-form	Imino-form	Amino-form	Imino-form
N(exo)-C(2)	0.3416	0.7213	0.3304	0.6382
N(1)-C(2)	0.6201	0.4696	0.6645	0.4587
C(2)-C(3)	0.6291	0.3672	0.5677	0.4999
C(3)-C(4)	0.6797	0.8650	0.7835	0.7786
C(4)-C(5 or 10)	0.6534	0.4187	0.5418	0.4909
C(5)-C(6) [or C(9)-C(10)]	0.6741	0.8403	0.5221	0.5487
C(6 or 9)-N(1)	0.6487	0.4321	0.5385	0.4168
C(5)-C(10)[b]	—	—	0.5605	0.5821
C(5)-C(6)[b]	—	—	0.7196	0.6994
C(6)-C(7)[b]	—	—	0.6076	0.6289
C(7)-C(8)[b]	—	—	0.7192	0.6919
C(8)-C(9)[b]	—	—	0.5620	0.6042
N(exo)-C(1′)	0.2875	0.3134	0.2873	0.3123
C(1′)-C(2′)	0.6371	0.6186	0.6371	0.6202
C(2′)-C(3′)	0.6728	0.6777	0.6728	0.6772
C(3′)-C(4′)	0.6626	0.6586	0.6626	0.6591

a) The lowest π-π^* transitions are given. b) Bonds in the carbocyclic ring of quinoline nucleus.

2-anilino-4-methylquinoline are similar to those of the corresponding 2-(*N*-methylanilino) derivatives and different considerably from those of the 1-methyl derivatives. This tendency is quite general when the spectra in aprotic solvents (given in Table 1) are compared. This suggests that 2-anilinopyridines (**2**) exist as amino tautomers at least in these solvents. Results of MO calculations on these tautomers are in accordance with the observations. In all cases, the amino structure is estimated to be more stable than the imino structure irrespective of the calculation methods.

The imino model compounds **4** and **7** possess intense bands at longer wavelengths. They are located at 372 and 383 nm, respectively in inert nonpolar solvents, and assigned to the π-π^* electronic transitions of the iminodiene chromophores from their intensities and locations. The imino tautomers are predicted to possess iminodiene characters judging from the bond alternation in the heterocyclic rings (as shown in the bond order values in Table 2). Considerable destablization of the imino tautomer might arise from

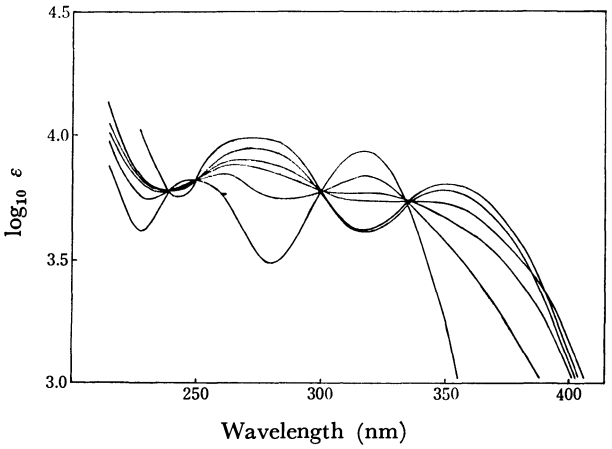

Fig. 2. The ultraviolet spectra of 1-methyl-2-phenyl-imino-1,2-dihydropyridine at various pH's.

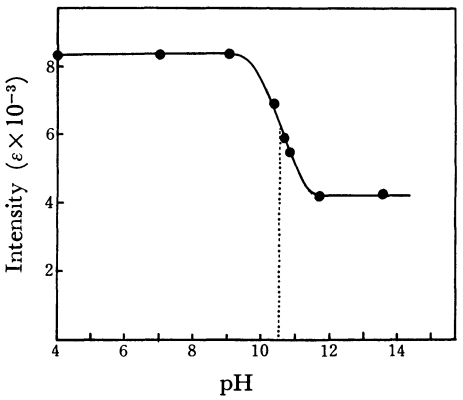

Fig. 3. The pH dependence of the intensity of the 318 nm-band of the anhydrobase (**4**).

the loss of aromaticity in the heterocyclic ring. The lowest π-π^* transition from the destablized ground state to the "aromatic" excited state should shift to the longer wavelength, and this actually occurs in the spectra of the imino model compounds **4** and **7**.

The absorption patterns of 2-anilinopyridine and 2-anilino-4-methylquinoline are similar to those of the corresponding amino model compounds **3**, **6**, and rather insensitive to the nature of the solvent. However, the lowest π-π^* bands of the 1-methyl derivatives **4** and **7** shift towards longer wavelengths with increase in the polarity of the solvents. By far larger hypsochromic shifts are observed when protic solvents are used for the measurement of the former imino compound, and this is assumed to arise from its protonation in this solvents. The anhydrobase (**4**) is expected to be enough basic to capture the hydroxylic protons from the protic solvents (alcohols and water). Existence of the acid-baseq euilibrium is assertained by observing the isosbestic points at 335, 300, and 249 nm in its ultraviolet spectra measured at different pH's (shown in Fig. 2).

Then, the ionization constant, pK_a, of the anhydrobase (**4**) is determined from the pH dependence of the ultraviolet spectra. Thus, the intensity of the its 318 nm peak is plotted against pH, and pK_a of **4** is estimated to be 10.5 from the curve shown in Fig. 3. The tauto-

meric equilibrium constant between the amino and the imino forms of 2-anilinopyridine is estimated according to the scheme proposed by Angyal *et al.*[1] for the estimation of the pK_a of 2-aminopyridine.

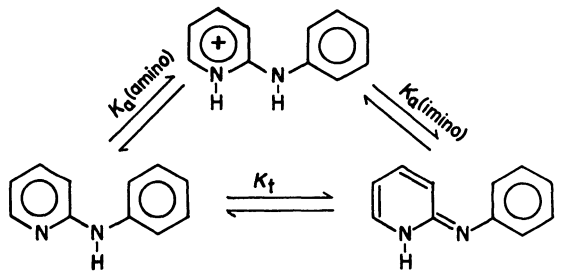

(**2a**) (**2b**)

If the pK_a's of the both forms (**2a** and **2b**) are known, the tautomeric equilibrium constant K_t is easily obtained by the following equation.

$$K_t = \frac{[\mathbf{2a}]}{[\mathbf{2b}]} = \frac{K_a(\text{amino})}{K_a(\text{imino})}$$ [17]

Since the K_a values of the amino and the imino tautomers could not be determined separately by any means, those of the model compounds are used instead for the calculation of the tautomeric equilibrium constant. The K_a values of **3** (6.0×10^{-6}) is comparable to that of 2-anilinopyridine (1.4×10^{-6}) itself. Moreover, the effect of *N*-methyl substitution is not serious upon the pK_a values of pyridone and its thio analogs,[18-20] the above assumption might be permissible. The K_t is then calculated to be 2×10^5. As expected, the predominance of the amino form is again proved.

NMR Spectra. The NMR spectra of the heterocyclic ring protons of 2-anilinopyridine, 2-anilino-4-methylquinoline and their *N*-methyl derivatives are given in Table 3. The assignments of the signals are based on the comparison with those of analogous heterocycles and on their lanthanide induced shifts.

As described in the preceding part of this report, a considerable decrease in aromaticity is predicted to the heterocyclic part of the imino tautomer. Jackman *et al.*[21] have assumed the low field shift by the "ring current" of aromatic ring structure to be 1.55 ppm, and have estimated the aromaticity of pyridones. The ring current theory has been criticized by several authors.[22] However, the chemical shift serves doubtlessly as an index for aromaticity, since there exists a close relationship between aromaticity and diamagnetic susceptibility. The heterocyclic protons of the imino compounds **4** and **7** resonate at remarkably higher fields. The high field shift of 0.95 ppm (in average) in the 2-anilinopyridine series corresponds to 41% of aromaticity if evaluated by Jackman's method, and loss of aromaticity is again significant. In 2-anilino-4-methylquinoline series, the high field shift is about half of that in the 2-anilinopyridine series. The loss of aromaticity is considerably less. This is in accordance with the fact that the anhydrobase (**7**) of the anilinoquinoline series is a weaker base with lesser extent of bond alternation.

Table 3. The NMR spectra (δ ppm in $CDCl_3$)

Compound	H(3)	H(4) or CH_3	H(5)	H(6)	N-CH_3
(**2**)	7.25	7.44	6.65	8.14	—
(**3**)	6.54	a)	6.47	8.16	3.47
(**4**)	6.35	a)	5.69	7.16	3.47
(**5**)	6.78	2.53	—	—	—
(**6**)	6.49	2.38	—	—	3.54
(**7**)	6.31	2.21	—	—	3.70

a) The H(4) signals of these compounds cannot be separated from the phenyl signals even when the shift reagent was added.

When compared with those of the parent anilino derivatives, the 3-H of the heterocyclic part resonates at a higher field in 2-(*N*-methylanilino) derivatives. As described in a previous paper of the present authors,[13] 2-anilinopyridines can exist either of the rotational isomers (A) or (B).

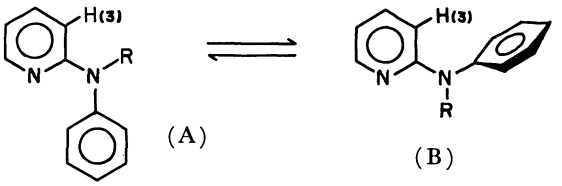

(A) (B)

In 2-anilino-pyridine and -4-methylquinoline, the rotamer (A) is somewhat more stable than the rotamer (B) probably because of the steric hindrance between the hydrogen atom at 3-position (3-H) and the phenyl. When the substituent R is methyl, the CH_3–H(3) interaction in conformer (A) prevent the planar arrangement of the heterocyclic ring and exocyclic nitrogen.[23] This enforces to take a twisted conformation about the exocyclic C_2–N bond which have larger double bond charactor than the N–Ph bond. On the other hand, the conformer (B) can still be coplanar by the sacrifice of the N–Ph coplanarity. Thus, the conformer (B) might become more favorable when the substituent on the anilino nitrogen is changed from hydrogen to methyl. In this conformation, the 3-H lies just above the phenyl ring and is subject to its diamagnetic effect which produce a high field shift.

Infrared Spectra. The tautomerism will affect profoundly the N–H stretching and the C=N stretching modes of vibration in the infrared region. The ν_{NH} spectra were discussed in the previous paper of the present authors.[13]

1-Methyl-2-pyridoneimine absorbs intensely at 1652 cm^{-1} and this band is assigned to the C=N stretching mode of vibration. 2-Anilinopyridine also has a weak absorption at 1650 cm^{-1} in the solid state, and Rud'ko *et al.* have concluded the existence of the imino tautomer. Thus, the spectra in the $\nu_{C=N}$ region are measured for a series of compounds investigated, and tabulated in Table 4. The absorption which appears at 1645 cm^{-1} is tentatively assigned to the C=N stretching mode; since it is very intense in the spectra of the imino model compound (**4**). As the solution spectra of 2-anilinopyridine shows no absorption in this region, this compound is supposed to take solely the amino form. However, since 2-anilinopyridinium salts have also the 1645 cm^{-1} bands (as shown in Table 4), the weak 1645 cm^{-1} band of 2-anilinopyridine in the solid state cannot necessarily related to the presence of

Table 4. The infrared spectra in the 1700 to 1600 cm^{-1} region

Compound	Medium	ν_{max} (cm^{-1})	ε_{max} (cm mol l^{-1})
(**2**)	KBr(solid)	1645	weak
	CCl_4	—	—
(**3**)	KBr(solid)	—	—
	CCl_4	—	—
(**4**)	KBr(solid)	1645	strong
	C_6H_{12}	1644	1200
	CCl_4	1644	1200
	CH_3CN	1645	1100
	$CHCl_3$	1644	960
		1652	620
	CH_3OH	1646	620
1-Methyl-2-anilino pyridinium iodide	KBr(solid)	1642	strong
	$CHCl_3$	1647	650
	CH_3OH	1647	60
(**5**)	KBr(solid)	1612	medium
(**6**)	KBr(solid)	1614	medium
(**7**)	KBr(solid)	1637	strong

a small amount of the imino tautomer. At present, the participation of a strongly hydrogen bonded dimeric structure (**2d**) also explains the infrared spectra, rather more adequately, since a remarkably lower NH stretching frequency is observed in the solid spectra of (**2**).

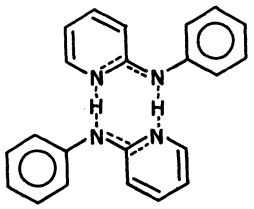

(**2d**)

In conclusion, 2-anilinopyridine (**2**) and 2-anilino-4-methylquinoline (**5**) exist as the amino tautomers. In solutions, the tautomeric equilibria are so preferable to the amino tautomers that no indications to the coexistence of the imino tautomer is obtained. Tautomeric equilibria in solids are not thoroughly studied; however, it is evident that the amino tautomer is by far more predominant than the imino tautomer.

The authors are grateful to Professor Hiroshi Kakiuchi, Yokohama National University, for his valuable advice and encouragement throughout this work. They also wish to express their hearty thanks to Mrs. Shigeko Yoshida for NMR measurement and to Miss Hiroko Endo for measurement of mass spectra.

References

1) S. J. Angyal and C. L. Angyal, *J. Chem. Soc.*, **1952**, 1461.
2) L. C. Anderson and N. V. Seeger, *J. Am. Chem. Soc.*, **71**, 340 (1949).
3) M. J. Cook, A. R. Katritzky, P. Linda, and R. D. Tack, *Chem. Commun.*, **1971**, 510.
4) C. L. Angyal and R. L. Werner, *J. Chem. Soc.*, **1952**, 2911.
5) J. D. S. Goulden, *J. Chem. Soc.*, **1952**, 2939.
6) D. J. Leis and B. C. Curran, *J. Am. Chem. Soc.*, **67**, 79 (1945).
7) K. Undheim and T. Grønneberg, *Org. Mass Spectrom.*, **6**, 823 (1972).
8) K. Undheim and T. Grønneberg, *Tetrahedron Lett.*, **1972**, 3193.
9) N. Boder, M. J. S. Dewar, and A. J. Harget, *J. Am. Chem. Soc.*, **92**, 2929 (1970).
10) M. J. Cook, S. O. Chua, and A. R. Katritzky, *J. Chem. Soc., Perkin Trans. 2*, **1973**, 2111.
11) M. G. W. Bell, M. Day, and T. Peters, *J. Chem. Soc., C*, **1967**, 132.
12) A. P. Rud'ko, I. N. Chernyuk, and Yu. S. Rozum, *Ukr. Khim. Zh.*, **34**, 1275 (1968).
13) T. Mizuno, M. Hirota, Y. Hamada, and Y. Ito, *Tetrahedron*, **27**, 6011 (1971).
14) O. Fischer, *Ber.*, **32**, 1302 (1899).
15) C. R. Hauser and M. J. Weiss, *J. Org. Chem.*, **14**, 310 (1949).
16) L. Knorr, *Justus Liebig's Ann. Chem.*, **236**, 103 (1886).
17) Since K_a(amino)=[**2a**][H^+]/[**3**] and K_a(imino)=[**2b**][H^+]/[**3**], this relation can be derived quite straightforwardly.
18) A. Albert and J. N. Phillips, *J. Chem. Soc.*, **1956**, 1294.
19) A. Albert and G. B. Borlin, *J. Chem. Soc.*, **1959**, 2384.
20) R. A. Jones and A. R. Katritzky, *J. Chem. Soc.*, **1958**, 3610.
21) L. M. Jackman and J. A. Elvidge, *J. Chem. Soc.*, **1961**, 859.
22) R. J. Abraham, R. C. Sheppard, W. A. Thomas, and S. Turner, *Chem. Commun.*, **1965**, 43.
23) Exocyclic anilino nitrogen must be sp^2-like and is supposed to take a planar conformation, since it carries an electron-withdrawing pyridyl substituent. See: M. Kasai, M. Hirota, Y. Hamada, and H. Matsuoka, *Tetrahedron*, **29**, 267 (1973).
24) The parameters proposed by Streitwieser Jr. (A Streitwieser Jr., "Molecular Orbital Theory for Organic Chemists," John Wiley & Sons, Inc., New York (1961), p. 135) were used for the HMO calculations. The semi-empirical SCF calculations were carried out by the method originally proposed by Pople (J. A. Pople, *Proc. Phys. Soc. (London)*, **A68**, 81 (1955)) using the integrals of Hinze *et al.* (*J. Am. Chem. Soc.*, **84**, 540 (1962)).

Carboxylation of Phenol Derivatives. XXII.[1] Formation of Alkali Alkyl Carbonate by the *O*-Carboxylation of Alcohol in the Presence of an Alkali Salt of a Weak Acid

Ichiro HIRAO, Taketoshi KITO, Takatomo FUNAMOTO, Taketoshi MURAKAMI, and Katsuyuki USAMI

Laboratory of Industrial Chemistry, Department of Chemical Engineering, Kyushu Institute of Technology, Tobata-ku, Kitakyushu-shi 804

(Received October 30, 1975)

O-Carboxylation of the alcohol (ROH) occurred to give alkali alkyl carbonate in a good yield when carbon dioxide was introduced into the mixture of an alkali salt of a weak acid, alcohol, and acetone (or THF) at room temperature under atmospheric pressure. Such alkali salts as PhOM, *p*-R'C_6H_4OM (R'=CH_3, CH_3O, or Br), Et_2NCSSM, NaCN, and $C_6H_4(CO)_2NK$ (M=K or Na) were effective. The mixture of HOC_6H_4COOM and ROCOOM was obtained from the reaction using MOC_6H_4COOM as an alkali salt. However, the mixture was composed of equimolar amounts of *p*-HOC_6H_4COOM and ROCOOM when *p*-MOC_6H_4COOM was used. In this reaction, two mechanisms have been examined.

Alkali alkyl carbonates, which are known as carboxylating agents of alkali phenoxide, are usually prepared by the introduction of carbon dioxide into the alcohol solutions of alkoxides which are obtained from a metallic alkali and alcohol or by the removal of the formed water from alkali hydroxide and alcohol at an azeotrope with alcohol.[2]

It has been well known that hydroxybenzoic acids are formed when alkali phenoxide is heated under carbon dioxide pressure at a high temperature and, on the other hand, the complex is formed when alkali phenoxide is brought into contact with carbon dioxide at a low temperature. The latter reaction has been studied by many authors.[3]

During the investigation of the complex, we discovered a new reaction that forms alkali alkyl carbonates from alcohol and carbon dioxide in the presence of an alkali salt of a weak acid.

Results and Discussion

When carbon dioxide was introduced into the methanol solution of alkali phenoxide, precipitates of alkali methyl carbonate were formed in good yields. This reaction was further examined and generalized as Eq. 1: where, AM represents an alkali salt of a weak acid.

$$AM + ROH + CO_2 \rightarrow AH + ROCOOM \quad (1)$$

The results with many alklali salts of weak acids are summarized in Tables 1 and 2.

Potassium and sodium hydroxides cannot be used as alkali sources because the water formed in the reaction decomposes the alkali alkyl carbonates according to Eq. 2:

$$ROCOOM + H_2O \rightarrow ROH + MHCO_3 \quad (2)$$

Alkali salts of weak acids, such as the sodium salt of phenol, *p*-cersol, *p*-methoxyphenol, *p*-bromophenol, diethyldithiocarbamic acid, or hydrogen cyanide and the potassium salt of phenol, diethyldithiocarbamic acid, or phthalimide, are effective, while alkali salts such as the sodium salt of nitrous acid, thiocyanic acid, sulfurous acid (mono salt), or hydrogen sulfide (di- and mono-salts), and potassium thiocyanate are not. The pK_a's of most of the parent acids of the uneffective alkali salts are lower than 7.2. For example, the pK_a's of some parent acids (in water at 25 °C) are as follows:[4] thiocyanic acid, 0.85; sulfurous acid, pK_1=1.90, pK_2=7.20; nitrous acid, 3.29; hydrogen sulfide, pK_1=6.88, pK_2=14.15. Among the parent acids of effective alkali salts, the strongest acid, is *p*-bromophenol, whose pK_a at 25 °C is 9.24 (*cf.* hydrogen cyanide, 9.32; phthalimide, 9.90, phenol, 9.99. Although there is no data for the pK_a of diethyl dithiocarbamic acid, it may be a weaker acid than *p*-bromophenol). Therefore, it can be concluded that an alkali salt whose parent acid has a pK_a of more than about 9 will be effective.

In most reactions, acetone or tetrahydrofuran (THF) was used as a solvent. Alkali phenoxides dissolve considerably in methanol and ethanol, but these salts and other alkali salts are practically insoluble in other higher alcohols. In addition, potassium methyl carbonate dissolves to some extent in methanol at room temperature (see Table 4). Acetone and THF were good solvents for the sodium and potassium salts of phenol and *p*-substituted phenols.

The products prepared according to Eq. 1 were confirmed to be alkali alkyl carbonates by the elementary analyses and by the comparison of each IR spectrum with that of an authentic sample. However, the elementary analyses of the carbon and hydrogen atoms of the potassium alkyl carbonates, in most cases, did not accord with the calculated values within ± 1%, and are not listed in Table 2.

Introduction of carbon dioxide into a mixture of sodium phenoxide, isobutyl alcohol, and acetone, followed by the addition of an excess of methanol, gave fine crystallines. The main component of the crystallines was found to be sodium methyl carbonate. The reaction of Eq. 3 might occur after the reaction of Eq. 1, where

$$i\text{-}C_4H_9OCOONa + CH_3OH \rightarrow CH_3OCOONa + i\text{-}C_4H_9OH \quad (3)$$

AM, R, and AH are PhONa, i-C_4H_9, and PhOH, respectively. In addition, sodium benzyl carbonate and sodium dodecyl carbonate, which are prepared only with difficulty by the previous method, were

Table 1. Sodium alkyl carbonates (Eq. 1)

Alkali salt (0.03 mol)	ROH[a] R	Solvent (100 ml)	Product	Yield (%)	Analyses (%)[b] C	H	Na
PhONa	CH_3	Acetone	$CH_3OCOONa$	98	24.39 (24.50)	3.08 (3.08)	23.20 (23.45)
PhONa	C_2H_5	EtOH (50 ml)	$C_2H_5OCOONa$	99	32.19 (32.16)	4.59 (4.50)	—
PhONa	*i*-C_4H_9	THF	*i*-$C_4H_9OCOONa$	63	40.80 (42.86)	5.40 (6.47)	15.54 (16.41)
PhONa	*i*-C_4H_9	Acetone	$CH_3OCOONa$[c]	58	25.47 (24.50)	2.77 (3.08)	25.34 (23.45)
PhONa	*s*-C_4H_9	Acetone	*s*-$C_4H_9OCOONa$	69	38.65 (42.86)	5.55 (6.47)	17.40 (16.41)
PhONa	*n*-C_5H_{11}	Acetone	*n*-$C_5H_{11}OCOONa$	93	46.30 (46.75)	7.26 (7.19)	—
PhONa	*n*-$C_{12}H_{25}$	Acetone	*n*-$C_{12}H_{25}OCOONa$	96	61.47 (61.82)	9.71 (9.91)	—
PhONa	$C_6H_5CH_2$	Acetone	$C_6H_5CH_2OCOONa$	58	55.39 (55.18)	4.03 (4.05)	13.24 (13.20)
p-$CH_3C_6H_4ONa$	C_2H_5	THF	$C_2H_5OCOONa$	91	—	—	19.61 (20.52)
p-$CH_3OC_6H_4ONa$	C_2H_5	EtOH (50 ml)	$C_2H_5OCOONa$	94	—	—	20.56 (20.52)
p-BrC_6H_4ONa	C_2H_5	EtOH (50 ml)	$C_2H_5OCOONa$	98	—	—	20.07 (20.52)
$Et_2NCSSNa$	CH_3	THF	$CH_3OCOONa$	51	—	—	23.48 (23.45)
$Et_2NCSSNa$	C_2H_5	THF	$C_2H_5OCOONa$	63	—	—	20.16 (20.52)
NaCN	CH_3	MeOH (50 ml)	$CH_3OCOONa$	81	—	—	23.06 (23.45)
$PhONa \cdot CO_2$[d]	CH_3	Acetone	$CH_3OCOONa$	87[e]	24.80 (24.50)	3.18 (3.08)	23.54 (23.45)

a) At least 0.06 mol of alcohol was used. b) The calcd values are shown in parentheses. The Na% was evaluated by the titration of the $NaHCO_3$ in the product with 1 M HCl ($ROCOONa + H_2O \rightarrow ROH + NaHCO_3$). c) After introducing carbon dioxide into the mixture of sodium phenoxide, isobutyl alcohol, and acetone, 50 ml of methanol was added. The IR spectrum of the product obtained from this reaction was nearly identical with that of authentic sodium methyl carbonate. d) The complex was prepared according to the procedure described before (Ref. 1), but light oil was replaced with hexane. e) The yield is based on the PhONa initially used.

Table 2. Potassium alkyl carbonates (Eq. 1)

Alkali salt (0.03 mol)	ROH[a] R	Solvent (100 ml)	Product	Yield (%)	Analysis[b] K (%)
PhOK	CH_3	THF	CH_3OCOOK[c]	79	—
PhOK	C_2H_5	EtOH (50 ml)	C_2H_5OCOOK	87	31.0 (30.5)
PhOK	*n*-C_3H_7	THF	*n*-C_3H_7OCOOK	98	27.1 (27.5)
PhOK	*n*-C_4H_9	THF	*n*-C_4H_9OCOOK[c]	96	—
PhOK	$C_6H_5CH_2$	$C_6H_5CH_2OH$	$C_6H_5CH_2OCOOK$	88	20.9 (20.6)
Et_2NCSSK	CH_3	MeOH (50 ml)	CH_3OCOOK[c]	63	—
$C_6H_4(CO)_2NK$[d]	CH_3	Acetone	CH_3OCOOK	94	32.0[e] (34.3)
$PhOK \cdot CO_2$	CH_3	Acetone	CH_3OCOOK	83	34.6 (34.3)

a) At least 0.06 mol of alcohol was used. b) The calcd values are shown in parentheses. The K% was evaluated by the titration of the $KHCO_3$ in the product with 1 M HCl ($ROCOOK + H_2O \rightarrow ROH + KHCO_3$). c) The IR spectra of these products were in good agreement with those of authentic ones. d) Potassium phthalimide. e) Although the K% deviated 2.24% from the calcd value, the IR spectrum was nearly identical with that of potassium methyl carbonate.

easily obtained by the present reaction.

Kwan and his co-workers reported that a carbon atom with an active hydrogen is carboxylated by carbon dioxide in *N,N*-dimethylformamide in the presence of potassium phenoxide.[5] However, the yields were less than 50%. In the present reaction an oxygen atom of alcohol is carboxylated to give alkali alkyl carbonate in good yield. As was mentioned already, not only alkali phenoxide but also many alkali salts of weak acids were available as alkali sources.

Two mechanisms for the present reaction, Eq. 1, can be considered. It is well known that alkali phenoxide forms a stable complex with carbon dioxide. We also reported that the complex is formed in good yield (about 80%) when the mixture of potassium phenoxide and light oil is stirred vigorously under a carbon dioxide atmosphere at room temperature for 30 min.[1] It will be reasonable to assume that the first product formed in the present reaction of Eq. 1, where AM is alkali phenoxide, is a complex, because alcohol does not react with carbon dioxide at room temperature. Two complexes ($PhOK \cdot CO_2$ and $PhONa \cdot CO_2$) were prepared from potassium phenoxide and sodium phenoxide plus carbon dioxide, and then methanol was added to each complex. Potassium methyl carbonate and sodium methyl carbonate were obtained in good yields (see the last columns of Tables 1 and 2). Therefore, the complexes may be considered as intermediates in the present reaction and this reaction process can be expressed by two equations, (4) and (5). In Eq. 5 the oxygen atom of the alcohol would attack the

$$AM + CO_2 \rightarrow AM \cdot CO_2 \quad (4)$$

$$AM \cdot CO_2 + ROH \rightarrow ROCOOM + AH \quad (5)$$

carbon atom of the carbon dioxide of the complex, and as a result, phenol and alkali alkyl carbonate would be formed.

The second mechanism can be formulated as Eqs. 6 and 7:

$$AM + ROH \rightleftharpoons AH + ROM \quad (6)$$

$$ROM + CO_2 \longrightarrow ROCOOM \quad (7)$$

Equation 6 is equlibrium state, while Eq. 7 is substantially irreversible at room temperature.

It was reported that methyl ω-methoxyalkanoate was formed at high temperatures from the reaction shown in Eq. 8.[6] Also when a mixture of sodium phenoxide (0.1 mol), benzyl chloride (0.1 mol), and

$$p\text{-}CH_3OOCC_6H_4ONa + Cl(CH_2)_nCOOCH_3 \xrightarrow{\text{in MeOH}} p\text{-}CH_3OOCC_6H_4O(CH_2)_nCOOCH_3 + NaCl \quad (8)$$

methanol (100 ml) was refluxed for 2 h, benzyl methyl ether was obtained in 12% yield. These two facts support the assertion that at high temperature a considerable amount of sodium methoxide is formed by the equilibrium shown in Eq. 9, although both methyl

$$p\text{-}RC_6H_4ONa + CH_3OH \rightleftarrows p\text{-}RC_6H_4OH + CH_3ONa \quad (R=H \text{ or } CH_3OOC\text{-}) \quad (9)$$

p-hydroxybenzoic acid ($pK_a=8.47$ at 25 °C) and phenol ($pK_a=10.0$ at 25 °C) are considerably stronger acids than methanol ($pK_a=15.5$ at 25 °C).[7] However, at room temperature, where the present reactions were carried out, the equilibrium will lie further to the left if we consider the pK_a values. Therefore, the second mechanism may be less important than the first one. Alkali alkyl carbonate will be formed mainly by the first mechanism.

The mixture of sodium cyanide or sodium diethyldithiocarbamate and cyclohexane was stirred under a carbon dioxide atmosphere; the insoluble product was filtered. After the carbon dioxide had been replaced by nitrogen, methanol and acetone (solvent) were added into the product, but sodium methyl carbonate was not obtained. However, we noticed that these alkali salts absorbed carbon dioxide under atmospheric pressure. The difference between alkali phenoxides and other alkali salts may be as follows: although alkali phenoxide can form a stable complex with carbon dioxide,[1] the other salts can not form such stable complexes. However, when an alcohol exists, the oxygen atom of the alcohol would attack the positively charged carbon atom of the carbonyl group of the complex and give alkali alkyl carbonate.

The difference of the reactivity toward sodium phenoxide in acetone between butyl alcohol and isobutyl alcohol was examined. The butyl alcohol reacted about 30 times faster than the isobutyl alcohol and 40 times faster than *s*-butyl alcohol. The oxygen atom of the branched alcohol must have difficulty in approaching the carbon atom of the carbonyl group of the complex. Therefore, the large differences of the reactivity between butyl alcohol and the branched alcohols (*i*-C_4H_9OH and *s*-C_4H_9OH), and between isobutyl alcohol and *s*-butyl alcohol are attributed to the steric hindrance of the branched alcohol. The electronic effect of the alkyl group of alcohol would scarcely influence its reactivity because the difference of the electronic effect between the three alkyl groups, especially between the butyl and isobutyl groups, will be small.

Both di-alkali salts of salicylic acid and *p*-hydroxybenzoic acid may be employed as an alkali source. These results are summarized in Table 3. It was found that the content of *p*-hydroxybenzoic acid in each precipitate was in good agreement with the value calculated on the assumption that the precipitate is composed of equimolar amounts of mono-potassium salt or mono-sodium salt of *p*-hydroxybenzoic acid and potassium methyl carbonate or sodium methyl carbonate respectively, when the di-potassium salt or the di-sodium salt of *p*-hydroxybenzoic acid is used as an alkali source. However, the content of salicylic acid in each precipitate deviated significantly from the calculated value and, moreover, differed in every run when *p*-hydroxybenzoic acid was replaced with salicylic acid.

Alkali salts of *p*-hydroxybenzoic acid and salicylic acid can be well dissolved in methanol, but the solubility of sodium methyl carbonate is poor, only 1.0 g in 50 ml of methanol (see Table 4).

The results summarized in Table 3 can be explained as follows: when carbon dioxide is introduced into the methanol solution of the di-potassium salt of *p*-hydroxybenzoic acid, potassium methyl carbonate and potassium *p*-hydroxybenzoate are formed. Further introduction

Table 3. Reactions using di-alkali salts of POB or SA[a]

Alkali salt[b] (g)		ppt (g)	POB or SA (wt%)[c] in product	pptd	Analyses (%)[d] C	H
POB di-K	4.94	2.75	51.9	(47.6)	—	—
POB di-K	5.07	2.78	52.0	(47.6)	—	—
POB di-Na	5.00	4.44	54.2	(53.5)	40.67	3.61
POB di-Na	2.89	3.27	55.8	(53.5)	40.74	3.37
SA di-K	6.50	0.37	76.1	(47.6)	—	—
SA di-Na	6.12	2.12	38.5	(53.5)	41.34	3.02

a) POB=*p*-Hydroxybenzoic acid, SA=Salicylic acid; di-K=di-potassium salt, di-Na=di-sodium salt. b) These salts are dissolved in 50 ml of methanol. c) The values in parentheses were calculated on the assumption that the precipitates were composed of equal molar amounts of mono-alkali salt of POB or SA and alkali methyl carbonate. For example, [POB(Mw. 138.1)]×100/[POB mono-K(Mw. 176.2)+CH_3OCOOK (Mw. 114.1)]=47.6(%). The determination of POB or SA was carried out by the UV technique. d) Calcd for (POB or SA mono-Na+$CH_3OCOONa$): C, 41.88%; H, 3.12%.

Table 4. Solubilities of alkali salts in methanol

Alkali salt[a]	Solubility[b] (g)	Alkali salt	Solubility (g)
POB di-K	12.0	POB di-Na	9.7
POB mono-K	10.0	POB mono-Na	5.0
SA di-K	6.5	SA di-Na	4.7
SA mono-K	7.0	SA mono-Na	10.5
CH_3OCOOK	9.5	$CH_3OCOONa$	1.0

a) See Table 3. b) Solubilities are defined as the amounts which dissolved easily in 50 ml of methanol at room temperature.

of carbon dioxide gives the complex composed of potassium *p*-hydroxybenzoate, carbon dioxide, and potassium methyl carbonate and the complex precipitates. However, carbon dioxide may escape from the complex during drying *in vacuo* after filtration. A similar explanation can be applied to the reaction using the di-sodium salt of *p*-hydroxybenzoic acid as an alkali source. There are other facts which support the above idea. When the methanol solutions of potassium *p*-hydroxybenzoate and of potassium methyl carbonate or the same solutions of sodium *p*-hydroxybenzoate and of sodium methyl carbonate were mixed, no precipitates were formed in either case. However, when carbon dioxide was introduced into each solution, precipitates were formed immediately from both.

The difference of the reactivity between the di-alkali salts of salicylic acid and of *p*-hydroxybenzoic acid was also observed in the Williamson ether syntheses. In the Williamson ether syntheses of the di-alkali salt of salicylic acid or *p*-hydroxybenzoic acid and benzylchloride in methanol at reflux temperature for 2 h, methyl benzyl ether was formed. Although di-alkali salts of *p*-hydroxybenzoic acid gave methyl benzyl ether only in about 4% yield, di-potassium and di-sodium salts of salicylic acid gave the same product in 67 and 47% yields, respectively. In addition, when the di-potassium salt of salicylic acid was recrystalized from methanol, the precipitate was the mono-potassium salt of salicylic acid (potassium salicylate). On the basis of these data, it was speculated that the di-potassium salt of salicylic acid easily changes into potassium salicylate. The reason may be due to the chelating structure of the salicylate; that is, the alkali atom of mono-alkali salicylate will be considerably neutralized and therefore the bonding force between the alkali atom of mono-alkali salicylate and the oxygen atom of carbon dioxide must be extremely weak.

Experimental

Authentic Alkali Alkyl Carbonate. Metallic potassium or sodium was dissolved in anhydrous alcohol and then carbon dioxide was introduced with vigorous stirring. From this mixture, excess alcohol was evaporated off at about 100 °C *in vacuo*.

Syntheses of Alkali Alkyl Carbonates by the Present Reaction. A typical example is as follows. Into a 200 ml four-necked flask, provided with a mechanical stirrer, a thermometer, and a gas-inlet tube whose top was connected to a calcium chloride tube, were placed sodium phenoxide (3.48 g, 0.03 mol), anhydrous methanol (3 ml), and anhydrous acetone (50 ml, as a solvent of sodium phenoxide). A sufficient volume of dry carbon dioxide was slowly introduced into the stirred acetone solution and white precipitates soon formed. These precipitates were collected on a glass filter, washed with dry ether, and then dried in *vacuo* at room temperature: yield, 98.0%.

In the preparations of the branched alkyl alkali carbonates, the mixture became a slurry when carbon dioxide was introduced into the mixture of sodium phenoxide, alcohol, and solvent (acetone or THF). Therefore, these carbonates might partially decompose into alcohol and sodium hydrogen carbonate by contact with the moisture in the air, since rapid filtration was very difficult. Another possibility is that these carbonates contain some amounts of solvent, because of the difficulty of the complete evaporation of the solvent from these carbonates in a slurry-state. Owing to the above reasons, the values of the elementary analyses of the branched alkyl alkali carbonates would deviate more than 1% from the calculated values.

Competitive Reactions. Carbon dioxide was introduced into a mixture of isobutyl alcohol (0.10 mol), butyl alcohol (0.10 mol) and sodium phenoxide (0.021 mol) in acetone (100 ml); the precipitates were filtered, washed with ether, and then decomposed with water into alcohols and sodium hydrogen carbonate. The resulting alcohol were extracted with ether, and butyl alcohol and isobutyl alcohol were determined by gas chromatography (internal standard compound, cyclohexane; instrument, Yanagimoto G80; column, PEG 20 M, 2.25 m; temp, 98 °C). The ratio of butyl alcohol/isobutyl alcohol was 33.

Similarly, the reaction was carried out using the mixture of *s*-butyl alcohol (0.10 mol), butyl alcohol (0.10 mol), sodium phenoxide (0.021 mol), and acetone (100 ml); the alcohols derived from sodium butyl carbonates were determined by gas chromatography (column temp, 90 °C). The ratio of butyl alcohol/*s*-butyl alcohol was 41.

Reactions using Di-alkali Salts of Hydroxybenzoic Acids as Alkali Sources. An example is as follows. Five grams of di-sodium salt of *p*-hydroxybenzoic acid were dissolved in 50 ml

of anhydrous methanol; into this mixture dry carbon dioxide was introduced. Within several minutes, white precipitates formed. After 30 min, the precipitates were filtered and dried *in vacuo* at room temperature: yield was 4.44 g. When di-potassium salt of salicylic acid was used, the formation of the precipitates was slower. Generally speaking, the readiness of the formation of the precipitates decreased in the following order: di-sodium salt of *p*-hydroxybenzoic acid>di-sodium salt of salicylic acid>di-potassium salt of *p*-hydroxybenzoic acid>di-potassium salt of salicylic acid.

The Formation of the Complex from Mono-alkali Salt of p-*Hydroxybenzoic Acid, Potassium Methyl Carbonate, and Carbon Dioxide.* Into a four-necked flask with a mechanical stirrer, 10.27 g of monopotassium salt of *p*-hydroxybenzoic acid and 50 ml of methanol were placed, and into this mixture carbon dioxide was introduced. The precipitates (perhaps mono-potassium salt of *p*-hydroxybenzoic acid) were filtered off. To the filtrate, a solution of 7.55 g of potassium methyl carbonate in 60 ml of methanol was added and then carbon dioxide was introduced. The precipitates were filtered and dried *in vacuo*: yield was 5.61 g. The content of *p*-hydroxybenzoic acid was 50.9% (determined by UV technique[2]). This value was in good agreement with the calculated one (47.6%, see Table 3), within experimental error. Therefore, this product must be composed of nearly equimolar amounts of mono-potassium salt of *p*-hydroxybenzoic acid and potassium methyl carbonate.

A similar reaction was carried out using sodium *p*-hydroxybenzoate and sodium methyl carbonate. The resulting content of *p*-hydroxybenzoic acid was 50.3%. This value is also in good agreement with the calculated one (53.5%, see Table 3), within experimental error.

Reactions of Alkali Salts with Benzyl Chloride. Into a 200 ml three-necked flask, with a mechanical stirrer and a reflux condenser whose top was connected to a calcium chloride tube, were placed 9.10 g of di-sodium salt of salicylic acid (0.05 mol), 6.35 g of benzyl chloride (0.05 mol), and 100 ml of methanol. The mixture was refluxed with vigorous stirring for 2 h. The volume of the solution was reduced to about half by evaporation of the methanol. The insoluble product was filtered off and then methyl benzyl ether was determined by gas chromatography (internal standard compound, dimethylaniline; column, PEG 20 M, 2.25 m; temp, 200 °C).

Thanks are due to Mr. Kazumi Hirakawa and Mr. Junji Anai for their assistance in the experimental work.

References

1) Part XXI of this series: I. Hirao and T. Kito, *Bull. Chem. Soc. Jpn.*, **46**, 3470 (1973).

2) I. Hirao, T. Kondo, and T. Kito, *Kogyo Kagaku Zasshi*, **72**, 692 (1969); T. Kito, Y. Hokamura, and I. Hirao, *ibid.*, **74**, 1651 (1971); T. Kito and I. Hirao, *Bull. Chem. Soc. Jpn.*, **44**, 3123 (1971).

3) J. L. Hales, J. I. Jones, and A. S. Lindsey, *J. Chem. Soc.*, **1954**, 3145; E. A. Shilov, I. V. Smirov-Zamkov, and K. I. Matkovskii, *Ukrain. Khim. Zhur.*, **21**, 484 (1955).

4) J. A. Dean, "Lange's Handbook of Chemistry," McGraw-Hill Book Company (1973), pp. 5—13.

5) T. Kwan, H. Yamamoto, H. Mori, and H. Samejima, *Kagaku Kogyo*, **74**, 1618 (1972).

6) T. Kito, H. Minami, and I. Hirao, *Kogyo Kagaku Zasshi*, **74**, 2313 (1971).

7) Z. Rappoport, "Handbook of Tables for Organic Compound Identification," 3rd ed., The Chemical Rubber Co. (1967), p. 434; J. A. Riddick and W. B. Bunger, "Organic Solvents," 3rd ed., Wiley-Interscience (1970), p. 145.

The Reactions of Sodium Diethyldithiocarbamate and Tetraethylthiuram Disulfide with Mercury(II) Chloride[1)]

Norio KOBAYASHI and Tamotsu FUJISAWA

Sagami Chemical Research Center, Nishi-Ohnuma, Sagamihara, Kanagawa 229

(Received December 17, 1975)

Sodium diethyldithiocarbamate (**1**) and tetraethylthiuram disulfide (**2**) have been found to react with excess mercury(II) chloride ($HgCl_2$) in water to give complexes with the general formula $Et_2NCS_2HgS_2CNEt_2 \cdot (HgCl_2)_{m-1}$, where the m value can be as high as five. The complex with $m=2$ was isolated and characterized. The reaction pathway was discussed in some detail. Also studied were the reactions of **2** with $HgCl_2$ in organic solvents.

While the strong metal-binding properties of dithiocarbamates, notably sodium diethyldithiocarbamate (**1**), are well recognized,[2)] the previous investigations of the interaction of dithiocarbamates with mercury compounds have been made almost exclusively from the viewpoints of analytical chemistry. The simple question of what amount of mercury salt can react with dithiocarbamates has been left unanswered. During the course of an investigation on the sulfur-containing polymers, it became highly desirable to determine the complex-forming ability of dithiocarbamates and their derivatives with mercury. Accordingly, we have studied the reaction of **1** with mercury(II) chloride ($HgCl_2$). It was found that the reaction proceeds according to Eq. 1, and that the m value

$$2Et_2NC(=S)SNa + mHgCl_2 \xrightarrow{-2NaCl} \underset{\mathbf{1}}{} Et_2NC(=S)SHgSC(=S)NEt_2 \cdot (HgCl_2)_{m-1} \quad (1)$$

in Eq. 1 can be as high as five. Tetraethylthiuram disulfide (**2**), an oxidation product of **1**, has also been found to react with $HgCl_2$ in a smilar manner.

Results and Discussion

Reaction of 1 with $HgCl_2$ The reaction of **1** with $HgCl_2$ was carried out in water for 22 h at room temperature. The solid product was filtered, washed with water, and then dried. The results are summarized in Table 1. As can be seen, the yields and the mercury contents of the products increased with an increase in the amount of $HgCl_2$ used. The IR spectra of the products varied depending on the mercury content, especially in the C–N partial double bond region (around 1500 cm^{-1}) (Fig. 1). In the case of the products with high mercury content, new bands appeared at 460, 1610, 3500, and 3560 cm^{-1} (Fig. 1c and 1d). The first band is characteristic of $HgCl_2$, thus indicating the presence of weakly bonded $HgCl_2$. No reasonable explanation could be given for the second band. The last two bands seem to be similar in nature to those observed for some tertiary amide–$HgCl_2$ complexes.[3)] The FIR spectra of these products showed two strong band at 300 and 345 cm^{-1}.

The product of the 1 : 0.5 reaction was a light yellow crystalline solid; its IR spectrum (Fig. 1a) was very close to that of bis(diethyldithiocarbamato)mercury (**3**). Recrystallization of the product from acetonitrile gave **3** in 85% yield.

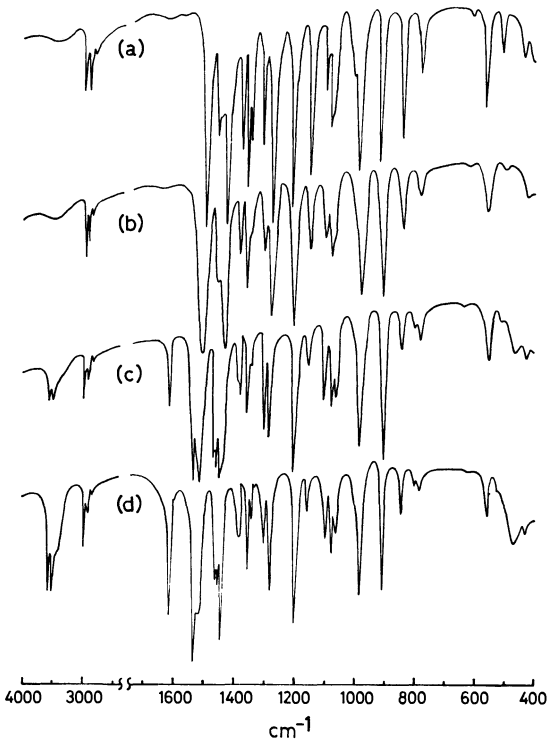

Fig. 1. The IR spectra of the mercury complexes formed in the reaction of **1** with $HgCl_2$ in water (KBr disks). **1**/$HgCl_2$; (a) 1: 0.5, (b) 1 : 1, (c) 1 : 2, and (d) 1 : 3.

The product of the 1 : 1 reaction was a faintly yellow solid and gave dichlorobis(diethyldithiocarbamato)-dimercury(II) (**4**) in 85% yield as colorless rod-like crystals on recrystallization from acetonitrile–acetone (4 : 1) below 60 °C. The confirmation of the structural formula of **4** was obtained by elemental analysis, IR, FIR, and NMR spectra, and independent synthesis; **4** was synthesized in high yields by the reaction of **3** with a stoichiometric quantity of $HgCl_2$ in acetone. It should be noted that **4** is a new type of stable mercury complex. The IR spectrum resembles that of dichlorotetrakis(diethyldithiocarbamato)trimercury(II), $Hg_3Cl_2(S_2CNEt_2)_4$.[4)] However, there are distinct differences in elemental composition and thermal properties between these two complexes.[5)]

All the other reaction products were white solids. Attempts to purify them were unsuccessful, because they were relatively unstable toward organic solvents;[6)]

Table 1. Reaction of **1** with $HgCl_2$ in water[a)]

$HgCl_2$ (g)	**1**/$HgCl_2$	Yield (g)	Mp (°C)	Analysis (%) C	H	Hg
1.36	1 : 0.5	1.91	110—114			
2.71	1 : 1	3.82	101—103			
4.07	1 : 1.5	5.07	100—104	11.85	1.85	57.20
5.42	1 : 2	6.27	—[b)]	9.34	1.68	58.99
6.78	1 : 2.5	7.17	—[b)]	9.08	1.44	61.80[c)]
8.13	1 : 3	7.99	—[b)]	7.57	1.11	63.11[d)]

a) Reaction conditions: **1** (as trihydrate) 2.55 g, H_2O 80 ml, stirring for 22 h at room temperature. b) A distinct mp was not observed. c) Calcd for $C_{10}H_{20}N_2S_4Hg_4Cl_6$: C, 9.16; H, 1.54; Hg, 61.17%. d) Calcd for $C_{10}H_{20}N_2S_4Hg_5Cl_8$: C, 7.59; H, 1.27; Hg, 63.35%.

Table 2. Reaction of **3** with $HgCl_2$ in water[a)]

$HgCl_2$ (g)	**3**/$HgCl_2$	Yield (g)	Mp (°C)	Hg/DEDC[b)]	$\nu_{C=N}$ (cm^{-1})	Hg (%)
0.54	1 : 1	1.48	107—109	0.95	1510	51.16
2.17	1 : 4	2.42	—[c)]	1.82	1515, 1530	61.32

a) Reaction conditions: **3** 0.99 g, H_2O 40 ml, stirring for 90 h at room temperature. b) Based on yield. c) A distinct mp was not observed.

Table 3. Reaction of **2** with $HgCl_2$ in water[a)]

$HgCl_2$ (g)	**2**/$HgCl_2$	Yield (g)	Mp (°C)	Hg/DEDC[b)]	$\nu_{C=N}$ (cm^{-1})	Hg (%)
0.54	1 : 1	0.94	109—113	0.44	1495	43.21
1.08	1 : 2	1.46	97—101	0.94	1515	53.19
1.63	1 : 3	2.01	100—104	1.44	1515, 1530	56.68
2.17	1 : 4	2.32	—[c)]	1.73	1515, 1530	58.77
2.71	1 : 5	2.52	—[c)]	1.92	1515, 1530	60.76
3.25	1 : 6	2.78	—[c)]	2.00	1515(sh), 1530	61.92

a) Reaction conditions: **2** 0.59 g, H_2O 40 ml, stirring for 90 h at room temperature. b) Based on yield. c) A distinct mp was not observed.

recrystallization from acetone lowered the mercury content, and repeated recrystallization resulted in the formation of **4**. The products of the 1 : 2.5 and 1 : 3 reaction had essentially the elemental analyses for $Et_2NCS_2HgS_2CNEt_2\cdot(HgCl_2)_3$ and $Et_2NCS_2HgS_2CNEt_2\cdot(HgCl_2)_4$, respectively.

From these findings, the following pathway for the reaction of **1** with $HgCl_2$ may be assumed. The initial step involves the condensation reaction giving rise

$$\underset{\mathbf{1}}{2Et_2NCSNa_2} + HgCl_2 \xrightarrow{-2NaCl} \underset{\mathbf{3}}{Et_2NCSHgSCNEt_2} \quad (2)$$

$$\mathbf{3} + HgCl_2 \longrightarrow \underset{\mathbf{4}}{Et_2NCSHgSCNEt_2\cdot HgCl_2} \quad (3)$$

$$\mathbf{4} + nHgCl_2 \longrightarrow Et_2NCSHgSCNEt_2\cdot(HgCl_2)_{n+1} \quad (4)$$

to **3**. Addition of another molecule of $HgCl_2$ to **3** gives a stable complex **4**. Further addition of $HgCl_2$ to **4** yields relatively unstable complexes with higher mercury contents. The net reaction is represented by Eq. 1. On the basis of the above assumptions the number of mercury atoms per diethyldithiocarbamate residue (DEDC), Hg/DEDC, in the product complex was calculated from the yield. The Hg/DEDC values were also calculated from the analytical values of carbon and mercury. In Fig. 2, Hg/DEDC in the product is plotted against the reactant ratio, $HgCl_2$/**1**. The Hg/DEDC values obtained from the yield are in

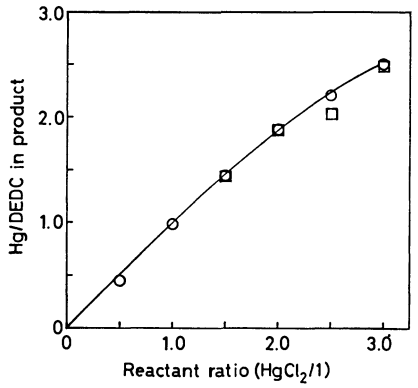

Fig. 2. Influence of reactant ratio on Hg/DEDC in product: ○ based on yield, □ based on analysis.

TABLE 4. REACTION OF 2 WITH $HgCl_2$ IN BENZENE–ETHANOL[a)]

$HgCl_2$ (g)	2/$HgCl_2$	Benzene (ml)	Ethanol (ml)	Yield (g)	Mp (°C)
2.71	1 : 1	50	70	2.64	133—138
5.42	1 : 2	50	70	7.94	134—137
8.13	1 : 3	50	70	8.26	132—135
10.80	1 : 4	70	100	8.30	134—137
13.55	1 : 5	70	100	8.28	131—133

a) Reaction conditions: **2** 2.96 g, stirring for 30 min at room temperature.

fair agreement with those obtained from the results of elemental analysis. Figure 2 also shows that the reaction proceeds almost quantitatively in the region $HgCl_2/\mathbf{1} < 1.5$, and that **1** can react with more than 2.5-mol of $HgCl_2$, that is, the *m* value in Eq. 1 can be as high as five.

Further support for these assumptions is the fact that the reaction of $HgCl_2$ with **3**, in place of **1**, proceeds in a similar manner to give the same mercury complexes as above (Table 2).

Reaction of 2 with $HgCl_2$ Since tetraethylthiuram disulfide (**2**) is practically insoluble in water, the reaction of **2** with $HgCl_2$ in water requires more than 50 h for completion.[7)] Thus the reaction was conducted by stirring a mixture of $HgCl_2$ and **2** in water for 90 h at room temperature. The results are summarized in Table 3. The yields and the mercury contents of the products increased with an increase in the amount of $HgCl_2$ used. It is clear that **2** can react with more than 4 mol of $HgCl_2$.[8)] The $\nu_{C=N}$ band shifted to a higher wavelength with mercury content. In addition, the products with higher mercury contents gave new bands at 1610, 3500, and 3560 cm^{-1}. This tendency is the same as that observed in the reaction of **1** with $HgCl_2$. It therefore seems reasonable to conclude that the reaction of $HgCl_2$ with **2** proceeds like the reaction with **1**, except that the first step is the insertion reaction of mercury into the S–S bond of **2**, as evidenced by the isolation of **3** from the 1 : 1 reaction product.

$$\underset{\mathbf{2}}{Et_2NC(=S)SSC(=S)NEt_2} + HgCl_2 \xrightarrow{-Cl_2} \underset{\mathbf{3}}{Et_2NC(=S)SHgSC(=S)NEt_2} \quad (5)$$

This type of reaction has been reported for several heavy metals, including mercury.[9–13)]

The literature contains some reports on the mercury complexes of thiuram disulfides, which were prepared in organic media and have elemental compositions that can not be explained by the reaction pathway described above.[14,15)] So the reaction of $HgCl_2$ with **2** was studied in several organic solvents.

A solution of **2** in benzene was added to a stirred solution of $HgCl_2$ in ethanol,[16)] and the mixture was stirred for 30 min. The precipitate was filtered, washed with ethanol, and dried. Table 4 lists the results of the reaction. Interestingly, all the products were essentially identical in physical appearance, thermal properties, and IR spectra. The IR spectra were characterized by a prominent band of $\nu_{C=N}$ at 1530 cm^{-1}. The results of the elemental analysis indicated the incorporation of about 2 atoms of mercury per molecule of **2**.

Table 5 summarizes the results of the reaction in acetone and ethanol. The 1 : 1 reaction in acetone gave the same product as that obtained in benzene–ethanol. On the other hand, an undertemined oily material was formed in ethanol. In both solvents, the use of excess $HgCl_2$ afforded products which resembled those obtained in water judging from IR spectra.

Conclusion. The reaction of **1** with $HgCl_2$ in water proceeds according to Eq. 1. The first step of the reaction is the formation of **3**, which can react with other molecules of $HgCl_2$ to give **4** and complexes with higher mercury content. The **4** complex is stable and it can be purified by recrystallization. The reaction of **2** with $HgCl_2$ proceeds in a similar manner. It is, however, to be emphasized that this is true only in water; the reaction is greatly affected by the solvent or solvent system used. These findings may be helpful in the design of heavy-metal adsorbing resins.

Experimental

Instrumentation. The following instruments were used in this study: a Hitachi EPI-G3 grating infrared spectrophotometer, a Hitachi FIS-3 far-infrared spectrophotometer, a Varian T-60 NMR spectrometer, a Perkin-Elmer DSC-2 differential scanning calorimeter, and a Yanaco micro melting point apparatus.

Materials. Sodium diethyldithiocarbamate (**1**) was prepared as trihydrate by the reaction of diethylamine with carbon disulfide in the presence of sodium hydroxide. Commercial tetraethylthiuram disulfide (**2**) was recrystallized from ethanol. $HgCl_2$ (Kanto Kagaku guaranteed reagent) was used as received.

Reaction of 1 with $HgCl_2$. The reaction of **1** with $HgCl_2$ was carried out in water. The results are summarized in Table 1. The following is an example of the general procedure. A mixture of 2.25 g of **1** (as trihydrate), a prescribed amount of $HgCl_2$, and 80 ml of water was stirred

TABLE 5. REACTION OF 2 WITH $HgCl_2$ IN ACETONE AND ETHANOL

2 (g)	$HgCl_2$ (g)	2/$HgCl_2$	Solvent (ml)	Time (h)	Yield (g)[a)]	$\nu_{C=N}$ (cm^{-1})
2.96	2.71	1 : 1	Acetone (50)	3	1.28[b)]	1530
1.48	6.78	1 : 5	Acetone (200)	20	1.11[c)]	1510, 1530
2.96	2.71	1 : 1	Ethanol (120)	3	—[d)]	
2.96	8.13	1 : 3	Ethanol (200)	20	6.71[c)]	1515(sh), 1530

a) For solid product precipitated during the reaction. b) Mp 128—132 °C. c) A distinct mp was not observed. d) An oily yellow material was formed.

magnetically for 22 h at room temperature. The solid was filtered off, washed thoroughly with water, and then dried at room temperature under a vacuum.

The 1 : 0.5 reaction product was recrystallized from acetonitrile to give **3** as a yellow crystal in 85% yield; mp 139—141 °C (lit,[13] mp 138—139 °C).

IR (KBr disk): 1500 cm^{-1} ($\nu_{C=N}$).

NMR ($CDCl_3$): δ 1.33 (t, J=7 Hz, 12H), 3.84 (q, J=7 Hz, 8H).

Found: C, 24.32; H, 4.19; Hg, 39.98%. Calcd for $C_{10}H_{20}N_2S_4Hg$: C, 24.16; H, 4.06; Hg, 40.35%.

The 1 : 1 reaction product was recrystallized from acetonitrile–acetone (4 : 1) below 60 °C to give **4** as a colorless rod in 85% yield: mp 105—107 °C.

IR (KBr disk): 1510 cm^{-1} ($\nu_{C=N}$).

FIR (Nujol mull): 334 cm^{-1} (ν_{Hg-Cl}).

NMR (d_6-acetone): δ 1.34 (t, J=7 Hz, 12H), 3.85 (q, J=7 Hz, 8H).

Found: C, 15.66; H, 2.68; S, 16.70; Hg, 52.27%. Calcd for $C_{10}H_{20}N_2S_4Hg_2Cl_2$: C, 15.63; H, 2.62; S, 16.69; Hg, 52.19%.

Recrystallization of 2.00 g of the 1 : 3 reaction product from 150 ml of acetone gave 0.99 g of white crystals. The IR spectrum showed a single band due to $\nu_{C=N}$ at 1510 cm^{-1}, but the bands at 460, 1530, 1610, 3500, and 3560 cm^{-1} characteristic of the original product (Fig. 1d) were completely absent.

Found: C, 12.59; H, 1.51; Hg, 56.34%.

*Reaction of **3** with $HgCl_2$ in Acetone.* A mixture of 4.96 g of **3** and 120 ml of acetone was heated at about 60 °C until it became homogeneous. To this solution was added 2.71 g of $HgCl_2$, and the mixture was stirred for 1 h under reflux. After cooling, the white crystals of **4** were collected and dried. From the filtrate a small amount of **4** was obtained by concentration, followed by crystallization. The total yield of **4** was 7.35 g (95%). Recrystallization of the raw product from acetonitrile–acetone gave 6.02 g (78%) of **4** in a pure form.

*Reaction of **3** with $HgCl_2$ in Water.* A mixture of 0.99 g of **3**, a prescribed amount of $HgCl_2$, and 40 ml of water was stirred for 90 h at room temperature. The work-up procedure was the same as that followed with **1**. The results are summarized in Table 2. The IR spectra were very close to those of the corresponding products obtained in the reaction of **1** with $HgCl_2$.

*Reaction of **2** with $HgCl_2$ in Water.* The results of the reaction are summarized in Table 3. The following is a typical example. A mixture of 0.59 g of **2**, 2.17 g of $HgCl_2$, and 40 ml of water was stirred for 90 h at room temperature. The solid product was filtered, washed thoroughly with water, and then dried at room temperature under a vacuum. The yield was 2.32 g. The IR spectrum revealed characteristic bands at 460, 1515, 1530, 1610, 3500, and 3560 cm^{-1}.

Found: C, 9.33; H, 1.22; Hg, 58.77%.

*Reaction of **2** with $HgCl_2$ in Benzene–Ethanol.* The results of the reaction are summarized in Table 4. The following is a typical example. To a stirred solution of 8.13 g of $HgCl_2$ in 70 ml of ethanol was added dropwise a solution of 2.96 g of **2** in 50 ml of benzene. A white crystalline precipitate started to separate almost immediately. The mixture was stirred for 30 min at room temperature and filtered. The filtered solid was washed with ethanol and then dried at room temperature under a vacuum. The yield was 8.26 g; mp 132—135 °C (dec.).

IR (KBr disk): 1530 cm^{-1} ($\nu_{C=N}$).

Found: C, 15.64; H, 2.67; S, 16.30; Cl, 11.14; Hg, 48.08%.

Repeated recrystallization of the product from acetonitrile gave a small amount of **4**: mp 105—107 °C.

Found: C, 15.35; H, 2.36; S, 16.63%. Calcd for $C_{10}H_{20}N_2S_4Hg_2Cl_2$: C, 15.63;, H, 2.62; S, 16.69%.

*Reaction of **2** with $HgCl_2$ (1 : 5) in Acetone.* To a stirred solution of 6.78 g of $HgCl_2$ in 150 ml of acetone was added a solution of 1.48 g of **2** in 50 ml of acetone. The mixture was stirred for 20 h at room temperature. The white precipitate was filtered and dried. The yield was 1.11 g. The IR spectrum showed characteristic bands at 460, 1510, 1530, 1610, 3500, and 3560 cm^{-1}. Essentially the same product was obtained from the filtrate by concentration, followed by treatment of the residue with acetone–ether. The yield was 2.44 g.

Found: C, 7.69; H, 1.23; S, 8.23%.

*Reaction of **2** with $HgCl_2$ (1 : 3) in Ethanol.* A solution of 8.13 g of $HgCl_2$ in 80 ml of ethanol was added to a stirred solution of 2.96 g of **2** in 120 ml of ethanol. In time, the system became cloudy, and then a viscous yellow material began to separate. The stirring was continued for 20 h. During this period the yellow material turned to a white crystalline solid. The solid was filtered, washed with ethanol, and dried. The yield was 6.71 g. The IR spectrum showed characteristic bands at 460, 1515 (sh), 1530, 1610, 3500, and 3560 cm^{-1}.

Found: C, 13.11; H, 2.16; S, 13.35; Hg, 50.50%.

The authors are indebted to Dr. Hitoshi Iwasaki of the Institute of Physical and Chemical Research for supplying a sample of $Hg_3Cl_2(S_2CNEt_2)_4$.

References

1) Sulfur-containing polymers Part XVII: Part XVI, N. Kobayashi, A. Osawa, and T. Fujisawa, *J. Polym. Sci. Polym. Chem. Ed.*, **13**, 2863 (1975).

2) G. D. Thorn and R. A. Ludwig, "The Dithiocarbamates and Related Compounds," Elsevier Publishing, New York (1962), pp. 157—168.

3) I. Baxter and G. A. Swan, *J. Chem. Soc.*, **1965**, 3011.

4) H. Iwasaki, *Chem. Lett.*, **1972**, 1105.

5) DSC analysis indicated two endotherm at 104.5 °C (ΔH=11.6 mcal/mg) and at 118.5 °C (ΔH=2.5 mcal/mg) for **4** and one endotherm at 117.5 °C (ΔH=15.0 mcal/mg) for $Hg_3Cl_2(S_2CNEt_2)_4$.

6) They were reasonably stable toward water. A sample of the 1 : 3 reaction product was stirred in water for 90 h. The mercury content of the sample before and after this treatment were 63.11 and 63.01%, respectively.

7) M. Ambe, K. Shimizu, A. Osawa, N. Kobayashi, and T. Fujisawa, unpublished results.

8) Application of thiuram disulfide to mercury removal: S. Otsuki, Japan Kokai 49-14315 (1974).

9) Ref. 2, pp. 71—72.

10) K. Lesz and T. Lipiec, *Roczniki Chem.*, **40**, 1117 (1966); *Chem. Abstr.*, **66**, 61360b (1967).

11) H. Shizuka and T. Azami, *Nippon Gomu Kyokai Shi*, **39**, 999 (1966).

12) T. Mukaiyama and T. Endo, *Bull. Chem. Soc. Jpn.*, **40**, 2388 (1967).

13) T. Mukaiyama, T. Endo, S. Ikenaga, and K. Osonoi, *J. Org. Chem.*, **33**, 2242 (1968).

14) S. Prasad and P. D. Sharma, *J. Proc. Inst. Chem.*, **30**, 259 (1958); *Chem. Abstr.*, **53**, 11086f (1959).

15) H. C. Brinkhoff, A. M. Grotens, and J. J. Steggerda, *Rec. Trav. Chim. Pays-Bas*, **89**, 11 (1970).

16) The reaction product of tetramethylthiuram disulfide and $HgCl_2$ in benzene–ethanol has been claimed to have a fungicidal and seed immunising action: J. R. Geigy A. G., Brit. 543089 (1942).

The Association Constants of Hexaamminechromium(III) and Tris-(ethylenediamine)chromium(III) Ions with Several Univalent Anions in Aqueous Solutions

Tatsuo TAKAHASHI and Takefumi KOISO

Department of Chemistry, Fukushima Technical College, Iwaki 970

(Received December 22, 1975)

The thermodynamic ion-association constants of hexaamminechromium(III) and tris(ethylenediamine)-chromium(III) with several univalent anions were determined in aqueous solutions at 25.0 °C. The log K_{con} values obtained by the conductometric method are 1.3_7 for $[Cr(NH_3)_6]^{3+}$–Cl^-, 1.5_8 for $[Cr(en)_3]^{3+}$–Cl^-, 1.5_7 for $[Cr(NH_3)_6]^{3+}$–Br^-, 1.5_0 for $[Cr(en)_3]^{3+}$–Br^-, 1.5_3 for $[Cr(NH_3)_6]^{3+}$–NO_3^-, and 1.4_9 for $[Cr(en)_3]^{3+}$–NO_3^-. The log K_{sp} values obtained by the spectrophotometric method are 1.6_5 for $[Cr(en)_3]^{3+}$–Cl^-, 1.4_6 for $[Cr(en)_3]^{3+}$–Br^-, and 0.9_0 for $[Cr(en)_3]^{3+}$–ClO_4^-; the value for $[Cr(en)_3]^{3+}$–ClO_4^- could be indirectly calculated from the apparent ion-association constant of $[Cr(en)_3]^{3+}$–Br^- determined in the solutions containing both bromide and perchlorate ions. Though the detailed comparison of the ion-association constants obtained in this study was limited, it could be concluded that the K_{con} values were in relatively good agreement with the K_{sp} values obtained on the given ion-pairs and that the ion-association constants of chromium(III) complex cations with several univalent anions are slightly less than those of the corresponding cobalt(III) complex cations with their anions.

In view of the fact that the theories for ion association proposed by Bjerrum,[1] Fuoss,[2] and other authors were not fully related to the Debye-Hückel[3] theory of electrolyte solutions, Yokoyama and Yamatera[4] showed that the ion-association constant could be derived in direct relation to the Debye-Hückel theory, reexamined to explain the ion-association. Meanwhile, the determination of the standard enthalpies and entropies for the ion-pair formation,[5] and the comparison of the ion-association constants obtained by the various types of measurements[6–9] were considered to provide some significant information concerning the interaction between the ions.

In this paper, a conductometric investigation of the ion-pairs, $[Cr(NH_3)_6]^{3+}$–X^-, $[Cr(en)_3]^{3+}$–X^- (X=Cl, Br, NO_3) and a spectrophotometric investigation of $[Cr(en)_3]^{3+}$–Br^-, $[Cr(en)_3]^{3+}$–Cl^-, $[Cr(en)_3]^{3+}$–ClO_4^- will be presented. The ion-association constants which were determined in this study and the previous study[10] (X=I, ClO_4) will be compared with the values reported for the corresponding cobalt(III) complex cations with several univalent anions, and will be briefly discussed in terms of Bjerrum's theory of ion-association.

Experimental

The compounds, $[Cr(NH_3)_6]Cl_3$, $[Cr(NH_3)_6]Br_3$, $[Cr(en)_3]Cl_3 \cdot 3.5H_2O$, $[Cr(NH_3)_6](NO_3)_3$, $[Cr(en)_3](NO_3)_3$, and $[Cr(en)_3]Br_3 \cdot 4H_2O$, were prepared according to the procedures described in the literature. Each compound was carefully recrystallized three times from redistilled water. The purity was examined by the method described in a previous paper;[10] the results were in very good agreement with the theoretical values. All the chemicals used were of an analytical reagent grade and were highly purified by recrystallization from redistilled water.

Solutions of various concentrations were carefully prepared by using conductivity water of a low specific conductance ($<4\times10^{-7}$ $\mho$ cm^{-1}). The electric conductivities were measured with a Yanagimoto conductivity outfit, Model MY-7, in an atmosphere of purified nitrogen over the surface of the solution, after the dissolved carbon dioxide in the solution had been removed by bubbling nitrogen gas through the solution. All the measurements were carried out within 30 min after the preparation of the solution, in a water-thermostat of 25.00±0.02 °C. The absorbancy measurements of solutions were made with a 124-type Hitachi spectrophotometer with a thermostated cell compartment (25.0±0.1 °C), using a 10-mm quartz cell, within 30 min after the preparation of the solution. Increasing quantities of sodium chloride or potassium bromide were added to each solution containing a small, constant concentration of the complex. The reference solutions used for the measurement had exactly the same concentration of Cl^- or Br^- as in the corresponding sample solutions.

Results and Discussion

The equivalent conductivities, Λ, of the complexes at various concentrations are summarized in Tables 1 and 2. The relations between the equivalent conductivities obtained and the ionic strength (I) are shown in Figs. 1—3. Table 3 presents the limiting equivalent conductivities, Λ°, of each complex, as determined by Onsager's method of extrapolation,[11] and also the limiting ionic equivalent conductivities, λ°, of each complex cation calculated from the Λ° values. Table 4 summarizes the so-called Stokes' radii, r_s, of $[Cr(NH_3)_6]^{3+}$ and $[Cr(en)_3]^{3+}$, as determined from the conductivity data in this study and those of the corresponding cobalt(III) complex cations.

Figures 1—3 show the plots of Λ against $I^{1/2}$; the broken lines indicate the theoretical Onsager lines[11] calculated. The slight deviation between the experimental conductivity lines and the theoretical lines was assumed to be due to the ion-pair formation between the cations and the anions:

$$M^{3+} + X^- \rightleftharpoons M^{3+}X^- \qquad (1)$$

$M = Cr(NH_3)_6$, $Cr(en)_3$

X = Cl, Br, NO_3

The degrees of dissociation, α, of the possible ion pairs were determined according to the successive approximation method described by Jenkins and Monk.[12] The thermodynamic ion-association constants, K, for Eq. 1 were calculated from both the

Table 1. Conductivities, Λ, degrees of dissociation, α, and thermodynamic association constants, K, of $[Cr(NH_3)_6]^{3+}$-X^- in aqueous solutions at 25.0 °C

Molar concn $\times 10^4$	Λ	α	log K
	(X=Cl)		
2.166	165.6_6	0.989_3	1.3_3
2.647	164.6_8	0.987_4	1.3_3
2.836	164.2_2	0.985_3	1.3_7
2.958	164.1_6	0.987_1	1.3_0
3.851	162.5_7	0.983_2	1.3_2
4.333	161.6_9	0.979_8	1.3_6
4.525	161.5_7	0.981_5	1.3_0
5.262	160.1_4	0.973_9	1.4_1
5.672	159.6_5	0.973_6	1.3_9
6.163	158.9_2	0.970_8	1.4_0
6.835	158.2_1	0.970_7	1.3_7
7.718	157.0_4	0.966_3	1.3_9
8.589	155.9_4	0.961_9	1.4_1
9.898	154.5_7	0.958_4	1.4_1
	(X=Br)		
1.887	168.3_7	0.986_4	1.4_9
1.935	168.2_3	0.985_8	1.5_0
2.748	166.1_5	0.977_1	1.5_8
2.960	165.7_7	0.976_5	1.5_7
3.880	163.9_2	0.969_5	1.5_8
4.828	162.0_9	0.960_9	1.6_2
5.039	162.0_9	0.964_4	1.5_6
5.168	161.8_9	0.963_7	1.5_6
5.280	161.3_7	0.958_2	1.6_2
5.846	160.7_6	0.958_6	1.5_8
6.983	159.5_4	0.958_2	1.5_2
7.813	158.1_0	0.949_0	1.5_8
9.019	156.6_9	0.944_3	1.5_7
9.973	155.3_9	0.937_0	1.5_9
	($X=NO_3$)		
1.508	162.6_5	0.989_1	1.4_8
1.861	161.7_0	0.986_1	1.5_1
2.296	160.6_1	0.982_2	1.5_4
2.830	159.5_8	0.980_3	1.5_0
3.462	158.4_2	0.977_4	1.4_9
3.839	157.5_7	0.972_7	1.5_4
4.594	156.3_1	0.968_6	1.5_4
5.283	155.4_1	0.967_5	1.5_0
5.996	154.2_0	0.961_3	1.5_4
6.692	152.9_9	0.954_2	1.5_8
7.483	152.2_4	0.954_6	1.5_4
8.724	150.4_1	0.944_1	1.5_8
9.782	149.2_2	0.939_7	1.5_8

Table 2. Conductivities, Λ, degrees of dissociation, α, and thermodynamic association constants, K, of $[Cr(en)_3]^{3+}$-X^- in aqueous solutions at 25.0 °C

Molar concn $\times 10^4$	Λ	α	log K
	(X=Cl)		
1.751	143.3_8	0.985_1	1.5_6
2.048	142.7_2	0.983_1	1.5_6
2.994	140.8_7	0.976_8	1.5_6
3.821	139.3_3	0.969_4	1.5_9
3.907	139.3_3	0.971_2	1.5_6
4.989	137.5_8	0.962_6	1.5_9
4.990	137.6_7	0.964_3	1.5_7
5.804	136.3_1	0.955_4	1.6_1
6.180	135.9_3	0.955_2	1.6_0
7.170	134.8_5	0.952_4	1.5_7
8.104	133.7_5	0.947_3	1.5_8
8.865	132.7_5	0.940_6	1.6_1
9.340	132.3_7	0.940_5	1.5_9
9.850	131.7_3	0.936_0	1.6_1
	(X=Br)		
1.877	144.8_8	0.986_4	1.4_9
2.121	144.3_0	0.983_9	1.5_2
2.999	142.5_5	0.977_6	1.5_4
3.914	141.3_1	0.977_1	1.4_5
4.255	140.7_8	0.975_1	1.4_6
4.938	139.6_5	0.969_3	1.5_0
5.901	138.0_9	0.959_8	1.5_6
6.052	138.1_7	0.963_7	1.5_1
7.031	137.1_4	0.962_1	1.4_7
7.939	136.0_2	0.956_4	1.5_0
8.954	134.9_6	0.952_6	1.5_0
8.991	134.5_2	0.945_2	1.5_6
9.933	134.4_9	0.958_1	1.4_1
10.040	133.5_6	0.942_6	1.5_5
	($X=NO_3$)		
1.526	138.3_1	0.991_3	1.3_8
1.915	137.4_4	0.989_0	1.3_9
2.868	135.5_9	0.983_2	1.4_3
3.327	134.5_3	0.975_8	1.5_4
3.789	133.8_0	0.973_4	1.5_3
4.537	132.6_8	0.969_3	1.5_3
5.378	131.7_8	0.969_5	1.4_7
5.986	130.9_8	0.966_1	1.4_8
6.722	130.0_1	0.961_2	1.5_0
7.487	129.0_4	0.956_0	1.5_2
8.520	127.9_6	0.952_1	1.5_2
9.793	126.6_2	0.945_6	1.5_3

degree of dissociation thus obtained and the activity coefficient, f, of ions as estimated from the Debye-Hückel limiting equation. The results are summarized in Tables 1 and 2. In the present calculation, the λ° values of ion-pairs were assumed to be equal to two-thirds of those of complex cations, and the actual ionic strength, I, is $(1+\alpha)C$, where C is the equivalent concentration of the complex. If the distance of the closest approach of the two ions of an ion-pair is assumed to be equal to the sum of their Stokes' radii, the ion-association constant of the ion-pair can be estimated by Bjerrum's theory.[1] Table 5 presents the log K values calculated theoretically.

It has generally been observed that, in the ultraviolet region, the ion-association is usually accompanied either by the appearance of a new absorption band or by a shift of an existing band. The present authors also found an increase in the optical densities of the charge-transfer band in the ultraviolet region of $[Cr(en)_3]Cl_3 \cdot 3.5H_2O$ and $[Cr(en)_3]Br_3 \cdot 4H_2O$ upon

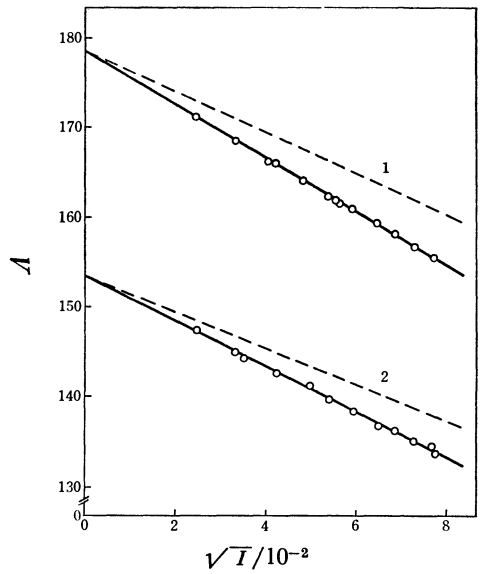

Fig. 1. The Onsager plots of hexaamminechromium-(III) bromide (1) and tris(ethylenediamine)chromium-(III) bromide (2) in aqueous solutions at 25.0 °C.

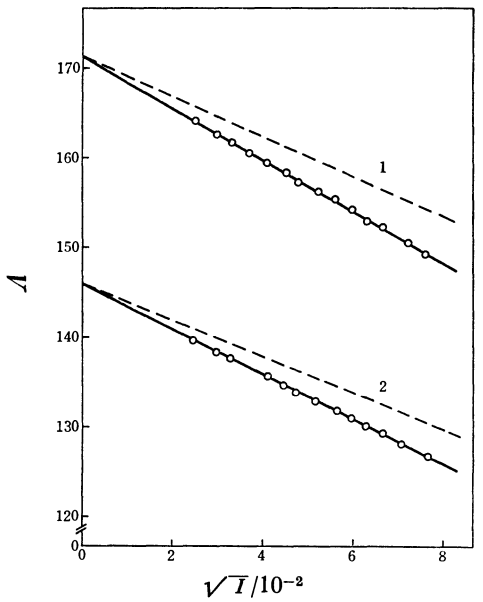

Fig. 2. The Onsager plots of hexaamminechromium-(III) nitrate (1) and tris(ethylenediamine)chromium-(III) nitrate (2) in aqueous solutions at 25.0 °C.

TABLE 3. THE LIMITING EQUIVALENT CONDUCTIVITY, Λ°, OF CHROMIUM(III) COMPLEXES AND THE LIMITING IONIC EQUIVALENT CONDUCTIVITY, λ°, OF CHROMIUM(III) COMPLEX CATIONS IN AQUEOUS SOLUTIONS AT 25.0 °C

Complex	Λ°	λ°
$[Cr(NH_3)_6](NO_3)_3$	170.1	98.6
$[Cr(NH_3)_6]Br_3$	176.9	98.8
$[Cr(NH_3)_6]Cl_3$	174.5	98.1
$[Cr(en)_3](NO_3)_3$	144.9	73.4
$[Cr(en)_3]Br_3 \cdot 4H_2O$	152.6	74.5
$[Cr(en)_3]Cl_3 \cdot 3.5H_2O$	150.9	74.5

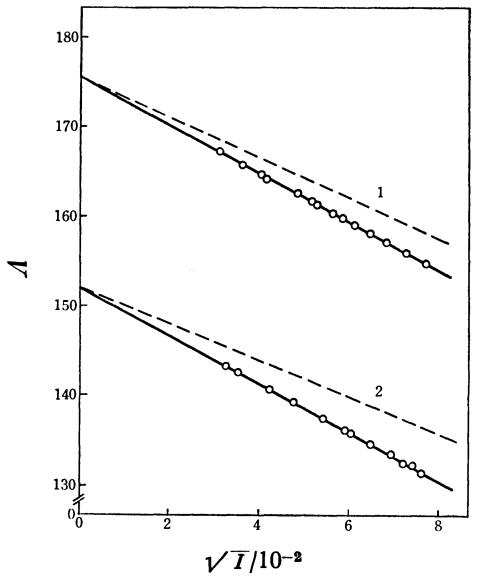

Fig. 3. The Onsager plots of hexaamminechromium-(III) chloride (1) and tris(ethylenediamine)chromium-(III) chloride (2) in aqueous solutions at 25.0 °C.

TABLE 4. THE LIMITING EQUIVALENT CONDUCTIVITY, λ°, AND THE STOKES' RADIUS, r_s, OF CHROMIUM(III) AND COBALT(III) COMPLEX CATIONS IN AQUEOUS SOLUTIONS AT 25.0 °C

Complex cations	λ°	r_s (Å)
$[Cr(NH_3)_6]^{3+}$	98.5	2.80
	98.5[10]	2.80[10]
$[Cr(en)_3]^{3+}$	74.1	3.72
	73.4[10]	3.75[10]
$[Co(NH_3)_6]^{3+}$	99.2[12]	2.77[12],a)
	99.0—99.7[7,15]	2.78—2.76[7,15]
$[Co(en)_3]^{3+}$	74.5[12]	3.68[12],a)

a) These values were calculated by means of this equation: $r_s = 91.6|Z_1|/\lambda_1^\circ$.

TABLE 5. LOGARITHMIC ASSOCIATION CONSTANTS OF THE ION-PAIRS CALCULATED BY BJERRUM'S THEORY IN AQUEOUS SOLUTIONS AT 25.0 °C

Ion-pair	log K
$[Cr(NH_3)_6]^{3+}$-NO_3^-	1.7_9
$[Cr(en)_3]^{3+}$-NO_3^-	1.6_5
$[Cr(NH_3)_6]^{3+}$-Br^-	1.8_1
$[Cr(en)_3]^{3+}$-Br^-	1.6_7
$[Cr(NH_3)_6]^{3+}$-Cl^-	1.8_1
$[Cr(en)_3]^{3+}$-Cl^-	1.6_7

the addition of Cl^- or Br^- as a result of the ion-association. When the Reaction 1 of ion-pair formation was in equilibrium, the spectrophotometric data could be approximately treated according to the following equation:

$$\frac{[X^-]_T}{\varepsilon_{obsd}-\varepsilon_M}\cdot\frac{f_M f_X}{f_{MX}} = \frac{1}{K(\varepsilon_{MX}-\varepsilon_M)} + \frac{[X^-]_T}{\varepsilon_{MX}-\varepsilon_M}\cdot\frac{f_M f_X}{f_{MX}} \quad (2)$$

where ε_{obsd} is the observed molar extinction coefficient;

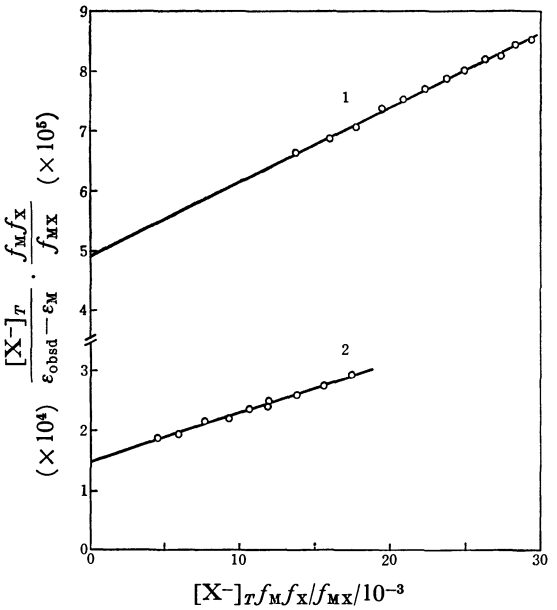

Fig. 4. Plots of the left-hand side of Eq. 2 against the $[X^-]_T f_M f_X/f_{MX}$ at 230 nm
(1): $[Cr(en)_3]^{3+}$–Br^-, (2): $[Cr(en)_3]^{3+}$–Cl^-.

ε_M and ε_{MX}, the molar extinction coefficients of M^{3+} and $M^{3+}X^-$, and f_M, f_X, and f_{MX}, the activity coefficients of M^{3+}, X^- and an ion-pair, $M^{3+}X^-$, respectively. The plot of the left-hand side of Eq. 2 *vs.* $[X^-]_T \cdot f_M f_X/f_{MX}$ gives a straight line, and the thermodynamic ion-association constant, K, can be determined from the ratio of its slope to the intercept. The activity coefficient was calculated from the following equation:

$$\log f_i = \frac{-0.5115\, Z_i^2\sqrt{I}}{1+0.329a\sqrt{I}} \qquad (3)$$

The ion-size parameters, a,[13] used in the calculation are 3.0 Å for Cl^- and Br^-, 3.5 Å for ClO_4^-, and 6.0 Å for $[Cr(en)_3]^{3+}$, $[Cr(en)_3]^{3+}$–Cl^-, and $[Cr(en)_3]^{3+}$–Br^-. The results of the experiments are shown in Fig. 4. The linear relationship in Fig. 4 suggests that no appreciable contribution of the ion-pair formations, such as $[Cr(en)_3]^{3+}$–$2Cl^-$, as $[Cr(en)_3]^{3+}$–$2Br^-$, were to be expected in these systems. The $\log K$ values thus obtained were 1.6_5 for $[Cr(en)_3]^{3+}$–Cl^- and 1.4_6 for $[Cr(en)_3]^{3+}$–Br^-. No change was found in the ultraviolet spectra of the $[Cr(en)_3](ClO_4)_3$ solution at higher concentrations of ClO_4^-. These results do not always indicate the lack of the $[Cr(en)_3]^{3+}$–ClO_4^-, ion-pair. On the basis of the conclusion from the conductometric investigation that the $[Cr(en)_3]^{3+}$ did also associate with the ClO_4^- added to adjust the ionic strength, the determination of the ion-association constant of $[Cr(en)_3]^{3+}$–ClO_4^- was carried out by the spectrophotometric method on a system containing both Br^- and ClO_4^-.[14]

Under such experimental conditions, the Eq. 2 is rewritten as:

$$\frac{[Br^-]_T}{\varepsilon_{obsd}-\varepsilon_M} = \frac{1}{K'_{c,MBr}(\varepsilon_{MBr}-\varepsilon_M)} + \frac{[Br^-]_T}{\varepsilon_{MBr}-\varepsilon_M} \qquad (4)$$

The apparent ion-association constant of $[Cr(en)_3]^{3+}$–Br^- determined at the given ionic strength, $K'_{c,MBr}$, is

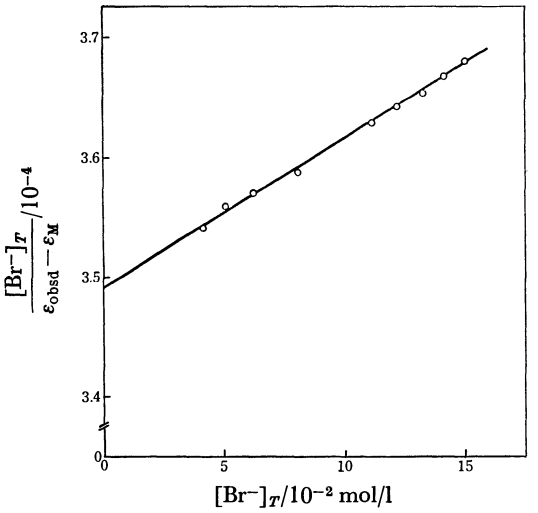

Fig. 5. Plot of the left-hand side of Eq. 4 against the total concentration of bromide ions at I=0.1530 at 230 nm.

given by:

$$K'_{c,MBr} = \frac{K_{c,MBr}}{1+K_{c,MClO_4}\cdot A}\left(1-\frac{K_{c,MClO_4}}{K_{c,MBr}}\right) \qquad (5)$$

where $K_{c,MBr}$ and $K_{c,MClO_4}$ are the concentration ion-association constants of $[Cr(en)_3]^{3+}$–Br^- and $[Cr(en)_3]^{3+}$–ClO_4^-, and where A indicates the values of $[Br^-]_T$ plus $[ClO_4^-]_T$, which was kept constant in this study. The value of $K'_{c,MBr}$ was found to be 3.6 from the analysis of the plot of Eq. 4 shown in Fig. 5. In this case, the activity coefficients of these ions are not a unit; therefore, the thermodynamic ion-association constant, K_{MBr}, determined by the spectrophotometric method was reduced to 6.0 ($K_{c,MBr}$) at the ionic strength of 0.1530. With the $K'_{c,MBr}$, $K_{c,MBr}$ and A values, $K_{c,MClO_4}$ was evaluated to be 1.6 with the aid of Eq. 5. The ion-association constant of $[Cr(en)_3]^{3+}$–ClO_4^- at an infinite dilution was calculated to be 8.0 after correction for the activity coefficients of the ions.

The K value for $[Cr(en)_3]^{3+}$–ClO_4^-, estimated indirectly by the spectrophotometric method, was in relatively good agreement with that of the conductometric method, showing that ClO_4^- acts as a counter anion for the ion-association. From these results, it might be considered that the ion-association constants determined by the conductometric method and the spectrophotometric method are not very different from each other. Similar conclusions were drawn in the case of the previous studies of the $[Cr(en)_3]^{3+}$–I^-, $[Cr(en)_3]^{3+}$–ClO_4^-, $[Cr(NH_3)_6]^{3+}$–I^-, and $[Cr(NH_3)_6]^{3+}$–ClO_4^- ion-pairs. On the basis of the assumption that most cations do not associate with ClO_4^- in aqueous solutions, spectrophotometric studies have been made by many investigators of solutions containing large amounts of sodium perchlorate. However, we found that there was a difference between the values obtained previously by the conductometric and spectrophotometric methods. The difference did not occur when a different method was used. However, it might be caused by the fact that the above assumption is in-

TABLE 6. LOGARITHMIC ASSOCIATION CONSTANTS AT AN INFINITE DILUTION AT 25.0 °C

Ion-pair	log K	Method[a)]	Investigators	Reference
$[Cr(NH_3)_6]^{3+}$–ClO_4^-	1.1_8	cond	Takahashi, Koiso and Tanaka (1974)	10
	1.0_0[c)]	sp	Takahashi, Koiso and Tanaka (1974)	10
$[Co(NH_3)_6]^{3+}$–ClO_4^-	1.4_0	cond	Katayama and Tamamushi (1968)	7
$[Cr(en)_3]^{3+}$–ClO_4^-	1.0_2	cond	Takahashi, Koiso and Tanaka (1974)	10
	1.2_0[c)]	sp	Takahashi, Koiso and Tanaka (1974)	10
	0.9_0[c)]	sp	The present study	
$[Cr(NH_3)_6]^{3+}$–I^-	1.2_9	cond	Takahashi, Koiso and Tanaka (1974)	10
	1.3_4	sp	Takahashi, Koiso and Tanaka (1974)	10
$[Co(NH_3)_6]^{3+}$–I^-	1.3_8	cond	Katayama and Tamamushi (1968)	7
$[Cr(en)_3]^{3+}$–I^-	1.4_2	cond	Takahashi, Koiso and Tanaka (1974)	10
	1.3_3	sp	Takahashi, Koiso and Tanaka (1974)	10
$[Cr(NH_3)_6]^{3+}$–Cl^-	1.3_7	cond	The present study	
$[Co(NH_3)_6]^{3+}$–Cl^-	1.4_9	cond	Jenkins and Monk (1951)	12
	1.5	cond	Tamamushi, Isono and Katayama (1967)	15
$[Cr(en)_3]^{3+}$–Cl^-	1.5_8	cond	The present study	
	1.6_5	sp	The present study	
$[Co(en)_3]^{3+}$–Cl^-	1.7_2	cond	Jenkins and Monk (1951)	12
$[Cr(NH_3)_6]^{3+}$–Br^-	1.5_7	cond	The present study	
$[Co(NH_3)_6]^{3+}$–Br^-	1.6_5	cond	Katayama and Tamamushi (1968)	7
$[Cr(en)_3]^{3+}$–Br^-	1.5_0	cond	The present study	
	1.4_6	sp	The present study	
$[Cr(NH_3)_6]^{3+}$–NO_3^-	1.5_3	cond	The present study	
$[Co(NH_3)_6]^{3+}$–NO_3^-	1.6_3	cond	Katayama and Tamamushi (1968)	7
$[Cr(en)_3]^{3+}$–NO_3^-	1.4_9	cond	The present study	
$[Cr(NH_3)_6]^{3+}$–SO_4^{2-}	3.1_4[b)]	pol	Tanaka, Ogino and Satô (1966)	16
$[Co(NH_3)_6]^{3+}$–SO_4^{2-}	3.2_1[b)]	pol	Tanaka, Ogino and Satô (1966)	16
	3.5_6	cond	Jenkins and Monk (1951)	12
	3.3_0	chron	Tanaka and Yamada (1967)	17
	3.2_6	sp	Tanaka, Kobayashi and Kamada (1967)	6
$[Co(en)_3]^{3+}$–SO_4^{2-}	3.1_0	sp	Tanaka, Kobayashi and Kamada (1967)	6

a) Method of measurement. cond: Conductivity, sp: Spectrophotometry, pol: Polarography, chron: Chronopotentiometry. b) The values calculated from concentration constants obtained at an ionic strength of 0.10. c) These values were determined indirectly.

correct, not by the different working principles of the various methods. The thermodynamic ion-association constants for the corresponding cobalt(III) complex cations with some anions have been determined by various methods and/or by various researchers; they are given in Table 6, together with the results obtained in this study and the previous study. It seems certain that the ion-pairs of the chromium(III) complex cations with some anions are slightly less stable than those of the corresponding cobalt(III) complex cations, even if the inaccuracy in the determination of the ion-association constants is taken into consideration. Table 6 also indicates that the ion-pairs formed between $[Cr(NH_3)_6]^{3+}$ and such a Br^-, ClO_4^-, or NO_3^- are much more stable than those of $[Cr(en)_3]^{3+}$ with their anions, whereas the ion-pairs, $[Cr(NH_3)_6]^{3+}$ with I^- or Cl^- are less stable than those of $[Cr(en)_3]^{3+}$ with their anions.

Since the Stokes' radii of $[Cr(en)_3]^{3+}$ are larger than that of $[Cr(NH_3)_6]^{3+}$, the lower tendency of $[Cr(NH_3)_6]^{3+}$ to associate with I^- or Cl^-, shown by the present and previous studies, seems rather unexpected, in so far as the ion-association is assumed to depend on only a pure electrostatic. The ion-association constants of the corresponding cobalt(III) complex cations with Cl^- or SO_4^{2-} were determined by various methods. Similar results were obtained regardless of the method used. That is, the value of $[Co(en)_3]^{3+}$–Cl^- is somewhat greater than that of $[Co(NH_3)_6]^{3+}$–Cl^-, whereas the value of $[Co(NH_3)_6]^{3+}$–SO_4^{2-} is greater than that of $[Co(en)_3]^{3+}$–SO_4^{2-}. Therefore, it seems appropriate to state that the electrostatic interaction between ions exerts a dominant influence, but also the internal conjugate base (ICB) effect[18] proposed in the complex formation mechanism should be considered in the ion-pair formation.

The authors wish to express their sincere thanks to Professor Nobuyuki Tanaka (Department of Chemistry, Faculty of Science, Tohoku University) for his kind guidance in the course of this work. The authors also wish to thank Mr. Eichi Ôsawa and Mr. Yasuaki Kobayashi for the computer calculations, all of which were performed on an OKITAC-4500 computer using a FORTRAN program.

References

1) N. Bjerrum, *Kgl. Danske Videnskab.*, **7**, No. 9 (1926).
2) R. M. Fuoss, *J. Am. Chem. Soc.*, **80**, 5059 (1958).
3) P. Debye and E. Hückel, *Physik. Z.*, **24**, 185 (1923).
4) H. Yokoyama and H. Yamatera, *Chem. Lett.*, **1973**, 337.
5) S. Katayama, *Bull. Chem. Soc. Jpn.*, **46**, 106 (1973).
6) N. Tanaka, Y. Kobayashi, and M. Kamada, *Bull. Chem. Soc. Jpn.*, **40**, 2839 (1967).
7) S. Katayama and R. Tamamushi, *Bull. Chem. Soc. Jpn.*, **41**, 606 (1968).
8) H. Yokoyama and H. Yamatera, The Proceedings of the 20th Conference on Coordination Chemistry of the Chemical Society of Japan, Tokyo, November, (1970), p. 57.
9) N. Tanaka and H. Kaneko, The Proceedings of the 20th Conference on Coordination Chemistry of the Chemical Society of Japan, Tokyo, November, (1970), p. 61.
10) T. Takahashi, T. Koiso, and N. Tanaka, *Nippon Kagaku Kaishi*, **1974**, 65.
11) L. Onsager, *Physik. Z.*, **28**, 277 (1927).
12) I. L. Jenkins and C. B. Monk, *J. Chem. Soc.*, **1951**, 68.
13) J. Kielland, *J. Am. Chem. Soc.*, **59**, 1675 (1937).
14) N. Tanaka and H. Kaneko, The Proceedings of the 27th Annual Meeting of the Chemical Society of Japan, Nagoya, October, Vol. II (1972), p. 493.
15) R. Tamamushi, T. Isono, and S. Katayama, *Bull. Chem. Soc. Jpn.*, **40**, 334 (1967).
16) N. Tanaka, K. Ogino, and G. Satô, *Bull. Chem. Soc. Jpn.*, **39**, 366 (1966).
17) N. Tanaka and A. Yamada, *Z. Anal. Chem.*, **224**, 117 (1967).
18) D. B. Rorabacher, *Inorg. Chem.*, **5**, 1891 (1966).

The Photochemical Reaction of 1,2-Naphthoquinones with Aldehydes. II.[1] The Photo-addition Reactions of Aliphatic Aldehydes to 1,2-Naphthoquinones

Akio TAKUWA

Department of Chemistry, Faculty of Literature and Science, Shimane University, Matsue 690

(Received January 12, 1976)

3-Acyl-1,2-naphthalenediols and 1,2-naphthalenediol monoacyl esters were obtained from the photochemical reactions of 1,2-naphthoquinones with aliphatic aldehydes. 3-Halogeno-1,2-naphthoquinones gave the corresponding 1,2-naphthalenediol monoacyl esters, 3-acyl-1,2-naphthalenediols, which are the same products as those from the photochemical reactions of 1,2-naphthoquinone with those aldehydes and 3-halogeno-4-acyl-1,2-naphthoquinone when they were irradiated in aldehydes. 3-Methyl-1,2-naphthoquinone, however, gave the corresponding 1,2-naphthalenediol monoacetate and 3-methyl-4-acetyl-1,2-naphthoquinone when it was irradiated in acetaldehyde. These photochemical reactions were applicable for syntheses of 3-acyl-1,2-naphthalenediols and 1,2-naphthalenediol monoacyl esters.

The wide variety of photo-induced reactions among quinones and aldehydes has been examined by several workers.[2] The photochemical reactions of *p*-benzoquinones and 1,4-naphthoquinones with aliphatic or aromatic aldehydes give acyl or aroylquinols (**1**) and quinol monoesters (**2**).

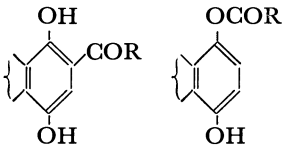

1 **2** **3** R=Alkyl or Aryl

On the other hand, *o*-quinones usually give the corresponding enediol monoesters (**3**) exclusively. For example, tetrachloro-1,2-benzoquinone yields tetrachlorocatechol monoacetate and monobenzoate when it is irradiated in the presence of acetaldehyde and benzaldehyde.[3] 9,10-Phenanthrenequinone reacts in a similar fashion with both aliphatic or aromatic aldehydes.[4] 4-Cyano-1,2-naphthoquinone, however, behaves differently, since with aromatic aldehydes it gives naphthalenediol monoesters, but the products from the reaction with acetaldehyde and propionaldehyde are reported to be the corresponding 1,2-dihydroxy-3-acyl-4-naphthalenecarbonitriles.[5] But no factor leading to monoesters of 1,2-naphthalenediol or to ring-acylated 1,2-naphthalenediols has been discovered yet. Therefore, it is necessary to scrutinize the photochemical reactions of 1,2-naphthoquinones with aliphatic aldehydes. In this work, the photochemical reactions of 1,2-naphthoquinone and its derivatives with a variety of aliphatic aldehydes were examined. It was found that 3-acyl-1,2-naphthalenediols and 1,2-naphthalenediol monoacyl esters were usually obtained with the exception of the cases in which the 3-position of a quinone ring was substituted.

Results and Discussion

The 1,2-naphthoquinones examined in this work are 1,2-naphthoquinone and its 3-chloro-, 3-bromo-, 3-methyl-, 4-cyano-, 6-bromo-, and 6-methyl-derivatives. The aldehydes used are acetaldehyde, propionaldehyde, butyraldehyde, isobutyraldehyde, valeraldehyde, isovaleraldehyde, hexanal, heptanal, octanal nonanal, and decanal.

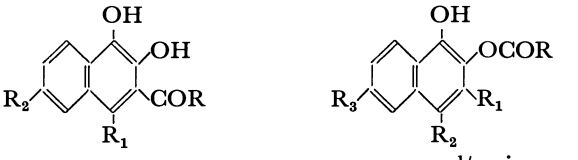

4 R=$CH_3(CH_2)_n$ **5** (n=0—8) and/or isomer

A benzene solution of 1,2-naphthoquinones and an aldehyde was irradiated by means of a 300-W high pressure Hg arc lamp through a 5 cm thick layer of flowing water. The structures of the photo-addition compounds were determined by the following procedures. As a typical example, the photochemical reaction of 1,2-naphthoquinone with acetaldehyde will be illustrated. After the usual work-up of the reaction mixture, orange colored prisms (**4a**: R=CH_3, R_1=R_2=H; 24%) and white crystals (**5a**: R=CH_3, R_1=R_2=R_3=H; 39%) were obtained. The compound, **4a**, has carbonyl (1652 cm^{-1}) and hydroxyl (3400 cm^{-1}) groups, judging from its infrared spectrum. The PMR of **4a** showed signals at δ: 2.76 (s, 3H, $COCH_3$), 5.91 (s, 1H), 7.18—8.08 (m, 5H, aromatic protons), and 11.48 (s, 1H). The signal at δ: 5.91 and 11.48 disappeared after shaking with deuterium oxide, so these two signals could be assigned to the hydroxyl groups. The signal which appears at δ: 11.48 should be assigned to the 2-hydroxyl group, which is intramolecularly hydrogen-bonded to the adjacent carbonyl of the neighboring acetyl group.

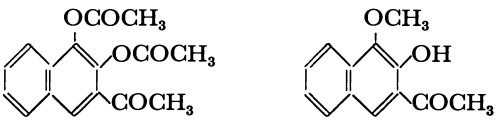

6 **7**

The acetylated or methylated derivatives were confirmed to be **6** and **7** by their IR and PMR analyses. From these results the orange-colored photo-addition compound should have structure **4a**. Such photo-addition compounds are colored yellow to orange. The IR of another white photo-adduct (**5a**) showed absorption bands at 3400 and 1743 cm^{-1}, corresponding to hydroxyl and carbonyl groups respectively. The white crystal was the nearly 1 : 1 mixture of two isomeric esters, since two sorts of methyl proton signals of acetoxyl

groups were observed at δ: 2.42 and 2.52 by PMR analysis.

3-Acyl-1,2-naphthalenediols and 1,2-naphthalenediol monoacyl esters were also obtained from the photochemical reactions of nonsubstituted 1,2-naphthoquinone, 4-cyano-, 6-bromo-, and 6-methyl-derivatives of 1,2-naphthoquinone with aliphatic aldehydes. Awad and Hafez have reported that when a strong electron attracting group such as the cyano group was introduced at position 4 of 1,2-naphthoquinone, 3-acylated 1,2-naphthalenediols were the products in the photochemical reactions with acetaldehyde or propionaldehyde.[6] Since 3-acylated 1,2-naphthalenediols were also obtained from the photochemical reactions of 1,2-naphthoquinone with aliphatic aldehydes, it is of interest to investigate the role of the cyano group in the reaction.

Photochemical reactions of 3-substituted 1,2-naphthoquinones, such as 3-chloro-, 3-bromo-, and 3-methyl-1,2-naphthoquinone, with aliphatic aldehydes were chosen for this purpose. Irradiation of 3-halogeno-1,2-naphthoquinone in acetaldehyde afforded, however, 3-halogeno-1,2-naphthalenediol monoacetates (**5**: R=CH_3, R_1=Cl or Br, R_2=R_3=H, 26%) as the main products, plus paraldehyde (*ca.* 90%) along with a little metaldehyde. The use of benzene as a solvent did not interfere with these photochemical reactions. Polymerization of acetaldehyde suggested that a hydrogen halide had been formed in the reaction system.

In view of these results, a detailed analysis of the minor products in these reactions was required. In fact, 3-acetyl-1,2-naphthalenediol (1—3%), which is the same product as in the photochemical reaction of 1,2-naphthoquinone with acetaldehyde, and 3-halogeno-4-acetyl-1,2-naphthoquinone (2—5%) were isolated. 3-Chloro-4-acetyl-1,2-naphthoquinone was identified by comparison with the authentic sample prepared by the chlorination of 4-acetyl-1,2-naphthoquinone. Analogous products were also obtained from the photochemical reactions of 3-halogeno-1,2-naphthoquinone with other aliphatic aldehydes. Irradiation of a benzene solution of 3-methyl-1,2-naphthoquinone and acetaldehyde gave 3-methyl-1,2-naphthalenediol monoacetate (17.7%) and 3-methyl-4-acetyl-1,2-naphthoquinone (6.6%). It is thought that 3-halogeno-4-acetyl-1,2-naphthalenediols and 3-methyl-4-acetyl-1,2-naphthalenediol converted into the corresponding quinones by oxidation with the original quinone in the reaction system or with air during the separation procedure, since 3-chloro-4-acetyl-1,2-naphthalenediol was easily auto-oxidized into 3-chloro-4-acetyl-1,2-naphthoquinone in silica gel or in benzene solution.

Even after a benzene solution of 1,2-naphthalenediol monoacetate [**5a**; λ_{max} (ε): 329 nm (2310)] was irradiated for 1—3 days, no 3-acetyl-1,2-naphthalenediol (**4a**) was detected by PMR analysis. However, the rearrangement of **5a** to **4a** might be sensitized by 1,2-naphthoquinone. This possibility was checked by irradiating a mixture of 1,2-naphthoquinone and **5a** in benzene, but no **4a** was detected. Therefore, under these conditions the photo-induced Fries rearrangement of **5a** to **4a** is unlikely. The detailed mechanism of the formation of these photo-adducts remains still unestablished, but the results examined so far have been described in this paper as a preliminary report.

Experimental

All melting points were determined on a Yanagimoto Micro-melting Point apparatus and are uncorrected. Yields were based on the amount of quinones used. PMR spectra were taken with a JEOL MH-100 spectrometer in CCl_4 or $CDCl_3$ solution using TMS as the internal standard. The coupling constants were 7.0—8.0 Hz in all compounds. Infrared spectra were obtained on a Hitachi 215 spectrometer, using a KBr disc. Ultraviolet spectra were recorded by means of a Hitachi 124 spectrophotometer.

Materials. 1,2-naphthoquinone (mp 121—122 °C) was prepared by the oxidation of 1-amino-2-naphthol hydrochloride with iron(III) chloride.[7] 3-Chloro (mp 171 °C)[8] and 3-bromo-1,2-naphthoquinone (mp 164 °C)[9] were prepared by chlorination or bromination of 1,2-naphthoquinone. 3-Methyl-1,2-naphthoquinone (mp 120 °C) was prepared by the oxidation of 3-methyl-α-tetralone with selenium dioxide.[10] 4-Cyano-1,2-naphthoquinone (mp 175—176 °C) was prepared by the oxidation of 1-amino-2-hydroxy-4-cyanonaphthalene with chromium trioxide.[11] 6-Bromo-1,2-naphthoquinone (mp 156 °C) was prepared by the oxidation of 6-bromo-2-naphthol with Fremy's salt.[12] 6-Methyl-1,2-naphthoquinone (mp 126—127 °C) was prepared by the oxidation of 6-methyl-2-naphthol with Fremy's salt at 15 °C.[14] All commercially available aldehydes were further purified by distillation under nitrogen.

General Procedures. A typical photochemical reaction was performed as follows: 1,2-naphthoquinone derivatives (200 mg, 0.84—1.27 mmol) and aldehydes (500 mg, 3—11 mmol) were dissolved in 25 ml of benzene, and the solution was irradiated from outside in an ordinary tube by a 300 W high-pressure mercury arc lamp through a 5 cm thick layer of flowing water at 15—20 °C. After 2—10 days, the characteristic color of 1,2-naphthoquinones faded to yellow. Benzene was removed under reduced pressure, and then the residue was chromatographed on silica gel, using benzene as the eluting solvent. Appropriate fractions were collected and concentrated and then light petroleum was added; these gave photo-adducts. The photo-adducts were further purified by recrystallization from benzene or benzene-light petroleum or by a florisil column.

Photo-addition Products of 1,2-Naphthoquinone with Aliphatic Aldehyde. (i) Acetaldehyde: 3-Acetyl-1,2-naphthalenediol [**4a**: R=CH_3, R_1=R_2=H]: orange prisms (60 mg, 24%), mp 135—136 °C. IR: ν_{OH} 3440; $\nu_{C=O}$ 1652 cm^{-1}. PMR (CCl_4), δ: 2.76 (s, 3H, CH_3), 5.91 (s, 1H, OH, removed by D_2O), 7.17—8.08 (m, 5H, aromatic-H), 11.48 (s, 1H, OH, removed by D_2O). UV($CHCl_3$): λ_{max} (ε), 409 (7330), 300(21500), 263(38500). Found: C, 71.07; H, 4.49%. Calcd for $C_{13}H_{10}O_3$: C, 71.28; H, 4.98%. Treatment with acetic anhydride afforded 3-acetyl-1,2-naphthalenediol diacetate (**6**): pale yellow crystals from ethanol, mp 155–157 °C. IR: $\nu_{C=O}$ 1770, 1687 cm^{-1}. PMR($CDCl_3$), δ: 2.37(s, 3H, $OCOCH_3$), 2.46 (s, 3H, $OCOCH_3$), 2.67(s, 3H, $COCH_3$), 7.28—8.18 (m, 5H, aromatic-H). Treatment with dimethylsulfate in aqueous sodium hydroxide afforded 1-methoxy-2-hydroxy-3-acetylnaphthalene (**7**): yellow crystals, mp 80—81 °C. IR: ν_{OH} 3420; $\nu_{C=O}$ 1655 cm^{-1}. PMR(CCl_4), δ: 2.78(s, 3H, $COCH_3$), 4.06(s, 3H, OCH_3), 7.16—8.05 (m, 5H, aromatic-H), 11.42(s, 1H, OH, removed by D_2O). 1,2-Naphthalenediol monoacetate [**5a**: R=CH_3, R_1=R_2=R_3=H]: white crystals (100 mg, 39%), mp 136—138 °C. IR: ν_{OH} 3400; $\nu_{C=O}$ 1740 cm^{-1}. PMR($CDCl_3$), δ: 2.40(s, 3H, CH_3),

2.52(s, 3H, CH_3), 7.13—7.88(m, 14H, aromatic-H+OH). UV($CHCl_3$): $\lambda_{max}(\varepsilon)$, 329(2310), 288(4960), 278 nm (6090). Found: C, 70.98; H, 4.76%. Calcd for $C_{12}H_{10}O_3$: C, 71.28; H, 4.98%. Treatment with acetic anhydride afforded 1,2-naphthalenediol diacetate: white crystals, mp 108—111 °C. It was identified (mixed melting point, IR and PMR spectra) by comparison with an authentic sample.

(ii) Propionaldehyde: 3-Propionyl-1,2-naphthalenediol [**4**: $R=CH_3CH_2$, $R_1=R_2=H$]: orange yellow prisms (51mg,19%), mp 129—130.5 °C. IR: ν_{OH} 3455; $\nu_{C=O}$ 1660 cm^{-1}. PMR (CCl_4), δ: 1.32 (t, 3H, CH_3), 3.20 (q, 2H, CH_2), 5.93 (s, 1H, OH, removed by D_2O), 7.16—8.11 (m, 5H, aromatic-H), 11.57 (s, 1H, OH, removed by D_2O). Found: C, 72.36; H, 5.62%. Calcd for $C_{13}H_{12}O_3$: C, 72.21; H, 5.59%. 1,2-Naphthalenediol monopropionate [**5**: $R=CH_3CH_2$, $R_1=R_2=R_3=H$]: white crystals (38 mg, 14%), mp 105—106 °C. IR: ν_{OH} 3440; $\nu_{C=O}$ 1750 cm^{-1}. PMR($CDCl_3$), δ: 1.32 (t, 3H, CH_3), 1.42 (t, 3H, CH_3), 2.72(q, 2H, CH_2), 2.84 (q, 2H, CH_2), 7.10—7.83(m, 14H, aromatic-H+OH). Found: C, 72.15; H, 5.80%. Calcd for $C_{13}H_{12}O_3$: C, 72.21; H, 5.59%.

(iii) Butyraldehyde: 3-Butyryl-1,2-naphthalenediol [**4**: $R=CH_3(CH_2)_2$, $R_1=R_2=H$]: orange prisms (59 mg, 20%), mp 98.0—99.5 °C. IR: ν_{OH} 3455; ν_{CH} 2980; $\nu_{C=O}$ 1655 cm^{-1}. PMR(CCl_4), δ: 1.06(t, 3H, CH_3), 1.82(sex, 2H, CH_2), 3.06 (t, 2H, $COCH_2$), 5.84 (s, 1H, OH), 7.06—7.98(m, 5H, aromatic-H), 11.45(s, 1H, OH). Found: C, 72.94; H, 6.02%. Calcd for $C_{14}H_{14}O_3$: C, 73.03; H, 6.13%. 1,2-Naphthalenediol monobutyrate [**5**: $R=CH_3(CH_2)_2$, $R_1=R_2=R_3=H$]: white crystals (21 mg, 7%), mp 77—78 °C. IR: ν_{OH} 3320; ν_{CH} 2980; $\nu_{C=O}$ 1725 cm^{-1}. PMR($CDCl_3$), δ: 1.08 (t, 3H, CH_3), 1.88 (sex, 2H, CH_2), 2.64 (t, 2H, $COCH_2$), 7.08—8.10 (m, 7H, aromatic-H+OH). Found: C, 73.58; H, 6.35%. Calcd for $C_{14}H_{14}O_3$: C, 73.03; H, 6.13%.

(iv) Isobutyraldehyde: 3-Isobutyryl-1,2-naphthalenediol [**4**: $R=(CH_3)_2CH$, $R_1=R_2=H$]: yellow crystals (15 mg, 5%), mp 105—107 °C. IR: ν_{OH} 3500; ν_{CH} 2985, 2950; $\nu_{C=O}$ 1655 cm^{-1}. PMR (CCl_4), δ: 1.30 (d, 6H, $(CH_3)_2$), 3.77 (sep, 1H, CH), 5.97(s, 1H, OH), 7.12—8.12 (m, 5H, aromatic-H), 11.80 (s, 1H, OH). Found: C, 72.81; H, 6.21%. Calcd for $C_{14}H_{14}O_3$: C, 73.03; H, 6.13%. 1,2-Naphthalenediol monoisobutyrate [**5**: $R=(CH_3)_2CH$, $R_1=R_2=R_3=H$]: white crystals (80 mg, 27.5%), mp 73—74 °C. IR: ν_{OH} 3350 (br), ν_{CH} 2955; $\nu_{C=O}$ 1742, 1725 cm^{-1}. PMR($CDCl_3$), δ: 1.37(d, 6H, $(CH_3)_2$), 1.46(d, 6H, $(CH_3)_2$), 2.78 (sep, 1H, CH), 3.00(sep, 1H, CH), 7.13—8.30 (m, 14H, aromatic-H+OH). Found: C, 72.83; H, 5.96%. Calcd for $C_{14}H_{14}O_3$: C, 73.03; H, 6.13%.

(v) Valeraldehyde: 3-Valeryl-1,2-naphthalenediol (**4**: $R=CH_3(CH_2)_3$, $R_1=R_2=H$]: orange yellow prisms (25 mg, 8.1%), mp 131—132 °C. IR: ν_{OH} 3455; ν_{CH} 2970; $\nu_{C=O}$ 1645 cm^{-1}. PMR(CCl_4), δ: 0.98 (t, 3H, CH_3), 1.24—1.88(m, 4H, $(CH_2)_2$), 3.05 (t, 2H, $COCH_2$), 5.92 (s, 1H, OH), 7.13—8.05 (m, 5H, aromatic-H), 11.44(s, 1H, OH). Found: C, 73.53; H, 6.71%. Calcd for $C_{15}H_{16}O_3$: C, 73.75; H, 6.60%. 1,2-Naphthalenediol monovalerate [**5**: $R=CH_3(CH_2)_3$, $R_1=R_2=R_3=H$]: white crystals (48 mg, 15.5%), mp 68.5—71.0 °C. IR: ν_{OH} 3410; ν_{CH} 2960, 2940; $\nu_{C=O}$ 1735 cm^{-1}. PMR (CCl_4), δ: 0.98 (t, 3H, CH_3), 1.29—1.94 (m, 4H, $(CH_2)_2$), 2.47 (t, 2H, $COCH_2$), 6.17(1H, OH, broad), 6.87—7.67 (m, 6H, aromatic-H). Found: C, 74.00; H, 6.48%. Calcd for $C_{15}H_{16}O_3$: C, 73.75; H, 6.60%.

(vi) Isovaleraldehyde: 3-Isovaleryl-1,2-naphthalenediol [**4**: $R=(CH_3)_2CHCH_2$, $R_1=R_2=H$]: orange yellow oil (23 mg, 8%). PMR(CCl_4), δ: 1.00(d, 6H, $(CH_3)_2$), 2.30(m, 1H, CH), 2.89(d, 2H, $COCH_2$), 5.85 (s, 1H, OH), 7.08—8.05 (m, 5H, aromatic-H), 11.67 (s, 1H, OH). 1,2-Naphthalenediol monoisovalerate [**5**: $R=(CH_3)_2CHCH_2$, $R_1=R_2=R_3=H$]:white crystals (50 mg, 16%), mp 79.0—81.5 °C. IR: ν_{OH} 3420; ν_{CH} 2960, 2940, 2875; $\nu_{C=O}$ 1735, 1725 cm^{-1}. PMR (CCl_4), δ: 1.05 (d, 6H, $(CH_3)_2$), 1.09 (d, 6H, $(CH_3)_2$), 2.10—2.45(m, 2H, CH), 2.42(d, 2H, $COCH_2$), 2.56(d, 2H, $COCH_2$), 6.06(OH, 2H, broad), 6.90—8.18(m, 10H, aromatic-H). Found: C, 73.28; H, 6.81%. Calcd for $C_{15}H_{16}O_3$: C, 73.75; H, 6.60%.

(vii) Hexanal: 3-Hexanoyl-1,2-naphthalenediol [**4**: $R=CH_3(CH_2)_4$, $R_1=R_2=H$]: orange yellow prisms (40 mg, 12.3%), mp 119—120 °C. IR: ν_{OH} 3450; ν_{CH} 2935, 2870; $\nu_{C=O}$ 1645 cm^{-1}. PMR ($CDCl_3$), δ: 0.80—1.95 (m, 9H, CH_3-$(CH_2)_3$), 3.07 (t, 2H, $COCH_2$), 5.97 (s, 1H, OH), 7.20—8.02 (m, 5H, aromatic-H), 11.60 (s, 1H, OH). Found: C, 74.31; H, 6.95%. Calcd for $C_{16}H_{18}O_3$: C, 74.40; H, 7.02%. 1,2-Naphthalenediol monohexanoate [**5**: $R=CH_3(CH_2)_4$, $R_1=R_2=R_3=H$]: white crystals (40 mg, 12.3%), mp 79.0—81.5 °C. IR: ν_{OH} 3410; ν_{CH} 2960, 2935, 2870; $\nu_{C=O}$ 1735 cm^{-1}. PMR($CDCl_3$), δ: 0.83—1.90 (m, 18H, $CH_3(CH_2)_3$), 2.57 (t, 2H, $COCH_2$), 2.70(t, 2H, $COCH_2$), 6.90—7.70 (m, 12H, aromatic-H+OH). Found; C, 74.56; H, 7.20%. Calcd for $C_{16}H_{18}O_3$: C, 74.40; H, 7.02%.

(viii) Heptanal: 3-Heptanoyl-1,2-naphthalenediol [**4**: $R=CH_3(CH_2)_5$, $R_1=R_2=H$]: yellow plates (35 mg, 10.2%), mp 105—106 °C. IR: ν_{OH} 3470; ν_{CH} 2975, 2945, 2855; $\nu_{C=O}$ 1645 cm^{-1}. PMR(CCl_4), δ: 0.92 (t, 3H, CH_3), 1.23—1.90 (m, 8H, $(CH_2)_4$), 3.04(t, 2H, $COCH_2$), 5.95 (s, 1H, OH), 7.13—8.07 (m, 5H, aromatic-H), 11.65 (s, 1H, OH). Found: C, 74.77; H, 7.30%. Calcd for $C_{17}H_{20}O_3$: C, 74.97; H, 7.40%. 1,2-Naphthalenediol monoheptanoate [**5**: $R=CH_3$-$(CH_2)_5$, $R_1=R_2=R_3=H$]: white needles (65 mg, 19%), mp 59 °C. IR: ν_{OH} 3460; ν_{CH} 2950, 2870; $\nu_{C=O}$ 1760, 1740 cm^{-1}. PMR(CCl_4), δ: 0.80—1.96 (m, 22H, $CH_3(CH_2)_4$), 2.64 (t, 2H, $COCH_2$), 2.76 (t, 2H, $COCH_2$), 7.12—8.32 (m, 14H, aromatic-H+OH). Found: C, 75.15; H, 7.47%. Calcd for $C_{17}H_{20}O_3$: C, 74.97; H, 7.40%.

(ix) Octanal: 3-Octanoyl-1,2-naphthalenediol [**4**: $R=CH_3$-$(CH_2)_6$, $R_1=R_2=H$]: orange prisms (40 mg, 14%), mp 98—99 °C. IR: ν_{OH} 3460; ν_{CH} 2945, 2872; $\nu_{C=O}$ 1650 cm^{-1}. PMR(CCl_4), δ: 0.90 (t, 3H, CH_3), 1.22—1.89 (m, 10H, $(CH_2)_5$), 3.05(t, 2H, $COCH_2$), 5.98 (s, 1H, OH), 7.11—8.04 (m, 5H, aromatic-H), 11.72(s, 1H, OH). Found: C, 75.32; H, 7.64%. Calcd for $C_{18}H_{22}O_3$: C, 75.50; H, 7.74%. 1,2-Naphthalenediol monooctanoate [**5**: $R=CH_3(CH_2)_6$, $R_1=R_2=R_3=H$]: white plates (75 mg, 26.2%), mp 53—54 °C. IR: ν_{OH} 3340; ν_{CH} 2920, 2855; $\nu_{C=O}$ 1755, 1735 cm^{-1}. PMR (CCl_4), δ: 0.82—1.82 (m, 26H, $CH_3(CH_2)_5$), 2.50 (t, 2H, $COCH_2$), 2.62 (t, 2H, $COCH_2$), 6.12 (2H, OH), 6.98—8.16 (m, 12H, aromatic-H). Found: C, 75.66; H, 7.70%. Calcd for $C_{18}H_{22}O_3$: C, 75.50; H, 7.74%.

(x) Nonanal: 3-Nonanoyl-1,2-naphthalenediol [**4**: $R=CH_3(CH_2)_7$, $R_1=R_2=H$]: yellowish orange prisms (38 mg, 10%), mp 99—100 °C. IR: ν_{OH} 3475; ν_{CH} 2975, 2945, 2855; $\nu_{C=O}$ 1647 cm^{-1}. PMR(CCl_4), δ: 0.87 (t, 3H, CH_3), 1.18—1.90 (m, 12H, $(CH_2)_6$), 3.06 (t, 2H, $COCH_2$), 5.91 (s, 1H, OH), 7.14—8.07 (m, 5H, aromatic-H), 11.64 (s, 1H, OH). Found: C, 75.63; H, 7.81%. Calcd for $C_{19}H_{24}O_3$: C, 75.97; H, 8.05%. 1,2-Naphthalenediol monononanoate [**5**: $R=CH_3(CH_2)_7$, $R_1=R_2=R_3=H$]: white needles (62 mg, 16.4 %), mp 62.5—63.5 °C. IR: ν_{OH} 3400, ν_{CH} 2935, 2863; $\nu_{C=O}$ 1730 cm^{-1}. PMR (CCl_4), δ: 0.80—1.90 (m, 15H, CH_3-$(CH_2)_6$), 2.77 (t, 2H, $COCH_2$), 7.12—7.84 (m, 7H, aromatic-H +OH). Found: C, 76.08; H, 7.94%. Calcd for $C_{19}H_{24}O_3$: C, 75.97; H, 8.05%.

(xi) Decanal: 3-Decanoyl-1,2-naphthalenediol [**4**: $R=CH_3(CH_2)_8$, $R_1=R_2=H$]: orange prisms (34 mg, 8.6 %), mp 88—89 °C. IR: ν_{OH} 3465; ν_{CH} 2945, 2857; $\nu_{C=O}$ 1648 cm^{-1}.

PMR(CCl_4), δ: 0.87 (t, 3H, CH_3), 1.15—1.89 (m, 14H, $(CH_2)_7$), 5.90 (s, 1H, OH), 7.14—8.06 (m, 5H, aromatic-H), 11.64 (s, 1H, OH). Found: C, 76.37; H, 8.27%. Calcd for $C_{20}H_{26}O_3$: C, 76.40; H, 8.33%. 1,2-Naphthalenediol monodecanoate [**5**: $R=CH_3(CH_2)_8$, $R_1=R_2=R_3=H$]: white needles (61 mg, 15.4%), mp 67—68 °C. IR: ν_{OH} 3385; ν_{CH} 2935, 2860; $\nu_{C=O}$ 1729 cm^{-1}. PMR (CCl_4), δ: 0.86—1.82 (m, 17H, $CH_3(CH_2)_7$), 2.85 (t, 2H, $COCH_2$), 7.08—7.80 (m, 7H, aromatic-H+OH). Found: C, 76.67; H, 8.42%. Calcd for $C_{20}H_{26}O_3$: C, 76.40; H. 8.33%.

Photo-addition Compounds of 4-Cyano-1,2-naphthoquinone with Aliphatic Aldehyde. *(i) Acetaldehyde*: 1,2-Dihydroxy-3-acetyl-4-naphthalenecarbonitrile [**4**: $R=CH_3$, $R_1=CN$, $R_2=H$]: orange yellow needles (56 mg, 22.5%), mp 213—217 °C. IR: ν_{OH} 3435; ν_{CN} 2225; $\nu_{C=O}$ 1640 cm^{-1}. PMR ($CDCl_3$), δ: 3.17 (s, 3H, CH_3), 6.73 (s, 1H, OH, removed by D_2O), 7.52—7.77, 8.10—8.52 (m, 4H, aromatic-H), 12.03 (s, 1H, OH, removed by D_2O). Found: C, 69.04; H, 3.99; N, 5.98%. Calcd for $C_{13}H_9NO_3$: C, 68.72; H, 3.99; N, 6.16%. Treatment with acetic anhydride afforded 1,2-diacetoxy-3-acetyl-4-naphthalenecarbonitrile; white needles from alcohol, mp 159—160 °C. IR: ν_{CN} 2240; $\nu_{C=O}$ 1780, 1700 cm^{-1}. PMR($CDCl_3$), δ: 2.33 (s, 3H, $OCOCH_3$), 2.50 (s, 3H, $OCOCH_3$), 2.78 (s, 3H, $COCH_3$), 7.66—8.00, 8.25—8.39 (m, 4H, aromatic-H). 1,2-Dihydroxy-4-naphthalenecarbonitrile monoacetate [**5**: $R=CH_3$, $R_1=R_3=H$, $R_2=CN$]: white needles (29 mg, 11.6 %), mp 172—174 °C. IR: ν_{OH} 3375; ν_{CN} 2235; $\nu_{C=O}$ 1745 cm^{-1}. PMR($CDCl_3$), δ: 2.46 (s, 3H, CH_3), 7.56—7.87, 8.08—8.50 (m, 5H, aromatic-H+OH). Found: C, 68.86; H, 3.89; N, 6.20%. Calcd for $C_{13}H_9NO_3$: C, 68.72; H, 3.99; N, 6.16%. The acetylate compound was identical with authentic 1,2-diacetoxy-4-naphthalenecarbonitrile (mixed melting point, IR and PMR).

(ii) Propionaldehyde: 1,2-Dihydroxy-3-propionyl-4-naphthalenecarbonitrile [**4**: $R=CH_3CH_2$, $R_1=CN$, $R_2=H$]: orange plates (131 mg, 49.5%), mp 171—174 °C. IR: ν_{OH} 3310; ν_{CN} 2220; $\nu_{C=O}$ 1640 cm^{-1}. PMR ($CDCl_3$), δ: 1.34 (t, 3H, CH_3), 3.57 (q, 2H, CH_2), 6.68 (s, 1H, OH), 7.46—7.60, 8.02—8.28 (m, 4H, aromatic-H), 11.90 (s, 1H, OH). Found: C, 69.64; H, 4.52; N, 5.86%. Calcd for $C_{14}H_{11}NO_3$: C, 69.70; H, 4.60; N, 5.81%. 1,2-Dihydroxy-4-naphthalenecarbonitrile monopropionate [**5**: $R=CH_3CH_2$, $R_1=R_3=H$, $R_2=CN$]: white needles (29 mg, 11%), mp 135—136 °C. IR ν_{OH} 3455; ν_{CN} 2230; $\nu_{C=O}$ 1740 cm^{-1}. PMR ($CDCl_3$), δ: 1.34 (t, 3H, CH_3), 2.75 (q, 2H, CH_2), 7.46—7.68, 8.00—8.30 (m, 6H, aromatic-H+OH). Found: C, 69.53; H, 4.67; N, 5.74%. Calcd for $C_{14}H_{11}NO_3$: C, 69.70; H, 4.60; N, 5.81%.

(iii) Butyraldehyde: 1,2-Dihydroxy-3-butyryl-4-naphthalenecarbonitrile [**4**: $R=CH_3(CH_2)_2$, $R_1=CN$, $R_2=H$]: orange plates (81 mg, 29%), mp 138.5—140 °C. IR: ν_{OH} 3300; ν_{CH} 2965, 2840; ν_{CN} 2230; $\nu_{C=O}$ 1640 cm^{-1}. PMR($CDCl_3$), δ: 1.07 (t, 3H, CH_3), 1.87(sex, 2H, CH_2), 3.50 (t, 2H, $COCH_2$), 6.74 (s, 1H, OH), 7.47—7.68, 8.12—8.34 (m, 4H, aromatic-H), 12.05(s, 1H, OH). Found: C, 70.50; H, 5.21; N, 5.44%. Calcd for $C_{15}H_{13}NO_3$: C, 70.58; H, 5.13; N, 5.49%. 1,2-Dihydroxy-4-naphthalenecarbonitrile monobutyrate [**5**: $R=CH_3(CH_2)_2$, $R_1=R_3=H$, $R_2=CN$]: colorless needles (8 mg, 3%), mp 110—111 °C. IR: ν_{OH} 3320; ν_{CN} 2220; $\nu_{C=O}$ 1738 cm^{-1}. PMR($CDCl_3$), δ: 1.07 (t, 3H, CH_3), 1.83 (sex, 2H, CH_2), 2.66 (t, 2H, $COCH_2$), 7.56—7.84, 8.06—8.44 (m, 6H, aromatic-H+OH). Found: C, 70.49; H, 5.06; N, 5.37%. Calcd for $C_{15}H_{13}NO_3$: C, 70.58; H, 5.13; N, 5.49%.

(iv) Isobutyraldehyde: 1,2-Dihydroxy-3-isobutyryl-4-naphthalenecarbonitrile [**4**: $R=(CH_3)_2CH$, $R_1=CN$, $R_2=H$]: orange plates (90 mg, 32%), mp 147—149 °C. IR: ν_{OH} 3330; ν_{CH} 2980, 2940; ν_{CN} 2220; $\nu_{C=O}$ 1640 cm^{-1}. PMR($CDCl_3$), δ: 1.34(d, 6H, $(CH_3)_2$), 4.42(sep, 1H, CH), 6.77(s, 1H, OH), 7.50—7.73, 8.15—8.40(m, 4H, aromatic-H), 11.45(s, 1H, OH). Found: C, 70.65; H, 5.10; N, 5.45%. Calcd for $C_{15}H_{13}NO_3$: C, 70.58; H, 5.13; N, 5.49%. 1,2-Dihydroxy-4-naphthalenecarbonitrile monoisobutyrate [**5**: $R=(CH_3)_2CH$, $R_1=R_3=H$, $R_2=CN$]: colorless crystals (15 mg, 5.4%), mp 126.5—127 °C. IR: ν_{OH} 3245; ν_{CH} 2990, 2950; ν_{CN} 2235; $\nu_{C=O}$ 1765 cm^{-1}. PMR($CDCl_3$), δ: 1.30 (d, 6H, $(CH_3)_2$), 2.97(sep, 1H, CH), 7.55—7.80, 8.09—8.40(m, 6H, aromatic-H+OH). Found: C, 70.44; H, 5.19; N, 5.53%. Calcd for $C_{15}H_{13}NO_3$: C, 70.58; H, 5.13; N, 5.49%.

(v) Valeraldehyde: 1,2-Dihydroxy-3-valeryl-4-naphthalenecarbonitrile [**4**: $R=CH_3(CH_2)_3$, $R_1=CN$, $R_2=H$]: orange plates (91 mg, 31%), mp 112.5—113.0 °C. IR: ν_{OH} 3340; ν_{CH} 2964, 2940, 2880; ν_{CN} 2220; $\nu_{C=O}$ 1638 cm^{-1}. PMR($CDCl_3$), δ: 0.98 (t, 3H, CH_3), 1.30—1.95 (m, 4H, $(CH_2)_2$), 3.50 (t, 2H, $COCH_2$), 6.80 (s, 1H, OH), 7.46—7.65, 8.04—8.20 (m, 4H, aromatic-H), 11.97(s, 1H, OH). Found: C, 71.24; H, 5.69; N, 5.13%. Calcd for $C_{16}H_{15}NO_3$: C, 71.36; H, 5.61; N, 5.20%. 1,2-Dihydroxy-4-naphthalenecarbonitrile monovalerate [**5**: $R=CH_3(CH_2)_3$, $R_1=R_3=H$, $R_2=CN$]: white needles (22 mg, 7.4%), mp 118—119 °C. IR: ν_{OH} 3275; ν_{CH} 2960, 2940, 2880; ν_{CN} 2235; $\nu_{C=O}$ 1753 cm^{-1}. PMR(CCl_4), δ: 0.98(t, 3H, CH_3), 1.27—1.90 (m, 4H, $(CH_2)_2$), 2.63 (t, 2H, $COCH_2$), 6.81 (s, 1H, OH), 7.40—8.25 (m, 5H, aromatic-H). Found: C, 71.40; H, 5.55; N, 5.26%. Calcd for $C_{16}H_{15}NO_3$: C, 71.36; H, 5.61; N, 5.20%.

(vi) Hexanal: 1,2-Dihydroxy-3-hexanoyl-4-naphthalenecarbonitrile [**4**: $R=CH_3(CH_2)_4$, $R_1=CN$, $R_2=H$]: orange plates (87 mg, 28%), mp 129.5—130.0 °C. IR: ν_{OH} 3300; ν_{CH} 2960, 2940, 2865; ν_{CN} 2220; $\nu_{C=O}$ 1640 cm^{-1}. PMR ($CDCl_3$), δ: 0.92 (t, 3H, CH_3), 1.35—1.88 (m, 6H, $(CH_2)_3$), 3.47 (t, 2H, $COCH_2$), 6.65 (s, 1H, OH), 7.13—8.18 (m, 4H, aromatic-H), 11.83 (s, 1H, OH). Found: C, 71.88; H, 6.10; N, 4.97%. Calcd for $C_{17}H_{17}NO_3$: C, 72.07; H, 6.05; N, 4.94%. 1,2-Dihydroxy-4-naphthalenecarbonitrile monohexanoate [**5**: $R=CH_3(CH_2)_4$, $R_1=R_3=H$, $R_2=CN$]: white needles (15 mg, 5.3%), mp 105.5—106.5 °C. IR: ν_{OH} 3275; ν_{CH} 2960, 2930, 2860; ν_{CN} 2220; $\nu_{C=O}$ 1760 cm^{-1}. PMR(CCl_4), δ: 0.94 (t, 3H, CH_3), 1.31—1.85 (m, 6H, $(CH_2)_3$), 2.61 (t, 2H, $COCH_2$), 6.85 (s, 1H, OH), 7.46—8.25 (m, 5H, aromatic-H). Found: C, 72.33; H, 6.18; N, 4.79%. Calcd for $C_{17}H_{17}NO_3$: C, 72.07; H, 6.05; N, 4.94%.

(vii) Heptanal: 1,2-Dihydroxy-3-heptanoyl-4-naphthalenecarbonitrile [**4**: $R=CH_3(CH_2)_5$, $R_1=CN$, $R_2=H$]: orange plates (94 mg, 28.8%), mp 108—109 °C. IR: ν_{OH} 3300; ν_{CH} 2960, 2930, 2860; ν_{CN} 2220; $\nu_{C=O}$ 1640 cm^{-1}. PMR ($CDCl_3$), δ: 0.90 (t, 3H, CH_3), 1.24—1.94 (m, 8H, $(CH_2)_4$), 3.45 (t, 2H, $COCH_2$), 6.60(s, 1H, OH), 7.17—8.12 (m, 4H, aromatic-H), 11.71(s, 1H, OH). Found: C, 72.65; H, 6.56; N, 4.67%. Calcd for $C_{18}H_{19}NO_3$: C, 72.71; H, 6.44; N, 4.71%. 1,2-Dihydroxy-4-naphthalenecarbonitrile monoheptanoate [**5**: $R=CH_3(CH_2)_5$, $R_1=R_3=H$, $R_2=CN$]: white needles (15 mg, 4.6%), mp 91—92 °C. IR: ν_{OH} 3290; ν_{CH} 2960, 2935, 2867; ν_{CN} 2235; $\nu_{C=O}$ 1765 cm^{-1}. PMR (CCl_4), δ: 0.90—1.90 (m, 11H, $CH_3(CH_2)_4$), 2.61 (t, 2H, $COCH_2$), 6.82(1H, OH), 7.46—8.25 (m, 5H, aromatic-H). Found: C, 72.29; H, 6.33; N. 4.72%. Calcd for $C_{18}H_{19}NO_3$: C, 72.71; H, 6.44; N, 4.71%.

(viii) Octanal: 1,2-Dihydroxy-3-octanoyl-4-naphthalenecarbonitrile [**4**: $R=CH_3(CH_2)_6$, $R_1=CN$, $R_2=H$]: orange plates (98 mg, 28.7%), mp 112.0—112.5 °C. IR: ν_{OH} 3315; ν_{CH} 2955, 2940, 2860; ν_{CN} 2215; $\nu_{C=O}$ 1640 cm^{-1}. PMR(CCl_4), δ: 0.86 (t, 3H, CH_3), 1.25—1.90 (m, 10H, $(CH_2)_5$), 3.42 (t, 2H, $COCH_2$), 6.46 (s, 1H, OH), 7.30—

propionate [**5**: R=CH_3CH_2, R_1=Cl, R_2=R_3=H]: white needles (75 mg, 28.9 %), mp 107—108 °C. IR: ν_{OH} 3300; $\nu_{C=O}$ 1740 cm^{-1}. PMR($CDCl_3$), δ: 1.36 (t, 3H, CH_3), 2.77 (q, 2H, CH_2), 7.33—8.22 (m, 6H, aromatic-H). Found: C, 62.37; H, 4.46%. Calcd for $C_{13}H_{11}ClO_3$: C, 62.29; H, 4.42%. 3-Propionyl-1,2-naphthalenediol (8 mg, 3.6%) was identical (IR spectrum) with the photo-adduct of 1,2-naphthoquinone and propionaldehyde.

(iii) Butyraldehyde: 3-Chloro-1,2-naphthalenediol monobutyrate [**5**: R=$CH_3(CH_2)_2$, R_1=Cl R_2=R_3=H): white needles (70 mg, 24.4%), mp 116.5—118 °C. IR: ν_{OH} 3360; ν_{CH} 2960, 2930, 2880; $\nu_{C=O}$ 1735 cm^{-1}. PMR ($CDCl_3$), δ: 1.10 (t, 3H, CH_3), 1.14 (t, 3H, CH_3), 1.88 (sex, 2H, CH_2), 1.92 (sex, 2H, CH_2), 2.75 (t, 2H, $COCH_2$), 2.79 (t, 2H, $COCH_2$), 7.29—8.15 (m, 12H, aromatic-H). Found: C, 63.54; H, 4.88%. Calcd for $C_{14}H_{13}ClO_3$: C, 63.52; H, 4.95%. 3-Butyryl-1,2-naphthalenediol (11.5 mg, 4.6%) was identical (IR and PMR spectra) with the photo-adduct of 1,2-naphthoquinone and butyraldehyde.

(iv) Isobutyraldehyde: 3-Chloro-1,2-naphthalenediol monoisobutyrate [**5**: R=$(CH_3)_2CH$, R_1=Cl, R_2=R_3=H]: white needles (92 mg, 33.5%), mp 116.0—117.5 °C. IR: ν_{OH} 3405; ν_{CH} 2990, 2940; $\nu_{C=O}$ 1735 cm^{-1}. PMR ($CDCl_3$), δ: 1.42 (d, 6H, $(CH_3)_2$), 1.46 (d, 6H, $(CH_3)_2$), 3.02 (sep, 1H, CH), 3.06 (sep, 1H, CH), 5.72 (1H, OH), 5.84 (1H, OH), 7.01—8.23 (m, 10H, aromatic-H). Found: C, 63.33; H, 4.99%. Calcd for $C_{14}H_{13}ClO_3$: C, 63.52; H, 4.95%. 3-Isobutyryl-1,2-naphthalenediol (15 mg, 5.9%) was identical (IR and PMR spectra) with the photo-adduct of 1,2-naphthoquinone and isobutyraldehyde.

(v) Valeraldehyde: 3-Chloro-1,2-naphthalenediol monovalerate [**5**: R=$CH_3(CH_2)_3$, R_1=Cl, R_2=R_3=H]: white needles (80 mg, 27.7%), mp 89—90 °C. IR: ν_{OH} 3275; ν_{CH} 2960, 2940; $\nu_{C=O}$ 1735 cm^{-1}. PMR (CCl_4), δ: 0.92 (t, 3H, CH_3), 1.30—1.88 (m, 4H, $(CH_2)_2$), 2.60 (t, 2H, $COCH_2$), 6.10 (1H, OH), 7.30—8.12 (m, 5H, aromatic-H). Found: C, 64.57; H, 5.46%. Calcd for $C_{15}H_{15}ClO_3$: C, 64.64; H, 5.42%. 3-Chloro-4-valeryl-1,2-naphthoquinone: orange plates (9 mg, 3.1%), mp 144.5—145.5 °C. IR: ν_{OH} 2969, 2940, 2883; $\nu_{C=O}$ 1704, 1688 cm^{-1}. PMR(CCl_4), δ: 0.97 (t, 3H, CH_3), 1.33—1.82 (m, 4H, $(CH_2)_2$), 6.91—8.08 (m, 4H, aromatic-H). MS, *m/e*: 276 (M^+), 241 (M−Cl), 213 (M−CO−Cl), 191 (M−COR). Found: C, 65.02; H, 4.81%. Calcd for $C_{15}H_{13}ClO_3$: C, 65.11; H, 4.74%. 3-Valeryl-1,2-naphthalenediol (15 mg, 5.9%) was identical (IR and PMR spectra) with the photo-adduct of 1,2-naphthoquinone and valeraldehyde.

(vi) Isovaleraldehyde: 3-Chloro-1,2-naphthalenediol monoisovalerate [**5**: R=$(CH_3)_2CHCH_2$, R_1=Cl, R_2=R_3=H]: white needles (93 mg, 32.2%), mp 125—125.5 °C. IR: ν_{OH} 3315, ν_{CH} 2972, 2922, 2880; $\nu_{C=O}$ 1735 cm^{-1}. PMR($CDCl_3$), δ: 1.08 (d, 6H, $(CH_3)_2$), 2.30 (m, 1H, CH), 2.60 (d, 2H, $COCH_2$), 7.40—8.20 (m, 6H, aromatic-H+OH). Found: C, 64.66; H, 5.38%. Calcd for $C_{15}H_{15}ClO_3$: C, 64.66; H, 5.42%. 3-Chloro-4-isovaleryl-1,2-naphthoquinone: reddish orange plates (12 mg, 4.2 %), mp 138—140 °C. IR: ν_{CH} 2970, 2942, 2885; $\nu_{C=O}$ 1704, 1687 cm^{-1}. PMR(CCl_4), δ: 1.07 (d, 6H, $(CH_3)_2$), 2.35 (m, 1H, CH), 2.70 (d, 2H, $COCH_2$), 6.94—8.10 (m, 4H, aromatic-H). Found: C, 65.00; H, 4.61%. Calcd for $C_{15}H_{13}ClO_3$: C, 65.11; H, 4.74%. 3-Isovaleryl-1,2-naphthalenediol(3.8 mg, 1.5%) was identical (PMR spectrum) with the photo-adduct of 1,2-naphthoquinone and isovaleraldehyde.

(vii) Hexanal: 3-Chloro-1,2-naphthalenediol monohexanoate [**5**: R=$CH_3(CH_2)_4$, R_1=Cl, R_2=R_3=H]: white needles (89 mg, 29.3%), mp 95.5—96.5 °C. IR: ν_{OH} 3200; ν_{CH} 2960, 2940; $\nu_{C=O}$ 1735 cm^{-1}. PMR($CDCl_3$), δ: 0.92 (t, 3H, CH_3), 1.30—1.90 (m, 6H, $(CH_2)_3$), 2.69 (t, 2H, $COCH_2$), 7.40—8.20 (m, 6H, aromatic-H+OH). Found: C, 65.73; H, 5.83%. Calcd for $C_{16}H_{17}ClO_3$: C, 65.64; H, 5.85%. 3-Chloro-4-hexanoyl-1,2-naphthoquinone: orange plates, mp 111—112 °C. IR: ν_{CH} 2960, 2935, 2870; $\nu_{C=O}$ 1705, 1680 cm^{-1}. 3-Hexanoyl-1,2-naphthalenediol was identical (IR spectrum) with the photo-adduct of 1,2-naphthoquinone and hexanal.

(viii) Heptanal: 3-Chloro-1,2-naphthalenediol monoheptanoate [**5**: R=$CH_3(CH_2)_5$, R_1=Cl, R_2=R_3=H]: white needles (103 mg, 32.4%), mp 80.5—82.0 °C. IR: ν_{OH} 3422; ν_{CH} 2958, 2935, 2870; $\nu_{C=O}$ 1735 cm^{-1}. PMR($CDCl_3$), δ: 0.92 (t, 3H, CH_3), 1.20—1.90 (m, 8H, $(CH_2)_4$), 2.70 (t, 2H, $COCH_2$), 5.80 (1H, OH), 7.40—8.20 (m, 5H, aromatic-H). Found: C, 66.71; H, 6.20%. Calcd for $C_{17}H_{19}ClO_3$: C, 66.56; H, 6.24%. 3-Chloro-4-heptanoyl-1,2-naphthoquinone: yellow crystals (12 mg, 3.8%), mp 105—106 °C. IR: ν_{CH} 2967, 2940, 2874; $\nu_{C=O}$ 1708, 1685 cm^{-1}. PMR (CCl_4), δ: 0.90 (t, 3H, CH_3), 1.23—1.84 (m, 8H, $(CH_2)_4$), 2.77 (t, 2H, $COCH_2$), 6.95—8.14 (m, 4H, aromatic-H). Found: C, 66.89; H, 5.57%. Calcd for $C_{17}H_{17}ClO_3$: C, 67.00; H, 5.62%. 3-Heptanoyl-1,2-naphthalenediol (23 mg, 8.2%) was identical (IR and PMR spectra) with the photo-adduct of 1,2-naphthoquinone and heptanal.

(ix) Octanal: 3-Chloro-1,2-naphthalenediol monooctanoate [**5**: R=$CH_3(CH_2)_6$, R_1=Cl, R_2=R_3=H]: white needles (47 mg, 14.1%), mp 79.5—80.5 °C. IR: ν_{OH} 3290, ν_{CH} 2960, 2935, 2860; $\nu_{C=O}$ 1737 cm^{-1}. PMR($CDCl_3$), δ: 0.88—1.90 (br. m, 13H, $CH_3(CH_2)_5$), 2.72 (t, 2H, $COCH_2$), 5.80 (1H, OH), 7.40—8.20 (m, 5H, aromatic-H). Found: C, 67.50; H, 6.30%. Calcd for $C_{18}H_{21}ClO_3$: C, 67.39; H, 6.60%. 3-Octanoyl-1,2-naphthalenediol (15 mg, 5.1%) was identical (IR and PMR spectra) with the photo-adduct of 1,2-naphthoquinone and octanal.

(x) Nonanal: 3-Chloro-1,2-naphthalenediol mononononanoate [**5**: R=$CH_3(CH_2)_7$, R_1=Cl, R_2=R_3=H]: white needles (72 mg, 20.7%), mp 76—77 °C. IR: ν_{OH} 3280; ν_{CH} 2970, 2945, 2870; $\nu_{C=O}$ 1735 cm^{-1}. PMR($CDCl_3$), δ: 0.88—1.90 (br. m, 15H, $CH_3(CH_2)_6$), 2.72 (t, 2H, $COCH_2$), 7.40—8.20 (m, 6H, aromatic-H+OH). Found: C, 68.15; H, 6.83%. Calcd for $C_{19}H_{23}ClO_3$: C, 68.15; H, 6.92%. 3-Chloro-4-nonanoyl-1,2-naphthoquinone: orange crystals (18 mg, 5.2%), mp 108—109 °C. IR: ν_{CH} 2967, 2938, 2870; $\nu_{C=O}$ 1720, 1680 cm^{-1}. PMR(CCl_4), δ: 0.88 (t, 3H, CH_3), 1.17—1.86 (br. m, 12H, $(CH_2)_6$), 2.78 (t, 2H, $COCH_2$), 6.92—8.07 (m, 4H, aromatic-H). Found: C, 68.64; H, 6.31%. Calcd for $C_{19}H_{21}ClO_3$: C, 68.57; H, 6.36%. 3-Nonanoyl-1,2-naphthalenediol (27 mg, 9.4%) was identical (IR and PMR spectra) with the photo-adduct of 1,2-naphthoquinone and nonanal.

(xi) Decanal: 3-Chloro-1,2-naphthalenediol monodecanoate [**5**: R=$CH_3(CH_2)_8$, R_1=Cl, R_2=R_3=H]: white needles (79 mg, 21.8%), mp 67—68 °C. IR: ν_{OH} 3290; ν_{CH} 2960, 2930, 2860; $\nu_{C=O}$ 1735 cm^{-1}. PMR($CDCl_3$), δ: 0.84 (t, 3H, CH_3), 1.10—1.90 (br. m, 14H, $(CH_2)_7$), 2.68 (t, 2H, $COCH_2$), 7.40—8.20 (m, 6H, aromatic-H+OH). Found: C, 69.10; H, 7.37%. Calcd for $C_{20}H_{25}ClO_4$: C, 68.86; H, 7.22%. 3-Chloro-4-decanoyl-1,2-naphthoquinone: orange plates (19 mg, 5.3%), mp 103—104 °C. IR: ν_{CH} 2986, 2935, 2865; $\nu_{C=O}$ 1718, 1678 cm^{-1}. PMR ($CDCl_3$), δ: 0.87 (t, 3H, CH_3), 1.17—1.85 (br. m, 14H, $(CH_2)_7$), 2.85 (t, 2H, $COCH_2$), 6.98—8.14 (m, 4H, aromatic-H). MS; *m/e* 346 (M^+), 311 (M−Cl), 283 (M−CO−Cl). Found: C, 69.33; H, 6.54%. Calcd for $C_{20}H_{23}ClO_3$: C, 69.26; H, 6.68%. 3-Decanoyl-1,2-naphthalenediol (18 mg, 5.5%) was identical (IR and PMR spectra) with the photo-adduct of 1,2-naphthoquinone and decanal.

Synthesis of 3-Chloro-4-acetyl-1,2-naphthoquinone. 4-Acetyl-1-naphthol (930 mg, 5 mmol) was dissolved in acetone (100 ml) and added to a solution of Fremy's salt (3 g) dissolved in water (200 ml) and M/6 KH_2PO_4 solution (50 ml). The solution became red after 30 min and an oily substance was separated. The solution was extracted with chloroform (70 ml×3), then the extract was washed with water and dried (Na_2SO_4). After the solvent was removed, the quinone was solidified. 4-Acetyl-1,2-naphthoquinone: red crystals from alcohol, mp 92—93 °C. Yield was theoretical. Dry chlorine was passed into the mixture of 4-acetyl-1,2-naphthoquinone (193 mg) and acetic acid (1.6 g) until the quinone was dissolved. Hot water (80—90 °C) was added into the reaction mixture, then the 3-chloro-4-acetyl-1,2-naphthoquinone which separated was collected and washed with water: reddish orange needles from chloroform, mp 194—197 °C. Its IR and PMR spectra were identical with the data of the corresponding quinone obtained from the photo-induced reaction of 3-chloro-1,2-naphthoquinone with acetaldehyde.

Auto-oxidation of 3-Chloro-4-acetyl-1,2-naphthalenediol The reduction of 3-chloro-4-acetyl-1,2-naphthoquinone with sodium hydrosulfite gave 3-chloro-4-acetyl-1,2-naphthalenediol. This was oxidized into the original quinone in benzene or through a silica gel column.

Photo-addition Products of 3-Bromo-1,2-naphthoquinone with Aliphatic Aldehydes. (i) Acetaldehyde: 3-Bromo-1,2-naphthalenediol monoacetate [**5**: R=CH_3, R_1=Br, R_2=R_3=H]: white needles (44 mg, 18.6%), mp 159.5—160.5 °C. IR: ν_{OH} 3310; $\nu_{C=O}$ 1745 cm^{-1}. PMR ($CDCl_3$), δ: 2.47 (s, 3H, CH_3) 7.32—8.23 (m, 6H, aromatic-H+OH). Found: C, 51.11; H, 3.28%. Calcd for $C_{12}H_9BrO_3$: C, 51.27; H, 3.23 %. 3-Bromo-4-acetyl-1,2-naphthoquinone (trace); IR: $\nu_{C=O}$ 1700, 1690 cm^{-1}. 3-Acetyl-1,2-naphthalenediol (4 mg, 2.4%) was identical (IR spectrum) with the photo-adduct of 1,2-naphthoquinone and acetaldehyde.

(ii) Propionaldehyde: 3-Bromo-1,2-naphthalenediol monopropionate [**5**: R=CH_3CH_2, R_1=Br, R_2=R_3=H]: white needles (20 mg, 8.1%), mp 112—114 °C. IR: ν_{OH} 3320 (br); ν_{CH} 2980; $\nu_{C=O}$ 1740 cm^{-1}. PMR($CDCl_3$), δ: 1.37 (t, 3H, CH_3), 2.78 (q, 2H, CH_2), 7.40—8.22 (m, 6H, aromatic-H). Found: C, 53.08; H, 3.87%. Calcd for $C_{13}H_{11}BrO_3$: C, 52.91; H, 3.76%. 3-Propionyl-1,2-naphthalenediol (15 mg, 8.3%) was identical (IR and PMR spectra) with the photo-adduct of 1,2-naphthoquinone and propionaldehyde.

(iii) Butyraldehyde: 3-Bromo-1,2-naphthalenediol monobutyrate [**5**: R=$CH_3(CH_2)_3$, R_1=Br, R_2=R_3=H]: white crystals (28 mg, 10.8%), mp 126—128 °C. IR: ν_{OH} 3360; ν_{CH} 2970, 2940, 2880; $\nu_{C=O}$ 1740 cm^{-1}. PMR($CDCl_3$), δ: 1.12 (t, 3H, CH_3), 1.90 (sex, 2H, CH_2), 2.72 (t, 2H, $COCH_2$), 7.32—8.00 (m, 6H, aromatic-H+OH). Found: C, 54.22; H, 4.21%. Calcd for $C_{14}H_{13}BrO_3$: C, 54.39; H, 4.24%. 3-Butyryl-1,2-naphthalenediol (8 mg, 4.2%) was identical (IR spectrum) with the photo-adduct of 1,2-naphthoquinone and butyraldehyde.

(iv) Isobutyraldehyde: 3-Bromo-1,2-naphthalenediol monoisobutyrate [**5**: R=$(CH_3)_2CH$, R_1=Br, R_2=R_3=H]: white needles (38 mg, 14.7%), mp 106—107 °C. IR: ν_{OH} 3380 (br); ν_{CH} 2980, 2940, 2880; $\nu_{C=O}$ 1730 cm^{-1}. PMR($CDCl_3$), δ: 1.41 (d, 6H, $(CH_3)_2$), 1.44 (d, 6H, $(CH_3)_2$), 2.95 (sep, 1H, CH), 2.98 (sep, 1H, CH), 7.24—8.20 (m, 12H, aromatic-H +OH). Found: C, 54.15; H, 4.12%. Calcd for $C_{14}H_{13}BrO_3$: C, 54.39; H, 4.24%. 3-Butyryl-1,2-naphthalenediol (10 mg, 5.2%) was identical (IR spectrum) with the photo-adduct of 1,2-naphthoquinone and isobutyraldehyde.

(v) Valeraldehyde: 3-Bromo-1,2-naphthalenediol monovalerate [**5**: R=$CH_3(CH_2)_3$, R_1=Br, R_2=R_3=H]: white needles (69 mg, 25.5%), mp 96—97 °C. IR: ν_{OH} 3250 (br); ν_{CH} 2965, 2935, 2870; $\nu_{C=O}$ 1728 cm^{-1}. PMR(CCl_4), δ: 0.88 —1.90 (m, 7H, $CH_3(CH_2)_2$), 2.60 (t, 2H, $COCH_2$), 6.61 (1H, OH), 7.30—8.10 (m, 5H, aromatic-H). Found: C, 55.55; H, 4.49%. Calcd for $C_{15}H_{15}BrO_3$: C, 55.75; H, 4.68%. 3-Bromo-4-valeryl-1,2-naphthoquinone: orange needles (8 mg, 3%), mp 141—142 °C. IR: ν_{CH} 2965, 2935, 2880; $\nu_{C=O}$ 1700, 1685 cm^{-1}. PMR(CCl_4), δ: 0.96 (t, 3H, CH_3), 1.30—1.80 (m, 4H, $(CH_2)_2$), 2.78 (t, 2H, $COCH_2$), 6.94—8.08 (m, 4H, aromatic-H). Found: C, 56.13; H, 4.21%. Calcd for $C_{15}H_{13}BrO_3$: C, 56.10; H, 4.08%. 3-Valeryl-1,2-naphthalenediol (18 mg, 8.8%) was identical (IR spectrum) with the photo-adduct of 1,2-naphthoquinone and valeraldehyde.

(v) Isovaleraldehyde: 3-Bromo-1,2-naphthalenediol monoisovalerate [**5**: R=$(CH_3)_2CHCH_2$, R_1=Br, R_2=R_3=H]: white needles (59 mg, 21.8%), mp 124.5—125.5 °C. IR: ν_{OH} 3335; ν_{CH} 2960, 2877; $\nu_{C=O}$ 1735 cm^{-1}. PMR($CDCl_3$), δ: 1.10 (d, 6H, $(CH_3)_2$), 1.13 (d, 6H, $(CH_3)_2$), 2.30 (m, 2H, CH), 2.54 (d, 2H, $COCH_2$), 2.57 (d, 2H, $COCH_2$), 5.60 (1H, OH), 5.90 (1H, OH), 7.23—8.20 (m, 10H, aromatic-H). Found: C, 55.68; H, 4.62%. Calcd for $C_{15}H_{15}BrO_3$: C, 55.75; H, 4.68%. 3-Bromo-4-isovaleryl-1,2-naphthoquinone: orange crystals (6 mg, 2.2%), mp 151—153 °C. IR: ν_{CH} 2975, 2885; $\nu_{C=O}$ 1700, 1685 cm^{-1}. PMR(CCl_4), δ: 1.14 (d, 6H, $(CH_3)_2$), 2.35 (m, 1H, CH), 2.65 (d, 2H, $COCH_2$), 6.95—8.09 (m, 4H, aromatic-H). 3-Isovaleryl-1,2-naphthalenediol (14 mg, 6.8%) was identical (IR and PMR spectra) with the photo-adduct of 1,2-naphthoquinone and isovaleraldehyde.

(vii) Hexanal: 3-Bromo-1,2-naphthalenediol monohexanoate [**5**: R=$CH_3(CH_2)_4$, R_1=Br, R_2=R_3=H]: white needles (57 mg, 20.1%), mp 89.5—90.5 °C. IR: ν_{OH} 3250; ν_{CH} 2950, 2875; $\nu_{C=O}$ 1730 cm^{-1}. PMR(CCl_4), δ: 0.92 (t, 3H, CH_3), 1.20—1.90(m, 6H, $(CH_2)_3$), 2.60(t, 2H, $COCH_2$), 6.10(1H, OH), 7.32—8.16(m, 5H, aromatic-H). Found: C, 56.83; H, 5.19%. Calcd for $C_{16}H_{17}BrO_3$: C, 56.99; H, 5.08%. 3-Bromo-4-hexanoyl-1,2-naphthoquinone: orange plates (7 mg, 2.5%), mp 100—101 °C. IR: ν_{CH} 2970, 2946, 2878; $\nu_{C=O}$ 1703, 1683 cm^{-1}. PMR(CCl_4), δ: 0.93(t, 3H, CH_3), 1.27—1.88(m, 6H, $(CH_2)_3$), 2.81(t, 2H, $COCH_2$), 6.87—8.04(m, 4H, aromatic-H). 3-Hexanoyl-1,2-naphthalenediol (15 mg, 6.9%) was identical(IR and PMR spectra) with the photo-adduct of 1,2-naphthoquinone and hexanal.

(viii) Heptanal: 3-Bromo-1,2-naphthalenediol monohexanoate[**5**: R=$CH_3(CH_2)_5$, R_1=Br, R_2=R_3=H]: white needles (30 mg, 10.2%), mp 78.5—79.5 °C. IR: ν_{OH} 3375; ν_{CH} 2958, 2940, 2860; $\nu_{C=O}$ 1725 cm^{-1}. PMR(CCl_4), δ : 0.94—1.88(br. m, 11H, $CH_3(CH_2)_4$), 2.62(t, 2H, $COCH_2$), 6.06 (1H, OH), 7.30—8.20(m, 5H, aromatic-H). Found: C, 58.24; H,5.44%. Calcd for $C_{17}H_{19}BrO_3$: C,58.13; H, 5.45%. 3-Heptanoyl-1,2-naphthalenediol(17 mg, 7.5%) was identical(IR and PMR spectra) with the photo-adduct of 1,2-naphthoquinone and heptanal.

(ix) Octanal: 3-Bromo-1,2-naphthalenediol monooctanoate[**5**: R=$CH_3(CH_2)_6$, R_1=Br, R_2=R_3=H]: white needles (20 mg, 6.5%), mp 65—66 °C. IR: ν_{OH} 3350(br); ν_{CH} 2930, 2860; $\nu_{C=O}$ 1735 cm^{-1}. PMR(CCl_4), δ: 0.82—1.90(br.m, 26H, $CH_3(CH_2)_5$), 2.64(t, 2H, $COCH_2$), 2.67(t, 2H, $COCH_2$), 5.96(2H, OH), 7.30—8.20(m, 10H, aromatic-H). Found: C,59.16; H,5.85%. Calcd for $C_{18}H_{21}BrO_3$: C, 59.19; H, 5.79%. 3-Octanoyl-1,2-naphthalenediol (5 mg, 2.1%) was identical(IR spectrum) with the photo-adduct of 1,2-naphthoquinone and octanal.

(x) Nonanal: 3-Bromo-1,2-naphthalenediol mononononanoate[**5**: R=$CH_3(CH_2)_7$, R_1=Br, R_2=R_3=H]: white needles (27 mg, 8.5%), mp 82—83 °C. IR: ν_{OH} 3275(br); ν_{CH} 2925, 2860; $\nu_{C=O}$ 1735 cm^{-1}. PMR(CCl_4), δ: 0.82—1.95

(br. m, 15H, $CH_3(CH_2)_6$), 2.66(t, 2H, $COCH_2$), 5.99(s, 1H, OH), 7.33—8.23 (m, 5H, aromatic-H). Found: C, 60.33; H, 6.10%. Calcd for $C_{19}H_{23}BrO_3$: C,60.17; H, 6.11%. 3-Bromo-4-nonanoyl-1,2-naphthoquinone: orange crystals (8 mg 2.5%), mp 87—88 °C. IR: ν_{CH} 2945,2870; $\nu_{C=O}$ 1715, 1675 cm^{-1}. PMR(CCl_4), δ: 0.86(t, 3H, CH_3), 1.29—1.90(br. m, 12H, $(CH_2)_6$), 2.76(t, 2H, $COCH_2$), 6.93—8.08(m, 4H, aromatic-H). Found: C,60.25; H,5.50%. Calcd for $C_{19}H_{21}BrO_3$: C, 60.49; H, 5.61%. 3-Nonanoyl-1,2-naphthalenediol(9 mg, 3.6%) was identical (IR spectrum) with the photo-adduct of 1,2-naphthoquinone and nonanal.

(xi) Decanal: 3-Bromo-1,2-naphthalenediol monodecanoate [**5**: $R=CH_3(CH_2)_8$, $R_1=Br$, $R_2=R_3=H$]: white needles (28 mg, 8.5%), mp 79—80 °C. IR: ν_{OH} 3250(br); ν_{CH} 2960, 2920, 2858; $\nu_{C=O}$ 1728 cm^{-1}. PMR(CCl_4), δ: 0.80—1.95(br. m, 17H, $CH_3(CH_2)_7$), 2.62 (t, 2H, $COCH_2$), 6.19(1H, OH), 7.30—8.10(m, 5H, aromatic-H). Found: C, 60.94; H, 6.44%. Calcd for $C_{20}H_{25}BrO_3$: C,61.08; H,6.41%. 3-Bromo-4-decanoyl-1,2-naphthoquinone: orange plates (10 mg, 3%), mp 89—90 °C. IR: ν_{CH} 2945, 2870; $\nu_{C=O}$ 1715, 1675 cm^{-1}. PMR(CCl_4), δ: 0.88(t, 3H, CH_3), 1.17—1.84 (br. m, 14H, $(CH_2)_7$), 2.84(t, 2H, $COCH_2$), 6.96—8.13 (m, 4H, aromatic-H). Found: C,61.35; H,5.82%. Calcd for $C_{20}H_{23}BrO_3$: C,61.39; H,5.92%. 3-Decanoyl-1,2-naphthalenediol (8 mg, 3%) was identical(IR spectrum) with the photo-adduct of 1,2-naphthoquinone and decanal.

Photo-addition Products of 3-Methyl-1,2-naphthoquinone with Acetaldehyde: 3-Methyl-1,2-naphthalenediol monoacetate [**5**: $R=CH_3$, $R_1=CH_3$, $R_2=R_3=H$]: white crystals (37 mg, 17%), mp 127—128 °C. IR: ν_{OH} 3340(br); $\nu_{C=O}$ 1739 cm^{-1}. PMR($CDCl_3$), δ: 2.28(s, 3H, CH_3), 2.37(s, 3H, CH_3), 2.40(s, 3H, $COCH_3$), 2.46(s, 3H, $COCH_3$), 5.47(1H, OH), 5.60(1H, OH), 7.29—8.15(m, 10H, aromatic-H). Found: C, 72.08; H, 5.59%. Calcd for $C_{13}H_{12}O_3$: C, 72.21; H, 5.59%. 3-Methyl-4-acetyl-1,2-naphthoquinone: orange crystals (14 mg, 6.5%), mp 180—182 °C. IR: $\nu_{C=O}$ 1700, 1675 cm^{-1}. PMR(CCl_4), δ: 1.90(s, 3H, CH_3), 2.44(s, 3H, $COCH_3$), 6.88—8.05 (m, 4H, aromatic-H). Found: C, 73.03; H, 4.83%. Calcd for $C_{13}H_{10}O_3$: C, 72.89; H, 4.71%.

The author wishes to express his gratitude to Professor Kazuhiro Maruyama of Kyoto University and Professor Osamu Soga of Shimane University for their invaluable suggestions and encouragement. Financial support from the Ministry of Education is acknowledged with pleasure.

References

1) Part I for this series. K. Maruyama and A. Takuwa, *Chem. Lett.*, **1974**, 471.
2) L. M. Bruce, *Quart. Revs.*, **21**, 405 (1967).
3) A. Schönberg, N. Latif, R. Moubasher, and A. Sina, *J. Chem. Soc.*, **1951**, 1364.
4) For example: K. Maruyama, A. Takuwa, T. Otsuki, and S. Kako, *Bull. Inst. Chem. Res., Kyoto Univ.*, **50**, 348 (1972).
5) A. Schönberg, W. I. Awad, and A, Mousa, *J. Am. Chem. Soc.*, **77**, 3850 (1955).
6) W. I. Awad and M. S. Hafez, *J. Am. Chem. Soc.*, **80**, 6057 (1957).
7) A. H. Blatt, *Org. Synth.*, Coll. Vol. II, 430 (1948).
8) T. Zincke, *Ber.*, **19**, 2497 (1886).
9) T. Zincke, *Ber.*, **19**, 2495 (1886).
10) F. Weygand and K. Schroder, *Ber.*, **74**, 1884 (1941).
11) W. Bradley and R. Robinson, *J. Chem. Soc.*, **1934**, 1484.
12) R. W. A. Oliver, R. M. Rashman, and A. W. Somerville, *Tetrahedron*, **24**, 4067 (1968).
13) K. Dziewonsky, J. Schoenowna, and E. Waldmann, *Ber.*, **58**, 1211 (1925).
14) H. J. Teuber and N. Götz, *Chem. Ber.*, **87**, 1236 (1954).

Doubly Charged Ion Mass Spectra of Monosubstituted Aromatic Compounds

Hiroshi SAKURAI, Akira TATEMATSU, and Hisao NAKATA*

Faculty of Pharmacy, Meijo University, Tempaku-ku, Nagoya 468

**Department of Chemistry, Aichi Kyoiku University, Kariya, Aichi 448*

(Received January 13, 1976)

The 2E doubly charged ion mass spectra of twelve simple monosubstituted aromatic compounds were recorded. The spectral pattern of these compounds can be classified into three types. When the substituent is strongly electron-donating such as the amino or dimethylamino group, a very intense molecular ion peak appears, no fragment ion peak being observed. Phenol, anisole, toluene, and chlorobenzene show both molecular and fragment ion peaks in varying intensities. The parent benzene itself behaves similarly. Only fragment ion peaks were observed for nitrobenzene and aromatic carbonyl compounds such as benzaldehyde, acetophenone, methyl benzoate, or benzoic acid. The major fragmentation reactions are discussed.

In the 2E doubly charged ion mass spectrum[1,2] we can observe singly charged ions arising from the charge exchange reaction between doubly charged ions and any neutral species in the first field-free region of a mass spectrometer. Under these spectral conditions, aromatic hydrocarbons[3,4] exhibit several peculiar fragmentations including drastic skeletal changes, the spectra showing strong similarity irrespective of hydrocarbon structure. On the other hand, the spectra of aromatic amines[5] and substituted aromatic carbonyl compounds[6] afford certain characteristic fragmentation patterns with structures. The purpose of the present work is to investigate the structure-spectrum correlation in more detail by using simple monosubstituted aromatic compounds.[7]

General Appearance of the Spectrum

The 2E spectra of twelve simple aromatic compounds are given in Table 1 and Fig. 1. The spectral pattern of these compounds can be classified into three types. When the substituent is strongly electron-donating such as the amino or dimethylamino group, a very intense molecular ion peak appears, no fragment ion peak being observed. This indicates that the substituent can accomodate two positive charges within the benzene ring and the molecular ion is stable enough to be detected.

The compounds with other electron-donating substituents, *e.g.*, phenol, anisole, or toluene, show both molecular and fragment ion peaks in varying intensities. The parent benzene itself behaves similarly. Chlorobenzene, in which the substituent is electron-withdrawing, also exhibits a strong molecular ion peak as well as several fragment ion peaks of comparable intensity. In this case, the presence of lone-pair

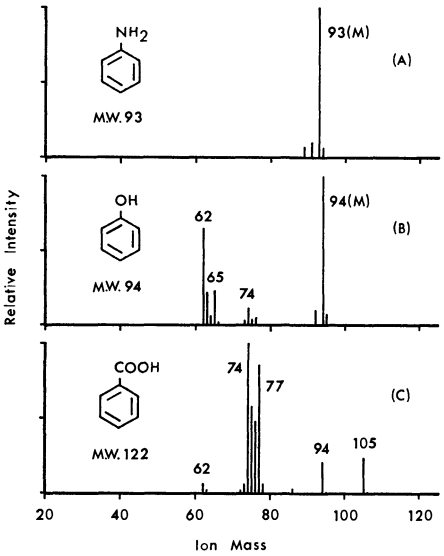

Fig. 1. 2E Doubly charged ion mass spectra of aniline (A), phenol (B), and benzoic acid (C).

TABLE 1. 2E DOUBLY CHARGED ION MASS SPECTRA OF MONOSUBSTITUTED AROMATIC COMPOUNDS[a] (RELATIVE INTENSITIES IN PARENTHESES)

C_6H_5-Z	[M]	[M-1]	$H-\overset{+}{C}(=C=)_x\overset{+}{C}-H$	Other fagment ion peaks
$Z=N(CH_3)_2$	121 (100)	120 (34)	74 (3)	104 (7), 117 (10), 119 (11), 122 (8)
OCH_3	108 (22)	—	62 (100), 74 (23)	63 (31), 64 (7), 65 (18), 75 (9), 79 (5)
CH_3	92 (21)	91 (38)	62 (3), 86 (43)	85 (3), 87 (10), 88 (7), 89 (6), 90 (100)
H	78 (100)	77 (8)	62 (3), 74 (74)	73 (5), 75 (44), 76 (46), 79 (8)
Cl	112 (100) 114 (31)	—	74 (44)	75 (33), 76 (79), 77 (5), 110 (5), 113 (6)
NO_2	123[b]	—	62 (38), 74 (100)	63 (7), 73 (5), 75 (55), 76 (15), 77 (8), 87 (12), 89 (5), 93 (6), 102 (4)
CHO	106 (8)	105 (5)	62 (6), 74 (100), 86 (39)	73 (7), 75 (40), 76 (39), 77 (39), 78 (34), 85 (6), 87 (9), 90 (5), 104 (6)
$COCH_3$	120[b]	—	74 (22), 86 (28), 98 (14)	75 (19), 76 (21), 77 (100), 87 (9), 91 (10), 99 (5), 102 (17), 105 (34)
$COOCH_3$	136[b]	—	62 (4), 74 (79)	73 (7), 75 (62), 76 (51), 77 (100), 78 (10), 105 (13), 118 (10)

a) Spectra of aniline, phenol, and benzoic acid are shown in Fig. 1. b) No molecular ion peak was observed.

electrons on the chlorine atom seems to be a dominant factor for stabilization of two positive charges.

On the other hand, only fragment ion peaks were observed for nitrobenzene and aromatic carbonyl compounds such as benzaldehyde, acetophenone, methyl benzoate, or benzoic acid. Since the substituents of these compounds are electron-withdrawing, two positive charges are not stable in the molecular framework. This might be responsible for the exclusive occurrence of fragmentations.

Major Fragmentation Patterns

Two peaks which might be due to the ions of $[M-H_2]$ and $[M-2H_2]$ appear in the spectra of aniline and *N,N*-dimethylaniline. These ions were also observed in the substituted aniline derivatives.[6] The [M−H] peak in *N,N*-dimethylaniline is also significant. On the other hand, phenol and anisole gave fragment ions at 62, 63, 64, and 65 mass units with expulsion of oxygen-containing fragments. In contrast to the case of aromatic amines,[5] elimination of hydrocarbon fragments does not seem to be very favorable for these compounds. Thus, the behavior of phenol and anisole seems to be similar to that in the ordinary singly charged ion spectrum.

The fragmentation of benzene and toluene has been discussed in detail in a previous paper.[4] Thus, the ions at 74 for benzene and 86 for toluene correspond to the allene-type dication of $H-\overset{+}{C}(=C=)_x\overset{+}{C}-H$ with x being 4 and 5, respectively. This series of hydrocarbon ions may appear at 62, 74, 86, 98, *etc.* The peak at 86 is usually observed if the compound has a side chain containing at least one carbon atom directly bound to an aromatic ring. The [M−H] and $[M-H_2]$ peaks were also prominent in benzene and toluene spectra.

Chlorobenzene showed a group of peaks at 74, 75, and 76 mass units as in benzene. These peaks are also characteristic of nitrobenzene and carbonyl compounds. Besides the usual ions of [M−NO] and $[M-NO_2]$, a moderately intense peak at 62 mass units appeared in the nitrobenzene spectrum. The origin of this peak would be the same as in phenol and anisole.

For aromatic carbonyl compounds, C_6H_5–CO–R, two successive fragmentations, [M−R] and [M−R−CO], which eventually give rise to a phenyl ion at 77, were commonly observed as in the ordinary mass spectrum.

On the other hand, the [M−CO] peak was also noticeable in the spectrum of benzaldehyde or benzoic acid (peaks at 78 and 94 mass units, respectively). This is ascribable to the novel fragmentation that involves a rearrangement reaction of the side chain, the peak being encountered in most of the *para*- and some of the *meta*-substituted aromatic carbonyl compounds.[6,8] Acetophenone and methyl benzoate exhibited a weak $[M-H_2O]$ peak. The mechanism of this fragmentation is obscure.

From these results, it is apparent that the fragmentation patterns of simple aromatic compounds clearly reflect the nature of the substituent. However, we have no evidence for the mechanism of these fragmentations. Due to the unusually drastic skeletal changes, the mechanistic interpretation in the 2E mass spectra may not be straightforward as in the ordinary mass spectra. Another difficulty in analyzing the fragmentation in the 2E spectrum is the involvement of collisional charge exchange process during the course of formation of each fragment ion. The relative intensities of individual peak should be examined with care, as Ast and Beynon have pointed out.[5] Empirically, however, the 2E doubly charged ion mass spectrum may prove useful in obtaining information on the structure of unknown compounds, or in discriminating the isomer pairs of certain molecules.[6]

Experimental

Materials. Commercial compounds were used. All the samples were characterized and checked for purity by conventional mass spectrometry prior to the determination of doubly charged ion mass spectra.

Doubly Charged Ion Mass Spectra. The spectra were recorded with an Hitachi RMU-7 double focusing mass spectrometer by the method previously described.[4] Standard operating conditions were as follows: ionizing energy 70 eV, ionizing current 80 μA, source temperature 250 °C, sample pressure $1—5\times10^{-6}$ Torr, and accelerating voltage 1.8 kV.

References

1) J. H. Beynon, A. Mathias, and A. E. Williams, *Org. Mass Spectrometry*, **5**, 303 (1971).

2) R. G. Cooks, J. H. Beynon, R. M. Caprioli, and G. R. Lester, "Metastable Ions," Elsevier, Amsterdam (1973), pp. 128—153.

3) T. Ast, J. H. Beynon, and R. G. Cooks, *Org. Mass Spectrometry*, **6**, 749 (1972).

4) A. Tatematsu, H. Sakurai, H. Nakata, and T. Goto, *Shitsuryo Bunseki*, **20**, 331 (1972).

5) T. Ast and J. H. Beynon, *Org. Mass Spectrometry*, **7**, 503 (1973).

6) H. Sakurai, A. Tatematsu, and H. Nakata, *Bull. Chem. Soc. Jpn.*, **47**, 2731 (1974).

7) The 2E doubly charged ion mass spectrum of some other compounds has also been reported: T. Blumenthal and J. H. Bowie, *Org. Mass Spectrometry*, **6**, 1083 (1972).

8) H. Sakurai, A. Tatematsu, and H. Nakata, *Org. Mass Spectrometry*, **7**, 1109 (1973).

Catalytic Dehydration of Ethers on Nickel Oxide–Silica–Alumina

Hisao IMAI

Research Laboratory of Engineering Materials, Tokyo Institute of Technology, Ookayama, Meguro-ku, Tokyo 152

(Received February 21, 1976)

The dehydration of diethyl ether was studied on synthetic nickel oxide–silica–alumina catalysts in the temperature range of 340—400 °C and at pressures less than 50 Torr. It was found that ethylene, butenes, water, and small amounts of carbon monoxide and methane were formed on the catalysts of lower nickel content. The rate constant for the formation of butenes showd a maximum on the catalyst of 10 atom% nickel. The mechanism of the formation of the butenes was discussed by studying the catalytic dehydration of various ethers.

The dehydration of alcohols or ethers on solid acid catalysts has been studied for many years.[1,2] However, the dehydration of alcohols or ethers on supported nickel oxide has been reported only rarely. In a series of papers, Pines *et al.*[3] studied the dehydration of alcohols in the presence of hydrogen over supported and unsupported nickel oxide catalysts, and found the following facts: In most of these dehydration reactions, ether is the main product, while the other dehydration products are the paraffins formed by hydrogenation of the olefins produced from the alcohol. Paraffins with one carbon less than the original alcohols are also formed in competition with the dehydration reaction.

In the present research, the reaction of diethyl ether on nickel oxide–silica–alumina catalysts was investigated. It was found that in addition to ethylene, which was a normal dehydration product of the ether, butenes were formed on the catalysts of lower nickel content. The mechanism of the formation of the butenes is studied by investigating the reaction products of various ethers and alcohol.

Experimental

Materials. Nickel oxide–silica–alumina catalysts were prepared by a co-precipitation method with sodium silicate and nickel nitrate solutions in the same way as described elsewhere[4]. The catalysts were sized (1—2 mm) and stored for use after the treatment in a stream of dried air for 16 h at 350°C. Some properties of the catalysts are summarized in Table 1. The specific surface area was obtained by applying the standard B. E. T. method to the adsorption isotherm of nitrogen at −196 °C.

Ethers and ethanol were of guaranteed grade. All of these reagents were distilled in a vacuum and stored in glass reservoirs for use in the reactions.

Apparatus and Procedures. The activities of the catalysts were measured by an all-glass circulatory flow system, 713 ml in total volume. Prior to the reaction, the catalyst was treated *in situ* in a stream of dried air for 16h at 400°C, and then evacuated for 3 h ($\approx 10^{-5}$ Torr) at the same temperature. After admitting 50 Torr of ether vapor to the gas circulation system, a small portion (*ca.* 2 ml) of the circulating gas was withdrawn at intervals from the system for the analysis. The analysis was made by gas chromatographs (6 m benzyl cyanide–$AgNO_3$, 5 m Carbowax 1500 and 1.5 m activated carbon columns) and by a Hitachi RMU-6E mass spectrometer.

TABLE 1. CATALYSTS

Catalyst	Composition 100 Ni/(Ni+Si)	Surface area m^2/g
NS-0	0	150
5	5.0	205
10	10	259
20	20	337
40	40	425
50	50	442
80	80	265

Results and Discussion

Figure 1 is an example of the reactions of diethyl ether on the catalysts of lower nickel content. Ethylene, butenes, water, and small amounts of carbon monoxide and methane were formed on the NS-20 catalyst at 360 °C; the initial pressure of the ether was 50.0 Torr. The composition of the reacting mixture, expressed as atom% of the carbon in each molecule, changed linearly with an increase in the reaction time. This fact indicates that all these reactions are zero order with respect to ether pressure. The butenes were produced as an almost equilibrium mixture of 1-butene, *cis*-2-butene, and *trans*-2-butene (1-butene: *cis*-2-butene : *trans*-2-butene=1.0 : 1.6 : 2.2). While carbon monoxide and methane were produced at small rates on the catalysts of lower nickel content, they were produced at much higher rates on the catalyst of NS-80, as shown in Fig. 2. Ethylene was formed only at the beginning of the reaction on this catalyst. No butene was found, but small amounts of ethane and carbon dioxide were found in the products. The ratio of carbon monoxide to methane was found to be almost unity on all the catalysts studied. A material

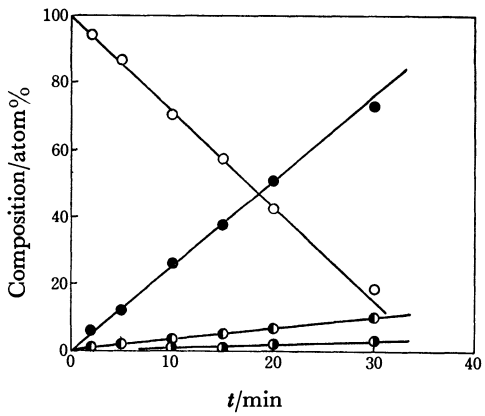

Fig. 1. Reaction of diethyl ether on NS-20 catalyst at 360 °C.
○: Ether, ●: ethylenes, ◑: butenes, ◑: $CO+CH_4$.

Table 2. Reactions of ethers and ethanol[a)]

Reactant	$[k_s/(\text{mol min}^{-1}\text{ m}^{-2})]\times 10^7$				
	Ethylene	Propene	Butenes	Pentenes	Hexenes
$C_2H_5OC_2H_5$	5.41	—	0.327	—	—
$C_2H_5OC_2H_5$ + Propene	5.32	—	0.301	—	—
$C_2H_5OC_3H_7$	3.20	5.26	0.231	0.107	0.025
$C_3H_7OC_3H_7$	—	28.9	—	—	0.027
C_2H_5OH	7.02	—	0.445	—	—

a) Catalyst: NS-20; temperature: 360 °C.

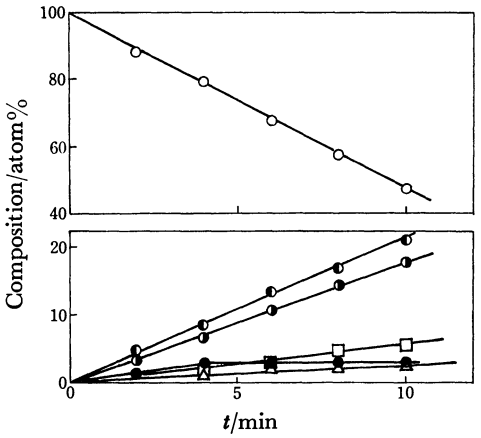

Fig. 2. Reaction of diethyl ether on NS-80 catalyst at 360 °C.
○: Ether, ◐: CO, ◑: CH_4, ●: ethylene, □: ethane, △: CO_2.

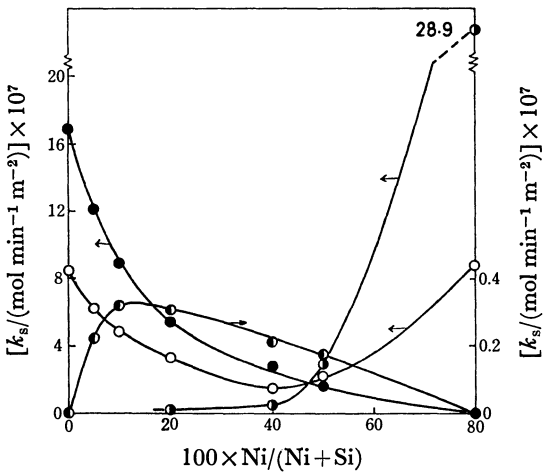

Fig. 3. k_s *vs.* catalyst composition.
○: Ether, ●: ethylene, ◐: butenes, ◑: $CO+CH_4$.

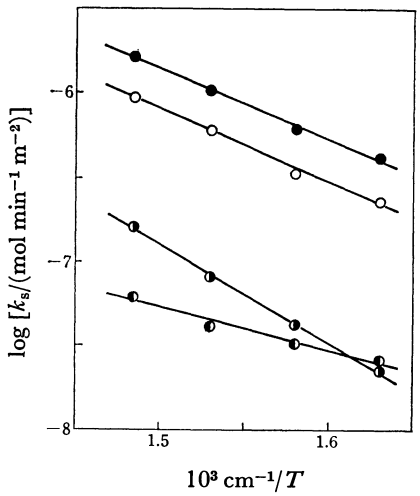

Fig. 4. Arrhenius plots.

		E/(kcal mol^{-1})
○:	Ether	20.6
●:	Ethylene	19.7
◐:	Butenes	12.2
◑:	$CO+CH_4$	27.7

balance of the products obtained at the reaction time of 10 min revealed that about 50% of the oxygen atoms in the products originated from the catalyst.

The effect of catalyst composition on the catalytic activity is shown in Fig. 3. In this figure, the zero order rate constant per unit surface area of the catalyst (k_s) is plotted against the catalyst composition (atom% of nickel). The rate constant for the consumption of the ether decreases with an increase in the nickel content and then increases with a further increase in the nickel content. This increase observed in the catalysts of higher nickel content (>50%) can be ascribed to the increase in the rates of formation of carbon monoxide and methane. The rate constant for the formation of ethylene decreases with increasing nickel content. On the other hand, the rate constant for the formation of butenes shows a maximum at a nickel content of about 10%.

The effect of temperature was studied by using the catalyst of NS-20, as shown in Fig. 4. The Arrhenius plots of the rate constants are linear and the apparent activation energies obtained are also shown in the figure. The fact that the activation energies of these reactions are different suggests that these reactions take place at different active sites or by different mechanisms. The value of the activation energy for the formation of ethylene falls within the range of the literature values (14—24 kcal/mol)[1)] obtained in the catalytic dehydration on silica and alumina surfaces. As shown in Fig. 3, the rate constant for the formation of ethylene decreases with increasing nickel content until its value becomes zero at the catalyst of NS-80. These facts may suggest that the formation of ethylene takes place on the surface of silica. The formation of carbon monoxide and methane, on the other hand, may take place on the surface of nickel oxide, because carbon monoxide and methane are produced as the main products on the catalyst of high nickel content (NS-80). As to the formation of butenes, it can be presumed that

the reaction takes place on the active sites of the dimerization of olefins, because the nickel oxide–silica–alumina is known to be active for the dimerization of olefins.[5-8]

The following three mechanisms can be considered for the formation of the butenes: (1) Ethylene is produced from the ether and desorbed to the gas phase. The desorbed ethylene is again adsorbed on the active sites for the dimerization to form butenes. (2) Ethylene is produced from the ether. The chemisorbed ethylene reacts, before desorption to the gas phase, on the active sites to form butenes. (3) Butenes are formed by the intramolecular dehydration condensation of diethyl ether.

The reactions of various ethers were studied on NS-20 catalyst at 360 °C in order to get an insight into the mechanism of the reaction. The results are summarized in Table 2. In all cases, the rate of formation of olefins could be expressed by a zero-order rate equation, as in the case of diethyl ether. The reaction products of diethyl ether were ethylene and butenes, as described before. Carbon monoxide and methane are not listed in the table, although small amounts of these molecules were produced in every case. When a mixture of diethyl ether (50.1 Torr) and propene (26.1 Torr) was in contact with the catalyst, ethylene and butenes were formed, but neither pentenes nor hexenes were formed. Moreover, the rate constant for the formation of butenes was almost the same as that obtained when only diethyl ether was the reactant. If the reaction takes place according to the first mechanism, it is expected that pentenes and hexenes will also be produced when the reactant is the mixture of diethyl ether and propene. Thus, it is concluded that the first mechanism, *i.e.*, the desorbed ethylene is adsorbed again to form butenes, does not hold in the present case. If the reaction takes place according to the third mechanism, *i.e.*, the intramolecular dehydration condensation, it is expected that only pentenes will be produced in the reaction of ethyl propyl ether. The experimental result obtained with ethyl propyl ether showed that butenes, pentenes, and small amount of hexenes were produced in the molar ratio of 1.0 : 0.46 : 0.11, respectively, in addition to ethylene and propene. This fact indicates that the third mechanism also does not hold in the present case. The result of the reaction with dipropyl ether was almost the same as that obtained for diethyl ether, except that the ratio of the formation of olefin dimer was smaller in the former case. When ethanol was used as the reactant, ethylene and butenes were produced, and the rate constant for the formation of butenes was comparable to that obtained in the reaction of diethyl ether—the former was 1.36 times of the latter. These facts suggest that the second mechanism, *i.e.*, the chemisorbed ethylene which was produced by the dehydration of ether reacts, before desorption, to form butenes, may hold in the present case.

References

1) M. E. Winfield, "Catalysis," Vol. 7, ed. by P. H. Emmett, Reinhold Pub. Corp., New York (1960), p. 93.
2) H. Pines and J. Manassen, "Advances in Catalysis and Related Subjects," Vol. 16, ed. by D. D. Eley *et al.*, Academic Press, New York & London (1966), p. 49.
3) H. Pines and P. Steingaszner, *J. Catal.*, **10**, 60 (1968); H. Pines and T. P. Kobylinski, *ibid.*, **17**, 375 (1970); T. P. Kobylinski and H. Pines, *ibid.*, **17**, 384 (1970); H. Pines and T. P. Kobylinski, *ibid.*, **17**, 394 (1970); J. Hensel and H. Pines, *ibid.*, **24**, 197 (1972); H. Pines, J. Hensel, and J. Simonik, *ibid.*, **24**, 206 (1972); J. Simonik and H. Pines, *ibid.*, **24**, 211 (1972); H. Pines and J. Simonik, *ibid.*, **24**, 220 (1972); E. Licht, Y. Schachter, and H. Pines, *ibid.*, **31**, 110 (1973).
4) H. Imai and H. Uchida, *Bull. Chem. Soc. Jpn.*, **38**, 925 (1965).
5) M. Koizumi, *J. Inst. Polytech., Osaka City Univ.* **4**, 1 (1953).
6) J. P. Hogan, R. L. Banks, W. C. Lanning, and A. Clark, *Ind. Eng. Chem.*, **47**, 752 (1955).
7) A. Ozaki, *Bull. Tokyo Inst. Technol., Ser. B*, 109 (1960).
8) H. Uchida and H. Imai, *Bull. Chem. Soc. Jpn.*, **35**, 989 (1962).

The Photoreaction of Pyrazine Derivatives

Kazutoshi YAMADA, Kiyoshi KATSUURA, Hideaki KASIMURA, and Hirotada IIDA

Department of Synthetic Chemistry, Faculty of Engineering, Chiba University, Yayoi-cho, Chiba 280

(Received February 27, 1976)

The irradiation of the pyrazine derivative with an α-carbonyl substituent (**1**) under a nitrogen atmosphere gave hydroxypyrazine (**2**) and two solvent adducts (**3** and **4**). In the case of **1e**, the charge-transfer complex of pyrazine and dihydropyrazine, produced by the reduction of the pyrazine, was isolated. The mechanism of this photoreaction was similar to that of flavine. The attack of oxygen on dihydropyrazine produced **2**. Furthermore, the photoreduction with DTT occurred through the intermediate, which was similar to the case of flavine. The reaction rates of various pyrazines were measured. The quenching studies indicate that the photoreaction proceeds *via* the n-π^* triplet state.

We have previously investigated the reactions of enaminoketone and have reported the relation between the conformation of the enaminoketone and its photoreaction. At that time, we planned also to study the photoreaction of the pyrazine derivative (**1**) as a model of enaminoketone with a fixed conformation.[1]

Several photoreactions of pyrazines have been studied, but the photoreaction of pyrazine with an α-carbonyl substituent is not known. Padwa and his co-workers prepared pyrazine by the photodimerization and the photoisomerization of azirine.[2] Chambers and his co-workers showed the rearrangement of pyridazine to pyrazine by irradiation.[3] Lahmani and Ivanoff irradiated pyrazine derivative and thus obtained the pyrimidine derivative.[4] Furthermore, in the case of phenazine, which had a pyrazine ring in a molecule, the photoreaction occurred in either an acidic or reducible condition, and 1-alkoxyphenazines were produced as photoproducts.[5]

We wish now to report the results on the photobehavior of the pyrazine derivative (**1**), which produced hydroxypyrazine (**2**) and two solvent adducts (**3** and **4**), and discuss the mechanism, which might be similar to that in the behavior of flavin. It was found that pyrazine exhibited photochromism and could be considered a model of the photoreaction of flavin.

Results and Discussion

Photolysis of Pyrazine Derivatives. The irradiation of the pyrazine derivative **1a** in diethyl ether with a 450-W high pressure mercury lamp (>330 nm) gave two significant photoproducts (**2a** and **3a**) (Scheme 1).

The structures of **2a** and **3a** were identified as methyl 3,6-dimethyl-5-hydroxypyrazine-2-carboxylate and a solvent adduct respectively on the basis of their physical data. The mass spectrum of **2a** gave a molecular ion at *m/e* 182 ($C_8H_{10}N_2O_3$). The UV spectrum showed absorptions at 236 (ε 13900) and 307 nm (ε 6650). The IR spectrum had a hydroxyl absorption at 3430 cm^{-1}. The NMR spectrum of **2a** in $CDCl_3$ showed three sharp singlets for the C(2), C(3), and C(6) methyl groups, and a broad singlet for the hydroxyl group. Moreover, the structure of **2a** was identified by the fact that the hydrolysis and further thermal degradation of **2a** gave 3,6-dimethyl-2-pyrazinol, identical with the independently prepared sample.[6] The mass spectrum of **3a** showed peaks at *m/e* 298 ($M^{+\cdot}$; $C_{14}H_{22}N_2O_5$) and 225 ($M^{+\cdot}-C_4H_9O$). The UV spectrum showed absorptions at 266 (ε 14000) and 322 nm (ε 5300). The NMR spectrum of **3a** in $CDCl_3$ showed three sharp singlets for the C(2), C(3), C(5), and C(6) methyl groups, and nine protons for the 1-ethoxyethyl group. The presence of a NH group was confirmed by the IR band at 3270 cm^{-1}. Thus, **3a** was identified as dimethyl 1,4-dihydro-3,6-dimethyl-1-(1-ethoxyethyl)-2,5-pyrazinedicarboxylate.

Using tetrahydrofuran as a solvent, **2a** and a solvent adduct (**4a**) were obtained. In each case of **1b**, **1c**, and **1d**, the corresponding hydroxyl compound (**2**) and a solvent adduct (**3** or **4**) were given. However, the physical data and yields of **3b**, **3d**, **4b**, and **4d** were hard to obtain, because the isolation of these compounds was difficult. The yields and physical data of **2**, **3**, and **4** are given in Table 1.

Spectrobehavior of Pyrazine Derivatives. The change in the absorption spectrum of **1a** during the photoreaction under an argon atomosphere was examined.

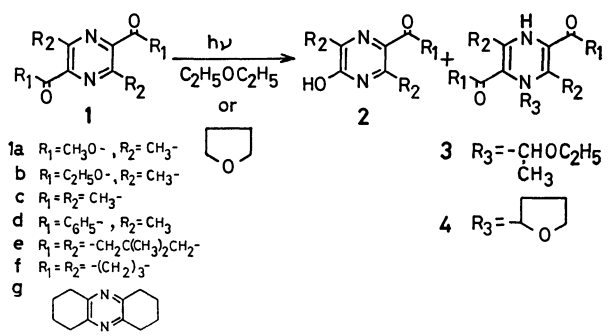

Scheme 1.

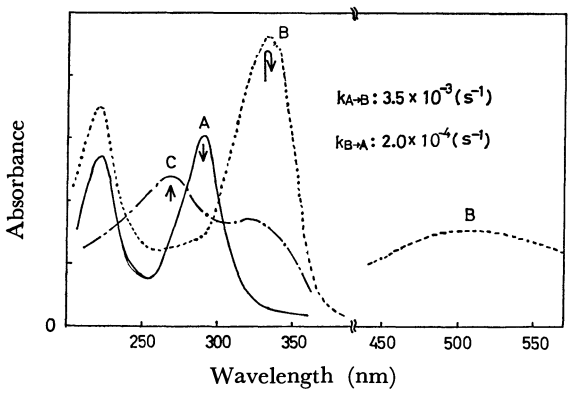

Fig. 1. Spectral change of **1a** in 2-propanol with irradiation.

5e: 372 and 504 nm). The mass spectra of **5c** and **5e** showed peaks more than that of **1c** and **1e** by two (**5c**: *m/e* 194 ($M^{+\cdot}+2$) and 192 ($M^{+\cdot}$); **5e**: *m/e* 274 ($M^{+\cdot}+2$) and 272 ($M^{+\cdot}$)). The NMR spectrum of **5e** in CD_3COOD showed a signal of the NH proton at δ 2.15. By D–H exchange, the signal of the hydroxyl proton of acetic acid at δ 11.30 soon appeared and increased with a decrease in the signal at δ 2.15. The above facts indicate that these colored compounds surely have the structure of dihydropyrazine. Also, in the photoreaction of phenazine, a similar colored compound obtained; it was reported to be a dimer of phenazine and dihydrophenazine.[8]

Mechanism. We may conclude from the experiments described above that this reaction includes both a reduction process and an oxidation process. Therefore we investigated the oxidations and reductions of several compounds with heteroenone structures such as **1**. Beinert reported that the spectral behavior of reduced flavine upon oxidation was similar to that of **1** upon irradiation.[9] The redox mechanism of flavine can also well explain the initial process of this reaction. It appears that **1** is reduced by irradiation to produce dihydropyrazine because, first, the molecular complex **5** of pyrazine and dihydropyrazine is obtained as a colored precipitate, and second, a solution of dihydropyrazine hydrochloride, **6**, dissociated to show a (B) absorption identical with that of the molecular complex **5**. The peak near 500 nm of (B) of **1** is characteristic of the charge-transfer complex, and the peaks in the wavelength region of about 320 to 400 nm are due to the semiquinone radical produced by the dissociation of the complex. The complex and radical coexist at equilibrium to form the (B) absorption. In fact, the ESR spectrum of **5e** in acetic acid was obtained, but the hyperfine structure was not clear. The reversibility between the (A) and (B) absorptions may be based on the instability of the radical to the oxidation with oxygen.

The continuous irradiation of the solution showing the (B) absorption gave a mixture containing the solvent adduct and came to show the (C) absorption. The nature of the mixture is not clear, but the precursor of **2** is surely present in this mixture because the mixture reacted with oxygen upon irradiation to give **2**. The hydroxyl compound **2** was not detected in the solution showing the (C) absorption, nor was it obtained by the bubbling of oxygen into the solution showing the (C) absorption. The formation of **2** from the solution required both oxygen and light. Furthermore, the irradiation of the solvent adduct (**3** and **4**) did not yield **2**. These results indicate that the formation of **2** is different from the reaction which gave **3** or **4**.

From the above results and the mechanism of the photo-oxidation of tetrahydropteridine reported by Mager,[10] we presumed that **2** was formed through the intermediate, **7**, which was produced by the attack of oxygen on the dihydropyrazine derivative. Therefore the mechanism for this reaction may be illustrated as is shown in Scheme 2.

Photobehavior of Pyrazine Derivatives with 1,4-Dimercapto-2,3-butanediol. Flavin derivatives, *e.g.*, flavin adenine dinucleotide (FAD) and lipoic acid, are included in the cycle of the decarboxylation of α-ketoacid in a living organism.[11] In this cycle, FAD oxidizes dihydrolipoic acid to lipoic acid and is then itself reduced to dihydroflavin ($FADH_2$). This reaction of flavin presumably passes through the 4-adduct of flavin, with dihydrolipoic acid as an intermediate.[12] In order to confirm the mechanism of the photoreaction of **1**, we presumed **1** to be a model of flavin and 1,4-dimercapto-2,3-butanediol (DTT; **8**) to be a model of dihydrolipoic acid, and we studied reaction of **1** and DTT.

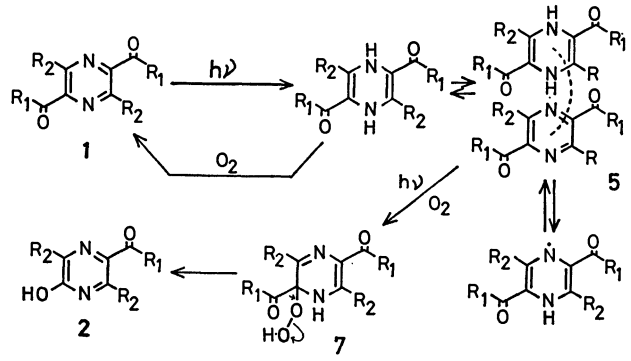

Scheme 2.

The change in the absorption spectrum during the photoreaction was examined. A solution of **1e** and DTT in 50% acetic acid in a quartz cell was irradiated under an argon atmosphere. All the original peaks diminished rapidly and were replaced by new peaks centered at 357 (ε 20900) and 500 nm (ε 1630), and the solution changed from colorless to red. The curves of the change in the absorption clearly defined two isosbestic points at 232 and 333 nm. The spectrum remained unchanged for at least several days in the dark. This suggests that there is no substantial dark side reaction and that the photoproduct is stable under these reaction conditions. After a four-hour irradiation the change in the spectrum almost entirely ceased. The resulting spectrum was identical in shape with that of the charge-transfer complex (**5e**). When the solution was then kept in the dark, the spectrum returned to the **1e** state upon air oxidation. The pseudo first-order rate constant of this reaction was measured from the decrease in the peak at 318 nm of **1e** and the increase in the peak at 357 nm (Table 3).

These results indicate that the photoreduction of **1** occurs in this system. We neglected the equilibrium between reactant and product and considered that **1** reacted with DTT to give a complex **9**, as is shown in Scheme 3. K_d was the dissociation constant of the equilibrium of the complex formation; k_1 and k_2 were

Table 3. Reversibility of the reaction of pyrazine derivatives in 50% acetic acid

λ_{max} (nm)	318	357
k_{photo}[a] s^{-1}	4.7×10^{-4}	5.1×10^{-4}
k_{oxi}[b] s^{-1}	6.5×10^{-5}	6.6×10^{-5}

a) The reaction rate of the photoreduction. b) The reaction rate of the oxidation reaction.

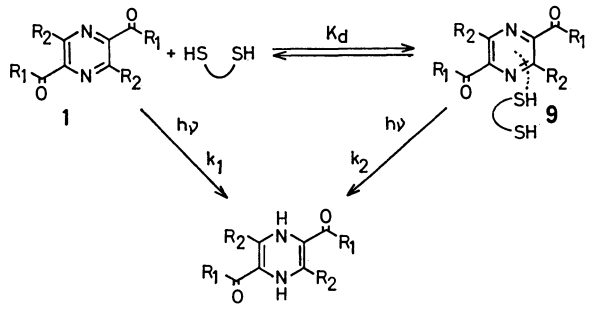

Scheme 3.

the rate constants for the reactions designated, and k_{obsd} was the observed rate constant. [DTT] was the concentration of DTT. When DTT existed in a larger quantity than **1e**, we obtained Eq. 1 (Lineweaver-Burk plots[13]):

$$(k_1-k_{obsd})^{-1} = (k_1-k_2)^{-1} + K_d(k_1-k_2)^{-1}[DTT]^{-1} \quad (1)$$

A series of measurements of the reaction rate with varying concentrations of DTT were carried out. A typical run was zero-order in the DTT and first-order in **1e**. The results, given in Fig. 2, were obtained by plotting 1/[DTT] *vs.* $1/(k_1-k_{obsd})$. From the good linearity of Fig. 2, we may conclude that the pyrazine derivatives, **1**, form the **9** complex with DTT such as do the flavin derivatives. From the intercept and slope of plotting, $K_d=5.1\times10^{-5}$ mol/l and $k_2=5.3\times10^{-5}$ s^{-1} were obtained. The DTT had a quenching effect, because k_2 was smaller than k_1 ($k_2/k_1\simeq10^{-3}$).

As the photoreaction of **1** was quenched by DTT, the quenching experiment was examined. The quantum yields were determined by using potassium tris(oxalato)ferrate(III) actinometry.[14] A Stern-Volmer plot of Φ against the concentration of DTT is given in Fig. 3, it shows good lineality, even in a large excess of DTT to **1** (DTT/**1**$>10^2$). Such examples are very few, but an instance has been shown in the photoreaction of pyridine; the quenching effect might be attributed to the reaction of pyridine and the quencher.[15] These data further indicate that the quenching effect of DTT occurs by the formation of a complex of pyrazine and DTT. The photoreaction of disulfide derivatives has been reported to produce dithiol derivatives ($\Phi=1$).[16] The low reactivity of the **9** complex on irradiation may be attributed to a difficulty on the

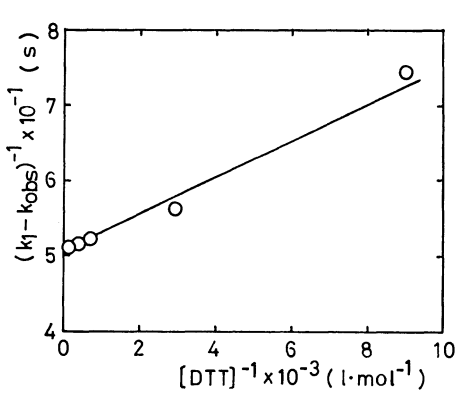

Fig. 2. Dependence of $1/(k_1-k_{obs})$ on the reciprocal of DTT. [**1e**]$=5\times10^{-5}$ mol/l.

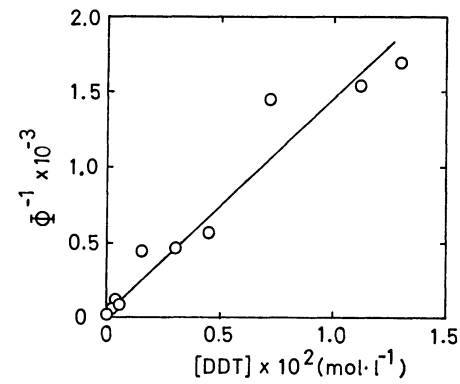

Fig. 3. Inverse quantum yields for photoreaction of **1e** (5×10^{-5} mol/l) against 1/[DTT].

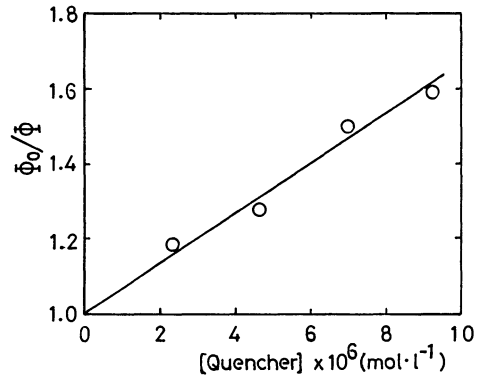

Fig. 4. Stern-Volmer plots of photoreduction of **1e** in 2-propanol solution (5×10^{-5} mol/l). The reaction was quanched by 9-fluorenone.

TABLE 4. SUBSTITUENT EFFECT ON THE PHOTOREACTION OF PYRAZINE DERIVATIVES WITH DTT IN 50% ACETIC ACID

Pyrazine	$k_1\times10^4$ s^{-1}	k_1/k_0
1a	5.22	1.0[a]
b	13.0	2.5
d	23.8	4.6
e	26.3	5.1
f	11.9	3.2

a) k_0.

formation of the disulfide derivative on irradiation.

The substituent effect of this reaction was studied, but no substituent effect was obtained, as is summarized in Table 4. This result indicates that the adduct of pyrazine with DTT as a **9** complex may have been formed.

Quenching Effects with 9-Fluorenone and Anthracene. In order to confirm the excited species, the quenching experiments were examined. The Stern-Volmer plots, which indicated a good linearity in the low-concentration areas of 9-fluorenone, are shown in Fig. 4. From the slope of Fig. 4, $k_q\tau=6.6\times10^4$ l/mol was obtained. Furthermore, from the quenching effect with anthracene, $k_q\tau=3.1\times10^4$ l/mol was obtained. As a result, a triplet state is proposed for this reaction, probably as a single excited species.

Experimental

All melting points were measured with a Yanagimoto micro melting point apparatus. The UV spectra were taken on a Hitachi ERS-3T or a Shimadzu UV-200 spectrometer. The IR spectra were measured using a Jasco IR-G spectrometer. The NMR spectra were measured with a Hitachi R-24 spectrometer using tetramethysilane as an internal standard. The mass spectra were recorded with a Hitachi RMU-6E mass spectrometer. The elementary analyses were performed at the Faculty of Pharmaceutical Sciences, Chiba University.

Materials. All materials, obtained from the Wako Pure Chemical Industries Ltd. and the Tokyo Kasei Co., were used without further purification. Dimethyl 3,6-dimethyl-2,5-pyrazinedicarboxylate (**1a**) and diethyl 3,6-dimethyl-2,5-pyrazinedicaboxylate (**1b**) were prepared by the method of Iida and his co-workers.[6]

*2,5-Diacetyl-3,6-dimethylpyrazine (**1c**).* To a solution of 200 g 2,4-pentanedione in 224 ml of acetic acid, a solution of 152 g of sodium nitrite in 270 ml of water was slowly added for 1 h below 7° C in ice bath. The solution was stirred for an hour at 30 °C and furthermore for two hours with 200 ml of water. The aqueous mixture was extracted with 200 ml of ether. The extracted liquor was neutralized, washed and dried with soldium sulfate. Romoval of the solvent gave 197 g (76 %) of white flaky crystals of 3-nitroso-2,4-pentanedione. A solution of 37.6 g of 3-nitroso-2,4-pentanedione in 120 ml of ethanol and 36 ml of acetic acid was reduced at room temperature using 4.0 g of 10% palladium charcoal as catalyst in 500 ml autoclave. The solution containing catalyst was filtered. The solvent of filtrate was removed and the residue was chromatographed on silica gel to give 14.2 g (16 %) of pale yellow needles of of **1c**, mp 99 °C, ν_{max} (KBr) 1699 cm^{-1}, λ_{max} (EtOH) 234 (ε 5200) and 298 nm (ε 8600), δ ($CDCl_3$) 2.67 (6H, s) and 2.79 (6H, s); *m/e* 192 ($M^{+\cdot}$). Found: C, 62.46; H, 6.63; N, 14.46%. Calcd for $C_{10}H_{12}N_2O_2$: C, 62.48; H, 6.63; N, 14.58%.

*2,5-Dibenzoyl-3,6-dimethylpyrazine (**1d**).* To a solution of 50 g of 1-phenyl-1,3-butanedione in 49 ml of acetic acid, a solution of 24 g of soldium nitrite in 47 ml of water was slowly added for about an hour below 25 °C in water bath. The solution was stirred for half an hour at 30 °C and was cooled to give white crystals of 1-phenyl-2-nitroso-1,3-butanedione. The solution containing the crystals was filtered and the filtrate was extracted with ether. The extracted liquor was concentrated and poured into a large quantity of water to give crystals of 57.5 g (97%) of 1-phenyl-2-nitroso-1,3-butanedione. The crystals were washed well. A solution of 17 g of 1-phenyl-2-nitroso-1,3-butanedione of 60 ml of ethanol and 20 ml of acetic acid was reduced at room temperature using 3.6 g of 10% palladium charcoal as catalyst in 500 ml autoclave. The solution containing catalyst was filtered. The solvent of filtrate was removed and the residue was dissolved in chloroform. The solution was neutralized, washed and dried with sodium sulfate. The chloroform was removed and the residue was dissolved in ethanol. Aeration of the solution for three hours gave 728 mg (2.6%) of white crystals of **1d**, mp 167—169 °C; λ_{max} (EtOH) 256 (ε 23300) and 290 nm (ε 21000); δ ($CDCl_3$) 2.59 (6H, s), 7.25—8.95 (10H, m); *m/e* 316 ($M^{+\cdot}$). Found: C, 75.97; H, 5.15; N, 8.79%. Calcd for $C_{20}H_{16}N_2O_2$: C, 75.93; H, 5.10; N, 8.86%.

*1,2,3,4,6,7,8,9-Octahydro-3,3,8,8-tetramethyl-1,6-phenazinedion (**1e**).* 5,5-Dimethyl-2-(hydroxyimino)-1,3-cyclohexanedione was prepared by the method of Hass.[17] A solution of 2 g of 5,5-dimethyl-2-(hydroxymino)-1,3-cyclohexanedione in 50 ml of ethanol was reduced using 0.2 g of 10% palladium charcoal as catalyst in 100 ml autoclave. The solution containing catalyst was filtered and the filtrate was aerated for three hours at 40—60 °C. After removal of the solvent, the separation of the reaction mixture by column chromatography gave 0.35 g (18%) of **1e**, mp 214—219 °C; λ_{max} (EtOH) 233 (ε 9400) and 317 nm (ε 9300); δ ($CDCl_3$) 1.17 (12H, s), 2.72 (4H, s), and 3.27 (4H, s); *m/e* 272 ($M^{+\cdot}$). Found: C, 70.17; H, 7.43; N, 10.11%. Calcd for $C_{16}H_{20}N_2O_2$: C, 70.17; H, 7.40; N, 10.29%.

Furthermore, **1e** was prepared by the following manner. Decahydro-3,3,8,8-tetramethyl-1,6-phenazinedione dihydrochloride (**6e**) in methanol was neutralized. The methanol was removed. The purification of the residue gave pale yellow crystals of **1e**.

*1,2,3,4,6,7,8,9-Octahydro-1,6-phenazinedione (**1f**).* Decahydro-1,6-phenazine dihydrochloride (**6f**) in methanol was neutralized. After the solvent was removed, the residue was chromatographed on silica gel to give **1f** (45%), mp 250—260 °C; λ_{max} (EtOH) 230 (ε 13700) and 317 nm (ε 15600); δ($CDCl_3$) 2.30 (4H, dt), 2.88 (4H, t), and 3.30 (4H, t); *m/e* 216 ($M^{+\cdot}$). Found: C, 66.38; H, 5.60; N, 12.75%. Calcd for $C_{12}H_{12}N_2O_2$: C, 66.65; H, 5.59; N, 12.96%

*1,2,3,4,6,7,8,9-Octahydrophenazine (**1g**).* 2-Chlorocyclohexanone was synthesized by the method of Organic Synthesis.[18] Ammonia was bubbled into a solution of 24 g of 2-chlorocyclohexanone in 350 ml of ethanol for about three hours below 7 °C in ice bath. The solution, which was added 40 ml of 3M-HCl, was extracted with four 80 ml portions of ether. Adjustment of the extracted liquor to pH 2 with sodium hydroxide gave white crystals in good yield. Upon recrystalization from acetone, **1g** was obtained as white plates, mp 108 °C; λ_{max} (EtOH) 290 nm (ε 10800), δ($CDCl_3$) 1.84 (8H, m) and 2.79 (8H, m); *m/e* 188 ($M^{+\cdot}$).

*Decahydro-3,3,8,8-tetramethyl-1,6-phenazinedione Dihydrochloride (**6e**).* 2-Amino-5,5-dimethyl-1,3-cyclohexanedion was prepared by the method of Regitz and Stadler.[19] A 10 g of 2-amino-5,5-dimethyl-1,3-cyclohexanedione was refluxed in 150 ml 15% HCl for few hours to obtain yellow crystals of **6f**. After filtration, same operation were repeated. **6f**, mp 177 °C; *m/e* 218 ($M^{+\cdot}-2HCl$). Found: C, 49.02; H, 5.48; N, 9.62; Cl, 23.94%. Calcd for $C_{12}H_{12}N_2O_2 \cdot 2HCl$: C, 49.50; H, 5.54; N, 9.62; Cl, 24.35%.

Irradiation of Pyrazine Derivatives. A solution of 2.0 g of **1a**—**d** in 2 l of diethyl ether was irradiated with a Ushio UM-425 450-W high pressure mercury lamp for six hours. After irradiation, the solvent was removed *in vacuo* at room temperature and the oily residue was chromatographed on silica gel to give **2a**—**d** and the viscous liquid of solvent adducts **3a** and **3c**. **3a** was crystalized very slowly from hexane–benzene. Using tetrahydrofuran as a solvent, **4a** and **4c** were obtained. The yields and physical data of **2**, **3**, and **4** were shown in Table 1.

*Determination of the Structure of **2**.* A solution of 200 mg of methyl 3,6-dimethyl-5-hydroxypyrazine-2-carboxylate (**2a**) in 5 ml of water containing 0.09 g of potassium hydroxide was stirred for an hour at room temperature and further for an hour at 40 °C. From the solution adjusted to pH 4—5 by dil. HCl, **2a** which had not reacted was removed by the extraction with ether. The residue was dried by repetition of azeotropy with benzene and extracted with ethanol in a Soxhlet extracter. Removal of the solvent gave 40 mg of residue. By thermolysis and sublimation of the mixture of this residue, a solid and

a liquid were obtained. Solid, mp 202 °C; λ_{max} (EtOH) 267 nm. The solid compound was identical with 3,6-dimethyl-2-pyrazinol from its melting point (lit,[7] 207 °C).

Measurement of the Reaction Rate of Pyrazine Derivatives with DTT. Equivolume of distilled water and dried acetic acid were mixed as the solvent. **1e** (3.19 mg, 1.15×10^{-5} mol) was dissolved in 50 ml of the solvent using a volumetric flask DTT (20 mg, 1.3×10^{-4} mol) was transferred to a volumetric flask and diluted to 20 ml with the solvent. From solution of DTT, an appropriate aliquot was further dilute to yield 10^{-4}—10^{-2} mol/l solution for spectral analysis. One ml of a solution of **1e** and 0—3 ml of solution of DTT were mixed in a 1 ml quartz cell and diluted to 4 ml with the solvent.

After bubbling of argon gas for an hour, a quartz cell was sealed. Consecutive irradiations of short duration were carried out with a Ushio UM-103B 100-W high pressure mercury lamp in a sealed quartz cell which was transferred periodically to the UV spectrometer for spectral recording.

The reaction rate calculated from the decrease of the peak at 318 nm (ε 12000) of **1e** or the increase of the peak at 357 nm (ε 21800) of **5e**.

Substituent Effects on the Reaction of Pyrazines. Equivolume of distilled water and dried acetic acid were mixed as the solvent. Pyrazine derivatives **1** (1.1×10^{-5} mol) was dissolved in 50 ml of the solvent. DTT (1.37 mg, 8.88×10^{-6} mol) was dissolved in 20 ml of the solvent. 1 ml of each solutions were mixed and diluted to 4 ml of the solvent in a quartz cell.

After bubbling of argon gas for an hour, irradiations were carried out with a 100-W high pressure mercury lamp. Periodically UV spectra were recorded. And the reaction rates were calculated from the decrease of the peak of the pyrazine.

Quenching of the Photoreaction of Pyrazine Derivatives. Pyrazine **1e** (3.67 mg, 1.35×10^{-5} mol) was dissolved in 50 ml of dried 2-propanol. 9-Fluorenone (3.33 mg, 1.85×10^{-5} mol) was dissolved in 100 ml of dried 2-propanol. From a solution of 9-fluorenone, an appropriate aliquot was further diluted for spectral analysis. One ml of a solution of **1e** and 0—3 ml of a diluted solution of 9-fluorenone were mixed in a 1 ml quartz cell and diluted to 4 ml with dried 2-propanol. In analogy with measurement of substituent effects, the reaction rates were measured: a linear Stern-Volmer plots of $\Phi_0/\Phi(=k_0/k)$ *vs.* concentration of quencher was obtained with $k_q\tau=6.6\times10^4$ l/mol.

From the quenching effect of **1e** (5.5×10^{-5} mol/l) with anthracene in dried acetic acid, $k_q\tau=3.1\times10^4$ l/mol was obtained.

References

1) K. Yamada, T. Konakahara, S. Ishihara, T. Itoh, K. Kimura, and H. Iida, *Tetrahedron Lett.*, **1972**, 2513; K. Yamada, T. Konakahara, and H. Iida, *Bull. Chem. Soc. Jpn.*, **46**, 2504 (1973); K. Yamada, M. Kamei, Y. Nakano, H. Kasimura, and H. Iida, *Tetrahedron Lett.*, **1974**, 1741.

2) A. Padwa and E. Glazer, *J. Am. Chem. Soc.*, **94**, 7788 (1972); A. Padwa, M. Dharan, J. Smolanoff, and S. I. Wetmore, Jr., *J. Am. Chem. Soc.*, **95**, 1945 (1973); *ibid.*, **95**, 1954 (1973).

3) R. D. Chambars, J. R. Maslzkiewicz, and K. C. Srivastava, *J. Chem. Soc. Perkin. Trans. 1*, **1975**, 1130.

4) F. Lahmank and N. Ivanoff, *Tetrahedron Lett.*, **1967**, 3913.

5) C. Dufraisse, A. Etienne, and E. Toromanoff, *C. R. Acad. Sci.*, **235**, 759 (1952); E. Toromanoff, *Ann. Chem. (Paris)*, **1**, 115 (1956); T. Iwaoka, S. Niizima, and M. Koizumi, *Bull. Chem. Soc. Jpn.*, **43**, 2786 (1970); D. N. Bailey, D. K. Roi, and D. M. Herucles, *J. Am. Chem. Soc.*, **90**, 6291 (1968); S. Wake, Y. Otuji, and E. Imoto, *Bull. Chem. Soc. Jpn.*, **47**, 1251 (1974).

6) H. Iida, K. Hayashida, M. Yamada, K. Takahashi, and K. Yamada, *Synth. Commun.*, **3**, 225 (1973).

7) W. Sparp and F. S. Spring, *J. Chem. Soc.*, **1948**, 1862.

8) S. M. Japar and E. W. Abrahamson, *J. Am. Chem. Soc.*, **93**, 4140 (1971).

9) H. Beinert, *J. Am. Chem. Soc.*, **78**, 5323 (1956); J. H. Swinehart, *ibid.*, **87**, 904 (1965); *ibid.*, **88**, 1056 (1966); Q. H. Gibson, V. Massey, and N. M. Atherton, *Biochem. J.*, **85**, 369 (1962); F. Muller, P. Hemmerrich, A. Ehrenberg, G. Palmer, and V. Massey, *Eur. J. Biochem.*, **14**, 185 (1970).

10) H. I. X. Mager and W. Berends, *Tetrahedron Lett.*, **1973**, 4051.

11) S. Shinkai, *Kagaku*, **30**, 39 (1975).

12) T. C. Bruice, L. Main, S. Smith, and P. Y. Bruice, *J. Am. Chem. Soc.*, **93**, 7327 (1971); E. L. Loecher and T. C. Hollocher, *ibid.*, **97**, 3235 (1975); I. M. Gascoigne and G. K. Radda, *Biochim. Biophys. Acta*, **131**, 498 (1967).

13) H. Lineweaver and D. Burk, *J. Am. Chem. Soc.*, **56**, 658 (1934).

14) C. G. Hatchard and C. A. Parke, *Proc. R. Soc. London, Ser. A*, **235**, 518 (1965).

15) T. J. van Berger and R. M. Kellogg, *J. Am. Chem. Soc.*, **94**, 8451 (1971).

16) C. C. Price, "Geometry of Molecule," McGraw-Hill, New York (1969).

17) P. Haas, *J. Chem. Soc.*, **91**, 1437 (1907).

18) M. S. Newman, M. D. Farbman, and H. Hipsher, *Org. Synth.*, Coll. Vol. III, 188 (1955).

19) M. Regitz and D. Stadler, *Justus Liebigs Ann. Chem.*, **687**, 214 (1965).

The Reaction of Monoketones with Manganese(III) Acetate

Masayoshi OKANO and Takaaki ARATANI

Faculty of Integrated Arts and Sciences, Hiroshima University, Higashisenda-machi, Hiroshima 730

(Received March 19, 1976)

When acetone, ethyl methyl ketone (EMK), and cyclohexanone were heated with manganese(III) acetate dihydrate in a mixed solvent of glacial acetic acid and acetic anhydride at 100 °C, acetoxy ketones were obtained as common products. Furthermore, ketone dimers (1,4-diketones) were obtained from acetone and cyclohexanone, which also gave 1,2,3,4-tetrahydrodibenzofuran. When mixtures of these ketones and 1-hexene were heated with the oxidant, saturated and unsaturated ketones and γ-acetoxy ketones were obtained as common products, and 2-propylchromene was obtained as a new product from the cyclohexanone–1-hexene mixture. The formation courses of these reaction products are discussed.

In the previous paper,[1] it was established that the reaction of alkenes with manganese(III) acetate in carboxylic acid solvents containing acid anhydride proceeds through a solvent-participating free radical reaction mechanism. α-Carboxyalkyl or acyloxy radicals are formed in the first step by abstraction of a hydrogen atom on the α-carbon or that in the carboxyl group of the carboxylic acid by an acetoxyl radical produced directly from the oxidant; then these redicals may add to the alkenes. Furthermore, acid anhydride accelerates the reaction rate by abstraction of hydrated water from the oxidant.

The reaction of ketones–alkenes mixtures[2,3] and ketones–enol esters mixtures[4] with manganese(III) acetate have been studied in considerable detail. Heiba *et al.*[3] reported that 2-undecanone, unstaurated ketone, and keto acetate were obtained from an acetone–1-octene mixture (27 : 1) at 85 °C in glacial acetic acid containing potassium acetate; they proposed an electron transfer mechanism (formation of carbonium ion) through a radical addition.

In the present investigation, the formation of the characteristic products, such as ketone dimers (**2** and **6**) and the acetoxy ketones (**2**, **3**, **4**, and **5**), requires the generation of the ketonyl radical and the manganese acetate radical(I)[1] which are not easily further oxidized. To account for these facts the reaction course in Scheme 1 is proposed as reasonable.

Results and Discussion

The Reaction of Monoketones with Manganese(III) Acetate. When acetone was heated with manganese(III) acetate in a mixture of glacial acetic acid and acetic anhydride (1 : 1, v/v, solvent A), acetonyl acetate (**1**, 30%) and acetonylacetone (**2**, 9%) were obtained. In the case of EMK, 1-acetoxy-2-butanone (**3**, 15%) and 3-acetoxy-2-butanone (**4**, 6%) were obtained, while in the case of cyclohexanone, 2-acetoxycyclohexanone (**5**, 18%), bicyclohexane-2,2′-dione (*meso*(**6a**): 3%, *dl*(**6b**): 5%), and 1,2,3,4-tetrahydrodibezofuran (**7**, 4%) were obtained. Thus, α-acetoxy ketones (**1**, **2**, **3**, **4**, **5**) and dimers (**2**, **6a**, **6b**) were obtained as the major products.

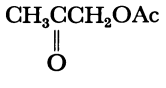

1

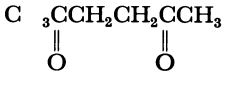

2

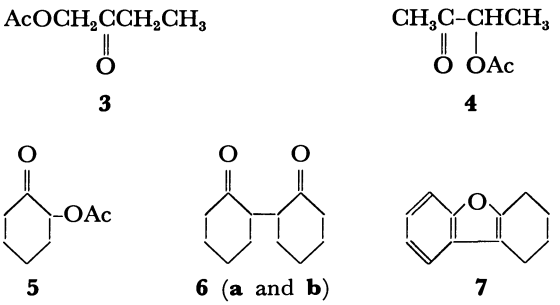

3 **4** **5** **6** (**a** and **b**) **7**

These results suggest the formation of α-keto radicals and an acetoxyl radical, which should be stabilized within the coordination sphere of the manganese(II) ion.[1] The α-acetoxy ketones may be formed by the addition of the acetoxyl radical to each α-keto radical, because the α-keto radical is not easily oxidized due to the electron-withdrawing character of the carbonyl group.[5]

The Reaction of Cyclohexanone–1-hexene Mixture with Manganese(III) Acetate. When the cyclohexanone–1-hexene mixture was heated with manganese(III) acetate in solvent A, a new type of 2-propylchromene (**8**, 13%) was obtained as a major product, in addition to the known types[2,3] of 2-(2-acetoxyhexyl)cyclohexanone (**9**, this is a mixture of the two diastereoisomeric **9a** and **9b** types, in the ratio 8% : 8%), 2-hexylcylohexanone (**10**, 6%), 2-(1-hexenyl)cyclohexanone (**11**, 8%), 2-(2-hexenyl)cyclohexanone (**12**, 4%), 4-acetoxyoctanoic acid (**13**, 4%), and 4-octanolide (**14**, 12%).

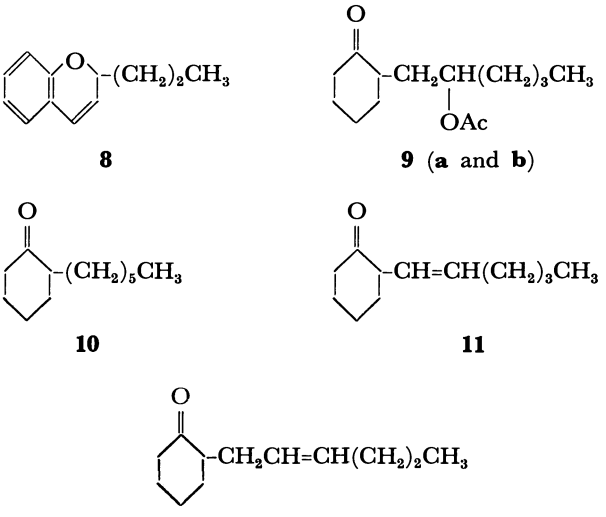

8 **9** (**a** and **b**) **10** **11** **12**

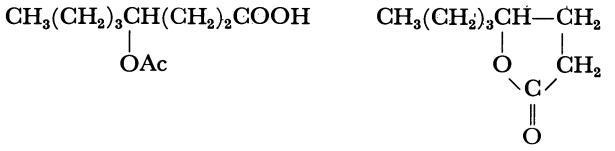

13 14

Of these products, **8**, **9a**, **9b**, **10**, **11**, and **12** may be obtained by the oxidative coupling of cyclohexanone and 1-hexene, and **13** and **14** by the reaction of solvent acetic acid and 1-hexene. Thus, the reaction might proceed through two pathways; the former would be predominant, because the total yield of the former is 47% and of the latter is 24%. The latter reaction may proceed through the radical course explained previously[1] and the former by a similar course.

When 1-decene was used instead of 1-hexene, 2-heptylchromene (**15**) and the known types of compounds were obtained. The formation of these chromene derivatives is very interesting because it is a novel tocopherol synthesis.

The products obtained by using 1-octene and 1-nonene instead of 1-hexene were identified as the same types of compounds as those obtained in the case of 1-hexene by their relative retention times in GLC.

The Reaction Course of Ketone–Alkene Mixtures. On the basis of the formation of α-acetoxyketones and ketone dimers, the reaction of ketones may proceed as shown in Scheme 1. First, manganese(III) acetate dihydrate is dehydrated by acetic anhydride or heating to give anhydrous manganese(III) acetate. By heating, the anhydrous manganese(III) acetate changes to a manganese acetate radical(I)[1] in which the acetoxyl radical is prevented from decomposing. The radical (I) then abstracts a hydrogen atom on the α-position or the caboxyl group in acetic acid to give carboxymethyl radical(II) or acetoxyl radical(III), which is somewhat stabilized by the formation of I. A hydrogen atom on the α-position of ketone also abstracted by the radical(I) to give an α-keto radical(IV or V). The keto radical may react with I to form α-acetoxy ketones (**1** or **5**) or react with each keto radical to form dimers (**2** or **6a** and **6b**). Furthermore, **6a** and **6b** may be enolized, dehydrated, and dehydrogenated in the allylic positions to give 1,2,3,4-tetrahydrodibenzofuran (**7**).

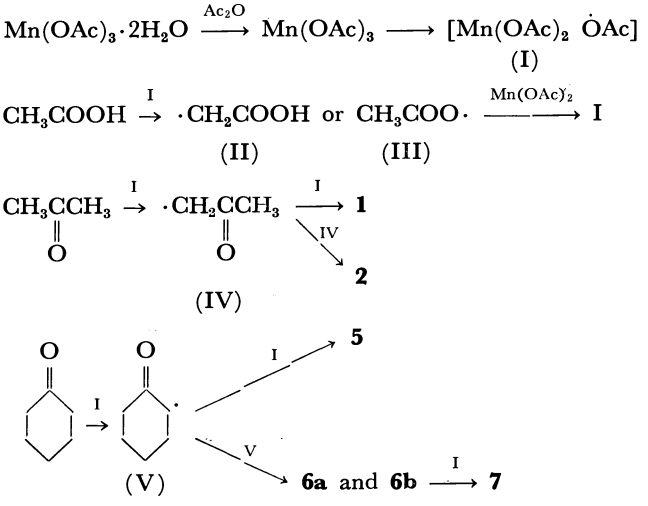

Scheme 1.

On the basis of the above results, the reaction of the ketone–alkene mixture may proceed as shown in Scheme 2. The α-keto radical(V) adds to the alkenes in the first step to form the radical intermediate(VI), which may be converted to γ-acetoxy ketones (**9a** and **9b**) by the reaction between VI and I. The intermediate(VI) may also be converted to unsaturated ketones (**11** and **12**) or to a saturated one (**10**) by abstraction or addition of a hydrogen atom. Furthermore, **12** may be converted to chromene derivatives (**8**) by cyclization of enol and abstraction of allylic hydrogens.

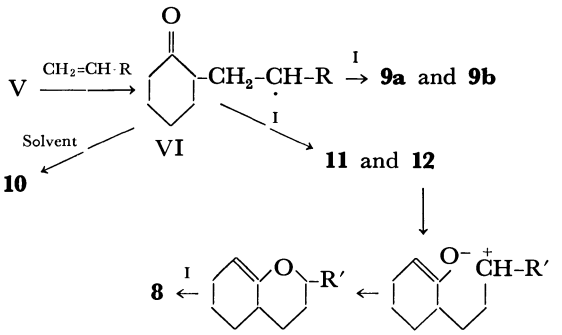

Scheme 2.

The formation of 4-acetoxyoctanoic acid (**13**) and the corresponding γ-lactone (**14**) suggests that the reaction of ketone-alkene mixtures proceeds through a pathway similar to that in the reaction of alkenes with manganese(III) acetate in solvent A,[1] in addition to the pathway in Scheme 2.

Experimental

The analytical and preparative GLC were carried out on a Hitachi 023 gas chromatograph equipped with a thermocouple detector in connection with a stainless steel column (3 mm in diameter) which was packed with Celite 545 (40—60 mesh) impregnated with 20% PEG-20 M or 25% DEGS. The NMR spectra were determined on a JEOL model JNM-MH-60 spectrometer in CCl_4 or $CDCl_3$ with an internal reference of tetramethylsilane. The mass spectra were taken on a Hitachi RMS-4 instrument at 70 eV ionization voltage and 200 °C ionization chamber temperature.

Preparation of Manganese(III) Acetate Dihydrate. $Mn(OAc)_2 \cdot 4H_2O$ was oxidized with potassium permanganate according to a modification of the procedure of Heiba.[3] The crystallized $Mn(OAc)_3 \cdot 2H_2O$ which filtered up from the reacted mixture was washed with ether and preserved over sodium hydroxide *in vacuo* for a week. The purity was 99%, according to iodometric titration.

Reaction of Acetone, EMK, and Cyclohexanone with Manganese(III) Acetate. Acetone(5.8 g, 100 mmol), EMK(7.2 g, 100 mmol), and cyclohexanone(9.8 g, 100 mmol) were each added to a solution of manganese(III) acetate (53.6 g, 200 mmol) in a mixed solvent of acetic acid and acetic anhydride(v/v, 1 : 1, solvent A, 400 ml) drop by drop at 70 °C in flowing nitrogen. The mixture was then heated up to 100 °C with stirring. When the brown color of the Mn(III) ions disappeared, the stirring was stopped and the reaction mixture was cooled, diluted with ether (*ca.* 300 ml), and neutralized with sodium carbonate. The precipitate was filtered off and washed with ether, and the mother liquor was evaporated away, leaving brown oily substances. The

oily substances were then separated by a combination of column chromatography (100—200 mesh silica gel, hexane-ethyl acetate(4:1, v/v)), and preparative gas chromatography into individual compounds. Their characterizations were carried out as follows:

*Reaction Products of Acetone. Acetonyl Acetate (**1**)*: This compound was isolated as a colorless liquid by preparative GLC(DEGS, 2m, 160 °C, t_R 1.8 min) from the reaction mixture. $C_5H_{18}O_3$(MS). *m/e* 116(42%, M^+), 73 (22%, $C_3H_5O_2$), 43(100%, C_2H_3O); $\delta^{CCl_4}_{ppm}$ 2.10 s (6H), 4.45 s (2H). The IR spectrum coincided with that of authentic acetonyl acetate.[6]

*Acetonylacetone (**2**)*: This compound was isolated as a colorless liquid. $C_6H_{10}O_2$(MS). *m/e* 114(40%, M^+), 99 (48%, M^+-CH_3), 71 (48%, $M^+-C_2H_3O$), 43 (100%, C_2H_3O); $\delta^{CCl_4}_{ppm}$ 2.10 s (6H), 4.45 s (4H). The IR spectrum coincided with that of authentic acetonylacetone.[6]

*Reaction Products of EMK. 1-Acetoxy-2-butanone (**3**)*: A colorless liquid. n_D^{25} 1.4189. $C_6H_{10}O_3$(MS). *m/e* 130 (4%, M^+), 73(8%, $M^+-C_3H_5O$), 57(63%, C_3H_5O), 43 (100%, C_2H_3O); $\delta^{CCl_4}_{ppm}$ 1.08 t (3H, J=7 Hz), 2.15 s (3H), 2.45 q (2H, J=7 Hz), 4.65 s (2H); ν^{neat}_{max} 1750(ester), 1735 (ketone), 1230(acetate).

*3-Acetoxy-2-butanone (**4**)*: A colorless liquid. $\delta^{CCl_4}_{ppm}$ 1.39 d (2H, J=7 Hz), 2.15 s (6H), 5.06 q (1H, J=7 Hz); ν^{neat}_{max} 1740(ester), 1235(acetate).

*Reaction Products of Cyclohexanone. 2-Acetoxycyclohexanone (**5**)*: A colorless liquid. n_D^{25} 1.4571. $C_8H_{12}O_3$(MS). *m/e* 156(12%, M^+), 113(56%, $M^+-C_2H_3O$), 96(14%, $M^+-C_2H_4O_2$), 43(100%, C_2H_3O); $\delta^{CCl_4}_{ppm}$ 2.05 s (3H), 4.95 t (1H, J=6 Hz); ν^{neat}_{max} 1750(ester), 1720(ketone), 1240(acetate).

meso-*Bicyclohexane-2,2'-dione (**6a**)*: A colorless crystal. mp 60—61 °C. $C_{12}H_{18}O_2$(MS). *m/e* 194(39%, M^+), 98 (100%, $M^+-C_6H_8O$), 97(73%, $M^+-C_6H_9O$); $\delta^{CCl_4}_{ppm}$ 1.85 m (12H), 2.21 t (4H, J=6 Hz), 2.74 d (2H, J=14 Hz); ν^{KBr}_{max} 1710(ketone).

dl-*Bicyclohexane-2,2'-dione (**6b**)*: A colorless liquid. $C_{12}H_{18}O_2$(MS). *m/e* 194 (3%, M^+), 98 (100%, $M^+-C_6H_8O$), 97(42%, $M^+-C_6H_9O$); $\delta^{CCl_4}_{ppm}$ 1.85 m (12H), 2.23 m (6H); ν^{neat}_{max} 1710(ketone). A mixture (0.1 g) of **6a** and **6b** was allowed to undergo a pyrrole reaction which gave 1,2,3,4,5,6,7,8-octahydrocarbazole(dark green crystal, mp 88—90 °C). $C_{12}H_{17}N$(MS). *m/e* 175 (100%, M^+); $\delta^{CCl_4}_{ppm}$ 1.63 bs (8H), 2.24 m (8H), 6.64 m (1H); ν^{Nujol}_{max} 3350(NH).

*1,2,3,4-Tetrahydrodibenzofuran (**7**)*: A colorless liquid. n_D^{25} 1.5732. $C_{12}H_{12}O$ (MS). *m/e* 172 (76%, M^+); λ^{EtOH}_{max} 252 (ε=12200), 279(ε=4700), 286(ε=4300) nm. This compound was refluxed in xylene with chloranil to give dibenzofuran, which was identified by comparing its t_R with that of the authentic one.

Reaction of Cyclohexanone-1-hexene Mixture with Manganese(III) Acetate. Cyclohexanone–1-hexene mixture (100 mmol : 100 mmol) was added to a solution of manganese(III) acetate(53.6 g, 200 mmol) in the solvent A (400 ml) drop by drop at 100 °C in flowing nitrogen; the mixture was carried out as in the reaction of ketone. The reaction products were identified as follows:

*2-Propylchromene (**8**)*: A colorless liquid. n_D^{25} 1.5199. $C_{12}H_{14}O$ (MS and elementary analysis). *m/e* 174.1045(62%, M^+, calcd *m/e*: 174.1045), 131(100%, $M^+-C_3H_7$); Found: C, 83.07; H, 8.16%. Calcd for $C_{12}H_{14}O$: C, 82.70; H, 8.11%. $\delta^{CCl_4}_{ppm}$ 0.95 t (3H, J=6 Hz), 1.23—1.70 m (4H), 2.16—2.83 m (2H), 6.27 bs (1H), 7.00—7.37 m (4H); ν^{neat}_{max} 3050 and 1600(aromatic), 1250(phenyl ether).

*2-(2-Acetoxyhexyl)cyclohexanone (**9a** and **9b**)*: **9a** and **9b**, diastereoisomers, were separated by a preparative GLC as colorless liquids. **9a**: $C_{14}H_{24}O_3$(MS). *m/e* 240(1%, M^+), 197 (3%, $M^+-C_2H_3O$), 180(25%, $M^+-C_2H_4O_2$), 98(100%, $C_6H_{10}O$), 43 (71%, C_2H_3O); $\delta^{CCl_4}_{ppm}$ 0.93 t (3H, J=5 Hz), 1.39 s (3H), 2.15 m (5H); ν^{neat}_{max} 1735(ester), 1710(ketone), 1250 (acetate). **9b**: $C_{14}H_{24}O_3$(MS). *m/e* 240 (1%, M^+), 197 (1%, $M^+-C_2H_3O$), 180(23%, $M^+-C_2H_4O_2$), 98(100%, $C_6H_{10}O$), 43 (71%, C_2H_3O); $\delta^{CCl_4}_{ppm}$ 0.93 t (3H, J=5 Hz), 1.37 m (12H), 1.96 s (3H), 2.24 m(5H), 4.80 m (1H); ν^{neat}_{max} 1735(ester), 1710(ketone), 1250(acetate).

A mixture of **9a** and **9b** (0.4 g) was treated with LAH (0.4 g) in dried ether to give two diols (0.35 g), which were separated by a preparative GLC. The easily moving diol (colorless oil): $C_{12}H_{24}O_2$(MS). *m/e* 182(6%, M^+-H_2O), 164(16%, M^+-2H_2O), 143(17%, C_4H_9), 125(64%, M^+-H_2O C_4H_9), 107(33%, $M^+-2H_2O-C_4H_9$), 98(100%, $C_6H_{10}O$), 57(26%, C_4H_9); $\delta^{CCl_4}_{ppm}$ 0.90 t (3H, J=5 Hz), 1.34 m (17H), 3.05—3.80 m (2H), 4.44 bs (2H, exchangeable for D_2O); ν^{neat}_{max} 3320 (associated OH). The slowly moving diol (colorless oil): $C_{12}H_{24}O_2$(MS). *m/e* 182(9%, M^+-H_2O), 164(11%, M^+-2H_2O), 143(17%, $M^+-C_4H_9$), 125(88%, $M^+-H_2O-C_4H_9$), 98(100%, $C_6H_{10}O$), 57(53%, C_4H_9); $\delta^{CCl_4}_{ppm}$ 0.90 t (3H, J=5 Hz), 1.33 m (17H), 3.00—3.83 m (2H), 4.65 m (2H, exchangeable for D_2O); ν^{neat}_{max} 3300(associated OH). A mixture of these diols(0.20 g) was treated with Jones reagent(0.6 ml) to give diketone (0.15 g): $C_{12}H_{20}O_2$ (MS). *m/e* 196 (24%, M^+), 139 (90%, $M^+-C_4H_9$), 111 (100%, $M^+-C_5H_9O$), 85(54%, C_5H_9O), 57(60%, C_4H_9); ν^{neat}_{max} 1710(ketone). Another mixture of **9a** and **9b** (0.4 g) was heated at 250 °C for 1 h to give acetic acid, **11**, and **12** which were identified by an admixing GLC of the autherntic samples.

*2-Hexylcyclohexanone (**10**)*: A colorless liquid. $C_{12}H_{22}O$(MS). *m/e* 182(10%, M^+), 98(100%, $C_6H_{10}O$); $\delta^{CCl_4}_{ppm}$ 0.93 t (3H, J=5 Hz), 1.25 bs(10H), 1.92 m (6H), 2.15 m (3H); ν^{neat}_{max} 1710(ketone).

*2-(1-Hexenyl)cyclohexanone (**11**)*: A colorless liquid. $C_{12}H_{20}O$(MS). *m/e* 180(39%, M^+), 98(100%, $C_6H_{10}O$); $\delta^{CCl_4}_{ppm}$ 0.89 t (3H, J=6 Hz), 1.3—1.9 m (12H), 2.22 m (3H), 5.35 m (2H); ν^{neat}_{max} 1710(ketone), 970(C=C).

*2-(2-Hexenyl)cyclohexanone (**12**)*: A colorless liquid. $C_{12}H_{20}O$(MS). *m/e* 180(33%, M^+), 98(100%, $C_6H_{10}O$); $\delta^{CCl_4}_{ppm}$ 0.91 t (3H, J=6 Hz), 1.3—1.9 m (12H), 2.20 m(3H), 5.34 m (2H); ν^{neat}_{max} 1710 (ketone), 970 (C=C). A mixture of **11** and **12** (0.30 g) was hydrogenated in ethanol (70 ml) at 45 °C for 2 h using Raney nickel (W-2, 0.5 g) under a hydrogen pressure of 55 kg/cm² to give **10** (*ca.* 0.2 g). Another mixture of **11** and **12** (0.1 g) was oxidized with potassium permanganate in water (50 ml) at 50 °C for 2 h. The reacted mixture was acidified with 10% sulfuric acid, extracted with ether, then methylated with diazomethane to give methyl esters of butanoic and pentanoic acids, which were identified by an admixing GLC of the authentic samples.

*4-Acetoxyoctanoic Acid (**13**)*: A colorless liquid. n_D^{25} 1.4563. The spectral data coincided with those of the authentic sample obtained by the reaction of 1-hexene with mangnese(III) acetate in the solvent A.[1] **13** (0.18 g) was treated with LAH (0.18 g) to give 1,4-octanediol (0.15 g): $C_8H_{18}O_2$(MS). *m/e* 115(26%, M^+-CH_3O), 71(71%, $M^+-C_4H_9$), 69(55%, $M^+-C_3H_7O$), 59(18%, C_3H_7O), 57(34%, C_4H_9); $\delta^{CCl_4}_{ppm}$ 0.91 t (3H, J=5 Hz), 1.36—1.53 m (12H), 3.55 m (3H), 4.54 bs (2H, exchangeable for D_2O); ν^{neat}_{max} 3325 (associated OH), 1055 (prim. OH). This diol (0.13 g) was oxidized with Jones reagent (0.5 ml) to give 4-octanolide (0.10 g), which was identified by an admixing GLC and by comparing the IR and mass spectra with those of the authentic sample.

*4-Octanolide (**14**)*: A colorless liquid. This compound was identified by an admixing GLC and by comparing

the IR spectrum with that of the authentic sample.

2-Heptylchromene(**15**, colorless liquid) was obtained by the reaction of cyclohexanone-1-decene mixture with the oxidant. $C_{16}H_{22}O$ (MS and elementary analysis). *m/e* 230.1692(29%, M^+, calcd for $C_{16}H_{22}O$: 230.1671), 131 (100%, $M^+-C_7H_{15}$); Found: C, 83.60; H, 9.67%. Calcd for $C_{16}H_{22}O$: C, 83.41%; H, 9.64%. $\delta_{ppm}^{CCl_4}$ 0.89 t (3H, $J=5$ Hz), 1.30 bs (12H), 2.47 t (2H, $J=7$ Hz), 6.29 s (1H), 7.0—7.5 m (4H); ν_{max}^{neat} 3050 and 1600(aromatic), 1255(phenyl ether).

References

1) M. Okano, *Bull. Chem. Soc. Jpn.*, **49**, 1041 (1976).

2) M. G. Vinogradov, S. P. Ve Cenchikov, and C. I. Nikishin, *Chem. Abstr.*, **75**, 5162 (1971).

3) E. I. Heiba and R. M. Dessau, *J. Am. Chem. Soc.*, **93**, 524 (1971).

4) E. I. Heiba and R. M. Dessau, *J. Am. Chem. Soc.*, **94**, 2888 (1972).

5) J. K. Kochi and D. M. Mog, *J. Am. Chem. Soc.*, **87**, 522 (1965).

6) C. J. Pouchert, "The Aldrich Library of Infrared spectra," (Aldrich Chemical Co., Inc., USA, 1970), p. 195 and p. 305.

Synthesis of 4-Amino-2-hydroxybutanoic Acid and Its 3-Methyl Derivative

Hiroko SATO, Takenori KUSUMI, Kyoto IMAYE, and Hiroshi KAKISAWA

Department of Chemistry, Tokyo Kyoiku University, Otsuka, Tokyo 112

(Received December 4, 1975)

1,3-Dipolar addition of the nitronic ester (**3**) to methyl acrylate afforded regiospecifically the isoxzolidine (**4**), which produced the oxime ether (**7**) on heating. Reduction of **7** followed by hydrolysis gave the hydroxy amino acid (**6**), which is known to improve anitibiotic activities. The nitronic ester (**3**) also reacted regio- and stereospecifically with methyl crotonate to produce the adduct (**8**). Pyrolysis of (**8**) followed by reduction and hydrolysis gave the *erythro* hydroxy amino acid (**11**).

Recent investigation of the modification of antibiotics disclosed that acylation of kanamycin with L-4-amino-2-hydroxybutanoic acid (**6**) at the C-1 amino group of deoxystreptamine moiety improved the antibiotic activities;[1] the acylated kanamycin inhibited some kanamycin resistant microorganisms including *Psudomonas* species. This amino acid, 4-amino-2-hydroxybutanoic acid (**6**), was discovered as a constituent of an antibiotic butyrosin,[2] and had been synthesized[2] from 2-hydroxybutyrolactone in conjunction with the synthesis of deoxyeritadenine. In the course of studies on the new annelation reaction we have found that, whereas the nitronic ester (**1**) was not cyclized by intramolecular 1,3-dipolar cycloaddition of the nitronic ester group to the isolated double bond,[4] **1** was regiospecifically condensed to an acrylate or acrylonitrile to give isoxazolidines (**2a** and **2b**). The fuctionalities in the adduct (**2a**), an oxygen atom at α-position and a nitrogen atom at γ-position to the carboxy ester group indicate a new synthetic route to the 4-amino-2-hydroxybutanoic acid (**6**).

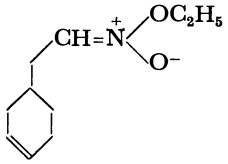

(**1**)

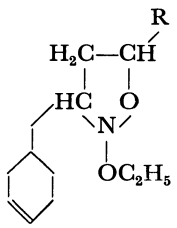

(**2a**; R=$COOCH_3$)
(**2b**; R=CN)

This paper deals with a new synthesis of 4-amino-2-hydroxybutanoic acid (**6**) and its 3-methyl derivative (**11**) from the adducts of the nitronic ester (**3**) with methyl acrylate and metyl crotonate.

Many methods are known for the preparation of nitronic esters. The *O*-alkylation of sodium, potassium, or silver salts of nitroalkanes with alkyl halides has been examined extensively. The initial product is found to be nitronic esters, but they decompose easily to form oximes and carbonyl compounds. The ester (**3**) was thus prepared by the ethylation of sodium salt of nitromethane with triethyloxonium fluoroborate at 0 °C,[6] the ester being used for the reaction with methyl acrylate without purification. The cycloaddition reaction proceeded smoothly at −10 °C to yield a 1 : 1-adduct. Although two structures, (**4**) and (**5**), were considered feasible for the adduct, the NMR spectrum and TLC showed the exclusive formation of **4**. The spectrum showed a double-doublet at 4,66 assignable to the proton at C-5 besides other signals consistent with structure (**4**).

The isoxazolidine (**4**) was quantitatively converted into a mixture of *syn*- and *anti*-oxime ethers (**7**) on heating at 100 °C. The NMR spectrum of the mixture showed two signals with almost equal intensities at 7.40 and 6.75, which are assignable to protons attached to imino carbon atoms of *syn*- and *anti*-oxime ethers, respectively. Catalytic hydrogenation of the oxime ethers over platinum oxide afforded methyl 4-amino-2-hydroxybutanoate in a good yield. Acid catalyzed hydrolysis and purification by ion exchange chromatography afforded the hydroxy amino acid (**6**) in 37% overall yield from adduct (**4**). The NMR spectrum and R_f value in paper chromatography of the synthetic hydroxy amino acid (**6**) were identical with those of natural 4-amino-2-hydroxybutanoic acid.

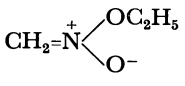

(**3**)

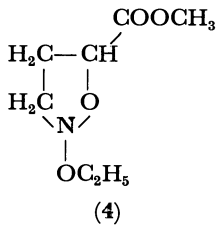

(**4**)

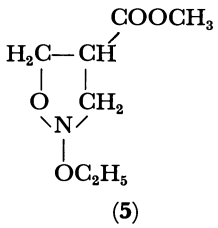

(**5**)

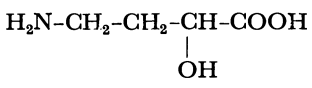

(**6**)

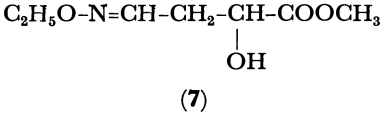

(**7**)

Regiospecificity of the 1,3-dipolar addition of the nitoronic ester (**3**) was also observed when **3** reacted with methyl crotonate. The structure of the cycloaddition product (**8**) was determined from the spectra, and the stereochemistry was assigned from the reaction mechanism. Huisgen *et al.*[7] reported that intermolecular cycloaddition of the nitrone (**9**) to methyl crotonate proceeds regiospecifically to give the isoxazolidine (**10**). The discrepancy in the regiospecificity of the two reactions would be explained in terms[8] o diffference of electron distribution in the nitronic ester and the nitrone.

The isoxazolidine (**8**) was converted into the *erythro* hydroxy amino acid (**11**) in the same manner as described above. Isomerization of **8** to the corresponding oxime ether at 200 °C, followed by catalytic hydrogenation and hydrolysis yielded 4-amino-*erythro*-2-hydroxy-3-methylbutanoic acid (**11**).

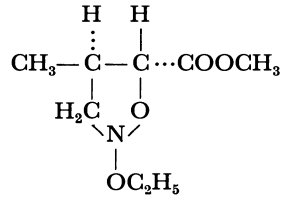

(**8**)

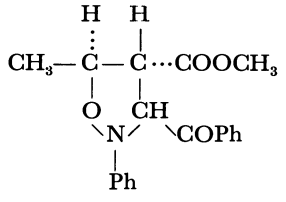

(**10**)

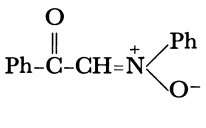

(**9**)

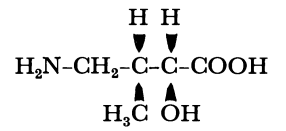

(**11**)

Experimental

NMR spectra were obtained with a Hitachi H-60 instrument using TMS as an internal standard. All the infrared spectra were taken on a Hitachi EPI-S2 spectrophotometer. Melting points and boiling points are uncorrected.

*Methyl 2-Ethoxy-5-isoxazolidinecarboxylate (**4**) and Methyl 4-Ethoxyimino-2-hydroxybutanoate (**7**).* A 1.8 M solution of sodium ethoxide in ethanol (300 ml; 0.54 mol) was added to nitromethane (30 g ; 0.50 mol) with stirring at room temperature. The mixture was stirred for 20 min, and the solvent was removed with a suction pump at 40°. The resulting sodium salt of nitromethane was dried *in vacuo* for 3 h. To this was added dry dichloromethane (400 ml), and the suspension was cooled at −5 °C. A solution of triethyloxonium fluoroborate (100 g ; 0.53 mol) in dichloromethane (80 ml) was added to the suspension under nitrogen atmosphere during 5 min, and the mixture was stirred for 15 min at −5 °C. Freshly distilled methyl acrylate (46.8 g ; 0.55 mol) was added to the ethyl nitronate solution, and the reaction mixrure was allowed to stand at −15 °C overnight. The precipitates were filtered away, and the filtrate was evaporated. Distillation yielded **4** (8.1 g) ; bp 95—99 °C/10 Torr; ν_{max} (CCl_4) : 1735 cm^{-1} ; δ(CCl_4) : 1.20 (3H, t, J=6 Hz), 2.2—3.3 (2H, m), 3.60 (2H, t, J=5.5 Hz), 3.78 (3H, s), 3.90 (2H, q, J=6 Hz), and 4.66 (1H, dd, J=5 and 9 Hz ; *m/e* 175 (M^+), 146 (M^+-OCH_3), 130 ($M^+-OC_2H_5$), and 129 ($M^+-HOC_2H_5$). Found: *m/e* 175.083. Calcd for $C_7H_{13}NO_4$: 175.084. Another fraction with higher boiling point, 78.5 °C/4 Torr, was found to be the oxime ether (**7**) (19.5 g); δ(CCl_4) : 1.25 (3H, t, J=6 Hz), 2.5—3.4 (1H, m), 3.80 (3H, s), 4.05 (1H, q, J=6 Hz), 4.10 (1H, q, J=6 Hz), 4.40 (1H, t, J=6.5 Hz), 6.75 (1/2H, t, J=5 Hz), and 7.40 (1/2H, t, J=6 Hz). Found : C, 48.04 ; H, 7.19 ; N, 8.32%. Calcd for $C_7H_{13}NO_4$: C, 47.99 ; H, 7.19 ; N, 8.00%. The adduct (4) was quantitatively converted to the oxime ether (**7**) on heating at 100 ° for 1 h.

*4-Amino-2-hydroxybutanoic Acid (**6**).* The oxime ether (**7**) (2.0 g ; 11.4 mmol) was hydrogenated over platinum oxide (400 mg) in methanol (8 ml) in the presence of concentrated hydrochloric acid (1.3 ml). Crude methyl 4-amino-2-hydroxybutanoate (1.8 g) was heated with 6M hydrochloric acid (20 ml) for 6 h. The product was adsorbed on a cation exchanger (Amberlite Type I CG 120) (13 g). Elution with water afforded the recovered methyl ester, and with 0.5% aqueous ammonia 4-amino-2-hydroxybutanoic acid (**6**) (469 mg ; 37% from **7**) ; mp 189—190 °C (lit,[1] 191—192 °C) ; δ(D_2O) : 2.08 (2H, m), 3.12 (2H, t), and 4.12 (1H, dd).

*Methyl 2-Ethoxy-4-methyl-5-isoxazolinecarboxylate (**8**).* The procedure was essentially the same as that for the preparation of **4**. Nitromethane (15 g) was converted to sodium salt, and treated with triethyloxonium fluoroborate (31 g) and methyl crotonate (17 ml). The mixture was allowed to stand at −15 °C overnight. Distillation afforded **8** (950 mg) ; bp 65—66 °C/0.9 Torr. The NMR spectrum of this material showed peaks at δ : 1.16 (3H, t), 1.33 (3H, d), 2.5—3.5 (3H, m), 3.7 (3H, s), and 4.3 (1H, d), and no others. Its TLC showed only one spot. Found : 189.098. Calcd for $C_8H_{15}NO_4$: 189.100.

*4-Amino-*erythro*-2-hydroxy-3-methylbutanonic Acid (**11**).* The isoxazolidine (**8**) was heated at 200 °C in a sealed tube for 10 min producing methyl 4-ethoxyimino-2-hydroxy-3-methylbutanoate in a quantitative yield ; ν_{max}(CCl_4) : 3500, 1735, and 1610 cm^{-1} ; δ(CCl_4) : 1.20 (3H, d), 1.20 (3H, t), 6.60 (1/3H, d), and 7.20 (2/3H, d). The oxime ether (317 mg ; 1.67 mmol) was hydrogenated over platinum oxide (60 mg) in methanol (5 ml) containing three drops of concentrated hydrochloric acid. The crude product was heated in 6M hydrochloric acid (20 ml), and the resulting mixture was chromatographed on a cation exchanger (Amberlite Type I CG 120) (13 g). Elution with 0.5% aqueous ammonia afforded **11** (176 mg) as a thick oil ; ν_{max} (KBr) : 3500 (br.), 1580 (br.), 1460, 1400, 1130, and 1060 cm^{-1}. Paper chromatography of this amino acid showed a single spot (water–butanol–acetic acid), and its NMR spectrum showed peaks at δ (D_2O) : 1.05 (3H, d, J=7Hz), 2.2 (1H, br.), 3.05 (2H, d, J=6 Hz), and 4.0 (1H, d, J=4 Hz). No other signals showing the presence of impurities were found in the spectrum. The amino acid was characterized as a *N*-phthaloyl derivative, which was prepared according to Nefken's method[9], and purified by chromatography on Sephadex LH 20. This phthaloyl derivative was an oil, showing one spot in its TLC. Its NMR spectrum exhibited peaks at δ : 1.15 (3H, d), 2.5 (1H, m), 4.15 (1H, d), 3.8 (2H, ABX), and 7.85 (5H, br.s), and no others. Found : 263.079. Calcd for $C_{13}H_{13}NO_5$: 263.081.

The authors thank Dr. T. Naito, Bristol-Banyu Research Laboratories, for providing the authentic sample of 4-amino-2-hydroxybutanoic acid.

References

1) H. Kawaguchi, T. Naito, S. Nakagawa, and K. Fujisawa, *J. Antibiotics*, **25**, 695 (1972); T. Naito, S. Nakagawa, Y. Abe, S. Toda, K. Fujisawa, Y. Miyaki H. Koshiyama, H. Ohkuma, and H. Kawaguchi, *ibid.*, **26**, 297 (1973).

2) P. W. K. Woo, H. W. Dion, and Q. R. Bartz, *Tetrahedron Lett.*, **1971**, 2625.

3) Y. Saito, M. Hashimoto, H. Seki, and T. Kamiya, *Tetrahedron Lett.*, **1970**, 4863.

4) C. Fukaya, T. Kusumi, K. Imaye, and H. Kakisawa, 26th Annual Meeting of the Chemical Society of Japan, Hiratsuka, 1972.

5) H. B. Hass and M. L. Bender, *J. Am. Chem. Soc.*, **71**, 1767 (1949); *Org. Synth.*, Coll. Vol. IV, 932 (1963).

6) N. Kornblum and R. A. Brown, *J. Am. Chem. Soc.*, **86**, 2681 (1964).

7) R. Huisgen, H. Seidl, and I. Bruning, *Chem. Ber.*, **102**, 1102 (1969).

8) K. N. Houk, *J. Am. Chem. Soc.*, **94**, 8953 (1972); J. Sims and K. N. Houk, *ibid.*, **95**, 5798 (1973).

9) G. H. L. Nefkens, G. I. Tesser, and R. J. F. Nivard, *Recl. Trav. Chim. Pays-Bas*, **79**, 688 (1960).

Retrograde Aldol Reaction of 3-(1-Hydroxy-2,2,2-trichloroethyl)-2,4-pentanedione Catalyzed by the Bivalent Metal Complexes of 2,4-Pentanedione[1]

Kaku UEHARA, Yoshiyuki OHASHI, and Makoto TANAKA

Department of Applied Chemistry, College of Engineering, University of Osaka Prefecture, Sakai-shi, Osaka 591

(Received March 29, 1976)

The bivalent metal complexes of 2,4-pentanedione($M(acac)_2$) catalyzes the conversion of 3-(1-hydroxy-2,2,2-trichloroethyl)-2,4-pentanedione(A) into chloral and acetylacetone(Hacac) in a chloroform solution. The order of activity of $M(acac)_2$ as the catalyst is: Mg(II), Mn(II)>Co(II)>Ni(II)>Cu(II)<Zn(II). It was found that the catalyzed reaction proceeds through saturation-type kinetics. The Lineweaver-Burk-type plots show linear relationships and are consistent with a mechanism in which a preequilibrium complex formation between $M(acac)_2$ and a substrate is followed by the rate-determining decomposition to give the products. Acetylacetone acts as a competitive inhibitor for the $Cu(acac)_2$-catalyzed reaction. The third stability constant for the Cu–Hacac chelate system can be evaluated from the inhibitor constant as $\log K_3=4.3$. The retrograde aldol reactions of 3-(1-hydroxy-2,2,2-trichloroethyl)-5-methyl-2,4-hexanedione and 3-(1-hydroxy-2,2,2-trichloroethyl)-4-phenyl-2,4-butanedione were studied in the same manner as 3-(1-hydroxy-2,2,2-trichloroethyl)-2,4-pentanedione. A possible mechanism for the catalysis is proposed.

A number of studies have been carried out on the catalysis of metal ions or chelates for the clarification of the role of metal ions in metalloenzymes. Sigman and Jorgensen[2] reported the zinc(II)-catalyzed transesterification of *N*-(2-hydroxyethyl)ethylenediamine by *p*-nitrophenyl picolinate which involved a reactive ternary complex analogous to metalloenzyme–substrate complexes. Breslow *et al.*[3] found that the mechanism of metal-catalyzed hydration of 2-cyano-1,10-phenanthroline is related to the "rack mechanism" proposed for some enzymatic processes.

These metal-catalyzed processes represent models for the catalytic role of metals in the active site and not for overall enzymatic processes, since catalysis of metal ions or chelates differs essentially from that of enzymes. However, the rate of the metal-catalyzed reaction can be described by saturation-type kinetics if the substrate(S) coordinates to a vacant site of metal ion or chelate(M) to give the complex(SM) which is decomposed to products(P) and M; $S+M \rightleftarrows SM \rightarrow P+M$. Tsuchida *et al.*[4] found that the oxidative polymerization of 2,6-xylenol with a copper–amine complex proceeds *via* a mechanism similar to that of a Michaelis-Menten-type reaction.

In the present paper it is shown that the rates of $M(acac)_2$-catalyzed retrograde aldol reaction (1) can be explained in terms of saturation-type kinetics, and that the third stability constant for the Cu–Hacac chelate system can be obtained from the kinetic parameters of the inhibitory action of acetylacetone on the $Cu(acac)_2$-catalyzed reaction as shown below.

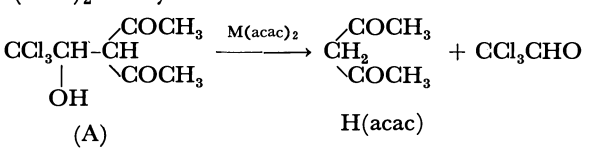

(A) H(acac) (1)

Experimental

Materials. 3-(1-Hydroxy-2,2,2-trichloroethyl)-2,4-pentanedione(A) was prepared according to the method described in the preceding paper.[5] Similarly, 3-(1-hydroxy-2,2,2-trichloroethyl)-5-methyl-2,4-hexanedione(B) was prepared from a mixture of 5.9 g (0.046 mol) of isobutyrylacetone,[6] 6.8 g (0.046 mol) of chloral and a few drops of piperidine in a yield of 20% (2.54 g). Mp 59 °C. Found: C, 39.19; H, 4.70%. Calcd for $C_9H_{13}O_3Cl_3$: C, 39.23; H, 4.76%. IR(KBr disk): 3380(s), 2920(m), 1720(s), 1690(s), 1460(s), 1350(s), 1290(m), 1150(m), 1100(m), 990(w), 810(s), and 710 cm^{-1} (s). UV($CHCl_3$): λ_{max} 290 nm(ε_{max} 137). 3-(1-Hydroxy-2,2,2-trichloroethyl)-4-phenyl-2,4-butanedione (C) was synthesized from 3.1 g (0.019 mol) of benzoylacetone and 2.8 g (0.019 mol) of chloral in the presence of piperidine (yield, 3.4 g(59%)). Mp 91 °C. Found: C, 46.14; H, 3.52%. Calcd for $C_{12}H_{12}O_3Cl_3$: C, 46.41; H, 3.89%. IR(KBr disk): 3370(s), 1705(s), 1680(s), 1450(m), 1360(s), 1290(s), 1180(s), 1100(s), 1050(w), 980(m), 840(m), 805(m), 790(s), 760(s), and 700 cm^{-1}(m). UV($CHCl_3$): λ_{max} 252 nm(ε_{max} 317). $M(acac)_n$ of GR grade reagents(Dojindo Co. Ltd., Research Laboratories, Kumamoto) were used without further purification. Copper(II) chelates of isobutyrylacetone and benzoylacetone were prepared by the method of Adams *et al.*[6] Commercial acetylacetone and chloroform were distilled before use.

Spectral Measurements. The IR spectra were measured with a Hitachi Model 215 grating spectrophotometer, the UV spectra with a Shimadzu UV-200 spectrophotometer, and the NMR spectra with a Hitachi Model R-20 spectrometer. Tetramethylsilane was used as an internal standard, deuteriochloroform being used as the solvent. Elemental analyses were carried out with a Yanagimoto Model MT-2 CHN analyzer.

Kinetic Measurements. Kinetic measurements were carried out spectrophotometrically by monitoring the spectral changes in the 250—350 nm region. The absorbance of a mixed solution of A(or either B or C) and $M(acac)_2$ increased with time, the spectrum being similar to that of acetylacetone (or the corresponding β-diketones) even at a very low conversion(below 2%) since absorbance of A and chloral is regarded as negligible as compared with that of acetylacetone. The chloroform solution containing only $M(acac)_2$ showed no observable spectral change during the course of measurement. An example of the time-dependent UV spectra of a reaction mixture is shown in Fig. 1. The initial rate of the retrograde aldol reaction can be followed conveniently by the measurement of UV absorption. The amount of produced acetylacetone, or consumed A, can be calculated as follows: where Abs(t) and $c_{Hacac}(t)$ denote absorbance and concentration, respectively, of acetylacetone at time t, c_A^0 and c_M^0 the initial concentrations of A and $M(acac)_2$, respectively, and ε_A, ε_M, ε_{Hacac}, and $\varepsilon_{chloral}$ the molar extinction coefficients of A, $M(acac)_2$, Hacac, and chloral,

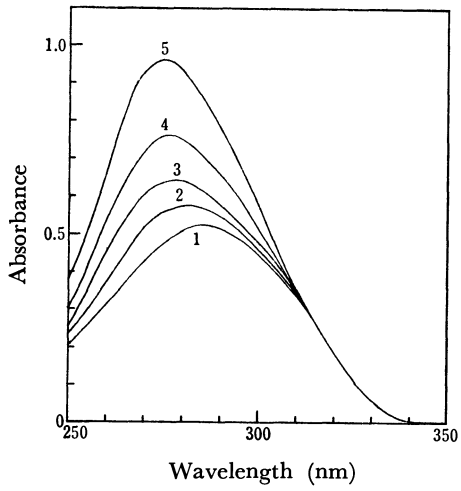

Fig. 1. Time-dependent UV spectra of a mixture of A and $Cu(acac)_2$ at 26 °C in chloroform after mixing. $[A]=3.53\times10^{-3}$ M, $[Cu(acac)_2]=5.83\times10^{-6}$ M, 1 : t=2 min, 2 : t=11 min, 3 : t=21 min, 4 : t=37 min, 5 : t=63 min (conversion=1.77%).

$$A + M(acac)_2 \rightarrow Hacac + chloral + M(acac)_2 \quad (2)$$

$$Abs(t) = \varepsilon_A c_A^0(1-x) + \varepsilon_M c_M^0 + \varepsilon_{Hacac} x c_A^0 + \varepsilon_{chloral} x c_A^0 \quad (3)$$

$$c_{Hacac}(t) = x c_A^0 = \frac{Abs(t) - \varepsilon_A c_A^0 - \varepsilon_M c_M^0}{\varepsilon_{Hacac} + \varepsilon_{chloral} - \varepsilon_A} \quad (4)$$

respectively. The initial rate of reaction can be calculated from the initial slope obtained from a time-conversion curve. For example, at 280 nm,

$$Rate = \frac{Abs(\Delta t) - Abs(0)}{\Delta t \times 2.598 \times 10^7} \quad (M\,s^{-1}) \quad (5)$$

At low conversions below 2%, time-conversion curves gave straight lines passing through the origin, suggesting that the ligand exchange reaction beween A and $M(acac)_2$ can be neglected.

Spectrometric Determination of Equilibrium Constant. The reaction (1) is reversible.[7] The formation of A was followed by means of NMR in a deuteriochloroform solution of chloral, acetylacetone, and $M(acac)_2$. 0.0013 g of $M(acac)_2$ was added to a 2 ml deuteriochloroform solution of chloral and acetylacetone($[CCl_3CHO]=[Hacac]=1.02$ M). The NMR spectrum of this solution was measured after it had been left to stand at room temperature for a few hours. Similarly, the NMR spectrum of a deuteriochloroform solution containing A ($[A]=1.02$ M) and 0.0013 g of $Mg(acac)_2$ was also measured after being left to stand for several hours. The two spectra agreed with each other. The equilibrium constant K of Eq. 6 was obtained to be 1.22 M^{-1} from the NMR data.

$$Chloral + Hacac \overset{K}{\rightleftharpoons} A \quad (6)$$

Results and Discussion

Rate Equation of Retrograde Aldol Reaction. Though the reaction took place without catalyst, the reaction rate in chloroform solution was low at room temperature. The rate of catalyzed reaction was found to be of pseudo-first order with respect to $M(acac)_2$ at constant initial concentration of A. Thus, the rate of disappearance of A is described as

$$Rate = k_{cat}[M(acac)_2] + E \quad (7)$$

Table 1. Pseudo-first-order rate constants catalyzed by $M(acac)_n$, second stability constants for metal complexes with acetylacetone, and force constants of $M(acac)_2$
$[A]=3.35\times10^{-3}$ M, at 26 °C in chloroform

$M(acac)_n$	$k_{cat}\times10^2$ s^{-1}	log K_2[8]	K(M-O)[12] N cm^{-1}
$Mg(acac)_2$	14.0	6.27	
$Mn(acac)_2$	14.0	7.35	
$Co(acac)_2$	6.5	9.54	1.50
$Ni(acac)_2$	1.8	10.77	2.05
$Zn(acac)_2$	1.2	8.81	1.50
$Cu(acac)_2$	0.08	16.34	2.20
$Co(acac)_3$	0		2.40
$Cr(acac)_3$	0		2.30

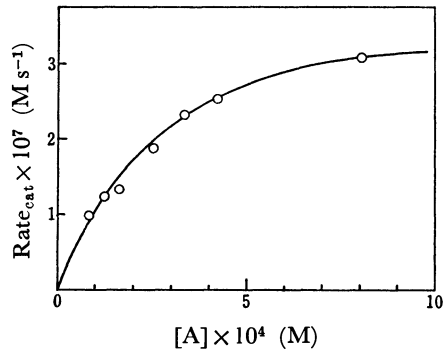

Fig. 2. Plot of initial rate of retrograde aldol reaction, catalyzed by $Co(acac)_2$ *vs.* concentration of A at 26 °C in chloroform. $[Co(acac)_2]=5.66\times10^{-6}$ M.

where E is the rate for the spontaneous reaction in the absence of $M(acac)_2$. The values of k_{cat} for various $M(acac)_2$ are given in Table 1. The trivalent metal complexes of 2,4-pentanedione such as $Co(acac)_3$ and $Cr(acac)_3$ were inactive as a catalyst. It was found that the order of activity of $M(acac)_2$ as the catalyst is: Mg(II), Mn(II) > Co(II) > Ni(II) > Cu(II) < Zn(II). $M(acac)_2$ having a stable O–M bond is unfavorable for a high catalytic activity. Thus, it is suggested that the present catalysis also proceeds *via* the dissociation of the O–M bond as shown for the metal-ion-catalyzed alcoholysis of β-diketones.[9]

Figure 2 shows a typical example of the plots of observed initial rates *vs.* concentrations of A. The observed saturation phenomenon can be analyzed in terms of saturation-type kinetics. The kinetics is based on the assumption that substrate A coordinates reversibly to a vacant site of $M(acac)_2$ to form a complex which is then decomposed, giving back the free $M(acac)_2$ and products(acetylacetone and chloral). The kinetic expression for the present reaction can be written as

$$A + M \underset{k_{-1}}{\overset{k_{+1}}{\rightleftharpoons}} AM \xrightarrow{k_2} M + P \quad (8)$$

where M stands for $M(acac)_2$, A is 3-(1-hydroxy-2,2,2-trichloroethyl)-2,4-pentanedione, and P is acetylacetone and chloral.

If the aldol reaction ($P \overset{M}{\rightarrow} A$) is neglected when

the concentration of P is sufficiently small, the catalyzed reaction rate ($Rate_{cat}$) is expressed as follows from the steady state of the intermediate AM.

$$Rate_{cat} = \frac{V[A]}{K_m + [A]} \tag{9}$$

where $V=k_2[M]^0$, $K_m=(k_{-1}+k_2)/k_{+1}$. This is of the same form as the Michaelis-Menten mechanism and explains the fact that the rate of the catalyzed reaction is proportional to the initial concentration of $M(acac)_2$ at a given concentration of A and that the initial rate *vs.* [A] curve shows a pronounced saturation. Equation 9 can be rearranged to give Eq. 10. If $1/Rate_{cat}$ is plotted against 1/[A] (Lineweaver-Burk plot),[10] the values of the maximum rate V and the constant K_m can be obtained from the intercepts of vertical and horizontal axis, respectively.

$$\frac{1}{Rate_{cat}} = \frac{1}{V} + \frac{K_m}{V}\frac{1}{[A]} \tag{10}$$

As shown in Fig. 3, the Lineweaver-Burk plot (Fig. 2) gives a straight line with intercepts of vertical axis of $1/V$ and of horizontal axis of $-1/K_m$, supporting the above hypothesis that the present reaction can be written by Eq. 8 and the aldol reaction is neglected presumably because of very low concentration of P in the initial stage of the reaction. The rate constant k_2 is evaluated from the maximum rate V, which is defined as $k_2[M]^0$. The values of K_m, k_2 and k_2/K_m obtained from Lineweaver-Burk plots for the various $M(acac)_2$-catalyzed reactions are given in Table 2. If $k_{-1} \gg k_2$, K_m can be defined as k_{-1}/k_{+1} (dissociation constant of complex AM), and if $k_{-1} \ll k_2$, $K_m=k_2/k_{+1}$. An approximate parallelism is observed between K_m and k_2 within a series of $M(acac)_2$-catalyzed retrograde aldol reactions of A(Table 2).

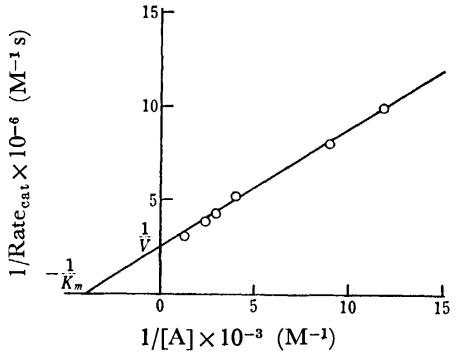

Fig. 3. Lineweaver-Burk-type plot of the data of Fig. 2.

Table 2. Kinetic parameters for the retrograde aldol reaction of A catalyzed by various $M(acac)_2$ at 26 °C in chloroform

$M(acac)_2$	$K_m \times 10^4$ M	$k_2 \times 10^2$ s^{-1}	k_2/K_m M^{-1} s^{-1}
$Mg(acac)_2$	37.0	14.0	38
$Co(acac)_2$	2.6	7.1	270
$Ni(acac)_2$	7.2	2.2	30
$Zn(acac)_2$	9.1	1.4	15
$Cu(acac)_2$	0.34	0.076	22

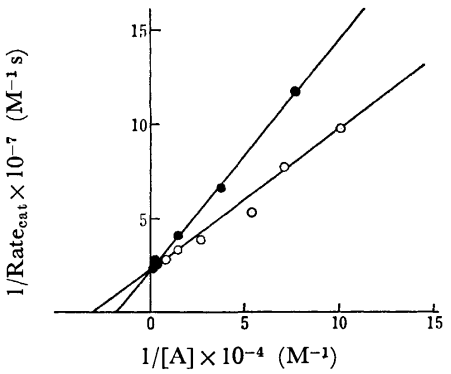

Fig. 4. Inhibitory action of acetylacetone on the $Cu(acac)_2$-catalyzed retrograde aldol reaction of A at 26 °C in chloroform. $[Cu(acac)_2]=5.92\times10^{-5}$ M.
—○—: In the absence of Hacac,
—●—: in the presence of Hacac ([Hacac]$=3.11\times10^{-5}$ M).

Inhibitory Action of Acetylacetone on the $Cu(acac)_2$-Catalyzed Reaction. It is highly probable that the catalytic action of $M(acac)_2$ will be suppressed in the presence of a compound which can coordinate to $M(acac)_2$. Conversely, observation of the inhibitory action should emphasize the validity of the proposed mechanism. Acetylacetone which is one of the reaction products is an effective ligand for the metal ions and should act as a competitive inhibitor. In the presence of acetylacetone, the initial rate of the $Cu(acac)_2$-catalyzed retrograde aldol reaction of A in chloroform was measured as a function of the concentration of A. Figure 4 shows the relationship between initial rate and substrate concentration [A] in the absence and presence of acetylacetone. Compared with the initial rate in the absence of the inhibitor, the initial rate in the presence of acetylacetone was somewhat reduced without alteration of the maximum rate. This suggests that acetylacetone behaves as a typical competitive inhibitor, *i.e.*, acetylacetone competes with A for occupation of the coordination site of $Cu(acac)_2$ to form a five-coordinated copper(II) complex. The whole reaction containing the inhibition of acetylacetone can be represented as follows.

$$A + M \underset{k_{-1}}{\overset{k_{+1}}{\rightleftharpoons}} AM \xrightarrow{k_2} Hacac + CCl_3CHO + M \tag{11}$$

$$Hacac + M \underset{k_{-1}}{\overset{k_{+1}}{\longrightarrow}} Hacac\cdot M \tag{12}$$

By applying the steady-state treatment to AM, we obtain the rate equation

$$Rate_{cat} = \frac{V[A]}{K_m(1+i/K_i)+[A]} = \frac{V[A]}{K_p+[A]} \tag{13}$$

where i is concentration of acetylacetone, and K_i is dissociation constant of Hacac·M, *viz.*, $K_i=k_{-1}/k_{+1}$. K_i is also called the inhibitor constant. The value of $K_p(=K_m(1+i/K_i))$ was found to be 5.6×10^{-5} M at $i=3.11\times10^{-5}$ M from Fig. 4, and the K_i value to be 4.8×10^{-5} M from K_p and K_m values.

Since the reciplocal of K_i should be the stability constant of Hacac·M, the value of log $(1/K_i)$, 4.3, corresponds to the third stability constant for the Cu–

Hacac chelate system. The first and second stability constants have been reported to be 8.22 and 6.73, respectively.[11]

Kinetics for Compounds B and C. The kinetics was studied for the retrograde aldol reactions of 3-(1-hydroxy-2,2,2-trichloroethyl)-5-methyl-2,4-hexanedione(B) and 3-(1-hydroxy-2,2,2-trichloroethyl)-4-phenyl-2,4-butanedione(C) in the same manner as for compound A. Copper(II) chelate of isobutyrylacetone and benzoylacetone were employed as catalyst for the reaction of B and C, respectively. The initial rate of the copper(II)-catalyzed reaction was found to be proportional to the initial concentration of copper(II) chelate at a given concentration of B or C. The saturation-type kinetics was again observed in the plots of initial rates *vs.* concentrations of B or C. The corresponding Lineweaver-Burk-type plots were found to be linear. Kinetic parameters for the reaction of A, B, and C are summarized in Table 3.

Table 3. Kinetic parameters for the reaction of A, B, and C at 26 °C in chloroform

Substrate	$K_m \times 10^4$ M	$k_2 \times 10^3$ s^{-1}	k_2/K_m M^{-1} s^{-1}
A	0.34	0.76	22
B	0.46	6.2	135
C	13	34	26

The k_2 values increase in the order A<B<C. This arises from replacement of the methyl group of acetylacetone by the isopropyl or phenyl group. The substituent effect can be attributed to an increased steric hindrance of intermediate. There is a tendency for the value of K_m to increase with increase in k_2. When the metal ion of $M(acac)_2$ changes as Cu→Ni→Mg, a similar variation in K_m and k_2 values (Cu<Ni<Mg) was observed. This parallelism in K_m and k_2 may be characteristic of the present retrograde aldol reaction, but it is impossible to understand its meaning.

Reaction Mechanism. On the basis of the results, a possible mechanism for the $M(acac)_2$-catalyzed retrograde aldol reaction of A may be proposed as follows. Compound A coordinates to a vacant site of $M(acac)_2$ to give the intermediate AM. The hydroxyl group of the complex is then deprotonated to give acetylacetone with the concomitant rearrangement of electrons in the intermediate leading to chloral elimination and regeneration of $M(acac)_2$.

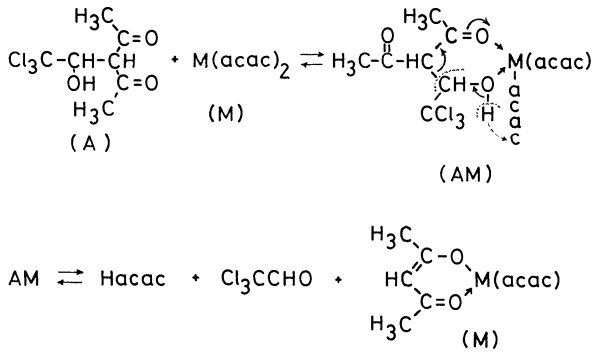

Fig. 5. Reaction scheme.

The present reaction is reversible, the equilibrium constant for the overall reaction being 1.22 M^{-1}. Reaction of acetylacetone with chloral by $M(acac)_2$ will occur with the opposite route of the retrograde aldol reaction to give an equilibrium mixture.

References

1) Part XXII in the series "Catalytic Behavior of Metal Chelate Compounds," Part XXI, K. Uehara, Y. Ohashi, and M. Tanaka, *Bull. Chem. Soc. Jpn.*, **49**, 1447 (1976).
2) D. S. Sigman and C. T. Jorgensen, *J. Am. Chem. Soc.*, **94**, 1724 (1972).
3) R. Breslow, R. Fairweather, and J. Keana, *J. Am. Chem. Soc.*, **89**, 2135 (1967).
4) E. Tsuchida, M. Kaneko, and H. Nishide, *Markomol. Chem.*, **151**, 221 (1972).
5) K. Uehara, Y. Ohashi, and M. Tanaka, *Bull. Chem. Soc. Jpn.*, **49**, 1447 (1976).
6) J. T. Adams and C. R. Hauser, *J. Am. Chem. Soc.*, **66**, 1220 (1944); R. Levine, J. A. Conroy, J. T. Adams, and C. R. Hauser, *ibid.*, **67**, 1510 (1945).
7) K. Uehara, Y. Ohashi, and M. Tanaka, *Chem. Lett.*, **1974**, 827.
8) J. A. Dean, "Lange's Handbook of Chemistry," eleventh ed., McGraw-Hill, New York (1973), pp. 5—51.
9) K. Uehara, F. Kitamura, and M. Tanaka, *Bull. Chem. Soc. Jpn.*, **49**, 493 (1976).
10 H. Lineweaver and D. Burk, *J. Am. Chem. Soc.*, **56**, 658 (1934).
11) R. M. Izatt, W. C. Fernelius, and B. P. Block, *J. Phys. Chem.*, **59**, 80 (1955).
12) K. Nakamoto, P. J. McCarthy, A. Ruby, and A. E. Martell, *J. Am. Chem. Soc.*, **83**, 1066 (1961); K. Nakamoto, P. J. McCarthy, and A. E. Martell, *ibid.*, **83**, 1272 (1961).

Preparation of Polyvinylamine by the Hofmann Degradation of Polyacrylamide[1)]

Hiroo TANAKA and Ryoichi SENJU

Department of Forest Products, Faculty of Agriculture, Kyushu University, Hakozaki, Higashi-ku, Fukuoka 812

(Received March 29, 1976)

Polyvinylamine which contained 95.6 mol% amine units was obtained when the Hofmann degradation was applied to polyacrylamide by use of a very slight excess of sodium hypochlorite and a large excess of sodium hydroxide at 0 to −15 °C for about 15 h. Polyvinylamine hydrochloride (PVAm·HCl) was isolated almost quantitatively as a white powder. PVAm·HCl was freely soluble in water, but insoluble in organic solvents such as methanol, acetone, dioxane, *N,N*-dimethylformamide (DMF), and dimethyl sulfoxide (DMSO). The desalting of PVAm·HCl was performed by passing its aqueous solution through columns of ion exchange resins. The product containing 30.5% nitrogen was obtained in reasonable yield. Polyvinylamine was freely soluble in water, acetic acid, or lower alcohols, but insoluble in solvents such as acetone, dioxane, DMF, and DMSO.

It is well known that *N*-haloamides are highly stable at a temperature as low as 0 °C and activation energy of the Hofmann degradation is about 30 kcal/mol. Therefore, the Hofmann degradation is generally carried out by dissolving the amide in a very slight excess of cold aqueous hypohalite solution, followed by rapid warming.[2)]

However, the Hofmann degradation of polyacrylamide (PAM) is exceptional. It has been previously shown in this laboratory that the Hofmann degradation of PAM is accelerated very much by the neighboring-group participation and the *N*-haloamide groups of PAM are easily converted to amino groups even at a temperature below 0 °C.[3)] According to this procedure, the partial amination of PAM was easily accomplished while limiting the formation of carboxyl groups to a very small percentage.[4)]

The present investigation was undertaken in order to find some suitable methods for increasing further the contents of amine units, and for the separation and the purification of polyvinylamine (PVAm). PVAm containing as much as 95.6 mol% amine units could be purely isolated almost quantitatively.

Experimental

Materials. Acrylamide and $K_2S_2O_8$ were recrystallized twice from benzene and water solution respectively. All of the other chemicals used were reagent grade.

Polymerization of acrylamide was carried out in 10% aqueous solution with the use of $K_2S_2O_8$-2-propanol redox initiator under nitrogen atmosphere at 60 °C for 60 min. The resulting polymer was purified by reprecipitating twice from water-methanol. The nitrogen content of PAM was 18.9% and the content of carboxyl groups was negligible small. The intrinsic viscosity of PAM was 2.1 dl/g at 30 °C.

Sodium hypochlorite solution was prepared by passing chlorine gas through a 7 M NaOH solution cooled with an ice bath. The concentration of NaOCl measured by the iodometry was 2.0 mol/l and that of NaOH by the acidmetry after removal of NaOCl with a small excess of H_2O_2 was 2.5 mol/l.

The ion exchange resins used were Amberlite IR-120B and IRA-400.

Reaction Procedure. Twenty-four grams of 10.3% PAM (1.4 mol/l per amide group) cooled to 0 °C were added into 10 ml of alkaline NaOCl cooled to about −5 °C with vigorous stirring. The resulting solution was cooled rapidly by dipping in a bath of −15 °C. When the temperature of the solution reached about −10 °C, a desirable amount (1—40 ml) of 10 mol/l NaOH cooled to −15 °C was added with stirring and maintained at −10 to −15 °C for 1—2 h. Then the reaction mixture was warmed to 0 °C and allowed to stand for 10—15 h.

Isolation and Purification. The polymer was isolated by pouring the mixture into about a 4-fold amount of methanol. The resulting precipitate was dissolved in about 25 ml of water and 6 M HCl was added dropwise to this solution with stirring. Although CO_2 gas evolved and the polymer precipitated once, it was soon dissolved completely by the continuous stirring, keeping the pH about 2. The resultant solution was poured into about a 4-fold amount of methanol again. The supernatant solution was decanted and the residual precipitate was filtered through the weighed sintered glass disk, then washed with methanol and ethanol successively and dried *in vacuo* over P_2O_5. The ash content of polyvinylamine hydrochloride (PVAm·HCl) obtained in this manner was less than 0.3%.

The repetition of the reprecipitations was undesirable because the purified PVAm·HCl was precipitated with great difficulty. Since PVAm·HCl is very hygroscopic, care had to be taken in handling it.

The aqueous solution (2—3%) of PVAm·HCl was passed through the columns of cation and anion exchange resins successively and the columns were washed with water about double in volume. The collected effluent from the columns was concentrated to about 5% under reduced pressure and the resultant solution was poured into a large amount of acetone. The precipitate obtained was filtered and dried *in vacuo*.

Analytical Method. Contents of both amino and carboxyl groups were measured by the colloid titration method.[5)] For details of the analyses the previous paper[3)] should be referred to.

The chlorine content of PVAm·HCl was determined as follows: Dilute sulfuric acid was added to 100 ml of the aqueous solution containing about 0.1 g PVAm·HCl to adjust the pH to about 2. A proper amount (50—100 ml) of 0.01 M potassium poly(vinyl sulfate)[5)] was added to this solution until the supernatant solution became clear, and the resulting precipitate was filtered off and washed several times with a small amount of water. The combined filtrate was neutralized and titrated by 0.05 M $AgNO_3$ (Mohr method). If the PVAm was not removed, the end point of the titration became imprecise and the content of chlorine was overestimated.

Table 1. Reaction conditions of the Hofmann degradation of PAM and the analytical results

No.	Reaction conditions			Analytical results			Analytical results of PVAm·HCl				
	PAM (mol/kg)	NaOCl (mol/kg)	NaOH (mol/kg)	Amino group (mol/kg)	Degree of amination (%)	Carboxyl group (mol%)	Yield (g)	Ash (%)	Chlorine (%)	Nitrogen (%)	Carboxyl group
1	0.740	0.751	1.16	0.395	53.4	5	1.49	0.3	25.9	17.2	neg. small
2	0.500	0.507	2.99	0.435	87.0	4	1.52	0.2	40.3	16.0	neg. small
3	0.385	0.394	4.14	0.354	92.0	3	1.54	0.3	43.0	16.0	neg. small
4	0.263	0.268	5.28	0.253	95.6	2	1.55	0.1	43.3	16·1	neg. small
5	0.288	0.294	8.15	0.273	94.8	2	1.54	0.1	42.9	15.9	neg. small
6	0.257	0.259	5.09	0.227	88.3	1	1.53	0.1	40.7	15.5	neg. small
7	0.255	0.261	5.09	0.205	80.4	1	1.51	0.2	38.3	16.0	neg. small
8	0.218	0.220	4.86	0.191	87.6	1	1.53	0.2	40.2	15.5	neg. small
						PVAm·HCl (calcd)	1.61	0	44.6	17.6	0

In the case of Nos. 6—8, 3 ml of dioxane (No. 6), 3 ml of methanol (No. 7) or 10 ml of water saturated with NaCl (No. 8) were added to 14 g of 10.3% PAM solution before mixing it with the alkaline NaOCl.

Nitrogen contents were determined by the Kjeldahl method.

Results and Discussion

Effect of NaOH Concentration on Yields of Amine Units. During the progress of the Hofmann degradation, the isocyanato groups which are formed as transient intermediates react with water to yield the objective amino groups on the polymer chain in the presence of excess alkali[2] On the other hand, a part of these resulting amino groups give the urea derivatives due to the reaction between the amino and isocyanato groups. These two reactions can be illustrated as follows:

$$R\text{-}CONH_2 \xrightarrow{OCl^-} R\text{-}CON^-Cl \longrightarrow [R\text{-}N{=}C{=}O] \xrightarrow{OH^-} R\text{-}NH_2 \quad (1)$$

$$R\text{-}N{=}C{=}O + R\text{-}NH_2 \longrightarrow R\text{-}NHCONH\text{-}R \quad (2)$$

Therefore the yields of amine increase with an increase in concentration of NaOH. When PAM was subjected to the Hofmann degradation in the presence of 4.2 mol/l NaOH, 88% of the amide units converted to amine, as described earlier[3]. Although the yields of amine units could be expected to increase further if an additional amount of NaOH was applied, the salting-out of the polymer, which took place on the occasion of mixing the PAM solution with alkaline aqueous NaOCl, precluded an experiment with a high concentration of NaOH.

After various attempts were made, it was found that the concentrations of NaOH could be increased still more, without any salting-out of the polymer, by adding the large amount of 10—20 mol/l NaOH to the mixrure of PAM and NaOCl prepared in the presence of a small amount of NaOH. This may be responsible for the fact that the *N*-chlorinated PAM salt outed with more difficulty than the PAM.

Results are shown in Table 1. The degrees of amination based on amide groups were 53.4 and 87.0% in the presence of 1.16 and 2.99 mol/kg NaOH respectively. Since these experimental data are similar to the results of the paper reported previously,[3] the degree of amination has been found to be little influenced by the addition procedures of NaOH.

The degree of amination increased further with increase of the concentration of NaOH and amounted to 95.6 mol% in the presence of 5.28 mol/kg NaOH. However, when an excess concentration of NaOH such as 8.15 mol/kg (No. 5) was applied, the degree of amination was limited to 94.8 mol% because the polymer salt outed as a pasty cake. The higher limit of NaOH concentration in the homogeneous reaction seemed to be 6—7 mol/kg.

In the cases shown above (No. 1—5), 2—5 mol% of carboxyl groups were formed, even though PAM cooled to 0 °C was used. It may be preferable to mix alkaline NaOCl with PAM at a lower temperature to reduce the formation of carboxyl groups[3]. Further, it has already been found that the degree of amination increases with decrease of the reaction temperature[3]. No. 6—8 were the cases in which PAM cooled to −5 to −10 °C after the addition of dioxane, methanol, or water saturated with NaCl was mixed with an alkaline NaOCl to −15 °C. As can be seen from Table 1, the formation of carboxyl groups was less than 1%. However, the degree of amination was reduced also, contrary to our expectation. That the degree of amination is particularly low in the presence of methanol may be due to the formation of some urethane linkages.

Isolation of PVAm·HCl and Analytical Results. Results are shown in Table 1. The products of 1.49—1.55 g were obtained from 1.44 g PAM. Since the molecular weight of monomer units of PAM and PVAm·HCl are 71.1 and 79.5 respectively, the theoretical yield of PVAm·HCl is 1.61 g. In the case of No. 4 in which 95.6% of the amide units converted to amine, 1.55 g of PVAm·HCl was obtained.

The ash contents of the products were very small (0.1—0.3%). The chlorine contents of the products increased with increase of amine units. The chlorine content (43.3%) of No.4 is 97.1% of the theoretical

Table 2. Analytical results of PVAm desalted from PVAm·HCl by ion exchange

No.	Yield (%) found	Yield (%) calcd	Nitrogen (%)	Molecular weight per nitrogen	Molecular weight per amino group	Carboxyl group
1	72.5	73.1	22.0	63.7	104.9	neg. small
2	57.3	58.4	25.0	56.0	59.1	neg. small
3	54.0	55.5	28.5	49.2	49.9	neg. small
4	53.7	55.4	30.5	45.9	46.5	neg. small
PVAm (calcd)		54.2	32.5	43.1	43.1	0

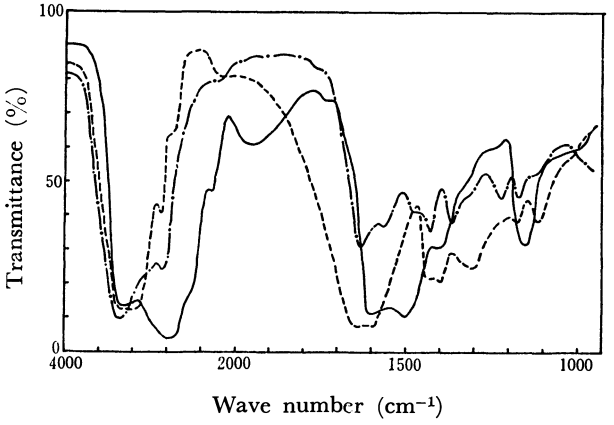

Fig. 1. IR spectra of PAM, PVAm·HCl(No. 4) and PVAm(No. 4).
----: PAM, ——: PVAm·HCl, ——: PVAm.

value (44.6%). This value agreed closely with the degree of amination (95.6%) determined by colloid titration.

The carboxyl contents were negligible small. The disappearance of carboxyl groups appeared to be due to the formation of methyl ester which occured during the isolations and purifications, because methanol was detected in the hydrolysis solutions of purified products by the gas chromatography.

PVAm·HCl was highly hygroscopic and freely soluble in water. However, it was insoluble in pure organic solvents such as methanol, acetone, dioxane, *N*,*N*-dimethylformamide (DMF), and dimethyl sulfoxide (DMSO), though soluble in methanol, DMF, or DMSO containing 10—20% water.

The infrared absorption spectrum of PVAm·HCl (No.4) in a KBr disk is shown in Fig. 1 and compared with that of PAM. The absorption band at 1640 cm^{-1} in PAM, which was assigned to $CONH_2$, diminished and new bands due to NH_3^+ appeared at 2800, 1950, and 1500 cm^{-1}. A very weak absorption band due to the ester was observed at 1700 cm^{-1}. The absorption bands due to NH_2 exist at 3335 and 1610 cm^{-1}.

Preparation of PVAm from PVAm·HCl. Attempts to obtain the pure PVAm by pouring the PVAm·HCl solution with a small excess of NaOH into various organic solvents were unsuccessful. Even if the above solution was added into a large amount of methanol the solids did not appear. Although some milky precipitates were obtained by pouring such a solution into ethanol or 2-propanol, the filtration was actually impossible. By using the acetone–ethanol (4 : 1) or dioxane–ethanol (2 : 1) mixture as precipitant, precipitates which could be filtered easily were obtained, but these contained as much as 30—60% ash.

The ion exchange resins were also applied to desalt PVAm·HCl. Results are shown in Table 2. The yields of products were satisfactory, as can be seen from comparison of found and calculated values, and accordingly the amount of PVAm bound to cation exchange resins was extremely small.

The nitrogen contents of the products were 22.0—30.5%. The latter value (30.5%) approximates adequately to the theoretical nitrogen content of PVAm (32.5%). Then the equivalent molecular weights per nitrogen (EW-N) were compared with those per amino group (EW-A) determined by colloid titration. In the case of No. 1, EW-N was 63.7 and EW-A 104.9. This serious difference shows that No. 1 contains a large amount of non-amine-type nitrogens. EW-N and EW-A are brought close together with increase of the degree of amination. In the case of No. 4 (degree of amination: 95.6%), the nitrogen was found to be virtually an amine-type one since EW-N was 45.9 and EW-A 46.5.

The contents of carboxyl groups were small enough to neglect. The ester seems not to be hydrolyzed by passing it through the ion exchange resins.

PVAm was hygroscopic and freely soluble in water, acetic acid, or lower alcohols such as methanol, ethanol, and 2-propanol. However, it was insoluble in organic solvents such as acetone, dioxane, tertahydrofuran, DMF, DMSO, benzene, and choroform.

The infrared absorption spectrum of PVAm in a KBr disk is shown in Fig. 1, in comparison with that of PVAm·HCl. The absorption bands due to NH_2 existed at 3340 and 1635 cm^{-1}, although the bands at 2800, 1950, and 1500 cm^{-1} in PVAm·HCl, which were assigned to NH_3^+, diminished.

The intrinsic viscosity of PVAm (No.4) measured at 30 °C in 0.1 M NaCl solution was 0.70 dl/g.

References

1) Preparation of Cationic Polymers and Their Applications. IV. Part III of this series: H. Tanaka, K. Suzuki, and R. Senju, *Jpn. Tappi*, **30**, 492 (1976).

2) E. S. Wallis and J. F. Lane, *Org. React.*, Vol. III, John Wiley & Sons, New York (1962).

3) H. Tanaka and R. Senju, *Kobunshi Ronbunshu*, **33**, 309 (1976).

4) H. Tanaka, K. Suzuki, and R. Senju, *Jpn. Tappi*, **30**, 392 (1976).

5) R. Senju, "Koroido Tekitei Ho," (in Japanese), Nankodo, Tokyo (1969).

The Reaction of Disodium Tetracarbonylferrate(−II) with Carboxylic Esters and Carbothioic Esters[1)]

Yoshihisa WATANABE, Masakazu YAMASHITA, Mineo IGAMI,
Take-aki MITSUDO, and Yoshinobu TAKEGAMI

Department of Hydrocarbon Chemistry, Faculty of Engineering, Kyoto University, Sakyo-ku, Kyoto 606

(Received April 5, 1976)

The reaction of carboxylic and carbothioic esters with disodium tetracarbonylferrate has been studied. Aryl and thiolic esters reacted with the ferrate under mild conditions to give aldehydes after the reaction mixture had been quenched with acetic acid, but alkyl esters did not. 3-Benzylidenephthalide and phthalide gave 2-phenyl-1,3-indanedione and a dimeric product respectively.

Recently, several works have demonstrated that alkali metal tetracarbonylferrate, $[Fe(CO)_4]^{2-}$ (**1**), is useful for the syntheses of aldehydes,[2-5)] carboxylic acid derivatives,[6)] and ketones[7,8)] from alkyl halides, acid chlorides, carboxylic anhydrides, and carboxylic carbonic anhydrides. Though these carboxylic acid derivatives have great reactivities to **1**, little attention has been paid to other carboxylic acid derivatives. In this paper, we wish to report that the ferrate (**1**) also has some reactivities as a nucleophile to carboxylic esters and carbothioic esters, which can be transformed into the corresponding acyl tetracarbonylferrate (**2**). This is the first example of an anionic metal carbonyl reacting with an ester linkage.

Results and Discussion

Reactions of Carboxylic Esters with 1. Aryl esters, such as phenyl benzoate and phenyl propionate, reacted with a tetrahydrofuran(THF) solution of **1** at room temperature, and the corresponding aldehydes and phenols were formed after the treatment of the reaction mixture with glacial acetic acid.

$$\mathrm{RCOOPh} \xrightarrow[\text{ii) } H^+]{\text{i) } Na_2Fe(CO)_4} \mathrm{RCHO} + \mathrm{PhOH}$$

Alkyl esters, such as ethyl propionate and benzyl benzoate, scarcely reacted at all with **1** even at rather higher temperatures. The results are summarized in Table 1.

In the case of the aryl esters, the infrared spectra of the reaction mixture show bands at 1890 and 1550—1600 cm^{-1} which are not detectable before the addition of the esters. This indicates that the corresponding acylcarbonylferrates (**2**) are formed as intermediates.[9)]

$$\mathrm{RCOOPh} + [Fe(CO)_4]^{2-} \rightarrow [\mathrm{R\text{-}C(=O)\text{-}Fe(CO)_4}]^- + \mathrm{PhO}^-$$

(**1**) (**2**)

2 is assumed to be formed by the uncleophilic attack of **1** on the carbonyl carbon of the ester. The remarkable difference in reactivity between the aryl esters and the alkyl ones appears to arise partly from the electronic effects of the phenoxyl and alkoxyl group. The electron-withdrawing property of the phenoxyl group is larger than that of the alkoxyl group. Therefore, the electron density on the carbonyl carbon of the aryl esters may be lower than that of alkyl carboxylates. This slight difference may make the aryl esters active in the nucleophilic attack of **1**. Such an influence of the electron density of the carbonyl carbon on the attack of **1** has also been observed in the reaction of mixed carboxylic anhydrides.[4)]

Reaction of Carbothioic Esters with 1. Carbothioic esters such as *S*-*p*-chlorophenyl benzenecarbothioate reacted readily with **1** to give the corresponding

Table 1. Reaction of carboxylic esters with disodium tetracarbonylferrate

Run	Carboxylic ester	Reaction conditions: Temp (°C)	Time	Solvent	Aldehyde[a)]	Yield (%)[c)]
1	Phenyl benzoate	25	6 (day)	THF	Benzaldehyde	27
2	Phenyl benzoate	25	6 (day)	THF-NMP(1 : 1)	Benzaldehyde	20
3	Phenyl benzoate	60	8 (h)	THF	Benzaldehyde	Trace[b)]
4	Phenyl *p*-toluate	25	10 (day)	THF	*p*-Tolualdehyde	32
5	Phenyl *p*-chlorobenzoate	25	8 (day)	THF	*p*-Chlorobenzaldehyde	39
6	Phenyl propionate	25	7 (day)	THF	Propionaldehyde	40
7	Phenyl nicotinate	25	6 (day)	THF	3-Pyridinecarbaldehyde	22
8	*p*-Chlorophenyl benzoate	25	6 (day)	THF	Benzaldehyde	25
9	*p*-Chlorophenyl propionate	25	6 (day)	THF	Propionaldehyde	35
10	Benzyl benzoate	25	7 (day)	THF	—[b)]	
11	Benzyl benzoate	60	5 (h)	THF	—[b)]	
12	Ethyl propionate	25	5 (day)	THF	—[b)]	

a) Product after the treatment of the reaction mixture with acetic acid. b) Almost quantitative amounts of starting materials were recovered. c) Based on the amount of esters used.

Table 2. Reaction of carbothioic esters with disodium tetracarbonylferrate[a)]

Run	Carbothioic ester	Aldehyde[b)]	Yield (%)[c)]
13	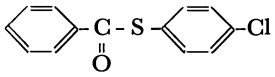	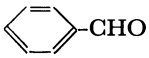	49
14	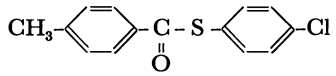	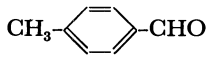	70
15	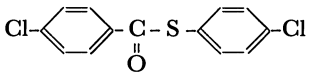	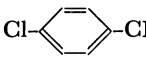	56
16	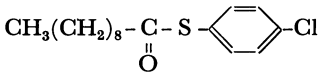	$CH_3-(-CH_2-)_8-CHO$	45

a) At 25 °C for 20 h in tetrahydrofuran. b) Product after the treatment of the reaction mixture with acetic acid. c) Based on the amount of esters used.

aldehydes in high yields after the treatment of the reaction mixture with glacial acetic acid. The results are shown in Table 2. In these reactions, the infrared spectra of the reaction mixture had bands at 1890 and 1550—1600 cm^{-1}. Therefore, the formation of the acyl tetracarbonylferrate (**2**) as an intermediate in this reaction is also strongly suggested.

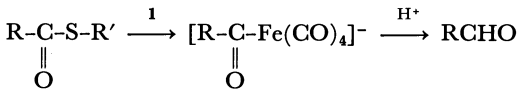

(**2**)

A comparison of the reaction conditions and the yields of the products in Tables 1 and 2 show that carbothioic esters have a greater reactivity to a nucleophilic attack of **1** than usual carboxylic esters. This agrees with the order of susceptibility of carboxylic acid derivatives to a nucleophilic attack.

Reaction of Cyclic Carboxylic Esters with ***1****.* The reaction of **1** with carboxylic esters was applied to cyclic esters. As the esters, phthalide, coumarin, 3,4-dihydrocoumarin, 3-benzylidenephthalide, and γ-butyrolactone were employed. If the reaction proceeds as expected, the corresponding aldehydes with a hydroxyl group will be produced, but the aldehydes were not obtained in these reactions. When coumarin, 3,4-dihydrocoumarin, and γ-butyrolactone were treated with **1**, some reaction took place, with a color change in the reaction mixture from pale-yellow to reddish-black. However, the formation of acyl carbonylferrate as an intermediate is not clear; the infrared absorption bands characteristic of the acyl carbonylferrate (**2**) were not detectable. In these reactions, only a black, tarry material was obtained even after treatment with acetic acid or methyl iodide.

3-Benzylidenephthalide gave 2-phenyl-1,3-indanedione in *ca.* a 50% yield by a reaction with **1**.

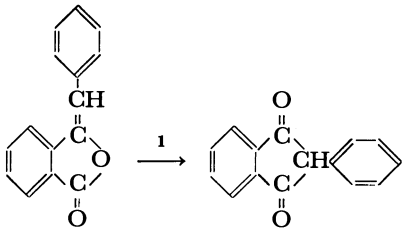

The reaction mechanism is not completely clear at the present time, but a plausible reaction scheme is that described in Scheme 1.

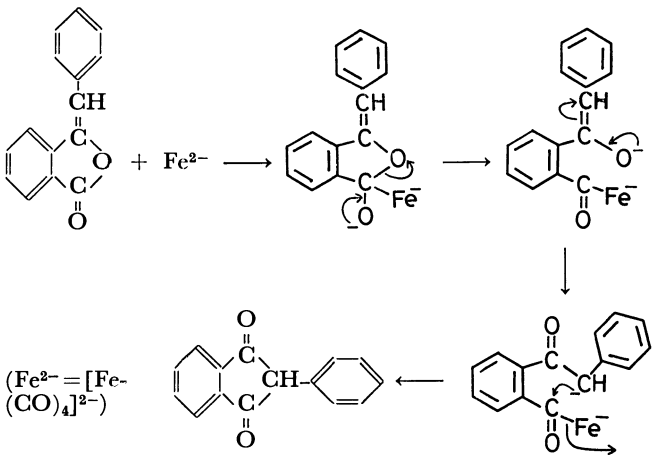

Scheme 1.

In this scheme, an acyl carbonylferrate is also considered to be an intermediate. Such a transformation of 3-benzylidenphthalide takes place in the presence of sodium alkoxide as the catalyst.[10)]

Phthalide also reacted with **1** to give white crystals in a 71% yield (based on the amount of phthalide); these crystals are soluble only in acetone and dimethyl sulfoxide. The infrared spectra of this compound had absorption bands at 3400 and 1740 cm^{-1}, characteristic of the hydroxyl group and of a carbonyl in a strained ring respectively. Thermolysis under reduced pressure (180 °C 1 Torr) and hydrolysis in a hot 3.5 M NaOH alcoholic solution gave phthalide in 85 and 70% yields respectively. From these results and elemental analysis, the structure of this compound is considered to be **3**.

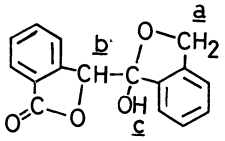

(**3**)

The mass spectrum did not exhibit a peak corresponding to the parent molecular ion, but the following peak

assignments were made: *m/e* 251[M−OH]$^+$, 135[M−$\overline{C_6H_4COOCH}$]$^+$, 134[$\overline{C_6H_4CH_2OCO}$]$^+$, 133[M−135]$^+$, 118[135−OH]$^+$. **3** may be a mixture of two diastereomers. In the NMR spectra, there are three types of signals besides that of the benzene ring: i) τ 5.04 and 4.90, both the AB type, assigned to a in **3**, ii) τ 4.09 and 4.25, both signlets, assigned to b, and iii) τ 3.75 and 3.70, both singlets, assigned to c, which disappeared upon the addition of D_2O. The fractional recrystallization of **3** from an acetone–water solution gave white needles (**4**), which have a similar infrared spectrum to, and the same composition as **3**. The NMR spectrum of **4** showed signals at τ 4.90 (AB type, 2H), 4.25 (singlet, 1H), and 3.70 (singlet, 1H). These results show that **4** is the one of the diastereomers of **3**, although its steric configuration is unknown at the present time.

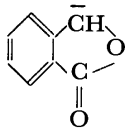

(**5**)

The mechanism of the formation of **3** is not clear at present, but the phthalide anion (**5**) is assumed to be formed by the reaction of phthalide with **1**; the anion will attack a carbonyl carbon of the second phthalide to give **3** after protonation. The phthalide anion (**5**) is also suggested to be formed by the treatment of phthalide with a basic reagent and to react with carbonyl compounds to give cross-adducts.[11] However, in the reaction of phthalide with **1** in the presence of such carbonyl compounds as benzyl benzoate, the cross-adducts were not obtained.

Experimental

The NMR spectra were obtained on a JEOL JNM-PMX 60 NMR spectrometer and a Varian Model HR-220 NMR spectrometer. The infrared spectra were measured on a Hitachi model 215 grating infrared spectrometer. The mass spectra were recorded on a JMS=OISG mass spectrometer. The melting points are uncorrected.

Materials. *p*-Chlorophenyl benzoate, *p*-chlorophenyl propionate, phenyl *p*-chlorobenzoate, phenyl *p*-toluate, *S*-*p*-chlorophenyl benzenecarbothioate, *S*-*p*-chlorophenyl *p*-toluenecarbothioate, *S*-*p*-chlorophenyl decanethioate, and *S*-*p*-chlorophenyl *p*-chlorobenzenecarbothioate were prepared according to the usual manner from acid chlorides and phenol, *p*-chlorophenol, or *p*-chlorothiophenol. The pentacarbonyliron, acetic acid, and other compounds employed in this study were all commercial products; their purities were checked by GLPC and found to be satisfactory for the reaction. Tetrahydrofuran was dried over lithium aluminium hydride and distilled before use.

*Preparation of Disodium Tetracarbonylferrate (**1**).* All the reactions were carried out in a 200-ml, three-necked flask equipped with a gas buret and a magnetic stirrer under an argon atmosphere. $Na_2[Fe(CO)_4]$ (**1**) was prepared according to the method described in a previous paper.[3] Six mmol of **1** in 30 ml of tetrahydrofuran were used in each run.

General Reaction Procedures and Analyses. To a solution of 6 mmol of **1** in tetrahydrofuran, an equimolar amount of an ester compound was added, and the reaction mixture was agitated at a desired temperature. After a certain reaction time, 0.6 ml of glacial acetic acid was poured in by means of a syringe and the mixture was stirred for an additional five minutes. A 0.2-ml sample of the solution was taken off and then submitted to GLPC analyses; column (3 mmϕ, 1.5 m) packed with Diethylene Glycol Adipate Polyester on chromosorb. The aldehydes were identified by a comparison of their retention times in GLPC with those of authentic samples, and the yields of the aldehydes were determined using internal standards.

*Reaction of 3-Benzylidenephthalide with **1**.* 3-Benzylidenephthalide (11 mmol) was added to a tetrahydrofuran solution of **1** (11 mmol) under an argon atmosphere, and the mixture was stirred for about 5 h at 40 °C. The mixture was acidified with 30 ml of 25% sulfuric acid, the tetrahydrofuran was removed *in vacuo*, and the residue was shaken with 100 ml of diethyl ether. The clean aqueous layer was discarded, and the green-black ether layer was shaken with two 70-ml portions of a 20% sodium cabonate solution. The acidification of the sodium carbonate solution with hydrochloric acid furnished white solids. The solid was terated with about 200 ml of diethyl ether, and the yellow-brown ether solution was left overnight at room temperature over sodium sulfate and then dried. After the removal of the solvent, 2-phenyl-1,3-indanedione (1.2 g, yield *ca.* 50%) was obtained and recrystallized from ethanol; mp 148 °C (literature mp 147—148 °C).[12] Found: C, 81.23; H, 4.34%. Calcd for $C_{15}H_{11}O_2$: C, 81.06; H, 4.54%. The IR and NMR spectra are identical with those of an authentic sample.

*The Reaction of Phthalide with **1**.* Into a tetrahydrofuran solution of **1** (11 mmol), we stirred 1.34 g (10 mmol) of phthalide in tetrahydrofuran at room temperature under argon. After 24 h, to the reaction mixture we added 3 ml of glacial acetic acid and the solvent was distilled off under reduced pressure. A 100-ml portion of a mixture of acetone and water, (5 : 1 v/v) was poured into the residue, and then 100 more ml of water were added. Diethyl ether (50 ml) was poured into the solution, and the organic layer was separated after vigorous shaking with the spearatory funnel. The organic solution was dried over sodium sulfate overnight, and the solvent was evaporated under reduced pressure. The white solids (**3**) thus obtained were recrystallized from acetone (0.95 g; yield 71% based on phthalide); mp 149.5—150.5 °C. Found: C, 71.52; H, 4.40%. Calcd for $C_{16}H_{12}O_4$: C, 71.63; H, 4.51%. Mass; *m/e* 251, 135, 134, 133, 118, 105. The fractional recrystallization of **3** was conducted as follows. 105 mg of **3** were dissolved in 15 ml of an acetone-water mixed solution (5 : 1 v/v), and the solution was permitted to stand in the open air. After about one week, the precipitated white crystals (**4**) were collected(28 mg). Found: C, 71.59; H, 4.61%.

References

1) This work was presented at the 33rd Annual Meeting of the Chemical Society of Japan, Fukuoka, October, 1975.

2) M. P. Cooke, Jr., *J. Am. Chem. Soc.*, **92**, 6080 (1970).

3) Y. Watanabe, T. Mitsudo, M. Tanaka, K. Yamamoto, T. Okajima, and Y. Takegami, *Bull. Chem. Soc. Jpn.*, **44**, 2569 (1971).

4) Y. Watanabe, M. Yamashita, T. Mitsudo, M. Igami, and Y. Takegami, *Bull. Chem. Soc., Jpn.*, **48**, 2490 (1975).

5) Y. Watanabe, M. Yamashita, T. Mistudo, M. Igami,

K. Tomi, and Y. Takegami, *Tetrahedron Lett.*, **1975**, 1063.
6) J. P. Collman, S. R. Winter, and R. G. Komoto, *J. Am. Chem. Soc.*, **95**, 249 (1973).
7) J. P. Collman, S. R. Winter, and D. R. Clark, *J. Am. Chem. Soc.*, **94**, 1788 (1972).
8) J. P. Collman and N. W. Hoffman, *J. Am. Chem. Soc.*, **95**, 2689 (1973).
9) W. O. Siegel and J. P. Collman, *J. Am. Chem. Soc.*, **94**, 2516 (1972).
10) S. L. Shaporo, K. Geiger, and L. Freedman, *J. Org. Chem.*, **25**, 1860 (1960).
11) W. Trueb and C. H. Engster, *Helv. Chim. Acta*, **55**, 969 (1972).
12) W. Dieckman, *Ber.*, **47**, 1439 (1914).

Studies of Enamines. VIII.[1] Reactions of Enamino Ketones with Benzoyl and Thiobenzoyl Isocyanates

Otohiko Tsuge* and Akitaka Inaba

Research Institute of Industrial Science, Kyushu University, Hakozaki, Higashi-ku, Fukuoka 812

(Received April 16, 1976)

The reaction of enamino ketone **1**, derived from acetylacetone, with benzoyl isocyanate (**4**) gave the isomeric benzoylcarbamoyl derivatives **6** and **9**, and/or 2-pyridone **7**, depending upon the reaction conditions. Similarly, enamino ketone **2**, derived from benzoylacetone, reacted with **4** to afford the isomeric benzoylcarbamoyl compounds **12**, **13**, and/or 2-pyrone **14**. It has been found that the carbamoyl compound **12** was thermally converted into **13** and **14**. Enamino ketones **1** and **2** reacted with thiobenzoyl isocyanate (**5**) at room temperature to yield the 2-pyridones **7** and **15**, respectively. On the other hand, enamino ketones **3**, derived from benzoylacetaldehyde and secondary amines, reacted with **4** to give the corresponding 2-benzoylcarbamoyl-2-penten-2-one compound **18**, while in the reaction with **5**, **3** gave the 1,3-thiazin-4-one **19** and/or (4+2) cycloaddut **20**.

In a previous paper,[1] we reported that enamino ketones, 4-(1-pyrrolidinyl)-3-penten-2-one (**1**) and 1-phenyl-3-(1-pyrrolidinyl)-2-buten-1-one (**2**), react with benzoyl isothiocyanate to yield 2-thiopyridone derivatives, **A**—**C**, and/or 3-benzoylthiocarbamoyl-3-penten-2-one compound **D** (R=Me), depending upon the nature of enamino ketones and the reaction conditions. Although a few reports are available on the reaction of simple enamines with acyl and thioacyl isocyanates,[2-4] the reaction of enamino ketones with these isocyanates has not been investigated.

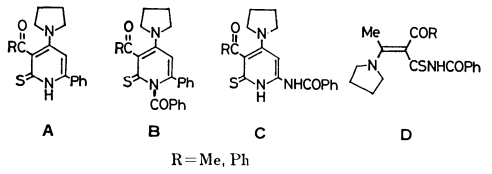

For a comparison with the reactions of enamino ketones with aryl isocyanates,[5] and with benzoyl isothiocyanate,[1] it seemed of interest to investigate the reaction of enamino ketones, **1** and **2**, with acyl and thioacyl isocyanates. It might be expected that enamino ketones, **3**, derived from benzoylacetaldehyde which were inactive toward phenyl isocyanate, would be able to react with acyl isocyanates, since acyl isocyanates are one of the most reactive systems among isocyanates. This paper deals with the reactions of enamino ketones, **1**—**3**, with benzoyl (**4**) and thiobenzoyl isocyanates (**5**).

Results and Discussion

Reaction of Enamino Ketone 1. When a solution of equimolar quantities of **1** and benzoyl isocyanate (**4**) in benzene was stirred at room temperature for 6 h, a product **7**, mp 264—266 °C (decomp), was obtained as colorless prisms in a 35% yield, together with 1,2-dibenzoylurea and benzamide.

On the basis of the following evidence, compound **7** was assigned to be 3-acetyl-6-phenyl-4-(1-pyrrolidinyl)-2-pyridone whose structure corresponds to that of a compound arising from 3-benzoylcarbamoyl-4-(1-pyrrolidinyl)-3-penten-2-one (**6**) by dehydration. The molecular formula of **7** agrees with that of the assigned structure, the IR spectrum showing bands at 2800—3000 (NH) and 1645 cm^{-1} (C=O), respectively. The NMR spectrum in $CDCl_3$ displays signals at δ 2.62 (3H, s, C**H**$_3$), 6.10 (1H, s, =C**H**), and 12.27 ppm (1H, br, N**H**), besides pyrrolidinyl and aromatic protons. **7** is identical with a sample prepared by the reaction of 3-acetyl-6-phenyl-4-(1-pyrrolidinyl)-2-thiopyridone (**8**)[1] with phosphoryl chloride, and the subsequent hydrolysis (Scheme 1).

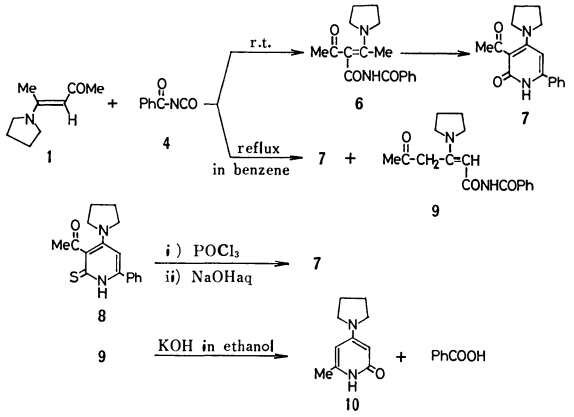

Scheme 1.

Although attempts to isolate the 1 : 1 adduct **6** were unsuccessful, it was confirmed by NMR spectroscopic study that the 1 : 1 adduct **6** is initially formed in the reaction of **1** with **4**. The NMR of a solution of equimolar quantities of **1** and **4** in $CDCl_3$ was measured at room temperature. The spectrum changed with time, and after about 30 min it showed only signals ascribable to the protons of **6**. That is, signals appeared at δ 1.95, 3.79 (each 4H, m, C**H**$_2$), 2.01, 2.51 (each 3H, s, C**H**$_3$), 7.2—8.2 (5H, m, aromatic protons), and 13.9 ppm (1H, br, N**H**). After 2 h, a singlet ascribable to a ring proton of **7** showed up at δ 6.10 ppm.

On the other hand, **1** reacted with **4** in refluxing benzene to afford **7** and 5-benzoylcarbamoyl-4-(1-pyrrolidinyl)-4-penten-2-one (**9**), mp 152—153 °C, in 12 and 15% yields respectively, together with 1,2-dibenzoylurea. The structure of **9** was assigned from the result of microanalysis and of spectral data. The

* To whom all correspondence shoud be addressed.

IR spectrum exhibited bands at 3240 (NH), 1690, 1720 (C=O), and 1635 cm^{-1} (C=C), and the NMR spectrum in $CDCl_3$ showed signals at δ 2.12 (3H, s, CH_3), 4.02 (2H, s, CH_2), 5.01 (1H, s, =CH), and 12.7 ppm (1H, br, NH), besides pyrrolidinyl and aromatic protons. Treatment of **9** with an ethanolic potassium hydroxide solution at room temperature for 5 h gave benzoic acid and 6-methyl-4-(1-pyrrolidinyl)-2-pyridone (**10**), mp 273—275 °C (decomp), in 37 and 76% yields, respectively (Scheme 1). In contrast to the 1 : 1 adduct **6**, however, the 1 : 1 adduct **9** remarkably resisted dehydration.

The reaction of **1** with thiobenzoyl isocyanate (**5**) at room temperature proceeded in the same manner as that with isocyanate **4**. After **1** was allowed to react with **5** at room temperature for 1 h, the reaction mixture was chromatographed on alumina to give pyridone **7** in only 3% yield, together with **1**. However, an initial product in the reaction was found to be 3-thiobenzoylcarbamoyl-4-(1-pyrrolidinyl)-3-penten-2-one (**11**), which was partially converted into **7** with time, by NMR spectroscopic study in nitrobenzene-d_5 (see Experimental).

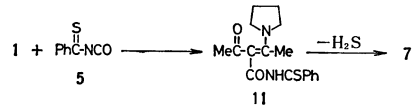

Reaction of Enamino Ketone **2**. Enamino ketone **2** reacted with an equimolar quantity of the isocyanate **4** in benzene at room temperature for 5 h to give 2-benzoylcarbamoyl-1-phenyl-3-(1-pyrrolidinyl)-2-buten-1-one (**12**), mp 133—134 °C (decomp), in a good yield. Since the 1 : 1 adduct **12** is liable to thermally decompose, **12** was recrystallized from a mixture of ethanol and petroleum ether (bp 40—60 °C) below 50 °C, and its structure was deduced from the spectral data.

On the other hand, the reaction of **2** with **4** in refluxing benzene afforded two compounds, **13** (mp 141—142 °C), and **14** (mp 187—188 °C), in 15 and 17.5% yields respectively, together with 1,2-dibenzoylurea. From the spectral data, compound **13** was assigned to 4-benzoylcarbamoyl-1-phenyl-3-(1-pyrrolidinyl)-3-buten-1-one.

The molecular formula of **14** agreed with that of a compound derived from an 1 : 2 adduct of **2** and **4** with the elimination of benzamide. The IR spectrum of **14** showed bands at 3240 (NH), 1650, 1670, and 1725 cm^{-1} (C=O), and the NMR spectrum in $CDCl_3$ displayed signals at δ 6.65 (1H, s, =CH) and 12.33 ppm (1H, br, NH), besides pyrrolidinyl and aromatic protons. Thus, compound **14** was deduced to be 3-benzoyl-6-benzamido-4-(1-pyrrolidinyl)-2-pyrone. Further support for this assignment of **14** was provided by its chemical conversions.

When a benzene solution of the 1 : 1 adduct **12** was refluxed for 1 h, the 1 : 1 adduct **13** and pyrone **14** were obtained in 17 and 15% yields, respectively, together with 1,2-dibenzoylurea and benzamide. This indicates that the 1 : 1 adduct **12** thermally dissociates into the starting materials **2** and **4**, giving **13** and **14**. On treatment with an ethanolic potassium hydroxide

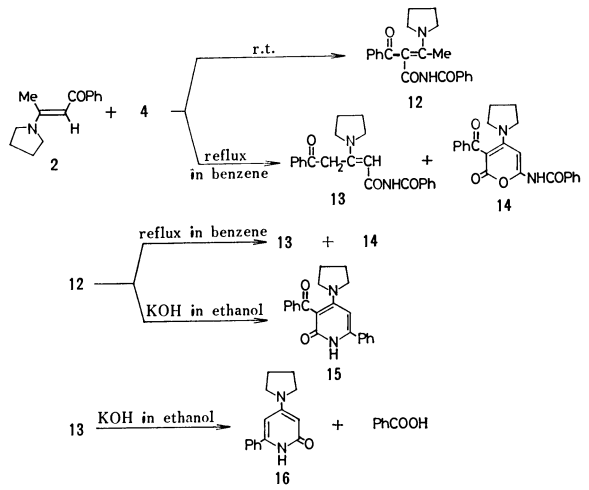

Scheme 2.

solution, the 1 : 1 adduct **12** was converted into 3-benzoyl-6-phenyl-4-(1-pyrrolidinyl)-2-pyridone (**15**) in a 42% yield. On the other hand, the same treatment of the 1 : 1 adduct **13** gave a 56% yield of 6-phenyl-4-(1-pyrrolidinyl)-2-pyridone (**16**) (Scheme 2).

In order to obtain further information on the structure of the pyrone **14**, its chemical conversions were attempted. On treatment with an ethanolic potassium hydroxide solution at room temperature, **14** was converted into 5-ethoxycarbonyl-6-phenyl-4-(1-pyrrolidinyl)-2-pyridone (**17**), mp 236—238 °C, in an 87% yield. The structure of **17** was assigned on the basis of the following evidence. The IR spectrum of **17** showed bands at 2800—3080 (NH), 1730 (C=O), and 1600—1630 cm^{-1} (C=O and C=C). The NMR spectrum in $CDCl_3$ displayed signals at δ 1.33 (3H, t, CH_2CH_3), 4.33 (2H, q, CH_2Me), 6.02 (1H, s, =CH), and 11.8—12.4 ppm (1H, br, NH), besides pyrrolidinyl and aromatic protons. The mass spectrum showed the parent peak (M^+) at *m/e* 312, together with major peaks at *m/e* (M^+-Et), 267 (M^+-OEt), and 239 (267^+-CO, base peak). The pathway for the formation of **17** from **14** could be interpreted as depicted in Scheme 3. 6-Amino-3-benzoyl-4-(1-pyrrolidinyl)-2-pyrone (**E**) would be initially formed by hydrolytic cleavage of benzamido group of **14**. This would be

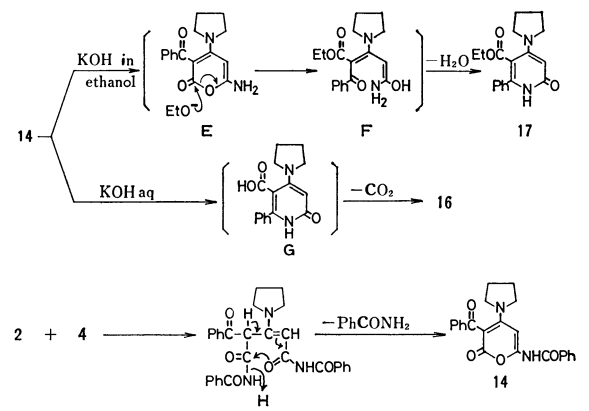

Scheme 3.

followed by attack of ethoxide ion to yield an open chain intermediate **F**, and the concurrent dehydration would give the final product **17**. On the other hand, **14** afforded the pyridone **16** in an 85% yield when treated with an aqueous potassium hydroxide solution. The formation of **16** from **14** could be reasonably interpreted by decarboxylation of 2-pyridone-5-carboxylic acid derivative **G** produced in a similar way to that for **17**.

Enamino ketone **1** reacts with aryl isocyanates to yield 1 : 2 adducts, 3,5-bis(arylcarbamoyl)-4-(1-pyrrolidinyl)-3-penten-2-ones.[5] Thus, the pathway for the formation of **14** can be viewed as depicted in Scheme 3. That is, enamino ketone **2** would react with two moles of **4** to form 1-phenyl-2,4-bis(phenylcarbamoyl)-3-(1-pyrrolidinyl)-3-buten-1-one(**H**).[6] A nucleophilic attack of the oxygen atom of 4-benzoylcarbamoyl group to the carbon atom of 2-benzoylcarbamoyl group, and the concurrent elimination of benzamide from **H** would give the pyrone **14**.

On the other hand, **2** reacted with thiobenzoyl isocyanate (**5**) in xylene at room temperature for 2 h gave 3-benzoyl-6-phenyl-4-(1-pyrrolidinyl)-2-pyridone (**15**) in a 12% yield, accompanied by the recovery of **2**.

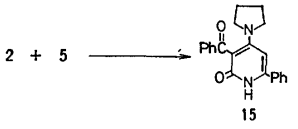

Reaction of Enamino Ketone ***3***. The reaction of 1-benzoyl-2-(1-pyrrolidinyl)ethylene (**3a**) with an equimolar quantity of benzoyl isocyanate (**4**) in benzene at room temperature for 2 h afforded 1-benzoyl-1-benzoylcarbamoyl-2-(1-pyrrolidinyl)ethylene (**18a**), mp 171—172 °C (decomp), almost quantitatively. Similarly, 1-benzoyl-2-(1-piperidyl)ethylene (**3b**) reacted with **4** to give the corresponding benzoylcarbamoyl compound **18b**, mp 140—141 °C, in a 75% yield. The structures of **18a** and **18b** were confirmed by the results of microanalyses and their spectral data.

The reaction of **3a** with thiobenzoyl isocyanate (**5**) at room temperature for 2 h afforded a 58% yield of 5-benzoyl-2-phenyl-1,3-thiazin-4-one (**19**), mp 180—181 °C, whose structure corresponded to that of a compound derived from a (4+2) cycloadduct with the elimination of pyrrolidine. **3b** reacted with **5** to give **19** and an 1 : 1 adduct **20**, mp 108—110 °C (decomp),

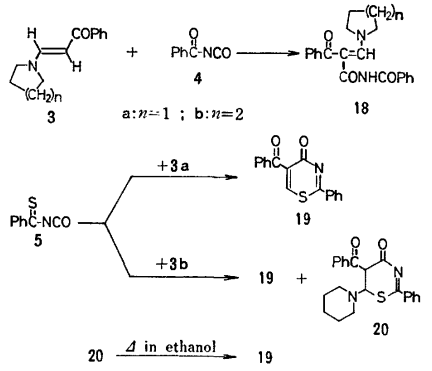

Scheme 4.

in 9 and 35.5% yields, respectively. The IR spectrum of the 1 : 1 adduct **20** showed no NH absorption bands, and the NMR spectrum in $CDCl_3$ displayed signals at δ 7.2—8.2 (11H, m, aromatic protons and $\rangle$**CH**) and 8.17 ppm (1H, d, $\rangle$**CH**, J=7 Hz), besides piperidyl protons. On heating in ethanol **20** was easily converted into the 1,3-thiazine **19**. Thus, **20** is concluded to be the (4+2) cycloadduct, 5,6-dihydro-5-benzoyl-2-phenyl-6-(1-piperidyl)-4*H*-1,4-thiazin-4-one.

Experimental

All the melting points are uncorrected. The NMR spectra were determined with a Hitachi R-20 Model spectrometer, with TMS as an internal standard. The IR spectra were measured as KBr disks, the mass spectra being obtained on a Hitachi RMS-4 mass spectrometer with a direct inlet and an ionization energy of 70 eV.

Materials. 4-(1-Pyrrolidinyl)-3-penten-2-one (**1**) was prepared from acetylacetone and pyrrolidine.[5]

1-Phenyl-3-(1-pyrrolidinyl)-2-buten-1-one (**2**): A solution of 18.0 g of sodium salt of benzoylacetone, prepared from sodium salt of acetophenone and ethyl acetate, and 10.0 g of hydrochloride of pyrrolidine in 100 ml of water was stirred at room temperature for 5 h, during which time crystals precipitated. Filtration gave crystals, which on recrystallization from a mixture of benzene and petroleum ether (bp 60—80 °C) afforded 18.7 g (87%) of enemino ketone **2**, mp 157—158 °C, as yellow prisms. IR spectrum: 1595 (C=O), 1520 cm^{-1} (C=C). NMR spectrum ($CDCl_3$): δ ppm 1.97, 3.43 (each 4H, m, CH_2), 2.68 (3H, s, CH_3), 5.62 (1H, s, =**CH**), 7.3—8.0 (5H, m, aromatic protons). Mass spectrum: *m/e* 215 (M^+). Found: C, 78.39; H, 7.87; N, 6.42%. Calcd for $C_{14}H_{17}NO$: C, 78.10; H, 7.96; N, 6.51%.

1-Benzoyl-2-(1-pyrrolidinyl)ethylene (**3a**) and 1-benzoyl-2-(1-piperidyl)ethylene (**3b**) were prepared from sodium salt of benzoylacetaldehyde prepared from sodium salt of acetophenone and ethyl formate, and the corrseponding hydrochlorides of amines. **3a**: Mp 118—119 °C, pale yellow prisms. IR spectrum: 1630 (C=O), 1540 cm^{-1} (C=C). NMR spectrum ($CDCl_3$): δ ppm 1.93, 3.90 (each 4H, m, CH_2), 6.10, 8.66 (each 1H, d, =**CH**, J=12Hz), 7.3—8.2 (5H, m, aromatic protons). Mass spectrum: *m/e* 201 (M^+). Found: C, 77.29; H, 7.36; N, 7.04%. Calcd for $C_{13}H_{15}NO$: C, 77.58; H, 7.51; N, 6.96%. **3b**: Mp 89—90 °C (lit,[7] mp 80—81 °C).

Benzolyl isocyanate (**4**) was prepared by the reported method.[8] In order to prepare thiobenzoyl isocyanate (**5**), a solution of 2-phenylthiazoline-4,5-dione in xylene was heated at 120 °C, giving a reddish-violet solution of **5** which was used *in situ*.[9]

Reaction of Enamino Ketone ***1*** *with Benzoyl Isocyanate (****4****).* *i*) A solution of 1.53 g (0.01 mol) of enamino ketone **1** and 1.47 g (0.01 mol) of the isocyanate **4** in 30 ml of benzene was stirred at room temperature for 6 h. Filtration gave 0.35 g of 1,2-dibenzoylurea. The filtrate was chromatographed on alumina using benzene as the eluent to give 0.98 g (35%) of 3-acetyl-6-phenyl-4-(1-pyrrolidinyl)-2-pyridone (**7**), mp 264—266 °C (decomp), as colorless prisms, 0.2 g of benzamide, and 0.25 g of unreacted **1** respectively.

The pyridone **7**: NMR spectrum ($CDCl_3$) δ ppm 1.92, 3.22 (each 4H, m, CH_2), 2.62 (3H, s, CH_3), 6.10 (1H, s, =**CH**), 7.3—8.0 (5H, m, aromatic protons), 12.27 (1H, br, **NH**). Mass spectrum: *m/e* 282 (M^+), 267 (M^+—NH, base peak), 254 (M^+—CO), 239 (M^+—HNCO). Found: C, 72.07; H, 6.41; N, 9.72%. Calcd for $C_{17}H_{18}N_2O_2$: C, 72.32;

H, 6.43; N, 9.92%.

Compound **7** was identical with a sample prepared from 3-acetyl-6-phenyl-4-(1-pyrrolidinyl)-2-thiopyridone (**8**).[1] After a solution of 30 mg of **8** in 2ml of phosphoryl chloride was refluxed for 1 h, the reaction mixture was poured into ice-water. The resulting solution was alkalized with aqueous potassium hydroxide solution, and then neutralized with hydrochloric acid to give 10 mg of **7**.

ii) After a solution of 1.53 g of **1** and 1.47 g of **4** in 30 ml of benzene was refluxed for 1 h, filtration gave 0.19 g of 1,2-dibenzolylurea. The filtrate was evaporated *in vacuo* and the residue was chromatographed on alumina using chloroform as the eluent to give 0.28 g (12%) of **7** and 0.45 g (15%) of 5-benzoylcarbamyl-4-(1-pyrrolidinyl)-4-penten-2-one (**9**), mp 152—153 °C, as colorless needles. Found: C, 67.88; H, 6.69; N, 9.34%. Calcd for $C_{17}H_{20}N_2O_3$: C, 67.98; H, 6.71; N, 9.33%.

Hydrolysis of the 1:1 Adduct ***9***. A solution of 0.1 g of **9** in 10 ml of 4% ethanolic potassium hydroxide solution was stirred at room temperature for 5 h. The reaction mixture was poured into water, giving crystals. Filtration gave crystals, which on recrystallization from ethanol afforded 45 mg (76%) of 6-methyl-4-(1-pyrrolidinyl)-2-pyridone (**10**), mp 273—275 °C (decomp), as colorless prisms. IR spectrum: 2800—3000 (NH), 1630 cm^{-1} (C=O). NMR spectrum ($CDCl_3$): δ ppm 1.95, 3.27 (each 4H, m, CH_2), 2.28 (3H, s, CH_3), 5.28, 5.51 (each 1H, d, =CH, J=2.5 Hz), 12.9 (1H, br, NH). Mass spectrum: *m/e* 178 (M^+, base peak), 177, 150 (M^+-CO), 135 (M^+-HNCO). Found: C, 67.09; H, 7.90; N, 15.60%. Calcd for $C_{10}H_{14}N_2O$: C, 67.38; H, 7.92; N, 15.72%.

The filtrate was acidified with hydrochloric acid to give 15 mg (37%) of benzoic acid.

Reaction of Enamino Ketone ***1*** *with Thiobenzoyl Isocyanate (****5****).* *i*) A solution of 3.06 g (0.02 mol) of **1** was added to the isocyante **5**, generated from 3.82 g (0.02 mol) of 2-phenylthiazoline-4,5-dione in 50 ml of xylene, and the solution was stirred at room tempreature for 1 h. The reaction mixture was concentrated *in vacuo* to leave a residue, which on chromatography on alumina using chloroform as the eluent gave 0.17 g (3%) of the 2-pyridone **7** and 1.90 g (62%) of unreacted **1**.

ii) The same reaction was followed by NMR spectroscopy. A solution of equimolar quantities of **1** and **5** in nitrobenzene-d_5 was prepared, and its NMR spectrum was measured at room temperature. After *ca.* 30 min, the spectrum showed only signals ascribable to the protons of 3-thiobenzoylcarbamoyl-4-(1-pyrrolidinyl)-3-penten-2-one (**11**) as follows: δ ppm 1.93, 3.0—4.0 (each 4H, m, CH_2), 2.45, 2.63 (each 3H, s, CH_3), 7.2—8.3 (5H, m, aromatic protons), 12.0 (1H, br, NH). After 1 h the formation of **7** was observed, crystals separating out within 5 h.

Reaction of Enamino Ketone ***2*** *with Benzoyl Isocyanate (****4****).* *i*) A solution of 1.0 g (4.65 mmol) of **2** and 0.75 g (5.1 mmol) of **4** in 30 ml of benzene was stirred at room temperature for 5 h, during which time crystals precipitated. Filtration gave crystals, which on recrystallization from a mixture of ethanol and petroleum ether (bp 40—60 °C) below 50 °C afforded 1.45 g (86%) of 2-benzoylcarbamoyl-1-phenyl-3-(1-pyrrolidinyl)-2-buten-1-one (**12**), mp 133—134 °C (decomp.), as colorless needles. IR spectrum: 2800—3000 (NH), 1705, 1655 cm^{-1} (C=O). NMR spectrum ($CDCl_3$): δ ppm 1.95, 3,66 (each 4H, m, CH_2), 2.12 (3H, s, CH_3), 7.2—8.3 (10H, m, aromatic protons), 13.74 (1H, br, NH). Found: C, 73.04; H, 6.06; N, 7.64%. Calcd for $C_{22}H_{22}N_2O_3$: C, 72.91; H, 6.12; N, 7.73%.

ii) A solution of 1.07 g (5 mmol) of **2** and 0.75 g (5.1 mmol) of **4** in 30 ml of benzene was refluxed for 1 h, during which time 0.25 g of 1,2-dibenzoylurea precipitated. The filtrate was concentrated *in vacuo* to leave a residue, which was dissolved in 10 ml of ethanol. The ethanol solution was allowed to stand overnight to give crystals. Filtration gave crystals, which on recrystallization from a mixture of chloroform and petroleum ether (bp 50—60 °C) afforded 0.33 g (17.5%) of 3-benzoyl-6-benzamido-4-(1-pyrrolidinyl)-2-pyrone (**14**), mp 187—188 °C, as colorless needles. NMR spectrum ($CDCl_3$): δ ppm 2.0, 3.65 (each 4H, m, CH_2), 6.65 (1H, s, =CH), 7.3—8.2 (10H, m, aromatic protons), 12.33 (1H, br, NH). Mass spectrum: *m/e* 388 (M^+), 283 (M^+-PhCO), 266 (283^+-OH), 241 ($M^+-PhCONCO$), 213 (241^+-CO), 184, 147 ($PhCONCO^+$), 105 ($PhCO^+$, base peak). Found: C, 70.92; H, 5.20; N, 7.25%. Calcd for $C_{23}H_{20}N_2O_4$: C, 71.12; H, 5.19; N, 7.21%.

The ethanol filtrate was concentrated *in vacuo*, and the reside was recrystallized from a mixture of ethanol and petroleum ether (bp 60—80 °C) to give 0.27 g (15%) of 4-benzoylcarbamoyl-1-phenyl-3-(1-pyrrolidinyl)-3-buten-1-one **13**), mp 141—142 °C, as pale yellow prisms. IR spectrum: 2800—3000 (NH), 1750 cm^{-1} (C=O). NMR spectrum ($CDCl_3$): δ ppm 2.02 4H, m, CH_2), 3.42, 4.0 (each 2H, m, CH_2), 4.22 (2H, s, CH_2), 5.79 1H, s, =CH), 7.3—8.3 (10H, m, aromatic protons), 12.66 (1H, br, NH). Mass spectrum: *m/e* 362 (M^+). Found: C, 72.71; H, 6.06; N, 7.67%. Calcd for $C_{22}H_{22}N_2O_3$: C, 72.91; H, 6.12; 7.73%.

Thermolysis of the 1:1 Adduct ***12***. A solution of 1.0 g of **12** in 20 ml of benzene was refluxed for 1 h. The reaction mixture was then allowed to stand overnight, giving 0.11 g (30%) of 1,2-dibenzoylurea. The filtrate was concentrated *in vacuo*, and the residue was chromatographed on alumina using chloroform as the eluent to give 0.17 g (17%) of **13** and 0.16 g (15%) of **14**. Further elution with ethanol afforded 60 mg (18%) of benzamide.

Hydrolysis of ***12***. A solution of 0.45 g of **12** in 10 ml of 13% ethanolic potassium hydroxide solution was stirred at room temperature for 1 h, during which time crystals precipitated. Filtration gave 0.11 g (33%) of 1,2-dibenzoylurea. The filtrate was neutralized with hydrochloric acid to give crystals, which on recrystallization from ethanol afforded 0.18 g (42%) of 3-benzoyl-6-phenyl-4-(1-pyrrolidinyl)-2-pyridone (**15**), mp 305—307 °C (decomp.), as pale orange needles. IR spectrum: 2800—3000 (NH), 1660 cm^{-1} (C=O). NMR spectrum (DMSO-d_6): δ ppm 1.9, 3.6 (each 4H, m, CH_2), 5.87 (1H, s, =CH), 7.2—8.7 (10H, m, aromatic protons), 11.7—12.0 (1H, br, NH). Mass spectrum: *m/e* 344 (M^+), 327 (M^+-OH), 315 (M^+-COH, base peak). Found: C, 76.95; H, 5.88; N, 7.98%. Calcd for $C_{22}H_{20}N_2O_2$: C, 76.72; H, 5.85; N, 8.13%.

Hydrolysis of the 1:1 Adduct ***13***. A solution of 0.23 g of **13** in 10 ml of 4% ethanolic potassium hydroxide solution was stirred at room temperature for 5 h, and then the reaction mixture was poured into water. The resulting solution was acidified with hydrochloric acid and filtration gave 20 mg (26%) of benzoic acid. The filtrate was neutralized with aqueous sodium hydroxide solution to give crystals, which on recrystallization from ethanol afforded 86 mg (56%) of 6-phenyl-4-(1-pyrrolidinyl)-2-pyridone (**16**), mp 267—269 °C (decomp.), as colorless prisms. IR spectrum: 2800—3000 (NH), 1600—1640 cm^{-1} (C=O and C=C). NMR spectrum ($CDCl_3$): δ ppm 2.0, 3.34 (each 4H, m, CH_2), 5.39, 5.99 (each 1H, d, =CH, J=2.5 Hz), 7.3—8.0 (5H, m, aromatic protons), 9.5—10.5 (1H, br, NH). Mass spectrum: *m/e* 240 (M^+). Found: C, 74.78; H, 6.83; N, 11.55%. Calcd for $C_{15}H_{16}N_2O$: C, 75.00 H, 6.67; N, 11.67%.

Hydrolysis of the Pyrone ***14***. *i*) A solution of 0.2 g of

14 in 10 ml of 13% ethanolic potassium hydroxide solution was stirred at room temperature for 2 h, and then the reaction mixture was poured into 20 ml of water. Filtration gave crystals, which on recrystallization from ethanol afforded 0.14 g (87%) of 5-ethoxycarbonyl-6-phenyl-4-(1-pyrrolidinyl)-2-pyridone (**17**), mp 236—238 °C, as colorless prisms. NMR spectrum ($CDCl_3$): δ ppm 1.33 (3H, t, CH_2CH_3, J=7.2 Hz), 1.96, 3.45 (each 4H, m, CH_2), 4.33 (2H, q, CH_2-Me), 6.02 (1H, s, =CH), 7.2—7.9 (5H, m, aromatic protons), 11.8—12.4 (1H, br, NH). Found: C, 69.01; H, 6.23; N, 9.18%. Calcd for $C_{18}H_{20}N_2O_3$: C, 69.23; H, 6.41; N, 8.97%.

ii) After a suspension of 0.2 g of **14** in 20 ml of 20% aqueous potassium hydroxide solution had been heated under reflux for 1 h, the reaction mixture was poured into water. The resulting solution was neutralized with hydrochloric acid to give crystals, which on recrystallization from ethanol afforded 105 mg (85%) of **16**.

Reaction of Enamino Ketone 2 with Thiobenzoyl Isocyanate (5). A solution of 2.15 g (0.01 mol) of **2** and **5**, generated from 1.91 g (0.01 mol) of 2-phenylthiazoline-4,5-dione, in 30 ml of xylene was stirred at room temperature for 2 h. The reaction mixture was concentrated *in vacuo* to leave a residue, which on fractional recrystallization from ethanol afforded 0.42 g (12%) of **15** and 0.85 g (40%) of **2**.

Reaction of Enamino Ketone 3 with Benzoyl Isocyanate (4). A solution of 0.4 g (2 mmol) of the enamino ketone **3a** and 0.3 g (2 mmol) of **4** in 10 ml of benzene was stirred at room temperature for 2 h, during which time crystals precipitated. Filtration gave crystals, which were recrystallized from a mixture of chloroform and petroleum ether (bp 40—60 °C) to give 0.68 g (98%) of 1-benzoyl-1-benzoylcarbamoyl-2-(1-pyrrolidinyl)ethylene (**18a**), mp 171—172 °C (decomp.), as colorless prisms. IR spectrum: 2800—3000 (NH), 1730, 1670 cm^{-1} (C=O). NMR spectrum ($CDCl_3$): δ ppm 1.87 (4H, m, CH_2), 3.21, 3.55 (each 2H, m, CH_2), 7.3—8.3 (11H, m, =CH and aromatic protons), 12.77 (1H, br, NH). Found: C, 72.47; H, 5.78; N, 8.01%. Calcd for $C_{21}H_{20}N_2O_3$: C, 72.39; H, 5.79; N, 8.04%.

Similaly, the reaction of 0.53 g (2.5 mmol) of the enamino keton **3b** with 0.37 g (2.5 mmol) of **4** in 10 ml of benzene afforded 0.68 g (75%) of 1-benzoyl-1-benzoylcarbamoyl-2-(1-piperidyl)ethylene (**18b**), mp 140—141 °C, as colorless prisms. IR spectrum: 2800—3000 (NH), 1720, 1660 cm^{-1} (C=O). NMR spectrum ($CDCl_3$): δ ppm 1.58 (6H, m, CH_2), 3.30 (4H, m, CH_2), 7.3—8.3 (11H, m, =CH and aromatic protons), 12.9 (1H, br, NH). Found: C, 73.11; H, 6.25; N, 7.58%. Calcd for $C_{22}H_{22}N_2O_3$: C, 72.91; H, 6.12; N, 7.73%.

Reaction of Enamino Ketone 3 with Thiobenzoyl Isocyanate (5). A solution of 1.01 g (5 mmol) of **3a** and **5**, generated from 0.95 g (5 mmol) of 2-phenylthiazoline-4,5-dione, in 30 ml of xylene was stirred at room temperature for 2 h. The reaction mixture was evaporated *in vacuo* to leave a residue, which was triturated with petroleum ether to give crystals. Recrystallization from ethanol afforded 0.85 g (58%) of 5-benzolyl-2-phenyl-1,3-thiazin-4-one (**19**), mp 180—181 °C, as colorless prisms. IR spectrum: 1670, 1630 cm^{-1} (C=O). NMR spectrum ($CDCl_3$): δ ppm 7.2—8.3 (10H, m, aromatic protons), 8.21 (1H, s, =CH). Found: C, 69.69; H, 3.72; N, 4.90%. Calcd for $C_{17}H_{11}NO_2S$: C, 69.62; H, 3.78; N, 4.72%.

Similarly, the reaction of 1.07 g (5 mmol) of **3b** with **5**, generated from 0.95 g (5 mmol) of 2-phenylthiazoline-4,5-dione, in 30 ml of xylene afforded 0.13 g (9%) of **19** and 0.67 g (35.5%) of 5,6-dihydro-5-benzoyl-2-phenyl-6-(1-piperidyl)-4*H*-1,3-thiazin-4-one (**20**), mp 108—110 °C (decomp.), as pale pink crystals. IR spectrum: 1670 cm^{-1} (C=O). NMR spectrum ($CDCl_3$): δ ppm 1.55 (6H, m, CH_2), 3.25 (4H, m, CH_2), 7.2—8.2 (11H, m, $\geqslant$CH and aromatic protons), 8.17 (1H, d, $\geqslant$CH, J=7 Hz). Found: C, 69.75; H, 5.83: N, 7.69%. Calcd for $C_{22}H_{22}N_2O_2S$: C, 69.82; H, 5.86; N, 7.40%.

References

1) Part VII of this series: O. Tsuge and A. Inaba, *Heterocycles*, **3**, 1081 (1975).

2) B. A. Arbuzov, N. N. Zobova, and F. B. Balabanova, *Izv. Akad. Nauk SSSR, Ser. Khim.*, **1972**, 2086; *Chem. Abstr.*, **78**, 29690w (1973).

3) J. Goerdeler and H. Schenk, *Chem. Ber.*, **98**, 3831 (1965).

4) E. Müller and H. Huber, *Chem. Ber.*, **96**, 2319 (1963).

5) O. Tsuge and A. Inaba, *Bull. Chem. Soc. Jpn.*, **46**, 286 (1973).

6) No further reaction of the 1:1 adduct **13** with the isocyanate **4** took place, but **13** was recovered. Similar phenomena were observed in the cases of the 1:1 adduct of **1** to 1-naphthyl isocyanate[5] and the 1:1 adduct of **1** to phenyl isothiocyanate.[10]

7) E. Benary, H. Meyer, and K. Charisius, *Ber.*, **59**, 108 (1926).

8) A. J. Speriale and L. R. Smith, *J. Org. Chem.*, **27**, 4361 (1962); *ibid.*, **28**, 1805 (1963).

9) J. Goerdeler and H. Schenk, *Chem. Ber.*, **98**, 2954 (1965).

10) O. Tsuge and A, Inaba, *Bull. Chem. Soc. Jpn.*, **46**, 2221 (1973).

Kinetics and Mechanism of the Reactions of Butenenitrile with Imidazoles

Fukiko YAMADA, Osamu KITANO, Soichi SHINDO, and Harunori UEDA

Department of Applied Chemistry, Faculty of Engineering, Kansai University, Senriyama, Suita, Osaka 564

(Received April 19, 1976)

The reaction kinetics of 3- and 2-butenenitriles with 2-alkylimidazoles were studied by using NMR, and a mechanism consistent with the results is proposed. The imidazoles were active in isomerizing 3-butenenitrile to 2-butenenitrile, and then reacted only with the 2-butenenitrile to give the corresponding 1-(2-cyano-1-methylethyl)imidazoles. These consecutive reactions, isomerization and cyanoethylation, are second-order over all. For example, in the reaction of 3-butenenitrile with imidazole, the rate measurements of the isomerization at various temperatures, ranging from 30 to 90 °C, afforded the activation parameters of E_a= 14.6 kcal/mol and ΔS^*= −35.3 cal/degree. On the other hand, in the case of 2-butenenitrile with imidazole, the measurements of the cyanoethylation at 60—100 °C gave these parameters; E_a= 15.3 kcal/mol and ΔS^*= −45.7 cal/degree. In this case, the rates of the isomerization ($k_1 = 6.0 \times 10^{-6}$ l/mol s at 60 °C) are approximately ten times larger than those of the cyanoethylation ($k_2 = 0.53 \times 10^{-6}$). A mechanism is discussed on the basis of their NMR spectral and kinetic data.

Recently, in our previous paper, the kinetic data on the reaction of acrylonitrile with imidazole have been reported.[1] By means of the NMR method, factors governing the points of the cyanoethylation and the polymerization of acrylonitrile are well understood. The studies have now been extended to unsaturated nitriles with a view to obtaining a clear picture of the reaction.

In this paper, we wish to describe the kinetics of the reactions of 3- and 2-butenenitriles (3-BN and 2-BN) with imidazole (Im), 2-ethylimidazole (EtIm), and 2-isopropylimidazole (*i*-PrIm) respectively, and their possible mechanism.

Experimental

Measurements. All the boiling and melting points are uncorrected. The NMR spectra were obtained at 60 MHz with a Japan Electron Optics Model JNM-3H-60 spectrometer at room temperature. The chemical shifts were reported in ppm downfield from the internal TMS (δ). The IR spectra were recorded on a Shimadzu Model 27-G grating spectrophotometer on a KBr disk for the solid materials or on a NaCl plate for the liquid ones. The GLC analysis was carried out on a Shimadzu gas chromatograph, Model GC-5AP$_3$T, using a 3.00-m column packed with silicone HV grease (20-wt%). The percentage composition of the product was estimated by means of the relative peak areas (uncorrected).

A constant-temperature bath with a temperature control of ±0.1 °C was employed.

Materials. Im, EtIm, and *i*-PrIm were recrystallized from benzene several times; mps, 88—89, 83—84, and 133—134.5 °C respectively. Imidazole-1-*d*[2] and 3-BN (bp 118—121 °C)[3] were prepared by the reported methods. 2-BN (bp 115—118 °C) was of a reagent quality and was used without further purification. In all the materials, the purities were determined by means of NMR and GLC analyses.

Kinetic Measurements. The reactions of the imidazoles with 3- or 2-BN were carried out in sealed tubes. The rate of the appearance of the product was followed by using NMR.[1] In a typical preparation, about 1.5 g of Im was placed in a 10-ml volumetric flask and weighed. Then the volume was quickly made up to 10 ml with the nitrile. This solution was transferred into ten separate tubes and sealed. The first NMR analysis was performed as soon as feasible after the sample preparation. The sealed tubes were shaken at a constant temperature for a given time. The rate measurements were then performed by means of the NMR method.[1] Each experiment was repeated in order to check the reproducibility.

Reaction Products. After the reaction had been completed, the reaction mixture collected from each run was treated and purified by the method reported previously.[1] The physical properties of the corresponding 1-(2-cyano-1-methylethyl)imidazoles thus obtained may be shown as follows:

Product 1. 1-(2-Cyano-1-methylethyl)imidazole (**1**); bp 128 °C/0.9 Torr. Picrate; mp 125.0—126.0 °C, Found: C, 42.73; H, 3.23; N, 23.25%. Calcd for $C_{13}H_{12}N_6O_7$: C, 42.84; H, 3.32; N, 23.08%. IR (C≡N) : 2254 cm^{-1}. NMR (CH_2Cl_2) : δ 1.53 (d, 3H, CH_3), 2.82 (d, 2H, $-CH_2CN$), 4.53 (sextet, 1H, N⩾CH), 6.97—7.05 (2H, ring-proton), 7.53 (s, 1H, ring).

Product 2. 1-(2-Cyano-1-methylethyl)-2-ethylimidazole (**2**); bp 105 °C/0.4 Torr. Picrate; mp 152.0—153.0 °C, Found: C, 46.16; H, 3.90; N, 22.03%. Calcd for $C_{15}H_{16}N_6O_7$: C, 45.92; H, 4.11; N, 21.42%. IR (C≡N): 2257 cm^{-1}. NMR (CH_2Cl_2) : δ 1.51 (d, 3H, CH_3), 2.81 (d, 2H, $-CH_2CN$), 4.54 (sextet, 1H, N⩾CH), 1.29 and 2.70 (t, 3H ; q, 2H, 2-C_2H_5), 6.90 and 7.02 (2H, ring).

Product 3. 1-(2-Cyano-1-methylethyl)-2-isopropylimidazole (**3**); mp 51.0—53.0 °C. Picrate ; mp 151.5—152.5 °C. Found: C, 47.41; H, 4.35; N, 20.95%. Calcd for $C_{16}H_{18}N_6O_7$: C, 47.27; H, 4.46; N, 20.68%. IR (C≡N) : 2248 cm^{-1}. NMR (CH_2Cl_2) : δ 1.54 (d, 3H, CH_3), 2.77 (d, 2H, $-CH_2CN$), 4.56 (sextet, 1H, N⩾CH), 1.24 and 1.32 (d, d, 3H, 3H, 2CH_3 of *i*-Pr), 3.01 (septet, 1H, ⩾CH of *i*-Pr), 6.88—6.95 (2H, ring).

Results and Discussion

Reactions. In the reaction between Im and 3-BN, the changes in the NMR spectra with the time are shown in Fig. 1. One-proton and two-proton singlets due to the ring protons of Im appear at 7.3 and 8.0 ppm respectively. In the earlier period of the reaction, the new singals of the methyl and olefinic protons due to 2-BN, the product of the isomerization, began to appear in the regions of 2.0—2.2 and 6.5—6.9 ppm respectively (after 60 min, in Fig. 1). Their intensities increased with the reaction time. After a considerable amount of 2-BN had been produced (900 min), the signals of Compound **1** appeared at 1.8 (CH_3), 3.1 ($-CH_2CN$), and 4.9 ppm (N⩾CH) respectively. Therefore, the progress of the reaction

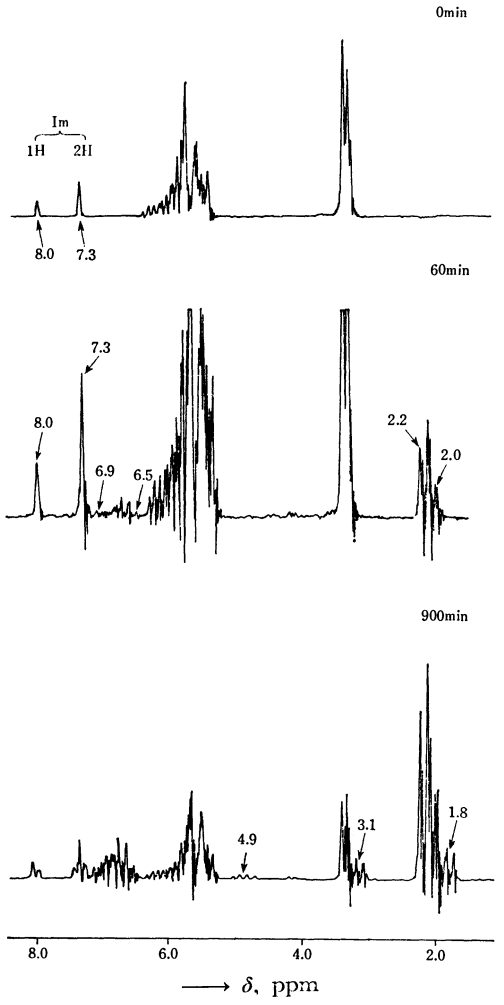

Fig. 1. Changes of the NMR spectra with reaction time, in the reaction of Im (1.325 mol/l) with 3-BN (11.396 mol/l) at 77 °C. After 900 min, the conversion of 3-BN to 2-BN was 67.4%.
3-BN, NMR (CCl_4): δ 3.23—3.38 (2H, CH_2) and 5.27—6.28 (3H, H_2C=CH–).
2-BN, NMR (CCl_4): δ 1.98—2.23 (3H, CH_3), and 5.44—5.74 and 6.47—7.18 ppm (2H, –CH=CH–).

was followed by observing the rates of the appearances of the signals of 2-BN and Compound **1**.

In this reaction at 90 °C, the time-conversion curves of the above two products and the plots of the NH shift and its content at the reaction time are shown in Fig. 2.

From these observations, it is clear that 3-BN is first converted to 2-BN in the presence of Im, and that then 2-BN reacts with Im to give Compound **1**. That is, Im is active in isomerizing 3-BN to 2-BN. It is also easily observable in Fig. 2 that the isomerization proceeds much faster than the cyanoethylation and that, during the proceeding of the isomerization, the NH signal moves downfield.

On the other hand, it was observed by means of the NMR method that, in the reaction of Im with 2-BN, Compound **1** was the sole product. Figure 3 shows both the conversion and NH shift curves in this reaction. The two curves show a similar tendency. The NH signal moves upfield with an increase in the yield of

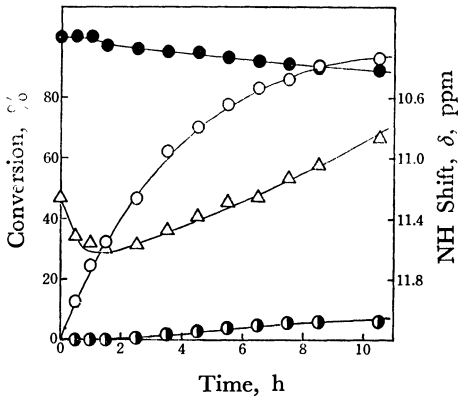

Fig. 2. Time-conversions and NH shift curves in the reaction of Im (1.679 mol/l) with 3-BN (11.110 mol/l) at 90 °C.
○: Conversion of isomerization, 3-BN to 2-BN;
◑: conversion for compound **1**;
△: NH shift; ●: NH content, %.

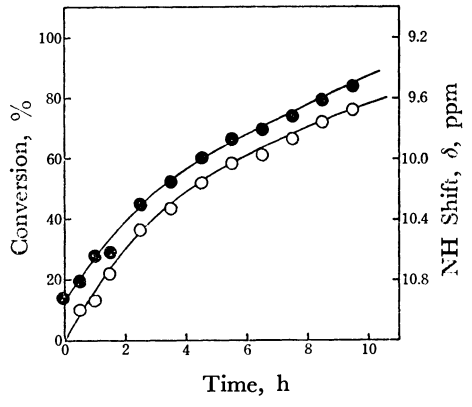

Fig. 3. Time-conversion and NH shift curves in the reaction of Im (1.736 mol/l) with 2-BN (10.800 mol/l) at 90 °C.
○: Conversion; ●: NH shift.

Compound **1**. On the contrary, in the isomerization (Fig. 2) the NH signal moves downfield. Thus, the reactions of the imidazoles with 2-BN yielded the corresponding 1-(2-cyano-1-methylethyl) imidazoles (**1**, **2**, and **3**).

Rates. From the above observations, this consecutive reaction can be represented as follows:

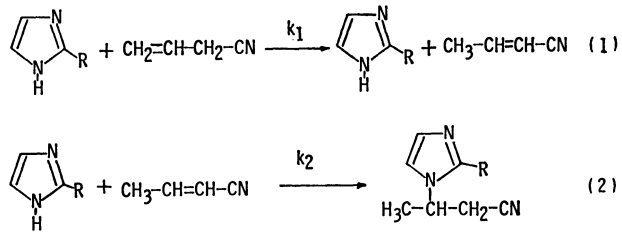

The isomerizaation (Eq. 1) was monitored by the NMR method to trace a time-conversion curve and may be expressed as:

$$d(2\text{-BN})/dt = k_1(3\text{-BN})^m(\text{Im})^n \quad (3)$$

When this process is carried out with an excess of 3-BN, the changes in the concentration of Im are

Table 1. Reaction rates[a] and activation parameters for the isomerization of 3-BN to 2-BN

Temp, °C	30	35	40	45	50	60	70	77	80	90	E_a[b]	ΔS^*[c]
Im	0.8	1.1	1.7	2.3	3.0	6.0	11.8	15.8	28.2	45.2	14.6	−35.3
EtIm					16.2	34.7	68.8		134.0		16.2	−35.1
i-PrIm						39.8		103.0		273.0	15.5	−37.1

a) Calculated by the least-squares method, $k_1 \times 10^6$ l/mol s. b) Activation energy, kcal/mol. c) Calculated at 70 °C, cal/degree.

Table 2. Reaction rates and activation parameters for the cyanoethylation of 2-BN with imidazoles

Imidazoles	$K_2 \times 10^6$ l/mol s (Temperature, °C)						kcal/mol E_a	ΔS^* cal/degree
Im	0.53 (60)	1.3 (70)	1.9 (80)	4.0 (90)	6.5 (100)		15.3	−45.7
EtIm	4.3 (110)	5.4 (120)	7.5 (130)	10.0 (140)			9.2	−63.6
i-PrIm	0.61 (100)	1.2 (120)	2.1 (140)	2.3 (150)	2.7 (160)	2.8 (170)	7.8	−70.1

negligible. Therefore, the apparent rate of the isomerization depends only on the concentration of 3-BN. Consequently, Eq. 3 can be written as:

$$d(2\text{-BN})/dt = k_{obsd}(3\text{-BN})^m \quad (4)$$

The orders, m and n, are determined by the initial-rates (V_0) method.[4] In fact, when the (3-BN) or (Im) concentrations are kept constant and the (Im) or (3-BN) concentrations (C_0) are varied, the plots of log V_0 against log C_0 are linear and their slopes are $m = 1.01$ and $n = 0.96$. That is, the orders are assumed to be 1.0. Consequently, we can rearrange Eqs. 3 and 4 by substituting the above values and can rewrite the equations as follows:

$$d(2\text{-BN})/dt = k_1(3\text{-BN})(\text{Im}) \quad (5)$$

$$= k_{obsd}(3\text{-BN}) \quad (6)$$

All the runs, carried out with an excess of 3-BN, gave excellent pseudo first-order kinetics to at least 70% completion. The rates were measured at various temperatures between 30 and 90 °C. The rate constants, k_1, derived for the isomerization and their activation parameters in the reactions of the imidazoles with 3-BN are listed in Table 1. In the case of 2-methylimidazole, it was difficult to get an accurate value because of its low solubility in the reaction mixture. As is obvious from the table, the rate constants increase with the change in R in the order of ethyl and isopropyl, while the values of E_a and ΔS^* are almost constant.

On the other hand, the reactions of the imidazoles with 2-BN were found to follow second-order rate equations[1]:

$$d(\text{product})/dt = k_2(2\text{-BN})(\text{Im}) \quad (7)$$

The values of the second-order rate constants, k_2, were obtained by a method reported previously.[1] Table 2 shows the rate constants at various temperatures, along with the values of the activation parameters. Small E_a values and large negative ΔS^* values are observed. In general, such facts indicate that the reaction involves a strongly polarized and/or crowded transition state. In this case, the above fact implies that not only a polar effect, but also a steric effect of R, is a controlling factor. Furthermore, the plot of E_a *vs.* ΔS^* for R of H, C_2H_5, and *i*-Pr shows a good compensation effect.

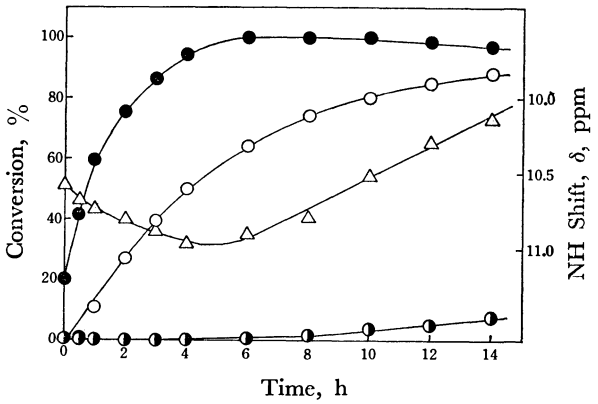

Fig. 4. Time-conversions and NH shift curves in the reaction of imidazole-1-d_1 (1.702 mol/l) with 3-BN (11.090 mol/l) at 70 °C.
○: Conversion of isomerization, 3-BN to 2-BN;
◑: conversion for compound **1**;
△: NH shift; ●: NH content, %.

Possible Reaction Mechanism. *(A) Isomerization.* To elucidate the mechanism, the reaction of imidazole-1-*d*, containing up to 19.2% NH, with 3-BN was performed by monitoring the NMR method. Plots of NH shift, its content, and the conversions against the reaction time are shown in Fig. 4. In the beginning of the reaction, the NH content of imidazole-*d* was 20%; it then increased with an increase in the reaction time. When its content approached 100%, the NH signal began to move upfield and the formation of Compound **1** was observed. The curves of the NH shifts and the conversions in Fig. 4, are identical with those illustrated in Fig. 2. As can be seen in both Figs. 2 and 4, the NH shift in each lowest field appeared at approximately 11 ppm. These phenomena support the idea that either the hydrogen of NH in the Im molecule is bonded to another mole-

cule, probably the 3-BN molecule, by a very weak bond such as a hydrogen bond, or, since the bonding energy of NH falls, the distance is sufficiently stretched. On the other hand, a hydrogen atom of the methylene group in the 3-BN molecule is activated by the −I-effect of the CN group.

We also attempted the reactions of pyrrole, pyrazole, and imidazole nitrate with 3-BN under the same conditions. However, no products could thus be obtained.

These considerations lead us to believe that the following reaction mechanism holds:

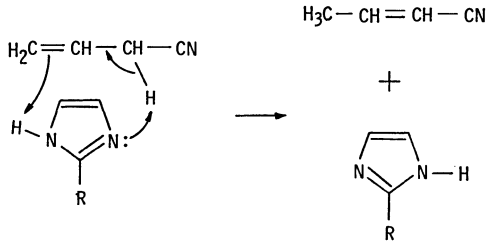

A. Isomerization mechanism

(B) Cyanoethylation. In the reaction of Im with acrylonitrile, we have already reported the value for the activation energy, $E_a = 12.0$ kcal/mol. In this work, the activation energy of the reaction of Im with 2-BN was 15.3 kcal/mol. This result suggests that the reaction of 2-BN with Im is somewhat more difficult than that of acrylonitrile. This may be due to the +I-effect of the metyl group in 2-BN. As can be seen in Fig. 3, the NH signal appears at around 11 ppm in the beginning of the reaction. On the basis of the results mentioned above and other considerations,[1] a possible mechanism for the cyanoethylation can be described as follows:

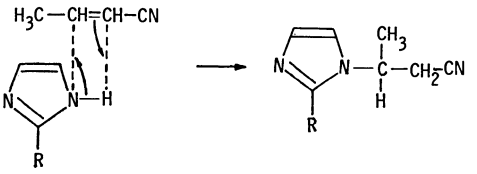

B. Cyanoethylation mechanism

We wish to thank the Shikoku Fine Chemicals Co., Ltd., for the supply of the imidazoles.

References

1) F. Yamada and Y. Fujimoto, *Bull. Chem. Soc. Jpn.*, **44**, 557 (1971).
2) J. H. Bowie, R. G. Cooks, S. O. Lawesson, and G. Schroll, *Aust. J. Chem.*, **20**, 1613 (1967).
3) J. V. Supniewski and P. L. Salzberg, *Org. Synth.*, Coll. Vol. I, 46 (1955).
4) M. Oiwa, "Hannosokudo Keisanho," Asakura Shoten, Tokyo (1973), p. 12.

Formation of Diorganostannylenes. I. Photolytic Reaction of Dibutyltin with Organic Halides

Sinpei KOZIMA, Kazuhiko KOBAYASHI,* and Mituyosi KAWANISI*

Department of Chemistry, School of Liberal Arts and Sciences, Kyoto University, Sakyo-ku, Kyoto 606

** Department of Industrial Chemistry, Faculty of Engineering, Kyoto University, Sakyo-ku, Kyoto 606*

(Received April 22, 1976)

The photochemical reactions of dibutyltin, $(Bu_2Sn)_m$, with alkyl monohalides, R'X, give $Bu_2R'SnX$-type compounds by the insertion of the intermediately formed dibutylstannylene to the C–X bond of alkyl halides. This provides a facile method for preparing $Bu_2R'SnX$ compounds, since the reaction proceeds quickly under mild conditions giving the products in good yields, the only by-product Bu_3SnX which can be distilled being obtained only in a low yield. The reactions with dihalomethanes were also successful. The reaction pathway is discussed in connection with the reactivities of the substrates.

In previous papers,[1,2] thermal reactions of polymeric diorganotins, $(R_2Sn)_m$, with alkyl halides, R'X, were reported to yield the insertion products, $R_2R'SnX$, together with a variety of disproportionation products, R_4Sn, R_3SnX, and $RR_2'SnX$. Kumada and his collabolators reported on the formation of silylenes, R_2Si:, by the photolysis of organopolysilanes.[3] Schroer and Neumann,[4] and Neumann and Schwarz[5] reported on the transient formation of dialkylstannylenes, R_2Sn:, by the thermal decomposition of 1,2-dichlorotetraalkylditin, and by the photolysis of dialkyltins, respectively. These reports have promped us to disclose our recent results of the photochemical reactions of dibutyltin with organic halides. This paper deals mainly with the reactions of dibutyltin with organic bromides and chlorides, giving a discussion on the reaction pathway comparing the results of the photolytic reactions with those of the thermal reactions.

A solution of dibutyltin, $(Bu_2Sn)_m$, in a large excess of alkyl bromides, R'Br, was irradiated with a high pressure mercury lamp through a Pyrex filter at 0 °C for 30 min to give $Bu_2R'SnBr$ in about 60% yield, together with a small amount of Bu_3SnBr (1—3%). From the distillation residue, bis(dibutylbromotin) oxide, $(Bu_2BrSn)_2O$, was isolated in about 30% yield. Yellow coloration of dibutyltin still remained when the solution was kept in the dark at room temperature for 10 days. Irradiation, therefore, apparently induced the reaction. The major product, $Bu_2R'SnBr$, could be formed by the insertion of transiently formed dibutylstannylene, Bu_2Sn:, into the C–Br bond of alkyl bromide. Since polymeric diorganotins are yellowish liquid or solids,[6] they have absorptions in the ultraviolet and visible regions (Fig. 1). The absorptions could be attributed to the polymeric Sn–Sn bonds. Thus, irradiation with UV light could cleave the Sn–Sn bonds of diorganotins. Photolysis of cyclic dibutyltin, $(Bu_2Sn)_m$, could produce dibutylstannylene, Bu_2Sn:, accompanied by the formation of cyclic dibutyltin, $(Bu_2Sn)_{m-1}$, and/or acyclic polydibutyltin biracdical (III) (Eq. 1). The spin state

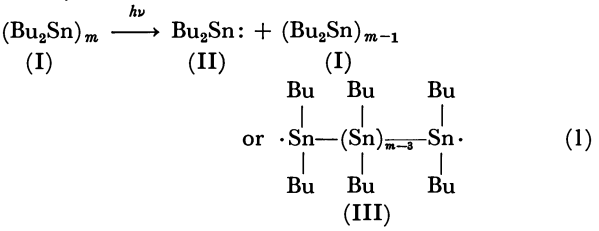

(1)

of the stannylene, singlet or triplet can not be discussed from our present results. A part of the stannylene thus formed undergoes insertion into the C–Br bond of the alkyl bromide (Eq. 2), and the rest of the stannylene could be inserted into the Sn–Sn bonds and/or C–Sn bonds of dibutyltin (Eqs. 3 and 4).[7] It is also probable that the stannylene abstracts two bromine atoms from alkyl bromide successively to form dibutyltin dibromide. No dibutyltin dibromide was found in the distillation product, however, a small amount of the dibromide (*ca.* 4%) was detected in the reaction mixture (Eq. 5). A part of the dibromide could be consumed by the reaction with the stannylene (Eq. 6).

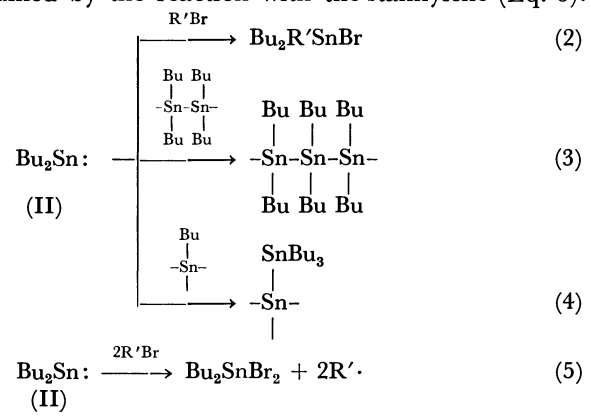

It has been confirmed that dibutyltin dibromide readily reacts with dibutyltin under the same irradiation

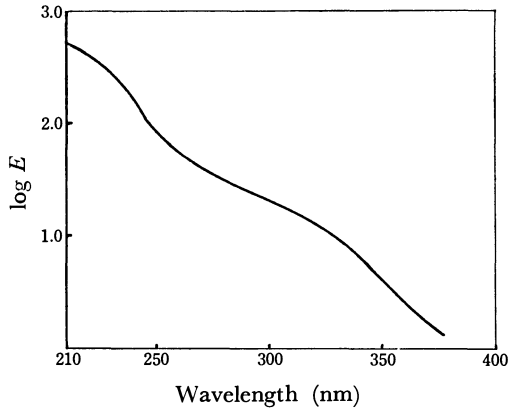

Fig. 1. Ultraviolet spectrum of dibutyltin in cyclohexane.

conditions to yield 1,2-dibromotetrabutylditin (IV) in 80% yield together with tributyltin bromide in 20% yield (Eq. 6). After the photolysis, the reaction mixture was exposed to air to oxidize the residual Sn–Sn bonds.[8] Thus, bis(dibutylbromotin) oxide (V) in the distillation residue should be formed by the air oxidation of 1,2-dibromotetrabutylditin (IV) (Eq. 7). Ditin compounds (IV) could be formed by the successive abstraction of two bromine atoms from alkyl bromide by tetrabutylditin biradical (Eq. 8), or by the reaction of dibutyltin dibromide with the stannylene (Eq. 6).

$$Bu_2SnBr_2 + (Bu_2Sn)_m \xrightarrow{h\nu} \underset{\text{(IV)}}{Br\text{-}Sn(Bu)_2\text{-}Sn(Bu)_2\text{-}Br} + Bu_3SnBr \quad (6)$$

(I)

$$\underset{\text{(IV)}}{Br\text{-}Sn(Bu)_2\text{-}Sn(Bu)_2\text{-}Br} \xrightarrow{O_2} \underset{\text{(V)}}{Br\text{-}Sn(Bu)_2\text{-}O\text{-}Sn(Bu)_2\text{-}Br} \quad (7)$$

$$\underset{\text{(IV)}}{\cdot Sn(Bu)_2\text{-}Sn(Bu)_2\cdot} \xrightarrow{2R'Br} \underset{\text{(IV)}}{Br\text{-}Sn(Bu)_2\text{-}Sn(Bu)_2\text{-}Br} + 2R'\cdot \quad (8)$$

The minor by-product, Bu_3SnBr, can be produced by the reaction of tributyltin radical with alkyl bromide. This reaction was found to occur in the dehalogenation of organic halides by organotin hydrides.[9] There might be several possible pathways for the formation of tributyltin radical. One of them is the insertion of dibutylstannylene into the Bu–Sn bond of dibutyltin to give tributyltin group (Eq. 4), which could be cleaved by the irradiation (Eq. 9). This insertion

$$-Sn(Bu)_2\text{-}Sn(Bu)_2\text{-}Sn(Bu)(SnBu_3)\text{-} \xrightarrow{h\nu} -Sn(Bu)_2\text{-}Sn(Bu)_2\text{-}\dot{S}n(Bu)\text{-} + Bu_3Sn\cdot \quad (9)$$

pathway, however, could be a minor one since the yield of Bu_3SnBr was independent of the concentration of $(Bu_2Sn)_m$.

Another one is the intramolecular transposition of butyl group to give the tributyltin group at the terminal position together with the monobutyltin group (Eq. 10). The possibility of this pathway has been con-

$$-Sn(Bu)_2\text{-}Sn(Bu)_2\text{-}\dot{S}n(Bu)_2 \xrightarrow{h\nu} -Sn(Bu)_2\text{-}Sn(Bu)\cdot\text{-}Sn(Bu)_2\text{-}Bu \quad (10)$$

firmed by the irradiation of polymeric dibutyltin in the absence of alkyl halide. By the photolysis of dibutyltin in benzene (0.503 g/8 ml) for 80 min, 9% of dibutyltin fragments were converted into tributyltin and monobutyltin fragments. In the case of the more dilute benzene solution (0.158 g/24 ml), the conversion proceeded more efficiently (23%). The disproportionation, therefore, would take place *via* the intramolecular process. This intramolecular transposition of butyl group might be a major pathway for the formation of tributyltin group. The tributyltin group thus formed is photochemically cleaved to afford tributyltin radical (Eq. 11).

$$-Sn(Bu)_2\text{-}Sn(Bu)_2\text{-}Sn(Bu)_2\text{-}Bu \xrightarrow{h\nu} -Sn(Bu)_2\text{-}\dot{S}n(Bu)\cdot + Bu_3Sn\cdot \quad (11)$$

The reaction of dibutylstannylene with the free butyl radical cleaved photochemically from dibutyltin might be also possible. A similar photochemical disproportionation was reported in the photolysis of bis[bis(trimethylsilyl)methyl]stannylene to give the trisubstituted stannyl radical.[10] The probability of this pathway can not be eliminated by our present results.

In the reaction with propyl chloride, a longer reaction time was required to achieve a good conversion than in the cases of alkyl bromides. The insertion product, $Bu_2PrSnCl$, and the disproportionation product, Bu_3SnCl, were obtained in 57 and 7.3% yield, respectively. It is to be noted that the photochemical reaction occurred at lower temperature (0 °C), in shorter reaction time (80 min), in contrast to the thermal reaction,[1] where the insertion product, $Bu_2PrSnCl$, was produced under drastic conditions in the presence of catalysts (160 °C, 15 h) accompanied by many thermally scrambled alkyltin products. No bis(dibutylchlorotin) oxide was detected in the distillation residue exposed to air, but organopolystannoxane containing more than two tin atoms, presumably a trimer or a tetramer, was found. Since the C–Cl bond of alkyl chloride is less reactive than the C–Br bond, the rate of the insertion of dibutylstannylene toward the C–Cl bond could be much lower. In the reaction with alkyl chloride, accordingly, the reformation of Sn–Sn bonds from the stannylene (Eq. 3) could be enhanced. Therefore, the chance for the formation of tributyltin fragments increases, and the relatively longer chains of Sn–Sn bonds remain in the reaction mixture.

Dibutylstannylene also undergoes the insertion reaction into C–X bonds of dichloro- and dibromomethane to afford analytically pure dibutyl(chloromethyl)tin chloride (58%)[11] and dibutyl(bromomethyl)-tin bromide (70%), respectively. No disproportionation products, Bu_3SnCl and Bu_3SnBr were detected in the reaction products. Since the stannylene was captured effectively by the dihalomethanes, the reformation reaction of polydibutyltin from the stannylene (Eq. 3) could be restricted, and the disproportionation to produce tributyltin fragment, therefore, might be extremely suppressed.

$$(Bu_2Sn)_m + XCH_2X \xrightarrow{h\nu} Bu_2SnCH_2X \quad (12)$$

(X)

Experimental

Reactions with Alkyl Monohalides. Dibutyltin was prepared from dibutyltin dihydride and dibutyltin dimethoxide by the method of Neumann, Pedain, and Sommer.[12] In all

the experiments, freshly prepared yellow liquid of dibutyltin was used. The ^{13}C-NMR spectra were recorded in the pulse Fourier transform mode with a JEOL-FX 60 spectrometer operating at a resonance frequency of 15.03 MHz. The parameters used were: pulse width 8 μs, spectral width 2500 Hz for 8 K data points.

In a typical procedure, a mixture of 1.106 g of dibutyltin and 8 ml of ethyl bromide in a sealed Pyrex glass ampoule was irradiated with a high pressure mercury lamp (450 W) externally at 0 °C under nitrogen atmosphere for 30 min. The reaction mixture was then exposed to air, and the excess of ethyl bromide was removed by distillation *in vacuo*. The product was distilled under reduced pressure to give 0.946 g of distillate (bp 96—98 °C/3 mmHg), containing 57% yield of dibutylethyltin bromide and 1.1% of tributyltin bromide. Dibutylethyltin bromide was identified by comparing the retention time on gas chromatography and the IR and ^{13}C-NMR spectra with those of the authentic samples.[1] ^{13}C-NMR($CDCl_3$): δ 9.6(Sn-**C**H_2CH_3 $J_{C-^{119}Sn}$=334 Hz), 10.3 (Sn-CH_2**C**H_3). The colorless crystals in the distillation residue (0.527 g, 35%) were recrystallized from acetone and identified as bis(dibutylbromotin) oxide, $(Bu_2BrSn)_2O$.[13]

In a similar procedure, the reaction of dibutyltin with propyl bromide gave dibutylpropyltin bromide (66%),[1] tributyltin bromide (2.5%) and bis(dibutylbromotin) oxide (26%). Dibutylpropyltin bromide: ^{13}C-NMR($CDCl_3$): δ 20.5 (Sn-**C**$H_2CH_2CH_3$ $J_{C-^{119}Sn}$=338 Hz), 19.4 (Sn-CH_2-**C**H_2CH_3), 18.3 (Sn-CH_2CH_2**C**H_3).

In the reaction with alkyl chlorides, the irradiation time was extended to 80 min. Thin-layer chromatography of the residual stannoxane developed with CH_2Cl_2 showed no detectable spot of bis(dibutylchlorotin) oxide, but those of longer chain stannoxanes in the lower R_f-values.

The reaction of 1.194 g of dibutyltin with 8 ml of propyl chloride gave dibutylpropyltin chloride (0.913 g, 57%),[1] tributyltin chloride (0.121 g, 7.3%) and residual stannoxane (0.412 g). Dibutylpropyltin chloride: ^{13}C-NMR($CDCl_3$): δ 20.3 (Sn-**C**$H_2CH_2CH_3$ $J_{C-^{119}Sn}$=338 Hz), 19.4 (Sn-CH_2**C**H_2CH_3), 18.3 (Sn-CH_2CH_2**C**H_3).

Tributyltin chloride (1.063 g, 69%) was obtained in pure form, together with the residual stannoxane (0.326 g), from 1.107 g of dibutyltin and 8 ml of butyl chloride.

Reactions with Dihalomethanes. Under similar conditions, a solution of 3.24 g of dibutyltin in 10 ml of dichloromethane was irradiated for 30 min. Excess dichloromethane was evaporated off. Distillation of the residue gave analytically pure dibutyl(chloromethyl)tin chloride (bp 80—82 °C/0.01 Torr) in 58% yield (n_D^{25} : 1.5087, lit[11]). The compound was identified by elemental analysis, IR, PMR and ^{13}C-NMR spectra. PMR($CDCl_3$) : δ 3.40 (s, 2H, CH_2Cl). ^{13}C-NMR($CDCl_3$) : δ 29.3 (CH_2Cl, $J_{C-^{119}Sn}$= 325 Hz). The reaction of dibutyltin and dibromomethane was carried out in a similar manner to give 70% yield of the new compound, dibutyl(bromomethyl)tin bromide, $Bu_2BrSnCH_2Br$, (bp 87—88 °C/0.009 Torr, n_D^{25} : 1.5395). PMR ($CDCl_3$) : δ 3.00 (s, 2H, CH_2Br). ^{13}C-NMR($CDCl_3$) : δ 11.8 (CH_2Br, $J_{C-^{119}Sn}$=293 Hz). Found: C, 26.30; H, 4.89%. Calcd for $C_9H_{20}Br_2Sn$: C, 26.56; H, 4.92%.

Reaction with Dibutyltin Dibromide. Dibutyltin dibromide (0.689 g) was added to the cyclohexane solution of dibutyltin (0.408 g) in a sealed Pyrex glass ampoule, and the mixture was irradiated under the same conditions. After the photolysis, the reaction mixture was exposed to air. A trace of organopolystannoxanes insoluble in $CDCl_3$ was removed by filtration. The gas chromatographic analysis and ^{13}C-NMR spectra showed that the reaction mixture consisted of bis(dibutylbromotin) oxide (80%) and tributyltin bromide (20%). The ratio of these compounds was determined by the integral values of their peaks assigned to the α-carbons of butyl groups in the ^{13}C-NMR spectra measured by gated decoupling technique without NOE. ^{13}C-NMR ($CDCl_3$) : δ 36.1, 36.3 (C(1) of $(Bu_2BrSn)_2O$), 17.3 (C(1) of Bu_3SnBr).

Photolysis of Dibutyltin in the Absence of Alkyl Halide. The benzene solution of dibutyltin (0.503 g/8 ml) was irradiated for 80 min under the same conditions as above. To the irradiation product was added a benzene solution of iodine at 0 °C to cleave the Sn–Sn bond completely. The mixture was stirred for 5 min at 0 °C, and was treated with a large excess of methylmagnesium iodide. The distribution of the three products, $BuMe_3Sn$, Bu_2Me_2Sn, Bu_3MeSn, was determined by gas chromatographic analysis to be 4.6, 91, and 4.2%, respectively. When the diluted solution (0.158 g/24 ml) was irradiated, the distribution of the methylated products were found to be 11, 77, and 12%, respectively.

References

1) K. Sisido, S. Kozima, and T. Isibasi, *J. Organomet. Chem.*, **10**, 439 (1967).
2) K. Sisido, T. Miyanisi, K. Nabika, and S. Kozima, *J. Organomet. Chem.*, **11**, 281 (1968).
3) M. Ishikawa, F. Ohi, and M. Kumada, *Tetrahedron Lett.*, **1975**, 645; *cf.* references cited therein.
4) U. Schroer and W. P. Neumann, *Angew. Chem.*, **87**, 247 (1975).
5) W. P. Neumann and A. Schwarz, *Angew. Chem.*, **87**, 844 (1975).
6) P. Pfeiffer, *Ber.*, **44**, 1269 (1911).
7) The insertion reactions of the stannylene into Sn–Sn and C–Sn bonds were reported in Ref. 5.
8) The oxidation of the residual polymeric dibutyltin into dibutyltin oxides could minimize the possible thermal disproportionation during the course of distillation.
9) H. G. Kuivila, L. W. Menapace, and C. R. Warner, *J. Am. Chem. Soc.*, **84**, 3584 (1962).
10) P. J. Davidson, A. Hudson, M. F. Lappert, and P. W. Lender, *J. Chem. Soc., Chem. Commun.*, **1973**, 829.
11) D. Seyferth and E. G. Rochow, *J. Am. Chem. Soc.*, **77**, 1302 (1954).
12) W. P. Neumann, J. Pedain, and R. Sommer, *Ann. Chem.*, **694**, 9 (1966).
13) A. J. Gibbons, A. K. Sawyer, and A. Ross, *J. Org. Chem.*, **26**, 2304 (1961).

The Synthesis of Benzannelated Annulenes. Dibenzo-tetrakisdehydro-[18]annulene, and Tribenzo-bisdehydro[14]annulene

Jūro Ojima,* Tadayoshi Yokomachi, and Akihiko Kimura
Faculty of Literature and Science, Toyama University, Gofuku, Toyama 930

(Received April 26, 1976)

In order to establish the effect of the annelation of benzene rings on [4*n*+2]annulenes, the syntheses of benzannelated dehydroannulenes were attempted. Dibenzo-tetrakisdehydro[18]annulenes (IIa and IIb) were prepared according to the reaction sequence developed in the synthesis of tetramethyltetrakisdehydro-[18]annulene (I) from *o*-ethynylbenzaldehyde (VIII); both of them proved to be unstable. Tribenzo-bisdehydro[14]annulene (XVII) was also prepared from VIII by a double Wittig reaction, followed by oxidative coupling. An examination of the NMR spectrum indicated that XVII is atropic.

The effect on the ring current of diatropic macrocyclic $(4n+2)\pi$-electron systems produced by the annelation of one or more benzenoid rings seems to be of considerable interest.[1]

In 1968, one of the present authors (J. O.) reported the synthesis of 1,5,10,14-tetramethyl-6,8,15,17-tetrakisdehydro[18]annulene (I).[2] The strong diatropicity observed in I prompted us to synthesize the corresponding dibenzo analogue, 11,16-dimethyldibenzo-[*a*,*g*]-3,5,12,14-tetrakisdehydro[18]annulene (IIa), in

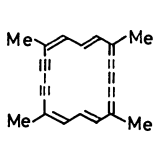

I

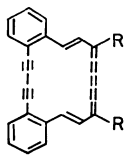

IIa R=Me
b R=Ph

order to examine the effect of the annelation of the benzene nuclei on the conjugated eighteen-membered ring system containing formal diacetylene and hexapentaene linkages.[3] To this end, a synthesis of *o*-ethynylbenzaldehyde (VIII) was required. VIII appeared to be a valuable intermediate for the synthesis of other conjugated macrocycles with fused benzene nuclei. Related experiments designed along similar lines have been reported in preliminary form by several workers after the completion of this work.[4]

Recently, Weavers and Sondheimer have reported the synthesis of benzo-1,3-bisdehydro[14]annulene (XIX) and showed that the fusion of one benzene ring reduces the diatropicity of the 1,3-bisdehydro[14]-annulene series.[4i] By the use of *o*-ethynylbenzaldehyde (VIII), we have prepared the corresponding tribenzo analogue, XVII, in order to examine the relative magnitude of the ring current in the "1,3-bisdehydro[14]annulene" system. In this paper, we wish to report the syntheses and properties of 11, 16-dimethyldibenzo[*a*,*g*]-3,5,12,14-tetrakisdehydro[18]annulene (IIa), the diphenyl derivative (IIb), and tribenzo[*a*,*e*,*i*,]-11,13-bisdehydro[14]annulene (XVII).

The key compound, *o*-vinylbenzaldehyde (IV), was prepared from phenethylamine (III) as has been described by Dale *et al.*[5] The reaction of *o*-vinylbenzaldehyde (IV) with a 1 molar equivalent of bromine in carbon tetrachloride gave *o*-(1,2-dibromoethyl)-benzaldehyde (V) in a 74% yield; this substance was converted with triethyl orthoformate into diethyl acetal (VI) in an 88% yield. The dehydrobromination of VI was effected by means of potassium hydroxide in boiling methanol to give *o*-ethynylbenzaldehyde diethyl acetal (VII). VIII was obtained in a good yield after the hydrolysis of the VII with dilute hydrochloric acid. The over all yield of VIII in the seven-step synthesis from I was *ca.* 20%.

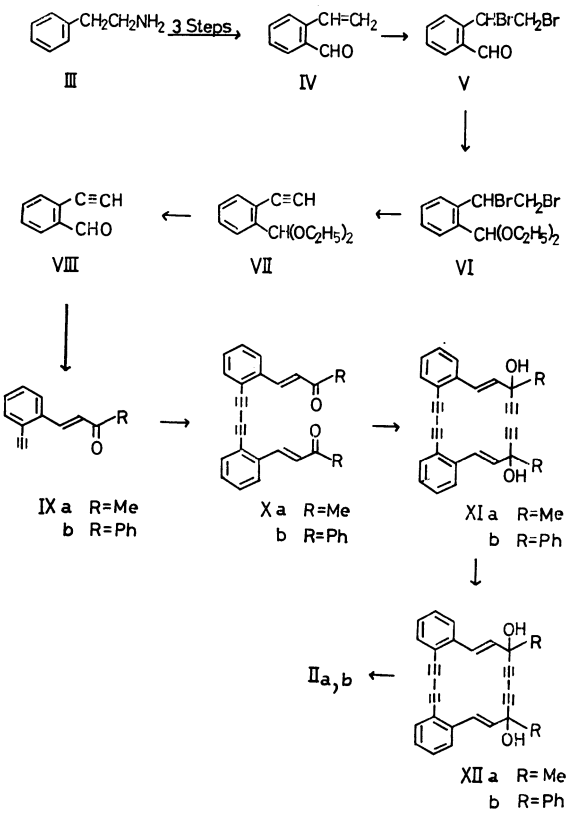

The conversion of VIII to IIa and IIb was performed according to the reaction sequence developed for the synthesis of tetramethyltetrakisdehydro-[18]annulene (I). The condensation of VIII with acetone gave the ketone (IXa) in a 52% yield; the ketone was oxidatively coupled to afford the diketone (Xa) in an 82% yield by the use of copper(II) acetate in a mixture of pyridine and methanol.[6] The reaction of IXa with the lithium acetylide–ethylenediamine complex[7] in tetrahydrofuran gave the glycol (XIa) as a yellow, viscous liquid in a 63% yield. The intramolecular oxidative coupling of XIa was per-

*To whom correspondence should be addressed.

formed under high-dilution conditions, using ether as the entraining agent, by Eglinton's method.[6] The dehydroxylation of cyclic glycol XIIa could be effected by tin(II) chloride in concentrated hydrochloric acid. The rapid color change of the resulting oil seemed to suggest the unstable nature of the dibenzannelated annulene (IIa). The substance could be kept at room temperature in a relatively dilute solution for less than half an hour. As all attempts to obtain IIa in the neat state or in a concentrated solution resulted in decomposition, we were unable to determine the well-defined IR, UV, NMR and mass spectra. The UV spectrum [$\lambda_{max}^{benzene}$ (>300 nm) 350, 418, 437, 510 sh nm] was similar to that of 1,6-dimethyl-1, 6-diphenylhexapentaene (XIV) [$\lambda_{max}^{benzene}$ 352, 419, 443 nm]. Consequently, it seemed that the product obtained was IIa. XIV was prepared from 2,7-diphenyl-3,5-octadiyne-2,7-diol (XIII) on treatment with tin(II) chloride in concentrated hydrochloric acid.[8] Since it was expected that the unstability of IIa might be reduced by the introduction of a substituent group bulkier than a methyl group, the synthesis of the diphenyl derivative was attempted by the same route. The oxidative coupling of IXb gave the diketone, Xb, in a 65% yield. However, as Xb was poorly soluble in usual solvents, XIb could be obtained only in a low yield by the bisethynylation of Xb. Therefore, the conversion of XIb to IIb was performed by using crude products. The IIb thus obtained proved to be as unstable as IIa.

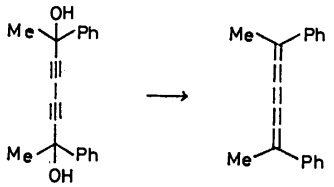

XIII XIV

Recently, Weavers and Sondheimer have reported the synthesis of benzobisdehydro[14]annulene (XIX) by the oxidative coupling of the acyclic compound (XVIII), which has been synthesized by a double Wittig reaction between *cis*-3-methyl-2-penten-4-ynal and the salt XV.[41] In order to examine the relative magnitude of the ring current in 1,3-bisdehydro[14]-annulene system, we decided to prepare the corresponding tribenzo analogue of this type, tribenzo[*a*,*e*,*i*]-11,13-bisdehydro[14]annulene (XVII), by using *o*-ethynylbenzaldehyde (VIII) according to the route developed for the synthesis of XIX. The Wittig reaction of 2 molar equivalents of *o*-ethynylbenzaldehyde (VIII) and 1 molar equivalent of α,α'-bis-(triphenylphosphonio)-*o*-xylene dibromide[9] (XV) in *N*,*N*-dimethylformamide with ethanolic lithium ethoxide led to a mixture of geometrical isomers which, upon chromatography on alumina, gave the di-*trans* isomer (XVI) in a 16% yield. The oxidative coupling of XVI with copper(II) acetate monohydrate in pyridine afforded the desired XVII in a 33% yield.

The chemical shifts of the protons of the XVI and XVII thus obtained are summarized in Table 1, along

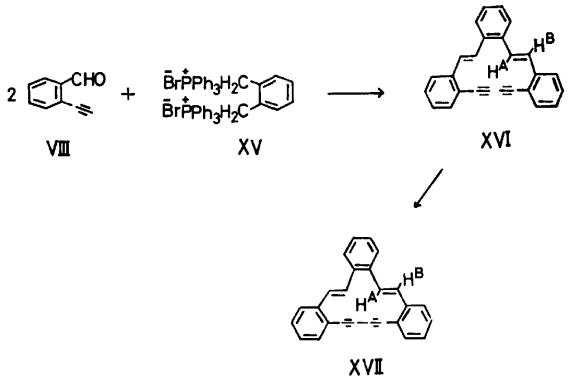

VIII XV XVI XVII

with those of XVIII and XIX reported by Weavers and Sondheimer.[41] As is shown in Table 1, there is not much difference in the NMR spectra between XVI and XVII, particularly on the chemical shift of the inner proton, H^A. That is, the observed chemical shift of H^A of XVII is in the normal region of the olefinic proton. Therefore, it is apparent that XVII is not diatropic, but atropic.

On the other hand, a comparison of the NMR spectra of XVIII and XIX suggests that compound XIX is diatropic, because the H^A resonance has moved to a higher field, and the H^B, H^C, and CH_3 resonances, to a lower field, as compared with the resonances of XVIII.

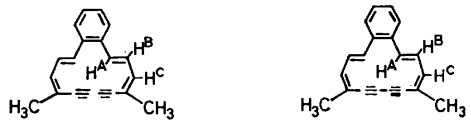

XVIII XIX

From these results, it may be concluded that the diatropic nature, which is revealed in the monobenzo-fused compound, XIX, is completely suppressed in the tribenzo-fused compound, XVII.

Table 1. ^{1}H-NMR parameters of XVI, XVII, XVIII, and XIX in $CDCl_3$
(τ-values; TMS as the internal standard)

Proton	XVI[a,c]	XVII[a,d]	XVIII[b]	XIX[b]
H^A	3.42[e]	3.33[e]	3.12	5.01
H^B	f)	f)	2.85	2.56
benzenoid	2.45—3.15	2.37—2.70		
H^C			3.51	2.92
CH_3			8.10	7.64

a) At 60 MHz. b) At 100 MHz. c) In addition, a singlet at 6.70 (-C≡CH). d) The ^{1}H-NMR spectrum of XVII was essentially temperature-independent in the range from −60 °C to 25 °C. e) We assigned the high-field signal to the H^A proton by referring to the chemical shifts of the related compound.[4e,f,h] However, some ambiguity remains because we do not have data definitely supporting this assignment. f) This proton signal is submerged by those of the benzenoid protons.

Experimental

All the melting and boiling points are uncorrected. Brockmann alumina (Act. II—III) was used for column

chromatography. The IR and UV spectra were taken on Hitachi EPI-S2 and Hitachi 124 spectrophotometers respectively. The shoulders in the UV spectra are indicated by sh. The NMR and mass spectra were taken on JEOL-C-60A and JEOL-JMS-OI-SG-2 spectrometers respectively. The chemical shifts are given in τ-values with respect to TMS as the internal standard, while the coupling constants are given in Hz.

o-Vinylbenzaldehyde (IV). *o*-Vinylbenzaldehyde was prepared by the reported method,[5] with slight modifications.

o-[1,2-Dibromoethyl]benzaldehyde (V). Bromine (43.2 g, 0.27 mol) was added, in one portion, to a solution of the aldehyde (IV, 34.1 g, 0.26 mol) in chloroform (280 ml) over a period of 1 h at 0 °C, after which the solution was stirred for a further 3 h at room temperature. After the addition of an aqueous sodium carbonate solution (150 ml) to the cooled mixture, the organic and benzene extracts of the aqueous layer were combined and worked up in the usual way. The dark red liquid thus obtained gave a solid mass of crystals (V, 70.4 g, 74%) on cooling. Recrystallization from light petroleum-benzene afforded pure V as colorless cubes; mp 74.5—75.1°C. IR (KBr disk): 1700 cm^{-1} (CHO), NMR (CCl_4): −0.18 (s, 1H, -CHO), 2.1—2.5 (m, 4H, phenyl H), 3.36 (t, J=8, 1H, -CHBr), 5.97 (d, J=8, 2H, $-CH_2Br$).

Found: C, 37.17; H, 2.69%. Calcd for $C_9H_8OBr_2$: C, 37.02; H, 2.76%.

o-Ethynylbenzaldehyde (VIII). A solution of dibromide (V, 82.6 g, 0.28 mol), triethyl orthoformate (55 g, 0.37 mol), and *p*-toluenesulfonic acid (1.6 g) in absolute ethanol (126 ml) was refluxed for 5 h. After pouring into 3M-aqueous ammonia, the mixture was extracted with ether. The extracts were then washed successively with 3M-aqueous ammonia (2 times) and a saturated sodium chloride solution (3 times), dried over potassium carbonate, and evaporated to give a dark red liquid (VI, 91 g). The liquid shows no IR absorption due to an aldehyde group, but it does show that due to an acetal group, IR (neat): 1100, 1070, 1050 cm^{-1} (C-O-C).

The crude product (VI, 91 g, 0.25 mol) in methanol (35 ml) was stirred into a solution of potassium hydroxide (159 g, 2.83 mol) in boiling methanol (247 ml) for 1 h. Crystals of potassium bromide deposited soon. The mixture was then heated under reflux for an additional 3 h, poured into water (1500 ml), and extracted with ether. The extracts were washed with a saturated sodium chloride solution and dried over potassium carbonate. The dark red liquid after the evaporation of the solvent was distilled under reduced pressure to give ethynyl acetal as a colorless liquid (VII, bp 85—97°C/2 Torr, 26.5 g, 52%); IR (neat): 3350 (-C≡CH), 2150 (-C≡C-), 1100, 1040 cm^{-1} (C-O-C).

The ethynyl acetal (VII, 26.5 g, 0.13 mol) in ether (82 ml) was stirred with 3M-hydrochloric acid (165 ml) at room temperature for 2 h. The organic and ethereal extracts from the aqueous layer were combined and worked up in the usual way. A partly crystallized liquid thus obtained was dissolved in benzene and absorbed on alumina (200 g).

Elution with light petroleum gave VIII (9.3 g, 55%).

Recrystallization from hexane afforded pure VIII as colorless needles; mp 62.5—63.5 °C, IR (KBr disk): 3250(-C≡CH), 2100 (-C≡C-), 1695 cm^{-1} (CHO), UV: λ_{max}^{EtOH} 250 (8800), 255 (9210), 305 (2370), 314 (2410), NMR ($CDCl_3$): −0.43 (s, 1H, -CHO), 2.0—2.7 (m, 4H, phenyl H), 6.54 (s, 1H, -C≡CH).

Found: C, 82.80; H, 4.58%. Calcd for C_9H_6O: C, 83.06; H, 4.65%.

4-(o-Ethynylphenyl)-1-buten-2-one (IXa). An ice-cooled mixture of 12% aqueous sodium hydroxide (16 ml) and ethanol (8 ml) was added to a stirred and ice-cooled solution of the aldehyde (VIII, 5.2 g, 0.04 mol) in acetone (5 ml). After being stirred for 90 min at the same temperature, the reaction was quenched with 1M-sulfuric acid (8 ml). A dark red liquid obtained from the ethereal extracts was chromatographed on alumina (200 g) with light petroleum-ether (8:2) to afford a pale yellow liquid (IXa, 3.5 g, 52%). Crystallization from hexane gave pure IXa as yellow plates; mp 64—65°C,[10] Mass: *m/e* 170 (M^+, 35%), 120 (base); mol. wt, 170.20, IR (KBr disk): 3250 (-C≡CH), 2100 (-C≡C-), 1700, 1615, 1595 (C=O, C=C), 990, 970 cm^{-1} (*trans* C=C), UV: λ_{max}^{EtOH} 230 sh (14400), 242 (17700), 247 (16200), 291 (13800), NMR ($CDCl_3$): 2.02 (d, J=16, 1H, olefinic H), 2.3—2.8 (m, 4H, phenyl H), 3.33 (d, J=16, 1H, olefinic H), 6.57 (s, 1H, -C≡CH), 7.59 (s, 3H, Me).

Found: C, 84.77; H, 6.21%. Calcd for $C_{21}H_{10}O$: C, 84.68; H, 5.92%.

1,4-Bis[o-(3-oxo-1-butenyl)phenyl]-1,3-butadiyne (Xa). A solution of the ketone (IXa, 8.4 g, 0.049 mol) in methanol (126 ml) and pyridine (210 ml) was stirred, drop by drop over a 2 h period at room temperature, into a solution of copper(II) acetate monohydrate (19 g, 0.095 mol) in methanol (660 ml) and pyridine (660 ml). The mixture was then stirred for an additional 3 h at the same temperature, concentrated under reduced pressure to a quarter volume, poured into 2M-sulfuric acid (1800 ml), and extracted with ether. The ethereal extracts were washed successively with water, aqueous sodium hydrogencarbonate, and saturated sodium chloride solutions, and dried over sodium sulfate. The dark red liquid obtained by evaporating the solvent was chromatographed on alumina (100 g) with benzene to give Xa (6.82 g, 82%). Recrystallization from methanol gave pure Xa as yellow needles; mp 144.0—145.5°C, IR (KBr disk): 2200 (-C≡C-), 1670—1630 (triplet, C=O), 995, 975 cm^{-1} (*trans* C=C), NMR ($CDCl_3$): 1.92 (d, J=16, 2H, olefinic H), 2.15—2.65 (m, 8H, phenyl H), 3.16 (d, J=16, 2H, olefinic H), 7.56 (s, 6H, Me).

Found: C, 84.93; H, 5.21%. Calcd for $C_{24}H_{18}O_2$: C, 85.18; H, 5.36%.

1,4-Bis[o-(3-hydroxy-3-methyl-1-penten-4-ynyl)phenyl]-1,3-butadiyne (XIa). To a mixture of the lithium acetylide-ethylenediamine complex (14.1 g, 0.153 mol) and tetrahydrofuran (500 ml) saturated with acetylene we added a solution of the diketone (IXa, 24.1 g, 0.14 mol) in the same solvent (150 ml) for 5 hr at 35°C under stirring and bubbling with acetylene. After the reaction mixture had been stirred vigorously for an additional 2 h under the slow introduction of acetylene, a cold saturated sodium chloride solution (200 ml) was added to the cooled reaction mixture. The organic layer, combined with ethereal extracts, was washed successively with 2M-hydrochloric acid, aqueous sodium hydrogencarbonate, and saturated sodium chloride solutions, and dried over sodium sulfate. After the solvents had been removed under reduced pressure, a dark red liquid thus obtained was chromatographed on alumina (500 g) with benzene-ether to give XIa (17.4 g, 63%) as a yellow liquid. All attempts to crystallize the liquid failed; the IR (neat) (3300 (-OH), 3250 (-C≡CH), 2200, 2100 (-C≡C-), 965 cm^{-1} (*trans* C=C)) and the NMR ($CDCl_3$) (2.5—3.0 (m, 8H, phenyl H), 3.04 (d, J=16, 2H, olefinic H), 3.87 (d, J=16, 2H, olefinic H), 6.8 (broad s, 2H, -OH), 7.42 (s, 2H, -C≡CH), 8.37 (s, 6H, Me)) were found to be in accord with the structure of XIa.

1,6-Dimethyl-9,10 : 15,16-dibenzocyclooctadeca-7,17-diene-2,4,11,

13-tetrayne-1,6-diol (XIIa). A high-dilution apparatus was used in this experiment. A solution of the acyclic glycol (XIa, 4.66 g, 0.012 mol) in ether (60 ml), methanol (72 ml), and pyridine (290 ml) was stirred, over a 15-h period, into a refluxing mixture of copper(II) acetate monohydrate (13.1 g, 0.066 mol) in ether (300 ml), methanol (360 ml) and pyridine (1400 ml). The reaction mixture was refluxed for an additional 1 h, concentrated to 300 ml under reduced pressure, and then poured into 2M-hydrochloric acid (1800 ml). The ethereal extracts from the aqueous layer were worked up in the usual way. The dark red liquid thus obtained was chromatographed on alumina (700 g) with ether–ethyl acetate to give XIIa (1.54 g, 33%). Recrystallization from acetone yielded pure XIIa as pale yellow plates; mp 160°C (dec). Although a satisfactory elemental analysis is not obtained, the IR (KBr disk) (3350 (-OH), 2200, 2140 (-C≡C-), 1595 (C=C), 965 cm^{-1} (*trans* C=C)), the NMR (DMSO-d_6) (2.65 (d, J=16.5, 2H, olefinic H), 2.05—2.75 (m, 8H, phenyl H), 3.48 (d, J=16.5, 2H, olefinic H), 6.40 (broad s, 2H, -OH), 8.40 (s, 6H, Me), and the mass (*m/e* 388 (M^+); mol. wt., 388.4) were found to be consistent with the assigned structure.

11,16-Dimethyldibenzo[a,g]*-3,5,12,14-tetrakisdehydro[18]annulene (IIa).* Into a suspension of cyclic glycol (XIIa, 550 mg, 1.4×10^{-3} mol) in pentane (20 ml) benzene (10 ml), we stirred at room temperatuer a solution of tin(II) chloride dihydrate (730 mg, 3.2×10^{-3} mol) in concentrated hydrochloric acid (8 ml). After 10 min, benzene (30 ml) was added in 5-ml portions for 15 min. The reddish reaction mixture was then poured into water (100 ml), and the layers were separated. The organic layer and ethereal extracts were combined, washed successively with water, aqueous sodium hydrogencarbonate and saturated sodium chloride solutions, dried over sodium sulfate, and evaporated under reduced pressure. The residue was chromatographed on alumina with light petroleum–benzene to give a reddish fraction which was concentrated to one-third its original volume. After the addition of benzene, this fraction was subjected to UV measurement. UV: $\lambda_{max}^{benzene}$ (>300 nm) 350 (relative optical density, 0.50), 418 (0.93), 437 (1.00), 510 sh nm. The further concentration of this eluent gave yellow substances which were insoluble in benzene.

3-(o-Ethynylphenyl)-1-phenyl-2-propen-1-one (IXb). To a stirred and ice-cooled solution of the aldehyde (VIII, 2.5 g, 0.019 mol) in ethanol (13 ml), we added, drop by drop, a 40% aqueous potassium hydroxide solution (10 ml) and acetophenone (2.3 g, 0.019 mol) simultaneously over a 15-min period; then the mixture was stirred for a further 3 h at room temperature. The reaction mixture was then poured into 3M-hydrochloric acid (100 ml) and extracted with ether. The ethereal extracts were worked up in the usual way. The dark red liquid thus obtained was chromatographed on alumina (200 g) with light petroleum–ether (8:2) to give Xb (1.1 g, 25%). Recrystallization from cyclohexane gave pure Xb as pale yellow cubes; mp 55.0—55.5°C, IR (KBr disk): 3300 (-C≡CH), 2100 (-C≡C-), 1660 (C=O), 1605, 1600 (C=C), 1020, 985 cm^{-1} (*trans* C=C), UV: λ_{max}^{EtOH} 249 (16300), 254 (16800), 308 (18200), NMR ($CDCl_3$): 1.57 (d, J=17, 1H, olefinic H), 1.8—2.6 (m, 10H, phenyl and olefinic H), 6.33 (s, 1H, -C≡CH), Mass: *m/e* 232 (M^+, 45%), 203 (base); mol. wt., 232.27.

Found: C, 87.72; H, 5.28%. Calcd for $C_{17}H_{12}O$:C, 87.90; H, 5.21%.

1,4-Bis[o-(*2-benzoylvinyl*)*phenyl*]*-1,3-butadiyne (Xb).* A solution of the ketone (IXb, 4.7 g, 0.021 mol) in methanol (19 ml) and pyridine (19 ml) was stirred, over a period of 30 min at room temperature, into a solution of copper(II) acetate monohydrate (12.2 g, 0.06 mol) in methanol (77 ml) and pyridine (77 ml), and then the mixture was stirred for a further 3 h at the same temperature. The reaction mixture was then poured into 3M-hydrochloric acid (600 ml). The resulting solids (Xb, 3.0 g, 65%) were collected on a filter and washed with water (300 ml). Recrystallization from benzene gave an analytical specimen; mp 192—194°C, IR (KBr disk): 1660 (C=O), 1600—1580 (triplet, C=C), 1010, 990 cm^{-1} (*trans* C=C), UV: λ_{max}^{THF} 267 (28700), 290 (21600), NMR ($AsCl_3$): 1.62 (d, J=16, 2H, olefinic H), 1.8—2.8 (m, 20H, phenyl and olefinic H), Mass: *m/e* 463 (M^+, 75%), 357 (base); mol. wt., 462.52.

Found: C, 88.26; H, 4.80%. Calcd for $C_{34}H_{22}O_2$: C, 88.29; H, 4.79%.

11,16-Diphenyldibenzo[a,g]*-3,5,12,14-tetrakisdehydro*[*18*]*annulene (IIb).* This experiment was carried out by almost the same procedure as that used in the preparation of IIa. However, as the Xb diketone was poorly soluble in usual solvents and was, hence, converted to XIb in only a very low yield, the crude products were used for the preparation of IIb as well as XIIb. The UV spectrum of IIb is as follows: $\lambda_{max}^{benzene}$ 417 (relative optical density, 1.00), 498 (0.46), 530 (0.48), 550 nm (0.45).

2,7-Diphenyl-3,5-octadiyne-2,7-diol (XIII). XIII was prepared by the ethynylation of acetophenone, followed by oxidative coupling; mp 194—195°C (lit, 194°C)[11] NMR ($CDCl_3$): 2.3—2.8 (m, 10H, phenyl H), 6.69 (broad s, 2H, -OH), 8.15 (s, 6H, Me).

Found: C, 82.61; H, 6.27%. Calcd for $C_{20}H_{18}O_2$: C, 82.73; H, 6.25%.

1,6-Dimethyl-1,6-diphenylhexapentaene (XIV). XIV was prepared like IIa. The UV spectrum of XIV is as follows: $\lambda_{max}^{benzene}$ 352 (relative optical density, 0.27), 419 (0.60), 443 nm (1.00).

o-*Bis*[trans-*2-(o-ethynylphenyl)vinyl*]*benzene (XVI).* Lithium ethoxide prepared from lithium (323 mg, 0.046 gatm) in ethanol (120 ml) was stirred, drop by drop under a nitrogen atmosphere at 80—85 °C for 1 h, into *o*-ethynylbenzaldehyde (VIII, 6.0 g, 0.046 mol) and α,α′-bis(triphenylphosphonio)-*o*-xylene dibromide[9] (XV, 18.6 g, 0.023 mol) in dry *N,N*-dimethylformamide (460 ml). After the completion of the addition, the reaction mixture was stirred under a nitrogen atmosphere at 80—85°C for further a 2 h; then it was poured into water (1500 ml) and extracted with ether (500 ml×3). The ethereal extracts were worked up in the usual way to give a dark red liquid. The liquid was passed through a column of alumina (200 g) with light petroleum to give a mixture of XVI and other geometrical isomers (4.5 g, 59%) as a dark red liquid. Repeated chromatography on alumina (100 g) with light petroleum afforded the *trans-trans* isomer, XVI (1.2 g, 16%). Recrystallization from hexane gave pure XVI as white needles; mp 107—108°C, IR (KBr disk): 3300 (-C≡CH), 2120 (-C≡C-), 1615, 1600 (C=C), 945 cm^{-1} (*trans* C=C), UV: λ_{max}^{THF} 259 (26500), 315 (20500), mass: *m/e* 330 (M^+, 100%); mol. wt., 330.40, NMR ($CDCl_3$): 3.42 (d, J=14.5, 2H, H_A) 2.45—3.15 (m, 14H, phenyl and H), and see Table 1.

The elementary analyses of XVI always afforded low values of carbon, but the spectral properties clearly support the structure of XVI.

Tribenzo[a,e,i]*-11,13-bisdehydro*[*14*]*annulene (XVII).* A solution of XVI (2.0 g, 0.006 mol) in pyridine (45 ml) was stirred, drop by drop over a 20 min period, into a solution of copper(II) acetate monohydrate (18 g) in pyridine (60 ml) kept at 50 °C; the mixture was then stirred for a further 2 h at 60—65 °C. Then the mixture was chilled, diluted with benzene (200 ml), and poured into 6% hydro-

chloric acid (1000 ml). The layers were separated, and the aqueous layer was extracted with ether (150 ml×2). The organic and ethereal extracts were combined, washed successively with aqueous sodium hydrogencarbonate and saturated sodium chloride solutions, dried over sodium sulfate, and evaporated *in vacuo*. The residue was chromatographed on alumina (200 g) with light petroleum–ether (8:2) to give XVII (650 mg, 33%). Recrystallization from hexaene–benzene gave pure XVII as colorless cubes; mp 202—203°C, IR (KBr disk): 2200 (-C≡C-), 950 cm^{-1} (*trans* C=C), UV: λ_{max}^{THF} 237 (24800), 256 (21400), 291 (34700), 330 (22800), 356 (11300), mass: *m/e* 328 (M^+, 100%); mol wt, 328.39, NMR ($CDCl_3$): 3.33 (d, J=14.5, 2H, H^A), 2.3—2.7 (m, 14H, phenyl and H^A), and see Table 1.

Found: C, 95.25; H, 5.01%. Calcd for $C_{26}H_{16}$: C, 95.09; H, 4.91%.

The authors wish to thank Professor Masazumi Nakagawa, Osaka University, for the mass spectral measurement, and Mr. Michiaki Takagi and Misses Michiko Enkaku and Miyako Ishiyama for their experimental help. This work was supported by a Grant-in-Aid (4089, 1970) for Scientific Research from the Ministry of Education, which is gratefully acknowledged.

References

1) K. Endo, Y. Sakata, and S. Misumi, *Tetrahedron Lett.*, **1970**, 2557; *Bull. Chem. Soc. Jpn.*, **44**, 2465 (1971).

2) J. Ojima, T. Katakami, G. Nakaminami, and M. Nakagawa, *Tetrahedron Lett.*, **1968**, 1115; *Bull. Chem. Soc. Jpn.*, **49**, 292 (1976).

3) For a preliminary report, see J. Ojima, T. Yokomachi, and T. Yokoyama, *Chem. Lett.*, **1972**, 633.

4) a) M. Iyoda, M. Morigaki, and M. Nakagawa, *Tetrahedron Lett.*, **1974**, 817, 3677; b) A. Yasuhara, T. Satake, M. Iyoda, and M. Nakagawa, *ibid.*, **1975**, 895; c) M. Iyoda and M. Nakagawa, *Chem. Lett.*, **1975**, 815; d) A. Yasuhara, M. Iyoda, T. Satake, and M. Nakagawa, *Tetrahedron Lett.*, **1975**, 3931; e) J. Ojima, Y. Yokoyama, and T. Yokoyama, *Chem. Lett.*, **1974**, 1261; f) J. Ojima, A. Kimura, and T. Yokoyama, *ibid.*, **1975**, 207; g) R. T. Weavers, R. R. Jones, and F. Sondheimer, *Tetrahedron Lett.*, **1975**, 1043; h) J. Ojima, M. Ishiyama, A. Kimura, and Y. Yokoyama, *ibid.*, **1975**, 1909; i) R. T. Weavers and F. Sondheimer, *Angew. Chem. Int. Ed. Engl.*, **13**, 141 (1974).

5) W. J. Dale, L. Starr, and C. W. Strobel, *J. Org. Chem.*, **26**, 2225 (1961).

6) G. Eglinton and A. R. Galbraith, *Chem. Ind.*, **1956**, 737; *J. Chem. Soc.*, **1959**, 889.

7) D. F. Beumel, Jr., and R. F. Harris, *J. Org. Chem.*, **28**, 2775 (1963); *ibid.*, **29**, 1872 (1964).

8) R. Kuhn and H. Krauch, *Chem. Ber.*, **88**, 309 (1955); F. Bohlmann and K. Kieslich, *ibid.*, **88**, 1211 (1955).

9) C. E. Griffin, K. R. Martin, and B. E. Douglas, *J. Org. Chem.*, **27**, 1627 (1962); C. E. Griffin and J. A. Peters, *ibid.*, **28**, 1715 (1963).

10) The melting point of IXa given in the preliminary report (Ref. 3) was erroneous.

11) J. B. Armitage, E. R. H. Jones, and M. C. Whiting, *J. Chem. Soc.*, **1954**, 44.

Nitration of Binary and Ternary Schiff Base Complexes of Cu(II)

B. T. THAKER and P. K. BHATTACHARYA

Chemistry Department, Faculty of Science, M.S. University of Baroda, Baroda 390002, India

(Received November 18, 1975)

Nitration of the coordinated ligands in the complexes bis[1-(2-hydroxyphenyl)ethylideneamine or its methyl derivative]Cu(II) and *N,N'*-ethylene or propylene bis[1-(2-hydroxyphenyl)ethylideneaminato]Cu(II) have been carried out. Similar nitration reactions of mixed diamine Schiff base complexes of Cu(II) have also been carried out. The substitution products have been characterized by elemental analyses, comparison with authentic samples in case of binary complexes and by means of magnetic moments, electronic and IR spectral studies. The orientation of incoming substituents in the chelates is found to be the same as that in uncomplexed 2-hydroxyacetophenone or methyl substituted 2-hydroxyacetophenone. Nitration reactions in case of mixed ligand complexes confirm the structure.

Nitration of metal salicylaldehyde and metal acetylacetonates using different nitrating agents such as N_2O_4, a mixture of copper nitrate, beryllium nitrate in acetic anhydride[1-3] or $N_2O_4 \cdot BF_3$[4] has been reported earlier. This paper describes the substitution of nitro groups in Schiff base present in binary and ternary Cu(II) complexes. The mild nitrating agent, acetyl nitrate used in the present reactions is formed *in situ* by the reaction of copper nitrate with acetic anhydride. This mild reagent has been used for many nitration reactions and in the case of coordinated ligands the reagent seems to have many advantages over other strong nitrating agents such as N_2O_4, HNO_3, and H_2SO_4 which cause decomposition of the Schiff base complexes. The mechanism of electrophilic substitution over a benzene ring in a coordinated ligand has been reported by Singh *et al.*[2]

In the present investigation nitrated compounds have been prepared by direct substitution of nitro groups, into the appropriate unsubstituted Schiff base complexes. These derivatives were characterized by comparison with authentic samples obtained by complexing appropriate nitrated 2-hydroxyacetophenone or methyl substituted 2-hydroxyacetophenone.

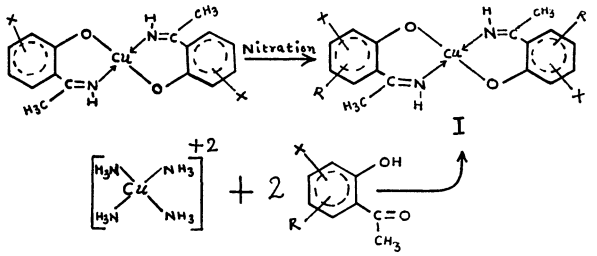

I

X=H or 4-CH_3, R=3-NO_2 and 5-NO_2
X=3-CH_3 or 5-CH_3, R=5-NO_2 or 3-NO_2

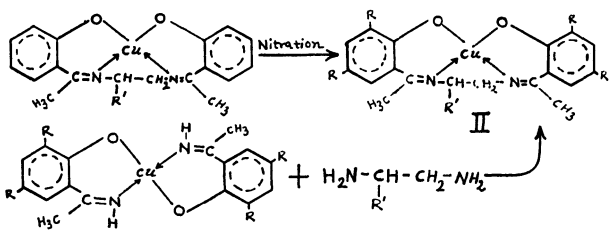

II

R=3-NO_2 and 5-NO_2
R'=H or -CH_3

The nitration reactions were further extended to the mixed Schiff base complexes reported by us earlier.[5] The reaction can be shown as follows:

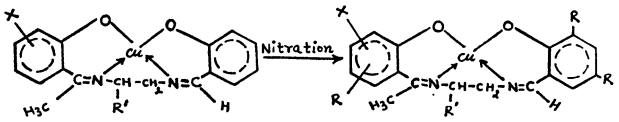

III

X=H or 4-CH_3, R=3-NO_2 and 5-NO_2
X=3-CH_3 or 5-CH_3, R=5-NO_2 or 3-NO_2
R'=H or -CH_3

Experimental

Material Used. Bis[1-(2-hydroxyphenyl)ethylideneamine or its methyl derivative]Cu(II), *N,N'*-ethylene or propylene bis[1-(2-hydroxyphenyl)ethylideneaminato]Cu(II) and mixed ligand *N,N'*-ethylene or propylene [salicylideneaminato, 1-(2-hydroxyphenyl)ethylideneaminato or its methyl derivative]Cu(II) were prepared as reported earlier.[5,6] Acetic anhydride (BDH), cupric nitrate trihydrate (Riedell, pure, Germany), and sodium acetate crystal (Pfiezer) were used. Ethanol was of analytical grade.

Method and Apparatus. The magnetic susceptibilities of the Cu(II) complexes were determined at room temperature by the Gouy method using $Hg[Co(NCS)_4]$ as a calibrant. TLC was carried out for most of the complexes. Infrared spectra in KBr disc were recorded on a Perkin Elmer model 427 infrared grating spectrophotometer in the range 4000—625 cm^{-1}. The reflectance spectra of the complexes have been taken on a DU2 Beckman Spectrophotometer.

Synthesis of bis[1-(2-hydroxy-3,5-dinitrophenyl)ethylideneamine]Cu(II), bis[1-(2-hydroxy-3,5-dinitro-*p*-tolyl)ethylideneamine]Cu(II), bis[1-(6-hydroxy-5-nitro-*m*-tolyl)ethylideneamine]Cu(II), bis[1-(2-hydroxy-5-nitro-*m*-tolyl)ethylideneamine]Cu(II), *N,N'*-ethylene or propylene bis[1-(2-hydroxy-3,5-dinitrophenyl)ethylideneaminato]Cu(II), *i.e.*, I and II R=3-NO_2 and 5-NO_2, R'=H or $-CH_3$, X=H, 3-CH_3, 4-CH_3, or 5-CH_3. 0.5 g of bis[1-(2-hydroxyphenyl)ethylideneamine or its methyl derivative]Cu(II) or *N,N'*-ethylene or propylene bis[1-(2-hydroxyphenyl)ethyleneaminato]Cu(II) Schiff base and acetic anhydride (14 ml) were taken in a 250 ml conical flask fitted with a calcium chloride drying tube and stirred magnetically over an ice bath for half an hour. Powedred $Cu(NO_3) \cdot 3H_2O$ (0.82 g) was added in small portions over a period of 30 min. The ice bath was removed after 4 h but the stirring was continued for additional 4 h. The resulting green substance was decomposed by pouring into 150 ml of ice-cold water containing sufficient amount of sodium acetate and stirring for 2 h. The precipi-

tate thus obtained was filtered, washed with water, then with ethanol.

The above bis complexes were also prepared by direct treatment of tetra ammine Cu(II) salt with nitrated 2-hydroxyacetophenone or its methyl derivatives. 2-Hydroxy-3,5-dinitroacetophenone, 2 - hydroxy - 5 - methyl - 3 - nitroacetophenone, 2-hydroxy-3-methyl-5-nitroacetophenone were prepared as described in the literature.[7] These nitrated 2-hydroxyacetophenone were converted into above shown Cu(II) Schiff base complexes by treating Cu–ammine solutions with 2 moles of appropriate ethanolic solutions of nitrated 2-hydroxyacetophenone or its methyl derivatives. The mixture was refluxed for half an hour. The precipitate thus obtained was filtered, washed with water, then with ethanol.

The above nitrated ethylideneamine and propylenediamine complexes were also prepared by direct treatment of nitrated imine Schiff base complex with ethylenediamine or propylenediamine.

Synthesis of mixed *N,N'*-ethylene or propylene[3,5-dinitrosalicylideneaminato, 1-(2-hydroxy-3,5-dinitro-*p*-tolyl) or (2-hydroxy-3,5-dinitrophenyl)ethylideneaminato]Cu(II), *N,N'*-ethylene or propylene[3,5-dinitro salicylideneaminato, 1-(2-hydroxy-5-nitro-*m*-tolyl)ethyleneaminato]Cu(II) and *N,N'*-ethylene or propylene[3,5-dinitro salicylideneaminato, 1-(6-hydroxy-5-nitro-*m*-tolyl)ethyleneaminato]Cu(II), *i.e.*, III R= 3-NO_2 and 5-NO_2, R'=H or $-CH_3$ and X=H, 3-CH_3, 4-CH_3 or 5-CH_3. The procedure is the same as that for binary Schiff base complexes.

Analysis. Cu(II) in the complexes was analyzed iodometrically, after the complexes had been decomposed in nitric acid. Carbon, hydrogen, and nitrogen were determined by the micro analytical method. The analytical data are given in Table 1.

The solubilities of nitrated binary and mixed Schiff base complexes of Cu(II) in organic solvents are very low. TLC of all the compounds have been carried out on silica gel G(Sichem) using chloroform: acetone (6 : 4) mixture as the solvent. Only one dot is obtained for dinitro and mononitro complexes indicating that the complex formed is a single compound.

Results and Discussion

In these reactions the nitronium ions produced from the acetyl nitrate act as electrophile to form two stable σ-complex intermediates (IV-a and b) (V-a and b) as follows:

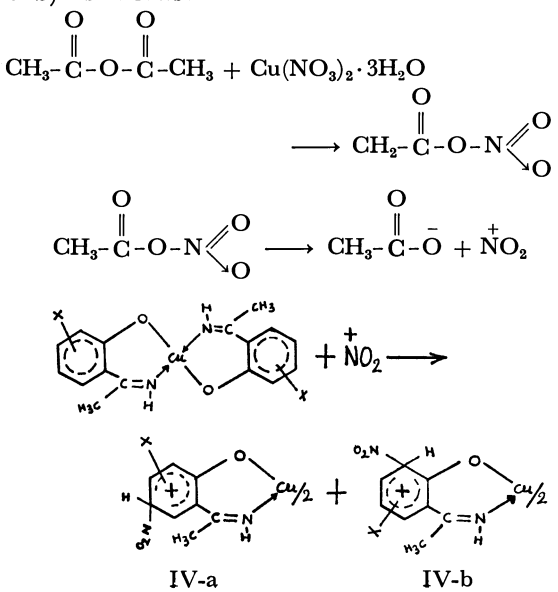

IV-a IV-b

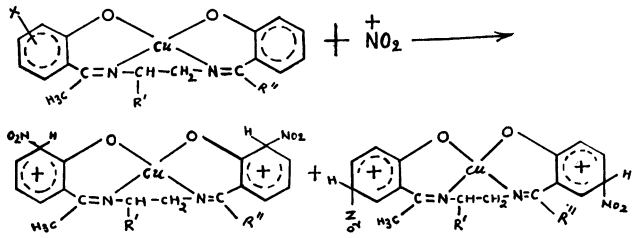

V-a V-b

X=H, 3-CH_3, 4-CH_3 or 5-CH_3 R'=R''=H or -CH_3

The proton is removed from each of these intermediates and the dinitro chelates further react with the NO^+_2 ion in the same manner resulting in the formation of the di-, tri, or tetranitro compounds I, II, or III. In the case of 3-methyl and 5-methyl substituted binary imine complexes, however, only mononitro complexes were formed, one of the positions 3 or 5 being already occupied by the methyl group. This shows that the nitration reaction takes place over benzene ring at positions 3 and 5 rather than positions 4 and 6. This is due to *ortho*, *para* orienting effect of phenolic O and *meta* directing effect of –C=N–. Thus the orientation of incoming substitutions in the binary Schiff base complexes is found to be the same as that for the uncomplexed 2-hydroxyacetophenone or methyl substituted 2-hydroxyacetophenone. The nitration reaction, however, requires a long time of refluxing. This shows that the electrophilic substitution reaction is retarded on the coordination of the ligand with the metal.

The analysis, magnetic moments and spectral properties of the above binary nitrated complexes and the corresponding binary complexes obtained by the reaction of metal with nitrated Schiff base are found to be similar.

In the case of complexes of ethylenediamine Schiff base coordinated at two ends with 2-hydroxy-4-methyl- or 2-hydroxyacetophenone and salicylaldehyde, tetranitro complexes were formed. Both salicylaldehyde and 2-hydroxy-4-methyl or 2-hydroxyacetophenone get nitrated at positions 3 and 5. In the case of diamine Schiff base, complexes of 2-hydroxy-3-methyl or 5-methyl acetophenone and salicylaldehyde trinitrated complexes were formed, since salicylaldehyde gets nitrated at positions 3 and 5 while 2-hydroxy-3-methyl and 5-methyl acetophenone gets nitrated only at positions 5 and 3, respectively, the other position being already occupied by the methyl group.

TLC shows only one dot indicating that nitro compounds are single compounds. This confirms the proposed structure[5] for these new Schiff base complexes with ethylenediamine condensed at two ends with aldehyde and ketone.

All nitrated Cu(II) Schiff base complexes are paramagnetic (μ=1.8 to 2.0 B.M.) indicating the presence of one unpaired electron. There is no change in the paramagnetic value of nitrated compounds of Cu(II) Schiff base complexes from those without nitro substitution. The reflectance spectra of nitrated compounds exhibit one broad band at ≈550 nm as expected for a square planar structure. This shows that the

square planar structure of the complex is retained even after the substitution of the nitro groups.

The IR spectra of the nitrated compounds show bands similar to those of unsubstituted Schiff base complexes.[5,6] However, there is a broadening in the bands showing the presence of nitro groups. The IR spectra of the nitro compounds obtained by the two methods are also almost superimposable indicating that the complexes are identical. Nitration of the coordinated ketone and aldehyde is thus confirmed.

Thanks are due to Prof. S. M. Sethna, Head, Department of Chemistry, M. S. University, Baroda, for providing necessary laboratory facilities.

References

1) J. P. Collman, R. L. Marshall, W. L. Young, III, and S. D. Goldby, *Inorg. Chem.*, **1**, 704 (1962).
2) P. R. Singh, R. Sahai, and I. J. Sharma, *J. Indian Chem. Soc.*, **49**, 211 (1972).
3) J. N. Patil and D. N. Sen., *Indian J. Chem.*, **12**(2), 189 (1974).
4) G. B. Backman and J. L. Dever, *J. Am. Chem. Soc.*, **80**, 5871 (1958).
5) B. T. Thaker and P. K. Bhattacharya, *J. Inorg. Nucl. Chem.*, **37**, 615 (1975).
6) B. T. Thaker and P. K. Bhattacharya, *J. Indian Chem. Soc.*, **52**, 454 (1975).
7) S. S. Joshi and H. Singh, *J. Am. Chem. Soc.*, **76**, 4996 (1954).

Sound Velocity in Aqueous Solutions of Ammonium Halides

Harumi Endo* and Otohiko Nomoto**

Department of Applied Physics, National Defense Academy, Yokosuka 239

(Received June 25, 1975)

The sound velocity in water aqueous solutions increases with increasing temperature and reaches the maximum velocity (V_p) at a peak temperature (T_p). In the present paper, the concentration dependence of T_p and V_p in ammonium halides are reported. It was found empirically that the relationship between the hydration number and the slope ($\Delta T_p/\mu$) of T_p at infinite dilution for many electrolytes is linear, but that for ammonium halides this is not the case.

The sound velocity in water increases with increasing temperatures and reaches a maximum velocity (V_p) at 74 °C, while the adiabatic compressibility of water has a minimum at 64 °C. This temperature for V_p is termed the peak temperature (T_p) of water. This behavior is characteristic of water and aqueous solutions. It is known that water is an associated liquid exhibiting structural equilibrium. The origin of the maximum velocity in water can be explained on the basis of a decrease in the structural compressibility and an increase in the instantaneous compressibility with increase in temperature.

When substances are dissolved in water, the values of T_p and V_p for the solutions shift from those of pure water, since the structural equilibrium of water is also affected by the solutes. Therefore, it is possible to study the effects of solutes on the water structure on the basis of the shifts of T_p and V_p from the values for pure water.

For aqueous solutions of electrolytes, the concentration dependences of T_p have been reported by many investigators.[1-6] In the case of solutions of NH_4I,[6] a unique behavior of the concentration dependence of T_p was observed, in which the temperature remained nearly constant up to about 4.5 mol %, and then decreased more and more sharply with increase in concentration. While the V_p in aqueous solutions usually increases as compared with that in pure water, it decreases in some cases, such as in solutions of $Pb(NO_3)_2$ and NH_4I.

In the present paper, measurements on NH_4Br and NH_4Cl solutions are extended.

Experimental

Apparatus. A crystal-controlled ultrasonic interferometer operating at a frequency of 5 MHz is used to measure the wavelength of standing waves. The measuring cell containing a solution is immersed in an oil bath controlled to within ±0.1 °C at moderate temperatures and to within ±0.4 °C at higher temperatures. To determine the wavelength one hundred standing waves are used. While the accuracy of the wavelength measurement is ±0.006%, the dominant cause of error in the sound velocity measurements is the temerature fluctuation. So the overall accuracy of the velocity measurements is about ±0.02%.

Materials. NH_4Cl, NH_4Br, and $(NH_4)_2SO_4$ were purified by recrystallization of reagent grade products from water.

* Present address: Department of Chemistry, The University of Oklahoma, Norman, Oklahoma 73069 USA.

** Kobayashi Institute of Physical Research, Kokubunji, Tokyo 185.

Results and Discussion

In Figs. 1 and 2, the sound velocities (V) for NH_4Cl and NH_4Br are respectively plotted against the concentration (μ: mol %) over the temperature (T) range from 20—100 °C at 5 °C intervals. In order to compare

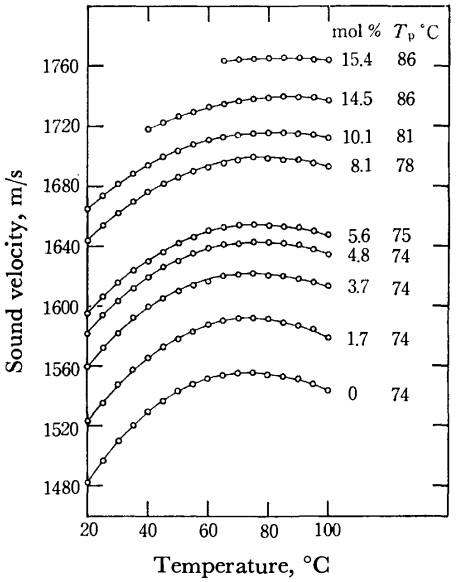

Fig. 1. Sound velocity *vs.* temperature in ammonium chloride aqueous solutions at various concentrations.

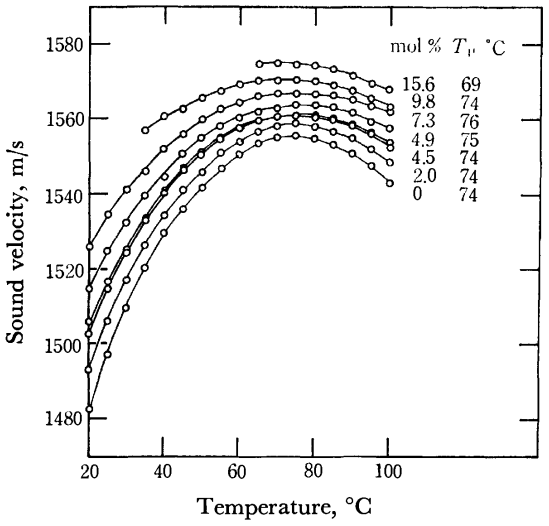

Fig. 2. Sound velocity *vs.* temperature in ammonium bromide aqueous solutions at various concentrations.

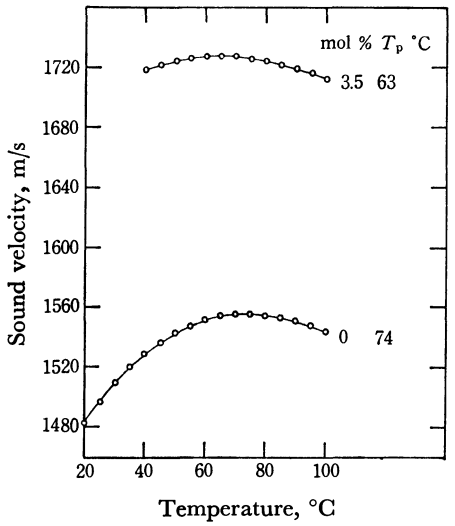

Fig. 3. Sound velocity *vs.* temperature in ammonium sulfate aqueous solutions at various concentrations.

with ammonium halides (NH_4X), the sound velocity in an $(NH_4)_2SO_4$ aqueous solution at 3.5 mol % was measured. These results are shown in Fig. 3.

In all cases of ionic or nonionic aqueous solutions, the $V(T)$-curves are of parabolic type like that of pure water. Except for solutions at high concentrations, the $V(T)$-curves are, within the limits of experimental error, the same as a displaced curve for water. Therefore, the template of curve for water was used to fix the T_p of the solutions, while the V_p in the solutions were also determined at the same time from the smoothed curve of the template. The accuracies of the T_p and V_p values at lower concentrations were within ± 1.5 °C and ± 1 m/s, respectively. For solutions at high concentrations, the T_p of solutions was successively determined from the smoothed curve for a lower concentration which was previously determined, starting from the template of the curve for water. The accuracies of the T_p and V_p values at high concentrations were within ± 2.0 °C and ± 1 m/s, respectively. Figures 4 and 5 show, respectively, the V_p and T_p values as functions of concentration for aqueous solutions of NH_4X together with other electrolytes.[6] The values of V_p in electrolytes usually increase with increasing concentration, but there are some exceptions such as NH_4I, $Pb(NO_3)_2$, *etc.*[7] These electrolytes have a heavy ion in the molecule. On the other hand, the values of T_p usually decrease, although there are some rare exceptional cases, with increasing concentration. The results obtained from Figs. 4 and 5 indicate that the slopes ($\Delta V_p/\mu$ and $\Delta T_p/\mu$) at infinite dilution are nearly constant.

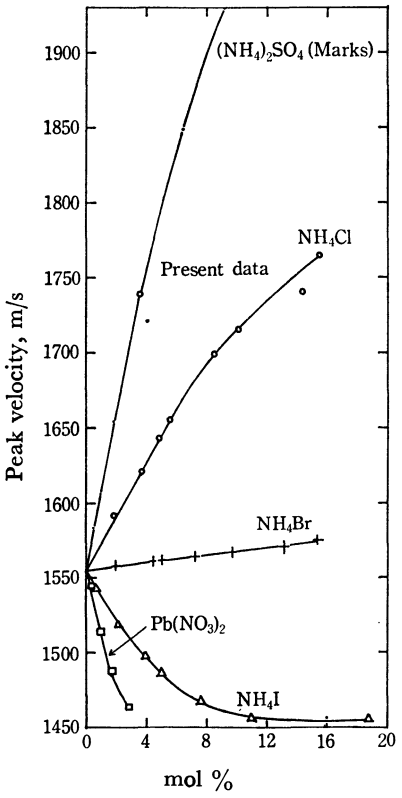

Fig. 4. Peak velocity *vs.* concentration for various solutes.

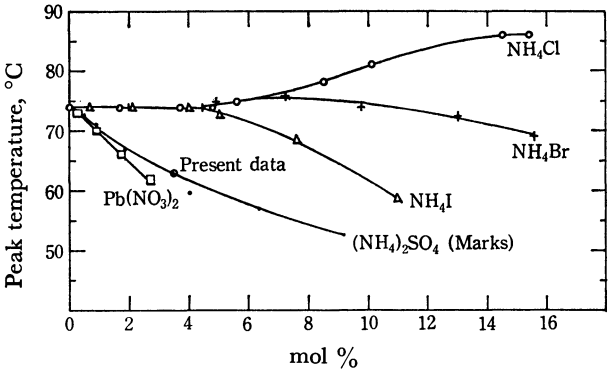

Fig. 5. Peak temperature *vs.* concentration for various solutes.

As can be seen in Fig. 5, the discrepancy between NH_4X and the other electrolytes is evident. First the T_p of NH_4X aqueous solutions are approximately constant to *ca.* 4.5 mol % regardless of the kind of anion,

Table 1. Values of $\Delta V_p/\mu$, $\Delta T_p/\mu$ and hydration number (h) for various electrolytes

	$\Delta V_p/\mu$ m/s/mol%		$\Delta T_p/\mu$ °C/mol%		h[a] at 25 °C
NH_4Cl	+18.0		0		4.2
NH_4Br	+ 1.2		0		3.7
NH_4I	−20.5		0		3.2
$(NH_4)_2SO_4$	+55.0		−3.8		11—12
Li_2SO_4	+66.5		−7.4		14—15
Na_2SO_4	+71.5	b)	−7.8	b)	17—18
K_2SO_4	+62.3		−7.0		15—16
$KHSO_4$	−35.9		−2.6		
$MgSO_4$	+55.0		−5.7		14.8
LiCl	+25.5		+1.2		6.0
NaCl	+27.0		−2.6		7.1
KCl	+26.5		−2.7		6.4
RbCl	+ 6.5	c)	−2.6	c)	
LiBr	+ 5.6		+4.2		5.4
LiI	−13.5		−2.0		4.7
LiOH	+41.0		−4.3		8.7
NaOH	+42.5	d)	−5.0	d)	9.9
KOH	+40.5		−3.8		9.2
$Pb(NO_3)_2$	−45.0		−4.4		10.8[6]

a) Ref. 8. b) Ref. 3. c) Ref. 5. d) Ref. 4.

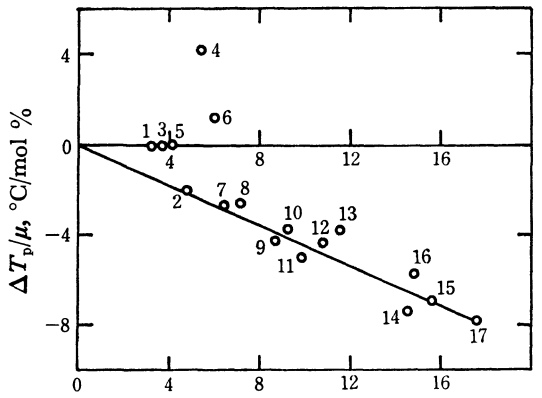

Fig. 6. $\Delta T_p/\mu$ *vs.* h for various electrolytes.
1: NH_4I, 2: LiI, 3: NH_4Br, 4: LiBr, 5: NH_4Cl, 6: LiCl, 7: KCl, 8: NaCl, 9: LiOH, 10: KOH, 11: NaOH, 12: $Pb(NO_3)_2$, 13: $(NH_4)_2SO_4$, 14: Li_2SO_4, 15: K_2SO_4, 16: $MgSO_4$, 17: Na_2SO_4.

and secondary, the behaviors of T_p (μ)-curves at higher concentrations beyond *ca.* 4.5 mol % are quite different depending on the anions. On the other hand, the T_p of $(NH_4)_2SO_4$ solutions monotonical decreases with increasing concentration as in many other electrolytes.

The values of $\Delta V_p/\mu$ and $\Delta T_p/\mu$ for various electrolytes[3-6] are summarized in Table 1 together with the hydration number[8] (h) of the solutes at 25 °C. Although there are many methods[9] for determining the hydration number, the values of the hydration numbers used here are the results of acoustical measurements obtained on the basis of Passynski's assumption.[10] Since it is necessary to investigate the relationship between h and $\Delta T_p/\mu$, in Fig. 6 $\Delta T_p/\mu$ is plotted against h for various electrolytes. A large part of them, except for NH_4X, are gathered about the straight line: $\Delta T_p/\mu = -0.44\,h$.

References

1) B. Kudriavtsev, *Soviet Phys. Acoust.*, **2**, 172 (1956).
2) K. Tamm and H. Haddenhorst, *Acustica*, **4**, 653 (1954).
3) G. Marks, *J. Acoust. Soc. Am.*, **31**, 936 (1956).
4) G. Marks, *J. Acoust. Soc. Am.*, **32**, 327 (1960).
5) S. Surahmanyan and S. Raghavan, *Acustica*, **28**, 215 (1973).
6) O. Nomoto and H. Endo, *Bull. Chem. Soc. Jpn.*, **44**, 16 (1971).
7) D. S. Allam and W. H. Lee, *J. Chem. Soc., Suppl.*, **1964**, 6049.
8) D. S. Allam and W. H. Lee, *J. Chem. Soc., A*, **1**, 5 (1966).
9) J. Hinton and E. Amis, *Chem. Rev.*, **71**, 627 (1971).
10) A. G. Passynski, *Acta Physicochim. U. R. S. S.*, **8**, 385 (1938).

Kinetics of Oxidation of α-Hydroxy Acids by Ceric Sulfate

K. C. TEWARI, H. N. SINGH, and V. S. SINGH
Department of Chemistry, Aligarh Muslim University, Aligarh, India
(Received November 7, 1975)

The mechanism of the oxidation of α-hydroxy acids by ceric sulfate in sulfuric acid medium has been re-examined in the temperature range 15—30 °C and the thermodynamic parameters have been calculated. The role of HSO_4^- ion as an active inhibitor has been discussed quantitatively.

Kinetics of the oxidation of α-hydroxy acids with ceric sulfate as oxidant has been the subject of several recent studies.[1-8] The mechanism of oxidation in presence of moderate sulfuric acid concentration, in general, involves a rapid formation of an activated complex between the hydroxy acid and the metal species which then decomposes slowly to yield organic radical and reduced metal ion. However, the present work on the oxidation of lactic, DL-malic, and mandelic acid by ceric sulfate was undertaken to re-examine the conflicting claims on the assumption of reactive species of cerium by different authors,[1,4,5] the effect of sulfuric acid on the reaction rate, particularly the role of HSO_4^- ion as an active inhibitor and to furnish further information on the little known temperature dependence of ceric oxidation.

Experimental

The materials used were of the highest purity available (AnalaR or E. Merck's Guaranteed Reagents).

A solution[9] of ceric sulfate in 1: 1 v/v sulfuric acid was diluted and standardized by titration against ferrous ammonium sulfate, *N*-phenylanthranilic acid being used as an indicator. The sulfuric acid contents were determined by the method reported by McAuley.[5] The solutions of organic acids were standardized by titration against sodium hydroxide. The progress of the reaction was followed as for the reaction between ceric ion and thallous ion.[10] The stoichiometry of the reaction was determined by allowing the reaction mixtures containing large excess of Ce(IV) to stand for several days in a thermostat-bath at 25 °C. The excess of Ce(IV) was then estimated by titration against ferrous ammonium sulfate. An average of five determinations in each case showed that one mol of mandelic, DL-malic, and lactic acid requires 2.0, 8.5, and 5.75 mol, respectively, of ceric ion.

Results

Our kinetic result on the oxidation of α-hydroxy acids by ceric sulfate, in presence of sulfuric acid of moderate concentration, are in agreement with that reported by Krishna and Tewari.[1] The concentration range 0.5—3.0 N of sulfuric acid is referred to as moderate concentration. The reaction is of simple kinetic order if the molar concentration of ceric sulfate is not greater than that of the hydroxy acid. The rate studies were made at temperatures 15—30 °C, in moderate sulfuric acid medium and found to be of first order with respect to each reactant. The second order rate constant, k_2, was derived from the plot of log $[(a-x)/(b-x/y)]$ against time t, where a and b are the initial concentrations of the reactants, x is the amount of ceric sulfate consumed after time t and y is the moles of ceric sulfate required for complete oxidation of one mole of the hydroxy acid.

The reaction rate depends inversely on the square of concentration of sulfuric acid present. Sulfuric acid was varied in the concentration range 0.5—3.0 N.

TABLE 1. VARIATION OF REACTION RATE WITH TEMPERATURE
$[Ce(SO_4)_2] = 1 \times 10^{-2}$ M
[Hydroxy acid] $= 1 \times 10^{-2}$ M

Hydroxy acid	$[H_2SO_4]$ M	Temperature °C	$k_2 \times 10^3$ 1 mol^{-1} s^{-1}
Lactic	0.6	20.0	3.23
		23.0	4.53
		25.0	5.69
		27.5	8.15
		30.0	10.89
	1.0	20.0	1.23
		25.0	2.39
		30.0	4.46
DL-Malic	1.0	20.0	6.80
		23.0	10.43
		25.0	12.93
		27.0	16.10
		30.0	23.50
Mandelic	2.0	15.0	32.75
		20.0	56.46
		25.0	96.26
		30.0	166.02

TABLE 2. THERMODYNAMIC PARAMETERS FOR CERIC OXIDATION AT 25 °C

Hydroxy acid	$[H_2SO_4]$ M	Frequency factor $\times 10^{-14}$ 1 mol^{-1} s^{-1}	Activation energy kcal mol^{-1}	ΔH^* kcal mol^{-1}	ΔF^* kcal mol^{-1}	ΔS^* e.u.	Ref.
Lactic	0.6	0.62	21.8	21.21	20.52	2.0	
	1.0	1.19	22.7	22.11	21.43	2.3	
DL-Malic	1.0	1.03	21.6	21.00	20.98	0.1	
Mandelic	2.0	0.11	19.1	18.51	18.31	0.7	
	1.0	0.18	18.9	18.30	18.40	−0.3	6
Glycollic	1.0	0.36	23.2	22.61	22.18	1.4	5

Addition of nitric or hydrochloric acid in small amounts produces only insignificant retardation. However, hydrogen sulfate and sulfate ions produce a marked retardation. Addition of potassium chloride or nitrate produces negative salt effect while thorium nitrate increases the reaction rate.

The dependence of the rate with temperature for lactic, DL-malic and mandelic acid is shown in Table 1. The values of the activation energy were calculated from the slope of the straight line obtained by plotting log k_2 against $1/T$. The calculated thermodynamic parameters are given in Table 2.

Discussion

Ceric sulfate in aqueous sulfuric acid medium is known to exist[11-14] in variety of complex ions. The composition of these solutions, in general, is governed by the following equilibria:

$$Ce(SO_4)_2 \rightleftharpoons Ce(SO_4)^{2+} + SO_4^{2-}$$
$$Ce(SO_4)_2 + SO_4^{2-} \rightleftharpoons Ce(SO_4)_3^{2-}$$
$$Ce(SO_4)_2 + HSO_4^- \rightleftharpoons HCe(SO_4)_3^-$$
$$\rightleftharpoons Ce(SO_4)_3^{2-} + H^+$$
$$HCe(SO_4)_3^- + HSO_4^- \rightleftharpoons H_2Ce(SO_4)_4^{2-}$$
$$\rightleftharpoons Ce(SO_4)_4^{4-} + 2H^+$$

$Ce(SO_4)_2$, $HCe(SO_4)_3^-$, and $Ce(SO_4)^{2+}$ have been postulated as the reactive species by different authors[1,4,5] in the oxidation of α-hydroxy acids by ceric sulfate in a moderate sulfuric acid medium. From the equilibrium constants of Hardwick and Robertson,[14] for the formation of various ceric sulfate species, the concentration of various species at different $[HSO_4^-]$ and at constant acidity can be estimated. The results along with the observed dependence of the reaction rate on sulfuric acid concentration indicate $Ce(SO_4)_2$ and $Ce(SO_4)^{2+}$ are the possible reactive species. In the presence of moderate sulfuric acid, the experimental results could best be explained by assuming $Ce(SO_4)_2$ as the dominant reactive species as postulated by Krishna and Tewari.[1] At high acid concentration the reaction rate depends inversely on the square of concentration of sulfuric acid present. McAuley[5] has discussed the influence of $[HSO_4^-]$ on the reaction velocity over a smaller concentration range and found that the linear relationship deviates markedly at higher pH values. Possible existence of the reactive ions of the type $Ce(SO_4)^{2+}$ could not be ruled out[14] in a narrower concentration range.

In a solution containing a moderate amount of sulfuric acid and small amount of ceric sulfate, the concentration of HSO_4^- ion would be practically equal to the concentration of sulfuric acid taken. Sulfuric acid dissociates in the following stages

$$(a)\ H_2SO_4 \rightleftharpoons H^+ + HSO_4^-$$
$$(b)\ HSO_4^- \overset{K}{\rightleftharpoons} H^+ + SO_4^{2-}$$

In the first stage the dissociation is cent percent while in the second stage the dissociation is determined by the magnitude of K which is equal to 0.01 at zero ionic strength and 0.075 at an ionic strength of one unit.[15] At higher ionic strengths the equilibrium constant will be the same but the equilibrium quotient of the second stage, *i.e.*$(C_{H^+}C_{SO_4^{2-}}/C_{HSO_4^-})$ will be slightly greater. In any case the dissociation in the second stage will be limited and the concentration of HSO_4^- ion will be equal to the initial concentration of sulfuric acid taken. The active ceric complex species which reacts in the rate determining step is $Ce(SO_4)_2$ formed from the following reaction steps which occur rapidly in succession.

$$(c)\ H_2Ce(SO_4)_4^{2-} \rightleftharpoons HCe(SO_4)_3^- + HSO_4^-$$
$$(d)\ HCe(SO_4)_3^- \rightleftharpoons Ce(SO_4)_2 + HSO_4^-$$

The scheme completely explains the inhibitory action of sulfuric acid and also the proportionality of the reaction rate to the ceric salt concentration. The assumption that most of the ceric salt in the presence of moderate concentration of sulfuric acid exists in the form $H_2Ce(SO_4)_4^{2-}$ in which hydrogen is tightly bound also explains why hydrogen ions from an external source, *i.e.* other than sulfuric acid, do not perceptibly affect the velocity of the reaction. This leads to the conclusion that HSO_4^- ion is the effective retarding agent. In the presence of a moderate sulfuric acid concentration the hydrogen ions added in small quantities, equilibrium (b) will shift very little from right to left and addition of hydrogen ion upto 0.1 M will be hardly perceptible. On the other hand, even a small quantity of SO_4^{2-} ion as will be available from K_2SO_4 up to 0.1 M due to the second dissociation of K_2SO_4 will produce a perceptible change in equilibrium from right to left with the consequent formation of HSO_4^- ions resulting in an appreciable inhibition of the reaction velocity. The observed lowering of reaction rate due to the addition of potassium sulfate could therefore be attributed partly to the increase in the ionic strength and partly to the dissociation in the following two stages.[16]

$$(e)\ K_2SO_4 \longrightarrow K^+ + KSO_4^-$$
$$(f)\ KSO_4^- \rightleftharpoons K^+ + SO_4^{2-}$$

The dissociation constant for the second stage is 0.151. Addition of K_2SO_4 to a solution of sulfuric acid will produce more of HSO_4^- ion due to the reaction

$$SO_4^{2-} + H^+ \rightleftharpoons HSO_4^-$$

causing the observed retardation in the reaction velocity. Another reason for retardation in velocity could be that only a small part of KSO_4^- formed gives rise to SO_4^{2-} ions and the rest remains undissociated and very likely forms a complex with $Ce(SO_4)_2$ according to the following reaction

$$(g)\ Ce(SO_4)_2 + 2KSO_4^- \rightleftharpoons K_2Ce(SO_4)_4^{2-}$$

thus reducing the active species. A similar reasoning could be given for the inhibitory action of $(NH_4)_2SO_4$.

The main inhibitory role of HSO_4^- ion can be examined quantitatively on the following consideration. In a solution containing sulfuric acid the increment in HSO_4^- will be equal to the concentration of $KHSO_4$ added. Since the velocity constant is inversely proportional to the square of the concentration of sulfuric acid, we may write

$$k_2 \propto \frac{1}{[H_2SO_4]^2}$$

or

$$k_2 \propto \frac{1}{[HSO_4^-]^2} = \frac{b}{[HSO_4^-]^2} \quad (1)$$

where b is the proportionality constant. Differentiating with respect to $[HSO_4^-]$ and rearranging, we obtain

$$-[HSO_4^-]^3 \frac{dk_2}{d[HSO_4^-]} = 2b = \text{constant} \quad (2)$$

Since the amount of $KHSO_4$ added is small in comparison to the total concentration of H_2SO_4 already present, we can make the approximations

$$d[HSO_4^-] \approx \Delta[HSO_4^-] = \Delta[KHSO_4]$$

$$dk_2 \approx \Delta k_2$$

therefore,

$$-[HSO_4^-]^3 \frac{\Delta k_2}{\Delta[HSO_4^-]} = \text{constant}$$

or

$$-[H_2SO_4]^3 \frac{\Delta k_2}{\Delta[KHSO_4]} = \text{constant} \quad (3)$$

where $[H_2SO_4]^3$ is the cube of the average concentration of H_2SO_4 initially taken, plus the concentration of $KHSO_4$ added, *i.e.* the average of the concentration of HSO_4^- ion between which Δk_2 is measured. The validity of Eq. 3 is shown in Table 3. The data both for mandelic and DL-malic acid have been taken from the oxidation studies reported by Krishna and Tewari.[1]

Table 3. Inhibitory effect of HSO_4^- ion[a]

Hydroxy acid	$[H_2SO_4]$ M	$[KHSO_4]$ M	Δk_2	$-[H_2SO_4]^3 \cdot \Delta k_2/\Delta[KHSO_4]$
Mandelic	1.01	0.02	−0.245	12.61
	1.02	0.04	−0.426	11.30
	1.04	0.08	−0.920	12.93
	1.05	0.10	−1.091	12.63
DL-Malic	0.400	0.05	−0.379	0.486
	0.425	0.10	−0.588	0.456
	0.450	0.15	−0.800	0.486

a) Data taken from Ref. 1.

We see from Table 3 that the values in the last column are practically constant. This justifies the assumption that the main inhibitory ion is HSO_4^-.

The small negative salt effect observed by the addition of potassium chloride or nitrate follows no mathematical regularity and is hard to visualize in the presence of high ionic strength. The observed increase in the reaction velocity due to the addition of thorium nitrate may be due to some kind of complex formation between thorium and any one of the reactants.

A comparison of the values of different thermodynamic parameters (Table 2) for the oxidation of different hydroxy acids by ceric sulfate in presence of moderate sulfuric acid medium suggests a common mechanism,[17] *viz.*, a rapid formation of an activated complex between Ce(IV) and organic acid and subsequent slow decomposition into organic radical.

The authors are indebted to Professor W. Rahman, Head, Department of Chemistry for providing necessary facilities. One of the authors (V.S.) thanks U.G.C., New Delhi, for a Junior Research Fellowship.

References

1) B. Krishna and K. C. Tewari, *J. Chem. Soc.*, **1961**, 3097.
2) K. P. Bhargawa, R. Shanker, and J. N. Joshi, *J. Sci. Ind. Res., India*, **216**, 573 (1962).
3) T. J. Kemp and W. A. Waters, *J. Chem. Soc.*, **1964**, 1192.
4) G. V. Bakore, R. Dayal, and P. Nath, *Z. Phys. Chem.*, **227**, 19 (1964).
5) A. McAuley, *J. Chem. Soc.*, **1965**, 4054.
6) A. McAuley and C. H. Brubaker, Jr., *J. Chem. Soc.*, **1966**, 960.
7) V. K. Grover, S. K. Mishra, and Y. K. Gupta, *J. Inorg. Nucl. Chem.*, **32**, 2677 (1970).
8) R. Dayal and G. V. Bakore, *Ind. J. Chem.*, **10**, 1165 (1972).
9) B. Krishna and B. P. Sinha, *Z. Phys. Chem. (Frankfurt)*, **212**, 149 (1959).
10) B. Krishna and B. P. Sinha, *Z. Phys. Chem. (Frankfurt)*, **212**, 155 (1959).
11) T. W. Moore and R. C. Anderson, *J. Am. Chem. Soc.*, **66**, 1476 (1944).
12) E. L. King and M. L. Pandow, *J. Am. Chem. Soc.*, **75**, 3063 (1953).
13) G. Hargreaves and L. H. Sutcliffe, *Trans. Faraday Soc.*, **51**, 1105 (1955).
14) T. J. Hardwick and E. Robertson, *Can. J. Chem.*, **29**, 828 (1951).
15) R. A. Whiteker and N. Davidson, *J. Am. Chem. Soc.*, **75**, 3081 (1953).
16) E. C. Righellato and C. W. Davies, *Trans. Faraday Soc.*, **26**, 592 (1930).
17) P. Lavesley and W. A. Waters, *J. Chem. Soc.*, **1955**, 217

A Comparative Study of Electrochemical Kinetic Parameters by the Potential Step Method. Electrode Reactions of CyDTA and EDTA Complexes of Cu(II) at DME

G. A. BHAT*

Department of Inorganic and Physical Chemistry, Indian Institute of Science, Bangalore 560012, India

(Received November 11, 1975)

By using the same current-time (*I-t*) curves, electrochemical kinetic parameters are determined by two methods, (a) using the ratio of current at a given potential to the diffusion-controlled limiting current and (b) curve fitting method, for the reduction of Cu(II)–CyDTA complex. The analysis by the method (a) shows that the rate determining step involves only one electron although the overall reduction of the complex involves two electrons suggesting thereby the stepwise reduction of the complex. The nature of *I-t* curves suggests the adsorption of intermediate species at the electrode surface. Under these circumstances more reliable kinetic parameters can be obtained by the method (a) compared to that of (b). Similar observations are found in the case of reduction of Cu(II)–EDTA complex.

The determination of electrochemical kinetic parameters of metal complexes by comparative methods is not found common. Particularly, such studies are lacking for the systems involving more than one electron in the reduction process. A comparative study of kinetic parameters of such systems by different methods of analysis could verify the reliability of the results obtained by each method and also throw some light on the mechanism of reduction of the complexes at the electrode interface. With this in view, kinetic parameters of two complexes, Cu(II)–*trans*-1,2-cyclohexanediamine-*N,N,N',N'*-tetraacetic acid (Cu–CyDTA) and Cu–EDTA, were determined by the potential step method. Current-time (*I-t*) curves were analyzed by the two different methods: method (a) using the ratio of current at a given potential to the diffusion-controlled limiting current, and method (b) using the curve fitting procedure. The details of the methods employed were reported elsewhere.[1-3]

The basic equations relating the conditional rate constant, $k_c^{\ominus}$, with the rate constants for the oxidizing (k_{ox}) and reducing (k_{red}) reactions, $O+ne \rightleftharpoons R$, can be written as follows:

$$k_{red} = k_c^{\ominus} \exp\left[-\frac{\alpha_c nF}{RT}(E-E^{\circ\prime})\right] \quad (1)$$

$$k_{ox} = k_c^{\ominus} \exp\left[\frac{\alpha_a nF}{RT}(E-E^{\circ\prime})\right] \quad (2)$$

where α_c and α_a are cathodic and anodic transfer coefficients respectively, $E^{\circ\prime}$ is the conditional potential, and R, T, n, F have their usual meaning. These equations can be used to determine the kinetic parameters from the current-time relationship at each potential.

Experimental

Apparatus and Chemicals. The electronic potential step generator along with a timer for dislodging the mercury drop was constructed by using operational amplifiers. The cell was of conventional type. The working electrode was a slowly dropping mercury electrode the drop time and the rate flow of mercury being 18.0 s and 0.624 mg s^{-1} respectively, measured at the height of the mercury column of 42 cm. A spiral of bright platinum was used as the counter electrode. The solution was deaerated with pure nitrogen and was kept under nitrogen atmosphere throughout the experiment. The temperature of the solution was kept constant at 25±0.2 °C. All solutions were prepared in double distilled water and all chemicals used were of analytical grade.

Cu(II)–CyDTA complex was prepared by mixing equimolar solutions of $CuCl_2$ and disodium salt of CyDTA.[4] Cu(II)–EDTA complex was prepared by mixing equimolar solutions of $CuCl_2$ and disodium salt of EDTA.[5]

Method of Measurement. The initial potential for the Cu(II)–CyDTA system was fixed at −0.200 V *vs.* SCE. The potential was stepped up at 14 s after the mercury drop starts growing. The current-time curves were photographed on a Tektronix oscilloscope, Type 564, with a Type 2A63 differential amplifier and Type 2B67 time-base unit. The difference between each potential step-up in subsequent steps was of the order of 5 mV along the rising portion of the reduction wave and 25 mV on the limiting current plateau. Enlarged prints were used for calculating the current. The calculation was programmed on a SOBAX ICC-2700 calculator.

For the Cu(II)–EDTA system the initial potential was fixed at −0.130 V *vs.* SCE and the rest of the measurement was the same as in the case of the Cu(II)–CyDTA system.

The ohmic resistance of the system was about 50Ω, and the effect of the ohmic drop was neglected in the present analysis. The uncertainty of the electrode potential due to the ohmic drop was estimated to be of the order of several millivolts at potentials near $E^{\circ\prime}$. However, this uncertainty will not affect the following discussion on the kinetic parameters of the systems or on the mechanism of reduction of the complexes.

Results and Discussion

Electrode Reaction of Cu(II)–CyDTA System. Analysis by the Method (a)[1,3]: Under the conditions where the current corresponds to a large value of t ($t=t_\infty$), and the potential is sufficiently negative so as to satisfy the conditions, $Q\sqrt{t}>5$ and $k_{red} \gg k_{ox}$, the following relationships can be obtained**

* Research Fellow of the Japan Society for the Promotion of Science in the Inorganic Chemistry Laboratory, The Institute of Physical and Chemical Research, Wako-shi, Saitama 351, Japan.

** The symbols and terminology are according to IUPAC recommendations.[6]

$$\frac{I(t)I_d(t_\infty)}{I(t_\infty)I_d(t)} = \sqrt{\pi}Q\sqrt{t}\ \exp(Q^2t)\ \mathrm{erfc}\ (Q\sqrt{t}) \quad (3)$$

$$k_{red} = Q\frac{I(t_\infty)}{I_d(t_\infty)}\sqrt{D_0} \quad (4)$$

$$k_{ox} = Q\left[1-\frac{I(t_\infty)}{I_d(t_\infty)}\right]\sqrt{D_R} \quad (5)$$

where $I_d(t)$ and $I_d(t_\infty)$ are the currents at far negative potentials and Q is the parameter at a given electrode potential E at which $I(t)$ and $I(t_\infty)$ were measured. For this system, t=400 μs and t_∞=1.0 s were used. The currents $I(t)$ and $I(t_\infty)$ were measured at several potentials in the neighbourhood of $E^{o\prime}$. Also, the diffusion-controlled currents, $I_d(t)$ and $I_d(t_\infty)$, were measured at several potentials on the diffusion current plateau. These values were substituted into Eq. 3 to get Q. By using these Q-values k_{red} and k_{ox} were obtained from Eqs. 4 and 5 assuming $D_0=D_R=6.8\times10^{-6}$ cm^2 s^{-1}, estimated from the polarographic diffusion current by the Ilkovic equation.

Figure 1 gives the typical plots of log k_{red} and log k_{ox} *vs.* potential for one value of I_d measured at a potential on the diffusion current plateau. The conditional rate constant $k_c^\ominus$ was obtained from the intersection of two straight lines and α_c and α_a were obtained from the slopes. In a similar way, by using other values of I_d's several $k_c^\ominus$-values were obtained and were plotted

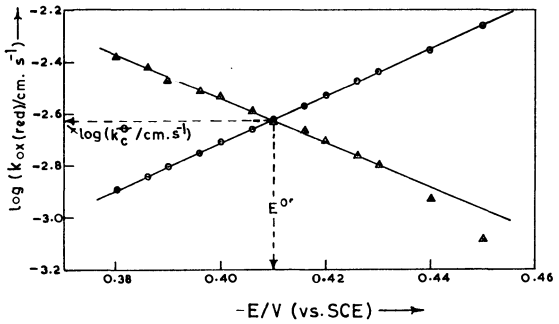

Fig. 1. Plots of log (k_{red}/cm s^{-1}) and log (k_{ox}/cm s^{-1}) *vs.* E; the rate constant obtained by the method (a) using diffusion-controlled limiting current. System: 6.0 mM Cu(II)–CyDTA complex in a 0.4 M KNO_3 solution containing 0.1 M acetate buffer and 3 μM polyoxyethylene lauryl ether (LEO).

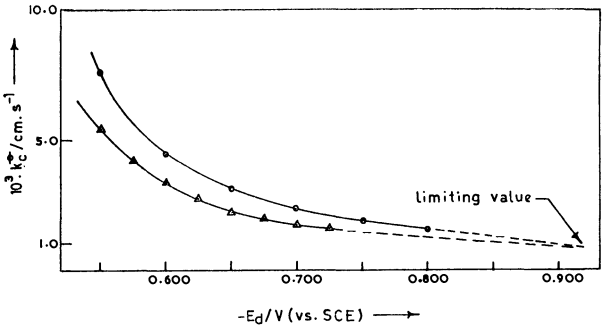

Fig. 2. Variation of $k_c^\ominus$ with potentials, E_d, at which I_d's are measured; analysis by the method (a). System: 4 mM (△) and 6 mM (○) Cu(II)–CyDTA in 0.4 M KNO_3 solutions containing 0.1 M acetate buffer and 3 μM LEO.

against the electrode potential, E_d, where the I_d-values were measured (Fig. 2).

It is obvious from Fig. 2 that the rate constant decreases as the potential becomes more and more negative and finally comes to a limiting value. However, at far negative potentials the distortion of *I-t* curves was noticed (broken lines in Fig. 2 correspond to the potentials where the distortion was observed). The curve, $k_c^\ominus$ *vs.* E_d, was extrapolated in this region to obtain the limiting value of $k_c^\ominus$ which is in reasonably good agreement with that obtained by other methods[7] (see, Table 1).

Table 1. Kinetic parameters obtained by different methods of analysis for Cu(II)–CyDTA and Cu(II)–EDTA complexes

System	Method	$n\alpha_c$	$n\alpha_a$	$k_c^\ominus\times10^3$ / cm s^{-1}
Cu(II)–CyDTA	Potential-step; method (a)	0.52	0.48	0.8
	Potential-step; method (b)	0.5	—	1.4
	Faradaic impedance method	—	—	0.63[a]
Cu(II)–EDTA	Potential-step; method (a)	0.53	0.48	1.7
	Potential-step; method[10]	0.54	0.46	4.0
	Faradaic impedance method	—	—	0.85[a]

a) To be published.

At all potentials of the I_d-measurement $n\alpha_c$ and $n\alpha_a$ obtained as slopes add up to one unlike in the case of Zn(II) system.[1] This suggests that the number of electrons involved in the rate determining step is only one although the overall reduction of the complex involves two electrons.[8] Therefore, the mechanism of reduction of the complex at DME can be written as follows.

$$\text{Cu(II)–CyDTA} + e \xrightarrow{\text{slow}} \text{Cu(I)–CyDTA}$$

$$\text{Cu(I)–CyDTA} + e \overset{\text{fast}}{\rightleftharpoons} \text{Cu}^o\text{(Hg)} + \text{CyDTA}$$

Analysis by the Curve Fitting Method (b)[1,2]: At any given potential the best values of $I(t=0)$ and Q were calculated by the trial-and-error method using Eq. 6:

$$I(t)/I(t=0) = \exp(Q^2t)\ \mathrm{erfc}\ (Q\sqrt{t}) \quad (6)$$

where

$$I(t=0) = -nFAk_{red}c_0 \quad (7)$$

$$Q = k_{red}/\sqrt{D_0} + k_{ox}/\sqrt{D_R} \quad (8)$$

By knowing the concentration c_o, of the complex, and surface area, A, of the mercury drop and by using Eq. 7, the values of k_{red} were calculated at several potentials in the neighborhood of $E^{o\prime}$ from the best values of $I(t=0)$, and were plotted against E. From the resulting straight line graph $k_c^\ominus$ was read at $E^{o\prime}$ obtained by the method (a). From the slope α_c was calculated. These values agree well with the values obtained by the method (a) (see Table 1). However, the values of k_{ox} obtained by using appropriate Q values employing expression (8) were found to be much higher than expected (of the order of 10^{-2} cm s^{-1}).

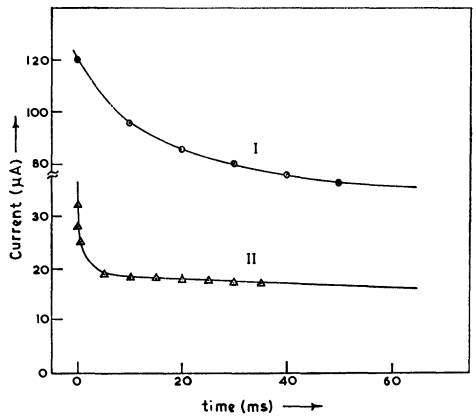

Fig. 3. (I) *I-t* curve for the reduction of zinc(II) at −0.994 V *vs.* SCE. 8.0 mM $Zn(NO_3)_2$ in a 0.5 M KNO_3 solution containing 0.2 mM HNO_3.
(II) *I-t* curve for the reduction of Cu(II)–CyDTA at −0.410 V *vs.* SCE. 6.0 mM Cu(II)–CyDTA in a 0.4 M KNO_3 solution containing 0.1 M acetate buffer and 3.0 μM LEO.

Figure 3 gives the *I-t* curves for the Cu(II)–CyDTA system and for the Zn(II) system near to their respective $E^{\circ\prime}$. A comparison of the *I-t* curves for these two systems shows that the decay of current with time is much faster in the case of the Cu–CyDTA complex than in the case of the Zn(II) system. According to Eqs. 6 and 7 the decay of current with time should be comparable for two systems if their conditional rate constants, α's and D's are comparable. However, in the above two cases their *I-t* curves are found to be quite different though their kinetic parameters are comparable. Because of this the curve fitting in the case of the Cu(II)–CyDTA system had to be carried out between 600 μs and 900 μs where exists a perceptible difference in the current with time. Such a behavior of the system is probably due to the adsorption of the short-lived intermediate species during reduction. This adsorption of intermediate species could act as a capacitance in parallel to the faradaic impedance and thereby shunts the latter to make the current decay more rapidly.[9]

Electrode Reaction of Cu(II)–EDTA System. Analysis by the Method (a): The procedure adopted in this case is the same as in the previous case. The two time limits chosen were, $t=350$ μs and $t_\infty=1.0$ s. The limiting value, $k_c^\ominus$, obtained by extrapolating $k_c^\ominus$ *vs.* E_d curve is given in Table 1. In this case also, the distortion of *I-t* curve was found at far negative potentials. The values of $n\alpha_c$ and $n\alpha_a$ add up to make one suggesting that the number of electrons involved in the rate determining step is one only. Therefore, the mechanism of the reduction process can be written as follows:

$$\text{Cu(II)-EDTA} + e \xrightarrow{\text{slow}} \text{Cu(I)-EDTA}$$

$$\text{Cu(I)-EDTA} + e \overset{\text{fast}}{\rightleftharpoons} \text{Cu}^{\circ}\text{(Hg)} + \text{EDTA}$$

The nature of *I-t* curves in this case, *i.e.*, the decay of current with time is similar to that of the Cu(II)–CyDTA system indicating the adsorption of intermediate species.

Conclusion. The reduction of Cu(II)–CyDTA and Cu(II)–EDTA complexes occurs at DME in two steps and each step involves one electron in the reduction process. When the reduction is further complicated by the adsorption of intermediate species the analysis of *I-t* curves by the curve fitting method introduces some uncertainty in the results. On the other hand, the analysis by the method (a) can be adopted to obtain more reliable kinetic parameters.

The author wishes to thank Dr. R. Tamamushi, Rikagaku Kenkyusho, Wako-shi, Saitama 351, Japan, for having provided the facility to carry out this work. He is also thankful to him and to Dr. K. Niki for helpful discussions. The financial assistance by the Japan Society for the Promotion of Science to carry out this work is gratefully acknowledged.

References

1) G. A. Bhat and R. Tamamushi, *Sci. Pap. Inst. Phys. Chem. Res.*, **70**, 16 (1975).
2) K. Niki, Y. Okuda, T. Tomonari, E. Buck, and N. Hackerman, *Electrochim. Acta*, **16**, 487 (1971).
3) N. Tanaka, Y. Aoki, and A. Yamada, *Electrochim. Acta*, **14**, 1155 (1969).
4) G. Schwarzenbach and H. Ackermann, *Helv. Chim. Acta*, **32**, 1682 (1949).
5) W. Furness, P. Crawshaw, and Cule Davies, *Analyst*, **74**, 629 (1949).
6) R. Parsons, *Pure Appl. Chem.*, **37**, No. 4 (1974).
7) To be published.
8) H. A. Laitinen and W. J. Subcasky, *J. Am. Chem. Soc.*, **80**, 2623 (1958).
9) Q. J. M. Slaiman and W. J. Lorenz, *Electrochim. Acta*, **19**, 791 (1974).
10) N. Tanaka, A. Kitani, A. Yamada, and K. Sasaki, *Sci. Repts. Tohoku Univ. Ser.*, **1**, 55 (1972).

Studies with Parchment Supported Membranes. VII. Application of Fick's Diffusion Law and Nernst-Planck Formulae for Electrical Potential—Consideration of Membrane Field Strength and Energetics of Permeation of Cations

Fasih A. SIDDIQI, M. Nasim BEG, Abdul HAQUE, and Surendra P. SINGH

Division of Physical Chemistry, Department of Chemistry, Aligarh Muslim University, Aligarh, India

(Received December 8, 1975)

Electrolytic transport processes occurring across parchment supported membranes have been described by Nernst-Planck flux equation taking into account the membrane resistance R_m, membrane potential E_m *etc.* E_m values for various electrolytes display very interesting phenomena. In the case of 1:1 electrolyte the E_m values are all positive, while in the case of (2:1) and (3:1) electrolytes surface charge reversal takes place. The diffusion rate sequence and selectivity of the membrane for different uni-, bi-, and tri-valent cations was found to be primarily dependent on the difference in the hydration energies of counter ions in the external solution. On the basis of Eisenman-Sherry theory the diffusion rate sequence of alkali metal cations point towards the weak field strength of the fixed charge groups. Various thermodynamic parameters, $\Delta H^{\neq}$, $\Delta F^{\neq}$, and $\Delta S^{\neq}$ were evaluated by applying the theory of absolute reaction rates to the diffusion process through parchment supported membranes. The values of $\Delta S^{\neq}$ were found to be negative, indicating that diffusion takes place with partial immobilization in the membrane phase. The relative partial immobility was found to increase with increase in the valence of the ions constituting the electrolyte. A formal relation between $\Delta H_{hydration}$, $\Delta F_{hydration}$, and $\Delta S_{hydration}$ of cations with the corresponding values of $\Delta H^{\neq}$, $\Delta F^{\neq}$, and $\Delta S^{\neq}$ for diffusion, was also found to exist for these membranes.

Transport processes occuring across membranes are of great interest for biologists, who use them as simple models for physiological membranes in order to understand the behavior of complex cell membranes in terms of established physico-chemical principles. It was demonstrated by Teorell[1] that the gastric mucosal membrane, in some formal aspects at least, behaved exactly like parchment membrane. His findings, that electrolytic transport processes in stomach could be handled by something similar to Fick's diffusion law and that Nernst-Planck formulae for electrical potential were applicable, has encouraged us to proceed further with the studies of (a) the parchment supported membranes[2-9] and (b) the asymmetric polymeric membranes[10-14] which mimic some of the properties of nerve cells[15,16] as models for biological system.

This paper deals with the studies of diffusion rate of biologically important electrolytes through parchment supported membranes. The results are discussed in the light of Eisenman-Sherry field strength model[17-20] and the theory of absolute reaction rates.[21-23]

Experimental

The parchment supported membranes of (i) silver (ii) cadmium hexacyanoferrate(II) and (iii) barium phosphate were prepared by the method of interaction described by Siddiqi *et al.*[2-9] In order to precipitate these substances in the interstices of the parchment paper, 0.2 M solution of potassium hexacyanoferrate(II) was kept inside a glass tube to one end of which was tied the parchment paper. This was suspended for 72 h in a 0.2 M solution of silver nitrate or cadmium chloride (for hexacyanoferrate(II) membranes). The two solutions were interchanged later and kept for another 72 h. A similar procedure was adopted for the preparation of barium phosphate membrane by taking 0.5 M solutions of barium chloride and potassium di-hydrogen orthophosphate. The membranes thus prepared were washed with deionized water for removal of free electrolytes.

The apparatus and procedures used to measure membrane potential E_m, membrane resistance R_m, and electrolyte concentrations were described by siddiqi *et al.*[2] The membrane was held between two half cells, each containing 125 ml of the electrolyte solution. Initially the concentrations C_1 and C_2 were 0.001 and 0.1 M, respectively. Each of the half cell was fitted with two platinized platinum electrodes firmly fixed to follow concentration changes and two anion reversible Ag–AgCl electrodes-one a disc type to pass a small d. c. current and the other a J-shaped wire electrode placed 1.7 cm apart from the membrane surface to measure membrane potential (Pye precision potentiometer No. 7568) and changes in membrane potential following current flow. The solutions in both the half cells were kept well stirred by magnetic stirrers. The whole cell assembly was immersed in a water thermostat maintained at 10, 15, 20, 25, and 30 °C (±0.1 °C).

Conductance changes on the dilute solution side was followed by means of the conductivity bridge (Cambridge Instrument Co. England No L-350140). The exact concentration of the solution at any given time was estimated from a calibration curve. The membrane resistance was determined by applying an external emf to the disc-type Ag–AgCl electrodes and measuring the change in potential across the membrane using J-type wire electrodes. The current passed through the membrane system was determined by measuring IR drop across a precision kilo-ohm resistor. The current was kept very low in order to minimize the ion transfer during the period (2—3 min) required for each resistance measurement. The direction of current flow was reversed in each successive measurement. The resistance measurements gave a value for the system electrolyte solution (R_e')-Membrane (R_m)-electrolyte solution (R_e''). In order to measure R_m directly, the wire electrodes should be placed strictly on the membrane surfaces. When this was done, resistance values were not reproducible This procedure was therefore abondoned in favor of the former and corrections for the electrolyte resistances R_e' and R_e'' were applied to derive a value for R_m. Since the geometry of the system (area=24.6 cm^2 and the distance at which wire electrode was placed from the membrane face=1.7 cm) and the specific conductance of the electrolyte solutions were known accurately (better than 0.5%), the sum ($R_e'+R_e''$) can be computed easily. Thus R_m, the membrane resistance only, can be derived as the difference between the measured total resistance and the sum of the

calculated electrolyte resistances ($R_e'+R_e''$). Although the membrane potential could be measured to a better accuracy than $\pm 1\%$, the estimation of membrane resistance was accurate to $\pm 3\%$.

Results and Discussion

The transport phenomena are often described by some extended form of the Nernst-Planck flux equation.[24] Evaluation of flows requires integration of these flux equations under suitable boundary conditions governing the behavior of the membrane system. Some time ago, Kittelberger[25] from the simple laws of electrolysis, developed the equation

$$\frac{dQ_+}{dt} = \frac{1}{Z_+FR_m}\left[\frac{RT}{Z_+F}\ln\frac{a_2}{a_1} - E_m\right] \times\left[\left(\frac{Z_+Z_-}{Z_++Z_-}\right)\left(\frac{E_m}{\frac{RT}{F}\ln\frac{a_2}{a_1}}\right)+\frac{Z_+}{Z_++Z_-}\right] \quad (1)$$

where Q_+ is the milli-equivalents of cations diffusing in time t s, Z_+, Z_- are the valencies of cation and anion, respectively, R_m is the resistance in ohm of the membrane, E_m is the membrane potential in millivolts, a_1 and a_2 are the activities of the two electrolyte solutions on either side of the membrane, R, T, and F have their usual meanings to describe the rate of flow of a charged species or electrolyte through a membrane.

$$\frac{Z_+Z_-}{Z_++Z_-}\frac{E_m}{\frac{RT}{F}\ln\frac{a_2}{a_1}}+\frac{Z_+}{Z_++Z_-} \quad (2)$$

is the cation transport number expressed in terms of observed membrane potential E_m. The term

$$\frac{RT}{Z_+F}\ln\frac{a_2}{a_1} - E_m \quad (3)$$

is the effective potential acting on the ion.

The emf measured across the membrane using the J-type Ag–AgCl electrodes is made up of two components, the electrode potential difference E_e due to the Ag–AgCl electrodes existing in the two chloride solutions of different activity a_1 and a_2, and the membrane potential E_m arising across the membrane due to flow of electrolyte through it. E_e is given by the equation

$$E_e = \frac{RT}{Z-F}\ln\frac{C_2\nu_2}{C_1\nu_1} \quad (4)$$

where ν's are the activity coefficients of the electrolyte solutions. Since (E_e+E_m) is measured directly, E_m can be evaluated by substraction.

Changes in E_m and R_m with time are shown in Figs. 1 and 2 for various electrolytes diffusing through a cadmium hexacyanoferrate(II) membrane. At any given time, the membrane resistance R_m increases in the order; KCl, NaCl, LiCl, for electrolytes (1: 1), $CaCl_2$, $MgCl_2$, $BaCl_2$ for electrolytes (2: 1), and electrolyte (3: 1) $AlCl_3$ produces the highest value for R_m.

E_m values for the various electrolytes display a very interesting phenomenon. In the case of (1: 1) electrolytes, the values are all positive (dilute solution side C_1 taken as positive) indicating thereby that the membrane is cation selective. In the case of (2: 1) and (3: 1) electrolytes, E_m changes sign. This indicates that the

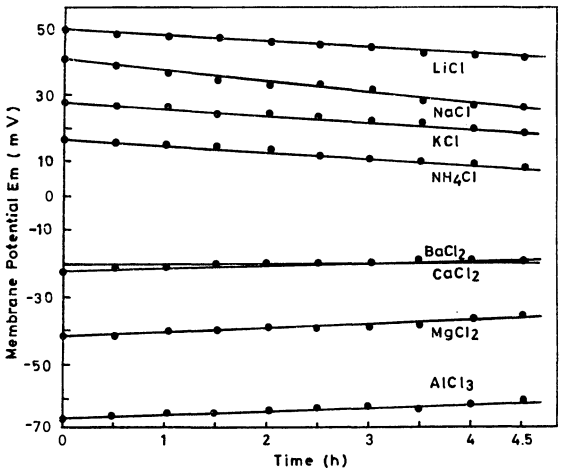

Fig. 1. Plots of membrane potential E_m against time for various electrolytes with cadmium hexacyanoferrate(II).

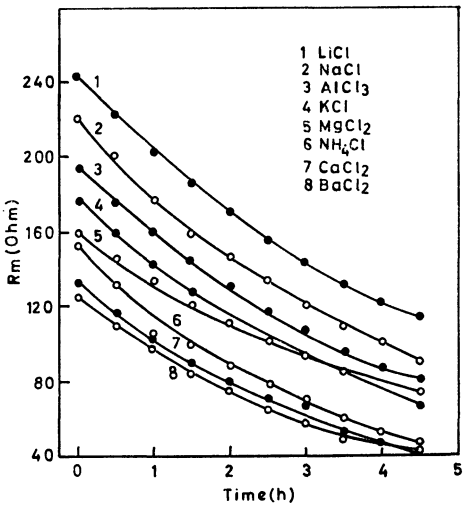

Fig. 2. Plots of R_m against time for various electrolytes with cadmium hexacyanoferrate(II).

membrane has become anion selective. The change in the selectivity character of the membrane is evidently due to adsorption of multivalent ions leading to a state where a net positive charge is left on the membrane surface taking it anion selective. Adsorption of Al^{3+} makes the membrane more anion selective than it is with the adsorption of other divalent cations. Such behavior seems to be observed with a number of other systems.[26–28]

The surface charge reversal occurred in every one of the membranes and electrolytes (2: 1) and (3: 1) and can be seen in the results given in Table 1 (a, b). E_m and R_m values are recorded.

With the help of Eq. 1, the rate at which various electrolytes diffuse through the membranes can be calculated. For electrolyte (1: 1), ($Z_+=Z_-=1$), Eq. 1 becomes

$$\frac{dQ_+}{dt} = \frac{dQ_-}{dt} = \frac{dQ}{dt} = \frac{1}{2FR_m}\left[59.16\log\frac{C_2\nu_2}{C_1\nu_1} - E_m\right] \times\left[\frac{E_m}{59.16\log\frac{C_2\nu_2}{C_1\nu_1}}+1\right] \quad (5)$$

For electrolyte (2: 1), ($Z_+=2$ and $Z_-=1$), it becomes

Table 1(a). Values of membrane potential E_m, membrane resistance R_m, and diffusion rate D_r at the end of 1/2 and 4 h periods at 25 °C[a)]

Membrane	Silver Hexacyanoferrate(II)						Cadmium hexacyanoferrate(II)					
Thickness	0.0381 cm						0.0279 cm					
Electrolyte	E_m (mV)		R_m (ohm)		D_r (μ mol/h)		E_m (mV)		R_m (ohm)		D_r (μ mol/h)	
	1/2 h	4 h	1/2 h	4 h	1/2 h	4 h	1/2 h	4 h	1/2 h	4 h	1/2 h	4 h
LiCl	77.5	61.4	260	143	3.7	6.3	48.5	43.0	223	123	7.0	9.2
NaCl	70.0	52.0	231	127	5.1	9.0	39.0	28.0	200	100	8.2	15.3
KCl	63.7	44.1	214	114	6.3	12.6	26.5	20.0	160	70	11.5	17.5
NH_4Cl	—	—	—	—	—	—	16.6	10.6	133	53	16.0	26.3
$BaCl_2$	−1.5	−20.9	117	55.5	5.0	8.5	−21.5	−17.3	118	50	6.3	11.5
$CaCl_2$	−11.6	−31.0	134	73.5	4.8	6.6	−21.6	−19.6	117	49	6.0	9.2
$MgCl_2$	−35.0	−40.4	181	108	4.0	5.0	−41.9	−35.0	147	79	5.0	6.3
$AlCl_3$	−67.4	−75.0	226	140	0.8	0.5	−65.6	−61.5	177	87	1.5	2.8

a) Area of membrane=24.6 cm^2.

Table 1(b). Values of membrane potential E_m, membrane resistance R_m, and diffusion rate D_r at the end of 1/2 and 3 h periods at 25 °C[a)]

Membrane	Barium phosphate					
Thickness	0.03612 cm					
Electrolyte	E_m (mV)		R_m (ohm)		D_r (μ mol/h)	
	1/2 h	3 h	1/2 h	3 h	1/2 h	3 h
KCl	12.72	7.10	155.0	55.0	10.483	22.70
NaCl	4.53	−0.73	180.2	84.0	7.894	15.624
LiCl	3.12	0.60	221.1	136.0	7.107	9.493

a) Area of membrane=24.6 cm^2.

$$\frac{dQ_+}{dt} = \frac{1}{2}\frac{dQ_-}{dt} = \frac{dQ}{dt} = \frac{1}{3FR_m}\left[29.58 \log \frac{C_2\nu_2}{C_1\nu_1} - E_m\right] \times \left[\frac{E_m}{59.16 \log \frac{C_2\nu_2}{C_1\nu_1}} + 1\right] \quad (6)$$

For electrolyte (3: 1), ($Z_+=3$ and $Z_-=1$), it becomes

$$\frac{dQ_+}{dt} = \frac{1}{3}\frac{dQ_-}{dt} = \frac{dQ}{dt} = \frac{1}{4FR_m}\left[19.72 \log \frac{C_2\nu_2}{C_1\nu_1} - E_m\right] \times \left[\frac{E_m}{59.16 \log \frac{C_2\nu_2}{C_1\nu_1}} + 1\right] \quad (7)$$

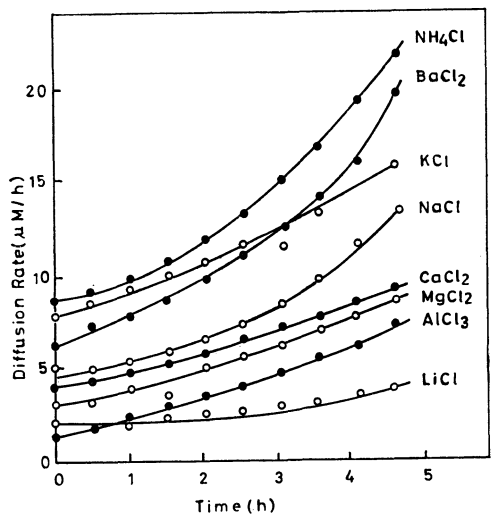

Fig. 3. Plots of diffusion rate *vs.* time through cadmium hexacyanoferrate(II).

The electrolyte fluxes dQ/dt *i.e.* D_r calculated from Eqs. 5—7 for various electrolytes at 25 °C are given in Table 1 for all the three membranes. The reproducibility of the results were within ±3% at a certain temperature. The changes in R_m, E_m, and D_r with time for cadmium hexacyanoferrate(II) membrane are shown in Figs. 1—3, while comparative values for various cations are given in Fig. 3a.

The diffusion rate derived from the electrometrically or conductometrically determined changes in the salt concentration of the test solution C_1 is called "observed diffusion rate," while the values computed from the measured concentration potential and electrolytic resistance of the membrane *i.e.* from Eqs. 5—7 is designated the "computed" diffusion rate. The "computed" and "observed" diffusion rates of KCl, NaCl, LiCl for barium phosphate membrane are shown in Fig. 4a. For

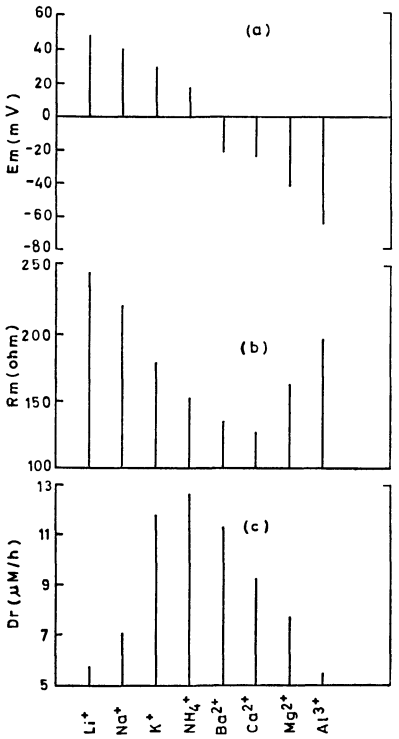

Fig. 3a. Plots of E_m, R_m, and D_r against the various electrolytes for cadmium hexacyanoferrate(II).

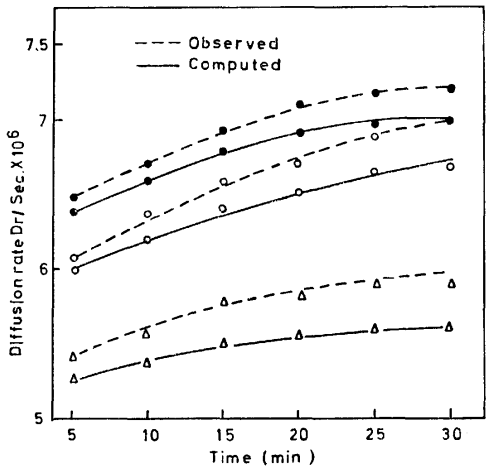

Fig. 4a. Plots of observed and computed diffusion rate against time for ●: KCl, ○: NaCl, and △: LiCl with barium phosphate membrane.

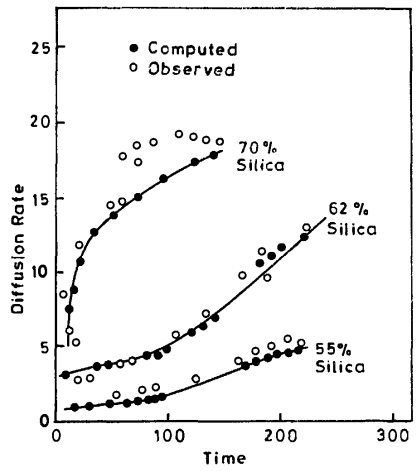

Fig. 4b. Plots of observed and computed diffusion rate against time for hydrochloric acid through polyvinyl butyral membrane.

the sake of comparison the rates of diffusion of hydrochloric acid through poly (vinyl butyral) membranes obtained by Kittelberger[25] are also given in Fig. 4b. Agreement is fair in both cases.

The diffusion of the electrolyte through the membrane is slower than in free solution. The order does not remain the same due to various reasons; (a) only a part of the frame work is available for free diffusion, (b) the diffusion paths in the membrane phase are more tortuous and therefore longer (*i.e.* the tortuousity factor), (c) the large hydrated ions in the narrow mesh region of the membrane might be impeded in their mobility by the frame work and (d) the interaction of the diffusing species with the fixed groups on the membrane matrix. Parchment paper, except for the presence of some stray and end carboxyl groups, contains very few fixed groups. Deposition of inorganic precipitate gives rise to a net negative charge on the membrane surface in the case of electrolyte (1: 1) leading to the type of ionic distribution associated with the electrical double layer. However, use of electrolyte (2: 1) or (3: 1) leaves a net positive charge on the membrane and results in the formation of the electrical double layer. The system is considered as having charged capillary structures or gels which can be judged in the light of classical fixed charge theory of Teorell,[29] Meyer and Sievers,[30] Sollner,[31] Gregor,[32] and Schmid.[33,34] Flow of electrolyte by diffusion because of the presence of a net charge ($-ve$ or $+ve$) on the membrane gives rise to the membrane potential as opposed to the liquid junction potential ordinarily observed under similar conditions in the absence of the membrane, which regulates the flow of electrolyte by increasing the speed of slow moving ion and by decreasing the speed of the faster moving ion. The regulated rate of flow (*i.e.* diffusion) measured for different electrolytes through the investigated membranes follow the sequence: $NH_4^+ > K^+ > Na^+ > Li^+$ and $Ba^{2+} > Ca^{2+} > Mg^{2+} > Al^{3+}$.

Depending on the size and electrical charge pattern of a pore, it may either admit or repel a solute particle. This is the basis of ion selectivity. Mullins[35] proposed that the hydration of the materials of the pores themselves may provide a favorable water environment for particular ions or molecules, so that they slip into the pores away from their previous water molecules. This could result in selection of a particular size with discrimination against both smaller and larger hydrated ions. In order to obtain a quantitative relation between the ease of penetration and the ion size, it is necessary to know the electrostatic force which acts between the ions and the material of the membranes, since this force provides energy to displace water of hydration. Eisenman *et al.*[17-19] pointed out that the order of the ease of penetration of cations depends on the energy available from the ion-fixed charge interaction. From a simplified model, in which field strength was taken as a controlling variable, the Coulomb energies of interaction of alkali cations with the charged sites were compared with the free energy of hydration of cations. A simplified theory of selectivity for four alkaline earths (Mg^{2+}, Ca^{2+}, Sr^{2+}, and Ba^{2+}) in a cation exchange membrane has been worked out by Sherry.[20] Specificity is determined by the difference between the free energy of hydration of

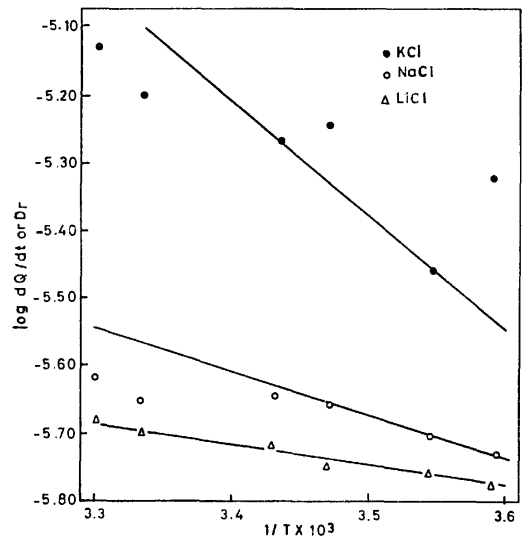

Fig. 5. Plots of log D_r *vs.* $1/T$ for different electrolytes with barium phosphate membrane.

Table 2(a). Experimental activation energy E_a and other thermodynamic parameters calculated from transition state theory of rate processes for various electrolytes diffusion, through membrane (Temperature=25 °C)

Membrane	Silver hexacyanoferrate(II)				Cadmium hexacyanoferrate(II)			
Electrolyte	E_a kcal mol^{-1}	ΔH^* kcal mol^{-1}	ΔF^* kcal mol^{-1}	ΔS^* e.u.	E_a kcal mol^{-1}	ΔH^* kcal mol^{-1}	ΔF^* kcal mol^{-1}	ΔS^* e.u.
LiCl	5.53	4.94	8.80	−13.0	6.36	5.77	8.79	−10.1
NaCl	5.97	5.38	8.85	−11.6	7.15	6.37	8.68	− 7.9
KCl	6.26	5.67	8.81	−10.5	7.50	6.95	8.58	− 5.8
NH_4Cl	—	—	—	—	7.65	7.06	8.56	− 5.1
$BaCl_2$	4.24	3.65	8.85	−17.5	4.61	4.02	8.95	−16.5
$CaCl_2$	3.68	3.09	9.90	−19.8	4.24	3.65	9.11	−18.3
$MgCl_2$	3.96	3.37	9.13	−19.4	4.61	4.02	9.25	−17.6
$AlCl_3$	3.41	2.82	9.72	−23.1	3.32	2.73	9.86	−23.9

Table 2(b). Experimental activation energy E_a and other thermodynamic parameters calculated from transition state theory of rate processes for various electrolytes diffusion, through membrane (Temperature=25 °C)

Membrane	Barium phosphate			
Electrolyte	E_a kcal mol^{-1}	ΔH^* kcal mol^{-1}	ΔF^* kcal mol^{-1}	ΔS^* e.u.
KCl	5.45	4.84	7.83	−10
NaCl	4.21	3.61	8.08	−15
LiCl	3.09	2.50	9.06	−22

alkaline earth cations and their Coulomb energies of interaction with the negatively charged sites. On the basis of Eisenman-Sherry theory,[17–20] the diffusion rate sequence obtained with the investigated membranes point towards the weak field strength of charged groups.

The theory of absolute reaction rates[21–23] has been applied to diffusion processes in membranes by several investigators.[36–39] According to Laidler *et al.*[22–23] the integral diffusion coefficient $\bar{D}$ is given by the expression

$$\bar{D} = Ae^{-E_a/RT} \tag{8}$$

where E_a is the observed activation energy for diffusion and A is the frequency factor. Thus, if log D is plotted against $1/T$, the slope gives (Fig. 5) the value of energy of activation for the diffusion process. These values of E_a were determined for a number of electrolytes and with all the three membranes, and are given in Tables 2 (a, b).

According to Zwolinski *et al.*,[21] we have

$$\bar{D} = \lambda^2\left(\frac{KT}{h}\right)\exp(\Delta S^*/R)\exp\left(\frac{-\Delta H^*}{RT}\right) \tag{9}$$

where λ is the distance between successive equilibrium positions of diffusing species, ΔS^* the entropy of activation, ΔH^* the enthalpy of activation, k, h, R, and T having their usual meanings.

The Eyring enthalpy of activation ΔH^* is calculated from the activation energy E_a (previously determined) by means of the relation

$$\Delta H^* = E_a - RT \tag{10}$$

Assuming λ to be equal to 3 Å for different electrolytes (values 1—5 Å for λ have been used by different investigators) and substituting the value of diffusion coefficient $\bar{D}$, the value of ΔS^* has been calculated. The free energy of activation ΔF^* is then calculated by the Gibbs-Helmholtz equation

$$\Delta F^* = \Delta H^* - T\Delta S^* \tag{11}$$

The values so derived for the different thermodynamic parameters are given in Tables 2 (a, b).

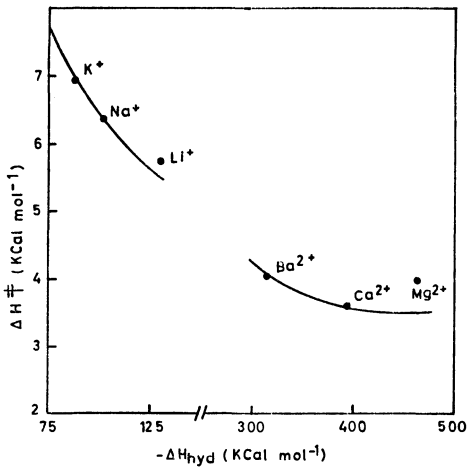

Fig. 6a. Plots of ΔH^* for the diffusion of various electrolytes (at 25 °C) against $-\Delta H_{hyd}$ for the respective cations through cadmium hexacyanoferrate(II).

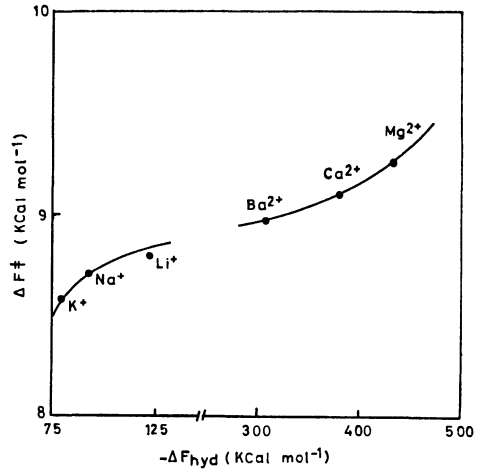

Fig. 6b. Plots of ΔF^* for the diffusion of various electrolytes (at 25 °C) against $-\Delta F_{hyd}$ for the respective cations through cadmium hexacyanoferrate(II).

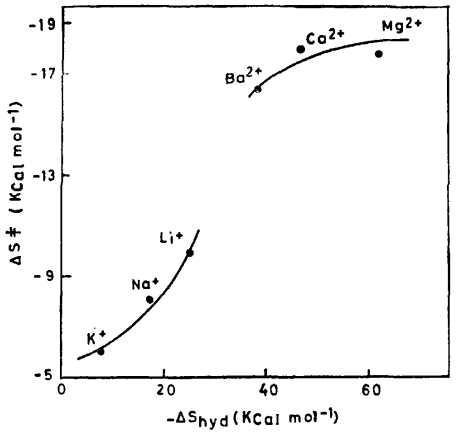

Fig. 6c. Plots of ΔS^* for the diffusion of various electrolytes (at 25 °C) against $-\Delta S_{hyd}$ for the respective cations through cadmium hexacyanoferrate(II).

The results indicate that electrolyte permeation gives rise to negative values of ΔS^*. The values of ΔS^* for all the three membranes show a similar behavior for different electrolytes. With increase in valence of the individual ion, the decrease in the values of ΔS^* is enhanced. It is believed that the membrane and not the solution-membrane interface controls the electrolyte diffusion process. The negative values of ΔS^* as suggested by Schular *et al.*[23] indicate electrolyte diffusion with partial immobilization in the membrane, the relative partial immobility increasing with increase in the valence of ions constituting the electrolyte. In Fig. 6 (a, b, c) the individual ionic contribution to the properties of aqueous ions given by Noyes[40] namely $\Delta H_{hydration}$, $\Delta F_{hydration}$, and $\Delta S_{hydration}$, of Li^+, Na^+, K^+, as well as those of Ba^{2+}, Ca^{2+}, and Mg^{2+} are plotted against the corresponding ΔH^*, ΔF^*, and ΔS^* values for diffusion through the membrane. It is found that at least some formal relationship exists between these thermodynamic parameters.

The authors are grateful to Prof. Wasiur Rahman, Head of Department of Chemistry, for providing research facilities and to C.S.I.R. (India) for financial assistance to A. H. and S. P. S.

References

1) T. Teorell in "Membrane Phenomena," *Discuss. Faraday Soc.*, **21**, 9 (1956).
2) F. A. Siddiqi and S. Pratap, *J. Electroanal. Chem.*, **23**, 137, 147 (1969).
3) F. A. Siddiqi, N. Lakshminarayanaiah, and S. K. Saksena, *Z. Phys. Chem., (Frankfurt)*, **72**, 298, 307 (1970).
4) F. A. Siddiqi, N. Lakshminarayanaiah, and M. N. Beg, *J. Polym, Sci.*, **9**, 2868 (1971).
5) F. A. Siddiqi, M. N. Beg, and S. P. Singh, *J. Polym. Sci.*, in press.
6) F. A. Siddiqi, M. N. Beg, and P. Prakash, *J. Electroanal. Chem.*, in press.
7) W. U. Malik and F. A. Siddiqi, *Proc. Indian Acad. Sci.*, **A56**, 206 (1962).
8) W. U. Malik and F. A. Siddiqi, *J. Colloid Sci.*, **18**, 161 (1963).
9) W. U. Malik, H. Arif, and F. A. Siddiqi, *Bull. Chem. Soc., Jpn.*, **40**, 1741 (1967).
10) N. Lakshminarayanaiah and F. A. Siddiqi, *Biophys. J.*, **11**, 603, 617 (1971).
11) N. Lakshminarayanaiah and F. A. Siddiqi, *Biophys. J.*, **12**, 540 (1972).
12) N. Lakshminarayanaiah and F. A. Siddiqi in "Membrane Processes in Industry and Biomedicine," ed. by M. Bier, Plenum Publishing Corporation, New York (1971).
13) N. Lakshminarayanaiah and F. A. Siddiqi, *J. Polym. Sci.*, **8**, 2949 (1970).
14) N. Lakshminarayanaiah and F. A. Siddiqi, *Z. Phys. Chem., (Frankfurt)*, **78**, 150 (1972).
15) A. M. Liquori and C. Botre, *Ric. Sci.*, **34**, 6 (1964).
16) A. M. Liquori and C. Botre, *J. Phys. Chem.*, **71**, 3765, (1967).
17) G. Eisenman in "Membrane Transport and Metabolism," ed. by A. Kleinzeller and A. Kobyk, Academic Press, New York (1961).
18) G. Eisenman, "The Glass Electrode," Interscience Publishers, Inc., New York (1965).
19) G. Eisenman, *Biophys. J.*, **2**, 259 (1962).
20) H. Sherry in "Ion Exchange," Vol. 2, ed. by J. A. Marinsky, Dekker, New York (1968).
21) B. J. Zwolinski, H. Eyring, and C. E. Reese, *J. Phys. Chem.*, **53**, 1426 (1949).
22) S. Glasston, K. J. Laidler, and H. Eyring, "The Theory of Rate Processes," McGraw-Hill, New York (1941).
23) E. K. Shuller, C. A. Dames, and K. J. Laidler, *J. Chem. Phys.*, **17**, 860 (1949).
24) R. Schlögl, "Estofftransport durch Membranen," Steinkopff, Darmstadt (1964); *Ber. Bunsenges Phys. Chem.*, **70**, 400 (1966).
25) W. W. Kittelberger, *J. Phys. Colloid Chem.*, **53**, 392 (1949).
26) N. W. Rosenberg, J. H. B. George, and W. D. Potter, *J. Electrochem. Soc.*, **104**, 111 (1957).
27) N. Lakshminarayanaiah, *J. Electrochem. Soc.*, **116**, 338 (1969).
28) G. Schulz, *Z. Anorg. Allgem. Chem.*, **301**, 97 (1959).
29) T. Teorell, *Proc. Soc. Exptl. Biol.*, **33**, 282 (1935); *Proc. Natl. Acad. Sci., (U.S.A.)*, **21**, 152 (1935); *Progr. Biophys. Chem.*, **3**, 305 (1953).
30) K. H. Meyer and J. F. Sievers, *Helv. Chim. Acta*, **19**, 649, 605, 987 (1936).
31) K. Sollner, *J. Phys. Chem.*, **49**, 47 171 (1945); *J. Electrochem. Soc.*, **97**, 139C (1950); *Ann. N. Y. Acad. Sci.*, **57**, 177 (1953).
32) H. P. Gregor, *J. Am. Chem. Soc.*, **70**, 1293 (1948); *ibid.*, **73**, 642 (1950).
33) G. Schmid, *Z. Elektrochem.*, **54**, 424 (1950); *ibid.*, **55**, 229 (1951); *ibid.*, **56**, 181 (1952).
34) G. Schmid and H. Schwarz, *Z. Elektrochem.*, **55**, 295 (1951); *ibid.*, **55**, 684 (1951); *ibid.*, **56**, 35 (1952).
35) L. J. Mullins in "Transport and Accumulation in Biological Systems,"ed. by E. J. Harris, Butterworths Scientific Publication, London (1960).
36) H. T. Tien and H. P. Ting, *J. Colloid Interface Sci.*, **27** 702 (1968).
37) R. M. Barrer, *Trans. Faraday Soc.*, **38**, 322 (1942).
38) R. M. Barrer and G. Skirrow, *J. Polymer Sci.*, **3**, 549 (1948).
39) R. M. Barrer and H. T. Chio, in "Transport Phenomena in Polymeric Films," ed. by C. A. Kumins, Interscience, New York (1965).
40) R. M. Noyes, *J. Am. Chem. Soc.*, **84**, 513 (1962).

Studies with Parchment Supported Membranes. VIII. Determination of the Thermodynamic Effective Fixed Charge Density of Barium Phosphate Membrane by Various Methods and Evaluation of Permselectivity

Fasih A. SIDDIQI, M. Nasim BEG, Surendra P. SINGH, and Abdul HAQUE
Physical Chemistry Division, Department of Chemistry, Aligarh Muslim University, Aligarh, India
(Received December 8, 1975)

The thermodynamic effective fixed charge density, the most important parameter governing transport phenomena in membranes, was estimated by methods of TMS, Altug and Hair and the most recent one of Kobatake based on the thermodynamics of irreversible processes. Kobatake's equation has also been utilized for the evaluation of permselectivity of membranes. The two limiting forms of his equation for dilute and concentrated ranges gave identical values of θ (charge density) for barium phosphate membrane. The theoretical predictions for membrane potential by the equation were borne out quite satisfactorily by experimental results obtained with the investigated membranes.

The theories of transport of charged or uncharged particles through membranes have been treated on the basis of the following: (a) the idealized theory of TMS[1-2] and its refinements,[3] (b) the pseudo thermodynamic approach due to Scatchard[4] and treatment based on the thermodynamics of irreversible processes,[5-8] and (c) a kinetic approach based on the theory of absolute reaction rates.[9-10] In the preceeding paper[11] we showed that the parchment supported membranes can generate potentials when they are used to separate electrolyte solutions of different concentrations. This is attributed to the presence of a net charge (negative in the case of 1:1 electrolyte and positive in the case of 2:1 or 3:1 electrolyte) on the membrane probably due to the adsorption of anions or cations.[12-19] This communication deals with the evaluation of membrane fixed charge density on the basis of various approaches of TMS,[1-2] Altug and Hair[20] and Kobatake *et al.*[21-26] based on the thermodynamics of irreversible processes.

Experimental

The barium phosphate parchment supported membrane was prepared as described in part VII of this series.[11] The potential developed across the cell was measured by using a Pye Precision Vernier Potentiometer (No. 7568) at 25 °C (±0.1 °C).

S.C.E. | Solution (C_1) | Membrane | Solution (C_2) | S.C.E.
Donnan potential; Donnan potential
← Diffusion potential →

Results and Discussion

The membrane potential data obtained with the barium phosphate parchment supported membrane in various 1:1 electrolyte solutions are plotted as a function of log $(C_1+C_2)/2$ with the ratio r of concentration C_2/C_1 fixed at 10 and are shown in Fig. 1.

The total membrane potential according to the Teorell[1] and Meyer-Sievers theories[2] consists of two Donnan potential at the two solution-membrane interfaces (π_1 and π_2) and a diffusion potential ($\phi_2-\phi_1$)

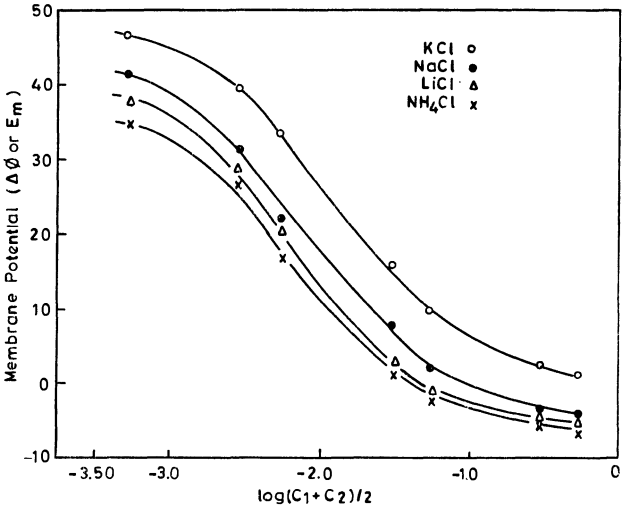

Fig. 1. Plots of observed potentials against log $(C_1+C_2)/2$ for various electrolytes with barium phosphate membrane.

arising from the unequal concentrations of the mobile ions at the two membrane surfaces. The membrane potential E_m or $\Delta\phi$ in millivolts according to TMS theory applicable to a highly idealized system is given by

$$E_m = 59.16\left[\log\frac{C_1(\sqrt{4C_2^2+\bar{X}^2}+\bar{X})}{C_2(\sqrt{4C_1^2+\bar{X}^2}+\bar{X})} + \bar{U}\log\frac{\sqrt{4C_1^2+\bar{X}^2}+\bar{X}\bar{U}}{\sqrt{4C_2^2+\bar{X}^2}+\bar{X}\bar{U}}\right] \quad (1)$$

where $$\bar{U} = \frac{\bar{u}-\bar{v}}{\bar{u}+\bar{v}}$$

$\bar{u}$ and $\bar{v}$ are the mobilities of cation and anion, respectively, in the membrane phase (the bars refer to the parameters in the membrane phase), $\bar{X}$ is the effective charge on the membrane expressed in equivalents/litre of the imbibed solution. In order to evaluate this parameter for the simple case of 1:1 electrolyte and membrane carrying a net negative charge of unity (*i.e.* $\bar{X}=1$) theoretical values for E_m were calculated as a function of C_2, the ratio r of C_2/C_1 being kept at 10 for the different values of the mobility ratio $\bar{u}/\bar{v}$ and plotted as shown in Fig. 2.

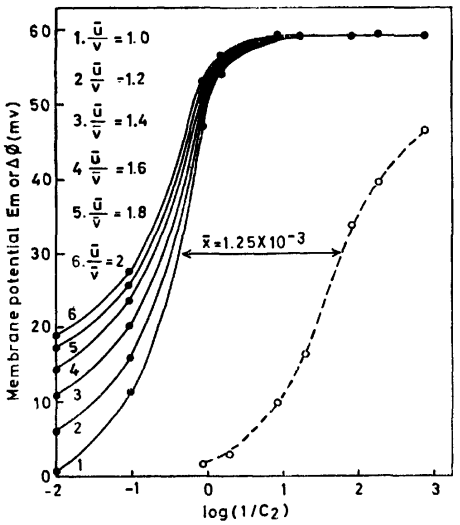

Fig. 2. Evaluation of membrane charge density x and the mobility ratio $\bar{u}/\bar{v}$ in the membrane phase. The different curves for different mobility ratio; O. The observed value E_m for barium phosphate membrane for KCl are plotted against log $(1/C_2)$.

The observed membrane potential values for barium phosphate membrane and KCl electrolyte are plotted in the same graph as a function of log $(1/C_2)$. The experimental curve shifts horizontally and runs parallel to one of the theoretical curves. The extent of this shift gives log $\bar{X}$ and the parallel theoretical curve the value $\bar{u}/\bar{v}$. The values of $\bar{X}$ and $\bar{u}/\bar{v}$ so derived for the barium phosphate membrane and various 1 : 1 electrolytes are given in Table 1.

Table 1. Values derived for the membrane parameters $\bar{X}$ and $(\bar{u}/\bar{v})$

Membrane	Parameter	KCl	NaCl	LiCl	NH_4Cl
Barium phosphate	$(\bar{X})\times 10^3$ eq/l	1.259	3.162	1.995	1.995
	$(\bar{u}/\bar{v})$	1.0	1.0	1.0	1.0

In a modification of this type of plotting, Altug and Hair[20] evaluated $\bar{X}$ on the glass membrane chosing the aqueous electrolyte solution values for $\bar{u}$ and $\bar{v}$ and calculating the values for E_m assigning different values for $\bar{X}$. The total membrane potential E_{calcd} is given by

$$E_{calcd} = (\pi_1+\pi_2) + (\phi_2-\phi_1) \tag{2}$$

where

$$\pi_1 = -\frac{RT}{F}\ln r_1 \tag{3a}$$

$$\pi_2 = \frac{RT}{F}\ln r_2 \tag{3b}$$

r_1 and r_2 are the Donnan distribution ratios, which are determined by means of the equation

$$r = \left\{1+\left(\frac{w\bar{X}}{2a}\right)^2\right\}^{1/2} - \left(\frac{w\bar{X}}{2a}\right) \tag{4}$$

where a is the external solution concentration. The diffusion potential $(\phi_2-\phi_1)$ for 1 : 1 electrolyte is given by

$$(\phi_2-\phi_1) = \frac{u-v}{u+v}\frac{RT}{F}\ln\left\{\frac{a_1(r_1u+v/r_1)}{a_2(r_2u+v/r_2)}\right\} \tag{5}$$

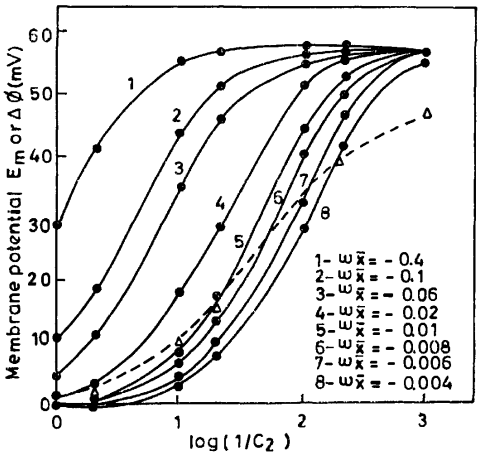

Fig. 3. Plots of membrane potential across barium phosphate membrane for KCl electrolyte of varying concentrations at fixed charge density against log $(1/C_2)$ (observed value are shown by brokenline).

where u and v are the cationic and anionic mobilities respectively, subscripts 1 and 2 referring to the solution on each side of membrane. Substitution in Eq. 2 gives

$$E_m = \frac{u-v}{u+v}\frac{RT}{F}\ln\frac{a_1\left(r_1u+\frac{v}{r_1}\right)}{a_2\left(r_2u+\frac{v}{r_2}\right)} + \frac{RT}{F}\ln\frac{r_2}{r_1} \tag{6}$$

Thus the membrane potentials are calculated by Eq. 6 for different values of fixed charge density $\bar{X}$. They are plotted in Fig. 3 as a function of the external solution concentration. The experimental values of membrane potential observed in the case of KCl for barium phosphate membrane are plotted against solution concentration. The theoretical curve which most nearly coincides with the experimental one gives the value of fixed charge density $\bar{X}$. The value of $\bar{X}$ thus calculated for KCl is given in Table 4.

Starting with the basic flow equations provided by the thermodynamics of irreversible processes Kobatake *et al.*[21] derived the following expression for the membrane potential $\Delta\phi$:

$$\Delta\phi = -\left(\frac{RT}{F}\right)\left[\frac{1}{\beta}\ln\frac{C_2}{C_1} - \left(1+\frac{1}{\beta}-2\alpha\right) \times \ln\left(\frac{C_2+\alpha\beta\theta}{C_1+\alpha\beta\theta}\right)\right] + \cdots \tag{7}$$

where

$$\alpha = \frac{l_+}{l_++l_-} \tag{8a}$$

and

$$\beta = 1 + (KF\theta/l_+). \tag{8b}$$

l_+ and l_- are the molar mobilities of $+ve$ and $-ve$ ions, respectively, defined in terms of the mass fixed frame of reference, K is a constant which is considered to depend on the viscosity of the solution and the structural details of the polymer net work of which the membrane is composed, θ is the charge density (in mol/cm^3) and F is the Faraday constant. These parameters have been assumed to be independent of salt concentration C_2 and C_1.

For the analysis of data, Eq. 7 can be used under two sets of conditions, two limiting forms thus being

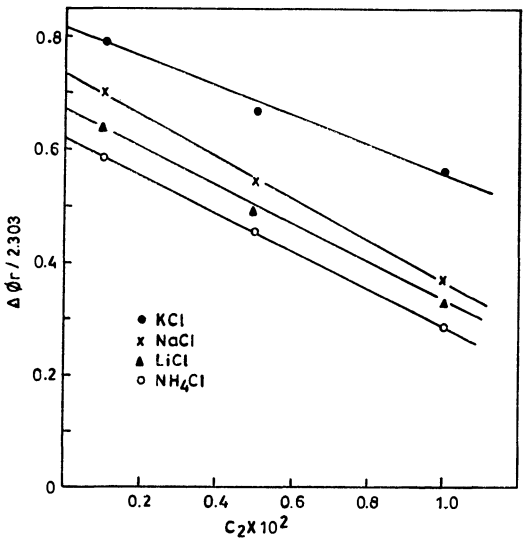

Fig. 4. $|\Delta\phi_r/2.303|$ *vs.* $C_2\times 10^2$ plots for various electrolytes with barium phosphate membrane.

obtained: (a) when concentration C_2 becomes sufficiently small, (extreme dilute range) Eq. 7 can be expanded to give

$$|\Delta\phi_r| = \frac{1}{\beta}\ln\nu - \frac{\nu-1}{\alpha\beta\nu}\left(1+\frac{1}{\beta}-2\alpha\right)\frac{C_2}{\theta} + \cdots \qquad (9)$$

where $|\Delta\phi_r|$ is the absolute value of reduced potential defined by

$$|\Delta\phi_r| = \frac{F\Delta\phi}{RT}. \qquad (10)$$

Equation 9 indicates that the value of β and a relation between α and θ can be obtained by evaluating the intercept and initial slope of a plot for $|\Delta\phi_r|$ against C_2. Figure 4 shows plots for $|\Delta\phi_r|$ *versus* C_2 in the region of very low concentration determined for four electrolytes with barium phosphate membrane. The values of the intercepts for all electrolytes were equal to $(1/\beta)\ln\nu$ from which the values of β were evaluated (Table 2).

Table 2. Values of parameters α, β, and θ for various electrolyte with barium phosphate membrane at $\nu=10$

Electrolyte	α	β	θ
KCl	0.51	1.23	0.008
NaCl	0.46	1.33	0.0071
LiCl	0.44	1.53	0.0020
NH_4Cl	0.44	1.69	0.0070

(b) It is well-known experimentally that at fixed ν the inverse of an apparent transference number, *i.e.* $t_{\bar{a}pp}$, for the co-ion species in a negatively charged membrane is proportional to the inverse of concentration C_2 in the region of high salt concentration. Here $t_{\bar{a}pp}$ is defined by the relation

$$|\Delta\phi_r| = (1-2t_{\bar{a}pp})\ln\nu \qquad (11)$$

Substituting for $\Delta\phi_r$ from Eq. 7 and expanding the resulting expression for $1/t_{\bar{a}pp}$ in powers of $1/C_2$ gives

$$\frac{1}{t_{\bar{a}pp}} = \frac{1}{(1-\alpha)} + \frac{(1+\beta-2\alpha\beta)(\nu-1)}{2(1-\alpha)^2\ln\nu}\left(\frac{\theta}{C_2}\right). \qquad (12)$$

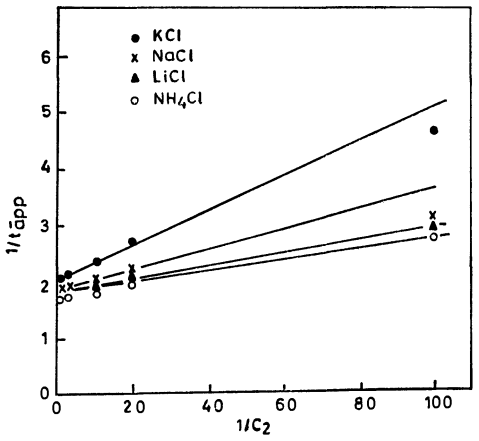

Fig. 5. $1/t_{\bar{a}pp}$ *vs.* $1/C_2$ plots for various electrolytes with barium phosphate membrane.

This indicates that intercept for a plot of $1/t_{\bar{a}pp}$ against $1/C_2$ at fixed ν allows the value of α to be determined. Plots of $1/t_{\bar{a}pp}$ against $1/C_2$ for various 1 : 1 electrolytes are shown in Fig. 5. The values of α are given in Table 2. There are two limiting cases for the evaluation of θ; (i) In the dilute range (1×10^{-3}M) using Eq. 9, the slope is given by

$$\frac{\nu-1}{\alpha\beta\nu}\left(1+\frac{1}{\beta}-2\alpha\right)\times\frac{1}{\theta}.$$

The graphical value of the slope determined from Fig. 4 is equated to the above equation, and the values of α and β are substituted. θ is thus evaluated, the value being designated as θ_d. (ii) In the concentration range (1.0 M) using Eq. 12, the slope is given by

$$\frac{(1+\beta-2\alpha\beta)(\nu-1)}{2(1-\alpha)^2\ln\nu}\times\theta.$$

The graphical value of slope determined from Fig. 5 is equated with the above expression and the values of α and β are substituted. θ is thus evaluated, the value being designated as θ_c.

In the present investigation with barium phosphate membrane, the two values of θ, *viz.* θ_c and θ_d, obtained from the opposite limits agree well with each other (Table 2) confirming the applicability of Kobatake's equation to this system. Also the value of α in Kobatake's treatment is defined by $u_+^0/(u_+^0+u_-^0)$ where u_+^0 and u_-^0 stand for the mobilities of cation and anion respectively in free solution. Thus, the value of α should be 0.5· KCl. The value of α obtained for KCl with barium phosphate membrane (Table 2) is 0.5. This implies that the assumption in the equation of Kobatake holds good for the barium phosphate membrane. It is evident that the constancy of the stoichiometric fixed charge density of the barium phosphate membrane is maintained, which is the basic assumption of the TMS theory[1-2] and its revised form given by Schlögl[3] and Kobatake *et al.*[21-26]

Comparison can be made between theoretical and experimental data and the applicability of Kobatake *et al.* equation to barium phosphate membrane can be tested by the following analytical technique suggested by Kobatake.

Equation 7 can be rewritten as

$$\frac{\nu-e^q}{e^q-1}=X \tag{13}$$

with q and X defined by

$$q=\frac{[|\Delta\phi_r|+(1-2\alpha)\ln\nu]}{1/\beta+(1-2\alpha)} \tag{14a}$$

$$X=\frac{C_2}{\alpha\beta\theta}. \tag{14b}$$

(The X is not the same as the one used in TMS or Altug and Hair method for the evaluation of charge density). Thus if Eq. 7 is valid, the values of log $(\nu-e^q)/(e^q-1)$ calculated from measured $\Delta\phi$ and the given value of ν must fall on a straight line, which has a unit slope and passes the coordinate origin when plotted against log X as shown in Fig. 6, the theoretical predictions from the Kobatake *et al.* membrane potential equation are borne out quite satisfactorily by our experimental results with barium phosphate membrane.

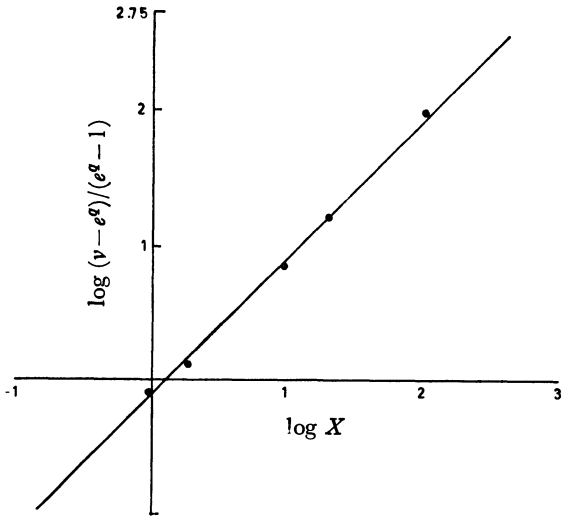

Fig. 6. Plot of log $(\nu-e^q)/(e^q-1)$ *vs.* log X for KCl with barium phosphate membrane.

A method of characterization of the membrane electrolyte system has been developed by Siddiqi and Pratap[12] for parchment supported membranes. Recently a general method of characterization applicable to any system irrespective of ion species has been developed by Kobatake.[26] Consider the present system of negatively charged membrane immersed in an electrolyte solution of average concentration C (*i.e.* $(C_1+C_2)/2$) for which Donnan equilibrium for small ions holds. The mass transference number τ_- of anions in the membrane is given by

$$\tau_-=1-\alpha\frac{(4\xi^2+1)^{1/2}+1}{(4\xi^2+1)^{1/2}+(2\alpha-1)} \tag{15}$$

where ξ and α stand for the relative concentration defined by $C/\phi X$ and $u_+^0/(u_+^0+u_-^0)$ respectively.

On the other hand the apparent transference number of anions in the membrane, *i.e.* t_{app}^-, is defined from the derived membrane potential by the Nernst equation

$$\Delta\phi=-\frac{RT}{F}(1-2t_{app}^-)\ln\frac{C_2}{C_1}. \tag{16}$$

The difference between τ_- (in Eq. 15) and t_{app}^- (in Eq. 16) was less than 2% within a wide range of salt concentration.[26] If τ_- is replaced by t_{app}^-, and C by $(C_1+C_2)/2$, Eq. 15 is applicable even when the concentration of the two sides of the membrane differs. Rearrangement of Eq. 15 leads to the following expression

$$\frac{1}{(4\xi^2+1)^{1/2}}=\frac{1-t_{app}^--\alpha}{\alpha-(2\alpha-1)(1-t_{app}^-)}\equiv P_s \tag{17}$$

where P_s is a measure of permselectivity of the membrane electrolyte system. The value of P_s takes a value between zero and unity depending on the external salt concentration for a given system of a membrane and an electrolyte pair. P_s can be calculated from the data of the membrane potential, while the left hand side of Eq. 17 is a function of the relative concentration $\xi=C/\phi X$ or $(C_1+C_2)/2\phi X$. Thus the values of the right hand side should be independent of the mobilities of ion species involved. Equation 17 implies that the plot of P_s against $(1+4\xi^2)^{-1/2}$ should give a straight line of unit slope.

For the evaluation of the effective fixed charge density, another procedure suggested by Kobatake[26] was also adopted for barium phosphate membrane. The various values of P_s were calculated by substituting the value of α (bulk) and t_{app}^- in Eq. 17 (*vide* Table 3) and then plotted against by log $(C_1+C_2)/2$. A curve was obtained as shown in Fig. 7 when the average concentration C, *i.e.* $(C_1+C_2)/2$, becomes equal to the effective fixed charge density ϕX, the value of ξ becomes equal

Table 3. Values of permselectivity P_s for various electrolytes of barium phosphate membrane at different concentrations

Electrolytes	Concentrations (M)						
	1	0.5	0.1	0.05	0.01	0.005	0.001
KCl	0.05	0.06	0.18	0.29	0.58	0.67	0.80
NaCl	0.12	0.14	0.23	0.32	0.53	0.66	0.78
LiCl	0.24	0.26	0.29	0.29	0.58	0.71	0.79
NH_4Cl	−0.08	−0.06	0.0	0.06	0.30	0.47	0.60

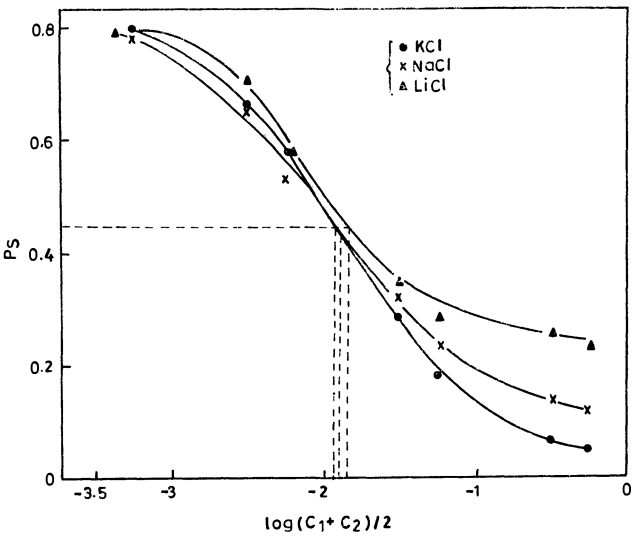

Fig. 7. Plots of P_s defined by Eq. 17 against log $(C_1+C_2)/2$ for various electrolyte with barium phosphate membrane.

Table 4. Comparison of charge density (ϕX or $W\bar{X}$ or $\bar{X}$) by different methods for KCl

Membrane	TMS $\bar{X}$	Altug and Hair $W\bar{X}$	Kobatake's Eq. 12 θ^*	Kobatake's Eq. 9 θ^*	Kobatake's P_s *vs.* log $(C_1+C_2)/2$ $\phi\bar{X}$
Barium phosphate	0.1259×10^{-2}	0.800×10^{-2}	0.8×10^{-2}	2.0×10^{-2}	1.14×10^{-2}

$$\theta^* = \text{slope}\frac{2(1-\alpha)^2 \ln \nu}{(1+\beta-2\alpha\beta)(\nu-1)\alpha} \qquad \theta^* = \frac{\nu-1(1+1/\beta-2\alpha)}{\text{slope }(\alpha\beta\nu)}$$

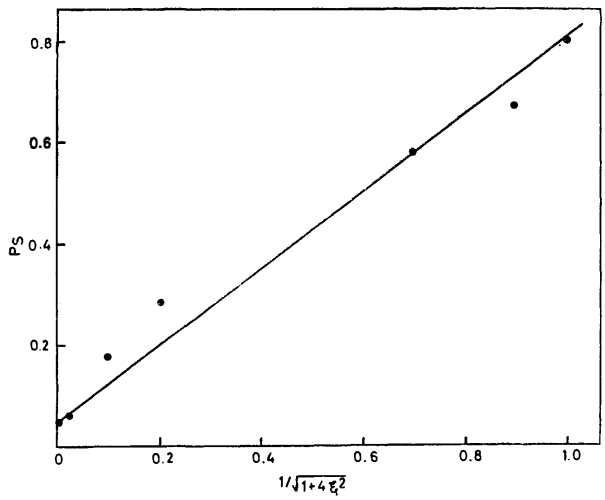

Fig. 8. Plots of P_s against $1/\sqrt{1+4\xi^2}$ for KCl electrolyte with barium phosphate membrane.

to unity, *i.e.* $C/\phi X=1$. Substituting this value of $\xi=1$ into $P_s=1/(4\xi^2+1)^{1/2}$, the value of P_s 0.448 is obtained. At this particular value of 0.448, the corresponding concentration is obtained from the curve P_s *versus* log C (Fig. 7). This value of concentration is equal to the fixed charge density (Table 4). The plot of P_s *versus* $(1+4\xi^2)^{-1/2}$ is drawn for barium phosphate membrane with KCl electrolyte is (Fig. 8). It is evident that the line passes through the origin with unit slope confirming the applicability of Kobatake's equation.

All the theories derived for the fixed charge membrane and used in these investigations give the effective fixed charge density θ or ϕX instead of X itself, when the charge density is evaluated from the data of membrane phenomena such as the membrane potential, ion permeability, electric resistance *etc.* Thus, the values of X do not differ from ϕX ($0<\phi<1$). For the evaluation of true X the titration and isotopic methods were tried. The titration method proved very inconvenient and inaccurate. The isotopic method was discarded in view of strong ionic adsorption phenomenon exhibited by these systems. Consequently the potentiometric method was used.

The authors are grateful to Professor W. Rahman, Head, Department of Chemistry for providing necessary facilities and also to Dr. N. Lakshminarayanaiah of the University of Pennsylvania U.S.A. for valuable discussions. The financial assistance from C.S.I.R. (New Delhi) India to two of us (S.P.S. and A.H.) is gratefully acknowledged.

References

1) T. Teorell, *Proc. Soc. Expt. Biol.*, **33**, 282 (1935); *Proc. Natl. Acad. Sci. U. S. A.*, **21**, 152 (1935); *Z. Elektrochem.*, **55**, 460 (1951); *Progr. Biophys. Chem.*, **3**, 305 (1953).
2) K. H. Meyer and J. F. Sievers, *Helv. Chim. Acta*, **19**, 649, 665, 987 (1936).
3) R. Schlögl, *Z. Elektrochem.*, **57**, 195 (1953); *Z. Physik. Chem. (Frankfurt)*, **1**, 305 (1954).
4) G.Scatchard, *J. Am. Chem. Soc.*, **75**, 2883 (1956).
5) G. J. Hills, P. W. M. Jacobs, and N. Lakshiminarayanaiah, *Proc. R. Soc. London, Ser. A*, **262**, 246 (1961).
6) Y. Kobatake, *J. Chem. Phys.*, **28**, 146 (1958).
7) J. W. Lorimer, E. I. Boterenbrood, and J. J. Hermans, *Discuss., Faraday Soc.*, **21**, 141 (1956).
8) A. J. Staverman, *Trans. Faraday Soc.*, **48**, 176 (1952).
9) M. Nagasawa and I. Kagawa, *Discuss. Faraday Soc.*, **21**, 52 (1956).
10) M. Nagasawa and Y. Kobatake, *J. Phys. Chem.*, **56**, 1017 (1952).
11) Fasih A. Siddiqi, Mohd Nasim Beg, Surendra P. Singh, and Abdul Haque, *Bull. Chem. Soc., Jpn.* **49**, 2858 (1976).
12) Fasih A. Siddiqi and S. Pratap, *J. Electroanal. Chem.*, **23**, 137, 147 (1969).
13) Fasih A. Siddiqi, N. Lakshminarayanaiah, and S. K. Saksena, *Z. Physik Chem. (Frankfurt)*, **72**, 298, 307 (1970).
14) Fasih A. Siddiqi, N. Lakshminarayanaiah, and M. N. Beg, *J. Polym. Sci.*, **9**, 2853, 2868 (1971).
15) Fasih A. Siddiqi, M. Nasim Beg, and Surendra P. Singh, *J. Polym. Sci.*, in press.
16) Fasih A. Siddiqi, M. Nasim Beg, and Poorna Prakash, *J. Electroanal. Chem.*, in press.
17) Wahid U. Malik and Fasih A. Siddiqi, *Proc. Indian Acad. Sci.*, **A56**, 206 (1962).
18) Wahid U. Malik and Fasih A. Siddiqi, *J. Colloid Sci.*, **18**, 161 (1963).
19) Wahid U. Malik, H. Arif, and Fasih A. Siddiqi, *Bull. Chem. Soc. Jpn.*, **40**, 1741 (1967).
20) I. Altug and M. L. Hair, *J. Phys. Chem.*, **72**, 599 (1968).
21) Y. Kobatake, N. Takeguchi, Y. Toyoshima, and H. Fujita, *J. Phys. Chem.*, **69**, 3981 (1965).
22) N. Kamo, Y. Toyoshima, and Y. Kobatake, *Kolloid-Z, Z-Polym.*, **249**, 1061 (1971).
23) N. Kamo, Y. Toyoshima, H. Nazaki, and Y. Kobatake, *Kolloid-Z, Z-Polym.*, **248**, 914 (1971).
24) Y. Toyoshima, M. Yuasa, Y. Kobatake, and H. Fujita, *Trans. Faraday Soc.*, **63**,2803, 2814 (1967).
25) M. Yuasa, Y. Kobatake, and H. Fujita, *J. Phys. Chem.* **72**, 2871 (1968).
26) N. Kamo, M. Oikawa, and Y, Kobatake, *J. Phys. Chem*, **77**, 92 (1973).

Dielectric Relaxation in Some Substituted Benzaldehydes in Benzene at Different Temperatures

Buta SINGH and J. K. VIJ

Department of Physics, Punjabi University, Patiala 147002, Punjab, India

(Received February 20, 1976)

Measurements of the relative permittivity at 1 MHz and 9.27 GHz, and of the refractive index for the sodium-D line have been made for (A) *o*-nitrobenzaldehyde, (B) *m*-nitrobenzaldehyde, (C) *m*-chlorobenzaldehyde, and (D) *p*-chlorobenzaldehyde, at 15, 25, 35, and 45 °C in dilute solutions of benzene. The dielectric relaxation times $\tau_{(1)}$ and $\tau_{(2)}$ have been calculated using the Higasi, Koga, and Nakamura method. The results suggest that the relaxation time for the overall rotation decreases at a greater rate than the one for the internal rotation. The thermodynamic energy parameters have been calculated. The results show that the freedom of rotation of the –CHO group increases around the C_{alip}–C_{arom} bond as an electronegative substituent moves from the *o*- to *m*- to *p*- positions.

The present work is an extension of the study previously undertaken on the dielectric relaxation mechanism in some substituted benzaldehydes[1] to include temperature as another variable. Since our previous communication, we have come across the results reported by Mountain and Walker[2] on benzaldehyde, *p*-fluoro-, *p*-chloro-, *p*-bromo-, and *p*-nitro-benzaldehydes in dilute solutions of *p*-xylene at a single temperature and *p*-chlorobenzaldehyde at five temperatures. On the whole, our results and some of the inferences drawn agree with them, though we studied the materials only at a single frequency in the dispersion region. This provides a good test for the Higasi, Koga, and Nakamura method[3,4] of analysing the relative permittivity data. Our results[1] showed that benzaldehydes interact with the benzene molecule through the π-electrons from the benzene molecule. Mountain and Walker's results[2] of benzaldehydes in *p*-xylene show a similar interaction. They have postulated it to be a weak hyderogen bonding of the type $-\overset{\overset{O}{\|}}{C}-H\cdots\pi$. On the other hand, our results,[1] on the study of the benzaldehyde–dioxane systems, indicated that the hyderogen bonding of the type $-\overset{\overset{O}{\|}}{C}-H\cdots O$, if at all, there is fairly weak. There is no confirmation to this fact as yet.

The temperature is introduced as another variable in making a comparative study of the benzaldehydes and their interactions with benzene.

Experimental and Results

The materials are of the same purity standard as previously discussed.[1] The relative permittivity and the refractive index measurements have been made by the same techniques. However, the dielectric cell used for the measurements at 1 MHz was a two terminal one with an air capacitance of 17.9 pF. The cell was calibrated

TABLE 1. VALUES OF a_0, a', a'', $a_{\infty 1}$, $a_{\infty 2}$, $\tau_{(1)}$, $\tau_{(2)}$, AND LIT. VALUES[2] OF τ_1 AND τ_2, AND $\mu_{int.,\,rot.}$, FOR THE SUBSTANCES A—D AT DIFFERENT TEMPERATURES

T(K)	a_0	a'	a''	$a_{\infty 1}$	$a_{\infty 2}$	$\tau_{(1)}$	$\tau_{(2)}$	τ_1 (lit)	τ_2 (lit)	$\mu_{int.,\,rot.}$
						ps				(D)
					o-Nitrobenzaldehyde					
288	15.70	6.75	5.54	0.297	3.32	14.7	27.7	—	—	1.99
298	14.75	7.21	5.40	0.315	3.35	13.5	24.0	—	—	2.04
308	14.10	7.33	5.18	0.312	3.36	12.7	22.4	—	—	2.10
318	13.05	7.45	4.88	0.303	3.20	11.7	19.7	—	—	2.10
					m-Nitrobenzaldehyde					
288	9.90	4.27	3.37	0.265	2.26	14.5	28.7	—	—	1.61
298	9.25	4.29	3.31	0.279	2.08	14.2	25.7	—	—	1.57
308	8.77	4.15	3.26	0.283	1.85	14.5	24.3	—	—	1.48
318	8.28	4.39	3.10	0.283	1.92	12.9	21.5	—	—	1.59
					m-Chlorobenzaldehyde					
288	6.43	3.65	2.46	0.254	1.47	12.4	19.4	—	—	1.21
298	6.12	3.72	2.37	0.241	1.38	11.4	17.4	—	—	1.21
308	5.81	3.65	2.26	0.254	1.29	11.4	16.4	—	—	1.19
318	5.33	3.60	2.17	0.260	0.88	11.1	13.7	—	—	0.95
					p-Chlorobenzaldehyde					
288	3.95	1.83	1.02	0.276	1.34	11.3	35.7	36.0	13.0	1.14
298	3.66	1.87	0.95	0.270	1.37	10.2	32.3	33.0	10.8	1.18
308	3.47	1.90	0.94	0.263	1.34	9.9	28.7	18.0 (40 °C)	9.0 (40 °C)	1.21
318	3.25	1.85	0.90	0.256	1.32	9.9	26.7	—	—	1.22

Table 2. Values of $\tau_{(2)}$, ΔF_ε, ΔF_ε (lit values[2]), ΔF_η, ΔH_ε, ΔH_η, ΔS_ε, ΔS_η, and $x(=\Delta H_\varepsilon/\Delta H_\eta)$ for the substances A—D at different temperatures

T(K)	$\tau_{(2)}$ (ps)	ΔF_ε	ΔF_ε (lit, values)	ΔF_η	ΔH_ε	ΔH_η	ΔS_ε	ΔS_η	$x=\Delta H_\varepsilon/\Delta H_\eta$
		kcal/mol					cal/deg mol		
				o-Nitrobenzaldehyde					
288	27.7	2.93	—	2.89			−5.00	−1.32	
298	24.0	2.97	—	2.91	1.49	2.51	−4.97	−1.34	0.59
308	22.4	3.05	—	2.93			−5.06	−1.36	
318	19.7	3.08	—	2.95			−5.00	−1.38	
				m-Nitrobepzaldehyde					
288	28.7	2.95	—	2.89			−5.80	−1.32	
298	25.7	3.01	—	2.91	1.28	2.51	−5.81	−1.34	0.51
308	24.3	3.10	—	2.93			−5.91	−1.36	
318	21.5	3.14	—	2.95			−5.85	−1.38	
				m-Chlorobenzaldehyde					
288	19.4	2.73	—	2.89			−5.14	−1.32	
298	17.4	2.78	—	2.91	1.25	2.51	−5.13	−1.34	0.50
308	16.4	2.85	—	2.93			−5.23	−1.36	
318	13.7	2.85	—	2.95			−4.94	−1.38	
				p-Chlorobenzaldehyde					
288	35.7	3.08	3.08	2.89			−6.60	−1.32	
298	32.3	3.15	3.15	2.91	1.18	2.51	−6.61	−1.34	0.47
308	28.7	3.20	2.97 (40°C)	2.93			−6.56	−1.36	
318	26.7	3.28	—	2.95			−6.60	−1.38	

Literature values of ΔF_ε for *p*-chlorobenzaldehyde are calculated from the values of the relaxation time for overall rotation (τ_1) reported by Mountain and Walker.[2]

for each temperature. The values of the slopes are calculated from the experimental plots of the data *versus* weight fraction. The dielectric relaxation times are calculated using the same techniques.[1]

Values of the parameters a_0, a', a'', $a_{\infty 1}$, $a_{\infty 2}$, $\tau_{(1)}$, and $\tau_{(2)}$ (defined already[1]), for all the four materials at each temperature, are given in Table 1. The table also includes the literatures values[2] of τ_1 and τ_2 for *p*-chlorobenzaldehyde in *p*-xylene as well as value of the dipole moment for internal rotation ($\mu_{\text{int., rot.}}$) which was calculated in the same way as described earlier[1] (Table 1).

The thermodynamic energy parameters are calculated using Eyring's equation[5,6] for the relaxation time $\tau_{(2)}$ since it has been shown[4] to be nearly equal to the relaxation time for overall rotation (τ_1). These values are given in Table 2.

Discussion

Comparing the present values of the dielectric realaxtion times $\tau_{(2)}$ with those of τ_1 given by Mountain and Walker,[2] for *p*-chlorobenzaldehyde in *p*-xylene, and also, keeping in view the accuracy of determination and a slight viscosity difference betweem the two solvents, we find that the agree is reasonably good. This establishes at least the fact that benzene and *p*-xylene have similar characteristics in so far as the interactions with benzaldehydes are concerned. Values of $\tau_{(1)}$ and $\tau_{(2)}$ for each material at a particular temperature are quite distinct from each other. This shows that these molecules possess more than one dielectric relaxation time.

A comparison of the enthalpy of activation (ΔH_ε) for the isomers shows an interesting aspect. The energy barrier for the dielectric relaxation mechanism decreases from *o*- to *m*- and from *m*- to *p*- isomers both for the chloro- and nitro-benzaldehydes.

Since the relaxation time involved is $\tau_{(2)}$, the energy barrier is a combination of barrier to the molecular and to the internal rotations. However, if one assumes, at the worst, that the barrier to the molecular rotation remains the same for the different isomers of a substituted benzaldehyde, the barrier to the internal rotation decreases in the order, *o*- to *m*- and from *m*- to *p*- substituents. This shows indirectly that the freedom of the –CHO group along the C_{alip}–C_{arom} bond increases when these substituents move from the *o*- to *p*- position through *m*- position. Mountain and Walker[2] have explained it in terms of inductive and mesomeric effects of the substituents on the electron density of the C_{alip}–C_{arom} bond. This concept successfully explain why the aldehyde group, when present alone, dose not rotate around the C_{alip}–C_{arom} bond.

Another interesting aspect of the results is that $\Delta H_\varepsilon < \Delta H_\eta$. The ratio $\Delta H_\varepsilon/\Delta H_\eta(=x)$ for the different materials is listed in Table 2. The values of this factor is 0.59 for *o*-nitrobenzaldehyde whereas it is $\approx$0.50 for the other materials. According to the classification of polar liquids, given by Krishnaji and Mansingh,[7] substances for which $x>0.55$ do not show solid rotator phase and those for which $x<0.45$ show such a phase. Since the values of x for the three materials B, C, and D are between the two limits, there is some possibility that these materials, particularly *p*-chlorobenzaldehyde, may show a solid rotator phase.

Values of $\mu_{int.,\,rot.}$ for a particular material remain constant with temperature within experimental error. This indicates that the internal rotations of the –CHO group and the nature of its interactions with the benzene molecule are independent of temperature.

The authors are thankful to Prof. B. S. Sood, Head of the Physics Department, for his valueable suggestions and interest in this work. They are also grateful to Dr. K. K. Srivastava of the Physics Department, Panjab University Chandigarh, for the fruitful discussions during the course of research.

References

1) B. Singh and J. K. Vij, *Bull. Chem. Soc. Jpn.*, **48**, 2551 (1975).
2) P. F. Mountain and S. Walker, *Can J. Chem.*, **52**, 3229 (1974).
3) K. Higasi, Y. Koga, and M. Nakamura, *Bull. Chem. Soc. Jpn.*, **44**, 988 (1971).
4) J. K. Vij, I. Krishan, and K. K. Srivastava, *Bull. Chem. Soc. Jpn.*, **46**, 17 (1973).
5) H. Eyring, *J. Chem. Phys.*, **4**, 283 (1936).
6) S. Glasstone, K. J. Laidler, and H. Eyring, "The Thory of Rate Process," McGraw-Hill, N. Y. (1941), pp. 544—551.
7) Krishnaji and Mansingh, *J. Chem. Phys.*, **44**, 1590 (1966).

Studies on Some Mixed Schiff's Base Complexes. V.

Rakesh Kumar KOHLI and P. K. BHATTACHARYA
Department of Chemistry, M. S. University, Baroda, 390002, India
(Received November 18, 1975)

As regards the preparation and characterization of some new mixed complexes of the type MLL′ where M= Cu(II), Ni(II); L=salicylaldimine and L′=(*o*-hydroxybenzyl)(ethylideneamine) or *o*-hydroxydiphenylenethyleneamine or their derivatives, we have carried out the preparation of a few similar types of complexes where L′=2-hydroxy-1-naphthylmethyleneamine. The mixed imine Schiff's base complexes have been prepared by treating the metal ammine complex with an equivalent amount of salicylaldehyde and 2-hydroxy-1-naphthaldehyde. Amine exchange reactions were also been carried out by treatment of mixed imine Schiff's base complex with ethylenediamine(en) or propylenediamine(pn). The complexes of new Schiff's base were formed where diamine have salicylaldehyde condensed at one end and 2-hydroxy-1-naphthaldehyde at the other end. The complexes have been characterized by elemental analysis, TLC analysis, conductance measurements, magnetic measurements, and spectral analysis.

The preparation of the compound of the type ML_2 where L=salicylaldehyde and their reactions with ammonia leading to the formation of the Schiff's base complexes have been reported.[1-5] Reactions of bis-salicylaldehyde complexes with ethylenediamine[6] and aniline[7] have also been reported. Transamination and transamidation reactions have been performed on the Schiff's base complexes.[3-8] The study of reactions of amines with bis 2-hydroxy-acetophenone or bis-2-hydroxy benzophenone complexes of Cu(II) and Ni(II) have also been prepared.[9-10] The possibility of the formation of Mixed-Schiff's base complexes has been indicated by Chakravorty and Holm,[11] on the basis of NMR studies. However, such complexes were not been isolated in solid state. Schiff's base formation reaction of mixed ligand complexes of the type MLL′, where L= salicylaldineamine and 1(*o*-hydroxyphenyl)ethylideneamine[12] or *o*-hydroxydiphenylmethyleneamine and their derivatives have been reported. The present paper deals with the preparation and reactions of a series of mixed ligand complexes of general formula MLL′ where M=Cu(II) or Ni(II), L=salicylideneamine, L′=2-hydroxy-1-naphthyleneamine.

The mixed Schiff's base complex was prepared by treating the metal ammine complex with one equivalent of salicylaldehyde and another of 2-hydroxy-1-naphthaldehyde.

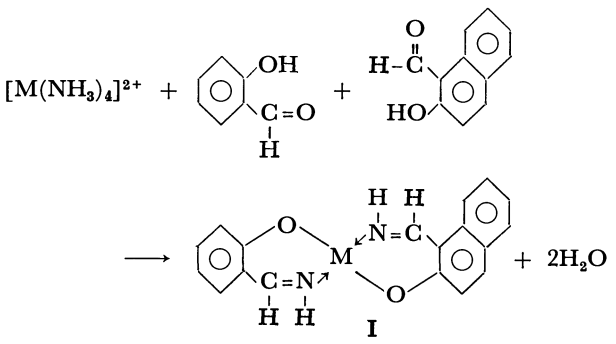

M=Cu(II) or Ni(II)

Complex(I) was treated with ethylenediamine(en) or propylenediamine(pn), leading to the formation of new Schiff's base complexes with the diamine condensed to one end with salicylaldehyde and at the other end with 2-hydroxy-1-naphthaldehyde.

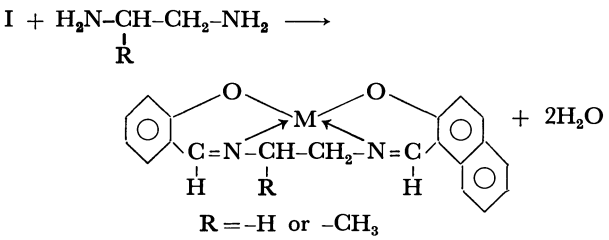

R=–H or –CH_3
M=Cu(II) or Ni(II)

Similar reactions were also carried out with methyl and ethyl amine and the following type of mixed complexes were obtained.

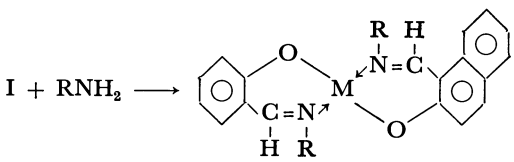

R=–CH_3 or –C_2H_5
M=Cu(II) or Ni(II)

When the en Schiff's base is treated with pn, en is slowly replaced by pn, as shown in the following equn.

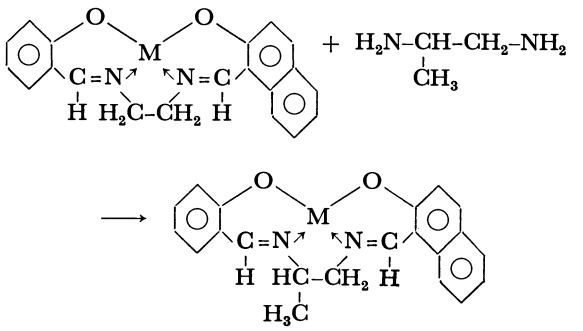

M=Cu(II) or Ni(II)

Experimental

Material. Ligand of AR quality and nickel nitrate and cupric chloride of Analar grade were used.

Preparation of Amine Schiff's Base Complex. (Salicylaldeneaminato)(2-hydroxy-1-naphthylmethyleneaminato)Cu(II) or Ni(II): To the metal chloride solution was added an excess of ammonia till the hydroxide formed dissolved resulting in the formation of metal ammine complex. To this was added one equi-

Structure of Cu(II) Complexes. All the Cu(II) complexes are paramagnetic showing the presence of one unpaired electron. The values of μ expected for one unpaired electron is 1.73 B.M., the slightly higher value obtained for the present complexes can be attributed to spin-orbit coupling.[13] The visible spectra show a broad band at ≈590 or ≈520 nm; and agree with the square planar geometry. The Cu(II) imine Schiff's base complex shows a band around ≈550 nm (ε=123) and the en and pn Schiff's base complexes exhibit at ≈560 (ε=410) and at ≈550 (ε=478), respectively. The spectrum of complex {*N*,*N*'-ethylene(salicylideneaminato-2-hydroxy-1-naphthylmethyleneaminato)}Cu(II) (No. 7) was compared with that of (bis-ethylene salicylideneaminato)Cu(II) and (bis-ethylene 2-hydroxy-1-naphthylmethylenediaminato)Cu(II) complexes. The complex (No. 7) shows one peak falling between the two bis compounds. This indicates the mixed nature of these complexes.

Structure of Ni(II) Complexes. All the complexes were recrystallized until constant magnetic susceptibility was obtained. They exhibit some paramagnetism. Anomalous magnetic behavior of Ni(II) Schiff's base complexes were studied and interpreted in detail.[14,15] The visible spectra of the imine Schiff's base complex in chloroform solution shows a shoulder at ≈550 nm with (ε=274). A similar spectrum was obtained in the case of en and pn Schiff's base complexes, the shoulder shifting to ≈530 nm and ≈550 nm with (ε=418) and (ε=343), respectively. The absence of bands beyond 600 nm confirms square geometry for the complexes.

In the IR spectra of all the compounds bands in the range ≈3400 cm^{-1} are absent indicating that O–H hydrogen of the aldehyde or the Schiff's base get dissociated after complexation. In the spectra of Cu(II) and Ni(II) complexes(I) a band at 1600 cm^{-1} corresponding to C=N stretch appears. There is a strong band at ≈3200 cm^{-1} corresponding to N=H stretching frequency. This is absent in the en and pn diamine Schiff's base and also in methyl and ethyl amines compounds showing the absence of free =NH group.

The authors wish to express their sincere thanks to Prof. S. M. Sethna, Head, Department of Chemistry, M. S. University of Baroda, for providing all the laboratory facilities. Thanks are also due to Malti-Chem Research Centre, Nandesari, Baroda, for the recording of the IR spectra of the complexes. One of the authors (R.K.K.) is grateful to U.G.C., New Delhi for awarding the Junior Research Fellowship.

References

1) H. Schiff., *Ann.*, **150**, 193 (1869).
2) C. Ettling, *Ann.*, **35**, 241 (1840).
3) P. Pfeffier, *Angew. Chem.*, **53**, 93 (1940).
4) P. Pfeffier, E. Buchholz, and O. Bouer, *J. Pract. Chem.*, **129**, 163 (1931).
5) R. H. Holm, G. W. Everett, and A. Chakravorty, *Prog. Inorg. Chem.*, **7**, 83 (1966).
6) B. O. West in "New Pathways in Inorganic Chemistry," ed. by Ebsworth and Sharpe, Cambridge University Press (1968), p. 309.
7) B. M. Higson, D. A. Lewton, and E. D. Makenzie, *J. Chem. Soc., Dalton Trans.*, **1974**, 1960.
8) H. S. Water and A. E. Frost, *J. Am. Chem. Soc.*, **82**, 85 (1960).
9) B. T. Thaker and P. K. Bhattacharya, *J. Ind. Chem. Soc.*, **52**, 454 (1975).
10) V. B. Mohan Kumar and P. K. Bhattacharya, *Indian J. Chem.*, **13**, 928 (1975).
11) A. Chakravorty and R. H. Holm, *J. Am. Chem. Soc.*, **86**, 3999 (1964).
12) B. T. Thaker and P. K. Bhattacharya, *J. Inorg. Nucl. Chem.*, **37**, 615 (1975).
13) A. Earnshaw, "Introduction to Magnetochemistry," Academic Press, New York (1969), p. 35.
14) R. H. Holm and M. J. O'Cooner, *Prog. Inorg. Chem.*, **14**, 252 (1971).
15) L. Sacconi, *Transition Metal Chem.*, **4**, 269 (1968).

BULLETIN OF THE CHEMICAL SOCIETY OF JAPAN, VOL. 49 (10), 2875—2876 (1976)

A Study of Self Oscillatory Chemical Reaction of Gallic Acid and Potassium Bromate System

J. Sreekantha Babu, M. M. Bokadia, and K. Srinivasulu
School of Studies in Chemistry, Vikram University, Ujjain 456010, India

(Received September 5, 1975)

Synopsis. The oscillatory phenomenon during oxidation of gallic acid with potassium bromate, catalyzed by cerium ion in acid medium with stirring was investigated. The cross section of a three dimensional graph for the regions where the oscillatory behavior can be observed is given. Effect of Ag^+ and Br^- on the oscillatory behavior was studied.

Oscillation in the concentrations of Br^- and Ce^{4+}/Ce^{3+} during the oxidation of malonic acid by bromate ion with cerium ion as a catalyst was studied by different workers.[1-7] Similar oscillatory phenomenon was observed in gallic acid-bromate system catalyzed by cerium ions.

Experimental

A freshly recrystallized gallic acid (GA)(Riedel), 1,10-phenanthroline ferrous sulphate complex (ferroin) solution (0.025 M)(BDH) and other BDH AR grade chemicals were used.

A requisite quantity of gallic acid was dissolved in distilled water, to which a ceric solution with sulphuric acid was added. The reaction was studied at constant temperature and with constant moderate stirring on addition of a requisite volume of bromate solution and a drop of ferroin indicator, the total volume being kept 10 ml. The color change from red to green, *i.e.*, Ce(III) to Ce(IV), takes place abruptly. The oscillations visually observed are reporducible within the limits of experimental error.

Results and Discussion

Important parameters for the occurrence of oscillations in the system are bromate, gallic acid and cerium ion concentrations. A minimum concentration of acid which depends upon the concentration of other reactants, is required to start the reaction. When the reactant concentrations are kept constant, the frequency of oscillations (n) increases, and the total time of oscillation (T) decreases with increasing acid concentration. A large number of oscillations were observed at an acid concentration of 2.57 N.

Effect of Individual Reactant. (Other Variables Being Kept Constant).

(a) Gallic Acid Variation.

($[BrO_3^-]=0.1$ M, $[Ce(IV)]=0.003$ M, [acid]=2.57 N). The total number of oscillations (N) is high at concentration of 0.03 M, and decreases when the concentration becomes greater or smaller than this value. The value of n decreases and T increases with a decrease in gallic acid concentration.

(b) Bromate Variation.

($[GA]=0.04$ M, $[Ce(IV)]=0.001$ M, [acid]=2.57 N). The value of N is maximum for $[BrO_3^-]=0.1$ M. Values of n and I (induction period) decrease while T increases when $[BrO_3^-]$ increases.

(c) Cerium Ion Variation.

($[GA]=0.04$ M, $[BrO_3^-]=0.1$ M, [acid]=2.57 N). In the concentration range 3.0×10^{-4}—1.0×10^{-4} M, a great number of oscillations were observed and outside the range the value of N decreased. With increase and decrease in concentrations of total cerium ion beyond the mentioned range, the n value increased and decreased respectively. The system showed 80 oscillations in 150 min before the oscillation ceased, when $[GA]=0.045$ M, $[BrO_3^-]=0.1$ M, $[Ce(IV)]=3.0\times10^{-4}$ M and [acid]=2.57 N.

The oscillatory cycle can be divided into two processes, the former is a trigger process and the latter is a recovery.

$$Ce^{3+} \xrightarrow[H^+]{BrO_3^-} Ce^{4+} \quad (1)$$

$$Ce^{4+} \xrightarrow{GA} Ce^{3+} \quad (2)$$

The products of bromate reduction in the trigger process (1) may brominate gallic acid. Bromide ion is formed as a result of decomposition of gallic acid-bromine derivatives induced by ceric ion oxidation (2). It was verified experimentally that bromide ion is a strong inhibitor of trigger process. Addition of Br^- inhibits the trigger process, resulting in the dampening of oscillation. At 0.005 M of $[Br^-]$, inhibition of oscillatory behavior was observed. Addition of Ag^+ which removes Br^- also dampens down and at 0.1M concentration inhibits the oscillation. This indicates that $[Br^-]$ plays an important role in the oscillatory behavior[7] (Fig. 1).

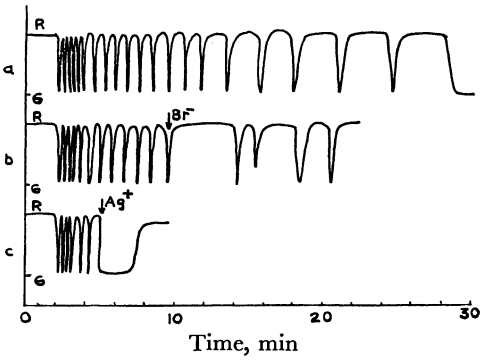

Fig. 1. Oscillatory curve with respect to time. (As indicated by ferroin.) R- Red and G- Green representing Ce(III) and Ce(IV) respectively.
(a) $[GA]=0.0425$ M, $[BrO_3^-]=0.1$ M, $[Ce(IV)]=0.0005$ M and [acid]=2.57 N.
(b) Effect of bromide ion. Concentrations similar as in (a) and [KBr]=0.05 M.
(c) Effect of silver ion. Concentrations similar as in (a) and $[AgNO_3]=0.05$ M.
Arrow indicates the point of addtion.

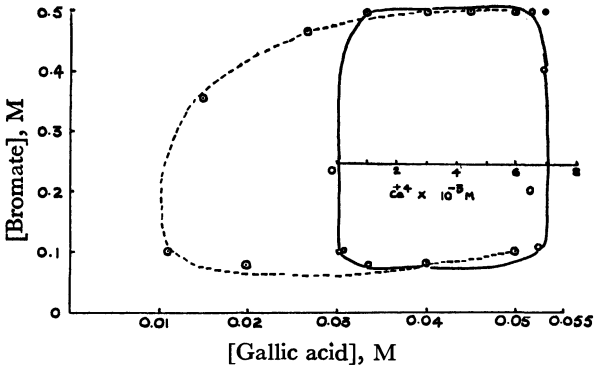

Fig. 2. Cross sections of three dimensional plot for the boundary region where oscillations are observed. Temperature 35 °C. [Sulfuric acid] 2.57 N. [GA]—X axis, $[BrO_3^-]$—Y axis and [Ce(IV)]—Z axis.
------ represents the curve of [GA] *vs.* $[BrO_3^-]$.
—— represents the curve of [Ce(IV)] *vs.* $[BrO_3^-]$ when [GA]=0.04 M.

Oscillations could be observed in the concentration range of reactants studied (Fig. 2). The boundary conditions of gallic acid, bromate and cerium ion concentrations were determined keeping temperature, acidity and stirring constant. The upper limit of [GA] could not be fixed due to its solubility limitation. As the concentrations of reactants approach the boundary conditions, the oscillations tend to cease and beyond it, they are not significant.

The authors are thankful to the Council of Scientific and Industrial Research, India, for the financial assistance.

References

1) B. P. Belousov, *Sb. ref. radiants. med. za.* 1958, Medgiz, Moscow (1959).
2) A. M. Zhabotinskii, *Biofizika*, **9**, 306 (1964).
3) A. M. Zhabotinskii, *Dokl. Akad. Nauk SSSR*, **157**, 392 (1964).
4) H. Degn, *Nature*, **213**, 589 (1967).
5) V. A. Vavilin, A. M. Zhabotinskii, and A. N. Zaikin, *Russ. J. Phys. Chem.*, **42**, 1649 (1968).
6) G. J. Kasperek and T. C. Bruice, *Inorg. Chem.*, **10**, 382 (1971).
7) H. G. Busse, *Nature Phys. Sci.*, **233**, 137 (1971).

BULLETIN OF THE CHEMICAL SOCIETY OF JAPAN, VOL. 49 (10), 2877—2878 (1976)

Some New β-Diketone Complexes of Ruthenium(III) with Triphenylphosphine and Triphenylarsine

K. NATARAJAN and Umesh AGARWALA

Department of Chemistry, Indian Institute of Technology, Kanpur 208016, U.P., India

(Received April 7, 1976)

Synopsis. The syntheses of some new β-diketone complexes of Ru(III) with triphenylphosphine and triphenylarsine have been described. Their spectral (IR and visible) and magnetic properties have been reported. Some of them show unusual magnetic moment.

Mixed complexes of ruthenium(II) with triphenylphosphine and β-diketones have been reported in the literature,[1] but no work has so far been done on similar complexes of ruthenium(III).

In this communication, we report the preparations of the ruthenium(III) complexes of the type $[RuX_2L_2(bdk)]$ (X=Cl, Br; L=PPh_3, $AsPh_3$; bdk=acetylacetonate, dibenzoylmethanate, benzoylacetonate) starting from $[RuCl_3(AsPh_3)_3]$,[2] $[RuBr_3(AsPh_3)_3]$,[3] $[RuCl_3(PPh_3)_3]$,[4] and $[RuBr_3(PPh_3)_2(MeOH)]$.[5] Their spectral and magnetic properties have also been studied.

The general procedure to prepare these complexes is as follows:

A solution of 0.4 g of $[RuX_3L_3]$ or $[RuX_3L_2(MeOH)]$ in 20 ml of benzene or dichloromethane was mixed with another solution of β-diketone (0.2 g) in 5 ml of ethyl alcohol. It was heated under reflux for 3—5 h whereby the desired complex was separated out on concentrating the refluxing solution. The colour in the case of chloro complexes was green while that of bromo ones, brown. All the compounds were recrystallized from dichloromethane–methanol mixture.

Magnetic susceptibilities of the complexes were determined with a Gouy balance. The electronic spectra of the complexes were recorded in chloroform solution with a Cary-14 recording spectrophotometer in the range of 1000—300 nm. The infrared spectra of the complexes were taken with the help of a Perkin-Elmer 521 grating infrared spectrophotometer in the range of 4000—300 cm^{-1} using KBr pellets of the samples. The major IR bands are given in Table 1.

TABLE 1.

Sl. No.	Complex	Mp °C	Magnetic moment B.M.	IR bands cm^{-1}
1	$RuCl_2(acac)(AsPh_3)_2$	267	2.54	1530, 1565
2	$RuCl_2(dbm)(AsPh_3)_2$	281	2.53	1540, 1610
3	$RuCl_2(ba)(AsPh_3)_2$	255	2.10	1530, 1570, 1610
4	$RuCl_2(acac)(PPh_3)_2$	215	2.00	1530, 1570
5	$RuCl_2(dbm)(PPh_3)_2$	230	2.71	1525, 1540, 1600
6	$RuCl_2(ba)(PPh_3)_2$	214	2.31	1540, 1560
7	$RuBr_2(acac)(AsPh_3)_2$	290	2.03	1530, 1570
8	$RuBr_2(dbm)(AsPh_3)_2$	267	2.07	1530, 1570
9	$RuBr_2(ba)(AsPh_3)_2$	231—233	2.02	1530, 1570, 1605
10	$RuBr_2(acac)(PPh_3)_2$	224	1.80	1545, 1575
11	$RuBr_2(dbm)(PPh_3)_2$	222	2.00	1535, 1550, 1610
12	$RuBr_2(ba)(PPh_3)_2$	206	1.91	1535, 1560, 1600

acac=acetylacetonate; dbm=dibenzoylmethanate; ba=benzoylacetonate.

The analytical data of carbon, hydrogen, ruthenium and halide ion of the complexes confirm the general formula $[RuX_2L_2(bdk)]$.

The IR spectra of the complexes showed all the bands due to triphenylphosphine or triphenylarsine. Besides these, two or three bands were also present in the region 1525—1610 cm^{-1}. These may be assigned to the characteristic bands of the coordinated β-diketones arising due to the normal coordinates having contributions from ν(C=O) and ν(C=C).[6,7] The molecular weight determination in bromoform solution of the complexes confirm monomeric structure for all the compounds.

The electronic spectra of all the complexes in chloroform solution showed two to three bands in the region 600—350 nm. The bands are very much characteristic of the octahedral surrounding of the ligand molecules around ruthenium(III) ions.[8-10] Generally in the visible region ruthenium(III) ion show charge transfer bands around 400 nm.[11,12] It is also clear by the shift in the positions of both the bands in the bromo complexes towards lower wavelength side because of the greater reducing power of Br than Cl.[12]

The values of the magnetic moments were a little abnormal (see Table 1). Since ruthenium(III) belongs to d^5 system, having one unpaired electron, it should normally show a value of the magnetic moment around 2.00 B. M. In some of the cases of β-diketone derivatives of ruthenium(III), the values of magnetic moment are found to be in the range of 2.3—2.7 B. M. This high value can not be explained by the presence of one unpaired electron and hence a spin-free system must be invoked.[13] In order to explain this, further studies on low temperature magnetic measurements and ESR are under progress. Preliminary ESR studies showed the presence of two lines, indicating distorted octahedral nature of the complexes.[14]

References

1) J. D. Gilbert and G. Wilkinson, *J. Chem. Soc., A*, **1969**, 1749.

2) R. K. Poddar, I. P. Khullar, and U. Agarwala, *Inorg. Nucl. Chem. Lett.*, **10**, 221 (1974).

3) K. Natarajan, R. K. Poddar, and U. Agarwala, *J. Inorg. Nucl. Chem.*, in press.

4) J. Chatt, G. J. Leigh, D. M. P. Mingos, and R. J. Paske, *J. Chem. Soc., A*, **1968**, 2636.

5) T. A. Stephenson and G. Wilkinson, *J. Inorg. Nucl. Chem.*, **28**, 945 (1966).

6) K. Nakamoto, "Infrared Spectra of Inorganic and Coordination Compounds," John Wiley & Sons, New York, N. Y.

(1964).
7) David M. Adams, "Metal-Ligand and Related Vibrations," New York, St. Martins Press (1968).
8) C. J. Ballhausen, "Introduction to Ligand Field Theory," McGraw Hill Book Co., New York (1962).
9) A. B. P. Lever, "Inorganic Electronic Spectroscopy," Elsevier Publishing Co., Amsterdam, London, New York (1968).
10) K. Natarajan, R. K. Poddar, and U. Agarwala, *J. Inorg. Nucl. Chem.*, **38**, 249 (1976).
11) A. E. Martell, "Coordination Chemistry," Vol. 1, Van Nostrand Reinhold, New York, N. Y. (1971).
12) B. N. Figgis, "Introduction to Ligand Field Theory," Interscience Publishers, New York, N. Y. (1966).
13) T. A. Stephenson and G. Wilkinson, *J. Inorg. Nucl. Chem.*, **28**, 2285 (1966).
14) J. Chatt, G. J. Leigh, and D.M.P. Mingos, *J. Chem. Soc., A*, **1969**, 1674.

BULLETIN OF THE CHEMICAL SOCIETY OF JAPAN, VOL. 49 (10), 2879—2880 (1976)

Thermogravimetric Analysis of Tetraalkylammonium Haloborates. I.

S. U. SHEIKH

Department of Chemistry, University of Islamabad, Islamabad, Pakistan

(Received April 28, 1976)

Synopsis. Thermogravimetric analysis of tetraalkylammonium haloborates lead to the formation of trialkylamine trihaloborane and dialkylamino dihaloborane followed by ill-predictable intermediates leading to the formation of boron-nitrogen polymers.

Pyrolysis and thermoanalytical techniques applied to tetraalkylammonium haloborates is a part of an extensive research investigation into the factors to develop chemically and thermally stable boron-nitrogen polymers.[1-2] Considerable interest is attached to prepare polymers in which main chain is composed of elements other than carbon, in the hope that the thermal stability would be greater than that of the known organic polymers. Although a number of useful thermally stable polymers have in fact been developed by organic chemists but the interest given to the development of some areas of organometallic chemistry has been inadequate. Our work which is being presented in this and succeeding papers is directed towards the preparation of boron-nitrogen polymers.

Polyborazynes $[XBNR]_n$ exist as cyclic dimers, trimers and linear polymers.[3-5] The great difficulty in the preparation of linear polyborazynes is the overwhelming propensity of polyborazynes to exist as small rings.[6] It was thought that one method to prevent the formation of small rings and constraining polymerization to only linear polymers was to introduce some measure of steric inhibition to ring formation. In our efforts to prepare linear polymers two approaches were devised. The first was to discover whether by a suitable choice of reactants or experimental conditions the formation of ring compounds might be suppressed in favor of linear polymers. The second approach was to devise means whereby ring compounds might be linked in linear chains either directly or through suitable bridging groups. This paper describes part of our work on the first approach namely the study of dealkylhalogenation of the 1:1 adducts tetraalkylammonium haloborates[7] selected as suitable models for the study of the possible inhibition of ring compound formation and for the preparation of linear polymers.

Experimental

Appropriate tetraalkylammonium haloborates were prepared by interaction of equimolar quantities of tetraalkylammonium halides and trihaloborane in dichloromethane. Tetraalkylammonium tetraphenylborates were prepared in aqueous medium.

$$R_4N^+X^- + BX_3 \longrightarrow R_4N^+BX_4^-$$

$$R_4N^+Cl^- + Na^+BPh_4^- \longrightarrow R_4N^+BPh_4^- + NaCl$$

R = Et, *n*-Pr and *n*-Bu

X = Cl, Br and $PhBCl_2$

Thermogravimetric analyses were carried out by using Stanton HT-SM Thermobalance. All samples of haloborates and haloboranes were subjected to heat in an atmosphere of nitrogen with a flow rate of 5 l/h. Nitrogen gas provided a blanket of an inert atmosphere by preventing ingress of air. Samples varied in weights from 0.1 g to 0.2 g were used. Platinum crucible with or without platinum lid was used and its capacity varied between 10 to 15 mm. To achieve better resolution heating rates from 0.5 to 6 °C per minute were employed depending on the relative rates of decomposition of each reaction intermediate.

Results and Discussion

Tetraalkylammonium haloborates $[R_4N^+BX_4^-]$ undergo interesting transformations. When in the above complex R was ethyl and X was chloride and phenylboron dichloride inflection corresponding to the ejection of one molecule of ethyl chloride was observed with the formation of 1:1 complex $[R_3NBX_3]$. When R was butyl and X was chloride and bromide in the complex $[R_4N^+BX_4^-]$, the complex ejected two molecules of butyl halide in one step with the formation of dibutylamino dihaloborane. When R was butyl and X was

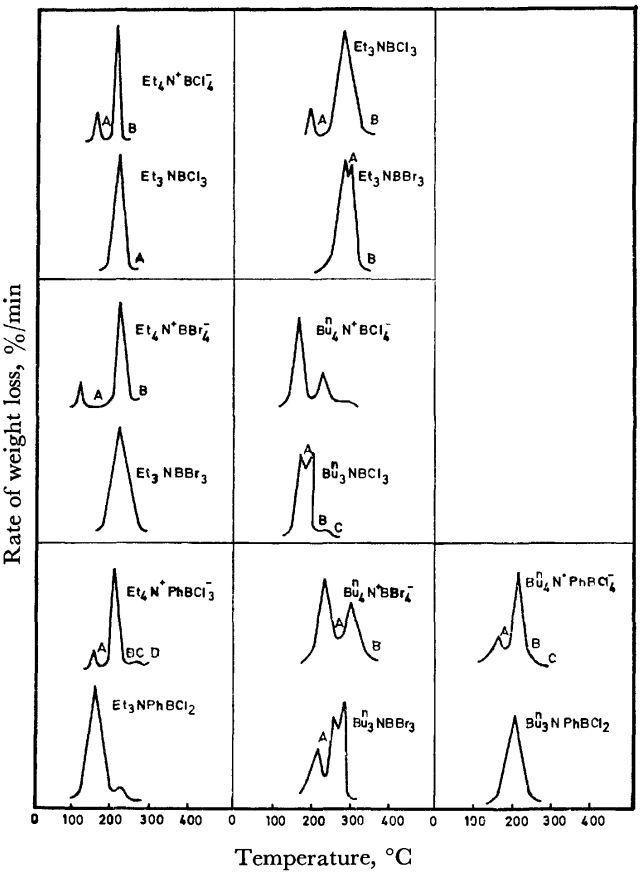

Fig. 1. Differential thermograms.

Table 1. Thermogravimetric analysis of tetraalkylammonium haloborate

Compound	Sample wt (mg)	% wt loss at inflection	% wt loss calculated for 1:1 complex	1:1 Complex formed
$Et_4N^+BCl_4^-$	178.2	22.4 at A	22.9	Et_3NBCl_3
		94.2 at B[a)]	—	—
$Et_4N^+BBr_4^-$	207.5	14.4 at A	23.6	—
		39.4 at B[a)]	—	—
$Et_4N^+BPhCl_3^-$	187.1	19.1 at A	19.7	$Et_3NBPhCl_2$
		37.8 at B	39.5	$Et_2NBPhCl$
		82.8 at C[a)]	—	—
		89.2 at D[a)]	—	—
$Et_4N^+BPh_4^-$	158.1	22.8 at A	23.6	Et_3NBPh_3
		88.6 at B[a)]	—	—
n-$Bu_4N^+BCl_4^-$	111.9	47.4 at A	46.9	n-Bu_2NBCl_2
		87.6 at B[a)]	—	—
n-$Bu_4N^+BBr_4^-$	156.9	48.4 at A	47.8	n-Bu_2NBBr_2
		89.8 at B[a)]	—	—
n-$Bu_4N^+BPhCl_3^-$	156.2	17.8 at A	21.1	n-$Bu_3NBPhCl_2$
		39.7 at B	40.2	n-$Bu_2NBPhCl$
		93.4 at C[a)]	—	—
n-$Bu_4N^+BPh_4^-$	100.4	No inflection	—	—

a) Undermined intermediates.

phenylboron dichloride, two molecules of butyl chloride were ejected in two separate steps with the formation of dibutylamino phenylchloride. The results are represented in the form of differential thermograms in Fig. 1 and Table 1.

$$Et_4N^+BCl_4^- \longrightarrow Et_3NBCl_3 + EtCl \quad (1)$$

$$Et_4N^+BPhCl_3^- \longrightarrow Et_3NBPhCl_2 + EtCl \quad (2)$$

$$Et_3NBPhCl_2 \longrightarrow Et_2NBPhCl + EtCl \quad (3)$$

$$Bu_4N^+BX_4^- \longrightarrow Bu_2NBX_2 + 2BuX \quad (4)$$

$$Bu_4N^+BPhCl_3^- \longrightarrow Bu_3NBPhCl_2 + BuCl$$

$$Bu_3NBPhCl_2 \longrightarrow Bu_2NBPhCl + BuCl. \quad (5)$$

Thermogravimetric analysis of tetrabutylammonium tetraphenylborate did not give any indication for the formation of any resolvable intermediate. However, in the case of tetraethylammonium tetraphenylborate system an intermediate, equivalent to $[Et_3NBPh_3]$ was indicated with possible loss of one molecule of ethylbenzene.

All the thermogravimetric analysis results were further supported by the differential thermal analysis. The latter technique afforded no identification of the thermal decomposition sequence beyond the point of formation of 1:1 complex except in the case of triethylamine and tributylamine trichloroboranes, where, there are some indications of the possible formation of diethylamino and dibutylamino dichloroborane respectively. These indications are obtained by comparison of relevant differential thermal analysis curves.

Helpful guidance of Dr. B. R. Currell during the course of this work is acknowledged.

References

1) W. Gerrard, *J. Oil. Col. Chem. Ass.*, **42**, 625 (1959).
2) W. Gerrard, *Soc. Chem. Ind. Mongr.*, No. 13 (1961).
3) M. F. Lappert and M. K. Majumdar, *Proc. Chem. Soc.*, **1963**, 88.
4) J. C. Sheldon and B. C. Smith, *Quart. Rev.*, **14**, 200 (1960).
5) A. B Burg and J. Banus, *J. Am. Chem. Soc.*, **76**, 3903 (1954).
6) C. A. Brown and A. W. Laubengayer, *J. Am. Chem. Soc.*, **77**, 3699 (1955).
7) I. M. Butcher and W. Gerrard, *J. Inorg. Nucl. Chem.*, **27**, 829 (1965).

BULLETIN OF THE CHEMICAL SOCIETY OF JAPAN, VOL. 49 (10), 2881—2882 (1976)

Oxidation of Flavanone Hydrazones with Manganese Dioxide

T. C. SHARMA, Amba LAL, and (Mrs) Vinita SAKSENA
School of Studies in Chemistry, Vikram University, Ujjain 456010, India

(Received January 27, 1976)

Synopsis. Oxidation of flavanone hydrazones(I) with active manganese dioxide gave a mixture of flavanones(II) and the azines(III).

The oxidation of hydrazones with manganese dioxide has been studied by many workers.[1-8] Scrutiny of literature shows that manganese dioxide oxidation of hydrazones gives different types of products depending upon the reaction conditions and the structure of the parent carbonyl compound. In the present investigations, we have examined the oxidation of flavanone hydrazones with manganese dioxide.

We found that when flavanone hydrazones(I) are shaken with manganese dioxide in chloroform at room temperature, a mixture of the parent ketone(II) and the corresponding azine(III) results in each case.

The identity of the ketones was confirmed by means of melting point and the mixture melting point with authentic samples. Azines were characterized from their elemental analysis and infrared spectra; azines show a strong absorption peak in the region 1605—1610 cm^{-1} due to the conjugated C=N stretching frequency.

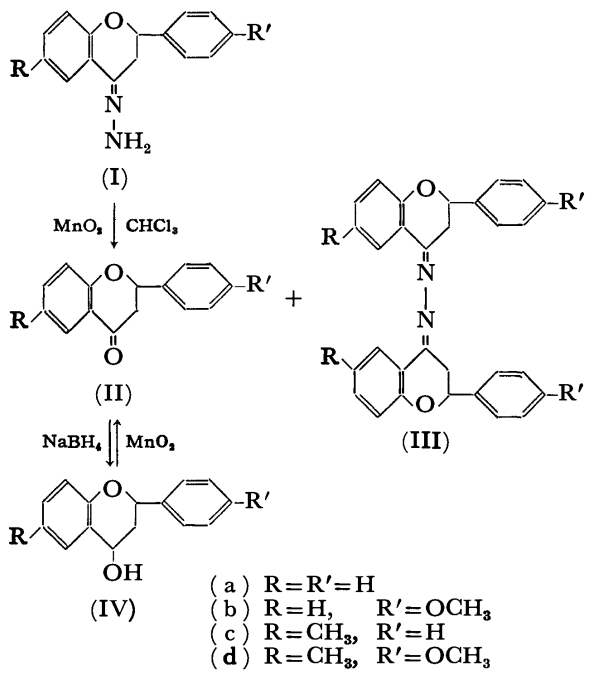

Maier and Heep[8] oxidized some hydrazones with manganese dioxide to the carbonyl compounds and suggested that diazoalkanes are the intermediates in these reactions. Thus, the formation of flavanone azines can be explained if it is assumed that the intermediate diazo compounds dimerize followed by the loss of nitrogen (Scheme 1).

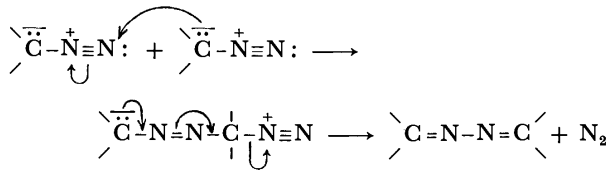

Scheme 1.

However, the conversion of the hydrazones into flavanones can also be explained by a free radical mechanism* (Scheme 2).

Experimental

All mps are uncorrected.

Flavanone Hydrazones (I). These compounds were synthesized following the reported procedure.[10]

Oxidation of Flavanone Hydrazone (Ia). A mixture of flavanone hydrazone (2 g) and manganese dioxide (10 g) in chloroform (160 ml) was shaken at room temperature for 6 h. The residue, obtained after removal of solvent and manganese dioxide, on fractional crystallization from a mixture of benzene and chloroform gave azine (IIIa) as yellow needles (0.45 g), mp 256—257 °C (lit[10] 254—260 °C). Found: C, 80.4; H, 5.8; N, 6.7%. Calcd for $C_{30}H_{24}N_2O_2$: C, 81.0; H, 5.4; N, 6.3%.

The IR spectrum (KBr) of this azine has absorption bands at 1617, 1607, 1523, 1460, 1380, 1320, 1238, 1220, 1150, 1115, 1070, 1027, 990, 907, 752, and 700 cm^{-1}.

From the mother liquor, flavanone (0.2 g) was also isolated which melted at 76 °C. Mixture melting point with an authentic sample gave no depression.

The oxidation of other flavanone hydrazones was similarly studied. Data for the new compounds are given in Table 1.

Oxidation of Flavan-4-ol (IVa). A mixture of flavan-4-ol

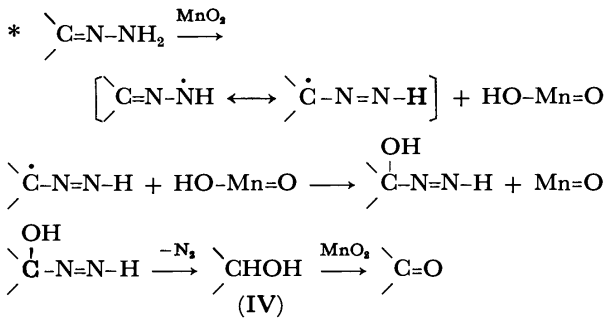

Scheme 2.

We propose this scheme since compounds containing C–N=N–H are usually unstable and decompose to C–H+N_2, possibly *via* a free radical mechanism. The proposed intermediates flavan-4-ols (IV), however, could not be isolated from the reaction mixture but we found that flavan-4-ols undergo oxidation to the corresponding flavanones under similar reaction conditions. The free radical mechanism was also suggested earlier[9] for the oxidation reactions of diamines, hydrazines and phenylhydrazones with manganese dioxide.

Table 1. Data for the new compounds

Compd No.	Formula	Mp °C	Solvent of crystallization	Yield (%)	Found (%) Required (%) C	H	N
Ib	$C_{16}H_{16}N_2O_2$	138—139	EtOH	48	—	—	10.2
					—	—	10.4
Ic	$C_{16}H_{16}N_2O_2$	129—130	EtOH	50	—	—	11.0
					—	—	11.1
Id	$C_{17}H_{18}H_2O_2$	130—131	EtOH	45	—	—	9.7
					—	—	9.9
IIIb	$C_{32}H_{28}N_2O_4$	254—255	C_6H_6–$CHCl_3$	20	76.2	5.8	5.7
					76.1	5.5	5.5
IIIc	$C_{32}H_{28}N_2O_2$	242—243	C_6H_6–$CHCl_3$	18	81.4	6.2	6.3
					81.3	5.9	6.8
IIId	$C_{32}H_{32}N_2O_4$	252—253	C_6H_6–$CHCl_3$	19	76.5	5.8	5.4
					76.7	6.0	5.3
IVc	$C_{16}H_{16}O_2$	127—128	EtOH–H_2O	80	79.8	6.5	—
					80.0	6.6	—

(2 g) and manganese dioxide (10 g) in chloroform was shaken for 6 h. The reaction mixture was worked up as usual to afford flavanone (1.2g), mp and mmp 76 °C.

The other flavan-4-ols[11,12] when oxidized similarly gave the corresponding flavanones in 50—55% yield.

The authors thank Professor M. M. Bokadia for providing laboratory facilities and to the authorities of Chemistry Department I. I. T. Kanpur for providing analytical and spectral data. One of us (V. S.) is grateful to U. G. C., New Delhi for the award of a research fellowship.

References

1) M. Z. Barakat, M. F. Abdel-wahab, and M. M. El-Sadr, *J. Chem. Soc.*, **1956**, 4685.
2) J. Diekmann, *J. Org. Chem.*, **28**, 2933 (1963).
3) N. L. Allinger, L. A. Freiberg, R. B. Hermann, and M. A. Miller, *J. Am. Chem. Soc.*, **85**, 1171 (1963).
4) J. H. Atkinson, A. W. Johnson, and W. Raudenbush, *J. Chem. Soc., C*, **1966**, 1155.
5) G. Wittig, A. Krebs, and R. Pohlke, *Angew. Chem.*, **72**, 324 (1960).
6) S. Hauptmann, M. Kluge, K. D. Seidig, and H. Wilde, *Angew. Chem. Int. Ed. Engl.*, **4**, 688 (1965).
7) H. Morrison, S. Danishefsky, and P. Yates, *J. Org. Chem.*, **26**, 2617 (1961).
8) G. Maier and U. Heep, *Angew. Chem. Int. Ed. Engl.*, **4**, 956 (1965).
9) I. Bhatnagar and M. V. George, *J. Org. Chem.*, **32**, 2252 (1967); *ibid.*, **33**, 2407 (1968).
10) F. Kallay, G. Janzso, and I. Koczar, *Tetrahedron*, **21**, 19 (1965).
11) M. M. Bokadia, B. R. Brown, and W. Cummings, *J. Chem. Soc.*, **1960**, 3308.
12) C. G. Joshi and A. B. Kulkarni, *Chem. Ind.*, **1954**, 1421.

An Application of Current-pulse Electrolysis to an Electro-initiated Polymerization of Acrylamide*

Zempachi OGUMI, Zenichiro TAKEHARA, and Shiro YOSHIZAWA

Department of Industrial Chemistry, Faculty of Engineering, Kyoto University, Yoshida, Sakyo-ku, Kyoto 606

(Received August 13, 1975)

A unidirectional current pulse was applied to the electro-initiated polymerization of acrylamide in a Kolbe system, and the behavior of intermediate was investigated. The formation rate of the oligomer during the current-on pulse was not affected by the pulse length, and it was almost the same as that under steady conditions. An oligomer was also formed during current-off pulse. The formation rate of the oligomer during the current-off pulse was calculated on the base of the mechanism presented in previous papers; the calculated results agreed well with the experimental results. The half-life time of intermediate radical, [RM·], was about 10 ms.

In previous papers[1,2] it was clarified that the concentration of an intermediate at an electrode interface had an important influence on the current efficiency of the oligomer formation and that the current density was more important than the electrode potential. Current-pulse electrolysis was applied to an electro-initiated polymerization of acrylamide in the system of Kolbe electrolysis based on the prediction that the intermediates had a finite lifetime.

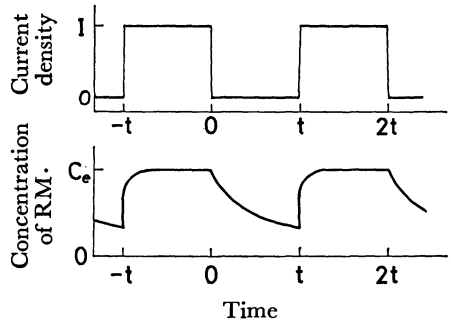

Fig. 1. The concentration change under unidirectional pulse conditions.

The concentration of an intermediate will be changed by electrolysis under unidirectional pulse conditions (Fig. 1). The concentration of the intermediate increases rapidly at the current-on pulse up to a steady value, C_e, depending on the current density and decreases at the current-off pulse depending on the rate of the following chemical reaction. If the pulse electrolysis is applied to the system in which a rise-up time is negligibly short compared with the length of the current-on pulse, the electrode reaction during the current-on pulse may be considered to be the same as that under steady conditions. In this case the formation rate of a product during the current-off pulse can be calculated. If the reaction mechanism is known, the concentration change of intermediate may be calculated using the formation rate obtained above. In the present paper, a unidirectional current pulse was applied to an electro-initiated polymerization of acrylamide in the Kolbe system.

* Studies of Electro-Initiated Polymerization. Part V.

Experimental

An H-shaped glass cell fitted with an anion-exchange membrane as a diaphragm was used as the electrolysis cell. A smooth platinum plate (3×1.5 cm^2) and a smooth platinum cylinder electrode (1.3 cm diameter, 3 cm height, 10 cm^2 area) were used as working electrodes. As a cathode, a smooth platinum electrode (3×3 cm^2) was used. The working electrodes were pretreated prior to use, as has been described before.[1] A solution prepared by dissolving 1 mol of acetic acid and 1 mol of potassium acetate in distilled water to 1 liter was used and will be designated as the 2 M acetate solution from now on. The electrolyte was prepared by dissolving a given amount of acrylamide in this solution. The acrylamide was refined by recrystallization. A current interrupter (Hokuto Denko CI253) was used as the current source. The details of the experimental procedure were described in a previous paper.[1]

The amount of the polymerized product, an oligomer, was measured as follows. When the anolyte was poured into 1 liter of methanol after electrolysis, a white precipitate of an insoluble polymerized product came out. This was filtered through a #4 glass filter, dried at 60—80 °C under reduced pressure, and weighed. The yield of the oligomer thus produced was also calculated as follows. The yield during electrolysis time, T_t, is Y_t. The real time of current flowing, T_{on}, is the sum of the current-on time. The yield per unit of time by electrolysis under steady conditions at the current density equal to it in the current-pulse electrolysis is Y_s. It is assumed that the rate of oligomer formation during the current-on pulse under pulse conditions is the same as under steady conditions. The yield for the total current in time Y_{on} is calculated from Y_s and T_{on}. The yield, Y_{off}, for the total current-off time, T_{off}, can also be calculated by means of Y_{on} and Y_t:

$$Y_{off} = Y_t - Y_{on} \quad (1)$$

$$Y_{on} = Y_s \times T_{on} \quad (2)$$

The yield per current-off pulse, y, is calculated as follows:

$$y = Y_{off}/(T_t/t_t) \quad (3)$$

t_t is the pulse length (on time+off time). The quantity of electricity passed through was measured by means of a hydrogen/oxygen coulometer and a transistorized coulometer manufactured by Hokuto Denko Co., Ltd.

Results and Discussion

Kolbe Reaction under Galvanostatic Pulse Conditions. Constant current pulse electrolysis was first of all applied

Table 1. The current efficiency of carbon dioxide in the case of current-pulse electrolysis at 200 mA/9 cm² in a 2 M acetate solution on a smooth platimum plate electrode
Current-on time/current-off time=1/1.

Pulse length (ms)		2	10	20	40
Current efficiency of CO_2 (%)	91.2[a]	89.7	90.8	91.0	91.2

a) Steady-current electrolysis.

to the Kolbe electrochemical reaction, and the effect of current pulse on the charge-transfer reaction in the system of the electro-initiated polymerization of acrylamide was investigated. The current efficiency of carbon dioxide was examined on a smooth platinum plate electrode in a 2 M acetate solution. The carbon dioxide was measured by using 0.1 M $Ba(OH)_2$. The current efficiency does not depend on the pulse length and is almost the same as that in steady-current electrolysis (Table 1). Wood[3] has reported that acetate is completely oxidized to carbon dioxide and water in an acidic aqueous solution on a platinum electrode at a potential less positive than that where the electrode surface is completely covered with oxide. Fleischmann *et al.*[4] have investigated the Kolbe electrolysis under pulse conditions where they have used the potential pulse between E_h (2.2 V *vs.* NHE) and E_l (−0.15 V *vs.* NHE). Under these conditions, the surface oxide formed on the electrode at E_h is reduced at E_l. The state of the electrode surface just after setting the potential at E_h is considered to be different from the state which is normally attained as the Kolbe reaction proceeds. Accordingly, the Kolbe reaction does not proceed at the beginning of the setting at E_h. Complete oxidation, as in Eq. 4, and surface-oxide formation proceed simultaneously until the surface state necessary for the Kolbe reaction is attained:

$$CH_3COO^- + 2H_2O \longrightarrow 2CO_2 + 7H^+ + 8e \quad (4)$$

Moreover, these reactions result in lowering the current efficiency of the Kolbe reaction and in decreasing the formation of carbon dioxide.** Hickling and Wilkins[5] and Wilson and Lippincott[6] have investigated the application of the alternating current pulse to the Brown-Walker and Kolbe reactions. They examined the effect of the pulse length on the current efficiency of the dimerized product and ascertained that the current efficiency was independent of the pulse length and was equal to that obtained by steady-state electrolysis when the reverse (cathodic) current was zero, that is, when the pulse current was applied instead of the alternating current. On the other hand, when the alternating pulse current with a small reverse current was applied, the current efficiency decreased and depended on the coulombic amount of reverse electricity. When the reverse electricity exceeded a critical value, the current efficiency again became high. However, in the present system, the current efficiency of carbon dioxide did not depend on the pulse length and almost coincided with the value obtained by steady-current electrolysis (Table 1). This fact indicates that the formation of surface oxide and the complete oxidation described by Eq. 4 do not occur, differing from the result of the potential pulse electrolysis of Fleischmann *et al.*[4] and also from results reported by Hickling and Wilkins,[5] and Wilson and Lippincott.[6] It is a possible to conclude that, under the present pulse conditions, a usual Kolbe reaction proceeds during the current-on pulse.

An Oligomer Production and the Effects of Some Electrolysis Conditions. The above investigation made it clear that, by electrolysis using a unidirectional pulse current, carbon dioxide was produced at the same current efficiency as with steady-current electrolysis. The change in the surface state under the pulse conditions was examined by measuring the electrode potential. The electrode potential is considered to change with the change in the electrode surface state and not to attain the steady-state value until the electrode surface reaches the steady state. The measurement was carried out by using a cathode-ray oscilloscope. The measuring circuit is shown diagramatically in Fig. 2. The potential was referred to SCE. The potential change is shown representatively in Fig. 3. The time, τ, which was required for attaining the steady potential and the potential difference, ΔE, were measured and tabulated in Table 2 in the system with and without the addition of acrylamide. The potential change, ΔE, increased with the pulse length; the time, τ, also increased in the

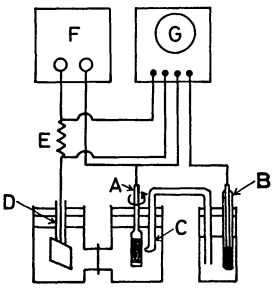

Fig. 2. Experimental equipment.
A: Working electrode. B: Reference electrode (SCE).
C: Luggin capillary. D: Counter electrode.
E: Standard resistor. F: Current pulse generator.
G: Cathode ray oscilloscope.

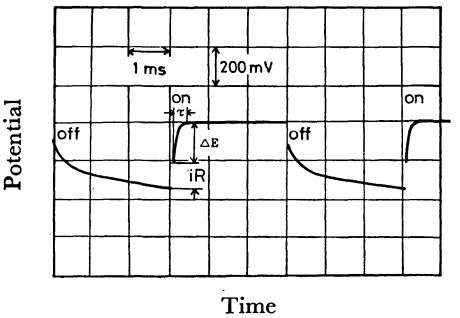

Fig. 3. Typical potential change in current pulse electrolysis at 200 mA/10 cm² on a rotating cylinder electrode (2000 rpm). *iR* means an ohmic drop.

** In Reaction 4, only 1 mol of CO_2 is produced by the electrolysis of 4 Faraday, but in the Kolbe reaction ($2CH_3COO^- \rightarrow CH_3-CH_3 + 2CO_2 + 2e$), 4 mol of CO_2 are produced by this electrolysis.

Table 2. Dependence of the rise-up time, τ, on the pulse length on a rotating cylinder electrode (2000 rpm) at 250 mA/10 cm² 2 M acetate solution, 100 ml.

Pulse length (ms)	Without acrylamide		With acrylamide (20 g)	
	ΔE (mV)	τ (ms)	ΔE (mV)	τ (ms)
0.4	160	0.08		
1	200	0.10	280	0.08
2	250	0.12	340	0.09
6	320	0.14	400	0.10
10	355	0.16	410	0.11
14	400	0.18	420	0.12
20	440	0.20	480	0.14
30	480	0.23	510	0.15
40	530	0.25	580	0.15
60	580	0.25	590	0.16
100	610	0.26		
	760	0.24		

same manner. The ratio of τ to the pulse length is easily calculated; its value is small and decreases as the pulse length becomes longer. The ratio is especially very small in the system with acrylamide added. Furthermore, the steady potential after the rise-up was independent of the pulse length and was 2.4 and 3.2 V in the systems with and without acrylamide respectively. As has been described above, the surface state required for the occurrence of the Kolbe reaction might be destroyed during the current-off pulse. This would lower the current efficiency of the Kolbe reaction. However, the potential drop during the current-off time, which is equal to ΔE, is so small, and the steady potential attained during the current-on time is so high (2.4 or 3.2 V), that the destruction of the surface state does not occur (Table 2). This consideration might allow us to conclude that the Kolbe reaction proceeds during the rise-up time, τ, except for a small current for the charging of the double layer. In addition to this, it has already been established that, in the electro-initiated polymerization of acrylamide in the Kolbe system, the formation rate of the polymerized product hardly depended on the current density at the potentials large enough for the Kolbe reaction.[1,2] Accordingly, it can reasonably be presumed that the formation rate of the oligomer during the rise-up time is almost the same as in the steady state. In order to confirm this assumption, the dependence of the oligomer-formation rate on the current-on pulse length was examined at a constant current-off pulse length. The measurement was carried out in a 2 M acetate solution containing 20 g of acrylamide by utilizing a rotating cylinder electrode (1450 rpm) at 200 mA/cm². The length of the current-on pulse had little effect on the yield (Fig. 4). This fact shows that the oligomer production during the rise-up time proceeds almost at the same rate as the steady state. From now on the ratio of the current-on time to the current-off time will be set at 1 unless specifically stated.

An effect of the rotation rate was next examined on a cylinder electrode and compared with the results

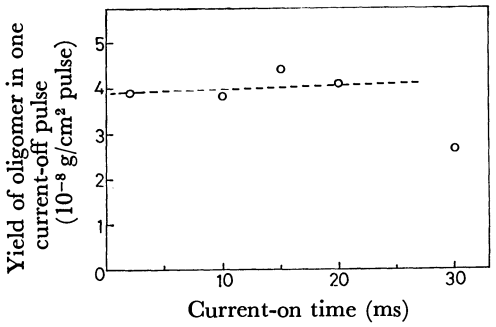

Fig. 4. The effect of current-on pulse length on the oligomer yield at 200 mA/10 cm² on a rotating cylinder electrode (1450 rpm) in the solution 2 M acetate solution 100 ml+acrylamide 20 g. Current-off pulse= 10 ms.

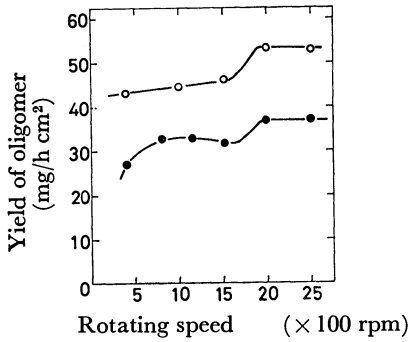

Fig. 5. Dependence of the yield on rotation rate on a rotating cylinder electrode at 200 mA/10 cm² in the solution 2 M acetate solution 100 ml+acrylamide 20 g. a —●—: With pulse current of 20 ms, b —○—: with steady current.

obtained by steady-current electrolysis (Fig. 5). Curve a in this figure represents the yield per hour, including the current-off time under pulse conditions of a 20 ms pulse length at 200 mA/10 cm². Curve b represents the yield under steady conditions at the same current density. On both curves an abrupt change is observed between 1500 and 2000 rpm; above and below this range, the change is not remarkable. The yield during the current-off pulse can be calculated from Fig. 5 (Fig. 6). The rotation rate has no effect on the yield except for a point at 400 rpm, and no abrupt change is observed in

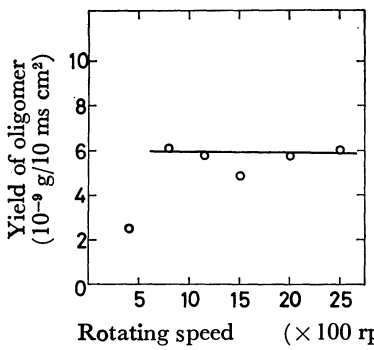

Fig. 6. The effect of rotation rate on the yield during current-off pulse in the solution 2 M acetate solution 100 ml+acrylamide 20 g on a rotating cylinder electrode at 200 mA/10 cm².

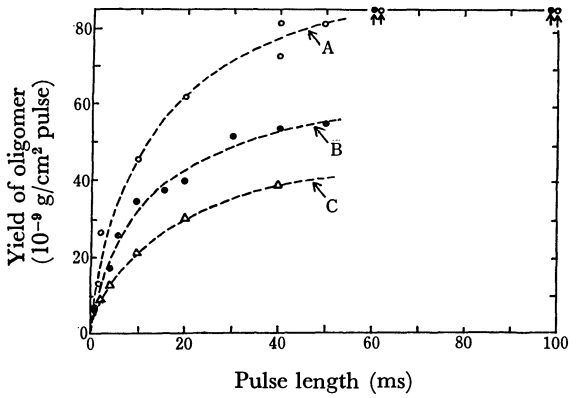

Fig. 7. Relationship between pulse length and the oligomer yield during one current-off pulse on a rotating cylinder electrode in the solution 2 M acetate solution 100 ml+acrylamide 20 g.
A: 250 mA/10 cm^2, 2000 rpm.
B: 200 mA/10 cm^2, 2000 rpm.
C: 200 mA/10 cm^2, 400 rpm.

Fig. 6. Thus, the formation of the oligomer during the current-off pulse is not remarkably affected by the mass-transfer rate to the electrode.

The relationship between the current-pulse length and the yield of the oligomer during the current-off pulse was also examined (Fig. 7). The yield increased with the pulse length in the region of short pulse lengths. However, the yield suddenly reached a high value at pulse lengths longer than 60 ms. In this case, a high polymer was observed besides an oligomer. The high polymer is considered to be formed through a different process, which is still ambiguous, from that of oligomer formation.

Behavior of Intermediate Radicals and a Theoretical Treatment of It. In the Kolbe system two intermediate radicals, $CH_3\cdot$ and $CH_3COO\cdot$, are considered to exist on or near an electrode surface. In spite of vigorous investigations by many workers, however these intermediates have never been directly detected. The electrode surface is covered with oxide and intermediates. Bruno and Dobois[7] reported that a hydrophobic polymer film like polyethylene covered the surface, and authors also found that, in an electro-initiated polymerization of acrylamide in an aqueous solution of trifluoroacetate, an electrode surface was covered with a hydrophobic film which was not easily removed.[9] Kolbe intermediates are considered to exist at the interface under interaction with the above species adsorbed on the surface. As has been reported in the previous papers,[1,2] the polymerized product in the Kolbe system is formed by the reactions of intermediates. A low current efficiency of polymerization was ascribed to that polymerization was initiated on or just near the electrode surface, where the radical concentration was high. The fact that an oligomer was formed during current-off pulse explicitly shows that some intermediate species which have the ability to initiate the polymerization have a finite lifetime. Taking this into consideration the mechanism of oligomer formation under pulse conditions was examined. The reaction proceeds as follows:[1]

$$CH_3COO^- \longrightarrow R\cdot + e \quad (5)$$

R· represents two Kolbe intermediate radicals, $CH_3\cdot$ and $CH_3COO\cdot$.

$$R\cdot + R\cdot \xrightarrow{k_1} R\text{-}R \quad (6)$$

$$R\cdot + M \xrightarrow{k_2} RM\cdot \quad (7)$$

$$R\cdot + RM\cdot \xrightarrow{k_3} RMR \quad (8)$$

M represents an acrylamide monomer. The RM· thus formed reacts further into polymerized products as follows:***

$$RM\cdot + M \xrightarrow{k_4} RMM\cdot \quad (9)$$

$$RMM\cdot + nM \xrightarrow{k_p} RM_{n+2}\cdot \dashrightarrow \text{Oligomer} \quad (10)$$

$$RM\cdot + RM\cdot \xrightarrow{k_5} RMMR \quad (11)$$

$$RM\cdot + B \xrightarrow{k_6} RMX + B' \quad (12)$$

B represents some impurity *etc.*, RMX includes a stable radical which can not initiate polymerization. B′ can not initiate polymerization, either. The formation rate of R·, v, is expressed as follows:

$$v = g\cdot I/F \quad (13)$$

I and g represent the current density and the current efficiency respectively. F is the Faraday constant. The change in the R· concentration is:

$$d[R\cdot]/dt = v - 2k_1[R\cdot]^2 - k_2[R\cdot][M] - k_3[RM\cdot][R\cdot] \quad (14)$$

The change in the RM· concentration is:

$$d[RM\cdot]/dt = k_2[R\cdot][M] - k_3[RM\cdot][R\cdot] - k_4[RM\cdot][M] - 2k_5[RM\cdot]^2 - k_6[RM\cdot][B] \quad (15)$$

In the above expressions, it was assumed that mass-transfer did not cause any probelms in any reaction. The rate of oligomer formation is:

$$v_p = k_4[RM\cdot][M] \quad (16)$$

It is considered for the sake of simplification, that all the R· formed in Eq. 5 proceeds Reaction 7 into RM·, because it was clarified in a previous paper[2] that no dimerized Kolbe product, R–R, was produced in this system, and the contributions of Reactions 8 and 12 are considered to be small when acrylamide is used at concentrations higher than 2.5 mol/l (see another previous paper).[2] In this experiment, the concentration of acrylamide was about 2.8 mol/l. Therefore, $k_3[RM\cdot]\times[R\cdot]$ and $k_6[RM\cdot][B]$ in Eqs. 14 and 15 can be neglected.

Then,

$$k_2[R\cdot][M] = v \quad (17)$$

By replacing [RM·] and [M] with C and m respectively, Eq. 15 is written as follows:

*** As lower-molecular-weight products are formed in our system, RMR, RMMR, and RMX were mainly detected.[2] The other reactions besides Eqs. 8, 11, and 12 (*e.g.*, $RM\cdot + RM_2\cdot \rightarrow RM_3R$) were thus not considered as terminating reactions.

$$dC/dt = v - (k_4'C + 2K_5C^2) \quad (18)$$

Here, $k'_4 = k_4 m$. The concentration at the interface should be taken as m. Under steady conditions at constant-current electrolysis,

$$dC/dt = 0. \quad (19)$$

Then C_e, the steady value of C, is

$$C_e = (-k_4' + \sqrt{k_4'^2 + 8k_5 v})/(4k_5). \quad (20)$$

At the current-off time under pulse conditions, $v=0$. Then, from Eq. 18 under the condition that $C=C_e$ at $t=0$,

$$C = k_4'/(2k_5 \times [\exp\{k_4'(K+t)\} - 1]). \quad (21)$$

$$K = \ln\{k_4'/(2k_5C_e) + 1\}/k_4' \quad (22)$$

Using the average molecular weight, M_0, the yield of the oligomer is:

$$y = M_0 \int_0^t v_p dt. \quad (23)$$

The yield at the current-off time is calculated from Eq. 23 using Eqs. 16 and 21 as follows:

$$y = M_0 \frac{k_4'}{2k_5} \ln \frac{1 - \exp\{-k_4'(K+t)\}}{1 - \exp(-k_4'K)} \quad (24)$$

When the pulse is very long,

$$y|_{t\to\infty} = M_0 \frac{k_4'}{2k_5} \ln\left(1 + \frac{2k_5C_e}{k_4'}\right). \quad (25)$$

On the other hand,

$$\left.\frac{dy}{dt}\right|_{t=0} = M_0 k_4' C_e = v_{p0} M_0. \quad (26)$$

Here v_{p0} represents the rate of oligomer formation at a steady current which is equal to the value at the current-on pulse. If the values of M_0, v_{p0}, v, $y|_{t\to\infty}$ are experimentally known, k'_4, k_5, and C_e can be calculated from Eqs. 20, 25, and 26. This calculation was carried out for Curve B (Fig. 7) as one example. Also, the relationship between the pulse length and the yield during the current-off pulse was obtained.

The molecular weight of the oligomer obtained under pulse conditions was almost the same as that obtained under steady conditions. Hence, M_0 was assumed to be 1000 based on the result by Yoshizawa *et al.*[8] v_{p0} was obtained from $dy/dt|_{t=0}$ or the observed rate of oligomer formation under steady conditions. v was calculated form the current density, assuming a 100% current efficiency. $dy/dt|_{t=0}$, can be obtained from Fig. 7. On the other hand, the yield suddenly became a high value beyond a pulse length at 60 ms (Fig. 7). It is impossible to obtain $y|_{t\to\infty}$ from the experimental results. Therefore, it is necessary to calculate the values of k'_4, k_5, and C_e based on the supposed $y|_{t\to\infty}$ (Table 3). In this calculation v_{p0} was obtained from Fig. 7 as 1.3×10^{-8} mol

Table 3. C_e, k_5, and k'_4 parameters at different $Y|_{t\to\infty}$ values

$Y\|_{t\to\infty}$ (10^{-8} g/cm^2)	C_e (10^{-10} mol/cm^2)	k_5 (10^{12} cm^2/mol/s)	k'_4 (10 s^{-4})	Fig. 8
3.4	1.6	0.35	12.5	a
5.4	2.9	1.2	4.5	b
9.5	5.4	3.3	2.4	c

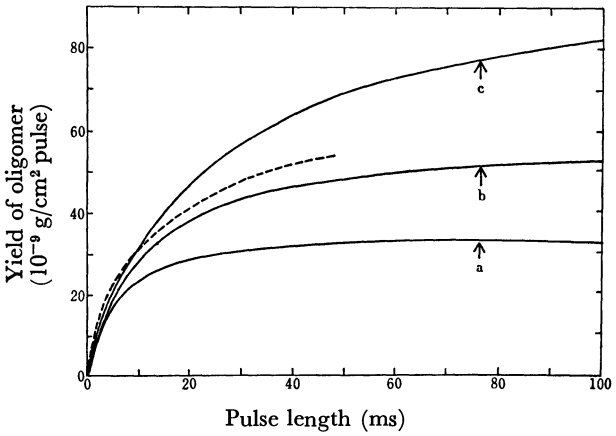

Fig. 8. Relationship between pulse length and the oligomer yield during one current-off pulse calculated by using Eq. 24. a, b, and c represent those in Table 3 respectively. A dotted line represents curve B in Fig. 7.

cm^{-2} s^{-1}, which agreed well with the value, 1.5×10^{-8} mol cm^{-2} s^{-1}, obtained from a steady-state electrolysis at 200 mA/10 cm^2. Using these values, the relationship between the yield, y, and the pulse length, t, was calculated (Fig. 8). The dotted line in this figure shows the experimental result. The calculated curves does not agree perfectly with the experimental results, but the agreement is fairly good. From these calculated results, the half-lifetime of the intermediate, RM·, can be calculated; it becomes about 10 ms. This value is much larger than the half-lifetime of $CH_3\cdot$ (10^{-10} s). An experiment to detect this intermediate was attempted by utilizing the cyclic voltammetry technique at a high scanning rate. However, the reduction current due to intermediates was never observed. Accordingly, the intermediates are considered to be electrochemically inactive.

Conclusion

The following results were obtained from an application of current-pulse electrolysis to an electro-initated polymerization of acrylamide by the Kolbe electrochemical reaction in an aqueous acetate solution.

(1) Under unidirectional current-pulse conditions, the current efficiency of the Kolbe reaction is independent of the pulse length and equal to that under steady conditions.

(2) In the electro-initiated polymerization under pulse conditions, polymerized products are formed not only during the current-on pulse, but also the current-off pulse.

(3) The behavior of intermediates, namely, the production path of polymerized products during the current-off pulse, can be explained well by assuming the rate-determining step to be a simple chemical reaction on or near an electrode.

(4) Intermediate species are electrochemically inactive and have a half-life of about 10 ms.

(5) The application of pulse electrolysis to electrode reactions, in which successive chemical reactions have a decisive influence on the current efficiency of the

intended reaction, allows us to improve the reaction selectivity and the current efficiency and, moreover, to analyze the following chemical reactions in more detail.

(6) In a current-pulse electrolysis the current loss for nonfaradaic processes, such as double-layer charging, *etc.*, has only an insignificant effect.

References

1) Z. Ogumi, I. Tari, Z. Takehara, and S. Yoshizawa, *Bull. Chem. Soc. Jpn.*, **47**, 1843 (1974)

2) Z. Ogumi, I. Tari, Z. Takehara, and S. Yoshizawa, *Bull. Chem. Soc. Jpn.*, **49**, 841 (1976).

3) R. Wood, *J. Electroanal. Chem.*, **21**, 457 (1969).

4) M. Fleischmann and A. Goodridge, *Discuss. Faraday Soc.*, **45**, 254 (1968); M. Fleischmann, J. R. Mansfield, and Lord Wynne-Jones, *J. Electroanal. Chem. Interfacial Electrochem.*, **10**, 522 (1965).

5) A. Hickling and R. Wilkins, *Discuss. Faraday Soc.*, **45**, 261 (1968).

6) C. L. Wilson and W. T. Lippincott, *J. Am. Chem. Soc.*, **78**, 4290 (1956); *J. Electrochem. Soc.*, **103**, 672 (1956).

7) F. Bruno and J. E. Dubois, *Electrochim. Acta*, **17**, 1161 (1972).

8) S. Yoshizawa, I. Tari, and M. Suhara, *Denki Kagaku.*, **40**, 650 (1972).

9) S. Yoshizawa, Z. Takehara, I. Tari, and Z. Ogumi, unpublished.

Cathodic Reduction of Nitrobenzene on the Packed-bed Copper Electrode

Shiro YOSHIZAWA, Zenichiro TAKEHARA, Zempachi OGUMI, and Toshio TSUJI

Department of Industrial Chemistry, Faculty of Engineering, Kyoto University, Yoshida, Sakyo-ku, Kyoto 606

(Received January 29, 1976)

An application of a packed-bed copper electrode to the formation of aniline by the cathodic reduction of nitrobenzene was investigated. As the particles for the packed-bed, spherical particles of an anion exchange resin chemically plated with copper were successfully used. Though the current efficiency for the aniline formation on the packed-bed electrode in a batch cell decreased with continuing electrolysis, the efficiency was improved by the electrolysis under a flowing electrolyte and became very high, *i.e.*, near 100%. This is due to the removal of the accumulated products on the electrode surface by the flowing electrolyte. The effective depth of the bed electrode on which the nitrobenzene reacted cathodically was also determined from the measurement of the potential profile in a packed-bed electrode: the result was about 3 mm. This low value of the effective depth is ascribed to the low conductivity of the electrolyte and to the high electronic conductivity of the packed-bed. This may be improved by using bed particles of lower electronic conductivity and a higher cell capacity may be expected.

The electrochemical production of organic compounds at a high rate is generally difficult due to the low exchange current density of the electrode reaction and the disturbance of the electrode reaction by the accumulation of the reaction products on the electrode surface, in the case of the formation of low solubility products. Thus, an application of a packed-bed electrode, which is a three-dimensional electrode may be considered. By its operation under a flowing electrolyte the accumulation of the reaction products on the electrode surface may be avoided. Such a packed-bed electrode was applied to the cathodic reduction of nitrobenzene in acidic solution, which is an electrode process which has a well-known reaction mechanism,[1] and the probability of scaling up the cell capacity was examined.

Experimental

Electrolytic Cell. The anode compartment of the electrolytic cell (Fig. 1) was separated from the cathode one by a diaphragm of an ion exchange membrane. A platinum plate was utilized as the counter electrode (anode), and the working electrode (cathode) was made from a packed-bed. The diameter of the working surface was 25 mm and the distance between the diaphragm and the current feeder was 40 mm. A copper net was used as the current feeder. A 2% (volume) aqueous sulfuric acid solution was used as an anolyte. A catholyte was prepared from an EWS solution, which consisted of 35 parts of ethanol, 10 parts of water, and two parts of sulfuric acid and nitrobenzene. The catholyte flowed through the bed from top to bottom and the anolyte was circulated. The electrolysis was operated at room temperature. The particles for the packed-bed electrode were prepared from an anion exchange resin, Amberlite IR-410 as follows:[2] Pretreatment: 1. Stir in ethanol. 2. Keep in a 15% aqueous solution of potassium carbonate for 15 min below 70 °C under stirring. 3. Wash with distilled water. 4. Keep in a solution composed of 1 part of 1% aqueous silver nitrate solution and 1 part of ethanol at room temperature for 5 min under stirring (surface activation). 5. Vacuum dry below 40 °C. Each particle thus pretreated was chemically plated. A plating bath was prepared by dissolving 180 g of glycerine and 180 g of copper carbonate in 1 liter of 20% NaOH solution. The solution was kept for a day before use. A 28% formaldehyde solution was used as a reducting reagent. One gram of particles was put in 10 ml of plating bath and a reducing reagent was added 1 ml at a time until the color of the copper ions disappeared. Particles plated with copper were dried under a reduced pressure after being washed with distilled water, and were kept in a desiccator.

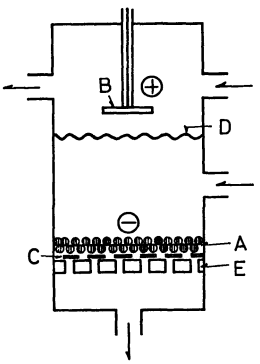

Fig. 1. Electrolytic cell.
A: Working bed electrode. B: Counter electrode.
C: Current feeder. D: Anion exchange membrane.
E: Plastics net.

Analysis. Each fraction of the effluent electrolyte was analyzed as follows: It was first neutralized by a NH_3 solution and then it was extracted by ether. The extract was analyzed by utilizing a liquid chromatography technique.

Potential Measurement. A probe was devised to measure the particle potential in a bed electrode. A copper wire of 0.5 mm diameter was covered with polyethylene. One end of it was bare only at an edge and the other was bare for the contact to the measuring circuit. This probe was supported by a glass pipe. A fine Luggin capillary was attached, with a porous porcelain tip on its edge to prevent bed particles from coming into the capillary. If that occurred, the solution potential measured by the capillary would be disturbed by the dissolution of copper.

Results and Discussion

Current-Potential Relationship. The potential on the copper-plate electrode where the nitrobenzene reacted in a mixed solution (EWS) was examined by cyclic voltammetry (Fig. 2). The reduction of nitrobenzene begins at about −0.2 V (*vs.* SCE) and hydrogen evolution begins at about −0.5 V. Accordingly, only the reduction of nitrobenzene occurs between −0.2 and −0.5 V.

Electrolysis in a Batch-Cell. The current efficiency for aniline formation was examined at a copper-plate

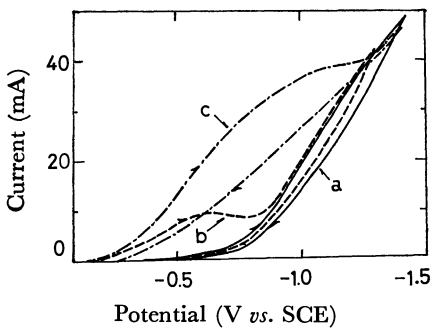

Fig. 2. Current-potential curves on the copper-plate electrode in EWS solution by a cyclic voltammetry with sweep rate of 0.1 V/s.
a: Without nitrobenzene, b: with 1% nitrobenzene, c: with 5% nitrobenzene.

electrode in an H-shaped batch-cell which was equipped with an ion exchange membrane as a diaphragm. At the early stage of electrolysis under a constant current, of 10 mA/cm^2, for example, the current efficiency of aniline formation was very high, about 70—80%. However, the electrode surface was covered by a colloidal product with continuing electrolysis and the current efficiency decreased with electrolysis time. After a few hours electrolysis the current efficiency decreased to 30—40% and hydrogen evolution occurred as a side reaction. Besides the copper plate, a copper-particle bed was used as the electrode in a batch-cell. As the latter electrode, 1 g of particles was inserted in a glass vessel (10 mm diameter, 10 mm height). A copper wire which was set at the bottom of the vessel was utilized as a current feeder. The rate of aniline formation on this electrode was examined under a constant current electrolysis (Fig. 3). A solid product accumulated on the bed electrode; it was identified as anilinium sulfate by its IR spectrum. No other compound was observed. A straight line in this figure represents the calculated rate of aniline formation by supposing that the current efficiency of aniline formation is 100%. The experimentally obtained rate was lower than the calculated one. This may be due to the hydrogen evolution as a

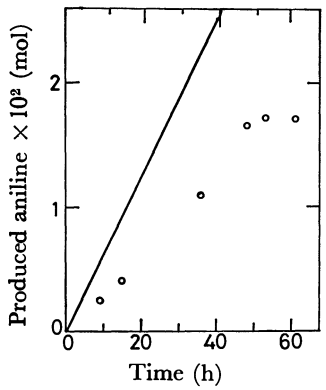

Fig. 3. Current efficiency for aniline formation at constant current (100 mA) electrolysis by using packed-bed copper electrode in a batch cell.
—: Calculated rate as 100% current efficiency,
○: observed value.

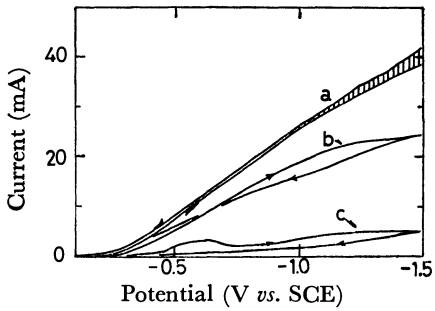

Fig. 4. Current-potential curves on the copper-plate electrode in EWS solution containing 5% nitrobenzene by a cyclic voltammetry with sweep rate 0.1 V/s.
a: By using copper electrode not covered by a colloidal product,
b: by the use of the solution added with 0.3% aniline after the measurement of "a",
c: by using copper electrode after 3 h electrolysis at 10 mA covered by a colloidal product.

side reaction. The rate of aniline formation hardly decreased after about 48 h electrolysis.

The potential-current curve by cyclic voltammetry on the copper-plate electrode covered by the colloidal product was measured (Fig. 4). The current in the potential region in which the reduction of nitrobenzene occurred decreased exceedingly after being covered by the colloidal product. By adding aniline, which is the reaction product, the decrease of current was also observed, but it was very slight. This may show that a colloidal product retards the cathodic reduction of nitrobenzene very much and accelerates the hydrogen evolution, due to the shift of the potential to a more negative value during the constant current electrolysis. Thus, the current efficiency for aniline formation may be decreased with continuing constant current electrolysis in a batch-cell.

Electrolysis at a Packed-Bed Electrode. By using a packed-bed electrode (Fig. 1), an EWS solution containing 5% nitrobenzene was electrolyzed at a constant current (100 mA) under flow. The effluent electrolyte was collected by 10 ml at a time. Each fraction was analyzed for the aniline content, and the rate of aniline

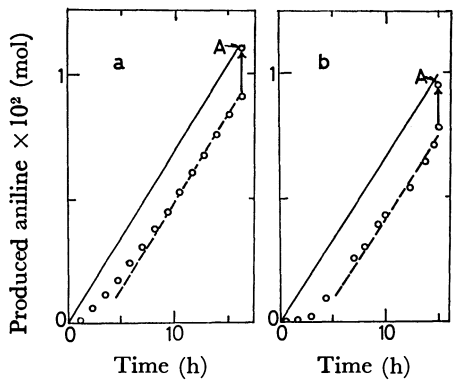

Fig. 5. Current efficiency for aniline formation at constant current (about 100 mA) electrolysis by using packed-bed copper electrode under flowing electrolyte.
a: bed depth, 30 mm, b: bed depth, 10 mm.
—: Calculated rate as 100% current efficiency,
○: observed value.

formation was calculated (Fig. 5). a and b in this figure represent results obtained by the cells of 30 and 10 mm heights, respectively. Straight lines represent results which were calculated by assuming that the current efficiency of aniline formation was 100%. At the early stage of electrolysis, the rate is apparently slow. This is due to the induction period before the flowing out of the solution under the bed electrode. The experimental results fell almost on the dotted lines which represent the current efficiency of 100%. It becomes clear from this fact that the current efficiency is very high. The electrolyte contained in the cell flowed out after electrolysis and was analyzed for the aniline content. Then the amount of aniline became point A in Fig. 5. These results also show that the current efficiency is very high, approximately 100%.

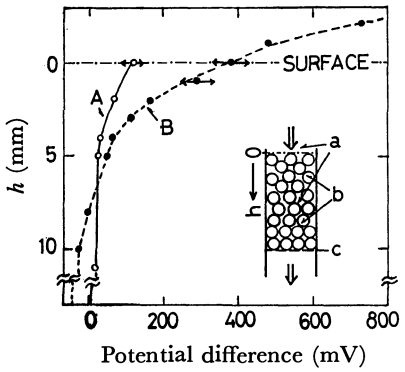

Fig. 6. Potential profile in a packed-bed copper electrode at 75 mA/cm² electrolysis under flowing electrolyte.
A: Potential difference between particles and feeder at various positions (b—c),
B: potential difference between solution and feeder at various positions (a—c).

Potential Profile in a Packed-Bed Electrode. The potential profile in a packed-bed electrode was examined under the conditions of constant current electrolysis (Fig. 6). The change of solution potential was measured along the bed depth by using a fine Luggin capillary. The change of particle potential was measured also along the bed depth by the probe described in the experimental section. Both potentials were referred to a current feeder which was at the furthest position from a counter electrode. In this experiment the total current was 100 mA and the apparent current density per cross sectional area of packed-bed electrode became 75 mA/cm². Potential changes became very small at the current densities lower than 10 mA/cm² and, on the other hand, the convection occurred in the bed at the current densities higher than 400 mA/cm². This convection is ascribed to the large Joule heat. Accordingly, the same profile as in Fig. 6 was observed between 10 mA/cm² and 400 mA/cm². The effective depth of the bed electrode on which nitrobenzene reacts is considered from Fig. 6 to be less than 3 mm, because the particle potential must be more negative by 200 mV than the solution potential for the reduction of nitrobenzene, as shown in Fig. 2. The low value of the effective depth is ascribed to the low conductivity of the electrolyte and to the high electronic conductivity of the packed-bed. At deeper positions in the packed-bed electrode, the potential of the particle electrode became more positive than the solution potential at the same position. This may cause the dissolution of copper. In order to increase the effective depth of the packed-bed electrode, bed particles of lower electronic conductivity must be used.

The authors wish to thank the staff of the Asahi Glass Foundation for the Contribution to Industrial Technology for their support of this work.

References

1) R. Glicksman and C. K. Morehouse, *J. Electrochem. Soc.*, **105**, 299 (1958).
2) V. I. Shorokhova, *Int. Chem. Eng.*, **4** (3), 451 (1964).

Absorption Spectra of Four Naphthalenediols with C_{2v} Symmetry. Interpretation by Means of Configuration Analysis

Tsuneo FUJII and Satoshi SUZUKI

Department of Industrial Chemistry, Faculty of Engineering, Shinshu University, Wakasato, Nagano 380

(Received January 12, 1976)

The electronic absorption spectra of four substituted naphthalenes with two electron-donating groups, 1,4-, 1,8-, 2,3-, and 2,7-naphthalenediols, have been investigated by means of configuration analysis, with particular attention paid to the dependence of the spectra on the positions of substitutions and on the molecular symmetry. The wave functions calculated by the Pariser-Parr-Pople method are analyzed in terms of locally-excited states and intramolecular charge-transfer states. The excited electronic wave functions of naphthalenediols have been expanded not only in terms of the electronic states of naphthalene, but also in terms of those of naphthol. The present configuration analysis shows that the electronic states of all these four naphthalenediols may reasonably interpreted in terms of locally-excited states of the parent compounds and charge-transfer states from the substituents to the parent compounds. The characteristic spectral changes in the L_b, L_a, and B_b bands caused by substitution are adequately explained in relation to the positions and to the molecular symmetry. The intensification of the L_b band caused by the introduction of the hydroxyl groups is interpreted as due to the mixing between the L_b and B_b bands. The B_b reference state interacts with the L_b and A_g^- reference states in 1,4- and 2,3-naphthalenediols, whereas it interacts with the L_b, B_{1g}^+, and B_{1g}^- reference states in 1,8- and 2,7-naphthalenediols.

The electronic absorption spectra of naphthalene derivatives show characteristic behavior depending on the position and the properties of the substituents. The electronic spectra of monosubstituted naphthalenes are now well understood both theoretically and experimentally.[1-8]

However, little attention has been directed to the electronic spectra of disubstituted naphthalenes, although some studies have been made from both theoretical and experimental points of view.[4,9-12]

The present paper will report on the results of configuration analysis (hereafter abbreviated to CA) for four naphthalenediols, 1,4-, 1,8-, 2,3-, and 2,7-naphthalenediols (hereafter abbreviated to 1,4-, 1,8-, 2,3-, and 2,7-diol respectively), based on two different types of reference compounds, naphthalene and naphthols. The 1,4- and 2,3-diols have a symmetry axis along the long(b) axis of the naphthalene ring while the 1,8- and 2,7-diols have a symmetry axis along the short(a) axis. The interaction scheme of the naphthalenediols is expected to be more simple than that of monosubstituted naphthalenes.

Calculation

The method of a semi-empirical LCAO-SCF-CI calculation and the procedure of the CA are the same as has been described previously.[6,7] It is assumed that the molecules studied have a planar structure and that the naphthalene ring consists of regular hexagons with every C–C bond length equal to 1.40 Å. The parameters, the bond lengths, r, the valence-state ionization potentials, I, the electron affinities, A, and the resonance integrals, β, are the same in a previous paper.[6] The C–C–O bond angle is assumed to be equal to 120°.

The SCF MO's are numbered in the order of increasing energy. In the CI calculation of 1,4-diol, the following eleven singly excited configurations are included: 7→8, 9, 10, 11; 6→8, 9, 10; 5→8, 9; 4→8, 9. One more configuration is added for the other diols. The added configuration is as follows: for 1,8-diol, 5→10; for the 2,3- and 2,7-diols, 6→11.

Experimental

The 1,4-, 2,3-, and 2,7-diols were purified by treating them with decolorizing carbon and by repeated crystallizations and subsequent sublimation *in vacuo* prior to use. Isooctane (2,2,4-trimethylpentane) was fractionally distilled and then passed through a column of silica gel. The absorption spectra were recorded on a Hitachi EPS-3 recording spectrophotometer.

Results

The calculated energies, the oscillator strengths(f), and the directions of the transition moments for the lower singlet states of naphthalenediols are presented in Table 1, together with the observed data. The data of naphthalene and naphthols used in the present study were given in a previous paper.[6] The symbols used in the present paper for denoting the electronic states and absorption bands have the same meaning as the corresponding symbols in that previous paper,[6] unless otherwise noted. The X-axis and Y-axis are taken along the long and short axes of the naphthalene ring respectively. The newly observed absorption spectra of three naphthalenediols are shown in Figs. 1, 2, and 3. The calculated energies are indicated in the figures by vertical lines, the lengths of which represent the relative values of the oscillator strength.

The results of the CA of naphthalenediols on the basis of the state functions of naphthalene are presented in Tables 2, 4, 6, and 8. The reference MO's employed in the present study are the SCF MO's of naphthalene ϕ_1°, ϕ_2°,……, ϕ_{10}°, and two MO's of the substituents, ϕ_{0+}° and ϕ_{0-}°, which are linear combinations of the two AO's, χ_{01} and χ_{02}, of the substituents:

$$\phi_{0+}^\circ = \frac{1}{\sqrt{2}}(\chi_{01}+\chi_{02}),$$

$$\phi_{0-}^\circ = \frac{1}{\sqrt{2}}(\chi_{01}-\chi_{02}).$$

Table 1. Excited states of naphthalenediols

Compound State function	Energy (eV) calcd	obsd	Oscillator strength calcd	obsd	Band assignment	Polarization
1,4-Naphthalenediol						
Ψ_G	0					
Ψ_1	3.87	3.80	0.092	0.082	I	X
Ψ_2	3.87	3.80	0.283		II	Y
Ψ_3	5.09		0.047			
Ψ_4	5.19	5.04	0.484	0.388	III	X
Ψ_5	5.56		0.007			
Ψ_6	5.95	6.39	1.220	0.912	IV	X
Ψ_7	6.32		1.120			Y
1,8-Naphthalenediol						
Ψ_G	0					
Ψ_1	3.99	3.7[a]	0.068		I	X
Ψ_2	4.14	4.2[a]	0.328		II	Y
Ψ_3	5.05		0.014			
Ψ_4	5.34		0.000			
Ψ_5	5.47		0.055			
Ψ_6	5.74	5.6[a]	1.732		III	X
Ψ_7	6.14		0.465			
2,3-Naphthalenediol						
Ψ_G	0					
Ψ_1	3.91	3.84	0.046	0.021	I	X
Ψ_2	4.22	4.43	0.158	0.091	II	Y
Ψ_3	5.27	5.19	0.470		III	X
Ψ_4	5.35		0.028			
Ψ_5	5.66	5.51	0.726	1.256	IV	Y
Ψ_6	5.68		1.583			X
Ψ_7	5.85		0.036			
2,7-Naphthalenediol						
Ψ_G	0					
Ψ_1	3.95	3.85	0.024	0.025	I	X
Ψ_2	4.19	4.41	0.189	0.086	II	Y
Ψ_3	5.24		0.092			
Ψ_4	5.26	5.06	0.558		III	X
Ψ_5	5.59		1.108			X
Ψ_6	5.88	5.41	0.481	1.461	IV	X
Ψ_7	5.96		0.733			Y

a) Estimated for an isooctane solution. See Text.

The reference states which were taken into account in this analysis are as follows: the ground reference state and thirteen excited reference states of naphthalene, Ψ_G°, Ψ_1°,……, Ψ_{13}°; six intramolecular charge-transfer reference states, and $\Psi_{CTO\to k+}^\circ$ and $\Psi_{CTO\to k-}^\circ$, which correspond to a one-electron excitation from ϕ_{0+}° and ϕ_{0-}° to ϕ_k° with $k=6$, 7, and 8. Of these nineteen excited reference states, the seven locally excited reference states and six intramolecular charge-transfer reference states are listed in Tables 2, 4, 6, and 8. The total weight means the sum of the weights of all the twenty reference states described above.

The CA of naphthalenediols calculated on the basis of the state functions of 1- or 2-naphthol can also be made in an analogous manner. These results are presented in Tables 3, 5, 7, and 9. In these cases, the reference MO's are the SCF MO's of naphthols ϕ_1°, ϕ_2°,……, ϕ_{11}°, and the π-AO of the substituent, ϕ_0°. In these calculations the reference states are as follows: the ground reference state, Ψ_G°, and the locally excited reference states of naphthol (13 states for 1-naphthol or 14 states for 2-naphthol), and the three intramolecular charge-transfer states, $\Psi_{CTO\to k}^\circ$, which correspond to a one-electron excitation from ϕ_0° to ϕ_k° with $k=7$, 8, and 9. The total weight means the sum of the weights of all the seventeen (or eighteen) reference states for 1,4- and 1,8- (or 2,3- and 2,7-) diols.

The band assignments are given in Tables 2—9. When a single reference state has a weight higher than 50%, the state notation of the state is indicated in the columns of the band assignments. The notations given in the columns of the reference absorption bands of Tables 3, 5, 7, and 9 are the same as the band assignments of 1- and 2-naphthols given in a previous paper.[6]

Discussion

It may be seen in Table 1 that the calculated energies for the naphthalenediols are in good agreement with the observed values.

Naphthalenediols, like monosubstituted naphthalene,[6,7] show absorption spectra characteristic of the positions of substituents. The first and second absorption bands (L_b and L_a in naphthalene) overlap strongly in 1,8-diol, and coalesce into one band in 1,4-diol. Two absorption bands appear in the region of the B_b band of naphthalene in 1,4-diol, while only one absorption band appears in the B_b band region in 1,8-diol. In contrast to this, the spectra of 2,3- and 2,7-diols resemble the naphthalene spectrum in the first and second absorption bands, although a weak absorption band appears on the lower side of the strong absorption band in the region of the B_b band of naphthalene.

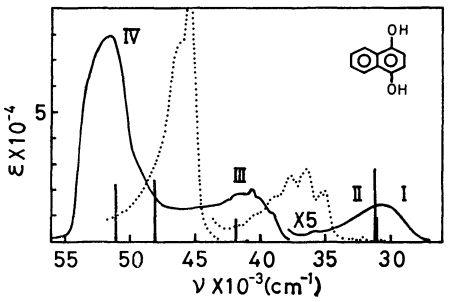

Fig. 1. Absorption spectrum in isooctane solution of 1,4-naphthalenediol. The dotted curve is the spectrum of naphthalene. Vertical lines represent theoretical spectra, with the lengths of lines indicating relative values of oscillator strengths.

1,4-Naphthalenediol. Figure 1 shows the absorption spectrum of 1,4-diol in isooctane, including the calculated data. With reference to the results shown in Tables 1 and 2, Bands I, II, and III may be assigned to the transitions to the Ψ_1, Ψ_2, and Ψ_4 while Band IV is actually composed of two absorption bands related to Ψ_6 and Ψ_7.

Table 2 shows that Bands I and II can reasonably be assigned to the L_b and L_a states respectively. The $\Psi_{CTO\to 7+}^\circ$ state makes an important weight contribution to the Ψ_1 state (11.4%). The $\Psi_{CTO\to 6+}^\circ$ state similarly

Table 2. Configuration analysis for 1,4-naphthalenediol from naphthalene (weight in percent)

Reference state		Absorption band (upper) and state function (lower)							
			I	II		III		IV	
Wave function[a]	Symmetry type	Ψ_G	Ψ_1	Ψ_2	Ψ_3	Ψ_4	Ψ_5	Ψ_6	Ψ_7
Ψ_G°	A_g^-	79.4	0.0			0.2		0.0	
Ψ_1°	B_{3u}^-, L_b	0.0	65.3			8.4		0.9	
Ψ_2°	B_{2u}^+, L_a			55.7	0.0		19.1		0.8
Ψ_3°	B_{1g}^+			0.4	57.9		6.7		0.0
Ψ_4°	A_g^-	0.0	0.9			40.3		20.5	
Ψ_5°	B_{3u}^+, B_b	0.0	2.1			15.7		55.8	
Ψ_6°	B_{1g}^-			8.0	5.3		38.3		5.4
Ψ_7°	B_{2u}^+			0.1	1.3		6.9		67.7
$\Psi_{CTO\to 8+}^\circ$				18.1	4.9		6.0		0.0
$\Psi_{CTO\to 7+}^\circ$		0.0	11.4			10.0		0.0	
$\Psi_{CTO\to 8+}^\circ$				0.8	12.8		3.7		1.0
$\Psi_{CTO\to 6-}^\circ$		8.9	0.0			2.7		1.0	
$\Psi_{CTO\to 7-}^\circ$				0.0	0.0		0.3		0.1
$\Psi_{CTO\to 8-}^\circ$		5.1	0.0			0.1		0.0	
Total weight[b]		93.5	81.0	83.1	84.0	78.8	82.7	80.0	80.6
Assignment[c]		[G]	[L_b]	[L_a]				[B_b]	[B_{2u}^+]

a), b), and c): See Text for definitions.

makes a large weight contribution to the Ψ_2 state (18.1 %). This large contribution is responsible for the large red shift of Band II. The 1,4-diol has C_{2v} symmetry, so that the L_b state does not interact with the L_a state but interacts with the B_b state, from which the intensity of Band I is derived.

The B_b state interacts with the A_g^- state and splits into two bands, Bands III and IV. The B_{2u}^+ state (Ψ_7) overlaps with the B_b (Ψ_6), yielding Band IV. This interaction is characteristic of the naphthalene derivatives with a substituent at the 1-position.[8] The $\Psi_{CTO\to 7+}^\circ$ state has a weight of 10.0% in the Ψ_4 state. There are no substantial contributions of charge-transfer states to the Ψ_6 and Ψ_7 states.

It may be seen from Table 3 that Bands I, II, III, and IV can also reasonably be assigned to Bands i, ii, iii, and iv of 1-naphthol. The $\Psi_{CTO\to 7}^\circ$ and $\Psi_{CTO\to 8}^\circ$ states make a important weight contributions to the Ψ_2 and Ψ_1 states (9.7 and 7.0% respectively). The results show that the hydroxyl group still has an electron-donating character with respect to 1-naphthol. The total weights of the individual excited states are about 90%; therefore, the electronic states of 1,4-diol can be well reproduced from the ground and the excited reference states of 1-naphthol and the intramolecular charge-transfer reference states.

1,8-Naphthalenediol. The observed values obtained by other authors between 220 and 350 nm in ethanol are used in the present study.[18] There are three bands, I, II, and III; their energies are 3.7, 4.1, and 5.5 eV respectively. The band shifts of Bands i, ii, and iii of 1-naphthol on going from an isooctane to an ethanol solution are 150, 750, and 700 cm^{-1} respectively. Provided that the band shifts of 1,8-diol are the same as those of 1-naphthol, the state energies of 1,8-diol in isooctane may be estimated to be 3.7, 4.2, and 5.6 eV

Table 3. Configuration analysis for 1,4-naphthalenediol from 1-naphthol (weight in percent)

Reference state		Absorption band (upper) and state function (lower)							
			I	II		III		IV	
Wave function[a]	Absorption band	Ψ_G	Ψ_1	Ψ_2	Ψ_3	Ψ_4	Ψ_5	Ψ_6	Ψ_7
Ψ_G°		88.9	0.0	1.0	1.5	0.0	0.0	0.0	0.0
Ψ_1°	i	0.0	79.1	1.9	0.1	2.9	0.0	0.1	0.0
Ψ_2°	ii	0.2	1.9	75.3	0.1	0.5	4.4	0.2	0.1
Ψ_3°		0.1	0.0	0.1	67.2	7.9	6.2	0.0	0.0
Ψ_4°	iii	0.0	0.9	0.1	6.9	68.2	0.1	0.7	0.0
Ψ_5°		0.0	0.0	1.7	4.7	0.2	70.9	2.4	0.5
Ψ_6°	iv	0.0	0.2	0.1	0.2	1.0	1.6	81.3	0.2
Ψ_7°		0.0	0.1	0.0	0.1	0.0	0.9	0.1	82.2
$\Psi_{CTO\to 7}^\circ$		4.4	0.0	9.7	1.4	1.6	3.9	0.5	0.0
$\Psi_{CTO\to 8}^\circ$		0.0	7.0	0.0	0.0	6.0	0.1	0.0	0.0
$\Psi_{CTO\to 9}^\circ$		3.5	0.0	0.5	6.9	0.0	2.0	0.0	0.6
Total weight[b]		97.2	90.3	90.8	90.2	89.1	90.9	89.5	89.6
Assignment[c]		[G]	[i]	[ii]		[iii]		[iv]	

a), b), and c): See Text for definitions.

TABLE 4. CONFIGURATION ANALYSIS FOR 1,8-NAPHTHALENEDIOL FROM NAPHTHALENE (WEIGHT IN PERCENT)

Reference state		Absorption band (upper) and state function (lower)							
			I	II				III	
Wave function[a]	Symmetry type	Ψ_G	Ψ_1	Ψ_2	Ψ_3	Ψ_4	Ψ_5	Ψ_6	Ψ_7
Ψ_G°	A_g^-	79.0		2.8		0.0			0.1
Ψ_1°	B_{3u}^-, L_b		72.0		0.2		0.2	4.6	
Ψ_2°	B_{2u}^+, L	0.5		69.9		1.7			0.1
Ψ_3°	B_{1g}^+		0.1		60.9		2.6	0.4	
Ψ_4°	A_g^-	0.0		0.6		60.6			0.0
Ψ_5°	B_{3u}^+, B_b		1.6		0.6		0.6	72.9	
Ψ_6°	B_{1g}^+		0.3		0.6		62.7	0.5	
Ψ_7°	B_{2u}^+	0.0		0.0		0.0			75.0
$\Psi_{CTO\to6+}^\circ$		9.2		8.4		0.7			1.0
$\Psi_{CTO\to7+}^\circ$			7.6		0.0		0.1	4.1	
$\Psi_{CTO\to8+}^\circ$			0.1		4.4		8.1	0.0	
$\Psi_{CTO\to6-}^\circ$			0.0		16.9		9.1	0.3	
$\Psi_{CTO\to7-}^\circ$		0.0		0.1		14.3			0.3
$\Psi_{CTO\to8-}^\circ$		5.1		0.5		0.0			1.9
Total weight[b]		93.9	81.7	82.5	83.8	79.0	83.4	82.9	79.6
Assignment[c]		[G]	[L_b]	[L_a]				[B_b]	

a), b), and c): See Text for definitions.

respectively.

According to Table 4, Bands I, II, and III can reasonably be assigned to the L_b, L_a, and B_b states respectively. As in the case of 1,4-diol, the L_b state interacts not with the L_a state, but with the B_b state, because of symmetry. The intensity of Band I is derived from the mixing with the B_b. The $\Psi_{CTO\to7+}^\circ$ and $\Psi_{CTO\to6+}^\circ$ states make weight contributions to the Ψ_1 and Ψ_2 states of 7.6 and 8.4% respectively.

The B_b state interacts not with the A_g^- state, but with the B_{1g}^+ and B_{1g}^- states. Hence, there is no interaction characteristic of naphthalene derivatives with a substituent at the 1-position. It is noteworthy that the interactions of the B_b state with the B_{1g}^+, A_g^-, and B_{1g}^- states are extremely small in extent in 1,8-diol compared with the other diols studied in this paper (see below).

Table 5 shows the results of the CA for 1,8-diol using the state functions composed of 1-naphthol and the OH substituent as the reference state functions. Band i of 1-naphthol contributes to the Ψ_1 state by a weight of 51.5%. Bands II and III have no reference states which singly exceed 50.0%. The total weights of 1,8-diol are smaller than those of 1,4-diol by about 20—30%.

2,3-Naphthalenediol. Figure 2 shows the absorption spectrum of 2,3-diol in isooctane, including the

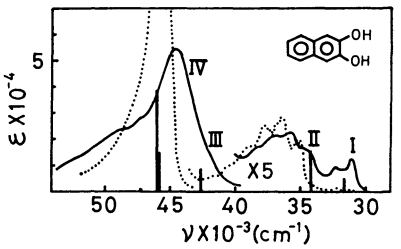

Fig. 2. Absorption spectrum in isooctane solution of 2,3-naphthalenediol. The dotted curve and the lengths of lines have the same meaning as in Fig. 1.

TABLE 5. CONFIGURATION ANALYSIS FOR 1,8-NAPHTHALENEDIOL FROM 1-NAPHTHOL (WEIGHT IN PERCENT)

Reference state		Absorption band (upper) and state function (lower)							
			I	II				III	
Wave function[a]	Absorption band	Ψ_G	Ψ_1	Ψ_2	Ψ_3	Ψ_4	Ψ_5	Ψ_6	Ψ_7
Ψ_G°		66.6	0.0	3.3	0.6	0.0	0.7	0.0	0.0
Ψ_1°	i	0.1	51.5	0.7	0.3	1.6	0.0	2.5	0.1
Ψ_2°	ii	1.1	1.0	48.3	2.9	0.5	2.8	0.2	0.1
Ψ_3°		1.8	0.1	1.9	45.9	3.4	0.8	0.3	0.4
Ψ_4°	iii	0.1	2.3	0.0	2.5	42.8	0.4	9.7	0.0
Ψ_5°		1.1	0.0	5.6	3.7	0.2	37.3	3.9	4.4
Ψ_6°	iv	0.3	0.0	0.4	0.9	9.5	2.9	47.1	0.0
Ψ_7°		0.0	0.1	0.3	0.0	0.1	3.8	0.2	59.4
$\Psi_{CTO\to7}^\circ$		4.1	0.0	3.9	7.4	0.3	4.7	0.1	0.4
$\Psi_{CTO\to8}^\circ$		0.0	3.4	0.1	0.0	5.1	0.0	1.8	0.1
$\Psi_{CTO\to9}^\circ$		2.3	0.0	0.1	2.8	0.0	2.6	0.0	0.7
Total weight[b]		85.4	62.5	71.1	69.2	64.7	62.2	69.8	66.7
Assignment[c]		[G]	[i]						

a), b), and c): See Text for definitions.

Table 6. Configuration analysis for 2,3-naphthalenediol from naphthalene (weight in percent)

Reference state		Absorption band (upper) and state function (lower)							
			I	II	III		IV		
Wave function[a]	Symmetry type	Ψ_G	Ψ_1	Ψ_2	Ψ_3	Ψ_4	Ψ_5	Ψ_6	Ψ_7
Ψ_G°	A_g^-	80.5	0.3		1.1			1.3	
Ψ_1°	B_{3u}^+, L_b	0.0	68.3		6.7			0.3	
Ψ_2°	B_{2u}^+, L_a			74.7		1.4	0.4		1.1
Ψ_3°	B_{1g}^+			0.5		74.0	1.1		0.0
Ψ_4°	A_g^-	0.0	1.1		45.2			15.4	
Ψ_5°	B_{3u}^+, B_b	0.2	0.6		10.8			54.7	
Ψ_6°	B_{1g}^-			0.2		0.0	1.4		74.3
Ψ_7°	B_{2u}^+			0.2		0.4	48.6		0.8
$\Psi_{CTO\to6+}^\circ$				5.7		2.4	1.5		2.6
$\Psi_{CTO\to7+}^\circ$		5.8	2.7		0.1			4.0	
$\Psi_{CTO\to8+}^\circ$				0.0		2.9	0.0		2.7
$\Psi_{CTO\to6-}^\circ$		3.9	10.1		8.2			2.0	
$\Psi_{CTO\to7-}^\circ$				2.0		0.6	21.5		0.6
$\Psi_{CTO\to8-}^\circ$		1.4	0.2		6.4			3.3	
Total weight[b]		91.9	83.5	83.5	79.6	82.1	84.1	82.2	82.6
Assignment[c]		[G]	[L_b]	[L_a]				[B_b]	

a), b) and c): See Text for definitions.

Table 7. Configuration analysis for 2,3-naphthalenediol from 2-naphthol (weight in percent)

Reference state		Absorption band (upper) and state function (lower)							
			I	II	III		IV		
Wave function[a]	Absorption band	Ψ_G	Ψ_1	Ψ_2	Ψ_3	Ψ_4	Ψ_5	Ψ_6	Ψ_7
Ψ_G°		89.5	0.1	0.7	0.3	0.4	0.8	0.3	0.1
Ψ_1°	i	0.0	75.3	9.2	0.9	0.2	2.5	0.0	0.0
Ψ_2°	ii	0.1	6.5	76.4	1.4	0.7	0.0	0.6	0.2
Ψ_3°		0.0	0.0	0.0	45.8	40.0	2.0	1.1	0.1
Ψ_4°		0.1	0.1	0.2	19.7	39.9	3.3	17.1	0.5
Ψ_5°	iii	0.0	0.4	0.2	9.8	5.5	2.7	47.0	19.7
Ψ_6°		0.0	0.3	0.0	2.5	0.2	13.5	6.0	58.6
Ψ_7°		0.1	0.3	0.1	0.1	0.1	50.0	11.7	6.8
$\Psi_{CTO\to7}^\circ$		2.8	5.6	2.8	5.0	1.2	0.6	1.8	1.4
$\Psi_{CTO\to8}^\circ$		2.7	1.6	0.7	0.0	0.2	11.6	2.0	0.2
$\Psi_{CTO\to9}^\circ$		0.8	0.2	0.0	3.8	1.4	0.0	1.9	1.5
Total weight[b]		96.2	91.6	90.5	89.9	89.9	91.4	90.9	90.4
Assignment[c]		[G]	[i]	[ii]					

a), b), and c): See Text for definitions.

calculated data.

From Table 6, the mixing between the B_b and A_g^- states is responsible for the Ψ_3 (Band III) and Ψ_6 (Band IV) states, and Band IV is composed of the two states which correspond to the transitions to the Ψ_5 and Ψ_6 states. Bands I and II are assigned to the L_b and L_a respectively. The $\Psi_{CTO\to6-}^\circ$ state makes contributions of 10.1 and 8.2% to the Ψ_1 and Ψ_3 states. The $\Psi_{CTO\to7-}^\circ$ state makes an important weight contribution to the Ψ_5 state of 21.5%.

Table 7 shows the results of the CA for 2,3-diol using the state functions composed of 2-naphthol and the OH substituent as the reference state functions. Bands I and II are assigned to Bands i and ii of 2-naphthol respectively. There is large mixing among the Ψ_3°, Ψ_4°, and Ψ_5° states and among the Ψ_5°, Ψ_6°, and Ψ_7° states. These mixings are responsible for Bands III and IV. The $\Psi_{CTO\to7}^\circ$ state makes contributions of 5.6, 2.8, and 5.0% to the Ψ_1, Ψ_2, and Ψ_3 states respectively. The $\Psi_{CTO\to8}^\circ$ state makes a contribution of 11.6% to the Ψ_5 state.

The total weights are about 90%, so that the electronic states of 2,3-diol are well expanded in terms of the electronic states of 2-naphthol and the charge-transfer states from the substituent to 2-naphthol, as in the case of 1,4-diol.

2,7-Naphthalenediol. The absorption spectrum of 2,7-diol in isooctane is shown in Fig. 3, together with the calculated data. Table 1 shows that Band IV is composed of the transitions of the Ψ_5, Ψ_6, and Ψ_7 states. From Table 8, Bands I and II may be assigned to the L_b and L_a states respectively. The Ψ_5 state is made from the interaction among the B_{1g}^+, B_b, and B_{1g}^- states. The $\Psi_{CTO\to6-}^\circ$ state contributes to the Ψ_1 state by a weight of 10.5% and to the Ψ_4 state by a weight of 6.4%.

Table 9 shows the results of the CA of the 2,7-diol

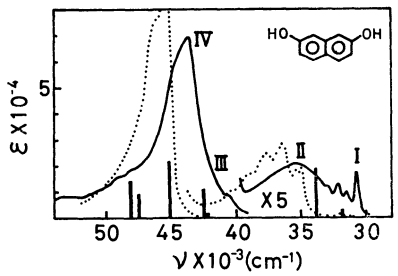

Fig. 3. Absorption spectrum in isooctane solution of 2,7-naphthalenediol. The dotted curve and the lengths of lines have the same meaning as in Fig. 1.

based on 2-naphthol. The results of the CA indicate that Bands I, II, and IV are closely connected with Bands i, ii, and iii of 2-naphthol respectively. The total weights of 2,7-diol are smaller than those of 2,3-diol by about 20—30%. This is analogous to the situation between 1,4- and 1,8-diol.

Remarks and Conclusions. When one chooses 1- or 2-naphthol as the parent compound in the CA, there is a marked difference in the total weight depending on the type of naphthalenediol. The total weights for the 1,4- and 2,3-diols, which have two substituents in the same benzene ring, are slightly larger on the naphthol basis than those on the naphthalene basis, whereas the total weights for 1,8- and 2,7-diols, which have one substituent in every benzene ring, are considerably smaller on the naphthol basis than those on the naphthalene basis. Such a marked difference indicates that the state functions of naphthols are a good basis for the expansion of the state functions of 1,4- and 2,3-diols; however, they are a poor basis for 1,8- and 2,7-diols. This suggests that the interaction between two substituents in diols differs depending on whether or not the two substituents lie on the same benzene ring.

Table 8. Configuration analysis for 2,7-naphthalenediol from naphthalene (weight in percent)

Reference state		Absorption band (upper) and state function (lower)							
			I	II		III	IV		
Wave function[a]	Symmetry type	Ψ_G	Ψ_1	Ψ_2	Ψ_3	Ψ_4	Ψ_5	Ψ_6	Ψ_7
Ψ_G°	A_g^-	79.0		1.9	0.0				2.0
Ψ_1°	B_{3u}^-, L_b		67.3			3.1	0.0	0.0	
Ψ_2°	B_{2u}^+, L_a	0.3		70.9	0.9				0.4
Ψ_3°	B_{1g}^+		1.0			51.4	17.6	2.5	
Ψ_4°	A_g^-	0.0		0.1	53.3				6.5
Ψ_5°	B_{3u}^+, B_b		0.3			13.6	36.0	18.4	
Ψ_6°	B_{1g}^-		0.0			0.8	15.5	55.9	
Ψ_7°	B_{2u}^+	0.2		0.0	3.4				61.2
$\Psi_{CTO\to6+}^\circ$		3.7		5.3	7.5				0.0
$\Psi_{CTO\to7+}^\circ$			2.4			3.4	2.4	1.1	
$\Psi_{CTO\to8+}^\circ$			0.1			2.1	4.0	2.0	
$\Psi_{CTO\to6-}^\circ$			10.5			6.4	4.0	0.3	
$\Psi_{CTO\to7-}^\circ$		6.5		0.6	5.6				8.6
$\Psi_{CTO\to8-}^\circ$		1.3		0.0	7.0				1.4
Total weight[b]		91.1	82.2	79.9	80.3	82.0	80.0	80.9	81.9
Assignment[c]		[G]	[L_b]	[L_a]		[B_{1g}^+]		[B_{1g}^-]	[B_{2u}^+]

a), b), and c) See Text for definitions.

Table 9. Configuration analysis for 2,7-naphthalenediol from 2-naphthol (weight in percent)

Reference state		Absorption band (upper) and state function (lower)							
			I	II		III	IV		
Wave function[a]	Absorption band	Ψ_G	Ψ_1	Ψ_2	Ψ_3	Ψ_4	Ψ_5	Ψ_6	Ψ_7
Ψ_G°		70.8	0.3	1.3	0.0	0.0	0.0	0.0	0.4
Ψ_1°	i	0.3	56.5	4.4	0.1	0.0	0.4	0.0	0.3
Ψ_2°	ii	0.0	4.6	55.8	2.0	0.9	0.0	0.0	0.0
Ψ_3°		0.5	0.0	1.0	21.1	30.4	0.5	0.5	2.0
Ψ_4°		0.1	1.6	0.1	27.3	23.7	3.9	0.4	0.2
Ψ_5°	iii	0.3	0.2	0.6	0.7	1.8	51.8	0.5	2.8
Ψ_6°		0.0	0.3	0.1	0.0	0.7	0.5	57.3	6.4
Ψ_7°		0.1	0.4	0.0	0.0	3.5	1.3	7.9	54.5
$\Psi_{CTO\to7}^\circ$		1.5	4.7	2.7	3.9	2.5	1.4	0.2	0.0
$\Psi_{CTO\to8}^\circ$		2.8	0.7	0.4	2.1	1.8	1.5	0.4	3.5
$\Psi_{CTO\to9}^\circ$		0.5	0.0	0.0	2.4	1.1	1.8	1.0	0.8
Total weight[b]		81.3	70.7	67.8	61.8	67.8	65.3	70.4	73.0
Assignment[c]		[G]	[i]	[ii]			[iii]		

a), b), and c) See Text for definitions.

References

1) H. Baba and S. Suzuki, *Bull. Chem. Soc. Jpn.*, **34**, 82 (1961).
2) K. Nishimoto, *J. Phys. Chem.*, **67**, 1443 (1963); *Theor. Chim. Acta*, **7**, 207 (1967).
3) L. S. Forster and K. Nishimoto, *J. Am. Chem. Soc.*, **87**, 1459 (1965).
4) Y. Tanizaki and S. Kubodera, *J. Mol. Spectrosc.*, **24**, 1 (1967).
5) S. M. Lyle and E. C. Lim, *Chem. Phys. Lett.*, **17**, 367 (1973).
6) S. Suzuki, T. Fujii, and H. Baba, *J. Mol. Spectrosc.*, **47**, 243 (1973).
7) S. Suzuki, T. Fujii, and T. Ishikawa, *J. Mol. Spectrosc.*, **57**, 490 (1975).
8) S. Suzuki and T. Fujii, *J. Mol. Spectrosc.*. **61**, 350 (1976).
9) C. Daglish, *J. Am. Chem. Soc.*, **72**, 4859 (1950).
10) D. M. Hercules and L. B. Rogers, *Spectrochim. Acta*, **1959**, 393.
11) K. Nishimoto and R. Fujishiro, *Bull. Chem. Soc. Jpn.*, **32**, 445 (1959); *ibid.*, **35**, 390 (1962).
12) K. Hara, T. Takemura, and H. Baba, *J. Mol. Spectrosc.*, **50**, 90 (1974).
13) H. Baba and S. Suzuki, *Bull. Chem. Soc. Jpn.*, **40**, 2457 (1967).
14) H. Baba, S. Suzuki, and T. Takemura, *J. Chem. Phys.*, **50**, 2078 (1969).
15) H. Baba and I. Yamazaki, *J. Mol. Spectrosc.*, **44**, 118 (1972).
16) T. Takemura, K. Hara, and H. Baba, *Bull. Chem. Soc. Jpn.*, **44**, 977 (1971).
17) S. Suzuki and T. Fujii, *Bull. Chem. Soc. Jpn.*, **48**, 835 (1975).
18) E. A. Hochstein, C. R. Stephen, L. H. Conover, P. P. Regna, R. Pasternack, P. N. Gordon, F. J. Pilglim, K. J. Brinigs, and R. B. Woodward, *J. Am. Chem. Soc.*, **75**, 5455 (1953).

The Surface Tension of Aqueous Solutions Saturated with Triacetin-Tributyrin Mixtures

Noriaki FUNASAKI and Sakae HADA

Kyoto College of Pharmacy, Yamashina, Kyoto 607

(Received March 12, 1976)

The surface tension of aqueous solutions saturated with triacetin–tributyrin mixtures was measured in order to study the phase equilibria among an adsorbed monolayer (m), an aqueous solution (w), and an oily mixture (l). The variation in the surface tension, γ, of saturated aqueous solutions with an increase in the number of moles, m_t, of the added mixtures depended on the mole fractions, x_2, of tributyrin in the mixtures; the γ value remained unchanged in the case of $x_2=0.0027$, decreased in the case of $x_2>0.0027$, and increased in the case of $x_2<0.0027$. The results of the theoretical analysis of the γ *vs.* m_t curves gave the mole fractions, x_2^l, of tributyrin in the oily mixtures. The x_2^l values thus evaluated agreed with those determined gas-chromatographically. It was found that all of the γ *vs.* x_2^m, γ *vs.* x_2^l, and γ *vs.* x_2^w curves have a minimum, at which the γ values are identical and at which $x_2^m=x_2^l>x_2^w$. The characteristics of these curves were explained thermodynamically on the basis of the assumption that triacetin and tributyrin form a regular mixture in a monolayer as well as in a liquid.

The overcompression and the dissolution of a spread monolayer often make it impossible to study the equilibrium state between the spread monolayer and the bulk of the film-forming substance on an aqueous surface.[1-4] When a film-forming substance is soluble in the underlying water, the equilibria among the adsorbed monolayer, the bulk, and the saturated aqueous solution are easily established.

Hence, the present authors measured the surface tension of aqueous solutions saturated with triacetin–tributyrin mixtures and discussed thermodynamically the results of the adsorbed monolayer-bulk equilibrium in comparison with those of the spread monolayer-bulk equilibrium.[2-6]

Theoretical

We consider a system composed of a liquid mixture of Component 1 and 2 (oily phase) and an aqueous solution (aqueous phase) in equilibrium with each other. The notations used hereafter are summarized in Table 1. The superscripts, w, l, and m mean the aqueous phase, the oily phase, and an adsorbed monolayer at the air-water interface. The superscript o means the pure substance or the standard state. The subscripts 1 and 2 mean triacetin and tributyrin, and the subscript t means the sum of the parts of triacetin and tributyrin.

Table 1. List of notations

γ: surface tension of an aqueous solution
F: surface pressure on an aqueous surface
V: total volume of water in the system
C: concentration of an aqueous solution
C_i^{ow}: solubility of a pure liquid, i, in water
Γ: adsorption amount at the air-water interface
$\bar{A}_i$: partial molecular area of Component i
μ_i: chemical potential of Component i
B: constant representing the intermolecular interaction
m: moles of triglyceride
R: gas constant
k: Boltzmann constant
T: absolute temperature
N: Avogadro number
$C_t=(m_1+m_2)/V$
$x_2^l=m_2^l/(m_1^l+m_2^l)$
$x_2^m=\Gamma_2/(\Gamma_1+\Gamma_2)$
$x_2^w=C_2^w/(C_1^w+C_2^w)$

Surface Tension of Saturated Aqueous Solutions. Although the following consideration is entirely general, we illustrate the γ *vs.* log C_t curves for triacetin–tributyrin mixtures in Fig. 1a. We consider the interrelation between the curves of γ *vs.* log C_t and γ *vs.* x_2^l in the presence of both aqueous and oily phases.

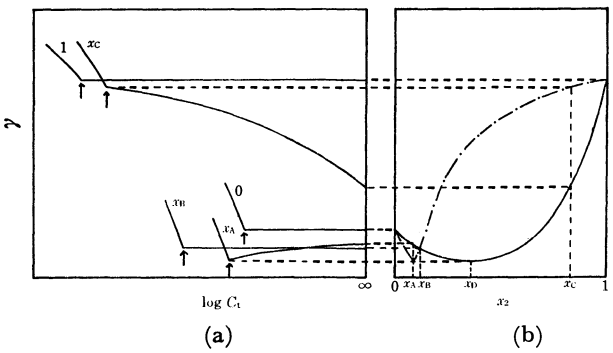

Fig. 1. Schematic interrelationship between curves of (a) γ *vs.* log C_t, and (b) γ *vs.* x_2^l (solid line) and x_2^w (chained line). Arrows indicate saturation.

When we drop a liquid mixture with the composition of x_2 into water of a given volume, V, we have a kinkpoint on the γ *vs.* log C_t curve, as is shown in Fig. 1a. The concentration at the kinkpoint, C_t^w (shown by an arrow), indicates the solubility. The relation between the surface tension and the mole fraction of Component 2 in the aqueous solution, x_2^w (equal to the value of the dropped-in liquid mixture, x_2) at the kinkpoint is shown by a chained line in Fig. 1b. When we drop in an infinite amount of a liquid mixture, though, we can neglect the amount dissolved into the water. Thus, we can obtain the relation between the surface tension at $C_t\to\infty$ and the mole fraction of Component 2 in the oily phase, x_2^l (equal to the value of the dropped-in liquid mixture, x_2), as is shown by a solid line in Fig. 1b. This relation can also be obtained through the simultaneous determination of the surface tension of the aqueous solution and the composition of the oily mixture

in equilibrium with the former.

As is shown in Fig. 1a, the surface tension of the aqueous solution saturated with the pure substance, 1 (Curve 0) or 2 (Curve 1), remains unchanged regardless of the presence of an excess of the substance. In particular, the liquid mixture with the composition, x_B, at which the solid and chained lines in Fig. 1b intersect each other, behaves as if it were a pure substance in this respect (Curve x_B). On the other hand, as the dropped-in amount of a liquid mixture at $x_2<x_B$ increases, the surface tension passes through a minimum (*e.g.*, Curve x_A). When a liquid mixture at $x_2>x_B$ is dropped in, the surface tension gradually decreases with an increase in the C_t (*e.g.*, Curve x_C). In the case of mixtures, a variation in the surface tension of aqueous solutions with an increase in C_t results from the simultaneous variation of the compositions in the aqueous and oily phases.

We can obtain the relation between x_2^w and x_2^l at an equilibrium state from Fig. 1b. If a horizontal line is drawn at a given surface tension in Fig. 1b, the points of the intersection of this line with a solid and a chained line give the mole fractions of Component 2 in the oily and aqueous phases respectively. For example, it is found that the aqueous solution with the composition of x_A is in equilibrium with the oily mixture with the composition of x_D.

When we drop a mixture with the composition of x_2 into water above its solubility, we can calculate the γ *vs.* log C_t relation, using the experimental values of γ, C_1^w, and C_2^w of the aqueous solution in equilibrium with the oily mixture with the composition of x_2^l. The total moles of Components 1 and 2 can be given by the following equations:

$$C_t x_1 V = C_1^w V + m^l x_1^l \quad (1)$$

$$C_t x_2 V = C_2^w V + m^l x_2^l \quad (2)$$

Eliminating m^l, the total moles of the oily mixtures, from Eqs. 1 and 2, we obtain Eq. 3:

$$C_t = \frac{C_1^w x_2^l - C_2^w x_1^l}{x_1 x_2^l - x_2 x_1^l} \quad (3)$$

Using Eq. 3, we can calculate a C_t value at a given surface tension for the saturated aqueous solution.

Conversely, we can also obtain the expression for x_2^l from Eq. 3:

$$x_2^l = \frac{C_t x_2 - C_2^w}{C_t - C_1^w - C_2^w} \quad (4)$$

Hence, we can calculate an x_2^l value (the composition of the oily mixture) at a given surface tension from Eq. 4, using the γ *vs.* log C_t relation.

Equilibria among Aqueous, Oily, and Surface Phases. Assuming that triacetin and tributyrin form a regular solution in an oily mixture as well as in an adsorbed monolayer, and that they behave as a dilute solution in an aqueous solution, we can express the chemical potentials, μ_i, of Component i (i=1 or 2) in the oily mixture, the adsorbed monolayer, and the aqueous solution as follows:

$$\mu_i^l = \mu_i^{ol} + RT \ln x_i^l + B^l(1-x_i^l)^2 \quad (5)$$

$$\mu_i^m = \mu_i^{om} + RT \ln x_i^m + B^m(1-x_i^m)^2 + N\bar{F}\bar{A}_i \quad (6)$$

$$\mu_i^w = \mu_i^{ow} + RT \ln C_i^w \quad (7)$$

where μ_i^{ol} is the chemical potential of the pure liquid, i; μ_i^{om} and μ_i^{ow} are the standard chemical potentials, and $\bar{A}_i$ is the partial molecular area of Component i. Equation 6 has also been used for a spread monolayer.[3-6]

Equilibrium between Aqueous and Oily Phases. From the equality of the chemical potential in the phase equilibria, we can obtain:

$$\mu_1^{ow} + RT \ln C_1^w = \mu_1^{ol} + RT \ln x_1^l + B^l(x_2^l)^2 \quad (8)$$

$$\mu_2^{ow} + RT \ln C_2^w = \mu_2^{ol} + RT \ln x_2^l + B^l(x_1^l)^2 \quad (9)$$

using Eqs. 5 and 7. When x_i^l is equal to 1, we obtain from Eqs. 8 and 9:

$$\mu_1^{ow} + RT \ln C_1^{ow} = \mu_1^{ol} \quad (10)$$

$$\mu_2^{ow} + RT \ln C_2^{ow} = \mu_2^{ol} \quad (11)$$

where C_i^{ow} represents the solubility of the pure liquid, i, in water. Using Eqs. 8—11, we obtain Eqs. 12—14:

$$C_1^w = C_1^{ow} x_1^l \exp\left[\frac{B^l}{RT}(x_2^l)^2\right] \quad (12)$$

$$C_2^w = C_2^{ow} x_2^l \exp\left[\frac{B^l}{RT}(x_1^l)^2\right] \quad (13)$$

$$C_t^w = C_1^{ow} x_1^l \exp\left[\frac{B^l}{RT}(x_2^l)^2\right] + C_2^{ow} x_2^l \exp\left[\frac{B^l}{RT}(x_1^l)^2\right] \quad (14)$$

If the B^l value is assumed appropriately, we can calculate the C_t^w *vs.* x_2^l curve from Eq. 14, and also the C_t^w *vs.* x_2^w curve from Eqs. 12 and 13.

Equilibrium between Oily and Surface Phases. In the equilibrium state of the two phases, we can obtain from Eqs. 5 and 6 the following equations:

$$\mu_1^{ol} + RT \ln x_1^l + B^l(x_2^l)^2 = \mu_1^{om} + RT \ln x_1^m + B^m(x_2^m)^2 + N\bar{F}\bar{A}_1 \quad (15)$$

$$\mu_2^{ol} + RT \ln x_2^l + B^l(x_1^l)^2 = \mu_2^{om} + RT \ln x_2^m + B^m(x_1^m)^2 + N\bar{F}\bar{A}_2 \quad (16)$$

Using Eqs. 15 and 16, as has been shown previously,[5] we can obtain the following equations:

$$x_1^l \exp\left[B^l (x_2^l)^2\right] = x_1^m \exp\left[\frac{B^m}{RT}(x_2^m)^2 + \frac{F\bar{A}_1 - F_{1e}A_{1e}}{kT}\right] \quad (17)$$

$$x_2^l \exp\left[\frac{B^l}{RT}(x_1^l)^2\right] = x_2^m \exp\left[\frac{B^m}{RT}(x_1^m)^2 + \frac{F\bar{A}_2 - F_{2e}A_{2e}}{kT}\right] \quad (18)$$

where F_{ie} and A_{ie} are the surface pressure and the molecular area at the interface between the air and an aqueous solution saturated with a pure substance, i. We can obtain the F *vs.* x_i^l and F *vs.* x_i^m relations by solving Eqs. 17 and 18 simultaneously if the $\bar{A}$ value is found and if the B^l and B^m values are assumed appropriately.

Equilibrium between Aqueous and Surface Phases. We can calculate the F *vs.* x_i^w curve using Eqs. 12, 13, 17, and 18 if the B^l and B^m values are assumed appropriately.

Experimental

Materials. The triacetin and tributyrin used were

obtained from Nakarai Chemicals.[7] The ion-exchanged water was twice distilled before use.

Measurement. A triacetin–tributyrin mixture was dropped into water of a given volume with a weight-pippete and the surface tension of the aqueous solution was measured at 37±0.2 °C by means of the Wilhelmy method.[7] The concentration, C, was expressed on a solute mole/water volume basis. When the amount of the oily mixture was relatively great, we measured the surface tension of the aqueous solution separated from the oily mixture.

The composition of the oily mixture separated from the aqueous solution was determined with a Shimadzu gas chromatograph, GC-3BT. The water content in the oily mixtures was found to be negligibly small.

Results

Figure 2 shows the plots of the surface tension of aqueous solutions, γ, against the logarithm of the total concentration, C_t, when a triacetin–tributyrin mixture with the composition of x_2 was dropped into the water. The kinkpoints (indicated by arrows) on the γ *vs.* log C_t curves indicate saturation.

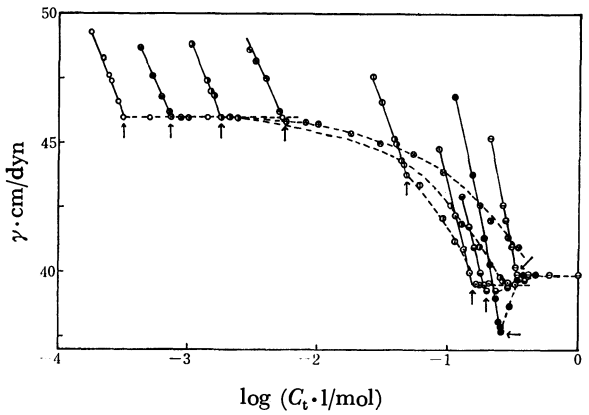

Fig. 2. The γ *vs.* log C_t relations at different compositions x_2: ○; 1, ⊗; 0.500, ◑; 0.234, ⊕; 0.0863, ⓘ; 0.010, ⊙; 0.0027, ◒; 0.0020, ●; 0.00059, ⊖; 0. Dotted lines are calculated from Eq. 3.

The surface tension above the concentration of the saturation points remained unchanged when the liquid dropped in was either a pure substance (triacetin or tributyrin) or a mixture at x_2=0.0027, which is nearly equal to the composition of the intersection of the solid lines in Fig. 4 to be described below. On the other hand, the γ value increased in the case of mixtures at $x_2<0.0027$, but decreased in the case of mixtures at $x_2>0.0027$, with an increase in the C_t.

Figure 3 shows the relation between the surface tension and the logarithm of the total concentration of triacetin, C_1, when triacetin was dropped into tributyrin solutions with the concentration of C_2. The kinkpoints (shown by arrows) indicate the saturation.

The open circles in Fig. 4 show the relation between the surface tension and the mole fraction of tributyrin in an aqueous solution, x_2^w. Furthermore, the closed circles in Fig. 4 show the relation between the surface tension of the aqueous solutions and the mole fraction of tributyrin in the oily phase (in equilibrium with the former), x_2^l, which was determined gas-chromatographically.

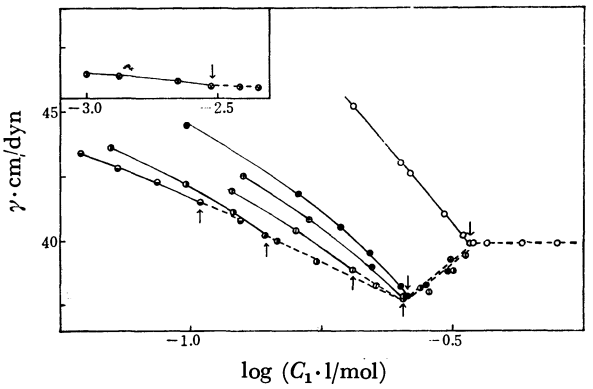

Fig. 3. The γ *vs.* log C_1 relations at different concentrations of tributyrin C_2 (mol/l)×10⁴: ⊗; 3.94, ◒; 3.31, ◑; 3.02, ⓘ; 1.89, ⊕; 1.46, ●; 1.13, ○; 0. Dotted lines are calculated from Eq. 22.

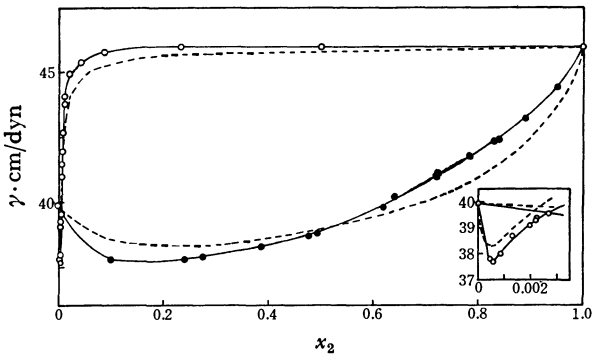

Fig. 4. The curves of γ *vs.* x_2^l (closed circles) and γ *vs.* x_2^w (open circles) with partial expansion of tributyrin-poor region as an insert. Dotted lines are calculated from Eqs. 12, 13, 17, and 18 with $B^l=0.5RT$ and $B^m=-1.9RT$.

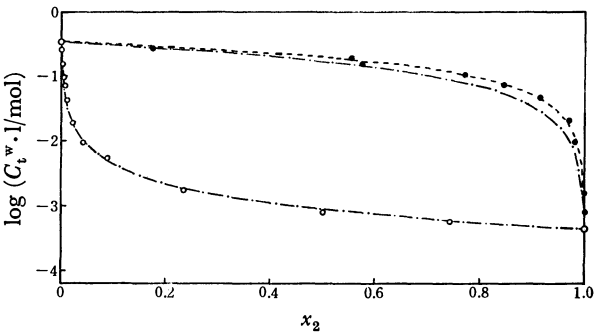

Fig. 5. The plots of log C_t^w *vs.* x_2^w (open circles) and *vs.* x_2^l (closed circles). Chained and dotted lines are calculated from Eqs. 12—14 with $B^l=0$ and $B^l=0.5RT$.

The open circles in Fig. 5 show the log C_t^w *vs.* x_2^w relation obtained from the kinkpoints (indicated by arrows) in Figs. 2 and 3. In addition, the closed circles in Fig. 5 show the log C_t^w *vs.* x_2^l curve determined from the x_2^l *vs.* x_2^w relation, which was obtained from the intersections of the horizontal line with the γ *vs.* x_2^w and γ *vs.* x_2^l curves in Fig. 4.

We can write the Gibbs adsorption equation in aqueous solutions of Components 1 and 2 as:[8]

$$-d\gamma = \Gamma_1 RT\, d\ln C_1^w + \Gamma_2 RT\, d\ln C_2^w \quad (19)$$

In the case of a constant C_1^w/C_2^w ratio, Eq. 19 is reduced to:

$$-d\gamma = (\Gamma_1+\Gamma_2)RT\, d\ln C_t^w \quad (20)$$

Hence, we can obtain the γ *vs.* $(\Gamma_1+\Gamma_2)$ relation for the adsorbed monolayers in equilibrium with oily mixtures; the respective values of γ and $(\Gamma_1+\Gamma_2)$ are evaluated at the kinkpoints in Fig. 2.

On the other hand, in the case of a constant C_2^w, Eq. 19 is reduced to:

$$-d\gamma = \Gamma_1 RT\, d\ln C_1^w \quad (21)$$

Hence, we can obtain the γ *vs.* Γ_1 relation for the adsorbed monolayers in equilibrium with oily mixtures; the respective values of γ and Γ_1 are evaluated at the kinkpoints in Fig. 3.

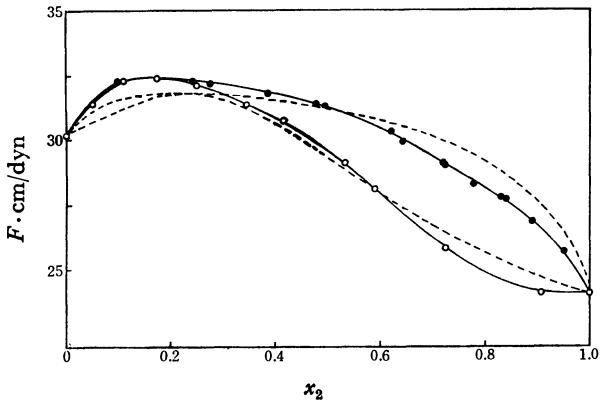

Fig. 6. The plots of F *vs.* x_2^1 (closed circles) and *vs.* x_2^m (open circles). Dotted lines are calculated from Eqs. 17 and 18 with $B^1=0.5RT$ and $B^m=-1.9RT$.

Thus, we can obtain the relation between the surface pressure, F, and the mole fraction, x_2^m, of tributyrin in an adsorbed monolayer from the combination of the γ *vs.* $(\Gamma_1+\Gamma_2)$ and γ *vs.* Γ_1 relations. This result, shown by open circles in Fig. 6, is found to be similar to that for the spread mixed monolayers of 1-hexadecanol and 1-octadecanol.[4] The upper and lower curves in Fig. 6 correspond to the curves of the equilibrium-spreading pressure and the collapse pressure respectively.

Discussion

Surface Tensions of Saturated Aqueous Solutions. We can calculate a C_t value by substituting into Eq. 3 the values of C_1^w and C_2^w (determined from the kinkpoints in Figs. 2 and 3) and x_2^1 (obtained from the upper solid curve in Fig. 6) at a given surface tension when a liquid mixture with the composition of x_2 is dropped in and when the aqueous and oily phases coexist in equilibrium. The γ *vs.* log C_t curves thus obtained are shown by dotted lines in Fig. 2. Similarly, when we drop triacetin into a tributyrin solution with the concentration of C_2, we can calculate the C_1 value by means of the following equation:

$$C_1 = C_1^w + \frac{(C_2-C_2^w)}{x_2^1} \times x_1^1 \quad (22)$$

Here, the experimental values of C_1^w, C_2^w, and x_2^1 at a given surface tension are substituted into Eq. 22. The γ *vs.* log C_1 curves thus obtained are shown by dotted lines in Fig. 3. The dotted lines in Figs. 2 and 3 were found to be in good agreement with the experimental results.

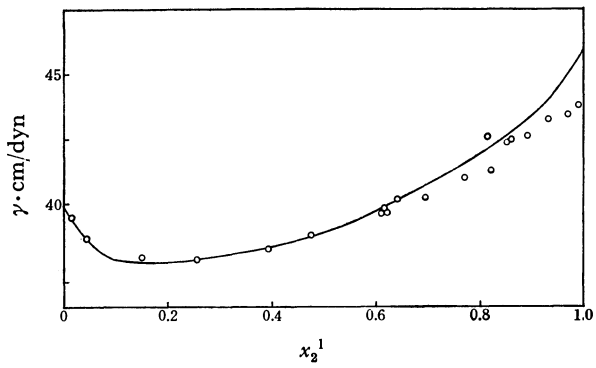

Fig. 7. The γ *vs.* x_2^1 relation in which a solid line is etermined gas-chromatographically and open circles are calculated from Eq. 4.

Conversely, we can calculate an x_2^1 value at a given surface tension by using Eq. 4 and the experimental results of the γ *vs.* log C_t curves in Fig. 2. The results thus calculated are plotted by open circles in Fig. 7. The solid line is drawn through the x_2^1 values determined gas-chromatographically. Thus, it was found that we can evaluate the composition of oily mixtures from the concentration dependence of the surface tension of aqueous solutions saturated with oily mixtures.

Equilibria among Aqueous, Oily, and Surface Phases. Assuming that $B^1=0.5RT$, we can calculate the log C_t^w *vs.* x_2^w (lower curve) and log C_t^w *vs.* x_2^1 (upper curve) relations from Eqs. 12—14. These relations, shown by dotted lines in Fig. 5, agree well with the experimental results. The chained lines in Fig. 5 show the relations calculated from Eqs. 12—14 with $B^1=0$, *viz.*, as an ideal solution in the oily mixture. It should be noted that the B^1 value has little effect on the log C_t^w *vs.* x_2^w relation.

Furthermore, assuming that $B^1=0.5RT$ and $B^m=-1.9RT$, we can calculate the F *vs.* x_2^m (lower curve) and F *vs.* x_2^1 (upper curve) relations from Eqs. 17 and 18. These relations are shown by dotted lines in Fig. 6. In the above calculation, we used the values of $F_{1e}=30.19$ dyn/cm, $F_{2e}=24.12$ dyn/cm, $A_{1e}=41.6$ Å^2/molec, $A_{2e}=81.3$ Å^2/molec, $C_1^{ow}=0.343$ mol/l, and $C_2^{ow}=4.41\times10^{-4}$ mol/l and assumed that the $\bar{A}$ value is equal to the molecular area in an adsorbed monolayer of the pure substance.

The dotted lines in Fig. 4 are reproduced from the dotted lines in Figs. 5 and 6.

The dotted lines in Figs. 4, 5, and 6 represent fairly well the trend of the experimental results; this means that the above thermodynamic treatment is approximately valid.

References

1) G. L. Gaines, Jr., "Insoluble Monolayers at Liquid-Gas Interfaces," Interscience Publishers, New York (1966), pp. 144—155.
2) M. Nakagaki, N. Funasaki, and K. Fujita, *Nippon Kagaku Zasshi*, **93**, 243 (1972).
3) M. Nakagaki and N. Funasaki, *Bull. Chem. Soc., Jpn.*, **47**, 2094 (1974).
4) N. Funasaki and M. Nakagaki, *Bull. Chem. Soc. Jpn.*, **48**, 2727 (1975).
5) M. Nakagaki and N. Funasaki, *Bull. Chem. Soc. Jpn.*, **47**, 2482 (1974).
6) N. Funasaki, *Nippon Kagaku Kaishi*, **1975**, 1841.
7) N. Funasaki, S. Hada, and K. Suzuki, *Chem. Pharm. Bull.*, **24**, 731 (1976).
8) R. Defay, I. Prigogine, A. Bellemans, and D. H. Everett, "Surface Tension and Adsorption," Longmans, London (1966), p. 86.

The Partial Molar Volumes of Normal Alkanols in Aqueous Sodium Dodecyl Sulfate Solutions

Masahiro MANABE, Keishiro SHIRAHAMA,* and Masaharu KODA

Department of Industrial Chemistry, Niihama Technical College, Niihama, Ehime 792
**Department of Chemistry, Faculty of Science and Engineering, Saga University, Saga 840*

(Received May 1, 1976)

The partial molar volumes of normal alkanols ($C_mH_{2m+1}OH$, $m=1$—10) in aqueous sodium dodecyl sulfate solutions were measured by a dilatometric method at 25 °C. For the alkanols ($m=4$—8), different constant partial molar volumes appeared below and above the CMC value, whereas no such difference was observed for lower alkanols ($m=1$—3), and for higher alkanols ($m=8$—10) the partial molar volumes above the CMC value are nearly identical with their own molar volumes. The partition coefficient of the alkanols between the bulk and micellar phases is estimated on the basis of the volumetric results.

It is known that the addition of small amounts of alkanol depresses the critical micelle concentration (CMC) of surfactants,[1-4] and some factors have been considered in order to explain the phenomenon from the viewpoint that the added alkanol is partitioned between the bulk and micellar phases. Few determinations, excepting a single work,[5] have ever been made of the amount of alkanol solubilized in micelles, in spite of the necessity of the quantity for estimating the factors contributing to solubilization phenomena. It is known that the partial molar volumes of alkyl derivatives[6-9] including surfactants[10-14] increase on passing from an aqueous environment to a nonpolar one. There have been, however, restricted investigations[15,16] of the volumetric behavior of solubilizates.

In the present study, the partial molar volumes of a series of normal alkanols were determined in sodium dodecyl sulfate solutions below and above CMC. On the basis of these results, a partition coefficient of alkanol between the bulk and micellar phases is estimated.

Experimental

The sodium dodecyl sulfate (SDS) were prepared as follows. Esterized dodecyl alcohol with sulfuric acid in absolute acetone was neutralized with a concentrated aqueous sodium hydroxide solution. The crude SDS crystal obtained from the acetone phase of the reaction mixture was recrystallized five times from acetone containing a small amount of water and then refluxed with petroleum ether. The CMC of the SDS in water was 8.30 mmol/kg[17] as determined by the conductivity method at 25 °C.

The methods of purification of water and normal alkanols used were the same as those described in an earlier paper.[9] Among the alkanols, nonyl alcohol was a commercially purified material (Tokyo Kasei Kogyo Co., Ltd., G. R. grade) and was used without further purification.

Partial molar volumes of alkanols in SDS solutions were measured using the same dilatometric method as shown in a previous paper,[9] in the alkanol-concentration range up to about 1 g/l. For higher alkanols, the solution in the dilatometer was stirred with each addition of alkanol for about one hour in order to insure sufficient dissolution. The dilatometer used in the measurements of the molar volumes of pure alkanols consits of only a glass capillary and injection parts.

Results and Discussion

Partial Molar Volumes of Normal Alkanols. The partial molar volume, V_a, of normal alkanols ($m=1$—10) was determined at different specific SDS concentrations, where m refers to the number of carbon atoms in the alkanol molecule. The results are plotted in Fig. 1 against the SDS concentration. It was found for alkanols with $m=4$—8 that a pair of almost constant V_a values appears: one below the CMC of SDS, expressed as V_a^D, and the other above CMC, V_a^M, where the CMC values are the ones in the presence of the added alkanols. This figure is coincident with the volumetric results of surfactants in water,[10] that is, in line with a pseudo-phase separation model of micelle formation.[18] Accordingly, the V_a^D value can be regarded as a partial molar volume of alkanol dissolved in a singly dispersed state, since the V_a in water cannot be distinguished from V_a^D, and V_a^M is probably contributed form the alkanol molecule dissolved in both the singly dispersed and solubilized states.

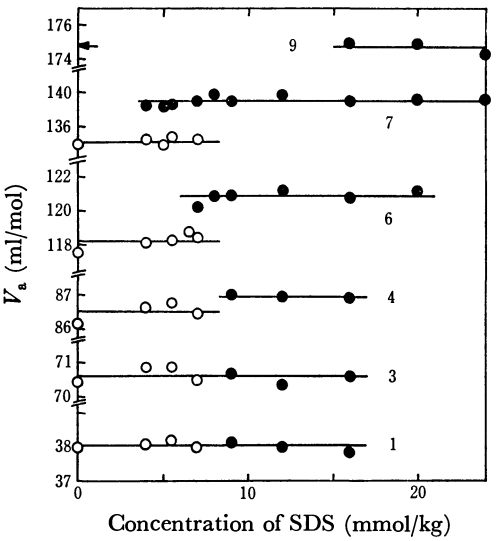

Fig. 1. Dependence of V_a on SDS concentration; ○: V_a below CMC, ●: V_a above CMC, and —: averaged V_a (V_a^D or V_a^M). The number indicates chain length of alcohol, and the arrow molar volume of nonyl alcohol.

For lower alkanols ($m=1$—3), however, all V_a values obtained here do not correspond to V_a^M but only to V_a^D even at SDS concentrations above the CMC value. During some determinations of the V_a^M of higher alkanols ($m=8$—10), the concentration of alkanol eventually

attained a maximum additive concentration (MAC),[19] at which turbidity appeared. The V_a^M in the absence of turbidity is little different from the partial molar volume determined in the presence of turbidity, and also from the molar volume of alkanol in the normal liquid state. The V_a^D value of alkanols (m=9, 10) could not be determined because of their very slight miscibility in water[20] and in SDS solutions below the CMC value. The almost constant V_a^D values as well as V_a^M values were averaged, respectively, and the mean values are shown in Table 1.

Table 1. The molar volumes and partial molar volumes of normal alkanols in SDS solutions, and the values of j and $j/(1-j)$

m	V_a^D (ml/mol)	V_a^M (ml/mol)	molar volume (ml/mol)	j	$j/(1-j)$
1	38.05		40.72[a]		
2	55.05		58.68[a]		
3	70.61		75.13		
4	86.48	86.90	91.85	0.077	0.084
5	102.3_4	103.5_4	109.0_3	0.196	0.244
6	118.1_9	120.9_3	124.7_0	0.402	0.672
7	134.1_5	139.0_4	141.5_9	0.660	1.94
8	149.9_0	157.5_3	157.9_1	0.93	13
9		174.7_0	174.7_1		
10		191.6_8	191.1_2		

a) Taken from Ref. 29.

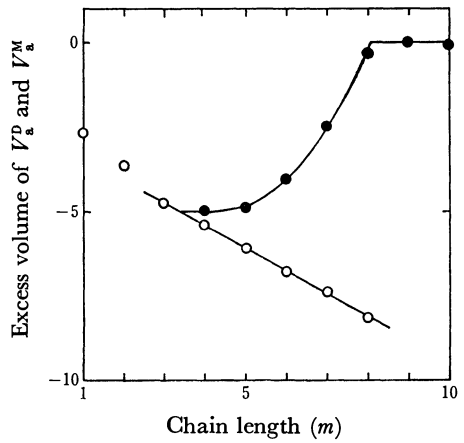

Fig. 2. Correlation of excess volumes with chain length of alcohol; ○: excess volume of V_a^D, ●: excess volume of V_a^M.

Figure 2 shows the dependence of both V_a^D and V_a^M on the chain length, m, in terms of the excess partial molar volume, the increment in the partial molar volume with respect to the molar volume, $V_a°$, which is calculated from the equation:

$$V_a° = 16.55m + 25.71 \quad (m=3—10). \qquad (1)$$

This equation is obtained by the least-squares method from the measured molar volumes given in Table 1. The excess volume of V_a^D is negative and decreases linearly with an increase in the chain length (m=3—8) except for lower alkanols (m=1, 2). Such a finding has also been made on the partial molar volumes of normal alkanols in water.[9] Hence the relation between V_a^D and the chain length is expressed by the least-squares method as

$$V_a^D = 15.87m + 23.02 \quad (m=3—8). \qquad (2)$$

The excess volume of V_a^M is negative and increases with an increase in the chain length for m=4—7 and then becomes zero at about m=8 or above. From the viewpoint of a pseudo-phase separation model of micelle formation, it is supposed that the added alkanol in the micellar solution is partitionally dissolved between the bulk and micellar phases. The solubilized fraction of added alkanol probably increases with the chain length of the alkanol molecule, and almost the entire amounts of these higher alkanols would be solubilized; the partial molar volume of the alkanol in the solubilized state should be identical with the molar volume in their normal liquid states.[16]

The curve for V_a^M, in Fig. 2, can be extrapolated to intersect with the one for V_a^D at about m=3.5. This critical chain length is comparable with that (C_3—C_5) estimated from the partial molar volume change of the surfactants on micellization as the shortest one needed for micellization according to Corkill *et al.*[12] It is likely that a solubilizate as well as surfactant with a normal alkyl chain shorter than four carbon atoms can hardly participate in the solubilization or micellization.

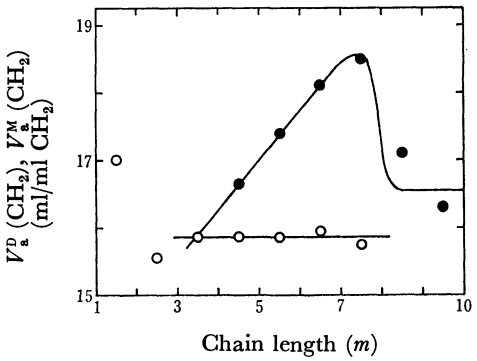

Fig. 3. Dependence of volume increment per methylene group on chain length of alcohol; ○: V_a^D (CH_2), ●: V_a^M (CH_2).

Volume Increment per Methylene Group. It is interesting and useful to discuss the increment in the partial molar volume per methylene group for normal alkanols with successive numbers of carbon atoms since the increment gives information about the environment of the group. As is shown in Fig. 3, the increment for V_a^D, denoted by $V_a^D(CH_2)$, except for lower alkanols (m=1, 2), has an almost constant value (15.87 ml/mol CH_2, *cf.* Eq. 2) which is in good agreement with the corresponding values of various normal alkyl chain derivatives in water (≈16 ml/mol CH_2).[21,22] The increment for V_a^M, $V_a^M(CH_2)$, indicates a nearly linear increase with an increase in the chain length (m=4—7) and then sharply decreases passing through a maximum to a probably constant value (16.55 ml/mol CH_2, *cf.* Eq. 1) above m=8, taking into account the identity of V_a^M and the molar volume. The $V_a^M(CH_2)$ attains the

constant $V_a^D(CH_2)$ at about $m=3.5$. These results for $V_a^M(CH_2)$ may be consistent with the interpretation on Fig. 2. The linear increase in the increment means that the V_a^M value is a quadratic function of the chain length:

$$V_a^M = 0.3675m^2 + 13.34m + 27.66 \quad (m=4—7), \quad (3)$$

where the coefficients were determined by the method of least squares.

Corkill *et al.*[12] supposed that the interior of the micelles is in a more expanded state than that in the normal liquid form of normal alkanes because the volume increment per methylene group of some homologous series of surfactants above CMC was 17.3 ml/mol CH_2, where the corresponding value of normal alkanes[12] and normal alkanols in their liquid states is identically 16.6 ml/mol CH_2 (*cf.* Eq. 1). However, the present results indicate that the $V_a^M(CH_2)$ of the higher alkanols ($m=8—10$) is rather comparable to the latter value. The apparent expansion of micelles formed with surfactant molecules alone may be caused, in addition to the volume increment per methylene group itself, by some other additional factors characteristic of micellization, which also depend linearly on the chain length of the surfactant. Because the volume increment per methylene group appears to be variable, as in the present case, $V_a^M(CH_2)$ increases even up to about 18.5 ml/mol CH_2, as is seen in Fig. 3.

Estimation of the Partition Coefficient. It is possible to estimate a partition coefficient for the alkanol in a solution with any composition, between the bulk and micellar phases, from the difference between V_a^D and V_a^M. The fraction of alkanol solubilized in one mol of added alkanol, j, may be related with the volumetric values, as follows:

$$V_a^M = \bar{V}_a^D(1-j) + \bar{V}_a^M j \quad (4)$$

where $\bar{V}_a^D$ and $\bar{V}_a^M$ are the partial molar volumes of alkanol in the singly dispersed and solubilized states, respectively, and the former is regarded as same as the V_a^D shown in Table 1. If the $\bar{V}_a^M$ value is identical with the molar volume for all alkanols, as in the case of higher alkanols ($m=8—10$), the equation can be calculated for j. The values obtained of j and $j/(1-j)$ which is the ratio of the fraction of alkanol solubilized to that dissolved monomerically are shown in Table 1.

The logarithmic values of j, $1-j$, and $j/(1-j)$ are plotted against chain length in Fig. 4. The curve of $\log j$ increases with an increase of m and attains zero at about $m=8$, whereas $\log(1-j)$ increases with decreasing m and attains zero at about $m=3.5$. These results are also consistent with the explanation given above. The $\log\{j/(1-j)\}$ *vs.* m plot is a straight line with a positive slope given by

$$\log\{j/(1-j)\} = 0.453m - 2.89 \quad (m=4—7), \quad (5)$$

which was obtained from a least-squares fit of the plots. If the decrease in the CMC value for the addition of alkanol is negligible, a partition coefficient, K, for alkanol between the bulk and micellar phases is defined in molar fraction units as

$$K = \{j/(C_s - C_s^\circ)\}/\{(1-j)/n_w\}, \quad (6)$$

where C_s is the total SDS concentration, C_s° is the CMC value in water, 8.30 mmol/kg, and n_w is molar number of water, 55.5 mole. It is noted that the K of a given alkanol depends on C_s although $j/(1-j)$ does not. Hayano and Hayase[5] have determined the partition coefficients of alkanols ($m=4—6$) by vapor pressure measurements in a 30 mmol/l SDS solution at 25 °C. The present calculated values of K for the respective alkanols at the same SDS concentrations are in fairly good agreement with their values, *e.g.*, for amyl alcohol, 6.24×10^2 was obtained here in comparison with their value of 7.29×10^2.

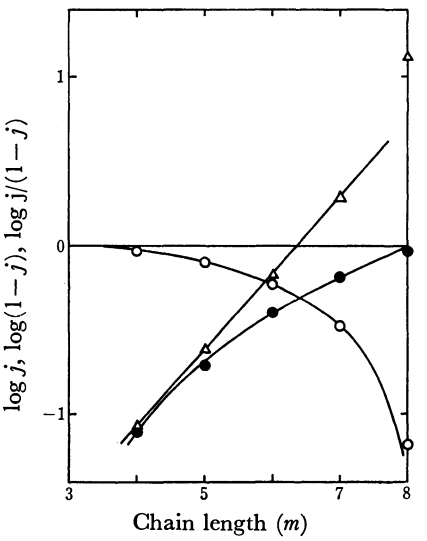

Fig. 4. Dependence of $\log j$, $\log(1-j)$, and $\log\{j/(1-j)\}$ on chain length of alcohol; ●: $\log j$, ○: $\log(1-j)$, △: $\log\{j/(1-j)\}$.

The standard free energy change of transfer for the methylene group of an alkanol molecule from the bulk to micellar phases can be calculated from the K values and was found to be −619 cal/mol CH_2. This value is independent of the SDS concentration, and is in good agreement with the corresponding values of various surfactants on their micellizations.[23-25]

The authors would like to acknowledge the continuing guidance and encouragement of Professor Ryohei Matuura and Assistant Professor Shoji Kaneshina of Kyushu University.

References

1) S. H. Herzfeld, M. L. Corrin, and W. D. Harkins, *J. Phys. Colloid Chem.*, **54**, 271 (1950).
2) K. Shinoda, *Bull. Chem. Soc. Jpn.*, **26**, 101 (1953); *J. Phys. Chem.*, **58**, 1136 (1954).
3) K. Shirahama and T. Kashiwabara, *J. Colloid Interface Sci.*, **36**, 65 (1971).
4) N. Nishikido, Y. Moroi, H. Uehara, and R. Matuura, *Bull. Chem. Soc. Jpn.*, **47**, 2634 (1974).
5) S. Hayano and M. Hayase, The Proceeding of the 28th Colloid and Interface Chemistry, Okayama, Japan (1975), p. 96.
6) M. E. Friedman and H. A. Scheraga, *J. Phys. Chem.*, **69**, 3795 (1965).
7) F. Franks and H. T. Smith, *Trans. Faraday Soc.*, **64**, 2962 (1968).
8) S. Cabani, G. Conti, and L. Lepori, *J. Phys. Chem.*, **76**,

1338 (1972); *ibid.*, **78** 1030 (1974).
9) M. Manabe and M. Koda, *Bull. Chem. Soc. Jpn.*, **48**. 2367 (1975).
10) K. Shinoda and T. Soda, *J. Phys. Chem.*, **67**, 2072 (1963).
11) L. Benjamin, *J. Phys. Chem.*, **70**, 3790 (1966).
12) J. M. Corkill, J. F. Goodman, and T. Walker, *Trans. Faraday Soc.*, **63**, 768 (1967).
13) F. Franks, M. J. Quickenden, J. R. Ravenhill, and H. T. Smith, *J. Phys. Chem.*, **72**, 2668 (1969).
14) G. M. Musbally, G. Perron, and J. E. Desnoyers, *J. Colloid Interface Sci.*, **48**, 494 (1974).
15) W. D. Harkins, R. W. Matton, and M. L. Corrin, *J. Colloid Sci.*, **1**, 105 (1946).
16) E. Hutchinson and C. S. Mosher, *J. Colloid Sci.*, **11**. 352 (1956).
17) P. Mukerjee and K. J. Mysels, "Critical Micelle Concentrations of Aqueous Surfactant Systems," Nat. Stand. Ref. Data Ser., N. B. S. (US), Washington, D.C. (1971), p 51.
18) K. Shinoda T. Nakagawa, B. Tamamushi, and T. Isemura, "Colloidal Surfactants," Academic Press, New York (1963) p. 27.
19) P. H. Elworthy, A. T. Florence, and C. B. Macfarlance, "Solubilization by Surface-Active Agents," Chapman and Hall Ltd., London (1968), p. 63.
20) K. Kinoshita, H. Ishikawa, and K. Shinoda, *Bull. Chem. Soc. Jpn.*, **31**, 1081 (1958).
21) M. Sakurai, *Bull. Chem. Soc. Jpn.*, **46**, 1596 (1973).
22) M. Sakurai, T. Komatu, and T. Nakagawa, *Bull. Chem. Soc. Jpn.*, **48**, 3491 (1975).
23) P. Molyneux, C. T. Rhodes, and J. Swarbrick, *Trans. Faraday Soc.*, **61**, 1043 (1965).
24) I. J. Lin and P. Somasundaran, *J. Colloid Interface Sci.*, **37**, 731 (1971).
25) I. Mandru, *J. Colloid Interface Sci.*, **41**, 430 (1972).
26) "International Critical Table," McGraw-Hill, New York (1928), Vol. III.

The Microwave Spectrum of Ethyl Isocyanate

Takeshi SAKAIZUMI, Osamu YAMADA, Kyoichi USHIDA, Osamu OHASHI, and Ichiro YAMAGUCHI

Department of Chemistry, Faculty of Science and Technology, Sophia University, Kioi-cho, Chiyoda-ku, Tokyo 102

(Received May 6, 1976)

The microwave spectrum of ethyl isocyanate, CH_3CH_2NCO, has been obtained in the frequency region from 8.5 to 35.5 GHz. The spectrum identified is attributed to the *cis* conformation, in which the methyl group eclipses the isocyanato group. The rotational constants in the ground vibrational state obtained are $A=14110\pm3$, $B=3067.91\pm0.02$, and $C=2605.01\pm0.02$ MHz. The dipole moment (μ_a) for this rotamer is 2.81 ± 0.02 D. Four sets of vibrational satellites were observed and assigned to the transitions in the first, second, third, and fourth excited states of the C–N torsional vibration.

We have previously reported the microwave spectrum of the *cis*-rotational isomer of ethyl isothiocyanate,[1] CH_3CH_2NCS, as an example of the rotational isomerism about single carbon-heteroatom bonds in mono-substituted ethanes. Kniseley *et al.* have studied the structure of ethyl isocyanate using infrared spectroscopy. They reported that the rotational isomerism about the C–N bond for alkyl isocyanate was not possible on the basis of these observation that, in the solid-state spectrum, the absorption band assigned to the NCO asymmetric stretching vibration decreased sharply in intensity and usually exhibited a poorly defined band envelope.

It is interesting to determine the conformation of the ethyl isocyanate molecule and compare the result with that for ethyl isothiocyanate.[1] In this paper, the microwave spectrum of ethyl isocyanate in the *cis*-conformation will be reported and the structure and the dipole moment will be discussed.

Experimental

The sample of ethyl isocyanate was obtained commercially (from the Tokyo Kasei Co.) and was purified by distillation *in vacuo*. The rotational spectrum was measured over the frequency range from 8.5 to 35.5 GHz with a conventional 100-kHz sinusoidal- and square-wave Stark modulation spectrometer. The wave-guide cell was cooled with Dry Ice in order to enhance the intensity of the absorption lines. The transition frequencies were measured with a Hewlett-Packard Model 5245 L frequency counter.

Results and Discussion

Microwave Spectrum and Assignment of the Vibrational Ground State. The observed spectrum was quite dense in appearance, consisting of a large number of absorption lines. This feature may be ascribed to the various rotational isomers and their vibrationally-excited states. Four rotational isomers may be considered for ethyl isocyanate, as for ethyl isothiocyanate, namely, the *cis*, *gauche*, *skew*, and *trans* forms, as is shown in Fig. 1. The moments of inertia calculated from the assumed structure, indicated that all the isomers are nearly prolate symmetric tops (the value of Ray's asymmetric parameter lie in the range from −0.995 to −0.920). A large a-component of the dipole moment can be expected for these isomers because the –N=C=O bond, with a large moment, lies close to the a-axis. Consequently, strong

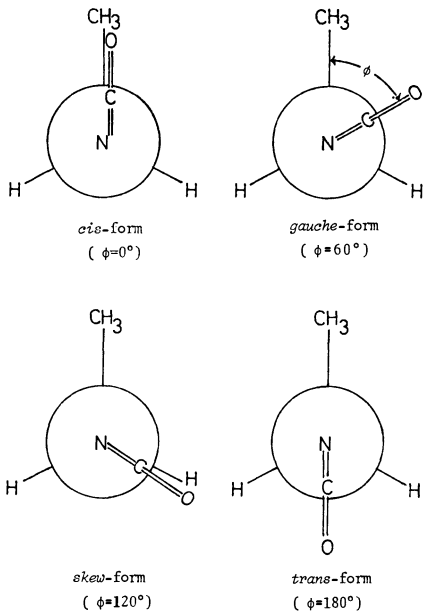

Fig. 1. Model of rotational isomers of ethyl isocyanate. ϕ: dihedral angle.

a-type R-branch transitions with $K_{-1}=0$ and 1 are to be expected. In the vicinity of the $K_{-1}=0$ line, absorption lines for K_{-1} equal to or larger than two should appear, and a large Stark effect should be observed.

The $J=3\leftarrow2$ transitions with $K_{-1}=2$ were first observed with a low Stark voltage, and next a $K_{-1}=0$ line in the vicinity of the $K_{-1}=2$ line was observed with a high Stark voltage. The transitions of $3_{13}\leftarrow2_{12}$, $3_{03}\leftarrow2_{02}$, and $3_{12}\leftarrow2_{11}$ were identified from their characteristic Stark behavior. The frequencies of the observed transitions in the ground vibrational state are listed in Table 1.

With the preliminary values of the rotational constants fitted to the low-J transition frequencies, the high-J transition frequencies were predicted by the rigid-rotor approximation. As the values of J and K_{-1} increased, the difference between the observed and calculated transition frequencies was found to become larger, in particular for the lines with K_{-1} values larger than one, as in the case of ethyl isothiocyanate. This deviation is probably attributable to the centrifugal distortion effect. Therefore, the observed transition frequencies given in Table 1 were fitted to the equation of the rotational energy, with correction for the first-order centrifugal

Table 1. Rotational transitions of the ethyl isocyanate in the ground state (MHz)

Transition	ν_{obsd}	$\nu_{obsd}-\nu_{calcd}$
$2_{12}\leftarrow 1_{11}$	10882.03	−0.03
$2_{02}\leftarrow 1_{01}$	11329.78	0.07
$2_{11}\leftarrow 1_{10}$	11805.85	−0.21
$3_{13}\leftarrow 2_{12}$	16313.97	−0.13
$3_{03}\leftarrow 2_{02}$	16958.99	0.07
$3_{22}\leftarrow 2_{21}$	17016.49	−0.06
$3_{21}\leftarrow 2_{20}$	17072.87	−0.36
$3_{12}\leftarrow 2_{11}$	17700.03	0.20
$4_{14}\leftarrow 3_{13}$	21735.52	−0.21
$4_{04}\leftarrow 3_{03}$	22545.76	−0.12
$4_{23}\leftarrow 3_{22}$	22677.20	0.01
$4_{32}\leftarrow 3_{31}$	22717.28	−0.12
$4_{31}\leftarrow 3_{30}$	22719.03	−0.01
$4_{22}\leftarrow 3_{21}$	22818.37	0.03
$4_{13}\leftarrow 3_{12}$	23582.47	−0.37
$5_{15}\leftarrow 4_{14}$	27144.07	−0.03
$5_{05}\leftarrow 4_{04}$	28078.99	−0.13
$5_{24}\leftarrow 4_{23}$	28327.93	−0.09
$5_{42}\leftarrow 4_{41}$	28395.99	0.20
$5_{41}\leftarrow 4_{40}$		0.17
$5_{33}\leftarrow 4_{32}$	28407.85	0.36
$5_{32}\leftarrow 4_{31}$	28412.84	−0.37
$5_{23}\leftarrow 4_{22}$	28608.04	0.17
$5_{14}\leftarrow 4_{13}$	29448.49	0.11
$6_{16}\leftarrow 5_{15}$	32537.13	0.27
$6_{06}\leftarrow 5_{05}$	33546.14	0.19
$6_{25}\leftarrow 5_{24}$	33966.30	−0.25
$6_{52}\leftarrow 5_{51}$	34075.60	−0.12
$6_{51}\leftarrow 5_{50}$		−0.12
$6_{43}\leftarrow 5_{42}$	34084.34	0.14
$6_{42}\leftarrow 5_{41}$		−0.02
$6_{34}\leftarrow 5_{33}$	34103.56	0.23
$6_{33}\leftarrow 5_{32}$	34118.36	−0.18
$6_{24}\leftarrow 5_{23}$	34448.91	−0.03
$6_{15}\leftarrow 5_{14}$	35293.30	−0.35

distortion effect.

The rotational and centrifugal distortion constants, as obtained by the least-squares method, are given in Table 2. The observed and calculated transition frequencies are in good agreement, as is shown in Table 1. The centrifugal distortion effect of ethyl isocyanate was similar in magnitude to that of ethyl isothiocyanate.[1)]

Conformation of the Molecule. If the molecule studied in this work has a plane of symmetry, *viz.*, a *cis* or *trans* conformation, four hydrogen atoms are located out of this plane. For this instance, the following relation is valid if the molecule is a rigid rotor:

$$8m_Hc_H^2 = I_a + I_b - I_c$$

where m_H is the mass of one hydrogen atom and c_H is its distance from the plane of symmetry. Using the assumed structural parameters given in Table 3, the value of

Table 3. Structural parameters[a)]

Distances	Angles
C–H: 1.091 Å[b)]	∠HCH: 108.8°[b)]
C_α–C_β: 1.520 Å[b)]	$\angle HC_\beta C_\alpha$: 109.6°[b)]
C_α–N: 1.461 Å	$\angle C_\beta C_\alpha H$: 112.0°[b)]
N=C: 1.207 Å[b)]	$\angle C_\beta C_\alpha N$: 109.14°
C=O: 1.171 Å[b)]	$\angle C_\alpha NC$: 142.11°
	∠N=C=O: 180°[b)]

a) The carbon atoms at the α- and β-positions are denoted as C_α and C_β respectively. The structural parameters are taken from the mono-substituted ethanes, CH_3CH_2X,[1)] for the ethyl group and from the methyl isocyanate for the isocyanato group.
b) Assumed parameters fixed for structural analysis. Three other were also determined.

$8m_Hc_H^2$ for the two forms, *cis* and *trans*, was calculated to be 6.344 amu Å^2. This is in good agreement with the value determined experimentally. This result suggests that the conformation of the molecule for which the transitions are assigned is a form having a plane of symmetry, namely, the *cis* or *trans* form. Moreover, comparing the rotational constants determined experimentally with those calculated from the assumed structures, as are shown in Table 4, the preferred conformation is clearly the *cis* form shown in Fig. 2.

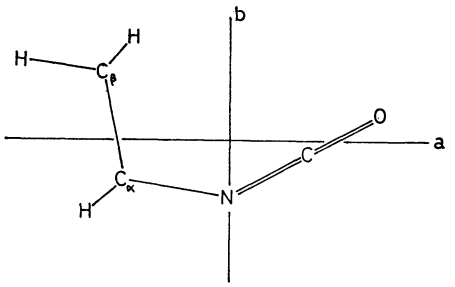

Fig. 2. Conformation of the *cis*-ethyl isocyanate.

Table 2. Rotational and centrifugal distortion constants and moments of inertia[a)] for ethyl isocyanate

	$v=0$	$v_t=1$	$v_t=2$	$v_t=3$	$v_t=4$
A(MHz)	14110±3	14657±20	15215±25	15919±56	16853±110
B(MHz)	3067.01±0.02	2982.36±0.09	2922.95±0.08	2861.01±0.12	2792.80±0.17
C(MHz)	2605.01±0.02	2578.47±0.09	2556.90±0.08	2533.53±0.14	2505.87±0.13
D_J(kHz)	4.17±0.22	5.69±1.04	7.15±0.99	9.38±1.44	11.48±1.73
D_{JK}(kHz)	−39.1±0.5	−69.3±2.9	−95.0±2.8	−145.5±6.2	−428.4±5.1
I_a(amu Å^2)	35.816±0.009	34.480±0.049	33.215±0.056	31.745±0.111	29.987±0.178
I_b(amu Å^2)	164.778±0.001	169.455±0.005	172.899±0.005	176.642±0.007	180.956±0.011
I_c(amu Å^2)	194.001±0.002	195.998±0.007	197.651±0.006	199.475±0.011	201.676±0.010
ΔI(amu Å^2)[b)]	6.593±0.012	7.937±0.061	8.463±0.067	8.912±0.129	9.267±0.199

a) Conversion factor=505376 MHz amu Å^2. b) $\Delta I=I_a+I_b-I_c$.

TABLE 4. OBSERVED AND PREDICTED ROTATIONAL CONSTANTS

	Obsd	Calcd			
		cis	*gauche*	*skew*	*trans*
A(MHz)	14110.25	14111.78	16091.99	24577.12	34937.53
B(MHz)	3067.01	3068.93	2796.52	2376.32	2242.26
C(MHz)	2605.01	2603.11	2499.49	2292.55	2164.28
κ	−0.919689	−0.919049	−0.956295	−0.992481	−0.995241
Δ(amu Å^2)[a]	−6.592	−6.344	−9.929	−12.791	−6.344
ϕ(°)[b]		0	60	120	180

a) $\Delta=I_c-I_b-I_a$. b) ϕ: dihedral angle about the C–N bond; see Fig. 1.

Ethyl isocyanate, as one of the rotational isomers, is in the *cis* conformation in the gas phase. This result is consistent with the case of ethyl isothiocyanate,[1] for which the spectrum identified is attributed to the *cis* conformation.

Three structural parameters, ($r_{C_\alpha-N}$, $\angle C_\beta C_\alpha N$, and $\angle C_\alpha NC$), of the ethyl isocyanate were obtained from the observed rotational constants, fixing the remaining parameters to the values assumed. The results thus obtained are given in Table 3.

Comparing the CNC angle obtained (142°) here for CH_3CH_2NCO with that (151°) obtained for CH_3CH_2NCS[1] in the previous work, a large increase in the angle (about 9°) is seen on the replacement of O by S. Similar trends are evident for the cases of the HNC angle of HNCO[3] (128°) and HNCS[4] (135°), and the CNC angle of CH_3NCO[5] (140°) and CH_3NCS[5] (147.5°).

The dense spectrum suggests the presence of other rotamers in appreciable concentrations. An attempt

TABLE 5. ROTATIONAL TRANSITIONS OF THE ETHYL ISOCYANATE IN THE TORSIONAL-EXCITED STATE (MHz)

Transition	$v_t=1$		$v_t=2$		$v_t=3$		$v_t=4$	
	ν_{obsd}	Δ[a]	ν_{obsd}	Δ[a]	ν_{obsd}	Δ[a]	ν_{obsd}	Δ[a]
$2_{12}\leftarrow1_{11}$	10717.74	0.04	10593.65	−0.10	10461.92	0.01	10311.08	−0.67
$2_{02}\leftarrow1_{01}$	11111.12	−0.04			10781.82[b]	−0.89	10592.92	0.29
$2_{11}\leftarrow1_{10}$	11525.60	−0.17	11326.06	−0.01			10887.73[b]	2.12
$3_{13}\leftarrow2_{12}$	16069.69	−0.42	15885.10	−0.21	15688.06	−0.47	15463.81	−0.44
$3_{03}\leftarrow2_{02}$	16640.77	0.02	16406.58	−0.02	16158.87	0.54	15877.61	0.21
$3_{22}\leftarrow2_{21}$	16683.81	0.25	16441.57[b]	0.50	16186.95[b]	0.81	15905.90[b]	0.84
$3_{21}\leftarrow2_{20}$	16724.11[b]	−0.60	16472.96	−0.30	16210.49	0.04	15922.36	−0.06
$3_{12}\leftarrow2_{11}$	17282.05[b]	−0.61	16983.88[b]	0.53	16671.60[b]	0.70	16326.50[b]	1.51
$4_{14}\leftarrow3_{13}$	21414.18	−0.36	21170.08	−0.38	20909.17[b]	−0.88	20612.06	−0.68
$4_{04}\leftarrow3_{03}$	22139.30	−0.01	21837.25	−0.04	21514.88	−0.24	21148.44	0.01
$4_{23}\leftarrow3_{22}$	22236.19	0.07	21914.48	0.11	21576.16	0.42	21202.93[b]	0.85
$4_{22}\leftarrow3_{21}$	22338.56	−0.11	21994.46	−0.20	21635.99	−0.42	21245.24	−0.20
$4_{13}\leftarrow3_{12}$	23029.79[b]	0.64	22634.29	0.28	22219.90	0.35	21762.61[b]	2.40
$5_{15}\leftarrow4_{14}$	26748.88	−0.05	26447.08	−0.35	26124.79	−0.16	25755.92	0.07
$5_{05}\leftarrow4_{04}$	27597.32	−0.07	27235.84	0.01	26846.78	−0.31	26400.98	−0.08
$5_{24}\leftarrow4_{23}$	27781.27	0.04	27381.68	0.07	26960.09	−0.28	26581.19	−0.40
$5_{42}\leftarrow4_{41}$, $5_{41}\leftarrow4_{40}$	27835.46	0.14, 0.13	27428.49	−0.31, −0.32	27004.85	0.01, 0.02	26565.18	−0.63, −0.63
$5_{33}\leftarrow4_{32}$	27842.20[b]	0.92						
$5_{32}\leftarrow4_{31}$	27884.07[b]	−0.67						
$5_{23}\leftarrow4_{22}$	27985.23	0.07	27541.47	0.01	27081.52	0.18	26581.19	−0.40
$5_{14}\leftarrow4_{13}$	28764.98	0.01	28275.56	0.18	27760.88	0.01	27191.40[b]	1.62
$6_{16}\leftarrow5_{15}$	32071.86	0.49	31715.34[b]	0.77	31332.74[b]	0.91	30893.68	0.79
$6_{06}\leftarrow5_{05}$	33006.90	−0.01	32595.20	−0.17	32148.90	0.17	31630.97	−0.32
$6_{25}\leftarrow5_{24}$	33317.01	−0.11	32841.24	−0.05	32338.95	0.11	31782.86	−0.27
$6_{52}\leftarrow5_{51}$, $6_{51}\leftarrow5_{50}$	33406.53	−0.12, −0.12	32921.65	0.05, 0.05				
$6_{43}\leftarrow5_{42}$, $6_{42}\leftarrow5_{41}$	33408.31	0.09, −0.17	32918.75	0.19, 0.19	32407.75	−0.06, −0.02		
$6_{34}\leftarrow5_{33}$	33420.30	0.58	32924.70	0.25	32406.87	0.51		
$6_{33}\leftarrow5_{32}$	33428.89	0.01	32930.45	−0.19	32410.19	−0.15	31853.70	0.30
$6_{24}\leftarrow5_{23}$	33670.10	−0.13	33118.75	−0.07	32549.29	0.01	31932.23[b]	−1.69
$6_{15}\leftarrow5_{14}$	34484.95[b]	−0.64	33904.21	−0.48	33292.10[b]	−0.64	32611.98[b]	−1.64

a) $\Delta=\nu_{obsd}-\nu_{calcd}$. b) Not included in the least-squares fitting.

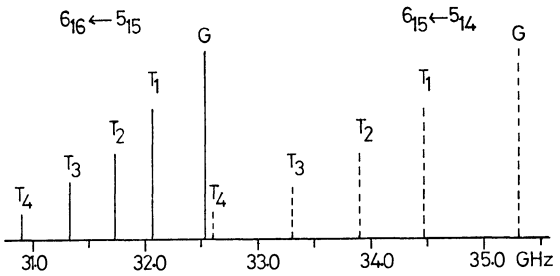

Fig. 3. Typical satellite pattern of $J=6\leftarrow5$ transitions of *cis*-ethyl isocyanate: dotted lines are $6_{15}\leftarrow5_{14}$ transition.

was made to find the transitions due to *skew* or *trans* forms. Measurements were carefully made near the transition frequencies predicted by the rotational constants of the models of the *skew* and *trans* forms calculated with the structural parameters in Table 3. However, no transition could be assigned which might be ascribed to the *skew* or *trans* form.

Vibrationally-excited State. Four sets of the spectrum due to the vibrationally-excited states were found. The satellite lines have essentially the same Stark effect behavior and the same K_{-1} series pattern as those of the ground state. Figure 3 illustrates same typical satellite patterns of $6_{16}\leftarrow5_{15}$ and $6_{15}\leftarrow5_{14}$ transitions. The vibrationally-excited states lines were assigned as is shown in Table 5. The effective rotational constants of the four excited vibrational states were obtained in a manner similar to that used for the ground state. These results are also given in Table 2.

From the relative intensities of the satellite lines with respect to the ground-state line, the vibrational frequency of 150 ± 50 cm^{-1} for $v_t=1$ was obtained. Referring to Kniseley's assignment of this molecule and to the study of ethyl isothiocyanate, the observed vibrational frequencies (100, 144, and 224 cm^{-1}) were assigned to the C–N torsion, CNC bending, and C–C torsion modes respectively, as is shown in Table 6. Because the value of $\Delta'I(I_c-I_b-I_a+8m_Hc_H^2)$ obtained for $v_t=1$ has a negative value,[6] the vibrational satellite corresponding to 150 cm^{-1} can be ascribed to the excited state of the C–N torsion mode.

Table 6. Far-infrared spectra (cm^{-1})

CH_3CH_2NCS	CH_3CH_2NCO	Assignment
70(w)	100(w)	C–N torsion
130(s)	144(s)	CNC bending
225(w)	224(w)	C–C torsion
380(s)	395(s)	CCN bending (in-plane)[a]
450(m)	595(m)	NCX bending (out-of-plane)[a]
540(s)	608(s)	NCX bending (in-plane)[a]

Abbreviations: s, strong; m, medium; w, weak.
a) Ref. 2.

From the relative intensities and the ΔI values of the remaining sets, $v_t=2$, $v_t=3$, and $v_t=4$, given in Table 2, these sets may be ascribed to the excited states of the C–N torsional vibrations. The variation in the rotational constants (A, B, and C) with the vibrational quantum

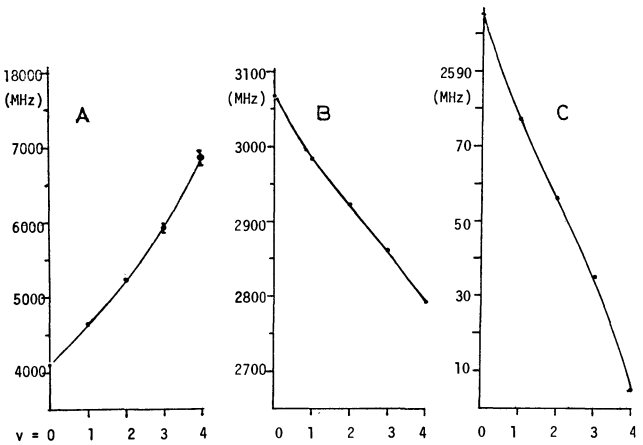

Fig. 4. Variation of rotational constants of *cis*-ethyl isocyanate with the quantum number.

Table 7. Stark coefficients[a] ($\Delta\nu/E^2$) and dipole moment (D)

Transition	M	$v=0$ obsd	$v=0$ calcd	$v_t=1$ obsd	$v_t=1$ calcd	$v_t=2$ obsd	$v_t=2$ calcd	$v_t=3$ obsd	$v_t=3$ calcd	$v_t=4$ obsd	$v_t=4$ calcd
$3_{03}\leftarrow2_{02}$	0	−0.902	−0.901	−1.15	−1.10	−1.14	−1.04	−1.19	−1.09		
	1	−0.256	−0.256	−0.326	−0.341	−0.259	−0.279	−0.289	−0.306		
	2	1.68	1.68	1.94	1.94	2.10	2.01	2.06	2.05		
$3_{12}\leftarrow2_{11}$	0	−0.240	−0.240								
	1	−3.03	−3.33	−4.64	−4.38	−4.70	−4.91	−5.57	−5.55		
	2			−16.0	−16.6	−18.5	−18.7	−21.1	−21.3		
$4_{04}\leftarrow3_{03}$	0									−0.467	−0.467
	1									−0.297	−0.296
	2									0.226	0.213
$4_{13}\leftarrow3_{12}$	1									−1.07	−0.864
	2									−2.86	−2.72
	3									−5.87	−5.81
μ_a	:	2.81±0.02		2.99±0.04		3.01±0.04		3.02±0.02		3.05±0.05	
μ_b	:	0.03		0.13		0.11		0.03		0.262	
μ_c	:	0 (assumed)		0 (assumed)		0 (assumed)		0 (assumed)		0 (assumed)	

a) [MHz/(V/cm)^2]$\times10^{-5}$.

number of the C–N torsion is non-linear, as is shown in Fig. 4. Therefore, this torsional vibration is rather anharmonic.

Dipole Moment. From the Stark coefficients of the $3_{03}\leftarrow 2_{02}$, and $3_{12}\leftarrow 2_{11}$ transitions for the ground state and the excited states, $v_t=1$, 2, and 3, and the $4_{04}\leftarrow 3_{03}$ and $4_{13}\leftarrow 3_{12}$ for $v_t=4$, the dipole moment of ethyl isocyanate was determined for both the ground and excited vibrational states. From the second-order Stark coefficients determined for the five Stark component lines, the dipole moments shown in Table 7 were obtained. The c-component of the dipole moment was assumed to be zero because of the symmetry, as has been discussed above. The b-component was not determined exactly, since no b-type transitions were observed. The electric-field strength in the absorption cell was calibrated using the $J=1\leftarrow 0$ transition of OCS.[7] The dipole moment (μ_a) for the ground state was determined to be 2.81 ± 0.02 D.

The authors wish to express their thanks to Professor Hiroaki Takahashi and Dr. Norio Kaneko of Waseda University for the use of Hitachi FIS-3 far-infrared spectrophotometer and for their helpful discussions.

References

1) T. Sakaizumi, O. Ohashi, and I. Yamaguchi, *Bull. Chem. Soc. Jpn.*, **49**, 948 (1976).
2) R. P. Hirschmann, R. N. Kniseley, and V. A. Fassel, *Spectrochim. Acta*, **21**, 2125 (1965).
3) L. H. Jones, J. N. Shoolery, R. G. Shulman, and D. M. Yost, *J. Chem. Phys.*, **18**, 990 (1950).
4) R. Kewley, K. V. L. N. Sastry, and M. Winnewisser, *J. Mol. Spectrosc.*, **10**, 418 (1963).
5) R. G. Lett and W. H. Flygare, *J. Chem. Phys.*, **47**, 4730 (1967).
6) D. R. Herschbach and V. W. Laurie, *J. Chem. Phys.*, **40**, 3142 (1964).
7) J. S. Muenter, *J. Chem. Phys.*, **48**, 4544 (1968).

The Dissociative Excitation and Dissociative Ionization of Simple Aliphatic Hydrocarbons by Controlled Electron Impact

Masaharu Tsuji,* Teiichiro Ogawa, Yukio Nishimura,* and Nobuhiko Ishibashi

Faculty of Engineering, Kyushu University, Hakozaki, Fukuoka 812

(Received May 12, 1976)

Photoemissions from the following excited species were observed from simple aliphatic hydrocarbons (CH_4, C_2H_2, C_2H_4, 1,3-C_4H_6) under controlled electron-impact excitation (0—400 eV) at wavelengths from 300 to 600 nm: H(Balmer), CH(A–X, B–X, C–X), CH^+(A–X, B–A, b–a), C_2(C–A, d–a; not from CH_4), and $C_4H_2^+$(A–X; not from CH_4). All the excited species except for $C_4H_2^+$ from C_2H_2 and C_2H_4 were confirmed to be primarily produced. The excitation function (0—400 eV) and the appearance potential of H, CH, and CH^+ produced from CH_4 and C_2H_2 were measured, and the corresponding processes of the fragmentation near the threshold were determined. The $CH_4+e\rightarrow CH^+(B)+H_2(X)+H(n=1)$ and $C_2H_2+e\rightarrow CH^+(B)+CH(X)$ processes were concluded to be responsible for the formation of CH^+(B). The formation of ionic species, H^+ and CH^+, can be considered as the limiting case of the dissociative excitation for producing H and CH. A triplet excitation process may contribute to the formation of CH(A) from C_2H_2. The observed threshold energies indicated that superexcited states were involved in the formation of excited neutral fragment species.

Spectroscopic investigations of the dissociative excitation of simple aliphatic hydrocarbons (CH_4, C_2H_2, C_2H_4, C_2H_6) have been extensively carried out by the irradiation of vacuum ultraviolet photons,[1,2] by the impact of an ion beam,[3,4] and by the impact of an electron beam,[5–11] and photoemissions from the excited atoms (H, CI, CII) and molecular fragments (C_2, CH, CH^+, CH_2) have been observed.

The electron-impact method is a very effective method, partly because the excitation energy is variable over a wider range and partly because a relatively intense photoemission can be obtained even at a low excitation energy near the threshold. Thus, the emission cross section, the excitation function, and the appearance potential of some fragment species of various molecules have been measured under the electron-impact excitation. Sroka[5] and Morgan and Mentall[10] have reported the excited atomic lines, H(Lyman), CI, and CII, from CH_4 in the VUV region. De Heer *et al.*[11] determined the emission cross sections of some excited fragments from simple aliphatic hydrocarbons (CH_4, C_2H_2, C_2H_4, C_2H_6) as a function of the electron-impact energy and clarified the dissociative-excitation processes. Recently, Finn *et al.*,[12] using time-of-flight techniques, investigated the production of hydrogen and carbon atoms in metastable and high-lying Rydberg states by electron impact on CH_4 and CD_4.

The CH^+ ion is an important species in astrophysics, mass spectroscopy, and radiation chemistry; three systems ($A^1\Pi$–$X^1\Sigma^+$, $B^1\Delta$–$A^1\Pi$, $b^3\Sigma^-$–$a^3\Pi$) have been known in the emission spectrum. The latter two systems were first observed and analyzed by Carré[4] under proton bombardment on CH_4 and C_2H_2; they were also identified by Beenakker and de Heer[11] under electron impact on CH_4, C_2H_2, C_2H_4, and C_2H_6. However, no studies have been carried out on the mechanism for the formation of CH^+ in the excited electronic state because of the weakness of the emission intensity. We have previously communicated the emission spectra of CH^+ produced from CH_4 and C_2H_2 by controlled electron impact.[13] The present paper will describe the emission spectra of simple aliphatic hydrocarbons (CH_4, C_2H_2, C_2H_4, 1,3-C_4H_6) and the mechanism for the fragmentation of H($n=4$), CH(A), and CH^+(B) from CH_4 and C_2H_2 under the electron-impact excitation.

Experimental

The apparatus and the experimental techniques used in this investigation were similar to those described previously.[14] The electrons emitted from a tungsten filament were accelerated and focused into the collision chamber, where they collided perpendicularly with a molecular jet introduced from a nozzle 0.1 mm in diameter. The electron-beam current in the collision chamber ranged between 0.1 and 3000 μA for electron energies from 0 to 400 eV. The pressure in the collision region was estimated to be of the order of 10^{-3} Torr when the sample gas was introduced.

The emission spectra in the 300—600 nm region were measured by use of a JASCO CT-50 monochromator equipped with an EMI 9558QB photomultiplier, which was connected to a DC amplifier. The spectral bandpass used in this experiment was in the 4—5 Å range.

For the measurements of the excitation function and the appearance potential, a cell whose inside wall was made of brass was employed to reduce the space-charge effect on the wall. In this case, photons modulated by a mechanical chopper were detected by the same monochromator equipped with a HTV R585 photomultiplier, which was connected to an NF PC545A photon counter. The excitation functions and the appearance potentials of N_2 (3371 Å; the (0, 0) band of the second positive system) and N_2^+ (3914 Å; the (0, 0) band of the first negative system) produced from N_2 were measured in order to check the efficiency of this apparatus and to calibrate the electron energy. The satisfactory agreement with the results by Stanton and John[15] indicated that our apparatus could be used for the measurements of the excitation function and the appearance potential.

The gas samples were of a Research Grade obtained from the Takachiho Trading Co.; their purities were specified as 99.95% for CH_4, 99.6% for C_2H_2, 99.8% for C_2H_4, and 99.5% for 1,3-C_4H_6. They were subjected to several freeze-pump-thaw cycles before use.

* Research Institute of Industrial Science, Kyushu University, Hakozaki, Fukuoka 812.

Results and Discussion

The Spectra of Methane and Acetylene. Photoemissions from excited fragments and a dimeric ion were found in the 300—600 nm region, as is shown in Figs. 1 and 2. In the longer wavelength region (above 390 nm) of both spectra, the Balmer series of the hydrogen atom ($H_{\beta,\gamma,\delta,\varepsilon,\zeta}$), and the 4300 Å system ($A^2\Delta$–$X^2\Pi$) and the 3900 Å system ($B^2\Sigma^-$–$X^2\Pi$) of CH are identified. In addition, the line at 423 nm, which is superimposed upon the intense band of CH(A–X), is assigned to the (0, 0) band of $CH^+(A^1\Pi$–$X^1\Sigma^+)$.[16] In the spectrum of C_2H_2, the $\Delta v=1$, 0, and -1 sequences of the Swan system of $C_2(d^3\Pi_g$–$a^3\Pi_u)$, and the (0, 0) sequence of the Schüler's T spectrum of $C_4H_2^+(A^2\Pi_g$–$X^2\Pi_u)$, designated as A,[16] are also identified.

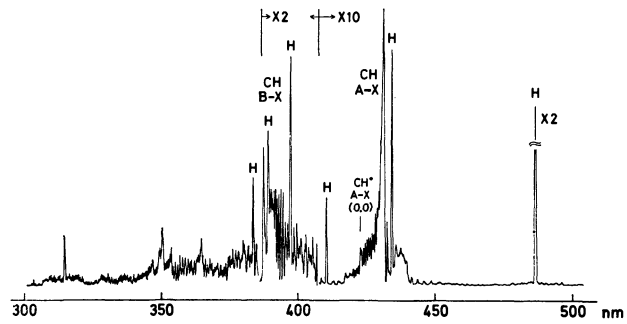

Fig. 1. Emission spectrum of CH_4 by controlled electron impact. Electron energy 200 eV, electron-beam current 800 μA.

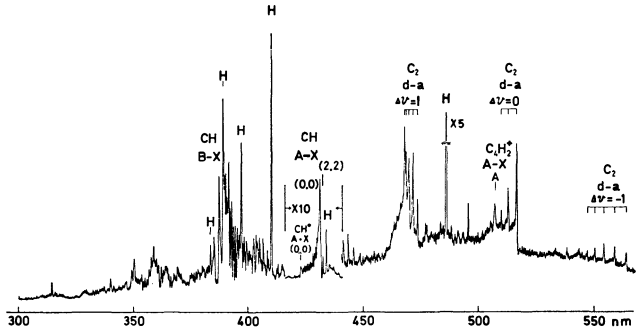

Fig. 2. Emission spectrum of C_2H_2 by controlled electron impact. Electron energy 200 eV, electron-beam current 500 μA.

In the shorter-wavelength region of both spectra, some weak features come out, as is shown in detail in Fig. 3. The $H_{\gamma,\delta}$ lines of the Balmer series of the hydrogen atom, the (1, 0) band of the CH(B–X), and the 3100 Å system ($C^2\Sigma^+$–$X^2\Pi$) of CH are identified in both spectra. In addition, the features at 347—362 nm, which are more clearly observed in the spectrum of CH_4, are assigned to the $B^1\Delta$–$A^1\Pi$ and $b^3\Sigma^-$–$a^3\Pi$ transitions of CH^+ by reference to Carré's results on CH_4 and C_2H_2 by proton bombardment.[4] The (0, 0) and (1, 1) bands of the B–A transition are observed at 350 and 347 nm. The (0, 0) band of the b—a transition is observed at 349—362 nm, superimposed upon the (0, 0) band of the B–A transition; the band head

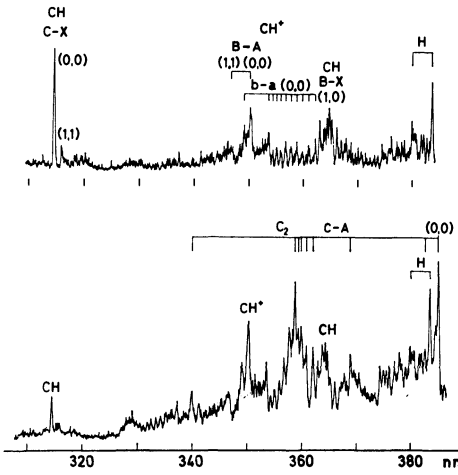

Fig. 3. Emission spectra of CH_4 and C_2H_2 in the 310—385 nm region by controlled electron impact (expanded for the detailed analysis). Top; CH_4, electron energy 300 eV, electron-beam current 800 μA. Bottom; C_2H_2, electron energy 200 eV, electron-beam current 600 μA.

is located at 349 nm, and its rotational structure extends towards the longer wavelengths (up to 362 nm). Some weak features at 327—347 nm are probably related to these two systems, as was observed by Carré.

Other numerous bands, which complicate the spectrum of C_2H_2, are ascribed to the Delandres-D'Azambuja system of $C_2(C^1\Pi_g$–$A^1\Pi_u)$; the (0, 0) band is found at 385 nm. Principal bands of this system, described in the Pearse and Gaydon table,[16] are indicated by the straight lines; most of the other features observed in C_2H_2 may be assigned to this system.

Mass-spectrometric studies have shown that the CH^+ ion is an important primary ion produced by electron impact on CH_4 and C_2H_2 and that it constitutes 2—3% of the total ions at a 50—500 eV electron impact on CH_4[17] and 2—4% of the total ions at a 50—500 eV electron impact on C_2H_2.[18] The calculated potential energy curves of the CH^+ ion show that the repulsive $c^3\Sigma^+$ state crosses with the $B^1\Delta$ and $b^3\Sigma^-$ states.[19] The weakness of the emission intensity of CH^+ compared with that of H and CH may be partly due to the competition of the predissociation with photoemission.

Current and Pressure Dependence of the Emission Intensity. The number of the electron and the molecule which participate in the formation of excited species can be determined by the dependence of the photoemission intensity on the electron-beam current and the gas pressure. The intensity of the CH^+ emission was measured on the band at 350 nm under the assumption that the band overlapping with the b–a transition is negligible. This assumption is supported by the finding that the triplet system did not affect the lifetime measurement of the (0, 0) band of the B–A system.[6]

Figures 4 and 5 show that the band intensities of H, CH, C_2, and CH^+ from C_2H_2 are proportional both to the electron-beam current and to the gas pressure at the constant electron energy. Similar linear relationships have been obtained for other fragment species (H, CH, CH^+) from CH_4, as was reported for H and CH by one of the present authors.[7] These results suggest

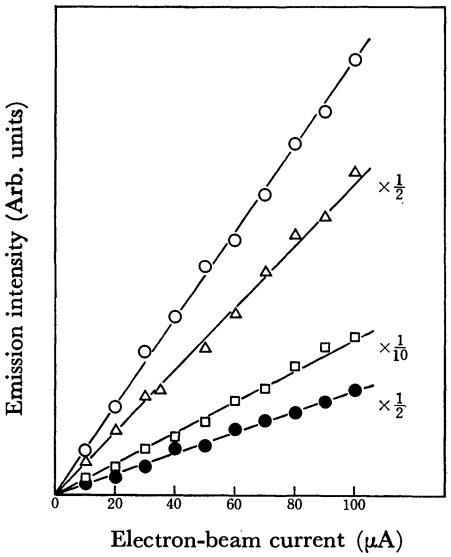

Fig. 4. Dependence of photoemission intensities of C_2H_2 on the electron-beam current. Electron energy 200 eV. ○: CH(431 nm), △: H_γ, □: CH^+ (350 nm), ●: C_2 (468 nm).

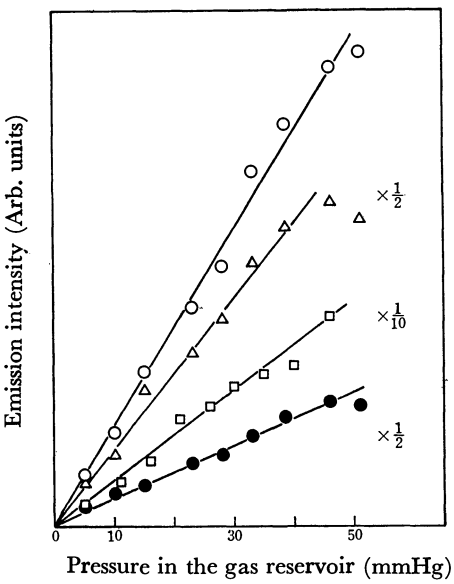

Fig. 5. Dependence of photoemission intensities of C_2H_2 on the pressure in the gas reservoir. Electron energy 200 eV, electron-beam current 50 μA. ○: CH(431 nm), △: H_γ, □: CH^+ (350 nm), ●: C_2 (468 nm).

that emitting excited species are produced through a primary collision of an incident electron with a molecule and that they are not collisionally deactivated within their radiative lifetimes. However, the behavior of the intensity of $C_4H_2^+$ from C_2H_2 to the electron-beam current is exceptional; it is probably produced in a dimerization-excitation process.[20]

Dissociation Processes from Methane. The dependence of the photoemission intensities of H_γ, CH(A–X), and CH^+(B–A) from CH_4 on the electron-impact energy up to 400 eV is shown in Figs. 6 and 7. The energy dependence of H_β was similar to that of H_γ. No discrete structure can be observed on these excitation functions,

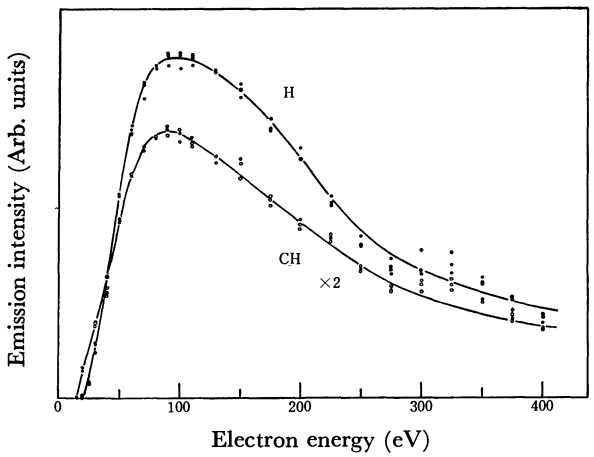

Fig. 6. Excitation functions of H and CH produced by electron impact on CH_4. ●: H_γ electron-beam current 3 μA, ○: CH(431 nm) electron-beam current 3 μA.

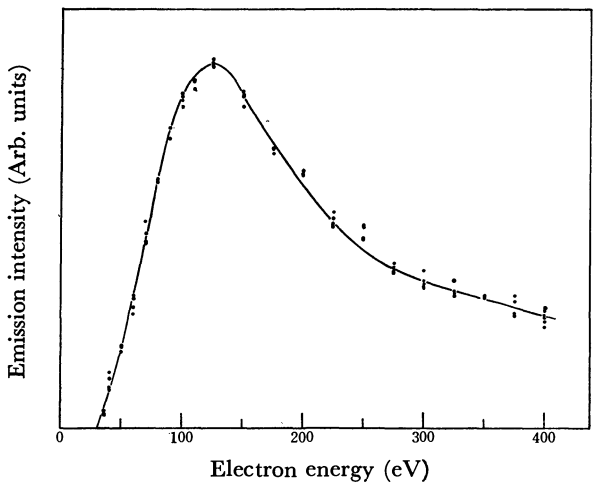

Fig. 7. Excitation function of CH^+ (350 nm) produced by electron impact on CH_4. Electron-beam current 15 μA.

and the maximum emission cross section is located at about 100 eV for H_γ, at about 90 eV for CH(A–X), and at about 130 eV for CH^+(B–A). The maximum positions of H_β and H_γ in the present study nearly agree with those of the previous investigations of the Balmer and Lyman series[5,8,10,11] and of the metastable and high Rydberg hydrogen fragments.[12] On the other hand, the maximum position of CH(A–X) is higher than the values reported by Aarts *et al.*[11] (about 60 eV) and by Fujita[8] (about 80 eV), while that of CH^+(B–A) is also higher than the maximum ionization cross section of CH^+ as measured by means of a mass spectrometer[17] (about 80 eV).

The appearance potentials of H_β, CH(A–X), and CH^+(B–A) were measured through the careful determination of the excitation function at a low energy; the results obtained are given in Table 1. Table 1 also enumerates the possible dissociative-excitation and dissociative-ionization processes for the formation of H(n=4), H(high Rydberg states), H^+, CH(A), CH^+(X), and CH^+(B); their minimum excitation energies were calculated by making use of the following dissociation

Table 1. Threshold energies for dissociative excitation and dissociative ionization of CH_4 by electron impact

Dissociation processes	Threshold energies (eV) (calcd)	(obsd) Present results	(obsd) Electron impact	(obsd) Photo-excitation	(obsd) Mass spectral data
$CH_4+e \longrightarrow CH_3(\tilde{X})+H(n=4)$	(1) 17.2				
$CH(X)+H(n=4)+H_2(X)$	(2) 22.0	21.0±1.0	21.8±0.5(H_β)[a]	19.8—20.3(H_β)[d]	
$CH_2(\tilde{X})+H(n=4)+H(n=1)$	(3) 22.1		21.7±0.8(Ly_γ)[b]		
$CH_3(\tilde{B})+H(n=4)$	(4) 22.9				
$CH_3(\tilde{X})+H(n=R)$	(5) 18.0		22.0±0.5(R)[c]		
$\longrightarrow CH_3(\tilde{X})+H^+$	(6) 18.0				
$CH(X)+H^++H_2(X)$	(7) 22.9				22.7±0.5[e]
$CH_2(\tilde{X})+H^++H(n=1)$	(8) 22.9				24.0±0.5[f]
$CH_3(\tilde{B})+H^+$	(9) 23.7				
$\longrightarrow CH(A)+H_2(X)+H(n=1)$	(10) 12.2				
$CH(A)+3H(n=1)$	(11) 16.6	14.5±0.5	14.6±0.5[a]	12.0[d]	
$CH(A)+H_2(X)+H(n=2)$	(12) 22.4				
$\longrightarrow CH^+(X)+H_2(X)+H(n=1)$	(13) 20.4				
$CH^+(X)+3H(n=1)$	(14) 24.9				22.4±0.1[g]
$CH^+(X)+H_2(X)+H(n=2)$	(15) 30.6				23.3±0.6[e]
$\longrightarrow CH^+(B)+H_2(X)+H(n=1)$	(16) 26.9				
$CH^+(B)+3H(n=1)$	(17) 31.3	30.2±1.0			
$CH^+(B)+H_2(X)+H(n=2)$	(18) 37.1				

a) Ref. 11. b) Ref. 5. c) Ref. 12. d) Ref. 1. e) Ref. 23. f) Ref. 24. g) Ref. 25.

(D) and ionization (I) energies: D(H–H)=4.48 eV,[21] D(CH_3–H)=4.41 eV,[22] D(CH_2–H)=4.90 eV,[22] D(CH–H)=4.46 eV,[11] and I(CH)=11.1 eV.[21] In the right column of Table 1, the threshold energies of $H_\beta(n=4-2)$ and CH(A–X) obtained by Aarts *et al.*,[11] of $Ly_\gamma(n=4-1)$ obtained by Sroka,[5] and of high Rydberg hydrogen fragments obtained by Finn *et al.*[12] under electron-impact excitation, and those of H_β and CH(A–X) obtained by Welch and Judge[1] under photo-excitation, are given, in addition to the appearance potentials of H^+[23,24] and CH^+.[23,25]

The observed threshold energy of H_β is slightly lower than those of H_β and Ly_γ reported by the other investigators, while it is higher by approximately 1 eV than that of H_β obtained by photo-excitation. By comparing the experimental value with the calculated energies, the most significant process for the formation of $H(n=4)$ near the threshold is concluded to be the process (1). The excess energy of 3.8±1.0 eV, which is close to the translational energy of high Rydberg hydrogen fragments (4.0±0.5 eV),[12] is imparted to the fragments as the rotational, vibrational, and translational energies. The coincidence of the excess energy may indicate that $H(n=4)$ and H(R) are produced by a similar process.

By photo-excitation Welch and Judge[1] observed the threshold energy of CH(A–X) near 12.0 eV. The present result, which agrees well with the finding of Aarts *et al.*, is higher by 2.5 eV than that obtained under photo-excitation. From the energy consideration, near the threshold it is believed that the process (10) is responsible for the formation of CH(A) and that about 2.3 eV is released as internal and kinetic energies.

The appearance potential of the CH^+(B–A) emission was observed at 30.2±1.0 eV. As to the dissociative-ionization process for CH^+(B), the three following mechanisms through highly excited states of methane designated as CH_4** and/or through the highly excited methane ion are possible:

$$CH_4 + e \longrightarrow (CH_4^{**}, CH_4^{+*}) \longrightarrow \begin{cases} CH^+(B^1\Delta) + H_2(X^1\Sigma_g^+) + H\ (n=1) \\ CH^+(B^1\Delta) + 3H\ (n=1) \\ CH^+(B^1\Delta) + H_2(X^1\Sigma_g^+) + H\ (n=2). \end{cases}$$

The most likely mechanism is the process (16), and the excess energy of about 3.3 eV is released to the fragments as internal and kinetic energies at the threshold.

The appearance potential of the ion upon mass spectroscopy gives information on the formation of ionic species in the ground state. Smith[23] and McDowell and Warren[25] found the appearance potential of CH^+ from CH_4 at 23.3±0.6 eV and 22.4±0.1 eV respectively. From Table 1, the energetically possible process at the threshold is the process (13) and the excess energy of 2—3 eV is imparted to the fragments. The most likely process for the formation of CH^+(B) in the present study is similar to that of CH^+(X).

Since the production of ionic species can be considered as a limiting case of the formation of the corresponding neutral excited species, a similar mechanism can be expected to be involved in the dissociative-excitation and related dissociative-ionization processes. The facts that the process for the formation of CH(A) is similar to that of CH^+(X) and that the excess energy of the former (2.3±0.5 eV) is close to that of the latter (2.0±0.1 eV,[25] 2.9±0.6 eV[23]) support the above expectation.

Four reactions can account for the formation of H^+ near the threshold, as is shown in Table 1. Smith[23] found the appearance potential of H^+ at 22.7 ± 0.5 eV, and recently Appell and Kubach[24] observed H^+ ions with kinetic energies between 1.4 and 3.4 eV at an appearance potential of 24.0 ± 0.5 eV. Both values indicate that the energetically possible process is the process (6), which is similar to the process (1).

Platzman pointed out that neutral primary products are formed in a radiation-induced reaction through a highly excited neutral state just above the first ionization potential (IP_1) of the molecule named the superexcited state, where dissociation and preionization are competitive.[26] The isotope effect of the Balmer emission from CH_4 under electron-impact excitation has been interpreted as support that excited hydrogen atoms originate from such a superexcited state.[8,11] Since the observed threshold energies of H_β and CH(A–X) are larger than the IP_1 of CH_4 (12.99 eV[22]) and the ionic fragment is not involved in the resulting species, it is concluded that they are produced through the superexcited states.

The superexcited state of CH_4 has been investigated on the basis of the difference between the absorption (energy loss) and ionization spectrum,[26–28] and recently Backx *et al.*[28] have found two regions of superexcited states by means of electron-electron and electron-ion coincidence measurements at keV electron impact. The first state ranged between the IP_1 and 17 eV, which was attributed to high vibrationally-excited Rydberg states converging to the ground state of CH_4^+, $(1t_2)^{-1}$, with reference to the interpretation of Nishikawa and Watanabe.[29] The second state occurred in the region of 22—24 eV, which was connected with the second ionic state, $(2a_1)^{-1}$. The observed threshold energy of CH(A–X) emission indicates that the formation of CH(A) near the threshold proceeds through the first superexcited states. The threshold energy of H_β in the present study and that of the Balmer and Lyman series,[1,5,10–12] and high Rydberg hydrogen fragments[12] are all in the range between 20 and 22 eV. Therefore, superexcited states can be expected to exist in this energy region, although the possibility of excitation to these superexcited states may be small because excited hydrogen atoms are formed by optically forbidden processes.[11] However, Backx *et al.*[28] found no superexcited states in the region of 17—22 eV, which is consistent with the works of Platzman[26] and Nishikawa and Watanabe.[29] Meanwhile, the results by Metzger and Cook,[30] and Rebbert and Ausloos (the ionization efficiency $\eta_i=0.96$ at 21.2 eV)[31] under photo-excitation, and by Ehrhards and Linder[27] under 70 eV electron-impact excitation, support the existence of superexcited states in the same energy range.

Dissociation Processes from Acetylene. The excitation functions of H_β, CH(A–X), and CH^+(B–A) from C_2H_2 are shown in Figs. 8 and 9. The excitation function of H_γ was nearly identical with that of H_β when it was normalized at the maximum. The excitation functions of H_β and CH^+(B–A) have no structure; the former has a maximum at about 100 eV, and the latter, at about 130 eV. The excitation function of CH(A–X) rapidly increases near the threshold; the second threshold can

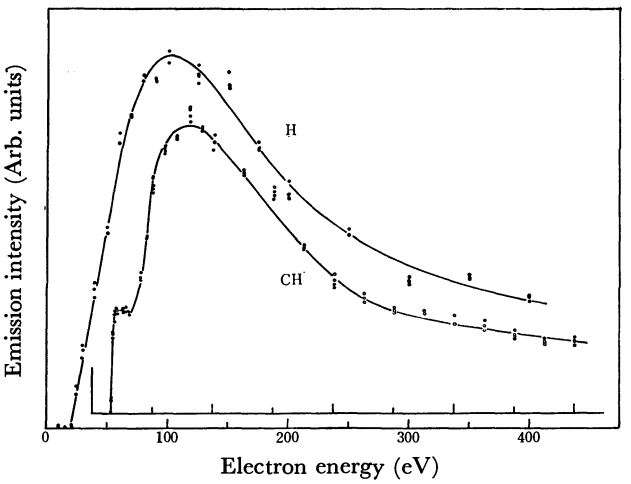

Fig. 8. Excitation functions of H and CH produced by electron impact on C_2H_2. ●: H_β electron-beam current 1.5 μA, ○: CH(431 nm) electron-beam current 1 μA.

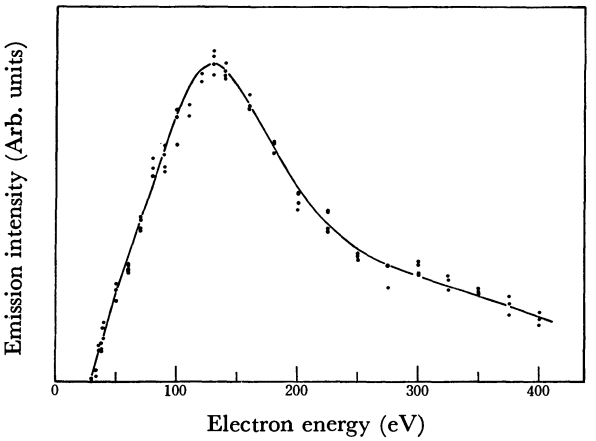

Fig. 9. Excitation function of CH^+ (350 nm) produced by electron impact on C_2H_2. Electron-beam current 5 μA.

be observed at about 30 eV, as was found by Beenakker and de Heer[11] at 28 ± 2 eV. The maximum position of the emission cross section of H_β agrees with the Beenakker and de Heer's result, while that of CH(A–X) is higher than theirs (about 60 eV). The maximum position of CH^+(B–A) is also higher than that of the ionization cross section of CH^+ as measured by a mass spectrometer (about 90 eV).[18] At present no explanation can be given for the discrepancy in the maximum positions of CH and CH^+ from CH_4 and C_2H_2 between the present work and the others; the excitation functions were measured with as low an electron-beam current as possible to avoid the space-charge effect, although higher currents are required for CH^+(B–A) because of the weakness of the intensity.

The appearance potentials and the predominant dissociation channels for the formation of H(n=4), CH(A), and CH^+(B) are enumerated in Table 2. Table 2 also shows the possible dissociative-ionization processes for H^+ and CH^+, and their appearance potentials as obtained in mass-spectrometric studies.[18,32] The threshold energies were calculated using data

Table 2. Threshold energies for dissociative excitation and dissociative ionization of C_2H_2 by electron impact

Dissociation processes	Threshold energies (eV) (calcd)	(obsd) Present results	(obsd) Beenakker *et al.*[a]	(obsd) Mass spectral data
$C_2H_2+e \longrightarrow C_2H(\tilde{X}) + H(n=4)$	(1) 18.1			
$C_2(X) + H(n=4) + H(n=1)$	(2) 23.4	20.6±1.0	20.6±1.0	
$C_2H^+(\tilde{X}) + H(n=4)$	(3) 30.1			
$\longrightarrow C_2H(\tilde{X}) + H^+$	(4) 19.0			
$C_2(X) + H^+ + H(n=1)$	(5) 24.2			21.7±1.0[b]
$C_2H^+(\tilde{X}) + H^+$	(6) 30.9			
$\longrightarrow CH(A) + CH(X)$	(7) 12.8			
$CH(A) + CH(A)$	(8) 15.6			
$CH(A) + C(^3P) + H(n=1)$	(9) 16.2	13.5±1.0	13.0±1.5	
$CH(A) + CH^+(X)$	(10) 23.9			
$CH(A) + C^+(^2P) + H(n=1)$	(11) 27.5			
$CH(A) + C(^3P) + H^+$	(12) 29.8			
$\longrightarrow CH^+(X) + CH(X)$	(13) 21.0			
$CH^+(X) + CH(A)$	(10) 23.9			21.9[c]
$CH^+(X) + C(^3P) + H(n=1)$	(14) 24.5			
$CH^+(X) + CH^+(X)$	(15) 32.1			
$\longrightarrow CH^+(B) + CH(X)$	(16) 27.5			
$CH^+(B) + CH(A)$	(17) 30.3	29.3±1.0		
$CH^+(B) + C(^3P) + H(n=1)$	(18) 30.9			
$CH^+(B) + CH^+(X)$	(19) 38.6			

a) Ref. 11. b) Ref. 18. c) Ref. 32.

identical with those employed by Beenakker and de Heer.[11] The observed appearance potentials of H_β and CH(A–X), which agree well with the work of Beenakker and de Heer,[11] indicate that the significant dissociative-excitation processes for $H(n=4)$ and CH(A) near the threshold are both the lowest-energy processes, (1) and (7). The excess energies of about 2.5 eV for $H(n=4)$ and about 0.7 eV for CH(A) are imparted to the resulting fragment species as the internal and kinetic energies. Meanwhile, mass-spectrometric studies show that the dissociative-ionization processes (4) and (13), which are similar to the dissociative-excitation processes for $H(n=4)$ and CH(A), contribute to the formation of H^+ and CH^+. It should be noticed that the excess energies of H^+ (2.7±1.0 eV) and CH^+ (0.9 eV) are in good agreement with those of $H(n=4)$ and CH(A) described above. Thus, the formation of H^+ and CH^+ from C_2H_2 can be considered as the limiting case of the excitation of H and CH.

The excitation function of CH(A–X) differs from that of the other fragments in the inclination near the threshold; it increases steeply and has the second threshold. The excitation function for a spin-forbidden transition is known to exhibit a sharp maximum at a slightly higher energy than the threshold and to drop rapidly at a still greater electron energy; meanwhile, the maximum cross section for an optically allowed transition is located at a fairly higher energy than the threshold, and the peak is not very sharp.[11] These features in the excitation functions for the excitation and the ionization of the parent molecule are also manifest in those for the dissociative excitation. The dissociative-excitation process (7) can proceed both through the singlet and the triplet states of the excited parent molecule, according to the spin-conservation rule. Thus, the steep increase and the first threshold of the excitation function of CH(A) from C_2H_2 can probably be interpreted as the contribution of the spin-forbidden process, and the further increase up to 80 eV, as that of one or a few optically allowed processes. The second threshold may be due to the superposition of the two excitation processes. The shape of the excitation function of CH(A) from CH_4 indicates that the contribution of the triplet excitation process is unimportant in the dissociative excitation of CH_4 into CH(A).

The threshold energy of the CH^+(B–A) emission was found at 29.3±1.0 eV. Above this threshold, CH^+(B) is probably formed in the process (16), which is the lowest-energy process, as in the case of CH^+(X), and the fragment species carry off an excess energy of about 1.8 eV.

Since the threshold energies of H_β and CH(A–X) emissions exceed the IP_1 of C_2H_2 (11.41 eV[22]) and no ions are produced in the reactions, they are produced through superexcited states of C_2H_2. It is noteworthy that all the dissociation processes of CH_4 in Table 1 need more excess energy than that required in the corresponding dissociation processes of C_2H_2 in Table 2, assuming that the calculated threshold energies are accurate. This can be interpreted by means of the fact that energy between the cross point of a repulsive potential with the primarily prepared highly-excited

states and the dissociation limit is larger in all cases of CH_4, where the energy of the cross point determines the observed appearance potential.

Ethylene and 1,3-Butadiene. The emission spectra of C_2H_4 and C_4H_6 in the 300—600 nm region were measured. The resulting spectra consist of H(Balmer), CH(A–X, B–X, C–X), CH^+(A–X, B–A, b–a), C_2(C–A, d–a), and $C_4H_2^+$(A–X), which are qualitatively identical with the spectrum of C_2H_2. However, the intensity of the CH^+ emission relative to the H and CH emissions is much weaker than that in the cases of CH_4 and C_2H_2. This is consistent with the lower fraction of the CH^+ ions relative to the total ions observed in the mass-spectrometric studies.[33]

The formation of excited H, CH, CH^+, and $C_4H_2^+$ except for $C_4H_2^+$ from C_2H_4[20] are confirmed to be primarily produced by the linear dependence of the intensities on both the electron-beam current and the gas pressure. A more sensitive device will make it possible to measure the excitation function and the threshold energy of the CH^+ emission.

The authors wish to thank Professor Fumiyuki Nakashio and Dr. Minoru Toyoda for their discussions. They are also indebted to Professor Tomoo Oyama for the use of his CT-50 monochromator.

References

1) A. R. Welch and D. L. Judge, *J. Chem. Phys.*, **57**, 286 (1972).
2) K. H. Becker, D. Haaks, and M. Schürgers, *Z. Naturforsch.*, **26a**, 1770 (1971).
3) C. Liu and H. P. Broida, *Phys. Rev. A*, **2**, 1824 (1970).
4) M. Carré, *Physica (Utrecht)*, **41**, 63 (1969).
5) W. Sroka, *Z. Naturforsch*, **24a**, 1724 (1969).
6) J. E. Hesser and B. L. Lutz, *Astrophys. J.*, **159**, 703 (1970).
7) T. Ogawa, I. Fujita, M. Hatada, and K. Hirota, *Bull. Chem. Soc. Jpn.*, **44**, 659 (1971).
8) I. Fujita, Thesis, Osaka University (1973).
9) V. T. Koppe, N. P. Danilevskiĭ, A. G. Koval, and D. V. Pilipenko, *Opt. Spectry. USSR, Engl. Transl.*, **36**, 347 (1974).
10) H. D. Morgan and J. E. Mentall, *J. Chem. Phys.*, **60**, 4734 (1974).
11) D. A. Vroom and F. J. de Heer, *J. Chem. Phys.*, **50**, 573 (1969); J. F. M. Aarts, C. I. M. Beenakker, and F. J. de Heer, *Physica*, **53**, 32 (1971); C. I. M. Beenakker and F. J. de Heer, *Chem. Phys.*, **6**, 291 (1974), **7**, 130 (1975); F. J. de Heer, *Int. J. Radiat. Phys. Chem.*, **7**, 137 (1975).
12) T. G. Finn, B. L. Carnahan, W. C. Wells, and E. C. Zipf, *J. Chem. Phys.*, **63**, 1469 (1975).
13) M. Tsuji, T. Ogawa, Y. Nishimura, and N. Ishibashi, *Chem. Lett.*, **1975**, 317.
14) T. Ogawa, M. Tsuji, M. Toyoda, and N. Ishibashi, *Bull. Chem. Soc. Jpn.*, **46**, 2637 (1973).
15) P. N. Stanton and R. M. S. John, *J. Opt. Soc. Am.*, **59**, 252 (1969).
16) R. W. B. Pearse and A. G. Gaydon, "The Identification of Molecular Spectra," Chapman and Hall, London (1965).
17) B. Adamczyk, A. J. H. Boerboom, B. L. Schram, and J. Kistemaker, *J. Chem. Phys.*, **44**, 4640 (1966).
18) J. T. Tate, P. T. Smith, and A. L. Vaughan, *Phys. Rev.*, **48**, 525 (1935).
19) A. J. Lorquet, J. C. Lorquet, H. Wankenne, and J. Momigny, *J. Chem. Phys.*, **55**, 4053 (1971).
20) M. Tsuji, T. Ogawa, T. Imasaka, Y. Nishimura, and N. Ishibashi, *Bull. Chem. Soc. Jpn.*, **49**, 53 (1976).
21) G. Herzberg, "Spectra of Diatomic Molecules," Van Nostrand, Princeton (1950).
22) G. Herzberg, "Electronic Spectra of Polyatomic Molecules," Princeton (1966).
23) L. G. Smith, *Phys. Rev.*, **51**, 263 (1937).
24) J. Appell and C. Kubach, *Chem. Phys. Lett.*, **11**, 486 (1971).
25) C. A. McDowell and J. W. Warren, *Disc. Faraday Soc.* **10**, 53 (1951).
26) R. L. Platzman, *Vortex*, **23**, 372 (1962); *Radiat. Res.*, **17**, 419 (1962).
27) H. Ehrhardt and F. Linder, *Z. Naturforsch.*, **22a**, 444 (1967).
28) C. Backx, G. R. Wight, R. R. Tol, and M. J. Van der Wiel, *J. Phys. B*, **18**, 3007 (1975); C. Backx and M. J. Van der Wiel, *ibid.*, **18**, 3020 (1975).
29) S. Nishikawa and T. Watanabe, *Chem. Phys. Lett.*, **15**, 590 (1973).
30) P. H. Metzger and G. R. Cook, *J. Chem. Phys.*, **41**, 642 (1964).
31) R. E. Rebbert and P. Ausloos, *J. Res. Nat. Bur. Stand.*, **75A**, 481 (1971).
32) J. L. Franklin and M. A. Haney, "Recent Developments in Mass Spectroscopy," ed. by K. Ogata and T. Hayakawa, University of Tokyo Press, Tokyo (1970), p 909.
33) E. Stenhagen, S. Abrahamsson, and F. W. McLafferty, "Registry of Mass Spectral Data," John Wiley & Sons (1974).

Localized Molecular Orbital Studies of Chemical Reaction. II. Abstraction and Addition Reactions of Triplet Methylene

Shigeru NAGASE and Takayuki FUENO

Department of Chemistry, Faculty of Engineering Science, Osaka University, Toyonaka, Osaka 560

(Received May 13, 1976)

Energy-localized molecular orbitals (LMO) generated from UHF–INDO wave functions have been used for the studies of the mechanistic details of the abstraction and addition reactions of triplet methylene. The UHF LMO mapping procedure which we have previously developed permits a clear understanding of the nature of the chemical bonds to be formed or broken on reaction. Significance of the three-stage mechanism, which should involve the successive β- and α-spin electron delocalizations between reactants and the concomitant spin polarization of the reacting bond, is emphasized. The whole aspects of the reactions are well in accord with the customarily accepted mechanistic schemes.

In the preceding paper of this series,[1] we dealt with mechanistic details of radical reactions in terms of the localized molecular orbitals (LMO). The results were found to be chemically meaningful in many respects. The success has encouraged us to take up the abstraction and addition reactions of triplet methylene, $CH_2(^3B_1)$. Specifically, we wish to elucidate the nature of the deformation of bonds due to the intermolecular interactions. To this end, we have carried out the LMO mapping analysis of the unrestricted Hartree-Fock (UHF) wave functions for the entire reacting systems on one hand and the schematic description of the movement of the LMO charge centroids with reaction on the other. Further, the UHF wave functions of the interacting systems were expanded as a superposition of various electronic configurations of reactant molecules, and their relative importances to the reaction were assessed. The results are found to be useful for the understanding of mechanistic features of the reactions in question.

Calculation Method

The canonical molecular orbitals (CMO) for isolated molecules as well as the reacting systems were calculated by the UHF method[2] in the INDO approximation.[3] The UHF LMO's were generated by the successive two-by-two rotation method[4] for α- and β-spin electrons separately. All possible two-orbital transformations were repeated until further increase in the sum of intraorbital Coulomb energies did not exceed 10^{-6} eV. Virtual CMO's were also localized by the same method.

The UHF LMO's $\boldsymbol{\phi}^\gamma$ for the entire reacting systems obtained at various reaction path points are mapped over the LMO's $\boldsymbol{\phi}^\gamma$ for the isolated reactant molecules:

$$\boldsymbol{\phi}^\gamma = \boldsymbol{\phi}^\gamma \boldsymbol{T}^\gamma \tag{1}$$

where $\boldsymbol{T}^\gamma$ is a unitary matrix pertinent to the mapping, the superscript γ denoting the α- or β-spin. The LMO mapping matrix $\boldsymbol{T}^\gamma$ was obtained by the same procedure as described in a previous paper.[1]

The UHF ground-state wave functions at given path points can be expanded into various electronic configurations:

$$\begin{aligned}\Psi_{\mathrm{UHF}} &= |\psi_1^\alpha \psi_1^\beta \cdots\cdots \psi_p^\alpha \psi_p^\beta \psi_{p+1}^\alpha| \\ &= C_{\mathrm{G}}\Phi_{\mathrm{G}} + \sum_{\mathrm{K}}\sum_i C_{\mathrm{K}i}\Phi_{\mathrm{K}i}\end{aligned} \tag{2}$$

where Φ_{G} is the ground configuration and where $\Phi_{\mathrm{K}i}$ is the i-th configuration of type K—local excitation (LE) of reactant molecule, charge transfer (CT) from reactant to $^3CH_2$, back charge transfer (BCT) from $^3CH_2$ to reactant, and so on.[1] The configurational coefficients, C_{G} and $C_{\mathrm{K}i}$'s, were calculated by the technique similar to the one used by Baba *et al.*[5] All computations were carried out on a FACOM 230-60 at the Kyoto University Computation Center.

Results and Discussion

A. Characteristics of the UHF–LMO's of Methylene. It is recognized that methylene (CH_2) can exist in both singlet ($^1A_1$) and triplet ($^3B_1$) states. The bond angles calculated by the INDO method for a fixed bond length (R_{CH}=1.094 A) are 107 and 132°, respectively,[3] which are both in good agreement with observations (102.4 and 136°, respectively[6-8]). The LMO's which we obtained at these calculated equilibrium angles are shown in Table 1, where $CH_2(^3B_1)$ is assumed to have two more α-spin electrons than β-spin ones. It can be seen that each LMO is certainly little delocalized (less than 1%).

The total energy E of methylene can be expressed as the sum of contributions from individual occupied LMO's, provided the nuclear charge of each atom is assumed to be expressible in the form[9-11]

$$Z_{\mathrm{A}} = \sum_i Z_{i,\mathrm{A}} \tag{3}$$

where $Z_{i,\mathrm{A}}$ is the part of the nuclear charge on atom A partitioned to the i-th LMO. The value of $Z_{i,\mathrm{A}}$ is taken to be equal to 1 for an unpaired LMO as well as an LMO localized mainly around two atoms, whereas $Z_{i,\mathrm{A}}$=2 for a lone-pair LMO. The component energies ε_i^γ thus derived are given by

$$\varepsilon_i^\gamma = \frac{1}{2}\langle\phi_i^\gamma|\boldsymbol{F}^\gamma + \boldsymbol{H}^c|\phi_i^\gamma\rangle + c_i\sum_j\sum_{\mathrm{A}}\sum_{\mathrm{B}} e^2 Z_{i,\mathrm{A}} Z_{j,\mathrm{B}}/R_{\mathrm{AB}} \tag{4}$$

where $\boldsymbol{F}^\gamma$ and $\boldsymbol{H}^c$ are the Hartree-Fock and core Hamiltonian operators, respectively; R_{AB} is the internuclear distance between atoms A and B; and c_i is a constant which is 1/2 for the i-th α-spin counterpart of a β-spin LMO and 1 for an unpaired radical-center LMO.

Figures 1 and 2 show the variations in ε_i^γ of various filled LMO's of the singlet and triplet methylenes, respectively, with the bond angle ∠HCH. The numbers

Table 1. Localized orbitals for the singlet and triplet methylenes

LMO[a]		AO coefficients					
		Cs	Cp_x	Cp_y	Cp_z	H_a	H_b
			CH_2 ($^1A_1$)				
Occupied	CH_a	0.399	0.353	0.475	0.000	0.700	−0.011
	L	0.715	−0.693	0.000	0.000	−0.060	−0.060
Vacant	CH_a*	0.307	0.380	0.506	0.000	−0.710	−0.012
	L*	0.000	0.000	0.000	1.000	0.000	0.000
			CH_2($^3B_1$)				
Occupied	CH_a^{α}	0.348	0.404	0.497	0.000	0.684	−0.027
	CH_a^{β}	0.518	0.129	0.471	0.000	0.701	−0.045
	$N_{\pm}$	0.517	−0.482	0.000	±0.707	0.023	0.023
Vacant	CH_a^{α}*	0.335	0.324	0.503	0.000	−0.728	−0.025
	CH_a^{β}*	0.411	0.236	0.527	0.000	−0.704	−0.038
	$N_{\pm}$*	0.250	−0.654	0.000	±0.707	−0.069	−0.069

a) See Figs. 1 and 2.

appended indicate the values of x for hybridization (sp^x)of the carbon orbitals involved.

Comparison of Fig. 1 with Fig. 2 shows that the energies ε_i^{γ} have a roughly similar pattern of angular variations for both spin states. The lone-pair (L) and unpaired (N) orbital energies have the greatest angular variations and are decreased as the bond angle decreases. On the contrary, the C–H bond energies for both spin states increase with the decreasing bond angle. In other words, the nonbonding orbitals tend to make the methylene molecule bent, while the C–H bond orbitals are energetically in favor of the linear geometry. The equilibrium bond angles would be a compromise between these two opposing contributions. The results are in accord with those obtained by the electrostatic force theory,[12] in which the former contribution is ascribed to the "atomic dipole" force and the latter, to the "exchange" force.

Here, considerations of the spatial arrangement of the C–H bond orbitals themselves seem to be in order. In the triplet methylene, the LMO's for the α-spin electrons can be described roughly as tetrahedral (sp^3) in type while those for the β-spin electrons as linear (sp). Pauling[13] pointed out qualitatively that the two $(C\text{-}H)^{\alpha}$ bond orbitals would tend to bring the HCH bond angle to 90° while the two $(C\text{-}H)^{\beta}$ bond orbitals, to 180°. The directions of the C–H bond orbitals obtained by the present treatment for varying bond angle are as illustrated in Fig. 3. Deviations of the direction of bond orbitals from that of the C–H bonds may be taken as reflecting the force with which the orbitals attract the H nucleus. It would then appear as though the bond angle were determined by the balance between the attractive forces from the $(C\text{-}H)^{\alpha}$ and $(C\text{-}H)^{\beta}$ bond orbitals. Thus, at the equilibrium bond angle, the hydrogen atom is situated nearly on the bisector of the angle between the bond orbitals. For the singlet state, things are much simpler; only when the equilibrium

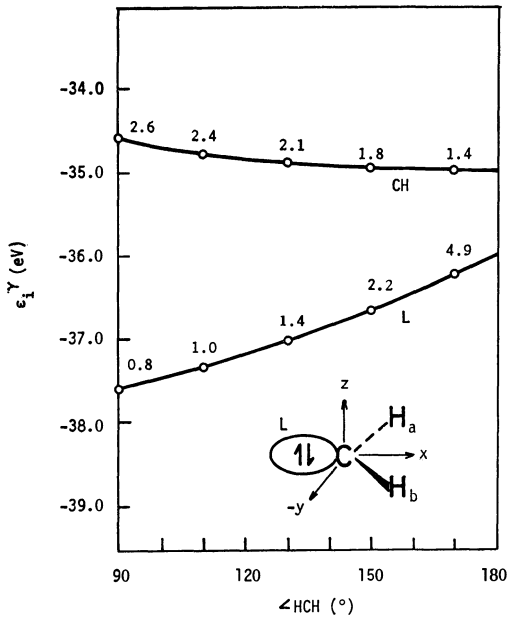

Fig. 1. Variations of the bond energy and hybridization with the bond angle (<HCH) for the singlet methylene.

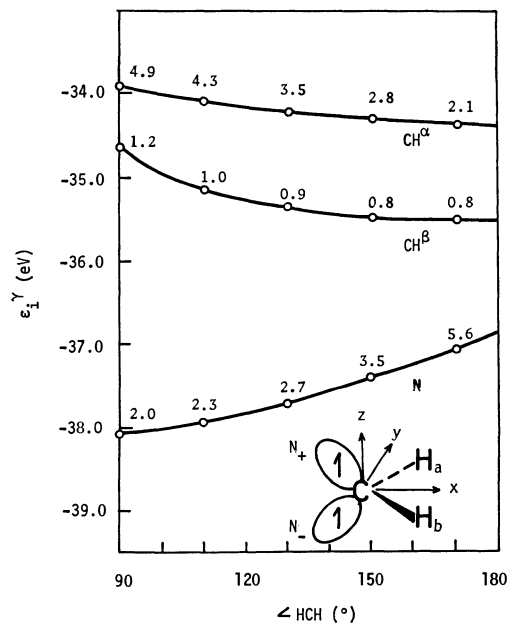

Fig. 2. Variations of the bond energy and hybridization with the bond angle (<HCH) for the triplet methylene.

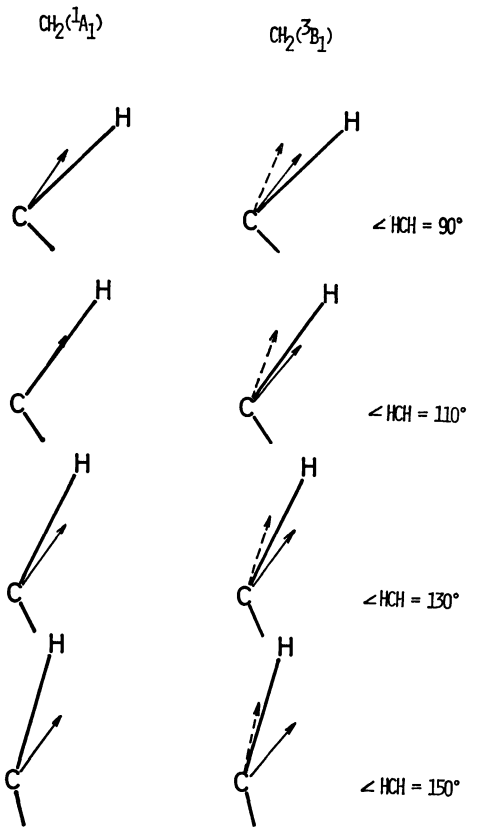

Fig. 3. Directions of the C–H bond orbitals for $^{1,3}CH_2$. The solid and broken arrows for $^3CH_2$ show the directions of the α- and β-spin C–H bond orbitals, respectively.

bond angle is reached, can the hydrogen atom locate itself in the direction of the (C–H) bond orbital. These results may serve as a useful guide for the prediction of the changes in nuclear motions during chemical reactions.

B. Abstraction Reaction. We wish to examine the reaction of triplet methylene with methane as a prototype of abstraction reactions. The reaction is considered to proceed *via* a linear transition state[14] as shown in Fig. 4. This was indeed confirmed by the calculations[15] of the intermolecular interaction energy based on our intermolecular perturbation method.[16] A similar transition state geometry has been assumed for the hydrogen abstraction reaction of triplet methylene from molecular hydrogen.[17]

The main purpose of this study is to analyze the alteration in electronic structure of molecules during

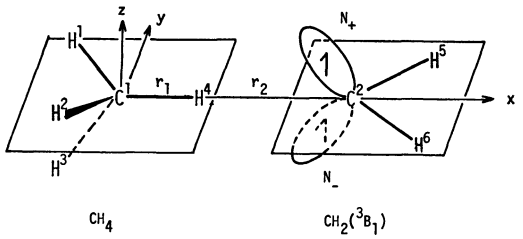

Fig. 4. Coordinate system for the abstraction reaction of methane by triplet methylene.

reaction rather than the change in the total energy, and to interpret it in an orderly manner in terms of the LMO mappings. We specify the reaction path with the notation (r_1, r_2), where r_1 is the distance in units of Å between carbon C^1 and hydrogen H^4, while r_2 is that between carbon C^2 and hydrogen H^4 (Fig. 4). Calculations were carried out at model path points A(1.09, 2.5), B(1.09, 2.0), C(1.09, 1.5), and D(1.29, 1.3),[18] where 1.09 Å is the equilibrium C–H distance of methane.[19]

Variations in hybridization during the reaction are shown in Table 2. It is seen that the bond orbitals C^1–H^1 and C^1–H^4 of methane suffer variations in hybridization in different manners. The α-spin C^1–H^4 bond destined to be cleaved diminishes in p character as the reaction proceeds. In the meantime, the remaining three α-spin C–H bonds gain p character to make up the decrease in p character of the α-spin C^1–H^4 bond. On the other hand, the β-spin C^1–H^4 bond gains p character, being accompanied by the decrease in p character of the remaining three β-spin C–H bonds. As for the methylene molecule, the p character of both the α- and β-spin C–H bonds tends to be increased while that for the unpaired α-spin orbitals is decreased. It is only the C^1–H^4 bond that suffers drastic change in form during the reaction.

TABLE 2. VARIATIONS IN HYBRIDIZATION[a] OF THE CARBON ATOMS IN THE CH_4–$^3CH_2$ SYSTEM[b]

Path point	CH_4				$^3CH_2$		
	C^1–H^1		C^1–H^4		C^2–H^5		N_+
	α-spin	β-spin	α-spin	β-spin	α-spin	β-spin	α-spin
∞[c]	2.68	2.68	2.68	2.68	3.45	0.89	2.73
(A)	2.68	2.66	2.66	2.69	3.45	0.89	2.73
(B)	2.72	2.62	2.59	2.76	3.46	0.91	2.69
(C)	2.87	2.47	2.31	3.10	3.66	0.99	2.53

a) The entries are the values of x for the hybridization sp^x. b) See Fig. 4. c) Isolated reactants.

Shown in Fig. 5 are the movements of the centroids of the LMO charge distributions with the progress of reaction. The approach of two unpaired electrons of the methylene carbon decouples the electron pairing in the C^1–H^4 bond. The β-spin electron moves toward the H^4 atom while the α-spin electron, in the opposite direction. This separation of the α- and β-spin electrons will effectively weaken (and eventually break) the bond. Meanwhile, the β-spin electron begins to be coupled with one of the α-spin electrons of CH_2. The situation is closely related to the conventional representation as follows:

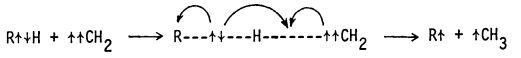

A better insight into the mechanism of bond rearrangement can be obtained from the results of LMO mapping analysis (Table 3). The bonds other than the C^1—H^4 bond of methane and the $N_\pm$ orbitals of methylene suffer little deformation during the reaction. The α-spin electrons in $N_\pm$ orbitals are delocalized mainly into the antibonding orbital $(C^1$–$H^4)^*$, which will weaken the C^1–H^4 bond. On the other hand, the β-spin orbital

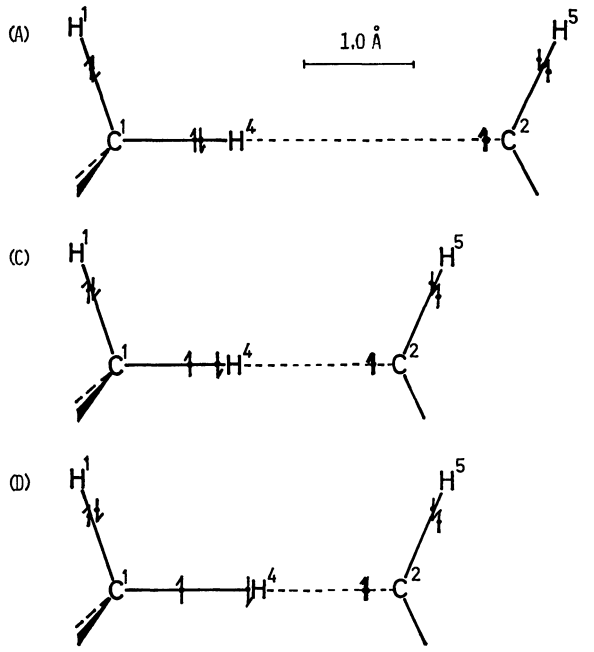

Fig. 5. Top view of the centroids of localized molecular orbitals in the CH_4–$CH_2(^3B_1)$ system at the path points (A), (C), and (D).

(C^1–H^4) mixes first with the vacant unpaired orbital N* of methylene in a strongly bonding way and then with the antibonding orbital (C^1–H^4)* with a negative sign. The corresponding α-spin orbital allows the orbital (C^1–H^4)* to mix into it with a positive sign. The mixing of the antibonding orbital (C^1–H^4)* into the corresponding α- and β-spin bonding orbitals (C^1–H^4) in different signs is what is usually called "spin polarization." The spin polarization induces an excess α-spin density around the carbon C^1 and an excess β-spin density around the hydrogen H^4.

All the above arguments converge into a concept of three-stage mechanism as follows: The main bond deformation caused at the initial stage of reaction is due to the mixing of the β-spin C^1–H^4 orbital into the vacant unpaired orbital $N_\pm$*. At the middle stage, the mixing of the α-spin $N_\pm$ orbital into the antibonding orbital (C^1–H^4)* develops, to form a three-center bond. As the reaction approaches the final stage, the mixing of the α-spin orbital (C^1–H^4) into the antibonding orbital (C^1–H^4)* becomes dominant. Thus, in the first place, a β-spin electron is transferred from methane to methylene; next, back transfer of an α-spin electron from methylene to methane takes place; and finally, local excitation in the bond to be broken becomes appreciable. The first stage can be termed the electrophilic stage of the reaction. From the viewpoint of spin properties, the first and second stages may be envisaged as the "spin delocalization" stage, which operates to drive the two reactant molecules close to each other, thus forming a three-center bond over C^1, H^4, and C^2. Cleavage of the old bond is effected primarily by the last stage, *i.e.*, the "spin polarization" stage. The spin polarization is in effect equivalent to the "triplet excitation" noted in the intermolecular configuration interaction treatments.[1,20]

In connection with the above statement, we briefly consider the reaction of the triplet methylene with CH_3X (X=F or Cl). Triplet methylene attacks substrates containing both hydrogen and halogen atoms in a selective manner; it abstracts a hydrogen atom rather than a halogen atom.[21] The calculated triplet excitation energies[22] from the bonding (C–H) to antibonding (C–H)* orbital are 17.1 and 17.3 eV for CH_3F and CH_3Cl, respectively. Those from (C–F) and (C–Cl) to (C–F)* and (C–Cl)* are 24.0 and 19.1 eV, respectively. Thus, we may anticipate the spin polarization effect to be larger in the C–H bond rather in the C–F or C–Cl bond. Spin density distributions in

Table 3. LMO mapping analysis of the hydrogen abstraction of $^3CH_2$ from CH_4

Spin	Path point	Mapped LMO[a]
		C^1–H^4
α	(A)	$0.999(C^1H^4)+0.005(C^1H^4)^*$
	(B)	$0.999(C^1H^4)+0.023(C^1H^4)^*-0.002[(N_+)+(N_-)]$
	(C)	$0.989(C^1H^4)+0.088(C^1H^4)^*-0.008[(N_+)+(N_-)]$
	(D)	$0.946(C^1H^4)+0.301(C^1H^4)^*-0.051[(N_+)+(N_-)]$
β	(A)	$0.998(C^1H^4)-0.003(C^1H^4)^*$ $+0.049[(N_+)^*+(N_-)^*]$
	(B)	$0.986(C^1H^4)-0.017(C^1H^4)^*$ $+0.115[(N_+)^*+(N_-)^*]$
	(C)	$0.937(C^1H^4)-0.056(C^1H^4)^*$ $+0.237[(N_+)^*+(N_-)^*]$
	(D)	$0.866(C^1H^4)-0.177(C^1H^4)^*$ $+0.326[(N_+)^*+(N_-)^*]$
		$N_\pm$
α	(A)	$0.999(N_\pm)-0.024(C^1H^4)^*$
	(B)	$0.998(N_\pm)-0.052(C^1H^4)^*+0.003(C^1H^4)$
	(C)	$0.992(N_\pm)-0.116(C^1H^4)^*+0.025(C^1H^4)$
	(D)	$0.962(N_\pm)-0.236(C^1H^4)^*+0.128(C^1H^4)$

a) For the LCAO expressions of the C^1–H^4 bond LMO's, (C^1H^4) and (C^1H^4),* of isolated methane, see Table 1 of Ref. 1

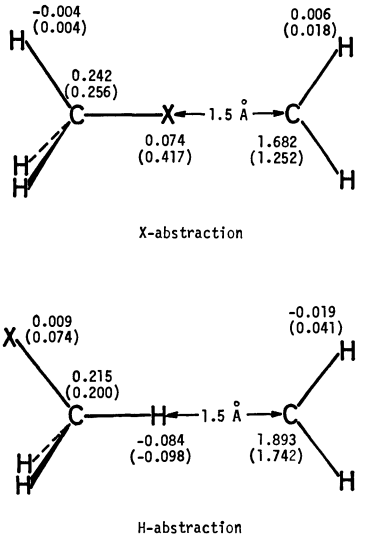

Fig. 6. Spin density distributions in the CH_3X–$CH_2(^3B_1)$ system (X=F or Cl). The entries given in parentheses are the values for the case of X=Cl.

the reaction systems lend support to this view (Fig. 6). Apparently, the distributions are $\overset{\alpha}{C}\cdots\overset{\alpha}{X}\cdots\overset{\alpha}{C}$ in the case of the halogen abstraction and $\overset{\alpha}{C}\cdots\overset{\beta}{H}\cdots\overset{\alpha}{C}$ for the hydrogen abstraction. Thus, the triplet excitation energy in the bond as well as the spin density distribution may be a useful guide for predicting the relative ease of the bond cleavage.

C. Addition Reaction. The reaction here studied is the addition of triplet methylene to the double bond of ethylene. Characteristics of this particular reaction was already investigated by Hoffmann[23] in terms of the extended Hückel molecular orbitals. The reaction path was more thoroughly examined by Bodor *et al.*[14] using the MINDO/2 method. We here choose to employ the path similar to that of Bodor *et al.* for our purpose.

The relative positions of methylene and ethylene during the reaction are specified as shown in Fig. 7. The middle of the ethylene double bond was taken as the origin of the coordinate. The carbons C^1 and C^2 of ethylene are put on the x axis, and the carbons C^1, C^2 and C^3 are placed on the xz plane. The entire system is assumed to be symmetric with respect to this plane. The geometry of the system is characterized by the notation $(r, \theta, \psi, \omega)$ in units of Å and degree. The path points considered are A(3.5, 90, 90, 0), B(2.4, 85, 90, 0), C(2.0, 80, 80, 0), D(1.9, 65, 75, 0), E(1.9, 50, 60, 0), and F(1.9, 50, 60, 30).

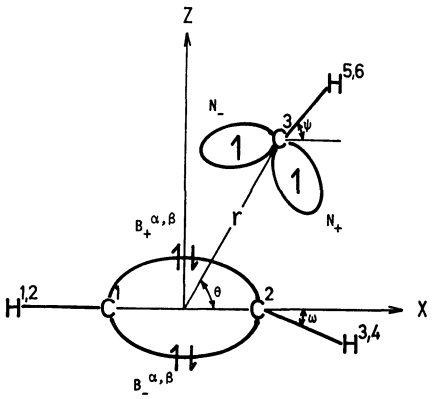

Fig. 7. Coordinate system (side view) for describing the relative position of $CH_2(^3B_1)$ and $CH_2{=}CH_2$.

The LMO calculations for the ethylene molecule provide two equivalent banana bonds for the description of the double bond; one (B_+) lies above the molecular plane while the other (B_-) below it. The banana bonds associated with the α- and β-spin electrons are specified as $B_\pm^\alpha$ and $B_\pm^\beta$, respectively. The triplet methylene has two unpaired orbitals N_+ and N_- as has been mentioned earlier.

When reaction takes place, these particular LMO's suffer the greatest deformation. Table 4 gives the results of the LMO mapping analysis at path points (B)

TABLE 4. LMO MAPPING ANALYSIS OF THE ADDITION OF $^3CH_2$ TOWARD C_2H_4

Spin	Path point	Mapped LMO[a]
		B_-
α	(B)	$1.000(B_-)$
	(C)	$0.982(B_-)+0.170(B_+)$
	(D)	$0.859(B_-)+0.508(B_+)$
	(E)	$0.819(B_-)+0.570(B_+)$
β	(B)	$0.990(B_-)+0.079(B_+)$
	(C)	$0.949(B_-)+0.303(B_+)$
	(D)	$0.882(B_-)+0.456(B_+)$
	(E)	$0.838(B_-)+0.527(B_+)$
		B_+
α	(B)	$0.998(B_+)-0.023(B_-)+0.017(B_+)^*-0.014(B_-)^*$
	(C)	$0.965(B_+)-0.150(B_-)+0.132(B_+)^*-0.116(B_-)^*$
	(D)	$0.762(B_+)-0.433(B_-)+0.333(B_+)^*-0.294(B_-)^*$
	(E)	$0.701(B_+)-0.467(B_-)+0.374(B_+)^*-0.344(B_-)^*$
β	(B)	$0.963(B_+)-0.046(B_-)-0.014(B_+)^*+0.011(B_-)^*+0.198(N_-)^*+0.174(N_+)^*$
	(C)	$0.857(B_+)-0.241(B_-)-0.069(B_+)^*+0.053(B_-)^*+0.298(N_-)^*+0.326(N_+)^*$
	(D)	$0.736(B_+)-0.354(B_-)-0.136(B_+)^*+0.113(B_-)^*+0.392(N_-)^*+0.353(N_+)^*$
	(E)	$0.679(B_+)-0.398(B_-)-0.157(B_+)^*+0.140(B_-)^*+0.433(N_-)^*+0.324(N_+)^*$
		N_+
α	(B)	$0.995(N_+)+0.001(N_-)$
	(C)	$0.950(N_+)+0.004(N_+)+0.066(B_+)-0.040(B_-)-0.218(B_+)^*+0.193(B_-)^*$
	(D)	$0.828(N_+)+0.176(N_-)+0.246(B_+)-0.160(B_-)-0.302(B_+)^*+0.282(B_-)^*$
	(E)	$0.712(N_+)+0.321(N_-)+0.289(B_+)-0.213(B_-)-0.302(B_+)^*+0.313(B_-)^*$
		N_-
β	(B)	$0.999(N_-)-0.002(N_+)$
	(C)	$0.996(N_-)-0.005(N_+)$
	(D)	$0.947(N_-)-0.265(N_+)$
	(E)	$0.869(N_-)-0.457(N_+)$

a) For the LCAO expressions of the banana bond LMO's $B_\pm$ and $B_\pm^*$ of isolated ethylene, see Table 4 of Ref. 1

to (E). As is naturally expected, the B$_-^{\alpha}$, B$_-^{\beta}$, B$_+^{\alpha}$, and N$_-$ bonds are responsible primarily for the intramolecular bond rearrangement, while the B$_+^{\beta}$ and N$_+$ orbitals, for the intermolecular bond formation. Here also, the mixing of the B$_+^{\alpha}$ and B$_+^{\beta}$ bonds with the anti-bonding B$_+$* and B$_-$* bonds takes place with opposite signs, a situation which is equivalent to an inducement of triplet excitation in the double bond.[1]

The addition reaction of triplet methylene also conforms to a three-stage mechanism. As can be inferred from Table 4, triplet methylene initially approaches ethylene as a β-spin acceptor. Next, it comes to behave as an α-spin donor. Finally, local excitation in the ethylene molecule becomes appreciable. The β- and α-spin electron transfers must be the major origin of the formation of the new C^2–C^3 bond. The local excitation, *i.e.*, spin polarization in the C^1—C^2 bond should be a factor most effective to the cleavage of the B$_+$ bond.

The results described above can be illustrated pictorially by the schematic representation of the centroids of LMO charge distributions (Fig. 8). Again, the schematic description is in accord with the conventional scheme:

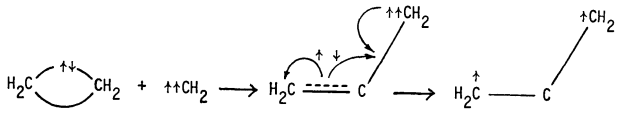

The paired electrons which existed in the B$_-$ bond are slightly decoupled and migrate toward the mid-point of the carbons C^1 and C^2 to form a single bond. The paired electrons which existed in the B$_+$ bond are highly decoupled; the α-spin electron migrates onto the carbon C^1 to form a radical center there, while the β-spin electron migrates toward the mid-point of the carbons C^2 and C^3 to make a pair with one of the two unpaired electrons of methylene, leaving the other unpaired electron to form another radical center on C^3.

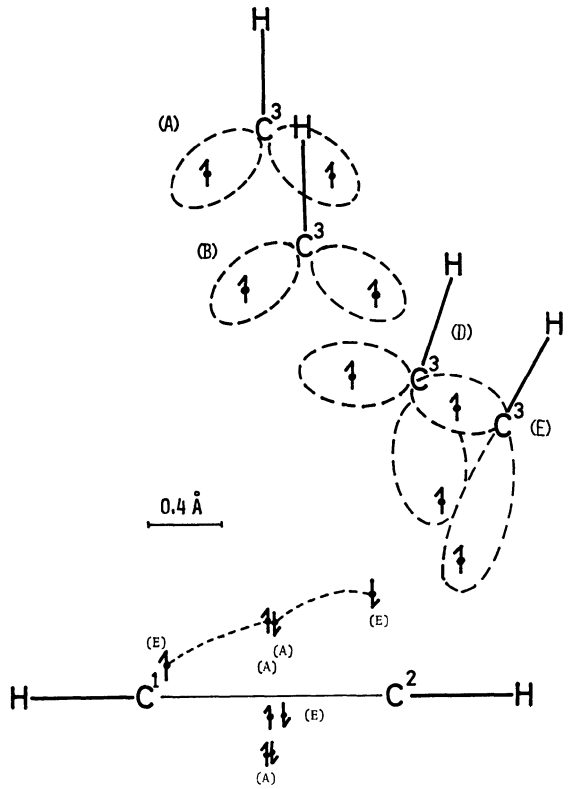

Fig. 8. Schematic representation of the centroids of LMO charge distributions at path points (A)—(E) in the addition reaction of triplet methylene to ethylene.

Listed in Table 5 are the total weights $\sum_i C_{Ki}^2$ of various types of configurations K contributing to Φ_{UHF} at different reaction path points. That the reaction proceeds by the three-stage mechanism can be perceived here even more clearly. Thus, the most dominant configuration to be mixed with Φ_G at initial stages of reaction is Φ_{CT}, the β-spin delocalization from ethylene to CH_2. This is followed up by the mixing of Φ_{BCT}, the α-spin delocalization from CH_2 to ethylene. Finally, the contribution of Φ_{LE} due to the α-spin, and hence triplet, excitation on ethylene becomes appreciable.

Table 5. Total weights of the composite configurations in the addition of triplet methylene (M) to ethylene (E)

Path point	Spin	C_G^2 (EM)	$\sum_i C_{LE.i}^2$ (E*M)	$\sum_k C_{CT.k}^2$ (E$^+$M$^-$)	$\sum_l C_{BCT.l}^2$ (E$^-$M$^+$)	$\sum_j C_{LE.j}^2$ (EM*)
(A)	α	0.998	0.000	0.000	0.000	0.000
	β		0.000	0.002	0.000	0.000
(B)	α	0.896	0.001	0.003	0.009	0.001
	β		0.001	0.085	0.000	0.001
(C)	α	0.648	0.026	0.010	0.073	0.008
	β		0.008	0.179	0.001	0.008
(D)[a]	α	0.354	0.082	0.005	0.178	0.001
	β		0.019	0.176	0.001	0.009

a) Other highly-transferred and highly-excited configurations are also mixed into the ground configuration.

If triplet methylene approached ethylene by way of the least motion with the C_{2v} symmetry ($\theta=\psi=90°$), no new pairing of opposite spins would be possible between them and the bonded electron pair in B$_+$ could not be decoupled with ease. This was in fact confirmed by separate calculations. The situation is much the same as in the addition of methyl radical to ethylene, which has been discussed previously.[1] The steric course of reaction should thus be dependent upon how smoothly the interchange of pairing of opposite spins can take place.

References

1) S. Nagase, K. Takatsuka, and T. Fueno, *J. Am. Chem. Soc.*, **98**, 3838 (1976).
2) J. A. Pople and R. K. Nesbet, *J. Chem. Phys.*, **22**, 571 (1954).
3) J. A. Pople and D. L. Beveridge, "Approximate Molecular Orbital Theory," McGraw-Hill, New York (1970).
4) C. Edmiston and K. Ruedenberg, *Rev. Mod. Phys.*, **35**, 457 (1963); *J. Chem. Phys.*, **43**, 597 (1965).
5) H. Baba, S. Suzuki, and T. Takemura, *J. Chem. Phys.*, **50**, 7078 (1969).
6) G. Herzberg and J. W. C. Johns, *Proc. R. Soc. London, Ser. A*, **295**, 107 (1966); *J. Chem. Phys.*, **54**, 2276 (1971).
7) E. Wasserman, V. J. Kuck, R. S. Hutton, and W. A.

Yager, *J. Am. Chem. Soc.*, **92**, 7491 (1970).
8) R. A. Bernheim, H. W. Bernard, P. S. Wang, L. S. Wood, and P. S. Skell, *J. Chem. Phys.*, **53**, 1280 (1970).
9) J. M. Parks and R. G. Parr, *J. Chem. Phys.*, **28**, 335 (1958).
10) T. L. Allen and H. Shull, *J. Chem. Phys.*, **35**, 1644 (1961).
11) W. England and M. S. Gordon, *J. Am. Chem. Soc.*, **93**, 4649 (1971).
12) H. Nakatsuji, *J. Am. Chem. Soc.*, **95**, 345, 354, 2084 (1973).
13) L. Pauling in "Molecular Orbitals in Chemistry, Physics, and Biology," P.-O. Löwdin and B. Pullman, Ed., Academic Press, New York (1964) p. 207.
14) N. Bodor, M. J. S. Dewar, and J. S. Wasson, *J. Am. Chem. Soc.*, **94**, 9095 (1972).
15) S. Nagase and T. Fueno, *Theor. Chim. Acta*, **41**, 59 (1976).
16) T. Fueno, S. Nagase, K. Tatsumi, and K. Yamaguchi, *Theor. Chim. Acta*, **26**, 431 (1972); S. Nagase and T. Fueno, *ibid.*, **35**, 217 (1974).
17) C. P. Baskin, C. F. Bender, C. W. Bauschlicher, Jr., and H. F. Schaefer III, *J. Am. Chem. Soc.*, **96**, 2709 (1974).
18) The points A to D, which have been selected rather arbitrarily in this work, may not fall exactly on the reaction path to be obtained by rigorous calculations of the potential energy surface. Nevertheless, we believe that the qualitative features of the reaction which are pointed out herewith would not be affected seriously by more rigorous treatments of the reaction.
19) H. C. Allen and E. K. Plyler, *J. Chem. Phys.*, **26**, 972 (1957).
20) A. D. McLachlan, *Mol. Phys.*, **5**, 51 (1962).
21) H. D. Roth, *J. Am. Chem. Soc.*, **93**, 1527, 4935 (1971); **94**, 1400 (1972).
22) As the INDO parametrization is not available in the original method for the second row atoms, we employed the CNDO approximation including d orbitals.[3]
23) R. Hoffmann, *J. Am. Chem. Soc.*, **90**, 1475 (1968).

The Crystal and Molecular Structure of 1-(2-Thiazolylazo)-2-naphthol

Masayasu KURAHASHI

National Research Institute for Metals, 3-12, 2-Chome, Nakameguro, Meguro-ku, Tokyo, 153

(Received May 14, 1976)

The crystal structure of 1-(2-thiazolylazo)-2-naphthol, $C_{13}H_9N_3OS$, has been determined from three-dimensional X-ray data collected by counter methods. The crystals are monoclinic with space group $P2_1/a$; cell dimensions: $a=17.721(1)$, $b=28.366(2)$, $c=4.699(1)$ Å, $\beta=91.78(1)°$, and $Z=8$. The structure was solved by the symbolic addition procedure and refined by the least-squares method to give an R value of 0.051 for 2150 observed reflections. There are two crystallographically independent molecules in an asymmetric unit; both of the molecules show a generally similar shape and size, but their structural details differ in planarity and distribution of the bond lengths. Both molecules have the azo and hydrazone character, but the equilibrium is shifted toward the azo tautomer.

The compound 1-(2-thiazolylazo)-2-naphthol (abbreviated as Htan) forms colored complexes with various metals, and has therefore been used as an analytical reagent. As part of a series of investigations of the structure of Htan and its metal chelates, the X-ray determination of Htan has been undertaken. The main purpose of the investigation is to establish the configuration of the ligand molecule; this will help to elucidate the structural change involved in the chelate ring formation.

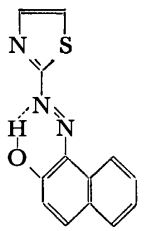

Htan

There is also interest in the tautomerism of this compound. It is well known that the azo and hydrazone tautomers frequently coexist in *ortho*-azophenol compounds.[1-5] An IR spectral study has suggested the azo-hydrazone tautomerism of Htan;[6] however, an explicit interpretation has never been made. Since the phenomenon of the tautomerism seemed to be important for understanding the reactions of this compound with metals, a detailed analysis of the structure has been undertaken. A preliminary note of this work has already been published.[7]

Experimental

The crystals of Htan were obtained from an ethanolic solution by slow evaporation. A crystal of dimensions $0.15\times0.3\times0.4$ mm was chosen for data collection. The crystal data are summarized in Table 1. The cell parameters were determined by the least-squares procedure from the 2θ values of 40 reflections measured on a diffractometer using monochromated Cu $K\alpha$ radiation. The density was determined by flotation in an aqueous solution of sodium iodide.

TABLE 1. CRYSTAL DATA

$C_{13}H_9N_3OS$	M. W. 255.3
Monoclinic	Space group $P2_1/a$
$a=17.721(1)$ Å	$D_m=1.44$ g cm^{-3}
$b=28.366(2)$ Å	$D_x=1.436$ g cm^{-3}
$c=4.699(1)$ Å	$Z=8$
$\beta=91.78(1)°$	$\mu=2.64$ cm^{-1} (for Mo $K\alpha$)
$V=2360.8$ Å^3	

The integrated intensities of the reflections were measured on a Rigaku automated four-circle diffractometer with Mo $K\alpha$ radiation monochromated by a graphite plate. The ω-2θ scan technique was employed at a scan speed of 4°/min in ω, and scanning was repeated up to four times when the $\sigma(|F|)$ due to the counting statistics was larger than 3% of $|F|$. The scan width was determined according to the formula $1.5°+0.6°\times\tan\theta$. Background was counted for 10 s at both sides of each peak. Three standard reflections were measured every fifty reflections during the data collection. The intensities of unique reflections with 2θ values less than 55° were collected and a total of 2150 reflections with $|F|>3\sigma(|F|)$ were obtained. The data were corrected for Lorentz and polarization factors, but no correction was made for absorption ($\mu r<0.1$).

Solution of the Structure and Refinement

The structure was determined by the symbolic addition procedure.[8] The distribution and statistics of $|E|$'s agree well with the theoretical values for the centrosymmetric case. Signs of 386 reflections could be determined by the usual symbolic addition procedure using three origin reflections and three symbols, and the resulting E map revealed the location of all 36 non-hydrogen atoms. Several cycles of least-squares refinement of the coordinates and isotropic temperature factors resulted in an $R(=\sum||F_o|-|F_c||/\sum|F_o|)$ of 0.092. Anisotropic thermal parameters were then introduced for all non-hydrogen atoms, and the R factor was reduced to 0.075. All the hydrogen atoms were located on the difference map. This map also revealed that the phenolic hydrogen atoms (H(O) and H(O')) are disordered or oscillate violently, especially the H(O') atom; the contour lines corresponding to the H(O') are elongated toward both O' and N(2') atoms. A second difference map, computed after three cycles of refinement in which all the hydrogen atoms except H(O) and H(O') were included with an isotropic temperature factor, showed the same tendency. Then various least-squares calculations were made, assuming the internal hydrogen bonding of the double minimum type [O–H(O)···H(N)–N]. For example, when the occupancy factors [H(O) to H(N) ratio] of 7 to 3 and 6 to 4,

estimated from the N(1)–N(2) and C(2)–O distances, were given to A (unprimed molecule) and B (primed molecule) respectively, R dropped to 0.052. However, the lowest R value, 0.051, was obtained when the single minimum model of the type O–H(O)···N(2) was assumed. Unit weight was given to all 2150 reflections. The atomic scattering factors used for S, O, N, and C were taken from International Tables for X-ray Cry-

TABLE 2. POSITIONAL AND THERMAL PARAMETERS

(a) Fractional atomic coordinates for the non-hydrogen atoms

	x	y	z		x	y	z
S	0.1994(1)	0.0125(1)	−0.0166(3)	S′	0.2008(1)	0.2967(2)	−0.3010(11)
O	0.2341(2)	0.1798(1)	0.4676(9)	O′	0.1158(2)	0.4517(1)	0.7121(8)
N(1)	0.1597(2)	0.0899(1)	0.3437(9)	N(1′)	0.1133(2)	0.3528(1)	0.8596(9)
N(2)	0.2196(3)	0.1010(1)	0.2085(9)	N(2′)	0.1615(2)	0.3793(1)	0.9965(9)
N(3)	0.3002(2)	0.0735(2)	−0.1381(9)	N(3′)	0.2600(3)	0.3782(2)	1.3353(10)
C(1)	0.1384(3)	0.1229(2)	0.5362(11)	C(1′)	0.0675(3)	0.3731(2)	0.6608(11)
C(2)	0.1712(3)	0.1660(2)	0.5953(12)	C(2′)	0.0692(3)	0.4220(2)	0.5846(11)
C(3)	0.1406(4)	0.1971(2)	0.7955(11)	C(3′)	0.0201(3)	0.4384(2)	0.3621(12)
C(4)	0.0772(3)	0.1862(2)	0.9297(12)	C(4′)	−0.0297(3)	0.4102(2)	0.2299(12)
C(5)	0.0383(3)	0.1431(2)	0.8819(11)	C(5′)	−0.0356(3)	0.3609(2)	0.3011(11)
C(6)	−0.0276(3)	0.1319(2)	1.0255(12)	C(6′)	−0.0885(3)	0.3320(2)	0.1594(12)
C(7)	−0.0624(4)	0.0897(2)	0.9827(13)	C(7′)	−0.0921(4)	0.2851(2)	0.2285(14)
C(8)	−0.0333(4)	0.0578(2)	0.7915(15)	C(8′)	−0.0440(3)	0.2665(2)	0.4354(14)
C(9)	0.0298(3)	0.0681(2)	0.6461(13)	C(9′)	0.0078(3)	0.2940(2)	0.5764(12)
C(10)	0.0680(3)	0.1110(2)	0.6841(11)	C(10′)	0.0139(3)	0.3425(2)	0.5146(11)
C(11)	0.2429(3)	0.0667(2)	0.0221(11)	C(11′)	0.2083(3)	0.3566(2)	1.1915(11)
C(12)	0.2539(3)	−0.0017(2)	−0.2641(12)	C(12′)	0.2747(3)	0.3019(2)	1.4948(12)
C(13)	0.3118(3)	0.0340(2)	−0.3010(11)	C(13′)	0.2978(3)	0.3467(2)	1.5083(14)

(b) Anisotropic thermal parameters for the non-hydrogen atoms ($\times 10^4$)

The anisotropic thermal parameters are in the form $\exp\{-(h^2B_{11}+k^2B_{22}+l^2B_{33}+hkB_{12}+hlB_{13}+klB_{23})\}$

	B_{11}	B_{22}	B_{33}	B_{12}	B_{13}	B_{23}		B_{11}	B_{22}	B_{33}	B_{12}	B_{13}	B_{23}
S	44(1)	11(1)	584(8)	−4(1)	50(4)	−18(2)	S′	41(1)	11(1)	552(8)	1(1)	0(4)	−5(2)
O	50(2)	13(1)	749(27)	−9(2)	82(12)	−46(7)	O′	47(2)	11(1)	603(23)	−5(2)	−20(10)	7(6)
N(1)	35(2)	10(1)	394(22)	3(2)	−13(10)	−2(6)	N(1′)	27(2)	12(1)	442(23)	2(2)	−10(10)	−1(6)
N(2)	36(2)	10(1)	421(23)	0(2)	−30(10)	−14(6)	N(2′)	31(2)	10(1)	506(25)	0(2)	−12(10)	14(7)
N(3)	31(2)	13(1)	534(26)	−2(2)	29(11)	22(7)	N(3′)	36(2)	14(1)	690(30)	−5(2)	−76(13)	−7(8)
C(1)	36(2)	10(1)	399(26)	5(2)	−14(12)	−21(7)	C(1′)	25(2)	11(1)	466(28)	2(2)	17(12)	−18(8)
C(2)	40(2)	11(1)	502(30)	3(2)	−5(14)	−10(8)	C(2′)	34(2)	12(1)	450(28)	5(2)	29(12)	−4(8)
C(3)	58(3)	11(1)	644(37)	−5(3)	28(17)	−38(9)	C(3′)	43(2)	13(1)	538(33)	4(2)	35(15)	44(9)
C(4)	54(3)	12(1)	537(33)	6(2)	39(16)	−23(8)	C(4′)	31(2)	18(1)	559(33)	10(2)	−7(14)	2(9)
C(5)	35(3)	11(1)	460(29)	9(2)	−31(13)	5(8)	C(5′)	27(2)	16(1)	494(31)	2(2)	24(12)	−4(9)
C(6)	42(3)	16(1)	565(33)	14(3)	30(15)	−13(9)	C(6′)	30(2)	23(1)	575(34)	−3(3)	−10(14)	−8(10)
C(7)	44(3)	19(1)	685(39)	5(3)	87(16)	13(11)	C(7′)	41(3)	23(1)	664(40)	−16(3)	−37(16)	−44(11)
C(8)	47(3)	16(1)	887(46)	−10(3)	91(18)	−38(11)	C(8′)	45(3)	14(1)	787(43)	−10(3)	54(17)	−38(10)
C(9)	41(3)	12(1)	657(36)	2(2)	18(15)	−20(9)	C(9′)	37(2)	13(1)	608(34)	−1(2)	31(14)	−13(9)
C(10)	34(2)	9(1)	439(28)	7(2)	−31(12)	−15(7)	C(10′)	28(2)	12(1)	441(27)	3(2)	22(12)	2(8)
C(11)	34(2)	11(1)	399(27)	3(2)	−24(12)	−3(8)	C(11′)	32(2)	13(1)	462(29)	2(2)	11(12)	4(8)
C(12)	48(3)	12(1)	511(30)	8(2)	−13(15)	−34(8)	C(12′)	46(3)	16(1)	551(33)	9(3)	−2(15)	2(10)
C(13)	32(2)	17(1)	483(30)	9(2)	−20(13)	−20(9)	C(13′)	37(2)	20(1)	698(37)	3(3)	−31(16)	−21(11)

(c) Positional and thermal parameters for the hydrogen atoms

	x	y	z	B		x	y	z	B
H(3)	0.168(3)	0.223(2)	0.827(10)	5.0(12)	H(3′)	0.024(3)	0.470(2)	0.316(10)	5.9(12)
H(4)	0.059(2)	0.207(2)	1.081(9)	4.8(11)	H(4′)	−0.064(3)	0.421(2)	0.067(10)	4.8(12)
H(6)	−0.049(3)	0.154(2)	1.165(11)	6.3(14)	H(6′)	−0.120(3)	0.345(2)	−0.003(12)	6.8(15)
H(7)	−0.105(3)	0.082(2)	1.090(10)	5.6(12)	H(7′)	−0.126(3)	0.265(2)	0.133(10)	5.4(13)
H(8)	−0.058(3)	0.026(2)	0.754(11)	6.0(13)	H(8′)	−0.046(3)	0.232(2)	0.481(11)	6.2(13)
H(9)	0.049(2)	0.048(2)	0.513(10)	4.8(11)	H(9′)	0.039(3)	0.285(2)	0.734(10)	4.9(13)
H(12)	0.261(3)	−0.032(2)	−0.354(11)	6.8(15)	H(12′)	0.289(3)	0.275(2)	1.601(10)	4.9(12)
H(13)	0.355(2)	0.035(1)	−0.439(9)	3.9(10)	H(13′)	0.335(3)	0.361(2)	1.632(11)	6.5(14)
H(O)	0.245(3)	0.155(2)	0.310(13)	9.0(17)	H(O′)	0.148(3)	0.429(2)	0.877(13)	9.1(17)

stallography,[9] for H, those of Stewart, Davidson, and Simpson were used.[10] The final atomic parameters based on the single minimum model are listed in Table 2. The observed and calculated structure factors are compared in Table 3.*

Description of the Structure and Discussion

The structure consists of two chemically similar but crystallographically independent molecules (referred to as A and B). The configuration of these molecules viewed normal to the naphthalene plane is shown in Fig. 1. The thermal ellipsoids are drawn at 50% probability. Both molecules show a generally similar shape and size, but some structural details are different, as described below. Each azo group adopts a *trans* conformation, and the phenolic oxygen atom, O, is linked to the azo nitrogen atom, N(2), by intramolecular hydrogen bonding; the O···N(2) distances are 2.548(6) and 2.556(6) Å for A and B, respectively.

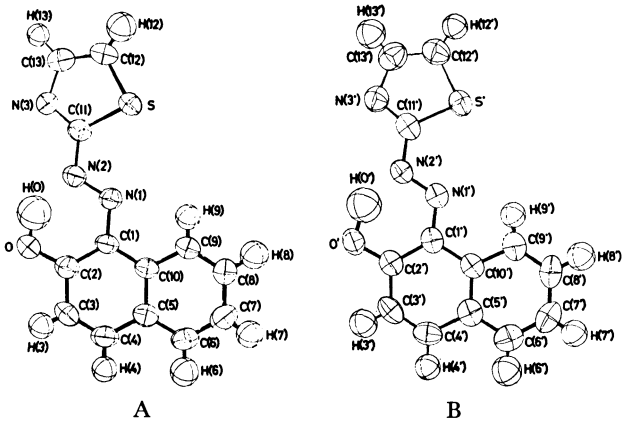

Fig. 1. The molecular structures viewed normal to each naphthalene plane. The thermal ellipsoids are drawn at 50% probability.

N(1) and N(3) are in *trans* positions with respect to the C(11)–N(2) bond. A similar conformation was observed for a bromo-derivative of Htan, 1-(2-thiazolylazo)-6-bromo-2-naphthol.[11] This will imply that the observed conformation is the most stable one for these molecules. A relatively short non-bonded distance of 2.87 Å, as shown in Fig. 2a, is observed between N(1) and S (and N(1′) and S′).

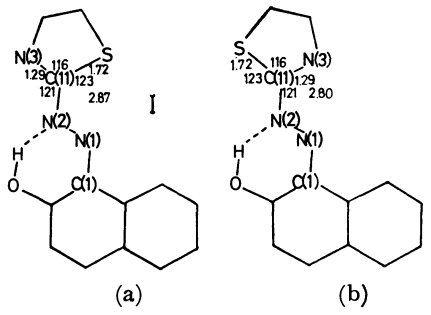

Fig. 2. Two possible planar configurations for Htan. (a) *trans* (b) *cis* (N(1)–N(2)–C(11)–N(3)).

If the thiazole ring is rotated by 180° around the C(11)–N(2) bond, that is, when N(1) and N(3) are in *cis* positions, the N(1)···N(3) distance will be about 2.80 Å (Fig. 2b). Inspection of MO calculations for this molecule[12] reveals that such a conformation is less stable in view of the electrostatic interaction, because the formal charges on N(1) and N(3) are both negative. On the other hand, the N(1)···S interaction in the observed conformation (Fig. 2a) is of the attractive type, since the formal charges on N(1) and S are negative and positive, respectively.

Bond lengths and angles are shown in Table 4 with their e.s.d.'s. The most significant differences between A and B are in the N(1)–N(2) and C(1)–C(10) distances; the other distances of both molecules agree well, within the limit of three times their corresponding e.s.d.'s.

The observed N(1)–N(2) distance of 1.278(7) Å lies between the standard distance of the azo form (–N=N–), 1.24±0.01 Å,[13–18] and that of the hydrazone form (–NH–N=), 1.39±0.01 Å,[16,19,20] and is closer to the value corresponding to the azo form. On the other hand, the observed value of 1.306(7) Å for N(1′)–N(2′) is almost intermediate between the azo and hydrazone

Table 4. Bond lengths and angles

(a) Bond lengths (l/Å)

	A (Unprimed atoms)	B (Primed atoms)
S–C(11)	1.728(6)	1.719(6)
S–C(12)	1.700(6)	1.702(6)
O–C(2)	1.325(7)	1.317(7)
N(1)–N(2)	1.278(6)	1.306(6)
N(1)–C(1)	1.371(7)	1.359(7)
N(2)–C(11)	1.382(7)	1.378(7)
N(3)–C(11)	1.285(7)	1.294(7)
N(3)–C(13)	1.372(8)	1.375(8)
C(1)–C(2)	1.412(8)	1.409(7)
C(1)–C(10)	1.416(8)	1.446(7)
C(2)–C(3)	1.413(9)	1.423(8)
C(3)–C(4)	1.323(9)	1.337(9)
C(4)–C(5)	1.418(8)	1.419(8)
C(5)–C(6)	1.395(8)	1.419(9)
C(5)–C(10)	1.418(8)	1.415(8)
C(6)–C(7)	1.345(9)	1.347(10)
C(7)–C(8)	1.389(10)	1.410(10)
C(8)–C(9)	1.348(9)	1.354(9)
C(9)–C(10)	1.405(8)	1.396(8)
C(12)–C(13)	1.332(9)	1.326(9)
C(3)–H(3)	0.88(5)	0.91(5)
C(4)–H(4)	0.97(5)	1.02(4)
C(6)–H(6)	1.00(5)	0.98(6)
C(7)–H(7)	0.93(5)	0.90(5)
C(8)–H(8)	1.02(5)	0.99(6)
C(9)–H(9)	0.92(5)	0.96(5)
C(12)–H(12)	0.95(6)	0.96(5)
C(13)–H(13)	1.00(4)	0.93(6)
O–H(O)	1.04(6)	1.17(6)
N(2)···H(O)	1.66(6)	1.50(6)
O···N(2)	2.548(6)	2.556(6)

* Table 3 is kept as Document No. 7629 at the Chemical Society of Japan, 1-5, Kanda-Surugadai, Chiyoda-ku, Tokyo.

(b) Bond angles (φ/°)

	A (Unprimed atoms)	B (Primed atoms)
C(11)–S–C(12)	88.3(3)	88.3(3)
N(2)–N(1)–C(1)	117.2(4)	117.1(4)
N(1)–N(2)–C(11)	115.2(4)	114.6(4)
C(11)–N(3)–C(13)	109.9(5)	108.4(5)
N(1)–C(1)–C(2)	123.4(5)	125.0(5)
N(1)–C(1)–C(10)	116.8(5)	114.9(4)
C(2)–C(1)–C(10)	119.8(5)	120.1(5)
O–C(2)–C(1)	123.6(5)	122.3(5)
O–C(2)–C(3)	117.8(5)	118.6(5)
C(1)–C(2)–C(3)	118.6(5)	119.1(5)
C(2)–C(3)–C(4)	121.4(6)	120.9(6)
C(3)–C(4)–C(5)	122.8(6)	122.2(6)
C(4)–C(5)–C(6)	122.5(5)	121.0(5)
C(4)–C(5)–C(10)	117.5(5)	119.4(5)
C(6)–C(5)–C(10)	120.0(5)	119.7(5)
C(5)–C(6)–C(7)	121.2(6)	120.2(6)
C(6)–C(7)–C(8)	119.5(6)	120.4(6)
C(7)–C(8)–C(9)	120.9(7)	120.1(6)
C(8)–C(9)–C(10)	121.8(6)	121.9(6)
C(1)–C(10)–C(5)	120.0(5)	118.3(5)
C(1)–C(10)–C(9)	123.4(5)	123.9(5)
C(5)–C(10)–C(9)	116.6(5)	117.8(5)
S–C(11)–N(2)	122.8(4)	122.8(4)
S–C(11)–N(3)	115.3(4)	116.1(4)
N(2)–C(11)–N(3)	121.9(5)	121.1(5)
S–C(12)–C(13)	110.7(5)	110.4(5)
N(3)–C(13)–C(12)	115.8(5)	116.9(6)
O–H(O)–N(2)	146(5)	140(5)

forms, but is slightly closer to the value corresponding to the azo form.

The C(2)–O and C(2′)–O′ distances of 1.325(7) and 1.317(7) Å observed for A and B respectively are congruent with neither the standard distance of the phenolic form (C–OH), 1.38±0.01 Å,[21,22] nor with that of the quinoid form (C=O), 1.22±0.01 Å.[21,23,24] The distances lie intermediate between these two values, but are slightly closer to the value corresponding to the phenolic C–OH distance.

Somewhat similar behaviors were observed in 1-(*p*-nitrophenylazo)-2-naphthol,[25] 4-chloro-2,5-dimethoxyanilide of 1-(2,5-dichlorophenylazo)-2-hydroxy-3-naphthoic acid,[26] and 1,2-naphthoquinone 1-(2-nitro-4-chlorophenylhydrazone).[27] In these compounds N–N (–N=N– or –NH–N=) and C–O (C=O or C–OH) distances range from 1.32 to 1.34 Å and from 1.25 to 1.26 Å, respectively. These reported values correspond more nearly to the hydrazone tautomer than to the azo tautomer.

In view of the bond length distribution for Htan, azo-like (phenol) character is predominant rather than the hydrazone-like (quinone) character in both A and B. However, B has more of a hydrazone-like character than A, since the N(1)–N(2) and C(1)–C(10) are longer and C(2)–O and N(1)–C(1) are shorter in B than in A.

The azo-hydrazone tautomerism of Htan was better established by the location of the relevant hydrogen

TABLE 5. LEAST-SQUARES PLANES

Plane 1	entire molecular plane	A
Plane 2	naphthalene ring plane	A
Plane 3	thiazole ring plane	A
Plane 4	entire molecular plane	B
Plane 5	naphthalene ring plane	B
Plane 6	thiazole ring plane	B

(a) equations of planes (a, b, c*)

Plane 1	$0.5431x-0.4202y+0.7270z=1.625$
Plane 2	$0.5357x-0.4203y+0.7324z=1.638$
Plane 3	$0.5867x-0.3738y+0.7184z=1.882$
Plane 4	$-0.6853x+0.1958y+0.7014z=3.466$
Plane 5	$-0.6956x+0.2099y+0.6871z=3.575$
Plane 6	$-0.6639x+0.1812y+0.7255z=3.556$

(b) Deviations of atoms from planes (l/Å)

	A		
	1	2	3
S	0.083*	0.044	−0.002*
O	0.042*	0.010	0.180
N(1)	−0.004*	−0.028	−0.035
N(2)	−0.024*	−0.060	0.012
N(3)	−0.079*	−0.135	−0.001*
C(1)	−0.005*	−0.021*	−0.021
C(2)	0.029*	0.009*	0.095
C(3)	0.033*	0.023*	0.107
C(4)	0.002*	0.002*	0.006
C(5)	−0.018*	−0.013*	−0.098
C(6)	−0.038*	−0.020*	−0.190
C(7)	−0.013*	0.008*	−0.246
C(8)	0.009*	0.021*	−0.234
C(9)	0.006*	0.006*	−0.168
C(10)	−0.010*	−0.014*	−0.101
C(11)	−0.015*	−0.059	0.002*
C(12)	0.044*	−0.010	0.002*
C(13)	−0.043*	−0.105	−0.001*

	B		
	4	5	6
S	0.003*	−0.109	0.004*
O	0.047*	0.048	−0.108
N(1)	0.028*	−0.019	−0.071
N(2)	0.055*	0.001	−0.021
N(3)	0.003*	−0.092	0.002*
C(1)	0.022*	0.005*	−0.124
C(2)	0.014*	0.021*	−0.160
C(3)	−0.045*	−0.017*	−0.278
C(4)	−0.055*	−0.012*	−0.301
C(5)	−0.016*	0.004*	−0.236
C(6)	−0.015*	0.013*	−0.258
C(7)	0.003*	0.008*	−0.215
C(8)	0.017*	−0.007*	−0.152
C(9)	0.021*	−0.012*	−0.125
C(10)	0.006*	−0.004*	−0.164
C(11)	0.023*	−0.061	−0.004*
C(12)	−0.058*	−0.196	−0.004*
C(13)	−0.043*	−0.169	−0.002*

* Only the atoms with asterisks were used in the plane calculation.

(c) Angles between planes (φ/°)

	1	2	3	4	5
2	0.8				
3	3.7	4.2			
4	87.0	86.2	88.6		
5	88.3	87.6	90.0	1.4	
6	84.8	84.1	86.5	2.2	3.5

atoms. The positions of H(O) and H(O'), which were located from the difference map (higher than 0.3 e Å^{-3}), were refined by the least-squares method as mentioned above. The observed O–H(O) and O'–H(O') distances are 1.04(6) and 1.17(6) Å respectively (the N(2)···H(O) and N(2')···H(O') distances are 1.65(6) and 1.55(6) Å respectively), indicating O–H(O)···N(2) [and O'–H(O')···N(2')] hydrogen bonding. This fact is sufficient to establish the azo form as the predominant tautomer in both A and B. It can also be seen from the hydrogen positions that B has more of a hydrazone-like character than A.

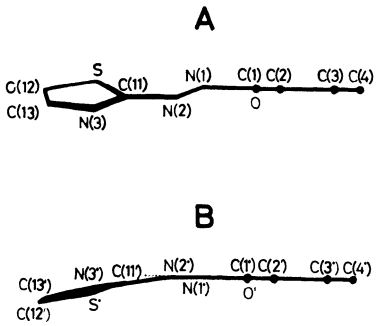

Fig. 3. Side view of the A and B molecules. The vertical scale is approximately eight times greater than the horizontal scale.

In studying the problem of the tautomerism, it is of interest to see the planarity of the molecules. The equations of the best planes through various sets of atoms in the respective molecules are presented in Table 5(a). The displacement of atoms from the planes and the angles between these planes are given in Tables 5(b) and 5(c). A view of the molecules which illustrates the planarity is shown in Fig. 3. The vertical scale is approximately eight times greater than the horizontal scale. Naphthol and thiazole rings of both molecules are planar within the experimental error. The A and B molecules are roughly planar within the deviations of $\pm$0.08 and $\pm$0.06 Å respectively, and each breaks the planarity in a different way, as can be seen in Figs. 1 and 3. The molecule A is twisted along the N(1)–C(1) bond, with 4.2° as the angle between the planes of the thiazole and naphthol rings. On the other hand, the molecule B is slightly folded at the N(2) atom and the thiazole ring plane makes an angle of 3.5° with the naphthol ring plane. The slight rotation along the N(1)–C(1) bond will indicate the single bond character, and accordingly the pronounced azo-like character in A. The slight pyramidal configuration (C(11')–N(2')$<^{N(1')}_{H(O')}$) around the N(2') atom is indicative of some hydrazone-like character in B.

From the X-ray evidence mentioned above, the following two models can be proposed for the real molecular structure of Htan. The first is to assume that the azo (I) and hydrazone (II) tautomers coexist in the crystals of Htan, but the azo tautomer predominates.

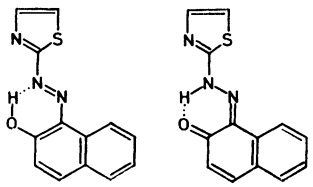

(I) (II)

Accordingly the molecules as a whole are disordered; the azo and hydrazone tautomers occupy statistically two slightly different positions with unequal probability. Elongation of the thermal ellipsoids, especially in the molecule B, along the N(1)–N(2), N(1)–C(1), C(2)–O, *etc.*, suggests this model. However, it seems that more elongated ellipsoids should appear in such a case.

The second is that there exists only one type of molecule, whose electronic structure is intermediate between the azo and hydrazone tautomer, but the contribution of the azo form is more pronounced. If the potential curve of the hydrogen bonding is of the single minimum type (IIIa), the hydrogen atom would vibrate violently in the potential well. If the potential is of the double minimum type (IIIb), only the hydrogen

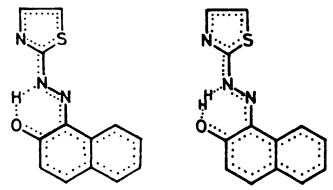

(IIIa) (IIIb)

atoms would be disordered. X-Ray evidence cannot distinguish these two cases. The potential well is clearly not the symmetric double minimum nor the symmetric single minimum type.

The average values of bond distances and angles in the thiazole ring are: S–C(11)=1.724, S–C(12)=1.701, N(3)–C(11)=1.290, N(3)–C(13)=1.374, and C(12)–C(13)=1.329 Å. C(11)–S–C(12)=88.3, C(11)–N(3)–C(13)=109.2, S–C(11)–N(3)=115.7, S–C(12)–C(13)=110.6, and N(3)–C(13)–C(12)=116.4°. Both S–C(11) and S–C(12) distances are significantly shorter than the standard distance of the paraffinic C–S bond, 1.817(5) Å.[28] This indicates that both C–S bonds have some double bond character and that the hybridization state of S is not sp^3.

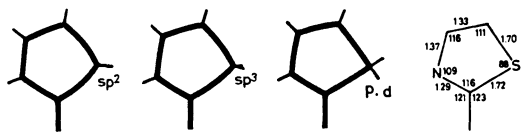

(a) (b) (c) (d)

Fig. 4. Framework molecular models (a, b, c) for thiazole and observed geometry (d). For S atom (a) sp^2, (b) sp^3 and (c) p (or d_{xy}) orbital skeleton was used.

Figure 4 shows the molecular models of a thiazole ring in which the valence state of S is assumed to be (a) sp^2, (b) sp^3, and (c) p (or some other orthogonal orbitals like d_{xy}). The observed distribution of bond angles, (d), corresponds more to that of model (c) than to (a) or (b). This may suggest that the valence state of S is not sp^2 either. In the case of thiophene, the C–S distance and the C–S–C angle are reported to be 1.718 Å and 92.2(1)° respectively,[29] and the d-electron orbitals are thought to be involved in the hybridization.[30] The observed values of C–S bond length and C–S–C angle for Htan are very close to the values for thiophene. Therefore, d-electron orbitals may be connected with the hybridization in the case of thiazole as well. If the hybridization state is purely sp^2 or sp^3, and if the accuracy of the analysis is high enough, lone pair electrons will appear in a residual map. An attempt to locate the relevant lone pair electrons for the sulfur atom in the final difference map failed; A more detailed analysis will be necessary to discuss this problem.

If the thiazole sulfur atom does not have lone pair electrons pointing to the bisector of C(11)–S–C(12), the sulfur atom will not participate in any chelate ring formation. Actually, there is no example of the participation of the thiazole sulfur atom in metal binding. X-Ray determinations of Fe(II)-, Co(III)-, Ni(II)-, Cu(II)-, and Pd(II)-chelates of the 1-(2-thiazolylazo)-2-naphtholato (tan) group have established that tan is coordinated to the metal through the phenolic oxygen atom, the azo nitrogen atom adjacent to the naphthol ring, and the thiazole nitrogen atom so as to form two five-membered chelate rings.[31–35]

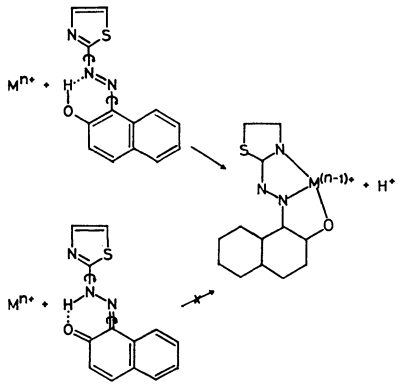

Fig. 5. Conformational changes on chelate ring formation.

Comparison of the structures of Htan and tan indicates that both thiazole and naphthol rings are rotated by 180° around the N(2)–C(11) and N(1)–C(1) bonds, as illustrated by Fig. 5. It should be noted that the rotation around the N(1)–C(1) bond will not usually occur when the N(1)–C(1) is a double bond (*i.e.* hydrazone form). Thus the reaction of the type $Htan+M^{n+}\longrightarrow M^{(n-1)+}\text{-tan}+H^+$ will occur through the azo tautomer.

The crystal structure projected along the c axis is shown in Fig. 6. Intermolecular distances shorter than 3.5 Å are given in Table 6. All distances are consistent with the van der Waals contacts, and there is no evidence of intermolecular hydrogen bonding.

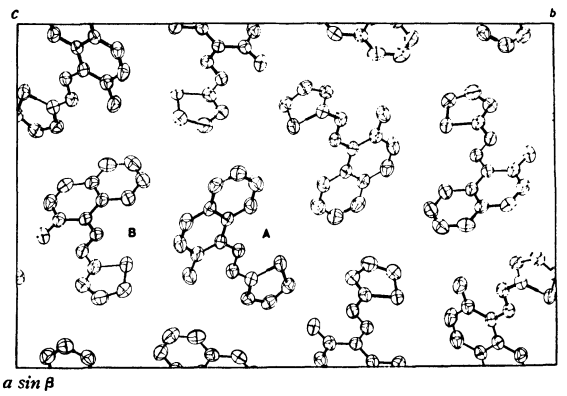

Fig. 6. Crystal structure projected along the c axis. The thermal ellipsoids are drawn at 50% probability.

Table 6. Interatomic distances shorter than 3.5 Å

		Symmetry operation	Distance (*l*/Å)
O	S′	1	3.50
O	C(7′)	3	3.46
N(1)	N(2)	1	3.44
N(1)	C(5)	2	3.37
N(1)	C(13)	1	3.48
N(2)	N(3)	1	3.43
N(2)	C(2)	2	3.50
N(2)	C(13)	1	3.36
N(3)	C(4′)	3	3.45
C(1)	C(4)	2	3.49
C(1)	C(11)	1	3.34
C(11)	C(13)	1	3.48
C(12)	O′	4	3.31
C(12)	N(3′)	5	3.44
C(13)	O′	4	3.31
N(1′)	C(5′)	1	3.40
N(2′)	C(2′)	1	3.46
N(2′)	C(3′)	1	3.50
N(2′)	C(13′)	2	3.50
C(1′)	C(4′)	1	3.39
C(1′)	C(11′)	2	3.40
C(6′)	C(9′)	2	3.43

Symmetry operations

1 (x y $1+z$) 4 ($\frac{1}{2}-x$ $\frac{1}{2}+y$ $-z$)
2 (x y $1-z$) 5 ($\frac{1}{2}-x$ $\frac{1}{2}+y$ $1-z$)
3 ($\frac{1}{2}+x$ $\frac{1}{2}-y$ z)

The author wishes to express his gratitude to Professor Yoshihiko Saito of the Univ. of Tokyo who kindly allowed him to use the diffractometer. He is also grateful to Dr. Akira Kawase of National Chemical Laboratory for Industry for his valuable discussions. Calculations were performed on the HITAC 5020F computer at the Computer Center of National Aerospace Laboratory and on the NEAC 3100 computer at this Institute. Some UNICS programs were used.[36] Figures 1 and 6 were drawn with the DEAM-4 program.[37]

References

1) D. Hadzi, *J. Chem. Soc.*, **1956**, 2143.
2) A. Buraway, A. G. Salen, and A. R. Thompson, *J. Chem. Soc.*, **1952**, 4793.

3) J. W. Dudek and E. P. Dudek, *J. Am. Chem. Soc.*, **88**, 2407 (1966).
4) V. Bekárak, K. Rothshein, P. Vetešnĭk, and M. Večeřa, *Tetrahedron Lett.*, **1968**, 3711.
5) J. E. Kuder, *Tetrahedron*, **28**, 1973 (1972).
6) A. Kawase, Doctor thesis, The University of Tokyo (1964).
7) M. Kurahashi, *Chem. Lett.*, **1974**, 181.
8) J. Karle and I. L. Karle, *Acta Crystallogr.*, **21**, 849 (1966).
9) "International Tables for X-Ray Crystallography," Vol. III, Kynoch Press, Birmingham, England (1962).
10) R. F. Stewart, E. R. Davidson, and W. T. Simpson, *J. Chem. Phys.*, **42**, 3175 (1965).
11) M. Kurahashi, M. Fukuyo, A. Shimada, and A. Kawase, *Bull. Chem. Soc. Jpn.*, **49**, 872 (1976).
12) K. Nishimoto, private communication.
13) C. J. Brown, *Acta Crystallogr.*, **B21**, 146; **B21**, 153 (1966).
14) H. Hope and D. Victor, *Acta Crystallogr.*, **B25**, 1849 (1969).
15) A. W. Hanson, *Acta Crystallogr.*, **B29**, 454 (1973).
16) J. W. Schilling and C. E. Nordman, *Acta Crystallogr.*, **B28**, 1635 (1972).
17) R. D. Gilardi and I. L. Karle, *Acta Crystallogr.*, **B28**, 1635 (1972).
18) J. P. Chesick, *Acta Crystallogr.*, **B29**, 2309 (1973).
19) D. J. Duchamp and C. G. Chidester, *Acta Crystallogr.*, **B28**, 1092 (1972).
20) J. W. Edmond and W. C. Hamilton, *Acta Crystallogr.*, **B28**, 1362 (1972).
21) T. Sakurai, *Acta Crystallogr.*, **B24**, 403 (1968).
22) P. C. Bois, *Acta Crystallogr.*, **B28**, 25 (1972).
23) J. Gaultier and C. Hauw, *Acta Crystallogr.*, **18**, 179 (1965).
24) P. B. Rees, *Acta Crystallogr.*, **B26**, 1292; **B26**, 1298 (1970).
25) C. T. Grainger and J. F. McConnell, *Acta Crystallogr.*, **B25**, 1262 (1969).
26) Von D. Kobelt, E. F. Paulus, and W. Kunstmann, *Acta Crystallogr.*, **B28**, 1319 (1972).
27) L. J. Guggenberger and G. Teufer, *Acta Crystallogr.*, **B31**, 785 (1975).
28) L. E. Sutton, "Tables of Interatomic Distances and Configuration in Molecules and Ions," p. S22s. The Chemical Society, London (1965).
29) B. Bak, D. Christensen, L. Hansen-Nygaard, and J. Rastrup-Andersen, *J. Mol. Spectrosc.*, **7**, 58 (1961).
30) H. C. Longuet-Higgins, *Trans. Faraday Soc.*, **45**, 173 (1949).
31) M. Kurahashi, A. Kawase, K. Hirotsu, M. Fukuyo, and A. Shimada, *Bull. Chem. Soc. Jpn.*, **45**, 1940 (1972).
32) M. Kurahashi, *Chem. Lett.*, **1974**, 1271.
33) M. Kurahashi, *Bull. Chem. Soc. Jpn.*, **47**, 2067 (1974).
34) M. Kurahashi and A. Kawase, *Bull. Chem. Soc. Jpn.*, **49**, 127 (1976).
35) M. Kurahashi, *Bull. Chem. Soc. Jpn.*, **47**, 2045 (1974).
36) "The Universal Crystallographic Computing System (I)," ed. by T. Sakurai, The Crystallographic Society of Japan (1967).
37) A. Takenaka, "Schematic Drawing of Crystal and Molecular Structures Containing Atomic Thermal Motions," APPLY 270/30-503-001, Fujitsu Ltd, Tokyo (1972).

The Penetration of Disodium Hexadecyl Phosphate to the Monolayers of Cholesterol and its Esters from the Underlyning Aqueous Solutions

Masayuki NAKAGAKI and Tetsurou HANDA

Faculty of Pharmaceutical Sciences, Kyoto University, Sakyo-ku, Kyoto 606

(Received May 15, 1976)

The surface pressure of the monolayers of cholesterol (CH), cholesteryl acetate(CA), and cholesteryl propionate (CP) on the aqueous solutions of disodium hexadecyl phosphate (SHP) was measured. The monolayer exhibited a more expanded state on the solution than on pure water. The curves showing the surface pressure against the area per molecule of each monolayer had a kink point, which was considered to indicate the collapse of the monolayer. The amount of SHP penetrating into the insoluble monolayer was calculated by means of the Gibbs adsorption equation. It was found that the relation between the penetration amount and the activity of SHP in the aqueous solution could be expressed by a modification of the Langmuir adsorption equation. It was also found that the saturated amount of the penetration decreased, and the Langmuir coefficient increased, with the compression of the monolayer.

To study the penetration of a physiologically active substances from its aqueous solution into an insoluble lipid monolayer is important and interesting. Many papers on this subject have been published on, *e.g.*, the penetration of surfactants into the cholesterol or long-chain alcohol monolayers,[1-3] the penetration of anesthetics into the phospholipid monolayers,[4] and the penetration of various proteins into the phospholipid monolayers.[5-7] These papers have presented valuable discussion related to the fundamental aspect of the drug action, the biomembrane structure, the interaction of antibodies with lipid antigens, the enzyme activation, and so forth.

When an insoluble monolayer is spread on an aqueous solution of a surface-active substance, the latter penetrates into the insoluble monolayer and a mixed monolayer of these components is formed. In our laboratory, the thermodynamics of mixed monolayers of insoluble components have been studied and the miscibility of components in the monolayer and the phase transition of the monolayer have been explained by applying the phase rule and the theory of regular solution to the monolayer.[8-9] Moreover, the surface tension of aqueous solutions of disodium dodecyl, tetradecyl, and hexadecyl phosphates have been measured. On the basis of the surface tension measurement, it has been found that the adsorption to the solution surface and the formation of micelles of these bi-valent anionic surfactants could be explained satisfactorily by using the activity, instead of the concentration, of these compounds in the solutions,[10] and also that, on the basis of the measurement of the surface tension of a mixed solution of these compounds, the mixed adsorption and the formation of the mixed micelle could be explained by assuming an ideal mixing at the adsorption layer and the micelle phase.[11] The penetration of the soluble component into the insoluble monolayer will be discussed here, with reference to the results of our previous papers.[8-10]

In order to discuss the above subjects quantitatively, the calculation of the penetration amount (the adsorption amount) of the soluble component into the insoluble monolayer is indispensable. The adsorption equation of the soluble component was presented by B. A. Pethica and applied to the system of cholesterol and sodium dodecyl sulfate (SDS).[2]

In this work, the surface pressure of the cholesterol (CH), cholesteryl acetate (CA), and cholesteryl propionate (CP) spread as monolayers on an aqueous solution of disodium hexadecyl phosphate (SHP), was measured by the Wilhelmy method at 25 °C, and the penetration amounts of SHP into the monolayers of cholesterol and its esters were calculated.

Experimental

Materials. The specimen of CH was from the Sigma Chemical Co. and the CP, from The Aldrich Chemical Co. Inc. the CA, from the Nakarai Chemical Co., was recrystallized from acetone. The specimen of SHP was the same as that used in a previous paper, which had been synthesized and dissolved in water, as was reported there.[10]

Surface-pressure Measurement. On the aqueous solution of SHP in a trough, the monolayer of CH, CA, or CP was spreaded by using benzene as the spreading solvent. The curves of the surface pressure against the area per molecule (the *F–A* curve) was measured by the Whilhelmy plate method by compressing the monolayer with a barrier, that means, by the surface-area-decreasing method (SAD method). Otherwise, *F–A* curve was obtained by dropping a benzene solution of an insoluble component onto a constant area, that means, by the insoluble-component-addition method (ICA method). The area per molecule, A, is S/nN_A, where S is the area of the aqueous surface between two barriers, n is the mole of the insoluble component spread in this area, and N_A is the Avogadro number. Therefore, A can be decreased either by decreasing S (SAD method) or by increasing n (ICA method). Details of the surface pressure measurement have been reported in a previous paper.[12]

Results

F–A Curves and γ–c_2 Curves of the Monolayers of CH on the Aqueous Solution of SHP. The surface pressure, F, was measured by changing the area per molecule of the insoluble component, A, on the aqueous solution of SHP at various concentrations, c_2. Both the SAD method and the ICA method were applied. The *F–A* curves of the CH monolayers are shown in Fig. 1, where the surface pressure, F, is defined as usual by:

$$F = \gamma_w - \gamma \quad (1)$$

where γ is the surface tension of the SHP solution, whose

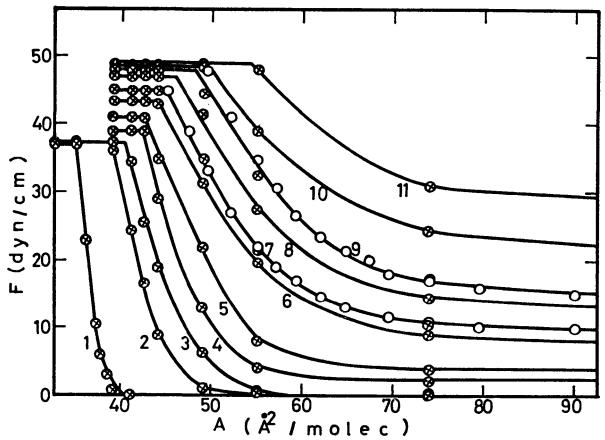

Fig. 1. *F–A* curves of the CH monolayers on the SHP solutions.
○: SAD method, ⊗: ICA method,
c_2: (1) 0 mM, (2) 0.02 mM, (3) 0.05 mM, (4) 0.1 mM, (5) 0.2 mM, (6) 0.4 mM, (7) 0.5 mM, (8) 0.8 mM, (9) 1 mM, (10) 2 mM, (11) 3 mM.

surface is covered with an insoluble monolayer, and γ_w is that of pure water. It is found that the monolayer is more expanded and is shifted to a higher surface pressure on a solution with a higher concentration of SHP, c_2. Even if the practical surface pressure, F', is calculated by subtracting the surface pressure of the SHP solution, the curves of F' against the area per molecule are also more expanded on a solution with a higher value of c_2.[9] This phenomenon is due to the penetration of the soluble component, SHP, into the insoluble monolayer. On the other hand, each curve in Fig. 1 has a kink point. It was found in our previous paper that this point indicates the collapse of the monolayer.[9]

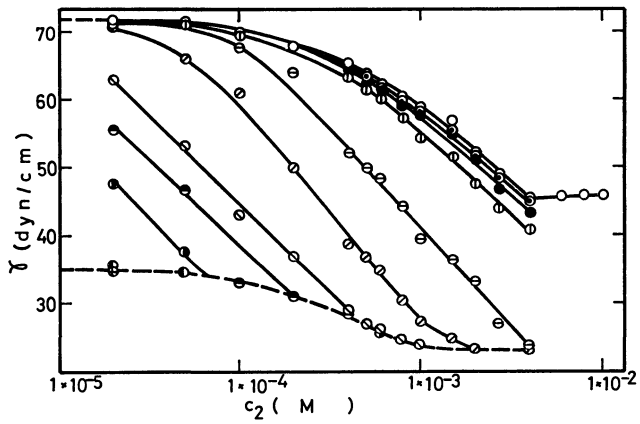

Fig. 2. The relations of surface tension, γ, and the concentration of SHP, c_2, at various values of A of CH.
A (Å²/molec): ○ no insoluble monolayer, ⊙ 220, ● 110, ⓘ 74, ⊖ 55, ⊘ 49, ⊗ 44, ◓ 42.5, ◑ 41, ◐ 39, ⊕ 35.

In Figure 2, the surface tension, γ, is plotted against the SHP concentration, c_2. Each line is drawn at a constant area per molecule of the insoluble component (CH), A. The data in Fig. 2 can be transcribed into the data in Fig. 1. The critical micelle concentration of SHP is 6 mM, and the insoluble monolayers were spread on a SHP solution of less than 6 mM. It was found that, at a constant value of A, the surface tension, γ, decreases with c_2, and that at a constant value of c_2, γ increases with A. The collapse points are shown by the broken line in Fig. 2.

γ–c_2 Curves of the Monolayer of CA. The *F–A* curves and the *F'–A* curves of CA on aqueous solutions of SHP with various values of concentration, c_2 were presented in our previous paper.[9] Both the SAD method and the ICA method were applied; the data based on these two methods were in good agreement. Each *F'–A* curve had a kink point, which was considered to be the collapse point, and the practical surface pressure of this point (the collapse pressure) was independent of c_2. As well as the monolayer of CH, the monolayer of CA was the more expanded on the SHP solution with a higher concentration.

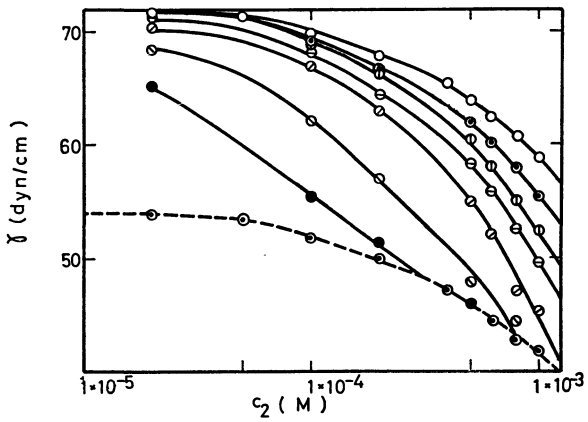

Fig. 3. The relations of surface tension, γ, and the concentration of SHP, c_2, at various values of A of CA.
A (Å²/molec): ○ no insoluble monolayer, ⊙ 100, ⓘ 80, ⊖ 70, ⊘ 60, ⊗ 50, ● 45, ◎ 40.

Figure 3 shows the relation between the surface tension, γ, and the SHP concentration, c_2, at various values of the area per molecule of CA, A. The collapse points of the monolayers are shown by the broken line. The general features of the CA monolayers on the SHP solutions are identical with those of the CH monolayers.

γ–c_2 Curves of the Monolayers of CP. The *F'–A* curves of the CP monolayer on the aqueous solution of SHP were also presented in our previous paper.[9] Both the SAD method and ICA method were applied here also. It is noticeable that the data based on these two methods were not in agreement. The monolayers of CP on the SHP solutions were easily supercompressed when the SAD method was applied. The value of the surface pressure of the kink point decreased with the time and was constant at $F'=7.5$ dyn/cm. On the other hand, the *F'–A* curves based on the ICA method showed no change with the time, agreed well with the curves obtained by the SAD method in the region of low F' values, and gave the collapse pressure $F'=7.2$ dyn/cm, which is practically equal to the above-mentioned value of the "equilibrium" collapse pressure obtained by the SAD method.

In Fig. 4, the relation between the surface tension, γ, and the SHP concentration, c_2 of the equilibrium

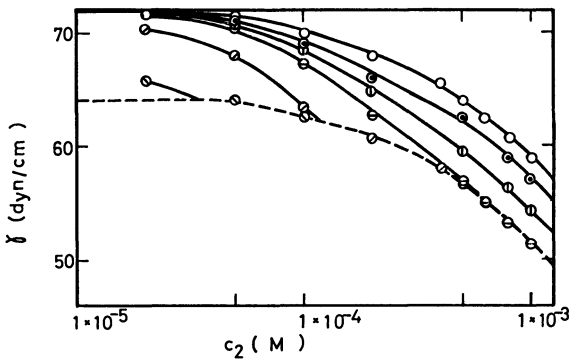

Fig. 4. The relations of surface tension, γ, and the concentration of SHP, c_2, at various values of A of CP. A (Å²/molec): ○ no insoluble monolayer, ⊙ 100, ⊕ 80, ⊖ 70, ⊘ 60, ⊗ 50.

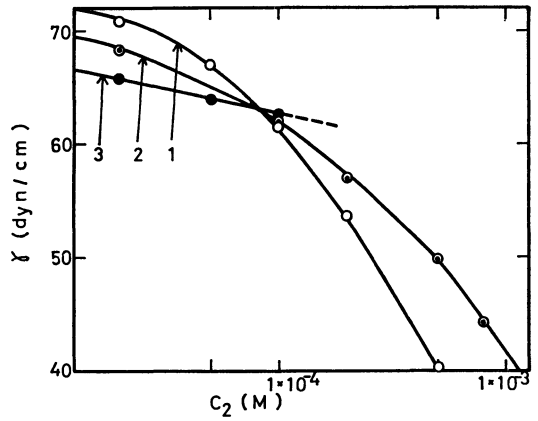

Fig. 5. The relations of surface tension, γ, and the concentration of SHP, c_2, at $A=50$ Å²/molec. Insoluble component: 1. CH, 2. CA, 3. CP.

monolayers of CP are shown. The equilibrium collapse points are shown by the broken line. The general features of the CH, CA, and CP monolayers on the SHP solution are similar. However, there is one noticeable aspect: in comparing at a constant area per molecule of the insoluble components, A, the surface tension is higher in the region of the lower value of c_2 in the order of CH, CA, and CP whereas the surface tension is lower in the region of the higher values of c_2 in the order of CH, CA, and CP. This aspect is shown in Fig. 5, at $A=50$ Å²/molec., as an example. This must affect the penetration isotherms of SHP into the insoluble monolayers of CH, CA, and CP.

Discussion

Mixed Monolayers of an Insoluble Component and a Soluble Component. Into the insoluble monolayer, the surface-active soluble component, SHP, penetrates and a mixed monolayer of these components is formed. The molecular interaction between the insoluble (CH, CA, or CP in this case) and soluble (SHP in this case) components is important in helping one to decide the general features of the mixed monolayer. Three typical cases, shown in Fig. 6, can be expected.

a) If these two components are completely miscible in the monolayer, the F–A curve of the mixed monolayer takes the shape of Type a. b) If these two components are only partially miscible, the F–A curve takes the shape of Type b. In the plateau region, two monolayer phases of different compositions co-exist under a constant pressure, a constant temperature, and a constant concentration of SHP, c_2. According to the surface-phase rule, the freedom of the system becomes zero and the surface pressure, F, does not change.[13,14] By the compression of the monolayer, one monolayer phase diminishes, after the complete disappearance of this monolayer phase, the surface pressure again increases. c) When the insoluble and soluble components are completely immiscible, the general feature of the F–A curve is Type c. The surface pressure does not change from F_{SHP} by the compression of the monolayer until the p point. At this point, the F–A curve is the same as that on pure water (the broken line in in Fig. 6).

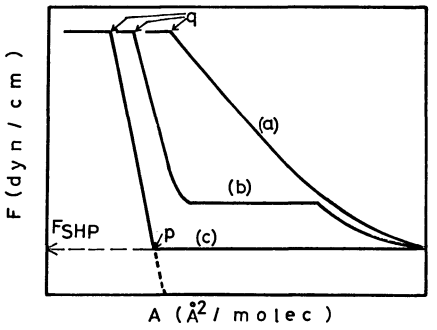

Fig. 6. The general features of F–A curves of the penetrated monolayers.

On the basis of the above discussion, all of the systems in this paper (CH–SHP, CA–SHP, and CP–SHP) can be identified as of Type a. Therefore, in the monolayers, the insoluble component and the soluble component are miscible. The q point is the collapse point of the monolayer.

The Calculation of the Amount of Penetration of SHP into the Insoluble Monolayer. SHP and the insoluble component (CH, CA, or CP) are designated as Components 2 and 3 (Component 1 is water). The Gibbs adsorption equation is given as:

$$\begin{aligned} dF &= \Gamma_2 d\mu_2 + \Gamma_3 d\mu_3^s \\ &= \Gamma_2 RT \, d\ln a_2 + \Gamma_3 d\mu_3^s \end{aligned} \quad (4)$$

where Γ_2 is the penetration amount (the adsorption amount) of SHP (mol/cm²), a_2 is the activity of SHP in the aqueous solution, Γ_3 is the mole of the insoluble component in the monolayer of 1 cm² and is equal to $1/AN_A$, and μ_3^s is the chemical potential of the insoluble component in the monolayer. The activity of SHP in the solution, a_2, is defined as:

$$a_2 = \gamma_\pm^3 c_2 (2c_2 + c')^2 \quad (5)$$

where $\gamma_\pm$ is the mean ionic activity coefficient, the latter can be calculated from the Güntelberg approximation of the Debye-Hückel theory:

$$\log \gamma_\pm = \frac{-B\sqrt{J}}{1+\sqrt{J}} \quad (6)$$

Here, J is the ionic strength, and B is a constant whose value is 1.022 for SHP at 25 °C.[15] c' is the concentration of the added electrolyte (in this case, $c'=0.01$ M NaOH). With respect to the chemical potential of the insoluble component in the monolayer, μ_3^s, we give the following equation:

$$d\mu_3^s = N_A\omega_3 dF + RT d\ln X_3 \quad (7)$$

Here, N_A is the Avogadro number, ω_3 is the partial molecule area of component 3, which is obtained from the F–A curve of the monolayer on pure water at the corresponding value of the surface pressure, and X_3 is the mole fraction of the insoluble component in the monolayer. X_3 is defined as:

$$X_3 = \frac{\Gamma_3}{\Gamma_2+\Gamma_3} \quad (8)$$

Because the surface-pressure measurement is performed by changing the concentration of SHP, c_2 (the activity of SHP, a_2), and the area per molecule of the insoluble component, A, under a constant temperature and constant pressure, F and X_3 are functions of $\ln a_2$ and A respectively.

$$dF = \left(\frac{\partial F}{\partial \ln a_2}\right)_A d\ln a_2 + \left(\frac{\partial F}{\partial A}\right)_{a_1} dA \quad (9)$$

$$dX_3 = \left(\frac{\partial X_3}{\partial \ln a_2}\right)_A d\ln a_2 + \left(\frac{\partial X_3}{\partial A}\right)_{a_1} dA \quad (10)$$

Under the constant area per molecule of the insoluble component, A, Eqs. 4, 7, 9, and 10 give the following equation:

$$\Gamma_2 = \frac{(1-\omega_3/A)(\partial F/\partial \ln a_2)_A}{1-(\partial \ln X_2/\partial \ln a_2)_A} \quad (11)$$

Because the value of $(\partial \ln X_2/\partial \ln a_2)_A$ is not directly known from the data (Figs. 2 and 4), we start the calculation of Γ_2 with an approximate equation and revise succesively. For this purpose, the following equation may be used instead of Eq. 11:

$$\Gamma_2 = (1-\omega_3/A)(\partial F/\partial \ln a_2)_A \quad (12)$$

if the following equation is used instead of Eq. 7:

$$d\mu_3^s = N_A\omega_3 dF \quad (13)$$

The same equation as Eq. 12 was used by Pethica[2] and other investigators[16] for the systems of cholesterol and SDS and of octadecanol and hexadecyl-trimethyl ammonium bromide. The calculation of Γ_2 from Eq. 11 is performed as follows:

1. Γ_2 is calculated by applying Eq. 12 to, for example, Fig. 3. 2. $\ln X_2$ is calculated by means of Eq. 8. 3. $(\partial \ln X_2/\partial \ln a_2)_A$ is calculated graphically. 4. Now, Γ_2 is recalculated by means of Eq. 11. 5. The successive approximation is repeated until the value of Γ_2 converges to a difined value.

In Fig. 7, the values of Γ_2 calculated from Eqs. 11 and 12 are shown for the $A=220$ Å^2/molec of CH as an example. In the region of low concentrations of SHP, c_2, an appreciable difference is recognized between the values calculated from these equations. This is caused by the comparatively large value of $(\partial \ln X_2/\partial \ln a_2)_A$ in this region of c_2. In Fig. 8, the converged values of Γ_2 are shown against the concentration of SHP at various values of the A of CH. The following points are found: 1. The relation of Γ_2 and c_2 at each value of A are, in appearance, those of the Langmuir adsorption. 2. The saturated amount of the penetration is larger at a larger value of A. 3. The initial increment of Γ_2 against c_2 is larger at a small value of A.

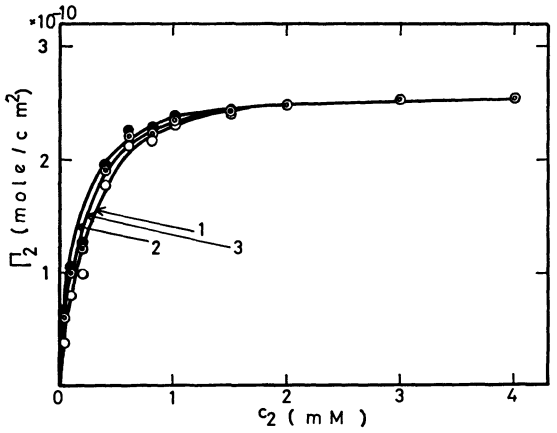

Fig. 7. The relations of the penetration amount, Γ_2, and the concentration of SHP, c_2, for $A=220$ Å^2/molec of CH. ○ 1st approximation by Eq. 12, ● 2nd approximation, ◎ the converged values by Eq. 11.

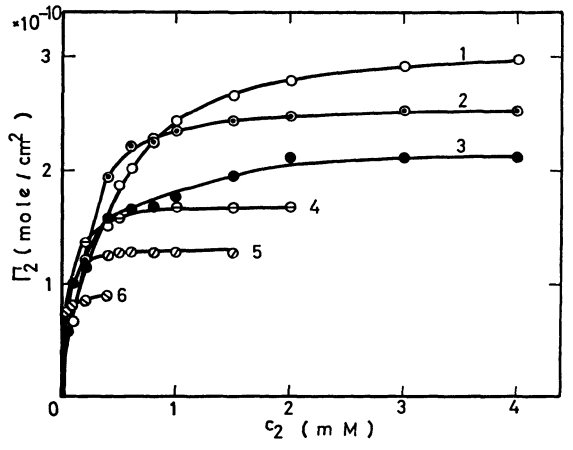

Fig. 8. The relations of the penetration amount, Γ_2, and the concentration of SHP, c_2.
The converged values, A (Å^2/molec): 1. no insoluble monolayer, 2. 220, 3. 110, 4. 55, 5. 49, 6. 44. the insoluble component is CH.

Because SHP is an electrolyte, we assumed the modified Langmuir adsorption equation by using the activity, a_2, instead of the concentration, c_2:

$$\Gamma_2 = \frac{\Gamma_s K a_2}{1+Ka_2} \quad (14)$$

where Γ_s is the saturated amount of the penetration of SHP and K is the modified Langmuir coefficient. If we, therefor, plot the value of (a_2/Γ_2) against a_2, a straight line is obtained: the values of Γ_s and K are obtained from the slope and the intersection in relation to the ordinate. In Fig. 9, (a_2/Γ_2)-a_2 plots for CH are shown for several values of A. All the plots shown a linear relation: the values of Γ_s and K thus obtained are shown in Fig. 10. The data of CA and CP as well as CH are shown in this figure.

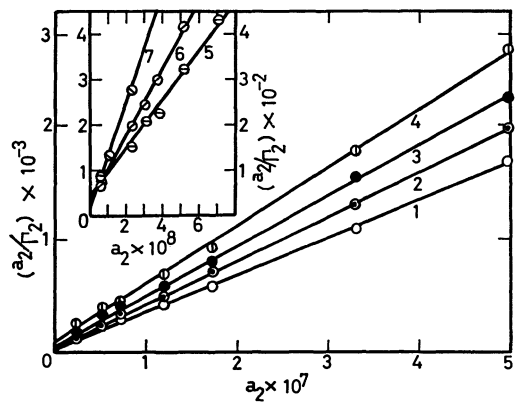

Fig. 9. The Langmuir plots, (a_2/Γ_2) *vs.* a_2.
The insoluble component is CH. A (Å²/molec): 1. no insoluble monolayer, 2. 220, 3. 110, 4. 74, 5. 55, 6. 49, 7. 44.

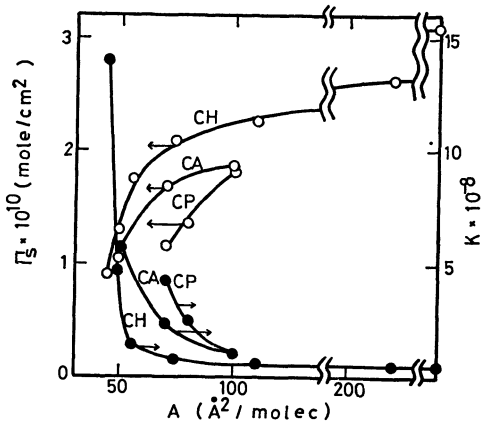

Fig. 10. The saturated penetration amount, Γ_s, or the modified Langmuir coefficient, K, *vs.* the area per molecule of the insoluble component, A.

The value of the saturated amount of the penetration, Γ_s, is 3.1×10^{-10} mol/cm² when surface is free from the insoluble component, and it decreases with a decrease in the value of A. At a constant value of A, the value of Γ_s is larger in the order of CH, CA, and CP. On the other hand, the value of K is nearly constant at the large value of A (A>100 Å²/molec); it is 0.5—1.0×10^8, which agrees with the value of 0.5×10^8 for the solution surface free from the insoluble component. When the value of A decreases further, the value of K steeply increases. The value of K is correlated with the strength of the penetration, and the increase in the value of K means a larger strength of the penetration of SHP into the insoluble monolayer and is caused by the greater amount of intermolecule interaction. The value of K for the system of CP–SHP is the largest, and that for the system of CH–SHP is smallest. This is caused by the hydrophobic nature of these compounds; the noticeable difference in Figs. 2, 3, 4, and 5 directly indicate these effect of the K and Γ_s of CH, CA, and CP.

References

1) E. G. Goddard and J. H. Schulman, *J. Colloid Sci.*, **8**, 309 (1953); *ibid.*, **8**, 329 (1953).
2) B. A. Pethica, *Trans. Faraday Soc.*, **51**, 1402 (1955); *ibid.*, **51**, 1080 (1955).
3) M. Matubara, *Bull. Chem. Soc. Jpn.*, **38**, 1245 (1964).
4) D. Papahadjopoulos, *Biochim. Biophys. Acta*, **265**, 169 (1972).
5) P. J. Quin and R. M. C. Dawson, *Biochem. J.*, **113**, 791 (1969); *ibid.*, **115**, 65 (1969); *ibid.*, **116**, 671 (1970).
6) P. D. Morse and D. Deamer, *Biochim. Biophys. Acta*, **298**, 769 (1973).
7) Y. London, R. A. Demel, W. S. M. G. Van Kessel, F. G. A. Vossenberg, and L. L. M. Van Deenen, *Biochim. Biophys. Acta*, **311**, 520 (1973).
8) M. Nakagaki and N. Funasaki, *Bull. Chem. Soc. Jpn.*, **47**, 2049 (1974); *ibid.*, **47**, 2482 (1974).
9) M. Nakagaki and T. Handa, *Bull. Chem. Soc. Jpn.*, **49**, 880 (1976).
10) M. Nakagaki, T. Handa and S. Shimabayashi, *J. Colloid Interface Sci.*, **43**, 521 (1973).
11) M. Makagaki and T. Handa, *Bull. Chem. Soc. Jpn.*, **48**, 630 (1975).
12) M. Nakagaki, N. Funasaki and M. Nishino, *Yakugaku Zasshi*, **90**, 1088 (1970).
13) R. Defay, I. Prigogine, A. Bellmans, and D. H. Everett, "Surface tension and adsorption," Longmans, London (1966), p. 166.
14) G. L. Gains Jr., "Insoluble Monolayers at the Liquid-gas Interface," Interscience Publisher (1966), p. 283.
15) E. Güntelberg, *Z. Phys. Chem.*, **123**, 199 (1962).
16) M. A. McGregor and G. T. Barnes, *J. Colloid Interface Sci.*, **54**, 439 (1976).

X-Ray Photoelectron Spectroscopy of Chloromethanes and Chloroethanes

Toshiaki OHTA and Haruo KURODA

Department of Chemistry, Faculty of Science, University of Tokyo, Hongo, Tokyo 113

(Received May 15, 1976)

X-Ray photoelectron spectra of chloromethanes ($CH_{4-n}Cl_n$, n=2,3,4) and chloroethanes ($CH_3CH_{3-n}Cl_n$, n=1,2,3) in vapor phase were observed employing Mg $K\alpha$ radiation. The observed Cls binding energies were analyzed by means of Siegbahn's electrostatic potential model and charge densities calculated by the CNDO/2 method, and the effects of inclusion and exclusion of Cl 3d atomic orbitals in the basis set of the CNDO/2 calculation is critically investigated. The assignment of all valence electron levels of above molecules were performed with the aids of the CNDO/2 calculations incorporated with Gelius' intensity model and the reported data of ultraviolet photoelectron spectroscopy.

X-Ray photoelectron spectroscopy (XPS) of free molecules in gas phase provides various useful informations concerning molecular electronic structures. By means of XPS, one can directly determine core-electron binding energies, which reflect charge distribution in molecule. As for valence-electron levels, XPS offers informations complementary to those obtainable by ultraviolet photoelectron spectroscopy (UPS) which employs the He I or He II line as the stimulating radiation; deep valence-electron levels, out of reach of UPS, are able to be studied by XPS, and, from the comparison between XPS and UPS spectra, one can obtain information concerning the s- and p-characters of ionizing molecular orbitals.

From the above point of view, we have previously investigated the gas-phase X-ray photoelectron spectra of mono-substituted benzenes,[1] and those of a series of molecules containing the C≡N group.[2]

In the present paper, we will describe the results obtained by gas-phase XPS of chloromethanes, $CH_{4-n}Cl_n$ (n=2, 3, and 4) and chloroethanes, $C_2H_{6-n}Cl_n$ (n=1, 2, and 3). On those series of chlorine-containing molecules, UPS studies have been carried out by other authors,[3-7] but no systematic investigation by gas-phase XPS has been hitherto reported.

We examined the correlation of the chemical shifts of Cls levels and charge distributions calculated by the CNDO/2 method. Discussion will be given on the effects of inclusion and exclusion of vacant 3d atomic orbitals of chlorine in the CNDO/2 calculations. We also intended to elucidate all of the valence-electron levels in these molecules from the analysis of XPS spectra with the aids of the reported UPS data and the CNDO/2 calculations.

Experimental

All materials used here were commercially obtained, and purified by distillation.

The gas-phase XPS spectra were measured with McPherson ESCA 36 electron spectrometer, equipped with a gas-iozination cell and gas-control system, by employing Mg $K\alpha$ (1253.6 eV) as the stimulating radiation. Details of experimental procedure were the same as those described in our previous papers.[1,2]

Binding energies of core-electron peaks were calibrated by using the Nls peak of nitrogen gas (409.9 eV) mixed in sample vapors as the reference. The weak Al $K\alpha$ radiation (1486.6 eV) which came out as the secondary X-ray from the Al window of the gas-ionization cell, gave weak core-electron peaks at the kinetic energies exactly higher by 233.0 eV than the kinetic energies of the corresponding peaks by Mg $K\alpha$. Some of them are located closely to the valence-electron spectrum due to Mg $K\alpha$. For example, Cl 2s peak induced by Al $K\alpha$ appears at the position corresponding to the binding energy of about 45 eV in the spectrum by Mg $K\alpha$. Thus we used this peak as a subsidiary reference for the calibration of binding energies of valence-electron peaks.

Measurement was carried out at least twice for each sample. Binding energies thus determined were reproducible within ±0.1 eV.

Results

For each material, we carried out measurement both for core- and valence-electron regions. In order to illustrate the general features of the XPS spectra of the chlorine-containing molecules studied here, three regions of the spectrum of chloroform are shown in Fig. 1. Note that the Cl 2s peak is apparently broader than C 1s peak, and that the C 1s and Cl 2s peaks induced by Al $K\alpha$ appear in the spectrum of valence-electron region.

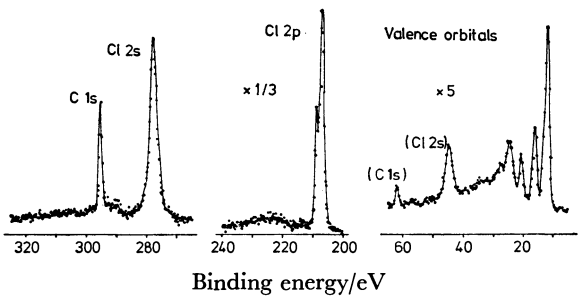

Fig. 1. Core and valence electron spectra of chloroform.

The C 1s spectra of chloromethanes and chloroethanes, observed with a higher resolution, are shown in Fig. 2. In the case of chloromethanes, the C 1s peak is markedly shifted to higher binding energy on increasing the number of chlorine atoms in a molecule, as it is expected from the high electronegativity of chlorine. In the case of chloroethanes, C 1s spectrum splits into two peaks of equal intensity, in which the one at higher binding energy (C 1s (a)) is attributable to the carbon atom of chlorine-substituted methyl group (hereafter, we denote this carbon atom as C(a)), and the one at lower binding energy (C 1s (b)) to the other carbon atom (we denote it as C(b)). C 1s (a) peak shows a marked shift

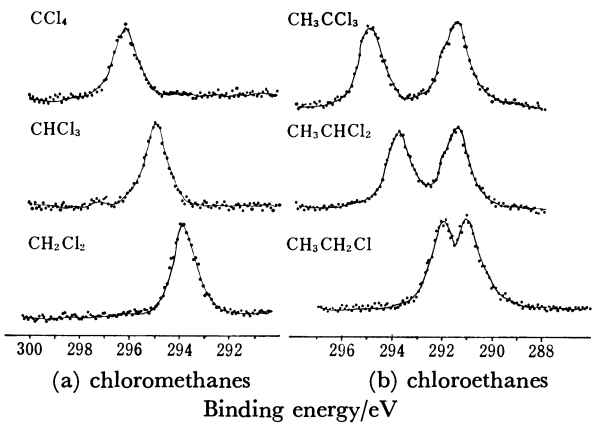

Fig. 2. C 1s spectra of (a) chloromethanes and (b) chloroethanes.

to higher binding energy on increasing the number of substituted chlorine atoms. The extent of this shift is almost the same as that found for the corresponding chloromethane.

As compared with the above change of C 1s binding energy, the changes of Cl2s and Cl2p binding energies are quite small, although these binding energies slightly increase with the number of chlorine atoms. The determined binding energies of core-electron levels are listed in Table 1.

TABLE 1. OBSERVED CORE ELECTRON BINDING ENERGIES OF CHLOROMETHANES AND CHLOROETHANES (eV)

	C 1s	Cl 2s	Cl $2p_{3/2}$
CH_3Cl	(292.4)*	(277.2)*	
CH_2Cl_2	294.0 (293.9)	277.6 (277.6)	206.7
$CHCl_3$	295.1 (295.1)	277.8 (277.7)	206.8
CCl_4	296.3 (296.3)	278.0 (278.0)	207.0
CH_3CH_2Cl	292.1, 291.1	276.8	206.0
CH_3CHCl_2	293.8, 291.5	277.2	206.4
CH_3CCl_3	295.0, 291.5	277.3	206.5

*) Figures in parentheses are from Thomas (Ref. 8).

Full width of half maximum (ΔE_{fwhm}) of C 1s peak was observed to be 1.2, 1.05, and 1.05 eV for dichloromethane, chloroform, and carbon tetrachloride, respectively. ΔE_{fwhm} of 1.05eV is likely to be the resolution limit under the present experimental condition, so that, among the above three cases, the C 1s peak of dichloromethane only can be concluded to be broader than the instrumental broadening. In the case of chloroethanes, ΔE_{fwhm} of C 1s (*a*) peak is almost constant at 1.1 eV, which is close to the resolution limit, but C 1s (*b*) peak is markedly asymmetric with ΔE_{fwhm} of about 1.3 eV, exhibiting a shoulder at about 0.4 eV from the main peak. The above asymmetry of C 1s (*b*) peak is very similar to that of the C 1s peak of methane reported by Gelius,[9] who explained the above asymmetry of the C 1s peak of methane as the effect of vibrational structure. It is also noteworthy that ΔE_{fwhm} of Cl 2s is as large as 2.6 eV. This can be attributed to the life-time broadening associated with the Coster-Kronig process.

It is of large value to know relative photoionization cross sections of core-electron levels, both from theoretical interest and from the interest to use XPS as a tool of quantitative analysis. However, as it has been pointed out by Siegbahn *et al.*,[10] relative intensities of photoelectron peaks could change, more or less, depending on the pressure of sample vapor, because of the effect of inelastic scattering. This pressure dependence of relative intensity is significant at higher sample pressure, but becomes almost negligible at sufficiently low pressure. We previousely observed the pressure dependence of the intensity ratio of the O 1s and C 1s peaks of methanol,[11] and found that the ratio was independent of sample pressure within the pressure region usually used in our experiments. By adopting such an experimental condition, we compared the integrated intensities of Cl 2s, Cl 2p, and C 1s peaks in the XPS spectra of chloromethanes and chloroethanes, and found that the relative intensities of these peaks can be quantitatively interpreted by assuming the ratios of apparent cross sections as follows;

$$\text{Cl 2s/C 1s} = 1.14$$
$$\text{Cl 2p/C 1s} = 2.02$$

The observed spectra of valence-electron region are shown in Figs. 3 and 4, where the observed data are shown by points, the solid lines being the calculated spectra which will be discussed later. The spectra of chloromethanes are very similar to each other. The same can be said also for the spectra of chloroethanes. We can roughly divide each spectrum into three parts; (1) The most intense peak at about 12 eV, which seems to be predominantly associated with Cl 3p lone pairs, (2) the peaks in the region of 15—22 eV, which are likely to be due to the orbitals associated with chemical bonds, and (3) the very broad bands with long tails in the region of 22—35 eV, where the peaks seem to be attributable to the molecular orbitals mainly associated with Cl 3s and C 2s atomic orbitals, possibly the long tails being due to shake-up or shake-off processes.

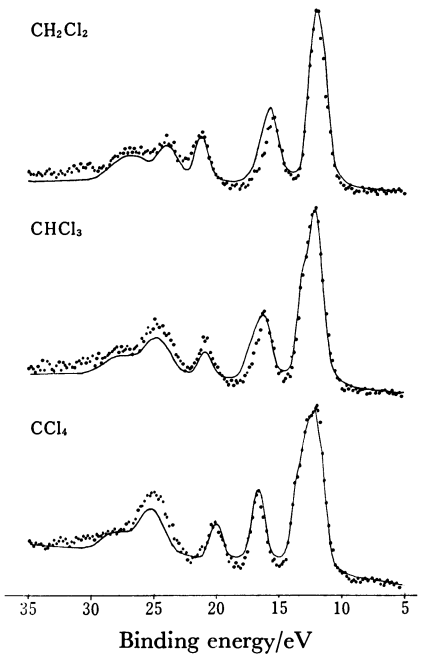

Fig. 3. Valence electron spectra of chloromethanes. Solid lines are the calculated spectra.

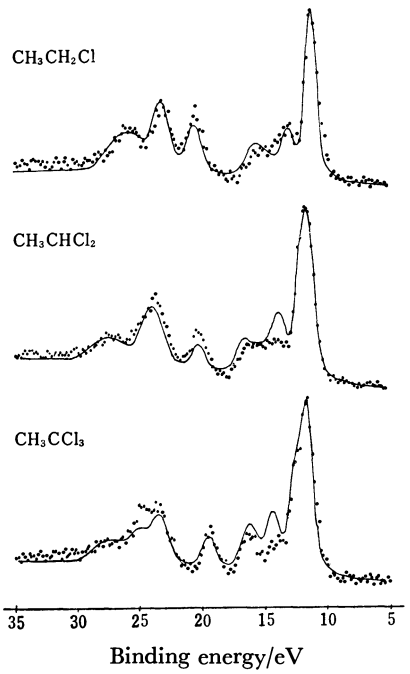

Fig. 4. Valence electron spectra of chloroethanes. Solid lines denote the calculated spectra.

Discussion

Binding Energies of Core-electron Levels. According to the electrostatic potential model, developed by Siegbahn and his co-workers,[10] core-electron binding energies can be correlated with charge distribution in molecule by the following relation;

$$E_i = E_0 + kq_i + \sum_{j \neq i}(q_j/R_{ij}) \qquad (1)$$

where E_i is the binding energy of a core-electron level of the atom i, q_j is the charge on the atom j, R_{ij} is the interatomic distance, and k is a constant characteristic of the kind of atom. In this equation, the second term gives the energy shift due to the charge on the atom i, and the third one is the contribution of the electrostatic potential due to surrounding atoms. This electrostatic potential model has been successfully used in conjunction with the charge density calculated by the CNDO/2 method.

Although the CNDO/2 method is widely used for a variety of organic molecules, the procedures of treating chlorine-containing molecules by the CNDO/2 method has not yet wholly established. There remains a problem concerned with the suitable extent of including vacant 3d atomic orbitals of chlorine in the CNDO/2 calculation of chlorine-containing molecules. In the present study, we carried out calculations by the two extreme methods; Method (a) is that proposed by Santry and Segal,[12] where the 3d orbitals of chlorine are included in the basis set, assuming their orbital exponents the same as those of the 3s and 3p atomic orbitals of chlorine, and Method (b) is the one which completely neglects the 3d orbitals of chlorine. The charge densities obtained by the above two methods are compared in Table 2. It should be noted that there is a significant difference between the charge distributions predicted by these two methods.

According to Eq. 1, we shall obtain a straight line when we plot $E_i - \sum_{i \neq j}(q_j/R_{ij})$ against q_i for a given kind of core-electron level, for example, for C 1s levels. The inclination of the line corresponds to the constant k and its intercept at $q_i=0$ gives the E_0 value. In Fig. 5, we have plotted $E_i(\text{obsd}) - \sum_{i \neq j}(q_j/R_{ij})$ against q_i, using the

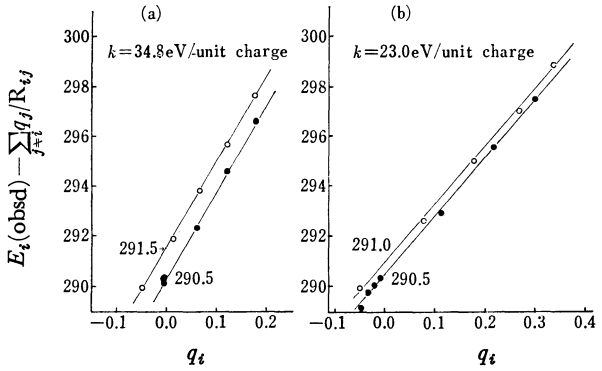

Fig. 5. Correlation between $E_i(\text{obsd}) - \sum_{j \neq i} q_i/R_{ij}$ and q_i.
(a) CNDO/2 including 3d orbitals.
(b) CNDO/2 excluding 3d orbitals.
Open and filled circles are for chloromethanes and chloroethanes, respectively.

Table 2. Charge densities obtained from CNDO/2 calculation

	Method (a)			Method (b)		
	C	Cl	H	C	Cl	H
CH_4	−0.050		0.012	−0.050		0.012
CH_3Cl	0.0125	−0.1233	0.0369	0.0756	−0.1288	0.0177
CH_2Cl_2	0.0633	−0.0905	0.0589	0.1765	−0.1107	0.0225
$CHCl_3$	0.1198	−0.0645	0.0738	0.2647	−0.0959	0.0231
CCl_4	0.1770	−0.0443		0.3367	−0.0842	

	Method (a)				Method (b)			
	C_a	C_b	Cl	H	C_a	C_b	Cl	H
CH_3CH_3	−0.09	−0.09		0.03	−0.09	−0.09		0.03
CH_3CH_2Cl	0.0595	−0.0055	−0.1452	0.0140	0.1143	−0.0237	−0.1513	0.0121
CH_3CHCl_2	0.1194	−0.0040	−0.1144	0.0233	0.2150	−0.0374	−0.1355	0.0233
CH_3CCl_3	0.1778	−0.0019	−0.0891	0.0305	0.3006	−0.0474	−0.1213	0.0369

observed binding energies of C 1s levels and calculated charge densities. The plots fall on a straight line for the charge densities obtained by Method (a) as well as for those by Method (b), but the inclination of line significantly differs between the two cases, giving the following k values, respectively;

Method (a); k(C 1s) = 34.8 eV/*unit charge*

Method (b); k(C 1s) = 23.0 eV/*unit charge*

In our previous paper, we obtained 22.67 eV/*unit charge* for k(C 1s) from the analysis of observed C 1s binding energies of benzene derivatives using CNDO/2 charge densities.[1] The k value of 23.0 eV/*unit charge* obtained here for the charge densities by the calculations with Method (b), is in good agreement with the above result, but the k value of 34.8 eV/*unit charge*, which was obtained for the charge densities calculated by Method (a), seems to be too large. The same conclusion has been derived recently by Clark *et al.*[13] from the study of XPS spectra of chlorobenzenes in solid phase. The equation of electrostatic potential model, (Eq. 1), can be reinterpreted quantum-mechanically for CNDO scheme.[14] According to this interpretation, the constant k corresponds to the Coulomb repulsion potential between a core electron and an electron in the valence shell, so that it can be theoretically calculated. When such a calculation is done for carbon atom by use of Slater AO's, we obtain 22.0 eV/*unit charge* for k(C 1s), which is close to the k value obtained here for the charge densities calculated by Method (b). However it should be noted that the point charge approximation, on which Siegbahn's electrostatic potential model has been derived, has a serious problem in the case of molecules which contain large atoms such as chlorine, because there can be a relatively large contribution of polarization in the electrostatic potential. At the same time, we have to consider that relaxation energy may appreciably increase by replacing hydrogen with chlorine.[15] Both of these effects are expected to reduce the apparent k value. In other words, the k value experimentally determined by the electrostatic potential model must be smaller than the theoretical value if the above effects are significant. When this situation is taken into account, the k value of 23.0 eV/*unit charge* seems to be already a little too large, and the k value of 34.8 eV/*unit charge* is apparently unreasonable. Therefore, we can conclude that Method (b), which neglects 3d orbitals of chlorine, gives better results than Method (a), at least for charge densities.

It should be noted in Fig. 5 that the plots for chloromethanes and those for chloroethanes are on separate lines with the same inclination. From the intercepts of these lines at $q_i=0$ in Fig. 5 (b), we obtain the following values for E_0 (Cls);

E_0(C 1s) = 291.0 eV for chloromethanes

E_0(C 1s) = 290.5 eV for chloroethanes

It is noteworthy that almost the same values are obtainable from Fig. 5 (a) which has used the charge densities calculated by Method (a).

We have previousely obtained 290.2 eV for E_0(C 1s) in the case of benzene derivatives.[1] As compared with this value, the E_0 value for chloromethanes is larger by 0.8 eV and that for chloromethanes is larger by 0.3 eV. Presumably, the above differences of E_0 values reflect the differences concerned with relaxation energy.

The binding energies of Cl 2s and Cl 2p levels slightly increase with the number of chlorine atoms. This change corresponds qualitatively to the decrease of the negative charges on chlorine atoms. However, the number of available data is so limited that it is not possible in these cases to quantify the correlation between binding energy and charge density.

Analysis of Valence-electron Spectra. The photoionization cross section of a molecular orbital is approximately given by the overlap integral between the molecular orbital and the photoelectron final-state wave function which can be expressed as a plane wave orthogonalized to the initial state. In the case of XPS, this overlap integral is almost entirely determined by the contributions from the parts very close to the nuclei, because of the short de Broglie wavelength of photoelectron. On the basis of this idea, Gelius[16] proposed that the molecular orbital cross section may be expressed as a sum over contributions from each atomic centers, as follows;

$$\sigma_j \propto (2+\beta/2)\sum_{A\lambda} P_{A\lambda}^{(j)}\sigma_{A\lambda} \qquad (2)$$

where $P_{A\lambda}^{(j)}$ denotes the probability of finding the electron in the j-th molecular orbital in an atomic orbital $A\lambda$, $\sigma_{A\lambda}$ is the cross section of the atomic orbital $A\lambda$, and β is the asymmetry parameter, $-1\leqq\beta\leqq 2$. In the case of chloromethanes and chloroethanes, one may use an average value of β instead of the true asymmetric parameters without significant influence on the calculated intensities. Thus, using relative atomic cross section $\sigma(A\lambda/\mathrm{C2s})=\sigma_{A\lambda}/\sigma_{\mathrm{C2S}}$, we can express the intensity of the peak associated with the photoionization of the j-th molecular orbital, as follows;

$$I_j \propto \sum_{A\lambda} P_{A\lambda}^{(j)}\sigma(A\lambda/\mathrm{C\,2s}) \qquad (3)$$

The simulation of valence-electron spectra, by use of the above intensity model, is useful for the analysis of valence-electron spectra.[16-20] In the present study, we carried out spectrum simulation adopting the following procedures:

(1) $P_{A\lambda}^{(j)}$ was calculated by CNDO/2 with neglect of 3d orbitals of chlorine (Method (b)). Incidentally, the CNDO/2 calculations including 3d orbitals of chlorine (Method (a)) gave the values of $P_{A\lambda}^{(j)}$ which are not significantly different from those obtained by Method (b).

(2) The shape of each photoelectron peak was assumed to be the one that is expressed by the modified Lorentzian function (Eq. 4).

$$f_j(\chi) = 0.5I_j\left\{\frac{1}{1+\left(\frac{2\chi}{w_j}\right)^2}+\frac{1}{1+\left(\frac{2\chi}{w_j}\right)^4}\right\} \qquad (4)$$

where χ is the energy measured from the center of the peak and w_j is the half-width. The value of w_j was fixed as 1.1 eV for peaks in the Cl 3p lone-pair region, and as 1.3 eV for those in the chemical-bonding region, but it was treated as an adjustable parameter for peaks in the Cl 3s region.

(3) The order of valence-electron levels was assumed the same as that predicted by the CNDO/2 calculation

TABLE 3. CALCULATED AND EXPERIMENTAL VALENCE ORBITALS OF CHLOROMETHANES

Molecule	Symmetry	CNDO/2 calculation: atomic population C 2s	C 2p	Cl 3s	Cl 3p	Orbital energy (eV)	Relative cross section	IP(obsd) (eV): UPS[a]	XPS	Peak width (eV)
CH_2Cl_2	$3b_2$	—	0.051	0.000	0.948	−14.09	0.95	11.40	11.4	1.1
	$2b_1$	—	0.046	—	0.840	−14.42	0.84			
	$4a_1$	0.001	0.075	0.000	0.874	−14.57	0.88	12.22	12.2	1.1
	$1a_2$	—	—	—	1.000	−15.17	1.00			
	$2b_2$	—	0.273	0.052	0.676	−17.66	0.75	15.30	15.3	1.3
	$3a_1$	0.024	0.247	0.078	0.612	−19.05	0.76	15.94	15.9	1.3
	$1b_1$	—	0.455	—	0.152	−22.94	0.19	16.77	16.8	1.3
	$2a_1$	0.099	0.133	0.542	0.040	−26.76	0.79	(20.3)	21.1	1.3
	$1b_2$	—	0.095	0.898	0.006	−29.28	0.91		23.9	2.0
	$1a_1$	0.411	0.000	0.334	0.058	−36.95	1.21		27.0	3.5
$CHCl_3$	$4a_1$	0.000	0.071	0.000	0.821	−14.49	0.83	11.48	11.5	1.1
	$1a_2$	—	—	—	1.000	−14.75	1.00	11.91	12.0	1.1
	4e	—	0.080	0.000	0.920	−14.14	2.37	12.01		
	3e	—	0.011	0.000	0.989	−15.72	1.98	12.85	12.9	1.1
	2e	—	0.230	0.074	0.622	−19.05	1.43	15.99	16.0	1.3
	$3a_1$	0.067	0.204	0.150	0.533	−20.87	1.67	16.96	17.0	1.3
	$2a_1$	0.102	0.201	0.354	0.100	−26.10	0.68	(19.8)	20.8	1.3
	1e	—	0.104	0.876	0.020	−29.79	1.81		24.6	2.5
	$1a_1$	0.372	0.000	0.453	0.083	−37.57	1.28		27.5	3.5
CCl_4	$1t_1$	—	—	—	1.000	−15.01	1.50	11.69	11.7	1.1
	$3t_2$	—	0.098	0.000	0.902	−14.14	1.37	12.44	12.5	1.1
	1e	—	—	—	1.000	−16.56	1.00	13.37	13.4	1.1
	$2t_2$	—	0.215	0.098	0.687	−20.03	1.21	16.58	16.6	1.3
	$2a_1$	0.214	—	0.404	0.382	−22.86	0.61	(20.0)	20.0	1.3
	$1t_2$	—	0.113	0.854	0.033	−30.25	1.35		24.8	2.4
	$1a_1$	0.337	—	0.552	0.111	−38.08	0.67		28.0	3.0

a) Ref. 4 Potts *et al.* Ionization potentials obtained with He II radiation are given in parentheses.

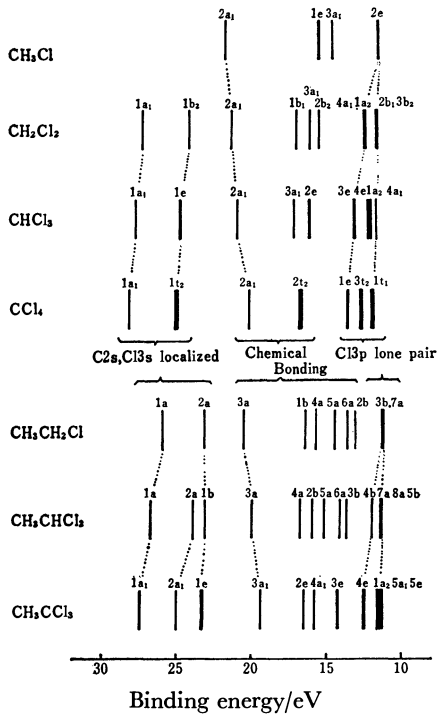

Fig. 6. Correlation diagram of observed valence electron energies for chloromethanes and chloroethanes.

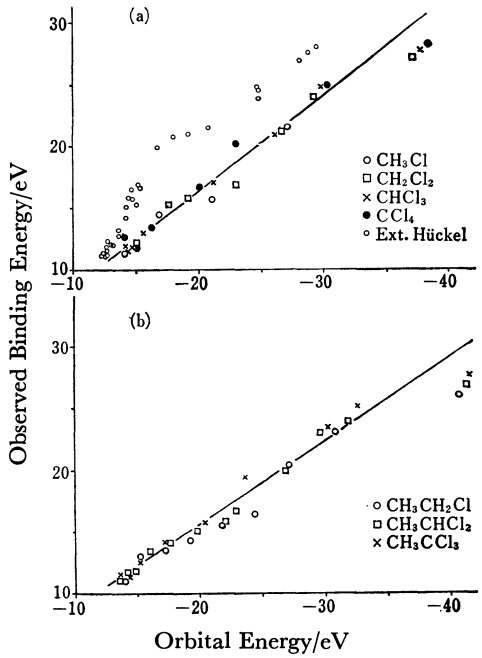

Fig. 7. Relation between observed ionization energies and CNDO/2 orbital energies.
(a) Chloromethanes, (b) chloroethanes.
Data obtained with extended Hückel type calculation by Hopfgarten and Manne are shown as small open circles in (a).

Table 4. Calculated and experimental valence orbitals of chloroethanes

Molecule	Symmetry	CNDO/2 calculation: Atomic population C 2s	C 2p	Cl 3s	Cl 3p	Orbital energy (eV)	Relative cross section	*IP*(obsd) (eV) UPS[a]	XPS	Peak width (eV)
CH_3CH_2Cl	7a	0.005	0.093	0.000	0.874	−13.98	1.00	11.06	11.1	1.1
	3b	—	0.046	—	0.842	−14.04	0.95			
	6a	0.003	0.307	0.010	0.476	−15.27	0.58	13.01	13.0	1.3
	2b	—	0.375	—	0.116	−17.32	0.17	13.51	13.5	1.3
	5a	0.000	0.675	0.014	0.131	−19.13	0.23	14.35	14.6	1.3
	4a	0.024	0.455	0.127	0.118	−21.81	0.37	15.60	15.6	1.3
	1b	—	0.563	—	0.037	−24.47	0.10	16.35	16.4	1.3
	3a	0.123	0.242	0.368	0.010	−27.28	0.72		20.4	1.5
	2a	0.255	0.124	0.373	0.016	−30.80	1.02		23.0	1.5
	1a	0.616	0.048	0.060	0.018	−40.78	1.47		25.8	3.5
CH_3CHCl_2	5b	—	0.073	0.000	0.913	−13.73	1.00	11.23	11.2	1.1
	8a	0.008	0.133	0.000	0.816	−14.09	0.92			
	7a	0.001	0.104	0.000	0.795	−14.27	0.88	11.92	11.9	1.1
	4b	—	0.014	0.000	0.965	−14.85	0.87			
	3b	—	0.229	0.010	0.628	−15.99	0.72	13.61	13.6	1.3
	6a	0.004	0.261	0.013	0.468	−17.42	0.56	14.03	14.0	1.3
	5a	0.005	0.536	0.042	0.250	−19.77	0.38	15.12	15.1	1.3
	2b	—	0.428	0.142	0.125	−22.00	0.33	15.93	15.9	1.3
	4a	0.072	0.417	0.171	0.146	−22.76	0.54	16.74	16.7	1.3
	3a	0.098	0.347	0.206	0.044	−26.77	0.52		19.9	1.3
	1b	—	0.164	0.800	0.012	−29.62	0.90		23.0	1.5
	2a	0.251	0.120	0.406	0.031	−31.81	1.03		23.8	1.5
	1a	0.598	0.049	0.117	0.036	−41.25	1.47		26.6	3.5
CH_3CCl_3	$5a_1$	0.11	0.178	0.000	0.880	−14.18	0.92	11.25	11.3	1.1
	5e	—	0.100	0.000	0.804	−13.82	1.63	11.58	11.6	1.1
	$1a_2$	—	—	0.000	1.000	−14.53	1.00			
	4e	—	0.037	0.000	0.924	−15.28	1.85	12.50	12.5	1.1
	3e	—	0.195	0.013	0.657	−17.32	1.37	14.24	14.2	1.3
	$4a_1$	0.026	0.354	0.091	0.494	−20.17	0.67	15.76	15.8	1.3
	2e	—	0.408	0.166	0.152	−22.49	0.71	16.44	16.4	1.3
	$3a_1$	0.182	0.289	0.275	0.144	−23.76	0.81		19.4	1.3
	1e	—	0.176	0.775	0.025	−30.19	1.63		23.3	1.5
	$2a_1$	0.250	0.119	0.420	0.044	−32.60	0.97		25.0	1.5
	$1a_1$	0.598	0.050	0.171	0.037	−41.60	1.41		27.4	3.0

a) Ref. 7.

with a few exceptions.[21] For the orbitals within reach of UPS, we used the binding energies reported by Pott *et al.*[4] for chloromethanes, and by Katsumata and Kimura[7] for chloroethanes. For the peaks at binding energies above 17 eV, we adjusted peak positions so as to give the best agreement between calculated and observed spectra.

In order to calculate the valence-electron spectra of chloromethanes and chloroethanes, we need to know three relative atomic cross sections, σ(C 2p/C 2s), σ(Cl 3s/C 2s) and σ(Cl 3p/C 2s), parametrized for CNDO/2 orbitals.[22] Banna *et al.*[20] has determined σ(C 2p/C 2s) from the analysis of the XPS spectrum of methane using CNDO/2 orbitals. Since the remaining two relative cross sections have not been known, we treat them as parameters, and found that the following values give the best over-all agreement between calculated and observed spectra for all chloromethanes and chloroethanes;[23]

$$\sigma(\text{Cl 3s/C 2s}) = 0.50$$

$$\sigma(\text{Cl 3p/C 2s}) = 0.50$$

The final results of spectrum simulation are shown by solid lines in Figs. 3 and 4 for chloromethanes and chloroethanes, respectively. The agreement with observed spectrum is very satisfactory in every case.

The binding energies and half-widths of photoelectron peaks finally employed in the above simulations are listed in Tables 3 and 4, together with the results of CNDO/2 calculations. It should be noted that the peaks at binding energies of 22—35 eV are very much broadened, having a width of 2.5—3.5 eV. These peaks are due to the molecular orbitals mainly associated with Cl 3s and C 2s atomic orbitals. Seemingly, the above phenomena are due to the life-time broadening, since a hole in these molecular orbitals is expected to decay rapidly by the Coster-Kronig process.

The photoelectron bands of chloromethanes at binding energies of about 20 eV were also studied by Potts *et al.* by means of UPS with He II resonance line.[4] The

binding energies reported by them are considerably different from our values, the discrepancies being as large as 1 eV. However, very recently, Katsumata and Kimura[24] carefully measured the UPS spectra of chloromethanes employing the He II line, and obtained the values which agree well with our XPS data.

Figure 6 shows the correlation diagram of valence electron levels of chloromethanes and chloroethanes. By examining the atomic populations, given in Tables 3 and 4, molecular orbitals can be roughly divided into three groups; (1) Cl 3p lone-pair orbitals (2) chemical-bonding orbitals, and (3) orbitals predominantly associated with Cl 3s and C2s. As it is naturally expected, Cl 3p lone-pair levels split wider on increasing the number of chlorine atoms in the case of chloromethanes as well as in the case of chloroethanes. The main features of this splitting are nearly the same between the two cases.

In Fig. 7, we have plotted the observed binding energies against the corresponding orbital energies obtained by CNDO/2 calculations. Most of the plots are on a straight line for each series of compounds, so that we can derive the following empirical relations between binding energy E_B and CNDO/2 orbital energy $\varepsilon_{CNDO/2}$; For chloromethanes,

$$E_B = 0.78(-\varepsilon_{CNDO/2}-2.9) \text{ eV},$$

and, for chloroethanes,

$$E_B = 0.72(-\varepsilon_{CNDO/2}-2.9) \text{ eV}.$$

Extended Hückel type (EHT) calculation is often used in the analysis of photoelectron spectrum. In Fig. 7(a), we have also plotted the observed binding energies against the orbital energies obtained with EHT calculation.[25] It should be noted that orbital energies by EHT calculations do not show such a simple correlation with observed binding energies as we have obtained for CNDO/2 orbital energies.

References

1) T. Ohta, T. Fujikawa, and H. Kuroda, *Bull. Chem. Soc. Jpn.*, **48**, 2017 (1975).

2) T. Fujikawa, T. Ohta, and H. Kuroda, *Bull. Chem. Soc. Jpn.*, **49**, 1486 (1976).

3) D. W. Turner, C. Baker, A. D. Baker, and C. R. Brundle, "Molecular Photoelectron Spectroscopy," Wiley-Interscience, New York (1970).

4) A. W. Potts, H. J. Lempka, D. G. Street, and W. C. Price, *Phil. Trans. Roy. Soc.*, **A268**, 59 (1970).

5) J. L. Ragle, I. A. Stenhouse, D. C. Frost, and C. A. McDowell *J. Chem. Phys.*, **53**, 178 (1970).

6) R. N. Dixon, J. N. Murrell, and B. Narayan, *Mol. Phys.*, **20**, 611 (1971).

7) S. Katsumata and K. Kimura, *J. Electron Spectrosc.*, **6**, 309 (1975).

8) T. D. Thomas, *J. Am. Chem. Soc.*, **92**, 4184 (1970).

9) U. Gelius, S. Svensson, H. Siegbahn, E. Basilier, A. Faxälv, and K. Siegbahn, *Chem. Phys. Lett.*, **28**, 1 (1974).

10) K. Siegbahn, C. Nordling, G. Johansson, J. Hedman, P. F. Heden, K. Hamrin, U. Gelius, T. Bergmark, L. Q. Werme, R. Manne, and Y. Baer, "ESCA Applied to Free Molecules," North-Holland, Amsterdam (1969).

11) T. Ohta, unpublished work.

12) D. P. Santry and G. A. Segal, *J. Chem. Phys.*, **47**, 158 (1967).

13) D. T. Clark, D. Kilcast, D. B. Adams, and W. K. Musgrave, *J. Electron Spectrosc.*, **6**, 117 (1975).

14) D. W. Davis and D. A. Shirley, *J. Electron Spectrosc.*, **3**, 137 (1974).

15) W. L. Jolly and W. B. Perry, *Inorg. Chem.*, **13**, 2686 (1974).

16) U. Gelius, "Electron Spectroscopy," ed. by D. A. Shirley, North-Holland, Amsterdam (1972), p. 311.

17) C. J. Allan, U. Gelius, D. A. Allison, G. Johansson, H. Siegbahn, and K. Siegbahn, *J. Electron Spectrosc.*, **1**, 131 (1972).

18) W. B. Perry and W. L. Jolly, *J. Electron Spectrosc.*, **4**, 219 (1974).

19) T. Fujikawa, T. Ohta, and H. Kuroda, *Chem. Phys. Lett.*, **28**, 433 (1974).

20) M. S. Banna, B. E. Mills, D. W. Davis, and D. A. Shirley, *J. Am. Chem. Soc.*, **61**, 4780 (1974).

21) There are some ambiguities in the assignment of MO's in the Cl 3p region. Although several possible cases were tried in the course of spectra simulation, we could not find a clear difference in these simulated curves. Accordingly, we have adopted the same assignment as those proposed by Hopfgarten and Manne (Ref. 25) for chloromethanes.

As for 1,1,1-trichloroethane, it would be reasonable to assign the first ionization potential to 5*a*, instead of 5*e* from the consideration of UPS spectral intensity. This assignment is contradicted with the CNDO/2 result.

22) As the cross section of H ls is much smaller than those of C 2s, 2p, Cl 3s, 3p in the XPS region, the contribution of H ls was neglected in the spectral simulation. (See for example, V. I. Nefedov *et al.*, *J. Electron Spectrosc.*, **2**, 383 (1973).

23) Most recently Berndtsson *et al.* (*Physica Scripta*, **12**, 235 (1975)) has measured XPS valence electron spectra of chloroethylenes and performed the spectral simulation by using extended Hückel type MO's. They determined the experimental relative cross sections for Cl 3s and Cl 3p, as follows,

$$\sigma(\text{Cl } 3s/\text{C } 2s) = 0.69$$

$$\sigma(\text{Cl } 3p/\text{C } 2s) = 0.58$$

These values are slightly higher than ours.

24) S. Katsumata and K. Kimura, private communication.

25) F. Hopfgarten and R. Mann, *J. Electron Spectrosc.*, **2**, 13 (1973).

Epoxide Rearrangement. VIII. The Acidic and Basic Properties of TiO_2-SiO_2-MgO and Its Catalytic Activities

Teruaki YAMADA, Kazushi ARATA,* Masayoshi ITOH, Hideshi HATTORI, and Kozo TANABE

Department of Chemistry, Faculty of Science, Hokkaido University, Sapporo 060
**Department of Chemistry, Hokkaido University of Education, Hachimancho, Hakodate 040*

(Received May 18, 1976)

Four kinds of TiO_2–SiO_2–MgO having different molar ratios, TiO_2–SiO_2–MgO (1: 1: 1, 10: 10: 1, 1: 10: 10, and 10: 1: 10), were prepared, their acidic and basic properties being examined by titration with butylamine and benzoic acid in benzene, respectively. The acidity of TiO_2–SiO_2–MgO was attributed to that of TiO_2–SiO_2 and SiO_2–MgO. The amount of strong acid sites of $H_0 \leqq -5.6$ decreased with the addition of MgO to TiO_2–SiO_2. The basicity of TiO_2–SiO_2–MgO was attributed to that of TiO_2–MgO and decreased with the increase in SiO_2 content. Catalytic activities for the isomerization of 1-butene and the decomposition of 4-hydroxy-4-methyl-2-pentanone are correlated with the acidity and basicity, respectively. For isomerization of 1-methylcyclohexene oxide and *d*-limonene oxide, TiO_2–SiO_2–MgO and TiO_2–SiO_2 showed high activities for the preferential formation of ketones except TiO_2–SiO_2–MgO (10: 1: 10) over which allyl alcohols were produced preferentially. The selectivities for the isomerization of two epoxides were interpreted in terms of the acidic and basic properties of the catalysts.

Binary metal oxides such as SiO_2–Al_2O_3,[2] TiO_2–Al_2O_3,[3] TiO_2–ZrO_2,[3] TiO_2–SiO_2,[4] SiO_2–MgO,[2,5] and TiO_2–MgO[6] have been investigated on acidic and basic properties and on their catalytic actions. Among the binary metal oxides, TiO_2–SiO_2 showed the highest acidic property; the acidity and acid strength of TiO_2–SiO_2 of a certain composition were found to be higher than those of SiO_2–Al_2O_3.[4] SiO_2–MgO is known to possess acid and base sites of moderate strength on the surface.[2,5] Recently, TiO_2–MgO has been found to show higher basicity than each component oxide. Thus, a mixed material of these three metal oxides, TiO_2–SiO_2–MgO, is expected to have both acid and base sites, the amount and strength of which may depend on the ratio of the three components.

No systematic investigation concerning both acidic and basic properties of multicomponent metal oxides except binary metal oxides has been performed, though many multicomponent metal oxides are often used as solid catalysts for many reactions. We have attempted to examine acidic and basic properties of TiO_2–SiO_2–MgO having different molar ratios and their relations to the catalytic actions for the isomerization of 1-butene, the decomposition of 4-hydroxy-4-methyl-2-pentanone and the isomerization of 1-methylcyclohexene oxide and *d*-limonene oxide.

Experimental

Catalyst Preparation. TiO_2–SiO_2–MgO with various compositions were prepared by kneading TiO_2–SiO_2 having different molar ratios of Ti to Si and magnesium hydroxide with a proper amount of water for 2 h, followed by drying at 120 °C for a day. TiO_2–SiO_2 was prepared by co-precipitation from a mixed solution of ethyl orthosilicate and titanium tetrachloride with aqueous ammonia.[4] The precipitate was aged over a water bath for 1 h, washed with distilled water until no chloride ion was detected and dried at 100 °C for a day. Magnesium hydroxide was prepared by the hydrolysis of magnesium chloride, followed by washing and drying as above.

All the catalysts were calcined in air at 500 °C for 3 h prior to reactions or measurements of surface properties.

Surface Area and X-Ray Analysis. A specific surface area was determined by applying the BET equation to the adsorption isotherm of nitrogen at −196 °C. X-Ray powder diffraction diagrams were recorded over the range of $2\theta = 20$—70° with an X-ray diffractometer (Toshiba ADG-301) by using nickel filtered Cu $K\alpha$ radiation.

Measurement of Acidic and Basic Properties. Acidity and basicity of catalysts at various strengths were measured by titrating with butylamine and benzoic acid in benzene, respectively, indicators of different pK_a's and pK_{BH} being used.[7,8]

Reaction Procedure. Isomerization reaction of 1-butene was carried out in a closed circulation system having a volume of about 900 ml at 200 °C.[4] 50 mg of a catalyst was placed in a reactor and evacuated at 200 °C for 2 h. The reactant (200Torr) was introduced and the products were analyzed periodically by gas chromatography. The analysis was carried out at 0 °C on a 4 m column containing 30 wt % propylene carbonate on Uniport C.

Decomposition of 4-hydroxy-4-methyl-2-pentanone to acetone was carried out at 30 °C for 10 min.[9] A mixture of 25 ml of 4-hydroxyl-4-methyl-2-pentanone and 0.5 g of a catalyst was stirred in a reaction vessel with a magnetic stirrer. For the analysis of products, a column packed with 10 wt% polyethylene glycol on chromsorb W and thermostated at 0 °C was used.

Isomerization of 1-methylcyclohexene oxide was carried out in the presence of toluene as a solvent at 108 °C for 2 h.[10] A mixture of 0.5 ml of the epoxide, 2.5 ml of toluene and about 0.3 g of a catalyst was stirred in a reaction vessel. The products were analyzed by gas chromatography, a 3 m column of polyethylene glycol 20M on Celite 545SK being used at 150 °C. For separation of two allyl alcohols, a 45 m capillary column of Ucon LB-500-X was used at 100 °C.

The procedure of reaction and analysis of products for the isomerization of *d*-limonene oxide[11] were similar to those for the isomerization of 1-methylcyclohexene oxide, except that a mixture of 1 ml of the epoxide and 5 ml of toluene was used.

Results and Discussion

Surface Area and X-Ray Analysis. Specific surface areas of catalysts are listed in Table 1. The values of

* Part VII; see Ref. 1

Table 1. Specific surface areas of catalysts

	TiO_2	SiO_2	MgO	TiO_2–SiO_2			TiO_2–SiO_2–MgO			
Mole ratio				(1:1)	(10:1)	(1:10)	(1:1:1)	(10:10:1)	(10:1:10)	(1:10:10)
Surface area ($m^2\,g^{-1}$)	85	227	145	358	227	201	181	299	222	168

Table 2. Acidity at various acid strengths of catalysts

Catalysts	Mole ratio	Acidity (μmol m^{-2})				
		$H_0 \leqq +3.3$	$H_0 \leqq +1.5$	$H_0 \leqq -3.0$	$H_0 \leqq -5.6$	$H_0 \leqq -8.2$
MgO[a]			0	0	0	0
TiO_2–MgO[a]	(1:2)	0	0	0	0	0
TiO_2–SiO_2	(1:1)	1.6	1.4	0.6	*[b]	*[b]
	(10:1)	2.7	3.5	0.1	*[b]	*[b]
	(1:10)	2.2	0.9	0.8	0.3	0
TiO_2–SiO_2–MgO	(1:1:1)	3.6	2.8	2.5	1.5	0.4
	(10:10:1)	2.1	1.9	1.7	1.0	0.8
	(10:1:10)	1.9	1.6	0	0	0
	(1:10:10)	1.6	1.3	0.5	0.3	0

a) Cited from Ref. 6. b) See text.

mixed oxides were larger than those of single component oxide except SiO_2.

According to X-ray diffraction pattern, TiO_2–SiO_2–MgO (1:1:1 and 10:10:1) were amorphous and TiO_2–SiO_2–MgO (1:10:10 and 10:1:10) showed only weak diffraction lines of TiO_2 (anatase) and MgO. Since no diffraction lines of the hydroxides were detected, calcination in air at 500 °C is considered to cause the dehydration to form TiO_2–SiO_2–MgO.

Acidic and Basic Properties. Acidity at various acid strengths of TiO_2–SiO_2–MgO calcined at 500 °C is given in Table 2, together with that of TiO_2–SiO_2 and TiO_2–MgO. The acidity at $H_0 \leqq -5.6$ and -8.2 of TiO_2–SiO_2 (10:1 and 1:1) could not be determined by the titration method, since the color of the acidic forms of indicators of $pK_a \leqq -5.6$ and -8.2 is yellow and that of the above mentioned TiO_2–SiO_2 is of the same tone. However, it was confirmed that TiO_2–SiO_2 (10:1 and 1:1) has high acidity at $H_0 = -5.6$ and -8.2 from experimental results which showed that larger amounts of basic molecules (ammonia, butylamine, and pyridine) remain after evacuation at high temperatures on TiO_2–SiO_2 than SiO_2–Al_2O_3 which shows high acidity at $H_0 \leqq -5.6$ and -8.2.[4]

The distribution of acidity on TiO_2–SiO_2 (1:1) and TiO_2–SiO_2–MgO (10:10:1 and 1:1:1) indicates that the acidity at lower acid strength of $-3.0 < H_0 \leqq +3.3$ increases with an increase in the Mg content. This is considered to be due to the acidity of SiO_2–MgO resulting from the mixing of MgO with TiO_2–SiO_2 (1:1). On the other hand, the acidity at $-3.0 < H_0 \leqq +3.3$ of TiO_2–SiO_2 (10:1) decreases with the addition of MgO. This may be attributed to the fact that TiO_2–MgO which has no acidity occupies the main part in TiO_2–SiO_2–MgO (10:1:10). Similarly, the acidity of TiO_2–SiO_2–MgO (1:10:10) might be explained in terms of the acidic characters of SiO_2–MgO and TiO_2–SiO_2. The acidity at higher acid strengths of $H_0 \leqq -5.6$ and -8.2 of TiO_2–SiO_2 (1:1 and 10:1) decreases with the addition of MgO. In all TiO_2–SiO_2–MgO systems, only TiO_2–SiO_2–MgO (10:1:10) showed no acidity at $H_0 \leqq -3.0$.

Table 3. Basicity and catalytic activity for decomposition of 4-hydroxy-4-methyl-2-pentanone (diacetone alcohol) at 30 °C

Catalysts	Mole ratio	Basicity[a] (μmol m^{-2})	Activity[b] ($\times 10^2$%m^{-2} min^{-1})
TiO_2–SiO_2	(1:1)	0	—
TiO_2–MgO[c]	(1:2)	19.4	3.9
	(5:1)	0	0
	(1:18)	51.6	8.2
TiO_2–SiO_2–MgO	(1:1:1)	1.5	0.5
	(10:10:1)	0	0
	(10:1:10)	1.6	1.0
	(1:10:10)	2.0	1.8

a) 2,4-Dinitroaniline ($pK_{BH} = 15.0$) was used as an indicator. b) Mole percentage of the product at 10 min of a reaction time per unit surface area of catalyst (m^{-2}) per unit time (min^{-1}). c) Cited from Ref. 6.

The basicity of TiO_2–SiO_2–MgO and TiO_2–MgO calcined at 500 °C is given in Table 3. The high basicity of TiO_2–MgO (1:2 and 1:18) greatly decreased with the addition of SiO_2, TiO_2–SiO_2–MgO (10:10:1) showing no basicity.

Isomerization of 1-Butene. The activity and selectivity (the ratio of *cis*- to *trans*-2-butene) of TiO_2–SiO_2–MgO, TiO_2–SiO_2, and MgO for the isomerization of 1-butene are given in Table 4. The active sites of TiO_2–SiO_2 for the reaction were ascribed to acid sites. In the reaction, the *cis*-/*trans*- ratios were 1—2 and the reaction proceeds *via* a butyl cation.[4] The ratio over TiO_2 was reported to be 4.2, suggesting a base-catalyzed isomerization *via* a π-allyl carbanion intermediate.[4] The ratios over TiO_2–SiO_2–MgO (1.7—2.1) indicate that the same acid-catalyzed isomerization as over TiO_2–SiO_2 takes place, the activity being correlated with acidity (see Table 2) and not basicity.

TABLE 4. CATALYTIC ACTIVITY AND SELECTIVITY (RATIO OF *cis*- TO *trans*-2-BUTENE) FOR ISOMERIZATION OF 1-BUTENE AT 200 °C

Catalysts	Mole raiio	Activity[a] ($\times 10^2$% m^{-2} min^{-1})	Selectivity[b]
MgO		0	—
TiO_2–SiO_2	(1: 1)	2.6	1.9
	(10: 1)	15.5	1.6
	(1: 10)	3.1	1.2
TiO_2–SiO_2–MgO	(1: 1: 1)	3.5	1.9
	(10: 10: 1)	2.9	1.9
	(10: 1: 10)	0.4	2.1
	(1: 10: 10)	1.1	1.7

a) Initial conversion per unit surface area of catalyst (m^{-2}) per unit time (min^{-1}).
b) Obtained by extrapolation to zero conversion.

Decomposition of 4-Hydroxy-4-methyl-2-pentanone. Catalytic activity as well as basicity of the catalysts are given in Table 3. A good correlation was observed between activity and basicity. Although TiO_2–SiO_2–MgO had acidic sites, the activity was small as compared with that of TiO_2–MgO which has no acidic sites. Thus, it is suggested that only basic sites are considered to be operative, and that the reaction proceeds as in the case of other solid base catalysts.[9]

Isomerization of 1-Methylcyclohexene Oxide. The reaction of 1-methylcyclohexene oxide over TiO_2–SiO_2–MgO, TiO_2–SiO_2, TiO_2, SiO_2, and MgO gave five main products: 2-methyl-cyclohexanone (III), 1-methylcyclohexanol (IV), 2-methyl-2-cyclohexene-1-one (V), 2-methylenecyclohexanol (VIa), and 2-methyl-2-cyclohexene-1-ol (VIb), with a small amount of 1-methylcyclohexene (I) and unidentified compound (II).

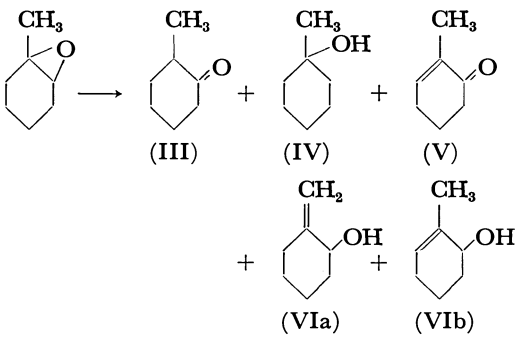

The activity and selectivity of catalysts in 2 h at 108 °C are shown in Table 5. The activity of three TiO_2–SiO_2 was higher than that of single component oxides. This fact is interpreted by taking into consideration the higher acidity of the former. It is of interest that TiO_2 formed the allyl alcohol (VI), but TiO_2–SiO_2 formed the ketone (III). Since formation of the ketone and the allyl alcohol is explained by isomerization over strong acid sites and acid-base bifunctional sites, respectively,[10] it is considered that comparatively weak acid sites and base sites exist on TiO_2 and strong acid sites exist on TiO_2–SiO_2.

Over TiO_2–SiO_2–MgO (1: 1: 1, 10: 10: 1, and 1: 10: 10), a high activity for the preferential formation of the ketone was observed. Although some basic sites were observed on TiO_2–SiO_2–MgO (1: 1: 1 and 1: 10: 10), they do not seem to be active. Only strong acid sites of $H_0 \leqq -3.0$ seem to be active. On the other hand, TiO_2–SiO_2–MgO (10: 1: 10) showed high activity and selectivity for the formation of the allyl alcohol. This suggests that TiO_2–SiO_2–MgO (10: 1: 10) has both base and acid sites at the proper acid strength to act as acid-base bifunctional sites; TiO_2–SiO_2–MgO (10: 1: 10) showed no acidity at higher acid strength of $H_0 \leqq -3.0$ (see Table 2).

Isomerization of d-*Limonene Oxide.* Isomerization of *d*-limonene oxide over the present catalysts gave the following products: cymene (II), 1-methyl-3-isopro-

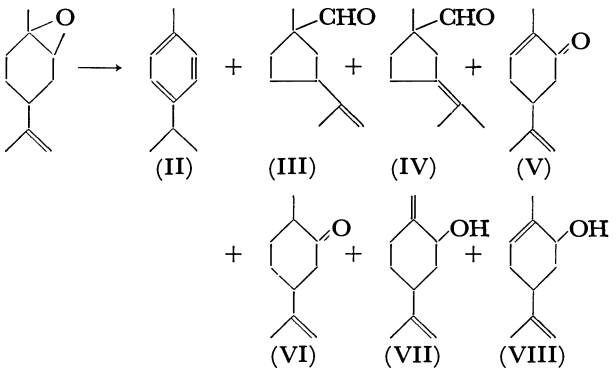

TABLE 5. CATALYTIC ACTIVITY AND SELECTIVITY FOR ISOMERIZATION OF 1-METHYLCYCLOHEXENE OXIDE AT 108 °C AT 2 h OF A REACTION TIME

Catalysts	Mole ratio	Amount of catalyst (g)	Conversion (%)	Products (%)[a] (II)	(III)	(IV)	(V)	VI(a, b)
SiO_2		0.20	6	0	31	0	5	64
TiO_2[b]		0.44	27	0	7	0	1	91(51, 40)
MgO[b]		0.23	2					
TiO_2–SiO_2	(1:1)	0.27	34	11	80	6	1	0
	(9: 1)	0.28	47	21	45	6	2	12
	(1: 9)	0.31	46	9	57	7	1	3
TiO_2–SiO_2–MgO	(1: 1: 1)	0.32	54	0	64	15	1	2
	(10:10: 1)	0.29	45	6	61	12	1	2
	(10: 1: 10)	0.32	63	0	12	14	14	58(24, 34)
	(1: 10: 10)	0.22	46	2	61	7	3	5

a) See text. b) Cited from Ref. 10.

Table 6. Catalytic activity and selectivity for isomerization of *d*-limonene oxide at 108 °C

Catalysts	Mole ratio	Amount of Catalyst (g)	Conversion (%)	Products (%)[a]							
				(I)	(II)	(III)	(IV)	(V)	(VI)	(VII)	(VIII)
SiO_2[b]		0.16	1								
TiO_2[b]		0.32	25	0	0	0	0	0	6	58	25
MgO[b,d]		0.24	1								
TiO_2–SiO_2	(1: 1)[c]	0.26	100	7	2	18	3	4	48	0	0
	(9: 1)[c]	0.35	98	3	1	17	1	3	30	21	19
	(1: 9)[c]	0.28	98	2	1	15	2	5	41	8	14
TiO_2–SiO_2–MgO	(1: 1: 1)[c]	0.18	98	4	1	19	1	4	44	11	11
	(10: 10: 1)[c]	0.28	100	6	2	22	1	4	47	9	2
	(10: 1: 10)[b]	0.17	31	0	0	0	0	4	22	30	41
	(1: 10: 10)[b]	0.21	90	5	0	30	2	4	43	6	9
	(1: 10: 10)[c]	0.21	51	0	0	21	4	5	48	7	12

a) See text. b) Reaction time: 75 min. c) Reaction time: 10 min. d) Cited from Ref. 11.

penyl-1-cyclopentanecarbaldehyde (III), 1-methyl-3-isopropylidene-1-cyclopentanecarbaldehyde (IV), carvone (V), dihydrocarvone (VI), *exo*-carveol (VII), *endo*-carveol (VIII), and an unidentified compound (I).

The activity and selectivity of TiO_2–SiO_2–MgO, TiO_2–SiO_2, TiO_2, SiO_2, and MgO in 10 or 75 min at 108 °C are listed in Table 6. TiO_2–SiO_2–MgO (1: 1: 1, 10: 10: 1, and 1: 10: 10) and all TiO_2–SiO_2 showed surprisingly high activity for the ketone (VI) formation, as in the case of SiO_2–Al_2O_3 and $LiClO_4$.[11] TiO_2–SiO_2–MgO (10: 1: 10) was less active than any other mixed oxide, the allyl alcohols (VII and VIII) being preferentially produced. The selectivity for the reaction is similar to that for the isomerization of 1-methylcyclohexene oxide in the sense that the ketone was produced over acidic sites and the allyl alcohols over bifunctional sites. The selectivity in the isomerization of *d*-limonene oxide can be explained by the acidic and basic properties of the catalysts, as in the case of 1-methylcyclohexene oxide.

The products of II and IV were obtained in small amounts on the present catalysts, though large amounts were formed over SiO_2–Al_2O_3[11] which have strong acid sites of the Brönsted type. Thus, TiO_2–SiO_2–MgO and TiO_2–SiO_2 are considered to have no strong Brönsted acid sites.

References

1) K. Arata and K. Tanabe, *Chem. Lett.*, **1976**, 321,
2) V. A. Dzisko, *Proc. Int. Congr. Catal.*, 3rd 1964 I-19, 422 (1965).
3) K. Shibata, T. Kiyoura, J. Kitagawa, T. Sumiyoshi, and K. Tanabe, *Bull. Chem. Soc. Jpn.*, **46**, 2985 (1973).
4) M. Itoh, H. Hattori, and K. Tanabe, *J. Catal.*, **35**, 225 (1974); H. Hattori, M. Itoh, and K. Tanabe, *ibid.*, **38**, 172 (1975).
5) Y. Okamoto, T. Imanaka, and S. Teranishi, *Bull. Chem. Soc. Jpn.*, **46**, 4 (1973).
6) K. Tanabe, T. Sumiyoshi, and H. Hattori, unpublished data.
7) O. Johnson, *J. Phys. Chem.*, **59**, 827 (1955).
8) K. Tanabe and T. Yamaguchi, *J. Res. Inst. Catal. Hokkaido Univ.*, **11**, 179 (1964); K. Tanabe, "Solid Acids and Bases," p. 38, Kodansha, Tokyo; Academic Press, New York (1970).
9) K. Yonai, S. Okazaki, Y. Fukuda, and K. Tanabe, *Nippon Kagaku Zasshi*, **92**, 815 (1971).
10) K. Arata, S. Akutagawa, and K. Tanabe, *Bull. Chem. Soc. Jpn.*, **48**, 1097 (1975).
11) K. Arata, S. Akutagawa, and K. Tanabe, *J. Catal.*, **41**, 173 (1976).

Deactivation of Triplet 2-Naphthol and 1-Anthrol by Aromatic *N*-Heterocycles

Sada-aki YAMAMOTO, Koichi KIKUCHI, and Hiroshi KOKUBUN

Department of Chemistry, Faculty of Science, Tohoku University, Aoba, Aramaki, Sendai 980

(Received May 20, 1976)

A flash-photolytic investigation was carried out on the hydrogen bonding interaction of triplet 2-naphthol and 1-anthrol with aromatic *N*-heterocycles such as 4-methylpyridine, quinoline, and benzo[*h*]quinoline. The deactivation of triplet 2-naphthol and 1-anthrol by aromatic *N*-heterocycles was found to be due to the hydrogen atom transfer reaction. The relationship between the reactivity and the reduction potential of aromatic *N*-heterocycles suggests that the electron transfer from the triplet to the quencher is the primary process of the hydrogen atom transfer reaction.

Previously, we studied the hydrogen bonding interaction of the π-electronic system such as 2-naphthol–pyridine, 1-anthrol–pyridine, and 1-anthrol–quinoline in the ground, the triplet and the excited singlet states.[1] On the basis of the results obtained, it was concluded that the hydrogen atom transfer reaction plays an important role in the dynamic deactivation through the hydrogen bonding interaction in the excited states and that the efficiency of the hydrogen atom transfer reaction in the excited state is affected by the acidity of the proton donor. In addition, the investigation of the triplet-triplet energy transfer from a suitable sensitizer to the hydrogen bonded species revealed that the triplet state of the hydrogen bonded species (^{3}DH–A) and the non-relaxed encounter complex (^{1}DH*···A) in the excited singlet state are the reaction state.[2]

$$^1\mathrm{DH}^* + \mathrm{A} \rightleftharpoons {}^1\mathrm{DH}^* \cdots \mathrm{A} \longrightarrow \dot{\mathrm{D}} + \dot{\mathrm{HA}}$$

$$^3\mathrm{DH} + \mathrm{A} \rightleftharpoons {}^3\mathrm{DH\text{–}A} \longrightarrow \dot{\mathrm{D}} + \dot{\mathrm{HA}}$$

However, the difference in the reactivity between the excited singlet state and the triplet state is still not fully elucidated.

To clarify the reaction mechanism, it is of prime importance to find out the factors which govern the reactivity. In the present paper, we have investigated the effect of the reduction potential of the quenchers on the reactivity by a conventional flash apparatus.

Experimental

Materials. 2-Naphthol (G. R. grade, Tokyo Kasei) was recrystallized twice from the water–ethanol mixture, and sublimed twice *in vacuo*. 1-Anthrol used was the same as described before.[1] Benzo[*h*]quinoline (G. R. grade, Tokyo Kasei) was recrystallized three times from the water–ethanol mixture, treated by thin-layer chromatography and sublimed *in vacuo*. 4-Methylpyridine (G. R. grade, Tokyo Kasei) was dried over barium oxide, distilled under reduced pressure and stored *in vacuo*. Quinoline (G. R. grade Tokyo Kasei) was distilled under reduced pressure and stored *in vacuo*. Cyclohexane was purified by the standard method.

Apparatus and Procedure. Absorption spectra were measured with a Hitachi EPS-3T spectrophotometer. The input energy of flash lamps was 65—130 J and its FWHM was about 10 μs. The combination of a Toshiba V-V40 and two plastic filters (cut off $\approx$380 nm) for the excitation of 1-anthrol and the combination of a Toshiba UV-D25 and a photographic plate glass for the excitation of 2-naphthol were used. Cyclohexane solutions were degassed by freeze-pump-thaw cycles. All measurements were made at about 25 °C.

Results and Discussion

A flashing of the deaerated cyclohexane solution of 2-naphthol gives the triplet-triplet absorption.[3] Both the decay rate of the triplet 2-naphthol and the yield of the 2-naphthoxyl radical ($\dot{\mathrm{D}}$) increase with increasing quinoline concentration [Qu] up to 10^{-4} M, where neither the formation of hydrogen bond in the ground state nor the interaction of the excited singlet 2-naphthol with quinoline occurs. Since the triplet level of quinoline (21800 cm^{-1})[4] is higher than that of 2-naphthol (21100 cm^{-1}), the deactivation of the triplet 2-naphthol is not due to the energy transfer but the hydrogen atom transfer reaction. The observed first order decay rate constant k_{obsd} is linear with respect to [Qu].

$$k_{\mathrm{obsd}} = k_{\mathrm{dt}} + k_{\mathrm{qt}}[\mathrm{Qu}] \qquad (1)$$

From the slope, the quenching rate constant k_{qt} was obtained as 3.3×10^9 M^{-1} s^{-1}. The reaction scheme is described as follows.

$$\mathrm{DH} \xrightarrow{I_{\mathrm{ab}}} \mathrm{DH}^* \xrightarrow{\phi_{\mathrm{st}}} {}^3\mathrm{DH} \underset{k_{-1}^{\mathrm{t}}}{\overset{k_1^{\mathrm{t}}[\mathrm{A}]}{\rightleftharpoons}} {}^3\mathrm{DH\text{–}A} \xrightarrow{k_{\mathrm{r}}^{\mathrm{t}}} \dot{\mathrm{D}} + \dot{\mathrm{HA}}$$

$$^3\mathrm{DH} \xrightarrow{k_{\mathrm{dt}}} \mathrm{DH} \qquad {}^3\mathrm{DH\text{–}A} \xrightarrow{k_{\mathrm{dt}}^{\mathrm{t}}} \mathrm{DH\text{–}A}$$

Reaction scheme 1.

where DH and A stand for the proton donor and acceptor, respectively.

The absorbance of the 2-naphthoxyl radical measured at the end of a flash, $D_{\mathrm{R}}{}^0(\lambda)$, is given by

$$\frac{1}{D_{\mathrm{R}}{}^0(\lambda)} = \frac{1}{\varepsilon_{\mathrm{R}}(\lambda)\mathrm{d}\phi_{\mathrm{ST}}I_{\mathrm{ab}}^0\phi_{\mathrm{R}}}\left(1+\frac{k_{\mathrm{dt}}}{k_{\mathrm{qt}}[\mathrm{Qu}]}\right) \qquad (2)$$

where $\phi_{\mathrm{R}}=k_{\mathrm{r}}{}^{\mathrm{t}}/(k_{\mathrm{r}}{}^{\mathrm{t}}+k_{\mathrm{dt}}{}^{\mathrm{t}})$ and $k_{\mathrm{qt}}=(k_{\mathrm{r}}{}^{\mathrm{t}}+k_{\mathrm{dt}}{}^{\mathrm{t}})\cdot k_1{}^{\mathrm{t}}/(k_{\mathrm{dt}}{}^{\mathrm{t}}+k_{\mathrm{r}}{}^{\mathrm{t}}+k_{-1}{}^{\mathrm{t}})$. The plot of $1/D_{\mathrm{R}}{}^{\mathrm{o}}$ (470 nm) *vs.* 1/[Qu] is linear, from which the ratio $k_{\mathrm{qt}}/k_{\mathrm{dt}}$ was found to be 2.0×10^5 M^{-1}. Since $k_{\mathrm{dt}}=1.5\times10^4$ s^{-1} is known,[3] k_{qt} was determined to be 3.0×10^9 M^{-1} s^{-1}, which agrees well with $k_{\mathrm{qt}}=3.3\times10^9$ M^{-1} s^{-1} obtained from the effect of quinoline concentration on the triplet decay. The reaction of the triplet 2-naphthol with quinoline yielding the 2-naphthoxyl radical occurs at one forth of the diffusion controlled rate; 1.1×10^{10} M^{-1} s^{-1} in cyclohexane.[5]

The triplet 2-naphthol also reacts with 4-methylpyri-

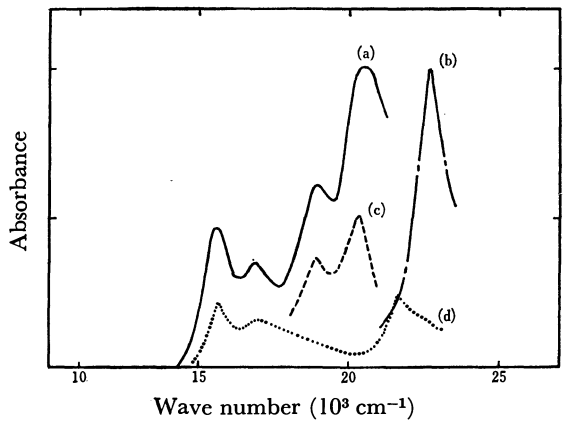

Fig. 1. Transient absorption spectra of 1-anthrol in cyclohexane. (a) [1-anthrol] = 1.0×10^{-4} M, [benzo[*h*]quinoline] = 1.0×10^{-3} M. (b) T-T absorption spectrum of 1-anthrol. (c) The spectrum of 1-anthroxyl radical. (d) The spectrum of benzo[*h*]quinoline radical.

Table 1. Quenohing rate constants of triplet 1-anthrol and 2-naphthol

Quencher	pK_a	k_{qt}/M^{-1} s^{-1}	Reduction potential in DMF[c]/V
		1-Anthrol	
Pyridine	5.23[a]	—	−2.76
Benzo[*h*] quinoline	4.25[a]	1.6×10^7	−2.23
Quinoline	4.94[a]	$(1.1—1.4)\times10^9$ [1]	−2.175
Acridine	5.5[a]	3.4×10^9 [1]	−1.62
		2-Naphthol	
4-Methylpyridine	6.02[b]	4.0×10^8	−2.86
Pyridine	5.23[a]	$(1.5—1.9)\times10^9$ [3]	−2.76
Quinoline	4.94[a]	$(3.0—3.3)\times10^9$	−2.175

a) A. Albert, R. Goldacre, and J. Phillips, *J. Chem. Soc.*, **1948**, 2240. b) H.C. Brown and X. Mihm, *J. Am. Chem. Soc.*, **77**, 1723 (1955). c) B. J. Tabner and J. R. Yandle, *J. Chem. Soc., A*, **1968**, 381.

dine to produce the 2-naphthoxyl radical. The value of k_{qt} was determined as 4.0×10^8 M^{-1} s^{-1} from both the 4-methylpyridine concentration effect on the triplet decay and the yield of the 2-naphthoxyl radical. This value is smaller than that for the 2-naphthol-quinoline pair by about one order of magnitude.

The investigation was extended to the triplet 1-anthrol and benzo[*h*]quinoline (BQ) pair. With the addition of BQ, the decay rate of the triplet 1-anthrol increases and the transient absorption spectrum shown in Fig. 1(a) appears. This spectrum seems to be the superposition of the spectrum of the 1-anthroxyl radical[1] and that of the BQ radical[6] (Fig. 1(c), (d)). The observed first order decay rate constant of the triplet 1-anthrol is linear with respect to BQ concentration (*cf.* Eq. 1) and the quenching rate constant was found to be 1.6×10^7 M^{-1} s^{-1}. It is obvious that the hydrogen atom transfer reaction occurs between the triplet 1-anthrol and BQ. However the rate constant is smaller by about three orders of magnitude than the diffusion controlled rate constant.

In Table 1 are collected the quenching rate constants for the triplet 1-anthrol and the triplet 2-naphthol, together with reduction potentials and acid dissociation constants of the proton acceptors.

In a previous paper, the difference in the reactivity of 1-anthrol and 2-naphthol in the excited singlet state was explained by the difference of their acidities;[1] the hydrogen atom transfer is suppressed in the systems where the proton transfer is considered to occur easier. In the triplet state, however, the reaction rate constant has no correlation with the acidity of the proton acceptor. But reduction potential is associated with the quenching rate constant, which increases with the lowering of reduction potential. The reaction rate seems to be dependent on the easiness of the electron transfer in the encounter complex.

Therefore it seems plausible that the hydrogen atom transfer reaction occurs initially by the electron transfer followed by the proton transfer.

$$^3DH\cdots A \longrightarrow {}^3\overset{+}{D}H\cdots \bar{A} \longrightarrow \dot{D} + H\dot{A}$$

References

1) S. Yamamoto, K. Kikuchi, and H. Kokubun, *J. Photochem.*, **5**, 469 (1976).
2) S. Yamamoto, K. Kikuchi, and H. Kokubun, *Chem. Lett.*, **1976**, 65.
3) K. Kikuchi, H. Watarai, and M. Koizumi, *Bull. Chem. Soc. Jpn.*, **46**, 749 (1973).
4) V. L. Ermolaev, *Opt. Spectrosk.*, **16**, 383 (1964).
5) S. L. Murov, "Handbook of Photochemistry," Marcel Dekker Inc., New York (1973), p. 55.
6) S. Yamamoto, K. Kikuchi, and H. Kokubun, to be submitted.

The Effect of Pressure on the Dissociation of Weak Acids in Aqueous Buffers

Motoyuki TSUDA, Ichimin SHIROTANI,* Shigeru MINOMURA,* and Yoshio TERAYAMA

Department of Physics, Sapporo Medical College, Sapporo 060

**Institute for Solid State Physics, The University of Tokyo, Roppongi, Tokyo 106*

(Received May 24, 1976)

The effect of pressure on the dissociation of boric acid, imidazole HCl, and $H_2PO_4^-$ in aqueous buffers has been investigated up to 6 kbars, using as optical indicators *p*-nitrophenol and Cresol Red. The limiting volume change on ionization at atmospheric pressure ($\Delta\bar{V}°$) and the compressibility change ($\Delta\bar{\kappa}°$) for these weak acids were obtained. The values of $\Delta\bar{V}°$ ($cm^3\ mol^{-1}$) and $\Delta\bar{\kappa}°$ ($cm^3\ mol^{-1}\ kbar^{-1}$) are -10.1 and -0.4 for Cresol Red, -30.2 and -4.3 for boric acid, and -2.4 and -0.6 for imidazole H^+.

A large number of measurements have been made of the dissociation constants of weak electrolytes under pressure using the method of the concentration cell e.m.f., and density and conductivity measurements.[1,2] They have shown that the dissociation of a weak acid HA in water, to form H^+ and A^- ions, is increased by pressure. Pressure lowers the free energy of solvation of the ions, because it is accompanied by a contraction, or electrostriction, of the surrounding solvent; water is much more densely packed around the ions than around the corresponding undissociated molecules. One important consequence of this is that the pH of aqueous buffer solutions varies with the pressure.[3] Biochemical systems are best studied under buffered conditions, and the conformation of biomolecules is sensitive to the pH. For the study of the pressure dependence of conformational change in biomolecules,[4-8] a detailed knowledge of pressure-induced changes in the buffer pH is required. The results obtained in this study have been extensively used in an investigation of pressure effects on the spectral changes in heme proteins and invertebrate rhodopsin.[9]

Gibson and Loeffer[10] attempted to measure the effects of pressure on the pH by the use of an optical indicator; however, no quantitative results were reported. Recently Newman *et al.*[3] extensively studied the pressure effects of weak acid ionization in aqueous buffers using as optical pH indicators 2,5-dinitrophenol and *p*-nitrophenol; they gave the values of the limiting volume change ($\Delta\bar{V}°$) and the compressibility change ($\Delta\bar{\kappa}°$) upon ionization for acetate, cacodylate, phosphate, and tris buffer. Here we wish to report on the effect of pressure on the acid dissociation of dihydrogen phosphate ($H_2PO_4^-$), boric acid, and imidazole HCl, using as optical pH indicators *p*-nitrophenol and Cresol Red up to 6 kbars. No data have been available for Cresol Red and imidazole HCl. However, the values of $\Delta\bar{V}°$ at atmospheric pressure for the ionization of boric acid have been reported on the basis of limited pressure studies utilizing a glass electrode;[11] they will serve as reference data for the optical experiments reported here.

Experimental

The *p*-nitrophenol was recrystallized from ethanol–water and given long needles were filtered and dried *in vacuo*. The Cresol Red was titrated with 0.1 M NaOH to pH 11 and filtered. The filtrate was then neutralized with 0.1 M HCl. The suspension was filtered, and the residue was washed with water. This procedure was repeated. The residue was then dried at 60 °C overnight. The imidazole, recrystallized from ethanol, was neutralized with hydrochloric acid. The other reagents, sodium borate, boric acid, sodium phosphate, and potassium dihydrogenphosphate, were reagent-grade chemicals, and were used without further purification. A stock solution of *p*-nitrophenol (0.01 M) was prepared by weighing it and by dissolving it in distilled deionized water. Solutions of this indicator in the various buffers were prepared just prior to use by diluting 1.2 ml of the stock to 10 ml with the appropriate buffer. A stock solution of Cresol Red (0.001 M) was prepared in water containing an equivalent amount of sodium hydroxide. Solutions of this indicator in various buffers were prepared just prior to use in the way described above.

The highpressure optical bomb is shown in Fig. 1(a). This bomb was constructed from hardened-steel and had three sapphire windows and a electrode for thermocouples. A

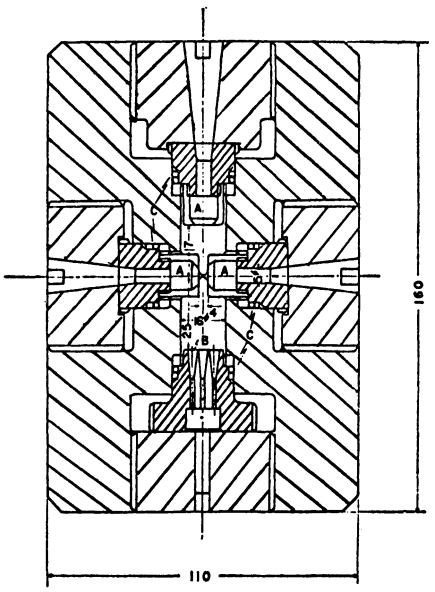

Fig. 1(a). The high pressure optical bomb.
A: sapphire window, B: electrode, C: O-ring (mm).

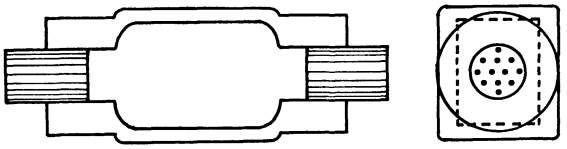

Fig. 1(b). The micro optical cell of quartz with Teflon piston.

hydrostatic pressure up to 6 kbars was applied by means of the pressuring fluid (silicone oil) through a pressure intensifier.

The pressure was determined by a Harwood manganine resistance gauge and a Heise Bourdon tube gauge. The indicator solutions were contained in an internal micro optical cell of quartz (0.3 cm path length and 1.0 cm overall length of the cell). The travelling Teflon piston in the separator served as a physical barrier to the mixing of the indicator solution with the pressuring fluid. The micro optical cell is exhibited in Fig. 1(b).

A thermostatting jacket was constructed for the high-pressure vessel. This was made of brass and was machined to fit snugly along the entire length of the highpressure vessel. The vessel, with its thermostatting jacket, was securely fastened into a metal supporting frame which was itself positioned directly into the sample compartment of a Shimadzu SV-50 spectrophotometer. The frame was designed so that the optical aperture of the cell automatically coincided with the light beam when the frame was in place.

The method of operating was to equilibrate the sample at a low pressure. After the data were obtained, the pressure was raised slightly and the system was allowed to reequilibrate. After the highest pressure had been attained, the system was returned to the initial low pressure to check for reversibility. The pH values of the buffers and the other solutions studied were measured using a Radiometer pH meter and Radiometer electrodes.

The absorbance of any solution in the optical cell of a fixed length will increase with an increase in the pressure due to compression. Before two-state equilibrium constants can be determined, the experimentally determined absorbances must be corrected for this effect. This correction** can be achieved by multiplying the experimental values by $OD_{I.P.}$ (1 atm)/ $OD_{I.P.}$ (P) for the isosbestic point of the absorption spectra of the indicator holds in its acid-base equilibrium. $OD_{I.P.}$-(P) implies the absorbance values at the wavelength at the isosbestic point under the pressure, P.

Methods

The molar equilibrium constant (K_a) for the ionization of weak acids is pressure- or volume-dependent. When the buffer concentration is sufficiently high, as it is these studies (0.05—0.10 M), pressure-induced changes in the pH of buffer solutions do not significantly alter the concentration ratio of the acid, HA, and its conjugate base A^-.

$$\frac{\partial \mathrm{pH}}{\partial P} = \frac{\partial \mathrm{p}K_a}{\partial P} + \frac{\partial}{\partial P}(\log([A^-]/[HA]) \simeq \frac{\partial \mathrm{p}K_a}{\partial P} \quad (1)$$

The pHs of solutions can be determined by an examination of the absorption spectra of pH indicators, using the following equation:

$$\mathrm{pH} = \mathrm{p}K_I - \log\left(\frac{\Delta OD}{OD}\right), \Delta OD = OD_I - OD \quad (2)$$

where pK_I is the dissociation constant of the acid form of the indicator, OD_I is the optical density at λ_{max} corresponding to the complete conversion of the indicator to its conjugate base, and OD is the observed optical density at the same wavelength due to the conjugate base of the indicator acid. The relation of the pressure dependence of pK_a and pK_I can thus be determined using Eq. 3, which arises from a combination of Eqs. 1 and 2.

$$\frac{\partial(\mathrm{p}K_a)}{\partial P} = \frac{\partial(\mathrm{p}K_I)}{\partial P} - \frac{\partial \log(\Delta OD/OD)}{\partial P} \quad (3)$$

The effect of the pressure on pK_I can be determined if the pressure dependence of pK_a is known. Equation 1 shows that the pressure-induced changes in pK_a can be attributed directly to changes in the pH. Thus, changes in the pH of the buffer with the pressure can be determined from the pressure dependence of the OD of the indicator.

The pressure dependencies of pK_a for boric acid and imidazole HCl were determined using as optical indicators p-nitrophenol (pK_I=7.05) and Cresol Red (pK_I= 8.3). The pressure dependence of pK_I for p-nitrophenol was determined but that of pK_I for Cresol Red is not known. Accordingly the pressure dependence for Cresol Red was calculated from data available for $H_2PO_4^-$.[3)]

The limiting volume change for the weak acid at atmospheric pressure ($\Delta\bar{V}°$) and the compressibility change ($\Delta\bar{\kappa}°$) during ionization may be readily obtained by means of thermodynamics. The change in the partial molar volume can be determined from the pressure derivative of the free energy, *i.e.*:

$$\left(\frac{\Delta\partial F°}{\partial P}\right) = -\left(\frac{\partial RT\ln K}{\partial P}\right)_T = \bar{V}°(H^+ + A^-) - \bar{V}°(HA) = \Delta\bar{V}° \quad (4)$$

where $\bar{V}°$ (HA) and $\bar{V}°$ ($H^+ + A^-$) are the partial molar volumes of acid and ionized forms of the weak acid. On the other hand, V varies with the pressure, the derivative

$$\left(\frac{\partial \Delta V°}{\partial P}\right)_T = -\Delta\bar{\kappa}° \quad (5)$$

being termed the standard partial molar isothermal compressibility on ionization. It follows that

$$\frac{RT\ln(K_p/K_o)}{P} = -\Delta\bar{V}° + \frac{1}{2}\Delta\bar{\kappa}°P, \quad (6)$$

where the $\Delta\bar{\kappa}°$ term accounts for the pressure dependence of $\Delta\bar{V}°$. Using the experimental data, the values of $\Delta\bar{V}°$ and $\Delta\bar{\kappa}°$ were obtained from the slope and intercept of $\log(K_p/K_o)/P$ *vs.* P (Eq. 6).

Results and Discussion

The absorption spectra of p-nitrophenol and Cresol Red in phosphate, borate and imidazole (Im) buffer were recorded at various pressures from 1 bar to 6 kbars. The absorption band of the alkali form of the indicators (λ_{max}; 570 nm for Cresol Red and 400 nm for p-nitrophenol) in phosphate and borate buffers increased in intensity and shifted slightly to a higher wavelength, but that of the indicator in the imidazole buffer decreased in intensity when it also shifted slightly to a higher wavelength under pressure. These changes were completely reversible upon the release of the pressure. An example is given in Fig. 2, which shows the absorption spectra of Cresol Red in the borate buffer (pH=8.4) recorded as a function of the pressure up to 6 kbars. The spectra are not corrected for contraction. The absorption band of

** As the pressure-induced shift of absorption maximum (λ_{max}) is small, this treatment may be correct for the present experimental accuracy.

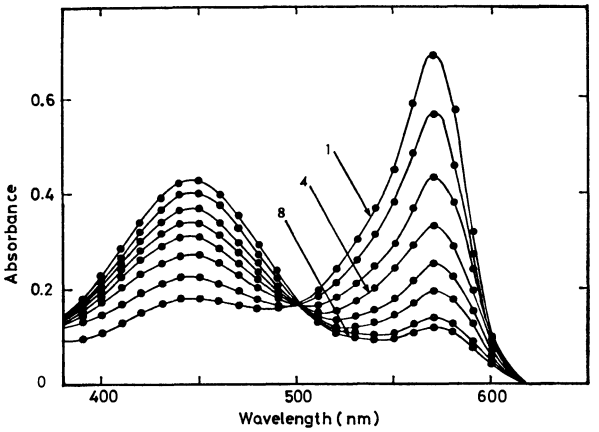

Fig. 2. The effect of pressure on the absorption spectrum of Cresol Red in the borate buffer (0.05 M, pH 8.4) and at appropriate pressures at 25 °C.
1: 1 bar, 2: 706 bar, 3: 1570 bar, 4: 2420 bar, 5: 3340 bar, 6: 4180 bar, 7: 5000 bar, 8: 5480 bar.

the alkali form of Cresol Red decreased, while that of the acid form increased, in intensity and shifted slightly to higher wavelength under pressure. The isosbestic point of the spectra shifted. This is due to the contraction of the sample under pressure. After the correction of the values of OD, the values of log (ΔOD/OD) were calculated for each buffer-indicator system; a summary of these data is presented in Fig. 3. These values of Δlog (ΔOD/OD) are equal to $\Delta pK_I - \Delta pK_a$, where the Δ symbol indicates the difference between the quantity at 1 bar and at a high pressure, P.

The values of Δlog(ΔOD/OD) for *p*-nitrophenol in the borate buffer and the imidazole buffer in conjunction with previously available data for the pressure dependence of pK_I for *p*-nitrophenol permitted the determination of the pressure dependence of pK_a for boric

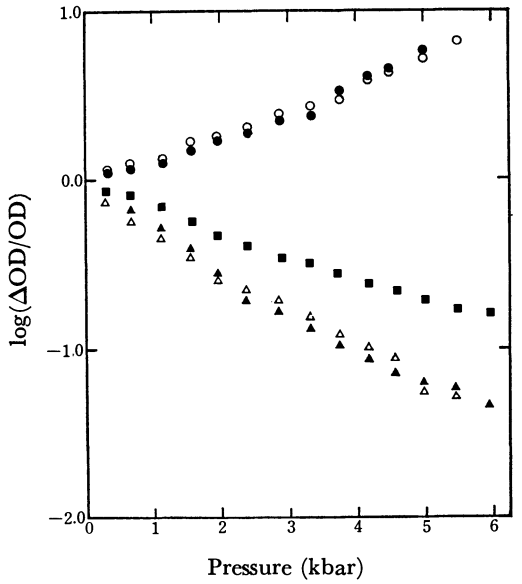

Fig. 3. Pressure dependence of log (ΔOD/OD) for the optical indicator Cresol Red in borate (●), phosphate (■) and imidazole (▲) buffers and for *p*-nitrophenol in borate (○), and imidazole (△) buffers.

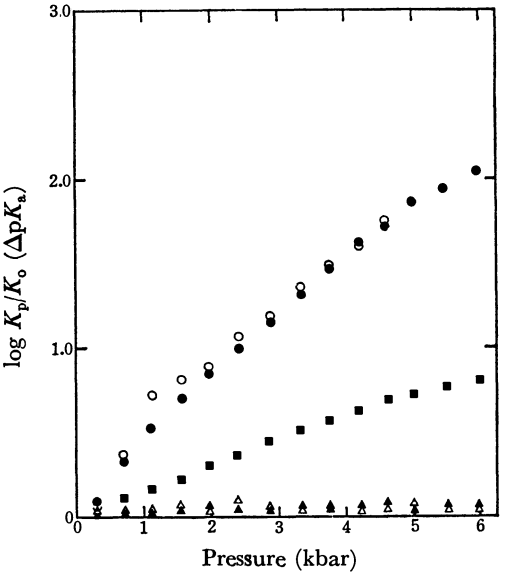

Fig. 4. Pressure dependence of calculated values of K_p/K_o for boric acid (○, ●), Cresol Red (■), and imidazole HCl (△, ▲).

acid and imidazole HCl. Further, the pressure dependence of the pK_a of boric acid and imidazole HCl was examined using Cresol Red as the indicator. The pressure dependence of the pK_I for the Cresol Red was calculated from the data available for $H_2PO_4^-$.[3] These pK_I values in conjunction with the data for Cresol Red in the borate and imidazole buffers, gave an alternate determination of ΔpK_a values for boric acid and imidazole HCl. The results are given in Fig. 4. With the exception of imidazole HCl, the dissociation of the acids is favored by pressure. The increases in the ΔpK_a value for Cresol Red are very similar to those for *p*-nitrophenol. The changes in the pK_a for boric acid are much greater. The results show that the pH of boric acid changes by more than two units up to the pressure of 6 kbars. On the other hand, the pH of imidazole HCl is almost pressure-insensitive up to 6 kbars.

The values of $\Delta\bar{V}°$ and $\Delta\bar{\kappa}°$ were calculated, using Eq. 6, from the experimental values of $\log(K_p/K_o)$ for *p*-nitrophenol, boric acid, and imidazole HCl. They are given in Table 1, along with the approximate values of $\Delta\bar{V}°$ for the imidazole HCl obtained. The values of $\Delta\bar{V}°$ for Cresol Red is close to the values previously

Table 1.

Weak acid	$\Delta\bar{V}°$(cm³/mol)	$\Delta\bar{\kappa}°$(cm³mol/kbar)	Coupled acid	pH
Cresol Red (CR)	−10.1	−0.4	$H_2PO_4^-$	7.60
Imidazole H^+	−2.4	−0.6	CR	7.84
	−2.0	−0.4	PNP	7.25
Boric acid	−30.2	−4.3	CR	8.26
	−30.9	−4.6	PNP	7.52
	(−31.4)[a]			
p-Nitrophenol (PNP)	(−11.3)[b]	(−1.43)[b]		

a) Observed by means of electrodes by A. Distèche and S. Distèche.[11] b) Observed by R. C. Neuman *et al.*[3]

reported for other phenols, that is, -11.3 cm^3 mol^{-1} [3] and -10.3 cm^3 mol^{-1} [2] for *p*-nitrophenol and -11.8 cm^3 mol^{-1} [13] and -11.3 cm^3 mol^{-1} [3] for 2,5-dinitrophenol. This fact supports the validity of the procedures used.

The value of $\Delta\bar{V}°$ for boric acid is considerably larger than those of the acids. The reason for the large $\Delta\bar{V}°$ value for the amine bases is that the positive charges of the cations are localized on the small nitrogen atoms.[1] Distèche[2] has suggested that this is probably also the reason why $\Delta\bar{V}°$ is very small for boric acid. We suggest that another contributive factor may be the existence of a preliminary hydration equilibrium for boric acid;

$$H_3BO_3 + H_2O \rightleftarrows H_3BO_3 \cdot H_2O$$

$$K_1 = \frac{[H_3BO_3 \cdot H_2O]}{[H_3BO_3]} \quad (7)$$

$$H_3BO_3 \cdot H_2O \rightleftarrows B(OH)_4^- + H^+$$

$$K_2 = \frac{[H^+][B(OH)_4^-]}{[H_3BO_3 \cdot H_2O]} \quad (8)$$

The dissociation constant, K, is based on the total concentration of boric acid, both free and hydrated, so that

$$K = \frac{[B(OH)_4^-] \cdot [H^+]}{[H_3BO_3] + [H_3BO_3 \cdot H_2O]} = \frac{K_1K_2}{1+K_1} \quad (9)$$

It follows that, when K_1 is very small, $K=K_1K_2$ and $\Delta\bar{V}°=\Delta\bar{V}°_1+\Delta\bar{V}°_2$, where the subscripts 1 and 2 refer to the hydration and ionization reactions, 7 and 8 respectively. Ellis correctly pointed out that the abnormally large values of $\Delta\bar{V}°$ for carbonic acid and sulforous acid can be ascribed to the contribution of $\Delta\bar{V}°_1$ since, at the atmospheric pressure, CO_2 and SO_2 are only slightly hydrated in solution.[14]

In striking contrast to these results is the fact that the pH of an imidazole buffer solution is almost pressure-insensitive, below 6 kbars. This is understandable in terms of the ionization equilibrium. Substances that are stronger bases than water are able to extract protons from water molecules, whereupon the conjugate acid of the base, BH^+, is formed, together with hydroxide ions:

$$Im + H_2O \rightleftarrows ImH^+ + OH^- \quad (10)$$

In an analogous way, acids such as BH^+ are able to react with water molecules, which then function as a base;

$$ImH^+ + H_2O \rightleftarrows Im + H_3O^+ \quad (11)$$

Reaction 10 may be taken as the basic dissociation of the base, Im, and the corresponding equilibrium constant is K_b. Reaction 11 is the acidic dissociation of acid BH^+, and the corresponding equilibrium constant is K_{bn}. K_b and K_{bn} are related by means of the ion-product constant of water, K_w:

$$K_w = K_bK_{bn}$$

Amines are usually characterized in terms of K_{bn}, because of the emphasis upon the hydrogen-ion concentration. The large volume changes for boric acid and amine bases with connected with Reaction 11 and with the effect of the pressure on K_b. The determinations of the pH yield $K_{bn}=K_w/K_b$, so that the effect of the pressure on K_b is cancelled by the corresponding effect on K_w, $\Delta\bar{V}°$ value for water being -20.4 cm^3 mol^{-1}. This explains why, for the imidazole buffer, the observed $\Delta\bar{V}°_{bn}$ value is -4.2 cm^3 mol^{-1}, which means that the $\Delta\bar{V}°_b$ value for Reaction 10 is -16.2 cm^3 mol^{-1}.

The authors wish to express their deep thanks to Mr. Tatsuo Takeda of the Institute for Solid State Physics, University of Tokyo, who constructed the delicate micro optical cell of quartz. We wish to express our thanks to Professor Hideo Yabu for his encouragement.

References

1) S. D. Hamann, "High Pressure Physics and Chemistry," R. S. Bradley, ed., Vol. 2, Academic Press, New York (1963).
2) A. Distèche, *Symp. Soc. Exp. Biol.*, **26**, 27 (1972).
3) R. C. Neuman, W. Kauzmann, and A. Zipp, *J. Phys. Chem.*, **77**, 2688 (1973).
4) K. Suzuki and Y. Taniguchi, *Symp. Soc. Exp. Biol.*, **26**, 103 (1972).
5) J. F. Brandts, R. J. Oliveira, and C. Westort, *Biochemistry.*, **9**, 1038 (1970).
6) A. Zipp and W. Kauzmann, *Biochemistry*, **12**, 4217 (1973).
7) A. A. Lamola, T. Yamane, and A. Zipp, *Biochemistry*, **13**, 738 (1974).
8) Q. H. Gibson and F. G. Carey, *Biochem. Biophys. Res. Commun.*, **67**, 747 (1975).
9) M. Tsuda *et al.*, unpublished data.
10) R. E. Gibson and O. H. Loeffler, *Trans. Am. Geophys. Un.*, **1941**, 503.
11) A. Distèche and S. Distèche, *J. Electrochem. Soc.*, **114**, 330 (1967).
12) D. A. Lown, H. R. Thirsk, and Lord Wynne-Jones, *Trans. Faraday Soc.*, **64**, 2073 (1968).
13) S. D. Hamann, *Division of Applied Chemistry, Technical Paper* No. 3, CSIRO, Australia (1972).
14) A. J. Ellis, *J. Chem. Soc.*, **1959**, 3689.

The γ-Radiolysis of a Cyclohexene-Carbon Dioxide Mixture in the Liquid Phase at −18 °C

Laszlo WOJNAROVITS,* Shun-ichi HIROKAMI, and Shin SATO

Department of Applied Physics, Tokyo Institute of Technology, Ookayama, Meguro-ku, Tokyo 152

(Received May 27, 1976)

The γ-radiolysis of a cyclohexene–carbon dioxide mixture in the liquid phase at −18 °C has been studied. When the mole fraction of carbon dioxide was low, carbon dioxide behaved as an electron scavenger and slightly suppressed the formation of the hydrogen and hydrocarbon products: 2,2′-bicyclohexenyl, cyclohexane, 3-cyclohexylcyclohexene, bicyclohexyl, 1-cyclohexylcyclohexene, and 1,3-cyclohexadiene. Along with this suppression, the formation of cyclohexanol was observed. At the high mole fraction of carbon dioxide, the main products were carbon monoxide and the oxygen atom-addition products: cyclohexene oxide, cyclohexanone, and cyclopentanecarbaldehyde. The material balance for oxygen atoms was good. The formation ratio of the addition products suggests that the precursors of the addition products are the ground-state oxygen atoms. These oxygen atoms are probably produced by the direct radiolysis of carbon dioxide. As the CO_2 mole frcation approached unity, the *G*-values of the addition products and other oxygenated compounds including 2-cyclohexenone and 2-cyclohexenol sharply increased. This suggests that there is another source of oxygen atoms which is suppressed by the presence of cyclohexene. The reactions may be $CO_2^+ + CO_2^- \rightarrow CO + O + CO_2$ and $CO_2^+ +$ cyclohexene$\rightarrow CO_2 +$ cyclohexene$^+$. The formation of 2-cyclohexenone and 2-cyclohexenol may be explained in terms of the reaction between the cyclohexenyl radicals and oxygen molecules eventually produced. To support the elucidation of the reaction mechanism, the radiolysis in the solid phase at 77K and the mercury-photosensitized reaction of a nitrous oxide–cyclohexene mixture in the gas phase have also been studied.

Carbon dioxide was used as an electron scavenger in the radiolysis of liquid hydrocarbon.[1,2] The formation of hydrogen was suppressed by the addition of carbon dioxide, but the yield of carbon monoxide was found to be very small.[1] In the radiolysis of pure liquid carbon dioxide, the observed products were carbon monoxide, oxygen, and ozone.[3] The oxygen atoms produced as intermediates were assumed to be in the ground state, $O(^3P)$. In the liquid-phase γ-radiolyses of benzene–CO_2[4] and of toluene–CO_2[5] mixtures at 0 °C, the main oxygenated products observed were phenol in the case of the benzene–CO_2 mixture and *o*-, *m*-, and *p*-cresols in the case of the toluene–CO_2 mixture. As the precursors of these oxygenated compounds, O^- and CO_3^- ions were considered because the addition of a small amount of SF_6 inhibited the formation of the oxygenated compounds. Sakurai *et al.* studied the γ-radiolysis of olefin–CO_2 mixtures and showed that the oxidizing species must be the ground-state oxygen atoms.[6]

The reactions of the ground-state oxygen atoms with simple olefins in the gas phase were extensively studied by Cvetanović and his co-workers, and a general reaction mechanism has been established.[7] The reaction of $O(^3P)$ atoms with simple olefins in the liquid and solid phases at cryogenic temperatures has also been studied.[8–10] These experimental results show that the general reaction mechanism proposed for the gas-phase reaction can equally apply to the liquid- and solid-phase reactions, although there are some ambiguities in the solid-phase reaction.

The reaction of O^- radical ions with simple olefins in the gas phase has been studied by Bohme and Young,[11] and a general reaction mechanism has been proposed, one which involves either the abstraction of a hydrogen atom to yield a hydroxide ion or the abstraction of a proton to yield a carbanion. The reaction of O^- radical ions in the liquid phase, however, has not been established. Neta and Schuler studied the reaction of O^- ions with organic compounds containing a double bond in an aqueous solution and concluded that the addition of O^- to the double bond is relatively slow, so that abstraction dominates addition.[12]

As has been described above, the reactions of $O(^3P)$ atoms and of O^- radical ions with cyclohexene may produce different types of products. With this prospect in mind, we have investigated the γ-radiolysis of the cyclohexene–CO_2 mixture in the liquid phase at −18 °C and in the solid phase at 77 K.

Experimental

Carbon dioxide and nitrous oxide supplied by the Takachiho Shoji Co. were used after thorough degassing and distillation. Cyclohexene supplied by the Tokyo Kasei Co. was distilled before use. The impurity was less than 1/200.

A conventional vacuum system was used for sampling. The measured amount of cyclohexene was introduced into a Pyrex tube (about 3 ml) with a breakable seal and was thoroughly degassed at the temperature of liquid nitrogen. Then a known amount of carbon dioxide was condensed in the tube, and the tube was sealed. The sample thus prepared was left for thirty minutes in a Dewar flask containing ice-sodium chloride slush at -18 ± 1 °C so that the carbon dioxide and cyclohexene were well mixed. The γ-irradiation was carried out at −18 °C or 77 K at the dose rate of 1.40×10^6 R h^{-1} usually for 3 or 6 h. The absorbed dose was estimated by Fricke dosimetry on the assumption of a proportionality between the absorbed dose and the electron fraction.

The gas noncondensable at the temperature of liquid nitrogen was collected in a gas buret by means of a Toepler pump. After the amount had been measured, the gas was introduced into a copper oxide furnace at about 270 °C, where CO and H_2 were converted into CO_2 and H_2O respectively.

* IAEA fellow 1975—76. Permanent address: Institute of Isotopes of the Hungarian Academy of Sciences, H-1525 Budapest, P. O. B. 77.

Both of them were trapped at 77 K. The amount of CO was measured by recovering CO_2 from the trap at −80 °C. In the radiolysis at 77 K, the formation of oxygen was observed; this was confirmed by using a gas chromatograph equipped with a 6 m column of a 5A molecular sieve at 40 °C.

The analysis of the condensable products was made by gas chromatography. The seal of the irradiated sample tube was broken in the atmosphere, and a certain amount of mesitylene was added as a standard. Two columns were used for the analysis; one was a 2-m PEG-600 column of 20% w/w on celite for C_6 hydrocarbons, while the other was a 2-m PEG-600 column connected in series with a 50-cm silicone SE-52 column for the C_{12} hydrocarbons and the oxygenated compounds. The identification of the products was made by seeding the gas chromatograph with authentic samples when available.

Results

γ-Radiolysis of Liquid CO_2–Cyclohexene Mixture at −18 °C. The *G*-values of the noncondensable products, hydrogen and carbon monoxide, are shown in Fig. 1 as a function of the electron fraction of CO_2. The small change in $G(H_2)$ from 1.25 to 0.75 at the low electron fraction of CO_2 and the rapid increase of $G(CO)$ in the range from 0.8 to 1.0 of the electron fraction of CO_2 are

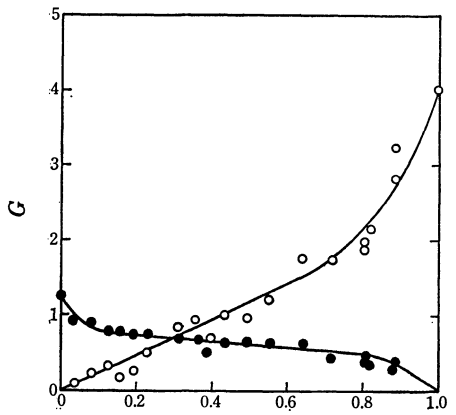

Fig. 1. *G*-values of hydrogen (●) and carbon monoxide (○) obtained at −18 °C in the liquid phase.

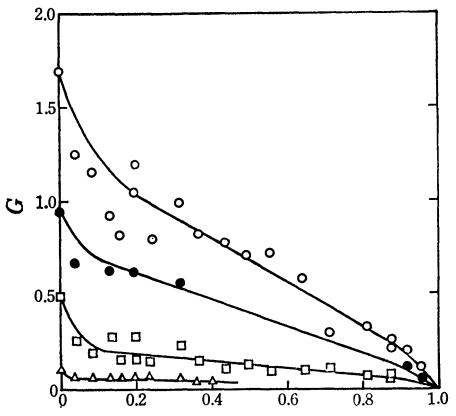

Fig. 2. *G*-values of 2,2′-bicyclohexenyl (○), cyclohexane (●), 3-cyclohexylcyclohexene (□), and 1,3-cyclohexadiene (△) obtained at −18 °C in the liquid phase.

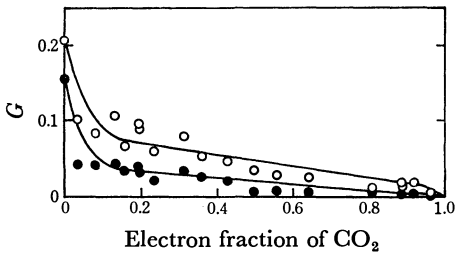

Fig. 3. *G*-values of bicyclohexyl (○) and 1-cyclohexylcyclohexene (●) obtained at −18 °C in the liquid phase.

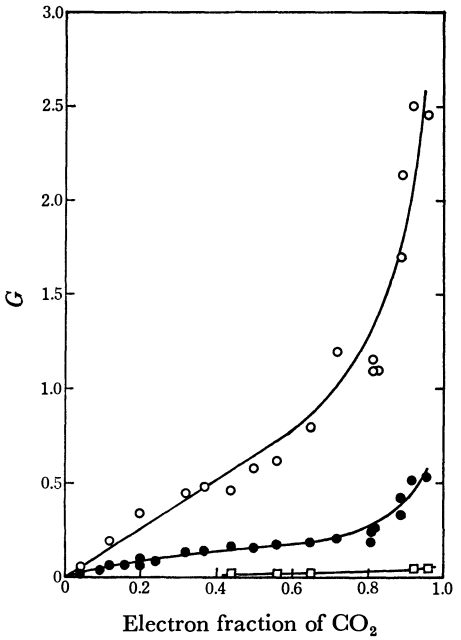

Fig. 4. *G*-values of cyclohexene oxide (○), cyclohexanone (●), and cyclopentanecarbaldehyde (□), obtained at −18 °C in the liquid phase.

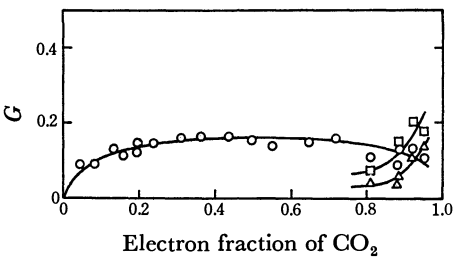

Fig. 5. *G*-values of cyclohexanol (○), cyclohexenol (□), and cyclohexenone (△) obtained at −18 °C in the liquid phase.

noticeable. It is also recognized that $G(H_2)$ does not linearly approach zero as the electron fraction of CO_2 approaches unity. These results suggest that some energy or charge-transfer processes between CO_2 and cyclohexene are involved in the formation of H_2 and CO. Figures 2 and 3 show the *G*-values of the hydrocarbon products. All of the curves are similar to one another. Figures 4 and 5 show the *G*-values of the oxygenated compounds. The rapid increase in the *G*-values of cyclohexene oxide, cyclohexanone, 2-cyclohexenone, and 2-cyclohexenol above 0.8 of the electron fraction of

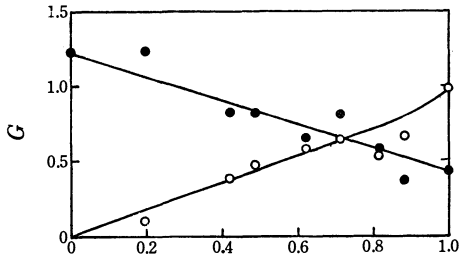

Fig. 6. *G*-values of the sum of hydrogen and oxygen (●) and of carbon monoxide (○) obtained at 77 K in the solid phase.

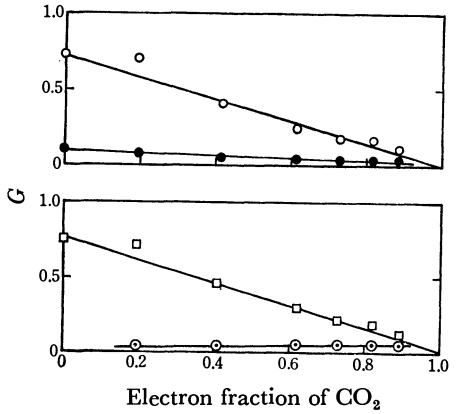

Fig. 7. *G*-values of bicyclohexenyl (○), bicyclohexyl (●), 3-cyclohexylcyclohexene (□), and cyclohexene oxide (⊙) obtained at 77 K in the solid phase.

CO_2 corresponds to the rapid increase in $G(CO)$ in the same region. Cyclohexanol seems to be quite different from the other oxygenated products in the mechanism of its formation.

γ-Radiolysis of Solid CO_2–Cyclohexene Mixture at 77 K. Figures 6 and 7 summarize the data obtained at 77 K. In the noncondensable products, oxygen was found; this was confirmed by gas chromatography but no quantitative measurement could be made. As Fig. 7 shows, the *G*-value of cyclohexene oxide was very small. This is quite different from the data obtained in the liquid phase. In the solid-phase radiolysis, it seems that there is no or very little interaction between CO_2 and cyclohexene.

Mercury-photosensitized Reaction of the Nitrous Oxide–Cyclohexene Mixture. In order to obtain the relative yield of the oxygen-atom-addition products, the mercury-photosensitized decomposition of nitrous oxide in the presence of cyclohexene was carried out. The experimental procedure was the same as that reported previously.[13] The relative yields obtained were as follows: cyclohexene oxide, 0.76; cyclohexanone, 0.19, and cyclopentanecarbaldehyde, 0.05.

Discussion

Radiolysis of Cyclohexene. The radiolysis of cyclohexene in the liquid phase at room temperature has been studied by several groups.[14–17] The most important reactions and the formation of products may be described as follows:

$$c\text{-}C_6H_{10} \rightsquigarrow c\text{-}C_6H_{10}^+ + e^- \quad (1a)$$
$$\searrow\ c\text{-}C_6H_{10}^* \quad (1b)$$
$$c\text{-}C_6H_{10}^+ + e^- \rightarrow c\text{-}C_6H_9 + H \quad (2a)$$
$$c\text{-}C_6H_{10}^* \rightarrow c\text{-}C_6H_8 + H_2 \quad (2b)$$
$$\rightarrow c\text{-}C_6H_{10} \quad (2c)$$
$$H + c\text{-}C_6H_{10} \longrightarrow H_2 + c\text{-}C_6H_9 \quad (3a)$$
$$\searrow\ c\text{-}C_6H_{11} \quad (3b)$$
$$2\ c\text{-}C_6H_9 \longrightarrow (c\text{-}C_6H_9)_2 \quad (4)$$
$$2\ c\text{-}C_6H_{11} \longrightarrow c\text{-}C_6H_{10} + c\text{-}C_6H_{12} \quad (5a)$$
$$\searrow\ (c\text{-}C_6H_{11})_2 \quad (5b)$$
$$c\text{-}C_6H_9 + c\text{-}C_6H_{11} \longrightarrow c\text{-}C_6H_8 + c\text{-}C_6H_{12} \quad (6a)$$
$$\searrow\ (c\text{-}C_6H_9)\text{-}(c\text{-}C_6H_{11}) \quad (6b)$$
$$c\text{-}C_6H_{11} + c\text{-}C_6H_{10} \longrightarrow (c\text{-}C_6H_{11})\text{-}(c\text{-}C_6H_{10}) \quad (7)$$

Hydrogen is formed by Reactions 2b and 3a. Wakeford and Freeman showed that Reaction 2b is less important than Reaction 3a in the formation of hydrogen. The radical formed by the abstraction of a hydrogen atom from cyclohexene is presumably of the allylic type. The disproportionation-combination ratio for allylic-type radicals has been measured in the condensed phase at 90 K by Klein and Kelly.[18] The combination takes place exclusively.

On the basis of the reaction mechanism proposed above and on the assumption that Reaction 7 is not important, we can estimate the *G*-values of the intermediate radicals, $c\text{-}C_6H_9$ and $c\text{-}C_6H_{11}$, by using these disproportionation-combination ratios: $k_{5a}/k_{5b}=1.2$ and $k_{6a}/k_{6b}=0.2$.[19,20] Here, the correction for the temperature of −18 °C has been made by using the activation-energy difference of 300 cal mol^{-1} between the combination and disproportionation established for ethyl and propyl radicals.[21] The radical yields thus calculated are shown in Fig. 8. If the reaction mechanism proposed above is correct, a half of the difference between $G(c\text{-}C_6H_9)$ and $G(c\text{-}C_6H_{11})$ should be equal to the *G*-value of hydrogen produced through the atomic reaction (3a). A comparison of $G(H_2)$ in Fig. 1 and $G(c\text{-}C_6H_9)$

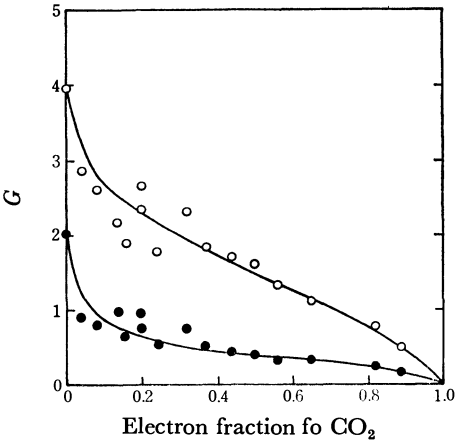

Fig. 8. *G*-values of cyclohexenyl (○) and cyclohexyl radicals (●) calculated from the data obtained at −18 °C in the liquid phase.

and $G(c\text{-}C_6H_{11})$ in Fig. 8 shows that most of hydrogen is produced through the atomic reaction; in other words, the formation of hydrogen by the unimolecular reaction (2b) is not important in the radiolysis of cyclohexene, as was suggested by Wakeford and Freeman.[15]

The formation of 2,2'-bicyclohexenyl, bicyclohexyl, 3-cyclohexyl-cyclohexene, 1,3-cyclohexadiene, and cyclohexane may be explained by Reactions 4—6b. The formation of a small amount of 1-cyclohexylcyclohexene may be explained in terms of the following disproportionation reaction:

$$(c\text{-}C_6H_{11})\text{-}(c\text{-}C_6H_{10}) + c\text{-}C_6H_{11} \longrightarrow \text{3-cyclohexylcyclohexene or 1-cyclohexylcyclohexene} + c\text{-}C_6H_{12} \quad (8)$$

Electron Scavenging by Carbon Dioxide. Upon the addition of a few mole percents of carbon dioxide to cyclohexene, the G-value of hydrogen and the G-values of the hydrocarbon products were reduced. This reduction may be explained in terms of the electron-scavenging reaction of carbon dioxide:

$$CO_2 + e^- \longrightarrow CO_2^- \quad (9)$$

$$CO_2^- + c\text{-}C_6H_{10}^+ \longrightarrow \text{no hydrogen} \quad (10)$$

As Fig. 5 shows, the formation of cyclohexanol was observed in place of the decrease in $G(H_2)$. This suggests that a part of Reaction 10 probably leads to the formation of the hydroxyl radical:

$$CO_2^- + c\text{-}C_6H_{10}^+ \longrightarrow CO + OH + c\text{-}C_6H_9 \quad (10a)$$

and that the OH radicals thus produced react with cyclohexene as follows:

$$OH + c\text{-}C_6H_{10} \longrightarrow c\text{-}C_6H_{10}OH \quad (11a)$$

$$\searrow\ H_2O + c\text{-}C_6H_9 \quad (11b)$$

Söylemez and Schuler studied the reaction of OH radicals with hydrocarbons in an aqueous solution[22] and reported that the addition-abstraction ratio for the reaction of OH radicals with cyclopentene is 4.0. Almost the same value may be applied to Reactions 11a and 11b. The $c\text{-}C_6H_{10}OH$ radicals thus formed will react with other radicals in the system through the disproportionation or combination reaction:

$$c\text{-}C_6H_{10}OH + c\text{-}C_6H_{11} \begin{cases} \nearrow\ c\text{-}C_6H_{11}OH + c\text{-}C_6H_{10} & (12a) \\ \longrightarrow\ c\text{-}C_6H_{10}O + c\text{-}C_6H_{12} & (12b) \\ \searrow\ (c\text{-}C_6H_{11}OH)\text{-}(c\text{-}C_6H_{11}) & (12c) \end{cases}$$

Similar reactions may occur between $c\text{-}C_6H_{10}OH$ and $c\text{-}C_6H_9$ radicals. A small part of cyclohexanone, the main process of the formation of which will be discussed below, must be produced by Reaction 12b.

Formation of Cyclohexene Oxide, Cyclohexanone, and Cyclopentanecarbaldehyde. As Fig. 4 shows, the most abundant oxygenated compound observed is cyclohexene oxide. If oxygen atoms in the ground state are produced in the present system, the formation of cyclohexene oxide can easily be explained, because it is well known that the main product between oxygen atoms and olefins is this type of oxide.[7] Since Cvetanović did not report the formation ratio of the oxygen atom-addition products—cyclohexene oxide, cyclohexanone, and cyclopentanecarbaldehyde, we have measured them, as was

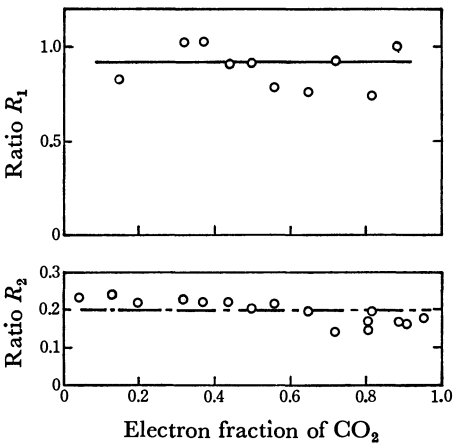

Fig. 9. The ratios of R_1 and R_2. R_1 is the ratio between the sum of the G-values of oxygenated compounds and the G-value of carbon monoxide. R_2 is the ratio between the G-value of cyclohexanone and the sum of the G-values of cyclohexene oxide and cyclohexanone. The dashed line shows the ratio, R_2, obtained in the mercury photosensitized decomposition of nitrous oxide in the presence of cyclohexene.

stated in the Results section. Figure 9 shows the ratio of cyclohexanone/(cyclohexene oxide+cyclohexanone). The ratios obtained in the radiolysis are in good agreement with that obtained in the photolysis. The small deviation at the low concentration of CO_2 may be due to the formation of cyclohexanone by other processes, such as Reaction 12b.

When the electron fraction of carbon dioxide is above 0.8, the amount of oxygen atom-addition products increases with the increase in the electron fraction. This suggests that there are two processes for the formation of oxygen atoms, and that one of them is suppressed by the presence of cyclohexene. They may be written as follows:

$$CO_2 \rightsquigarrow CO_2^* \longrightarrow CO + O \quad (13a)$$

$$\searrow\ CO_2^+ + e^- \quad (13b)$$

$$e^- + CO_2 \longrightarrow CO_2^- \quad (9)$$

$$CO_2^+ + CO_2^- \longrightarrow CO + O + CO_2 \quad (14a)$$

$$\searrow\ 2\,CO + O_2 \quad (14b)$$

$$CO_2^+ + c\text{-}C_6H_{10} \longrightarrow CO_2 + c\text{-}C_6H_{10}^+ \quad (15)$$

$$O + c\text{-}C_6H_{10} \longrightarrow \text{ 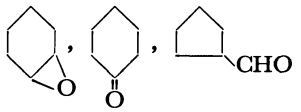 } \quad (16)$$

Formation of 2-Cyclohexenol and 2-Cyclohexenone. At the high concentrations of carbon dioxide, the formation of 2-cyclohexenol and 2-cyclohexenone has been observed. These compounds may be explained in terms of the reaction of cyclohexenyl radicals with the oxygen molecules produced.

$$c\text{-}C_6H_9 + O_2 \longrightarrow c\text{-}C_6H_9O_2 \quad (17)$$

$$2\,c\text{-}C_6H_9O_2 \longrightarrow c\text{-}C_6H_9OH + c\text{-}C_6H_8O + O_2 \quad (18)$$

Material Balance for Oxygen Atoms. As Fig. 9 shows, the ratio between the sum of the oxygenated compounds and carbon monoxide was about 93%

throughout the range of the electron fraction of CO_2. The ratio between the sum of the oxygen-atom-addition products and carbon monoxide was about 74%.

γ-Radiolysis at 77 K. As Figs. 6 and 7 show, the interaction between CO_2 and cyclohexene at the temperature of liquid nitrogen seems to be very little. The formation of cyclohexene oxide was very small. According to the experiment by Hughes *et al.*,[10] the reaction of oxygen atoms, which are produced in the gas phase, with olefins in the solid state is similar to that in the gas phase. This discrepancy might be due to the inhomogeneity in the solid in the present system or to the melting of the solid olefin surface by the collision of gas molecules in the experiment of Hughes *et al.* This problem is obviously subject to further investigations.

References

1) S. Sato, T. Terao, M. Kono, and S. Shida, *Bull. Chem. Soc. Jpn.*, **40**, 1818 (1967).
2) P. P. Infelta and R. H. Schuler, *J. Phys. Chem.*, **76**, 987 (1972).
3) P. Harteck and S. Dondes, *J. Chem. Phys.*, **23**, 902 (1955); *ibid.*, **26**, 1727 (1957); D. L. Baulch, F. S. Dainton, and R. L. S. Willix, *Trans. Faraday Soc.*, **61**, 1146 (1965).
4) S. Sato, K. Hosoya, S. Shishido, and S. Hirokami, *Bull. Chem. Soc. Jpn.*, **45**, 2308 (1972).
5) K. Ishizaki and S. Sato, *Chem. Lett.*, **1975**, 123.
6) H. Sakurai, K. Akimoto, S. Toki, and S. Takamuku, *Chem. Lett.*, **1975**, 469.
7) R. J. Cvetanović, *Advan. Photochem.*, **1**, 115 (1963).
8) W. B. DeMore, *Chem. Phys. Lett.*, **16**, 608 (1972); *J. Phys. Chem.*, **73**, 391 (1969).
9) S. Hirokami and R. J. Cvetanović, *Can. J. Chem.*, **51**, 373 (1973); *J. Am. Chem. Soc.*, **96**, 3738 (1974).
10) A. N. Hughes, M. D. Scheer, and R. Klein, *J. Phys. Chem.*, **70**, 798 (1966); M. D. Scheer and R. Klein, *ibid.*, **74**, 2732 (1970).
11) D. K. Bohme and L. B. Young, *J. Am. Chem. Soc.*, **92**, 3301 (1970).
12) P. Neta and R. H. Schuler, *J. Phys. Chem.*, **79**, 1 (1975).
13) S. Tsunashima and S. Sato, *Bull. Chem. Soc. Jpn.*, **41**, 284 (1968).
14) W. G. Burns and J. H. Winter, *Disc. Faraday Soc.*, **36**, 124 (1963).
15) B. R. Wakeford and G. R. Freeman, *J. Phys. Chem.*, **68**, 2635 (1964).
16) J. Y. Yang and I. Marcus, *J. Chem. Phys.*, **42**, 3315 (1965).
17) W. A. Cramer and G. J. Piet, *Trans. Faraday Soc.*, **66**, 850 (1970).
18) R. Klein and R. D. Kelley, *J. Phys. Chem.*, **79**, 1780 (1975).
19) W. A. Cramer, *J. Phys. Chem.*, **71**, 1112 (1967).
20) C. W. Larson, B. S. Rabinovitch, and D. C. Tardy, *J. Chem. Phys.*, **47**, 4570 (1967).
21) H. A. Gillis, *Can. J. Chem.*, **49**, 2861 (1971).
22) T. Söylemez and R. H. Schuler, *J. Phys. Chem.*, **78**, 1052 (1974).

Charge-Transfer Bands of the Mixed Molecular Complex, (Anthracene)$_{1-x}$(Phenanthrene)$_x$(1,2,4,5-Tetracyanobenzene)

John D. WRIGHT,* Toshiaki OHTA, and Haruo KURODA

Department of Chemistry, Faculty of Science, University of Tokyo, Hongo, Bunkyo-ku, Tokyo 113

(Received May 29, 1976)

A series of crystalline mixed molecular complexes of composition, (anthracene)$_{1-x}$(phenanthrene)$_x$(TCNB), with $0.17 \leq x \leq 0.63$, has been prepared from solutions containing mixtures of the three components. A linear relationship is observed between solution and solid composition, and the melting point data and powder X-ray diffraction patterns suggest the formation of a continuous series of mixed molecular complexes of closely related crystal structure. Polarized crystal spectra of these crystals show two charge-transfer bands characteristic of the interaction between anthracene and TCNB and that between phenanthrene and TCNB, respectively. Their intensity ratio is linearly dependent on composition, and constant for different crystals of the same composition. Discussion is given on these results by using the results of semi-empirical SCF-MO-CI calculations on the three-molecule model, anthracene/TCNB/phenanthrene.

Although physical properties of mixed molecular crystal composed of aromatic hydrocarbons have been widely studied, relatively little work has been reported[1,2] on crystals of mixed molecular complexes of the type (Donor 1)$_x$(Donor 2)$_{1-x}$(Acceptor). Extensive studies of the crystal structures of molecular complexes suggest that the relative orientation of donor and acceptor is influenced by lattice packing requirements in addition to intermolecular attractive forces.[3] Therefore, for a given donor/acceptor pair, the relative orientation of the donor and acceptor molecules can be different from the one found in the crystal of the pure molecular complex, if the pair is incorporated in the crystal lattice of mixed molecular complex. Thus, one could examine the effects of relative orientation of donor and acceptor on charge-transfer interaction by comparing the structures and properties of the crystals of mixed molecular complexes with those of pure molecular complexes.

The present work is an investigation of the crystal spectra and other physical properties of the mixed molecular complex system which involves anthracene and phenanthrene as the donors and 1,2,4,5-tetracyanobenzene (TCNB) as the acceptor, undertaken primarily to elucidate the nature of this mixed complex system. We were able to confirm that anthracene–TCNB and phenanthrene–TCNB complexes form a homogeneous solid-solution over the whole composition range. Discussion will be given on the nature of the charge-transfer bands which were observed in the single crystals of mixed molecular complexes.

Experimental

Anthracene was purified by chromatography and multiple zone refining. Phenanthrene, purified by successive treatment with maleic anhydride, KOH and sodium, followed by sublimation and multiple zone-refining,[4] was kindly supplied by Professor Y. Matsunaga. TCNB was synthesized from pyromellitic dianhydride,[5] and purified by recrystallization and sublimation. Crystals of the anthracene–TCNB and phenanthrene–TCNB (pure) complexes were grown by slow cooling of glacial acetic acid and 2-methoxyethanol solutions, respectively, containing 100 mg of each component in 5 ml of solvent. Crystalline powders of the apparent compositions, (anthracene)$_x$(phenanthrene)$_{1-x}$(TCNB) with $0.17 \leq x \leq 0.63$, were obtained from 2-methoxyethanol solutions containing 100 mg TCNB with varying ratios of anthracene and phenanthrene. The anthracene and phenanthrene contents of those powders were determined by ultraviolet spectrophotometry of their ethanol solutions: The optical densities of several solutions of different known concentrations in ethanol were measured at 356, 339, and 282 nm, for each sample of mixed complex, using a Hitachi EPS-3 recording spectrophotometer, and the data were interpreted assuming 1 : 1 mol ratio of (phenanthrene+anthracene)/TCNB, using previously determined values of the extinction coefficients of anthracene, phenanthrene and TCNB at these wavelengths.

X-Ray powder diffraction patterns were recorded for all samples using a diffractometer, Geigerflex, quartz being used as the internal standard. Differential scanning calorimetry (DSC) was carried out by means of a Rigaku TG-DSC apparatus on powdered samples sealed in small aluminium capsules.

The polarized absorption spectra in the visible region, were measured on small plate crystals, typically 20×10 μ in size and less than 1 μ thick, by using a microspectrophotometer, Olympus MSP-IV. The details of the apparatus and the procedures of measurement were described elsewhere.[6]

Results and Discussion

Structural Aspects of the Mixed Molecular Complex.
The anthracene/phenanthrene ratio of a crystalline powder of mixed complex varied depending on the anthracene/phenanthrene ratio initially mixed in the solution from which the sample was prepared. In Fig. 1, we have plotted the mol fraction of anthracene, x= [anthracene]/{[anthracene]+[phenanthrene]}, in the powder sample against the corresponding value for the solution. This plot shows a linear relationship, indicating that anthracene and phenanthrene form a continuous series of mixed molecular complexes with TCNB, with no particularly stable phase of fixed stoichiometric ratio of two donors.

In Fig. 2, the melting point is plotted against the composition. Accurate determination of melting point was not possible because of the thermal decomposition which was apparent at temperatures far below the melting point. The data shown in Fig. 2 were obtained by means of a conventional method of melting-point measurement with visual observation using a rapid heating

* On leave from University of Kent at Canterbury, Canterbury, Kent CT2 7NH, U. K.

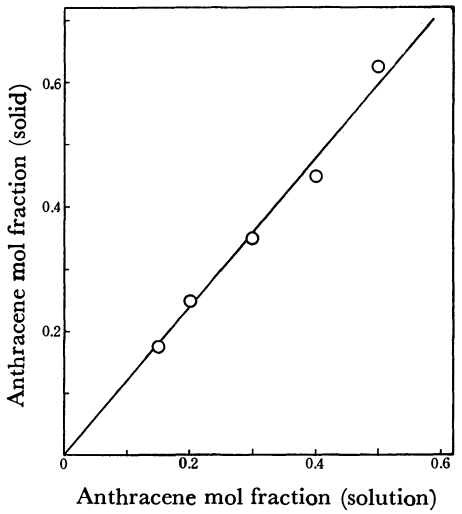

Fig. 1. Mol fraction of anthracene of mixed crystalline complexes, $(\text{Anthracene})_x(\text{phenanthrene})_{1-x}(\text{TCNB})$, as a function of composition of the solutions used to obtain the complexes.

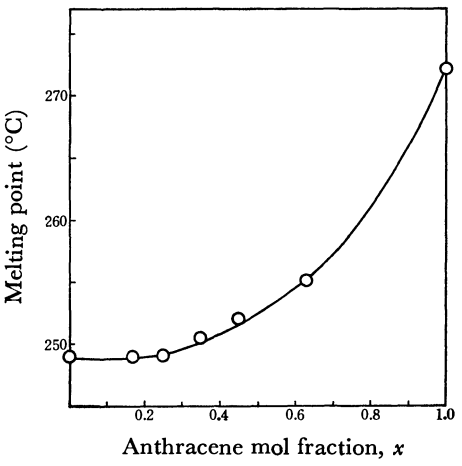

Fig. 2. Dependence of melting point on composition.

condition to minimize thermal decomposition. For each sample, melting occurred rapidly over a temperature range of about 1 °C, suggesting that all crystals in a given sample of mixed complex have almost identical composition. The plot of melting point *vs.* composition is a smooth curve, as shown in Fig. 2, with no evidence for a eutectic. None of the samples of (anthracene, phenanthrene)/TCNB showed any indication of a phase transition in their DSC curves, at least in the range above room temperature. Melting point can be determined also from DSC curves. The melting point data obtained by this method were 2—4 °C higher than those shown in Fig. 2, but their dependence on composition was essentially the same as found for the latter.

The X-ray powder diffraction patterns of mixed complexes and those of the two pure complexes are all very similar (see Fig. 3). Although the positions and intensities of several diffraction peaks are dependent on the composition, they vary continuously with the anthracene/phenanthrene ratio without showing any indication of discrete change of crystal lattice. We can also con-

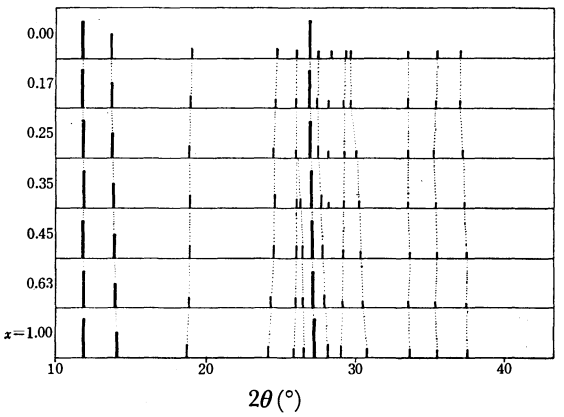

Fig. 3. X-Ray powder diffraction patterns of mixed complexes.

clude from the X-ray powder diffraction patterns that each powder sample of mixed complex in a given preparation is composed of crystals of almost uniform composition and structure.

All of the results mentioned above indicate that the $(\text{anthracene})_x(\text{phenanthrene})_{1-x}(\text{TCNB})$ system is indeed a homogeneous solid solution over the whole composition range, $0 \leq x \leq 1$.

The crystal structure of anthracene–TCNB complex was determined by Tsuchiya *et al.*[7] The crystal is monoclinic with space group C*m*, the lattice parameters being $a=9.505$ Å, $b=12.748$ Å, $c=7.417$ Å, and $\beta=92.45°$. Anthracene and TCNB molecules are alternately stacked on each other to form molecular columns parallel to the c-axis. It was pointed out that there exists a disorder concerning the orientation of anthracene molecule; Anthracene molecules are taking, with equal probability, one of the two orientations rotated by $\pm 8.6°$ within their molecular plane from the mean position. We are currently determining the crystal structure of phenanthrene–TCNB complex. The crystal data have been found to be as follows: monoclinic with possible space group C2/*m* or C2 and the lattice parameters, $a=9.413$ Å, $b=13.104$ Å, $c=7.260$ Å, and $\beta=93.06°$. Phenanthrene and TCNB molecules are alternately stacked along the c-axis and phenanthrene molecules are disordered so as to conform to the apparent site symmetry required for the space groups mentioned above. Thus the crystal lattice of phenanthrene–TCNB is very similar to that of anthracene–TCNB. This similarity of lattice structures suggests that the donor sites in the mixed complexes can be occupied with equal facility by anthracene or phenanthrene, and this may be a requirement for the formation of a continuous series of mixed molecular complexes.

Crystal Spectra of Anthracene–TCNB and Phenanthrene–TCNB. The polarized absorption spectra of single crystals of the two pure complexes are shown in Fig. 4.[8] In the crystal spectrum of anthracene–TCNB (Fig. 4a), the first absorption band at 20.5×10^3 cm^{-1} is almost completely polarized in the direction parallel to the c-axis, along which anthracene and TCNB are alternately stacked on each other. This absorption band can be assigned to the charge transfer from the highest occupied orbital of anthracene to the lowest vacant orbital of

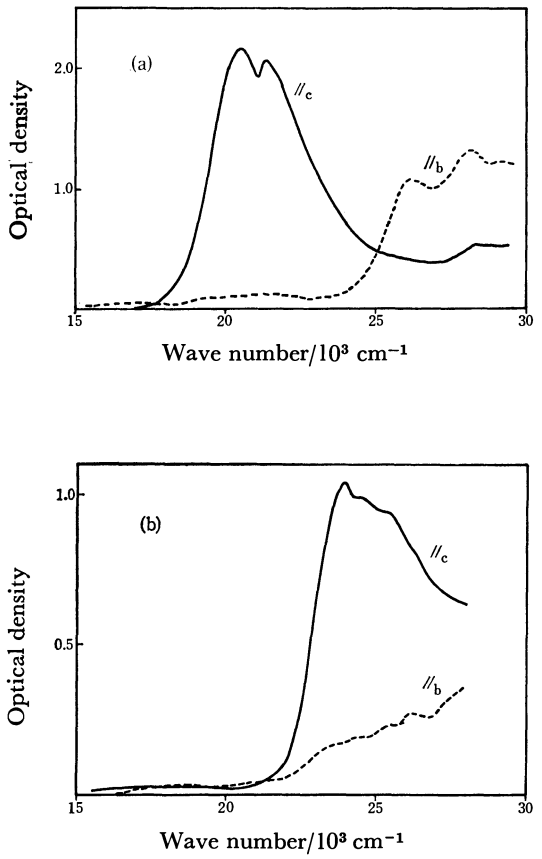

Fig. 4. Polarized absorption spectra of single crystals of pure complexes; (a) Anthracene–TCNB, (b) Phenanthrene–TCNB

TCNB. Incidentally, the corresponding charge-transfer band appears at 20.1×10^3 cm^{-1} in the case of the anthracene–TCNB (1:1) complex in chloroform solution.[9] In the crystal spectrum shown in Fig. 4a, there is another absorption band, polarized in the b-axis direction in the region above 25×10^3 cm^{-1}. This absorption band can be attributed to the local-excitation band mainly associated with the $^1B_{2u}\leftarrow{}^1A_g$ (short-axis polarized) transition of anthracene. Since the short-axis of the anthracene molecule is almost parallel to the b-axis, the above absorption band is expected to be strongly polarized in the b-axis direction. This is consistent with the observed results.

In the case of phenanthrene–TCNB, only one absorption band is found in the observed region (below 28×10^3 cm^{-1}) of crystal spectrum (see Fig. 4b). This absorption band shows its maximum at 23.8×10^3 cm^{-1}, and is strongly polarized in the c-axis direction. Since no local-excitation band is expected to appear in this region, we can safely attribute it to a charge-transfer band. The phenanthrene–TCNB (1:1) complex in chloroform solution exhibits a charge-transfer band at 25.0×10^3 cm^{-1}.[9] When it is compared with the charge transfer band of the anthracene–TCNB (1:1) complex in chloroform solution, the energy difference between them, 0.41 eV, closely agrees with the difference of the first ionization potentials of phenanthrene and anthracene, which have been determined as 7.86 and 7.47 eV, respectively, by means of photoelectron spectroscopy.[10] Thus the 25.0×10^3 cm^{-1} band of the solution spectrum of phenanthrene–TCNB complex can be assigned to the charge transfer from the highest occupied orbital of phenanthrene to the lowest vacant orbital of TCNB, although, in phenanthrene, the second highest occupied orbital is located rather close to the highest occupied orbital. Seemingly, the 23.8×10^3 cm^{-1} band of the crystal of phenanthrene–TCNB complex is also attributable to the charge transfer from the highest occupied orbital of phenanthrene to TCNB.

In measuring the crystal spectra of anthracene–TCNB and phenanthrene–TCNB complexes, we noted that the extinction coefficient of the charge-transfer band is very much lower in the latter than in the former, although we were not able to carry out a quantitative comparison because of the difficulty of determining crystal thickness. As we will describe later, this was confirmed to be the case from the studies of the crystal spectra of mixed molecular complexes.

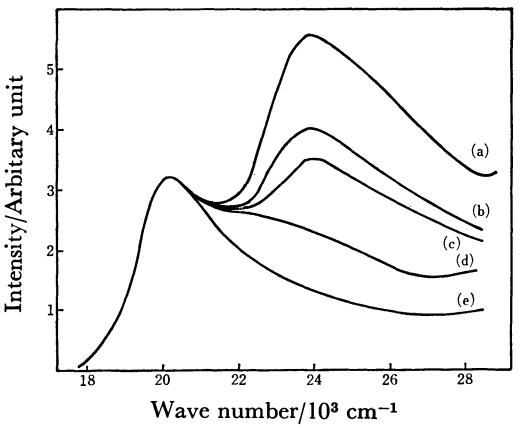

Fig. 5. Charge-transfer bands in the single-crystal spectra of mixed complexes, (Anthracene)$_x$(Phenanthrene)$_{1-x}$(TCNB); (a) $x=0.17$, (b) $x=0.25$, (c) $x=0.35$, (d) $x=0.45$, (e) $x=0.63$.

Charge-transfer Bands of Mixed Complexes. The crystals of mixed complexes all show broad absorption bands extending from 18×10^3 to 28×10^3 cm^{-1}, when the spectra are measured with light polarized parallel to the elongated direction of crystal, which is the crystal axis along which donor and acceptor molecules are alternately stacked on each other. The observed spectra are shown in Fig. 5, where the ordinate (optical density) has been scaled so that all spectra coincide in the region of the first absorption maximum (at about 20×10^3 cm^{-1}). As can be seen in Fig. 5, the observed spectra exhibit two absorption maxima, one at about 20×10^3 cm^{-1} and the other at about 24×10^3 cm^{-1}, and their intensity ratio varies as a function of anthracene/phenanthrene ratio. We have confirmed that the above intensity ratio is almost the same for all crystals in a given preparation of mixed complex. The intensity ratios observed for three different crystals taken from the crystalline powder whose apparent composition is (anthracene)$_{0.25}$(phenanthrene)$_{0.75}$(TCNB), agreed within 5%, indicating that the composition of the crystals in any given preparation is indeed uniform.

The positions of the two absorption maxima mention-

Table 1. Intensity ratios of the two charge-transfer bands in the crystal spectra of mixed complexes, $(\text{Anthracene})_x$-$(\text{Phenanthrene})_{1-x}(\text{TCNB})$

Composition x	Melting point [°C]	Intensity ratio[a] I_2/I_1
0.17	249	1.47
0.25	249	0.94
0.35	251	0.82
0.45	252	0.38
0.63	255	0.18

a) I_1 and I_2 are the integrated intensities of the 20×10^3 cm^{-1} and 24×10^3 cm^{-1} bands, respectively (see text).

ed above correspond closely to those of the first charge-transfer bands of the two pure complexes. This fact, together with the dependence of their intensity ratio on composition, suggests that the 20×10^3 cm^{-1} maximum is due to the charge transfer from anthracene to TCNB, and the 24×10^3 cm^{-1} maximum is due to the charge transfer from phenanthrene to TCNB. The observed charge-transfer bands of the mixed complexes can be reproduced well by superposing the charge-transfer bands of the crystals of the two pure complexes, assuming an appropriate intensity ratio. Table 1 includes the intensity ratios of the two bands of mixed complexes, obtained by the graphical decomposition of observed spectra.

If we assume that the intensities of the two charge-transfer bands of a mixed complex are simply proportional to the probabilities of finding anthracene/TCNB and phenanthrene/TCNB pairs in the crystal, the following relation is expected for the intesnity ratio,

$$\frac{I_2}{I_1}=\frac{I_{\text{phen/TCNB}}}{I_{\text{anth/TCNB}}}\cdot\frac{1-x}{x} \qquad (1)$$

where I_1 and I_2 are the intensities of the bands at 20×10^3 and 24×10^3 cm^{-1}, respectively, and $I_{\text{anth/TCNB}}$ and $I_{\text{phen/TCNB}}$ are the constants corresponding to the extinction coefficients of the charge-transfer bands of anthracene/TCNB and phenanthrene/TCNB pairs, respectively. In Fig. 6, we have plotted the observed intensity ratio against $(1-x)/x$. The points can be fitted well by a single straight line, showing that the intensity ratio is actually proportional to the phenanthrene/anthracene ratio, with $I_{\text{phen/TCNB}}/I_{\text{anth/TCNB}}=0.3$.

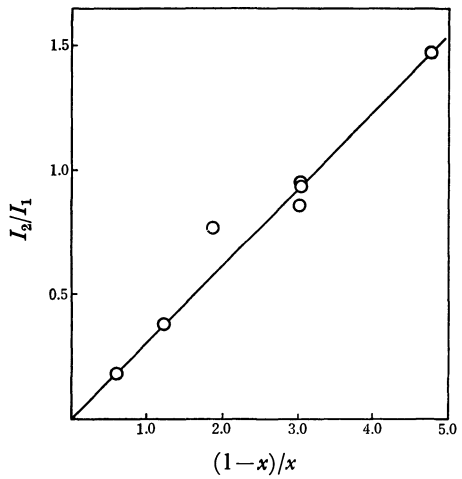

Fig. 6. Intensity ratio of the two charge transfer bands as a function of mol ratio of the two donors.

Molecular-orbital Calculations. Since the oscillator strength of a charge-transfer transition is usually quite small, charge-transfer excitons in a molecular complex crystal can be regarded as rather localized in nature, so that one may neglect the effects of long-range interaction between them. However, it should be noted that, in the crystal of mixed complex, there are sites where an acceptor molecule is sandwiched between two different donors, and, at those sites, the charge-transfer states associated with the two donors could appreciably interact with each other. Therefore, a crystal of mixed molecular complex could exhibit charge-transfer bands considerably different from those observed in pure complexes. However, the crystals of mixed complexes show two charge-transfer bands corresponding very well to those of anthracene–TCNB and phenanthrene–TCNB complexes, and their intensity ratio is simply proportional to the anthracene/phenanthrene ratio.

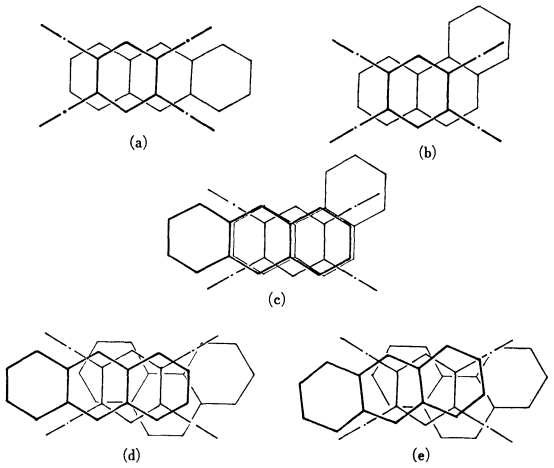

Fig. 7. Relative orientations of donor and acceptor, assumed for the models used in MO calculations. (The mean interplanar spacing between electron donor and acceptor molecules is 3.43 Å in all cases).

In order to examine the nature of charge-transfer bands of the crystals of (anthracene, phenanthrene)/TCNB mixed complexes, we carried out molecular-orbital calculations. Since the main purpose is to examine the short-range interactions of donor and acceptor molecules, calculations were made on simplified models, which are the three-molecule system, anthracene/TCNB/phenanthrene, and the two-molecule systems, anthracene/TCNB and phenanthrene/TCNB. The relative arrangements of donor and acceptor molecules assumed for these models are shown in Fig. 7. For the anthracene/TCNB pair (Fig. 7(a)) the relative orientation and mean separation were taken as those found in the crystal structure analysis of anthracene-TCNB complex, with the anthracene molecule occupying a position corresponding to the mean of the observed disordered arrangement. A model for the phenanthrene/TCNB pair (Fig. 7(b)) retained an orientation of TCNB relative to two of the aromatic rings of phenanthrene similar to

that in the crystal of anthracene–TCNB complex, with the same intermolecular spacing. The first trial model for anthracene/TCNB/phenanthrene (the model (c) in Fig. 7) consists of a combination of the models (a) and (b). However, since the experimental data suggest that anthracene and phenanthrene can be readily interchanged without appreciably disturbing the crystal lattice, two further models (d) and (e) (see Fig. 7) were adopted, in which phenanthrene molecule was rotated and translated so as to occupy a space as similar as possible to that occupied by the anthracene molecule. The two models, (d) and (e), differ only in that the latter contains anthracene occupying one of its extreme positions in the disordered model, rotated in the molecular plane by 8.6° from the orientation in model (d). Seemingly, model (e) is the most realistic one for the relative arrangement of molecules in the crystal of mixed complex.

We carried out calculations on the models described above, by the semiempirical molecular orbital method which was essentially the same as that previously described by Ohta, Kuroda, and Kunii,[11] but extended to permit calculation of a three-molecule system. In this calculation, the orbitals of the system composed of three molecules, D_1, A, and D_2, are calculated as linear combinations of 2p AO's of the atoms in the system as follows;

$$\psi_i = \sum_{\mu}^{(D_1)} c_{i\mu}\phi_\mu + \sum_{\mu'}^{(A)} c_{i\mu'}\phi_{\mu'} + \sum_{\mu''}^{(D_2)} c_{i\mu''}\phi_{\mu''} \qquad (2)$$

where the first, second and third summations are those over the AO's in D_1, A and D_2, respectively. In order to see the character of each orbital, we calculated the following quantities;

$$D_1^{(i)} = \sum_{\mu}^{(D_1)} c_{i\mu}^2, \quad A^{(i)} = \sum_{\mu'}^{(A)} c_{i\mu'}^2, \quad D_2^{(i)} = \sum_{\mu''}^{(D_2)} c_{i\mu''}^2 \qquad (3)$$

These show the contribution of each molecule in the i-th orbital of the system. The results of the calculation on model (e) are partly listed in Table 2. It should be noted that the highest three occupied orbitals are strongly localized on one of the three constituent molecules, although deeper occupied orbitals are considerably delocalized over the whole system. We can see also that vacant orbitals are localized on individual molecules. Similar results were obtained for other models.

Table 2. Characters of molecular orbitals of the three-molecule system, anthracene/TCNB/phenanthrene (Model (e))

Orbital number	Character of MO's[a]				Orbital energy (eV)
	TCNB	Anthracene	Phenanthrene		
12	0.133	0.615	0.253	Occupied	−11.924
13	0.117	0.315	0.568		−11.395
14	0.202	0.321	0.477		−10.757
15	0.131	0.414	0.455		−10.217
16	0.567	0.170	0.263		−9.939
17	0.052	0.923	0.024		−9.711
18	0.328	0.489	0.183		−9.666
19	0.027	0.002	0.971		−9.037
20	0.014	0.006	0.980		−8.655
21	0.034	0.958	0.008		−8.120
22	0.951	0.035	0.014	Vacant	−3.763
23	0.949	0.039	0.013		−2.868
24	0.902	0.060	0.038		−2.656
25	0.082	0.912	0.005		−2.310
26	0.957	0.006	0.037		−1.808
27	0.062	0.003	0.935		−1.693
28	0.043	0.001	0.957		−1.362
29	0.013	0.986	0.001		−0.965
30	0.837	0.126	0.037		−0.834
31	0.120	0.876	0.004		−0.713

a) Defined by Eq. 3 in the text.

We calculated the transitions in the three-molecule system by taking into account the lowest forty singly-excited configurations in the configuration interaction calculation. The results obtained for charge-transfer transitions using different models are compared in Table 3. For the three models of anthracene/TCNB/phenanthrene, (models (c), (d), and (e) of Fig. 7), the calculations gave nearly the same results. In all cases, the lowest-energy transition is predicted at 17.1×10^3—17.7×10^3 cm^{-1} with the character almost entirely associated with the charge transfer from the highest occupied orbital of anthracene to the lowest vacant orbital of TCNB, and the next transition is predicted at about 21×10^3 cm^{-1} with the character of the charge transfer from the highest occupied orbital of phenanthrene to the lowest vacant orbital of TCNB. There is little interac-

Table 3. Energies and oscillator strengths of charge-transfer bands, obtained from the calculations for different models

Model[a]	$\tilde{\nu}$ 10^3 cm^{-1}	f[b]	Contribution of HOMO(A)→LUMO(T)[c] %	$\tilde{\nu}$ 10^3 cm^{-1}	f[d]	Contribution of HOMO(P)→LUMO(T)[e] %
(a)	17.13	0.155(0.144)	97.9			
(b)				20.64	0.055	97.4
(c)	17.72	0.174(0.161)	97.9	21.57	0.041	97.2
(d)	17.45	0.164(0.155)	97.9	21.11	0.024	97.6
(e)	17.12	0.146(0.133)	98.0	20.99	0.028	97.1

(a) See Fig. 7. b) The transition moment of this transition has a small component (5—10%) parallel to the short-axis of anthracene molecule. The oscillator-strength component perpendicular to the molecular plane is given in the parenthesis. c) Contribution of the charge transfer from HOMO of anthracene to LUMO of TCNB, estimated by the procedure given in Ref. 11. d) The component parallel to the molecular plane is negligible. e) Contribution of the charge transfer from HOMO of phenanthrene to LUMO of TCNB.

tion between these two charge-transfer states.

Since model (c) has been formed simply by combining model (a) of the anthracene/TCNB pair and model (b) of the phenanthrene/TCNB pair, it is interesting to compare the results obtained for model (c) with those obtained separately for models (a) and (b). We can see in Table 3, that the two charge-transfer transitions predicted for model (c) of the anthracene/TCNB/phenanthrene very closely correspond to the charge-transfer transition predicted for the anthracene/TCNB pair and that for the phenanthrene/TCNB pair, respectively, although there are small differences as regards the predicted energies and oscillator strengths.

All of the results of the above calculations suggest that the nature of charge-transfer transitions in the mixed complex system should not differ appreciably from those found in the crystals of pure complexes.

TABLE 4. $I_{\text{phen·TCNB}}/I_{\text{anth·TCNB}}$ ESTIMATED FROM THE CALCULATIONS ON THE TWO- AND THREE-MOLECULE MODELS

	$I_{\text{phen·TCNB}}/I_{\text{anth·TCNB}}$
Model (b)/Model (a)	0.38
Model (c)	0.25
Model (d)	0.15
Model (e)	0.20
Expl.	0.30

The intensity ratio of the two charge-transfer bands of anthracene/TCNB/phenanthrene system can be calculated from the predicted oscillator strengths. As shown in Table 4, the predicted ratios[12] fall in the range of 0.15—0.25. If the intensity ratio is estimated by using the results calculated separately for the anthracene/TCNB and phenanthrene/TCNB pairs, (models (a) and (b) of Fig. 7), it becomes 0.38, which is a little larger than the values obtained by the calculations on the three-molecule models. The intensity ratios mentioned above correspond to $I_{\text{phen/TCNB}}/I_{\text{anth/TCNB}}$ in Eq. 3. As we have already mentioned, we obtained 0.3 as the experimental value of $I_{\text{phen/TCNB}}/I_{\text{anth/TCNB}}$ from the observed linear relationship between intensity ratio of two charge-transfer bands and composition of mixed complex. This experimental value is in reasonable agreement with the results of calculations.

Conclusion. The studies reported above show that anthracene and phenanthrene form a particularly ideal series of mixed molecular complexes with TCNB. This may be a consequence of the similar overall size of the three molecules. One interesting consequence of this ideality of (anthracene, phenanthrene)/TCNB solid solution is that it is possible to introduce a large amount of second donor, having different electronic properties, into the crystal lattice of a molecular complex without introducing appreciable lattice perturbations. In this respect the crystals of (anthracene, phenanthrene)/TCNB mixed complex seem to be of particular interest for the purpose of investigating energy transfer and electron transfer in molecular crystals. Studies of the electrical conductivity of this mixed molecular complex are now planned from the above point of view.

One of the authors (JDW) thanks the Royal Society for the award of an Overseas Fellowship.

References

1) S. K. Lower, *Mol. Cryst. Liq. Cryst.*, **5**, 363 (1969).
2) S. Koizumi and Y. Matsunaga, *Bull. Chem. Soc. Jpn.*, **47**, 9 (1974).
3) B. Mayoh and C. K. Prout, *J. Chem. Soc., Faraday Trans. 2*, **6**, 1072 (1972).
4) S. Iwashima, M. Kuramachi, T. Sawada, T. Kobayashi, M. Takekawa, S. Fujisawa, and J. Aoki, *Nippon Kagaku Kaishi*, **1974**, 841.
5) A. S. Bailey, B. R. Henn, and J. M. Langdon, *Tetrahedron*, **19**, 161 (1963).
6) H. Kuroda, T. Kunii, S. Hiroma, and H. Akamatu, *J. Mol. Spectrosc.*, **22**, 60 (1967).
7) H. Tsuchiya, F. Marumo, and Y. Saito, *Acta Crystallogr., Sect B*, **28**, 1935 (1972).
8) The absorption spectra of anthracene–TCNB and phenanthrene–TCNB solid complexes have been previously observed by means of diffuse-reflectance measurement of powder samples; A. S. Bailey, R. J. P. Williams, and J. D. Wright, *J. Chem. Soc.*, **1965**, 2579.
9) A. Zweig, J. E. Lehnsen, W. G. Hodgson, and W. A. Jura, *J. Am. Chem. Soc.*, **85**, 3937 (1963).
10) R. Boschi, J. N. Murrell, and W. Schmidt, *Faraday Discuss.*, **54**, 116 (1973).
11) T. Ohta, H. Kuroda, and T. L. Kunii, *Theoret. Chim. Acta*, **19**, 167 (1970).
12) These are the values obtained by using the oscillator-strength components perpendicular to the molecular plane.

The Absorption and Fluorescence Spectra of the Ion-Pairs of 1,2,4,5-Tetracyanobenzene with Several Methyl Substituted Benzenes

Satoru MATSUMOTO, Saburo NAGAKURA, and Takayoshi KOBAYASHI*

The Institute for Solid State Physics, The University of Tokyo, Roppongi, Minato, Tokyo 106
**The Institute of Physical and Chemical Research, Wako, Saitama 351*

(Received May 31, 1976)

The absorption and fluorescence spectra and the fluorescence decay times were measured at 77 K for the photo-irradiation products of the 1,2,4,5-tetracyanobenzene (TCNB) complexes with hexamethylbenzene (HMB), durene, mesitylene, and toluene. The absorption spectra of the photoproducts are similar in shape to that of the TCNB anion and have maxima at 469, 467, 466, and 465 nm for the TCNB complexes with HMB, durene, mesitylene, and toluene, respectively. The fluorescence maximum wavelengths and decay times of the photoproducts are also similar to those of the TCNB anion (505 nm, 19.6 ns for the TCNB–mesitylene system; 505 nm, 20.7 ns for the TCNB-toluene system). The red shift of the absorption maximum and the decrease in the fluorescence decay time by changing the electron donors from toluene to HMB are discussed in terms of ion-pair formation.

Only a few electron donor–acceptor (EDA) complexes have been found to emit fluorescence in fluid solutions and even those which are fluorescent in nonpolar fluid solutions become nonfluorescent in polar fluid solutions.[1,2] In connection with the fluorescence quenching, the ionic dissociation of EDA complex in their excited states has been studied.[3] Sofue and Nagakura[4] reported that flash irradiation of 1,2,4,5-tetracyanobenzene (abbreviated hereafter to TCNB) in such polar solvents as diethyl ethyl ether and acetonitrile at room temperature produces the TCNB anion. Achiba *et al.*[5] studied in more detail the TCNB complexes with tetrahydrofuran and other complexes (in dichloromethane) and observed charge-transfer (CT) bands. Furthermore, they found that the ionization takes place by the excitation in the CT band. Masuhara *et al.*[6] reported that such weak CT complexes as the TCNB–toluene system dissociate spontaneously into ions in their excited CT singlet states in polar solvents.

In the present paper, we report that TCNB complexes with methyl substituted benzenes in diethyl ether–isopentane (1: 1) mixed solvent produce stable ion-pairs at 77 K by excitation in their CT bands.[7] Subsequent to our study, Achiba and Kimura also obtained similar results for TCNB–2-methyltetrahydrofuran.[8]

Experimental

Commercially available TCNB (Frinton, GR grade) used as an electron acceptor was purified by sublimation *in vacuo*. Hexamethylbenzene (abbreviated hereafter to HMB) (Tokyo Kasei, GR grade) was purified by repeated recrystallizations and thereafter by sublimation *in vacuo*. Durene (Tokyo Kasei, GR grade) was purified by repeated recrystallizations from ethanol, and thereafter by repeated zone refinings (about 50 times). Spectrograde toluene (Dotite) was used without further purification. Commercially available mesitylene (Tokyo Kasei, GR grade) was purified by distillation. Diethyl ether and isopentane were purified by the usual methods. The samples in a mixed solvent of diethyl ether–isopentane (1: 1) (hereafter abbreviated to EP) were excited by a 100 W high-pressure mercury lamp at 77K. By using appropriate filters, the samples were exposed to and excited by light with a frequency corresponding to the CT band. The absorption spectra of the photoproducts were measured by the use of a Cary recording spectrophotometer, model 14R. The fluorescence spectra were measured with a grating monochromator (Spex model 1704) with an EMI 9558B photomultiplier as a detector and a 100 W high-pressure mercury lamp as the excitation source. Fluorescence lifetimes were measured by using a dye laser (4-methylumbelliferone; 460 nm) pumped by an Avco Everett model 950 nitrogen laser (peak power, 100 kW; pulse width, 10 ns) as a pulsed excitation light source and by using an HTV 1P28 photomultiplier combined with an oscilloscope (Hitachi, model V1000) as a detector.

Results and Discussion

TCNB in EP at 77 K was directly irradiated by a 100 W high-pressure mercury lamp. Several minutes after the excitation, the irradiated portion of the sample was colored. The absorption and emission spectra of the photoproduct are shown in Figs. 1 and 2, respectively. The absorption spectrum with a maximum at 460 nm[9] and with a vibrational structure is quite similar to that of the TCNB anion in acetonitrile.[4] Therefore the photoproduct can safely be assigned to the TCNB anion. The fluorescence spectrum is broad and structureless, with a maximum at 500 nm. The fluorescence lifetime was found to be 21.3 ns.

The TCNB–HMB system in EP was irradiated at 77 K by a 100 W high-pressure mercury lamp through a Toshiba UV-39 filter and a TCNB (in methylene chloride) solution filter. With these filters, the complex was

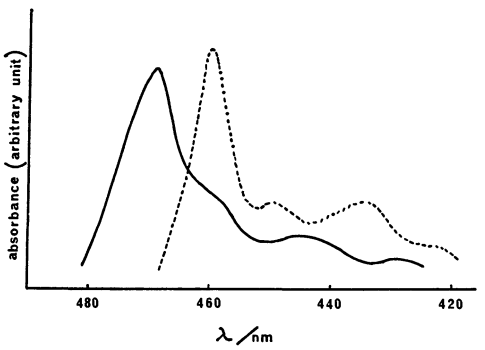

Fig. 1. The absorption spectra of the irradiated EP solution of TCNB (---) and the TCNB–HMB complex (—) at 77 K.

excited only in its CT band. After the irradiation of the sample for several minutes, we obtained a photoproduct with an absorption maximum at 469 nm (Fig. 1). The absorption spectrum of the photoproduct resembles that of the TCNB anion, although the former slightly shifts to longer wavelengths and is a little broader than the latter. The concentrations of the photoproducts were found to be proportional to the exciting light intensity. Therefore, the photo-process is a one photon process.

TABLE 1. THE MAXIMUM WAVELENGTHS OF THE ABSORPTION AND FLUORESCENCE SPECTRA (λ_a AND λ_f, RESPECTIVELY), STOKES SHIFTS ($\Delta\nu$), AND THE FLUORESCENCE LIFETIMES (τ_f) OBSERVED WITH THE TCNB ANION AND THE ION-PAIRS OF THE TCNB ANION AND THE METHYL SUBSTITUTED BENZENE CATIONS

Donor	λ_a(nm)	λ_f(nm)	$\Delta\nu(10^3\,cm^{-1})$	τ_f(ns)
HMB	469			
Durene	467			
Mesitylene	466	505	1.66	19.6
Toluene	465	505	1.70	20.7
TCNB anion only	460	500	1.74	21.3

Similar measurements have been made with the systems containing TCNB as an electron acceptor and durene, mesitylene, and toluene as electron donors; their absorption maxima were observed at 467, 466, and 465 nm, respectively (see Table 1). Thus, the absorption maxima of the photoproducts shift to longer wavelengths with the increasing number of the methyl groups in the donor.

The photoproducts have another common feature: they emit intense fluorescence. The fluorescence spectra and decay times of the photoproducts were measured for the TCNB–mesitylene and TCNB–toluene systems.[10] The observed fluorescence spectra are shown in Fig. 2, and the maximum wavelengths, Stokes shifts, and decay times are given in Table 1. The fluorescence spectra of the photoproducts[11] shift only slightly to longer wavelengths and their fluorescence decay times are only a little shorter compared with the corresponding quantities of the TCNB anion in EP. The Stokes shifts obtained from the absorption and emission spectra of the photoproducts are 1660 and 1700 cm^{-1} for the TCNB–mesitylene and TCNB–toluene systems, respectively. These values are similar to the value for the TCNB anion, 1740 cm^{-1}. The fluorescence excitation spectra were measured with the TCNB–mesitylene and TCNB–toluene systems. Their maximum positions agree well with those of absorption spectra of the respective systems within the limitations of experimental error and their vibrational structures are similar to that of the corresponding absorption spectra.

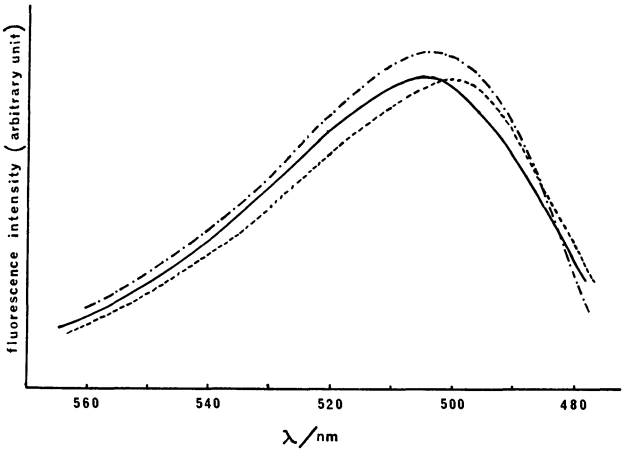

Fig. 2. The fluorescence spectra of the TCNB anion (------) and of the ion-pairs: $TCNB^-$–$toluene^+$(——) and $TCNB^-$-$mesitylene^+$(-·-·-) at 77 K.

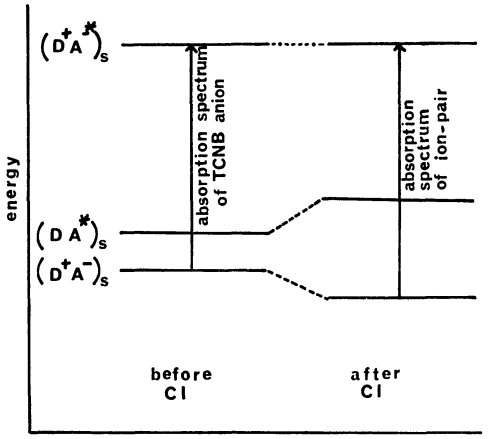

Fig. 3. The schematic energy diagrams of the ion-pair before and after configuration interaction.
( )s indicates the state after solvation.

The above-mentioned results for the absorption and fluorescence spectra, the fluorescence decay times, and the fluorescence excitation spectra show that the photoproducts are the TCNB anion perturbed by some chemical species. From the fact that a counter cation is formed in a pair with the TCNB anion for the electron-donor-acceptor system at 77 K in the rigid medium, it is reasonable to consider that the perturbing chemical species is the donor cation which forms an ion-pair with the TCNB anion. The identification of the photoproducts is supported by the following considerations about the peak wavelengths of the absorption spectra and the fluorescence decay times.

(i) In the ion-pair, the zero-order locally (within TCNB) excited state (DA*) is probably located above the zero-order ion-pair state (D^+A^-), and the two can interact. This interaction stabilizes the ion-pair state and increases the transition energy of the absorption band of the TCNB anion (see Fig. 3). The interaction depends on the energy separation, ΔE, and overlap, S, between the appropriate orbitals belonging to D and A. With the decreasing ionization potential, I_p, of the donor, namely, with the increase in the number of the methyl groups on the donor, $n(CH_3)$, the D^+A^- state becomes lower and ΔE increases. Furthermore, with the increase in $n(CH_3)$, the distance between the TCNB anion and the donor cation may increase because of the increasing steric hindrance, and S is expected to decrease.[12] Thus, we can expect that the stabilization of

the D^+A^- state due to the interaction with the DA* state decreases with the increase in $n(CH_3)$. From this we can explain the observed shift of the absorption maximum with $n(CH_3)$ of the donor.[13]

(ii) The decrease in the fluorescence decay time with the decreasing I_p of the donor may be tentatively explained in the following way: The radiative transition moment may decrease with the increasing DA* character of the ion-pair in the ground state, which is represented by D^+A^-, since the observed fluorescence corresponds to an allowed transition of the TCNB anion. As described above, the contribution of the DA* state to the ground state of the ion-pair increases with the decrease in $n(CH_3)$. Thus, the decrease in the radiative lifetime of S_1 with the decreasing I_p of donor can be explained. A similar tendency was also observed for the TCNB complexes with methyl substituted benzenes in both fluid and rigid nonpolar solvents, and was explained in the same way.[2]

Thus the TCNB complexes with methyl substituted benzenes produce stable ion-pairs at 77 K by excitation in their CT bands.

References

1) N. Mataga and Y. Murata, *J. Am. Chem. Soc.*, **91**, 3144 (1969).

2) T. Kobayashi, K. Yoshihara, and S. Nagakura, *Bull. Chem. Soc. Jpn.*, **44**, 2603 (1971) and Refs. 1—9 therein.

3) S. Nagakura, "Excited States," ed. by E. C. Lim, Vol. 2, Academic Press, New York (1975), p. 321.

4) M. Sofue and S. Nagakura, *Bull. Chem. Soc. Jpn.*, **38**, 1048 (1965).

5) Y. Achiba, S. Katsumata, and K. Kimura, *Bull. Chem. Soc. Jpn.*, **45**, 1272 (1972).

6) H. Masuhara, M. Shimada, N. Tsujino, and N. Mataga, *Bull. Chem. Soc. Jpn.*, **44**, 3310 (1971).

7) S. Matsumoto, S. Nagakura, and T. Kobayashi, Preprint for the 24th Annual Meeting of the Chemical Society of Japan, Osaka, March, 1971.

8) Y. Achiba and K. Kimura, *Chem. Phys. Lett.*, **36**, 65 (1975).

9) The absorption band at 460 nm shifts to 462 nm at room temperature (295 K) for a degassed solution.

10) The fluorescence spectra of the photoproducts could not be measured for the TCNB–HMB and TCNB–durene systems. It is difficult to separate them from the fluorescence spectra of the corresponding molecular complexes because of the large overlap.

11) The fluorescence spectra are broad (bandwidth 1700—1800 cm^{-1}) and structureless while the corresponding absorption spectra show a vibrational structure. This implies that a rather large change in the geometrical configuration of the photoproduct and in the orientation of the surrounding solvent molecules takes place in the excited state.

12) Since the ion-pair is formed by the excitation in the charge-transfer absorption band of the complexes in the rigid solvents, it is reasonable to consider that no solvent molecule intervenes between the TCNB anion and the donor cation. The molecular planes of the components in the ion-pair may be parallel with each other as are those in the parent complex. The exchange interaction between the components may exist in both the ion-pair and the parent CT complex, although it may decrease in the former.

13) The fact that the photoproduct of the TCNB–EP system shows its absorption maximum at a shorter wavelength (460 nm) than the TCNB–toluene complex can be explained by the interaction between D^+A^- and DA*. The ΔE value may conceivably be larger for the TCNB–diethyl ether than for the TCNB–toluene. The finding that the fluorescence decay time is longer for the TCNB–EP system than for the TCNB–toluene system can be explained along the same lines.

Selective Hydrogen Atom Abstraction by Hydrogen Atoms in Photolysis and Radiolysis of Alkane Mixtures at 77 K

Tetsuo MIYAZAKI,* Kazuhisa KINUGAWA, Masao EGUCHI, and Selma M. L. GUEDES**

Department of Synthetic Chemistry, Faculty of Engineering, Nagoya University, Chikusa-ku, Nagoya 464
***Coordenadoria de Radioquimica, Instituto de Energia Atômica, C.P. 11049 (Pinheiros), 01000 São Paulo, SP, Brazil*

(Received June 1, 1976)

A selective hydrogen atom abstraction reaction by H atoms, which are produced at 77K by radiolysis of alkane or photolysis of hydrogen halides, has been found in isobutane, 2,2,3,3-tetramethylbutane (TMB), and cyclopropane matrices as well as in the neopentane matrix. The selective hydrogen atom abstraction reaction is caused by H atoms which have initial kinetic energies in the range from 15 to 67 kcal/mol. The reaction is caused also by D atoms. The competitive reaction between *c*-C_6H_{12} and HI for H atoms has been studied in the radiolysis and photolysis of *neo*-C_5H_{12}–*c*-C_6H_{12}–HI mixture at 77K. The rate constants of these reactions in the neopentane matrix are quite different from those of a thermal H atom reaction, but similar to those of a hot H atom reaction. The importance of the selective hydrogen atom abstraction reaction by H atoms is pointed out in the radical formation in the radiolysis of pure TMB at 77K.

We can easily investigate solid-state reactions at 77 K by irradiation with ultraviolet light or γ rays. Recently quite interesting phenomena have been found in the radiolysis of a neopentane–alkane mixture in the solid phase at 77 K.[1] When neopentane containing a small amount of alkane is γ-irradiated at 77 K, alkyl radicals from solute alkanes rather than neopentyl radicals are selectively formed.

Since the formation of the solute alkyl radical is not affected by the addition of an electron scavenger or a hole scavenger, it was concluded that the alkyl radical is formed by a nonionic process.[1b] The following observations obtained previously showed that the solute alkyl radical is not formed by the excitation transfer from the irradiated neopentane to the solute, but by the selective hydrogen atom abstraction from the solute by H atoms.[1c] (1) The mechanism of excitation transfer promotes the formation of D_2 in the radiolysis of *neo*-C_5H_{12}–*i*-C_4H_9D at 77 K. Though much HD is formed in this system, D_2 is not formed at all.[1c] (2) When a *neo*-C_5H_{12}–*c*-C_6H_{12} (1 mol %) mixture is irradiated at 77 K by γ-rays, cyclohexyl radicals are mainly formed. When propylene is added to the mixture, the formation of the cyclohexyl radicals is suppressed, while C_3H_7 radicals are produced complementarily by the addition of H atoms to propylene.[2] (3) H atoms, which are produced by the photolysis of hydrogen iodide in neopentane containing a small amount of alkane, react selectively with the solute slkane at 77 K.[1c,3]

The selective hydrogen atom abstraction reaction by H atoms has new problems in its reaction kinetics in the solid phase at 77 K. When H atoms are hot, we must assume that they migrate a long distance at 77 K through the neopentane crystal without losing their kinetic energies. When H atoms are thermal, we must assume that the activation energy for hydrogen atom abstraction is nearly zero in the neopentane matrix at 77 K, though the value amounts to 7—10 kcal/mol in the gas phase.[4,5] The research described herein was undertaken in order to obtain further information about the nature of the reactive H atoms.

* All correspondence should be addressed.

The previous studies of the selective hydrogen atom abstraction have been limited only to the neopentane matrix and to the reactions of H atoms. In the present paper the study will be extended to other alkane matrices, such as isobutane, 2,2,3,3-tetramethylbutane (TMB), and cyclopropane, and to the reactions of H and D atoms.

The formation of radicals in the radiolysis of pure TMB and of a TMB–alkane mixture is discussed here in terms of the selective hydrogen atom abstraction by H atoms.

Experimental

Neopentane, isobutane, and propane were more than 99.9 mol% pure, while cyclopropane and ethane were respectively more than 99.0 and 99.7% pure. Spectrograde cyclohexane was passed through a 1-m column packed with silica gel and then distilled on a vacuum line before use. 2,2,3,3-Tetramethylbutane (TMB) was of a high purity and purified by sublimation on a vacuum line before use. To prepare hydrogen halides (HX), such as HI, HBr, DBr, and HCl, the aqueous solution of each hydrogen halide was passed through P_2O_5 and subjected to several trap-to-trap sublimations on the vacuum line.

UV illumination was provided by Toshiba medium-pressure or low-pressure mercury lamps. γ-Irradiation was done by Co-60 at a dose rate of 4.2×10^{19} eV/h.

The free radicals were measured at 77 K with a JES-3BX ESR spectrometer.

Results

Table 1 shows the yields of radicals by the reaction of hydrogen (or deuterium) atoms in the radiolysis or photolysis of alkane mixtures in the solid phase at 77 K. *t*-C_4H_9 radical is mainly formed in the photolysis of *neo*-C_5H_{12}(or TMB)–*i*-C_4H_{10}–hydrogen halide(HX), while a small amount of *i*-C_4H_9 radical is also produced. Since the ratio of the amounts of *i*-C_4H_9 radicals to those of *t*-C_4H_9 radicals increases with increasing the illumination time of ultraviolet light, *i*-C_4H_9 radical is formed by the isomerization of *t*-C_4H_9 radical, which absorbs ultraviolet light.[6] The amounts of C_4H_9 radicals re-

Table 1. Formation of solute radicals by the reaction of hydrogen (or deuterium) atoms in the radiolysis or photolysis of alkane mixtures at 77K[a)]

Sample	Species of radical	Methods of production of H (or D) atoms				
		γ-Irradiation[b)]	Ultraviolet illumination[c)]			
			HI	HBr	DBr	HCl
neo-C_5H_{12}–*i*-C_4H_{10}(2)[d)]	C_4H_9	Clearly observed[e)]	10.0	4.0	3.1	0.9
neo-C_5H_{12}	*neo*-C_5H_{11}	Clearly observed[e)]	10.0	3.0	4.1	<0.5
i-C_4H_{10}–C_3H_8(2)[d)]	C_3H_7	Clearly observed[e)]	10.0	2.0	1.9	
i-C_4H_{10}	*i*-C_4H_9	Clearly observed[e)]	10.0	2.6	5.5	
TMB–*i*-C_4H_{10}(5)[d)]	C_4H_9	Clearly observed[f)]	10.0	2.1	2.6	
c-C_3H_6–C_2H_6(4)[d)]	C_2H_5	Clearly observed[f)]	—	—	—	

a) Yields are averages of two or more runs. b) Alkane mixtures in the absence of hydrogen halide were irradiated at 77 K with γ-rays. H atoms are produced by the radiolysis of solvent alkane. c) H (or D) atoms are produced by the photolysis of hydrogen halide with ultraviolet light. Concentrations of hydrogen halide in *neo*-C_5H_{12}, *i*-C_4H_{10}, TMB, and *c*-C_3H_6 matrices are 0.5, 0.2, 0.5, and 0.5 mol/100 mol of solvent alkane. The yield of the radical in HI system is taken as 10. Illumination times of *neo*-C_5H_{12}, *i*-C_4H_{10}, TMB, and *c*-C_3H_6 matrices with UV light from a low-pressure mercury lamp are 5, 5, 20, and 30 min respectively. d) Unit of concentration is mol/100 mol of solvent alkane. e) ESR spectra are shown in Ref. 1a. f) ESR spectra are shown in Figs. 3 and 4.

present a sum of *t*-C_4H_9 and *i*-C_4H_9 radicals, and are measured by double integration of the first-derivative ESR signal of the radicals. Since only C_4H_9 radicals are formed selectively in the photolysis of *neo*-C_5H_{12}(or TMB)–*i*-C_4H_{10}–HX, overlapping of the spectra of the solute radical and the neopentyl radical does not occur. *neo*-C_5H_{11}, C_3H_7, *i*-C_4H_9, and C_2H_5 radicals do not isomerize under the illumination by ultraviolet light. Therefore the relative yields of these radicals are obtained from the heights of their peaks in the ESR spectrum. The yields of solute radicals increase linearly with increasing irradiation time. The yield of radical in the photolysis of HI is much higher than that in the photolysis of HBr, DBr, or HCl. This is because the absorbance of the ultraviolet light by HI is stronger than that by other hydrogen halides.[7)] H atoms in the previous studies have been produced only by the photolysis of HI with 253.7 nm. The present study has been undertaken in order to obtain qualitative information as to whether H atoms with various energies produced from different compounds also react selectively with solute alkanes or not. Since the absolute yields of radicals was not necessary, the effect of HX concentration on the radical yields has not been studied systematically, except for a few runs of different concentrations. The results of the photolysis in Table 1 have been obtained by the illumination in the air with UV light from a low pressure Hg lamp. It was found by using a filter that the photolysis of HI is caused mainly by light of 253.7 nm, while that of HBr or DBr is caused by light of 184.9 nm along with 253.7 nm.

In order to examine the effect of different wavelengths on the photolysis of HBr, two experiments have been undertaken. First, a filter which completely cuts off any light shorter than 190 nm has been used, and thus the photolysis was caused only by light of 253.7 nm. Second, the illumination with a low pressure Hg lamp has been done in the vacuum. The photolysis is caused mainly by light of 184.9 nm, because the decomposition of HBr by light of 253.7 nm is much smaller than that by light of 184.9 nm. Both H atoms, produced by the photolysis of HBr with the light of 184.9 nm or 253.7 nm, react selectively with the solute alkane in the *neo*-pentane matrix at 77 K.

The photolysis of HI has been done with a medium-pressure Hg lamp through a Toshiba UV31 filter, which cuts off all light shorter than 305 nm. The yields of radicals in the photolysis with the UV31 filter are much higher than those in the photolysis with a glass filter which cuts off all light shorter than 330 nm. Therefore the photolysis with the UV31 filter is caused mainly by the light from 330 nm to 305 nm. H atoms produced by the photolysis with the light from 330 nm to 305 nm also react selectively with the solute alkanes in the *neo*-pentane matrix at 77 K.

Figure 1 shows the effect of HI on the formation of cyclohexyl radicals in the radiolysis of *neo*-C_5H_{12}–*c*-C_6H_{12}–HI at 77 K. When *neo*-C_5H_{12} containing *c*-C_6H_{12} of 0.5, 1.0, and 2.0 (mol/100 mol of *neo*-C_5H_{12}) is γ-irradiated in the absence of HI, the yields of cyclohexyl radicals are approximately the same in the three systems; they are taken as 10.

Figure 2 shows the effect of HI on the formation of cyclohexyl radicals in the photolysis of *neo*-C_5H_{12}–*c*-C_6H_{12}–HI at 77 K. The yields of cyclohexyl radicals at HI concentration of 0.25 (mol/100 mol of *neo*-C_5H_{12}) are taken as 10

Figure 3a shows the ESR spectrum of γ-irradiated

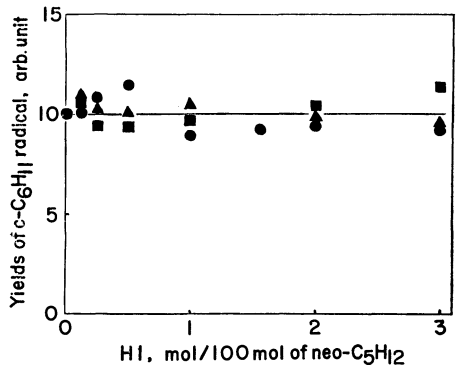

Fig. 1. Effect of HI on the yield of c-C_6H_{11} radicals in the radiolysis of *neo*-C_5H_{12}–c-C_6H_{12} mixture at 77 K with a dose of 2.1×10^{19} eV/g.
■, Concentration of c-C_6H_{12} is 0.5 mol/100 mol of *neo*-C_5H_{12}.
●, Concentration of c-C_6H_{12} is 1.0 mol/100 mol of *neo*-C_5H_{12}.
▲, Concentration of c-C_6H_{12} is 2.0 mol/100 mol of *neo*-C_5H_{12}.

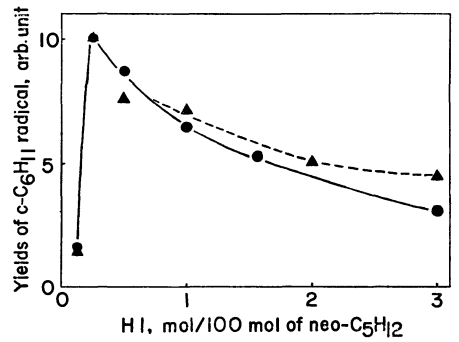

Fig. 2. Effect of HI on the yield of c-C_6H_{11} radicals in the photolysis of *neo*-C_5H_{12}–c-C_6H_{12}–HI mixture at 77 K.
●—●, c-C_6H_{12} concentration is 1.0 mol/100 mol of *neo*-C_5H_{12}.
▲---▲, c-C_6H_{12} concentration is 2.0 mol/100 mol of *neo*-C_5H_{12}.

pure TMB at 77 K. The spectrum is similar to that reported by Gerola *et al.*[8] The spectrum of three broad lines, indicated by ⇩, is ascribed to the $(CH_3)_3CC(CH_3)_2\dot{C}H_2$ (TMB·) radical. The other unidentified spectrum, indicated by ⇣, has been ascribed to an isomerized radical, *i.e.* $(CH_3)_3CCH_2\dot{C}(CH_3)_2$,[8] or a mixture of t-C_4H_9 and $(CH_3)_3C\dot{C}(CH_3)_2$ radicals.[9] When TMB containing a small amount of isobutane or cyclohexane are γ-irradiated at 77 K, quite different spectra are obtained (Figs. 3b and c). The spectrum in Fig. 3b consists of three broad lines, which are attributable to the TMB· radical, and eight narrow lines, indicated by ↓, with a splitting constant of 22 G. The spectrum of the eight lines is consistent with the reported spectrum for the t-C_4H_9 radical.[10,11] The spectrum in Fig. 3c consists of three broad lines, which are attributable to the TMB· radical, and six broad lines, indicated by ↓, with a splitting constant of 22 G. The spectrum of the six lines is consistent with the reported spectrum

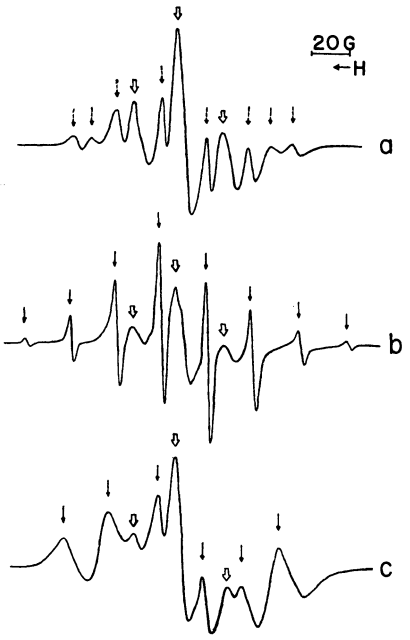

Fig. 3. ESR spectra of γ-irradiated TMB and TMB-alkane mixtures at 77 K with a dose of 1.8×10^{19} eV/g. Relative sensitivities of spectrometer for a, b, and c are approximately the ratios of 2: 1: 1.5 respectively. a, pure TMB; b, TMB–i-C_4H_{10}(5.4 mol/100 mol of TMB); c, TMB–c-C_6H_{12} (5.8 mol/100 mol of TMB).

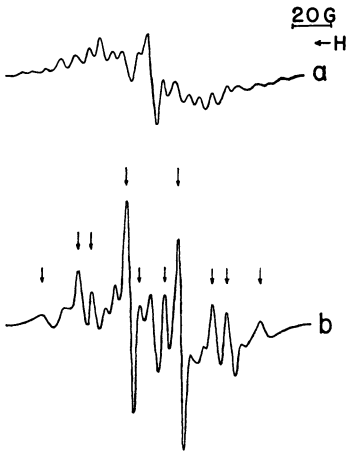

Fig. 4. ESR spectra of γ-irradiated c-C_3H_6 and c-C_3H_6–C_2H_6 mixtures at 77 K with a dose of 1.8×10^{19} eV/g. Sensitivities of spectrometer for a and b are approximately the same. a, pure c-C_3H_6; b, c-C_3H_6–C_2H_6 (4 mol/100 mol of c-C_3H_6).

for the cyclohexyl radical.[10,12] When TMB containing a small amount of C_3H_8, i-C_4H_8, or C_3H_6 is γ-irradiated at 77 K, C_3H_7, t-C_4H_9, or C_3H_7 radical is clearly observed.

Figure 4a shows the ESR spectrum of γ-irradiated pure cyclopropane at 77 K. The spectrum may be ascribed to C_3H_5 radical.[10] When cyclopropane containing a small amount of ethane is γ-irradiated at 77 K, a typical spectrum of an ethyl radical,[10,11] indicated by ↓, is clearly observed, as in Fig. 4b.[13]

Discussion

Selective Formation of Solute Radicals in the Radiolysis and Photolysis of Alkane Mixtures at 77 K. Table 1 shows that the selective formations of solute radicals in the radiolysis of alkane mixtures are observed also in isobutane, 2,2,3,3-tetramethylbutane (TMB), and cyclopropane matrices as well as in the neopentane matrix. All of the matrix alkanes are polycrystalline at 77 K. H atoms, produced by the photolysis of HI or HBr, react selectively with a small amount of the solute alkane in the *neo*-C_5H_{12}, *i*-C_4H_{10}, and TMB matrices. It is concluded that the selective hydrogen atom abstraction reaction is not limited to the neopentane matrix, but can be found also in other polycrystalline alkanes.

When H atoms are produced by the photolysis of HI with light of 330—305 nm, they react selectively with the solute alkane in the neopentane matrix. The 330—305 nm radiation corresponds to 86.6—93.7 kcal/mol, while the bond strength of HI is 71.3 kcal/mol.[14] To conserve momentum essentially all of the energy from the primary process in excess of that used in bond rupture must appear as translational energy of the H atom, because I atoms produced by the photolysis with 330—305 nm are mainly in the ground state.[15] Therefore the energies of the H atoms are 15—22 kcal/mol. The bond strength of HBr is 87.6 kcal/mol.[14] When H atoms are produced by the photolysis of HBr with light of 184.9 nm, the energies of the H atoms are 67 kcal/mol, because Br atoms produced by the photolysis are mainly in the ground state.[16] The H atoms also react selectively with the solute alkanes in the neopentane matrix. It is concluded that the H atoms, which have initial kinetic energies ranging from 15 to 67 kcal/mol, migrate a long distance through the neopentane matrix without reacting with the neopentane molecules and react selectively with the solute alkanes.

Though the C_2H_5 radical is mainly formed in the radiolysis of *c*-C_3H_6–C_2H_6 (Fig. 4), it is not observed in the photolysis of *c*-C_3H_6–C_2H_6–HI (HBr or DBr). Since the concentration of HX in cyclopropane and the method of illumination with UV light are the same as those in neopentane, the condition of the absorption of the light in cyclopropane must be the same as in neopentane, where the formation of radicals by the photolysis can be observed clearly. At present we cannot give a suitable explanation for the phenomenon that radicals are not formed by the photolysis in cyclopropane. One plausible reason would be as follows: that the amount of the H atoms produced by the photolysis of hydrogen halide in cyclopropane is extremely small. This might be because the ultraviolet light is reflected at the surface of the cyclopropane crystal and does not penetrate into the crystal, or because the decomposition of HX is suppressed by the cage effect in the cyclopropane crystal. The following results were observed during our experiments. Firstly, neither the C_3H_5 radical nor any other radical is produced by the illumination of *c*-C_3H_6–HX, where C_2H_6 does not exist, with ultraviolet light at 77 K. Secondly, when *c*-C_3H_6–C_2H_6–HI is illuminated with ultraviolet light, the color of I_2, produced by the decomposition of HI, is observed only at the surface of the crystal.

Table 1 shows that D atoms, produced by the decomposition of DBr, also react selectively with the solute alkanes. Therefore the selective hydrogen atom abstraction reaction is not limited only to H atoms.

Nature of Reactive Hydrogen Atom. In order to elucidate the mechanism of the selective hydrogen atom abstraction reaction by H atoms, it is important to get some information about the nature of the H atoms.

(I) Competitive reaction of H atoms with HI and *c*-C_6H_{12} in the *neo*-C_5H_{12} matrix at 77 K.

Figure 1 shows that the yields of cyclohexyl radicals in the radiolysis of *neo*-C_5H_{12}–*c*-C_6H_{12} mixtures are not affected by the addition of HI. As described in the Introduction, the previous studies[1] of the radiolysis of neopentane–alkane mixtures at 77 K have concluded that excited neopentane, formed by γ-irradiation, produces a H atom and a neopentyl radical. The H atom migrates through the neopentane matrix and reacts selectively with the solute cyclohexane. The ionic process and the excitation transfer are not responsible for the formation of *c*-C_6H_{11} radicals.[1] When HI is

$$\textit{neo}\text{-}C_5H_{12} \rightsquigarrow \textit{neo}\text{-}C_5H_{11} + H \quad (1)$$

$$H + c\text{-}C_6H_{12} \xrightarrow{k_{c\text{-}C_6H_{12}}} c\text{-}C_6H_{11} + H_2 \quad (2)$$

present in the *neo*-C_5H_{12}–*c*-C_6H_{12} system, occurrence of Reaction 3 is expected, because both hot and thermal H atoms react easily with HI in the gas phase. H

$$H + HI \xrightarrow{k_{HI}} I + H_2 \quad (3)$$

atoms produced by the radiolysis of *neo*-C_5H_{12} at 77 K, however, do not react with HI, but with *c*-C_6H_{12} (Fig. 1). It can be estimated from the results in Fig. 1 that $k_{HI}/k_{c\text{-}C_6H_{12}}$ is less than 0.05; the value is given in the first line in Table 2.

Figure 2 shows that the yields of cyclohexyl radicals in the photolysis of the *neo*-C_5H_{12}–*c*-C_6H_{12}–HI mixture reach a maximum at the HI concentration of 0.25 (mol/100 mol of *neo*-C_5H_{12}) and then decrease gradually with increasing concentration of HI. Such results can be explained in terms of competitive reactions between HI and cyclohexane for H atoms. A possible kinetic scheme is as follows:

$$HI \xrightarrow{h\nu} H + I \quad (4)$$

$$H + c\text{-}C_6H_{12} \xrightarrow{k_{c\text{-}C_6H_{12}}} c\text{-}C_6H_{11} + H_2 \quad (5)$$

$$H + HI \xrightarrow{k_{HI}} I + H_2 \quad (6)$$

If the rate of Reaction 4 is represented by r, the following kinetic equation is obtained:

$$\frac{1}{[c\text{-}C_6H_{11}]} = \frac{1}{r} + \frac{k_{HI}[HI]}{r\,k_{c\text{-}C_6H_{12}}[c\text{-}C_6H_{12}]}$$

The linear relationship between $1/[c\text{-}C_6H_{11}]$ and $[HI]/[c\text{-}C_6H_{12}]$ is obtained for the HI concentrations higher than 0.25 (mol/100 mol of *neo*-C_5H_{12}). When concentrations of *c*-C_6H_{12} are 1.0 and 2.0 (mol/100 mol of *neo*-C_5H_{12}), $k_{HI}/k_{c\text{-}C_6H_{12}}$ are 1.2 and 1.0 respectively. The mean value for $k_{HI}/k_{c\text{-}C_6H_{12}}$ is given in the second line in Table 2.

There are many studies of the reaction of hot atoms produced by the photolysis of hydrogen halides in the gas phase. Carter *et al.*[17] reported that $k_{DI}/k_{C_2H_6}$ is

Table 2. Competitive reaction between HI and c-C_6H_{12} for H atoms at 77 K

Species of H atom	$k_{HI}/k_{c-C6H12}$
H atom produced by radiolysis of *neo*-C_5H_{12} at 77 K	<0.05
H atom produced by photolysis of HI in *neo*-C_5H_{12} matrix at 77 K	1.1
Hot H atom[a]	0.23—1.1
Thermal H atom (A)[b]	10^{20}—10^{23}
Thermal H atom (B)[c]	10^{11}—10^{14}

a) Hot H atoms were produced by photolysis of HI in the gas phase. b) $k_{HI}/k_{c-C_6H_{12}}$ was estimated from the data in the gas phase. c) $k_{HI}/k_{c-C_6H_{12}}$ was estimated from the reaction of the thermal methyl radical in the solid phase at 77 K.

1.45 for reactions of hot D atoms with DI and C_2H_6. Hong *et al.*[18] reported that $k_{HI}/k_{C_2D_5H}$ is 7.0 for reactions of hot H atoms with HI and C_2D_5H. Rebbert *et al.*[19] reported that $k_{C_2D_6}/k_{c-C_6D_{12}}$ is 0.16 for reactions of hot CH_3 radicals with C_2D_6 and c-C_6D_{12}. Therefore $k_{HI}/k_{c-C_6H_{12}}$ ranges approximately from 1.45×0.16 (=0.23) to 7.0×0.16 (=1.1). These values are given in the third line in Table 2.

Thermal H atoms react quite easily with HI in the gas phase. According to the study by Sullivan,[20] the rate constant of this reaction can be expressed by $k_{HI}=10^{12.05}T^{0.5}\exp(-E/RT)$. The activation energy (E) is nearly zero, 0.48 kcal/mol. The activation energy for a reaction of thermal H atoms with cyclohexane is, however, about 8 kcal/mol.[4,5] If it is assumed that the pre-exponential factor of $k_{c-C_6H_{12}}$ is approximately the same as that of k_{HI} and that the activation energy for the reaction of H atoms with HI is 0—1 kcal/mol, $k_{HI}/k_{c-C_6H_{12}}$ at 77 K amounts to 10^{20}—10^{23}; this is given in the 4th line in Table 2.

Recently it has been reported that a thermal CH_3 radical abstracts H atoms from CH_3OH[21] and 3-methylpentane[22,23] at 77 K by quantum mechanical tunneling. The rate constant of the reaction can be estimated from the decay time of the CH_3 radical to be about 10^{-1} mol^{-1} ml s^{-1} at 77 K. Assuming that the thermal H atom reacts with cyclohexane by the quantum mechanical tunneling and that the rate constant of the thermal H atom is the same order of magnitude as that of the thermal CH_3 radical, $k_{HI}/k_{c-C_6H_{12}}$ at 77 K may be 10^{11}—10^{14}; this is given in the 5th line in Table 2.

Though a number of studies of the reaction rate have been undertaken in the gas and liquid phases at temperatures higher than room temperature, studies in the solid phase at 77 K are quite few. At present we have no information about the possibility that the activation energy changes drastically in the solid alkane at 77 K, as compared with the gas or liquid phases. If the activation energy obtained in the gas phase may be used also in the solid phase, the following discussion may be fruitful. The results in Table 2 show that $k_{HI}/k_{c-C_6H_{12}}$ of H atoms produced by the radiolysis or photolysis in the neopentane matrix at 77 K are quite different from the values expected from the reaction of thermal H atoms, but approximately similar to the value expected from the hot H atom reaction.

If the activation energy in the gas phase is quite different from that in the solid phase at 77 K, we cannot exclude the possibility that the H atoms produced by the radiolysis or photolysis in the neopentane matrix at 77 K are thermal. In this case, the thermal H atoms react more easily with cyclohexane than with hydrogen halide, though the activation energy for the former reaction is 8 kcal/mol and that for the latter reaction is nearly zero.

(II) Possibility of H atom abstraction by a thermal radical in the neopentane matrix at 77 K.

Since the activation energies for the hydrogen atom abstraction reaction from alkanes by thermal atoms or radicals are 7—10 kcal/mol,[4,5] it may be concluded from the previous theory of reaction kinetics that the reaction does not occur at all at 77 K.

Recent findings,[21-23] however, indicate that thermal methyl radicals abstract hydrogen atoms from the solvent molecules even at 77 K. We have examined here the possibility that thermal methyl radicals react in *neo*-C_5H_{12}–alkane mixtures at 77 K. When *neo*-C_5H_{12}–C_2H_6(2 mol/100 mol of *neo*-C_5H_{12})–CH_3Br(0.1 mol/100 mol of *neo*-C_5H_{12}) is irradiated with UV light at 77 K, a CH_3 radical is formed by the photolysis of CH_3Br. The thermal CH_3 decays very slowly at 77 K. The half-life for decay is about 150 h, which is extremely long as compared with 0.2—0.3 h in 3-methylpentane at 77 K.[22,23] When the CH_3 radicals decrease, the formation of *neo*-C_5H_{11} or C_2H_5 radicals cannot be observed at all, while unknown radicals increase complementarily. Therefore it is concluded that the hydrogen atom abstraction reaction from alkane by thermal methyl radicals does not occur in the *neo*-C_5H_{12}–C_2H_6 mixture at 77 K.

(III) Selective hydrogen atom abstraction by H atoms in the i-C_4H_{10}–C_3H_8 mixture at 77 K.

When i-C_4H_{10} containing HI is irradiated with UV light at 77 K, the H atom produced by the photolysis of HI abstracts a hydrogen atom from the primary C–H bond of i-C_4H_{10} to form an i-C_4H_9 radical. When a small amount of C_3H_8 is added to the mixture, the H atom react selectively with the solute propane (Table 1 and Ref. 3) and the formation of the i-C_4H_9 radical is suppressed.

$$HI \xrightarrow{h\nu} H + I \quad (4)$$

$$H + i\text{-}C_4H_{10} \longrightarrow i\text{-}C_4H_9 + H_2 \quad (7)$$

$$H + C_3H_8 \longrightarrow C_3H_7 + H_2 \quad (8)$$

The H atom produced by the photolysis of HI has an initial kinetic energy of 20 or 41 kcal/mol, depending on whether the iodine atom is produced in the excited state or in the ground state. In the radiolysis of i-C_4H_{10}–HI, it was found that the H atom, which is produced by dissociative electron attachment to HI, preferentially abstracts the tertiary H atom from i-C_4H_{10}.[24]

$$e^- + HI \longrightarrow H + I^- \quad (9)$$

$$H + i\text{-}C_4H_{10} \longrightarrow t\text{-}C_4H_9 + H_2 \quad (10)$$

The H atom produced by dissociative electron attachment has a kinetic energy of 5—6 kcal/mol, if HI captures a thermal electron. Therefore it can be concluded that the hot H atom with high energy abstracts a pri-

mary H atom from i-C_4H_{10}, while the H atom with low energy abstracts a tertiary H atom. The hot H atom reacts selectively with C_3H_8 when C_3H_8 is present in the system.

(IV) Migration of H atoms in the crystal.

It can be summarized from the present and previous studies[1] that the reactive H atoms in the crystalline alkane at 77 K have the following characteristics: (a) The activation energy for the reaction of the H atoms with solute alkane is nearly zero, though that in the gas phase is 7—10 kcal/mol. The H atoms produced by radiolysis of neopentane at 77 K do not react with HI, though the activation energy for this reaction is nearly zero in the gas phase. (b) The selective reaction of H atoms in the neopentane–isobutane mixture occurs efficiently in the solid phase at 77 K, while it does not occur at all in the liquid phase.[1c] The selective reaction has been found only in polycrystalline matrices (Table 1).

At present we cannot give a clear answer to the question whether the reactive H atoms are thermal or hot. Though the possibility of hot H atoms cannot be excluded a priori, only the reaction of thermal H atoms has been discussed in the previous paper.[1c] The possibility of hot H atoms will be described here in order to supplement the previous discussion.[1c]

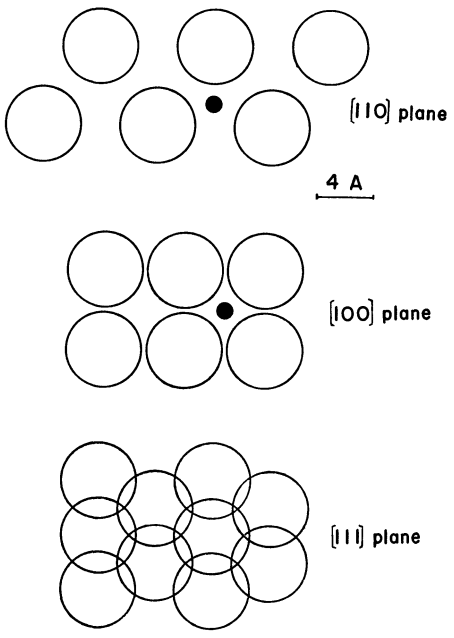

Fig. 5. Molecular arrangement of the three principal planes of fcc lattice of crystalline neopentane at 77 K.

One plausible explanation will be given by the idea of "channeling."[25-27] The crystalline structure of neopentane at 77 K consists of face-centered cubic unit cells with a lattice constant of 11.4 Å.[28] Since the chemical structure of neopentane is symmetrical, the structure is depicted here as a sphere. Projections of the molecular arrangements of the three principal planes of the fcc lattice of neopentane are shown in Fig. 5. A neopentane molecule is represented by a large circle, where a line of the circle is the most probable position of the electrons of H atoms in neopentane molecules. Top and second layers are depicted in the projections of the [110] and [100] planes, because the third and fourth layers are repetitions of the top and second layers. Top, second, and third layers are depicted in the projection of the [111] plane. A smaller circle, depicted by ●, represents a hot hydrogen atom with a Bohr radius. It is clear that the surface layers of the [110] and [100] orientations exhibit transparent regions to the incident hot H atoms. When hot H atoms produced by the radiolysis of neopentane or by the photolysis of hydrogen halide are incident upon the transparent regions of [110] and [100] planes, the hot H atoms may travel a long distance by a succession of glancing collisions with the channel walls of neopentane molecules and then react with a solute alkane which may exist as a defect in the neopentane crystal.

The selective hydrogen atom abstraction reaction by hot H atoms in neopentane–alkane mixtures is not observed in the liquid phase.[1c] This phenomenon can be explained by the channeling hypothesis. Since a random arrangement of molecules in the liquid phase does not contain transparent regions, *i.e.* channels, the hot H atom collides head-on with a solvent molecule in the liquid phase and loses its energy by chemical reaction or deactivation. It is expected from this hypothesis that the selective reaction will be found in the crystal, but not in the glass.

Radical Formation in the Radiolysis of Pure 2,2,3,3-Tetramethylbutane (TMB) and TMB–Alkane Mixture at 77 K. Gerola *et al.*[8] reported the ESR spectrum of γ-irradiated TMB at 77 K. Since $(CH_3)_3CC(CH_3)_2\dot{C}H_2$ (TMB·) and $(CH_3)_3CCH_2\dot{C}(CH_3)_2$ radicals are formed, they considered that first a C–H bond rupture occurs in the radiolysis of TMB and then the isomerization of the TMB· radical produces the $(CH_3)_3CCH_2\dot{C}(CH_3)_2$ radical. Shiraishi *et al.*[9] reported t-C_4H_9, $(CH_3)_3C\dot{C}$-$(CH_3)_2$, and TMB· radicals in the radiolysis of solid TMB. They considered that the free radicals are formed by C–C bond ruptures as well as C–H bond ruptures in the radiolysis of TMB.

The ESR spectrum in Fig. 3a consists of TMB· and an unidentified radical which has been ascribed to $(CH_3)_3CCH_2\dot{C}(CH_3)_2$[8] or a mixture of t-C_4H_9 and $(CH_3)_3C\dot{C}(CH_3)_2$.[9] When a small amount of alkane or olefin is added to TMB, the formation of the unidentified radical is suppressed and the solute alkyl radical is formed complementarily (Fig. 3b and c). Therefore it seems that the unidentified radical is neither formed by the isomerization of the TMB· radical nor by the direct C–C bond rupture, but by a secondary process of some active species which reacts also with the solute alkane or olefin.

The following observations obtained here show that the solute alkyl radical is not formed by the energy transfer from the irradiated TMB to the solute, but by the selective hydrogen atom abstraction by H atoms from the solute alkane.

(1) When TMB containing a small amount of propane is γ-irradiated at 77 K, the propyl radical is formed. The ionization potential of TMB has not been reported previously. But if we assume that the value is approximately the same as that of 2,2,4-trimethyl-

pentane, which is an isomer of TMB and has a structure similar to that of TMB, the ionization potential of TMB may be 9.86 eV,[29] which is lower than the ionization potential (11.07 eV)[29] of propane. The energy level of the first excited state of TMB is 8.0 eV,[30] which is lower than that (8.9 eV)[30] of propane. Therefore, assuming that the relative magnitude of the ionization potential and the first excited state is kept in the solid phase, the ordinary charge or excitation transfer from TMB to C_3H_8 cannot occur.

(2) When TMB containing a small amount of isobutene or propylene is irradiated with γ-rays at 77 K, the formation of the unidentified radical is suppressed, while t-C_4H_9 or C_3H_7 radical is produced complementarily by the addition of H atoms to isobutene or propylene.

(3) When TMB–i-C_4H_{10} (5 mol/100 mol of TMB)–HX (0.5 mol/100 mol of TMB) is irradiated with UV light at 77 K, the H atoms produced by the photolysis of hydrogen halide react selectively with i-C_4H_{10} to form the t-C_4H_9 radical (Table 1).

Therefore the mechanism of radical formation in the radiolysis of TMB at 77 K can be represented as follows:

$$\text{TMB} \rightsquigarrow \text{TMB}\cdot + \text{H} \quad (11)$$

$$\text{H} + \text{S} \longrightarrow (CH_3)_3CCH_2\dot{C}(CH_3)_2,\ t\text{-}C_4H_9, \text{ or } (CH_3)_3C\dot{C}(CH_3)_2 \quad (12)$$

$$\text{H} + \text{RH} \longrightarrow \text{R}\cdot + H_2 \quad (13)$$

Reactive H atoms produced by the decomposition of TMB (Reaction 11) react selectively with impurities (S) to form $(CH_3)_3CCH_2\dot{C}(CH_3)_2$, t-C_4H_9, or $(CH_3)_3C\dot{C}(CH_3)_2$ in the radiolysis of pure TMB. When an alkane (RH), such as C_3H_8, i-C_4H_{10}, or c-C_6H_{12}, is added to TMB, the H atoms react selectively with the solute to form an alkyl radical (R·).

The authors wish to express their appreciation to Professor Fausto W. Lima of Instituto de Energia Atômica in São Paulo for his encouragement. The authors also wish to express their appreciation to Professor Noriaki Ito and Dr. Kenji Morita of Nagoya University for their fruitful discussions.

References

1) a) T. Miyazaki, T. Wakayama, M. Fukaya, Y. Saitake, and Z. Kuri, *Bull. Chem. Soc. Jpn.*, **46**, 1030 (1973); b) M. Kato, Y. Saitake, T. Miyazaki, and Z. Kuri, *ibid.*, **46**, 2004 (1973); c) T. Miyazaki and T. Hirayama, *J. Phys. Chem.*, **79**, 566 (1975).

2) M. Kato, T. Miyazaki, and Z. Kuri, unpublished results.

3) T. Wakayama, T. Miyazaki, K. Fueki, and Z. Kuri, *J. Phys. Chem.*, **77**, 2365 (1973).

4) B. A. Thrush, *Progr. React. Kinet.*, **3**, 89 (1965).

5) T. Kagiya, Y. Sumida, I. Inoue, and F. S. Dyachkovskii, *Bull. Chem. Soc. Jpn.*, **42**, 1812 (1969).

6) M. Iwasaki and K. Toriyama, *J. Chem. Phys.*, **46**, 2852 (1967).

7) a) J. R. Bates, J. O. Halford, and L. C. Anderson, *J. Chem. Phys.*, **3**, 531 (1935); b) C. F. Goodeve and A. W. C. Taylor, *Proc. R. Soc.*, **A152**, 221 (1935); c) C. F. Goodeve and A. W. C. Taylor, *ibid.*, **A154**, 181 (1936); d) J. Romand, *Ann. Phys. (Paris)*, **4**, 527 (1948); e) M. A. Neiss and J. E. Willard, *J. Phys. Chem.*, **79**, 783 (1975).

8) J. Gerola, B. Lamotte, and R. Marx, *J. Chim. Phys.*, **66**, 216 (1969).

9) H. Shiraishi, H. Kadoi, K. Hasegawa, Y. Tabata, and K. Oshima, *Bull. Chem. Soc. Jpn.*, **47**, 1400 (1974).

10) R. W. Fessenden and R. H. Schuler, *J. Chem. Phys.*, **39**, 2147 (1963).

11) P. B. Ayscough and C. Thomson, *Trans. Faraday Soc.*, **58**, 1477 (1962).

12) B. Smaller and M. S. Matheson, *J. Chem. Phys.*, **28**, 1169 (1958).

13) A preliminary experiment was done by M. Fukaya and T. Miyazaki.

14) V. I. Vedeneyev, L. V. Gurvich, V. N. Kondratyev, V. A. Medvedev, and Ye. L. Frankevich, "Bond Energies, Ionization Potentials, and Electron Affinities," translated in English by W. C. Price, London, Edward Arnold LTD. (1966).

15) R. M. Martin and J. E. Willard, *J. Chem. Phys.*, **40**, 2999 (1964).

16) R. M. Martin and J. E. Willard, *J. Chem. Phys.*, **40**, 3007 (1964).

17) R. J. Carter, W. H. Hamill, and R. R. Williams, *J. Am. Chem. Soc.*, **77**, 6457 (1955).

18) K. Hong and G. J. Mains, *J. Phys. Chem.*, **76**, 3337 (1972).

19) R. E. Rebbert and P. Ausloos, *J. Chem. Phys.*, **48**, 306 (1968).

20) J. H. Sullivan, *J. Chem. Phys.*, **30**, 1292 (1959); **36**, 1925 (1962).

21) A. Campion and F. Williams, *J. Am. Chem. Soc.*, **94**, 7633 (1972).

22) E. D. Sprague, *J. Phys. Chem.*, **77**, 2066 (1973).

23) M. A. Neiss and J. E. Willard, *J. Phys. Chem.*, **79**, 783 (1975).

24) T. Wakayama, T. Miyazaki, K. Fueki, and Z. Kuri, *Bull. Chem. Soc. Jpn.*, **44**, 2619 (1971).

25) H. Lutz and R. Sizmann, *Phys. Lett.*, **5**, 113 (1963).

26) G. R. Piercy, F. Brown, J. A. Davies, and M. McCargo, *Phys. Rev. Lett.*, **10**, 399 (1963).

27) M. T. Robinson and O. S. Oen, *Phys. Rev.*, **132**, 2385 (1963).

28) A. H. Mones and B. Post, *J. Chem. Phys.*, **20**, 755 (1952).

29) K. Watanabe, T. Nakayama, and J. Mottl, *J. Quant. Spectrosc. Radiat. Transfer*, **2**, 369 (1962).

30) J. W. Raymonda and W. T. Simpson, *J. Chem. Phys.*, **47**, 430 (1967).

Relation between Amounts of Chemisorbed Water and Ammonia on Zinc Oxide

Mahiko NAGAO and Tetsuo MORIMOTO

Department of Chemistry, Faculty of Science, Okayama University, Tsushima, Okayama 700

(Received June 7, 1976)

The adsorption isotherm of NH_3 was measured at 25 °C on ZnO surfaces with a controlled amount of surface hydroxyls. It was found that NH_3 can be chemisorbed at 25 °C on the dehydroxylated sites of ZnO in a 1:1 molecular ratio of adsorbed NH_3 to desorbed H_2O. H_2O can be chemisorbed for prechemisorbed NH_3 through exchange reaction to form surface hydroxyls and gaseous NH_3. The physisorption of NH_3 at 25 °C can take place only on a limited part of ZnO surfaces which were fully hydroxylated or ammoniated.

Adsorption studies with the use of NH_3 as a basic adsorbate provide valuable information on the acidic properties of solid surfaces. Many workers have endeavored to investigate the surface properties of silica–alumina and related compounds.[1-6] The principal technique employed was the infrared spectroscopy of NH_3 adsorbed on solid surfaces, giving information on the adsorbed state of the molecules. H_2O molecules are chemisorbed on metal oxides and form surface hydroxyls even at room temperature. They can be desorbed gradually by heating.[7-14] Thus, the surface acidity of a solid is expected to be considerably affected by the existence of surface hydroxyls.[1,15]

The amount of NH_3 adsorbed on hydrated surfaces of MgO or SiO_2 is larger than that on dehydrated ones, since the surface hydroxyls act as the adsorption sites for NH_3.[16,17] Blyholder and Richardson[18] concluded from infrared studies that the sites for chemisorption of NH_3 on α-Fe_2O_3 are the same as those for the chemisorption of H_2O. However, no quantitative relation between the amounts of chemisorbed NH_3 and desorbed hydroxyl has been given.

We have investigated the infrared spectroscopy of NH_3 and H_2O adsorbed on ZnO surfaces with controlled amount of surface hydroxyls.[19] It was found that the adsorbed state of NH_3 depends largely upon the amount of hydroxyls on the surface. We found that the chemisorption of CO_2 occurs on the dehydrated sites of ZnO in such a way that one molecule of CO_2 can be chemisorbed for the removal of two hydroxyls.[20,21] The surface hydroxyls on the fully hydroxylated $(10\bar{1}0)$ planes of ZnO having a wurtzite structure give rise to closed hydrogen bondings with each other, resulting in the appearance of discontinuity in the adsorption isotherm of H_2O because of weakened adsorption force of the surfaces for coming H_2O molecules.[22]

The present work has been undertaken to investigate quantitatively the adsorption of NH_3 on ZnO in connection with the amount of surface hydroxyls, *i.e.*, to investigate the relation between the amounts of chemisorbed NH_3 and dehydroxylated sites on the surfaces of ZnO with controlled amount of surface hydroxyls.

Experimental

Materials. The ZnO sample mainly used was Kadox15 (ZnO–K), prepared by the New Jersey Zinc Co., being the same as that used for infrared studies.[19] Another sample (ZnO–S) prepared by the Sakai Chemical Co. and employed for various examinations,[10,13,22-25] was used for the sake of comparing the data with those of ZnO–K. Both samples gave almost the same adsorption data (Table 1), though their transmittance for infrared beam differs substantially.[19,21]

Measurement of Specific Surface Area. The specific surface area of the samples was measured by the BET method with N_2 adsorption at the temperature of liquid N_2; assumption for the cross-sectional area of a molecule of N_2 was made to be 16.2 Å^2.

Measurement of Adsorption Isotherm. For samples pretreated at 450 °C in a vacuum of 10^{-5} Torr for 4 h, the adsorption isotherms of H_2O and NH_3 were determined volumetrically at 25 °C with a conventional adsorption apparatus equipped with greaseless cocks for NH_3 adsorption and oil-manometer for H_2O adsorption. The pretreatment of the sample at 450 °C *in vacuo* resulted in the removal of almost all the chemisorbed CO_2 and H_2O, leaving only a small amount of chemisorbed H_2O (1.00 OH groups/100 Å^2). The sample was then exposed to saturated H_2O vapor at 25 °C for 12 h, followed by evacuation at 25 °C, which left the fully hydroxylated surfaces with little amount of physisorbed H_2O.[10,13] The last sample was subjected to evacuation at various temperatures from 100 to 400 °C in order to obtain samples of different degrees of hydroxylation, which were used for the measurement of adsorption isotherms of NH_3.

Measurement of Surface H_2O and NH_3 Content. The amount of H_2O or NH_3 chemisorbed was determined by the successive-ignition-loss method.[11] The vapor liberated by heating the NH_3-adsorbed sample was analyzed in the following way. All the vapor evolved in a given temperature range, *e.g.*, 300—400 °C, was condensed in a trap kept in liquid N_2, reevaporated in a closed system at room temperature for measurement of the total pressure, and recondensed in a trap cooled at the dry ice–ethanol temperature at which the pressure of uncondensed gas of NH_3 was measured. After the sample was reevacuated at the dry ice–ethanol temperature, the remaining condensed H_2O, if present, was measured after reevaporation at room temperature. The same procedure was repeated by raising the temperature at appropriate intervals from 25 to 1000 °C. The surface H_2O content, which implies the amount of chemisorbed H_2O remaining on the surface, was calculated by summing the amount of H_2O evolved over the temperature indicated and by assuming that the H_2O content of the sample treated at 1000 °C is nil. The surface NH_3 content was similarly calculated.

Results and Discussion

Adsorption Isotherms of H_2O and NH_3 on ZnO. Figure 1 shows the adsorption isotherms of H_2O and NH_3 on the ZnO–K sample. Curves a and b are the adsorption isotherms of H_2O on the dehydroxylated and fully

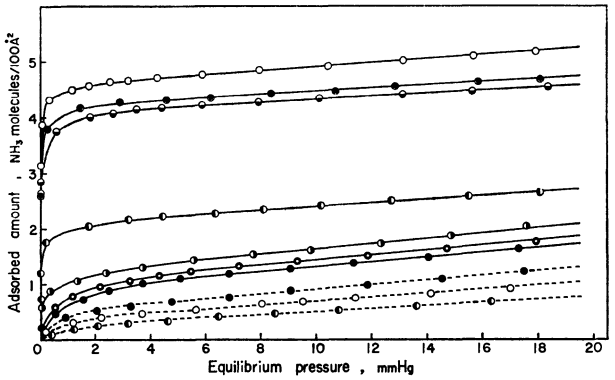

Fig. 3. Adsorption isotherms of NH_3 at 25 °C on differently hydroxylated ZnO prepared by degassing at various temperatures: ●, 25 °C; ◎, 100 °C; ◑, 200 °C; ◐, 300 °C; ◒, 350 °C; ⊙, 400 °C; ○, 450 °C. Solid line, first adsorption; broken line, second adsorption.

Recently, a similar exchange reaction was discovered on a system including H_2O vapor and the ZnO surface covered with chemisorbed CO_2, where CO_2 vapor was liberated from the surface in contact with H_2O vapor.[21]

Adsorption of NH_3 on ZnO with Controlled Amount of Surface Hydroxyls. The calculations (Table 1) suggest that one molecule of NH_3 can be chemisorbed on the sites formed by the desorption of H_2O. Figure 3 shows the adsorption isotherms of NH_3 at 25 °C on the ZnO samples on which the amount of surface hydroxyls was controlled by degassing the fully hydroxylated surfaces at different temperatures. Solid lines indicate the first adsorption isotherms and broken lines the second ones; some of the latter are omitted but they are all in this narrow range of adsorption amount. The results show that the amount of adsorbed NH_3 increases with increasing temperature of degassing and therefore with decreasing amount of the remaining hydroxyls. We can calculate the monolayer capacity of NH_3, $V_{m(h)}$, by applying the Langmuir equation to the isotherms (Fig. 3), and the amount of chemisorbed NH_3 by substracting the $V_{m(h)}$ value of the second adsorption from that of the first adsorption. The results obtained for the chemisorbed amount of NH_3 are plotted against the degassing temperature (Fig. 4), where the H_2O content of the same sample is also given. We see that the chemisorption of

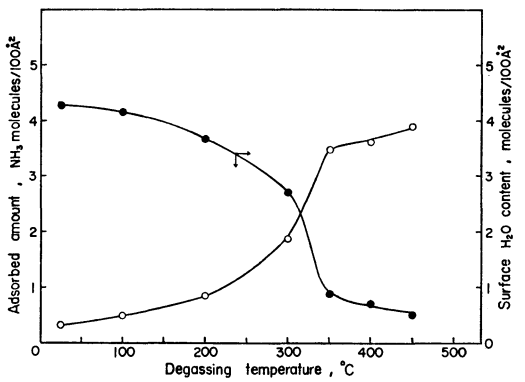

Fig. 4. Dependence of the amount of chemisorbed NH_3 and the surface H_2O content on degassing temperature.

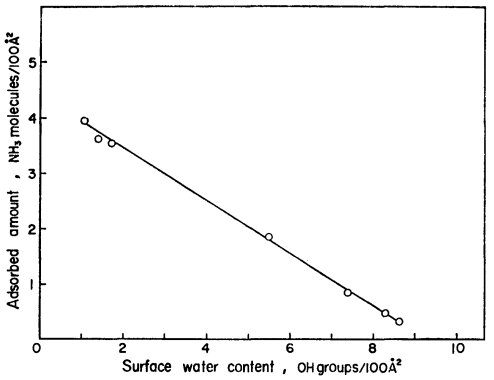

Fig. 5. Relation between the amount of chemisorbed NH_3 and the surface H_2O content.

NH_3 increases with the degassing temperature of the hydroxylated sample, a sharp increase being observed near 300—350 °C which corresponds to a sharp decrease in H_2O content of the sample, and that the sum of the H_2O content and the amount of chemisorbed NH_3 is almost kept constant. This can be seen more clearly from Fig. 5, where the amount of chemisorbed NH_3 is plotted against the remaining surface H_2O content, the linear relationship being observed between the two quantities. This strongly suggests that the chemisorption of NH_3 occurs on the dehydroxylated sites of ZnO in the ratio of one molecule of adsorbed NH_3 to one molecule of desorbed H_2O. A similar relation has been discovered on the chemisorption of CO_2 on ZnO surfaces.[20,21]

Physisorption of NH_3 on ZnO Surfaces. It might be of interest to infer the nature of a small number of physisorption sites for NH_3 at room temperature. The number of H_2O molecules physisorbed in the first layer on ZnO (Table 1) is identical to that of underlying hydroxyls,[13,22,25] while the number of physisorbed NH_3 molecules is less than half the number of underlying chemisorbed NH_3. For the surface hydroxyls, the number of physisorbed NH_3 molecules can be calculated from curve e (Fig. 1). This was found to be 1.50 molecules/100 Å^2, which is approximately the same as 1.35 for the surface with chemisorbed NH_3 (Table 1).

Infrared spectroscopy shows that the adsorption of NH_3 on the fully hydroxylated surface of ZnO takes place through hydrogen bonding and formation of NH_4^+ ions.[19] The hydroxylated (0001) or (000$\bar{1}$) planes of ZnO will be more active for physisorption of H_2O than the hydroxylated (10$\bar{1}$0) planes,[22] since they have isolated hydroxyls in contrast to the latter which have closed hydrogen bonding between surface hydroxyls. The former will also be more active for the physisorption of NH_3 than the latter, the sites on the surface defects such as corners, edges and steps being still more active. It seems that the adsorption of NH_3 occurs through hydrogen bonding on the isolated hydroxyls and through formation of NH_4^+ ions on the more active sites as stated above.

References

1) J. E. Mapes and R. P. Eischens, *J. Phys. Chem.*, **58**, 1059 (1954).

2) A. N. Sidorov, *Zhur. Fiz. Khim.*, **30**, 995 (1956).
3) L. M. Roev, V. N. Filimonov, and A. N. Terenin, *Optika Spektrosk.*, **4**, 328 (1958).
4) D. E. Nicholson, *Nature*, **186**, 630 (1960).
5) J. J. Fripiat, A. Léonard, and J. B. Uytterhoeven, *J. Phys. Chem.*, **69**, 3274 (1965).
6) M. R. Basila and T. R. Kantner, *J. Phys. Chem.*, **71**, 467 (1967).
7) G. J. Young, *J. Colloid Sci.*, **13**, 67 (1958).
8) C. M. Hollabaugh and J. J. Chessick, *J. Phys. Chem.*, **65**, 109 (1961).
9) J. J. Jurinak, *J. Colloid Sci.*, **19**, 477 (1964).
10) T. Morimoto, M. Nagao, and F. Tokuda, *Bull. Chem. Soc. Jpn.*, **41**, 1533 (1968).
11) T. Morimoto, M. Nagao, and F. Tokuda, *J. Phys. Chem.*, **73**, 243 (1969).
12) T. Morimoto, M. Nagao, and J. Imai, *Bull. Chem. Soc. Jpn.*, **44**, 1282 (1971).
13) M. Nagao, *J. Phys. Chem.*, **75**, 3822 (1971).
14) T. Morimoto, M. Nagao, and J. Imai, *Bull. Chem. Soc. Jpn.*, **47**, 2994 (1974).
15) E. P. Parry, *J. Catal.*, **2**, 371 (1963).
16) St. Malinowski, S. Szczepańska, A. Bielański, and J. Sloczyński, *J. Catal.*, **4**, 324 (1965).
17) V. I. Kvlividze, R. A. Brants, V. F. Kiselev, and G. M. Bliznakov, *J. Catal.*, **13**, 255 (1969).
18) G. Blyholder and E. A. Richardson, *J. Phys. Chem.*, **66**, 2597 (1962).
19) T. Morimoto, H. Yanai, and M. Nagao, *J. Phys. Chem.*, **80**, 471 (1976).
20) T. Morimoto and K. Morishige, *Bull. Chem. Soc. Jpn.*, **47**, 92 (1974).
21) T. Morimoto and K. Morishige, *J. Phys. Chem.*, **79**, 1573 (1975).
22) T. Morimoto and M. Nagao, *J. Phys. Chem.*, **78**, 1116 (1974).
23) T. Morimoto, M. Nagao, and M. Hirata, *Kolloid-Z. Z. Polym.*, **225**, 29 (1968).
24) M. Nagao and T. Morimoto, *J. Phys. Chem.*, **73**, 3809 (1969).
25) T. Morimoto and M. Nagao, *Bull. Chem. Soc. Jpn.*, **43**, 3746 (1970).

A Consideration on the Energy Efficiency of Agitation in Emulsion

Hisao HIDAKA, Shun'ichi NORO*, Akira TAKAMURA,* and Masumi KOISHI**

Department of Science and Engineering, Meisei University, Hodokubo, Hino-shi, Tokyo 191
**Meiji College of Pharmacy, Yato-cho, Tanashi-shi, Tokyo 188*
***Faculty of Pharmaceutical Science, Science University of Tokyo, Ichigaya Funakawara-machi, Shinjuku-ku, Tokyo 162*

(Received June 9, 1976)

The effects of mechanical factors on the energy efficieucy of agitation in o/w-type emulsions were investigated. The impeller diameters used were 49.0, 65.0, 80.1, and 89.9 mmϕ and the number of revolution was set at 200, 330, 400, 530, 660, or 812 rpm. The viscosity ratios (μ_d/μ_c) were 0.836: 1, 0.0861: 1, 0.000777: 1, and 0.000173: 1. The size of the dispersed liquid droplets was measured by the microphotographic method. The mean diameter of the droplets, their size distribution, and the agitation torque were determined, and the energy efficiency of agitation was evaluated. When the viscosity ratio was near 0.00861: 1, the energy efficiency of agitation showed a maximum. Furthermore, the energy efficiency decreased as the mean surface-volume diameter became smaller.

Agitation is one of the most important factors affecting the formation of emulsions when a specific emulsification method and specific emulsifying equipment are used:[1,2] more efficient agitation gives better emulsions. Now, the energy consumption related to agitation is considered to be due not only to the creation of new interfaces but also to setting the liquid in motion against viscous resistance in an emulsifying machine.[3,4] That is, the required input power of an agitator will depend upon various factors,[5] so it is very difficult to give a complete theoretical formula for agitation power. Even if the flow pattern is unknown, however, the relationship between agitation power and many mechanical factors may be formulated by the method of dimensional analysis, if the latter can be expressed in terms of such physical parameters as the diameter of the impeller and its rate of revolution.[6]

In this study, therefore, agitation power is first calculated from the torque value[7] and then the agitation energy[8] is evaluated as the product of agitation power and agitation time in the case of a liquid-liquid dispersion.[9] Secondly, the total interfacial energy of the emulsion is calculated as the product of the interfacial area and the interfacial tension.[8] The interfacial area is considered to be the most important factor[10] in the formation of emulsions and it is strongly affected by mechanical stirring. If the total interfacial energy and the agitation energy are calculated, the energy efficiency of agitation is then defined as the ratio of these two quantities.[8]

In this paper, therefore, the energy efficiency of agitation in the emulsion formation will be experimentally examined in relation to the impeller diameter, the revolution number, agitation torque, agitation power, the mean diameter of the dispersed phase, and interfacial tension.

Experimental

Equipment. The apparatus employed was the same one as described in our previous report.[11] The clear acrylate resin agitation tanks with 4 baffles were 150—200 mmϕ in diameter and 120—200 mm in depth. The stainless-steel agitation impeller (49.0—89.8 mmϕ) was of the standard Rushton-type with 6 blades. The tank was surrounded by a water jacket in order to keep the temperature of the liquid in it at 20.0 °C. The values of the tank diameter, the impeller diameter, and the number of revolution are summarized in Table 1.

TABLE 1. VALUES OF D_T, D_h, D_I, D_A, AND D_B OF THE APPARATUS EMPLOYED AND OF THE REVOLUTION NUMBER USED IN AGITATION

Tank size		Impeller size			Revolution number
D_T (mm)	D_h (mm)	D_I (mm)	D_A (mm)	D_B (mm)	N (rpm)
150	120	49.0	13.3	9.5	200, 330, 400,
		65.0	17.0	12.9	530, 660, 812
		80.1	19.9	15.9	
		89.8	24.9	17.1	
200	160	49.0	13.3	9.5	200, 330, 400,
		65.0	17.0	12.9	530, 660, 812
		80.1	19.9	15.9	
		89.8	24.9	17.1	
250	200	49.0	13.3	9.5	200, 330, 400,
		65.0	17.0	12.9	530, 660, 812
		80.1	19.9	15.9	
		89.8	24.9	17.1	

Measurement of Agitation Torque. The rotary torque meter used was of the Yamazaki SS-IR type (Yamazaki Seiki Laboratories) and was equipped with a stroboscope of the Sugawara PS-240 type (Sugawara Laboratory). The torque meter was tightly bound to the middle of the rotary shaft of the agitator, to prevent any precessional motion. Shortly after a liquid-liquid dispersion was formed, the torque was directly read with the light beam the stroboscope, which was exactly synchronized with the revolution of the impeller.

Measurement of Physical Properties. Mixtures of sodium silicate (Kishida Chemical Co.) and distilled water in varying ratios were used as the continuous phase. The total concentration of sodium silicate in the mixture ranged from 52.0 to 96.3% (w/w). The dispersed phase was made by mixing n-C_7H_{16} and CCl_4 in various volume ratios; the density was adjusted so as to be the same as that of the continuous phase (1.000—1.610 g/cm^3). Tween-20 (Tōhō Chemical Industry Co.) was employed as the emulsifying agent; its concentration was 0.1% (w/w). Interfacial tensions were measured by the ring method, and the viscosities of the liquid were measured by a rotating viscometer at 20.0±0.1 °C. The viscosity ratio, μ_d/μ_c, was widely varied, from 0.836: 1 to 0.000173: 1. The concentration of sodium silicate, the density of the continuous phase, the density ratio, the viscosity of the continuous phase,

TABLE 2. PHYSICAL PROPERTIES OF EACH CONTINUOUS PHASE

Concentration of sodium silicate (%, w/w)	Concentration of Tween-20 (%, w/w)	Density of continuous phase ρ_c (g/cm^3)	Density ratio ρ_d/ρ_c (—)	Viscosity of continuous phase μ_c (g/cm s)	Viscosity ratio μ_d/μ_c (—)	Interfacial tension $\lvert\gamma_d-\gamma_c\rvert$ (dyn/cm)
0.0	0.1	1.000	1.000	1.005	0.836	22.85
52.0	0.1	1.317	1.000	9.755	8.61×10^{-2}	15.62
75.0	0.1	1.486	1.000	97.60	8.61×10^{-3}	19.00
88.0	0.1	1.560	1.000	1082.0	7.77×10^{-4}	21.58
96.3	0.1	1.610	1.000	4860.0	1.73×10^{-4}	22.00

the viscosity ratio, and the interfacial tension are summarized in Table 2.

Experimental Procedure. The experiments were carried out under the following conditions:

(1) The viscosity ratios, μ_d/μ_c, used were 0.836: 1, 0.0861: 1, 0.00861: 1, 0.000777: 1, and 0.000173: 1.

(2) The tank diameters were 150, 200, and 250 mmϕ.

(3) The impeller diameters were 49.0, 65.0, 80.1, and 89.8 mmϕ.

(4) The revolution numbers of 200, 330, 400, 530, 660, and 812 rpm were employed.

The agitation tank was filled with 1960 ml of an aqueous sodium silicate solution, the continuous phase, containing Tween-20 as an emulsifying agent. The impeller was set at the center of the tank. In the middle of the impeller were gently placed 40 ml of a mixed solvent, the dispersed phase, to form a spherical drop.

The concentration of the dispersed phase was kept at 2.0% (w/w). Sixty minutes after agitation started, the liquid was sampled with a glass tube (5 mmϕ).

Each sample was photographed with a Nikon AFM camera equipped with a microscope. The diameters of the droplets were measured with a micrometer scale which had been photographed and enlarged under the same conditions. The number of droplets measured was one thousand in all cases. The mean length diameter, the mean surface diameter, the mean volume diameter, the standard deviation, and the particle size distribution were calculated by means of a Seiko-301 computer.

Calculation of Agitation Torque and Agitation Energy. The agitation power, P, can generally be represented, as shown below, by a function of the impeller diameter (D_I), revolution number (N), density of continuous phase (ρ_c), and viscosity of continuous phase (μ_c), when the dimensional analysis is applied to the case of turbulent flow.[12]

$$P = N_p(\rho_c N^3 D_I^5) \tag{1}$$

Here N_p is called the power number and is a function of impeller shape and Reynolds number.[13]

When the angular velocity of the impeller and the agitation torque are ω (rad/s) and T (kgw m), respectively, the agitation power P (kgw m/s) can be written as:

$$P = \omega T \tag{2}$$

Since the angular velocity is given by

$$\omega = 2\pi N \tag{3}$$

the agitation power can be written as:

$$\omega = 2\pi NT \tag{4}$$

Accordingly, if the agitation torque and the revolution number are exactly measured, the agitation power can be evaluated from Eq. 4.

When the agitation power is expressed in watts, the agitation energy E_A is given as the product of agitation power P and agitation time θ:

$$E_A = P\theta \tag{5}$$

Combining Eqs. 4 and 5,

$$E_A = 2\pi NT\theta \tag{6}$$

Consequently, the agitation energy can be obtained explicitly from Eq. 6.

Determination of the Energy Efficiency of Agitation. When the total interfacial area of the emulsion increases from S_1 to S_2, the increase in the total interfacial energy is calculated by the following equation:

$$E_s = \gamma(S_2-S_1) = \frac{6\gamma}{\rho_d}\left(\frac{1}{d_{sv_2}}-\frac{1}{d_{sv_1}}\right) \tag{7}$$

In order to investigate to what extent the agitation energy affects the increase in the total interfacial energy, the energy efficiency of agitation is defined as:

$$\eta = \frac{E_s}{E_A} = \frac{\gamma(S_2-S_1)}{P\theta} \tag{8}$$

Equation 8 gives the ratio of the total interfacial energy to the agitation energy, this is named the energy efficiency of agitation in mechanical dispersion. If the energy efficiency can be calculated under a certain agitation condition, it will be very useful for the research which looks for the optimum physical and mechanical conditions to obtain a good emulsion.

Results and Discussion

Relationship between Agitation Torque and Agitation Intensity. Agitation torques were measured at various impeller sizes and revolution numbers for two tank diameters, under a constant viscosity ratio in the range of μ_d/μ_c=0.836: 1—0.000173: 1. Figure 1 gives the relation between the agitation torque and the value of $\rho_c N^2 D_I^5$. The viscosity of the continuous phase was in the range of 1.005—4860 centi-poise, and its Reynolds number ranged from 2.63 to 110000. The log-log plot gives roughly the following experimental equation:

$$\log T = \alpha \log(\rho_c N^2 D_I^5) + \beta \tag{9}$$

where α is the slope of the straight line and β is the intercept on the ordinate.

From the data of previous reports, it is also quite certain that the agitation torque is approximately proportional to the agitation intensity,[14] $\rho_c N^2 D_I^5$, as obtained above. Table 3 gives the values of α and β calculated from Eq. 9 by the least-squares method. The interrelation coefficients are also listed in the same table. From Fig. 1, it is found that the agitation torque has a slightly higher value over the whole range of agitation

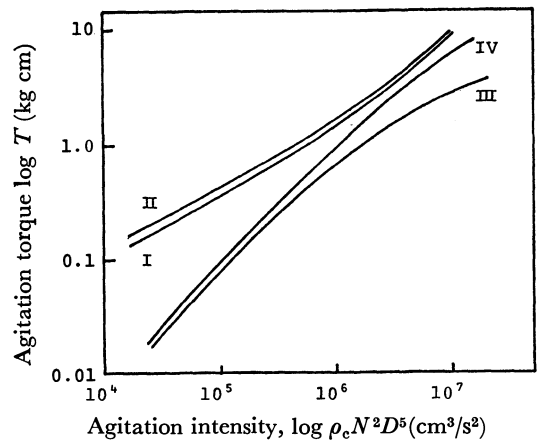

Fig. 1. Relation between agitation torque and agitation intensity at two tank diameters.
I: μ_c=4860 C.P., D_T=150 mmϕ, II: μ_c=4860 C.P., D_T=250 mmϕ, III: μ_c=1.005 C.P., D_T=150 mmϕ, IV: μ_c=1.005 C.P., D_T=250 mmϕ, Tween-20: 0.1% (w/w).

Table 3. The values of α and β calculated from Eq. 9 and of the interrelation coefficient

Viscosity ratio μ_d/μ_c	Tank diameter D_T (mm)	Slope α	Intercept at $\rho_c N^2 D_I^5=1$ β	Interrelation coefficient
8.36×10^{-1}	150	0.793	−5.003	0.991
	200	0.913	−5.629	0.994
	250	1.004	−6.131	1.000
8.61×10^{-2}	150	0.864	−5.332	0.992
	200	0.957	−5.828	0.997
	250	1.000	−6.065	0.999
8.61×10^{-3}	150	0.920	−5.645	0.998
	200	1.000	−6.085	1.000
	250	0.990	−6.010	0.999
7.77×10^{-4}	150	0.867	−5.194	0.999
	200	0.862	−5.155	0.999
	250	0.863	−5.157	1.000
7.77×10^{-5}	150	0.683	−3.868	0.997
	200	0.668	−3.740	0.997
	250	0.678	−3.788	0.996

intensity in the tank having a larger diameter. Furthermore, the agitation torque increases noticeably with increasing viscosity of the continuous phase, indicating that it is greatly affecting by the viscosity.

Effect of the Impeller Diameter on the Particle Size Distribution. The particle size distributions after 60 min of agitation, calculated from the length diameters of particles at three different impeller diameters, are shown in Fig. 2. At each impeller diameter, the size distribution had only one peak, at a particle size of about 12.5 μm. However, as the impeller diameter became smaller, the size distribution spread over a wider range of 5 to 50 μm.

Figure 3 shows changes in the mean surface-volume diameter of droplets at four impeller diameters and at three different viscosity ratios. At two viscosity ratios, 0.00861: 1 and 0.000173: 1, a plot of the mean surface-volume diameter against the impeller diameter gave

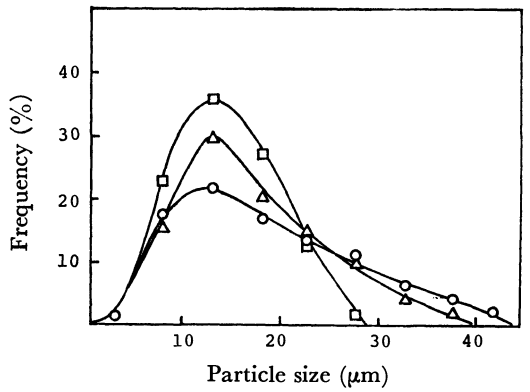

Fig. 2. Particle size distributions at three different impeller diameters.
N: 400 rpm, θ: 60 min, Tween-20: 0.1% (w/w), μ_d/μ_c: 8.61×10^{-3}: 1,
○: D_I=49.0 mm, △: D_I=65.0 mm, □: D_I=89.8 mm.

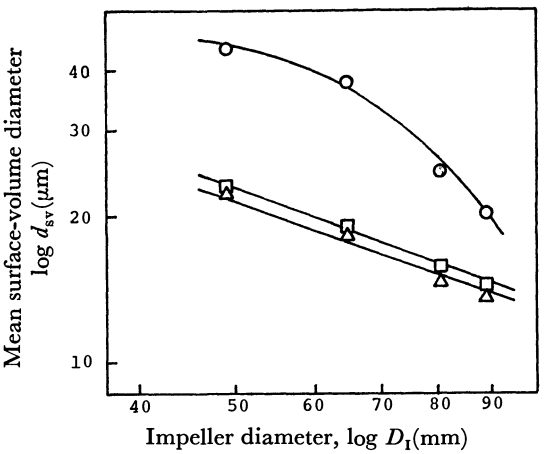

Fig. 3. Relation between mean surface-volume diameter and impeller diameter.
D_T: 150 mmϕ, N: 400 rpm, Tween-20: 0.1% (w/w), ○: μ_d/μ_c=0.836: 1, △: $\mu_d/\mu_c=8.61\times10^{-3}$: 1, □: $\mu_d/\mu_c=1.73\times10^{-4}$: 1.

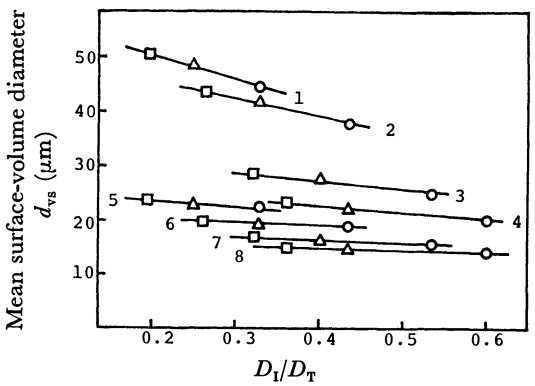

Fig. 4. Relation between mean surface-volume diameter and value of D_I/D_T.
N': 400 rpm, θ: 60 min, Tween-20: 0.1% (w/w).
○: D_T=150 mm, △: D_T=200 mm, □: D_T=250 mm.
1: μ_1, D_I=49.0 mm, 2: μ_1, D_I=65.0 mm, 3: μ_1, D_I=80.1 mm, 4: μ_1, D_I=89.8 mm, 5: μ_5, D_I=49.0 mm, 6: μ_5, D_I=65.0 mm, 7: μ_5, D_I=80.1 mm, 8: μ_5, D_I=89.8 mm.

approximately a straight line, while a convex curve was obtained at 0.836: 1, as illustrated in Fig. 3. The mean surface-volume diameter as measured at the same impeller diameter showed the smallest value when the viscosity ratio was 0.00861: 1. The relation between the mean surface-volume diameter and the diameter ratio of impeller to tank, D_I/D_T, is shown in Fig. 4. It was generally found that the mean surface-volume diameter decreased linearly with increase in the value of D_I/D_T. However, the slope of the straight line became smaller as both the impeller diameter and the viscosity of the continuous phase increased.

Effect of the Revolution Number on the Particle Size Distribution. The particle size distributions calculated by using the length diameters measured at three different revolution numbers are shown in Fig. 5. At each revolution number, the size distribution had only one peak, at a particle size of about 12.5 μm. However, the size distribution took a narrower and sharper shape with increase in the revolution number.

Figure 6 shows the relation between the mean surface-volume diameter of the droplets and the revolution number. When the continuous phase consisted of distilled water (μ_d/μ_c=0.836: 1) alone, a convex curve was observed. On the contrary, when the continuous phase consisted of a mixture of distilled water and sodium silicate (μ_d/μ_c=0.00861: 1 or 0.000173: 1), concave curves could be seen in the figure. In addition, the dependency of the mean surface-volume diameter on the viscosity ratio decreased remarkably at the highest revolution number (N'=812 rpm).

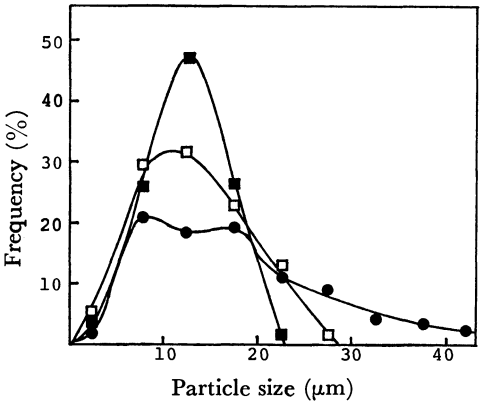

Fig. 5. Particle size distributions at three different revolution numbers.
D_I: 65.0 mm, D_T: 150 mm, θ: 60 min, Tween-20: 0.1% (w/w), $\mu_d/\mu_c=8.61\times10^{-3}$.
●: 330 rpm, □: 660 rpm, ■: 812 rpm.

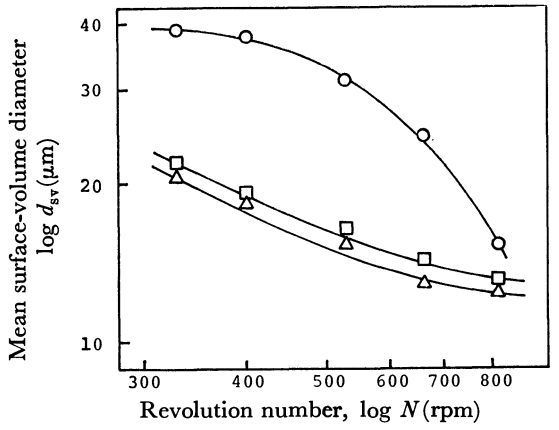

Fig. 6. Relation between mean surface-volume diameter and revolution number.
D_I: 65.0 mm, D_T: 150 mmϕ, Tween-20: 0.1% (w/w).
○: μ_d/μ_c=0.836: 1, △: $\mu_d/\mu_c=8.61\times10^{-3}$: 1, □: $\mu_d/\mu_c=1.73\times10^{-4}$: 1.

Effect of the Viscosity Ratio on the Particle Size Distribution. Changes in the mean surface-volume diameter with viscosity ratio are shown in Fig. 7. At each revolution number, the mean surface-volume diameter increased abruptly as the viscosity ratio approached unity. This tendency was particularly notable at two low revolution numbers, 330 and 400 rpm. On the other hand, the curves had a minimum value at a viscosity ratio of 10^{-2}: 1. In the region where the viscosity ratio is below 10^{-2}: 1, the curves were almost flat.

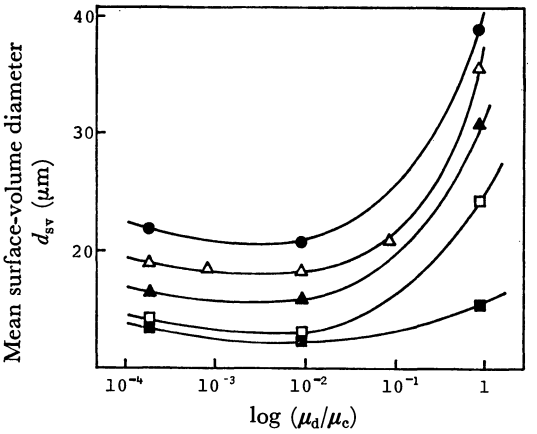

Fig. 7. Relation between mean surface-volume diameter and viscosity ratio.
D_I: 65.0 mm, D_T: 150 mm, θ: 60 min, Tween-20: 0.1% (w/w).
●: 330 rpm, △: 400 rpm, ▲: 530 rpm, □: 660 rpm, ■: 812 rpm.

Energy Efficiency of Agitation in Emulsion. In the present study, the agitation torque, the agitation power, and Reynolds number are as given below:

T: 0.025—8.5 (kgw cm), P: 0.045—73 (watt)

N_{Re}: 2.6—110000 (—)

Under the above conditions, we can now discuss the relation between the energy efficiency of agitation and the agitation conditions in order to obtain a valuable guide for finding the optimum conditions for making emulsions. In this study, the parameters characterizing agitation are chosen to be the viscosity ratio, the mean surface-volume diameter, and the agitation power.

First, the effect of the viscosity ratio on the energy efficiency is shown in Fig. 8. As can be seen from the figure, the relation gave a convex curve at each revolution number and each of the curves had a maximum value near μ_d/μ_c=0.00861: 1, except for the case of the high revolution number of 812 rpm. This means that the agitation power increases and, therefore, the agitation energy becomes higher as the viscosity of the conti-

nuous phase rises. On the other hand, the cohesion and coalescence of droplets during the agitation are obstructed by the high viscosity of the continuous phase, since subdivision of droplets occurs frequently and easily. Accordingly, when the viscosity ratio aproaches 0.00861: 1, the agitation energy and the interfacial energy are balanced.

Secondly, Fig. 9 shows the relation between the mean surface-volume diameter and the energy efficiency. It was found that the value of energy efficiency (μ_d/μ_c= 0.00861: 1 and 0.000173: 1) decreased linearly as the mean surface-volume diameter became smaller, while a concave curve was obtained at a viscosity ratio of 0.836: 1. This tendency can be interpreted as follows. For large droplets, break-up may be possible by only weak shear forces of agitation, while in small ones break-up may be impossible unless the droplets are subjected to strong shear forces of agitation. Thus, the probability for small droplets to burst may be low.

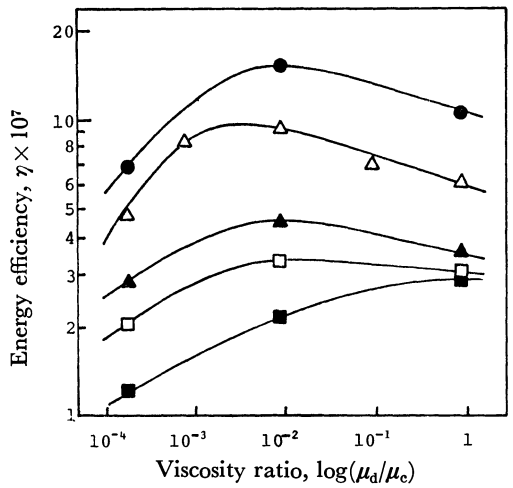

Fig. 8. Relation between energy efficiency and viscosity ratio.
D_I: 65.0 mm, D_T: 150 mmϕ, θ: 60 min, Tween-20: 0.1% (w/w).
●: 300 rpm, △: 400 rpm, ▲: 530 rpm, □: 660 rpm, ■: 812 rpm.

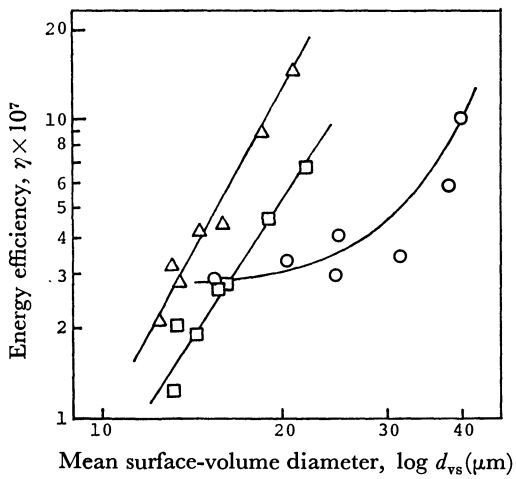

Fig. 9. Relation between energy efficiency and mean surface-volume diameter.
D_I: 65.0 mm, D_T: 150 mmϕ, θ: 60 min, Tween-20: 0.1% (w/w).
○: μ_d/μ_c=0.836: 1, △: $\mu_d/\mu_c=8.61\times10^{-3}$: 1, □: $\mu_d/\mu_c=1.73\times10^{-4}$: 1.

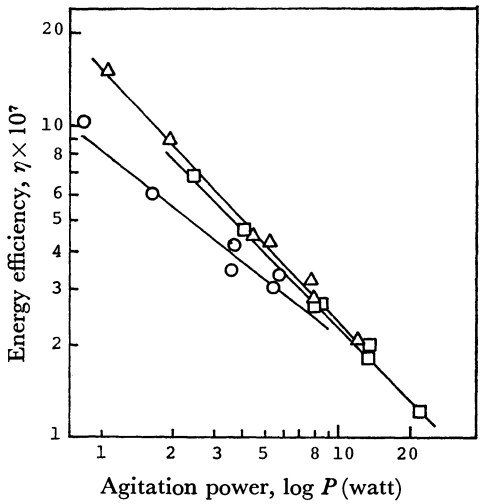

Fig. 10. Relation between energy efficiency and agitation power.
D_I: 65.0 mm, D_T: 150 mmϕ, θ: 60 min, Tween-20: 0.1% (w/w).
○: μ_d/μ_c=0.836: 1, △: $\mu_d/\mu_c=8.61\times10^{-3}$: 1, □: $\mu_d/\mu_c=1.73\times10^{-4}$: 1.

Finally, the relation between the energy efficiency and agitation power is shown in Fig. 10. The agitation power ranged from 1 to 20 watts. The energy efficiency decreased linearly as the agitation power increased. Thus, it is preferable to use as low an agitation power as possible in the formation of emulsions. In addition, the energy efficiency increased in the order of the viscosity ratios, μ_d/μ_c=0.00861: 1>μ_d/μ_c=0.000173: 1>μ_d/μ_c= 0.836: 1. Consequently, the effect of increasing the viscosity ratio is to decrease the rate of cohesion of the droplets, thereby raising the stability of the emulsions.

References

1) J. P. Ward and J. G. Knudsen, *AIChE J.*, **13**, 356 (1967).
2) A. A. Farugui, J. W. Finningan, C. H. Wright, and J. G. Knudsen, *AIChE J.*, **8**, 335 (1962).
3) P. Sherman, "Emulsion Science," Academic Press, New York (1968), p. 21.
4) S. V. Subramanyam and E. S. R. Gopal, *Ind. J. Technol.*, **5**, 139 (1968).
5) J. H. Rushton, E. W. Costich, and H. J. Everett, *Chem. Eng. Progr.*, **46**, 395 (1950).
6) T. Sasaki, *Kagaku Kogaku*, **31**, 432 (1967).
7) S. Tsukiyama and A. Takamura, *Chem. Pharm. Bull.*, **22**, 2607 (1974).
8) S. Tsukiyama, H. Takahashi, I. Takashima, and S. Hatano, *Yakugaku Zasshi*, **91**, 305 (1971).
9) S. Tsukiyama, A. Takamura, Y. Wakamatsu, and I. Takashima, *Yakugaku Zasshi*, **93**, 191 (1973).
10) M. Shigeta, T. Hayakawa, and S. Fujita, *Kagaku Kogaku*, **36**, 211 (1972).
11) S. Tsukiyama, A. Takamura, Y. Fukuda, and M. Koishi, *Bull. Chem. Soc. Jpn.*, **48**, 3561 (1975).
12) J. H. Rushton, D. E. Mack, and H. J. Everett, *Trans. Am. Inst. Chem. Engrs.*, **42**, 441 (1946).
13) S. Nagata, *Chem. Eng.*, **18**, 228 (1954).
14) S. Tsukiyama and A. Takamura, *Chem. Pharm. Bull.*, **23**, 616 (1975).

Copper Nuclear Quadrupole Resonance Spectra of Tris(tetramethylthiourea)copper(I) Tetrafluoroborate and Perchlorate

Yukio HIYAMA, Noriyuki WATANABE, and Eiji NIKI

Department of Industrial Chemistry, Faculty of Engineering, The University of Tokyo, Bunkyo-ku, Tokyo 113

(Received June 10, 1976)

^{63}Cu, ^{65}Cu NQR spectra of tris(tetramethylthiourea)copper(I) tetrafluoroborate ($[Cu(tmtu)_3]BF_4$) and tris(tetramethylthiourea)copper(I) perchlorate ($[Cu(tmtu)_3]ClO_4$) have been observed. The resonance frequencies are 27.390 MHz and 25.341 MHz in the BF_4 compound, 27.390 MHz and 25.340 MHz in the ClO_4 compound (23.0 °C). These results indicate that the crystal structure of $[Cu(tmtu)_3]ClO_4$ is very similar to that of $[Cu(tmtu)_3]BF_4$ and the copper valence has sp^2 hybridization with $p\pi$–$d\pi$ bonding. The temperature dependence of ^{63}Cu NQR of $[Cu(tmtu)_3]BF_4$ has been studied from −100 to +100 °C. A discontinuous point has been discovered at −11 °C.

Recently, copper(I) coordination compounds have been studied because of biochemical or stereochemical interest.

Tris(thiourea)copper(I) tetrafluoroborate[4] is a sulfur-bridged dimer with tetrahedral Cu(I), while bis(thiourea)copper(I) chloride contains trigonal planar CuS_3 in a chain structure. Several copper NQR spectra[1-3] of these compounds, for example $KCu(CN)_2$, have been studied. $[Cu(tmtu)_3]BF_4$ is a trigonal planar Cu(I) monomer,[4] and its chemical bonding is also very interesting. So we synthesized $[Cu(tmtu)_3]BF_4$ and $[Cu(tmtu)_3]ClO_4$, and measured the copper NQR of these compounds. Furthermore, the temperature dependence of the resonance frequency in the BF_4 complex was carefully studied.

Experimental

Materials. Tetramethylthiourea and copper(II) tetrafluoroborate were commercially obtained. Copper(II) perchlorate was prepared from copper(II) carbonate and perchloric acid.

Preparation of Compounds. $[Cu(tmtu)_3]BF_4$ was prepared by a method given by Weininger and Amma.[4] $[Cu(tmtu)_3]ClO_4$ was prepared by the same method except for copper(II) perchlorate. These compounds are quite pale and polycrystalline.

Analysis. The composition of these compounds was ascertained by C–H–N analysis. $[Cu(tmtu)_3]BF_4$—Found: C, 33.22; H, 6.90; N, 15.69%. Calcd for C, 32.94; H, 6.63; N, 15.36%. $[Cu(tmtu)_3]ClO_4$—Found: C, 32.15; H, 6.57; N, 14.92%. Calcd for: C, 32.19; H, 6.48; N, 15.01%.

Spectrometer. The search spectrometer was a noise-controlled superregenerative spectrometer that was built in our laboratory. The frequency measurement was made by use of the regenerative spectrometer that has been described[5] by Tsukada *et al.* The total error may amount to approximately 2 KHz.

Results and Discussion

^{63}Cu NQR spectra of $[Cu(tmtu)_3]BF_4$ are shown in Fig. 1. The observed resonance frequencies of the two compounds at 23.0 °C are given in Table 1.

Since ^{63}Cu or ^{65}Cu has a nuclear spin $I=3/2$, only a single NQR frequency $\nu=(e^2Qq/2h)(1+(\eta^2/3))^{1/2}$ is observed. Thus we cannot determine the coupling constant and the asymmetric parameter independently without a Zeeman study.

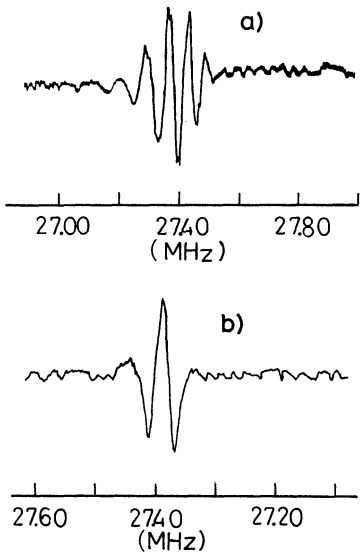

Fig. 1. ^{63}Cu NQR spectra of $[Cu(tmtu)_3]BF_4$. a) superregenerative spectrometer, b) regenerative spectrometer.

Table 1. Resonance frequency (MHz)

Compound	Temp	^{63}Cu	^{65}Cu
$[Cu(tmtu)_3]BF_4$	23.0°C	27.390	25.341
$[Cu(tmtu)_3]ClO_4$	23.0°C	27.390	25.340

According to the X-ray analysis by Weininger and Amma,[4] $Cu(tmtu)_3^+$ is distorted from a trigonal configuration. But we assume the asymmetric parameter η is zero for simplicity. On this assumption, we calculated the EFG (electric field gradient; q) of these compounds in Table 2. The EFG due to a 4p electron

Table 2. Value of the observed EFG

Compound	$q(\times 10^{15}$ esu cm$^{-3})$	
$[Cu(tmtu)_3]BF_4$	4.80	$Q(^{63}Cu)=-0.16$ barn
$[Cu(tmtu)_3]ClO_4$	4.80	
4p electron[6,a]	3.1	

a) determined from the constant of the magnetic hyperfine splitting, using the nuclear moment obtained by the nuclear induction method.

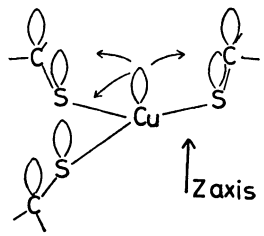

Fig. 2. $p\pi$—$d\pi$ bonding in $Cu(tmtu)_3^+$ ion. $3d_{z^2}$ (Cu) electron backdonates to π orbital (tmtu).

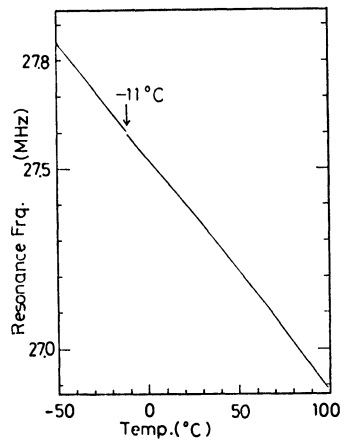

Fig. 3. Temperature dependence of ^{63}Cu NQR in $[Cu(tmtu)_3]BF_4$ (−50 to +100 °C). 28.763 MHz (−196 °C).

of the copper atom calculated by Korol'kov[6] is also shown in Table 2. So the EFG due to a sp^2 configuration (4s, 4p, $S=33\%$) is 3.1×10^{15} esu cm^{-3}. Since the BF_4^- ion is well separated from the copper atom, the EFG due to the negative ion is negligibly small.

The EFG observed around the copper atom in the $Cu(tmtu)_3^+$ is greater than that calculated for the sp^2 hybrid, quite covalent bond. We explain this by saying that the $3d_{z^2}$ electron of the copper backdonates to the π orbital of the ligands, and as a result the vacant $3d_{z^2}$ orbital enhances the EFG around the copper atom. Consequently we conclude that the EFG observed is due to sp^2 hybridization with $p\pi$–$d\pi$ bonding (Fig. 2).

The crystal structure of $[Cu(tmtu)_3]ClO_4$ has not yet been resolved. But we suggest that the crystal structure of the ClO_4 complex is close to that of the BF_4 complex, because of the similarity between the two EFG's.

Temperature Dependence. The temperature dependence of ^{63}Cu NQR in $[Cu(tmtu)_3]BF_4$ is shown in Fig. 3. The observed frequency gradient is very large ($d\nu/dT=-6.5$ kHz/°C) compared with that of Cu_2O (−3.3 kHz/°C). A discontinuous point has been discovered at −11 °C, but we could not ascertain any phase transition.

References

1) J. D. Graybeal and G. L. McKown, *Inorg. Chem.*, **5**, 1909 (1966).
2) G. A. Bowmaker, L. D. Brockliss, and R. Whiting, *Aust. J. Chem.*, **26**, 29 (1973).
3) G. A. Bowmaker, L. D. Brockliss, C. D. Earp, and R. Whiting, *Aust. J. Chem.*, **26**, 2593 (1973).
4) M. S. Weininger and E. L. Amma, *J. Chem. Soc., Chem. Commun.*, **1972**, 1140.
5) T. Tsukada, Y. Hiyama, N. Watanabe, and E. Niki, *Bunseki Kagaku*, **24**, 787 (1975).
6) V. S. Korol'kov and A. G. Makhanek, *Opt. Spektrosk.*, **12**, 87 (1962).

Associated Complex Formation in a Binary Solution and the Concentration Fluctuation: The Chloroform–Diethyl Ether System

Kenji IWASAKI, Yumiko KATAYANAGI, and Tsunetake FUJIYAMA

Department of Chemistry, Faculty of Science, Tokyo Metropolitan University, Setagaya-ku, Tokyo 158

(Received June 12, 1976)

The relations between the associated complex formation and the concentration fluctuation in a binary solution were derived. The concentration fluctuation of a chloroform–diethyl ether system was determined by observing light-scattering spectra at various concentrations. The theoretical values of the concentration fluctuation of this system were calculated from the proposed relation by the use of the shape and the number population of the associated complex, as determined from the infrared absorption intensity measurements. The observed and calculated concentration fluctuations agreed quite well.

The local fluctuation of the concentration is considered to afford information which is useful in understanding *mixing* from a molecular point of view. Based on this belief, a series of studies have been planned on analyses of the concentration dependence of the concentration fluctuation in solution through observation of the light-scattering spectra.[1)]

First, the relation between the concentration fluctuation and the Rayleigh intensities has been theoretically established.[2)] The concentration fluctuations for the chloroform–carbon disulfide system observed by this light-scattering method were compared with those obtained from the band-width of the infrared spectrum for the ν_1 fundamental of chloroform.[3)] The observed concentration dependence of the concentration fluctuation in the chloroform–carbon disulfide system indicated an associative tendency between the chloroform and carbon disulfide molecules.[2)]

The present report will concern itself with a study of the concentration dependence of the concentration fluctuation for a binary solution of the chloroform–diethyl ether system through the observation of light-scattering and infrared-absorption spectra. This system was chosen because (1 : 1)-complex formation between chloroform and diethyl ether has been well established with this dissociation equilibrium:

$$CHCl_3 : (C_2H_5)_2O \rightleftarrows CHCl_3 + (C_2H_5)_2O$$

Our main interest lies in the relation between the complex formation and the concentration fluctuation.

Theoretical

Ideal Solution. We start by considering the concentration fluctuation in an ideal binary solution whose components, A and B, behave as simple particles. In order to express the concentration fluctuation in terms of the number fluctuation of Component A, the volume area containing a constant quantity of Component B is to be considered. The volume of such an area changes in magnitude momentarily around its mean value. Therefore, the fluctuation of the mole fraction, x_A, of Component A arises from two factors: The exchange of A molecules between the inside and the outside of the area due to thermal motion of A molecules and the volume change in the area due to thermal motion of the B molecules. As the molecular number, n_B, of Component B is constant within the area under consideration, the fluctuation of x_A is expressed by the fluctuation of n_A. The mean fluctuation in n_A, $\langle(\Delta n_A)^2\rangle$, has been given as:[4)]

$$\langle(\Delta n_A)^2\rangle = \frac{kT}{(\partial\mu_A/\partial n_A)_{T,P}} \tag{1}$$

where k is the Boltzmann constant; T, the temperature; μ_A, the chemical potential of Component A, and P, the pressure. By definition,

$$x_A = \frac{n_A}{n_A + n_B} \tag{2}$$

Therefore,

$$dx_A = \frac{x_B}{n_A + n_B} dn_A \tag{3}$$

because n_B is constant. If the mixture of Components A and B is considered to be ideal, the chemical potential of Component A is given by:

$$\mu_A = \mu_A^\circ + kT \ln x_A \tag{4}$$

where μ_A° is the standard chemical potential. Equations 1, 3, and 4 are combined to become:

$$N\langle(\Delta x_A)^2\rangle = x_A(1 - x_A) \tag{5}$$

where

$$N = n_A + n_B$$

is the total number of molecules in the area under consideration.

Associated Complex Model. In the above discussion for an ideal solution, all the molecules in the solution are assumed to behave independently. In actual solutions, however, molecular species may be affected by a molecular species of the central molecule under consideration. This arises from the intermolecular interactions between the component molecules. In order to simplify the theoretical treatment, we wish to introduce the concept of an associated complex instead of considering intermolecular interactions explicitly. We will consider the formation of an associated complex, such as B_l or AB, in a binary solution of A and B components, where the suffix l indicates the number of molecules which form an associated complex. The associated complex, B_l or AB, is assumed to behave independently from the species A or B. In other words, the associated complex formation is considered to arise from strong intermolecular interactions, and the resultant complex is considered to have no interaction abilities with the other molecular species, A and B. Under these assumptions, we first calculate the concent-

ration fluctuation in a system of complete association, because such a system can be treated as a two-component system of A and B_l or A and AB.

Case I (A and B_l): Consider a case where strong intermolecular interactions are expected between B molecules in a binary solution of A and B molecules. We assume that a mixture of Components A and B is a two-component system of A molecules and associated complex molecules, B_l. If the effect of the volume difference between A and B_l is neglected, the binary mixture of A and B_l is an ideal solution. Therefore, the following relation is obtained directly from Eq. 5:

$$N'\langle(\Delta x_A')^2\rangle = x_A'(1-x_A') \tag{6}$$

where:

$$x_A' = \frac{n_A}{n_A+n_{B_l}} \tag{7}$$

and:

$$N' = n_A + n_{B_l} \tag{8}$$

and where n_A is the mean quantity of Component A in a small volume area which contains a constant number, n_{B_l}, of the B_l complex. As the $\Delta x_A'$, x_A', and N' which appear in Eqs. 6—8 are fictitious quantities, we have to rewrite these quantities in terms of real quantities, like Δx_A, x_A, and N. The true mole fraction, x_A, of Component A and the total number of molecules, N, in the volume range under consideration are expressed by these relations:

$$x_A = \frac{n_A}{n_A+ln_{B_l}} \tag{9}$$

and:

$$N = n_A + ln_{B_l} \tag{10}$$

From Eqs. 7—10, we obtain:

$$x_A' = \frac{lx_A}{(l-1)x_A+1}$$

or:

$$dx_A' = \frac{l}{\{(l-1)x_A+1\}^2}dx_A$$

and:

$$N' = \frac{(l-1)x_A+1}{l}N$$

Substituting the last three relations into Eq. 6, we finally obtain this relation:

$$N\langle(\Delta x_A)^2\rangle = -(l-1)x_A^3 + (l-2)x_A^2 + x_A \tag{11}$$

In Fig. 1 the results obtained from Eq. 11 are illustrated for various l values. The result for $l=1$ is identical with the result for an ideal binary solution of Eq. 5. It may be seen from the figure that the concentration fluctuation increases in magnitude as the association number, l, increases. The maximum of the fluctuation curve moves to the larger-mole-fraction side as the association number increases, until it arrives at $x_A=2/3$ for an infinite l. This may be understood reasonably by the following intuitive image. When x_A is large, that is, when n_B is small, a local concentration fluctuates mainly as a result of thermal motion of associated species in and out of the volume area. When x_A is small, on the other hand, a local concentration fluctuates mainly as a result of motion of non-associated species. The effect on the local concentration of the coming in and going out of one species may be supposed to be much larger in the former case than in the latter.

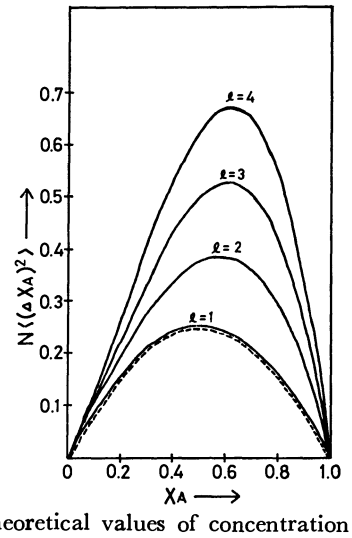

Fig. 1. Theoretical values of concentration fluctuation calculated from Eq. 11 for $l=1, 2, 3, 4$. The dashed line corresponds to the concentration fluctuation expected for an ideal binary solution.

Case II (A_l and B_l): Consider a case where strong intermolecular interactions are expected between A molecules and between B molecules. We assume that a mixture of Component A and B is a two-component system of associated complex molecules, A_l and B_l. Then, the calculation procedure is the same as that of Case I and the result is:

$$N\langle(\Delta x_A)^2\rangle = lx_A(1-x_A) \tag{12}$$

In Fig. 2 the results obtained from Eq. 12 are illustrated for various l values. In this case, the value of the concentration fluctuation is l times as large as that for an ideal binary solution.

Case III (A and AB): Consider a case where (1: 1) association between different species occurs in a binary mixture of Components A and B. The binary mixture of

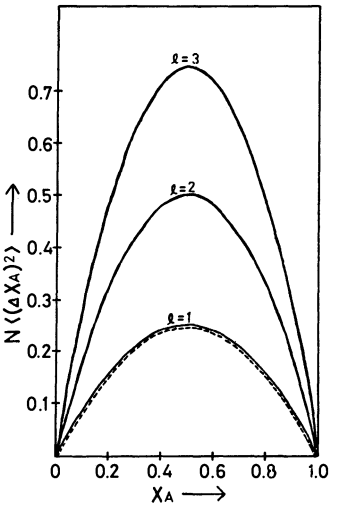

Fig. 2. Theoretical values of concentration fluctuation calculated from Eq. 12 for $l=1, 2, 3$. The dashed line corresponds to the concentration fluctuation expected for an ideal binary solution.

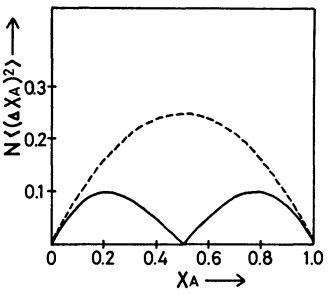

Fig. 3. Theoretical values of concentration fluctuation calculated from Eq. 13. The dashed line corresponds to the concentration fluctuation expected for an ideal binary solution.

A and B is composed of A and AB molecules for $x_A>0.5$ and of B and AB molecules for $x_A<0.5$. $N\langle(\Delta x_A)^2\rangle$ can be calculated similarly:

$$N\langle(\Delta x_A)^2\rangle = -2x_A{}^3 + 3x_A{}^2 - x_A \tag{13}$$

The results of Eq. 13 are shown in Fig. 3. It may be seen from the figure that the magnitude of the concentration fluctuation is smaller than that of an ideal solution for all the x_A values and that the concentration fluctuation has two maxima and takes a zero value at $x_A=1/2$.

Thus, we can understand roughly the relation between the shape of the associated complex and the concentration dependence of $N\langle(\Delta x_A)^2\rangle$ from the calculation of $N\langle(\Delta x_A)^2\rangle$ for the system of complete association. Association between the same species brings a larger $N\langle(\Delta x_A)^2\rangle$ than that of an ideal solution, while association between different species brings a smaller $N\langle(\Delta x_A)^2\rangle$.

Complex Formation with Association Equilibrium. Thus far we have discussed the concentration fluctuation for the system of complete association. In actual solutions, however, we have to take into account the association equilibrium between an associated complex and the component molecules. Consider a case where an association equilibrium of the form:

$$A + B \rightleftarrows AB$$

exists in a binary mixture of Components A and B. We assume that Components A and B and the AB complex behave as simple particles in the mixture. In other words, we consider an ideal ternary solution of A, B, and AB molecules. Under this assumption, we calculate the number fluctuation in the three-component system, and the result is reduced to the concentration fluctuation $N\langle(\Delta x_A)^2\rangle$.

Consider the fluctuations of the quantities, n_A and n_B, of A and B species in a small volume area which contains a constant number, n_{AB}, of the AB complex. The total number of molecules, N, in the volume area under consideration and the mole fraction, x_A, of Component A are expressed as:

$$x_A = (n_A+n_{AB})/N \tag{14}$$

and:

$$N = n_A + 2n_{AB} + n_B \tag{15}$$

From Eq. 14,

$$(\partial x_A/\partial n_A)_{n_B} = x_B/N \tag{16}$$

$$(\partial x_A/\partial n_B)_{n_A} = -x_A/N \tag{17}$$

Therefore,

$$\begin{aligned} dx_A &= (\partial x_A/\partial n_A)_{n_B}dn_A + (\partial x_A/\partial n_B)_{n_A}dn_B \\ &= (x_B/N)dn_A - (x_A/N)dn_B \end{aligned} \tag{18}$$

From Eq. 18, the mean square value of Δx_A is given as:

$$\langle(\Delta x_A)^2\rangle = \frac{x_B{}^2}{N^2}\langle(\Delta n_A)^2\rangle - 2\frac{x_Ax_B}{N^2}\langle\Delta n_A\Delta n_B\rangle + \frac{x_A{}^2}{N^2}\langle(\Delta n_B)^2\rangle, \tag{19}$$

In order to calculate $\langle(\Delta n_A)^2\rangle$, $\langle\Delta n_A\Delta n_B\rangle$, and $\langle(\Delta n_B)^2\rangle$, we define three imaginary mole fractions:

$$x_A' = n_A/N',\ x_B' = n_B/N',\ x_{AB}' = n_{AB}/N' \tag{20}$$

and:

$$N' = n_A + n_{AB} + n_B$$

In an ideal ternary solution of A, B, and AB, the corresponding chemical potentials are given as:

$$\mu_A = \mu_A{}^\circ + kT\ln x_A',$$

$$\mu_B = \mu_B{}^\circ + kT\ln x_B',$$

and:

$$\mu_{AB} = \mu_{AB}^\circ + kT\ln x_{AB}' \tag{21}$$

where $\mu_A{}^\circ$, $\mu_B{}^\circ$, and μ_{AB}° are the standard chemical potentials. Using the chemical potentials of Eq. 21, the number fluctuations are calculated to be:

$$\begin{aligned} &\langle\Delta n_A\rangle = \langle\Delta n_B\rangle = 0 \\ &\langle(\Delta n_A)^2\rangle = kTF_{BB}/(F_{AA}F_{BB}-F_{AB}{}^2) \\ &\langle(\Delta n_B)^2\rangle = kTF_{AA}/(F_{AA}F_{BB}-F_{AB}{}^2) \\ &\langle\Delta n_A\Delta n_B\rangle = -kTF_{AB}/(F_{AA}F_{BB}-F_{AB}{}^2) \end{aligned} \tag{22}$$

where:

$$F_{AA} \equiv \frac{\partial\mu_A}{\partial n_A},\ F_{BB} \equiv \frac{\partial\mu_B}{\partial n_B},\ F_{AB} \equiv \frac{\partial\mu_A}{\partial n_B} \tag{23}$$

Substituting Eq. 21 into Eq. 23, we obtain:

$$F_{AA} = \frac{kT(n_{AB}+n_B)}{n_AN'}$$

$$F_{BB} = \frac{kT(n_{AB}+n_A)}{n_BN'}$$

$$F_{AB} = \frac{-kT}{N'}$$

$$F_{AA}F_{BB}-F_{AB}{}^2 = \frac{(kT)^2n_{AB}}{n_An_BN'} \tag{24}$$

Now Eq. 22 can be rewritten as:

$$\langle(\Delta n_A)^2\rangle = \frac{n_A(n_A+n_{AB})}{n_{AB}}$$

$$\langle(\Delta n_B)^2\rangle = \frac{n_B(n_B+n_{AB})}{n_{AB}}$$

$$\langle\Delta n_A\Delta n_B\rangle = \frac{n_An_B}{n_{AB}} \tag{25}$$

The combination of Eq. 19 and 25 leads to:

$$\langle(\Delta x_A)^2\rangle = \frac{1}{N}x_A(1-x_A)(1-2n_{AB}/N)$$

Using the $x_{AB}=n_{AB}/N$ relation, we finally obtain the expression for the concentration fluctuation:

$$N\langle(\Delta x_A)^2\rangle = x_A(1-x_A)(1-2x_{AB}) \tag{26}$$

The x_{AB} can take the values from 0 to 0.5. When no complexes are formed, x_{AB} should be zero. Put $x_{AB}=0$, then Eq. 26 becomes:

$$N\langle(\Delta x_A)^2\rangle = x_A(1-x_A)$$

which is identical with Eq. 5. In the case of a complete (1:1) complex formation, x_{AB} can be replaced by either x_A or x_B. Then Eq. 26 is reduced to:

$$N\langle\Delta(x_A)^2\rangle = x_A(1-x_A)(1-2x_A)$$

which is identical with Eq. 13.

Experimental

In order to check the validity of the present theory, we have to observe the concentration fluctuation from the light-scattering spectra and the association equilibrium constant from infrared-absorption intensities.

Light-Scattering Measurements. The light-scattering spectra were recorded with a spectrometer designed and constructed in our laboratory.[1] The spectrometer is composed of a He-Ne gas laser source (NEC, GLG 108) and a pressure-scanning Fabry-Perot interferometer. The spacer between the interferometer etalons is 6 mm thick, giving a free spectral range of 0.82 cm^{-1} and an over-all instrumental half-width of about 0.042 cm^{-1}. The temperature inside the sample cell was maintained at 25.0±1.0 °C. The samples used in this experiment were commercially available reagents: Diethyl ether used without further purification and chloroform purified by column chromatography on alumina. The binary solutions of diethyl ether and chloroform were made dust-free by the use of a Millipore-filter FG (0.2 μm). The dust-free state was checked by comparing the observed L-P ratio of diethyl ether with the standard L-P ratio; the ratio of 0.41 was obtained by the present experiment, and that of 0.35 by Cummins.[5] The preparation (filtration and injection of a sample into cell) of the sample was repeated three times or more, and the sample which showed the best L-P ratio was used for further experiments. The refractive index of the sample was measured by means of a Shimadzu-Bausch-Lomb-Abbe refractometer 3L. The composition derivative of the refractive index at the mole fraction x was estimated from the difference between refrative indices measured at $x\pm0.05$.

Infrared-absorption Measurement. The chloroform-*d* was purchased from the Merck and Co., Ltd., and was dehydrated by zeorite A-3. The diethyl ether was purified by distillation with calcium hydride after the elimination of water by the use of zeorite A-3. The infrared-absorption spectra were recorded with a Perkin-Elmer 180 infrared spectrometer at the temperature of 25±1 °C. A sample cell with NaCl windows was used, and the thickness of a sample was determined by the interference-fringe method. The absorption spectra of the C-D stretching vibration for the frequency region of 2100—2400 cm^{-1} were measured under the resolution of 0.5 cm^{-1} and at the scanning speed of 7.0 cm^{-1}/min.

Results and Discussion

Light-scattering Spectra. The observed spectra for chloroform–diethy lether system are given in Fig. 4. It may be seem from the figure that the intensity of a Rayleigh line increases on passing from pure liquids to the binary solutions. The intensity of Brillouin lines, on the other hand, is largest for pure diethyl ether and smallest for pure chloroform. The intensity of a Rayleigh wing is weak and nearly constant along the frequency axis.

Concentration Fluctuation. Since the concentration fluctuation contributes only to a Rayleigh line, we can determine the concentration fluctuation from a Rayleigh intensity in a binary solution. In the previous report[2] we have shown the relation between the Rayleigh intensity of the light-scattering spectrum and the concentration fluctuation. The Rayleigh ratio for a Rayleigh line, $(R_{90})_R$, can be written approximately as:

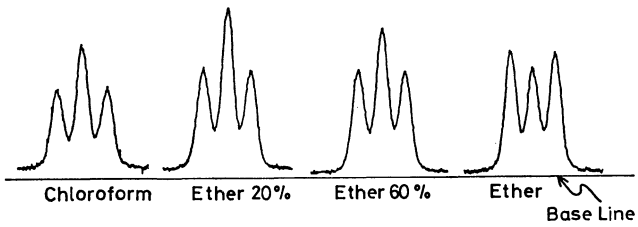

Fig. 4. Observed spectra for chloroform–diethyl ether system at 25 °C.

$$(R_{90})_R = \begin{pmatrix}\text{entropy-fluctuation}\\ \text{term}\end{pmatrix} + \begin{pmatrix}\text{concentration-}\\ \text{fluctuation term}\end{pmatrix}$$

Therefore, the concentration fluctuation, $V^*\langle(\Delta x_2)^2\rangle$, is given by:

$$V^*\langle(\Delta x_2)^2\rangle = (\lambda_i^4/\pi^2)\frac{1}{4n^2(\partial n/\partial x_2)^2_{T,P}}\{(R_{90})_R-(R_{90})_S\}, \quad (27)$$

where V^* is the fluctuation volume; x_2, the mole fraction of Component 2; λ_i, the wavelength of the incident light, and n, the refractive index. $(R_{90})_S$ is the Rayleigh ratio for entropy fluctuation and is given by:

$$(R_{90})_S = (\pi^2/\lambda_i^4)\frac{4kn^2T^2}{C_{Pg}\rho}(\partial n/\partial T)^2_{P,x_i} \quad (28)$$

where C_{pg} is the isobar heat capacity per gram, and ρ, the density.

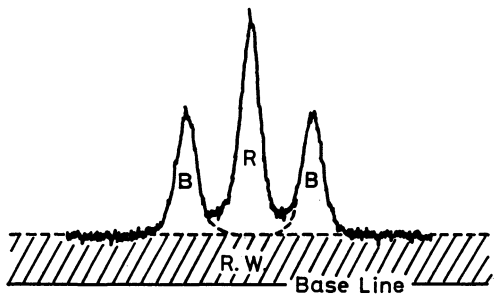

Fig. 5. Separation of Rayleigh line from light scattering spectra (schematic). R: Rayleigh line. B: Brillouin line. R.W.: Rayleigh wing.

The procedure of separating a Rayleigh line from Brillouin lines and a Rayleigh wing is illustrated in Fig. 5. A Rayleigh wing is assumed to be almost flat along a frequency axis. The outer halves of the Brillouin lines are assumed to be equal to non-overlapping line shapes. Thus, the intensity of a Rayleigh line was determined by eliminating the areas corresponding to the Rayleigh wing and the Brillouin lines.

Since the observed Rayleigh intensities are relative values, we have to express the observed relative intensities, I_R, in terms of Rayleigh ratios. A Rayleigh ratio is defined as Ir^2/I_0V_S, where I_0 is the incident-light intensity; I, the scattered-light intensity; r, the distance from scattering point to observing point, and V_S, the scattering volume. We first calculate $(R_{90})_S^{CHCl_3}$ for pure

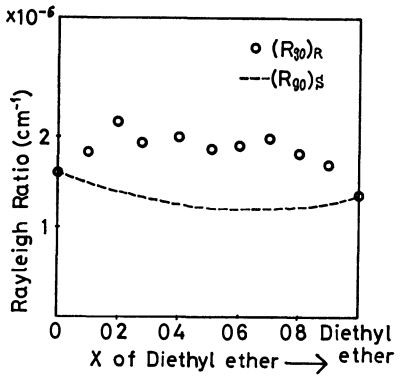

Fig. 6. Concentration dependence of Rayleigh intensity of chloroform–diethyl ether system. The open circles corresponds to $(R_{90})_R$ and the broken line $(R_{90})_S$.

chloroform by the use of Eq. 28. Then, the Rayleigh ratio for binary mixtures, $(R_{90})_R$, is calculated to be:

$$(R_{90})_R = I_R \times \frac{(R_{90})_S^{CHCl_3}}{I_R^{CHCl_3}} \tag{29}$$

where $I_R^{CHCl_3}$ is a relative Rayleigh intensity for pure chloroform. The calculated Rayleigh ratios are plotted by open circles in Fig. 6.

The theoretical values of $(R_{90})_S$ at each mole fraction were calculated by substituting the observed values of λ_i, n, T, ρ, and $(\partial n/\partial T)_{p,x_2}$, and C_{pg} values from the

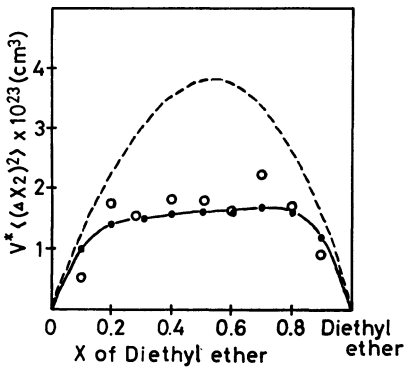

Fig. 7. Concentration dependence of concentration fluctuation for chloroform–diethyl ether system at 25 °C: ---; expected for an ideal binary solution, ○; observed by light scattering spectra, —●—●—; calculated from Eq. 26 by the use of the infrared data.

standard table[6] into Eq. 28 (see Table 1). Then, the fluctuation ability, $V^*\langle(\Delta x_2)^2\rangle$, was calculated at each concentration from Eq. 27. The calculated $V^*\langle(\Delta x_2)^2\rangle$ values are plotted by open circles in Fig. 7. The dashed line of Fig. 7 corresponds to the concentration fluctuation expected for an ideal binary solution. The procedure of converting $N\langle(\Delta x_2)^2\rangle$ into $V^*\langle(\Delta x_2)^2\rangle$ will be described later. It may be seen from the figure that the observed concentration fluctuation is smaller than that expected for an ideal binary solution throughout all concentrations. This tendency indicates the existence of molecular association, not between the same species (see Case I and II), but between different species (see Case III), in this mixture. Therefore, we will try to explain the observed concentration-fluctuation curve by the use of Eq. 26, because association equilibrium is taken into account in Eq. 26.

Determination of the Relative Population of (1: 1) Complex by Infrared-Absorption Measurements. The relative population of (1: 1) complex, x_{AB}, can be determined from the infrared-absorption-intensity measurement of the C-D stretching band (ν_1) of chloroform-*d*, because the ν_1 band increases in intensity in a diethyl ether solution by the formation of hydrogen bonding between chloroform-*d* and diethyl ether. The relative intensity of the ν_1 band of the chloroform-*d* in solution is defined as:

$$I_S = \frac{f_d}{l}\int_{band} \ln(I_0/I)\,d(\ln\nu) \tag{30}$$

in cm^{-1}, and the absolute intensities of the ν_1 bands of free and bonded chloroform-d are defined, respectively, as:

$$\Gamma_F = \frac{f_d}{C_F l}\int_{band} \ln(I_0/I)\,d(\ln\nu) \tag{31}$$

and:

$$\Gamma_B = \frac{f_d}{C_B l}\int_{band} \ln(I_0/I)\,d(\ln\nu) \tag{32}$$

in (cm^2/mole), where l is the thickness of the sample; C_F and C_B, the concentrations in moles per cm^3; I_0, the energy of the incident light; I, the energy of the transmitted light, and ν, the frequency of the light, and where the integration covers the whole band area. The subscript "B" refers to the chloroform-*d* forming a complex or to an associated complex. The f_d factor is

Table 1. Evaluation of concentration fluctuation from light-scattering spectra for the diethyl ether–chloroform system

Mole fraction of $(C_2H_5)_2O$	$(R_{90})_R$ (cm^{-1}) (25°C)	$(R_{90})_S$ (cm^{-1}) (25°C)	$\{(R_{90})_R-(R_{90})_S\}$ (cm^{-1})	n_D^{25}	$(\partial n/\partial x)_{T,P}$ (24°C)	$V^*\langle(\Delta x_2)^2\rangle$ (cm^3)
0	1.60×10^{-6}	1.60×10^{-6}	0×10^{-6}	1.4431	—	$-\times10^{-23}$
0.096	1.83	1.49	0.34	1.4345	0.105	0.60
0.198	2.16	1.40	0.76	1.4244	0.093	1.78
0.282	1.93	1.33	0.60	1.4168	0.089	1.54
0.395	1.99	1.26	0.73	1.4066	0.090	1.83
0.512	1.86	1.22	0.64	1.3980	0.086	1.79
0.597	1.90	1.22	0.67	1.3896	0.094	1.63
0.700	1.98	1.22	0.75	1.3810	0.085	2.23
0.802	1.82	1.24	0.58	1.3727	0.086	1.70
0.902	1.70	1.26	0.44	1.3621	0.106	0.88
1.000	1.35	1.27	0.08	1.3496	—	—

introduced to consider the intensity correction for the local-field effect,[7] which is defined as:

$$f_d = \frac{9n_D}{(n_D^2+2)^2} \tag{33}$$

where n_D is the refractive index of the sample. The three intensity parameters, I_S, Γ_F, and Γ_B, are related with each other as:

$$I_S = C_F\Gamma_F + C_B\Gamma_B \tag{34}$$

When chloroform-*d* and diethyl ether form a (1:1) complex, the analytical concentrations of free chloroform-*d* and diethyl ether, C_F° and C_E°, are related to the equilibrium concentrations by:

$$C_F = C_F^\circ - C_B \tag{35}$$

$$C_E = C_E^\circ - C_B \tag{36}$$

where C_E is the equilibrium concentration of diethyl ether. Notice that weak hydrogen bonding between chloroform-d molecules is neglected. Equations 34 and 35 are then combined to give:

$$I_S = C_F^\circ\Gamma_F + (\Gamma_B - \Gamma_F)C_B \tag{37}$$

Γ_F is directly measured in pure chloform-*d*, and I_S, in solution. As the frequency shift of the ν_1 band due to hydrogen bonding is about 10 cm^{-1}, ν_1 bands corresponding to the free and the bonded states overlap greatly with each other. Therefore, Γ_B cannot be determined directly from the intensity measurement of the ν_1 band corresponding to the bonded state. The value of Γ_B was obtained from the slope of the plots of I_S against C_F° in the low-concentration range of C_F° (see Fig. 8). It is assumed here that all the chloroform-*d*

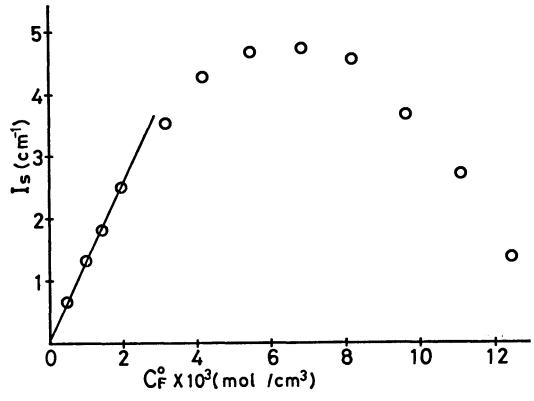

Fig. 8. I_S *vs.* C_F° plot for the chloroform-*d*-diethyl ether system.

molecules are hydrogen-bonded in the low-concentration range of C_F°. The Γ_B value of 1360 (cm^2/mol) and the Γ_F value of 109 (cm^2/mol) were obtained in the present work. As C_F° is known, C_B can be determined from I_S, Γ_F, Γ_B, and C_F° with the help of Eq. 37. C_B is reduced to x_{AB} as:

$$x_{AB} = \frac{C_B}{C_F^\circ + C_E^\circ} \tag{38}$$

Thus, we determined the relative population of the x_{AB} complex from the infrared-absorption measurements (see the 2nd column of Table 2).

Table 2. Evaluation of concentration fluctuation from Eq. 26 by the use of the infrared data for the diethyl ether–chloroform system

x_A [a]	x_{AB}	$N\langle(\Delta x_A)^2\rangle$	$V^*\langle(\Delta x_A)^2\rangle$ (cm^3)
0.10	0.10	0.072	0.99×10^{-23}
0.20	0.18	0.102	1.43
0.30	0.25	0.105	1.51
0.40	0.28	0.106	1.56
0.51	0.29	0.105	1.60
0.61	0.28	0.105	1.63
0.70	0.24	0.109	1.74
0.81	0.18	0.098	1.61
0.90	0.10	0.072	1.22

a) The subscript "A" refers to diethyl ether.

Comparison of Observed and Calculated $V^*\langle(\Delta x_2)^2\rangle$. As x_{AB} is obtained experimentally, $N\langle(\Delta x_2)^2\rangle$ can be calculated from Eq. 26. $N\langle(\Delta x_2)^2\rangle$ is related to $V^*\langle(\Delta x_2)^2\rangle$ by this relation:

$$V^*\langle(\Delta x_2)^2\rangle = \frac{N}{\rho_n}\langle(\Delta x_2)^2\rangle = \frac{N}{(\rho/M_{AV.})N_A}\langle(\Delta x_2)^2\rangle \tag{39}$$

and:

$$M_{AV.} = x_{ether}M_{ether} + x_{CHCl_3}M_{CHCl_3} \tag{40}$$

where ρ_n is the number density; N_A, Avogadro's number; x_{ether} and x_{CHCl_3}, the mole fractions of diethyl ether and chloroform respectively, and M_{ether} and M_{CHCl_3}, the molecular weights. In Fig. 7 the $V^*\langle(\Delta x_2)^2\rangle$ values calculated from Eqs. 39 and 40, using x_{AB} values determined by the infrared-intensity measurements, are compared with those obtained from the light-scattering data. It may be seen from the figure that these two sets of $V^*\langle(\Delta x_2)^2\rangle$ values agree quite well; this shows the validity of the present theoretical treatment of the concentration fluctuation.

Concluding Discussion. The present theoretical study has shown that the concentration dependence of the concentration fluctuation in a binary solution is quite sensitive to the formation of local structures or intermolecular interactions. If molecules of same chemical species have a tendency to get together, the concentration fluctuation takes larger values than those in an ideal binary solution. On the other hand, if molecules of different chemical species have a tendency to get together, the concentration fluctuation takes smaller values than those in an ideal binary solution. For a binary solution of chloroform–diethyl ether, the theoretical treatment corresponds to the calculation of the concentration fluctuation in a ternary solution. The pivotal point of the theory is the introduction of the shape and the number population of an associated complex. In the case of a chloroform–diethyl ether system, the shape and the number population can be determined by means of the infrared-absorption spectra. The very good agreement between the concentration fluctuation observed by the light-scattering spectra and the concentration fluctuation calculated using the infrared data shows that intensity measurements of light-scattering spectra can determine the shape and the number population of an associated complex which is

formed in a binary solution. It must be emphasized that the concept of an associated complex was introduced so as to simplify the theoretical treatment; therefore, the concept of complex formation is a rather fictitious concept. In other words, the present theory postulates the usefulness of light-scattering measurements for the study of local structures which are formed in solutions by intermolecular interactions between component molecules.

References

1) K. Iwasaki, M. Tanaka, and T. Fujiyama, *Bunko Kenkyu*, **25**(3), 134 (1976).
2) K. Iwasaki, M. Tanaka, and T. Fujiyama, *Bull. Chem. Soc. Jpn.*, **49**, 2719 (1976).
3) T. Fujiyama, M. Kakimoto, and T. Suzuki, *Bull. Chem. Soc. Jpn.*, **49**, 606 (1976).
4) L. D. Landau and E. M. Lifshitz, "Statistical Physics," Pergamon Press, London (1958).
5) H. Z. Cummins and R. W. Gammon, *J. Chem. Phys.*, **44**, 2785 (1966).
6) "International Critical Tables," McGraw-Hill, New York (1926).
7) S. R. Polo and M. K. Wilson, *J. Chem. Phys.*, **23**, 2376 (1955).

The Primary Process of the Photochemical Formation of 1-Nitrenopyrene

Minoru SUMITANI, Saburo NAGAKURA, and Keitaro YOSHIHARA*,**

Institute for Solid State Physics, The University of Tokyo, Roppongi, Minato, Tokyo 106
**Institute of Physical and Chemical Research, Wako, Saitama 351*

(Received June 18, 1976)

The primary process of the photo-decomposition of 1-azidopyrene (Py–N_3) was studied with the aid of nanosecond time-resolved laser photolysis. An excited singlet 1-nitrenopyrene (Py–N) was identified as an intermediate for the formation of the ground triplet nitrene. The direct photo-decomposition of 1-azidopyrene occurs through Py–N_3* (singlet)→Py–N* (singlet)→Py–N (triplet). The lifetime of the excited singlet nitrene was found to be 22 ns at room temperature in benzene and was found to be slightly longer at 77 K.

Organic azides decompose photochemically or thermochemically to corresponding nitrenes which are known as intermediates in various kinds of reactions; cyclization, reduction, oxidation, and dimerization.[1,2] The ground states of the nitrenes produced by the photo-decomposition of the azides are known to be in the triplet state;[3-5] the eliminated nitrogen molecule is in the singlet state.[6] The existence of the triplet nitrenes as reaction intermediates has been confirmed by flash-photolysis experiments[7-11] and also by measurements of the electronic absorption and ESR spectra of the rigid solutions at low temperature.[3-5,12-16] From the spin conservation rule for the reaction, two paths are conceivable for triplet nitrene formation. One of them is the "singlet mechanism" occurring through the excited singlet nitrene (R–N*(singlet)) and the other is the "triplet mechanism" through the excited triplet azide (R–N_3(triplet)).

$$\begin{array}{ccccc} \text{R–N}_3 & \xrightarrow{h\nu} & \text{R–N}_3\text{*(singlet)} & \longrightarrow & \text{R–N*(singlet)} + \text{N}_2 \\ & & \downarrow & & \downarrow \\ & & \text{R–N}_3\text{ (triplet)} & \longrightarrow & \text{R–N (triplet)} + \text{N}_2 \\ & & \text{azide} & & \text{nitrene} \end{array}$$

From quenching experiment Reiser and Leyshon[17] showed that phenyl azide in the excited singlet state directly decomposes to the singlet nitrene and nitrogen before it is transferred to the triplet azide by intersystem crossing. In the flash-photolysis experiment Lehman and Berry[11] found that the decay time from the excited singlet state to the ground triplet state was shorter than 6 μs for some organic nitrenes, but they could not detect any singlet nitrenes. The excited singlet nitrenes spectroscopically observed so far are limited to such simple nitrenes as NH, NF, and NCN[18-23] in the gaseous state.

The main purpose of the present study is to observe directly the excited singlet 1-nitrenopyrene (Py–N) by nanosecond laser photolysis and to elucidate the mechanism of the photo-decomposition of 1-azidopyrene (Py–N_3). The compound is suitable for this purpose since the photo-decomposition quantum yield is very large and the absorption peaks characteristic of Py–N_3 and the ground triplet and excited singlet Py–N can easily be distinguished from one another.

**Present address: Institute for Molecular Science, Myodaiji, Okazaki 444.

Experimental

The details of laser photolysis experiment were reported elsewhere.[24] We used a coaxial type N_2 laser (peak power at 337.1 nm, 100 kW; pulse duration, 7 ns FWHM) as a light source for the direct excitation of samples. A monitor light (an EG and G FX-131 flash lamp) was detected with a Hamamatsu TV R666 photomultiplier and a Tektronix 465 oscilloscope.

The sensitized photo-decomposition experiment of Py–N_3 was carried out by using biacetyl as a triplet sensitizer. Biacetyl purified by distillation under a nitrogen atmosphere was excited with a dye laser at 423.0 nm (peak powder, 70 kW; pulse duration, 6 ns FWHM). For the excitation of dye, we constructed a travelling-wave type N_2 laser (peak power, 1 MW; pulse duration, 6 ns FWHM) originally designed by Godard.[25] The dye laser is of a Hänsch type,[26] a Bausch and Lomb grating of 600 grooves per mm and with a blaze wavelength of 500 nm being used. POPOP (1,4-bis(5-phenyl-2-oxazolyl)benzene) in a methanol–dioxane 1:1 mixture was used as a lasing dye. The photolysis system with the dye laser is shown in Fig. 1.

1-Azidopyrene[27] was purified with alumina column chromatography under red light. The effect of oxygen on the reaction was carefully investigated. We observed no oxygen effect on the primary process; therefore, the sample was used

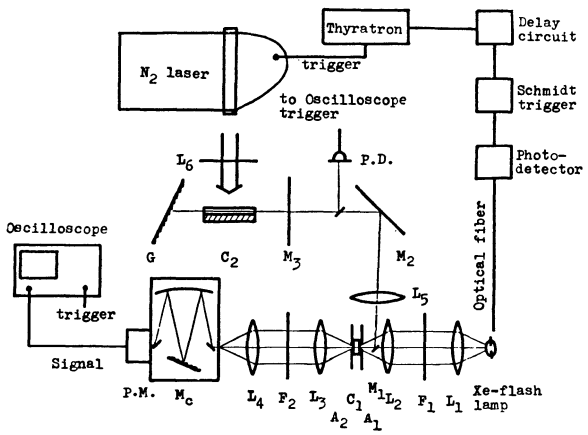

Fig. 1. Block diagram of the flash photolysis apparatus with the dye laser.
$A_{1,2}$: Apertuer, L_6: cylindrical lens, C_1: sample cell, $M_{1,2}$: 100% mirror, C_2: dye cell, M_3: 20% mirror, $F_{1,2}$: filter, M_c: monochromator, G: grating, P.M.: photomultiplier, L_{1-5}: Spherical lens, P.D.: biplanar photodiode.

with no deaeration. Since the overall reaction was completed with a single laser shot and gave a final product, sample solutions were either flowed through a sample cell or replaced by a new one at each experiment.

Results and Discussion

Direct Photolysis of Py–N_3 with an N_2 Laser. The time-resolved absorption spectra for the direct photolysis of Py–N_3 (3.6×10^{-4}M) in benzene were measured at room temperature. The results are shown in Fig. 2. We can see that two different absorptions appear at 450 nm and at 415 nm with an isosbestic point at 425 nm and that the 415 nm band increases in intensity with the decay of the 450 nm band. The time dependence of the absorption intensities was measured at various wavelengths. The results measured at 415, 430, and 450 nm are shown as examples in Figs. 3(a), (b), and (c), respectively. The absorption maximum at 415 nm of the long-lived component increases in intensity quickly at first, gradually approaches a constant value, and hardly exhibits any decay in the observed time range of 5 μs (Fig. 3a). On the other hand, the absorption maximum at 450 nm of the short-lived component decays quickly to reach a constant value (Fig. 3c). The intensity at 430 nm near the isosbestic point is almost time-independent (Fig. 3b). The absorptions of both components overlap each other in the observed wavelength region. But, by the deconvolution of oscilloscope traces we could determine the rise-time constant for the long-lived component to be 4.5×10^7 s^{-1} and the decay-time constant for the short-lived component to be 4.4×10^7 s^{-1}. Both values agree well with each other. This leads us to the conclusion that the short-lived component is the precursor of the long-lived component.

The absorption spectrum of the long-lived component

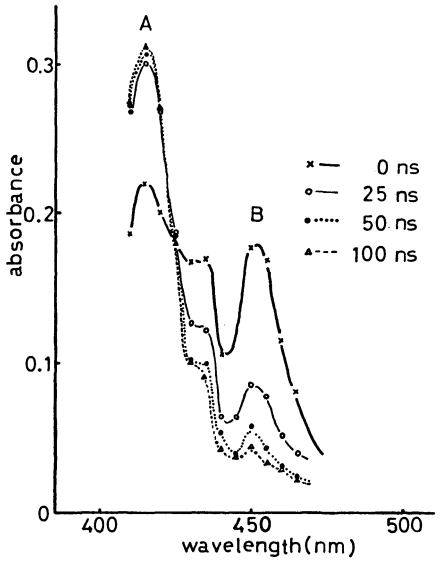

Fig. 2. Time-resolved transient absorption spectra for the direct decomposition of Py–N_3 (3.6×10^{-4} M in benzene): —×—, immediately after; —○—, 25 ns after; ···●···, 50 ns after; and ···△···, 100 ns after an N_2 laser pulse reached its maximum intensity.

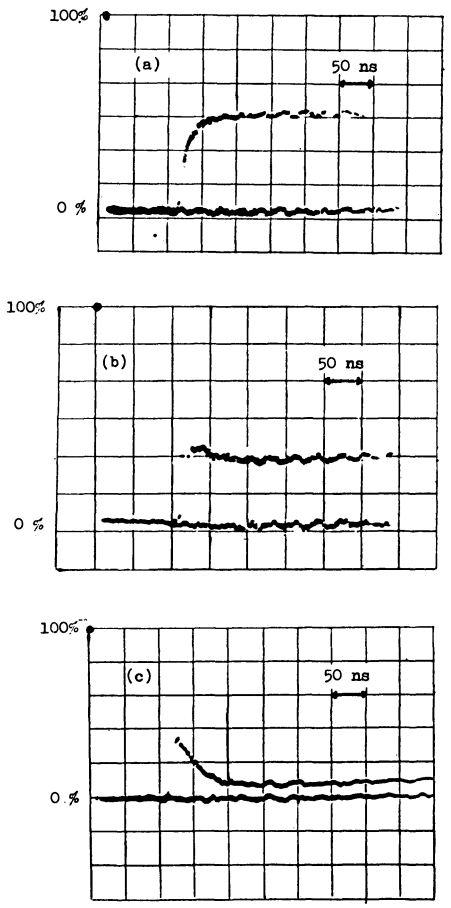

Fig. 3. Oscilloscope traces of transient absorption intensities in the direct photo-decomposition of Py–N_3 observed at (a) 415 nm, (b) 430 nm, and (c) 450 nm.

is the same as that of the ground triplet Py–N observed by Yamaoka *et al.*[10] Therefore it is concluded that the ground triplet Py–N is produced through the short-lived species with the absorption maximum at 450 nm.

The molar extinction coefficient at 450 nm of the short-lived component was determined to be $\approx2\times10^4$ cm^{-1} M^{-1} from comparison with that of the $T_1\leftarrow T_0$ absorption at 415 nm.[10] This value was estimated on the reasonable assumption that all the short-lived component molecules were transferred to T_0.

$T_1\rightarrow T_0$ Fluorescence of Nitrene. At the liquid nitrogen temperature, Py–N was produced photochemically with the N_2 laser and its emission was observed for the solution in the methylcyclohexane–isopentane 1 : 1 mixed solvent with the result shown in Fig. 4. The emission spectrum holds a mirror-image relationship to the $T_1\leftarrow T_0$ absorption spectrum of the ground triplet nitrene. This means that the observed emission is due to the $T_1\rightarrow T_0$ fluorescence of Py–N. The fluorescence-decay time was found to be shorter than 7 ns. Therefore the lifetime of the excited triplet states of Py–N is much shorter than the lifetime of the 450 nm species (22 ns). This clearly demonstrates that the precursor (the 450 nm species) of the ground triplet nitrene is not the excited triplet nitrene.

Quenching Experiment. In order to elucidate the role of the triplet state in the photo-decomposition of

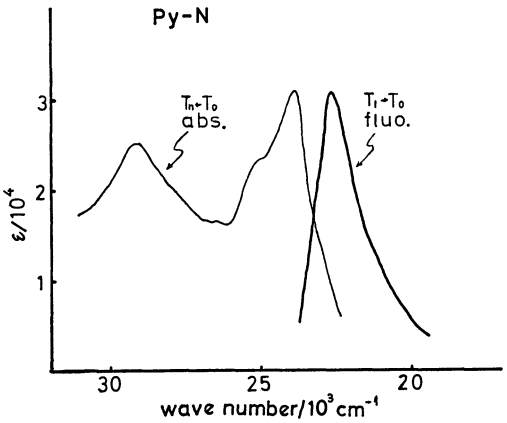

Fig. 4. The $T_1 \rightarrow T_0$ fluorescence (77 K) and absorption spectra of Py-N. The absorption spectrum is taken from Ref. 10.

$Py-N_3$, we examined the effect of triplet quenchers. The lowest triplet state of $Py-N_3$ has never been observed spectroscopically,[28] but its energy may roughly be estimated to be 56—46 kcal/mol. This is because in most of the organic azides the lowest triplet state is located 20—30 kcal/mol lower than the singlet state[29] and the singlet state energy (E_S) is 76 kcal/mol for $Py-N_3$. Thus, 1,3,5-cycloheptatriene ($E_T \approx 50$ kcal/mol), *trans*-stilbene ($E_T = 47$ kcal/mol), and oxygen can be used as triplet quenchers for the photo-decomposition of $Py-N_3$. The quenching experiment using these three molecules as quenchers exhibited no definite effect. Therefore, we concluded that the main reaction path is not *via* the triplet $Py-N_3$ and that the singlet mechanism is applicable to the direct photo-decomposition of $Py-N_3$. Lewis and Saunders[30] also observed no effect of the triplet quencher upon the direct photolysis of some alkyl azides.

Sensitized Photolysis of $Py-N_3$ with a Dye Laser. In order to obtain further support for the singlet mechanism, we induced the N_2 elimination reaction by the selective excitation to the triplet state of $Py-N_3$. Biacetyl ($E_S = 65.0$, $E_T = 56.0$ kcal/mol) is one of the sensitizers for the triplet excitation of $Py-N_3$ (see Fig. 5). We selectively excited biacetyl at 423.0 nm with a dye laser. The reaction occurred and the ground triplet nitrene was produced efficiently. This was confirmed by detecting the $T_1 \leftarrow T_0$ absorption at 415 nm. The oscilloscope trace for this experiment is shown in Fig.

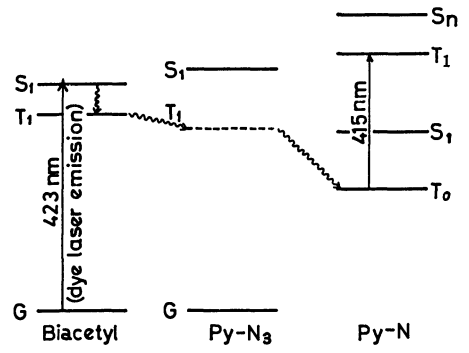

Fig. 5. Energy level diagrams of $Py-N_3$, biacetyl, and Py-N.

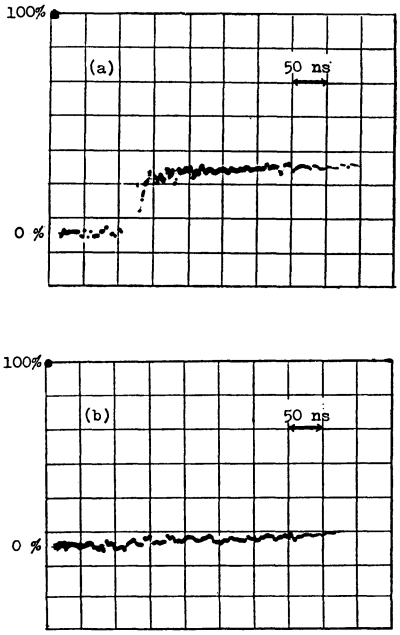

Fig. 6. Oscilloscope traces of transient absorption intensities in the sensitized decomposition of $Py-N_3$ (8.7×10^{-2} M in benzene) observed at (a) 415 nm and (b) 450 nm.

6(a). We can see that in the sensitized photolysis of $Py-N_3$ the short-lived absorption at 450 nm can not be observed (Fig. 6(b)).

The present experimental results of the lifetime of the excited triplet nitrene, the effect of the triplet quenchers on the photo-decomposition, and the sensitized photolysis completely obviate the triplet mechanism for the direct photo-decomposition of $Py-N_3$ and support the singlet mechanism. This means that the short-lived species with the absorption at 450 nm is the excited singlet state of either $Py-N_3$ or Py-N. In general, the lifetime of the excited singlet state of azide can be expected to be much shorter than 7 ns (the limitation of the time resolution of the present experimental apparatus), in view of the fact that it is not fluorescent. The observed lifetime is 22 ns for the 450 nm species. This safely eliminates the possibility that the 450 nm species is the excited singlet state of $Py-N_3$. Thus, the absorption band at 450 nm is due to an excited singlet state of Py-N.

$S_1 \rightarrow T_0$ Fast Intersystem Crossing of Py-N. The excited singlet nitrene is relaxed by the $S_1 \rightarrow T_0$ intersystem crossing to the ground triplet nitrene with a lifetime of 22 ns. The singlet nitrene is known as a strong hydrogen abstracting agent in protic solvents. In benzene, however, we did not detect 1-aminopyrene. The excited singlet Py-N in this solvent dimerizes to form azo compounds (*cis*- and *trans*-azopyrene) after the relaxation to the ground triplet Py-N.[10] Furthermore, we observed that the lifetime becomes longer (34 ns) only slightly in a rigid solution (methylcyclohexane–isopentane = 1 : 1) at 77 K. These results lead us to the conclusion that the lifetime is not determined by the chemical reaction rate but mainly by physical processes such as intersystem crossing. Lehman and Berry[11] estimated the rate of intersystem crossing for the excited singlet phenyl-

nitrene and naphthylnitrene to be faster than 6 μs but could not succeed in observing the nitrenes spectroscopically. The present experiment is the first direct observation of the excited singlet state of organic nitrene in solution.

The authors would like to express their thanks to Dr. Tsuguo Yamaoka, Chiba University, for his kindness in preparing 1-azidopyrene.

References

1) G. Lábbe, *Chem. Rev.*, **68**, 345 (1968).
2) W. Lwowski, ed., "Nitrenes," Interscience, New York, N. Y. (1970).
3) G. Smolinsky, L. G. Snyder, and E. Wasserman, *Rev. Mod. Phys.*, **35**, 576 (1963).
4) G. Smolinsky, E. Wasserman, and W. A. Yager, *J. Am. Chem. Soc.*, **84**, 3220 (1962).
5) J. A. R. Coope, J. B. Farmer, G. L. Gardner, and C. A. McDowell, *J. Chem. Phys.*, **42**, 54 (1965).
6) D. W. Cornell, R. S. Berry, and W. Lwowski, *J. Am. Chem. Soc.*, **87**, 3626 (1965).
7) R. S. Berry, D. Cornell, and W. Lwowski, *J. Am. Chem. Soc.*, **85**, 1199 (1963).
8) A. Reiser, G. C. Terry, and F. W. Willets, *Nature*, **211**, 410 (1966).
9) A. Reiser, F. W. Willets, G. C. Terry, V. Williams, and R. Marley, *Trans. Faraday Soc.*, **64**, 3265 (1968).
10) T. Yamaoka, H. Kashiwagi, and S. Nagakura, *Bull. Chem. Soc. Jpn.*, **45**, 361 (1972).
11) P. A. Lehman and R. S. Berry, *J. Am. Chem. Soc.*, **95**, 8614 (1973).
12) A. Reiser and V. Fraser, *Nature*, **208**, 682 (1965).
13) A. Reiser, H. Wagner, and G. Bowes, *Tetrahedron Lett.*, **1966**, 2635.
14) A. Reiser, G. Bowes, and R. J. Horne, *Trans. Faraday Soc.*, **62**, 3162 (1966).
15) A. Reiser, H. M. Wagner, R. Merley, and G. Bowes, *Trans. Faraday Soc.*, **63**, 2403 (1967).
16) A. Reiser and R. Marley, *Trans. Faraday Soc.*, **64**, 1806 (1968).
17) A. Reiser and L. J. Leyshon, *J. Am. Chem. Soc.*, **93**, 4051 (1971).
18) A. E. Douglas and W. E. Jones, *Can. J. Phys.*, **44**, 2251 (1966).
19) H. W. Kroto, *J. Chem. Phys.*, **44**, 831 (1966).
20) L. J. Schone, *J. Chem. Phys.*, **45**, 2773 (1966).
21) A. Gilles, J. Masanet, and C. Vermell, *Chem. Phys. Lett.*, **25**, 346 (1974).
22) B. Gelernt, S. V. Filseth, and T. Carrington, *Chem. Phys. Lett.*, **36**, 238 (1975).
23) C. Zetzsch and F. Stuhl, *Chem. Phys. Lett.*, **33**, 375 (1975).
24) K. Yoshihara, M. Sumitani, K. Nishi, I. Yokoyama, and S. Nagakura, *Oyo Butsuri*, **43**, 335 (1974).
25) B. Godard, *IEEE J. Quant. Electron.*, **QE-10**, 147 (1974).
26) T. W. Hänsch, *Appl. Phys. Lett.*, **18**, 108 (1971).
27) 1-Azidopyrene was prepared by Dr. T. Yamaoka, Chiba University. The authors are greatly indebted to him for his kindness in giving them the sample.
28) We attempted in vain to measure $T_1 \leftarrow S_0$ absorption making use of a heavy atom solvent (ethyl iodide).
29) F. D. Lewis and W. H. Saunders, Jr., *J. Am. Chem. Soc.*, **90**, 7033 (1968).
30) F. D. Lewis and W. H. Saunders, Jr., *J. Am. Chem. Soc.*, **90**, 7031 (1968).

Vibration Spectra and Rotational Isomerism of Chain Molecules. I. Methyl Propyl Ether, Ethyl Propyl Ether, and Butyl Methyl Ether

Takehiko SHIMANOUCHI, Yoshiki OGAWA, Masahiro OHTA, Hiroatsu MATSUURA, and Issei HARADA

Department of Chemistry, Faculty of Science, University of Tokyo, Hongo, Bunkyo-ku, Tokyo 113

(Received June 18, 1976)

The Raman and infrared spectra of methyl propyl ether, ethyl propyl ether, and butyl methyl ether were measured for the gaseous, liquid, glassy and crystalline states. The normal vibration frequencies were calculated, a consistent set of force constants explaining the frequencies of basic aliphatic ethers being assumed. The rotational isomerism was studied and the following conclusions were obtained. (1) Only the all-*trans* form exists in the crystalline state. (2) Another form which takes the *gauche* conformation about the OC–CC axis and the *trans* conformation about the CC–CC and CO–CC axes exists in the glassy state. (3) Other forms also exist in the liquid state. These results confirmed that the repulsive force between nonbonded hydrogen atoms was one of the important factors influencing the stability of molecular conformations. The stable conformations of the ether molecules were correlated with those of polyether chains.

The existence of rotational isomers has been clearly shown from the observation of Raman spectral changes on crystallization of 1,2-dichloroethane[1] and the rotational isomerism of small molecules has been studied in detail for various compounds.[2–4] The quantum mechanical treatment has also shown that the approximation of rotational isomerism can be practically applied.[5]

The rotational isomers of longer chain molecules have not yet been fully explored, since infrared and Raman spectra show too many bands to be assigned to each of possible rotational isomers. Recently we succeeded in estimating the force constants of chain molecules consisting of the CH_3, CH_2, O, S, F, Cl, Br, and I units and in calculating the vibrational frequencies of possible rotational isomers accurately enough to give reliable band assignments for longer chain molecules.[6]

This procedure provides us with a reliable method of determining the rotational isomers existing in the solid, liquid and other states. Accordingly, we started a series of research in which the rotational isomerism of longer chain molecules was studied. This paper is the first of this series and deals with the isomerism of methyl propyl ether $CH_3OCH_2CH_2CH_3$, ethyl propyl ether $CH_3CH_2OCH_2CH_2CH_3$ and butyl methyl ether $CH_3OCH_2CH_2CH_2CH_3$ and the results are correlated with those of other ethers[7–11] and the stable conformations of polyether chains.[12,13]

Notation

The conformation of a chain molecule is expressed with respect to the backbone axes and the symbols c, g^+, s^+, t, s^-, and g^- are used for the approximate internal-rotation angles of 0, 60, 120, 180, 240, and 300°, respectively,[3,14,15] where c, g, s, and t are the abbreviations of *cis*, *gauche*, *skew*, and *trans*. For saturated compounds, t, g^+, and g^- are stable.[2,4,16] In this series of papers, we use the generic symbols T, G, and G′ to represent the conformation of rotational isomers, since some of the molecular conformations expressed by t, g^+ and g^- are indistinguishable by vibrational spectroscopy. The symbol T corresponds simply to t, and G and G′ correspond to one and the other of g^+ and g^-. Thus, for example, g^+g^+ and g^-g^- are represented generically as GG, and g^+g^- and g^-g^+ as GG′. The conformations of longer chain molecules are defined by arranging the conformation symbols, T, G, and G′. Table 1 shows the generic names for accessible rotational isomers of the molecules which are studied in this series of papers.

Experimental

Samples of methyl propyl ether, ethyl propyl ether, and butyl methyl ether were purchased from Tokyo Kasei Kogyo Co., Ltd. and were distilled prior to the measurements. The Raman and infrared spectra were measured for the gaseous, liquid, glassy and crystalline states.

The Raman spectra were recorded on a JEOL JRS-400D spectrophotometer with a Coherent Radiation CR-3 argon ion laser in the region below 1600 cm^{-1}. A multireflection accessory and a gas cell with a heater were used for the measurements of the spectra in the gaseous state. The Raman spectra in the liquid state were measured at room and lower temperatures. The glassy state was obtained by putting into liquid nitrogen the sample enclosed in an ampoule and cooling it rapidly, and the crystalline state by inserting a copper wire in the sample and cooling it slowly with liquid nitrogen.

The infrared spectra were recorded on a Hitachi EPI-G2 double beam grating spectrometer in the region 1600—400 cm^{-1} and on a Hitachi EPI-L double beam grating spectrometer in the region 700—250 cm^{-1}. For the measurements in the region 700—250 cm^{-1}, the spectrometer was flushed with dry air to get rid of the interference of water vapor absorptions. The spectra in the gaseous state were measured with a 10 cm gas cell with KBr windows in the region 1600—400 cm^{-1}. For the measurements of the spectra in the liquid state, a 0.025 mm fixed cell with KBr windows and a variable cell with KRS-5 windows were used. The infrared spectra in the glassy and crystalline states were measured by the method previously reported.[17]

Normal Coordinate Treatment

The normal coordinate treatment of the unbranched ethers (see Table 2) was carried out with a computer program NCTB2[6] and a HITAC 8700/8800 computer system at the Computer Center of the University of Tokyo. The calculation made it possible to assign the observed Raman and infrared bands to individual rotational isomers and to determine a consistent set of

TABLE 2. PROCEDURE OF THE LEAST-SQUARES CALCULATION

Step	$CH_3OC_2H_5$[a]	$C_2H_5OC_2H_5$[b]	$CH_3OC_3H_7$[c]	$C_2H_5OC_3H_7$[c]	$CH_3OC_4H_9$[c]	$CH_3OC_2H_4OCH_3$[d]
1	T(22)	TT(27)				
2			TT(27)	TTT(33)	TTT(31)	
3	G(10)	TG(8)				
4			TG(14)	TTG(17)	TGT(18)	
5			GT(5)	TGT(8)	TTG(9)	
			GG(7)	TGG(4)	GTT(5)	
				GTG(4)	GTG(6)	
6						TGT(29)
						TTT(10)
7						TGG(15)
						TTG(12)
8	$CD_3OC_2H_5$[e] T(22) G(7)			$CH_3OCHDCH_3$[f] T(20) G(5)		
	$CH_3OCD_2CH_3$[g] T(21) G(7)			$CH_3OCH_2CD_3$[e] T(21) G(6)		
	$CD_3OCH_2CD_3$[f] T(19) G(5)			$CD_3OCHDCD_3$[f] T(21) G(4)		
	$CH_3OC_2D_5$[e] T(22) G(5)					
	$CD_3CH_2OCH_2CD_3$[h] TT(25) TG(12)			$CH_3CD_2OCD_2CH_3$[h] TT(25) TG(13)		
	$C_2D_5OC_2D_5$[i] TT(24) TG(8)			$C_2H_5OC_2D_5$[j] TT(22) TG(5)		
9	$(-OCH_2CH_2-)_n$[k] TGT (30)			$(-OCD_2CD_2-)_n$[j] TGT (20)		

The least-squares calculation begins with the simplest ethers given in the first step and the first set of orce constants is determined so as to give the best fit between the observed and calculated frequencies. This set of force constants gives the definite vibrational assignments of the ethers given in the second step and the second set of force constants is subsequently determined from the observed frequencies in this step in addition to those in the first step. By repeating this procedure, the final set of force constants is obtained. The figures in parentheses give the numbers of observed frequencies used for the least-squares calculation.

The observed frequencies of the CH and CD stretching vibrations are not included in the calculation and accordingly the force constants associated with these vibrations are not refined.

a) Refs. 7, 10a, 10b, 11, and 21. b) Refs. 7, 9, 10b, 10c, and 22. c) This study. d) This study and Ref. 7. e) Refs. 10a, 10b, and 11. f) Refs. 10a and 10b. g) Refs. 10a and 11b. h) Refs. 9 and 10c. i) Refs. 9, 10b, and 10c. j) Refs. 10b and 10c. k) Refs. 12, 13, 24, and 25. l) Ref. 13.

The following spectral features are observed for the three ethers in common. (1) The spectra in the various states are distinctly different, especially in the 600—200 cm^{-1} region of the skeletal deformation and torsional vibrations and in the 1200—800 cm^{-1} region of the skeletal stretching and the methyl and methylene rocking vibrations. (2) The spectral pattern of the crystalline state is the simplest and the smallest number of bands is observed. (3) In the glassy state, more bands appear in addition to those which persist in the crystalline state. (4) The liquid-state spectra have further more bands. As temperature is lowered, the intensities of the additional bands decrease rapidly relative to those of the bands which persist in the glassy state. (5) The gaseous-state spectra are essentially the same as the corresponding liquid-state spectra at room temperature.

In the following subsections, the rotational isomerism of the individual ethers is described.

Methyl Propyl Ether. Since this molecule has two internal-rotation axes associated with the rotational isomerism, there are five possible isomers, TT, TG, GT, GG, and GG′, as given in Table 1. The observed and calculated frequencies in the 600—250 cm^{-1} region are compared in Fig. 3.

The spectra in the crystalline state show that only the TT form exists. The number of the observed bands is just what is expected for one form. The frequencies, especially in the region below 600 cm^{-1}, can only be explained by the TT form.

The glassy-state spectra show that the TT and TG forms coexist. The bands at 506, 357, and 308 cm^{-1} which appear newly in the glassy state can only be explained by the TG form.

In the liquid and gaseous states, the observed spectra are explained by the coexistence of the TT, TG, GT and GG forms. The Raman band at 375 cm^{-1} and the infrared band at 495 cm^{-1} are assigned to the GT form, while the weak Raman band at 530 cm^{-1} in the gaseous state and the Raman and infrared bands at 285—292 cm^{-1} in the liquid and gaseous states are assigned to the GG form. The existence of the GG form is also confirmed by the observation of the Raman and infrared bands at 852 cm^{-1} which are assigned only to this form.

It is not likely that the GG′ form exists, since no Raman or infrared bands to be assigned to this form are detected. Furthermore, the distance between the two terminal methyl groups is too short for the GG′ form to be stable.

Ethyl Propyl Ether. This molecule has two C–O axes and a C–C axis which determine the molecular conformation. Accordingly, fourteen rotational isomers listed in Table 1 are derived as possible. Of these, the forms with a sequence of GG′ conformation, *i.e.* TGG′, GG′T, GGG′, GG′G, and GG′G′ are rejected because of the same reason as stated above for the GG′ form of methyl propyl ether.

Figure 6 indicates that the Raman and infrared

TABLE 3. OBSERVED FREQUENCIES AND VIBRATIONAL ASSIGNMENTS OF METHYL PROPYL ETHER

Observed frequency (cm^{-1})[a]								
Gas		Liquid		Glass		Crystal		Assignment[b]
R	IR	R	IR	R	IR	R	IR	
						1533VW		Origin unknown
	1475M, b	1480W, sh	1478M, sh	1486W 1475VW, sh	1480M	1498S 1476M	1482M 1473M, sh	CH_2 scis CH_2 scis
							1469VS	CH_3 ip-d-deform
1462M, vb			1463S, b	1465W, sh	1460M	1463W	1463VS	CH_3 s-deform
	1460M, vb	1451S, vb				1460W	1457VS, sh	CH_3 op-d-deform
			1452S	1454M	1449M	1450VS	1448W, sh	CH_3 op-d-deform
			1438M, sh	1439W, sh	1438M, sh	1443VW, sh	1440VW, sh	CH_3 ip-d-deform
	1396M	1389VW	1389S	1396VW	1388M	1403VW	1390VS	CH_2 wag (**TT**, TG)
	1386M		1381M, sh	1389VW	1381W, sh	1385VW	1381W	CH_3 s-deform (**TT**), CH_2 wag (GT, GG)
	1373VW, sh	1376VW	1374W, sh	1374VW	1371W			CH_3 s-deform (**TG**, GT, GG)
	1345VW	1343VW	1345W	1343VW	1344VW			CH_2 wag (**TG**, GG)
1312VW, sh	1308VW, sh	1305VW, sh	1309VW	1305VW	1307W	1307VW	1308W	CH_2 wag (**TT**, GT), CH_2 twist (GT)
1292VW	1292VW	1284W	1287W	1288W	1286W	1289S	1288VW	CH_2 twist (**TT**, TG, GG)
1272VW, sh	1268VW		1268VW					CH_2 twist (GT, GG)
							1263VW	Origin unknown
1249VW, sh	1251VW	1249VW	1251W	1249VW	1249W	1249VW	1251M	CH_2 twist (**TT**, TG)
1212VW	1212M					1212VW	1214VS	CH_3 ip-rock (**TT**)
	1204M	1204VW	1204VS	1205VW	1205S			CH_3 ip-rock (**TG**, GT, GG)
1178VW, sh	1178VW, sh	1174VW, sh	1174M, sh	1174VW, sh	1174VW, sh	1173VW	1175W	CH_3 op-rock (**TT**), CH_2 rock (GT)
1167VW, sh	1168VW, sh	1163VW	1165S	1166VW	1166W			CH_3 op-rock (**TG**, GT, GG)
1152VW, sh		1150VW, sh		1151VW, sh		1152VW	1152VW, sh	CH_3 op-rock (**TT**)
1147W	1148VS, sh	1141VW, sh	1144VS, sh	1144VW	1144M			CH_3 op-rock (**TG**)
1135VW, sh	1134VS	1131W	1132VS	1131W	1130VS	1126S	1132VS	CC stretch (**TT**)
1115VW	1118VS, sh	1116VW	1119VS	1114VW	1114VS			CO stretch (**TG**), CH_3 ip-rock (GT)
	1110VS	1103VW	1104VS, sh					CH_3 ip-rock (**GG**)
1096VW, sh	1098W, sh	1096VW, sh	1096VS, sh	1100VW	1100VS	1096W	1098VS	CO stretch (**TT**), CH_3 ip-rock (TG)
		1077VW, sh	1077VW, sh					CC stretch (**GG**)
	1062W							CO stretch (**GT**)
1058VW	1052M	1050VW, sh	1050S	1050VW, sh	1050S			CC stretch (**TG**)
1047W	1038VW, sh	1040W	1040W, sh	1042W	1042W, sh	1039VS	1042M	CC stretch (**TT**, GT)
1030VW, sh	1030VW, sh	1026VW	1026W					CO stretch (**GG**)
965VW, sh		958VW	959M	960VW	960S	961M	960VS	CO stretch (**TT**)
			942M, sh					CO stretch (**GT**)
938VW	938M, vb	933W	935S	935W	935S			CO stretch (**TG**), CH_3 ip-rock (GG)
		911VW, sh	913M	913VW, sh	912S			CH_2 rock (**TG**)
			903M, sh		905M, sh	911VW, sh	909VW	CH_2 rock (**TT**)
905W		902W	897W, sh	904W	897VW, sh	902VS	897S	CH_3 ip-rock (**TT**), CH_3 op-rock (GT), CH_2 rock (GG)
879VS		876VS	879W	879VS	879M			CC stretch (**TG**, GT)
855W		852W	852VW					CC stretch (**GG**)
759VW	760VW	756VW	759VW	758VW	760W	764VW	764M	CH_2 rock (**TT**, TG, GT, GG)
530VW								OCC deform (**GG**)
508M		505W	505VW, sh	506W	505VW			CCC deform (**TG**)
			495VW					OCC deform (**GT**)
447M		443W	441VW	442M	441VW	443M	442VW	COC bend (**TT**)
422W		418VW	414VW	416VW	414VW	424M	409VW	CCC deform (**TT**), COC bend (GG)
375VW, sh		375VW, sh						COC bend (**GT**)
355M		358VW	358VW	357W	357VW			COC bend (**TG**)
		312VW	305VW, sh	308VW	305VW			OCC deform (**TG**), CCC deform (GT)
287VW		292VW	285VW					CCC deform (**GG**)
223VW						223VW		CH_3 torsion (**TT**)
		195VW, b		205VW, b		205VW		OCC deform (**TT**), CH_3 torsion (TG)
						131VW		
						123W		
						110W		
						87VW		Torsions (**TT**) and lattice vibrations
						76W		
						68VW		
						55M		

a) VS: very strong, S: strong, M: medium, W: weak, VW: very weak, vb: very broad, b: broad, sh: shoulder. The broadness of the band shapes in the gaseous state does not always allow us to correlate the individual bands in the liquid state to those in the gaseous state. Only approximate correlations are made in such cases and in other cases of similar situations. b) The band is assigned preferentially to the isomer(s) given by boldface. For the notation and definition of the local symmetry coordinates, see Ref. 26.

TABLE 4. OBSERVED FREQUENCIES AND VIBRATIONAL ASSIGNMENTS OF ETHYL PROPYL ETHER

Observed frequency (cm^{-1})[a]								Assignment[b]
Gas		Liquid		Glass		Crystal		
R	IR	R	IR	R	IR	R	IR	
		1490W	1490W, sh	1492W	1490W, sh	1497W	1484W, sh	CH_3 scis
			1487W		1486W		1480M	CH_3 scis
			1473M	1473VW, sh	1472W, sh	1478VW, sh	1476W, sh	CH_3 scis
			1464M, sh	1460M, sh	1462W, sh	1468VW	1464M	CH_3 ip-d-deform
1462M, vb	1465M, vb	1458M, vb	1460M	1457M	1457W	1457M	1457M	CH_3 op-d-deform
			1452M, sh	1450M, sh	1449W, sh	1452W, sh	1456M	CH_3 ip-d-deform
			1443M	1439W, sh	1438W	1447W, sh	1442W	CH_3 op-d-deform
		1415VW, sh	1408W	1415VW	1418VW	1415VW	1416VW	CH_2 wag (**TTT**)
					1408W			CH_2 wag (**TTG**, TGT, TGG, GTG)
	1382M		1379S	1379VW	1378M		1378M	CH_3 s-deform (**TTT**, TTG, TGT, TGG, GTG), CH_2 wag (TGT, TGG, GTG)
	1366M	1380VW	1370M, sh	1372VW	1368M, sh	1371VW	1370M	CH_3 s-deform (**TTT**, TGT, TGG, GTG)
	1356M		1356M	1356VW	1354W	1355VW	1357W	CH_2 wag (**TTT**, TTG)
	1344VW, sh	1345VW	1345W	1344VW	1344W			CH_2 wag (**TTG**, TGG, GTG)
	1303W, b	1303VW, sh	1304W	1304VW	1303W	1308VW	1308W	CH_2 wag (**TTT**, TGT), CH_2 twist (TGT)
			1283W	1292VW, sh	1292VW, sh	1292W	1295VW	CH_2 twist (**TTT**, TGG, GTG)
				1285W, sh	1282W			CH_2 twist (**TTG**)
1284W, vb	1279W	1277W, b	1275W, sh	1276W	1274W, sh	1276W	1274VW	CH_2 twist (**TTT**, TTG, TGG)
			1265W					CH_2 twist (TGT, GTG)
	1264W, b	1250VW	1252W	1252VW, sh	1254VW, sh			CH_2 twist (**TTG**, TGT, TGG, GTG)
				1246VW	1246W	1245VW	1247W	CH_2 twist (**TTT**)
	1180W, sh		1182M, sh					CH_2 rock (**TGT**)
1170VW, sh	1168M, sh	1170VW, sh	1168M, sh	1170VW, sh	1172W, sh	1172VW	1172W	CH_2 rock (**TTT**)
		1165VW, sh			1165W			CH_2 rock (**TTG**, TGG), CH_3 op-rock (GTG)
1156W		1154W	1154S	1155M	1152M	1152M	1155S	CH_3 ip-rock (**TTT**, GTG), CH_2 rock (GTG), CH_3 op-rock (**TTT**, TTG, TGT, TGG)
			1133VS	1133VW	1131M, sh			CH_3 ip-rock (**TTG**),CO stretch (TGT, TGG)
1133W	1135VS, b	1124VW, b	1118VS	1119VW	1117VS			CO stretch (**TTG**), CH_3 ip-rock (TGT, TGG)
1110VW			1110VS, sh	1110VW, sh	1109W, sh	1110W	1112VS	CO stretch (**TTT**), CC stretch (TGT)
1098VW, sh	1090M, b	1099VW	1096S	1098VW	1098W	1101VW, sh	1098VS	CC stretch (**TTT**), CO stretch (GTG)
1085W		1085W	1086S	1085W	1087W			CC stretch (**TTG**, GTG)
1075VW, sh		1075VW, sh	1074M, sh					CC stretch (**TGG**)
	1059W, sh		1062M	1062VW	1063M			CC stretch (**TTG**)
1050VW, b		1048VW	1051M	1048VW	1051W	1050VW	1050S	CC stretch (**TTT**, TGG, GTG)
		1040VW, sh	1042VW, sh					CC stretch (**TGT**)
1017VW	1017W	1017VW	1017W	1017VW	1018W	1020M	1020S	CC stretch (**TTT**, TGT)
990VW, b	986W	985VW	986M	985VW	985M			CC stretch (**TTG**), CO stretch (TGG)
	962VW, sh	961VW	962W					CO stretch (**GTG**)
918VW, sh		918VW, sh	920VW, sh	918VW, sh	918VW			CH_2 rock (**TTG**, TGG, GTG), CH_3 op-rock (TGT)
908W, sh		908VW, sh	908VW, sh	908VW, sh	908VW, sh	908VW, sh	906W, sh	CH_3 ip-rock (**TTT**)
902W, sh		902W	902W	903VW	902W	901W	900M	CH_3 op-rock (**TTT**)
884VS	885W, vb	883VS		885VS	896W, sh			CO stretch (**TTG**), CH_3 ip-rock (TGT, GTG)
			883M		884M	885W	883M	CO stretch (**TTT**), CC stretch (**TTG**, GTG)
871W, sh		871VW, sh	873W, sh					CC stretch (**TGG**)
849W		844W	846W					CO stretch (TGT), CH_3 ip-rock (TGG)
820VW, sh	820VW	820VW, sh	818VW	819VW	818VW	826VW	826VW	CH_2 rock (**TTT**, TGT), CH_3 op-rock (TTG, TGG, GTG)
761VW	760VW, b	761VW	762VW	763VW	768VW, sh	769VW	767W	CH_2 rock (**TTT**, TGG, GTG)
					762W			CH_2 rock (**TTG**)
753VW, sh		753VW, sh	753VW, sh					CH_2 rock (**TGT**)
		546VW, sh	545VW					COC bend (TGT), CCC deform (TGG)
520VW		518VW	518VW					OCC deform (**GTG**)
496VW, sh	490VW	496VW, sh	494VW	498VW, sh	495VW	498VW	494VW	OCC deform (**TTT**)
488VW		489VW	486VW, sh	490VW	488VW, sh			OCC deform (**TTG**)
439M	439VW	439M	438VW	439M	438VW			COC bend (**TTG**, TGG)
408M	408VW	410M	409VW	410M	408VW	410VS	409VW	COC bend (**TTT**), OCC deform (GTG)
360W		363VW	361VW					OCC deform (**TGT**)
				335VW	331VW			CCC deform (**TTG**), OCC deform (TGG), COC bend (GTG)
328W		330VW	328VW					CCC deform (**TGT**)
				314VW	315VW	314VW	315VW	CCC deform (**TTT**), OCC deform (GTG)
						266VW	266VW	CH_3 torsion (**TTT**)
				257VW				CH_3 torsion (**TTG**)
						237VW		CH_3 torsion (**TTT**)
				195VW, sh		199VW		CH_2CH_2 torsion (**TTT**)
				165VW		160VW		OCC bend (**TTT**), torsions (**TTT**), and lattice vibrations
						147VW, sh		
						121VW, sh		
						103VW		
						80W, sh		
						78M		
						60VW		
						43VW		

a), b) See a) and b), respectively, of Table 3.

TABLE 5. OBSERVED FREQUENCIES AND VIBRATIONAL ASSIGNMENTS OF BUTYL METHYL ETHER

Observed frequency (cm^{-1})[a]								Assignment[b]
Gas		Liquid		Glass		Crystal		
R	IR	R	IR	R	IR	R	IR	
					1484W, sh	1498VW	1482M	CH_3 scis
		1480W, b	1480M, sh	1486W	1480M	1486W	1475W, sh	CH_3 scis
			1474M, sh	1470W, sh	1474W, sh	1477W	1471S	CH_3 ip-d-deform
			1467S, sh		1464S, sh	1463VW, sh	1462S	CH_2 scis
1457M, vb	1460M, vb		1461S	1461S, sh	1460S	1460W, sh	1458S, sh	CH_3 s-deform, CH_3 op-d-deform
		1452S, b	1452S		1452S	1452W	1452W, sh	CH_3 op-d-deform
			1444M, sh	1452S	1447M, sh	1448W, sh	1442W, sh	CH_3 ip-d-deform
			1432W	1434W	1430W, sh			Origin unknown
		1395VW	1395W, sh	1395VW	1395W, sh	1395VW	1395S	CH_2 wag (**TTT**, TTG)
1390VW, b		1385VW, sh	1387S	1385VW	1385M			CH_2 wag (**TGT**, GTT, GTG)
	1385M, b	1378VW, sh	1379M, sh	1378VW	1376M, sh	1381VW	1377M	CH_3 s-deform (**TTT**, TGT, TTG, GTT, GTG)
1367VW		1367VW	1367VW, sh	1368VW	1367VW, sh	1364VW	1366VW	CH_2 wag (**TTT**, TGT)
	1345VW	1342VW, sh	1342VW					CH_2 wag (TTG, GTT, GTG)
	1312VW	1318VW, sh	1313VW, sh					CH_2 wag (TTG, GTG), CH_3 twist (GTT)
1300W	1304VW	1304W	1305VW	1305M	1304W	1305VW		CH_2 twist (**TTT**, TGT, GTG)
		1286VW, sh		1286VW, sh	1287VW, sh	1284VW	1290VW	CH_2 twist (**TTT**, GTT), CH_2 wag (TGT)
		1270VW, sh	1271VW, sh		1271W, sh	1272VW, sh	1276W	CH_2 wag (**TTT**, GTT), CH_2 twist (TTG)
1265VW, sh	1260W	1260VW	1260W	1259VW	1261W			CH_2 twist (**TGT**, TTG, GTG)
		1233VW	1237W	1236VW	1236M			CH_2 twist (**TGT**, TTG, GTT, GTG)
1231VW, sh	1230W	1225VW, sh	1227VW, sh	1225VW, sh	1227W, sh	1227VW	1231VW	CH_2 twist (**TTT**)
	1208M					1206VW	1214S	CH_3 ip-rock (**TTT**)
1204VW	1200M	1200VW	1200S	1202VW	1202VS			CH_3 ip-rock (**TGT**, TTG, GTT, GTG)
1172VW, sh	1172M, sh	1171VW, sh	1172M, sh	1172VW, sh	1172W, sh	1172VW	1173W	CH_3 rock (**TTT**, GTT, GTG), CH_3 op-rock (TTG)
1162VW, sh	1162M, sh	1162VW, sh	1163S, sh	1165VW	1164M			CH_3 op-rock (**TGT**, GTT, GTG)
1150W, sh	1150S, sh	1148VW, sh	1149S, sh	1149VW, sh	1149W, sh	1149VW	1151VW, sh	CH_3 op-rock (**TTT**, TTG)
1142W		1142W	1144S, sh	1145W	1143S			CH_2 rock (**TGT**), CH_3 op-rock (TTG)
1131W, sh	1135VS	1130W	1132VS	1130W	1132VS, sh	1126W	1132VS	CC stretch (**TTT**)
1120W, sh		1121W, sh	1120VS	1120W	1122VS			CC stretch (**TGT**, TTG), CH_3 ip-rock (GTT)
1115W	1112S, sh	1115W	1112VS	1112W	1112VS			CO stretch (**TGT**)
1103VW, sh	1104M, sh	1103VW, sh	1103S, sh	1103VW, sh	1103VS, sh	1103VW	1107VS	CO stretch (**TTT**), CH_3 ip-rock (GTG)
1095VW, sh	1095M, sh	1098VW, sh	1098S, sh					CO stretch (**TTG**)
1067VW	1061M	1065VW	1066M	1063VW	1065W	1065W	1067VW	CC stretch (**TTT**, TTG, GTG), CO stretch (GTT, GTG)
1055VW		1054VW	1055W	1053VW	1053S			CC stretch (**TGT**, GTT)
1028VW	1024VW, sh	1022VW, sh	1024VW, sh	1025VW, sh	1026W, sh	1024W	1026M	CC stretch (**TTT**)
1019W	1016W	1016W	1017W	1019W	1019S			CC stretch (**TGT**, GTT)
		991VW	990W	991VW	989VW			Origin unknown
973W, sh		970W, sh		970VW, sh				CH_3 ip-rock (**TGT**, TTG), CH_3 op-rock (GTG) CC stretch (GTG)
966W		962W	960M	963VW	961S	962M	962VS	CO stretch (**TTT**), CH_2 rock (TTG)
955VW, sh	954W, b	952W, sh	952M, sh					CO stretch (TTG), CH_3 op-rock (GTT)
						945VW, sh	947W	CH_3 op-rock (**TTT**)
945W		942W	941M	940W	938S			CH_3 op-rock (**TGT**)
926VW, sh		924VW	920W					CO stretch (GTT, GTG)
898VW	895VW	897VW	896W	899VW	895W	900VW	895S	CH_3 ip-rock (**TTT**), CC stretch (GTT, GTG)
880VW		879VW	877VW, sh					CC stretch (**TTG**)
840VS	838W	839VS	838W, sh	841VS	838W			CO stretch (**TGT**)
831W, sh	828W	829M, sh	828W	828W	827S			CH_2 rock (**TGT**)
820W, sh		818W						CH_2 rock (**TTG**)
	813VW, sh	810W	813VW, sh	813VW, sh	813VW	813VW	813VW	CH_2 rock (**TTT**, TTG, GTT, GTG)
791VW, sh		791VW, sh						Other isomers
	753VW		756VW					CH_3 rock (GTG, TTG)
						747VW	745M	CH_3 rock (**TTT**, GTT)
739VW	740VW	740VW	738VW	740VW	739W			CH_3 rock (**TGT**)
550VW, sh		549VW	545VW	551VW	549VW			CCC deform (**TGT**)
525VW		525VW	529VW					Other isomers
509VW		509VW	505VW, sh					COC bend (**GTG**)
494VW		496VW	492VW	495VW	494VW	497VW	494VW	COC bend (**TTT**), OCC deform (GTT)
						485VW		Origin unknown
460VW, sh		460VW	459VW					CCC deform (**TTG**)
449VW		449VW						COC bend (**TTG**)
			425VW					Other isomers
		408VW	410VW					CCC deform (GTT, GTG)
383W		387W	386VW	385W	383VW	391VS	382VW	OCC deform (**TTT**)
349S		352M	352VW, sh	352W	352VW			COC bend (**TGT**, GTT), OCC deform (GTG)
				323VW	324VW, sh	324W	322VW	CCC deform (**TTT**, TTG)
323W		326W	322VW	315VW, sh	315VW			OCC deform (**TGT**)
				275VW	275VW			CCC deform (**TGT**)
		250VW, vb		250VW		247VW	252VW	CH_3 torsion (**TTT**, TTG)
						184VW		CCC deform (**TTT**), torsions (**TTT**), and lattice vibrations
						170VW		
						108VW		
						90M, sh		
						86M		
						57VW		
						49VW		

a), b) See a) and b), respectively, of Table 3.

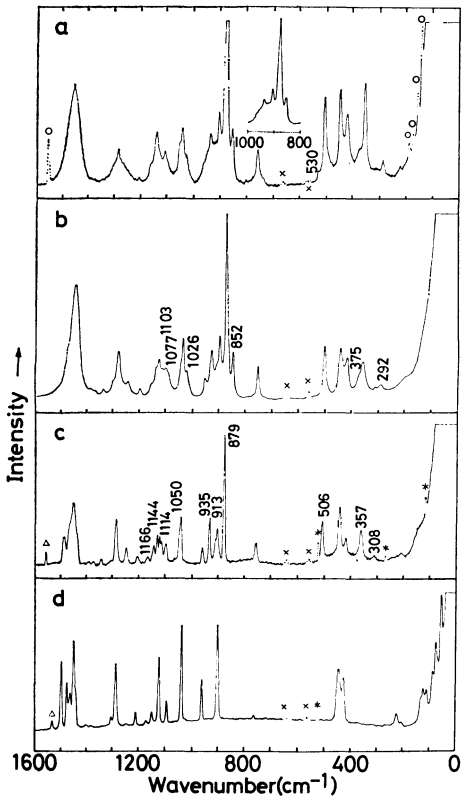

Fig. 1. Raman spectra of methyl propyl ether.
a: Gas (room temperature),
b: liquid (room temperature),
c: glass (liquid nitrogen temperature),
d: crystal (liquid nitrogen temperature).
Following symbols are used in Figs. 1—9. *: emission line of Ar^+, ○: rotational or vibrational Raman band of O_2 or N_2, □: librational infrared band of H_2O, ×: impurity, △: origin unknown.

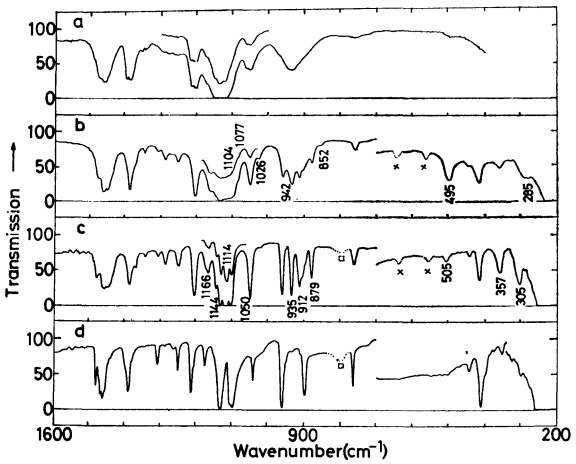

Fig. 2. Infrared spectra of methyl propyl ether.
a: Gas, b: liquid, c: glass, d: crystal.
The symbols are explained in the caption of Fig. 1.

bands observed in the crystalline state are explained only by the calculated result for the TTT form. The additional bands observed in the glassy state are assigned to the TTG form on the basis of the calculated frequencies.

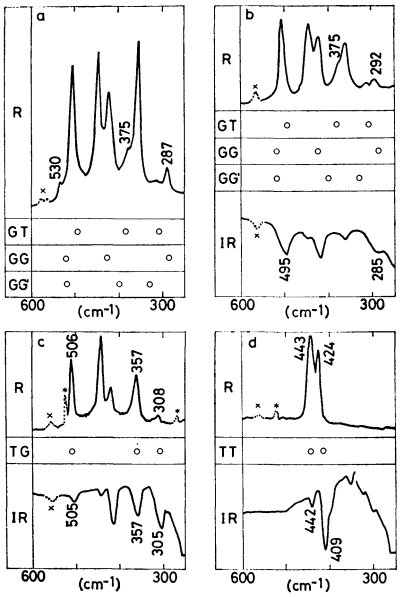

Fig. 3. Observed and calculated frequencies of methyl propyl ether in the 600—250 cm^{-1} region.
a: Gas, b: liquid, c: glass, d: crystal.
The symbols are explained in the caption of Fig. 1.

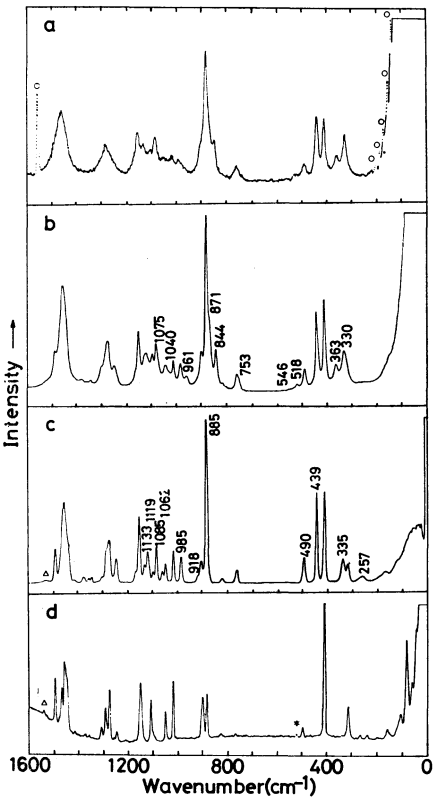

Fig. 4. Raman spectra of ethyl propyl ether.
a: Gas (room temperature),
b: liquid (room temperature),
c: glass (liquid nitrogen temperature),
d: crystal (liquid nitrogen temperature).
The symbols are explained in the caption of Fig. 1.

In the liquid state, several new Raman and infrared bands appear. The temperature dependence of the

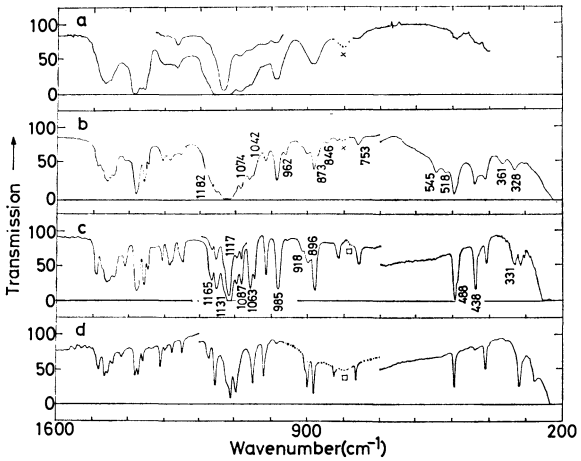

Fig. 5. Infrared spectra of ethyl propyl ether.
a: Gas, b: liquid, c: glass, d: crystal.
The symbols are explained in the caption of Fig. 1.

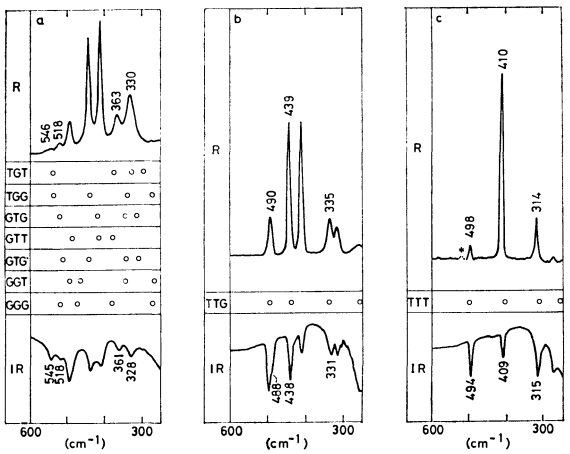

Fig. 6. Observed and calculated frequencies of ethyl propyl ether in the 600—250 cm^{-1} region.
a: Liquid, b: glass, c: crystal.
The symbols are explained in the caption of Fig. 1.

spectra and the calculated results show that the liquid-state spectra are explained by the TGT, TGG, and GTG forms in addition to the TTT and TTG forms which persist in the glassy state.

Existence of the GTT and GTG′ forms is uncertain, since all of their calculated frequencies are almost coincident with those of the other forms mentioned above. The GGT and GGG forms do not seem to exist in the liquid state, since no bands are observed around their characteristic frequencies of about 470 cm^{-1}.

Butyl Methyl Ether. This molecule has two C–C axes and a C–O axis associated with the rotational isomerism. Accordingly, fourteen isomers listed in Table 1 are derived as possible. The GG′T, GG′G and GG′G′ forms are unlikely because of the same reason as stated for methyl propyl ether. However, the TGG′ and GGG′ forms are not ruled out, since unlike the GG′ sequence of the CO–C–CC part in methyl propyl ether or ethyl propyl ether, the GG′ sequence of the OC–C–CC part is not expected to give rise to very large steric hindrance.

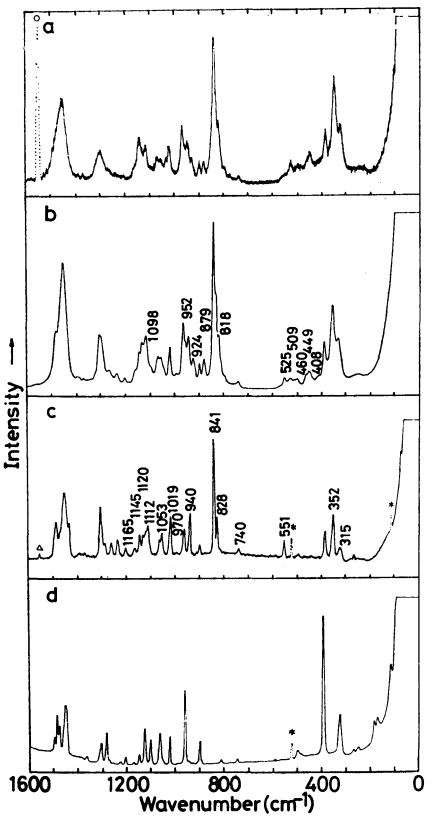

Fig. 7. Raman spectra of butyl methyl ether.
a: Gas (room temperature),
b: liquid (room temperature),
c: glass (liquid nitrogen temperature),
d: crystal (liquid nitrogen temperature).
The symbols are explained in the caption of Fig. 1.

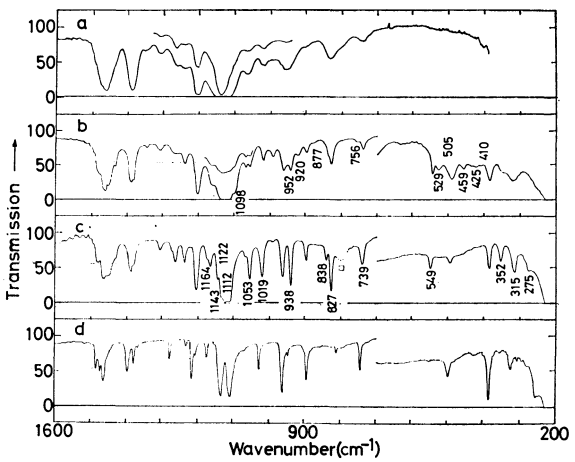

Fig. 8. Infrared spectra of butyl methyl ether.
a: Gas, b: liquid, c: glass, d: crystal.
The symbols are explained in the caption of Fig. 1.

The comparison with the calculated results (Fig. 9) shows that the crystalline-state spectra can be explained only by the TTT form and the glassy-state spectra by the TTT and TGT forms. The spectra in the liquid state have several new bands. Their frequencies are close to the frequencies calculated for the TTG, GTT, and GTG forms. In the liquid-state infrared spectrum,

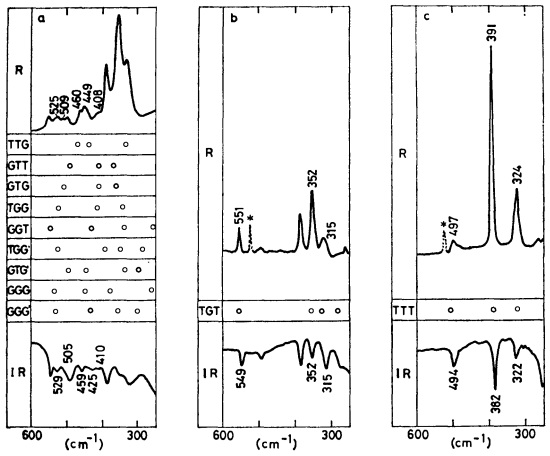

Fig. 9. Observed and calculated frequencies of butyl methyl ether in the 600—250 cm^{-1} region.
a: Liquid, b: glass, c: crystal.
The symbols are explained in the caption of Fig. 1.

several weak bands are observed in the region 450—400 cm^{-1}, which are not assignable to the isomers mentioned above. Accordingly, there are possibilities that other forms such as TGG, GGT, TGG' ,GTG', GGG, and GGG' isomers exist in the liquid state. The Raman band at 525 cm^{-1} and the infrared band at 529 cm^{-1} are assigned to either one or both of the TGG and TGG' forms.

Rotational Isomerism. In Table 6, the rotational isomerism of the ethers studied in this work is summarized, together with that of ethyl methyl ether and diethyl ether which has been established in earlier studies.[7,9-11] The symbol $\tilde{G}$ is used to specialize the *gauche* conformation about the C–C axis directly adjoining the O–C axis.

Discussion

The following results were obtained for the three ethers in common. (1) Only the all-*trans* form exists in the crystalline state. (2) An additional form coexists in the glassy state. This form takes the *gauche* conformation ($\tilde{G}$) about the OC–CC axis and the *trans* conformation about other axes. (3) More forms exist in the liquid state than in the glassy state. The temperature dependence of the Raman intensities indicates that the additional forms are much less stable than the two forms which persist in the glassy state, while the energy difference between the latter two is not appreciable. (4) It is likely that the molecules in the gaseous state take the same conformations as in the liquid state.

The stability of the *trans* conformation over the *gauche* conformation may be explained, in a way similar to the case of paraffins, in terms of the weaker nonbonded interactions. In fact, it has been shown that the *trans* conformation about the CO–CC axis is more stable than the *gauche* conformation by 1.1—1.5 kcal/mol as obtained for ethyl methyl ether[10a,11a,11c] and diethyl ether.[9,10c] The existence of the all-*trans* form in the crystal is ascribable also to the requirement of the molecular packing which is determined primarily by intermolecular forces.

In addition to the all-*trans* form, the second isomer with the $\tilde{G}$ conformation exists in the glassy state of the three ethers at liquid nitrogen temperature. This isomer was found to be as stable as the all-*trans* form in the liquid state. The stability of the $\tilde{G}$ conformation is also shown by the fact that ethylene glycol dimethyl ether $CH_3O–CH_2–CH_2–OCH_3$ takes the T$\tilde{G}$T conformation in the crystalline state.[7,23] Thus, it is now established that the $\tilde{G}$ conformation (*gauche* about the OC–CC or OC–CO axis) is much more stable than the *gauche* conformation about other axes such as CC–CC and CO–CC.

The stability of the $\tilde{G}$ conformation is understood in the following way by taking the case of the $C_1–O–C_2–C_3–C_4–C_5$ bond system. When the $C_1O–C_2C_3$ or $C_2C_3–C_4C_5$ axis takes the G conformation, appreciable repulsive forces are expected between the nonbonded hydrogen atoms attached to C_1 and C_3, or between those attached to C_2 and C_5. On the other hand, the $\tilde{G}$ conformation about the $OC_2–C_3C_4$ axis does not give rise to such forces, since the hydrogen atoms attached to C_4 have no counterpart hydrogen atoms. The absence of this type of nonbonded interaction is suggested to be one of the principal factors to stabilize the $\tilde{G}$ conformation.

In connection with the stable $\tilde{G}$ conformation, it is important to examine the structure of polyethers.[12,13]

Table 6. Rotational isomers of the ethers

	CH_3OCH_2-CH_3[a]	$CH_3CH_2OCH_2$-CH_3[b]	CH_3OCH_2-CH_2CH_3	$CH_3CH_2OCH_2$-CH_2CH_3	$CH_3OCH_2CH_2$-CH_2CH_3
Gas	**T G**	**TT TG**	**TT T$\tilde{G}$ GT** **G$\tilde{G}$**	**TTT TT$\tilde{G}$** TGT TG$\tilde{G}$ GT$\tilde{G}$ (GTT) (GTG')	**TTT T$\tilde{G}$T** TTG GTT GTG (T$\tilde{G}$G) (G$\tilde{G}$T) (T$\tilde{G}$G') (GTG') (G$\tilde{G}$G) (G$\tilde{G}$G')
Liquid	**T G**	**TT TG**	**TT T$\tilde{G}$ GT** **G$\tilde{G}$**	**TTT TT$\tilde{G}$** TGT TG$\tilde{G}$ GT$\tilde{G}$ (GTT) (GTG')	**TTT T$\tilde{G}$T** TTG GTT GTG (T$\tilde{G}$G) (G$\tilde{G}$T) (T$\tilde{G}$G') (GTG') (G$\tilde{G}$G) (G$\tilde{G}$G')
Glass	—	—	**TT T$\tilde{G}$**	**TTT TT$\tilde{G}$**	**TTT T$\tilde{G}$T**
Crystal	**T**	**TT**	**TT**	**TTT**	**TTT**

The isomers given by boldface are confirmed to exist. The existence of the isomers in parentheses is uncertain. For more details, see text.
a) Refs. 7, 10a, 10b, 11, and 21. b) Refs. 7, 9, 10b, 10c, and 22.

It has been shown that poly(oxyethylene) $(-OCH_2-CH_2-)_n$ and poly(oxytrimethylene) $(-OCH_2CH_2CH_2-)_n$ have several crystal modifications. In the most stable modification, the molecule takes the $T\tilde{G}T$ conformation for the series of O–C–C–O bonds in the former polymer and the $T\tilde{G}\tilde{G}T$ conformation for the series of O–C–C–C–O bonds in the latter polymer. In other modifications, the poly(oxyethylene) molecule takes the TTT conformation, and the poly (oxytrimethylene) molecule takes the $TT\tilde{G}TTT\tilde{G}'T$ and $(TTTT)_2$ conformations for the series of O–C–C–C–O–C–C–C–O bonds. These facts suggest that the $\tilde{G}$ conformation plays an important role in stabilizing molecular conformations of crystalline polymers.

References

1) S. Mizushima, Y. Morino, and S. Nojiri, *Sci. Pap. Inst. Phys. Chem. Res. Tokyo*, **29**, 63 (1936).

2) S. Mizushima, "Structure of Molecules and Internal Rotation," Academic Press, New York (1954).

3) Y. Morino and E. Hirota, *Ann. Rev. Phys. Chem.*, **20**, 139 (1969).

4) E. B. Wilson, *Chem. Soc. Rev.*, **1**, 293 (1972).

5) S. Mizushima, T. Shimanouchi, I. Harada, Y. Abe, and H. Takeuchi, *Can. J. Phys.*, **53**, 2085 (1975).

6) T. Shimanouchi, H. Matsuura, Y. Ogawa, and I. Harada, *J. Phys. Chem. Ref. Data.*, to be submitted.

7) R. G. Snyder and G. Zerbi, *Spectrochim. Acta*, **23A**, 391 (1967).

8) A. D. H. Clague and A. Danti, *Spectrochim. Acta*, **24A**, 439 (1968).

9) H. Wieser, W. G. Laidlaw, P. J. Krueger, and H. Fuhrer, *Spectrochim. Acta*, **24A**, 1055 (1968).

10) a) J. P. Perchard, *Spectrochim. Acta*, **26A**, 707 (1970); b) J. P. Perchard, *J. Mol. Structure*, **6**, 457 (1970); c) J. P. Perchard, J. C. Monier, and P. Dizabo, *Spectrochim. Acta*, **27A**, 447 (1971).

11) a) T. Kitagawa and T. Miyazawa, *Bull. Chem. Soc. Jpn.*, **41**, 1976 (1968); b) T. Kitagawa, K. Ohno, H. Sugeta, and T. Miyazawa, *ibid.*, **45**, 969 (1972); c) T. Kitagawa, K. Kusaki, and T. Miyazawa, *ibid.*, **46**, 3685 (1973).

12) T. Miyazawa, K. Fukushima, and Y. Ideguchi, *J. Chem. Phys.*, **37**, 2764 (1962).

13) T. Yoshihara, H. Tadokoro, and S. Murahashi, *J. Chem. Phys.*, **41**, 2902 (1964); H. Tadokoro, Y. Takahashi, Y. Chatani, and H. Kakida, *Makromol. Chem.*, **109**, 96 (1967); Y. Takahashi, I. Sumita, and H. Tadokoro, *J. Polym. Sci. Polym. Phys.*, **11**, 2113 (1973); Y. Takahashi and H. Tadokoro, *Macromolecules*, **6**, 672 (1973).

14) P. J. Flory, "Statistical Mechanics of Chain Molecules," Interscience, New York (1969).

15) T. Shimanouchi, *Discuss. Faraday Soc.*, **1970**, 60.

16) S. Mizushima and T. Shimanouchi, *J. Am. Chem. Soc.*, **86**, 3521 (1964).

17) F. Inagaki, M. Sakakibara, I. Harada, and T. Shimanouchi, *Bull. Chem. Soc. Jpn.*, **48**, 3557 (1975).

18) I. Harada, H. Takeuchi, M. Sakakibara, H. Matsuura, and T. Shimanouchi, *Bull. Chem. Soc. Jpn.*, to be published.

19) T. Shimanouchi, I. Nakagawa, C. Tanaka, I. Suzuki, H. Takahashi, T. Fujiyama, Y. Abe, T. Ueda, M. Mikami, M. Oka, A. Y. Hirakawa, and A. Kurokawa, Symposium on Molecular Structure, Osaka, 1966.

20) H. Matsuura and T. Miyazawa, *Bull. Chem. Soc. Jpn.*, **41**, 1798 (1968).

21) M. Hayashi and K. Kuwada, *J. Mol. Structure*, **28**, 147 (1975).

22) M. Hayashi and K. Kuwada, *Bull. Chem. Soc. Jpn.*, **47**, 3006 (1974).

23) Y. Ogawa, M. Ohta, M. Sakakibara, H. Matsuura, I. Harada, and T. Shimanouchi, to be published.

24) R. F. Schaufele, *Trans. New York Acad. Sci.*, **30**, 69 (1967).

25) J. L. Koenig and A. C. Angood, *J. Polym. Sci., Pt. A-2*, **8**, 1787 (1970).

26) T. Shimanouchi, "Tables of Molecular Vibrational Frequencies," Consolidated Vol. 1, U. S. Govt. Printing Office, No. C13.48: 39 (1972).

Carbon Monoxide Oxidation over Chromium Sesquioxide. I. Nature of Oxygen Adsorbed on Cr_2O_3

Masayoshi KOBAYASHI and Haruo KOBAYASHI

Department of Chemical Process Engineering, Faculty of Engineering, Hokkaido University, Sapporo 060

(Received August 4, 1975)

The nature of oxygen species adsorbed on Cr_2O_3 surface in the temperature range 131—163 °C was studied in detail by application of the transient response method with simultaneous measurements of the electrical conductivity of the catalyst as a p-type semiconductor. The distribution of oxidation power of the adsorbed oxygen species was also measured. The mode of the distribution curve of oxidation power indicates that the oxygen can be classified into two groups which differ in oxidation power as well as in the catalytic activity for the oxidation of CO. From the comparison between the results of the transient response and the oxidation power measurements, it is concluded that the rapidly and slowly adsorbed oxygen groups observed by the transient response method correspond to those of oxygen species of higher and lower oxidation power, respectively. Kinetic analysis of the conductivity response curve caused by the adsorption of oxygen leads to the conclusion that the dissociative adsorption of oxygen associated with electron transfer from the catalyst takes place simultaneously on two different kinds of adsorption sites at substantially different rates.

The adsorption of oxygen on Cr_2O_3 has been studied by a number of investigators[1,2] with special reference to the nature of adsorbed oxygen. It is widely accepted that the adsorption of oxygen on the surface is dissociative, even at room temperature. However, infrared studies[3,4] of the adsorbed oxygen on Cr_2O_3 revealed that there exist several different adsorption bands due to the different vibrations of bonds between the surface cation and oxygen, produced as a results of the dissociative chemisorption. The existence of the variety of surface oxygen may result in a complexity of reactions in which the surface oxygen takes part.

In order to provide necessary information on the role of adsorbed oxygen participating in the CO oxidation over Cr_2O_3, this paper deals with the nature of surface oxygen species and their activity for this reaction. The transient response method was used together with measurement of the distribution of oxidation power of the surface oxygen species.

Experimental

The chromium sesquioxide was prepared by decomposing chromium trioxide in an air flow at 450 °C for 5 h. The X-ray diffraction analysis of the sample indicated that the sample was in the form of α-Cr_2O_3. The sample used as the catalyst was in 24—32 mesh granule and was found to have a BET surface area of 21 m^2/g. The catalyst is a p-type semiconductor under the whole range of experimental conditions, showing an increase in electrical conductivity with increasing amount of adsorbed oxygen.

The experiments were carried out with either oxidized or reduced catalysts. The oxidized catalyst was prepared by pretreatment in a stream of O_2(20%)-N_2 mixture at 131 °C for more than 24 h and the reduced catalyst was prepared by reduction with a CO(6%)-nitrogen stream at the same temperature until no carbon dioxide in the effluent stream was detected. The electrical conductivity of the oxidized catalyst thus prepared was constant and no change in the conductivity could be observed with prolonged oxidation. The conductivity thus attained was 3.2×10^{-6} ohm^{-1} cm^{-1}. For the reduced catalyst, the electrical conductivity was found to be negligibly small as compared to that of the oxidized catalyst.

Commercial CO, CO_2, and N_2 were carefully purified through a dry ice-methanol trap to remove water vapor. A Pyrex glass tube reactor containing 55.2 g catalyst was immersed in an oil bath. The temperature of the catalyst bed was kept uniform within $\pm$0.1 °C at desired temperatures.

A flow system was employed in all the experiments and the total flow rate of the gas stream was always kept constant at 160$\pm$2 ml/min. In applying the transient response method, the concentration of one or two components in the inlet gas stream was changed stepwise by using nitrogen as a balancing gas. The reaction conditions were always chosen in such a way that the total conversion of carbon monoxide did not exceed ten percent in all the runs.

The gases were analyzed by gas chromatography and the conductivity of the catalyst bed was measured with a d.c. bridge. The amount of surface oxygen species was analyzed with a potassium iodode solution as a reducing agent and the distribution of oxidation power was determined by measurements at various pH's. More detailed descriptions of the transient response method,[5,6] conductivity measurement[5] and the analysis of surface oxygen species[7-9] can be found elsewhere.

Results and Discussion

Nature and Amount of Surface Oxygen Species. The nature of oxygen species adsorbed on the metal oxides varies a great deal with respect to the oxidation power and catalytic activity as in the case of NiO,[8] MnO_2,[5,7] and Pb_3O_4.[10] In order to determine the catalytically active oxygen species on Cr_2O_3 surfaces for carbon monoxide oxidation, the distribution of oxidation power of the surface oxygen species was measured with a potassium iodide solution at various pH for the catalysts exposed to various gas stream. The results are shown in Fig. 1. The amount of oxygen species on the oxidized surface shows a bimodal distribution with respect to the oxidation power similar to those adsorbed on MnO_2[5] and Pb_3O_4[10] (curve I, Fig. 1). One group of oxygen species has an oxidation power (O.P) higher than 9.0 and another with one lower than 9.0. We designate the surface oxygen species in the two groups O_s^h and O_s^l, respectively.

When the oxidized surface was exposed to a stream of CO(6%)-N_2 mixture for 30 min at 163 °C, the

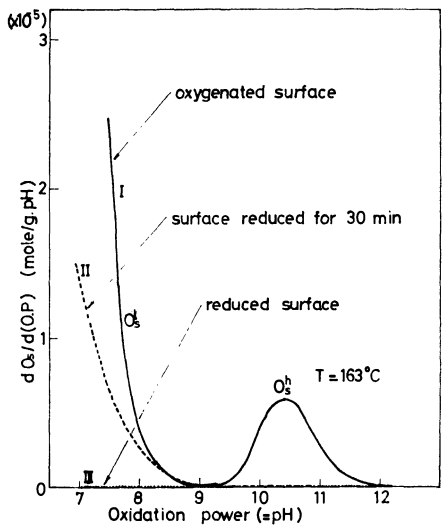

Fig. 1. Variation of the distribution of oxidation power by the reduction with CO.

newly measured distribution curve showed complete disappearance of O_s^h accompanying an appreciable decrease of O_s^l (curve II, Fig. 1). The partly reduced catalyst showed no variation in the amount of O_s^l when it was kept standing in pure nitrogen stream for different periods of time, indicating that no transformation between O_s^l and O_s^h took place.

When the oxidized surface was completely reduced for 24 h by the same gas mixture until no carbon dioxide was detected in the effluent gas stream, no more oxygen species were detected by the KI method on this reduced surface (curve III, Fig. 1).

Based on these results it may reasonably be concluded that both O_s^h and O_s^l are active for the reaction with carbon monoxide and the rate of the reaction is high with O_s^h and low with O_s^l.

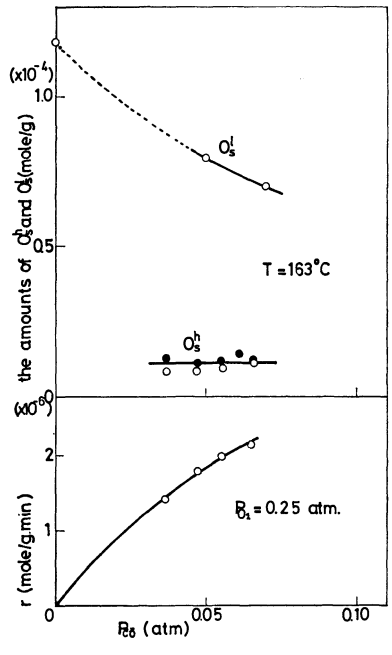

Fig. 2. The amounts of O_s^h and O_s^l and the rate of CO_2 formation on Cr_2O_3 as a function of P_{CO}.

The total amount of the surface oxygen species was determined with hydrazine solution,[7] which is a stronger reducing reagent than potassium iodide solution, and the amount was found to be 1.3×10^{-4} mol/g.

After the steady states of the reaction were attained at 163 °C with the feed streams of various partial pressure of carbon monoxide, the amounts of O_s^h and O_s^l existing on the surface were analyzed. The results are shown in Fig. 2 together with the reaction rate at each steady state. In this case, the amount of O_s^l was determined as the difference between the total amount determined by the hydrazine method and the amount of O_s^h determined by the potassium iodide method. The amount of O_s^h remains constant irrespective of the partial pressure of carbon monoxide in the feed, with which the reaction rate varies considerably (Fig. 2). The open and solid circles for O_s^h curve represent the repeated runs, indicating the satisfactorily good reproducibility of the data. The amount of O_s^l, on the other hand, decreases with increasing partial pressure of carbon monoxide in the feed stream. The results suggest that the rate of the reproduction of O_s^h from gaseous oxygen is sufficiently rapid as compared with the rate at which O_s^h is removed by the reaction with carbon monoxide, while the rate of the reproduction of O_s^l is not great enough and eventually the amount of O_s^l decreases with increasing partial pressure of carbon monoxide, where the reaction rate are higher. The deviation of the reaction rates from the first-order dependence in carbon monoxide can be explained by the diminution of O_s^l.

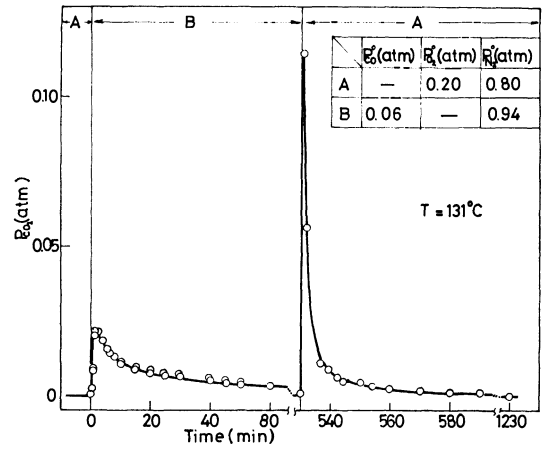

Fig. 3. CO–CO_2 response.

Amount of Surface Oxygen Determined by the Transient Response Method. After the catalyst was completely oxidized in the stream of O_2(20%)–N_2 mixture, the feed was suddenly replaced by the stream of CO(6%)–N_2 mixture and the CO(inc., 0)–CO_2 response was followed for 530 min until no more desorption of carbon dioxide was observed. The results are shown in Fig. 3. Since no oxygen is present in the gas phase after changing the feed composition, the graphical integration of the CO(inc., 0)–CO_2 response curve gives the amount of carbon dioxide produced by the reaction between surface oxygen species and carbon monoxide and then released

from the surface. It is estimated to be 2.5×10^{-4} mol/g.

In the subsequent run, the feed stream of CO(6%)–N_2 mixture was replaced by the stream of O_2(20%)–N_2 mixture and additional outflow of carbon dioxide was observed (Fig. 3, righthand-side). This addional release of carbon dioxide can be attributed to the desorption of irreversibly adsorbed carbon dioxide due to the competitive adsorption of oxygen on the same adsorption site. The behavior of adsorbed carbon dioxide will be discussed in detail in a subsequent paper (part II).[11] The amount of the irreversibly adsorbed carbon dioxide is estimated to be 5.2×10^{-5} mol/g. Hence the total amount of carbon dioxide produced by the reaction between surface oxygen species and carbon monoxide should be 3×10^{-4} mol/g, corresponding to 1.5×10^{-4} mol/g of surface oxygen species. The value is in good agreement with that estimated by the hydrazine method.

On the assumption that the cation layer in the undistorted (001) plane of α-chromia is associated with the surface, the number of surface chromium ions was calculated by McIver and Tobin[12] to be 9.8×10^{14} atom/cm^2. The oxygen adsorption on Cr_2O_3 surface might be dissociative. The amount of oxygen species adsorbed on the surface by the response method corresponds to 8.6×10^{14} atom/cm^2 by using BET surface area of 21 m^2/g. The value is very close to that of surface chromium ions, indicating that each of the dissociatively adsorbed oxygen is bonded to a chromium ion and the surface chromium ions are almost entirely covered with adsorbed oxygen atoms. The fact that the total amount of adsorbed oxygen does not change even when the oxidized surface is exposed to a stream of pure nitrogen at 131 °C for 60 min indicates that the adsorption of oxygen to the surface is fairly strong.

Adsorption of Oxygen on the Reduced Surface. After the reduced catalyst had been kept in a stream of pure nitrogen, the stream was replaced by a stream of O_2(20%)–N_2 mixture and the responce in the oxygen concentration in the effluent stream and the electrical conductivity of the catalyst were followed simultaneously. The results of the response in the conductivity (open circle) are shown in Fig. 4. Owing to the adsorption of oxygen the electrical conductivity of the catalyst

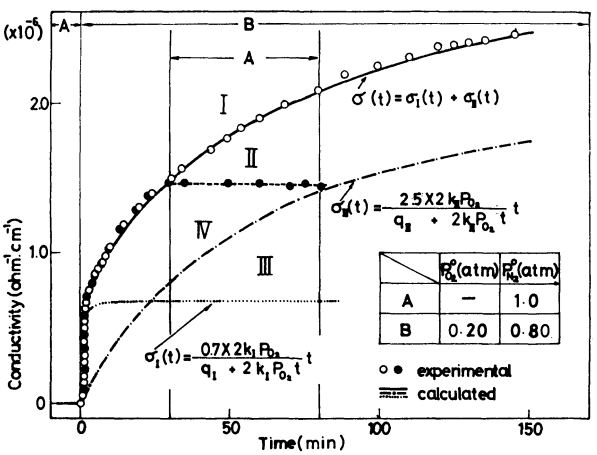

Fig. 4. O_2 (inc., 0)-σ response.

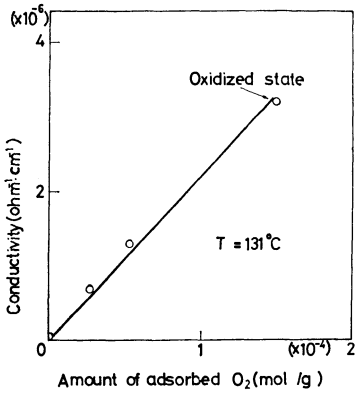

Fig. 5. Linear relationship between the amount of adsorbed O_2 and the conductivity.

increases very rapidly at the initial stage but becomes very slow in the following period of time. Since the catalyst is a p-type semiconductor, the increase in conductivity indicates the shift of electron from the catalyst to the adsorbed oxygen probably bringing about the formation of oxygen anions.

From the response in the oxygen concentration in the effluent stream, we can estimate the amount of adsorbed oxygen at each instant. When the conductivity of the catalyst is plotted against the amount of adsorbed oxygen at each instance, a linear relationship is obtained (Fig. 5). The linearity differs slightly from that obtained by Weller and Voltz,[13] who found that the conductivity was proportional to the 1.2 power of the amount of adsorbed oxygen. Although they stated that the precision of this relationship was not high because of the absolute changes in conductivity observed, the difference in the method of pretreatment of the sample might have caused the disagreement.

The observed response data show at first very rapid and then gradual increases in conductivity. This characteristic behavior of the response curve strongly suggests that the change is due to two different steps. Possible cases are; 1) the successive two-step electron transfer at different rates to the adsorbed oxygen from the catalyst, 2) adsorption of oxygen followed by bulk diffusion into the body of oxide associated with successive electron transfer as suggested by Burwell *et al.*,[2] and 3) the parallel adsorption of oxygen onto two different kinds of active sites at different adsorption rates associated with electron transfer. If 1) or 2) were the case, a gradual increase in the conductivity should be observed when the O_2(20%)–N_2 stream is replaced by a pure nitrogen stream during the course of response measurement. However, the experimental results (solid circles) showed no such changes in conductivity, remaining constant (Fig. 4). Thus the most probable case should be 3). The constancy of the conductivity of the catalyst, which was kept in the pure nitrogen stream, indicates the irreversibility of the oxygen adsorption on both types of active site.

Let us thereby assume the following two parallel elementary steps for the adsorption of oxygen.

$$O_2(g) + S_I \xrightarrow{k_I} O_s^-\cdot S_I \qquad \text{(very fast)} \qquad (1)$$

$$O_2(g) + S_{II} \xrightarrow{k_{II}} O_s^-\cdot S_{II} \qquad \text{(slow)} \qquad (2)$$

where S_I and S_{II} denote the different sites for the adsorption of oxygen with different activities, and O_s^- denotes the negatively charged oxygen spcies. One can roughly estimate the total amounts of $O_s^- \cdot S_I$ and $O_s^- \cdot S_{II}$ by using conductivity data (Fig. 4) and the linear relationship (Fig. 5). Let us suppose that the initial rapid increase in conductivity up to 0.7×10^{-6} ohm^{-1} cm^{-1} is mainly due to the rapid adsorption on site S_I and the gradual increase thereafter results from the slow adsorption on sites S_{II}. Since the conductivity of the catalyst reaches a maximum, 3.2×10^{-6} ohm^{-1} cm^{-1}, with the saturated amount of adsorbed oxygen (Fig. 5), the saturated amounts of $O_s^- \cdot S_I$ and $O_s^- \cdot S_{II}$ are estimated to be 3.3×10^{-5} mol/g and 1.17×10^{-4} mol/g, respectively.

Assuming the dissociative adsorption of oxygen, the rates of adsorption on S_I and S_{II} are given, respectively, by

$$\frac{d\theta_I}{dt} = \frac{2k_I}{q_I}(1-\theta_I)^2 P_{O_2} \quad (3)$$

$$\frac{d\theta_{II}}{dt} = \frac{2k_{II}}{q_{II}}(1-\theta_{II})^2 P_{O_2} \quad (4)$$

where q_I and q_{II} are the saturated amounts of $O_s^- \cdot S_I$ and $O_s^- \cdot S_{II}$, respectively, and θ_I and θ_{II} are the coverage fractions of respective sites.

The rates of oxygen adsorption on sites S_I and S_{II}, respectively, can be easily estimated from the graphical differentiation of the response curve in two portions, from zero to 0.7×10^{-6} ohm^{-1} cm^{-1} and from that to 3.2×10^{-6} ohm^{-1} cm^{-1}. For this purpose, the response curves of P_{O_2} and σ at initial stage are shown in Fig. 6. $d\theta_I/dt$ and $d\theta_{II}/dt$ thus obtained at each instance are plotted against $(1-\theta_I)^2$ and $(1-\theta_{II})^2$, respectively, and linear relationships are obtained (Fig. 7), where $(1-\theta_I)^2$ and $(1-\theta_{II})^2$ are denoted by θ_V^2, indicating Eqs. 3 and 4 fit the data satisfactorily. From the slopes

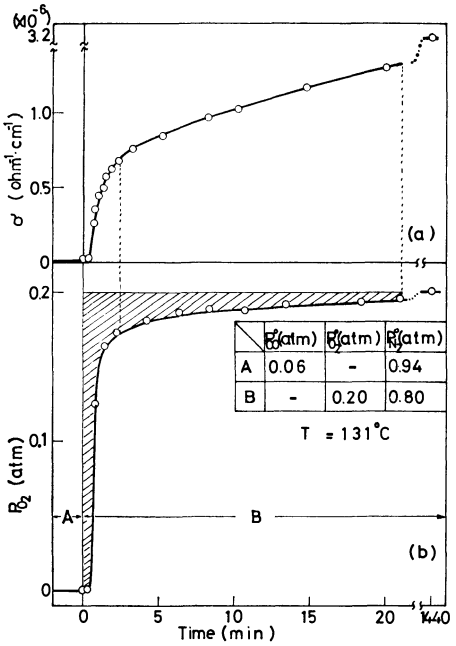

	$P_{O_2}^0$(atm)	P_{O_2}(atm)	$P_{O_2}^{\infty}$(atm)
A	0.06	-	0.94
B	-	0.20	0.80

Fig. 6. CO(dec., 0) and O_2(inc., 0)-O_2 and σ response; Initial stage.

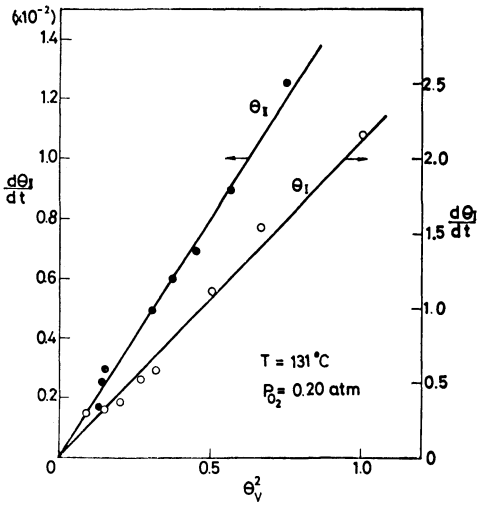

Fig. 7. Plots of $d\theta_I/dt$ and $d\theta_I/dt$ *vs.* θ_V^2.

of both straight lines, two adsorption rate constants, k_I and k_{II}, are calculated, respectively, as

$$k_I = 1.75 \times 10^{-4} \text{ mol/g atm min}$$

$$k_{II} = 4.8 \times 10^{-6} \text{ mol/g atm min}$$

Equations 3 and 4 can be easily integrated with the initial conditions, $\theta_I=0$, $\theta_{II}=0$ at $t=0$, to give

$$\theta_I(t) = \frac{at}{1+at} \quad (5)$$

$$\theta_{II}(t) = \frac{bt}{1+bt} \quad (6)$$

where $a=2k_I P_{O_2}/q_I$ and $b=2k_{II}P_{O_2}/q_{II}$. These equations give the time variation of fractional coverage of sites S_I and S_{II}, and can easily be transformed into the time variation of conductivity owing to the oxygen adsorption on both sites.

$$\sigma_I(t) = \frac{0.7at}{1+at} \quad (7)$$

$$\sigma_{II}(t) = \frac{2.5at}{1+at} \quad (8)$$

σ_I and σ_{II} are the conductivity contribution due to the adsorption of oxygen on sites S_I and S_{II}, respectively. With the values of $q_I=3.3 \times 10^{-5}$, $q_{II}=1.17 \times 10^{-4}$ mol/g and $P_{O_2}=0.2$ atm, Eqs. 7 and 8 are calculated as illustrated by curves III and IV in Fig. 4, respectively. Superposition of curves III and IV gives the calculated curve I, indicating an excellent agreement with the observed data. We might conclude that oxygen is adsorbed dissociatively on two different kinds of adsorption sites with simultaneous charge transfer from the catalyst.

The results showing that O_s^h is much more quickly reproduced than O_s^l from gaseous oxygen suggest that O_s^h and O_s^l correspond to $O_s^- \cdot S_I$ and $O_s^- \cdot S_{II}$, respectively. q_I (the amount of $O_s^- \cdot S_I$) and q_{II} (the amount of $O_s^- \cdot S_{II}$) correspond fairly well to the amount of oxygen species which produce irreversibly adsorbed CO_2 and reversibly adsorbed CO_2, respectively. The carbon dioxide formed on S_I seems to be adsorbed irreversibly and that formed on S_{II} reversibly.

Davydov, Shchekochikhin and Keier[14] demonstrated

that the reaction of CO takes place primarily with oxygen combined with Cr ions exhibiting the lowest degree of coordinative saturation with respect to oxygen. The surface compounds produced in the process, however, form slightly stronger bonds with the surface than the suface compounds combined with the Cr ions exhibiting the higher degree of coordinative saturation with respect to oxygen. The correspondence mentioned above seems to be reasonable.

References

1) E. R. S. Winter, *Adv. Catal.*, **10**, 196 (1958).
2) R. L. Burwell, G. L. Haller, K. C. Taylor, and J. F. Read, *Adv. Catal.*, **20**, 1 (1969).
3) Yu. M. Shchekochikhin, G. I. Panow, and N. A. Akulich, *Kinet. Katal.*, **9**, 1315 (1968).
4) A. Zecchina, S. Coluccia, L. Cerruti, and E. Borello, *J. Phys. Chem.*, **75**, 2783 (1971).
5) M. Kobayashi and H. Kobavashi. *J. Catal.*, **27**, 100 (1972).
6) H. Kobayashi and M. Kobayashi, *Catal. Rev.*, **10**, 139 (1974).
7) M. Kobayashi and H. Kobayashi, *J. Catal.*, **21**, 48 (1971).
8) T. Uchijima, M. Takahashi, and Y. Yoneda, *J. Catal.*, **9**, 402 (1967).
9) T. Uchijima, M. Takahashi, and Y. Yoneda, *Bull. Chem. Soc. Jpn.*, **40**, 2767 (1972).
10) M. Kobayashi and H. Kobayashi, *J. Catal.*, **36**, 74 (1975).
11) M. Kobayashi, T. Date, and H. Kobayashi, *Bull. Chem. Soc. Jpn.*, **49**, 3014 (1976).
12) D. S. McIver and H. H. Tobin, *J. Phys. Chem.*, **64**, 451 (1960).
13) S. W. Weller and S. E. Voltz, *Adv. Catal.*, **9**, 315 (1957).
14) A. A. Davydov, Yu. M. Shchekochikhin, and N. P. Keier, *Kinet. Katal.*, **10**, 1341 (1969).

Carbon Monoxide Oxidation over Chromium Sesquioxide. II. Adsorption Behavior of CO and CO_2

Masayoshi KOBAYASHI, Tomoyuki DATE, and Haruo KOBAYASHI

Department of Chemical Process Engineering, Faculty of Engineering, Hokkaido University, Sapporo 060

(Received August 4, 1975)

The adsorption behavior of carbon monoxide and carbon dioxide on oxidized and reduced surface of α-Cr_2O_3 catalyst was studied experimentally by the application of a transient response method. From the analysis of response curves obtained for the concentration of effluent gas component and for the electrical conductivity of catalysts, it was shown that neither carbon monoxide nor carbon dioxide can be adsorbed on the oxidized surface, but they are adsorbed on the reduced surface without electron transfer between adsorbates and the catalysts. Adsorption of carbon monoxide is almost reversible, but that of carbon dioxide is both reversible and irreversible. Oxygen markedly accelerates the desorption of both carbon monoxide and carbon dioxide. It is concluded that this can be attributed to the effect of adsorbed oxygen in lowering the degree of coordinative unsaturation of Cr^{3+} ions.

The adsorption of carbon monoxide and carbon dioxide on Cr_2O_3 surface has been studied by many investigators.[1-3] It was found that the adsorption behavior of both gases on Cr_2O_3 surface is strongly affected by the oxidation state of the surface as pointed out by Dawden and Garner.[1] In recent years, IR spectroscopy has been successfully applied to reveal the surface properties of Cr_2O_3 and the adsorbed states of CO and CO_2 on its surface.[4,5] It was demonstrated in this line of studies that the degree of coordination unsaturation of Cr^{3+} ions plays as important role in the adsorption behavior of these gases. Zecchina, Colluccia, Guglielminotti and Ghiotti[5] concluded that CO is adsorbed on coordinatively unsaturated (coord. unsatd.) Cr^{3+} ions and CO_2 is adsorbed mainly on Cr^{3+} (coord. unsatd.)–O^{2-} (coord. unsatd.) couples resulting in the formation of bidentate carbonate, and partly on Cr^{3+} (coord. unsatd.) ions or O^{2-}(coord. unsatd.) ions forming linearly bonded CO_2 or monodentate carbonate, respectively. The forms of adsorbed CO_2 and the strength of their bonding to the surface are strongly dependent on the coordination heterogeneity as well as on the ligand heterogeneity. Because of the variety of the adsorbed states it will be worthwhile to reveal the dynamic behavior of the surface complexes and the effect of oxygen on the dynamic behavior.

In the present study, the transient response method[6-8] was utilized for this purpose.

Experimental

α-Cr_2O_3 samples and the method of experiments are the same as described in part I.[9]

The responses of the electrical conductivity, σ, of the catalyst and of the concentration of component Y in the outlet gas stream to a step change in the concentration of component X in the inlet gas mixture are denoted by X-σ and X-Y, respectively. When X is increased from nil, X(inc., 0)-σ and X(inc., 0)-Y; when decreased down to nil, X(dec., 0)-σ and X(dec., 0)-Y.

Results and Discussion

Behavior of CO and CO_2 on the Oxidized Surface

After the catalyst had been completely oxidized in a stream of O_2(20%)–N_2 mixture at 131 °C, CO_2 was introduced stepwise into the feed stream without changing the concentration of oxygen, and the CO_2 (inc., 0)–CO_2 and the CO_2(inc., 0)–σ responses were followed simultaneously. Subsequently, the CO_2 in the feed stream was cut off and the CO_2(dec., 0)–CO_2 and the CO_2(dec., 0)–σ responses were followed. The CO_2–CO_2 responses obtained in both runs were instantaneous and the CO_2–σ responses showed no appreciable change in conductivity (Fig. 1). The CO–CO and the CO–σ responses were also measured in the same way and exactly the same results were observed. The results indicate that neither CO_2 nor CO can be adsorbed on the oxidized surface when prepared in the way used in this experiment. The oxidized sample used in our experiments contains saturated amounts of oxygen on the surface, and hence the oxidized surface has no activity for the additional adsorption of CO and CO_2.

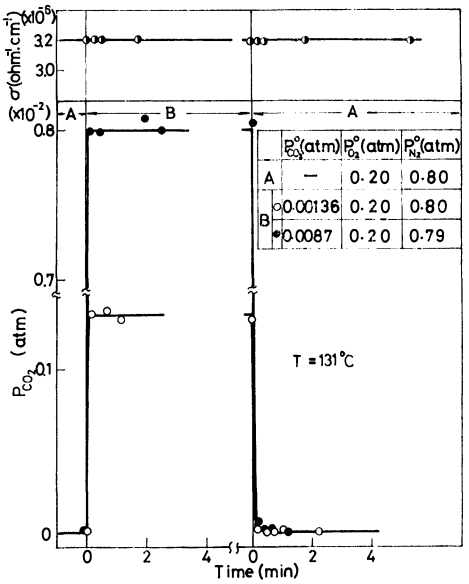

Fig. 1. CO_2–CO_2 response on the oxidized surface.

Behavior of CO_2 on the Reduced Surface. For the preparation of a reduced surface, a stream of CO(6%)–N_2 mixture was allowed to flow through the catalyst bed at 131 °C until no carbon dioxide was detected in the effluent stream. The electrical conductivity of the catalyst fell down to as low as 1×10^{-8} ohm^{-1} cm^{-1}. Carbon dioxide (0.85%) was then introduced into the

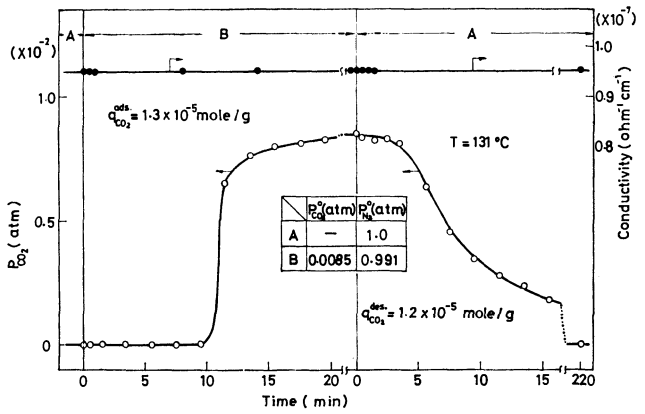

Fig. 2. CO_2–CO_2 response on the reduced surface.

inlet gas stream and the CO_2(inc., 0)–CO_2 and the CO_2(inc., 0)–σ responses were followed until a steady state was reached. Subsequently, the CO_2 in the feed stream was cut off and the CO_2(dec., 0)–CO_2 and the CO_2(dec., 0)–σ responses were followed. The results are shown in Fig. 2. The transient state of the CO_2–CO_2 response was observed in both cases for 30—220 min, indicating the adsorption of CO_2 on the reduced surface. The integrated amount of adsorbed CO_2 is estimated to be 1.3×10^{-5} mol/g from the CO_2 (inc., 0)–CO_2 response and that of desorbed CO_2 is estimated to be 1.2×10^{-5} mol/g from the CO_2(dec., 0)–CO_2 response. Both amounts are nearly the same. It seems that the adsorption of CO_2 under the present conditions is almost reversible.

During these response periods, the electrical conductivity of the catalyst remained constant (Fig. 2), indicating that no electron transfer is accompanied by the adsorption of carbon dioxide, *i.e.* the adsorbed carbon dioxide is electrically neutral.

After the CO_2(inc., 0)–CO_2 response had been followed as described above, the feed stream of CO_2(0.85%)–N_2 mixture was switched over to a stream of O_2(20%)–N_2 mixture instead of pure nitrogen and the CO_2-(dec., 0)–CO_2 response was followed. The results are shown in Fig. 3. A large amount of carbon dioxide was desorbed at the initial period of the response, it decreased steeply and then tailed until no carbon dioxide was detected after 220 min. No carbon monoxide was detected in the effluent stream during the course of response. The integrated amount of the desorbed CO_2 during this run was estimated to be 6.2×10^{-5} mol/g. Since the amount of desorbed CO_2 estimated in the foregoing run was 1.2×10^{-5} mol/g, the desorbed amount of CO_2 estimated in this run is much larger than that in the nitrogen stream. Since the adsorbed CO does not react with gaseous oxygen, the difference in the two amounts can be attributed to the existence of irreversibly adsorbed CO_2 which had been produced during the course of reduction of the surface with CO and remained during the subsequent treatment in the pure nitrogen stream. This suggests that the desorption of the irreversibly adsorbed CO_2 can be attributed to the competitive adsorption of oxygen onto Cr^{3+} (coord. unsatd.) ions. The amount of irreversibly adsorbed CO_2 is estimated to be 5.0×10^{-5} mol/g. This value is in good agreement with that estimated in Part I.

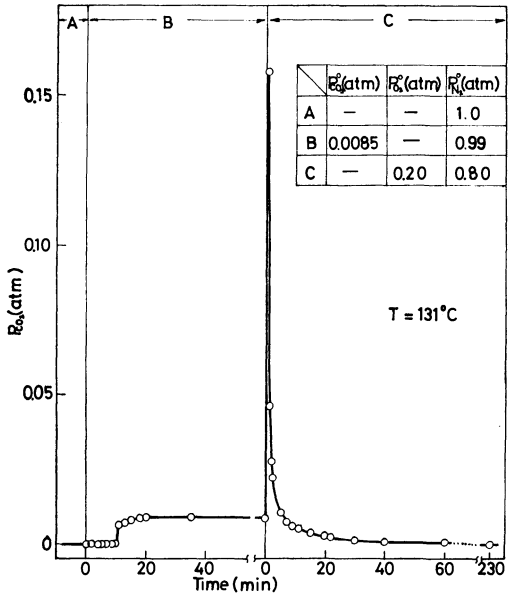

Fig. 3. CO_2–CO_2 response.

It was suggested in Part I that the carbon dioxide produced on site S_I is irreversibly adsorbed while that produced on site S_{II} is reversibly adsorbed. Since the adsorption of oxygen onto site S_I is very rapid, the desorption of the irreversibly adsorbed carbon dioxide from S_I due to the competitive adsorption of oxygen should also be rapid. Comparing the period of the initial rapid desorption of carbon dioxide (Fig. 3) with the time required for the initial rapid adsorption of oxygen (Fig. 6, Part I), we see that the time required for both processes are consistent with each other.

We might conclude that when oxygen is present in the gas phase, the site S_I is always free from retardation by adsorbed carbon dioxide, and $O^-\cdot S_I$, which is very active for CO oxidation, is rapidly regenerated, contributing substantially to the reaction. This might explain the fact that the amount of $O^-\cdot S_I$ remains constant in the steady state of the reaction with a variety of P_{CO}.

The rate of oxygen adsorption on S_{II} is very small and the same effect of oxygen can not be expected for the carbon dioxide produced on S_{II}. Eventually the amount of $O^-\cdot S_{II}$ is lowered at a steady state with higher partial pressure of CO where the rates of CO_2 formation on S_{II} are higher.

According to the results obtained by Zecchina *et al.*[5] the irreversibly adsorbed CO_2 observed in this study will probably be in the form of bidentate carbonate produced by the adsorption of CO_2 on the Cr^{3+} (coord. unsatd.)–O^{-2} (coord. unsatd.) couples which are present on the highly reduced surface. Another possibility is that the bicarbonate ions produced by the adsorption of CO_2 on hydroxyl ions remain on the surface. The reversibly adsorbed CO_2, on the other hand, will mainly correspond to CO_2 coordinated to Cr^{3+} (coord. unsatd.) ions in the linear form which is predominant when the degree of coordinative unsaturation of Cr^{3+} is low.

Behavior of CO on the Reduced Surface. After the

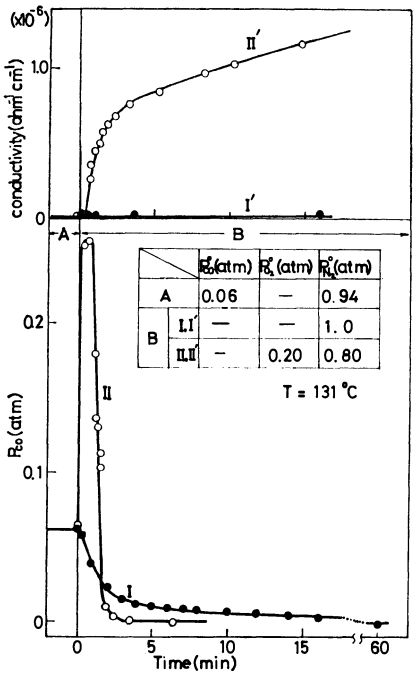

Fig. 4. CO-CO and CO-σ responses.

catalyst had been reduced in the same way as described in the foregoing section, the feed stream was switched over to a stream of either pure nitrogen or a mixture of $O_2(20\%)$–N_2, and the CO-CO and the CO-σ responses were followed simultaneously. The results are shown in Fig. 4.

When the feed stream was replaced by the stream of pure nitrogen, the desorption of CO was observed for about 60 min as shown by curve I in Fig. 4. From the graphical integration of curve I, the total amount of adsorbed carbon monoxide is estimated to be 3.0×10^{-5} mol/g. During the same run, the electrical conductivity of the catalyst was kept entirely constant (line I', Fig. 4). These results imply that CO can be adsorbed on the reduced surface without electron transfer between the adsorbed CO and the catalyst. Since the adsorption of CO can take place only on the reduced surface, the sites for the adsorption should be Cr^{3+} (coord. unsatd.) ions.

When the feed stream was replaced by a stream of $O_2(20\%)$–N_2 mixture, on the other hand, the desorption of a large amount of CO took place at the initial stage of the response and the desorption was completed within 3 min (curve II in Fig. 4). The integrated amount of desorbed CO is estimated to be 3.6×10^{-5} mol/g, being slightly higher than the amount of CO desorbed into the pure nitrogen stream. If the carbon monoxide adsorbed on the surface can react with the oxygen introduced, the amount of the desorbed CO in the $O_2(20\%)$–N_2 stream should be lower than the amount of the desorbed CO in the pure nitrogen stream. The results suggest that the adsorbed CO does not react with the introduced oxygen.

The difference in the amounts of desorbed CO into the $O_2(20\%)$–N_2 stream and the pure N_2 stream may also be ascribed to the same reason as in the case of CO_2.

It has been stated by Zecchina *et al.*[5] that the adsorption of CO on the reduced surface is reversible. Presumably, however, the adsorption of CO under the conditions in this study will not be completely reversible, and the adsorbed CO at a very low coverage will remain on highly coordinatively unsaturated Cr^{3+} ions, and these residual adsorbed CO molecules will be desorbed only by the adsorption of oxygen onto Cr^{3+} (coord. unsatd.) ions, with which the degree of coordinative unsaturation of Cr^{3+} (coord. unsatd.) ions is lowered and eventually the desorption of CO is enhanced.

The change in the electrical conductivity was observed (curve II', Fig. 4). Since no electron transfer takes place in the case of CO desorption into the pure nitrogen stream, the change in the electrical conductivity in this case should be due to the adsorption of oxygen.[9]

So far we have discussed the nature of adsorption sites on the surface only in terms of coordinative heterogeneity of Cr^{3+} ions, but ligand heterogeneity may also play some role in characterizing the nature of those sites. OH^- on the surface might have some effects on the behavior of CO and CO_2 on the surface.

Behavior of CO and CO_2 during the CO Oxidation at Steady States. When a mixture of CO–O_2–N_2 is allowed to flow through the bed of oxidized catalyst, oxidation of CO takes place, the reaction rate varying

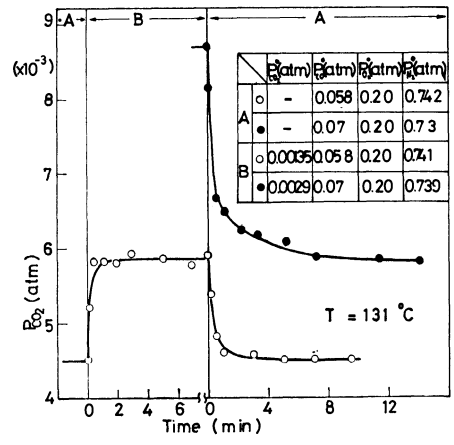

Fig. 5. CO_2-CO_2 response during the reaction.

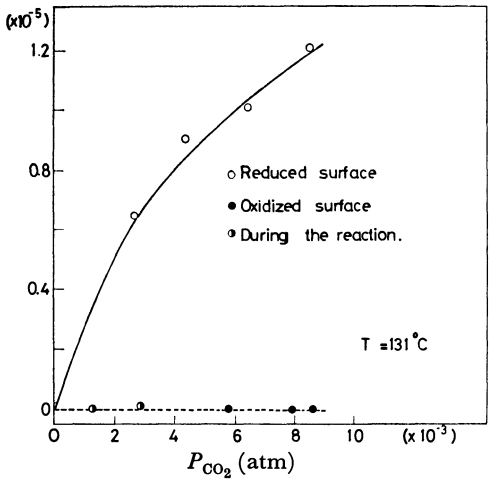

Fig. 6. Adsorption isotherm for CO_2.

very slowly until it reaches a steady state after 15 h. After the steady state was attained, the CO in the feed was cut off and CO(dec., 0)–CO response was followed. The response was instantaneous, indicating that no carbon monoxide was adsorbed on the surface in the steady state during the course of reaction. On the other hand, the CO_2(inc., 0)–CO_2 and the CO_2(dec., 0)–CO_2 responses obtained in the same steady state indicates the occurrence of adsorption and the desorption of CO_2 on the same surface (Fig. 5). The amount of adsorbed CO_2 estimated from the graphical integration of the CO_2(dec., 0)–CO_2 response curve was presented in Fig. 6 with those on the reduced surface and on the oxidized surface. As can be seen from Fig. 6, the amount of CO_2 adsorbed on the surface during the reaction was two orders of magnitude smaller than that adsorbed on the reduced surface and rather close to that on completely oxidized surface. From the result, it can be concluded that the catalyst surface during the course of reaction in the steady state is in highly oxidized state.

References

1) D. A. Dawden and W. E. Garner, *J. Chem. Soc.*, **1929**, 893.
2) D. S. MacIver and H. H. Tobin, *J. Phys. Chem.*, **64**, 451 (1960).
3) R. L. Burwell, G. L. Haller, K. C. Taylor, and J. F. Read, *Adv. Catal.*, **20**, 1 (1969).
4) A. A. Davydov, Yu. M. Shchekochikhin, and N. P. Keier, *Kinet. Katal.*, **10**, 1341 (1969).
5) A. Zecchina, S. Coluccia, E. Guglielminotti, and G. Ghiotti, *J. Phys. Chem.*, **75**, 2774, 2790 (1971).
6) M. Kobayashi and H. Kobayashi, *J. Catal.*, **27**, 100, 108, 114 (1972), *Shokubai*, **16**, No. 2, 8 (1974).
7) H. Kobayashi and M. Kobayashi, *Catal. Rev.*, **10**(2), 139 (1974).
8) M. Kobayashi, Doctoral Thesis, Hokkaido Univ., 1975.
9) M. Kobayashi and H. Kobayashi, *Bull. Chem. Soc. Jpn.*, **49**, 3009 (1976).

Carbon Monoxide Oxidation over Chromium Sesquioxide. III. Kinetics of the Reaction

Masayoshi KOBAYASHI and Haruo KOBAYASHI

Department of Chemical Process Engineering, Faculty of Engineering, Hokkaido University, Sapporo 060

(Received August 4, 1975)

Based on the experimental findings in Parts I and II, mechanisms of carbon monoxide oxidation over α-Cr_2O_3 were proposed with which the reaction takes place simultaneously through two parallel reaction paths. Overall reaction consists of five elementary steps, and the rate constants of all ellementary stepes were determined from the analysis of appropriate transient response data. The simulation of transient response with these rate constants proved the validity of these mechansims and the results of kinetic analyses.

The reaction mechanism of carbon monoxide oxidation over Cr_2O_3 has been studied by several investigators and the conclusions reached by these investigators are rather divergent. Winter[1] thought that the rate determining step was the adsorption of oxgen. Tarama, Teranishi, and Hattori[2] worked out the kinetic analysis of the data obtained in a closed recycle reaction system and suggested that the overall reaction was controlled by the reaction between adsorbed carbon monoxide and adsorbed atomic oxygen. Recently, Davydov, Shchekochikhin, and Keier[3] suggested, on the basis of IR spectroscopic study of surface complexes formed on α-Cr_2O_3, that the rate determing step was not the adsorption of oxygen but either the reaction of gaseous carbon monoxide with surface oxygen species or the desorption of surface complexes formed in the course of the reaction.

Voltz and Weller[4] pointed out in early days that the catalytic activity of Cr_2O_3 was affected by the oxidation states of the surface. Recently, the complexity of the characteristics of Cr_2O_3 surface has been revealed in detail by IR spectroscopic studies.[5-9] The divergent conclusions drawn by many investigators for the kinetics of CO oxidation over Cr_2O_3, therefore, may be attributable to the different characteristics of samples, which is highly sensitive to pretreatments, temperature, and ambient gas atmosphere.

In our previous paper, Part I,[10] it was concluded that oxygen is adsorbed dissociatively on coordinatively unsaturated chromium ions forming oxygen anions, and that the oxygen anions consist of two groups, $O^-\cdot S_I$ and $O^-\cdot S_{II}$, the former is very rapidly generated and easily reacts with CO while the latter is produced very slowly and is less active for the reaction with CO. It was also shown[11] that CO could not be adsorbed on α-Cr_2O_3 surface when it was either fully oxidized or in steady states where CO oxidation was taking place. These results lead to a conclusion that the oxidation of CO over α-Cr_2O_3 proceeds through the reaction between gaseous CO and oxygen anions on the surface.

In the present paper, we are concerned with how the different groups of the oxygen anions take part in the oxidation of CO, and also with the detailed kinetic analysis of the reaction.

Reaction Mechanism for Kinetic Analysis

According to the results and the discussion in the previous paper, the mechanism of the oxidation of CO over Cr_2O_3 catalyst can be summarized as follows.

a) Two kinds of dissociatively adsorbed oxygen anions, $O^-\cdot S_I$ and $O^-\cdot S_{II}$, are present on the surface and both are active for the oxidation of CO. $O^-\cdot S_I$ has a higher oxidation power and can be rapidly regenerated by gaseous oxygen. Therefore, S_I is always saturated with adsorbed oxygen anions under the steady states of the reaction at various partial pressure of CO. On the other hand, $O^-\cdot S_{II}$ has a lower oxidation power and the rate of its regeneration is slow and hence the concentration of $O^-\cdot S_{II}$ decreased with higher partial pressure of CO with which the reaction rates are higher.

b) Under the steady states of the reaction, the reaction proceeds through the simultaneous reactions of gaseous CO with both $O^-\cdot S_I$ and $O^-\cdot S_{II}$ with different reaction rates.

c) Carbon dioxide produced by the reaction between CO and $O^-\cdot S_I$ is adsorbed irreversibly on S_I when oxygen is not present in the gas phase, but when oxygen exists in the gas phase the adsorbed CO_2 on S_I is very rapidly desorbed due to the competitive adsorption of oxygen onto S_I. On the other hand, the desorption of carbon dioxide produced by the reaction between CO and $O^-\cdot S_{II}$ is not affected by the presence of oxygen in the gas phase. Under the steady states of the reaction, the amount of adsorbed CO_2 on S_{II} is negligibly small.

d) The adsorbed CO_2 on S_I and S_{II} is not ionized.

The reaction mechanism suggested above for the catalytic oxidation of CO over Cr_2O_3 can be represented in the sequence of the following steps.

Reaction path I:

$$CO(g) + O^-\cdot S_I \xrightarrow{k_1} CO_2\cdot S_I + e \quad (1)$$

$$O_2(g) + 2CO_2\cdot S_I + 2e \xrightarrow{k_2} 2CO_2(g) + 2O^-\cdot S_I \quad (2)$$

Reaction path II:

$$CO(g) + O^-\cdot S_{II} \xrightarrow{k_3} CO_2\cdot S_{II} + e \quad (3)$$

$$CO_2\cdot S_{II} \xrightarrow{k_4} CO_2(g) + S_{II} \quad (4)$$

$$O_2(g) + 2S_{II} + 2e \xrightarrow{k_5} 2O^-\cdot S_{II} \quad (5)$$

Although non-ionized adsorption of CO_2 was suggested in the previous paper[11], one can see another evidence in the results shown in Fig. 1, which indicate that the shift of electrons takes place when gaseous CO reacts with the surface oxygen anions.

Let us examine the results shown in Fig. 1. After the catalyst had been completely oxidized by a stream

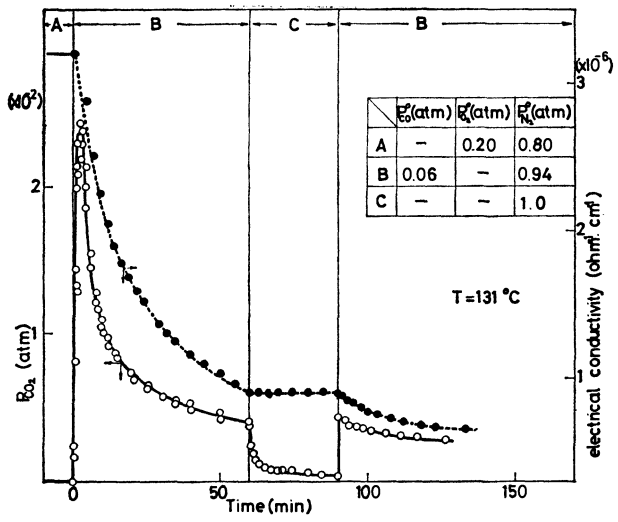

Fig. 1. CO-CO_2 and CO-σ response.

of O_2(20%)-N_2 mixture, the stream was suddenly replaced by a stream of CO(6%)-N_2 mixture and the responses in the outlet CO_2 concentration and in the electrical conductivity of the catalyst were followed for 60 min. The CO_2 concentration reached a maximum in a very short time and then fell down steeply and afterwards it gradually decreased to very low values. The electrical conductivity, on the other hand, decreased monotonously due to the formation of gaseous CO_2 with the expense of oxygen anions on the surface. Since the catalyst is a p-type semiconductor, the picking up of surface oxygen by CO in the form of CO_2 results in the decrease in the conductivity, due to the shift of electrons from the oxygen anions back to the catalyst. After 60 min, the feed was replaced by a stream of pure nitrogen. Even with no carbon monoxide in the feed, CO_2 could be detected for a certain period of time due to the desorption of CO_2 which had been produced and accumulated on the surface during the foregoing reduction period. The electrical conductivity, on the other hand, was kept entirely constant during this run. These results substantiate the Steps (1) and (2) which indicate that the electron transfer back to the catalyst occurs when the surface compounds are formed by the reaction of CO with surface oxygen anions, and not when the surface compound decomposes to give gaseous CO_2 as has been suggested by Matsushita, Nakata[12] and Courtois and Teichner.[13]

Determination of Rate Constants

The rate constants k_2 and k_5 have been already determined in Part I[10] as k_I and k_{II}, respectively.

$$k_2 = k_I = 1.75 \times 10^{-4} \text{ mol/g min atm}$$

$$k_5 = k_{II} = 4.8 \times 10^{-6} \text{ mol/g min atm}$$

Determination of k_4. The value of k_4 can be determined from the CO(dec., 0)-CO_2 response during the reaction under steady states. An example of the CO-(dec., 0)-CO_2 response data is shown in Fig. 2. As has been discussed in Part II,[11] the desorption of CO_2 produced by gaseous CO and $O^- \cdot S_I$ on the surface

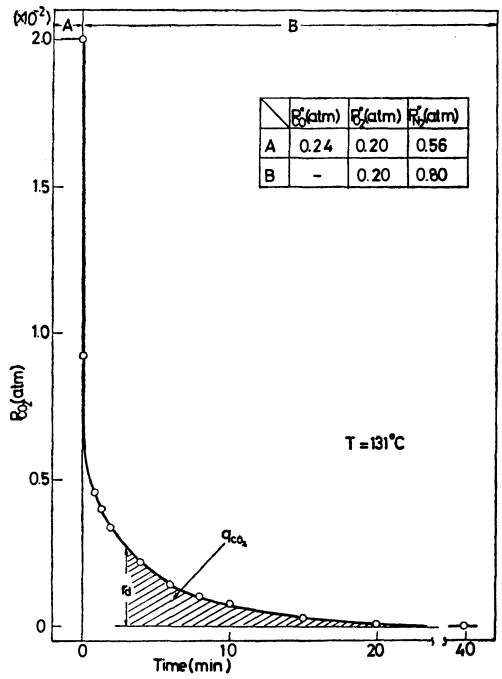

Fig. 2. CO(dec., 0)-CO_2 response during the reaction.

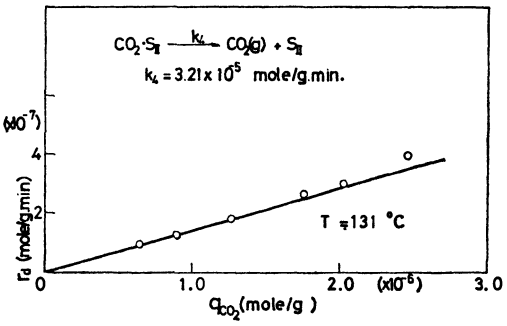

Fig. 3. Plot of the desorption rate of CO_2 *vs.* q_{CO_2} estimated from the graphical analyses of the curve presented in Fig. 2.

is very rapid due to the competitive adsorption of oxygen, then the slow desorption of CO_2 as can be seen in the later part of the response may be attributed solely to the desorption of CO_2 from $CO_2 \cdot S_{II}$. Furthermore, it is known that the amount of CO_2 readsorbed from gas phase on S_{II} during the reaction is negligible.[11] Therefore, the rates of CO_2 desorption measured in the later part of the response can be considered to give true rates of CO_2 desorption from $CO_2 \cdot S_{II}$. From the response data, one can estimate the amounts of adsorbed $CO_2 \cdot S_{II}$ and the corresponding desorption rates of CO_2. A plot of desorption rates against the adsorbed amounts of CO_2 gives a straight line as presented in Fig. 3. The rate of CO_2 desorption from $CO_2 \cdot S_{II}$ can be given by

$$r_d = k_4 \cdot \theta_{II} \cdot CO_2 \qquad (6)$$

where k_4 is the desorption rate constant of CO_2 from S_{II} and $\theta_{II \cdot CO_2}$ is the fractional coverage of S_{II} with CO_2. Assuming linear form of adsorbed CO_2 on S_{II}, as has been discussed in Part II,[11] the saturated amount of $CO_2 \cdot S_{II}$, $q_{CO_2 \cdot max}$, may be taken as equivalent to that of $O^- \cdot S_{II}$ as estimated in Part I, which is equal

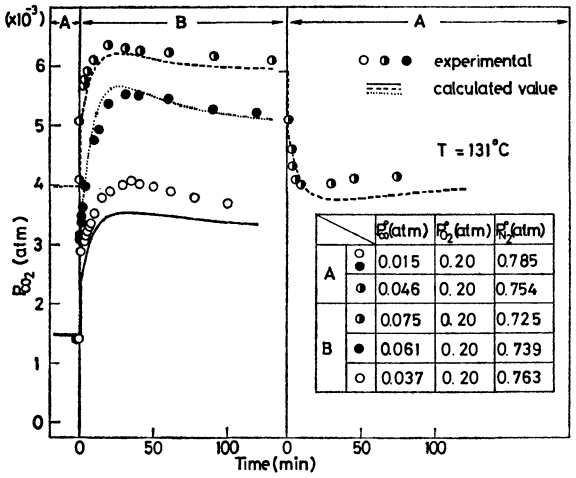

		P^0_{CO}(atm)	$P^0_{O_2}$(atm)	$P^0_{N_2}$(atm)
A	○	0.015	0.20	0.785
	◑	0.046	0.20	0.754
B	◑	0.075	0.20	0.725
	●	0.061	0.20	0.739
	○	0.037	0.20	0.763

Fig. 4. CO–CO_2 response.

to 2.34×10^{-4} mol/g. Using this value and the slope of the straight line in Fig. 3, one can estimate the value of k_4 as

$$k_4 = 3.21\times10^{-5} \text{ mol/g min}$$

Under the conditions given in Fig. 2, $\theta_{II\cdot CO_2}$ for the catalyst having been operated in the gas mixture A under the steady state was also estimated as

$$\theta_{II\cdot CO_2} = 0.017$$

Determination of k_1. k_1 can be determined from the CO–CO_2 response during the reaction at steady states. An example of such response is given in Fig. 4, which shows an instantaneous increase in P_{CO_2} followed by a gradual increase to a maximum and then approaches a new steady state. The initial instantaneous increase in P_{CO_2} may be ascribed to the rapid desorption of incremental CO_2 produced by the reaction of $O^-\cdot S_I$ and the increment of the partial pressure of CO. Because, as has been discussed in Part II, the CO_2 produced on S_I can be desorbed very rapidly by the competitive adsorption of oxygen while that produced on S_{II} desorbs gradually as we have seen in the foregoing sections. A plot of Δr_1 *vs.* ΔP_{CO} gives a linear relationship as presented in Fig. 5. Thus the initial increase in the production rate of CO_2, namely the rate of Step (1), can be given as

$$\Delta r_1 = k_1\cdot\theta_I\cdot\Delta P_{CO} \tag{8}$$

where θ_I is the fractional coverage of S_I with oxygen. Since it is known that θ_I can be taken to be unity, the valu of k_1 can be estimated from the slope of the straight line in Fig. 5 as

$$k_1 = 4.15\times10^{-6} \text{ mol/g min atm.}$$

Determination of k_3. At the reaction steady state, the rate of CO_2 formation canbe expressed by the sum of both Eqs. 1 and 3 as follows:

$$r_{st} = k_1P_{CO}\theta_I + k_3P_{CO}\theta_{II} = r_I + r_{II} \tag{7}$$

where $r_I=k_1P_{CO}\theta_I$ and $r_{II}=k_3P_{CO}\theta_{II}$. Using the values of k_1 and θ_I estimated in the foregoing section, one can calculate r_I and determine r_{st} from the experimental data at various partial pressures of

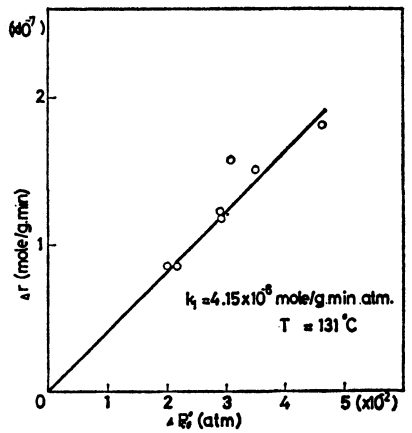

Fig. 5. Plot of Δr *vs.* ΔP^0_{CO}.

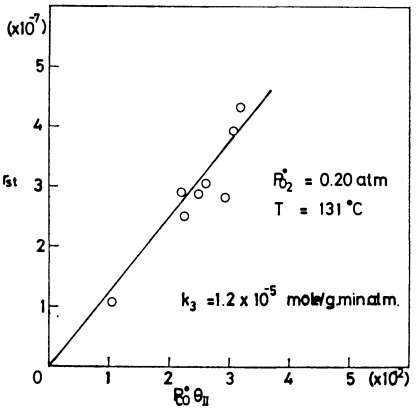

Fig. 6. Plot of r_{st} *vs.* $P^0_{CO}\theta_{II}$.

CO. Therefore, r_{II} at various partial pressures of CO is estimated easily from the difference between r_{st} and r_I at corresponding conditions.

On the other hand, the values of θ_{II} at the corresponding steady states can be roughly estimated from the electrical conductivity at the same conditions, which shows the amount of $O^-\cdot S_{II}$ since S_I is fully occupied by oxygen anions due to its rapid adsorption during the reaction. A plot of r_{II} against θ_{II} gives a straight line as shown in Fig. 6. From the slope of the straight line, the value of k_3 can be estimated as

$$k_3 = 1.2\times10^{-5} \text{ mol/g min atm.}$$

Simulation of Response Data

From the analyses presented in the foregoing section, it is seen that k_2 is very much larger than k_1, *i.e.* the Step (1) is the rate determining step of the reaction path I. Hence the rate of CO_2 formation through reaction path I can be expressed by the following equation.

$$\frac{dP_{CO_2}}{dt} = k_2\theta_IP_{CO} \tag{9}$$

Based on this simplification, the unsteady-state mass balance equations for each component for over-all reaction can be given by[14]

$$\frac{dP_{CO}}{dt} = \frac{2U}{\varepsilon L}(P^0_{CO}-P_{CO}) - \frac{2\rho_cRT}{\varepsilon}(k_1P_{CO}\theta_I+k_3P_{CO}\theta_{II}) \tag{10}$$

$$\frac{dP_{CO_2}}{dt}=\frac{2U}{\varepsilon L}(P^0_{CO_2}-P_{CO_2})+\frac{2\rho_c RT}{\varepsilon}\times(k_1P_{CO}\theta_I+k_4\theta_{II\cdot CO_2}) \quad (11)$$

$$\frac{dP_{O_2}}{dt}=\frac{2U}{\varepsilon L}(P^0_{O_2}-P_{O_2})-\frac{2\rho_c RT}{\varepsilon}\times\left(\frac{1}{2}k_1P_{CO}\theta_I+k_5P_{O_2}\theta^2_{II\cdot v}\right) \quad (12)$$

$$\frac{d\theta_{II}}{dt}=\frac{1}{q_{O_2}}(2k_5P_{O_2}\theta^2_{II\cdot v}-k_3P_{CO}\theta_{II}) \quad (13)$$

$$\frac{d\theta_{II\cdot CO_2}}{dt}=\frac{1}{q_{CO_2}}(k_3P_{CO}\theta_{II}-k_4\theta_{II\cdot CO_2}) \quad (14)$$

where ε abd ρ_c are, respectively, void fraction and apparent density of the catalyst bed, and U is the superficial velocity of the feed, L the length of the catalyst bed. $\theta_{II\cdot v}$ is the fraction of vacant site S_{II} and this is given by

$$\theta_{II\cdot v}=1-(\theta_{II}+\theta_{II\cdot CO_2}) \quad (15)$$

Suppose the reaction system is in the steady state with a feed containing CO and O_2 as the reactants, and the partial pressure of CO in the feed is suddenly increased from P^{io}_{CO} to P^{no}_{CO}, then the inital conditions for the transient response will be given by these equations

$$\left.\begin{array}{l}\left.\begin{array}{l}P^0_{CO}=P^{no}_{CO}\\P^0_{CO_2}=0\\P^0_{O_2}=P^{io}_{O_2}\end{array}\right\}\text{inflow}\\\left.\begin{array}{l}P_{CO}=P^{is}_{CO}\\P_{CO_2}=P^{is}_{CO_2}\\P_{O_2}=P^{is}_{O_2}\end{array}\right\}\text{outflow}\\\left.\begin{array}{l}\theta_{II}=\theta^{is}_{II}\\\theta_{II\cdot CO_2}=\theta^{is}_{II\cdot CO_2}\end{array}\right\}\text{on the surface}\end{array}\right\}\text{at } t=0 \quad (16)$$

In order to examine the validity of the k_j values estimated so far, let us simulate the CO–CO_2 response data given in Fig.4. Although P^{is}_{CO}, $P^{is}_{CO_2}$, and $P^{is}_{O_2}$ can be obtained experimentally, these values are also calculated from initial inflow conditions given in Fig. 4 with k_j values using Eqs. 10—14 under steady state conditions. For this calculation θ^{is}_{II} and $\theta^{is}_{II\cdot CO_2}$ are not known experimentally but can be calculated as follows as a function of P^{is}_{CO} and $P^{is}_{O_2}$.

Under the initial steady state,

$$\frac{d\theta_{II}}{dt}=0 \quad (17)$$

Then from Eq. 13,

$$2k_5P^{is}_{O_2}(1-\theta^{is}_{II}-\theta^{is}_{II\cdot CO_2})^2-k_3P^{is}_{CO}\theta^{is}_{II}=0 \quad (18)$$

Since $\theta_{II\cdot CO_2}$ is very small as has been stated in a previous section, Eq. 18 can be simplified as

$$(\theta^{is}_{II})^2-(2+a)\theta^{is}_{II}+1=0 \quad (19)$$

where

$$a=k_3P^{is}_{CO}/2k_5P^{is}_{O_2} \quad (20)$$

Solving Eq. 19, one can obtain

$$\theta^{is}_{II}=\frac{1}{2}(2+a-\sqrt{a^2+4a}) \quad (21)$$

In the same way, $\theta^{is}_{II\cdot CO_2}$ can be obtained from Eq. 21 and Eq. 14 under steady states.

$$\theta^{is}_{II\cdot CO_2}=\frac{k_3}{2k_4}P_{CO}(2+a-\sqrt{a^2+4a}) \quad (22)$$

By these calculations the initial conditions, Eq. 16, for the response can be obtained. With these initial conditions, Eqs. 10—14 can be solved numerically. The time courses of the P_{CO_2} change thus calculated for four different cases are shown in Fig. 4. The characteristic nature of the response data is simulated fairly well and this would indicate the validity of the proposed mechanisms and the values of k_j estimated so far.

Discussion

Here we shall summerize the values of k_j.

$k_1=4.15\times10^{-6}$ mol/g min atm

$k_2\ (=k_{II})=1.75\times10^{-4}$ mol/g min atm

$k_3=1.2\times10^{-5}$ mol/g min atm

$k_4=3.21\times10^{-5}$ mol/g min

$k_5\ (=k_{II})=4.8\times10^{-6}$ mol/g min atm

It is seen that k_2 is much larger than k_1 and this fact is quite consistent with the conclusion reached experimentally in Part II that the regeneration of $O^-\cdot S_I$ is very rapid and $O^-\cdot S_I$ always contributes to the reaction. It is seen also that k_5 is much smaller than k_3 and k_4. These results are also consistent with the conclusion drawn from the experimental findings in Parts I and II that the regeneration of $O^-\cdot S_{II}$ is slow and the concentration of $O^-\cdot S_{II}$ during the reaction under steady states is lowered when the reaction is opperated under higher partial pressures of CO, where the rates of picking up of $O^-\cdot S_{II}$ are higher.

Since k_1 and k_3 include the total number of $O^-\cdot S_I$ and $O^-\cdot S_{II}$, respectively, the true activity of each oxygen should be compared by the activity of single oxygen. Total amount of $O^-\cdot S_I$ is 3.3×10^{-5} mol/g and that of $O^-\cdot S_{II}$ is 1.17×10^{-4} mol/g and hence the true activity of each oxygen would be

$$k_1'=k_1/3.3\times10^{-5}=1.26\times10^{-1}\ \text{min}^{-1}\ \text{atm}^{-1}$$

$$k_3'=k_3/1.17\times10^{-4}=1.02\times10^{-1}\ \text{min}^{-1}\ \text{atm}^{-1}$$

k_1' is only slightly larger than k_3' and it seems to be not exactly consistent with the experimental findings in Part I, which suggest the higher reactivity of $O^-\cdot S_I$ compared to that of $O^-\cdot S_{II}$. The reason for this inconsistency may be ascribed to the difference in the activation energy of both types of oxygen species because the temperatures of reaction were different in both experiments. At the present moment, however, this problem is still open to the question and will need further investigations.

Nomenclature

a: defined in Eq. 20.

k_j: rate coefficient for step j, arbitrary unit.

L: total length of the catalyst bed (cm).

P_{O_2}, P_{CO}, P_{CO_2}: partial pressure of oxygen, carbon monoxide, and carbon dioxide at the outlet of the catalyst bed at the un-

steady state, respectively (atm).

$P^0_{O_2}$, P^0_{CO}, $P^0_{CO_2}$: partial pressure of oxygen, carbon monoxide, and carbon dioxide at the inlet of the catalyst bed, respectively (atm).

$P^{i0}_{O_2}$, P^{i0}_{CO}: partial pressure of oxygen and carbon monoxide at the inlet of the catalyst bedat initial steady state, respectively (atm).

P^{n0}_{CO}: newly set partial pressure of carbon monoxide at the inlet of the catalyst bed (atm).

$P^{is}_{O_2}$, P^{is}_{CO}, $P^{is}_{CO_2}$: partial pressure of oxygen, carbon monoxide, and carbon dioxide at the outlet of the catalyst bed at initial steady state, respectively (atm).

q_{CO_2}, q_{CO_2}: total amounts of O_2 and CO_2 adsorbed on active site S_{II}, respectively (mol/g).

R: gas constant, consistent units.

S_I, S_{II}: active sites on the surface denoted in earlier paper.[10]

t: time elapsed after the step change of gas composition (min).

T: temperature (K).

U: superficial gas velocity (cm/min).

Greek Symbols

ε: void fraction of packed bed of reactor (—).

θ_{II}, $\theta_{II\cdot CO_2}$: coverage averaged in the catalyst bed for $O^-\cdot S_{II}$ and $CO_2\cdot S_{II}$, respectively (—).

θ^{is}_{II}, $\theta^{is}_{II\cdot CO_2}$: coverage averaged in the catalyst bed for $O^-\cdot S_{II}$ and $CO_2\cdot S_{II}$ at the steady state of reaction, respectively (—).

$\theta_{II\cdot v}$: fraction of vacant active sites S_{II} (—).

ρ_c: catalyst bed density (g/cm^3).

Refereences

1) E. R. S. Winter, *J. Chem. Soc.*, **1955**, 2726.

2) K. Tarama, S. Teranishi, and K. Hattori, *Kogyo Kagaku Zasshi*, **63**, 714 (1960).

3) A. A. Davydov, M. Yu. Shchekochikhin, and P. N. Keier, *Kinet. Katal.*, **10**, 1341 (1969).

4) S. E. Voltz and S. W. Weller, *J. Phys. Chem.*, **59**, 566 (1955).

5) M. Yu. Shchekochikhin, G. I. Panov, and N. A. Akulich, *Kinet. Katal.*, **9**, 1315 (1968).

6) A. A. Davydov, M. Yu. Schekochikhin, P. N. Keier, and A.P. Zeif, *Kinet. Katal.*, **10**, 1125 (1969).

7) A. Zecchina, S. Coluccia, E. Guglielminotti, and G. Ghiotti, *J. Phys. Chem.*, **76**, 2774 (1971).

8) A. Zecchina, S. Coluccia, L. Cerruti, and E. Borello, *J. Phys. Chem.*, **76**, 2783 (1971).

9) A. Zecchina, S. Coluccia, E. Guglielminotti, and G. Ghiotti, *J. Phys. Chem.*, **76**, 2790 (1971).

10) M. Kobayashi and H. Kobayashi, *Bull. Chem. Soc. Jpn.*, **49**, 3009 (1976).

11) M. Kobayashi, T. Date, and H. Kobayashi, *Bull. Chem. Soc. Jpn.*, **49**, 3014 (1976).

12) S. Matsushita and T. Nakata, *J. Chem. Phys.*, **36**, 665 (1962).

13) M. Courtois and S. T. Teichner, *J. Catal.*, **1**, 121 (1962).

14) H. Kobayashi and M. Kobayashi, *Catal. Rev.*, **10**, 139 (1974).

The Complexing of Indium(III) by Cysteine: Evidence for Sulfur-bridged and Protonated Complexes

Nakao KOJIMA, Yukio SUGIURA, and Hisashi TANAKA

Faculty of Pharmaceutical Sciences, Kyoto University, Kyoto 606

(Received October 18, 1975)

The complex formation of the cysteine–In(III) system has been investigated by potentiometric titration and by PMR, IR, and UV spectroscopic measurements. The InL, InL_2, and InLH species are predominantly formed at the metal concentrations from 0.00025 to 0.0005 M. At higher concentrations of the metal ion (0.0025—0.005 M), however, the InL species is negligible and the InL_2, InL_3, InL(LH), and $In(LH)_2$ species are predominant. The formation constants calculated with a non-linear, least-squares program were log $\beta_{110}=14.12$, log $\beta_{120}=27.26$, log $\beta_{130}=32.20$, log $\beta_{11-1}=18.46$, log $\beta_{12-1}=31.78$, and log $\beta_{12-2}=35.74$ for InL, InL_2, InL_3, InLH, InL(LH), and $In(LH)_2$ respectively. The IR and UV spectra revealed that the amino group of the coordinating cysteine was protonated. The $[In_3L_4(OH)(H_2O)]$ complex was isolated.

The study of the complex formation of In(III) with various ligands is needed for the development of new radiopharmaceuticals for clinical diagnosis by the use of ^{113m}In or ^{111}In, which are favorable radioisotopes and which can effectively be used with several chelating agents. We have studied the complex formation of In(III) with penicillamine.[1] In this paper, we will discuss the complex formation of In(III) with cysteine in comparison with that with penicillamine.

Experimental

Materials. All the details of the preparation and standardization of the metal and KOH solutions for pH titration have been reported in a preceding paper.[1] Indium sulfate, $In_2(SO_4)_3 \cdot 9H_2O$, was used for the PMR and UV measurements and for the isolation of the complex. L-Cysteine hydrochloride was dried under a vacuum over diphosphorus pentoxide, and the solution was standardized potentiometrically. The D_2O, DCl, and NaOD (99.5% isotopically pure) were obtained from E. Merck. All the other reagents used were of a reagent grade.

IR Spectra. The IR spectra of the solid were measured in a KBr disk by means of a Hitachi grating infrared spectrophotometer, Model 215. The IR measurements were also made on a D_2O solution of the 0.1 M ligand with or without 0.05 M In(III), in a KRS-5 cell with a light path of 0.1 mm. All the pD values were obtained by the addition of 0.44[2] to the pH values determined using a Hitachi-Horiba pH meter, Model F-7.

PMR Spectra. The PMR spectra were recorded with a Varian A-60 NMR spectrometer at an ambient probe temperature of 33 °C. The concentration of the In(III) ion was 0.052M, and the chemical shifts were measured with sodium 3-(trimethylsilyl)propionate-2,2,4,4-d_4 as the internal standard.

Optical Spectra. The optical spectra were measured in an aqueous solution by means of a Shimadzu recording spectrophotometer, Model Double-40R. Sample solutions were composed of cysteine hydrochloride (0.00016M) and a small amount of 1 M hydrochloric acid, with or without In(III) (0.00008 M), and were neutralized with 1 M potassium hydroxide.

Potentiometric Titrations and Calculations. The potentiometric titrations were performed with standard carbonate-free potassium hydroxide solutions(1.002 M and 0.1001 M) at 21.00±0.05 °C in the presence of 0.1 M potassium nitrate. The total volume was adjusted to 20.00 ml. The apparatus and procedure have been described.[1]

The titrations were carried out for solutions with a wide range of total metal concentrations in order to investigate the formation of hydroxo, protonated, and/or polynuclear species. The system containing polynuclear species does not give coincident formation curves. If hydroxo and/or protonated species are formed, complicated formation curves are to be expected since the free ligand concentration [L] calculated by the usual manner is incorrect. In such cases, a non-linear, least-squares computer program was used for the calculation of the stability constants, β_{lmn}:

$$\beta_{lmn} = [M_lL_mH_{-n}]/[M]^l[L]^m(H^+)^{-n}$$

where n is positive for a hydrolyzed species and negative for a protonated species, and where the parentheses denote activity. The calculations were carried out in a manner previously described[1] by the use of a FACOM 230-75 computer, Kyoto University. This program was also used for the calculation of the dissociation constants of the ligand. The values of $pK_w=14.130$[3] at 21 °C and $[H^+]=10^{-pH}$ were used in the calculation.

Results

Elemental Analysis and IR Spectra of an Isolated In(III) Complex. When a solution containing cysteine hydrochloride (0.1 M) and In(III) (0.052 M) in the ligand-to-metal ratio of 1.9: 1 was titrated with 8 M KOH, a large quantity of a white precipitate which was different from simple In(III) hydrolysate was formed at pH 3.9 and which redissolved at pH 5.2, whereas no precipitation was observed in the system containing the ligand (0.1 M) and In(III) (0.05 M) in the ligand-to-metal ratio of 2: 1. The precipitate formed at pH 4.8 was isolated and dried under a vacuum over diphosphorus pentoxide. Elemental analysis showed that the ligand: metal ratio was 1.3: 1: Found: C, 15.54; H, 3.19; N, 6.12; In, 38.29%. Calcd for $[In_3L_4(OH)(H_2O)\cdot 3H_2O]$: C, 15.83; H, 3.19; N, 6.16; In, 37.85%.

Table 1 shows some significant IR absorption bands of the isolated complex, together with those of the free ligand and the In(III) hydrolysate. In the isolated In(III)-cysteine complex, the coordination of the ligand to In(III) *via* the thiol, amino, and carboxyl groups is assumed on the basis of the disappearance of the SH, NH_3^+, and COOH absorptions, and the presence of NH_2 and COO^- absorptions. The coordina-

Table 1. Infrared spectra of the isolated In(III)-cysteine complex, cysteine hydrochloride and simple In(III) hydrolysate (cm^{-1})[a]

In(III) Complex	Cysteine Hydrochloride	In(III) Hydrolysate	Assignments
3210 s			NH_2 str.
	2980 s, b		NH_3^+ str.
	2560 m		SH str.
	1745 s		C=O str.
1610 s			COO^- anti. str.
	1600 w		NH_3^+ deg. def.
1590 s			NH_2 bend.
	1520 m		NH_3^+ sym. def.
	1405 m		C–O str., OH bend.
1390 m			COO^- sym. str.
	1230 s		NH_3^+ rock.
	1205 s		OH bend., C–O str.
1120 m		1120 s	InOH bend.
1060 m		1060 s	InOH bend.
	935 w		SH bend.

a) Abbreviations: s=strong, m=medium, w=weak, b=broad.

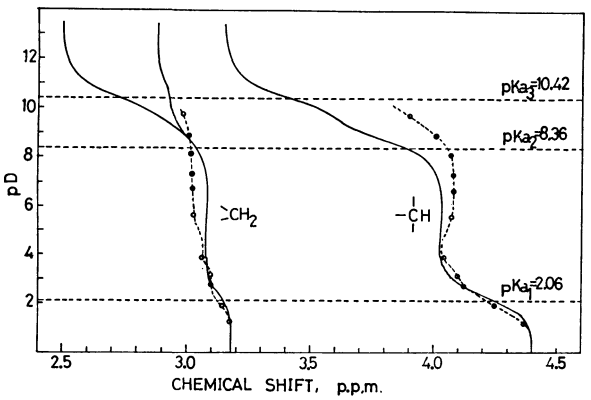

Fig. 1. Chemical shift data for cysteine (0.1 M) with (dashed lines) or without (solid lines) In(III) (0.052 M) at various pD values.

tion of the amino group indicates that the complex is not a non-charged protonated complex. In addition, the In(III) complex and the In(III) hydrolysate showed absorptions near 1100 cm^{-1}, which are assigned to the M–O–H bending mode.[4]

PMR Spectra of the 1.9: 1 Cysteine-In(III) System. Figure 1 shows the chemical-shift values of the CH and CH_2 protons of cysteine *versus* pD.[5] The dashed lines represent the titration curves of the 1.9: 1 cysteine-In(III) system. The constant chemical-shift values in the pD region from 5.5 to 8 reflect the $\widehat{SNO}$ coordination of the InL_2 complex species. In the higher pD region, the chemical-shift data suggest that some coordinated groups are released from the coordination sphere. The values of the chemical shift at about pD 4, obtained from the supernatant of the sample, are similar to those of the ligand. This indicates that the free ligand is present predominantly in the supernatant.

Potentiometric Titrations of the Cysteine-In(III) Systems. The acid dissociation constant for the carboxyl group of cysteine was obtained from the potentiometric titration data on the 0.05 M cysteine hydrochloride solution. The two remaining ionization constants, $pK_{a2}=8.36$ and $pK_{a3}=10.42$, were determined from the titration data for the 0.0015 M ligand solution by the usual linear least-squares method. These three constants were then refined by the non-linear FORTRAN IV computer program. The final values, with the standard deviations, are $\log \beta_{01-1}=10.42\pm0.01$, $\log \beta_{01-2}=18.78\pm0.01$, and $\log \beta_{01-3}=20.84\pm0.01$, at 21 °C and $I=0.1(KNO_3)$. The standard deviation in titre was 0.0029 ml. The pK_{a1} value of 2.06 was obtained from the $\log \beta_{01-3}$ and $\log \beta_{01-2}$ values. These constants are in good agreement with the reported values of $\log \beta_{01-1}=10.498$ and $\log \beta_{01-2}=18.833$ at 20 °C and $I=0.1(NaClO_4)$[6] and $pK_{a1}=1.96$ at 20 °C and $I=0.01$.[7]

The titration curve of the 4: 1 cysteine·HCl-In(III) system shows two distinct pH inflections, at $a=2$ and $a=2.75$, reflecting the formations of the InL_2 species and another species (probably InL_3) respectively; the latter was not observed in the penicillamine-In(III) system. Calculations of the stability constants for two simple species, InL and InL_2, were attempted by the Irving-Rossotti method,[8] but the consistency of the values obtained at each point was unsatisfactory. The pH titrations were carried out in the systems with various metal concentrations and metal-to-ligand ratios. The total metal concentrations $[In]_T$ were 0.00025, 0.0005, 0.0025, and 0.005 M, and the total ligand concentrations $[L]_T$ were 0.001, 0.001, 0.01, and 0.01 M respectively. The titration curves are shown in Fig. 2. Table 2 contains some data (94 points) relating to the four titration curves. The formation curves calculated in the usual manner, without assuming any hydroxo and protonated complexes, failed to be superimposed, and were not parallel to one another. The formations of the mononuclear hydroxo and protonated species were thus considered on the basis of the similarity to the penicillamine systems. These species were InL, InL_2, InLH, InL(LH), InL(OH), and $InL(OH)_2$. The best fit to the experimental results was sought for by the use of a non-linear computer program with an automatic

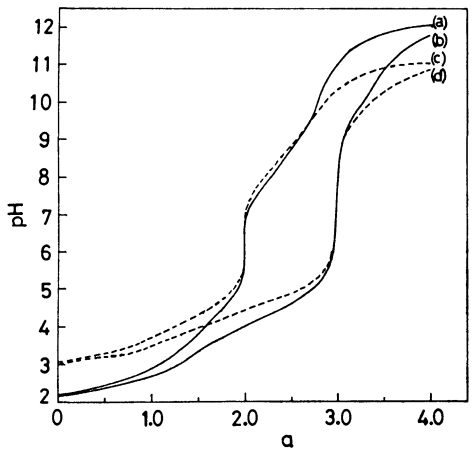

Fig. 2. Titration curves of the cysteine·HCl-In(III) systems. a=moles of KOH added per mole of the ligand. Experimental conditions for each curves ((a)—(d)) are given in Table 2.

TABLE 2. POTENTIOMETRIC DATA[a)]

Curve (a)			Curve (b)			Curve (c)			Curve (d)		
pH	V[b)]	Vc[c)]	pH	V[b)]	Vc[c)]	pH	V[b)]	Vc[c)]	pH	V[b)]	Vc[c)]
2.42	0.12	0.121	2.44	0.18	0.182	3.28	0.12	0.124	3.26	0.18	0.178
2.48	0.14	0.139	2.50	0.20	0.201	3.34	0.14	0.141	3.31	0.20	0.195
2.55	0.16	0.158	2.56	0.22	0.218	3.40	0.16	0.158	3.37	0.22	0.215
2.64	0.18	0.179	2.63	0.24	0.237	3.48	0.18	0.177	3.43	0.24	0.234
2.74	0.20	0.199	2.72	0.26	0.257	3.56	0.20	0.195	3.50	0.26	0.253
2.86	0.22	0.220	2.82	0.28	0.277	3.67	0.22	0.218	3.58	0.28	0.274
3.00	0.24	0.239	2.93	0.30	0.296	3.78	0.24	0.239	3.67	0.30	0.296
3.19	0.26	0.261	3.08	0.32	0.318	3.91	0.26	0.262	3.76	0.32	0.317
3.40	0.28	0.281	3.25	0.34	0.341	4.04	0.28	0.283	3.87	0.34	0.340
3.60	0.30	0.301	3.41	0.36	0.361	4.16	0.30	0.302	3.98	0.36	0.363
3.79	0.32	0.321	3.57	0.38	0.382	4.28	0.32	0.320	4.08	0.38	0.383
3.96	0.34	0.339	3.71	0.40	0.402	4.41	0.34	0.399	4.18	0.40	0.404
4.16	0.36	0.359	3.84	0.42	0.423	4.54	0.36	0.359	4.27	0.42	0.423
4.41	0.38	0.381	3.94	0.44	0.439	4.70	0.38	0.380	4.35	0.44	0.440
			4.05	0.46	0.459				4.44	0.46	0.460
			4.16	0.48	0.479				4.52	0.48	0.480
7.92	0.48	0.466	4.28	0.50	0.500	8.12	0.48	0.472	4.60	0.50	0.502
8.10	0.49	0.482	4.39	0.52	0.519	8.27	0.49	0.485	4.69	0.52	0.522
8.25	0.50	0.498	4.51	0.54	0.539	8.41	0.50	0.498	4.80	0.54	0.540
8.41	0.51	0.514	4.66	0.56	0.561	8.55	0.51	0.511	4.90	0.56	0.561
8.57	0.52	0.529	4.81	0.58	0.581	8.69	0.52	0.523	5.04	0.58	0.580
8.71	0.53	5.540	5.00	0.60	0.601	8.83	0.53	0.535	5.20	0.60	0.600
8.86	0.54	0.549	5.28	0.62	0.622	8.97	0.54	0.545	5.44	0.62	0.620
9.04	0.55	0.558				9.12	0.55	0.554			
9.25	0.56	0.566				9.28	0.56	0.563			
9.50	0.57	0.574				9.44	0.57	0.571			

a) About half of the data used for the calculation are shown. Composition of solutions: Curve (a): $[In]_T$= 0.0025 M, $[L]_T$=0.01 M, [HCl]=0.0013 M, [KOH]=1.002 M. Curve (b): $[In]_T$=0.005 M, $[L]_T$=0.01 M, [HCl]=0.0026 M, [KOH]=1.002 M. Curve (c): $[In]_T$=0.00025 M, $[L]_T$=0.001 M, [HCl]=0.00013 M, [KOH]=0.1001 M. Curve (d) $[In]_T$=0.0005 M, $[L]_T$=0.001 M, [HCl]=0.00026 M, [KOH]=0.1001 M. b) V=experimental titres (ml). c) Vc=calculated titres (ml).

TABLE 3. VALUES(LOGARITHMIC UNITS) OF THE FORMATION CONSTANTS IN THE SUCCESSIVE TRIALS FOR THE In(III) (0.005 M)-CYSTEINE HYDROCHLORIDE (0.01 M) SYSTEM[a)]

Trial	Complex species							Std. dev. in titre (ml)
	InL	InL_2	InLH	InL(LH)	$In(LH)_2$	InL(OH)	$InL(OH)_2$	
1	14.872 (0.025)	27.263 (0.027)	18.473 (0.024)					0.0047
2	14.759 (0.020)	27.049 (0.023)	18.521 (0.036)			10.255 (0.014)		0.0030
3	14.683 (0.022)	26.49 (0.36)	18.543 (0.011)			10.464 (0.034)	5.40 (0.23)	0.0023
4	14.662 (0.026)	27.197 (0.014)	18.548 (0.012)	31.548 (0.039)				0.0024
5		27.197 (0.014)	18.541 (0.013)	31.936 (0.015)	35.703 (0.033)			0.0023
6		27.150 (0.026)	18.536 (0.013)	31.916 (0.021)	35.728 (0.035)	9.05 (0.20)		0.0023
7	14.679 (0.026)	27.142 (0.025)	18.544 (0.012)	31.464 (0.078)		9.62 (0.21)		0.0023

a) Standard deviations in parentheses.

refinement of the stability constants. The approximate estimates, 14.92 and 28.12, obtained from the Irving-Rossotti method were used as the initial values of the unknown constants for the InL and InL_2 complexes respectively. The other estimates were obtained from the values of the corresponding penicillamine-In(III) complexes. The calculation was started in the system of 0.005 M In(III) and 0.01 M cysteine hydrochloride, assuming that three species, InL, InL_2, and InLH (Table 3, Trial 1), were formed. The agreement

between the experimental and calculated values is fairly good, as compared to the non-convergence in the chemical model of InL and InL_2. The fit was further improved by the introduction of InL(OH) into Trial 1 (Trial 2). However, the introduction of InL(OH) into the chemical model of InL and InL_2 was non-converged. The system was not consistent with the non-chelating complex, $InLH_2$. The further inclusion of the $InL(OH)_2$ species (Trial 3) increased the standard deviation of the log β_{120} value. The standard deviation in titre was appreciably improved by the introduction of the InL(LH) into Trial 1 (Trial 4). The further inclusion of the $In(LH)_2$ species in Trial 4, however, led to non-convergence, as had been expected. Trials 5, 6, and 7 gave good results, in agreement with the experimental and calculated values. The presence of the InL(OH) species was doubtful, because the constants obtained from Trials 2, 3, 6, and 7 varied considerably. Trial 5 gave a slight improvement over Trial 4. Under the condition of $[In]_T=0.05$ M (see Fig. 6), Trial 4 became non-converged. A similar investigation was carried out with various other polynuclear and hydrolyzed species: In_2L_2, $In_2L_2(LH)_2$, $InL_2(OH)$, $InL_2(OH)_2$, $In_2L_2(OH)$, $In_2L_2(OH)_2$, $In_2(LH)_4(OH)_2$, $In_3L_4(OH)$, $In_3L_4(OH)_2$, *etc.*, but the results showed the absence of these species. The same treatments on the other three curves indicated that the InL(LH) and $In(LH)_2$ species became negligible, and that the InL, InL_2, and InLH species were predominant, as the concentration of the metal ion decreased. A final refinement of all these constants over the range of experimental data (4 experiments, 166 points, <pH 6) yielded the constants listed in Table 4. The calculated and experimental titres agreed with each other within a standard deviation of 0.0059 ml. The constant of the InL_3 species is also shown in the table. This value was obtained from the higher pH regions (>pH 7) of the two 4: 1 (ligand-to-metal) titration curves (2 experiments, 26 points). In these regions, the $InL_2(OH)$ species was not detected. The calculated titres are listed in Table 2. Figure 3 shows the distribution diagram of the InL_2, InL_3, InLH, InL(LH), and $In(LH)_2$ species, which was obtained from the system of 0.0025 M In(III) and 0.01 M cysteine hydrochloride.

TABLE 4. STABILITY CONSTANTS OF In(III) COMPLEXES WITH CYSTEINE HYDROCHLORIDE AT 21°C AND I=0.1 (KNO_3)[a]

InL	Log β_{110} =14.12±0.06
InL_2	Log β_{120} =27.26±0.02
InLH	Log β_{11-1}=18.46±0.02
InL(LH)	Log β_{12-1}=31.78±0.05
$In(LH)_2$	Log β_{12-2}=35.74±0.06
InL_3	Log β_{130} =32.20±0.09

a) The uncertainty intervals associated with all values are the standard deviations.

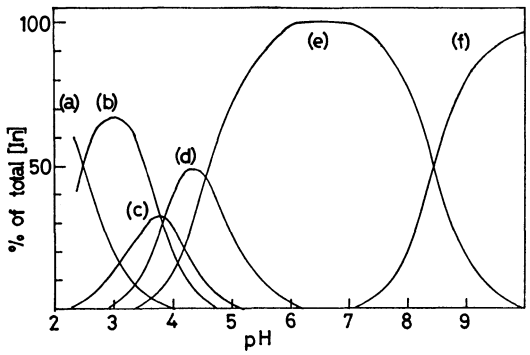

Fig. 3. Distribution diagram for the cysteine hydrochloride (0.01 M)–In(III) (0.0025 M) system: (a) In^{3+}; (b) InLH; (c) $In(LH)_2$; (d) InL(LH); (e) InL_2; (f) InL_3.

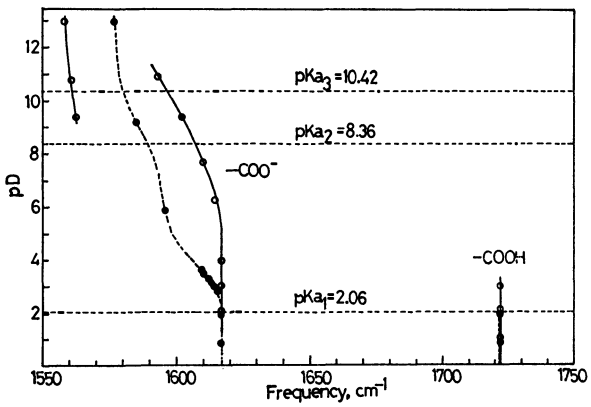

Fig. 4. IR data for cysteine (0.1 M) with (dashed line) or without (solid lines) In(III) (0.05 M) for various pD values.

IR and UV Spectra of the 2: 1 Cysteine–In(III) System. Figure 4 shows the carboxylate absorption bands of cysteine (0.1 M) in a D_2O solution in the absence (solid lines) and in the presence (dashed lines) of In(III) (0.05 M). In the lower pD region, the free ligand gives two bands, at 1617 and 1722 cm^{-1}, which are assigned to dissociated and undissociated carboxyl groups respectively. The carboxylate band shifts from 1617 to 1560 cm^{-1} with an increase in the pD, and a splitting of the band at about pD 10.5 was observed. The shift ($\Delta\nu$=57 cm^{-1}) is attributed to the electrostatic effect on the basis of the dissociation of the amino ($\Delta\nu$=42 cm^{-1}) and thiol groups ($\Delta\nu$=15 cm^{-1}), as deduced from Table 5. The electron delocalization of the carboxylate ion, $-C\overset{O}{\underset{O}{\langle}}\ominus$, could be more accelerated by the dissociation of these groups. In the solution containing the ligand and the metal ion, the carboxylate band appears

TABLE 5. CARBOXYLATE BANDS IN THE INFRARED ABSORPTION SPECTRA OF THE VARIOUS COMPOUNDS AT pD 7 AND 10 IN THE D_2O SOLUTION (cm^{-1})

Compounds	pD 7	pD 10	$\Delta\nu$[a]
α-Alanine[b]	1618	1570	48
β-Alanine[b]	1567	1567	0
S-Methyl-L-cysteine	1615	1573	42
N-Acetyl-L-cysteine	1592	1577	15
Cysteine	1617	1559	58

a) $\Delta\nu=\nu_{pD7}-\nu_{pD10}$. b) Ref. 16.

in a lower pD region in comparison with that of the ligand, indicating the coordination of the carboxyl group. The shift of the carboxylate band occurred at about pD 3, whereas about 40% of the ligand was already coordinated to the metal at pH 2, as is shown in Fig. 6. Consequently, the shift suggests the coordination of the amino group. In the pD region lower than 3, therefore, the presence of the $\widehat{S\ O}$-type complex is taken into account. The shift reaches its maximum at pD 6—7, where the InL_2 species is formed predominantly. The shift of the carboxylate band in the higher pD region (>pD 8) reveals the elimination of the carboxyl group from the coordination sphere, which is consistent with the PMR results.

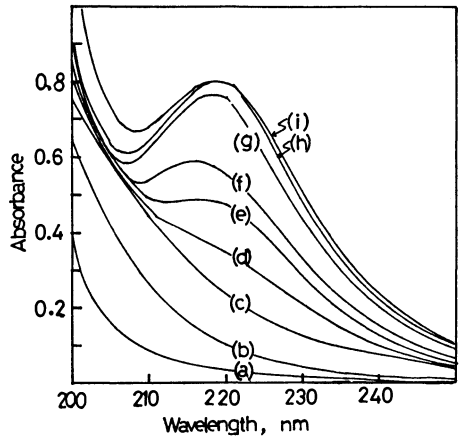

Fig. 5. Absorption spectra of the cysteine (0.00016 M)-In(III) (0.00008 M) system at various pH values: (a) pH 2.12; (b) pH 3.10; (c) pH 4.04; (d) pH 4.40; (e) pH 4.69; (f) pH 4.83; (g) pH 5.97; (h) 7.48; (i) pH 9.58.

The UV absorption of cysteine in the 228—229 nm region is based on the form of the RS^- ion.[9] The absorption spectra of the cysteine-In(III) complex as a function of the pH (Fig. 5) exhibit a maximum at 217 nm, and they are quite different from those of the ligand. On the other hand, the In(III) ion(d^{10}) shows no absorption bands. The absorption band of the complex is attributed to $d\pi$ back-donation from the d^{10} metal ion to the empty d orbitals of the sulfur. In the pH region lower than 4.5, the absorption band at 217 nm does not appear, although the absorbance at about 200 nm increases with an increase in the pH. The absorption spectra of the In(III)-cysteine methyl-ester complex ($\widehat{S\ N}$ type) exhibit a maximum in the 214—219 nm region, whereas the absorption band of the In(III)-*N*-acetyl-L-cysteine complex ($\widehat{S\ O}$ type) appears in the wavelength region lower than 200 nm. Accordingly, the protonated cysteine complex InLH ($\widehat{S\ O}$ type) is formed in the pH region lower than 4.5. These findings also indicate that the charge-transfer bands based on the $In\begin{matrix}S\\N\end{matrix}$ and $In\begin{matrix}S\\O\end{matrix}$ bonds appear at about 217 nm and in the wavelength region lower than 200 nm respectively.

Discussion

The white precipitate which was not observed in the case of penicillamine(I) was formed during titration when the cysteine(II): metal ratio was smaller than 2: 1, as in 2,3-dimercapto-1-propanol(III).

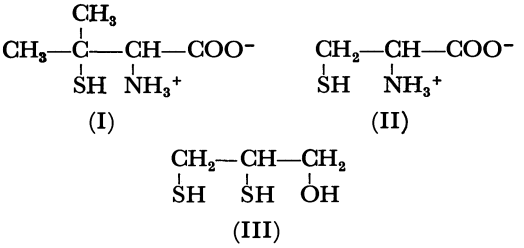

The steric effect on the thiol group may be the cause of the difference among these ligands. Some sulfur-bridged polynuclear metal complexes have been reported[6,10-12] in the (II) and (III) ligands. The IR spectra suggest that the isolated cysteine-In(III) complex is hydrolyzed, but not protonated. The elemental analysis indicates that the ligand: metal ratio of the complex is 4: 3 and that the total charge of the complex is zero. The following structure can reasonably be postulated from these results:

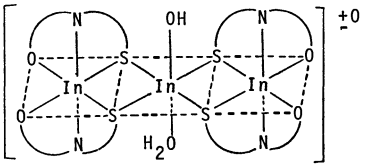

A little excess of the metal ion causes the disruption of the equilibrium established because of the insolubility of the trimeric complex. Consequently, about 30% of the ligand will remain in the supernatant of the solution. In fact, the PMR spectra of the supernatant were similar to that of the ligand. When more of the base was added, the coordination of another hydroxide ion causes a change of the charge from zero to −1. Accordingly, the trimer is dissolved, and then the free ligand in the solution coordinates to the central metal in the trimer to form InL_2, together with the small amount of the metal hydrolysate. Based on this postulate, the sulfur-bridged trimer should have a *cis*-form. The In–S bond is stabilized by the $d\pi$ back-donation.[6,10,13-15] The higher stability constant of the sulfur-containing ligand than those of the corresponding oxygen- and nitrogen-containing ligands may be regarded as a reflection of this stabilization (cf. β-hydroxypropionic acid: log K_1=3.75, log K_2=3.04; β-aminopropionic acid: log K_1=2.72, log K_2=2.54, at 25 °C and I=0.1[13]). For the first molecule of the ligand which coordinates to In(III), the d_{xy} and d_{yz} orbitals of In(III) are used for the π bonding with the d orbital of the sulfur on the x coordinate. These orbitals of the metal ion may become less available for the bonding with the second molecule of the ligand on the $-x$ coordinate. Consequently, a *trans*-form may be unfavorable for the complex.

In the 2: 1 cysteine-In(III) system, the $In_3L_4(OH)$

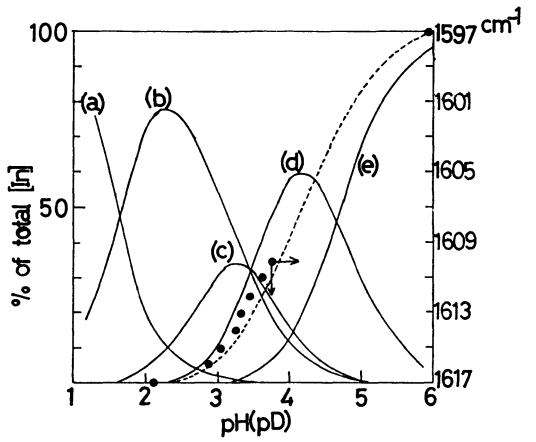

Fig. 6. Distribution diagram and IR data (●, in D_2O) for the cysteine hydrochloride (0.1 M)-In(III) (0.05M) system. Dashed line is given by $(1/2[InL(LH)]+[InL_2])/[In]_T$. (a) In^{3+}; (b) InLH; (c) $In(LH)_2$; (d) InL(LH); (e) InL_2.

and $In_3L_4(OH)_2$ trimer were not detected by the caluclation, as had been predicted. In the cysteine-In(III) system, the protonated complexes are more readily formed than in the penicillamine system, where the $In(LH)_2$ species is absent and InLH is not always formed. At the higher metal concentrations, therefore, the InL species is negligible in the cysteine system. These differences are due to the higher stability constants of the penicillamine complexes, *e.g.*, $\log \beta_{110}=15.330$ and $\log \beta_{120}=29.789$.

The results of the potentiometric and IR measurements support the formation of the three protonated species, InLH, InL(LH), and $In(LH)_2$. Figure 6 shows the distribution diagram of the solution containing 0.1 M cysteine hydrochloride and 0.05 M In(III). The dashed line represents the sum of the distribution ratios for the two species, InL(LH) and InL_2. This is obtained by $(1/2[InL(LH)]+[InL_2])/[In]_T$. The line reflects the coordination ratio of the amino group of the ligand to the metal. Each point in the figure is a plot of the absorption frequency of the carboxylate group against the pD obtained under the same conditions, assuming the complete formation of the InL_2 species at 1597 cm^{-1}. The shift of the absorption band is considered to be caused mainly by the coordination of the amino group. Each absorption point is approximately superimposable on the dashed line. The slight deviation is probably due to the small effect on the shift of the coordination of the thiol group. This finding indicates the presence of $In(LH)_2$ and the absence of InL under these conditions. The presence of the InLH species, and the conclusion that the amino group of the coordinating cysteine is protonated, are supported by the following observations: (1) the absence of the shift of the IR band in the pD region lower than 2.5 and (2) the absence of the band of the UV absorption based on the $In\begin{pmatrix}S\\N\end{pmatrix}$ bond in the pH region lower than 4.5. In the higher pH region, the final species, InL_3, is detected by the calculation. The IR and PMR spectra indicate that the carboxyl group does not coordinate to the metal in the complex. In the case of the penicillamine complex, the steric effect of the methyl groups of the ligand prevents the attack of the third ligand molecule. At the higher metal concentrations, the following coordination process is proposed:

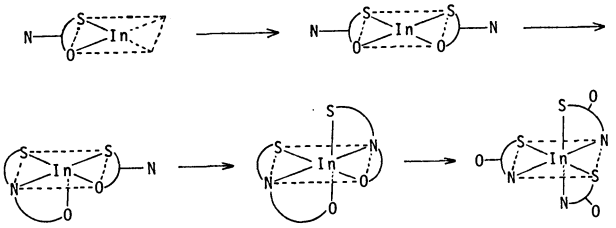

The authors wish to thank Dr. H. Aiba of the School of Medicine, Kyoto University, for his helpful advice, the staff of the Data Processing Center, Kyoto University, for the use of a FACOM 230-75 computer, and Dr. Y. Kuroda and Mrs. M. Uobe for their PMR measurements.

References

1) N. Kojima, Y. Sugiura, and H. Tanaka, *Bull. Chem. Soc. Jpn.*, **49**, 1294 (1976).
2) K. Mikkelsen and S. O. Nielsen, *J. Phys. Chem.*, **64**, 632 (1960).
3) H. S. Harned and B. B. Owen, "The Physical Chemistry of Electrolytic Solutions," 3rd ed., Reinhold Publishing Corp., New York, N. Y. (1958).
4) K. Nakamoto, "Infrared Spectra of Inorganic and Coordination Compounds," John Wiley & Sons, New York, N. Y. (1963), p. 159.
5) D. B. Walters and D. E. Leyden, *Anal. Chim. Acta*, **72**, 275 (1974).
6) D. D. Perrin and I. G. Sayce, *J. Chem. Soc., A*, **1968**, 53.
7) A. Albert, *Biochem. J.*, **50**, 690 (1952).
8) H. Irving and F. J. C. Rossotti, *J. Chem. Soc.*, **1953**, 3397.
9) G. E. Clement and T. P. Hartz, *J. Chem. Educ.*, **48**, 395 (1971).
10) D. D. Perrin and I. G. Sayce, *J. Chem. Soc., A*, **1967**, 82.
11) D. L. Leussing, *J. Am. Chem. Soc.*, **81**, 4208 (1959).
12) H. F. DeBrabander, L. C. Van Poucke, and Z. Eeckhout, *Anal. Chim. Acta*, **70**, 401 (1974).
13) R. Sarin and K. N. Munshi, *Aust. J. Chem.*, **25**, 929 (1972).
14) R. Sarin and K. N. Munshi, *J. Inorg. Nucl. Chem.*, **34**, 581 (1972).
15) R. Sarin and K. N. Munshi, *J. Inorg. Nucl. Chem.*, **35**, 201 (1973).
16) H. Lenormant, *C. R. Acad. Sci.*, 234, 1959 (1952); H. Lenormant, *J. Chim. Phys. Phys.-Chim. Biol.*, **49**, 635 (1952).

Spectrophotometric Study of the Zirconium-Pyrocatechol Violet-Tridodecylethylammonium Ternary Complex

Yoshio SHIJO

Department of Industrial Chemistry, Faculty of Engineering, University of Utsunomiya, Ishii-machi, Utsunomiya 321-21

(Received March 25, 1976)

The zirconium-pyrocatechol violet chelate anion is extracted with tridodecylethylammonium bromide in butyl acetate to form a ternary complex. The ternary complex has an absorption maximum at 586 nm in the organic layer. The optimum pH range for the extraction is from 5 to 6. Beer's law holds for 0.4—9 μg of zirconium in 5 ml of the organic phase. The molar absorptivity of the ternary complex is 3.9×10^4 cm^{-1} mol^{-1} l at 586 nm. The composition of the ternary complex is estimated to be $Zr(pv)_2(R-\overset{\overset{R}{|}}{N}-R')_3$.

The ternary complexes formed by the ionic association of the metal-Pyrocatechol Violet (PV) chelate anions and the bulky organic cations such as diphenylguanidine and quaternary ammonium salt have been studied by many workers. Kohara *et al.*[1] extracted ion pairs such as molybdenum-Pyrocatechol Violet(PV)-dialkylmethylbenzylammonium. Extraction of the indium-PV-hexadecylpyridinium system was reported by Ishito and Tonosaki.[2] The gallium-PV-diphenylguanidine system was studied by Akhmedli *et al.*[3] The gallium-PV-hexadecylpyridinium system was extracted in 1-butanol by Ishito.[4] The iron(III)-PV-diphenylguanidine system was studied by Yuryavichus and Valyukyavichyus.[5] Moreover, studies of the ternary complexes of the aluminum-PV-diphenylguanidine,[6] the bismuth-PV-diphenylguanidine,[7] and the titanium-PV-diphenylguanidine[8] systems have been reported. The water soluble metal-PV-quaternary ammonium ternary complexes in the micelle solution have been applied to the spectrophotometric determination of aluminum,[9] antimony and molybdenum,[10] niobium,[11] and tantalum.[12]

In the process of investigating the extraction of the metal chelate anions with an oleophilic quaternary ammonium salt such as tridodecylethylammonium bromide (TDEA), we reported an extraction spectrophotometric method for scandium[13] and yttrium[14] as Xylenol Orange chelate and for iron[15] as Eriochrome Cyanine R chelate and for copper,[16] tin,[17] and aluminum[18] as Pyrocatechol Violet chelate. In this paper, the fundamental conditions for the extraction of zirconium as the zirconium-PV-TDEA ternary complex with tridodecylethylammonium bromide in butyl acetate and the composition of the ternary complex will be discussed.

Experimental

Reagent. A 2.5×10^{-3} M zirconium solution was prepared by the following procedure. 0.1140 g of zirconium was placed in a platinum crucible and to this was added 6 ml of hydrofluoric acid (1+1). After the zirconium had been dissolved, 2 ml of sulfuric acid was added and evaporated to fuming sufur trioxide on a hot plate. Ater cooling, 137 ml of sulfuric acid was added and diluted to 500 ml with de-ionized water. A working standard solution was prepared as needed by the dilution of the 2.5×10^{-3} M solution with de-ionized water to each desired concentration. A 5×10^{-4} M PV solution was prepared by dissolving the Dotite PV in de-ionized water without any further purification. TDEA was prepared by the reflux to ethanolic solution of tridodecylamine and ethyl bromide for 4 h. After evaporation of the solvent, the salt was recrystallized two times from butyl acetate. A 6×10^{-4} M TDEA solution was prepared by dissolving the above TDEA in butyl acetate. All the other chemicals used were of a guaranteed reagent quality.

Apparatus. All the measurements of the absorbance were made with a Hitachi manual spectrophotometer, mode Epu-2A. Matched 10-mm absorption cells were used. The pH measurements were made with a Hitachi-Horiba model M-5 glass electrode pH meter.

Standard Procedure. Up to 9 μg of zirconium were placed in a 50 ml polyethylene beaker to which were added a definite amount of 0.1 M sulfuric acid and 2 ml of 5×10^{-4}M PV solution. pH of the solution was adjusted to 5 by the addition of 2 ml of 2 M sodium acetate solution and then the solution was diluted to 25 ml with de-ionized water. The solution was transferred into a 35 ml test tube and 5 ml of 6×10^{-4} M TDEA in butyl acetate was added. The extraction was carried out for 5 min by turning the test tube upside down at two times per 5 s. After the complete phase separation, the organic layer was taken out and centrifuged for 2 min at 3000 rpm. The extract was transferred into an absorption cell and the absorbance at 586 nm was measured against the reagent blank obtained in the same way.

Results and Discussion

Absorption Spectra. Absorption spectra of the ternary complex extracted into butyl acetate and of the zirconium-PV chelate anion in an aqueous solution are given in Fig. 1, along with that of the reagent blank. The ternary complex and the zirconium-PV chelate anion have an absorption maximum at 586 and 595 nm respectively.

Effect of pH. The aqueous solution was adjusted to various pH values with the acetate buffer solution and the extraction was carried out by the above procedure. Although formation of the zirconium-PV chelate should occur at a lower pH, about 2, the optimum pH range for the extraction of the ternary complex is found to be from 5 to 6. It is thought that the extractable higher cordination chelate anion forms at pH values from 5 to 6. The absorbance of the reagent blank

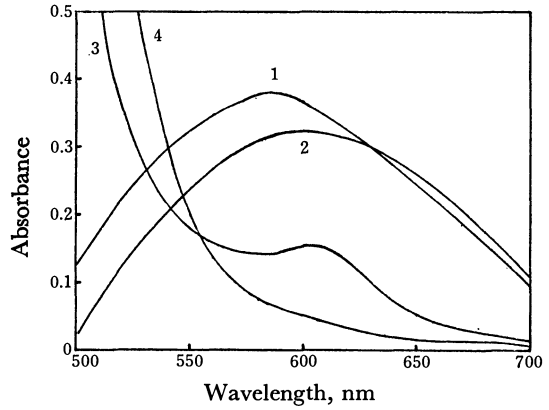

Fig. 1. Absorption spectra of the Zr–PV–TDEA in butyl acetate and the Zr–PV in aqueous solution.
pH=5, V_w(volume of aq. layer)=25 ml, V_o(volume of org. layer)=5 ml,
(1) Zr–PV–TDEA in butyl acetate $[Zr]_w=2\times10^{-6}$ M.
(2) Zr–PV in aq. soln. $[Zr]_w=10^{-5}$ M.
(3) PV–TDEA in butyl acetate $[PV]_w=4\times10^{-5}$ M
(4) PV in aq. soln. $[PV]_w=2\times10^{-4}$ M.

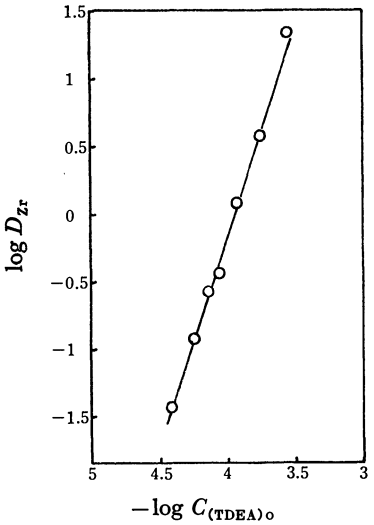

Fig. 2. Equilibrium-shift method applied to the Zr–PV–TDEA system.
$[Zr]_w=2\times10^{-6}$ M, $[PV]_w=2\times10^{-4}$ M, $[Br^-]_w=5\times10^{-4}$ M, pH=5, $V_w=25$ ml, $V_o=5$ ml, 586 nm.

in the organic layer increases very much with an increase in the pH value.

Organic Solvents. Several kind of organic solvents were tested in order to achieve a quantitative extraction of zirconium. The ternary complex can be extracted in such solvents as butyl acetate, carbon tetrachloride, benzene, toluene, xylene, and carbon disulfide. Absorbances of the ternary complex are much the same in these solvents. But the lowest absorbance of reagent blank is obtained in butyl acetate. The ternary complex can not be extracted in such solvents as 1-butanol, methyl isobutyl ketone, nitrobenzene, and chloroform.

The Effect of the PV Concentration. The effect of the PV concentration in the aqueous phase on the extraction of the ternary complex was examined by varying the PV concentration while other variables were held constant. The absorbance of the extract is constant when the PV in the initial aqueous phase is in the concentration range from 2×10^{-5}—6×10^{-5} M. The absorbance of the extract gradually decreases upon further addition of PV.

The Effect of the TDEA Concentration. The effect of the concentration of TDEA in butyl acetate on the extraction of the ternary complex was examined. The constant and maximum absorbance of the extract is obtained with a concentration higher than 4×10^{-4} M.

The Effect of the Mixing Time. The mixing time was varied from 10 sec to 15 min. The absorbance of the extract is constant for the mixing times from 3 to 15 min.

Extractability and Molar Absorptivity. The extractability of the ternary complex under the optimum conditions was examined by spectrophotometric determination of zirconium with Xylenol Orange in the extract after evaporating the organic layer. When a 250 ml portion of an aqueous layer containing 45.6 μg of zirconium is mixed with 50 ml of butyl acetate solution of TDEA, 97.8% of the zirconium is extracted by one extraction. The distribution ratio and the molar absorptivity are 2.22×10^2 and 3.9×10^4 cm^{-1} mol^{-1} l respectively.

Calibration Curve. A calibration curve for the determination of zirconium was made under the optimum conditions. A good linear relationship is obtained over the concentration range from 0.45 to 9 μg of zirconium per 5 ml of butyl acetate.

The Composition of the Ternary Complex. The molar ratio of PV to zirconium in the ternary complex was estimated to be 1 : 2 by the continuous-variation method. The molar ratio of zirconium to TDEA in the ternary complex was established by the equilibrium-shift method. All the equilibrium concentration and distribution ratios were estimated by measuring the absorbances of the organic or aqueous phase. The plot of log D_{Zr} against log $[TDEA]_o$ gives the number of TDEA which are involved in forming the ternary complex. The number is given by the slope. The slope of the straight line shows that the ratio of zirconium to TDEA is 1 : 3, as is shown in Fig. 2. According to these results, the composition of the ternary complex is estimated to be

$$Zr\,(pv)_2\left(R-\underset{\displaystyle R}{\overset{\displaystyle R}{N}}-R'\right)_3.$$

References

1) H. Kohara, N. Ishibashi, and K. Abe, *Bunseki Kagaku*, **19**, 48 (1970).
2) T. Ishito and K. Tonosaki, *Bunseki Kagaku*, **20**, 689 (1971).
3) M. K. Akhmedli, E. L. Glushchenko, and Z. L. Gasanova, *Zh. Anal. Khim.*, **26**, 1947 (1971).
4) T. Ishito, *Bunseki Kagaku*, **21**, 752 (1972).
5) R. U. Yuryavichus and C. A. Valyukyavichyus, *Zh. Anal. Khim.*, **27**, 1125 (1972).
6) M. M. Tananaido, O. P. Vdovenko, and V. M. Zatsarevnyi, *Zh. Anal. Khim.*, **29**, 1724 (1974).

7) N. L. Shestidesyatnaya, N. M. Milyaeva, and L. I. Kotelyanskaya, *Zh. Anal. Khim.*, **30**, 522 (1975).
8) R. Jurevicius, I. Blazis, and C. Valiukevicius, *Zh. Anal. Khim.*, **30**, 708 (1975).
9) J. E. Chester, R. M. Dagnall, and T. S. West, *Talanta*. **17**, 13 (1970).
10) B. W. Bailey, J. E. Chester, R. M. Dagnall, and T. S. West, *Talanta*, **15**, 1359 (1968).
11) R. Nakashima, S. Sasaki, and S. Shibata, *Bunseki Kagaku*, **22**, 723 (1973).
12) R. Nakashima, S. Sasaki, and S. Shibata, *Bunseki Kagaku*, **22**, 729 (1973).
13) Y. Shijo, *Nippon Kagaku Kaishi*, **1974**, 889.
14) Y. Shijo, *Bunseki Kagaku*, **23**, 884 (1974).
15) Y. Shijo, *Bull. Chem. Soc. Jpn.*, **48**, 2793 (1975).
16) Y. Shijo, *Bull. Chem. Soc. Jpn.*, **47**, 1642 (1974).
17) Y. Shijo, *Nippon Kagaku Kaishi*, **1974**, 1658.
18) Y. Shijo, *Nippon Kagaku Kaishi*, **1974**, 1912.

Glass Formation and Crystallization in Ternary Phosphate Systems Containing Al_2O_3

Akira KISHIOKA, Masao HAYASHI,* and Makio KINOSHITA

Department of Chemistry, Faculty of Science and Technology, Sophia University, Kioicho, Chiyoda-ku, Tokyo 102

(Received April 9, 1976)

Glass formation and crystallization were investigated in two types of three-component systems, M_2O–Al_2O_3–P_2O_5 (M=Li, Na, and K) and MO–Al_2O_3–P_2O_5 (M=Mg, Ca, and Ba). In the Li_2O–Al_2O_3–P_2O_5 and MO–Al_2O_3–P_2O_5 systems, wide regions of glass formation were found in compositions containing more than 50 mol% of P_2O_5. In the Na_2O–Al_2O_3–P_2O_5 and K_2O–Al_2O_3–P_2O_5 systems, the two peaks in Al_2O_3 content were found in the regions of glass formation corresponding to about 35 and 65 mol% of P_2O_5. In the devitrified products of the glasses with 60 and 70 mol% of P_2O_5, $AlPO_4$, $Al(PO_3)_3$, and alkaline earth metaphosphate (in the MO–Al_2O_3–P_2O_5 system) were found by X-ray powder diffractometry. The crystalline phases in the samples obtained as mixtures of glass and crystal consisted of $AlPO_4$ in the composition containing 60 mol% of P_2O_5, while those with a P_2O_5 composition of 70 mol% consisted of $Al(PO_3)_3$. By heating those samples at 700—900 °C, the X-ray diffractions of $AlPO_4$ and $Al(PO_3)_3$ were intensified. On the other hand, in the samples with 37.5, 40, and 50 mol% of P_2O_5, all the crystalline phases consisted of $AlPO_4$, and the intensities of these X-ray diffractions decreased after the samples were heated at 600—700 °C. Thus, there is a marked structural difference between the two peak-regions in the Na_2O–Al_2O_3–P_2O_5 and K_2O–Al_2O_3–P_2O_5 systems.

The addition of Al_2O_3 to phosphate glass results in an improvement in the chemical durability, a decrease in the thermal expansion coefficient, and an increase in the deformation temperature of the glass, that is, the stabilization of the glass structure.[1] It has been suggested that these changes in properties are due to the formation of a ($AlPO_4$) group in the glass. There have been many investigations of the role of the Al^{3+} ion in silicate glass. On the Al^{3+} ion in phosphate glass, however, only a few investigations have been reported. Recently, Sakka investigated the coordination number of the Al^{3+} ion in silicate, phosphate, borate, and other glasses on the basis of measurements of the chemical shift of the Al $K\alpha$ line by X-ray emission spectroscopy,[2] while Watanabe *et al.* proposed the existence of –P–O–Al– linkage in the glass of the $NaPO_3$–Al_2O_3 system.[3]

In a previous paper, the authors reported the regions of glass formation in multicomponent phosphate systems containing TiO_2.[4] However, no investigations of those in aluminophosphate systems have been reported. The glass-forming region in a three-component diagram is important in the investigation of the glass structure, because it is determined by the role of cations in the glass. Therefore, it may be worthwhile to determine the glass-forming regions in ternary phosphate systems containing Al_2O_3.

In this paper, the regions of glass formation in three-component diagrams were determined for six kinds of phosphate systems containing Al_2O_3—the M_2O–Al_2O_3–P_2O_5 (M=Li, Na, and K) and MO–Al_2O_3–P_2O_5 (M=Mg, Ca, and Ba) systems. In addition, the devitrified products of the glasses and the crystalline phases in these systems were investigated by X-ray powder diffractometry. From the results obtained, the glass structure and the action of Al^{3+} ion in it were discussed in connection with the P_2O_5 content in the glass.

* Present address: Meidensha Electric Mfg. Co., Ltd., Osaki, Shinagawa-ku, Tokyo 141.

Experimental

Preparation of Glass. The materials used were the following reagents. Aluminum oxide and orthophosphoric acid (85%) were used in all the systems, lithium hydroxide monohydrate was used in the Li_2O–Al_2O_3–P_2O_5 system, sodium dihydrogenphosphate dihydrate, sodium triphosphate, and anhydrous sodium carbonate in the Na_2O–Al_2O_3–P_2O_5 system, potassium dihydrogenphosphate and anhydrous potassium carbonate in the K_2O–Al_2O_3–P_2O_5 system, magnesium oxide in the MgO–Al_2O_3–P_2O_5 system, calcium hydrogenphosphate dihydrate in the CaO–Al_2O_3–P_2O_5 system, and barium hydroxide octahydrate in the BaO–Al_2O_3–P_2O_5 system. All the chemicals except sodium triphosphate were of a reagent grade. Commercial reagent-grade sodium triphosphate was purified by recrystallization and dehydrated.[5] A mixture obtained by mixing the necessary amounts of compounds selected from the compounds listed above was placed in platinum dishes or alumina crucibles. The former were used in the case of P_2O_5 contents up to 50 mol%, the latter, in the case of more than 50 mol%. In the case of a Na_2O/P_2O_5 or K_2O/P_2O_5 ratio of 1 as in the Na_2O–P_2O_5 or K_2O–P_2O_5 two-component system, $NaH_2PO_4 \cdot 2H_2O$ or KH_2PO_4 was used respectively. The weight of each batch was about 20 g.

Samples were heated in a Siliconit electric furnace BSH-1530 (Siliconit Konetsukogyo Co.) equipped with a platinum platinum-rhodium thermocouple with an automatic thermoelectric regulator. The temperature was slowly raised to 1350 °C over about a 7-h period and then kept at this temperature for 1 h. The melts of batches containing up to 55 mol% of P_2O_5 were poured out and quenched by pressing them with copper plate cooled with water. The other melts of a high viscosity were taken out from the furnace together with the alumina crucible and rapidly cooled by cold air flow generated by an electric fan. The homogeneity of the formed glass was immediately observed by the naked eye and also under a microscope or a polarizing microscope.

Because of the loss of P_2O_5 by vaporization during heating, the final copomistoin of the phosphate glass usually deviates to some extent from the initial composition, where the deviation depends on the condition of preparation. Therefore, all the diagrams for the glass formation were expressed in terms of the initial composition. In order to measure the volatiliza-

tion loss of P_2O_5, the three components in the MgO–Al_2O_3–P_2O_5 glasses in the range from 50 to 80 mol% of P_2O_5 in the batch composition were determined gravimetrically—MgO and P_2O_5 as $Mg_2P_2O_7$ and Al_2O_3 as $AlPO_4$.

Devitrification of Glass. Glass grains (0.25—1 mm in diameter) of about 2 g placed in a small porcelain crucible were heated for 10 h at the temperatures given in Tables 1—7. The temperature at which the glass in each system was devitrified was in the range from 600 to 900 °C; this temperature increased with the increase in the P_2O_5 content.

X-Ray Powder Diffractometry. The obtained samples were finely pulverized with an alumina mortar and their diffraction patterns were taken by a Rigaku Denki Geigerflex diffractometer with nickel-filtered Cu $K\alpha$ radiation. The identification of the crystalline products was carried out by comparing the X-ray diffraction peaks of the sample with those of the ASTM data file.

Results and Discussion

The experimetal results for the glass formation in each system are given in Figs. 1—6. The ranges of the glass formation in the M_2O–P_2O_5 and MO–P_2O_5 two-component systems were in agreement with the data presented by Takahashi,[6] except for the K_2O–P_2O_5 system, in which the glass formation was found in the composition containing less than 50 mol % of P_2O_5. In the composition at which the transparent homogeneous glass was not formed, the following three types of products were obtained; (1) a mixture of glass and crystal (when the melt was partly devitrified and when the crystalline substance was separated out in the melt), (2) a crystalline product (when the melt was devitrified and when the sample was not melted), and (3) the fused mass consisting of a crystal and glassy substance. No liquid-liquid-phase separation in the melt was found in any system.

In the MgO–Al_2O_3–P_2O_5 glasses with 50 to 80 mol % of P_2O_5, the amount of the loss of P_2O_5 by the volatilization was in the range from 1.0 to 16.5 mol %; it increased with an increase in the P_2O_5 content in the batch composition. The results of the gravimetric determination of three components in the glass of this system showed that the contents of water in the glasses were in the range from 0.5 to 1.5 wt %. Similar results may also be affirmed in the other systems.

The chemical formula of the crystalline products in the M_2O–Al_2O_3–P_2O_5 and MO–Al_2O_3–P_2O_5 systems, as identified by X-ray diffractometry, are listed in Tables 1—6, while those of the Al_2O_3–P_2O_5 two-component system are listed in Table 7.

Glass Formation in M_2O–Al_2O_3–P_2O_5 System. In the Li_2O–Al_2O_3–P_2O_5 system (Fig. 1), Al_2O_3 was incorporated into the glass composition when the P_2O_5 content exceeded about 35 mol %; the peak of the Al_2O_3 content appeared in the range from 60 to 70 mol % of P_2O_5. As can be seen from Figs. 1 and 4—6, the shape of the glass-forming region in this system is analogous to that in the MO–Al_2O_3–P_2O_5 system. As the properties of the Li^+ ion are similar to those of the alkaline earth ions, and as the electrostatic-bond strength of the Li^+ ion is larger than that of the Na^+ or K^+ ion, it may be considered that the Li^+ ion plays a role similar to that of the alkaline earth ion in the phosphate glass.

On the other hand, as is shown in Figs. 2 and 3, a large amount of Al_2O_3 was incorporated into the glass in composition of both about 35 as well as 65 mol %

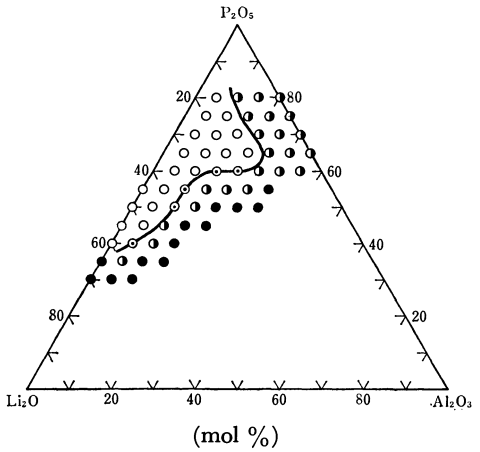

(mol %)

Fig. 1. Glass-forming region in Li_2O–Al_2O_3–P_2O_5 system.
○: Homogeneous glass, ⊙: trace amounts of crystal in glass, ◑: glass and crystal, ●: crystal.

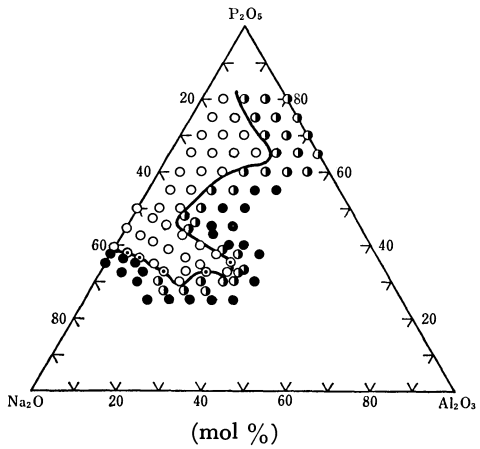

(mol %)

Fig. 2. Glass-forming region in Na_2O–Al_2O_3–P_2O_5 system.

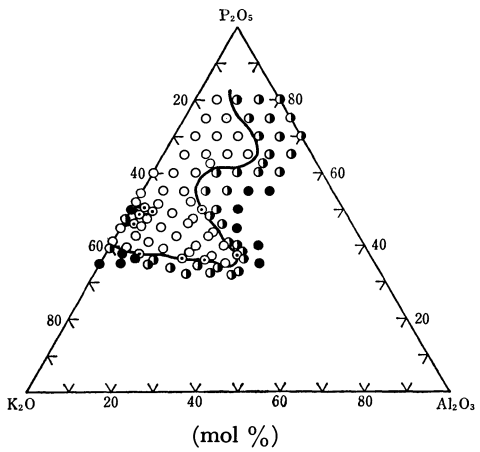

(mol %)

Fig. 3. Glass-forming region in K_2O–Al_2O_3–P_2O_5 system.

of P_2O_5 in the Na_2O–Al_2O_3–P_2O_5 and K_2O–Al_2O_3–P_2O_5 systems. This is a marked difference from the Na_2O–TiO_2–P_2O_5 and K_2O–TiO_2–P_2O_5 systems,[4] where only a small amount of TiO_2 is introduced into the glass even when the content of P_2O_5 exceeds 50 mol %. This fact indicates a difference between Al^{3+} and Ti^{4+} ions in their behavior in the phosphate glass. Since the Al^{3+} ion has been regarded as an intermediate ion, it is able to act as a network modifier as well as a network former in the glass structure. According to Sakka,[2] most of the Al^{3+} ions in the glass with a higher P_2O_5 content ($P/O \approx 0.33$) are 6-fold coordinated, while those with a lower P_2O_5 content ($P/O \lesssim 0.25$) are 4-fold coordinated. The existence of two peaks of Al_2O_3 content of the glass region in both the Na_2O–Al_2O_3–P_2O_5 and K_2O–Al_2O_3–P_2O_5 systems suggests the above-noted change in the coordination number of the Al^{3+} ion with the P_2O_5 content in the phosphate glass.

In the K_2O–P_2O_5 two-component system, the glass was not formed at $K_2O/P_2O_5=1$ (50 mol % of P_2O_5 in Fig. 3), but at $K_2O/P_2O_5>1$. Presumably a break in the long –P–O–P– straight-chain of potassium metaphosphate ($K_2O/P_2O_5=1$) by the excess K^+ ion favored the glass formation. The glass formation in the composition along the line of $K_2O/P_2O_5=1$ in the K_2O–Al_2O_3–P_2O_5 system was more extensive than that in the same composition in the K_2O–TiO_2–P_2O_5 system.[4] This fact also suggests that the network-forming and glass-forming abilities of the Al^{3+} ion differ in some degree from those of the Ti^{4+} ion in the phosphate glass.

Glass Formation in MO–Al_2O_3–P_2O_5 System. In the systems of MgO–Al_2O_3–P_2O_5, CaO–Al_2O_3–P_2O_5, and BaO–Al_2O_3–P_2O_5 (Figs. 4, 5, and 6), the content of Al_2O_3 incorporated into the glass increased with an increase in the P_2O_5 content, and the peak of Al_2O_3 content was found in the range from 60 to 70 mol % of P_2O_5. As has been described above, the glass-forming regions in these systems were similar to that in the Li_2O–Al_2O_3–P_2O_5 system. The difference between Al_2O_3 and TiO_2 in the glass formation was observed also in the BaO–Al_2O_3–P_2O_5 and BaO–TiO_2–P_2O_5 systems, because in the latter system the amount of TiO_2 within the composition limits of glass formation decreased with an increase in the P_2O_5 content.[4]

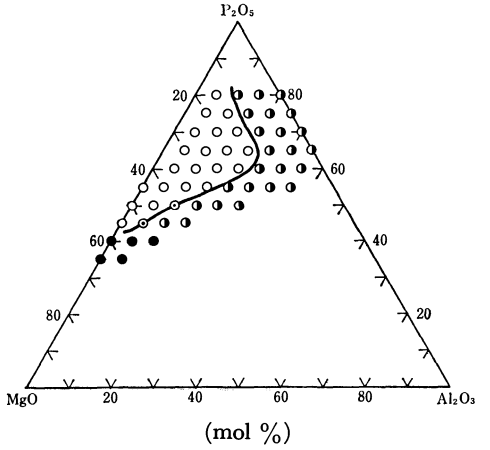

Fig. 4. Glass-forming region in MgO–Al_2O_3–P_2O_5 system.

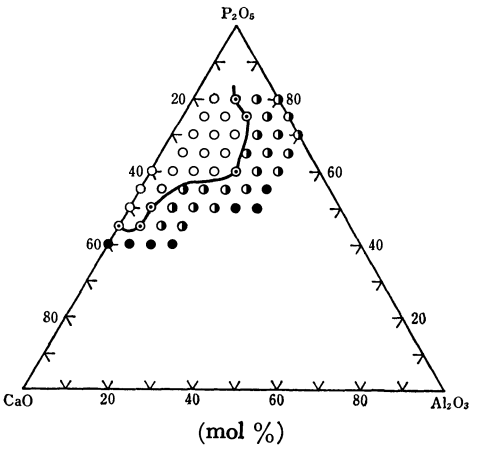

Fig. 5. Glass-forming region in CaO–Al_2O_3–P_2O_5 system.

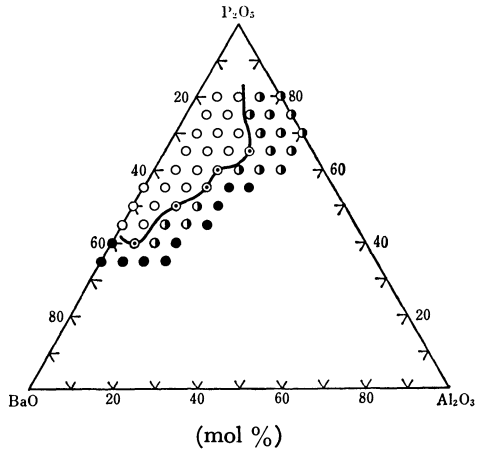

Fig. 6. Glass-forming region in BaO–Al_2O_3–P_2O_5 system.

X-Ray Powder Diffractometry. The devitrified products of the glasses obtained in the glass-forming region of the M_2O–Al_2O_3–P_2O_5 system were mainly aluminum metaphosphate in the composition containing 70 mol % of P_2O_5, aluminum metaphosphate and aluminum orthophosphate in 60 mol % of P_2O_5, and alkali metaphosphate (sodium trimetaphosphate in the Na_2O–Al_2O_3–P_2O_5 system) and aluminum orthophosphate in 50 mol % of P_2O_5 (Tables 1, 2, and 3). In each of the MO–Al_2O_3–P_2O_5 systems, alkaline earth metaphosphate as well as aluminum orthophosphate or aluminum metaphosphate was found in the compositions containing 50, 60, and 70 mol % of P_2O_5 (Tables 4, 5, and 6).

The crystalline phases in the samples outside the boundary for the glass formation in the M_2O–Al_2O_3–P_2O_5 and MO–Al_2O_3–P_2O_5 systems consisted mainly of aluminum metaphosphate in the composition containing 70 mol % of P_2O_5, aluminum orthophosphate and aluminum metaphosphate in 60 mol % of P_2O_5, and aluminum orthophosphate in 50 mol % of P_2O_5 (Tables 1—6). In the Na_2O–Al_2O_3–P_2O_5 system containing 37.5 mol % of P_2O_5 and the K_2O–Al_2O_3–P_2O_5 system containing 40 mol % of P_2O_5, the crystalline phases consisted mainly of aluminum orthophosphate (Tables 2 and 3).

As is marked with (+) sign in Tables 1—7, in all the samples outside the glass-forming range of 70 mol % of P_2O_5, the X-ray diffraction patterns of aluminum metaphosphate increased in intensity upon heating at 800—900 °C, while in the composition containing 60 mol % of P_2O_5 the crystallization of aluminum orthophosphate was promoted by heating at 700—900 °C. The same phenomena were also observed in the Al_2O_3–P_2O_5 two-component system (Table 7). The devitrified product of $25Al_2O_3 \cdot 75P_2O_5$ glass consisted predominantly of aluminum metaphosphate. These facts suggest that the network consisting of aluminum, oxygen, and phosphorous ions in the M_2O–Al_2O_3–P_2O_5 and MO–Al_2O_3–P_2O_5 glasses containing 60 mol % or more P_2O_5 is analogous to that in the Al_2O_3–P_2O_5 two-component glass. According to Pauling and Sherman,[7] the alumi-

Table 1. Crystalline phases in Li_2O–Al_2O_3–P_2O_5 system

Sample (batch composition)	Crystalline phase after quenching	Heat treatment (°C)	Crystalline phase after heat treatment
$15Li_2O \cdot 15Al_2O_3 \cdot 70P_2O_5$ (glass)		800	$Al(PO_3)_3$
$5Li_2O \cdot 25Al_2O_3 \cdot 70P_2O_5$ (glass & crystal)	$Al(PO_3)_3$, $AlPO_4$	800	$Al(PO_3)_3$(+),[a] $AlPO_4$(+)
$30Li_2O \cdot 10Al_2O_3 \cdot 60P_2O_5$ (glass)		700	$Al(PO_3)_3$, $AlPO_4$
$20Li_2O \cdot 20Al_2O_3 \cdot 60P_2O_5$ (glass)		700	$Al(PO_3)_3$, $AlPO_4$
$15Li_2O \cdot 25Al_2O_3 \cdot 60P_2O_5$ (glass & crystal)	$AlPO_4$	700	$AlPO_4$(+), $Al(PO_3)_3$
$40Li_2O \cdot 10Al_2O_3 \cdot 50P_2O_5$ (glass)		600	$LiPO_3$, $AlPO_4$
$35Li_2O \cdot 15Al_2O_3 \cdot 50P_2O_5$ (crystal & glass)	$AlPO_4$	600	$AlPO_4$(−),[b] $LiPO_3$

a) Intensity of X-ray diffraction increased. b) Intensity of X-ray diffraction decreased.

Table 2. Crystalline phases in Na_2O–Al_2O_3–P_2O_5 system

Sample (batch composition)	Crystalline phase after quenching	Heat treatment (°C)	Crystalline phase after heat treatment
$15Na_2O \cdot 15Al_2O_3 \cdot 70P_2O_5$ (glass)		800	$Al(PO_3)_3$, $AlPO_4$
$5Na_2O \cdot 25Al_2O_3 \cdot 70P_2O_5$ (glass & crystal)	$Al(PO_3)_3$	800	$Al(PO_3)_3$(+), $AlPO_4$
$30Na_2O \cdot 10Al_2O_3 \cdot 60P_2O_5$ (glass)		700	$Al(PO_3)_3$, $AlPO_4$
$20Na_2O \cdot 20Al_2O_3 \cdot 60P_2O_5$ (glass & crystal)		700	$Al(PO_3)_3$, $AlPO_4$
$15Na_2O \cdot 25Al_2O_3 \cdot 60P_2O_5$ (glass & crystal)	$AlPO_4$	700	$AlPO_4$(+), $Al(PO_3)_3$
$40Na_2O \cdot 10Al_2O_3 \cdot 50P_2O_5$ (glass)		600	$(NaPO_3)_3$, $AlPO_4$
$35Na_2O \cdot 15Al_2O_3 \cdot 50P_2O_5$ (glass & crystal)	$AlPO_4$	600	$(NaPO_3)_3$, $AlPO_4$(−)
$42.5Na_2O \cdot 20Al_2O_3 \cdot 37.5P_2O_5$ (glass)		600	Unknown
$32.5Na_2O \cdot 30Al_2O_3 \cdot 37.5P_2O_5$ (crystal& glass)	$AlPO_4$	600	Unknown
$27.5Na_2O \cdot 35Al_2O_3 \cdot 37.5P_2O_5$ (crystal)	$AlPO_4$	600	$AlPO_4$(−), Unknown

Table 3. Crystalline phases in K_2O–Al_2O_3–P_2O_5 system

Sample (batch composition)	Crystalline phase after quenching	Heat treatment (°C)	Crystalline phase after heat treatment
$15K_2O \cdot 15Al_2O_3 \cdot 70P_2O_5$ (glass)		900	$Al(PO_3)_3$
$5K_2O \cdot 25Al_2O_3 \cdot 70P_2O_5$ (glass & crystal)	$Al(PO_3)_3$	900	$Al(PO_3)_3$(+), $AlPO_4$
$30K_2O \cdot 10Al_2O_3 \cdot 60P_2O_5$ (glass)		800	$Al(PO_3)_3$, $AlPO_4$
$20K_2O \cdot 20Al_2O_3 \cdot 60P_2O_5$ (glass & crystal)		800	$Al(PO_3)_3$, $AlPO_4$
$15K_2O \cdot 25Al_2O_3 \cdot 60P_2O_5$ (glass & crystal)	$AlPO_4$	800	$AlPO_4$, $Al(PO_3)_3$
$40K_2O \cdot 10Al_2O_3 \cdot 50P_2O_5$ (glass)		600	KPO_3, $AlPO_4$, Unknown
$35K_2O \cdot 15Al_2O_3 \cdot 50P_2O_5$ (glass)		600	KPO_3, $AlPO_4$, Unknown
$30K_2O \cdot 20Al_2O_3 \cdot 50P_2O_5$ (glass & crystal)	$AlPO_4$	600	$AlPO_4$(−), KPO_3, Unknown
$40K_2O \cdot 20Al_2O_3 \cdot 40P_2O_5$ (glass)		600	Unknown
$30K_2O \cdot 30Al_2O_3 \cdot 40P_2O_5$ (glass &crystal)	Unknown	600	Unknown
$25K_2O \cdot 35Al_2O_3 \cdot 40P_2O_5$ (crystal)	$AlPO_4$	600	$AlPO_4$

Table 4. Crystalline phases in MgO–Al_2O_3–P_2O_5 system

Sample (batch composition)	Crystalline phase after quenching	Heat treatment (°C)	Crystalline phase after heat treatment
$15MgO \cdot 15Al_2O_3 \cdot 70P_2O_5$ (glass)		900	$Al(PO_3)_3$, $Mg(PO_3)_2$
$10MgO \cdot 20Al_2O_3 \cdot 70P_2O_5$ (glass & crystal)	$Al(PO_3)_3$	900	$Al(PO_3)_3$(+), $AlPO_4$, $Mg(PO_3)_2$
$20MgO \cdot 20Al_2O_3 \cdot 60P_2O_5$ (glass)		900	$Al(PO_3)_3$, $AlPO_4$, $Mg(PO_3)_2$
$15MgO \cdot 25Al_2O_3 \cdot 60P_2O_5$ (glass & crystal)	$AlPO_4$	900	$AlPO_4$(+), $Al(PO_3)_3$, $Mg(PO_3)_2$
$40MgO \cdot 10Al_2O_3 \cdot 50P_2O_5$ (glass)		750	$Mg(PO_3)_2$, $AlPO_4$
$35MgO \cdot 15Al_2O_3 \cdot 50P_2O_5$ (glass & crystal)	$AlPO_4$		

TABLE 5. CRYSTALLINE PHASES IN CaO–Al_2O_3–P_2O_5 SYSTEM

Sample (batch composition)	Crystalline phase after quenching	Heat treatment (°C)	Crystalline phase after heat treatment
$15CaO \cdot 15Al_2O_3 \cdot 70P_2O_5$ (glass)		900	$Al(PO_3)_3$, $Ca(PO_3)_2$
$10CaO \cdot 20Al_2O_3 \cdot 70P_2O_5$ (glass & crystal)	$Al(PO_3)_3$, $AlPO_4$	900	$Al(PO_3)_3(+)$, $AlPO_4$, $Ca(PO_3)_2$
$20CaO \cdot 20Al_2O_3 \cdot 60P_2O_5$ (glass)		900	$Al(PO_3)_3$, $AlPO_4$, $Ca(PO_3)_2$
$15CaO \cdot 25Al_2O_3 \cdot 60P_2O_5$ (glass & crystal)	$AlPO_4$	900	$AlPO_4(+)$, $Al(PO_3)_3$, $Ca(PO_3)_2$
$35CaO \cdot 15Al_2O_3 \cdot 50P_2O_5$ (glass & crystal)	$AlPO_4$		

TABLE 6. CRYSTALLINE PHASES IN BaO–Al_2O_3–P_2O_5 SYSTEM

Sample (batch composition)	Crystalline phase after quenching	Heat treatment (°C)	Crystalline phase after heat treatment
$15BaO \cdot 15Al_2O_3 \cdot 70P_2O_5$ (glass)		800	$Al(PO_3)_3$, $AlPO_4$, $Ba(PO_3)_2$
$10BaO \cdot 20Al_2O_3 \cdot 70P_2O_5$ (glass & crystal)	$Al(PO_3)_3$	800	$Al(PO_3)_3(+)$, $AlPO_4$, $Ba(PO_3)_2$
$30BaO \cdot 10Al_2O_3 \cdot 60P_2O_5$ (glass)		750	$Ba(PO_3)_2$, $Al(PO_3)_3$, $AlPO_4$
$20BaO \cdot 20Al_2O_3 \cdot 60P_2O_5$ (glass & crystal)		800	$Ba(PO_3)_2$, $Al(PO_3)_3$, $AlPO_4$
$15BaO \cdot 25Al_2O_3 \cdot 60P_2O_5$ (glass & crystal)	$AlPO_4$	800	$AlPO_4(+)$, $Al(PO_3)_3$, $Ba(PO_3)_2$
$40BaO \cdot 10Al_2O_3 \cdot 50P_2O_5$ (glass)		700	$Ba(PO_3)_2$, $AlPO_4$
$35BaO \cdot 15Al_2O_3 \cdot 50P_2O_5$ (glass & crystal)	$AlPO_4$	700	$Ba(PO_3)_2$, $AlPO_4(-)$

TABLE 7. CRYSTALLINE PHASES IN Al_2O_3–P_2O_5 SYSTEM

Sample (batch composition)	Crystalline phase after quenching	Heat treatment (°C)	Crystalline phase after heat treatment
$20Al_2O_3 \cdot 80P_2O_5$ (crystal & glass)	$Al(PO_3)_3$	900	$Al(PO_3)_3(+)$, $AlPO_4$
$25Al_2O_3 \cdot 75P_2O_5$ (glass)[a]		900	$Al(PO_3)_3$, $AlPO_4$
$30Al_2O_3 \cdot 70P_2O_5$ (crystal & glass)	$Al(PO_3)_3$, $AlPO_4$	900	$Al(PO_3)_3(+)$, $AlPO_4(+)$
$40Al_2O_3 \cdot 60P_2O_5$ (crystal & glass)	$AlPO_4$, $Al(PO_3)_3$	900	$AlPO_4(+)$, $Al(PO_3)_3(+)$

a) This glass was prepared by heating the mixture of aluminum orthophosphate and orthophosphoric acid (85%) at 1500 °C.

num metaphosphate consists of AlO_6 octahedra and rings of four PO_4 tetrahedra. Gill and Riaz reported that the ultraphosphate glasses with M/P=0.7—1.0 consisted of trimetaphosphate rings, polyphosphate chains, and branched chains.[8] Consequently, the AlO_6 octahedra seem to stabilize these glass structures by linking them to the rings of PO_4 tetrahedra and the branching points of phosphate chains.

On the other hand, the X-ray diffraction gave rather complex patterns for the devitrified samples of the Na_2O–Al_2O_3–P_2O_5 glasses with 37.5 mol % of P_2O_5 and K_2O–Al_2O_3–P_2O_5 glasses with 40 mol % of P_2O_5. In the diffraction patterns for the samples outside the glass-forming range in the systems of 37.5, 40, and 50 mol % of P_2O_5, the diffraction patterns of aluminum orthophosphate weakened upon heating at 600—700 °C. These facts suggest that the structure of the glass in the range from 37.5 to 50 mol % of P_2O_5 differs markedly from that in the composition containing more than 50 mol % of P_2O_5 (ultraphosphate). Therefore, the above results also suggest that the action of the Al^{3+} ion the glass structure varies with the P_2O_5 content in the glasses of the Na_2O–Al_2O_3–P_2O_5 and K_2O–Al_2O_3–P_2O_5 systems.

In the composition containing less than 50 mol % of P_2O_5 (polyphosphate), the structures of the Na_2O–Al_2O_3–P_2O_5 and K_2O–Al_2O_3–P_2O_5 glasses may be regarded as random aggregates of the –P–O–P– and –P–O–Al– chains (clusters) consisting of PO_4 and AlO_4 tetrahedra and the Na^+ or K^+ ions.

References

1) H. Rawson, "Inorganic Glass-Forming Systems," Academic Press, London (1967), p. 173.
2) S. Sakka, *Bull. Inst. Chem. Res., Kyoto Univ.*, **49**, 349 (1971).
3) M. Watanabe, S. Sato, and H. Saito, *Bull. Chem. Soc. Jpn.*, **48**, 893 (1975).
4) A. Kishioka, M. Haba, and M. Amagasa, *Bull. Chem. Soc. Jpn.*, **47**, 2493 (1974).
5) R. N. Bell, A. R. Wreath, and W. T. Curless, *Anal. Chem.*, **24**, 1997 (1952).
6) S. Sakka, T. Sakaino, and K. Takahashi, ed., "Garasu Hando-Bukku," Asakura Publishing Co. Ltd., Tokyo (1975), p. 882.
7) L. Pauling and J. Sherman, *Z. Kristallogr.*, **96**, 481 (1937).
8) J. B. Gill and S. A. Riaz, *J. Chem. Soc., A*, **1969**, 843.

The Conformations of Copper(II) Complexes with edda-Type Optically Active Polyamino Carboxylic Acids in Aqueous Solutions

Tasuku MURAKAMI and Masahiro HATANO

Chemical Research Institute of Non-Aqueous Solutions, Tohoku University, 2-1-1 Katahira, Sendai 980

(Received April 19, 1976)

A copper(II) complex with (*S,S*)-1,1′-ethylenedipyrrolidine-2,2′-dicarboxylic acid (H_2epro) was prepared, and its absorption and CD spectra were measured in an aqueous solution. A weak absorption band at 9500 cm^{-1} was indicative of the apical coordination of the carboxylate group. Furthermore, from the fact that the effect of unidentate bases, such as pyridine and ammonia, on the absorption and CD spectra of the epro complex was quite different from that of bidentate bases, the epro complex was expected to take a *Λ*-uns-*cis* conformation. In addition, the base-addition effect was measured for the complexes of (*S,S*)-α,α′-dimethyl-*N,N′*-ethylenediaminediacetic acid(H_2eddp), (*S,S*)-α,α′-diisopropyl-*N,N′*-ethylenediaminediacetic acid(H_2eddv), and (*S,S*)-α,α′-dibenzyl-*N,N′*-ethylenediaminediacetic acid(H_2eddc). The conformations of these complexes are also discussed on the basis of the information obtained for the epro complex.

In the previous paper,[1] we have reported that the copper(II) complexes with ethylenediamine-*N,N′*-diacetic acid(H_2edda)-type optically active polyamino carboxylic acids, such as (*S,S*)-α,α′-dimethyl-*N,N′*-ethylenediaminediacetic acid(H_2eddp),[2,3] (*S,S*)-α,α′-diisopropyl-*N,N′*-ethylenediaminediacetic acid(H_2eddv), and (*S,S*)-α,α′-dibenzyl-*N,N′*-ethylenediaminediacetic acid(H_2eddc), exhibited quite different circular dichroism(CD) spectra from each other and that, hence, these complexes might adopt different conformations in aqueous solutions.

In order to obtain further information on the conformations of the edda-type copper(II) complexes, we have now prepared a new edda-type complex of a copper(II) ion with (*S,S*)-1,1′-ethylenedipyrrolidine-2,2′-dicarboxylic acid (abbreviated to H_2epro). As may be seen in Fig. 1, this acid has two pyrrolidinyl groups in its inner parts and, hence, may be expected to coordinate to a metal ion with a large stereospecificity. In this paper, we wish to report the absorption and CD spectra of the epro complex of copper(II) and, in addition, the effects of unidentate and bidentate bases on the CD spectra of other edda-type complexes. The conformations of these complexes will be discussed on the basis of the behavior of the spectra.

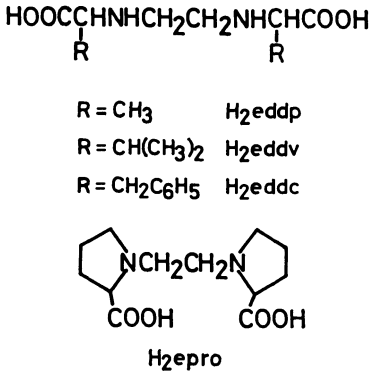

Fig. 1. Optically active edda-type polyamino carboxylic acids.

Results and Discussion

Conformation of [Cu(epro)] and Other edda-Type Complexes. Figure 2 shows the absorption and CD spectra of the epro complex in the region of 7000 to 22000 cm^{-1}, together with those of the eddp, eddv, and eddc complexes which have been reported previously.[1] The epro complex exhibited a main absorption at 15400 cm^{-1} and a weak band at about 9500 cm^{-1}. Corresponding to these two bands, two CD bands were observed with the opposite sign. The existence of this weak absorption band plays an important role when discussing the conformation of the epro complex, as will be described below.

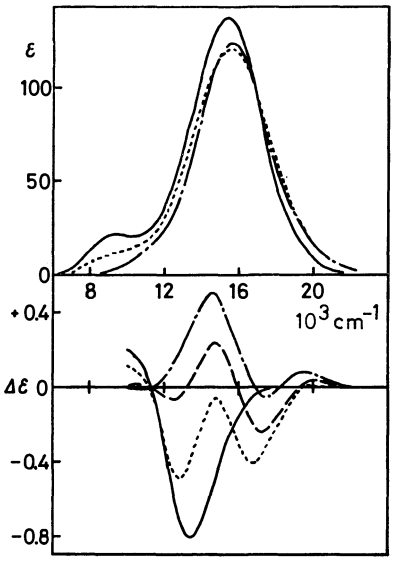

Fig. 2. Absorption and CD spectra of [Cu(epro)] (——), [Cu(eddp)] (— - —), [Cu(eddv)] (------), [Cu(eddc)] (— — —) in aqueous solutions.

In general, copper(II) complexes typically consist of four nearby donor atoms arranged approximately in a plane around the central metal ion, with the possibility of one or two more distant apical donors. A stronger ligation to the copper(II) ion along the tetragonal axis would cause the d-d absorption band to shift to a lower energy.[4-7] In many cases, a shoulder band appears at about 10000 cm^{-1} as a result of such a ligation.[7-9] Therefore, the weak band observed for the epro complex leads us to expect the apical ligation of one or two carboxylate group(s) of epro, that is, a *cis*-type coordination of epro to the copper(II) ion.[10] The chelated

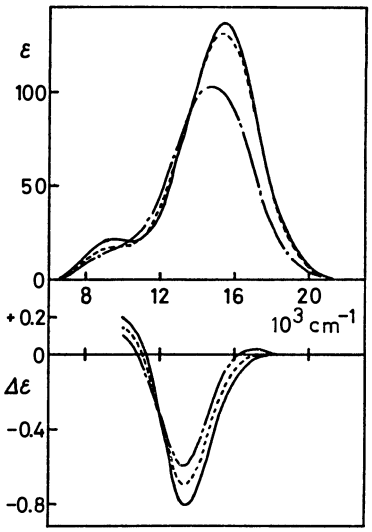

Fig. 3. The pH-dependent absorption and CD spectra of [Cu(epro)].
——: pH 5.3—9.0, ------: pH 10.5, —·—: pH 11.8.

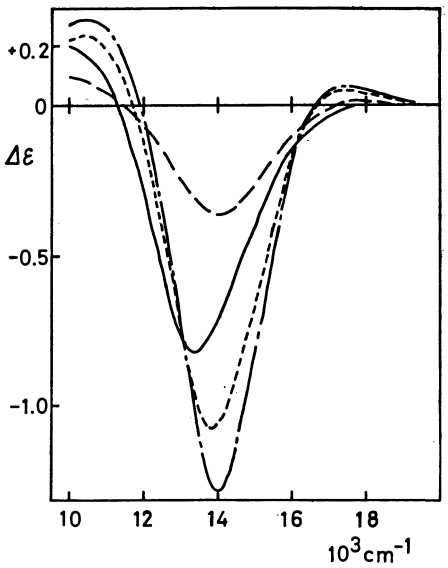

Fig. 4. Base-induced variation of the CD spectrum of [Cu(epro)] (mole ratio; in base/complex).
——: (0), ------: py (15), —·—: py (700), ——: bipy (5).

carboxylate group will possess a stronger ligand field than water, in spite of having the same coordination atom. Thus, the weak band is thought to become visible.

It has been observed that the optical activity of the ternary mixed complexes of copper(II) with diethylenetriamine and L-α-amino acids decreases in a high pH region.[7] This extreme decrease in the optical activity was concluded to result from the displacement of the carboxylate group coordinated at an apical position by a hydroxide ion. Therefore, if the epro complex contains an apical ligation, the intensity of the CD band is expected to decrease significantly in a high pH region. Figure 3 shows the variable-pH absorption and CD spectra of the epro complex. These spectra varied little in the pH 5 to 9 region. However, as the pH was further increased, the intensities of the absorption and CD bands appreciably decreased. Therefore, this is some evidence for the apical ligation of the carboxylate group in the epro complex. On the other hand, the absorption and CD spectra of the epro complex did not vary with the temperature (0—70 °C) and the concentration (2×10^{-3}—5×10^{-2} M) in a neutral pH region, indicating that the epro complex exists not as an equilibrium mixture, but as a single species in a neutral solution.

An examination of molecular models showed that epro hardly coordinates in a plane because of the rigid pyrrolidinyl groups. This is supported by the fact that some tetraamines, which have two pyrrolidinyl groups in their inner parts as well as epro, did not form planar species of the nickel(II) ion, but formed only octahedral ones.[11-13] Not only epro, but also other edda-type polyamino carboxylic acids seem to have primarily a certain characteristic that they hardly coordinate to a metal ion in a plane.[14] For example, as of now, no cobalt(III) complex with an edda-type acid in the planar configuration has been reported. Only s-*cis* and uns-*cis* isomers have actually been obtained.[10,15-17] Also, in the case of the edda-type complexes of the nickel(II) ion, the configuration in solution has been assigned to an s-*cis* form on the basis of NMR measurements.[18,19] Thus, the apical ligation of the one or two carboxylate group(s) which is derived from the absorption spectrum is also supported from the stereochemical point of view for epro.

In order to discriminate whether only one or both of the two carboxylate groups of epro coordinate(s) at the apical position, the effects of unidentate bases, such as pyridine and ammonia, added to the complex solution on the absorption and CD spectra were compared with those of bidentate bases, such as 2,2′-bipyridyl and ethylenediamine.

When a great excess of pyridine or ammonia was added to a solution of the epro complex, the absorption and CD bands became appreciably intense, but, in particular, the CD shape varied only to a lesser extent, as is shown in Fig. 4. However, when excess 2,2′-bipyridyl or ethylenediamine was added, the absorption spectral shape changed entirely and the intensity of the CD band decreased considerably. These findings indicate that the conformation of the epro complex remains essentially unaltered by the coordination of the unidentate bases, but the coordination of the bidentate bases alters the conformation.

The spectral behavior observed can be reasonably explained by supposing that the epro complex takes a conformation in which only one of the two carboxylate groups coordinates at an apical position, that is, a uns-*cis* form. It is expected that the bidentate base occupies two positions in the square plane about the copper(II) ion and displaces the carboxylate group coordinated in the plane, and that, consequently, the original conformation of epro is destroyed. On the other hand, the unidentate base probably coordinates to one position in the square plane and to one apical position, neither of which is occupied by epro; hence, the unidentate base may not alter the conformation

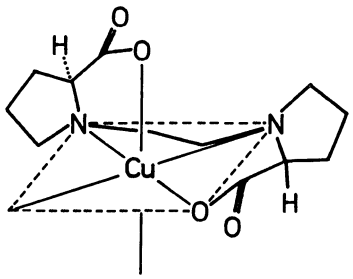

Fig. 5. Schematic drawing of a uns-*cis* structure proposed for [Cu(epro)].

of the epro complex. 2,2'-Bipyridyl or 1,10-phenanthroline act little as a unidentate base; the effect of α-methyl substituted pyridines such as α-picoline and 2,6-lutidine has been much smaller than that of pyridine.[20]

There are only two structures with apical ligation possible for the epro complex: *Λ*-uns-*cis* and Δ-s-*cis*,[21] because of the large strain originating from the pyrrolidine rings in epro. Therefore, the epro complex may be on the basis of the spectral behavior described above expected to take a *Λ*-uns-*cis* form. This structure is illustrated in Fig. 5. Each of the two tertiary nitrogen atoms in the epro complex has an *R* configuration, and the central ethylenediamine-like chelate ring seems to become an envelope.

As may be seen from Fig. 2, the eddv complex also exhibited a shoulder band at about 10000 cm^{-1} as a tailing of the main band. This implies that the apical ligation of the carboxylate group takes place to some extent in the eddv complex as well as in the epro complex. In addition, a high temperature dependence has been observed for the CD spectrum of the eddv complex.[1] This is apparently based on a binary equilibrium, as derived from the presence of isosbestic points. In the previous paper,[1] the temperature dependence observed for the eddv complex was expected to result from an equlibrium between two types of planar forms, in which the ring substituent groups are equatorial or axial. However, the contribution of the form in which the substituents are axial is probably small. The apical ligation of the carboxylate group appears to be a more plausible explanation of the weak band observed for the epro and eddv complexes.

The CD spectra of the four copper(II) complexes with optically active edda-type polyamino carboxylic acids are quite different from each other, as is shown in Fig. 2. The negative components of the CD spectra increase in this order; [Cu(eddp)]<[Cu(eddc)]<[Cu(eddv)]<[Cu(epro)]. This order is the same as that of the intensity of the shoulder band at about 10000 cm^{-1}. When excess unidentate bases, such as pyridine and ammonia, were added to the aqueous solutions of the copper(II) complexes with eddp, eddv and eddc, the intensities of these CD spectra increased extremely and their CD shapes became almost the same. In addition, the shoulder band at about 10000 cm^{-1} became very intense (see Figs. 6 and 7).[22] Furthermore, this CD shape is identical with the CD curve of the epro complex, which is affected to a lesser extent by the addition of the unidentate bases.

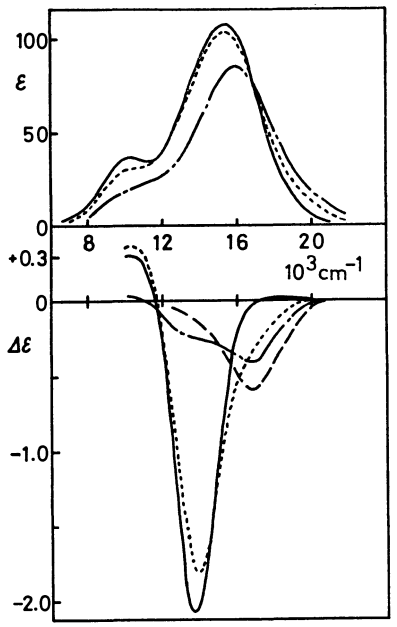

Fig. 6. Base-induced variation of the absorption and CD spectra of [Cu(eddv)] (mole ratio; in base/complex).
——: py (60), ----: NH_3 (5), — — —: en (1), – – –: bipy (5).

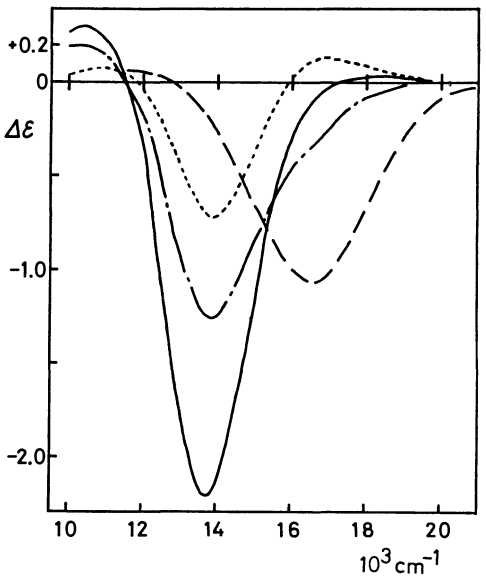

Fig. 7. Base-induced variation of the CD spectra of [Cu(eddp)] and [Cu(eddc)] (mole ratio; in base/complex).
——: [Cu(eddc)], py(100); — — —: [Cu(eddc)], NH_3 (5); – – –: [Cu(eddc)], bipy(6); ------: [Cu(eddp)], py (13300).

This spectral behavior, especially the conformity in the CD spectra, is very significant when discussing the conformations of these complexes. From these findings, the mixed complexes of eddp, eddv, and eddc with pyridine or ammonia may be expected to take the same conformation as the epro complex, that is, the *Λ*-uns-*cis* form. The remarkable augmentation of the intensity of the CD band is evidence in support of the occurrence of the dissymmetry about the metal ion. If the mixed

complexes take the *A*-uns-*cis* form, each of the two secondary nitrogen atoms has an *R* configuration as well as those of the epro complex. Thus, the unidentate base may be expected to convert the *trans*-type configuration of the edda-type acids into a uns-*cis*-type one. This conversion of the planar form into the uns-*cis* form may result from the stereospecific characteristic of the edda-type acids that they form a planar configuration only with difficulty.

The amount of unidentate bases necessary for the conversion of the eddp complex was much more than those needed for the addc and eddv complexes, as can be seen from Fig. 7. This may be a reflection on the higher stability of the planar configuration of eddp. This stability is probably related to the bulkiness of the substituent groups. Thus, the planar configuration of the edda-type acids is thought to become unstable with an increase in the bulkiness of the substituent groups. On the other hand, the effect of the bidentate bases on the spectra was entirely different from that of the unidentate bases, as is shown in Figs. 6 and 7. This finding is similar to the case of the epro complex.

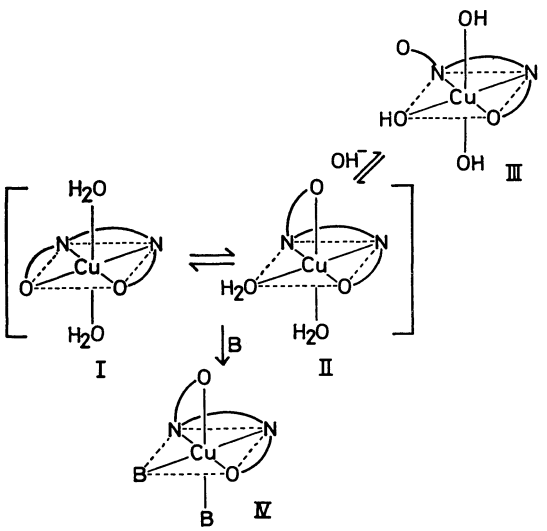

Fig. 8. Proposed equilibrium scheme for the edda-type copper(II) complexes in aqueous solutions. O–N–N–O represents edda-type ligands and B is a unidentate base. The charges on the central metal ion and coordinating groups are omitted for the simplicity.

Equilibrium Scheme. In conclusion, the equilibrium scheme for the edda-type copper(II) complexes in aqueous solutions is represented by Fig. 8, which is derived from the spectral results described above. Species (I) and (II) are predominant in a neutral pH region, which constitute an equilibrium state. In particular, however, the epro complex which exhibits the weak absorption band at 9500 cm^{-1} takes the uns-*cis* form (II) completely, and the eddp complex, almost the planar form (I). The eddv and eddc complexes may be equilibrium mixtures of these two forms. In a high pH region, the carboxylate group coordinated at the apical position is displaced by a hydroxide ion, and then Species (III) may be formed.

When an excess of the unidentate bases is added to the complex solutions, these complexes are converted from Form (I) or (II) into Form (IV). This is verified by the finding that, on the addition of unidentate bases, the CD spectra of these complexes become the same shape as that of the epro complex. Furthermore, the fact that the CD shape of the epro complex changes little on the addition of the unidentate bases is very important when introducing the above conclusion.

However, no data suitable for determining the structure of these edda-type complexes in the solid state has yet been obtained. In the near future, the structure in the solid state will be clarified in more detail.

Assignment of the CD Bands. In general, the absorption spectra observed for copper(II) complexes should consist of three d-d transitions, $d_{z^2}\rightarrow d_{x^2-y^2}$ $d_{xy}\rightarrow d_{x^2-y^2}$, and d_{xz}, $d_{yz}\rightarrow d_{x^2-y^2}$, if the molecular symmetry is taken as D_{4h}. In the case of the complexes with the stronger ligation along the tetragonal axis, the $d_{z^2}\rightarrow d_{x^2-y^2}$ transition is the lowest energy, as is well-known.[23,24] The weak band at about 10000 cm^{-1} observed for the epro complex and the mixed complexes with pyridine or ammonia apparently corresponds to the $d_{z^2}\rightarrow d_{x^2-y^2}$ transition. These complexes imposed the positive CD band for this transition, as can be seen from the figures.

On the other hand, within the main absorption band were observed a large negative CD band a very small positive band at the lower- and higher-wavenumber sides respectively. These CD bands should correspond to the other two transitions, $d_{xy}\rightarrow d_{x^2-y^2}$, and d_{xz}, $d_{yz}\rightarrow d_{x^2-y^2}$. The former transition seems to have a lower energy than the latter;[23] hence, the large negative band may be the $d_{xy}\rightarrow d_{x^2-y^2}$ transition. However, since these complexes apparently possess a molecular symmetry much lower than D_{4h}, the degenerate transition may split into two bands in practice. In this case, the main band consists of three transitions; consequently, the assignment of the two CD bands becomes more difficult. The following two descriptions may be convincing arguments: the split of the degenerate transition is probably small, or one of the three transitions may contribute little to the optical activity.

Experimental

Materials. The copper(II) complexes of eddp, eddv, and eddc were prepared as has been described in the previous paper.[1] The epro complex was isolated in the following manner. Basic copper(II) carbonate was mixed with an equimolar amount of the dimethyl ester of (*S*, *S*)-1,1′-ethylenedipyrrolidine-2 2′-dicarboxylic acid (H_2epro), which had been previously prepared,[11] in an aqueous solution. The solution was then allowed to stand at room temperature. Within a few days, a blue product was precipitated. The product was washed with ethanol and then reprecipitated from water. Found: C, 43.69; H, 5.89; N, 8.52%. Calcd for $[Cu(C_{12}H_{18}N_2O_4)]\cdot 1/2(H_2O)$: C, 44.10; H, 5.86; N, 8.57%.

The pyridine, ethylenediamine, 2,2′-bipyridyl, and 1,10-phenanthroline which were added to the complex solution were of commercial grades and were purified, if necessary, by the usual procedures. In the case of ammonia, equimolar amounts of ammonium chloride and sodium hydroxide were added to the complex solution.

Measurements. The absorption spectra were obtained by means of a Hitachi EPS-3T spectrophotometer, while the CD measurements in the region of 400 to 1000 nm were made on a Jasco J-20A spectropolarimeter. To follow the solution of the epro complex with a change in the pH, additional drops of 0.1 or 1.0 M sodium hydroxide were added. The pH of the solution was measured with a Toa HM-20B digital pH meter.

References

1) T. Murakami and M. Hatano, *Bull. Chem. Soc. Jpn.*, **46**, 3116 (1973).

2) The systematic names for these edda-type polyamino carboxylic acids, according to the IUPAC Rules (1971) are as follows: H_2eddp, (*S,S*)-2,2′-(ethylenediimino)dipropionic acid; H_2eddv, (*S,S*)-3,3′-dimethyl-2,2′-(ethylenediimino)dibutyric acid; H_2eddc, (*S,S*)-3,3′-diphenyl-2,2′-(ethylenediimino)dipropionic acid; H_2epro, (*S,S*)-1,1′-ethylenedipyrrolidine-2,2′-dicarboxylic acid.

3) *R* and *S* refer to the configurations about the asymmetric carbon or nitrogen atoms of ligands, according to the sequence rules of R. S. Cahn, C. K. Ingold, and V. Prelog, *Angew. Chem., Int. Ed. Engl.*, **5**, 385 (1966).

4) J. Bjerrum, C. J. Ballhausen, and C. K. Jørgensen. *Acta Chem. Scand.*, **8**, 1275 (1954).

5) R. L. Belford, M. Calvin, and G. Belford, *J. Chem. Phys.*, **26**, 1165 (1957).

6) A. A. G. Tomlinson and B. J. Hathaway, *J. Chem. Soc., A*, **1968**, 1685.

7) T. Murakami, T. Nozawa, and M. Hatano, *Bull. Chem. Soc. Jpn.*, **46**, 2456 (1973).

8) F. A. Cotton and G. Wilkinson, "Advanced Inorganic Chemistry," 2nd ed., Interscience Publishers, New York (1966), p. 906.

9) H. Ojima and K. Nonoyama, *Z. Anorg. Allgem. Chem.*, **401**, 207 (1973).

10) The nomenclature (*trans*, s-*cis*, and uns-*cis*) used here is employed in order to express three geometrical isomers of the edda-type complexes. This was suggested by J. H. Worrell and D. H. Busch, *Inorg. Chem.*, **8**, 1563 (1969).

11) S. Kitagawa, T. Murakami, and M. Hatano, *Inorg. Chem.*, **14**, 2347 (1975).

12) S. Kitagawa, T. Murakami, and M. Hatano, *Chem. Lett.*, **1974**, 925.

13) T. Murakami, S. Kitagawa, and M. Hatano, *Inorg. Chem.*, **15**, 1953 (1975).

14) G. R. Brubaker, D. P. Schaefer, J. H. Worrell, and J. I. Legg, *Coord. Chem. Rev.*, **7**, 161 (1971).

15) P. J. Garnett, D. W. Watts, and J. I. Legg, *Inorg. Chem.*, **8**, 2534 (1969).

16) P. F. Coleman, J. I. Legg, and J. Steele, *Inorg. Chem.*, **9**, 937 (1970).

17) K. D. Gailey, K. Igi, and B. E. Douglas, *Inorg. Chem.*, **14**, 2956 (1975), and the references therein.

18) F. F.-L. Ho, L. E. Erickson, S. R. Watkins, and C. N. Reilley, *Inorg. Chem.*, **9**, 1139 (1970).

19) T. Murakami, I. Hirako, and M. Hatano, *Bull. Chem. Soc. Jpn.*, to be published.

20) T. Murakami and M. Hatano, presented at the 21st Symposium on Coordination Chemistry, Nagoya, October, 1971.

21) Δ and *A* refer to the absolute configulations about the central metal atom as defined in *Inorg. Chem.*, **9**, 1(1970).

22) T. Murakami and M. Hatano, presented at the 22nd Symposium on Coordination Chemistry, Osaka, November, 1972.

23) Y. Nishida and S. Kida, *Bull. Chem. Soc. Jpn.*, **43**, 3814 (1970), and the references therein.

24) T. Murakami and M. Hatano, *Inorg. Chem.*, **14**, 999 (1975).

The Crystal and Molecular Structure of Chloro-α,β,γ,δ-tetraphenylporphinatocobalt(III)

Tosio SAKURAI, Kiyoko YAMAMOTO, Hirobumi NAITO,* and Nobuaki NAKAMOTO*

The Institute of Physical and Chemical Research, Wako-shi, Saitama 351
**Department of Engineering Chemistry, College of Science and Engineering, Nihon University, Kanda, Chiyoda-ku, Tokyo 101*

(Received May 10, 1976)

The structure of the title compound, $C_{44}H_{28}N_4CoCl$, has been determined by single-crystal X-ray diffraction. The crystals are body-centered tetragonal, with $a=b=13.693(2)$, $c=9.701(2)$ Å, and $Z=2$. The space group was determined to be $I4$ from the measurement of the anomalous dispersion effect. The structure was predicted prior to the X-ray analysis from the calculation of the intermolecular van der Waals energy; the result agreed quite well with the experimentally determined structure. A tetragonal pyramidal five coordination with the chlorine atom at the apex was found for the cobalt atom. The cobalt–chlorine distance is 2.149 (6) Å, about 0.1 Å shorter than those found in ordinary octahedral coordinations.

Previously, cobalt(III) α,β,γ,δ-tetraphenylporphin complexes with a nitrogenous base, $Cl(L)_nCoTPP$ ($n=1,2$),** were prepared[1] by treating Co(II)TPP with L in an alcoholic solution containing hydrochloric acid, and the octahedral six coordination about the cobalt atom of Cl(pyridine)CoTPP was confirmed by X-ray diffraction.[2] Recently, from a solution without L investigators could isolate single crystals of chloro-α,β,γ,δ-tetraphenylporphinatocobalt(III), ClCoTPP,*** whose coordination remained ambiguous from a study of the electronic absorption spectra in various solvents and the solid state.[4] The present paper will deal with the determination of the structure of this compound by the X-ray diffraction technique. The results show a tetragonal pyramidal five coordination about the cobalt atom, with the chlorine atom at the apex.

Experimental

Preparation of Chloro-α,β,γ,δ-tetraphenylporphinatocobalt(III) (ClCoTPP). Co(II)TPP[5] (0.3 g) was suspended in methanol (297 ml) containing concentrated hydrochloric acid (3 ml). When the suspension was stirred at room temperature in an open flask for several hours, the solution gradually changed to reddish purple, and then the whole became a clear solution. The solution was filtered and concentrated under reduced pressure at about 50 °C. The separated crystalline precipitates were collected, washed with water, and then with a small amount of a methanol–water mixture (2:1), dried at room temperature, and recrystallized from methanol and then chloroform–ether (yield, 0.2 g). The crystals thus obtained were again dissolved in a small amount of chloroform, and the solvent was allowed to evaporate slowly to yield ClCoTPP as violet, lustrous, single crystals.

Found: C, 73.45; H, 4.17; N, 7.85; Co, 8.24; Cl, 5.00%. Calcd for $C_{44}H_{28}N_4CoCl$: C, 74.73; H, 3.99; N, 7.92; Co, 8.33; Cl, 5.01%.

Electronic absorption spectrum (methanol), λ/nm (ε/10³): 575_{sh} (3.8), 541_{max} (14.4), 505_{max} (3.5), 425.5_{max} (250), and 313_{max} (17.0).

Magnetic susceptibility measurements showed diamagnetism.

Measurements of X-Ray Diffraction Intensities and the Space Group Determination. The preliminary Weissenberg photographs showed that the crystals belong to the tetragonal system and that the systematic absences are $h+k+l=2n+1$. Therefore, the possible space groups are $I4$, $I\bar{4}$, or $I4/m$. The diffraction intensities were collected on a Rigaku AFC four-circle diffractometer, with graphite-monochromatized Cu $K\alpha$ radiation, within the range of $2\theta \leq 140°$. The size of the crystal was $0.6\times0.4\times0.2$ mm³. The ordinary Lorentz and polarization corrections were applied. The effect of the absorption was corrected by North, Phillips, and Mathews's experimental method.[6] The linear absorption coeffecient is 49.8 cm^{-1}. The succssive averaging of equivalent reflections yielded 855 independent reflections with $l \leq 0$. Both cobalt and chlorine atoms have considerably large $\Delta f''$ components for Cu $K\alpha$ radiation. The values of $\Delta f''$ are 3.8 and 0.7 for the cobalt and chlorine atoms respectively.[7] Therefore, in order to determine the space group, all the equivalent reflections were measured for some reflections. A few examples are shown in Table 1. These F_o values have a four-fold symmetry in the reciprocal space. Therefore, the space group is $I4$.

Crystal data $a=b=13.693(2)$, $c=9.701(2)$ Å, $V=1818.9$ (6) Å³. Space group $I4$, $Z=2$. $D_c=1.292$ g cm^{-3}.

Prediction of the Structure

The number of general equivalent positions is eight for the $I4$ space group. The number of the molecule in the cell is two. Therefore, the molecule must be located on a special position with a four-fold symmetry. From the shape of the complex, the cobalt atom was taken as the point of origin. The symmetry of the TPP group is 4. The approximate geometry of the porphinato core is well known. The most probable dihedral angle between the porphinato plane and the phenyl plane is about 72°.[2] Therefore, freedom remains in the rotation of the TPP group about the c axis. The van der Waals energy between the TPP groups was calculated in relation to the rotation angle. The energy curve showed two very sharp minima when the Co–N

** This formula represents the composition. TPP: dianion of α,β,γ,δ-tetraphenylporphin. L: nitrogenous base (example, pyridine, *p*-toluidine, *etc.*).

*** The crystal structure of ClCoTPP was previously reported, in Fleischer's review article,[3] to be $I4/m$ with $a=b=13.41$ and $c=9.82$ Å. However, as far as the present authors are aware, no written report about the structure has been published.

TABLE 1. OBSERVED STRUCTURE FACTORS, F_o'S, EXHIBITING 4-FOLD SYMMETRY

Index {h k l}	F_o							
	h k l	−k h l	−h −k l	k −h l	−h −k −l	k −h −l	h k −l	−k h −l
4 4 2	32	33	33	32	24	24	24	24
6 4 2	33	34	34	33	33	33	33	33
2 3 3	31	31	31	30	35	36	36	35
6 5 3	20	20	20	20	26	27	27	26
1 5 4	29	28	28	28	29	30	30	29
4 3 5	23	24	23	23	18	19	19	18

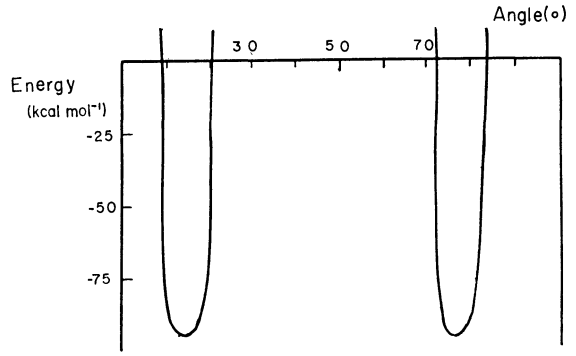

Fig. 1. Van der Waals energy of the tetraphenylporphin molecule. The abscissa is the angle between the Co–N vector and the a axis.

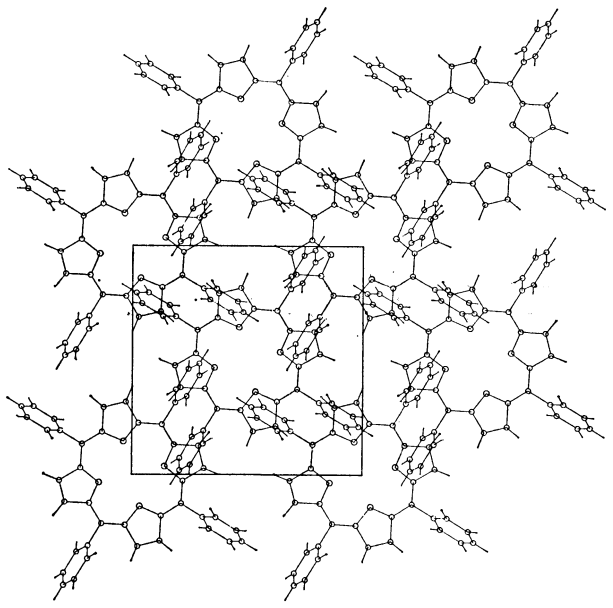

Fig. 2. The predicted structure. c axis projection.

vector makes an angle of 14° or 76° from the a axis (Fig. 1). These two orientations are energetically equivalent for the TPP group. Thus, the packing of the TPP groups in the unit cell was predicted to be as is shown in Fig. 2, or its equivalent, before the diffraction intensities were observed.

Structure Analysis

The structure was easily solved by the ordinary heavy-atom·method, independent from the predicted structure, and was refined by the block-diagonal least-squares method. In a difference Fourier map, the peaks corresponding to the hydrogen atoms were very broad; thus, the hydrogen atoms were not included in the structure-factor calculation. The refinement was performed using 855 unique reflections. The final R index, with anisotropic temperature factors, was 8.8%. In order to determine the absolute configuration and verify the space group, the structure factors of the Friedel pair reflections were also calculated. Some of the results are shown in Table 2, while the atomic parameters are given in Table 3. The structure factors

TABLE 2. STRUCTURE FACTORS OF FRIEDEL PAIRS

Index	F_o	F_c
4 4 2	32	33
−4 −4 −2	24	23
6 4 2	33	33
−6 −4 −2	33	32
2 3 3	31	34
−2 −3 −3	35	41
6 5 3	20	19
−6 −5 −3	26	27
1 5 4	29	27
−1 −5 −4	29	30
4 3 5	23	22
−4 −3 −5	18	19

TABLE 3. FRACTIONAL COORDINATES AND ANISOTROPIC THERMAL PARAMETERS ($\times 10^4$)

Standard deviations are given in parentheses.
The anisotropic parameters are in the form:
$\exp\{-(B_{11}h^2+B_{22}k^2+B_{33}l^2+2B_{12}hk+2B_{23}kl+2B_{13}hl)\}$

Atom	x	y	z
Co	0(0)	0(0)	0(0)
Cl	0(0)	0(0)	2216(7)
N	1396(7)	387(7)	−57(17)
C(1)	1762(8)	1318(9)	−53(19)
C(2)	2833(9)	1317(10)	10(23)
C(3)	3078(9)	356(10)	65(22)
C(4)	2206(8)	−205(9)	−24(20)
C(5)	2180(8)	−1216(9)	−40(20)
C(6)	3140(8)	−1770(9)	−64(23)
C(7)	3672(11)	−1806(13)	1282(23)
C(8)	4568(12)	−2354(14)	1269(29)
C(9)	4882(10)	−2786(10)	−116(34)
C(10)	4350(13)	−2742(12)	−1255(23)
C(11)	3449(12)	−2218(12)	−1251(21)

TABLE 3. (Continued)

Atom	B_{11}	B_{22}	B_{33}	B_{12}	B_{13}	B_{23}
Co	4(0)	4(0)	9(0)	0(0)	0(0)	0(0)
Cl	5(0)	5(0)	7(1)	0(0)	0(0)	0(0)
N	5(1)	5(1)	11(1)	0(0)	0(1)	0(1)
C(1)	5(1)	6(1)	12(2)	0(1)	2(1)	2(1)
C(2)	5(1)	7(1)	19(2)	0(1)	5(1)	−2(2)
C(3)	5(1)	6(1)	17(2)	0(1)	2(1)	2(1)
C(4)	5(1)	5(1)	13(2)	0(1)	3(1)	0(1)
C(5)	5(1)	6(1)	12(2)	0(1)	1(1)	−1(1)
C(6)	5(1)	6(1)	18(2)	0(1)	2(1)	−3(1)
C(7)	5(1)	10(1)	23(4)	1(1)	−2(2)	6(2)
C(8)	7(1)	10(1)	29(4)	2(1)	1(2)	2(2)
C(9)	5(1)	7(1)	31(3)	1(1)	2(2)	−2(2)
C(10)	7(1)	6(1)	31(4)	1(1)	6(2)	0(2)
C(11)	7(1)	6(1)	25(4)	0(1)	6(2)	−2(1)

are given in Table 4.****

Discussion of the Structure

The lattice parameters of the present crystals are significantly different from those referred to by Fleischer.[3] This difference is attributable to the order and disorder structures. For the disorder structure, the chlorine atoms are distributed randomly on both +z and −z sides of the cobalt atom, so that the apparent space group is $I4/m$. We also obtained disordered crystals with $a=13.489$ and $c=9.779$ Å from the same crystallization condition. So far, all known five-coordinate structures are disordered. The only known order structure is the six-coordinate Cl_2Sn(IV)TPP.[8] Therefore, the present structure is the first example of an order structure with a five coordination. The method of distinguishing between the order and disorder structures was fully discussed by us previously.[9]

The crystal structure is shown in Fig. 3. The cobalt-nitrogen bond makes an angle of 15° from the a axis. The dihedral angle between the phenyl plane and the mean porphinato plane is 75°. These values agree quite well with the predicted structure.

The shortest intermolecular carbon–carbon distance, 3.64 Å, is between the C(2) of the pyrrole group of a molecule and the C(11) of the phenyl group of the neighbouring molecule at the body center position (Fig. 4). The rapid increase in the intermolecular energy against the rotation of the molecule from the equilibrium position is due to the repulsion between phenyl groups of the neighbouring molecules.

The bond distances and angles within the TPP group, averaged over chemically equivalent bonds, are shown in Fig. 5, while the thermal ellipsoids are shown in Fig. 6. In contrast to the previous structure,[2] the porphinato group is quite flat. The maximum deviation of the atom from the mean plane is 0.08 Å for C(3) and less than 0.03 Å for the others. The angle between the mean pyrrole plane and the mean porphinato plane is 2.1°.

**** Table 4 has been submitted to, and is kept, by the office of the Chemical Society of Japan, 1-5 Kanda-Surugadai, Chiyoda-ku, Tokyo 101 (Document No. 7632).

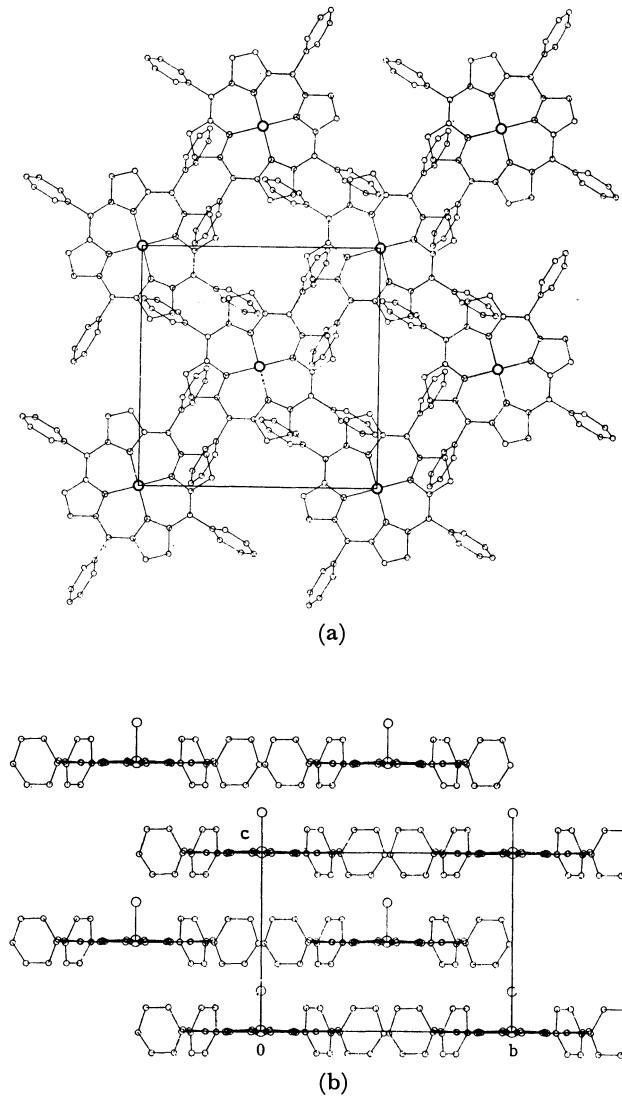

Fig. 3. The crystal structure.
(a) c axis projection. (b) a axis projection.

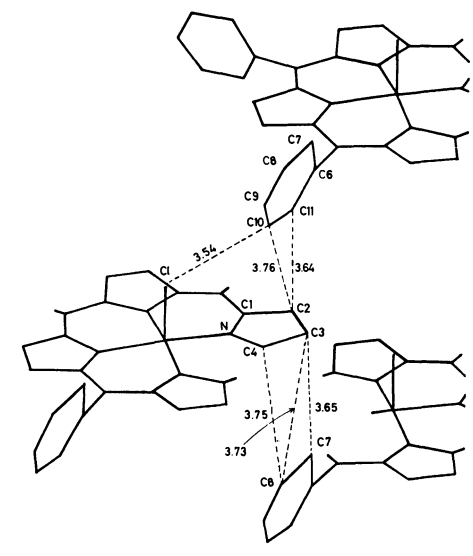

Fig. 4. Intermolecular atomic distances (Å).

Table 5. Coordination about the metal atom

Parameters of cobalt complexes.					
Complex	Coordination	Co–Ct[a] (Å)	Equatorial Co–N(Å)	Co–Cl (Å)	Ref.
ClCo(III)TPP	Five	0.05	1.985	2.145	This work
Co(III)(N_4)Cl[b]	Five	0.19		2.509	10
Cl(pyridine)Co(III)TPP	Six	0.	1.98	2.251	2
(1-Methylimidazole)Co(II)TPP	Five	0.13	1.977		11
(NO)Co(II)TPP	Five	0.09	1.978		12
(Piperidine)$_2$Co(II)TPP	Six	0.	1.987		13

Parameters of other five-coordinate metalloporphyrins.			
Complex	M–Ct[a] (Å)	Equatorial M–N (Å)	Ref.
(NO)Fe(II)TPP	0.211	2.001	14
(MeO)Fe(III)(Meso-P-IX DME)[c]	0.48	2.073	15
(Pyridine)Zn(II)TPyP[d]	0.33	2.073	16
(H_2O)Mg(II)TPP	0.273	2.072	17
(Me)Rh(III)OEP[e]	0.051	2.03	18
ClFe(III)TPP	0.38	2.049	19

a) Ct: Center of the plane of porphin nitrogen atoms. b) See footnote . c) Mesoporphyrin-IX dimethyl ester. d) α, β, γ, δ-Tetrapyridylporphin. e) 1, 2, 3, 4, 5, 6, 7, 8-Octaethylporphin.

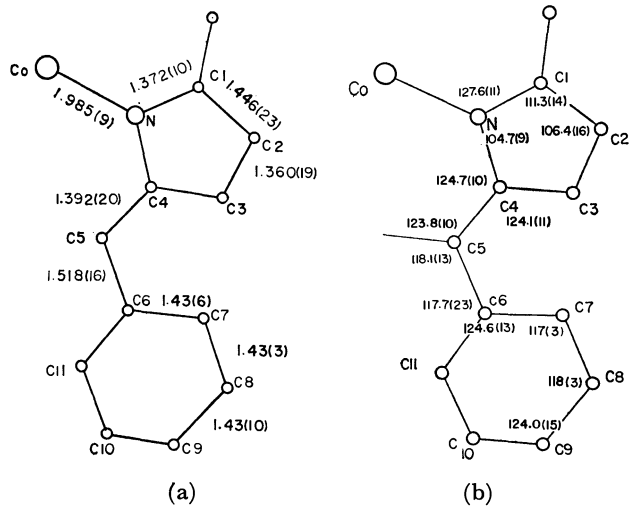

Fig. 5. (a) Bond distances (Å). (b) Bond angles (°).

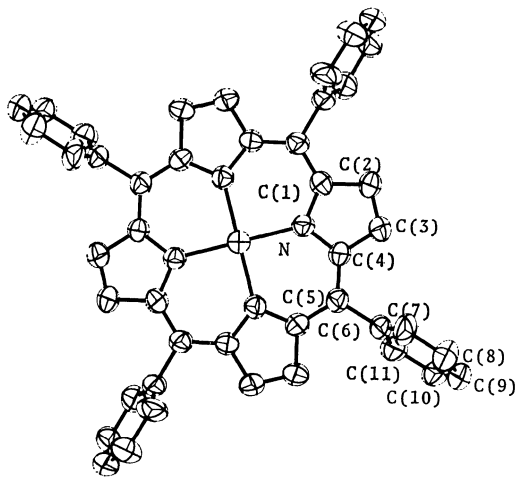

Fig. 6. Thermal ellipsoids of the molecule.

The coordination about the cobalt atom is the tetragonal pyramid, as is shown in Fig. 7. The ordinary cobalt(III) complex has been known to form an octahedral coordination. Recently, Bailey *et al.*[10] presented a tetragonal pyramidal structure for the cobalt(III) complex Co(N_4)Cl.† This complex is paramagnetic, in contrast to the present diamagnetism. Several other five-coordinate metalloporphyrins are known. The parameters of these complexes are compared in Table 5. In the present complex, the deviation of the cobalt atom from the mean plane of the nitrogen atoms is very small, and the Co–Cl distance, 2.15 Å, is shorter by about 0.1 Å than those of the ordinary six-coordinate cobalt(III) complexes.[2] Since the $d_{x^2-y^2}$ orbital of the central cobalt(III) ion is not occupied in the diamagnetic state and thus the effective radius is reduced, the cobalt ion can be in the central hole of the porphyrin. On the other hand, an occupation of $d_{x^2-y^2}$ orbital in chloro-α,β,γ,δ-tetraphenylporphinatoiron(III) gives rise to a shift of the central metal ion out of the porphinato plane.[19] The shortening of Co–Cl bond found in the present work is attributed to an enhanced donation of coordinating Cl^- ion. For an electroneutrality, the axial ligand in the five-coordinate configuration should donate much more than the one in an ordinary six-coordinate configuration. This shortening might be also due to an enhanced donation promoted by a vacancy of d_{z^2} orbital in this diamagnetic complex. In fact, the Co–Cl bond found in a paramagnetic five-coordinate cobalt(III) complex[10] is longer by about 0.25 Å than the normal bond. A similar shortening of the axial coordination in a diamagnetic d^6 five-coordinate complex has been reported on the Rh–C-

† (N_4) represents

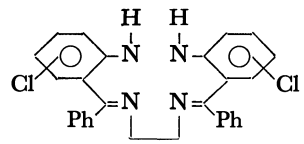

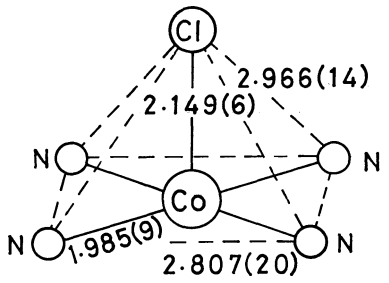

Fig. 7. Coordination about the cobalt atom.

(methyl) bond in octaethylporphinato(methyl)rhodium-(III).[18]

The structure of this complex corresponds to a geometry of an intermediate of the S_N1 substitution reaction of six-coordinate cobalt(III) complexes.

The calculations were carried out on the FACOM 230-75 computer of this Institute, using UNICS II program system.[20] The authors are grateful to Professor Hiroshi Kobayashi and Dr. Youkoh Kaizu of the Tokyo Institute of Technology for the discussion on an electronic state of this complex and the measurement of the magnetic properties. The research was supported, in part, by a Scientific Grant (034085) from the Ministry of Education.

References

1) K. Yamamoto and S. Tonomura, *Sci. Papers Inst. Phys. Chem. Res.*, **58**, 122 (1964).
2) T. Sakurai, K. Yamamoto, N. Seino, and M. Katsuta, *Acta Crystallogr.*, **B31**, 2514 (1975).
3) E. B. Fleischer, *Acc. Chem. Res.*, **3**, 105 (1970).
4) K. Yamamoto, 25th Symposium of Coordination Chemistry, Tokyo, October, 1975, p. 331.
5) G. D. Dorough, J. R. Miller, and F. M. Huennekens, *J. Am. Chem. Soc.*, **73**, 4315 (1951).
6) A. C. T. North, D. C. Phillips, and F. S. Mathews, *Acta Crystallogr.*, **A24**, 351 (1968).
7) C. H. MacGillavry and G. D. Rieck, ed., "International Tables for X-Ray Crystallography," The Kynoch Press, Vol. III, Birmingham (1962), p. 214.
8) D. M. Collins, W. R. Scheidt, and J. L. Hoard, *J. Am, Chem. Soc.*, **94**, 6689 (1972).
9) T. Sakurai and K. Yamamoto, *Sci. Papers Inst. Phys. Chem. Res.*, **70**, 31 (1976).
10) N. A. Bailey, E. D. McKenzie, and J. M. Worthington, *Inorg. Chim. Acta*, **12**, L31 (1975).
11) W. R. Scheidt, *J. Am. Chem. Soc.*, **96**, 90 (1974).
12) W. R. Scheidt and J. L. Hoard, *J. Am. Chem. Soc.*, **95**, 8281 (1973).
13) W. R. Scheidt, *J. Am. Chem. Soc.*, **96**, 84 (1974).
14) W. R. Scheidt and M. E. Frisse, *J. Am. Chem. Soc.*, **97**, 17 (1975).
15) J. L. Hoard, M. J. Hamor, T. A. Hamor, and W. S. Caughey, *J. Am. Chem. Soc.*, **87**, 2312 (1965).
16) D. M. Collins and J. L. Hoard, *J. Am. Chem. Soc.*, **92**, 3761 (1970).
17) R. Timkovich and A. Tulinsky, *J. Am. Chem. Soc.*, **91**, 4430 (1969).
18) A. Takenaka, S. K. Syal, Y. Sasada, T. Omura, H. Ogoshi, and Z. Yoshida, *Acta Crystallogr.*, **B32**, 62 (1976).
19) J. L. Hoard, G. H. Cohen, and M. D. Glick, *J. Am. Chem. Soc.*, **89**, 1992 (1967).
20) T. Sakurai, H. Iwasaki, Y. Watanabe, K. Kobayashi, Y. Bando, and Y. Nakamichi, *Rep. Inst. Phys. Chem. Res.*, **50**, 75 (1974).

A Potentiometric Study on Complex Formation of Cadmium(II) and Lead(II) Ions with *N*-(2-Hydroxyethyl)ethylenediamine-*N*,*N*′,*N*′-triacetic Acid

Noboru OYAMA, Takehide SHIRATO, Hiroaki MATSUDA, and Hitoshi OHTAKI

Department of Electronic Chemistry, Tokyo Institute of Technology, O-okayama, Meguro-ku, Tokyo 152

(Received May 13, 1976)

The complex formation of cadmium(II) and lead(II) ions with *N*-(2-hydroxyethyl)ethylenediamine-*N*,*N*′,*N*′-triacetic acid (HEDTA) has been studied potentiometrically in a 1.0 M $NaClO_4$ medium at 25.0 °C by using glass and metal–amalgam electrodes. The emf data obtained over the pH range 1 to 10 were explained in terms of the formation of the following species: for the Cd–HEDTA system, CdL^- (log $\beta_{101}=13.21\pm0.04$), CdHL (log $\beta_{111}=15.61\pm0.02$) and CdH_2L^+ (log $\beta_{121}=16.68\pm0.04$); for the Pb–HEDTA system, PbL^- (log $\beta_{101}=14.83\pm0.02$), PbHL (log $\beta_{111}=16.97\pm0.02$), PbH_2L^+ (log $\beta_{121}=17.89\pm0.02$) and PbH_3L^{2+} (log $\beta_{131}=18.67\pm0.02$), where $\beta_{pqr}=[M_pH_qL_r^{(2p+q-3r)+}]/[M^{2+}]^p[H^+]^q[L^{3-}]^r$ and L denotes the unprotonated molecule of HEDTA. Protonation constants of HEDTA were determined as log $\beta_{011}=9.20\pm0.01$, log $\beta_{021}=14.72\pm0.01$, log $\beta_{031}=17.06\pm0.01$, log $\beta_{041}=18.52\pm0.01$ and log $\beta_{051}=18.65\pm0.05$.

The complex formation reaction of Cd(II) and Pb(II) ions with polyamino-*N*-polycarboxylic acids has been quantitatively studied by many investigators, and numerous results for the formation constants of unprotonated complexes have been reported.[1] Nevertheless, a relatively few attentions have been focused on the formation reactions of protonated complexes.

Earlier works on equilibrium studies of metal–HEDTA compounds have been described for systems of some divalent heavy metals and rare-earth elements.[2,3] The complexes of Cd(II) and Pb(II) ions with HEDTA have also been examined by some investigators, but formation constants of protonated complexes have scarcely been reported.[2,4,5] Although protonated complexes are expected to be present in an acidic region, most of previous experiments have only been performed in a relatively high pH region where no protonated complexes were formed.

Recently, we have studied the electrode reactions of Cd(II) and Pb(II) complexes with HEDTA and it was concluded from the d.c. polarographic behavior of the complexes in these systems that the protonated complexes MH_2L and MHL should significantly participate in the charge transfer processes.[6,7] Therefore, it is expected that such protonated complexes are also present in the bulk of the solution. The aim of the present investigation is to search the formation of protonated complexes in these systems, and thus to carry out potentiometric measurements on complex equilibrium over a wide range of pH, especially in an acidic region.

Symbols

h	Concentration of hydrogen ion at equilibrium
m	Concentration of metal ion at equilibrium
H	Analytical excess of hydrogen ion in a test solution
H_1^T	Analytical excess of hydrogen ion in the T_1 solution
c_B^T	Hydroxide ion concentration in the T_2 solution
M	Cd(II) or Pb(II)
c_M	Total concentration of M
L	*N*-(2-Hydroxyethyl)ethylenediamine-*N*,*N*′,*N*′-triacetate anion ($hedta^{3-}$)
c_L	Total concentration of L
l	Concentration of free L
X	Degree of neutralization of H_3L: $(-H+[H]-[OH])/c_L$
p	Number of metal atoms bound to complex species
q	Number of protons bound to complex species
r	Number of ligands bound to complex species
β_{pqr}	Equilibrium constant for the reaction $pM+qH+rL=M_pH_qL_r$
$\bar{n}$	Average number of protons bound to one L
y_h, y_m	Activity coefficients of hydrogen and metal ions, respectively
E_g, E_m	Emf of the cells defined by the subscripts of Eqs. 1 and 2
$E_j(h,m)$	Liquid junction potential as a function of h and m
[ ]	Concentration

All charges are omitted for the sake of convenience.

Experimental

Reagents. *N-(2-Hydroxyethyl)ethylenediamine*-N,N′,N′-*triacetic acid* was purchased from Dojindo Laboratories, recrystallized from distilled water and dried under a reduced pressure in a desiccator over silica gel. Found: C, 43.41%; H, 6.74%; N, 10.16%; O, 39.78%. Calcd for $C_{10}H_{18}N_2O_7$: C, 43.17%; H, 6.52%; N, 10.07%; O, 40.25%.

Cadmium(II) perchlorate was prepared by dissolving CdO (99.99%, Mitsuwa Pure Chemicals Co.) in a $HClO_4$ solution and was purified by recrystallizing twice from water. The stock solution contained a small amount of perchloric acid to prevent the hydrolysis of cadmium ion. The concentration of cadmium ion in the stock solution was determined by electrogravimetry. The concentration of excess $HClO_4$ in the solution was determined from the location of the end point of neutralization by means of a Gran-plot.

Lead(II) perchlorate was prepared by dissolving $PbCO_3$ in $HClO_4$ solution and purified by recrystallizing twice from water. The concentration of lead(II) ion in the stock solution was determined by electrogravimetry as PbO_2.

Sodium perchlorate was prepared according to Biedermann and Civatta.[8]

Sodium hydroxide solution was prepared by electrolysis of sodium perchlorate solution. A 1.0 M sodium perchlorate solution was taken in a polyethylene bottle and electrolyzed at about 4 mA cm^{-2} with platinum foil electrodes. The concentration of hydroxide ion was determined by titrating the stock solution with a standard perchloric acid using a bromcresol green-methyl red mixed indicator.

Perchloric acid solution was used without further purification of $HClO_4$ (E. Merck Co., reagent grade). The concentration of hydrogen ion in the stock solution was determined by means

of titration with a standard $KHCO_3$ solution using the same mixed indicator as described above. The total concentration of ClO_4^- in the $HClO_4$ solution was adjusted to 1.0 M by the addition of some $NaClO_4$ crystals.

Potassium hydrogen carbonate was prepared by recrystallizing $KHCO_3$ (reagent grade) twice from water and kept in a vessel filled with CO_2 gas.

Silver perchlorate solution used for preparation of Ag–AgCl electrodes was prepared from $HClO_4$ and Ag_2CO_3, the latter being precipitated from $AgNO_3$ solution with Na_2CO_3 and then thoroughly decanted.

Cadmium- and lead-amalgams were prepared by electrolysis of cadmium(II) perchlorate and lead(II) nitrate solution respectively, with a Metrohm E211A type coulometer. The metal content of the amalgams was about 3% (weight). Before each experiment, the tap in the amalgam delivery line was opened to supply the amalgam and an appropriate amount of the amalgam was then transferred to a separate glass tube of the J-shape. This J-type amalgam electrode was originally described by Holloway and Reilley[4] and used with slight modification. Oxidation of the amalgam was avoided by preparing and storing it in an atmosphere of nitrogen.

The measurements were performed in a paraffin-oil thermostat at 25.00±0.02 °C, which was kept in a room thermostated at 25.0±1.0 °C.

Apparatus. *Glass electrodes* (Beckman Nos. 40495 and 40498) were used.

A silver–silver chloride electrode was made according to Brown.[9] The half-cell of the "Kawai" type[10] was set for emf measurements.

A digital pH/mV meter (Orion Research, Model 801) was used for pH measurements. Potentials at each point of measurements were determined with an accuracy of±0.1 mV.

A digital voltmeter (Takeda Riken, Model TR-6656) was used for measurements of potentials of the amalgam electrodes. The potentials were determined with an accuracy of ±0.01 mV.

The titration vessel was set with a glass electrode, an amalgam electrode, an Ag–AgCl reference electrode, burets, and glass tubes for nitrogen gas inlet and outlet. Nitrogen gas was freed from O_2 and CO_2 by passing through bottles containing 10% NaOH, 10% H_2SO_4–VSO_4–Zn–amalgam and 1.0 M $NaClO_4$ solutions. The titration vessel and burets were filled with nitrogen gas before the test and titrating solutions were introduced. A stream of nitrogen gas was passed through the test solution during the course of the titration.

Methods of emf Measurements. The concentrations of hydrogen and metal (II) ions were measured with the following cell:

Indicator Electrode	Test Solution	1.00 M $NaClO_4$ aqueous solution	0.01 M $AgClO_4$ 0.99 M $NaClO_4$ aqueous solution	AgCl–Ag

where the glass or amalgam electrode was used as the indicator electrode. The emf at equilibrium can be written by the following equation at 25 °C:

$$E_g = E_g^{\circ\prime} + 59.16 \log h + 59.16 \log y_h + E_j(h, m) \quad (1)$$

$$E_m = E_m^{\circ\prime} + 29.58 \log m + 29.58 \log y_m + E_j(h, m) \quad (2)$$

where $E_g^{\circ\prime}$ and $E_m^{\circ\prime}$ are constants.

In a constant ionic medium, y_h and y_m may reasonably be assumed to be constant. The liquid junction potential $E_j(h,m)$ which is given as a function of the concentrations of hydrogen and metal ions may be independent of m, as long as the concentration of metal ion is low. Under the present experimental conditions Eqs. 1 and 2 may be rewritten, respectively, as

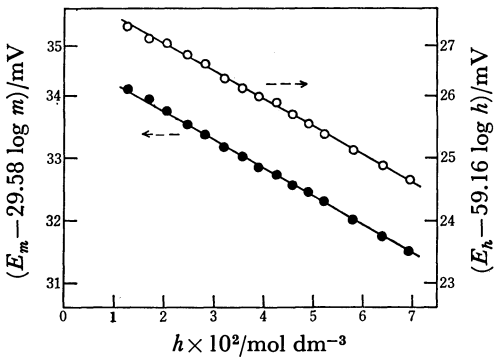

Fig. 1. Plots of $E_g - 59.16 \log h$, (○), and $E_m - 29.58 \log m$, (●), against h in 1.0 M (Na, H) ClO_4.

$$E_g = E_g^{\circ} + 59.16 \log h + E_j(h) \quad (3)$$

$$E_m = E_m^{\circ} + 29.58 \log m + E_j(h) \quad (4)$$

where $E_g^{\circ} = E_g^{\circ\prime} + 59.16 \log y_h$ and $E_m^{\circ} = E_m^{\circ\prime} + 29.58 \log y_m$. Equations 3 and 4 are transformed to

$$E_g - 59.16 \log h = E_j(h) + E_g^{\circ} \quad (5)$$

$$E_m - 29.58 \log m = E_j(h) + E_m^{\circ} \quad (6)$$

The values of $E_j(h)$, E_g° and E_m° were experimentally determined before each titration. $E_j(h)$ was estimated to be $-45\,h$ mV/mol dm^{-3}, as seen in Fig. 1, independent of the indicator electrodes used. Substituting the value of $E_j(h)$ thus obtained into Eqs. 3 and 4, the values of E_g° and E_m° were determined by means of Gran-plots. After the determination of E_g° and E_m° of the electrodes in a given solution, a suitable amount of HEDTA was added to allow to form complexes in the test solution, which has the following composition:

$$|c_M\ Cd^{2+} \text{ or } Pb^{2+},\ c_L\ HEDTA,\ H\ H^+,$$
$$(1.0 - 2c_M - H)\ NaClO_4| \quad (7)$$

During the course of the potentiometric titrations, equal volumes of T_1 and T_2 solutions,

$$T_1 = 2c_M\ Cd^{2+} \text{ or } Pb^{2+},\ 2c_L\ HEDTA,\ H_1^T\ H^+,$$
$$(1.0 - 4c_M - H_1^T)\ NaClO_4$$
$$T_2 = c_B^T\ OH^-,\ (1.0 - c_B^T)\ NaClO_4$$

were added into the test solution in order to keep constant the total concentrations of the metal ion c_M and the ligand c_L during the titration. The total concentration of perchlorate ion was also kept constant, 1.0 M. The values of h and m were obtained by using Eqs. 3 and 4, successive approximations being employed.

An emf of the amalgam electrode required about 5 min to attain a constant value after the addition of the titrants, while an emf of the glass electrode became constant within a few minutes. The potentials remained unchanged for several hours. The emf's of the amalgam electrode were determined within an accuracy of ±0.02 mV at $-\log h$ below 3.0, but at $-\log h$ above 3.5 the emf's became unstable so that the results obtained by the amalgam electrode were rather unreliable.

Results and Discussion

Evaluation of Protonation Constans of HEDTA. Overall protonation constants of the HEDTA base, β_{0q1}, were determined from the formation function $\bar{n}$. A generalized least squares method was applied to make the error squares sum $U = \sum(\bar{n} - \bar{n}_{calc})^2$ a minimum for the set of overall acid association (protonation) constants,

β_{011}, β_{021}, β_{031}, β_{041} and β_{051}. The calculation was performed with the help of an electronic computer HITAC 8700 at the Computer Center of the Tokyo Institute of Technology. $\bar{n}_{calc}$ and $\bar{n}$ denote

$$\bar{n}_{calc} = \frac{(\beta_{011}h+2\beta_{021}h^2+3\beta_{031}h^3+4\beta_{041}h^4+5\beta_{051}h^5)}{(1+\beta_{011}h+\beta_{021}h^2+\beta_{031}h^3+\beta_{041}h^4+\beta_{051}h^5)} \quad (8)$$

and

$$\bar{n} = \frac{3c_L + H - h + (K_W/h)}{c_L} \quad (9)$$

where K_W is the autoprotolysis constant of water in 1 M $NaClO_4$ solution: $10^{-13.95}$.[11] The protonation constants thus obtained were log β_{011}=9.20±0.01, log β_{021}=14.72±0.01, log β_{031}=17.06±0.01, log β_{041}=18.52±0.01 and log β_{051}=18.65±0.05. Bhat *et al.*[12] reported the values of log β_{011}=8.65, log β_{021}=13.76 and log β_{031}=16.06 in a 1.0 M $NaClO_4$ medium at 25 °C but not those of log β_{041} and log β_{051}.

Determination of the Composition and the Stability Constants of Complexes. Titration curves of the Cd(II)- and Pb(II)–HEDTA solutions are shown in Figs. 2 and 3.

From the material balance for the metal ion, we obtained Eq. 10:

$$c_M = [M] + \sum_p\sum_q\sum_r p\,[M_pH_qL_r]$$
$$= m + \sum_p\sum_q\sum_r p\beta_{pqr}m^p h^q l^r \quad (10)$$

The summation may include hydrolyzed species of the metal ion and the metal complexes ($q<0$).

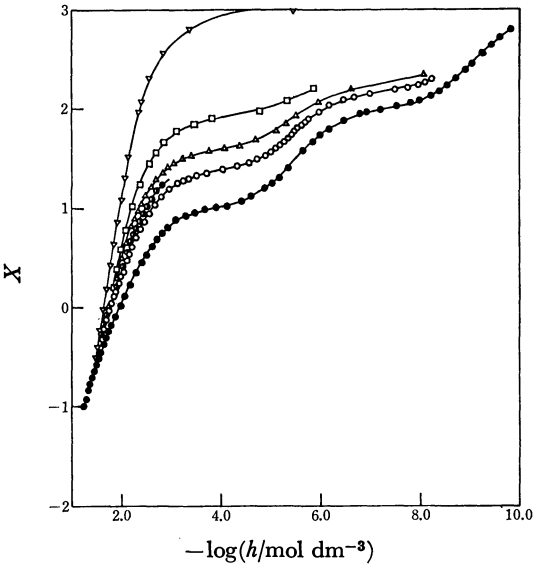

Fig. 2. Degrees of neutralization, X, of *N*-(2-hydroxyethyl)ethylenediamine-*N*,*N*′,*N*′-triacetic acid (HEDTA) solutions for the Cd(II)–HEDTA system.
(●); c_M=0.0 M, c_L=0.01351 M:
(○); c_M=0.002701 M, c_L=0.01252 M:
(◑); c_M=0.003440 M*, c_L=0.012771 M*:
(△); c_M=0.002699 M, c_L=0.007508 M:
(□); c_M=0.002564 M, c_L=0.005000 M:
(▽); c_M=0.007508 M, c_L=0.007579 M.
Solid lines are the values of X calculated by the use of the stability constants in Table 1. *c_M and c_L are the initial concentrations of the metal and the ligand, and c_M and c_L are slightly changed during the course of titration by the addition of the titrants.

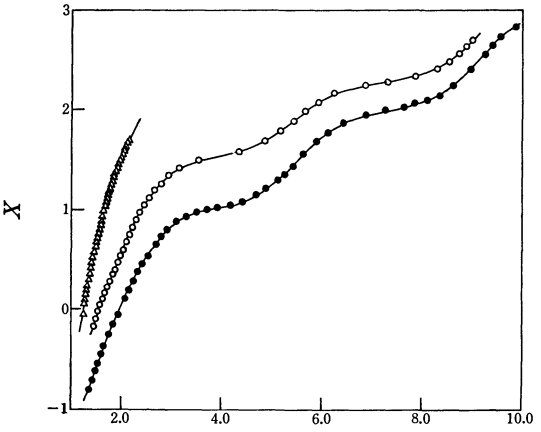

Fig. 3. Degrees of neutralization, X, of HEDTA solutions for the Pb(II)–HEDTA system.
(●); c_M=0.0 M, c_L=0.007050 M:
(○); c_M=0.002650 M, c_L=0.01008 M:
(△); c_M=0.01007 M, c_L=0.01523 M.
Solid lines are the values of X calculated by the use of the stability constants in Table 1.

Thus, we derive Eqs. 11 and 12:

$$\eta = \log(c_M/m) = \log\{1 + \sum_p\sum_q\sum_r p\beta_{pqr}m^{p-1}h^q l^r\} \quad (11)$$

and

$$\xi = \log\{(c_M - m)/m\} = \log\{\sum_p\sum_q\sum_r p[M_pH_qL_r]/[M]\}$$
$$= \log\{\sum_p\sum_q\sum_r p\beta_{pqr}m^{p-1}h^q l^r\} \quad (12)$$

The quantity η is a measure of the degree of complexation of the metal ion and $\eta>0$ at $-\log h>1.5$ (see Fig. 4). This fact shows that the complexes between the metal ions and HEDTA are formed even in an acid solution of minimum pH examined in this experiment.

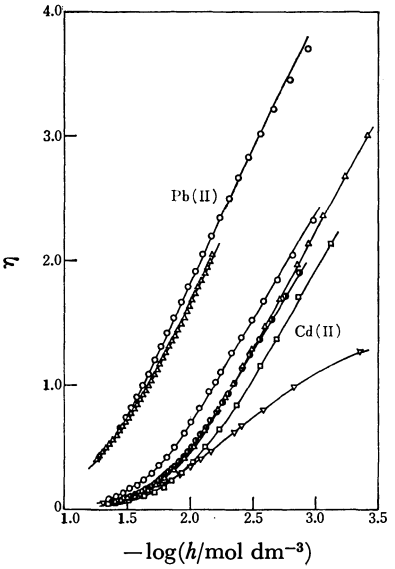

Fig. 4. Relationships between η and $-\log h$ for the Cd(II) and Pb(II) systems.
Symbols are the same as those in Figs. 2 and 3.
Solid lines are curves calculated by the use of the stability constants in Table 1.

As the first approach for analyzing data, we assume that only one kind of the complex $M_pH_qL_r$ is formed in the solution. Thus, Eq. 12 may be simplified as follows:

$$\xi = \log p\beta_{pqr} + (p-1)\log m + q\log h + r\log l \quad (13)$$

Since $c_M < c_L$ in most cases and the degree of complexation is rather small in a relatively low and narrow pH range, we can assume that l is proportional to c_L at a constant pH and inversely proportional to h^n at a given c_L; that is,

$$c_L \simeq l + \sum_{n=1}^{N}\beta_{0n1}lh^n \quad (14)$$

$$l \simeq c_L/(1+\sum_{n=1}^{N}\beta_{0n1}h^n) \simeq c_L/\beta_{0n1}h^n \quad (15)$$

From the knowledge of the association constants of the HEDTA molecules with protons, we know that most of the ligand molecules are present in the form of H_3L and H_2L^- and partially H_4L^+ in the pH range of 1.5 to 3. Therefore, the value of n may become 2—3 and may slightly change with pH. However, the assumption of an averaged constant value of n over this pH range may not introduce a serious error in the following argument at the stage of the first approximation.

Substitution of Eq. 15 into Eq. 13 leads to Eq. 16:

$$\xi \simeq \log p\beta_{pqr} + (p-1)\log m + (q-n)\log h + r\log c_L - \log\beta_{0n1} \quad (16)$$

The plots ($\xi - \log c_L$) *vs.* $-\log h$ are shown for the Cd(II)-system in Fig. 5. Points obtained at different c_L fell on an approximately single curve and the points were practically independent of c_M except for the case where $c_M = c_L$ and $-\log h > 2$. Thus, we conclude that the main species formed in this pH range has the composition of $p=1$ and $r=1$, and thus MH_qL. The slope of the line corresponds to $-(q-n)$ according to the above consideration, and we have found from Fig. 5 that the slope is about 2. Since $n=2\sim3$, q would become 0—1. Therefore, we can estimate the composition of the main species to be MHL and/or ML in the pH range discussed.

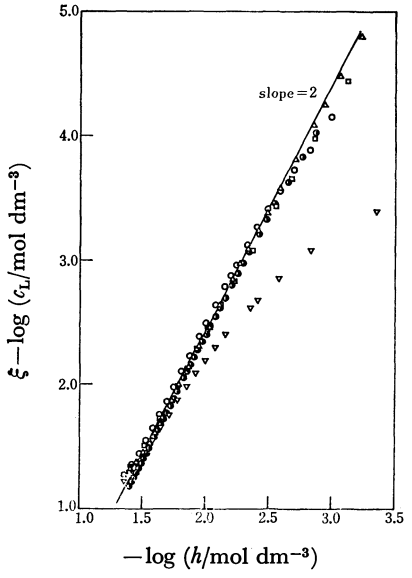

Fig. 5. Relationships between $\xi - \log c_L$ and $-\log h$ for the Cd(II)–HEDTA system.

The estimation for the compositions of the complexes formed in the solution may be made more quantitatively than in the above treatment, if the formation of mononuclear and monoligand complexes with various numbers of protons is assumed.

From the assumption, we obtained the following relationships:

$$c_M = m + \sum_{q=0}^{Q}[MH_qL] \quad (17)$$

$$c_L = l + \sum_{n=1}^{N}[H_nL] + \sum_{q=0}^{Q}[MH_qL] \quad (18)$$

Insertion of Eq. 17 into Eq. 18 and rearrangement lead to Eq. 19:

$$l = (c_L - c_M + m)/(1+\sum_{n=1}^{N}\beta_{0n1}h^n) \quad (19)$$

A function F_0 is defined as follows:

$$F_0 = (c_M - m)/ml = \sum_{q=0}^{Q}[MH_qL]/ml = \sum_{q=0}^{Q}\beta_{1q1}h^q \quad (20)$$

The plot of $\log F_0$ against $-\log h$ is shown in Fig. 6 for both systems of Cd(II)- and Pb(II)-HEDTA. In each system a single curve was obtained and the curve was independent of c_M, c_L and c_M/c_L. Therefore, the assumption of the formation of a series of MH_qL complexes is confirmed to be reasonable.

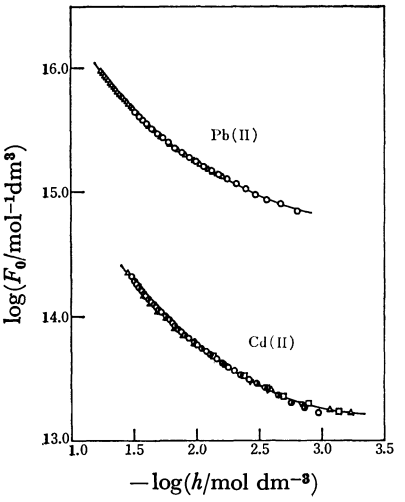

Fig. 6. Plot of $\log F_0$ against $-\log h$ for both systems. Each solid line is the curve calculated with the values of the stability constants in Table 1.

The plot of F_0 against h was extrapolated toward $h=0$ to give an intercept corresponding to β_{101}.

A new function

$$F_1 = (F_0 - \beta_{101})/h = \sum_{q=1}^{Q}\beta_{1q1}h^{q-1} \quad (21)$$

was plotted against h and then extrapolated toward $h=0$ in order to obtain β_{111}. The procedure was repeated until a horizontal line was obtained. The sets of the plots carried out to obtain β_{1q1} are shown in Figs. 7 and 8 for the Cd(II) and Pb(II) systems, respectively. The values of β_{1q1} thus found are given for the Cd(II)–HEDTA complexes as follows:

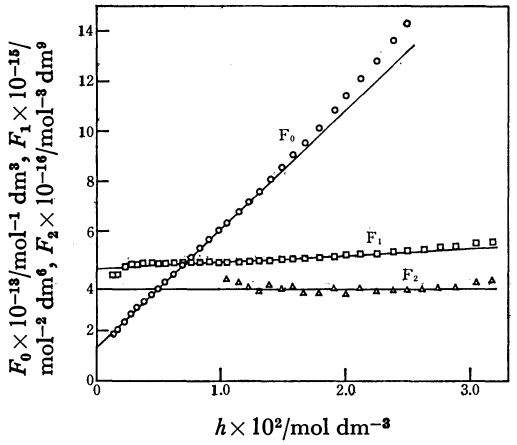

Fig. 7. A typical set of the plot of F_q *vs.* h in the system of Cd(II)–HEDTA complexes (c_M=0.002873 M, c_L= 0.01021 M). (○): F_0; (□): F_1; (△): F_2.

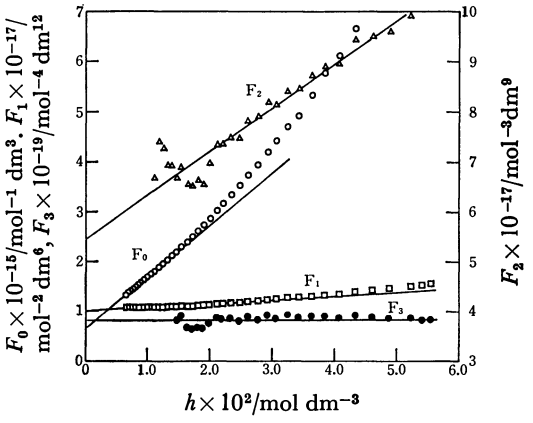

Fig. 8. A typical set of the plot of F_q *vs.* h in the system of Pb(II)–HEDTA complexes (c_M=0.01007 M, c_L= 0.01523 M). (○): F_0; (□): F_1; (△): F_2; (●): F_3.

$$\beta_{101} = 1.5\times10^{13}\ \text{mol}^{-1}\ \text{dm}^3$$
$$\beta_{111} = 4.4\times10^{15}\ \text{mol}^{-2}\ \text{dm}^6$$
$$\beta_{121} = 3.7\times10^{16}\ \text{mol}^{-3}\ \text{dm}^9$$

and for the Pb(II)–HEDTA complexes

$$\beta_{101} = 6.7\times10^{14}\ \text{mol}^{-1}\ \text{dm}^3$$
$$\beta_{111} = 1.0\times10^{17}\ \text{mol}^{-2}\ \text{dm}^6$$
$$\beta_{121} = 5.5\times10^{17}\ \text{mol}^{-3}\ \text{dm}^9$$
$$\beta_{131} = 8.0\times10^{18}\ \text{mol}^{-4}\ \text{dm}^{12}$$

The formation constants of the complexes were refined by means of a generalized least squares method. The method was applied to make the error squares sum $U=\sum\{\log F_0-\log F_{0,\text{calcd}}\}^2$ minimum for the set of the formation constants over the pH range 1.5 to 3, where $F_{0,\text{calcd}}$ denotes the value of F_0 calculated for a particular set of the formation constants. The formation constants thus determined are given in Table 1.

Since the metal amalgam electrode did not function well at a high pH range, data of X obtained in the high pH range were not analyzed by the extrapolation method described above. However, the constants reproduced the experimental results fairly well as seen from Figs. 2 and 3, and no polynuclear, polyligand and hydrolyzed species are formed.

Table 1. Stability constants of Cd(II)- and Pb(II)-HEDTA complexes (log β_{pqr})
log β_{011}=9.20±0.01, log β_{021}=14.72±0.01, log β_{031}= 17.06±0.01, log β_{041}=18.52±0.01, log β_{051}=18.65±0.05

Complexes	ML^-	MHL^0	MH_2L^+	MH_3L^{2+}
Cd(II)	13.21±0.04	15.61±0.02	16.68±0.04	—
Pb(II)	14.83±0.02	16.97±0.02	17.89±0.02	18.67±0.02

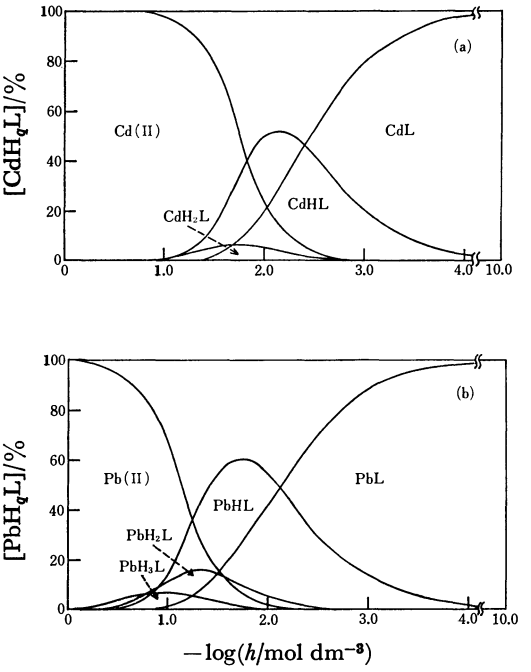

Fig. 9. The distribution of metal–HEDTA complexes *vs.* −log h (c_M=0.001M, c_L=0.01M).
(a): for the Cd(II)–HEDTA system. (b): for the Pb(II)–HEDTA system.

The distributions of the Cd(II)- and Pb(II)–HEDTA complexes are graphically represented in Fig. 9.

The Pb(II)–HEDTA complexes are stronger by 1—1.5 in log β unit than the corresponding Cd(II)–HEDTA complexes, like in other cases of the complexes of these metals with ligands containing oxygen or oxygen and nitrogen as the ligating atoms. Lead(II) ion forms the PbH_3L complex at a high concentration of hydrogen ion, whereas cadmium(II) ion does not.

The stepwise association constants of the complexes with protons are log K_H^{ML}=log {[MHL]/[ML][H]}= 2.40 and log $K_H^{MH_2L}$=log {[MH_2L]/[MHL][H]}=1.07 for the Cd(II)–HEDTA complexes and log K_H^{ML}= 2.13, log $K_H^{MH_2L}$=0.92 and log $K_H^{MH_2L}$=0.78 for the Pb(II)–HEDTA complexes. The association constants may be compared with the corresponding values of the ligand; log $K_H^{H_2L}$=log (β_{031}/β_{021})=log {[H_3L]/ [H_2L][H]}=2.34, log $K_H^{H_2L}$=log (β_{041}/β_{031})=1.46 and log $K_H^{H_2L}$=log (β_{051}/β_{041})=0.13.

The authors wish to thank Dr. Takayoshi Kawai for his kind help in potentiometric measurements.

References

1) L. G. Sillén and A. E. Martell, "Stability Constants," Chemical Society, London (1964), Supplement No. 1, (1971).
2) S. Chaberek and A. E. Martell, *J. Am. Chem. Soc.*, **77**, 1477 (1955).
3) F. H. Spedding, J. E. Powell, and E. J. Wheelwright, *J. Am. Chem. Soc.*, **78**, 34 (1956).
4) J. H. Holloway and E. N. Reilley, *Anal. Chem.*, **32**, 249 (1960).
5) M. Kodama, K. Namekawa, and T. Horiuchi, *Bull. Chem. Soc. Jpn.*, **47**, 2011 (1974).
6) N. Oyama and H. Matsuda, *J. Electroanal. Chem.*, in press.
7) N. Oyama, T. Shirato, and H. Matsuda, *J. Electroanal. Chem.*, in press.
8) G. Biedermann and L. Civatta, *Acta Chem. Scand.*, **15**, 1347 (1961).
9) A. S. Brown, *J. Am. Chem. Soc.*, **56**, 646 (1934).
10) H. Tsukuda, T. Kawai, M. Maeda, and H. Ohtaki, *Bull. Chem. Soc. Jpn.*, **48**, 691 (1975).
11) G. Anderegg, *Helv. Chim. Acta*, **50**, 2333 (1967).
12) T. R. Bhat, R. K. Iyer, and J. Schankar, *Z. Anorg. Chem.*, **343**, 329 (1966).

The Crystal Structure of Bis[1-(2-thiazolylazo)-2-naphtholato]-cobalt(III) Perchlorate

Masayasu KURAHASHI

National Research Institute for Metals, 3-12, 2-Chome, Nakameguro, Meguro-ku, Tokyo 153

(Received May 14, 1976)

The crystal structure of bis[1-(2-thiazolylazo)-2-naphtholato]cobalt(III) perchlorate, $[Co^{III}(C_{13}H_8N_3OS)_2]ClO_4$ was determined from X-ray reflection data collected by counter methods. The crystals are monoclinic, space group $P2_1/c$, with $a=10.348(2)$, $b=21.066(5)$, $c=13.072(5)$ Å, $\beta=112.35(3)°$, and $Z=4$. The structure was determined by the heavy-atom method and refined by the least-squares technique to give an R value of 0.051 for 2696 observed reflections. The cobalt atom is six-coordinate and exhibits octahedral coordination. The 1-(2-thiazolylazo)-2-naphtholato group is coordinated as a terdentate ligand with the cobalt atom through the phenolic oxygen atom, the azo nitrogen atom adjacent to the naphthol ring and the thiazole nitrogen atom giving two five-membered chelate rings. Short intraligand contacts of 2.24(6) and 2.28(6) Å are observed between the azo nitrogen and naphthol hydrogen atoms.

1-(2-Thiazolylazo)-2-naphthol (Htan) was first used for the detection of metals by Boni and Hemmeler in 1958.[1] Since then, a number of applications of this dye as a spectrophotometric reagent or a complexometric indicator have been reported.[2-6] The proposed structures for some tan complexes with divalent metals were confirmed by X-ray analysis.[7-10] For the cobalt(III)–tan complex, however, there was an ambiguity concerning the structure.[3,4] X-Ray analysis was therefore carried out, a preliminary letter of the work being reported.[11]

Experimental

Single crystals of $[Co^{III}(tan)_2]ClO_4$ were grown from an ethanol solution by slow evaporation. The crystal data are given in Table 1. The unit-cell dimensions were determined by the least-squares technique using the 2θ angles of 11 reflections measured by a diffractometer. The density was determined by flotation in an aqueous solution of sodium iodide.

Table 1. Crystal data
$[Co^{III}(C_{13}H_8N_3OS)_2]ClO_4$, F.W. 667.0

Monoclinic	Space group $P2_1/c$
$a=10.348(2)$ Å	$D_m=1.67$ g cm^{-3}
$b=21.066(5)$ Å	$D_x=1.68$ g cm^{-3}
$c=13.072(5)$ Å	$Z=4$
$\beta=112.35(3)°$	$\mu=9.9$ cm^{-1} (for Mo $K\alpha$)
$V=2635.4$ Å^3	

The intensity data were collected on a Rigaku automated four-circle diffractometer with Mo $K\alpha$ radiation monochromated with a graphite plate. The dimension of the crystal was $0.2\times0.2\times0.15$ mm. The ω-2θ scan technique was employed with a scan speed of 4°/min in ω. Scan range was calculated by the formula $1.5°+0.8°\times\tan\theta$. Measurement was automatically repeated until $\sigma(|F|)/|F|$ became less than 0.03, where $\sigma(|F|)$ is the standard deviation of $|F|$ due to the counting statistics. The maximum number of repetition was limited to four. The intensities of independent reflections

Table 2. Positional and thermal parameters
(a) Fractional atomic coordinates for the non-hydrogen atoms.

	x	y	z		x	y	z
Co	0.0510(1)	0.0674(1)	0.2312(1)	N(1′)	−0.0205(3)	0.0919(2)	0.0817(5)
S	−0.1067(1)	0.1600(1)	0.4501(2)	N(2′)	−0.1250(3)	0.0611(2)	0.0124(4)
O	0.1827(2)	0.0112(2)	0.2133(4)	N(3′)	−0.0931(3)	0.0048(2)	0.1758(5)
N(1)	0.1296(3)	0.0442(2)	0.3807(5)	C(1′)	0.0521(4)	0.1383(2)	0.0577(6)
N(2)	0.0858(3)	0.0709(2)	0.4512(4)	C(2′)	0.1645(3)	0.1586(3)	0.1543(6)
N(3)	−0.0615(3)	0.1191(2)	0.2842(5)	C(3′)	0.2583(4)	0.2049(3)	0.1453(6)
C(1)	0.2327(4)	0.0014(3)	0.4048(6)	C(4′)	0.2457(4)	0.2264(3)	0.0447(7)
C(2)	0.2562(4)	−0.0151(3)	0.3065(6)	C(5′)	0.1349(4)	0.2701(3)	−0.0546(6)
C(3)	0.3608(4)	−0.0613(3)	0.3131(6)	C(6′)	0.1274(4)	0.2310(3)	−0.1552(7)
C(4)	0.4336(4)	−0.0889(3)	0.4107(7)	C(7′)	0.0183(5)	0.2127(3)	−0.2512(7)
C(5)	0.4134(4)	−0.0735(3)	0.5104(6)	C(8′)	−0.0816(4)	0.1717(3)	−0.2472(7)
C(6)	0.4944(4)	−0.1036(3)	0.6116(7)	C(9′)	−0.0769(4)	0.1455(3)	−0.1491(6)
C(7)	0.4749(4)	−0.0880(3)	0.7067(6)	C(10′)	0.0338(4)	0.1631(2)	−0.0495(6)
C(8)	0.3798(4)	−0.0429(3)	0.7060(7)	C(11′)	−0.1621(4)	0.0150(3)	0.0683(6)
C(9)	0.2996(4)	−0.0125(3)	0.6098(6)	C(12′)	−0.2590(4)	−0.0713(3)	0.1359(7)
C(10)	0.3135(4)	−0.0274(3)	0.5103(6)	C(13′)	−0.1468(4)	−0.0450(3)	0.2130(7)
C(11)	−0.0182(4)	0.1127(3)	0.3933(6)	Cl	0.5762(1)	0.3043(1)	0.4394(2)
C(12)	−0.2055(4)	0.1887(3)	0.3212(7)	O(1)	0.5593(5)	0.3566(4)	0.4935(10)
C(13)	−0.1666(4)	0.1622(3)	0.2444(6)	O(2)	0.7128(4)	0.2841(3)	0.4847(6)
S′	−0.3002(1)	−0.0358(1)	0.0105(2)	O(3)	0.4857(6)	0.2627(4)	0.4409(13)
O′	0.1789(2)	0.1344(2)	0.2489(4)	O(4)	0.5423(7)	0.3133(6)	0.3273(8)

b) Anisotropic thermal parameters for the non-hydrogen atoms($\times 10^4$). The anisotropic thermal parameters are in the form $\exp\{-(h^2B_{11}+k^2B_{22}+l^2B_{33}+hkB_{12}+hlB_{13}+klB_{23})\}$.

	B_{11}	B_{22}	B_{33}	B_{12}	B_{13}	B_{23}
Co	76(1)	16(1)	40(1)	−5(1)	48(1)	−8(1)
S	116(2)	25(1)	66(1)	9(2)	94(3)	−11(1)
O	80(5)	22(1)	45(3)	6(4)	46(7)	−5(3)
N(1)	73(6)	18(1)	53(4)	−5(5)	52(8)	−4(4)
N(2)	96(6)	22(1)	40(4)	10(6)	53(8)	−3(4)
N(3)	87(6)	18(1)	39(4)	−1(5)	38(8)	−3(4)
C(1)	85(7)	19(2)	51(5)	0(6)	61(10)	−8(5)
C(2)	73(8)	22(2)	66(5)	−11(6)	48(10)	−6(5)
C(3)	113(8)	27(2)	63(5)	−14(7)	73(11)	−18(6)
C(4)	79(8)	28(2)	86(6)	0(6)	51(12)	−12(5)
C(6)	73(7)	24(2)	70(5)	−4(6)	52(10)	−7(6)
C(6)	99(9)	26(2)	91(6)	27(7)	24(13)	16(6)
C(7)	131(9)	36(3)	59(5)	−8(8)	43(12)	19(6)
C(8)	123(9)	34(2)	62(6)	−2(7)	71(12)	0(6)
C(9)	106(9)	26(2)	49(5)	19(7)	49(11)	14(5)
C(10)	80(7)	20(2)	53(5)	−2(6)	39(10)	1(5)
C(11)	107(8)	20(2)	55(5)	−7(6)	80(10)	−7(5)
C(12)	118(9)	27(2)	89(6)	28(7)	100(13)	7(6)
C(13)	102(8)	21(2)	78(6)	0(7)	76(12)	−4(5)
S′	113(2)	23(1)	75(1)	−37(2)	48(3)	−16(1)
O′	88(5)	18(1)	48(3)	−14(4)	54(7)	−11(3)
N(1′)	91(6)	20(1)	45(4)	−13(5)	64(8)	−15(4)
N(2′)	92(6)	18(1)	52(4)	−19(5)	42(8)	−10(4)
N(3′)	100(7)	18(1)	54(4)	−16(5)	60(8)	−7(4)
C(1′)	86(7)	19(2)	47(5)	−22(6)	60(10)	−9(4)
C(2′)	88(8)	19(2)	57(5)	−9(6)	68(10)	−13(5)
C(3′)	102(8)	24(2)	61(5)	−5(6)	49(11)	−10(5)
C(4′)	104(9)	20(2)	81(6)	−17(6)	70(12)	−5(5)
C(5′)	105(8)	18(2)	53(5)	−2(6)	50(11)	6(5)
C(6′)	142(10)	18(2)	96(6)	−14(7)	102(14)	14(5)
C(7′)	168(12)	25(2)	44(5)	6(8)	23(13)	10(5)
C(8′)	171(11)	21(2)	63(6)	−25(7)	81(13)	−3(6)
C(9′)	128(9)	25(2)	59(5)	−18(7)	72(11)	−4(5)
C(10′)	112(8)	15(2)	50(5)	6(6)	75(11)	2(5)
C(11′)	114(9)	21(2)	39(5)	−22(6)	45(11)	−11(5)
C(12′)	111(9)	25(2)	111(6)	−44(7)	121(12)	−32(6)
C(13′)	117(9)	20(2)	81(6)	−11(6)	102(12)	−10(5)
Cl	111(3)	42(1)	132(2)	−8(2)	53(4)	−32(2)
O(1)	239(12)	84(3)	319(12)	146(11)	−106(20)	−172(11)
O(2)	157(9)	84(3)	141(7)	65(9)	15(13)	−88(8)
O(3)	447(21)	93(4)	619(24)	−223(16)	821(40)	−120(17)
O(4)	461(23)	176(7)	145(8)	22(19)	−14(22)	91(13)

(c) Positional and thermal parameters for the hydrogen atoms.

	x	y	z	B
H(3)	0.372(3)	−0.073(2)	0.247(5)	3.8(13)
H(4)	0.508(3)	−0.119(2)	0.413(5)	4.2(14)
H(6)	0.574(4)	−0.133(3)	0.605(6)	4.7(15)
H(7)	0.507(5)	−0.113(3)	0.777(7)	11.4(21)
H(8)	0.372(3)	−0.037(2)	0.785(5)	2.2(11)
H(9)	0.227(3)	0.018(2)	0.602(5)	4.0(14)
H(12)	−0.288(4)	0.222(3)	0.314(6)	7.4(16)
H(13)	−0.209(3)	0.174(2)	0.158(5)	5.4(14)
H(3′)	0.339(3)	0.224(2)	0.211(5)	4.6(14)
H(4′)	0.300(4)	0.260(2)	0.039(6)	2.6(14)
H(6′)	0.198(3)	0.258(2)	−0.154(5)	2.7(13)
H(7′)	0.017(3)	0.236(2)	−0.319(6)	6.5(15)
H(8′)	−0.162(3)	0.149(3)	−0.323(6)	6.0(15)
H(9′)	−0.145(3)	0.120(2)	−0.142(5)	2.8(13)
H(12′)	−0.324(4)	−0.109(3)	0.148(6)	6.7(16)
H(13′)	−0.094(3)	−0.058(2)	0.293(5)	3.5(12)

with $2\theta \leq 55°$ were measured and weak reflections with $|F| < 3\sigma(|F|)$ were excluded. A total of 2696 independent reflections were obtained and used for the structure determination. The intensities were corrected for Lorentz and polarization effects, but not for absorption because of the small size of the crystal.

Solution of the Structure and Refinement

The structure was determined by the heavy-atom method. The location of the cobalt and two sulfur atoms was determined by the Patterson method. A Fourier map phased on these atoms yielded the positions of all the non-hydrogen atoms. Structural parameters were refined by the block-diagonal least-squares calculations, until $R(=\sum||F_o|-|F_c||/\sum|F_o|)$ was reduced to 0.083. The function minimized was $w(|F_o|-|F_c|)^2$, where w equals unity. 15 of 16 hydrogen atoms were clearly detected on a difference Fourier map, the remaining hydrogen position (H(7)) being evaluated by calculation. After inclusion of the hydrogen atoms, a final set of least-squares calculations was carried out, and the R value reached 0.051 for the 2696 observed reflections. Atomic scattering factors for the non-hydrogen atoms were taken from the International Tables for X-ray Crystallography,[12] and those for the hydrogen atom from Stewart, Davidson and Simpson.[13] Table 2 gives the final atomic parameters together with their estimated standard deviations. Observed and calculated structure factors are compared in Table 3.*

Description of the Structure and Discussion

The thermal ellipsoids and the numbering of atoms are given in Fig. 1. The complex cation, $[Co^{III}(tan)_2]^+$, has approximately C_2 symmetry. The cobalt atom is surrounded octahedrally by two ligand anions (referred to as A, unprimed atoms and B, primed atoms) in the mer configuration. The configuration coincides with that of $[Fe^{II}(tan)_2]$[7] and $[Ni^{II}(tan)_2]$[8] but differs from that of $[Cu^{II}(tan)(H_2O)_2]^+$,[9] or $[Pd^{II}Cl(tan)]$.[10]

The 1-(2-thiazolyazo)-2-naphtholato group (tan) acts as a terdentate ligand, being coordinated to the metal through the phenolic oxygen atom, the azo nitrogen atom adjacent to the naphthol ring and the thiazole nitrogen atom to form two five-membered chelate rings. Such mode of coordination is commonly observed in all the tan-complexes studied. No participation of the thiazole sulfur atom in metal binding has been found.

The thiazole sulfur atom is not involved in chelate ring formation because of (1) the positive charge on the thiazole sulfur atom, predicted by MO calculation for π-electron density of Htan,[14] the metal ion binding with the positively charged sulfur atom being unfavorable; and (2) the angular distortion of the chelate rings. Two possible molecular models for chelation, where the hybridization state of the ligating atoms was assumed to be sp^2, are shown in Fig. 2. The angular distortion of the chelate rings in model (a) is smaller than that in model (b). The difference arises from the fact that C(11)–S is longer than C(11)–N(3) by 0.4 Å and that C(11)–S–C(12) angle is less than C(11)–N(3)–C(13) by

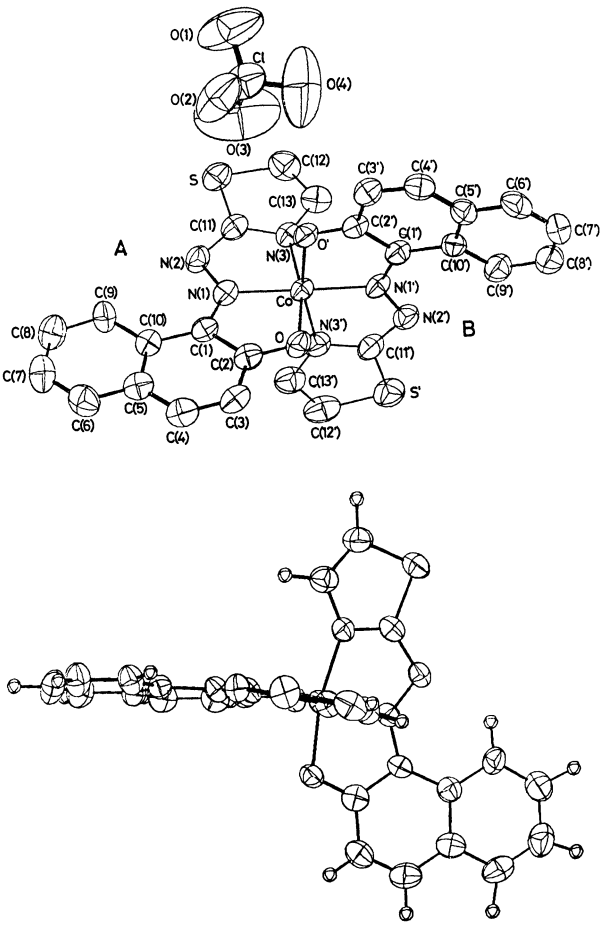

Fig. 1. (a) Thermals ellipsoids and numbering of atoms. The thermal ellipsoids are drawn at 50% probability. (b) The structure of the complex cation viewed perpendicular to the plane through Co and unprimed tan group.

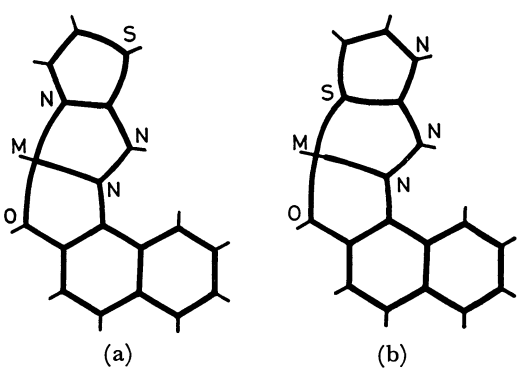

Fig. 2. Framework molecular models for the two linkage isomers.
(a) Coordination through O, N(1) and N(3). (Observed). (b) Coordination through O, N(1) and S. (Unobserved).

* Table 3 is kept as Document No. 7633 at the Chemical Society of Japan, 1-5, Kanada-Surugadai, Chiyoda-ku, Tokyo.

11°. If the hybridization state of the sulfur atom is not sp^2 and d-electron orbitals are involved in hybridization as indicated from the observed C(11)–S–C(12) angle of 90°, a larger angular distortion will occur, or chelation will not occur.[15]

The bond lengths and angles for the complex cation and the perchlorate anions are given in Table 4 with their e.s.d.'s. The geometries of the two moieties in the complex agree within the limit of three times their corresponding e.s.d.'s. The average Co–O distance of 1.888(4) Å is acceptable. The Co–N distances range from 1.874(5) to 1.918(6) Å, being significantly shorter than the Co–NH_3 distance observed in hexaamminecobalt(III) complex (1.972(1) Å).[16] The average O–Co–N(1) and N(1)–Co–N(3) angles are 85.0(2) and 81.4(2)° respectively, being compressed from the normal valence angles. On the other hand, average N(2)–N(1)–C(1), N(1)–C(1)–C(10), S–C(11)–N(2), and Co–N(3)–C(13) angles are enlarged to 125.7(5), 128.0(5), 124.6(5) and 139.0(4)°, respectively. Such an angular distortion is usually observed in the metal-tan complexes. The average N(1)–N(2), C(1)–N(1), and C(2)–O distances of 1.301(7), 1.349(8), and 1.291(8) Å, respectively, are between the corresponding single and double bonds. This will indicate the presence of some delocalization of π-electrons.

It is of interest to see the structural changes on chelate ring formation. Figure 3 shows a comparison of the structures of Htan and $[Co^{III}(tan)_2]^+$. Since there exist two crystallographically independent tan groups in an asymmetric unit, average values for bond lengths and angles are given. There is a notable difference in the conformation about the azo group; the two ring systems attached to the central azo group are rotated

TABLE 4. BOND LENGTHS AND ANGLES

(a) Bond lengths (l/Å).

		Unprimed atoms	Primed atoms
Co	–O	1.886(4)	1.889(4)
Co	–N(1)	1.874(5)	1.875(5)
Co	–N(3)	1.909(5)	1.918(6)
S	–C(11)	1.703(7)	1.706(7)
S	–C(12)	1.709(8)	1.715(8)
O	–C(2)	1.291(8)	1.291(8)
N(1)	–N(2)	1.307(7)	1.294(7)
N(1)	–C(1)	1.347(8)	1.350(8)
N(2)	–C(11)	1.377(8)	1.369(9)
N(3)	–C(11)	1.323(8)	1.324(9)
N(3)	–C(13)	1.367(9)	1.368(9)
C(1)	–C(2)	1.432(9)	1.416(9)
C(1)	–C(10)	1.441(9)	1.438(9)
C(2)	–C(3)	1.436(10)	1.417(9)
C(3)	–C(4)	1.337(10)	1.341(10)
C(4)	–C(5)	1.412(10)	1.418(10)
C(5)	–C(6)	1.417(10)	1.387(10)
C(5)	–C(10)	1.414(9)	1.428(10)
C(6)	–C(7)	1.376(11)	1.361(12)
C(7)	–C(8)	1.369(11)	1.383(12)
C(8)	–C(9)	1.370(10)	1.375(11)
C(9)	–C(10)	1.394(9)	1.400(10)
C(12)	–C(13)	1.344(11)	1.338(11)
Cl	–O(1)	1.369(12)	
Cl	–O(2)	1.380(9)	
Cl	–O(3)	1.296(16)	
Cl	–O(4)	1.390(15)	
C(3)	–H(3)	0.98 (5)	1.04 (6)
C(4)	–H(4)	1.05 (6)	1.02 (6)
C(6)	–H(6)	1.05 (6)	1.02 (5)
C(7)	–H(7)	1.03 (7)	1.05 (6)
C(8)	–H(8)	1.06 (5)	1.08 (6)
C(9)	–H(9)	1.01 (6)	0.97 (5)
C(12)	–H(12)	1.11 (6)	1.10 (6)
C(13)	–H(13)	1.05 (6)	1.05 (5)

(b) Bond angles (φ/°).

			Unprimed atoms	Primed atoms
O	–Co	–N(1)	85.4(2)	84.6(2)
N(1)	–Co	–N(3)	81.3(2)	81.5(2)
C(11)	–S	–C(12)	89.6(3)	90.0(3)
Co	–O	–C(2)	110.1(4)	110.4(4)
Co	–N(1)	–N(2)	120.3(4)	119.7(4)
Co	–N(1)	–C(1)	114.4(4)	114.1(4)
N(2)	–N(1)	–C(1)	125.2(5)	126.1(5)
N(1)	–N(2)	–C(11)	106.7(5)	107.8(5)
Co	–N(3)	–C(11)	109.3(4)	108.5(4)
Co	–N(3)	–C(13)	138.1(4)	139.8(4)
C(11)	–N(3)	–C(13)	112.5(5)	111.7(5)
N(1)	–C(1)	–C(2)	109.2(5)	110.2(5)
N(1)	–C(1)	–C(10)	128.7(5)	127.2(5)
C(2)	–C(1)	–C(10)	122.1(5)	122.4(5)
O	–C(2)	–C(1)	121.1(5)	120.7(5)
C(1)	–C(2)	–C(3)	118.7(6)	119.0(5)
C(2)	–C(3)	–C(4)	118.8(6)	119.0(6)
C(3)	–C(4)	–C(5)	124.1(6)	123.8(6)
C(4)	–C(5)	–C(6)	121.4(6)	121.4(6)
C(4)	–C(5)	–C(10)	120.1(6)	119.7(6)
C(6)	–C(5)	–C(10)	118.5(6)	119.0(6)
C(5)	–C(6)	–C(7)	120.8(6)	121.1(7)
C(6)	–C(7)	–C(8)	119.8(6)	120.7(7)
C(7)	–C(8)	–C(9)	121.2(6)	120.0(7)
C(8)	–C(9)	–C(10)	120.9(6)	120.5(6)
C(1)	–C(10)	–C(5)	116.2(5)	116.0(5)
C(1)	–C(10)	–C(9)	125.0(6)	125.3(6)
C(5)	–C(10)	–C(9)	118.8(6)	118.7(6)
S	–C(11)	–N(2)	124.5(5)	124.7(5)
S	–C(11)	–N(3)	113.2(5)	112.8(5)
N(2)	–C(11)	–N(3)	122.3(5)	122.5(6)
S	–C(12)	–C(13)	111.1(5)	110.9(5)
N(3)	–C(13)	–C(12)	113.6(6)	114.7(6)
O(1)	–Cl	–O(2)	109.8(5)	
O(1)	–Cl	–O(3)	108.0(7)	
O(1)	–Cl	–O(4)	114.0(7)	
O(2)	–Cl	–O(3)	114.9(7)	
O(2)	–Cl	–O(4)	107.7(6)	
O(3)	–Cl	–O(4)	102.4(8)	
O	–Co	–N(1′)	93.5(2)	
N(3)	–Co	–N(1′)	99.7(2)	
O′	–Co	–N(1)	93.4(2)	
N(3′)	–Co	–N(1)	100.4(2)	

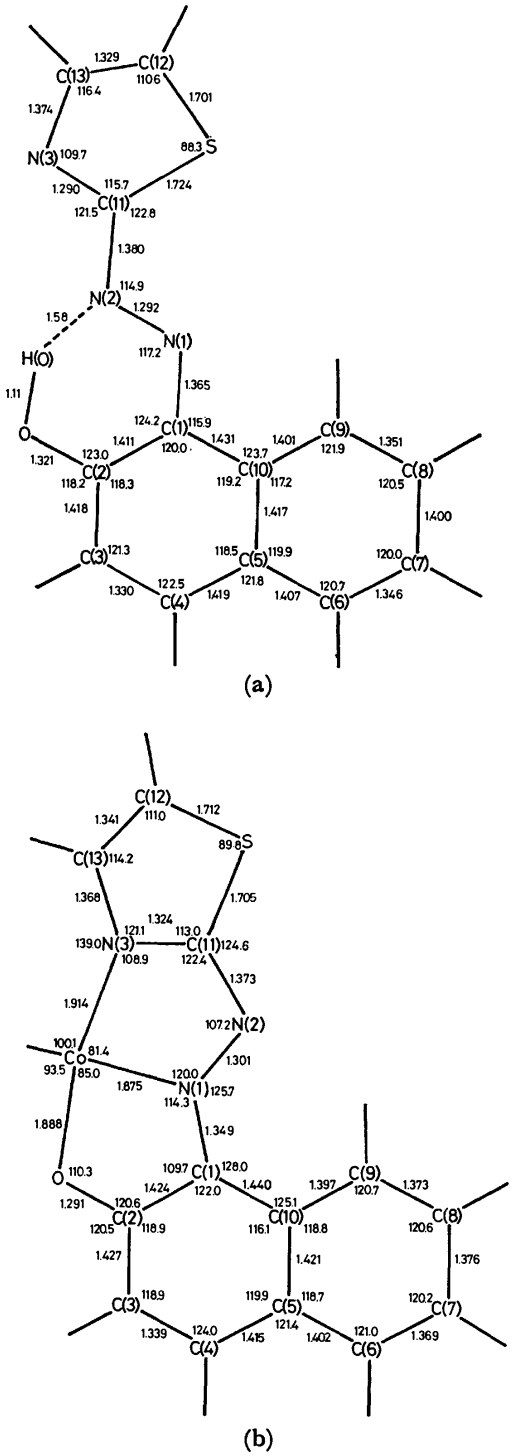

Fig. 3. Comparison of the structures between Htan and $[Co^{III}(tan)_2]^+$.
(a) Htan. (b) $[Co^{III}(tan)_2]^+$.

by 180° around the N(1)–C(1) and N(2)–C(11) bonds. As for the bond length distribution, all the corresponding distances in Htan and $[Co^{III}(tan)_2]^+$ agree within ±0.03 Å.

Comparison of N(1)–C(1)–C(10), C(1)–N(1)–N(2) and N(1)–N(2)–C(11) angles in Htan and $[Co^{III}(tan)_2]^+$ indicates that these angles are distorted by chelate ring formation. If these angles in $[Co^{III}(tan)_2]^+$ are the same as those observed in Htan, the N(2)···H(9) distance will be less than 1.8 Å. The observed distances are 2.24(6) and 2.28(6) Å for A and B, respectively. It is apparent that the tan deforms so as to relieve the N(2)···H(9) repulsion on chelate ring formation. Using the following potential function proposed by Giglio,[17]

$$V(r) = \{52100 \exp(-2.04r)\}/r^6 - 132/r^6$$

the N···H interaction energies $V(r)$ were calculated, and the values of 35.1 kcal/mol for $r=1.8$ Å and 2.3 kcal/mol for $r=2.3$ Å were obtained. This may indicate that the repulsion energy present in the complex is not too large; however, the steric effect would play an important role on chelate ring formation. A similar intraligand repulsion occurs in a complex of 2-(2-thiazolylazo)-3-methylphenol (I), as can be seen in I'.

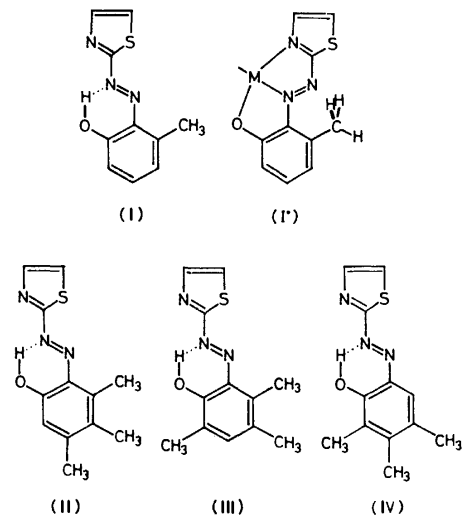

In the course of studying the extraction of nickel(II) chelates of 2-(2-thiazolylazo)-3,4,5-trimethylphenol (II), 2-(2-thiazolylazo)-3,4,6-trimethylphenol (III) and 2-(2-thiazolylazo)-4,5,6-trimethylphenol (IV) into benzene, Fujiwara and Kawase[18,19] found that stability constants, K, for the nickel chelates of II and III are lower than the values expected from the pK_a (acid dissociation constant) *vs* $\log K$ relation.[20] This implies a steric repulsion between the azo nitrogen and the methyl group at 3-position on the phenyl group.

It is likely that the magnitudes of the N(2)···H(9)

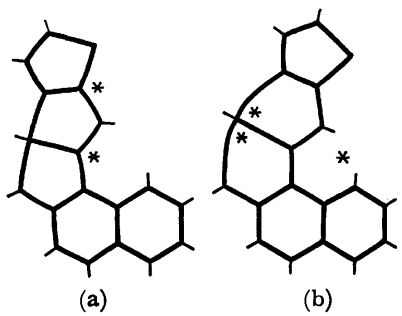

Fig. 4. Framework molecular models for the tan-complex, showing that the magnitudes of the N(2)···H(9) repulsion and the angular distortion depend on the size of the central metal atom.
(a) Small metal ion. (b) Large metal ion.

repulsion and the angular distortion depend on the size of the metal ion. Inspection of the molecular model (Fig. 4) reveals that in the complex of metal with small ionic radius the N(2)···H(9) repulsion and the angular distortion of O–M–N(1) and N(1)–M–N(3) will be small but the distortion of N(2)–N(1)–C(1) and S–C(11)–N(2) will be very large, whereas in the complex of metal with large ionic radius the former will be large and the latter small. This fact might be related to the selectivity of this reagent, that is, tan will not form a complex with metal having too small or too large ionic radius. It can be shown that the tan will not form a complex with metal whose coordination configuration is tetrahedral, so far as the tan acts as a planar terdentate ligand.[10]

A knowledge on structures may be useful for the prescription of a new analytical reagent. If one wishes to control the solubility, stability or absorbance of the complex, some functional groups are usually introduced in the ring system. In this case, it is important to take the effect of intramolecular repulsion into consideration. The present study revealed that the substitution of H(9) atom with a non-hydrogen atom or a large functional group will prevent the formation of a stable chelate ring. This means that it is unable to introduce a hydrophilic group or auxochromic group into 8-position (H(9) position) in the case of tan chelate. A similar argument holds for the substitution of H(13) atom (4-position of thiazole) with a large functional group.

The mean planes through Co and the unprimed tan

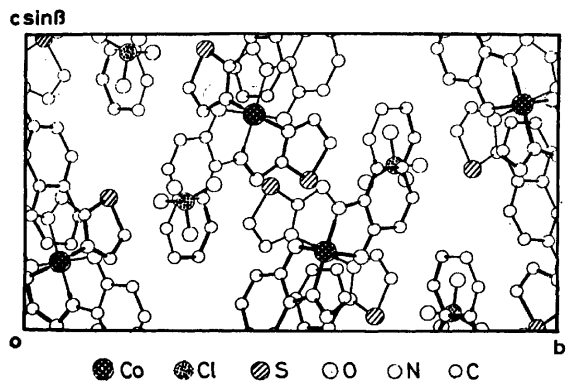

(a)

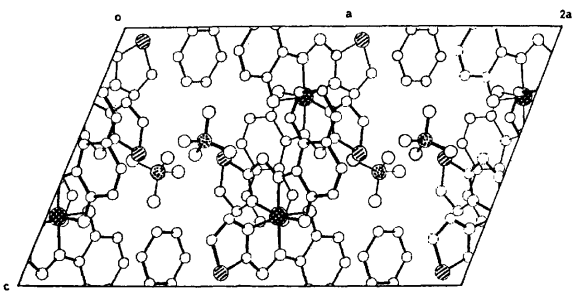

(b)

Fig. 5. (a) The crystal structure projected along the a axis.
(b) The crystal structure projected along the b axis.

TABLE 5. INTERATOMIC DISTANCES LESS THAN 3.5 Å

		Symmetry operation	Distance (l/Å)
S	O(2)	1	3.34
O	N(2′)	2	3.17
O	C(9′)	2	3.50
C(2)	C(6)	3	3.47
C(3)	C(9′)	2	3.42
C(4)	C(10)	3	3.45
C(6)	O′	3	3.24
C(6)	O(3)	3	3.44
C(7)	C(12)	4	3.41
C(8)	C(12)	4	3.50
C(9)	C(13′)	4	3.48
C(12)	C(8′)	5	3.48
C(12)	O(2)	6	3.26
C(13)	O(1)	7	3.44
C(13)	O(2)	7	3.33
C(13)	C(7′)	5	3.26
S′	O(1)	8	3.49
O′	C(6′)	5	3.23
C(4′)	O(3)	9	3.27
C(5′)	C(12′)	2	3.44
C(6′)	O(3)	9	3.44
C(8′)	C(13′)	2	3.47
C(9′)	C(13′)	2	3.46
C(12′)	O(1)	8	3.28

Symmetry operations

1	$(-1+x$	y	$z)$	6 $(1+x$	y	$z)$
2	$(-x$	$-y$	$-z)$	7 $(-1+x$	$\frac{1}{2}-y$	$-\frac{1}{2}+z)$
3	$(1-x$	$y-$	$1-z)$	8 $(-x$	$-\frac{1}{2}+y$	$\frac{1}{2}-z)$
4	$(-x$	$-y$	$1-z)$	9 $(x$	$\frac{1}{2}-y$	$-\frac{1}{2}+z)$
5	$(x$	$\frac{1}{2}-y$	$\frac{1}{2}+z)$			

and through Co and the primed tan are roughly planar (the maximum deviations being 0.08 and 0.17 Å, respectively) and these planes make an angle of 89°. The large displacements from the planes are due partly to non-bonded N(2)···H(9) repulsion and partly to intermolecular interaction. The structure of the complex cation viewed normal to the plane through the Co and the primed tan is given in Fig. 1(b).

The crystal structures projected along the a and b axes are illustrated in Fig. 5. The intermolecular distances less than 3.5 Å are listed in Table 5. There is no indication of hydrogen bonding.

The author wishes to express his sincere thanks to Professor Yoshihiko Saito of the University of Tokyo for use of the X-ray diffractometer. He is also grateful to Dr. Akira Kawase of National Chemical Laboratory for Industry for his valuable discussions. Part of the calculations was carried out on the HITAC 5020F computer at the Computer Center of the National Aerospace Laboratory, using SFR-5 and HBLS-4 programs in UNICS system.[21] The other calculations were performed on the NEAC 3100 computer of this Institute. Figures 1 and 5 were produced by DEAM-4 program.[22]

References

1) I. E. Boni and A. Hemmeler, *Chimica(Milan)*, **34**, 443 (1958).

2) A. Kawase, *Bunseki Kagaku*, **11**, 628 (1962); **12**, 810 (1963); **13**, 553 (1964).
3) A. Kawase, *Bunseki Kagaku*, **12**, 904 (1963).
4) G. Nakagawa and H. Wada, *Nippon Kagaku Zgsshi*, **83**, 1185 (1962).
5) G. Nakagawa and H. Wada, *Nippon Kagaku Zasshi*, **85**, 202 (1964).
6) H. Wada and G. Nakagawa, *Bunseki Kagaku*, **14**, 28 (1965).
7) M. Kurahashi and A. Kawase, *Bull. Chem. Soc. Jpn.*, **49**, 1419 (1976).
8) M. Kurahashi, *Bull. Chem. Soc. Jpn.*, **47**, 2045 (1974).
9) M. Kurahashi, *Bull. Chem. Soc. Jpn.*, **47**, 2067 (1974).
10) M. Kurahashi and A. Kawase, *Bull. Chem. Soc. Jpn.*, **49**, 127 (1976).
11) M. Kurahashi, *Chem. Lett.*, **1974**, 1271.
12) "International Tables for X-ray Crystallography," Vol. III, Kynoch Press, Birmingham, England (1962).
13) R. T. Stewart, E. R. Davidson, and W. T. Simpson, *J. Chem. Phys.*, **42**, 3175 (1965).
14) K. Nishimoto, Private comunication.
15) M. Kurahashi, *Bull. Chem. Soc. Jpn.*, **49**, 2927 (1976).
16) M. Iwata and Y. Saito, *Acta Crystallogr.*, **B29**, 822 (1973).
17) E. Giglio, *Nature*, **222**, 339 (1969).
18) J. Fujiwara and A. Kawase, *Bunseki Kagaku*, **22**, 564 (1973).
19) J. Fujiwara and A. Kawase, Private communication.
20) J. G. Jones, J. B. Pooles, J. C. Tomkinson, and R. T. P. Williams, *J. Chem. Soc.* **1958**, 2001.
21) "The Universal Crystallographic Computing System (I)," ed. by T. Sakurai, The Crystallographic Society of Japan (1967).
22) A. Takenaka, "Schematic Drawing of Crystal and Molecular Structures Containing Atomic Thermal Motions," APPLY 270/30—503—001, Fujitsu Ltd., Tokyo (1972).

Circular Dichroism Spectra of Cobalt(III) Complexes Containing One or Two Azido, Isothiocyanato, and Nitro Ligands. I. The Bis(ethylenediamine) Complexes of *cis* Type

Kiyoshi YAMASAKI,* Jinsai HIDAKA,** and Yoichi SHIMURA

Department of Chemistry, Faculty of Science, Osaka University, Toyonaka, Osaka 560

(Received May 24, 1976)

Circular dichroism spectra have been measured for the *cis*-$[Co(X)(NH_3)(en)_2]^{2+}$, *cis*-$[Co(X)_2(en)_2]^+$, and *cis*-$[Co(X)(X')(en)_2]^+$ complexes in the visible and ultraviolet region (X and X'=N_3^-, NCS^-, or NO_2^-). The absolute configurations of the complexes have been assigned from the circular dichroism pattern in the first d-d absorption band, region and correlated with that in the near ultraviolet region of the so-called specific absorption band. The origin of the specific absorption band has been discussed.

It is well known that transition metal complexes with some particular ligands, such as azido N_3^-, isothiocyanato NCS^-, nitro NO_2^-, and sulfito SO_3^{2-}, show characteristic intense absorption bands in the near-ultraviolet region. These characteristic absorption bands were named at first "special bands,"[1,2] and later "specific bands."[3] The specific absorption bands, which are specific for the particular ligands, have been investigated by many authors, but alternative characterizations have been assigned to the origin, that is, the one attributed the bands to intraligand transitions,[1,4] and the other to charge transfer transitions.[5-9] Recently Miskowsky and Gray[10] attributed most of the specific bands of $[Co(CN)_5X]^{n-}$ or $[CoX(NH_3)_5]^{n+}$ complexes to ligand-to-metal charge transfer transitions (X= NCS^-, SCN^-, and SO_3^{2-}), but assigned the specific bands of $[Co(CN)_5(NO_2)]^{3-}$ and $[Co(NO_2)(NH_3)_5]^{2+}$ which are located at 35200 and 30700 cm^{-1}, respectively, to a metal-to-ligand charge transfer transition. The latter metal-to-ligand transition has also been assumed for the specific bands of some hexanitro metallates.[11]

The present paper deals with circular dichroism (CD) spectra of *cis*-$[Co(X)(NH_3)(en)_2]^{2+}$, *cis*-$[Co(X)_2(en)_2]^+$, and *cis*-$[Co(X)(X')(en)_2]^+$ complexes (X and X'=N_3^-, NCS^-, or NO_2^-), to find the relationship between the CD behavior in the specific band region and the absolute configuration of the complexes, and furthermore to interpret, if possible, the origin of the specific bands on the basis of the CD spectra. A preliminary letter about some of the results has been reported.[12]

Experimental

Preparation and Optical Resolution. *(1)* $(-)_{589}$-cis-$[Co(N_3)(NH_3)(en)_2]Cl_2\cdot 0.5H_2O$: To a solution containing 6.0 g of *cis*-$[CoCl(NH_3)(en)_2]Cl_2$[13] in 30 cm^3 of water were added a few drops of glacial acetic acid and 1.4 g of sodium azide. The solution was heated on a water bath and concentrated until the surface of the solution was covered with a thin crystalline product. After the resulted mixture had been allowed to stand at room temperature for an hour, the crystals were collected by filtration. 4.0 g. Recrystallization was carried out from water (60 °C). The pure crystals deposited were filtered and washed with methanol, and then acetone, and air-dried. Found: C, 15.49; H, 6.14; N, 35.75 %. Calcd for $[Co(N_3)(NH_3)(C_2H_8N_2)_2]Cl_2$: C, 15.54; H, 6.20; N, 36.25%.

The optical resolution of this complex was achieved by a modified procedure of that of Buckingham, Olsen, and Sargeson[14] using NH_4*d*-bcs as a resolving agent (*d*-bcs stands for $(+)_{589}$-(1*R*, 3*S*, 4*S*, 7*R*)-3-bromocamphor-9-sulfonate ion). The less soluble diastereomer was recrystallized from water until it showed a constant rotation. $[\alpha]_{589}=-10°$, $[\alpha]_{546}=+15°$, $[\alpha]_{467}=+371°$. Found: C, 33.34; H, 5.52; N, 12.85%. Calcd for $[Co(N_3)(NH_3)(C_2H_8N_2)_2](C_{10}H_{14}O_4BrS)_2\cdot 0.5H_2O$: C, 33.23; H, 5.58; N, 12.92%. A solution of the diastereomer was passed through a column containing Dowex 1×8 strong-base anion exchange resin (Cl^- form) and the resulted solution was evaporated to dryness below 30 °C. The deposited fine reddish-violet crystals were suspended in methanol to eliminate a contaminant, filtered, washed with methanol and acetone, and dried in a desiccator over $CaCl_2$. $[\alpha]_{589}=-210°$, $[\alpha]_{546}=-116°$. Found: C, 15.06; H, 6.35; N, 34.01%. Calcd for $[Co(N_3)(NH_3)(C_2H_8N_2)_2]Cl_2\cdot 0.5H_2O$: C, 15.10; H, 6.34; N, 35.23%.

(2) $(+)_{589}$-cis-$[Co(N_3)_2(en)_2]ClO_4$: To a solution (50 °C) of 3.0 g of *rac*-$[Co(N_3)_2(en)_2]N_3$[15] in 80 cm^3 of water was added a solution of 1.8 g of $K_2[Sb_2(d\text{-tart})_2]\cdot 3H_2O$ in 20 cm^3 of water (*d*-tart stands for $(+)_{589}$-tartrate(4−) ion). The mixture was kept in a refrigerator for two days. The resulting dark reddish-violet prismatic crystals were filtered, washed with a little water, methanol, and then acetone, and dried in air. 2.6 g. $[\alpha]_{589}=+140°$, $[\alpha]_{546}=-539°$. The less soluble diastereomer was converted to the perchlorate by adding a large excess of solid $LiClO_4\cdot 3H_2O$ (5 g) to a suspension of the diastereomer in 80 cm^3 of water (40 °C) and stirring sufficiently (1 h). The red violet fine crystals separated were filtered, washed with a little water, methanol, and then acetone, and dried in a vacuum desiccator over $CaCl_2$. 0.5 g. Recrystallization was carried out from a minimum amount of water (40 °C). $[\alpha]_{589}=+237°$, $[\alpha]_{546}=-962°$. Found: C, 13.39; H, 4.46; N, 38.98%. Calcd for $[Co(N_3)_2(C_2H_8N_2)_2]ClO_4$: C, 13.25; H, 4.45; N, 38.62%.

The perchlorate of the $(-)_{589}$ isomer was obtained by the addition of a solution containing 0.7 g of $NaClO_4$ in 10 cm^3 of water to the above filtrate. By recrystallization from hot water this isomer gave the same rotation with the opposite sign as the $(+)_{589}$ perchlorate.

(3) $(+)_{589}$-cis-$[Co(NCS)(NH_3)(en)_2]Br_2\cdot 0.5H_2O$: $(-)_{589}$-$[CoCl(NCS)(en)_2]Cl$ (0.9 g, see below (10)) was placed in a 250 cm^3 cylinder and purged with ammonia gas in a Dry Ice–methanol bath to condense about 10 cm^3 of ammonia over the complex. The cylinder was tightly covered and allowed to stand at room temperature for about half an hour.

* Present address: Osaka Prefectural Industrial Research Institute, Enokojima, Nishi-ku, Osaka 550

** Present address: Department of Chemistry, The University of Tsukuba, Ibaraki 300-31

When the color of the ammonia solution was changed from dark red to deep orange, the ammonia was evaporated by a stream of dry nitrogen. The resulted orange product (0.9 g) was dried in a vacuum desiccator over P_2O_5 to remove the remaining ammonia. A portion (0.45 g) of the dried product was dissolved in 4 cm^3 of water, and 0.9 g of NaBr was added to the solution. After it had been kept in a refrigerator overnight, the first precipitate was filtered off (this was optically almost inactive). After the filtrate had been kept in a refrigerator for another day, the second precipitate (partly resolved complex) was filtered. When the filtrate was kept in a refrigerator for further four days, the orange prisms resulted. They were filtered, washed with ethanol and acetone, and dried in a vacuum desiccator over $CaCl_2$. 37 mg. $[\alpha]_{589}=+43°$, $[\alpha]_{546}=+83°$. Found: C, 14.32; H, 4.87; N, 20.12%. Calcd for $[Co(NCS)(NH_3)(C_2H_8N_2)_2]Br_2\cdot 0.5H_2O$: C, 14.47; H, 4.86; N, 20.25%. The $(-)_{589}$ isomer was obtained from $(+)_{589}$-$[CoCl(NCS)(en)_2]Cl$.

(4) $(-)_{589}$-cis-$[Co(NCS)_2(en)_2]Cl$: The racemic chloride monohydrate[16] (3.5 g) and the resolving agent $K_2[Sb_2(d\text{-tart})_2]\cdot 3H_2O$ (1.7 g) were dissolved in 300 cm^3 of water at 60 °C. After cooling the mixed solution to the room temperature, it was allowed to stand overnight in a refrigerator. The less soluble diastereomer deposited as red orange crystals, and it was recrystallized from hot water (300 cm^3, 60 °C). 1.1 g. $[\alpha]_{589}=-61°$, $[\alpha]_{546}=+165°$. To a suspension of 1.0 g of the recrystallized diastereomer in 80 cm^3 of water was added 200 cm^3 of aqueous solution containing 15 g of lithium chloride. The mixture was stirred for half an hour to transform the diastereomer into the reddish-orange chloride, and this was filtered, washed with 50% ethanol, ethanol and then acetone, and dried in a vacuum desiccator over $CaCl_2$. 0.5 g. $[\alpha]_{589}=-25°$, $[\alpha]_{546}=+134°$. It was confirmed that the optical rotation was not increased by recrystallization. Found: C, 21.77; H, 4.97; N, 25.44%. Calcd for $[Co(NCS)_2(C_2H_8N_2)_2]Cl$: C, 21.79; H, 4.88; N, 25.41%.

(5) $(-)_{589}$-cis-$[Co(NO_2)(NH_3)(en)_2]SO_4\cdot H_2O$: The racemic dithionate[13] was converted to the nitrate by an ion-exchange method with Dowex 2×8 resin (NO_3^- form, 50—100 mesh). The racemic nitrate, $[Co(NO_2)(NH_3)(en)_2](NO_3)_2$ (3.2 g), was dissolved in 17 cm^3 of water (40 °C), and 1.4 g of NH_4*d*-bcs was added to it.[17] The mixed solution was kept in a refrigerator for about four days. Orange yellow needles separated were filtered, washed with 50% ethanol, ethanol, and then acetone, and air-dried. 0.65 g. $[\alpha]_{589}=+44°$, $[\alpha]_{546}=+33°$, $[\alpha]_{436}=+386°$. The needles were occasionally contaminated with orange yellow prisms. The prisms were the racemic nitrate. The undesired prisms were easily removed by hand picking. The diastereomer was recrystallized from water (50 °C), and filtered, washed with a little ice-cold water, 50% ethanol, and then acetone, and dried in air. 0.5 g. $[\alpha]_{589}=+53°$, $[\alpha]_{546}=+49°$, $[\alpha]_{438}=+440°$. The diastereomer was converted to the sulfate by passing the aqueous solution through a column containing an anion-exchange resin (SO_4^{2-} form) and by evaporating the resulting solution to dryness below 30 °C. After suspending the sulfate in a methanol–water (4:1) mixture and stirring it enough, the sulfate of the $(-)_{589}$ isomer was filtered, washed with methanol and acetone, and dried in a vacuum desiccator over $CaCl_2$. $[\alpha]_{589}=-18°$, $[\alpha]_{546}=-49°$. Found: C, 13.73; H, 5.88; N, 23.21%. Calcd for $[Co(NO_2)(NH_3)(C_2H_8N_2)_2]SO_4\cdot H_2O$: C, 13.49; H, 5.94; N, 23.59%.

(6) $(-)_{589}$-cis-$[Co(NO_2)_2(en)_2]Cl$: To the solid complex, $[CoCO_3(en)_2]NO_3\cdot H_2O$[18] (32 g), was poured carefully 225 cm^3 of 4% of nitric acid. The complex was dissolved with the evolution of CO_2 gas to give a solution containing *cis*-$[Co(en)_2(OH_2)_2]^{3+}$ complex. After the solution had been stirred for a while to complete the aquation, 20.7 g of $NaNO_2$ was added, and the mixed solution was gradually heated on a water bath and stirred at 70 °C for an hour. The color of solution changed from red to dark orange, and the nitrate of the desired complex separated out. The crystals were filtered and washed with water, and then ethanol. 20 g. The nitrate was recrystallized from water (60 °C) and the fine crystals obtained were filtered, washed with water, and then ethanol, and dried in a vacuum desiccator over $CaCl_2$. Found: C, 14.74; H, 5.10; N, 29.27%. Calcd for $[Co(NO_2)_2(C_2H_8N_2)_2]NO_3$: C, 14.42; H, 4.84; N, 29.42%.

The perchlorate was obtained in a similar way from $[CoCO_3(en)_2]ClO_4$.[19] Found: C, 13.18; H, 4.23; N, 22.66%. Calcd for $[Co(NO_2)_2(C_2H_8N_2)_2]ClO_4$: C, 12.96; H, 4.35; N, 22.68%.

The nitrate was resolved in a usual way using $K_2[Sb_2(d\text{-tart})_2]\cdot 3H_2O$ as resolving agent.[20] The less soluble diastereomer yielded the $(-)_{589}$-$[Co(NO_2)_2(en)_2]Cl$.

(7) $(+)_{589}$-cis-$[Co(N_3)(NCS)(en)_2]Cl\cdot 0.5H_2O$: To a 60 °C solution of 6.0 g of *cis*-$[CoCl(NCS)(en)_2]ClO_4$[13] in 45 cm^3 of water was added 1.2 g of NaN_3, and the resulting solution was stirred at 60 °C for about 80 min. After the solution had been diluted with an appropriate amount of water, it was poured on a column (27×800 mm) containing Dowex 50 W×8 cation-exchange resin (200—400 mesh, H^+ form). The adsorbed band was eluted first with 0.2 M LiCl solution at a rate of 1.5—2.0 cm^3/min for a week. The eluates were discarded, because it was confirmed from the absorption measurement that the eluates contained some *trans* complexes. After these operations, the remaining colored band which was placed on the upper half of the column was eluted with 0.5 M LiCl (about 13 dm^3 in total) during the next week. The broad bands eluted were fractionated by 200 cm^3 portions. The eluted ten fractions which have the first absorption band at 510—509 nm were combined and concentrated to a volume as little as possible (about 50 cm^3) in a vacuum evaporator at 35 °C. After the mixture had stood in a refrigerator overnight, the resulting precipitates, *cis*-$[Co(N_3)(NCS)(en)_2]Cl\cdot 1.5H_2O$ and LiCl, were filtered. To remove the LiCl, the mixture was suspended in 200 cm^3 of ethanol and the suspension was stirred enough. The dark reddish-violet precipitate was filtered, washed with five 20 cm^3 portions of ethanol, and then ether, and dried in a vacuum desiccator. 0.41 g. This was recrystallized from water (50 °C), and the product was washed with ethanol and ether, and dried in a vacuum desiccator over $CaCl_2$. Found: C, 17.63; H, 5.67; N, 32.28%. Calcd for $[Co(N_3)(NCS)(C_2H_8N_2)_2]Cl\cdot 1.5H_2O$: C, 17.58; H, 5.60; N, 32.79%.

The resolving agent $K_2[Sb_2(d\text{-tart})_2]\cdot 3H_2O$ (120 mg) was dissolved in 40 cm^3 of water at 60 °C, and 220 mg of *cis*-$[Co(N_3)(NCS)(en)_2]CH_3CO_2$, which was obtained from the chloride by the usual ion-exchange method, was added to it with stirring. After cooling the mixed solution to room temperature, it was kept in a refrigerator overnight. The fine dark reddish-violet crystals separated were filtered, washed with ethanol and ether, and air-dried. 115 mg. $[\alpha]_{589}=+135°$, $[\alpha]_{546}=+60°$. The less soluble diastereomer (110 mg) was dissolved in 3 cm^3 of water at 45 °C. After the solution had stood for two weeks in a refrigerator, the resulted crystals were filtered, washed with a little water, ethanol and ether, and air-dried. 18 mg. $[\alpha]_{589}=+178°$, $[\alpha]_{546}=+50°$. The recrystallized diastereomer (18 mg) was dissolved in 10 cm^3 of water, and the solution was passed through an anion-exchange resin column (Cl^- form). The chloride solution obtained was evaporated to dryness in a vacuum desiccator over P_2O_5.

$[\alpha]_{589}=+125°$, $[\alpha]_{546}=-138°$. Found: C, 18.70; H, 5.29; N, 34.52%. Calcd for $[Co(N_3)(NCS)(C_2H_8N_2)_2]Cl\cdot 0.5H_2O$: C, 18.55; H, 5.29; N, 34.62%.

(8) $(+)_{589}$-cis-$[Co(N_3)(NO_2)(en)_2]ClO_4$: To a solution of 5.7 g of *cis*-$[CoCl(NO_2)(en)_2]Cl$ in 90 cm³ of water at 70 °C was added 1.3 g of NaN_3. The mixture was heated on a steam bath in a draft chamber. When the solution was concentrated to 10—15 cm³, a solution containing 2.4 g of $Na_2S_2O_6\cdot 2H_2O$ in 10 cm³ of water was added to it with stirring. After cooling the mixture to room temperature and then keeping it in an ice bath for an hour, the reddish-orange fine crystals precipitated were filtered, washed with a little water, and dried in air. 2.8 g. This was recrystallized twice from water (60 °C) and washed with a little water, ethanol, and then ether, and air-dried. Found: C, 13.70; H, 4.63; N, 31.87%. Calcd for $[Co(N_3)(NO_2)(C_2H_8N_2)_2]_2S_2O_6$: C, 13.84; H, 4.65; N, 32.27%.

The racemate, *cis*-$[Co(N_3)(NO_2)(en)_2]_2S_2O_6$ (6.0 g), was dissolved in 600 cm³ of water at 60 °C, and transformed into the chloride solution by an ion-exchange method. The resulted chloride solution was evaporated at 40 °C to 75 cm³ in a vacuum evaporator, and a solution of 2.6 g of NH_4*d*-bcs in 20 cm³ of water was added to it. After the mixed solution had been cooled in a refrigerator for two days, the red orange needles separated were filtered, washed with a little water, methanol and ether, and air-dried. 2.7 g. $[\alpha]_{589}=+77°$, $[\alpha]_{546}=+80°$, $[\alpha]_{472}=-542°$. The diastereomer was recrystallized from water (45 °C, 160 cm³). 0.9 g. $[\alpha]_{589}=+68°$, $[\alpha]_{546}=+72°$, $[\alpha]_{472}=-598°$. Found: C, 29.11; H, 5.26; N, 18.68%. Calcd for $[Co(N_3)(NO_2)(C_2H_8N_2)_2](C_{10}H_{14}O_4BrS)$: C, 29.13; H, 5.24; N, 19.41%. The recrystallized diastereomer (0.5 g) was dissolved in a minimum amount of water (35 cm³) at 40 °C, and 10g of $NaClO_4$ was added to it with stirring. After the mixture had stood for two hours, the resulted fine red orange lustrous prisms were filtered, washed with ethanol and ether, and air-dried. 144 mg. $[\alpha]_{589}=+32°$. $[\alpha]_{546}=+43°$. The perchlorate was recrystallized from water (40 °C, 6 cm³). 66 mg. It was confirmed that the optical rotation of this isomer was not increased by the recrystallization. Found: C, 13.27; H, 4.30; N, 30.61%. Calcd for $[Co(N_3)(NO_2)(C_2H_8N_2)_2]ClO_4$: C, 13.10; H, 4.40; N, 30.56%.

(9) $(+)_{589}$-cis-$[Co(NCS)(NO_2)(en)_2]Cl$: To a solution of 1.6 g of barium acetate in 200 cm³ of water (60 °C) was added 3.9 g of *cis*-$[Co(NCS)(NO_2)(en)_2]_2SO_4$.[13] After the mixture had been stirred for half an hour at 60 °C, the barium sulfate deposited was removed by filtration. The filtrate was evaporated to dryness with a vacuum evaporator, and the resulted fine yellow orange crystals were collected and washed with 70% ethanol, ethanol and then ether, and air-dried. 3.5 g. Found: C, 24.54; H, 5.62; N, 24.48%. Calcd for $[Co(NCS)(NO_2)(C_2H_8N_2)_2]CH_3CO_2$: C, 24.57; H, 5.60; N, 24.55%. The racemic acetate, *cis*-$[Co(NCS)(NO_2)(en)_2]CH_3CO_2$ (2.0 g), was dissolved in 10 cm³ of water at 40 °C, and a solution of 1.0 g of $K_2[Sb_2(d\text{-tart})_2]\cdot 3H_2O$ in 10 cm³ of water at 40 °C was added to it. A large amount of yellow orange precipitate separated soon, and was filtered after an hour (the filtrate was used for separating the $(-)_{589}$-isomer), washed with ethanol and ether, and air-dried. 1.5 g. $[\alpha]_{589}=+110°$, $[\alpha]_{546}=+160°$. This was recrystallized from water (45 °C, 500 cm³). Yellow orange needles. 0.9 g. $[\alpha]_{589}=+125°$, $[\alpha]_{546}=+191°$.

The recrystallized diastereomer (0.3 g) was dissolved in 150 cm³ of water at 40 °C, and was converted into the chloride solution by an ion-exchange method. The resulted chloride solution was evaporated to dryness below 30 °C in a vacuum evaporator. After being suspended in ethanol with stirring, the fine yellow orange prisms were filtered, washed with ethanol and ether, and dried in air. 0.13 g. $[\alpha]_{589}=+87°$, $[\alpha]_{546}=+197°$. Recrystallization of the chloride caused no increase in the optical rotation. Found: C, 18.89; H, 5.05; N, 26.29%. Calcd for $[Co(NCS)(NO_2)(C_2H_8N_2)_2]Cl$: C, 18.85; H, 5.06; N, 26.37%.

The $(-)_{589}$ optical isomer appeared soon after a solution of 1.0 g of LiCl in 2 cm³ of water was added to the above mentioned filtrate freed from the diastereomer. The crystals were filtered after about 5 min, washed with ethanol and ether, and air-dried. 0.41 g. $[\alpha]_{589}=-82°$, $[\alpha]_{546}=-186°$. This was recrystallized from water (45 °C, 16 cm³). 0.22 g.

(10) $(-)_{589}$-cis-$[CoCl(NCS)(en)_2]ClO_4$: The racemic perchlorate was prepared from *trans*-$[CoCl_2(en)_2]Cl$ by the Werner's method.[13] The perchlorate obtained was contaminated with the diisothiocyanato complex, and then purified as follows. The crude perchlorate salt was fractionally extracted with water, and to each extract was added one-fourth volume of 70% $HClO_4$ and the resulted solution was cooled in an ice bath for several hours. The fine orange crystals of the contaminant, $[Co(NCS)_2(en)_2]ClO_4$, precipitated from the earlier extracts, whereas the dark red crystals of *cis*-$[CoCl(NCS)(en)_2]ClO_4$ precipitated from the later extracts. No crystallization occurred from the middle extracts. The crystals of the desired complex were recrystallized from water by the addition of perchloric acid as described above, and filtered, washed with ethanol and ether, and sucked dry. Found: C, 16.00; H, 4.18; N, 18.74%. Calcd for $[CoCl(NCS)(C_2H_8N_2)_2]ClO_4$: C, 16.14; H, 4.33; N, 18.82%.

A solution of 12 g of racemic *cis*-$[CoCl(NCS)(en)_2]ClO_4$ in 160 cm³ of water (50 °C) and a solution of 5.3 g of NH_4*d*-bcs in 30 cm³ of water (50 °C) were mixed. The mixture was allowed to stand at room temperature for an hour, and then cooled gradually to 10 °C. The dark reddish violet crystalline precipitate was filtered, washed with ethanol and ether, and dried in air. 8.6 g. The filtrate was used for obtaining the $(+)_{589}$-isomer. $[\alpha]_{589}=+11°$, $[\alpha]_{546}=+226°$. This was recrystallized from water (45 °C). $[\alpha]_{589}=+27°$, $[\alpha]_{546}=+317°$. Found: C, 30.37; H, 5.43; N, 11.57%. Calcd for $[CoCl(NCS)(C_2H_8N_2)_2](C_{10}H_{14}O_4BrS)\cdot H_2O$: C, 29.98; H, 5.37; N, 11.66%. The recrystallized diastereomer (3.5 g) was stirred with 6 cm³ of 70% $HClO_4$ for an hour. After the mixture had been stirred in an ice bath for another hour, the separated fine crystals of the perchlorate were filtered, washed with ethanol and ether. 1.2 g. $[\alpha]_{589}=-31°$, $[\alpha]_{546}=+389°$. The perchlorate was dissolved in a minimum amount of water (20 cm³), and 4 cm³ of 70% $HClO_4$ was added to it. After the mixture had stood overnight, the reddish violet crystals separated were filtered, washed with ethanol and ether, and dried in a vacuum desiccator over $CaCl_2$. 0.7 g. $[\alpha]_{589}=-39°$, $[\alpha]_{546}=+440°$. Found: C, 16.34; H, 4.31; N, 18.45%. Calcd for $[CoCl(NCS)(C_2H_8N_2)_2]ClO_4$: C, 16.14; H, 4.33; N, 18.82%.

The filtrate freed from the less soluble diastereomer was evaporated at 25 °C to 170 cm³, and after cooling the solution in an ice bath, the second crop of the diastereomer was removed. The filtrate was evaporated further to 55 cm³, and 18 cm³ of 70% $HClO_4$ was added to it. After cooling the mixture by ice, the precipitated perchlorate was filtered. This was found to be an optically impure perchlorate of the $(+)_{589}$-isomer. The filtrate was kept in a refrigerator for three days, and then the dark reddish violet needles separated. The crystals were filtered, washed with ethanol and ether, and air-dried. 0.4 g. These showed the same optical rotation with the opposite sign in comparison with the $(-)_{589}$ perchlorate.

Measurements. The absorption spectra were measured by a Shimadzu UV-200 or a Beckman DU spectrometer. The CD spectra were recorded with a Jasco Model ORD/UV-5,

J-10, or J-20 spectropolarimeter, and the optical rotation by a Yanagimoto Model 185 or a Jasco Model ORD/UV-5 spectropolarimeter. The measurements were made at room temperature in aqueous solutions. The concentration of the solution ranged from 0.005 to 0.0001 M. The cell length was 1, 2 cm, or 1 mm.

Results and Discussion

Absorption and CD Spectra. The absorption and CD data are listed in Tables 1 and 2. In Fig. 1 the CD spectra of $(-)_{589}$-$[Co(N_3)(NH_3)(en)_2]^{2+}$ and $(+)_{589}$-$[Co(N_3)_2(en)_2]^+$ complexes are shown together with their absorption spectra. In the "azido-specific band" region around 33000 cm^{-1}, the ammineazido complex shows a single CD band with its peak in almost the same position as that of the absorption peak, while the diazido complex shows two CD bands of opposite signs. This observation supports that the broadening of the specific absorption band in the diazido complex is due to the overlapping of two split components of the band. The weak negative CD band at 26100 cm^{-1} of the ammineazido complex and the positive CD band at 25800 cm^{-1} of the diazido complex correspond to the second d-d absorption band ($^1A_{1g}\rightarrow{}^1T_{2g}$ in O_h symmetry). The positive CD band of the diazido complex has the intensity comparable to the CD band in the first d-d absorption band ($^1A_{1g}\rightarrow{}^1T_{1g}$ in O_h symmetry) region. This is unusual, but this behavior should be considered to be only the result of the contiguity of the intense

Table 1. Absorption and CD data of *cis*-$[Co(X)(NH_3)(en)_2]^{2+}$ and *cis*-$[Co(X)_2(en)_2]^+$ complexes

Complex ion	σ_{max}[a] (log ε)	σ_{ext}[a] ($\Delta\varepsilon$)
$(-)_{589}$-$[Co(N_3)(NH_3)(en)_2]^{2+}$	19.8(2.52)	19.4(−0.60)
	≈27 sh[b]	26.1(−0.15)
	33.3(3.90)	33.5(+1.9)
		≈43 sh(+)
	48.1(4.28)	
$(+)_{589}$-$[Co(N_3)_2(en)_2]^+$	19.3(2.52)	17.6(+0.80) 20.0(−1.17)
	≈26 sh	25.8(+1.92)
	33.1(4.06)	30.8(+5.8) 36.9(−6.0)
		≈42 sh(−)
	46.5(4.30)	46.3(+12)
$(-)_{589}$-$[Co(NCS)(NH_3)(en)_2]^{2+}$	20.5(2.32)	20.0(−0.28)
	≈28 sh	27.7(−0.05)
	33.2(3.23)	34.9(+0.18)
		41.8 (+1.2)
$(-)_{589}$-$[Co(NCS)_2(en)_2]^+$	20.4(2.54)	17.9(−0.12) 20.5(+0.32)
	≈28 sh	25.3(−0.04) 27.3(+0.10)
	32.5(3.46)	30.8(−0.45) 35.2(+0.12)
		40.7(−1.2) 43.7(+1.0)
$(-)_{589}$-$[Co(NO_2)(NH_3)(en)_2]^{2+}$	22.3(2.08)	21.1(−0.67) 23.9(+0.16)
	31.1(3.23)	31.0(−0.19) 36 sh(+)
	42.1(4.23)	40.8(+2.5)
$(-)_{589}$-$[Co(NO_2)_2(en)_2]^+$	22.8(2.23)	21.7(−1.66) 24.6(+0.62)
	31.1(3.56)	29.6(+2.48) 35 sh(−)
	41.7(4.32)	37.8(−3.7) 43.2(+16)

a) Wave numbers are given in 10^3 cm^{-1}. b)"sh" means a shoulder band.

Table 2. Absorption and CD data of *cis*-$[Co(X)(X')(en)_2]^+$ complexes

Complex ion	σ_{max}[a] (log ε)	σ_{ext}[a] ($\Delta\varepsilon$)
$(+)_{589}$-$[Co(N_3)(NCS)(en)_2]^+$	19.6(2.51)	18.4(+0.39) 20.9(−0.20)
		27.0(+0.26)
	32.4(3.91)	32.8(−1.3)
		41.7(−0.5)
$(+)_{589}$-$[Co(N_3)(NO_2)(en)_2]^+$	20.4(2.65)	19.8(+0.74) 22.5(−1.07)
		28.4(+1.05)
		31.0(−0.7)
	33.1(3.92)	33.9(+3.0)
	≈41 (4.05)	38.6(−5.1)
		45.8(−11)
$(+)_{589}$-$[Co(NCS)(NO_2)(en)_2]^+$	21.2(2.48)	20.3(+0.58) 23.0(−0.20)
		26.8(−0.31)
	31.0(3.52)	30.2(+2.44)
	≈41 (4.1)	37.8(−3.7)
		43.3(−1.4)
		46.0(+1.4)
$(-)_{589}$-$[CoCl(NCS)(en)_2]^+$	≈18 (2.1sh)[b] 19.9(2.24)	17.4(−0.36) 20.3(+0.59)
		27.9(+0.18)
	≈32 (3.2)	32.6(−0.6)
		37.1(+0.3)
	44.4(4.25)	45.0(−5.0)

a) Wave numbers are given in 10^3 cm^{-1}. b) "sh" means a shoulder band.

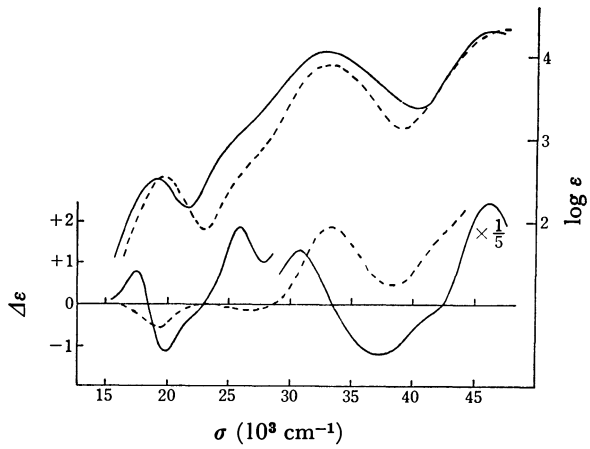

Fig. 1. Absorption and CD spectra of $(+)_{589}$-*cis*-$[Co(N_3)_2(en)_2]ClO_4$ (——) and $(-)_{589}$-*cis*-$[Co(N_3)(NH_3)(en)_2]Cl_2\cdot H_2O$ (------).

positive CD band of the specific band. In Fig. 2 the CD spectra of isothiocyanato complexes are shown with their absorption spectra. Concerning their specific bands the CD behavior similar to the azido complexes are observed; A single weal CD band is observed at 34900 cm^{-1} for the ammineisothiocyanato complex, while two CD bands of opposite signs are observed for the diisothiocyanato complex. This fact suggests the band splitting of the diisothiocyanato complex. The nagative CD band of the ammineisothiocyanato complex at 27700 cm^{-1} and the two CD bands of the diisothiocyanato complex at 25300 and 27300 cm^{-1} are assigned to the second d-d transitions.

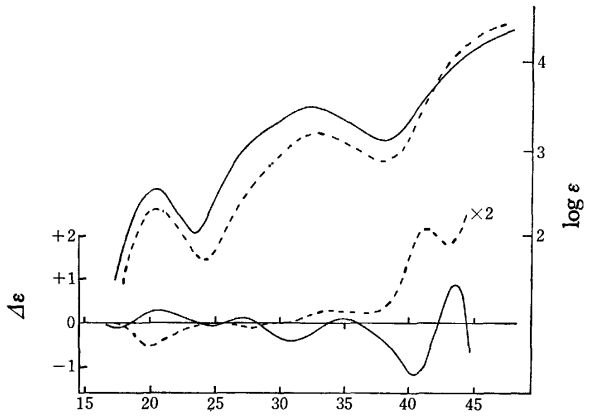

Fig. 2. Absorption and CD spectra of $(-)_{589}$-*cis*-[Co$(NCS)_2(en)_2$]Cl (——) and $(-)_{589}$-*cis*-[Co$(NCS)(NH_3)$-$(en)_2$]$Br_2 \cdot 0.5H_2O$ (------).

The azido and isothiocyanato complexes show very similar absorption curves to each other (Figs. 1 and 2). The specific absorption band at 33000 cm^{-1} of *cis*-$[Co(N_3)_2(en)_2]^+$ is 1.23 times as broad (and 1.45 times as intense) as that of *cis*-$[Co(N_3)(NH_3)(en)_2]^{2+}$. The same situation is also found for the isothiocyanato complexes, that is, the specific band at 32700 cm^{-1} of *cis*-$[Co(NCS)_2(en)_2]^+$ is 1.23 times as broad (and 1.70 times as intense) as that of *cis*-$[Co(NCS)(NH_3)(en)_2]^{2+}$. This absorption behavior concerning the band width of the azido and isothiocyanato complexes is quite a contrast to that of the corresponding nitro complexes, where the *cis* dinitro complex shows the specific band similar in width to the ammineniro one (Fig. 3). The absorption band broadening in the diazido and diisothiocyanato complexes suggests a band splitting, and this is confirmed from the CD spectra as above. It has been pointed out in earlier days for isothiocyanato complexes of chromium(III),[1] and isothiocyanato[3] and nitro[2] complexes of cobalt(III) that the specific band intensity is proportional to the number of the coordinated particular ligand, and this has been taken as an evidence for the theory that the specific band is due to the intraligand transition. As for the present complexes the (dianiono/ammineaniono) ratio of integrated intensities of the specific bands is approximately 2 for all of the azido, isothiocyanato, and nitro ligands. It is significant, however, in the case of the diazido and diisothiocyanato complexes, that the specific bands

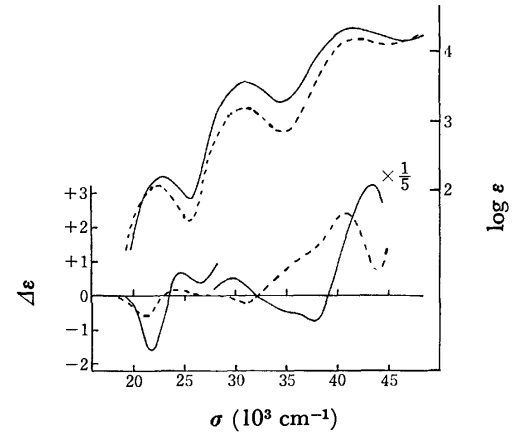

Fig. 3. Absorption and CD spectra of $(-)_{589}$-*cis*-[Co$(NO_2)_2(en)_2$]Cl (——) and $(-)_{589}$-*cis*-[Co$(NO_2)(NH_3)$-$(en)_2$]$SO_4 \cdot H_2O$ (------).

are shifted to the lower energy side than the corresponding ammineaniono complexes, and that the shift direction is the same as that of the first d-d absorption bands. The parallel shift of the specific and the first d-d bands may be taken as an evidence of the theory that the specific absorption band is due to the ligand-to-metal charge transfer transition, because the wider is the separation between the occupied d_π and the empty d_σ orbitals, the higher should be the energy of the charge transfer transition from the almost unaffected ligand orbital to the empty d_σ orbital.

Miskowsky and Gray[10] assigned the isothiocyanato specific band to the π(ligand)$\rightarrow d_{z^2}$(metal) transition as in the case of the longer wavelength charge transfer bands of amminehalogeno cobalt(III) complexes. As for the latter halogeno charge transfer bands, Yamatera[21] established the assignments that the longer and the shorter wavelength charge transfer bands are due to the p_π(ligand)$\rightarrow d_{z^2}$(metal) and p_σ(ligand)$\rightarrow d_{z^2}$(metal) transitions, respectively. The p_π(ligand)$\rightarrow d_{z^2}$(metal) transition of a C_{4v} complex such as $[CoX(NH_3)_5]^{2+}$ is expected to split into two transitions for a C_{2v} complex such as *cis*-$[CoX_2(NH_3)_4]^+$.[22] If it is presumed that the chelate ring effect of ethylenediamine is negligible, and the ligand fields of the diamine and the ammine are quite the same, the symmetry of *cis*-$[CoX(NH_3)(en)_2]^{2+}$ is approximated to C_{4v} and that of *cis*-$[CoX_2(en)_2]^+$ to C_{2v}. Then, the splitting of the specific absorption band in the diisothiocyanato complex can reasonably be explained by the theory that the isothiocyanato specific bands are due to the charge transfer transitions from π orbitals of the pseudohalogeno ligand to the lower empty d_σ orbital (d_{z^2}) of the central cobalt(III) ion. The similarity of the azido and isothiocyanato complexes in the CD and absorption spectra may be related to the fact that both the ligands are linear triatomic pseudohalide ions having sixteen valence electrons.[23] Therefore the azido specific band is also considered to be the ligand-to-metal charge transfer band.

In Fig. 3 the CD curves of the remaining pair of the mono- and dianiono type complexes, $(-)_{589}$-$[Co(NO_2)(NH_3)(en)_2]^{2+}$ and $(-)_{589}$-$[Co(NO_2)_2(en)_2]^+$, are shown with their absorption curves. In these complexes the second d-d absorption band is completely overlapped

with the nitro specific band. Both the dinitro and amminenitro complexes show two CD bands of opposite signs in the region. However, if the weak CD band of the amminenitro complex in the lower energy side is assumed to correspond to a component of the second d-d absorption band, the more intense CD band in the higher energy side corresponds to the specific band. It may be unreasonable to consider the nitro specific band in the same way as the pseudohalogeno specific band, because the NO_2^- ligand is much different from the N_3^- and NCS^- ligands, that is, the latter two ions are linear pseudohalides which have no absorption band in the near ultraviolet region,[23] while the former nonlinear ion has two weak absorption bands in this region, which have been assigned to $n\rightarrow\pi^*$ transitions.[24] Nevertheless, it is found experimentally that the CD behavior in the nitro specific band region rather resembles that in the pseudohalogeno specific band region.

For the second intense absorption band in the higher energy region (38000—45000 cm^{-1}) of the $(-)_{589}$ nitro complexes, a positive CD band is observed for the amminenitro complex and two CD bands of opposite signs, negative and positive from lower energy side, are observed for the dinitro one (Fig. 3). A similar splitting of the shorter wavelength CD band is also observed for the diisothiocyanato complex. That is, the complex has two CD bands of opposite signs in the region of 37000—44000 cm^{-1}, while the corresponding ammineisothiocyanato complex has only one CD band in this region (Fig. 2 and Table 1).

In Figs. 4—6 the absorption and CD curves of the three mixed complexes of the *cis*-$[Co(X)(X')(en)_2]^+$ type containing different two of N_3^-, NCS^-, and NO_2^- are shown together with the absorption curves of the "parent complexes," *cis*-$[Co(X)_2(en)_2]^+$ and *cis*-$[Co(X')_2(en)_2]^+$. The d-d absorption band positions of the mixed complexes are nearly intermediate between those of the parent ones, but the d-d band intensities are not necessarily intermediate. In the region of specific absorption bands, the absorption curves of the mixed complexes are nearly intermediate between those of the parent ones, but not exactly so, especially for the azidoisothiocyanato complexes. The deviation seems to suggest an interaction between two aniono ligands in the *cis* positions through the central cobalt(III) ion.

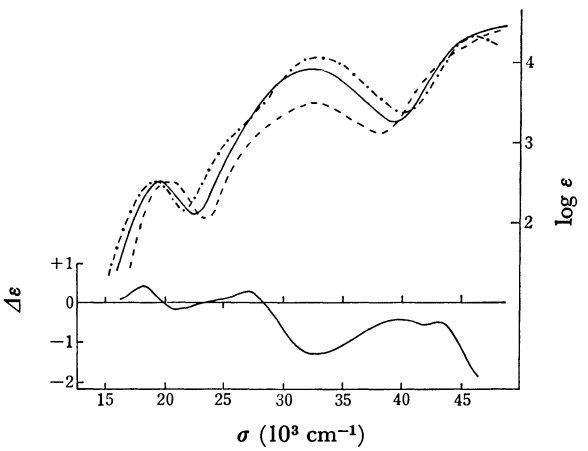

Fig. 4. Absorption and CD spectra of $(+)_{589}$-*cis*-$[Co(N_3)(NCS)(en)_2]Cl\cdot 0.5H_2O$ (——), and absorption spectra of *cis*-$[Co(N_3)_2(en)_2]ClO_4$ (-·-·-) and *cis*-$[Co(NCS)_2(en)_2]Cl\cdot H_2O$ (------).

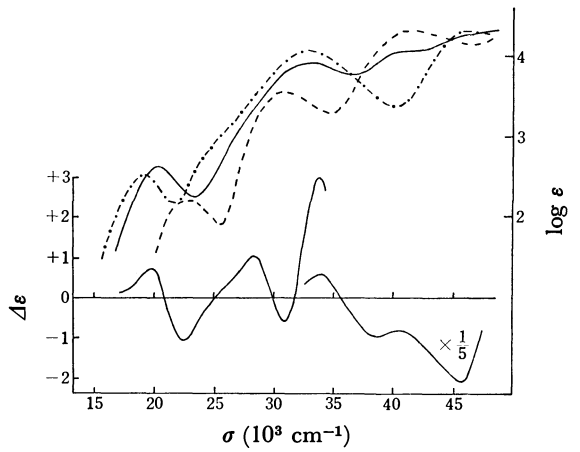

Fig. 5. Absorption and CD spectra of $(+)_{589}$-*cis*-$[Co(N_3)(NO_2)(en)_2]ClO_4$ (——), and absorption spectra of *cis*-$[Co(N_3)_2(en)_2]ClO_4$ (-·-·-) and *cis*-$[Co(NO_2)_2(en)_2]ClO_4$ (------).

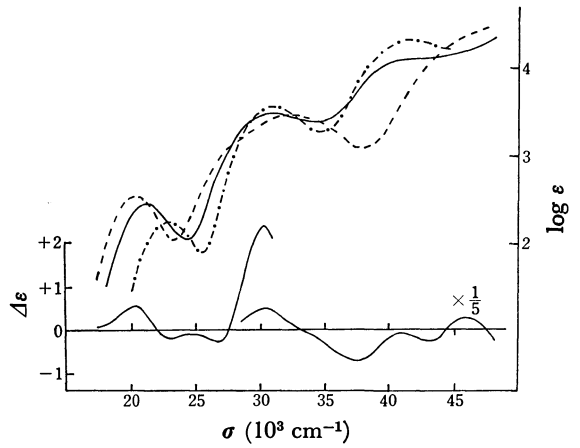

Fig. 6. Absorption and CD spectra of $(+)_{589}$-*cis*-$[Co(NCS)(NO_2)(en)_2]Cl$ (——), and absorption spectra of *cis*-$[Co(NCS)_2(en)_2]Cl\cdot H_2O$ (------) and *cis*-$[Co(NO_2)_2(en)_2]ClO_4$ (-·-·-).

The ultraviolet CD of the mixed complexes is too complicated to interpret systematically, and this may be also the reflection of the symmetry lowering and the interaction between the ligands. A comparison of the CD curves of the mixed complexes with those of the parent complexes having the same absolute configuration and further with their average CD curves was attempted on trial, but any simple regularity was not found.

Absolute Configurations of the Complexes. McCaffery *et al.*[25] have correlated the CD pattern in the first d-d absorption band of a bis(ethylenediamine) cobalt(III) complex with its absolute configuration by employing a model, in which a *cis*-$[Co(X)_2(en)_2]^+$ complex with C_2 symmetry is regarded as an intermediate between $[Co(en)_3]^{3+}$ with D_3 symmetry and *cis*-$[Co(X)_2(NH_3)_4]^+$ with C_{2v} symmetry. When the ligand X lies far above or below the ethylenediamine ligand in the spectro-

chemical series, the complex is near the C_{2v} limit, and the major one of the two CD components is observed closer in energy to the first d-d absorption band of $[Co(en)_3]^{3+}$ than the minor CD component. Then the positive major CD component is correlated to the positive E_a component of Λ-$(+)_{589}$-$[Co(en)_3]^{3+}$.[26] From this criterion and the CD data in Table 1, the absolute configuration Δ was assigned to the two present dianiono complexes, $(+)_{589}$-diazido and $(-)_{589}$-dinitro complexes, and Λ to the remaining $(-)_{589}$-diisothiocyanato complex. The absolute configuration of $(-)_{589}$-dinitro complex has been determined as Δ by an X-ray analysis.[27]

The same treatment can be applied to the mixed complexes of the *cis*-$[Co(X)(X')(en)_2]^+$ type by regarding them as the *cis*-$[Co(Z)_2(en)_2]^+$ complexes, where Z is an imaginary unidentate ligand having the average ligand strength of X and X', if X and X' are not so different in the ligand strength from each other. Thus the $(-)_{589}$ isomer of *cis*-$[CoCl(NCS)(en)_2]^+$, which has the major positive CD component at the higher energy side in the first absorption band region, was assigned to Λ. The $(+)_{589}$ isomer of *cis*-$[Co(N_3)(NCS)(en)_2]^+$ complex was assigned to Δ, because the higher energy CD component of the this isomer has a negative sign ($\Delta\varepsilon=-0.20$), though this negative component is not the major one.

As for the ammineaniono complexes, the isomers having a negative CD band in the first d-d absorption band region, that is, $(-)_{589}$-ammineazido and $(-)_{589}$-ammineisothiocyanato, were assigned to the Δ configuration according to Norman's proposal.[28] The Λ configuration of $(+)_{589}$-ammineisothiocyanato complex is consistent with the fact that this isomer was derived from the Λ-$(-)_{589}$-chloroisothiocyanato complex.

Garbett and Gillard[29] derived the $(+)_{589}$ isomer of ammineitro complex from the Λ-$(-)_{589}$-$[CoCl(NCS)(en)_2]^+$ through $(+)_{589}$-$[Co(NCS)(NO_2)(en)_2]^+$. This means that the configuration of $(-)_{589}$-ammineitro isomer in Table 1 is Δ, which has a major negative CD component at the lower energy side in the first absorption band region. It is consistent with the results for the other Δ nitro mixed complexes such as $(-)_{589}$-dinitro,[27] $(-)_{589}$-chloronitro,[29] and $(-)_{546}$-cyanonitro[30] complexes. In this relation, the present two mixed complexes, $(+)_{589}$-$[Co(N_3)(NO_2)(en)_2]^+$ and $(+)_{589}$-$[Co(NCS)(NO_2)(en)_2]^+$, were assigned to the Λ absolute configuration, because both the two complexes have a positive CD component at the lower energy side in the first absorption band region (Table 2).

Table 3. Absolute configurations of the optical isomers forming the less soluble diastereomers

Complex ion	Resolving agent	Optical rotation	Absolute configuration
(1) *cis*-$[Co(N_3)(NH_3)(en)_2]^{2+}$	a)	$(-)_{589}(-)_{546}$	Δ
(2) *cis*-$[Co(N_3)_2(en)_2]^+$	b)	$(+)_{589}(-)_{546}$	Δ
(3) *cis*-$[Co(NCS)(NH_3)(en)_2]^{2+}$	c)	$(+)_{589}(+)_{546}$	Λ
(4) *cis*-$[Co(NCS)_2(en)_2]^+$	b)	$(-)_{589}(+)_{546}$	Λ
(5) *cis*-$[Co(NO_2)(NH_3)(en)_2]^{2+}$	a)	$(-)_{589}(-)_{546}$	Δ
(6) *cis*-$[Co(NO_2)_2(en)_2]^+$	b)	$(-)_{589}(-)_{546}$	Δ
(7) *cis*-$[Co(N_3)(NCS)(en)_2]^+$	a)	$(+)_{589}(-)_{546}$	Δ
(8) *cis*-$[Co(N_3)(NO_2)(en)_2]^+$	a)	$(+)_{589}(+)_{546}$	Λ
(9) *cis*-$[Co(NCS)(NO_2)(en)_2]^+$	b)	$(+)_{589}(+)_{546}$	Λ
(10) *cis*-$[CoCl(NCS)(en)_2]^+$	a)	$(-)_{589}(+)_{546}$	Λ

a) NH_4(*d*-bcs). b) $K_2[Sb_2(d\text{-tart})_2]\cdot 3H_2O$. c) Derived from Λ-$(-)_{589}$-$[CoCl(NCS)(en)_2]^+$.

The assignments of absolute configurations for the present ten complexes are collected in Table 3. From this table and the CD signs of the "specific band" (Tables 1 and 2), the following relationship is obtained. In the ammineaniono complexes, all the Λ isomers show a negative CD band in the regions of the specific absorption bands, if a weak CD band of the amminenitro complex at 31000 cm^{-1} is neglected. As mentioned already, this longer-wavelength weak CD band may be due to the second d-d absorption band, which is completely overlapped with the nitro specific band. In the dianiono complexes, Λ isomers show regularly a CD pattern of negative and then positive signs in the order of increasing energy (Figs. 1—3). In the mixed type complexes, *cis*-$[Co(X)(X')(en)_2]^+$ (X and X'=N_3^-, NCS^-, or NO_2^-), the CD patterns are complicated, but the following regularity is found out for the specific band region; that is, the dominant CD band in this region is positive for all of their Λ isomers (Figs. 4—6).

The authors are grateful to Dr. Wasuke Mori of Osaka University, and Dr. Keiji Matsumoto of Osaka City University for their help in the measurements of CD spectra.

References

1) R. Tsuchida and M. Kobayashi, *Bull. Chem. Soc. Jpn.*, **13**, 471 (1938).
2) H. Kuroya, *J. Inst. Polytech., Osaka City Univ.*, **1**, No. 1, Ser. C, 29 (1950).
3) Y. Shimura, *J. Am. Chem. Soc.*, **73**, 5079 (1951).
4) C. K. Jørgensen, "Absorption Spectra and Chemical Bonding in Complexes," Pergamon Press, Oxford (1962), p. 196.
5) M. Linhard and M. Weigel, *Z. Anorg. Chem.*, **267**, 113 (1951).
6) M. Linhard and M. Weigel, *Z. Anorg. Chem.*, **267**, 121 (1951).
7) H. -H. Schmidtke, *Ber. Bunsenges. Phys. Chem.*, **71**, 1138 (1967).
8) H. -H. Schmidtke and D. Garthoff, *J. Am. Chem. Soc.*, **89**, 1317 (1967).
9) D. F. Gutterman and H. B. Gray, *J. Am. Chem. Soc.*, **93**, 3364 (1971).
10) V. M. Miskowski and H. B. Gray, *Inorg. Chem.*, **14**, 401 (1975).
11) K. G. Caulton and R. F. Fenske, *Inorg. Chem.*, **6**, 562 (1967).
12) K. Yamasaki, J. Hidaka, and Y. Shimura, *Chem. Lett.*, **1972**, 1143.
13) A. Werner, *Ann.*, **386**, 1-272 (1912).
14) D. A. Buckingham, I. I. Olsen, and A. M. Sargeson, *J. Am. Chem. Soc.*, **90**, 6654 (1968).

15) P. J. Staples and M. L. Tobe, *J. Chem. Soc.*, **1960**, 4812.
16) A. Werner and F. Braunlich, *Z. Anorg. Chem.*, **22**, 123 (1900).
17) K. Garbett, R. D. Gillard, and P. J. Staples, *J. Chem. Soc.*, **1966**, 201.
18) P. Pfeiffer and O. Angern, *Ber.*, **60**, 308 (1927).
19) M. Linhard and G. Stirn, *Z. Anorg. Chem.*, **268**, 105 (1952).
20) F. P. Dwyer and F. L. Garvan, *Inorg. Synth.*, **6**, 195 (1960).
21) H. Yamatera, *J. Inorg. Nucl. Chem.*, **15**, 50 (1960).
22) K. Nakamoto, J. Fujita, M. Kobayashi, and R. Tsuchida, *J. Chem. Phys.*, **27**, 439 (1957).
23) J. W. Rabalais, J. M. McDonald, V. Scherr, and S. P. McGlynn, *Chem. Rev.*, **71**, 73 (1971).
24) H. J. Maria, D. Larson, M. E. McCarville, and S. P. McGlynn, *Acc. Chem. Res.*, **3**, 368 (1970).
25) A. J. McCaffery, S. F. Mason, and B. J. Norman, *J. Chem. Soc.*, **1956**, 5094.
26) Y. Saito, K. Nakatsu, M. Shiro, and H. Kuroya, *Bull. Chem. Soc. Jpn.*, **30**, 795 (1957).
27) K. Matsumoto and H. Kuroya, *Bull. Chem. Soc. Jpn.*, **45**, 1755 (1972).
28) B. J. Norman, *Inorg. Chim. Acta*, **1**, 177 (1967).
29) K. Garbett and R. D. Gillard, *J. Chem. Soc.*, **1965**, 6084.
30) K. Ohkawa, J. Hidaka, and Y. Shimura, *Bull. Chem. Soc. Jpn.*, **40**, 2830 (1967).

Studies of the Cobalt(III) Complexes of 8-Amino-3,6-diazaoctanate Ion. II.[1] The Preparation and Some Properties of the Complexes with a Carbonate, Oxalate, or Malonate Ligand

Kiyokatsu WATANABE

Department of Chemistry, Faculty of Science, Ehime University, Matsuyama, Ehime 790

(Received June 12, 1976)

The following new cobalt(III) complexes containing the quadridentate 8-amino-3,6-diazaoctanate ion (adao) have been prepared: α-[Co(adao)(ox)], α-[Co(adao)(mal)] (mal, malonate ion), *β-mer(N)*-[Co(adao)(CO_3)], *β-mer(N)*-[Co(adao)(mal)], *β-fac(N)*-[Co(adao)(CO_3)], *β-fac(N)*-[Co(adao)(ox)], and *β-fac(N)*-[Co(adao)(mal)]. The geometrical isomers have been separated by the chromatographic technique. The configurations of the complexes have been identified by means of the electronic absorption spectra and the proton NMR spectra.

The 8-amino-3,6-diazaoctanate ion (adao)* can coordinate with four coordination modes in an octahedral complex, as is shown in Fig. 1-a. These modes were designated as *α,β-mer(N)*, *β-fac(N)*, and *trans* by Schneider and Collman.[2] The two optical isomers (*Δ* and *Λ*) which arise from the contribution of a configurational chirality may exist in each of three coordination modes (*α,β-mer(N)*, and *β-fac(N)*) of their four coordination modes. When we consider the configuration of the secondary amine nitrogen atom (*s*-N) in adao, further discrimination is possible in the *β-mer(N)*, *β-fac(N)*, and *trans* forms. This is illustrated in Fig. 1-b. The configuration of the chiral *s*-N atom is described by the *R* or *S* rule proposed by Cahn, Ingold, and Prelog.[3] For the respective *β-mer(N)*, *β-fac(N)*, and *trans* racemic isomers, the existence of isomers, (*SR,RS*) and (*SS,RR*), is possible. However, such isomers are impossible to exist for the α racemic isomer. Thus, five geometrical isomers *α,β-mer(N)*-(*SR,RS*), *β-mer(N)*-(*SS, RR*), *β-fac(N)*-(*RS,SR*), and *β-fac(N)*-(*RR,SS*), are possible when a symmetrical bidentate ligand occupies the residual sites.

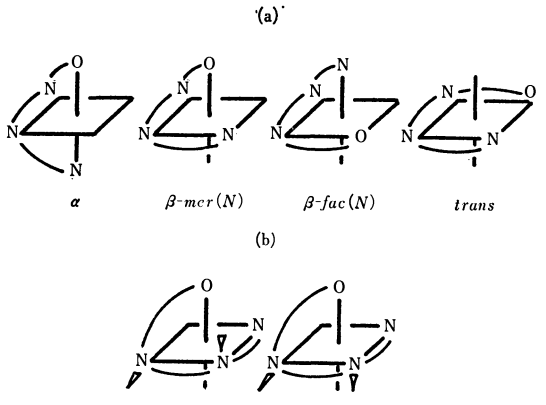

Fig. 1. Coordination modes of adao (a) and configurations around the *s*-N of adao in *Δ-β-mer(N)* coordination mode (b).

* The following abbreviations are used for the ligands: adao, 8-amino-3,6-diazaoctanate; edda, ethylenediamine-*N,N'*-diacetate; ed3a, ethylenediamine-*N,N,N'*-triacetate; *i*-dtma, 4-diethylenetriaminemonoacetate; ox, oxalate; mal, malonate.

If an unsymmetrical bidentate ligand occupies, the number of the isomers increase. Schneider *et al.*,[2] Fukuhara *et al.*,[4] and the present author[1] have studied the cobalt(III) complexes containing the quadridentate ligand. It was shown in these studies that most complexes isolated were the *β-mer(N)* isomers, although the existence of the α and the *β-fac(N)* isomers is also to be expected. In order to clarify this problem, the isolation of the isomers with a symmetrical bidentate ligand was attempted. Thus, we succeeded in isolating some of the α and *β-fac(N)* isomers for the carbonato, oxalato, and malonato complexes.

Experimental

Materials. Diethylenetriamine (Nakarai Chemicals), oxalic acid, malonic acid and all the other reagent-grade chemicals were used without further purification. Column chromatography was carried out by the use of Dowex 50 W-X8 cation-exchange resin.

Preparations. (1) *Isomers of (8-Amino-3,6-diazaoctanato)-carbonatocobalt(III)*, [*Co(adao)(CO_3)*]: The carbonato complex (5 g), which had been isolated by the method of Schneider *et al.*,[2] was dissolved in 30 cm^3 of water. The solution was then poured into a column (50 mm × 350 mm) containing Dowex 50W-X8 (200—400 mesh, sodium form). By elution with water, the adsorbed bands were gradually separated into two bands: the first was dark-red (Eluate I, ≈100 cm^3), and the second was red-violet (Eluate II, ≈300 cm^3). Eluate I was concentrated to about 15 cm^3 in a rotary evaporator below 40 °C and then kept in a refrigerator for two days. The red precipitate thus deposited (Precipitate I) was collected. Although it is possible to obtain the considerable precipitate from the mother filtrate, the precipitate does not consist of only one isomer. Precipitate I was recrystallized from warm water (≈3 cm^3, 65 °C) and subsequently washed with ethanol and ether. Yield, 0.25 g. Eluate II was reduced to about 5 cm^3 in a rotary evaporator, and then concentrated to nearly dryness over silica gel in a vacuum desiccator. The red-violet deposit was collected and recrystallized from 1 cm^3 of warm water. It was washed with ethanol and acetone. Yield, 0.12 g.

(2) *Isomers of (8-Amino-3,6-diazaoctanato)oxalatocobalt(III)*, [*Co(adao)(ox)*]: A solution of oxalic acid dihydrate (0.6 g) in 5 cm^3 of warm water (≈55 °C) was added to a suspension of Schneider's carbonato complex, [Co(adao)(CO_3)], (1.4 g) in 15 cm^3 of water, and then the mixture was heated at ≈75 °C for 4 h with continuous stirring. To the resulting product, which contained an appreciable amount of a precipitate, was added 40 cm^3 of water, and the precipitate was dissolved by

heating (≈70 °C). The solution was cooled, and then it was filtered. The red filtrate was poured into a column (20 mm × 700 mm) containing Dowex 50 W-X8 (100—200 mesh, hydrogen form), and the adsorbed sustance was eluted with water. The red band which was adsorbed at the top of the column, separated cleanly into three bands with red, pink-red, and red-violet color in the order of the elution. Each of three eluates (≈100 cm³, ≈100 cm³, and ≈120 cm³) was concentrated to about 5 cm³ in a rotary evaporator at ≈55 °C, and then cooled. Each deposit was recrystallized from hot water (5—7 cm³, ≈70 °C) and was washed with methanol and ether. The yields were 1.0 g for the red, 0.05 g for the pink-red, and 0.05 g for the red-violet isomer.

(3) *Isomers of (8-Amino-3,6-diazaoctanato)malonatocobalt(III), [Co(adao)(mal)]*: The reaction product was obtained and separated by a similar procedure to that described in (2) using malonic acid instead of oxalic acid. When three elutes (≈300 cm³, ≈250 cm³, and ≈300 cm³) were concentrated to dryness, dark-red, pink-red, and red-violet products were obtained respectively. Each product was washed with acetone. The pink-red product was hygroscopic; hence, it was difficult to handle. The yields were 1.0 g for the dark-red, 0.05 g for the pink-red, and 0.1 g for the red-violet isomer. The red-violet isomer can be obtained in a better yield by the reaction at a higher temperature (≈80 °C), but the yield of the pink-red isomer decreases.

Measurements. The visible and ultraviolet absorption spectra were measured with a Hitachi EPS-3T Recording Spectrophotometer or a Shimadzu UV-200 Recording Spectrophotometer. The proton NMR spectra were recorded with a Varian XL-100 spectrometer in deterium oxide, with *t*-butyl alcohol as the internal reference.

Results and Discussion

The analytical data for the complexes prepared are summarized in Table 1.

Electronic Spectra. The electronic spectra are shown in Figs. 2—4, while the numerical values of the absorption maxima are summarized in Table 2. If the configuration of the ligating nitrogen atom of adao is not considered, three geometrical isomers (*α,β-mer(N)*, and *β-fac(N)*) are possible for the complexes of [Co(adao)(AA)] (AA=CO_3, ox, and mal). The *α* and the *β-fac(N)* isomers belong to a *fac* type of $[CoN_3O_3]$, and the *β-mer(N)* to a *mer* one. As regards the complex of $[CoN_3O_3]$ type, it is well known that the first band of the *mer* isomer is broader than that of the *fac* isomer.[5] As may be seen in Fig. 3, which shows the spectra of the oxalato complexes, the first band of the red isomer is broader than those of the other two. From this spectral difference, the red isomer is identified as having the *β-mer(N)* structure. Although the two remaining isomers must belong to the *fac* isomer, it is difficult to determine their structures on the basis of the spectral data alone. However, it is observed that the absorption intensity of the first band of the red-violet isomer is stronger than that of the pink-red one. Similar features are observed among the spectra of the malonato com-

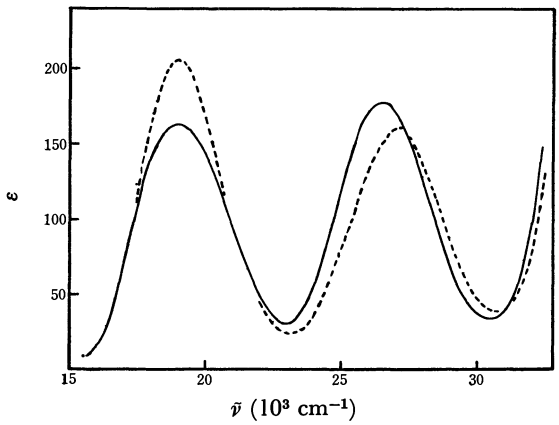

Fig. 2. Absorption spectra of [Co(adao)(CO_3)] complexes.
——: *β-mer(N)*-[Co(adao)(CO_3)] (red),
------: *β-fac(N)*-[Co(adao)(CO_3)] (red-violet).

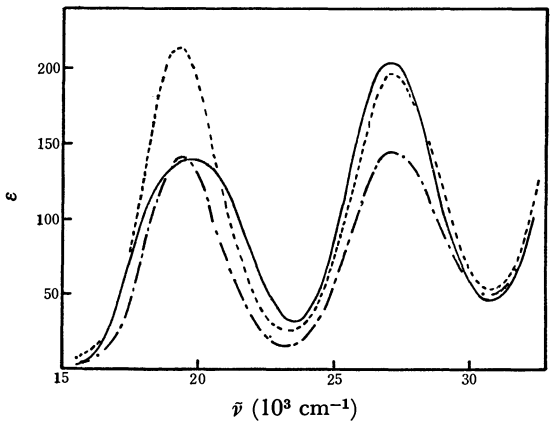

Fig. 3. Absorption spectra of [Co(adao)(ox)] complexes.
-·-·-: α-[Co(adao)(ox)] (pink-red),
——: *β-mer(N)*-[Co(adao)(ox)] (red),
------: *β-fac(N)*-[Co(adao)(ox)] (red-violet).

Table 1. Elemental analyses

	Color	C (%)		H (%)		N (%)	
		Found	Calcd	Found	Calcd	Found	Calcd
α-[Co(adao)(ox)]·1.5H_2O	Pink-red	29.06	28.75	4.85	5.13	12.50	12.57
α-[Co(adao)(mal)]·0.5H_2O	Pink-red	32.75	32.74	5.10	5.19	12.44	12.73
β-mer(N)-[Co(adao)(CO_3)]·H_2O	Red	28.14	28.29	5.43	5.43	14.25	14.14
β-mer(N)-[Co(adao)(ox)]	Red	30.98	31.28	4.61	4.59	13.51	13.68
β-mer(N)-[Co(adao)(mal)]·2.5H_2O	Dark-red	29.71	29.52	5.76	5.78	11.50	11.47
β-fac(N)-[Co(adao)(CO_3)]·2H_2O	Red-violet	26.39	26.68	5.78	5.76	13.25	13.33
β-fac(N)-[Co(adao)(ox)]	Red-violet	31.07	31.28	4.65	4.59	13.51	13.68
β-fac(N)-[Co(adao)(mal)]·0.5H_2O	Red-violet	33.16	32.74	5.14	5.19	13.13	12.73

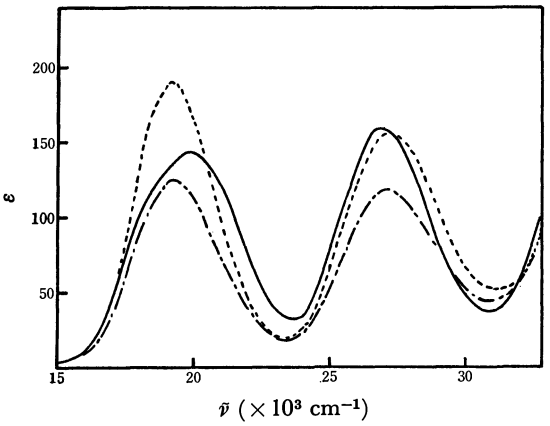

Fig. 4. Absorption spectra of [Co(adao)(mal)] complexes.
----: α-[Co(adao)(mal)] (pink-red),
——: *β-mer(N)*-[Co(adao)(mal)] (dark-red),
------: *β-fac(N)*-[Co(adao)(mal)] (red-violet).

TABLE 2. ABSORPTION DATA OF THE adao-Co(III) COMPLEXES (Wave numbers are in 10^3 cm^{-1})

	Color	I $\bar{\nu}_{max}$ (ε)	II $\bar{\nu}_{max}$ (ε)
α-[Co(adao)(ox)]	Pink-red	19.30(142)	27.10(145)
α-[Co(adao)(mal)]	Pink-red	19.23(125)	27.06(118)
β-mer(N)-[Co(adao)-(CO_3)]	Red	19.00(162)	26.39(177)
β-mer(N)-[Co(adao)-(ox)]	Red	≈19.9 (140)	27.03(204)
β-mer(N)-[Co(adao)-(mal)]	Dark-red	≈19.9 (143)	27.00(160)
β-fac(N)-[Co(adao)-(CO_3)]	Red-violet	19.00(206)	27.10(160)
β-fac(N)-[Co(adao)-(ox)]	Red-violet	19.23(213)	27.17(196)
β-fac(N)-[Co(adao)-(mal)]	Red-violet	19.12(190)	27.17(155)

plexes (Fig. 4), and it is inferred that the dark-red isomer is the *β-mer(N)*, while the pink-red and red-violet ones are the α or the *β-fac(N)*. Among the isomers of the carbonato complex, it is found that the intensity of the first band of the red-violet isomer is stronger and narrower than that of the red one.

Proton NMR Spectra. The proton NMR spectra of the two isomers of the carbonato complex and the red isomer of the oxalato complex are shown in Fig. 5. The PMR spectra of the dark-red and red-violet isomers of the malonato complex are shown in Fig. 6. It was difficult to measure the spectra of the other two isomers of the oxalato complex because of their low solubilities. For the pink-red isomer of the malonato complex, the PMR spectrum was not obtained satisfactorily. As can be inferred from the coordination modes of adao in Fig. 1-a, these isomers may be classified into two groups from the standpoint of the disposition of adao's glycinate ring: one group consists of the isomers with out-of-plane glycinate (α and *β-mer(N)*), and the other, of those with in-plane glycinate (*β-fac(N)* and *trans*). Therefore, the PMR spectra of the former

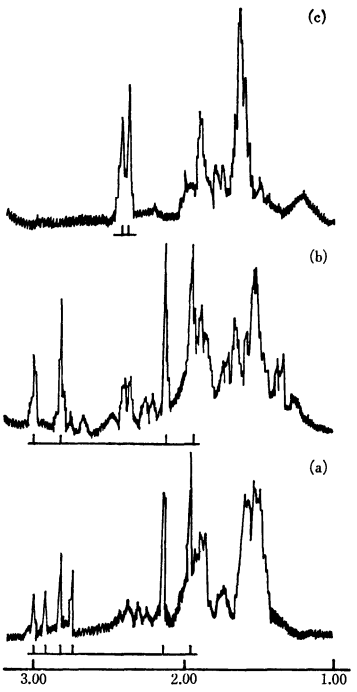

Fig. 5. Proton NMR spectra.
(a): *β-mer(N)*-[Co(adao)(ox)](red),
(b): *β-mer(N)*-[Co(adao)(CO_3)] (red),
(c): *β-fac(N)*-[Co(adao)(CO_3)](red-violet).

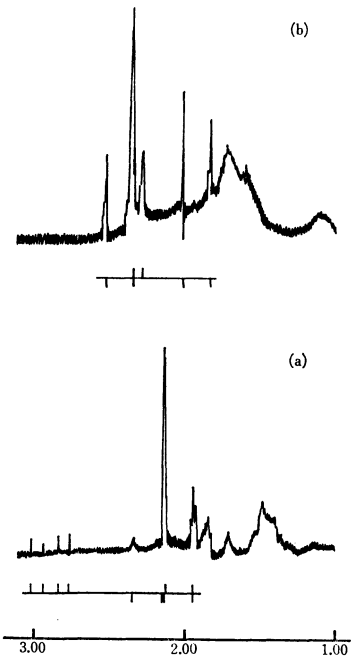

Fig. 6. Proton NMR spectra.
(a): *β-mer(N)*-[Co(adao)(mal)] (dark-red),
(b): *β-fac(N)*-[Co(adao)(mal)] (red-violet).

isomers may be expected to be different from those of the latter isomers at the resonances of the glycinate protons. It has been reported that a considerable difference exists between the isomers of [Co(edda)-(AA)]$^{1\pm}$ (AA=$(NH_3)_2$, en, ox, and mal)[6] and

$[Co(adao)(AA)]^{2+}$ ($AA=(NH_3)_2$, en)[1]; that is, a AB quartet appears for the out-of-plane ring (R-ring) protons and an apparent singlet for the in-plane ring (G-ring) protons. It has also been observed in the spectra of the edda and ed3a Co(III) complexes that the value of $\delta_{AB}(=\delta_A-\delta_B)$ for the R-ring protons is in the range of 0.7 to 1.0 ppm, while that for the G-ring protons is in the range of 0.0 to 0.4 ppm.[7] As may be seen in Fig. 5, the red isomer of the oxalato complex, which has been inferred to be the *β-mer(N)* structure on the basis of the electronic spectrum, shows one AB quartet in the range of 1.96 to 3.00 ppm, although the two resonances at the lower field split into doublet. A pair of doublets in the range of 2.74 to 3.00 ppm is considered to be due to the coupling with the amine proton, which is not completely exchanged at the time of the measurement. The value of the δ_{AB} is about 0.76 ppm ($J_{AB}=18$ Hz).

The red isomer of the carbonato complex shows one clear AB quartet in the range of 1.94 to 3.00 ppm. The δ_{AB} is calculated to be 0.86 ppm. On the other hand, the red-violet isomer of the carbonato complex exhibits two resonances at 2.37 and 2.41 ppm. If it is assumed that the J_{AB} is 16 Hz,[8] the δ_{AB} is 0.12 ppm. From these spectral patterns, it can be found that the glycinate ring's disposition of the red isomer is out-of-plane, while that of the red-violet one is in-plane. Consequently, it is reasonable to assign the red isomer to the *β-mer(N)*, and the red-violet one, to the *β-fac(N)*.

The malonato isomers show more complicated spectra than those of the oxalato and carbonato isomers because of the existence of the malonate ring protons. For the dark-red isomer, it was found that the four peaks in the range of 2.77 to 3.02 ppm (Fig. 6-a) are reduced to two peaks upon the addition of Na_2CO_3 to the solution. Thus, the resonances of the dark-red malonato isomer consist of two AB quartets: one is the resonances centered at about 2.45 ppm and the other is those centered at 2.145 ppm. The δ_{AB} and J_{AB} of the quartet with the center at 2.45 ppm are 0.80 ppm and 18 Hz respectively. From the similarity of these values (δ_{AB} and J_{AB}) between the dark-red isomer and the *β-mer(N)*-ox isomer, this AB quartet is attributed to the glycinate protons of adao. The other quartet may be considered to be due to the methylene protons of the malonate ring. Therefore, the dark-red isomer is assigned to the *β-mer(N)*. The PMR spectrum of the red-violet isomer consists, in the lower field, of a doublet with the center at 2.32 ppm and a quartet with the center at 2.18 ppm. The δ_{AB} of the former is about 0.16 ppm and that of the latter, 0.48 ppm. The chemical shift and the δ_{AB} of the doublet of this isomer are similar to those of the *β-fac(N)* isomer of the carbonato complex. The quartet is obviously due to the malonate ring protons. From these facts, the red-violet isomer is assigned to the *β-fac(N)* structure.

The cobalt-malonate ring is six-membered and is necessarily conformationally bent: three conformations, chair, boat, and skew-boat, are possible. Buckingham *et al.*[9] proposed that the boat and skew-boat conformations are more stable than the chair one, on the basis of the theory in which the dipole interaction between electron pairs on the ligating oxygen and on the adjacent carbonyl oxygen is more important in the chair form. Moreover, they suggested that the skew-boat conformation is more stable than the boat one, when there is interaction between the malonate hydrogen atom and another ligating group. The theory and the results of the PMR spectra indicated that the malonate rings in the complex ions such as $[Co(mal)(en)_2]^+$ and $[Co(mal)_2(en)]^-$ take the skew-boat conformation. On the other hand, when the absolute configuration of $(-)_{589}$-Na$[Co(mal)_2(en)]$ was studied by Butler and Snow by the X-ray method, they showed that the malonate rings in the complex ion adopt the boat conformation.[10] Furthermore, Matsumoto and Kuroya, in investigating the crystal structure of $(-)_{589}$-$[Co(NO_2)_2(en)_2]\cdot(+)_{589}$-$[Co(mal)_2(en)]$ by the X-ray method, showed that the two malonate rings are nearly planar.[11] From these facts and the theory proposed by Buckingham *et al.*, the existence of the chair conformers seems to be impossible for the Co(III)-complex with the malonate ring. When the molecular models of the *β-mer(N)*-[Co(adao)(mal)] isomer are examined, it seems to be impossible that the malonate ring takes the boat conformation because of the interactions between the malonate hydrogen atoms and the adao's NH and NH_2 hydrogen atoms.

Three conformations, boat, skew-boat, and planar, are possible for the *β-fac(N)*-[Co(adao)(mal)]. When the symmetry of only the malonate ring is considered, the chemical environments of two malonate hydrogen atoms are equivalent in the skew-boat and the planar conformation, but not in the boat one. Therefore, it may be expected that the δ_{AB}'s of the malonate protons for the formers are smaller than that for the latter. As may be seen in Fig. 6, the δ_{AB} of the malonate protons of the *β-fac(N)* isomer is larger than that of the *β-mer(N)* isomer. Consequently, it may be inferred that the malonate chelate ring in the *β-mer(N)* isomer adopts the skew-boat or the planar conformation and that in the *β-fac(N)* isomer the boat one.

The possible existence of the two *β-mer(N)* isomers arising from the configuration of *s*-N atom of adao is shown in Fig. 1-b. From the examination of molecular models, it may be expected that the PMR spectrum of *β-mer(N)*-(*SR,RS*) isomer is different from that of the *β-mer(N)*-(*SS,RR*) at the resonances of the glycinate ring protons. Thus, if the *β-mer(N)* complex isolated is a mixture, a pair of doublet at the high field portion of the AB quartet pattern may be observed in the PMR spectrum. However, the PMR spectrum with a pair of doublet at the region mentioned above, is not obtained. Thus, the PMR evidences indicate that the respective *β-mer(N)* complexes isolated consist of one configuration for *s*-N atom of adao. However, it is difficult to assign the configuration of the *s*-N on the basis of the PMR spectra. On the other hand, the examination of molecular models for the two possible *β-fac(N)* isomers shows that the *β-fac(N)*-(*RS,SR*) configuration is more favoured than the *β-fac(N)*-(*RR,SS*), because the latter configuration exhibits the interaction between the hydrogen atom of the glycinate ring and the terminal amino hydrogen atom of adao. Furthermore, the PMR

spectrum shows only one clear doublet pattern. Thus, it may be inferred that the *β-fac(N)* isomers prefer the (*RS,SR*) configuration.

Besides the well-known *β-mer(N)* coordination mode, the α and the *β-fac(N)* modes are established for the oxalato and malonato complexes. Although the configuration (whether (*SR,RS*) or (*SS,RR*)) of the *s*-N in the *β-mer(N)* isomers can not be decided, it is found that the *β-mer(N)* complex isolated in this work adopts only one of the two configurations. For the malonate complexes, it is difficult to decide the ring conformation exactly. It has been inferred, however, that the conformation is the skew-boat in the *β-mer(N)* isomer and the chair in the *β-fac(N)* one. From Table 2, it may be seen that the apparent maximum of the first absorption band in the *β-mer(N)* isomer is at the same or a higher wave number than those in the corresponding α and *β-fac(N)* isomers. It was found that there are some differences in the absorption and PMR spectra between the author's *β-mer(N)*-carbonato complex and Collman's. Also, the carbonato complex isolated by Collman's method was separated cleanly into two bands by the chromatography. These facts suggest that Collman's *β-mer(N)*-carbonato complex contained another species. It is noticeable that the second band maximum of the author's *β-mer(N)* carbonato isomer is at considerably the lower wave number than that of the *β-fac(N)* one. Such difference in the second band maxima between isomers of $[CoN_3O_3]$ type have not been recognized previously,[5,12] although it has been reported that the second band of the *mer(trans)*-$[Co(CO_3)(gly)(NH_3)_2]$[13] or *mer(N)*-[Co(*i*-dtma)(CO_3)][14] exhibits a splitting.

The author expresses sincere thanks to Professor Yoichi Shimura of Osaka University for his kind guidance and to Professor Kashiro Kuroda of Ehime University for his encouragement during the course of this work.

References

1) Part I of this series: K. Watanabe and K. Kuroda, *Nippon Kagaku Kaishi*, **1972**, 1409; In the paper, the abbreviation, "DTMA," proposed by Schneider *et al.*[2] was used instead of "adao."

2) P. W. Schneider and J. P. Collman, *Inorg. Chem.*, **7**, 2010 (1968).

3) R. S. Cahn, C. K. Ingold, and V. Prelog, *Angew. Chem. Int. Ed. Engl.*, **5**, 385 (1966).

4) A. Fukuhara, E. Kyuno, and R. Tsuchiya, the 20th Symposium on Coordination Chemistry (1970), Abstracts, p. 29.

5) (a) Y. Shimura and R. Tsuchida, *Bull. Chem. Soc. Jpn.*, **29**, 311 (1956); (b) N. Matsuoka, Y. Shimura, and R. Tsuchida, *Nippon Kagaku Zasshi*, **82**, 1637 (1961); (c) N. Matsuoka, J. Hidaka, and Y. Shimura, *Bull. Chem. Soc. Jpn.*, **39**, 1257 (1966).

6) (a) J. I. Legg and D. W. Cook, *Inorg. Chem.*, **4**, 1576 (1965); (b) K. Kuroda and K. Watanabe, *Bull. Chem. Soc. Jpn.*, **44**, 1034 (1971); (c) K. Kuroda, *Chem. Lett.*, **1972**, 719.

7) P. F. Coleman, J. I. Legg, and J. Steele, *Inorg. Chem.*, **9**, 937 (1970).

8) G. L. Blackmer and J. L. Sudmeier, *Inorg. Chem.*, **10**, 2019 (1971).

9) D. A. Buckingham, L. Durham, and A. M. Sargeson, *Aust. J. Chem.*, **20**, 257 (1967).

10) K. R. Butler and M. R. Snow, *Chem. Commun.*, **1971**, 550.

11) K. Matsumoto and H. Kuroya, *Bull. Chem. Soc. Jpn.*, **45**, 1755 (1972).

12) K. Kuroda, Y. Mori, H. Matsunaga, K. Kunigita, and K. Watanabe, *Bull. Chem. Soc. Jpn.*, **48**, 234 (1975).

13) S. Kanazawa and M. Shibata, *Bull. Chem. Soc. Jpn.*, **44**, 2424 (1971).

14) S. Nakashima and M. Shibata, *Bull. Chem. Soc. Jpn.*, **47**, 2069 (1974).

Effects of the Anion on the Extraction of Cobalt with 8-Quinolinol into Chloroform

Eiichi SEKIDO and Kazuhiko FUJITA

Department of Chemistry, Faculty of Science, Kobe University, Nada, Kobe 657

(Received June 14, 1976)

The effects of the anions, especially the perchlorate ion, on the extraction of cobalt into chloroform with 8-quinolinol (Hql) were examined. Two kinds of cobalt(II) 8-quinolinol complexes, species A and B, are extracted into the chloroform phase from the aqueous cobalt(II) solution containing perchlorate ions. Species A contains no perchlorate ion and is extracted above pH 7.7; species B is an ion-pair complex containing a perchlorate ion and is predominantly extracted below pH 5.1. The compositions of species A and B were estimated to be $Co_2ql_4(Hql)_2$ and $Co_2ql_3(Hql)_3ClO_4$, respectively. These dimer complexes are related by the following equilibrium, with $\log K_{AB} = -7.2$:

$$[Co_2ql_3(Hql)_3]^+ClO_{4(o)}^- \rightleftharpoons Co_2ql_4(Hql)_{2(o)} + ClO_4^- + H^+$$

The species extracted into the chloroform phase from the aqueous cobalt(II) solution containing sulfate ions does not contain any sulfate ions. The formation of the species containing anions increases in the order: $ClO_4^- > NO_3^- > Cl^- > SO_4^{2-}$, which is also the general order of the extent of forming the ion-pair compounds. The ion-pair complex tends to prevent the oxidation from cobalt(II) 8-quinolinol complex to cobalt(III) 8-quinolinol complex.

The stoichiometric behavior of the extraction of cobalt into chloroform containing 8-quinolinol (Hql) has been studied by several investigators.[1-4] In these studies it was reported that the species extracted into chloroform is not the simple cobalt 8-quinolinol chelate, $Coql_2$, but the self-adduct, such as $Coql_2(Hql)_2$,[1,2] or $Coql_2Hql$.[3,4] These stoichiometric studies, of course, were carried out under the condition of a constant ionic strength, which was adjusted by the addition of a salt such as sodium perchlorate or potassium chloride. On the other hand, Ōki *et al.* recently reported that an ion-pair complex is extracted into chloroform when a zinc solution containing perchlorate ions is shaken with a chloroform solution containing 8-quinolinol.[5] They suggested the formation of an ion-pair complex for nickel as well as for zinc.[6] Moreover, Sekido *et al.* studied the effects of various kinds of anions on the extraction of zinc with the chloroform solution of 8-quinolinol;[7] the compositions of the zinc 8-quinolinol complexes extracted were also determined.[8] Consequently, it will be assumed that the extraction of cobalt with chloroform containing 8-quinolinol may also be affected by the kind of anion contained in the aqueous solution. Thus, in this study, the extraction behavior of the cobalt with the chloroform solution of 8-quinolinol from an aqueous solution containing one of such anions as the perchlorate, nitrate, sulfate, or chloride ion have been reexamined.

Experimental

Reagents. 8-Quinolinol was recrystallized twice from ethanol (mp 73—73.5 °C). The chloroform was shaken with dilute hydrochloric acid solution, sodium hydroxide solution, and demineralized water, dried with anhydrous sodium sulfate, and then distilled twice. Cobalt perchlorate and nitrate in analytical-reagent grade were used to prepare stock solutions of cobalt; their concentrations were determined by chelatometric titrations. Carrier-free ^{60}Co radiotracer was added to the stock solutions when the distribution ratio of cobalt was determined. The sodium salts of perchlorate, nitrate, sulfate, and chloride and the buffer components were all of analytical-reagent grade.

Apparatus. Extraction was carried out in a Taiyo M incubator at 25±0.1 °C. A Japan Radio well-type NaI(Tl) scintillation detector connected with a Toshiba UDS-24202 B universal scalar was used for the radioactivity counting. Ultraviolet and visible absorption spectra of the chloroform phase were taken with a Hitachi 124 double beam spectrophotometer and the pH of the aqueous phase was measured with a Hitachi-Horiba M-5 pH meter.

Extraction of Cobalt. Into a 50 ml glass cylindrical tube with a glass stopper was introduced 1.00 ml of 1×10^{-3} M cobalt(II) perchlorate or nitrate solution, adjusted to the desired pH with a small amount of a buffer solution. Then the sodium salt solution of the appropriate anion, whose effect was to be examined, was added, so that 10.00 ml of the final cobalt solution could be kept at the ionic strength of 0.1 or 1.0. The buffer solution was made with the mineral acid having the appropriate anion, sodium hydroxide, or such a small amount of acetic acid or boric acid that we could ignore the effect of the acetate or borate anion. After the addition of 10 ml of 0.1 M chloroform solution of 8-quinolinol, the mixture was completely equilibrated by shaking for 10 min at 200 strokes/min at 25±0.1 °C. After the mixture was centrifuged for 2 min, 5 ml of the aqueous and of the chloroform phases were taken in order to measure the radioactivity. The residual aqueous phase was used for the measurement of pH. The absorption spectra of the chloroform phase, which was extracted by the procedure described above using the cobalt solution which does not contain ^{60}Co, were measured in the range of 300 to 500 nm.

Determination of the Perchlorate Ion in the Chloroform Extract. The extracted chloroform phase was shaken for 2 min with 8 ml of 0.01 M EDTA solution adjusted to pH 5.8 and then the amount of perchlorate ion back-extracted in the aqueous solution was absorptiometrically determined by Uchikawa's method.[9]

Estimation of Cobalt(II) and (III) 8-Quinolinol Complexes in the Chloroform Phase. It is important to determine the oxidation state of cobalt in the cobalt 8-quinolinol complexes extracted into the chloroform phase. The oxidation state of cobalt was judged by the following manner as proposed by Ōki.[3] 1) Cobalt(II) 8-quinolinol complexes in the chloroform solution are readily back-extracted into aqueous EDTA solution, while cobalt(III) complexes are not. 2) The absorption spectrum of cobalt(III) 8-quinolinol complex in the

chloroform solution has an absorption maximum at 420 nm. The practical procedure is as follows: Cobalt(II) and (III) 8-quinolinol complexes which might be contained in a chloroform phase are shaken for one min with 0.001 M EDTA solution at a pH in the range of 4.0 to 5.0. The cobalt(II) 8-quinolinol complexes are completely back-extracted into the aqueous solution, whereas cobalt(III) 8-quinolinol complex remains in the chloroform phase. The absorbance of the chloroform phase back-extracted at 420 nm is measured by using the calibration curve made from the chloroform solutions of known amounts of cobalt(III) 8-quinolinol complex.

Results and Discussion

Extraction of Cobalt into Chloroform with 8-Quinolinol from an Aqueous Solution Containing Perchlorate, Nitrate, or Sulfate Ions. The relationship between the logarithm of the distribution ratio, log D, and the pH of the aqueous phase containing 0.1 M perchlorate, nitrate, or sulfate ion is shown in Fig. 1. In the part where $D<K_{Dc}$ in the acidic region (K_{Dc}: distribution coefficient of cobalt 8-quinolinol complexes), the distribution curve for sulfate ion gives a straight line with the slope +2, but for perchlorate or nitrate ions, especially for perchlorate ions, the data do not give a linear relationship. Furthermore, it is observed that their distribution ratios decrease in the order of $ClO_4^->NO_3^->SO_4^{2-}$ at an arbitrary pH below 5. On the other hand, the distribution curves for the three anions start to overlap in the region above pH 8.

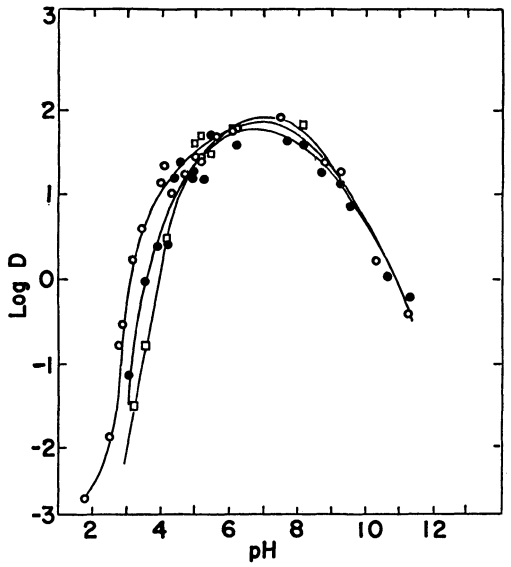

Fig. 1. Plots of log D *vs.* pH.
Initial concentration; cobalt 1.15×10^{-4} M, 8-quinolinol 0.1 M.
—○—; 0.1 M ClO_4^-, —●—; 0.1 M NO_3^-, —□—; 0.1 M SO_4^{2-}.

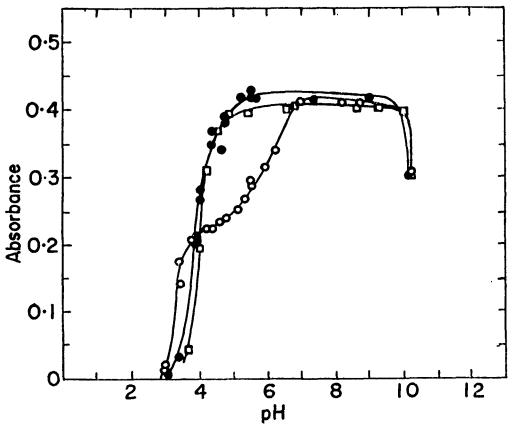

Fig. 2. Absorbance of the chloroform extracts as a function of pH. Wavelength; 410 nm, —○—; 0.1 M ClO_4^-, —●—; 0.1 M NO_3^-, —□—; 0.1 M SO_4^{2-}.

Values of the absorbance at 410 nm of the extracted chloroform phase as a function of pH of the aqueous phase containing 0.1 M perchlorate, nitrate, or sulfate ion are shown in Fig. 2. The absorbance change in the range of pH 4 to 7 for perchlorate ion shows significant differences from those for sulfate and nitrate ions, although the total concentrations of cobalt in the chloroform phase for three anions are not so appreciably different in this pH range, as seen in Fig. 1. Actually, the apparent molar absorptivity at 410 nm of the species extracted at various pH values can be calculated from the values of the distribution ratio and the absorbance. The results are shown in Table 1. The values of the

Table 1. Apparent molar absorptivity of chloroform extract at 410 nm

pH[a]	0.1M ClO_4^-			0.1M NO_3^-			0.1M SO_4^{2-}		
	$[Co]_0\times10^4$ [b]	Abs.[c]	E_{410}[d]	$[Co]_0\times10^4$ [b]	Abs.[c]	E_{410}[d]	$[Co]_0\times10^4$ [b]	Abs.[c]	E_{410}[d]
3.5	0.816	0.175	2150	0.306	0.075	2450	—	—	—
4.0	0.908	0.210	2310	0.816	0.220	2700	0.569	0.230	4140
4.5	0.938	0.225	2400	0.918	0.350	3810	0.891	0.370	4150
5.0	0.985	0.240	2440	0.959	0.400	4170	0.969	0.390	4020
5.5	1.00	0.260	2600	0.980	0.420	4290	0.993	0.400	4030
6.0	1.01	0.310	3070	0.980	0.425	4340	1.00	0.410	4100
6.5	1.02	0.350	3430	1.00	0.430	4300	1.00	0.410	4100
7.0	1.02	0.415	4070	1.02	0.430	4220	1.01	0.410	4060
8.0	1.02	0.420	4120	1.02	0.425	4170	1.00	0.410	4100
9.0	0.979	0.420	4290	0.979	0.420	4290	0.979	0.410	4190

a) pH of the aqueous phase after extraction. b) Total concentration of cobalt in chloroform extract.
c) Absorbance at 410 nm. d) Apparent molar absorptivity at 410 nm $\left(=\frac{Abs}{[Co]_0}\right)$.

apparent molar absorptivity for perchlorate ion seem to vary in two steps with pH. These facts suggest that two species of cobalt 8-quinolinol complexes exist in the chloroform phase: one is species A with $\varepsilon=4.1—4.2\times10^3$ extracted in the range of pH 7.0 to 9.0, and the other is species B with $\varepsilon=\approx2.4\times10^3$, extracted in the range of pH 4.0 to 9.0 for sulfate ions and in the range of pH 5.0 to 9.0 for nitrate ions, this species may be identical to species A extracted into the chloroform in the range of pH 7.0 to 9.0 for perchlorate ions. It was confirmed that no cobalt(III) 8-quinolinol complex, $Coql_3$, exists in the chloroform phase immediately after the extraction from an aqueous cobalt(II) solution below pH 7.0 containing 0.1 M perchlorate, nitrate, or sulfate ion, although several percents of cobalt are also extracted as a cobalt(III) 8-quinolinol complex at a pH above 7.0.

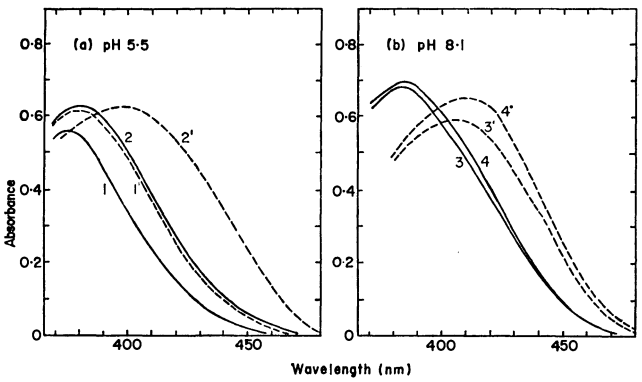

Fig. 3. Absorption spectra of the chloroform extracts from the aqueous solutions containing 0.1 M anion.
(*a*); pH 5.5, 1 and 1′; 0.1 M ClO_4^-, 2 and 2′; 0.1 M NO_3^-, Standing time; 1 and 2: 0 h, 1′ and 2′: 20 h.
(*b*); pH 8.1, 3 and 3′; 0.1 M ClO_4^-, 4 and 4′; 0.1 M NO_3^-, Standing time; 3 and 4: 0 h, 3′ and 4′: 16 h.

Absorption Spectra of Cobalt 8-Quinolinol Complexes Extracted into Chloroform. When the chloroform phase, which has been separated with a centrifuge from the aqueous phase, is allowed to stand in the dark at room temperature, its absorption maximum around 380 nm shifts to longer wavelengths and finally reaches 420 nm. The changes of the absorption spectra with time at pH 5.5 and 8.1 are shown Figs. 3a and 3b respectively. It is considered that the shift to the longer wavelength is due to the oxidation of the cobalt(II) 8-quinolinol complex to the cobalt(III) 8-quinolinol complex for the following reasons: 1) the wavelength of the finally reached absorption maximum, 420 nm is in accord with that for the cobalt(III) 8-quinolinol complex oxidized by hydrogen peroxide; 2) when the chloroform extracts were allowed to stand for an appropriate time, followed by back-extraction with the EDTA solution, the absorption maximum of the back-extracted chloroform phase was located at 420 nm; and 3) when nitrogen gas is passed through the chloroform phase, the shift to longer wavelengths is prolonged with time. The solid lines in Figs. 3a and 3b show absorption spectra of the chloroform phase immediately after the extraction at pH 5.5 and 8.1 from the cobalt(II) solution containing 0.1 M perchlorate or nitrate ion. These absorption spectra have their absorption maxima at 380 nm or below. This fact indicates that species A and species B extracted into the chloroform phase are not the normal 1:2 cobalt(II) 8-quinolinol complex, $Coql_2$, because its absorption maximum is located at 400 nm in chloroform.[10,11] The broken lines in Figs, 3a and 3b indicate the absorption spectra after the chloroform extracts were allowed to stand for a fixed time. When the chloroform phase extracted at pH 5.5 for perchlorate ions is allowed to stand for 20 h, no appreciable shift to longer wavelengths is observed. On the other hand, an appreciable shift to longer wavelengths is observed for nitrate ions at pH 5.5 as well as for perchlorate and nitrate ions at pH 8.1. These results lead to the conclusion that species A is apt to be oxidized in air, while species B is difficult to oxidize.

Tendency of the Formation of Species A or Species B with the Kind of Anions. The effect of the anion on the formation of species A and species B in the chloroform phase was examined by using various kinds of anions, such as perchlorate, nitrate, chloride, and sulfate ions, in 1.0 M solutions. The relationships of the standing time and the change of the absorption spectra of the chloroform phases extracted at pH 6.5 and 8.1 from the cobalt solution containing an anion in 1.0 M concentration are shown in Figs. 4 and 5 respectively. The

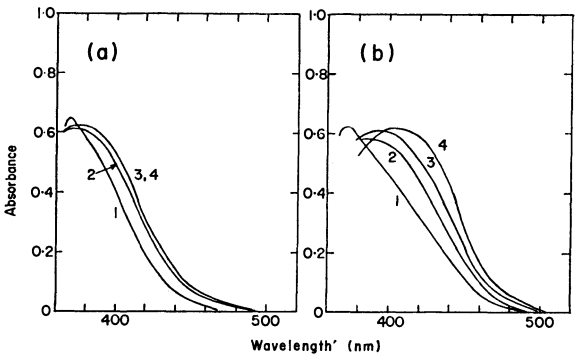

Fig. 4. Absorption spectra of the chloroform extracts from the aqueous solutions containing 1 M anion at pH 6.5.
(*a*); Immediately after extraction. (*b*); after standing for 20 h. 1; ClO_4^-, 2; NO_3^-, 3; Cl^-, 4; SO_4^{2-}.

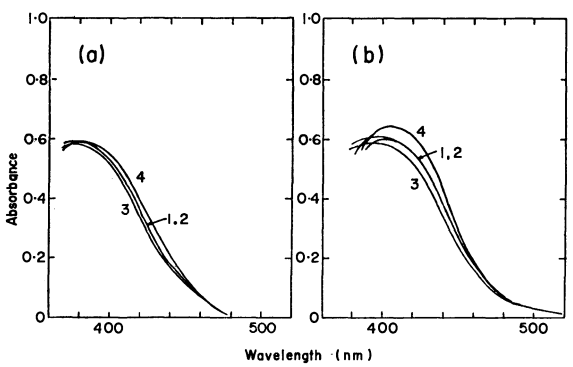

Fig. 5. Absorption spectra of the chloroform extracts from the aqueous solutions containing 1 M anion at pH 8.1.
(*a*); Immediately after extraction. (*b*); After standing for 20 h. 1; ClO_4^-, 2; NO_3^-, 3; Cl^-, 4; SO_4^{2-}.

absorption spectra after standing for 20 h for the extracts at pH 6.5 are located at longer wavelengths, in the order of $ClO_4^- < NO_3^- < Cl^- < SO_4^{2-}$ (Figs. 4a and 4b). This is the order for the rate of the oxidation to cobalt(III) 8-quinolinol complex, in other words, the order of the increase of species A, and the decrease of species B in the chloroform phase. On the other hand, for the extraction at pH 8.1, the absorption curves immediately after extraction are similar to those obtained 20 h after extraction, regardless of the kind of anion, and the oxidation seems to occur rapidly in all cases (Figs. 5a and 5b). These results indicate that species A is probably formed in the chloroform phase.

TABLE 2. CONCENTRATIONS OF COBALT AND PERCHLORATE IN THE CHLOROFORM EXTRACTS

pH[a]	$[Co]\times10^4$ (M)[b]	$[ClO_4^-]\times10^5$ (M)[c]	$[ClO_4^-]/[Co]$
3.85	1.00	5.13	0.513
4.20	1.05	5.20	0.495
4.40	1.08	5.73	0.513
5.10	1.12	5.68	0.508
5.30	1.13	4.67	0.413
5.40	1.13	4.33	0.383
6.05	1.14	3.88	0.340
7.70	1.15	0.533	0.046
8.50	1.13	0.465	0.041
	—	0.330	—

a) pH of the aqueous phase after extraction. b) Concentration of cobalt in the chloroform extracts. c) Concentration of perchlorate ion in the chloroform extracts.

Compositions of Species A and Species B. The perchlorate ion in species A and species B extracted into chloroform from the aqueous cobalt solution containing perchlorate ions was determined. The results are shown in Table 2. The chloroform phases extracted below pH 5.1 contain cobalt and perchlorate ions in the ratio of 2 to 1, but the concentration of perchlorate ions decreases gradually with increasing pH and becomes very low above pH 7.7, although the concentration of cobalt remains constant above pH 5.1. Therefore, the species extracted below pH 5.1, species B, might be an ion-pair complex, similar to that for zinc described in a previous report.[8] On the other hand, the species extracted above pH 7.7, species A, may be a complex containing no perchlorate ions. The prediction that the species extracted into chloroform to form the cobalt solution containing 1.0 M sulfate ion may be not species B but species A was confirmed by the follow. The aqueous solution containing 3.05×10^{-4} M cobalt and 1.0 M sulfate ions is extracted with 0.1 M 8-quinolinol chloroform solution at pH 3.7. The extracts in the chloroform phase can be back-extracted with 1.0 M hydrochloric acid, and then 0.1 M barium sulfate solution is added into the aqueous phase. No turbid material and no precipitate forms, so the extracts contain no sulfate ions.

On the basis of the above mentioned results, the compositions of species A and species B extracted from the cobalt solution containing perchlorate ions are represented by the formulae, $Co_nql_m(Hql)_l$ and $Co_{2s}ql_t(Hql)_u(ClO_4)_s$ respectively; then the reactions of extraction for species A and species B will be represented by the following equations:

$$nCo^{2+} + (m+l)Hql_{(o)} \rightleftarrows Co_nql_m(Hql)_{l(o)} + mH^+ \quad (1)$$

$$2sCo^{2+} + (t+u)Hql_{(o)} + sClO_4^- \rightleftarrows Co_{2s}ql_t(Hql)_u(ClO_4^-)_{s(o)} + tH^+ \quad (2)$$

where l, m, n, s, t, and u are integers. The equilibrium constants of Eqs. 1 and 2, that is, the exraction constants, K_{ex}^A and K_{ex}^B are represented as follows:

$$K_{ex}^A = \frac{[Co_nql_m(Hql)_l]_o[H]^m}{[Co]^n[Hql]_o^{m+l}} \quad (3)$$

$$K_{ex}^B = \frac{[Co_{2s}ql_t(Hql)_u(ClO_4^-)_s]_o[H]^t}{[Co]^{2s}[Hql]^{t+u}[ClO_4^-]^s} \quad (4)$$

where the charge of the chemical species was abbreviated. The distribution ratios of species A and species B, D_A and D_B, are represented by Eqs. 5 and 6 respectively:

$$D_A = \frac{n[Co_nql_m(Hql)_l]_o}{[Co]_T} \quad (5)$$

$$D_B = \frac{2s[Co_{2s}ql_t(Hql)_u(ClO_4^-)_s]_o}{[Co]_T} \quad (6)$$

Here $[Co]_T$ represents the analytical concentration of cobalt(II) in the aqueous phase. If the hydrolysis of cobalt ions and the complex formation of cobalt ions with other anions can be neglected in the aqueous phase, Eq. 7 is obtained:

$$[Co]_T = [Co](1+\sum_{i,j}\beta_{i,j}[ql]^i[Hql]^j) + [Co]\sum_{p,q}\beta_{p,q}[ql]^p[Hql]^q = [Co](1+N) \quad (7)$$

Here, $\beta_{i,j}$ and $\beta_{p,q}$ represent the formation constants of the mononuclear cobalt 8-quinolinol complex and the binuclear complex respectively, and N represents the sum of the second and third terms in the parentheses on the right-hand side of Eq. 7. When Eqs. 3 and 4 are replaced by Eqs. 5, 6, and 7 and both sides of the equations are made logarithmic, Eqs. 8 and 9 can be deduced.

$$\log D_A = (n-1)\log[Co]_T + m\mathrm{pH} + (m+l)\log[Hql]_o - n\log(1+N) + \log n + \log K_{ex}^A \quad (8)$$

$$\log D_B = (2s-1)\log[Co]_T + t\mathrm{pH} + (t+u)\log[Hql]_o - 2s\log(1+N) + s\log[ClO_4^-] + \log 2s + \log K_{ex}^B \quad (9)$$

Under the conditions that the terms except for $\log[Co]_T$ on the right-hand side of Eqs. 8 and 9 are constant, the plots of $\log D$ *vs.* $\log[Co]_T$ should give a straight line having the slope $n-1$ or $2s-1$. When $[Co]_T=[Co]_{int.}/(1+D)$, where $[Co]_{int.}$ is the initial concentration of cobalt, is placed Eqs. 8 and 9, the following Eqs. 10 and 11, which are into convenient for obtaining the values of m, l and t, u, can be deduced.

$$\log D_A + (n-1)\log(1+D_A) = m\mathrm{pH} + (m+l)\log[Hql]_o + (n-1)\log[Co]_{int.} - n\log(1+N) + \log n + \log K_{ex}^A \quad (10)$$

$$\log D_B + (2s-1)\log(1+D_B) = t\,\mathrm{pH} + (t+u)\log[\mathrm{Hql}]_o + s\log[ClO_4^-] + (2s-1)\log[\mathrm{Co}]_{int.} - 2s\log(1+N) + \log 2s + \log K_{ex}^B \quad (11)$$

The following three conditions are selected in order to determine the compositions of the extracted species A and species B: 1) the condition under which only one of species A and species B is extracted 2) the hydrolysis and the complex formation with the other anions for the cobalt ion can be neglected; 3) N can be neglected in comparison with 1 in Eq. 7. For condition 1), the extraction in the presence of sulfate ions was selected as a condition in which only species A is extracted, and the extraction in the presence of perchlorate ions at a low pH was selected as a condition in which only species B is extracted. For condition 2), the hydrolysis of cobalt ions can be neglected at low pH and the use of a low concentration of the buffer($<1\times10^{-3}$ M acetate) allows us to neglect the effect of the complex formation. For condition 3), the extraction at a pH below 3.6 satisfies the the condition of 3), according to the calculation of the concentrations of cobalt 8-quinolinol complexes.

The plots of log D *vs.* log[Co]$_T$ from Eqs. 8 and 9 are shown in Figs. 6a and 6b respectively. Both curves give straight lines with the slope of +1 in the vicinity of $[\mathrm{Co}]_{int.}=10^{-4}-10^{-5}$ M. The plots in Fig. 6a, however, seem to deviate from a straight line. Perhaps the condition of 3) is less satisfied at the higher pH in the extraction, 3.8, than at 3.6. It is suggested that both species A and species B may be dimer complexes, because $n=2$ for species A and $s=1$ for species B. In the regions of high and low concentrations of cobalt, the slopes are close to zero, which suggests that a mononuclear complex is extracted. This suggestion was supported by Table 3, which gives the data for the absorption spectra of the chloroform extracts from the cobalt solutions of various concentrations corresponding to Fig. 6a. As the concentration of cobalt becomes higher, the absorption maximum shifts to longer wavelengths. For the concentration of $[\mathrm{Co}]_{int.}=1.15\times10^{-3}$ M, the absorption maximum is located at 400 nm and the apparent molar absorptivity at 410 nm is 2000. It was confirmed that the shift to longer wavelengths can not be attributed to the oxidation to a cobalt(III) 8-quinolinol complex, because of the fact that the chloroform phase back-extracted with 1.0 M hydrochloric acid is clolorless. It is well-known that the absorption maximum of the chloroform solution of 1:2 cobalt 8-quinolinol complex is located at 395 nm and its molar absorptivity is 2200 at 410 nm, which agrees with the above results, so that the species extracted at 1×10^{-3} M of $[\mathrm{Co}]_{int.}$ may be the normal 1:2 cobalt 8-quinolinol complex.

The relationships of log $D(1+D)$ and log$[\mathrm{Hql}]_o$, according to Eqs. 10 and 11, are plotted in Figs. 7a and 7b. Straight lines with the slope +6 are obtained for both species A and B, so that $m+l=6$ for species A, and $t+u=6$ for species B. The plot of log D *vs.* pH for species A, and the plot of log $D(1+D)$ *vs.* log[ClO$_4$] for

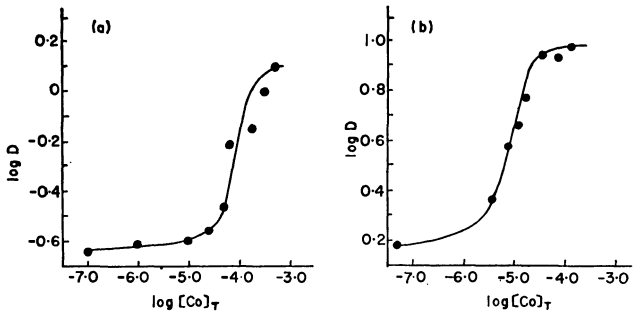

Fig. 6. Effect of the concentration of cobalt on extraction of species A and B.
(a); For species A, pH 3.80, Initial concentration; 8-quinolinol 0.1 M, SO_4^{2-} 0.1 M.
(b); For species B, pH 3.20, Initial concentration; 8-quinolinol 0.1 M, ClO_4^- 0.1 M.

Table 3. Effect of concentration of cobalt on absorption spectra of chloroform extracts

$[\mathrm{Co}]_{int.}$[a] (M)	%E	$[\mathrm{Co}]_o$ (M)	Abs. (410 nm)	ε_{410}[b]	λ_{max}[c] (nm)
3.45×10^{-4}	91.7	3.16×10^{-4}	0.840	2660	380
6.90×10^{-4}	94.2	6.50×10^{-4}	1.550	2380	390
1.15×10^{-3}	91.3	1.05×10^{-3}	2.10	2000	400

a) Initial concn. of cobalt in aqueous phase. b) Apparent molar absorptivity at 410 nm. c) Wavelength of absorption maximum.

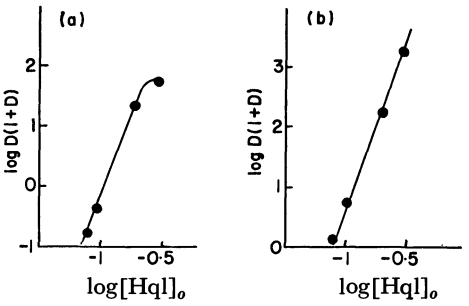

Fig. 7. Plot of log $D(1+D)$ *vs.* log[Hql].
(a); For species A, pH 3.50, Initial concentration; cobalt 1.02×10^{-4} M, SO_4^{2-} 0.1 M.
(b); For species B, pH 2.90, Initial concentration; cobalt 1.15×10^{-4} M, ClO_4^- 0.1 M.

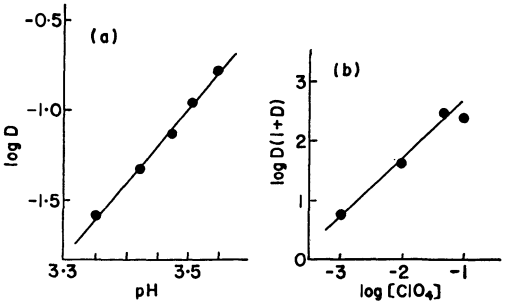

Fig. 8(a). Plot of log D *vs.* pH for species A. Initial concentration; cobalt 1.02×10^{-4} M, 8-quinolinol 0.1 M and SO_4^{2-} 0.1 M.
Fig. 8(b). Plot of log D *vs.* log $[ClO_4^-]$ for the species B. Initial concentration; cobalt 1.15×10^{-4} M, 8-quinolinol 0.1 M. Ionic strength; 0.1(ClO_4^- and SO_4^{2-}).

species B are also shown in Figs. 8a and 8b, respectively. Straight lines were obtained with the slope +2 for the former and +1 for the latter. From these results it is concluded that $n=2$, $m=4$, and $l=2$ for species A and $s=1$, $t=3$, and $u=3$ for species B, so that the composition of species A and species B can be represented by $Co_2ql_4(Hql)_2$ and $Co_2ql_3(Hql)_3ClO_4$, respectively.

Equilibrium between Species A and Species B. The following equilibrium can be considered between species A, $Co_2ql_4(Hql)_2$, and species B, $Co_2ql_3(Hql)_3ClO_4$, in the chloroform phase.

$$B_{(o)} \rightleftarrows A_{(o)} + H^+ + ClO_4^- \qquad (12)$$

$A_{(o)}$ and $B_{(o)}$ represent species A and species B in the chloroform phase. The equilibrium constant, K_{AB}, for Eq. 12 is shown in Eq. 13.

$$K_{AB} = \frac{[A]_o[H^+][ClO_4^-]}{[B]_o} \qquad (13)$$

$[A]_o$ and $[B]_o$ represent the concentrations of species A and species B in the chloroform phase. As species A and species B are both assumed to be dimer complexes, their molar absorptivities at 410 nm, ε^A_{410}, and ε^B_{410}, can be estimated to be double the values of the apparent molar absorptivities of the species which are extracted at pH 4.0 and 7.0, respectively, in the presence of of 0.1 M perchlorate ions, that is, $\varepsilon^A_{410}=8140$ and $\varepsilon^B_{410}=4620$.

The analytical concentration of cobalt in the chloroform phase, $[Co]_o$, is represented by Eq. 14 and the apparent molar absorptivity at a particular pH, ε_{410}, is represented by Eq. 15.

$$[A]_o + [B]_o = \frac{1}{2}[Co]_o \qquad (14)$$

$$[A]_o\varepsilon^A_{410} + [B]_o\varepsilon^B_{410} = \varepsilon_{410}[Co]_o \qquad (15)$$

When the values of $[A]_o$ and $[B]_o$ obtained from Eqs. 14 and 15 are placed in Eq. 13 and both sides of the equation are made logarithmic, Eq. 16 is obtained.

$$\log\frac{2\varepsilon_{410}-\varepsilon^B_{410}}{\varepsilon^A_{410}-2\varepsilon_{410}} = pH + p[ClO_4^-] + \log K_{AB} \qquad (16)$$

The plots of $\log\{(2\varepsilon_{410}-\varepsilon^B_{410})/(\varepsilon^A_{410}-2\varepsilon_{410})\}$ against $p[ClO_4^-]$ at pH=5.50 and against pH at $p[ClO_4^-]=1$ are shown in Figs. 9a and 9b, respectively. A straight line with the slope +1 was obtained in each figure, which indicates that the equilibrium represented by Eq. 12 is valid. $\log K_{AB}=-7.2$ was obtained as the average of −7.1 and −7.3, which were derived from the intercepts in Figs. 9a and 9b.

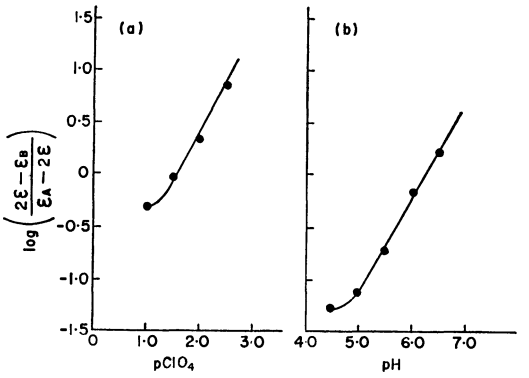

Fig. 9(a). Plot of $\log\{(2\varepsilon-\varepsilon_B)/(\varepsilon_A-2\varepsilon)\}$ *vs.* pH. Initial concentration; cobalt 1.02×10^{-4} M, 8-quinolinol 0.1 M, and ClO_4^- 0.1 M.

Fig. 9(b). Plot of $\log\{(2\varepsilon-\varepsilon_B)/(\varepsilon_A-2\varepsilon)\}$ *vs.* $p[ClO_4^-]$ a pH 5.50. Initial concentration; cobalt 1.15×10^{-4} M, 8-quinolinol 0.1 M. Ionic strength; 0.1 (ClO_4^- and NO_3^-).

The equilibrium constant, K_{AB} was also derived from the ratio of the extraction constants K^A_{ex} to K^B_{ex}. The extraction constant of species A, $K^A_{ex}=10^{-4.61}$ was obtained by using the intercept of Fig. 7a and Eq. 10, and that of species B, $K^B_{ex}=10^{2.60}$ by Fig. 7b and Eq. 11. Therefore, $\log K_{AB}=\log K^A_{ex}-\log K^B_{ex}=-4.61-2.60=-7.21$. This value is in good accord with the value obtained absorptiometrically, −7.2.

References

1) J. Stary, *Anal. Chim. Acta*, **28**, 132 (1963).
2) N. M. Kuz'min and Yu. A. Zolotov, *Zh. Neorg. Khim.*, **11**, 2316 (1966).
3) S. Ōki, *Anal. Chim. Acta*, **50**, 465 (1970).
4) H. Akaiwa, H. Kawamoto, and T. Saito, *Nippon Kagaku Zasshi*, **92**, 1156 (1971).
5) S. Ōki and I. Terada, *Anal. Chim. Acta*, **66**, 201 (1973).
6) S. Ōki and I. Terada, *Anal. Chim. Acta*, **69**, 220 (1974).
7) E. Sekido, Y. Yoshimura, and Y. Masuda, *J. Inorg. Nucl. Chem.*, **38**, 1183 (1976).
8) E. Sekido and Y. Yoshimura, *J. Inorg. Nucl. Chem.*, **38**, 1187 (1976).
9) O. Uchikawa, *Bull. Chem. Soc. Jpn.*, **40**, 798 (1967).
10) K. Sone, *J. Am. Chem. Soc.*, **75**, 5207 (1953).
11) E. Sekido, *Nippon Kagaku Zasshi*, **80**, 871 (1959).

Preparation and Ligand Isotopic Exchange of Tris(acetylacetonato)-tin(IV) Perchlorate in Acetonitrile

Akira NAGASAWA and Kazuo SAITO

Chemistry Department, Faculty of Science, Tohoku University, Aoba, Aramaki, Sendai 980

(Received June 19, 1976)

Tris(acetylacetonato)tin(IV) perchlorate $[Sn(acac)_3]ClO_4$ was prepared in crystalline state in acetylacetone (Hacac) and its structure was verified. It is stable in dehydrated acetonitrile (AN) at room temperature. It undergoes hydrolysis in the presence of a large amount of water (*e.g.*, 10^{-4} mol dm^{-3} complex against 10^{-1} mol dm^{-3} water) in two steps: The first, fast step gives a product $[Sn(acac)_2(OH)(H_2O)]ClO_4$, which slowly undergoes further hydrolysis or polymerization to give eventually a gelatinous precipitate. The ligand isotopic exchange with Hacac[^{14}C] can be measured in $\simeq 10^{-2}$ mol dm^{-3} complex solution in AN containing 0.03—0.12 mol dm^{-3} water below −20 °C. The rate is independent of free Hacac concentration. The dependence of the rates of the hydrolysis and the ligand isotopic exchange on water concentration is expressed by: rate$=A$[complex][H_2O]^2/(1+B[H_2O]), where the A values are 0.15 and 0.30 dm^6 mol^{-2} s^{-1} at −20 °C, ΔH^* and ΔS^* being (50±8) and (36±20) kJ mol^{-1}, and (−60±20) and (111±40) J mol^{-1}K^{-1}, respectively. There seems to be a common rate-determining step in which one acac$^-$ ligand dissociates with the action of water. The intermediate gives rapidly the original complex in the presence of excess Hacac. Otherwise it undergoes further hydrolysis in the presence of an overwhelming amount of water. The large ionic radius of tin(IV) should be responsible for the rapid water substitution as compared with the corresponding octahedral silicon(IV) and germanium(IV).

Tris(β-diketonato) complexes are common for a wide variety of transition and non-transition metal ions, and their structures and properties have been studied intensively.[1] Several workers[2] including ourselves[3,4] have investigated the kinetics of ligand substitution (including racemization and isomerization) of tris(β-diketonato) complex cations of Group 4 elements, *i.e.* silicon(IV), germanium(IV) and titanium(IV). It seems interesting to compare their properties with those of tin(IV) analogue, for which tris-bidentate octahedral complexes of β-diketonates are left unknown.

The tin(IV) complex containing acetylacetonate (acac$^-$) was first prepared by Dilthey,[5] and it was formulated as a salt of the cation $[Sn(acac)_3]^+$. However, Rosenheim *et al.*[6] gave the formula $[Sn(acac)_2Cl_2]$ to the complex, and this form was confirmed by White.[7] Similar complexes of the type $[Sn(acac)_2X_2]$ (X=halide, methyl, and phenyl) were synthesized and their rapid site-exchange was examined by NMR.[8] Tropolonate (trop$^-$), one of the related diketonates, gave chargeless complexes with coordination numbers 7 and 8, $[Sn(trop)_3X]$ (X=chloride and phenyl) and $[Sn(trop)_4]$.[9]

We have synthesized a new compound tris(acetylacetonato)tin(IV) perchlorate $[Sn(acac)_3]ClO_4$ in crystalline state and studied its hydrolysis and ligand isotopic exchange in acetonitrile.

Experimental

Materials. *Tris(acetylacetonato)tin(IV) Perchlorate*: Dichlorobis(acetylacetonato)tin(IV) (4.1 g, 0.011 mol) prepared by the method of Morgan and Drew[10] was dissolved in Hacac (60 cm^3) and treated with silver perchlorate (4.3 g, 0.021 mol) in Hacac (50 cm^3). The precipitate (silver chloride) was filtered off, and diethyl ether (120 cm^3) was added to the filtrate to give colorless needles. They were filtered off, washed with diethyl ether, dried, and recrystallized from Hacac solution (110 cm^3) by adding diethyl ether (250 cm^3). Yield, 50% on the basis of $[Sn(acac)_2Cl_2]$. The colorless crystals melt at 221—223 °C with decomposition. Found: C, 34.94; H, 4.11; Sn, 23.3%. Calcd for $C_{15}H_{21}O_{10}ClSn$: C, 34.95; H, 4.10; Sn, 23.0%. This compound contained no chloride ions.

The complex is insoluble in diethyl ether, tetrahydrofuran, chlorobenzene, acetic acid, and hexane. It is soluble in Hacac and was recrystallized from it. It is also soluble in the following solvents: easily in acetone, acetonitrile (AN), nitromethane, and dichloromethane; slightly in ethanol, ethyl acetate, and 1,1,2,2-tetrachloroethane. In all the seven solvents the recrystallization was unsuccessful, presumably owing to water contained as an impurity. Water, chloroform, and dimethyl sulfoxide rapidly decomposed the complex to give white precipitate and Hacac.

Hydrolysis Product: An AN solution (20 cm^3, containing *ca.* 0.1 M water; M=mol dm^{-3}) of the complex ($\simeq 10^{-2}$ M) was mixed with diethyl ether (60 cm^3) and set aside for 1 h. Colorless precipitate appeared gradually. They were filtered off, washed with diethyl ether, and dried *in vacuo*. This product (Product A) absorbed the moisture from air and decomposed into Hacac and brownish white solid.

Other Reagents: Acetonitrile was refluxed with diphosphorus pentoxide and distilled. The procedure was repeated until the water content fell to *ca.* 0.005 M. Commercially available pure hexane was used without further purification. The labeled compound Hacac[^{14}C] was prepared as in reference.[11] The specific activity was 0.01 mCi/g.

Kinetic Procedure. *Hydrolysis in Acetonitrile*: Kinetic runs were carried out in a quartz cell in a thermostated jacket, which was placed in a spectrophotometer Hitachi 124. A co-necked glass tube with two branched bottoms containing the complex solution ($\simeq 10^{-4}$ M, 5 cm^3) and AN (containing 0.01 to 0.6 M water, 5 cm^3) was cooled to −25 °C and both liquids were mixed. The solution was pippeted into the quartz cell at given temperatures (−11.8, −13.7, −17.3, and −20.0 °C). Methanol was used as coolant which was circulated through the jacket from HAAKE KT 33 thermostat. Dry nitrogen was blown on the surface of the cell to avoid freezing. The change in absorption was followed at 315 or 250 nm.

Ligand Isotopic Exchange: The complex solution in AN (0.05 to 0.1 M, 5 cm^3) containing 0.05 M Hacac and the radioactive Hacac solution in AN (0.01 to 0.1 M, 5 cm^3) were introduced separately into the two branched bottoms of a co-necked flask with a stopper, and cooled in a thermostat. Both solutions were mixed after *ca.* 30 min to let the exchange reaction start.

At appropriate time intervals, portions (*ca.* 1 cm³ each) were pippeted quickly into chilled hexane (*ca.* 5 cm³) in a thin glass tube at −55 °C. (Only the enol tautomer is partly extracted into the hexane phase.[4]) After 30 to 40 s, the hexane layer (*ca.* 3 cm³) was separated and allowed to stand for 24 h at room temperature until the keto-enol equilibrium was reached. One cm³ portion was diluted 10 folds with hexane and the extinction measured at 273 nm to find the concentration of Hacac. Another 1 cm³ portion was mixed with anisole containing 0.4% *p*-terphenyl and 0.01% *p*-bis(5-phenyl-2-oxazolyl)benzene (POPOP) to be submitted to *β*-activity counting. The specific activity (x) of the extracted Hacac was known from these data.

Calculation of the Exchange Rate. The rate of isotopic exchange was calculated according to McKay's formula (Eq. 1).

$$R = -[3ab/(3a+b)][\ln(1-F)]/t \quad (1)$$

where a and b are the complex and the ligand concentration, respectively, and t and F are the lapse of time and the extent of reaction at time t, respectively. The F values were calculated by $(x_0-x_t)/(x_0-x_\infty)$ where the suffixes denote the time lapse until the quenching of reaction.

Acetylacetone is present in tautomeric enol-keto equilibrium in AN, and the percentages of enol form are 62 and 67 in AN, at room temperature and −10 °C, respectively. The interconversion rate constant between enol and keto is *ca.* 10^{-5} s^{-1} at −10 °C, being much slower than the present isotopic exchange.[12] The experimental x_∞ coincided with the value calculated on the assumption that only the enol form of free Hacac participates in the exchange. All the calculations were therefore made on this assumption, the b values being set to be equal to 0.62 time of the gross free Hacac concentration. This factor is based upon the enol percentage of Hacac in AN at room temperature. (The Hacac solution for kinetic runs were prepared, set aside for more than 24 h at room temperature, and cooled immediately before use.) The log $(1-F)$ *vs.* t diagrams are linear until *ca.* half exchange time, and seems to concave on further progress of the reaction. The R values used in the following discussion are those obtained at the initial linear part of McKay plots.

Apparatuses. Hitachi 124 Spectrophotometer with a low temperature jacket and Hitachi 323 were used for recording the UV absorption spectra at −10 to −20 °C, and at room temperature, respectively. Nuclear Chicago Unilux II-A Liquid Scintillation Counter was employed for recording the *β*-activity of ^{14}C. The water content was measured by Karl Fischer titration. Metrohm E 365 B Konduktoskop with EA 608 bright platinum electrodes was used for conductivity measurements. Hitachi EPI-2G Infrared Spectrophotometer and Varian A-60 Spectrometer were used for recording the IR absorption and NMR spectra, respectively.

Results and Discussion

Structure and Ultraviolet Absorption. The properties of the complex are summarized in Table 1. The relation between molar conductivity and concentration showed that the tin(IV) complex was a 1:1 electrolyte as those of silicon(IV), germanium(IV) and titanium(IV). The IR absorption (KBr disk) was very similar to those of the corresponding silicon(IV) and germanium(IV) complexes, with C=O stretching and ClO_4^- bands in 1500—1570 cm^{-1} region and at 1100 cm^{-1}, respectively. Proton NMR spectrum in acetonitrile[$^2H_3$] (CD_3CN) gave two singlets at 2.32 and 6.18 ppm (*vs.* TMS), corresponding to methyl and methylidyne protons of the coordinated acetylacetonates. These properties suggest

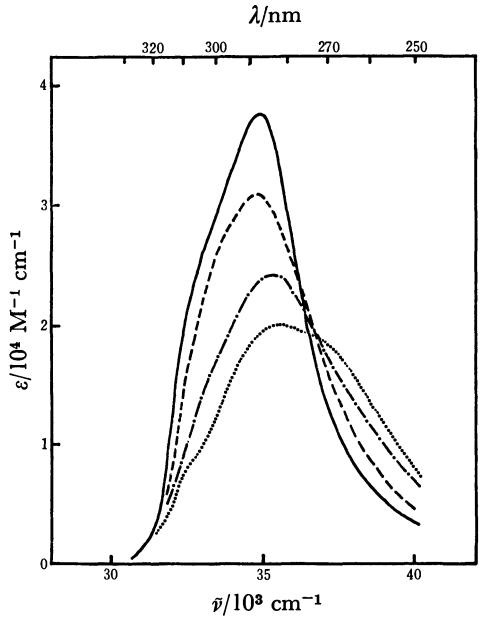

Fig. 1. Ultraviolet absorption spectrum of $[Sn(acac)_3]$-ClO_4 in acetonitrile. Complex, ≃10^{-4} M; water, 0.1 M; at 25 °C.
——Freshly prepared, -----1 h after,
-·-·-3 h after, ------10 h after.

Table 1. Properties of $[M(acac)_3]ClO_4$ (M=Si, Ge, and Sn) and $[Sn(acac)_2Cl_2]$

Central ion	Si(IV)[c]	Ge(IV)[e]	Sn(IV)	$[Sn(acac)_2Cl_2]$
Molar conductivity[a]				
Λ (complex)/S cm² M⁻¹	161	152	153	
UV absorption peak[b]				
$\bar{\nu}$/10³ cm⁻¹	32.7 (sh)	32.8 (sh)	32.5 (sh)	32.2 (sh)[f]
(ε/10⁴ M⁻¹ cm⁻¹)	34.4 (≈3.5)	34.7 (3.55)	34.7 (≈3.8)	33.3 (≈1.5)[f]
IR absorption peak[c]				
$\bar{\nu}$/cm⁻¹ C=O-M	1550—1570	1530—1570	1530—1570	
ClO_4^-	1100	1100	1100	
NMR peak (solvent)[d]	($CDCl_3$)	($CDCl_3$)	(CD_3CN)	($CDCl_3$)
δ/ppm CH_3	2.30	2.33	2.32	2.11, 2.20
=CH-	6.28	6.18	6.18	5.97 (or 5.69[g])

a) Complex concentration: 5×10^{-4} M, at 25 °C. b) In acetonitrile, at 25 °C. c) In KBr disk.
d) Tetramethylsilane: δ=0.0 ppm. e) Ref. 3. f) In benzene. g) Ref. 13.

that the tin(IV) complex has a common octahedral tris-chelate type structure.

The UV absorption spectrum is shown in Fig. 1. The pattern of a freshly prepared AN solution is very similar to those of silicon(IV) and germanium(IV) analogues in the absence of water (<0.01 M). There is an absorption peak at 34700 cm^{-1} (288 nm) with a shoulder at 32500 cm^{-1} (305 nm). In a complex solution ($\simeq 10^{-4}$ M) containing >0.1 M water at room temperature, the extinction coefficient decreased with time in the wavelength range 280—330 nm, and increased at 250—275 nm. Such a change seems to be due to hydrolysis of the complex cation. An isosbestic point at 278 nm was observed only in the initial period.

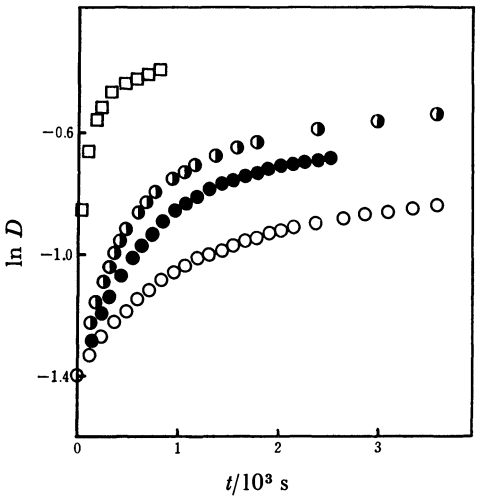

Fig. 2. Increase in extinction at 250 nm in acetonitrile at −17.3 °C. Complex, 7.4×10^{-5} M; water, 0.070 M (○), 0.094 M (●), 0.106 M (◑), 0.267 M (□).

Hydrolysis. The increase in extinction at 250 nm is illustrated in Fig. 2. At least two steps should be involved. The rate of the first fast step, which is apparent up to *ca.* 15 min in the diagram (−17.3 °C), increases with increase in water content, while the second step seems to be rather insensitive to it under the given conditions. Electrolytic conductivity of the solution remained unchanged throughout these periods.

Product of the First Step of Hydrolysis: Product A (see Experimental) seems to be a salt of hydrolysis product in the first step. This colorless solid deteriorated in atmosphere and its properties were not correctly known. The UV absorption spectrum in AN gave a peak at 34100 cm^{-1} (293 nm) with a shoulder around 33000 cm^{-1} (305 nm). The overall pattern is similar to that of the original complex, but the location and the intensity of the peak (ε=*ca.* 15000 M^{-1} cm^{-1} respect to the metal)are obviously different. The IR absorption in Nujol mull and KBr pellet indicated the presence of OH and/or H_2O, coordinated C=O of acetylacetonate, and perchlorate.

The proton NMR spectrum in CD_3CN (*ca.* 0.05 M) gave a group of peaks at *ca.* 2.2, and apparently broad peaks at *ca.* 3.7 and 6.1 ppm *vs.* TMS at room temperature. The signals at *ca.* 2.2 and 6.1 ppm seem to come from methyl and methylidyne of coordinated acac⁻, respectively. These chemical shifts are similar to those of *cis*-$[Sn(acac)_2Cl_2]$.[13]

One sample of Product A gave an analytical result, C, 25.10; H, 3.85; and ash 38.7%. (Calcd for $[Sn(OH)(acac)_2(H_2O)]ClO_4$, $C_{10}H_{17}O_{10}ClSn$: C, 26.6; H, 3.8; ash as SnO_2, 33.4%). There seems to be an overall trend that the carbon content decreases but the hydrogen and the ash percentages increase with increase in time lapse between the initiation of reaction and precipitation of Product A from AN solution. These results and constant electrolytic conductivity seem to indicate that the hydrolysis proceeds as Eq. 2 at the initial stage.

$$[Sn(acac)_3]^+ + 2H_2O \rightleftharpoons [Sn(OH)(acac)_2(H_2O)]^+ + Hacac \quad (2)$$

Product A should consist mainly of the perchlorate salt of this cation or its hydrate and contains small amounts of the products of further hydrolysis.

Reverse Reaction of the First Step: When the solution of Product A in CD_3CN ($\simeq$0.05 M) was treated with Hacac to produce *ca.* 1 M solution at room temperature, six sharp proton peaks appeared immediately in NMR spectrum. Four of them, at 2.05, 2.18, 3.65 and 5.61 ppm, correspond to the signals of free Hacac, and two remaining singlets coincided with the coordinated $acac^-$ in the original complex $[Sn(acac)_3]^+$ (Table 1). When Product A (*ca.* 2 g) was dissolved in Hacac (*ca.* 5 cm^3) at room temperature and immediately treated with diethyl ether (20 cm^3), crystalline $[Sn(acac)_3]ClO_4$ was obtained.

All these facts tell that the reverse reaction of Eq. 2 is very rapid in the presence of a large excess of Hacac. (UV absorption spectroscopy is not useful, because excessive Hacac gives an intense absorption in $\simeq$300 nm region).

Kinetics of the First Step: Apparent rate constants of the first "fast step," k_h, were obtained by the Guggenheim plot of the absorbance at 250 or 315 nm in AN. When the water concentration was less than 0.05 M in the presence of *ca.* 10^{-4} M complex, the hydrolysis was very slow below −10 °C, and the rate was measured

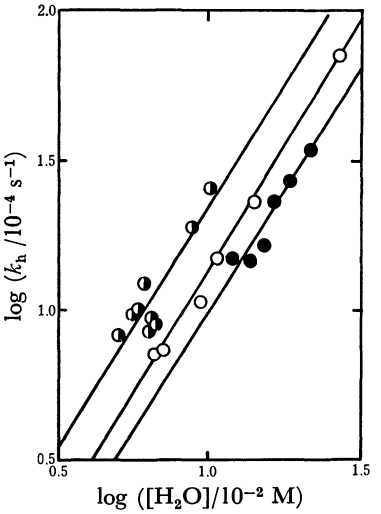

Fig. 3. Apparent hydrolysis rate constant k_h *vs.* water content in acetonitrile in log-log scale.
● −20.0 °C, ○ −17.3 °C, ◑ −11.8 °C.

in AN containing more than 0.05 M water at −10 to −20 °C. First order rate law was obeyed with respect to the complex concentration; rate=k_h[complex].

The observed k_h increases with increase in water content, as illustrated in the log-log plot of Fig. 3. The overall gradient is *ca.* 1.7 in the water concentration range 0.05 to 0.3 M. Various attempts were made to find an appropriate formula which fits the observed data. Linear plot of $[H_2O]/k_h$ *vs.* $1/[H_2O]$ indicated that Eq. 3 is a good approximation for the kinetic data in the given water concentration region.

$$k_h = A[H_2O]^2/(1+B[H_2O]) \quad (3)$$

The A values were calculated to be 0.15, 0.20, 0.27 and 0.34 $M^{-2}\,s^{-1}$ at −20.0, −17.3, −13.7 and −11.8 °C, respectively, and ΔH^* and ΔS^* therefore (50±8) kJ mol^{-1} and (60±20) J $mol^{-1}\,K^{-1}$, respectively. The observed deviation from 2 in the gradient of Fig. 3 seems to be due to the contribution of $B[H_2O]$ term in the denominator, which remains in the vicinity of unity.

The Second Step: The "slow step" of the hydrolysis was not investigated in detail. Since the electrolytic conductivity remained unchanged in this step, either further hydrolysis to give *e. g.* $[Sn(OH)_2(acac)(H_2O)_2]^+$ or polymerization to give *e.g.* $[(acac)_2Sn(\mu\text{-}OH)_2Sn(acac)_2]^{2+}$ may take place. The apparent rate constant which was rather insensitive to the water concentration (Fig. 2) was *ca.* $1\times10^{-5}\,s^{-1}$ at −20 °C. When the complex solution (≃10^{-2} M) was set aside in atmosphere for 24 h or treated with a large amount of water, gelatinous precipitate appeared, which were found to be hydrated tin(IV) hydroxide, *i.e.* olation product of tin(IV). Hence the product of the second step can be a binuclear tin(IV) complex.

Ligand Isotopic Exchange. Figure 4 gives log $(1-F)$ *vs.* t diagrams, in which Hacac in enol form is reckoned to participate in the exchange (see Experimental). These diagrams are linear without intercepts for at least $F<0.7$. The UV absorption of the reaction mixture remained unchanged during these periods. Therefore isotopic exchange must take place exclusively whenever the water concentration is of the same order with the complex concentration (≃10^{-2} M).

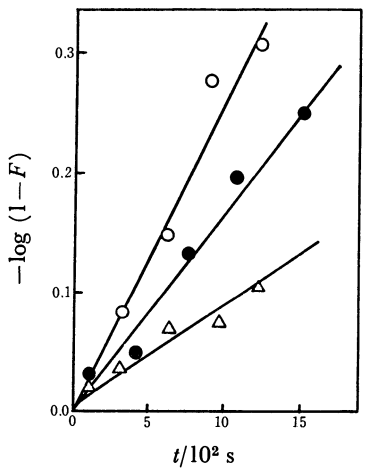

Fig. 4. McKay plots for ligand isotopic exchange of $[Sn(acac)_3]ClO_4$ in acetonitrile at −20.4 °C. Complex, 0.03 M; Hacac (enol), 0.06 M; water, 0.027 M (△), 0.045 M (●), 0.058 M (○).

Table 2. McKay's R values and the rate constants k_x of ligand isotopic exchange of $[Sn(acac)_3]ClO_4$ in acetonitrile at −20.4 °C[a)]

[Sn] 10^{-2}M	[L] 10^{-2}M	[H_2O] 10^{-2}M	R 10^{-6} M s^{-1}	k_x 10^{-4} s^{-1}	[Acid] 10^{-2}M
2.3	0.90	4.4	8.6±0.9	3.8±0.4	
2.6	1.8	2.6	4.1±0.3	1.6±0.2	
3.9	1.9	2.6	5.3±1.0	1.4±0.3	
6.7	1.8	5.9	32.9±4.3	4.9±0.6	
2.4	2.1	3.6	8.3±1.8	3.6±0.8	
2.4	2.1	4.4	6.1±0.3	2.5±0.1	
3.0	4.4	2.7	4.0±1.4	1.4±0.5	
2.5	5.2	3.6	8.8±1.3	3.6±0.5	
2.5	6.1	5.8	18.3±5.6	7.2±2.2	
2.9	6.2	2.7	5.1±2.5	1.7±0.9	
3.0	6.2	3.1	4.7±0.9	1.6±0.3	
3.0	6.2	7.1	32.5±3.5	11.0±1.2	
3.0	6.2	12.1	56.1±1.8	19.0±0.6	
5.1	6.1	2.9	11.1±4.1	2.2±0.8	
3.0	6.9	3.3	10.0±3.9	3.4±1.3	
5.6	7.2	4.2	28.4±2.6	5.1±0.5	
3.9	7.7	3.1	10.9±2.0	2.8±0.5	
5.6	10.1	6.9	48.2±5.1	8.7±0.9	
3.9	7.7	3.2	16.8±0.9	4.3±0.2	1.5[b)]
3.2	6.4	3.5	17.2±0.6	5.5±0.2	5.1[c)]
3.2	6.4	3.8	18.6±1.4	5.9±0.5	10.2[c)]

a) Concentration: complex, [Sn]; enol form of Hacac, [L]; water, [H_2O]; acid, [Acid]. b) Acetic acid. c) Trichloroacetic acid.

Adjustment of water concentration was extremely difficult at a low temperature, and the experimental error is larger than the ordinary kinetic studies. Table 2 gives McKay's R values obtained in the presence of varying concentration of the complex, Hacac and water, at −20.4 °C. They are proportional to the complex concentration, and first order rate constant k_x is expressed by Eq. 4.

$$k_x = R/a \quad (4)$$

The ligand concentration gives only a small influence on the rate constant. On the other hand, the water concentration gives greater effect on k_x than others do; Fig. 5 shows the plot of k_x *vs.* the water concentration on log-log scale. The overall gradient calculated by the method of least squares is *ca.* 1.7 in the range from 0.03 to 0.12 M water. A similar plot at −28.1 °C gave a similar pattern.

There seems to be a remarkable trend, however, that the gradient becomes greater than unity in <0.05 M water. This tendency can be more clearly expressed by the plot of $k_x/[H_2O]$ *vs.* [H_2O] in Fig. 6. The $k_x/[H_2O]$ values increase almost linearly with increase in water concentration in <0.05 M solution, and seem to approach a limiting value in the range >0.05 M. Such an observation leads to two possible interpretations of participation of water as in the following.

If the original complex interacts with one mole of water to give an encounter complex, which undergoes isotopic exchange with the aid of another mole of water, the rate formula can be written as Eq. 5.

$$k_x = A'[H_2O]^2/(1+B'[H_2O]) \quad (5)$$

When the water concentration is small, Eq. 5 is reduced

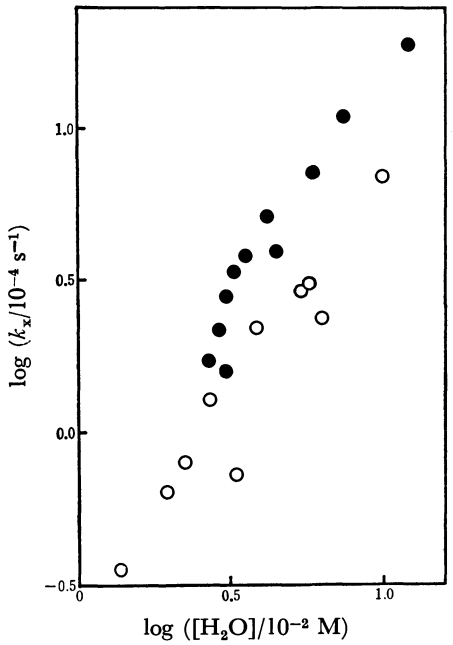

Fig. 5. Influence of water concentration on ligand isotopic exchange rate constant k_x at −28.1 (○) and − 0.4 °C (●). Complex, 0.03 M: Hacac (enol), 0.06 M.

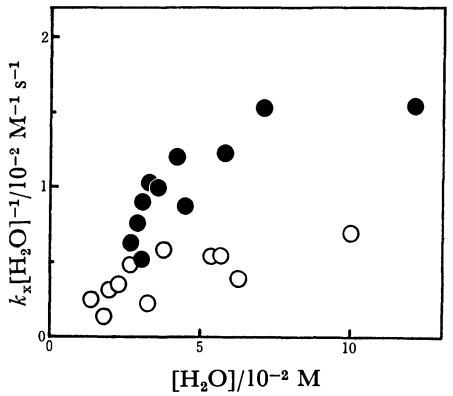

Dig. 6. Plots of $k_x/[H_2O]$ against $[H_2O]$ at −28.1 (○), and −20.4 °C (●). Complex, 0.03 M; Hacac (enol), 0.06 M.

to a second order rate formula as Eq. 6.

$$k_x = A'[H_2O]^2 \quad (6)$$

On the other hand, when the water concentration becomes >0.05 M, the term $B'[H_2O]$ in the denominator becomes sufficiently large and the $k_x/[H_2O]$ approaches a limiting value.

$$k_x/[H_2O] = (A'/B') \quad (7)$$

Equation 5 has the same pattern as Eq. 3 for the hydrolysis of the present complex. The A' value is *ca.* 0.3 M^{-2} s^{-1} in the water concentration range 0.05 to 0.12 M at −20.4 °C. (*cf.* A=0.15 M^{-2} s^{-1} for the hydrolysis). The activation enthalpies and entropies for the A' are $\Delta H^{\ddagger}=(36\pm20)$ kJ mol^{-1} and $\Delta S^{\ddagger}=(111\pm40)$ J mol^{-1} K^{-1}, respectively. They have rather large experimental errors since the data were obtained only at −28.1 and −20.4 °C.

Another interpretation can be encountered by assuming significant change in activity coefficient of water in AN.[14] Nevertheless we tend to favor the first consideration on the basis of the discussions given below.

Acetic and trichloroacetic acid enhance the isotopic exchange as seen in Table 2. The extent of the catalytic action of these weak and strong acids does not differ much from each other, and does not depend on their concentration. It seems the acid catalysis has reached almost saturation under the given conditions.

The Reaction Mechanism. The isotopic exchange does not proceed appreciably in the absence of water below 0 °C, and the original complex itself does not seem to undergo ligand isotopic exchange. The hydrolysis and the isotopic exchange were studied in different concentration regions of the complex and water in AN. However, the apparent exchange rate constant A' is only twice as large as the apparent hydrolysis rate A at −20 °C, and the activation parameters are similar to each other within the experimental errors. These facts suggest that these two reactions might proceed *via* a common route. A plausible mechanism is visualized in Fig. 7.

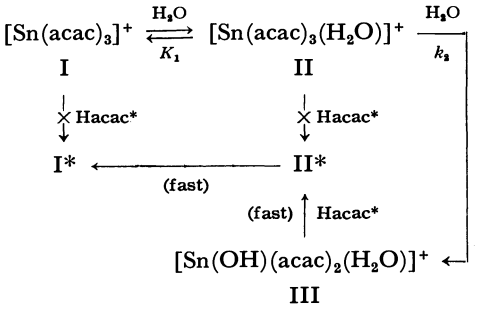

Fig. 7. Plausible mechanism of hydrolysis and ligand isotopic exchange of $[Sn(acac)_3]^+$ ion in acetonitrile. I* and II* are the same species with I and II respectively with labeled $acac^-$.

The original complex interacts rapidly with water to give an intermediate (II, for the structure, *vide infra*). Then II undergoes reaction with another molecule of water to give III, the main component of Product A (see Experimental). In the isotopic exchange reaction, excessive free Hacac rapidly reacts with III to restore II*. In the absence of free Hacac and in the presence of a large excess of water (experimental condition for the hydrolysis), III is subject to further reaction with water or to polymerization, to make the hydrolysis irreversible. Thus the isotopic exchange and hydrolysis seem to have a common intermediate and a common rate-determining step ($A=k_2K_1=A'$).

The rate-determining step II→III should involve the break of a metal-ligand bond with the aid of water. The water molecule should play a unique role, because the solvent AN brings about neither solvolysis nor isotopic exchange.

Structure and Role of Intermediate II: Intermediate II can be either a six-coordinated species with one unidentate and two bidentate $acac^-$ and a water molecule as ligands, or a seven-coordinated species with three bidentates and a water molecule. In the former case the break of the remaining bond with the aid of water would be the rate-determining step. If II were seven-coordinated, water-assisted break of a metal-ligand bond

followed by rapid break of another Sn–O bond of the same acac$^-$ would be rate-controlling. Alternatively, the seven-coordinated species can be in rapid equilibrium to give a small amount of the six-coordinated species with one unidentate acac$^-$ which can behave similarly as in the former case.

Present experimental data cannot discriminate these possible mechanisms, and we can only discuss the most probable route by analogie. Seven- and eight-coordinated tin(IV) complexes with oxygen donors are known in crystalline state,[9] and the presence of a seven-coordinated intermediate is not unlikely. Homologous complexes $[Si(acac)_3]^+$ and $[Ge(acac)_3]^+$ are claimed to produce intermediates with a unidentate acac$^-$ on racemization and isotopic exchange. It was discussed that unidentate acac$^-$ is stabilized in the complexes with highly charged central metal ions such as aluminium(III), gallium(III), silicon(IV), and germanium(IV).[3,15] Thus we tend to consider that intermediate II would be mostly present as seven-coordinated species and produce a small amount of unidentate acac$^-$ by rapid equilibrium, and that the break of the remaining Sn–O bond of the unidentate acac$^-$ would be responsible in determining the rate of hydrolysis and isotopic exchange. Assistance of water at this step can be substantiated either by attacking the intermediate as nucleophile or by blocking the vacant coordination site of the intermediate to retard the recombination of Sn–O.

Comparison with Related Complexes. Other members of 4B family, silicon(IV) and germanium(IV), give homologous complexes $[M(acac)_3]^+$ with acetylacetonate, and the structures are very similar to $[Sn(acac)_3]^+$. However, those two complexes are much more inert than the corresponding tin(IV) complex, and the ligand isotopic exchange is measurable over 100 °C in AN. The dependence of their rates upon various factors is significantly different from the present complex, and they are resistive against hydrolysis even at elevated temperatures.[3] They were resolved into enantiomers, and their racemizations were found to proceed similarly at a measurable rate without the assistance of water between 40 and 60 °C, presumably *via* an intermediate with a unidentate acac$^-$.

Frazer and Haines found that the related tin(IV) complexes $[Sn(acac)_2X_2]$ (X=Cl, Br, and I) undergo hydrolysis below 0 °C to liberate acac$^-$ in chloroform. The rate law was:

$$\text{rate} = k[H_2O][Sn(acac)_2X_2] \quad (8)$$

where the complex and water concentration were $\simeq 5\times10^{-5}$ and 0.005—0.01 M, respectively. They proposed a mechanism involving an association pre-equilibrium between the complex and water, and a rate-determining attack of this water molecule to break Sn–O bond.[16] The role of water molecule seems to be different from that in the present reactions, but the labile interaction with water is common. The large octahedral ionic radius of tin(IV) ion may be responsible for the difference among silicon(IV), germanium(IV), and tin(IV).

Titanium(IV), a member of 4A family, also gives a tris(acetylacetonato) complex $[Ti(acac)_3]^+$ with a similar structure, which readily undergoes hydrolysis in hydrous solvents. The rate of ligand isotopic exchange is measurable in the same temperature region as the tin(IV) complex, although details of the kinetic behavior remains unknown.[4] The similar lability towards hydrolysis and isotopic exchange seems to owe to the similarity in the octahedral ionic radius.

An iso-electronic cation indium(III) also gives a complex $[In(acac)_3]$, which is very sensitive to hydrolysis. Its ligand isotopic exchange is immeasurably fast at −20 °C in tetrahydrofuran.[17] Another d^{10} cation, gallium(III) gives also $[Ga(acac)_3]$ and the ligand isotopic exchange rate is measurable at $\simeq$0 °C. However, the dependence on various factors is different from the present case.[18] It seems as if the charge and the ionic radius of the central metal ion is very important in determining the kinetic behavior of non-transition metal complexes.

The authors wish to thank the Ministry of Education for Grant-in-Aid.

References

1) J. P. Fackler, Jr., *Progr. Inorg. Chem.*, **7**, 361 (1966). R. M. Pike, *Coord. Chem. Rev.*, **2**, 163 (1967).
2) S. K. Dhar, V. Doron, and S. Kirschner, *J. Am. Chem. Soc.*, **81**, 6372 (1959); R. G. Pearson, D. N. Edgington, and F. Basolo, *ibid.*, **84**, 3233 (1962).
3) T. Inoue and K. Saito, *Bull. Chem. Soc. Jpn.*, **46**, 2417 (1973); A. Nagasawa and K. Saito, *ibid.*, **47**, 131 (1974).
4) M. Nishizawa, H. Kido, I. Kinoshita, Y. Soma, and K. Saito, *Bull. Chem. Soc. Jpn.*, **49**, 819 (1976).
5) W. Dilthey, *Ber.*, **36**, 923 (1903).
6) A. P. Rosenheim, W. Loewenstamm, and L. Singer, *Ber.*, **36**, 1833 (1903).
7) E. White, *J. Chem. Soc.*, **1928**, 1413.
8) R. W. Jones, Jr. and R. C. Fay, *Inorg. Chem.*, **12**, 2599 (1973); N. Serpone and K. A. Hersh, *ibid.*, **13**, 2901 (1974); D. G. Bickley and N. Serpone, *ibid.*, **13**, 2908 (1974).
9) E. L. Muetterties and C. M. Wright, *J. Am. Chem. Soc.* **86**, 5132 (1964).
10) G. T. Morgan and H. D. K. Drew, *J. Chem. Soc.*, **124**, 372 (1925).
11) K. Saito and K. Masuda, *Bull. Chem. Soc. Jpn.*, **41**, 384 (1968).
12) M. T. Rogers, *Can. J. Chem.*, **43**, 1516 (1965); G. Allen, *J. Chem. Soc., B*, **1966**, 161; H. Watarai and N. Suzuki, *J. Inorg. Nucl. Chem.*, **36**, 1815 (1974).
13) W. H. Nelson, *Inorg. Chem.*, **6**, 1509 (1967).
14) If the exchange proceeds *via* an entirely different route involving only one mol of water, the rate formula can be written as: $k_x=k_f\gamma[H_2O]$ where γ stands for the activity coefficient of water in AN. If γ decreases in $<$0.05 M solution, k_x *vs.* $[H_2O]$ diagrams can assume apparently second order dependence as shown in Fig. 5. No information is available concerning the activity coefficient of a very small concentration of water in AN at −20 °C. However, such a solution may be approximated to an AN solution of ice and a significant decrease in activity coefficient cannot be necessarily unreasonable.
15) K. Saito and K. Masuda, *Bull. Chem. Soc. Jpn.*, **43**, 119 (1970); K. Matsuzawa and K. Saito, *ibid.*, **46**, 2777 (1973); A. Nagasawa and K. Saito, to be published.
16) M. J. Frazer and L. I. B. Haines, *J. Chem. Soc., Dalton Trans.*, **1975**, 1471.
17) K. Saito, *Pure Appl. Chem.*, **38**, 325 (1974).
18) C. Chatterjee, K. Matsuzawa, H. Kido, and K. Saito, *Bull. Chem. Soc. Jpn.*, **47**, 2809 (1974).

Keto-Enol Tautomerism. I. The Calorimetrical Determination of the Equilibrium Constant for Keto-Enol Tautomerism for Cyclopentanone

Jack HINE and Kazushi ARATA*

The Evans Laboratory of Chemistry, The Ohio State University, Columbus, Ohio, U.S.A.

(Received May 31, 1975)

The enol content of cyclopentanone was determined by calorimetrical measurement of the enthalpy of hydrolysis of cyclopentenyl methyl ether to cyclopentanone with the assumption that the thermodynamics of hydrolysis of any ROMe to ROH is the same as that for any other ROMe. The enthalpy of the ketonization of cyclopentenol was determined to be -7.87 kcal/mol in the liquid phase and -11.66 kcal/mol in the gas phase, at 25 °C. The enol content of cyclopentanone in the gas phase at 25 °C was found to be 2.5×10^{-7}%.

The equilibrium enol content of simple ketones (RR'HC·COR": R, R', and R"=H or allyl groups) is known to be very low, both in the neat substances and in aqueous solution. The enol content has been determined by several methods. Most of the measurements were based on the classical method in which the enol content was estimated by the rapid reaction of enol with bromine.

Schwarzenbach and Wittwer determined the enol content of cyclopentanone, cyclohexanone and acetone to be 0.0048, 0.02, and 0.00025%, respectively, by running a ketone solution of known concentration and a bromine solution of steadily increasing concentration at controlled rates through a reaction vessel and determining potentiometrically the moment at which excess bromine appears.[1]

Gero improved the bromine titration by the use of the most polar halogen available (iodine monochloride) instead of bromine, because the rate of the addition reaction is essential in order to obtain accurate information on the enol content. His values for cyclopentanone, cyclohexanone and acetone were 0.088, 1.2, and 0.00015 %, respectively.[2]

A careful work by Bell and Smith on the bromine titration[3] shows what large errors the method can lead to when the proper precautions are not taken. They found that the enol contents for cyclopentanone and cyclohexanone are, respectively, 0.0013 and 0.00041%, of which the latter is 3000 times as small as that reported by Gero.

Ultraviolet[4] and infrared[5] spectroscopy were also used as a mean of studying the keto-enol equilibria.

Calorimetry for Determining Equilibrium Constants for Keto-Enol Tautomerism. For simple ketones whose enol contents are relatively small, we planned to use an indirect method based on thermochemical measurements. This method is similar to that used by Sunner, who measured the heats of hydrolysis of *iso*-propenyl acetate and *m*-cresyl acetate.[6] He assumed that the heats of hydrolysis are identical for both of the esters and therefore claimed that the extra heat liberated in the hydrolysis of isopropenyl acetate is due to the subsequent ketonization of the initially formed enol. He got a value of the enthalpy change of 7 kcal/mol for ketonization in the liquid phase.

Jencks and co-workers have shown that the free energy of hydrolysis of ROAc's changes by 14.0±0.5 kcal/mol as R is changed from ethyl through phenyl and *p*-nitrophenyl to acetyl.[7] We believe that this method could be improved upon by eliminating the assumption that the heat of hydrolysis of one ROAc to ROH is the same as that of another. It is better to assume that the thermodynamic parameters of hydrolysis of any ROMe (or ROEt or ROPr-n, *etc.*) to ROH are approximately the same whether R is changed. In support of this assumption is the fact that as R is changed from methyl through phenyl to acetyl[8] the free energy of hydrolysis of ROMe changes by 1.7 kcal/mol.[9] Therefore, we shall measure the heats of hydrolysis of various enol methyl ethers and assume the heat of hydrolysis to ROH is the same as that for some ROMe for which the heat of hydrolysis is known reliably (and if possible for an ROMe that is structurally as closely related as possible to the enol methyl ether in question), *e.g.*,

$$CH_2{=}CROMe + H_2O \longrightarrow CH_3CRO + MeOH \quad \Delta H_1 \quad (1)$$

$$R'OMe + H_2O \longrightarrow R'OH + MeOH \quad \Delta H_2 \quad (2)$$

$$CH_2{=}CROMe + H_2O \longrightarrow CH_2{=}CROH + MeOH \quad \Delta H_3 \quad (3)$$

$$CH_2{=}CROH \longrightarrow CH_3CRO \quad \Delta H_4\ (\text{Ketonization}) \quad (4)$$

obviously

$$\Delta H_1 = \Delta H_3 + \Delta H_4\ (\text{Ketonization})$$

Since it is assumed that ΔH_3 is equal to ΔH_2

$$\Delta H_4\ (\text{Ketonization}) = \Delta H_1 - \Delta H_2$$

Both ΔH_1 and ΔH_2 can be determined experimentally and therefore ΔH_4 (Ketonization) may be calculated.

The following four values are experimentally determined in order to get ΔH_1 in the liquid phase;

$$CH_2{=}CROMe(liq) + H_2O{\cdot}S + S \longrightarrow CH_3CRO{\cdot}S + CH_3OH{\cdot}S \quad \Delta H_5 \quad (5)$$

$$H_2O(liq) + S \longrightarrow H_2O{\cdot}S \quad \Delta H_6 \quad (6)$$

$$CH_3CRO(liq) + S \longrightarrow CH_3CRO{\cdot}S \quad \Delta H_7 \quad (7)$$

$$CH_3OH(liq) + S \longrightarrow CH_3OH{\cdot}S \quad \Delta H_8 \quad (8)$$

where S's are solvents. The actual reaction taking place in the calorimeter is represented by Eq. 5. In order to obtain the isothermal ideal hydrolysis reaction, as defined by Eq. 9 or 1, it is necessary to calculate as follows:

* Present address: Hokkaido University of Education, Hachiman-cho 1-2, Hakodate 040.

Eq. 5+Eq. 6−Eq. 7−Eq. 8

$$CH_2{=}CROMe(liq) + H_2O(liq) \longrightarrow CH_3CRO(liq) + CH_3OH(liq) \quad \Delta H_9 = \Delta H_1 \qquad (9)$$

Experimental

Water used in making up solutions in this study was double-distilled. Traces of potassium permanganate and potassium hydroxide were added to the distilled water before the second distillation. Baker Analyzed reagent grade tetrahydrofuran was distilled over ferrous sulfate.[10]

Cyclopentenyl Methyl Ether. The preparation of cyclopentanone dimethyl ketal was based on the method of Arbuzov and Mikhailova.[11] Cyclopentanone (168 g) and trimethyl orthoformate (212 g) were placed into a 1 l round-bottomed flask fitted with a magnetic stirrer, a condenser, and an ice bath. Six drops of concentrated sulfuric acid were added, and the reaction proved to be exothermic, causing the colorless mixture to become brown. The ice bath was removed after an hour, and the reaction allowed to continue overnight. After the reaction mixture was allowed to stir for an hour with solid potassium bisulfite (80 g) and then filtered, the product was fractionally distilled to give 204.3 g (78.5% yield) of cyclopentanone dimethyl ketal, bp 60—63 °C at 50 mmHg. Cyclopentenyl methyl ether was prepared by pyrolysis of cyclopentanone dimethyl ketal. The dimethyl ketal (108 g) was boiled overnight while resulting methanol collected, and the product was fractionated to give 52.3 g (64%) of cyclopentenyl methyl ether, bp 108—109 °C, which was found by gas chromatographic (GLC) analysis to be 90.5% pure. The purer product, 99.5%, was obtained by preparative GLC. The NMR spectrum showed at τ 5.77, a singlet (1H), assigned to the olefinic proton: τ 6.62, a singlet (3H), assigned to methoxy protons, τ 7.88, a multiplet (4H), assigned to allylic methylene protons; τ 8.22, a multiplet (2H), assigned to homoallylic methylene protons.

Calorimetric Measurements. The Bunsen ice calorimeter was used. The apparatus and the experimental procedure were similar to those described previously[12] with the following exception: the outer jacket (chamber C) was evacuated to insulate internal chambers A and B from the surrounding medium after draining of water.

In order to confirm its reliability, the apparatus was first used to determine the enthalpy of neutralization of sodium hydroxide with hydrochloric acid. Three determinations gave values of 14.45, 14.62, and 14.50 kcal/mol. The average value, 14.52±0.09 kcal/mol, is in good agreement with the reported values,[13-15] and is 5.6% smaller than the value that should have been obtained as calculated from the calorimetrically determined heat of dissociation of water at 0 °C and infinite dilution[16] and the heats of dilution[17] of sodium hydroxide, hydrochloric acid, and sodium chloride.

Determination of Heats of Hydrolysis for Cyclopentenyl Methyl Ether. In these studies an ampoule containing about 1 g of enol methyl ether was broken in a solution of 1.817 g of distilled water and 0.411 g of 96.5% sulfuric acid in 24.747 g of tetrahydrofuran [30 ml of 91.67% THF–H_2O (0.15 mol/l H_2SO_4)]. Five determinations of heat evolved gave values of 4367, 4417, 4521, 4380, and 4404 cal/mol. The average value was 4418±61 cal/mol.

The reaction solution was analyzed by GLC. The reaction solution of 0.175 g (1.78×10^{-3} mol) cyclopentenyl methyl ether in 5 ml of 91.67% THF–H_2O (0.15 M H_2SO_4), which is almost the same concentration as that used in the calorimetrical measurements, was analyzed on a 10% Carbowax and 2% KOH column (2 m). From the ratios of the area of cyclopentanone to that of THF and area of methanol to that of THF, concentrations of the products, methanol and cyclopentanone, were obtained as 1.82×10^{-3} mol and 1.72×10^{-3} mol which were 102 and 96.7%, respectively, compared with the theoretical yields.

The reaction solution of 0.146 g (1.49×10^{-3} mol) cyclopentenyl methyl ether in 25 ml of 91.67% THF–H_2O (0.15 M H_2SO_4) was also analyzed on a 5% Carbowax 20 M on Chromosorb P column (2 m). The ratio of the area of methanol to that of cyclopentanone gave 1: 1.18 as the mole ratio calculated from the estimated standard values.

The reaction solution was analyzed by UV spectrometry. From the absorbance at 281 nm of 0.042 M solution of cyclopentenyl methyl ether in THF–H_2O (0.15 M H_2SO_4), the conversion was calculated to be 106, 97.7, and 107% (103% in the average).

Determination of Heats of Solution for Cyclopentanone. In these studies an ampoule containing about 1—2 g of ketone was broken in a solution of 30 ml of 91.67% THF–H_2O (0.15 M H_2SO_4). Four determinations of heat absorbed gave values of 232, 319, 405, and 294 cal/mol. The average value was 312±72 cal/mol.

Determination of Heats of Solution for Methanol. In these studies an ampoule containing about 1 g of methanol was broken in a solution of 30 ml of 91.67% THF–H_2O (0.15 M H_2SO_4). Five determinations of heat evolved gave values of 21, 16, −8, 27, and 13 cal/mol. The average value was 14±13 cal/mol.

Determination of Heats of Solution for Water. In these studies an ampoule containing about 1 g of water was broken in a solution of 30 ml of 91.67% THF–H_2O (0.15 M H_2SO_4). Five determinations of heat evolved gave values of 198, 204, 190, 197, and 238 cal/mol. The average value was 206±19 cal/mol.

Discussion

All values determined calorimetrically are as follows,

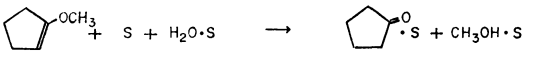

$$\Delta H_{10} = -4418 \pm 61 \text{ cal/mol} \qquad (10)$$

$$H_2O + S \longrightarrow H_2O{\cdot}S$$

$$\Delta H_{11} = -206 \pm 19 \text{ cal/mol} \qquad (11)$$

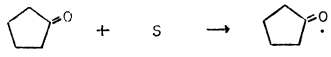

$$\Delta H_{12} = +312 \pm 72 \text{ cal/mol} \qquad (12)$$

$$CH_3OH + S \longrightarrow CH_3OH{\cdot}S$$

$$\Delta H_{13} = +14 \pm 13 \text{ cal/mol} \qquad (13)$$

where S's are solvents, and the ± figures are standard deviations. The actual reaction taking place in the calorimeter is represented by Eq. 10. In order to obtain the isothermal, ideal hydrolysis reaction (defined by Eq. 14) it is necessary to subtract Eq. 12 and 13 from 10 and to add 11. The following result is obtained.

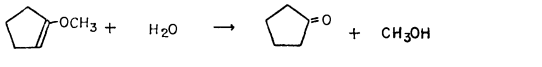

$$\Delta H_{14} = -4950 \pm 165 \text{ cal/mol} \qquad (14)$$

This value, −4950±165 cal/mol, is the heat of hydrolysis of the idealized reaction at 0 °C.

In order to obtain the heats of reaction at 25 °C, the

Kirchhoff's thermodynamic equation is used. The difference in the mean heat capacities at constant pressure of the products and reactants, ΔC_p, was estimated to be -4.9 cal/mol K.[18] Therefore, $\Delta H'_{14}$ (liq) $=-5072\pm165$ cal/mol, which is the heat of hydrolysis of the idealized reaction at 25 °C in the liquid phase for cyclopentenyl methyl ether, was obtained.

In order to calculate the heat of hydrolysis when both reactants and reaction are in the gaseous state it is necessary to know the heats of vaporization for all the compounds at 25 °C. The heat of vaporization of water, methanol,[20] cyclopentanone[22] and cyclopentenyl methyl ether[23] have been determined to be 10.47, 8.91, 9.67, and 9.4 kcal/mol, respectively.

The following five equations were used to calculate the heat of hydrolysis for cyclopentenyl methyl ether in the gas phase;

$$H_2O(liq) \longrightarrow H_2O(g)$$
$$\Delta H_{15} = +10.47 \text{ kcal/mol} \quad (15)$$
$$CH_3OH(liq) \longrightarrow CH_3OH(g)$$
$$\Delta H_{16} = +8.91 \text{ cal/mol} \quad (16)$$

$$\Delta H_{17} = +9.67 \text{ kcal/mol} \quad (17)$$

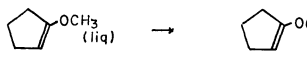

$$\Delta H_{18} = +9.4 \text{ kcal/mol} \quad (18)$$

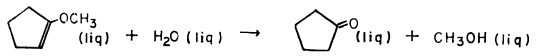

$$\Delta H_{19} = -5.07 \text{ kcal/mol} \quad (19)$$

Then, $-(15)+(16)+(17)-(18)+(19)$ gives the equation in the gaseous state. Therefore, $\Delta H'_{19}(g)=-6.36$ kcal/mol, which is the heat of hydrolysis for cyclopentenyl methyl ether at 25 °C in the gas phase, is obtained.

Heats of Ketonization. The hydrolysis of enol methyl ethers to ketones may be split into two consecutive steps, *viz.* the hydrolysis to enols, and the prototropic isomerization of enols to ketones:

$$R'R''C{=}CR'''OMe + H_2O \longrightarrow R'R''CHCOR''' + MeOH \quad \Delta H_{20} \quad (20)$$
$$R'R''C{=}CR'''OMe + H_2O \longrightarrow R'R''C{=}CR'''OH + MeOH \quad \Delta H_{21} \quad (21)$$
$$R'R''C{=}CR'''OH \longrightarrow R'R''CHCOR''' \quad \Delta H_{22}\text{ (Ketonization)} \quad (22)$$

A knowledge of the value of ΔH_{21} makes it possible to obtain a value of ΔH_{22} (ketonization), which is the reverse of the enolization reaction of ketones. The reaction for ΔH_{21} is of course not experimentally accessible; it is therefore necessary to estimate the accompanying change in enthalpy indirectly from the following reaction;

$$ROMe + H_2O \longrightarrow ROH + MeOH \quad \Delta H_{23} \quad (23)$$

When R is methyl ΔH_{23} is 5.6 kcal/mol and when R is phenyl ΔH_{23} is 5.3 kcal/mol in the gas phase at 25 °C.[9] These two values were estimated to be 2.80 kcal/mol in the liquid phase.[24] Therefore, ΔH_{22} (Ketonization) can be obtained by $\Delta H_{20}-\Delta H_{23}$. In the liquid phase, value of ΔH_{22}(Ketonization) for cyclopentanone is -7.87 kcal/mol. In the gas phase, ΔH_{22} (Ketonization) for cyclopentanone can be estimated to be -11.66 kcal/mol, by taking the value of ΔH_{23} for phenyl which structurally resembles cyclopentenyl more than methyl does.

Free Energies for Ketonization. Benson and Buss have pointed out that entropies of compounds may be calculated reliably from structural contributions. Calculations, using the first-order approximation to the law of additivity of bond properties, gave $+0.13$ e.u. for the entropy of ketonization of cyclopentenol in the gas phase at 25 °C.[26,27] Therefore, free energy for the ketonization of cyclopentenol in the gas phase was -11.70 kcal/mol, which made the calculation of the equilibrium constant for the ketonization, K, and its reverse, $1/K$, which is the equilibrium constant for the enolization. They were 4.0×10^{8} and 2.5×10^{-9}, respectively. Thus, the enol content of cyclopentanone was obtained to be 2.5×10^{-7}% in the gas phase at 25 °C.

References

1) G. Schwarzenbach and C. Wittwer, *Helv. Chim. Acta*, **30**, 669 (1947).
2) A. Gero, *J. Org. Chem.*, **19**, 1960 (1954).
3) R. P. Bell and P. W. Smith, *J. Chem. Soc., B*, **1966**, 241.
4) A. S. N. Murthy, A. Balasubramanian, and C. N. R. Rao, *Can. J. Chem.*, **40**, 2267 (1962); G. S. Hammond, W. G. Borduin, and G. A. Giuter, *J. Am. Chem. Soc.*, **81**, 4682 (1959).
5) R. Mecke and E. Funck, *Z. Elektrochem.*, **60**, 1124 (1956); L. J. Bellamy and L. Beecher, *J. Chem. Soc.*, **1954**, 4487; J. Osugi, T. Mizukami, and T. Tachibana, *Rev. Phys. Chem. Jpn.*, **36**, 8 (1966).
6) S. Sunner, *Acta Chem. Scand.*, **11**, 1757 (1957).
7) W. P. Jencks and M. Gilchrist, *J. Am. Chem. Soc.*, **86**, 4631 (1964); J. Gerstein and W. P. Jencks, *ibid.*, **86**, 4655 (1964); W. P. Jencks, F. Barley, R. Barnett, and M. Gilchrist, *ibid.*, **86**, 4464 (1964).
8) In making this calculation it was necessary to assume that the equilibrium constant for the hydrolysis of methyl acetate is the same as that for ethyl acetate.
9) J. Hine and R. D. Weimar, Jr., *J. Am. Chem. Soc.*, **87**, 3387 (1965).
10) J. Schurz and H. Stuebchen, *Angew. Chem.*, **68**, 182 (1956).
11) A. E. Arbuzov and B. M. Mikhailova, *Zh. Obshch. Khim.*, **6**, 290 (1936).
12) J. Hine and F. E. Rogers, *J. Am. Chem. Soc.*, **90**, 6701 (1968).
13) J. B. Speakman and E. Stott, *Trans. Faraday Soc.*, **34**, 1204 (1938).
14) P. Bender and W. J. Biermann, *J. Am. Chem. Soc.*, **74**, 322 (1952).
15) G. Kegeles, *J. Am. Chem. Soc.*, **62**, 3230 (1960).
16) V. P. Vasilev and G. A. Lobanov, *Zh. Fiz. Khim.*, **41**, 838 (1967); *Russ. J. Phys. Chem., (English Transl.)*, **41**, 434 (1967).
17) The heats of dilution used were determined at 25 °C. H. S. Harned and B. B. Owen, "The Physical Chemistry of Electrolytic Solutions," 3rd ed., Reinhold Publishing Corp., New York, N. Y. (1958), pp. 707, 708.
18) Mean heat capacities of water, methanol, and cyclo-

hexanone are 75.7, 78.2, and 177.8 J/K mol, respectively in the liquid phase.[19] Mean heat capacity of phenyl methyl ether, 200.8 J/K mol, was used instead of the value of cyclopentenyl methyl ether, and the value for cyclopentanone was taken as that cyclohexanone. To use the heat capacity of phenyl methyl ether for cyclopentenyl methyl ether may cause a large error, however, we believe that to take the value of cyclohexanone for cyclopentanone make this error minimized.

19) "International Critical Tables," Vol. 5, p. 106 (1929). Water: 4.220 at 0 °C, 4.210 at 5 °C, 4.199 at 10 °C, 4.190 at 15 °C, and 4.184 J/K g at 20 °C. Mean=4.200 J/K g. Methanol: 2.37 at 0 °C, 2.51 J/K g at 20 °C, mean=2.44 J/K g. Cyclohexanone: 1.812 J/K g at 15—18 °C. Phenyl methyl ether: 1.697 at 0 °C, 2.021 J/K g at 20—152 °C. Mean= 1.859 J/K g.

20) International Critical Tables, V. 5, p. 138 (1929). The heat of vaporization for methanol at 25 °C was calculated from that at 20 °C, 8.95 kcal/mol, and the heat capacities for the liquid and vapor, 80.3 J/K mol at 20 °C[19] and 43.9 J/K mol[21] at 25 °C, respectively.

21) D. R. Stull, E. F. Westrum, Jr., and G. C. Sinke, "The Chemical Thermodynamics of Organic Compounds," John Wiley and Sons; Inc., New York, N. Y. (1969), p. 422.

22) E. C. Baughan, A. L. Jones, and K. Stewart, *Proc. R. Soc. London, Ser. A.*, **225**, 478 (1954).

23) F. Klages, *Chem. Ber.*, **82**, 358 (1949). The heat of vaporization, ΔH_v, of any unassociated liquid at 25 °C is given as $\Delta H_v = 5.4 + 0.036\ t$ (kcal/mol), where t is its normal boiling point, t °C. Boiling point used was 111 °C for cyclopentenyl methyl ether.

24) In order to calculate ΔH_3 in the liquid phase at 25 °C, the heat of vaporization of methyl ether, and of phenyl methyl ether were estimated from Klages equation[23] to be 4.55, 10.9 kcal/mol, respectively. Boiling points used were −23.6 °C for methyl ether and 155 °C for phenyl methyl ether.[25] The heat of vaporization of phenol was calculated to be 15.0 kcal/mol from another equation, $\Delta H_v = 6.8 + 0.045\ t$ kcal/mol, given by Klages where t is its normal boiling point, t °C. The boiling point is 182 °C. Those of water and methanol used were 10.47 and 8.95 kcal/mol,[20] respectively.

25) "Dictionary of Organic Compounds," Vol. 2, p. 1169, Vol. 1, p. 248, Vol. 4, p. 2660, Eyre and Spottiswoode (Publishers) Ltd., 22 Henrietta Street, London (1965).

26) S. W. Benson and J. H. Buss, *J. Chem. Phys.*, **29**, 546 (1958).

27) The value of −2.5 for C_{vi}–O bond was estimated from values of −16.4 and −14.3 for C–C and C_{vi}–C, 12.9 and 13.8 for C–H and C_{vi}–H, and −4.0 for C–O, respectively.

Keto-Enol Tautomerism. II.[1] The Calorimetrical Determination of the Equilibrium Constants for Keto-Enol Tautomerism for Cyclohexanone and Acetone

Jack HINE and Kazushi ARATA*

The Evans Laboratory of Chemistry, The Ohio State University, Columbus, Ohio, U.S.A.

(Received May 31, 1975)

The vapor phase enol contents of cyclohexanone and acetone were determined by calorimetric measurements of the enthalpies of hydrolysis of their corresponding enol methyl ethers to ketones and methanol in 91.67% THF-H_2O (0.15 M H_2SO_4). The relative order of enol content, together with cyclopentanone in our previous study, was cyclohexanone>cyclopentanone≧acetone, which was the same as that reported by Gero and by Schwarzenbach, but different from Bell's observed order (cyclopentanone>cyclohexanone>acetone). The enthalpies calculated from Benson's correlation of thermodynamic properties for the enolization reactions of these ketones and for the hydrolysis reactions of enol methyl ethers agreed with our relative ordering. Furthermore, data on reactions of compounds with 5- and 6-membered rings lead to the prediction that cyclohexanone contains more enol than cyclopentanone does. The kinetics of hydrolysis of enol methyl ethers was also discussed.

In an earlier paper[1] we described methods for determining the equilibrium enol content of simple ketones (RR'HC·COR": R, R', and R"=H or allyl groups) by calorimetric measurements of the enthalpies of hydrolysis of their corresponding enol methyl ethers to ketones and methanol, and by assuming that the thermodynamic parameters of hydrolysis of any ROMe to ROH are approximately the same whether R is changed. The enol content of cyclopentanone was obtained to be 2.5×10^{-7}% in the vapor phase at 25 °C.

The same method has been applied to cyclohexanone and acetone, and the relative order of enol content of these three ketone is discussed.

Experimental

Experiments which do not overlap with those reported in our previous paper[1] are described here.

Cyclohexenyl Methyl Ether. The preparation of cyclohexenyl methyl ether was analogous to that of cyclopentenyl methyl ether.[1] Pyrolysis of 43 g of cyclohexanone dimethyl ketal, bp 63—67 °C at 40 mmHg, gave 28.0 g (83% yield) of cyclohexenyl methyl ether, bp 140 °C, which was found by GLC analysis to be 92.2% pure. The purer product, 99.6%, was obtained by preparative GLC. Its NMR spectrum was identical with the reported spectra;[2] τ 5.5, a triplet (1H), assigned to the olefinic proton: τ 6.6, a singlet (3H), assigned to methoxy protons; τ 8.1, a multiplet (4H), assigned to allylic methylene protons; τ 8.5, a multiplet (4H), assigned to homoallylic methylene protons.

Isopropenyl Methyl Ether. The preparation of isopropenyl methyl ether was based on Kaufmann's method of preparation of propyl isopropenyl ether.[3] A mixture of 107 g of 2,2-dimethoxypropane, 7 g of quinoline, and 0.4 g of *p*-toluenesulfonic acid was allowed to reflux under a nitrogen blanket in a Todd distillation column and 34 g of the fraction boiling 34—52 °C was collected. This reaction was repeated in order to get more product. These mixtures were placed in a reflux set-up equipped with magnetic stirrer, condenser, and drying tube, and excess potassium metal carefully added through the condenser. After 2 h, the mixture was again distilled with the fraction boiling at 33.0—33.5 °C collected. This procedure was repeated to get the sufficiently pure (99.9%) isopropenyl methyl ether, bp 35.5 °C; [lit,[4] bp 35.2—35.6 °C/752 Torr, n_D^{20} 1.3824, d_4^{20} 0.7645]. NMR spectrum: τ 6.88, a singlet (2H), assigned to olefinic protons; 7.23, a singlet (3H), assigned to methoxy protons; τ 8.93, a singlet (2H), assigned to methyl protons.

Determination of Enthalpies of Hydrolysis for Enol Methyl Ethers. In these studies an ampoule containing about 1 g of enol methyl ether was broken in a solution of 1.817 g of distilled water and 0.411 g of 96.5% sulfuric acid in 24.847 g of tetrahydrofuran [30 ml of 91.67% THF-H_2O (0.15 mol/l H_2SO_4)].

Enthalpy of Hydrolysis of Cyclohexenyl Methyl Ether: Five determinations of heat evolved gave values of 2686, 2629, 2695, 2884, and 2888 cal/mol. The average value was 2756±121 cal/mol.

Ethalpy of Hydrolysis of Isopropenyl Methyl Ether: four determinations of heat evolved gave values of 5127, 5077, 5166, and 5174 cal/mol. The average value was 5136±44 cal/mol.

Determination of Heats of Solution for Ketones. In these studies an ampoule containing about 1—2 g of ketone was broken in a solution of 30 ml of 91.67% THF-H_2O (0.15 M H_2SO_4).

Enthalpy of Solution of Cyclohexanone: three determinations of heat absorbed gave values of 145, 170, and 162 cal/mol. The average value was 159±13 cal/mol.

Enthalpy of Solution of Acetone: five determinations of heat absorbed gave values of 162, 114, 145, 188, and 202 cal/mol. The average value was 162±35 cal/mol.

Results and Discussion

All values determined calorimetrically are as follows,

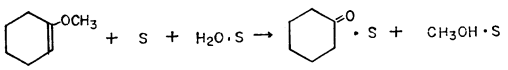

$$\Delta H_{1a} = -2756 \pm 121 \text{ cal/mol} \quad (1a)$$

$$CH_2{=}C(OCH_3)CH_3 + S + H_2O{\cdot}S \longrightarrow CH_3\overset{\overset{O}{\|}}{C}CH_3{\cdot}S + CH_3OH{\cdot}S$$

$$\Delta H_{1b} = -5136 \pm 44 \text{ cal/mol} \quad (1b)$$

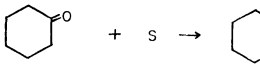

$$\Delta H_{2a} = +159 \pm 13 \text{ cal/mol} \quad (2a)$$

* Present address: Hokkaido University of Education, Hachiman-cho 1-2, Hakodate 040.

$$CH_3\overset{O}{\overset{\|}{C}}CH_3 + S \longrightarrow CH_3\overset{O}{\overset{\|}{C}}CH_3\cdot S$$

$$\Delta H_{2b} = +162 \pm 35 \text{ cal/mol} \quad (2b)$$

$$H_2O + S \longrightarrow H_2O\cdot S$$

$$\Delta H_3 = -206 \pm 19 \text{ cal/mol}^{1)} \quad (3)$$

$$CH_3OH + S \longrightarrow CH_3OH\cdot S$$

$$\Delta H_4 = +14 \pm 13 \text{ cal/mol}^{1)} \quad (4)$$

where S's are solvents, and the ± figures are standard deviations. In order to obtain the isothermal, ideal hydrolysis reaction it is necessary to subtract Eq. 2 and 4 from 1 and to add 3. Thus, the heats of hydrolysis of the idealized reaction in the liquid phase at 0 °C are −3135±166 and −5518±111 cal/mol for cyclohexenyl methyl ether and isopropenyl methyl ether, respectively.

These two values were corrected to those at 25 °C by following thermodynamic equation. Calculations[5] gave −3257±166 and −5745±111 cal/mol for cyclohexenyl and isopropenyl methyl ethers, respectively. These values are the heats of hydrolysis of the idealized reaction at 25 °C in the liquid phase.

In order to calculate the enthalpy of hydrolysis when both reactants and reaction are in the gaseous state it is necessary to know the heats of vaporization for all the compounds at 25 °C. Those of water, methanol, cyclohexanone, acetone, cyclohexenyl methyl ether and isopropenyl methyl ether were 10.47, 8.91,[1] 10.61,[7] 7.61,[8] 10.62, and 6.68[9] kcal/mol, respectively. Therefore, the heats of hydrolysis for cyclohexenyl methyl ether and that for isopropenyl methyl ether at 25 °C in the gas phase were obtained to be −4.83 and −6.38 kcal/mol, respectively.

The hydrolysis of enol methyl ethers to ketones may be split into two consecutive steps, *viz.* the hydrolysis to enols, and the prototropic isomerization of enols to ketones. The heat of ketonization of RR'C=CR"OH can be estimated by assuming that, as carried out in the previous paper,[1] the heat of hydrolysis of RR'C=CR"-OMe to RR'C=CR"OH is the same as that of ROMe for which the heat of hydrolysis is known reliably to be 5.6 and 5.3 kcal/mol in gas phase when R is methyl and phenyl, respectively.[11] The heat of hydrolysis of ROMe was estimated to be 2.80 kcal/mol in the liquid phase.[1] Therefore, enthalpies of ketonization were −6.06 and −8.54 kcal/mol in the liquid phase for cyclohexanone and acetone, respectively. In the gas phase, depending on whether R is taken as methyl which is reasonable for isopropenyl, or phenyl which seems structurally a better model for cyclohexenyl, they were −10.13 and −11.98 kcal/mol for cyclohexanone and acetone, respectively.

The entropies of ketonization of cyclohexenol and isopropenol were estimated to be +0.13 and −0.87 e.u., respectively, in the gas phase at 25 °C by calculations using the first-order approximation to the law of additivity of bond properties by Benson and Buss.[1,12] Therefore, free energies for the ketonization of cyclohexenol and isopropenol at 25 °C in the gas phase were −10.17 and −11.72 kcal/mol, respectively, which made the calculation of the equilibrium constant for the ketonization, K, and its reverse, $1/K$, which is the equilibrium constant for the enolization. They are summarized in Table 1, together with our previous study for cyclopentanone.[1]

Table 1. Equilibrium constant of ketonization, K, and enolization, $1/K$, in the gas phase at 25 °C

	K	$1/K$
Cyclopentanone[1]	4.0×10^{8}	2.5×10^{-9}
Cyclohexanone	3.0×10^{7}	3.3×10^{-8}
Acetone	4.2×10^{8}	2.4×10^{-9}

Kinetics of Reactions. It is interesting to note that one can find data from the literature to suggest that the reaction we studied should have been very rapid under our conditions. The hydrolysis of isopropenyl methyl ether was studied by Salomaa *et al.*[10] From their second-order rate constant at 25 and 35 °C in water, a second-order rate constant of 120 $M^{-1}\,s^{-1}$ may be calculated (from the Arrhenius equation) at 0 °C. In the presence of 0.15 M H_2SO_4 it would hydrolyze with a first-order rate constant of about 18 s^{-1} if the solvent was water. If the rate of protonation of the ether is the same in water and in 91.67% THF-8.33% water, then the half-life of the reaction we studied would be 0.04 s. Even if the real half-life is 1000 times as long as this, the reaction should be fast enough to study satisfactorily by the method we used. In the case of cyclohexenyl methyl ether, Lienhard and Wang have determined the second-order rate constant as 2810 $M^{-1}\,min^{-1}$ in water at 25 °C.[13] Similarly, it would give about 0.098 s for the half-life of the reaction in the presence of 0.15 M H_2SO_4 at 25 °C.

We must also be concerned as to whether there is any ketal present at the end of the reaction, due to the establishment of the following equilibrium. This

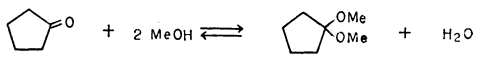

equilibrium was studied in aqueous methanol by Bell *et al.*[14] From their values of K at 10 and 25 °C, a value of 8.6×10^{-4} M^{-1} at 0 °C may be calculated. Starting with 0.35 M ether and 3.3 M water, $8.6\times10^{-4}=[\text{ketal}]\cdot[H_2O]/[\text{ketone}][MeOH]^2=[\text{ketal}]\cdot3/[0.35]^3$. Thus about 0.003% of the ketone would be in the form of ketal at equilibrium. This is certainly negligible. Similarly, in the cases of cyclohexanone and acetone, equilibrium constants of 2.14×10^{-2} for cyclohexanone and 9.3×10^{-4} for acetone at 0 °C were calculated from their values of K at 10 and 25 °C. These led to calculations that 0.058% and 0.0001%, respectively, would be in ketal forms at equilibrium.

Enol Contents of Ketones. Enol contents of cyclopentanone, cyclohexanone and acetone investigated by the auther are assembled in Table 2, together with the results by other workers for comparison. The most interesting phenomenon is the relative ordering of enol contents of cyclohexanone>cyclopentanone>acetone in the data by Schwarzenbach, Gero, and the author, which is the opposite tendency to that found by Bell, who reported that cyclopentanone contains more enol than does cyclohexanone.

Shechter and his co-workers have found that the rate

Table 2. Enol contents of ketones at 25 °C

Investigator	Compound Enol contents, %		
	Cyclohexanone	Cyclopentanone	Acetone
G. Schwarzenbach[15]	2.0×10^{-2},a)	4.8×10^{-3},a)	2.5×10^{-4},a)
A. Gero[16]	1.2b)	8.8×10^{-2},b)	1.5×10^{-4},b)
R. P. Bell[17]	4.1×10^{-4},c)	1.3×10^{-3},c)	$<10^{-4}$,c)
Author	3.3×10^{-6},d)	2.5×10^{-7},d)	2.4×10^{-7},d)
S. Sunner[18]	—	—	1.6×10^{-4},e)
J. Osugi[19]	2.0f)	—	4.0×10^{-2},f)
Calculated value	4.9×10^{-4},g)	—	2.8×10^{-6},g)

a) In aqueous solution. b) In 75% methanol–water. c) In aqueous solution. d) Idealized gas state. e) In 60% by volume ethanol–water. f) In toluene solution. g) Values calculated by the assumption of Lienhard and Wang.[13]

for enolization of cycloalkanones as a function of ring size is 6>8>5>7>4, and interpreted the rate order for acid-catalyzed enolization of cycloalkanones primarily on the basis of differences in steric requirements in conversion of the ketones to transition states having endocyclic unsaturated character.[20] If the rates of acid-catalyzed enolization of alkanones are related to the enol contents at equilibrium, cyclohexanone is considered to contain more enol than cyclopentanone.

Brown *et al.*[21] have reported that exocyclic double bonds stabilize a 5-membered ring and destabilize a 6-membered ring, and they made the generalization that reactions will proceed in such a manner as to favor the formation or retention of an exocyclic double bond in a 5-membered ring and to avoid the formation or retention of an exocyclic double bond in a 6-membered ring. It was also pointed out that reactions involving a change in coordination number from three to four proceed slowly in 5-membered and rapidly in 6-membered rings.

The proposal that an exocyclic double bond in 5-membered ring systems is more stable toward changes involving loss of the exocyclic double bond than the corresponding exocyclic double bond in 6-membered ring systems was supported by the higher heat of hydrogenation of cyclohexanone as compared to cyclopentanone; $\Delta H=-12.50$ kcal/mol for cyclopentanone and −15.42 for cyclohexanone.[22]

The generalization may be further illustrated by a consideration of the structures of the stable forms of the carbethoxy derivatives of cyclopentanone and cyclohexanone. The cyclopentanone derivative exists primarily in the form of the Keto derivative (5% enol) whereas the cyclohexanone compound exists primarily as the enol (57%) in 95% ethanol.[23]

In conclusion it may be reasonable to state that cyclohexanone contains more enol than cyclopentanone does. Heats of formation of three ketones and their enol forms in the gas phase at 25 °C were calculated by use of Benson and co-workers' second-order approximation which is the law of additivity of group properties. They were −53.10 kcal/mol for cyclohexanone, −45.50 for cyclopentanone, and −51.70 for acetone, and the values of their enol forms were −37.01, −27.56 and −31.40 kcal/mol, respectively. The differences for the reactions of enolization, $\Delta\Delta H°_f$, were +16.1 kcal/mol for cyclohexanone, +17.94 for cyclopentanone and +20.30 for acetone, while our observed values were 10.13, 11.66 and 11.98 kcal/mol, respectively.[24]

Heats of formation of three enol ethers, their corresponding ketones and methanol in the gas phase at 25 °C were calculated by use of Benson and co-workers' group property approach. They were −40.50 kcal/mol for cyclohexenyl methyl ether, −31.09 for cyclopentenyl methyl ether, −34.90 for isopropenyl methyl ether, −53.10 for cyclohexanone, −45.50 for cyclopentanone, −51.70 for acetone, and −48.0 for methanol. From these values, heats of hydrolysis for the enol ethers were obtained. The calculated values, $\Delta\Delta H°_f$, were −2.8 kcal/mol for cyclohexenyl methyl ether, −4.4 for cyclopentenyl methyl ether and −7.0 for isopropenyl methyl ether, while our observed values were −4.83, −6.36, and −6.38, respectively.[25] Heats of formation of enol ethers were also obtained from our values of ΔH for hydrolysis and other observed values.[24] They were −38.47 kcal/mol for cyclohexenyl methyl ether, −29.14 for cyclopentenyl methyl ether, and −35.52 for isopropenyl methyl ether in the gas phase at 25 °C.

References

1) Part I: J. Hine and K. Arata, *Bull. Chem. Soc. Jpn.*, **49**, 3085 (1976).

2) D. G. Lindsay and C. B. Reese, *Tetrahedron*, **21**, 1673 (1965).

3) J. C. Kaufmann, M. S. Thesis, Ohio State University, 1969.

4) P. Salomaa, A. Kankaanperä, and M. Lajunen, *Acta Chem. Scand.*, **20**, 1790 (1966).

5) The difference in the heat capacities at constant pressure of products and reactants, ΔC_p's, were obtained to be −20.5 and −38.1 J/K mol for cyclohexenyl and isopropenyl methyl ether, respectively. Mean heat capacity used was 124.3 J/K mol for acetone.[6] Mean heat capacities of phenyl methyl ether and ethyl ether, 200.8[1] and 164.8[6] J/K mol respectively, were used instead of the values of cyclohexenyl methyl ether and of isopropenyl methyl ether, respectively.

6) "International Critical Tables," Vol. 5, p. 106 (1929). Acetone: 2.134 at 0 °C, 2.151 J/K g at 3—22.6 °C. Mean= 2.142. Ethyl ether: 2.205 at −5 °C, 2.189 and 2.214 at 0 °C, 2.289 J/K g at 30 °C. Mean=2.228 J/K g.

7) K. R. Buck and H. N. M. Stewart, *Chem. Ind. (London)*, **1961**, 586.

8) E. C. Baughan, A. L. Jones, and K. Stewart, *Proc. R.*

Soc. London, Ser. A., **225**, 478 (1954).

9) For enol methyl ethers, the heat of vaporization was estimated from Klages equation. F. Klages, *Chem. Ber.*, **82**, 358 (1949). The heat of vaporization, ΔH_v, of any unassociated liquid at 25 °C is given as $\Delta H_v = 5.4 + 0.036\ t$ (kcal/mol), where t is its normal boiling point, t °C. Boiling points used were 145 °C for cyclohexenyl methyl ether and 35.5 °C for isopropenyl methyl ether (literature value 35.2—35.6 °C/752 Torr.[10]).

10) P. Salomaa, A. Kankaanperä, and M. Lajunen, *Acta Chem. Scand.*, **20**, 1790 (1966).

11) J. Hine and R. D. Weimar, Jr., *J. Am. Chem. Soc.*, **87**, 3387 (1965).

12) S. W. Benson and J. H. Buss, *J. Chem. Phys.*, **29**, 546 (1958).

13) G. E. Lienhard and T. Wang, *J. Am. Chem. Soc.*, **91**, 1146 (1969).

14) J. M. Bell, D. G. Kubler, P. Sartnell, and R. G. Zepp, *J. Org. Chem.*, **30**, 4284 (1965).

15) G. Schwarzenbach and C. Wittwer, *Helv. Chim. Acta*, **30**, 669 (1947).

16) A. Gero, *J. Org. Chem.*, **19**, 1960 (1954).

17) R. P. Bell and P. W. Smith, *J. Chem. Soc., B*, **241** (1966).

18) S. Sunner, *Acta Chem. Scand.*, **11**, 1757 (1957).

19) J. Osugi, T. Mizukami, and T. Tachibana, *Rev. Phys. Chem. Jpn.*, **36**, 8 (1966).

20) H. Schechter, M. J. Collis, R. Dessy, Y. Okuzumi, and A. Chen, *J. Am. Chem. Soc.*, **84**, 2905 (1962).

21) H. C. Brown, J. H. Brewster, and H. Schechter, *J. Am. Chem. Soc.*, **76**, 467 (1954); H.C. Brown, *J. Org. Chem.*, **22**, 439 (1957).

22) J. B. Conn, G. B. Kistiakowsky, and E. A. Smith, *J. Am. Chem. Soc.*, **61**, 1868 (1939).

23) G. Schwarzenbach, M. Zimmermann, and V. Prelog, *Helv. Chim. Acta*, **34**, 1954 (1951).

24) S. W. Benson, F. R. Cruickshank, D. M. Golden, G. R. Haugen, H. E. O'Neal, A. S. Rodgers, R. Shaw, and R. Walsh, *Chem. Rev.*, **69**, 279 (1969). O-(C_d)(H) and C-$(H)_3(C_d)$ were assigned values identical to O-(C)(H) and C-$(H)_3$(C), respectively.

25) The heat of formation for water in the gas phase at 25 °C, $\Delta H_f° = -57.80$ kcal/mol, was obtained from "Selected Values of Physical and Thermodynamic Properties of Hydrocarbons and Related Compounds," p. 464, F. D. Rossini *et al.*, Carnegie Press, Carnegie Institute of Technology, Pittsburgh, Pennsylvania, 1953.

Preparation and Properties of 7-Formyl-8-hydroxy-5-quinolinesulfonic Acid

Konomu MATSUMURA, Shin-ichi SASAKI, and Eiko TADA

Department of Chemistry, Kitasato University, Sagamihara, Kanagawa

(Received October 21, 1975)

8-Hydroxy-5-quinolinesulfonic acid (I), on condensation with formaldehyde in aqueous ammonia, produced 8-hydroxy-7-hydroxymethyl-5-quinolinesulfonic acid (IV), which, on oxidation with manganese (IV) oxide, gave 7-formyl-8-hydroxy-5-quinolinesulfonic acid (V). On treatment with boiling 6 M hydrochloric acid, V produced bis[α-hydroxy-(8-hydroxy-5-sulfo-7-quinolyl)methyl] ether (VIII).

It is known that 8-hydroxy-5-quinolinesulfonic acid (I), on condensation with formaldehyde and secondary amine, produces the corresponding Mannich base.[1] In the present study, it was found that 8-hydroxy-5-quinolinesulfonic acid (I), on heating at 90 °C for 3 h with formaldehyde in aqueous ammonia, afforded 8-hydroxy-7-hydroxymethyl-5-quinolinesulfonic acid (IV) in a 60% yield. In the course of our investigation, it was found that when this reaction was allowed to proceed at 90 °C for 40 min instead of 3 h, the major product was bis(8-hydroxy-5-sulfo-7-quinolylmethyl)amine (VII), admixed with a minute amount of IV, showing that the hydroxymethylation proceeded by way of the intermediate formation of the Mannich base (VII), which subsequently underwent hydrolysis on further heating at 90 °C. When the reaction of I with hexamethylenetetramine in aqueous ammonia was allowed to proceed at 90 °C for 3 h, a result similar to that of the formaldehyde–aqueous ammonia method was obtained.

On the other hand, when this reaction was allowed to proceed at 36 °C for 2 weeks, a mixture of IV and the Mannich base (VII), which was predominant, was formed. IV was converted to 7-formyl-8-hydroxy-5-quinolinesulfonic acid (V)[2] by oxidation with manganese(IV) oxide. The presence of a formyl group in V was confirmed by its infrared spectrum, which displayed two bands, at 2650 and 2800 cm^{-1}, indicating the characteristic carbon-hydrogen stretching frequency associated with the C–H of the formyl group. On the other hand, when a solution of I and formaldehyde in aqueous sodium hydroxide was heated at 90 °C for 3 h, contrary to our expectation of obtaining IV, 8,8′-dihydroxy-7,7′-methylenedi(5-quinolinesulfonic acid) (II) was produced in a 97% yield.

As was expected, on heating II with 50% sulfuric acid 7,7′-methylenedi(8-quinolinol) (III) was formed; on the same treatment IV also afforded III, the identity having been established by mixed mp and IR. The preparation of III by another route has already been reported by Ozawa and Shibuya.[3] The identity of the two compounds was proved by the mp and IR and mp of the diacetyl derivatives.

On heating V with 6 M hydrochloric acid at 100 °C for several minutes, a paste of well-defined crystal was formed in a good yield. This product was inferred to possess the (VIII) structure in consideration of its elemental composition and a mass-spectrometric examination.

The PMR spectrum of VIII showed no –CH(OH)– signals, perhaps because of deuteration during the examination.

VIII would be formed upon the elimination of water between two molecules of the aldehyde hydrate. Such a dimerization is not unusual with formaldehyde or chloral. The tendency of V to form aldehyde anhydride (VIII) in a 6 M hydrochloric acid solution may be due to the fact that the electron-attracting character of sulfo group may favor the formation of a hydrate form.

Mass Spectrometry. The characteristic features are that all the compounds examined underwent thermolyses prior to ionization. The mass-spectral data are listed in Table 1.

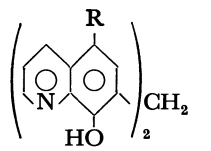

II R=SO_3H
III R=H

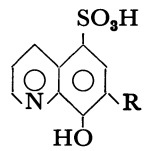

I R=H
IV R=CH_2OH
V R=CHO
VI R=CH=CH-COOH

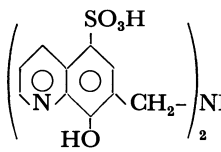

VII

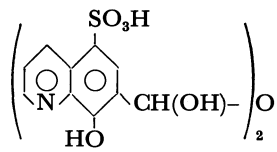

VIII

TABLE 1.

Compd	eV	°C	Peaks
II	75	230	302(100%), 298(15), 285(30), 283(38), 255(20), 158(83), 149(30), 145(88), 142(25), 136(18), 129(15), 117(25), 80(63), 64(158)
IV	70	210	302(100%), 298(9), 285(41), 283(26), 255(26), 158(81), 149(41), 145(70), 142(22), 136(19), 129(11), 117(22), 80(30), 64(63)
V	75	340	314(5%), 300(6), 299(30), 298(100), 270(40), 242(16), 241(16), 214(11), 188(13), 149(15), 135(24)
VII	70	230	327(3%), 312(6), 171(26), 170(94), 159(100), 158(69), 149(19), 145(36), 142(74), 130(84), 117(26), 115(36), 80(16), 64(96), 39(21)
VIII	75	180	336(28%), 261(22), 260(37), 259(67), 258(63), 232(13), 230(22), 195(76), 194(28), 193(59), 182(113), 178(81), 158(37), 152(37), 145(72), 143(100), 122(19), 117(85)

The relative intensities are given within parentheses. The mass spectra were recorded with a JEOL JMS-D100 mass spectrometer.

Experimental*

8,8'-Dihydroxy-7,7'-methylenedi(5-quinolinesulfonic Acid) (II). A solution of 5-sulfo-8-quinolinol dihydrate (10.44 g, 0.04 mol) and 36% formalin (30 g, 0.36 mol) in a 2.5 M sodium hydroxide solution (26 ml, 0.065 mol) was heated at 90 °C for 2 h. After cooling, the solution was acidified (T.B. 1.4) with hydrochloric acid; the crystals thus separated were filtered after the solution had stood for 2 days and then been dried at room temperature, yield, 9.3 g (97%) as monohydrate. Recrystallization from three hundred times its weight of boiling water yielded prismatic needles; mp 290—292 °C (foaming). It gives a dark green color with iron (III) chloride. IR (cm^{-1}, KBr), 3400 ($-SO_3H$), 3100 (-OH), 2950 ($-CH_2-$).

Found**: C, 47.44; H, 3.39; N, 5.76%. Calcd for $C_{19}H_{14}O_8N_2S_2\cdot H_2O$: C, 47.50; H, 3.33; N, 5.83%.

Found: C, 48.72; H, 3.35; N, 5.77%. Calcd for $C_{19}H_{14}O_8N_2S_2\cdot 0.5H_2O$: C, 48.41; H, 3.18; 5.94%.

8-Hydroxy-7-hydroxymethyl-5-quinolinesulfonic Acid (IV). (**A**) A solution of 5-sulfo-8-quinolinol dihydrate (10.44 g, 0.04 mol) and 36% formaldehyde (3.7 ml, 0.044 mol) in 7% aqueous ammonia (40 ml, 0.08 mol) was heated at 90 °C for 3 h and acidified (T.B. 1.4) while hot with 6 M hydrochloric acid; the crystals thus separated were filtered after the solution had stood for 4 days. The suspension of this crude product in 3 M hydrochloric acid (30 ml) was triturated at 90 °C for several minutes, filtered hot (filtrate F), washed with water and dried at 80 °C; yield, 6.12 g (60%). It forms as yellow thick plates (mp 289 °C(foaming)) and gives a deep green color with iron (III) chloride. For analysis, it was recrystallized from 300 times its weight of hot water. IR (cm^{-1}, KBr), 3450 ($-CH_2OH$), 3400 ($-SO_3H$), 3100 (-OH).

Found: C, 46.99; H, 3.36; N, 5.75%. Calcd for $C_{10}H_9O_5NS$: C, 47.06; H, 3.53; N, 5.49%.

Diacetyl Derivative of IV. This was made by heating a mixture of IV (260 mg), acetic anhydride (1 ml), and pyridine (1 ml) at 135 °C for 3 h, evaporating it *in vacuo* to dryness, acidifying with hydrochloric acid in cold, and washing with cold water; yield, 270 mg; mp 300 °C (foaming). It forms short needles.

Found***: C, 45.99; H, 3.97; N, 4.13%. Calcd for $C_{14}H_{13}O_7NS\cdot 1.5H_2O$: C, 45.90; H, 4.37; N, 3.83%.

Dibenzoyl Derivative of IV. A mixture of IV (260 mg), benzoyl chloride (420 mg), and pyridine (0.5 ml) was triturated at an ice-cold temperature for 0.5 h, allowed to stand at room temperature overnight, and then acidified (T.B. 1.8) with hydrochloric acid. The separated solid was filtered and treated with ethanol to give colorless prisms (300 mg), mp 288—290 °C (dec).

Found***: C, 57.58; H, 3.56; N, 3.35%. Calcd for $C_{24}H_{17}O_7NS\cdot 2H_2O$: C, 57.71; H, 4.21; N, 2.80%.

The filtrate, F, on concentration afforded fine needles (20 mg) mp 312 °C. It gives a dark violet color with iron(III) chloride and was identified as the Mannich base (VII) by IR.

(**B**) A solution of I dihydrate (5.22 g, 0.00 mol) and hexamethylenetetramine (0.51 g, $1/6\times 0.02$ mol) in 7% aqueous ammonia (20 ml) was heated at 90 °C for 2 h. The further treatment was similar to that used for (**A**). IV; yield, 2.92 g (57%); mp 289 °C (foaming). VII; yield, 50 mg; mp 312 °C. The two products were identified as IV and VII respectively by IR.

7,7'-Methylenedi(8-quinolinol) (III). A solution of II (200 mg) in 50% sulfuric acid (0.4 ml) was heated at 140 °C for one h. After cooling, on alkalifying with ammonia, the product was obtained as colorless, soft, thin plates; yield, 120 mg (86%).

On recrystallization from methanol, it formed compact prismatic needles; mp 185 °C; lit,[3] mp 170—180 °C, IR (cm^{-1}, KBr), 3100 (-OH), 2950, 1440 ($-CH_2-$).

Found: C, 75.26; H, 4.67; N, 9.04%. Calcd for $C_{19}H_{14}O_2N_2$: C, 75.50; H, 4.64; N, 9.27%.

Diacetyl Derivative of III. This crystallized as prisms from benzene; mp 170—172 °C; Lit,[3] mp 170—220 °C.

Found: C, 71.76; H, 4.81; N, 7.17%. Calcd for $C_{23}H_{17}O_4N_2$: C, 71.69; H, 4.42; N, 7.27%.

Monopicrate of III. This crystallized as rectangular thick plates from methanol; mp 245—246 °C (foaming).

Found: C, 56.30; H, 3.21; N, 12.88%. Calcd for $C_{19}H_{14}O_2N_2\cdot C_6H_3O_7N_3$: C, 56.50; H, 3.20; N, 13.18%.

A solution of IV (500 mg) in 50% soufuric acid (1 ml) was heated at 140—145 °C for 2.5 h. On further working, the product (310 mg) was obtained as prisms (mp 185 °C) and identified as III by a mixed mp and by IR.

Bis(8-hydroxy-5-sulfo-7-quinolylmethyl)amine (VII). (**A**) On heating a mixture of I dihydrate (5.22 g, 0.02 mol), hexamethylenetetramine (0.51 g, $1/6\times 0.022$ mol), and 7% aqueous ammonia (20 ml) at 80 °C for a few minutes, a clear solution was obtained. It was allowed to stand at 36 °C for 2 weeks. When the reaction mixture was then acidified (T.B. 1.4) with hydrochloric acid, soft precipitates with a gelatinous appearance were separated. The precipitates were filtered with suction, washed with water, and dried at 80 °C; yield, 3.76 g. On recrystallization from one thousand times its weight of boiling water, 2.17 g. (44.2%) of fine needles (mp 312 °C) were obtained. VII gives a dark violet color with iron (III) chloride. IR (cm^{-1}, KBr), 3400 ($-SO_3H$), 3200, 2850 (O–H), 1540, 1140 ($-CH_2-NH-CH_2-$).

Found: C, 48.52; H, 3.53; N, 8.38%. Calcd for $C_{20}H_{17}O_8N_3S_2$: C, 48.88; H, 3.46; N, 8.55%.

From the filtrate of the recrystallization, thick plates (1.16 g) were isolated on concentrating. They were after further recrystallization, identified as IV by IR and mp.

(**B**) A solution of I dihydrate (10.44 g, 0.04 mol) and 36% formalin (3.7 g, 0.044 mol) in 7% aqueous ammonia (40 ml, 0.08 mol) was heated at 90 °C for 40 min and acidified (T.B. 1.4) with 6 M hydrochloric acid; a yellow gelatinous solid thus separated was filtered after standing overnight in a refrigerator, washed well with water, and dried on a plate; yield, 5.9 g.

A portion of it, on recrystallization from hot water, yielded fine yellow needles; mp 312 °C. It gives a dark violet color with iron (III) chloride and was identified as VII by IR and mp.

7-Formyl-8-hydroxy-5-quinolinesulfonic Acid (V). To a hot solution of IV (4.1 g, 0.016 mol) and sodium acetate hydrate (2.2 g, 0.016 mol) in water (300 ml), commercial manganese dioxide (16 g) was added; the mixture was then heated at 95 °C for 2 h with vigorous stirring and filtered hot (charcoal). From the filtrate, the product was obtained as colorless thin plates on concentrating up to 150 ml, acidifying (T.B. 1.4) with hydrochloric acid, and standing overnight. It was recrystallized from fifty times its weight of hot water; yield,

* All the elemental analyses, unless stated otherwise, were performed after the material had been dried at 120 °C *in vacuo* over P_2O_5.

** Dried at room temperature over potassium hydroxide *in vacuo*.

*** Vacuum-dried at room temperature over potassium hydroxide.

1.96 g (48.2%). It turned to a black solid at 317 °C with preliminary darkening. It gives no color† reaction with iron(III) chloride; however, the mixture gradually developed a light green color after standing for 3 h at room temperature. IR (cm^{-1}, KBr), 2400 (-SO_3H), 3100 (OH), 2800, 2650 (H-CO-), 1740 (HC-O).

Found***: H_2O, 12.41; C, 41.63; H, 3.69; N, 5.06%. Calcd for $C_{10}H_7O_5NS \cdot 2H_2O$: H_2O, 12.46; C, 41.52; H, 3.81; N, 4.84%. Found: C, 47.20; H, 2.95; N, 5.76%. Calcd for $C_{10}H_7O_5NS$: C, 47.43; H, 2.77; N, 5.53%.

Mono-sodium salt of V. This was crystallized from water as colorless, soft, fine needles.

Found: C, 43.53; H, 2.66; N, 5.29%. Calcd for $C_{10}H_6O_5NSNa$: C, 43.64; H, 2.18; N, 5.09%.

3-(8-Hydroxy-5-sulfo-7-quinolyl)acrylic Acid (VI). A solution of V (0.5 g, 0.002 mol), malonic acid (0.32 g, 0.003 mol), and potassium hydroxide (0.5 g) in water (8 ml) was heated at 80 °C for 12 h and then at 95 °C for 5 h, thereafter it was acidified with hydrochloric acid; yield, 0.3 g (51%). Recrystallization from 300 times its weight of hot water afforded glistening thick plates; mp 287 °C (with foaming). VI gives a deep green color with iron(III) chloride.

Found***: C, 47.01; H, 3.36; N, 4.54%. Calcd for $C_{12}H_9O_6NS \cdot 0.5H_2O$: C, 47.37; H, 3.29; N, 4.64%.

Bis[α-hydroxy-(8-hydroxy-5-sulfo-7-quinolyl)methyl] Ether (VIII). A mixture of V dihydrate (1.16 g, 0.004 mol) and 6 M hydrochloric acid (8 ml), on heating with stirring at 100 °C, soon turned to a clear solution; it began to become turbid after 6 min and became a crystal paste after 10 min further heating.

It was diluted with water (8 ml), filtered after standing in a refrigerator overnight, washed with water, and dried at room temperature; yield, 0.96 g (80%).

Recrystallization from 55 times its weight of hot water, with the addition of a small amount of 3 M hydrochloric acid, afforded stout prismatic needles; mp 250—255 °C (foaming).

† A very concentrated solution gives a faint brownish yellow color.

VIII gives a deep green color with iron(III) chloride. It is unaltered when the solution in 1% sodium hydroxide is heated over free flame for a few min.

^1H NMR (Me_2SO-d_6): H-3: δ 7.95 (2H, dd, $J_{3,2}=5.0$; $J_{3,4}=9.0$), H-6: δ 8.00 (2H, s), H-2: δ 9.05 (2H, dd, $J_{2,3}=5.0$; $J_{2,4}=1.5$), H-4: δ 9.52 (2H, dd, $J_{4,2}=1.5$; $J_{4,3}=9.0$). IR (cm^{-1}, KBr), 3420, 2500 (O-H), 1180 (C-O-C).

Found***: C, 39.67; H, 3.48; N, 4.93%. Calcd for $C_{20}H_{16}O_{11}N_2S_2 \cdot 4H_2O$: C, 40.26; H, 4.03; N, 4.70%.

Found: C, 42.18; H, 2.87; N, 5.16%. Calcd for $C_{20}H_{16}O_{11}N_2S_2 \cdot 2H_2O$: C, 42.86; H, 3.57; N, 5.00%.

Tetraacetyl Derivative of VIII. A mixture of VIII (200 mg), acetic anhydride (2 ml), and concentrated sulfuric acid (one drop) was heated at 130 °C for 3 h and evaporated *in vacuo*, and the residue was treated with ice. The thick plates were filtered, washed with cold water, and dried *in vacuo* at room temperature; mp 263 °C (dec).

Found: C, 46.27; H, 3.11; N, 3.46%. Calcd for $C_{28}H_{24}O_{15}N_2S_2 \cdot 2H_2O$: C, 46.15; H, 3.85; N, 3.85%.

We wish to thank Dr. Yoshio Matsumoto for generously allowing one of us (K.M.) to complete this work in his laboratory and Dr. Chiji Yamazaki for his helpful interpretation of the physical data and for the NMR spectral measurements.

References

1) A. B. Sen and Y. D. Kulkarni, *J. Indian Chem. Soc.*, **33**, 326 (1956).

2) Fiedler reported the formation of V through another route of preparation, but without any characterization of this compound H. Fiedler, *Archiv. Pharmaz.*, **297**, 108 (1964). To our knowledge, II, IV, VII, and VIII have not heretofore been reported.

3) T. Ozawa and S. Shibuya, *Yakugaku Zasshi*, **83**, 498 (1963).

Water-Participation in the Crystalline-State Photodimerization of Cinnamic Acid Derivatives. A New Type of Organic Photoreaction

Fusae NAKANISHI, Hachiro NAKANISHI, Michio TSUCHIYA, and Masaki HASEGAWA

Research Institute for Polymers and Textiles, 4-Sawatari, Kanagawa-ku, Yokohama 221

(Received November 21, 1975)

A new type of organic photoreaction, a water-participation reaction in the crystalline state, has been investigated. The photoirradiation of *p*-formylcinnamic acid (*p*-FCA) crystals in the presence of water leads to 4,4′-diformyl-*β*-truxinic acid (*p*-FCA dimer) which has one molecule of crystal water. A comparison of the photodimerization carried out in the presence/absence of water revealed the effects of the water molecule on the reaction. That is, the water molecule is incorporated into the *p*-FCA dimer during the photodimerization process. Furthermore, the water accelerates the reaction rate of photodimerization, leading to the formation of the crystalline dimer, whereas only the water-free amorphous dimer results in the absence of water. In addition, by heating at 100—110 °C, the *p*-FCA dimer with a water molecule is converted into a water-free crystalline dimer, which is not attainable from a water-free amorphous dimer. The photodimerization of several *β*-form crystals of cinnamic acid derivatives has been examined from the viewpoint of water-participation: *p*-nitro, *p*-chloro, and 3,4-dichlorocinnamic acid were found to photodimerize in the same manner as *p*-FCA.

Schmidt and his co-workers[1] studied extensively the photodimerization of cinnamic acid in the crystalline state and established the field of a typical topochemical reaction in which the crystal structure of the compound plays a decisive role in the reactivity. In preparation for preparing the dimer of the *p*-phenylenediacrylic acid diethyl ester,[2] we have attempted the photodimerization of *p*-formylcinnamic acid (*p*-FCA) in the crystalline state and found that it was converted into the dimer with one molecule of crystal water if it was irradiated in the presence of water.[3]

Although a few dimers from cinnamic acid derivatives, for example α-truxillic acid, and its dichloride have been reported[4] to include a solvent molecule by the procedure of crystallization, the reaction is a new type of photoreaction in which water is incorporated into the dimer during the photodimerization process.

In this paper, further details of the reaction will be presented in order to reveal the overall view of characteristics of the crystalline-state water-participation reaction.

Experimental

Preparation of Cinnamic Acid Derivatives. *p*-FCA[5] was prepared by the condensation of terephthalaldehyde and malonic acid in the presence of piperidine and was separated from its by-product, *p*-phenylenediacrylic acid, by the extraction of crude product with acetone.

Other cinnamic acid derivatives were prepared according to the Reference.[1] All these compounds were recrystallized from the suitable solvents for preparing *β*-form crystals and were confirmed not to include any water in the original crystals.

Photodimerization. As a typical experiment, the photodimerization of *p*-FCA will be described.

Photodimerization in the Presence of Water. *p*-FCA crystals (0.3 g) were dispersed in water (100 ml) in a Pyrex flask. The flask was then irradiated with a 450-W high pressure mercury lamp at room temperature. Upon 60 minutes' irradiation the absorpotion maximum of *p*-FCA (295 nm) shifted to 254 nm and *p*-FCA was converted into the dimer quantitatively. NMR (DMSO-d_6) ppm: 3.8—4.5 (m 4, CH) 7.1—7.7 (m 8, C_6H_4) 9.8 (s 2, CHO). Found: C, 64.76; H, 4.76%. Calcd for $C_{20}H_{18}O_6+H_2O$: C, 64.86; H, 4.90%.

When the dimer was heated at 100—110 °C *in vacuo* for 10 h its elemental analysis changed as follows. Found: C, 68.48 H, 4.25%. Calcd for $C_{20}H_{18}O_6$: C, 68.18; H, 4.58%. The dimer can be recrystallized from ethanol–water.

Photodimerization in the Absence of Water. Method 1: *p*-FCA crystals were placed over phosphorus pentoxide in a petri dish with a glass cover. The dish was then irradiated with sun-light or a 450-W high-pressure mercury lamp until no further change was observed in the UV spectrum. Found: C, 67.71; H, 4.44%. Calcd for $C_{20}H_{18}O_6$: C, 68.18; H, 4.58%. *Method 2*: *p*-FCA crystals (0.3 g) were dispersed in thoroughly dried hexane (100 ml) and irradiated for 2 h in the way described above.

Identification and Quantitative Analysis of Water in the Dimer. All the crude dimers, which has been prepared in the presence of water and has been confirmed to be free from monomers by a study of their UV spectra, were dried in a dessicator over phosphorus pentoxide for 2 days at room temperature *in vacuo*. Differential scanning calorimetry (DSC) and thermogravimetric (TG) analysis were carried out with a Rigaku Standard DSC-TGA instrument at the heating rate of 10 °C/min under nitrogen.

The amounts of water in the dimer were determined by titration with Karl Fischer reagent (Mitsubishi Kasei). An accurately weighed dimer was dissolved in a dehydrated solvent (Mitsubishi Kasei) and titrated with a Karl Fischer reagent. The amounts of water in the dimer were calculated by means of the following equation:

$$\text{Weight (\%) of water in the dimer} = \text{ml of Karl Fischer reagent consumed } x \text{ factor of Karl Fischer reagent/weight of the dimer}$$

Formation of Anhydride Dimer. The dimer (0.3 g) was refluxed in acetic anhydride for 5 h. After removal of acetic anhydride, the residue was washed with ethanol and dried. The obtained product showed the absorption peaks at 1880 and 1790 cm^{-1} on the IR spectrum.

Results and Discussion

Crystalline Modification of p-*FCA.* Two crystalline modifications were found in *p*-FCA crystals, depending on the crystallization procedure. From an ethanol solution, photo-active crystals (*β*-form) are obtained, while photostable crystals (*γ*-form) are obtained from an

acetone solution. The two crystals give different intensities of absorption peaks (940, 990, and 1210—1230 cm^{-1}) in the IR spectra which are due to a carboxylic acid residue. The X-ray diffraction patterns are also different from each other (β-form, 17.2, 26.6°, γ-form, 16.9, 19.3, 23.6, 25.4, 26.8, 28.7°). However, both crystals show the same melting point (249 °C) and no phase-transition points have been observed by DSC analysis over the temperature range from room temperature to melting point.

Photodimerization of p-*FCA.* The product obtained by the irradiation of *p*-FCA crystals in the presence of water was identified as its dimer on the basis of the following data.

1. The IR spectrum of the product (Fig. 1) shows the disappearance of double bonds (1640 cm^{-1}, νC=C aliphatic).

2. In the NMR spectrum of the product, cyclobutane ring protons appear at 3.8—4.5 ppm.

However, the results of the elemental analysis of the product do not agree with the calculated value of the dimer and suggest the presence of one molecule of water in each dimer. The DSC diagram (Fig. 2-A) of the dimer shows three endothermic peaks at 105, 178, and 180 °C. The 105 °C peak which is broad and is accompanied by a weight loss, is considered to be the elimination of water from the dimer since the results of the elemental analysis of heat-treated dimer show that it has no water molecule and the DSC diagram shows two peaks at 178 and 180 °C, and no peak at 105 °C. The amounts of water in the dimer was determined to be 4.9% by means of the Karl Fischer reagent. This value indicates that each dimer has one molecule of water (Calcd 4.8%). Thus the presence of water in the *p*-FCA dimer was concluded. The peak at 178 °C was found to be due to the formation of cyclic anhydride from carboxylic acid residues; this was confirmed by the IR spectrum of the dimer heated up to 178 °C. The peak at 180 °C is its melting point. The IR spectrum of the water-free dimer is given in Fig. 1-B. The difference in the peaks at 3500, 1730, and 1350 cm^{-1} from those of the dimer with water (Fig. 1-A) is concluded to be due to the elimination of water. The X-ray diffraction patterns of the water-free dimer become different from those of the dimer with water.

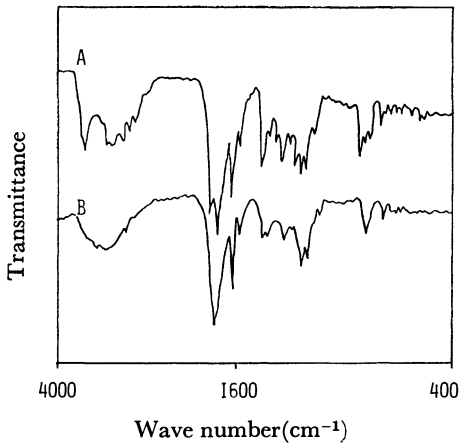

Fig. 1. IR spectra of *p*-FCA dimers.
A: The dimer obtained in the presence of water,
B: the water-free dimer obtained by heating above dimer.

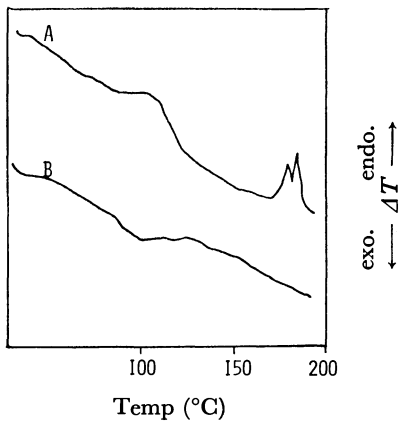

Fig. 2. DSC diagrams of *p*-FCA dimers.
A: The dimer obtained in the presence of water,
B: the dimer obtained in the absence of water.

The structure of the dimer was dertermined by anhydride formation from carboxylic acid residues. The IR spectrum of anhydride dimer indicates the formation of five-membered-ring anhydride and the NMR spectrum of its cyclobutane-ring protons is symmetrical. These data indicate the formation of a β-truxinic acid type dimer (4,4'-diformyl-β-truxinic acid).

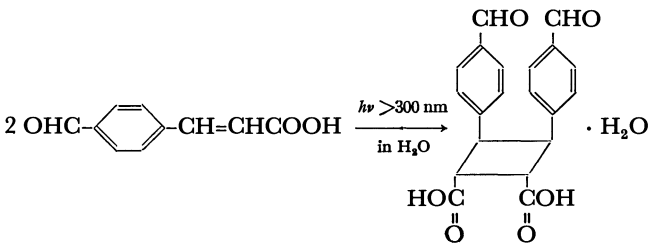

When the dimer in an ethanol or a dimethyl sulfoxide solution was irradiated with light (251 nm), it decomposed into *p*-FCA with cyclobutane-ring cleavage (Fig. 3).

The photodimerization of *p*-FCA crystals in the absence of water proceeds very differently in several points. The product obtained in the absence of water shows almost the same IR spectrum as that of the water-free dimer (Fig. 1-B) and the same NMR spectrum as that obtained in the presence of water.

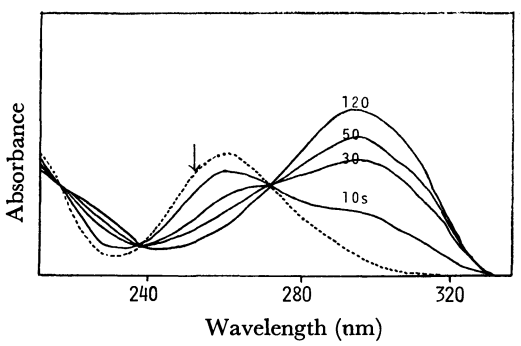

Fig. 3. Change in UV spectrum on irradiation of *p*-FCA dimer in ethanol solution.
------: Before irradiation, ——: after irradiation.

In the DSC diagram (Fig. 2-B) only the exothermic peak (100—110 °C) was observed, and there was no weight loss. The elemental analysis of the product agreed with the calculated value of the dimer without water molecule. From these data it may be concluded that the product obtained in the absence of water is the same β-truxinic acid-type dimer, but without water.

Remarkable differences connected with both dimers were found in the rates of photodimerization and crystallinity. It is interesting to note that photodimerization proceeds very rapidly, forcibly taking up the surrounding water. For example, *p*-FCA crystals embedded in the KBr pellet photodimerize in about 10 min, with the incorporation of the water which is absorbed in KBr.

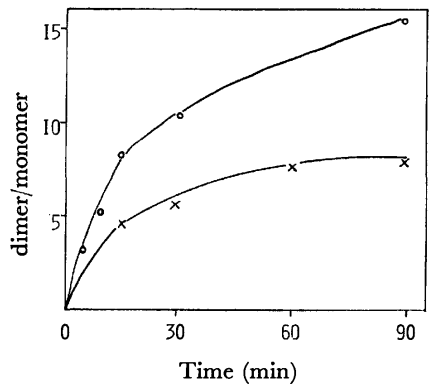

Fig. 4. Plot of dimer/monomer *vs.* time.
—○—: In water, —×—: in hexane.

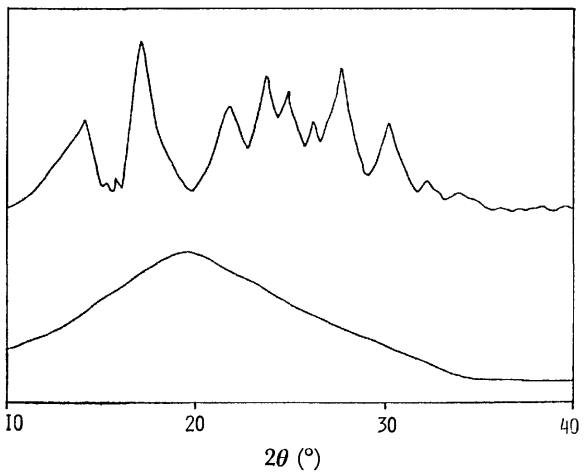

Fig. 5. X-Ray diffraction patterns of *p*-FCA dimers.
A: The dimer obtained in the presence of water,
B: the dimer obtained in the absence of water.

The plot of the dimer/monomer rate *vs.* the reaction time in water and hexane is shown in Fig. 4. The presence of water apparently accelerates the reaction. With respect to the crystallinity there is a prominent difference between two dimers (Fig. 5). The crystalline dimer was obtained in the presence of water, while amorphous one was obtained in the absence of water. It seems that the water molecule assists to crystallize the dimer, as is often observed in protein molecules.

The relationship of these two kinds of dimers is shown in Scheme 1.

(1) The dimer with one molecule of water (I) can be converted into the water-free crystalline dimer (II) by heating 100—110 °C *in vacuo*.

(2) The water-free amorphous dimer (II′) becomes the crystalline dimer with water (I′) by dispersing it in water as long as the irradiation time or by recrystallization from a water–ethanol solution. This process is not affected by light. The IR spectrum and X-ray diffraction patterns of the dimer (I) and the dimer (I′) are nearly identical; however, their thermal behavior is peculiarly different. The DSC diagram of the dimer (I′) shows only an endothermic peak at 100—110 °C, and it is dehydrated at that temperature not into the dimer (II) but into the water-free amorphous dimer (II′). In this point, the dimer (I′) is different from the dimer (I).

(3) The DSC diagram (Fig. 2-B) of the water-free amorphous dimer (II′) shows only an exothermic peak at 100—110 °C, which may be due to crystallization. However, it could not be converted into the water-free crystalline dimer (II) by heating at that temperature.

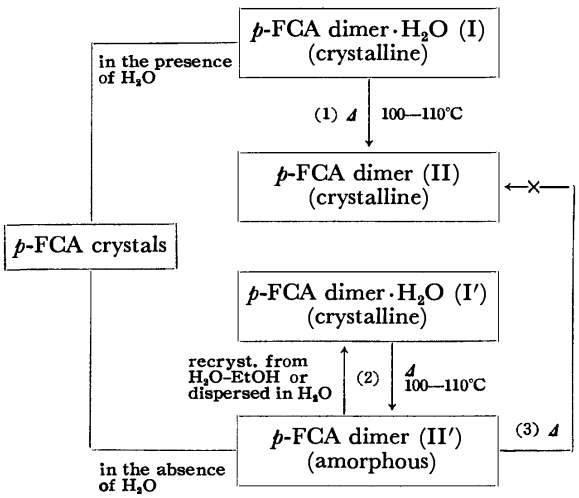

Scheme 1.

The observation (2) and the fact that a water solution saturated with *p*-FCA does not yield the dimer on irradiation imply that water molecule is incorporated into the dimer not after the formation of the dimer but during the photodimerization process.

Though the details of the reaction mechanism are not established yet, it is probably similar to that proposed for the solid-gas reaction of carboxylic acid and ammonia.[6] That is, if *p*-FCA crystals are exposed to light in an atmosphere of water, a dimer would be formed with the incorporation of the water molecule; at the same time, the disorientation of the crystal layer occurs sufficiently to permit the water molecule to diffuse into the next layer of *p*-FCA crystals, where the process is repeated.

Survey of Water Participation Crystalline Photodimerization of Other Cinnamic Acid Derivatives. In order to extend this new type of photodimerization of *p*-FCA to other compounds, the photodimerization of several other cinnamic acid derivatives was reinvestigated from the

Table 1. Photodimerization of cinnamic acid derivatives

X-C$_6$H$_4$-CH=CHCOOH	Elemental analysis (%)	Endo peaks on DSC diagrams (°C)	Amounts of water (%)
Photodimerization with water participation			
p-CHO–	C, 64.86, H, 4.90[a]	100—120,[e] 178,[f] 180[g]	4.9 (4.8)[a]
	C, 64.74, H, 4.76[b]		
p-NO_2–	C, 53.47, H, 3.99, N, 6.93[a]	100—120,[e] 216,[f] 226[g]	5.4 (4.5)[a]
	C, 53.52, H, 3.95, N, 6.71[b]		
p-Cl–	C, 58.03, H, 4.00[c]	85—100,[e] 200[b]	3.0 (4.7)[a]
	C, 57.60, H, 4.42[b]		
3,4-diCl–	C, 48.79, H, 2.69[c]	90—100,[e] 149[h]	2.5 (4.0)[a]
	C, 48.86, H, 2.82[b]		
Photodimerization without water participation			
p-H	—	212—213[h]	
p-Br	C, 47.60, H, 3.11[d]	212—214,[f] 224[g]	
	C, 47.36, H, 3.36[b]		
m-NO_2–	C, 55.96, H, 3.65, N, 7.25[d]	206[h]	
	C, 54.12, H, 3.66, N, 6.89[b]		
o-Cl–	C, 59.08, H, 3.73[d]	215—216[h]	
	C, 59.20, H, 3.87[b]		
2,4-diCl–	C, 49.80, H, 2.80[d]	240[h]	
	C, 50.39, H, 2.65[b]		
2,6-diCl–	C, 49.80, H, 2.80[d]	224[h]	
	C, 49.22, H, 2.45[b]		

a) Calcd as including one molecule of H_2O. b) Found. c) Calcd as including 1/2 molecule of H_2O. d) Calcd for dimer. e) Peak due to dehydration. f) Peak due to formation of anhydride. g) Melting point of anhydride. h) Melting point of dimers

viewpoint of water participation. Since the 1,2-*cis* conformation of carboxylic acid residues on a cyclobutane ring seems to be important factor in the incorporation of water, the photodimerization of several β-form crystals of cinnamic acid derivatives has been attempted in a water dispersant. The water participation was checked by the method described before. The results are given in Table 1. *p*-Nitro, *p*-chloro, and 3,4-dichlorocinnamic acid were found photodimerize in essensially the same way as *p*-FCA. The dimers from these monomers have more or less the same properties as those described in Scheme 1. However, the amounts of water incorporated into the dimer are different depending on the dimer. The dimers from β-form crystals of cinnamic acid, *o*-chloro, *m*-nitro, *p*-bromo, 2,4-, and 2,6-dichlorocinnamic acid did not incorporated any water during the photodimerization process.

Summarizing the results of the survey on the compounds which photodimerize with water participation, it can reasonablly be suggested that there is a possibility that the β-form crystals of *para*-substituted cinnamic acids photodimerize in this manner.

References

1) M. D. Cohen, G. M. Schmidt, and F. I. Sonntag, *J. Chem. Soc.*, **1964**, 2000.
2) H. Nakanishi, F. Nakanishi, Y. Suzuki, and M. Hasegawa, *J. Polym. Sci., Polym. Chem. Ed.*, **11**, 2501 (1973).
3) F. Nakanishi, T. Tasai, Y. Suzuki, and M. Hasegawa, *Chem. Lett.*, **1974**, 525.
4) F. K. Beilstein, "Handbuch d. Org. Chem.," **9**, 953, 955.
5) R. H. Wiley and P. H. Hobson, *J. Am. Chem. Soc.*, **71**, 2429 (1949).
6) R. S. Miller, D. V. Curtin, and I. C. Paul, *J. Am. Chem. Soc.*, **96**, 6329 (1974).

The Finkelstein Reaction in Acetonitrile-Glycol Mixtures.* An Approach by a Concurrent Monodentate and Bidentate Solvation Model of the Halide Ion

Yasuhiko KONDO, Kazuo TANAKA, and Niichiro TOKURA

Department of Applied Chemistry, Faculty of Engineering, Osaka University, Suita, Osaka 565

(Received February 23, 1976)

The rate constant of the reaction of methyl iodide with the bromide ion showed a characteristic dependence on the composition of solvent mixtures. In five solvent mixtures, *i.e.*, acetonitrile–ethylene glycol, –1,2-propanediol, –1,3-butanediol, –1,4-butanediol, and –2,3-butanediol, its dependence was fairly well reproduced by the theoretical equations derived on the basis of the concept of the concurrent monodentate and bidentate solvation of the halide ion by glycol. In contrast, the rate constants in acetonitrile–diethylene glycol and –triethylene glycol mixtures were better reproduced by the modified theoretical equations allowing for a self-association of glycol.

In the previous paper[1] the behavior of the rate constant of the Finkelstein reaction in acetonitrile–alcohol mixtures was discussed in terms of the multi-step solvation of anions in solvent mixtures. Several properties of the solvent which might influence the solvation energy of the anion changed simultaneously from one system to another, and this introduced extracomplexities into the treatment. In the present work, in order to understand better the concept of the multi-step solvation of anions, we intended to reduce the number of exposed parameters involved in the treatment as far as possible and to set up a visualized model of the solvation of anions in solvent mixtures.

In this paper the rate of the reaction of methyl iodide with the bromide ion in acetonitrile–glycol mixtures will be discussed on the basis of the concept of the concurrent monodentate and bidentate solvation of the anion.

Experimental

The tetrabutylammonium bromide, methyl iodide, and acetonitrile were treated as has been described elsewhere.[1] Commercial ethylene glycol, 1,2-propanediol, 1,3-butanediol, 1,4-butanediol, and diethylene glycol (all of purity>99% by GLPC) were dried over anhydrous sodium sulfate and distilled twice under reduced pressure. Commercial 2,3-butanediol (*dl*: 52.3%, *meso*: 46.6% by GLPC) and triethylene glycol (>96% by GLPC) were treated similarly.

The densities of the solvent mixtures were measured with a single-stem pycnometer with a capacity of *ca.* 30 ml; the interpolated values are summarized in Table 1.

The rate measurements were performed as has been described elsewhere.[1]

The experimental uncertainties of the rate constant were estimated to be less than ±2% from duplicate or triplicate runs. The average values are summarized in Table 2.

TABLE 1. DENSITIES OF SOLVENT MIXTURES (30 °C)

X_{CH_3CN}[a]	MeCN –Ethylene glycol	MeCN –1,2-Propanediol	MeCN –2,3-Butanediol	MeCN –1,3-Butanediol	MeCN –1,4-Butanediol	MeCN –Diethylene glycol	MeCN –Triethylene glycol	pure MeCN
0.95	0.7902	0.7892	0.7894	0.7897	0.7920	0.8030	0.8156	0.7711[1]
0.90	0.8092	0.8066	0.8061	0.8072	0.8112	0.8318	0.8529	
0.80	0.8461	0.8395	0.8371	0.8390	0.8461	0.8831	0.9140	
0.60	0.9174	0.8977	0.8880	0.8841	0.9031	0.9638	0.9977	
0.40	0.9870	0.9483	0.9288	0.9349	0.9480	1.0254	1.0520	
0.20	1.0489	0.9918	0.9618	0.9692	0.9824	1.0727	1.0893	
0	1.1066	1.0288	0.9892	0.9976	1.0093	1.1097	1.1163	

a) X_{CH_3CN} stands for the mole fraction of acetonitrile.

TABLE 2. RATE CONSTANTS FOR THE REACTION OF THE BROMIDE ION WITH METHYL IODIDE IN SOLVENT MIXTURES AT 30 °C; $k \times 10^4$ l mol^{-1} s^{-1} (in pure MeCN $k \times 10^4$: 2580[1])

X_{CH_3CN}	MeCN –Ethylene glycol	MeCN –1,2-Propandiol	MeCN –2,3-Butanediol	MeCN –1,3-Butanediol	MeCN –1,4-Butanediol	MeCN –Diethylene glycol	MeCN –Triethylene glycol
0.95	93.0	122	199	172	217	244	386
0.90	38.7	52.0	91.5	72.9	91.6	114	218
0.80	17.6	23.1	40.9	31.8	40.3	60.1	128
0.60	8.51	11.5	22.8	17.5	18.5	32.9	90.3
0.40	5.75	7.99	15.0	10.8	12.6	28.8	85.8
0.20	4.49	5.89	10.8	7.70	8.13	27.9	92.7
0	3.76	4.34	8.32	5.62[a]	6.03[a]	30.4	109

a): value estimated from the plot of log k_{mix} *vs.* X_4

* This should be referred to as "Reaction Rates in Binary Mixed Solvents. VIII."

Results and Discussion

Rate Constants in Acetonitrile–Glycol Mixtures. In acetonitrile–glycol mixtures the logarithmic rate constants show a marked negative deviation from the line connecting the values in pure solvents, *i.e.*, $x_1 \ln k_1 + x_4 \ln k_4$, where k_1 and k_4 stand for the rate constant in Solvents 1 and 4, while x_1 and x_4 correspond to the mole fractions of Solvents 1 and 4. This type of behavior can be ascribed to the specific solvation of a reactant by the solvent, tending to lower the rate of reaction.[1,2]

For the purpose of reducing the complexity of the derived final equations, we set up the following scheme for the solvation of the halide ion in acetonitrile–glycol mixtures:

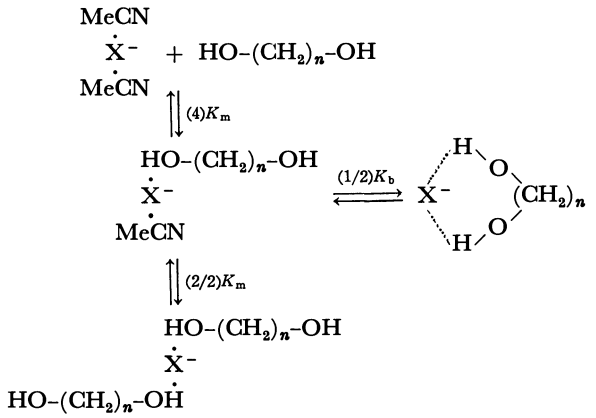

Scheme 1.

where K_m and K_b stand for the parameters corresponding to a monodentate and bidentate interaction of the glycol molecule with the halide ion and where the numbers in parentheses are the statistical factors of the reaction. Two such factors are combined to give the equilibrium constant of the reaction.

According to the same line of treatment as has been described in the previous papers,[1,3] the rate constants of

$$CH_3I + Br^- \longrightarrow CH_3Br + I^-$$

the reaction in mixed solvents, k_{mix}, are given by these equations:

$$\ln k_{mix} = \ln k_1 + \ln\{2K_m(2K_m+K_b)\} - \ln\{(x_4+2K_m x_1)^2+2K_m K_b x_1\} + \ln(V_{mix}/V_1) \quad (1)$$

$$(k_4/k_1) = 2K_m(2K_m+K_b)(V_4/V_1) \quad (2)$$

where V_1, V_4, and V_{mix} stand for the molar volumes of pure Solvent 1, of pure Solvent 4, and of a mixed solvent respectively. In the present series of solvent mixtures, k_4 is always the rate constant in acetonitrile.

Two parameters are included in these equations as a consequence of the proposed model. Since Eq. 2 serves as a boundary condition for the parameters, there is only one parameter left to be adjusted in reproducing the data. In Figs. 1 and 2 the theoretical values are compared with the experimental values.

One noticeable trend shown in Table 3 is that, as the distance between the hydroxyl groups gets larger and as the hydrocarbon moiety around the hydroxyl group becomes more bulky, the unidentate solvation mode takes the place of a bidentate solvation mode. This

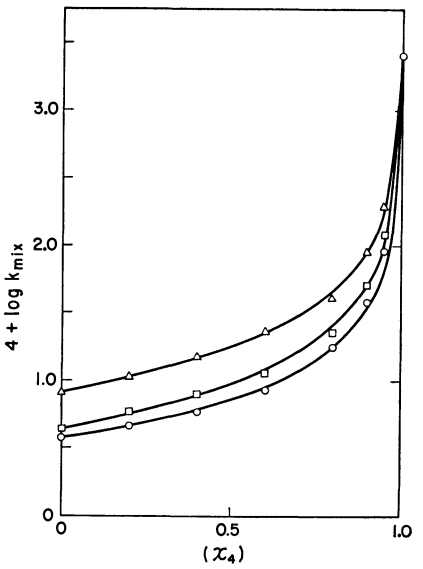

Fig. 1. Comparison of experimental and calculated data. ——; calculated, ○; MeCN–ethylene glycol, □; MeCN–1,2-propanediol, △; MeCN–2,3-butanediol.

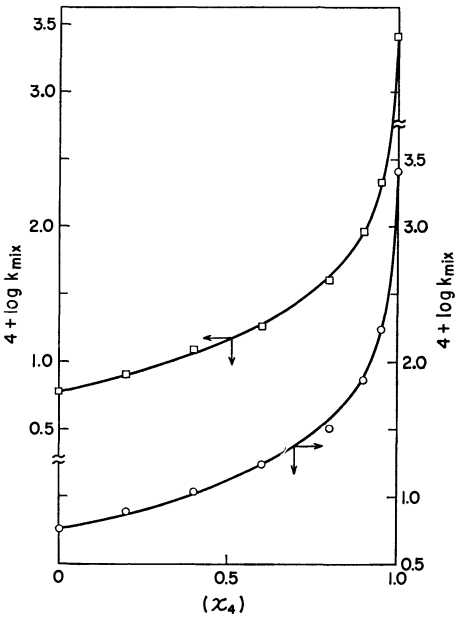

Fig. 2. Comparison of experimental and calculated data. ——; calculated, ○; MeCN–1,3-butanediol, □; MeCN–1 4-butanediol.

Table 3. Experimentally determined parameters in acetonitrile–glycol mixtures at 30 °C

Glycol	$2K_m/(2K_m+K_b)$	K_m	K_b	(K_b/K_m)
Ethylene glycol	723	0.5	722	1444
1,2-Propanediol	826	10.0	21.3	2.1
2,3-Butanediol	531	8.7	13.1	1.5
1,3-Butanediol	779	11.5	10.9	0.9
1,4-Butanediol	717	11.5	8.19	0.7

TABLE 4. EXPERIMENTALLY DETERMINED PARAMETERS AT 30 °C

	$\frac{2K_m\{2K_m+K_b(1+K)\}}{(1+K)^3}$	K	K_m	K_b	(K_b/K_m)
MeCN–Diethylene glycol	152	1.2	18.6	2.92	0.16
MeCN–Triethylene glycol	59.8	1.2	10.7	3.8	0.3

feature is in accord with our chemical intuitions.

Rate Constants in Acetonitrile–Diethylene Glycol and –Triethylene Glycol Mixtures. In contrast to the results shown above, the rate constants in diethylene glycol and triethylene glycol–acetonitrile mixtures exhibit marked negative deviations from the values estimated on the basis of the above treatment (Fig. 3).

One of the factors not taken into account in the above treatment, but which is likely to be operating in the present systems, is a self-association of the glycol through the hydrogen bonding of a hydroxyl group to an ether linkage.

For the system in which a glycol forms acyclic long-chain polymers through self-association,[4] the mole fractions of a monomer glycol and of acetonitrile, defined in terms of moles in solution, *i.e.*, y_1 and y_4, are related to the stoichiometric mole fractions of glycol and of acetonitrile, *i.e.*, x_1 and x_4, by the following equations, as will be described in the Appendix:

$$y_1 = \frac{1}{2K(1+K)x_1}\{2Kx_1+1-(4Kx_1x_4+1)^{1/2}\} \quad (3)$$

$$y_4 = \frac{1-(K+1)y_1}{1-Ky_1} \quad (4)$$

where K stands for the equilibrium constant of the self-association.

$$[HO\text{-}(CH_2CH_2O)_m\text{-}H]_{n-1} + HO\text{-}(CH_2CH_2O)_m\text{-}H \rightleftarrows [HO\text{-}(CH_2CH_2O)_m\text{-}H]_n$$

According to a line of treatment described elsewhere,[1,3] except for the additional assumption that only a monomer glycol, and not polymers, can participate in the specific solvation of the halide ion, the activity coefficient of a halide ion in a solvent mixture, $\beta_{2,\mathrm{mix}}$ is given by Eq. 5 (see Appendix). The rate constant in these mixtures, k_{mix}, is given by Eq. 6, and the k_4/k_1 ratio is now defined by Eq. 7:

$$\beta_{2,\mathrm{mix}} = \frac{1+\frac{Ky_1^2}{(1-Ky_1)^2}}{[1+K_0\{(y_4+2K_my_1)^2+2K_mK_by_1\}]}\left(\frac{f_2^\circ V_{\mathrm{mix}}}{RT}\right) \quad (5)$$

$$\ln k_{\mathrm{mix}} = \ln k_1 + \ln [2K_m\{2K_m+K_b(1+K)\}/(1+K)^3] - \ln \{(y_4+2K_my_1)^2+2K_mK_by_1\}/[1+\{Ky_1^2/(1-Ky_1)^2\}] + \ln (V_{\mathrm{mix}}/V_1) \quad (6)$$

$$(k_4/k_1) = \frac{2K_m\{2K_m+K_b(1+K)\}}{(1+K)^3}(V_4/V_1) \quad (7)$$

The calculations were performed as follows: (1) the values of y_1 and y_4 were calculated as functions of x_1 and x_4 from Eqs. 3 and 4, using an assumed value of K; (2) making use of these values, the rate constants were calculated by means of Eqs. 6 and 7 for an assumed value of (K_b/K_m), and (3) the procedures were repeated until the optimum fit to the experimental results was obtained.

The value found for the equilibrium constant, *i.e.*, $K=1.2$, is not unexpected, since, for the hydrogen bonding between ethanol and ether, an equilibrium constant of the same order of magnitude can be estimated from the pK_{Hb} values after correcting for its solvent dependence.[5–7]

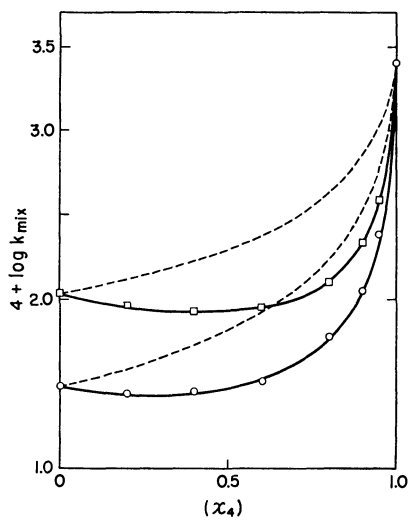

Fig. 3. Comparison of experimental and calculated data. ----; estimated values on the basis of Eqs. (1) and (2) assuming $(K_b/K_m)=0.7$, ——; calculated, ○; MeCN–diethylene glycol, □; MeCN–triethylene glycol.

As has been shown above, the values of the rate constant derived theoretically, on the basis of the solvation of the halide ion and the self-association of glycol, are in good agreement with the values observed in the various solvent mixtures. Even the phenomenon of a shallow minimum in the rate plots given in Fig. 3 is accounted for. However, although such features can be reproduced using the particular model, this does not constitute proof of the model. We feel, though, that the model is useful in accounting for the general trends observed.

We wish to thank Dr. M. H. Abraham, University of Surrey, for his discussions and for his comments on the manuscript.

Appendix

The material balances, mole fractions and equilibrium constants used in the treatment are given by these equations.

(1). Material balances,

$$N_1 = M_1 + \sum_{j=0}^{2} jM_{j2} + M_{b2} + \sum_{k=2}^{n} kM_{Ak} \quad (A\text{-}1)$$

$$N_2 = M_2 + \sum_{j=0}^{2} M_{j2} + M_{b2} \quad (A\text{-}2)$$

$$N_4 = M_4 + \sum_{j=0}^{2} (2-j)M_{j2} \quad (A\text{-}3)$$

where N_i, M_i, M_{j2}, M_{b2}, and M_{Ak} stand for the number of moles of species i before mixing, of species i in solution, of the

halide ion solvated by j mol of glycol in a monodentate way, of the halide ion solvated by glycol in a bidentate way, and of acyclic k-mer of glycol respectively.

(2). Mole fractions.

$$x_i = N_i/(N_1+N_2+N_4) \quad \text{(A-4)}$$

$$y_i = M_i/M_t \quad \text{(A-5)}$$

$$y_{j2} = M_{j2}/M_t \quad \text{(A-6)}$$

$$y_{b2} = M_{b2}/M_t \quad \text{(A-7)}$$

$$y_{Ak} = M_{Ak}/M_t \quad \text{(A-8)}$$

$$M_t = M_1 + M_2 + M_4 + M_{b2} + \sum_{j=0}^{2} M_{j2} + \sum_{k=2}^{n} M_{Ak} \quad \text{(A-9)}$$

(3). Equilibrium constants.

$$K_0 = y_{02}/(y_2 y_4^2) \quad \text{(A-10)}$$

$$4K_m = y_{12}y_4/(y_{02}y_1) \quad \text{(A-11)}$$

$$(2/2)K_m = y_{22}y_4/(y_{12}y_1) \quad \text{(A-12)}$$

$$(1/2)K_b = y_{b2}y_4/(y_{12}) \quad \text{(A-13)}$$

$$K = y_{Ak}/(y_1 y_{Ak-1}) \quad \text{(A-14)}$$

When $N_2=0$, the following relations are obtained:

$$\sum_{k=2}^{n}(k-1)y_{Ak} = Ky_1^2/(1-Ky_1)^2 \quad (\because n\to\infty) \quad \text{(A-15)}$$

$$y_1 + \sum_{k=2}^{n} k y_{Ak} = y_1/(1-Ky_1)^2 \quad (\because n\to\infty) \quad \text{(A-16)}$$

Combining Eqs. A-1, A-3, A-4, A-5, A-9, A-14, A-15, and A-16, two kinds of mole fraction are related to each other by these equations:

$$x_1 = N_1/(N_1+N_4) = y_1/\{(1-Ky_1)^2+Ky_1^2\} \quad \text{(A-17)}$$

$$x_4 = N_4/(N_1+N_4) = y_4(1-Ky_1)^2/\{(1-Ky_1)^2+Ky_1^2\} \quad \text{(A-18)}$$

Solving Eqs. A-17, and A-18 under the condition $x_1+x_4=1$, y_1 and y_4 are given by:

$$y_1 = \frac{1}{2K(1+K)x_1}\{2Kx_1+1-(4Kx_1x_4+1)^{1/2}\} \quad \text{(A-19)}$$

$$y_4 = \{1-(K+1)y_1\}/(1-Ky_1) \quad \text{(A-20)}$$

From Eqs. A-2, A-5, A-9, A-10, A-11, A-12, A-13, and A-15, we obtain:

$$\lim_{x_2\to 0}(y_2/x_2) = \{1+\sum_{k=2}^{n}(k-1)y_{Ak}\}/\{1+\sum_{j=0}^{2}(y_{j2}/y_2)+(y_{b2}/y_2)\} = \frac{1+\dfrac{Ky_1^2}{(1-Ky_1)^2}}{1+K_0\{(y_4+2K_m y_1)^2+2K_m K_b y_1\}} \quad \text{(A-21)}$$

According to the definition of $\beta_{2,\mathrm{mix}}$ previously described,[3] the activity coefficient of a solute in a solvent mixture is given by:

$$\beta_{2,\mathrm{mix}} = \lim_{x_2\to 0}(y_2/x_2)(f_2^\circ V_{\mathrm{mix}}/RT) = \frac{1+\dfrac{Ky_1^2}{(1-Ky_1)^2}}{1+K_0\{(y_4+2K_m y_1)^2+2K_m K_b y_1\}}\left(\frac{f_2^\circ V_{\mathrm{mix}}}{RT}\right) \quad \text{(A-22)}$$

References

1) Y. Kondo, T. Kato, and N. Tokura, *Bull. Chem. Soc. Jpn.*, **48**, 285 (1975).

2) Y. Kondo, Y. Honjo, and N. Tokura, *Bull. Chem. Soc. Jpn.*, **41**, 987 (1968).

3) Y. Kondo and N. Tokura, *Bull. Chem. Soc. Jpn.*, **45**, 818 (1972).

4) I. Prigogine and R. Defay, transl. by D. H. Everett, "Chemical Thermodynamics," Longmans (1954).

5) D. Gurka and R. W. Taft, Jr., *J. Am. Chem. Soc.*, **91**, 4794 (1969).

6) R. W. Taft, Jr., D. Gurka, L. Joris, P. von R. Schleyer, and J. W. Rakshys, *J. Am. Chem. Soc.*, **91**, 4801 (1969).

7) L. Joris, J. Mitsky, and R. W. Taft, Jr., *J. Am. Chem. Soc.*, **94**, 3438 (1972).

Studies on Reactions of the *N*-Phosphonium Salts of Pyridines. XIX. Carbonylation of Amines with Carbon Dioxide by Means of Phosphorus Chlorides in Tertiary Amines

Noboru YAMAZAKI, Tatsuya TOMIOKA, and Fukuji HIGASHI

Department of Polymer Science, Tokyo Institute of Technology, Ookayama, Meguro-ku, Tokyo 152

(Received March 2, 1976)

Reactions of carbon dioxide and disulfide with primary amines in the presence of phosphorus chlorides gave the corresponding symmetrically disubstituted ureas and thioureas in high yields under atmospheric conditions. Phosphorus trichloride and di- and mono-chlorophosphites were remarkably effective for the reactions, whereas phosphorus pentachloride and phosphoryl chloride were ineffective. The presence of tertiary amines such as pyridine satisfactorily favored the reactions. The reaction seems to proceed *via* the *N*-phosphonium salts of pyridines as those obtained from diphenyl and triaryl phosphites, on the basis of their IR spectroscopic analyses, stoichiometric relationship between reactants and the steric effect of tertiary amines.

Phosphorous acid hexaalkyltriamide (**1**) prepared from phosphorus trichloride and secondary amines afforded the corresponding carbamoyloxy compounds (**2**) by inserting carbon dioxide.[1] **2** was aminolysed with primary amines into ureas, but not with secondary amines.[2]

$$PCl_3 + 6R_2NH \longrightarrow \underset{(\mathbf{1})}{P(NR_2)_3} \xrightarrow{CO_2} \underset{(\mathbf{2})}{P(OCONR_2)_x(NR_2)_{3-x}}\ (x=1, 2)$$

$$\xrightarrow{R_2NH} R_2NCONR_2 \qquad \xrightarrow{RNH_2} RNHCONR_2$$

Some primary amines also reacted with phosphorus trichloride to give the phosphorus–nitrogen compounds such as phosphenimidous amide derivatives (RNH–P=NR) from the aromatic amines,[3] and the amides (P-(NHR)$_3$) from the alkylamines.[4] However, these phosphorus–nitrogen compounds have not been fully investigated, nor has the insertion reaction of carbon dioxide been reported.

The phosphorus–nitrogen bonds in these phosphorous amides and imides were expected to bring about the reaction with carbon dioxide, yielding ureas by aminolysis with amines as those in **1**. Ureas were, in fact, obtained in high yields using PCl_3 and chlorophosphites ($RO-PCl_2$, $(RO)_2-PCl$) in pyridine,[5] and the reaction was successfully applied to the preparation of polyureas under mild conditions.[6]

This paper gives detailed results of the reactions of phosphorus chloride and primary amines with carbon dioxide and disulfide in the presence of tertiary amines.

$$CX_2 + 2RNH_2 + \begin{cases} PCl_3 \\ RO-PCl_2 \\ (RO)_2-PCl \end{cases} \longrightarrow RNHC(X)NHR \quad (X=O, S)$$

Results and Discussion

When carbon dioxide was passed at 60 °C for 6 h into a cylindrical flask[7] containing phosphorus trichloride and aniline (4 equiv.) in pyridine, *N,N'*-diphenylurea was obtained in 93% yield based on aniline. The yield was lowered to 21%, when the reaction was carried out in the absence of pyridine by using 7 equivalents of aniline (3 equivalent excess as HCl scavenger) in toluene, suggesting that pyridine significantly facilitates the reaction.

Table 1. *N,N'*-Diphenylurea from carbon dioxide and aniline by use of phosphorus trichloride in various tertiary amines at 60 °C for 6 h

Tertiary amine	pK_a	Yield, %[a]
None	—	21[b]
Pyridine	5.19	93
γ-Picoline	6.08	88
β-Picoline	5.52	85
α-Picoline	6.20	73
2,4-Lutidine	6.99	77
2,6-Lutidine	6.99	28
Triethylamine	10.87	50[c]

a) Based on aniline used. b) In toluene.
c) In an autoclave at 20 atm of CO_2.

In order to elucidate the favorable effect of tertiary amines on the reaction, the reaction of carbon dioxide with aniline was investigated in several tertiary amines (Table 1). The presence of tertiary amines favored the reaction; of the tested amines, pyridine and β- and γ-picolines with smaller steric hindrance around the nitrogen atom gave satisfactory yields, whereas the yield was lowered in sterically hindered amines such as α-picoline and 2,4-lutidine, and strikingly low in 2,6-lutidine with the largest hindrance in pyridine derivatives. The unsatisfactory result in highly basic triethylamine even under severe reaction conditions indicated that the steric hindrance was more influential than the basicity.

Various ureas were prepared using phosphorus trichloride in pyridine (Table 2). In the reactions of amines more basic than pyridine, 7 equivalents of the amines were used, since 3 equivalents were consumed as HCl scavenger. Primary amines afforded the corresponding *N,N'*-disubstituted ureas, whereas secondary amines gave no ureas.

Table 2. *N,N'*-Disubstituted ureas from amines and carbon dioxide by use of phosphorus trichloride in pyridine at 60 °C for 6 h

Amine (mol)		Yield	
		mol	%[a]
Aniline	(4.0)	1.86	93
Cyclohexylamine	(7.0)[b]	1.64	82
Benzylamine	(7.0)[b]	1.40	70
Isopropylamine	(7.0)[b]	0.92	46
Piperidine	(7.0)[b]	0	—
Diphenylamine	(4.0)	0	—
N-Methylaniline	(4.0)	0	—

a) Based on amines (4 mol). b) Three equivalents were used as HCl scavenger.

Table 3. *N,N'*-Diphenylurea from aniline and carbon dioxide by use of various phosphorus chlorides in pyridine at 60 °C for 6 h

Phosphorus chloride (mol)		Aniline (mol)	Yield	
			mol	%[a]
$PhO-PCl_2$	(0.01)	0.02	0.009	90.0
		0.04	0.0173	86.5
$EtO-PCl_2$	(0.01)	0.02	0.0087	87.0
		0.04	0.0123	61.5
$Ph-PCl_2$	(0.01)	0.04	0.0050	25.0
$(PhO)_2-PCl$	(0.01)	0.02	0.0020	20.0
$(EtO)_2-PCl$	(0.01)	0.02	0.0028	28.0
		0.04	0.0047	23.5
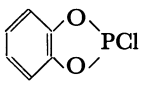	(0.01)	0.02	0.0030	30.0
$O=PCl_3$	(0.01)	0.05	0	—
$Ph-P(O)Cl_2$	(0.01)	0.05	0	—
PCl_5	(0.01)	0.05	0	—

a) Yield (%) based on aniline used.

Other phosphorus chlorides were tested in the reaction of carbon dioxide with aniline in pyridine (Table 3). Phenyl dichlorophosphite gave the best results, giving a nearly quantitative yield of *N,N'*-diphenylurea from both 2 and 4 equivalents of aniline. Monochlorophosphites gave moderate results. On the other hand, phosphorus(V) chlorides afforded no urea, but the corresponding phosphorus amides; phosphoryl chloride and phenylphosphinylidene dichloride yielded phosphoric trianilide and phenylphosphinic dianilide in 69 and 60% yields, respectively. These anilides unreactive to carbon dioxide gave no urea.

Similar to the reaction of carbon dioxide, carbon disulfide reacted with aniline in pyridine with use of phosphorus trichloride and phenyl dichlorophosphite, yielding thioureas in high yields (Table 4).

The reaction of carbon dioxide with aniline was carried out by varying the molar ratios of aniline to phosphorus chlorides, in order to examine how many mols of aniline can be converted into urea by one mol of phosphorus chloride. Figure 1 shows the variation of the produced amount of *N,N'*-diphenylurea with the ratio, indicating an increase of amount until a limiting value of *ca.* 4. Above this value, no substantial increase was found by additional aniline.

The results are represented in another way in terms of the yields based on phosphorus chloride (Fig. 2). Nearly quantitative yields were obtained at the ratio of 4 for phosphorus trichloride, and at both ratios of 2 and 4 for phenyl dichlorophosphite.

The results in Figs. 1 and 2 indicate that the trichloride can transform 4 mol of aniline into 2 mol of *N,N'*-diphenylurea, whereas the dichlorophosphite can react with 2 mol of aniline into 1 mol of the urea, and also with 4 mol of aniline into 2 mol of the urea.

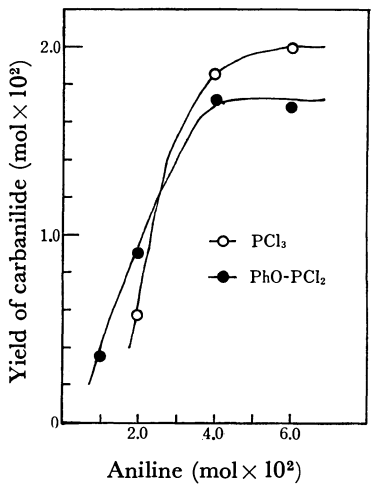

Fig. 1. Variation of urea yield with the amount of aniline employed: PCl_3=$PhO-PCl_2$=0.01 mol; temperature=60 °C; time=6 h.

Table 4. Thioureas from carbon disulfide and amines by use of phosphorus chlorides in pyridine at 40 °C for 6 h

Phosphorus chloride (mol)		Amide (mol)		Yield	
				mol	%[a]
PCl_3	(0.01)	Aniline	(0.04)	0.0175	87.5
PCl_3	(0.01)	Benzylamine	(0.07)[b]	0.0113	56.5
PCl_3	(0.01)	Cyclohexylamine	(0.07)[b]	0.0158	79.0
$PhO-PCl_2$	(0.01)	Aniline	(0.02)	0.0066	66.0
$PhO-PCl_2$	(0.01)	Aniline	(0.04)	0.0169	84.5

a) Yield (%) based on amines used. b) Three equivalents of amines were used as HCl scavenger.

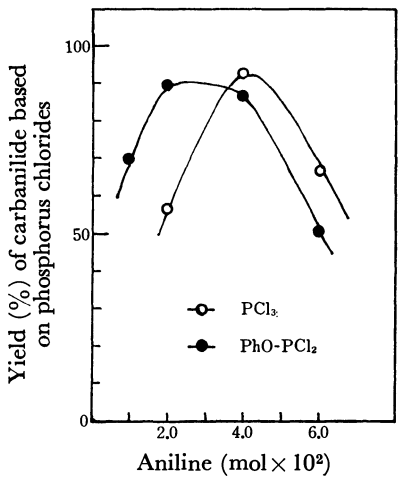

Fig. 2. Variation of urea yield with the amount of aniline employed: PCl_3=PhO-PCl_2=0.01 mol; temperature=60 °C; time=6 h.

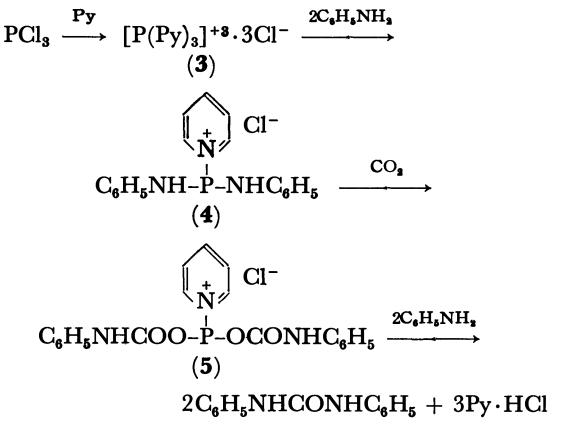

Scheme 1.

The results can explain the reaction with phosphorus trichloride in the following way (Scheme 1). The chloride in pyridine first forms a phosphonium salt (**3**), which then reacts with aniline to give **4**. The salt is also called *N*-phosphonium salt of pyridine[7] but it could be named pyridinium salt. Insertion of carbon dioxide into the phosphorus-nitrogen bonds in **4** results in a carbamoyloxy *N*-phosphonium salt (**5**) which is similar to that obtained from diphenyl phosphite.[8] Aminolysis of **5** with additional aniline gives urea.

In order to confirm the proposed mechanism, **4** was obtained as a syrup contaminated with pyridine hydrochloride, after the reaction mixture of phosphorus trichloride and aniline in pyridine had been extracted with ether until no detectable amounts of pyridine and aniline were found in the ether layer.

In the IR spectrum of the syrup, a peak at 1630 cm^{-1} is due to ν C=N+ of the *N*-phosphonium salt of pyridine, and is in good agreement with that of the phosphonium salts[7] given by the oxidation of phosphites in pyridine followed by aminolysis. Although the band is overlapped with that of pyridine hydrochloride, the latter intensity contained in the band is less than half, judging from the medium intensity of a couple of other peaks due to hydrochloride.

The syrup was decomposed in 1 M-sodium hydroxide, and the liberated pyridine and aniline were extracted with ether. The results of GLC analyses of the extract indicate that 3 mol of pyridine and 2 mol of aniline are present in the syrup. According to Scheme 1, **4** was contaminated with 2 mol of pyridine hydrochloride. Thus 1 mol of pyridine and 2 mol of aniline are involved in **4**.

In the reaction with amines more basic than pyridine such as cyclohexylamine, 3 mol of pyridine of **3** may be replaced by the amines to form triamide, and the amine hydrochloride, and 7 mol of the amine added can theoretically produce only 1 mol of the urea. However, better yield (1.64 mol) of the urea excluded the involvement of the triamide intermediate, although it is not clear why **3** did not react with 3 mol of the amine.

Another possible intermediate is a phosphenimidous derivative (**6**), which was proposed in amidation of carboxylic acids as shown before:[9]

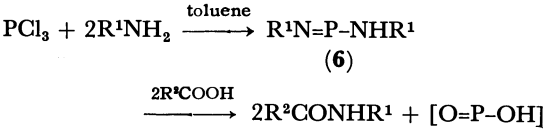

However, it can not be a dominant one in the reaction of carbon dioxide, since only a small amount (12% yield based on aniline) of **6** was obtained from the reaction mixture of phosphorus trichloride and aniline in pyridine. A separate reaction of **6** with carbon dioxide and aniline gave *N*,*N*′-diphenylurea in 38% yield as compared to 93% in the standard procedure in this study.

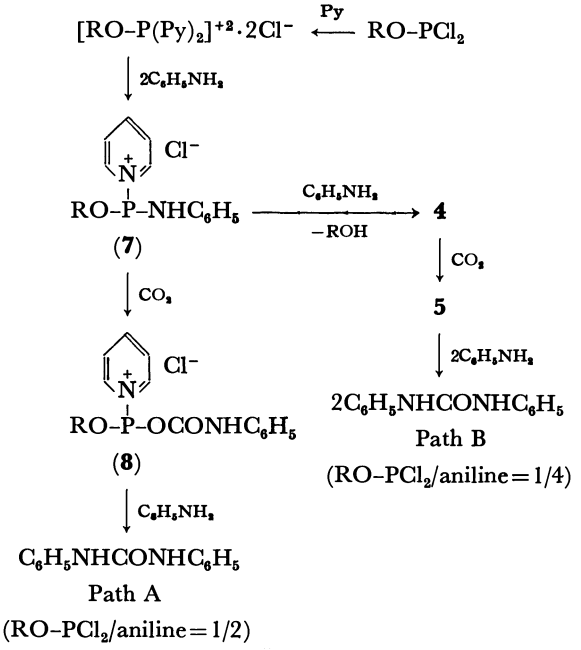

Scheme 2.

Similarly, dichlorophosphites might bring about two different reactions involving 2 and 4 equivalents of aniline (Scheme 2). In Path A phosphites react initially with 1 equivalent of aniline to give the *N*-phosphonium

salt (**7**) like **4**, which is converted into *N,N'*-diphenylurea by treating with carbon dioxide and then with aniline (RO–PCl_2/aniline=1/2). In Path B (RO–PCl_2/aniline=1/4), **7** reacts further with additional aniline to afford **4** by releasing phenol or alcohols. Insertion of carbon dioxide into the P–N bonds of **4** followed by aminolysis yields *N,N'*-diphenylurea. Actually, phenol (R=C_6H_5–) was obtained in 42% yield in the reaction by Path B. Better results with phenyl dichlorophosphite than with ethyl dichlorophosphite in Path B (Table 3) may be due to easier dephenoxylation than deethylation which promotes the formation of **4**.

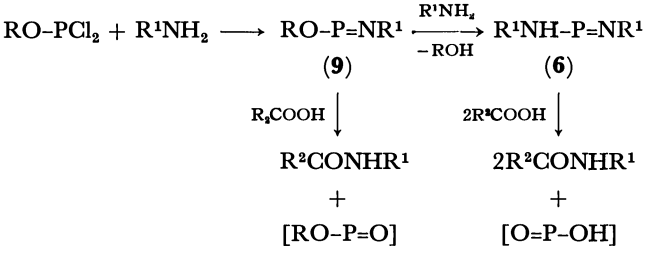

Scheme 3.

An alternative mechanism[11] *via* a phosphinimidite **6** and **9** proposed for amidation of carboxylic acids may not be reasonable, because of the lower reactivity of **6** to carbon dioxide (Scheme 3).

Similarly, the reaction with monochlorophosphites may proceed *via* the *N*-phosphonium salts of pyridine (**7** and **8**, or **4** and **5**) by releasing alcohols and phenol. Phenol was found in 47% yield (about a half of two phenoxy groups in the phosphite) in the reaction mixture with diphenyl monochlorophosphite.

An amidophosphite[11] also can be considered as an intermediate. In a separate experiment, diethyl anilidophosphite (**10**) gave the urea in 25% yield which is comparable to 29% obtained by the reaction with diethyl chlorophosphite.

Thus the reaction with monochlorophosphites may involve two paths as above (Scheme 4).

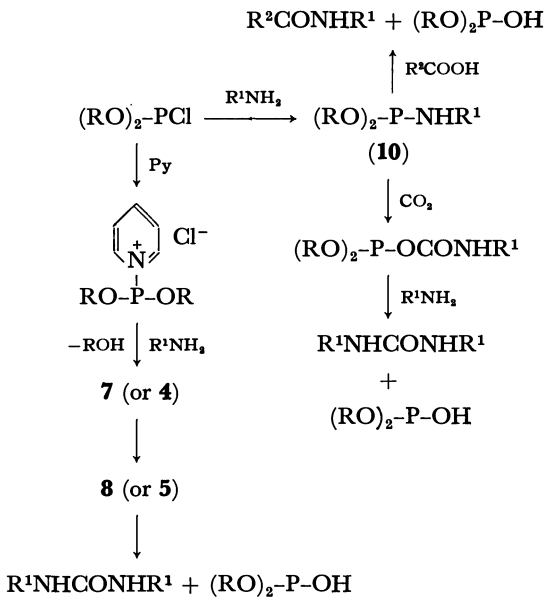

Scheme 4.

Experimental

N,N'-Diphenylurea from Carbon Dioxide and Aniline by Use of Phosphorus Trichloride in Various Tertiary Amines. Gaseous carbon dioxide was introduced at 60 °C for 6 h into a cylindrical flask containing a mixture of phosphorus trichloride (0.01 mol) and aniline (0.04 mol) in 30 ml of tertiary amines. In volatile triethylamine, the reaction was carried out in an autoclave at the pressure (20 atm) of carbon dioxide. The reaction was also carried out in 40 ml of toluene by using phosphorus trichloride (0.01 mol) and aniline (0.04 mol). The reaction mixture was condensed to a syrup under reduced pressure, and then treated with 20 ml of 50% aqueous ethanol, yielding *N,N'*-diphenylurea in high yields (Table 1).

Separation and Decomposition of **4**. A mixture of phosphorus trichloride (0.01 mol) and aniline (0.04 mol) in 30 ml of pyridine was heated at 40 °C for 1 h, and the mixture was extracted with dry ether until no pyridine and aniline were detected in the ether solution. **4** was separated as an ether-insoluble syrup, and was decomposed in 20 ml of 1 M-sodium hydroxide at ambient temperature for 1 h. The aqueous solution was extracted well with ether, and the combined ether solution was subjected to gas-liquid chromatographic analyses.

N,N'-Disubstituted Ureas from Carbon Dioxide and Various Amines by Use of Phosphorus Trichloride in Pyridine. Similarly, carbonylation of amines (0.04 mol) or amines (0.07 mol) more basic than pyridine was carried out at 60 °C for 6 h by adding the amines in pyridine to a mixture of phosphorus trichloride (0.01 mol) and pyridine (30 ml). Ureas were obtained by working up as above.

N,N'-Diphenylurea from Aniline and Carbon Dioxide by Use of Various Phosphorus Chlorides in Pyridine. The urea was obtained by the reaction at 60 °C for 6 h in 30 ml of pyridine with use of phosphorus chlorides (0.01 mol) and aniline (0.02—0.05 mol).

Thioureas from Carbon Disulfide and Amines by Use of Phosphorus Chlorides in Pyridine. A mixture of amines (0.02—0.07 mol) and phosphorus chlorides (0.01 mol) in 30 ml of pyridine was heated at 40 °C for 6 h. The resulting mixture was evaporated to a syrup under reduced pressure. Thioureas were obtained by treating the syrup with 20 ml of 50% aqueous ethanol.

References

1) G. Oertel, H. Malz, and H. Holtschmidt, *Chem. Ber.*, **97**, 891 (1964).
2) N. Yamazaki, T. Tomioka, and F. Higashi, *Synthesis*, **1975**, 384.
3) For example, H. W. Grimmel, A. Guenther, and J. F. Morgan, *J. Am. Chem. Soc.*, **68**, 539 (1946).
4) For example, A. Michaelis, *Justus Liebigs Ann. Chem.*, **326**, 129 (1903); R. B. Flint and P. L. Salzberg, U. S. Pat., 2151380 (1937).
5) N. Yamazaki, T. Tomioka, and F. Higashi, Preprint of the 32nd Annual Meeting of the Chemical Society of Japan, III-1596 (1975), April, Tokyo.
6) N. Yamazaki, T. Tomioka, and F. Higashi, *J. Polym. Sci. Polym. Lett. Ed.*, **14**, 55 (1976).
7) N. Yamazaki and F. Higashi, *Bull. Chem. Soc. Jpn.*, **46**, 3824 (1973).
8) N. Yamazaki, T. Iguchi, and F. Higashi, *Tetrahedron Lett.*, **1974**, 1191; *Tetrahedron*, **31**, 3031 (1975).
9) H. G. Grimmel, *J. Am. Chem. Soc.*, **68**, 529 (1946).
10) St. Goldschmidt, *Justus Liebigs Ann. Chem.*, **588**, 24 (1954).
11) R. W. Young, *J. Am. Chem. Soc.*, **74**, 5304 (1952).

Reactions of 2-Guanidino-1-cyclohexanol with Ketals and Acetals

Yasushi TAKAGI, Osamu KAWASHIMA,* Tsutomu TSUCHIYA, Hiroshi SANO, and Sumio UMEZAWA

Institute of Bioorganic Chemistry, 1614 Ida, Nakahara-ku, Kawasaki 211
**Department of Applied Chemistry, Faculty of Engineering, Keio University, Hiyoshi, Kohoku-ku, Yokohama 223*

(Received March 13, 1976)

Reactions of 2-guanidino-1-cyclohexanols (**1**, $\mathbf{1}_d$, $\mathbf{1}_l$) with 1,1-dimethoxycyclohexane in *N,N*-dimethylformamide in the presence of *p*-toluenesulfonic acid gave the *N,O*-cyclohexylidene derivatives (**5**, $\mathbf{5}_d$, $\mathbf{5}_l$), respectively. Similar reactions of $\mathbf{1}_l$ with 2,2-dimethoxypropane and with dimethyl acetals of *p*-tolualdehyde and *p*-bromobenzaldehyde also gave an *N,O*-isopropylindene, *N,O*-(*p*-methylbenzylidene) and *N,O*-(*p*-bromobenzylidene) derivative ($\mathbf{8}_l$, $\mathbf{9}_l$, $\mathbf{10}_l$), respectively. From IR and PMR spectral studies of $\mathbf{9}_l$ *p*-toluenesulfonate, seven-membered structures as exemplified by **9A** were assigned. The *N,O*-blocked derivatives (**5**,**9**) are stable in weakly acidic or alkaline media, but in stronger media, they are cleaved to **1**. The usefulness of the protective groups was also examined. **9** was found to resist tosylation or mesylation in pyridine but not acylation. The numerical values of optical rotations of the guanidinocyclohexanols were greatly enhanced by *N,O*-blocking.

During the course of synthetic studies on dihydrostreptomycin and related compounds, we undertook to protect the hydroxyl groups of the antibiotic by conversion into acetals or ketals. When 2″-*N*-benzyloxycarbonyldihydrostreptomycin[1] was treated with 1,1-dimethoxycyclohexane, a ketal reagent, in *N,N*-dimethylformamide (DMF) in the presence of acid catalyst, we obtained a tetracyclohexylidenated derivative. The product was found to contain no *O*-(1-methoxycyclohexyl) group[6] as judged by the PMR spectrum, although it was not isolated in crystalline state. This fact was unusual, since the starting material has only three sets of hydroxyl groups for the ketal formation. The fourth cyclohexylidene group might be formed between the guanidino and hydroxyl groups in the streptidine moiety of the dihydrostreptomycin. In order to clarify the above structure, we chose *trans*-2-guanidino-1-cyclohexanol (**1**) as a model compound and treated it with 1,1-dimethoxycyclohexane in the presence of acid catalyst. Since the compound has *trans*-diequatorial guanidino and hydroxyl groups attached to a cyclohexane ring, the compound can be deemed as a model compound for the streptidine portion of dihydrostreptomycin.

The *dl-trans*-2-guanidino-1-cyclohexanol (**1**) was prepared from *dl-trans*-2-amino-1-cyclohexanol by the reaction with *S*-methylisothiourea as described by Bannard *et al.*[2] The optically active isomers ($\mathbf{1}_d$, $\mathbf{1}_l$) were also prepared from *d*- and *l*-2-amino-1-cyclohexanol,[3,4] respectively. Since the guanidino compounds were scarcely soluble in common organic solvents, they were converted into the salts of *p*-toluenesulfonic acid which are fairly soluble in organic solvents. These *p*-toluenesulfonates were treated with 1,1-dimethoxycyclohexane in DMF in the presence of *p*-toluenesulfonic acid. The reaction was carried out to completion[5] under reduced pressure in order to remove the generated methanol. The products ($\mathbf{5}_d$, $\mathbf{5}_l$, and **5**) obtained in good yields were confirmed to have a cyclohexylidene group by elementary analyses and PMR spectral studies. Absence of the methoxyl group shown by PMR spectra ruled out the presence of the 1-methoxycyclohexyl group which is often formed[6] in the reaction between a single hydroxyl group and 1,1-dimethoxycyclohexane. These results show that the cyclohexylidene group is bifunctionally coupled to the hydroxyl and guanidine groups, or to the amino and imino groups of the guanidine portion. The presumption is also supported[7] by the difference of the color reactions of **5** and **1** for Sakaguchi reagent; **5** was negative, whereas **1** was positive, suggesting that compound **5** is a di- or tri-*N*-substituted guanidine.

As control experiments, the *p*-toluenesulfonates of guanidinocyclohexane,[2] 2-amino-1-cyclohexanol, and 2-methylamino-1-cyclohexanol[8] were each treated with 1,1-dimethoxycyclohexane. However, no reaction took place.

In order to confirm the absence of a free hydroxyl group in **5**, **5** *p*-toluenesulfonate was treated with acetic anhydride in pyridine in the presence of triethylamine. A mixture of two products, which could not be separated by silica gel column chromatography due to their unstable nature, was obtained. However, the IR spectrum of the mixture showed no absorption peaks between 1700—1800 cm^{-1} indicating the absence of the *O*-acetyl group. On the other hand, a similar acetylation of **1** *p*-toluenesulfonate gave a triacetyl derivative (**4**), which showed an absorption peak at 1730 cm^{-1}. When the salt of **1** was acetylated with acetic anhydride in pyridine without addition of triethylamine, a mono-*O*-acetyl derivative (**3**) was formed. These results and the aforementioned result that no reaction occurs between 1-guanidinocyclohexane and 1,1-dimethoxycyclohexane indicated that **5** has a cyclohexylidene group attached to N and O, but not to N and N.

Methoxycarbonylation of **5** *p*-toluenesulfonate with methyl chloroformate and sodium hydride afforded an *N*-methoxycarbonyl derivative (**6**) in a 29% yield. Acetylation of **6** with acetic anhydride in pyridine readily gave an *N*(or *N*′**)-acetyl-*N*(or *N*′)-methoxycarbonyl derivative (**7**) as judged from their IR spectra.

$\mathbf{1}_l$ *p*-Toluenesulfonate was treated with another ketal, 2,2-dimethoxypropane in a similar manner to that for **5** to give an *N,O*-isopropylidene derivative ($\mathbf{8}_l$) in a low yield. This may be ascribed[5] to the closeness of the

** For the sake of convenience the nitrogen directly attached to the cyclohexane ring is denoted by N and the other nitrogens by N′.

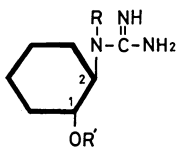

1 R = H R' = H
2 = CH_3 = H
3 = H = Ac

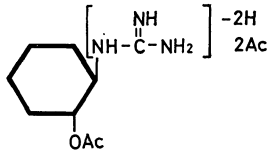

4

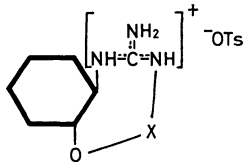

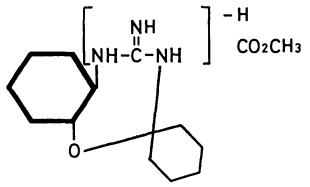

5 X =
8 =
9 = 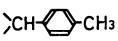
10 = 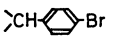

6

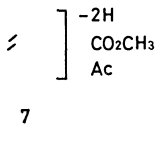

7

boiling points of 2,2-dimethoxypropane and methanol liberated. The structure of $\mathbf{8}_l$ was also confirmed by the acetylation of $\mathbf{8}_l$ as for **5**.

Determination of the position of nitrogen attached to the cyclohexylidene group was attempted. For this purpose, *p*-methylbenzylidene and *p*-bromobenzylidene derivatives ($\mathbf{9}_l$, $\mathbf{10}_l$)*** of $\mathbf{1}_l$ were prepared, since they were expected to have a structure similar to the cyclohexylidene derivatives (**5**, $\mathbf{5}_d$, and $\mathbf{5}_l$), and the benzylidene methine protons of the derivatives were expected to couple, in the PMR spectra, with the NH protons of the guanidine groups attached to the methine, thus revealing the position of the nitrogen in question. In the PMR spectrum of $\mathbf{9}_l$ *p*-toluenesulfonate in deuteriochloroform, the methine proton appeared as a doublet at δ 5.50. On irradiation at δ 8.34, or on deuteration, the doublet collapsed to a singlet. This suggests that the *p*-methylbenzylidene group is attached to a nitrogen bearing one hydrogen atom. However, it is still not possible to decide which one of the three nitrogens of the guanidine group is the nitrogen in question, since both **9A** and **9B** satisfy the above PMR spectral results.

Successful result was obtained from further PMR study on $\mathbf{9}_l$. Nuclear Overhauser effect was observed between the benzylidene methine proton (δ 5.50) and one of the methine protons (δ 3.2) of the cyclohexane ring. Examination of the stereomodels of **9A** and **9B** showed that only the structure **9A** can take the structure in which H-1 or H-2 of the cyclohexane ring and the methine hydrogen of the benzylidene group approach near enough for interaction. These observations suggest the structure **9A** for **9**. The IR spectra of $\mathbf{5}_d$, $\mathbf{8}_l$, $\mathbf{9}_l$, and $\mathbf{10}_l$ also supported the seven-membered structure as depicted in **9A** by the differences (75—95 cm^{-1}) in wavelength of two kinds of peaks at $\approx$1670 and $\approx$1590 cm^{-1} assignable to guanidinium ions as reported by Goto *et al.*[9]

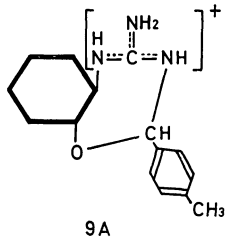

9A

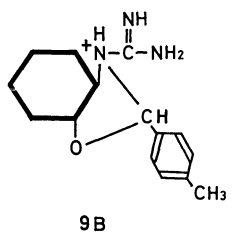

9B

In order to further confirm the structure, we prepared 2-(1-methylguanidino)-1-cyclohexanol (**2**, racemic), which has no hydrogen atom at N-1 of the guanidine portion, from 2-methylamino-1-cyclohexanol (racemic), and the **2** *p*-toluenesulfonate was treated with 1,1-dimethoxycyclohexane in a similar manner to that described above. However, this experiment was unsuccessful since no reaction occurred, suggesting that the 1-*N*-methyl group sterically hinders the ring formation or that the presence of the methyl group reduces the resonance stabilization of the guanidinium ion.

X-Ray crystallographic analysis[10] of $\mathbf{5}_d$ *p*-toluenesulfonate has been carried out and the result also supports the seven-membered structure.

In order to see if the above mentioned cyclohexylidenation, isopropylidenation, and benzylidenation can provide novel instances for *N,O*-protection, we first examined the stability of the protective groups in acidic or alkaline media. The compounds were fairly stable in weak acidic or weak alkaline media, but in moderately acidic or alkaline media, they were cleaved to the starting material (**1**) in a fairly short period.

In order to examine the usefulness of protection in synthesis, $\mathbf{9}_l$, selected as a model compound, was treated in pyridine with *p*-toluenesulfonyl or methanesulfonyl chlorides. The starting material ($\mathbf{9}_l$) was recovered in good yields showing that the *p*-methylbenzylidene group, as well as the guanidine portion, can resist the reaction. However, when $\mathbf{9}_l$ was treated in pyridine with acetic anhydride or benzoyl chloride at room temperature overnight, $\mathbf{9}_l$ was found to change, although the product was not identified. In the reaction of $\mathbf{9}_l$ with 50% sodium iodide in DMF at 100 °C, $\mathbf{9}_l$ resisted for 5 min, but gradually changed to **1** in a longer period. On the catalytic hydrogenation with palladium black or Raney nickel at room temperature, **5** and $\mathbf{9}_l$ were found to be stable at least for 10 h.

The *N,O*-blocked derivatives show high enhancement of the rotational value in magnitude as compared with **1**

Table 1.

Compound as *p*-toluenesulfonate	$[\alpha]_D$ (in methanol)
$\mathbf{1}_d$	−14°
$\mathbf{1}_l$	+14°
$\mathbf{5}_d$	−88°
$\mathbf{5}_l$	+84°
$\mathbf{8}_l$	+114°
$\mathbf{9}_l$	+123°
$\mathbf{10}_l$	+121°

*** By acetal formation, an asymmetric center is produced at the benzylidene methine carbon. However, in the present case, we can discuss the structures ($\mathbf{9}_l$ and $\mathbf{10}_l$) without taking the configuration of the methine into consideration.

(Table 1). This could be utilized for assigning the absolute configurations of compounds related to **1**.

Experimental

PMR spectra were recorded at 60 and 100 MHz on Hitachi R-24A and Varian XL-100 spectrometers. Thin-layer chromatography (TLC) was performed on plates of Wakogel B-5 with sulfuric acid spray for detection. For column chromatography, silica gel (Wakogel C-200) was used. When the solvent system of chloroform–methanol–28% ammonia was used with varying the ratio, the lower layers were used.

1-Guanidinocyclohexane p-*Toluenesulfonate.* A mixture of cyclohexylamine (4.75 g), *S*-methylisothiouronium sulfate (6.65 g), and water (19 ml) was treated in a similar way to that described by Bannard *et al.*,[2] and worked up as follows: After concentration to approximately two-thirds of the original volume, the reaction mixture was charged on a column of Dowex 1×2 resin (OH form, 250 ml) and developed with water. The strongly alkaline fractions were neutralized with *p*-toluenesulfonic acid and concentrated to give a solid, which was recrystallized from water to give needles, 6.65 g (44%), mp 67—69 °C. IR (KBr): 1670, 1640 cm^{-1}.

Found: C, 53.84; H, 7.35; N, 13.55; S, 10.18%. Calcd for $C_7H_{15}N_3 \cdot C_7H_7SO_3H$: C, 53.65; H, 7.40; N, 13.41; S, 10.23%.

d-, l-, *and* dl-trans-*2-Guanidino-1-cyclohexanol (**1**$_d$, **1**$_l$, and **1**)* p-*Toluenesulfonates.* These were prepared from *d*-, *l*-, and *dl-trans*-2-aminocyclohexanols and *S*-methylisothiouronium sulfate according to the method of Bannard *et al.*[2] The reaction mixture was concentrated, and the residue was boiled with methanol. The methanol solution was filtered and the filtrate was concentrated to give a solid. The solid was chromatographed on a column of Dowex resin as described above. The products, *p*-toluenesulfonates of **1**$_d$, **1**$_l$, and **1** were obtained in approximately 40% yield. They were recrystallized from methanol–ether to give plates. Each compound is soluble in water, methanol, pyridine, DMF, hot chloroform and hot acetone, but sparingly soluble in benzene, ether, and ethyl acetate. IR (KBr): 1660 and 1635 cm^{-1} (monosubstituted guanidinium[9]). **1**$_d$ *p*-Toluenesulfonate: mp 138—139 °C; $[\alpha]_D^{17}$ +6° (*c* 1, water), −14° (*c* 0.3, methanol), −6° (*c* 0.3, aqueous pyridine 1: 1). Found: C, 51.16; H, 7.06; N, 12.96; S, 9.58%. Calcd for $C_{14}H_{23}N_3O_4S$: C, 51.05; H, 7.04; N, 12.76; S, 9.73%.

1$_l$ *p*-Toluenesulfonate: mp 138—140 °C; $[\alpha]_D^{12}$ −7° (*c* 1, water), +14° (*c* 0.3, methanol), +3° (*c* 0.3, aqueous pyridine 1: 1). Found: C, 51.12; H, 6.98; N, 12.64; S, 9.64%.

1 *p*-Toluenesulfonate: mp 151—153.5 °C; $[\alpha]_D^{17}$ 0° (*c* 1, water).

dl-trans-*2-(1-Methylguanidino)-1-cyclohexanol (**2**)* p-*Toluenesulfonate.* *dl-trans*-2-Methylamino-1-cyclohexanol (2 g) prepared from cyclohexene oxide and methylamine according to the method reported[8] was dissolved in water (20 ml) and the solution was partially neutralized with *p*-toluenesulfonic acid to pH 9. Cyanamide (1.05 g) was added and the solution was heated at 60 °C for 3 h. After neutralization with *p*-toluenesulfonic acid to pH ≈7, the reaction mixture was concentrated by evaporating with ethanol and benzene. The residue was dissolved in ethanol and the solution was filtered, and evaporated. The residue was dissolved in a mixture of chloroform–methanol–28% ammonia (2: 1: 1) and the insoluble matter was removed by filtration and discarded. The filtrate was evaporated to give a residue, which was washed with water to afford a solid (2.02 g, 38%). The solid was recrystallized from chloroform–methanol–ether to give **2** *p*-toluenesulfonate as plates. It was positive to biacetyl but negative to Sakaguchi reagent. Mp 210—211 °C; IR(KBr): 1670, 1620 cm^{-1}; PMR (dimethyl-d_6 sulfoxide) δ: 2.85 (3H s, NCH_3).

Found: C, 52.38; H, 7.10; N, 12.38; S, 9.14%. Calcd for $C_8H_{17}N_3O \cdot C_7H_7SO_3H$: C, 52.46; H, 7.34; N, 12.23; S, 9.33%.

dl-trans-*1-Acetoxy-2-guanidinocyclohexane (**3**)* p-*Toluenesulfonate.* Acetic anhydride (0.17 ml) was added to a solution of **1** (305 mg) in pyridine–DMF (1: 1, 18 ml) which was then allowed to stand at room temperature for 40 h. On being subjected to TLC with chloroform–methanol–28% ammonia (1: 1: 1), the solution showed a spot at R_f 0.43. After addition of water (0.1 ml), the solution was concentrated by evaporation with toluene under reduced pressure to give a syrup. The syrup was chromatographed on a short column of silica gel with chloroform–methanol (10: 1) to give a solid of **3** *p*-toluenesulfonate, 283 mg (82%). IR (KBr): 1745 (OAc); 1680 and 1630 cm^{-1} (monosubstituted guanidinium[9]); PMR ($CDCl_3$) δ: 1.97 (3H s, OAc), 2.36 (3H s, Ts (CH_3)), 3.1—3.6 (1H m, H-2), 4.2—4.8 (1H m, H-1).

Found: C, 51.52; H, 6.68; N, 11.13; S, 8.66%. Calcd for $C_9H_{17}N_3O_2 \cdot C_7H_7SO_3H$: C, 51.74; H, 6.78; N, 11.31; S, 8.63%.

dl-trans-*1-Acetoxy-2-*[N,N′ *(or* N′,N′*)-diacetylguanidino]-cyclohexane (**4**).* Acetic anhydride (0.57 ml) and triethylamine (0.84 ml) were added to a solution of **1** *p*-toluenesulfonate (101 mg) in pyridine (2 ml), and the resulting solution was kept at room temperature for 18 h. On being subjected to TLC with benzene–ethanol (10: 1), the solution showed a spot at R_f 0.57 (**1**: R_f 0). The solution was poured into an ice-cold mixture of chloroform (25 ml) and water (25 ml) with stirring and the organic layer separated was washed with cold water, dried over magnesium sulfate and evaporated to dryness under reduced pressure. The residue was dissolved in benzene–ethanol (10: 1) and the solution was chromatographed as described above to give slightly brown crystals, 79 mg (93%), mp 66—68 °C. IR (KBr): 1730 (OAc), 1700, 1620 (s), 1560 cm^{-1}; PMR ($CDCl_3$) δ: 2.03, 2.14, and 2.18 (each 3H s, Ac), 4—4.5 (1H m, H-1?), 4.6—5.1 (1H m, H-2?), 9.15 (1H? m, broad; disappeared on deuteration).

Found: C, 54.86; H, 7.39; N, 14.65%. Calcd for $C_{13}H_{21}N_3O_4$: C, 55.11; H, 7.47; N, 14.83%.

d-, l-, *and* dl-trans-N′, O-*Cyclohexylidene-2-guanidino-1-cyclohexanol (**5**$_d$, **5**$_l$, and **5**)* p-*Toluenesulfonates.* *p*-Toluenesulfonic acid (175 mg) and 1,1-dimethoxycyclohexane (3.34 ml) were added to a solution of **1**$_d$ *p*-toluenesulfonate (1.53 g) in DMF (12 ml). The solution was heated at 50 °C for 2 h under reduced pressure (25 Torr). During this period, some solvent (≈1 ml) of the reaction mixture was distilled off. On being subjected to TLC with chloroform–methanol–28% ammonia (3: 1: 1), the solution gave a single spot at R_f 0.25. After triethylamine (3 ml) had been added, ether was gradually added until precipitation ceased. The precipitate was filtered, washed thoroughly with ether and with water to give colorless needles of **5**$_d$ *p*-toluenesulfonate (1.70 g), which were recrystallized from ethanol, 1.47 g (77%). It is soluble in aqueous pyridine (1: 1), pyridine–DMF (1: 2), chloroform–methanol (1: 1), hot pyridine, hot DMF, and hot ethanol but sparingly soluble in water even at reflux temperature. It was positive to biacetyl but negative to Sakaguchi reagent. Mp 203—205 °C, $[\alpha]_D^{21}$ −88° (*c* 0.16, methanol), $[\alpha]_D^{16}$ −110° (*c* 0.25, aqueous pyridine 1: 1). IR (KBr): 1675 and 1580 (disubstituted guanidinium[9]), 1650, 1505 cm^{-1}; PMR (pyridine-d_5–D_2O 1: 1) δ: 1.0—2.5 (≈18H), 2.30 (3H s, Ts(CH_3)), 2.5—3.2 (1H), 3.2—3.8 (1H), one AB q (4H) centered at 7.72 ($SO_2C_6H_4CH_3$).

Found: C, 58.46; H, 7.60; N, 10.43; S, 7.68%. Calcd for

$C_{13}H_{23}N_3O \cdot C_7H_7SO_3H$: C, 58.65; H, 7.63; N, 10.26; S, 7.83%.

l-Isomer, **5**$_l$ *p*-toluenesulfonate, was similarly prepared starting from **1**$_l$ *p*-toluenesulfonate. Mp 203—205 °C; $[\alpha]_D^{22}$ +84° (*c* 0.13, methanol); $[\alpha]_D^{16}$ +101° (*c* 0.25, aqueous pyridine 1:1). Other characteristics were the same as those of **5**$_d$.

Found: C, 58.47; H, 7.50; N, 10.52; S, 7.95%.

dl-Isomer, **5** *p*-toluenesulfonate, was similarly prepared from **1** *p*-toluenesulfonate, $[\alpha]_D^{22}$ 0° (*c* 0.1, methanol). Mp 196—200 °C.

Found: C, 58.81; H, 7.51; N, 10.03; S, 7.52%.

dl-trans-N′, O-*Cyclohexylidene-2*-[N *(or* N′*)-methoxycarbonylguanidino*]-*1-cyclohexanol* (**6**). To a solution of **5** *p*-toluenesulfonate (501 mg) in dry pyridine–DMF (1:1, 30 ml) was added 50% oily sodium hydride (130 mg) at room temperature under a nitrogen atmosphere. After stirring for 1 h, methyl chloroformate (0.12 ml) was added and the stirring was continued for 30 min. The reaction mixture was then similarly treated as above twice with the hydride (60 mg×2) and methyl chloroformate (0.1 ml×2; added 5 min after the addition of the hydride). Chloroform (300 ml) was added with stirring to the resulting mixture, and the organic layer was washed thoroughly with water, dried over magnesium sulfate and the solvent was removed by co-evaporation with toluene. The brown syrup was chromatographed on a column of silica gel (45 g) with chloroform–ethyl acetate (2:1) as a developer. The fractions containing the main product (R_f 0.14 with the above solvent mixture) were concentrated to give a pale-yellow syrup (106 mg, 29%), which crystallized on standing. It was recrystallized from ethyl acetate to give prisms of **6**, mp 166.5—167 °C. An additional minor product (R_f 0.4, 64 mg) was also obtained. This product was presumed to be a trimethoxycarbonyl derivative as judged by its PMR spectrum, but no further study was carried out. Compound **6** was negative to biacetyl and Sakaguchi reagents. IR(KBr): 1630, 1500 cm^{-1}; PMR ($CDCl_3$) δ: 3.70 (3H s, CO_2CH_3).

Found: C, 60.83; H, 8.36; N, 13.97%. Calcd for $C_{15}H_{25}N_3O_3$: C, 60.99; H, 8.53; N, 14.23%.

dl-trans-N′, O-*Cyclohexylidene-2*-[N *(or* N′*)-acetyl*-N *(or* N′*)-methoxycarbonylguanidino*]-*1-cyclohexanol* (**7**). Acetic anhydride (0.13 ml) was added to a solution of **6** (82 mg) in pyridine (1.6 ml), and the resulting solution was kept at room temperature for 30 h. This was poured into a mixture of chloroform and saturated sodium hydrogencarbonate solution with stirring and the organic layer was washed thoroughly with water, dried over magnesium sulfate and concentrated to give a syrup, 73 mg (79%). It is soluble in most of organic solvents including hexane. IR (KBr): 1690 (shoulder), 1655, 1615 cm^{-1}; PMR ($CDCl_3$) δ: 2.25 (3H s, Ac), 3.81 (3H s, CO_2CH_3).

Found: C, 60.26; H, 8.13; N, 12.75%. Calcd for $C_{17}H_{27}N_3O_4$: C, 60.51; H, 8.07; N, 12.45%.

l-trans-*2-Guanidino*-N′, O-*isopropylidene-1-cyclohexanol* (**8**$_l$) p-*Toluenesulfonate*. *p*-Toluenesulfonic acid (23 mg) and 2,2-dimethoxypropane (0.32 ml) were added to a solution of **1**$_l$ *p*-toluenesulfonate (204 mg) in DMF (1.6 ml) which was heated at 50 °C for 1 h under reduced pressure (100 Torr). A few drops of the reaction mixture were taken and were poured into a mixture of triethylamine and methanol. TLC of the solution with chloroform–methanol–28% ammonia (3:1:1) showed a weak spot at R_f 0.2 (**8**$_l$). Repeated addition of 2,2-dimethoxypropane (0.32 ml) to the above reaction mixture every 30 min and working up as above did not raise the yield of **8**$_l$ as judged by TLC. Application of a higher reduced pressure (25 Torr) also did not improve the yield. After addition of triethylamine (0.3 ml), the reaction mixture was evaporated to give a syrup, which was chromatographed on a column of silica gel with chloroform–methanol–28% ammonia (3:2:2) to give a syrup (38 mg) containing **8**$_l$. Repetition of the chromatography as above gave a pure solid of **8**$_l$ (10 mg). It is soluble in methanol, benzene, chloroform, acetone, and ethyl acetate, but sparingly soluble in ether and water $[\alpha]_D^{15}$ +114° (*c* 1, methanol). IR (KBr): 1670, 1590 (disubstituted guanidinium[9]); 1510 cm^{-1}; PMR ($CDCl_3$) δ: 1.50 (6H s, $(CH_3)_2C$), 2.40 (3H s, Ts(CH_3)).

Found: C, 54.91; H, 7.25; N, 11.22; S, 8.39%. Calcd for $C_{10}H_{19}N_3O \cdot C_7H_7SO_3H$: C, 55.26; H, 7.37; N, 11.37; S, 8.68%.

l-trans-*2-Guanidino*-N′, O-p-*methylbenzylidene-1-cyclohexanol* (**9**$_l$) p-*Toluenesulfonate*. *p*-Toluenesulfonic acid (116 mg) and *p*-tolualdehyde dimethyl acetal (2.53 ml) were added to a solution of **1**$_l$ *p*-toluenesulfonate (1.02 g) in DMF (8 ml), and the resulting solution was heated at 50 °C for 2 h under reduced pressure (25 Torr). After addition of triethylamine (2 ml), the solution was concentrated. Addition of ether gave precipitates, which were washed successively with ether containing triethylamine and water to give a solid of **9**$_l$ *p*-toluenesulfonate, 911 mg (66%). The solid was recrystallized from methanol–ether to give needles. It is soluble in methanol, chloroform, and pyridine, but sparingly soluble in benzene, acetone, ethyl acetate, ether, and water. It was positive to biacetyl but negative to Sakaguchi reagent. Mp 195.5—197 °C, $[\alpha]_D^{15}$ +123° (*c* 0.2, methanol). IR (KBr): 1670, 1595 (disubstituted guanidinium), 1510 cm^{-1}; PMR ($CDCl_3$) δ: 2.33 and 2.37 (each 3H s, $C\underline{H}_3C_6H_4SO_3H$ and $C\underline{H}_3C_6H_4CH$=), 3.0—3.3 (2H, broad, H-1,2), 5.50 (1H d, $CH_3C_6H_4C\underline{H}$; J= 3 Hz; collapsed to a sharp singlet on deuteration); two AB q (each 4H) centered at 7.27 and 7.30 (J=≈8.5 Hz); 7.73 (1H incomplete d, NH; J=≈2.5 Hz; disappeared on deuteration), 8.00 (2H s, NH; disappeared on deuteration), 8.34 (1H incomplete t, NH; J=2—3 Hz, disappeared on deuteration).

Irradiation at δ 5.50 collapsed the triplet at δ 8.34 to an incomplete doublet. Irradiation at δ 8.34 collapsed the doublets at δ 5.50 and 7.73 to a singlet, respectively.

Irradiation of the solution, after introducing nitrogen, at δ 3.15 (H-1,2) caused a 5% increase in the area of the signals at δ 5.50 ($CH_3C_6H_4C\underline{H}$).

Found: C, 61.42; H, 6.88; N, 9.56; S, 7.49%. Calcd for $C_{15}H_{21}N_3O \cdot C_7H_7SO_3H$: C, 61.23; H, 6.77; N, 9.74; S, 7.43%.

l-trans-N′, O-p-*Bromobenzylidene-2-guanidino-1-cyclohexanol* (**10**$_l$) p-*Toluenesulfonate*. *p*-Toluenesulfonic acid (42 mg) and *p*-bromobenzaldehyde dimethyl acetal (1.4 ml) were added to a solution of **1**$_l$ *p*-toluenesulfonate (402 mg) in DMF (3.2 ml), and the resulting solution was heated at 50 °C for 2 h under reduced pressure (25 Torr). On being subjected to TLC with chloroform–methanol–28% ammonia (1:1:1), the solution showed main spot at R_f 0.45 but **1**$_l$ still remained. Above acetal (0.7 ml) was further added and the reaction was continued for 3 h. After addition of triethylamine (0.1 ml), the solution was processed as described for **9** to give a solid of **10**$_l$ *p*-toluenesulfonate, 379 mg (62%). The solid was recrystallized from chloroform–methanol (1:1) to give needles. It is soluble in methanol, pyridine, DMF, but sparingly soluble in chloroform, benzene, acetone, ethyl acetate, ether, and water. It was positive to Beilstein's test for halogen. Mp 224—226 °C, $[\alpha]_D^{24}$ +121° (*c* 0.2, methanol). IR (KBr): 1670, 1595 (disubstituted guanidinium); 1520 cm^{-1}; PMR (DMSO-d_6) δ: 1.0—2.2 (8H), 2.29 (3H s, Ts(CH_3)), 5.66 (1H s, $BrC_6H_4C\underline{H}$=), 7.0—8.2 (12H, $CH_3C_6\underline{H}_4SO_3$, $BrC_6\underline{H}_4CH$=, and NH (4H), the last disappeared on deuteration).

Found: C, 51.02; H, 5.33; N, 8.20%. Calcd for $C_{14}H_{18}BrN_3O \cdot C_7H_7SO_3H$: C, 50.81; H, 5.28; N, 8.46%.

Stability of **5** *and* **9**$_l$ *in Acidic and Alkaline Media*. Com-

pound $\mathbf{9}_l$ was found stable on treating its chloroform solution with saturated sodium hydrogencarbonate or 5% *p*-toluenesulfonic acid at room temperature for 5 min, as judged by TLC with chloroform–methanol–28% ammonia (1: 1: 1). Compound **5** could not be examined under the same conditions since it is scarcely soluble in chloroform. When solutions of **5** and of $\mathbf{9}_l$ in aqueous pyridine (1: 1) were kept at room temperature for 48 h, a slight conversion of $\mathbf{9}_l$ to **1** occurred, whereas **5** remained unchanged. Complete conversion of $\mathbf{9}_l$ was found to occur by keeping its aqueous methanol (1: 10) solution saturated with sodium carbonate at room temperature for 30 min, whereas, by the same treatment, less than half the amount of **5** turned to **1**. When 1.5% solutions of **5** and $\mathbf{9}_l$ in chloroform–methanol (1:1) containing 1.1 molecular equivalents (based on **5** and $\mathbf{9}_l$) of *p*-toluenesulfonic acid were kept at room temperature for 2 h, **5** completely turned to **1**, while the conversion of $\mathbf{9}_l$ to **1** was about 50%.

Reactions of $\mathbf{9}_l$ *with* p-*Toluenesulfonyl and Methanesulfonyl Chlorides.* To a solution of $\mathbf{9}_l$ *p*-toluenesulfonate (49 mg) in dry pyridine (1 ml) was added *p*-toluenesulfonyl chloride (69 mg) or methanesulfonyl chloride (45 mg) and the solution was kept at room temperature overnight. On being subjected to TLC with chloroform–methanol–28% ammonia (3: 1: 1) and chloroform-ethanol (4: 1), the solution showed a single spot (R_f 0.25 and 0.4, respectively) of $\mathbf{9}_l$. After addition of water (0.1 ml), the solution was concentrated and the resulting syrup was dissolved in chloroform. The solution was washed successively with aqueous sodium hydrogencarbonate, saturated sodium *p*-toluenesulfonate solution, water, dried over sodium sulfate and concentrated to give $\mathbf{9}_l$ *p*-toluenesulfonate, 36 mg (74%) and 36 mg (74%), respectively. Their PMR and IR spectra were indistinguishable from those of $\mathbf{9}_l$ *p*-toluenesulfonate.

The authors are grateful to Dr. Hamao Umezawa, Director of the Institute of Microbial Chemistry, for his support and encouragement, to Dr. Hiroshi Naganawa of the Institute for carrying out the NOE experiment and for his kind discussions, and to Mr. Saburo Nakada of Keio University for carrying out elementary analysis.

References

1) S. Umezawa, Y. Takahashi, T. Usui, and T. Tsuchiya, *J. Antibiot.*, **27**, 997 (1974).
2) R. A. B. Bannard, A. A. Casselman, W. F. Cockburn, and G. M. Brown, *Can. J. Chem.*, **36**, 1541 (1958).
3) T. Suami, S. Ogawa, and S. Umezawa, *Bull. Chem. Soc. Jpn.*, **36**, 459 (1963).
4) Absolute configurations of $\mathbf{1}_d$ and $\mathbf{1}_l$ were determined as 1S: 2S and 1R: 2R, respectively, according to S. Umezawa, T. Tsuchiya, and K. Tatsuta, *Bull. Chem. Soc. Jpn.*, **39**, 1235 (1966).
5) F. H. Bissett, M. E. Evans, and F. W. Parrish, *Carbohyd. Res.*, **5**, 184 (1967).
6) D. Ikeda, T. Suzuki, T. Tsuchiya, and S. Umezawa, *Bull. Chem. Soc. Jpn.*, **46**, 3210 (1973).
7) J. D. Mold, J. M. Ladino, and E. J. Schantz, *J. Am. Chem. Soc.*, **75**, 6321 (1953).
8) J. B. Kay and J. B. Robinson, *J. Chem. Soc., C*, **1969**, 248.
9) T. Goto, K. Nakanishi, and M. Ohashi, *Bull. Chem. Soc. Jpn.*, **30**, 723 (1957).
10) H. Nakamura, H. Umezawa, and Y. Iitaka, the details will be described in the near future.

Studies of Peptide Antibiotics. XXXIII.[1] Syntheses of Gramicidin S Analogs Containing *N*-Methyl-L-valine in Place of L-Valine

Hayao ABE,* Kazuki SATO, Tetsuo KATO, and Nobuo IZUMIYA

Laboratory of Biochemistry, Faculty of Science, Kyushu University, Hakozaki, Higashi-ku, Fukuoka 812

(Received March 29, 1976)

Two analogs of gramicidin S, [1-*N*-methyl-L-valine]-gramicidin S and [1,1'-di-*N*-methyl-L-valine]-gramicidin S, were prepared for the purpose of investigating the contribution of NH group of L-valyl residue in gramicidin S to antibacterial activity. They exhibit weak activity as compared with gramicidin S in the antibacterial test toward microorganisms. The optical rotatory dispersions of these analogs and gramicidin S were measured in ethanol and 8 M urea. It was suggested that both analogs have a different molecular conformation from that of gramicidin S, and that the NH group of valyl residues is necessary for stabilizing the conformation to exhibit biological activity.

Several models have been proposed[2] for the conformation of gramicidin S (GS) in solid state and solution. The most favorable model is the intramolecular antiparallel β-form with four hydrogen bondings between the valyl and the leucyl residues.[3] A simplified structure of the model is shown in Fig. 1. In studies of the structure-activity relationship of GS, it has been proposed that the specific conformation is necessary for molecules of GS and its analogs to exhibit biological activity.[2]

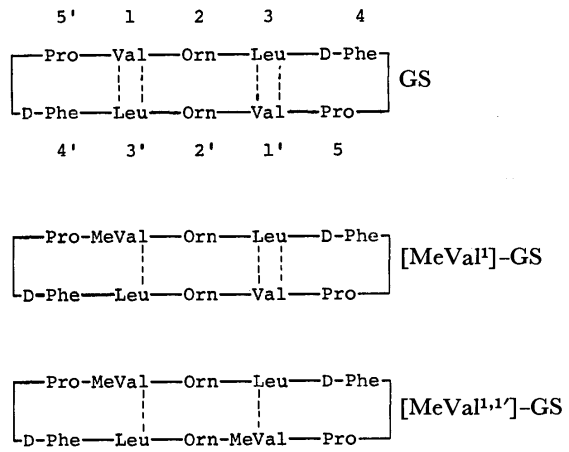

Fig. 1. Structure of GS and its analogs.

[3-*N*-Methyl-L-leucine]-gramicidin S ([MeLeu³]-GS) and [MeLeu³,³']-GS which lack some of the four hydrogen bondings in GS were synthesized in order to investigate to what extent the changes in the number of these hydrogen bondings vary the level of antibacterial activity and influence the conformations.[4] It was observed that the antibacterial activity of [MeLeu³]-GS and [MeLeu³,³']-GS is identical with that of GS and the optical rotatory dispersion (ORD) curves are similar to the curve of GS. Recent studies on the two analogs by proton magnetic resonance spectroscopy showed that the analogs might have a different conformation from that of GS in spite of the apparent resemblance between GS and the analogs in their ORD curves.[5] In other words, similarity of ORD patterns do not always guarantee similar conformation. The results led us to investigate other analogs which contain *N*-methylamino acid residue other than *N*-methyl-L-leucyl.

The present paper deals with the syntheses, antibacterial properties, and ORD measurements of [MeVal¹]-GS and [MeVal¹,¹']-GS, in which the L-valyl residues in positions 1 and 1' are replaced, singly or together, by *N*-methyl-L-valyl residues. These analogs lack one or two of the four hydrogen bondings in GS as shown in Fig. 1.

The syntheses of [MeVal¹]-GS and [MeVal¹,¹']-GS are outlined in Schemes 1 and 2.[6] The principle of the synthesis was to locate the leucyl residue at the C-terminal in order to achieve the cyclization in a good yield. In *B. brevis*, GS is synthesized enzymatically with the cyclization of a pentapeptide (H-D-Phe-Pro-Val-Orn-Leu-OH).[7] According to this finding, Tanaka *et al.* synthesized the protected GS chemically with a protected pentapeptide azide of the same amino acid sequence in a high yield of 30—36%.[8] Furthermore, the results of recent studies in this laboratory on the cyclization reaction of a pentapeptide *via* several active esters show that an *N*-hydroxysuccinimide method is excellent because of high yield, experimental simplicity, and no racemization.[1]

In order to avoid racemization of *N*-methyl-L-valyl residue, the stepwise elongation procedure was employed for the synthesis of X and XII for the following reason. McDermott and Benoiton observed that *N*-methyl-L-leucyl residue in Z-L-Ala-L-MeLeu-OH partially racemized in a coupling reaction with an amine-component by the DCC-HONSu method in spite of no racemization of Z-L-Ala-L-Leu-OH under the same conditions.[9] They reported absence of racemization of alkyloxycarbonyl-*N*-methyl-L-amino acid during the course of coupling reactions.[9]

For the synthesis of protected [MeVal¹]-GS (XIX), Boc-pentapeptide-ONSu (IX) and pentapeptide (XVI) were prepared by the stepwise elongation from the carboxyl toward the amino end as shown in Scheme 1. Coupling of these IX and XVI afforded Boc-decapeptide acid (XVII) which was converted into a decapeptide-ONSu. A key intermediate (XIX) was derived by the cyclization of the decapeptide-ONSu in a satisfactory yield of 56%. As shown in Scheme 2, Boc-decapeptide acid (XXII) was converted into the corresponding decapeptide-ONSu. A Z-substituted intermediate (XXIV) was derived by the cyclization of the decapep-

* Present address: Institute of Biological Science, Mitsui-Toatsu Chemicals, Inc., Mobara 297

Table 1. Antibacterial activity of GS and its analogs
(Minimum inhibitory concentration, μg/ml)

Strain	GS·2HC	[MeVal[1]]-GS·2HCl	[MeVal[1,1']]-GS·2HCl
Staphylococcus aureus 209p	12.5	25	50
Staphylococcus aureus Terajima	1.56	12.5	25
Enterococcus hemolyticus Hoshi	6.25	50	50
Bacillus subtillis ATCC 6633	1.56	25	50
Escherichia coli K 12	50	50	50
Proteus vulgaris OX 19	50	50	50

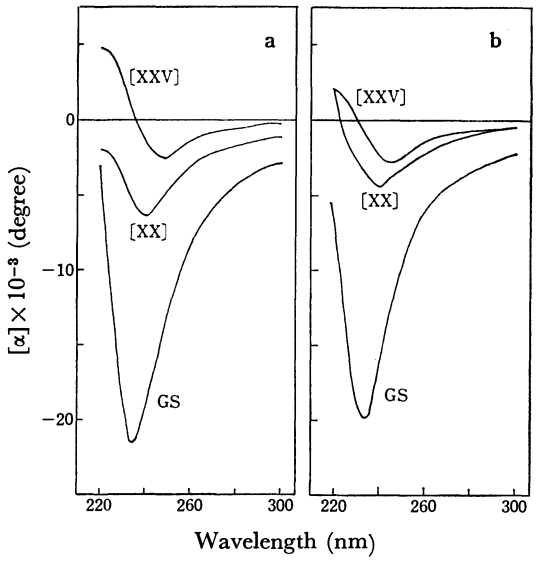

Fig. 2. ORD curves of [MeVal[1]]-GS (XX), [MeVal[1,1']]-GS (XXV), and GS.
Solvent: a, ethanol; b, 8 M aqueous urea.

analog (Table 1). The results indicate the importance of the NH's of L-valyl residues in GS for exhibiting the activity.

The ORD curves of the two analogs in ethanol as well as of GS are shown in Fig. 2-a. The trough of [MeVal[1]]-GS and of [MeVal[1,1']]-GS is at 240 and 248 nm, respectively, whereas that of GS is at 236 nm. The troughs of the analogs are shallower than the trough of GS. [MeVal[1,1']]-GS shows a greater shift in position and a shallower trough than [MeVal[1]]-GS. In 8 M aqueous urea which causes denaturation of various polypeptides, the position of the trough of [MeVal[1,1']]-GS shifts from 248 to 245 nm, but that of [MeVal[1]]-GS at 240 nm remains unchanged as in the case of GS (Fig. 2-b). The results of ORD measurements indicate that the conformation of the analogs differs from that of GS, and the stability of the analogs decreases as the number of *N*-methylvalyl residues increases. The tendency is comparable with the biological activity. We proposed that the biologically active analogs of GS show a similar ORD curve to that of GS.[10] The two analogs containing *N*-methylvalyl residues show a different ORD curve from that of GS and exhibit weak biological activity as had been expected. These results indicate that the destruction of intramolecular hydrogen bondings by substitution of valyl residues for *N*-methylvalyl residues cause the change and instabilization of conformation and decrease the biological activity consequently.

Experimental

Melting points are uncorrected. Thin-layer chromatography (TLC) was carried out on silica gel G (Merck) with the solvent system: chloroform–methanol (5: 1, v/v). The NMR spectra were recorded on a Hitachi R-20B spectrometer at 60 MHz with tetramethylsilane as an internal standard. The optical rotations were measured on a Yanagimoto polarimeter, OR-20.

Boc-Orn(Z)-Leu-OEt (I). To a solution of Boc-Orn(Z)-OH[11] (10.99 g, 30 mmol) and TEA (4.20 ml, 30 mmol) in THF (30 ml) was added isobutyl chloroformate (3.93 ml, 30 mmol) at −5 °C. After 15 min, a mixture of H-Leu-OEt·HCl (5.87 g, 30 mmol) and TEA (30 mmol) in chloroform (30 ml) was added. The mixture was left to stand overnight at room temperature, evaporated *in vacuo*, and the oily residue was dissolved in ethyl acetate. The solution was washed successively with 4% sodium hydrogencarbonate, 10% citric acid and water, and then dried over sodium sulfate. The solvent was evaporated under reduced pressure. The residual oil was solidified by the addition of ether and petroleum ether. The product was recrystallized from methanol–ether–petroleum ether; yield, 13.15 g (86%); mp 100—101 °C, $[\alpha]_D^{20}$ −21.6° (*c* 1, ethanol).

Found: C, 61.65; H, 8.02; N, 8.32%. Calcd for $C_{26}H_{41}O_7N_3$: C, 61.52; H, 8.14; N, 8.28%.

H-Orn(Z)-Leu-OEt·HCl (II). Compound I (12.69 g, 20 mmol) was dissolved in 96 ml of 2.6 M hydrogen chloride in ethyl acetate. The solution was allowed to stand for 1 h at room temperature and then evaporated. The oily residue was solidified by the addition of ether and petroleum ether, and the crude product was recrystallized from ethanol–ether–petroleum ether; yield, 10.66 g (96%); mp 126—129 °C; $[\alpha]_D^{20}$ −1.4° (*c* 1, ethanol).

Found: C, 57.13; H, 7.69; N, 9.43%. Calcd for $C_{21}H_{34}O_5N_3Cl$: C, 56.81; H, 7.72; N, 9.47%.

Boc-Val-Orn(Z)-Leu·OEt (III). A reaction mixture of Boc-Val-OH (1.87 g, 8.6 mmol), TEA (8.6 mmol) and isobutyl chloroformate (8.6 mmol) in THF (9 ml) was treated with a solution of II (3.84 g, 8.6 mmol) and TEA (8.6 mmol) in chloroform (9 ml) as described for I. The crude product was recrystallized from methanol–ether–petroleum ether; yield, 4.80 g (92%); mp 152—154 °C; $[\alpha]_D^{20}$ −38.6° (*c* 1, ethanol).

Found: C, 60.65; H, 8.13; N, 9.41%. Calcd for $C_{31}H_{50}O_8N_4\cdot1/2H_2O$: C, 60.46; H, 8.35; N, 9.10%.

H-Val-Orn(Z)-Leu-OEt·HCl (IV). Compound III (4.41 g, 7.3 mmol) was dissolved in 2.6 M hydrogen chloride in ethyl acetate (28 ml) and treated as described for II. The product was recrystallized from ethanol–ether–petroleum ether; yield, 3.57 g (90%); mp 205—207 °C; $[\alpha]_D^{20}$ −19.6° (*c* 0.5, ethanol).

Found: C, 56.72; H, 7.88; N, 10.27%. Calcd for $C_{26}H_{43}O_6N_4\cdot1/2H_2O$: C, 56.56; H, 8.03; N, 10.15%.

Boc-Pro-Val-Orn(Z)-Leu-OEt (V). A mixture of Boc-Pro-OH (1.29 g, 6 mmol), TEA (6 mmol) and isobutyl chloroformate (6 mmol) in THF (6 ml) was treated with IV (3.26 g, 6 mmol) and TEA (6 mmol) in chloroform (6 ml) as described for I. The product was recrystallized from

methanol–ether–petroleum ether; yield, 3.65 g (90%); mp 158—160 °C; $[\alpha]_D^{20}$ −69.0° (*c* 1, ethanol).

Found: C, 61.12; H, 8.04; N, 10.00%. Calcd for $C_{36}H_{57}O_9N_5$: C, 61.43; H, 8.16; N, 9.95%.

H–Pro–Val–Orn(Z)–Leu–OEt·HCl (VI). Compound V (3.52 g, 5 mmol) was treated with 2.6 M hydrogen chloride in ethyl acetate (19 ml) as described for II. The product was recrystallized from ethanol–ether–petroleum ether; yield, 3.07 g (96%); mp 187—189 °C; $[\alpha]_D^{20}$ −60.0° (*c* 0.5, ethanol).

Found: C, 57.58; H, 8.04; N, 11.01%. Calcd for $C_{31}H_{50}O_7N_5Cl$: C, 58.15; H, 7.87; N, 10.94%.

Boc–D–Phe–Pro–Val–Orn(Z)–Leu–OEt (VII). A mixture of Boc–D–Phe–OH (1.19 g, 4.5 mmol), TEA (4.5 mmol) and isobutyl chloroformate (4.5 mmol) in THF (4.5 ml) was treated with VI (2.88 g, 4.5 mmol) and TEA (4.5 mmol) in chloroform (4.5 ml) as described for I. The product was recrystallized from methanol–ether–petroleum ether; yield, 3.25 g (84%); mp 94—98 °C; $[\alpha]_D^{20}$ −76.0° (*c* 0.5, ethanol).

Found: C, 62.75; H, 8.05; N, 9.65%. Calcd for $C_{45}H_{66}O_{10}N_6\cdot 1/2H_2O$: C, 62.84; H, 7.85; N, 9.77%.

Boc–D–Phe–Pro–Val–Orn(Z)–Leu–OH (VIII). To a solution of VII (1.72 g, 2 mmol) in a mixture of methanol (10 ml) and dioxane (5 ml) was added 1 M sodium hydroxide (3.4 ml) and the solution was allowed to stand for 3 h at room temperature. After the addition of water (30 ml), the solution was concentrated *in vacuo* at a low temperature, and the residual solution was acidified with 10% citric acid and extracted with ethyl acetate. The organic layer was washed with water, dried over sodium sulfate, and evaporated. The residual oil was triturated with a mixture of ether and petroleum ether, and the powder was recrystallized from methanol–ether–petroleum ether; yield, 1.50 g (90%); mp 120—123 °C; $[\alpha]_D^{20}$ −80.1° (*c* 1, methanol).

Found: C, 61.96; H, 7.67; N, 9.98%. Calcd for $C_{43}H_{62}O_{10}N_6\cdot 1/2H_2O$: C, 62.07; H, 7.63; N, 10.10%.

Boc–D–Phe–Pro–Val–Orn(Z)–Leu–ONSu (IX). To a solution of VIII (832 mg, 1 mmol) in dioxane (5 ml) were added HONSu (115 mg, 1 mmol) and DCC (206 mg, 1 mmol) at 0 °C. After being left to stand at room temperature for 12 h, dicyclohexylurea formed was filtered off, the filtrate was evaporated, and the residual oil was solidified by the addition of ether. The product was recrystallized from dioxane–ether; yield, 643 mg (69%); mp 136—138 °C; $[\alpha]_D^{20}$ −74.1° (*c* 0.54, ethyl acetate).

Found: C, 60.83; H, 7.18; N, 10.50%. Calcd for $C_{47}H_{65}O_{12}H_7\cdot 1/2H_2O$: C, 60.76; H, 7.16; N, 10.55%.

Boc–MeVal–Orn(Z)–Leu–OEt (X). A reaction mixture of Boc–MeVal–OH[12] (4.63 g, 20 mmol), *N*-methylmorpholine (2.20 ml, 20 mmol) and isobutyl chloroformate (20 mmol) in THF (20 ml) was treated with II (8.88 g, 20 mmol) and *N*-methylmorpholine (20 mmol) in THF (20 ml) as described for I. The product was obtained as an oil; yield, 11.42 g (92%).

H–MeVal–Orn(Z)–Leu–OEt·HCl (XI). Compound X (11.17 g, 18 mmol) was treated with 2.6 M hydrogen chloride in ethyl acetate (139 ml) as described for II. The product was recrystallized from methanol–ether; yield, 7.42 g (74%); mp 174—175 °C; $[\alpha]_D^{20}$ −29.0° (*c* 0.52, methanol).

Found: C, 57.87; H, 8.15; N, 10.13%. Calcd for $C_{27}H_{45}O_6N_4Cl$: C, 58.20; H, 8.14; N, 10.06%.

Boc–Pro–MeVal–Orn(Z)–Leu–OEt (XII). To a solution of Boc–Pro–OH (2.80 g, 13 mmol), HOBt (1.76 g, 13 mmol), XI(7.24 g, 13 mmol) and TEA (13 mmol) in DMF (40 ml) was added WSCI (2.49 g, 13 mmol) at −5 °C. After stirring had been continued at −5—0 °C for 2 h, the mixture was left to stand overnight at room temperature. It was then evaporated and the residue was diluted with ethyl acetate (300 ml). The solution was washed with 4% sodium hydrogencarbonate, 10% citric acid and water, and dried over sodium sulfate. The solvent was evaporated to leave an oil; yield, 3.64 g (39%). Amino acid ratios in acid hydrolyzate; Pro 1.06, Orn 0.96, Leu 1.00.

H–Pro–MeVal–Orn(Z)–Leu–OEt·HCl (XIII) Compound XII (2.52 g, 3.5 mmol) was treated with 2.6 M hydrogen chloride in ethyl acetate (27 ml) as described for II. The oily product was purified with a column (4.9×33 cm) with silica gel 60 (Merck) as follows. The oily product was applied on the column, and the column was washed with ethyl acetate (1000 ml) and eluted with a mixture of ethyl acetate and ethanol (1: 1, v/v) (500 ml). Each fraction was assayed by TLC, and the fractions containing the desired product were evaporated to leave an oil which was crystallized by the addition of ether and petroleum ether; yield, 1.75 g (76%); mp 85—90 °C; $[\alpha]_D^{20}$ −86.6° (*c* 1.1, methanol).

Found: C, 58.28; H, 8.00; N, 10.55%. Calcd for $C_{32}H_{52}O_7N_5Cl$: C, 58.74; H, 8.01; N, 10.71%.

Boc–D–Phe–Pro–MeVal–Orn(Z)–Leu–OEt (XIV). To a solution of XIII (1.64 g, 2.5 mmol) and TEA (2.5 mmol) in dioxane (15 ml) at 5 °C was added Boc–D–Phe–ONSu[13] (1.09 g, 3 mmol) in dioxane (5 ml). The mixture was left to stand for 30 min at 5 °C and overnight at room temperature, and a few drops of 1-(2-aminoethyl)piperazine were added. After 30 min, the solution was evaporated and the residue was diluted with ethyl acetate (100 ml). The solution was washed with 4% sodium hydrogencarbonate, 10% citric acid and water, and dried over sodium sulfate. The solvent was evaporated to leave an oil; yield, 1.99 g (92%). Amino acid ratios in acid hydrolyzate; Phe 1.02, Pro 1.05, Orn 0.93, Leu 1.00.

Boc–D–Phe–Pro–MeVal–Orn(Z)–Leu–OH (XV). A solution of XIV (1.73 g, 2 mmol) in methanol (12 ml) was treated with 1 M sodium hydroxide (2.4 ml) as described for VIII. The product was recrystallized from methanol–ether–petroleum ether; yield, 1.37 g (82%); mp 95—97 °C; $[\alpha]_D^{20}$ −97.4° (*c* 0.51, methanol).

Found: C, 62.85; H, 7.72; N, 10.14%. Calcd for $C_{44}H_{64}O_{10}N_6$: C, 63.13; H, 7.71; N, 10.01%. NMR ($CDCl_3$); 1.36 (s, 9H, $(CH_3)_3C$–), 2.78 (s, 3H, CH_3N–), 5.06 (s, 2H, –O–CH_2–C_6H_5), 7.18—7.28 (m, 10H, phenyl protons).

H–D–Phe–Pro–MeVal–Orn(Z)–Leu–OH·HCl (XVI). Compound XV (840 mg, 1 mmol) was treated with 2.6 M hydrogen chloride in ethyl acetate (8 ml) as described for II. The oily product was purified with a column (4.9×38 cm) with silica gel 60 (Merck) as follows. The oily product was applied on the column, and the column was washed with a mixture of chloroform and methanol (19: 1, v/v) (500 ml) and eluted with a mixture of chloroform and methanol (9: 1, v/v) (1000 ml). The fraction with the desired product were evaporated and the residual oil was crystallized by the addition of ether; yield, 557 mg (72%); mp 136—140 °C; $[\alpha]_D^{20}$ −48.4° (*c* 0.49, methanol).

Found: C, 59.59; H, 7.32; N, 10.61%. Calcd for $C_{39}H_{57}O_8N_6Cl\cdot H_2O$: C, 59.19; H, 7.51; N, 10.62%.

Boc–D–Phe–Pro–Val–Orn(Z)–Leu–D–Phe–Pro–MeVal–Orn(Z)–Leu–OH (XVII). To a solution of XVI (162 mg, 0.21 mmol) and TEA (0.42 mmol) in DMF (1 ml) at 0 °C was added IX (195 mg, 0.21 mmol) in DMF (1 ml). The mixture was left to stand for 30 min at 0 °C and overnight at room temperature, a few drops of 1-(2-aminoethyl)piperazine were added, the solution was evaporated, and the residue was diluted with ethyl acetate (100 ml). The solution was washed with 4% sodium hydrogencarbonate, 10% citric acid and

water, dried over sodium sulfate, and the solvent was evaporated to leave an oil, which was solidified by the addition of ether. The product was recrystallized from methanol–ether; yield, 215 mg (66%); mp 133—134 °C; $[\alpha]_D^{20}$ −118° (*c* 0.33, methanol). Amino acid ratios in acid hydrolyzate; Phe 1.96, Pro 2.02; Val 0.98; Orn 1.98; Leu 2.00.

Found: C, 62.92; H, 7.54; N, 10.80%. Calcd for $C_{82}H_{116}O_{17}N_{12}\cdot H_2O$: C, 63.13; H, 7.63; N, 10.78%.

Boc–D–Phe–Pro–Val–Orn(Z)–Leu–D–Phe–Pro–MeVal–Orn(Z)–Leu–ONSu (XVIII). To a solution of XVII (185 mg, 0.12 mmol) in DMF (2 ml) were added HONSu (28 mg, 0.24 mmol) and WSCI (46 mg, 0.24 mmol) at 0 °C. After being left to stand at room temperature for 12 h, ethyl acetate (50 ml) was added, and the solution was washed with 4% sodium hydrogencarbonate, 10% citric acid and water. After drying over sodium sulfate, the solvent was evaporated to leave an oil which was solidified by the addition of ether. The product was reprecipitated from ethyl acetate–ether; yield, 186 mg (95%); mp 130—132 °C; $[\alpha]_D^{20}$ −146° (*c* 0.13, ethyl acetate).

Found: C, 61.93; H, 7.34; N, 10.95%. Calcd for $C_{86}H_{119}O_{19}N_{13}\cdot 2H_2O$: C, 61.66; H, 7.40; N, 10.87%.

cyclo(–D–*Phe–Pro–Val–Orn(Z)–Leu–D–Phe–Pro–MeVal–Orn(Z)–Leu–*) *(XIX).* Compound XVIII (164 mg, 0.1 mmol) was dissolved in TFA (3 ml) at 0 °C. After 20 min, the solution was evaporated, the residual oil was triturated with ether, and the precipitate was collected by filtration (yield, 160 mg). The *N*-hydroxysuccinimide ester trifluoroacetate thus obtained was dissolved in DMF (2 ml), the solution was added drop by drop to pyridine (50 ml) at room temperature, and the mixture was stirred for 12 h and evaporated. The residual oil was dissolved in a mixture (25 ml) of methanol and water (5: 1, v/v), and the solution was passed through columns (1.8×20 cm, each) of Dowex 1 (OH^- form) and Dowex 50 (H^+ form). The columns were washed with the same solvent (500 ml), and the combined effluent was evaporated to leave an oily product which was precipitated by the addition of water (yield, 98 mg). A part (63 mg) of the precipitate dissolved in methanol (1 ml) was applied on a column (1.8×110 cm) with Sephadex LH-20 and the developing was continued with methanol. The fractions with the desired product were evaporated and the residual solid was recrystallized from methanol–ether–petroleum ether; yield, 51 mg (56% from XVIII); mp 218—219 °C; $[\alpha]_D^{20}$ −211° (*c* 0.17, methanol).

Found: C, 63.19; H, 7.45; N, 11.39%; mol wt, 1455.[14] Calcd for $C_{77}H_{106}O_{14}N_{12}\cdot 2H_2O$: C, 63.35; H, 7.60; N, 11.52%; mol wt, 1460.

cyclo(–D–*Phe–Pro–Val–Orn–Leu–D–Phe–Pro–MeVal–Orn–Leu–*)·2*HCl ([MeVal*[1]*]-GS·2HCl) (XX).* Compound XIX (40 mg, 0.028 mmol) dissolved in 0.01 M hydrogen chloride in methanol (7 ml) was hydrogenated using palladium black as a catalyst. After removal of the catalyst, the filtrate was evaporated and the residual oil was precipitated by the addition of 1 M hydrochloric acid (1 ml). The product was recrystallized from ethanol–1 M hydrochloric acid; yield, 24 mg (70%); 226—228 °C; $[\alpha]_D^{20}$ −141° (*c* 0.12, ethanol). Amino acid ratios in acid hydrolyzate; Phe 2.06, Pro 2.10, Val 1.08, Orn 1.92, Leu 2.00.

Found: C, 57.75; H, 7.85; N, 13.21%. Calcd for $C_{61}H_{94}O_{10}N_{12}\cdot 2HCl\cdot 2H_2O$: C, 57.94; H, 7.97; N, 13.30%.

Boc–D–Phe–Pro–MeVal–Orn(Z)–Leu–ONSu (XXI). Compound XV (670 mg, 0.8 mmol) in dioxane (4 ml) was treated with HONSu 184 mg, 1.6 mmol) and WSCI (307 mg, 1.6 mmol) as described for XVIII. The product was reprecipitated from ethyl acetate–ether–petroleum ether; yield, 677 mg (91%); mp 105—107 °C; $[\alpha]_D^{20}$ −67.8° (*c* 0.26, ethyl acetate).

Found: C, 61.33; H, 7.17; N, 10.47%. Calcd for $C_{18}H_{67}O_{12}N_7$: C, 61.72; H, 7.23; N, 10.50%.

Boc–(D–Phe–Pro–MeVal–Orn(Z)–Leu)$_2$–OH (XXII). A solution of XVI (600 mg, 0.78 mmol) and TEA (1.56 mmol) in DMF (3 ml) was treated with XXI (654 mg, 0.7 mmol) in DMF (3 ml) as described for XVII. The product was recrystallized from methanol–ether–petroleum ether; yield, 943 mg (87%); mp 125—127 °C; $[\alpha]_D^{20}$ −46.8° (*c* 0.80, methanol). Amino acid ratios in acid hydrolyzate; Phe 1.02, Pro 1.01, Orn 1.12, Leu 1.00.

Found: C, 63.13; H, 7.73; N, 10.71%. Calcd for $C_{83}H_{118}O_{17}N_{12}\cdot H_2O$: C, 63.33; H, 7.69; N, 10.68%.

Boc–(D–Phe–Pro–MeVal–Orn(Z)–Leu)$_2$–ONSu (XXIII). Compound XXII (902 mg, 0.58 mmol) was converted into the active ester (XXIII) by the method described for XVIII; yield, 865 mg (90%); mp 115—117 °C $[\alpha]_D^{20}$ −70.6° (*c* 0.28, ethyl acetate).

Found: C, 63.00; H, 7.42; N, 10.92%. Calcd for $C_{87}H_{121}O_{19}N_{13}$: C, 63.21; H, 7.38; N, 11.02%.

cyclo(–(D–*Phe–Pro–MeVal–Orn(Z)–Leu)$_2$–*) *(XXIV).* Compound XXIII (826 mg, 0.5 mmol) was treated with TFA (10 ml) and pyridine (500 ml), successively, as described for XIX. The crude product dissolved in a mixture of methanol and water (5: 1, v/v) was treated with Dowex 1 and 50, and an oily product was precipitated by the addition of water (yield, 552 mg). A part (100 mg) of the precipitate dissolved in methanol (20 ml) was purified by column chromatography using Sephadex LH-20 (2.8×158 cm) and the residual solid was recrystallized from methanol–ether–petroleum ether; yield, 86 mg (66% from XXIII); mp 280—285 °C; $[\alpha]_D^{20}$ −50.6° (*c* 0.29, methanol).

Found: C, 64.32; H, 7.56; N, 11.51%; mol wt, 1427.[14] Calcd for $C_{78}H_{108}O_{14}N_{12}\cdot H_2O$: C, 64.35; H, 7.62; N, 11.55%; mol wt, 1438.

cyclo(–(D–*Phe–Pro–MeVal–Orn–Leu)$_2$–*)·2*HCl ([MeVal*[1,1']*-GS·2HCl) (XXV).* Compound XXIV (50 mg, 0.035 mmol) was hydrogenated as in the case of XX; yield, 41 mg (95%); mp 218—220 °C; $[\alpha]_D^{20}$ −51.9° (*c* 0.18, ethanol). Amino acid ratios in acid hydrolyzate; Phe 1.00, Pro 1.05, Orn 1.10, Leu 1.00.

Found: C, 54.25; H, 7.74; N, 11.92%. Calcd for $C_{62}H_{96}O_{10}N_{12}\cdot 2HCl\cdot 7H_2O$: C, 54.40; H, 8.25; N, 12.28%.

Paper Electrophoresis. In order to confirm the purity of the analogs of gramicidin S synthesized, paper electrophoresis was carried out.[15] The peptide (XX and XXV) revealed a single spot, and their mobility were comparable with that of GS·2HCl.

Microbiological Assays. The minimum amount of the compounds necessary for the complete inhibition of growth of several microorganisms was determined by a dilution method using a nutrient agar, the results being shown in Table 1.

ORD Measurements. The measurements were performed on a JASCO spectropolarimeter model ORD/UV-5 over the wavelength range 220—300 nm at an ambient temperature. A cell of path length 0.1 cm was used. Patterns in ethanol and 8 M urea are shown in Figs. 2-a and 2-b, respectively.

The authors wish to express their thanks to Drs. M. Miyoshi and H. Sugano of Tanabe Seiyaku Co. Ltd., Osaka, for their helpful discussions. Thanks are also due to the staff of Institute of Biological Science, Mitsui-Toatsu Chemicals, Inc., Chiba, for the biological assays.

References

1) Part XXXII: S. Matsuura, H. Takiguchi, M. Waki,

and N. Izumiya, *Mem. Fac. Sci. Kyushu Univ., C*, **9**, 277 (1975).

2) T. Kato and N. Izumiya, "Chemistry and Biochemistry of Amino Acids, Peptides, and Proteins," Vol. 2, ed. by B. Weinstein, Marcel Dekker, New York (1974), pp. 1—39.

3) D. C. Hodgkin and B. M. Oughton, *Biochem. J.*, **65**, 752 (1957), and the references cited in Ref. 2.

4) H. Sugano, H. Abe, M. Miyoshi, T. Kato, and N. Izumiya, *Bull. Chem. Soc. Jpn.*, **47**, 698 (1974).

5) N. G. Kumar, N. Izumiya, M. Miyoshi, H. Sugano, and D. W. Urry, *Biochemistry*, **14**, 2197 (1975); *J. Am. Chem. Soc.*, **97**, 4105 (1975).

6) The abbreviations recommended by the IUPAC-IUB Commission of Biochemical Nomenclature (*J. Biol. Chem.*, **247**, 977 (1972)) have been used throughout. Additional abbreviations: DCC, dicyclohexylcarbodiimide; DMF, *N,N*-dimethylformamide; HOBt, 1-hydroxy-benzotriazole; HONSu, *N*-hydroxysuccinimide; MA, mixed anhydride method; TEA, triethylamine; TFA, trifluoroacetic acid; THF, tetrahydrofuran; WSCI, 1-ethyl-3-(3-dimethylaminopropyl)-carbodiimide. Amino acid symbols except D-Phe denote the L-configuration.

7) F. Lipmann, *Acc. Chem. Res.*, **6**, 361 (1973).

8) K. Tanaka, A. Shichiho, and S. Sakakibara, The 20th Ann. Meeting of Chem. Soc. Japan, Tokyo, April, Abst. III, p. 661 (1967).

9) J. R. McDermott and N. L. Benoiton, *Can. J. Chem.*, **51**, 2551, 2562 (1973).

10) T. Kato, M. Waki, S. Matsuura, and N. Izumiya, *J. Biochem.*, **68**, 751 (1970).

11) E. Schnabel, *Justus Liebigs Ann. Chem.*, **702**, 188 (1967).

12) K. Okamoto, H. Abe, K. Kuromizu, and N. Izumiya, *Mem. Fac. Sci. Kyushu Univ., C*, **9**, 131 (1974).

13) G. W. Anderson, J. E. Zimmerman, and F. M. Callahan, *J. Am. Chem. Soc.*, **86**, 1839 (1964).

14) Molecular weight was determined on a Hitachi Osmometer, type 115, using methanol as a solvent.

15) H. Aoyagi, T. Kato, M. Waki, O. Abe, R. Okawa, S. Makisumi, and N. Izumiya, *Bull. Chem. Soc. Jpn.*, **42**, 782 (1969).

Substrate Specificity in the Cyclodextrin-catalyzed Cleavage of Organic Phosphates and Monothiophosphates in Alkaline Solutions

Kazuo MOCHIDA, Yoshihisa MATSUI, Yoshio OTA, Koji ARAKAWA, and Yoshio DATE

Department of Agricultural Chemistry, Shimane University, Nishikawazu, Matsue 690

(Received April 10, 1976)

Cyclodextrin accelerates the phenol release from organic phosphates such as dialkyl 4-nitrophenyl phosphates, but it decelerates the reactions of the corresponding monothiophosphates in alkaline solutions. Each reaction proceeds *via* the prior formation of a cyclodextrin–substrate inclusion complex, followed by the nucleophilic attack of the cyclodextrin alkoxide ion or the hydroxide ion on the reaction site of the included substrate. The equilibrium and kinetic parameters involved in the reaction processes were determined and discussed in connection with the geometry of a cyclodextrin–substrate complex.

Substrate specificity is one of the most important characteristics of enzyme-catalyzed reactions. A little modification in the structure of substrates results in pronounced changes in both the binding and catalytic processes of an enzymatic reaction. A similar feature has been observed in relatively simple enzyme-model systems such as cyclodextrin.[1] For example, the cyclodextrin-induced rate acceleration of the phenol release from *meta*-substituted phenyl acetates is much greater than that from the corresponding *para*-substituted phenyl acetates.[2] The process includes the prior complexation of a substrate with cyclodextrin, and the specific spatial orientation of a substrate in a cyclodextrin complex causes a marked substrate specificity.

During the course of an investigation of the catalytic action of cyclodextrin, we found that the cyclodextrin-catalyzed cleavage of some organophosphorus pesticides in alkaline solutions reveals a characteristic substrate specificity: cyclodextrin accelerates the phenol release from the phosphates, **1a**, **1b**, and **1c**, but decelerates the release from the corresponding monothiophosphates, **2a** and **2b**.

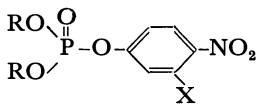

1a: R=CH_3, X=CH_3
1b: R=CH_3, X=H
1c: R=C_2H_5, X=H

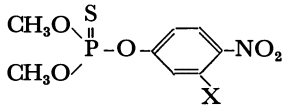

2a: X=CH_3
2b: X=H

The present study was undertaken in order to elucidate the catalytic modes of the cyclodextrin and the hydroxide ion by means of a close determination of the equilibrium and kinetic parameters involved in the reaction processes. The rate effect of cyclodextrin was also examined on the alkaline hydrolysis of a few phenyl acetates, such as *o*- and *m*-acetoxybenzoic acids (**3a** and **3b** respectively), in order to compare the equilibrium and kinetic parameters with those of the organophosphorus compounds.

Experimental

Materials. The α- and β-cyclodextrins were prepared by the method of Lane and Pirt.[3] They were separated and purified according to the directions of Cramer and Henglein.[4] Methyl α-D-glucopyranoside of a reagent grade was used without further purification. 3-Methyl-4-nitrophenol (**4**) was prepared by the method of Koelsch[5] and was purified by means of chromatography on an activated alumina column with benzene, ether, and ether–ethanol (4: 1, v/v) as eluants. The ether and ether–ethanol fractions were collected and concentrated by evaporation. The residue was recrystallized from water. Mp 127—129 °C (lit, mp 128 °C[6]). **1a** was prepared by the reaction of **4** with dimethyl chlorophosphate.[7] Crude **1a** was purified by chromatography on a silica gel column, with hexane, benzene, and ether as eluants. The ether fractions were collected and concentrated by evaporation. The residue was distilled *in vacuo*. **1b** was prepared by the reaction of sodium 4-nitrophenoxide with dimethyl chlorophosphate.[8] The **1c**, **2a**, and **2b** were provided by Sumitomo Chemical Co. and were used without further purification. The purity of these organophosphorus compounds was estimated to be 95% for **1a**, 100% for **1b**, 95% for **1c**, 97% for **2a**, and 94% for **2b** by the spectrophotometric determination at 400 nm of the phenolate anions afforded by the alkaline hydrolysis of the compounds. **3a** of a reagent grade was used without purification. **3b** was prepared by the reaction of *m*-hydroxybenzoic acid with acetic anhydride in dry pyridine and was recrystallized from chloroform.

Kinetics. The reaction rates of the esters were measured by following the appearance of the absorption of the corresponding phenoxide anions at 410 nm for the phosphates and monothiophosphates and at 300 and 310 nm for **3a** and **3b** respectively in aqueous NaOH solutions, the ionic strength (I_c) of which was maintained at 0.65 M with Na_2SO_4. In a typical run, 3.00 ml of a base solution was pipetted into a pair of 1.00-cm quartz cells, one of which was used as a reference cell and the other, as a sample cell in a Hitachi spectrophotometer, Model 124. After thermal equilibrium at 25.0±0.1 °C had been reached, 5 to 15 μl of a 8 to 55 mM ester in ethanol or methanol was added to the sample cell and the change in absorbance was followed. The results for various reaction times were treated according to the ordinary first-order rate equation. The rate constants were graphically determined. All the reactions examined obeyed good first-order kinetics with respect to substrates in both the absence and presence of cyclodextrin.

Determination of the Dissociation Constants and Rate Constants of Cyclodextrin–Substrate Complexes. As is shown in Table 1 as an example, the observed pseudo first-order rate constant (k_{obsd}) for each substrate examined approached a maximum or minimum value as the cyclodextrin concentration ([CD]) is increased. This saturation behavior, as well as the fact that methyl α-D-glucopyranoside had only a slight effect on the reaction rate, suggests that the rate process involves the prior formation of the inclusion complex of cyclodextrin with each substrate. Upon the assumption of the formation of an 1: 1

Table 1. Pseudo-first-order rate constants for the phenol release from **1a** and **2a** in alkaline solutions containing carbohydrates at 25.0 °C and I_c=0.65 M

Carbohydrate	Concn. (mM)	$k_{obsd} \times 10^2$, min^{-1}	
		1a[a]	**2a**[b]
None	—	1.33	3.14
Methyl α-D-glucopyranoside	35.0	1.30	3.06
α-Cyclodextrin	1.00	1.30	2.77
	10.0	1.15	2.65
β-Cyclodextrin	1.00	1.58	2.22
	2.50	1.74	1.64
	5.00	1.96	1.22
	7.50	2.07	1.01
	10.0	2.19	0.87

a) 0.0094 M NaOH. b) 0.20 M NaOH.

cyclodextrin–substrate complex, k_{obsd} is represented by Eq. 1[1,2] if [CD] is much higher than that of a substrate ([S]):

$$k_{obsd} = K_{diss}(k_{un}-k_{obsd})/[CD] + k_c \quad (1)$$

In this equation, K_{diss} is the dissociation constant of an inclusion complex, and k_{un} and k_c, the rate constants for free and complexed substrates respectively. The plot of k_{obsd} *vs.* $(k_{un}-k_{obsd})/[CD]$ was virtually linear for each cyclodextrin–substrate system, and the values of K_{diss} and k_c were calculated from the slope and the intercept of the line respectively.

Calculation of Equilibrium and Kinetic Parameters from the pH Dependence of the Cyclodextrin-rate Effects. We postulated the reaction scheme shown below in order to explain the pH dependence of the cyclodextrin-rate effect:

Equilibrium Processes:

$$\begin{array}{ccc} \text{CDOH} + \text{S} & \overset{K_{diss}}{\rightleftharpoons} & \text{CDOH}\cdot\text{S} \\ K_a \uparrow\downarrow \text{OH}^- & & K_a \uparrow\downarrow \text{OH}^- \\ \text{CDO}^- + \text{S} & \overset{K_{diss}}{\rightleftharpoons} & \text{CDO}^-\cdot\text{S} \end{array}$$

Reaction Processes:

$$\text{S} + \text{OH}^- \xrightarrow{k_f} \text{P}$$

$$\text{CDO}^-\cdot\text{S} \xrightarrow{k_s} \text{P}$$

$$\text{CDOH}\cdot\text{S} + \text{OH}^- \xrightarrow{k_b} \text{P}$$

$$\text{CDO}^-\cdot\text{S} + \text{OH}^- \xrightarrow{k_b} \text{P}$$

where CDOH and CDO^- represent the unionized and ionized cyclodextrins respectively; S, a substrate; P, products; K_a, the first ionization constant of cyclodextrin; k_s, the first-order rate constant for the reaction of a completed substrate with the cyclodextrin alkoxide ion, and k_f and k_b, the second-order rate constants for the reactions of free and complexed substrates respectively with OH^-. We assumed that (1) the ionization of cyclodextrin has approximately no effect on the K_{diss} and k_b values; (2) the inclusion of a substrate also has little effect on the K_s value, and (3) the reaction of a substrate with the unionized cyclodextrin is negligible. Then, the rate constants, k_{un} and k_c, may be represented as is shown below:

$$k_{un} = k_f[OH^-] \quad (2)$$

$$k_c = k_s\{K_a[OH^-]/(K_a[OH^-]+K_w)\} + k_b[OH^-] \quad (3)$$

where K_w is the ion product of water and where the term, $K_a[OH^-]/(K_a[OH^-]+K_w)$, corresponds to the fraction of the ionized cyclodextrin. To calculate the values of k_s, k_b, and K_s in Eq. 3 from the $[OH^-]$ dependence of k_c observed, we used a computerized statistical technique of regression analysis. The calculated values excellently well explained the measured values of k_c at various OH^- concentrations with the correlation coefficients of 0.986 to 0.999, as is illustrated in Figs. 1 and 2.

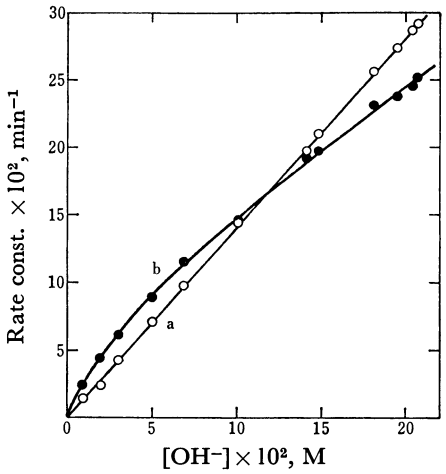

Fig. 1. Plots of k_{un} (a) and k_c (b) *vs.* $[OH^-]$ for **1a** at 25 °C and I_c=0.65 M. The solid lines were computed using the parameters in Table 3 and correspond to the best fit.

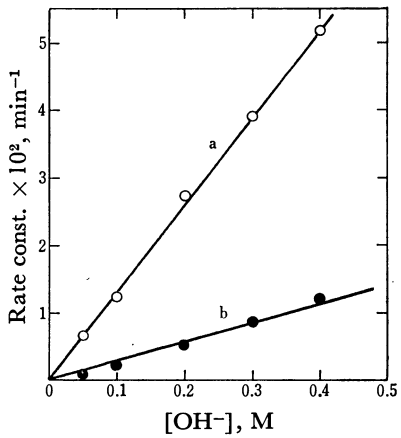

Fig. 2. Plots of k_{un} (a) and k_c (b) *vs.* $[OH^-]$ for **2a** at 25 °C and I_c=0.65 M. The solid lines were computed using the parameters in Table 3 and correspond to the best fit.

Determination of the Dissociation Constant of a Cyclodextrin–4 Complex. A 0.20 M NaOH solution (I_c=0.65 M) containing 1.33×10^{-5} M **4** and 0.0, 1.0, 2.5, 5.0, 7.5, or 10.0 mM α- or β-cyclodextrin was added to a 1.00-cm quartz cell. After the cell had been maintained at 25.0±0.1 °C, the absorption spectrum of each solution was measured by means of a Hitachi Model 124 spectrophotometer. The K_{diss} value was determined on the basis of the well-known equation:[9]

$$[CD][S]/\Delta Abs = K_{diss}/\Delta\varepsilon + [CD]/\Delta\varepsilon \quad (4)$$

where ΔAbs is the decrease in the absorbance at 380 nm of a **4** solution on the addition of cyclodextrin, and $\Delta\varepsilon$, the difference in the molar absorption coefficient at 380 nm between the free and the complexed **4** anions. The plot of $[CD][S]/\Delta Abs$ *vs.* [CD] gave an approximately straight line for a β-cyclodextrin–**4**

system, and the $\Delta\varepsilon$ and K_{diss} values were determined to be 2.8×10^{3} $M^{-1}cm^{-1}$ and 6.5×10^{-3} M respectively from the slope and the intercept of the line. The spectrum of **4** was not changed by the addition of α-cyclodextrin up to 10.0 mM.

Results

The dissociation constants (K_{diss}) of cyclodextrin–substrate-inclusion complexes and the first-order rate constants, k_{un} and k_c, of the free and included substrates respectively were measured or evaluated by the use of Eq. 1; they are summarized in Table 2. The rate effect of α-cyclodextrin on the reactions of **1a**, **2a**, and **2b** was not large enough for the corresponding k_c and K_{diss} values to be determined.

Table 2. Rate constants and dissociation constants for cyclodextrin–organic ester systems at 25.0 °C and I_c=0.65 M

Compound	[OH⁻], M	k_{un}, min^{-1},	k_c, min^{-1},	K_{diss}, mM
		α-Cyclodextrin		
1b	0.019	0.0457	0.076	4.0
1c	0.020	0.0123	0.053	18
3a	0.010	0.116	2.3	23
3b	0.0092	0.686	6.6	10
		β-Cyclodextrin		
1a	0.0094	0.0135	0.024	3.4
1b	0.021	0.0496	0.085	6.3
1c	0.019	0.0120	0.036	11
2a	0.20	0.0314	0.0046	1.9
2b	0.24	0.0591	0.011	1.1
3a	0.010	0.114	0.87	12
3b	0.0069	0.515	2.2	4.4

To learn the role of OH^- in the reactions of the esters, the reaction rates were measured at various alkaline concentrations in the absence and in the presence of cyclodextrin. The resulting rate constants, k_{un} and k_{obsd}, as well as the K_{diss} values given in Table 2, were used to calculate the k_c values at various OH^- concentrations on the basis of Eq. 1. The rate constants, k_c, thus obtained, together with the k_{un} values, were then plotted against [OH^-], as is illustrated in Figs. 1 and 2 for the β-cyclodextrin-**1a** and -**2a** systems respectively. The plot of k_{un} *vs.* [OH^-] for each substrate gave a good straight line through the point of origin. On the other hand, the plot of k_c *vs.* [OH^-] gave a hyperbolic curve for each phosphate or acetate system: The k_c values at lower OH^- concentrations were larger than the corresponding k_{un} values, but the slope of the curve decreased with an increase in the OH^- concentration until it reached a constant value. In some cases, the k_c value became smaller than the corresponding k_{un} value in a high OH^- concentration region (Fig. 1). The k_c values for the monothiophosphates were always smaller than the corresponding k_{un} values and increased linearly with an increase in the OH^- concentration over the whole [OH^-] range studied.

It is impossible to explain these [OH^-] dependencies of k_c in terms of the reaction scheme proposed by Van-Etten *et al.*[10] for cyclodextrin–phenyl benzoate systems. They neglected the contribution of the k_b term to k_c in Eq. 3 and thought $k_c=k_a\{K_a[OH^-]/(K_a[OH^-]+K_w)\}$. Then, k_c should asymptotically approach a constant value of k_a with an increase in the OH^- concentration. This is not the case at present. On the contrary, the [OH^-] dependencies of k_c observed can be well explained by the use of Eq. 3 which involves the k_b term, too. Thus, when [OH^-] is low enough to be $K_a[OH^-]\ll K_w$, k_c in Eq. 3 becomes proportional to [OH^-]:

$$k_c = [(k_aK_a/K_w)+k_b]\cdot[OH^-] \quad (5)$$

When [OH^-] is high enough to be $K_a[OH^-]\gg K_w$,

$$k_c = k_a + k_b[OH^-] \quad (6)$$

This may be the case for the phosphate and acetate systems. If the k_a term is negligibly small compared with the k_b term in Eq. 3, k_c is given by:

$$k_c = k_b[OH^-] \quad (7)$$

This may be the case for the monothiophosphate systems. The actual values of K_a, k_a, and k_b for each reaction system were calculated by means of regression analysis with a computer (Table 3). The solid lines in Figs. 1 and 2 were drawn on the basis of the values in Table 3. They are in excellent agreement with the experimental values with correlation coefficients above 0.999.

Table 3. Equilibrium and kinetic parameters for cyclodextrin–organic ester systems at 25.0 °C and I_c=0.65 M

Compound	pK_a	k_f ($min^{-1}M^{-1}$)	k_a (min^{-1})	k_b ($min^{-1}M^{-1}$)	k_a/k_f (M)	k_b/k_f
			α-Cyclodextrin			
1b	11.4	2.42	0.024	2.67	0.001	1.11
1c	12.4	0.625	0.105	0.38	0.17	0.61
3a	12.1	11.6	6.52	0.00	0.56	0.00
3b	12.3	74.6	21.0	17.0	0.28	0.23
			β-Cyclodextrin			
1a	12.6	1.41	0.087	0.86	0.062	0.61
1b	12.4	2.42	0.113	1.32	0.047	0.55
1c	12.1	0.625	0.051	0.23	0.081	0.36
2a	—	0.130	0.000	0.029	0.000	0.22
2b	—	0.233	0.000	0.047	0.000	0.20
3a	12.3	11.6	2.83	4.45	0.25	0.38
3b	12.3	74.6	8.70	42.3	0.12	0.57

Discussion

The rates of the phenol release from the phosphates, monothiophosphates, and acetates in the absence of cyclodextrin showed a first-order dependence on the substrates and also on OH^-. The reactions may involve a nucleophilic attack of OH^- at the phosphorus atoms of the phosphates and monothiophosphates or at the carbonyl carbon atoms of the acetates. The water-catalyzed hydrolysis of the esters may be negligible under the present reaction conditions.

Both α- and β-cyclodextrins significantly affected the reaction rates of the esters, while methyl α-D-glucopyranoside did not. This fact, as well as the fact that the rate effect is saturated with an increase in the cyclodextrin concentration, indicates that the prior formation of an inclusion compound between cyclodextrin and a substrate is essential to the rate effect.

A marked substrate specificity was found for the cyclodextrin-catalyzed cleavage of the esters studied. Thus, β-cyclodextrin accelerates the phenol release from the **1a**, **1b**, and **1c** phosphates and the **3a** and **3b** acetates at low OH^- concentrations, while it decelerates the corresponding reactions of the monothiophosphates, **2a** and **2b**. α-Cyclodextrin also accelerates the phenol release from the **1b** and **1c** phosphates and the **3a** and **3b** acetates, whereas it only slightly decelerates the corresponding reactions of **1a**, **2a**, and **2b**.

These specific rate effects of α- and β-cyclodextrins may be related to the stereochemistry of cyclodextrin–substrate complexes.[1,2] Thus, a spectrophotometric study (see the Experimental section), together with a study with the Corey-Pauling-Koltum scale molecular models, suggests that the 3-methyl-4-nitrophenyl moiety of **1a** or **2a** is too large to be included in the α-cyclodextrin cavity, but it is small enough to be included in the β-cyclodextrin cavity. The 4-nitrophenyl moiety of **1b**, **1c**, or **2b** and the carboxyphenyl moiety of **3a** or **3b** are small enough to be included in both the α- and β-cyclodextrin cavities.[2] Therefore, the relatively small effect of α-cyclodextrin on the rates of the reactions of **1a** and **2a** may be due to the binding to the α-cyclodextrin cavity of the parts other than the 3-methyl-4-nitrophenyl moiety of the substrate molecules. In such cases, the reaction sites of the substrates may be located too far from the catalytic site of α-cyclodextrin for them to react with each other.

The kinetic and equilibrium parameters determined by the regression analysis of the $[OH^-]$ dependency of k_c also serve as a basis for speculation about the geometry of a cyclodextrin-substrate complex. As VanEtten *et al.*[2] suggested, the ratio of k_a/k_f may be a measure of the proximity between the reaction site of a substrate and the catalytic site (the alkoxide ion) of cyclodextrin in a cyclodextrin-substrate complex. Furthermore, the ratio of k_b/k_f may depend on how much the reaction site of an included substrate is protected from the nucleophilic attack of OH^- compared with the free substrate.

The k_a/k_f values for β-cyclodextrin–monothiophosphate systems are virtually zero, and the k_b/k_f values for these systems are significantly smaller than those for β-cyclodextrin–phosphate systems. This fact suggests that the phosphorus atoms of the monothiophosphates are located in the middle of the cyclodextrin cavity. The electronegativity of sulfur (2.44[11]) is less than that of oxygen (3.50[11]), and the atomic radius of sulfur (1.27 Å[11]) is larger than that of oxygen (0.6 Å[11]). Therefore, the monothiophosphate group may be more hydrophobic than the corresponding phosphate group, and the former may be included more deeply in the β-cyclodextrin cavity than the latter. This presumption is supported by the fact that the inclusion complexes of β-cyclodextrin with monothiophosphates are more stable than those with the corresponding phosphates (compare the K_{diss} values in Table 2). On the other hand, the phosphorus atoms of the phosphates or the carbonyl carbon atoms of the acetates may be located in the vicinity of the secondary hydroxyl groups which are arranged around one edge of the torus of cyclodextrin. Hence, the k_a/k_f values are appreciably large for the phosphates and the acetates. The k_a/k_f values for α-cyclodextrin–phosphate and –acetate systems are generally larger than those for the corresponding β-cyclodextrin systems. This fact may be a result of the size of α-cyclodextrin being smaller than that of β-cyclodextrin.[2]

The pK_a values determined for various cyclodextrin–organic ester systems varied within a relatively small range of 12.1 to 12.7, with the one exception of pK_a= 11.4 for an α-cyclodextrin–**1b** system. VanEtten *et al.*[10] and Van Hooidonk and Groos[12] also estimated the pK_a value of α-cyclodextrin to be 12.1 and 12.6 respectively. The small variation in the pK_a value may be due either to experimental error or to a substrate-induced pK_a change, such as has often been observed for enzyme systems. Further accurate experiments may be necessary to determine which of them is the case.

Only in the case of an α-cyclodextrin–**1b** system is the pK_a value unusually small and the k_b/k_f value unusually large. A study with the scale molecular models suggested the possibility that the phosphonyl oxygen (>P→O) of **1b** included in α-cyclodextrin is located in the vicinity of one of the secondary hydroxyl groups of α-cyclodextrin close enough to form the hydrogen bonding between them. Upon the formation of such bonding, the acid dissociation of the cyclodextrin hydroxyl group may be facilitated, and at the same time the ester linkage of the substrate may be weakened to make it susceptible to the nucleophilic attack of OH^-. Cramer *et al.*[13,14] have also postulated the formation of hydrogen bonding between cyclodextrin and a substrate to explain the catalytic effect of cyclodextrin. However, the definite meaning of k_b/k_f remains to be ascertained.

The authors wish to acknowledge the technical assistance afforded by Messrs. Yoriyoshi Asano, Takashi Doi, and Tamotsu Shimizu.

References

1) D. W. Griffiths and M. L. Bender, *Adv. Catal.*, **23**, 209 (1973).

2) R. L. VanEtten, J. F. Sebastian, G. A. Clowes, and M. L. Bender, *J. Am. Chem. Soc.*, **89**, 3242 (1967).

3) A. G. Lane and S. J. Pirt, *J. Appl. Chem. Biotechnol.*, **21**,

330 (1971).
4) F. Cramer and F. M. Henglein, *Chem. Ber.*, **91**, 308 (1958).
5) C. F. Koelsch, *J. Am. Chem. Soc.*, **66**, 2019 (1944).
6) W. J. Hickinbottom, "Chemistry of Carbon Compounds," Vol. 3, ed. by E. H. Rodd, Elsevier, Amsterdam (1951), p. 445.
7) W. Lorenz and G. Schrader, Belg. Pat. 609802 (1962); *Chem. Abstr.*, **58**, 11402e (1963).
8) A. M. DePoos and H. J. Toet, *Rec. Trav. Chim. Pays-Bas*, **77**, 946 (1958).
9) F. Cramer, W. Saenger, and H. -Ch. Spatz, *J. Am. Chem. Soc.*, **89**, 14 (1967).
10) R. L. VanEtten, G. A. Clowes, J. F. Sebastian, and M. L. Bender, *J. Am. Chem. Soc.*, **89**, 3253 (1967).
11) A. J. Gordon and R. A. Ford, "The Chemist's Companion," John Wiley & Sons, New York (1972), pp. 84—85.
12) C. Van Hooidonk and C. C. Groos, *Rec. Trav. Chim. Pays-Bas*, **89**, 845 (1970).
13) F. Cramer and W. Kampe, *J. Am. Chem. Soc.*, **87**, 1115 (1965).
14) N. Hennrich and F. Cramer, *J. Am. Chem. Soc.*, **87**, 1121 (1965).

The Thermal Decomposition of *N*-Thiocarbonyl Diphenylsulfimides

Hiroshi Yoshida, Hitoshi Taketani, Tsuyoshi Ogata, and Saburo Inokawa

Department of Synthetic Chemistry, Faculty of Engineering, Shizuoka University, Johoku, Hamamatsu 432

(Received April 19, 1976)

N-Thiocarbonyl diphenylsulfimides, Ia—i (R = Ph, *p*- and *m*-MeC_6H_4, *p*- and *m*-$MeOC_6H_4$, MeO, EtO, MeNH, and Me_2N), were prepared, and their thermal decomposition were studied. At 70 °C, Ia—h decomposed easily to give nitriles (or their derivatives), together with diphenyl sulfide and sulfur. Contrary to these results, the oxygen analog of Ia, g showed no decomposition even upon heating at 140 °C. The thermolysis of Ia—e in the presence of excess acetylenes(III) gave isothiazoles(IV) in moderate yields. Thiazirine(V) and nitrile sulfide(VI) may be supposed, on the basis of the kinetic experiments, to be possible intermediates for the thermal decomposition of Ib—e.

Recently a number of workers have reported on the preparation and reactions of free sulfimides[1-3] and their *N*-substituted derivatives, such as *N*-acetyl,[2,4,5] and *N*-tosyl.[3,6,7] In the course of our studies of the thiocarbonyl-stabilized *P*- and *S*-ylides and imides, we have found an interesting thermal decomposition of *N*-thiocarbonyl diphenylsulfimides(I):

$$Ph_2S{=}N{-}C(=S)R$$

I

We wish to report here on the thermal decomposition of I in the presence and in the absence of acetylenes(III).

Results and Discussion

It has been reported that free diphenylsulfimide reacts with acylating reagents, such as acid chloride and acid anhydride, to give *N*-acylsulfimides.[1,2] Here we have found the reactions of free diphenylsulfimide with methyl dithiobenzoates and xanthates to give *N*-thiocarbonyl substituted sulfimide(I) in moderate yields. The results are shown in Table 1. The sulfimides, Ia—e, decomposed slowly, even at room temperature.

The thermal decomposition of some sulfimides which have α- or β-hydrogen has been studied.[4-6] The thermolysis of *N*-acetyl dialkylsulfimide having β-hydrogen gives olefin and *N*-(alkylthio)acetamide.[4,5] However, *N*-acetyl dimethylsulfimide gives dimethyl sulfide, bis-(methylthio)methane, *N*,*N*′-methylenebisacetamide, and *N*,*N*′,*N*″-methylenetrisacetamide, which are formed by a mechanism involving a Pummerer-type rearrangement.[4,5]

N-Benzoyl and ethoxycarbonyl diphenylsulfimides (oxygen analogs of Ia and Ig) were highly stable, and did not decompose even under heating at 140 °C for 10 h. Contrary to these results, *N*-thiocarbonyl sulfimides(I) were thermally unstable, as is shown in Table 1. All the reaction products were identified by comparing their NMR and IR spectra with those of the authentic samples. Generally *N*-thiocarbonyl sulfimides(I) decomposed to give nitriles(II) (or their derivatives), together with diphenyl sulfide and sulfur. The thermolysis of If and Ig gave methyl and ethyl cyanates respectively as the initial products (NMR observation),

$$Ph_2S{=}N{-}C(=S)R \longrightarrow RCN + Ph_2S + (1/8)S_8$$

I II

but they easily rearranged to isocyanates and trimerized to tri(alkyl isocyanates). The instability of alkyl cyanates is well known.[8]

The thermolysis of Ia—e in the presence of excess acetylenes(III) gave isothiazoles(IV), together with nitrile(II), diphenyl sulfide, and sulfur. The structure of IV was confirmed by comparing the NMR and IR spectra with those of the authentically prepared samples and by elemental analyses (Table 2).

Table 1. Preparation and thermal decomposition of I

	R	Acylating reagent	Yield (%)	Mp (°C)	NMR (δ in $CDCl_3$) R[a]	Thermal decomposition at 70°C: Solvent	Time (min)	Product[b] (Yield %)
Ia	Ph	RCS_2Me	38	109—112		PhH	5	RCN(95)
Ib	*p*-MeC_6H_4	RCS_2Me	58	107	2.38(Me)	PhH	5	RCN(93)
Ic	*m*-MeC_6H_4	RCS_2Me	45	90—91	2.34(Me)	PhH	5	RCN(96)
Id	*p*-$MeOC_6H_4$	RCS_2Me	45	117—119	3.80(MeO)	PhH	5	RCN(97)
Ie	*m*-$MeOC_6H_4$	RCS_2Me	49	68—70	3.74(MeO)	PhH	5	RCN(95)
If	MeO	RCS_2Me	37	87—88	4.02(Me)	PhH	15	$(MeNCO)_3$(67), MeNCO(27)
Ig	EtO	RCS_2Me	34	78—79	1.37(t, Me, J=7) 4.45(q, CH_2)	PhH	15	$(EtNCO)_3$(45), EtNCO(37)
Ih	MeNH	MeNCS	44	130—131	3.03 (d,Me, J=5) 6.35(d, H)	$CHCl_3$	200	$(MeNHCN)_3$(75)
Ii	Me_2N	RCSCl	42	156—157	3.35(Me_2N)	$CHCl_3$	900	Recovery

a) Phenyl ring protons were observed at 6.7—8.5 as multiplets. b) Diphenyl sulfide and sulfur were obtained in quantitative yields.

Table 2. Physical properties of isothiazoles IV

	IV Ar	IV R′	Mp (°C)[a]	MS (M^+)	Anal % Found (Calcd) C	H	N	NMR (δ in $CDCl_3$)
IVa	Ph	CO_2Me[b]	73(A)	277	55.87 (56.32)	3.92 (4.00)	4.87 (5.05)	3.82 (s, MeO), 3.84 (s, MeO), 7.1—7.7 (m, Ar)
	Ph	COPh	149—150(B)	369	75.11 (74.79)	4.05 (4.09)	3.72 (3.79)	7.2—8.5 (m, Ar)
IVb	*p*-MeC_6H_4	CO_2Me[c]	91—92(A)	291	57.48 (57.73)	4.58 (4.50)	4.62 (4.82)	2.33 (s, Me), 3.83 (s, MeO), 3.84 (s,MeO), 6.9—7.5 (m, Ar)
	p-MeC_6H_4	COPh	142—143(B)	383	75.19 (75.18)	4.21 (4.47)	3.67 (3.65)	2.20 (s, Me), 6.9—8.0 (m, Ar)
IVc	*p*-$MeOC_6H_4$	CO_2Me	88—90(A)	307	54.65 (54.72)	3.93 (4.26)	4.03 (4.56)	3.63 (s, MeOPh), 3.73 (s, 2MeOCO) 6.7—7.5 (m, Ar)
	p-$MeOC_6H_4$	COPh	166—168(B)	399	72.30 (72.17)	4.13 (4.29)	3.49 (3.51)	3.57 (s, MeO), 6.7—7.8 (m, Ar)

a) Recrestallization solvents: A petroleum ether; B benzene-petroleum ether. b) Lit,[9,10] mp 72—73°C. c) Lit,[9] mp 90—91 °C.

Table 3. Effect of the concentration of III ($R'=CO_2Me$) on the product composition (IIb: IVb) for the thermal decomposition of Ib benzene at 50 °C

Ib mol/l	III($R'=CO_2Me$) mol/l	Ib/III	IVb($R'=CO_2Me$): IIb
0.130	0.106	0.815	25:75
0.100	0.132	1.32	25:75
0.130	0.201	1.55	27:73
0.144	0.482	3.34	28:72

Table 4. The effect of the substituents of I and III on the product composition (II: IV) for the decomposition of Ib—e in benzene I: 0.05—0.30 mol/l, III: 0.13—0.7 mol/l.

Temp (°C)	III R′	Ib IIb:IVb	Ic IIc:IVc	Id IId:IVd	Ie IIe:IVe
50	COPh	54:46	48:52	51:49	48:52
	CO_2Me	73:27	70:30	72:28	66:34
	Ph	100:0	100:0	100:0	100:0
35	COPh	54:46			

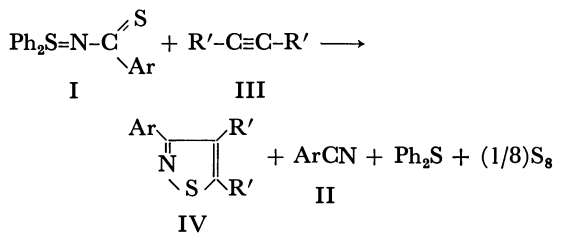

Tables 3 and 4 show the effects of the concentrations and the substituents of I and III on the product compositions, II: IV, as determined by means of the NMR spectrum. The total yields(II+IV) were quantitative, and the II: IV ratios were independent of the concentration of III.

On ultraviolet irradiation in the presence of acetylenedicarboxylate, 4-aryl-1,3,2-oxathiazoline 5-oxides give isothiazole derivatives, together with nitrile and sulfur.[9] Thiazirine and nitrile sulfide are supposed to be intermediates for this photolysis. It has also been reported that benzonitrile sulfide is a possible intermediate for the thermolysis of 5-phenyl-1,3,4-oxathiazol-2-one in the presence of dimethyl acetylenedicarboxylate to give an isothiazole derivative.[10] We similarly supposed that nitrile sulfide was a probable intermediate for the thermolysis of Ia—e.

We have performed kinetic experiments to find a possible mechanism for the thermal decomposition of I. The decomposition of I gave a good first-order rate constant(k_1), as followed by NMR spectroscopy, and k_1 was independent of the concentration of I(0.08—0.25 mol/l). The results are summarized in Table 5. The effects of solvents and substituents ($\rho=+0.22$ to Hammett's σ in benzene at 50 °C) are very small, and positive activation entropies are observed.

Table 5. First-order rate constants for the thermal decomposition of Ib—f

I	Temp (°C)	Solvent	$k_1\times10^4$ s^{-1} [a]	
Ib	50.0	PhH	3.43	E_a=24.8kcal/mol
	43.0	PhH	1.47	ΔS=13.2eu
	34.5	PhH	0.377	
	50.0	PhCN	3.07	
	50.0	$PhNO_2$	2.90	
	50.0	*o*-$C_6H_4Cl_2$	3.84	
Ic	50.0	PhH	3.76	
Id	50.0	PhH	2.94	
	50.0	PhCN	2.63	
Ie	50.0	PhH	3.91	
If	60.2	PhH	5.55	E_a=29.3kcal/mol
	50.0	PhH	1.46	ΔS=13.5eu
	43.0	PhH	0.50	

a) Errors are within 5%.

When the reaction of Ib with III(R′=COPh) was carried out in a benzene solution, and followed by NMR spectroscopy, the product ratio, IIb/IVb (R′=COPh), was nearly constant while the reaction proceeded. Two representative kinetic runs are shown in Table 6, and the results are collected in Table 7. The results in the table indicate that k_{disapp}(I) is equal to k_{app}(II)+k_{app}(IV), that k_{app}(II) is constant in either the presence orabsence of III, and that, moreover, k_{app}(IV) is unaffected by the concentration of III, but highly de-

Table 6. Examples of the reaction of Ib with III (R=COPh) in benzene at 50 °C as followed by the NMR spectral changes of the methyl signals of Ib, IIb, and IVb (R′=COPh)

Example A. Initial concn: Ib 0.150; III (R′=COPh) 0.126 mol/l.

Time (min)	Composition (%) Ib	IIb	IVb	IIb/IVb	Disapp. Ib $k_1\times10^4$ s^{-1}
6	77.9	11.8	10.3	1.15	6.94
11	63.6	20.1	16.3	1.23	6.86
16	52.4	26.1	21.6	1.21	6.73
21	44.4	30.1	25.5	1.18	6.44
26	36.1	33.6	30.3	1.11	6.53
31	30.0	38.1	32.0	1.19	6.47
150	0.0	53.8	46.2	1.17	
		Aver.		1.18±0.03	6.73±0.21

k_{app}(IIb) $=3.64\pm0.11\times10^{-4}$ s^{-1}
k_{app}(IVb) $=3.09\pm0.10\times10^{-4}$ s^{-1}

Example B. Initial concn: Ib 0.123; III (R′=COPh) 0.260 mol/l.

Time (min)	Composition (%) Ib	IIb	IVb	IIb/IVb	Disapp. Ib $k_1\times10^4$ s^{-1}
8	70.4	16.5	13.1	1.26	7.31
13	59.2	22.4	18.4	1.22	6.72
23	42.7	31.7	25.6	1.24	6.17
29	34.2	35.6	30.3	1.17	6.17
37	25.3	40.4	34.3	1.18	6.19
150	0.0	54.5	45.5	1.20	
		Aver.		1.21±0.03	6.51±0.45

k_{app}(IIb) $=3.57\pm0.24\times10^{-4}$ s^{-1}
k_{app}(IVb) $=2.94\pm0.21\times10^{-4}$ s^{-1}

Table 7. Representative rate data for the decomposition of Ib, c in benzene at 50 °C

	III R′	Concn I mol/l	Concn III mol/l	Disapp. I $k_1\times10^4$ s^{-1}	App. II $k_1\times10^4$ s^{-1}	App. IV $k_1\times10^4$ s^{-1}
Ib	—	0.142		3.43	3.43	
	COPh	0.150	0.126	6.73	3.65	3.08
	COPh	0.123	0.260	6.51	3.57	2.94
	CO_2Me	0.133	0.116	4.72	3.47	1.25
	CO_2Me	0.133	0.244	5.06	3.61	1.44
	Ph	0.138	0.210	3.51	3.51	0.0
Ic	—	0.145		3.76	3.76	
	COPh	0.163	0.223	8.01	3.78	4.32

pendent on the electrophilic activity of III (R″: PhCO >MeOCO>Ph) as dipolarophiles with nitrile sulfides.

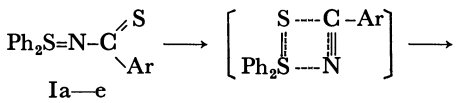

Ia—e

$$ArCN + Ph_2S{=}S \longrightarrow Ph_2S + (1/8)S_8$$

II

The explanation that II is formed by a simple four-membered cyclic transition state seems improbable,

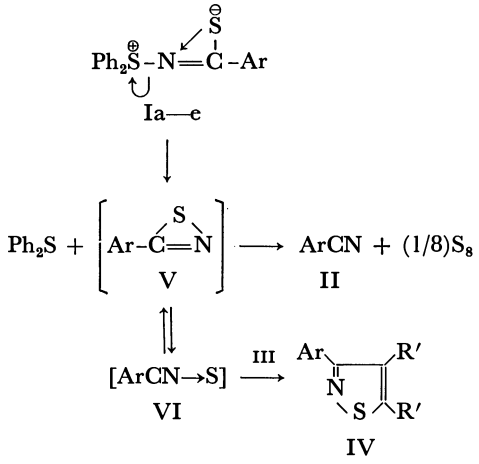

Scheme 1.

since the thermolysis of I showed positive activation entropies (Table 5) and I gave IV in the presence of III.

The mechanism we suggest is shown in Scheme 1: the initial formation of thiazirine(V), followed by two reaction paths. One is a rate-limiting cheletropic reaction of V to give II and sulfur, while the other is the ring opening of V to afford nitrile sulfide(VI), which then undergoes 1,3-dipolar cycloaddition to acetylene(III). A direct path from VI to yield II seems improbable, since rate for the appearance of II(k_{app} (II)) was unaffected by the III added (Table 7). Thus, we propose a rapid equilibrium between V and VI.

Another possible mechanism or intermediate is the formation of thiocarbonyl nitrene(VII), followed by the formation of thiazirine(V):

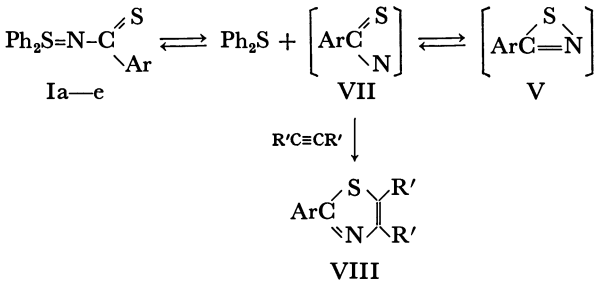

Ia—e VII V

VIII

Acyl nitrenes have proposed as intermediates in the Curtius rearrangement of carbonyl azides to isocyanates.[11] Some addition reactions of acyl nitrenes with sulfoxides, olefins, and acetylenes have been reported.[11] At present we have no positive evidence for the existence of the intermediate(VII). In the thermolysis of Ia—e, no isothiocyanate was observed. No addition product was isolated from the attempted reaction of Ib with dimethyl sulfoxide, cyclohexene, dimethyl fumarate, and maleate. Moreover, the result that the reaction of Ia—e with acetylenes gave isothiazoles, not thiazoles-(VIII), seems to show an intermediate(VII) having no possibility of existence or any significant lifetime.

Experimental

Preparation of Ia—i. Free diphenylsulfimide was prepared according to the literature.[3] A general procedure for the preparation of I is as follows: a mixture of diphenylsulfi-

mide (2.01 g (0.01 mol)) and methyl dithiobenzoate (2.02 g (0.012 mol)) in 50 ml of dry benzene was stirred for 3 h at room temperature. The resulting solution was treated with charcoal, and condensed *in vacuo* to give an oil, which gave needles Ia from benzene–hexane (without heat). Similarly, Ia—h were prepared in moderate yields.

Ii was prepared as follows: to a solution of diphenylsulfimide (2.01 g (0.01 mol)) and 0.9 g (0.012 mol) of pyridine in dry ether (30 ml), we slowly added 1.23 g (0.01 mol) of dimethylthiocarbamoyl chloride in ether (30 ml) at room temperature. After the mixture was stand for 4 h, the oily precipitate was separated and the resulting solution was dried *in vacuo* to give a crystalline mass, which afforded needles (Ii) from ethyl acetate–petroleum ether. The physical properties are shown in Table 1.

Thermal Decomposition of I. All the reactions were followed by NMR spectroscopy and TLC. The reaction products were identified by comparing their NMR and IR spectra with those of the authentic samples. The yields of the products were determined by VPC (IIa—e) or NMR (IIf—h), using mesityrene as the internal standard. The thermal decomposition of If, g in benzene was followed by NMR spectroscopy. The methyl signal of If, which appeared at δ 4.14, decreased in its intensity, giving new three peaks at 2.25 (MeNCO), 2.56 (MeOCN), and 3.08 [$(MeNCO)_3$]. Finally, the signals at 4.14 and 2.56 disappeared entirely. Similarly, on the thermolysis of Ig a methylene quartet (J=7 Hz) at 4.14 for Ig gave methylene quartets at 2.20(EtNCO), 3.31 (EtOCN), and 3.74 [$(EtNCO)_3$].

The yields of the products are collected in Table 1.

Thermal Decomposition of Ia—e in the Presence of Acetylene-(III). All the reactions were followed by means of the NMR spectral changes. The product compositions, II: IV were obtained by NMR spectroscopy. The isothiazoles were separated as follows: the resulting mixture was condensed *in vacuo*, and elemental sulfur was precipitated by the addition of petroleum ether. The subsequent condensation of the petroleum ether solution *in vacuo* (100 °C/1 Torr) afforded an oil which gave crystals upon the addition of a small amount of petroleum ether. The physical properties and analytical results of isothiazoles (IV) are collected in Tables 2 and 3.

Attempted Reactions of Ib with Olefins and DMSO. The reactions were followed by means of the NMR spectral changes. A solution of Ib (15 mg) and dimethyl fumarate or maleate or cyclohexene (30 mg) in benzene (0.4 ml) was heated in an oil bath at 70 °C for 15 min. The product was *p*-tolunitrile.

A solution of Ib (20 mg) in DMSO (0.5 ml) was heated at 70 °C for 20 min. Then the solution was quenched in 5 ml of water and extracted with 1 ml of chloroform. The extract was dried over sodium carbonate, and the product was found by NMR and VPC analyses to be a mixture of *p*-tolunitrile and diphenyl sulfide.

Kinetic Studies. A solution of I (0.05—0.25 mol/l) and III (0.0—0.45 mol/l) in dry benzene (or other solvents) was sealed in an NMR sample tube; the rate was followed at suitable time intervals by analyzing the NMR spectra of the methyl groups of I, II, and IV. The results are summarized Tables 5—7.

References

1) N. Furukawa, T. Yoshimura, T. Omata, and S. Oae, *Chem. Ind. (London)*, **1974**, 702.

2) Y. Tamura, K. Sumoto, H. Matsushima, H. Taniguchi, and M. Ikeda, *J. Org. Chem.*, **38**, 4324 (1973).

3) N. Furukawa, T. Omata, T. Yoshimura, T. Aida, and S. Oae, *Tetrahedron Lett.*, **1972**, 1619.

4) H. Kise, G. F. Whitfield, and D. Swern, *J. Org. Chem.*, **37**, 1125 (1972); *Tetrahedron Lett.*, **1971**, 1761.

5) G. F. Whitfield, H. S. Beilan, D. Saika, and D. Swern, *Tetrahedron Lett.*, **1970**, 3543.

6) S. Oae, K. Harada, K. Tsujihara, and N. Furukawa, *Bull. Chem. Soc. Jpn.*, **46**, 3482 (1973), and the references cited therein.

7) T. Aida, N. Furukawa, and S. Oae, *Chem. Lett.*, **1975**, 29.

8) K. A. Jensen and A. Holm, *Acta Chem. Scand.*, **18**, 826 (1964); K. A. Jensen, M. Due, and A. Holm, *ibid.*, **19**, 438 (1965).

9) H. Gotthardt, *Tetrahedron Lett.*, **1971**, 1277; *Chem. Ber.*, **105**, 188 (1972).

10) J. E. Franz and L. L. Black, *Tetrahedron Lett.*, **1970**, 1381; R. K. Howe and J. E. Franz, *J. Chem. Soc., Chem. Commun.*, **1973**, 524.

11) W. Lwowski, ed., "Nitrenes," Interscience Publishers, New York (1970).

The Preparation and Reactions of α-Thiocarbonyl Dimethyloxosulfonium Ylides

Hiroshi YOSHIDA, Terutaka YAO, Tsuyoshi OGATA, and Saburo INOKAWA

Department of Synthetic Chemistry, Faculty of Engineering, Shizuoka University, Johoku, Hamamatsu 432

(Received April 19, 1976)

α-Thiocarbonyl dimethyloxosulfonium ylides IIIa—e were prepared in moderate yields. The ester-stabilized ylides, IIIa—c, were mixtures of *E* and *Z* isomers, and IIIe was *Z*. The methylation of III with methyl iodide gave *S*-methylated products, IV, in quantitative yields. The thermal decomposition of IVa and IVe gave I(R=Me) and V respectively in good yields. The treatment of IIIb—e with carbon disulfide afforded 1,2-dithiole-3-thiones VIIIb—e in moderate yields.

The physical and chemical properties of carbonyl-stabilized sulfur ylides, such as I and II, have been widely studied in recent years.

I II

In the course of our studies of α-thiocarbonyl-stabilized[1] *P*- and *S*-ylides and imines, we have found interesting results on α-thiocarbonyl-stabilized dimethyloxosulfonium ylides, III. Here we will report our experimental observations of the structure and reactions of III. Some α-thiocarbonyl-stabilized sulfonium ylides are isolated as unstable compounds.[2]

Results and Discussion

Preparation of Ylides, III. A number of carbonyl-stabilized ylides, I, have previously been prepared from dimethyloxosulfonium methylide with such acylating reagents as acid chloride, acid anhydride, and alkyl carboxylate.[3] However, the reaction of dimethyloxosulfonium methylide with such thionoesters as dimethyl trithiocarbonate or methyl dithiobenzoate gives olefinic products.[4] We also could not isolate any ylide from the reaction of dimethyloxosulfonium methylide with alkyl xanthates. However, the action of the methylide with thioacylating reagents, such as xanthic anhydride, tetramethylthiuram monosulfide, and thiobenzoyl chloride, afforded α-thiocarbonyl dimethyloxosulfonium methylides, IIIa—e, in moderate yields (Table 1). The use of good leaving groups may give the expected products.

IIIa—e

a b c d e

R: MeO EtO *i*-PrO Me_2N Ph

X=RCS_2 or Cl

Structure and Methylation of IIIa—e. Evidence for the resonance interaction of ylide carbanion with a thiocarbonyl group can be obtained by an examination of the infrared spectra of thioacyl ylides, III. The S=O and C=S streching frequencies of III occurred at 1020—1030 and 1160—1190 cm^{-1} respectively, as is shown in Table 1. Considering the C=S stretching frequencies of the model compounds (*O*-ethyl thioacetate (1250—1260 cm^{-1}),[5] diaryl thioketone (≈1220 cm^{-1}),[6] dialkyl thioketones (≈1260 cm^{-1}),[7] *N*,*N*-dimethylthioacetamide(1122 cm^{-1})[8]], the shift of 50—100 cm^{-1} for IIIa—c,e may be attributed to the increased single-bond character to the delocalization of the carbanion electrons through the thiocarbonyl groups (*i.e.*, betain forms). A shift to the higher frequency for IIId may diminish the

Table 1. Preparation of III's and their physical properties

		IIIa	IIIb	IIIc	IIId	IIIe
Acylating reagent		$(MeOCS)_2S$	$(EtOCS)_2S$	$(i\text{-}PrOCS)_2S$	$(Me_2NCS)_2S$	PhCSCl
Yield (%)		35	60	60	38	30
Mp (°C)		67.5—70.5	76.5—78.5	120.5—122	124—125	140
IR (KBr) cm^{-1}	$\nu_{S=O}$	1030	1025	1025	1015	1020
	$\nu_{C=S}$	1125	1145	1135	1165	1180
NMR ($CDCl_3$)	Conf.	*Z* *E*	*Z* *E*	*Z* *E*	*Z*	*Z*
	(%)	33 67	30 70	28 72	100	100
	CH	5.21 4.90	5.20 4.88	5.16 4.80	4.18	6.04
	$SOMe_2$	3.35 3.63	3.38 3.68	3.32 3.68	3.72	4.12
	R	3.98 3.87	4.59q 4.41q	5.57sept	3.24	7.7—8.3m
	(*J*(Hz))		1.44t 1.32t (7.0) (7.0)	1.41d 1.27d (6.5) (6.5)		
Found (%) (Calcd)	C	36.01 (36.12)	39.79 (39.97)	43.38 (43.27)	40.25 (40.19)	56.33 (56.57)
	H	6.15 (6.06)	6.80 (6.71)	7.40 (7.26)	7.16 (7.31)	5.54 (5.70)
	N				7.59 (7.81)	

Table 2. Physical properties of IV

		IVa		IVb		IVc		IVd	IVe
Mp (°C)		114—5		108—9		96—8		126—8	104—6
Conf.		*Z*	*E*	*Z*	*E*	*Z*	*E*	*Z*	*Z*
(%)		42	58	39	61	26	74	100	100
NMR δ	CH	6.62	6.13	6.64	6.24	6.68	6.28	5.86	7.15
	$SOMe_2$	4.08	4.03	4.12	4.08	4.04	3.99	3.98	4.39
	SMe	2.47	2.77	2.49	2.78	2.40	2.75	2.50	2.23
	R	4.18	4.15	4.48q	4.51q		5.03sept	3.35	7.4—7.9m
	(*J*(Hz))			1.48t (7.0)	1.50t (7.0)	1.54d (6.5)	1.48d (6.5)		

double-bond character of the thioamide resonance form, $^{\ominus}S\rangle C{=}\overset{\oplus}{N}Me_2$. This observation accords with the appearance of only one peak for two *N*-methyl groups in the NMR spectrum of IIId.[9]

The structure of the III ylide was confirmed on the basis of NMR spectroscopic studies and methylation reaction. These ylides, IIIa—e, reacted easily with methyl iodide to give only *S*-methylation products, IVa—e, in good yields. IIIa—c were mixtures of *E* and *Z* isomers, while IIId,e were composed of only *Z* isomers.

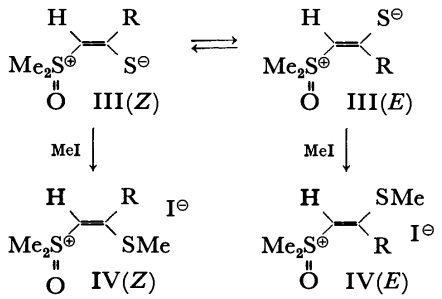

The NMR spectra of the carbonyl-stabilized sulfur ylides, I and II, have been widely studied in recent years. Much of this interest has involved the observation of geometrical isomers in these compounds.[4] Ester-stabilized ylides, I(R=alkyl–O)[10] and II(R=alkyl–O),[11] are known to be mixtures of *E* and *Z* isomers at lower temperatures.

The NMR spectra of ester-stabilized ylides, IIIa—c, at 34.5 °C showed peaks of two groups corresponding to the *E* and *Z* isomers. The stereochemistry of IIIa—c was assigned on the assumption that the methine proton *cis* to the thiolate sulfur may appear at a higher field than the methine proton *trans* to the thiolate sulfur as a result of the anisotropic shielding by the thiolate sulfur.[12] The results are shown in Table 1. The *E* isomers are much more favored than the *Z* isomers in $CDCl_3$. The methylation reactions of IIIa—c with methyl iodide to give IVa—c also support the structure determination of IIIa—c. The stereochemistry of the methylation products, IVa—c, was assigned on the basis of the chemical shifts of the vinyl protons using the values of Pascuel, Meier, and Simon.[13] Table 2 indicates that the *Z*/*E* ratio for IVc agrees well with that for IIIc. The marked deviation of the *Z*/*E* value for IVa, b from that of IIIa, b is caused by the partial decomposition of IVa, b during the methylation reaction, since IVa, b decomposes much faster than does IVc (the thermal decomposition of IVa—c will be described later). As a result, IIIa—c and IVa—c exist mainly in *E* forms.

Table 3. Solvent effects on the *Z*:*E* isomer ratios in IIIa-c at 34.5 °C

Solvent (ε)	IIIa *Z*:*E*	IIIb *Z*:*E*	IIIc *Z*:*E*
PhH (2.27)	16:84	15:85	16:84
$CDCl_3$ (4.7)	33:67	30:70	28:72
PhCl (5.61)	16:84	18:82	21:79
PhCN (25.2)	33:67	34:66	36:64
$PhNO_2$ (34.8)	28:72	32:68	38:62

The *Z*/*E* isomer ratios for IIIa—c in a variety of solvents at 34.5 °C are summarized in Table 3.

The solvent effect on the isomer ratios for ester-stabilized *P*-ylides has been widely studied.[14] The population of the *E* isomer increases consistently with an increase in the solvent polarity and with the bulkiness of the alkoxyl group; also, the *Z*/*E* ratio is governed by the dipole interaction between $P^{\oplus}$ and $O^{\ominus}$, and by the solvation of the carbonyl group.

Unlike the ester-stabilized *P*-ylides, the oxosulfonium ylides, IIIa—c, show no solvent dependence (Table 3), and *E* isomers were favoured in all the solvent used. Some keto-stabilized *S*-ylides have been shown to be mixtures of *E* and *Z* isomers.[10] Simple *keto*-stabilized ylides, such as I (R=Me, Ph)[10] and II(R=Ph),[15] show no evidence of the restricted rotation on the NMR spectra; however, they are believed to be *Z* isomers, since the following reasons may favor the *Z* form: i) steric repulsion between the sulfonium and R groups, and ii) electrostatic attraction between the positive sulfur and the negative enolate oxygen. Moreover, the alkylation of *keto*-stabilized sulfur-ylides[15,16] with trialkyloxonium tetrafluoroborate gives a mixture of *E* and *Z* *O*-alkylation products. This result indicates that the alkylation reaction does not necessarily support the presence of rotational isomers.

The methylation of IIId, e with methyl iodide gave only one isomer in quantitative yields (Table 2). The isomer was supposed to be *Z* on the basis of the following two results.

Some reports[17] show the good correlation between the chemical shifts of olefinic protons situated at the *cis* position to R and Hammett's σ_p for R: $\begin{matrix} H & R \\ \rangle{=}\langle \end{matrix}$ Similar treatments for IIIa—e and IVa—e (Figs. 1 and 2) gave straight lines for IIIa—c (*Z*), and IIId,e and for IVa—c (*Z*), and IVd,e respectively.

the conjugate acids of ylide carbanions.[19] Thus, the reaction of III with carbon disulfide may proceed as is shown below to give stable 6π compounds, VII.

Experimental

Preparation of III. Method A (in a mixture of DMSO and THF). Dimethyloxosulfonium methylide (0.15 mol) in DMSO (25 ml) was prepared from DMSO, NaH (0.15 mol), and trimethyloxosulfonium iodide (0.15 mol) according to the literature.[3] To a solution diluted with 70 ml of dry THF, we added methylxanthic anhydride (0.075 mol) in 15 ml of THF, portion by portion, for 15 min in an ice-water bath; stirring was then kept up for 2 h. The resulting mixture was quenched in ice water and extracted with 200 ml of chloroform. The chloroform extract was dried over magnesium sulfate and condenced *in vacuo* to give an oily product, which gave crystals (IIIa) from chloroform–petroleum ether. The yield and physical properties are shown in Table 1.

IIIb—e were prepared similarly.

Method B(in THF). Dimethyloxosulfonium methylide (0.15 mol) in THF (250 ml) was prepared from trimethyloxosulfonium chloride and NaH according to the literature.[3] To the solution we added tetramethylthiuram monosulfide (0.075 mol) in benzene (50 ml), portion by portion, at room temperature. The reaction mixture was stirred for 24 h, and then the precipitates were filtered off. The filtrate was condensed and chromatographed over silica gel with benzene–ethyl acetate (2: 1 v/v) to give IIId.

Reaction of III with Methyl Iodide. A solution of III in chloroform was treated with an excess of methyl iodide at room temperature for a few hours. The addition of benzene to the solution afforded IV in good yields (Table 2).

The decomposition of IV was run in $CDCl_3$ at 34.5 °C, the process being followed by NMR spectroscopy. IVa gave ylide I(R=SMe) and methyl iodide in quantitative yields after one day. I(R=SMe): Mp 109—110 °C (chloroform–ether). NMR (δ in $CDCl_3$): 2.30 (s, 3H, MeS), 3.42 (s, 6H, Me_2S), and 4.54 (s, 1H, C<u>H</u>-CO). Found: C, 36.01; H, 5.92%. Calcd for $C_5H_{10}O_2S_2$: C, 36.12; H, 6.06%.

IVe gave V in about a 90% yield and methyl iodide in a quantitative yield. V: Mp 68.5—70 °C (ether). NMR (δ in $CDCl_3$): 2.06 (s, 3H, SMe), 2.76 (s, 3H, SOMe), and 6.61 (s, 1H, C<u>H</u>=C). Found: C, 56.03; H, 5.97%. Calcd for $C_{10}H_{12}OS_2$: C, 56.57; H, 5.70%.

Photoisomerization was run in $CDCl_3$, with the NMR spectral change being followed. On irradiation with a high-pressure mercury lamp, V gave an equilibrium mixture of V and VI (1: 2) after 18—20 h. Subsequent condensation and the addition of a small amount of petroleum ether afforded VI. VI: Mp 138—140.5 °C. NMR (δ in $CDCl_3$): 2.41 (s, 3H, SMe), 2.66 (s, 3H, SOMe), and 6.15 (s, 1H, C<u>H</u>=C). Found: C, 56.43; H, 5.57%. Calcd for $C_{10}H_{12}OS_2$: C, 56.57; H, 5.70%.

A similar irradiation of VI in $CDCl_3$ afforded again a mixture of V and VI (1: 2).

The Reaction of III with Carbon Disulfide. A solution of IIIb (1.0 g) and carbon disulfide (2.0 g) in chloroform (20 ml) was refluxed for 3 h in a stream of nitrogen. The resulting mixture was condensed and chlomatographed over silica gel with hexane–ethyl acetate (6: 1). VIIb was isolated and crystallized from benzene–ether. Yield, 0.27 g; Mp 82—82.5 °C. Ms: 178(M^+).

VIIc was similarly isolated. VIIc: Mp 59.5—60.5 °C. MS: 192 (M^+). Found: C, 37.56; H, 4.22%. Calcd for $C_6H_8OS_3$: C, 37.50; H, 4.17%.

VIId, e were isolated from a crude reaction mixture and confirmed by comparison with known samples.[20,21] The results are collected in Table 4.

References

1) H. Yoshida, H. Matsuura, T. Ogata, and S. Inokawa, *Bull. Chem. Soc. Jpn.*, **48**, 2907 (1975).

2) Y. Hayashi, T. Akazawa, K. Yamato, and R. Oda, *Tetrahedron Lett.*, **1971**, 1781.

3) For example, see E. J. Corey and M. Chaycovsky, *J. Am. Chem. Soc.*, **86**, 1640 (1964).

4) D. Lecadet, D. Paquet, and A. Thuillier, *C. R. Acad. Sci., Ser. C*, **276**, 875 (1973).

5) R. Reynaud and R. C. Morean, *Bull. Soc. Chim. Fr.*, **1964**, 2999.

6) A. Fuson, M. L. Josien, and E. M. Shelton, *J. Am. Chem. Soc.*, **75**, 2526 (1954).

7) C. Andrien, M. Demuynck, and Y. Mollier, *C. R. Acad. Sci., Ser A*, **265B**, 127 (1967).

8) C. S. Marvel, P. DeRadzitzky, and J. J. Brader, *J. Am. Chem. Soc.*, **77**, 5997 (1955).

9) Restricted rotation about the C–N bond for amide and thioamide has been widely studied, and two isomers, E and Z, have been observed, See, for example, R. C. Neuman and V. Jones, *J. Org. Chem.*, **39**, 929 (1974).

10) K. Kondo and D. Tunemoto, *J. Chem. Soc., Chem. Commun.*, **1970**, 1361, and Ref. cited therein.

11) J. Casanova, Jr. and D. A. Rutolo, *J. Chem. Soc., Chem. Commun.*, **1967**, 1224.

12) R. C. Neuman and L. B. Young, *J. Phys. Soc.*, **69**, 1777 (1965).

13) C. Pascual, J. Meier, and W. Simon, *Helv. Chim. Acta*, **49**, 164 (1966).

14) H. Yoshida, H. Matsuura, T. Ogata, and S. Inokawa, *Chem. Lett.*, **1974**, 1065, and Ref. cited therein.

15) S. H. Smallcombe, R. J. Holland, R. H. Fish, and M. C. Caserio, *Tetrahedron Lett.*, **1968**, 5987.

16) C. R. Johnson and P. E. Rogers, *J. Org. Chem.*, **38**, 1798 (1973).

17) J. Niwa and H. Kasiwagi, *Bull. Chem. Soc. Jpn.*, **36**, 1414 (1963), and Ref. cited therein.

18) J. R. Neff, R. R. Gruetzmacher, and J. E. Nodlander, *J. Org. Chem.*, **39**, 3814 (1974), and Ref. cited therein.

19) C. Kissel, R. J. Holland, and M. C. Caserio, *J. Org. Chem.*, **37**, 2720 (1972). S. Fliszar, R. F. Hudson, and G. Salvadori, *Helv. Chim. Acta*, **46**, 1580 (1963).

20) T. Mukaiyama, S. Aizawa, and T. Yamaguchi, *Bull. Chem. Soc. Jpn.*, **40**, 2641 (1967).

21) E. Kingsbery, *J. Am. Chem. Soc.*, **83**, 2934 (1961).

The Photochemical Reaction of 1,1,4,4-Tetramethyl-2,3-tetralindione with Hydrogen Donors

Kazuhiro MARUYAMA and Tomoji TAKAHASHI

Department of Chemistry, Faculty of Science, Kyoto University, Kyoto 606

(Received April 23, 1976)

The photochemical reaction of 1,1,4,4-tetramethyl-2,3-tetralindione, **1**, with hydrogen donors, such as xanthene and aldehyde, in the liquid phase has been investigated. When xanthene was selected as the hydrogen donor, the main products were the "1,2-adduct," photo-reduced α-keto alcohol, and 9,9′-bixanthenyl. The photolysis of **1** and an aldehyde gave the mixture of the "1,2-adduct" and the "1,4-adduct." However, in the reaction with isobutyraldehyde another type of "1,2-adduct" was obtained, *i.e.*, a combination product between the semidione radical and the isopropyl radical resulting from the decarbonylation of the isobutyryl radical, together with propene and carbon monoxide. The usual type of "1,2-adduct," the "1,4-adduct," and the photo-reduced product (α-keto alcohol) were the minor products in the reaction. It was also confirmed that the original "1,4-adduct" obtained from **1** and acetaldehyde rearranged photochemically to a different type of "1,2-adduct," but no reverse rearrangement was observed under the present conditions. The mechanisms of the reactions were discussed on the basis of product analysis and the examination of the reaction by means of CIDNP.

The photo-excited α-diketone abstract the hydrogen atom from the suitable hydrogen donor, giving the semidione radical.[1] In our previous study,[2] it was reported that 3,3-dimethyl-1,2-indandione also abstracts the hydrogen atom from aldehydes. However, no appreciable amounts of products were obtained in most cases because of the occurrence of a back reaction from the unstable intermediates produced by the attack of the acyl radicals on the aromatic ring of the conjugated semidione radical. This paper will deal with the photochemistry of 1,1,4,4-tetramethyl-2,3-tetralindione **1** as a non-enolizable α-diketone whose dicarbonyl group can not conjugate with aromatic π-electrons.

A few papers have appeared on the photochemical reaction of 1,1,4,4-tetramethyl-2,3-tetralindione, **1**, with some hydrogen donors.[3,4] However, the mechanism of the reaction has not yet been discussed. In order to understand the characteristics of the photochemical reaction, the mechanism of the reaction has now been investigated by means of the CIDNP technique.

Results and Discussion

In all of the photochemical reactions described below, a benzene solution of **1** and a hydrogen donor in a usual glass tube was irradiated from the outer side by means of a 300W high-pressure mercury arc lamp at room temperature.

The irradiation of **1** and xanthene gave a "1,2-adduct," 3-hydroxy-1,1,4,4-tetramethyl-3-xanthenyl-2-tetralone, **2**; as a photo-reduced product, 3-hydroxy-1,1,4,4-tetramethyl-2-tetralone, **3**, and 9,9′-bixanthenyl, **4**, in yields of 42, 50, and 45% respectively. As Fig. 1 shows, the polarized absorption signals which were

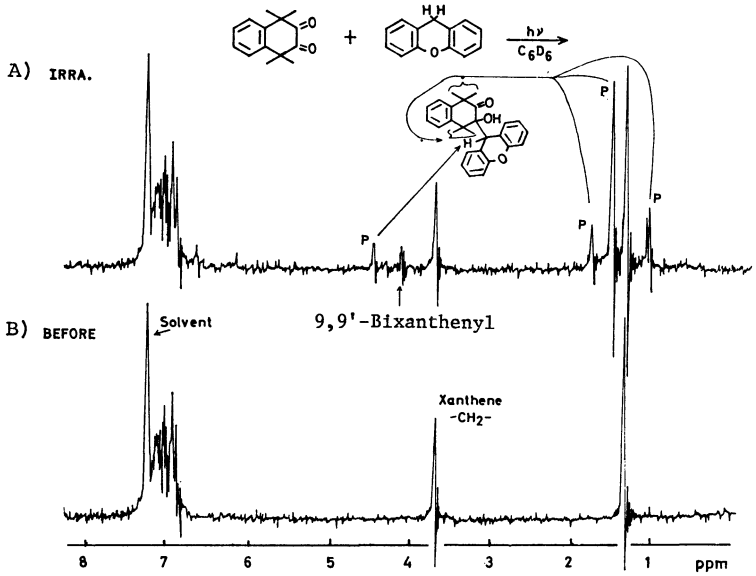

Fig. 1. A): PMR signals observed in the course of the photochemical reaction of 1,1,4,4-tetramethyl-2,3-tetralindione with xanthene during irradiation. P, polarized signals.
B): PMR signals observed before irradiation.

assigned to protons of the "1,2-adduct," **2**, were observed in the course of the photochemical reaction. It can be explained by Kaptein's simple rule[5] that the "1,2-adduct," **2**, results from the in-cage combination of the semidione radical, **5** ($g\simeq2.0046$[6]), and the xanthenyl radical, **6** ($g\simeq2.0057$[7]), from the triplet pair.[8] However, the semidione radical, **5**, and the xanthenyl radical, **6**, might partly escape from the cage and encounter another xanthene molecule, giving the reduced product, **3**, and 9,9'-bixanthenyl.

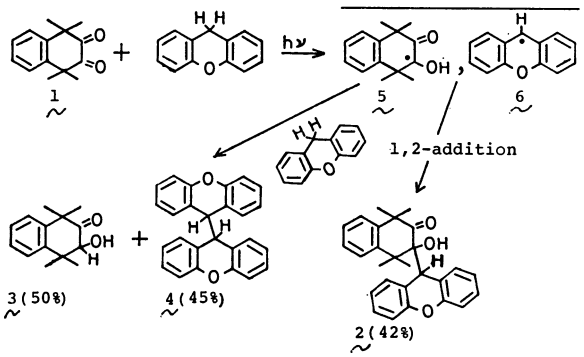

Scheme 1. Proton written with Gothic letter showed polarization.

When acetaldehyde was used as the hydrogen donor, a "1,2-adduct," 3-acetyl-3-hydroxy-1,1,4,4-tetramethyl-2-tetralone, **7a**, and a ketonization product after 1,4-addition, 3-acetoxy-1,1,4,4-tetramethyl-2-tetralone, **8a**, were obtained in yields of 32 and 34% respectively. The "1,2-adduct," **7a**, was identified by means of its spectral properties and by an iodoform test. The last procedure changed **7a** to 2-hydroxy-1,1,3,3-tetramethylindan-2-carboxylic acid, **9** (mp 181—184 °C[9]), quantitatively *via* the formation of 3-hydroxy-2-oxo-1,1,4,4-tetramethyl-2-tetralin-3-carboxylic acid, **10**, which was then easily decarboxylated to give **1**.[10] In fact, a benzilic-acid rearrangement converted **1** to **9** quantitatively under the same conditions. The product, **9**, was esterified with diazomethane, giving methyl 2-hydroxy-1,1,3,3-tetramethylindan-2-carboxylate, **11** (mp 77.5—78.5 °C[11]), quantitatively. The other product, **8a**, was identified by means of its spectral properties and by comparison with an authentic sample prepared by the acetylation of 3-hydroxy-1,1,4,4-tetramethyl-2-tetralone, **3**, in the presence of pyridine.

On irradiation for two days, 3-acetoxy-1,1,4,4-tetramethyl-2-tetralone, **8a**, was slowly changed to **7a** in a 17% yield, whereas no reverse conversion could be observed. A filter solution[12] was employed to cut the light of the wavelengths shorter than 330 nm. On irradiation with the light through the filter solution, **8a** remained unchanged. This is similar to the case with **7a**. Under the same conditions, **1** and acetaldehyde reacted photochemically to give **7a** and **8a** in yields of 34 and 41% respectively. In the course of the photochemical reaction of **1** and acetaldehyde, the CIDNP technique gave a only limited information because of the contingent coincidence of the acetyl protons of **7a** and **8a** in their chemical shifts in benzene-d_6. On irradiation with the light through the filter solution, **1** and other

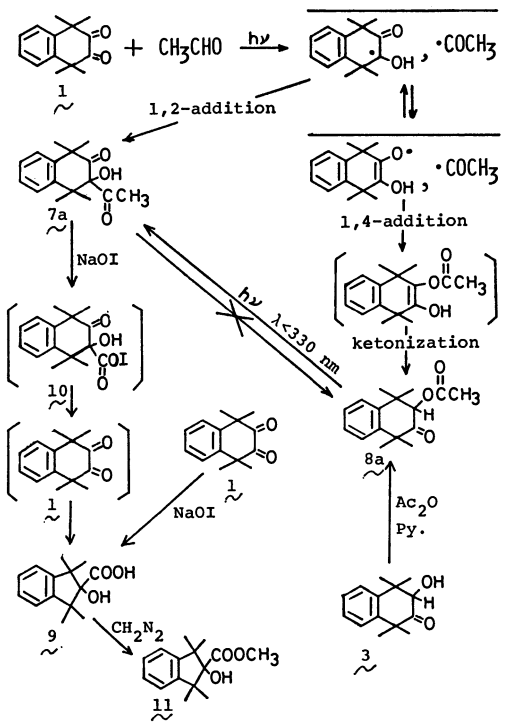

Scheme 2.

Table 1. Yield of 3-acyl-3-hydroxy-1,1,4,4-tetramethyl-2-tetralone and 3-acyloxy-1,1,4,4-tetramethyl-2-tetralone

	Yield (%) of **7**	Yield (%) of **8**
a	34	41
b	34	39
c	17	77
d	41	20
e	66	32
f	38	13
g	26	15

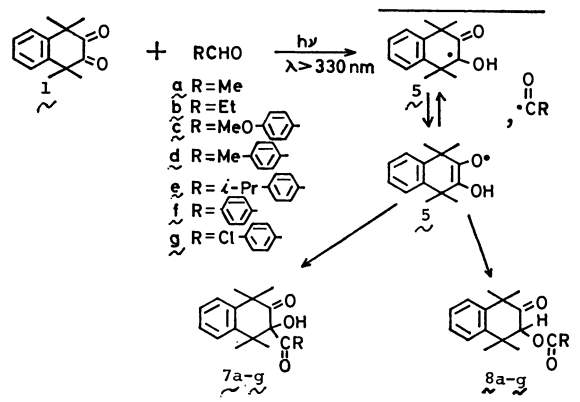

Scheme 3.

aldehydes, propionaldehyde, *p*-anisaldehyde, *p*-tolualdehyde, *p*-isopropylbenzaldehyde, benzaldehyde, and *p*-chlorobenzaldehyde, reacted photochemically, giving the corresponding "1,2-adducts," 3-acyl-3-hydroxy-1,1,4,4-tetramethyl-2-tetralone, **7b**—**g**, and the respective "1,4-adducts," 3-acyloxy-1,1,4,4-tetramethyl-2-tetralone, **8b**—**g**. The yields of **7a**—**g** and **8a**—**g** are

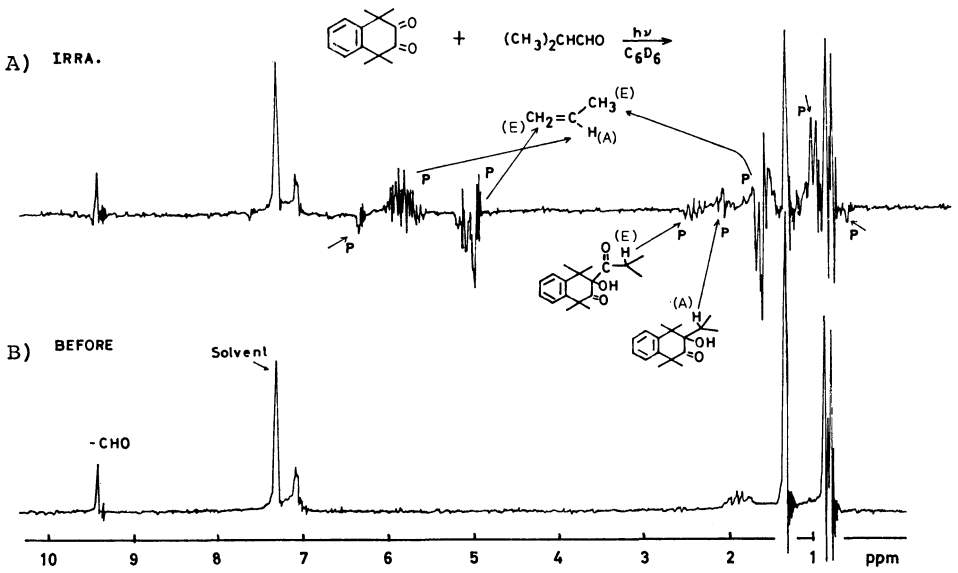

Fig. 2. A): PMR signals observed in the course of the photochemical reaction of 1,1,4,4-tetramethyl-2,3-tetralindione with isobutyraldehyde during irradiation. P, polarized signals.
B): PMR signals observed before irradiation.

summarized in Table 1. In conclusion, the photochemical reactions of **1** with aldehydes can be described as are shown in Scheme 3.

On the other hand, the irradiation of **1** with isobutyraldehyde gave a "1,2-adduct"; 3-hydroxy-3-isobutyryl-1,1,4,4-tetramethyl-2-tetralone, **7h** (17%), a "1,4-adduct"; 3-isobutyryloxy-1,1,4,4-tetramethyl-2-tetralone, **8h** (47%), a 1,2-addition product resulting from the decarbonylation, **12** (10%), a reduced product, **3** (11%), an oxidized product; α,α,α',α'-tetramethyl-*o*-phenylenediacetic anhydride **13** (5%), and propene (7—10%), accompanied by the evolution of carbon monoxide (45—63%). Carbon monoxide was identified by the use of palladium chloride-test paper. The product, **13**, could be formed by the reaction of the semidione radical, **5**, with oxygen.[11] As Fig. 2 shows, in the course of the photochemical reaction of **1** with isobutyraldehyde, a multiplet emission signal was observed in the region corresponding to the methine proton of the "1,2-adduct,' **7h**. In addition, a multiplet absorption signal was observed corresponding to the methine proton of the other "1,2-adduct," **12**, accompanied by the other strongly polarized signals corresponding to the signals of propene;[13] these signals assigned by comparison with the signals of the synthesized authentic sample. Thus, the "1,2-adduct," **7h**, might result from the in-cage combination of the semidione radical, **5**, and the isobutyryl radical *via* the triplet pair. Similarly, **12** may be formed from the in-cage combination of the semidione radical, **5**, with the isopropyl radical ($g \cong 2.0032$[14]) *via* the triplet pair. Propene and the reduced product, **3**, might result from the dehydrogenation of the isopropyl radical by **5** *via* the triplet pair. The reaction mechanism is shown in Scheme 4. The decarbonylation and 1,2-addition reactions may be competitive, and the relative rates may depend on the stabilities of the related radicals.[15] Although the combination, disproportionation, or escape of the related radicals may occur competitively, depending on the stability of the radicals concerned, the steric repulsion between the related radicals in the radical pair could be another controlling factor. The combination of the semidione radical, **5**, with the isopropyl radical or xanthenyl radical would be more hindered sterically than that of **5** with acyl radicals. This is the reason for the formation of the reduction product, **3**, in the reactions with isobutyraldehyde and with xanthene.

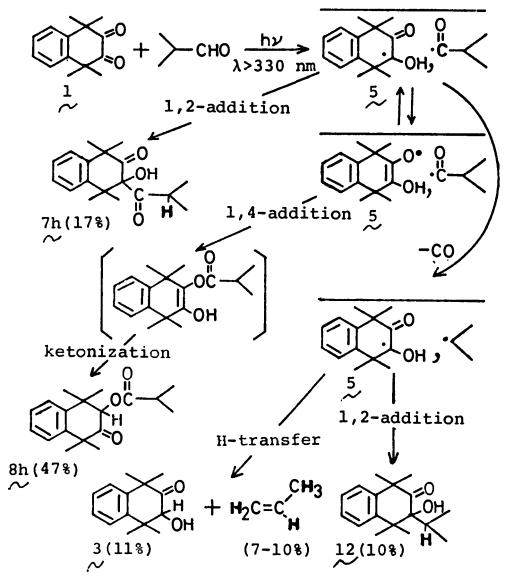

Scheme 4. Protons written with Gothic letter showed polalization.

Experimental

The melting points described are uncorrected. The infrared spectra (KBr disk or a liquid film) were taken with a JASCO

IR-G spectrometer. The PMR spectra were measured with a JEOL PS-100 MHz spectrometer, using TMS as the internal standard. The ultraviolet and visible spectra were recorded by means of a Shimadzu UV-200 spectrometer. The CIDNP spectra were observed using a JEOL PS-100 MHz spectrometer, equipped with a modified NMR probe for irradiation.[16]

Materials. 1,1,4,4-Tetramethyl-2,3-tetralindione, **1**, was prepared by the oxidation of 1,1,4,4-tetramethyl-2-tetralone with selenium dioxide[17] and was purified by sublimation; mp 59—61 °C (lit,61—62 °C[17]). IR(KBr): 1710 cm^{-1} (C=O). PMR (CCl_4): δ; 1.24 (s, 12H), 7.12 ppm (s, 4H). UV_{max} (EtOH): 286 nm (ε: 443), 387 (10), 396 (15). The xanthene was commercially obtained and was purified by recrystallization from ethanol. The acetaldehyde was prepared by the depolymerization of paraldehyde. The other aldehydes were commercially obtained and were distilled before use.

General Procedure. **1** (0.5—1.0 mmol) and 2—6 equivalents of a hydrogen donor were dissolved in 20 ml of dry benzene, and then the solution was irradiated from the outer side by means of a 300W high-pressure mercury arc lamp through a water layer 5 cm thick or a filter solution 1 cm thick at room temperature. After the solution had become colorless, irradiation was stopped. After the removal of the solvent, the total product was separated by TLC, using a benzene and hexane mixture as the developing solvent. The filter solution used for light-cutting was an aqueous solution (50 ml) of sodium bromide (24.45 g) and lead nitrate (0.15 g).

Photochemical Reaction of 1 with Xanthene. A benzene solution of **1** (244 mg, 1.1 mmol) and two equivalents of xanthene was irradiated for about 5 h. 9,9'-Bixanthenyl, **4** (363 mg, 45%), 3-hydroxy-1,1,4,4-tetramethyl-3-xanthenyl-2-tetralone, **2** (486 mg, 42%), and 3-hydroxy-1,1,4,4-tetramethyl-2-tetralone, **3** (180 mg, 50%), were thus obtained. **2**; white plates; mp 149 °C. IR (KBr): 3450 (OH), 1695 cm^{-1} (C=O). PMR (CCl_4): δ; 0.75 (s, 3H), 0.94 (s, 3H), 1.48 (s, 3H), 1.84 (s, 3H), 3.02 (s, 1H; OH), 4.12 (s, 1H), 5.8—7.1 ppm (m, 12H). Found: C, 81.52; H, 6.64%. Calcd for $C_{27}H_{26}O_3$: C, 81.38; H, 6.58%. **3**; white crystals; mp 39.0—41.0 °C (lit, 40—42 °C[3]). IR (KBr): 3450 (OH), 1710 cm^{-1} (C=O). PMR (CCl_4): δ; 0.87 (s, 3H), 1.40 (s, 3H), 1.44 (s, 3H), 1.49 (s, 3H), 3.52 (d, 1H; OH), 4.20 (d, 1H), 6.9—7.2 ppm (m, 4H). **4**; white crystals; mp 211 °C.

Photochemical Reaction of 1 with Acetaldehyde. A solution of **1** (82 mg, 0.4 mmol) and acetaldehyde (77 mg, 1.8 mmol) was irradiated for about 6 h. 3-Acetyl-3-hydroxy-1,1,4,4-tetramethyl-2-tetralone, **7a** (34 mg, 34%), and 3-acetoxy-1,1,4,4-tetramethyl-2-tetralone, **8a** (32 mg, 32%), were thus obtained. **7a**; white plates; mp 80.5—81.0 °C. IR (KBr): 3400 (OH), 1700 cm^{-1} (C=O). PMR (CCl_4): δ; 0.91 (s, 3H), 1.33 (s, 3H), 1.40 (s, 3H), 1.43 (s, 3H), 2.00 (s, 3H), 4.63 (s, 1H; OH), 6.9—7.1 ppm (m, 4H). UV_{max} (EtOH): 315 nm (ε; 150). Found: C, 73.77; H, 7.77%. Calcd for $C_{16}H_{20}O_3$: C, 73.86; H, 7.76%. **8a**; white plates; mp 106.5—107.0 °C. IR (KBr): 1735, 1716 cm^{-1} (C=O). PMR (CCl_4): δ; 1.03 (s, 3H), 1.36 (s, 3H), 1.44 (s, 3H), 1.48 (s, 3H), 2.13 (s, 3H), 5.24 (s, 1H), 6.9—7.1 ppm (m. 4H). UV_{max} (EtOH): 285 nm (ε: 38), 300 (23). Found: C, 73.69; H, 7.91%. Calcd for $C_{16}H_{20}O_3$: C, 73.86; H, 7.76%.

Iodoform Reaction of 7a. To a solution of iodine (77 mg) and sodium hydroxide (141 mg) in water (10 ml), we added a solution of **7a** (24 mg) in ether (3 ml). After stirring at room temperature for 24 h, the solution was acidified with hydrochloric acid and extracted with ether. The ethereal solution was dried over sodium sulfate and evaporated, giving white crystals of 2-hydroxy-1,1,3,3-tetramethylindan-2-carboxylic acid, **9** (21 mg); mp 181—184 °C (lit, 188—189 °C[9]). IR-(KBr): 3450 (OH), 1690 cm^{-1} (C=O). PMR ($CDCl_3$): δ; 1.34 (s, 6H), 1.68 (s, 6H), 7.0—7.4 ppm (m, 4H).

Esterification of 9 with Diazomethane. A ethereal solution of diazomethane was added to a solution of **9** (13 mg) in ether at room temperature. After the removal of the solvent, white crystals of methyl 2-hydroxy-1,1,3,3-tetramethylindan-2-carboxylate, **11** (14 mg), were obtained; mp 72.0—74.0 °C (lit, 77.5—78.5 °C[11]). IR(KBr): 3450 (OH), 1705 cm^{-1} (C=O). PMR (CCl_4): δ; 1.16 (s, 6H), 1.30 (s, 6H), 3.52 (s, 3H), 6.9—7.1 ppm (m, 4H). Mass: *m/e*; 248 (M^+), 189 ($M^+ - COOCH_3$, base), 171 ($M^+ - COOCH_3 \cdot H_2O$).

Benzilic Acid Rearrangement of 1. **1** (22 mg) was converted to **9** (24 mg) under the conditions described in "*Iodoform Reaction of 7a.*"

Acetylation of 3. A mixture of **3** (26 mg), acetic anhydride (10 ml), and pyridine (10 ml) was warmed for 3 h at 80 °C. After the subsequent evaporation of the liquid phase, white crystals of **8a** (29 mg) were obtained; mp 107 °C.

Irradiation of 7a and 8a. The irradiation of a benzene solution of **8a** (13 mg) for 2 days gave a mixture of the starting material, **8a** (8 mg, 60%), and **7a** (2 mg, 17%). However, the irradiation of **7a** under the same conditions gave no reaction. On irradiation through the filter solution[13] (transmitting the light $\geq$330 nm) for 4 days, **8a** remained unchanged. **7a** was also recovered unchanged.

Photochemical Reaction of 1 with Acetaldehyde with the Use of the Filter Solution. On irradiation through the filter solution, **1** (108 mg, 0.5 mmol) and acetaldehyde (75 mg, 1.7 mmol) reacted to give **7a** (96 mg, 34%) and **8a** (102 mg, 41%).

Photochemical Reaction of 1 with Propionaldehyde. A benzene solution of **1** (119 mg, 0.6 mmol) and propionaldehyde (166 mg, 2.9 mmol) was irradiated through the filter solution to give 3-hydroxy-3-propionyl-1,1,4,4-tetramethyl-2-tetralone, **7b** (52 mg, 34%), and 3-propionyloxy-1,1,4,4-tetramethyl-2-tetralone, **8b** (59 mg, 39%). **7b**; white plates; mp 116.0—118.0 °C. IR (KBr): 3400 (OH), 1695 cm^{-1} (C=O). PMR (CCl_4): δ; 0.84 (t, 3H), 0.92 (s, 3H), 1.31 (s, 3H), 1.36 (s, 3H), 1.44 (s, 3H), 2.24 (q, 2H), 4.64 (s, 1H; OH), 6.9—7.1 ppm (m, 4H). Found: C, 74.41; H, 7.82%. Calcd for $C_{17}H_{22}O_3$: C, 74.42; H, 8.08%. **8b**; white plates; mp 67.0—68.0 °C. IR(KBr): 1745, 1725 cm^{-1} (C=O). PMR (CCl_4): δ; 1.07 (s, 3H), 1.24 (t, 3H), 1.40 (s, 3H), 1.48 (s, 3H), 1.53 (s, 3H), 2.49 (q, 2H), 5.36 (s, 1H), 7.0—7.4 ppm (m, 4H). Found: C, 74.13; H, 8.31%. Calcd for $C_{17}H_{22}O_3$: C, 74.42; H, 8.08%.

Photochemical Reaction of 1 with p-*Anisaldehyde.* A benzene solution of **1** (146 mg, 0.7 mmol) and *p*-anisaldehyde (341 mg, 2.5 mmol) was irradiated through the filter solution to give 3-hydroxy-3-*p*-methoxybenzoyl-1,1,4,4-tetramethyl-2-tetralone, **7c** (41 mg, 17%), and 3-*p*-methoxybenzoyloxy-1,1,4,4-tetramethyl-2-tetralone, **8c** (190 mg, 77%). **7c**; white needles; mp 153.5—154.5 °C. IR (KBr): 3350 (OH), 1703 cm^{-1} (C=O). PMR (CCl_4): δ; 0.96 (s, 3H), 1.23 (s, 3H), 1.52 (s, 3H), 1.57 (s, 3H), 3.77 (s, 3H), 4.64 (s, 1H; OH), 6.64—7.64 (dd, 4H), 6.9—7.1 ppm (m, 4H). Found: C, 74.69; H, 7.04%. Calcd for $C_{22}H_{24}O_4$: C, 74.97; H, 6.86%. **8c**; white prisms; mp 132.5—133.0 °C. IR (KBr); 1735, 1705 cm^{-1} (C=O). PMR (CCl_4): δ; 1.16 (s, 3H), 1.40 (s, 3H), 1.52 (s, 3H), 1.56 (s, 3H), 3.76 (s, 3H), 5.52 (s, 1H), 6.74—7.86 (dd, 4H), 6.9—7.1 ppm (m, 4H). Found: C, 74.73; H, 6.87%. Calcd for $C_{22}H_{24}O_4$: C, 74.97; H, 6.86%.

Photochemical Reaction of 1 with p-*Tolualdehyde.* The irradiation of **1** (124 mg, 0.6 mmol) and *p*-tolualdehyde (321 mg, 2.7 mmol) in benzene by the use of the filter solution gave 3-hydroxy-3-*p*-toluoyl-1,1,4,4-tetramethyl-2-tetralone, **7d** (79 mg, 41%), and 3-*p*-toluoyloxy-1,1,4,4-tetramethyl-2-tetralone, **8d** (39 mg, 20%). **7d**; white needles; mp 171.5—173.0 °C.

Biogenetic Model Reactions of Epoxygermacrones

Masatake NIWA, Masanobu IGUCHI, and Shosuke YAMAMURA*

Faculty of Pharmacy, Meijo University, Showa-ku, Nagoya 468

(Received April 21, 1976)

From a biogenetic point of view, acid- or base-catalyzed cyclizations of epoxygermacrones (**2**, **23**, and **33**) were carried out. In most cases, the stereospecific cyclizations of these epoxygermacrones took place to give many compounds with an 11-oxabicyclo[5.3.1]undecane system, cadinane-type, selinane-type or guaiane-type compounds depending on the kinds of reagents and solvents. The formation process of each cyclization product will be discussed in detail.

In the preceding paper,[1] we described the regio- and stereo-specific cyclizations of the germacrones in detail. Our interests are also focused on the biogenetic model reactions of the epoxygermacrones. In the present paper, we describe the acid-catalyzed cyclizations of three different kinds of epoxygermacrones leading to the formation of various cyclization products depending on the kinds of reagents and solvents. In addition, the base-catalyzed cyclizations of these epoxygermacrones are also discussed.

When treated with *m*-chloroperbenzoic acid (1.06 equiv.) (0 °C, 20 h), isoacoragermacrone (**1**)[2] was readily converted into the expected monoepoxide (**2**) (mp 55 °C; $C_{15}H_{24}O_2$; λ_{max} 243 nm), in a quantitative yield, which has an *E*-epoxide ring at the position corresponding to the isolated trisubstituted double bond of the original ketone (**1**). Epoxyisoacoragermacrone (**2**) thus obtained is used for the biogentic model reactions, as follows.[3]

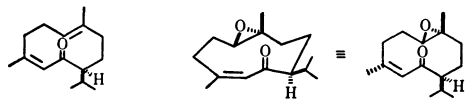

1 2

Fig. 1.

Acid-catalyzed Cyclizations of Epoxyisoacoragermacrone (2)

On treatment with 80% aq. HCOOH (−20 °C, 10 min), **2** was converted into a dihydroxy ketone (**3**) and a *cis*-selinate-type compound (**4**) in 47.5 and 34.2% yields, respectively. Of these two products, the structure of the former is based on its spectral data, which indicate the presence of a $-CH_2CH(OH)-\overset{Me}{\overset{|}{C}}(OH)-$grouping [$\nu_{max}$ 3400 br. cm^{-1}; δ 1.22 (3H, s) and 3.48 (1H, dd, J=4.0 and 6.0 Hz) ppm] in addition to the original α,β-unsaturated carbonyl system [ν_{max} 1685 and 1645 cm^{-1}; λ_{max} 238 nm (ε, 4200); δ 1.87 (3H, d, J=1.2 Hz) and 5.98 (1H, br.s) ppm]. The configuration of the tertiary OH group remains unsolved from the spectral data of **3**. However, this hydroxyl group must be in an α-configuration from a stereochemical aspect, as shown in Scheme 1.

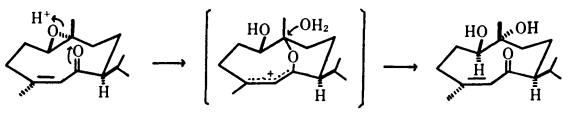

2 3

Scheme 1. Formation process of the dihydroxy compound (**3**).

* To whom all correspondence should be addressed.

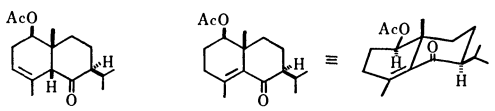

5 6

Fig. 2.

The structure of the *cis*-selinane-type compound (**4**) is unambiguously determined by its spectral data and the chemical evidences, as follows. The cyclization product (**4**) as a colorless liquid [$C_{15}H_{24}O_2$ (*m/e* 236 (M^+))] has each one of OH and CO groups (ν_{max} 3430 br. and 1705 cm^{-1}), the NMR spectrum of which indicates the presence of a $MeC(OH)=CH-$ grouping [δ 1.58 (3H, br.s) and 5.44 (1H, br.s) ppm] in addition to a tertiary methyl group [δ 1.02 (3H, s) ppm]. Acetylation of **4** with Ac_2O-pyridine (room temp, overnight) afforded the corresponding acetoxy compound (**5**) ($C_{17}H_{26}O_3$; ν_{max} 1740 and 1710 cm^{-1}). In its NMR spectrum, the triplet at δ 3.53 (1H, J=5.0 Hz) ppm in **4** is observed at δ 4.80 (1H, t, J=4.5 Hz) ppm. The remaining signals are nearly identical in both compounds. Furthermore, the ORD curve of **5** showed a negative Cotton effect ($[\phi]^T_{318nm}$ $-72°\times10^2$; $[\phi]^P_{276nm}+63°\times10^2$; $A=-135$), strongly suggesting that the acetate **5** is a *cis*-selinane-type ketone. This is further confirmed by the following acid-catalyzed isomerization with 100% HCOOH: when treated with 100% HCOOH under reflux for 10 h, the acetoxy compound **5** was converted into a fully substituted α,β-unsaturated ketone (**6**) [$C_{17}H_{26}O_3$; λ_{max} 246 nm (ε, 4800); δ 1.71 (3H, br.s) ppm], whose ORD curve has a strong positive peak ($[\phi]^P_{264nm}+150°\times10^2$) as seen in that of cholest-4-en-6-one. Finally, in comparison of the NMR spectra between **5** and **6**, the coupling constant for the proton attached to the carbon atom bearing the acetoxyl group in the latter [δ 4.85 (1H, dd, J=6.2 and 9.0 Hz) ppm] is different from that of **5** [δ 4.80 (1H, t, J=4.5 Hz) ppm]. Clearly, the configuration of the acetoxyl group should be axial in **5** and equatorial in **6**. Therefore, the stereostructures of the cyclization product and the acid-isomerization compound can be represented by **4**

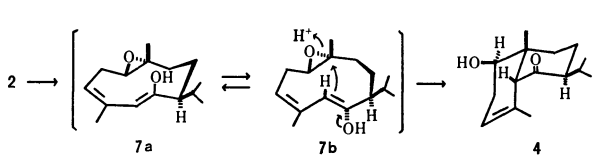

7a 7b 4

Scheme 2. Possible pathway from epoxyisoacoragermacrone (**2**) to the *cis*-selinane-type compound (**4**).

and **6**, respectively. In the above acid-catalyzed cyclization, a conjugated dienol (**7**) is a possible intermediate as shown is Scheme 2, and the stereochemistry of the cyclization product (**4**) must be led by the more favorable conformation of **7b** than that of **7a**.

We further examined the acid-catalyzed reactions of epoxyisoacoragermacrone (**2**) using 100% HCOOH in thiophenol. When treated with 100% HCOOH in thiophenol (room temp, 40 min) instead of 80% aq. HCOOH, epoxyisoacoragermacrone (**2**) was readily converted into an enol ether (**8**) with an 11-oxabicyclo-[5.3.1]undec-1-ene system, in a 65.5% yield. This compound has two tertiary methyl groups (δ 1.21 and 1.35 ppm) and the original isopropyl group (δ 0.86 and 0.88 ppm). Furthermore, the compound **8** has a PhS group [δ 7.30 (5H, complex) ppm] as well as an enol ether system (–Ċ–CH=Ċ–O–) [ν_{max} 1665 cm^{-1} and δ 4.75 (1H, s) ppm], in addition to one secondary OH group [ν_{max} 3420 br. cm^{-1} and δ 4.25 (1H, br.t, $J\simeq$6.0 Hz) ppm] which can be easily acetylated with Ac_2O–pyridine to give the corresponding acetate [**9**; ν_{max} 1735 cm^{-1} and δ 5.57 (1H, br.t, $J\simeq$6.8 Hz) ppm].

In the above reaction, the regio- and stereospecific cyclization of **2** takes place in a concerted mechanism, leading to the formation of **8**, as shown in Scheme 3.

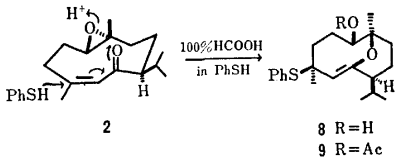

2 8 R=H 9 R=Ac

Scheme 3. Reaction of epoxyisoacoragermacrone (**2**) with 100% HCOOH in thiophenol.

Furthermore, the acid-catalyzed cyclization of **2** with $AlCl_3$ in absolute ether were carried out at −18 °C for 20 min to give three products **10**, **11**, and **12** in 18, 47, and 33% yields, respectively.

The compound **10** is a colorless liquid [$C_{15}H_{24}O_2$ (*m/e* 236 (M^+))] with a conjugated diene system [–CH_2–CH=C(Me)–CH=Ċ–O–] [ν_{max} 1650 cm^{-1}; λ_{max} 243 nm (ε, 7500); δ 1.79 (3H, br.s), 5.15 (1H, s) and 5.34 (1H, t, J=6.8 Hz) ppm]. The presence of each one of secondary OH and tertiary methyl groups is also confirmed by its spectral data [ν_{max} 3430 br. cm^{-1} and δ 3.45 (1H, dd, J=5.8 and 3.7 Hz) ppm; δ 1.35 (3H, s) ppm]. Other two compounds (**11**, mp 159.5—160.5 °C; **12**, mp 143.5—144.5 °C) with the same molecular formula ($C_{30}H_{48}O_4$) are dimeric and regarded as double bond isomers to each other, which are converted into the corresponding acetates **13** and **14**, respectively, on acetylation with Ac_2O–pyridine. The results indicate the presence of two secondary OH groups. The structures of these two dimeric compounds are also determined on the basis of their spectral data, as follows. Similarly, the NMR spectra of both compounds have three methyl singlets in addition to signals due to two isopropyl groups. However, a remarkable difference is seen in the NMR signals assigned to three olefinic protons: **11** has two singlets at δ 4.46 and 5.15 ppm and one triplet at δ 5.41 (1H, t, J=7.0 Hz) ppm, while **12** has three singlets at δ 4.79, 5.33 and 5.96 ppm. In addition, the UV spectra of these two compounds show different chromophores [**11**, λ_{max} 247 nm (ε, 6670); **12**, λ_{max} 254 nm (ε, 22400)]. From these data, the structures **11** and **12** should be given to the two dimeric compounds with mp 159.5—160.5 and 143.5—144.5 °C, respectively.

In the case of $AlCl_3$, clearly, the acid-catalyzed reaction of **2** must be initiated by cleavage of the epoxide ring with $AlCl_3$ followed by simultaneous participation of the carbonyl group, as shown in Scheme 4.

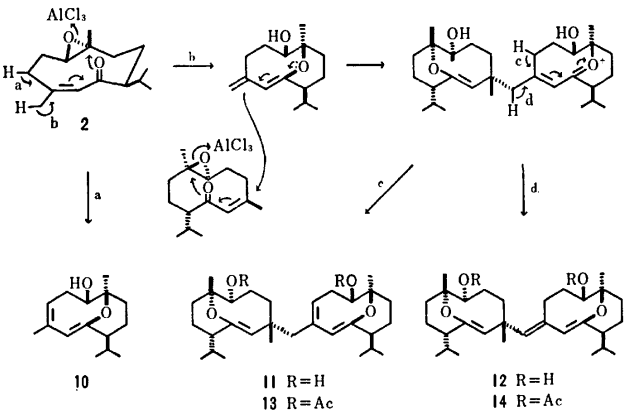

10 11 R=H 13 R=Ac 12 R=H 14 R=Ac

Scheme 4. Reaction of epoxyisoacoragermacrone (**2**) with $AlCl_3$.

Base-catalyzed Cyclizations of Epoxyisoacoragermacrone (2). In the case of the acid-catalyzed cyclization with $AlCl_3$, the driving force of the intramolecular cyclization at the initial step may be attributable to the epoxide ring openning. In contrast, the different results were obtained in the case of the base-catalyzed reactions, as described below.

When treated with *t*-BuOK in *t*-BuOH (1.1 equiv.) under a nitrogen atmosphere (room temp, 2 h), the epoxide (**2**) was readily converted into an α,β-unsaturated ketone **15** ($C_{15}H_{24}O_2$) in a 75% yield, which was further converted into the known acetate (**6**) on acetylation with Ac_2O–pyridine. In the above cyclization using *t*-BuOK, **16** is regarded as a possible intermediate, and the stereochemistry of **15** must be led by the corresponding conformation **16b**, as shown in Scheme 5.

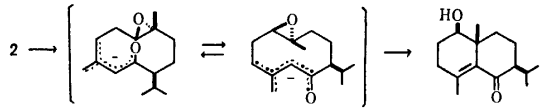

16a 16b 15

Scheme 5. Chemical conversion of **2** into the selinane-type compound **15**.

In connection with acolamone and isoacolamone,[2,4] both of which are included in the plant together with acoragermacrone,[2] this α,β-unsaturated ketone (**15**) was converted into the thermal isomerization product (**17**) of acolamone, in three steps, as follows. On treatment with mesyl chloride–pyridine (room temp, 2 h), the compound **15** was converted into the corresponding mesylate (**18**) [δ 3.07 (3H, s) and 4.21 (1H, t, J=7.5 Hz) ppm] in an almost quantitative yield. Further treatment of **18** with NaI in methyl ethyl ketone (under

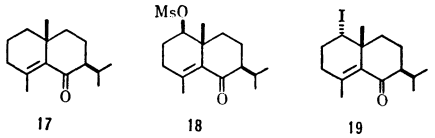

17 18 19

Fig. 3.

reflux, 15 h) afforded the corresponding iodide (**19**) [δ 4.31 (1H, dd, J=7.0 and 2.0 Hz) ppm]. which was directly reduced with n-Bu_3SnH in toluene (under reflux, 4 h) to give the compound **17**.

We further examined the base-catalyzed cyclization of **2** using basic alumina, as follows. Epoxyisoacoragermacrone (**2**) was directly absorbed on basic alumina (150—250 mesh), and then eluted with hexane-benzene (1 : 3) to give an isomer **20** with a CO group (ν_{max} 1715 cm^{-1}), in a 34% yield. Further elution with ether gave a fairly unstable isomer **21**, which has a secondary OH group [ν_{max} 3400 br. cm^{-1}; δ 4.32 (1H, dd, J=6.5 and 9.5 Hz) ppm], in a 46% yield. The structures of these two reaction products are based on their spectral data and the chemical evidences, as follows. Either of these compounds has a tertiary methyl group (δ 1.18 ppm in **20**; δ 1.27 ppm in **21**) in addition to the original isopropyl group. However, the former has a MeC=CH–CH–O– grouping [δ 1.86 (3H, br.s), 3.77 (1H, br.d, J=7.9 Hz) and 5.88 (1H, br.d, J=7.9 Hz) ppm], which was hydrogenated over 5% Pd-C to give the corresponding dihydro-compound **22**, mp 37—40 °C; $C_{15}H_{26}O_2$: δ 1.08 (3H, d, J=6.5 Hz) and 3.27 (1H, m) ppm. On the other hand, the alcohol **21** has a conjugated diene system (CH_2=C–CH=C–O–), as judged by its IR, UV and NMR spectra: ν_{max} 1650 and 1600 cm^{-1}; λ_{max} 240 nm (ε, 16160); δ 4.67 (1H, br.m), 4.79 (1H, d, J=2.4 Hz) and 5.58 (1H, s) ppm.

21 22

Fig. 4.

In the above reaction using basic alumina, an intramolecular H^- transfer may take place, leading to the formation of **20**, as shown in Scheme 6.

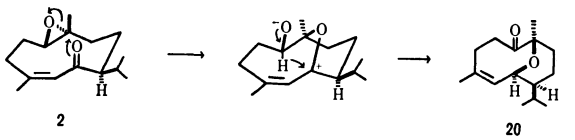

2 20

Scheme 6. Formation process of the keto compound (**20**).

In the next experiment, epoxidation of isoacoragermacrone (**1**) was carried out using 30% H_2O_2–5% NaOH aq. solution (room temp, overnight) to afford an epoxygermacrone (**23**) in a 92% yield (mp 85.5—86 °C; $C_{15}H_{24}O_2$; ν_{max} 1720 cm^{-1}: δ 1.42 (3H, s) and 3.43 (1H, s) ppm], which has an epoxide ring[5] at the position corresponding to the conjugated double bond of isoacoragermacrone (**1**). This epoxide (**23**) was also submitted to the biogenetic model reactions,[6] as seen in the case of **2**.

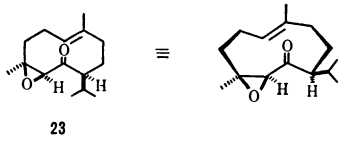

23

Fig. 5.

Acid-catalyzed Cyclizations of the Epoxygermacrone (23). This epoxide (**23**) is quite stable to 80% aq. AcOH at room temperature. However, when heated at 60 °C for 3 h, **23** was converted into a cadinane-type compound **24** [mp 195 °C (decomp.); $C_{15}H_{26}O_3$] in a 48% yield. This cyclization product **24** was also obtained in an 8% yield together with the corresponding formate (**25**) [ν_{max} 1720 cm^{-1}; δ 8.04 (1H, s) ppm] in a 15% yield, on treatment of **23** with 80% aq. HCOOH (room temp, 10 min). The latter (**25**) was readily converted into **24** on hydrolysis with 10% methanolic KOH. The structure of the cadinate-type compound (**24**) was determined by its spectral data [ν_{max} 3400 br. cm^{-1}; δ 1.32 (3H, s), 1.73 (3H, br.s), 3.90 (1H, br.s) and 5.64 (1H, m) ppm] and the following chemical evidence. When treated with $NaIO_4$ in aq. MeOH (room temp, overnight), the compound **24** was converted into a diketone (**26**) as a colorless liquid [ν_{max} 1720 br. cm^{-1} and no OH band; δ 1.26 (3H, s), 2.12 (3H, s) and 8.00 (1H, s) ppm]. This oxidation product (**26**) was further treated with NaOMe–MeOH (under reflux, 4 h) to give an α,β-unsaturated ketone in a high yield, whose structure was proved to be **27** by its spectral data: ν_{max} 1710 and 1660 cm^{-1}; λ_{max} 243 nm (ε, 10300); δ (C_6D_6) 1.56 (3H, s), 1.72 (3H, s), 2.30 (2H, t, J=7.8 Hz), and 2.65 (2H, t, J=7.8 Hz) ppm.

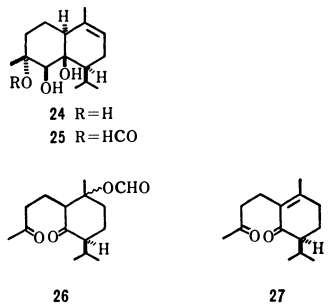

24 R=H
25 R=HCO

26 27

Fig. 6.

Probably, the intramolecular cyclization of **23** takes place after cleavage of the epoxide ring. From a biogenetic point of view, the formation of the trisubstituted olefins (**24** and **25**) is interesting. The further acid-catalyzed cyclization of the epoxygermacrone (**23**) was carried out using $AlCl_3$ in absolute ether.

On treatment with $AlCl_3$ in absolute ether (0 °C, 10 min), the epoxide (**23**) afforded a mixture of several compounds, from which two cyclization products **28** and **29** were isolated in 27 and 32% yields, respectively. The former (**28**) is an aldehyde [$C_{15}H_{24}O_2$ (m/e 236 (M^+)); ν_{max} 2700 and 1720 cm^{-1}; δ 9.75 (1H, s) ppm], and has no OH group. The NMR spectrum of **28** indicates the presence of two tertiary methyl groups (δ 1.25 and 1.52 ppm)[7] in addition to the original isopropyl group. On reduction with $LiAlH_4$ in THF (room temp, overnight). the aldehyde (**28**) was converted

into the corresponding alcohol **30** ($C_{15}H_{26}O_2$) which was a tertiary hydroxymethyl group [ν_{max} 3400 cm^{-1}: δ 3.56 (1H, d, J=12 Hz) and 3.76 (1H, d, J=12 Hz) ppm]. It was acetylated with Ac_2O–pyridine to give an acetate (**31**); $C_{17}H_{28}O_3$; ν_{max} 1740 cm^{-1}; δ 2.07 (3H, s) and 4.10 (2H, br.s) ppm. This alcohol was easily reconverted into the original aldehyde (**28**), in a 52% yield, on oxidation with Jones reagent (room temp, 1.5 h). From the above spectral and chemical data, the structure of the aldehyde can be represented by **28**.

The compound **29** has the same molecular formula as that of **28**. However, the former has no CO group, but instead a hydroxyl group (ν_{max} 3560 cm^{-1}). As described above, the aldehyde (**28**) has two tertiary methyl groups, while **29** has one methyl group [δ 1.67 (3H, s) ppm] and one exocyclic double bond [δ 4.66 (1H, br.s) and 4.86 (1H, br.s) ppm] that can be converted into a secondary methyl group on catalytic hydrogenation leading to the formation of the corresponding dihydro-compound (**32**); $C_{15}H_{26}O_2$ [m/e 238 (M^+)]; δ 1.10 (3H, d, J=8 Hz) and 2.85 (1H, m) ppm. From a structural point of view, particularly, it is important that the NMR spectra of **29** and **32** both have the two sharp doublets with a geminal coupling constant (J= 12 Hz) which can be assigned to the isolated methylene group (δ 2.90 and 3.31 ppm in **29**; δ 2.86 and 3.18 ppm in **32**). From these data, the structure of the alcohol may be represented by **29**.

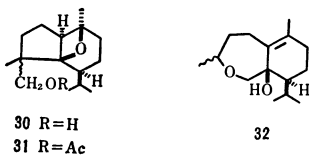

Fig. 7.

In the above reaction of the epoxygermacrone (**23**) with $AlCl_3$, these two cyclization compounds **28** and **29** may be produced according to the following pathways, as shown in Scheme 7.

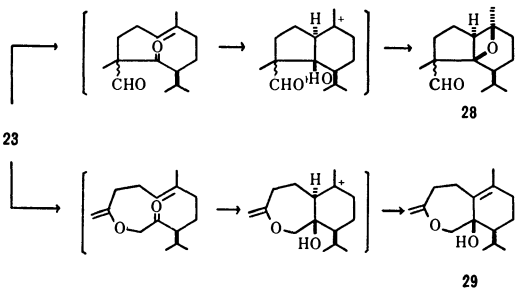

Scheme 7. Possible pathways from **23** to the compounds **28** and **29**.

Finally, we used the oxidation product (**33**) of shiromodiolmonoacetate[8] as an (*E*,*E*)-epoxygermacrone, as will be described below. This epoxide (**33**) is also stable to 80% aq. AcOH at room temperature, as seen in the case of the (*Z*,*E*)-epoxygermacrone (**23**). However, when heated at 80 °C for 4 h, the epoxide (**33**) was converted into a mixture of many products, from which a guaiane-type compound (**34**) was isolated in a low yield (*ca.* 15%). The structure of **34** is based on its mass, IR and NMR spectra: $C_{17}H_{26}O_4$ [m/e 276 (M^+-18) and 234 (M^+-60)]; ν_{max} 3420, 1735 and 1710 cm^{-1}; δ 0.98 (3H, d, J=7 Hz) and 1.05 (3H, d, J= 7 Hz) [*i*-Pr], 1.36 (3H, s) [Me–C(OH)–], 1.71 (3H, br.s) [Me–C=C–], 2.05 (3H, s) and 5.30 (1H, m) [AcO–CH–] and 3.54 (1H, br.s) ppm [=C–CH–C=O]. This guaiane-type compound (**34**) was also produced in a 40% yield on treatment with $AlCl_3$ in absolute ether (−5 °C, 15 min). These results are quite similar to that of shiromodiol monoacetate (**35**), the acid-catalysed cyclization of which has afforded the corresponding guaiane-type compound (**36**).[8]

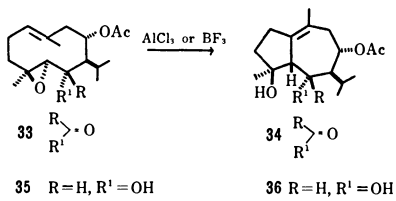

Scheme 8. Acid-catalyzed cyclization of the (*E*,*E*)-epoxygermacrone or -germacrene.

Experimental

All the mps are uncorrected. GLC were recorded on a Shimadzu GC-1C gas chromatograph with a flame-ionizer detector (stationary phase: 5% PEG 20 M on Celite 545 (100 mesh); column (ϕ 3 mm × 1.5 m (stainless steel)] temp: 90 °C; carrier gas: nitrogen (85 ml/min); inlet pressure: 1.2 Kg/cm^2], unless otherwise stated. IR spectra were recorded on a Hitachi-215 spectrophotometer. UV spectra were taken on a Hitachi-124 spectrophotometer, using MeOH as the solvent. NMR spectra were recorded on a Varian Associate A-60 (60 MHz), a Nihondenshi JNM-C60H (60 MHz) or JNM-PS 100 (100 MHz), using $CDCl_3$ as the solvent, unless otherwise stated. The chemical shifts are given in ppm relative to the internal TMS, and only prominent signals are cited (d, doublet; m, multiplet; q, quartet; s, singlet; t, triplet). Mass spectra were obtained on a Hitachi RMU-6D mass spectrometer operating at an ionization energy of 70 eV. ORD curves were recorded on a JASCO ORD/UV spectrophotometer, using MeOH as the solvent. Preparative TLC were carried out on Kieselgel PF_{254} (E. Merck, A. G.), unless otherwise stated.

Epoxidation of Isoacoragermacrone (1) with m-*Chloroperbenzoic Acid.* To a solution of **1** (1.10 g) in ether (40 ml) was added, with stirring, *m*-chloroperbenzoic acid (920 mg) at 0 °C. The resulting solution was further stirred at 0 °C for 20 h, and then washed successively with sat. Na_2SO_3, sat. $NaHCO_3$ and sat. NaCl aq. solutions, and then dried over anhydrous Na_2SO_4. Removal of the solvent afforded a crystalline solid of **2** (1.18 g), which was recrystallized from hexane to give colorless columns; mp 55 °C; ν_{max} (KBr) 1675 and 1620 cm^{-1}; λ_{max} 243 nm (ε, 6400); δ 0.93 (3H, d, J=6.5 Hz), 0.97 (3H, d, J=6.5 Hz), 1.21 (3H, s), 1.91 (3H, d, J=1.3 Hz) and 6.20 (1H, br.s) ppm; m/e 236 (M^+), 193 and 175 (Found: C, 76.30; H, 10.47%. Calcd for $C_{15}H_{24}O_2$: C, 76.22; H, 10.24%).

Reaction of 2 with 80% aq. HCOOH. The compound **2** (260 mg) was dissolved, with stirring, in 80% aq. HCOOH (8 ml) at −18—−20 °C. The resulting solution was further stirred at the same temperature for 10 min, and then diluted with ice water (*ca.* 40 ml) and extracted with CH_2Cl_2. The extract was washed successively with a sat. $NaHCO_3$ aq. solu-

tion and water, and then dried over anhydrous $MgSO_4$. Evaporation of the solvent under reduced pressure afforded crude crystals, which were washed with ether to leave insoluble crystals of the dihydroxy ketone **3** (94 mg). The ethereal solution was concentrated under reduced pressure to give an oil, which was separated by preparative TLC using alumina [GF_{254} (type E), E. Merck, A. G.] and hexane–ether (2: 1) to give **3** (39 mg) and the *cis*-selinane-type compound **4** (89 mg).

3: mp 155—157 °C (from Et_2O–MeOH); ν_{max} (KBr) 3400 br., 1680 and 1645 cm^{-1}; λ_{max} 238 nm (ε, 4200); δ 0.93 (6H, d, J=6.5 Hz), 1.22 (3H, s), 1.87 (3H, d, J=1.2 Hz), 3.48 (1H, dd, J=4.0 and 6.0 Hz), and 5.98 (1H, br. s) ppm; *m/e* 236 (M^+-18) and 210 (Found: C, 70.81; H, 10.57%. Calcd for $C_{15}H_{26}O_3$: C, 70.83; H, 10.30%).

4 as a colorless viscous liquid: ν_{max} (film) 3430 br. and 1705 cm^{-1}; δ 0.91 (6H, d, J=5.0 Hz), 1.02 (3H, s), 1.58 (3H, br. s), 3.53 (1H, t, J=5.0 Hz), and 5.44 (1H, br. s) ppm; *m/e* 236 (M^+) and 193 (Found: *m/e* 236.17726. Calcd for $C_{15}H_{24}O_2$: *m/e* 236.17762).

Acetylation of the Selinane-type Compound (4). A solution of **4** (85 mg) in Ac_2O–pyridine (2: 5) (7 ml) was stirred at room temperature overnight, and then poured into a cooled 5% HCl aq. solution, and extracted with ether. The ethereal extract was washed successively with water, 5% $NaHCO_3$ aq. solution and water, and then dried over anhydrous $MgSO_4$. Removal of the solvent under reduced pressure gave an oil, which was purified by preparative TLC using alumina [GF_{254} (type E), E. Merck, A. G.] and hexane–ether (5: 1) to afford **5** (53 mg) as a colorless viscous liquid; ν_{max} (film) 1740, 1710, and 1245 cm^{-1}; δ 0.90 (6H, d, J=5.1 Hz), 0.98 (3H, s), 1.62 (3H, br. s), 2.03 (3H, s), 4.80 (1H, t, J=4.5 Hz), and 5.45 (1H, br. s) ppm; *m/e* 278 (M^+), 237, and 219 (Found: 278.18864. Calcd for $C_{17}H_{26}O_3$: *m/e* 278.18818).

Acid-catalyzed Isomerization of the Acetate (5) with 100% HCOOH. A solution of **5** (50 mg) in 100% HCOOH (3 ml) was refluxed for 10 h under a nitrogen atmosphere, and then slowly poured into a sat. $NaHCO_3$ aq. solution and extracted with ether. The ethereal extract was washed with water, and then dried over anhydrous $MgSO_4$. Removal of the solvent left a brown oil (42 mg) which was separated by preparative TLC using alumina [GF_{254} (type E), E. Merck, A. G.] and hexane–ether (4: 1) to give the starting material **5** (8 mg) and the α,β-unsaturated ketone **6** (10 mg) as a colorless viscous liquid; ν_{max} (film) 1745, 1690, 1630, and 1250 cm^{-1}; λ_{max} 246 nm (ε, 4800); δ 0.89 (3H, d, J=6.8 Hz), 0.95 (3H, d, J=6.8 Hz), 1.01 (3H, s), 1.71 (3H, br. s), 2.07 (3H, s). and 4.85 (1H, dd, J=6.2 and 9.0 Hz) ppm; *m/e* 278 (M^+), 237, and 219 (Found: *m/e* 278.18670. Calcd for $C_{17}H_{26}O_3$: *m/e* 278.18818).

Acid-catalyzed Reaction of Epoxyisoacoragermacrone (2) in Thiophenol. To a solution of **2** (160 mg) in thiophenol (2 ml) was added, with stirring, 5 drops of 100% HCOOH at room temperature. The resulting solution was further stirred at room temperature, and then diluted with a cooled 10% NaOH aq. solution (20 ml) and extracted with ether. The ethereal extract was washed successively with a cooled 10% NaOH aq. solution and water, and then dried over anhydrous $MgSO_4$. Removal of the solvent afforded an almost colorless liquid, which was purified by preparative TLC using alumina [GF_{254} (type E), E. Merck, A. G.] and hexane–benzene (1: 1) to give the enol ether **8** (165 mg) as a colorless viscous liquid; ν_{max} (film) 3420 br., 3060 sh., 3950, 1665, 1580, 745, and 690 cm^{-1}: δ 0.86 (3H, d, J=6.0 Hz), 0.88 (3H, d, J=6.0 Hz), 1.21 (3H, s), 1.35 (3H, s), 1.49 (1H, s, OH), 4.25 (1H, br. t, $J\simeq$6.0 Hz), 4.75 (1H, s), and 7.30 (5H, complex) ppm; *m/e* 236 (M^+-PhSH) and 221 (Found: *m/e* 236.17410. Calcd for $C_{15}H_{24}O_2$ ($C_{21}H_{30}O_2S-C_6H_6S$)*: *m/e* 236.17762).

Acetylation of 8 with Ac_2O–Pyridine. To a solution of **8** (60 mg) in pyridine (2 ml) was added Ac_2O (0.5 ml) at 0 °C. The solution was allowed to stand at the same temperature overnight, and then diluted with ice water (*ca.* 20 ml) and extracted with ether. The ethereal extract was washed successively with a cooled 10% HCl aq. solution and water, and then dried over anhydrous $MgSO_4$. Removal of the solvent under reduced pressure left a colorless viscous liquid (61 mg) in an almost pure state, which was further purified by preparative TLC using benzene to give **9** (58 mg) as a colorless viscous liquid; ν_{max} (film) 3050, 1735, 1665, 1580, 1240, 745, and 690 cm^{-1}; δ 0.87 (6H, d, J=6.0 Hz), 1.25 (3H, s), 1.37 (3H, s), 2.00 (3H, s), 4.82 (1H, s), 5.57 (1H, br. t, $J\simeq$6.8 Hz), and 7.35 (5H, complex) ppm; *m/e* 279 (M^+-109) and 278 (M^+-110) (Found: *m/e* 279.19579. Calcd for $C_{17}H_{27}O_3$ ($C_{23}H_{32}O_3S-C_6H_5S$)*: *m/e* 279.19601).

Reaction of 2 with $AlCl_3$ in Absolute Ether. To a solution of **2** (325 mg) in absolute ether (15 ml) was added, with stirring, a solution of $AlCl_3$ (200 mg) in absolute ether (4 ml) at −18 °C. The solution was further stirred at −18—−20 °C for 20 min, and then diluted with ether saturated with water. The ethereal solution was washed successively with a sat. potassium sodium tartarate aq. solution and a sat. NaCl aq. solution, and then dried over anhydrous Na_2SO_4. Removal of the solvent afforded a residue, which was dissolved in ether (2 ml). Precipitated colorless crystals of the dimer **11** (95 mg) was collected by filtration. The filtrate was concentrated, and the residue was subjected to preparative TLC using alumina [GF_{254} (type E), E. Merck, A. G.] and hexane–ether (1: 1) giving two fractions. From the less polar fraction, the compound **10** (60 mg) was isolated as a colorless liquid; ν_{max} (film) 3430 br., 3030 sh. and 1650 cm^{-1}; λ_{max} 243 nm (ε, 7500); δ 0.95 (6H, d, J=5.3 Hz), 1.35 (3H, s), 1.79 (3H, br. s), 1.69 (1H, s, OH), 3.45 (1H, dd, J=3.7 and 5.8 Hz), 5.15 (1H, s) and 5.34 (1H, t, J=6.8 Hz) ppm: *m/e* 236 (M^+ for $C_{15}H_{24}O_2$), 221, 218, and 175. Elemental analysis of **10** was not carried out because of its instability, but its structure was supported by the above-mentioned physical data.

From the more polar fraction, a colorless oil was obtained, which was further separated by preparative TLC using $CHCl_3$–MeOH (100: 5) to give two dimers **11** (59 mg) and **12** (107 mg). Their physical data are shown below.

11: mp 159.5—160.5 °C (from hexane–ether); ν_{max} (KBr) 3450 br., 1680 and 1660 cm^{-1}; λ_{max} 247 and 205 nm (ε, 6670 and 13680, respectively); δ 0.96 (12H, complex), 1.01 (3H, s), 1.28 (3H, s), 1.39 (3H, s), 3.21 (1H, t, J=4.0 Hz), 3.93 (1H, t, J=6.1 Hz), 4.46 (1H, s), 5.15 (1H, s), and 5.41 (1H, t, J=7.0 Hz) ppm; *m/e* 472 (M^+), 238, 237, 236, and 219 (Found: *m/e* 472.35658. Calcd for $C_{30}H_{48}O_4$: *m/e* 472.35524).

12: mp 143.5—144.5 °C (from hexane–ether); ν_{max} (KBr) 3390 br., 1680, and 1650 cm^{-1}; λ_{max} 254 and 203 nm (ε, 22400 and 11800, respectively); δ 0.90 (12H, complex), 1.08 (3H, s), 1.18 (3H, s), 1.23 (3H, s), 1.51 (2H, s, OH), 3.32 (1H, br. m), 4.26 (2H, br. m), 4.79 (1H, s), 5.33 (1H, s), and 5.96 (1H, s) ppm; *m/e* 472 (M^+), 238, 237, 236, and 219 (Found: *m/e* 472.35714. Calcd for $C_{30}H_{48}O_4$: *m/e* 472.35524).

Acetylation of the Dimer 11. To a solution of **11** (100 mg) in pyridine (5 ml) was added Ac_2O (2 ml) at 0 °C. The resulting solution was further stirred at 0 °C overnight, and then poured into ice water and extracted with ether. The ethereal extract was washed successively with a cooled 5% HCl aq. solution, a cooled sat. $NaHCO_3$ aq. solution, and water, and then dried over anhydrous Na_2SO_4. After evaporation of the solvent, the residue was purified by preparative TLC using

* No molecular ion peak was observed.

alumina [GF_{254} (type E), E. Merck, A. G.] and benzene to give **13** (62 mg) as a colorless viscous liquid; ν_{max} (film) 3040, 1740, 1670, and 1250 cm^{-1}; δ 0.83—1.00 (12H, complex), 1.00 (3H, s), 1.27 (6H, s), 2.00 (3H, s), 2.06 (3H, s), 4.64 (1H, s), 5.26 (1H, s), and 4.87—5.74 (3H, complex) ppm (Found: *m/e* 556.37888. Calcd for $C_{34}H_{52}O_6$: *m/e* 556.37637).

Acetylation of the Dimer ***12***. To a solution of **12** (90 mg) in pyridine (5 ml) was added Ac_2O (2 ml) at 0 °C. The resulting solution was stirred at 0 °C overnight, and then treated according to the same procedure as that for **11** to give an oil, which was purified by preparative TLC using AcOEt–benzene (1: 10) to give **14** (61 mg) as a colorless viscous liquid; ν_{max} (film) 1740, 1680, 1650, and 1240 cm^{-1}; δ 0.90 (12H, complex), 1.11 (3H, s), 1.22 (3H, s), 1.28 (3H, s), 2.02 (6H, s), 3.48 (1H, m), 4.87 (1H, s), 5.38 (1H, s), 5.31—5.67 (2H, m), and 5.99 (1H, s) ppm (Found: *m/e* 556.37982. Calcd for $C_{34}H_{52}O_6$: *m/e* 556.37637).

Base-catalyzed Reaction of ***2*** *with* t-*BuOK*. To a solution of potassium metal (25 mg) in *t*-BuOH (4 ml) was added, with stirring, a solution of **2** (137 mg) in *t*-BuOH (1 ml) at 25 °C under a nitrogen atmosphere. The solution was further stirred at 25 °C for 2 h, and then diluted with water (10 ml) and extracted with ether. The ethereal extract was washed with water, and then dried over anhydrous Na_2SO_4. Removal of the solvent gave an oil which was purified by preparative TLC using alumina [GF_{254} (type E), E. Merck, A. G.] and hexane–ether (1: 1) to give a colorless viscous liquid of **15** (103 mg); ν_{max} (film) 3450 br., 1680, and 1630 cm^{-1}; λ_{max} 248 nm (ε, 4600); δ 0.90 (3H, d, J=6.9 Hz), 0.95 (3H, d, J=6.9 Hz), 0.94 (3H, s), 1.69 (3H, br. s) and 3.61 (1H, dd, J=6.5 and 9.0 Hz) ppm; *m/e* 236 (M^+) and 193 (Found: *m/e* 236.17911. Calcd for $C_{15}H_{24}O_2$: *m/e* 236.17762).

Acetylation of the α,β-Unsaturated Ketone ***(15)***. A solution of **15** (84 mg) in pyridine (5 ml) and Ac_2O (1 ml) was allowed to stand at room temperature overnight, and then poured into a cooled 5% HCl aq. solution and extracted with ether. The ethereal extract was washed successively with water, 5% $NaHCO_3$ aq. solution and water, and then dried over anhydrous $MgSO_4$. Removal of the solvent afforded an oil, which was purified by preparative TLC using alumina [GF_{254} (type E), E. Merck, A. G.] and hexane–ether (5: 1) to give a colorless viscous liquid (69 mg), which was completely identical with the acetoxy compound **6** (TLC and IR spectrum).

Mesylation of ***15***. To a solution of **15** (93 mg) in pyridine (3 ml) was added dropwise, with stirring, mesyl chloride (50 mg) at 0 °C. The resulting solution was further stirred at 0 °C for 1 h, and then at room temperature for 2 h. After addition of ice–water (*ca.* 10 ml), the solution was extracted with ether. The extract was washed successively with a cooled 5% HCl aq. solution, water and a sat. NaCl aq. solution, and then dried over anhydrous Na_2SO_4. Removal of the solvent under reduced pressure afforded the mesylate **18** (124 mg) in a pure state as a colorless viscous liquid; ν_{max} (film) 1690, 1630, 1350, and 1170 cm^{-1}; λ_{max} 246 nm (ε, 4200); δ 0.89 (3H, d, J=6.5 Hz), 0.95 (3H, d, J=6.5 Hz), 1.00 (3H, s), 1.70 (3H, s), 3.07 (3H, s), and 4.21 (1H, t, J=7.5 Hz) ppm; *m/e* 314 (M^+), 218 and 175 (Found: *m/e* 314.15690. Calcd for $C_{16}H_{26}O_4S$: *m/e* 314.15517).

Reaction of the Mesylate ***18*** *with NaI*. A mixture of **18** (112 mg) and NaI (530 mg) in methyl ethyl ketone (7 ml) was refluxed, with stirring, for 15 h under a nitrogen atmosphere, and then concentrated under reduced pressure to leave a reddish residue, which was diluted with water (30 ml) and then extracted with ether. The ethereal extract was washed with water, and then dried over anhydrous Na_2SO_4. Removal of the solvent left a reddish oil (120 mg) which was purified by preparative TLC using hexane–benzene (1: 3) to give **19** (36 mg) as a colorless liquid; ν_{max} (film) 1690 and 1630 cm^{-1}; δ 0.88 (3H, d, J=6.3 Hz), 0.93 (3H, d, J=6.3 Hz), 1.11 (3H, s), 1.67 (3H, s), and 4.31 (1H, dd, J=7.0 and 2.0 Hz) ppm; *m/e* 346 (M^+ for $C_{15}H_{23}IO$) and 219 (M^+—I). This iodide was directly used for the next experiment.

Reduction of the Iodide ***19*** *with* n-Bu_3SnH. To a solution of **19** (36 mg) in toluene (3 ml) was added *n*-Bu_3SnH (26 mg) under a nitrogen atmosphere. The solution was refluxed for 4 h, and then concentrated under reduced pressure to give a yellow oil, which was purified by preparative TLC using hexane–benzene (1: 1) to give a pale yellow liquid (22 mg) which was completely identical with an authentic sample of the isomerization product (**17**) of acolamone[4] (GLC, TLC, and IR spectrum).

Reaction of Epoxyisoacoragermacrone ***(2)*** *with Basic Alumina*. The compound **2** (980 mg) was dissolved in hexane–benzene (1: 3), and directly chromatographed on basic alumina (Katayama Chemical Co., Ltd., 150—250 mesh) (50 g). Elution with the same solvent system afforded **20** (330 mg) in a pure state as a colorless oil; ν_{max} (film) 3030, 1715, and 1650 cm^{-1}; δ 0.99 (6H, d, J=6.9 Hz), 1.18 (3H, s), 1.86 (3H, br. s), 3.33 (1H, m), 3.77 (1H, br. d, J=7.9 Hz) and 5.88 (1H, br. d, J=7.9 Hz) ppm; *m/e* 436 (M^+), 193, 175, and 165 (Found: *m/e* 236.17941. Calcd for $C_{15}H_{24}O_2$: *m/e* 236.17762).

Further elution with ether afforded a pale yellow oil (450 mg) in an almost pure state, which was further purified by preparative TLC using alumina [GF_{254} (type E), E. Merck, A. G.] and benzene to give **21** in a pure state as a colorless viscous liquid; λ_{max} (film) 3400 br., 3080, 1650, 1600, 915, and 880 cm^{-1}; λ_{max} 240 nm (ε, 16160); δ 0.89 (3H, d, J=6.3 Hz), 0.92 (3H, d, J=6.3 Hz), 1.27 (3H, s), 3.38 (1H, br. m), 4.32 (1H, dd, J=6.5 and 9.5 Hz), 4.67 (1H, br. m), 4.79 (1H, d, J=2.4 Hz), and 5.58 (1H, s) ppm; *m/e* 236 (M^+ for $C_{15}H_{24}O_2$), 221 and 193. Elemental analysis of **21** was not carried out because of its instability, but its structure may be supported by the above-mentioned physical data.

Catalytic Hydrogenation of ***20***. Catalytic hydrogenation of **20** (45 mg) in MeOH (10 ml) was carried out over 5% Pd–C (150 mg) at room temperature for 40 min, and then filtered to remove the catalyst. The filtrate was concentrated under reduced pressure to give a colorless viscous liquid which was chromatographed on alumina and eluted with ether to give the dihydro compound **22** (38 mg) as colorless crystals; mp 37—40 °C (by sublimation); ν_{max} (KBr) 1705 cm^{-1}; δ 0.94 (6H, d, J=7.1 Hz), 1.08 (3H, d, J=6.5 Hz), 1.23 (3H, s), and 3.27 (1H, m) ppm; *m/e* 238 (M^+), 210, 195, 182, and 167 (found: *m/e* 238.19233. Calcd for $C_{15}H_{26}O_2$: *m/e* 238.19327).

Epoxidation of Isoacoragermacrone ***(1)*** *with 30% H_2O_2–5% aq. NaOH*. To a solution of **1** (440 mg) in MeOH (30 ml) was slowly added a mixed solution of 30% H_2O_2 (2 ml) and 5% NaOH aq. solution (10 ml) at 0 °C, and then the reaction temperature was gradually elevated to room temperature. The solution was further stirred at room temperature overnight, and then diluted with water (60 ml) and extracted with ether. The ethereal extract was washed with water, and then dried over anhydrous $MgSO_4$. Removal of the solvent afforded a colorless viscous liquid (436 mg), which was crystallized from hexane to give colorless prisms of **23**; mp 85.5—86 °C; ν_{max} (KBr) 1720 cm^{-1}; δ 0.90 (3H, d, J=7 Hz), 1.04 (3H, d, J=7 Hz), 1.42 (3H, s), 1.44 (3H, s), 3.43 (1H, s) and 5.20 (1H, t, J=7 Hz) ppm (Found: *m/e* 236.17474. Calcd for $C_{15}H_{24}O_2$: *m/e* 236.17762).

Reaction of ***23*** *with 80% aq. AcOH*. A solution of **23** (23 mg) in 80% aq. AcOH (0.5 ml) was heated at 60 °C for 3 h,

with stirring. After addition of ether (20 ml), the solution was washed successively with a sat. $NaHCO_3$ aq. solution and a sat. NaCl aq. solution, and then dried over anhydrous $MgSO_4$. Removal of the solvent afforded a colorless liquid (25 mg), which was recrystallized from ether to give colorless crystals (10 mg). The remaining ethereal solution was concentrated, and then separated by preparative TLC to give colorless crystals (2 mg). Recrystallization from $CHCl_3$ afforded colorless prisms of **24**; mp 195 °C (decomp.); ν_{max} (KBr) 3400 cm^{-1}; δ 0.92 (3H, d, J=7 Hz), 0.94 (3H, d, J=7 Hz), 1.32 (3H, s), 1.56 (1H, s, OH), 1.73 (3H, br. s), 2.16 (2H, s, OH), 3.90 (1H, br. s) and 5.64 (1H, m) ppm; *m/e* 254 (M^+) and 236 (Found: C, 70.27; H, 10.50%. Calcd for $C_{15}H_{26}O_3$: C, 70.83; H, 10.30%).

*Reaction of **23** with 80% aq. HCOOH.* A solution of **23** (120 mg) in 80% aq. HCOOH (2 ml) was stirred at room temperature for 10 min, and then diluted with ether (40 ml). The ethereal solution was washed successively with water, a sat. $NaHCO_3$ aq. solution and a sat. NaCl aq. solution, and then dried over anhydrous $MgSO_4$. Removal of the solvent afforded a colorless viscous liquid which was dissolved in ether (0.5 ml) to give the triol **24** (10 mg) as colorless crystals. After filtration of the crystals, the filtrate was subjected to preparative TLC using $CHCl_3$ to give the formate **25** (22 mg) as a colorless viscous liquid; ν_{max} (film) 3470 and 1720 cm^{-1}; δ 0.93 (3H, d, J=7 Hz), 0.96 (3H, d, J=7 Hz), 1.66 (3H, s), 1.74 (3H, br.s), 2.49 (1H, s, OH), 3.96 (1H, d, J=5.4 Hz), 5.65 (1H, m), and 8.04 (1H, s) ppm; *m/e* 236 (M^+−HCOOH), 218, and 200. Without purification this formate was used for the next experiment.

*Hydrolysis of the Formate (**25**) with 10% Methanolic KOH.* A solution of **25** (22 mg) in 10% methanolic KOH (5 ml) was stirred at room temperature overnight, and then diluted with ether (30 ml). The ethereal solution was washed with water, and then dried over anhydrous Na_2SO_4. Removal of the solvent gave colorless crystals of **24** (mp and IR spectrum).

*Oxidation of the Triol (**24**) with $NaIO_4$.* To a solution of **24** (90 mg) in MeOH (6 ml) was added, with stirring, a solution of $NaIO_4$ (230 mg) in water (3 ml). The resulting solution was further stirred at room temperature overnight, and then diluted with water (20 ml) and extracted with ether. The ethereal extract was washed successively with water and a sat. NaCl aq. solution, and then dried over anhydrous $MgSO_4$. After evaporation of the solvent, the oily residue was separated by preparative TLC using $CHCl_3$ to give the oxidation product **26** (18 mg) in addition to the starting material (20 mg) (TLC and IR spectrum).

26. A colorless viscous liquid: ν_{max} (film) 1720 br.cm^{-1}; δ 0.86 (3H, d, J=6.5 Hz), 0.93 (3H, d, J=6.5 Hz), 1.26 (3H, s), 2.12 (3H, s), 3.03 (1H, dd, J=10 and 2 Hz) and 8.00 (1H, s) ppm; *m/e* 222 [M^+($C_{15}H_{24}O_4$)−HCOOH]. This compound was further used for the next experiment.

*Formation of an α,β-Unsaturated Ketone **27**.* A solution of **26** (18 mg) in MeOH (4 ml) containing NaOMe (10 mg) was refluxed for 4 h under a nitrogen atmosphere, and then diluted with water (10 ml) and extracted with ether. The ethereal solution was washed with water, and then dried over anhydrous $MgSO_4$. Evaporation of the solvent gave a colorless oil, which was purified by preparative TLC using $CHCl_3$ to afford **27** (14 mg) in a pure state as a colorless liquid; δ (C_6D_6) 0.86 (3H, d, J=7.0 Hz), 0.91 (3H, d, J=7.0 Hz), 1.56 (3H, s), 1.72 (3H, s), 2.30 (2H, t, J=7.8 Hz), and 2.65 (2H, t, J=7.8 Hz) ppm (Found: *m/e* 222.16433. Calcd for $C_{14}H_{22}O_2$: *m/e* 222.16197).

*Reaction of **23** with $AlCl_3$.* To a solution of **23** (190 mg) in absolute ether (10 ml) was added, with stirring, a solution of $AlCl_3$ (118 mg) in absolute ether (2 ml) at 0 °C. The solution was further stirred at 0 °C for 10 min, and then the reaction was quenched by addition of ice-water (0.5 ml). After addition of a sat. potassium sodium tartarate aq. solution (10 ml), the ethereal layer was separated. The aqueous solution was further extracted with ether. The combined ethereal extracts were washed with water, and then dried over anhydrous $MgSO_4$. Evaporation of the solvent afforded a colorless viscous liquid, which was separated by preparative TLC using benzene to give **28** (52 mg) and **29** (60 mg).

28. A colorless viscous liquid: ν_{max} (film) 2700 and 1720 cm^{-1}; δ 0.91 (3H, d, J=7 Hz), 0.98 (3H, d, J=7 Hz), 1.25 (3H, s), 1.52 (3H, s), and 9.75 (1H, s) ppm (Found: *m/e* 236.17748. Calcd for $C_{15}H_{24}O_2$: *m/e* 236.17762).

29. A colorless viscous liquid: ν_{max} (film) 3560, 3090, and 1650 cm^{-1}; δ 0.87 (3H, d, J=7 Hz), 0.90 (3H, d, J=7 Hz), 1.67 (3H, s), 2.90 (1H, d, J=12 Hz), 3.31 (1H, d, J=12 Hz), 4.66 (1H, br. s), and 4.86 (1H, br. s) ppm (Found: *m/e* 236.17253. Calcd for $C_{15}H_{24}O_2$: *m/e* 236.17762).

*Reduction of the Aldehyde (**28**) with $LiAlH_4$.* To a solution of **28** (55 mg) in absolute THF (5 ml) was added, with stirring, $LiAlH_4$ (20 mg) at room temperature. The reaction mixture was further stirred at room temperature overnight. After decomposition of an excess of the reagent with water, the reaction mixture was diluted with 5% HCl aq. solution, and then extracted with ether. The ethereal extract was washed with water, and then dried over anhydrous $MgSO_4$. After evaporation of the solvent, a colorless oil was purified by preparative TLC using $CHCl_3$ to give **30** (35 mg) as a colorless viscous liquid; ν_{max} (film) 3400 cm^{-1}; δ 0.98 (3H, d, J=6 Hz), 1.03 (3H, d, J=6 Hz), 1.24 (6H, s), 3.56 (1H, d, J=12 Hz), and 3.76 (1H, d, J=12 Hz) ppm (Found: *m/e* 238.19307. Calcd for $C_{15}H_{26}O_2$: *m/e* 238.19327).

*Acetylation of the Alcohol (**30**).* A solution of **30** (35 mg) in pyridine (3 ml) and Ac_2O (1 ml) was stirred at room temperature overnight, and then treated as usual to give a pale yellow oil, which was purified by preparative TLC using $CHCl_3$ to give **31** (25 mg) as a colorless viscous liquid; ν_{max} (film) 1740 and 1240 cm^{-1}; δ 0.94 (3H, d, J=7 Hz), 0.97 (3H, d, J=7 Hz), 1.24 (3H, s), 1.28 (3H, s), 2.07 (3H, s), and 4.10 (2H, br. s) ppm (Found: *m/e* 280.20383. Calcd for $C_{17}H_{28}O_3$: *m/e* 280.20433).

*Hydrolysis of the Acetate (**31**).* A solution of **31** (25 mg) in 5% methanolic KOH (2 ml) was stirred at room temperature overnight, and then diluted with water (10 ml) and extracted with ether. The ethereal extract was washed with water and then dried over anhydrous $MgSO_4$. Removal of the solvent afforded the original alcohol (**30**) (TLC and IR spectrum) as a colorless liquid.

*Oxidation of **30**.* Jones' reagent was carefully added to a solution of **30** (25 mg) in acetone (4 ml) until a brown color appeared persistently. The mixture was stirred at room temperature for 1.5 h, and then diluted with water (10 ml) after decomposition of an excess of the reagent with 30% ascorbic acid aq. solution. The aqueous solution was extracted with ether. The ethereal extract was washed with water, and then dried over anhydrous $MgSO_4$. Removal of the solvent gave an almost colorless oil, which was purified by preparative TLC using benzene to afford **28** (13 mg) (TLC and IR spectrum) as a colorless viscous liquid.

*Catalytic Hydrogenation of **29**.* Catalytic hydrogenation of **29** (28 mg) in AcOEt (3 ml) was carried out over PtO_2 at room temperature for 1.5 h, and then filtered to remove the catalyst. The filtrate was concentrated under reduced pressure to give a colorless viscous liquid, which was purified by preparative TLC using hexane–benzene (1: 1) to give the

dihydro compound (**32**) as a colorless viscous liquid; ν_{max} (film) 3560 cm^{-1}; δ 0.90 (3H, d, J=7 Hz), 0.92 (3H, d, J=7 Hz), 1.10 (3H, d, J=8 Hz), 1.64 (3H, s), 2.85 (1H, m), 2.86 (1H, d, J=12 Hz), and 3.18 (1H, d, J=12 Hz) ppm (Found: *m/e* 238.19088. Calcd for $C_{15}H_{26}O_2$: *m/e* 238.19327).

*Reaction of **33** with 80% aq. AcOH.* A solution of **33** (60 mg) in 80% aq. AcOH (1 ml) was heated, with stirring, at 80 °C for 4 h, and then diluted with water (15 ml) and extracted with $CHCl_3$. The extract was washed successively with water, a sat. $NaHCO_3$ aq. solution and water, and then dried over anhydrous $MgSO_4$. Removal of the solvent afforded a pale brown oil, which was separated by preparative TLC using benzene–ether (3: 1) to give **34** (9 mg) as a colorless viscous liquid; *m/e* 276 (M^+-H_2O), 234 (M^+—AcOH), and 216 (Found: *m/e* 234.16179. Calcd for $C_{15}H_{22}O_2$ ($C_{17}H_{26}O_4$–AcOH): *m/e* 234.16197).

*Reaction of **33** with $AlCl_3$ in Absolute Ether.* To a solution of **33** (120 mg) in absolute ether (20 ml) was added, with stirring, a solution of $AlCl_3$ (60 mg) in absolute ether (10 ml) at −5 °C. The solution was further stirred at −5 °C, and then the reaction was quenched by addition of ice–water (*ca.* 1 ml). The ethereal layer was separated, and dried over anhydrous $MgSO_4$. After evaporation of the solvent, an oily residue was separated by preparative TLC using benzene–ether (3: 1) to give **34** (48 mg) (TLC and IR spectrum) as a colorless viscous liquid.

The authors wish to thank Prof. Y. Hirata (Nagoya University) for his invaluable suggestions. Thanks are also due to Prof. K. Munakata and Dr. K. Wada (Nagoya University) for the sample and IR spectrum of shiromodiol diacetate, and Prof. M. Noro (Meijo University) for collection of the plant *Parabenzoinn trilobum* Nakai. They are also indebted to Drs. M. Kurono and M. Toda (Ono Pharmaceutical Co., Ltd.) for measurements of high resolution mass spectra. This research has been supported in part by grants from the Ministry of Education, to which greatful acknowledgement is made.

References

1) M. Niwa, M. Iguchi, and S. Yamamura, *Bull. Chem. Soc. Jpn.*, **49**, 3148 (1976).
2) M. Niwa, A. Nishiyama, M. Iguchi, and S. Yamamura, *Bull. Chem. Soc. Jpn.*, **48**, 2930 (1975).
3) M. Iguchi, M. Niwa, and S. Yamamura, *J. Chem. Soc., Chem. Commun.*, **1972**, 689.
4) M. Niwa, A. Nishiyama, M. Iguchi, and S. Yamamura, *Chem. Lett.*, **1972**, 823.
5) A 12% NOE is observed between 5-Me and 6-H.
6) M. Niwa, M. Iguchi, and S. Yamamura, *Tetrahedron Lett.*, **1975**, 3661.
7) The methyl singlet at δ 1.52 ppm in **28** is shifted to δ 1.24 ppm in **30**.
8) K. Wada, Y. Enomoto, and K. Munakata, *Agr. Biol. Chem. Jpn.*, **34**, 946 (1970) and references cited therein.

Chemical Correlations of α-Santonin with (+)-Junenol and Acolamone

Masatake NIWA, Masanobu IGUCHI, and Shosuke YAMAMURA*

Faculty of Pharmacy, Meijo University, Showa-ku, Nagoya 468

(Received April 21, 1976)

The chemical transformation of the acetoxy ketone (**5**), which has previously been obtained from α-santonin, to (+)-junenol (**1**) and acolamone (**3**) has been carried out. In addition, isojunenol (**2**) was also derived from **5** *via* the trisubstituted olefin (**9**) which was obtained as the main product from the α- and β-oriented mesylates (**8** and **11**) on treatment with NaI in HMPA.

From a biogenetic point of view, the selinane-type sesquiterpenes [(+)-junenol (**1**),[1] isojunenol (**2**), acolamone (**3**) and isoacolamone (**4**)[2]] should be produced from such a common intermediate as a ten-membered ring compound with an (*E,E*)-1,5-cyclodecadiene system, as is shown in Scheme 1.[2] Of these four selinane-type compounds, isojunenol (**3**) has not yet been found. In the present paper, we describe the chemical transformation of the known acetoxy ketone (**5**)[3] to these selinane-type sesquiterpenes. The results indicate that they have the same absolute configuration as α-santonin.

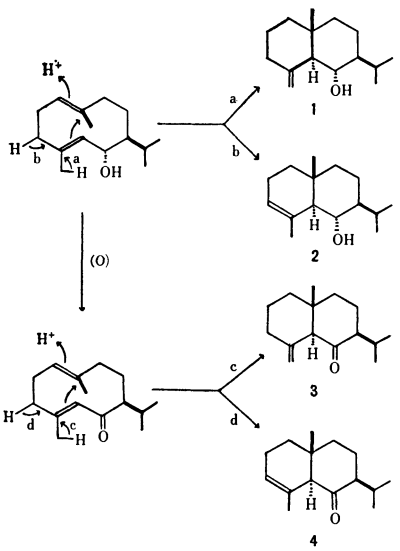

Scheme 1.

The acetoxy ketone (**5**) was reduced with $NaBH_4$ in EtOH (room temp, overnight) to give a mixture of α- and β-hydroxy compounds in a 98% yield (**6**, 27%; **7**, 71%). The further treatment of the latter with mesyl chloride-pyridine afforded the corresponding mesylate (**8**) in a 98% yield; it was directly converted into a trisubstituted olefin (**9**) and a disubstituted olefin (**10**), in 65 and 22% yields respectively, on treatment with NaI in HMPA (80 °C, 3 h) under a nitrogen atmosphere [**9**, δ 1.65 (3H, br.s) and 5.32 (1H, br.s) ppm; **10**, δ 1.01 (3H, d, J=6.5 Hz) and 5.45 (2H, complex) ppm]. Furthermore, the mesylate (**11**) obtainable from **6** in a 92% yield was also treated with NaI in HMPA to give **9** and **10** in 54 and 20% yields respectively. The trisubstituted olefin (**9**) which was obtained from **5** in a 56% overall yield was used for the next experiment, as will be described below.

* To whom all correspondence should be addressed.

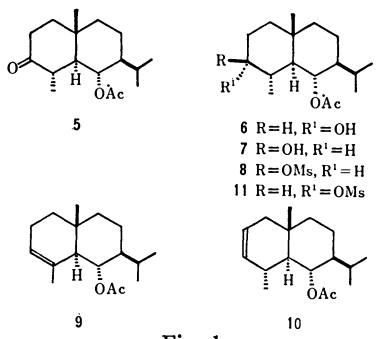

Fig. 1.

The epoxidation of **9** with *m*-chloroperbenzoic acid (under reflux, 3 h), followed by $LiAlH_4$ reduction, afforded a dihydroxy compound (**12**) *via* an epoxide (**13**); the compound was further converted into an acetate (**14**) in an 87.4% overall yield on acetylation with Ac_2O-pyridine (100 °C, overnight).

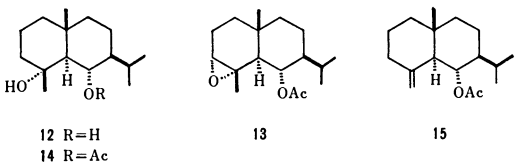

Fig. 2.

Finally, compound **14** was converted into (+)-junenol (**1**) and then into acolamone (**3**) as follows. When treated with $POCl_3$-pyridine at 0 °C for 1 h and then at room temperature overnight, **14** was converted into the corresponding dehydration product, (**15**) [δ 4.45 (1H, br.s) and 4.73 (1H, br.s)ppm], in a 94% yield; it was then reduced with $LiAlH_4$ in ether (under reflux, 2 h) to give, in a quantitative yield, (+)-junenol (**1**); mp 61—61.5 °C (lit, mp 60 °C); $[\alpha]_D^{23}$ +53.1 ° (c=1.07 MeOH) (lit, +52°).[1] The further oxidation of **1** with pyridinium chlorochromate in CH_2Cl_2 (room temp, 30 h) afforded acolamone (**3**) as a colorless, viscous liquid in a 78% yield.

The chemical correlation between acolamone (**3**) and isoacolamone (**4**) has already been established.[2] Surprisingly, though, isojunenol (**2**) has not been isolated from any source. However, on treatment with $LiAlH_4$ in ether (under reflux, 2 h), the olefin (**9**) was readily converted, in a quantitative yield, into isojunenol (**2**); mp 77—78.5 °C; $C_{15}H_{26}O$; ν_{max} 3380 br. cm^{-1}; δ 1.91 (3H, br.s), 3.51 (1H, br.t, J=10.0 Hz), and 5.36 (1H, br.s) ppm.

Experimental

All the mps are uncorrected. IR spectra were recorded on a Hitachi-215 spectrophotometer. NMR spectra were obtained on a Nihondenshi JNM-PS 100 (100 MHz) NMR spectrometer, using $CDCl_3$ as the solvent, unless otherwise stated. The chemical shifts are given in ppm relative to the internal TMS, and only prominent signals are cited (d, doublet; m, multiplet; q, quartet; s, singlet; t, triplet). Mass spectra were obtained on a Hitachi RMU-6D mass spectrometer operating at an ionization energy of 70 eV. Preparative TLC were carried out on Kieselgel PF_{254} (E. Merck, A. G., Germany), unless otherwise stated.

Reduction of the Acetoxy Ketone (5) with $NaBH_4$. Into a solution of **5** (140 mg) in EtOH (4 ml) we stirred $NaBH_4$ (20 mg). The resulting solution was further stirred at room temperature overnight, and then diluted with ether (30 ml) and washed with water. After having been dried over anhydrous Na_2SO_4, the ethereal solution was concentrated under reduced pressure to give a crystalline solid (140 mg), which was subsequently separated by preparative TLC using 5% Et_2O–$CHCl_3$ to give an α-hydroxy acetate, **6** (38 mg), and a β-hydroxy acetate, **7** (100 mg).

6 as colorless prisms: mp 115—116 °C (from hexane); ν_{max} (KBr) 3510, 1720, and 1270 cm^{-1}; δ 0.81 (3H, d, J=6.5 Hz), 0.87 (3H, s), 0.88 (3H, d, J=6.5 Hz), 1.98 (3H, s), 2.14 (1H, br. s, OH), 3.66 (1H, br. s), and 4.86 (1H, br. t, J=9.0 Hz) ppm (Found: C, 72.31; H, 10.95%. Calcd for $C_{17}H_{30}O_3$: C, 72.30; H, 10.71%).

7 as colorless needles: mp 126—126.5 °C (from hexane); ν_{max} (KBr) 3220 br., 1735, and 1250 cm^{-1}; δ 0.82 (3H, d, J=7.0 Hz), 0.89 (3H, d, J=7.0 Hz), 0.90 (3H, s), 0.98 (3H, d, J=6.5 Hz), 2.01 (3H, s), 3.03 (1H, dt, J=5.2 and 10.0 Hz), and 4.92 (1H, t, J=9.5 Hz) ppm (Found: C, 72.09; H, 11.06%. Calcd for $C_{17}H_{30}O_3$: C, 72.30; H, 10.71%).

Reaction of the β-Hydroxy Acetate (7) with Mesyl Chloride–Pyridine. Into a solution of **7** (150 mg) in pyridine (1 ml) we stirred mesyl chloride (67 mg), and then the solution was further stirred at room temperature for 3 h and diluted with ether (30 ml). The ethereal solution was washed successively with 10% aq. HCl, water, and a sat. NaCl aq. solution, and then dried over anhydrous Na_2SO_4. The removal of the solvent under reduced pressure afforded colorless prisms of **8** (182 mg); mp 97—100 °C (from hexane); δ 0.82 (3H, d, J=7.0 Hz), 0.89 (3H, d, J=7.0 Hz), 0.92 (3H, s), 0.98 (3H, d, J=6.5 Hz), 1.99 (3H, s), 2.98 (3H, s), 4.16 (1H, dt, J=6.0 and 10.0 Hz), and 4.88 (1H, br. t, J=9.0 Hz) ppm (Found: C, 59.91; H, 9.30%. Calcd for $C_{18}H_{32}O_5S$: C, 59.97; H, 8.95%).

Reaction of the α-Hydroxy Acetate (6) with Mesyl Chloride–Pyridine. Using the same procedure as that used for **7**, the **6** acetate (170 mg) was treated with mesyl chloride (76 mg)-pyridine (2 ml) (room temp, 3 h) to afford colorless prisms of **11** (200 mg); mp 102—103 °C (from hexane–ether); ν_{max} (KBr) 1730, 1250, and 1185 cm^{-1}; δ 0.82 (3H, d, J=7.5 Hz), 0.89 (3H, d, J=7.5 Hz), 0.90 (3H, s), 1.01 (3H, d, J=6.0 Hz), 2.00 (3H, s), 3.02 (3H, s), 4.20 (1H, br. q, J=2.0 Hz), and 4.89 (1H, br. t, J=9.5 Hz) ppm (Found: C, 59.73; H, 9.13%. Calcd for $C_{18}H_{32}O_5S$: C, 59.97; H, 8.95%).

Formation of Two Olefins, 9 and 10. Into a solution of the **8** mesylate (400 mg) in HMPA (5 ml) we stirred NaI (330 mg) under a nitrogen atmosphere. The reaction mixture was further stirred at 80 °C for 3 h and then diluted with AcOEt. The solution was washed with water, and then dried over anhydrous Na_2SO_4. The removal of the solvent under reduced pressure afforded a reddish oil (290 mg), which was separated by preparative TLC [10% $AgNO_3$–SiO_2; hexane–benzene (3:2)] to give **9** (185 mg) and **10** (63 mg).

9 as a colorless viscous liquid: ν_{max} (film) 1740, 1640, and 1250 cm^{-1}; δ 0.82 (3H, s), 0.85 (3H, d, J=5.5 Hz), 0.92 (3H, d, J=5.5 Hz), 1.65 (3H, br. s), 2.04 (3H, s), 4.95 (1H, br. t, J=9.5 Hz), and 5.32 (1H, br. s) ppm; *m/e* 204 (M^+—AcOH), 198 and 161. No elemental analysis of this oil has been carried out, but its structure must be supported by the above-mentioned spectral data, coupled with those of the next experiment, as will be described below.

10 as colorless needles: mp 35—36 °C (by sublimation); ν_{max} (KBr) 1730, 1660, and 1255 cm^{-1}; δ 0.81 (3H, d, J=7.0 Hz), 0.90 (3H, d, J=7.0 Hz), 0.91 (3H, s), 1.01 (3H, d, J=6.5 Hz), 2.06 (3H, s), 5.01 (1H, br. t, J=10.0 Hz), and 5.45 (2H, complex) ppm (Found: C, 76.67; H, 10.93%. Calcd for $C_{17}H_{28}O_2$: C, 77.22; H, 10.67%).

Reaction of 11 with NaI in HMPA. Using the same procedure as that used for **8**, a solution of **11** (180 mg) and NaI (150 mg) in HMPA (3 ml) was heated at 80 °C for 3 h with stirring, and then treated as usual to give **9** (71 mg) and **10** (27 mg).

Epoxidation of the Trisubstituted Olefin (9). To a solution of **9** (70 mg) in CH_2Cl_2 (5 ml) we added *m*-chloroperbenzoic acid (50 mg). The resulting solution was refluxed for 3 h, then washed successively with 10% aq. Na_2SO_3, 10% aq. $NaHCO_3$, and sat. NaCl aq. solutions, and then dried over anhydrous Na_2SO_4. The removal of the solvent under reduced pressure gave white crystals (70 mg), the sublimation of which afforded colorless prisms of **13**; mp 81—82 °C; ν_{max} (KBr) 1735 and 1250 cm^{-1}; δ 0.84 (3H, s), 0.85 (3H, d, J=5.0 Hz), 0.92 (3H, d, J=5.0 Hz), 1.22 (3H, s), 2.08 (3H, s), 2.87 (1H, br. t, J=2.0 Hz) and 4.92 (1H, dd, J=11.0 and 9.0 Hz) ppm (Found: C, 72.57; H, 10.18%. Calcd for $C_{17}H_{28}O_3$: C, 72.82; H, 10.06%).

Reduction of the Epoxide (13) with $LiAlH_4$. A mixture of **13** (140 mg) and $LiAlH_4$ (10 mg) in ether (10 ml) was refluxed for 2 h with stirring. After decomposition with ether saturated with water, the reaction mixture was filtered. The filtrate was concentrated under reduced pressure to give colorless needles of **12**; mp 142.5—143 °C; ν_{max} (KBr) 3200 br. cm^{-1}; δ 0.86 (3H, s), 0.87 (3H, d, J=7.0 Hz), 0.94 (3H, d, J=7.0 Hz), 1.34 (3H, s), 3.61 (1H, br. t, J=8.5 Hz), and 4.19 (2H, br. s, OH) ppm (Found: C, 74.96; H, 12.06%. Calcd for $C_{15}H_{28}O_2$: C, 74.95; H, 11.74%).

Acetylation of the Diol (12). A solution of **12** (94 mg) in Ac_2O (0.5 ml) and pyridine (1 ml) was stirred at 100 °C overnight, and then diluted with water (10 ml) and extracted with ether. The ethereal extract was washed successively with 10% aq. HCl, 10% aq. NaOH, water, and a sat. NaCl aq. solution, and then dried over anhydrous Na_2SO_4. The removal of the solvent under reduced pressure gave white crystals (102 mg), which were recrystallized from hexane to give colorless needles of **14**; mp 85—86 °C; ν_{max} (KBr) 3330 br., 1735, and 1250 cm^{-1}; δ 0.85 (3H, d, J=7.0 Hz), 0.90 (3H, d, J=7.0 Hz), 0.91 (3H, s), 1.19 (3H, s), 2.06 (3H, s), 2.91 (1H, br. s, OH), and 5.19 (1H, br. t, J=10.0 Hz) ppm (Found: C, 71.95; H, 10.63%. Calcd for $C_{17}H_{30}O_3$: C, 72.30; H, 10.71%).

Dehydration of the Monoacetate (14). Into a solution of **14** (85 mg) in pyridine (2 ml), we stirred $POCl_3$ (0.5 ml) at 0 °C. The resulting solution was further stirred at 0 °C for 1 h, and at room temperature overnight, and then slowly poured into ice-water and extracted with ether. The ethereal extract was washed successively with 10% aq. HCl and water, and then dried over anhydrous Na_2SO_4. The removal of the solvent under reduced pressure afforded a crystalline solid, which was subsequently purified by preparative TLC using benzene to give white crystals of **15** (75 mg); mp 37—40 °C

(by sublimation); ν_{max} (KBr) 1730, 1655, and 1255 cm^{-1}; δ 0.76 (3H, s), 0.87 (3H, d, J=7.0 Hz), 0.92 (3H, d, J=7.0 Hz), 2.02 (3H, s), 4.45 (1H, br. s), 4.73 (1H, br. s), and 5.00 (1H, br. t, J=9.5 Hz) ppm (Found: C, 76.73; H, 10.88%. Calcd for $C_{17}H_{28}O_2$: C, 77.22; H, 10.67%).

Formation of (+)-Junenol (1). A mixture of **15** (125 mg) and $LiAlH_4$ (10 mg) in absolute ether (10 ml) was refluxed for 2 h with stirring. After the decomposition of the excess amounts of the reagent with ether saturated with water, the reaction mixture was filtered. The filtrate was concentrated under reduced pressure to give white crystals (104 mg), the sublimation of which afforded colorless needles of (+)-junenol (mp, optical rotation, and IR spectrum)[1]; δ 0.73 (3H, s), 0.87 (3H, d, J=7.5 Hz), 0.94 (3H, d, J=7.5 Hz), 1.95 (1H, s, OH), 3.63 (1H, br. t, J=10.0 Hz), 4.63 (1H, br. s), and 4.93 (1H, br. s) ppm (Found: C, 80.72; H, 12.03%. Calcd for $C_{15}H_{26}O$: C, 81.02; H, 11.79%).

Oxidation of (+)-Junenol (1). Into a suspension of pyridinium chlorochromate (680 mg) in CH_2Cl_2 (7 ml) we stirred a solution of **1** (70 mg) in CH_2Cl_2 (3 ml) at room temperature. The reaction mixture was further stirred at room temperature for 30 h, and then diluted with absolute ether and filtered. The filtrate was concentrated under reduced pressure to give a brown liquid, which was subsequently separated by preparative TLC using hexane–benzene (1:2) to afford a colorless liquid of acolamone (31 mg) (TLC and IR spectrum) and white crystals of the starting material (30 mg) (mp and IR spectrum).

Reduction of the Acetoxy Olefin (9) with $LiAlH_4$. Into a solution of **9** (112 mg) in absolute ether (10 ml) we stirred $LiAlH_4$ (10 mg), and then the reaction mixture was refluxed for 2 h. After the decomposition of the excess amounts of the reagent with ether saturated with water, the reaction mixture was filtered. The filtrate was concentrated under reduced pressure to give white crystals (93 mg), the sublimation of which afforded colorless prisms of isojunenol (**2**); mp 77—78.5 °C; ν_{max} (KBr) 3380 br. cm^{-1}; δ 0.78 (3H, s), 0.87 (3H, d, J=7.0 Hz), 0.96 (3H, d, J=7.0 Hz), 1.91 (3H, br. s), 3.51 (1H, br. t, J=10.0 Hz), and 5.36 (1H, br. s) ppm (Found: C, 80.50; H, 12.11%. Calcd for $C_{15}H_{26}O$: C, 81.02; H, 11.79%).

References

1) V. Herout, O. Motl, and F. Sǒrm, *Coll. Czech. Chem. Commun.*, **22**, 785 (1957); S. C. Bhattacharyya, A. S. Rao, and A. M. Shaligram, *Chem. Ind.*, **1960**, 469; *Tetrahedron*, **18**, 969 (1962); D. W. Theobald, *ibid.*, **20**, 2593 (1964).

2) M. Niwa, A. Nishiyama, M. Iguchi, and S. Yamamura, *Bull. Chem. Soc. Jpn.*, **48**, 2930 (1975).

3) K. Kato, Y. Hirata, and S. Yamamura, *Tetrahedron*, **27**, 5987 (1971).

Regio- and Stereospecific Cyclizations of Germacrones

Masatake NIWA, Masanobu IGUCHI, and Shosuke YAMAMURA*

Faculty of Pharmacy, Meijo University, Showa-ku, Nagoya 468

(Received April 21, 1976)

From a biogenetic point of view, the acid-catalyzed cyclizations of germacrones (**1**, **2**, and **3**) were carried out, using several kinds of reagents and solvents (80% aq AcOH, 80% aq HCOOH, $AlCl_3$ in absolute ether, AcOH in PhSH, 100% HCOOH in PhSH, and concd H_2SO_4 in PhSH). In all cases, the stereospecific cyclizations of these germacrones took place to give cadinane-type, selinane-type or guaiane-type compounds depending on the kinds of reagents and solvents. The formation process of each compound will be presented in detail.

From a biogentic point of view, many sesquiterpenes are known to be derived from germacrenes or germacrones, which are regarded as an important precursor. Our interests are focused on the biogenetic-type reactions of these ten-membered ring sesquiterpenes and their derivatives. In the present paper, we describe the regio- and stereospecific cyclizations of these germacrones with some acids, leading to the formation of cadinane-type, selinane-type or guaiane-type compounds. In addition, some naturally occurring sesquiterpenes were synthesized from these germacrones.

As described in the previous papers,[1,2] many sesquiterpenes have been isolated from the plant *Acorus calamus* L. and their structures also been established. Of these sesquiterpenes, acoragermacrone (**1**) is regarded as the most important compound, which has been chemically converted into isoacoragermacrone (**2**), preisocalamendiol (**3**) and other sesquiterpenes.[2] In our experiments, mainly, three germacrones **1**, **2** and **3** were used for the biogenetic-type reactions.

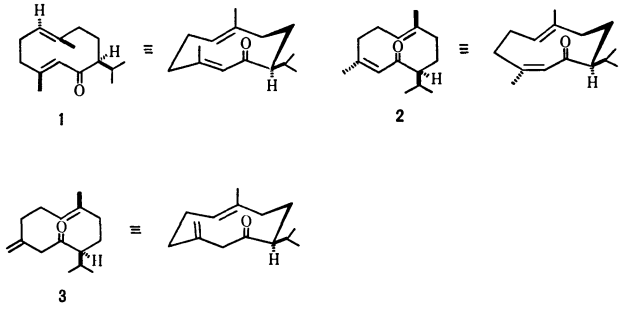

Fig. 1.

Acid-catalyzed Cyclizations of Acoragermacrone (1). Biogenetically, *trans*-selinane-type sesquiterpenes are produced from the corresponding germacrenes with an (*E*,*E*)-1,5-cyclodecadiene system, while cadinane-type compounds must be stereochemically produced from the corresponding ten-membered ring compounds with an (*E*,*Z*)-1,5-cyclodecadiene system which may be directly derived from a (*Z*,*E*)-farnesyl pyrophosphate or produced on *cis-trans* isomerization of the corresponding (*E*,*E*)-1,5-cyclodecadienes: the formation process of junenol (**4**)[3] as well as of α-cadinol (**5**)[4] is demonstrated in Scheme 1. Quite recently, 5-epi-junenol (**6**) was isolated from *Ferula galbaniflua*.[5] Probably, this sesquiterpene is produced on double-bond isomerization of the (*E*,*E*)-1,5-cyclodecadienyl cation, followed by acid-catalyzed cyclization together with simultaneous hydration, as shown in Scheme 1.

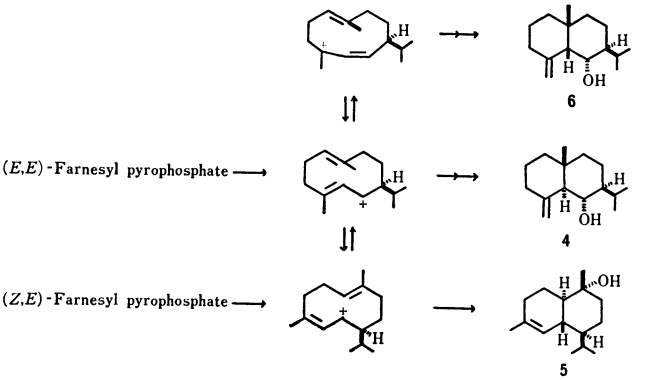

Scheme 1. Biogenesis of *cis*- and *trans*-selinane-type and cadinane-type sesquiterpenes.

It is interesting to examine the acid-catalyzed cyclization of acoragermacrone (**1**), because the protonated form (A) of **1** is expected to show the same behavior as that of the (*E*,*E*)-1,5-cyclodecadienyl cation (B), as shown in Scheme 1. Thus, the acid-catalyzed reactions of acoragermacrone (**1**) were carried out under various conditions.[6]

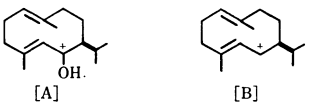

Fig. 2.

As described earlier,[2] $AlCl_3$ converted **1** into two *trans*-selinane-type sesquiterpenes, acolamone (**7**) and isoacolamone (**8**), in 55 and 23% yields, respectively. Both of them are included in the plant together with acoragermacrone (**1**).

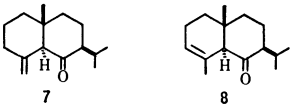

Fig. 3.

Acoragermacrone (**1**) is fairly stable toward 80% aq AcOH at room temperature. However, when heated at 75°C for 50 min, the compound **1** afforded isocalamendiol (**9**),[1] in a 28% yield. Clearly, acoragermacrone with an (*E*,*E*)-1,5-cyclodecadiene system must be converted into preisocalamendiol (**3**) which is further subjected to the regio- and stereospecific cyclization giving the

* To whom all correspondence should be addressed.

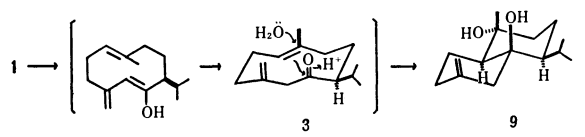

Scheme 2. Conversion of acoragermacrone into isocalamendiol.

cadinane-type compound (**9**), as shown in Scheme 2.

Furthermore, the acid-catalyzed cyclization of acoragermacrone (**1**) was carried out using 80% aq HCOOH instead of 80% aq AcOH. In this case, the cyclization reaction takes place under much milder conditions (room temp, 10 min) to give three cyclization products **9**, **10** and **11**, in 19, 17 and 17% yields, respectively, one of which is identical with isocalamendiol (mp and IR spectrum). Other two compounds both are selinane-type compounds (**10**, mp 45—48 °C; **11**, mp 83—85 °C) with the same molecular formula ($C_{16}H_{26}O_3$), whose structures are based on their spectral data, as will be discussed below. Both cyclization compounds show an IR absorption band at 1720 cm^{-1}, and an intense fragment peak at *m/e* 220 (M^+—HCOOH). The NMR spectra of both compounds are also quite similar to each other: they have two methyl singlets (δ 0.90 and 1.88 ppm in **10**; δ 0.96 and 1.91 ppm in **11**) in addition to one isopropyl group. Furthermore, these compounds have two singlets due to a C_5-methine proton and a HCOO–grouping (δ 2.87 and 8.04 ppm in **10**; δ 2.93 and 8.03 ppm in **11**). From the above data, these two products must be selinane-type compounds and stereoisomers to each other. In fact, a remarkable difference is observed in their ORD curves: the *trans*-selinane-type compound (**10**) has a positive Cotton effect ($[\phi]^{P}_{320nm}$ $+14°\times10^2$, $[\phi]^{T}_{277nm}$ $-28°\times10^2$, $A=+42$), while the *cis*-isomer (**11**) has a negative Cotton effect $[(\phi]^{T}_{324nm}$ $-56°\times10^2$, $[\phi]^{P}_{278nm}$ $+61°\times10^2$, $A=-117$). In particular, the formation of the *cis*-selinane-type compound (**11**)is interesting in connection with Scheme 1. As seen in Scheme 3, two possible pathways from **1** to the *trans*-isomer (**10**) are suggested, and any of them can not be ruled out. The *cis*-isomer (**11**) seems to be derived directly from one of the ten-membered ring conformers, since these two selinane-type compounds are not interconvertible under mild reaction conditions. We further examined the acid-catalysed cyclization of acoragermacrone (**1**) using 100% HCOOH in thiophenol, as follows.

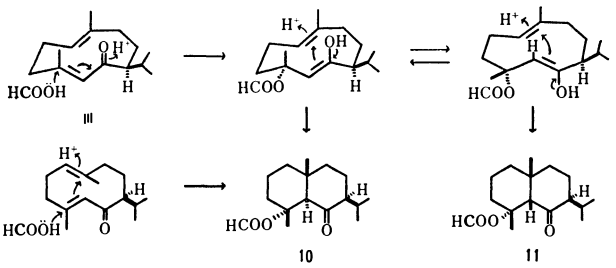

Scheme 3. Acid-catalyzed cyclization of acoragermacrone with 80% aq HCOOH.

When treated with 100% HCOOH in thiophenol (room temp, 1 h), the compound **1** was readily converted into a selinne-tyape compound (**12**), in *ca.* 60% yield. This compound (**12**) is a colorless oil with molecular formula $C_{21}H_{30}OS$, whose structure has been elucidated on the basis of its spectral data and chemical evidence: desulfurization of **12** with Raney Ni(W-4) gave dihydroacolamone (**13**)[2] in a 26% yield. In particular, the NMR signal at δ 3.01 (1H, dd, J=6.5 and 8.8 Hz) ppm indicates that the PhS group should be in an equatorial configuration. As shown in Scheme 4, the regio- and stereospecific cyclization of **1** may not take place in an ionic mechanism, but probably in a radical manner.[7]

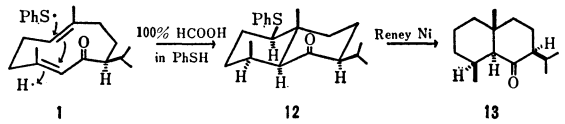

Scheme 4. Regio- and sterespecific cyclization of acoragermacrone with 100% HCOOH in thiophenol.

Acid-catalyzed Cyclization of Isoacoragermacrone (2). It is quite reasonable to suppose that the protonated form(C) of isoacoragemacrone (**2**) is equivalent to the (*Z,E*)-1,5-cyclodecadienyl cation (D) in their chemical behavior. Furthermore, from a stereochemical aspect, isoacoragermacrone, which has been obtained from acoragermacrone (**1**) as well as from preisocalamendiol (**3**),[2] seems to be converted into cadinane-type compounds, as shown in Scheme 1. In fact, when treated with 80% aq AcOH at room temperature for 5 min, **2** was readily converted into two dienes **14** and **15**, in 43 and 23% yields, respectively.[8] The structures of these products are based on their spectral data [**14**,

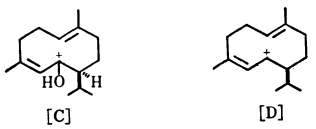

Fig. 4.

$C_{15}H_{24}O$; ν_{max} 3350 (br) cm^{-1}; λ_{max} 247 and 241 nm (ε, 11100 and 10900, respectively); δ 1.06 (3H, s), 1.80 (3H, br.s) and 6.24 (1H, br.s) ppm. **15**, $C_{17}H_{26}O_2$; ν_{max} 1730 cm^{-1}; λ_{max} 247 and 241 nm (ε, 10500 and 10300, respectively); δ 1.35 (3H, s), 1.79 (3H, br.s), 1.99 (3H, s) and 6.25 (1H, br.s) ppm], in which the configuration of the asterisked carbon atom will be discussed later. The different point between **14** and **15** is that the former has a hydroxyl group, while an acetoxyl group is present in **15**. Thus, treatment of the latter with $LiAlH_4$ afforded **14** in a high yield. In the above experiment, the regio- and stereospecific cyclization of isoacoragermacrone (**2**) takes place in a concerted

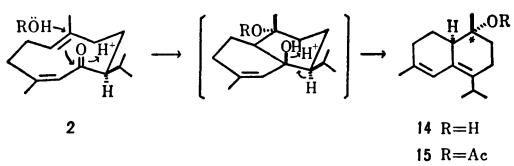

Scheme 5. Reaction of isoacoragermacrone (**2**) with 80% aq AcOH.

manner, leading to the formation of **14** and **15**, as shown in Scheme 5.

On the other hand, when treated with $AlCl_3$ in absolute ether (0 °C, 10 mil), isoacoragermacrone (**2**) was converted into an isomer of **14** in a 72% yield. The spectral data of this isomer (**16**) are quite similar to those of **14** except for the chemical shift of the tertiary methyl signal (δ 1.06 ppm in **14**; δ 1.28 ppm in **16**). Clearly, the axial methyl signal in the former should be observed in higher magnetic field than that of the equatorial isomer.[8,9] In the case of $AlCl_3$, the stereospecific reaction of **2** takes place in a stepwise manner, as demonstrated in Scheme 6, which includes an intramolecular oxygen-transfer.[8]

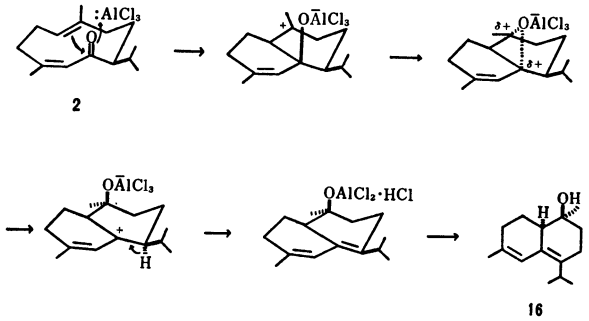

Scheme 6. Reaction of isoacoragermacrone (**2**) with $AlCl_3$.

We further examined the acid-catalyzed cyclization of isoacoragermacrone (**2**) in thiophenol.[10] Interestingly, when treated with AcOH in thiophenol (room temp, 24 h), isoacoragermacrone (**2**) was converted into a guaiane-type compound (**17**, mp 90—91 °C; $C_{21}H_{30}OS$), in a 50% yield, whose structure was determined by its spectral data and the following chemical evidence. This compound has a CO group (ν_{max} 1700 cm^{-1}) and each one of secondary and tertiary methyl groups [δ (CCl_4) 0.95 (3H, d, J=7.5 Hz) and 1.22 (3H, s) ppm] in addition to the original isopropyl group. Treatment of **17** with MeI in acetone (under reflux, 8 h) afforded an α,β-unsaturated ketone in a 66% yield [**18**, $C_{15}H_{24}O$; ν_{max} 1670 and 1610 cm^{-1}; λ_{max} 256 nm (ε, 8270); δ 2.05 (3H, s) ppm]. On desulfurization with Raney Ni (W-4) in EtOH, the guaiane-type compound **17** was readily converted, in an 86% yield, into the corresponding reduction product (**19**, mp 55—57.5 °C; $C_{15}H_{26}O$) which has a newly formed secondary methyl group in addition to the three secondary methyl groups (δ 0.83, 0.87, 0.92 and 1.13 ppm). In addition, a methine doublet at δ 2.92 (1H, d, J= 8.5 Hz) ppm in **17** became double doublets at δ 2.86 (1H, dd, J=7.8 and 4.8 Hz) ppm in **19**. Finally, this reduction product **19** was converted into the more stable *trans*-isomer (**20**) on treatment with NaOMe–MeOH (under reflux, 3 h).[11] The stereostructures of these two isomers (**19** and **20**) are also supported by measurements of their ORD curves: the *cis*-isomer (**19**) has a positive Cotton effect ($[\phi]^{P}_{321nm}$ +14°×10², $[\phi]^{P}_{276nm}$ −39°×10², A=+53), while the *trans*-isomer (**20**) has a negative Cotton effect ($[\phi]^{T}_{312nm}$ −46°×10², $[\phi]^{P}_{272nm}$ +57°×10², A=−103).

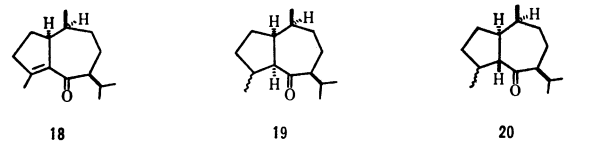

Fig. 5.

The formation process of the guaiane-type compound (**17**) is shown in Scheme 7, indicating that the regio- and stereospecific cyclization of **2** takes place in a radical mechanism.

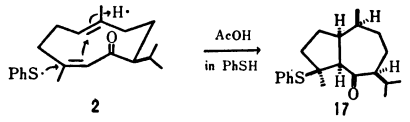

Scheme 7. Reaction of isoacoragermacrone with AcOH in thiophenol.

In the case of 100% HCOOH in thiophenol (room temp, 15 h), four cyclization products were obtained from isoacoragermacrone (**2**), in low yields (**17**, 15%; **21**, 5%; **22a**+**22b**, 12%). One of them is completely identical with the guaiane-type compound (**17**) which has been already obtained in the case of AcOH in thiophenol, as described earlier (mp and IR spectrum). The other three products (**21**, **22a** and **22b**) are cadinane-type compounds, whose structures are based on their spectral data and chemical evidences. The compound **21** is a colorless viscous liquid ($C_{21}H_{28}S$) and has two methyl groups [δ 1.09 (3H, s) and 1.76 (3H, br.s) ppm] in addition to the original isopropyl group. In addition, one broad singlet at δ 6.13 ppm due to an olefinic proton is observed in the NMR spectrum of **21**.

The compound **22**, a colorless viscous liquid, is an inseparable mixture consisting of two epimers (**22a** and **22b**), both of which have two PhS groups [δ 7.10—7.70 (10H, complex) ppm] and one olefinic proton (δ 5.35 and 5.43 ppm). Finally, these compounds (**21**, **22a** and **22b**) were chemically interconvertible, as follows.

When treated with conc. H_2SO_4 in thiophenol (0 °C, 30 min), the compound **21** was readily converted into the mixture of **22a** and **22b**, in a 75% yield. On the other hand, the mixture (**22a** and **22b**) reacted with excess amounts of MeI (under reflux, 4 h) to give **21** and calamenene (**23**), in 45 and 29% yields, respectively.

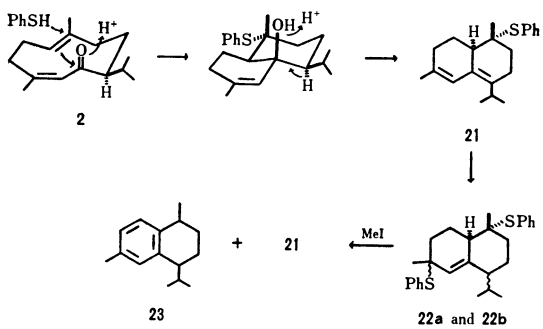

Scheme 8. The formation of cadinane-type compounds (**21**, **22a** and **22b**) from isoacoragermacrone (**2**).

We further examined the acid-catalyzed cyclization of isoacoragermacrone (**2**) in thiophenol using concd H_2SO_4 instead of 100% HCOOH (0 °C, 30 min). In this case, the cadinane-type compounds were only isolated from the reaction mixture (**21**, 4%; **22a**+**22b**, 67%). In the above experiment using such a strong acid as concd H_2SO_4, clearly, the regio- and stereospecific cyclization of **2** giving these cadinane-type compounds must take place in an ionic mechanism (see Scheme 8) in contrast to the formation process of the guaiane-type compound (**17**).

From a biogenetic point of view, such an allyl alcohol as **24** is also attractive to us for the biogenetic model reactions (see Scheme 1). However, reduction of isoacoragermacrone (**2**) with diisobutylaluminium hydride (0—5 °C, 2 h) did not afford the desired alcohol (**24**), but a saturated ketone (**25**) in a 72% yield, which could be converted into the known cadinane-type compound (**26**)[1] in a 20% yield on treatment with 80% aq AcOH (room temp, 5 min).

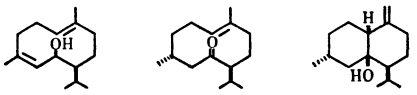

24 25 26

Fig. 6.

Regio- and Stereospecificity in the Cyclizations of Preisocalamendiol (3) and its Derivatives. As reported in the previous paper,[1] action of 80% aq AcOH on preisocalamendiol (**3**) converted it into isocalamendiol (**9**) in a good yield. However, any amount of calamendiol (**27**), an isomer of **9**, has not been obtained.[8] We further examined the acid-catalyzed cyclization of **3** with $AlCl_3$ in absolute ether, which was carried out at 0 °C for 10 min to give the dienol (**28**)[1] in a 54% yield. The compound **28** was also obtained, in a high yield, by thermal reaction of **3** at 180 °C, as described in Table 1. Probably, a chair-like transition state must be included in the course of the stereospecific cyclization, as demonstrated in Scheme 9.[12]

Table 1. Thermal isomerization of preisocalamendiol (**3**)

Time (min)	**3** (%)	**28** (%)	Other products (%)
0	100	0	0
7.5	99	1	0
22	83	17	0
42	48	46	6
90	3	86	11

Peak-heights in gas chromatogram (PEG 20 M, N_2, 115 °C, flame-ionizer detector) were served as approximate values of the content (%)

The Formation of ε-Cadinene. Preisocalamendiol (**3**) is quite stable toward $NaBH_4$. However, when treated with excess amounts of $LiAlH_4$ (room temp, 30 h), **3** was converted into the corresponding hydroxy compound in a quantitative yield [**29**, $C_{15}H_{26}O$; ν_{max} 3360 br·cm^{-1}; δ 3.60—3.92 (1H, m) ppm]. Further

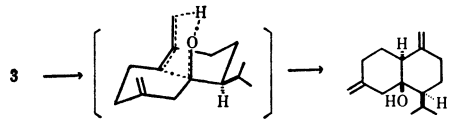

28

Scheme 9. Thermal isomerization of preisocalamendiol (**3**) to the dienol (**28**).

treatment of **29** with 80% aq HCOOH (0 °C, 2 h) did not afford any cyclization product, but the corresponding formate in a high yield [**30**, ν_{max} 1720 cm^{-1}; δ 3.66—3.90 (1H, m) and 8.11 (1H, s) ppm]. On reduction with $LiAlH_4$, this formate was reconverted into the original alcohol (**29**).

Finally, dehydration of **29** with mesyl chloride-pyridine (room temp, 7 h) afforded ε-cadinene (**31**) in a 35% yield, which was further subjected to catalytic hydrogenation (PtO_2 in AcOEt) giving the corresponding tetrahydro compound (**32**).[13] The IR spectrum of **32** was completely identical with that of an authentic sample of tetrahydrocadinene.[14]

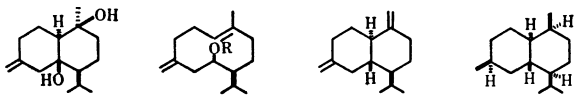

27 29 R=H 31 32

30 R=CHO

Fig. 7.

Experimental

All the mps are uncorrected. GLC were recorded on a Shimadzu GC-1C gas chromatograph with a flame-ionizer detector [stationary phase: 5% PEG 20M on Celite 545 (100 mesh); column [ϕ 3 mm × 1.5 m (stainless steel)] temp: 90 °C; carrier gas: nitrogen (85 ml/min); inlet pressure: 1.2 kg/cm^2], unless otherwise stated. IR spectra were recorded on a Hitachi-215 spectrophotometer. UV spectra were taken on a Hitachi-124 spectrophotometer, using MeOH as the solvent. NMR spectra were recorded on a Varian Associate A-60 (60 MHz), a JEOL JNM-C60H (60 MHz) or JNM-PS 100 (100 MHz), using $CDCl_3$ as the solvent, unless otherwise stated. The chemical shifts are given in ppm relative to the internal TMS, and only prominent signals are recorded (d, doublet; m, multiplet; q, quartet; s, singlet; t, triplet). Mass spectra were obtained on a Hitachi RMU-6D mass spectrometer operating at an ionization energy of 70 eV. ORD curves were recorded on a JASCO ORD/UV-5 spectrophotometer, using MeOH as the solvent. Preparative TLC were carried out on Kieselgel PF_{254} (E. Merck, A. G.), unless otherwise stated.

Reaction of Acoragermacrone (1) with 80% aq AcOH. A solution of **1** (27 mg) in 80% aq AcOH (0.5 ml) was heated at 75 °C for 50 min with stirring, and then diluted with water (2 ml). The solution was neutralized with a dil. $NaHCO_3$aq solution, and then extracted with ether. The ethereal extract was washed with water, and then dried over anhydrous Na_2SO_4. Removal of the solvent gave a colorless viscous liquid, which was subsequently separated by preparative TLC using benzene–ether (4: 1) to give isocalamendiol (**9**) (8 mg) (mp and IR spectrum).

Reaction of Acoragermacrone (1) with 80% aq HCOOH. A solution of **1** (90 mg) in 80% aq HCOOH (0.9 ml) was

stirred at room temperature for 10 min, and then diluted with water (5 ml). The solution was neutralized with a sat. $NaHCO_3$ aq solution, and then extracted with ether. The ethereal extract was washed with water and dried over anhydrous Na_2SO_4. The solvent was evaporated under reduced pressure to give a pale yellow liquid (106 mg), which was separated by preparative TLC using benzene–ether (4: 1) to give three main fractions in the following order: **9** (18 mg), **10** (19 mg), and **11** (19 mg). The compound **9** was identical with an authentic sample of isocalamendiol (mp and IR spectrum). The physical data of the other two products are shown below.

trans-*Selinane-type Compound (10)*: mp 45—48 °C (from hexane); ν_{max} (film) 1720 cm^{-1}; δ 0.88 (3H, d, J=6.5 Hz), 0.92 (3H, d, J=6.5 Hz), 0.90 (3H, s), 1.88 (3H, s), 2.87 (1H, s) and 8.04 (1H, s) ppm; *m/e* 266 (M^+) and 220 (Found: *m/e* 266.18862. Calcd for $C_{16}H_{26}O_3$: *m/e* 266.18818).

cis-*Selinane-type Compound (11)*: mp 83—85 °C (from hexane); ν_{max} (film) 1720 cm^{-1}; δ 0.85 (3H, d, J=6.0 Hz), 0.98 (3H, d, J=6.0 Hz), 0.96 (3H, s), 1.91 (3H, s), 2.93 (1H, s), and 8.03 (1H, s) ppm; *m/e* 266 (M^+) and 220 (Found: *m/e* 266.19067. Calcd for $C_{16}H_{26}O_3$: *m/e* 266.18818).

Reaction of Acoragemacrone (1) with 100% HCOOH in Thiophenol. To a solution of **1** (125 mg) in thiophenol (2 ml) was added 5 drops of 100% HCOOH with stirring. The resulting solution was further stirred at room temperature for 1 h, and then diluted with a lot of ether. The ethereal solution was washed successively with 10% NaOH aq solution and water, and then dried over anhydrous Na_2SO_4. Removal of the solvent under reduced pressure left a pale yellow liquid (190 mg), which was purified by preparative TLC using hexane–benzene (1: 1) to give a pale yellow liquid of **12** (109 mg), ν_{max} (film) 3060, 1710, 1580, 735, and 690 cm^{-1}; δ 0.83 (3H, s), 0.85—1.00 (9H, complex), 3.01 (1H, dd, J=6.5 and 8.8 Hz) and 7.18—7.69 (5H, complex) ppm; *m/e* 330 (M^+) and 220 (Found: *m/e* 330.20388. Calcd for $C_{21}H_{30}OS$: *m/e* 330.20173).

Desulfurization of 12. To a solution of **12** (80 mg) in EtOH (3 ml) was added Raney Ni (W-4) (100 mg), and then the reaction mixture was refluxed for 3 h under a nitrogen atmosphere. After removal of the catalyst, the filtrate was concentrated under reduced pressure to give a colorless viscous liquid (51 mg) which was purified by preparative GLC at 120 °C to give a colorless liquid of dihydroacolamone (14 mg) (GLC, TLC and IR spectrum).

Reaction of Isoacoragermacrone (2) with 80% aq AcOH. Isoacoragermacrone (40 mg) was dissolved in 80% aq AcOH (5 ml) with stirring. The resulting solution was further stirred at room temperature for 5 min, and then diluted with ice-water (*ca.* 10 ml). After neutralization with $NaHCO_3$ powder, the solution was extracted with ether. The ethereal extract was washed with a sat. NaCl aq solution and dried over anhydrous Na_2SO_4, and then concentrated under reduced pressure to give a colorless oil, which was separated by preparative TLC using petroleum ether–ether (1: 3) to give two fractions. From the more polar fraction, the alcohol **14** (17 mg) was isolated as a colorless viscous liquid. From the less polar fraction, the acetate **15** (11 mg) was also obtained as a colorless viscous liquid.

14: ν_{max} (film) 3350 br. and 1640 br. cm^{-1}; λ_{max} 247 and 241 nm (ε, 11100 and 10900, respectively); δ 0.96 (3H, d, J=7.0 Hz), 0.98 (3H, d, J=7.0 Hz), 1.06 (3H, s), 1.80 (3H, br. s) and 6.24 (1H, br. s) ppm; *m/e* 220 (M^+), 187 and 159 (Found: *m/e* 220.18096. Calcd for $C_{15}H_{24}O$: *m/e*220.18270).

15: ν_{max} (film) 1730 and 1660 br. cm^{-1}; λ_{max} 247 and 241 nm (ε, 10500 and 10300, respectively); δ 0.96 (3H, d, J=7.0 Hz), 0.98 (3H, d, J=7.0 Hz), 1.35 (3H, s), 1.79 (3H, br. s), 1.99 (3H, s), 4.77 (1H, br. s) and 6.25 (1H, br. s) ppm; *m/e* 262 (M^+), 220, 202, 187, 177, and 159 (Found: *m/e* 262.19634. Calcd for $C_{17}H_{26}O_2$: *m/e* 262.19327).

Reduction of the Acetate 15 with $LiAlH_4$. To a solution of **15** (18 mg) in anhydrous ether (5 ml) was added $LiAlH_4$ (4 mg) with stirring, and then the reaction mixture was heated under reflux for 4 h. After decomposition of an excess of the reagent with water, 20% potassium sodium tartarate aq solution was added to the reaction mixture, which was extracted with ether. The ethereal extract was dried over anhydrous Na_2SO_4, and then concentrated under reduced pressure to give a colorless oil (14 mg), which was purified by preparative TLC using petroleum ether–ether (1: 3) to give the alcohol **14** (GLC, TLC, and IR spectrum).

Reaction of Isoacoragermacrone (2) with $AlCl_3$. To a solution of **2** (39 mg) in absolute ether (5 ml) was added a solution of $AlCl_3$ (24 mg) in absolute ether (1.5 ml) at 0 °C, with stirring. The resulting solution was further stirred at 0 °C for 10 min, and then poured into ice water and extracted with ether several times. The combined ethereal extracts were washed with a sat. NaCl aq solution, and then dried over anhydrous Na_2SO_4. Removal of the solvent under reduced pressure afforded a colorless oil,* which was purified by preparative TLC using alumina [GF_{254} (type E), E. Merck A. G.] and benzene to give **16** as a colorless viscous liquid (20 mg); ν_{max} (film) 3570 sh., 3450 and 1640 cm^{-1}; λ_{max} 246 and 241 nm (ε, 16300 and 16200, respectively); δ 1.00 (6H, d, J=7.0 Hz), 1.28 (3H, s), 1.77 (3H, br. s) and 6.27 (1H, br. s) ppm; *m/e* 220 (M^+), 202, 187, and 159 (Found: *m/e* 220.18247. Calcd for $C_{15}H_{24}O$: *m/e* 220.18271).

The Formation of the Guaiane-type Compound (17). To a solution of isoacoragermacrone (245 mg) in thiophenol (2 ml) was added, with stirring, 10 drops of AcOH at room temperature, and then the resulting solution was further stirred at room temperature for 24 h. After addition of a cooled 10% NaOH aq solution, the solution was extracted with ether. The ethereal extract was washed successively with a cooled 10% NaOH aq solution and water, and then dried over anhydrous $MgSO_4$. Removal of the solvent under reduced pressure gave an almost colorless liquid, which was chromatographed on silica gel (20 g) and eluted with benzene to give **17** as colorless crystals (184 mg); mp 90—91 °C (from hexane); ν_{max} (KBr) 3060, 1700, 1580, 745, and 690 cm^{-1}; δ (CCl_4) 0.91 (3H, d, J=6.4 Hz), 0.95 (3H, d, $J\simeq$7.5 Hz), 0.96 (3H, d, J=6.4 Hz), 1.22 (3H, s), 2.92 (1H, d, J=8.5 Hz) and 7.08—7.57 (5H, m) ppm; *m/e* 330 (M^+) and 221 (Found: C, 76.53; H, 9.26%. Calcd for $C_{21}H_{30}OS$: C, 76.31; H, 9.15%).

Formation of the α,β-Unsaturated Ketone (18). A solution of **17** (100 mg) and freshly distilled MeI (1 ml) in acetone (4 ml) was refluxed under a nitrogen atmosphere for 8 h, and then concentrated under reduced pressure to give a crude residue which was purified by preparative TLC using hexane–benzene (1: 1) to give **18** as a colorless liquid (44 mg); ν_{max} (film) 1670 and 1610 cm^{-1}; λ_{max} 256 nm (ε, 8270); δ 0.72 (3H, d, J=6.5 Hz), 0.88 (3H, d, J=6.4 Hz), 0.92 (3H, d, J=6.4 Hz), 2.05 (3H, br. s) and 3.24 (1H, m) ppm; *m/e* 220 (M^+) and 215 (Found: 220.18108. Calcd for $C_{15}H_{24}O$: *m/e* 220.18271).

Desulfurization of 17. To a solution of **17** (137 mg) in absolute EtOH (5 ml) was added, with stirring, Raney Ni (W-4) (*ca.* 1 g) at room temperature, and then the reaction mixture was refluxed under a nitrogen atmosphere for 6 h. After filtration of the catalyst, the filtrate was concentrated

* Peak-area of analytical GLC was served as approximate values of the content (%), indicating that this oil contained the alcohol **16** (28.2 mg).

under reduced pressure to give a crystalline solid (79 mg), the sublimation of which afforded **19** as colorless needles; mp 55—57.5 °C; ν_{max} (KBr) 1700 cm^{-1}; δ 0.83 (3H, d, J=6.7 Hz), 0.87 (3H, d, J=6.5 Hz), 0.92 (3H, d, J=6.5 Hz), 1.13 (3H, d, J=6.3 Hz) and 2.86 (1H, dd, J=7.8 and 4.8 Hz) ppm; *m/e* 222 (M^+), 207 and 166 (Found: *m/e* 222.19849. Calcd for $C_{15}H_{26}O$: *m/e* 222.19836).

Epimerization of ***19***. A solution of **19** (44 mg) and NaOMe (27 mg) in absolute MeOH (3 ml) was refluxed for 3 h under a nitrogen atmosphere, and then concentrated under reduced pressure. After addition of water (5 ml), the reaction mixture was extracted with ether. The ethereal extract was dried over anhydrous $MgSO_4$. Evaporation of the solvent afforded a colorless liquid (39 mg), which was separated by preparative TLC using hexane–benzene (1: 1) to give two fractions. From the less polar fraction, the starting material of **19** (8 mg) was recovered (mp and IR spectrum). From the polar fraction, a colorless viscous liquid **20** (28 mg) was isolated; ν_{max} (film) 1695 cm^{-1}; δ 0.84—1.06 (12H, complex) ppm; *m/e* 222 (M^+), 207 and 166 (Found: *m/e* 222.19846. Calcd for $C_{15}H_{26}O$: *m/e* 222.19836).

Reaction of Isoacoragermacrone (2) with 100% HCOOH in Thiophenol. To a solution of **2** (480 mg) in thiophenol–benzene [30 ml (1: 1)] was added, with stirring, 20 drops of 100% HCOOH at room temperature. The resulting solution was further stirred at room temperature for 15 h, and then washed successively with 10% NaOH aq solution and water, and then dried over anhydrous $MgSO_4$. Removal of the solvent under reduced pressure afforded a viscous liquid which was chromatographed on silica gel. Elution with hexane–benzene (1: 1) gave a colorless oil (347 mg), which was rechromatographed on silica gel and eluted with hexane and then with hexane–benzene (9: 1) to give **21** (33 mg) and **22** (110 mg), respectively.

Further elution of the above viscous liquid with hexane–benzene (1: 1) gave a colorless viscous liquid (179 mg) of undetermined structure. Continuous elution with the same solvent system afforded the guaiane-type compound **17** (110 mg) (mp and IR spectrum).

21. A colorless viscous liquid; ν_{max} (film) 3070 sh., 3060, 1580 br., 745 and 690 cm^{-1}; δ (CCl_4) 0.93 (6H, d, J=7.0 Hz), 1.09 (3H, s), 1.76 (3H, br. s), 2.99 (1H, m, J=7.0 Hz), 6.13 (1H, br. s) and 7.30 (5H, complex) ppm; *m/e* 312 (M^+), 202, 187, and 159 (Found: *m/e* 312.19197. Calcd for $C_{21}H_{28}S$: *m/e* 312.19116).

22. A colorless viscous liquid; ν_{max} (film) 3070, 1585 br., 750 and 695 cm^{-1}; δ (CCl_4) 0.76—0.98 (6H, complex), 1.12 (3H, s), 1.24 and 1.26 (total 3H), 5.35 and 5.43 (total 1H) and 7.10—7.70 (10H, complex) ppm; *m/e* 312 (M^+—110), 202 and 159 (Found: *m/e* 312.19105. Calcd for $C_{27}H_{34}S_2$–C_6H_6S; *m/e* 312.19116).

Reaction of Isoacoragermacrone (2) with concd H_2SO_4 in Thiophenal. To a solution of **2** (380 mg) in thiophenol (12 ml) was added, with stirring, 10 drops of conc. H_2SO_4 at 0 °C, and the solution was further stirred at 0 °C for 30 min, and then extracted with ether after addition of a cooled 10% NaOH aq. solution (40 ml). The ethereal extract was washed successively with 10% NaOH aq solution and water, and then dried over anhydrous $MgSO_4$. Removal of the solvent afforded a pale yellow liquid, which was chromatographed on silica gel (15 g) and eluted with hexane to give a colorless viscous liquid of **21** (22 mg) (TLC and IR spectrum). Further elution with hexane–benzene (9: 1) also gave a colorless viscous liquid **22** (491 mg) (TLC and IR spectrum).

Formation of the Dithio Compounds (22a and 22b) from the Conjugated Diene (21). To a solution of **21** (12 mg) in thiophenol (1 ml) was added, with stirring, one drop of concd H_2SO_4 at 0 °C. The solution was further stirred at 0 °C for 30 min, and then extracted with hexane after addition of a cooled 10% NaOH aq solution. The extract was washed successively with a cooled 10% NaOH aq solution and water, and then dried over anhydrous $MgSO_4$. After evaporation of the solvent, the residue was purified by preparative TLC using hexane to give a mixture of dithio compounds (**22a** and **22b**) as a colorless viscous liquid (9 mg) (TLC and IR spectrum).

Conversion of the Dithio Compounds (22a and 22b) into the Conjugated Diene (21). A solution of the dithio compounds (100 mg) in acetone containing MeI (2 ml) was refluxed for 4 h under a nitrogen atmosphere, and then concentrated under reduced pressure to give a pale yellow liquid which was separated by preparative TLC using hexane to give two fractions. From the first fraction, calamenene (14 mg) was isolated (GLC, TLC, and IR spectrum). From the second fraction, **21** (39 mg) was obtained (TLC and IR spectrum) as a colorless viscous liquid.

Reduction of Isoacoragermacrone (2) with Diisobutylaluminium Hydride (DBAH). To a solution of **2** (27 mg) in absolute benzene (2 ml) was added, with stirring, a solution of DBAH (100 mg) in heptane at 0 °C under a nitrogen atmosphere. The solution was further stirred at 0 °C for 1.5 h and at 5 °C for 30 min, and then cooled to 0 °C again. After addition of MeOH–benzene (1: 1) (5 ml), the solution was concentrated under reduced pressure to dryness. The residue was diluted with benzene with shaking, and then filtered. The filtrate was concentrated under reduced pressure to give a colorless oil (26 mg),** which was purified by preparative TLC using alumina [GF_{254} (type E), E. Merck A. G.] and benzene to give the corresponding dihydro compound **25** (7.5 mg) as a colorless viscous liquid; ν_{max} (film) 1700 cm^{-1}; δ 0.87 (3H, d, J=6.9 Hz), 0.92 (3H, d, J=6.9 Hz), 0.96 (3H, d, J=6.9 Hz), 1.45 (3H, br. s) and 5.16 (1H, t, J=6.5 Hz) ppm; *m/e* 222 (M^+) and 207 (Found: *m/e* 222.19837. Calcd for $C_{15}H_{26}O$: *m/e* 222.19836).

Reaction of the Dihydro Compound (25) with 80% aq AcOH. A solution of **25** (54 mg) in 80% aq AcOH (4 ml) was stirred at room temperature for 5 min, and then diluted with ice–water (*ca.* 10 ml). After neutralization with $NaHCO_3$ powder, the solution was extracted with ether. The ethereal extract was washed with a sat. NaCl aq solution, and then dried over anhydrous Na_2SO_4. Removal of the solvent afforded a colorless oil which was separated by preparative TLC using alumina [GF_{254} (type E), E. Merck A. G.] and benzene to give **26** (11 mg) as a colorless viscous liquid, which was identical with an authentic sample of dihydro-dehydroisocalamendiol.[1]

Reaction of Preisocalamendiol (3) with $AlCl_3$. To a solution of **3** (27 mg) in absolute ether (5 ml) was added, with stirring, a solution of $AlCl_3$ (23 mg) in absolute ether (1.5 ml) at 0 °C. The resulting solution was further stirred at 0 °C for 10 min, and then poured into ice–water. After separation of the ethereal layer, the aqueous solution was extracted with ether. The combined extracts were washed with a sat. NaCl aq. solution, and then dried over anhydrous Na_2SO_4. Removal of the solvent afforded a yellow oil***, which was subjected to preparative TLC using alumina [GF_{254} (type E), E. Merck A. G.] and benzene, giving a colorless viscous liquid, the dienol **28** (6.6 mg) (GLC, TLC, and IR spectrum).[1]

** Peak-area of analytical GLC was served as approximate values of the content (%), indicating that this oil contained the dihydro compound (19.6 mg).

*** Peak-area of analytical GLC was served as an approximate value of the content (%), indicating that this oil contained the dienol (14.6 mg).

Thermal Isomerization of Preisocalamendiol (3). A colorless viscous liquid of **3** (*ca.* 10 mg) in a sealed tube was heated at 180 °C, and the composition of the reaction mixture was checked by analytical GLC, as already described in Table 1.

Reduction of Preisocalamendiol (3) with $LiAlH_4$. To a solution of **3** (220 mg) in absolute ether (20 ml) was slowly added, with stirring, $LiAlH_4$ (40 mg) at room temperature, and then the reaction mixture was further stirred at room temperature for 30 h. After decomposition of an excess of the reagent with water, 20% potassium sodium tartarate aq solution was added to the reaction mixture, which was extracted with ether. The ethereal extract was washed with a sat. NaCl aq solution, and then dried over anhydrous Na_2SO_4. Removal of the solvent under reduced pressure afforded **29** (220 mg)† as a colorless liquid; ν_{max} (film) 3360 br. and 1640 cm^{-1}; δ 0.95 (6H, d, J=6.8 Hz), 1.60 (3H, br. s), 3.60—3.92 (1H, m), 4.92 (2H, br. s) and 5.25 (1H, m) ppm; *m/e* 222 (M^+), 204 and 161 (Found: *m/e* 222.19700. Calcd for $C_{15}H_{26}O$: *m/e* 222.19836).

Reaction of 29 with 80% aq HCOOH. The alcohol **29** (36 mg) was dissolved in 80% aq HCOOH (1 ml) at 0 °C. The resulting solution was stirred at 0 °C for 2 h, and then poured into a cooled sat. $NaHCO_3$ aq solution and extracted with ether. The ethereal extract was washed with a sat. NaCl aq solution, and then dried over anhydrous Na_2SO_4. Removal of the solvent gave a colorless oil (39 mg) in an almost pure state, which was purified by preparative GLC at 110 °C to afford a pure sample of the formate **30** (13 mg); ν_{max} (film 1720 and 1645 cm^{-1}; δ 0.93 (3H, d, J=6.9 Hz), 0.98 (3H, d, J=6.9 Hz), 1.66 (3H, d, J=1.3 Hz), 3.66—3.90 (1H, m), 4.97 (2H, br. s), 5.28 (1H, br. m) and 8.11 (1H, s) ppm; *m/e* 204 (M^+-46) and 161. Elemental analysis of this formate has not been carried out, but its structure (**30**) is supported by the above-mentioned spectral data coupled with the next experimental results.

Recoversion of the Formate (30) into the Alcohol (29). To a solution of **30** (13 mg) in absolute ether (3 ml) was added, with stirring, $LiAlH_4$ (4 mg). The reaction mixture was further stirred at room temperature for 3 h, and then an excess of the reagent was decomposed by addition of ether saturated with water. The reaction mixture was diluted with 20% potassium sodium tartarate aq solution (5 ml), and then extracted with ether. The ethereal extract was washed with a sat. NaCl aq solution, and then dried over anhydrous Na_2SO_4. Removal of the solvent afforded a colorless oil (11 mg) which was purified by preparative TLC using petroleum ether–ether (5:3) to give **29** (6 mg) in a pure state (GLC and IR spectrum).

Formation of ε-Cadinene (31). To a solution of **29** (164 mg) in absolute pyridine (10 ml) was slowly added, with stirring, a solution of mesyl chloride (100 mg) in pyridine (5 ml) at 0 °C. The resulting solution was further stirred at 0 °C for 1 h, and then at room temperature for 7 h. The solution was poured into ice water, and then extracted with ether. The ethereal extract was washed throughly with a sat. NaCl aq solution, and then dried over anhydrous Na_2SO_4. Removal of the solvent under reduced pressure gave an almost colorless oil (135 mg), which was purified by preparative TLC using hexane to give ε-cadinene (51 mg) as a colorless viscous liquid; ν_{max} (film) 3070 and 1645 cm^{-1}; δ 0.71 (3H, d, J=6.7 Hz), 0.91 (3H, d, J=6.7 Hz) and 4.72—4.48 (4H, complex) ppm; *m/e* 204 (M^+ for $C_{15}H_{24}$), 176 and 161.

Catalytic Hydrogenation of ε-Cadinene (31). Catalytic hydrogenation of **31** (10 mg) in AcOEt (1 ml) was carried out over PtO_2 (3 mg) at room temperature for 2 h. After filtration of the catalyst, the solvent was evaporated under reduced pressure to give a colorless oil (10.1 mg) in a pure state; δ 0.73 (3H, d, J=6.6 Hz), 0.82 (6H, d, J=7.0 Hz) and 0.97 (3H, d, J=6.6 Hz) ppm; *m/e* 208 (M^+ for $C_{15}H_{28}$), 165 and 109. The IR spectrum of this oil was completely identical with that of an authentic sample of tetrahydrocadinene.[14]

† GLC of this liquid showed only one peak.

The authors wish to thank Professor Yoshimasa Hirata (Nagoya University) for his invaluable suggestion. Thanks are also due to Drs. Masayasu Kurono and Masaaki Toda (Ono Pharmaceutical Co. Ltd.) for measurements of high resolution mass spectra. This research has been supported in part by grants from the Ministry of Education, to which greatful acknowledgement is made.

References

1) S. Yamamura, M. Iguchi, A. Nishiyama, M. Niwa, H. Koyama, and Y. Hirata, *Tetrahedron*, **27**, 5419 (1971) and references cited therein.

2) M. Niwa, A. Nishiyama, M. Iguchi, and S. Yamamura, *Bull. Chem. Soc. Jpn.*, **48**, 2930 (1975).

3) V. Herout, O. Motl, and F. Sǒrm, *Coll. Czech. Chem. Commun.*, **22**, 785 (1957); S. C. Bhattacharyya, A. S. Rao, and A. M. Shaligram, *Chem. Ind.*, **1960**, 469, and *Tetrahedron*, **18**, 969 (1962); D. W. Theobald, *Tetrahedron*, **20**, 2593 (1964).

4) O. Motl, V. Sykora, V. Herout, and F. Sǒrm, *Coll. Czech. Chem. Commun.*, **23**, 1297 (1958).

5) A. F. Thomas, M. Ozainne, R. Decorzant, F. Näf, and C. Lukacs, *Tetrahedron*, in press.

6) M. Iguchi, M. Niwa, and S. Yamamura, *Tetrahedron Lett.*, **1973**, 4367.

7) J. G. Traynham, G. R. Frauzen, G. A. Knesel, and D. J. Northington Jr., *J. Org. Chem.*, **32**, 3285 (1967); J. G. Traynham, and H. H. Hsieh, *ibid.*, **38**, 868 (1973); J. K. Sutherland, *Tetrahedron*, **30**, 1651 (1974).

8) M. Iguchi, M. Niwa, and S. Yamamura, *J. Chem. Soc., Chem. Commun.*, **1971**, 974.

9) M. Ōki, "Jikken Kagaku Koza," Supplement Vol. XII, ed. by The Chemical Society of Japan, Maruzen Publishing Co. Ltd., Tokyo (1967), p. 252.

10) M. Iguchi, M. Niwa, and S. Yamamura, *Tetrahedron Lett.*, **1973**, 1687.

11) G. Büchi, W. Hofheinz, and J. V. Paukstelis, *J. Am. Chem. Soc.*, **91**, 6473 (1969) and references cited therein.

12) M. Iguchi, A. Nishiyama, S. Yamamura, and Y. Hirata, *Tetrahedron Lett.*, **1970**, 855.

13) L. Westfelt, *Acta Chem. Scand.*, **20**, 2865 (1966).

14) We are most grateful to Drs. Y. Hirose and Y. Ohta (The Institute of Food Chemistry) for their discussion, and identification of the synthetic tetrahydrocadinene with an authentic sample.

A Single-step Synthesis of 2-Substituted 2-Thiazolines[1)]

Nobutaka SUZUKI and Yasuji IZAWA*

Department of Industrial Chemistry, Faculty of Engineering, Mie University, Tsu 514

(Received April 23, 1976)

2-Phenyl-2-thiazoline (**4b**) and its derivatives: [4-carboxylic acid (**4c**), 4-carboxylic acid methyl ester (**4d**), and 5,5-dimethyl-4-carboxylic acid (**4e**)], 2-(*p*-chlorophenyl)-2-thiazoline (**4f**) and its 4-carboxylic acid (**4g**), and 2-methyl-2-thiazoline (**4h**) were obtained by treating $RCS_2CH_2CO_2H$ [R=Phenyl (**1b**), *p*-chlorophenyl (**1d**), or methyl (**1e**)] or $MeCS_2Et$ (**1f**) with the corresponding 2-aminoethane thiols, *i.e.*, cysteamine (**6a**), cysteine (**6b**), cysteine methy ester (**6c**), and/or penicillamine (**6d**). **4b** was also obtained from $PhCS_2Et$ (**1c**) and **6a** with a rate approximately equal to that from **1b** and **6a**. The attempted synthesis of 2-methyl-2-thiazoline-4-carboxylic acid (**4i**) using a similar method gave only *N*-acetylcysteine (**7**).

There have been numerous reports concerning the synthesis of 2-aryl- and 2-alkyl-2-thiazolines. The known synthetic methods can be classified as follows: (a) condensation of nitriles (R–C≡N)[2-4)] or isonitriles (R–N=C:)[5a)] with 2-aminoethane thiols (H_2N–CH_2CH_2–SH), or intramolecular cyclization of 2-mercapto isonitriles [R–CH(SH)CHR′–N=C:];[5b)] (b) dehydration of *N*-acyl-2-aminoethane thiols (R–$CONHCH_2CH_2$–SH)[2,6)] or *N*-thioacyl-2-aminoethanols (R–$CSNHCH_2$–CH_2–OH);[7)] and (c) condensation of thioamides or imino thiols [R–(C=NH)SH] with 1,2-dihalides (X–CH_2CH_2–X) or 2-haloethylamines (H_2N–CH_2CH_2–X),[8)] where R and R′=alkyl, aryl, or H, and X=Br or Cl. However, most of these require several steps and/or drastic conditions, such as high temperature and strongly acidic or basic media, to synthesize relatively unstable thiazolines.

Suzuki and Goto have found in the course of the studies on the firefly bioluminescence[9)] that (carbamoylthiocarbonylthio)acetic acid (**1a**)[10)] readily condensed with *o*-phenylenediamine (**2**) at room temperature and pH *ca.* 8 to give 2-carbamoylbenzimidazole (**3**); similar reactions were expected to be applicable to the preparation of other five-membered heterocycles.

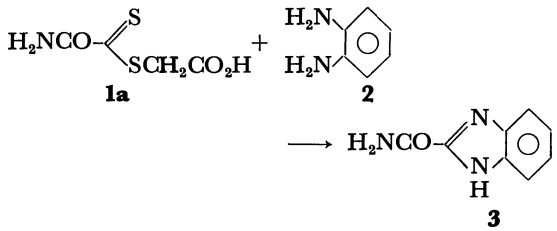

1a **2** **3**

White *et al.* reported an effective synthesis of an unstable thiazoline, firefly luciferin (**4a**), by condensation of 2-cyano-6-hydroxybenzothiazole (**5a**) with cysteine (**6b**) under mild conditions, *i.e.*, at room temperature at pH *ca.* 8.[4)] However, we found that although 2-phenyl-2-thiazoline (**4b**) could be prepared by treating benzonitrile (**5b**) with cysteamine (**6a**)

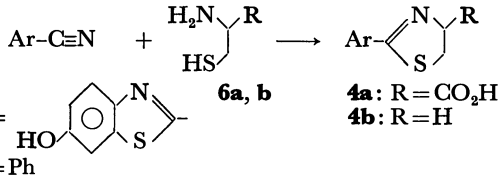

6a, b **4a**: R=CO_2H **4b**: R=H

5a: Ar=

5b: Ar=Ph

* To whom all correspondence should be addressed.

according to the above method (required reflux in EtOH), attempted condensation of the nitrile (**5b**) with other 2-aminoethane thiols (**6b**, **6c**, and **6d**) under similar conditions did not give the corresponding thiazolines (**4c**, **4d**, and **4e**).

In the present paper we wish to report on a convenient preparation of 2-substituted 2-thiazolines and their derivatives (**4b—4h**),[1)] which were obtained by the condensation of dithioates (**1b—1f**) with the corresponding 2-aminoethane thiols (**6a—6d**) under slightly alkaline conditions; a probable reaction pathway is also discussed.

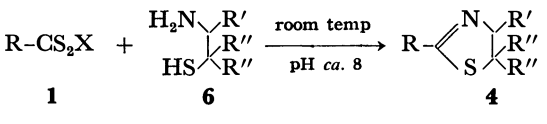

1 **6** **4**

1

	R	X
1b:	Ph	CH_2CO_2H
1c:	Ph	Et
1d:	*p*-Cl-Ph	CH_2CO_2H
1e:	Me	CH_2CO_2H
1f:	Me	Et

6

	R′	R″
6a:	H	H
6b:	CO_2H	H
6c:	CO_2Me	H
6d:	CO_2H	Me

4

	R	R′	R″
4b:	Ph	H	H
4c:	Ph	CO_2H	H
4d:	Ph	CO_2Me	H
4e:	Ph	CO_2H	Me
4f:	*p*-Cl-Ph	H	H
4g:	*p*-Cl-Ph	CO_2H	H
4h:	Me	H	H

Methods and Results

Syntheses of the 2-phenyl-2-thiazolines (**4b—4e**) which gave good yields were performed by the condensation of the dithioate (**1b**)[11)] with the corresponding 2-aminoethane thiols (**6a—6d**) at room temperature in slightly alkaline media. **4b** was also obtained by the condensation of **6a** with **1c**[12)] in place of **1b**.

Similarly, **4f** and **4g** were obtained from **1d**[13)] and the corresponding 2-aminoethane thiols (**6a** and **6b**). Although 2-methyl-2-thiazoline (**4h**) was obtained in an unsatisfactory yield by the similar condensation of **1e**[11)] or **1f**[12)] with **6a**, the attempted synthesis of the 4-carboxylic acid (**4i**) by treating **1e** or **1f** with **6b** was unsuccessful; *N*-acetylcysteine (**7**), mp 106 °C,[14)] as

Table 1. Synthesis of the 2-thiazolines (**4b**—**4h**) and **7**

Product	**4b**		**4c**	**4d**	**4e**	**4f**	**4g**	**4h**	**7**	
Reagents										
RCS_2X	**1b**	**1c**	**1b**	**1b**	**1b**	**1d**	**1d**	**1e**	**1e**	**1f**
2-Aminoethane thiols	**6a**	**6a**	**6b**	**6c**	**6d**	**6a**	**6b**	**6a**	**6b**	**6b**
Reaction Time (h)	5	5	23	3.5	22	22	20	22	48	28
Solvent[a]	E(2:1)		E(2:1)	M	E(2:1)	E(1:1)	E(1:1)	E(1:1)	E(1:1)	
Isolation[b]	A		B	C	C	C	D	C	C	
Recryst. Solvent[c]	—		C	A	A	B	B	—	—	
Cryst. Form and Color[d]	C-Liq.		C–N	C–FN	C–P	PY–L	C–FN	PY–Liq.	C–N	
Yield (%)	87	84	79	84	88	66	53	25	65	45
Mp (bp) (°C)	(129—130.5 °C/ 10 Torr)		121.5— 122.5 °C	112— 114 °C	120— 121.5 °C	50— 52 °C	169— 171 °C	(144 °C)	106— 108 °C	
[lit.]	(110 °C/5 Torr)		122 °C	113— 114 °C	—	—	—	(143— 145 °C)	107— 107.5 °C	
Reference	2)		7a)	7a)	—	—	—	19)	14)	

a) E (n: 1): EtOH–H_2O (n: 1); M: MeOH. b) A: Extd. with CH_2Cl_2 and ether, followed by distn.; B: Extd. with EtOAc and ether; C: Extd. with EtOAc; D: Collected by filtration. c) A: Ether; **B**: EtOH; C: Benzene–hexane. d) C: Colorless; PY: Pale yellow; N: Needles; L: Leaflets; FN: Fine needles.

Table 2. Physical properties of the 2-thiazolines (**4b**—**4h**) and **7**

Compd	ν_{max}^{KBr} (cm^{-1})		δ (ppm)			
	C=N	C=O	Solv.[b]	C_4	C_5	Others
4b	1605S[a]		C	4.42, t,[c] J 8 Hz	3.35, t, J 8	7.45, 3H, m 7.89, 2H, m
4c	1605S	1740sh 1730S	D	5.24, t, 9	3.56, d, 9 3.65, d, 9	7.48, 3H, m 7.76, 2H, m
4d		1745S 1225	C	5.26, t, 9	3.61, d, 9 3.66, d, 9	7.40, 3H, m 7.82, 2H, m
4e	1590	1735	D	4.81, s	1.44, s, 1.72, s	7.50, 3H, m 7.78, 2H, m
4f	1605S		C	4.46, t, 8.4	3.44, t, 8.4	7.39, 2H, d, J 8.6 7.79, 2H, d, 8.6
4g	1600S	1725S	D	5.32, t, 8.8	3.65, d, 8.8 3.68, d, 8.8	7.56, 2H, d, 8.2 7.82, 2H, d, 8.2
4h	1630S		C	4.12, br. t	3.32, t, 10	2.16, 3H, t, 2
7		1720M 1635S	D	4.40, m	2.80, m	1.91, 3H, s 8.11, 1H, d, 8.0(NH)

a) S: strong; M: medium. b) C: chloform-d_1; D: dimethyl-d_6 sulfoxide. c) s: singlet; d: doublet; t: triplet; m: multiplet; br: broad.

colorless crystals was however obtained in moderate yields (44% for **1e** and 65% for **1f**).

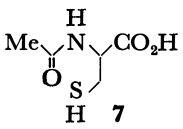

7

The results and the physical properties of the products are summarized in Table 1 and 2.

Discussion

To account for the observed products, especially *N*-acetylcysteine (**7**), a stepwise reaction pathway may be considered as the possible reaction scheme rather than a concerted reaction pathway. The product (**7**) is regarded as a rearrangement product of *S*-acetylcysteine derived from a hydrolysis of *S*-thioacetylcysteine;[14] this is supported by the moderate stability of **4e** reported by Smith and Gorin.[14] The production of *N*-acetyl-*o*-aminophenol (**8**) in the synthesis of 2-methylbenzoxazole (**9**)[15] may also support the stepwise reaction pathway.

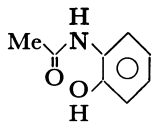

8

The first step in this reaction should be a nucleophilic attack of one of two nucleophiles, *i.e.*, the amino group or the sulfide anion.

$-SCH_2CO_2H$ **10** $-SEt$ **11**

It is well known that the carboxymethylthio group (**10**) is an effective leaving group in aqueous alkaline

media. We expected to get some mechanistic information about the first step of the present reaction when the group **10** was replaced by the ethylthio group (**11**), which is supposed to be a less effective leaving group than **10**.[16,17] When **1b** and **1c** were treated with **6a**, the disappearance rates of **1b** and **1c** were almost identical and the products were identified by GLC and IR spectra to be **4b**. This fact implies that there is little effect from the leaving groups on this reaction (see Fig. 1), and also that the sulfide anion is so strong a nucleophile that no significant effect from the leaving group could be determined.

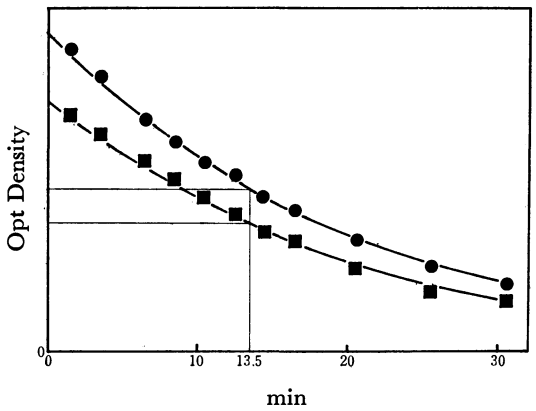

Fig. 1. Optical densities of **1b** and **1c** on treatments with **6a** at λ_{max} 488 nm in aqueous EtOH (1: 1).
—●—: **1b**, —■—: **1c**.

Lawson and Searle have shown that in the absence of any steric hindrance to the approach of the amino-nitrogen atom to the thion-carbon atom of **1b**, the ease of thiobenzoylation of amino compounds depends largely on the nucleophilicity of the amino-nitrogen atom.[7b] Thus, the lower yield of 2-methyl derivative (**4h**) and the unsuccessful attempt to prepare **4i** may be explained by the lowering of the electrophilicity of the thion-carbon atom caused by an electronic effect of the methyl substituent in the second step of the present reaction.

Some of the cyclizations to yield 2-thiazolines were reported to be acid catalysed.[2,5b,7a-c,12] The cyclization in the present reaction, however, occurs in basic conditions.

Provided that the present reaction proceeds through a stepwise mechanism, and since the acidities of –SH and $-NH_2$ are

$$-SH \gg -NH_2,^{18)}$$

we suggest that the cyclization may proceed as follows:

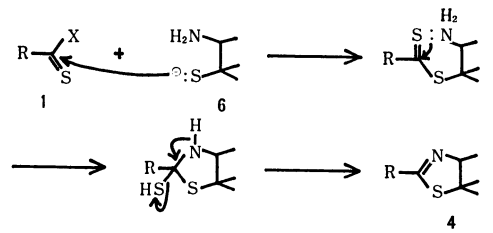

Chart 1.

Experimental

All mps and bps were uncorrected. The following spectrometers were used for spectral measurements: UV: Shimadzu UV-200; IR: JASCO IR-G; NMR: JEOL JNM-MH-100 (100 MHz); MS: JEOL JMS-D-100. The spectral data are presented as follows: UV: in nm and ε in parentheses; IR in cm^{-1}; NMR: chemical shifts (δ) in ppm from int. TMS and coupling constants (J) in Hz (accuracy $\pm$0.5 Hz); the solvents used are given in parentheses. GLC conditions used were as follows: Yanagimoto Yanaco G-1800F; Silicone SE-GE-31 (10%) on Diasolid L (60—80 mesh), in stainless steel column (2 m $\times$ ϕ 2.25 mm); col. temp 215 °C, inj. temp 170 °C, carrier gas (N_2) 20 ml/min. TLC conditions used were as follows: Silica gel PF_{254}-gipshaltig (E. Merck A. G.); thickness: 2.2 mm, 20 cm $\times$ 20 cm, hexane.

Benzonitrile (**5b**), acetonitrile, cysteine (**6b**), cysteine methyl ester (**6c**), penicillamine (**6d**), and *N*-acetyl-L-cysteine (**7**) were purchased from Nakarai Chem. Co., and cysteamine (**6a**) was from Tokyo Kasei Chem. Co.

*Carboxymethyl dithiobenzoate (**1b**)*[11] and *carboxymethyl p-chlorodithiobenzoate (**1d**)*[13] were prepared according to the method of Kurzer *et al.*[11] **1b**: Red fine prisms; mp 121—123 °C [lit,[11] 125 °C], λ_{max} [EtOH–H_2O (1: 1)] 487 nm (ε 120), 294 (12000), no change occurred after the addition of 1 M NaOH. **1d**: Reddish orange leaflets; mp 120—121 °C [lit,[13] 115—117 °C]; Found: C, 44.09; H, 2.76%. Calcd for $C_9H_7ClO_2S_2$: C, 43.81; H, 2.86%.

*Ethyl dithioacetate (**1f**)*,[12] *ethyl dithiobenzoate (**1c**)*,[12] and *carboxymethyl dithioacetate (**1e**)*[13] were prepared according to the methods of Meijer *et al.*[12] **1c**: Red liq.; bp 113—118 °C/1.2 mmHg [lit,[13] 164 °C/12 Torr], λ_{max} [EtOH–H_2O (1: 1)] 488 nm (100), 298 (10800), no change occurred after the addition of 1 M NaOH. **1e**: Yellow needles; mp 76—79 °C [lit,[7a] 80—81 °C]. **1f**: Orange-yellow liq.; bp 47—50 °C/12 mm [lit,[12] 52 °C/12 mm].

Authentic samples of **4c**, **4d**, **4h** were prepared by the methods described in the lit. **4c**: Colorless needles; mp 116—117 °C [lit,[7a] mp 122 °C]. **4d**: Colorless fine needles; mp 112—114 °C [as HCl salt; lit,[7a] mp 113—114 °C]. **4h**: Pale-yellow liq. bp 142—144 °C [lit,[19] bp 143—145 °C].

General Synthetic Procedure of the Thiazolines. The dithioate (**1b—f**) (1.0 mmol) and the aminothiol (**6a—d**) (1.1 mmol) were dissolved in aqueous MeOH or aqueous EtOH (1: 1; 25 ml); the pH was adjusted to *ca.* 8 with aqueous 1 M NaOH. The mixture was stirred at room temp under slightly reduced pressure (aspirator) to remove H_2S generated until the red color of the dithioate disappeared. The reaction was also monitored by TLC (E. Merck A. G.; Silica gel PF_{254}-gipshaltig, *ca.* 0.25 mm, hexane–acetone, 3: 1). The pH of the mixture was checked occasionally and kept *ca.* 8 by intermittent additions of the aqueous alkali. After the mixture was acidified (pH *ca.* 3) with aqueous 1 M HCl and concentrated *in vacuo* below 40 °C, the resulting aqueous mixture was extracted with $CHCl_3$ or EtOAc. Evaporation of the extracts and/or crystallization gave a liquid (**4b** or **4h**) or crystalline product (**4c**, **4d**, **4e**, **4f**, or **4g**) in good yield. The results and their properties are shown in Tables 1 and 2. The products of each condensation were checked with GLC and/or TLC before and after the acidification of the reaction mixtures. The products were identical before and after the work-up.

The thiazoline (**4b**) synthesized was identical with that from **5b** and **6a** (IR and NMR), and its bp was identical with that which appears in the lit.[11] The carboxylic acid (**4c**) and its methyl ester (**4d**) were identified by comparing with mp, IR, and NMR of the authentic samples.[7a] 2-Methyl-2-thiazoline

(**4h**) synthesized was identical with that of the authentic sample.[19] The *N*-acetylcysteine (**7**) obtained was assigned by comparing its mp, IR, and NMR with the authentic sample.[14]

*2-Phenyl-5,5-dimethyl-2-thiazoline-4-carboxylic Acid (**4e**).* Found: C, 61.39; H, 5.58%. Calcd for $C_{12}H_{13}NO_2S$: C, 61.25; H, 5.57%. Its IR spectrum was very similar to that of **4c**; MS showed a molecular peak at *m/e* 235 and NMR spectral data showed two methyls (1.44s and 1.72s), a methine (4.81s), and monosubstituted benzene protons (7.50 m and 7.78 m), which support the structure assignment (**4e**).

*2-(p-Chlorophenyl)-2-thiazoline (**4f**).* Found: C,54.44; H, 3.79%. Calcd for C_9H_8ClNS: C, 54.68; H, 4.08%. Its IR spectrum was very similar to that of **4b**; MS showed a molecular peak at *m/e* 197 and its NMR spectrum showed two methylenes (3.44 t and 4.46 t), and *p*-disubstituted benzene protons (7.39 d and 7.79 d), which support the structure assignment (**4f**).

*2-(p-Chlorophenyl)-2-thiazoline-4-carboxylic Acid (**4g**).* Found: C, 49.82; H, 3.23; N, 5.64%. Calcd for $C_{10}H_8ClNO_2S$: C, 49.70; H, 3.34; N, 5.80%. Its IR spectrum was very similar to that of **4c**; MS showed a molecular peak at *m/e* 241 and its NMR spectrum showed two methylene protons (3.65 d and 3.68 d), a methine (5.32 t), and *p*-disubstituted benzene protons (7.56 d and 7.82 d), which support the structure assignment (**4g**).

*Relative Rate of Reaction of **1b** or **1c** with **6d**.* Into the aqueous ethanolic (1:1; 3 ml) solutions of **1b** or **1c** (0.1 mmol/15 ml) were added an aqueous 1 M NaOH (60 μl) and then an aqueous ethanolic solution (2 ml) of **6a** (0.11 mmol/10 ml). Their optical densities at *ca.* 488 nm were measured at intervals (16 °C). The relative reaction rate was calculated based on the results to be about unity ($\tau_{1/2}$=13.5 min). The generation of **4b** was confirmed by GLC. (See Fig. 1).

We thank Professor Toshio Goto and his co-laborators of Nagoya University for the measurements of Mass spectra.

References

1) Preliminary communication: N. Suzuki and Y. Izawa, *Tetrahedron Lett.*, **1974**, 1863.

2) J. C. Sheehan and J. J. Ryan, *J. Am. Chem. Soc.*, **73**, 4367 (1951).

3) (a) R. Kuhn and F. Drawert, *Justus Liebigs Ann. Chem.*, **590**, 55 (1954); (b) W. Stoffel and L. C. Craig, *J. Am. Chem. Soc.*, **83**, 145 (1961); (c) H. Baganz and L. Domaschke, *Chem. Ber.*, **95**, 1842 (1962).

4) E. H. White, F. McCapra, and G. F. Field, *J. Am. Chem. Soc.*, **85**, 337 (1963).

5) (a) Y. Ito, Y. Inubushi, M. Zenbayashi, S. Tomita, and T. Saegusa, *J. Am. Chem. Soc.*, **95**, 4447 (1973); (b) U. Schöllkopf and D. Hoppe, *Angew. Chem. Int. Ed. Engl.*, **12**, 1006 (1973).

6) (a) S. Michels, *Ber.*, **25**, 3051 (1892); (b) R. E. Basford and F. M. Hünnekens, *J. Am. Chem. Soc.*, **77**, 3878 (1955); (c) A. K. Bose, G. Spiegelman, and M. S. Manhas, *ibid.*, **90**, 4506 (1968).

7) (a) J. C. Crawhall and D. F. Elliott, *J. Chem. Soc.*, **1951**, 2071; (b) A. Lawson and C. E. Searle, *ibid.*, **1957**, 1556; (c) D. A. Tomalia and J. N. Paige, *J. Org. Chem.*, **38**, 3949 (1973).

8) (a) S. Gabriel and C. F. V. Hirsch, *Ber.*, **29**, 2610 (1896); (b) Shell Research Ltd., Belg., 623714 (1963): *Chem. Abstr.*, **60**, 9299a (1964); (c) J. Yates, H. P. Rosinger, and J. T. Hackmann, Ger., 1262667 (1968): *Chem. Abstr.*, **70**, 57823V (1969); (d) J. Yates and E. Haddock, U. S., 3418331 (1968): *Chem. Abstr.*, **70**, 57824W (1969).

9) N. Suzuki and T. Goto, *Agr. Biol. Chem.*, **36**, 2213 (1972).

10) S. Seto, K. Ogura, and Y. Nishiyama, *Bull. Chem. Soc. Jpn.*, **36**, 331 (1963).

11) F. Kurzer and A. Lawson, *Org. Synth.*, Coll. Vol. V, p. 1046 (1973); F. Kurzer, *Chem. Ind. (London)*, **1961**, 1333.

12) J. Meijer, P. Vermeer, and L. Brandsma, *Recl. Trav. Chim. Pays-Bas*, **92**, 601 (1973).

13) K. A. Jensen and C. Pedersen, *Acta Chem. Scand.*, **15**, 1087 (1961).

14) H. A. Smith and G. Gorin, *J. Org. Chem.*, **26**, 820 (1961).

15) N. Suzuki, T. Yamabayashi, and Y. Izawa, *Bull. Chem. Soc. Jpn.*, **49**, 353 (1976).

16) (a) E. S. Gould, "Mechanism and Structure in Organic Chemistry," Dryden, New York, N. Y. (1959), p. 261; (b) G. Maccagnani and G. Mazzanti, "The Chemistry of the Thiol Group," ed. by S. Patai, Interscience Pub., New York, N. Y. (1974), p. 417.

17) G. Kortuem, N. Vogel, and K. Andrussow, "Dissociation Constants of Organic Acids in Aqueous Solution," Butterworths, London (1961).

18) D. D. Perrin, "Dissociation Constsants of Organic Bases in Aqueous Solution," Butterworths, London (1965).

19) G. Pinkus, *Ber.*, **26**, 1083 (1893).

Hetera-*p*-carbophane. VIII. The Change in Binding Sites of NMR Shift Reagents in Polyoxadioxo[*n*]paracyclophanes and Their Open-chain Analogs[1)]

Kazuhiko SAKAMOTO and Michinori ŌKI*

Department of Chemistry, Faculty of Science, The University of Tokyo, Hongo, Bunkyo-ku, Tokyo 113

(Received May 7, 1976)

A series of polyoxadioxo[*n*]paracyclophanes were prepared by condensation of polyethylene glycols with the corresponding 2,5-disubstituted *p*-phenylenediacetyl dichlorides under high dilution conditions. ^{1}H NMR spectra of these compounds were recorded in the presence and absence of lanthanoid shift reagents and the results are compared with those of the open-chain analogs. The change in binding sites of the shift reagents is observed as the number of ethylenedioxy units increases, and the result is discussed from the standpoint of electronic and steric effects.

The usefulness of NMR shift reagents for the determination of the ester conformations, *s-cis* and *s-trans*, has been reported from this laboratory.[2)] As a combined extension of this and other studies on hetera-*p*-carbophanes, it was of interest to investigate the binding sites of the shift reagent for polyoxadioxo[*n*]paracyclophanes.

A literature search revealed that, although ether oxygen is usually a very weak binding site for the shift reagent,[3)] polyglyme does form a complex at the end of the chain[4)] and several aromatic compounds which possess two ether groups *ortho* to each other bind more strongly to the shift reagent at the ethers than to the ester groups.[5)] Therefore, if an ansa chain contains ethylenedioxy units there is a possibility that competition takes place among the binding sites including the ethylenedioxy and the ester groups.

Therefore, a series of polyoxadioxo[*n*]paracyclophanes and open-chain analogs were prepared and their ^{1}H NMR spectra were observed in the presence of the shift reagents. This paper describes an interesting result which suggests that a change in the binding sites occurs according to the chain length of the polyoxyethylene compounds.

Experimental

The syntheses of a series of disubstituted polyoxadioxo[*n*]-paracyclophanes (III^R_m, where *m* is the number of oxyethylene units and R the substituent) and open-chain analogs (IV_m, where *m* is the number of oxyethylene units) were accomplished by the condensation of polyoxaalkane-α,ω-diols (polyethylene glycols) with the corresponding acyl chlorides (Scheme 1). The polyoxaalkane-α,ω-diols were of commercial origin except for 3,6,9,12-tetraoxatetradecane-1,14-diol (II_5) which was prepared according to a method described in the literature.[6)] The acid chlorides were synthesized in a manner reported previously.[7)]

Syntheses of Polyoxadioxo[n]*paracyclophanes (III^R_m) and Bis(*2,5-*dimethylphenylacetate)s (IV_m) of Polyoxaalkane-α,ω-diols.* The condensation between the chlorides (I) and the diols (II_m) was carried out in essentially the same manner as that reported previously,[8)] except for the omission of the base. A chromatograph of the crude products on silica gel using a hexane–ether mixture as the eluent gave pure compounds. Esterification of II with 2,5-dimethylphenylacetyl chloride proceeded normally. Analytical and other pertinent data are summarized in Table 1.

Measurement of Spectra. The infrared spectra were recorded on a Hitachi EPI-G2 infrared spectrometer with KBr discs for III^R_m and with a neat liquid for IV_m. The ^{1}H NMR spectra were measured at 34 °C on a Hitachi R-20B spectrometer operating at 60 MHz. Samples were dissolved in deuteriochloroform for conventional measurements and the chemical shifts were recorded relative to an internal TMS. Lanthanoid [Eu(dpm)$_3$ and Eu(fod)$_3$-d_{27}] induced shifts were measured with deuteriochloroform solutions in a manner analogous to that reported previously.[2)] The mass spectra were recorded on a Hitachi RMU-6L spectrometer.

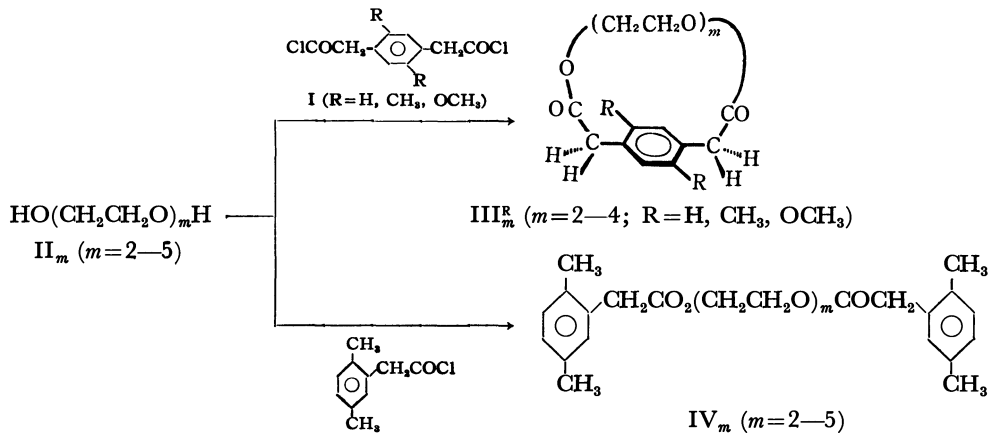

Scheme 1.

TABLE 1. POLYOXADIOXO[*n*]PARACYCLOPHANES (III^R_m) AND BIS(2,5-DIMETHYLPHENYLACETATE)S (IV_m) OF POLYOXAALKANE-α,ω-DIOLS[a]

Compound	*m*	R	Molecular formula	Mp (°C)	Analytical data C(%)	Analytical data H(%)	Mol wt	Recrystallization solvent	IR ν_{CO} (cm^{-1})
III^R_m	2	H	$C_{14}H_{16}O_5$	158.5—159.5	64.11	6.21	264	CH_2Cl_2	1725
					63.62	6.10	264.3		
	2	Me	$C_{16}H_{20}O_5$	96.0— 97.0	66.09	7.26	292	ether–hexane	1725
					65.74	6.90	292.3		
	3	H	$C_{16}H_{20}O_6$	39.0— 40.0	62.37	6.30	308	ether–hexane	1720[b]
					62.33	6.54	308.3		
	3	Me	$C_{18}H_{24}O_6$	70.5— 71.0	64.51	7.11	336	ether–hexane	1730[b]
					64.27	7.19	336.4		
	4	H	$C_{18}H_{24}O_7$	95.5— 96.5	61.37	6.83	352	CH_2Cl_2	1735
					61.35	6.87	352.4		
	4	Me	$C_{20}H_{28}O_7$	85.5— 86.5	63.23	7.53	380	ether	1720
					63.14	7.42	380.4		
	4	OMe	$C_{20}H_{28}O_9$	94.5— 95.0	58.23	6.64	412	ether	1725
					58.24	6.84	412.4		
IV_m	2		$C_{24}H_{30}O_5$	oil	72.12	7.50			1740
					72.34	7.59			
	3		$C_{26}H_{34}O_6$	oil	70.77	7.61			1725
					70.56	7.74			
	4		$C_{28}H_{38}O_7$	oil	69.30	7.64			1745
					69.11	7.87			
	5		$C_{30}H_{32}O_8$	oil	68.06	8.09			1730
					67.90	7.99			

a) The numerical values in the upper column are those found experimentally and those in the lower column are calculated values. b) A broad or bifurcated absorption.

TABLE 2. ^1H NMR DATA FOR POLYOXADIOXO[*n*]PARACYCLOPHANES (III^R_m) AND BIS(2,5-DIMETHYLPHENYLACETATE)S (IV_m) OF POLYOXAALKANE-α,ω-DIOLS IN DEUTERIOCHLOROFORM AT 34 °C (δ)[a]

Protons	Compounds										
	III^H_2	III^{Me}_2	IV_2	III^H_3	III^{Me}_3	IV_3	III^H_4	III^{Me}_4	III^{OMe}_4	IV_4	IV_5
1-CH_2	3.52	3.60	3.61	3.60	3.58	3.61	3.63	3.59	3.65	3.61	3.63
	s	AB-q[b]	s	s	AB-q[c]	s	s	s	s	s	s
	4H	4H	8H*	8H*	8H*	12H*	16H*	8H*	8H*	16H*	16H*
4-CH_2	4.07	4.03	4.20	4.21	4.19	4.24	4.29	4.24	4.27	4.25	4.26
	AA′	AA′	AA′	AA′	AA′	AA′	AA′	AA′	AA′	AA′	AA′
	4H	4H	4H	4H	4H	4H	4H	4H	4H	4H	4H
5-CH_2	3.21	3.21	3.58	3.53	3.54	3.63	3.63	3.62	3.65	3.66	3.68
	BB′	BB′	BB′	BB′	BB′	BB′	BB′	BB′	BB′	BB′	BB′
	4H	4H	8H*	8H*	8H*	12H*	16H*	8H*	8H*	16H*	16H*
7-CH_2				3.15	3.14	3.54					
				s	s	s					
				4H	4H	12H*	3.50	3.41	3.44	3.59	3.60
8-CH_2							m	m	m	s	s
							16H*	8H*	8H*	16H*	16H*
10-CH_2											
Ar–H	7.20	6.94	7.00	7.25	7.02	7.00	7.30	7.02	6.78	7.00	7.02
	s	s	s	s	s	s	s	s	s	s	s
	4H	2H	6H	4H	2H	6H	4H	2H	2H	6H	6H
Ar–CH_3		2.26	2.27		2.28	2.27		2.28	(3.80)	2.27	2.28
(or–OCH_3)		s	bs		s	bs		s	bs	bs	bs
		6H	12H		6H	12H		6H	6H	12H	12H

a) s=singlet, AB-q=AB-quartet, m=multiplet, AA′=AA′ part of AA′BB′ type signal, BB′=BB′ part of AA′BB′ type signal, and bs=broad signal. b) J_{AB}=14.0 Hz, $\Delta\delta_{AB}$=16.8 Hz. c) J_{AB}=14.5 Hz, $\Delta\delta_{AB}$=14.5 Hz. *) Since there was so much overlapping of the methylene protons at δ 3.4—3.7 in III^R_m and IV_m that it was difficult to estimate the intensities separately, the intensity of all protons contributing to the overlapped signals was shown.

Results and Discussion

Peak Assignments of Bridge Methylene Protons. The ^1H NMR spectral data of polyoxadioxo[n]paracyclophanes (III^R_m) and bis(2,5-dimethylphenylacetate)s (IV_m) of polyoxaalkane-α,ω-diols are summarized in Table 2.

The benzylic protons of III^{Me}_2 and III^{Me}_3 give signals of the AB type at δ *ca.* 3.60, suggesting a slow internal rotation of the aromatic ring on the NMR time scale, whereas those of III^R_m other than III^{Me}_2 and III^{Me}_3 and IV_m give signals of the A_2 type at δ 3.52—3.65. AA'BB' signals appearing at δ 4.0—4.3 and 3.2—3.7 for III^R_m and IV_m are assigned to 4- and 5-methylene protons,

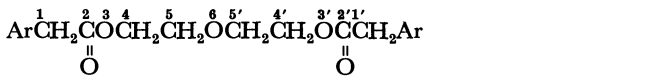

III^R_2 and IV_2

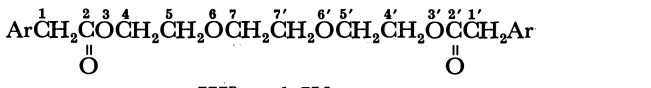

III^R_3 and IV_3

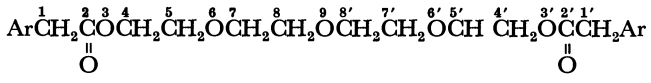

III^R_4 and IV_4

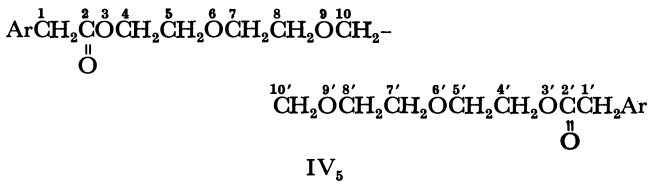

IV_5

respectively, from a comparison of the chemical shifts with those for α-methylene protons of the corresponding dioxadioxo[n]paracyclophanes (V_n, where n is the number of atoms in the ansa chain) and open-chain analogs,[8] and by taking advantage of a known chemical shift rule.[9] The singlets observed at δ *ca.* 3.15 for III^R_3 and at δ 3.54 for IV_3 were then assigned to 7-methylene protons. Similarly, the multiplets centered at δ *ca.* 3.5 for III^R_4 and the broad singlet at δ *ca.* 3.6 for IV_4 were attributed to 7- and 8-methylene protons. IV_5 has a singlet signal for 7-, 8-, and 10-methylene protons.

Table 3. High-field shift induced by a diamagnetic ring current[a]

m	Position of bridge methylenes			
	4	5	7	8
2	0.17	0.37		
3	0.05	0.09	0.40	
4	0.01	0.04		0.18

a) For the numbering of the bridge methylene, see text.

On the basis of the above assignments, the difference in chemical shifts of the corresponding methylene protons can be calculated, as $\Delta\delta_{CH_2}=\delta_{CH_2}(IV_m)-\delta_{CH_2}(III^{Me}_m)$, and the results are shown in Table 3. The results are believed to be a reflection of the ring current effect of the benzene ring and, indeed, are in close agreement with the expected values from a calculation using the Johnson-Bovey method.[10] An increase in the number of oxyethylene units causes a decrease in $\Delta\delta_{CH_2}$ indicating that the mobility of the ansa chain is increased and the ring current effect is increasingly cancelled out.

Lanthanoid-induced Shifts [LIS] and Assignment of the Binding Site. The shift reagents, Eu(dpm)$_3$ and Eu(fod)$_3$-d_{27}, were added to solutions containing the substrate and the molar ratios were changed from 0 to 0.5. The LIS was plotted against [L]/[S], where [L] and [S] have their usual meanings,[3] indicating proper linearity. Relative slopes of the straight lines were obtained by taking the slope of the straight line due to methylene protons in the α-position of the carbonyl group as a reference and are shown in Table 4.

The assignment of straight lines obtained by plotting

Table 4. Relative slopes of LIS vs. [L]/[S] lines obtained for polyoxadioxo[n]paracyclophanes (III^R_m) and bis(2,5-dimethylphenylacetate)s (IV_m) of polyoxaalkane-α,ω-diols[a]

Protons	Compounds										
	III^H_2	III^{Me}_2	IV_2	III^H_3	III^{Me}_3	IV_3	III^H_4	III^{Me}_4	III^{OMe}_4	IV_4	IV_5
1-CH_2	1.0	1.0	1.0	1.0	1.0	1.0 (1.0)	1.0	1.0	1.0	1.0 (1.0)	1.0 (1.0)
4-CH_2	1.0_4	1.0_3	1.1_7	0.1_9	0.1_8	1.0_9 (1.4_1)	0.6_8	0.6_4	0.5_9	1.0_9 (1.4_6)	1.1_6 (1.7_9)
5-CH_2	0.5_7	0.5_3	0.7_5	2.0_8	1.8_9	2.1_5 (3.8_6)	1.9_8	2.0_1	2.0_0	1.8_3 (3.9_2)	1.8_3 (3.9_2)
7-CH_2				8.1_0	7.9_5	5.7_9 (8.8_2)	5.0_4	5.1_0	5.1_0	4.3_2 (6.4_6)	4.2_3 (6.3_9)
8-CH_2							6.6_6	6.6_7	6.5_0	5.5_5 (7.9_4)	4.9_2 (9.0_6)
10-CH_2											5.1_2 (9.6_0)
Ar-H	0.5_0	0.5_3		1.1_9	1.1_8		1.3_3	1.3_0	1.3_8		
Ar-Me (or-OMe)		0.4_2	0.3_8		0.9_1	0.5_3 (0.6_6)		1.0_9	0.8_0	0.5_5 (0.6_4)	0.5_6 (0.7_3)
			0.0_9			0.3_1 (0.5_3)				0.3_2 (0.5_2)	0.2_9 (0.5_0)

a) Values in parentheses are those obtained using Eu(fod)$_3$-d_{27} while the others were obtained using Eu(dpm)$_3$.

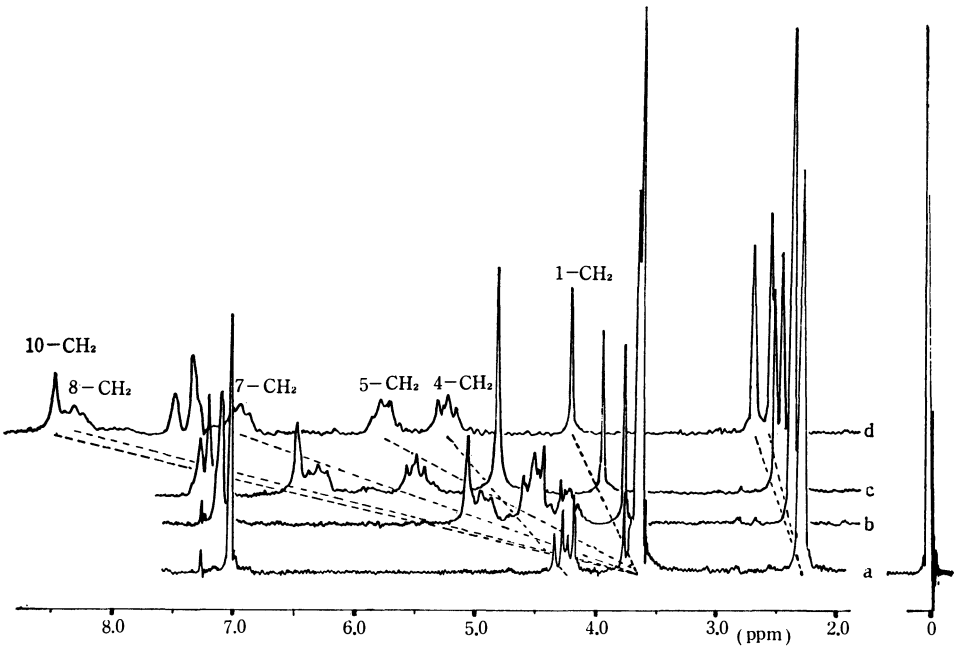

Fig. 1. ^{1}H NMR spectra of IV_5 with various amounts of Eu(fod)$_3$-d_{27} in $CDCl_3$ at 34 °C. Curves a, b, c, and d correspond to [L]/[S] of 0, 0.17, 0.29, and 0.52, respectively.

LIS *vs.* [L]/[S] is straightforward when the number of oxyethylene groups is 2 or 3, because they result in a set of independent signals for each pair of protons. However, it is necessary to carefully assign those signals which appear separately after the addition of the shift reagent, but which overlap in the absence of the reagent.

The ^{1}H NMR spectra of IV_5 for varying amounts of Eu(fod)$_3$-d_{27} in deuteriochloroform at 34 °C are shown in Fig. 1. The apparent singlet at δ 3.60 in the absence of the reagent separates into a singlet and two multiplets with an increase in the value of [L]/[S]. The singlet at the lowest field is necessarily assigned to 10-methylene protons because the neighboring methylene group is equivalent and no coupling with other protons is expected. From the 7- and 8-methylene protons, the latter produces the lower field signal because the 10-methylene protons give the signal at the lowest field and the shift reagent must be coordinated closer to the 8-methylene than to the 7-methylene protons.

The assignments of signals due to III_2^R and IV_4 were carried out analogously. The chemical shifts of 4- and 5-methylene protons are known even in the absence of the shift reagent. For the 7- and 8-protons, it must be the 8-protons that result in the lower field signals for the addition of the shift reagent, because if a complex is formed using the 6′- and 9-oxygens, the 8-protons are closer to the shift reagent than the 7-protons. Although the binding site may change as discussed later, the situation still holds because if the binding sites are 6- and 9-oxygens, the effect should be equal for the 7- and 8-protons.

The relative slopes of 1-methylene protons in III_2^R are in good agreement with the data for 13,16-dimethyl-3,9-dioxa-2,10-dioxo[11]paracyclophane (V_{11})[5] which has an ansa chain with the same number of atoms and is known to form a complex with the shift reagent at the oxygen of the ester carbonyl. IV_2 showed a similar tendency. Thus, it may be concluded that the reagent binds to the ester carbonyl in III_2^R and IV_2.

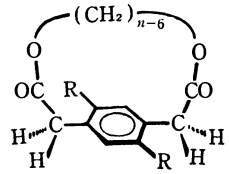

V_{11}: n=11, R=CH_3
V_{14}: n=14, R=CH_3

In contrast, the relative slopes of 1-methylene protons in III_3^R are different from those of V_{14} to a great extent, although similar values are expected if III_3^R binds at the carbonyl oxygen, as does V_{14}.[8] IV_3 behaves similarly to III_3^R. Therefore, the results must be attributed to the presence of (a) binding site(s) other than the carbonyl.

Although lactarorufin is known to bind preferentially to the shift reagent at an ether oxygen rather than at an ester carbonyl,[11] this anomaly is caused because of steric blocking of the carbonyl oxygen and such a steric factor is not expected in these compounds (III_m^R). Rather, it is reasonably assumed that the ethylenedioxy unit is a preferred binding site for the shift reagent, because two ether oxygens *ortho* to each other in the aromatic system are known to bind as a bidentate ligand to the shift reagent more readily than the ester group,[5] and because polyglyme binds to the shift reagent.[4]

Judging from the failure of complex formation at the ethylenedioxy units in III_2^R and IV_2, it is concluded that the ethylenedioxy unit, one oxygen of which is a part of the ester moiety, is inferior to the ester carbonyl for complexation. Thus the order of binding ease is $ROCH_2CH_2OR > RCOOR > ROCH_2CH_2OCOR$.

Since the slopes of LIS *vs.* [L]/[S] for the methylenes

in III_3^R and IV_3 become steeper as the methylene becomes closer to the center of the chain, it is reasonable to assume that the shift reagent forms a complex at the 6,6′-positions. Indeed, it is generally accepted that in ^1H NMR an LIS results by complexation to an oxygen function of an organic compound predominantly from the pseudocontact interaction.[3]

The data for III_4^R may be interpreted as the result of rapid equilibrium between the two equivalent complexes as has been pointed out for polyglyme,[4] because there are two equally good binding sites. The LIS values observed for a compound with only one strong binding site may be taken to represent "intrinsic" shifts for protons of such complexes. Then the observed shifts in a molecule with two or more good complexing sites can be taken as weighted means of the "intrinsic" shifts, and are determined by the populations of the complexes. Since IV_4 has two equivalent binding sites, it may be assumed that two complexes exist in equal populations and exchange rapidly on the NMR time scale. By analogy to the cases of III_3^R and IV_3, these two complexes are shown by $IV_4(6,9)$ and $IV_4(6',9)$.

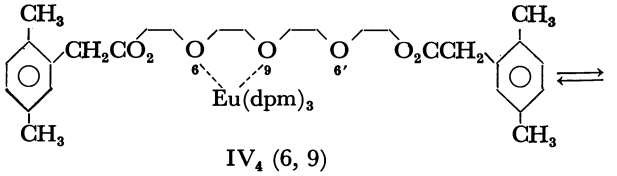

IV_4 (6, 9)

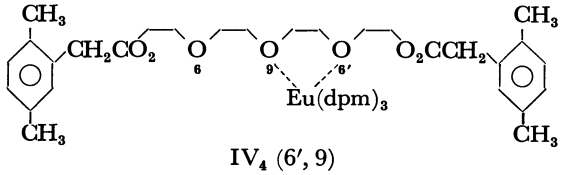

IV_4 (6′, 9)

According to the above assumption, the relative slopes of the LIS *vs.* [L]/[S] lines for $IV_4(6,9)$ and $IV_4(6',9)$ can be taken as almost the same as those in the IV_3–lathanoid complex $IV_3(6,6')$; the 7- and 8-methylenes in $IV_4(6,9)$ give a slope of 5.8, since these are equivalent to the 7- and 7′-methylenes in $IV_3(6,6')$. Then 5- and 8′-methylenes in $IV_4(6,9)$ will give a slope of 2.2, since these are equivalent to the 5- and 5′-methylenes in $IV_3(6,6')$, *etc.* Using the above assumption, we can calculate the relative slopes as shown in Fig. 2. The calculated values are in good agreement with those observed.

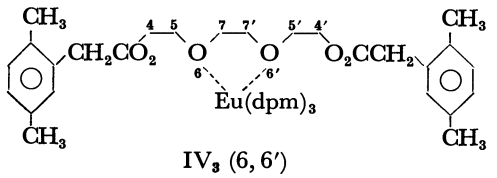

IV_3 (6, 6′)

Similarly, the observed values of IV_5 are reasonably well reproduced by the assumption of equal populations of complexes $IV_5(6,9)$, $IV_5(9,9')$, and $IV_5(6',9')$ (see Fig. 2). Since, if we assume that there is only one complex $IV_5(9,9')$ or only two complexes, $IV_5(6,9)$ and $IV_5(6',9')$, we obtain much less satisfactorily calculated values, it may be assumed that the three complexing

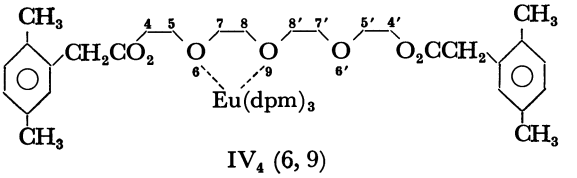

IV_4 (6, 9)

	4	5	7	8	8′	7′	5′	4′
IV_4 (6, 9)	(1.1	2.2	5.8	5.8	2.2	1.1	∼1	∼1)×1/2
IV_4 (6′, 9)	+(∼1	∼1	1.1	2.2	5.8	5.8	2.2	1.1)×1/2
	(2.1	2.3	6.9	8.0	8.0	6.9	2.3	2.1)×1/2
Ratio of relative slopes Calcd			1.0	0.86	0.40	0.26		
Ratio of relative slopes Obsd			1.0	0.77	0.32	0.20		

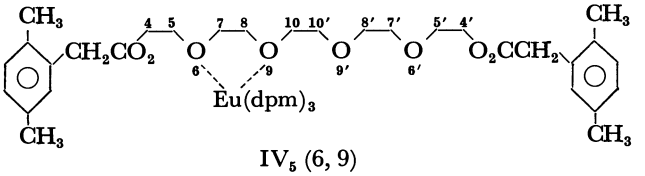

IV_5 (6, 9)

	4	5	7	8	10	10′	8′	7′	5′	4′
IV_5(6, 9)	(1.1	2.2	5.8	5.8	2.2	1.1	∼1	∼1	∼1	∼1)×1/3
IV_5(9, 9′)	(∼1	∼1	1.1	2.2	5.8	5.8	2.2	1.1	∼1	∼1)×1/3
IV_5(9′, 6′)	+(∼1	∼1	∼1	∼1	1.1	2.2	5.8	5.8	2.2	1.1)×1/3
	(3.1	4.2	7.9	9.0	9.1	9.1	9.0	7.9	4.2	3.1)×1/3
			10′	8′	7′	5′	4′			
Ratio of relative slopes Calcd			1.0	0.99	0.87	0.46	0.37			
Ratio of relative slopes Obsd			1.0	0.96	0.82	0.35	0.24			

Fig. 2. Calculations of the relative slopes of straight lines, LIS *vs.* [L]/[S], on an assumption of "intrinsic" slopes.

sites contribute almost equally.*

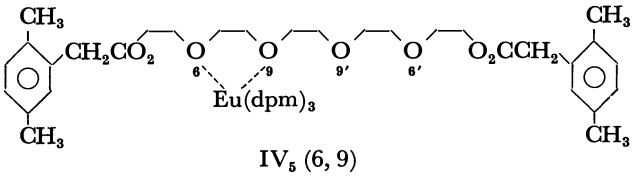

IV_5 (6, 9)

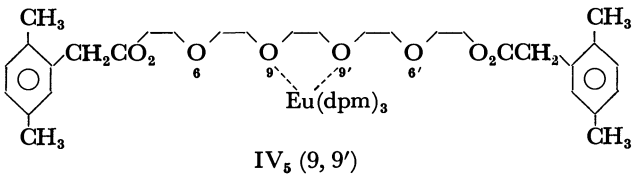

IV_5 (9, 9′)

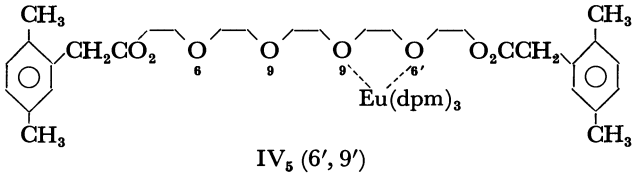

IV_5 (6′, 9′)

IV_5 (9, 9′)

IV_5 (6, 9) ⇌ IV_5 (6′, 9′)

It is concluded, by taking advantage of the results with open-chain analogs, that the polyoxadioxo[n]-paracyclophanes with long ansa chains behave similarly

* Although the above simple calculation gives satisfactory results for flexible molecule, it appears that the method is not applicable to less mobile molecules. Thus, application of the method to the cyclophanes (III_m^R) gives results far from satisfactory.

toward the shift reagent. The binding sites in these compounds are changing rapidly among the favored ethylenedioxy units. The chemical shifts of the methylene protons and the slopes of LIS *vs.* [L]/[S] lines are in agreement with this conclusion.

Origin for the Change in Binding Sites. It is clear from the above discussion that the ester carbonyl is an inferior binding site for the shift reagent with respect to the ethylenedioxy unit, unless one of the oxygens in the latter is a part of the ester moiety. The inferiority of the $ROCH_2CH_2O_2CR$ moiety can be attributed to the low electron density of the ether oxygen in the ester group.

Among the ethylenedioxy units referred to in this paper, the binding ability appears to be invariant irrespective of the position of the unit. This is in sharp contrast to the fact that polyglymes bind to the shift reagent at the terminal ethylenedioxy units. It is proposed that this difference be ascribed to steric and electronic effects for the following reasons. Firstly, the methyl group is known to be smaller than the ethyl group and other long chain alkyls, the most noted example being the reactivity of the carbonyl group in ketones toward hydrogen sulfite.[12] In complex formation also, the heat of formation and the entropy term will be unfavorable when the chain becomes longer. Secondly, the oxygen in position 2 of polyoxaalkanes will have the highest basicity, since the oxygens in the inner positions are substituted by an "ethyl" group which carries an oxygen atom in the β-position. In fact, 3-methoxypropionic acid is known to be a stronger acid than acetic acid by an order of magnitude, indicating that the $CH_3OCH_2CH_2$ group is electron-withdrawing relative to the CH_3.[13]

References

1) Part VII of this series; K. Sakamoto and M. Ōki, *Chem. Lett.*, **1976**, 257.
2) K. Sakamoto and M. Ōki, *Bull. Chem. Soc. Jpn.*, **47**, 2623 (1974).
3) A. Cockerill, G. L. O. Davies, R. C. Harden, and D. M. Rackham, *Chem. Rev.*, **73**, 553 (1973).
4) A. M. Grotens, C. W. Hilbers, E. de Boer, and J. Smid, *Tetrahedron Lett.*, **1972**, 2067.
5) G. E. Wright and T. Y. Tang Wei, *Tetrahedron*, **29**, 3775 (1973).
6) C. J. Pederson, *J. Am. Chem. Soc.*, **89**, 7017 (1967).
7) K. Sakamoto and M. Ōki, *Bull. Chem. Soc. Jpn.*, **46**, 270 (1973); **48**, 497 (1975).
8) K. Sakamoto and M. Ōki, *Bull. Chem. Soc. Jpn.*, **47**, 2739 (1974).
9) K. Nukada, O. Yamamoto, T. Suzuki, M. Takeuchi, and M. Ohnishi, *Anal. Chem.*, **35**, 1892 (1963).
10) C. E. Johnson, Jr., and F. A. Bovey, *J. Chem. Phys.*, **29**, 1012 (1958).
11) R. Caple and S. C. Kuo, *Tetrahedron Lett.*, **1971**, 4413.
12) M. A. Gubareva, *Zh. Obshch. Khim.*, **17**, 2259 (1947); *Chem. Abstr.*, **42**, 4820a (1948).
13) H. S. Harned and B. B. Owen, *J. Am. Chem. Soc.*, **52**, 5091 (1930).

N-Halogen Compounds of Cyanamide Derivatives. VI.[1] The Preparation and Reaction of 2-Carbonimidoyl-3-imino-Δ^4-1,2,4-thiadiazolines

Toshio FUCHIGAMI and Keijiro ODO

Department of Electronic Chemistry, The Graduate School, Tokyo Institute of Technology, Ookayama, Meguro-ku, Tokyo 152

(Received May 11, 1976)

The reactions of potassium methyl cyanoiminodithiocarbonate (I), potassium methoxy and ethoxythiocarbonylcyanamide (IIa and IIb) with *N*-chloroamidines in various solvents were investigated. Δ^4-1,2,4-Thiadiazolines (TDZ), IIIa—d, were obtained from I in good yields, whereas the 1,3,5-triazines obtained as by-products in addition to TDZ were formed from II and *N*-chlorobenzamidine (NCB) in chloroform and dichloromethane. In the latter reaction, desulfrization occurred completely to give 1,3,5-triazine and/or a chain intermediate to 1,3,5-triazine in dipolar solvents. The TDZ were readily cleft at the N-S link by hydrogen sulfide and recyclized to 1,3,5-triazines. By alkaline hydrolysis, the TDZ were transformed to 2-amino-1,3,5-triazin-4-ols.

1,2,4-Thiadiazole derivatives have been known since 1821,[2] and many of them are important compounds as dyes, medicines, and agricultural chemicals. However, there have been few reports on the preparation of 1,2,4-thiadiazolines, especially on that of Δ^4-1,2,4-thiadiazolines. In our previous works,[3,4] we found that 2-carbonimidoyl-3-imino-5-methylthio-Δ^4-1,2,4-thiadiazolines could easily be prepared by the reaction of *N*-chloroamidino compounds with I and clarified their properties.

In this paper, we wish to describe the preparation of TDZ using *N*-chloroamidines, I, and II, and the desulfurization in the reaction of II with NCB, together with the reactivities of TDZ in alkaline solutions.

Results and Discussion

Preparation of Potassium Methoxythiocarbonylcyanamide (IIa). According to the method of preparing IIb,[5] IIa was prepared by the reaction of cyanamide with *O,S*-dimethyl dithiocarbonate in the presence of potassium hydroxide in ethanol. The yield was 40%, and the melting point was 192—195 °C (dp).

Reaction of I with N-*Chloroamidines.* *N*-Chloroamidine reacted exothermically with I in chloroform below 5 °C. After 1—2 h, an active chlorine disappeared and TDZ were formed. In the case of NCB, the yield of the TDZ increased when the solvent was acetonitrile. The structures of the TDZ, IIIa—d, were confirmed by means of elemental analyses and by studies of the IR and mass spectra. The results are summarized in Table 1.

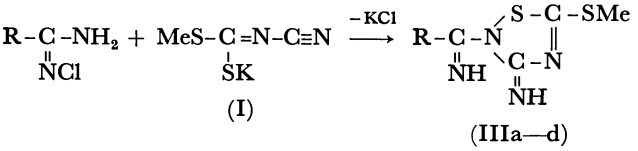

(I) (IIIa—d)

Reaction of IIa and IIb with N-*Chloroamidines.* NCB and IIa reacted readily in chloroform at 10—15 °C. After about 1 h, the active chlorine disappeared and an oily material was obtained instead of the TDZ. A small amount of a crystal (A), the oily material (B), and sulfur could be separated from it.

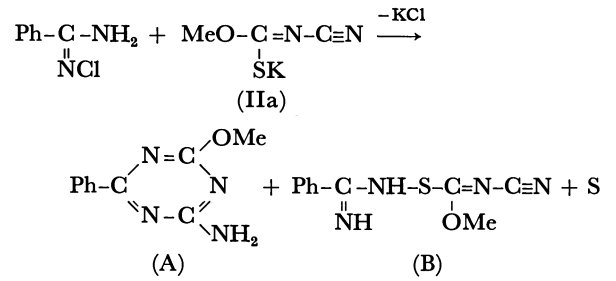

(IIa) (A) (B)

The A product was 2-amino-4-methoxy-6-phenyl-1,3,5-triazine, whose structure was determined by the elemental analysis and by a study of its IR spectrum, in which the characteristic absorption of 1,3,5-triazine ring was observed at 830 cm^{-1}. The other product, B, which contained sulfur and showed a strong absorption of a nitrile group at 2200 cm^{-1} in the IR spectrum, was supposed to be the open-chain intermediate to the TDZ, the ring closure of B was attempted by acid catalysis. Expectedly, TDZ (IV) could be obtained as corresponding salts by the treatment of B at room temperature using hydrochloric acid, picric acid, and copper (II) chloride.

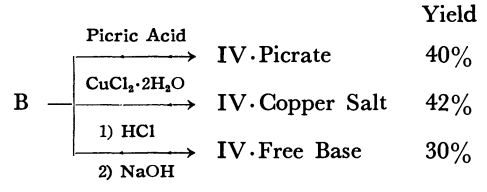

Table 1. PREPARATION OF TDZ FROM I AND *N*-CHLQOOAMIDINES

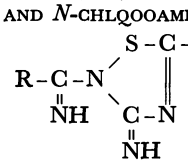

TDZ No	TDZ R	Solvent	Reaction time (min)	Yield (%)
IIIa	Ph	$CHCl_3$	100	64
IIIa	Ph	MeCN	50	76
IIIb	*p*-tol	$CHCl_3$	120	58
IIIc	Bzl	$CHCl_3$	110	57
IIId	Me	$CHCl_3$	180	58

The reaction of NCB with IIb was likewise examined

using various kinds of solvents. As is shown in Table 2, a remarkable solvent effect was observed. In dichloromethane, the products were a TDZ (Va) and C, whose IR spectrum showed the absorption of a nitrile group at 2200 cm^{-1}. Only 2-amino-4-ethoxy-6-phenyl-1,3,5-triazine (D) was formed in acetonitrile and ethyl acetate, while C was the sole product in acetone. C was *N*-benzimidoyl-*N'*-cyano-*O*-ethylisourea, whose structure was confirmed by means of elemental analysis, by studies of the IR and mass spectra, and also by the following reaction. C, which was stable at room temperature, was converted into 1,3,5-triazine under reflux in acetone.

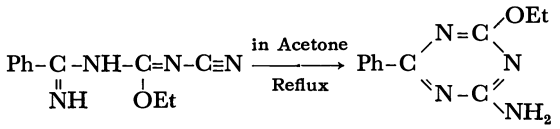

(C) (D) quant.

Thus, it was found that desulfurization took place completely in the above three solvents. On the other hand, no desulfurization was observed in the case of *N*-chloroacetamidine, and the corresponding TDZ (Vb) was obtained in a low yield. This desulfurization may occur by means of the oxidation with a positive chlorine from NCB and may be accelerated in polar solvents.

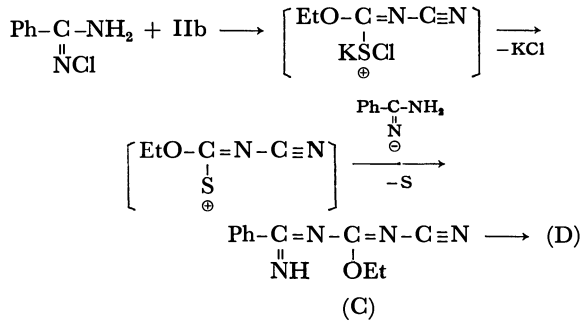

(C)

Table 2. Reaction of IIb with *N*-chloroamidines

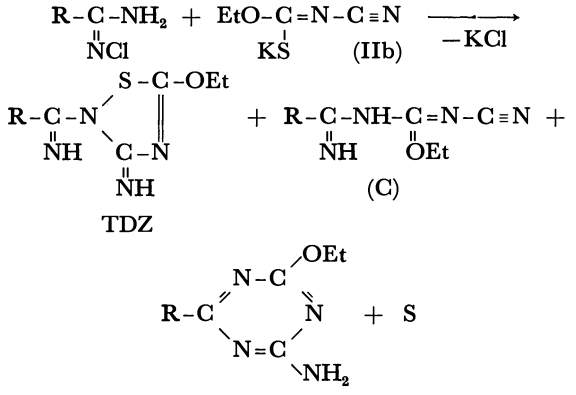

TDZ (C)

(D)

R	Solvent	Reaction time (min)[a]	Product (%) TDZ	C	D	S
Ph	CH_2Cl_2	60(40)	47	18	—	+
	AcOEt	90(60)	—	—	62	++
	MeCN	35(15)	—	—	78	++
	Me_2CO	60(40)	—	98	—	++
Me	MeCN	270	38	—	—	—

a) Active chlorine disappeared.

The decay time of an active chlorine decreased considerably in acetonitrile, as is shown in Table 2.

The TDZ derivatives thus prepared are mono acidic bases, and their basicity is weaker than that of the starting compounds, amidino compounds. Therefore, a TDZ ring seems to be an electron-withdrawing group. A copper salt, whose color is blue or green, is formed from TDZ and copper (II) chloride, but its structure has not yet been established. The physical properties and analytical data of TDZ and the copper salts are summarized in Tables 3 and 4.

Table 3. Physical properties and analytical data of TDZ

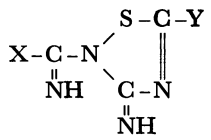

No.	X	Y	Free base Mp (°C)	Found (Calcd) % C	H	N	UV Spectra $\lambda_{max}^{H_2O}$ ($\varepsilon \times 10^{-4}$)	Picrate Mp (°C)	Found (Calcd) % C	H	N
IIIa	Ph	SMe	138—139	47.68 (47.98)	3.87 (4.03)	22.56 (22.38)	256(3.2)	192—194 (Dp)	40.08 (40.09)	2.62 (2.73)	20.19 (20.46)
IIIb	*p*-tol	SMe	181—182	49.78 (49.98)	4.51 (4.58)	21.19 (21.19)	263(3.5)	204—205 (Dp)	41.53 (41.39)	2.94 (3.06)	19.57 (19.87)
IIIc	Bzl	SMe	148—149 (Dp)	49.80 (49.98)	4.45 (4.58)	20.85 (21.18)	247(2.8)	183—185	41.55 (41.39)	2.95 (3.06)	19.52 (19.87)
IIId	Me	SMe	155—158	31.63 (31.90)	4.22 (4.28)	29.59 (29.76)	243(2.3)	—	—	—	—
IV	Ph	OMe	124—128	51.08 (51.27)	4.32 (4.30)	23.51 (23.91)	278(1.3)	183—185	41.91 (41.47)	2.64 (2.83)	21.29 (21.16)
Va	Ph	OEt	138—139	52.74 (53.21)	4.70 (4.87)	22.38 (22.56)	278(1.2)	193—195	42.98 (42.77)	3.08 (3.19)	20.22 (20.54)
Vb	Me	OEt	80— 81	36.76 (36.91)	5.36 (5.68)	28.29 (28.70)[a]	271(0.9)	148—149	34.53 (34.70)	3.15 (3.15)	23.65 (23.61)

a) Calcd for $C_6H_4N_4SO \cdot 1/2\ H_2O$: S content 16.75% (16.42%).

Table 4. Physical properties and analytical data of copper salts of TDZ

$TDZ \cdot CuCl_2 \cdot (H_2O)_n$

TDZ No.	Dp (°C)	Color	*n*	N Found (Calcd %)
IIIa	246	Yellowish green	1	13.89(13.89)
IIIb	253	Green	1	13.40(13.47)
IIIc	172—174	Dark blue	2	12.86(12.91)
IV	266	Green	1	14.46(14.48)
Va	270	Blue	2	13.46(13.40)

TDZ was readily cleft at the N–S link by hydrogen sulfide, and the elimination of methanethiol or hydrogen sulfide from the intermediate gave 1,3,5-triazines. Although 5-methylthio-TDZ gave two kinds of 1,3,5-triazines, 5-ethoxy-TDZ gave only one kind of 1,3,5-triazine.

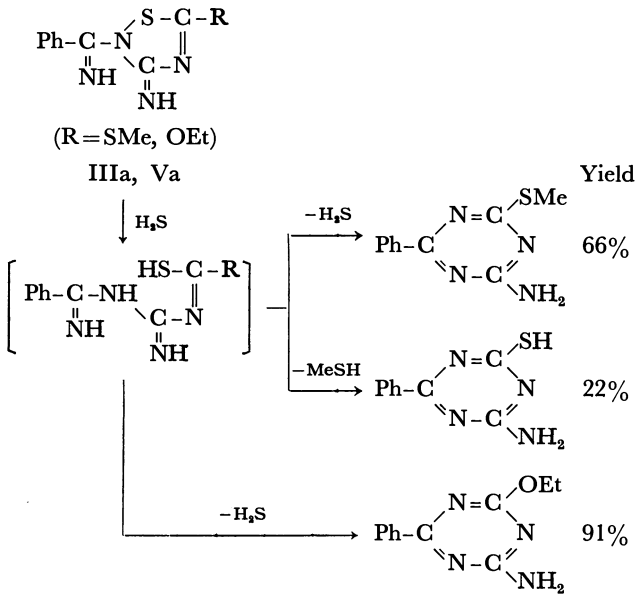

The low stability of TDZ seems to be related to its structure, in which the aromatic character is absent.

5-Methylthio-TDZ, IIIa was treated with ethanolic sodium hydroxide to give 5-ethoxy-TDZ, Va in a low yield.

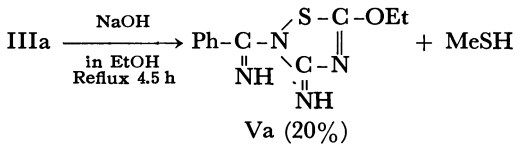

We found that the ring cleavage of TDZ by alkaline hydrolysis gave rise to 1,3,5-triazine, also. The TDZ were refluxed with sodium hydroxide in aqueous alcohol to give 2-amino-1,3,5-triazin-ol in high yields.

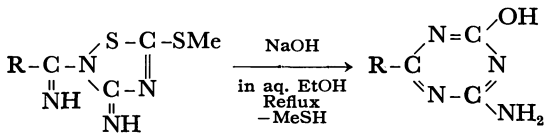

(IIIa, b)

	Yield
R=Ph	85%
R=*p*-tol	64%

However, the detailed mechanism of the transformation has not yet been made clear.

The physical properties and analytical data of 1,3,5-triazines are summarized in Table 5.

Experimental

Materials. Potassium Methyl Cyanoiminodithiocarbonate (I): To a stirred solution of cyanamide (8.40 g, 20 mmol) and potassium hydroxide (22.40 g, 40 mmol) in water–acetone (60—30 ml), we gradually added, drop by drop, carbon disulfide (15.20 g, 20 mmol) at 0—5 °C. After the addition, the mixture was stirred at room temperature for 1.5 h; it was cooled below 5 °C again, and then methyl iodide was added, drop by drop. After the addition, the mixture was stirred at room temperature for 2 h. The residue obtained by the removal of the solvent was extracted with hot ethanol (80 ml). After the extract had been concentrated under reduced pressure, the crude product of I was obtained (24 g, 71%). Re-

Table 5. Physical properties and analytical data of 1,3,5-triazines

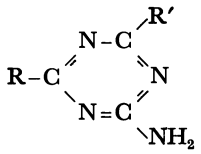

R	R′	Free base Mp (°C)	Free base Found (Calcd) % C	H	N	Picrate Mp (°C)	Picrate Found (Calcd) % C	H	N
Ph	MeO	161—164	57.10 (56.86)	5.07 (5.25)	26.63 (26.53) [a]	—	—	—	—
Ph	EtO	153—154	58.93 (58.68)	5.89 (5.78)	24.89 (24.88) [b]	193—195	45.66 (45.85)	3.30 (3.40)	22.04 (22.02)
Ph	OH	327—328 (320—321) [b] (dp)	57.53 (57.44)	4.24 (4.28)	30.09 (29.77)	278—280	43.27 (43.17)	2.62 (2.66)	23.52 (23.50)
p-tol	OH	320 (dp)	59.03 (59.40)	4.91 (4.98)	27.72 (27.71)	295 (Dp)	44.11 (44.56)	3.02 (3.04)	22.53 (22.73)

a) Calcd for $C_{10}H_{10}N_4O \cdot 1/2H_2O$. b) Calcd for $C_{11}H_{12}N_4O \cdot 1/2H_2O$.

crystallization from ethanol gave pure I; mp 213—214 °C (214—216 °C).[7]

Potassium Methoxythiocarbonylcyanamide (IIa): According to the method of preparing potassium ethoxythiocarbonylcyanamide (IIb),[5] IIa was prepared by the reaction of cyanamide with *O,S*-dimethyl dithiocarbonate and potassium hydroxide in ethanol. Two recrystallizations from ethanol gave pure IIa (yield 40%, dp 192—195 °C). Found: C, 23.30; H, 1.96; N, 18.14%. Calcd for $C_3H_3N_2OSK$: C, 23.36; H, 1.96; N, 18.16%.

The *N*-chloroamidines were prepared by a previously described method.[8]

Reaction of I with N-Chloroamidines. 2-Benzimidoyl-3-imino-5-methylthio-TDZ (IIIa): To a stirred suspension of I (3.40 g, 20 mmol) in acetonitrile (20 ml), we gradually added a solution of NCB (3.09 g, 20 mmol) in acetonitrile (20 ml), the temperature being kept below 10 °C. After about 50 min of continued stirring, the solvent was removed by distillation under reduced pressure. The titled compound was obtained by washing the residue with water to remove potassium chloride; 3.78 g, 76%, mp 129—135 °C. Pure IIIa: mp 138—139 °C (from acetone). The above reaction, when carried out in chloroform by a similar method, gave IIIa in a 64% yield.

2-p-Toluimidoyl-3-imino-5-methylthio-TDZ (IIIb): To a stirred mixture of I (5.95 g, 35 mmol) and chloroform (55 ml) we gradually added, drop by drop, a solution of *N*-chloro-*p*-toluamidine (5.90 g, 35 mmol) in chloroform (55 ml). After about 2 h of continued stirring, the active chlorine disappeared and potassium chloride was precipitated. After the salt had been removed by filtration, the filtrate was concentrated. When the residue was washed with a small amount of acetone, 4.90 g of crude IIIb remained; 53%, mp 181—182 °C. Recrystallization from acetone gave pure IIIb; mp 181—182 °C. To the washings, we added a methanolic solution of copper (II) chloride. The copper salt of IIIb thus precipitated was collected by filtration; dp 253 °C. The yield was 5%.

Similarly, reactions with other *N*-chloroamidines were carried out.

Reaction of IIa with NCB. Cyclization by Picric Acid: To a stirred suspension of IIa (4.62 g, 30 mmol) in chloroform (40 ml), we added, drop by drop, a solution of NCB (4.62 g, 30 mmol) in chloroform (20 ml). After 1 h of stirring, the reaction mixture was poured into water (25 ml). The organic layer was separated, and then the aqueous layer was extracted twice with 5 ml portions of chloroform. After the combined chloroform extracts had been dried over sodium sulfate, filtered off, and concentrated under reduced pressure, an oily material remained. On standing for 5 days at room temperature, part of 2-amino-4-methoxy-6-phenyl-1,3,5-triazine (A) crystallized out of the oil. On the addition of a small amount of ethyl acetate, the resulting A was separated by filtration (0.83 g, 13%). The oily product (B) obtained by the concentration of the filtrate was dissolved in ether, and a saturated ethereal solution of picric acid was added. The picrate of 2-benzimidoyl-3-imino-5-methoxy-TDZ (IV) thus precipitated was collected and recrystallized from water; mp 183—185 °C. The yield was 5.53 g (40%). When A was recrystallized from methanol, a small amount of sulfur was separated. Purified A; mp 161—164 °C.

Cyclization by Copper(II) Chloride: A (0.80 g, 13%) and B were obtained by the same procedure as above. The copper salt of IV was precipitated on the addition of a methanolic solution of copper(II) chloride ($CuCl_2 \cdot 3H_2O$) to a methanolic solution of B. The yield was 4.83 g (42%); dp 266 °C.

Cyclization by Hydrochloric Acid: To a methanolic solution of A, we added 15 ml of 2 M hydrochloric acid, and then the mixture was stirred for 20 min at room temperature. After the addition of 2 M sodium hydroxide to make the reaction mixture neutral, the methanol was almost entirely removed by concentration. The oily material thus obtained was left for a while, whereupon, crystals (IV) were obtained as a free base. The yield was 2.11 g (30%); mp 124—128 °C (from acetone–water).

Reaction of IIb with NCB. The Reaction in Dichloromethane: To a stirred suspension of IIb (10.08 g, 60 mmol) in dichloromethane (60 ml), we added, drop by drop, a solution of NCB (9.27 g, 60 mmol) in dichloromethane (60 ml) below 10 °C. After about 1 h of continued stirring, the reaction mixture was poured into 30 ml of water; then sulfur was separated. The organic layer was separated, and the aqueous layer was extracted twice with 10 ml portions of dichloromethane. The combined extracts were dried over sodium sulfate, filtered, and concentrated. To the residual oily material, we added a small amount of ethyl acetate and rubbed the sirup with a grass rod. The resulting crystals were filtered off and recrystallized from ethanol to give 2-benzimidoyl-3-imino-5-ethoxy-TDZ (Va); mp 138—139 °C. The yield was 6.16 g (41%). The filtrate and mother liquor were then combined, and an ethanolic solution of copper(II) chloride was added. The copper salt of Va thus precipitated was collected by filtration (1.50 g, 6%, dp 270 °C). By removing the copper from the filtrate, 2-amino-4-ethoxy-6-phenyl-1,3,5-triazine (D) was obtained; 2.34 g (18%); mp 153—154 °C (from ethanol).

The Reaction in Acetonitrile: The reaction (15 mmol scale) in 30 ml of acetonitrile was carried out according to the same procedure. Desulfurization occurred at the time of the addition of NCB, and after about 15 min the active chlorine disappeared. The insoluble matter was removed by filtration, and the filtrate was evaporated to dryness under reduced pressure. D was obtained by washing the residual crystals with ether: 2.37 g, 73%, mp 153—156 °C. To the washings, we added a saturated ethereal solution of picric acid. The picrate of D was thus precipitated; 0.37 g (5%), dp 193 °C. The total yield was 78%.

The reaction in ethyl acetate was carried out similarly.

The Reaction in Acetone-Formation of N-Benzimidoyl-N′-cyano-O-ethylisourea (C): According to the same procedure, the reaction (17 mmol scale) in acetone (34 ml) was carried out. The insoluble matter was removed by filtration, and the filtrate was evaporated to dryness under reduced pressure. The residue, C, was washed with petroleum ether and a small amount of ether. The yield of C was 3.60 g (98%); mp 120 °C. Recrystallization from ethanol gave pure C; mp 125—126 °C. IR spectrum (cm^{-1}): 3200, 3300 (νNH); 2200 (νC≡N); 1600 (νC=N). Found: C, 60.93; H, 5.58; N, 25.41%. Calcd for $C_{11}H_{12}N_4O$: C, 61.10; H, 5.59; N, 25.91%.

Reaction of IIb with N-Chloroacetamidine. According to the same procedure, a reddish brown reaction mixture was obtained. The insoluble matter was removed by filtration, and the concentration of the filtrate afforded a reddish brown oily material, which was then dissolved in hot water and treated with charcoal. The addition of a saturated aqueous solution of picric acid to it afforded the picrate of 2-acetimidoyl-3-imino-5-ethoxy-TDZ (Vb). The yield was 7.93 g (38%); mp 144—148 °C. Recrystallization from water gave pure Vb; mp 148—149 °C. The free base of Vb was obtained by the treatment of the picrate with concd hydrochloric acid; mp 80—81 °C (from dichloromethane–petroleum ether).

Reduction of TDZ by Hydrogen Sulfide. Reduction of IIIa: Hydrogen sulfide was passed through a solution of IIIa (2.00

g, 8 mmol) in ethanol–chloroform (40—40 ml). The solution was left at room temperature for about 1 h and the resulting precipitate (P-1) was separated by filtration. After the filtrate had been evaporated to dryness, the residual yellowish crystals were dissolved in 5% ammonium hydroxide (20 ml), and then the insoluble matter was removed by filtration. The filtrate was neutralized with 3 M acetic acid, and the precipitate (P-1) was separated by filtration. The matter insoluble in ammonium hydroxide was extracted with hot ethanol (20 ml), and the residual sulfur was removed by filtration. After cooling, the precipitate (P-2) was obtained. P-1 was 2-amino-4-mercapto-6-phenyl-1,3,5-triazine; yield 0.36 g (22%); dp 278 °C (from DMF–water). P-2 was 2-amino-4-methylthio-6-phenyl-1,3,5-triazine; 1.15 g, 66%, mp 170—172 °C (from acetone).

Reduction of Va: In the same way, hydrogen sulfide was passed through. The precipitated sulfur was removed by filtration, and the filtrate was evaporated to dryness. The recrystallization of the residue from ethanol gave pure D; 91%, mp 153—154 °C.

Reaction of IIIa with Potassium Hydroxide in Ethanol. IIIa (2.50 g, 10 mmol) and potassium hydroxide were refluxed in ethanol (20 ml) for 4.5 h. Methanethiol was evolved and an insoluble matter was precipitated after about 1 h of reflux. The unidentified precipitate was removed by filtration, and the concentration of the filtrate gave an oily material. It was dissolved in chloroform; the subsequent removal of an insoluble matter by filtration and the concentration of the filtrate gave a sirup. It was solidified by treatment with a small amount of ether, and the solid was collected by filtration. Two recrystallizations from ethanol gave Va; 0.23 g (9%). The addition of a saturated ethereal solution of picric acid to an ethereal solution of the filtrate gave the picrate of Va; 0.51 g (11%). The total yield of Va was 20%. A mixed-melting-point determination with the authentic sample prepared from IIb and NCB showed no depression.

Reaction of IIIa with Sodium Hydroxide in Aqueous Ethanol. A mixture of IIIa (2.50 g, 10 mmol) and 3 M sodium hydroxide (30 ml)–ethanol (30 ml) was refluxed for 1.5 h. TDZ, IIIa was thus gradually dissolved, with the evolution of methanethiol. When the reaction mixture was evaporated under reduced pressure to remove almost all the ethanol and was neutralized with 3 M hydrochloric acid, the resulting precipitate, 2-amino-4-hydroxy-6-phenyl-1,3,5-triazine, was filtered out; yield, 1.60 g (85%): dp 327—328 °C (from DMF–ethanol).

Reaction of IIIb with Sodium Hydroxide in Aqueous Ethanol. 2-Amino-4-hydroxy-6-*p*-tolyl-1,3,5-triazine was obtained by a similar method. The yield was 64%, dp 327—329 °C (from DMF–water).

References

1) Part 103 of "Studies of Cyanamide Derivatives."
2) F. Wohler and Gilbert's, *Ann. Physik.*, **69**, 273 (1821).
3) T. Fuchigami and K. Odo, *Chem. Lett.*, **1973**, 917.
4) T. Fuchigami and K. Odo, *Bull. Chem. Soc. Jpn.*, **48**, 310 (1975).
5) T. Suyama and K. Odo, *Yuki Gosei Kagaku Kyokai Shi*, **29**, 65 (1971).
6) H. Nagasaka and K. Odo, *Yuki Gosei Kagaku Kyokai Shi*, **25**, 1048 (1967).
7) R. Timmons and L. Wittenbrook, *J. Org. Chem.*, **32**, 1566 (1967).
8) T. Fuchigami, E. Ichikawa, and K. Odo, *Bull. Chem. Soc. Jpn.*, **46**, 1765 (1973).

N-Halogen Compounds of Cyanamide Derivatives. VII.[1] The Preparation and Amidination of 5-Ethoxy-Δ^4-1,2,4-thiadiazolines

Toshio FUCHIGAMI, Tsutomu NONAKA, and Keijiro ODO

Department of Electronic Chemistry, The Graduate School, Tokyo Institute of Technology, Ookayama, Meguro-ku, Tokyo 152

(Received May 11, 1976)

2-Methoxycarbonimidoyl and 2-amidino-3-imino-5-ethoxy-Δ^4-1,2,4-thiadiazolines (I and II) were prepared by the reaction of potassium ethoxythiocarbonylcyanamide (III) with *N*-chloro compounds of *O*-methylisourea and guanidine. Δ^4-1,2,4-Thiadiazoline, I reacted with aliphatic amine to give 2-amidino-Δ^4-1,2,4-thiadiazolines and 1,3,5-triazines in the presence of both the free amines and amine hydrochlorides. The ring opening of Δ^4-1,2,4-thiadiazoline, which finally results in the formation of 1,3,5-triazine, was found to be catalyzed mainly by a base and also by an acid.

Our previous papers[2-4] described that 2-imidoyl-3-imino-5-methylthio and 5-alkoxy-Δ^4-1,2,4-thiadiazolines were prepared in good yields by the reaction of *N*-chloroamidino compounds; we also described their reactivities for sodium hydroxide, amine, hydrogen chloride, and hydrogen sulfide.

In this paper, we wish to report on the preparation of two new Δ^4-1,2,4-thiadiazolines (TDZ), I and IIa, from III[4] and *N*-chloro compounds of *O*-methylisourea and guanidine, and on the amidination of I, together with the ring opening of TDZ, catalyzed by the amine, to give 1,3,5-triazine (IV).

Results and Discussion

Preparation of 5-Ethoxy-TDZ (I and II). *N*-Chloro compounds of *O*-methylisourea and guanidine readily reacted with III in acetonitrile to form I and IIa. The structures of I and IIa were confirmed by means of elemental analysis and by a study of the IR spectrum.

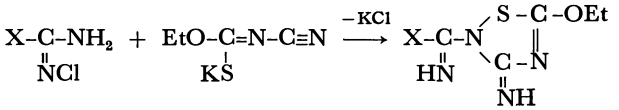

(III)

X	Yield (%)
MeO	I (80)
H_2N	IIa (60)

Amidination of I. Since compound I can be regarded as *N,N*-disubstituted *O*-alkylisourea with a reactive imidate group, the amidination of I was examined using various kinds of amines. The amidination of I proceeded under reflux in ethanol in the presence of both amine and its hydrochloride to give 2-amidino-TDZ and 1,3,5-triazine (IV). 1,3,5-Triazine, IV has a composition in which sulfur can be excepted from TDZ. In the case of methylamine, desulfurization occurred almost completely, so IV and an unidentified product were obtained instead of 2-amidino-TDZ. In the case of benzylamine, when the amount of free amine was reduced by half, desulfurization was considerably inhibited. Therefore, free amine seemed to participate in the conversion of 2-amidino-TDZ to IV. In the case of a weak base such as aniline, neither the amidination nor ring opening of TDZ occurred, and 2-carbamoyl-TDZ (V) was obtained. Compound V was also obtained quantitatively by the treatment of I with excess dry hydrogen chloride in methanol.

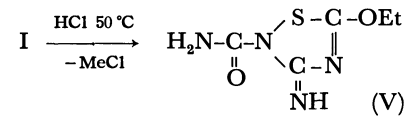

As is shown in Table 1, the ethoxyl group of I was found not to be reactive.

The physical properties and analytical data of TDZ are summarized in Table 2.

TABLE 1. AMIDINATION OF I

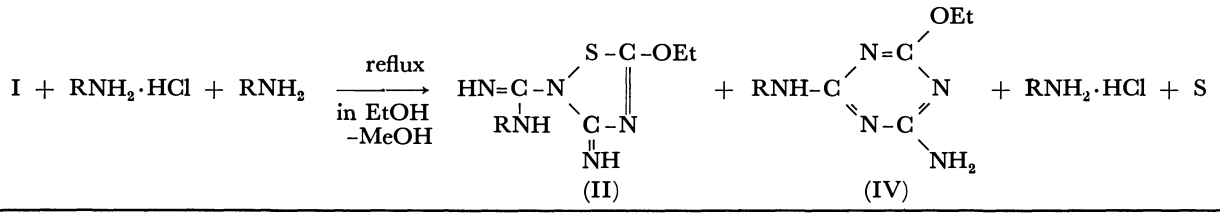

Amine			Reaction time (h)	Products (Yield %)			
R	Free base[a]	Salt[a]		TDZ(II)	1,3,5-Triazine(IV)	S	Others
Me	2	1	3.0	0	10(IVd)	94	+[b]
n-Pr	2	1	2.5	20(IIb)	39(IVb)	55	—
Bzl	2	1	3.0	50(IIc)	19(IVc)	25	—
Bzl	1	1	3.0	40(IIc)	Trace(IVc)	6	I
Ph	2	1	3.0	0	0	0	86[c]

a) Molar ratio. b) The structure could not be determined. c) Yield of IV.

Table 2. Physical properties and analytical data of Δ^4-1,2,4-thiadiazolines

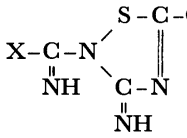

Compound No	X	Mp (°C)	UV Spectra λ_{max}^{MeOH} ($\varepsilon \times 10^{-4}$)	Found (Calcd) % C	H	N
I	MeO	143	263 (1.0)	34.66 (35.63)	4.99 (4.98)	27.40 (27.70)
IIa	H_2N	177—180	242 (0.7)	32.12 (32.08)	4.99 (4.85)	37.31 (37.41)
IIb	*n*-PrNH	161—162	272 (1.1)	41.72 (41.91)	6.29 (6.59)	30.24 (30.54)
IIc	BzlNH	143—145	267 (1.0)	52.21 (51.97)	5.53 (5.45)	25.30 (25.25)
V	HO	300	272 (1.3)	31.54 (31.91)	3.98 (4.28)	29.45 (29.77)

Table 3. Conversion of TDZ to 1,3,5-triazines

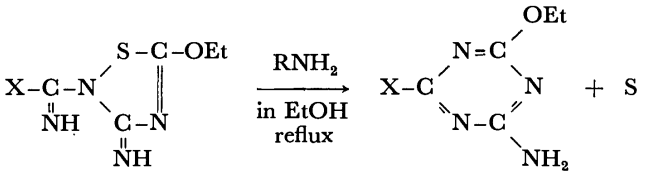

X	Amine R	R′	Free base[a]	Salt[a]	Reaction time (h)	1,3,5-Triazine (IV) Yield (%)	Mp (°C)	
MeO	Ph	H	4	0	3	0		
MeO	H	H	4	0	3	54 (46)[b]		
MeO	Me	H	1	0	3	83	102—103	(IVe)
MeO	Et	Et	1	0	3	Trace		
MeO	Et	Et	4	0	3	Quant.		
MeO	[c]		4	0	2	0		
H_2N	Et	H	4	0	3	Quant.	182 (182)[5]	(IVa)
BzlNH	zBl	H	3	0	4	0		
BzlNH	Bzl	H	2	1	3	Quant.	181—183	(IVc)

a) Molar ratio. b) Yield of recovered TDZ. c) Triethylamine.

Conversion of TDZ into 1,3,5-Triazine. Since the above results suggest that free amine participates in the ring opening of TDZ, the conversion of TDZ into 1,3,5-triazine was examined using various kinds of TDZ and amines. Methylamine reacted with I under reflux in ethanol to give IV, as expected, in a good yield. In the case of a bulky amine such as diethylamine, traces of IV were obtained in the presence of an equivalent of the base, and, finally, four equivalents of the base were needed for the quantitative conversion. In the case of triethylamine, no ring opening occurred, and the starting TDZ was recovered. The result may be due to the steric hindrance of triethylamine. Ammonium chloride reacted also with I to give V in about a 50% yield. In the reaction with a weak base such as aniline, no reaction occurred. TDZ (IIc) did not react with free benzylamine, while in the presence of the hydrochloride the reaction occurred to give IVc quantitatively. Amine was found to act as a catalyzer, because the amine used as a neucleophile is not included in IV. The above results showed that the conversion of TDZ to IV depends on the bulkiness and basicity of the amine and on the presence of acid.

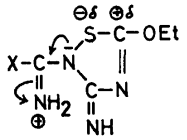

Fig. 1.

The conversion may be initiated by the attack of the free amine on the 5-carbon. The cleavage of the C–S bond, the loss of sulfur from the resulting intermediate, and the recyclization take place to give IV. In the presence of acid, protonation may occur at the imino group. The electron density at the 5-carbon may be

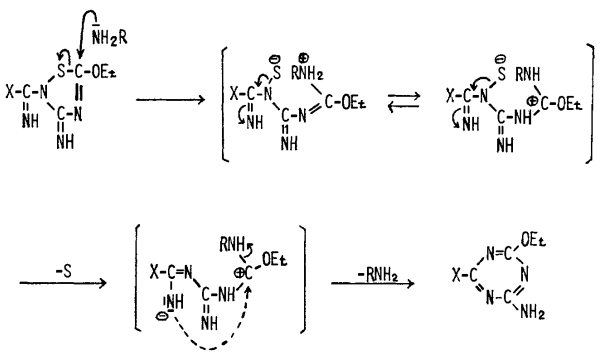

Scheme 1. Conversion of TDZ to 1,3,5-triazine.

reduced by the effect of the protonated imino group, and so the attack of the amine may be easier (Fig. 1).

Experimental

2-Methoxycarbonimidoyl-3-imino-5-ethoxy-Δ^4-1,2,4-thiadiazoline (I). To a stirred mixture of III[4] (6.27 g, 40 mmol) and acetonitrile (40 ml), we added a solution of *N*-chloro-*O*-methylisourea (4.34 g, 40 mmol) in acetonitrile (20 ml). The temperature was maintained below 5 °C during the reaction. After 1.75 h of continued stirring, the reaction mixture was evaporated to dryness under reduced pressure. The title compound was obtained by washing the residue with water 6.45 g; 80%; mp 138—143 °C. Recrystallization from ethanol gave a pure product; mp 143 °C. Picrate: mp 137 °C (from water). Found: C, 33.32; H, 2.97; N, 22.78%. Calcd for $C_{12}H_{13}N_7SO_9$: C, 33.42; H, 3.04; N, 22.73%.

2-Amidino-3-imino-5-ethoxy-Δ^4-1,2,4-thiadiazoline (IIa). The title compound was prepared according to approximately the same procedure as that described previously.[3] Recrystallization from methanol–water gave pure IIa; mp 177—180 °C. Picrate: mp 288 °C (from water). Found: C, 31.77; H, 2.93; N, 26.80%. Calcd for $C_{11}H_{12}N_8SO_8$: C, 31.74; H, 2.91; N, 26.92%.

Amidination of I. *Amidination of I with Benzylamine*: A solution of I (2.02 g, 10 mmol), benzylamine (2.14 g, 20 mmol), and benzylamine hydrochloride (1.44 g, 10 mmol) in ethanol (25 ml) was refluxed for 3 h. After the reaction mixture had been evaporated to dryness under reduced pressure, the residue was washed with ether (10 ml). TDZ, IIc containing sulfur was obtained by washing the residue with water: 1.39 g; 50%; mp 137—140 °C (from MeOH). The addition of petroleum ether to the ethereal washings afforded 2-amino-4-benzylamino-6-ethoxy-1,3,5-triazine (IVc) (0.47 g; 19%; mp 181—183 °C (from DMF). Found: C, 58.61; H, 6.26; N, 28.45%. Calcd for $C_{12}H_{15}N_5O$: C, 58.76; H, 6.16; N, 28.55%. Picrate: mp 174—175 °C (from EtOH). Found: C, 45.45; H, 3.83; N, 23.51%. Calcd for $C_{18}H_{18}N_8O_8$: C 45.57; H, 3.82; N, 23.62%.

Amidination of I with n-*Propylamine*: Using the same procedure as above (20 mmol scale), after the sulfur had been removed, the filtrate was concentrated. The residual oily material was crystallized from water (20 ml), subsequent recrystallization from ethanol (15 ml) afforded two kinds of products. IIb: 0.92 g; 20%; mp 162—163 °C (from EtOH). 2-Amino-4-ethoxy-6-*n*-propylamino-1,3,5-triazine (IVb): 1.53 g; 39%; mp 132—134 °C (from aq MeOH). Found: C, 48.59; H, 7.45; N, 35.31%. Calcd for $C_8H_{15}N_5O$: C, 48.72; H, 7.67; N, 35.51%.

2-Amino-4-ethoxy-6-methylamino-1,3,5-triazine (IVd) was obtained in a similar manner by the reaction of I with methylamine: 10%; mp 171—172 °C (170—171 °C)[6] (from water). Picrate: dp 202—203 °C (from water). Found: C, 36.26; H, 3.74; N, 27.70%. Calcd for $C_{12}H_{14}N_8O_8$: C, 36.19; H, 3.54; N, 28.13%.

2-Carbamoyl-3-imino-5-ethoxy-Δ^4-1,2,4-thiadiazoline (V). A slow stream of dry hydrogen chloride was passed through a solution of I (2.02 g, 10 mmol) in methanol (30 ml) at 50 °C for 40 min. A small amount of a brown precipitate was removed by filtration, and the filtrate was evaporated to dryness under reduced pressure. The title compound was obtained by washing the residue with ether; 1.84 g, 98%; dp> 300 °C (from DMF–EtOH).

Reaction of TDZ with Free Amines. *Reaction of I with Aqueous Ammonia*: A solution of I (1.01 g, 5 mmol) and 5% ammonium hydroxide (8 ml, 20 mmol) in ethanol (15 ml) was refluxed for 3 h. After the precipitated sulfur had been filtered off, the filtrate was cooled and I was precipitated; 0.46 g, 46%. After the filtration of I, the concentration of the filtrate afforded 2-amino-4-ethoxy-6-methoxy-1,3,5-triazine (IVe): 0.46 g, 54%; mp 102—103 °C. Found: C, 41.92; H, 6.03; N, 32.62%. Calcd for $C_6H_{10}N_4O_2$: C, 42.35; H, 5.92; N, 32.92%.

Reaction of IIc with Benzylamine: A mixture of IIb (0.55 g 2 mmol), benzylamine (0.72 g, 4 mmol), and benzylamine hydrochloride (0.29 g, 2 mmol) was refluxed in ethanol (6 ml) for 3 h. After the reaction mixture had been concentrated, the residue was washed with ether and water; 1,3,5-triazine (IVc) was thus obtained; 0.49 g; quant.

References

1) Part 104 of "Studies of Cyanamide Derivatives."
2) T. Fuchigami and K. Odo, *Chem. Lett.*, **1973**, 917.
3) T. Fuchigami and K. Odo, *Bull. Chem. Soc. Jpn.*, **48**, 310 (1975).
4) T. Fuchigami and K. Odo, *Bull. Chem. Soc. Jpn.*, **49**, 3165 (1976).
5) J. Controulis and C. Banks, *J. Am. Chem. Soc.*, **67**, 1946 (1945).
6) W. Pearlmann, J. Mitsulski, and C. Banks, *J. Am. Chem. Soc.*, **71**, 3248 (1949).

The Wolff Rearrangement and 1,3-Dipolar Cycloaddition of 2-Diazo-3,4-bis(diphenylmethylene)cyclobutanone[1]

Kozaburo UEDA, Masanori IGAKI, and Fumio TODA

Department of Industrial Chemistry, Faculty of Engineering, Ehime University, Matsuyama 790

(Received May 12, 1976)

The first example of the Wolff rearrangement of α-diazocyclobutanone, the title diazo ketone (**2**), into the three-membered cyclic ketene (**4**) was observed. The ketene intermediate (**4**) could be trapped by its reaction with alcohols, aniline, azobenzene, and *N*-benzylideneaniline to afford 1-alkoxycarbonyl- (**5a**—**c**) and 1-phenylcarbamoyl-2,3-bis(diphenylmethylene)cyclopropane (**5e**), and 1,2-bis(diphenylmethylene)-5,6-diphenyl-5,6-diaza- (**9**) and 1,2-bis(diphenylmethylene)-5,6-diphenyl-5-azaspiro[2,3]hexan-4-one (**10a**), respectively. In contrast to the rearrangement, **2** directly reacted with *p*-benzoquinone and nitrosobenzene, affording the corresponding 1,3-dipolar cycloadducts (**14** and **15**).

The Wolff rearrangements of six- and five-membered α-diazocycloalkanones have been extensively applied to the synthesis of highly strained compounds.[2] However, no such rearrangement of α-diazocyclobutanone has yet been reported, because the synthesis of the α-diazocyclobutanone is difficult.[3] We wish now to report the first synthesis of the α-diazocyclobutanone, 2-diazo-3,4-bis-(diphenylmethylene)cyclobutanone (**2**), and its Wolf rearrangement into the three-membered cyclic ketene (**4**).

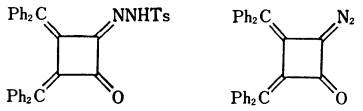

1 **2**

Diazo ketone (**2**) was prepared by the treatment of 3,4-bis(diphenylmethylene)cyclobutanedione tosylhydrazone (**1**), which had been derived from 3,4-bis-(diphenylmethylene)cyclobutanedione[4] and tosylhydrazine, with basic aluminum oxide; the overall yield was 95%. The irradiation of **2** in the presence of water, ROH, and an aniline afforded 1-carboxy-(**5d**), 1-alkoxycarbonyl-(**5a**—**c**), and 1-phenylcarbamoyl-2,3-bis(diphenylmethylene)cyclopropane (**5e**) respectively in the yields summarized in Table 1. Although the photolysis of **2** in the presence of water afforded **5d** in a very low yield, the thermal decomposition of **2** in aqueous dioxane afforded **5d** in a relatively high yield (52%). The above trapping reactions support the intermediacy of **4** in both the photolysis and thermolysis of **2**.

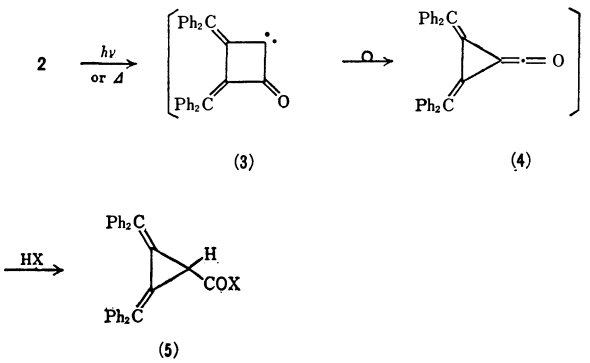

(3) (4) (5)

Scheme 1.

The structures of all the rearrangement products (**5a**—**e**) were elucidated on the basis of their spectral data (Table 1). In the mass spectra, all the esters (**5a**—**c**) showed a fragment ion ($C_{23}H_{15}^+$, *m/e* 291) as the base peak; a reasonable fragment pattern of **5** is as follows: The rearrangement of the cation radical (**a**) into **b** is similar to the cyclopropylidene-allene rearrangement.[5] In the UV spectra, the absorption bands of **5a**—**e** (λ_{max} 370—374 nm) appeared at a longer wavelength region than that of **8**[6] (λ_{max} 357 nm). This bathochromic shift is probably due to a ring strain of **5**.

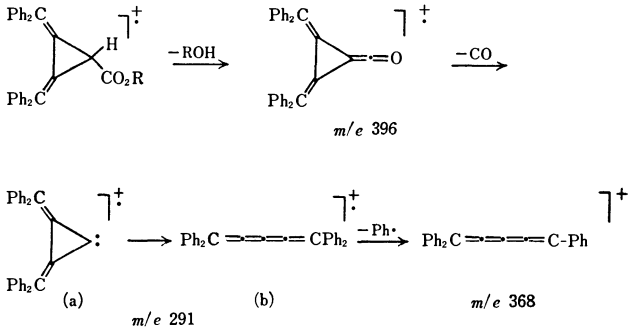

m/e 396

(a) *m/e* 291 (b) *m/e* 368

Scheme 2.

The treatment of 2,3-bis(diphenylmethylene)-cyclopropylmethanol (**6**), which had been obtained by the reduction of **5a** with $LiAlH_4$, with thionyl chloride afforded 3-chloro-1,2-bis(diphenylmethylene)cyclobutane (**7**). The formation of **7** can be interpreted by a ring expansion accompanied by chlorination.[7]

The photolysis of **2** in the presence of azobenzene gave 1,2-bis(diphenylmethylene)-5,6-diphenyl-5,6-diazaspiro-[2.3]hexan-4-one (**9**) in a 75% yield. The photolysis and thermolysis of **2** in the presence of benzylideneaniline and *N*-(diphenylmethylene)aniline afforded 5,6-

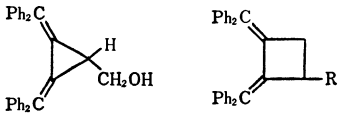

6 **7** R=Cl **8** R=H

TABLE 1. PHYSICAL PROPERTIES, YIELDS, ANALYTICAL DATA OF **5a–e**

Compd	X	Yield (%)	Mp (°C)	$\nu_{C=O}^{KBr}$ (cm^{-1})	$\lambda_{max}^{CHCl_3}$ nm ($\varepsilon \times 10^{-2}$)	τ_{C-H} [b]	Found (Calcd) (%) C	H
5a	OMe	87	157—159	1725	262 (282)	6.72	86.67	5.40
					373 (360)		(86.89	5.65)
5b	OEt	65	128—129	1720	264 (298)	6.70	86.62	5.87
					374 (376)		(86.85	5.92)
5c	O*i*-Pr	75	161—162	1710	260 (297)	6.75	86.64	6.12
					370 (360)		(86.81	6.18)
5d	OH	13 (52) [a]	217—218	1695	263 (259)	6.75	86.70	5.07
					373 (360)		(86.93	5.35)
5e	NHPh	45	171—172	1645	254 (332)	6.63	88.14	5.52
					373 (339)		(88.31	5.56)

a) Yield obtained by thermolysis in aq dioxane. b) Chemical shift of the ring proton.

diphenyl- (**10a**) and 5,6,6-triphenyl-1,2-bis(diphenylmethylene)-5-azaspiro[2.3]hexan-4-one (**10b**) respectively. These reactions can be interpreted in terms of the cycloaddition of the ketene (**4**) with azobenzene and imines, because it has been known that the reaction of ketene with N=N or C=N bonds affords the corresponding cycloaddition product.[8] The thermolysis of diazetidinone (**9**) easily afforded 1,2-bis(diphenylmethylene)-3-phenyliminocyclopropane (**11**) quantitatively; on hydrolysis, this afforded 1,1,4,4-tetraphenyl-2-phenylcarbamoyl-1,3-butadiene (**12**, 75%).

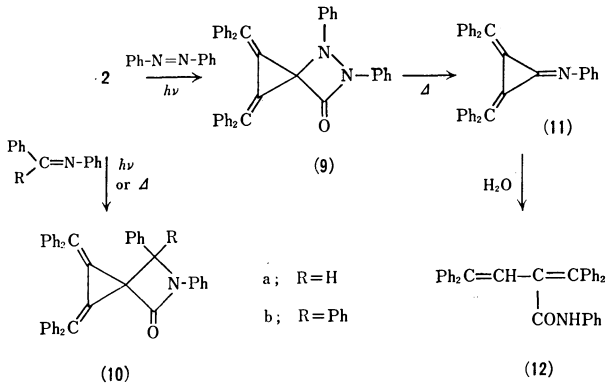

Scheme 3

On the contrary, the photolysis and thermolysis of **2** in the presence of *p*-benzoquinone afforded 2,3-bis(diphenylmethylene)-4,4-(3,6-dioxo-4-cyclohexen-1,2-ylene)cyclobutanone (**13**) in 45 and 59% yields respectively. However, when a mixture of **2** and *p*-benzoquinone in benzene was kept at room temperature, 5,6-diaza-7,8-(1,4-dioxo-2-butylene)-2,3-bis(diphenylmethylene)spiro[3,4]octan-1-one (**14**) was obtained in an 80% yield. The heating of **14** easily afforded **13** quantitatively. Finally, it is clear that the conversion of **2** into **13** proceeds *via* **14**. Similarly, the reaction of **2** with nitrosobenzene afforded 2,3-bis(diphenylmethylene)-8-phenyl-5,6,8-triaza-7-oxaspiro[3.4]oct-5-en-1-one (**15**) and 2,3-bis(diphenylmethylene)-4-phenyliminocyclobutan-1-one *N*-oxide (**16**) in 15 and 50% yields respectively. The 1,3-dipolar cycloadduct (**15**) was thermally unstable and was easily converted into

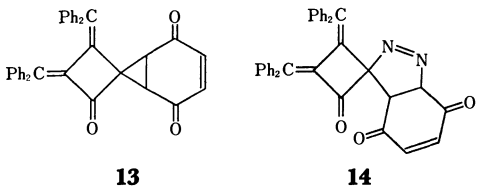

13 **14**

16 at room temperature. To our best knowledge, no such 1,3-cycloadduct as **15** has yet been isolated in any reaction of diazoketone with nitrosobenzene.[9]

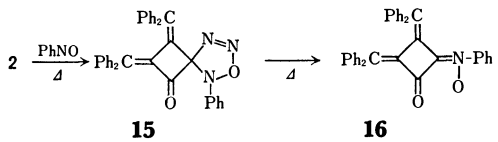

15 **16**

Experimental

All the melting points are uncorrected. Photolysis was carried out at room temperature under a nitrogen atmosphere, using light from a 100-W high-pressure mercury lamp (Riko Kagaku Sangyo Co), with filtered Pyrex glass. The IR, UV, and NMR spectra were measured in a KBr disk, $CHCl_3$, and $CDCl_3$ respectively, unless otherwise stated. The mass spectra were obtained with an ionization energy of 75 eV.

Preparation of Diazo Ketone (2). A mixture of 3,4-bis(diphenylmethylene)cyclobutanedione[3] (4.12 g, 10 mmol), tosylhydrazine (2.05 g, 11 mmol), and concd HCl (1 ml) in CH_2Cl_2–MeOH (1: 1, 200 ml) was kept at room temperature for 4 h. The crude crystals thus formed were recrystallized from AcOEt to give **1** as red needles; 5.80 g (100%); mp 145—146 °C. IR (Nujol): 3240 (NH), 1750 (C=O), 1170 (SO_2), 755 cm^{-1} (Ph); λ_{max}: 281 (28000), 398 (24000), 440 sh (8400), 515 nm (ε, 10000); NMR: 0.10 (s, 1H, NH), 2.35—2.9 (m, 14H), 3.17 (s, 5H), 3.24 (s, 5H), 7.62 τ (s, 3H).

Found: C, 76.46; H, 4.53%. Calcd for $C_{37}H_{28}O_3N_2S$: C, 76.54; H, 4.86%.

To a stirred solution of **1** (1.16 g, 2 mmol) in $CHCl_3$ (50 ml), we added aluminum oxide (20 g, Woelm, basic activity I) at 0 °C over a period of 30 min; the stirring was continued for a further hour. The mixture was then passed through the short column packed with basic aluminum oxide (30 g) described above, using $CHCl_3$ (200 ml) as the eluent. The crude crystals left after the evaporation of the solvent were recrystal-

lized from ether–light petroleum to afford **2** as orange prisms; 0.81 g (95%); mp 123—124 °C. IR: 2050 (N_2), 1745 cm^{-1} (C=O); λ_{max}: 262 (10000), 271 (11000), 338 (6700), 420 nm (ε, 5100).

Found: C, 84.65; H, 4.60%. Calcd for $C_{30}H_{20}ON_2$: C, 84.88; H, 4.75%.

*Photolysis of **2** in the Presence of Alcohols, Aniline, and Water.* A mixture of **2** (424 mg, 1 mmol) and MeOH (20 ml) in benzene (150 ml) was irradiated for 2 h. The oily material left after the evaporation of the solvent was chromatographed on silica gel, using benzene as the eluent, to afford crude crystals. The recrystallization from EtOH afforded **5a** as colorless prisms; 372 mg (87%). The photochemical reactions of **2** with EtOH, *i*-PrOH, and aniline, according to the same procedure as above, afforded **5b**, **5c**, and **5e** respectively. The photochemical reaction of **2** with water was carried out in dioxane for 12 h. The oily material left after the evaporation of the solvent was taken up in ether, from which **5d** was extracted with an aqueous Na_2CO_3 solution. The physical properties, yields, and analytical data of **5a**—**e** are summarized in Table 1.

*Thermal Reaction of **2** in Aqueous Dioxane.* A solution of **2** (424 mg, 1 mmol) in 10%-aqueous dioxane (30 ml) was refluxed for 1 h. The reaction mixture was then treated by the procedure used for the reaction mixture of the photolysis of **2** in aqueous dioxane to afford **5d**; 215 mg (52%).

*Reduction of **5a** with $LiAlH_4$.* To a stirred solution of **5a** (200 mg, 0.47 mmol) in ether (20 ml), we added an excess of $LiAlH_4$. The reaction mixture was stirred for a further hour, decomposed with dil-HCl, and then extracted with ether. The crude crystals left after the evaporation of the solvent were recrystallized from CH_2Cl_2–EtOH to give **6** as colorless prisms; 180 mg (95%); mp 141—142 °C. IR (Nujol): 3400 and 1070 cm^{-1} (OH); λ_{max} 260 (23700), 375 nm (ε, 28600); NMR; 2.48 (s, 10H), 3.05 (s, 5H), 3.12 (s, 5H), 6.03 (d, J=9 Hz, 2H), 7.13 (t, J=9 Hz, 1H), 8.75 τ (br s, 1H, OH).

Found: C, 89.65; H, 5.88%. Calcd for $C_{30}H_{24}O$: C, 89.96; H, 6.04%.

*Chlorination of **6** with $SOCl_2$.* To a solution of 6 (100 mg, 0.25 mmol) in ether (10 ml), we added an excess of $SOCl_2$, after which the mixture was refluxed for 1 h. The oily material left after the evaporation of the solvent was chromatographed on silica gel, using benzene as the eluent, to give **7** as orange prisms; 42 mg (40%); mp 183—184 °C. NMR: 2.60 (s, 5H), 2.65 (s, 5H), 3.07 (s, 10H), 4.83 (t, J=5.5 Hz, 1H), 6.55—67.5 τ (m, 2H).

Found: C, 85.87; H, 5.42%. Calcd for $C_{30}H_{23}Cl$: C, 86.00; H, 5.53%. The spectral data of **7** were identical with those of an authentic sample prepared by the addition of HCl to 3,4-bis(diphenylmethylene)-1-cyclobutene.[4]

*Preparation of **9**.* A solution of **2** (424 mg, 1 mmol) and azobenzene (200 mg, 1.1 mmol) in benzene (150 ml) was irradiated for 10 h. The oily material left after the evaporation of the solvent was chromatographed on silica gel. Elution with benzene afforded **9** as yellow prisms; 435 mg (75%); mp 186.5—187 °C. IR: 1760 cm^{-1} (C=O); λ_{max}: 270 (27200), 404 nm (ε, 28000); NMR: 2.30—3.40 (m); MS: *m/e* (rel intensity) 578 (M^+, 91), 501 (80), 459 (M^+—PhNCO, 34), 167 (100).

Found: C, 86.88; H, 5.15%. Calcd for $C_{42}H_{30}ON_2$: C, 87.17; H, 5.23%.

*Preparation of **11** and Its Hydrolysis.* A solution of **9** (580 mg, 1 mmol) in xylene (30 ml) was refluxed for 4 h. The subsequent evaporation of the solvent under reduced pressure afforded **11** as a red liquid; 460 mg (100%). IR (neat): 1600 and 1030 cm^{-1} (C–N); λ_{max}: 272 (37500), 395 nm (ε, 32000); NMR: 2.45—3.30 (m). **11** is very sensitive to water and is easily hydrolyzed. For example, when a solution of **11** (230 mg, 0.5 mmol) in AcOEt (10 ml) was kept at room temperature for 1 day, **12** was obtained as colorless prisms after recrystallization from AcOEt; 180 mg (75%); mp 224—225 °C. IR (Nujol): 3330, 1655, and 1520 cm^{-1} (CONH); λ_{max}: 245 (21200), 337 nm (ε, 14000); NMR: 2.30—2.95 (m, 25H), 3.32 τ (br s, 2H); MS: *m/e* (rel intensity) 477 (M^+, 56), 385 (M^+—PhNH, 76), 357 (M^+—PhNHCO, 74), 279 (100).

Found: C, 87.85; H, 5.70%. Calcd for $C_{35}H_{27}ON$: C, 88.02; H, 5.70%.

*Preparation of **10a**. By Photolysis*: A solution of **2** (424 mg, 1 mmol) and *N*-benzylideneaniline (200 mg, 1.1 mmol) in benzene (150 ml) was irradiated for 8 h. The crude crystals left after the evaporation of the solvent were recrystallized from AcOEt to afford **10a** as yellow prisms; 376 mg (65%); mp 190—191 °C. IR: 1750 and 1260 (C=O), 1170 cm^{-1} (C–N); 2.35—3.7 (m, 30H), 4.68 τ (s, 1H); λ_{max}: 260 (36200), 383 nm (ε, 29500); MS: *m/e* (rel intensity) 578 (M^+, 20), 459 (M^+—PhNCO, 20), 397 (M^+—PhCH=NPh, 80), 396 (100).

Found: C, 89.10; H, 5.22%. Calcd for $C_{43}H_{31}ON$: C, 89.40; H, 5.41%.

By Thermolysis: A solution of **2** (424 mg, 1 mmol) and *N*-benzylideneaniline (200 mg, 1.1 mmol) in dioxane (30 ml) was heated under reflux for 1 h; thereafter it was worked up in a manner similar to that described above to afford **10a**; 237 mg (41%).

*Preparation of **10b**. By Photolysis*: A solution of **2** (424 mg, 1 mmol) and *N*-(diphenylmethylene)aniline (314 mg, 1.1 mmol) in benzne (150 ml) was irradiated for 10 h. The oily material left after the evaporation of the solvent was chromatographed on silica gel, using benzene as the eluent, to give **10b** as yellow prisms; 530 mg (81%); mp 242—246 °C. IR: 1740 and 1250 (C=O), 1170 (C–N), 740 cm^{-1} (Ph); λ_{max}: 263 (30000), 383 nm (ε, 23900); MS: *m/e* 653 (M^+, 100), 396 (M^+—Ph_2C–NPh, 30), 291 (70).

Found: C, 89.75; H, 5.38%. Calcd for $C_{49}H_{35}ON$: C, 90.01; H, 5.40%.

By Thermolysis: A solution of 2 (424 mg, 1 mmol) and *N*-(diphenylmethylene)aniline (314 mg, 1.1 mmol) in dioxane (30 ml) was refluxed for 1 h. The oily material left after the evaporation of the solvent was chromatographed on silica gel, using benzene as the eluent, to afford **10b**, 260 mg (40%).

*Preparation of **13**. By Photolysis*: A solution of **2** (424 mg, 1 mmol) and *p*-benzoquinone (126 mg, 1.1 mmol) in benzene (150 ml) was irradiated for 6 h. The crude crystals left after the evaporation of the solvent were recrystallized from AcOEt to give **13** as yellow prisms; 227 mg (45%); mp 218.5—220 °C. IR: 1760 and 1670 cm^{-1} (C=O); λ_{max}: 246 (25400), 265 (22600), 350 (14000), 455 nm (ε, 7400)0 NMR: 2.54 (s, 10H), 3.00 (s, 5H), 3.17 (s, 5H), 3.35 (s, 2H), 7.13 τ (s, 2H); MS; *m/e* (rel intensity) 504 (M^+, 100), 427 (M^+—Ph, 20).

Found: C, 85.49; H, 4.98%. Calcd for $C_{36}H_{24}O_3$: C, 85.69; H, 4.79%.

By Thermolysis: A solution of **2** (424 mg, 1 mmol) and *p*-benzoquinone (126 mg, 1.1 mmol) in dioxane (30 ml) was refluxed for 2 h. The crude crystals left after the evaporation of the solvent were recrystallized from AcOEt to afford **13**; 298 mg (59%).

*Preparation of **14** and Its Thermal Decomposition.* A solution of 2 (424 mg, 1 mmol) and *p*-benzoquinone (126 mg, 1.2 mmol) in benzene (30 ml) was kept for 12 h at 0 °C. The crude crystals left after the evapotation of the solvent were recrystallized from CH_2Cl_2–EtOH to afford **14** as orange prisms; 425 mg (80%); mp 290 °C. IR: 1760 and 1695 cm^{-1} (C=O); λ_{max}: 283 (26000), 362 (17000), 450 nm (ε, 10000);

NMR: 2.25—3.7 (m, 22H), 7.40 τ(s, 2H).

Found: C, 80.94; H, 4.28%. Calcd for $C_{36}H_{24}O_3N_2$: C, 81.18; H, 4.54%.

A solution of **14** (200 mg, 0.38 mmol) in xylene (50 ml) was heated at reflux for 4 h. The crude crystals left after the evaporation of the solvent were recrystallized from AcOEt to afford **13**; 180 mg (95%).

*Preparation of **15** and **16**.* A solution of **2** (848 mg, 2 mmol) and nitrosobenzene (630 mg, 4 mmol) in benzene (50 ml) was kept for 10 h at room temperature. The crude crystals left after the evaporation of the solvent were recrystallized from CH_2Cl_2–EtOH to afford a mixture of pale yellow (**15**; 160 mg (15%); mp 120 °C dec) and brilliant black crystals (**16**; 475 mg (50%); mp 211—213 °C), which were separated mechanically. When a solution of the former (**15**, 100 mg, 0.19 mmol) in AcOEt was heated at reflux for 10 min and then kept for 12 h, the latter crystals were obtained; they were subsequently recrystallized from AcOEt to afford **16**; 76 mg (80%) **15**. IR: 1780 (C=O), 1195 cm^{-1} (C–N); λ_{max}: 242 (27000), 315 nm (ε, 14500); NMR: 2.35—2.75 (m, 10H), 2.85—2.95 (m, 5H), 3.0—3.4 τ (m, 10H).

Found: C, 80.92; H, 4.48%. Calcd for $C_{36}H_{25}O_2N_3$: C, 81.33; H, 4.74%.

16. IR: 1750 (C=O), 1290 cm^{-1} (N-O); λ_{max} 241 (17200), 280 (16300), 408 (10000), 505 (11700), 585 sh (3700), 640 nm (ε, 2300); MS: *m/e* (rel intensity) 503 (M^+, 9), 487 (M^+—O, 28), 382 (67), 189 (100).

Found: C, 85.60; H, 5.12%. Calcd for $C_{36}H_{25}O_2N$: C, 85.86; H, 5.00%.

References

1) A preliminary report has been published previously: K. Ueda and F. Toda, *Chem. Lett.*, **1975**, 779.

2) a) W. Kirmse, "Carbene Chemistry," Academic Press, New York, N. Y. (1971), p. 475. b) H. Meier and K. P. Zeller, *Angew. Chem. Int. Ed. Engl.*, **14**, 32 (1975).

3) M. P. Cava and R. P. Stein, *J. Org. Chem.*, **31**, 1866 (1966).

4) F. Toda and K. Akagi, *Tetrahedron*, **27**, 2801 (1971).

5) W. M. Jones, *J. Am. Chem. Soc.*, **82**, 6200 (1960).

6) F. Toda, K. Kumada, N. Ishiguro, and K. Akagi, *Bull. Chem. Soc. Jpn.*, **43**, 3535 (1971).

7) J. D. Roberts and R. H. Mazur, *J. Am. Chem. Soc.*, **73**, 2509 (1951).

8) a) H. Staudinger, *Chem. Ber.*, **41**, 1355 (1908); b) L. Horner, E. Spietschka, and A. Gross, *Ann. Chem.*, **573**, 17 (1951); c) W. Kirmse and L Horner, *Chem. Ber.*, **89**, 2759 (1956); d) L. L. Muller and J. Hamer, "1,2-Cycloaddition Reaction," Interscience Publications, New York, N. Y. (1967), p. 173.

9) For example, see a) O. Tsuge, I. Shinkai, and M. Koga, *Org. Prep. Proced. Int.*, **4**, 169 (1972); b) A. W. Johnson, *J. Org. Chem.*, **28**, 252 (1963).

Nucleophilic Displacement Catalyzed by Transition Metal. III.[1] Kinetic Investigation of the Cyanation of Iodobenzene Catalyzed by Palladium(II)

Kentaro TAKAGI, Tadashi OKAMOTO,* Yasumasa SAKAKIBARA,** Atsuyoshi OHNO,* Shinzaburo OKA,* and Naomi HAYAMA

College of Liberal Arts and Science, Okayama University, Tsushima, Okayama 700

(Received May 26, 1976)

The nucleophilic displacement of iodobenzene with potassium cyanide was carried out in HMPA in the presence of palladium(II) acetate. The reaction obeys the following kinetics;

$$d[C_6H_5CN]/dt = k[Pd(OAc)_2]_0(M_{KCN})^{2/3}$$

A reaction scheme composed of two cycles has been proposed: in one cycle Pd^0 activates iodobenzene and in the other cycle Pd^{2+} assists the dissolution of potassium cyanide.

In a previous paper,[2] we reported that the nucleophilic displacement of non-activated aryl halides by cyanide anions takes place in the presence of palladium-

$$ArX + KCN \xrightarrow{Pd(II)} ArCN + KX$$

(II) salts. The scope of the reaction revealed that the palladium(II) salt is initially reduced to a lower-valent species, which plays the role of an active catalyst, and that the cyanide ligand retards the reduction. It is particularly interesting to note that a cyanide anion in the solution is a retarder of the reaction. In order to obtain an insight into the mechanism of the reaction, we studied the reaction from the kinetic viewpoint. The results and the most plausible scheme for the reaction will be presented in this paper.

Results and Discussion

The reaction of iodobenzene with potassium cyanide

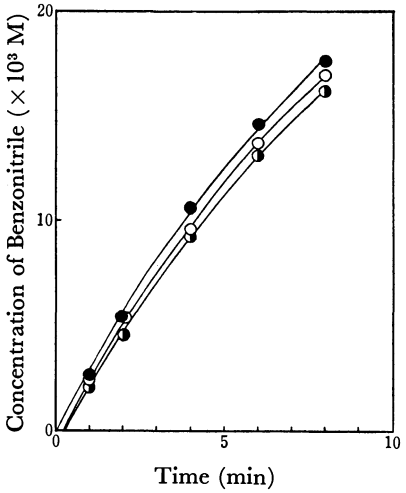

Fig. 1. Effect of concentration of iodobenzene.
KCN 1.03 mmol, $Pd(OAc)_2$ 1.03×10^{-3} M, HMPA 7.7 ml, 102±1 °C, under N_2 C_6H_5I ● 7.07×10^{-2} M ○ 4.36×10^{-2} M ◑ 2.36×10^{-2} M.

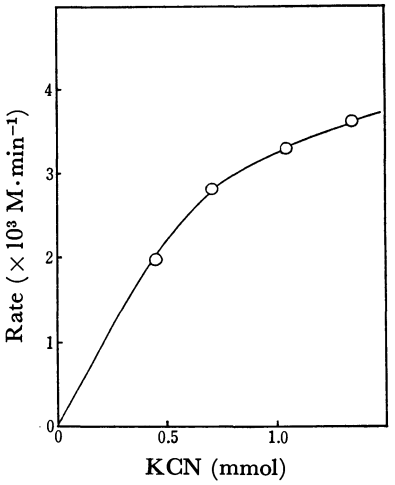

Fig. 2. Effect of amount of potassium cyanide on reaction rate.
$Pd(OAc)_2$ 1.74×10^{-3} M, C_6H_5I 4.36×10^{-2} M, HMPA 7.7 ml, 102±1 °C, under N_2.

was carried out in hexamethylphosphoric triamide (HMPA) at 102 °C using palladium(II) acetate as a catalyst. Benzonitrile was obtained in a quantitative yield, and by-products such as biphenyl were not detected on GLC. Since the reaction system is heterogeneous and there remains an undetermined variable (*vide infra*), we resigned to calculate numerical values for the rate constants.

Effect of Concentrations of Reactants. As is shown in Fig. 1, the initial rate for the appearance of benzonitrile was independent of the initial concentration of iodobenzene, which ranged from 2.36×10^{-2} M to 7.07×10^{-2} M. On the other hand, the rate increased non-linearly with the amount (weight) of potassium cyanide, as illustrated in Fig. 2. The analysis of the order with the method of integration[3] revealed that the kinetics obeys a two-thirds-order (r=0.992) for the amount of potassium cyanide. A linear relationship directed at the origin was observed between the rate and the concentration of palladium(II) acetate, provided that the concentration was greater than 1.04×10^{-3} M (Fig. 3).

Thus, Eq. 1 shows the rate expression determined experimentally, where $[Pd(OAc)_2]_0$ stands for the initial concentration of palladium(II) acetate and M_{KCN}

* Institute for Chemical Research, Kyoto University, Uji, Kyoto 611.

** Chemical Laboratory of Textile Fibers, Kyoto University of Industrial Arts and Textile Fibers, Kyoto 606.

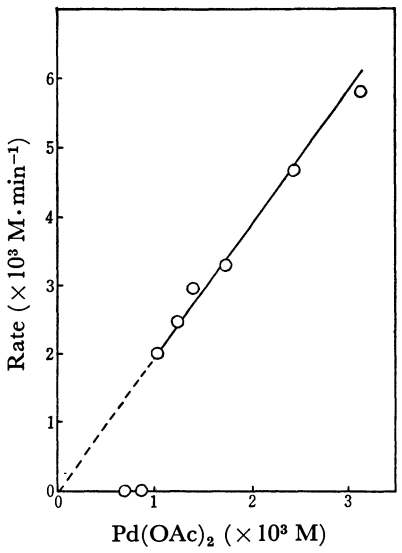

Fig. 3. Effect of concentration of palladium(II) acetate on reaction rate.
KCN 1.01 mmol, C_6H_5I 4.36×10^{-2} M, HMPA 7.7 ml, 102±1 °C, under N_2.

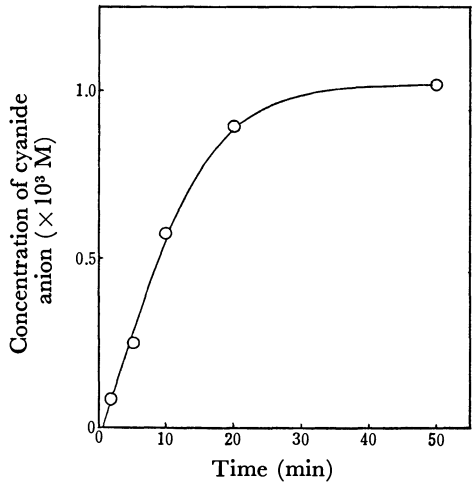

Fig. 4. Dissolution of potassium cyanide in HMPA.
(Plot of concentration of cyanide anion *vs.* time)
KCN 2.02 mmol, HMPA 15.4 ml, 102±1 °C, under N_2.

means the amount of potassium cyanide in the reaction mixture.

$$d[C_6H_5CN]/dt = k[Pd(OAc)_2]_0(M_{KCN})^{2/3}$$
$$[Pd(OAc)_2]_0 \geq 1.04 \times 10^{-3}M$$

Rate of Dissolution of Potassium Cyanide into HMPA. Concentrations of potassium cyanide in HMPA at 102 °C were measured at appropriate time intervals after mixing both materials; the result is shown in Fig. 4. It is noteworthy that the concentration-time profile has an asymptote of about 1×10^{-3} M, which is almost identical to the minimum concentration of palladium(II) acetate necessary for the catalytic reaction. This observation seems to reveal that the cyanide anion in the solution[4] is trapped rapidly by a palladium(II) acetate at the very initial stage of the reaction to form the cyanide salt, which is inactive for initiation of the reaction.

$$Pd(OAc)_2 + CN^- \xrightarrow[\text{fast}]{} Pd^{2+}(CN^-)L_n \not\rightarrow Pd^0$$
$$\downarrow \qquad\qquad \uparrow$$
$$Pd^0 \qquad KCN_{solid}$$

L; ligand(OAc^-, solvent, *etc.*)

The fact that potassium tetracyanopalladate(II) or palladium(II) cyanide is an inactive catalyst under the present conditions[2,5] supports this idea. Thus, in order to have a catalytic reaction, the initial concentration of palladium(II) acetate must exceed that of potassium cyanide in the solution.

The initial rate of dissolution of potassium cyanide into HMPA can be calculated to be 6×10^{-5} M·min^{-1}, which is far smaller (1/30—1/100) than the rates of the appearance of benzonitrile (2×10^{-3}—6×10^{-3} M·min^{-1}, *cf.* Figs. 1—3). This result suggests that the cyanide anions which contribute to the reaction comes directly from the potassium cyanide in the solid state, if not all.

Reaction Scheme. The results and discussion presented above leads to the following scheme as the most plausible mechanism for the reaction:

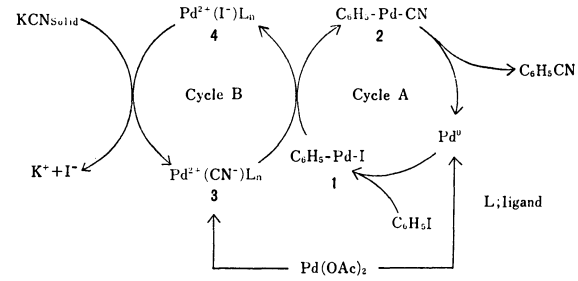

The low-valent palladium species (Pd^0) which comes from palladium(II) acetate[6] reacts with iodobenzene to give an oxidative-addition adduct (**1**). A methathesis of **1** with the cyanopalladium complex (**3**) produces the phenylcyanopalladium(II) complex (**2**), which subsequently yields benzonitrile and regenerates Pd^0 to ensure the catalytic cycle A. This is the well-known sequence of oxidative addition, methathesis, and reductive elimination in transition metal catalysis.[7] Supporting evidence for this is presented by the reaction of arylmercury(II) compound with potassium cyanide in the presence of palladium(II) chloride.

$$p\text{-}CH_3\text{-}C_6H_4\text{-}HgCl + KCN + PdCl_2 \longrightarrow$$
$$p\text{-}CH_3\text{-}C_6H_4\text{-}CN\ (+\ KCl + HgCl_2 + Pd)$$

In this case *p*-methylbenzonitrile was obtained quantitatively based on palladium(II) chloride.[8]

The cycle B represents a cyanide-carrier. Palladium-(II) species draws the cyanide anion away from solid potassium cyanide and transfers it to **1** in methathesis.

The fact that the overall reaction rate is independent of the concentration of iodobenzene implies that the rate-determining step is the process for the abstraction of cyanide anions from the solid surface by palladium(II) species. Under such a circumstance the reaction rate is proportional to the stoichiometric concentration of

palladium(II) acetate and to the surface area of potassium cyanide in solid state, that is, the two-thirds-order of the amount of potassium cyanide; thus the experimentally derived Eq. 1 is consistent with the reaction scheme.

It should be noted that, in constructing the reaction scheme, we have assumed that almost all the palladium species in the reaction mixture is used as a cyanide-carrier (cycle B) and that the steady-state concentration of palladium species in cycle A is quite low.

That a cyano-complex such as **3** can provide the cyanide anions to form another complex, **2**, has been confirmed with a control experiment: when palladium(II) acetate ($[Pd(OAc)_2]/[KCN]=1/4$) was added into a homogeneous solution of iodobenzene and potassium cyanide in HMPA containing a small amount of water and the solution was heated at 102 °C for 30 min, no reaction took place. However, when additional palladium(II) acetate (half the amount to the initial palladium(II) acetate) was added to this reaction solution and the solution was kept at 102 °C for 30 min, benzonitrile was obtained in a 86% yield (based on potassium cyanide used). Since all palladium(II) cations initially added were consumed to form tetracyanopalladate(II) anions, there remained no species to yield Pd^0, whereas Pd^0 could be produced from the second portion of palladium(II) acetate because there remained scarcely any cyanide anions in the solution.

The existence of an appreciable amount of an iodo-complex, **4**, in the reacting solution can be shown from the absorption spectra. A pale-yellow reaction solution turns to reddish brown during the reaction, then comes back to pale-yellow at the end of the reaction. The reddish brown solution exhibits absorption similar to that of palladium(II) iodide solution at 500 nm or higher wavelengths, as is illustrated in Fig. 5.[9]

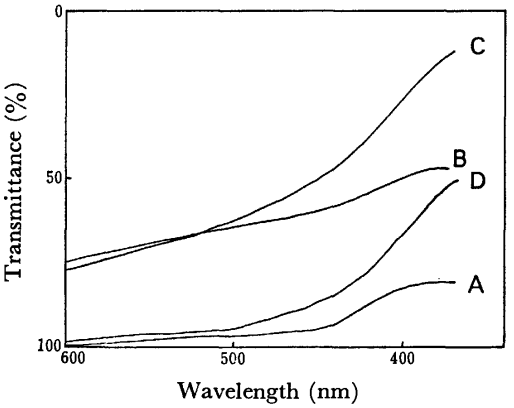

Fig. 5. Electronic spectra.
(A) $Pd(OAc)_2$, (B) PdI_2, (C) Reaction solution-in progress, (D) Reaction solution-terminate.
The concentrations of palladium(II) salts and other reaction conditions (C,D) are identical with those of Fig. 2.

Experimental

Materials. Palladium(II) acetate was prepared according to the literature.[10] HMPA and iodobenzene were commercial reagents and were dried over Molecular Sieves-(3A). Potassium cyanide was recrystallized from water and was ground by the use of a mortar.

Procedure. All reactions were performed in a 30-ml flask equipped with a magnetic stirrer and a three-way trap under a nitrogen stream. A mixture composed of potassium cyanide, iodobenzene, naphthalene (internal standard), and HMPA was stirred for 30 min at 102±1 °C. Then, a HMPA solution of palladium(II) acetate was added at once to start the reaction. Each aliquot (0.4 ml) taken out at appropriate time intervals was quenched with 5 ml of 12.5% aqueous sodium chloride, and the organic materials were extracted with 3 ml of ether. The ether layer was washed with 5 ml of 12.5% aqueous sodium chloride, dried over sodium sulfate, and subjected to the analysis on GLC (Hitachi Perkin-Elmer F6D, 35% silicon DC 200 on celite 545, 2 m, 140 °C, 0.8 kg·cm^{-2} of N_2).

The standard reaction mixture was composed of 1.01 mmol of potassium cyanide, 0.34 mmol of iodobenzene, 0.011 mmol of palladium(II) acetate, and 7.7 ml of HMPA. The concentration of each reagent was changed as indicated in Figs. 1—3.

The reaction rates were computed based on the amount of benzonitrile yielded at 2 min after the initiation.

Reaction of Arylmercury(II) Compound with Potassium Cyanide in the Presence of Palladium(II) Chloride. Into a solution of 65.8 mg (0.2 mmol) of *p*-chloromercuritoluene and 13.0 mg (0.2 mmol) of potassium cyanide in DMF (2.5 ml) was added 2.5 ml of 0.02 M solution of palladium(II) chloride in DMF. The mixture was kept at 50 °C for 1 h. The analysis by GLC revealed 5.8 mg (0.05 mmol) of *p*-methylbenzonitrile (a 99% yield based on $PdCl_2$) and a small amount of *p,p'*-bitolyl.

Solubility of Potassium Cyanide. To 2.02 mmol of potassium cyanide kept at 102 °C under nitrogen was added 15.4 ml of HMPA preheated to 102 °C; the concentrations of cyanide anions in the stirred mixture were measured at appropriate time intervals by the aid of a cyanide-ion electrode (Toa Electronic Ltd., CN-125).

Absorption Spectra. The spectra were recorded on a Hitachi Spectrophotometer 124. The reaction mixture was diluted with HMPA by a factor of 3 when it was submitted to the spectroscopy.

One of the authors (K. T.) wishes to thank the Ministry of Education for the support of this work with Grant No. 074167.

References

1) Part II. K. Takagi, T. Okamoto, Y. Sakakibara, A. Ohno, S. Oka, and N. Hayama, *Chem. Lett.*, **1975**, 951.

2) K. Takagi, T. Okamoto, Y. Sakakibara, A. Ohno, S. Oka, and N. Hayama, *Bull. Chem. Soc. Jpn.*, **48**, 3298 (1975); K. Takagi, T. Okamoto, Y. Sakakibara, and S. Oka, *Chem. Lett.*, **1973**, 471.

3) K. J. Laidler, "Chemical Kinetics," 2nd ed., McGraw-Hill, New York (1965), p. 5.

4) The mixture composed of potassium cyanide, iodobenzene, and HMPA was stirred for 30 min at 102 °C (see Experimental). Thus, the palladium(II) acetate was added to the mixture containing about 1×10^{-3} M of cyanide anions.

5) P. M. Maitlis, "Organic Chemistry of Palladium," Vol. 1, Academic Press, New York (1971), p. 32.

6) In a previous paper,[2] the reduced palladium species (Pd^0) was supposed to be the active catalyst for this palladium-

(II)-catalyzed cyanation from the following observations:

(1) The catalytic activity was greatly enhanced by the addition of a reductant such as potassium hydroxide or potassium carbonate.

(2) The cyanide ($Pd(CN)_2$ or $K_2Pd(CN)_4$), which is reduced with difficulty, was a less effective catalyst than the other palladium(II) salts examined.

(3) Palladium(II) acetate was spontaneously reduced to palladium metal on standing in HMPA under nitrogen.

7) L. Cassar, S. Ferra, and M. Foa, "Homogeneous Catalysis-II," Advances in Chemistry Series No. 132, American Chemical Society, Washington (1974), p. 252; D. G. Morrell and J. K. Kochi, *J. Am. Chem. Soc.*, **97**, 7262 (1975) and references cited therein.

8) An early report concerning a similar reaction described only unsatisfactory results (<20% yield); P. M. Henry, *J. Org. Chem.*, **36**, 1886 (1971).

9) Normally, organopalladium complexes (containing iodide ligand) are white; J. K. Klabunde and J. Y. E. Low, *J. Am. Chem. Soc.*, **96**, 7674 (1974).

10) T. A. Stephenson, S. M. Morehouse, A. R. Powell, J. P. Heffer, and G. Wilkinson, *J. Chem. Soc., A*, **1965**, 3632.

The Synthetic Reactions of Aliphatic Nitro Compounds. XI. The Synthesis of β-Amino-α-hydroxycarboxylic Acids and γ-Aminocarboxylic Acids[1]

Eisuke KAJI, Akira IGARASHI, and Shonosuke ZEN

School of Pharmaceutical Sciences, Kitasato University, Shirokane, Minato-ku, Tokyo 108

(Received May 31, 1976)

The *O*-alkylation of some nitroparaffins, 2-nitropropane, 2-nitrobutane, 1-nitropropane, and phenylnitromethane, with methyl bromoacetate in dipolar aprotic solvent led to α-hydroxy-β-nitrocarboxylates, which were converted into β-amino-α-hydroxycarboxylic acids. Several γ-aminocarboxylic acids were synthesized from the corresponding γ-nitrocarboxylates which were obtained *via* *C*-alkylation of the nitroparaffins with methyl β-bromopropionate.

The ambident reactivity of aliphatic nitro compounds has been known to undergo unique reactions with several electrophiles.[2-4] We have found that alkylation of α-carbon atom in nitroparaffins is useful for the formation of a C–C bond, considering that carbon alkylation is applicable to a rather limited case where some nitroparaffins are alkylated with α-halonitroparaffins or some benzyl halides.[5-7]

It has been already reported by Hass *et al.*[8] that oxygen alkylation is available for the synthesis of aldehydes. However, practical investigation of the ambident nitronate anion is limited to the field of a reaction involving radical anion intermediates.[9,10]

Recently we have found that the use of dipolar aprotic solvents such as *N,N*-dimethylacetamide in this reaction promotes carbon alkylation of nitroacetate anion, and that the orientation of alkylation depends on the kind of the electrophiles used. We have reported that several α-amino acids[11,12] and 4-substituted isoxazoline *N*-oxides[13] can be synthesized *via* alkylation of nitroacetate. Recent developments on amino acids of β- or γ-series which are themselves biologically active or the important components of several antibiotics[14-16] prompted us to explore new and general syntheses of these series of amino acids *via* alkylation of nitroparaffins.

For our purposes, attempted alkylation of several nitroparaffins, 2-nitropropane (**1a**), 2-nitrobutane (**1b**), 1-nitropropane (**1c**), and phenylnitromethane (**1d**), with bromoacetic ester and β-bromopropionic ester was carried out. The reaction of two equivalents of the aci-nitro compounds with methyl bromoacetate in a dipolar aprotic solvent produced α-hydroxy-β-nitroesters (**5**) which would be produced by the condensation of excess nitroparaffin with methyl glyoxylate (**4**) formed by the initial *O*-alkylation followed by degradation, as illustrated in Chart 1. This scheme was supported by the isolation of α-benzaldoxime (**3d**, $R^1=C_6H_5$, $R^2=H$) from the reaction mixture of **5d**, which was identified with an authentic sample. The structure of **5** was confirmed from the IR and NMR spectra and elemental analyses (Tables 1 and 2).

It seems that this reaction is well suited for secondary rather than primary nitroparaffins except for phenylnitromethane. In the alkylation of nitromethane or nitroethane with methyl bromoacetate, similar products that were expected were not obtained under analogous conditions, since the products from primary nitro compounds would still have an active hydrogen which would undergo subsequent alkylation or side reaction.

The compound **5b** or **5c** was confirmed by NMR to be a diastereomeric mixture consisting of *erythro* and *threo* isomers in a ratio of *ca.* 1 : 1, as shown in Table 2. This result agreed well with a previous report on the ethyl ester of **5c**.[17]

Catalytic hydrogenation of **5** in methanol usually gave a mixture of products which could not be purified further. Subsequently *O*-acetyl derivatives (**6**) of **5** were prepared and subjected to hydrogenation over a Raney nickel catalyst to yield the corresponding β-amino-esters (**7**). From the spectroscopic data of **7**, *O*→*N* migration of acetyl group seems to be occurred to give

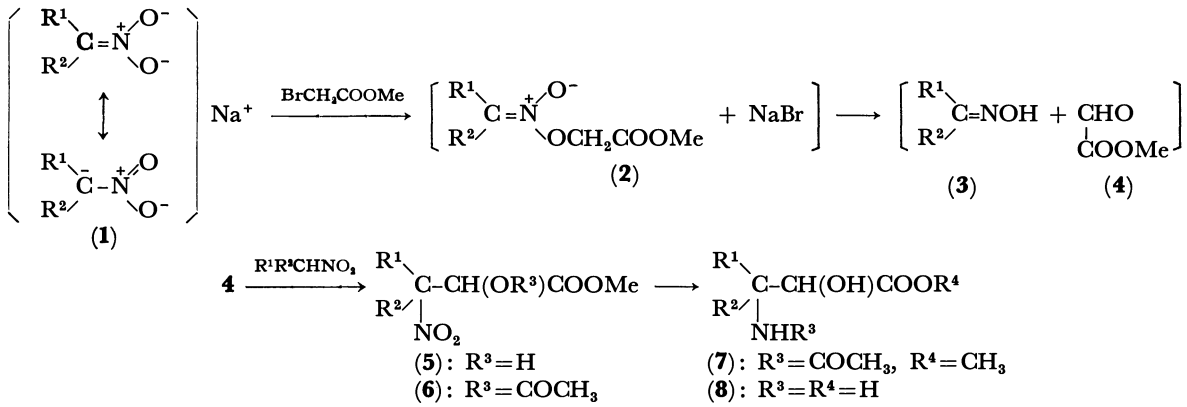

a: $R^1=R^2=CH_3$; **b**: $R^1=C_2H_5$, $R^2=CH_3$; **c**: $R^1=C_2H_5$, $R^2=H$; **d**: $R^1=C_6H_5$, $R^2=H$

Chart 1.

TABLE 1. METHYL α-HYDROXY- AND α-ACETOXY-β-NITROCARBOXYLATES (**5** and **6**)

Compound No.	R^1	R^2	Bp °C/Torr (Mp °C)	Yield (%)	Formula	Found (%)			Calcd (%)		
						C	H	N	C	H	N
5a	CH_3	CH_3	75.7—77.5/0.3	48	$C_6H_{11}NO_5$	40.56	6.23	7.57	40.68	6.26	7.91
5b	C_2H_5	CH_3	74—75/0.3	52	$C_7H_{13}NO_5$	43.72	6.72	6.93	43.42	6.63	7.33
5c	C_2H_5	H	85—87/0.3	11	$C_6H_{11}NO_5$	40.41	6.33	7.64	40.68	6.26	7.91
5d	C_6H_5	H	(109—110)	68	$C_{10}H_{11}NO_5$	53.18	4.89	6.26	53.33	4.92	6.22
6a	CH_3	CH_3	(67—68)	63	$C_8H_{13}NO_6$	43.84	5.98	6.39	44.04	6.09	6.34
6b	C_2H_5	CH_3	74—75/0.04	54	$C_9H_{15}NO_6$	46.08	6.44	5.85	46.35	6.48	6.01
6c	C_2H_5	H	85—90/0.02	85	$C_8H_{13}NO_6$	43.58	5.97	6.14	43.84	5.98	6.39
6d	C_6H_5	H	(64—65)	85	$C_{12}H_{13}NO_6$	53.85	5.01	5.02	53.93	4.90	5.24

TABLE 2. IR AND NMR DATA OF METHYL α-HYDROXY- AND α-ACETOXY-β-NITROCARBOXYLATES (**5** and **6**)

Compound No.	ν (liquid film) cm^{-1}			δ (100 MHz) in $CDCl_3$				Composition[a] *erythro : threo*
	C-NO_2	C=O	OH	α-H	β-H or -CH_3	OH or $COCH_3$	CO_2CH_3	
5a	1545, 1350	1750	3450	4.65 (d)	1.63 (s) 1.67 (s)	3.47 (d)	3.87 (s)	—
5b	1550, 1360	1740	3460	4.59 (d) 4.65 (s)	1.46 (s) 1.54 (s)	3.27 (d)	3.78 (s) 3.82 (s)	1 : 1
5c	1550, 1370	1750	3500—3400	4.40 (d—d)[b] *ca.* 4.6 (?)[c]	4.5—4.8 (m)	3.18 (d)	3.84 (s)	1 : 1
5d[f]	1550, 1350	1750	3450	4.90 (broad)	5.80 (d)	*ca.* 3.6 (broad)	3.73 (s)	?
6a[f]	1550, 1350	1750	—	5.57 (s)	1.68 (s)	2.13 (s)	3.78 (s)	—
6b	1555, 1380	1755	—	5.56 (s) 5.60 (s)	1.60 (s) 1.64 (s)	2.10 (s) 2.17 (s)	3.76 (s) 3.79 (s)	1 : 1
6c	1560, 1380	1750	—	5.40 (d)[d] 5.61 (d)[e]	4.65—4.95 (m)	2.16 (s)	3.79 (s)	1 : 1
6d[f]	1550, 1350	1750	—	5.83 (s)	5.83 (s)	2.13 (s)	3.50 (s)	?

a) The composition was determined by the signal intensity of α-H or β-CH_3. b) $J_{\alpha,\beta}$ =4.0 Hz. c) $J_{\alpha,\beta}$ was not observed because of the overlapping to β-H. d) e) $J_{\alpha,\beta}$ were 6.8 and 4.2 Hz respectively. f) IR spectrum was measured in KBr disk.

TABLE 3. METHYL γ-NITROCARBOXYLATES (**10**)

Compound No.	R^1	R^2	Bp (°C/Torr)	n_D^{20}	Yield (%)
10a	CH_3	CH_3	57/0.1	1.4408[a]	85
10b	CH_3	H	51/0.1	1.4361[b]	24
10c	C_2H_5	H	52/0.2	1.4368[c]	34
10d	C_6H_5	H	113/0.04	1.5150[d]	37

a) Reported[18] bp. 79 °C/1 Torr, n_D^{20} 1.4408. b) Reported[19] bp. 91 °C/4 Torr, n_D^{25} 1.436. c) Reported[20] bp. 97 °C/2 Torr, n_D^{20} 1.4371. d) Reported[21] bp. 128—134 °C/1 Torr, n_D^{18} 1.5164.

methyl β-acetamido-α-hydroxycarboxylates (**7**). The IR spectra of **7** showed a strong absorption at 1640—1650 cm^{-1}, typical of an amide, and a broad NH peak appeared at δ 5.8—6.1 region in its NMR spectra. **7** was readily hydrolyzed by treatment with 6 M hydrochloric acid under refluxing for 16 h, giving β-amino-α-hydroxycarboxylic acid hydrochloride as a viscous oil. Deionization through an ion-exchange resin (IR-45, OH form or Dowex 50 W, Na form) column followed by recrystallization gave free amino acids (**8**) as colorless crystals.

The composition of the isomers of **8b** and **8c** was observed to be almost one isomer on the basis of NMR signals for β-CH_3 proton (δ 1.27) for **8b** and α-proton (δ 4.08) for **8c**, whereas crude products (**8b** and **8c**) consist of a mixture of two diastereomers in which β-CH_3 proton was observed at δ 1.27 and 1.23 for **8b** and α-proton at δ 4.08 and 4.16 for **8c**. β-Phenylisoserine (**8d**) was separated into two isomers under ion-

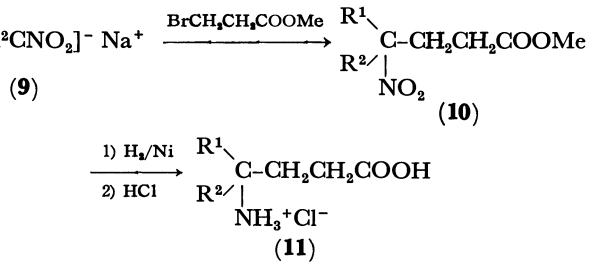

(**9**) (**10**) (**11**)

a: $R^1=R^2=CH_3$; **b**: $R^1=CH_3$, $R^2=H$;
c: $R^1=C_2H_5$, $R^2=H$; **d**: $R^1=C_6H_5$, $R^2=H$

Chart 2.

exchange chromatography, and its results are shown in Table 4. On the other hand, the alkylation reaction of **9a—9d** with methyl β-bromopropionate in *N,N*-dimethylacetamide proceeds preferentially *via* carbon alkylation to yield methyl γ-nitrocarboxylates (**10a—d**) as shown in Chart 2. **10a—d** showed physical constants identical with reported values as well as in IR and NMR spectra and elemental analyses. The catalytic reduction products of **10a—d** were obtained as chromatographically homogeneous syrups. These products were subsequently hydrolyzed with 6 M hydrochloric acid to the corresponding γ-amino acids (**11a—c**) as their hydrochloride and purified by recrystallization. The results are summarized in Table 4.

Table 4. β-Amino-α-hydroxycarboxylic acids (**8**) and γ-aminocarboxylic acid hydrochlorides (**11**)

Compound No.	R^1	R^2	Mp (°C)	R_f [a]	Yield [b] (%)
8a	CH_3	CH_3	278—279 (dec.) [c]	0.56	42
8b	C_2H_5	CH_3	217—218 (dec.) [d]	0.72	54
8c	C_2H_5	H	267—268 (dec.) [e]	0.37	31
8d	C_6H_5	H	240 (dec.) [f]	0.79	24
8d	C_6H_5	H	265 (dec.) [g]	0.70	28
11a	CH_3	CH_3	178—179 [h]	0.49	51
11b	CH_3	H	139—140 [i]	0.49	77
11c	C_2H_5	H	118—119 [h]	0.53	75

a) Paper chromatography on Toyo Roshi filter paper No. 525; solvent, 1-butanol: acetic acid: water (4: 1: 1). b) Based on the corresponding α-hydroxy-β-nitroesters or γ-nitroesters. c) Reported[22] mp. 276.5—277 °C (dec.). d) Found: C, 48.96; H, 8.94; N, 9.45%. Calcd for $C_6H_{13}NO_3$: C, 48.97; H, 8.90; N, 9.52%. e) Found: C, 44.88; H, 8.26; N, 10.28%. Calcd for $C_5H_{11}NO_3$: C, 45.10; H, 8.33; N, 10.52%. f) Reported[23] mp. 230—232 °C. g) Reported[23] mp. 275—280 °C. h) The free amino acid has been reported in the literature[15]. i) Reported[19] mp. 135 °C.

Experimental

All boiling and melting points are uncorrected. The IR spectra were measured on a JASCO Model IRA-1 spectrometer. The NMR spectra were recorded with a 100 MHz JEOL PS-100 spectrometer. Tetramethylsilane was used as an internal standard for deuteriochloroform and tetradeuteriomethanol solution and sodium 2,2-dimethyl-2-silapentane-5-sulfonate was used in deuterium oxide solution. The peak positions are given in δ value.

Typical Procedure. *Methyl α-Hydroxy-β-nitroisovalerate (5a)*: 1 M sodium methoxide (10 ml) was added to a stirred solution of 2-nitropropane (1.73 g, 20 mmol) and methyl bromoacetate (1.53 g, 10 mmol) in 30 ml of *N,N*-dimethylacetamide. After agitation at room temperature overnight, the reaction mixture was poured into 150 ml of ice-cold water covered with 50 ml of benzene. The aqueous phase was extracted four more times with 50 ml portions of benzene. After the benzene extract had been washed with four 50 ml portions of water, benzene layer was dried over anhydrous sodium sulfate. The benzene was removed under reduced pressure. Rectification of the residue yielded 0.85 g of **5a** in 48% yield. Bp, elemental analysis, and spectroscopic data were shown in Table 1 and 2. **5b—5d** were also obtained in a similar procedure. **5c** and **5d** were purified by column chromatography on silica gel (hexane/ethyl acetate as eluant) before distillation.

Methyl α-Acetoxy-β-nitroisovalerate (6a). Concds ulfuric acid (0.05 ml) was added to a stirred solution of **5a** (1 g, 5.65 mmol) in 10 ml of acetic anhydride under ice-cooling. When stirring was continued for an additional 1 h, all the starting material was consumed as shown by silica gel TLC (hexane–ethyl acetate, 2: 1). The reaction mixture was poured into 50 ml of water and extracted with diethyl ether (3×25 ml). The combined extracts were washed with water, dried over anhydrous sodium sulfate, and solvent was evaporated. Recrystallization or sublimation of the resultant solid-residue gave 0.78 g (63%) of colorless crystals. **6b—6d** were also obtained under analogous conditions. The results are summarized in Table 1 and 2.

β-Amino-α-hydroxyisovaleric Acid (8a). A methanolic slurry of Raney nickel T-1 catalyst (1.5 ml) was added to a solution of **6a** (0.73 g, 3.33 mmol) in 40 ml of methanol. The mixture was hydrogenated at room temperature under 3.5 kg/cm² of hydrogen atmosphere in a Parr low-pressure hydrogenator. The catalyst was filtered and the filtrate was evaporated to afford 0.73 g of deep yellow oil (**7a**). **7a** was subjected to next step without further purification except **7b** and **7c** which were passed through ion-exchange resin (Dowex 50 W, H form).

A 0.5 g (2.64 mmol) portion of **7a** was refluxed with 6 M hydrochloric acid (8 ml) for 16 h. After evaporation of the solvent the residual oil was dissolved in water and deionized through a column of basic resin (IR-45, OH form, water as an eluant). Concentration of the eluant gave 0.4 g of amorphous solid. The crude solid was recrystallized from aqueous ethanol to yield 0.15 g of colorless crystals in 42% yield. **8b—8d** were prepared in a similar way as **8a** from the corresponding α-acetoxy-β-nitro esters (**6b—6d**). The results are summarized in Table 4.

Methyl γ-Nitroisocaproate (10a) To a stirred solution of 2-nitropropane (1.0 g, 11.24 mmol) and methyl β-bromopropionate (1.88 g, 11.24 mmol) in 20 ml of anhydrous *N,N*-dimethylacetamide, was added 11.24 ml of 1 M sodium methoxide. The mixture was stirred at room temperature overnight. The resultant yellow liquid was worked up as in the procedure for **5a**. The crude yellow oil was purified by distillation to yield 1.67 g (85%) of colorless oil (**10a**). **10b—10d** were also obtained in analogous way. The results are summarized in Table 3.

γ-Aminoisocaproic Acid (11a). **10a** (1.5 g, 8.57 mmol) was hydrogenated in 80 ml of methanol in the presence of Raney nickel T-1 (2 ml of methanolic slurry) with a low pressure hydrogen (3.5 kg/cm²) for 1.5 h at room temperature. The catalyst was filtered off and the solvent was removed. The residue was subsequently hydrolyzed without further purification. Hydrolysis was carried out by refluxing with 6 M hydrochloric acid for 16 h. After evaporation the residual solid was washed with anhydrous ether and acetone. Recrystallization from methanol–ether afforded 0.73 g (51%) of analytically pure **11a**. **11b—11c** were also obtained in a similar way. The results are summarized in Table 4.

The authors are indebted to Miss Kazuko Shibuya, Messrs. Kazuo Yamaji and Toshihide Kamiya for their technical assistance.

References

1) Part X, *Yuki Gosei Kagaku Kyokai Shi*, **34**, 503 (1976).

2) H. B. Hass and M. L. Bender, *J. Am. Chem. Soc.*, **71**, 3482 (1949).
3) N. Kornblum, R. A. Smiley, R. K. Blackwood, and D. C. Iffland, *J. Am. Chem. Soc.*, **77**, 6269 (1955).
4) N. Kornblum, P. Pink, and K. V. Yorka, *J. Am. Chem. Soc.*, **83**, 2779 (1961).
5) L. W. Seigle and H. B. Hass, *J. Org. Chem.*, **5**, 100 (1940).
6) H. B. Hass, E. J. Berry, and M. L. Bender, *J. Am. Chem. Soc.*, **71**, 2290 (1949).
7) R. C. Kerber, G. W. Urry, and N. Kornblum, *J. Am. Chem. Soc.*, **87**, 4520 (1965).
8) H. B. Hass and M. L. Bender, *J. Am. Chem. Soc.*, **71**, 1767 (1949).
9) N. L. Holy and J. D. Marcum, *Angew. Chem. Int. Ed. Engl.*, **10**, 115 (1971).
10) N. Kornblum, S. D. Boyd, and N. Ono, *J. Am. Chem. Soc.*, **96**, 2580 (1974)
11) S. Zen and E. Kaji, *Bull. Chem. Soc. Jpn.*, **43**, 2277 (1970).
12) E. Kaji and S. Zen, *Bull. Chem. Soc. Jpn.*, **46**, 337 (1973).
13) S. Zen and E. Kaji, *Chem. Pharm. Bull.*, **22**, 477 (1974).
14) J. P. Greenstein and M. Winitz, "Chemistry of the Amino Acids," Vol. I, John Wiley & Sons, Inc., New York (1961), p. 18.
15) E. L. Schumann, L. A. Paquette, R. V. Heinzelman, D. P. Wallach, J. P. DaVanzo, and M. E. Greig, *J. Med. Pharm. Chem.*, **5**, 464 (1962).
16) P. W. K. Woo, H. W. Dion, and Q. R. Bartz, *Tetrahedron Lett.*, **1971**, 2625.
17) C. Shin, Y. Yonezawa, and J. Yoshimura, *Nippon Kagaku Kaishi*, **1974**, 718.
18) R. B. Moffett, *Org. Synth.*, Coll. Vol. IV, p. 652 (1963).
19) J. Colonge and J. M. Pouchol, *Bull. Soc. Chim. Fr.*, **1962**, 596.
20) M. C. Kloetzel, *J. Am. Chem. Soc.*, **70**, 3571 (1948).
21) A. A. Smirnova, V. V. Perekalin, and V. A. Scherbakov, *Zh. Org. Khim.*, **4**, 2245 (1968).
22) T. Kaneko and T. Inui, *Kogyo Kagaku Zasshi*, **82**, 743 (1961).
23) J. P. Fourneau and R. Marechal, *Bull. Soc. Chim. Fr.*, **12**, 990 (1945).

Conformationally Stable 1-Substituted 1-Methyl-4-*t*-butyl-1-silacyclohexanes, a New Organosilicon System Suitable for Stereochemical Studies

Hideki SAKURAI and Masashi MURAKAMI

Department of Chemistry, Faculty of Science, Tohoku University, Sendai 980

(Received June 7, 1976)

Ten 1-methyl-4-*t*-butyl-1-silacyclohexyl derivatives ($C_{10}H_{21}Si$–X, X=H, Cl, $OCH(CH_3)_2$, OCH_3, $OC(CH_3)_3$, C_6H_5, *p*-Br–C_6H_4, *p*-Cl–C_6H_4, $Si(CH_3)_2H$, F) were synthesized and separated into conformationally stable *cis* and *trans* isomers. The stereochemistry of these compounds has been determined on the basis of NMR and GLC. They were found to behave stereochemically like acyclic optically active silanes.

Sommer and Frye prepared the first optically active organosilicon compounds, 1-naphthylphenylmethylsilane derivatives (1-NaPhMeSi*X) in 1959.[1]

Since then several reports have been made on other optically active organosilicon compounds.[2–5] They are of importance for the study of the stereochemical behavior of reactions at silicon centers. Several other types of optically active ring compounds are also known.[6,7] However, the majority of optically active organosilicon compounds so far prepared have at least one bond between an aromatic moiety and silicon. Such a structure is often inconvenient for a certain stereochemical research of reactions in which the bond of silicon to aromatic groups cleaves or forms. Cleavage of the bond of silicon to aromatic groups with electrophiles (desilylation)[8] and substitution reactions of silyl radicals on an aromatic nucleus (homolytic aromatic silylation)[9] are examples of such reactions. Moreover, accurate measurement of optical activity requires a large amount of pure sample. In some cases, separation of optically active product(s) from a reaction mixture is infeasible because of extensive racemization.[10]

Conformationally stable compound such as *t*-butylcyclohexane derivatives are also useful in stereochemical investigations. However, no silicon analog of such a class of compounds has been prepared. During the course of a study on the stereochemistry of unstable organosilicon intermediates such as silyl radicals and silylenes,[11] it became necessary to find aliphatic silicon compounds suitable for the stereochemical study. This paper describes the synthesis and reactions of new 4-*t*-butyl-1-methyl-1-silacyclohexane derivatives.[12] Numerous stereochemical studies on the corresponding carbon analogs, 4-*t*-butylcyclohexanes, have been published since the first proposal of the *t*-butyl function as a holding group.[13] The conformationally stable organosilicon compounds are also proved to be useful in the stereochemical study of almost all kinds of reactions on silicon.

Results and Discussion

Preparation and Stereochemistry. The reaction of the di-Grignard reagent from 3-*t*-butyl-1,5-dibromopentane (**1**)[14] with methyldichlorosilane and with methyltrichlorosilane afforded 4-*t*-butyl-1-methyl-1-silacyclohexane (**2**, *cis*/*trans*=1.0) and 4-*t*-butyl-1-methyl-1-chloro-1-silacyclohexane (**3**, *cis*/*trans*=1/2.3), respectively.

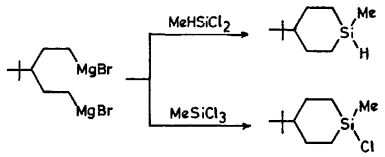

Since all the compounds so far prepared have a methyl group on silicon, 4-*t*-butyl and 1-methyl groups are referred to as *cis* and *trans* respectively, throughout this paper. Suffix a is added to the *cis* compounds and b to the *trans*, as illustrated in the following.

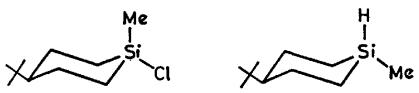

3a (*cis*) 2b (*trans*)

By reduction of **3** (*cis*/*trans*=1/2.3) with lithium aluminum hydride, **2** (*cis*/*trans*=2.8/1) was obtained. The *cis* and *trans* mixtures of **2** and **3** could not be separated into individual isomers by means of GLC. However, alkoxy derivatives, prepared by the direct alcoholysis of **3** or alcoholysis of **2** catalyzed by palladium on charcoal, can be used for separation. The isopropoxysilane (**4**) was the most convenient for separation of *cis* and *trans* isomers by preparative TLC. These isomeric alkoxysilanes can be reduced to **2** with lithium aluminum hydride with retention of configuration as in reduction of optically active alkoxysilanes.[2] Several derivatives were prepared from **2** and **3** the usual organosilicon transformations (Table 1).

The *cis* and *trans* structures of hydrosilanes (**2**) can be identified unequivocally even as a mixture by NMR, and spectral assignment done with the mixture was confirmed again with pure isomers, **2a** and **2b**. Figure 1 shows the NMR spectra of **2**. Figures 2 and 3 show Si–H region of NMR spectra of **2b**, and **2a**, respectively.

The structures of **2a** and **2b** were assigned as follows from SiH–CH_2 coupling constants. Irradiation of the $SiCH_3$ signal of **2b** revealed $J_{SiH(ax)CH(ax)}$ and $J_{SiH(ax)CH(eq)}$ to be 6.5 and 1.7 Hz, respectively, and $J_{SiH(ax)CH(ax)}$ to be *ca.* 1.0 Hz for **2a**. The value of $J_{SiH(ax)CH(ax)}$ observed in the present compound is relatively smaller than the $J_{SiH(ax)CH(ax)}$ values (8—13 Hz) observed for carbon analogs. It should be noted that the present analysis of the coupling constants may not be accurate for complex systems such as AA'BB'X. Thus, we do not claim accuracy of the absolute values of the coupling constant. However, the relative values are sufficient to

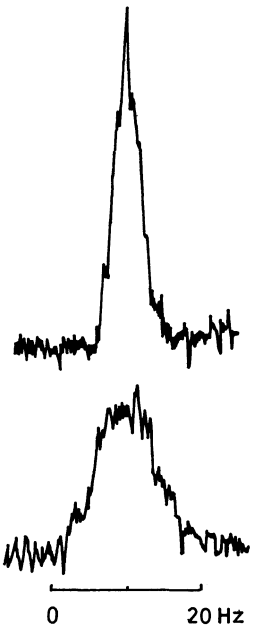

Fig. 3. SiH signal of **2a** (lower) and SiH signal irradiated at the $SiCH_3$ signal of **2a** (upper).

Table 2. Chemical shifts and configuration of functional group attached to six-membered ring in the chair conformation

Group	Relationship in 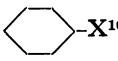	Relationship in 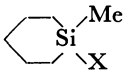
Me	Equatorial upfield	Equatorial upfield
OMe	Equatorial upfield[a]	Equatorial upfield
H	Axial upfield	Axial upfield
	$J_{CHax-CHax}$ 8—13 Hz	$J_{SiHax-CHax}$ 6.5 Hz
	$J_{CHax-CHeq}$ 2—6 Hz	$J_{SiHax-CHeq}$ 1.7 Hz
		$J_{SiHeq-CHax}$ 1 Hz

a) Some exceptions have been given.[16]

field is the *cis* isomer.

Reaction. The isomeric alkoxy derivatives were reduced to **2** with lithium aluminum hydride with retention of configuration. It seems of interest that the *cis* isopropoxysilane, **4a**, was more reactive than the *trans* one, **4b**, toward reduction. Thus, **4a** was reduced easily with lithium aluminum hydride by reflux for a few hours in ether. However, **4b** could not be reduced completely at the temperature of refluxing ether even

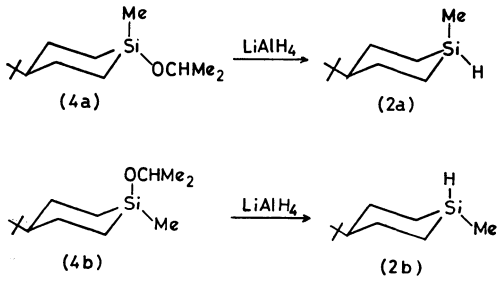

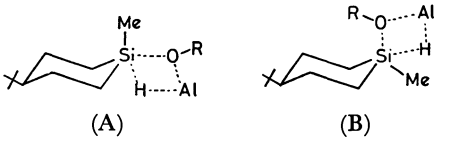

after 10 h, and was only reduced in refluxing tetrahydrofuran. To this type of reaction, Sommer and coworkers[17] suggested a four-centered mechanism. The present result on the silacyclohexane series can also be explained in terms of such a four-centered mechanism. The reaction intermediate or the transition state (B) leading to **2b** should be much more crowded than (A) which should lead to **2a**. Thus it is reasonable to consider that **4b** is less reactive than **4a** toward reduction.

The free radical chlorination of **2** with carbon tetrachloride in the presence of benzoyl peroxide gave **3** in almost quantitative yields with retention of configuration.

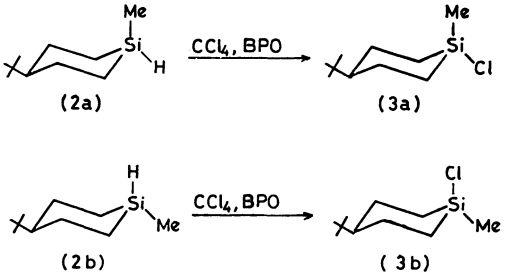

Since the free-radical chlorination in this reaction has been shown to go through a silyl radical intermediate with retention of configuration,[18] the chlorosilane (**3**) should have the same configuration as **2**.[7] This is a strong indication that the stereochemical assignments based on NMR are valid.

Reactions of **3** (*cis*/*trans*=1/2.3) with lithium aluminum hydride gave **2** (*cis*/*trans*=2.8/1), namely, an inversion of configuration. 4-*t*-Butyl-1-methyl-1-phenyl-1-silacyclohexane (**7**, *cis*/*trans*=1.6/1) was also prepared from **3** (*cis*/*trans*=1/2.3) by phenylation with phenyllithium. Methanolysis of **3** (*cis*/*trans*=1/2.3) gave 4-*t*-butyl-1-methyl-1-methoxy-1-silacyclohexane (**5**, *cis*/*trans*=1.7/1), with inversion of configuration in both reactions. Thus, the stereochemical courses of these three reactions were in good agreement with the results studied by using optically active silicon compounds.[2] Recently it has been demonstrated that the angle-strained asymmetric silicon center shows remarkable stereochemical crossover to retention of configuration.[7] However, it can be concluded that the strainless silicon centers in six-membered rings behave stereochemically like acyclic organosilicon compounds.

Several derivatives listed in Table 4 were prepared and separated by preparative GLC. As an example, phenyl derivatives **7a** and **7b** could be separated by GLC, typical examples of GLC and NMR spectra being shown in Fig. 4. The ratio of **7a** and **7b** determined by GLC agreed completely with that obtained by NMR. Silacyclohexyl derivatives which have bulky groups attached to silicon at the equatorial position, *i.e. cis* compounds, were separated systematically from

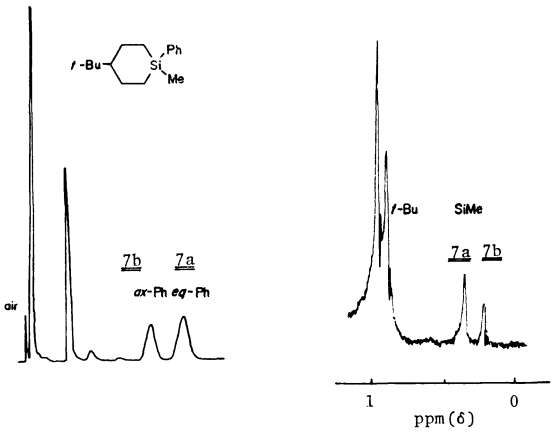

Fig. 4. GLC chart (left) and NMR spectrum (right) of 4-*t*-butyl-1-methyl-1-phenyl-1-silacyclohexane (**7**).

their *trans* compounds on GLC with a longer retention time as observed for carbon analogs.[12]

It should be noted that the compounds possess some advantages as substrates in the stereochemical study; (a) separation of *cis* and *trans* isomer is relatively easy: (b) the stereochemical course can be monitored by NMR and/or GLC; hence each reaction requires only a small amount of reactant: (c) a mixture simply enriched with either of the two isomers can be used satisfactorily: (d) absence of the phenyl or naphthyl group makes some reactions, such as photolysis in the presence of **2** and halodesilylation of **7**, possible.

Experimental

Materials. Reduction of *t*-butylphenol followed by chromic acid oxidation was employed for the preparation of 4-*t*-butylcyclohexanone according to the literature.[19] Preparation of 1,5-dibromo-3-*t*-butylpentane (**1**) has been described elsewhere.[20] Other materials were commercially available and were used without further purification.

NMR spectra were obtained at 100 MHz using a Varian HA-100 spectrometer. IR spectra were taken with a Hitachi EPI spectrometer.

Preparation of 4-t-Butyl-1-methyl-1-silacyclohexane (2). *Method A*: A mixture of 5 g (0.2 g-atom) of magnesium and 100 ml of tetrahydrofuran (THF) was placed in a 500 ml three-necked flask. Then 28.6 g (0.10 mol) of **1** and 11.5 g (0.10 mol) of methyldichlorosilane in 100 ml of THF were added over a period of 1 h. The mixture was stirred with reflux for several hours to complete the reaction. The mixture was then hydrolyzed and extracted with petroleum ether. After the solvent was removed, fractional distillation gave 5 g (0.03 mol, 29% yield) of **2** (*cis*/*trans*=1) as a colorless oil, bp 95 °C (35 mmHg); n_D^{20} 0.8424; IR (neat, cm^{-1}): 2120 (ν_{SiH}), 1250 (δ_{SiMe}) 800 (ν_{Si-Me}). Found: C, 70.37; H, 12.89%. Calcd for $C_{10}H_{22}Si$: C, 70.50; H, 13.01%.

Method B: Reduction of 1 g (4 mmol) of **3** (*cis*/*trans*=1/2.3) with 1 g (26.3 mmol) of lithium aluminum hydride gave **2** (*cis*/*trans*=2.8/1) in an almost quantitative yield (by GLC). The compound was identified by comparing its NMR and IR spectra and GLC with those of **2** prepared by method A.

Preparation of 4-t-Butyl-1-methyl-1-chloro-1-silacyclohexane (3). A mixture of 4 g (0.2 g-atom) of magnesium and 100 ml of THF was placed in a 500 ml three-necked flask. Then 28.5 g (0.10 mol) of **1** and 15 g (0.10 mol) of methyltrichlorosilane in 100 ml of THF were added in a period of 1 h. After the reaction was completed, THF was distilled as completely as possible and 200 ml of diethyl ether was added. The precipitated magnesium salts were filtered from the ethereal solution. After the solvent was removed, fractional distillation gave 10 g (0.148 mol, 48% yield) of **3** (*cis*/*trans*=1/2.3) as a colorless oil, bp 103 °C (20 mmHg). Found: C, 58.32; H, 10.6%. Calcd for $C_{10}H_{21}SiCl$: C, 58.64; H, 10.33%.

Preparation of 4-t-Butyl-1-methyl-1-fluoro-1-silacyclohexane (11). A volatile residue in the preparation of **3** [5.8 g bp ≈120 °C (3 mmHg)] was added drop by drop to 50 ml of concd sulfuric acid at −10 °C with vigorous stirring over a period of 30 min. After additional stirring for 1 h, 4 g (0.07 mol) of ammonium hydrogen fluoride was added several portions. The organic layer was extracted with petroleum ether. Evaporation of the solvent gave 5.1 g of a residue. Fractional distillation of the residue gave 3.7 g of **11** (*cis*/*trans*=1) as a colorless oil, bp 98 °C (55 mmHg); n_D^{20} 0.9127. IR (neat cm^{-1}): 1260 (ν_{SiMe}), 800 (ν_{SiMe}). Found: F, 10.3%. Calcd for $C_{10}H_{21}SiF$: F, 10.1%.

Preparation and Separation of 4-t-Butyl-1-methyl-1-methoxy-1-silacyclohexane (5). *Method A*: Methanolysis of 0.99 g (4.9 mmol) of **3** (*cis*/*trans*=1/2.3) with 10 ml (0.25 mol) of methanol in the presence of 20 ml (0.2 mol) of cyclohexylamine in 50 ml of petroleum ether gave 1.03 g of a crude product. This was purified by chromatography on a silica gel column to yield 0.65 g (3.3 mmol, 67% yield) of **5** (*cis*/*trans*=1.7/1). The *cis* and *trans* mixture can be separated into each isomer by preparative GLC (PEG 20 M, ratio of the retention times: *cis*/*trans*=1.14). Physical data are: **5a**, n_D^{20} 1.4530; d_4^{20} 0.8891 and **5b**, n_D^{20} 1.4520; d_4^{20} 0.8908. IR (neat, cm^{-1}): 1090 (ν_{SiO}), 1255 (ν_{SiMe}), 820 (ν_{SiMe}). Found **5a**: C, 66.14; H, 12.25%. **5b**: C, 66.18; H, 11.86%. Calcd for $C_{11}H_{24}SiO$: 65.93; H, 12.07%.

Method B: Methanolysis of 1.39 g (8.19 mmol) of **2** (*cis*/*trans*=1) with 0.35 ml (8.7 mmol) of methanol in dry pentane in the presence of 0.09 g of 10% palladium on charcoal (10% Pd-C) gave **5** (1.7 g) as a crude product, which was subsequently treated with a silica gel column. Fractional distillation gave 0.89 g (4.5 mmol, 54% yield) of pure **5**, bp 120 °C (70 mmHg). The substance was identified by comparing its NMR, IR, and GLC with those of **5** prepared by method A.

Preparation and Separation of 4-t-Butyl-1-methyl-1-isopropoxy-1-silacyclohexane (4). 3.69 g (21.6 mmol) of **2** (*cis*/*trans*=1) was treated with 2 g (*ca.* 20 mmol) of isopropyl alcohol in 50 ml of dry pentane in the presence of 0.5 g of 10% Pd-C. After further work-up as described above, fractional distillation gave 2.60 g (10.7 mmol, 49.5% yield) of **4**, bp 108 °C (24 mmHg). The product was isolated and purified by preparative GLC (Apiezon L, ratio of retention times: **4a**/**4b**=1.25) to give 0.49 g of **4b**, n_D^{20} 1.4483; d_4^{20} 0.8714 and 0.57 g of **4a**, n_D^{20} 1.4486; d_4^{20} 0.8710, IR (neat cm^{-1}) 1030 (ν_{SiO}), 1255 (ν_{SiMe}), 815 (ν_{SiMe}). Found **4a**: C, 68.14; H, 12.25%. **4b**: C, 68.32; H, 12.25%. Calcd for $C_{13}H_{23}SiO$: C, 68.35; H, 12.35%.

Preparation and Separation of 4-t-Butyl-1-methyl-1-t-butoxy-1-silacyclohexane (6). 25 ml of pentane, 0.4 ml (2.5 mmol) of triethylsilane and 3 ml (30 mmol) of *t*-butyl alcohol were treated with 0.5 g of 10% Pd-C. When vigorous evolution of hydrogen ceased 1.7 g (9.8 mmol) of **2** (*cis*/*trans*=1) was added to the mixture which was kept standing overnight under nitrogen. After a similar work-up, fractional distillation gave 2.1 g (8.7 mmol, 85% yield) of **6**, bp 145 °C (70 mmHg). This was separated to each isomer with preparative GLC (Apiezon L, ratio of retention times: **6a**/**6b**=1.22), giving 0.41 g of **6a**, n_D^{20} 1.4484, d_4^{20} 0.8680; and 0.22 g of **6b**, n_D^{20} 1.4510, d_4^{20} 0.8727.

IR (neat cm^{-1}) 1050 (ν_{Si-O}), 1250 (ν_{SiMe}), 820 (ν_{SiMe}). Found: **6a**: C, 69.69, H, 12.56%. **6b**: C, 69.14; H, 12.45%. Calcd for $C_{14}H_{30}SiO$: C, 69.35; H, 12.47%.

Preparation and Separation of 4-t-Butyl-1-methyl-1-phenyl-1-silacyclohexane (7). *Method A*: Phenylation of 3.1 g (16.4 mmol) of **11** with 25 ml (0.87 M, 20.1 m eq.) of phenyllithium in ether, followed by fractional distillation, gave 2.5 g (9.5 mmol, 58% yield) of **7**, bp 145 °C (35 mmHg). This was further purified by preparative GLC (Apiezon L, ratio of retention times: **7a**/**7b**=1.26) to give 0.78 g of **7a**: n_D^{20} 1.5173; d_4^{20} 0.9345, and 0.36 g of **7b**: n_D^{20} 1.5174; d_4^{20} 0.9333, IR (neat, cm^{-1}): 1436, 1115 (SiPh); 1250 (ν_{SiMe}), 800 (ν_{SiMe}). Found **7a**: C, 77.79, H, 10.72%. **7b**: C, 77.72; H, 10.92%. Calcd for $C_{16}H_{26}Si$: C, 77.97; H, 10.63%.

Preparation and Separation of 4-t-Butyl-1-methyl-1-(p-bromophenyl)-1-silacyclohexane (8). *p*-Bromophenyllithium was prepared from 10.5 g (10.5 mmol) of 1,4-dibromobenzene and 10 m eq. of butyllithium in ether by Gilman's method.[21] To the ethereal solution of *p*-bromophenyllithium was added 1.5 g (8.0 mmol) of **11**. The reaction mixture was refluxed overnight under nitrogen. Further work-up and evaporation of the solvent gave 3.3 g of a residual material. This was purified with a silica gel column to give 2.6 g (8.0 mmol, 100% yield) of **8** (*cis*/*trans*=1.86/1) as a pale yellow oil which solidified readily. Further purification of 1.2 g of **8** by preparative GLC (Apiezon L, ratio of retention times: **8a**/**8b**=1.24) gave 176 mg of **8a** (mp 39—40 °C after recrystallization from ethanol) and 77 mg of **8b** (mp 84—85 °C, after recrystallization from ethanol). Found **8a**: C, 59.24; H, 7.78%. **8b**: C, 59.31; H, 8.01%. Calcd for $C_{16}H_{25}SiBr$; C, 59.06; H, 7.74%.

Preparation and Separation of 4-t-Butyl-1-p-Chlorophenyl-1-methyl-1-silacyclohexane (9). *p*-Chlorophenylmagnesium chloride in THF was prepared from 7 g (47.5 mmol) of 1,4-dichlorobenzene and 1 g (40 mg-atom) of magnesium. By a similar procedure to that given above, followed by purification by preparative GLC (Apiezon L, ratio of retention times: **9a**/**9b**=1.20), 0.85 g (4.5 mmol) of **11** gave *ca.* 40 mg of **9a** (mp 30 °C) and 10 mg of mixture of **9a** and **9b**. Calcd for $C_{16}H_{25}SiCl$: C, 68.41; H, 9.06%. Mixture of **8a** and **8b**; C, 68.49; H, 9.20%.

Preparation of cis-*4-t-Butyl-1-methyl-1-silacyclohexane (2a).* A mixture of 0.56 g (2.26 mmol) of **4a** and 1 g (26.4 mmol) of lithium aluminum hydride in 100 ml of ether was refluxed for 10 h and hydrolyzed. After work-up, 0.26 g (1.54 mmol, 68% yield) of pure **2a** was obtained. The structure of **2a** was confirmed by its IR and NMR spectra, and retention time of GLC.

Preparation of trans-*4-t-Butyl-1-methyl-1-silacyclohexane (2b).* Reduction of 0.44 g (1.8 mmol) of **4b** with 1 g (26.4 mmol) of lithium aluminum hydride by refluxing in THF for 10 h gave 0.23 g (1.3 mmol 75% yield) of pure **2b**. The structure of **2b** was confirmed by its IR and NMR spectra, and retention time of GLC.

The authors are grateful to Toshiba Silicone Co. Ltd., for a gift of chlorosilanes.

References

1) L. H. Sommer and C. L. Frye, *J. Am. Chem. Soc.*, **81**, 1013 (1959).
2) L. H. Sommer, "Stereochemistry, Mechanism and Silicon," McGraw-Hill, New York (1965).
3) a) C. Eaborn and O. W. Steward, *Proc. Chem. Soc.*, **1963**, 59; b) C. Eaborn and O. W. Steward, *J. Chem. Soc.*, **1965**, 521; c) R. Baker, R. W. Bott, C. Eaborn, and P. W. Jones, *J. Organometal. Chem.*, **1**, 37 (1963).
4) a) A. G. Brook and C. M. Warner, *Tetrahedron Lett.*, **1962**, 815; b) A. G. Brook and W. W. Limburg, *J. Am. Chem. Soc.*, **85**, 832 (1963).
5) L. H. Sommer, L. A. Ulland, and G. A. Parker, *J. Am. Chem. Soc.*, **94**, 3469 (1972) and previous papers.
6) a) R. Corriu and G. Royo, *J. Organometal. Chem.*, **14**, 291 (1968); b) R. Corriu and J. Masse, *Bull. Soc. Chim. Fr.*, 3491 (1969).
7) D. N. Roak and L. H. Sommer, *J. Am. Chem. Soc.*, **95**, 969 (1973).
8) a) C. Eaborn, *Pure Appl. Chem.*, **19**, 375 (1969); b) R. O. C. Norman and R. Taylor, "Electrophilic Substitution in Benzenoid Compounds," Elsevier (1965).
9) H. Sakurai and A. Hosomi, *J. Am. Chem. Soc.*, **93**, 1709 (1971).
10) H. Sakurai, M. Murakami, and M. Kumada, *Bull. Chem. Soc. Jpn.*, **41**, 1973 (1968).
11) H. Sakurai, "Free Radicals," Vol. 2, ed. by J. K. Kochi, John Wiley, New York, N. Y. (1973) Chap. 25.
12) A preliminary account of part of this work has been reported: H. Sakurai and M. Murakami, *J. Am. Chem. Soc.*, **94**, 5080 (1972).
13) S. Winstein and N. J. Holness, *J. Am. Chem. Soc.*, **77**, 5562 (1955).
14) C. R. Johnson and D. McCants, Jr., *J. Am. Chem. Soc.*, **87**, 1109 (1965).
15) R. West, *J. Am. Chem. Soc.*, **76**, 6015 (1954).
16) L. M. Jackman and S. Sternhell, "Application of Nuclear Magnetic Resonance Spectroscopy in Organic Chemistry," 2nd ed., Pergamon Press, Elmsform, New York (1969) Chap. 3—8.
17) a) L. H. Sommer, C. L. Frye, C. A. Parker, and K. W. Michael, *J. Am. Chem. Soc.*, **86**, 3271 (1964); b) L. H. Sommer, W. D. Korte, and P. G. Rodewald, *ibid.*, **89**, 862 (1967); see also Ref. 2.
18) a) H. Sakurai, M. Murakami, and M. Kumada, *J. Am. Chem. Soc.*, **91**, 519 (1969); b) C. H. Sommer and L. A. Ulland, *J. Org. Chem.*, **37**, 3837 (1972).
19) L. Schmerling, *J. Am. Chem. Soc.*, **69**, 1121 (1947).
20) H. Sakurai and M. Murakami, *Org. Prep. Proc. Int.*, **5**, 1 (1973).
21) R. G. Jones and H. Gilman, *Org. React.*, Vol. VI, John Wiley and Sons, Inc., New York (1951) p. 355.

Syntheses of 2-Amino-2,3-dideoxy-L- and -D-Ribohexose by Utilizing an O→N Acetyl Migration

Tetsuro YAMASAKI,* Yutaka KUBOTA,* Tsutomu TSUCHIYA, and Sumio UMEZAWA

Institute of Bioorganic Chemistry, 1614 Ida, Nakahara-ku, Kawasaki 211
**Department of Applied Chemistry, Faculty of Engineering, Keio University, Hiyoshi, Yokohama 223*

(Received June 10, 1976)

2-Amino-2,3-dideoxy-L- and -D-ribohexose ($\mathbf{1}_L$ and $\mathbf{1}_D$) were synthesized from 2-amino-2-deoxy-L- and -D-glucose, respectively, through a reaction sequence which involves 3-O→2-N acetyl migration of methyl 3,4,6-tri-*O*-acetyl-2-amino-2-deoxy-β-L- and -D-glucopyranoside ($\mathbf{3}_L$ and $\mathbf{3}_D$). A preparative method of methyl 4,6-di-*O*-acetyl-2-amino-2-deoxy-β-D-glucopyranoside ($\mathbf{11}_D$) is given.

In a program directed towards the synthesis of deoxy variants of streptomycin, Sano *et al.*[1] reported a novel method for the preparation of 2-amino-2,3-dideoxy-L-ribohexose ($\mathbf{1}_L$) from 2-amino-2-deoxy-L-glucose achieved without protection of the anomeric hydroxyl group throughout the reaction sequence. In the present paper we wish to report an alternative method for the preparation of $\mathbf{1}_L$ from 2-amino-2-deoxy-L-glucose by utilizing O→N acetyl migration. The same synthesis for the D-sugar ($\mathbf{1}_D$) is also described.

Results and Discussion

2-Amino-2-deoxy-L-glucose ($\mathbf{2}_L$) was prepared from L-arabinose by the method of Kuhn and Kirschenlohr.[2] Treatment of the hydrochloride of $\mathbf{2}_L$ with acetyl bromide followed by treatment with methanol according to the method for the corresponding D-sugar described by Irvine *et al.*[3] and Wolfrom and Shen Han[4] gave methyl 3,4,6-tri-*O*-acetyl-2-amino-2-deoxy-β-L-glucopyranoside ($\mathbf{3}_L$) hydrobromide. Treatment of the hydrobromide with 5% aqueous sodium carbonate gave the free base ($\mathbf{3}_L$) in 93% yield, O→N acetyl migration being successfully avoided. Fodor and Oetvoes[5] obtained the corresponding D-sugar base from its hydrobromide by treatment with sodium methoxide in chloroform in 97% yield.

The regiospecific removal of the acetyl group at C-3 of $\mathbf{3}_L$ by utilizing O→N acetyl migration was studied in detail. Fodor *et al.*[5,6] reported that the behavior of ethyl 3,4,6-tri-*O*-acetyl-2-amino-2-deoxy-β-D-glucoside in organic solvents (methanol, ethanol, and acetone) is complicated and that O→N acetyl migration or deacetylation occurs as the main reaction, depending on the reaction conditions (solvents, their dryness, and temperature). We further attempted the O→N acetyl migration of $\mathbf{3}_L$ in pyridine,[7] toluene, and diglyme, but without success. However, we found that, with *N,N*-dimethylformamide (DMF) at reflux temperature, $\mathbf{3}_L$ was converted into the migration product, methyl 2-acetamido-4,6-di-*O*-acetyl-2-deoxy-β-L-glucopyranoside ($\mathbf{4}_L$) in a high yield (72%).

It should be noted that, in ethanol at room temperature, deacetylation at C-3 of methyl 3,4,6-tri-*O*-acetyl-2-amino-2-deoxy-β-D-glucopyranoside ($\mathbf{3}_D$) takes place almost completely to afford methyl 4,6-di-*O*-acetyl-2-amino-2-deoxy-β-D-glucopyranoside ($\mathbf{11}_D$) in a 93% yield, in accord with the result reported by Fodor and Oetvoes.[5]

Tosylation or mesylation of $\mathbf{4}_L$ was readily achieved by the conventional method to give the 3-*O*-tosylate ($\mathbf{5}_L$) or 3-*O*-mesylate ($\mathbf{6}_L$). Iodination with sodium iodide in DMF gave the 3-iodo derivative ($\mathbf{7}_L$), which was then hydrogenolyzed with Raney nickel to afford methyl 2-acetamido-4,6-di-*O*-acetyl-2,3-dideoxy-β-L-ribohexopyranoside ($\mathbf{8}_L$). To confirm the structure, $\mathbf{8}_L$ was de-*O*-acetylated and the *N*-acetyl derivative ($\mathbf{9}_L$) was acetonated with 2,2-dimethoxypropane to give $\mathbf{10}_L$. The position of the isopropylidene group in the derivative was determined by PMR studies; the large coupling constants of H-3_{ax} ($J=\approx 11$ Hz) indicated the 3-deoxy-4,6-*O*-isopropylidene, not 4-deoxy-3,6-*O*-isopropylidene, structure.

Finally acid hydrolysis of $\mathbf{8}_L$ was carried out in 1 M hydrochloric acid at 110 °C to afford 2-amino-2,3-dideoxy-L-ribohexose ($\mathbf{1}_L$), which shows a specific rotation numerically compatible with that of D-isomer[8] but opposite in direction.

2-Amino-2,3-dideoxy-D-ribohexose ($\mathbf{1}_D$) and the intermediates of D-series were prepared in a similar manner to that described in the preparation of the corresponding L-series.

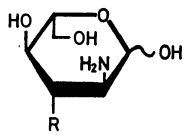

1L R = H
2L R = OH

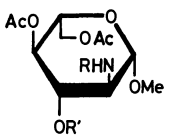

3L R = H, R' = Ac
4L R = Ac, R' = H
5L R = Ac, R' = Ts
6L R = Ac, R' = Ms

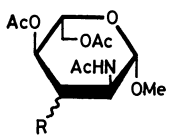

7L R = I
8L R = H

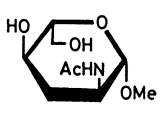

9L

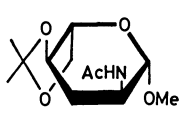

10L

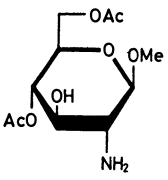

11D

Experimental

General. Melting points were determined on a Kofler block and are uncorrected. Infrared spectra were recorded for potassium bromide pellets with a Hitachi Model 285 grating

infrared spectrophotometer. PMR spectra were recorded a 60 and 100 MHz with Hitachi R-24A and Varian XL-100 spectrometers. Thin layer chromatography was performed on Wakogel B-5 with sulfuric acid spray for detection. For column chromatography, silica gel (Wakogel C-200) was used.

*Methyl 3,4,6-Tri-*O*-acetyl-2-amino-2-deoxy-β-*L*- and* D*-glucopyranoside (**3**$_L$ and **3**$_D$).* Acetyl bromide (15.4 ml) was added to a well dried (dried *in vacuo* at 60 °C for 2 h in the presence of P_2O_5) 2-amino-2-deoxy-L-glucose (**2**$_L$) hydrochloride (4.8 g), and the mixture in a sealed tube was allowed to stand at room temperature for 3 days. Deposition of deep-brown needles was observed. The reaction mixture was concentrated *in vacuo*. To the resulting solid were added methanol (200 ml) and pyridine (20 ml) and the solution was allowed to stand for 30 min at room temperature. After concentration of the solution, the residue hydrobromide was suspended in chloroform (250 ml) and the mixture was washed with 5% aqueous sodium carbonate and water. The chloroform layer was dried over sodium sulfate, and concentrated to give crystals (6.3 g, 93%). Recrystallization from hexane–chloroform gave needles of **3**$_L$; mp 152.5—153 °C, $[\alpha]_D^{24}$ −17.5° (*c* 1, methanol). IR: 1750 (OAc), 1605 (NH_2) cm^{-1}. PMR ($CDCl_3$): δ 1.40 (2H s, disappeared on deuteration), 2.05 (3H s, Ac), 2.10 (6H s, Ac), 2.95 (1H q, *J*=8 and 10.5 Hz, H-2), 3.61 (3H s, OCH_3), 4.0—4.55 (2H double q, *J*=3, 4.5, and 12 Hz, H-6,6′), 4.21 (1H d, *J*=8 Hz, H-1), 4.99—5.17 (2H m, H-3, 4). Irradiation at δ 5.1 caused the quartet at 2.95 to collapse to a doublet. Irradiation at δ 2.95 caused the doublet at δ 4.21 to collapse to a singlet.

Found: C, 48.84; H, 6.56; N, 4.29%. Calcd for $C_{13}H_{21}NO_8$: C, 48.90; H, 6.63; N, 4.39%.

3$_D$: mp 151—152 °C (lit,[5] 152 °C), $[\alpha]_D^{27}$ +15° (*c* 1, methanol) (lit,[5] +10° (methanol)).

Found: C, 49.20; H, 6.58; N, 4.14%.

*Methyl 2-Acetamido-4,6-di-*O*-acetyl-2-deoxy-β-*L*- and* D*-glucopyranoside (**4**$_L$ and **4**$_D$).* A solution of **3**$_L$ (4.30 g) in dry DMF (86 ml) was refluxed for 4 h. On being subjected to TLC with chloroform–acetone (1: 1), **3**$_L$ (R_f 0.5) almost disappeared and **4**$_L$ (R_f 0.25) appeared. Concentration of the solution under reduced pressure gave a residue, which was dissolved in methanol (200 ml). The solution was decolorized with charcoal and concentrated to give a solid, which was recrystallized from hexane–chloroform to give needles (2.36g). Concentration of the mother liquor gave a syrup, which was chromatographed on a silica gel column with chloroform–acetone (2: 1) as a developer to give **4**$_L$ (720 mg) and **3**$_L$ (111 mg). Total yield of **4**$_L$ was 72%. Mp 172.5—173 °C, $[\alpha]_D^{24}$ +35° (*c* 1, methanol). IR: 3430 (OH), 1740 (OCO); 1620, 1560 (NHCO) cm^{-1}. PMR ($(CD_3)_2SO$): δ 1.81 (3H s, Ac), 2.02 and 2.03 (each 3H s, Ac), 3.33 (3H s, OCH_3), 3.35—3.75 (3H m, H-2,3,5), 3.85—4.25 (2H double q, *J*=3, 5, and 12 Hz, H-6,6), 4.35 (1H d, *J*=8 Hz, H-1), 4.63 (1H q, *J*=8 and 10 Hz, H-4), 5.28 (1H d, *J*=5 Hz, disappeared on deuteration), 7.75 (1H d, *J*=8 Hz, disappeared on deuteration). Irradiation at δ 3.5 caused the doublets at δ 4.35, 5.28, and 7.75 collapsed to singlets, respectively.

Found: C, 48.93; H, 6.58; N, 4.25%. Calcd for $C_{13}H_{21}NO_8$: C, 48.89; H, 6.64; N, 4.39%.

4$_D$: mp 173—173.5 °C, $[\alpha]_D^{27}$ −38° (*c* 1, methanol).

Found: C, 48.98; H, 6.50; N, 4.33%.

*Methyl 2-Acetamido-4,6-di-*O*-acetyl-2-deoxy-3-*O*-tosyl-β-*L*- and* D*-glucopyranoside (**5**$_L$ and **5**$_D$).* *p*-Toluenesulfonyl chloride (840 mg) was added to a cold solution of well dried **4**$_L$ (700 mg) in dry pyridine (14 ml), and the solution was allowed to stand at −10 °C overnight. The solution showed a single spot at R_f 0.57 on being subjected to TLC with chloroform–tacetone (2: 1). After addition of water (0.2 ml), the mixture was concertrated and coevaporated with toluene. The residue was extracted with ethyl acetate. The solution was washed successively with 0.4 M potassium hydrogensulfate, aqueous sodium hydrogencarbonate, and water, dried over sodium sulfate and concentrated. The residue was recrystallized from hexane–ethyl acetate to give needles, 638 mg (61%); mp 137—138.5 °C (dec), $[\alpha]_D^{24}$ +18° (*c* 1, methanol). PMR ($CDCl_3$): δ 1.91 (6H s, Ac), 2.06 (3H s, Ac), 2.46 (3H s, $C_6H_4CH_3$), 3.54 (3H s, OCH_3), 4.90 (1H d, *J*=8.5 Hz, H-1). 5—5.5 (2H m, H-3,4).

Found: C, 50.57; H, 5.73; N, 2.71; S, 6.91%. Calcd for $C_{20}H_{27}NO_{10}S$: C, 50.73; H, 5.75; N, 2.96; S, 6.77%.

5$_D$: mp 138—139 °C (dec), $[\alpha]_D^{27}$ −22° (*c* 1, methanol).

Found: C, 50.87; H, 5.79; N, 2.74; S, 6.61%.

*Methyl 2-Acetamido-4,6-di-*O*-acetyl-2-deoxy-3-*O*-mesyl-β-*L*- and* D*-glucopyranoside (**6**$_L$ and **6**$_D$).* Compounds **4**$_L$ and **4**$_D$ were treated as described above for **5**$_L$ using methanesulfonyl chlororide instead of *p*-toluenesulfonyl chloride to give **6**$_L$ and **6**$_D$ (~80%), respectively.

6$_L$: mp 157—158 °C (dec), $[\alpha]_D^{23}$ +20° (*c* 1, methanol).

Found: C, 42.47; H, 5.65; N, 3.23; S, 8.17%. Calcd for $C_{14}H_{23}NO_{10}S$: C, 42.31; H, 5.83; N, 3.52; S, 8.07%.

6$_D$: mp 158—159.5°C (dec), $[\alpha]_D^{27}$ −20° (*c* 1, methanol).

Found: C, 42.25; H, 5.65; N, 3.35; S, 8.24%.

*Methyl 2-Acetamido-4,6-di-*O*-acetyl-2,3-dideoxy-3-iodo-β-*L*- and* D*-gluco and/or allopyranoside (**7**$_L$ and **7**$_D$).* To a solution of **5**$_L$ (1.01 g) in dry DMF (20 ml) was added dry sodium iodide (10 g) and after displacement of the air in the reaction vessel with nitrogen, the mixture was heated in a tightly stoppered vessel at 100 °C for 2 h. Chloroform (200 ml) was added and the mixture was filtered. The organic layer was washed successively with water, aqueous 20% sodium thiosulfate, and water, and dried over sodium sulfate. The solution showed, on being subjected to TLC with chloform–ether (1: 1), a single spot at R_f 0.15 (*cf.* **5**$_L$: R_f 0.1). Concentration of the solution gave a solid of **7**$_L$, 677 mg (74%); mp 186—188 °C (dec), $[\alpha]_D^{24}$ +5° (*c* 1, methanol).

Found: C, 36.35; H, 4.63; N, 3.20; I, 29.20%. Calcd for $C_{13}H_{20}INO_7$: C, 36.38; H, 4.70; N, 3.26; I, 29.51%.

7$_D$: mp 184—186 °C (dec), $[\alpha]_D^{26}$ −7.5° (*c* 1, methanol).

Found: C, 36.75; H, 4.80; N, 2.95; I, 29.24%.

*Methyl 2-Acetamido-4,6-di-*O*-acetyl-2,3-dideoxy-β-*L*- and* D*-ribohexopyranoside (**8**$_L$ and **8**$_D$).* To a solution of **7**$_L$ (582 mg) in aqueous dioxane (1: 9, 10 ml) was added sodium hydrogencarbonate (40 mg) and the mixture was hydrogenated over Raney nickel under pressure (50 lb/in²) at room temperature for 3 h. Filtration followed by evaporation gave a syrup, which was chromatographed on a silica gel column with ethyl acetate to give a solid of **8**$_L$, 298 mg (72%), mp 150—150.5 °C, $[\alpha]_D^{24}$ +43° (*c* 1, methanol). PMR (DMF-d_7): δ 1.60 (1H q, *J*=≈11.5 Hz, H-3_{ax}), 1.88 (3H s, Ac), 2.07 (6H s, AcO), 2.37 (1H double t, *J*=5 and 12 Hz, H-3_{eq}), 3.43 (3H s, OCH_3), octet centered at 4.22 (q in higher field, *J*=3 and 12 Hz; q in lower field, *J*=5 and 12 Hz, H-6,6′), 4.49 (1H d, *J*=8 Hz, H-1), 4.72 (1H octet, *J*=5, 10, and 11 Hz, H-4), 7.97 (1H broad d, *J*=≈8 Hz, NH). Irradiation of H-4 caused the signal of H-3_{ax} and H-3_{eq} to collapse to a triplet (*J*=≈11 Hz) and a quartet (*J*=5 and 12 Hz), respectively.

Found: C, 51.65; H, 6.92; N, 4.53%. Calcd for $C_{13}H_{21}NO_7$: C, 51.48; H, 6.98; N, 4.62%.

8$_D$: mp 149—149.5 °C, $[\alpha]_D^{27}$ −44° (*c* 1, methanol).

Found: C, 51.41; H, 6.91; N, 4.53%.

*Methyl 2-Acetamido-2,3-dideoxy-β-*L*-ribohexopyranoside (**9**$_L$).* To a solution of **8**$_L$ (64 mg) in dry methanol (2 ml) was added a piece of sodium metal. After 5 min, the solution was

neutralized with Amberlite CG 50 (H form, pretreated with methanol) and concentrated. The residue was recrystallized from ethanol–ether to give needles of $\mathbf{9}_L$, 39 mg (85%); mp 152—153 °C, $[\alpha]_D^{23}$ +58° (*c* 1, methanol). IR: 1560, 1650 cm^{-1}. PMR ($CDCl_3$): δ 1.92 (3H s, Ac), 4.28 (1H d, J=8 Hz, H-1).

Found: C, 49.09; H, 7.73; N, 6.16%. Calcd for $C_9H_{17}NO_5$: C, 49.31; H, 7.82; N, 6.39%.

*Methyl 2-Acetamino-2,3-dideoxy-4,6-O-isopropylidene-β-L-ribo-hexopyranoside (**10**$_L$).* To a solution of $\mathbf{9}_L$ (27 mg) in DMF (1 ml) were added 2,2-dimethoxypropane (0.1 ml), molecular sieves 5A, and a trace amount of *p*-toluenesulfonic acid and the solution was allowed to stand at 25 °C for 3 h. The solution showed, on being subjected to TLC with chloroform–methanol (5: 1), a single spot at R_f 0.42 (*cf.* $\mathbf{7}_L$: R_f 0.1). After addition of triethylamine (0.1 ml), the mixture was filtered and concentrated. The residue was purified by passing through a short column of silica gel with chloroform–methanol (15: 1) to give a syrup, which, on standing, crystallized into prisms, 30 mg (95%); mp 148—149 °C, $[\alpha]_D^{23}$ +81° (*c* 1, methanol). PMR ($CDCl_3$): δ 1.41 and 1.50 (each 3H s, $C(CH_3)_2$), 1.54 (1H q, J=12 Hz, H-3_{ax}), 1.99 (3H s, Ac), 2.36 (1H double t, J=≈4.5×2 and 12 Hz, H-3_{eq}), 3.48 (3H s, OCH_3), 4.34 (1H d, J=8 Hz, H-1).

Found: C, 55.31; H, 7.97; N, 5.30%. Calcd for $C_{12}H_{21}NO_5$: C, 55.58; H, 8.16; N, 5.40%.

*2-Amino-2,3-dideoxy-L- and D-ribohexose (**1**$_L$ and **1**$_D$) Hydrochloride.* A solution of $\mathbf{8}_L$ (100 mg) in 1 M hydrochloric acid (2 ml) was heated at 110 °C for 2 h in the atmosphere of nitrogen in a sealed tube. Water (20 ml×2) was added to the reaction mixture which was then concentrated. To the concentrate (~0.5 ml) were added methanol and acetone to give a syrup, which was dissolved in methanol and decolorized with charcoal. The solution was concentrated to give a residue which was recrystallized from methanol–acetone to give needles of $\mathbf{1}_L$ hydrochloride, 31 mg. Another crop (15 mg) was obtained from the mother liquor. Total yield was 72%, mp 150—160 °C (gradually decomposes), $[\alpha]_D^{23}$ −49° (*c* 1, water, final value). R_f 0.30 (TLC with ethyl acetate–pyridine–acetic acid–water 5: 5: 1: 3) (*cf.* 2-amino-2-deoxy-L-glucose hydrochloride: R_f 0.27).

Found: C, 36.32; H, 6.94; N, 6.89; Cl, 17.81%. Calcd for $C_6H_{13}NO_4 \cdot HCl$: C, 36.10; H, 7.07; N, 7.02; Cl, 17.76%.

$\mathbf{1}_D$: $[\alpha]_D^{23}$ +43° (*c* 0.3, water, final value) (lit,[8] +43.9° (water)).

*Methyl 4,6-Di-O-acetyl-2-amino-2-deoxy-β-D-glucopyranoside (**11**$_D$).* A solution of $\mathbf{3}_D$ (1.83 g) in ethanol (200 ml) was kept at room temperature for 2 days. Concentration of the solution gave a residue, which was recrystallized from hexane–chloroform to give plates, 1.71 g (93%), mp 138—139 °C, $[\alpha]_D^{23}$ −37° (*c* 1, methanol). PMR ($CDCl_3$): δ 2.08 and 2.13 (each 3H s, Ac), 2.35 (3H s, disappeared on deuteration, NH_2 and OH), 2.75 (1H q, J=8 and 10 Hz, H-2), 3.48 (1H t, J=10 Hz, H-3), 3.55 (3H s, OCH_3), 3.65 (1H m, H-5), 4.12 (1H d, J=8 Hz, H-1), 4—4.55 (2H double q, J=3, 4.5 and 12 Hz, H-6,6′), 4.87 (1H t, J=10 Hz, H-4). Irradiation of H-2 caused the signals of H-1 (δ 4.12) and H-3 (δ 3.48) to collapse to a singlet and a doublet, respectively, but the signals of H-4 (δ 4.87) remained unchanged.

Found: C, 47.35; H, 6.62; N, 4.76%. Calcd for $C_{11}H_{19}NO_7$: C, 47.65; H, 6.91; N, 5.05%.

References

1) H. Sano, T. Tsuchiya, Y. Ban, and S. Umezawa, *Bull. Chem. Soc. Jpn.*, **49**, 313 (1976).
2) R. Kuhn and W. Kirschenlohr, *Justus Liebigs Ann. Chem.*, **600**, 115 (1956).
3) J. C. Irvine, D. McNicoll, and A. Hynd, *J. Chem. Soc.*, **99**, 250 (1911).
4) M. L. Wolfrom and T. M. Shen Han, *J. Org. Chem.*, **26**, 2145 (1961).
5) G. Fodor and L. Oetvoes, *Chem. Ber.*, **89**, 701 (1956).
6) G. Fodor, F. Letourneau, and N. Mandava, *Can. J. Chem.*, **48**, 1465 (1970).
7) T. Kurisu, M. Yamashita, Y. Nishimura, T. Miyake, T. Tsuchiya, and S. Umezawa, *Bull. Chem. Soc. Jpn.*, **49**, 285 (1976).
8) T. Oda, T. Mori, and Y. Kyotani, *J. Antibiot.*, **24**, 503 (1971).

Aminocyclitols. 34. Synthesis of Inosadiamine-1,4 Derivatives

Kinnichi TADANO, Takaaki SHIRATORI, and Tetsuo SUAMI*

Department of Applied Chemistry, Faculty of Engineering, Keio University, Hiyoshi, Yokohama 223

(Received June 19, 1976)

Three new inosadiamine-1,4 derivatives have been prepared by nitromethane cyclization of a dialdehyde obtained by periodate oxidation of 1,4-di-*O*-methyl-(1,2,3,4,5/0)-5-acetamido-1,2,3,4-cyclopentanetetrol. The cyclization product was catalytically hydrogenated and subsequently acetylated to give three inosadiamine derivatives. Their structures were established by PMR spectra as *myo*-2,5, *epi*-1,4, and *cis*-inosadiamine-1,4 derivatives.

In connection with the results given in the preceding paper,[1] we have prepared three inosadiamine-1,4-derivatives: 1,3-di-*O*-methyl-*myo*-inosadiamine-2,5 (**6**), 3,5-di-*O*-methyl-*epi*-inosadiamine-1,4 (**7**) and 3,5-di-*O*-methyl-*cis*-inosadiamine-1,4 derivatives (**8**), by the nitromethane cyclization of dialdehyde (**5**).

When the starting material 2,3-*O*-cyclohexylidene-1,4-di-*O*-mesyl-(1,4/2,3,5)-5-acetamido-1,2,3,4-cyclopentanetetrol[2] (**1**) was subjected to displacement of the sulfonyloxy groups by heating in water in the presence of sodium acetate, 2,3-*O*-cyclohexylidene-(1,2,3,4,5/0)-5-acetamido-1,2,3,4-cyclopentanetetrol (**2**) was obtained in 72% yield. *O*-Methylation of **2** afforded the 1,4-di-*O*-methyl derivative (**3**), which was further converted to 1,4-di-*O*-methyl-(1,2,3,4,5/0)-5-acetamido-1,2,3,4-cyclopentanetetrol (**4**) by hydrolysis. Oxidation of **4** by sodium metaperiodate yielded the dialdehyde (**5**) as a syrup. Cyclization of **5** with nitromethane in the presence of sodium methoxide gave deoxynitroinosamine derivatives, which were catalytically hydrogenated and subsequently acetylated. The product was purified by column chromatography to give the three products **6**, **7**, and **8**.

Results and Discussion

Since three new chiral centers are introduced in the products, it is possible for six diastereomers to occur in the reaction: *allo*-2,5, *cis*-1,4, *epi*-1,4, *epi*-3,6, *myo*-2,5 and *neo*-inosadiamine-2,5 derivative.

The PMR spectrum of **6** revealed three signals due to the four acetyl groups. Unequivocal distinction between the signal of an acetoxyl and that of an acetamido group was established by means of deuterioacetylation technique.[3] The two signals at δ 1.85 and 2.00 are attributable to the two acetamido groups and the signal at δ 2.04 is ascribed to the two equatorial acetoxyl groups.[4] The results are summarized in Table 1. The two methoxyl groups revealed their signal at δ 3.38 as a singlet. This indicates that these

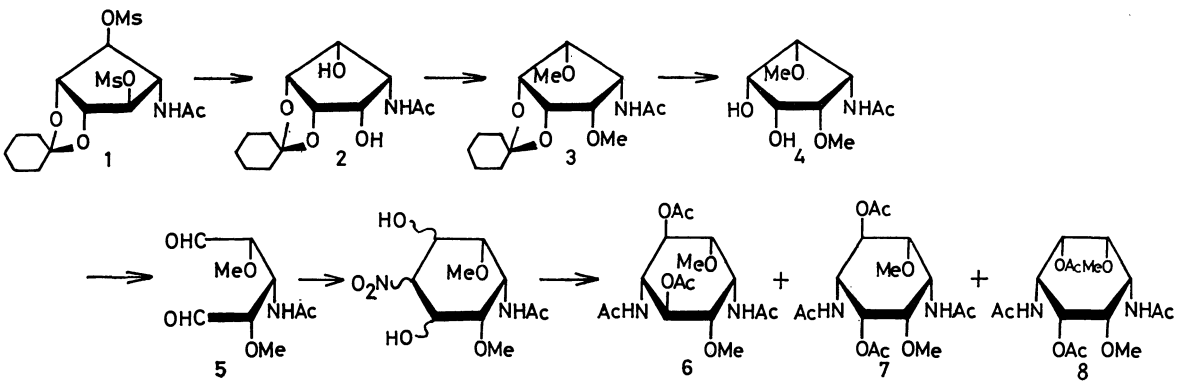

Scheme 1.

TABLE 1. CHEMICAL SHIFTS OF METHYL PROTONS IN DMSO-d_6

Compound	Acetamido		Acetoxyl		Methoxyl
	equatorial	axial	equatorial	axial	
6: *myo*-2,5	1.85 (3H)[a]	2.00 (3H)	2.04 (6H)		3.38 (6H)
12	1.84 (3H)	2.00 (3H)			3.34 (6H)
7: *epi*-1,4	1.87 (3H)	2.02 (3H)	2.05 (3H)	2.23 (3H)	3.38 (3H), 3.39 (3H)
13	1.87 (3H)	2.03 (3H)			3.40 (3H), 3.42 (3H)
8: *cis*-1,4	1.85 (3H)	2.02 (3H)	2.09 (6H)		3.51 (6H)
14	1.85 (3H)	2.02 (3H)			3.51 (6H)

a) Peak positions are given in δ values, the number of protons being given in parentheses.

* To whom correspondence should be addressed.

methoxyl groups are located in an equivalent state. Hence, *myo*-2,5 and *cis*-1,4 configurations are conceivable. The signal of the two ring protons on the carbons which bear the acetoxyl groups appeared at δ 5.35 (J=10 Hz) as a triplet, indicating that *trans* configurations exsist between the acetoxyl and the methoxyl groups, and between the acetoxyl and the newly introduced acetamido groups. Furthermore, the two ring protons on the carbons which bear the methoxyl groups revealed their signal at δ 3.62 as double doublet (J=10 and 3 Hz), suggesting a *cis*-configuration between the methoxyl and another acetamido group. Thus, the configuration of *myo*-inosadiamine-2,5 was established for **6**.

The PMR spectrum of **7** revealed four signal at δ 1.87, 2.02, 2.05, and 2.23 for the four acetyl groups. The first two peaks are attributed to an equatorial and an axial acetamido group, respectively, the last two peaks to an equatorial and an axial acetoxyl group, respectively. The two methoxyl groups showed their signals at δ 3.38 and 3.39, indicating a nonequivalent conformation of the surroundings. Thus, **7** was assigned to be *epi*-inosadiamine-1,4 derivative.

The PMR spectrum of **8** revealed two signals at δ 1.85 and 2.02 for the two acetamido groups, and a signal at δ 2.09 for the two acetoxyl groups. The signal of the two methoxyl groups appeared at δ 3.51. These data indicate a symmetrical structure of **8**, *cis*-inosadiamine-1,4 being proposed for the configuration.

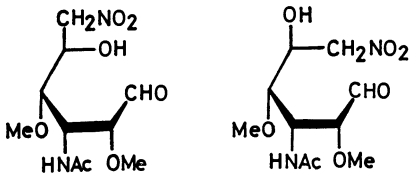

D-*allo* L-*talo*

Scheme 2.

The analogous reaction mechanism[1,5] is proposed for the present nitromethane cyclization. That is the initial step of the reaction is an addition between nitromethane and one of the two aldehyde groups of **5**, giving two diastereomers: D-*allo* and L-*talo* type intermediates. The second step of the reaction is an intramolecular cyclization of the intermediates to give *cis*-1,4 and *epi*-1,4 from the D-*allo*, and *epi*-1,4 and *myo*-2,5 from the L-*talo* intermediate.

Experimental

All the melting points were determined in capillary tubes, and are uncorrected. Solutions were evaporated under reduced pressure. De-*O*-acetylation was carried out in methanolic ammonia at ambient temperature. PMR spectra were measured at 60 MHz on a Varian A-60D spectrometer in dimethyl-d_6 sulfoxide with tetramethylsilane as an internal standard. The peak positions are given in δ values.

2,3-O-Cyclohexylidene-(1,2,3,4,5/0)-5-acetamido-1,2,3,4-cyclopentanetetrol (2). 2,3-*O*-Cyclohexylidene-1,4-di-*O*-mesyl-(1,4/2,3,5)-5-acetamido-1,2,3,4-cyclopentanetetrol[2] (**1**, 20.0 g) and sodium acetate (97.0 g) were heated in boiling water (300 ml) under reflux for 16 h. After cooling to ambient temperature, the solution was repeatedly extracted with chloroform. The resulting solution was dried over anhydrous sodium sulfate and evaporated. The residue was recrystallized from ethyl acetate to give 9.20 g (72%) of **2**, mp 170—171 °C.

Found: C, 57.80; H, 7.81; N, 5.11%. Calcd for $C_{13}H_{21}NO_5$: C, 57.55; H, 7.80; N, 5.16%.

1,4-Di-O-methyl-(1,2,3,4,5/0)-5-acetamido-1,2,3,4-cyclopentanetetrol (4). A mixture of **2** (10.8 g), methyl iodide (11.0 ml) and silver oxide (22.0 g) in *N,N*-dimethylformamide (100 ml) was stirred for 10 h in the dark, and an insoluble matter was removed by filtration. The filtrate was evaporated to give 2,3-*O*-cyclohexylidene-1,4-di-*O*-methyl-(1,2,3,4,5/0)-5-acetamido-1,2,3,4-cyclopentanetetrol (**3**) as a syrup (13.4 g). PMR ($CDCl_3$) δ 1.99 (s, 3, NAc), 3.40 (s, 6, $2OCH_3$).

Compound **3** (13.4 g) was heated under reflux for 2 h in 0.1 M hydrochloric acid (105 ml), and the solution was evaporated to give a crystalline residue (10.1 g). Recrystallization from benzene afforded 6.28 g (72% from **2**) of **4**, mp 123—125 °C.

Found: C, 49.03; H, 7.60; N, 6.17%. Calcd for $C_9H_{17}NO_5$: C, 49.30; H, 7.82; N, 6.39%.

*3-Acetamido-2,4-di-O-methyl-3-deoxy-*ribo*-pentodialdose (5).* Compound **4** (1.50 g) was added with mechanical agitation under ice cooling to a solution of sodium metaperiodate (1.61 g) in cold water (20 ml). The solution was left to settle overnight at ambient temperature. After being neutralized with sodium hydrogen carbonate, the solution was filtered. The filtrate was evaporated to give **5** as a crude residue. The product was used for a successive reaction without purification.

Nitromethane Cyclization of 5. To a solution of **5** (1.48 g) and nitromethane (0.74 ml) in methanol (6.0 ml), 1.4 M methanolic sodium methoxide (10 ml) was added under ice cooling with agitation. After being left to settle in a refrigerator overnight, the solution was evaporated. The residue was hydrogenated in 20% aqueous acetic acid (12 ml) in the presence of Raney nickel T-4[6] at 3.4 kg/cm^2 of hydrogen atmosphere with a Parr apparatus for 16 h. After the catalyst was removed by filtration, the filtrate was evaporated. The residue was acetylated with acetic anhydride in pyridine in the usual manner. The product was dissolved in 10 ml of benzene–ethanol (4: 1, v/v), and the solution was stored in a refrigerator for a few days to give 244 mg of tetra-*N,O*-acetyl-3,5-di-*O*-methyl-*cis*-inosadiamine-1,4 (**8**) as crystals.

The mother liquor was evaporated, and the residue was fractionated on a silica gel column (28×380 mm) in benzene–ethanol (5: 1, v/v). Each aliquot was monitored on TLC with the same solvent. The fractions (R_f 0.37 on TLC) were combined and evaporated to give 309 mg (12% from **4**) of tetra-*N,O*-acetyl-1,3-di-*O*-methyl-*myo*-inosadiamine-2,5 (**6**). A part of the product was recrystallized from ethanol to give an analytical sample, mp 203—205 °C.

Found: C, 51.50; H, 6.93; N. 7.35%. Calcd for $C_{16}H_{26}N_2O_8$: C, 51.33; H, 7.00; N, 7.48%.

The fractions (R_f 0.30 on TLC) gave 417 mg (16% from **4**) of tetra-*N,O*-acetyl-3,5-di-*O*-methyl-*epi*-inosadiamine-1,4 (**7**) as a syrup.

Found: C, 51.14; H, 6.88; N, 7.34%. Calcd for $C_{16}H_{26}N_2O_8$: C, 51.33; H, 7.00; N, 7.48%.

The fractions (R_f 0.22 on TLC) gave another crop (202 mg) of **8**. The total yield (446 mg) was 17% from **4**. A part of the product was recrystallized from benzene–ethanol (4: 1, v/v) to give an analytical sample, mp 290—292 °C.

Found: C, 51.06; H, 6.91; N, 7.33%. Calcd for $C_{16}H_{26}N_2O_8$: C, 51.33; H, 7.00; N, 7.48%.

*2,5-Di-*N*-acetyl-1,3-di-*O*-methyl-*myo*-inosadiamine-2,5 (9).*

Compound **6** (180 mg) was de-*O*-acetylated, and the product was recrystallized from ethanol to give 76 mg (54%) of **9**, mp 240—242 °C.

Found: C, 49.76; H, 7.57; N, 9.48%. Calcd for $C_{12}H_{22}N_2O_6$: C, 49.65; H, 7.64; N, 9.65%.

A 50 mg portion of **9** was acylated with acetic anhydride-d_6 (0.2 ml) in pyridine (1 ml), and the product was recrystallized from ethyl acetate to give 35 mg (53%) of 4,6-di-*O*-acetyl-d_3 derivative (**12**), mp 203—205 °C.

1,4-Di-N-*acetyl-3,5-di*-O-*methyl*-epi-*inosadiamine-1,4 (**10**).* Compound **7** (340 mg) was de-*O*-acetylated, and the product was recrystallized from ethyl acetate–ethanol (10: 1, v/v) to give 210 mg (80%) of **10**, mp 207—208°C.

Found: C, 49.45; H, 7.42; N, 9.76%. Calcd for $C_{12}H_{22}N_2O_6$: C, 49.65; H, 7.64; N, 9.65%.

An 80 mg portion of **10** was acylated with acetic anhydride-d_6 in pyridine, and the product was purified on a silica gel column in benzene–ethanol (5: 1, v/v) to give 83 mg (79%) of 2,6-di-*O*-acetyl-d_3 derivative (**13**) as a syrup.

1,4-Di-N-*acetyl-3,5-di*-O-*methyl*-cis-*inosadiamine-1,4 (**11**).* Compound **8** (400 mg) was de-*O*-acetylated, and the product was recrystallized from methanol to give 188 mg (61%) of **11**, mp above 295 °C.

Found: C, 49.40; H, 7.54; N, 9.48%. Calcd for $C_{12}H_{22}N_2O_6$: C, 49.65; H, 7.64; N, 9.65%.

A 50 mg portion of **11** was acylated with acetic anhydride-d_6 in pyridine, and the product was recrystallized from ethanol to give 32 mg (49%) of 2,6-di-*O*-acetyl-d_6 derivative (**14**), mp 290—292 °C.

References

1) T. Suami, K. Tadano, and S. Horiuchi, *Bull. Chem. Soc. Jpn.*, **48**, 2895 (1975).

2) T. Suami, Y. Sakota, K. Tadano, and S. Nishiyama, *Bull. Chem. Soc. Jpn.*, **44**, 222 (1971).

3) D. Horton, J. B. Hughes, J. S. Jewell, K. D. Philips, and W. N. Turner, *J. Org. Chem.*, **32**, 1073 (1967); D. Horton, W. E. Mast, and K. D. Philips, *ibid.*, **32**, 1471 (1967); T. Suami, S. Ogawa, Y. Naito, and H. Sano, *ibid.*, **33**, 2831 (1968).

4) F. W. Lichtenthaler and P. Emig, *Carbohyd. Res.*, **7**, 121 (1968).

5) J. Kovář and H. H. Bear, *Carbohyd. Res.*, **39**, 19 (1975).

6) S. Nishimura, *Bull. Chem. Soc. Jpn.*, **32**, 61 (1959).

New Sesquiterpene Lactones of Eremophilane-Type from *Ligularia Fauriei* (Fr.) Koidz.[1]

Yoshihiko Moriyama and Takeyoshi Takahashi

Department of Chemistry, Faculty of Science, The University of Tokyo, Bunkyo-ku, Tokyo 113

(Received June 21, 1976)

Two new sesquiterpene lactones of eremophilane-type were isolated from *Ligularia Fauriei* (Fr.) Koidz., and their structures including absolute stereochemistry were shown to be 8β-hydroxyeremophil-7(11)-ene-12,8α;14β,6α-diolide (**1**) and eremophil-7(11)-ene-12,8α;14β,6α-diolide (**2**), respectively. The isolation of the two known lactones, 6β,8β-dihydroxyeremophil-7(11)-en-12,8α-olide (**3**) and 6β-hydroxyeremophil-7(11)-en-12,8α-olide (**4**), is also described. The photosensitized autoxidation of the known furanoeremophilan-14β,6α-olide (**5**) gave **1** and 8β-methoxyeremophil-7(11)-ene-12,8α;14β,6α-diolide (**18**).

During chemical investigation on plants of the genus *Ligularia* (Compositae) and related plants,[2] two new sesquiterpene lactones were isolated from *Ligularia Fauriei* (Fr.) Koidz. In the present communication, the structure determination leading to 8β-hydroxyeremophil-7(11)-ene-12,8α; 14β,6α-diolide (**1**) and eremophil-7(11)-ene-12,8α; 14β,6α-diolide (**2**) for these sesquiterpenes is described.

A benzene extract of the roots of the plant was subjected to separation by column chromatography on silica gel to give four sesquiterpene lactones (**1**, **2**, **3**, and **4**) in addition to the previously reported furanoeremophilan-14β,6α-olide (**5**).[3,4]

The lactone (**1**), mp 253.5—254 °C (dec), $[\alpha]_D$ +94° ($CHCl_3$), crystallized from a mixture of benzene and chloroform as colorless needles. The molecular formula of $C_{15}H_{18}O_5$ was determined by elemental analysis and the appearance of the molecular ion peak at *m/e* 278 in the mass spectrum. The IR, UV, and PMR spectra indicated the presence of a tertiary methyl, an olefinic methyl, an α,β-unsaturated γ-lactone,[5,6] a γ-lactone, and a hydroxyl group; signals due to a secondary methyl were absent (*cf.* Experimental). Acetylation of the lactone (**1**) with acetic anhydride in pyridine gave a monoacetate (**6**) showing no hydroxyl absorption in its IR spectrum. Based on these spectral data, the structure (**1**) is suggested for this lactone (**1**), providing that the lactone belongs to a sesquiterpene of eremophilane-type. The following evidence provides support for the proposed structure (**1**).

It has been reported that the autoxidation of atractylon (**7**) gives a lactone (**8**) and a hydroxylactone (**9**), and that the latter compound (**9**) in turn affords an unsaturated enol lactone (**10**) by dehydration.[7] Oxidation of atractylon (**7**) with dichlorodicyanobenzoquinone (DDQ) to yield **10** has also been described.[8] Furanoeremophilan-14β,6α-olide (**5**) with the known absolute stereochemistry[3] was treated with DDQ in dioxane to give an unsaturated enol lactone (**11**). The same compound (**11**) was obtained by dehydration of the lactone (**1**) with phosphorus oxychloride in pyridine. Irradiation of **5** in methanol with a high pressure mercury lamp under an oxygen atmosphere in the presence of Rose Bengal gave a compound identical with the lactone (**1**). The observation described above shows that the lactone (**1**) can be formulated as 8ξ-hydroxyeremophil-7(11)-ene-12,8α; 14β,6α-diolide. The β-configuration of the hydroxyl group at $C_{(8)}$ was suggested by the presence in the lactone (**1**) of a long-range spin-coupling (J=2 Hz) between the olefinic methyl ($C_{(11)}$–CH_3) protons and the allylic proton ($C_{(6\beta)}$)–H) at the lactone terminus. An examination of the stereostructure of **1** with 8β-OH by the use of Dreiding model shows that the angle between $C_{(6\beta)}$–H and $C_{(11)}$–CH_3 is around 90°, in agreement with the observed homoallylic spin-coupling constant.[9] In an alternative structure with 8α-OH, the angle lies around 30° and the corresponding homoallylic spin-coupling would be negligible.[9] This received support from the following observation.[10] Naya *et al.*[10] reported the presence of a homoallylic spin-coupling (J=1.0—1.5 Hz) between $C_{(6\alpha)}$–H and $C_{(11)}$–CH_3 in 6β-hydroxy-8α-methoxyeremophil-7(11)-en-12,8β-olide (**12**) and 6β-acetoxy-8α-methoxyeremophil-7(11)-en-12,8β-olide (**13**) whose structures were firmly established, while the absence of this long-range spin-coupling in 6β-hydroxy-8β-methoxyeremophil-7(11)-en-12,8α-olide (**14**) and 6β-acetoxy-8β-methoxyeremophil-7(11)-en-12,8α-olide(**15**). The angles between $C_{(6\alpha)}$–H and $C_{(11)}$–CH_3 were reported to be 90° and 20° for the 8α- (**12** and **13**) and 8β-methoxy (**14** and **15**) derivatives, respectively. Therefore, the structure including absolute stereochemistry of the lactone (**1**) should be represented by 8β-hydroxyeremophil-7(11)-ene-12,8α;14β,6α-diolide (**1**).

The molecular formula of $C_{15}H_{18}O_4$ was given for the lactone (**2**), mp 186—186.5 °C (dec.), $[\alpha]_D$+93°

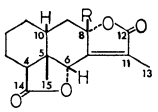

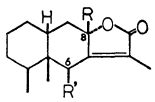

1 R = OH

2 R = H

6 R = OAc

18 R = OMe

3 R = OH, R' = OH

4 R = H, R' = OH

16 R = OAc, R' = OAc

17 R = H, R' = H

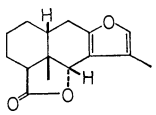

5

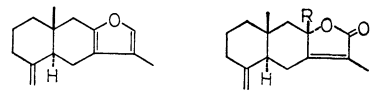

7 8 R = H 9 R = OH

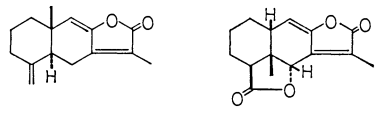

10 11

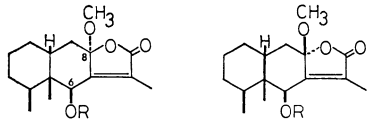

12 R=H 13 R=Ac 14 R=H 15 R=Ac

($CHCl_3$). The spectral data suggested the presence of a tertiary methyl, an olefinic methyl, an α,β-unsaturated γ-lactone, and a γ-lactone grouping (*cf.* Experimental). No hydroxyl absorption was observed in the IR spectrum. In the PMR spectrum of the lactone (**2**) the signals due to the proton ($C_{(8)}$–H) at the unsaturated lactone terminus appeared at δ 4.75 as a multiplet, while the corresponding signals were absent in the spectrum of the lactone (**1**). Treatment of the lactone (**1**) with sodium borohydride in methanol containing sodium hydroxide gave the lactone (**2**). These results show that the lactone (**1**) contains one hydroxyl group more than the lactone (**2**), and that the hydroxyl group at $C_{(8)}$ of **1** must be replaced by a hydrogen atom in the case of the lactone (**2**). PMDR experiments revealed the presence in the lactone (**2**) of long-range spin-couplings of the olefinic methyl ($C_{(11)}$–CH_3) protons to the allylic proton ($C_{(6\beta)}$–H; J=2 Hz) and to the other allylic proton ($C_{(8)}$–H; J=2 Hz). This observation leads to the 8β-H configuration for the lactone (**2**).[9] Thus, the structure including absolute stereochemistry of the lactone (**2**) is shown to be eremophil-7(11)-ene-12,8α; 14β,6α-diolide (**2**).

The lactone (**3**), mp 217—218 °C (dec), $[\alpha]_D$ +82° (EtOH), gave a diacetate (**16**), mp 120.5—121 °C, by acetylation with acetic anhydride in pyridine. This lactone (**3**) proved to be identical with 6β,8β-dihydroxyeremophil-7(11)-en-12,8α-olide (**3**),[10] recently reported by Naya *et al.* The lactone (**4**), mp 207—207.5 °C, $[\alpha]_D$ +213° ($CHCl_3$), was found to be identical with 6β-hydroxyeremophil-7(11)-en-12,8α-olide (**4**).[6,10,11] The lactone (**3**) was treated with sodium borohydride in methanol containing sodium hydroxide to yield two products, which were shown to be **4** and eremophil-7(11)-en-12,8α-olide (**17**),[12,13] respectively. The similar treatment of **4** gave **17**.

The photosensitized autoxidation of **5** in methanol gave a compound (**18**), $C_{16}H_{20}O_5$, mp 184.5—185 °C, besides the lactone (**1**). The PMR spectrum of **18** indicated the presence of a methoxyl group. The multiplet due to 8β-H appeared in the spectrum of **2** is absent in that of **18**. The other spectral data of **2** and **18** were almost identical, showing the presence of the common groupings: a tertiary methyl, an olefinic methyl, an α,β-unsaturated γ-lactone, and a γ-lactone grouping (*cf.* Experimental). The extra methoxyl group of **18** must be located on $C_{(8)}$ of the structure moiety of **2**. The presence of a long-range spin-coupling (J=2 Hz) of the olefinic methyl ($C_{(11)}$–CH_3) protons to the allylic proton ($C_{(6\beta)}$–H) at the lactone terminus was observed for **18**.[9] Therefore, the structure of the photoproduct (**18**) should be represented by 8β-methoxyeremophil-7(11)-ene-12,8α; 14β,6α-diolide (**18**).

The two lactones (**1** and **2**)[14] represent the first examples of eremophilane-type sesquiterpenes with two lactone rings in their molecules.

Experimental

All mps were determined on a hot block and reported uncorrected. IR, UV, and mass spectra were recorded on Hitachi EPI-G2, Hitachi EPS-3, and Hitachi RMU-6 spectrometers, respectively. Measurements of optical rotation were carried out using a JASCO DIP-SL polarimeter. PMR spectra were taken on a Hitachi R-20 or a JEOL JNM-PS-100 spectrometer, using TMS as internal standard. Kieselgel G nach Stahl and Kieselgel 60 PF_{254} (Merck) were used for analytical and preparative TLC, respectively. For column chromatography Wakogel C-200 (Wako Pure Chemicals) was used.

Isolation of the Lactones (1, 2, 3, and 4). Dried roots (900 g) of *L. Fauriei* were extracted twice with hot benzene (2 l). The residue obtained after removal of the solvent was chromatographed on a column of silica gel (180 g). Elution with petroleum ether–ether (20: 1, 1 l) gave furanoeremophilan-14β, 6α-olide (**5**)[3,4] (5.40 g). After elution of **5**, more polar constituents were eluted with ether. The residue obtained after evaporation of the solvent was subjected to chromatographic separation on a column of silica gel (100 g).

Elution with benzene (1.2 l) gave, on removal of the solvent, a solid, which was crystallized from ether to afford eremophil-7(11)-ene-12, 8α; 14β, 6α-diolide (**2**; 204 mg) as needles, mp 186—186.5 °C (dec.); $[\alpha]_D$ +93° (*c* 0.91, $CHCl_3$); UV (EtOH) λ_{max} 217 nm (ε 19300); IR (Nujol) 1786, 1739, and 1684 (sh) cm^{-1}; PMR ($CDCl_3$) δ 1.29 (3H, s; $C_{(5)}$–CH_3), δ 2.00 (3H, t, $J_{6\beta,13}$=2 and $J_{8\beta,13}$=2 Hz; $C_{(11)}$–CH_3), δ 4.75 (1H, m, $J_{8\beta,13}$=2, $J_{8\beta,9\alpha}$=13, and $J_{8\beta,9\beta}$=5 Hz (by PMDR experiments); $C_{(8\beta)}$–H), and δ 5.05 (1H, q, $J_{6\beta,13}$=2 Hz (confirmed by PMDR experiments); $C_{(6\beta)}$–H); mass spectrum *m/e* 262 (relative intensity 73%; M^+), *m/e* 152 (100%). Found: C, 69.13; H, 7.14%. Calcd for $C_{15}H_{18}O_4$: C, 68.68; H, 6.92%.

Subsequent elution with benzene–ether (10: 1, 400 ml) and evaporation of the solvents gave a residue, which was crystallized from benzene to yield 6β-hydroxyeremophil-7(11)-en-12, 8α-olide[6,10,11] (**4**; 40 mg) as needles, mp 207—207.5 °C (lit, mp 208 °C[6,11] and mp 204—205 °C[10]); $[\alpha]_D$ +213° (*c* 1.19, $CHCl_3$) (lit, $[\alpha]_D$ +205.8° ($CHCl_3$),[6] $[\alpha]_D$ +203° ($CHCl_3$),[10] and $[\alpha]_D$ −35.4° ($CHCl_3$)[11,15]); UV (EtOH) λ_{max} 218 nm (ε 14400) [lit, λ_{max} 218.5 nm (ε 13700) (EtOH)[6] and λ_{max} 220 nm (log ε 4.12)[11]]; IR (Nujol) 3440, 1739, 1709 (sh), and 1690 cm^{-1}; PMR ($CDCl_3$) δ 0.80 (3H, d-like; $C_{(4)}$–CH_3), δ 1.13 (3H, s; $C_{(5)}$–CH_3), δ 1.85 (3H, d, $J_{8\beta,13}$=2 Hz; $C_{(11)}$–CH_3), δ 4.80 (1H, s; $C_{(6\alpha)}$–H), δ *ca.* 5.1 (1H, m; $C_{(8\beta)}$–H), and

δ 2.23 (1H, s, disappeared on addition of D_2O; $C_{(6\beta)}$-OH); mass spectrum *m/e* 250 (7%, M^+), *m/e* 126 (100%). Found: C, 72.00; H, 8.90%. Calcd for $C_{15}H_{22}O_3$: C, 71.97; H, 8.86%. This lactone was found to be identical (mp, mixed mp, $[\alpha]_D$, IR, UV, PMR, and mass spectra) with an authentic specimen of **4**.[6]

Fractions eluted with benzene–ether (5: 1, 400 mg) gave, on removal of the solvents, a solid, which was crystallized from chloroform–benzene to afford 8β-hydroxyeremophil-7(11)-ene-12, 8α; 14β, 6α-diolide (**1**; 250 mg) as needles, mp 253.5—254 °C (dec); $[\alpha]_D$ +94° (*c* 0.88, $CHCl_3$); UV (EtOH) λ_{max} 214 nm (ε 12400); IR (Nujol) 3260, 1787, and 1710 cm^{-1}; PMR (acetone-d_6) δ 1.28 (3H, s; $C_{(5)}$-CH_3), δ 1.86 (3H, d, $J_{6\beta,13}$=2 Hz; $C_{(11)}$-CH_3), δ 5.18 (1H, q, $J_{6\beta,13}$=2 Hz (confirmed by PMDR experiments); $C_{(6\beta)}$-H), and δ 6.51 (1H, s, disappeared on addition of D_2O; $C_{(8\beta)}$-OH); mass spectrum *m/e* 278 (44%, M^+), *m/e* 109 (100%). Found: C, 65.08; H, 6.42%. Calcd for $C_{15}H_{18}O_5$: C, 64.73; H, 6.52%.

Successive elution with the same solvents [benzene–ether (5: 1), 500 ml] and the evaporation of the solvents gave a residue. This was crystallized from chloroform–benzene to yield 6β,8β-dihydroxyeremophil-7(11)-en-12, 8α-olide (**3**; 567 mg)[10] as plates, mp 217—218 °C (dec) (lit, mp 211—212 °C); $[\alpha]_D$ +82° (*c* 0.98, EtOH) [lit, $[\alpha]_D$ +169° ($CHCl_3$)[10]]; UV (EtOH) λ_{max} 219 nm (ε 11800); IR (Nujol) 3480, 3230, and 1721 cm^{-1}; ($CHCl_3$) 3530, 1761, 998, and 980 (sh) cm^{-1} (lit, ($CHCl_3$) 3525, 3250, 1760, 1005, and 990 cm^{-1} [10]); PMR (acetone-d_6) δ 0.80 (3H, d-like; $C_{(4)}$-CH_3), δ 1.12 (3H, s; $C_{(5)}$-CH_3), δ 1.83 (3H, s, $C_{(11)}$-CH_3), and δ 4.64 (1H, br. s; $C_{(6\alpha)}$-H); ($CDCl_3$) δ 0.82 (3H, unresolved signals; $C_{(4)}$-CH_3), δ 1.13 (3H, s, $C_{(5)}$-CH_3), δ 1.88 (3H, s; $C_{(11)}$-CH_3), δ 2.09 (2H, s; $C_{(9)}$-H_2), δ 2.96 and δ 3.10 (each 1H, s, disappeared on addition of D_2O; $C_{(6\beta)}$-OH and $C_{(8\beta)}$-OH), and δ 4.62 (1H, s; $C_{(6\alpha)}$-H); [lit, ($CDCl_3$) δ 0.78 (3H, unresolved signals; $C_{(4)}$-CH_3), δ 1.11 (3H, s; $C_{(5)}$-CH_3), δ 1.87 (3H, s; $C_{(11)}$-CH_3), δ 2.07 (2H, s; $C_{(9)}$-H_2), δ 2.70 (2H, br. s; $C_{(6\beta)}$-OH and $C_{(8\beta)}$-OH), and δ 4.60 (1H, s; $C_{(6\alpha)}$-H)[10]]; mass spectrum *m/e* 248 (6%, $(M-18)^+$], *m/e* 109 (100%) (no molecular ion peak was observed). Found: C, 67.89; H, 8.53%. Calcd for $C_{15}H_{22}O_4$: C, 67.65; H, 8.33%. This lactone proved to be identical with **3**, recently reported by Naya *et al.*[10]

Acetylation of the Lactone (1). The lactone (**1**; 36 mg) was acetylated with acetic anhydride (2 ml) in pyridine (3 ml) at room temperature. Treatment as usual gave a residue, which was chromatographed on a column of silica gel (5 g). Fractions eluted with benzene (14 ml) gave an oil, which was purified by preparative TLC. Crystallization of the oil from petroleum ether afforded a monoacetate (**6**; 17 mg) as needles, mp 183—184 °C; IR (Nujol) 1800, 1784, 1773, and 1707 cm^{-1}; PMR ($CDCl_3$) δ 1.32 (3H, s; $C_{(5)}$-CH_3), δ 2.06 (3H, d, $J_{6\beta,13}$=2 Hz; $C_{(11)}$-CH_3), δ 2.13 (3H, s; -$COCH_3$), and δ 5.04 (1H, q, $J_{6\beta,13}$=2 Hz; $C_{(6\beta)}$-H); mass spectrum *m/e* 320 (3%, M^+), *m/e* 278 [100%, $(M-42)^+$]. Found: C, 63.66; H, 6.26%. Calcd for $C_{17}H_{20}O_6$: C, 63.74; H, 6.29%.

Acetylation of the Lactone (3). To a solution of **3** (30 mg) in pyridine (2 ml) was added acetic anhydride (1 ml), and the solution was left for 3 days at room temperature. After working up in the usual manner, a crystalline product was obtained. Recrystallization from petroleum ether gave a diacetate (**16**; 38 mg), as needles, mp 120.5—121 °C (lit, 119.5—120.5 °C[10]); IR (Nujol) 1770, 1751, 1733, and 1248 cm^{-1}; PMR ($CDCl_3$) δ 0.82 (3H, unresolved signals; $C_{(4)}$-CH_3), δ 1.00 (3H, s; $C_{(5)}$-CH_3), δ 1.96 (3H, s; $C_{(11)}$-CH_3), δ 1.98 (3H, s; -$COCH_3$), δ 2.02 (3H, s; -$COCH_3$), and δ 5.88 (1H, s; $C_{(6\alpha)}$-H); mass spectrum *m/e* 308 [3%, $(M-42)^+$], *m/e* 109 (100%) (no molecular ion peak was observed). Found: C, 65.24; H, 7.45%. Calcd for $C_{19}H_{26}O_6$: C, 65.12; H, 7.48%.

Oxidation of the Lactone (5) with DDQ. A mixture of furanoeremophilan-14β,6α-olide (**5**; 500 mg) and DDQ (1.2 g) in dioxane (10 ml) was heated at 80 °C for 1 h, and then the solvent was evaporated under reduced pressure. The residue was extracted with hot benzene. The reaction mixture obtained after removal of the benzene was chromatographed on a column of silica gel (50 g). Elution with benzene–ether (5: 1, 1 l) gave a mixture of crystalline products (227 mg, recrystallized from benzene), which was subjected to sublimation. From the sublimated material (119 mg), a product (34 mg) with R_f value 0.62 (benzene–ether, 1: 1) on TLC (silica gel) was collected by repeated preparative TLC. Crystallization of the product from ether gave an unsaturated enol lactone (**11**; 23 mg) as an amorphous solid, IR (neat) 1785 and 1665 cm^{-1}; PMR ($CDCl_3$) δ 1.38 (3H, s; $C_{(5)}$-CH_3), δ 2.12 (3H, br. s; $C_{(11)}$-CH_3), δ 2.65 (1H, dd, $J_{3\alpha,4\alpha}$=2 and $J_{3\beta,4\alpha}$= 12 Hz; $C_{(4\alpha)}$-H), δ 2.96 (1H, m; $C_{(10\beta)}$-H), δ 5.28 (1H, q, $J_{6\beta,13}$=1.5 Hz; $C_{(6\beta)}$-H), and δ 5.65 (1H, d, $J_{9,10\beta}$=3 Hz; $C_{(9)}$-H) (the presence of these spin-couplings was confirmed by PMDR experiments); mass spectrum *m/e* 260 (9%, M^+ related to a molecular formula of $C_{15}H_{16}O_4$], *m/e* 67 (100%). This compound is very unstable and most of the compound decomposed within 1 day on leaving it in a solution. The purity was checked before and after the measurement of these spectra. The UV (EtOH) spectra showed the absorption maximum at 280 nm.[7,8] However, the ε value could not be determined precisely due to fragility of the compound. Appearance of the maximum at 222 nm during the measurement would be due to the decomposition of the compound. Elemental analysis gave an unsatisfactory result probably due to the unstability of the compound.

Dehydration of the Lactone (1). To a stirred solution of **1** (51 mg) in pyridine (2 ml), phosphorus oxychloride (0.2 ml) was added at 0 °C, and the stirring was continued for 1 h at 0 °C, then for 4 h at room temperature. After addition of crushed ice, the reaction mixture was extracted with chloroform (50 ml). The extract was dried over anhydrous sodium sulfate, and the solvent was evaporated under reduced pressure. From the reaction mixture, the unsaturated enol lactone (**11**; 9 mg) was obtained by preparative TLC, which was found to be identical (TLC, IR, PMR, and mass spectra) with the sample (**11**) prepared by oxidation of **5**.

Photosensitized Autoxidation of the Lactone (5) in Methanol. Rose Bengal (53 mg) was added to a solution of **5** (308 mg) in methanol (600 ml), and the resulting solution was irradiated with a high pressure mercury lamp (100W, Rikosha) under oxygen atmosphere at 0 °C for 1 h. The residue obtained after removal of the methanol under reduced pressure, was chromatographed on a column of silica gel (50 g). Elution with benzene–ether (10: 1) gave two principal fractions: the less polar fraction (269 mg) and the more polar fraction (21 mg). From the more polar fraction, a crystalline product (9.5 mg) was obtained after recrystallization from benzene–chloroform, which was found to be identical (mp, TLC, IR, and PMR spectra) with 8β-hydroxyeremophil-7(11)-ene-12, 8α;14β,6α-diolide (**1**).

The less polar fraction was repeatedly chromatographed on a column of silica gel (50 g). Elution with benzene–ether (20: 1, 200 ml) gave 8β-methoxyeremophil-7(11)-ene-12,8α;14β,6α-diolide (**18**; 111 mg, recrystallized from petroleum ether), mp 184.5—185 °C; UV (EtOH) λ_{max} 216 nm (ε 14700); IR (Nujol) 1790, 1765, and 1690 cm^{-1}; PMR ($CDCl_3$) δ 1.29 (3H, s; $C_{(5)}$-CH_3), δ 2.01 (3H, d, $J_{6\beta,13}$=2 Hz; $C_{(11)}$-CH_3), δ 3.21 (3H, s; -OCH_3), and δ 4.88 (1H, q, $J_{6\beta,13}$=2 Hz; $C_{(6\beta)}$-H); mass spectrum *m/e* 292 (35%, M^+), *m/e* 67 (100%). Found: C, 65.67; H, 6.66%. Calcd for $C_{16}H_{20}O_5$: C, 65.74; H,

6.90%.

When the lactone (**5**) in methanol was either left for 3 days under bubbling of oxygen or irradiated with ultraviolet rays for 5 h under oxygen atmosphere, **5** suffered no change.

Reduction of the Lactone (1) with Sodium Borohydride. To a mixture of **1** (30 mg) and aqueous sodium hydroxide (10%, 0.3 ml) in methanol (3 ml), sodium borohydride (51 mg) was added at 0 °C with stirring, and the stirring was continued for 1 h at 0 °C, then for 2 h at room temperature. After evaporation of the methanol under reduced pressure, the residue was acidified with sulfuric acid (0.5 M), and extracted with ether. The ethereal solution was dried over anhydrous sodium sulfate and the solvent was removed to give a residue, which was chromatographed on a column of silica gel (7 g), using benzene–ether (10:1) as eluent. A crystalline product (5 mg) was obtained, which was purified by crystallization from ether. This compound (2 mg) was found to be identical (mp, TLC, IR, PMR, and mass spectra) with eremophil-7(11)-ene-12,8α; 14β,6α-diolide (**2**).

Reduction of the Lactone (3) with Sodium Borohydride. The lactone (**3**; 30 mg) was treated with sodium borohydride (50 mg) in methanol containing sodium hydroxide according to the procedures described in the reduction of **1**. The residue was chromatographed on a column of silica gel (20 g). Elution with benzene (120 ml) gave an oily product, which then solidified (10 mg). This compound proved to be identical with eremophil-7(11)-en-12,8α-olide (**17**),[12,13] mp 107—111 °C; IR (Nujol) 1740, 1687, and 1035 cm^{-1}; PMR ($CDCl_3$) δ 0.80 (3H, d-like; $C_{(4)}$–CH_3), δ 1.05 (3H, s; $C_{(5)}$–CH_3), δ 1.80 (3H, t, $J_{6\beta,13}$=2 Hz and $J_{8\beta,13}$=2 Hz; $C_{(11)}$–CH_3), δ 2.90 (1H, d, $J_{6\alpha,6\beta}$=15 Hz; $C_{(6\alpha)}$–H) (signals due to $C_{(6\beta)}$–H is overlapped with other signals), and δ 4.61 (1H, m; $C_{(8\beta)}$–H); mass spectrum *m/e* 234 (8%, M^+ related to a molecular formula of $C_{15}H_{22}O_3$), *m/e* 123 (100%).

Successive elution with benzene–ether (5: 1, 90 ml) gave a product (3 mg), mp 207—207.5 °C, whose IR, PMR, and mass spectra were found to be identical with those of 6β-hydroxyeremophil-7(11)-en-12,8α-olide (**4**).[6]

Reduction of the Lactone (4) with Sodium Borohydride. Treatment of the lactone (**4**; 13 mg) with sodium borohydride (55 mg) in methanol containing sodium hydroxide, according to the procedures described in the reduction of **3**, gave a residue, which was chromatographed on a column of silica gel (5 g). Elution with benzene (150 ml) gave a crystalline compound (3 mg). This compound was found to be identical (mp, TLC, IR, and PMR spectra) with **17** described above. Further elution with ether (30 ml) afforded the unchanged starting material (**4**; 10 mg).

The authors wish to thank Prof. K. Naya, Kwansei Gakuin University, for a generous gift of authentic samples of 6β,8β-dihydroxyeremophil-7(11)-en-12,8α-olide (**3**) and the diacetate (**16**), together with their PMR and IR spectra. The authors are also grateful to Dr. H. Ishii, Shionogi Research Laboratory, for a kind supply of an authentic sample of 6β-hydroxyeremophil-7(11)-en-12,8α-olide (**4**).

References

1) A preliminary account of this paper: Y. Moriyama and T. Takahashi, *Chem. Pharm. Bull.*, **24**, 360 (1976). A part of this work was presented at the 26th Annual Meeting of the Chemical Society of Japan, Hiratsuka, April, 1972 (Proceedings, Vol. III, p. 1227).

2) T. Sato, Y. Moriyama, H. Nagano, Y. Tanahashi, and T. Takahashi, *Bull. Chem. Soc. Jpn.*, **48**, 112 (1975). And references cited therein.

3) Y. Ishizaki, Y. Tanahashi, T. Takahashi, and K. Tori, *Chem. Commun.*, **1969**, 551.

4) Y. Moriyama, T. Tsuyuki, T. Takahashi, and H. Koyama, *Phytochemistry*, **13**, 288 (1974).

5) K. Takeda, H. Minato, M. Ishikawa, and M. Miyawaki, *Tetrahedron*, **20**, 2655 (1964).

6) H. Ishii, T. Tozyo, and H. Minato, *J. Chem. Soc.*, **1966**, 1545.

7) H. Hikino, Y. Hikino, and I. Yoshioka, *Chem. Pharm. Bull.*, **12**, 765 (1964). And references cited therein.

8) K. Takeda, M. Ikuta, M. Miyawaki, and K. Tori, *Tetrahedron*, **22**, 1159 (1966): The same type of reaction has also been described to proceed in the case of linderene and its derivatives.

9) N. S. Bhacca and D. H. Williams, "Applications of NMR Spectroscopy in Organic Chemistry," Holden-Day (1964), p. 110.

10) K. Naya, R. Kanazawa, and M. Sawada, *Bull. Chem. Soc. Jpn.*, **48**, 3220 (1975). And references cited therein.

11) L. Novotný, V. Herout, and F. Šorm, *Coll. Czech. Chem. Commun.*, **29**, 2189 (1964).

12) L. Novothý, J. Jizba, V. Herout, and F. Šorm, *Coll. Czech. Chem. Commun.*, **27**, 1393 (1962); M. Horák, O. Motl, J. Pliva, and F. Šorm, "Die Terpene," Teil II, Akademie-Verlag (1963), p. S I 28.

13) The $C_{(8\beta)}$–H configuration of **17** was determined by X-ray study: C. Kabuto, N. Takada, S. Meada, and Y. Kitahara, *Chem. Lett.*, **1973**, 371.

14) These lactones might be considered as artifacts produced from **5** during isolation procedures. Although the fresh extract of the plant was examined by thin layer chromatography, no conclusive evidence was obtained due to the complexity of a mixture of the constituents. The subsequent separation led to the isolation of **1** and **2** as described in Experimental.

15) This reported $[\alpha]_D$ value seems to be erroneous.

The Lanthanoid-Induced Shifts of Proton NMR Spectra and the Conformations of β-(2-Thienyl)acrylic Esters and Related Compounds

Minoru HIROTA, Shigeko YOSHIDA, Yoshinobu NAGAWA, Makoto ONO, Hiroko ENDO, and Hajime SATONAKA*

Department of Applied Chemistry, Faculty of Engineering, Yokohama National University, Minami-ku, Yokohama 233
**Industrial Research Institute of Kanagawa Prefecture, 3173, Showa-machi, Kanazawa-ku, Yokohama 236*

(Received June 23, 1976)

The most predominant conformation of 4-(2-thienyl)-3-butene-2-one and methyl β-(2-thienyl)acrylates were determined by the analysis of their LIS's. The LIS's toward higher fields were observed with some ring protons (H_3's and some of H_4's), and were best interpreted by assuming that about 20% of the shift reagent coordinates on the methoxyl oxygen atom and the rest on the carbonyl oxygen atom.

β-(2-Thienyl)acrylic esters are considered to take a planar conformation in order to minimize pi-electronic energy of the whole conjugated system. However, the rotation about the two C(sp^2)–C(sp^2) single bonds (C_β–C_2 and C_α–$C_{carbonyl}$) produces the possibility to exist as the four conformers **1**a—**1**b. As the rotational barriers around these essential single bonds are relatively low,[1] the interconversion among these occurs rapidly, and the ester exists as an equilibrium mixture in which the most stable conformer predominates over the others. Thus, it is of considerable significance to determine which of the four is the most predominant conformer. The stereochemistry of conjugated unsaturated ketones have been discussed by several authors,[2,3] and it is concluded that the *s-trans* conformation is, in general, more stable than *s-cis* one from the ultraviolet spectroscopic evidences. However, the conformation around the other essential single bond is less certain. The molecular models and the molecular diagrams[2] suggest that the conformer (a or b) in which the C_2–C_3 bond of the thiophene ring is *s-trans* with respect to the ethylenic bond of the enone system is considerably less hindered than the *s-cis* one (c or d), since the H_α–H_3 repulsion operating in the *s-cis* conformer is substituted by much less H_β–H_3 repulsion in the former conformer.

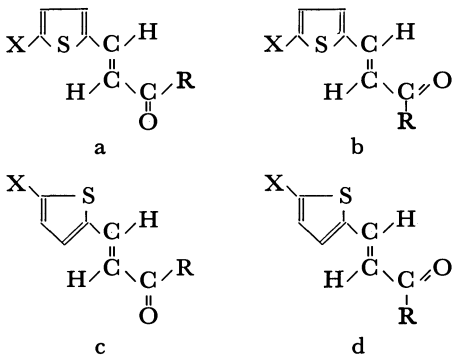

a b c d

Thus, the stereochemistry of some *trans*-β-(2-thienyl)-acrylic esters (**1**) and *trans*-4-(2-thienyl)-3-buten-2-one (**2**) has been investigated by measuring the LIS (lanthanoid induced shift) values of their proton NMR spectra.

Experimental

Materials used in this investigation were synthesized according to the methods previously reported,[10] or obtained by purification of commercially available materials. Proton NMR spectra were measured in carbon tetrachloride employing a JNM C-60H spectrometer operating at 60 MHz. The concentrations of the solutions were adjusted approximately at 0.3 mol l^{-1} with respect to substrates. Tris(dipivaloylmethanato)europium [=Eu(dpm)$_3$] was used as a shift reagent throughout this investigation, and it was added in small portions to a solution containing an excess of the substrate in order to obtain the $\Delta\delta$ *vs.* [shift reagent]/[substrate] plots.

Results and Discussion

The LIS values and their proportions to the largest were given in Table 1. In order to determine the privileged conformation of *trans*-4-(5-bromo-2-thienyl)-3-buten-2-one, the most probable locations of the Eu(III) ion to reproduce the observed LIS values of 2 were calculated with all of four conformations **2**a—**2**d (where X is Br) by evaluating the agreement factors (*R*-values) defined by Eq. 1,[4] where $(S_{obsd})_i$ and $(S_{calcd})_i$ are the observed and the calculated LIS's of proton *i*, respectively.

$$R = \left\{ \frac{[(S_{obsd})_i - (S_{calcd})_i]^2}{(S_{obsd})_i^2} \right\}^{1/2} \quad (1)$$

Reasonable results given in Fig. 1 were obtained only when the substrate molecule takes the *s-trans*, *s-trans* conformation (**2**a). As shown in Fig. 1, the location of Eu(III) in the enone–Eu(dpm)$_3$ complex is 2.3 Å apart from the carbonyl oxygen atom and not so far from the C=O axis.

The relative values of the LIS's of the thienylacrylic esters, as a whole, are similar to those of the thienylbutenone (**2**). However, a remarkable differences are observed with the signs of the LIS's of some ring protons (H_3's and some H_4's in Table 1) and with the relative magnitudes of the LIS's of α- and β-protons. The difference is interpreted by assuming that the complexation of Eu(dpm)$_3$ also occurs on the methoxyl oxygen atom to some extent. To estimate roughly the relative abundances of the complexes in which the Eu(III) ions are bonded to the carbonyl and the alkoxyl oxygen atoms, the LIS's of the equimolar mixture of acetone and diethyl ether is measured and, by comparing with the LIS's of each component under the same conditions, the 80% of the shift reagent is shown to coordinate to the carbonyl oxygen atom of acetone.[5] Employing the results of the intermolecular competition, the LIS's of the thienylacrylic ester (**1**) were estimated as

TABLE 1. THE LIS'S OF METHYL β-(5-SUBSTITUTED-2-THIENYL)-ACRYLATES AND RELATED COMPOUNDS

Compounds		(O)CH_3	H_α	H_β	H_3	H_4	5-CH_3
$BrC_4H_3SCH{=}CHCOCH_3$	S_i[a]	15.48	13.50	12.70	1.48	0.90	
	$S_i/(S_i)_{max}$	1.00	0.87	0.82	0.096	0.058	
$BrC_4H_3SCH{=}CHCOOCH_3$	S_i	15.44	12.26	13.72	−1.04	−0.16	
	$S_i/(S_i)_{max}$	1.00	0.79	0.89	−0.067	−0.010	
$ClC_4H_3SCH{=}CHCOOCH_3$	S_i	15.50	12.25	13.30	−1.05	−0.14	
	$S_i/(S_i)_{max}$	1.00	0.79	0.86	−0.068	−0.009	
$CH_3C_4H_3SCH{=}CHCOOCH_3$	S_i	15.59	12.47	13.72	−0.76	0.00	0.42
	$S_i/(S_i)_{max}$	1.00	0.80	0.88	−0.046	0.00	0.027
$BrC_4H_3SCH{=}CMeCOOCH_3$	S_i	13.84	(8.90)	12.52	−0.26	0.24	
	$S_i/(S_i)_{max}$	1.00	(0.64)	0.90	−0.019	0.017	
$BrC_4H_3OCH{=}CHCOOCH_3$	S_i	15.04	13.06	13.48	−0.82	0.13	
	$S_i/(S_i)_{max}$	1.00	0.87	0.89	−0.054	0.009	
$C_6H_5CH{=}CHCOOCH_3$	S_i	15.62	12.18	13.63	0.78	0.14	
	$S_i/(S_i)_{max}$	1.00	0.78	0.87	0.05	0.01	
Estimated value[b] for $XC_4H_3SCH{=}CHCOOCH_3$	$S_i/(S_i)_{max}$	1.00	0.71	0.79	−0.03	0.03	

a) S_i refers to the LIS value of proton i, which is defined as $S_i = \Delta\delta/([Eu(dpm)_3]/[Substrate])$.
b) See text.

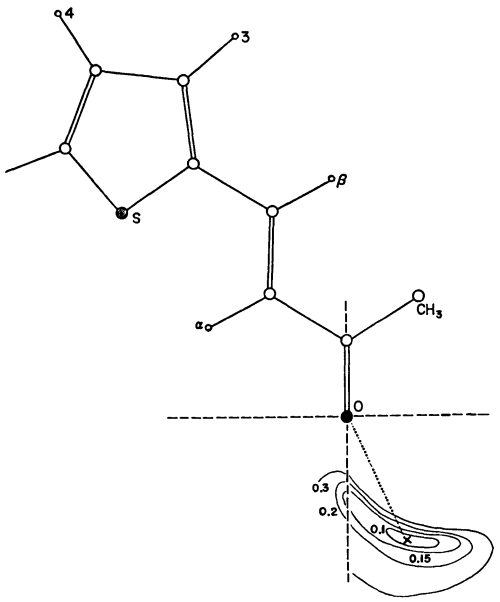

Fig. 1. The most probable position of the Eu(III) ion (x) determined by evaluating the R-values from Eq. 1 for 4-(2-thienyl)-3-buten-2-one.
(The figures show the R-values.)

the weighted sums of the contribution of the Eu(III) ions in two sites calculated by the McConnell Robertson equation,[6] $\Delta\delta = K(1-3\cos^2\theta)r^{-3}$, by assuming (i) that the shift reagent coordinates to the carbonyl and the methoxyl oxygen atoms of the ester in the ratio of 4: 1, (ii) that the Eu(III) ion is located on the extension of the C=O bond or on the bisector of the C–O–C angle of the methoxyl group, and (iii) that the Eu–O distance is 2.5 Å for the carbonyl oxygen and 3.0 Å for the methoxyl oxygen of the ester group. A conformation in which the two alkyl groups are antiperiplanar, termed "*trans*", is demonstrated to be the most favorable conformation of the carboxylic ester,[7] and the same conformation is also assumed in the calculation. As the location of the second Eu(III) ion coordinating on the methoxyl oxygen atoms is too close (about 1.9 Å) to realize, its location is modified to be on a line 19° out side from the bisector line and 3.0 Å distant from the oxygen atom (so as to keep the nearest Eu···H distance farther than 2.5 Å). This modification gives a reasonable set of the calculated LIS's of **1** showns together with the observed values, in Table 1. The position of the methoxyl protons are chosen to be the center of gravity of its three protons. In spite of this oversimplification and uncertainty of the position of the methyl group, the agreement between the relative values of the observed and the calculated LIS's are good, and the LIS's of the thienylacrylic esters can be explained by taking into accounts the participation of the alkoxyl oxygen atom in the formation of the shift reagent–substrate complex. The β-(5-bromo-2-furyl)-acrylic esters behave quite similarly with their thia-analogs towards the shift-reagent, and, in consequence with the previous reports,[8,9] the intra-ring oxygen atom does not participate in the complex formation with the shift-reagent. The LIS's of cinnamic esters are also similar and the participation of the alkoxyl-oxygen atom might be quite general in esters.

References

1) Low rotational barriers of single bonds are reported, for example, in the following paper. J. G. Aston, G. Szasz, H. W. Woolley, and F. G. Brickwedde, *J. Chem. Phys.*, **14**, 67 (1946).

2) a) E. A. Braude and C. J. Timmons, *J. Chem. Soc.*, **1955**, 3766; b) A. Bienenue and J. -E. Dubois, *Bull. Soc. Chim. Fr.*, **1969**, 391.

3) G. Montaudeo, V. Librando, S. Caccamese, and P. Maravigna, *J. Am. Chem. Soc.*, **95**, 6365 (1973).

4) M. R. Willcott, III, R. E. Lenkinski, and R. E. Davis, *J. Am. Chem. Soc.*, **94**, 1744, 1749 (1972).

5) M. Hirota, S. Aizawa, Y. Nagawa, and K. Hara,

Zairyo-Kisokogaku Kenkyu, (Yokohama National Univ.), **9**, 55 (1974).

6) H. M. McConnell and R. E. Robertson, *J. Chem. Phys.*, **29**, 1361 (1958).

7) C. P. Smyth, "Dielectric Behavior and Structure," McGraw-Hill, New York (1954), p. 305. See also M. Ōki and H. Nakanishi, *Bull. Chem. Soc. Jpn.*, **43**, 2558 (1970).

8) H. Hart and G. M. Love, *Tetrahedron Lett.*, **1971**, 625.

9) N. Platzer, C. Lang, J. J. Basselier, and P. Demerseman, *Bull. Soc. Chim. Fr.*, **1975**, 227.

10) T. Shimura, Z. Saito, and H. Satonaka, *Nippon Kagaku Zasshi*, **90**, 716, 1173 (1969).

Layered Compounds. XXXVI.[1] Structure and Properties of Triple-layered Metaparacyclophanes

Naoki KANNEN, Tetsuo OTSUBO, Yoshiteru SAKATA, and Soichi MISUMI*

The Institute of Scientific Industrial Research, Osaka University, Suita, Osaka 565

(Received June 7, 1976)

The geometrical structures of triple-layered metaparacyclophanes are discussed on the basis of the chemical shifts of the NMR spectra and their temperature dependence. [2.2]Metacyclo(4,7)[2.2]paracyclophane **1** and [2.2]metacyclo(12,15)[2.2]metaparacyclophane **2** proved to be mixtures of conformational isomers due to arrangement of meta-substituted ring. [2.2]Paracyclo(4,6)[2.2]metaparacyclophane **3** was confirmed to be a staircase-shape (*anti*-form), in contrast to a platform-shape (*syn*-form) of [2.2]metacyclo(4,6)[2.2]metaparacyclophane **5**. In their electronic spectra, **1** and **2** exhibit a transannular electronic interaction between the benzene rings similar to that of multilayered [2.2]paracyclophanes; **3** and **5** show one similar to that of multilayered [2.2]metacyclophanes. The difference between the former and the latter groups seems to arise from the substitution modes of methylene bridges attached to the inside benzene of triple-layered metaparacyclophanes.

In the preceding paper we reported the syntheses of triple-layered [2.2]metaparacyclophanes **1**—**6**.[1] The compounds are expected to consist of mixtures of conformational isomers due to fixation of meta-substituted benzene rings. In compounds **3**—**6** there seem to be two types of stacking which characterize either a staircase-shape (*anti*-form) or a platform-shape (*syn*-form) conformer. In this paper we discuss the assignment of the structures in detail and the conformational flipping of the meta ring at high temperature on the basis of NMR study. The transannular electronic interactions between benzene rings are considered in comparison with the electronic spectra of multilayered paracyclophane or metacyclophane.

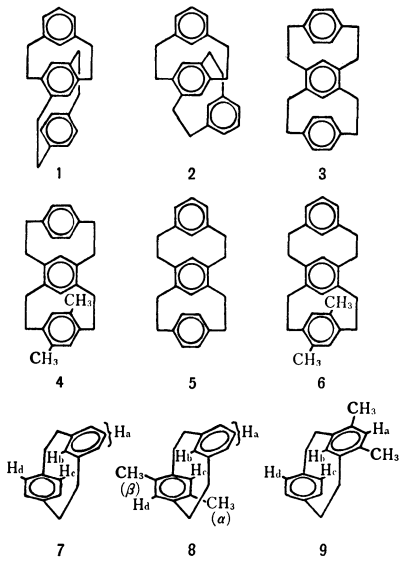

Scheme 1.

Results and Discussion

Structure and NMR Spectra. The NMR spectra of layered metaparacyclophanes **1**—**9** are summarized in Table 1. The high field shift of the inner aromatic proton Hb of [2.2]metaparacyclophane **7** suggests that the proton is situated just above the faced para-substituted ring. The aromatic protons, Hc and Hd, of the para ring are nonequivalent at room temperature, becoming equivalent at higher temperature (T_c, *ca.* 140 °C). The behavior is interpreted in terms of conformational flipping of the meta ring which is fixed at room temperature.[2] The activation energy calculated is about 21 kcal/mol. Similarly two dimethyl derivatives **8** and **9** show the fixation of the meta ring at room temperature.

The triple-layered metaparacyclophane **1** exhibits a NMR pattern similar to those of **7**—**9** except high field shifts of the protons, Hb, Hc, and Hd, due to the anisotropy of the additional third benzene ring. Figure 1

Table 1. NMR SPECTRA OF METAPARACYCLOPHANES

Compound	δ Value in deuterochloroform
1	6.6 (m, 3H, Ha), 6.30 (bs, 4H, He), 6.17 (s, 1H, Hd), 5.12 (bs, 1H, Hb), 4.90 (s, 1H, Hc), 1.5—3.6 (m, 16H, CH_2)
2	6.4—7.1 (m, 12H, Ha and Ha'), 6.87 (s, 1H, Hc'), 5.60 (s, 2H, Hc), 5.37 (bs, 1H, Hb), 5.28 (bs, 1H, Hb'), 4.39 (s, 1H, Hd'), 1.5—3.5 (m, 32H, CH_2)
3	7.12 (bs, 4H, Ha), 5.66 (bs, 4H, Hb), 4.94 (s, 2H, Hc), 1.5—3.3 (m, 16H, CH_2)
4	7.09 (d, J=1 Hz, 2H, Ha), 6.79 (s, 1H, Hf), 5.63 (d, J=1 Hz, 2H, Hb), 5.48 (s, 1H, He), 5.05 (s, 1H, Hc), 4.90 (s, 1H, Hd), 1.7—3.2 (m, 16H, CH_2), 2.39 (s, 3H, CH_3-β), 1.44 (s, 3H, CH_3-α)
5	7.46 (d, J=2 Hz, 2H, Hf), 7.3 (m, 3H, Ha), 6.48 (d, J=2 Hz, 2H, He), 5.70 (bs, 1H, Hb), 5.62 (s, 1H, Hd), 3.66 (s, 1H, Hc), 1.5—3.5 (m, 16H, CH_2)
6	6.9—7.3 (m, 7H, Ha, Ha', and Hf), 6.87 (s, 1H, Hf'), 6.21 (s, 1H, He), 5.80 (bs, 1H, Hb), 5.60 (s, 1H, He'), 5.39 (s, 1H, Hd), 5.07 (bs, 1H, Hb'), 4.20 (s, 1H, Hd'), 3.71 (s, 2H, Hc and Hc'), 1.7—3.2 (m, 32H, CH_2), 2.58 (s, 3H, CH_3-β), 2.44 (s, 3H, CH_3'-β), 1.98 (s, 3H, CH_3-α), 1.49 (s, 3H, CH_3'-α)
7	7.18 (d, J=2 Hz, 2H, Hd), 6.8 (m, 3H, Ha), 5.85 (d, J=2 Hz, 2H, Hc), 5.42 (bs, 1H, Hb), 2.0—3.3 (m, 8H, CH_2)
8	6.6—7.0 (m, 3H, Ha), 6.78 (s, 1H, Hd), 5.09 (s, 1H, Hc), 5.51 (bs, 1H, Hb), 1.9—3.4 (m, 8H, CH_2) 2.43 (s, 3H, CH_3-β), 1.65 (s, 3H, CH_3-α)
9	7.16 (d, J=1 Hz, 2H, Hd), 6.65 (bs, 1H, Ha), 5.83 (d, J=1 Hz, 2H, Hc), 5.22 (s, 1H, Hb), 1.7—3.3 (m, 8H, CH_2), 2.22 (s, 6H, CH_3)

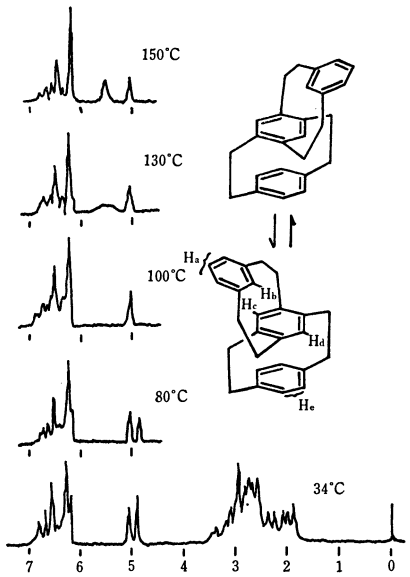

Fig. 1. NMR spectra of **1** in hexachlorobutadiene at various temperatures.

shows NMR spectra at various temperatures. The conformational flipping of meta ring occurs at 100 °C, a relatively low temperature which corresponds to 18 kcal/mol of activation energy. The difference in 3 kcal/mol as compared with [2.2]metaparacyclophane **7** is considered to arise from twisting of the inside ring, which is pulled up and down by two pairs of methylene bridges, to lower the steric energy barrier to the flipping of the meta ring.

For **2**, fixation of the meta ring is expected to give two conformational isomers, **2a** and **2b**, which should show quite different NMR spectra. In fact **2** reveals the NMR spectrum corresponding to 1 : 1 equilibrium mixture of the two isomers at room temperature (Fig. 2). Thus the inner aromatic protons, Hb and Hb', of meta rings appear at slightly different positions (δ 5.28 and 5.37 ppm) with equal integral intensity. Also, as expected from the structures in Fig. 2, the aromatic protons Hc at the inside ring of **2a** are equivalent (δ 5.60), but not those (Hc' and Hd') of **2b** (δ 4.39 and 6.87). The extraordinary upfield shift of the proton Hd' is explained in terms of an additive shielding effect of two meta rings, between which the proton is sandwiched. The energy barrier for the conformational flipping of the meta rings is relatively low (19 kcal/mol). Above the coalescence temperature (116 °C) the inner aromatic protons of meta rings and the aromatic protons of the inside ring appear as a singlet at δ 5.63 and 5.30, respectively.

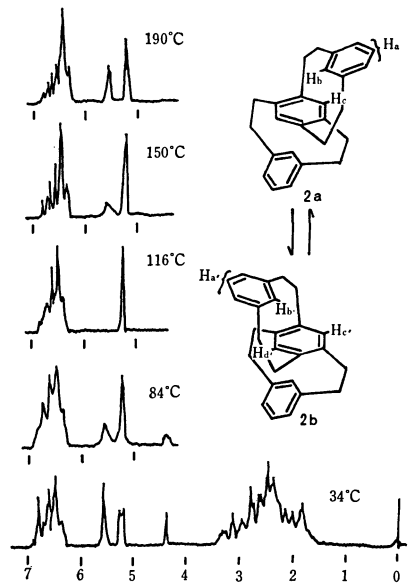

Fig. 2. NMR spectra of **2** in hexachlorobutadiene at various temperatures.

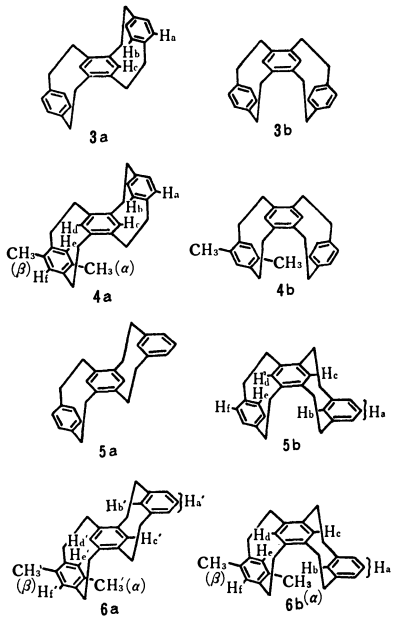

Scheme 2.

Two conformations, **3a** and **3b**, are possible for the structure of **3**. However, the NMR spectrum of **3** is very simple, suggesting that the compound consists of a symmetrical isomer. Dimethyl derivative **4** was prepared in order to facilitate the structure assignment of the parent compound **3**. Examination of the *syn*-form **3b** with a molecular model indicates that the *endo* aromatic protons of the two para rings are sterically crowded. When methyl groups are substituted to **3b**, more severe crowding is expected in the resulting *syn*-form **4b**. On the other hand, such methyl substitution in *anti*-form **3a** does not seem to influence the parent structure. The actual compound **4** is also composed of a single isomer and should have the same geometry as **3** since the aromatic protons, Ha and Hb, of nonsubstituted para ring of **4** show chemical shifts very close to those of **3**. *endo* Methyl protons CH_3-α (δ 1.44) of **4** appear at a slightly higher field than the corresponding protons (δ 1.65) of 12,15-dimethyl[2.2]metaparacyclophane **8**. If the geometry is of *syn*-form, the methyl signal should shift to downfield due to the deshielding effect of the third benzene ring or nonsubstituted para ring. Consequently, the staircase-shape (*anti*-form) structure is assigned to both **3** and **4**. Recently the validity of this assignment has been confirmed by X-ray crystallo-

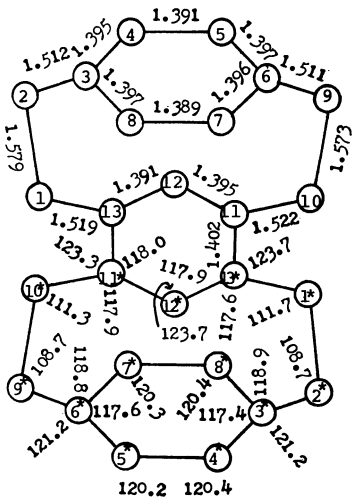

Fig. 3. Profile of triple-layered metaparacyclophane **3**. Bond lengths and angles.

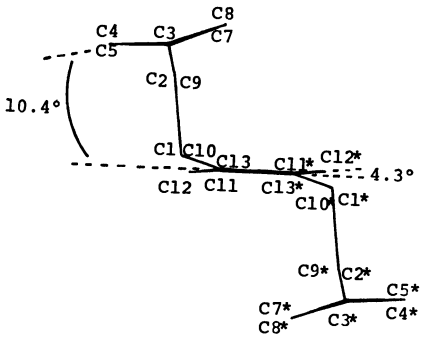

Fig. 4. Projection viewed down the vector C(1)–C(10).

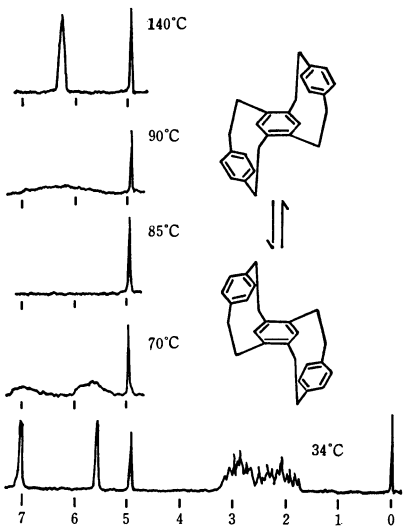

Fig. 5. NMR spectra of **3** in hexachlorobutadiene at various temperatures.

graphic analysis.[3] The inside benzene is slightly overlapped with two para rings at *ca.* 10° angle, as shown in Figs. 3 and 4. By steric repulsion with the two para rings arranged in *anti*-form, the inside benzene ring is bent into a chair shape. This is the first example of a chair-shape benzene. There is a conformational flipping at elevated temperature also for compound **3** (Fig. 5). The nonequivalent aromatic protons, Ha and Hb, of para rings coalesce at 85 °C and appear as a singlet just in the middle of their initial positions at higher temperature. This spectrum indicates that the conformational change occurs between two *anti*-forms by means of double flipping of the two para rings, but not between *anti*- and *syn*-forms by one ring flipping.

A different conformational behavior was observed in the case of **5**. Two conformational isomers, *anti*-form **5a** and *syn*-form **5b**, are also possible for **5**. However, compound **5** shows no temperature dependence in its NMR spectrum, suggesting that it is composed of a single isomer, **5a** or **5b**. Methyl substitution makes the *syn*-form structure unstable as in the case of **3**. Actually the dimethyl derivative **6** was obtained as a mixture of two conformational isomers, **6a** and **6b**, in a 1 : 1 ratio (Table 1). The results may be explained by assuming that the *syn*-form conformer **5b** is assigned to the structure of compound **5** and the methyl substitution equalizes the stabilities of *syn*- and *anti*-forms by lowering the stability of the former. The assumption was confirmed by X-ray crystal analysis of **5** (Figs. 6 and 7).[3] Differing from **3**, the inside benzene of **5** is bent into a boat shape.

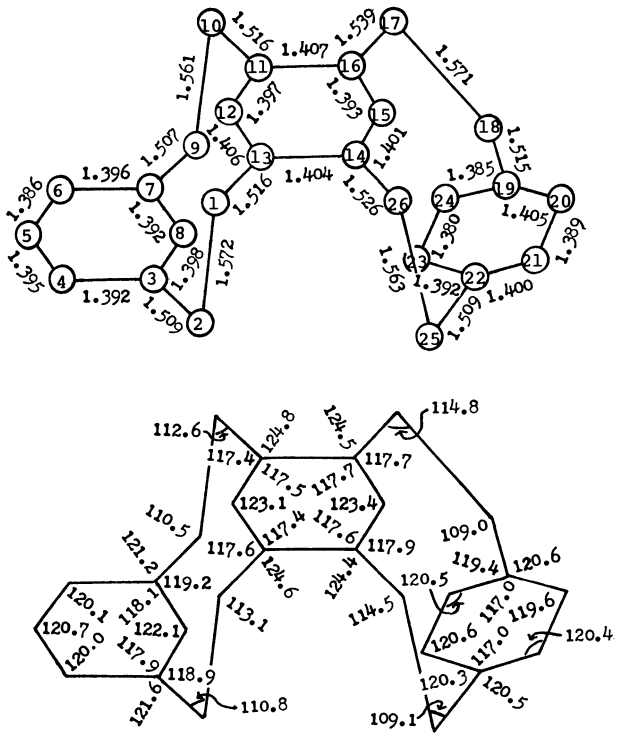

Fig. 6. Profile of triple-layered metaparacyclophane **5**. Bond lengths and angles.

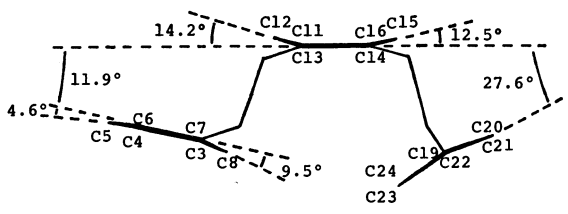

Fig. 7. Projection viewed down the vector C(3)–C(7).

Let us discuss the stereochemical difference between the two triple-layered metaparacyclophanes **3** and **5**. In a series of multilayered [2.2]metacyclophanes, the platform conformer is thermally more stable than the staircase one.[4] This seems to be related to the strained structure of the inside benzene ring. Thus the inside ring is bent into a boat form in the former and into a chair form in the latter. Molecular orbital calculation revealed that the boat-shape benzene is much more stable than the chair-shape one, mainly due to the difference in the resonance integral term.[5] The stability of *syn*-form **5b** can be explained in the same manner. On the other hand, molecular model examination of *syn*-form **3b** indicates that steric crowding between two para benzenes should be considerably large. The steric overcrowding energy presumably overcomes the energy difference between boat and chair forms of the inside benzene, making the *anti*-form geometry favorable for compound **3**.

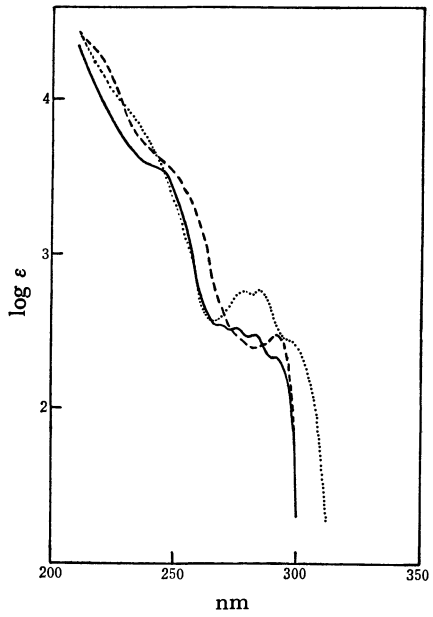

Fig. 8. Electronic spectra of [2.2]metaparacyclophane **7** (—) and the dimethyl derivatives **8**(···) and **9** (---) in cyclohexane.

Electronic Spectra. Electronic spectra of [2.2]-metaparacyclophane **7** and its dimethyl derivatives **8** and **9** are shown in Fig. 8. The most marked features are broadening and bathochromic shift of the absorption bands associated with B_{1u} and B_{2u} transitions of benzene. Such features were generally observed in the spectra of layered cyclophanes and mainly explained by π-electronic interaction between benzene rings.[6] In addition, bending of the benzene ring is responsible to some extent.[7] This is also the case for [2.2]metapara-cyclophane, since its para ring is severely bent into a boat shape as demonstrated by X-ray crystal analyses.[3,8] Although [2.2]paracyclophane shows strong π-electron interaction due to sufficient overlapping of two faced benzenes, such a strong interaction can not be expected for the parent compound **7** of [2.2]metaparacyclophane series because of partial overlapping. However, the interaction in this cyclophane system is evidently realized by methyl substitution. Thus, two dimethyl derivatives **8** and **9** show rather different spectra from that of **7** besides the normal substituent effect. It is especially remarkable in the long wavelength region of **8**, *viz.*, the substitution at para ring is more effective than that at meta ring. This suggests that the transition of the para ring makes relatively large contribution to the transannular electronic interaction of [2.2]meta-paracyclophane.

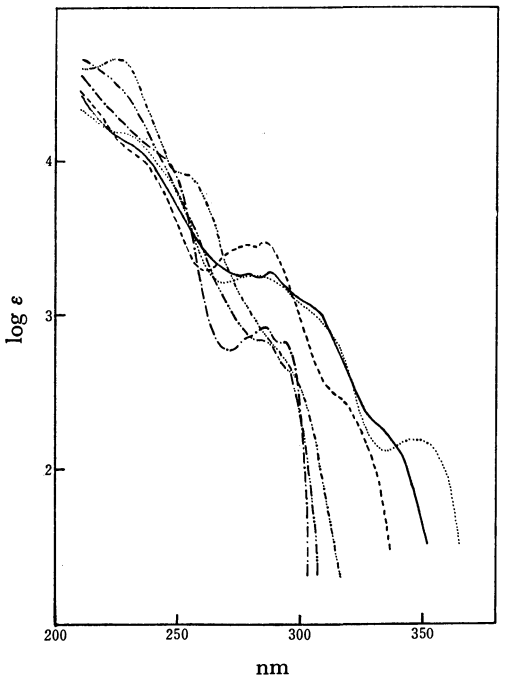

Fig. 9. Electronic spectra of triple-layered [2.2]meta-paracyclophanes **1** (——), **2** (----), **3** (-·-·-), and **5** (-··-), together with triple-layered [2.2]paracyc-lophane **10** (·····) and metacyclophane **11** (-·-·-) in cyclohexane.

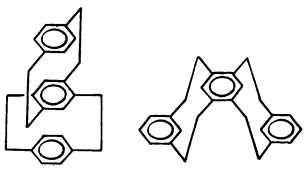

10 **11**

Scheme 3.

A similar consideration can be extended to the present triple-layered metaparacyclophanes. As seen in Fig. 9, the electronic spectra of **1** and **2** show new bands around 330 and 315 nm, respectively, and an increase of intensity of the bands in the 260—310 nm region as compared with that of [2.2]paracyclophane or [2.2]-metaparacyclophane. Thus their absorption curves are similar to the curve of triple-layered [2.2]paracyclophane **10**,[9] indicating that a marked transannular electronic interaction also exists between the meta and para rings. On the other hand, the electronic spectra of **3** and **5** are similar to that of triple-layered [2.2]metacyclophane **11**[10] indicative of a weak electronic interaction. This is in marked contrast to the phenomenon of **1** and **2**.

There is no essential difference in the spectra due to conformational difference between *anti*- and *syn*-forms. Substitution modes of methylene bridges attached to the inside ring of triple-layered [2.2]metaparacyclophane serve as an important factor on overlapping of benzene rings and hence, on the electronic interaction.

The present work was partially supported by a Grant-in-Aid (754096, 1972) for Scientific Research from the Ministry of Education.

References

1) Part XXXV, N. Kannen, T. Otsubo, Y. Sakata, Y. Sakata, and S. Misumi, *Bull. Chem. Soc. Jpn.*, **49**, 3307 (1976).

2) D. T. Hefelfinger and D. J. Cram, *J. Am. Chem. Soc.*, **92**, 1073 (1970); **93**, 4767 (1971); F. Vögtle, *Chem. Ber.*, **102**, 3077 (1969); S. Akabori, S. Hayashi, M. Nawa, and K. Shiomi, *Tetrahedron Lett.*, **1969**, 3727; S. A. Sherrod and V. Boekelheide, *J. Am. Chem. Soc.*, **94**, 5513 (1972); S. A. Sherrod, R. L. da Costa, R. A. Barner, and V. Boekelheide, *ibid.*, **96**, 1565 (1974).

3) Y. Koizumi, T. Toyoda, N. Kannen, H. Horita, and S. Misumi, presented at the Symposium on Molecular Structure, November, 1975 in Osaka (Japan), Abstract p. 455.

4) T. Umemoto, T. Otsubo, and S. Misumi, *Tetrahedron Lett.*, **1974**, 1573.

5) H. Iwamura, H. Kihara, S. Misumi, Y. Sakata, and T. Umemoto, *Tetrahedron Lett.*, **1976**, 615.

6) D. J. Cram, N. L. Allinger, and H. Steinberg, *J. Am. Chem. Soc.*, **76**, 6132 (1963); M. T. Vara, Jr., I. H. Hiller, S. A. Rice, and J. Jortner, *J. Chem. Phys.*, **44**, 23 (1966); S. Iwata, K. Fuke, M. Sasaki, S. Nagakura, T. Otsubo, and S. Misumi, *J. Mol. Spectrosc.*, **46**, 1 (1973).

7) N. L. Allinger, L. A. Freiberg, R. B. Hergmann, and M. A. Miller, *J. Am. Chem. Soc.*, **85**, 1171 (1963); N. L. Allinger and T. J. Walter, *ibid.*, **94**, 9267 (1972); N. L. Allinger, J. T. Sprague, and T. Liljefors, *ibid.*, **96**, 5100 (1974); A. D. Wolf, V. V. Kane, R. H. Levin, and M. Jones, Jr., *ibid.*, **95**, 1680 (1973); V. V. Kane, A. D. Wolf, and M. Jones, Jr., *ibid.*, **96**, 2643 (1974).

8) A. W. Hansen, *Acta Crystallogr.*, **B27**, 197 (1971).

9) T. Otsubo, S. Mizogami, I. Otsubo, Z. Tozuka, A. Sakagami, Y. Sakata, and S. Misumi, *Bull. Chem. Soc. Jpn.*, **46**, 3519 (1973).

10) T. Umemoto, T. Otsubo, Y. Sakata, and S. Misumi, *Tetrahedron Lett.*, **1973**, 593.

Layered Compounds. XXXVII.[1] Syntheses and Properties of Quadruple-layered Metaparacyclophanes

Naoki KANNEN, Tetsuo OTSUBO, and Soichi MISUMI

The Institute of Scientific and Industrial Research, Osaka University, Suita, Osaka 565

(Received June 24, 1976)

Six quadruple-layered [2.2]metaparacyclophanes have been synthesized by photo-induced desulfurization or the Hofmann elimination method. Their electronic spectra exhibit stronger transannular electronic interactions than those of the corresponding triple-layered [2.2]metaparacyclophanes and considerable dependence on the bridge substitution mode of the inside ring. The absorption spectra of the charge transfer complexes of a series of layered metaparacyclophanes and tetracyanoethylene have been studied with regard to the donor characters. It is concluded that the electron release from meta to para ring is significant, while the reverse is less effective.

In preceding papers we reported the syntheses, structures, and properties of triple-layered [2.2]metaparacyclophanes **1**—**4**.[1] Although double-layered [2.2]-metaparacyclophanes **5**—**7** show no remarkable transannular electronic interaction between benzene rings,[1] compounds **1** and **2**, the inside ring of which is doubly *para*-substituted with two pairs of methylene brigdes, exhibit strong interaction as in the case of multilayered [2.2]paracyclophanes. On the other hand, compounds **3** and **4** with doubly *meta*-substituted benzene reveal weak interaction as in the case of multilayered [2.2]-metacyclophanes. In this paper we report the syntheses and properties of some quadruple-layered [2.2]metaparacyclophanes. The compounds are expected to give us further information on the relationship between structures and spectra.

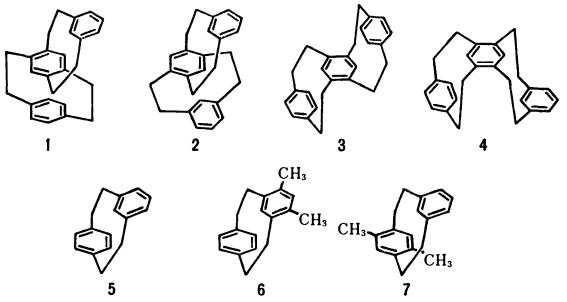

Scheme 1.

Results and Discussion

Syntheses and Structures. Dimethyl derivative **8**[2] of triple-layered [2.2]paracyclophane was brominated with *N*-bromosuccinimide and the resulting dibromide **9** was coupled with 1,3-bis(mercaptomethyl)benzene **10** to afford dithia compound **11** in 16% overall yield.

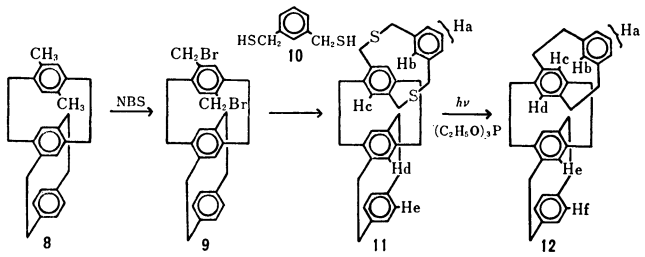

Scheme 2.

Compound **11** was then converted into the desired quadruple-layered metaparacyclophane **12** in an excellent yield (81%) using photodesulfurization developed by Bruhin *et al.*[3] The structure of **12** was determined by its NMR spectrum. Most of the aromatic protons appear at high field due to the shielding effect of the other benzene rings. Hc and Hd protons are not equivalent, indicating fixation of meta ring as in the case of [2.2]metaparacyclophane **5**.[4]

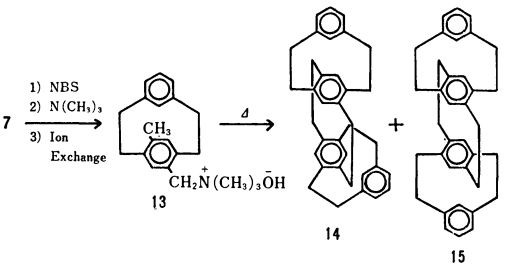

Scheme 3.

Hofmann elimination reaction, a convenient method for approach of multilayered [2.2]paracyclophanes,[2,5] was applied to the syntheses of quadruple-layered metaparacyclophanes **14** and **15**. 12,15-Dimethyl[2.2]-metaparacyclophane **7**[1] was brominated with *N*-bromosuccinimide followed by treatment with trimethylamine and then ion exchange resin to give the quaternary ammonium hydroxide **13**. Pyrolysis of **13** in boiling xylene afforded a mixture of the desired cyclophanes **14** and **15**, which could be separated by utilizing the large difference in their solubility. In the same manner as for quadruple-layered [2.2]paracyclophanes,[2] the more soluble isomer was assigned to the structure **14**, and the less soluble one to the structure **15**. The eclipse of methylene bridges at two inside rings of **15** may be responsible for the lower yield (2.7%) than that of **14** (12%). Fixation of the meta rings of **14** gives two possible conformational structures **14a** and **14b**. They

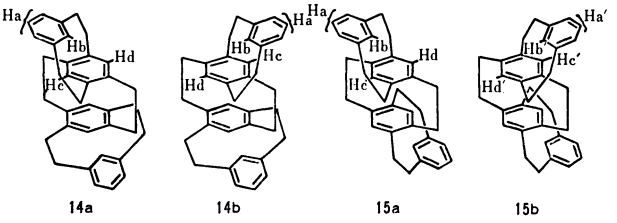

Scheme 4.

are not enantiometric with each other, but can not be distinguished on NMR analysis due to the equivalence of the corresponding aromatic protons. Two conformational structures are expected also for **15**. In this case the NMR spectrum demonstrates two sets of signals for aromatic protons, which correspond to **15a** and **15b**. The ratio was evaluated to be 1 : 1 on the basis of the integral intensities.

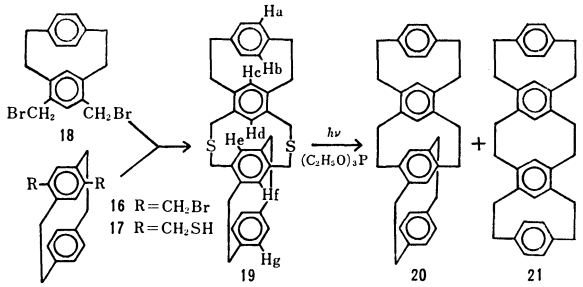

Scheme 5.

4,7-Bis(bromomethyl)[2.2]paracyclophane **16**[1] was led to the corresponding dithiol **17** in 74% yield. Condensation of **17** with 4,6-bis(bromomethyl)[2.2]-metaparacyclophane **18**[1] gave dithia compound **19** in 25% yield. Photodesulfurization of **19** in triethyl phosphite afforded the desired quadruple-layered metaparacyclophane **20** in 40% yield and its isomer **21** in 33% yield. From the fact that triple-layered metaparacyclophane **1** is easily photo-isomerized to **4**,[1] **20** seems to isomerize to **21** during the photolysis.

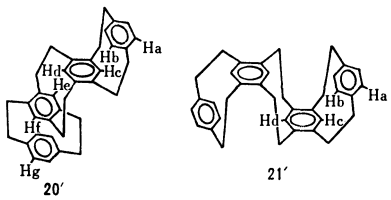

Scheme 6.

The geometry of **3** was confirmed to be a staircase-shape on the basis of NMR analysis[1] and X-ray crystallographic analysis.[6] Similarly, the structure of **20** is expected to have a staircase-shape as shown in **20′**. The NMR spectrum is in good accord with the present structure **20′**. In the same manner as in the case of multilayered[2.2]paracyclophanes,[7] the chemical shifts of the aromatic protons in **20** can be successfully evaluated by considering the anisotropy of the stacked rings. Three stereoisomers are possible for **21**. However, its NMR spectrum is simple and suggests that there is only one conformational isomer having a symmetrical structure. The structure was determined to be **21′** by comparison of the NMR spectrum with that of **4** which has a platform-shape differing from **3**.[1]

Condensation of 4,6-bis(bromomethyl)[2.2]metacyclophane **22**[8] with 4,7-bis(mercaptomethyl)[2.2]-paracyclophane **17** gave coupling compound **23** in 29% yield. Photodesulfurization of **23** afforded **24** in 30% yield. The product **24** is considered to be derived from **25** which was initially desired. Unfortunately **25**

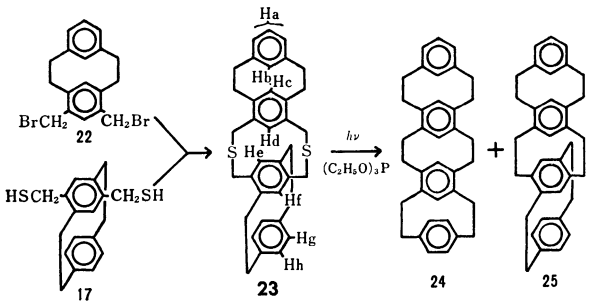

Seheme 7.

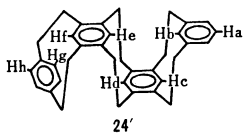

Scheme 8.

could not be isolated because of contamination with oily by-products. Four conformational isomers are possible for **24**, but the NMR spectrum can be explained on a single isomer of zigzag structure **24′**. The assignment is consistent with the fact that in multilayered metacyclophanes, the structure of platform-shape is thermodynamically stable.[9]

Electronic Spectra. The electronic spectra of quadruple-layered [2.2]metaparacyclophanes are shown in Fig. 1. The explanation that bridge substitution mode is important for transannular electronic interaction of triple-layered metaparacyclophane[5] is also applicable to the present case. Compounds **12**, **14**, and **15** are formally regarded as if they are given by stacking another meta or para substituted benzene on the outside para ring of triple-layered metaparacyclophane **1**. As expected, their spectra exhibit much more bathochromic

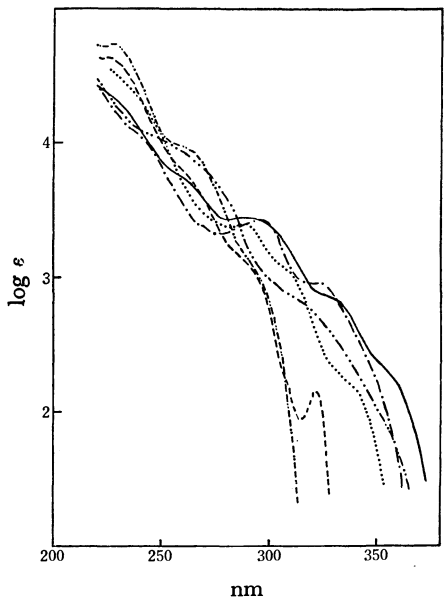

Fig. 1. Electronic spectra of quadruple-layered metaparacyclophanes **12** (——), **14** (-·-·-) in cyclohexane and **15** (-···-), **20** (·····), **21** (– – –), **24** (------) in tetrahydrofuran.

shifts and stronger transannular electronic interactions than that of **1**. On the other hand, stacking of another *para*-substituted benzene on the outside meta ring of **1** gives the structure **20**, which is expected to provide spectral properties of both meta and para bridged types. In fact, the electronic spectrum of **20** is, in a short wavelength region, similar to that of **3** (meta type) and, in a long wavelength region, identical with that of **1** (para type). Compounds **21** and **24** are classified as a meta bridged type. Their spectra exhibit just a weak transannular electronic interaction as seen in multilayered [2.2]metacyclophanes.[8]

Charge Transfer Spectra. It is well-known that an aromatic hydrocarbon forms a charge transfer complex with tetracyanoethylene (TCNE) and that absorption maximum of its charge transfer band gives information on π-basicity of the donor.[10] The increased transannular electronic interaction of multilayered [2.2]paracyclophanes was observed to be reflected in the increase of π-basicity.[2,5] Thus with increasing number of layers, the donor character of the cyclophanes increases and the absorption maximum of the charge transfer complex with TCNE shifts to longer wavelength.

It is interesting to study which of the two benzene rings in [2.2]metaparacyclophane **5** tends to more easily form a complex with TCNE and which of two types of transannular electron release in TCNE complexes is more effective, *viz.*, from the non-complexed meta or para ring to the complexed face ring. Absorption maximum wavelengths of layered metaparacyclophane–TCNE complexes are summarized in Table 1. The charge transfer complex of *m*-xylene with TCNE shows a CT absorption maximum at 440 nm in dichloromethane, and the complex of *p*-xylene two absorption maxima at 420 nm and 465 nm.[2] The CT absorption maximum of [2.2]metaparacyclophane **5** with TCNE is at 457 nm which is situated between the above values of *m*-xylene and *p*-xylene. This suggests that both the meta and para benzenes form complexes with TCNE. The CT complexes of dimethyl derivatives **6** and **7** give us further information. Their absorption maxima appear around 490 nm, with an additional shoulder at 570 nm for **7**. This is considered to arise from the complex of the durene moiety with TCNE. Since durene–TCNE complex shows a CT band at 480 nm,[2] the transannular electron release from the meta ring to the complexed durene moiety is more significant, whereas that from the para ring is less effective.

Table 1. Absorption maxima of layered [2.2]-metaparacyclophane–TCNE complexes in dichloromethane

Compound	λ_{max} (nm)
[2.2]MPC[a]	
5	457
6	497
7	486, 570[b]
MPC[a] having meta-rings at both outsides	
2	473
14	472
15	476
MPC[a] having para-rings at both outsides	
3	451, 547
20	545
MPC[a] having a para- and a meta-rings at both outsides	
1	483, 585[b]
4	428, 520[b]
12	486, 710

a) Metaparacyclophanes. b) Shoulder.

In the case of multilayered metaparacyclophanes having meta rings on both outsides, TCNE exclusively forms a complex with the outside meta ring since TCNE is sterically unable to face the inside ring. Evidently these compounds have very weak π-basicity although their own electronic spectra exhibit remarkable transannular electronic interactions. It can be concluded that electron release from the para ring to the meta ring is less effective.

On the other hand, compounds **3** and **20** have para rings at both ends which exclusively face TCNE. The two absorption maxima of **3** at 451 and 547 nm exhibit outstanding bathochromic shifts as compared with the corresponding peaks of *p*-xylene–TCNE complex. Evidently there is reasonable electron release from the meta to the para ring as described in dimethyl[2.2]-metaparacyclophanes. In the case of **20**, the [2.2]-paracyclophane moiety is considered to form TCNE complex with relative ease. Comparing the CT absorption maximum (545 nm) with that (521 nm) of [2.2]-paracyclophane itself,[2] we might expect some contribution of electron release from the third stacked benzene ring to the complexed face ring of the [2.2]paracyclophane moiety in TCNE complex of **20**.

Compounds **1** and **12** contain double- and triple-layered [2.2]paracyclophane moieties, respectively, which have more increased donor character than [2.2]-metaparacyclophane. In fact, the long wavelength maxima of the TCNE complexes shift to longer wavelength like multilayered [2.2]paracyclophanes[2] and the donor characters of these cyclophanes increase progressively. The transannular electron release of **12** is particularly significant. The case of **4** seems to be more complicated because its structure is a platform-shape and the inside ring is also capable of forming a complex. Probably its CT spectrum appears as a mixture of all possible complexes.

Experimental

Mps are uncorrected. All the solvents are of reagent grade unless otherwise specified. NMR spectra were taken with a Hitachi-Perkin Elmer R-20 spectrometer (60 MHz) using tetramethylsilane as an internal std, electronic spectra with a Hitachi EPS-3T spectrophotometer, and mass spectra with a Hitachi RMU-7 spectrometer at 70 eV using a direct insertion technique.

Bis(bromomethyl)triple-layered[2.2]paracyclophane (9). A mixture of dimethyl derivative **8**[2] (1.00 g, 2.7 mmol) of triple-layered [2.2]paracyclophane, *N*-bromosuccinimide (0.97 g, 5.4 mmol), and a small amount of benzoyl peroxide in 20 ml of carbon tetrachloride was refluxed for 3 h. After removal of insoluble succinimide by filtration, the soln was washed with water and dried over anhyd sodium sulfate. The solvent was evaporated to give the desired product as an oil (1.65 g). This was used in the next step without purification.

*Dithia Compound (**11**).* A soln of the above dibromide **9** in 35 ml of benzene and a soln of 1,3-bis(mercaptomethyl)-benzene **10** (0.54 g, 3 mmol) and sodium hydroxide (0.26 g, 6.5 mmol) in water (2 ml) and ethanol (33 ml) were added dropwise and simultaneously over a period of 2.5 h to a refluxing ethanol (100 ml) in a nitrogen atmosphere. After the solvent was removed, the residue was taken up in benzene and chromatographed on alumina (40 g) using benzene–hexane (1:1) for elution. The initial fraction gave the desired coupling compd **11** (0.23 g, 16% based on **8**), colorless needles from 1:1 benzene–ethanol, mp 217—218 °C.

Found: C, 81.29; H, 6.67; S, 12.16%. Calcd for $C_{36}H_{36}S_2$: C, 81.14; H, 6.87; S, 12.03%. NMR ($CDCl_3$, δ) 2.0—3.9 (m, 24H, CH_2), 5.29 (bs, 1H, Hb), 5.48 (s, 2H, Hd), 5.64 (s, 2H, Hc), 6.17 (s, 4H, He), 6.82 (m, 3H, Ha). MS *m/e* 532 (M^+), 104.

*Quadruple-layered Metaparacyclophane (*m-p,p-p,p-p*) (**12**).* The above coupling compd **11** (100 mg, 0.19 mmol) in 13 ml of purified triethyl phosphite was irradiated through a quartz tube with a high pressure mercury lamp for 3 h under a nitrogen atmosphere. The solvent was evaporated and the residue was chromatographed over silica gel (20 g) using 1:4 benzene–hexane for elution. The first fraction gave the desired product **12** (71 mg, 81%), colorless plates from 1:1 benzene–ethanol, mp 117—118 °C.

Found: C, 92.10; H, 7.60%. Calcd for $C_{36}H_{36}$: C, 92.24; H, 7.76%. NMR ($CDCl_3$, δ) 1.5—3.4 (m, 24H, CH_2), 4.67 (s, 1H, Hc), 5.05 (bs, 1H, Hb), 5.27 (s, 2H, He), 5.90 (s, 1H, Hd), 6.15 (s, 4H, Hf), 6.5 (m, 3H, Ha). MS *m/e* 468 (M^+), 234.

*Quadruple-layered Metaparacyclophane (*m-p,p-p,p-m*) (**14** and **15**).* A mixture of 12,15-dimethyl[2.2]metaparacyclophane **7**[1] (2.98 g, 13 mmol), *N*-bromosuccinimide (2.24 g, 13 mmol), and a small amount of benzoyl peroxide in 20 ml of carbon tetrachloride was refluxed for 5 h. After removal of succinimide by filtration, the soln was washed with water, dried over anhyd sodium sulfate, and then mixed with excess trimethylamine in ether. The mixture was stirred with ice cooling overnight. The resulting white ppt of quaternary ammonium bromide was extracted with a small amount of water. The aq soln was filtered, washed with xylene, and passed through a column containing strongly basic anion exchange resin, Dowex I-X8, 50—100 mesh. The aq soln of the quaternary ammonium hydroxide **13** was mixed with phenothiazine (100 mg) and xylene (50 ml). The mixture was heated with stirring under a nitrogen atmosphere, and water was removed by azeotropic distillation using a Dean-Stark type of water separator. After removal of water, the reflux was continued for additional 6 h. The solvent was removed and the residue was chromatographed over silica gel using 1:4 benzene–hexane for elution. The first fraction gave a mixture of **14** and **15**, which then separated by treatment with carbon tetrachloride. The more soluble isomer **14** (366 mg, 12%) was recrystd from toluene, colorless fine crystals, mp 191—192 °C.

Found: C, 92.27; H, 7.88%. Calcd for $C_{36}H_{36}$: C, 92.24; H, 7.76%. NMR ($CDCl_3$, δ) 1.2—3.4 (m, 24H, CH_2), 4.73 (s, 2H, Hc), 5.06 (bs, 2H, Hb), 5.94 (s, 2H, Hd), 6.4—7.0 (m, 6H, Ha). MS *m/e* 468 (M^+), 234, 104.

The less soluble isomer **15** (82 mg, 2.7%) was recrystd from toluene, colorless fine crystals, mp 265 °C (dec).

Found: C, 92.36; H, 7.61%. Calcd for $C_{36}H_{36}$: C, 92.24; H, 7.76%. NMR ($CDCl_3$, δ) 1.0—3.0 (m, 48H, CH_2), 4.68 (s, 2H, Hc′), 4.79 (s, 2H, Hc), 5.10 (bs, 4H, Hb, and Hb′), 5.94 (s, 2H, Hd), 6.07 (s, 2H, Hd′), 6.4—6.9 (m, 12H, Ha and Ha′). MS *m/e* 468 (M^+), 234.

*4,7-Bis(mercaptomethyl)[2.2]paracyclophane (**17**).* 4,7-Bis(bromomethyl)[2.2]paracyclophane **16**[1] (11.82 g, 30 mmol) was added portionwise to a boiling soln of thiourea (4.60 g, 61 mmol) in 50 ml of ethanol. The mixture was refluxed for 2 h and concd to dryness. The crude thiouronium salt was refluxed with potassium hydroxide (20 g) in 50 ml of water for 15 h. After filtration, the soln was acidified with dil sulfuric acid and the resulting solid was extracted with chloroform. The extract was washed with water, dried over anhyd sodium sulfate, and subjected to alumina column chromatography. Elution with 1:1 benzene–hexane gave the desired mercaptan **17** (6.70 g, 74%), colorless prisms from benzene–hexane, mp 92—93 °C.

Found: C, 72.23; H, 6.79; S, 21.03%. Calcd for $C_{18}H_{20}S_2$: C, 71.94; H, 6.72; S, 21.34%. NMR ($CDCl_3$, δ) 1.53 (t, J=8 Hz, 2H, SH), 2.6—4.0 (m, 12H, bridged CH_2 and CH_2-S), 6.25 (s, 2H, ArH), 6.40 and 6.63 (A_2B_2, J=8 Hz, 4H, ArH). MS *m/e* 300 (M^+).

*Dithia Compound (**19**).* A soln of 4,6-bis(bromomethyl)-[2.2]metaparacyclophane **18**[1] (1.30 g, 3.3 mmol) in 35 ml of benzene and a soln of 4,7-bis(mercaptomethyl)[2.2]paracyclophane **17** (0.99 g, 3.3 mmol) and potassium hydroxide (0.38 g, 5.8 mmol as 85% content) in water (7 ml) and ethanol (28 ml) were added dropwise and simultaneously over a period of 3 h to boiling ethanol (100 ml) in a nitrogen atmosphere. Reflux was continued for additional 12 h and the solvent was removed. The residue was taken up in benzene and chromatographed over alumina using 1:1 benzene–hexane for elution. The first fraction gave the desired product **19** (0.44 g, 25%), colorless fine crystals from toluene, mp 260 °C (with dec).

Found: C, 81.24; H, 6.67; S, 11.90%. Calcd for $C_{36}H_{36}S_2$: C, 81.14; H, 6.82; S, 12.03%. NMR ($CDCl_3$, δ) 1.8—4.2 (m, 24H, CH_2), 4.86 (s, 1H, Hc or Hd), 5.06 (s, 1H, Hd or Hc), 6.03 (bs, 2H, Hb), 6.15 (s, 1H, He or Hf), 6.43 (s, 1H, Hf or He), 6.3—6.7 (m, 4H, Hg), 7.13 (bs, 2H, Ha). MS *m/e* 532 (M^+).

*Quadruple-layered Metaparacyclophane (*p-m,m-p,p-p*) (**20**) and (*p-m,m-m,m-p*) (**21**).* The dithia compd **19** (100 mg, 0.19 mmol) and triethyl phosphite (14 ml) were placed in a quartz tube and irradiated with a high pressure mercury lamp for 3 h under bubbling nitrogen. The solvent was evaporated and the residue was treated with 1:4 benzene–hexane. The insoluble solid was filtered and washed with hexane to give the pure isomer **21** (29 mg, 33%), colorless plates from toluene, mp$>$300 °C.

Found: C, 91.99; H, 7.48%. Calcd for $C_{36}H_{36}$: C, 92.24; H, 7.76%. NMR ($CDCl_3$, δ) 1.5—3.5 (m, 24H, CH_2), 5.26 (s, 2H, Hd), 5.72 (s, 2H, Hc), 6.35 (bs, 4H, Hb), 7.47 (bs, 4H, Ha). MS *m/e* 468 (M^+).

The filtrate was subjected to silica gel column chromatography. Elution with 1:4 benzene–hexane afforded the other isomer **20** (35 mg, 40%), colorless plates from 1:1 benzene–hexane, mp 242—243 °C.

Found: C, 91.99; H, 7.54%. Calcd for $C_{36}H_{36}$: C, 92.24; H, 7.76%. NMR ($CDCl_3$, δ) 1.5—3.5 (m, 24H, CH_2), 4.62 (s, 1H, Hd), 4.69 (s, 1H, He), 4.75 (s, 1H, Hc), 5.55 (bs, 2H, Hb), 6.11 (s, 1H, Hf), 6.29 (bs, 4H, Hg), 7.09 (bs, 2H, Ha). MS *m/e* 468 (M^+), 364, 104.

*Dithia Compound (**23**).* A soln of 4,6-bis(bromomethyl)-[2.2]metacyclophane **22**[8] (1.36 g, 3.5 mmol) in 40 ml of benzene and a soln of 4,7-bis(mercaptomethyl)[2.2]paracyclophane **17** (1.04 g, 3.5 mmol) and potassium hydroxide (0.55 g, 8.3 mmol as 85% content) in water (10 ml) and ethanol (30 ml) were added dropwise and simultaneously over a period of 3.5 h to boiling ethanol (100 ml) in a nitrogen atmosphere.

Reflux was continued for additional 12 h. The solvent was removed, and the residue was taken up in benzene and subjected to alumina column chromatography. Elution with 1:1 benzene–hexane gave an oil which was then treated with hexane to solidify. The product **23** was filtered and washed with hexane (0.52 g, 29%), colorless fine crystals from toluene, mp 230—231 °C.

Found: C, 81.26; H, 6.68; S, 11.94%. Calcd for $C_{36}H_{36}S_2$: C, 81.14; H, 6.82; S, 12.03%. NMR ($CDCl_3$, δ) 2.5—4.1 (m, 25H, CH_2 and Hc), 4.52 (bs, 1H, Hb), 5.23 (s, 1H, Hd), 6.20 (s, 2H, He and Hf), 6.40 and 6.60 (A_2B_2, J=7 Hz, 4H, Hh, and Hg, respectively), 7.1 (m, 3H, Ha). MS *m/e* 532 (M^+).

Quadruple-layered Metaparacyclophane (m-m,m-m,m-p) ***(24)***. The dithia compd **23** (50 mg, 0.09 mmol) and triethyl phosphite (13 ml) was placed in a quartz tube and irradiated with a high pressure mercury lamp (400 W) for 2 h under nitrogen. The solvent was evaporated and the residue was chromatographed over silica gel using 1:4 benzene–hexane for elution. After a mixture of **25** and an unknown oily compd, the desired product **24** was eluted (13 mg, 30%), colorless fine crystals from toluene, mp>300 °C.

Found: C, 92.23; H, 7.50%. Calcd for $C_{36}H_{36}$: C, 92.24; H, 7.76%. NMR ($CDCl_3$, δ) 1.5—3.7 (m, 24H, CH_2), 4.19 (s, 1H, Hc), 4.58 (s, 1H, He), 5.01 (bs, 1H, Hb), 5.62 (s, 1H, Hd), 5.71 (s, 1H, Hf), 6.50 (d, J=2 Hz, 2H, Hg), 7.1—7.4 (m, 3H, Ha), 7.50 (d, J=2 Hz, 2H, Hh). MS *m/e* 468 (M^+).

The present work was partially supported by a Grant-in-Aid (754096, 1072) for Scientific Research from the Ministry of Education, to which the authors' thanks are due.

References

1) Part XXXV and XXXVI, N. Kannen, T. Otsubo, Y. Sakata, and S. Misumi, *Bull. Chem. Soc. Jpn.*, **49**, 3307, 3203 (1976).

2) T. Otsubo, S. Mizogami, I. Otsubo, Z. Tozuka, A. Sakagami, Y. Sakata, and S. Misumi, *Bull. Chem. Soc., Jpn.* **46**, 3519 (1973).

3) J. Bruhin, W. Kneubühler, and W. Jenny, *Chimia*, **27**, 277 (1973); J. Bruhin and W. Jenny, *Tetrahedron Lett.*, **1973**, 1215.

4) D. T. Hefelfinger and D. J. Cram, *J. Am. Chem. Soc.*, **92**, 1073 (1970); **93**, 4767 (1971); F. Vögtle, *Chem. Ber.*, **102**, 3077 (1969); S. Akabori, S. Hayashi, M. Nawa, and K. Shiomi, *Tetrahedron Lett.*, **1969**, 3727; S. A. Sherrod, R. L. daCosta, R. A. Barnes, and V. Boekelheide, *J. Am. Chem. Soc.*, **96**, 1565 (1974).

5) D. T. Longone and H. S. Chow, *J. Am. Chem. Soc.*, **92**, 994 (1970).

6) Y. Koizumi, T. Toyoda, N. Kannen, H. Horita, and S. Misumi, presented at the Symposium on Molecular Structure, November, 1975 in Osaka (Japan), Abstract p. 455.

7) T. Otsubo, S. Mizogami, Y. Sakata, and S. Misumi, *Bull. Chem. Soc. Jpn.*, **46**, 3831 (1973).

8) T. Umemoto, T. Otsubo, Y. Sakata, and S. Misumi, *Tetrahedron Lett.*, **1973**, 593.

9) T. Umemoto, T. Otsubo, and S. Misumi, *Tetrahedron Lett.*, **1974**, 1573; H. Iwamura, H. Kihara, S. Misumi, Y. Sakata, and T. Umemoto, *ibid.*, **1976**, 615.

10) R. E. Merrifield and W. D. Phillip, *J. Am. Chem. Soc.*, **80**, 2778 (1958).

Arjungenin, Arjunglucoside I, and Arjunglucoside II. A New Triterpene and New Triterpene Glucosides from *Terminalia arjuna*[1]

Tadashi HONDA, Tatsushi MURAE, Takahiko TSUYUKI, Takeyoshi TAKAHASHI, and Masanobu SAWAI*

Department of Chemistry, Faculty of Science, The University of Tokyo, Bunkyo-ku, Tokyo 113
**Chemical Research Laboratory, Teikoku Hormon Manufacturing Co., Ltd., Shimosakunobe, Kawasaki 213*

(Received June 25, 1976)

Arjungenin, a new triterpene isolated from *Terminalia arjuna*, is shown to be 2α,3β,19α,23-tetrahydroxyolean-12-en-28-oic acid (**1**). The structures of two new triterpene glucosides, arjunglucoside I and arjunglucoside II, isolated from the same plant, were determined to be β-D-glucopyranosyl 2α,3β,19α,23-tetrahydroxyolean-12-en-28-oate (**2**) and β-D-glucopyranosyl arjunolate (**3**), respectively.

It has been reported that *Terminalia arjuna* (Combretaceae) contains ellagic acid, D(+)-mannitol, (+)-leucocyanidin, (+)-leucodelphinidin, β-sitosterol, oleanolic acid, arjunic acid, arjunolic acid, arjunetin, and a saponin ($C_{42}H_{68}O_{15}\cdot 2H_2O$).[2,3] The methanol extract of the bark of the plant was recently examined, and a new sapogenin which we named arjungenin was isolated. In the present communication, we wish to report the structure determination leading to the structure **1** for arjungenin. An isolation of two new saponins named arjunglucoside I (**2**) and arjunglucoside II (**3**) from the same plant is also described.

The molecular formula of $C_{30}H_{48}O_6$ was given for arjungenin (**1**), mp 293—294 °C (dec), $[\alpha]_D$ +29° (EtOH), based on its elemental analysis and mass spectral data. Arjungenin was treated with diazomethane to give a methyl ester (**4**), mp 162—165 °C, which on acetylation with acetic anhydride in pyridine afforded an ester triacetate (**5**), mp 137—138 °C. Treatment of **5** with acetic anhydride in the presence of perchloric acid gave an ester tetraacetate (**6**), an amorphous solid, which shows no IR absorption due to a hydroxyl group. Therefore, the nature of all six oxygen atoms involved in arjungenin is characterized. Arjungenin is a tetrahydroxy carboxylic acid.

In the mass spectra of arjungenin (**1**), **4**, **5**, and of **6**, characteristic peaks due to a retro-Diels-Alder-type cleavage of the olean-12-ene skeleton[4,5] appear at *m/e* 264, *m/e* 278, *m/e* 278, and *m/e* 320, respectively, showing the presence of a hydroxyl group at the D/E ring of arjungenin. The ester triacetate (**5**) was heated under reflux with phosphoryl chloride in pyridine to give a mixture of dienes (**7** and **8**), which was then treated with dry hydrogen chloride in chloroform to afford a single product (**8**), mp 115—118 °C (UV and PMR spectral data: *cf.* Experimental). This product (**8**) was found to be identical with the diene (**8**) derived from methyl tri-*O*-acetylarjunolate (**9**)[6] according to the procedures described by King *et al.*[3] The Collins oxidation of **5** gave a ketone (**10**), an amorphous solid, whose ORD curve (a=+102) was almost identical with that (a=+102) of a 19-keto derivative (**11**)[2a] prepared from arjunic acid (**12**).[2a] Arjungenin is thus suggested to be 2α,3β,19ξ,23-tetrahydroxyolean-12-en-28-oic acid.

The structure of tomentosic acid has been determined to be 2α,3β,19β(equatorial), 23-tetrahydroxyolean-12-en-28-oic acid (**13**).[7] As the physical constants of arjungenin and its methyl ester are not identical with those[7] of **13** and its methyl ester, respectively, the hydroxyl group at C-19 of arjungenin (**1**) is considered to be in an α(axial) configuration. This received support from the following evidence.

Reduction of a ketone (**14**) with sodium borohydride has been reported to yield a 19α(axial)-ol (**15**; methyl arjunate) almost quantitatively.[2a] On reduction with sodium borohydride, the ketone (**10**) gave arjungenin ester triacetate (**5**) as a sole product. The PMR spectrum

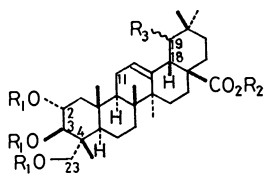

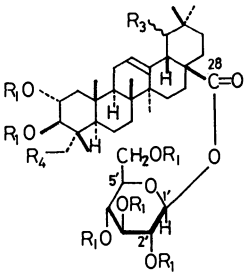

	R_1	R_2	R_3
1	H	H	α-OH
4	H	CH_3	α-OH
5	Ac	CH_3	α-OH
6	Ac	CH_3	α-OAc
9	Ac	CH_3	H
13	H	H	β-OH
24	H	H	H
27	CH_3	H	H

	R_1	R_3	R_4
2	H	α-OH	OH
3	H	H	OH
22	Ac	α-OH	OAc
25	Ac	H	OAc
26	CH_3	H	OCH_3
28	H	α-OH	H
29	Ac	α-OH	H

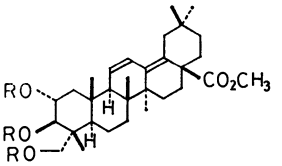

8 R=Ac
30 R=H

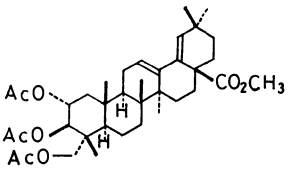

7

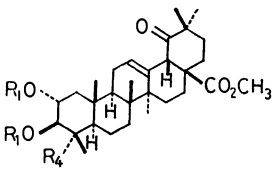

	R_1	R_4
10	Ac	CH_2OAc
11	Ac	CH_3
14	H	CH_3

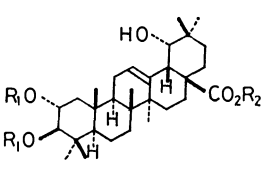

	R_1	R_2
12	H	H
15	H	CH_3
20	Ac	CH_3

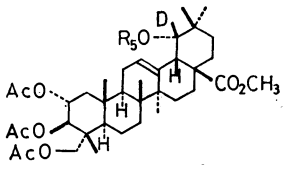

16 R_5=H
17 R_5=Ac

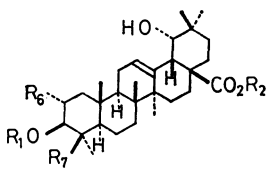

	R_1	R_2	R_6	R_7
18	H	H	H	CH_3
19	H	H	OH	CH_2OH
21	Ac	CH_3	OAc	CH_2OAc

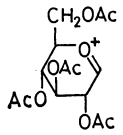

23

of **5** shows a broad signal ($W_{1/2}$=6 Hz) at δ 3.10 due to a proton on C-18 (β, axial) and a multiplet at δ 3.35 due to a proton on C-19 (Table 1). When deuterium oxide was added, this multiplet changed into a doublet ($J_{18\beta,19\beta}$=4 Hz) suggesting an equatorial (β) nature for the proton on C-19. The presence of the same coupling constant ($J_{18\beta,19\beta}$=4 Hz) was observed in the spectrum of arjungenin ester tetraacetate (**6**) (Table 1). The ketone (**10**) was reduced with sodium borodeuteride (in dioxane, room temperature) to give a 19β-deuterated product (**16**). In the PMR spectrum of **16**, the signal at δ 3.10 due to a proton on C-18 appears as a broad singlet ($W_{1/2}$=3 Hz), while the multiplet at δ 3.35 is absent. When treated with acetic anhydride in the presence of perchloric acid, **16** yielded a 19β-deuterated tetraacetate (**17**). The signal due to a proton on C-18 of **17** is shifted and appears at δ 3.30 The evidence described above confirms the assignment for signals due to the protons on C-18 and C-19, and leads to an α(axial)-configuration for the hydroxyl group at C-19. The structure including absolute configuration of arjungenin should be represented by 2α,3β,19α,23-tetrahydroxyolean-12-en-28-oic acid (**1**).

Siaresinolic acid (**18**),[8,9] arjunic acid (**12**),[2a] and sericic acid (**19**)[10] are triterpene acids which have the same structure moiety (19α-hydroxyolean-12-en-28-oic acid structure) around the C/D/E rings as that of arjungenin (**1**). The assignments hitherto reported for the PMR signals due to the protons on C-18β and C-19β of methyl di-*O*-acetylarjunate (**20**) and of methyl tri-*O*-acetylsericate (**21**) seem to be erroneous. In the PMR spectrum of **20**, a triplet at δ 3.35 and a broad signal at δ 3.10 were described to be due to a proton on C-19β and a hydroxyl group on C-19α, respectively.[2a] However, we found that the latter signal (δ 3.10) remained unchanged after addition of deuterium oxide. The signal at δ 3.10 must be due to the proton on C-18β in accordance with our spectral data for arjungenin ester triacetate (**5**) (*cf.* Table 1). Bombardelli *et al.* reported that in the PMR spectrum of **21** a broad doublet at δ 3.16 (J=3 Hz) and a doublet at δ 3.34 (J=3 Hz) are due to the protons on C-19β and C-18β, respectively.[10] These assignments are considered to be reversed based on the observation described for **5** (*cf.*

Table 1. PMR spectral data (in δ values)

Compounds	**5**[a]	**6**[a]	**22**[b]	**25**[b]
t-CH_3	0.69s	0.68s	0.70s	0.75s
	0.91s	0.82s	0.92s	0.92s
	0.99s	0.90s	0.96s	0.92s
	0.99s	1.06s	0.99s	0.92s
	1.10s	1.06s	1.10s	1.10s
	1.25s	1.27s	1.25s	1.12s
-$OCOCH_3$	1.99s	1.99s	2.00s	1.99s
	2.01s	2.01s	2.02s	2.01s
	2.09s	2.08s	2.04s	2.03s
		2.10s	2.04s	2.03s
			2.04s	2.03s
			2.08s	2.06s
			2.11s	2.08s
-CO_2CH_3	3.62s	3.65s	—	—
$C_{(18\beta)}$-H	3.10[c]	3.35br.d J=4	3.08[c]	2.85[c]
$C_{(19\beta)}$-H	3.35m[d]	4.92d J=4	3.34[c]	—[e]
-$C_{(23)}H_2$-OAc	3.58[f] 3.82[g]	3.58[f] 3.82[g]	3.61[f] 3.83[g]	3.59[f] 3.85[g]
$H_{(5')}$-H	—	—	3.80m	3.80m
-$C_{(6')}H_2$-OAc	—	—	4.06[h] 4.28[i]	4.06[h] 4.28[i]
$C_{(3\alpha)}$-H, $C_{(2\beta)}$-H	*ca.* 5.10[j]	*ca.* 5.10[j]	—[k]	—[k]
$C_{(2')}$-H, $C_{(3')}$-H, $C_{(4')}$-H	—	—		
$C_{(12)}$-H	5.45t	5.50t	5.44[c]	5.32[c]
$C_{(1')}$-H	—	—	5.60d J=8	5.58d J=8

a) Determined in $CDCl_3$ at 60 MHz. Coupling constants are expressed in Hz. s: singlet; d: doublet; br. d: broad doublet; t: triplet; m: multiplet. b) Determined in $CDCl_3$ at 100 MHz. c) Broad signal. d) On addition of D_2O, this multiplet changes into a doublet (J=4 Hz). e) Unresolved signal. f) A-part of AB-type quartet (J_{AB}=12 Hz). g) B-part of AB-type quartet. h) A-part of ABX-spin system (J_{AB}=12 Hz; J_{AX}=2 Hz). i) B-part of ABX-spin system (J_{AB}=12 Hz; J_{BX}=4 Hz). j) These signals are overlapped. k) These signals are overlapped and appear at δ 4.96—δ 5.30.

Table 1).

Arjunglucoside I (**2**) crystallized from aqueous methanol as colorless needles, mp 231 °C, $[\alpha]_D$ +17° (EtOH). Elemental analysis indicates the formula $C_{36}H_{58}O_{11}\cdot 2H_2O$. Acid-catalyzed methanolysis of **2** afforded arjungenin (**1**) and methyl D-glucoside. An alkaline hydrolysis of **2** yielded **1** and D-glucose. The IR spectrum of **2** shows an ester carbonyl absorption at 1730 cm^{-1} and no carbonyl absorption due to a free carboxylic acid. Therefore the presence of an ester glucoside linkage is suggested for **2**. Acetylation of **2** with acetic anhydride and pyridine gave a heptaacetate (**22**). The mass spectrum of **22** shows a peak at *m/e* 331 due to a fragment ion (**23**)[11] formed by cleavage of

the glucoside linkage; the appearance of a series of peaks at *m/e* 331, *m/e* 211, *m/e* 169, and *m/e* 109[11] suggests the presence of a tetra-*O*-acetylglucopyranosyl group for **22**. As the tetra-*O*-acetyl-D-glucopyranosyl group preferentially exists as a Cl form, the PMR spectrum of **22** ($J_{1',2'}$=8 Hz; Table 1) indicates the presence of a β-glucosyl linkage in the molecule.[12] The presence of an ester glucoside linkage in **22** received support from the appearance of signals due to a proton on C-1′ at δ 5.60 (Table 1). The structure of arjunglucoside I is thus shown to be β-D-glucopyranosyl 2α,3β,19α,-23-tetrahydroxyolean-12-en-28-oate (**2**).

The elemental analysis of arjunglucoside II (**3**; crystallized from aqueous methanol), mp 252 °C, $[\alpha]_D$ +37° (EtOH), fitted best for the molecular formula $C_{36}H_{58}O_{10}\cdot H_2O$.[13] On acid-catalyzed methanolysis, **3** yielded arjunolic acid (**24**) and methyl D-glucoside. An alkaline hydrolysis of **3** gave **24** and D-glucose. The IR spectrum of **3** shows the presence of an ester carbonyl group (1730 cm^{-1}) and the absence of a free carboxylic acid. Acetylation of **3** with acetic anhydride and pyridine gave a heptaacetate (**25**). When treated with methyl iodide in *N,N*-dimethylformamide in the presence of silver oxide, **3** gave a heptamethyl ether (**26**). On hydrolysis of **26**, arjunolic acid trimethyl ether (**27**) was obtained. Therefore, the presence of an ester glucoside linkage is suggested for **3**. The mass spectrum of **25** shows a series of peaks at *m/e* 331, *m/e* 211, *m/e* 169, and *m/e* 109[11] characteristic for the presence of a tetra-*O*-acetylglucopyranosyl group. The presence of a β-glucosyl linkage is suggested from the PMR spectrum of **25** ($J_{1',2'}$=8 Hz; Table 1). The structure of β-D-glucopyranosyl 2α,3β,23-trihydroxy-olean-12-en-28-oate (**3**; β-D-glucopyranosyl arjunolate) is thus given for arjunglucoside II.

Experimental

IR spectra were measured using a Hitachi EPI-G2 spectrometer. UV spectra were determined on a Hitachi EPS-3 spectrophotometer. ORD measurements were carried out on a JASCO Model J-20 spectrometer. Optical rotations were measured on a JASCO DIP-SL polarimeter. Mass spectra were taken on a Hitachi RMU-6-Tokugata mass spectrometer with a direct inlet system operating at 70 eV. PMR spectra were measured using a JEOL 4H-100 (100 MHz) or a Hitachi R-20 (60 MHz) spectrometer. Chemical shifts were expressed in δ downfield from TMS as an internal standard, and coupling constants in Hz. Thin layer chromatography (TLC) was carried out on Kieselgel G nach Stahl, Kieselgel GF_{254} nach Stahl, and Kieselgel 60 PF_{254} (E. Merck, Darmstadt). For column chromatography Wakogel C-200 (Wako Pure Chemical Ind.) was used. All mps were determined on a hot block and reported uncorrected.

Isolation. The bark (1.3 kg) of *Terminalia arjuna* were sliced and ground into powder and extracted with methanol (total 4 l) at room temperature. To the extract was added lead acetate (100 g) and a precipitated material then formed was filtered off. Water (*ca.* 12 l) was added to the filtrate to give a greenish-yellow precipitate which was separated by filtration. The mother liquor was concentrated under reduced pressure to give another crop of the greenish-yellow precipitate. The combined greenish-yellow material (material A; total 4 g) showed six spots on TLC and was subjected to separation on a column of silica gel (450 g). Eluted fractions were examined by TLC (silica gel).

Elution with chloroform–methanol (47: 3) gave *arjunic acid*[2a] (**12**; 260 mg), mp >280 °C (dec), $[\alpha]_D$ +28° (*c* 3.1, EtOH), characterized as its methyl ester diacetate[2a] (**20**), mp 234—235 °C (crystallized from methanol), $[\alpha]_D$ +4° (*c* 1.6, EtOH); IR (Nujol) 3540, 1740, and 1640 cm^{-1}; PMR ($CDCl_3$) δ 0.69, δ 1.06, and δ 1.25 (each 3H, s; *t*-CH_3), δ 0.91 and δ 0.99 (each 6H, s; 2×*t*-CH_3), δ 1.98 and δ 2.05 (each 3H, s; 2×$OCOCH_3$), δ 3.62 (3H, s; CO_2CH_3), δ 3.10 (1H, m; $C_{(18\beta)}$-H), δ 3.35 (1H, d, J=4 Hz; $C_{(19\beta)}$-H), δ 4.75 (1H, d, J=11 Hz; $C_{(3\alpha)}$-H), δ 5.15 (1H, ddd, J=11, J=11, and J=4 Hz; $C_{(2\beta)}$-H), and δ 5.45 (1H, t; $C_{(12)}$-H); mass spectrum *m/e* 586 (M^+), *m/e* 568, *m/e* 527, *m/e* 278, *m/e* 260, *m/e* 245, *m/e* 219, and *m/e* 201 (base peak).

Found: C, 71.69; H, 9.54%. Calcd for $C_{35}H_{54}O_7$: C, 71.64; H, 9.28%.

Subsequent elution with chloroform–methanol (23: 2) yielded *arjunolic acid*[6,14] (**24**; 230 mg), mp 296—297 °C (dec.) (from aqueous methanol), $[\alpha]_D$ +61° (*c* 2.9, EtOH), characterized as its methyl ester,[6] mp 210—213 °C, $[\alpha]_D$ +61° (*c* 1.3, EtOH); IR (KBr) 3430, 1730, and 1640 cm^{-1}; PMR ($CDCl_3$) δ 0.73, δ 0.85, δ 1.03, and δ 1.15 (each 3H, s; *t*-CH_3), δ 0.95 (6H, s; 2×*t*-CH_3), δ 3.63 (3H s; CO_2CH_3), and δ 5.30 (1H, m; $C_{(12)}$-H); mass spectrum *m/e* 502 (M^+), *m/e* 484, *m/e* 466, *m/e* 262, *m/e* 249, *m/e* 203 (base peak), *m/e* 189, and *m/e* 133.

Found: C, 74.19; H, 10.12%. Calcd for $C_{31}H_{50}O_5$: C, 74.06; H, 10.03%. This methyl ester was found to be identical (mp, $[\alpha]_D$, IR, PMR, and mass spectrum) with an authentic sample of methyl arjunolate.[14]

Successive elution with chloroform–methanol (9: 1) gave *arjungenin* (**1**; 20 mg), mp 293—294 °C (dec.)(from aqueous methanol), $[\alpha]_D$ +29° (*c* 2.6, EtOH), IR (KBr) 3400, 1690, and 1630 cm^{-1}; PMR (pyridine-d_5) δ 1.08 and δ 1.11 (each 6H, s; 2×*t*-CH_3), δ 1.19 and δ 2.09 (each 3H, s; *t*-CH_3), δ 3.59 (2H, s), δ 3.76 (1H, s), δ 4.15 (2H, m), and δ 5.52 (1H, s; $C_{(12)}$-H); mass spectrum *m/e* 504 (M^+), *m/e* 486, *m/e* 468, *m/e* 264, *m/e* 246, *m/e* 231, and *m/e* 201 (base peak).

Found: C, 71.41; H, 9.56%. Calcd for $C_{30}H_{48}O_6$: C, 71.39; H, 9.59%.

Elution with chloroform–methanol (43: 7) yielded *arjunetin*[2b] (**28**; β-D-glucopyranosyl arjunate; 1.8 g), mp 232—234 °C (from aqueous methanol), $[\alpha]_D$ +15° (*c* 1.3, EtOH); IR (Nujol) 3370, 1730, and 1640 cm^{-1}; mass spectrum *m/e* 488, *m/e* 470, *m/e* 452, *m/e* 264, *m/e* 246, *m/e* 231, and *m/e* 201 (base peak) (no molecular ion peak was observed), characterized as its hexaacetate (**29**)[2b], mp 235—237 °C (from ethanol), $[\alpha]_D$ +1° (*c* 1.5, $CHCl_3$); IR (Nujol) 3510, 1760, 1730, and 1710 cm^{-1}; PMR ($CDCl_3$) δ 0.69, δ 0.90, δ 0.92, δ 0.95, δ 0.98, δ 1.06, and δ 1.25 (each 3H, s; *t*-CH_3), δ 1.99 (3H, s; $OCOCH_3$), δ 2.02 (9H, s; 3×$OCOCH_3$), δ 2.07 (6H, s; 2×$OCOCH_3$), δ 3.06 (1H, br. signal; $C_{(18\beta)}$-H), δ 3.34 (1H, br. signal; $C_{(19\beta)}$-H), δ 3.80 (1H, m; $C_{(5')}$-H), δ 4.06 (1H, as A part of ABX-system: $J_{6',6'}$=12 and $J_{5',6'}$=2 Hz; $C_{(6')}$-H), δ 4.28 (1H, as B part of ABX-system: $J_{6',6'}$=12 and $J_{5',6'}$=4 Hz; $C_{(6')}$-H), δ 4.74 (1H, d, $J_{2\beta,3\alpha}$=10 Hz; $C_{(3\alpha)}$-H), δ 5.44 (1H, m; $C_{(12)}$-H), and δ 5.60 (1H, d, $J_{1',2'}$=8 Hz; $C_{(1')}$-H); mass spectrum *m/e* 570, *m/e* 554, *m/e* 526, *m/e* 331, *m/e* 271, *m/e* 264, *m/e* 246, *m/e* 231, *m/e* 211, *m/e* 169, *m/e* 109, and *m/e* 43 (base peak) (no molecular ion peak was observed).

Found: C, 64.07; H, 8.06%. Calcd for $C_{48}H_{70}O_{16}$: C, 63.85; H, 7.76%. Alkaline hydrolysis (4% KOH–EtOH, reflux, 5 h) of **28** gave arjunic acid (**12**) and D-glucose.

Subsequent elution with chloroform–methanol (21: 4) gave *arjunglucoside II* (**3**; β-D-glucopyranosyl arjunolate; 1 g), mp 252 °C (from aqueous methanol), $[\alpha]_D$ +37° (*c* 2.3, EtOH); IR (KBr) 3400, 1730, and 1630 cm^{-1}; mass spectrum *m/e* 488,

m/e 470, *m/e* 452, *m/e* 248 (base peak), *m/e* 233, *m/e* 203, *m/e* 189, and *m/e* 133 (no molecular ion peak was observed).

Found: C, 61.13; H, 8.83%. Calcd for $C_{36}H_{58}O_{10}\cdot 3H_2O$: C, 61.34; H, 9.15%.

Five among six constituents contained in material A were thus separated. The sixth constituent corresponding to the most polar spot on the TLC could be obtained from material B, rather than from material A, as described below. The mother liquor after separation of material A was treated with hydrogen sulfide to precipitate lead sulfide which was removed by filtration. The resulting filtrate gave, on evaporation of the solvent, a residue (material B; 3.2 g), containing the sixth constituent mentioned above as a main constituent (examined by TLC). Material B was subjected to separation on a column of silica gel (250 g). Elution with chloroform–methanol (83: 17) gave *arjunglucoside I* (**2**; 450 mg), mp 231 °C (from aqueous methanol), $[\alpha]_D$ +17° (*c* 2.8 EtOH); IR (KBr) 3410, 1730, and 1640 cm^{-1}; mass spectrum *m/e* 504, *m/e* 486, *m/e* 468, *m/e* 264, *m/e* 246, *m/e* 231, and *m/e* 201 (base peak) (no molecular ion peak was observed). Found: C, 63.16; H, 9.13%. Calcd for $C_{36}H_{58}O_{11}\cdot H_2O$: C, 63.14; H, 8.83%.

Methylation of Arjungenin (1). To arjungenin (**1**, 217 mg) in ether was added diazomethane in ether. The reaction mixture was treated as usual to give a residue (215 mg), which was crystallized from ether to yield arjungenin methyl ester (**4**), mp 162—165 °C; IR (KBr) 3430, 1720, and 1640 cm^{-1}; mass spectrum *m/e* 518 (M^+), *m/e* 500, *m/e* 482, *m/e* 278, *m/e* 260, *m/e* 245, *m/e* 219, and *m/e* 201 (base peak). Found: *m/e* 518.3503 (M^+). Calcd for $C_{31}H_{50}O_6$: *m/e* 518.3604.

Acetylation of Arjungenin Methyl Ester (4). Arjungenin methyl ester (**4**; 100 mg) dissolved in pyridine (1 ml) was treated with acetic anhydride (1 ml) overnight at room temperature. After the usual work-up, acetylated product (100 mg) was obtained and purified by column chromatography to give arjungenin methyl ester triacetate (**5**) mp 137—138 °C, $[\alpha]_D$ +8° (*c* 1.8, EtOH); IR (Nujol) 3520, 1740, and 1630 cm^{-1}, PMR (Table 1); mass spectrum *m/e* 644 (M^+), *m/e* 626, *m/e* 585, *m/e* 278, *m/e* 260, *m/e* 245, *m/e* 219, and *m/e* 201 (base peak). Found: C, 68.73; H, 8.89%. Calcd for $C_{37}H_{56}O_9$: C, 68.91; H, 8.75%.

Acetylation of Arjungenin Methyl Ester Triacetate (5). To arjungenin methyl ester triacetate (**5**; 23 mg) in acetic anhydride (2 ml) was added a drop of perchloric acid at −10 °C. The reaction mixture was kept at room temperature for 15 min, and poured into water. Extraction with ether and removal of the solvent gave a residue (22 mg), which was purified by preparative TLC to yield arjungenin methyl ester tetraacetate (**6**; 9 mg), an amorphous solid, IR (Nujol) 1730, and 1230 cm^{-1}, PMR (Table 1; signals due to four acetoxyl groups were observed); mass spectrum *m/e* 626 [(M−AcOH)$^+$], *m/e* 567, *m/e* 507, *m/e* 320, *m/e* 260, *m/e* 245, and *m/e* 201 (base peak)(no molecular ion peak was observed). Found: *m/e* 626.3820 [(M−AcOH)$^+$]. Calcd for ($C_{39}H_{58}O_{10}-C_2H_4O_2$): *m/e* 626.3815.

Dehydration of Arjungenin Methyl Ester Triacetate (5). Arjungenin methyl ester triacetate (**5**; 30 mg) in pyridine (0.5 ml) was treated with phosphoryl chloride (0.2 ml) under reflux for 6 h. The reaction mixture was treated in the usual manner to give a residue which was chromatographed to afford a mixture (24 mg) of dienes (**7** and **8**), an amorphous solid, UV (EtOH) λ_{max} 243, 252, and 261 nm, mass spectrum *m/e* 626 and *m/e* 201 (base peak). The fact that the product was a mixture of dienes (**7** and **8**) is suggested by the PMR spectrum. There appear signals at δ 5.40 (s; $C_{(19)}$–H) and δ 5.48 (m; $C_{(12)}$–H) due to olefinic protons of a 12,18-diene[2a] system, besides those at δ 5.53 (d, J=11 Hz; $C_{(12)}$–H) and δ 6.43 (dd, J=11 and J=2 Hz; $C_{(11)}$–H) due to olefinic protons of the 11,13(18)-diene (**8**) (*vide infra*).

Treatment of the Mixture of Dienes (7 and 8) with Dry Hydrogen Chloride. Dry hydrogen chloride was passed through a solution of the mixture (24 mg) of dienes (**7** and **8**) in chloroform (3 ml) at room temperature for 1 h. After the usual work-up, a residue was obtained and purified by preparative TLC to give methyl 2α,3β,23-triacetoxyoleana-11,13(18)-dien-28-oate (**8**; 15 mg), mp 115—118 °C, $[\alpha]_D$ −120° (*c* 0.2, EtOH); UV (EtOH) λ_{max} 243.5 nm (log ε 4.41), 251.5 (4.47), 260.5 (4.27); IR (KBr) 1735 and 1630 cm^{-1}, PMR ($CDCl_3$) δ 0.80 (6H, s; 2×*t*-CH_3), δ 0.90, δ 0.94, δ 0.97, and δ 1.10 (each 3H, s; *t*-CH_3), δ 2.00, δ 2.01, and δ 2.10 (each 3H, s; $OCOCH_3$), δ 3.66 (3H, s; CO_2CH_3), δ 3.60 and δ 3.80 (each 1H, d, J=12 Hz; $C_{(23)}$–H_2), δ 5.15 (2H, m; $C_{(2\beta)}$–H and $C_{(3\alpha)}$–H), δ 5.53 (1H, d, J=11 Hz; $C_{(12)}$–H), and δ 6.43 (1H, dd, J=11 and J=2 Hz; $C_{(11)}$–H); mass spectrum *m/e* 626 (M^+), *m/e* 567, *m/e* 507, *m/e* 447, *m/e* 387, and *m/e* 187 (base peak). Found: C, 70.75; H, 8.81%. Calcd for $C_{37}H_{54}O_8$: C, 70.90; H, 8.68%.

Oxidation of Methyl Tri-O-acetylarjunolate (9) with Selenium Dioxide. This oxidation was effected according to the procedures described by King *et al.*,[3] which include alkaline hydrolysis at the final stage to give methyl 2α,3β,23-trihydroxyoleana-11,13(18)-dien-28-oate (**30**). Methyl tri-*O*-acetylarjunolate[6] (**9**; 51 mg) in acetic acid (2 ml) was heated with selenium dioxide (9 mg) under reflux for 17 h. After cooling, the reaction mixture was poured into water and extracted with ether. Removal of the solvent gave a residue (42 mg), which was purified by preparative TLC to afford 2α,3β,23-triacetoxyoleana-11,13(18)-dien-28-oate (**8**; 18 mg). This compound proved to be identical (mp, $[\alpha]_D$, IR, UV, PMR, TLC, and mass spectrum) with the diene (**8**) obtained from **5** by dehydration and by subsequent treatment with dry hydrogen chloride.

The Collins Oxidation of Arjungenin Methyl Ester Triacetate (5). To a solution prepared from chromium trioxide (260 mg), pyridine (0.5 ml), and dichloromethane (4 ml), was added a solution of arjungenin methyl ester triacetate (**5**; 220 mg) in dichloromethane (2 ml), and the whole was stirred at room temperature for 30 min. After the usual work-up a residue (200 mg) was obtained. The residue was purified by preparative TLC to yield methyl 2α,3β,23-triacetoxy-19-oxo-olean-12-en-28-oate (**10**, 150 mg), an amorphous solid; IR (Nujol) 1745 and 1710 (sh) cm^{-1}; PMR ($CDCl_3$) δ 0.74, δ 0.88, δ 0.98, and δ 1.19 (each 3H, s; *t*-CH_3), δ 1.09 (6H, s; 2×*t*-CH_3), δ 1.98, δ 2.00, and δ 2.07 (each 3H, s; $OCOCH_3$), δ 3.68 (3H, s; CO_2CH_3), δ 3.58 and δ 3.90 (each 1H, d, J=12 Hz; $C_{(23)}$–H_2), δ 5.10 (2H, m, $C_{(2\beta)}$–H and $C_{(3\alpha)}$–H), and δ 5.30 (1H, m; $C_{(12)}$–H); ORD (*c* 0.06, EtOH) $[\phi]_{315}$ +5300° and $[\phi]_{265}$ −4900° (a=+102); mass spectrum *m/e* 642 (M^+), *m/e* 582, *m/e* 522, *m/e* 462, *m/e* 276, and *m/e* 217 (base peak). Found: C, 69.11; H, 8.58%. Calcd for $C_{37}H_{54}O_9$: C, 69.13; H, 8.47%.

The Jones Oxidation of Methyl Di-O-acetylarjunate (20). To a solution of methyl di-*O*-acetylarjunate (**20**; 200 mg) in acetone (15 ml) was added the Jones reagent (2.2 ml), and the mixture was stirred at 0 °C for 20 min. After the usual treatment, a residue was crystallized from methanol to afford methyl 2α,3β-diacetoxy-19-oxo-olean-12-en-28-oate[2a] (**11**; 120 mg), mp 200—201 °C; IR (KBr) 1720, 1440, 1360, and 1240 cm^{-1}; PMR ($CDCl_3$) δ 0.78, δ 1.00, and δ 1.20 (each 3H, s; *t*-CH_3), δ 0.91 and δ 1.10 (each 6H, s; 2×*t*-CH_3), δ 2.00 and δ 2.05 (each 3H, s; $OCOCH_3$), δ 3.70 (3H, s; CO_2CH_3), δ 4.77 (1H, d; J=11 Hz; $C_{(3\alpha)}$–H), δ 5.05 (1H, ddd; J=11, J=11, and J=4 Hz; $C_{(2\beta)}$–H), and δ 5.28 (1H, m; $C_{(12)}$–H); ORD (*c* 0.04, EtOH) $[\phi]_{315}$ +4900° and $[\phi]_{265}$ −5300° (a=+102); mass spectrum *m/e* 584 (M^+), *m/e* 525, *m/e* 464, *m/e* 405, *m/e* 276,

and *m/e* 217 (base peak). Found: C, 71.69; H, 9.23%. Calcd for $C_{35}H_{52}O_7$: C, 71.88; H, 8.96%.

*Reduction of the Ketone (**10**) with Sodium Borohydride.* The ketone (**10**; 16 mg) in dioxane (1.5 ml) was treated with sodium borohydride (76 mg) under stirring at room temperature for 2 h. The reaction mixture was diluted with water, acidified with diluted sulfuric acid, and extracted with ether. Removal of the solvent gave a residue (11 mg), showing one spot (on TLC) corresponding to the 19α-ol (**5**). This residue was passed through a column of silica gel [elution with benzene–acetone (47: 3)] to afford arjungenin methyl ester triacetate (**5**; 8 mg) (identified by mp, mixed mp, $[\alpha]_D$, IR, PMR, and mass spectra).

Similar reduction of the ketone (**10**; 20 mg) in dioxane (1.2 ml) with sodium borodeuteride (102 mg) gave a residue (16 mg), which was purified by preparative TLC to yield 19β-deuterated arjungenin methyl ester triacetate (**16**; 13 mg). The IR spectrum of **16** is almost superimposable with that of **5**.

In the PMR spectrum ($CDCl_3$) of **16**, a broad singlet (1H, $W_{1/2}$=3 Hz; $C_{(18\beta)}$-H) appears at δ 3.10. The multiplet signal at δ 3.35 (1H; $C_{(19\beta)}$-H) observed for **5** is absent in the spectrum of **16**. The other PMR spectral data of **16** and **5** are identical. The mass spectrum of **16** shows the following peaks: *m/e* 645 (M^+), *m/e* 627, *m/e* 586, *m/e* 279, *m/e* 261, *m/e* 246, *m/e* 220, and *m/e* 202 (base peak).

*Acetylation of the 19β-Deuterated Product (**16**).* The 19β-deuterated product (**16**; 11 mg) was acetylated according to the procedures described for the acetylation of **5**. 19β-Deuterated arjungenin methyl ester tetraacetate (**17**; 6 mg) was obtained as an oil. The IR spectra of **17** and arjungenin methyl ester tetraacetate (**6**) are almost identical. The PMR spectrum ($CDCl_3$) of **17** shows a broad singlet (1H) at δ 3.30 due to $C_{(18\beta)}$-H; no signal due to $C_{(19\beta)}$-H was observed. The other PMR spectral data of **17** and **6** are the same. The mass spectrum of **17** shows the following peaks: *m/e* 627 [(M−AcOH)$^+$], *m/e* 568, *m/e* 508, *m/e* 321, *m/e* 261, *m/e* 246, and *m/e* 202 (base peak) (no molecular ion peak was observed).

*Methanolysis of Arjunglucoside I (**2**).* To a solution prepared from methanol (6 ml), water (2 ml) and sulfuric acid (0.3 ml), was added arjunglucoside I (**2**; 77 mg), and the resulting mixture was heated under reflux for 4 h. The reaction mixture was poured into water and extracted with ether. The ethereal layer was treated as usual to give a residue, which was crystallized from aqueous methanol to afford arjungenin (**1**; 45 mg) (identified by mp, mixed mp, $[\alpha]_D$, IR, PMR, TLC, and mass spectrometry). The aqueous layer was passed through a column of Dowex 1-X2 (OH^-) and a column of Dowex 50W-X8 (H^+), successively, and concentrated under reduced pressure to give a residue. The residue (methyl D-glucoside) was trimethylsilylated and subjected to examination by GLC [column: 2% Silicone OV 17 on Chromosorb WAW, 4(mm)×1.5(m), column temperature: 160 °C; detection: FID, detector temperature: 190 °C, carrier gas: N_2 45 ml/min; instrument: Shimadzu GC-4A PF] to identify the silylated product as methyl tetra-*O*-trimethylsilyl-D-glucoside (retention time: 8.6 min).

*Alkaline Hydrolysis of Arjunglucoside I (**2**).* To a solution prepared from methanol (5 ml), water (3 ml) and potassium hydroxide (0.3 g), was added arjunglucoside I (**2**; 170 mg). The resulting mixture was heated under reflux for 5 h, poured into water, acidified by addition of hydrochloric acid, and extracted with ether. From the ethereal layer arjungenin (**1**; 100 mg) (identified by mp, mixed mp, $[\alpha]_D$, IR, PMR, TLC, and mass spectrometry) was obtained. The aqueous layer was passed through a column of Dowex 1-X2 (OH^-) and then a column of Dowex 50W-X8 (H^+), and concentrated under reduced pressure to give a residue, which was identified to be D-glucose (R_f=0.52) [on Avicel plate (Funakoshi Pharmaceutical Co., Ltd.), developing with pyridine–ethyl acetate–acetic acid–water (5: 5: 1: 3), visualized by aniline hydrogen phthalate at 80 °C].

*Acetylation of Arjunglucoside I (**2**).* Arjunglucoside I (**2**; 38 mg) in pyridine was treated with acetic anhydride overnight at room temperature. The reaction mixture was treated as usual to give a residue, which was purified by column chromatography to afford arjunglucoside I heptaacetate (**22**; 30 mg), mp 147—149 °C, $[\alpha]_D$ −7° (*c* 1.4, EtOH); IR (KBr) 3520, 1740, and 1630 cm^{-1}; PMR (Table 1); mass spectrum *m/e* 331, *m/e* 271, *m/e* 264, *m/e* 246, *m/e* 231, *m/e* 211, *m/e* 201, *m/e* 169, *m/e* 109, and *m/e* 43 (base peak) (no molecular ion peak was observed). Found: C, 62.08; H, 7.59%. Calcd for $C_{50}H_{72}O_{18}$: C, 62.49; H, 7.55%.

*Methanolysis of Arjunglucoside II (**3**).* A mixture of arjunglucoside II (**3**; 130 mg), methanol (5 ml), water (1 ml), and sulfuric acid (0.2 ml), was heated under reflux for 4 h. Water was added to the reaction mixture and the resulting mixture was extracted with ether. From the ethereal layer arjunolic acid[6] (**24**; 85 mg) was obtained (identified by mp, $[\alpha]_D$, IR, TLC, and mass spectrometry). The aqueous layer was treated as described in the methanolysis of **2** to give a residue, which proved to be methyl D-glucoside (identified by its conversion to methyl tetra-*O*-trimethylsilyl-D-glucoside; detection by GLC).

*Alkaline Hydrolysis of Arjunglucoside II (**3**).* A mixture of arjunglucoside II (**3**; 100 mg), methanol (4 ml), water (2 ml), and potassium hydroxide (0.2 g), was heated under reflux for 4 h. The reaction mixture was poured into water, acidified by addition of hydrochloric acid, and extracted with ether. The ethereal layer gave, after the usual work-up, arjunolic acid[6] (**24**; 60 mg) (identified by mp, $[\alpha]_D$, IR, TLC, and mass spectrometry). The aqueous layer was treated as described in the alkaline hydrolysis of **2** to give a residue, which proved to be identical with D-glucose.

*Acetylation of Arjunglucoside II (**3**).* Arjunglucoside II (**3**; 40 mg) in pyridine was acetylated with acetic anhydride overnight at room temperature. After the usual work-up, a residue was obtained. The residue was chromatographed to yield arjunglucoside II heptaacetate (**25**; 46 mg), mp 136—140 °C, $[\alpha]_D$ +26° (*c* 2.0, $CHCl_3$); IR (Nujol) 1740 and 1630 cm^{-1}; PMR (Table 1), mass spectrum *m/e* 331, *m/e* 271, *m/e* 248, *m/e* 233, *m/e* 211, *m/e* 203, *m/e* 189, *m/e* 169, *m/e* 133, *m/e* 109, and *m/e* 43 (base peak) (no molecular ion peak was observed). Found: C, 62.33; H, 7.54%. Calcd for $C_{50}H_{72}O_{17}\cdot H_2O$: C, 62.35; H, 7.74%.

*Methylation of Arjunglucoside II (**3**).* To a solution of arjunglucoside II (**3**; 110 mg) in *N*,*N*-dimethylformamide (3 ml), were added methyl iodide (4 ml) and silver oxide (1.2 g), and the whole was stirred at 60 °C for 24 h. After cooling, the reaction mixture was filtered to remove insoluble material, which was washed several times with chloroform. The washings were combined with the filtrate. Evaporation of the solvents gave a residue, which was dissolved in chloroform. This chloroform solution was washed successively with water, aqueous sodium thiosulfate solution, and with brine, and dried over calcium chloride. Removal of the solvent gave a residue, which was chromatographed to give arjunglucoside II heptamethyl ether (**26**; 30 mg), an amorphous solid, IR (KBr) 1740 and 1635 cm^{-1}; PMR ($CDCl_3$) δ 0.68, δ 0.78, δ 0.98, and δ 1.16 (each 3H, s; *t*-CH_3), δ 0.94 (6H, s; 2×*t*-CH_3), δ 3.33, δ 3.38, δ 3.43, and δ 3.65 (each 3H, s; OCH_3), δ 3.54 (9H, s; 3×OCH_3), δ 5.32 (2H, m; $C_{(12)}$-H and $C_{(1')}$-H); mass spectrum *m/e* 748 (M^+), *m/e* 704, *m/e* 584, *m/e* 530, *m/e* 528, *m/e* 498, *m/e* 497, *m/e* 248, *m/e* 219, *m/e* 203, *m/e* 187 (base peak), and *m/e* 155. Found: C, 67.53; H, 9.79%. Calcd for $C_{43}H_{72}O_{10}\cdot H_2O$: C,

67.33; H, 9.72%.

*Acid Hydrolysis of Arjunglucoside II Heptamethyl Ether (**26**).* A mixture of the heptamethyl ether (**26**; 100 mg), methanol (8 ml), and hydrochloric acid (0.3 ml), was heated under reflux for 7 h. The reaction mixture was poured into water and extracted with ether. Evaporation of the solvent gave a residue, which was chromatographed to afford arjunolic acid trimethyl ether (**27**; 43 mg), mp 140—150 °C (dec); IR (Nujol) 1690 cm^{-1}; PMR ($CDCl_3$) δ 0.65, δ 0.72, and δ 1.12 (each 3H, s; t-CH_3), δ 0.94 (9H, s; $3\times t$-CH_3), δ 3.31, δ 3.42, and δ 3.52 (each 3H, s; OCH_3), δ 5.27 (1H, br. signal; $C_{(12)}$–H); mass spectrum *m/e* 530 (M^+), *m/e* 528, *m/e* 498, *m/e* 466, *m/e* 453, *m/e* 248 (base peak), *m/e* 233, *m/e* 203, *m/e* 189, and *m/e* 133. Found; *m/e* 530.3887. Calcd for $C_{33}H_{54}O_5$: *m/e* 530.3968.

References

1) A preliminary account of this paper: T. Honda, T. Murae, T. Tsuyuki, and T. Takahashi, *Chem. Pharm. Bull.*, **24**, 178 (1976).

2) a) L. R. Row, P. S. Murty, G. S. R. S. Rao, C. S. P. Sastry, and K. V. J. Rao, *Indian J. Chem.*, **8**, 716 (1970); b) L. R. Row, P. S. Murty, G. S. R. S. Rao, C. S. P. Sastry, and K. V. J. Rao, *ibid.*, **8**, 772 (1970); c) L. R. Row and G. S. R. S. Rao, *J. Indian Chem. Soc.*, **39**, 89 (1962).

3) F. E. King, T. J. King, and J. M. Rose, *J. Chem. Soc.*, **1954**, 3995.

4) H. Budzikiewicz, J. M. Wilson, and C. Djerassi, *J. Am. Chem. Soc.*, **85**, 3688 (1963).

5) An alternative urs-12-ene skeleton for these compounds [arjungenin (**1**), **4**, **5**, and **6**] can be eliminated as described later.

6) F. E. King, T. J. King, and J. D. White, *J. Chem. Soc.*, **1958**, 2830.

7) L. R. Row and G. S. R. S. Rao, *Tetrahedron*, **18**, 827 (1962).

8) D. H. R. Barton, N. J. Holness, K. H. Overton, and W. J. Rosenfelder, *J. Chem. Soc.*, **1952**, 3751.

9) R. T. Aplin, W. H. Hui, C. T. Ho, and C. W. Yee, *J. Chem. Soc. C*, **1971**, 1067. In connection with the structure study of spinosic acid A, an examination of the PMR spectrum of methyl siaresinolate was reported. A doublet at δ 3.32 (J= 5 Hz) was described to be due to a proton on C-19β in agreement with our spectral data for **5**.

10) E. Bombardelli, A. Bonati, B. Gabetta, and G. Mustich, *Phytochemistry*, **13**, 2559 (1974).

11) K. Biemann, D. C. DeJongh, and H. K. Schnoes, *J. Am. Chem. Soc.*, **85**, 1763 (1963).

12) R. U. Lemieux, R. K. Kulling, H. J. Bernstein, and W. G. Schneider, *J. Am. Chem. Soc.*, **80**, 6098 (1958).

13) L. R. Row *et al.* (ref. 3c) reported an isolation of a saponin, mp 219—220 °C, $[\alpha]_D$ +86°, $C_{42}H_{68}O_{15}\cdot 2H_2O$, which gave arjunolic acid (**24**) and glucose on acid hydrolysis. No further information was described on this diglucoside of arjunolic acid.

14) Authentic sample of methyl arjunolate was kindly supplied by Professor E. Ritchie, the University of Sydney, to whom the authors' sincere thanks are due. *Cf.* S. Sasaki, H. C. Chiang, K. Habaguchi, H. Y. Hsü, and K. Nakanishi, *Bull. Chem. Soc. Jpn.*, **39**, 1816 (1966).

Micellar Activation of Nucleophilic Reactivity of Coenzyme A and Glutathione toward *p*-Nitrophenyl Acetate*

Seiji SHINKAI and Toyoki KUNITAKE

Department of Organic Synthesis, Faculty of Engineering, Kyushu University, Fukuoka 812

(Received June 26, 1976)

The reaction of coenzyme A(CoASH) and glutathione (GSH) with *p*-nitrophenyl acetate was studied in aqueous media at 30 °C. The reaction is highly accelerated in the presence of hydrophobic aggregates such as hydrophobic oligocations and CTABr micelles. Nonionic and anionic micelles were ineffective. The pK_a of CoASH is lowered by 0.5 pK_a unit in 2 mM of CTABr, while that of GSH is hardly affected. The second-order rate constant for CoASH is improved (290-fold) more than that of GSH(100-fold), relative to the nonmicellar system. Enhanced reactivities are efficiently suppressed by addition of KCl. These results are the first example of the marked activation of sulfhydryl coenzymes by the micellar microenvironment, and explicable by the concept of *hydrophobic ion pairs*: the coenzymes are bound onto the cationic micelle and the thiol anions form ion pairs with surfactant cations at the relatively hydrophobic environment of the micelle.

The reactivity of thiol groups has been of much concern in relation to functions of some sulfhydryl enzymes and enzymes requiring coenzyme A(CoASH) or glutathione (GSH).[1,2]

Nucleophilic reactions of thiol anions toward *p*-nitrophenyl acetate (NpAc: Eq. 1) have been evaluated by several investigators. Schonbaum and Bender[3] reported the hydrolysis of NpAc by *o*-mercaptobenzoic acid, and Jencks and Carriuolo[4] determined second-order rate constants (k_a) for the reaction of 2-mercaptoethanol and mercaptoacetate with NpAc. Subsequently, Whitaker[5] and Ogilvie and coworkers[6] reported the rate constants for the reaction of biologically important thiols such as cysteine and glutathione (GSH) with NpAc. However, the nucleophilic reactivity of thiol groups *in vivo* is incomparably enhanced relative to those observed *in vitro*. It is known that the active site of sulfhydryl enzymes is situated in the hydrophobic region,[7] but the essential role of the hydrophobic environment is not established. Heitmann[8] demonstrated that the nucleophilicity of *N*-dodecanoyl-DL-cysteinate mixed with a cationic micelle is appreciably improved (6—7 fold toward chloroacetamide, 100—200 fold toward NpAc). Tagaki and coworkers[9] also reported that a micellar solution of octadecyltrimethylammonium bromide markedly enhanced the reaction rate of alkanethiols and NpAc.

The possibility thus arises that the nucleophilic reactivity of a number of biological cofactors containing thiol groups is commonly affected by the micellar environment. One may anticipate that the reactions of coenzymes occurring in micelles are akin to those occurring in apoenzymes. That is, coenzymes may be activated by the micellar environment as done by apoenzymes. In this study, we examined the effect of micellar environments on the nucleophilic reactivity of coenzyme A(CoASH) and GSH toward NpAc. These coenzymes have additional anionic charges other than the thiol group and are expected to be easily bound onto the cationic micelles. We have discovered that the nucleophilicity of these biological cofactors toward NpAc (Eq. 1) is pronouncedly enhanced in the presence of a cationic micelle of hexadecyltrimethylammonium bromide (CTABr) and analogous hydrophobic aggregates (tetracationic detergents), and that the rate enhancement is attributed to the formation of *hydrophobic ion pairs*.[10-12] This is probably the first example that the nucleophilicity of coenzymes is markedly improved by the microenvironmental effect.

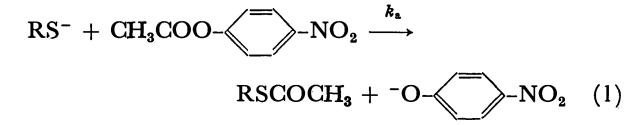

$$RS^- + CH_3COO\text{-}C_6H_4\text{-}NO_2 \xrightarrow{k_a} RSCOCH_3 + {}^-O\text{-}C_6H_4\text{-}NO_2 \quad (1)$$

Surfactants[1]: CTABr, $CH_3(CH_2)_{15}N^+(CH_3)_3Br^-$

$(N\text{-R})_4Br_4$, $H_3C\text{-}\overset{\overset{CH_3}{|}}{\underset{\underset{R}{|}}{N^+}}\text{-}(CH_2CH_2\overset{\overset{CH_3}{|}}{\underset{\underset{R}{|}}{N^+}})_3\text{-}CH_3\ 4Br^-$

SDS, $CH_3(CH_2)_{11}OSO_3Na$

POOA, $CH_3(CH_2)_7CH{=}CH(CH_2)_7CH_2\text{-}(OCH_2CH_2)_{10}OH$

Experimental

Materials. Coenzyme A and glutathione were purchased from Kojin and Wako Pure Chem. Ind., respectively, and used without further purification. These cofactors were assayed by the reaction with NpAc(see Results Section). Hexadecyltrimethylammonium bromide was the product of wako Pure Chem. Ind., and recrystallized from ethanol before use. Other surfactants (sodium dodecylsulfate, polyoxyethylene ($n=10$) oleyl alcohol, trioctylmethylammonium chloride) were used without further purification. Quaternized triethylenetetramine derivatives were prepared and characterized by Mr. Y. Okahata.

Kinetics. The kinetic measurements for the reaction of coenzyme A and glutathione with NpAc were carried out in 3 vol% aqueous ethanol at 30 ± 0.1 °C at a calculated ionic strength ($\mu=0.01$ with KCl) unless otherwise stated. The buffer solutions (0.02 M borate below pH 9.3 and ammonium above pH 9.3) were prepared in twice-distilled water under nitrogen. In order to avoid air oxidation of thiols, the kinetic runs were performed under anaerobic conditions(N_2). A typical example of the reaction procedure is as follows: 2.8 ml of a buffer solution containing an appropriate surfactant were placed in a modified Thunberg cuvette, and was degassed for 15 min by bubbling N_2. An aqueous solution (0.1 ml) of coenzyme was added, and 0.1 ml of an ethanol solution of NpAc was deposited in the side-arm of the cell. Both solutions

* Nucleophilic Ion Pairs. III. Contribution No. 407 from this department.

were degassed for 15 min by passing N_2. The cell was closed and equilibrated at 30 °C, and the content of the side-arm was rapidly mixed with the buffer solution. The progress of the reaction was followed by monitoring the *p*-nitrophenolate ion released (401 nm) on a Hitachi 124 spectrophotometer equipped with a thermostated cell-housing. In runs in the presence of surfactants, excess substrates were employed in order to lower the concentration of thiols as far as possible, since addition of polyanionic species may significantly affect the catalysis of the cationic micelle. On the other hand, excess thiols were employed in the absence of the surfactant. The pseudo-first-order rate constants were calculated with a Sharp Compet 364 for up to 3—4 half-lives. The pH of the reaction mixture was confirmed not to vary before and after the reaction by pH measurements (TOA Digital pH Meter, model HM-15A).

Results

Burst Release of p-*Nitrophenolate and Stoichiometry.* The reaction under anaerobic conditions was initiated by mixing of a surfactant solution containing coenzymes and an ethanol solution of NpAc. Figure 1 gives the time course of the absorbance change at 401 nm for the reaction of GSH and NpAc in the presence of 2 mM of CTABr. The burst release of *p*-nitrophenolate at pH 9.20 almost concluded within 10 s, and the slow, linear increase in the absorbance ensued. Since the absorbance increase in the second stage of the reaction was parallel to (or, under the insufficiently anaerobic condition, slightly slower than) that observed in the absence of the coenzyme moiety, the decomposition of the thiol ester (turnover) is negligibly slow, and the second stage should correspond to the spontaneous decay of NpAc (k_{spont}).

The magnitude of the initial burst was plotted against the concentration of CoASH and GSH in Fig. 2. The slopes of Fig. 2 were evaluated by the least-squares method to be 15000 for CoASH and 16600 for GSH,

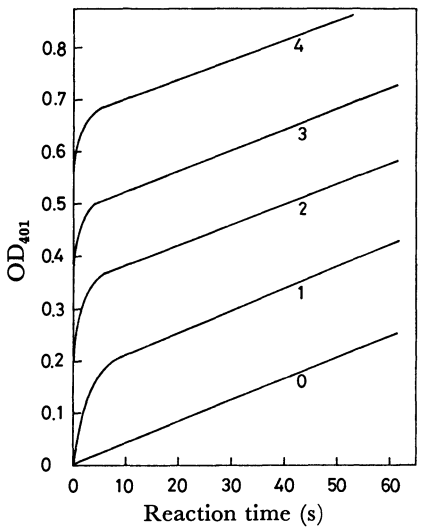

Fig. 1. Time-course of the absorption of *p*-nitrophenolate ion (401 nm) for the reaction of GSH and NpAc. pH 9.20, $[NpAc]=4.00\times10^{-4}$ M, $[CTABr]=2.0\times10^{-3}$ M. $[GSH]_T\times10^5$ M: (0) 0; (1) 1.00; (2) 2.00; (3) 3.00; (4) 4.00.

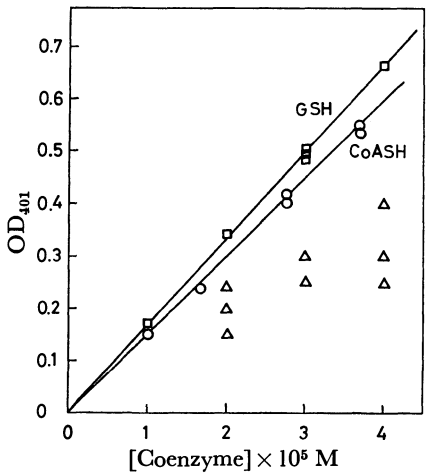

Fig. 2. $[CoASH]_T$ and $[GSH]_T$ *vs.* OD_{401} of the initial burst stage; △, N_2 was not bubbled prior to initiation of the reaction of GSH and NpAc.

respectively. These values are close to the molar absorption coefficient of the *p*-nitrophenolate anion ($\varepsilon=17800$) in the presence of 2 mM of CTABr. Thus, the coenzymes bound onto the CTABr micelle must react quantitatively with NpAc. The slight discrespancy observed would be due to the loss of the thiol function by air oxidation. When nitrogen was not bubbled prior to the reaction, the data lacked in reproducibility and a smaller slope (*ca.* 7500) resulted (Fig. 2). The influence of cationic micelles on the oxidation of thiols will be discussed elsewhere.

Results of Figs. 1 and 2 now enable us to depict reaction scheme 1 and the corresponding rate equation (Eq. 2),

$$v_{obsd}=k_{spont}[NpAc]+v_a \quad (2)$$

where v_{obsd} is the reaction rate at the initial burst stage and v_a the reaction rate for the acyl transfer from NpAc to the coenzyme.

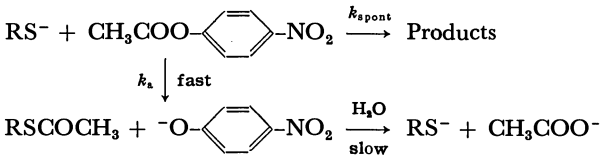

Scheme 1.

Determination of Second-Order Rate Constants. The rate constants for the initial burst reaction were determined at pH 8.78. The increase in absorbance at 401 nm satisfied the pseudo-first-order rate equation at least up to 3 half-lives, and the pseudo-first-order rate constants ($k_{a,obsd}$) thus evaluated were proportional to the concentration of NpAc (Fig. 3). Evidently, the reaction is first-order both in coenzyme and in substrate, giving the kinetic expressions of Eqs. 3 and 4,

$$v_a=k_{a,obs}[CoASH\text{ or }GSH]_T$$
$$=k_a'[CoASH\text{ or }GSH]_T[NpAc] \quad (3)$$

$$k_a'=k_a\left(\frac{K_a}{K_a+a_H}\right) \quad (4)$$

where K_a is the acid dissociation constant of thiol groups

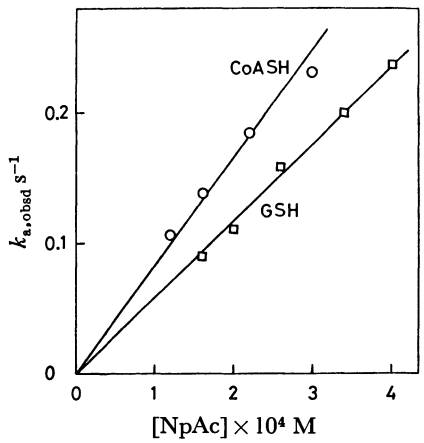

Fig. 3. [NpAc] *vs.* $k_{a,obsd}$. pH 8.78±0.03, [CTABr]= 2.0×10^{-3} M, $[CoASH]_T=2.00\times10^{-5}$ M, $[GSH]_T=2.19\times10^{-5}$ M.

Table 1. Apparent and true second-order rate constants

Surfactant	mM	k'_a at pH 8.78 $M^{-1}s^{-1}$	k_a $M^{-1}s^{-1}$	pK_a[c]
For CoASH:				
None		1.06	11	9.8
CTABr	2.0	863	3160	9.3
(N-OctDe)$_4$Br$_4$	0.52	885		
(N-Dod)$_4$Br$_4$	1.8	6.90		
(N-Oct)$_4$Br$_4$	1.9	2.21		
SDS	10	0.81		
POOA	0.11	1.11		
POOA	0.43	1.22		
POOA[a]	0.43	1.18		
POOA[b]	0.43	2.90		
For GSH:				
None		7.60	16	9.1
CTABr	2.0	530	1590	9.2
SDS	3.0	7.10		
	10	4.88		
POOA	0.11	9.61		
	0.32	10.1		

a) $[Oct_3MeNCl]=2.0\times10^{-4}$ M b) $[CTABr]=2.0\times10^{-4}$ M c) Estimated kinetically.

and $[CoASH]_T$ and $[GSH]_T$ are the total concentration of coenzymes. Typical examples of the apparent second-order rate constants (k_a') for the reaction of CoASH and GSH with NpAc in the presence and the absence of surfactants are recorded in Table 1.

Surfactant Concentration-Rate Profiles. In the non-micellar system, the apparent second-order rate constants at pH 8.78 were 1—8 $M^{-1}s^{-1}$ (Table 1). These values are not much different from those of alkane thiols,[5,6] indicating that the nucleophilic reactivity of biological cofactors toward NpAc is not anomalous in the nonenzymatic system.

In Figs. 4 and 5, the apparent second-order rate constants were plotted against the concentration of CTABr and quaternized triethylenetetramine derivatives. Plots of k_a' against the concentration of CTABr

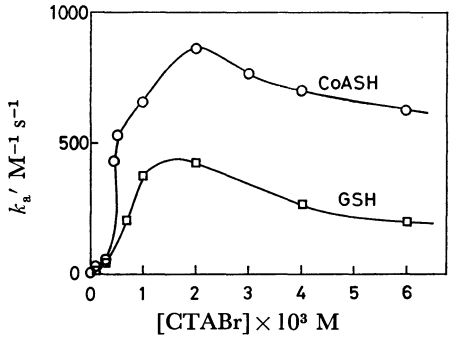

Fig. 4. Apparent second-order rate constants plotted against the concentration of CTABr. For CoASH+NpAc: $[CoASH]_T=2.00\times10^{-5}$ M, $[NpAc]=1.60\times10^{-4}$ M, pH 8.78±0.03. For GSH+NpAc: $[GSH]_T=2.05\times10^{-5}$ M, $[NpAc]=3.35\times10^{-4}$ M, pH 8.65±0.03.

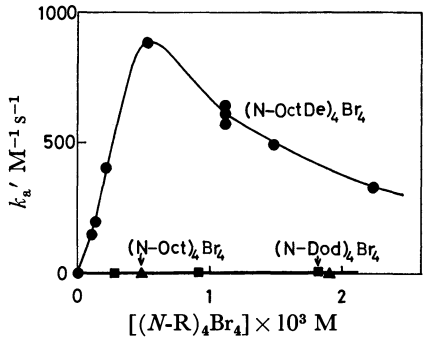

Fig. 5. Apparent second-order rate constants for the reaction of CoASH and NpAc plotted against the concentration of (N-R)$_4$Br$_4$. $[CoASH]_T=2.00\times10^{-5}$ M, $[NpAc]=2.00\times10^{-4}$ M, pH 8.78±0.03.

(Fig. 4) give multiphasic curves: around the CMC (9.2×10^{-4} M at 25 °C[13]: 8.0×10^{-4} M under the kinetic condition; Okahata, unpublished) the rate constants rise rapidly with increasing concentration of CTABr. Further increase in the CTABr concentration rather suppresses the rate constants, resulting in rate maxima at 2×10^{-3} M of CTABr. At the optimal CTABr concentration (2 mM), rate augmentations of 810-fold for CoASH and 75-fold for GSH are observed. Plots of k_a' against the concentration of (N-OctDe)$_4$ showed a similar concentration-rate profile with a rate maximum at 5×10^{-3} M, except that the reaction rates are significantly improved at very low concentration of (N-OctDe)$_4$Br$_4$ (Fig. 5). The rate augmentation in the presence of (N-OctDe)$_4$Br$_4$ for the reaction of CoASH and NpAc was 840-fold at the optimal concentration as compared with the typical non-micellar system. In contrast, the aqueous solutions of (N-Dod)$_4$ and (N-Oct)$_4$ did not accelerate this reaction (Fig. 5). Addition of anionic (SDS) and nonionic (POOA) surfactants above their CMC was also ineffective (Table 1). Addition of hydrophobic ammonium ions such as CTABr (below the CMC) and Oct_3MeNCl to the nonionic micellar system did not increase the rate, either (Table 1).

Effects of Ionic Strength and pH. The rate of micelle-catalyzed reaction is influenced by the ionic strength of the medium.[14,15] Apparent second-order rate constants (k_a') for the reaction of CoASH and GSH

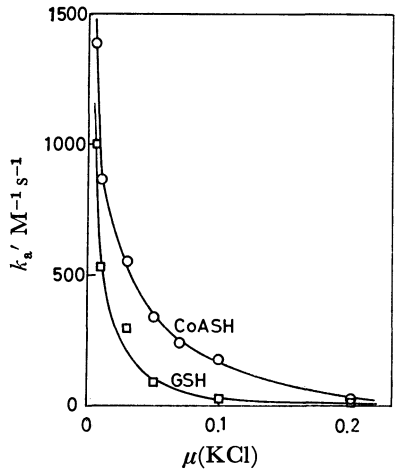

Fig. 6. Effect of ionic strength. [CTABr]$=2.0\times10^{-3}$ M, pH 8.78±0.03. Other reaction conditions are recorded under Fig. 4.

bound to the CTABr micelle were evaluated as a function of ionic strength (μ(KCl)$=0.006-0.2$; Fig. 6). The reaction rates for both coenzymes are markedly suppressed with increasing salt concentration. Fig. 6 proves that the reactivity of GSH is more susceptible to ionic strength than that of CoASH, and the rate difference amounts to 54-fold for CoASH and 110-fold for GSH. At $\mu=0.2$, the k_a' value for the reaction of GSH and NpAc is 9.05 M^{-1} s^{-1}, which is almost equal to the non-micellar value (7.60 M^{-1} s^{-1}).

The pH dependence of the rate is illustrated in Fig. 7. The acid dissociation constants (K_a) and the true second-order rate constants (k_a) were determined by fitting of the theoretical curves (Eq. 4) to the experimental plots. The solid curves in Fig. 7 were obtained

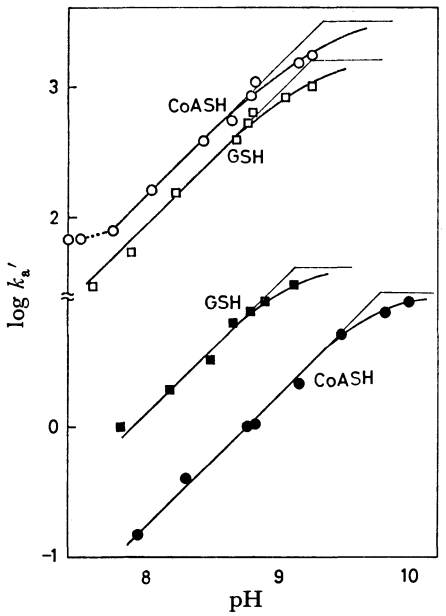

Fig. 7. pH Dependence. [CTABr]$=2.0\times10^{-3}$ M for ○ and □; other reaction conditions are recorded under Fig. 4. CTABr are not added for ● and ■; [CoASH]$_T=2.00\times10^{-4}$ M, [GSH]$_T=4.02\times10^{-4}$ M, [NpAc]$=2.00\times10^{-5}$ M.

by using Eq. 4 for k_a and pK_a values recorded in Table 1. The reactive species in this acyl transfer reaction is undoutedly the dissociated fraction of the thiol groups. The true second-order constants (k_a) in the presence of 2 mM of CTABr are thus estimated to be $(1-3)\times10^3$ M^{-1} s^{-1} (Table 1). Therefore, the cationic micelle of CTABr enhances the nucleophilicity of CoASH and GSH anions by 290-fold and 100-fold respectively. It is also worth while mentioning that the pK_a value of CoASH is considerably lowered (0.5 pK_a unit), while that of GSH is not.

As shown in Fig. 7, the rate constant for the reaction of CoASH and NpAc in the presence of CTABr deviates upwards at pH 7.4—7.6. A similar trend has been noticed in the polysoap-catalyzed reaction of CoASH with NpAc.[16] We consider that the adenine moiety of CoASH is responsible for the deviation, but the detail is not clear at present.

Discussion

It is frequently said that the micellar catalyses provide appropriate model systems of the enzymatic catalyses.[15,17] For instance, micelles significantly influence rates and equilibria of biologically important reactions. One of the recent, novel findings in the micellar catalysis is the fact that the nucleophilicity of a variety of anionic nucleophiles is unusually enhanced in cationic micelles (Ref. 10 and references cited therein) as well as in cationic polysoap.[18-20] Since this phenomenon is not limited to the conventional cationic micelle, it was proposed that the rate acceleration is largely derived from the formation of hydrophobic ion pairs between anionic species and cationic surfactant in a micellar, hydrophobic environment.[10-12] The anion included in a hydrophobic ion pair will attain its high reactivity from desolvation (dehydration), as already known for the ionic reactions in organic solvents.[21]

The apparent second-order rate constants (k_a') for CoASH and GSH at pH 8.78 were evaluated to be 863 and 530 M^{-1} s^{-1}, respectively (Table 1). On the other hand, the k_a' values for the reaction of dodecanethiol and NpAc are 417 M^{-1} s^{-1} ([octadecyltrimethylammonium bromide]$=ca.$ 10^{-3} M, pH 9.0)[9] and 462 M^{-1} s^{-1} ([partially laurylated poly(2-ethyl-1-vinylimidazole)]$=2.25\times10^{-3}$ M, pH 8.93).[20] The nucleophilicity of the micellar GSH is comparable to that of the hydrophobic ion pair of dodecanethiol, and that of CoASH is still higher. In the previous examples, some hydrophobic functions such as long alkyl chain, aromatic ring, and/or polymer backbone were indispensable for forming highly nucleophilic ion pairs.[18,22-24] In contrast, CoASH and GSH are polyanions with phosphate and carboxylate groups, and expected to be bound onto the cationic micellar surface mainly due to the electrostatic interaction. It is unlikely, by considering the poor solubility of these coenzymes in organic solvents, that the thiol groups are buried deeply in the hydrophobic core of the micelle. Therefore, the formation of reactive hydrophobic ion pairs is possible in a region fairly close to the surface of the micelle.

We previously showed that the nucleophilicity of

hydrophobic hydroxamate anions in the presence of nonionic micelles is markedly enhanced by the addition of hydrophobic ammonium salts.[10-12] As listed in Table 1, rate increases could not be observed by addition of CTABr below the CMC and Oct_3MeNCl. Supposedly, the hydrophobic interaction between these hydrophobic ammonium salts and the biological cofactors is not strong enough to bring the latter to the micellar phase of the nonionic micelle.

It is probable that the higher reactivity of CoASH relative to that of GSH is associated with the efficient binding of CoASH to the micellar phase. According to Cordes and Dunlap,[14] typical surfactant concentration-rate profiles such as Figs. 4 and 5 can be rationalized on the basis of (1) adsorption of progressively greater fractions of the nucleophile to the micellar phase until that fraction approaches unity (in the CTABr micellar system, NpAc is hardly concentrated in the micellar phase)[25] and (2) inhibition of the micellar catalysis by the counterions of the surfactant itself. Thus, Cordes and Dunlap[14] state that, when 50% of the nucleophile is associated with the micellar phase, about 50% of the maximum catalysis experienced. Figure 4 shows that the concentration of CTABr at the 50% reactivity is 0.9 mM for CoASH and 1.5 mM for GSH, so that CoASH possesses association constant several times larger than that of GSH. In a separate study, we estimated the binding constants of CoASH and GSH with 29 mol % laurylated poly(2-ethyl-1-vinylimidazole) to be 1100 and 240 M^{-1}, respectively.[16]

A similar trend is found for the effect of ionic strength (Fig. 6). The salt effect in the micellar system primarily arises from competitive occupation of the counterion site.[26] Figure 6 suggests that GSH is expelled out of the micellar phase more easily than CoASH by the counteranion binding.

In conclusion, the reactivity of sulfhydryl coenzymes can be enhanced remarkably in the presence of cationic micelles. This is explained by the formation of reactive ion pairs between CoASH and GSH anions and cationic CTABr molecules in the micellar phase. Since the coenzyme binding site of apoenzymes is said to be situated in relatively hydrophobic regions,[7] the CTABr micelle may serve as a model of apoenzymes.

References

1) Abbreviations employed are: coenzyme A, CoASH; glutathione, GSH; *p*-nitrophenyl acetate, NpAc; hexadecyltrimethylammonium bromide, CTABr; sodium dodecylsulfate, SDS; polyoxyethylene ($n=10$) oleyl alcohol, POOA; hexamethyl-N^1,N^2,N^3,N^4-tetraalkyl-triethylenetetramine tetrabromide, $(N\text{-R})_4Br_4$, where alkyl groups are octyl(Oct), dodecyl(Dod), and Octadecyl(OctDe).

2) S. A. Bernhard, "The Structure and Function of Enzymes," W. A. Benjamin, New York, N. Y. (1968).

3) G. R. Schonbum and M. L. Bender, *J. Am. Chem. Soc.*, **82**, 1900 (1960).

4) W. P. Jencks and J. Carriuolo, *J. Am. Chem. Soc.*, **82**, 1778 (1960).

5) J. R. Whitaker, *J. Am. Chem. Soc.*, **84**, 1900 (1962).

6) J. W. Ogilvie, J. T. Tildon, and B. S. Strauch, *Biochemistry*, **3**, 754 (1964).

7) O. Tsolas and B. L. Horecker, "The Enzymes," Vol 8, P. D. Boyer Ed., Academic Press, New York, N. Y. (1972) p. 276.

8) P. Heitmann *Eur. J. Biochem.*, **5**, 305 (1968).

9) W. Tagaki, T. Amada, Y. Yamashita, and Y. Yano, *J. Chem. Soc., Chem. Commun.*, **1972**, 1131.

10) T. Kunitake, S. Shinkai, and Y. Okahata, *Bull. Chem. Soc. Jpn.*, **49**, 540 (1976).

11) S. Shinkai and T. Kunitake, *Chem. Lett.*, **1976**, 109.

12) S. Shinkai and T. Kunitake, *J. Chem. Soc., Perkin Trans. 2*, **1976**, 980.

13) E. J. Fendler and J. H. Fendler, *Adv. Phys. Org. Chem.*, **8**, 271 (1970).

14) E. H. Cordes and R. B. Dunlap, *Acc. Chem. Res.*, **2**, 329 (1969).

15) J. H. Fendler and E. J. Fendler, "Catalysis in Micellar and Macromolecular Systems," Academic Press, New York, N. Y., 1975.

16) S. Shinkai and T. Kunitake, *Polymer Preprints, Japan*, **25**, No. 1, 55 (1976).

17) E. H. Cordes and C. Gitler, *Prog. Bioorg. Chem.*, **2**, 1. (1973).

18) T. Kunitake, S. Shinkai, and S. Hirotsu, *J. Polym. Sci., Polym. Lett. Ed.*, **13**, 377 (1975).

19) T. Kunitake, S. Shinkai, and S. Hirotsu, *Biopolymers*, **15**, 1143 (1975).

20) S. Shinkai and T. Kunitake, *Makromol. Chem.*, in press.

21) A. J. Parker, *Chem. Rev.*, **69**, 1 (1969).

22) A. K. Yatsimirski, K. Martinek, and I. V. Berezin, *Tetrahedron*, **27**, 2855 (1971).

23) H. Chaimovich, A. Blanco, L. Chayet, L. M. Costa, P. M. Monteiro, C. A. Bunton, and C. Paik., *Tetrahedron*, **31**, 1139 (1975).

24) Yu. E. Kirsh, A. A. Rahnanskaya, G. M. Lukovkin, and V. A. Kabanov, *Eur. Polymer J.*, **10**, 393 (1974).

25) K. Martinek, A. P. Osipov, A. K. Yatsimirski, and I. V. Berezin, *Tetrahedron*, **31**, 709 (1975).

26) M. Grätzel and J. K. Thomas, *J. Am. Chem. Soc.*, **95**, 6885 (1973).

The *N*-Alkylation of Xanthine Derivatives with Trialkyl Phosphates

Toshizumi TANABE, Kiyoshi YAMAUCHI, and Masayoshi KINOSHITA

Department of Applied Chemistry, Osaka City University, Sumiyoshi-ku, Osaka 558

(Received June 26, 1976)

The *N*-alkylation of xanthine, theophylline, and theobromine with trimethyl, triethyl, and triallyl phosphates in a weak alkaline aqueous solution is described. Especially, trimethyl phosphate converted these heterocycles to the corresponding *N*-methyl derivatives in good yields.

Xanthine and its methylated derivatives, such as theophylline and theobromine, occur in living systems, especially in plants. Since these methylated purines and other alkyl analogs are biologically and physiologically important, the *N*-alkylation of this class of heterocycles has been studied actively.

Various alkylating agents, such as dialkyl sulfate,[1-3] alkyl *p*-toluenesulfonate,[3] and alkyl halide,[4,5] have been used for the *N*-alkylation of xanthine and its derivatives. Although the site of alkylation is influenced by various conditions, it has been generally established that, under alkaline conditions, alkylation takes place in the following order, that of the decreasing acidity of the replaced proton: N-3, N-7, and then N-1. Under neutral or acidic conditions, on the other hand, only imidazole ring-nitrogens are alkylated, converting the purine into quaternised or betaine forms.

In previous papers, we reported the *N*-alkylation of purines,[6] imidazoles,[7,8] and pyrimidines[9] by heating with alkyl esters of phosphoric acid at about 200 °C. Since this procedure would be too vigorous for many natural products, however, we continued our search for mild conditions, using xanthine, theophylline, and theobromine. This paper will show a facile *N*-alkylation of this class of heterocycles in a weak alkaline aqueous solution at 25—60 °C. Unlike reactions with other alkylating agents, which in most cases are insoluble in water, the present reaction can be carried out successfully in an aqueous environment because of the water-soluble property of a trialkyl phosphate.

Results and Discussion

The reactions were carried out by stirring a mixture of a purine and a 2—5 molar excess of trialkyl phosphate in water (pH 9—10) at 25—60 °C. The products were isolated through extraction and recrystallization. The results are summarized in Table 1.

The reaction of xanthine (**1**) with trimethyl phosphate (**a**) at 25 °C for 48 h afforded four ultraviolet absorbing products (**2**—**5**). The **2** and **3** products were produced mainly, and identified as caffeine and theobromine respectively through their physical constants. Compounds **4** and **5** were identified as 3-methylxanthine and 7-methylxanthine respectively according to their ultraviolet absorption spectra. With an increase in the reaction temperature and the reaction time, **1** tends to be methylated effectively at the N-1, N-3, and N-7 positions to produce 1,3,7-trimethylxanthine (**2**, caffeine), while at low temperatures and short reaction times **3** is isolated as the only product. Ethylation and allylation took place also in **1** to give 3,7-dialkyl derivatives (**6**, **7**). These results suggest that the N-1 position of **1** is less reactive than the N-3 and N-7 positions.

This trend was observed also in the alkylation of theobromine (**3**) and theophylline (**10**). Thus, although **10** was alkylated with triethyl phosphate (**b**) or triallyl phosphate (**c**) to give the corresponding 7-alkyl derivatives (**11** and **12**) quantitatively, **3** was transformed to the 1-alkyl derivatives (**8** and **9**) in only low yields.

Table 1. Reactions of purines with trialkyl phosphates[a]

Purine	R of O=P $(OR)_3$	Mole ratio (Ester/Purine)	Temp (°C)	Time (h)	Product	Yield (%)
Xanthine (**1**)	Me	6	60	48	Caffeine (**2**)	73
1	Me	6	25	48	**2**	17
					3	9
					3-Methylxanthine (**4**)	Trace
					7-Methylxanthine (**5**)	Trace
1	Et	3	80	48	3,7-Diethylxanthine (**6**)	6
1	Allyl	3	60	48	3,7-Diallylxanthine (**7**)	15
Theophylline (**10**)	Me	6	25	48	**2**	83
10	Me	3	60	8	**2**	92
10	Et	3	60	48	7-Ethyltheophylline (**11**)	26
10	Allyl	3	60	48	7-Allyltheophylline (**12**)	50
Theobromine (**3**)	Me	6	25	100	**2**	87
3	Me	3	60	24	**2**	93
3	Et	3	60	48	1-Ethyltheobromine (**8**)	10
3	Allyl	3	60	48	1-Allyltheobromine (**9**)	16

a) The reactions were carried out in an aqueous solution at pH 9—10.

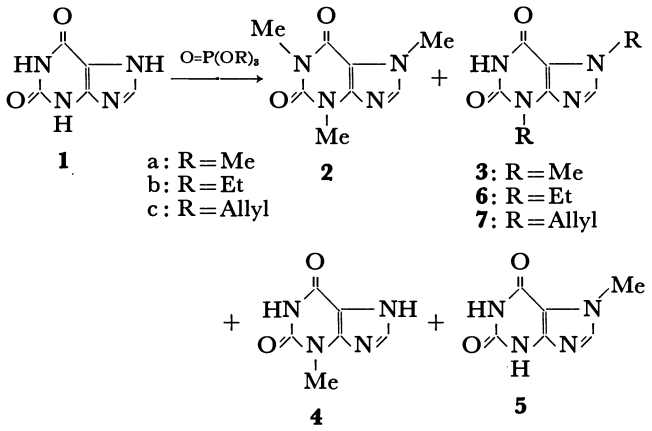

The low reactivity of the N-1 position towards alkylation might be attributed to the decreased nucleophilicity of the N-1 nitrogen atom and the steric hindrance around the N-1 position towards the alkyl groups of phosphate esters by two adjacent carbonyl groups at the 2 and 6 positions.

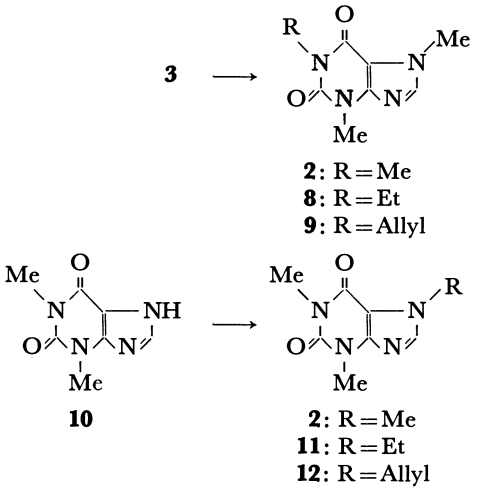

The order of the reactivity of trialkyl phosphates in aqueous solutions was $O=P(OCH_3)_3$ (**a**)>$O=P(OCH_2-CH=CH_2)_3$ (**c**)>$O=P(OCH_2H_5)_3$ (**b**). The high reactivity of **a** may result partly from its low steric hindrance at the reaction site. The unexpected high reactivity of **c**, in spite of its decreased solubility in water, may originate from its conjugated structure.

The above results indicate that trialkyl phosphate, especially **a**, may be a useful alkylating agent, allowing an alkylation reaction to proceed under mild conditions.

Experimental

The UV and IR spectra were measured with Hitachi EPS-3T and Jasco IR-G spectrometers respectively. The NMR spectra were recorded on a Hitachi-Perkin Elmer R-20 spectrometer, with a dilute solution in deuteriochloroform or dimethyl-d^6 sulfoxide and tetramethylsilane as the internal and outside standards. Thin-layer chromatography was performed on silica gel [GF_{254} (type 60), Merck] using a mixture of chloroform and methanol (7: 1). Commercially available xanthine, theophylline, and theobromine, as well as trimethyl and triethyl phosphates, were used without further purification. The triallyl phosphate was prepared by the procedure of Toy and Costello.[10]

The following preparations are typical. The reaction conditions are listed in Table 1.

Alkylation of Xanthine (1). *A. With Trimethyl Phosphate (a)*: *Procedure 1*: A mixture of **1** (1.38 g, 9.1 mmol) and **a** (7.50 g, 54.0 mmol) in water (10 ml) was stirred at 60 °C. The solution was maintained at pH 9—10 throughout the reaction by the occasional addition of 4 M sodium hydroxide. After 48 h of stirring, the reaction mixture was extracted with chloroform. The subsequent evaporation of the solvent from the organic extract gave caffeine (**2**) as crystals; mp 233—234 °C (from THF–ethanol) (lit,[11] mp 235 °C), (1.28 g, 73%).

Procedure 2: A mixture of **1** (1.35 g, 8.9 mmol) and **a** (7.50 g, 54.0 mmol) in water (20 ml, pH 9—10, NaOH) was stirred at 25 °C for 48 h. Thin-layer chromatography of the reaction mixture showed four ultraviolet absorbing products; R_f: **5**= 0.27, **4**=0.31, **3**=0.46, and **2**=0.69 (chloroform–methanol 7: 1). The subsequent evaporation of the solvent from the organic layer gave **2** as crystals; (0.29 g, 17%). The aqueous layer was neutralized with concentrated hydrochloric acid and extracted with chloroform. Upon the concentration of the organic layer, **3** was obtained as a white powder and was identified as theobromine by a comparison of its physical properties with those of an authentic sample (0.14 g, 9%). The ultraviolet spectra of the aqueous extract of the corresponding spots for **5** and **4** coincided with those of 7-methyl- and 3-methylxanthine respectively; 7-methylxanthine: λ_{max} (H_2O) nm: 265 (pH 1), 269 (pH 7), 283 (pH 13) [lit,[12] 266 (pH 0.8), 268 (pH 4), 268 (pH 7), 288 (pH 13)], 3-methylxanthine: λ_{max} (H_2O) nm: 269 (pH 1), 272 (pH 7), 275 (pH 13) [lit,[11] 270 (pH 6), 274 (pH 14)].

B. With Triallyl Phosphate (c): The treatment of **1** (1.52 g, 10.0 mmol) with **c** (5.10 g, 30 mmol) in water (10 ml, pH 9—10, NaOH) gave 3,7-diallylxanthine (**7**, 0.38 g, 15%) after the reaction mixture had been stirred at 60 °C for 48 h; mp 182.5—184 °C (from ethanol); IR (KBr): 3000 (m), 2800 (w), 1680 (s), 1585 (m), 1540 (m), 1375 (m), 1295 (w), 1265 (m), 1130 (m), 990 (s), 920 (s), 840 (m), 750 (w), and 620 cm^{-1} (m); NMR (DMSO-d^6): 4.43 (complex m, 2H, $-C\mathbf{H}_2-CH=CH_2$), 4.60—5.30 (complex m, 2H, $-CH_2-CH=C\mathbf{H}_2$), 5.45—6.25 (complex m, 1H, $-CH_2-C\mathbf{H}=CH_2$), and 7.92 ppm (δ) (s, 1H, H^8); UV, λ_{max} (H_2O) nm: pH 1, 269 (log ε 4.13), pH 7, 273 (log ε 3.96), pH 13, 275 (log ε 4.00); Found: C, 56.54; H, 5.08; N, 23.74%. Calcd for $C_{11}H_{12}N_4O_2 \cdot 0.1H_2O$: C, 56.54; H, 5.22; N, 23.95%.

Alkylation of Theophylline (10). *A. With Trimethyl Phosphate (a)*: A mixture of **10** (1.54 g, 8.6 mmol) and **a** (3.75 g, 27.0 mmol) was stirred in water (10 ml, pH 9—10, NaOH) at 60 °C for 8 h. After the reaction mixture had then been allowed to stand at room temperature, **2** appeared as crystals from the solution (1.28 g, 79%). The organic layer was concentrated to give another crop of **2** (0.20 g, 12%).

B. With Triallyl Phosphate (c): A reaction of **10** (1.81 g, 10.0 mmol) with **c** (5.10 g, 30.0 mmol) in water (10 ml, pH 9—10, NaOH) at 60 °C for 48 h afforded 7-allyltheophylline (**9**, 1.11 g, 50%) after a procedure similar to that described above; mp 101—103 °C (from hexane) (lit,[13] 101—102 °C); IR (KBr): 3100 (m), 2950 (w), 1700 (s), 1655 (s), 1550 (m), 1480(m), 1370 (w), 1230 (m), 1030 (m), 940 (w), 760 (s), 750 (s), and 620 cm^{-1} (m); NMR ($CDCl_3$): 3.48 (s, 3H, $-C\mathbf{H}_3$), 3.67 (s, 3H, $-C\mathbf{H}_3$), 5.03 (complex m, 2H, $-C\mathbf{H}_2-CH=CH_2$), 5.20—5.53 (complex m, 2H, $-CH_2-CH=C\mathbf{H}_2$), 5.70—6.45 (complex m, 1H, $-CH_2-C\mathbf{H}=CH_2$), and 7.65 ppm (δ) (s, 1H, $\mathbf{H}^8$); UV, λ_{max} (H_2O) nm: pH 1, 273 (log ε 3.98), pH 7, 275 (log ε 3.94), pH 13, 275 (log ε 3.94); Found: C, 54.47; H, 5.43; N, 26.00%. Calcd for $C_8H_{10}N_4O_2$: C, 54.54;

H, 5.49; N, 25.44%.

Alkylation of Theobromine (3) with Triallyl Phosphate (c). A reaction of **3** (1.81 g, 10.0 mmol) with **c** (5.20 g, 30.0 mmol) in water (10 ml, pH 9—10, NaOH) at 60 °C for 48 h afforded 1-allyltheobromine (**9**, 0.29 g, 16%) upon the treatment of the reaction mixture in a manner similar to that described above; mp 139—142 °C (sublime); IR (KBr): 3200 (m), 2900 (w), 1700(s), 1640 (s), 1540 (m), 1450 (m), 1360 (m), 1275 (w), 1230 (m), 1100 (w), 920 (s), 860 (w), 760 (s), 740 (s), 650 (w), and 620 cm^{-1} (m); NMR ($CDCl_3$): 3.58 (s, 3H, $-CH_3$), 4.00 (s, 3H, $-CH_3$), 4.63 (complex m, 2H, $-CH_2-CH=CH_2$), 5.03—5.47 (complex m, 2H, $-CH_2-CH=CH_2$), 5.48—5.96 (complex m, 1H, $-CH_2-CH=CH_2$), and 7.53 ppm (δ) (s, 1H, H^8); UV, λ_{max} (H_2O) nm: pH 1, 274 (log ε 4.03), pH 7, 275 (log ε 4.01), pH 13, 275 (log ε 4.01); Found: C, 54.77; H, 5.40; N, 25.88%. Calcd for $C_8H_{10}N_4O_2$: C, 54.54; H, 5.49; N, 25.44%.

References

1) H. Bredereck, H. G. von Schuh, and A. Martini, *Chem. Ber.*, **83**, 201 (1950).
2) H. Bredereck and H. G. von Schuh, Ger. Pat. 864869 (1953).
3) J. W. Jones and R. K. Robins, *J. Am. Chem. Soc.*, **84**, 1914 (1962).
4) E. Fischer, *Justus Liebigs Ann. Chem.*, **215**, 309 (1882).
5) E. Fischer, *Justus Liebigs Ann. Chem.*, **215**, 253 (1882).
6) K. Yamauchi, M. Hayashi, and M. Kinoshita, *J. Org. Chem.*, **40**, 385 (1975).
7) K. Yamauchi and M. Kinoshita, *J. Chem. Soc., Perkin, Trans. 1*, **1973**, 2506.
8) M. Hayashi, K. Yamauchi, and M. Kinoshita, *Bull. Chem. Soc. Jpn.*, **49**, 283 (1976).
9) K. Yamauchi and M. Kinoshita, *J. Chem. Soc., Perkin, Trans. 1*, **1973**, 391.
10) A. D. F. Toy and J. R. Costello, U. S. Pat. 2754315 (1950).
11) W. Pfleiderer and G. Nübel, *Justus Liebigs Ann. Chem.*, **647**, 155 (1961).
12) J. A. Hains, C. B. Reese, and L. Todd, *J. Chem. Soc.*, **1962**, 5281.
13) R. Zelnik, *Bull. Soc. Chim. Fr.*, **1960**, 1917.

An Anion Radical Precursor in the Nucleophilic Substitution of *o*-Dinitrobenzene

Takehiro ABE and Yusaku IKEGAMI*

College of General Education, Tohoku University, Kawauchi, Sendai 980
**Chemical Research Institute of Non-Aqueous Solutions, Tohoku University, Katahira-2-chome, Sendai 980*

(Received July 12, 1976)

By visible and ESR spectroscopies, the appearance of *o*-dinitrobenzene anion radical has been demonstrated for the replacement of one nitro group of *o*-dinitrobenzene by hydroxide ion in aqueous dimethyl sulfoxide. Kinetic studies have supported the suggestion that the anion radical is a precursor in the substitution reaction.

According to the electron transfer theory proposed by Nagakura and Tanaka,[1,2] nucleophilic aromatic substitution should proceed *via* the anion radical resulting from one-electron transfer from the highest occupied orbital of a nucleophilic reagent to the lowest vacant orbital of an aromatic molecule. Here the energy level of the highest occupied orbital must be higher than that of the lowest vacant orbital. Recently, some anion radicals observed during the course of nucleophilic substitution have been supposed to be precursors in the substitution mechanisms.[3-10] As described by Bernasconi,[10] there has been no evidence that the anion radicals are the precursors in the nucleophilic substitution rather than the products resulting from competing side reactions. We now present the experimental results strongly supporting that an *o*-dinitrobenzene anion radical is the precursor in the replacement of one nitro group of *o*-dinitrobenzene by hydroxide ion in aqueous dimethyl sulfoxide (DMSO).

Experimental

o-Dinitrobenzene was obtained commercially and purified by recrystallization. DMSO was kept in contact with barium oxide for a week and fractionated two times under reduced pressure. *N,N*-Dimethylformamide was treated with sodium hydroxide pellets and barium oxide, and distilled at 1 Torr. This solvent was kept with Molecular Sieves 4A after degassed.

Unless otherwise stated, all the mixings of degassed solutions of *o*-dinitrobenzene with degassed solutions of sodium hydroxide were carried out in sealed cells in order to obtain the electronic and ESR spectra. Electronic-spectral changes were recorded with a Cary 14 recording spectrophotometer equipped with a thermostated cell compartment. ESR spectra were recorded with a Varian E-4 EPR spectrometer.

Results and Discussion

When a DMSO solution of *o*-dinitrobenzene was mixed with an aqueous DMSO solution of sodium hydroxide, the resultant reaction system showed absorption spectral changes shown in Figs. 1 and 2. Curve e in Fig. 1 is obtained by correcting curve a for the absorption of DMSO, because DMSO absorbs above 700 nm as shown in Fig. 1. The reaction system, therefore, shows the absorption curve of e in the region 800—1200 nm. The bands at 325 and 800—1200 nm increased in intensity and gradually disappeared later on.

The initial 420 nm band (curve a in Fig. 2) differs from the final 430 nm band (curve f) in peak position. In the case of the similar reaction system open to the air, it was distinctly observed with a Hitachi rapid scan spectrophotometer RSP-2 that at the initial stage the 420 nm band increased in intensity in the same way as the 325 nm band. The time courses of absorption-coefficient changes at 900 and 430 nm are shown in Fig. 3. Curve b in Fig. 3 indicates that the whole course of increasing absorption coefficient at 430 nm is not due to one species, since the increase in the coefficient is abruptly slow down at *ca.* 5 min after mixing. Accordingly, the initial 420 nm band is assigned to the labile

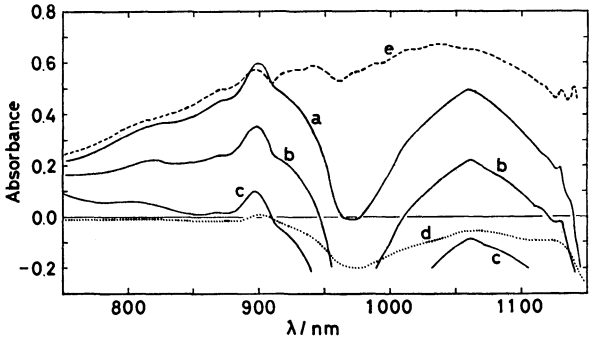

Fig. 1. Spectral change of the DMSO solution containing *o*-dinitrobenzene (3.30×10^{-4} M), sodium hydroxide (1.00×10^{-2} M) and 4% (v/v) water (25 °C). Time after mixing: a, 4.4 min; b, 15 min; c, 41 min. Curve e is obtained by correcting curve a for the absorption of DMSO (curve d). Path length was 2.87 cm except the case of d, whose path length was 1.00 cm.

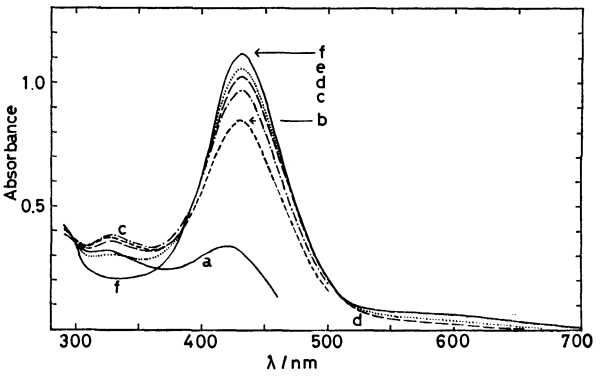

Fig. 2. Spectral change of the same solution as in Fig. 1 (25 °C). Time after mixing: a, 15 s; b, 1.3 min; c, 4.6 min; d, 11 min; e, 30 min; f, 100 min. Path length was 0.390 cm.

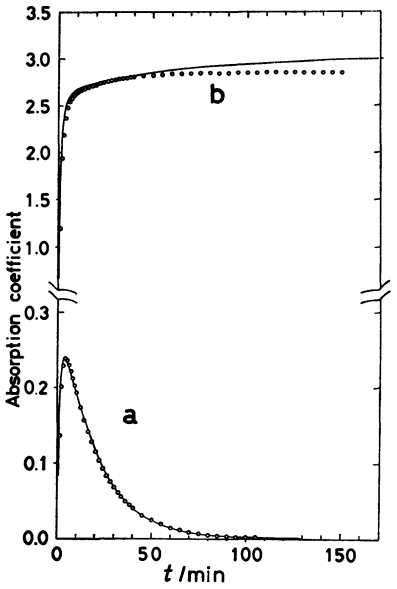

Fig. 3. Time course (full lines) of absorption coefficient of the same solution as in Fig. 1 (25.0 °C). a, 900 nm; b, 430 nm. Circles show the values calculated according to Eqs. 1 and 2 or to Eqs. 3 and 4.

species showing the bands at 325 and 800—1200 nm.

The bands at 325 and 420 nm do not correspond to the 430 and 455 nm bands, respectively, of the π-electronic structure (*i.e.*, 1-nitropentadienate) of 1-amino-1-methoxy-2-nitrocyclohexadienate formed from *o*-nitroaniline and methoxide ion in dichloromethane.[11] The bands at 325, 420, and 800—1200 nm correspond to those at 350, 440, and 1090 nm, respectively, assigned to the *o*-dinitrobenzene anion radical in a γ-irradiated rigid solution in 2-methyltetrahydrofuran at 77 K.[12] We, therefore, assign the labile species showing these bands to the anion radical.

It is well-known that the reaction of *o*-dinitrobenzene with hydroxide ion yields *o*-nitrophenol and nitrite ion.[13] Sodium nitrite (4.5×10^{-4} M) in DMSO containing 4% (v/v) water and sodium hydroxide (1.00×10^{-2} M) absorbed very weakly in the region above 400 nm. The final 430 nm band of the reaction system (curve f in Fig. 2) differed in peak position from the 450 nm band of the similar solution of *o*-nitrophenol, while the similar DMSO solution of *p*-dinitrobenzene finally showed the band identical with that of the similar solution of *p*-nitrophenol in the peak position and shape.[8] When the reaction system containing *o*-dinitrobenzene (0.3 M) and sodium hydroxide (0.7 M) in aqueous DMSO-d_6 was stood for 4 h in the dark at room temperature, the system showed the ^{1}H NMR spectrum of *o*-nitrophenoxide ion at the range δ 5—8 ppm.[14] The reaction of *o*-dinitrobenzene (0.745 g, 0.12 M) with sodium hydroxide (0.26 M) in DMSO containing 19% (v/v) water at room temperature afforded a yellowish-orange crude substance (0.485 g) after dilution with water, neutralization, and extraction with diethyl ether. The IR spectrum of the crude substance exhibited the absorption bands corresponding to *o*-nitrophenol. The results of thin-layer chromatography for the aqueous DMSO solution of *o*-dinitrobenzene (7.2×10^{-2} M) and sodium hydroxide (1.8×10^{-1} M), allowed to stand overnight in the dark at room temperature, showed the major product of *o*-nitrophenol and the absence of unaltered *o*-dinitrobenzene, though there was the small spot which could not be eluted with benzene containing a small amount of methanol. From the above results, the final species showing the 430 nm band was identified as *o*-nitrophenoxide ion. The production of nitrite ion was confirmed by the brown ring test.

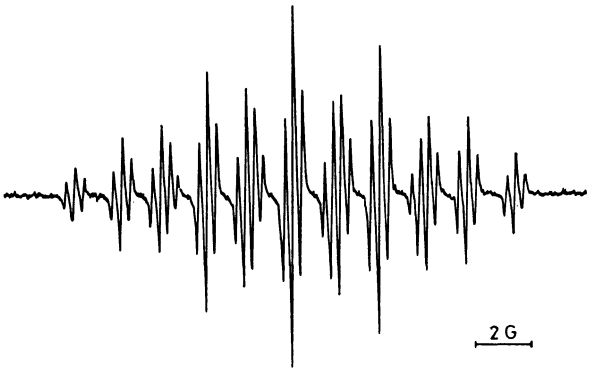

Fig. 4. ESR Spectrum of the same solution as in Fig. 1 (*ca.* 21 °C).

The formation of the labile *o*-dinitrobenzene anion radical in the reaction system was confirmed by ESR spectroscopy. The reaction system showed a strong ESR signal. Hyperfine structure of the ESR spectrum (Fig. 4) is consistent with that of the *o*-dinitrobenzene anion radical having the two equivalent nitrogen atoms. The splitting constants, $a_N=3.02$, $a_H(3,6)=0.30$, and $a_H(4,5)=1.64$ gauss, agreed well with the reference values.[15] The time course of relative ESR-signal intensity of the anion radical in the reaction system at *ca.* 21 °C resembled that of the absorption coefficient change at 900 nm in Fig. 3.

No other radical species was found in the ESR spectrum of the reaction system, even if the system kept at 19 °C for 3 min after mixing was suddenly cooled to −130 °C and then warmed gradually over recording the spectrum. This result indicates that any long-lived radical other than the *o*-dinitrobenzene anion radical was not present in the reaction system, and eliminates any mechanism including persisting radicals other than the *o*-dinitrobenzene anion radical. Thus, the result eliminates the following schemes in which the hydroxyl radical produced reversibly should long live together with the anion radical.

o-Dinitrobenzene

$\uparrow\downarrow$ OH^-

A Meisenheimer-type intermediate $\longrightarrow$ *o*-Nitrophenol

$\uparrow\downarrow$

[*o*-Dinitrobenzene anion radical ··· $\dot{O}H$]

The formation of the *o*-dinitrobenzene anion radical in DMSO is not due to electron transfer from methylsulfinyl methanide[16] to *o*-dinitrobenzene, because the

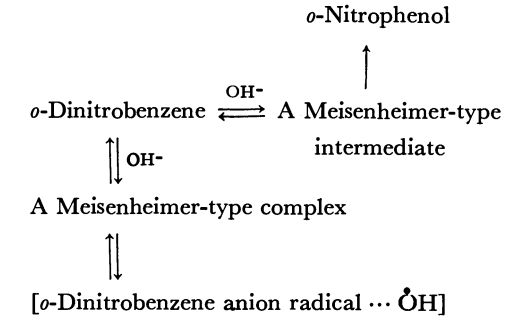

mixture obtained by mixing two drops of aqueous solution of sodium hydroxide (5 M) with an *N*,*N*-dimethylformamide solution of *o*-dinitrobenzene (1×10^{-2} M) also showed the ESR spectrum of the *o*-dinitrobenzene anion radical with $a_N=3.25$, $a_{H3}=0.40$, and $a_{H4}=1.68$ gauss.

The mixture of *o*-dinitrobenzene (1.00×10^{-2} M) and sodium 1,1-dimethoxy-2,4,6-trinitrocyclohexadienate (9.21×10^{-3} M)[17] in DMSO did not show any ESR signal at the temperatures of 0° and 25 °C. This fact suggests that an electron transfer does not occur between *o*-dinitrobenzene and the Meisenheimer-type intermediate in the reaction system under study. Since the Meisenheimer intermediate has the stable π-electronic structure of pentadienate, the highest-occupied energy level of the intermediate would be lower than the lowest-vacant energy level of *o*-dinitrobenzene, so that the electron transfer can not occur.[1,2]

Thus, the formation of *o*-dinitrobenzene anion radical is probably due to the direct electron transfer from hydroxide ion to *o*-dinitrobenzene. The lowest-vacant energy level of *o*-dinitrobenzene can be estimated to be −5.84 eV from the values[18] of the lowest π-π^* transition energy (4.43 eV) and ionization potential (10.27 eV) of *o*-dinitrobenzene. The energy level is sufficiently lower than the occupied energy level of OH^- (−2.1 eV[1]). According to Nagakura and Tanaka's theory, therefore, the anion radical can be formed as a result of the direct electron transfer from hydroxide ion to *o*-dinitrobenzene. In the case of the aqueous DMSO solution of *p*-dinitrobenzene and hydroxide ion, the production of the short-lived hydroxyl radical has been confirmed by spin-trapping with 2-nitroso-2-methylpropane.[9]

Here we denote the initial concentrations of *o*-dinitrobenzene and sodium hydroxide by $[o\text{-DNB}]_0$ and $[NaOH]_0$, respectively. The rate of decrease in the 900 nm absorption coefficient of the DMSO solution containing 4% (v/v) water, $[o\text{-DNB}]_0=3.31\times10^{-4}$ M, and $[NaOH]_0=1.00\times10^{-2}$ M was faster than that for the same solution except for $[NaOH]_0=5.0\times10^{-3}$ M at 25 °C. When $3\times[o\text{-DNB}]_0<[NaOH]_0=1.00\times10^{-2}$ M, the decrease in the 900 nm absorption coefficient obeyed the pseudo-first order kinetics and was relatively fast. In the case of $[o\text{-DNB}]_0:[NaOH]_0=1:2$ where $[NaOH]_0=1.00\times10^{-2}$ M, the decrease in the 900 nm absorption coefficient was extremely slow. The radical species in this solution lived for a few days at room temperature after mixing. The thin-layer chromatography of the reaction system, stood overnight in the dark at room temperature, distinctly showed the presence of unaltered *o*-dinitrobenzene for the case of $2.5\times[o\text{-DNB}]_0>[NaOH]_0$. All these facts mean that the relatively fast decomposition of the anion radical requires hydroxide ion. The further reaction of the anion radical with hydroxide ion is possibly the formation of a dianion radical such as proposed by Shein *et al.*[4,10] The question, however, remains, since the formation of the dianion radical is unfamiliar. Hydroxide ion will be further consumed for ionizing *o*-nitrophenol, because *o*-nitrophenol in the DMSO solution containing 4% (v/v) water in the absence of sodium hydroxide did not show any absorption band above 400 nm.

In view of the above results, the reaction scheme for the present reaction may be written below under the condition of $3\times[o\text{-DNB}]_0<[NaOH]_0$.

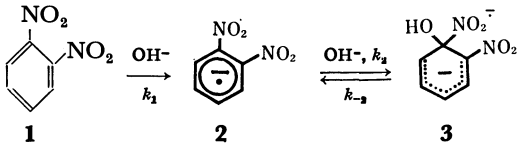

Scheme 1.

Here k_i denotes the rate constant for the ith step. The first-order rate constants of k_1 and k_2 contain $[NaOH]_0$. The authors propose Scheme 2 or 3 for the further reactions of **3**.

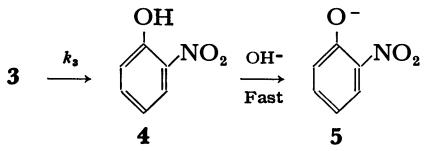

Scheme 2.

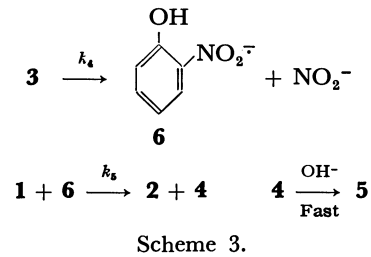

Scheme 3.

According to one of the mechanisms proposed by Schein *et al.*,[4,10] **3** should undergo the reaction indicated in Scheme 4.

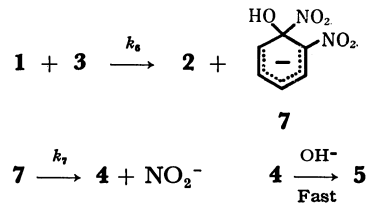

Scheme 4.

Dianion radical **3** seems very labile, because any Meisenheimer-type complex, in which the nucleophilic reagent attacks the carbon atom carrying a nitro group, has never been observed. Dianion radical **3** is,

therefore, likely to decompose rather than to exchange an electron with *o*-dinitrobenzene. Moreover, Scheme 4 would give the concentration changes different from those for Schemes 2 and 3, which can explain the experimental data shown in Fig. 3, as described below. Accordingly, Scheme 4 is ignored here.

Since no band other than those of **2** and **5** is found in Fig. 2, we can assume the restrictions of $k_2 \ll k_3$ and $k_2 \ll k_4$ or k_5 in Schemes 2 and 3, respectively. Then, the steady state treatment was applied for the concentrations of **3** and **6**. The absorption-coefficient changes for 900 and 430 nm with time t are expressed below. For Schemes 1 and 2,

$$a(900\,\text{nm}) = \frac{k_1}{k_1-k_2'}\varepsilon_R[o\text{-DNB}]_0\{\exp(-k_2't)-\exp(-k_1t)\} \quad (1)$$

$$a(430\,\text{nm}) = \varepsilon_{NP}[o\text{-DNB}]_0-\frac{k_1}{k_1-k_2'}(\varepsilon_{NP}-\varepsilon_R')[o\text{-DNB}]_0 \times\exp(-k_2't)-\frac{k_1\varepsilon_R'-k_2'\varepsilon_{NP}}{k_1-k_2'}[o\text{-DNB}]_0\exp(-k_1t) \quad (2)$$

where $k_2'=k_2\{1-k_{-2}/(k_3+k_{-2})\}$. Here ε_R and ε_{NP} are molar absorption coefficients of **2** and **5**, respectively. For Schemes 1 and 3,

$$a(900\,\text{nm}) = \frac{k_1}{r_1-r_2}\varepsilon_R[o\text{-DNB}]_0\{\exp(-r_2t)-\exp(-r_1t)\} \quad (3)$$

$$a(430\,\text{nm}) = \varepsilon_{NP}[o\text{-DNB}]_0-\frac{r_1\varepsilon_{NP}-k_1\varepsilon_R'}{r_1-r_2}[o\text{-DNB}]_0\exp(-r_2t) -\frac{k_1\varepsilon_R'-r_2\varepsilon_{NP}}{r_1-r_2}[o\text{-DNB}]_0\exp(-r_1t) \quad (4)$$

where $r_1=k_1/2+\{(k_1/2)^2-k_1k_2k_3/(k_{-2}+k_3)\}^{1/2}$ and $r_2=k_1/2-\{(k_{1/2})^2-k_1k_2k_3/(k_{-2}+k_3)\}^{1/2}$. Instead of the last two steps in Scheme 3, the following steps are also possible and give the same results.

$$\mathbf{6} + OH^- \xrightarrow{\text{Fast}} \mathbf{8} + H_2O$$

$$\mathbf{1} + \mathbf{8} \xrightarrow{k_5} \mathbf{2} + \mathbf{5}$$

The values calculated for the absorption coefficients according to Eqs. 1 and 2, are plotted in Fig. 3 by assuming the following values: $k_1=0.638\ \text{min}^{-1}$, $k_2'=0.0519\ \text{min}^{-1}$, $\varepsilon_R(900\,\text{nm})=9.05\times10^2$, $\varepsilon_R'(430\,\text{nm})=7.63\times10^3$, and $\varepsilon_{NP}(430\,\text{nm})=8.62\times10^3$. Equations 3 and 4 also give the identical plot by assuming the following values: $k_1=0.690\ \text{min}^{-1}$, $r_1=0.638\ \text{min}^{-1}$, $r_2=0.0519\ \text{min}^{-1}$, $\varepsilon_R(900\,\text{nm})=8.37\times10^2$, $\varepsilon_R'(430\,\text{nm})=7.05\times10^3$, and $\varepsilon_{NP}(430\,\text{nm})=8.62\times10^3$.

The calculated values of absorption coefficients for 430 nm are somewhat lower than the found ones after 50 min. The values finally found may be made up by the small superposition of absorption coefficients of nitrite ion and a minor by-product upon that of *o*-nitrophenoxide ion at 430 nm. The molar absorption coefficients of 440 and 1090 nm bands of the anion radical in the rigid solution at 77 K are 6×10^3 and 4×10^3, respectively.[12] The values of $\varepsilon_R'(430\,\text{nm})$ are comparable to 6×10^3, while the values of $\varepsilon_R(900\,\text{nm})$ are considerably smaller than 4×10^3.

Now we can not select one of Schemes 2 and 3. In Scheme 2, the decomposition of **3** should yield the dianion radical $NO_2\cdot^{2-}$. The formation $NO_2\cdot^{2-}$ is unfamiliar, though it has been identified by ESR spectroscopy in KCl crystals dropped with KNO_2.[19] As shown in Fig. 3, the two sets of Eqs. 1 and 2 and of Eqs. 3 and 4 can well reproduce the experimental data to the same extent. In conclusion, the kinetic results strongly support that the *o*-dinitrobenzene anion radical is the precursor in the reaction under study, though the further reaction of the anion radical is not established.

It is unlikely that the primary step of formation of **2** in Scheme 1 is an elementary reaction. The step may be accounted for below. In the case of photosubstitution reaction of 3,5-dinitroanisole with hydroxide ion to produce 3,5-dinitrophenol, a primary reaction step is the formation of intermediate [3,5-dinitroanisole···ȮH] owing to an electron transfer from hydroxide ion to the π-π^* triplet state of 3,5-dinitroanisole.[20,21] The half-lifetime of the intermediate is *ca.* 5×10^{-7} s.[20] Therefore, the corresponding intermediate (**9**) is reasonably supposed to be formed in the present reaction. On the other hand, the rate constant for the reaction of hydroxyl radical with DMSO in aqueous DMSO ($HO\cdot + CH_3SOCH_3 \rightarrow CH_3\cdot + CH_3SO\cdot OH$) is $5\times10^9\ M^{-1}\,s^{-1}$ (25 °C).[22] The reaction between DMSO and hydroxyl radical in **9** is probably faster than that of **9**. Thus, the persisting *o*-dinitrobenzene anion radical in the present reaction system may be generated as follows:

$$\mathbf{1} + OH^- \rightleftharpoons \mathbf{9}$$

$$\mathbf{9} + CH_3SOCH_3 \longrightarrow \mathbf{2} + CH_3\cdot + CH_3SO\cdot OH$$

The methyl radical will undergo a rapid reaction.

References

1) S. Nagakura and J. Tanaka, *J. Chem. Phys.*, **22**, 563 (1954); *Bull. Chem. Soc. Jpn.*, **32**, 734 (1959).
2) S. Nagakura, *Tetrahedron*, **19**, Suppl. 2, 361 (1963).
3) K. A. Bilevitch, N. N. Pubnov, and O. Yu. Okhlobystin, *Tetrahedron Lett.*, **1968**, 3465.
4) S. M. Shein, L. V. Bryukhovetskaya, V. F. Starichenko, and T. M. Ivanova, "Organic Reactivity," Vol. 6, Tartua (SSSR) (1969), p. 1087.
5) L. A. Blyumenfeld, L. V. Bryukhovetskaya, G. V. Fomin, and S. M. Shein, *Zh. Phys. Khim*, **44**, 931 (1970).
6) S. M. Shein, L. V. Bryukhovetskaya, and T. M. Ivanova, *Izv. Acad. Nauk SSSR, Ser. Khim*, **1973**, 1596.
7) L. V. Bryukhovetskaya, L. V. Mironova, and S. M. Shein, *Izv. Acad. Nauk SSSR, Ser. Khim*, **1973**, 1601.
8) T. Abe, *Chem. Lett.*, **1973**, 1339.
9) I. I. Bilkis and S. M. Shein, *Tetrahedron*, **31**, 969 (1975).
10) C. F. Bernasconi, "Aromatic Compounds," H. Zollinger, ed., Butterworths, London (1973), p. 33.
11) S. Ohsawa, *Nippon Kagaku Kaishi*, **1973**, 1486.
12) T. Shida and S. Iwata, *J. Phys. Chem.*, **75**, 2591 (1971).

13) L. F. Fieser and M. Fieser, "Advanced Organic Chemistry," Reinhold, New York, N. Y. (1961), p. 678.
14) The authors wish to thank Professor Toyonobu Asao of Tohoku University for the NMR measurement, which was carried out with a Hitachi high-resolution NMR spectrometer, Model R-22 (90 MHz).
15) D. H. Geske, J. L. Ragle, M. A. Bambenek, and A. L. Balch, *J. Am. Chem. Soc.*, **86**, 987 (1964).
16) G. A. Russell, E. G. Janzen, and E. T. Strom, *J. Am. Chem. Soc.*, **86**, 1807 (1964).
17) The Meisenheimer complex was crystallized from the methanolic solution of 2,4,6-trinitroanisole and sodium methoxide.
18) M. D. Gordon and J. F. Neumer, *J. Phys. Chem.*, **78**, 1868 (1974).
19) J. R. Morton, *Chem. Rev.*, **64**, 453 (1964).
20) G. P. de Gunst and E. Havinga, *Tetrahedron*, **29**, 2167 (1973).
21) W. G. Dauben, L. Salem, and N. J. Turro, *Acc. Chem. Res.*, **8**, 41 (1975).
22) B. C. Gilbert, R. O. C. Norman, and R. C. Sealy, *J. Chem. Soc., Perkin Trans.* 2, **1975**, 303.

A Simple Method for the Synthesis of Lignan Skeleton.[1] Syntheses of (±)-Parabenzlactone and (±)-Hinokinin

Yuzo Asano, Tadao Kamikawa, and Takashi Tokoroyama

Faculty of Science, Osaka City University, Sugimotocho, Sumiyoshiku, Osaka 558

(Received July 14, 1976)

The reaction of 2-aryl-2-lithio-1,3-dithianes with 2-butenolide followed by quenching with benzyl halides gave lignan skeleton in fairly good yield.

In connection with the total synthesis of a novel class of antileukemic lignan lactone, steganacin (**1**),[2] we needed the efficient synthetic method for constructing the *seco*-lactone skeleton (**2**). We have studied the addition of 2-aryl-2-lithio-1,3-dithianes to 2-butenolide, hoping to find a new method leading to **2**. Although synthetic applications of 2-lithio-1,3-dithianes as an acyl anion equivalent had been widely explored,[3] little investigation existed for the Michael addition of it to α,β-unsaturated lactones, when we started on this project. Since then Ziegler and Schwartz[4] reported the synthesis of lignans by means of a conjugate addition of aryl dithiane anion to 2-butenolide. In this paper we wish to report on the results of our own independent studies which based on the essentially the same idea as theirs.

Results and Discussion

Treatment of 2-aryl-1,3-dithianes (**3**)[5] in THF with butyllithium at −40 °C followed by addition of 2-butenolide at −78 °C gave the Michael addition products (**4**). Concerning the effect of substituents, it was shown that the addition was facilitated by the presence of electron-releasing groups **4b**—**4e**, as shown in Table 1. Neither 2-lithio-1,3-dithiane nor 2-lithio-2-aryl-1,3-dithiolane added to 2-butenolide. Desulfurization of **4** with *N*-chlorosuccinimide and silver nitrate gave β-aroyl-γ-lactones (**5**), as shown in Table 2.

Table 1. Formation of dithiane lactones

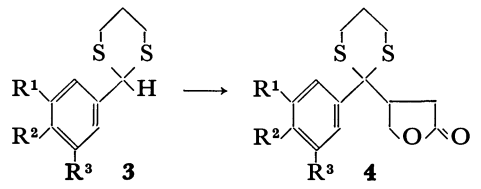

Dithiane **3**	Product Mp (°C)	Yield (%)[a]
a ; $R^1=R^2=R^3=H$	109 —110	13
b ; $R^1=R^3=H$; $R^2=OMe$	98.5—100	88
c ; $R^1=R^2=OMe$; $R^3=H$	130 —131	71
d ; $R^1=R^2=-OCH_2O-$; $R^3=H$	158.5—160	78
(lit,[4])	154 —155)	
e ; $R^1=R^2=R^3=OMe$	161 —163	68
f ; $R^1=OBz$; $R^2=OMe$; $R^3=H$	130 —131.5	79

a) Isolated yield.

Table 2. Desulfurization of dithiane lactones

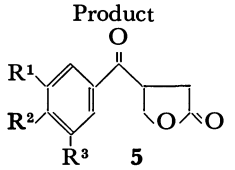

Product **5**	Condition Temp (°C)	Time (min)	Mp (°C)	Yield (%)
b ; $R^1=R^3=H$; $R^2=OMe$	rt	60	68.5— 69.5	80
c ; $R^1=R^2=OMe$; $R^3=H$	40	30	118 —119.5	67
d ; $R^1=R^2=-OCH_2O-$; $R^3=H$	50	30	118 —119	100
e ; $R^1=R^2=R^3=OMe$	0→rt	45	93 — 95	61
f ; $R^1=OBz$; $R^2=OMe$; $R^3=H$	rt	60	150 —151	72

Attempted alkylation of **4d** with lithium cyclohexylisopropylamide and piperonyl bromide (THF–HMPA, −78 °C, 2 h) led to the recovery of the starting material.* We then carried out indirect alkylation. Treatment of the lactone **4d** with dimethyl carbonate and sodium hydride without solvent gave the α-carbomethoxy lactone (**6**). The NMR spectrum showed peaks at 3.94 ppm (d, J=9.0 Hz) due to $-CO-\underline{CH}-CO_2Me$, suggesting the *trans* configuration of substituents. This was alkylated with piperonyl bromide to give the trisubstituted lactone (**7**) in 74% yield from **4d**. The IR spectrum of **7** showed the presence of a γ-lactone (1780 cm^{-1}) and an ester group (1750 cm^{-1}). The NMR spectrum of **7** showed signals at 3.00 (H_e, dd, J=8.2 and 11.3 Hz), 3.31 (H_c, H_d, AB_q, J=16.1 Hz), 3.92 (H_b, t, J=8.2 and 10.2 Hz) and 4.55 ppm (H_a, dd, J=10.2 and 11.3 Hz). Hydrolysis of the ester **7** with ethanolic potassium hydroxide followed by acidification gave the bis-benzyl-substituted lactone (**8**) in 80% yield. The IR spectrum of **8** showed a characteristic band at 1770 cm^{-1}. The NMR spectrum of **8** showed signals at 2.91 (H_c, m), 3.86 (H_b, q, J=8.2 and 9.8 Hz), 4.54 (H_a, q, J=4.2 and 9.8 Hz), 5.86 ($-OCH_2O-$, q, J=2 Hz) and 5.96 ppm ($-OCH_2O-$, q, J=2 Hz). The characteristic feature of the NMR spectrum is the non-equivalence of both methylenedioxy groups, probably due to the stretched and rather rigid *trans* orientation[6] of the two methylenedioxy benzyl residue to avoid the steric repulsion of large 1,3-dithiane group and to the presence of hindered rotation.

We have also observed that the intermediate lactone enolate generated by the Michael addition can be

* Ziegler and Schwartz[4] alkylated **4d** with lithium diisopropylamide and 3,4,5-trimethoxybenzyl chloride in THF–HMPA at −78 °C for 3 h and then at room temperature for 18 h.

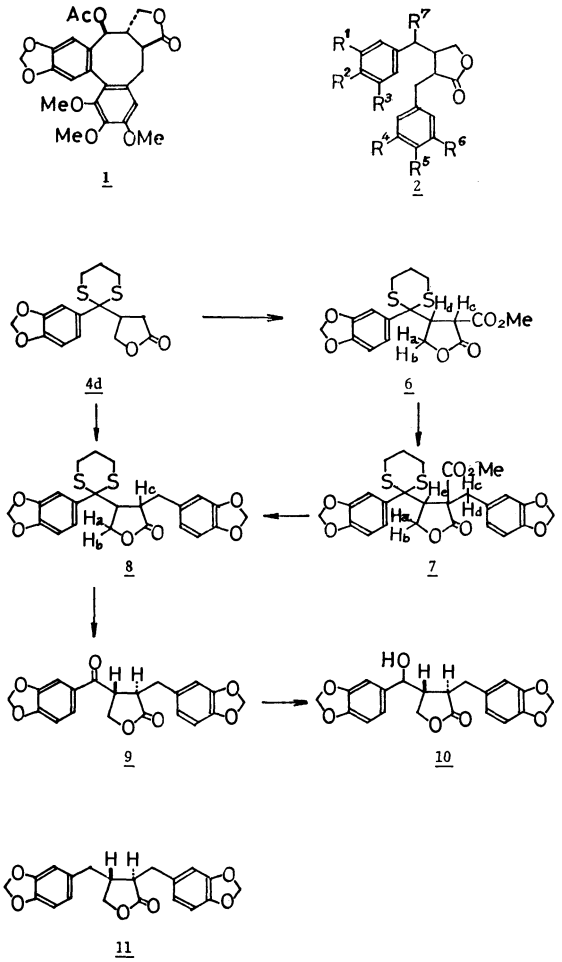

trapped with piperonyl bromide to give **8** in 78% yield. Cleavage of the dithioketal group of **8** gave the keto lactone **9**. The NMR spectrum ($CDCl_3$–C_6D_6 1: 1) of **9** showed three protons multiplet between 2.52—3.36 ppm (Fig. 1). The multiplets centered at 2.76 and 3.30 ppm were assigned as H_A and H_B, and H_X, respectively. Two benzylic protons forming the AB part of an ABXY system with $J_{AY}=J_{BY}=0$ Hz and the proton α to the lactone carbonyl forming the X part. Analysis of the spectrum revealed the following coupling constants: $|J_{AB}|=14.2$ Hz; $|J_{AX}|=3.4$ Hz; $|J_{BX}|=9.0$ Hz; and $|J_{XY}|=8.5$ Hz. As the coupling constants of flexible five-membered ring might be of little diagnostic value, we then carried out equilibration experiments. Equilibration of **9** with potassium *t*-butoxide in *t*-butyl alcohol gave unchanged material, suggesting the thermodynamically more stable, *trans* stereochemistry of the two substituents at the lactone ring. The keto lactone **9** was identical with oxo-parabenzlactone[7] (IR, UV, NMR, and TLC) derived from natural (—)-parabenzlactone by means of Jones' oxidation.

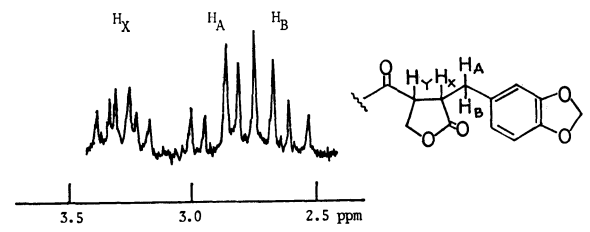

Fig. 1 The NMR spectrum of 9 in $CDCl_3$-C_6D_6 (1:1).

Fig. 1. The NMR spectrum of **9** in $CDCl_3$–C_6D_6 (1: 1).

Reduction of **9** with $NaBH_4$ or $Zn(BH_4)_2$ gave (±)-parabenzlactone (**10**), which was identical with the natural product[7] (IR, UV, NMR, and TLC). Since it has been known that the reduction with $Zn(BH_4)_2$ does not change the configuration at the lactone ring,[8] the synthetic parabenzlactone also takes the *trans* stereochemistry. Thus the synthesis unambiguously established the *trans* stereochemistry of (—)-parabenzlactone which accords with the conclusion derived from CD experiments.[9]

Reductive desulfurization of **8** with Raney Ni gave the amorphous lactone (**11**), whose IR and NMR spectra were superimposable with those of (—)-hinokinin.[9]

Experimental

All the melting points are uncorrected. The IR spectra were measured with JASCO IRA-1 spectrophotometer. The NMR spectra were recorded in $CDCl_3$, with TMS as the internal standard, using JEOL PS-100 spectrophotometer.

General Procedure for the Preparation of Dithiane Lactones **4**. Butyllithium (6.5 ml of a 15% hexane solution, 0.0105 mol) was added to a solution of 2-aryl-1,3-dithiane **3** (0.01 mol) in THF (30 ml) and HMPA (0.01 mol) at −75 °C under nitrogen atmosphere. The mixture was stirred for an additional hour at −40 °C. After cooling at −75 °C, the mixture was treated with 2-butenolide (1.26 g; 0.015 mol) in 3 ml of THF, stirred for two hours at −75 °C, and then treated with 10% hydrochloric acid. Extractive work-up and chromatography on silicic acid gave pure dithiane lactone.

Dithiane Lactone **4a**. IR (Nujol) 1780, 1770 (sh), 1600, 1490, 1180, 770, and 710 cm^{-1}; NMR ($CDCl_3$) 1.84 (m, 2), 2.16—3.12 (m, 6), 4.0—4.42 (m, 2), 7.2—7.48 (m, 3), and 7.84—7.94 (m, 2); Found: C, 60.05; H, 5.82%. Calcd for $C_{14}H_{16}O_2S_2$: C, 59.97; H, 5.75%.

Dithiane Lactone **4b**. IR ($CHCl_3$) 1775, 1605, and 1025 cm^{-1}; NMR ($CDCl_3$) 1.7—2.0 (m, 2), 2.21—3.16 (m, 7), 3.84 (s, 3), 4.04—4.44 (m, 2), 6.90 (m, 2), and 7.82 ppm (m, 2); Found: C, 58.06; H, 5.84%. Calcd for $C_{15}H_{18}O_3S_2$: C, 58.03; H, 5.84%.

Dithiane Lactone **4c**. IR ($CHCl_3$) 1775, 1600, 1590, and 1025 cm^{-1}; NMR ($CDCl_3$) 1.8—2.04 (m, 2), 2.29—3.24 (m, 7), 3.97 (s, 6), 4.10—4.52 (m, 2), 6.94 (d, 1, J=9 Hz) and 7.49—7.60 ppm (m, 2); Found: C, 56.55; H, 5.94%. Calcd for $C_{16}H_{20}O_4S_2$: C, 56.44; H, 5.92%.

Dithiane Lactone **4d**. IR (Nujol) 1775, 1500, 1040, and 930 cm^{-1}; NMR ($CDCl_3$–DMSO-d_6) 1.8—2.01 (m,2), 2.24—3.16 (m, 7), 4.06—4.46 (m, 2), 6.02 (s, 2), 6.80 (d, 1, J=9 Hz), and 7.31—7.48 ppm (m, 2); Found: C, 55.51; H, 4.95%. Calcd for $C_{15}H_{16}O_4S_2$: C, 55.53; H, 4.97%.

Dithiane Lactone **4e**. IR (Nujol) 1780, 1500, 1585, and 1130 cm^{-1}; NMR ($CDCl_3$) 1.96 (m, 2), 2.28—3.22 (m, 7), 3.91 (s, 9), 4.11—4.61 (m, 2), and 7.28 (s, 2); Found: C, 55.06; H, 5.99%. Calcd for $C_{17}H_{22}O_5S_2$: C, 55.11; H, 5.99%.

Dithiane Lactone **4f**. IR ($CHCl_3$) 1770, 1600, 1585, and 1020 cm^{-1}; NMR ($CDCl_3$) 1.80—2.02 (m, 2), 2.26—3.20 (m, 7), 3.90 (s, 3), 4.08—4.50 (m, 2), 5.17 (s, 2), 6.92 (d, 1, J=8 Hz), and 7.30—7.56 (m, 8).

General Procedure for the Desulfurization of Dithiane Lactones **4**. To a mixture of NCS (0.004 mol) and silver nitrate (0.0045 mol) in 4 ml of CH_3CN and 2 ml of water was added a solution of **4** (0.001 mol) in CH_3CN. The mixture was stirred under

the condition shown in Table 2, then poured into sat NaCl soln and extracted with ether. The extract was washed with $NaHSO_3$ soln and NaCl soln and dried. Evaporation and chromatography gave pure β-aroyl-γ-lactone **5**.

β-(4-Methoxybenzoyl)butyrolactone ***5b***. IR ($CHCl_3$) 1770, 1670, 1595, 1570, 1210, and 1025 cm^{-1}; NMR ($CDCl_3$) 2.56—3.10 (m, 2), 3.86 (s, 3), 4.12—4.64 (m, 3), 6.94 (m, 2), and 7.87 ppm (m, 2); Found: C, 65.46; H, 5.49%. Calcd for $C_{11}H_{12}O_4$: C, 65.44; H, 5.49%.

β-(3,4-Dimethoxybenzoyl)butyrolactone ***5c***. IR ($CHCl_3$) 1775, 1670, 1590, 1585, 1260, and 1020 cm^{-1}; NMR ($CDCl_3$) 2.60—3.15 (m, 2), 3.93 (s, 3), 3.96 (s, 3), 4.27—4.70 (m, 3), 6.94 (d, 1, J=9 Hz), and 7.44—7.61 (m, 2); Found: C, 62.37; H, 5.68%. Calcd for $C_{13}H_{14}O_5$: C, 62.39; H, 5.64%.

β-(3,4-Methylenedioxybenzoyl)butyrolactone ***5d***. IR (Nujol) 1780, 1680, 1620, and 1040 cm^{-1}; NMR ($CDCl_3$) 2.57—3.12 (m, 2), 4.08—4.64 (m, 3), 6.04 (s, 2), 6.84 (d, 1, J=8 Hz) and 7.35—7.50 ppm (m, 2); Found: C, 61.40; H, 4.28%. Calcd for $C_{12}H_{10}O_5$: C, 61.54; H, 4.30%.

β-(3,4,5-Trimethoxybenzoyl)butyrolactone ***5e***. IR ($CHCl_3$) 1780, 1680, 1590, 1030, and 1000 cm^{-1}; NMR ($CDCl_3$) 2.90 (m, 2), 3.93 (s, 9), 4.48 (m, 3), and 7.16 ppm (s, 2).

β-(3-Benzyloxy-4-methoxybenzoyl)butyrolactone ***5f***. IR ($CHCl_3$) 1775, 1670, 1590, 1580, 1260, and 1020 cm^{-1}; NMR ($CDCl_3$) 2.55—3.12 (m, 2), 3.91 (s, 3), 4.20—4.62 (m, 3), 5.20 (s, 2), 6.89 (d, 1, J=9 Hz), 7.27—7.42 (m, 6), and 7.46 ppm (d, 1, J=9 Hz); Found: C, 69.84; H, 5.49%. Calcd for $C_{19}H_{18}O_5$: C, 69.93; H, 5.56%.

Carbomethoxylation of ***4***. To 0.275 g (0.0057 mol) of 50% mineral oil dispersion of NaH (twice washed with anhyd. hexane) suspended in 5 ml of dry Me_2CO_3 was added 713 mg of **4** in 11 ml of Me_2CO_3 and 5 ml of anhyd. THF, and the mixture was refluxed for 10 h. After the excess reagent had been destroyed with MeOH, the mixture was poured into water and extracted with $CHCl_3$. The organic layer was washed with $NaHCO_3$ soln, dried and evaporated to give 813 mg (97%) of the carbomethoxy lactone **6**, mp 168—170 °C (from EtOH), IR (Nujol) 1770 and 1735 cm^{-1}; NMR ($CDCl_3$) 1.94 (m, 2), 2.72 (m, 4), 3.58 (m, 1, H_d), 3.68 (s, 3), 3.94 (d, 1, J=9 Hz, H_c), 4.32 (q, 1, J=8 and 10 Hz), 6.82 (d, 1, J=9 Hz), and 7.44 ppm (m, 2); Found: C, 53.35; H, 4.72%. Calcd for $C_{17}H_{18}O_6S_2$: C, 53.39; H, 4.74%.

Alkylation of ***6***. To a soln of 654 mg (0.00171 mol) of **6** in 30 ml of DME was added 115 mg (0.00239 mol) of NaH mineral oil dispersion (50%) under a nitrogen atmosphere. Several drops of dried *t*-BuOH were added, the mixture was stirred for 40 min at room temp, then a soln of 386 mg (0.00171 mol) of piperonyl bromide in 7 ml of DME was added and the resulting mixture was refluxed for 3 h. After removal of the solvent under reduced pressure, water was added to this mixture and extracted with ether. The crude product was chromatographed over neutral Al_2O_3 (Act II), and elution with C_6H_6–ether (95: 5) afforded 674 mg (76%) of **7**, mp 206—208 °C (from EtOH), IR ($CHCl_3$) 1780, 1750, 1610, and 940 cm^{-1}; NMR ($CDCl_3$) 1.91 (m, 2), 2.64 (m, 4), 3.00 (q, 1, J=8.2 and 8.5 Hz, H_e), 3.31 (q, 2, J=15 Hz, H_c, H_d), 3.81 (s, 3), 3.92 (q, 1, J=8.2 and 10 Hz, H_b), 4.55 (q, 1, J=8.5 and 10 Hz, H_a), 5.91 (s, 2), 6.06 (s, 2), and 6.74—7.56 ppm (m, 6); Found: C, 58.04; H, 4.67%. Calcd for $C_{25}H_{24}O_8S_2$: C, 58.12; H, 4.68%.

Decarboxylation of ***7***. Hydrolysis of **7** (260 mg) with 1 M ethanolic KOH (15 ml) at 50 °C for an hour followed by acidification with acetic acid gave **8** (205 mg; 80%), mp 153—155 °C (from EtOH); IR ($CHCl_3$) 1770, 1610, and 940 cm^{-1}; NMR ($CDCl_3$) 1.84 (m, 2), 2.56 (m, 7), 2.96 (m, 1, H_c), 3.86 (q, 1, J=8.2 and 10 Hz, H_b), 4.54 (q, 1, J=4.2 and 10 Hz, H_a), 5.86 (q, 2, J=2.0 Hz) and 5.96 ppm (q, 2, J=2.0 Hz); Found: C, 60.12; H, 4.83%. Calcd for $C_{23}H_{22}O_6S_2$: C, 60.24; H, 4.84%.

One-pot Synthesis of ***8***. Butyllithium (3.3 ml of a 15% hexane soln, 5.29×10^{-3} mol) was added to a soln of **3d** (1.211 g; 5.04×10^{-3} mol) in THF (25 ml) at −78 °C under nitrogen atmosphere. The mixture was stirred for 1.5 h at −40 °C. After cooling at −78 °C, the mixture was treated with 2-butenolide (0.423 g; 5.04×10^{-3} mol) in 5 ml of abs. THF. After stirring for 2 h at −60 °C, the mixture was treated with 10% HCl. Extractive work-up and chromatography on silicic acid and elution with C_6H_6–AcOEt (95: 5) gave pure **8** in 77% yield.

Equilibration of ***8***. The lactone **8** (50 mg) was added to a 3% soln of *t*-BuOK in *t*-BuOH (10 ml). The mixture was stirred for 5 h at 60 °C and then for 12 h at room temp. After quenching the reaction with dil HCl, extractive work-up gave the starting material (TLC, NMR, and IR).

Desulfurization of ***8***. To a mixture of NCS (0.567 g; 97%; 4.12×10^{-3} mol) and silver nitrate (0.787 g; 4.63×10^{-3} mol) in 4 ml of CH_3CN and 2 ml of water was added a soln of **8** (474 mg; 1.03×10^{-3} mol) in 6 ml of CH_3CN. The mixture was heated for 30 min at 50 °C, then poured into sat. NaCl soln and extracted with ether. The extract was washed with $NaHSO_3$ soln and NaCl soln and dried. Evaporation of the solvent gave the keto lactone **9**, (370 mg; 100%), mp 140—142 °C (from EtOH); IR ($CHCl_3$) 1780, 1675, 1610, and 940 cm^{-1}; NMR ($CDCl_3$) 2.92 (m, 2, AB part of ABXY system), 3.38 (m, 1, X part of ABXY system), 3.79—4.40 (m, 3), 5.84 (s, 2), and 6.01 ppm (s, 2). This compound was identical with the oxo-parabenzlactone derived from natural (−)-parabenzlactone[7] by oxidation with Jones' reagent (IR, NMR, UV and TLC).

Reduction of ***9***. (a) To a chilled (0 °C) soln of **9** (36 mg; 9.78×10^{-5} mol) in 5 ml of MeOH and 5 ml of THF was added 4 mg (9.78×10^{-5} mol) of $NaBH_4$. The mixture was stirred for 40 min and then the excess reagent was destroyed with few drops of acetic acid. The solvent was removed *in vacuo* (50 °C), the residue was diluted with water and worked up by extraction with $CHCl_3$ giving **10** (16 mg), mp 156—158 °C (from MeOH). This was identical with natural parabenzlactone[7] (IR, NMR, and TLC).

(b) To a soln of **9** (60 mg; 1.63×10^{-4} mol) in 2.5 ml of dry C_6H_6 was added 1.63×10^{-4} mol of zinc borohydride[8] in 11.2 ml of abs ether. After 24 h at room temp the mixture was treated with water and then with dil acetic acid. Extractive work-up gave an oil (65 mg), which was purified by chromatography on silicic acid. Elution with AcOEt–C_6H_6 (1: 4) gave pure **10** (50 mg).

Reductive Desulfurization of ***8***. The mixture of **8** (150 mg) and 2 g of Raney Ni (W-2) in 50 ml of abs EtOH was refluxed overnight. Filtration of the catalyst and evaporation of the solvent gave **11** as a viscous oil. The IR and NMR spectra of **11** were superimposable with those of (−)-hinokinin.[9]

The authors wish to express their thanks to Dr. K. Wada, Nagoya University, for provinding the sample of (−)-parabenzlactone and to Dr. S. Nishibe, Higashinippon Gakuen University, for informing us the stereochemistry of (−)-parabenzlactone, and for kindly supplying the IR and NMR spectra of (−)-hinokinin.

References

1) A preliminary report of this paper was presented at the 34th National Meeting of the Chemical Society of Japan, Tokyo, April, 1976.

2) S. M. Kupchan, R. W. Britton, M. F. Ziegler, C. J.

Gilmore, R. J. Restivo, and R. F. Bryan, *J. Am. Chem. Soc.*, **95**, 1335 (1973).

3) D. Seebach, *Synthesis*, **1969**, 17; D. Seebach and M. Kolb, *Chem. Ind. (London)*, **1974**, 689.

4) F. E. Ziegler and J. A. Schwartz, *Tetrahedron Lett.*, **1975**, 4643.

5) D. Seebach and E. J. Corey, *J. Org. Chem.*, **40**, 231 (1975).

6) It has been reported that *trans*-isomers are more thermodynamically stable than *cis*-ones in 2,3-disubstituted-γ-lactones. S. A. M. Hussain, W. D. Ollis, C. Smith, and J. F. Stoddart, *J. Chem. Soc. Perkin Trans. 1*, **1975**, 1480.

7) K. Wada and K. Munakata, *Tetrahedron Lett.*, **1970**, 2017.

8) W. J. Gensler, F. Johnson, and A. D. B. Sloan, *J. Am. Chem. Soc.*, **82**, 6074 (1960).

9) S. Nishibe, private communication.

Studies of the Removal of Oily Soil by Rolling-up in Detergency. II. On Binary Soil Systems Consisting of Oleic Acid and Liquid Paraffin

Keizo OGINO and Ken-ichi SHIGEMURA

Faculty of Science and Technology, Science University of Tokyo, Noda, Chiba 278

(Received February 28, 1976)

The rolling-up mechanism of oily soil from the surface of a polypropylene (PP) sheet in an aqueous solution of sodium dodecylbenzenesulfonate (LAS) was studied by the observation of the contact angle (θ). A binary system consisting of *cis*-9-octadecenoic acid (oleic acid)–liquid paraffin (Nujol) was used as an example of oily soil. The time required for the removal of the oily soil mixture from the PP sheet by rolling-up became shorter with the increase in the liquid paraffin content of the mixture. The oily soil with binary components was more easily removed from the substrate than a single-component oily soil.

Although the mechanism of the practical cleaning of oily soil is extremely complicated, it is well known that the cleaning consists of three basic processes that may occur simultaneously or in succession: rolling-up, solubilization, and emulsification.[1]

The process of rolling-up may be explained as follows. As soon as the soil-substrate system of air is purged and the solution/soil/substrate interfaces become stable, the contact angle at the soil/substrate interface begins to increase and attains the intrinsic equilibrium state. At the same time, the force acting between the oily soil and the substrate decreases; when the contact angle reaches 180°, the oily soil is completely removed from the substrate.

Smith *et al.*[2] have reported a change in the contact angle of an oily soil/substrate system in detergent solutions of various concentrations in the course of time, using mineral oil as the oily soil and fiber as the substrate. On the other hand, Stevenson[3] found that polar oil was far more easily removed from fiber than was mineral oil and that the addition of polar substances to mineral oil greatly facilitated the removal. However, their studies were only presented qualitatively by photographs; the inter-relations of the changes among the components of the soil, the concentration of the detergent in the solution, and other factors were not described.

In the previous report, we studied the removal of single-component oily soil from a low-energy surface.[4] In this study, the rolling-up process of oily soil on a polypropylene surface in a detergent solution was examined in terms of the change in the contact angle with time, using mixtures of polar and non-polar soils in certain proportions (by weight), and the interaction between the oily soil and surfactant was speculated upon.

Experimental

Materials. *Substrate*: A polypropylene (PP) sheet from Mitsui Noblene J. H. G. was used as the substrate. The preparation of the specimen from the obtained sheet was described in the previous report.[4] The sheet was cut into specimens of $10\times10\times1.2$ mm, and the surface was cleaned several times with a commercial detergent solution at 35 °C, rinsed with distilled water for 60 min, soaked into absolute ethanol for 5 min, dried in a vacuum for 3 h, and stored in a dessicator at room temperature till use.

Surface-active Agents: The sodium dodecylbenzenesulfonate (LAS) was of commercial grade from the Wako Chemical Co., Ltd.

Oily Soil: Oily soil of a binary system was prepared by mixing oleic acid (reagent grade from Tokyo Kasei Co.) and liquid paraffin (reagent grade from Wako Pure Chemical Co., Ltd.) in the ratios of 1:0, 3:1, 1:1, 1:3, and 0:1 (by weight).

Apparatus. The contact angle and its change with the time were measured by means of a Goniometer (Erma Kogaku Co., Ltd., M 2010, A-a, G-type), while the surface tension of the oily soil was measured by means of a Wilhelmy-type Surface Tensionmeter ST-1 (Shimadzu Seisakusho).

Procedure. A volume of 1.5×10^{-3} ml of the oily soil was dropped on a PP sheet by means of a microsyringe connected with a micrometer. Then the sheet with a drop of the soil on it was set in a glass cell ($40\times25\times15$ mm). The glass cell was placed on the table of the Goniometer, and then the surfactant solution was poured slowly onto it. The change in the contact angle with the time and the time required for the removal of the oily soil from the surface by rolling-up were measured as in the previous report.[4]

Results and Discussion

Wetting of the Polypropylene Sheet with Organic Liquids. Figure 1 shows the contact angle and the surface tension of the binary oily soil on a PP sheet in the air. Both the contact angle and the surface tension decreased with an increase in the proportion of liquid paraffin in the soil and reached the highest value at 100 per cent oleic acid. This result is consistent with that of Zisman[5] that the contact angle of organic liquid on a low-energy

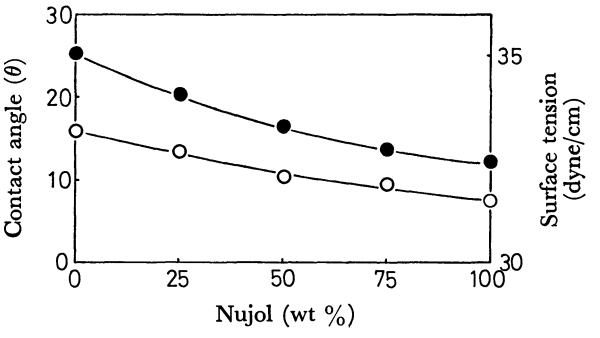

Fig. 1. Contact angle on PP sheets and surface tension of oleic acid–liquid paraffin binary systems in air (at 30 °C).
●: Contact angle,
○: Surface tension.

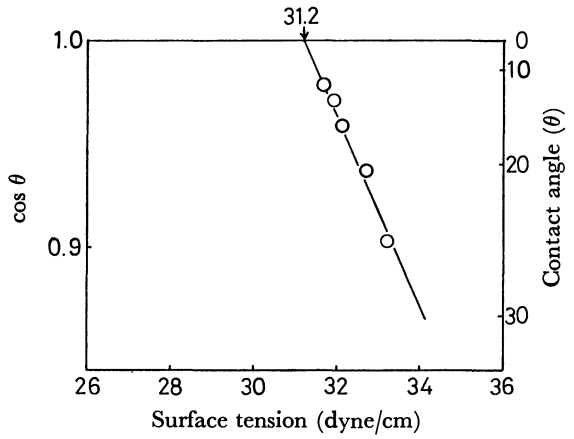

Fig. 2. Surface tension *vs.* cosine of the contact angle of the same mixed liquids as Fig. 1 on polypropylene.

surface tends to decrease with a decrease in the surface tension for a homologous series of liquids.

From the results shown in Fig. 1, the relation between the contact angle and the surface tension was derived; it is plotted in Fig. 2, which indicates a linear relationship between the two properties; the critical surface tension of PP, γ_c, is 31.2 dyne/cm, a calculated from the relationship extrapolated to $\cos\theta=1$.

Change in the Appearance of Oily Soil in a Detergent Solution. The change in the appearance of oily soil which had been dropped onto the PP sheet was observed in accordance with the time-course of the change in the contact angle in LAS solutions of various concentrations. The results for the binary oily soil systems are shown in Figs. 3, 4, and 5. Similar results have been obtained for the single-component systems of oleic acid or liquid paraffin, as has been described in the previous paper.[4] The change in the appearance of oily soils of various compositions in LAS solutions is illustrated in Fig. 6.

As may be seen in Figs. 3, 4, and 5, the contact angle changed with the time in oleic acid–liquid paraffin binary systems; the cause of this change is considered

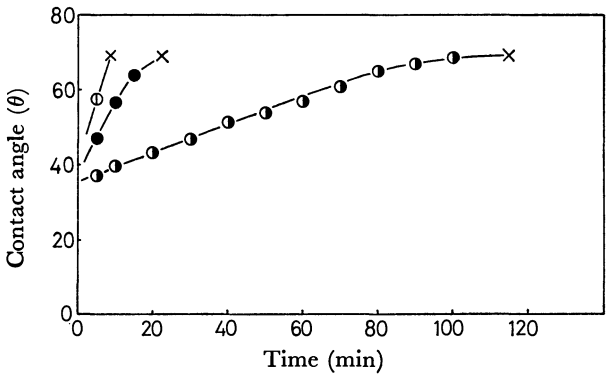

Fig. 3. Contact angle of a mixture of oleic acid and liquid parafin (3: 1) in aqueous solution of LAS (at 30 °C).
◑: 0.125 (wt% of LAS),
●: 0.115 (wt% of LAS),
◑: 0.100 (wt% of LAS),
×: rolling-up.

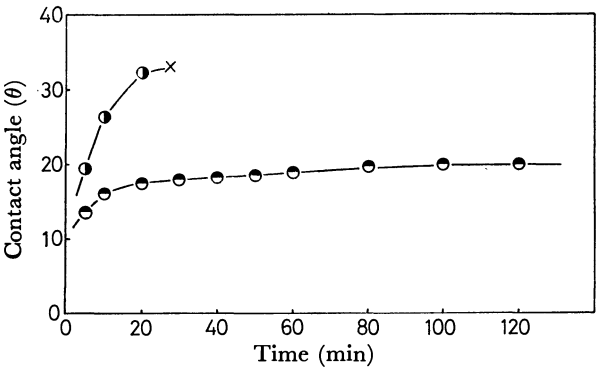

Fig. 4. Contact angle of a mixture of oleic acid and liquid paraffin (1: 1) in aqueous solution of LAS (at 30 °C).
◑: 0.100 (wt% of LAS),
◓: 0.075 (wt% of LAS),
×: rolling-up.

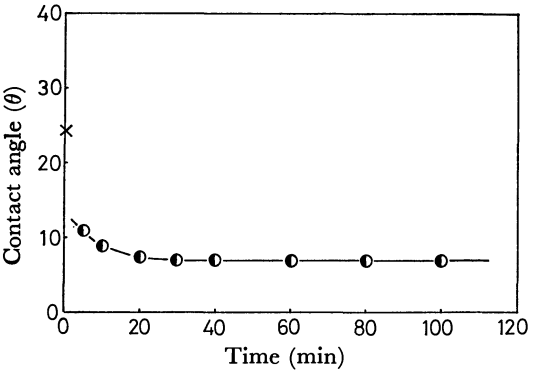

Fig. 5. Contact angle of a mixture of oleic acid and liquid paraffin (1: 3) in aqueous solution of LAS (at 30 °C).
×: Rolling-up (0.100 wt% of LAS),
◐: 0.065 (0.100 wt% LAS).

to be the adsorption of a surface-active agent on the oily soil surface. When the droplet of oleic acid on the substrate was brought into the surfactant solution, the contact angle rapidly increased and rolled back, as was shown in the previous paper.[4] After about 20 min in the 0.150 per cent LAS solution, the droplet was constricted and floated away.

For a mixture of oleic acid and liquid paraffin in the proportion of 3: 1, the addition of a 0.115 per cent LAS solution causes the roll back of the droplet, much as with oleic acid alone; necking begins after about 22 min of rolling-up, but a portion of the soil remains intact on the PP sheet after the removal of the droplet (Figs. 3 and 6). In contrast to the soil of oleic acid alone, the binary soil of oleic acid and liquid paraffin rolls up in a more dilute solution of LAS; for example, the time required for rolling-up was 114.9 min in 0.100 per cent, 22.3 min in 0.115 per cent, and 8.7 min in 0.125 per cent solutions of LAS.

Similarly, the rolling-up phenomena were observed for the mixtures of oleic acid and liquid paraffin in the ratios of 1: 1 (Figs. 4 and 6) and 1: 3 (Figs. 5 and 6). Both mixed soils were removed incompletely from the PP surface; the time for the removal was 27.6 min for the former and about 30 s for the latter in an LAS

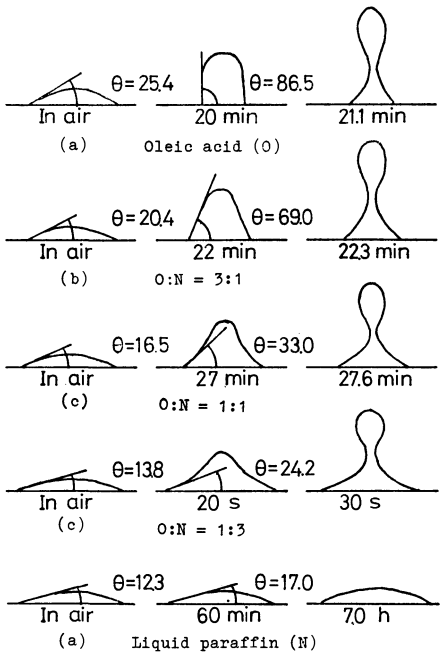

Fig. 6. Rolling-up process in aqueous solution of LAS.
(a): 0.150 (wt% of LAS),
(b): 0.115 (wt% of LAS),
(c): 0.100 (wt% of LAS).

TABLE 1. REMOVAL OF OILY SOILS

Oily soils	In air (at 30 °C)		In aq. solution of LAS (at 30 °C)		
	Contact angle (θ)	Surface tension (dyne/cm)	Contact angle (θ)	Rolling up[a]	Rolling up time (min)
Oleic acid (O)	25.4	33.2	86.5	○	21.1[b]
O:N=3:1	20.4	32.7	69.0	○	22.3[c]
O:N=1:1	16.5	32.1	33.0	○	27.6[d]
O:N=1:3	13.8	31.9	24.2	○	0.5[d]
Liquid paraffin (N)	12.3	31.5	17.0	×	—[b]

a) ○: Rolling up, ×: No rolling up. b) Measured in 0.150 percent level of LAS solution. c) Measured in 0.115 percent level of LAS solution. d) Measured in 0.100 percent level of LAS solution.

solution at a 0.100 per cent concentration.

As presented in the previous study and in Fig. 6, non-polar liquid paraffin was the only material which showed no appreciable changes in the contact angle in the detergent solutions.

In Table 1, the values of the contact angle and the time required to remove the mixed oily soil from the PP sheet by rolling-up in an LAS solution are shown. It is apparent from these results that the rolling-up phenomenon occurs for the mixed oily soil, but not for the liquid paraffin alone. On the other hand, both the value of the final contact angle of the oily soil to the PP sheet in a LAS solution and the time required to remove oily soil by rolling-up decrease with an increase in the proportion of liquid paraffin in the soil. Besides, it is confirmed that the addition of paraffin to oleic acid facilitates the rolling-up of the droplets.

For the mixture of oleic acid-liquid paraffin placed as an oily soil on a low-energy surface such as polypropylene, the rolling-up occurs at the contact angle of $0°<\theta<90°$. It is noteworthy that, on a high-energy surface, rolling-up occurs only when $\theta=180°$.[6]

From Fig. 6, the adsorbed concentration of LAS molecules at the solution/oily soil interface seems to be larger than that at the solution–substrate interface. On the other hand, in the mixed oily soil systems, the contact angle in a LAS solution decreases, while the contact area does not decrease, with the increase in the proportion of liquid paraffin. These differences between the soils of the binary components and oleic acid alone are presumed to be due to the difference in the orientation of the oleic acid and liquid paraffin molecules.

The intermolecular force in the bulk of liquid oily soil is strongly exerted by the polar molecules, and the intervention of non-polar molecules with the polar molecules causes a decrease in the intermolecular forces. As a result, the reduction of the cohesive force of the molecules in the oily soil gives rise to rolling-up in spite of the small contact angle in the LAS solution. It was clarified in the previous paper[4] that polar oils interact with a surfactant more strongly than non-polar substances. This must be the reason for the easier rolling-up of the polar soils.

When a drop of oily soil placed onto a substrate was immersed into a solution of the surface-active agent, the contact angle increased and approached equilibrium, and the oily soil underwent necking and rolling-up depends on three forces: the cohesive force of the oily soil itself, the buoyancy, and the adhesive force between the substrate and the oily soil. For instance, a droplet of oleic acid rolls up because the horizontal tension nearly disappears at a contact angle, θ of 86.5° (nearly 90°).[4] It is presumed that the balance of the above three forces is shifted in a solution of a surface-active agent by the adsorption and desorption of LAS molecules at the oil/solution/substrate triple interfaces.

From these results, it may be speculated that, in all oily-soil systems of multiple components except those of paraffin alone, one of the three forces which exert influence on the oily soil, buoyancy, exceeds the other two forces; the reduction of cohesive force between the molecules in the soil is considered to be the inherent reason for the rolling-up process. Also, on a low-energy surface such as polypropylene, oily soil including polar components tends to roll up. The presence of polar components in the soil is one of the factor controlling the rolling-up.

References

1) A. M. Schwartz, *J. Am. Oil Chem. Soc.*, **48**, 566 (1971).
2) S. Smith, B. Johannessen, and P. O. Sherman, *Text. Chem. Color.*, **5** (7), 138 (1973).
3) D. G. Stevenson, *J. Textile Inst.*, **44**, T12 (1953).
4) K. Ogino and W. Agui, *Bull. Chem. Soc. Jpn.*, **46**, 1703 (1976).
5) H. W. Fox and W. A. Zisman, *J. Colloid Sci.*, **5**, 514 (1950); *ibid.*, **7**, 109, 428 (1952).
6) W. Kling, E. Langer, and I. Haussen, *Melliand Textilber*, **25**, 198 (1944).

Sulfoxonium Ylide Chemistry. VII.[1] Reductive Cleavage of Dimethylsulfoxonium Allylides

Junya IDE and Yukichi KISHIDA

Central Research Laboratories, Sankyo Co., Ltd., 1-2-58 Hiromachi, Shinagawa-ku, Tokyo 140

(Received June 14, 1976)

Reductive cleavage of dimethylsulfoxonium allylides with zinc in acetic acid or by hydrogenation over platinum at high pressure (120 atm) has been investigated. Reduction of dimethylsulfoxonium 3-ethoxycarbonyl-2-phenylallylide (**1**) with zinc gave predominantly ethyl 3-phenyl-3-butenoate (**2**) together with ethyl (*E*)-3-phenyl-2-butenoate (**3**) (90: 10). However, under the more acidic conditions (pH 2), **3** was the exclusive product. Hydrogenation of **1** over platinum afforded a mixture of **3** and ethyl 3-phenylbutanoate (**4**). Reduction of dimethylsulfoxonium 3-ethoxycarbonyl-2-phenyl-1-(phenylcarbamoyl)allylide (**6**) either with zinc or by hydrogenation gave ethyl (*Z*)-3-phenyl-4-phenylcarbamoyl-2-butenoate (**7**). Hydrogenation of dimethylsulfoxonium 1-benzoyl-3-ethoxycarbonyl-2-phenylallylide (**9**) at room temperature provided ethyl (*Z*)-3,5-diphenyl-5-oxo-2-pentenoate (**10**) and 4,6-diphenyl-2-pyrone (**11**), and at 80 °C **11** and ethyl 3,5-diphenyl-5-oxopentanoate (**12**).

In the continuation of our studies on sulfoxonium ylides to clarify the chemical behavior of carbon–sulfur ylide bond, the reduction of sulfoxonium ylides by a dissolving metal or catalytic hydrogenation is of interest from a synthetic view point. It is already known that desulfurizations of allyl sulfide and thioacetals are effected by dissolving metal such as Raney-Ni or sodium. Additionally, dissolving metal reduction either in the presence of a proton donor or followed by treatment with a proton donor offers the advantage of selectivity in reduction or of stereoselectivity. There has been, however, only one report on the reduction of a sulfoxonium ylide reported by Corey and Chaykovsky.[2]

In the present paper, we would like to describe the reduction of sulfoxonium allylides with zinc in acetic acid and by catalytic reduction over platinum in acetic acid at high pressure, along with certain mechanistic aspects of these processes.

Results and Discussion

Treatment of dimethylsulfoxonium 3-ethoxycarbonyl-2-phenylallylide (**1**) with zinc powder in acetic acid (pH 4.7) at 16—18 °C under an argon atmosphere gave ethyl 3-phenyl-3-butenoate (**2**) and ethyl (*E*)-3-phenyl-2-butenoate (**3**) in a ratio of 90: 10 (by GLC analysis) in 92% yield. On the contrary, under more acidic conditions using a small amount of hydrochloric acid (pH 2), **1** afforded **3** exclusively. Reduction of **1** over platinum in acetic acid at 120 atm of hydrogen at room temperature gave a mixture of **3** and ethyl 3-phenylbutanoate (**4**) in 88% yield. However, under atmospheric pressure the reduction was not effected and the starting material (**1**) was recovered.

Base-catalysed isomerization of **2** was readily effected with alumina or triethylamine to give the more stable isomer (**3**). Catalytic hydrogenation of **2** or **3** over 5% palladium–charcoal afforded **4**, which was hydrolysed to the corresponding acid (**5**).

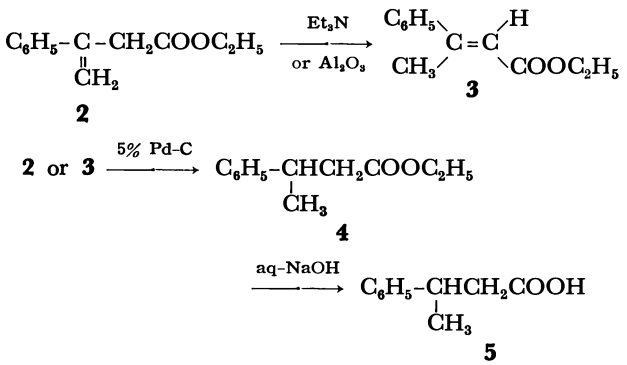

The NMR, UV, and IR spectral data of **2**, **3**, and **4** also support their structures. Terminal methylene protons of **2** appeared at δ 5.21 and 5.48 ppm (J=1.2 Hz). The UV spectrum of **2** showed λ_{max} (EtOH) 243 nm (ε 10600), which was very similar to that of α-methylstyrene (λ_{max} (EtOH) 240 nm (ε 12000)),[3] and its IR spectrum exhibited a band at 909 cm^{-1} characteristic of terminal methylene group. The *E*-configuration was assigned to **3** based on the UV spectrum showing its absorption maximum at 265 nm (ε 15860).[4] From a synthetic view point this method seems to be preferable for the preparation of the unconjugated ester (**2**) which is hardly accessible because of its chemical instability.

Reduction of dimethylsulfoxonium 3-ethoxycarbonyl-2-phenyl-1-(phenylcarbamoyl)allylide (**6**) either with zinc in acetic acid or over platinum in acetic acid under

120 atm of hydrogen at room temperature afforded ethyl β-(phenylcarbamoylmethyl)cinnamate (**7**), mp 169—170 °C, in 66% and 73% yield, respectively.

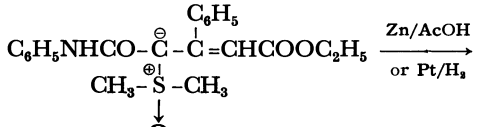

6

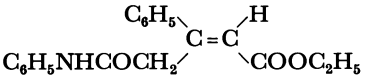

7

In the NMR spectrum of **7**, methylene and vinyl protons appeared as singlets at δ 4.16 and 6.57 ppm, respectively. The UV spectrum of **7** showed λ_{max} (EtOH) 224 (ε 13880), 247 (ε 22200), and 270 nm (ε 15850) which was similar to the additive chromophore of ethyl (*E*)-phenyl-2-butenoate (**3**) and acetanilide (λ_{max} (EtOH) 242 nm (ε 13200)),[5] whereas the UV spectrum of *trans*-cinnamanilide (**8**) showed λ_{max} (EtOH) 221 (ε 18600), 240 (ε 4800), and 295 nm (ε 25800),[6] which would be appropriate for that of the other double bond isomer (**7'**).

7' **8**

Treatment of dimethylsulfoxonium 1-benzoyl-3-ethoxycarbonyl-2-phenylallylide (**9**) with zinc in acetic acid at 16—18 °C resulted in a complex mixture, whereas its reduction over platinum in acetic acid under 120 atm at room temperature afforded ethyl *(Z)*-β-(benzoylmethyl)cinnamate (**10**), mp 85—86 °C and 4,6-diphenyl-2-pyrone (**11**), mp 136—137 °C (lit, mp 142 °C)[7] in 20 and 13% yield, respectively. However, in the reduction of **9** at 80 °C, the pyrone (**11**) and ethyl 3,5-diphenyl-5-oxobutanoate (**12**), mp 61—62 °C, were obtained in 60 and 9% yield, respectively.

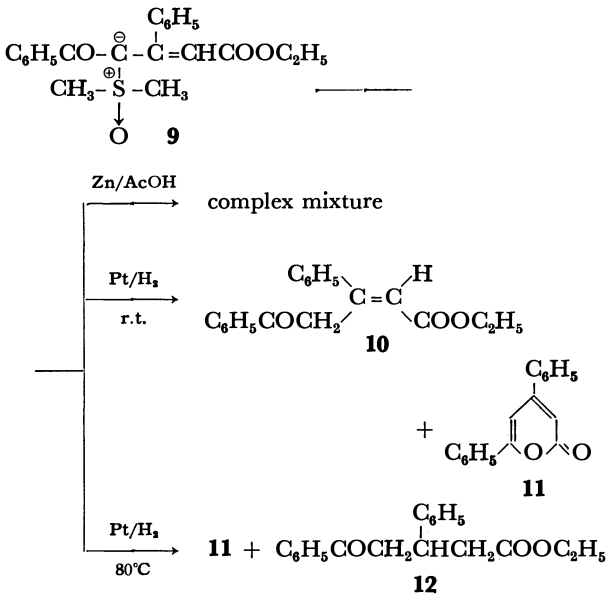

9 **10** **11** **12**

The assignment of the position of the double bond and *Z*-configuration to **10** was based on the NMR and UV spectral data. In the NMR spectrum of **10** methylene and vinyl protons appeared at δ 4.87 (singlet) and 6.40 ppm (singlet), respectively. Its UV spectrum showed λ_{max} (EtOH) 246 (ε 21750) and 268 nm (ε 16630), which is in good agreement with the chromophore bearing acetophenone (λ_{max} (EtOH) 243 nm (ε 13200)[8]) and ethyl (*E*)-3-phenyl-2-butenoate (**3**). Another possible structure (**13**) which should have a similar chromophore with (*E*)-1,3-diphenyl-2-buten-1-one (**14**) (λ_{max} (EtOH) 227.5 (ε 9600), 262.5 (ε 10500) (sh), and 295 nm (ε 16000)),[9] can be excluded by comparing with that of **10**. Its IR spectrum revealed the carbonyl band at 1715 cm^{-1} which is appropriate for an α,β-unsaturated ester, but not for an α,β-unsaturated benzoyl group.

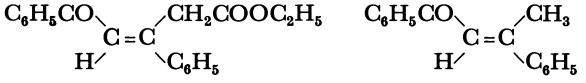

13 **14**

The NMR spectrum of **11** showed two vinyl protons as AB quartet with a small coupling constant at δ 6.48 and 6.98 ppm (J=1.3 Hz) and its UV spectrum exhibited λ_{max} (EtOH) 229 (ε 10880), 236 (ε 11200), 262 (ε 23100), and 344 nm (ε 10200).[10] The pyrone (**11**) was directly compared with an authentic sample prepared according to the method of Schulte *et al.*[7] The structure of **12** was determined by the examination of its UV and NMR spectra (see Experimental) and elemental analysis. The UV spectrum of **12** showed λ_{max} (EtOH) 243 nm (ε 12930), which was very close to that of acetophenone (*vide supra*),[8] supporting the existence of $C_6H_5COCH_2$ moiety.

Reduction of a sulfoxonium ylide with zinc in acetic acid could be well interpreted as proceeding through an anion radical (**15**) produced by electron transfer from the metal surface to sulfur of ylide (type "**a**"), or radical (**17**) produced by electron transfer to the sulfoxonium ion (**16**) fromed by protonation to ylide in acidic conditions (type "**b**").[11] A further electron transfer to the resulting radical (**17**) leads to the cleavage of carbon–sulfur bond. This reductive cleavage reaction

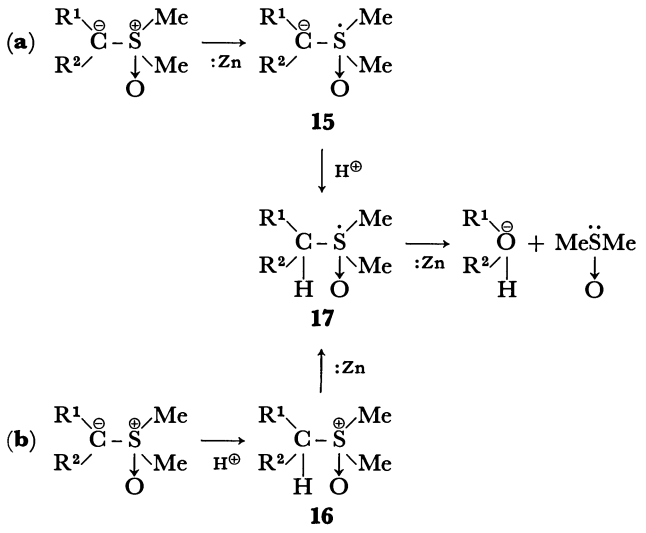

15 **17** **16**

of type "**b**" by dissolving metal has been found in ammonium, sulfonium, and phosphonium salts.[11]

On the other hand, the sulfoxonium allylide over platinum in acidic medium at high pressure of hydrogen is likely to undergo hydrogenolysis of allylsulfoxonium salt (**18**) produced by protonation to the ylide, and the resulting allyl group could be further hydrogenated partially to the saturated product depending upon the reaction conditions and/or the character of the substituents on the double bond.

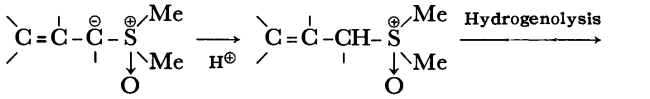

18

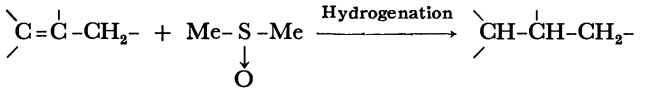

It is noteworthy that in the reduction of **1** with zinc the non-conjugated ester (**2**) and the conjugated ester (**3**) are obtained selectively depending on the acidity of reaction medium. This would be attributed to the mode of protonation of the plausible reaction intermediate (**19**), in which weak acids lead to the kinetically-controlled product (**2**) by proton attack at the central position of the enolate anion, and strong acids or equilibrating conditions give the thermodynamically-controlled one (**3**) by attack of the proton at the terminal position according to the Ingold's theory.[12]

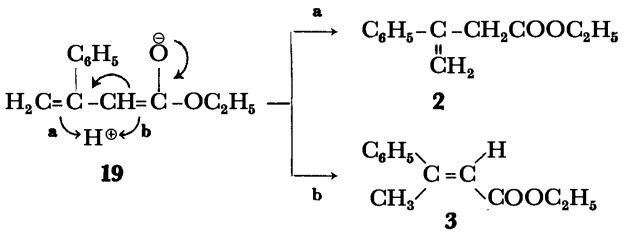

19

2

3

Experimental

All the melting points were uncorrected. NMR spectra were recorded on a Varian A-60 and HA-100 spectrometers using TMS as an internal standard, IR spectra were taken on a Hitachi EPI-G3, and UV spectra were obtained with Beckman DK-2 spectrophotometer.

Reduction of Dimethylsulfoxonium 3-Ethoxycarbonyl-2-phenylallylide (1) with Zinc in Acetic Acid. *a) At pH 4.7*: To a solution of **1** (15 g, 57 mmol) in glacial acetic acid (160 ml) was added zinc powder (39 g, 570 mmol) in many portions so as to control the inner temperature at 16—18 °C with external cooling, and the reaction mixture was stirred at room temperature for 8 h. The inorganic substances were filtered and washed with ether. The filtrate was concentrated under reduced pressure. The residue was dissolved in ether (500 ml), and the ethereal solution was washed successively with 5% $NaHCO_3$ solution, water and saturated NaCl solution, and dried over anhydrous Na_2SO_4. After the evaporation of the solvent under reduced pressure, the residue was chromatographed on silica gel (220 g). Elution with hexane–benzene (5: 1) gave ethyl (*E*)-3-phenyl-2-butenoate (**3**) (990 mg; 9.2% yield), bp 105—106 °C/1 Torr; IR (Liquid): ν 1710, 1625, and 1170 cm^{-1}; NMR ($CDCl_3$): δ 1.15 (3H, t, J=7 Hz; $COOCH_2$-$C\underline{H}_3$), 4.05 (2H, q, J=7 Hz; $COOC\underline{H}_2CH_3$), 2.54 (3H, d, J=1.2 Hz; =C–CH_3), 6.07 (1H, q, J=1.2 Hz; =C–H), 7.3 ppm (5H, m; C_6H_5–); UV (EtOH): λ_{max} 265 nm (ε 15860); Found: C, 75.84; H, 7.54%. Calcd for $C_{12}H_{14}O_2$: C, 75.76; H, 7.42%. Elution with hexane–benzene (3: 1) gave ethyl 3-phenyl-3-butenoate (**2**) (9.84 g, 90.8% yield), bp 98—100 °C/1 Torr; IR (Liquid): ν 1735 (–$COOC_2H_5$) and 909 cm^{-1} (=CH_2); NMR ($CDCl_3$): δ 1.15 (3H, t, J=7 Hz; $COOCH_2$-$C\underline{H}_3$), 4.08 (2H, q, J=7 Hz; $COOC\underline{H}_2CH_3$), 3.41 (3H, d, J_{AX}=1.2 Hz, =C–$C\underline{H}_{2X}$–$COOC_2H_5$), 5.21 (1H, q, J_{AB}=J_{AX}=1.2 Hz; =C–H_A (*trans* to phenyl group)), 5.48 (1H, d, J_{AB}=1.2 Hz; =C–H_B (*cis* to phenyl group)), and 7.3 ppm (5H, m; C_6H_5); UV (EtOH): λ_{max} 243 nm (ε 10600); Found: C, 75.60; H, 7.55%. Calcd for $C_{12}H_{14}O_2$: C, 75.76; H, 7.42%.

b) At pH 2 Containing Hydrogenchloride: The Ylide (**1**) (5 g, 19 mmol) was dissolved in glacial acetic acid (70 ml), and pH value was adjusted at 1.8—2.0 by adding small amount of concd HCl (*ca.* 2 ml). To the solution was added zinc powder (13 g, 200 mmol) in many portions so as to control the inner temperature at 16—18 °C with external cooling and the reaction mixture was stirred at room temperature for 8 h. After the same work-up as described in **a**), the residue was distilled *in vacuo* to give **3**, bp 105—106 °C/1 Torr (3.2 g, 90% yield).

Catalytic Hydrogenolysis of Dimethylsulfoxonium 3-Ethoxycarbonyl-2-phenylallylide (1) over Platinum in Acetic Acid. A solution of **1** (8.8 g, 33 mmol) in glacial acetic acid (60 ml) was hydrogenated over PtO_2 (1.8 g) in an autoclave at 120 atm of hydrogen at room temperature for 10 h. The catalyst was removed by filtration and the filtrate was concentrated under reduced pressure. The residue was chromatographed on silica gel (140 g). Elution with hexane–benzene (5: 1) afforded **3** (4.04 g, 64.4% yield) and elution with hexane–benzene (3: 1) gave ethyl 3-phenylbutanoate (**4**) (1.52 g, 24% yield), bp 95—97 °C/2 Torr; IR (Liquid): ν 1735 cm^{-1} ($COOC_2H_5$); NMR ($CDCl_3$): δ 1.14 (3H, t, J=7 Hz; $COOCH_2C\underline{H}_3$), 4.06 (2H, q, J=7 Hz; $COOC\underline{H}_2CH_3$), 1.3 (3H, d, J=7 Hz; H_X in C_6H_5–$\underset{H_Y}{\overset{CH_{3X}}{C}}$–$\underset{H_B}{\overset{H_A}{C}}$–), 2.41 (1H, dd, J_{AY}=2 Hz, J_{AB}=15.5 Hz; H_A), 2.71 (1H, d, J_{AB}=15.5 Hz; H_B), 3.30 (1H, dq, J_{AY}=2 Hz, J_{XY}=7 Hz; H_Y), 7.25 ppm (5H, m; $C_6\underline{H}_5$); Found: C, 75.41; H, 8.32%. Calcd for $C_{12}H_{16}O_2$: C, 74.96; H, 8.39%.

Isomerization of Ethyl 3-Phenyl-3-butenoate (2) to Ethyl (E)-3-Phenyl-2-butenoate (3). *a) With Alumina*: A solution of **2** (2.5 g) in hexane (10 ml) was placed on Al_2O_3 (Woelm grade I) (50 g) and eluted with hexane–benzene (1: 1) to give 2.3 g of **3**.

b) With Triethylamine: A solution of **2** (2.5 g) and triethylamine (500 mg) in benzene (10 ml) was heated under reflux for 1 h. After evaporation under reduced pressure, the residue was distilled *in vacuo* to give 2.2 g of **3**, bp 105—106 °C/1 Torr.

Hydrogenation of Ethyl 3-Phenyl-3-butenoate (2) or Ethyl (E)-3-Phenyl-2-butenoate (3). A solution of **2** or **3** (1.4 g) and Pd-charcoal (5%) (500 mg) in ethyl acetate (10 ml) was hydrogenated in hydrogen atmosphere under ordinary pressure. After removal of the catalyst, the solution was concentrated under reduced pressure. The residue was distilled *in vacuo* to afford **4**, bp 95—97 °C/2 Torr.

Hydrolysis of Ethyl 3-Phenylbutanoate (4). The ester (**4**) (1.2 g) was dissolved in ethanol (10 ml) and 10% NaOH (6 ml), and the solution was heated at 50 °C for 3 h. The reaction mixture was neutralized with acetic acid and concentrated under reduced pressure. After the addition of water (10 ml) and extraction with ethyl acetate, the organic layer was dried over anhydrous Na_2SO_4 and evaporated under reduced pres-

sure. The residue was distilled *in vacuo* to give 850 mg of the corresponding acid (**5**), bp 132—136 °C/2 Torr (bath temp); Found: C, 73.45; H, 7.41%. Calcd for $C_{10}H_{12}O_2$: C, 73.14; H, 7.36%.

*Reduction of Dimethylsulfoxonium 3-Ethoxycarbonyl-2-phenyl-1-(phenylcarbamoyl)allylide (**6**) with Zinc in Acetic Acid.* To a solution of **6** (15.6 mmol, 6 g) in glacial acetic acid (60 ml) was added zinc powder (10 g, 160 mmol) in many portions so as to control the inner temperature at 16—18 °C with external cooling. The reaction mixture was stirred at room temperature for 15 h. The inorganic substances were filtered and washed with CH_2Cl_2 (100 ml). The filtrate was concentrated under reduced pressure. The residue was dissolved in chloroform (400 ml), and the solution was washed successively with 5% $NaHCO_3$ solution, water and saturated NaCl solution, and dried over Na_2SO_4. After the evaporation of the solvent under reduced pressure, the residue was chromatographed on silica gel (50 g). Elution with benzene gave ethyl β-(phenylcarbamoylmethyl)cinnamate (**7**; 3.18 g, 66% yield), mp 169—170 °C (from EtOH); IR (Nujol): ν 3100—3300 (NH), 1700, 1650, 1620, and 1600 cm^{-1} (CONH, $=CCOOC_2H_5$); NMR ($CDCl_3$): δ 1.37 (3H, t, J=7 Hz; $COOCH_2C\underline{H}_3$), 4.41 (2H, q, J=7 Hz; $COOC\underline{H}_2CH_3$), 4.15 (2H, s; $COC\underline{H}_2C=$), 6.56 (1H, s; =CH–), and 7.65 ppm (10H, m; C_6H_5); UV (EtOH): λ_{max} 224 (ε 13880), 247 (ε 22200), and 270 nm (ε 15850) (shoulder); Found: C, 73.48; H, 6.18; N, 4.53%. Calcd for $C_{19}H_{19}NO_3$: C, 73.76; H, 6.19; N, 4.53%.

*Catalytic Hydrogenolysis of Dimethylsulfoxonium 3-Ethoxycarbonyl-2-(phenylcarbamoyl)allylide (**6**) over Platinum in Acetic Acid.* A solution of **6** (2.1 g, 5.4 mmol) and PtO_2 (500 mg) in glacial acetic acid (20 ml) was hydrogenated in an autoclave at 125 atm of hydrogen at room temperature for 12 h. The catalyst was removed by filtration and the filtrate was concentrated under reduced pressure. The residue was chromatographed on silica gel (20 g). Elution with benzene gave **7** (1.22 g, 73% yield), mp 169—170 °C (from EtOH).

*Catalytic Hydrogenolysis of Dimethylsulfoxonium 1-Benzoyl-3-ethoxycarbonyl-2-phenylallylide (**9**).* *a) At Room Temperature*: A solution of **9** (4 g, 11 mmol) in glacial acetic acid (45 ml) was hydrogenated over PtO_2 (800 mg) in an autoclave at 125 atm of hydrogen at room temperature for 10 h. The catalyst was removed by filtration and the solvent was evaporated under reduced pressure. The residue was chromatographed on silica gel (70 g). Elution with hexane–benzene (2: 1) gave ethyl (*Z*)-β-(benzoylmethyl)cinnamate (**10**, 0.64 g, 20.2% yield), mp 85—86 °C (colorless needles, from EtOH); IR (Nujol): ν 1715 cm^{-1} ($C_6H_5C=CHCOOC_2H_5$); NMR ($CDCl_3$) δ 1.26 (3H, t, J=7 Hz; $COOCH_2C\underline{H}_3$), 4.18 (2H, q, J=7 Hz; $COOC\underline{H}_2CH_3$), 4.87 (2H, s; $COCH_2C=$), 6.40 (1H, s; =CH–), 7.4 (8H, m; aromatic protons), and 8.1 ppm (2H, m; aromatic protons); UV (EtOH): λ_{max} 246 (ε 21750), and 268 nm (ε 16630); Found: C, 77.21; H, 7.21%. Calcd for $C_{19}H_{18}O_3$: C, 77.52; H, 7.16%. Elution with hexane–benzene (1: 1) afforded 4,6-diphenyl-2-pyrone (**11**, 350 mg, 13% yield), mp 137—138 °C (lit, mp 142 °C;[7] 138—139 °C;[10b] IR (Nujol): ν 1702 cm^{-1} (pyrone CO); NMR ($CDCl_3$): δ 6.47 (1H, d, J=1.5 Hz; =CH), 6.97 (1H, d, J=1.5 Hz; =CH), and 7.4—8.0 ppm (10H, m); UV (EtOH): λ_{max} 229 (ε 10880), 236 (ε 11200), 262 (ε 23100), and 344 nm (ε 10200); Found: C, 82.17; H, 4.80%. Calcd for $C_{17}H_{12}O_2$: C, 82.24; H, 4.87%. The mixed melting point of **11** with the authentic sample prepared by the method[7] showed no depression.

b) At 80 °C: A solution of **9** (7.1 g 19.2 mmol) in glacial acetic acid (50 ml) was hydrogenated over PtO_2 (1.2 g) in an autoclave at 125 atm of hydrogen at 80 °C for 10 h. The catalyst was removed by filtration and the solvent was concentrated under reduced pressure. The residue was chromatographed on silica gel (120 g). Elution with hexane–benzene (3: 1) gave ethyl 3,5-diphenyl-5-oxobutanoate (**12**, 500 mg, 8.8% yield), mp 61—62 °C (colorless crystals, from hexane–EtOH): IR (Nujol): ν 1745 ($COOC_2H_5$) and 1680 cm^{-1} (CO); NMR (100 Mc. $CDCl_3$); for $PhCO-\overset{H_A}{\underset{H_B}{C}}-\overset{H_X}{\underset{Ph}{C}}-\overset{H_C}{\underset{H_D}{C}}-COOEt$: δ 1.10 (3H, t, J=7 Hz; $COOCH_2C\underline{H}_3$), 4.0 (2H, q, J=7 Hz; $COOC\underline{H}_2CH_3$), 2.80 (H_C, q, J_{CD}=15 Hz, J_{CX}=7 Hz), 2.61 (H_D, q, J_{CD}=15 Hz, J_{DX}=8 Hz), 3.39 (H_A, q, J_{AB}=15 Hz, J_{AX}=6.5 Hz), 3.24 (H_B, q, J_{AB}=15 Hz, J_{BX}=8 Hz), 3.86 (H_X, m: about 9 lines containing splittings matching J_{AX}, J_{BX}, J_{CX}, and J_{DX}), 7.22 (5H, s; C_6H_5), and 7.9 and 7.5 ppm (5H, m: C_6H_5CO); UV (EtOH): λ_{max} 243 nm (ε 12930); Found: C, 77.46; H, 6.66%. Calcd for $C_{19}H_{20}O_3$: C, 77.00; H, 6.80%.

The authors are very grateful to Dr. M. C. Woods of Varian Associates at Tohoku University for measuring 100 Mc NMR spectra and for his valuable comments, and to Dr. T. Hiraoka of our Laboratories for his helpful suggestions. Thanks are also due to Mr. M. Ishida for his technical assistance.

References

1) Sulfoxonium Ylide Chemistry. VI: J. Ide and Y. Yura, *Bull. Chem. Soc. Jpn.*, **49**, 3341 (1976). A part of this work has been published in preliminary form: J. Ide and Y. Kishida, *Tetrahedron Lett.*, **1966**, 1787.

2) E. J. Corey and M. Chaykovsky, *J. Am. Chem. Soc.*, **86**, 1640 (1964).

3) a) P. Ramart-Lucas and P. Amagat, *Bull. Soc. Chim. Fr.*, **1932**, 119; b) W. G. Young, *J. Am. Chem. Soc.*, **75**, 4094 (1953).

4) A. Psarrea, C. Sandris, and G. Tsatsas, *Bull. Soc. Chim. Fr.*, **1961**, 2145: Butyl β-methylcinnamate, λ_{max} 269 nm (ε 16000); β-Methylcinnamic acid; λ_{max} 266 nm (ε 14800); α-Methylcinnamic acid, λ_{max} 246 nm (ε 9000).

5) H. E. Ungnade, *J. Am. Chem. Soc.*, **75**, 432 (1953).

6) a) N. I. Latosh and Z. V. Pushkareva, *Trudy Ural Politekh. Inst. in. S. M. Kirova*, **1959**, 42 (*Chem. Abstr.*, **55**, 8038e (1961)); b) P. Grammatickis, *Bull. Soc. Chim. Fr.*, **1948**, 979.

7) K. E. Schulte, J. Reisch, and O. Heine, *Arch. Pharm.*, **294**, 234 (1961).

8) Y. Hirota, "Interpretation of Ultraviolet and Infrared Spectra," ed. by Kyoritsu Shuppan K. K. Tokyo, (1965), p. 67.

9) W. B. Black and R. E. Rutz, *J. Am. Chem. Soc.*, **77**, 5134 (1955).

10) a) λ_{max} (EtOH): 236 (ε 13900), 262 (ε 46670), and 340 nm (ε 11420): I. E. El-Kholy, F. K. Rafla, and M. M. Mishrikey, *J. Chem. Soc., C*, **1970**, 1578; b) E. P. Kohler, *J. Am. Chem. Soc.*, **44**, 379 (1922).

11) H. O. House, "Modern Synthetic Reactions," 2 nd Ed., ed. by W. A. Benjamin, Inc., (1972), p. 145, references cited therein.

12) a) C. K. Ingold, "Structure and Mechanism in Organic Chemistry," ed. by Cornell University Press, Ithaca, N. Y. (1953), p. 554; b) S. K. Malhotra and H. J. Ringold, *J. Am. Chem. Soc.*, **85**, 1538 (1963).

Sulfoxonium Ylide Chemistry. VIII.[1] A Novel Rearrangement of Dimethylsulfoxonium Ylides

Junya IDE, Tetsuo HIRAOKA, and Yukichi KISHIDA

Central Research Laboratories, Sankyo Co., Ltd., 1-2-58 Hiromachi, Shinagawa-ku, Tokyo 140

(Received June 14, 1976)

Reduction of dimethylsulfoxonium 3-ethoxycarbonyl-1-[1,2-bis(methoxycarbonyl)vinyl]-2-phenylallylide (**1**) and dimethylsulfoxonium 3-ethoxycarbonyl-1-[2-(ethoxycarbonyl)vinyl]-2-phenylallylide (**5**) with zinc in acetic acid gave (*Z*)- and (*E*)-3-methoxycarbonyl-4-ethoxycarbonyl-5-phenyl-3,5-hexadienoic acid methyl ester (**6a** and **6b**), and (*Z*)- and (*E*)-4-ethoxycarbonyl-5-phenyl-3,5-hexadienoic acid ethyl ester (**7a** and **7b**), respectively, whose structures were determined by the NMR spectral data and further chemical transformations. The reaction mechanism of the reductive rearrangement was proposed to proceed through an anion radical to form a four membered intermediate (**11**), which cleaved to non-conjugated dienes leading to *Z* and *E* conjugated products.

In the preceding paper,[1] we have reported that the reductive cleavage of sulfoxonium allylides with dissolving metal such as zinc in acetic acid proceeds through an anion radical produced by electron transfer from the metal surface to the sulfur atom of ylides followed by cleavage of carbon–sulfur bond to produce a carbanion. Furthermore, we reported on the photolysis of several dimethylsulfoxonium allylides,[2] in which the vinylallylide (**1**) afforded naphthalene derivatives supposedly produced through a carbene intermediate (**2**) followed by complex rearrangement.

In the continuation of our studies on sulfoxonium ylides to clarify the chemical character of the carbon–sulfur ylide bond, it would be of interest to compare the chemical behavior of divinyl carbene (**2**) presumably generated by photolysis of the corresponding ylide (**3**) with divinyl carbanion (**4**) produced by dissolving metal reduction of **3**.

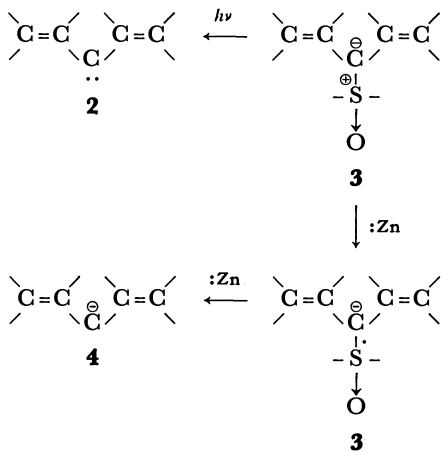

In the present paper we wish to describe a novel type of rearrangement of sulfoxonium vinylallylides *via* divinyl carbanion by dissolving metal reduction.

Results and Discussion

Treatment of dimethylsulfoxonium 3-ethoxycarbonyl-1-[1,2-bis(methoxycarbonyl)vinyl]-2-phenylallylide (**1**)[3] and dimethylsulfoxonium 3-ethoxycarbonyl-1-[2-(ethoxycarbonyl)vinyl]-2-phenylallylide (**5**)[3] with zinc in acetic acid at room temperature afforded a mixture of two geometrical isomers, (**6a** and **6b**) in 74% and (**7a** and **7b**) in 51% yield, respectively. The products obtained from **1** were successfully separated by silica gel column chromatography into **6a** and **6b** with a ratio of 88: 12 which was determined by the NMR spectroscopy. However, the separation of the mixture obtained from **5** was unsuccessful even by repeated column chromatography on silica gel or alumina. The ratio of two geometrical isomers (**7a** and **7b**) consisted of 40: 60 determined by the NMR spectroscopy.

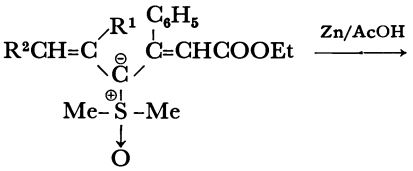

1: $R^1=R^2=COOMe$
5: $R^1=H$, $R^2=COOEt$

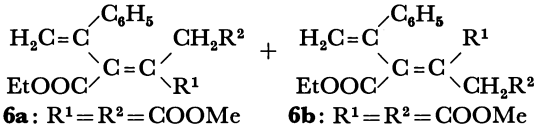

6a: $R^1=R^2=COOMe$ **6b**: $R^1=R^2=COOMe$
7a: $R^1=H$, $R^2=COOEt$ **7b**: $R^1=H$, $R^2=COOEt$

In the NMR spectra of **6a** and **6b**, terminal methylene protons were observed characteristically as AB quartet at δ 5.43 and 5.83 ppm (J=0.4 Hz), and δ 5.25 and 5.62 ppm (J=0.8 Hz), respectively. Likewise, terminal methylene protons of **7a** and **7b** appeared as AB quartet at δ 5.13 and 5.74 ppm (J=1.5 Hz), and δ 5.27 and 5.36 ppm (J=1.5 Hz), respectively. These terminal methylenes in **6a**, **b** and **7a**, **b** were chemically identified as 2,4-dinitrophenylhydrazone of formaldehyde liberated by ozonolysis.

The methylene protons (=C–$\underline{CH_2}$–COOMe) of **6a** and **6b** appeared at δ 3.39 and 3.78 ppm as sharp singlet, respectively. The fact that the chemical shift of the methylene protons of **6b** appeared at lower field than that of **6a**, is apparently caused by anisotropic effects of the ethoxycarbonyl group at the β-position. Therefore, the geometry between the methoxycarbonylmethyl (–CH_2COOMe) and ethoxycarbonyl group in **6b** is assignable to *Z*-configuration, and in **6a** to *E*-configuration. The *E*-isomer (**6a**) is likely to be thermodynamically more stable than the *Z*-isomer (**6b**) because of less interraction between methoxycarbonyl methyl and ethoxycarbonyl group. This observation

reflects the product distribution of **7**.

For **7a** the methylene (-$\underline{CH_2}$COOEt) and vinyl protons exhibited doublet at δ 3.19 ppm (J=7.5 Hz) and triplet at δ 7.1 ppm (J=7.5 Hz), respectively, and for **7b** doublet at δ 3.55 ppm (J=7 Hz) and triplet at δ 6.37 ppm (J=7 Hz), respectively. The chemical shifts of the vinyl proton of **7a** and the methylene protons (=C-$\underline{CH_2}$-COOMe) of **7b** appeared at lower field than those of **7b** and **7a**, respectively, due to the anisotropic effect of the ethoxycarbonyl group at the β-position. These observations indicate that the geometry between the methoxycarbonylmethyl (-CH_2COOMe) and ethoxycarbonyl group of **7a** is assigned to E-, and that of **7b** to Z-configuration.

Another possible structures (**6a'** and **6b'**) and (**7a'** and **7b'**) could be written for the reduction products obtained from sulfoxonium ylides (**1**) and (**5**), respectively. However, further chemical transformations and mechanistic consideration definitely excluded this possibility (*vide infra*).

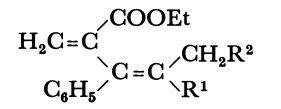

6a': R^1=R^2=COOMe **6b'**: R^1=R^2=COOMe
7a': R^1=H, R^2=COOEt **7b'**: R^1=H, R^2=COOEt

Treatment of the pure E-isomer (**6a**) with triethylamine in benzene furnished stereospecifically only one isomerized product (**8**), whose geometrical configuration was not clear. In its NMR spectrum, methyl and one vinyl protons appeared at δ 2.58 ppm (sharp singlet) and at δ 6.61 ppm (singlet), respectively, in addition to the peaks due to the two methoxycarbonyl and ethoxycarbonyl groups.

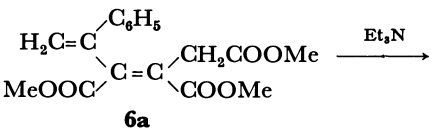

6a

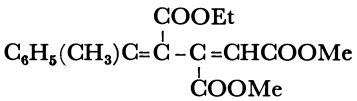

8

Analogously, base-catalysed isomerization of a mixture of **7a** and **7b** (36: 65) with triethylamine gave a mixture of two geometrical isomers (**9a**, and **9b**) in a ratio of 76: 24, which was determined by the NMR spectroscopy. In the NMR spectrum of **9a**, methyl protons appeared at δ 2.24 ppm as doublet (J=1 Hz), vinyl proton (H_A) at δ 5.88 ppm as doublet (J=16 Hz) and vinyl proton (H_B) at δ 7.30 ppm as quartet (J=16 and 1 Hz), and in that of **9b**, methyl protons appeared at δ 2.33 ppm as singlet, vinyl proton (H_C) at δ 6.07 ppm as doublet (J=16 Hz) and vinyl proton (H_D) at δ 7.76 ppm as doublet (J=16 Hz). The geometry of two vinyl protons in both **9a** and **9b** should be assigned to E-configuration from their coupling constant of J=16 Hz. The chemical shifts of the methyl (δ 2.33 ppm) and vinyl proton (H_D at δ 7.76 ppm) of **9b** appeared at lower field than that of **9a** (2.23 and 7.30 (H_B), respectively) due to the anisotropic effects of the ethoxycarbonyl and phenyl groups of **9b**. These facts indicate that the methyl group of **9b** preserves Z-configuration to the β-ethoxycarbonylgroup, and that of **9a** E-configuration.

7a+**7b**

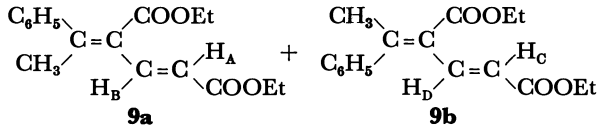

9a **9b**

Ozonolysis of **8** in dichloromethane followed by treatment with zinc liberated acetophenone, which was identified as 2,4-dinitrophenylhydrazone, together with acetaldehyde,[4] whereas a mixture of **9** (a mixture of Z

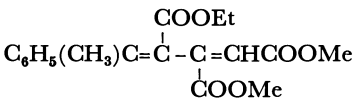

8

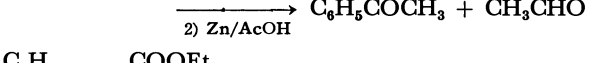

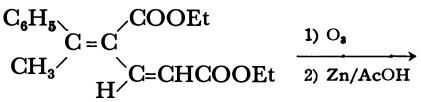

9

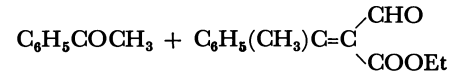

10

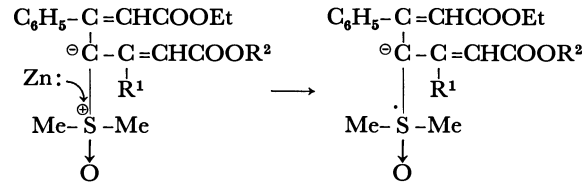

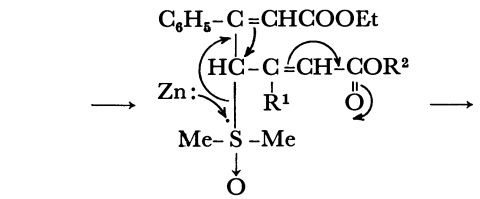

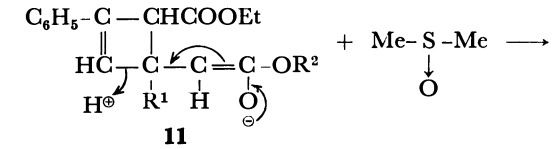

11

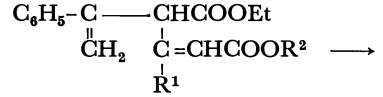

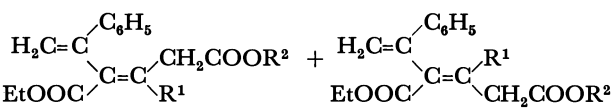

6: R^1=COOMe, R_2=Me; **7**: R^1=H, R^2=Et

and *E* (76: 24)) by ozonolysis yielded acetophenone and 2-formyl-3-phenyl-2-butenoate (**10**), which was confirmed as 2,4-dinitrophenylhydrazone (mp 194—195 °C). Thus, other possible structures (**6a'**, **6b'**, **7a'**, and **7b'**) as reduction products from **1** and **5** were firmly excluded.

The reaction pathway for the present reductive cleavage of dimethylsulfoxonium vinylallylides is likely to proceed through an anion radical to form a four membered intermediate (**11**), which would be cleaved to an unstable non-conjugated diene leading finally to conjugated products. On these novel and complex reactions the proposed mechanism can only be viewed tentatively. The mechanistic investigation in detail is under continuation.

It seems to be quite interesting that divinyl carbanion and carbene system derived by dissolving metal reduction and photolysis from the corresponding sulfoxonium ylides, respectively, possess remarkably outstanding chemical bihavior, which are now under studying.

Experimental

All the melting points were uncorrected. NMR spectra were recorded on a Varian A-60 and HA-100 spectrometers using TMS as an internal standard, IR spectra were taken on a Hitachi EPI-G3 and UV spectra were obtained with Beckman DK-2 spectrophotometer.

*Reduction of Dimethylsulfoxonium 3-Ethoxycarbonyl-1-[1,2-bis-(methoxycarbonyl)vinyl]-2-phenylallylide (**1**).* To a solution of **1** (15.5 g, 38 mmol) in acetic acid (150 ml) was added zinc powder (25 g, 380 mmol) in many portions under controlling inner temperature at 18—20 °C with cold water, and the reaction mixture was stirred at room temperature for 10 h. The inorganic substrance was filtered and washed with ether. The filtrate was concentrated under reduced pressure. The residue was dissolved in ether (*ca.* 500 ml), and the ethereal solution was washed successively with 5% $NaHCO_3$ solution, water and saturated NaCl solution, and dried over anhydrous Na_2SO_4. After the evaporation of the solvent under reduced pressure, the residue was chromatographed on silica gel (80 g). Elution with hexane–benzene (3: 1) gave 1.11 g (8.8% yield) of methyl (*Z*)-4-ethoxycarbonyl-3-methoxycarbonyl-5-phenyl-3,5-hexadienoate (**6b**), bp 140—143 °C/10^{-4} Torr (bath temp); IR (liquid): ν 1745, 1720, 1718, and 905 cm^{-1} (=CH_2); NMR ($CDCl_3$): δ 1.03 (3H, t, J=7 Hz; $COOCH_2C\underline{H}_3$), 4.10 (2H, q, J=7 Hz; $COOC\underline{H}_2CH_3$), 3.56 (3H, s; $COOCH_3$), 3.74 (3H, s; $COOCH_3$), 3.78 (2H, s; CH_2COOMe), 5.25 (1H, d, J=0.8 Hz; -CH), 5.62 (1H, d, J=0.8 Hz; =CH) and 7.4 ppm (5H, m; C_6H_5); Found: C, 65.21; H, 6.03%. Calcd for $C_{18}H_{20}O_6$: C, 65.02; H, 6.07%. Elution with hexane–benzene (1: 1—1: 3) afforded 7.99 g (63.3% yield) of methyl (*E*)-3-ethoxycarbonyl-4-methoxycarbonyl-5-phenyl-3,5-hexadienoate (**6a**), bp 140—141 °C/10^{-4} Torr (bath temp); IR (Liquid): ν1745, 1720, 1705, and 905 cm^{-1} (=CH_2); NMR ($CDCl_3$): δ 1.18 (3H, t, J=7 Hz; $COOCH_2C\underline{H}_3$), 4.22 (2H, q, J=7 Hz; $COOC\underline{H}_2CH_3$), 3.60 (3H, s; $COOCH_3$), 3.81 (3H, s; $COOCH_3$), 5.43 (1H, d, J=0.4 Hz; -CH), 5.83 (1H, d, J=0.4 Hz; =CH) and 7.4 ppm (5H, m; C_6H_5); Found: C, 64.78; H, 6.11%. Calcd for $C_{18}H_{20}O_6$: C, 65.02; H, 6.07%.

*Reduction of Dimethylsulfoxonium 3-Ethoxycarbonyl-1-[2-(ethoxycarbonyl)vinyl]-2-phenylallylide (**5**).* To a solution of **5** (8.4 g, 23 mmol) in acetic acid (100 ml) was added zinc powder (15 g, 230 mmol) in many portions under controlling inner temperature at 18—20 °C with cold water, and the reaction mixture was stirred over night (13 h). The inorganic substance was filtered and washed with ether. The filtrate was concentrated under reduced pressure. The residue was dissolved in ether (*ca.* 300 ml), and the ethereal solution was washed successively with 5% $NaHCO_3$ solution, water, and saturated NaCl solution, and dried over anhydrous Na_2SO_4. After the evaporation of the solvent under reduced pressure, the residue was distilled *in vacuo* to give 3.4 g (51.2% yield) of a mixture of ethyl (*Z*)- and (*E*)-4-ethoxycarbonyl-5-phenyl-3,5-hexadienoate (**7a** and **7b**) in a ratio of 40: 60, bp 120—121 °C/10^{-4} Torr; IR (Liquid): ν 1745, 1720, and 903 cm^{-1} (=CH_2); UV (EtOH): λ_{max} 238 nm (ε 12440); NMR (100 Mc, $CDCl_3$): For *Z*-isomer (7a): δ 1.10 and 1.23 (6H, t, J=7 Hz; $COOCH_2C\underline{H}_3$), 4.08 and 4.21 (4H, q, J=7 Hz; $COOC\underline{H}_2CH_3$), 3.19 (2H, d, J=7.5 Hz; =C-$C\underline{H}_2$COOEt), 7.10 (1H, t, J=7.5 Hz; =C$\underline{H}$-CH_2-), 5.13 (1H, d, J=1.5 Hz; =CH), 5.74 (1H, d, J=1.5 Hz; =CH), and 7.25 ppm (5H, s; C_6H_5); For *E*-isomer (**7b**): δ 1.01 and 1.27 (6H, t, J=7 Hz; $COOCH_2C\underline{H}_3$), 4.12 and 4.17 (4H, q, J=7 Hz; $COOC\underline{H}_2CH_3$), 3.55 (2H, d, J=7 Hz; =C-CH_2COOEt), 6.37 (1H, t, J=7 Hz; =C$\underline{H}$-CH_2), 5.27 (1H, d, J=1.5 Hz; =CH), 5.36 (1H, d, J=1.5 Hz; =CH), and 7.25 ppm (5H, s; C_6H_5); Found: C, 70.69; H, 7.15%. Calcd for $C_{17}H_{20}O_4$: C, 70.81; H, 6.99%.

*Ozonolysis of a Mixture of Methyl(Z)- and (E)-4-Ethoxycarbonyl-3-methoxycarbonyl-5-phenyl-3,5-hexadienoate (**6a** and **6b**).* Into a solution of **6** (a mixture of **6a** and **6b** (88: 12)) (1.5 g, 4.5 mmol) in acetic acid (50 ml) containing small amount of KI freshly generated ozone was passed under cooling at 15—18 °C with cold water until iodine deposited. To the reaction mixture was added zinc (1 g) and water (20 ml), and stirred at room temperature for 2 h. The reaction mixture was submitted to steam-distillation, and the distilate was passed into a saturated solution of 2,4-dinitrophenylhydrazine in 2 M-HCl (150 ml). Deposited yellow precipitate was collected by filtration, and recrystallized from ethyl acetate to give 250 mg (26.5% yield) of 2,4-dinitrophenylhydrazone of formaldehyde, mp 162—163 °C, which was identified with an authentic sample in the mixed melting point and in their IR spectra.

*Ozonolysis of a Mixture of Ethyl (Z)- and (E)-4-Ethoxycarbonyl-5-phenyl-3,5-hexadienoate (**7a** and **7b**).* Into a solution of **7** (a mixture of **7a** and **7b** (40: 60)) (1 g, 3.46 mmol) in acetic acid (40 ml) containing small amount of KI, freshly generated ozone was passed under cooling at 15—18 °C with cold water until iodine deposited. The same work-up as described above afforded 240 mg (33% yield) of 2,4-dinitrophenylhydrazone of formaldehyde, mp 162—163 °C.

*Isomerization of Methyl (E)4-Ethoxycarbonyl-3-methoxycarbonyl-5-phenyl-3,5-hexadienoate (**6a**) to Methyl 4-Ethoxycarbonyl-3-methoxycarbonyl-5-phenyl-2,4-hexadienoate (**8**).* A solution of **6a** (3.0 g, 9 mmol) and triethylamine (9 ml) in benzene (75 ml) was heated under reflux for 30 h. After the evaporation of the solvent, the residue was chromatographed on silica gel (100 g). Elution with benzene afforded 1.15 g (38.3% yield) of **8**, bp 142—143 °C/10^{-4} Torr (bath temp); IR (Liquid): ν 1720, 1718, and 1715 cm^{-1}; NMR ($CDCl_3$): δ 1.24 (3H, t, J=7 Hz; $COOCH_2C\underline{H}_3$), 4.22 (2H, q, J=7 Hz; $COOC\underline{H}_2CH_3$), 2.58 (3H, s; =CCH_3), 3.60 (3H, s; $COOCH_3$), 3.69 (3H, s, $COOCH_3$), 6.61 (1H, s; =CH), and 7.25 (5H, m; C_6H_5); Found: C, 64.78; H, 6.26%. Calcd for $C_{18}H_{20}O_6$: C, 65.02; H, 6.07%. Further elution with benzene–ethyl acetate (3: 1) gave a mixture of **6a** and **8** (1.12 g).

*Isomerization of a Mixture of Ethyl (Z)- and (E)-4-Ethoxycarbonyl-5-phenyl-3,5-hexadienoate (**7a** and **7b**) to a Mixture of Ethyl (Z)- and (E)-4-Ethoxycarbonyl-5-phenyl-2,4-hexadienoate (**9a** and **9b**).* A solution of **7** (a mixture of **7a** and **7b** (40: 60)) (1.6 g, 5.5 mmol) and triethylamine (5 g, 50 mmol)

in benzene (25 ml) was heated under reflux for 2 h. After the evaporation of the solvent, the residue was distilled *in vacuo* to give 1.2 g (75% yield) of a mixture of **9a** and **9b**, bp 140—141 °C/10^{-4} Torr; IR (liquid): ν 1720, 1718 cm^{-1}; NMR ($CDCl_3$): For *E*-isomer (**9a**): δ 1.22 and 1.38 (6H, t, J=7 Hz; $COOCH_2C\underline{H}_3$), 4.14 and 4.40 (4H, q, J=7 Hz; $CO\text{-}OC\underline{H}_2CH_3$), 2.24 (3H, s; CH_3), 5.88 (1H, d, J=16 Hz; =CHCOOEt), 7.30 (1H, d, J=16 Hz; =CH), and 7.35 ppm (5H, m; C_6H_5); For *Z*-isomer (**9b**): δ 0.87 and 1.30 (6H, t, J=7 Hz; $COOCH_2C\underline{H}_3$), 3.94 and 4.27 (4H, q, J=7 Hz; $COOC\underline{H}_2CH_3$), 2.33 (3H, s; CH_3), 6.07 (1H, d, J=16 Hz; =CHCOOEt), 7.76 (1H, d, J=16 Hz; =CH), and 7.25 ppm (5H, m; C_6H_5); UV (EtOH) λ_{max} 234 (ε 11160), and 285 nm (ε 14660); Found: C, 70.86; H, 7.02%. Calcd for $C_{17}H_{20}O_4$: C, 70.81; H, 6.99%.

Ozonolysis of Methyl 4-Ethoxycarbonyl-3-methoxycarbonyl-5-phenyl-2,4-hexadienoate (8). Into a solution of **8** (800 mg, 2.4 mmol) in dichloromethane (12 ml) was passed freshly generated ozone (250 mg, 5.2 mmol) at −50 °C. To the reaction mixture was added zinc powder (800 mg), acetic acid (0.4 ml) and water (0.2 ml), and stirred at room temperature for 2 h. After filtration of the inorganic substance, the filtrate was concentrated under reduced pressure. To the residue was added a solution of 2,4-dinitrophenylhydrazine (2.4 g in H_2SO_4 (12 ml), H_2O (18 ml) and EtOH (150 ml)), and heated under reflux for 30 min. After addition of water (200 ml) and extraction with ethyl acetate, the organic layer was washed with water and dried over anhydrous Na_2SO_4. After evaporation of the solvent under reduced pressure, the residue was chromatographed on silica gel (30 g). Elution with benzene gave 2,4-dinitrophenylhydrazone of acetophenone (110 mg, 15.2% yield), mp 253—255 °C, which showed no depression in mixed melting point with an authentic specimen. Further elution with benzene gave 2,4-dinitrophenylhydrazone of acetaldehyde (400 mg, 74% yield),[4] mp 159—161 °C (from EtOH), which showed no depression in mixed melting point with an authentic samples; NMR ($CDCl_3$): δ 2.16 (3H, d, J=6 Hz; N=CH-$C\underline{H}_3$), 7.69 (1H, q, J=6 Hz; N=CH-CH_3), 8.01 (1H, d, J=10 Hz; 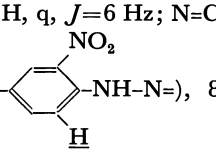
-NH-N=), 8.40 (1H, dd, J=2.5 and J=10 Hz; 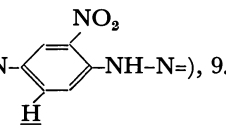
-NH-N=), 9.19 (1H, d, J=2.5 Hz: 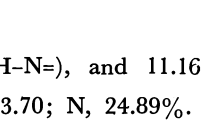
-NH-N=), and 11.16 (1H, m, NH); Found: C, 42.62; H, 3.70; N, 24.89%. Calcd for $C_8H_8N_4O_4$: C, 42.86; H, 3.59; N 24.99%.

Ozonolysis of a Mixture of Ethyl (Z)- and (E)-4-Ethoxycarbonyl-5-phenyl-2,4-hexadienoate (9a and 9b). Into a solution of **9** (a mixture of **9a** and **9b** (76: 24)) (1.0 g, 3.5 mmol) in dichloromethane (55 ml) was passed freshly generated ozone (*ca.* 8 mmol) at −50 °C. To the reaction mixture was added zinc powder (840 mg, 14 mmol), acetic acid (0.5 ml) and water (0.1 ml), and stirred at room temperature for 2 h. After the same procedure as described above, the crude hydrazone was chromatographed on silica gel (30 g). Elution with benzene gave 36 mg of 2,4-dinitrophenylhydrazone of acetophenone, mp 253—255 °C (from EtOH), which showed no depression with an authentic sample in mixed melting point; Further elution with benzene gave 148 mg (10.7% yield) of orange crystals of 2,4-dinitrophenylhydrazone of ethyl 2-formyl-3-phenyl-2-butenoate (**10**), mp 194—195 °C (decomp) (from ethyl acetate): NMR ($CDCl_3$): δ 1.48 (3H, t, J=7 Hz; $COOCH_2C\underline{H}_3$), 4.50 (2H, q, J=7 Hz; $COOC\underline{H}_2CH_3$), 2.30 (3H, s; $=CCH_3$), 7.42 (5H, m; C_6H_5), 7.69 (1H, s; =CH-), 7.80 (1H, d, J=9 Hz; 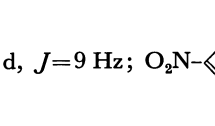
-NHN=), 8.32 (1H, dd, J=9 and J=3 Hz; 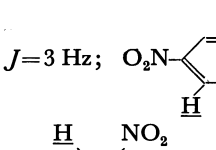
-NHN=), 9.07 (1H, d, J=3 Hz; 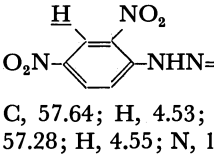
-NHN=), and 10.98 ppm (1H, m; NH); Found: C, 57.64; H, 4.53; N, 13.93%. Calcd for $C_{19}H_{18}N_4O_6$: C, 57.28; H, 4.55; N, 14.07%.

The authors wish to thank Messrs. N. Ishida and T. Miyamura for their technical assistance.

References

1) Sulfoxonium Ylide Chemistry. VII: J. Ide and Y. Kishida, *Bull. Chem. Soc. Jpn.*, **49**, 3239 (1976).

2) a) Y. Kishida, T. Hiraoka, and J. Ide, *Tetrahedron Lett.*, **1968**, 1139; b) Y. Kishida, T. Hiraoka, and J. Ide, *Chem. Pharm. Bull.*, **17**, 1991 (1969).

3) J. Ide, and Y. Kishida, *Chem. Pharm. Bull.*, **16**, 784 (1968).

4) In addition to acetophenone, a significant amount of acetaldehyde was obtained (see Experimental), which was presumably produced by phenyl migration on the decomposition of the ozonide of **9** with zinc in acidic conditions.

Self-Immolative Asymmetric Synthesis. III. Allylic Rearrangement of Optically Active Trichloroacetimidate

Yukio YAMAMOTO, Hiroshi SHIMODA,* Jun'ichi ODA, and Yuzo INOUYE

Institute for Chemical Research, Kyoto University, Uji, Kyoto 611
**Research Laboratory, Fumakilla Co. Ltd., Ohno-cho, Hiroshima 739-04*

(Received May 26, 1976)

The [3,3]sigmatropic rearrangement of (2*E*)-(1*R*)-1-methyl-3-phenyl-2-propenyl trichloroacetimidate to give *N*-[(2*E*)-(1*R*)-1-phenyl-2-butenyl]trichloroacetamide was effected thermally with nearly complete transfer of chirality *via* a doubly suprafacial transition state. The application of the self-immolative asymmetric synthesis to optically active carveols afforded carveylamines of the predicted configuration.

In the previous papers, we reported transfer of chirality from tetracoordinate nitrogen to trigonal carbon[1] and from tetrahedral carbon to trigonal carbon[2] with nearly quantitative conservation of chirality. These findings not only indicate that the reaction proceeds *via* [2,3]sigmatropic rearrangement but also offer a novel method for stereo-specific synthesis of alcohols from amine oxides with allylic inversion. The reverse transformation, allylic alcohols to amines with allylic inversion, can be achieved by the Chapman-type rearrangements,[3] which are classified as [3,3]sigmatropic rearrangement according to the Woodward-Hoffmann rule. The conversion of an allylic phenylurethane into an *N*-phenylallylamine by Hill was the sole precedent in which the stereochemistry was thoroughly elucidated.[4] In spite of the reasonable stereochemical outcome in favor of a doubly suprafacial mode, the optical yield obtained (65%) was rather moderate in view of the general observations in this type of rearrangements.[5] This may presumably be due to the radical by-path. Recently, the rearrangement of allylic trichloroacetimidates to trichloroacetamides was reported by Overman.[6] This process would be advantageous in enabling one to ensure high yields of primary amines over those which are limited by substituents on nitrogen.

We now present another self-immolative asymmetric synthesis of amines from chiral allylic alcohols by the use of trichloroacetimidic ester as an intermediary. The substrate used in the present study was the chiral trichloroacetimidate, (*E*)-(+)-1-methyl-3-phenyl-2-propenyl trichloroacetimidate [(+)-2].

By the treatment with sodium hydride and trichloroacetonitrile, (*E*)-(+)-4-phenyl-3-buten-2-ol [(+)-**1**, $[\alpha]_D^{20}$ 17.3°][7a,b] was converted to (+)-**2** having $[\alpha]_D^{20}$ 34.7° in 94% yield, whose purity proved to be 85% as assessed by NMR. The trichloroacetimidate (+)-**2** was heated in toluene under reflux to give the [3,3] shift product, (+)-*N*-[(*E*)-1-phenyl-2-butenyl]trichloroacetamide [(+)-**3**, $[\alpha]_D^{20}$ 15.1°] in 74% yield. The *E*-geometry of double bond in resulting (+)-**3** was established by IR and NMR spectra. Neither *Z*-isomer nor [1,3] shift product was detected in the reaction mixture. Hydrogenation of (+)-**3** over palladium charcoal resulted in the formation of the saturated dichloroacetamide [(+)-**4**, $[\alpha]_D^{20}$ 32.7°], one of the 3 chlorine atoms having been simultaneously replaced by hydrogen during the reaction process.

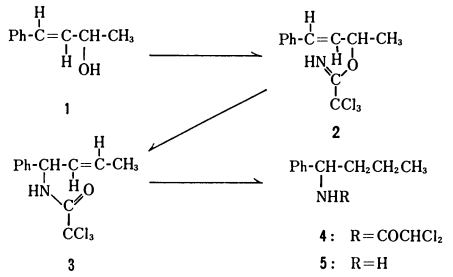

Scheme 1.

The absolute configuration as well as the enantiomeric purity of **4**, crucial to the mechanistic picture of the present rearrangement, were obtained by the conversion of optically pure (−)-1-phenyl-1-aminobutane [(−)-**5**, $[\alpha]_D^{25}$ −22.2°] of the well-defined *S*-configuration[8] into (−)-**4**, $[\alpha]_D^{25}$ −71.7°. Consequently, the end product (+)-**4** and the parent rearrangement product (+)-**3** can be safely assigned the *R*-configuration and should be of 45.6% optical purity.

Since the *R*-configuration of the starting (+)-**1** has been unambiguously established by the correlation to (*R*)-(−)-4-phenyl-2-butanol,[7a,c] and the NMR spectroscopy with the use of a chiral shift reagent showed the chiral alcohol (+)-**1** to be of 45±2% enantiomeric purity, the present thermal rearrangement proceeded with complete retention of chirality.

The finding that the complete transfer of chirality was achieved during the [3,3] shift and that the [1,3] shift product was not detected at all corroborates the concertedness of the process and excludes radical dissociation-recombination. Two transition states would be conceivable for doubly suprafacial fasion in thermally allowed [3,3]sigmatropic rearrangement: 4-centered chair-form and 6-centered boat-form. In view of the Cope[5a,9] and the Claisen[5b,10] rearrangements attained so far, we can reasonably formulate the transition state topology of choice for the allylic rearrangement of trichloroacetimidate as the former in agreement with Overman. Furthermore, the finding that the *R-E* trichloroacetimidate (+)-**2** rearranged to give the *R-E* trichloroacetamide (+)-**3** cogently supports the fashion **6**. The *S-Z* product, which would be expected from the alternative 4-centered mode **7**, was not detected at all in the present rearrangement. The preference of fashion **6** to **7** could be rationalized by the unfavorable non-bonded interaction between methyl group and hydrogen atom which orient *syn*-axial in the latter,

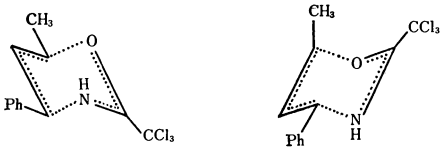

6 7

Fig. 1. Transition state topology predicted for the rearrangement of (2*E*)-(1*R*)-1-methyl-3-phenyl-2-propenyl trichloroacetimidate [(+)-**2**].

while both methyl and phenyl groups orient equatorial in the former, therefore thermodynamically more favorable.

As a probe of synthetic utility, the present rearrangement was successfully applied to the naturally derived allylic alcohols whose configurations have been known. According to Scheme 2, (+)-*trans*-carveol [(+)-**8**, α_D^{20} 172°][11] was converted into the corresponding trichloroacetimidate [(+)-**9**, $[\alpha]_D^{22}$ 72°] in 85% yield. It is noted in this system that the allylic group is tied back in a 6-membered ring, which *a priori* compels the transition state topology to assume nothing but a doubly suprafacial mode.

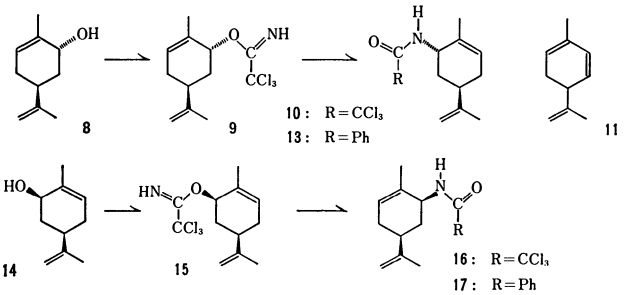

Scheme 2.

Upon heating, (+)-**9** gave (−)-*N*-carveyl trichloroacetamide [(−)-**10**, $[\alpha]_D^{23}$ −117°] in 44% yield. The observed lowering in the yield of rearrangement product may be attributed to the elimination side process, as actually indicated by the formation of the triene (**11**, 18%) and trichloroacetamide (**12**, 41%).[12] The transformation of (−)-**10** by the consecutive alkaline hydrolysis and benzoylation gave (−)-*N*-*trans*-carveylbenzamide [(−)-**13**, $[\alpha]_D^{18}$ −245°, mp 112—113 °C]. The absolute configuration of (−)-**13** can be safely assigned as depicted in Scheme 2 by the comparison of physical constants in agreement with those in the literature.[13]

In the case of the (−)-*cis* counterpart [(−)-**15**, $[\alpha]_D^{23}$ −48 °], (−)-*N*-carveyltrichloroacetamide [(−)-**16**,$[\alpha]_D^{23}$ −43.6°] was obtained in 42% yield along with **12** (35%). By exactly the same work-up as for (−)-*trans* isomer, (−)-**16**, was transformed into (−)-*N*-*cis*-carveylbenzamide [(−)-**17**, $[\alpha]_D^{20}$ −95.2°, mp 169 °C].[13]

In both cases, the absolute configurations of the rearrangement products coincided with those predicted from the doubly suprafacial transition state. The stereospecific 1,3-transposition of alcohol and amine functions was thus achieved by the present self-immolative asymmetric synthesis.

Experimental

All melting and boiling points were uncorrected. IR spectra were recorded with a Hitachi 215 and NMR spectra on a Varian EM-360. Elemental analyses were carried out with a Yanagimoto CHN-corder TM-1. Optical rotations were observed with a Yanagimoto OR-50 or a Perkin Elmer R-241.

Assessment of the Enantiomeric Purity of (E)-(+)-4-Phenyl-3-buten-2-ol [(+)-1]. Chemical shift non-equivalence of the enantiomers was observed on the following conditions; carbon tetrachloride solution of (+)-**1** (0.45 M, $[\alpha]_D^{20}$ 17.3°)[7a,b] and tris-[3-(trifluoromethylhydroxymethylene)-*d*-camphorato]-europium (III) (**18**, 0.06 M) using JEOL MH-100 (100 MHz). Methyl doublets of enantiomers appeared at (δ 2.31, 2.37) and (δ 2.34, 2.40) respectively. The enantiomeric purity of (+)-**1** proved to be 45±2% by the calculation from peak heights and areas.

(E)-(+)-1-Methyl-3-phenyl-2-propenyl Trichloroacetimidate [(+)-2]. A solution of (+)-**1** [1.8 g, 12 mmol, $[\alpha]_D^{20}$ 17.3° (*c* 5.1, $CHCl_3$)] in dry ether (20 ml) was treated with sodium hydride (110 mg, 47% in mineral oil, 2.1 mmol) which had been previously washed 3 times with dry hexane. The resulting mixture was added to trichloroacetonitrile (1.8 g, 12 mmol) in dry ether (10 ml) at −15 °C in nitrogen atmosphere. After stirring at 0 °C for 1.5 h, the solution was concentrated under reduced pressure. Pentane (40 ml) containing methanol (0.8 ml, 2.1 mmol) was added and the mixture was shaken for 1 min. Successive filtration and evaporation gave (+)-**2** (3.3 g, 94%) whose purity proved to be 85% as assessed by NMR; $[\alpha]_D^{20}$ 34.7° (*c* 5.0, $CHCl_3$); IR (liquid): NH 3350, C=N 1650, =CH (*E*) 960 cm^{-1}; NMR (CCl_4): δ 1.63 (d, 3H, CH_3), 5.77—6.28 (m, 1H, CH), 6.39—7.33 (m, 2H, CH=CH), 7.57—8.00 (m, 5H, phenyl), 8.70—9.00 (broad, 1H, NH).

[3,3] Rearrangement of (+)-2. The trichloroacetimidate (+)-**2** (3.2 g, purity 85%) in toluene (35 ml) was heated under reflux for 4 h. Distillation gave (+)-*N*-[(*E*)-1-phenyl-2-butenyl]trichloroacetamide [(+)-**3**, 2.0 g, 74%]; bp 121—124 °C/0.06 Torr; mp 62—64 °C; $[\alpha]_D^{20}$ 15.1° (*c* 2.7, $CHCl_3$); IR (KBr): NH 3400, C=O 1680, =CH (*E*) 962 cm^{-1}; NMR (CCl_4): δ 1.70—1.91 (m, 3H, CH_3), 5.28—5.87 (m, 3H, CH, and CH=CH), 6.44—7.00 (broad, 1H, NH), 7.31 (s, 5H, phenyl).

Found: C, 49.30; H, 4.18; N, 4.76%. Calcd for $C_{12}H_{12}NOCl_3$: C, 49.26; H, 4.13; N, 4.79%.

Hydrogenation of (+)-3. The trichloroacetamide (+)-**3** (1.0 g, 3.4 mmol) was hydrogenated over 5% palladium-charcoal (200 mg) in ethanol (100 ml) and 2 equivalent amounts of hydrogen (170 ml at room temperature) were absorbed. The reaction mixture was neutralized with aqueous potassium carbonate. Distillation gave (+)-*N*-(1-phenylbutyl)dichloroacetamide [(+)-**4**, 740 mg, 83%]; bp 116 °C/0.03 Torr; mp 92—93.5 °C; $[\alpha]_D^{20}$ 32.7° (*c* 3.0, $CHCl_3$); IR (KBr): NH 3280, C=O 1660 cm^{-1}; NMR ($CDCl_3$): δ 0.78—1.12 (m, 3H, CH_3), 1.13—2.08 (m, 4H, CH_2CH_2), 4.78—5.20 (m, 1H, CH), 5.98 (s, 1H, $CHCl_2$), 7.41 (s, 5H, phenyl).

Found: C, 55.34; H, 6.07; N, 5.39%. Calcd for $C_{12}H_{15}NOCl_2$: C, 55.40; H, 5.81; N, 5.38%.

(−)-1-Phenyl-1-aminobutane [(−)-5]. The racemic amine[14] (136 g, 0.91 mol) was added to (−)-*N*-acetylleucine (158 g, 0.91 mol) in methanol (1200 ml) and the salt formed was recrystallized 4 times from methanol to yield colorless fine needles (4.6 g); mp 196—198 °C; $[\alpha]_D^{25}$ −1.8° (*c* 5.0, methanol). The physical constants did not alter on further recrystallizations. The amine liberated from the salt had bp 105—107 °C/20 Torr, $[\alpha]_D^{25}$ −22.2° (*c* 5.1, $CHCl_3$). The racemic **5** exhibited an apparent chemical shift non-equiva-

lence for the methine proton in carbon tetrachloride solution of (±)-**5** (0.4 M) and **18** (0.02 M), whereas no separation of the same signal was observed with the resolved amine under the same conditions.

(−)-N-(1-Phenylbutyl)dichloroacetamide [*(−)-4*]. To the solution of dichloroacetyl chloride (1.5 g, 10 mmol) in benzene (10 ml), the mixture of (−)-**5** (1.5 g, 10 mmol) and pyridine (1.6 g, 20 mmol) in benzene (10 ml) was added dropwise at 0 °C. After stirring at room temperature overnight, the resulting dichloroacetamide was extracted with benzene. Distillation gave (−)-**4** (1.7 g, 56%); $[\alpha]_D^{25}$ −71.7° (*c* 3.1, $CHCl_3$).

*(+)-*trans*-Carveyltrichloroacetimidate* [*(+)-9*]. The reaction of (+)-*trans*-carveol [(+)-**8**, 1.5 g, 10 mmol, α_D^{20} 172° (neat) (lit,[11] α_D^{20} 185.8°)] and trichloroacetonitrile (1.4 g, 10 mmol) was conducted with potassium hydride (500 mg, 23.8% in mineral oil, 2 mmol) in place of sodium hydride. The subsequent work-up in exactly the same manner as described for (+)-**2** yielded (+)-**9** (2.5 g, 85%). In this case, the unreacted (+)-**8** was not detected in NMR spectrum; $[\alpha]_D^{22}$ 72° (*c* 3.0, $CHCl_3$); IR (liquid): NH 3350, C=N 1650 cm^{-1}; NMR (CCl_4): δ 0.68—2.75 (m, 5H, ring protons), 1.78 (s, 3H, CH_3), 1.82 (s, 3H, CH_3), 4.78—4.99 (m, 2H, $=CH_2$), 5.41—5.66 (m, 1H, CH–O), 5.77—6.07 (m, 1H, =CH–), 8.33—8.63 (broad, 1H, NH).

[3,3] Rearrangement of (+)-9. The trichloroacetimidate (+)-**9** (2.5 g) in toluene (25 g) was heated under reflux for 10 h. The reaction mixture was concentrated and treated with warm hexane. After removal of the insoluble material, trichloroacetamide (**12**, 560 mg, 41%), the solution was evaporated. After 1,5,8(9)-*p*-menthatriene (**11**, 200 mg, 18%) was removed, (−)-*N*-carveyltrichloroacetamide [(−)-**10**, 1.1 g, 44%] distilled at 114—115 °C/0.15 Torr. The analytical sample was obtained by recrystallization from hexane; mp 91—93 °C; $[\alpha]_D^{23}$ −117° (*c* 3.0, $CHCl_3$); IR (KBr): NH 3310, C=O 1690 cm^{-1}; NMR (CCl_4): δ 1.20—2.58 (m, 5H, ring protons), 1.80 (s, 6H, $2CH_3$), 4.28—4.66 (m, 1H, CH–N), 4.85—5.00 (m, 2H, $=CH_2$), 5.79—6.01 (m, 1H, =CH–), 6.40—6.83 (broad, 1H, NH).

Found: C, 48.55; H, 5.58; N, 4.69%. Calcd for $C_{12}H_{16}NOCl_3$: C, 48.59; H, 5.44; N, 4.72%.

*(−)-N-*trans*-Carveylbenzamide* [*(−)-13*]. Sodium hydroxide (1.6 g, 40 mmol) in water (8 ml) was added to (−)-**10** (400 mg, 1.4 mmol) in ethanol (13 ml). The reaction mixture was stirred in nitrogen atmosphere at room temperature for 40 h. The amine extracted with ether was treated with benzoyl chloride (420 mg, 3 mmol) in pyridine (3 ml). The resulting benzamide (−)-**13** was extracted with chloroform and recrystallized from methanol-water; mp 112—113 °C; $[\alpha]_D^{18}$ −245° (*c* 3.0, $CHCl_3$) (lit,[13a] mp 103 °C; $[\alpha]_D^{21}$ −175.4°, lit,[13b] 114 °C; $[\alpha]_D$ −250°).

Found: C, 79.76; H, 8.36; N, 5.41%. Calcd for $C_{17}H_{21}NO$: C, 79.96; H, 8.29; N, 5.49%.

*(−)-*cis*-Carveyltrichloroacetimidate* [*(−)-15*]. By the same procedure as described for the (+)-*trans* counterpart, (−)-*cis*-carveol [(−)-**14**, α_D^{24} −22° (neat) (lit,[15a] α_D^{25} −22.8°)] was converted to (−)-**15** (99%); $[\alpha]_D^{23}$ −48° (*c* 3.0, $CHCl_3$); IR (liquid): NH 3350, C=N 1660 cm^{-1}; NMR (CCl_4): δ 0.87—2.80 (m, 5H, ring protons), 1.85 (s, 6H, $2CH_3$), 4.97—5.18 (m, 2H, $=CH_2$), 5.71—6.19 (m, 2H, CH–O and =CH–), 8.71—8.95 (broad, 1H, NH).

[3,3] Rearrangement of (−)-15. The trichloroacetimidate (−)-**15** (2.6 g) in xylene (26 ml) was heated under reflux for 8 h. The reaction mixture was worked up in exactly the same manner as described for (−)-**10**. Along with **12** (500 mg, 35%), (−)-*N*-carveyltrichloroacetamide [(−)-**16**] was obtained (1.1 g, 42%); bp 109—110 °C/0.1 Torr; mp 87—89° C; $[\alpha]_D^{23}$ −43.6° (*c* 3.0, $CHCl_3$); IR (KBr): NH 3270, C=O 1680 cm^{-1}; NMR (CCl_4): δ 1.05—2.63 (m, 5H, ring protons), 1.73 (s, 3H, CH_3), 1.77 (s, 3H, CH_3), 4.26—4.75 (m, 1H, CH–N), 4.73—4.93 (m, 2H, $=CH_2$), 5.52—5.87 (m, 1H, =CH–), 6.35—6.93 (broad, 1H, NH).

Found: C, 48.82; H, 5.54; N, 4.77%. Calcd for $C_{12}H_{16}NOCl_3$: C, 48.59; H, 5.44; N, 4.72%.

*(−)-N-*cis*-Carveylbenzamide* [*(−)-17*]. By the same procedure as described for (−)-**14**, (−)-**16** was converted to (−)-**17**; mp 169 °C; $[\alpha]_D^{20}$ −95.2° (*c* 4.7, $CHCl_3$) (lit,[13a] mp 169 °C; $[\alpha]_D^{19}$ −91.9°, lit,[13b] mp 169 °C; $[\alpha]_D$ −96°).

Found: C, 79.97; H, 8.24; N, 5.66%. Calcd for $C_{17}H_{21}NO$: C, 79.96; H, 8.29; N, 5.49%.

The authors are indebted to Dr. Larry E. Overman of the University of California for his valuable suggestion to this work.

References

1) M. Moriwaki, Y. Yamamoto, J. Oda, and Y. Inouye, *J. Org. Chem.*, **41**, 300 (1976).

2) Y. Yamamoto, J. Oda, and Y. Inouye, *J. Org. Chem.*, **41**, 303 (1976).

3) a) R. M. Roberts and F. A. Hussein, *J. Am. Chem. Soc.*, **82**, 1950 (1960); b) J. W. Schulenberg and S. Archer, "Organic Reactions," Vol. 14, John Wiley & Sons, New York (1965), p. 28; c) O. Mumm and F. Möller, *Ber.*, **70**, 2214 (1937); d) W. M. Lauer and C. S. Benton, *J. Org. Chem.*, **24**, 804 (1959).

4) M. E. Synerholm, N. W. Gilman, J. W. Morgan, and R. K. Hill, *J. Org. Chem.*, **33**, 1111 (1968).

5) a) R. K. Hill and N. W. Gilman, *Chem. Commun.*, **1967**, 619; b) R. K. Hill, R. Soman, and S. Sawada, *J. Org. Chem.*, **37**, 3737 (1972).

6) a) L. E. Overman, *J. Am. Chem. Soc.*, **96**, 597 (1974); b) L. E. Overman, *Tetrahedron Lett.*, **1975**, 1149; c) L. E. Overman, private communication.

7) a) J. Kenyon, S. M. Partridge, and H. Phillips, *J. Chem. Soc.*, **1936**, 85; b) H. L. Goering, G. S. Koermer, and E. C. Linsay, *J. Am. Chem. Soc.*, **93**, 1230 (1971); c) O. Červinka, E. Kroupová, and O. Bělovský, *Collect. Czech. Chem. Commun.*, **33**, 3551 (1968).

8) a) P. A. Levene, A. Rothen, and M. Kuna, *J. Biol. Chem.*, **120**, 777 (1937); b) O. Červinka, V. Suchan, O. Kotýnek, and V. Dudek, *Collect. Czech. Chem. Commun.*, **30**, 2484 (1965).

9) a) W. E. Doering and W. R. Roth, *Tetrahedron*, **18**, 67 (1962); b) M. Simonetta, G. Favini, C. Mariani, and P. Gramaccioni, *J. Am. Chem. Soc.*, **90**, 1280 (1968).

10) a) E. N. Marvell, J. L. Stephenson, and J. Ong, *J. Am. Chem. Soc.*, **87**, 1267 (1965); b) Gy. Fráter, A. Habich, H.-J. Hansen, and H. Schmid, *Helv. Chim. Acta*, **52**, 335 (1969).

11) S. Schroeter, *Justus Liebigs Ann. Chem.*, **674**, 118 (1964).

12) The yield of **11** lower than that of **12** can be ascribed to the loss during the purification work-up because of the high volatility of **11**.

13) a) H. Goldschmidt and A. Fischer, *Ber.*, **30**, 2069 (1897); b) S. Schroeter and E. L. Eliel, *J. Am. Chem. Soc.*, **86**, 2066 (1964).

14) The racemic amine was obtained from *n*-butyrophenone and ammonium formate; bp 109—111 °C/21 Torr. [bp 107—109 °C/16 Torr; M. Busch and L. Leefhelm, *J. Prakt. Chem.*, **77**, 1 (1908)].

15) a) R. G. Johnston and J. Read, *J. Chem. Soc.*, **1934**, 233; b) R. H. Reitsema, *J. Am. Chem. Soc.*, **75**, 1996 (1953).

Studies on the Reactions of Bis(acetylacetonato)platinum(II) with Lewis Bases. I. Reactions with Tertiary Phosphines Leading to a Complex Containing Carbon-Bonded Unidetate Acetylacetonato Ligand and Preparation of New Alkylplatinum Complexes

Takashi Ito, Takashi Kiriyama, and Akio Yamamoto

Research Laboratory of Resources Utilization, Tokyo Institute of Technology, Ookayama, Meguro-ku, Tokyo 152

(Received June 23, 1976)

Addition of tertiary phosphines (PR_3) to [Pt(acac)$_2$] (acac=acetylacetonato-*O,O'*) causes the rearrangement of one of the O-bonded chelate acac ligands to a C-bonded form giving [Pt(acac)(γ-acac)PR_3] (γ-acac=acetylacetonato-*C*[3]) (PR_3=PPh_3, **1a**, and $P(C_6H_{11})_3$, **2a**). Complexes **1a** and **2a** were isolated and characterized by means of elemental analysis, infrared and ^{1}H- and ^{13}C-NMR spectroscopy. Some reactions involving complex **1** were investigated. The mechanism of formation of a diethylplatinum complex in the reaction of [Pt(acac)$_2$] with Al(OEt)Et_2 and PPh_3 is discussed taking into account the rearrangement of the acac ligand from the O-bonded chelate to a C-bonded form.

Various alkyl-transition metal complexes have been isolated from the systems consisted of transition metal acetylacetonates, [M(acac)$_n$],[1] alkylaluminium compounds and ligand molecules such as tertiary phosphines or amines.[2] Some of these systems also afford hydrido complexes or zero-valent complexes by decomposition of intermediate unstable alkyltransition metal complexes. The mechanism of formation of the carbon-to-metal σ bond in these systems, however, has not been studied extensively. In the course of our study on the syntheses of alkyl complexes of palladium(II) and platinum(II) from systems consisted of [M(acac)$_2$] (M=Pd and Pt), alkylaluminium compound, and Lewis bases,[3] we found that [Pt(acac)$_2$] itself reacts with a tertiary phosphine to yield the complexes **1a** and **2a** in which acetylacetonato ligand is coordinated with platinum in a unidentate form *via* central (γ-) carbon atom.

Several kinds of ionic platinum(II) complexes with a central carbon bonded acetylacetonato ligand[4-6] have been reported by Lewis *et al.* More recently, Baba *et al.* reported the preparation of palladium(II) analog of **1a** by the reaction of [Pd(acac)$_2$] with Lewis bases such as PPh_3, pyridine, and secondary amines.[7] Here we report isolation, characterization, and some reactions of complexes **1a**, **2a**, and **2b** with special reference to the alkylation reaction mentioned above.

[M(acac)$_2$][1] [M(acac)(γ-acac)PR_3][1]

{M=Pt; PR_3=PPh_3 (**1a**), $P(C_6H_{11})_3$ (**2a**)
{M=Pd; PR_3=PPh_3 (**1b**)[7], $P(C_6H_{11})_3$ (**2b**)

Results and Discussion

Reaction of [Pt(acac)$_2$] with Triphenylphosphine, PPh_3.

The reaction of [Pt(acac)$_2$] with an equimolar amount of triphenylphosphine in toluene at room temperature afforded a diamagnetic pale yellow compound, which was identified as (2,4-pentanedionato-*C*[3])(2,4-pentanedionato-*O,O'*)triphenylphosphineplatinum(II), [Pt(acac)(γ-acac)PPh_3],[1] **1a**, on the basis of its infrared and NMR spectra and elemental analysis. The product is soluble in most aromatic solvents, chlorinated organic solvents, and ethers, and can be recrystallized from these solvents. As is shown in Table 1, complex **1a** possesses intense infrared bands which are characteristic of an enol-type bidentate acac ligand (1575, 1550, and 1525 cm^{-1}) and diketo-type γ-acac ligand (1685 and 1650 cm^{-1}),[5,8,9] and are very similar to the analogous palladium complex, [Pd(acac)(γ-acac)PPh_3], **1b**. A medium band at 445 cm^{-1} was assigned to ν(Pt–C) since the band lacks in the spectra of [PtX(acac)PPh_3] (X= Cl, Br and I) and [Pt(acac)$(PPh_3)_2$]BPh_4 which are derived from complex **1a** (*vide post*).

The ^{1}H-NMR spectral data of complex **1a** are listed in Table 2 together with **1b** and **2a**. Fig. 1a shows the ^{1}H-NMR spectrum of **1a** as a typical spectrum of this type of complexes. Assignment of each signal has been achieved by comparing it with the one reported for anionic Pt(II) complexes,[5,8] Pt(IV) complexes,[9] and analogous Pd(II) complexes[7] with γ-acac ligands. Of the two singlets due to methyl protons in the chelate acac ligand, the lower field signal was assigned to that trans to the phosphorus ligand according to the assign-

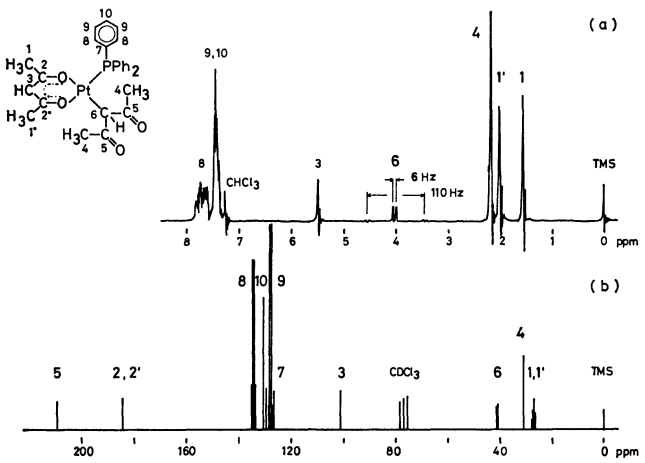

Fig. 1. ^{1}H- and ^{13}C-NMR spectra of [Pt(acac)(γ-acac)-PPh_3], **1a**, in $CDCl_3$, at room temperature.

Table 1. Relevant infrared data (in cm^{-1}) for some acetylacetonato complexes (KBr disc)

Complexes		acac Bands			γ-acac Bands	
[Pt(acac)(γ-acac)PPh$_3$]	**1a**	1575s	1550s	1525s	1685s	1650s
[Pd(acac)(γ-acac)PPh$_3$][a]	**1b**	1570s	1540m	1520s	1670s	1640s
[Pt(acac) (γ-acac)PCy$_3$]	**2a**	1580s	1550sh	1515vs	1645s	
[Pd(acac)(γ-acac)PCy$_3$]	**2b**	1585s	1540m	1515s	1675s	1665m
[PtI(acac)PPh$_3$]	**3a**	1565s	1560s	1524vs		
[PdI(acac)PPh$_3$]	**3b**	1575s	1560s	1510vs		
[Pt(acac)(PPh$_3$)$_2$]BPh$_4$	**4a**	1585sh	1565s	1530s		
[Pd(acac)(PPh$_3$)$_2$]BPh$_4$	**4b**	1580m	1565s	1520s		

a) The compound was prepared by the reported method.[7]

Table 2. ^{1}H-NMR spectral data of acetylacetonato complexes[a]

Complexes		acac ligand		γ-acac ligand				L[h]
		δ(CH$_3$)	δ(CH)	δ(CH$_3$)	δ(CH)	J[e]	J[f]	
[Pt(acac)(γ-acac)PPh$_3$]	**1a**	1.58(s, 3H) 2.04(s, 3H)	5.48(s, 1H)	2.20(s, 6H)	4.04(ds, 1H)	6	110	*o*- ~7.7(m, 6H) *m,p*- ~7.5(m, 9H)
[Pt(acac)(γ-acac)PPh$_3$]	**1a**[b]	1.52(s, 3H) 1.96(s, 3H)	5.44(s, 1H)	2.36(s, 6H)	4.28(ds, 1H)	6	109	—[i]
[Pt(acac)(γ-acac)PPh$_3$]	**1a**[c]	1.34(s, 3H) 1.82(s, 3H)	5.18(s, 1H)	2.52(s, 6H)	4.44(ds, 1H)	6	109	*o*- ~7.9(m, 6H) *m,p*- ~7.1 (m, 6H)
[Pd(acac)(γ-acac)PPh$_3$][d]	**1b**	1.54(s, 3H) 2.06(s, 3H)	5.30(s, 1H)	2.18(s, 6H)	3.54(d, 1H)	6	—	*o*- ~7.7(m, 6H) *m,p*- ~7.5(m, 9H)
[Pt(acac)(γ-acac)PCy$_3$]	**2a**	2.00(s, 3H) 2.08(s, 3H)	5.47(s, 1H)	2.21(s, 6H)	3.99(d, 1H)	4	—[g]	1.1—2.5(m, br)
[Pd(acac)(γ-acac)PCy$_3$]	**2b**	1.93(s, 3H) 2.03(s, 3H)	5.39(s, 1H)	2.35(s, 6H)	3.44(d, 1H)	4	—	1.2—2.6(m, br)

a) In $CDCl_3$ unless otherwise stated, 100 MHz, at 25 °C. Chemical shifts are in δ values (ppm) with respect to tetramethylsilane as internal standard. Coupling constants are in Hz. In the parentheses are multiplicity and number of protons. Multiplicity symbols are as follows: s, singlet; ss, singlet with satellites due to ^{195}Pt; d, doublet; ds, doublet with satellites due to ^{195}Pt; q, quintet; sex, sextet; m, multiplet; br, broad. b) In C_5H_5N. c) In C_6D_6. d) The compound was prepared by the method described in the literature.[7] e) $|^3J(PH)|$. f) $|^2J(^{195}PtH)|$. g) ^{195}Pt-Satellites were not obtained due to low S/N ratio. h) L corresponds to tertiary phosphine ligand. i) Not observable due to overlapping with solvent signals.

ment by Baba *et al.*[7] Protons in the chelate acac ligand in complex **1a** exhibit upfield shift when the solvent was changed from $CDCl_3$ through pyridine to benzene, whereas those in the C-bonded γ-acac ligand shift towards downfield. The chemical shift of the methine proton in the γ-acac ligand in **1a** is somewhat lower than in the corresponding palladium complex, **1b** (δ=3.54 ppm[7]). The phosphorus–hydrogen coupling constant for this proton ($|^3J(P-H)|$=6 Hz) is almost the same as the reported value of 6.1 Hz for *trans*-[Pt(CH$_3$)Cl(PEt$_3$)$_2$][10] and 6.3 Hz for **1b**.[7] The methine proton attached to the platinum-bonded carbon atom in γ-acac ligand is known to accompany satellite signals due to ^{195}Pt. The fairly large coupling constant of $|^2J(^{195}Pt-H)|$=110 Hz for complex **1a** is similar to the reported values for K$^+$[Pt(acac)(γ-acac)-Cl]$^-$ (120 Hz) and K$^+$[Pt(acac)(γ-acac)$_2$]$^-$ (123 Hz).[5]

The ^{31}P{^{1}H}-NMR spectrum of **1a** in $CDCl_3$ showed a singlet at 11.8 ppm (downfield from the external reference of PPh$_3$ in C_6D_6/C_6H_5Cl) with the satellite bands due to ^{195}Pt. The analogous Pd complex, **1b**, showed the ^{31}P resonance at 37.8 ppm. The coupling constant, $|^1J(^{195}Pt-P)|$, of 4490 Hz for **1a** does not greatly differ from reported values of 3875 Hz for *cis*-[PtCl$_2$(PPh$_3$)$_2$][11] and of 3500—3600 Hz for *cis*-[PtCl$_2$(PR$_3$)$_2$],[12] and much larger than those of *ca.* 2400 Hz for *trans*-[PtCl$_2$(PR$_3$)$_2$].[12]

Table 3 summarizes the ^{13}C-NMR data of complex **1a** and its palladium analog, **1b**, together with those of [Pd(acac)$_2$], which were used to assist the assignment of the phosphine complexes. Fig. 1b compares the ^{13}C-NMR spectrum with ^{1}H-NMR spectrum for the typical complex **1a**. Although satellite bands due to ^{195}Pt could not be observed except for *ortho*-carbons (C^8) (as for the carbon numbering, refer to Fig. 1) of PPh$_3$ in the spectrum of complex **1a**, the assignment was made with the aid of supplementary information on the ^{13}C-NMR of [Pt(acac)(γ-acac)py] (py=pyridine)[13] which shows varying magnitudes of $|J(^{195}Pt-^{13}C)|$ values corresponding to the positions of the carbon atoms with respect to the central platinum. As is seen in Table 3, carbon signals due to the bidentate enol-acac ligand (C^1–C^3) are almost unchanged from those of [Pd(acac)$_2$] and their chemical shifts are very similar to those reported for acetylacetonato complexes of Be,[14] Al,[14] Co,[14,15] Ir,[16] and Ni.[17] Two methyl- and two keto-carbons of the bidentate acac ligand (C^1 and $C^{1'}$, and C^2 and $C^{2'}$, respectively) in **1b** are observed as non-equivalent carbons on coordination of PPh$_3$ as in the case for methyl protons in the ^{1}H-NMR spectrum. Resolution of the

Table 3. ^{13}C-NMR spectral data of [M(acac)(γ-acac)PPh_3] (M=Pt and Pd) and [$Pd(acac)_2$][a)]

Assignment[b)]			[Pt(acac)(γ-acac)PPh_3], **1a**	[Pd(acac)(γ-acac)PPh_3], **1b**	[$Pd(acac)_2$]
acac	CH_3	*1*	27.2 c	26.9 s	25.4 s
	CH_3	*1'*		28.3 d (7.6, n=4)	
	C=O	2	184.4 c	186.5 s	187.2 s
	C=O	*2'*		186.0 d (21.4, n=3)	
	H–C	*3*	101.2 s	99.6 s	101.6 s
γ-acac	CH_3	*4*	31.1 s	31.4 s	—
	>C=O	*5*	209.2 s	206.4 s	—
	–C–H	*6*	41.3 d (3.1, n=2)	51.1 d (4.6, n=2)	—
PPh_3	P-C	*7*	128.2 d (62.6, n=1)	128.7 d (51.9, n=1)	—
	o-C	*8*	134.6 ds (10.7, n=2)	134.1 d (10.7, n=2)	—
	m-C	*9*	128.2 d (10.7, n=3)	128.4 d (10.7, n=3)	—
	p-C	*10*	139.0 s	131.0 s	—

a) In $CDCl_3$ at room temperature. 25.2 MHz, Chemical shifts are in ppm, downfield positive, from tetramethylsilane as an internal reference. Coupling constants $|^nJ(^{31}P-^{13}C)|$ in Hz are in parentheses. Multiplicity abbreviations are: s, singlet; d, doublet; ds, doublet with satellite bands due to ^{195}Pt; c, complex pattern. b) See Fig. 1 for numbering of the carbon atoms. c) $|^3J(^{195}Pt-^{13}C)|=35.1$ Hz.

fine structure of the NMR spectrum for these carbons in complex **1a** was not sufficient and a complicated pattern due to the coupling with ^{195}Pt resulted. A large upfield shift is observed for the methine carbon in the γ-acac ligand (C^6) compared to that in the bidentate enol-acac ligand (C^3), and the C^6 carbon in the Pt complex resonates at a higher field than in its Pd analog. All these features parallel with those of the ^{1}H-NMR spectra. Appearance of a single C^5 signal at a lower field than for C^2 indicates that C^5 carbons belong to intact keto groups which are free from coordination to the central metal. Cheney *et al.* reported that ^{31}P–^{13}C coupling constants of the Pt-bonded methyl carbon in *cis*-[$PtMe_2(PMe_2Ph)_2$] are 104 and 9 Hz for mutually trans and cis ^{31}P and ^{13}C nuclei, respectively.[18] The small $|^2J(^{31}P-^{13}C)|$ values (5—9 Hz) of the methyl carbon cis to the phosphorus ligands were also reported for the cationic *trans*-monomethylbis(tertiaryl phosphine)-platinum(II) complexes.[19] A small value of the ^{31}P–^{13}C coupling constants for C^6 methine carbon suggests that γ-acac ligand occupies the cis position with respect to PPh_3 in complexes **1a** and **1b**. Furthermore, fairly large values of $|J(^{31}P-^{13}C)|$ observed for $C^{1'}$ and $C^{2'}$-carbons in **1b** indicate the presence of a large trans effect of PPh_3, the fact in accord with the observation in dimethylplatinum complex mentioned above. Chemical shifts and ^{31}P–^{13}C coupling constants of the *ortho*-, *meta*-, and *para*-carbons (C^8, C^9, and C^{10}) of the coordinated PPh_3 are similar to those of free PPh_3.[20] On the other hand, the carbon atom (C^7) attached to phosphorus moves upfield considerably (*ca.* 10 ppm) upon coordination accompanying an increase in the magnitude of the ^{31}P–^{13}C coupling constant (from 21 Hz for free PPh_3[20] to 62.6 Hz for **1a**). These facts may reflect an increase in M→P back donation in complexes **1a** and **1b**.

When more than one mole equivalent of PPh_3 was allowed to react with [$Pt(acac)_2$] at an elevated temperature in tetrahydrofuran, a creamy white compound was isolated, whose infrared spectrum shows ν(C=O) bands at 1653 and 1600 cm^{-1}. The ^{1}H-NMR spectrum and elemental analysis of this diamagnetic compound suggest the composition of [$Pt(CH_2COCHCOCH_3)(PPh_3)_2$]. The detailed study of this unusual complex will be reported elsewhere.

Reaction of [*Pt(acac)$_2$*] *and* [*Pd(acac)$_2$*] *with Tricyclohexylphosphine, PCy$_3$.* Tricyclohexylphosphine reacted with an equimolar amount of [$Pt(acac)_2$] in diethyl ether at room temperature to yield a white compound which was identified as (2,4-pentanedionato-C^3)(2,4-pentanedionato-O,O')tricyclohexylphosphineplatinum(II), [Pt(acac)(γ-acac)PCy_3], **2a**, on the basis of its infrared and ^{1}H-NMR spectra. Similarly obtained was its Pd-analog, [Pd(acac)(γ-acac)PCy_3], **2b**, by the reaction in benzene. Both complexes **2a** and **2b** are quite soluble in most common organic solvents to render the purification by recrystallization somewhat difficult. The infrared absorptions of **2a** and **2b** in the region of 1500 1700 cm^{-1}, listed in Table 1, indicate the presence of both acac and γ-acac ligands. Detection of the metal–carbon stretching bands for these complexes failed due to the complicated absorptions in the low frequency region.

The ^{1}H-NMR spectral data for complexes **2a** and **2b** are listed in Table 2. Signals due to the acac and γ-acac ligands are essentially the same as those of the analogous PPh_3 complexes **1a** and **1b**. Differences of the chemical shifts between two acac-CH_3 protons are less in PCy_3 complexes (0.08 ppm in **2a** and 0.10 ppm in **2b**) than in the PPh_3 complexes (0.46 ppm in **1a** and 0.50 ppm[7] in **1b**) indicating a weaker trans effect of PCy_3 as compared with PPh_3. The chemical shift of the γ-acac methine proton is lower by 0.55 ppm in Pt complex, **2a**, than in the corresponding Pd complex, **2b**, as was the case in the PPh_3 complexes, **1a** and **1b**. Unlike the Pt–PPh_3 complex, **1a**, no satellite bands due to ^{195}Pt were observed for the methine proton of γ-acac ligand in the PCy_3 complex **2a**. This may be attributable to a low S/N ratio encountered in the spectrum of **2a**.

The reaction of [$Pt(acac)_2$] with an excess amount of PCy_3 also yielded complex **2a** and the complex

analogous to [Pt($CH_2COCHCOCH_3$)(PPh_3)$_2$] was not obtained.

Some Reactions of the Complexes [M(acac)(γ-acac)PPh$_3$] (M=Pt, 1a and Pd, 1b). In order to get some information on chemical properties of the C-bonded acetylacetonato ligand, several reactions were carried out on complexes **1a** and **1b**. The reaction of **1a** with an excess amount of acetyl or benzoyl chloride afforded the known complex [PtCl(acac)(PPh_3)];[21] the similar reaction has been reported for the Pd analog, **1b**.[7] Methyl iodide reacted with **1a** and **1b** at ambient temperature to give [MI(acac)(PPh_3)] (M=Pt, **3a**; Pd, **3b**) whose characteristic infrared absorptions are included in Table 1. Similarly was obtained [PtBr(acac)(PPh_3)] by the reaction between **1a** and ethyl bromide. A cationic complex of the type [M(acac)(PPh_3)$_2$]$^+BPh_4^-$ (M=Pt, **4a**; Pd, **4b**) was obtained upon treatment of **1a** or **1b** with $NaBPh_4$ in the presence of an equimolar amount of PPh_3 in tetrahydrofuran at room temperature. These reactions accompany formation of sodium salt of acetylacetonate which was isolated and identified by means of its infrared spectrum and elemental analysis.

$$[M(acac)(\gamma\text{-acac})(PPh_3)] + PPh_3 + NaBPh_4 \longrightarrow [M(acac)(PPh_3)_2]^+BPh_4^- + \text{Na-acac}$$

1a (M=Pt), **1b** (M=Pd); **4a** (M=Pt), **4b** (M=Pd)

Absence of bands at 1600—1700 cm^{-1} in the infrared spectra of **4a** and **4b** (Table 1) indicates that the C-bonded acac ligand in **1a** and **1b** is replaced by PPh_3. The ^{1}H-NMR spectrum of **4b** in $CDCl_3$ at room temperature shows a single methyl resonance at δ 1.51 ppm (6H) and the methine resonance at δ 5.41 ppm (singlet, 1H). Complex **4b** was also obtained by a successive reaction of [Pd(acac)$_2$] with 2 molar equivalents of PPh_3 followed by $NaBPh_4$ treatment in refluxing EtOH.

Preparation of Alkyl Complexes from the System of [Pt(acac)$_2$], Alkylaluminium Compounds, and Tertiary Phosphines. A variety of mono- or di-alkyl complexes of Pt(II) or Pd(II) have been prepared by the use of alkyllithium compounds or Grignard reagents.[22,23] However, application of alkylaluminium compounds for such synthesis has been relatively limited. Formation of hydrido complexes has been reported when [M(acac)$_2$] (M=Pd or Pt) was treated with $AlEt_3$ in the presence of $P(C_6H_{11})_3$.[24] A zero-valent ethylene complex, [Pd(C_2H_4)(PR_3)$_2$], and a σ-diethyl complex, [$PdEt_2$($R_2PCH_2CH_2PR_2$)], have been prepared by the reaction of Al(OEt)Et_2 with [Pd(acac)$_2$] in the presence of an appropriate tertiary phosphine.[25] In our attempts to obtain new alkyl complexes of Pt(II) and Pd(II) using alkylaluminium compound as an alkylating agent, we succeeded in the isolation of a series of dialkylpalladium complexes[3] and some alkylplatinum complexes.

The reaction of [Pt(acac)$_2$] with a large excess of diethylmonoethoxyaluminium in the presence of 2 mol of PPh_3 in diethyl ether at room temperature yielded a white solid whose elemental analysis was close to the value for [$PtEt_2$(PPh_3)$_2$], **5a**. The infrared spectrum of the product shows aliphatic C–H stretching bands at 2800—2940 cm^{-1} in a complicated pattern and no bands due to acetylacetonato ligand were observed. There are two relatively strong bands at 460 and 425 cm^{-1} which disappear on thermolysis of the complex. These bands are absent in the spectrum of *cis*-[$PtCl_2$(PPh_3)$_2$]. Hence either one of the two or both bands may be assignable to ν(Pt–C). The ^{1}H-NMR spectrum of **5a** in toluene-d_8 at room temperature showed a complicated multiplet at δ 0.4—1.8 ppm assignable to the ethyl group together with signals at 7—8 ppm due to the phenyl protons. Upon thermolysis *in vacuo* at 160 °C, the complex evolved quantitative amounts of ethylene and ethane in a ratio of 1 : 1. Although a diethyl complex of the type [$PtEt_2L_2$] has been reported for L=PMe_3 and PEt_3,[22] this is the first example of the isolation of the ethylplatinum complex with L=PPh_3.

$$[Pt(acac)_2] + 2PPh_3 \xrightarrow{10\,Al(OEt)Et_2} [PtEt_2(PPh_3)_2]\ \mathbf{5a}$$

$$[Pt(acac)_2] + 2PPh_3 \xrightarrow{2\,Al(OEt)Et_2} [PtEt(\gamma\text{-acac})(PPh_3)_2]\ \mathbf{6a}$$

$$\mathbf{6a} \xrightarrow[-C_2H_6]{\text{recrystallized from THF}} [Pt(CH_2COCHCOCH_3)(PPh_3)_2]$$

When a smaller amount of Al(OEt)Et_2 (2—6 mol per mol of [Pt(acac)$_2$]) was employed, a pale yellow solid of **6a** precipitated. The solid evolved ethylene and ethane (0.5: 1) on thermolysis at 145 °C, the total amount of which was 105% on the basis of the formula, [$PtEt(\gamma$-acac)(PPh_3)$_2$]. Its infrared spectrum shows strong bands at 1670 and 1635 cm^{-1} indicating the acetylacetonato ligand coordinated *via* the central carbon atom. Interestingly, attempted crystallization of this monoethyl complex from tetrahydrofuran at room temperature yielded the afore-mentioned unique acetylacetonato complex, [Pt($CH_2COCHCOCH_3$)(PPh_3)$_2$], as supported by infrared and ^{1}H-NMR spectra and elemental analysis.

In alkylations of nickel(II) acetylacetonate, with alkylaluminium compounds in the presence of appropriate tertiary phosphine ligands, intermediate alkylation products having both acac and alkyl ligands have been isolated.[26,27] Therefore, it is evident that the acac ligands in the starting complexes can be replaced with alkyl ligands in a stepwise manner. In considering the replacement mechanism of the acac ligand by an alkyl group, it is natural to assume that the acac ligand in a unidentate form may be replaced more easily than the chelated acac ligand. We have observed that the methyl groups in acac ligand of [NiEt(acac)(PPh_3)],[17b] [Ni(COEt)(acac)(PPh_3)],[28] and [Pd(acac)(γ-acac)(py)][13] give rise to a singlet ^{1}H-NMR resonance in some solvents and accounted for the results by assuming an exchange process proceeding through partial dissociation of the acac ligand to give an O-bonded unidentate form. Furthermore, we have recently isolated a platinum complex, [Pt(2,4-pentanedionato-*O*)$_2$(PEt_3)$_2$], which possesses two unidentate O-bonded acetylacetonato ligands.[29]

On the basis of these results we propose the processes

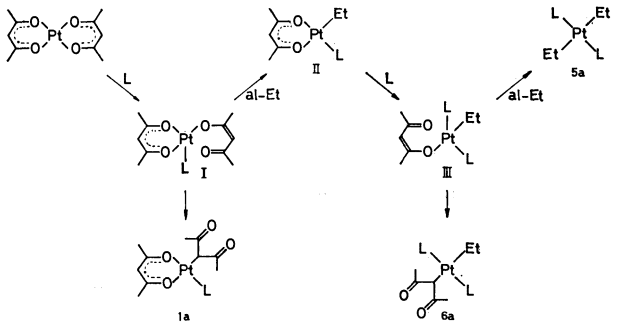

Scheme.
L=PPh_3, al-Et=Al(OEt)Et_2

as represented in the Scheme as the likely alkylation mechanism of [Pt(acac)$_2$] by an alkylaluminium compound. [Pt(acac)$_2$] may be converted to a unidentate O-bonded form I in the presence of a tertiary phosphine ligand. The intermediate I may give the [Pt(acac)(γ-acac)L] type complex **1a** in the absence of an alkylating agent, but the alkylating agent such as diethylmonoethoxyaluminium may replace the unidentate O-bonded acac ligand by the ethyl group to afford II. Although the intermediate II was not isolated in the present case, the corresponding nickel analogs were isolated and fully characterized.[17,26,27,30] The intermediate complex II may further rearrange by attack of another tertiary phosphine ligand to the isolated complex, [PtEt(γ-acac)(PPh_3)$_2$] **6a** by a process as shown in the Scheme.[31] The presence of a larger amount of the alkylating agent gives rise to the dialkylplatinum complex **5a**. In view of the isolation of complexes **1a** and **6a** an alternative line of alkylation processes involving the replacement of the γ-acac ligand by an alkyl group is also conceivable, although such a mechanism seems less straightforward as compared with the one presented in the Scheme.

Experimental

All manipulations were carried out under an atmosphere of deoxygenated nitrogen or argon, or *in vacuo*. Solvents were dried in the usual manner, distilled, and stored under a nitrogen atmosphere.

Infrared spectra were recorded on Hitachi EPI-G3 and 295 spectrometers using KBr pellets prepared under an inert atmosphere. NMR spectra were measured on a JEOL PS-100 spectrometer by Mr. Y. Nakamura of our research laboratory to whom we are indebted. Measurements of ^{1}H-NMR spectra (100 MHz) were carried out in deuteriochloroform at 25 °C unless otherwise stated and ^{1}H chemical shifts are reported with tetramethylsilane as the internal standard. Proton noise decoupled ^{31}P- and ^{13}C-NMR spectra were measured on the same spectrometer operating in the Fourier transform mode at 40.5 (^{31}P) and 25.2 MHz (^{13}C), respectively. Using 10 mm sample tubes, the spectra were taken on deuteriochloroform solutions and were calibrated with triphenylphosphine (in a mixture of C_6D_6 and C_6H_5Cl) as the external reference (for ^{31}P spectra) and with tetramethylsilane as the internal reference (for ^{13}C spectra). Microanalyses were carried out by Mr. T. Saito of our research laboratory.

Bis(2,4-pentanedionato)platinum(II)[32] and -palladium (II),[33] and (2,4-pentanedionato-*C*^{3}) (2,4-pentanedionato-*O*,*O*′)triphenylphosphinepalladium(II)[7] were prepared according to the reported method. Triphenylphosphine was kindly donated by Ihara Chemical Industry Co. Ltd., and used without further purification. Tricyclohexylphosphine was prepared as described in the literature.[34] Commercially available methyl iodide, benzoyl chloride, acetyl chloride, ethyl bromide and sodium tetraphenylborate were used without further purification. Diethylmonoethoxyaluminium was prepared from triethylaluminium and ethanol by the usual method.

Analytical data of new compounds prepared in this report are listed in Table 4.

*Preparation of (2,4-Pentanedionato-*C^3*)(2,4-pentanedionato-O,O′)triphenylphosphineplatinum(II)*, **1a**. On stirring the mixture of [Pt(acac)$_2$] (0.41 g, 1.05 mmol), PPh_3 (0.29 g, 1.09 mmol) and toluene (5 cm^3) at room temperature, the initial pale yellow suspension turned to a pale yellow clear solution in 1 h. The system was stirred for another 1.5 h. Then, the solution was concentrated to 2 cm^3 to leave a yellow oily solution, from which a creamy white precipitate was yielded on digestion with hexane. The precipitate was filtered off, washed with hexane and dried *in vacuo* to give 0.61 g (89%) of crude product. Recrystallization of the creamy white powder from diethyl ether afforded 0.40 g (58%) of [Pt(acac)(γ-acac)PPh_3] as a white microcrystalline solid. The reaction could be carried out similarly in diethyl ether, but in this case much longer reaction period (*ca.* 40 h) was necessary to complete the reaction.

*Preparation of (2,4-Pentanedionato-*C^3*)(2,4-pentanedionato-O,O′)tricyclohexylphosphineplatinum(II)*, **2a**. On stirring the heterogeneous pale yellow mixture of [Pt(acac)$_2$] (0.37 g, 0.95 mmol), tricyclohexylphosphine (0.27 g, 0.95 mmol), and diethyl ether (20 cm^3) at room temperature, the amount of precipitate gradually decreased, and in 21 h of stirring, an almost clear yellow solution resulted. Then, the solvent was

Table 4. Melting points and analytical results of some new acetylacetonato complexes

Complexes		Appearance	Mp, °C[a]	Analysis[b], % C	H
[Pt(acac)(γ-acac)PPh_3]	**1a**	white crystals	148—153	51.3 (51.3)	5.3 (4.5)
[Pt(acac)(γ-acac)PCy_3]	**2a**	creamy white crystals	180—182	48.9 (49.9)	7.1 (7.0)
[Pd(acac)(γ-acac)PCy_3]	**2b**	pale yellow crystals	178—181	56.5 (57.5)	8.6 (8.1)
[PtI(acac)PPh_3]	**3a**	orange-yellow powder[c]	—	—	—
[PdI(acac)PPh_3]	**3b**	orange needles	184—188	47.4 (46.5)	3.9 (3.7)[d]
[Pt(acac)(PPh_3)$_2$]BPh_4	**4a**	white crystals	183—187	68.1 (67.6)	5.6 (5.2)
[Pd(acac)(PPh_3)$_2$]BPh_4	**4b**	yellow crystals	160—164	74.4 (74.4)	5.9 (5.5)

a) Melting points (with decomposition) were measured on a hot stage with a sample in a small capillary sealed under vacuum and are uncorrected. b) Calculated values are in parentheses. c) Not obtained pure. d) I, 20.3% (21.3%).

partially evaporated in the stream of nitrogen with stirring, which caused precipitation of a white powder. The precipitate was filtered off at about −20 °C, washed with diethyl ether at the same temperature and dried *in vacuo* at room temperature to give 0.49 g (76%) of crude product. Recrystallization of a white powder from CH_2Cl_2–hexane at low temperature yielded 0.17 g (26.5%) of pure [Pt(acac)(γ-acac)PCy_3] as a creamy white crystalline solid. The yield of recrystallization was low due to too high solubility of the product in the common organic solvents.

Similarly obtained is its Pd-analog, (2,4-pentanedionato-C^3)-(2,4-pentanedionato-*O*, *O'*) tricyclohexylphosphinepalladium-(II), **2b**, from [Pd(acac)$_2$] (0.38 g, 1.23 mmol) and PCy_3 (0.35 g, 1.25 mmol). The reaction was carried out in benzene (5 cm^3) and completed in 1 h to give, on working up, 0.42 g (58%) of the product as a pale yellow microcrystalline solid.

*Reactions of [Pt(acac)(γ-acac)PPh_3], **1a**. With Benzoyl Chloride*: Complex **1a** (0.21 g, 0.32 mmol) was allowed to react with 2.0 cm^3 (17.1 mmol) of PhCOCl in benzene (2 cm^3) at room temperature for 4 h. The initial clear yellow solution turned to heterogeneous. The amount of the precipitate was increased on addition of hexane to the system. The precipitate was filtered off, washed with hexane and dried *in vacuo*. The yellowish brown powder thus obtained was crystallized from benzene and was identified as [PtCl(acac)PPh_3] on the basis of the infrared spectrum and elemental analysis. Similarly carried out was the reaction of **1a** with neat acetyl chloride to give the same product.

With Methyl Iodide: To the flask containing 0.20 g (0.31 mmol) of complex **1a** was added 5 cm^3 of methyl iodide by means of trap-to-trap method in a vacuum. The yellow solution was stirred at room temperature for 10 days. The unreacted methyl iodide was evaporated off *in vacuo* to leave an orange solid, which was reprecipitated from toluene–hexane. The orange-yellow powder of [PtI(acac)PPh_3], **3a**, thus obtained weighed 0.11 g (58%). The reaction of **1a** with ethyl bromide was similarly carried out to give an orange-yellow powder of [PtBr(acac)PPh_3].

With Sodium Tetraphenylborate: To the yellow solution of complex **1a** (0.46 g, 0.70 mmol) and PPh_3 (0.19 g, 0.70 mmol) in tetrahydrofuran (7 cm^3), 0.24 g (0.70 mmol) of $NaBPh_4$ was added. On stirring the mixture at room temperature for a day, a white fine powder, possibly of sodium acetylacetonate, was yielded. The solvent was evaporated off *in vacuo* to leave an off-white solid, which was washed with ethanol and dried *in vacuo*. The crude white powder thus obtained was recrystallized from THF–EtOH to give white microcrystals of [Pt(acac)$(PPh_3)_2$]$^+BPh_4^-$ **4a** (0.46 g, 58%).

*Reaction of [Pd(acac)(γ-acac)PPh_3], **1b**. With Methyl Iodide*: Into the yellow suspension of **1b** (0.30 g, 0.53 mmol) in toluene (5 cm^3), 0.114 g (0.803 mmol) of methyl iodide was added by means of a microsyringe. The mixture was stirred at room temperature for 6 h to yield a pale red solution. The solvent was evaporated *in vacuo* into almost dryness. The residual orange-yellow solid was washed with hexane and dried *in vacuo*. The crude product, weighed 0.18 g (57%), was crystallized from CH_2Cl_2–hexane to afford orange needles of [PdI(acac)PPh_3], **3b**, (0.07 g, 22%).

With Sodium Tetraphenylborate: Into a clear yellow solution of **1b** (0.22 g, 0.39 mmol) and PPh_3 (0.11 g, 0.39 mmol) in tetrahydrofuran, was added 0.14 g (0.39 mmol) of $NaBPh_4$. On stirring the solution at room temperature the system became turbid in about one minute and a colorless precipitate gradually came out. After being stirred for 1.5 h, the white precipitate was removed by filtration and was identified as sodium 2,4-pentanedionate (0.04 g, 84%) on the basis of infrared spectrum and microanalysis. Found: C, 49.1; H, 6.5%. Calcd for $C_5H_7O_2Na$: C, 49.2; H, 5.8%. From the yellow filtrate, the solvent was evaporated off *in vacuo* to leave a pale yellow mass, which was washed with ethanol and hexane, and dried *in vacuo*. The crude product (0.38 g, 93%) was recrystallized from tetrahydrofuran to give a yellow crystalline solid of [Pd(acac)$(PPh_3)_2$]$^+BPh_4^-$, **4b** (0.22 g, 84%). Compound **4b** was also obtained by the direct reaction of [Pd(acac)$_2$] (0.20 g, 0.65 mmol) and PPh_3 (0.34 g, 1.31 mmol) in the presence of $NaBPh_4$ (0.23 g, 0.67 mmol) in refluxing ethanol (8 cm^3) for 2 h. The crude product of **4b** weighed 0.62 g (90%).

*Preparation of Diethylbis(triphenylphosphine)platinum(II), **5a**.* Into a cooled (−60 °C) mixture of [Pt(acac)$_2$] (1.0 g, 2.6 mmol), PPh_3 (1.35 g, 5.2 mmol) and diethyl ether (40 cm^3), 3.9 cm^3 (26 mmol) of Al(OEt)Et_2 was added by means of a syringe. The temperature of the mixture was allowed to raise gradually and the system was stirred at room temperature for 75 h, to yield a white precipitate with an accompanying evolution of ethane. The precipitate was filtered off, washed with hexane and crystallized from toluene to afford a colorless microcrystalline powder. (0.50 g, 25% based on [Pt(acac)$_2$] used.) (Found: C, 60.4; H, 5.3%. Calcd for $C_{40}H_{40}P_2Pt$: C, 61.8; H, 5.2%). A low stability of the product in solution prevented from obtaining an analytically pure compound.

Thermolysis of 0.1398 g (0.1798 mmol) of the product *in vacuo* at 160 °C evolved 0.360 mmole of gas (as measured with a Toepler pump) which consists of equimolar amounts of ethylene and ethane as analyzed by GLC.

*Preparation of Ethyl(2,4-pentanedionato-C^3)bis(triphenylphosphine)platinum(II), **6a**.* To a mixture of [Pt(acac)$_2$] (1.89 g, 4.80 mmol), PPh_3 (2.52 g, 9.63 mmol) and 50 cm^3 of diethyl ether, Al(OEt)Et_2 (3.76 g, 8.79 mmol) was added at −70 °C. The mixture was stirred at room temperature for 74 h to yield a white precipitate, which was filtered off, washed with hexane and dried *in vacuo*. The pale yellow powder thus obtained had an analytical value close to that for [PtEt(γ-acac)$(PPh_3)_2$] (0.92 g, 23%). (Found: C, 62.0; H, 5.1%. Calcd for $C_{43}H_{42}O_2P_2Pt$: C, 60.9; H, 5.0%). On thermolysis of the product (115.1 mg, 0.1358 mmol) at 145 °C, evolution of ethylene and ethane (0.5: 1), the total amount of which was 0.143 mmol (105%), was observed.

We thank the Kawakami Foundation for support.

References

1) Throughout this paper, abbreviation acac is used to indicate the enol type 2,4-pentanedionato (acetylacetonato) ligand which is coordinated to the central metal in a bidentate fashion through two oxygen atoms, whereas γ-acac represents the 2,4-pentanedionato ligand coordinated to the metal in a unidentate way through the central (γ-) carbon atom.

2) *E. g.*, T. Mole and E. A. Jeffery, "Organoaluminium Compounds," Elsevier, Amsterdam (1972), Chap. 15; A. Yamamoto, and S. Ikeda, *J. Macromol. Sci. Chem.*, **A9**, 931 (1975).

3) T. Ito, H. Tsuchiya, and A. Yamamoto, submitted for publication.

4) B. N. Figgis, J. Lewis, R. F. Long, R. Mason, R. S. Nyholm, P. J. Pauling, and G. B. Robertson, *Nature (London)*, **195**, 1278 (1962); R. Mason, G. B. Robertson, and P. J. Pauling, *J. Chem. Soc., A*, **1969**, 485.

5) J. Lewis, R. F. Long, and C. Oldham, *J. Chem. Soc.*, **1965**, 6740.

6) J. Lewis and C. Oldham, *J. Chem. Soc., A*, **1966**, 1456.

7) S. Baba, T. Ogura, and S. Kawaguchi, *Bull. Chem. Soc. Jpn.*, **47**, 665 (1974).

8) G. T. Behnke and K. Nakamoto, *Inorg. Chem.*, **7**, 330 (1968).
9) J. R. Hall and G. A. Swile, *J. Organomet. Chem.*, **47**, 195 (1973).
10) F. H. Allen and A. Pidcock, *J. Chem. Soc.*, **1968**, 2700.
11) K. B. Dillon, T. C. Waddington, and D. Younger, *J. Chem. Soc. Dalton Trans.*, **1975**, 790.
12) S. O. Grim, R. L. Keiter, and W. McFarlane, *Inorg. Chem.*, **6**, 1133 (1967).
13) T. Ito, T. Kiriyama, Y. Nakamura, and A. Yamamoto, *Bull. Chem. Soc. Jpn.*, **49**, 3257 (1976).
14) J. C. Hammel and J. A. S. Smith, *J. Chem. Soc., A*, **1970**, 1855.
15) T. Ikariya, Y. Nakamura, and A. Yamamoto, *J. Organomet. Chem.*, **118**, 101 (1976).
16) R. Bonnaire and N. Platzer, *J. Organomet. Chem.*, **104**, 107 (1976).
17) (a) F. A. Cotton, B. A. Frenz, and D. L. Hunter, *J. Am. Chem. Soc.*, **96**, 4820 (1974). (b) T. Yamamoto, T. Saruyama, Y. Nakamura, and A. Yamamoto, *Bull. Chem. Soc. Jpn.*, **49**, 589 (1976).
18) A. J. Cheney, B. E. Mann, and B. L. Shaw, *Chem. Commun.*, **1971**, 431.
19) M. H. Chisholm, H. C. Clark, E. Manzer, J. B. Stothers, and J. E. H. Ward, *J. Am. Chem. Soc.*, **95**, 8574 (1973).
20) O. A. Gansow and B. Y. Kimura, *Chem. Commun.*, **1970**, 1621.
21) G. Hulley, B. F. G. Johnson, and J. Lewis, *J. Chem. Soc., A*, **1970**, 1732.
22) J. Chatt and B. L. Shaw, *J. Chem. Soc.*, **1959**, 705; 4020.
23) G. Calvin and G. E. Coates, *J. Chem. Soc.*, **1960**, 2008.
24) K. Kudo, M. Hidai, and Y. Uchida, *J. Organomet. Chem.*, **56**, 413 (1973).
25) R. van der Linde and R. O. de Jongh, *Chem. Commun.*, **1971**, 563.
26) P. W. Jolly, K. Jonas, C. Krüger, and Y. -H. Tsay, *J. Organomet. Chem.*, **33**, 109 (1971).
27) A. Yamamoto, T. Yamamoto, T. Saruyama, and Y. Nakamura, *J. Am. Chem. Soc.*, **95**, 4073 (1973).
28) T. Saruyama, T. Yamamoto, and A. Yamamoto, *Bull. Chem. Soc. Jpn.*, **49**, 546 (1976).
29) T. Ito, T. Kiriyama, and A. Yamamoto, *Chem. Lett.*, **1976**, 835.
30) K. Maruyama, T. Ito, and A. Yamamoto, *J. Organomet. Chem.*, **90**, C28 (1975).
31) Although the configurations of complexes **5a** and **6a** have not been established, only trans structures are illustrated in the Scheme for clarity.
32) A. Werner, *Ber.*, **34**, 2584 (1901).
33) A. A. Grinberg and L. K. Simonova, *Zhur. Priklad. Khim. (Leningrad)*, **26**, 880 (1953); *Chem. Abstr.*, **47**, 11060g (1953).
34) K. Issleib and A. Brack, *Z. Anorg. Chem.*, **227**, 258 (1954).

Studies on the Reacions of Bis(acetylacetonato)platinum(II) with Lewis Bases. II. Reaction with Pyridine Leading to Complexes Containing Uni- and Bis-Carbon Bonded Acetylacetonato Ligand(s).

Takashi Ito, Takashi Kiriyama, Yoshiyuki Nakamura, and Akio Yamamoto

Research Laboratory of Resources Utilization, Tokyo Institute of Technology, Ookayama, Meguro-ku, Tokyo 152

(Received June 23, 1976)

Heating a pyridine solution of [Pt(acac)$_2$] (acac=2,4-pentanedionato-*O,O'*) at 100 °C afforded central C-bonded complexes, [Pt(acac)(γ-acac)py], **1**, and [Pt(γ-acac)$_2$py$_2$], **2** (γ-acac=2,4-pentanedionato-*C*^{3}). Complexes **1** and **2** were isolated and characterized by means of elemental analysis, infrared and ^{1}H- and ^{13}C-NMR spectroscopy. Heating **1** in pyridine yielded **2**, and conversely, heating **2** in $CDCl_3$ yielded **1**. All these reactions were monitored by ^{1}H-NMR spectroscopy and were found to obey the first-order rate law. From the rate constants at various temperatures, activation parameters were calculated for each reaction. Existence of isokinetic relationship among these three reactions suggests the presence of a common reaction intermediate. Observation of the variable temperature ^{1}H-NMR spectra of [Pd(acac)(γ-acac)py] in pyridine suggests that the activated intermediate may be a species having an oxygen-bonded unidentate acac ligand ("dangling" enolate ligand).

Participation of a central(γ-) carbon atom in an acetylacetonato ligand in coordination to the metal was disclosed for the first time by Hazell *et al.* in 1959 for a dimeric β-diketonato complex of platinum(IV).[1] Soon after, Mason *et al.*[2] reported that Werner's K[Pt(acac)$_2$Cl][3,4] was in fact K[Pt(acac)(γ-acac)Cl][4] in which one of two acetylacetonato ligands is coordinated to Pt(II) *via* the central(γ-) carbon atom. Since then several kinds of γ-acac complexes of platinum(II) have been reported including $Na_2[Pt(\gamma\text{-acac})_2X_2]$ (X= halogen),[5] K[Pt(acac)(γ-acac)$_2$],[5] and [(acac)ClPt(γ-acac)M(II)(γ-acac)PtCl(acac)] where M(II) stands for a divalent metal ion,[6,7] as well as those of Pt(IV) such as [Pt(CH$_3$)$_3$(γ-acac)(L-L)] where L-L is 2,2'-bipyridine (bpy),[8,9] and 1,10-phenanthroline (phen).[9] However, non-ionic Pt(II) complex with a carbon-bonded acetylacetonato ligand has not been known except for poorly soluble [Pt(γ-acac)X(L-L)] where L-L is a bidentate ligand such as bpy, phen, ethylenediamine (en) and 1,2-bis(diphenylphosphino)ethane (dpe).[10] In a preceding paper, we described the isolation and characterization of new, non-ionic γ-acac complexes of the type [Pt(acac)(γ-acac)L] (L=PPh_3 and $P(C_6H_{11})_3$), which are formed by the reaction of bis(acetylacetonato)platinum with an equimolar amount of the tertiary phosphine.[11] The reaction of [Pt(acac)$_2$] with an excess of pyridine, on the other hand, yielded the complex in which both acetylacetonato ligands are coordinated to platinum *via* central carbon atoms, *i.e.*, [Pt(γ-acac)$_2$(py)$_2$)], **2**, together with a mono-γ-acac complex, [Pt(acac)(γ-acac)(py)], **1**, which exist as an equilibrium mixture. There is no precedent of the observation of a direct rearrangement of the acetylacetonato ligand coordinated to platinum metal from the bidentate enol type mode of coordination (acac) to the diketo type (γ-acac), although such a rearrangement has been reported for mercury(II)[12,13] and palladium(II).[14] The present report describes isolation and characterization of γ-acac complexes **1** and **2** and some results of mechanistic study on their rearrangement reaction observed by means of the ^{1}H-NMR spectroscopy.

Results and Discussion

Reaction of Bis(acetylacetonato)platinum with Pyridine. When [Pt(acac)$_2$] was heated at 100 °C in pyridine (py), a homogeneous brown solution resulted, from which colorless prisms were produced on allowing it to stand still at room temperature. The prisms were characterized as bis(2,4-pentanedionato-*C*^{3})bispyridineplatinum(II), [Pt(γ-acac)$_2$(py)$_2$], **2**, on the basis of microanalysis, and infrared and NMR spectral results. Although a steric configuration of **2** is uncertain, the fact that 2,2'-bipyridine does not react with [Pt(acac)$_2$] is in favor of the *trans*-configuration as is shown in the following equation.

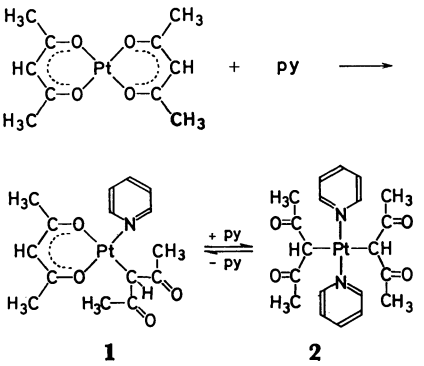

1 **2**

From the solution part of the reaction mixture, an off-white crystalline powder of (2,4-pentanedionato-*C*^{3})-(2,4-pentanedionato-*O,O'*)pyridineplatinum(II), [Pt(acac)(γ-acac)py], **1**, was precipitated on addition of hexane. If the solution is heated again at 100 °C after removal of the prisms, instead of precipitating out **1**, a further crop of prisms of **2** was obtained. Thus, repetition of these procedures for 5 times or more makes the total yield of **2** to be almost quantitative. This fact indicates that complexes **1** and **2** exist in equilibrium in a pyridine solution in agreement with the result obtained by a ^{1}H-NMR spectral study (*vide infra*).

The complexes analogous to **1**, but having tertiary phosphines with a formula of [Pt(acac)(γ-acac)L] (L=

Table 1. Melting points, micro analyses, and infrared spectral data for complexes **1** and **2**

Complex		Mp[a] (°C)	Analysis[b] (%) C	H	N	IR Absorptions (cm^{-1}) γ-acac bands	acac bands
[Pt(acac)(γ-acac)py]	**1**	162—164	37.8	3.92	3.01	1700s	1565s, 1545sh
			(38.1)	(4.05)	(2.97)	1655m	1525s
[Pt(γ-acac)$_2$(py)$_2$]	**2**	174—165	43.6	4.26	5.07	1650vs	
			(43.6)	(4.39)	(5.08)	1610s	

a) Melting points (with decomposition) were measured on a hot stage with a sample in a small capillary sealed under vacuum and are uncorrected. b) Calculated values are in parentheses.

PPh_3 and $P(C_6H_{11})_3$) have been obtained by the reaction of [Pt(acac)$_2$] with an equimolar amount of the corresponding tertiary phosphine.[11] It is interesting to note, however, that the reaction with an excess amount of triphenylphosphine at an elevated temperature resulted in the formation of another type of platinum(II) complex of a composition [Pt($CH_2COCHCOCH_3$)(PPh_3)$_2$],[11] instead of yielding the bis-γ-acac complex analogous to **2**. Complex **2** is the first example of a neutral Pt(II) complex in which two acetylacetonato ligands are coordinated to the metal *via* central (γ-) carbon atoms. The reaction of bis(acetylacetonato)-palladium with pyridine is known to afford only the complex analogous to **1**, *i.e.*, [Pd(acac)(γ-acac)py].[14] The formation of the palladium complex similar to **2**, [Pd(1-ethoxy-1,3-dioxobut-2-yl)$_2$L$_2$] was reported quite recently, where L stands for a substituted or unsubstituted p ridine.[15]

Infrared and ^1H- and ^{13}C-NMR Spectra of the Complexes. In Table 1, characteristic infrared absorptions due to the acetylacetonato ligands in complexes **1** and **2** are listed together with melting points and analytical data. A pattern of the spectrum of complex **1** in the region of 1500—1700 cm^{-1} is very similar to those reported for [Pt(acac)(γ-acac)PPh_3][11] and K[PtCl(acac)(γ-acac)].[16] In addition to bands listed in Table 1, there is an extra band in the spectrum of complex **1** at 1615 cm^{-1} which is assignable to the coordinated pyridine moiety. Two bands due to the γ-acac ligand in **1** appeared at a higher wave number by 15—20 cm^{-1} than in palladium analog of **1**, [Pd(acac)(γ-acac)py].[14] Absence of a band in the region of 1500—1600 cm^{-1} in complex **2** strongly suggests that it has no O-bonded chelate acac ligand. Two bands at 1650 and 1610 cm^{-1} can be assigned to ν(C=O) of the carbon bonded γ-acac ligand by comparing them with the reported values of 1652 and 1626 cm^{-1} for $Na_2[PtCl_2(\gamma\text{-acac})_2]$.[16] These lines of infrared spectral evidence are in accord with the bis(γ-acac) type of structure proposed for **2**.

The ^{1}H-NMR parametrs of complexes **1** and **2** are listed in Table 2. Assignments of their signals have been made simply by comparing them with those reported for the similar complexes.[5,9,11,14] Two methyl groups in the chelated enol acac ligand in **1** appear as non-equivalent signals owing to difference in the influence of the ligands *trans* to the chelate oxygen, as is the case reported for [MX(acac)L] (M=Pt[10] and Pd[14]) and [M(acac)(γ-acac)L] (M=Pd[14] and Pt[11]). According to the assignment made by Baba *et al.* for [Pd(acac)(γ-acac)-L] (L=PPh_3, py, and *N*-methylbenzylamine),[14] the signal at higher field (δ=1.87 ppm) is tentatively assigned to the methyl group *cis* to the pyridine ligand. The methine proton of the γ-acac ligand in complex **1** resonates at a lower field than that in [Pt(acac)(γ-acac)-

Table 2. The ^{1}H-NMR data for [Pt(acac)(γ-acac)py], **1**, and [Pt(γ-acac)$_2$(py)$_2$], **2**[a]

Complexes	Assignments		δ ppm	Multiplicity[d]	Relative intensity[b]	J Hz
1	acac	$-CH_3$	1.87	s	2.8(3)	
		$-CH_3$	1.96	s	2.6(3)	
		>CH	5.50	s	1.0(1)	
	γ-acac	$-CH_3$	2.24	ss	5.5(6)	$\lvert^4J(\text{Pt-H})\rvert$=9
		>CH	5.05	ss	1.0(1)	$\lvert^2J(\text{Pt-H})\rvert$=129
	py	α-H	8.70	ds[e]	2.1(2)	$\lvert^3J(\text{Pt-H})\rvert$=43
		β-H	7.35	t[e]	2.9(2)[c]	
		γ-H	7.80	t[e]	1.1(1)	
2	γ-acac	$-CH_3$	1.87	ss	6.1(6)	$\lvert^4J(\text{Pt-H})\rvert$=11
		>CH	4.29	ss	1.0(1)	$\lvert^2J(\text{Pt-H})\rvert$=102
	py	α-H	8.45	ds[e]	2.0(2)	$\lvert^3J(\text{Pt-H})\rvert$=39
		β-H	7.44	t[e]	2.1(2)[c]	
		γ-H	7.80	t[e]	1.1(1)	

a) 100 MHz. in $CDCl_3$ at room temperature, tetramethylsilane as an internal standard. b) Required values in parentheses. c) Signals due to solvent impurities are overlapping. d) Muliplicity abbreviations: s, singlet; ss, singlet with satellites due to ^{195}Pt; ds, doubelt with satellites due to ^{195}Pt, t, triplet. e) $\lvert^3J(\text{H—H})\rvert \approx 6$ Hz.

Table 3. ^{13}C-NMR spectral data of [Pt(acac)(γ-acac)py], **1**, and [Pt(γ-acac)$_2$(py)$_2$], **2**[a]

Assignment[b]			[Pt(acac)(γ-acac)py], **1**			[Pt(γ-acac)$_2$(py)$_2$], **2**		
			δ / ppm	Multiplicity[c]	J / Hz	δ / ppm	Multiplicity[c]	J / Hz
acac	CH_3	*1*	27.1	s				
	CH_3	*1′*	27.2	s				
	C=O	*2*	183.8	s				
	C=O	*2′*	184.8	s				
	H–C	*3*	102.0	ss	$\|^3J(\text{Pt–C})\|=68$			
γ-acac	CH_3	*4*	30.7	s		30.5	s	
	>C=O	*5*	207.9	ss	$\|^2J(\text{Pt–C})\|=65$	203.1	ss	$\|^2J(\text{Pt–C})\|=49$
	–C–H	*6*	41.7	ss	$\|^1J(\text{Pt–C})\|=619$	60.3	ss	$\|^1J(\text{Pt–C})\|=369$
py	α-C	*7*	153.6	s		153.0	s	
	β-C	*8*	125.5	ss	$\|^3J(\text{Pt–C})\|=49$	126.0	ss	$\|^3J(\text{Pt–C})\|=49$
	γ-C	*9*	137.6	ss	$\|^4J(\text{Pt–C})\|=14$	138.0	s	

a) In $CDCl_3$ at room temperature, 25.1 MHz. Tetramethylsilane as an internal standard.
b) Numbering for the carbon atoms is as follows:

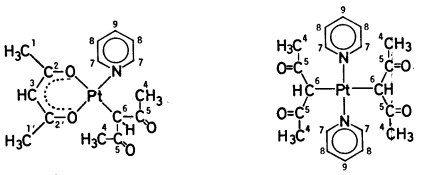

c) Multiplicity abbreviations: s, singlet; ss, singlet with satellite bands due to ^{195}Pt.

PPh_3] (4.04 ppm[11]) by *ca.* 1 ppm whereas that in **2** resonates at the similar field. These methine protons accompanied satellite bands due to ^{195}Pt with a larger coupling constant for **1** than for **2**. Although no data are available for the ^{195}Pt–H coupling constant of the methine proton of the mutually *trans* bis(γ-acac) ligands, the $|^2J(^{195}\text{Pt–H})|$ values for **1** and **2** listed in Table 2 are similar to those reported for K[Pt(acac)(γ-acac)Cl] (120 Hz) and K[Pt(acac)(γ-acac)$_2$] (123 Hz).[5] Assignments of the signals due to the pyridine ligand(s) were achieved by examination of their relative intensities and multiplicities. A doublet assignable to the α-proton in the coordinated pyridine accompanied satellite bands due to a coupling with ^{195}Pt.

The structures of complexes **1** and **2** are further supported by their ^{13}C-NMR spectra which are summarized in Table 3. The spectrum of complex **1** is similar to that of the analogous complex [Pt(acac)-(γ-acac)PPh_3].[11] Absence of the phosphorus nucleus in **1** made the spectrum more simplified than the PPh_3 analog. Assignment of each signal was further confirmed by recording a half decoupled spectrum,[17] in which the signals assigned to C^3, C^6, C^7, C^8, and C^9 split into doublets while those to C^2, $C^{2'}$, and C^5 remained as singlets. (As for the numbering of the carbon atoms, refer to the foot note of Table 3). A singlet signal due to C^4 split into a quartet on half decoupling and those of C^1 and $C^{1'}$ changed to a complex pattern which is consisted of basically 8 lines. The $|^1J(^{195}\text{Pt–}^{13}\text{C})|$ value of 619 Hz for the methine carbon of the γ-acac ligand in complex **1** is similar to the reported values for *cis*-[Pt(CH_3)$_2$L$_2$] (594 Hz for L=PMe_2Ph,[18] 689 Hz for L=$AsMe_3$,[19] and 685 Hz for L=$AsMe_2Ph$.[18] On the other hand, an exceptionally small $|^1J(^{195}\text{Pt–}^{13}\text{C})|$ value (369 Hz) was observed for complex **2**. Such a small ^{195}Pt–^{13}C coupling constant has been reported only for the methyl carbon attached to platinum atom at a *trans* position with respect to the carbene ligand, *i.e.*, *trans*-[Pt(CH_3)(cb)($AsMe_3$)$_2$][PF_6], where cb stands for carbene ligands (385 Hz for cb=:CMe(NMe_2), 381 Hz for cb=:CMe(NHMe), 380 Hz for cb=:CMe(NH_2), and 360 Hz for cb=:CMe(OMe)).[19,20] This decrease in $|^1J(\text{Pt–C})|$ value when going from **1** to **2** parallels a decrease in $|^2J(\text{Pt–H})|$ value suggesting a stronger Pt–C bond in complex **1** than in **2**. Interestingly, the slope of the line connecting two points plotted for $|^1J(\text{Pt–C})|$ *vs* $|^2J(\text{Pt–H})|$ coincided fairly well with those reported for serieses of platinum–methyl complexes.[20,21] The keto-carbon (C^5) in the γ-acac ligand in **1** and **2** showed ^{195}Pt-satellite bands with $|^2J(\text{Pt–C}^5)|=65$ and 49 Hz, respectively. Although there are no available data on the ^{13}C-NMR spectral parameters for this type of ligand, these values are within the range of values reported for $|^2J(\text{Pt–C})|$, *e.g.*, 50 and 86 Hz have been reported for $|^2J(\text{Pt–As–C})|$ and $|^2J(\text{Pt–C–C})|$, respectively, in the carbene complex, *trans*-[PtMe{C(OMe)-Me}($AsMe_3$)$_2$][PF_6].[20,21] Furthermore, ^{195}Pt-satellite bands are observed for the methine carbon (C^3) of acac ligand with $|^3J(\text{Pt–C}^3)|=68$ Hz, which is larger than $|^2J(\text{Pt–C}^5)|$. This effect may reflect the conjugate character of the chelate acac ligand. Intensities of unequivalent C^2 and $C^{2'}$ signals were reduced considerably as compared with that of the C^3 signal due to the absence of NOE effect (C^3 being tertiary carbon), hence a discernment of its satellite bands from the noise signals might have become impossible. Among three signals due to the pyridine ligand, the signal with the smallest intensity at *ca.* 138 ppm was assigned to the

γ-carbon. Assignments of the other two signals were made by comparing their chemical shifts with those of free pyridine (149.6, 123.5 and 135.6 ppm for α, β, and γ-carbons, respectively in $CDCl_3$).[22] It should be noticed that the α-carbon signal does not accompany satellite bands due to ^{195}Pt in spite of the presence of the distinct satellite bands for β- (in **1** and **2**) and γ- (in **1**) carbon atoms. This fact may be correlated to the reported data on the phenylplatinum complex, *cis*-$[PtPh_2(PEt_3)_2]$, where the ^{195}Pt–C coupling constant due to the phenyl *ortho* carbon is less than that for *meta* carbon (36 and 64 Hz, respectively).[21] A poor resolution of the spectrum of **2** prevented the accurate measurement of the coupling constant for the γ-carbon satellite bands.

Kinetic Study on the Formation of 1 and 2. Kinetic studies on the formation of **1** and **2** and their interconversions were achieved by following the ^1H-NMR spectral change in either pyridine or chloroform at various temperatures.

The ^1H-NMR spectrum of $[Pt(acac)_2]$ in pyridine at 60 °C consists of a single methyl resonance at 1.79 ppm and a methine resonance at 5.48 ppm. (Fig. 1A). On keeping the sample at this temperature, several new signals which are assignable to the protons of γ-acac ligand(s) in **1** and **2** appeared at the expense of the initial two singlets and they grew gradually with time. Figure 1B illustrates the spectrum of the system taken after 9 h at 60 °C. Assignments of the signals were confirmed by comparing them with the spectra of the isolated complexes **1** and **2**. The rate of conversion of $[Pt(acac)_2]$ into **1** (reaction (i) in Eq. 2) obeyed the first-order rate law with respect to $[Pt(acac)_2]$. The first-order rate constants (k_1) thus obtained for reaction (i) at various temperatures are listed in Table 4. Similarly were obtained the first-order rate relationship for reactions (ii) and (iii) in Eq. 2. For reaction (ii) the

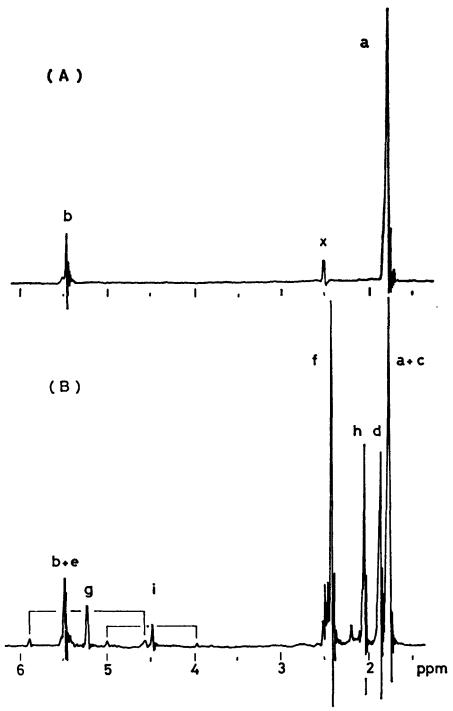

Fig. 1. Change of the ^1H-NMR spectrum (methyl and methine proton region) of $[Pt(acac)_2]$ in pyridine at 60 °C. (A) Initial spectrum. (B) After 9 h.

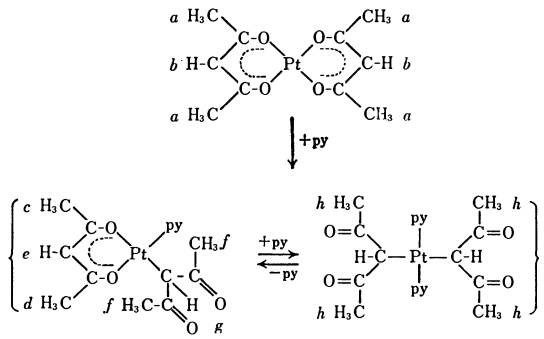

The signal **x** is assignable to γ-picoline present in the solvent as an impurity.

Table 4. First-order rate constants for the reactions (i), (ii), and (iii) (Eq. 2)

Temp. (°C)	40	50	60	70	80	90	100
$k_1\times10^5/s^{-1}$	—	—	4.55	13.2	28.7	54.4	118
$k_2\times10^5/s^{-1}$	—	1.36	2.94	6.23	12.1	—	—
$k_3\times10^5/s^{-1}$	0.410	—	5.10	17.1	53.7	—	—

$$[Pt(acac)_2] + py \xrightarrow[(i)]{k_1}$$

$$\{[Pt(acac)(\gamma\text{-acac})py \underset{-py,\ k_3(iii)\ \text{in}\ CDCl_3}{\overset{+py,\ k_2(ii)}{\rightleftharpoons}} [Pt(\gamma\text{-acac})_2py_2]\} \quad (2)$$

isolated complex **1** was dissolved in pyridine and the rate of growth of the methyl signal in the γ-acac ligand of **2** in pyridine was monitored (Fig. 2) and the first-order rate constants, k_2, thus obtained are listed in Table 4. The reverse reaction (iii) was followed by observing the spectral change of **2** in $CDCl_3$, where signals due to **1** appeared and grew gradually with time as is

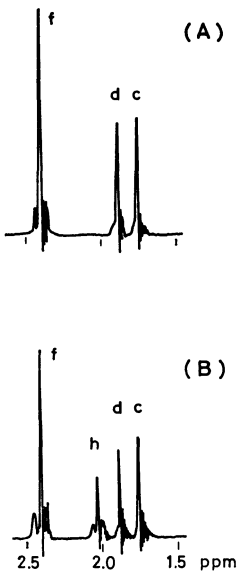

Fig. 2. Change of the ^1H-NMR spectrum (methyl proton region) of $[Pt(acac)(\gamma\text{-acac})py]$ in pyridine-d_5 at 50 °C. (A) Initial spectrum. (B) After 4 h. Proton notations are as shown in Fig. 1.

Table 5. Activation parameters for the reactions (i)—(iii) (Eq. 2) and (iv) (Eq. 3)

Reaction	E_a / kcal mol^{-1}	log A	ΔH^* / kcal mol^{-1}	ΔS^* / cal K^{-1} mol^{-1}	ΔG^* (60 °C) / kcal mol^{-1}
(i)	20.9±0.1	9.34±0.07	19.3±0.1	−20.7±0.2	26.2±0.2
(ii)	16.3±0.0	6.17±0.01	15.6±0.0	−32.7±0.1	26.5±0.1
(iii)	26.6±0.0	13.2±0.0	26.0±0.0	−0.36±0.10	26.1±0.1
(iv)	6.16±0.07	5.67±0.05	5.82±0.06	−33.7±0.2	16.2±0.1[a]

a) ΔG^* at 35° C.

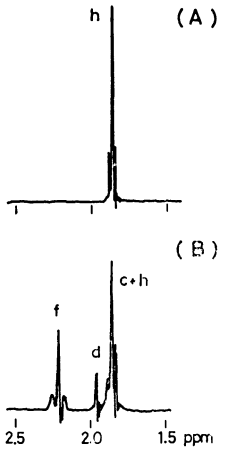

Fig. 3. Change of the ^{1}H-NMR spectrum (methyl region) of [Pt(γ-acac)$_2$py$_2$] in $CDCl_3$ at 60 °C. (A) Initial spectrum. (B) After 4.5 h. Proton notations are as shown in Fig. 1.

illustrated in Fig. 3. Deuteriochloroform was used as a reaction solvent in reaction (iii) because of a poor solubility of **2** in pyridine. The first-order rate law was again observed and the rate constants, k_3, obtained at various temperatures, are also included in Table 4. Arrhenius activation energies, E_a, and frequency factors, A, for reactions (i), (ii), and (iii) were obtained from the slopes and intercepts, respectively, of the least-square straight lines of log k *vs.* $1/T$ plots. Activation enthalpies, ΔH^*, and activation entropies, ΔS^*, were obtained similarly from the least-square treatment for the Eyring plots of log k/T *vs.* $1/T$. The free energy of activation, ΔG^*, was calculated from the equation $\Delta G^* = \Delta H^* - T\Delta S^*$. The activation parameters are liested in Table 5.

In spite of numerous studies concerning the configurational rearrangement of octahedral enolate acetylacetonato complexes of transition and non-transition metals,[23-27] scarcely has been reported the mechanistic study of the ligand exchange in the square planar acetylacetonato complex.[28] This may be ascribed to the slow rate of exchange in the latter compared to the six-coordinate complex, which renders the study of dynamic behavior of these complexes by NMR measurement inapplicable. Furthermore, little has been studied on the rearrangement of acetylacetonato complex between a chelated enol form and a central carbon bonded diketo form. Fish has made an NMR study on the dynamic behavior of bis(1,1,1,2,2,3,3-heptafluoro-7,7-dimethyl-4,6-dioxooctan-5-yl)mercury in acetone-d_6, in which the following exchange has been observed.[13] The Arrhenius activation energy, E_a, and the free

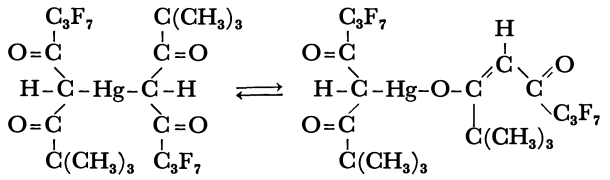

energy of activation, ΔG^*, for this process were estimated as 9.90 and 10.35 (at 25 °C) kcal/mol*, respectively, which are much lower than the values of, respectively, 16—27 and *ca.* 26 kcal/mol for the present system, indicating a less labile character of the acac ligand in the present platinum complexes in the keto-enol exchange as compared to the mercury complex in agreement with the prediction by Fish.[13]

Observation that the reactions (i), (ii), and (iii) obey the first-order rate law suggests that these reactions proceed *via* unimolecular processes with respect to the complexes involved. Furthermore, observation of constant ΔG^* values for the three reactions, despite the considerable variance of ΔH^* and ΔS^* values, suggests the presence of an isokinetic relationship. Figure 4 demonstrates the presence of the compensation effect between ΔH^* and ΔS^* values in the three reactions. In a strict sense, comparison of the reactions (i) and (ii) with reaction (iii) may not be quite adequate because of the difference in the solvent employed. (Employment of $CDCl_3$ in reactions (i) and (ii) was not feasible because of occurence of unexpected, not fully studied reaction

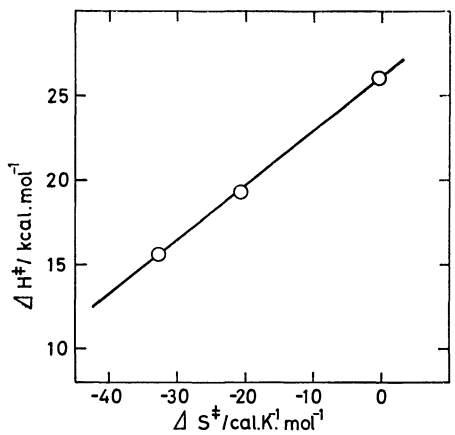

Fig. 4. Isokinetic relationship for the reactions, [Pt(acac)$_2$] $\xrightarrow{py}$ [Pt(acac)(γ-acac)py] $\underset{-py}{\overset{py}{\rightleftharpoons}}$ [Pt(γ-acac)$_2$(py)$_2$].

* Throughout this paper 1 cal=4.184 J.

between $CDCl_3$ and pyridine in the presence of the platinum complex.) However, the results suggest that, in spite of the difference in solvents, the three reactions proceed through a similar activated species in the rearrangement reactions from the acac form to the γ-acac form and *vice versa*. The isokinetic temperature, the temperature at which the rates of three processes become equal, was estimated as 323 K (50 °C).

In contrast to the platinum complex, the reaction of bis(acetylacetonato)palladium with pyridine has been reported to give only [Pd(acac)(γ-acac)py] even under rigorous conditions.[14] No bis(γ-acac) complex of palladium, analogous to **2**, has been isolated. The variable temperature ^{1}H-NMR measument of [Pd(acac)(γ-acac)py], **3**, in pyridine, however, revealed the presence of equilibria as follows:

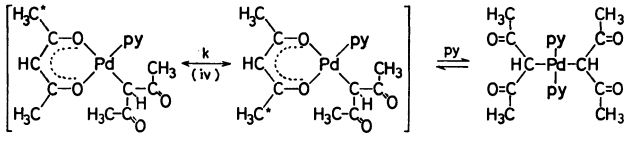

A **3** B **4** (3)

Two singlets at 2.08 and 1.94 ppm at −20 °C due to the two methyl groups of the chelated acetylacetonato ligand in **3** broaden on raising the temperature and coalesce at 46 °C. Above the temperature, the coalesced singlet signal sharpens with temperature increase. This spectra change may be interpreted by assuming the acceleration of the exchange rate between species A and B on raising the temperature (Eq. 3). In Fig. 5, the relevant spectra in the temperature range of 20—46 °C are reproduced, together with the one at −20 °C. The rate constants k, for the exchange were calculated from the separation of two singlets as are recorded in Figure 5. An Arrhenius plot of these k values leads to activation parameters which are included in Table 5. A very small peak is observed at 1.99 ppm at −20 °C and it grows gradually on raising the temperature (Figure 5). This may be due to the methyl protons of bis(γ-acac) type complex **4**, which is in equilibrium with **3** (Eq. 3). All attempts to isolate **4** from the equilibrium mixture were unsuccessful.

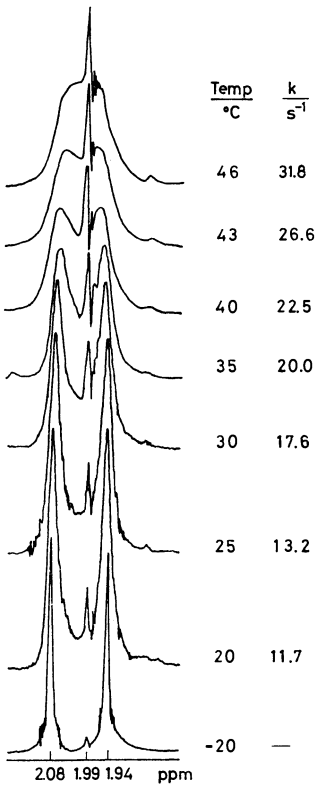

Fig. 5. Temperature dependence of the ^{1}H-NMR spectra (methyl proton region) of [Pd(acac)(γ-acac)py] in pyridine-d_5.

Saito and Takahashi have reported the Arrhenius activation energy E_a of 23 kcal/mol for the palladium–oxygen bond rupture in the exchange reaction of $[Pd(acac)_2]$ and ^{14}C-labelled acetylacetone in anisole.[28] Much smaller value (6.2 kcal/mol) obtained in the present study implies that the presence of a large excess of pyridine may facilitate the palladium–oxygen bond rupture. The presence of large negative $\Delta S^{\ddagger}$ values for the forward (bidentate enol→unidentate diketo) transformations and a very small $\Delta S^{\ddagger}$ value for the reverse process with regards to platinum complexes also may be taken as an indication of the solvent participation in the forward processes. The mechanism of the interchange may involve the solvent assisted partial M–O bond rupture as shown below, rotation of the unidentate acac around the M–O bond and recoordination *via* the carbonyl group to the metal.

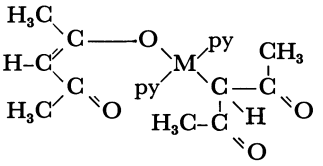

M=Pd, Pt

The similar value of E_a, *ca.* 10 kcal/mol, has been reported for the exchange of a bidentate enol acac ligand in [NiEt(acac)PPh_3][29] and in the various six-coordinate acac complexes.[23,24]

In a separate reaction of $[Pt(acac)_2]$ with triethylphosphine we have isolated another type of a complex, bis(2,4-pentanedionato-*O*)bis(triethylphosphine)platinum(II) containing two unidentate acac ligands, which are singly bonded to platinum through enol oxygen atoms.[30]

In view of these results it is tempting to speculate on the rearrangement mechanisms of the acac ligand. In the forward reaction starting from the bidentate enol type complex to the γ-acac type complex three reaction pathways are conceivable. A bimolecular mechanism involving the direct transfer of the chelate acac ligand to another platinum complex is unlikely on the basis of the observed first-order rate law. The second mechanism where a unimolecular "flipping" of the bidentate enol ligand to the γ-acac ligand takes place seems less likely than the third mechanism which involves the partial dissociation of the bidentate enol ligand to a singly bonded form with participation of the solvent. The further process might involve an oxoallyl intermediate through which a new M–C bond is formed as shown below in the following scheme:

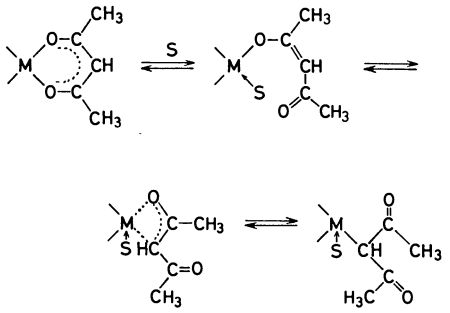

(S=solvent molecule)

The reverse process starting from the γ-diketo form leading to the enol chelate could be accounted for by assuming common intermediates presented above.

Although the evidence supporting this mechanism is circumstantial at best, it is compatible with various features of the rearrangement reaction.

Formation of a γ-acac type complex also may have implications related to the polymerization activities of various transition metal acetylacetonates for some vinyl monomers.[31,32] A typical initiator [Mn(acac)$_3$] can be reduced to [Mn(acac)$_2$] in the presence of a vinyl monomer which is polymerized by a radical $CH_3CO\dot{C}HCOCH_3$[31-33] liberated by homolytic splitting of Mn–C bond from a possible intermediate complex such as [Mn(acac)$_2$(γ-acac)·S]. In fact, the reduction of [Mn(acac)$_3$] in the presence of 1,10-phenanthroline gave a phen-complex [Mn(acac)$_2$(phen)].[33,34] Another implication of the partial dissociation of the enol chelate concerning the alkylation mechanism of transition metal acetylacetonates has been discussed in the previous paper.[11]

Experimental

Procedures, materials, and instruments used are as reported in a preceding paper.[11] Guaranteed grade pyridine was used for the reaction without further purification.

Reaction of Bis(acetylacetonato)platinum(II) with Pyridine. The pale yellow suspension of [Pt(acac)$_2$] (0.60 g, 1.53 mmol) in pyridine (3.4 cm^3) was heated at 100—110 °C under nitrogen for 1 h resulting in a brown solution. After cooling, 20 cm^3 of hexane was added to the solution to yield a creamy white precipitate, which was filtered off, washed with hexane and dried *in vacuo*. The crude product (0.54 g) thus obtained is a mixture of [Pt(acac)(γ-acac)py], **1**, and [Pt(γ-acac)$_2$(py)$_2$], **2**, which can be separated from each other by extraction with diethyl ether (20 cm^3×5). The extract was concentrated to *ca.* 10 cm^3 *in vacuo*. To the concentrated solution was added hexane (20 cm^3) to give a creamy white precipitate which was filtered off, washed with hexane and dried *in vacuo*. The off-white powder thus obtained (0.34 g, 40%) was identified as [Pt(acac)(γ-acac)py], **1**, on the basis of infrared and NMR spectroscopy (see text). The product thus obtained is analytically pure, but can be recrystallized from toluene.

The white residue of extraction was found to be analytically pure [Pt(γ-acac)$_2$(py)$_2$], **2** (0.12 g, 17%). The results of micro analysis for complexes **1** and **2** are listed in Table 1.

In order to obtain **2** in a much higher yield, the following procedure is recommendable. The yellow solution of [Pt(acac)$_2$] (0.90 g, 2.29 mmol) in pyridine (10 cm^3) was heated at 100—110 °C under nitrogen for 6 h. The system was cooled down to room temperature and kept at the temperature overnight. The colorless prisms of **2** thus yielded were isolated by decantation, washed with diethyl ether and dried *in vacuo*. (0.16 g). The supernatant was again heated at 110 °C for 3 h. On working up as above, 0.20 g of the prisms of **2** were obtained. Repetition of this procedure 5 times gave the total amount of 0.91 g (72%) of **2** obtained as colorless prisms; the procedure may be continued further until the quantitative yield of **2** is attained.

Kinetic Measurements. The kinetic measurements of the rearrangement of acetylacetonato ligand were made using a JEOL PS-100 NMR spectrometer equipped with a JES-VT-3 variable-temperature controller. The temperature of the probe was calibrated (±0.5 °C) by measuring the reading of the thermometer inserted directly into a probe. The sample solution made up with the concentration of 0.18—0.27 M was used for each run.

The extent of conversion (x) of the reactions (i), (ii), and (iii) (Eq. 2 in the text) was calculated by the equations, $x_{\mathrm{i}}=\{2[f]+[h]\}/\{[a+c]+[d]+[f]+[h]\}$, $x_{\mathrm{ii}}=[h]/\{[c]+[d]+[f]+[h]\}$, and $x_{\mathrm{iii}}=2[f]/\{[c]+[d]+[f]+[h]\}$, respectively, where an alphabet in a square blacket means the relative intensity of the corresponding signal shown in Figs. 1—3. First-order rate constants were obtained from the slope of the linear plots of $\ln 1/(1-x)$ *vs.* t.

The rates of the interchange of the enol acetylacetonato ligand in [Pd(acac)(γ-acac)py] in pyridine-d_5 were calculated from the differences in the chemical shifts of two methyl singlets below the coalescence temperature using Gutowsky and Holm's equation.[35] The singlet signal above the coalescence temperature could not be used for the purpose of the kinetic analyses because of the overlapping of the signal in question with that ascribable to the methyl proton of [Pd(γ-acac)$_2$(py)$_2$] (see text).

We thank the Kawakami Foundation for support.

References

1) A. C. Hazell, A. G. Swallow, and M. R. Truter, *Chem. Ind. (London)*, **1959**, 564.
2) B. N. Figgis, J. Lewis, R. F. Long, R. Mason, R. S. Nyholm, P. J. Pauling, and G. B. Robertson, *Nature (London)*, **195**, 1278 (1962); R. Mason, G. B. Robertson, and P. J. Pauling, *J. Chem. Soc., A*, **1969**, 485.
3) A. Werner, *Ber.*, **34**, 2584 (1901).
4) Abbreviations acac and γ-acac are used throughout this paper to indicate the chelate O-bonded enol type and unidentate central (γ-) carbon bonded diketo type 2,4-pentanedionato (acetylacetonato) ligands, respectively.
5) J. Lewis, R. F. Long, and C. Oldham, *J. Chem. Soc.*, **1965**, 6740.
6) J. Lewis and C. Oldham, *J. Chem. Soc., A*, **1966**, 1456.
7) Y. Nakamura and K. Nakamoto, *Inorg. Chem.*, **14**, 63 (1975).
8) A. G. Swallow and M. R. Truter, *Proc. R. Soc. London, Ser. A*, **266**, 527 (1962).
9) J. R. Hall and G. A. Swile, *J. Organomet. Chem.*, **47**, 195 (1973).
10) G. Hulley, B. F. G. Johnson, and J. Lewis, *J. Chem. Soc., A*, **1970**, 1732.
11) T. Ito, T. Kiriyama, and A. Yamamoto, *Bull. Chem. Soc. Jpn.*, **49**, 3250 (1976).
12) K. Flatau and H. Musso, *Angew. Chem.*, **82**, 390 (1970).
13) R. H. Fish, *J. Am. Chem. Soc.*, **96**, 6664 (1974).
14) S. Baba, T. Ogura, and S. Kawaguchi, *Bull. Chem. Soc. Jpn.*, **47**, 665 (1974).
15) S. Okeya, S. Kawaguchi, N. Yasuoka, Y. Kai, and N.

Kasai, Abstr. No. 85, 23rd Symposium on Organometallic Chemistry, Japan, Tokyo, October 1975.

16) G. T. Behnke and K. Nakamoto, *Inorg. Chem.*, **7**, 330 (1968).

17) White-noise decoupled and half decoupled ^{13}C-NMR spectra of complex **2** were recorded on JEOL FX-60 by Mr. K. Kosaka of JEOL Ltd., to whom we are indebted.

18) A. J. Cheney, B. E. Mann, and B. L. Shaw, *Chem. Commun.*, **1971**, 431.

19) M. H. Chisholm, H. C. Clark, L. E. Manzer, and J. B. Stothers, *Chem. Commun.*, **1971**, 1627.

20) M. H. Chisholm, H. C. Clark, L. E. Manzer, J. B. Stothers, and J. E. H. Ward, *J. Am. Chem. Soc.*, **95**, 8574 (1973).

21) B. E. Mann, *Adv. Organomet. Chem.*, **12**, 135 (1974).

22) R. J. Cushley, D. Naugler, and C. Ortiz, *Can. J. Chem.*, **53**, 3419 (1975).

23) N. Serpone and D. G. Bickley, *Prog. Inorg. Chem.*, **17**, 391 (1972), and references cited therein.

24) (a) N. Serpone and R. Ishayek, *Inorg. Chem.*, **13**, 52 (1974); (b) N. Serpone and K. A. Hersh, *ibid.*, **13**, 2901 (1974).

25) D. R. Herrington and L. J. Boucher, *Inorg. Chem.*, **12**, 2378 (1973).

26) R. C. Fay and R. N. Lowry, *Inorg. Chem.*, **13**, 1309 (1974).

27) (a) K. Saito and M. Murakami, *Bull. Chem. Soc. Jpn.*, **45**, 2472 (1972); (b) T. Inoue and K. Saito, *ibid.*, **46**, 2417 (1973); (c) K. Matsuzawa and K. Saito, *ibid.*, **46**, 2777 (1973); (d) A. Nagasawa and K. Saito, *ibid.*, **47**, 131 (1974); (e) C. Chatterjee, K. Matsuzawa, H. Kido, and K. Saito, *ibid.*, **47**, 2809 (1974); (f) T. Inoue, J. Fujita, and K. Saito, *ibid.*, **48**, 1228 (1975); (g) M. Nishizawa, H. Kido, I. Kinoshita, Y. Soma, and K. Saito, *ibid.*, **49**, 819 (1976).

28) K. Saito and M. Takahashi, *Bull. Chem. Soc. Jpn.*, **42**, 3462 (1969).

29) T. Yamamoto, T. Saruyama, Y. Nakamura, and A. Yamamoto, *Bull. Chem. Soc. Jpn.*, **49**, 589 (1976).

30) T. Ito, T. Kiriyama, and A. Yamamoto, *Chem. Lett.*, **1976**, 835.

31) C. H. Bamford and D. J. Lind, *Proc. R. Soc. London, Ser. A*, **302**, 145 (1968).

32) K. Kaeriyama, *Bull. Chem. Soc. Jpn.*, **43**, 1511 (1970).

33) K. Kaeriyama, *Makromol. Chem.*, **150**, 189 (1971).

34) K. Kaeriyama, *Bull. Chem. Soc. Jpn.*, **47**, 753 (1974).

35) H. S. Gutowsky and C. H. Holm, *J. Chem. Phys.*, **25**, 1228 (1956).

The Constitution of $NaPO_3$-Cr_2O_3 Melts

Makoto WATANABE, Shoji SATO, and Hajime SAITO*

Department of Industrial Chemistry, Chubu Institute of Technology, Matsumoto-cho, Kasugai-shi, Aichi 487

**Department of Applied Chemistry, Faculty of Engineering, Nagoya University, Chikusa-ku, Nagoya 464*

(Received May 8, 1976)

Glassy and crystalline thermal products were made by heating a mixture of sodium metaphosphate glass and chromium(III) oxide with P/Cr ratios in the range from 1.0 to 300 at 1000 °C for 3 h in a platinum crucible and by then rapidly quenching the resulting melt. The crystalline substances were present in the products with P/Cr ratios smaller than 50 and were, except for chromium(III) oxide, an unknown substance and chromium(III) tripolyphosphate. The colorimetric determination and the measurement of the average chain length of polyphosphate anions present in the water-soluble parts of the products with P/Cr ratios larger than 50 showed that chromium(III) oxide reacts with sodium metaphosphate glass to make Cr–O–P linkages. Assuming that the glass has P–O–P, P–O^-, Cr–O–P, and Cr–O^- linkages, a theoretical treatment of the degree of polymerization of condensed phosphates were made and compared with the data. It was concluded that the most reasonable chemical structure of the glassy thermal products of the $NaPO_3$–Cr_2O_3 system is $Cr(OP)_3$.

Several attempts to prepare condensed phosphates containing oxoacid anions of some elements other than phosphorus have been made. The investigated systems were arsenate–phosphates,[1] silicate–phosphates,[2] vanadate–phosphates,[3] and borate–phosphates.[4,5] It was reported that condensed compounds of this type have P–O–As, P–O–Si, P–O–V, and P–O–B linkages, respectively. The authors also have studied thermal products in antimonate–phosphate,[6–8] molybdate–phosphate,[9] tungstate–phosphate,[9] and aluminate–phosphate[10] systems. It was concluded that they have P–O–Sb, P–O–Mo, P–O–W, and P–O–Al linkages, respectively, and the most reasonable chemical structure of the glassy products is proposed.

In the present paper, glassy and crystalline substances of the $NaPO_3$–Cr_2O_3 system with various P/Cr ratios were prepared by heating a mixture of Graham's salt and chromium(III) oxide at 1000 °C for 3 h in order to obtain some information on the chemical composition and structure of the system. The compositions of condensed phosphates were determined by the paper-chromatographic analysis of their aqueous solutions. The identification of the crystalline products was made by X-ray diffractometry and the chemical structure of the glassy products was studied by the theoretical treatment of the degree of polymerization of the condensed phosphates contained in the glassy products.

Experimental

Materials and Procedure. Sodium metaphosphate glass was prepared by heating monosodium orthophosphate dihydrate in a platinum crucible at 1000 °C for 3 h and then by quenching the melt by placing the crucible in ice water. The chromium(III) oxide was of a commercial grade. A mixture of sodium metaphosphate glass and chromium(III) oxide with P/Cr ratios in the range from 1.0 to 300 was heated in a platinum crucible at 1000 °C for 3 h. The resulting product was quenched by the same method as that for the preparation of sodium metaphosphate.

Chromium(III) Pyro- and Tripolyphosphates. The X-ray diffraction data for chromium(III) orthophosphate are listed in the "A. S. T. M. Diffraction Data File," while those for chromium(III) pyro- and tripolyphosphates are not. Chromium(III) pyro- and tripolyphosphates were prepared by the following method for the purpose of referring the X-ray diffraction data for chromium(III) pyro- and tripolyphosphates with those for the thermal products. Chromium(III) pyro- and tripolyphosphates were made by adding chromium(III) nitrate to an aqueous solution of sodium pyro- and tripolyphosphates. The precipitate was filtered off and washed with water.[11] The hydrated compound was heated first at 500 °C for 1 h and then at 1000 °C for 1 h. The X-ray diffraction patterns of the dehydrated compounds were taken with a powder method. The determination of the chemical compositions of the compounds were made by paper-chromatographic analysis of the phosphates present in the precipitates and the quantitative analysis of chromium and phosphorus of the dehydrated compounds. The dehydrated compounds were insoluble in water. About one gram of these water-insoluble compounds was mixed completely with 10 g of potassium carbonate and then heated at 800 °C for 20 min in a platinum crucible. Chromium is oxidized to chromate and these water-insoluble compounds are converted to water-soluble compounds. The chromate and phosphate ions in the aqueous solution of the water-soluble compounds were determined by the colorimetric method of analysis;[12] for chromate, the diphenylcarbazide method was used and for phosphate the molybdenum blue method. In the case of the colorimetric analysis of phosphates, 2 ml of the Mo reagent and 1 ml of the reducing solution were used because this method is more suitable than that described in textbooks for the colorimetric analysis of the phosphates contained in water-soluble compounds. Accordingly, the colorimetric measurement of phosphorus must be made under the condition that the concentration of phosphorus is less than 10 γ/50 ml.

The crystalline thermal products of the $NaPO_3$–Cr_2O_3 system were also insoluble in water. The determination of chromium and phosphorus of the crystalline thermal products were made by using the same method as that for chromium(III) pyro- and tripolyphosphates. The quantitative analysis of the phosphates present in the water-soluble thermal products was made as follows.

Paper Chromatography and Colorimetric Determination of Phosphates in the Water-soluble Thermal Products. One-dimensional paper chromatography was used for the separation of the phosphate species contained in the water-soluble thermal products by using the solvents described in a previous paper.[10] About one gram of the product was placed in 50 ml of water and the mixture was stirred for one hour at room temperature. The insoluble part was then filtered off, dried, and weighed for

the purpose of measuring the solubility of the product. About 8 μl of the sample solution was placed on the starting point of Toyo No. 51A filter paper (2 by 50 cm) and developed for 40 h at 5 °C. The identifications and determinations of each phosphate spot on a chromatogram were carried out by using the same method as that described in a previous paper.[6]

The Measurement of the Average Chain Length of Phosphates in Glassy Thermal Products. The method used in a previous paper[6] was adopted for the measurement of the average chain length of polyphosphates contained in the thermal products. The measurement of the average chain length of polyphosphates was achieved for sample solutions of the thermal products with P/Cr ratios larger than 80 and no appreciable effect of chromium ions on the measurement of the average chain length of polyphosphates was observed.

X-Ray Diffractometry. The samples were ground to powder which could pass through a 150 mesh sieve. Their X-ray diffraction patterns were taken by using a powder method on a Toshiba X-ray diffractometer, ADG-102.

Infrared Spectral Measurement. The infrared spectra of the products were recorded on a JASCO infrared spectrophotometer, model IR-G, by using a KBr tablet method.

Results and Discussion

Chromium(III) Pyro- and Tripolyphosphates. The P/Cr ratios of the chromium(III) pyro- and tripolyphosphates obtained by adding chromium(III) nitrate to an aqueous sodium pyro- or tripolyphosphate solution were 1.5 and 1.8, respectively. The values of the P/Cr ratios correspond to the theoretical values of the P/Cr ratios of $Cr_4(P_2O_7)_3$ and $Cr_5(P_3O_{10})_3$. The X-ray diffraction diagrams of the dehydrated chromium(III) pyro- and tripolyphosphates are shown in Fig. 1.

Amount of the Water-soluble Parts in the Thermal Products and Identification of the Thermal Products by X-Ray Diffractometry. The thermal products with P/Cr ratios larger than 80 were amorphous, while those with P/Cr ratios in the range from 1.0 to 50 contained crystalline substances. The X-ray diffraction diagrams of the crystalline thermal products with P/Cr ratios in the range from 1.0 to 3.0 are shown in Fig. 1. The X-ray diffraction diagrams of the thermal products with P/Cr ratios of 1.0 and 2.0 contain peaks of chromium(III) oxide and an unknown crystalline substance. The peaks due to chromium(III) oxide and chromium(III) tripolyphosphate appear in the X-ray diffraction pattern of the thermal product with a P/Cr ratio of 3.0. The X-ray diffraction diagrams for the products with P/Cr ratios in the range from 5.0 to 50 were the same as that for chromium(III) tripolyphosphate and hence chromium(III) tripolyphosphate is the only crystalline substance contained in the thermal products with P/Cr ratios in the range from 5.0 to 50. Accordingly, it could be concluded that the P–O–P linkages of high-polyphosphate in this system are broken to make chromium(III) tripolyphosphate. It is noteworthy that chromium(III) oxide reacts with $NaPO_3$ glass to produce chromium(III) tripolyphosphate and not to make chromium(III) ortho- and pyrophosphates. The unknown crystalline substance and chromium(III) tripolyphosphate present in the thermal products were insoluble in water. The amount of water-soluble parts in the products are listed in Table 1. The results of identification of the crystalline products by X-ray diffractometry are also shown in Table 1.

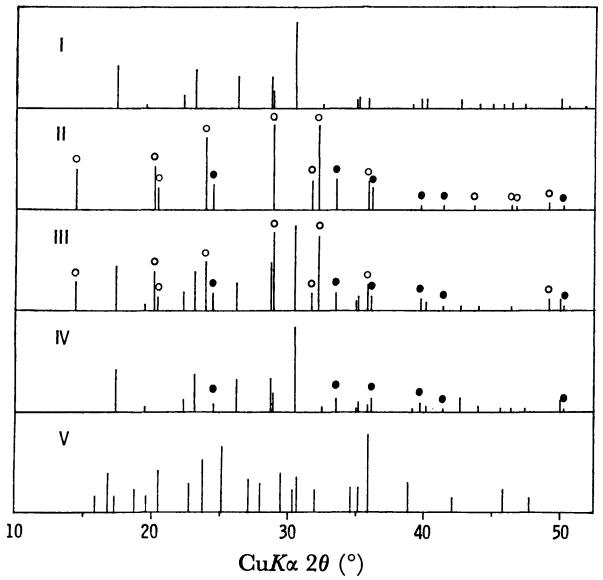

Fig. 1. X-Ray diffractograms of the thermal products, $Cr_4(P_2O_7)_3$, and $Cr_5(P_3O_{10})_3$.
I: $Cr_5(P_3O_{10})_3$, II: product with the P/Cr ratio of 1.0, III: product with the P/Cr ratio of 2.0, IV: product with the P/Cr ratio of 3.0, V: $Cr_4(P_2O_7)_3$.
○: Unknown peak for assignment, ●: peak attributable to Cr_2O_3 (Ref. ASTM card 6-504).

Table 1. Amount of water-soluble parts in the products and identification of the thermal products by X-ray diffractometry

P/Cr	X-Ray diff.	Water-soluble parts (%)
1.0	Unknown, Cr_2O_3	5.7
2.0	Unknown, Cr_2O_3, $Cr_5(P_3O_{10})_3$	29
3.0	Cr_2O_3, $Cr_5(P_3O_{10})_3$	52
5.0—50	$Cr_5(P_3O_{10})_3$	67—98
80—300	Glassy	100

Unknown: unknown crystalline product (see Fig. 1).

Distribution of Phosphates. The results of quantitative analysis of the phosphates contained in the water-soluble parts of the thermal products are listed in Table 2. The contents of ortho-, pyro-, and tripoly-

Table 2. Distribution of phosphates of water-soluble parts in the products

P/Cr	Ortho	Pyro	Tri	Tri-meta	Tetra-meta	Higher
1.0	3.0	11.1	33.1			52.8
2.0	1.0	4.1	17.0			77.9
3.0	1.1	2.5	11.2	1.3	0.8	83.1
5.0	0.8	1.7	6.2	1.2	0.8	89.3
7.0	0.5	0.8	3.1	2.0	1.5	92.1
10	0.7	0.6	1.0	3.0	1.4	93.3
15	0.4	0.5	0.7	3.3	1.3	93.8
20—300				2—4	1—3	93—97

phosphates decrease with an increase in the P/Cr ratio, while those of high-polyphosphates increase with an increase in the P/Cr ratio. This result is in good agreement with those of the other systems described in previous papers.[6-10] By the same considerations as in previous papers, it can reasonably be concluded that chromium(III) oxide reacts with sodium metaphosphate to make a Cr–O–P linkage at 1000 °C and that the Cr–O–P linkage of the water-soluble products is readily hydrolyzed to produce chromium and phosphate ions in water solutions. The contents of trimeta- and tetrametaphosphates do not change much with the variation in the P/Cr ratio and hence the formation of trimeta- and tetrametaphosphates may be little affected by chromium.

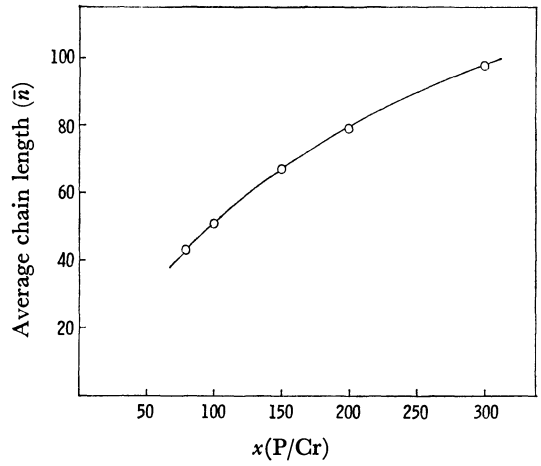

Fig. 2. Variation of average chain length of polyphosphates present in the thermal products with P/Cr ratios larger than 80.

Average Chain Length of Polyphosphates and the Chemical Structure of Glassy Products. The behavior of chromium contained in the glassy and water-soluble thermal products can be examined by measuring the correlation between the average chain length of polyphosphates and the P/Cr ratio of the products,[2,6-10] because the chain length of the polyphosphates present in the thermal products is affected by the coordination number of chromium. To obtain the correlation, it is necessary that the thermal product dissolves completely in water. Therefore, the average chain length of the polyphosphates present in the glassy products with P/Cr ratios larger than 80 was measured. The result is shown in Fig. 2 and indicates that the average chain length of the polyphosphates contained in the glassy products increases with an increase in the P/Cr ratio. This tendency is the same as that of the distribution of polyphosphates obtained by quantitative analysis. Accordingly, it can be concluded that this result is one proof of the presence of the Cr–O–P linkage in the glassy products. The correlation between the chromium coordination number and the average chain length of polyphosphates in the glassy products can be discussed theoretically employing the method described in previous papers.[2,6-10] Depending upon the method, the average chain length, $\bar{n}$, of the polyphosphates in the glass of the $NaPO_3$-Cr_2O_3 system is given by the following equation:

$$(\bar{n}+2)/\bar{n} = (x+y-z+fx)/x \quad (1)$$

where, x, y, and z are respectively the number of phosphorus atoms, P–O–Cr linkages, and Cr–O^- linkages per atom of chromium and where f is the factor shortening the chain length of the polyphosphates, given with respect to an atom of phosphorus. The previous results[2,6-10] indicate that the value of f is in the range from 0.01 to 0.025 under the conditions employed in this experiment. There are three possible structures containing P–O–Cr and Cr–O^- linkages, which are as follows:

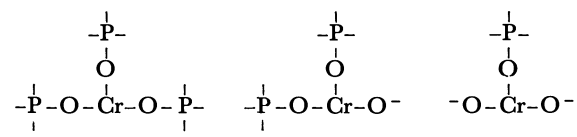

The average chain length of the polyphosphates present in the glassy products can be calculated on the basis of these chemical structures. The calculated values are listed in Table 3. When the f factor is 0.01, the calculated values of $\bar{n}$ based on Structure A are very close to the measured ones throughout the range of P/Cr ratios from 80 to 300. From these results, it may be reasonably concluded that the chemical structure of the glassy thermal products of the Cr_2O_3–$NaPO_3$ system with P/Cr ratios larger than 80 is the Structure A and hence the valence of chromium which contributes to the shortening of the chain length of polyphosphates is three. The chromium coordination number in the glassy products may be larger than three (in general, the coordination number of chromium is six or four). The coordination numbers which do not contribute to the shortening of the chain length of polyphsophates cannot be discussed by using the method described above. The P–O–Cr linkage which does not affect the average chain length of polyphosphates may be produced by the interaction between chromium and the oxygen atom of a P=O bond.

Table 3. Average chain length of polyphosphates of the $NaPO_3$-Cr_2O_3 system with P/Cr ratios larger than 80

x (P/Cr)	$\bar{n}$ Found	$\bar{n}$ calcd by Eq. 1 (f=0.01) Structure A (y=3, z=0)	Structure B (y=2, z=1)	Structure C (y=1, z=2)
80	43	42	89	—
100	51	50	100	∞
150	67	67	120	600
200	79	80	133	400
300	98	100	150	300

Infrared Spectra. The infrared spectra of sodium metaphosphate glass, chromium(III) oxide, chromium(III) tripolyphosphate, and the thermal products with P/Cr ratios in the range from 1.0 to 15 are shown in Fig. 3. Since the infrared spectra of the thermal products with P/Cr ratios larger than 20 are the same as that of sodium metaphosphate glass, the existence of the absorptions of the Cr–O–P linkage in the glassy products

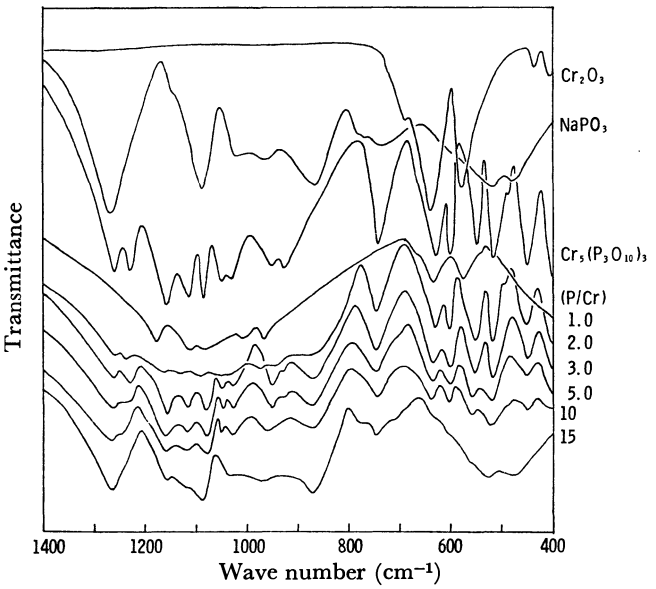

Fig. 3. IR spectra of Cr_2O_3, $NaPO_3$, $Cr_5(P_3O_{10})_3$, and the products with P/Cr ratios from 1.0 to 15.

cannot be discussed. The infrared spectrum of the thermal product with a P/Cr ratio of 1.0 contains the absorptions due to chromium(III) oxide (absorptions at 640 and 580 cm^{-1}) and does not contain an absorption due to chromium(III) tripolyphosphate, while the infrared spectra of the thermal products with P/Cr ratios larger than 2.0 exhibit an absorption attributable to chromium(III) tripolyphosphate. The absorption of chromium(III) tripolyphosphate becomes gradually ambiguous with an increase in the P/Cr ratio from 3.0 to 15. The infrared spectra of the water-insoluble parts which were obtained by treating with water the thermal products with P/Cr ratios of 5.0—50 are the same as that of chromium(III) tripolyphosphate. These results agree well with those obtained above.

References

1) K-H. Jost, H. Worzalla, and E. Thilo, *Z. Anorg. Allg. Chem.*, **325**, 98 (1963).
2) S. Ohashi and F. Oshima, *Bull. Chem. Soc. Jpn.*, **36**, 1489 (1963).
3) S. Ohashi and T. Matsumura, *Bull. Chem. Soc. Jpn.*, **35**, 501 (1962).
4) T. Nakamura and S. Ohashi, *Bull. Chem. Soc. Jpn.*, **40**, 110 (1967).
5) K. Honma and K. Honma, *Nippon Kagaku Kaishi*, **1972**, 856.
6) M. Watanabe, K. Tanabe, T. Takahara, and T. Yamada, *Bull. Chem. Soc. Jpn.*, **44**, 712 (1971).
7) M. Watanabe and M. Kato, *Bull. Chem. Soc. Jpn.*, **45**, 1058 (1972).
8) M. Watanabe, *Bull. Chem. Soc. Jpn.*, **46**, 2468 (1973).
9) M. Watanabe, *Nippon Kagaku Kaishi*, **1974**, 1407, 1412.
10) M. Watanabe, S. Sato, and H. Saito, *Bull. Chem. Soc. Jpn.*, **48**, 893 (1975).
11) The precipitate produced from an aqueous tripolyphosphate solution was too fine to filter and was centrifuged.
12) G. Muto, "Hishoku Bunseki Ho," Kyoritsu, Tokyo (1966), pp. 153, 168.

Photoinduced One-Electron Reduction of 1-Benzyl-3-carbamoylpyridinium Chloride and 3,5-Bis(ethoxycarbonyl)-2,6-dimethylpyridine[1)]

Koji KANO and Taku MATSUO*

Department of Organic Synthesis, Faculty of Engineering, Kyushu University, Hakozaki, Higashi-ku, Fukuoka 812

(Received May 7, 1976)

Photolysis of 1-benzyl-3-carbamoylpyridinium chloride (BNA^+) in aqueous solution in the presence of diethylamine and/or ethylenediaminetetraacetate gives the 6,6′-dimer (**1**), a coupled product of the pyridyl radicals generated by one-electron transfer from alkylamine to photoexcited BNA^+. Thermal one-electron reduction of BNA^+ either with zinc dust/copper sulfate or with magnesium powder in aqueous alkaline medium yields the 4,6′-dimer (**2**) together with a small amount of **1**. In the case of 3,5-bis(ethoxycarbonyl)-2,6-dimethylpyridine (HE_{ox}), the 2,2′-dimer (**3**) is formed as an initial photoreduction product, which is converted into the 4,4′-dimer (**4**) and 1,2-dihydropyridine (**5**) upon prolonged irradiation.

The non-enzymatic reduction of NAD^+ and its analogues is classified into one- and two-electron reductions.[2)] Sodium dithionite and hydroborate are two-electron reducing agents, the former affording 1,4-dihydronicotinamides and the latter 1,2- and 1,6-isomers.[3,4)] On the other hand, the one-electron reduced species (pyridyl radicals) of 1-substituted 3-carbamoylpyridinium ions are obtained either by electrolysis in DMSO[5)] or radiolysis in aqueous 2-propanol,[6,7)] The pyridyl radicals give 6,6′-dimers (Scheme 1) as the final product.[5)] From a synthetic

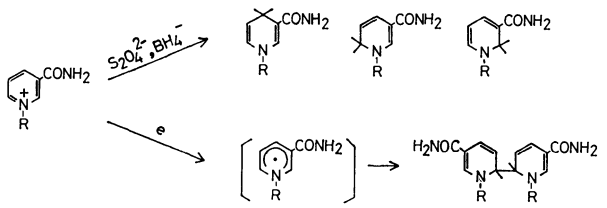

Scheme 1.

viewpoint, however, neither electrolysis nor radiolysis is a convenient method for preparing the reduced pyridines. In 1959, Wallenfels and Gellrich reported that the reduction of 1-benzyl- and 1-(2,6-dichlorobenzyl)-3-carbamoylpyridinium chlorides either with magnesium powder or with zinc dust/copper sulfate in aqueous alkaline solution gave the 6,6′-dimers in 20—26% yields.[8)]

In the present paper, a new type of one-electron reduction of pyridinium and pyridine compounds is reported.[9)] The compounds investigated are 1-benzyl-3-carbamoylpyridinium chloride (BNA^+) and 3,5-bis(ethoxycarbonyl)-2,6-dimethylpyridine (HE_{ox}), which are also useful as NAD^+ models. Diethylamine (DEA) and ethylenediaminetetraacetate (EDTA) were used as the reducing agents under photo-irradiation. The thermal reduction of BNA^+ was also carried out according to the method of Wallenfels and Gellrich. 4,6′-Dimer (**2**) was obtained as the main reduction product accompanied by a small amount of 6,6′-dimer (**1**). This result differs from that reported by Wallenfels and Gellrich.[8)]

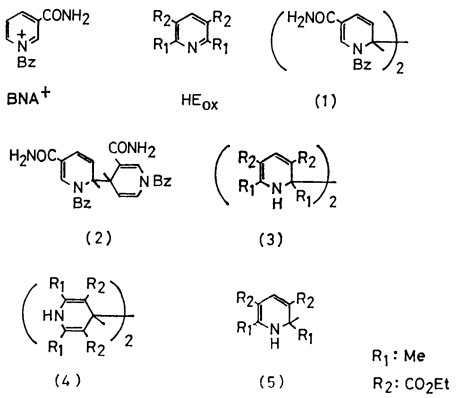

Yellow solid materials adhered to the surface of the lamp upon irradiation of a solution of BNA^+ in water

TABLE 1. SPECTRAL AND PHYSICAL DATA OF DIMERS

Compound	Mp, °C	λ_{max}, nm (log ε)	F_{max}, nm[a)]	IR, cm^{-1} (KBr) NH	IR, cm^{-1} (KBr) C=O	Mass	Anal[Found (Calcd)] C	H	N
6,6′-Dimer (**1**)	164—165 (dec)	277 (3.44), 354.5 (3.89) in MeOH		3440, 3320 1640, 1630	1678	214, 213 (1/2M·+)	72.76 (73.21)	6.12 (6.14)	13.03 (13.14)
4,6′-Dimer (**2**)	168.7—169.2 (dec)	273 (4.17), 360 (3.96) in MeOH		3480, 3320 1660, 1650 1640, 1630	1679	214, 213 (1/2M·+)	72.63 (73.21)	6.16 (6.14)	12.96 (13.14)
2,2′-Dimer (**3**)	175.8—176 (dec)	387 (3.86) in pyridine	445 in pyridine	3300	1695, 1686 1670, 1652	252 (1/2M·+)	61.60 (61.89)	7.12 (7.19)	5.54 (5.55)
4,4′-Dimer (**4**)	>200 (sublim.)	240 (4.31), 275 (4.00) 360 (3.93) in MeOH	450 in MeCN	3300	1692, 1655	252 (1/2M·+)	61.84 (61.89)	7.16 (7.19)	5.61 (5.55)

a) Fluorescence maximum.

containing DEA with a high-pressure mercury lamp. Based on spectroscopic data, the solid material was identified to be the 6,6′-dimer (**1**) as obtained by the coupling of the pyridyl radicals generated by the one-electron reduction of BNA$^+$. The yield of **1** was 50% as calculated on the basis of consumed BNA$^+$. 6,6′-Dimer (**1**) was synthesized by Wallenfels and Gellrich,[8] its UV and NMR spectroscopic data being reported.[8,10] The UV and NMR spectra of **1** obtained in the present experiment are in good agreement with those reported,[8,10] although the mp (164—165 °C (dec)) of **1** we obtained differs distinctly from that given by Wallenfels and Gellrich (mp 191—193 °C (dec)).[11] An attempt was made to prepare the 6,6′-dimer (**1**) by the receipe of Wallenfels and Gellrich.[8] Reduction was carried out either with zinc dust/copper sulfate or with magnesium powder in aqueous ammonia solution, the main product with mp 169 °C (dec) being obtained (yield, 6—20%) in both cases.[11] The UV and NMR spectra (Table 1) suggest that the thermal reduction product is not the 6,6′-dimer (**1**). By means of NMR spectroscopy, the compound was confirmed to be the 4,6′-dimer (**2**) (see Experimental). As in the case of 6,6′-dimer (**1**), 4,6′-dimer (**2**) was rapidly oxidized by methyl viologen in methanol. In the case of Zn/Cu system, a small amount of byproduct (mp 164—165.5 °C (dec), 0.3%) was also isolated together with **2** (20%). Both the spectroscopic data and mp (dec) proved that the byproduct is the same 6,6′-dimer (**1**) as obtained by photoreduction. In spite of the fact that experiment was carried out very carefully, **1** was obtained only in a low yield.

DEA could be replaced with EDTA. In this case, the solution should be made slightly alkaline since **1** decomposes to an unknown compound either in neutral or in acidic medium.

Benzyl and methyl viologens were analogously photoreduced to the corresponding cation radicals in the Ar-flushed aqueous solution (pH 7.9) containing EDTA:

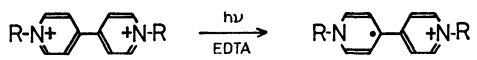

R: CH_2Ph λ_{max} 371, 388, 400, 550, 560, 599, and 660 (sh) nm.
R: CH_3 λ_{max} 367, 384, 395, 570 (sh), 600, and 660 nm.[12]

The pyridine ring itself could also be photoreduced by the above method devised for pyridinium ions. Upon irradiation of a mixture of HE_{ox}, EDTA, and potassium carbonate in 40% (v/v) aqueous acetonitrile, the 2,2′-dimer (**3**) precipitated as very pure, lemon yellow crystals, its yield being 51% as calculated on the basis of consumed HE_{ox}. The 2,2′-dimer (**3**) is hardly soluble in organic solvents, such as acetonitrile, dimethyl sulfoxide, carbon tetrachloride, chloroform, ethanol, methanol, acetone, and benzene, but easily soluble in basic solvents such as pyridine and DEA. Its structure was deduced from the following spectroscopic data. In the NMR spectrum of **3** in pyridine-d_5, the proton signals due to methyl groups at the 6,6′- and

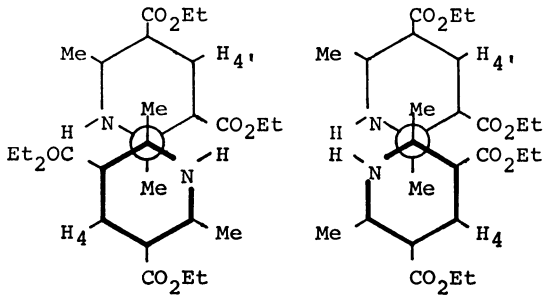

Fig. 1. Steric isomers of the 2,2′-dimer (**3**).

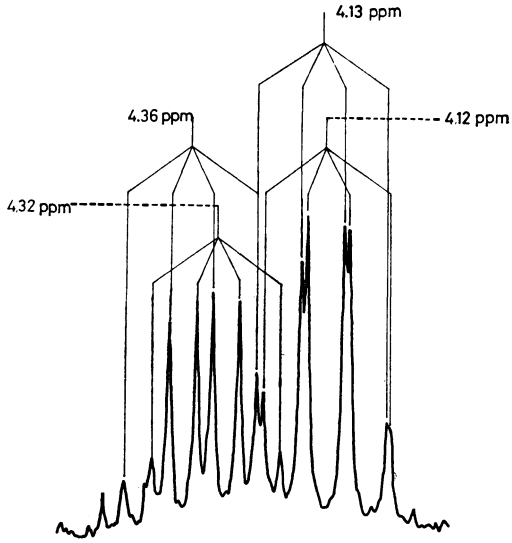

Fig. 2. NMR spectrum of $CO_2CH_2CH_3$ of the 2,2′-dimer(**3**) in DMSO-d_6 (90 MHz).

2,2′-positions are observed at δ 2.11 and 2.58 ppm, respectively, and those due to the ethoxycarbonyl groups at 1.03 and 1.26 ppm. The proton at the 4-position can not be detected because the signal overlaps with that of non-deuterated pyridine (7.68 ppm) in the solvent. As to the methylene protons of the ethoxycarbonyl group, the four quartet signals were observed (Fig. 1). Since **3** contains two asymmetric carbon atoms, it is expected that *meso* and racemic isomers are present (Fig. 2) and that the chemical shift of the methylene protons of the ethoxycarbonyl groups in the two isomers differs. Judging from the distance between the asymmetric center and the protons in question, the difference in the chemical shift for the ethoxycarbonyl groups at 5- and 5′-positions should be less than that for the 3- and 3′-positions. Therefore, the two quartet signals at δ 4.12 and 4.13 ppm should be assigned to the methylene protons at 5(5′)-positions of the *meso* and racemic isomers. The ones at lower magnetic field (δ 4.32 and 4.36 ppm) are thus ascribed to the methylene protons at 3(3′)-positions of these isomers. In agreement with the assignment of the NMR spectra, four different carbonyl absorptions are observed for **3** (Table 1).

2,2′-Dimer (**3**) could not be isolated by the photolysis of HE_{ox} in aqueous acetonitrile containing large

Table 2. Effects of irradiation time on yields of 4 and 5[a)]

Run No.	Irradiation time, h	4, %[b)]	5, %[b)]
1	3	14	12
2	6	19	13
3	6.25	19	17
4	14	3	27

a) A mixture of HE_{ox} (1.0 g) and DEA (20 ml) in 50% (v/v) aqueous acetonitrile (200 ml) was irradiated with a 30W low-pressure mercury lamp under nitrogen atmosphere. b) Except for Run No. 3, the yields of **4** and **5** were determined by NMR spectra of the mixture of **4** and **5** which were obtained by the evaporation of acetonitrile from the photolyzed solution. In Run No. 3, the yields were calculated from the weight of **4** and **5** isolated.

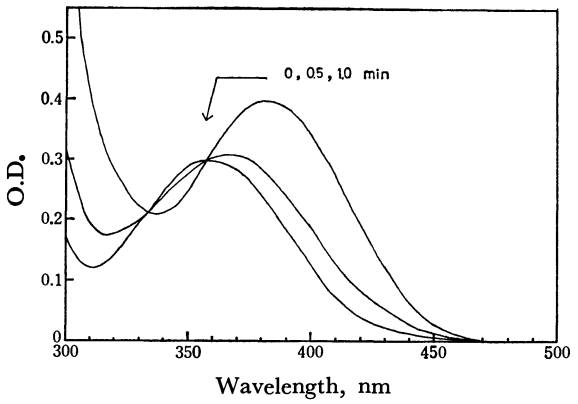

Fig. 3. Photoisomerization of the 2,2′-dimer (**3**) to the 4,4′-dimer (**4**). The 2,2′-dimer (**3**) in methanol was flushed with argon gas and irradiated with beams of light (>420 nm, a Toshiba V-Y42 filter) obtained from a Ushio 500 W super high-pressure mercury lamp.

excess of DEA. Instead, the 4,4′-dimer (**4**) and 3,5-bis(ethoxycarbonyl)-2,6-dimethyl-1,2-dihydropyridine (**5**) were obtained in 19 and 17% yields, respectively. It should be noted that dihydropyridine (**5**) is a two-electron reduced product. The effect of irradiation time on the yield of **4** and **5** is given in Table 2. It is seen that prolonged irradiation increases the yield of **5** at the expense of **4**. This suggests that **5** is formed *via* **4**. 4,4′-Dimer (**4**) (λ_{max} 360 nm) was verified to be almost quantitatively converted to **5** (λ_{max} 373 nm) upon irradiation of the aqueous acetonitrile solution in the presence of DEA, although **5** was not obtained in the absence of DEA.

2,2′-Dimer (**3**) precipitated during irradiation (17%) when the photoreaction of HE_{ox} was carried out in the presence of low concentration of DEA. It is suggested that **3** is an intermediate of the photochemical reactions. Figure 3 shows the spectral change along the photolysis of **3** in methanol. Upon irradiation (>420 nm, Ar), the absorption maximum at 382 nm due to **3** shifts to 358 nm which is ascribed to **4**. This is a 1,3-sigmatropic rearrangement, which is considered to proceed quantitatively since isosbestic points are observed at 257, 333, and 358 nm. The scheme of the photoreduction of HE_{ox} in the presence of DEA can be summarized as follows (Scheme 2):

$$HE_{ox} \xrightarrow[DEA]{h\nu} [HE_{ox}H\cdot] \longrightarrow \mathbf{3} \xrightarrow{h\nu} \mathbf{4} \xrightarrow[DEA]{h\nu} \mathbf{5}$$

Scheme 2.

No photoreduction products of HE_{ox} (**3**, **4**, and **5**) in methanol are oxidized by methyl viologen.

The photolysis of either BNA^+ or HE_{ox} in aqueous media containing DEA and/or EDTA afforded the corresponding dimers of one-electron reduced species. In the case of BNA^+, the one-electron transfer from alkylamine to photoexcited BNA^+ should yield a radical **6**. On the basis of both quantum mechanical calculation[13)] and stereochemical consideration, it seems that coupling of the radical takes place at the 6-position.

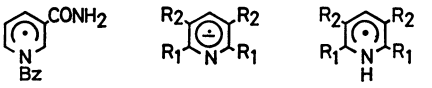

(6) (7) (8)

In the case of HE_{ox}, on the other hand, a pyridyl radical anion **7** should be a primary photoproduct. According to Brühlmann and Hayon, the pK_a-values for radical anions of nicotinamide analogues are generally larger than 13.[7)] The radical anion **7** can be immediately protonated to yield a free radical **8** under the present experimental conditions. The free radical **8** will afford the dimer **3** as the final product. The pyridyl radicals are thus proposed as the common intermediates in the photoreduction of both BNA^+ and HE_{ox}. The presence of the pyridyl radicals has also been verified by the kinetic study of the reduction of the Hemin pyridine complex (one-electron acceptor) coupled with the photoreduction of BNA^+, HE_{ox}, and other related compounds in the presence of *N,N,N′,N′*-tetramethylethylenediamine.[14)]

In connection with the redox property of the pyridine derivatives, it should be mentioned that the Hemin complex was also reduced by all the above-described dimers (**1**, **2**, **3**, and **4**) although the rates were somewhat lower than those with the pyridyl radicals. On the other hand, the Hemin complex was hardly reduced by two-electron reduced NAD^+-model compounds such as 1-benzyl-1,4-dihydronicotinamide[15)] and 3,5-bis(ethoxycarbonyl)-2,6-dimethyl-1,4-dihydropyridine (Hantzsch ester). This difference may be useful in elucidating the mechanism of redox-systems where pyridine derivatives play important roles.

Experimental

Melting points were determined on a hot-stage apparatus and are corrected. Spectroscopic measurements were made with Shimadzu UV-200 and Hitachi 124 recording spectrophotometers, Varian A-60 and Bruker WH-90 FT NMR spectrometers, a Hitachi RML-6E mass spectrometer, and a JASCO DS-403 G grating IR spectrophotometer. A Shimadzu Baush & Lomb Spectronic 505 recording spectro-

photometer was modified for the fluorescence measurements. BNA^{+}[16] and HE_{ox}[17] were prepared according to the procedures given in the literature. Reagent grade DEA (Wako Pure Chem.) and disodium ethylenediaminetetraacetate dihydrate (Dohzin Pharm. Co.), DMSO-d_6 (Stohler Isotope Chem., 99.5%), and pyridine-d_5 (Merck, 99.5%) were used. Water was distilled and deionized with a column of ion-exchange resin. The photolysis in a preparative scale was carried out by the use of Riko immersion-type 100W high-pressure and 30W low-pressure mercury lamps.

Reduction of 1-Benzyl-3-carbamoylpyridinium Chloride with Zinc Dust-Copper Sulfate in Aqueous Ammonia.[8] A solution of 2.5 g copper sulfate pentahydrate in 20 ml of water was gradually poured into water containg 6 g of zinc dust under vigorous stirring at room tempreature. A mixture of 10 ml of 28% aqueous ammonia and 50 ml of methanol was added to it and then 5 g (20 mmol) of BNA^{+} in 20 ml of water was poured into the solution. At this time, the reaction mixture turned yellow. After stirring was continued for 20 min at room temperature, the yellow precipitates and inorganic materials were collected by filtration. The residue was extracted with 20 ml of boiling methanol in nitrogen atmosphere and the insoluble matter was filtered. The residue was further extracted with 30 ml of boiling methanol. The former extract was kept in a refrigerator (*ca.* −5 °C) overnight to give lemon yellow crystals (0.85 g), which was identified to be 4,6′-dimer (**2**) (yield, 20%); mp 168.5—169 °C (dec); NMR (DMSO-d_6): δ 7.38 (s, aromatic ring), 7.18 (s, 2,2′H), 6.78 and 6.38 (broad s, $CONH_2$), 6.36 (d, 4′H or 6H, $J_{4',5'}$ or $J_{5,6}$ 8.0 Hz), 6.20 (d, 6H or 4′H, $J_{5,6}$ or $J_{4',5'}$ 8.0 Hz), 4.79 (q, 5′H, $J_{5',6'}$ 5.0 Hz), 4.66 (q, 5H, $J_{4,5}$ 4.4 Hz), 4.42 (s, NCH_2), 4.00 (d, 4H), and 3.28 ppm (d, 6′H). The NMR spectrum (5 mg/1 ml of DMSO-d_6) was obtained after 100 scans with the Bruker WH-90 FT NMR spectrometer.

When nitrogen was bubbled into a methanolic solution of the latter extract, 13 mg (0.3%) of the 6,6′-dimer (**1**) separated out of the solution; mp 164—165.5 °C (dec). The analytical date are given in Table 1 and in the photochemical section (*vide infra*).

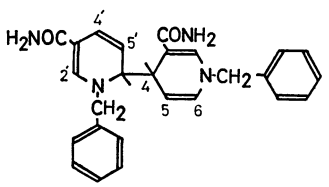

Reduction of 1-Benzyl-3-carbamoylpyridinium Chloride with Magnesium Powder in Aqueous Ammonia.[8] Magnesium powder (3 g) was gradually added into a 1.1% aqueous ammonia solution (100 ml) of BNA^{+} (5 g, 20 mmol) and ammonium chloride (9 g) under vigorous stirring at 48—50 °C, about 1.5 h being required for the addition. Stirring was continued for additional 30 min at 48—50 °C after all of magnesium powder had been consumed. When the reaction was completed, the reaction mixture was cooled with an ice-bath and the yellow precipitates and colorless inorganic solid were collected by filtration. The residue was dissolved into 100 ml of methanol in order to remove inorganic matter and the methanolic layer was concentrated to *ca.* 50 ml. The residue was gradually poured into 200 ml of 2.8% aqueous ammonia under cooling with an ice-bath. The pale yellow precipitates (3 g) were filtered and recrystallized from acetonitrile to give crude 4,6′-dimer (**2**) (mp 144—145.5 °C (dec)). Further recrystallization from methanol afforded the pure 4,6′-dimer (**2**) (0.27 g, 6%); mp 168.7—169 °C (dec).

Photoreduction of 1-Benzyl-3-carbamoylpyridinium Chloride in the Presence of Diethylamine. A solution of BNA^{+} (2 g, 8.0 mmol) and DEA (10 ml, *ca.* 96 mmol) in 140 ml of water was irradiated with a 100W high-pressure immersion lamp under nitrogen bubbling for 2 h. Orange yellow precipiates (119 mg) were collected by filtration. The filtrate was further irradiated for 2 h after the solid covering the lamp wall had been removed. The second precipitates (212 mg) were collected and combined with the former. The NMR spectrum indicated that the precipitates were mainly 6,6′-dimer (**1**) (19%). The crude **1** (67 mg) was recrystallized from methanol and the pale yellow plates obtained were dried at 50 °C overnight to give 42 mg of pure **1**; mp 164—165 °C (dec); NMR (DMSO-d_6): δ 7.29 (s, aromatic ring), 7.18 (s, 2H), 6.97 (broad s, $CONH_2$), 6.04 (d, 4H, $J_{4,5}$ 7.6 Hz), 4.34 (s, NCH_2), 4.33 (q, 5H), and 3.18 ppm (d, 6H, $J_{5,6}$ 5.0 Hz). The NMR spectrum was measured with the Bruker WH-90 FT NMR spectrometer. After the second photolysis, unreacted BNA^{+} was recovered (1.23 g, 61%) from the filtrate.

Photoreduction of 1-Benzyl-3-carbamoylpyridinium Chloride in the Presence of Ethylenediaminetetraacetate. A solution of BNA^{+} (0.5 g, 2 mmol), disodium ethylenediaminetetraacetate dihydrate (1.1 g, 3 mmol), and potassium carbonate (2 g) in 200 ml of water was irradiated with a 30W low-pressure mercury lamp under argon bubbling for 10 h. The precipitates (63 mg, 15%) were filtered and recrystallized from methanol to give the 6,6′-dimer (**1**).

Photoreduction of 3,5-Bis(ethoxycarbonyl)-2,6-dimethylpyridine in the Presence of Ethylenediaminetetraacetate. A solution of HE_{ox} (0.5 g, 2 mmol), disodium ethylenediaminetetraacetate dihydrate (2.25 g, 6 mmol), and potassium carbonate (2 g) in 40% (v/v) aqueous acetonitrile (250 ml) was irradiated with a 30W low-pressure mercury lamp under nitrogen bubbling and stirring for 9.5 h. The lemon yellow precipitates of the 2,2′-dimer (**3**) (171 mg, 34%) were collected by filtration; mp 178—179 °C (dec). HE_{ox} (166 mg, 33%) was recovered by the evaporation of acetonitrile from the filtrate. 2,2′-Dimer (**3**) can be recrystallized from pyridine; mp 175.8—176 °C (dec); NMR (pyridine-d_5): δ 8.98 (braod s, NH), 7.68 (s, 4H?), 4.36 and 4.32 (q, 3,3′-$CO_2CH_2CH_3$), 4.13 and 4.12 (q, 5,5′-$CO_2CH_2CH_3$), 2.58 (s, 2,2′-CH_3), 2.11 (s, 6,6′-CH_3), 1.26 (t, 3,3′-$CO_2CH_2CH_3$, J 7.0 Hz), and 1.03 ppm (t, 5,5′-$CO_2CH_2CH_3$, J 7.0 Hz). The NMR spectrum (10 mg/0.6 ml of pyridine-d_5) was obtained after 35 scans with the Bruker WH-90 FT NMR spectrometer.

Photoreduction of 3,5-Bis(ethoxycarbonyl)-2,6-dimethylpyridine in the Presence of Diethylamine. a) A solution of HE_{ox} (1 g, 4 mmol) and DEA (20 ml, 192 mmol) in 50%(v/v) aqueous acetonitrile (120 ml) was irradiated with a 30W low-pressure mercury lamp under nitrogen bubbling for 6.25 h. The reaction mixture was concentrated *in vacuo* to *ca.* 50 ml. Yellow precipitates were collected by filtration. Unreacted HE_{ox} was recovered from the filtrate as brown oil, which was purified by silica gel column chromatography with ethyl acetate and recrystallized from acetonitrile (284 mg, 28%). The yellow precipitates were recrystallized from acetonitrile to give 193 mg of the 4,4′-dimer (**4**) (19%); mp>200 °C (sublim.). The filtrate was concentrated and the residue obtained was purified by silica gel column chromatography with ethyl acetate to give 172 mg of 3,5-bis(ethoxycarbonyl)-2,6-dimethyl-1,2-dihydropyridine (**5**) (17%); mp 149—153 °C (dec).

The 4,4′-dimer (**4**); NMR (DMSO-d_6): δ 8.35 (broad s, NH), 3.97 (s, 4,4′H), 3.97 (q, $CO_2CH_2CH_3$, J 7.0 Hz), 2.05 (s, CH_3), and 1.18 ppm (t, $CO_2CH_2CH_3$).

3,5-Bis(ethoxycarbonyl)-2,6-dimethyl-1,2-dihydropyridine (**5**); Mass: 253 (M^{+}); UV: λ_{max}^{MeOH} 212, 283, and 373.5

nm; fluorescence: F^{MeOH}_{max} 490 nm; NMR (DMSO-d_6): δ 7.70 (s, 4H), 6.93 (broad s, NH), 4.52 (q, 2H, $J_{2,Me}$ 6.5 Hz), 4.18 (q, $CO_2CH_2CH_3$, J 7.0 Hz), 2.39 (s, $6CH_3$), 1.30 (t, $CO_2CH_2CH_3$), and 1.18 ppm (d, $2CH_3$). The NMR spectrum of **4** and **5** were measured with the Varian A-60 spectrometer.

b) A mixture of HE_{ox} (0.5 g, 2 mmol), DEA (1 g, 14 mmol), and 100 ml of a phosphate buffer solution (1/15 M, pH 8.0) was disolved into 150 ml of 67%(v/v) aqueous acetonitrile. The HE_{ox} solution was irradiated with a 30W low-pressure mercury lamp under nitrogen bubbling and stirring for 4 h. The lemon yellow precipitates were collected by filtration and washed with water and acetonitrile to give pure 2,2′-dimer (**3**) (84 mg, 17%); mp 176—176.5 °C (dec).

References

1) Contribution No. 406 from the Department of Organic Synthesis, Faculty of Engineering, Kyushu University.

2) H. Sund, H. Diekmann, and K. Wallenfels, "Advances in Enzymology," Vol. 26, Interscience, New York, London (1964), p. 115.

3) K. Wallenfels and H. Schuly, *Angew. Chem.*, **67**, 617 (1955); **69**, 505 (1957).

4) K. Wallenfels and H. Schuly, *Justus Liebigs Ann. Chem.*, **621**, 106 (1959).

5) K. S. V. Santhanam and P. J. Elving, *J. Am. Chem. Soc.*, **95**, 5482 (1973).

6) R. L. Willson, *Chem. Commun.*, **1970**, 1005; *Trans. Faraday Soc.*, **67**, 3020 (1971).

7) U. Brühlmann and E. Hayon, *J. Am. Chem. Soc.*, **96**, 6169 (1974).

8) K. Wallenfels and M. Gellrich, *Chem. Ber.*, **92**, 1406 (1959).

9) A preliminary communication: K. Kano and T. Matsuo, *Tetrahedron Lett.*, **1975**, 1389.

10) H. Diekmann, G. Engert, and K. Wallenfels, *Tetrahedron*, **20**, 291 (1964).

11) The melting points (decomposition points) of **1** (164—165.5 °C) and **2** (169 °C) were reproducible as far as the measurement was made on a hot-stage apparatus. However, **1** and **2** decomposed at >187 °C and 180—182 °C, respectively, and turned into brown resins when the measurement was carried out with degassed samples in capillary tubes and a heating bath. Both resins gradually melted at 210—220 °C. **1** and **2** might have been oxidized by air during the course of mesurement on the hot-stage, the resulting oxidation products decomposing at 164—165.5 °C (**1**) and 169 °C (**2**). The difference in the mp (dec) of **1** between the present experiment and that by Wallenfels and Gellrich seems to be due to the difference in the method of measurement.

12) E. M. Kosower and J. L. Cotter, *J. Am. Chem., Soc.*, **86**, 5524 (1964).

13) B. Pullman and A. Pullman, *Proc. Natl. Acad. Sci. U.S.A.*, **45**, 136 (1972).

14) K. Kano, T. Shibata, M. Kajiwara, and T. Matsuo, *Tetrahedron Lett.*, **1975**, 3693.

15) A. Ohno, T. Kimura, S. Oka, Y. Ohnishi, and M. Kagami, *Tetrahedron Lett.*, **1975**, 2371.

16) P. Karrer and F. J. Stare, *Helv. Chim. Acta*, **20**, 418 (1937).

17) A. Singer and S. M. McElvain, *Org. Synth.*, Coll. Vol. II, 860 (1943).

Synthesis of Dihalogenobis(2-pyridinethiolato)tin(IV) by the Oxidative Addition of Disulfide to Tin(II) Halides—Consideration on the Coordination Structure[1]

Mitsuo MASAKI and Satoshi MATSUNAMI

Polymer Research Laboratory, Ube Industries, Ltd., Minami-Kaigan, Goi, Ichihara, Chiba 290

(Received May 11, 1976)

The reaction of di-2-pyridyl disulfide with tin(II) halides was found to give dihalogenobis(2-pyridinethiolato)-tin(IV). The oxidative addition reaction was successfully extended to the preparation of other dihalogenodithiolatotin(IV) complexes. Dichlorobis(2-pyridinethiolato)tin(IV) was also prepared by the reaction of 2(1*H*)-pyridinethione with tin(IV) chloride and proposed to be a monomeric, octahedral complex with a four-membered (Sn, S, C, and N) chelate ring from its molecular weight and IR spectral data. Dichlorobis(2-quinolinethiolato)tin(IV) could be isolated similarly as a stable complex. However, attempts to isolate the dichlorodithiolatotin(IV) in which an intramolecular chelation seems hardly possible were unsuccessful. The great stability of bis(2-pyridinethiolato)- and bis(2-quinolinethiolato)-dihalogenotin(IV) could be ascribed to the intramolecular four-membered chelate ring formation for the six-coordination of tin atom.

In a previous paper, an isolation of a stable complex, dichlorobis(2-pyridinethiolato)tin(IV) (**1**) was reported.[2] Several types of stable dihalogenodithiolatotin(IV) complexes, formed with dithiocarbamato,[3] phosphinodithionito,[4] alkoxycarbonylmethanethiolato,[5] 1,3-diphenyl-3-thioxo-1-propanonato[6] and 2-pyridinethiolato *N*-oxide[7] are known. These ligands act as a bidentate in the complexes and allow the intramolecular chelation for six-coordination of tin atom. Six-membered(Sn, S, 3 C, and O), five-membered (Sn, S, C, C or N, and O) and four-membered (Sn, S, C or P, and S) chelate ring structures have been proposed for the complexes. Six-coordination of the tin atom seems possible for the complex **1** by a coordination of the pyridine nucleus through nitrogen. Such a coordination, however, would lead to the formation of a new type four-membered (Sn, S, C, and N) chelate ring.

This paper deals with the synthesis of dihalogenobis-(2-pyridinethiolato)tin(IV) by the oxidative addition reaction of di-2-pyridyl disulfide to tin(II) halides, an extension of the reaction to prepare other dihalogenodithiolatotin(IV) complexes, and an observation on the structure of **1**, as well as a consideration on a relationship between the stability of dihalogenodithiolatotin-(IV) complex and its coordination structure.

Results and Discussion

Synthesis. When tin(II) chloride was mixed with an equimolar or excess amount of di-2-pyridyl disulfide in an organic solvent such as 1,2-dichloroethane or benzene at room temperature, an exothermic reaction occurred and dichlorobis(2-pyridinethiolato)-tin(IV) (**1**) was produced in a high yield. The product was identified by IR spectrum with the specimen prepared from the reaction of 2(1*H*)-pyridinethione with tin(IV) compounds. Analogous reactions of the disulfide with tin(II) bromide and tin(II) iodide afforded dibromobis(2-pyridinethiolato)tin(IV) and diiodobis(2-pyridinethiolato)tin(IV) in high yields. The reactions of bis(substituted 2-pyridyl) disulfides with tin(II) chloride proceeded in a similar way to give the corresponding dichlorodithiolatotin(IV) complexes. The results are given in Table 1.

Treatment of di-2-pyridyl disulfide *N,N'*-dioxide with tin(II) chloride or fluoride in an aqueous hydrohalogenic acid gives the complex of the dioxide with the tin(II) halide.[8] Dihalogenobis(2-pyridinethiolato *N*-oxide)-tin(IV) was prepared from 2-pyridinethiol *N*-oxide and tin(IV) halide.[7] In contrast, the treatment of di-2-pyridyl disulfide with tin(II) chloride in an aqueous hydrochloric acid afforded neither the tin(II) complex nor **1**, but 2(1*H*)-pyridinethione in 75% yield. No report seems to have appeared on such an oxidative addition of disulfide to tin(II) halide.[9]

The reaction was successfully extended to the preparation of other dihalogenodithiolatotin(IV) complexes. Dichlorobis(ethoxycarbonylmethanethiolato)tin(IV) was obtained from the reaction of bis(ethoxycarbonylmethyl) disulfide with tin(II) chloride in refluxing ethanol. The reaction of bis(dialkylthiocarbamoyl) disulfide with tin(II) chloride or fluoride in 1,2-dichloroethane afforded the corresponding dihalogenobis(dialkyldithiocarbamato)tin(IV), respectively. Since tin(II) halides are almost insoluble in 1,2-dichloroethane or benzene, the use of a soluble complex of tin(II) halide with an inert organic ligand such as triphenylphosphine oxide or hexahydro-2*H*-azepin-2-one was attempted with successful results. The advantage of this method lies in the fact that the reaction can be carried out smoothly in a homogeneous system affording a highly pure product in a good yield without purification process. Dichlorobis(2-pyridinethiolato *N*-oxide)-tin(IV) was prepared readily from the corresponding disulfide and the complex of tin(II) chloride with the ligand mentioned above. The results are given in Table 1.

Complex **1** can be obtained from the reaction of 2(1*H*)-pyridinethione with dichlorobis(organo-oxy)tin-(IV) such as bis(acetylacetonato)dichlorotin(IV).[2] It was also prepared either by the reaction of 2(1*H*)-pyridinethione with tin(IV) chloride in the presence of base, or by the treatment of tetrachlorobis[2(1*H*)-pyridinethione]tin(IV) with a large excess of water. The treatment of **1** with hydrogen chloride under anhydrous conditions afforded tetrachlorobis[2(1*H*)-pyridinethione]tin(IV). The results are illustrated in Scheme 1.

TABLE 1. DICHLORODITHIOLATOTIN(IV) $[(RS)_2SnX_2]$

Compound R	X	Reaction conditions: Method[a]	Solvent	Temp	Time h	Mp °C [lit]	Yield %	Anal, % Found (Calcd) C	H	N	S	X
2-Pyridyl	Br	A	EDC	r. t.	5	278—280	81	24.30	1.69	5.62	12.78	
								(24.08)	(1.62)	(5.62)	(12.85)	
	I	A	EDC	r. t.	3	271—273	84	20.18	1.24	4.95	10.63	43.09
								(20.26)	(1.36)	(4.73)	(10.82)	(42.81)
3-(CN)-4,6-Me_2-2-pyridyl	Cl	A	PhH	r. t.	1	259—260 (dec)	74	37.29	2.72	10.87	12.29	14.15
								(37.24)	(2.73)	(10.86)	(12.43)	(13.74)
	Cl	C	PhH	r. t.	12		93					
3-(CN)-4-Me-6-Ph-2-pyridyl	Cl	A	PhH	r. t.	12	304—305 (dec)	88	49.40	2.93	8.72	10.12	10.87
								(48.79)	(2.83)	(8.75)	(10.02)	(11.08)
	Cl	C	PhH	r. t.	12		90					
4,6-Me_2-2-pyridyl	Cl[b]	A	PhH	r. t.	12	198—201	55	36.06	3.40	6.19	13.47	15.04
								(36.08)	(3.46)	((6.01)	(13.76)	(15.22)
	Cl	C	Xylene[c]	refl.	2		90					
	Cl	B	PhH	refl.	2		57					
3-(CN)-6-Me-2-pyridyl	Cl	A	PhH	refl.	1	262—265 (dec)	78	34.79	2.13	11.95	13.38	14.30
								(34.47)	(2.07)	(11.48)	(13.14)	(14.53)
	Cl	C	Xylene	refl.	1		97					
3-(COOEt)-6-Me-2-pyridyl	Cl	A	PhH (CCl_4)[d]	r. t.	2.5	165.5—166.0	84	37.20	3.37	4.96	11.04	12.37
								(37.14)	(3.46)	(4.81)	(11.02)	(12.18)
3-(COOEt)-4,6-Me_2-2-pyridyl	Cl	C	PhH	refl.	1	202—203	84	39.25	3.71	4.52	10.45	11.62
								(39.38)	(3.97)	(4.59)	(10.51)	(11.62)
5-(NO_2)-2-pyridyl	Cl	A	PhH (CCl_4-*i*-PrOH)[d]	r. t.	0.5	260—262 (dec)	67	24.33	1.30	11.38	13.07	14.14
								(24.03)	(1.20)	(11.21)	(12.83)	(14.18)
1-Oxido-2-pyridyl	Cl	A	PhH	r. t.	3	300.5—302.0 (dec) [297—298.5][7]	94					
	Cl	C	PhH	70 °C	0.3		91					
2-Quinolyl	Cl	C	PhH	refl.	0.5	313—319 (dec)	97	42.51	2.29	5.60	12.84	14.14
								(42.39)	(2.37)	(5.49)	(12.57)	(13.90)
4-Me-2-quinolyl	Cl	C	EDC	refl.	0.5	291—293 (dec)	87	44.45	2.93	5.46	11.83	13.06
								(44.64)	(3.00)	(5.21)	(11.91)	(13.18)
Ethoxycarbonyl-methyl	Cl	A	EtOH	r. t.	5	163—163.5	66	22.53	3.12		14.60	16.55
								(22.45)	(3.30)		(14.99)	(16.57)
Dimethylthio-carbamoyl	Cl	A	EDC (PhH)[d]	r. t.	8.5	266—268 (dec) [244—246][3c]	94					
	F	A	EDC	refl.	6	300	90	18.64	3.19	7.25	32.54	
								(18.15)	(3.05)	(7.05)	(32.29)	
Diethylthio-carbamoyl	Cl	A	EDC	r. t.	48	211—212 [200—201][3c]	49					
	F[3b]	A	EDC (EtOAc)[d]	refl.	11	196—197 (dec)	70	26.70	4.39	6.21	28.31	
								(26.51)	(4.45)	(6.18)	(28.30)	
2-Benzothiazolyl	Cl	A	$PhCH_3$	refl.	7		trace[e]					

a) A and B indicate procedures similar to methods *a*) and *b*) for **1**, respectively, C indicates a procedure similar to the method reported for **1**.[2] b) Mol wt: Found: 481; Calcd: 466. c) refl.: refluxing temperature. d) The solvent in parentheses was used for separation of the products after termination of the reaction. e) The product could be confirmed only by mass spectrum; *m/e* 522(M^+).

Observation on Structure. Complex **1** is monomeric in dilute methyl isobutyl ketone (osmometry) at ambient temperature. The mass spectrum of **1** exhibits the monotin-containing, polyisotopic molecular ion (*m/e* 410) as the highest mass feature, which corresponds to the parent peak of the monomer. The remaining major peaks (*m/e* 375, 340, 300, 265, and 230) in the spectrum can be assigned to species resulting from the loss of one or two chlorine and/or a pyridinethiolato group from the parent molecular ion. However, no molecular ion corresponding to ditin-containing species was observed. This suggests that **1** is the monomeric tin(IV) complex.

The IR spectrum of **1** exhibits four bands due to

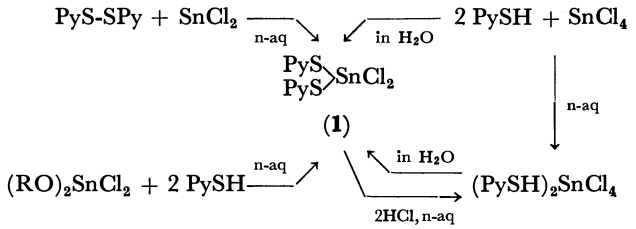

Py: pyridyl, n-aq: in non-aqueous organic solvent

Scheme 1.

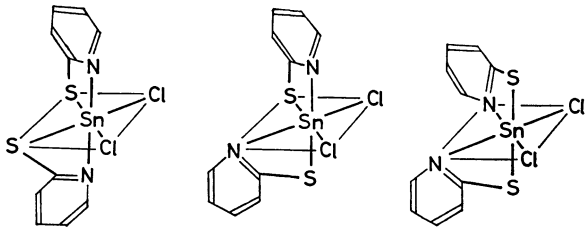

Fig. 1. Three possible structures for **1**. The enantiomers are possible for the respective structures.

ring vibration (C=C/C=N stretching) at 1580(s), 1550 (m), 1435(s), and 1420 cm^{-1}(s) in the 1600—1400 cm^{-1} region. This absorption pattern corresponds to that of di-2-pyridyl disulfide [1570(s), 1555(m), 1440(s), and 1410 cm^{-1} (s)], rather than to that of 2(1*H*)-pyridinethione [1610(m), 1575 (s; N–H bending), 1500(w), and 1435 cm^{-1} (m)]. The spectrum of **1** exhibits no remarkable band in C=S stretching spectral region, while a very strong intensity absorption band at 1136 cm^{-1} is observed in the spectrum of 2(1*H*)-pyridinethione. This indicates that the two 2-pyridinethiolato ligands in **1** exist not in an unequivocal thione form but rather in the thiol form like di-2-pyridyl disulfide. On the other hand, a difference in the spectra between **1** and di-2-pyridyl disulfide is observed in the absorption bands due to ring vibrations and C–H bending vibrations. The ring vibration frequencies which are present at 990 and 610 cm^{-1} in di-2-pyridyl disulfide shift to 1010 and 650 cm^{-1} in **1**, respectively. The shift to higher frequency region confirms the coordination of pyridine nucleus through nitrogen to tin atom.[10] The C–H out of plane bending vibration bands in **1** are at 770(m), 755(m), and 720 cm^{-1} (m), while the absorptions are at 750 (s; doublet) and 710 cm^{-1} (m) in the disulfide. The shift to higher frequency region in **1** can be interpreted again by the coordination of pyridine nucleus through nitrogen, which are likely to cause a depletion of π-electron density on the pyridine ring.[11] Additional information is available in the 500—200 cm^{-1} spectral region. Since a decisive assignment of all the bands in this region is difficult, dimethylbis(2-pyridinethiolato)tin(IV) was synthesized for comparison from dichlorodimethyltin(IV) and 2(1*H*)-pyridinethione. It was found that the three strong absorption bands at 310, 300, and 270 cm^{-1} are characteristic of **1**. The former two bands can be assigned to the Sn–Cl vibrations, since the frequency range is quite close to that of six-coordinated octahedral tin(VI) complexes[10,12–14] and absorption due to Sn–N vibration should be in a lower frequency region.[14] Two Sn–Cl stretching bands suggest *cis* configuration for the chlorine atoms in this complex, since only one Sn–Cl stretching band is expected for the *trans* configuration.[2,12]

Thus, six possible structures can be envisaged for **1**, *cis* Sn–S and *trans* Sn–N, *cis* Sn–S and *cis* Sn–N, and *trans* Sn–S and *cis* Sn–N, and their respective enantiomers. Three possible structures are shown in Fig. 1. However, it is not clear which structure is favorable, since no decisive information is available as to whether the two sulfur–tin bonds are *cis* or *trans*.

Consideration on Stability. Dihalogenobis(2-pyridinethiolato)tin(IV) is not sensitive to hydrolysis, being energetically so stable that it can be readily obtained under mild conditions from various starting materials including highly stable bis(acetylacetonato)dichlorotin(IV).[15] All the monomeric, octahedral dihalogenodithiolatotin(IV) complexes reported hitherto[3–7] are similarly stable. However, there has been no report on the dihalogenodithiolatotin(IV) complexes in which an intramolecular chelation is absent, except bis(benzenethiolato)dichlorotin(IV). Klages *et al.* reported that bis(benzenethiolato)dichlorotin(IV) can be obtained by the thermal dehydrochlorination of the complex prepared from 2 equiv of benzenethiol and tin(IV) chloride.[16]

In the course of repeated experiments on the reaction of benzenethiol with tin(IV) chloride in molar ratio 2 : 1 under several conditions, we could not isolate bis(benzenethiolato)dichlorotin(IV) but obtained diphenyl disulfide and tin(II) chloride together with tetrakis(benzenethiolato)tin(IV). This suggests that bis(benzenethiolato)dichlorotin(IV) is so unstable as to decompose giving diphenyl disulfide and tin(II) chloride or to disproportionate to tetrakis(benzenethiolato)-tin(IV) and tin(IV) chloride.

The stability of the dihalogenobis(2-pyridinethiolato)-tin(IV) could be ascribed to the octahedral structure with the four-membered chelate ring condensed with pyridine ring. In order to confirm this, syntheses of several dichlorodithiolatotin(IV) were attempted.

The reaction of bis(acetylacetonato)dichlorotin(IV) with 2(1*H*)-quinolinethione or 4-methyl-2(1*H*)-quinolinethione gave dichlorobis(2-quinolinethiolato)tin(IV) or its 4-methyl homolog as a stable complex in a good yield, as expected. Attempts to prepare dichlorotin-(IV) derivatives of five-membered heterocyclethiol[17] were then made by reactions of bis(acetylacetonato)-dichlorotin(IV) or dichlorobis(hexahydro-2*H*-azepin-2-onato)tin(IV) with the various thiols or by reactions of tin(II) chloride with the corresponding disulfides. However, all the attempts were unsuccessful except for dichlorobis(2-benzothiazolethiolato)tin(IV), which could be obtained from either of the reactions as a very unstable product.

The unsuccessful syntheses can be ascribed to the unstability of the desired products. Dichlorotin(IV) derivative of the five-membered heterocyclethiols would not take an octahedral structure, since an intramolecular chelation would be hardly possible owing to the strain of four-membered chelate ring condensed with the five-membered cycle.[18] The unstability of a dichlorodi-

Table 2. Substituted dipyridyldisulfides [RSSR]

Compound	Solvent for recryst.	Mp °C	Yield %	Anal, % Found (Calcd) C	H	N	S
3-(CN)-4-Me-6-Ph-2-pyridyl	C_6H_6	200—201	97	69.46 (69.31)	3.70 (4.02)	12.65 (12.43)	14.16 (14.23)
4,6-Me_2-2-pyridyl	MeOH-H_2O	84.0—84.5	84	60.83 (60.83)	5.93 (5.83)	10.19 (10.13)	23.04 (23.20)
3-(COOEt)-6-Me-2-pyridyl	CCl_4	138—140	73	54.88 (55.08)	5.06 (5.14)	7.31 (7.14)	16.14 (16.34)
3-(CN)-6-Me-2-pyridyl	*i*-PrOH	172—173.5	68	56.47 (56.36)	3.43 (3.38)	18.29 (18.78)	21.99 (21.49)

thiolatotin(IV) which is not octahedral was also supported by an unsuccessful preparation of dichlorotin(IV) derivative of ethanethiol or phenylmethanethiol.

The results suggest that six-coordination with an intramolecular chelation is of considerable importance for stabilization of a monomeric dihalogenodithiolatotin(IV) complex.

Experimental

All the melting points were determined in a liquid bath and are uncorrected. The products were identified, unless otherwise stated, by comparison of the melting points and IR spectra with those of authentic samples as well as elemental analyses. The IR spectra were measured in KBr disk with a Hitachi Perkin-Elmer 225 Grating Infrared Spectrometer and a JASCO IR-G Grating Infrared Spectrometer. The molecular weight was determined in methyl isobutyl ketone with a Hitachi 115 Vapor Pressure Osmometer.

Materials. Commercial anhydrous $SnCl_2$ was used after drying over sulfuric acid. Substituted pyridyl disulfides were prepared from the corresponding substituted pyridinethiol by a procedure midified from that described for the preparation of di-2-pyridyl disulfides.[19] Appropriate thiol (0.1 mol) was dissolved in a solution of sodium ethoxide (0.1 mol) in ethanol (80—160 ml). To the resulting solution was added dropwise a solution of iodine (0.05 mol) in ethanol (90—190 ml). The precipitated product was collected and recrystallized. When the reaction mixture was homogeneous, it was concentrated under reduced pressure, and the residue was treated with water (120 ml) to give the crude disulfide, which was recrystallized. The results for new compounds are given in Table 2.

Dichlorobis(2-pyridinethiolato)tin(IV) **1**. *a) Reaction of Di-2-pyridyl Disulfide with $SnCl_2$*: A solution of di-2-pyridyl disulfide (19.40 g, 88.1 mmol) in 1,2-dichloroethane (EDC, 70 ml) was added drop by drop to a suspension of $SnCl_2$ (13.76 g, 72.6 mmol) in EDC (50 ml) at 10 °C and the mixture was stirred at room temperature for 12 h. The precipitate was collected by filtration, washed with EDC(200 ml), and dried to give 28.86 g of a slightly pale yellow powdery solid; mp 275—277 °C (dec). The solid (6 g) was recrystallized from methyl isobutyl ketone (650 ml) to give slightly pale yellow prisms (4.33 g); mp 275—277 °C (dec). The product was identified with the specimen reported previously.[2] Yield, 97%. Mol wt: Found: 385; Calcd: 410.

The use of a solution of triphenylphosphine oxide–tin(II) chloride (41.22 g, 88.1 mmol) complex or hexahydro-2*H*-azepin-2-one–tin(II) chloride (36.64 g, 88.1 mmol) complex in EDC in place of the suspension of $SnCl_2$ gave a similar result.

b) Treatment of Tetrachlorobis[2(1H)-pyridinethione]tin(IV) with Triethylenediamine: A solution of trietylenediamine (2.81 g, 25 mmol) in benzene (30 ml) was added drop by drop to a suspension of tetrachlorobis[2(1*H*)-pyridinethione]tin(IV) (12.07 g, 25 mmol) in benzene (120 ml) at room temperature. After completion of the addition, the mixture was refluxed by heating for 2 h. The reaction mixture was filtered to give 14.69 g of a mixture of **1** and triethylenediamine dihydrochloride. The mixture was washed repeatedly with ice-water and then dried to give 10.04 g (98%) of **1**; mp 275—277 °C (dec).

c) Treatment of Tetrachlorobis[2(1H)-pyridinethione]tin(IV) with Water: Tetrachlorobis[2(1*H*)-pyridinethione]tin(IV) (4.83 g 10 mmol) was suspended in water (100 ml) and the mixture was stirred vigorously at room temperature for 20 min. The suspension was filtered, washed with water, and dried to give 3.45 g (84%) of **1**; mp 275—277 °C (dec).

Dichloro(triphenylphosphine oxide)tin(II). To a solution of triphenylphosphine oxide (5.56 g, 20 mmol) in benzene (40 ml) was added $SnCl_2$ (3.78 g, 20 mmol), and the mixture was heated with stirring to the refluxing temperature. The resulting solution was filtered and left to stand at room temperature under nitrogen atmosphere. The precipitated crystals were collected and washed with a small amount of benzene to give 9.92 g of dichloro(triphenylphosphine oxide)tin(II)–benzene adduct (1 : 1) as colorless crystals; mp 81—84 °C (sinter at 67 °C). Found: C, 52.97; H, 3.89; Cl, 12.91%. Calcd for $C_{30}H_{26}Cl_2OPSn$; C, 52.89; H, 3.70; Cl, 13.01%.

The adduct was dried at 50 °C under reduced pressure to give the benzene free adduct; mp 96—97 °C.

Found: C, 46.13; H, 3.37; Cl, 15.14%. Calcd for $C_{24}H_{20}Cl_2OPSn$: C, 46.16; H, 3.21; Cl, 15.18%.

4,6-Dimethyl-2-pyridinethiol. A suspension of 3-cyano-4,6-dimethyl-2-pyridinethiol[20] (48.21 g, 294 mmol) in 250 ml of aqueous hydrobromic acid (48%) was heated with refluxing for 4 h and left to stand at room temperature for several hours. The resulting precipitate was filtered and recrystallized from ethanol (1700 ml) to give 9.31 g (17%) of 2-mercapto-4,6-dimethyl-3-pyridinecarboxylic acid; mp 253—254 °C (dec). Found: C, 52.40; H, 4.99; N, 7.57; S, 17.70%. Calcd for $C_8H_9NO_2S$: C, 52.44; H, 4.95; N, 7.64; S, 17.50%.

The filtrate separated from the carboxylic acid was diluted with water (1500 ml) and allowed to stand overnight at room temperature to give 11.64 g of yellow precipitate. Recrystallization from acetonitrile (800 ml) gave 7.50 g (18%) of the title compound as yellow prisms; mp 239—241 °C. Found: C, 60.42; H, 6.52; N, 10.18; S, 22.74%. Calcd for C_7H_9NS: C, 60.39; H, 6.52; N, 10.06; S, 23.03%.

Ethyl 2-Mercapto-6-methyl-3-pyridinecarboxylate. Into a suspension of 2-mercapto-6-methyl-3-pyridinecarboxylic acid[21] (14.44 g, 85.3 mmol) and ethanol (200 ml) was passed dry hydrogen chloride with refluxing by heating for

5 h and the mixture was allowed to stand at room temperature overnight. The resulting crystalline precipitate was collected (9.60 g) and neutrallized by treating with an aqueous solution of sodium hydrogen carbonate. Recrystallization from diisopropyl ether (1500 ml) gave 5.41 g (32%) of yellowish prisms; mp 129—131 °C. Found: C, 54.69; H, 5.40; N, 7.11; S, 16.23%. Calcd for $C_9H_{11}NO_2S$: C, 54.80; H, 5.62; N, 7.10; S, 16.22%.

Ethyl 2-Mercapto-4,6-dimethyl-3-pyridinecarboxylate. Into a homogeneous mixture of ethyl cyanoacetate (80 g, 0.7 mol), pyridine (80 ml) and triethylamine (50 ml) was passed dry hydrogen sulfide at room temperature for 7 h. The reaction mixture was poured into water (250 ml) and extracted three times with diisopropyl ether. The combined extracts were concentrated and the residue was chromatographed on a silica gel (Wakogel C-200) column, immersed in benzene. Elution with benzene–1-butanol (4 :1) afforded ethyl thiocarbamoylacetate (55.33 g) as the first running substance. A mixture of the thiocarbamoylacetate (40.22 g, 0.27 mol), acetylacetone (54.7 g, 0.55 mol) and triethylamine (10 g) was heated at 50 °C for 5 h, and then treated with diisopropyl ether (100 ml). The crystalline product was recrystallized twice from isopropyl alcohol (350 ml)–diisopropyl ether (150 ml) to give 35 g (61%) of pale brown needles; mp 154.5—155.5 °C. Found: C, 57.05; H, 6.25; N, 6.76; S, 15.00%. Calcd for $C_{10}H_{13}NO_2S$: C, 56.85; H, 6.20; N, 6.63; S, 15.17%.

Reaction of **1** *with Hydrogen Chloride.* Into a suspension of **1** (4.10 g, 10 mmol) in EDC (100 ml) was passed dry hydrogen chloride (400 ml) below −20 °C. The reaction mixture was concentrated under reduced pressure, and the residue was treated with EDC (100 ml). Filtration followed by drying at 100 °C under reduced pressure for 5 h gave 4.83 g (100%) of tetrachlorobis[2(1*H*)-pyridinethione]tin(IV), which was identified with the authentic specimen described below.

Tetrachlorobis[2(1H)-pyridinethione]tin(IV). A solution of tin(IV) chloride (3.13 g, 12 mmol) in EDC (20 ml) was added drop by drop to a solution of 2(1*H*)-pyridinethione (2.67 g, 24 mmol) in EDC (80 ml) with stirring at room temperature. After the addition, the mixture was stirred for 15 h. The resulting solid was collected by filtration, washed with EDC (30 ml), and dried to give 5.79 g (100%) of yellow crystalline powder; mp 224—226 °C. Found: C, 25.22; H, 2.12; N, 6.11; S, 13.34; Cl, 29.10%. Calcd for $C_{10}H_{10}Cl_4N_2S_2Sn$: C, 24.87; H, 2.09; N, 5.80; S, 13.28; Cl, 29.37%.

Dimethylbis(2-pyridinethiolato)tin(IV). To a solution of sodium ethoxide (30.4 mmol) in ethanol (150 ml) was added 2(1*H*)-pyridinethione (3.38 g, 30.4 mmol) and then dimethyldichlorotin(IV) (1.82 g, 15.2 mmol). After being stirred at room temperature for 2 h, the mixture was concentrated and the residue was treated with water (200 ml). The insoluble substance was collected by filtration, washed with water (30 ml) and dried to give 2.96 g of crude product, which was recrystallized from isopropyl alcohol (40 ml) to give 2.62 g (47%) of colorless needles; mp 139 °C. IR (KBr): 1570, 1550, 1445, 1410, 990, 740, 720, 620, 395, and 360 cm^{-1}. Found: C, 39.00; H, 3.77; N, 7.39; S, 17.41%. Calcd for $C_{12}H_{14}N_2S_2Sn$: C, 39.05; H, 3.82; N, 7.59; S, 17.38%.

An Attempted Synthesis of Bis(benzenethiolato)dichlorotin(IV). A solution of bis(benzenethiol)tetrachlorotin(IV),[16] prepared by adding a solution of tin(IV) chloride (10.42 g, 40 mmol) in EDC (50 ml) to a solution of benzenethiol (8.82 g, 80 mmol) in EDC (100 ml) below −20 °C, was refluxed by heating for 8 h, during which dry nitrogen gas was passed through a capillary in the mixture, in order to remove hydrogen chloride formed. Eighty percent of hydrogen chloride based on benzenethiol was trapped in 0.5 M aqueous sodium hydroxide solution from the exhaust nitrogen gas. The product precipitated in the reaction mixture was collected by filtration and confirmed to be $SnCl_2$ (1.20 g, 16% based on $SnCl_4$) by being converted into dichloro(triphenylphosphine oxide)tin(II), which was identified with the authentic sample. To the filtrate was added triphenylphosphine oxide (9.39 g, 33.7 mmol), and the mixture was stirred for 0.5 h. The mixture was then concentrated and the residue was treated with benzene (150 ml). The resulting precipitate was collected by filtration, washed with benzene (70 ml), and dried to give 13.72 g (42% based on $SnCl_4$ used) of tetrachlorobis(triphenylphosphine oxide)tin(IV); mp 330—332 °C (lit,[22] mp 323 °C). The filtrate separated from the tin(IV) complex and the washing were combined and concentrated, and to the residue was added hexane (30 ml). The insoluble yellow crystals were collected by filtration and washed with hexane (15 ml×2). Crude tetrakis(benzenethiolato)-tin(IV) (**2**) was obtained: 6.40 g. The combined filtrate and washings were concentrated and the residue was chromatographed on a silica gel column (Wakogel C-300) immersed in hexane. Elution with hexane afforded 1.35 g (7.7% based on benzenethiol) of diphenyl disulfide; mp 58—60 °C (lit,[23] mp 60—62 °C). Subsequent elution with benzene gave 1.26 g of **2**, which was identified by its IR spectrum. Two crops of **2** were combined and recrystallized from isopropyl alcohol (220 ml). Pale yellow needles, 4.06 g (18% based on $SnCl_4$); mp 65—66.5 °C (lit,[24] 63—64 °C).

The authors wish to express their gratitude to Dr. Masao Horio, Prof. Emeritus, Kyoto University, and Dr. Shotaro Sugiura, President, Polymer Research Laboratory, Ube Industries, for their encouragement.

References

1) A part of this work was presented at the 30th Annual Meeting of Chemical Society of Japan, Osaka, April, 1974. Preprint, Part III, p. 1238.

2) M. Masaki, K. Fukui, I. Uchida, and H. Yasuno, *Bull. Chem. Soc. Jpn.*, **48**, 2310 (1975).

3) a) F. Bonati and R. Ugo, *J. Organomet. Chem.*, **10**, 257 (1967); b) J. L. K. F. DeVries and R. H. Herber, *Inorg. Chem.*, **11**, 2458 (1972); c) F. Bonati, G. Mingetti, and S. Cenini, *Inorg. Chim. Acta*, **2**, 375 (1968).

4) W. Kuchen, A. Jadat, and J. Metten, *Chem. Ber.*, **98**, 3981 (1965); H. W. Roesky and M. Dietl, *Z. Anorg. Allg. Chem.*, **376**, 230 (1970); F. Bonati, S. Cenini, and R. Ugo, *Rend. Inst. Lombardo Sci. Lett.*, **A99**, 825 (1965); *Chem. Abstr.*, **65**, 1749c (1966).

5) Y. Yamaji, Y. Nakagawa, H. Matsuda, and S. Matsuda, *Kogyo Kagaku Zasshi*, **73**, 2222 (1970); *Chem. Abstr.*, **74**, 141999x (1971).

6) H. Schnorr, V. Pohl, E. Uhlemann, and P. Thomas, *Z. Chem.*, **13**, 143 (1973); E. Uhlemann and P. Thomas, *Z. Anorg. Allg. Chem.*, **356**, 71 (1967).

7) D. Petridis, F. P. Mullins, and C. Curpan, *Inorg. Chem.*, **9**, 1270 (1970).

8) B. A. Starrs, U. S. Patent 3027372; *Chem. Abstr.*, **57**, 12441i (1962); A. F. Langlykke, J. Bernstein, and L. La. Via. Milltown, U. S. Patent 3346578; *Chem. Abstr.*, **67**, 111459i (1967).

9) After this work had been completed,[1] the following reports appeared on oxidative addition reactions of organotin(II): K. D. Bos, E. J. Bulten, and J. G. Noltes [*J. Organo-*

met. Chem., **67**, C13 (1974)] on the reactions of organotin(II), such as dicyclopentadienyltin(II), diethyltin(II), and dimethoxytin(II), with diphenyl disulfide; W. P. Neuman and A. Schwarz [*Angew. Chem.*, **87**, 844 (1975)] on the reaction of dialkyltin(II) with peroxides or disulfides.

10) R. C. Paul, H. S. Makhni, P. Singh, and S. L. Chadha, *Z. Anorg. Allg. Chem.*, **337**, 108 (1970), and the references cited therein.

11) The depletion of π-electron density of aromatic nucleus is known to lead to a decreased ability of the carbon bonding orbitals to follow the out-of-plane movement of the hydrogen atoms, resulting in higher bending vibration frequencies: R. D. Kross, V. A. Fassel, and M. Margoshes, *J. Am. Chem. Soc.*, **78**, 1332 (1956). A similar phenomenon should be observed for the pyridine ring in complex **1**, since the resulting four-membered chelate ring would be on the same plane as the pyridine ring.

12) R. C. Paul and S. L. Chandha, *Aust. J. Chem.*, **22**, 1381 (1969).

13) I. R. Beattie and M. Milne, *J. Inorg. Nucl. Chem.*, **30**, 664 (1968).

14) N. Ohkaku and K. Nakamoto, *Inorg. Chem.*, **12**, 2440, 2446 (1973).

15) Y. Kawasaki, T. Tanaka, and R. Okawara, *Bull. Chem. Soc. Jpn.*, **40**, 1562 (1967).

16) F. Klages, A. Gleissner, and R. Ruhnau, *Chem. Ber.*, **92**, 834 (1959).

17) The thiols attempted for the reaction were 2-imidazolinethione, 4-methyl-, 4-phenyl-, and unsubstituted thiazole-2-thiol, 5-amino-1,3,4-thiadiazole-2-thiol, 1-methylimidazole-2-thiol, benzoxazole-2-thiol, benzimidazole-2-thiol, and benzothiazole-2-thiol.

18) Dimeric or polymeric octahedral structures also seem unfavorable owing to the bulkiness of the ligands.

19) W. Marckwald, W. Klemm, and H. Trabert, *Chem. Ber.*, **33**, 1556 (1900).

20) U. Schmidt and H. Kubitzek, *Chem. Ber.*, **93**, 1959 (1960).

21) V. G. Zhiryakov and P. I. Abramenko, *Khim. Geterotsikl. Soedin.*, **1965**, 334; *Chem. Abstr.*, **63**, 13231d (1965).

22) P. A. Yeats, J. R. Sams, and F. Aubke, *Inorg. Chem.*, **9**, 740 (1970).

23) H. Lecher, *Chem. Ber.*, **48**, 525 (1915).

24) W. E. Leistner and O. H. Knoepke, U. S. Patent 2726227; *Chem. Abstr.*, **50**, 6095d (1956).

Resolution of Amino Acids. XII. Preparation of L-2-Amino-5-arylpentanoic Acids, Constituent Amino Acids in AM-Toxins[1,2]

Yasuyuki SHIMOHIGASHI, Sannamu LEE, and Nobuo IZUMIYA

Laboratory of Biochemistry, Faculty of Science, Kyushu University, Hakozaki, Higashi-ku, Fukuoka 812

(Received May 13, 1976)

The L-forms of 2-amino-5-(*p*-methoxyphenyl)pentanoic acid (Amp), 2-amino-5-phenylpentanoic acid (App), and 2-amino-5-(*p*-hydroxyphenyl)pentanoic acid (Ahp) are constituent amino acids in AM-toxins. The *O*-methyl linkage of L-Amp was hydrolyzed gradually by heating with hydrochloric acid. A procedure without drastic acid treatment is given for the synthesis and resolution of Amp. Diethyl [3-(*p*-methoxyphenyl)propyl]acetamidomalonate (**3a**) was saponified to the corresponding malonic acid (**5a**), and **5a** was converted into acetyl-DL-Amp (DL-**6a**) by decarboxylation. The DL-**6a** and acetyl-DL-App were resolved by acylase to afford L-Amp and L-App, respectively. The L-Ahp was prepared from L-Amp by acid treatment.

A toxic substance isolated from *Alternaria mali* was named alternariolide by Okuno *et al.*[3] and AM-toxin I by Ueno *et al.*[4] They confirmed the structure to be a cyclic tetradepsipeptide which contains L-2-amino-5-(*p*-methoxyphenyl)pentanoic acid (L-Amp, L-**1a**) as a constituent.[3,4] Later Ueno *et al.* clarified the structures of AM-toxin II[4] and III,[5] indicating that II contains L-2-amino-5-phenylpentanoic acid (L-App, L-**1b**) and III L-2-amino-5-(*p*-hydroxyphenyl)pentanoic acid (L-Ahp, L-**1c**).[6] We

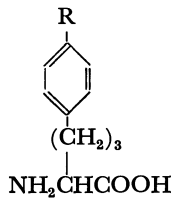

	R
Amp (**1a**)	OMe
App (**1b**)	H
Ahp (**1c**)	OH

undertook to synthesize AM-toxin I, II, and III with the intention of preparing three L-amino acids (L-**1a, b, c**). This paper deals with the synthesis of acetyl-DL-Amp and acetyl-DL-App, their subsequent optical resolution by acylase to afford L-Amp and L-App, and the preparation of L-Ahp from L-Amp by demethylation.

Okuno *et al.* reported the synthesis of DL-Amp by Strecker method which involves heating with hydrochloric acid.[7] There has been no report on the synthesis of L-Amp. Ueno *et al.*[4] and Okuno *et al.*[7] described the isolation of L-Amp by heating AM-toxin I with 6 M hydrochloric acid at 110 °C for 20 h, but they reported neither occurrence nor isolation of Ahp in the acid hydrolysate. The results indicate that *O*-methyl linkage in Amp is quite stable during the course of acid treatment. Izumiya and Nagamatsu prepared D-tyrosine from *O*-methyl-D-tyrosine (*O*-Me-D-Tyr) by refluxing in 48% hydrobromic acid.[8] Hirota *et al.* also isolated D-tyrosine together with *O*-Me-D-Tyr by heating Cyl-2, a cyclic tetrapeptide containing *O*-Me-D-Tyr residue as a constituent,[9] with 6 M hydrochloric acid at 115 °C for 15 h. These reports stimulated us to study the stability of *O*-methyl group of Amp against acid treatment. Both L-Amp and *O*-Me-L-Tyr were heated with 6 M hydrochloric acid at 110 °C for certain intervals, and the resulting solution was subjected to an amino acid analysis for determination of the amount of Ahp or tyrosine. The result is shown in Fig. 1. Unexpectedly the rate of demethylation of L-Amp was slightly greater than that of *O*-Me-L-Tyr.

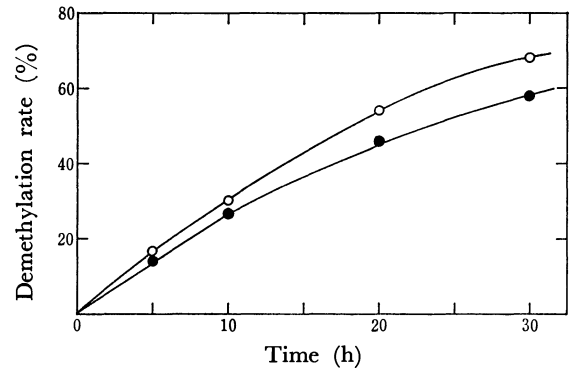

Fig. 1. Time course of demethylation of *O*-methyl-α-amino acids with 6 M HCl at 110 °C.
○: L-Amp, ●: *O*-Me-L-Tyr.

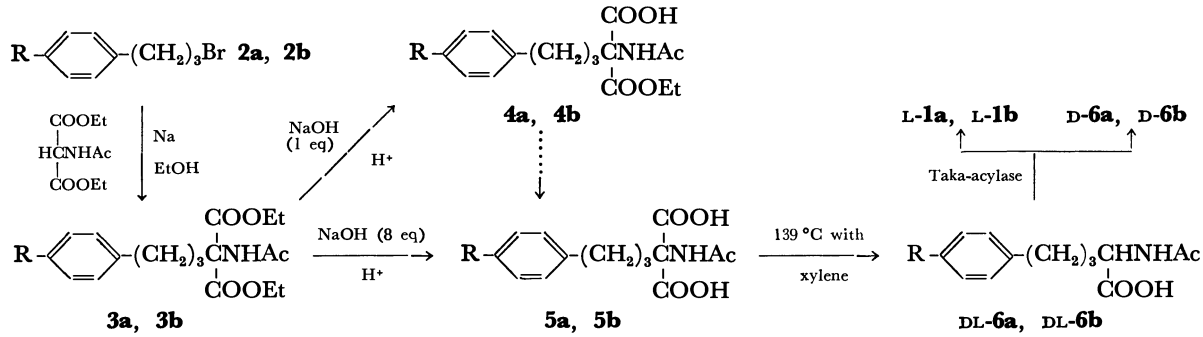

Scheme 1. Synthesis and resolution of acetyl-DL-amino acids (DL-**6a**, DL-**6b**).
a: R=OMe, **b**: R=H.

Table 1. Proteolytic coefficients (C_0) of acetylamino acids by Taka-acylase

Substrate	C_0[a]	
	0.05M[b]	0.01M[b]
Ac-DL-Phe	1.21	2.26
Ac-DL-Amp (DL-**6a**)	0.32	1.19
Ac-DL-App (DL-**6b**)	0.23	1.70

a) $C_0 = K_0/E$ where K_0 = % hydrolysis × min^{-1} and E = mg protein $N \times ml^{-1}$; pH 7.3, temp 38 °C. b) Concentration of L-form of substrate.

For the synthesis and optical resolution of Amp, we designed a route which involves no heating with a mineral acid. As shown in Scheme 1, diethyl [3-(*p*-methoxyphenyl)propyl]acetamidomalonate (**3a**) was prepared from alkyl bromide (**2a**) and diethyl acetamidomalonate in a yield of 64%. When **3a** was subjected to saponification with excess sodium hydroxide at 38 °C, TLC indicated that **3a** rapidly turned to **4a**, and that **3a** or **4a** finally turned to [3-(*p*-methoxyphenyl)propyl]acetamidomalonic acid (**5a**) after ten days; **5a** was obtained from **3a** in a yield of 95%. Pure **4a** was easily prepared from **3a** by the use of one equivalent of sodium hydroxide. Acetyl-DL-Amp (DL-**6a**) was obtained from **5a** by heating in xylene in a yield of 95%. Andrako *et al.* prepared a series of alkylacetamidomalonic acids (**7**) from the corresponding diethyl malonates with sodium hydroxide at 100 °C. They used it for the next step without isolating **7**; a suspension of **7** in water was heated to give the corresponging acetyl-DL-amino acid.[10] When we applied the procedure of Andrako *et al.* to **3a**, we could only isolate DL-**6a** in poor yield because of high hydrophobicity of a series of compounds (**3a**, **5a**, DL-**6a**).

Acetyl-DL-App (DL-**6b**) was also prepared in good yield by decarboxylation of **5b** (Scheme 1). Nakashima *et al.* reported the preparation of DL-**6b** by acetylation of DL-App which was synthesized from **3b** with refluxing hydrochloric acid.[11]

Prior to the preparative resolution of DL-**6a** and DL-**6b** by Taka-acylase, the rates of hydrolysis of two substrates were determined using acetyl-DL-Phe as a reference substrate. The results are given in Table 1. For the preparation of Taka-acylase from Takadiastase powder,[12] the procedure of Masaki *et al.*[13] was slightly modified. Although both L-**6a** and L-**6b** were less susceptible than Ac-L-Phe, the results indicate that optical resolution of DL-**6a** and DL-**6b** is achieved with a slightly increased amount of Taka-acylase. DL-**6a** or DL-**6b** was subjected to the action of Taka-acylase, the desired L-amino acid (L-**1a** or L-**1b**) being obtained in a yield of 83% or 82% (Scheme 1). Acetyl-D-amino acid (D-**6a** or D-**6b**) was isolated from the mother liquor after removal of L-amino acid. Nakashima *et al.* also isolated L-App from the reaction mixture of Ac-DL-App and aminoacylase.[11]

For the preparation of L-Ahp, the L-Amp was heated with 6 M hydrochloric acid for 80 h (Fig. 1), L-Ahp being isolated in a yield of 82%. We suspected the occurrence of partial racemization in Ahp during prolonged heating with hydrochloric acid. For the detection of possible racemate in L-Ahp isolated, the method of Manning and Moore[14] was applied with slight modification; benzyloxycarbonyl-L-leucine succinimide ester (Z-L-Leu-OSu) was used instead of L-leucine *N*-carboxyanhydride. DL-Ahp prepared from Ac-DL-Amp was coupled with Z-L-Leu-OSu, and the resulting Z-L-Leu-DL-Ahp was hydrogenated to afford L-Leu-DL-Ahp substance (**8**). In a similar manner, L-Leu-L-Ahp substance (**9**) was prepared from Z-L-Leu-OSu and the L-Ahp. A chromatogram of an amino acid analyzer is shown in Fig. 2. We assumed that a peptide showing peak C is L-Leu-L-Ahp while the one showing peak D is L-Leu-D-Ahp. Since **9** afforded peak C but no D, the L-Ahp is optically pure. In contrast, Manning and Moore reported that L-Leu-L-Tyr, which is a homolog of L-Leu-L-Ahp, is eluted more slowly than L-Leu-D-Tyr.[14] We obtained the same results[14] in the preparation of L-Leu-L-Tyr substance and L-Leu-DL-Tyr substance using Z-L-Leu-OSu, and subsequent chromatographic studies.

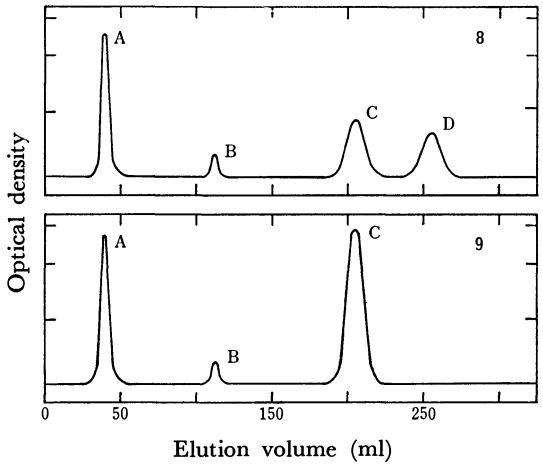

Fig. 2. Chromatogram of L-Leu-DL-Ahp substance (**8**) and L-Leu-L-Ahp substance (**9**). Buffer: pH 5.28 throughout. A: Leu, B: Ahp, C: L-Leu-L-Ahp, D: L-Leu-D-Ahp.

The synthesis of AM-toxin I by utilization of L-Amp has been reported.[2]

Experimental

All the melting points are uncorrected. TLC was carried out on silica gel G (Merck) with the solvent system; R_f^1, *n*-BuOH(1-butanol)–AcOH–pyridine–H_2O (4:1:1:2,v/v). Paper chromatography was carried out on Toyo Roshi No. 51 with the solvent system: R_f^2, the same solvent as that used for TLC; R_f^3, *n*-BuOH–AcOH–H_2O (4:1:2, v/v). Amino acids and peptides were determined with a Hitachi amino acid analyzer KLA-5 with spherical resin under the following conditions: flow rate, 60 ml/h; jacket temperature, 55 °C. Specific rotation was measured with a Union high sensitivity polarimeter PM-71.

*3-(p-Methoxyphenyl)propyl Bromide (**2a**).* The procedure of Catch *et al.*[15] was slightly modified as follows. Ethyl *p*-methoxycinnamate (65 g)[15] in EtOH (300 ml) was treated with hydrogen in the presence of Pd black (5 g). Absorption of hydrogen (7.1 l) ceased after about 18 h.

The catalyst was removed and the filtrate was distilled under reduced pressure to afford ethyl 3-(*p*-methoxyphenyl)propionate (**10**) (59.7 g, 91%), bp 148—149 °C/8 mmHg. The **10** (59.3 g) was reduced with $LiAlH_4$ (6.88 g), and the resulting 3-(*p*-methoxyphenyl)-1-propanol (48.2 g, 90%) was treated with PBr_3 (33.1 g) and **2a** was distilled (bp 117—119 °C/5 mmHg).[15] Yield of **2a**, 49.8 g (75%).

*3-Phenylpropyl Bromide (**2b**).* The procedure of Norris *et al.*[16] was slightly modified as follows. A mixture of 3-phenyl-1-propanol (54.8 g) and 48% hydrobromic acid (192 ml) was refluxed for 36 h. After being cooled the solution was diluted with water, and extracted with ether. The extract was washed successively with 4% Na_2CO_3 solution and water, and then dried (Na_2SO_4). After removal of the solvent, distillation under reduced pressure gave **2b** (71.5 g, 89%), bp 84—85 °C/5 mmHg.

*Diethyl [3-(p-Methoxyphenyl)propyl]acetamidomalonate (**3a**).* To a solution of Na (2.08 g, 90.4 mmol) in absolute EtOH (70 ml) was added diethyl acetamidomalonate (16.4 g, 75.5 mmol) under stirring. A solution of **2a** (17.3 g, 75.5 mmol) in absolute EtOH (30 ml) was added within 30 min. The brown solution was stirred under reflux for 8 h. The precipitate filtered off was washed with EtOH. The combined filtrates were evaporated *in vacuo* to give an oil which crystallized with the addition of water. The crystals collected were washed successively with water and ether–petroleum ether (1:1, v/v); yield, 17.6 g (64%); mp 97—99 °C; R_f^1 0.94.

Found: C, 62.44; H, 7.33; N, 3.89%. Calcd for $C_{19}H_{27}O_6N$: C, 62.45; H, 7.45; N, 3.83%.

*Diethyl (3-Phenylpropyl)acetamidomalonate (**3b**).* This was prepared from **2b** (50 g, 251 mmol) as described for **3a**; yield, 65.0 g (77%); mp 86—87 °C; R_f^1 0.95 (Found: C, 64.47; H, 7.56; N, 4.18%). Andrako *et al.* synthesized **3b** with mp 87—88 °C in 14% yield by the same method.[10]

*2-Acetamido-2-ethoxycarbonyl-5-(p-methoxyphenyl)pentanoic Acid (**4a**).* To a solution of **3a** (730 mg, 2 mmol) in EtOH (8 ml) was added 1 M NaOH (2 ml) at 0 °C. After being left to stand for 18 h at room temperature, the solution was evaporated and acidified with 1 M HCl (2.2 ml). The oil separated was extracted with AcOEt. The extract was washed with water, dried and evaporated. The residual solid was recrystallized from AcOEt–ether–petroleum ether; yield, 517 mg (77%); mp 126 °C; R_f^1 0.73.

Found: C, 60.37; H, 6.93; N, 4.11%. Calcd for $C_{17}H_{23}O_6N$: C, 60.52; H, 6.87; N, 4.15%.

*2-Acetamido-2-ethoxycarbonyl-5-phenylpentanoic Acid (**4b**).* This was prepared from **3b** (1.68 g, 5 mmol) as described for **4a**; yield, 1.09 g (71%); mp 129—130 °C; R_f^1 0.79.

Found: C, 62.30; H, 6.88; N, 4.68%. Calcd for $C_{16}H_{21}O_5N$: C, 62.52; H, 6.88; N, 4.56%.

*[3-(p-Methoxyphenyl)propyl]acetamidomalonic Acid (**5a**).* To a solution of **3a** (14.2 g, 38.9 mmol) in MeOH (350 ml) was added 2 M NaOH (160 ml). The solution was allowed to stand at 38 °C for 10 days until no **3a** or **4a** was detected in the reaction mixture; TLC was used as a monitor. The solution was evaporated, and acidified with 6 M HCl (55 ml). The liberated oil was extracted with AcOEt. The extract was washed with water, dried and evaporated. The residual solid was recrystallized from AcOEt–ether–petroleum ether; yield, 11.4 g (95%); mp 109—110 °C; R_f^1 0.61. Compound **5a** is less stable than **5b**; on being left to stand at room temperature for several days, purified crystals of **5a** gave a small amount of decarboxylated material (DL-**6a**) as detected by TLC. The values of elemental analysis of **5a** deviated from the calculated ones.

*(3-Phenylpropyl)acetamidomalonic Acid (**5b**).* This was prepared from **3b** (16.8 g, 50 mmol) with 2 M NaOH (200 ml) as described for the preparation of **5a**. The rate of saponification of **3b** was slightly greater than that of **3a**. Yield, 12.6 g (90%); mp 119—120 °C; R_f^1 0.64.

Found: C, 60.19; H, 6.16; N, 5.03%. Calcd for $C_{14}H_{17}O_5N$: C, 60.20; H, 6.14; N, 5.02%.

*Ac-DL-Amp (DL-**6a**).* Compound **5a** (8.47 g, 27.4 mmol) suspended in *p*-xylene (100 ml) was refluxed for 2 h. After being cooled at 0 °C, crystals were collected and washed with petroleum ether; yield, 6.91 g (95%); mp 132—133 °C; R_f^1 0.79.

Found: C, 63.45; H, 7.24; N, 5.19%. Calcd for $C_{14}H_{19}O_4N$: C, 63.38; H, 7.22; N, 5.28%.

*Ac-DL-App (DL-**6b**).* This was prepared from **5b** (12.0 g, 42.9 mmol) as described for DL-**6a**; yield, 9.10 g (90%); mp 148—149 °C; R_f^1 0.80 (Found: C, 66.47; H, 7.40; N, 5.82%). Reported value, mp 147—148 °C.[10]

Partially Purified Enzyme (Taka-acylase). Preparation of Taka-acylase: Takadiastase powder (100 g) was suspended in water (550 ml) and the insoluble material was filtered off at 0 °C. The filtrate was treated with $(NH_4)_2SO_4$ (92 g, 0.26 saturation) and centrifuged (10000 rpm, 20 min) at 0 °C. The supernatant phase was brought to 0.85 saturation with $(NH_4)_2SO_4$ (209 g) and centrifuged (10000 rpm, 20 min) at 0 °C. The sediment was suspended in 30% acetone (200 ml) at −5 °C and the suspension was centrifuged (12000 rpm, 30 min). The sediment was dissolved in a small amount of water, dialyzed and lyophilized; yield of powder(Taka-acylase), 397 mg.

Determination of Proteolytic Coefficient (C_0) *by Taka-acylase*: In a 2-ml flask, an acetyl-DL-amino acid and one equivalent of 0.5 M NaOH were added. Further 0.1 M sodium barbital buffer (1 ml) of pH 7.3, 1/80 M $CoCl_2$ (0.2 ml), and an aqueous enzyme solution (0.2 ml) containing Taka-acylase (4 mg) were added. The solution was made up to 2.0 ml with water. The reaction mixture was incubated at 38 °C, aliquots being withdrawn at selected intervals. The rate of appearance of free amino acid was followed by the amino acid analyzer: column, 0.9×10 cm; buffer, standard 0.2 M sodium citrate at pH 5.28. It was found that the hydrolysis of substrates follows zero-order kinetics within experimental error. The result is shown in Table 1.

*Resolution of Ac-DL-Amp (DL-**6a**). L-Amp (L-**1a**)*: DL-**6a** (5.31 g, 20 mmol) was dissolved in 0.2 M NaOH (110 ml), the pH being adjusted to 7.3 with AcOH. To the solution were added 128 mg of Taka-acylase in 0.2 M sodium acetate (20 ml) and 20 ml of 1/80 M $CoCl_2$. Water was added to bring the volume to 200 ml. After a few drops of toluene had been added, the solution was left to stand at 38 °C for 10 days. The precipitate formed was collected by filtration and washed with 100 ml of water (the precipitate was dissolved in a small amount of 1 M HCl and the solution was subjected to column chromatography). The pH of the combined filtrates was adjusted to 5 with 6 M HCl, a small amount of Norit was added, and the mixture was maintained at 50—60 °C for 10 min. The filtrate was evaporated to a small volume, its pH being adjusted to 3. The mixture was extracted with AcOEt, and the extract was washed with water (the extract was used for the preparation of Ac-D-Amp). The combined aqueous layers and the solution of the above precipitate in 1 M HCl were put on a column (2.2×20 cm) of Dowex 50×8 (H^+ form). The column was washed with water and eluted with 2 M NH_4OH (300 ml). The eluate was evaporated, and the residue was recrystallized from dilute HCl–Et_3N; yield, 1.85 g (83%); mp 232—234 °C (dec); $[\alpha]_D^{21}$ +31.8° (*c* 2.0, 5 M HCl–DMF);[17] R_f^2 0.88, R_f^3 0.76.

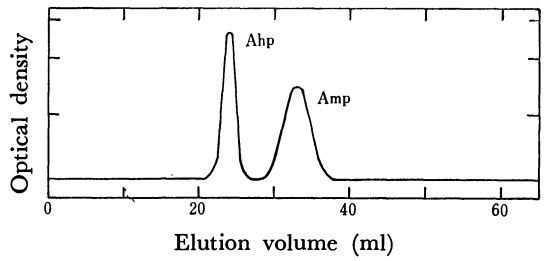

Fig. 3. Chromatogram of a solution after 20 h heating at 110 °C with 6 M HCl of L-Amp.

Found: C, 64.45; H, 7.60; N, 6.05%. Calcd for $C_{12}H_{17}O_3N$: C, 64.55; H, 7.68; N, 6.27%.

Ac-D-Amp (D-**6a**): The extract obtained above was dried (Na_2SO_4) and evaporated. Residual solid was recrystallized from EtOH–water; yield, 2.50 g (94%); mp 145 °C; $[\alpha]_D^{21}$ −16.1 ° (*c* 2.0, EtOH); R_f^1 0.79.

Found: C, 63.27; H, 7.18; N, 5.24%. Calcd for $C_{14}H_{19}O_4N$: C, 63.38; H, 7.22; N, 5.28%.

Resolution of Ac-DL-App (DL-**6b**). L-*App* (L-**1b**): DL-**6b** (5.88 g, 25 mmol) was treated with Taka-acylase as mentioned above. L-App was obtained from the reaction mixture, and an extract with AcOEt was set aside for the next step. Yield, 1.98 g (82%); mp 227—229 °C (dec); $[\alpha]_D^{21}$ +33.5 ° (*c* 2.0, 5 M HCl–DMF); R_f^2 0.91, R_f^3 0.77 (Found: C, 68.29; H, 7.79; N, 7.24%). Reported value, $[\alpha]_D^{21}$ +25.7 ° (1 M HCl).[11]

Ac-D-App (D-**6b**): The extract obtained above was treated as described for Ac-D-Amp; yield, 2.54 g (86%); mp 148—149 °C; $[\alpha]_D^{21}$ −11.0 ° (*c* 2.0, EtOH); R_f^1 0.80.

Found: C, 66.34; H, 7.29; N, 5.97%. Calcd for $C_{13}H_{17}O_3N$: C, 66.36; H, 7.28; N, 5.95%.

Demethylation of L-*Amp and* O-*Me*-L-*Tyr*. L-Amp (1.12 mg, 5 μmol) and O-Me-L-Tyr (0.98 mg, 5 μmol)[8] were each heated in a sealed tube with 6 M HCl (1 ml) at 110 °C for certain intervals. A solution in the tube was subjected to amino acid analysis. Determination of the two components in the solution was carried out under the following conditions: column, 0.9×10 cm; buffer, standard 0.2 M citrate buffer at pH 5.28; effluent volume, 24 ml (Ahp) and 33 ml (Amp), 18 ml (Tyr) and 22 ml (*O*-Me-Tyr). The percentage of demethylation of these *O*-methyl-α-amino acids is plotted against time (Fig. 1), and the chromatogam of a solution after 20 h heating of L-Amp is shown in Fig. 3. Amp was converted completely into Ahp after heating for 70—80 h.

DL-*Ahp* (DL-**1c**). A suspension of DL-**6a** (220 mg, 0.83 mmol) in 6 M HCl (20 ml) was refluxed on an oil bath at 110 °C for 80 h. The solution was evaporated *in vacuo* several times by the addition of water. The residual solid was recrystallized from dilute HCl–Et_3N–EtOH; yield, 134 mg (77%); mp 272—273 °C (dec); R_f^2 0.78, R_f^3 0.66.

Found: C, 62.66; H, 7.21; N, 6.63%. Calcd for $C_{11}H_{15}O_3N$: C, 63.14; H, 7.23; N, 6.69%.

L-*Ahp* (L-**1c**). This was prepared from L-Amp (1.12 g, 5 mmol) as described above; yield, 0.86 g (82%); mp 242—243 °C (dec); $[\alpha]_D^{21}$ +36.1 ° (*c* 2.0, 5 M HCl–DMF); R_f^2 0.78, R_f^3 0.66.

Found: C, 62.65; H, 7.22; N, 6.50%. Calcd for $C_{11}H_{15}O_3N$: C, 63.14; H, 7.23; N, 6.69%.

Racemization Test of L-*Ahp*. L-*Leu*-DL-*Ahp Substance* (**8**): To a solution of DL-Ahp (10 mg, 48 μmol), dioxane (1 ml), water (1 ml), and Et_3N (6.7 μl, 48 μmol) was added Z-L-Leu-OSu[18] (26 mg, 72 μmol) in dioxane (1 ml) at 0 °C. The mixture was allowed to stand overnight at room temperature and then evaporated. The residue dissolved in MeOH–AcOH–H_2O (5:1:1, v/v) was hydrogenated in the presence of Pd black, and the filtrate was evaporated to dryness. The residue was designated **8**.

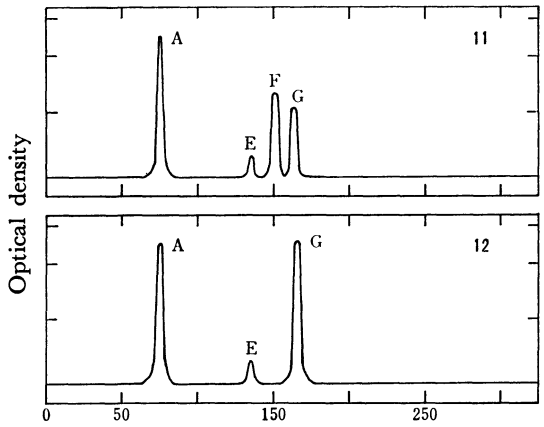

Fig. 4. Chromatogram of L-Leu-DL-Tyr substance (**11**) and L-Leu-L-Tyr substance (**12**). Buffer: pH 4.25 for 0—40 ml and pH 5.28 after 40 ml. A: Leu, E: Tyr, F: L-Leu-D-Tyr, G: L-Leu-L-Tyr.

L-*Leu*-L-*Ahp Substance* (**9**): This was obtained from L-Ahp (10 mg, 48 μmol) as described above.

Chromatography with Amino Acid Analyzer: **8** and **9** were each dissolved in 0.2 M citrate buffer of pH 2.2, and an aliquot (1 μmol) of the solution was subjected to amino acid analysis. The following conditions were sufficient to permit the separation of two diastereomers; column, 0.9× 55 cm; buffer, the standard citrate at pH 5.28. The chromatograms are shown in Fig. 2.

Chromatography of L-*Leu-Tyr*. The L-Leu-DL-Tyr substance (**11**) and L-Leu-L-Tyr substance (**12**) were prepared as described for the preparation of **8** and **9**. **11** was eluted as one peak (effluent volume, 75 ml) which was faster than L-Leu-L-Ahp (effluent volume, 203 ml) when analysis was carried out under the same conditions for the separation of **8**. It was possible under the following conditions to separate two diastereomers in **11**; **11** was eluted with pH 4.25 buffer for 40 min, thereafter with pH 5.28 buffer. As shown in Fig. 4, L-Leu-L-Tyr substance (**12**) showed a peak of G, but the view that a peptide showing G might be *O*-leucyl peptide was not excluded. The possibility was eliminated by the following experiment. Z-L-Leu-OSu was coupled with *O*-benzyl-L-Tyr[19] and the peptide substance obtained by hydrogenation gave a peak identical with that of G.

References

1) Part XI of this series: N. Nishino, H. Nishikawa, and N. Izumiya, *Memoirs Fac. Sci. Kyushu Univ., C*, **9**, 311 (1975).

2) Part of this work has been briefly communicated: S. Lee, H. Aoyagi, Y. Shimohigashi, N. Izumiya, T. Ueno, and H. Fukami, *Tetrahedron Lett.*, **1976**, 843.

3) T. Okuno, Y. Ishita, K. Sawai, and T. Matsumoto, *Chem. Lett.*, **1974**, 635.

4) T. Ueno, T. Nakashima, Y. Hayashi, and H. Fukami, *Agric. Biol. Chem.*, **39**, 1115 (1975).

5) T. Ueno, T. Nakashima, Y. Hayashi, and H. Fukami, *Agric. Biol. Chem.*, **39**, 2081 (1975).

6) Ueno *et al.* isolated Amp from a hydrolysate of AM-

toxin I and confirmed by several experiments that the Amp possesses an L-configuration. However, they reported no $[\alpha]_D$ because the amount of the L-Amp isolated was very small. For the L-configuration of App and Ahp in AM-toxin II and III, they gave no experimental evidence and made the assumption from an analogy of L-Amp in I.

7) T. Okuno, K. Sawai, Y. Mori, R. Suzuki, and T. Matsumoto, Abstr. No. 44, 19th Symposium on the Chemistry of Natural Products, Hiroshima, October 1975.

8) N. Izumiya and A. Nagamatsu, *Bull. Chem. Soc. Jpn.*, **25**, 265 (1952).

9) A. Hirota, A. Suzuki, and S. Tamura, *Agric. Biol. Chem.*, **37**, 1185 (1973).

10) J. Andrako, J. D. Smith, and W. H. Hartung, *J. Pharm. Sci.*, **50**, 337 (1961).

11) R. Nakashima, K. Aoki, and T. Matsuura, Abstr. No. 3P23, 30th National Meeting of Chemical Society of Japan, Osaka, April 1974.

12) We indebted to the Sankyo Co., Tokyo, for the supply of Takadiastase Sankyo.

13) M. Masaki, T. Kato, and N. Izumiya, *Memoirs Fac. Sci. Kyushu Univ., C*, **8**, 89 (1972).

14) J. M. Manning and S. Moore, *J. Biol. Chem.*, **243**, 5591 (1968).

15) J. R. Catch, H. P. W. Huggill, and A. R. Somerville, *J. Chem. Soc.*, **1953**, 3028.

16) J. F. Norris, M. Watt, and R. Thomas, *J. Am. Chem. Soc.*, **38**, 1071 (1916).

17) 5 M HCl–DMF represents a mixture of 5 M HCl: *N*,*N*-dimethylformamide=1:1 by vol. L-**1a**, **b**, and **c** dissolved easily in this solvent. The L-amino acids did not dissolve sufficiently in either 5 M HCl or AcOH; thus accurate determination of specific rotation was difficult.

18) G. W. Anderson, J. E. Zimmerman, and F. M. Callahan, *J. Am. Chem. Soc.*, **86**, 1839 (1964).

19) E. Wünsch, G. Fries, and A. Zwick, *Chem. Ber.*, **91**, 542 (1958).

Oxidation of Olefins with Thallium(III) Acetate in Diols[1)]

Sakae UEMURA,* Haruo MIYOSHI, Akio TOSHIMITSU, and Masaya OKANO

Institute for Chemical Research, Kyoto University, Uji, Kyoto 611

(Received May 19, 1976)

The oxidation of styrene, α- and β-methylstyrene, and 1-octene with thallium(III) acetate in diols, $HO(CH_2)_nOH$ (n=2, 3, and 4), has been investigated. From styrene the derivatives of 1,3-dioxolane, 1,3-dioxane, and 1,3-dioxepane were mainly obtained for n=2, 3, and 4 respectively, while the reaction of 1-octene in 1,2-ethanediol afforded 1-acetoxy-2-(2-hydroxyethoxy)octane as the main product. A new alkoxythallate of styrene, $C_6H_5CH(OCH_2CH_2OH)CH_2Tl(OAc)_2$, has been isolated under milder conditions.

Extensive data are available on the oxidation of olefins with metal salts in alcohols. However, there are only a few reports[2)] on the reaction with the use of a diol as an alcohol component. As an extension of studies on the alkoxythallation of olefins[3)] we now report the first example of the oxidation of olefins with thallium(III) acetate in various diols, $HO(CH_2)_nOH$ (n=2, 3, and 4), where an intramolecular substitution of thallium moiety by hydroxy oxygen may be expected in the intermediate ω-hydroxyalkoxythallate of olefins. Isolation of a new alkoxythallate of styrene and its reactions are also reported.

Results and Discussion

Reaction of styrene (**1a**) with thallium(III) acetate in 1,2-ethanediol, 1,3-propanediol, and 1,4-butanediol at 80 °C for 4 h gave 2-benzyl-1,3-dioxolane (**2a**, 36% yield), 2-benzyl-1,3-dioxane (**2d**, 33% yield), and 2-benzyl-1,3-dioxepane (**2e**, 17% yield) respectively, together with small amounts of phenylacetaldehyde and acetophenone in each case. Similarly, 2-methyl-2-benzyl-1,3-dioxolane (**2b**, 81% yield) and 2-(α-methylbenzyl)-1,3-dioxolane (**2c**, 23% yield) were formed from α- (**1b**) and β-methylstyrene (**1c**) respectively, by the use of 1,2-ethanediol as solvent. The ring products clearly arise from phenyl migration (Scheme 1). When the reaction of styrene with thallium(III)

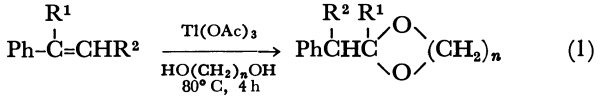

(1)

1a(R^1=R^2=H) **2a**(R^1=R^2=H, n=2)
b(R^1=Me, R^2=H) **b**(R^1=Me, R^2=H, n=2)
c(R^1=H, R^2=Me) **c**(R^1=H, R^2=Me, n=2)
d(R^1=R^2=H, n=3)
e(R^1=R^2=H, n=4)

acetate in 1,2-ethanediol was carried out at room temperature, a new organothallium(III) compound (**3**) was isolated together with **2a** (Scheme 2). In

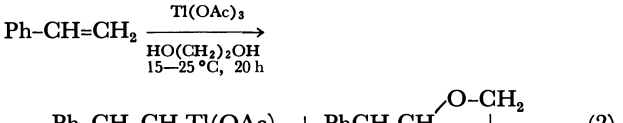

(2)

3 **2a**

order to ascertain **3** to be the intermediate for **2a**, the isolated **3** was heated in 1,2-ethanediol at 80 °C for 4 h. As expected, **2a** was obtained as the sole product.

*To whom correspondence should be addressed.

This indicates that **2a** was formed through a 1,2-shift of the phenyl group with dethallation and a simultaneous or successive nucleophilic attack of hydroxy oxygen on the carbon bearing alkoxyl group (Scheme 3a) as was noted in thermal decomposition of methoxythallate of styrene in methanol,[3c)] with no intramolecular attack of oxygen on carbon bearing thallium moiety to give 2-phenyl-1,4-dioxane (Scheme 3b) taking place at all. Formation of **2b—e** can also be explained by a similar scheme. On the other hand, when **3** was heated in 1,2-ethanediol in the presence of palladium(II) salt, 2-methyl-2-phenyl-1,3-dioxolane (**4**) was readily obtained almost quantitatively. Formation of **4** can be explained by Scheme 3c which involves hydride shift instead of phenyl migration as has been proposed in the reactions of alkoxymercurials[2b)] and alkoxythallates[3a)] of olefins with palladium(II) salts.

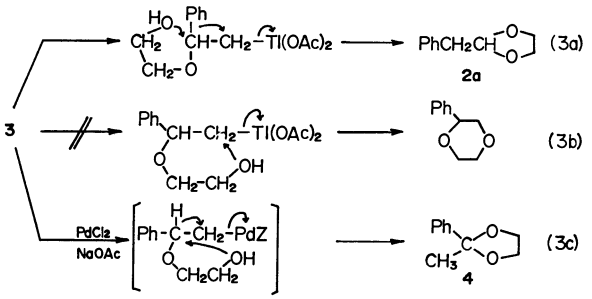

If the phenyl group which easily migrates to give **2a—e** is replaced by the alkyl group, the formation of the reaction product by Scheme 3b can be expected since the alkyl group does not migrate as easily as the phenyl group. We chose 1-octene as a substrate and carried out its oxidation in 1,2-ethanediol at 80 °C for 4 h, the oxidation with thallium(III) acetate in methanol having been reported in detail.[4)] As a result one major product and three minor ones were identified (Scheme 4) together with smaller amounts of some

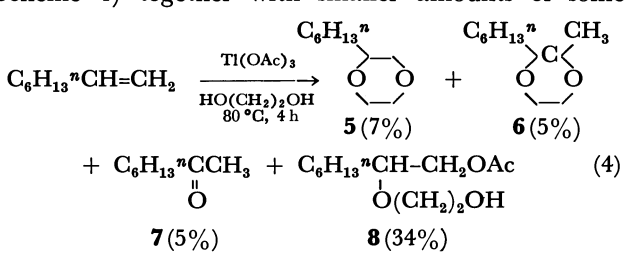

(4)

7(5%) **8**(34%)

unidentified compounds. 2-Heptyl-1,3-dioxolane or 1-octanal which arises from hexyl group migration was not formed in the reaction products. Formation of 2-hexyl-1,4-dioxane (**5**) shows that the reaction corresponding to Scheme 3b is partly operative in this case. A similar reaction in 1,3-propanediol gave no compound corresponding to **5**.

Although thallium(III) was almost completely reduced to thallium(I) in these reactions, the yields of the products were generally low. This may be due to the consumption of thallium(III) for the oxidation of diols as was noted by Kabbe in the case of some 1,2-diols.[5] We also confirmed that when thallium(III) acetate (10 mmol) is heated in 1,2-ethanediol (7.5 ml) at 82 °C for 4 h, 65% of thallium(III) is reduced to thallium(I) (by iodometry).

Experimental

Commercial organic and inorganic materials were used. The IR and NMR spectra were recorded with a Hitachi EPI-S2 and a Varian EM-360 apparatus, respectively. Gas chromatography was carried out on Shimadzu 4BMPF and 5APTF apparatus using EGSS-X(15%)-Chromosorb-W (1 m and 3 m) and PEG-6000(25%)-Chromosorb-W (3 m) columns (N_2 as a carrier gas).

Oxidation of Olefin with $Tl(OAc)_3$ in Diol. A typical experimental procedure is as follows. A mixture of styrene (4.1 g, 40 mmol), $Tl(OAc)_3$ (7.7 g, 20 mmol), and 1,2-ethanediol (15 ml) was heated at 80 °C for 4 h under stirring. After the usual work-up, GLC analysis of benzene extract revealed the presence of 7.2 mmol (36% yield based on Tl^{3+} charged) of 2-benzyl-1,3-dioxolane (**2a**) and small amounts of phenylacetaldehyde and acetophenone as the products, butyrophenone being used as an internal standard. Distillation gave 0.5 g of pure **2a**. Thallium(III) was almost completely reduced to thallium(I). Authentic samples of **2a—e**, **4**, and **6** were prepared by the acetalization or ketalization of phenylacetaldehyde, 2-phenylpropionaldehyde, acetophenone and 2-octanone in the corresponding diols[6] and their structures were confirmed by NMR; **2a** bp 80—93 °C/2 Torr, **2b** bp 81 °C/2 Torr, **2c** bp 93—95 °C/4 Torr, **2d** bp 100—104.5 °C/4 Torr, **2e** bp 106—110 °C/4 Torr, **4** bp 83—84 °C/15 Torr, **6** bp 78—79°C/15 Torr. **5** was prepared by the alkaline dehydrobromination of 1-bromo-2-(2-hydroxyethoxy)octane which was synthesized from 1-octene, 1,2-ethanediol, and *N*-bromosuccinimide.[7] **8** was prepared by the reaction of 1-bromo-2-(2-hydroxyethoxy)octane with KOAc in DMSO; bp 120—123 °C/5 Torr, NMR (CCl_4) δ 0.67—1.07 (m. 3H), 1.07—1.73 (m. 10H), 1.98(s. 3H), 2.3(br. 1H), 3.23—3.67(m. 5H), and 3.67—4.23(m. 2H). No 2-acetoxy-1-(2-hydroxyethoxy)octane (positional isomer of **8**) was detected by NMR in the oxidation products of 1-octene.

*Isolation of **3**.* A mixture of styrene (4.1 g, 40 mmol), $Tl(OAc)_3$ (7.7 g, 20 mmol), and 1,2-ethanediol (15 ml) was stirred at 15—25 °C for 20 h. To this was added 500 ml of petroleum ether and the mixture was then left to stand for 3 days in a refrigerator to give a white crystal of **3** as a precipitate. **3** was collected by filtration [4.2 g, 43% yield; mp 133—135 °C(dec)]. The treatment of organic filtrate as described above revealed the presence of 28% yield of **2a**. **3** is soluble in pyridine, DMSO, DMF, hot $CHCl_3$, and hot ethanol, but insoluble in water, THF, ether, benzene, CCl_4, acetonitrile, and acetic acid. IR(hexachlorobutadiene and paraffin mulls): 3250(s), 2950(m), 2920(m), 2860(m), 1625(sh), 1610(s), 1530(s), 1430(s), 1360(s), 1320(s), 1110(m), 1090(m), 1067(m), 974(m), 762(m), 695(m), and 685(m) cm^{-1}. NMR(pyridine-d_5): δ 2.09(s. 6H), 3.10(d. 1H, J_{Tl-H} = 732 Hz), 3.14(d. 1H, J_{Tl-H} = 875 Hz), 3.53(t. 2H), 3.76 (t. 2H), 5.01(d. 1H, J_{Tl-H} = 739 Hz), 5.76(s. 1H), and 6.9—7.6 (m. 5H). Found: C, 34.48; H, 4.11; Tl, 41.28%. Calcd for $C_{14}H_{19}O_6Tl$: C, 34.48; H, 3.93; Tl, 41.91%.

*Reaction of **3** with Palladium(II) Salt.* **3** (0.98 g, 2 mmol) was added to a hot mixture (75—80 °C) of $PdCl_2$ (0.36 g, 2.03 mmol), NaOAc (0.33 g, 4.02 mmol), and 1,2-ethanediol (10 ml) and the resulting mixture was stirred for 20 min. A black precipitate formed was filtered off. Saturated aq. NaCl was added to the filtrate which was then extracted with benzene. GLC analysis of the benzene extract revealed the presence of acetophenone (0.19 mmol) and 2-methyl-2-phenyl-1,3-dioxolane (**4**, 1.81 mmol) together with a trace amount of **2a**, *p*-methylacetophenone being used as an internal standard.

References

1) Presented at the 33rd Annual Meeting of the Chemical Society of Japan, Fukuoka, October 19, 1975.

2) a) R. Jira and W. Freiesleben, "Organometallic Reactions," Vol. 3, ed. by E. I. Becker and M. Tsutsui, Wiley-Interscience, New York, N. Y. (1972), pp. 157—158; b) D. F. Hunt and G. T. Rodeheaver, *Tetrahedron Lett.*, **1972**, 3595.

3) a) S. Uemura, K. Zushi, M. Okano, and K. Ichikawa, *J. Chem. Soc., Chem. Commun.*, **1972**, 234; b) S. Uemura, A. Tabata, and M. Okano, *J. Chem. Soc., Chem. Commun.*, **1972**, 517; c) S. Uemura, K. Zushi, A. Tabata, A. Toshimitsu, and M. Okano, *Bull. Chem. Soc. Jpn.*, **47**, 920 (1974); d) S. Uemura, A. Toshimitsu, M. Okano, and K. Ichikawa, *Bull. Chem. Soc. Jpn.*, **48**, 1925 (1975).

4) A. Lethbridge, R. O. C. Norman, and C. B. Thomas, *J. Chem. Soc., Perkin Trans. 1*, **1974**, 1929.

5) H. J. Kabbe, *Justus Liebigs Ann. Chem.*, **656**, 204 (1962).

6) S. R. Sandler and W. Karo, "Organic Functional Group Preparations," Part III, Academic Press, New York, N. Y. (1972), Chap. 1.

7) A. Iovchev, H. Reinheckel, L. Stoilov, and K. Haage, *Monatsh. Chem.*, **102**, 114 (1971).

The Stereoselective Synthesis of *threo*-3-Hydroxy-4-amino Acids

Tsutomu KATSUKI and Masaru YAMAGUCHI

Department of Chemistry, Faculty of Science, Kyushu University, Higashi-ku, Fukuoka 812

(Received May 31, 1976)

Two *threo*-3-hydroxy-4-amino acids, *dl*-4-amino-3-hydroxy-6-methylheptanoic acid (**1**) and *dl*-4-amino-3-hydroxy-2-methyl-5-(3-pyridyl)pentanoic acid (**2**), the optically active forms of which had been isolated by the acid hydrolysis of some antibiotics, were synthesized stereoselectively from L-leucine and DL-3-(3-pyridyl)-alanine respectively through 2-pyrrolidinone intermediates.

Two unusual *threo*-type hydroxy amino acids, (3*S*,4*S*)-4-amino-3-hydroxy-6-methylheptanoic acid (**1**) and (2*R*,3*S*,4*S*)-4-amino-3-hydroxy-2-methyl-5-(3-pyridyl)pentanoic acid (**2**), have been isolated by the acid hydrolysis of various pepstatins[1a-e] and pyridomycin[2] respectively. The first synthesis of **1** was carried out by Morishima *et al.* in a *non*-stereoselective way.[3] Kinoshita *et al.* recently synthesized **1** and **2** in a highly stereospecific manner starting from the appropriate optically active deoxy-sugar derivatives.[4,5]

The present authors have now attempted the synthesis of this type of hydroxy amino acid according to a general plan starting from common amino acids and involving the stereoselective reduction of 4-hydroxy-3-pyrrolin-2-one intermediates, such as **6** (Scheme 1) or **13** (Scheme 2). The *dl*-**1** could be synthesized smoothly along those lines. In the case of **2**, the reduction of the 4-hydroxy-3-pyrrolin-2-one (**13**) proceeded in the desired manner, but the subsequent steps led to a mixture of two *dl*-hydroxy amino acids, epimeric at the C-2 carbon atom. The major (90%) *non*-natural-type isomer (**23**) could easily be obtained in a pure form, but the isolation of the minor (10%) natural-type isomer (**2**) was so tedious that no crystalline sample could be obtained.

Results and Discussion

dl-*4-Amino-3-hydroxy-6-methylheptanoic Acid (1) (Scheme 1).* The *N*-(ethoxycarbonylacetyl)leucine ethyl ester (**4**) derived from **3** was subjected to Dieckmann condensation in a usual way[6] to give 3-ethoxycarbonyl-4-hydroxy-5-isobutyl-3-pyrrolin-2-one (**5**), which was then decarboxylated to 5-isobutyl-2,4-pyrrolidinedione (**6**) in an 87.7% overall yield from **4**. The pyrrolidinedione (**6**) thus obtained was a racemate, and it was used without resolution.

When **6** was hydrogenated with Raney nickel, it gave a mixture of 4-hydroxy-5-isobutyl-2-pyrrolidinone (**7**) and 5-isobutyl-2-pyrrolidinone (**8**). Compound (**7**) could be separated from **8** by crystallization and was proved, from the results of the subsequent hydrolysis, to be the *cis*-compound with regard to the two substituents at C-4 and C-5.

The hydrogenation of **6** in the presence of platinum oxide in ethyl acetate gave mostly **7**, but in a mixture of ethanol and acetic acid, it led to the hydrogenolyzed product (**8**) quantitatively. Alternatively, **6** was converted into 4-methoxy-5-isobutyl-3-pyrrolin-2-one (**9**) by diazomethane and was hydrogenated with Raney nickel to give *cis*-4-methoxy-5-isobutyl-2-pyrrolidinone (**10**) in an 87% yield.

The hydrolysis of **7** or **10** with 48% hydrobromic acid, followed by chromatographic purification on a Dowex 50 column, gave the *dl*-**1**[7] in a fair yield (74% from **10**). The NMR spectrum of synthetic *dl*-**1** agreed with that of the natural specimen.[3]

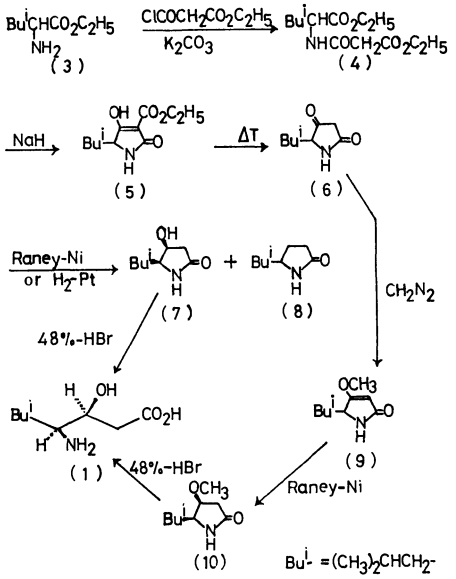

Scheme 1.

dl-*4-Amino-3-hydroxy-2-methyl-5-(3-pyridyl)pentanoic Acid (2) (Scheme 2).* DL-3-(3-Pyridyl)alanine[8] was converted to its methyl ester (**11**), which was then condensed with 2-ethoxycarbonylpropionyl chloride. The *N*-(2-ethoxycarbonylpropionyl)-3-(3-pyridyl)alanine methyl ester (**12**) thus obtained was subjected to Dieckmann condensation with sodium methoxide to afford 4-hydroxy-3-methyl-5-(3-pyridylmethyl)-3-pyrrolin-2-one (**13**) in a 32% overall yield from pyridylalanine.

The catalytic hydrogenation of **13**, its methyl ether (**14**), or its acetate (**15**) was, however, unsuccessful because of the hydrogenolysis of the *O*-function at C-4 and/or of the reduction of the pyridine nucleus, leading to the formation of **16**, for example. Compound (**13**) was then reduced with sodium borohydride in 2-propanol to give, stereoselectively, a single compound, bis[4-methyl-5-oxo-2-(3-pyridylmethyl)-3-pyrrolidinyl]-boronate, which was considered to have the desired *cis*-configuration, as represented by **17**. Unfortunately, the compound was unstable to heat, and, on recrystallization from a mixture of chloroform and ethyl acetate, it isomerized into the more stable isomer (**18**).

The compound (**17** or **18**) was hydrolyzed with

48% hydrobromic acid at 50 °C. The product obtained was a mixture of the boron complexes of the two isomeric hydroxy amino acids with the composition represented by **19**.

The elimination of boric acid from **19** was effected by treatment with 48% hydrobromic acid, followed by ion-exchange chromatography, thus giving a mixture of two racemic hydroxy amino acids (**21**, a mixture of **2** and **23**, 30% from **13**). The isomer with the configuration corresponding to the natural amino acid (**2**) in the mixture was the minor component (10% from NMR). Alternatively, boron was removed by the acetylation of **18** with acetic anhydride and pyridine, and the acetate (**20**) was hydrolyzed by hydrobromic acid to give **21** with the same isomeric ratio as above in a 40% overall yield from **13**.

The *non*-natural-type major isomer (**23**) could be easily separated from the minor counterpart by the recrystallization of the mixture from ethanol, whereupon

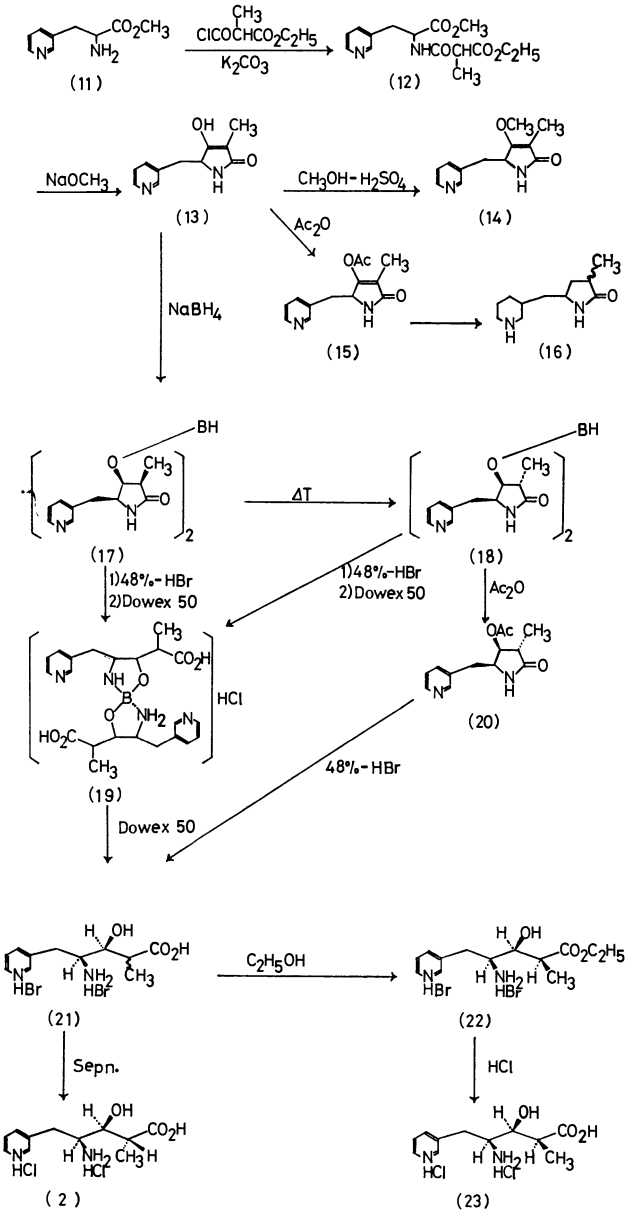

Scheme 2.

the isomer crystallized out as its ethyl ester (**22**);[9] the hydrolysis of the ester gave pure **23**. The isolation of the natural-type isomer (**2**) was, however, very tedious. The above hydroxy amino acid mixture (**21**) was repeatedly chromatographed on the Dowex-50 column, and finally a small amount of an almost pure sample was obtained in the form of a *non*-crystalline concentrate, which gave the same NMR spectrum as that of authentic natural amino acid (**2**).

Experimental

The melting points are uncorrected. The IR spectra were taken on a Hitachi R-215 spectrometer. The NMR spectra were recorded on Hitachi R-20B and Hitachi R-22 spectrometers.

N-(Ethoxycarbonylacetyl)leucine Ethyl Ester (4), 3-Ethoxycarbonyl-4-hydroxy-5-isobutyl-3-pyrrolin-2-one (5), and 5-Isobutyl-2,4-pyrrolidinedione (6). Compounds (**4** and **5**) were prepared from the L-leucine ethyl ester in a way similar to that described by Achiwa and Yamada for the preparation of 5-ethyl-5-methyl-2,4-pyrrolidinedione.[6] **4** (60% from **3**); bp 145 °C/2 mmHg. **5** (87% from **4**), NMR (CD_3OD): δ 0.96(d, 6H), 1.31(t, 3H), 1.40—2.05 (m, 3H), 4.08(t, 1H), 4.3(q, 2H). The recrystallization of **5** from a mixture of ethyl acetate and ligroin gave **6** as colorless needles. Mp 124 °C. IR: ν_{max} 3180, 2960, 1765, 1680, 1384, 1290, 1240, 853, 800, 682 cm^{-1}. NMR ($CDCl_3$):[10] δ 0.96(d, 6H), 1.45—2.10(m, 3H), 3.03(s, 2H), 4.06(m, 1H), 7.85 (broad s, 1H). Found: C, 61.57; H, 8.42; N, 8.86%. Calcd for $C_8H_{13}NO_2$: C, 61.91; H, 8.44; N, 9.03%.

4,5-cis-4-Hydroxy-5-isobutyl-2-pyrrolidinone (7). a) A mixture of **6** (97 mg), excess Raney nickel, and ethanol (10 ml) was refluxed for 3 h. The Raney nickel was then removed by filtration, and the solvent was removed *in vacuo* to give a colorless solid. Subsequent recrystallization from a mixture of dichloromethane and hexane gave **7** as colorless prisms (48 mg, 48%). Mp 131—132 °C. NMR ($CDCl_3$): δ 0.96(d, 6H), 1.58(m, 3H), 2.51(m, 2H), 3.70 (m, 1H), 4.40(m, 1H), 6.28(broad s, 1H). Found: C, 60.95; H, 9.62; N, 8.76%. Calcd for $C_8H_{15}NO_2$: C, 61.12; H, 9.62; N, 8.91%.

b) Compound (**6**, 32 mg) was dissolved in ethyl acetate (20 ml) and hydrogenated over the platinum oxide catalyst. After the removal of the catalyst, the solution was concentrated and the residue was crystallized from a mixture of dichloromethane and hexane to give **7** as colorless prisms (31 mg, 94%).

5-Isobutyl-2-pyrrolidinone (8). Compound (**6**, 29 mg) was dissolved in a mixture of ethanol(9 ml) and acetic acid (1 ml) and then hydrogenated over the platinum oxide catalyst. After the removal of the catalyst and the solvent, the residue was sublimed at 80 °C/20 mmHg to afford **8** as colorless needles (26 mg, quantitative). Mp 74.5—75°C. NMR ($CDCl_3$): δ 0.94 (d, 6H), 1.29—1.85 (m, 3H), 2.18—2.52(m, 4H), 3.70(m, 1H), 6.60(1H). Found: C, 67.88; H, 10.65; N, 9.83%. Calcd for $C_8H_{15}NO$: C, 68.04; H, 10.71; N, 9.92%.

4-Methoxy-5-isobutyl-3-pyrrolin-2-one (9) and 4,5-cis-4-Methoxy-5-isobutyl-2-pyrrolidinone (10). The ethereal diazomethane was added to a solution of **6** in methanol at 0 °C. After the removal of the excess diazomethane and the solvent, **9** was obtained as colorless needles quantitatively. NMR ($CDCl_3$): δ 0.96(d, 6H), 1.32—1.95 (m, 3H), 3.78(s, 3H), 4.05 (m, 1H), 5.00 (d, 1H), 6.95 (broad s, 1H). The ether (**9**) was used without purification in the following reaction. A mixture of **9** (139 mg) and excess Raney nickel

in ethanol was refluxed for 5 h. The mixture was then filtered and concentrated under reduced pressure. The residue was recrystallized from a mixture of dichloromethane and hexane to give **10** as colorless needles (120 mg, 86%). Mp 87—88 °C. NMR ($CDCl_3$): δ 0.95(6H), 1.35—1.70 (m, 3H), 2.44 (d, 2H), 3.32 (s, 3H), 3.69—4.10 (m, 2H), 7.35(broad s, 1H). Found: C, 62.97; H, 10.03; N, 8.04%. Calcd for $C_9H_{17}NO_2$: C, 63.13; H, 10.00; N, 8.18%.

dl-*4-Amino-3-hydroxy-6-methylheptanoic Acid (1).*

a) A mixture of **10** (60 mg) and 48% hydrobromic acid (5 ml) was stirred for 10 h at 78 °C. The mixture was then concentrated to dryness under reduced pressure, redissolved in water (5 ml), and applied to a column of Dowex 50(0.8 cm × 25 cm). The column was washed with water until the eluent became neutral, and then the amino acid was eluted with 2 M-ammonia. The eluate was concentrated under reduced pressure, and the residue was recrystallized from a mixture of methanol and ethanol to afford *dl*-**1** as colorless crystals (45 mg, 74%). Mp 211.5—213.5 °C (dec). NMR (D_2O): δ 0.98 (d, 6H), 1.38—1.72 (m, 3H), 2.44—2.62(m, 2H), 3.13—3.47(m, 1H), 3.88—4.22(m, 1H). The NMR spectrum ($J_{3,4}$=5.5 Hz) of *dl*-**1** agreed with that ($J_{3,4}$=5.5 Hz)[3] of natural amino acid. Found: C, 54.66; H, 9.68; N, 7.99%. Calcd for $C_8H_{17}NO_3$: C, 54.83; H, 9.68; N, 7.99%.

b) By the same procedure as was used in the hydrolysis of **10**, **7** was hydrolyzed to give *dl*-**1** (80%).

N-*(2-Ethoxycarbonylpropionyl)-3-(3-pyridyl)alanine Methyl Ester (12).* By the same procedure as was described for the preparation of **4**, **11** (2.8 g) was *N*-acylated with 2-ethoxycarbonylpropionyl chloride. The crude product was purified by chromatography (silica gel, ethyl acetate) to give **12** (3.99 g, 88%). It was then recrystallized from diisopropyl ether. Colorless needles; mp 70.5—71.5 °C. IR: ν_{max} 3300, 3100, 3000, 2940, 1740, 1640, 1550, 1200, 1100, 1045, 1000, 960, 830, 810, 770, 715 cm^{-1}. NMR ($CDCl_3$): δ 1.22(t, 3H), 1.35(d, 3H), 3.05—3.43(m, 3H), 3.72(s, 3H), 4.14(q, 2H), 4.87(m, 1H), 7.15—7.70 and 8.30—8.60(m, 4H), 9.42(brosd s, 1H). Found: C, 58.43; H, 6.67; N, 8.80%. Calcd for $C_{15}H_{20}N_2O_5$: C, 58.43; H, 6.54; N, 9.09%.

4-Hydroxy-3-methyl-5-(3-pyridylmethyl)-3-pyrrolin-2-one (13). Sodium (3 g) was dissolved in absolute methanol (100 ml). To this solution, **12** (3 g) was added, after which the whole mixture was refluxed for 10 h. After the removal of the solvent under reduced pressure, the residue was dissolved in water (10 ml) and applied to a column of Dowex 50 (3 cm × 40 cm). After the column had then been washed with water, the **13** was eluted with 2 M-ammonia. Fractions containing **13** were concentrated, and the residue was recrystallized from methanol to give **13** as colorless prisms (1.1 g, 41%). Mp 172—174 °C. IR: ν_{max} 1665, 1600, 1580, 1490, 1225, 760, 700 cm^{-1}. NMR (CD_3SOCD_3): δ 1.39(s, 3H), 2.87—3.05(m, 2H), 4.13(m, 1H), 7.24—7.75 and 8.32—8.55 (m, 4H). Found: C, 64.52; H, 5.90; N, 14.10%. Calcd for $C_{11}H_{12}N_2O_2$: C, 64.69; H, 5.92; N, 13.72%.

4-Methoxy-3-methyl-5-(3-pyridylmethyl)-3-pyrrolin-2-one (14). A mixture of **13** (67 mg) and concentrated sulfuric acid (0.1 ml) in anhydrous methanol was refluxed for 30 h. This solution was then neutralized with dry Dowex 1 (OH-type). After filtration, the whole solution was concentrated to an oil (47 mg, 76%). NMR ($CDCl_3$): δ 1.78(s, 3H), 2.75—3.01(m, 2H), 3.90—4.20(m, 1H), 3.97(s, 3H), 6.80—7.56 and 8.20—8.50(m, 4H).

4-Acetoxy-3-methyl-5-(3-pyridylmethyl)-3-pyrrlolin-2-one (15). A mixture of **13** (45 mg) and acetic anhydride (0.4 ml) was stirred for 3 h. The solution was then concentrated, and the residue was recrystallized from a mixture of chloroform and diisopropyl ether to give colorless needles (50 mg, 89%). Mp 134—134.5 °C. IR: ν_{max} 3180, 3080, 1780, 1700, 1575, 1480, 1420, 1200, 760, 705 cm^{-1}. NMR ($CDCl_3$): δ 1.57 (d, 3H), 2.16(s, 3H), 2.73—2.96(m, 2H), 4.40—4.68(m, 1H), 5.65(broad s, 1H), 7.05—7.65 and 8.22—8.48(m, 4H). Found: C, 63.16; H, 5.83; N, 11.45%. Calcd for $C_{13}H_{14}N_2O_3$: C, 63.40; H, 5.73; N, 11.38%.

*Bis[4-methyl-5-oxo-2-(3-pyridylmethyl)-3-pyrrolidinyl]boronate (17, 3,4-*cis*-4,5-*cis*) and (18, 3,4-*trans*-4,5-*cis*).* Sodium borohydride (200 mg) was added to a solution of **13** (200 mg) in 2-propanol (20 ml), after which the mixture was stirred at room temperature for 48 h. The mixture was then diluted with water and extracted with chloroform. The extract was washed with water, dried over anhydrous sodium sulfate, and concentrated under a vacuum to give **17** as colorless oil (165 mg, 82%). NMR (CD_3OD): δ 1.16(d, 3H, J= 6.5 Hz), 2.30(m, 1H), 2.79—3.15 (m, 2H), 3.70—4.18 (m, 2H), 7.20—7.90 and 8.26—8.60(m, 4H). The recrystallization of **17** from a mixture of methanol and diisopropyl ether afforded a stable isomer, **18**, as colorless prisms. Mp 210—218 °C. IR: ν_{max} 1710, 1585, 1485, 1115, 780, 720, 710 cm^{-1}. NMR (CD_3OD): δ1.15(d, 3H, J=7.5 Hz), 2.29 (m, 1H), 2.80—3.10(m, 2H), 3.53—4.20(m, 2H), 7.24—7.90 and 8.25—8.57(m, 4H). Found: C, 62.45; H, 6.67; N, 13.21%. Calcd for $C_{22}H_{27}N_4O_4B$: C, 62.57; H, 6.44; N, 13.27%.

Boron Complex of 4-Amino-3-hydroxy-2-methyl-5-(3-pyridyl)-pentanoic Acid (19). Compound (**18**, 100 mg) was dissolved in 48% hydrobromic acid, and the solution was stirred at 70 °C for 72 h. The solution was then concentrated and applied to an ion-exchange column of Dowex 50 (0.8 cm × 25 cm). The amino acid was eluted by 3 M-hydrochloric acid, and the residue of the eluate was recrystallized from a mixture of ethanol and 2-propanol to give **19** as colorless needles (70 mg, 60%). Mp 211.5—212 °C. IR: ν_{max} 1700, 1575, 1475, 1105, 1040, 773, 720, 700 cm^{-1}. Found: C, 53.78; H, 6.20; N, 11.49%. Calcd for $C_{22}H_{30}N_4O_6$-BCl: C, 53.62; H, 6.14; N, 11.37%.

*3,4-*trans*-4,5-*cis*-4-Acetoxy-3-methyl-5-(3-pyridylmethyl)-2-pyrrolidinone (20).* A mixture of **18** (125 mg), pyridine (2 ml), and acetic anhydride (2 ml) was stirred at room temperature for 24 h, diluted with water, and extracted with chloroform. The extract was dried over anhydrous sodium sulfate and concentrated to give a residue which was then recrystallized from a mixture of methanol and diisopropyl ether. Colorless needles (80 mg, 54.5%); mp 143.5—144 °C. IR: ν_{max} 1730, 1710, 1580, 1485, 1218, 785, 710 cm^{-1}. NMR (CD_3OD): δ 1.17 (d, 3H), 2.10 (s, 3H), 2.46 (m, 1H), 2.82 (d, 2H), 4.20 (q, 1H), 5.01 (t, 1H), 7.25—7.88 and 8.30—8.60 (m, 4H). Found: C, 62.91; H, 6.52; N, 11.33%. Calcd for $C_{13}H_{16}N_2O_3$: C, 62.89; H, 6.50; N, 11.28%.

4-Amino-3-hydroxy-2-methyl-5-(3-pyridyl)pentanoic Acid Dihydrochloride (21, a Mixture of 2 and 23). a) The complex (**19**, 120 mg) was dissolved in 48% hydrobromic acid in the presence of ion-exchange resin (Dowex 50, 5 g). The mixture was stirred for 10 h, and the solvent was removed under reduced pressure. The resin was washed with water, and the amino acid was eluted with 3 M-hydrochloric acid. The concentration of the eluate gave **21**, an isomeric mixture of the dihydrochlorides of **2** and **23**, in the form of a viscous syrup (90 mg, 62%). The NMR spectrum of the sample gave an approximate ratio of **23** : **2**=9 : 1.

b) The acetate (**20**, 200 mg) was dissolved in 48% hydrobromic acid. The mixture was stirred at 70 °C for 40 h and then concentrated to a viscous syrup in the form of

dihydrobromide, with the same isomeric ratio as above (280 mg, 90%).

*Ethyl 4-Amino-3-hydroxy-2-methyl-5-(3-pyridyl)pentanoate Dihydrobromide (**22**).* The above dihydrobromide (**21**, 250 mg) was crystallized from ethanol to give **22** as colorless needles (150 mg, 56%). Mp 191 °C (dec). IR: ν_{max} 1725, 1610, 1590, 1510, 1204, 1095, 790, 675 cm^{-1}. NMR (CD_3OD): δ 1.24 (t, 3H), 1.25 (d, 3H), 2.85 (m, 1H), 3.25—3.50 (m, 2H), 3.65—4.20 (m, 2H), 4.14 (q, 2H), 8.00—8.30 and 8.61—9.10 (m, 4H). Found: C, 37.41; H, 5.30; N, 6.75%. Calcd for $C_{13}H_{20}N_2O_3 \cdot 2HBr$: C, 37.70; H, 5.35; N, 6.76%.

*4-Amino-3-hydroxy-2-methyl-5-(3-pyridyl)pentanoic Acid Dihydrochloride (**23**).* The ethyl ester (**22**, 100 mg) was stirred with 4 M-hydrochloric acid (25 ml) at room temperature for 10 h; then the mixture was concentrated, and the residue was treated with dioxane. As the precipitate was very hygroscopic, it was filtered with the exclusion of moisture, washed with dioxane, and dried to yield **23** (68.5 mg, 90%). IR: ν_{max} 1710, 1605, 1548, 1466, 1185, 780, 673 cm^{-1}. NMR (D_2O): δ 1.14 (d, 3H, J=7.0 Hz), 2.80 (m, 1H), 3.18—3.42 (m, 2H), 3.58—3.94 (m, 2H), 7.91—8.21 and 8.44—8.84 (m, 4H). Found: C, 42.21; H, 6.21; N, 8.87%. Calcd for $C_{11}H_{16}N_2O_3 \cdot 2HCl \cdot H_2O$: C, 41.92; H, 6.40; N, 8.89%.

*4-Amino-3-hydroxy-2-methyl-5-(3-pyridyl)pentanoic Acid Dihydrochloride (**2**).* A hydroxy amino acid mixture (**21**, 185 mg) which contained *dl*-**2** (10%) and its diastereomer (**23**, 90%) was applied to a column of Dowex 50 (H-form, 100—200 mesh, 0.8 cm × 50 cm). The column was washed with water, and then the amino acid was eluted with 2M-hydrochloric acid. The diastereomer (**23**) was eluted a little faster than **2**. The fractions containing *dl*-**2** were combined and concentrated. The concentrate was, again, applied to the column; this process was repeated five times. The glassy concentrate thus obtained (4 mg) gave an NMR spectrum identical with that of natural (−)-**2**. NMR (D_2O): δ 1.13 (d, 3H, J=7.0 Hz), 2.80 (quintet, 1H), 3.18—3.44 (m, 2H), 3.67—3.91 (m, 2H), 7.95—8.25 (m, 1H), 8.50—8.85 (m, 3H).

The authors wish to express their thanks to Dr. Hiroshi Ogawara, National Institute of Health of Japan, and Professor Mitsuhiro Kinoshita, Keio University, who kindly offered the NMR spectrum of (−)-**2**. This work was supported in part by a grant from the Ministry of Education.

References

1) (a) H. Umezawa, T. Aoyagi, H. Morishima, M. Hamada, and T. Takita, *J. Antibiot.* (*Tokyo*), **23**, 259 (1970); (b) H. Morishima, T. Takita, T. Aoyagi, T. Takeuchi, and H. Umezawa, *ibid.*, **23**, 263 (1970); (c) S. Murao and S. Satoi, *Agric. Biol. Chem.*, **34**, 1265 (1970); (d) T. Miyano, M. Tomiyasu, H. Iizuka, S. Tomisaka, T. Takita, T. Aoyagi, and H. Umezawa, *J. Antibiot.* (*Tokyo*), **25**, 489 (1972); (e) T. Aoyagi, Y. Yagisawa, M. Kumagai, M. Hamada, H. Morishima, T. Takeuchi, and H. Umezawa, *ibid.*, **26**, 539 (1973).

2) H. Ogawara, K. Maeda, G. Koyama, H. Nagawara, and H. Umezawa, *Chem. Pharm. Bull.*, **16**, 679 (1968).

3) H. Morishima, T. Takita, and H. Umezawa, *J. Antibiot.* (*Tokyo*), **26**, 115 (1973).

4) M. Kinoshita, A. Hagiwara, and S. Aburaki, *Bull. Chem. Soc. Jpn.*, **48**, 570 (1975).

5) M. Kinoshita and S. Mariyama, *Bull. Chem. Soc. Jpn.*, **48**, 2081 (1975).

6) K. Achiwa and S. Yamada, *Chem. Pharm. Bull.*, **14**, 537 (1966).

7) *dl*-**1** was converted into its diastereomer as follows. *dl*-**1** was *N*-benzoylated, and the product was treated with diazomethane and then with thionyl chloride. The imino ester thus obtained was a mixture of two diastereomers (50 : 50), which was then hydrolyzed to give a mixture of *dl*-**1** and its diastereomer.

8) R. K. Griffith and H. J. Harwood, *J. Org. Chem.*, **29**, 2658 (1964).

9) The ethyl ester (**22**) was converted with silver oxide to 4-hydroxy-3-methyl-5-(3-pyridyl)methyl-2-pyrrolidinone, the hydrolysis of which gave an amino-acid mixture (**21**).

10) The 2,4-pyrrolidinedione (**6**) existed in the keto-form in chloroform, but in the enol-form in methanol (NMR).

Carbonylation of Dienes and Diols in the Presence of Copper(I) Carbonyl Catalysts

Yoshie SOUMA, Jun IYODA, and Hiroshi SANO

Government Industrial Research Institute, Osaka Midorigaoka, Ikeda, Osaka 563

(Received May 4, 1976)

Dienes and diols having carbon numbers of 6 to 12 reacted with carbon monoxide to give mixtures of lactones, dicarboxylic acids and monocarboxylic acids in the presence of copper(I) carbonyl catalysts at room temperature and at 1 atm of carbon monoxide. Dienes and diols having carbon numbers larger than 10 gave isomers of dicarboxylic acid, the main component of which was tetramethyl-substituted tertiary carboxylic acid. The yield increased for an increase of the carbon number. All starting materials gave mixtures of 1,4- and 1,5-lactones. Larger amounts of the lactones were obtained from diols than from dienes. Cyclic monocarboxylic acid and saturated monocarboxylic acid were obtained by the carbonylation of 1,7-octadiene. The appropriate reaction temperature of the dienes and diols was 0—10 and 20—30 °C, respectively.

Several results of carbonylation catalyzed by copper(I) carbonyl ion giving tertiary-carboxylic acids in high yields from olefins and alcohols at room temperature and in pure carbon monoxide at 1 atm were described in previous paper.[1-5]

For the carbonylation of dienes and diols, strong acid catalysts and metal carbonyl catalysts were used. Schauerte and Koch have studied the carbonylation of dienes and diols in concd H_2SO_4 and $BF_3 \cdot H_2O$, and obtained mixtures of dicarboxylic acids, monocarboxylic acids and lactones.[6,7] On the other hand, Kuvaev *et al.* have studied the carbonylation of butadiene in the presence of a $Co_2(CO)_8$ catalyst at 160—220 °C at 250 atm of carbon monoxide, and obtained mixtures of adipic, methylglutaric and alkylsuccinic acids.[8] Paulik has also synthesized C_5—C_{22} dicarboxylic acids by the carbonylation of C_3—C_{20} non-vicinal glycols in the presence of rhodium and iridium complex catalysts at 200 °C at 70 atm of carbon monoxide.[9] In all these reactions, the carbonylation was carried out at elevated pressures of carbon monoxide.

In this paper, carbonylation of dienes and diols in the presence of copper(I) carbonyl catalysts in strong acids at room temperature and at 1 atom of carbon monoxide are described. The effect of the carbon number of the starting materials upon the formation of the dicarboxylic acid or lactone was studied using C_6—C_{12} dienes and diols. The reaction mechanisms are briefly discussed.

Results and Discussion

An unstable copper(I) carbonyl ion $Cu(CO)_n^+$ is formed by the absorption of carbon monoxide in an H_2SO_4 or H_2SO_4–FSO_3H solution of cuprous oxide.[10] Dienes and diols easily react with carbon monoxide at atmospheric pressure in the presence of copper(I) carbonyl ions.

$$Cu^+ + CO \rightarrow Cu(CO)^+ \xrightarrow{CO} Cu(CO)_n^+ \quad n=3, 4$$

$$Cu(CO)_n^+ \rightleftharpoons Cu(CO)^+ + (n-1)CO$$

The copper(I) carbonyl ion behaves as a CO carrier from the gas phase to the H_2SO_4 solution, and has the same effect on the carbonylation as for elevated pressures of carbon monoxide. In general, the carbonylation of dienes in acid solutions is difficult because of their strong tendency to polymerization. However, the application of copper(I) carbonyl catalysts renders possible the carbonylation of diene in high yields even in strong acid solutions.

Dienes and diols having carbon numbers from 6 to 12 react with carbon monoxide and gave mixtures of monocarboxylic acids, dicarboxylic acids and lactones. The ratio of these components in the mixture varied with the carbon number of the starting material. The results are shown in Table 1. Dicarboxylic acids were obtained from starting materials having carbon numbers larger than 10. Lactones were obtained from all compounds. In general, larger amounts of lactones were obtained from diols than from dienes. Cyclic monocarboxylic acid and saturated monocarboxylic acid were obtained by the carbonylation of 1,7-octadiene. No hydroxycarboxylic acid and unsaturated carboxylic acid were identified in the strong acid solution. The carbonylation of diols was carried out at 20—30 °C, on the other hand, the carbonylation of dienes was carried out at 0—10 °C in order to prevent polymerization.

The reaction schemes are explained as follows. The reaction pathways of the dienes and diols are almost the same. A carbonium ion (I) is formed by protonation to the double bond of the diene, or by protonation and successive dehydration of the diol.

$$CH_2{=}CH{-}(CH_2)_n{-}CH{=}CH_2 \xrightarrow{H^+} CH_3{-}\overset{+}{C}H{-}(CH_2)_n{-}\overset{+}{C}H{-}CH_3$$

$$HO{-}(CH_2)_{n+4}{-}OH \xrightarrow{H^+} H_2\overset{+}{O}{-}(CH_2)_{n+4}{-}\overset{+}{O}H_2 \xrightarrow{-H_2O} CH_2{-}(CH_2)_{n+2}{-}\overset{+}{C}H_2$$

(I)

When the carbon number of I is larger than 10, the carbonium ion (I) isomerizes to the more stable *t*-carbonium ion (II) by Wagner-Meerwein rearrangement, and reacts with carbon monoxide. By this mechanism, *t*-dicarboxylic acid is obtained from a diene or diol having a carbon number larger than 10. In this case, the carbon number for the two tertiary carbonium ions is larger than 4. The yield of *t*-dicarboxylic acid increases when the carbon numbers of the starting materials increases to between

Table 1. Carbonylation products of dienes and diols[a)]

Substrates	Time h	Temp °C	Products	Abbr.	Yield %
1,5-Hexadiene	2	0— 5	2-Ethyl-4-pentanolide	(I)	46
1,7-Heptanediol	3	20—30	2,2-Dimethyl-4-hexanolide	(II)	40
			2-Methyl-2-ethyl-5-pentanolide	(III)	30
			2,2-Dimethyl-5-hexanolide	(IV)	10
1,7-Octadiene	2.5	3— 8	2,2-Dimethyl-4-heptanolide	(V)	15
			2,2-Dimethyl-5-heptanolide	(VI)	8
			2,2-Dimethylheptanoic acid		14
			2-Methyl-2-ethylhexanoic acid		6
			1,4-Dimethylcyclohexanecarboxylic acid		35
1,8-Octanediol	2.5	20—25	2,2-Dimethyl-4-heptanolide	(V)	35
			2,2-Dimethyl-5-heptanolide	(VI)	40
1,9-Nonanediol	3	15—25	2,2-Dimethyl-4-octanolide	(VII)	35
			2,2-Dimethyl-5-octanolide	(VIII)	25
			2,2-Diethyl-4-hexanolide		10
1,9-Decadiene[b)]	2.5	5—10	2-Methyl-2-ethyl-4-octanolide	(IX)	20
			2-Methyl-2-ethyl-5-octanolide	(X)	15
			2,2,7,7-Tetramethyloctanedioic acid	(XI)	45
			2-Ethyl-2,6,6-trimethylheptanedioic acid		10
1,10-Undecadiene[b)]	2	4— 8	1,4- and 1,5-Lactone[c)]		25
			2,2,8,8-Tetramethylnonanedioic acid	(XII)	49
			2-Ethyl-2,7,7-trimethyloctanedioic acid		8
1,12-Dodecanediol	3	20	1,4- and 1,5-Lactone[c)]		50
			2,2,9,9-Tetramethyldecanedioic acid	(XIII)	38
			2-Ethyl-2,8,8-trimethylnonanedioic	(XIV)	9

a) Reactions were carried out using 30 ml of 98% H_2SO_4, 1.144 g of Cu_2O and 30 mmol of dienes or diols.
b) During the carbonylation, 10 ml of FSO_3H was added. c) The structure of this substance was not determined.

C_{10} and C_{12}. The dicarboxylic acids obtained consist of structural isomers of which the main product is tetramethyl-substituted dicarboxylic acid and the by-product is ethyl-substituted dicarboxylic acid.

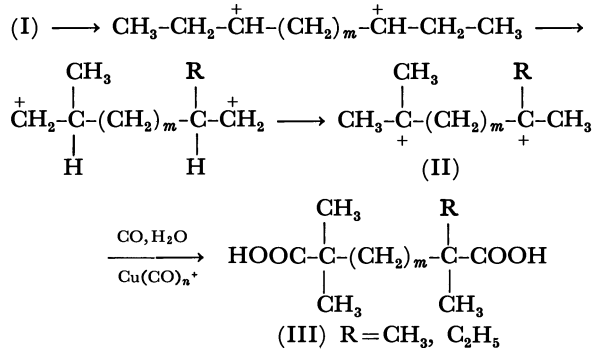

Lactone was always obtained for the carbonylation of the dienes or diols. The lactone obtained is a mixture of five-membered 1,4-lactones and six-membered 1,5-lactone derivatives. No four-membered lactones or large-ring lactones were obtained. In the formation of stable 1,4-lactone derivatives, the carbonium ions (I) rearrange to resonance-stabilized allyl cation intermediates (V′). The carbonium ions (V) undergo carbonylation and hydration, and subsequently 1,4-lactones are formed by intramolecular esterification. During the isomerization process to V, carbonium ions (IV) react with carbon monoxide, and then stable 1,5-lactone derivatives are obtained. Generally, the amount of 1,4-lactone is larger than the quantity of 1,5-lactone. Lactonization to five- and six-membered rings is fast, however ring-closure reactions to seven- and eight-membered rings are slow. Furthermore, the isomerization rate is higher than the ring-closure rate to large-ring lactones. For these reasons, it is understood that no large-ring lactones or four-membered lactone are obtained. In all lactones, the α-carbon of the carbonyl group has two alkyl substituents, and the carbon atom adjacent to the oxygen atom has one alkyl substituent.

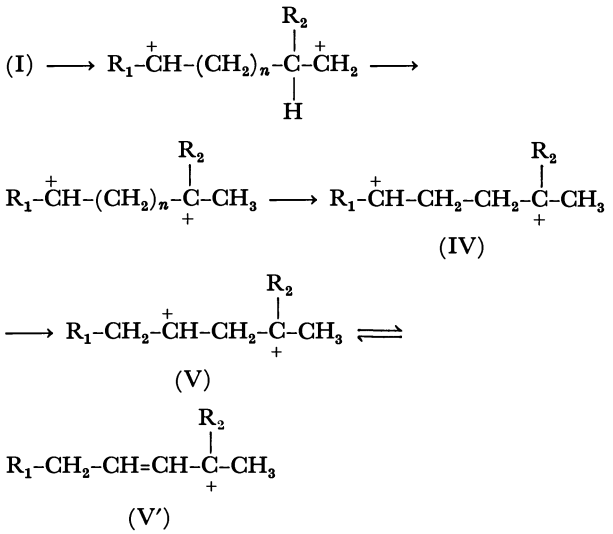

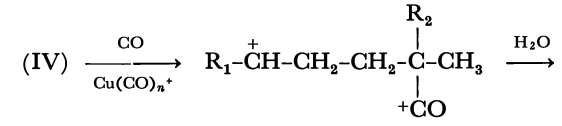

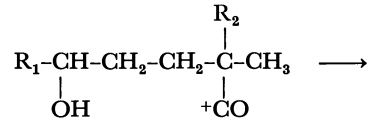

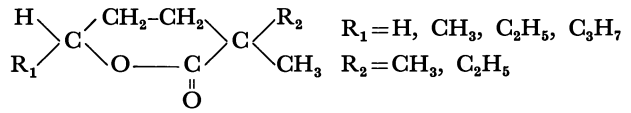

(VI)

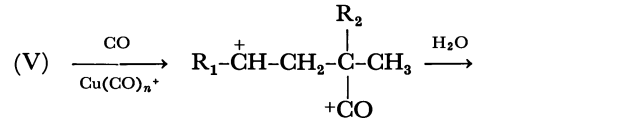

(VII)

R_1=CH_3, C_2H_5, C_3H_7, C_4H_9
R_2=CH_3, C_2H_5

Cyclic monocarboxylic acid and *t*-monocarboxylic acid are obtained by the carbonylation of 1,7-octadiene. In the formation of cyclic monocarboxylic acid, the carbonium ion (VIII) undergoes a ring-closure reaction by means of the intramolecular attack of the cation on the double bond. After rearrangement from IX to X, the carbonium ion (X) reacts with carbon monoxide producing 1,4-dimethylcyclohexanecarboxylic acid.

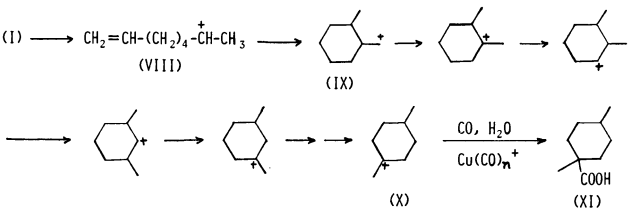

To form saturated *t*-monocarboxylic acid, some of the carbonium ions (I) are saturated by hydride abstraction from other molecules. It appears that the secondary carbonium ions are more susceptible to saturation than *t*-carbonium ions.

Actually, the main alkyl chain of the carboxylic acid obtained is linear.

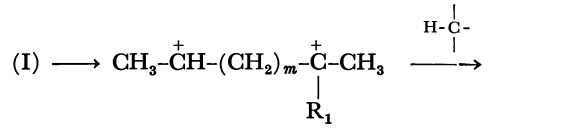

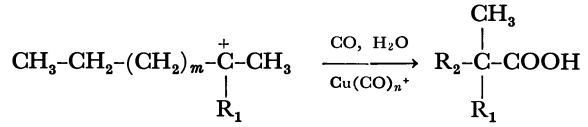

R_1=CH_3, C_2H_5
R_2=C_4H_9, C_5H_{11}

(XII)

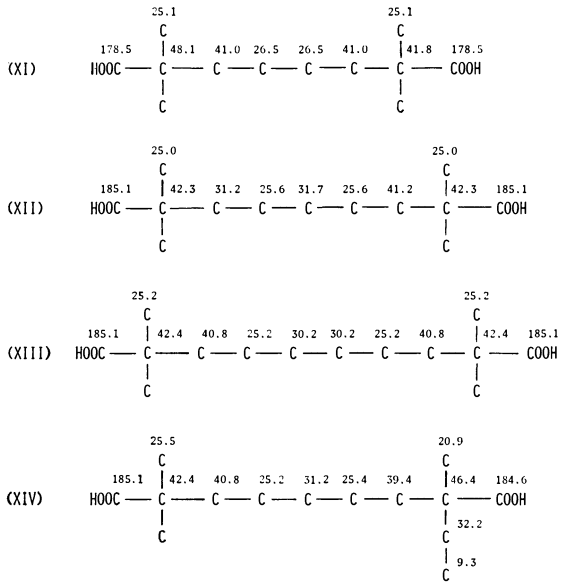

Chart 1. ^{13}C NMR chemical shifts of tertiary-dicarboxylic acids.

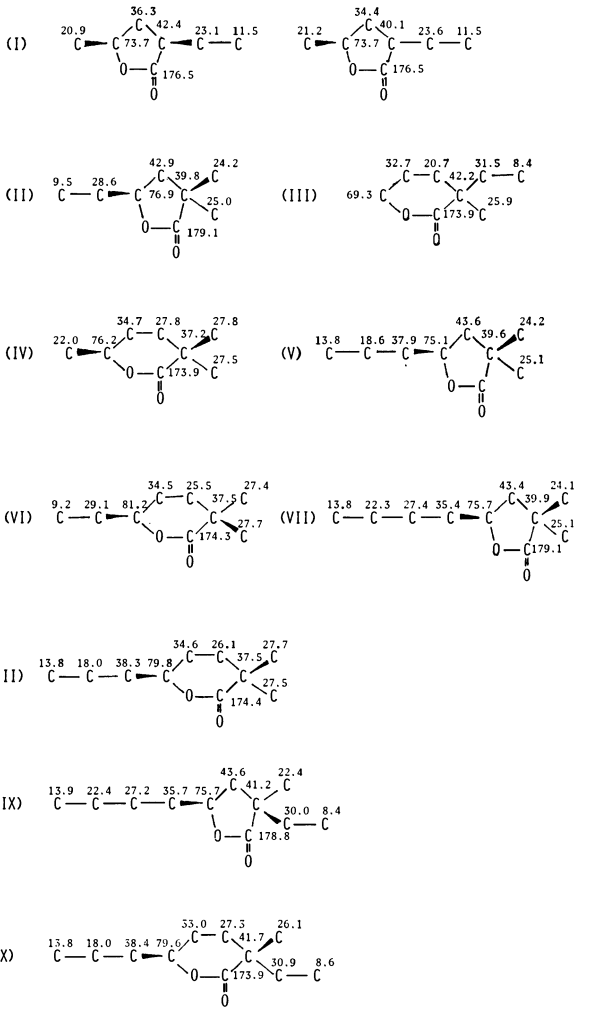

Chart 2. ^{13}C NMR chemical shifts of lactones.

Dicarboxylic acid was separated as crystals from lactone and recrystallized from a mixed solvent of petroleum ether and acetone. Since the isomers of

the dicarboxylic acids could not be separated, the mixtures were analyzed by ^{13}C NMR. Lactone and monocarboxylic acid were isolated by preparative GLPC, and the structures were determined by ^{1}H NMR, ^{13}C NMR, IR, GC-MS and elemental analysis. The ^{13}C NMR chemical-shift assignments of the dicarboxylic acids and lactones are shown in Charts 1 and 2. From the ^{13}C NMR analysis, other isomers coexisted with the compound shown in Charts 1 and 2, however, the amount of other isomers was so few that the determination of their structures was not successful.

Several characteristics are clarified by the results of the analysis of the lactones. On the GLPC chromatogram, two large peaks were observed for every sample. The first peak corresponds to the 1,4-lactone derivatives, and the second peak to the 1,5-lactone derivatives. In the IR spectra, the $\nu_{C=O}$ of 1,4-lactone and 1,5-lactone were observed at 1775 and 1725 cm^{-1}, respectively. In the ^{1}H NMR chemical shifts of 1,4-lactones, characteristic signals for methylene of the lactone ring were observed at 2.0—2.3 ppm as the AB part of the ABX spin system. From ^{13}C NMR analysis, the chemical shifts for the carbonyl carbons of 1,4-lactone and 1,5-lactone were determined to be at 176—179 ppm and at *ca.* 174 ppm, respectively.

Using silver carbonyl ions instead of copper(I) carbonyl ions as catalysts, the same catalytic effect was observed and the same reaction products were obtained.

Experimental

GLPC analysis was performed using a 3-m Free Fatty Acid Polyester column. The infrared spectra were taken with neat samples using a JASCO IRA-1 spectrophotometer. The ^{1}H NMR spectra were taken using a JEOL PS-100 at 100 MHz with CCl_4 as the solvent. Chemical shifts are given in δ units (ppm) downfield from the tetramethylsilane internal standard. The ^{13}C NMR spectra were measured using the pulsed Fourier-transform technique with a JEOL PS-100 instrument, an FT-100 FT unit, a DP-1 pulse programmer, and an EC-100 computer, at a resonance frequency of 25.15 MHz. Proton noise decoupling was normally used. Mass spectra were obtained using a JEOL JMS-06 gas chromatograph-mass spectrometer with a 20-eV ionizing voltage.

Preparation of the Cu(I) Carbonyl Catalysts. In a 300-ml three-necked flask equipped with a thermometer and a carbon monoxide gas burette, 1.144 g of Cu_2O and 30 ml of 98% H_2SO_4 were placed: The apparatus was evacuated by a rotary pump, and then carbon monoxide was introduced from the gas burette. The mixture was stirred vigorously and a heterogeneous solution of $Cu(CO)_n^+$ was prepared.

Carbonylation of Dienes and Diols. From a syringe, 30 mmol of dienes or diols were added dropwise to the Cu(I) carbonyl catalyst solution for 2 h. Absorption of the carbon monoxide was completed within 2 — 3 h, and the reaction mixture was poured over ice-water. The mixture was shaken with hexane, and the reaction products were isolated by preparative GLPC or by recrystallization. The structures of the products were determined by ^{1}H NMR, ^{13}C NMR, IR and mass spectra and by elemental analysis.

In order to determine the monocarboxylic acid, dicarboxylic acid and lactone yield in the mixture, first the total amount of the carboxylic acids was determined by titrating a 1/10 volume of hexane extract with a 1/10 M NaOH ethanol solution. The monocarboxylic acid yield was determined using gas chromatography by adding a known amount of an internal standard. The dicarboxylic acid yield was calculated from the difference between the total carboxylic acid yield and the monocarboxylic acid yield. The lactone yield was determined by measuring the saponification value. The excess of the 1/10 M NaOH ethanol solution was added to the hexane extract, and the mixture was refluxed for 3 h, then titrated with a standard 1/10 M HCl solution. The lactone yield was found from the difference between saponification value and the total amount of carboxylic acids.

2,2-Dimethyl-4-hexanolide was obtained from 1,7-heptanediol. IR: 2960, 1760 (C=O), 1460, 1205 cm^{-1}. NMR δ 0.98 (3H, t, J=7Hz, $-CH_2-CH_3$), 1.20 (6H, s, $-\overset{|}{\underset{|}{C}}-CH_3$) 1.43—1.80 (2H, m, $-CH_2-CH_2$), 2.00—2.30 (2H, m, $-OCH-CH_2-$), 4.25(1H, m, $-O-CH-CH_2-$). Found: C, 67.23; H, 9.78%. Calcd for $C_8H_{14}O_2$: C, 67.57; H, 9.92%.

2-Methyl-2-ethyl-5-heptanolide was obtained from 1,7-heptanediol. IR: 2980, 1735 (C=O), 1380, 1260, 1140 cm^{-1}. NMR (CCl_4) δ 0.90 (3H, t, J=7Hz, $-CH_2-CH_3$), 1.20 (3H, s, $-\overset{|}{\underset{|}{C}}-CH_3$), 1.40—2.00 (6H, m, $-CH_2-$), 4.28 (2H, m, $-O-CH_2-$). Mass spectrum *m/e* (%) 142 (M^+, 8) 127(9), 113(100), 55(46). Found: C, 67.11; H, 9.89%. Calcd for $C_8H_{14}O_2$; C, 67.57; H, 9.92%.

2,2-Dimethyl-4-heptanolide was obtained from 1,7-octadiene and 1,8-octanediol. IR: 2970, 1770 (C=O), 1460, 1385, 1205, 1115 cm^{-1}. NMR (CCl_4) δ 1.00 (3H, t, J=7 Hz, $-CH_2-CH_3$), 1.20 (6H, s, $CH_3-\overset{|}{\underset{|}{C}}-CH_3$), 1.36—2.20 (6H, m, $-CH_2-$), 4.35 (1H, m, $-CH-O-$). Mass spectrum *m/e* (%) 156 (M^+, 21), 113(100), 85(82), 69(86). Found: C, 69.07; H, 10.64%. Calcd for $C_9H_{16}O_2$: C, 69.19; H, 10.32%.

2,2-Dimethyl-5-heptanolide was obtained from 1,7-octadiene and 1,8-octanediol. IR: 2970, 1725(C=O), 1385, 1280, 1120 cm^{-1}. NMR (CCl_4) δ 1.02 (3H, t, J=7 Hz, $-CH_2-CH_3$), 1.22 (6H, s, $CH_3-\overset{|}{\underset{|}{C}}-CH_3$), 1.40—1.95 (6H, m, $-CH_2-$), 4.14 (1H, m, $-CH-O-$). Mass spectrum *m/e* (%) 156 (M^+, 9), 127(14), 81(28) 70(25), 56(100). Found: C, 69.22; H, 10.73%. Calcd for $C_9H_{16}O_2$: C, 69.19; H, 10.32%.

2,2-Dimethyl-4-octanolide was obtained from 1,9-nonanediol. IR: 2960, 1765 (C=O), 1460, 1200, 1115 cm^{-1}. NMR (CCl_4) δ 0.94 (3H, t, J=6Hz, $-CH_2-CH_3$), 1.20 (6H, s, $CH-\overset{|}{\underset{|}{C}}-CH_3$), 1.40—2.40 (8H, m, $-CH_2-$), (1H, m, $-CH-O-$). Mass spectrum *m/e* (%) 170(M^+, 14), 140(13), 112 (76), 70(100). Found: C, 70.35; H, 10.46%. Calcd for $C_{10}H_{18}O_2$: C, 70.55; H, 10.65%.

2,2-Dimethyl-5-octanolide was obtained from 1,9-nonanediol. IR: 2960, 1725 (C=O), 1380, 1120 cm^{-1}. NMR (CCl_4) δ 0.98 (3H, t, J=7 Hz, $-CH_2-CH_3$), 1.20 (6H, s, $CH_3-\overset{|}{\underset{|}{C}}-CH_3$), 1.40—1.80 (8H, $-CH_2-$), 4.20 (1H, m, $-CH-O-$). Mass spectrum *m/e* (%) 170 (M^+, 10), 126 (33), 70 (55), 56(100). Found: C, 70.48; H, 10.49%. Calcd for $C_{10}H_{18}O_2$: C, 70.55; H, 10.65%.

C_{12} t-Dicarboxylic Acids (a mixture of 2,2,7,7-tetramethyloctanedioic acid and 2-ethyl-2,6,6-trimethylheptanedioic acid) were obtained from 1,9-decadiene. Mp 152—156 °C. IR (KBr): 2970, 1680 (C=O), 1465, 1380, 1250, 1170 cm^{-1}. NMR (CCl_4) δ 0.88 (t, J=7 Hz, CH_3-CH_2-), 1.08, 1.12, 1.16 (s, $\overset{|}{\underset{|}{C}}-CH_3$), 1.20—1.95 (m, $-CH_2-$), 12.5

(br. s, -COOH). Found: C, 62.28; H, 9.75%. Calcd for $C_{12}H_{22}O_4$: C, 62.58; H, 9.63%.

C_{13} t-Dicarboxylic Acids (a mixture of 2,2,8,8-tetramethylnonanedioic acid and 2-ethyl-2,7,7-trimethyloctanedioic acid) were obtained from 1,10-undecadiene. Mp 132—134°C. IR(KBr): 2970, 1680 (C=O), 1400, 1250, 1193, 920 cm^{-1}. NMR (CCl_4) δ 0.84 (t, J=7Hz, CH_3-CH_2-), 1.04 (s, CH_3-C-), 1.14 (s, CH_3-C-CH_3), 1.26—1.88 (m, -CH_2-), 11.2 (br. s, -COOH). Found: C, 64.29; H, 10.38%. Calcd for $C_{13}H_{24}O_4$: C, 63.91; H, 9.90%.

C_{14} t-Dicarboxylic Acids (a mixture of 2,2,9,9-tetramethyldecanedioic acid and 2-ethyl-2,8,8-trimethylnonanedioic acid) were obtained from 1,12-dodecanediol. Mp 114—118°C. IR(KBr): 2970, 1680 (C=O), 1460, 1250, 1180, 920 cm^{-1}. NMR (CCl_4) δ 0.86 (t, J=7Hz, CH_3-CH_2-), 1.08, 1.14 (s, CH_3-C-), 1.20—1.80 (m, -CH_2-), 12.2 (br. s, -COOH). Found: C, 65.47; H, 10.57%. Calcd for $C_{14}H_{26}O_4$: C, 65.09; H, 10.14%.

2-Ethyl-4-pentanolide, *2,2-Dimethylheptanoic Acid*, *2-Methyl-2-ethylhexanoic Acid* and *1,4-Dimethylcyclohexanecarboxylic Acid* were identified using authentic samples obtained by the carbonylation of 1,5-hexadiene, 1-octene and 1,4-dimethylcyclohexane, respectively.[1,3]

References

1) Y. Souma, H. Sano, and J. Iyoda, *J. Org. Chem.*, **38**, 2016 (1973).
2) Y. Souma and H. Sano, *Bull. Chem. Soc. Jpn.*, **46**, 3237 (1973).
3) Y. Souma and H. Sano, *J. Org. Chem.*, **38**, 3633 (1973).
4) Y. Souma and H. Sano, *Bull. Chem. Soc. Jpn.*, **47**, 1717 (1974).
5) N. Yoneda, T. Fukuhara, Y. Takahashi, and A. Suzuki, *Chem. Lett.*, **1974** 607.
6) K. Schauerte and H. Koch, *Brennstoff Chem.*, **49**, 263 (1968).
7) K. Schauerte and H. Koch, *Brennstoff Chem.*, **49**, 302 (1968).
8) B. E. Kuvaev, N. S. Imyanitov, and D. M. Rudkovskii, *Zh. Prikl. Khim. (Leningrad)*, **40**(6), 1359; *Chem. Abstr.*, **67**, 99587g (1967).
9) F. E. Paulik, A. Hershman, W. R. Knox, and J. F. Roth, *Ger. Offen.*, 1941448; *Chem. Abstr.*, **73**, 34811n (1970).
10) Y. Souma, J. Iyoda, and H. Sano, *Inorg. Chem.*, **15**, 968 (1976).

Carbonylation of Olefins, Alcohols, and Saturated Hydrocarbons Using $Cu(CO)_n^+$ and $Ag(CO)_2^+$ Catalysts in BF_3–H_2O

Yoshie Souma and Hiroshi Sano

Government Industrial Research Institute, Osaka, Midorigaoka, Ikeda, Osaka 563

(Received May 4, 1976)

Olefins, alcohols, and saturated hydrocarbons reacted with carbon monoxide to give *t*-carboxylic acids in high yields using copper carbonyl and silver carbonyl catalysts at room temperature and in carbon monoxide at atmospheric pressure in BF_3–H_2O solutions. Dienes and diols also reacted with carbon monoxide to give mixtures of monocarboxylic acids, dicarboxylic acids and lactones. The concentration ratio of H_2O/BF_3 was maintained between 1 and 2 during the carbonylation reaction. There was no difference between the catalytic behavior of $Cu(CO)_n^+$ and that of $Ag(CO)_2^+$. The reaction rates for primary alcohols were very low in BF_3–H_2O, although they increased with the addition of H_2SO_4. The reaction rates for *s*-alcohol, *t*-alcohol and olefins in BF_3–H_2O remained unchanged upon the addition of H_2SO_4.

In previous papers, the authors have reported that olefins, alcohols, and saturated hydrocarbons reacted with carbon monoxide and produced *t*-carboxylic acids in the presence of $Cu(CO)_n^+$ catalysts in H_2SO_4 at room temperature and at atmospheric pressure.[1-4] Similarly, carbonylation reactions of diisobutylene and 1-octene have been reported by Yoneda *et al.* using $Cu(CO)_n^+$ catalysts in BF_3–H_2O.[5] It has been reported that Ag_2O was not effective in the carbonylation.[6] In this case, no silver carbonyl ions appear to be formed, because silver compounds are easily reduced to metal silver when BF_3–H_2O is added to Ag_2O in a CO atmosphere at room temperature. However, the formation of $Ag(CO)_2^+$ was possible by adding Ag_2O to cold BF_3–H_2O.[7] Therefore, it was clarified that the catalysis of $Ag(CO)_2^+$ was the same as that of $Cu(CO)_n^+$ in BF_3–H_2O. This paper describes the carbonylation of olefins, alcohols, and saturated hydrocarbons using $Ag(CO)_2^+$ and $Cu(CO)_n^+$ catalysts in BF_3–H_2O.

Results and Discussion

Cu(I) compounds absorb carbon monoxide and form unstable copper carbonyl ions $Cu(CO)_4^+$, in BF_3–H_2O, as described in a preceding paper.[7]

$$Cu^+ + CO \rightleftharpoons Cu(CO)_4^+ \quad (1)$$

$$Cu(CO)_4^+ \rightleftharpoons Cu(CO)^+ + 3CO \quad (2)$$

In BF_3–H_2O, $Cu(CO)_4^+$, and $Cu(CO)^+$ coexist in equilibrium. The effect of temperature and BF_3 concentration on the formation of $Cu(CO)_4^+$ has been reported by Matsushima *et al.*[8] As the temperature decreases, the equilibruim is shifted toward the left hand side of Reaction 2.

As has been described previously, Ag carbonyl ions are also formed by the absorption of carbon monoxide by silver compounds in cold BF_3–H_2O solutions.[7]

$$Ag^+ + CO \rightleftharpoons Ag(CO)_2^+ \quad (3)$$

$Ag(CO)_2^+$ and Ag^+ also coexist in equilibrium. The effect of the temperature and concentration of BF_3–H_2O on the formation of $Ag(CO)_2^+$ is shown in Fig. 1. Silver carbonyl ions are formed in concentrated BF_3–H_2O solutions, when the H_2O/BF_3 molar ratio of the solution is between 1 and 2. The equilibirum is shifted toward the right hand side of Reaction 3 as the temperature decreases. IR absorption ($\nu_{C=O}$) of $Cu(CO)_4^+$, $Cu(CO)^+$, and $Ag(CO)_2^+$, in BF_3–H_2O occur at 2185, 2160, and 2193 cm^{-1}, respectively.[7] The ^{13}C NMR chemical shifts of $Cu(CO)_4^+$, $Cu(CO)^+$, and $Ag(CO)_2$ are 169.5, 169.0, and 173.4 ppm, respectively.[7]

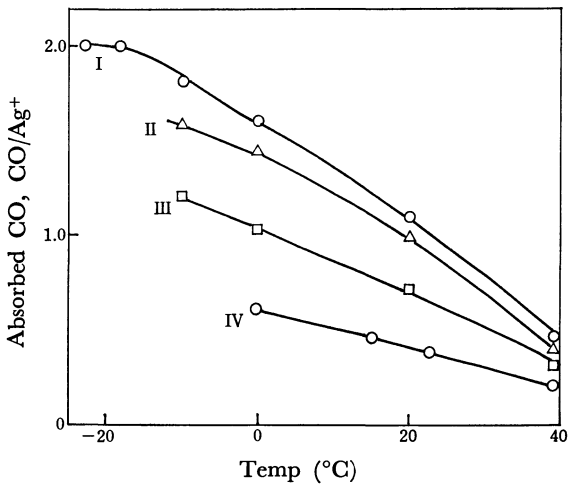

Fig. 1. The formation of $Ag(CO)_2^+$ in BF_3–H_2O solution.
I: BF_3–H_2O, II: BF_3–$1.2H_2O$, III: BF_3–$1.5H_2O$, IV: BF_3–$2.0H_2O$.

Table 1. Carbonylation of 1-octene catalyzed by $Cu(CO)_n^+$ and $Ag(CO)_2^+$ in BF_3–H_2O[a]

H_2O/BF_3 mole ratio	$Cu(CO)_n^+/Cu^+$	Yield of C_9-*t*-acid	$Ag(CO)_2^+/Ag^+$	Yield of C_9-*t*-acid
1.0	2.8	92	1.2	93
1.2	2.5	95	1.1	96
1.5	1.8	68	0.7	80
1.7	1.4	50	0.6	55
2.0	1.1	7	0.4	5

a) In all cases, 20 ml of BF_3–H_2O, 572 mg of Cu_2O, 928 mg of Ag_2O and 3.15 ml of 1-octene were used. The reaction was carried out at 20°C in 1 atm of carbon monoxide. b) The product was a 4 : 2 : 1 mixture of 2,2-dimethylheptanoic acid, 2-methyl-2-ethylhexanoic acid and 2-methyl-2-propylpentanoic acid.

The results of the carbonylation reaction of 1-octene in various concentrations of BF_3–H_2O using $Cu(CO)_n^+$ and $Ag(CO)_2^+$ catalysts are shown in Table 1.

Table 2. The carbonylation of olefins, alcohols, and saturated hydrocarbons[a)]

Compound	Catalyst	Time	Products	Yield	(total)
1-Hexene	$Cu(CO)_4^+$	1 h	2,2-Dimethylpentanoic acid	60	80
			2-Methyl-2-ethylbutanoic acid	20	
1-Octene	$Ag(CO)_2^+$	1 h	2,2-Dimethylheptanoic acid	55	92
			2-Methyl-2-ethylhexanoic acid	26	
			2-Methyl-2-propylpentanoic acid	13	
1-Decene	$Ag(CO)_2^+$	1 h	2,2-Dimethylnonanoic acid	47	86
			2-Methyl-2-ethyloctanoic acid	23	
			2-Methyl-2-propylheptanoic acid	11	
			2-Methyl-2-buthylhexanoic acid	5	
Cyclohexene	$Cu(CO)_4^+$	1 h	1-Methylcyclopentanecarboxylic acid		75
2-Propanol	$Cu(CO)_4^+$	3 d	2-Methylpropionic acid		15
2-Methyl-2-propanol	$Cu(CO)_4^+$	2 h	2,2-Dimethylpropionic acid		94
1-Hexanol	$Ag(CO)_2^+$	1 d	2,2-Dimethylpentanoic acid	12	16
			2-Methyl-2-ethylbutanoic acid	4	
2-Hexanol	$Ag(CO)_2^+$	2 h	2,2-dimethylpentanoic acid	72	95
			2-Methyl-2-ethylbutanoic acid	23	
3-Methyl-3-pentanol	$Ag(CO)_2^+$	2 h	2,2-Dimethylpentanoic acid	16	95
			2-Methyl-2-ethylbutanoic acid	79	
1-Octanol	$Ag(CO)_2^+$	7 d	2,2-Dimethylheptanoic acid	20	35
			2-Methyl-2-ethylhexanoic acid	10	
			2-Methyl-2-propylpentanoic acid	5	
		1 d	same as above		16
Methylcyclohexane (Coexist. with 1-octene)	$Cu(CO)_4^+$	2 h	1-Methylcyclohexanecarboxylic acid		30
			C_9 *t*-carboxylic acid		60
Methylcyclopentane (Coexist. with 2-hexanol)	$Ag(CO)_2^+$	2 h	1-Methylcyclopentanecarboxylic acid		30
			C_7 *t*-carboxylic acid		50

a) The reaction was carried out using 20 ml of BF_3–H_2O, 572 mg of Cu_2O, 928 mg of Ag_2O, and 20 mmol of the compound, at 25 °C in carbon monoxide, at 1 atm.

The yield of *t*-carboxylic acids and the reaction rate decrease with a decrease in the BF_3 concentration. This tendency of the yield to decrease corresponds to the decrease of the amount of $Cu(CO)_4^+$ or $Ag(CO)_2^+$ present in the BF_3–H_2O solution. The carbonylation does not proceed at H_2O/BF_3 molar ratio larger than 2. The best results were obtained at H_2O/BF_3 molar ratios of 1.0—1.2.

The reaction scheme is the same as that for H_2SO_4. The olefin is protonated in the BF_3–H_2O solution and is rearranged to a tertiary carbonium ion with the migration of an alkyl group. The tertiary carbonium ion reacts with carbon monoxide and forms *t*-carboxylic acid in the presence of $Cu(CO)_4^+$ or $Ag(CO)_2^+$ as a catalyst.

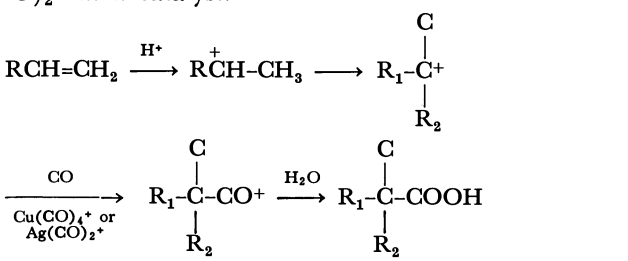

$R_1 = CH_3$, C_2H_5, *n*-C_3H_7, *n*-C_4H_9, *n*-C_5H_{11}, *n*-C_6H_{13}, *n*-C_7H_{15}
$R_2 = CH_3$, C_2H_5, *n*-C_3H_7

The results of the carbonylation of olefins, alcohols, and saturated hydrocarbons are shown in Table 2.

The rate and the conversion of the reaction with primary alcohols were low, and most of the primary alcohol was recovered. The dehydration of primary alcohol appears to be difficult.

Table 3. The influence of the BF_3–H_2O concentration on the carbonylation of saturated hydrocarbons[a)]

Yield of carboxylic acid	H_2O/BF_3 molar ratio			
	1.0	1.2	1.5	1.7
1-Methylcyclohexane-carboxylic acid	30	8	1	0
C_9 *t*-carboxylic acid	60	84	65	57

a) The reactions were carried out using 20 ml of BF_3–H_2O, 527 mg of Cu_2O, 2.56 ml of methylcyclohexane, and 3.14 ml of 1-octene at 20 °C.

Saturated hydrocarbons react with carbon monoxide in the presence of olefins and alcohols. The hydride ion is abstracted from the saturated hydrocarbon by the carbonium ion formed from the olefin or alcohol. Then the carbonium ion forms *t*-carboxylic acid. Saturated hydrocarbons which have no tertiary hydrogens do not react with carbon monoxide.

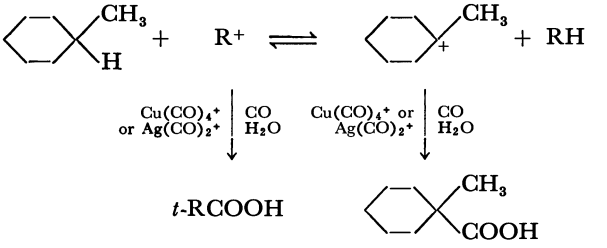

Hydride transfer takes place only in concentrated BF_3–H_2O solutions. The results of the carbonylation

of 1-methylcyclohexane in the presence of 1-octene in various concentrations of BF_3–H_2O are shown in Table 3.

The results of carbonylation reactions of diene and diol are shown in Table 4. Mixtures of *t*-monocarboxylic acids or *t*-dicarboxylic acids and lactones were obtained. The lactones have alkyl branches on α-carbon. The structural analysis of each compound will be reported elsewhere.[9]

The reaction scheme proposed is as follows.

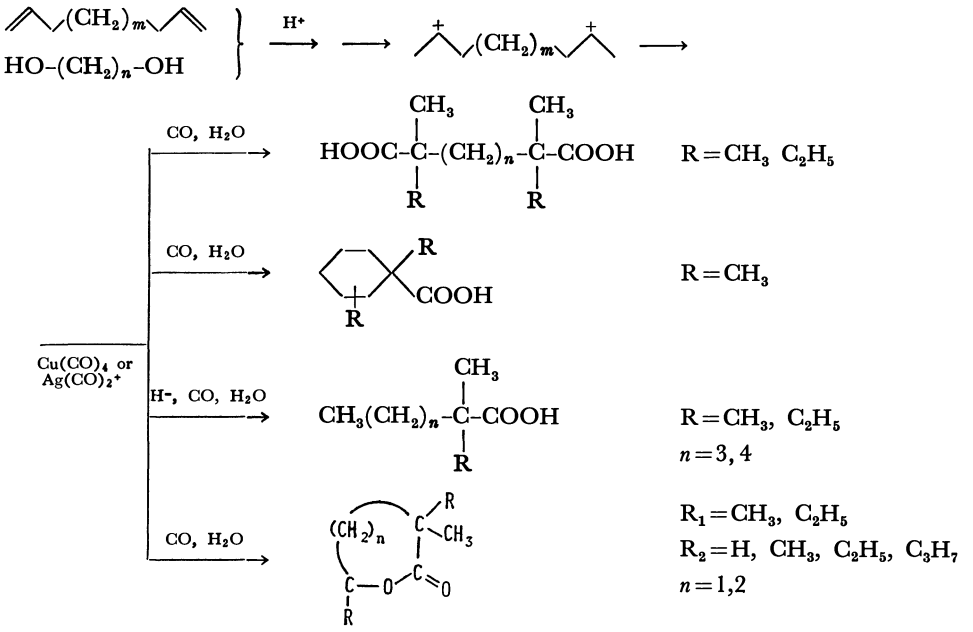

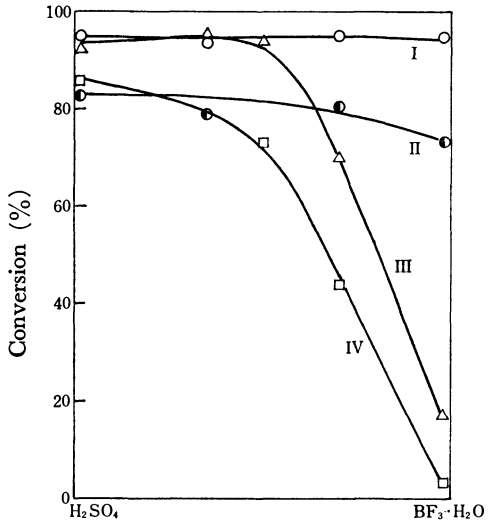

Fig. 2. Carbonylation in BF_3–H_2O~H_2SO_4 system. I: 1-Octene, II: 1,9-decadiene, III: 1-octanol, IV: 1,2-dodecanediol.

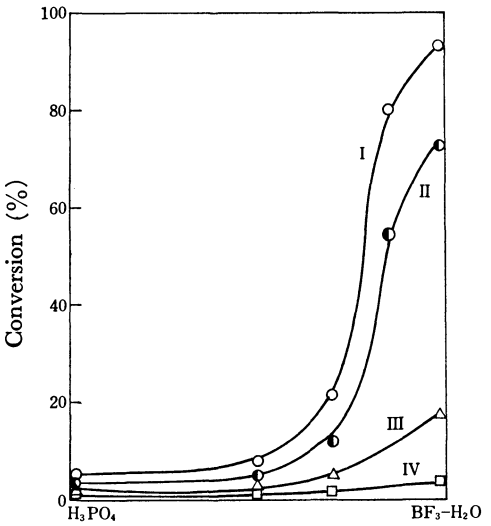

Fig. 3. Carbonylation in BF_3–H_2O~H_3PO_4 system. I: 1-Octene, II: 1,9-decadiene, III: 1-octanol, IV: 1,12-dodecanediol.

The effect of the addition of H_2SO_4 or H_3PO_4 to the BF_3–H_2O solution is shown in Figs. 2 and 3. The addition of H_2SO_4 accelerates the carbonylation reaction of primary alcohols such as 1-octanol and 1,12-dodecanediol, but is not effective in the reactions of olefins and *s*- or *t*-alcohols. The addition of H_2SO_4 appears to promote the dehydration of primary alcohols. The addition of H_3PO_4 decreases the carboxylic acid yield and the reaction rate.

The catalytic behavior of $Ag(CO)_2^+$ and $Cu(CO)_4^+$ are the same for the carbonylation reactions in BF_3–H_2O.

Experimental

Preparation of $Cu(CO)_n^+$ and $Ag(CO)_2^+$ in BF_3–H_2O. The BF_3–H_2O solution was preparared by introducing BF_3 gas into water.

In a 300 ml three-necked flask, equipped with a thermometer and a CO gas burette, 572 mg of Cu_2O were placed. The apparatus was evacuated by a vacuum pump and CO was introduced from the gas burette. The mixture was stirred after the addition of BF_3–H_2O. Colorless copper(I) carbonyl ions were formed by the absorption of CO by the Cu_2O.

Table 4. Carbonylation of dienes and diols[a)]

Compound	Catalyst	Temp, °C	Time, h	Products	Yield, %
1,5-Hexadiene	$Cu(CO)_4^+$	5—10	2	2-Ethyl-4-pentanolide	35
1,7-Octadiene	$Ag(CO)_2^+$	20—30	2	1,4-Dimethylcyclohexanecarboxylic acid	30
				2,2-Dimethyl-4-heptanolide	35
				2,2-Dimethyl-5-heptanolide	8
1,9-Decadiene	$Cu(CO)_4^+$	6—10	2	2,2,7,7-Tetramethyloctanedioic acid	30
				2-Ethyl-2,6,6-trimethylheptanedioic acid	5
				2-Methyl-2-ethyl-4-octanolide	40
				2-Methyl-2-ethyl-5-octanolide	20
1,12-Dodecanediol	$Cu(CO)_4^+$	20—30	3	No reaction	
1,12-Dodecanediol	$Cu(CO)_4^+$	20—25	3	2,2,9,9-Tetramethyldecanedioic acid	30
				2-Ethyl-2,8,8-trimethylnonanedioic acid	10
				1,4- and 1,5-Lactone	45

a) The reactions were carried out using 30 ml of BF_3–H_2O, 6 mmol of Cu_2O or Ag_2O, and 30 mmol of the compound. b) An additional 30 ml of 98% H_2SO_4 were used.

For the preparation of silver carbonyl ions, 928 mg of Ag_2O were placed in a three-necked flask containing ice-cold BF_3–H_2O. Colorless silver carbonyl ions were formed by the absorption of CO by the Ag_2O for a period of 10 min.

Carbonylation of Olefins, Alcohols, and Saturated Hydrocarbons. From a syringe, 20 mmol of an olefin (an alcohols or an equimolar mixture consisting of saturated hydrocarbons and an alkyl cation source) were added drop by drop to the copper(I) carbonyl (or silver carbonyl) catalyst solution. Immediately, carbon monoxide reacted with these compounds. The reaction mixture was poured into ice-water, and the product was extracted with hexane.

The yields of monocarboxylic acid, dicarboxylic acid and lactone in the mixtures were determined as follows. First, a 1/5 volume of an hexane extract of the mixture was titrated with a 1/10 N NaOH ethanol solution to determine the total amount of carboxylic acid. The amount of monocarboxylic acid was determined by gas chromatography in the presence of a known amount of prim-carboxylic acid as an internal standard. The amount of dicarboxylic acid was found from the difference between the total amount of carboxylic acids and the amount of monocarboxylic acid. The amount of lactone was determined by measuring the saponification value as follows. The excess of the 1/10 N NaOH ethanol solution was added to the hexane extract, and the mixture was refluxed for 3 h and then titrated using a standard 1/10 N HCl solution. The amount of lactone was calculated from the difference between the saponification value and the total amount of carboxylic acid. GLPC analysis was performed using a 3-m FFAP column (10% on chromosorb WAW).

All identifications were carried out using authentic samples obtained and characterized previously by the carbonylation of olefins, alcohols, and saturated hydrocarbons in H_2SO_4 systems.[1-3,9)]

References

1) Y. Souma, H. Sano, and J. Iyoda, *J. Org. Chem.*, **38**, 2016 (1973).
2) Y. Souma and H. Sano, *Bull. Chem. Soc. Jpn.*, **46**, 3237(1973).
3) Y. Souma and H. Sano, *J. Org. Chem.*, **38**, 3633(1973).
4) Souma and H. Sano, *Bull. Chem. Soc. Jpn.*, **47**, 1717 (1973).
5) N. Yoneda, T. Fukuhara, Y. Takahashi, and A. Suzuki, *Chem. Lett.*, **1974** 607.
6) T. Fukuhara, Y. Takahashi, N. Yoneda, and A. Suzuki, presented at the Summer Meeting of the Chemical Society of Japan, Hokkaido, July 25, 1974, Abstract p. 43.
7) Y. Souma, J. Iyoda, and H. Sano, *Inorg. Chem.*, **15**, 968 (1976).
8) Y. Matsushima, T. Koyano, T. Kitamura, and S. Wada, *Chem. Lett.*, **1973**, 433.
9) Y. Souma and H. Sano, *Bull. Chem. Soc. Jpn.*, **49**, 3291 (1976).

Layered Compounds. XXXIV.[1] Molecular and Crystal Structure of a Polycyclic Compound from Novel Cycloaddition Reaction of Triple-layered Anthracenophane

Toshihiro TOYODA, Akio IWAMA, Tetsuo OTSUBO, and Soichi MISUMI*

The Institute of Scientific and Industrial Research, Osaka University, Suita, Osaka 565

(Received May 15, 1976)

An unusual Diels-Alder reaction was observed to give intramolecular cycloadducts during the syntheses of triple-layered cyclophanes containing anthracene nucleus. The structure of the product was determined by spectral and X-ray crystal analyses. The crystal is monoclinic, $P2_1/c$, with $a=15.896$, $b=8.937$, $c=18.575$ Å, $\beta=120.31°$, $Z=4$. The crystal structure was determined by the direct method using the MULTAN program and refined by the block-diagonal least-squares method to an R index of 0.081. The structure of the molecule is fairly strained.

Layered cyclophanes in which benzene rings are closely fixed face-to-face by methylene bridges have been studied as suitable models for examining transannular π-electron interactions.[2] Reports appeared on the double-layered compounds containing anthracene nuclei as carbophanes of extended aromatic π-system, and their anomalous physical and chemical behaviors.[3] In order to study further the transannular π-electron interaction anthracenophanes, we have undertaken the syntheses of triple-layered compounds (**5**) containing anthracene nucleus. In this paper we report on an unusual reaction which takes place to give cycloadducts (**6**) in place of the desired anthracenophanes. The structures of the products were determined by spectroscopic and X-ray crystallographic analyses.

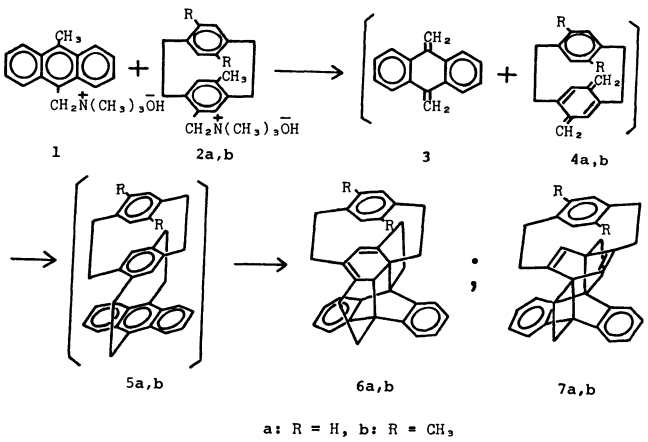

Scheme 1.

Syntheses and Properties. A quaternary ammonium hydroxide (**1**) was obtained by treatment of 9-chloromethyl-10-methylanthracene[4] with trimethylamine in ether followed by anion exchange with a resin IRA-400. Pyrolysis of an equimolar mixture of the ammonium hydroxide (**1**) and (7-methyl-4-[2.2]-paracyclophanylmethyl)trimethylammonium hydroxide (**2a**)[5] was carried out in boiling xylene in the presence of a catalytic amount of phenothiazine. After removal of water by azeotropic distillation, and separation of solid material by filtration, the reaction mixture was chromatographed twice on alumina to afford pure colorless product in 7.8% yield along with quadruple-layered cyclophanes[5] derived by self-coupling of an intermediate quinodimethane derivative **4a**. The recrystallized product showed a molecular formula $C_{34}H_{30}$ coinciding with the structure **5a** from elemental analysis, mass spectrum, and osmometric molecular weight determination. However, its electronic spectrum shows only a tailing absorption in a wavelength region longer than 350 nm, indicating the absence of anthracene nucleus (Fig. 1). Its PMR spectrum reveals an olefinic proton at δ 4.36 and an increase of aliphatic protons at the expense of two aromatic protons as compared with the proton ratio expected from formula **5a** (Table 1). The spectral data indicate that the intermediate **5a** undergoes a certain intramolecular reaction to give a structural isomer.

Two structures (**6a** and **7a**) are possible for the product on the basis of spectral data and examination with molecular models. Structure **6a** is regarded as a $(4\pi+2\pi)$ cycloadduct of the anthracene and the inner benzene moieties of **5a**, and structure **7a** as a $(4\pi+4\pi)$ one. The PMR data (Table 1) is not consistent with **7a** having C_2 symmetry. Consequently, the remaining **6a** is presumed as the structure of intramolecular cycloadduct. Similarly, the product $C_{36}H_{34}$ which was obtained by cross-breeding pyrolysis of a mixture of **1** and **2b** shows spectra consistent with **6b** (Fig. 1 and

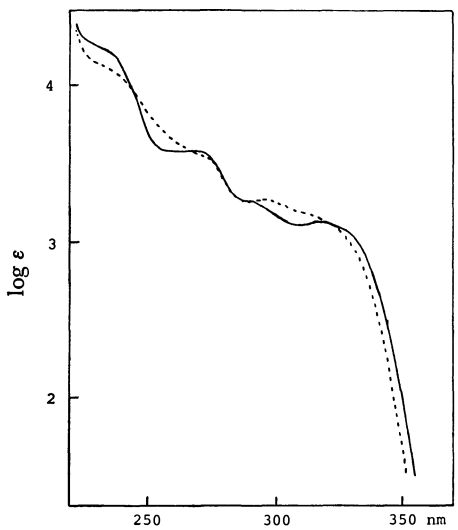

Fig. 1. Electronic spectra of the compounds **6a** (——) and **6b** (----) in tetrahydrofuran.

Table 1. PMR spectra of pyrolysis products

1+**2a** → $C_{34}H_{30}$			**1**+**2b** → $C_{36}H_{34}$		
Chemical shift ppm	Number of protons		Chemical shift ppm	Number of protons	
1.0—3.0 (m)	17	CH_2, CH	0.9—3.3 (m)	23	CH_3, CH_2, CH
4.36 (bs)	1	=CH	4.52 (bs)	1	=CH
6.7—7.4 (m)	12	ArH	6.42 (s)	1	ArH
			6.55 (s)	1	ArH
			6.7—7.2 (m)	8	ArH

Table 1). Two singlets at δ 6.42 and 6.55 on its PMR spectrum are assigned to the aromatic protons of paracyclophane moiety. A considerable high-field shift of the protons as compared to the corresponding ones of **6a** is attributed to the enhanced ortho shift σ_{OE}.[6]

Attempts to prepare the triple-layered anthracenophane **5** by retro-Diels-Alder reaction of **6** under various thermal and photochemical conditions were unsuccessful.

Experimental

Physical Methods. Melting points are uncorrected. PMR spectra were taken on Hitachi Perkin-Elmer R-20 (60 MHz) and JEOL JNM-TS-100 (100 MHz) spectrometers on dilute solution in deuteriochloroform using tetramethylsilane as an internal standard. UV spectra were measured on Hitachi EPS-3T spectrometer, MS on Hitachi RMU-7 spectrometer, and molecular weights on Knauer vapor pressure osmometer using methylene chloride.

(9-Methyl-10-anthrylmethyl)trimethylammonium Chloride. An excess of trimethylamine (4 g) in ether (50 ml) was added with stirring to a solution of 9-chloromethyl-10-methylanthracene (6.5 g, 27 mmol), obtained by chloromethylation of 9-methylanthracene,[4] in benzene (800 ml) at room temp. After prolonged stirring, the resulting yellow ppt was filtered, washed with benzene and dried *in vacuo*. The yield of quaternary ammonium chloride was 7.3 g (90%).

*Cross-breeding Pyrolysis of Ammonium Bases, **1** and **2**. Compound **6a**.* An aq solution (1.5 l) of equimolar mixture of (9-methyl-10-anthrylmethyl)trimethylammonium chloride (4.0 g, 13.3 mmol) and (7-methyl-4-[2.2]paracyclophanylmethyl)trimethylammonium bromide[5] (4.6 g, 13.3 mmol) was passed through a column of anion exchange resin IRA-400 to give aq solution of two ammonium bases, **1** and **2a**. The aq soln was added dropwise for 15 h to a boiling solution of phenothiazine (100 mg) in xylene (200 ml) placed in a three-necked, pear-shaped flask fitted with a mechanical stirrer and a Dean-Stark type water separator. After complete removal of water, insoluble solid was filtered and the filtrate was condensed to *ca.* 5 ml *in vacuo*. Precipitated solid was filtered and the filtrate was chromatographed on neutral alumina (Sumitomo KCG-30). Elution with benzene–hexane (1 : 9) gave 0.51 g (8.7% yield) of **6a**. Compound **6a** was recrystallized from benzene, colorless prisms, mp 238.0—240.5 °C with decomposition near 240 °C.

MS (*m/e*) 438 [M+], 334, 234, 204. Found: C, 92.98; H, 6.81%; mol wt 428 (vapor pressure osmometry). Calcd for $C_{34}H_{30}$: C, 93.12; H, 6.90%; mol wt 438.6.

*Compound **6b**.* Pyrolysis of two ammonium bases, **1** and **2b**, derived from an equimolar solution (1.5 l) of (9-methyl-10-anthrylmethyl)trimethylammonium chloride (3.35 g, 11.2 mmol) and (4,7,12-trimethyl-15-[2.2]paracyclophanylmethyl)trimethylammonium bromide[5] (5.0 g, 12.4 mmol), was carried out in the same manner as that for **6a** to afford a 1.5% yield (78 mg) of **6b**. Compound **6b** was recrystallized from benzene to give colorless prisms, mp 220—235 °C with decomposition over 180 °C.

MS (*m/e*) 466 [M+], 334, 262, 204, 132. Found: C, 92.65; H, 7.23%; mol wt 458 (vapor pressure osmometry). Calcd for $C_{36}H_{34}$: C, 92.66; H, 7.35%; mol wt 466.7.

X-Ray Structure Determination

The crystal of compound **6a** crystallized in colorless prisms from benzene was used for the measurement of intensities. The space group was determined to be $P2_1/c$ from oscillation and Weissenberg photographs. The cell constant was determined by the least-squares method (Sakurai, 1967)[7] based on the Bragg angles of 30 reflections. The density was measured by floatation in aq zinc bromide at room temperature.

Crystal Data. $C_{34}H_{30}$ MW=438.61; monoclinic, space group $P2_1/c$, a=15.896(3), b=8.937(2), c=18.575(3) Å, β=120.31 °(1), V=2278.0(6) Å^3), Mo $K\alpha$ radiation λ=0.71069 Å, D_m=1.275 g/cm^3, Z=8, D_x=1.279 g/cm^3.

Systematic absences $h0l$ when l is odd
$0k0$ when k is odd

Three-dimensional intensity data were collected on a Rigakudenki automatic four-circle diffractometer with Mo $K\alpha$ radiation. The crystal selected for the data collection was 0.33×0.17×0.20 mm in size. The relative intensities were measured with the θ-2θ scan technique (scan speed 2 °/min(2θ)) in a range from $\{2\theta(\alpha_1)-1.0\ °\}$ to $\{2\theta(\alpha_2)+1.0\ °\}$. During the course of data collection, the three standard reflections were monitored at every 50 reflections in order to examine the stability of the electronics and the crystal. A total of 5669 independent reflections were measured in the range $0<\sin\theta/\lambda<0.7$, of which 3054 were recorded as observed. The intensities were corrected for Lorentz and polarization factors, but not for absorption. Background intensities were measured for ten seconds at both ends of a scan.

Structure Refinement. The structure was determined by the direct method using the MULTAN program[8] with 494 reflections having E's>1.5. The sets of phases selected by the program were:

h	k	l	Phase	
4	1	$\bar{1}$	0	origin fixing
4	1	$\bar{2}$	0	
5	4	$\overline{23}$	0	

Table 2. Atomic fractional coordinates and anisotropic thermal parameters ($\times 10^4$) of the carbon atoms
Anisotropic thermal parameters are expressed in the form of $\exp[-(\beta_{11}h^2+\beta_{22}k^2+\beta_{33}l^2+\beta_{12}hk+\beta_{13}hl+\beta_{23}kl)]$.
The estimated standard deviation, given in parentheses, refers to the last significant figure.

Atom	x/a	y/b	z/c	β_{11}	β_{22}	β_{33}	β_{12}	β_{13}	β_{23}
C(1)	3002(3)	7648(5)	3835(2)	58(2)	127(6)	29(1)	−33(6)	39(3)	15(5)
C(2)	4135(3)	7673(5)	4388(3)	56(2)	122(6)	44(2)	−41(6)	67(4)	−16(6)
C(3)	4485(3)	7996(4)	5296(2)	41(2)	106(6)	44(2)	−37(5)	54(3)	−5(5)
C(4)	4176(3)	9253(5)	5525(3)	49(2)	108(6)	43(2)	−33(6)	38(3)	−12(5)
C(5)	4159(3)	9277(5)	6267(3)	49(2)	122(6)	42(2)	−35(6)	39(3)	−52(6)
C(6)	4471(3)	8054(5)	6793(2)	47(2)	147(7)	29(1)	−62(6)	29(3)	−35(5)
C(7)	5002(3)	6966(5)	6660(2)	36(2)	152(7)	34(2)	−28(6)	13(3)	6(6)
C(8)	5003(2)	6932(5)	5913(3)	29(2)	134(6)	47(2)	−6(5)	36(3)	−6(6)
C(9)	3991(3)	7687(6)	7298(3)	61(3)	225(9)	33(2)	−88(8)	46(4)	−52(7)
C(10)	3126(3)	6555(6)	6787(2)	64(3)	249(10)	32(2)	−120(8)	57(4)	−61(7)
C(11)	2795(2)	6489(5)	5864(2)	36(2)	169(7)	26(1)	−66(6)	34(3)	−32(5)
C(12)	2184(3)	7713(5)	5307(2)	39(2)	133(6)	42(2)	−18(6)	43(3)	−53(6)
C(13)	1971(2)	7857(4)	4519(2)	38(2)	95(5)	39(2)	20(5)	28(3)	−6(5)
C(14)	2380(2)	6793(4)	4145(2)	32(2)	92(5)	24(1)	1(5)	21(2)	8(4)
C(15)	2877(2)	5436(4)	4671(2)	30(2)	77(4)	26(1)	6(4)	28(2)	11(4)
C(16)	3034(2)	5366(4)	5528(2)	32(2)	133(6)	24(1)	−41(5)	19(2)	5(5)
C(17)	3369(3)	3767(5)	5809(2)	64(3)	150(7)	31(2)	−7(7)	21(3)	41(6)
C(18)	3004(3)	2860(5)	4974(3)	56(2)	98(6)	46(2)	14(6)	42(4)	33(6)
C(19)	2325(2)	3931(4)	4284(2)	34(2)	86(5)	36(2)	−15(5)	39(3)	−9(5)
C(20)	2155(2)	3882(4)	3400(2)	37(2)	112(6)	36(2)	−25(5)	44(3)	−27(5)
C(21)	2492(3)	2777(5)	3078(3)	56(2)	144(7)	60(3)	−44(7)	79(4)	−61(7)
C(22)	2295(3)	2900(6)	2262(3)	78(3)	214(9)	64(3)	−96(9)	106(5)	−114(8)
C(23)	1773(4)	4092(6)	1778(3)	95(4)	252(10)	43(2)	−123(10)	96(5)	−82(8)
C(24)	1439(3)	5214(6)	2091(3)	69(3)	182(8)	31(2)	−70(8)	44(4)	−21(6)
C(25)	1632(3)	5118(4)	2909(2)	44(2)	107(5)	28(1)	−19(5)	36(3)	−20(5)
C(26)	1369(2)	6258(4)	3366(2)	37(2)	115(6)	26(1)	15(5)	18(3)	2(5)
C(27)	830(2)	5367(5)	3709(2)	35(2)	133(6)	32(2)	−19(5)	30(3)	−53(5)
C(28)	−102(3)	5679(6)	3563(3)	36(2)	199(8)	54(2)	−1(7)	32(4)	−91(7)
C(29)	−524(3)	4750(7)	3888(3)	48(2)	296(11)	68(3)	−100(9)	78(4)	−167(9)
C(30)	−36(3)	3531(6)	4352(3)	75(3)	277(11)	53(2)	−177(9)	96(5)	−136(8)
C(31)	908(3)	3192(6)	4514(3)	71(3)	190(8)	43(2)	−103(8)	73(4)	−52(7)
C(32)	1325(2)	4122(4)	4183(2)	38(2)	121(6)	28(1)	−41(5)	36(3)	−34(5)
C(33)	897(3)	7780(5)	2999(3)	57(3)	127(7)	39(2)	42(7)	5(3)	21(6)
C(34)	1162(3)	8753(5)	3790(3)	54(2)	120(6)	48(2)	59(6)	12(4)	−7(6)

Table 3. Atomic fractional coordinates ($\times 10^3$) and isotropic thermal parameters (in Å^2) of the hydrogen atoms
The numbering follows that of the carbon atoms to which the hydrogens are attached.

Atom	x/a	y/b	z/c	B	Atom	x/a	y/b	z/c	B
H(1A)	284(3)	724(5)	330(3)	4(1)	H(1B)	276(3)	874(5)	371(3)	4(1)
H(2A)	437(3)	664(5)	432(3)	4(1)	H(2B)	433(3)	862(5)	414(3)	4(1)
H(4)	378(3)	999(5)	506(3)	4(1)	H(5)	378(3)	1009(5)	634(3)	4(1)
H(7)	528(3)	602(5)	705(3)	4(1)	H(8)	528(3)	603(5)	578(3)	4(1)
H(9A)	443(3)	721(6)	781(3)	5(1)	H(9B)	367(3)	867(6)	737(3)	5(1)
H(10A)	335(3)	553(5)	704(3)	4(1)	H(10B)	259(3)	681(5)	687(3)	4(1)
H(12)	189(3)	837(5)	552(3)	4(1)	H(15)	352(3)	531(5)	471(2)	3(1)
H(17A)	409(3)	370(5)	621(3)	4(1)	H(17B)	305(3)	343(5)	611(3)	4(1)
H(18A)	358(3)	261(5)	490(3)	4(1)	H(18B)	272(3)	184(5)	498(3)	4(1)
H(21)	284(3)	188(5)	343(3)	4(1)	H(22)	251(3)	199(6)	199(3)	5(1)
H(23)	163(3)	422(6)	119(3)	5(1)	H(24)	105(3)	605(5)	177(3)	5(1)
H(28)	−45(3)	649(5)	325(3)	5(1)	H(29)	−121(3)	498(6)	377(3)	5(1)
H(30)	−26(3)	281(5)	461(3)	5(1)	H(31)	119(3)	229(5)	479(3)	5(1)
H(33A)	120(3)	830(6)	265(3)	5(1)	H(33B)	16(3)	765(6)	264(3)	5(1)
H(34A)	146(3)	981(6)	378(3)	5(1)	H(34B)	63(3)	887(6)	393(3)	5(1)

8	2	$\bar{2}$	0
2	2	$\bar{8}$	0
12	1	$\overline{15}$	0, π
12	4	$\bar{2}$	0, π
1	5	$\overline{12}$	0, π
1	8	$\bar{1}$	0, π

by Σ_1 formula

Of the 16 possible solutions, one set of phases (12,1, $\overline{15}$ and 1,5,$\overline{12}=0$;12,4,$\bar{2}$ and $18\bar{1}=\pi$) giving the figure of merit of 1.23 seemed to be correct. An E map generated from this set of phases gave starting positions for all carbon atoms which gave an initial $R=0.27$. After refinement with the block-diagonal least-squares method ($R=0.17$), a difference synthesis revealed the positions of all the hydrogen atoms. The refinement with isotropic thermal parameters for all the atoms, followed by further cycles of refinement using the block-diagonal least-squares method[9] with carbon atoms anisotropic and hydrogen atoms isotropic temperature factors, yielded the final residual R of 0.081. The final atomic coordinates, thermal parameters, and the corresponding standard deviations are listed in Tables 2 and 3.* Computation was done on a NEAC 2200-700 computer at Osaka University. Atomic scattering factors were taken from those of Suzuki.[10]

Results and Discussion

The molecular geometry is shown in Fig. 2. The structure obtained is in complete agreement with that of **6a** determined by spectroscopy. For the dimethyl derivative $C_{36}H_{34}$, structure **6b** can be assigned on the basis of the fact that it shows electronic and PMR spectra similar to those of **6a** and that the cell constant and the reflection pattern of the crystal of **6b** (space group $P2_1/c$) closely resemble those of **6a**.

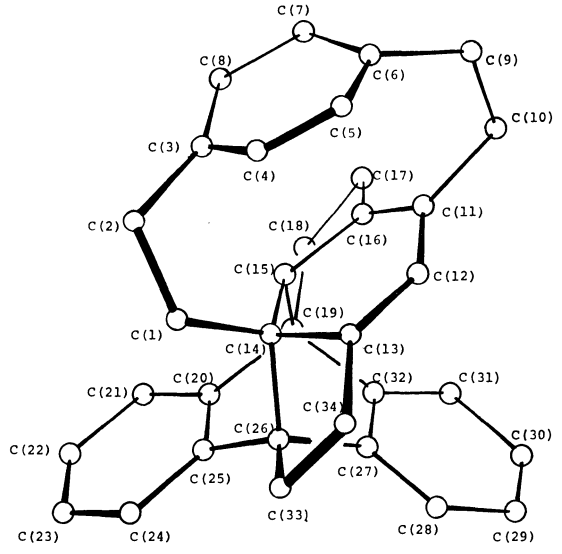

Fig. 2. Projection of the molecular structure along the b-axis.

* A list of structure factors has been deposited with the Chemical Society of Japan, 1-5 Kanda-Surugadai, Chiyoda-ku, Tokyo 101 (Document No. 7630).

The bond distances and angles for the molecule of **6a** are given in Tables 4 and 5 with their estimated standard deviations. The C–C bond lengths of the benzene ring, C(3)—C(8), are normal. On the other hand, the two aromatic C–C bonds, C(22)–C(23) and C(29)–C(30), are slightly shorter, which is probably attributable to intermolecular repulsions and/or the inaccuracy of the present crystal analysis.

In the cyclohexadiene moiety C(11)—C(16), the bond lengths of the double bonds, C(11)–C(16) and C(12)–C(13), and the single bond C(11)–C(12) are normal as compared to the common butadiene system (C=C 1.31—1.34 Å and C–C 1.37—1.53 Å), whereas the single bonds, C(14)–C(15) and C(15)–C(16), are appreciably shorter than the normal values (C–C 1.54 Å and C–C= 1.51 Å). As shown in Fig. 3 and Table 6, the marked steric compressions of C(15) and H(15) by benzene C(3)—C(8) and the bridged methylene, C(2) and C(18), are responsible for the shortening of these two single bonds. Other two single bonds,

Table 4. Bond lengths and their estimated standard deviations

C(1)---C(2)	1.562(6)	C(1)---C(14)	1.571(6)
C(2)---C(3)	1.513(6)	C(3)---C(4)	1.375(7)
C(3)---C(8)	1.393(6)	C(4)---C(5)	1.392(7)
C(5)---C(6)	1.381(6)	C(6)---C(7)	1.389(6)
C(6)---C(9)	1.515(7)	C(7)---C(8)	1.388(6)
C(9)---C(10)	1.581(7)	C(10)---C(11)	1.519(7)
C(11)---C(12)	1.482(6)	C(11)---C(16)	1.335(6)
C(12)---C(13)	1.332(6)	C(13)---C(14)	1.504(6)
C(13)---C(34)	1.539(7)	C(14)---C(15)	1.506(5)
C(14)---C(26)	1.600(5)	C(15)---C(16)	1.484(5)
C(15)---C(19)	1.567(5)	C(16)---C(17)	1.523(6)
C(17)---C(18)	1.579(7)	C(18)---C(19)	1.527(6)
C(19)---C(20)	1.523(6)	C(19)---C(32)	1.513(6)
C(20)---C(21)	1.394(7)	C(20)---C(25)	1.406(6)
C(21)---C(22)	1.389(8)	C(22)---C(23)	1.369(8)
C(23)---C(24)	1.393(8)	C(24)---C(25)	1.394(6)
C(25)---C(26)	1.512(6)	C(26)---C(27)	1.526(6)
C(26)---C(33)	1.538(6)	C(27)---C(28)	1.393(7)
C(27)---C(32)	1.390(6)	C(28)---C(29)	1.381(8)
C(29)---C(30)	1.362(8)	C(30)---C(31)	1.409(7)
C(31)---C(32)	1.387(6)	C(33)---C(34)	1.527(6)
C(1)---H(1A)	0.97(5)	C(1)---H(1B)	1.03(5)
C(2)---H(2A)	1.03(5)	C(2)---H(2B)	1.00(5)
C(4)---H(4)	1.01(5)	C(5)---H(5)	0.99(5)
C(7)---H(7)	1.06(5)	C(8)---H(8)	1.01(5)
C(9)---H(9A)	0.95(5)	C(9)---H(9B)	1.05(5)
C(10)---H(10A)	1.01(5)	C(10)---H(10B)	0.97(5)
C(12)---H(12)	0.96(5)	C(15)---H(15)	0.99(4)
C(17)---H(17A)	1.00(5)	C(17)---H(17B)	0.97(5)
C(18)---H(18A)	1.01(5)	C(18)---H(18B)	1.02(5)
C(21)---H(21)	1.00(5)	C(22)---H(22)	1.10(5)
C(23)---H(23)	1.00(5)	C(24)---H(24)	0.96(5)
C(28)---H(28)	0.92(5)	C(29)---H(29)	1.02(5)
C(30)---H(30)	0.97(5)	C(31)---H(31)	0.94(5)
C(33)---H(33A)	1.08(5)	C(33)---H(33B)	1.03(5)
C(34)---H(34A)	1.06(5)	C(34)---H(34B)	1.01(5)

Table 5. Bond angles and their estimated standard deviations

C(2)-C(1)-C(14)	119.7(4)	C(1)-C(2)-C(3)	112.9(4)
C(2)-C(3)-C(4)	120.9(4)	C(2)-C(3)-C(8)	121.1(4)
C(4)-C(3)-C(8)	117.3(4)	C(3)-C(4)-C(5)	120.5(4)
C(4)-C(5)-C(6)	120.6(4)	C(5)-C(6)-C(7)	117.5(4)
C(5)-C(6)-C(9)	119.7(4)	C(7)-C(6)-C(9)	120.1(4)
C(6)-C(7)-C(8)	120.0(4)	C(3)-C(8)-C(7)	120.6(4)
C(6)-C(9)-C(10)	108.9(4)	C(9)-C(10)-C(11)	113.8(4)
C(10)-C(11)-C(12)	119.5(4)	C(10)-C(11)-C(16)	122.6(4)
C(12)-C(11)-C(16)	117.9(4)	C(11)-C(12)-C(13)	123.6(4)
C(12)-C(13)-C(14)	121.1(4)	C(12)-C(13)-C(34)	130.7(4)
C(14)-C(13)-C(34)	106.7(4)	C(1)-C(14)-C(13)	111.1(3)
C(1)-C(14)-C(15)	114.1(3)	C(1)-C(14)-C(26)	110.1(3)
C(13)-C(14)-C(15)	114.7(3)	C(13)-C(14)-C(26)	97.9(3)
C(15)-C(14)-C(26)	107.7(3)	C(14)-C(15)-C(16)	118.5(3)
C(14)-C(15)-C(19)	113.9(3)	C(16)-C(15)-C(19)	102.0(3)
C(11)-C(16)-C(15)	122.6(4)	C(11)-C(16)-C(17)	132.7(4)
C(15)-C(16)-C(17)	104.3(3)	C(16)-C(17)-C(18)	104.7(4)
C(17)-C(18)-C(19)	104.8(4)	C(15)-C(19)-C(18)	99.1(3)
C(15)-C(19)-C(20)	105.8(3)	C(15)-C(19)-C(32)	105.7(3)
C(18)-C(19)-C(20)	123.6(4)	C(18)-C(19)-C(32)	115.4(4)
C(20)-C(19)-C(32)	105.4(3)	C(19)-C(20)-C(21)	125.8(4)
C(19)-C(20)-C(25)	113.6(4)	C(21)-C(20)-C(25)	120.5(4)
C(20)-C(21)-C(22)	119.2(5)	C(21)-C(22)-C(23)	120.5(5)
C(22)-C(23)-C(24)	121.2(5)	C(23)-C(24)-C(25)	119.4(5)
C(20)-C(25)-C(24)	119.2(4)	C(20)-C(25)-C(26)	114.0(3)
C(24)-C(25)-C(26)	126.7(4)	C(14)-C(26)-C(25)	105.9(3)
C(14)-C(26)-C(27)	107.3(3)	C(14)-C(26)-C(33)	100.3(3)
C(25)-C(26)-C(27)	104.8(3)	C(25)-C(26)-C(33)	124.0(4)
C(27)-C(26)-C(33)	113.3(3)	C(26)-C(27)-C(28)	125.6(4)
C(26)-C(27)-C(32)	115.1(4)	C(28)-C(27)-C(32)	119.4(4)
C(27)-C(28)-C(29)	119.9(5)	C(28)-C(29)-C(30)	120.7(5)
C(29)-C(30)-C(31)	120.8(5)	C(30)-C(31)-C(32)	118.2(5)
C(19)-C(32)-C(27)	113.2(3)	C(19)-C(32)-C(31)	125.8(4)
C(27)-C(32)-C(31)	121.1(4)	C(26)-C(33)-C(34)	103.5(4)
C(13)-C(34)-C(33)	104.2(4)		
C(14)-C(1)-H(1A)	107.8(28)	C(14)-C(1)-H(1B)	108.1(27)
C(2)-C(1)-H(1A)	107.0(28)	C(2)-C(1)-H(1B)	107.9(27)
C(1)-C(2)-H(2A)	106.4(27)	C(1)-C(2)-H(2B)	102.2(28)
C(3)-C(2)-H(2A)	110.8(27)	C(3)-C(2)-H(2B)	110.0(28)
C(6)-C(9)-H(9A)	111.4(32)	C(6)-C(9)-H(9B)	109.2(30)
C(10)-C(9)-H(9A)	106.5(32)	C(10)-C(9)-H(9B)	106.4(30)
C(9)-C(10)-H(10A)	108.0(29)	C(9)-C(10)-H(10B)	108.0(30)
C(11)-C(10)-H(10A)	108.6(29)	C(11)-C(10)-H(10B)	110.6(30)
C(16)-C(17)-H(17A)	112.5(29)	C(16)-C(17)-H(17B)	106.5(30)
C(18)-C(17)-H(17A)	114.0(29)	C(18)-C(17)-H(17B)	111.5(30)
C(17)-C(18)-H(18A)	109.7(28)	C(17)-C(18)-H(18B)	113.2(28)
C(19)-C(18)-H(18A)	108.8(28)	C(19)-C(18)-H(18B)	116.0(28)
C(26)-C(33)-H(33A)	112.1(28)	C(26)-C(33)-H(33B)	109.4(30)
C(34)-C(33)-H(33A)	109.2(28)	C(34)-C(33)-H(33B)	109.9(30)
C(33)-C(34)-H(34A)	112.9(29)	C(33)-C(34)-H(34B)	115.6(31)
C(13)-C(34)-H(34A)	106.9(29)	C(13)-C(34)-H(34B)	104.7(31)
C(16)-C(15)-H(15)	107.8(25)	C(19)-C(15)-H(15)	104.5(25)
C(14)-C(15)-H(15)	109.1(25)	C(3)-C(4)-H(4)	115.7(27)
C(5)-C(4)-H(4)	121.3(27)	C(4)-C(5)-H(5)	117.2(28)
C(6)-C(5)-H(5)	120.7(28)	C(6)-C(7)-H(7)	121.6(26)
C(8)-C(7)-H(7)	117.1(26)	C(7)-C(8)-H(8)	119.1(27)
C(3)-C(8)-H(8)	119.4(27)	C(11)-C(12)-H(12)	116.4(29)
C(13)-C(12)-H(12)	119.8(29)	C(20)-C(21)-H(21)	119.0(29)

TABLE 5. (Continued)

C(22)-C(21)-H(21)	121.7(29)	C(21)-C(22)-H(22)	118.9(28)
C(23)-C(22)-H(22)	120.5(28)	C(22)-C(23)-H(23)	122.6(31)
C(24)-C(23)-H(23)	116.2(31)	C(23)-C(24)-H(24)	124.1(32)
C(25)-C(24)-H(24)	116.4(31)	C(27)-C(28)-H(28)	120.8(33)
C(29)-C(28)-H(28)	119.3(33)	C(28)-C(29)-H(29)	119.3(30)
C(30)-C(29)-H(29)	120.0(30)	C(29)-C(30)-H(30)	128.3(30)
C(31)-C(30)-H(30)	110.9(30)	C(30)-C(31)-H(31)	117.9(31)
C(32)-C(31)-H(31)	123.5(31)		
H(1A)-C(1)-H(1B)	105.5(39)	H(2A)-C(2)-H(2B)	114.3(39)
H(9A)-C(9)-H(9B)	114.2(44)	H(10A)-C(10)-H(10B)	107.8(42)
H(17A)-C(17)-H(17B)	107.4(42)	H(18A)-C(18)-H(18B)	104.3(39)
H(33A)-C(33)-H(33B)	112.3(41)	H(34A)-C(34)-H(34B)	111.5(42)

TABLE 6. SOME INTRAMOLECULAR NONBONDING DISTANCES AROUND C(15) AND H(15) WITH e.s.d.'s

C(15)...C(2)	3.055(6)	H(15)...C(2)	2.53(4)
C(15)...C(3)	3.182(6)	H(15)...C(3)	2.77(4)
C(15)...C(8)	3.266(6)	H(15)...C(8)	2.71(4)
C(15)...H(18A)	2.70(5)	H(15)...H(18A)	2.42(7)

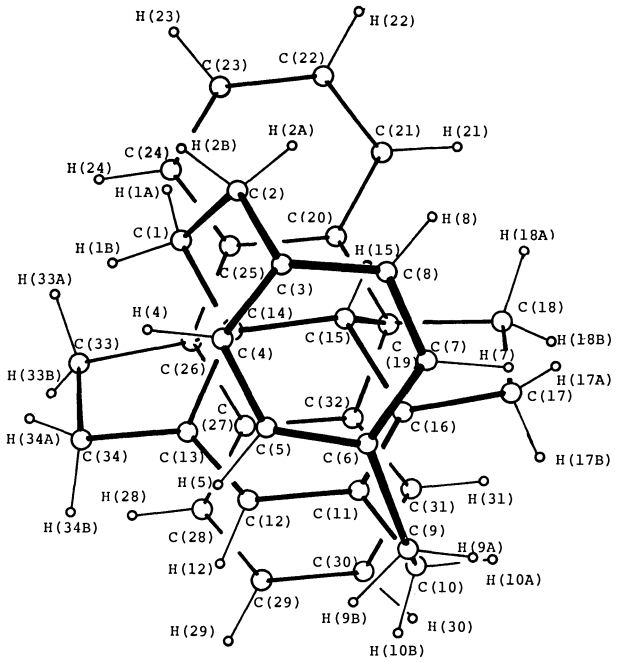

Fig. 3. A view of the molecule along the normal to the plane defined by four carbon atoms, C(20), C(25), C(27), and C(32).

C(14)–C(26) and C(15)–C(19), formed by the intramolecular Diels-Alder reaction are considerably elongated to 1.600 and 1.567 Å, respectively, from the normal value. This may be caused by the steric repulsions acting on methylene C(1) and the cyclohexadiene moiety C(11)—C(16) from the dihydroanthracene moiety C(19)—C(32) (Table 7). As shown in Fig. 4, the cyclohexadiene moiety has a nearly planar structure in spite of a severe overlapping of the π-electron cloud with that of the benzene ring C(3)—C(8). Intramolecular nonbonding distances are given in

TABLE 7. SOME INTRAMOLECULAR NONBONDING DISTANCES AROUND C(1) AND BETWEEN CYCLOHEXADIENE C(11)—C(16) AND TWO BENZENE RINGS, C(20)—C(25) AND C(27)—C(32), WITH e.s.d.'s

C(1)...C(3)	2.563(6)	C(12)...C(27)	3.375(6)
C(1)...C(13)	2.536(6)	C(13)...C(27)	2.785(6)
C(1)...C(15)	2.582(6)	C(14)...C(20)	2.883(6)
C(1)...C(25)	3.005(6)	C(14)...C(25)	2.484(5)
C(1)...C(26)	2.598(6)	C(14)...C(27)	2.517(5)
C(1)...C(33)	2.894(6)	C(14)...C(32)	2.938(5)
C(1)...C(34)	3.047(7)	C(15)...C(20)	2.465(6)
		C(15)...C(25)	2.856(5)
		C(15)...C(27)	2.813(5)
		C(15)...C(32)	2.455(5)
		C(16)...C(32)	2.829(6)

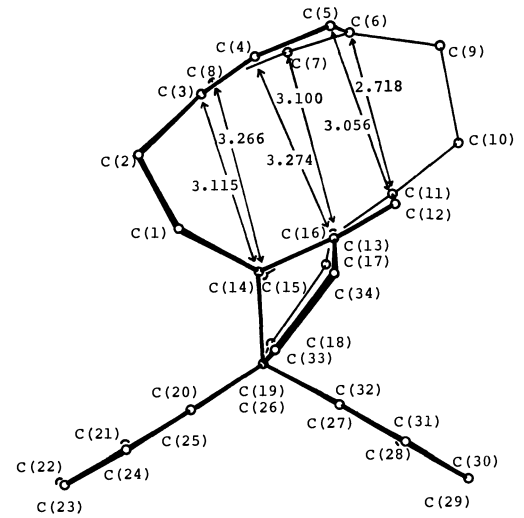

Fig. 4. A view of the molecule along the bond C(19)–C(26).

Table 8. Such unexpected planarity of the cyclohexadiene moiety can be explained by a compensation of the repulsions acting on both upper and lower sides of the diene moiety. An unsymmetrical boat-shape deformation of the para-substituted benzene ring C(3)—C(8) is observed (Fig. 5), which may result from the π-electron repulsion between the benzene ring and the diene moiety (Table 8). The repulsion would also affect the bond lengths of the

Table 8. Intramolecular nonbonding distances between benzene ring C(3)—C(8) and cyclohexadiene ring C(11)—C(16) with e.s.d.'s

C(3)...C(14)	3.115(6)	C(6)...C(11)	2.718(6)
C(3)...C(15)	3.182(6)	C(6)...C(12)	3.287(6)
C(4)...C(12)	3.285(6)	C(6)...C(16)	3.331(6)
C(4)...C(13)	3.274(6)	C(7)...C(11)	3.072(6)
C(5)...C(11)	3.135(6)	C(7)...C(16)	3.100(6)
C(5)...C(12)	3.056(6)	C(8)...C(15)	3.266(6)
		C(8)...C(16)	3.165(6)

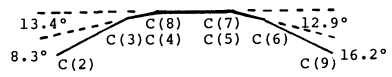

Fig. 5. The distortion angles of benzene.

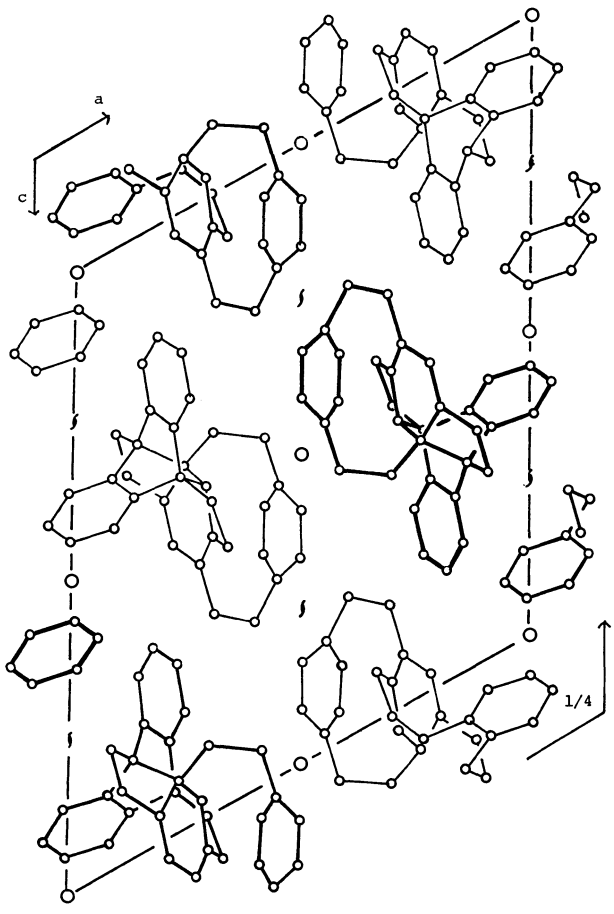

Fig. 6. Molecular arrangement in the crystal.

two bridged single bonds, C(1)–C(2) and C(9)–C(10), both of them, especially the latter, being longer than the normal C–C bond length.

The molecular arrangement in the crystal is shown in Fig. 6. Some intermolecular nonbonding distances are so short that will cause the strain of the molecule.

In conclusion, it is shown from spectral and X-ray crystal analyses that the unexpected cycloadducts **6** were formed in place of the desired triple-layered anthracenophane **5** by cross-breeding pyrolysis of the ammonium bases **1** and **2**. The formation of **6** is explainable by the intramolecular Diels-Alder addition of the inner benzene ring as a dienophile to the 9,10-positions of the anthracene moiety in the intermediate **5**. Recently, Korte and his co-workers[11] reported the first example of benzene and its derivatives being allowed to react as dienophile with hexachlorobutadiene under the high pressure of 10 kbar to afford 1:2 adducts. The unusual cycloaddition reaction of the intermediate **5** under ordinary conditions can be explained by the close fixing of the anthracene against the inner benzene moieties with short methylene bridges, and by the severe molecular strain of the intermediate as seen in the structures of triple-[12] and quadruple-layered cyclophanes.[13] In other words, strain releasing forces would act as a driving force for the unusual reaction.

The authors are greatly indebted to Professors M. Kakudo and N. Kasai of Osaka University for the X-ray crystallographic analysis. The research was supported by a Grant-in-Aid for Scientific Research from the Ministry of Education.

References

1) Part XXXIII, M. Yoshida, H. Tatemitsu, Y. Sakata, S. Misumi, H. Masuhara, and N. Mataga, *J. Chem. Soc., Chem. Commun.*, **1976**, 587.

2) For reviews: D. J. Cram and J. M. Cram, *Acc. Chem. Res.*, **4**, 204 (1971); F. Vögtle, *Chem.-Ztg.*, **95**, 668 (1971); S. Misumi, *Mem. Inst. Sci. & Ind. Res., Osaka Univ.*, **33**, 53 (1976).

3) J. H. Golden, *J. Chem. Soc.*, **1961**, 3741; T. Toyoda, I. Otsubo, T. Otsubo, Y. Sakata, and S. Misumi, *Tetrahedron Lett.*, **1972**, 1731; A. Iwama, T. Toyoda, T. Otsubo, and S. Misumi, *Chem. Lett.*, **1973**, 587; *Tetrahedron Lett.*, **1973**, 1725.

4) M. W. Miller, R. W. Amiden, and P. O. Tawney, *J. Am. Chem. Soc.*, **77**, 2845 (1955).

5) T. Otsubo, S. Mizogami, I. Otsubo, Z. Tozuka, A. Sakagami, Y. Sakata, and S. Misumi, *Bull. Chem. Soc. Jpn.*, **46**, 3519 (1973).

6) H. J. Reich and D. J. Cram, *J. Am. Chem. Soc.*, **91**, 3534 (1969); T. Otsubo, S. Mizogami, Y. Sakata, and S. Misumi, *Bull. Chem. Soc. Jpn.*, **46**, 3831 (1973).

7) "The Universal Crystallographic Computation Program System (I)," ed. by T. Sakurai, The Crystallographic Society of Japan, Tokyo (1967), p. 45.

8) G. Germain, P. Main, and M. M. Woolfson, *Acta Crystallogr.*, **A27**, 368 (1971).

9) T. Ashida, "The Universal Crystallographic Computing System-Osaka," the Computation Center, Osaka University (1973), p. 20.

10) T. Suzuki, *Nippon Butsuri Gakkai Shi*, **13**, 793 (1958).

11) W. Jarre, D. Bieniek, and F. Korte, *Angew. Chem.*, **87**, 201 (1975).

12) Y. Koizumi, T. Toyoda, H. Horita, and S. Misumi, The 32nd National Meeting of The Chemical Society of Japan, Abstr. Vol. I, p. 184, Tokyo, April 1975.

13) H. Mizuno, K. Nishiguchi, T. Toyoda, T. Otsubo, S. Misumi, and N. Morimoto, *Tetrahedron Lett.*, **1972**, 4981.

Layered Compounds. XXXV.[1] Syntheses of Triple-layered Metaparacyclophanes

Naoki KANNEN, Tetsuo OTSUBO, Yoshiteru SAKATA, and Soichi MISUMI*
The Institute of Scientific and Industrial Research, Osaka University, Suita, Osaka 565
(Received June 7, 1976)

Six triple-layered [2.2]metaparacyclophanes have been prepared using general synthetic methods such as the Stevens rearrangement-Raney nickel desulfurization method, pyrolysis of bissulfone, and photo-induced desulfurization. The pyrolysis of bissulfone has turned out to be the most useful and convenient method for preparation of the intermediate double-layered [2.2]metaparacyclophanes because of simple experimental process and excellent yields. The unexpected formation of compound **9** during the photo-induced desulfurization of **7** was explained by a unique skeletal rearrangement of the intermediate **8** on irradiation.

Since [2.2]metaparacyclophane **2** in which meta-substituted benzene is stacked at some angle on the para-substituted benzene by double methylene bridges was first synthesized in 1966,[2] its unique structure has become of great interest. Earlier efforts were made to study the NMR spectrum which showed temperature-dependence due to the flipping of the meta-ring.[2-5] On the other hand, as observed in the electronic spectra, there are few unambiguous evidences supporting the originally expected transannular electronic interaction between two benzene rings. In earlier papers of this series, multilayered para- and meta-cyclophanes were reported to exhibit stronger electronic interactions in their physical and chemical properties than the corresponding double-layered cyclophanes.[6]

One may expect that, in the same manner as multilayered meta- and para-series, multilayered metaparacyclophanes should offer further informations concerning the interaction between meta- and para-rings. However, there are a number of possible structual isomers according to the combination modes of meta- and para-rings in this series of multilayered cyclophanes. The present paper describes the syntheses of six triple-layered metaparacyclophanes containing a durene ring as the inner benzene nucleus along with several [2.2]metaparacyclophane derivatives.[7]

The nomenclature of cyclophanes proposed by Hirayama[8] is very useful also for the present series of multilayered cyclophanes, but not so familiar with us. Therfore, in this paper, we tentatively call the triple-layered cyclophanes as derivatives of double-layered one. For example, the compound **8** is regarded as a metacyclo derivative of [2.2]paracyclophane. In addition, we use a brief and convenient notation affixed after the name of compounds, *e.g.*, m-p,p-p for **8**, where m and p indicate meta and para bridging of methylene chains, respectively.

Results and Discussion

Synthesis: *[2.2]Metaparacyclophane (2).* From acid-catalyzed rearrangement of [2.2]paracyclophane, [2.2]-metaparacyclophane **2** was first prepared by Cram and his co-workers.[2] As alternate routes, Boekelheide and his co-workers developed the Stevens rearrangement-Hofmann elimination method and dithiane alkylation-Raney nickel desulfurization method.[9] Also Vögtle obtained the same compound **2** by pyrolysis of bissulfone.[3] We investigated photo-induced desulfurization according to Jenny and his co-workers[10] as an alternate synthetic method of **2**. On irradiation of 2,11-dithia-[3.3]metaparacyclophane **1**[9] in triethyl phosphite with a 400w high pressure mercury lamp, **2** was obtained in 40% yield together with a by-product, 2-thia[3.2]metaparacyclophane **3** in 9% yield.

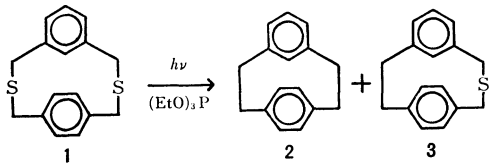

Scheme 1.

[2.2]Metacyclo(4,7)[2.2]paracyclophane (m-p,p-p) *(8).* Treatment of 4,7-dimethyl[2.2]paracyclophane **4**[6a] with *N*-bromosuccinimide (NBS) gave the corresponding bis(bromomethyl) compound **5** in 76% yield. Condensation of **5** with 1,3-bis(mercaptomethyl)benzene **6** smoothly afforded 18,27-dithia[3.3]metacyclo(4,7)[2.2]-paracyclophane **7** in 56% yield. The desired triple-layered metaparacyclophane (m-p,p-p) **8** was obtained in only 12% yield by the Stevens rearrangement of **7** followed by desulfurization with Raney nickel. On the other hand, direct photodesulfurization of **7** in triethyl phosphite gave **8** in 26% yield together with a small amount of another isomer (m-m,m-p) **9**. The structure of **9** was confirmed by comparison with the authentic sample synthesized by alternate routes as described later. The unexpected formation of **9** provides an interesting problem whether **9** is formed

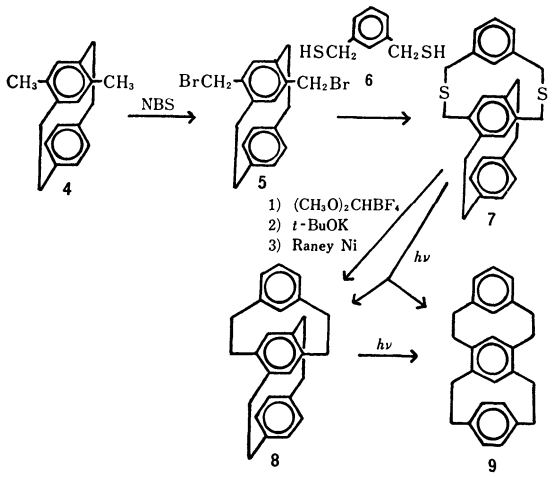

Scheme 2.

directly from **7** or through the main product **8**. A plausible mechanism is that the initially produced **8** isomerizes to **9** by exchanging the bridge positions at the inside benzene ring during irradiation. This assumption was supported by the facts that prolonged irradiation of **7** resulted in an increased yield (23%) of **9** with a decreased yield of **8** and that irradiation of **8** in degassed cyclohexane produced the isomer **9**.

[2.2]Metacyclo(12,15)[2.2]metaparacyclophane (m-p,p-m) ***(17)***. Condensation of 2,5-bis(chloromethyl)-*p*-xylene **10** with **6** gave 14,17-dimethyl-2,11-dithia[3.3]metaparacyclophane **11** in a good yield (71%) together with its dimer **12** in 6% yield. Pyrolysis of bissulfone **13** at about 900 °C, which was derived by oxidation of the dithiacyclophane **11** in a quantitative yield, afforded 12,15-dimethyl[2.2]metaparacyclophane **14** in an excellent yield (86%). Treatment of **14** with NBS gave the corresponding bis(bromomethyl) compound **15** in 88% yield. As usual, 18,27-dithia[3.3]metacyclo(12,15)[2.2]metaparacyclophane **16** was obtained by condensation of **15** with **6** in 32% yield and then converted to the desired cyclophane (m-p,p-m) **17** in a low yield (9.4%) by the Stevens rearrangement-Raney nickel desulfurization method. Direct photodesulfurization of **16** to **17** was unsuccessful.

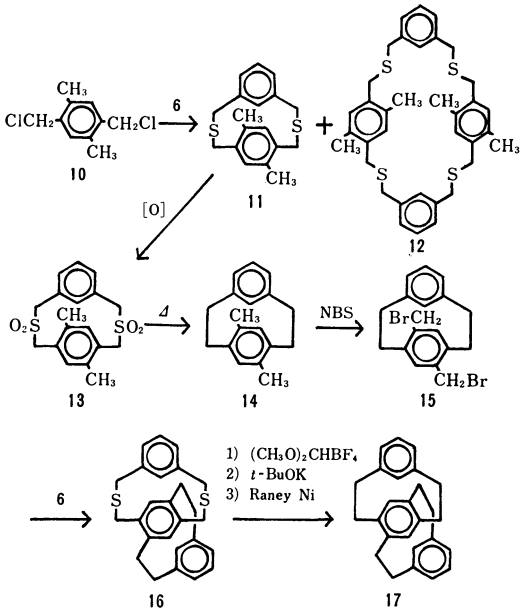

Scheme 3.

[2.2]Paracyclo(4,6)[2.2]metaparacyclophane (p-m,m-p) ***(28)***. Condensation of 4,6-bis(chloromethyl)-*m*-xylene **18** with 1,4-bis(mercaptomethyl)benzene **19** gave 5,6-dimethyl-2,11-dithia[3.3]metaparacyclophane **20** and its cyclic dimer **21** in 68 and 18% yields, respectively. Oxidation of **20** and pyrolysis of the resulting bissulfone **22** afforded 4,6-dimethyl[2.2]metaparacyclophane **23** in a satisfactory yield (91%). Surprisingly, pyrolysis of tetrakissulfone **24** derived from **21** produced rather strained metaparacyclophane **23** in 74% yield instead of the expected [2.2.2.2]metaparametaparacyclophane **25**. 4,6-Bis(bromomethyl)[2.2]metaparacyclophane **26**, which was derived from bromination of **23** with NBS in 78% yield, was coupled with dimercaptan **19** to give 18,27-dithia[3.3]paracyclo(4,6)[2.2]metaparacyclophane **27** in 35% yield. The Stevens rearrangement-Raney nickel desulfurization treatment of **27** afforded the desired cyclophane (p-m,m-p) **28** in only 6.8% yield. On the other hand, direct photodesulfurization of **27** in triethyl phosphite under a nitrogen atmosphere provided the same cyclophane **28** in a better yield of 55%.

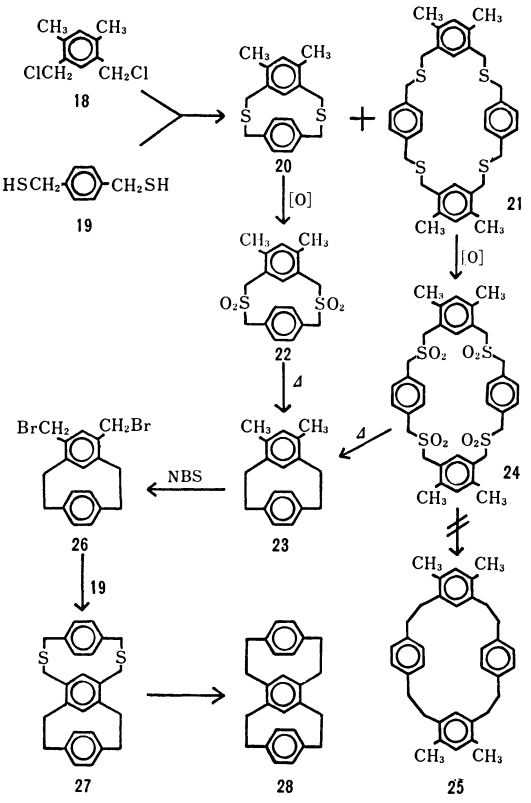

Scheme 4.

12,15-Dimethyl[2.2]paracyclo(4,6)[2.2]metaparacyclophane (dimethyl p-m,m-p) ***(31)***. 4,6-Bis(bromomethyl)[2.2]-metaparacyclophane **26** was converted to the corresponding bis(mercaptomethyl) compound **29** in 96% yield in the usual way. The reaction of **29** with **10** gave dimethyl dithia compound **30** in 70% yield. Irradiation of **30** in triethyl phosphite under bubbling nitrogen afforded the desired dimethylcyclophane **31** in 60% yield and half-desulfurized cyclophane **32** in 24% yield.

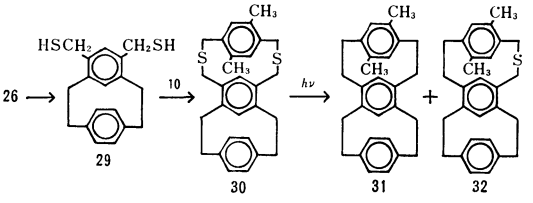

Scheme 5.

[2.2]Metacyclo(4,6)[2.2]metaparacyclophane (m-m,m-p) ***(9)***. Treatment of 4,6-bis(bromomethyl)[2.2]metacyclophane **33**[6b] with dimercaptan **19** gave 18,27-dithia-[3.3]paracyclo(4,6)[2.2]metacyclophane **34** in 34%

yield. Then **34** was led to the desired cyclophane **9** by the Stevens rearrangement-Raney nickel method (19%) or the photochemical method (35%).

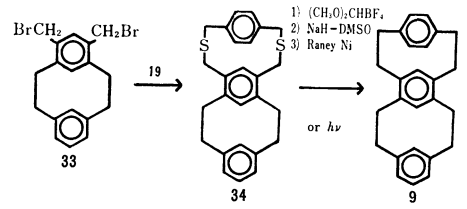

Scheme 6.

12,15-Dimethyl[2.2]metacyclo(4,6)[2.2]metaparacyclophane (dimethyl m-m,m-p*)* (**37**). The above dibromide **33** was transformed to the corresponding dimercaptan **35** in 85% yield. As usual, the reaction of **35** with **10** smoothly gave dimethyl dithia compound **36** in 74% yield. Desulfurization of **36** was carried out using the Stevens rearrangement-Raney nickel reaction to prepare the desired cyclophane **36** in 15% yield, while photochemical desulfurization of **35** failed to provide **37** because of a large amount of oily contaminant.

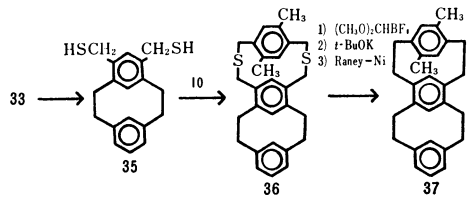

Scheme 7.

Experimental

Mps are uncorrected. All solvents are of reagent grade unless otherwise specified. Photodesulfurizations were carried out in triethyl phosphite degassed or under nitrogen bubbling at room temp using a quartz tube and a 400 W high pressure mercury lamp. PMR spectra were taken with a Hitachi-Perkin Elmer R-20 spectrometer (60 MHz) using TMS as an internal std, and MS with a Hitachi RMU-7 spectrometer at 70 eV using a direct insertion technique.

*Photodesulfurization of 2,11-Dithia[3.3]metaparacyclophane (**1**).* A soln of 250 mg (0.93 mmol) of 2,11-dithia[3.3]metaparacyclophane **1** in 6 ml of triethyl phosphite purified by distillation over sodium metal was degassed by the freeze-pump-thaw method in a quartz tube and then the tube was sealed. The soln was irradiated with a 400 W high pressure mercury lamp for 7 days at room temp. The solvent was evaporated and the residue was chromatographed on neutral alumina (40 g, Woelm activity I-II). First elution with hexane gave [2.2]metaparacyclophane **2** (79 mg, 40%), then with hexane-benzene (1 : 1) a mixture of 2-thia[3.2]metaparacyclophane **3** and *O,O,O*-triethyl phosphorothioate, and finally with benzene **1** (20 mg) was recovered. [2.2]Metaparacyclophane was recrystd from methanol to give colorless fine crystals, mp 79—80 °C [lit, 79—81 °C (Cram,[2] Vögtle[3]), 81—81.5 °C (Boekelheide[9])]. The compd **3** was purified by rechromatography on silica gel (30 g, Merck activity I-II) using hexane-benzene (4 : 1) (20 mg, 9%). Recrystallization from ethanol gave colorless plates, mp 224—224.5 °C.

Found: C, 80.22; H, 6.66; S, 13.19%. Calcd for $C_{16}H_{16}S$: C, 79.95; H, 6.71; S, 13.34%. PMR (CCl_4, δ) 2.67 (A_2B_2, 4H, CH_2), 3.26 (s, 2H, CH_2), 3.70 (s, 2H, CH_2), 5.32 (bs, 1H, meta internal ArH), 6.34 (d, J=9 Hz, 2H, para ArH), 6.82 (d, J=9 Hz, 2H, para ArH). MS *m/e* 240 (M^+), 104.

*4,7-Bis(bromomethyl)[2.2]paracyclophane (**5**).* A mixture of 4,7-dimethyl[2.2]paracyclophane **4** (4.72 g, 20 mmol) and *N*-bromosuccinimide (7.12 g, 40 mmol) was refluxed in 100 ml of carbon tetrachloride for 4 h. After removal of succinimide by filtration, the filtrate was evaporated and the residue was recrystd from carbon tetrachloride to give the desired dibromide **5** (5.95 g, 76%), colorless prisms, mp 166—168 °C.

Found: C, 54.62; H, 4.67; Br, 40.23%. Calcd for $C_{18}H_{18}Br_2$: C, 54.85; H, 4.60; Br, 40.55%. PMR (CCl_4, δ) 2.6—3.6 (m, 8H, bridged CH_2), 4.16 and 4.40 (A_2B_2, 4H, CH_2Br), 6.29 (s, 2H, ArH). MS *m/e* 396, 394, 392 (M^+), 315, 313, 234, 104.

*18,27-Dithia[3.3]metacyclo(4,7)[2.2]paracyclophane (**7**).* A soln of 1,3-bis(mercaptomethyl)benzene **6** (0.90 g, 5.3 mmol) and sodium hydroxide (0.43 g, 11 mmol) in 35 ml of 95% ethanol, and a soln of the dibromide **5** (1.97 g, 5 mmol) in 35 ml of benzene were added dropwise and simultaneously over a period of 4 h to refluxing and stirring abs ethanol (100 ml) placed in a 300 ml three necked flask under a nitrogen atmosphere. Refluxing was continued for additional 12 h. The mixture was concd and the residue was extracted with chloroform. The extract was washed, dried, and evaporated. The residual solid was chromatographed on neutral alumina (Woelm act. II) with hexane-benzene (1 : 1) to give the dithia compd (1.12 g, 56%). Recrystallization from benzene-ethanol (1 : 1) afforded colorless fine crystals, mp 163—164 °C.

Found: C, 77.49; H, 6.37; S, 15.74%. Calcd for $C_{26}H_{26}S_2$: C, 77.55; H, 6.52; S, 15.92%. PMR ($CDCl_3$, δ) 2.1—4.0 (m, 16H, CH_2) 5.39 (bs, 1H, meta inner ArH), 5.89 (s, 2H, ArH of inner benzene), 6.34 and 6.50 (A_2B_2, 4H, para ArH), 6.9 (m, 3H, meta ArH). MS *m/e* 402 (M^+), 104.

[2.2]Metacyclo(4,7)[2.2]paracyclophane (m-p,p-p) *(**8**).*

a) By the Stevens Rearrangement-Raney Nickel Desulfurization. A mixture of the above dithia compd **7** (0.40 g, 1 mmol) and dimethoxycarbonium fluoroborate[11] (0.65 g, 4 mmol) was refluxed with magnetic stirring in 30 ml of dichloromethane for 6 h. After evaporation of the solvent and decomposition of the excess reagent, the residual solid was powdered and then refluxed with potassium *t*-butoxide (1.1 g, 10 mmol) in 30 ml of dry tetrahydrofuran for 16 h. The mixture was filtered and the filtrate was evaporated. The resulting rearrangement product was refluxed with Raney nickel (6 ml) in 50 ml of abs ethanol for 19 h. Raney nickel was removed by filtration and washed with benzene. The filtrate and the washings were combined and evaporated. The residue was chromatographed on neutral alumina (50 g, Woelm act. II) eluted with hexane-benzene (9 : 1) to give the desired triple-layered metaparacyclophane **8** (40 mg, 12%). For analysis, **8** was recrystd from ethanol, colorless plates, mp 144—145 °C.

Found: C, 92.40; H, 7.68%. Calcd for $C_{26}H_{26}$: C, 92.24; H, 7.76%. PMR ($CDCl_3$, δ) 1.5—3.6 (m, 16H, CH_2), 4.90 (s, 1H, ArH of inner benzene), 5.12 (bs, 1H, meta inner ArH), 6.17 (s, 1H, ArH of inner benzene), 6.30 (bs, 4H, para benzene), 6.6 (m, 3H, meta benzene). MS *m/e* 338 (M^+), 234, 104.

b) By Photodesulfurization. The dithia compd **7** (95 mg, 0.24 mmol) was dissolved in 10 ml of freshly distd triethyl phosphite in a quartz tube and the tube was externally irradiated for an hour bubbling a slow stream of nitrogen

through the soln. The solvent was evaporated and the residue was chromatographed over silica gel (40 g, Merck act. II-III) with hexane–benzene (4 : 1) to give 23 mg (28%) of **8**. When the irradiation was continued for 15 h, an isomeric triple-layered metaparacyclophane **9** was obtained in 23% yield, accompanied with **8** and an unknown oily substance. A 98 h irradiation produced **9** in the highest yield (34%). A soln of **8** (43 mg) in 10 ml of freshly purified cyclohexane was irradiated in a quartz tube for 28 h under an argon atmosphere and worked up in the usual way to give a mixture of **8** and **9** (26 mg).

*14,17-Dimethyl-2,11-dithia[3.3]metaparacyclophane (**11**) and 14,-17,32,35-Tetramethyl-2,11,20,29-tetrathia[3.3.3.3]metaparametaparacyclophane (**12**).* A soln of 1,3-bis(mercaptomethyl)-benzene **6** (3.40 g, 20 mmol) and sodium hydroxide (1.60 g, 40 mmol) in a mixture of water (5 ml) and ethanol (245 ml) and a soln of 2,5-bis(chloromethyl)-*p*-xylene **10** (4.06 g, 20 mmol) in 250 ml of benzene–ethanol (1 : 1) were added dropwise and simultaneously over a period of 4 h with stirring to refluxing alcohol (1 l) in a nitrogen atmosphere. Refluxing was continued for additional 12 h. The solvent was evaporated and the residue was extracted with benzene. The benzene extract was condensed and chromatographed over silica gel (100 g, Merck act. II-III). Elution with hexane–benzene (1 : 1) gave the dithia compd **11** (4.72 g, 71%), colorless columns from benzene–ethanol (1 : 1), mp 130—131 °C.

Found: C, 71.84; H, 6.79; S, 20.94%. Calcd for $C_{18}H_{20}S_2$: C, 71.94; H, 6.72; S, 21.34%. PMR ($CDCl_3$, δ) 2.16 (s, 6H, CH_3), 3.48 (s, 4H, CH_2), 3.71 and 3.96 (A_2B_2, 4H, CH_2), 5.63 (bs, 1H, ArH), 6.69 (s, 2H, ArH), 7.03 (m, 3H, ArH). MS *m/e* 300 (M^+).

Then elution with benzene gave the tetrathia compd **12** (0.36 g, 5.5%), which was recrystd from hexane–benzene (1 : 1), colorless fine crystals, mp 206—207 °C.

Found: C, 71.77; H, 6.60; S, 21.05%. Calcd for $C_{36}H_{40}S_4$: C, 71.94; H, 6.70; S, 21.34%. PMR ($CDCl_3$, δ) 2.13 (s, 12H, CH_3), 3.59 (s, 8H, CH_2), 3.61 (s, 8H, CH_2), 6.89 (bs, 4H, ArH), 7.08 (bs, 2H, ArH), 7.32 (m, 6H, ArH). MS *m/e* 600 (M^+), 132.

*12,15-Dimethyl[2.2]metaparacyclophane (**14**).* To a suspension of 15 g (50 mmol) of the above dithia compd **11** in 100 ml of acetic acid was added slowly an excess (30 ml, 0.34 mol) of hydrogen peroxide (35%) with stirring and then the soln was warmed at 100 °C for 5 h. The resulting ppt was filtered, washed repeatedly with water, and dried to give a quantitative yield of the corresponding bissulfone **13**. Pyrolysis of the bissulfone **13** to the corresponding [2.2]cyclophane **14** was carried out according to the general method described below. The bissulfone **13** (2.0 g) was placed into a Pyrex bulb and plugged lightly with glass wool. In order to prevent a loss of the product, some absorbent cotton was placed near the end of a glass tube which was connected to an aspirator to absorb sulfur dioxide generated. The Pyrex bulb was inserted into a furnance pre-heated at 900 °C and the reaction was completed within 1 min. The trapped product **14** was chromatographed over neutral alumina (10 g, Woelm act. II) with hexane (1.12 g, 86% based on **11**), colorless plates from pentane, mp 65—66 °C.

Found: C, 91.25; H, 8.68%. Calcd for $C_{18}H_{20}$: C, 91.45; H, 8.55%. PMR ($CDCl_3$, δ) 1.65 (s, 3H, CH_3), 1.9—3.4 (m, 8H, CH_2), 2.43 (s, 3H, CH_3), 5.51 (s, 1H, meta inner ArH), 5.69 (s, 1H, para ArH), 6.78 (s, 1H, para ArH), 6.86 (m, 3H, meta ArH). MS *m/e* 236 (M^+), 104.

*12,15-Bis(bromomethyl)[2.2]metaparacyclophane (**15**).* By the usual way from **14** (1.00 g, 4 mmol), *N*-bromosuccinimide (1.51 g, 8 mmol), and a small amount of benzoyl peroxide in 20 ml of carbon tetrachloride, 1.46 g (88%) of **15** was obtained as an yellow oil. The dibromide was used in the next coupling reaction without purification.

PMR ($CDCl_3$, δ) 2.0—4.5 (m, 8H, CH_2), 4.60 (s, 4H, CH_2), 5.55 (bs, 1H, meta ArH), 5.82 (s, 1H, para ArH), 6.9 (m, 3H, meta ArH), 7.22 (s, 1H, para ArH). MS *m/e* 396, 394, 392 (M^+), 315, 313.

*18,27-Dithia[3,3]metacyclo(12,15)[2.2]metaparacyclophane (**16**).* A soln of the dibromide **15** (1.46 g, 3.7 mmol) in 35 ml of benzene and a soln of 1,3-bis(mercaptomethyl)-benzene **6** (0.63 g, 3.7 mmol) and sodium hydroxide (0.30 g, 7.5 mmol) in a mixture of 2 ml of water and 33 ml of ethanol were added dropwise and simultaneously to 100 ml of refluxing ethanol for 4 h in a nitrogen atmosphere and refluxing was continued for additional 12 h. The solvent was evaporated and the residue was chromatographed on neutral alumina (60 g, Woelm act. II) with hexane–benzene (1 : 1). The initial eluate gave 0.47 g (32%) of **16** as an oil.

PMR ($CDCl_3$, δ) 1.5—4.3 (m, 16H, CH_2), 5.22 (bs, 1H, ArH of [2.2]bridged *m*-xylene moiety), 5.42 (s, 1H, ArH of durene moiety), 5.53 (bs, 1H, ArH of S-bridged *m*-xylene moiety), 6.54 (s, 1H, ArH of durene moiety), 6.5—7.2 (m, 6H, ArH of both *m*-xylene moieties). MS *m/e* 402 (M^+).

[2.2]Metacyclo(12,15)[2.2]metaparacyclophane (m-p,p-m) *(**17**).* The synthesis of **17** was carried out in the same manner as that of **8**. The reaction conditions were as follows; methylation of the dithia compd **16** (1.10 g, 2.7 mmol) with the Borch reagent[11] (2.30 g, 14 mmol) in dichloromethane (20 ml) under reflux for 15 h; the Stevens rearrangement with potassium *t*-butoxide (3.50 g, 31 mmol) in 25 ml of dry tetrahydrofuran under reflux for 4 h; desulfurization with Raney nickel (6 ml) in 60 ml of benzene–ethanol (1 : 5) under reflux for 15 h. The desired cyclophane **17** was purified by column chromatography over silica gel (50 g, Merck act. II) using hexane–benzene (9 : 1) (87 mg, 9.4%) and recrystd from benzene–ethanol (1 : 1), colorless plates, mp 170—171 °C.

Found: C, 92.04; H, 7.67%. Calcd for $C_{26}H_{26}$: C, 92.24; H, 7.76%. PMR ($CDCl_3$, δ) 1.5—3.5 (m, 32H, CH_2), 4.39 (s, 1H, ArH of durene moiety), 5.28 (bs, 1H, meta ArH), 5.37 (bs, 1H, meta ArH), 5.60 (s, 2H, ArH of durene moiety), 6.4—7.1 (m, 12H, meta ArH), 6.87 (s, 1H, ArH of durene moiety). MS *m/e* 338 (M^+).

*5,7-Dimethyl-2,11-dithia[3.3]metaparacyclophane (**20**) and 5,7,-23,25-Tetramethyl-2,11,20,29-tetrathia[3.3.3.3]metaparametaparacyclophane (**21**).* A soln of 4,6-bis(chloromethyl)-*m*-xylene **18** (10.15 g, 50 mmol) in 250 ml of benzene–alcohol (1 : 4) and a soln of 1,4-bis(mercaptomethyl)benzene **19** (8.50 g, 50 mmol) in 10 ml of water and 240 ml of alcohol were added dropwise and simultaneously over a period of 4 h to boiling ethanol (1 l) with stirring under a nitrogen atmosphere and refluxing was continued for additional 12 h. After removal of the solvent the residue was extracted with chloroform and the extract was evaporated to dryness. The resulting solid was chromatographed over silica gel (200 g, Merck act. II). Elution with benzene–hexane (1 : 1) gave the dithia compd **20** (10.14 g, 68%), which was recrystd from benzene, colorless columns, mp 215—216 °C.

Found: C, 71.90; H, 6.85; S, 21.08%. Calcd for $C_{18}H_{20}S_2$: C, 71.94; H, 6.72; S, 21.34%. PMR ($CDCl_3$, δ) 2.15 (s, 6H, CH_3), 3.42 (s, 4H, CH_2), 3.86 (s, 4H, CH_2), 5.30 (s, 1H, ArH of durene moiety), 6.92 (bs, 1H, ArH of durene moiety), 7.00 (s, 4H, ArH of *p*-xylene moiety). MS *m/e* 300 (M^+).

Elution with benzene gave the tetrathia compd **21** (2.76 g, 18%) which was recrystallized from toluene, colorless needles, mp 235—236 °C.

Found: C, 72.02; H, 6.69; S, 21.08%. Calcd for $C_{36}H_{40}S_4$: C, 71.94; H, 6.72; S, 21.34%. PMR ($CDCl_3$, δ) 2.37 (s, 12H, CH_3), 3.55 (s, 8H, CH_2), 3.63 (s, 8H, CH_2), 6.87 (bs, 2H, ArH), 7.04 (bs, 2H, ArH). MS *m/e* 600 (M^+).

*4,6-Dimethyl[2.2]metaparacyclophane (**23**).* The cyclophane **23** was synthesized from **20** by the same method as **14**. Thus a suspension of the dithiacyclophane **20** (3.0 g, 10 mmol) in 20 ml of acetic acid was oxidized with 10 ml of hydrogen peroxide (35%) at 100 °C for 5 h with stirring to give the bissulfone **22** in a quantitative yield. Pyrolysis of the bissulfone **22** at 900 °C under 0.1 mmHg followed by chromatography gave **23** (91% based on **20**), colorless plates from pentane, mp 63—64 °C. On the other hand, the same cyclophane **23** was obtained in a good yield of 74% by oxidation-pyrolysis of the tetrathiacyclophane **21**.

Found: C, 91.25; H, 8.63%. Calcd for $C_{18}H_{20}$: C, 91.45; H, 8.55%. PMR ($CDCl_3$, δ) 2.22 (s, 6H, CH_3), 1.7—3.3 (m, 8H, CH_2), 5.22 (s, 1H, ArH of durene moiety), 5.83 (d, J=1 Hz, 2H, ArH of *p*-xylene moiety), 6.65 (bs, 1H, ArH of durene moiety), 7.16 (d, J=1 Hz, 2H, ArH of *p*-xylene moiety). MS *m/e* 236 (M^+), 132, 104.

*4,6-Bis(bromomethyl)[2.2]metaparacyclophane (**26**).* A mixture of **23** (0.50 g, 2 mmol), *N*-bromosuccinimide (0.76 g, 4 mmol), and a small amount of benzoyl peroxide in 20 ml of carbon tetrachloride was refluxed for 3.5 h and worked up in the usual way. The resulting crystals were washed with methanol to give 0.65 g (78% yield) of **26**, colorless plates from carbon tetrachloride, mp 151—152 °C.

Found: C, 55.02; H, 4.51; Br, 40.14%. Calcd for $C_{18}H_{18}Br_2$: C, 54.85; H, 4.60; Br, 40.55%. PMR ($CDCl_3$, δ) 1.8—3.4 (m, 8H, CH_2), 4.46 (s, 4H, CH_2Br), 5.45 (s, 1H, ArH of durene moiety), 6.14 (d, J=2 Hz, 2H, ArH of *p*-xylene moiety), 7.12 (s, 1H, ArH of durene moiety), 7.24 (d, J=2 Hz, 2H, ArH of *p*-xylene moiety). MS *m/e* 396, 394, 392 (M^+), 315, 313, 104.

*18,27-Dithia[3.3]paracyclo(4,6)[2.2]metaparacyclophane (**27**).* A soln of the dibromide **26** (0.6 g, 1.7 mmol) in 35 ml of benzene and a soln of 1,4-bis(mercaptomethyl)benzene **19** (0.28 g, 1.6 mmol) and sodium hydroxide (0.14 g, 3.5 mmol) in water (2 ml) and alcohol (35 ml) were added dropwise and simultaneously to 100 ml of boiling ethanol for 4 h under a nitrogen atmosphere. The mixture was refluxed for 12 h and worked up in the usual way. The desired dithiacyclophane **27** was purified by column chromatography (0.30 g, 35%) and recrystd from benzene, colorless prisms, mp 265—266 °C (sealed tube).

Found: C, 77.71; H, 6.35; S, 15.74%. Calcd for $C_{26}H_{26}S_2$: C, 77.55; H, 6.52; S, 15.92%. PMR ($CDCl_3$, δ) 1.0—4.0 (m, 16H, CH_2), 5.01 (s, 1H, ArH of durene moiety), 5.14 (s, 1H, ArH of durene moiety), 5.91 (bs, 2H, ArH of [2.2]bridged *p*-xylene moiety), 7.02 (bs, 2H, ArH of S-bridged *p*-xylene moiety), 7.14 (bs, 2H, ArH of [2.2]-bridged *p*-xylene moiety), 7.30 (bs, 2H, ArH of S-bridged *p*-xylene moiety). MS *m/e* 402 (M^+), 104.

[2.2]Paracyclo(4,6)[2.2]metaparacyclophane (p-m,m-p) *(**28**).*
a) By the Stevens Rearrangement-Raney Nickel Desulfurization. In the same manner as the synthesis of **8**, 1.53 g (3.8 mmol) of the dithiacyclophane **27** and 1.50 g (9.3 mmol) of the Borch reagent[11] in 20 ml of dichloromethane were refluxed with stirring for 15 h. The resulting ppt was filtered and then refluxed with 2.0 g (18 mmol) of potassium *t*-butoxide in 30 ml of dry tetrahydrofuran for 5 h. The mixture was filtered and the filtrate was condensed. The residue was refluxed with Raney nickel (10 ml) in benzene (5 ml) and ethanol (60 ml) for 17 h. After removal of Raney nickel the soln was worked up in the usual way. Chromatography over silica gel (50 g, Merck act. II) gave **28** (87 mg, 6.8%) from hexane–benzene (9 : 1) eluate. The cyclophane **28** was recrystd from toluene, colorless plates, mp 259—260 °C (sealed tube).

Found: C, 92.20; H, 7.73%. Calcd for $C_{26}H_{26}$: C, 92.24; H, 7.76%. PMR ($CDCl_3$, δ) 1.5—3.3 (m, 16H, CH_2), 4.94 (s, 2H, ArH of durene moiety), 5.66 (bs, 4H, ArH of *p*-xylene moiety), 7.12 (bs, 4H, *p*-xylene moiety). MS *m/e* 338 (M^+), 104.

b) By Photodesulfurization. A suspension of the dithiacyclophane **27** (30 mg, 0.075 mmol) in 15 ml of freshly distd triethyl phosphite was placed in a quartz tube and the tube was externally irradiated with a 400 W high pressure mercury lamp under bubbling of nitrogen for 13 h. After removal of the solvent the residue was adsorbed on silica gel (15 g, Merck act. II) and eluted with hexane–benzene (4 : 1) to give **27** (15 mg, 55%).

*4,6-Bis(mercaptomethyl)[2.2]metaparacyclophane (**29**).* 4,6-Bis(bromomethyl)[2.2]metaparacyclophane **26** (6.61 g, 17 mmol) was added portionwise to a warm soln of thiourea (2.60 g, 34 mmol) dissolved in 50 ml of ethanol and then the mixture was refluxed for 3 h. The solvent was evaporated and the residual thiouronium salt was refluxed with 85% potassium hydroxide (18 g) in 50 ml of water for 8 h. The cold soln was filtered and acidified with hydrochloric acid to ppt the dithiol **29**. The mixture was extracted with chloroform and the extract was washed with water, dried over anhyd sodium sulfate, and evaporated to dryness. The resulting solid was chromatographed on neutral alumina (20 g) using hexane–benzene (1 : 1) to give the desired thiol **29** (4.83 g, 96%), colorless fine crystals from hexane–benzene (1 : 1), mp 112—113 °C.

Found: C, 72.23; H, 6.68; S, 21.08%. Calcd for $C_{18}H_{20}S_2$: C, 71.94; H, 6.72; S, 21.34%. PMR ($CDCl_3$, δ) 1.78 (t, J=8 Hz, 2H, SH), 1.7—3.3 (m, 8H, CH_2), 3.70 (d, J=8 Hz, 4H, CH_2), 5.36 (s, 1H, ArH of durene moiety), 6.03 (d, 2H, ArH of *p*-xylene moiety), 6.97 (s, 1H, ArH of durene moiety), 7.23 (d, 2H, ArH of *p*-xylene moiety). MS *m/e* 300 (M^+).

*21,24-Dimethyl-18,27-dithia[3.3]paracyclo(4,6)[2.2]metaparacyclophane (**30**).* A soln of 2,5-bis(chloromethyl)-*p*-xylene **10** (1.02 g, 5 mmol) in 40 ml of benzene and a soln of the above dithiol **29** (1.50 g, 5 mmol) and 85% potassium hydroxide (0.66 g, 10 mmol) in 40 ml of 80% aq ethanol were added dropwise and simultaneously over a period of 3 h to 300 ml of boiling ethanol under a nitrogen atmosphere. The mixture was refluxed for additional 12 h and worked up in the same manner as the synthesis of **7**. Chromatography of the product over silica gel (50 g, Merck act. II) with hexane–benzene (1 : 1) gave the dithiacyclophane **30** (1.44 g, 70%), colorless plates from ethanol, mp 201—202 °C.

Found: C, 78.14; H, 6.91; S, 14.84%. Calcd for $C_{28}H_{30}S_2$: C, 78.23; H, 6.98; S, 14.90%. PMR ($CDCl_3$, δ) 1.96 (s, 3H, CH_3), 2.45 (s, 3H, CH_3), 2.5—4.4 (m, 16H, CH_2), 4.89 (s, 1H, ArH), 5.08 (s, 1H, ArH), 5.76 (bs, 2H, ArH of *p*-xylene moiety), 6.76 (s, 1H, ArH), 7.00 (s, 1H, ArH), 7.10 (bs, 2H, ArH of *p*-xylene moiety). MS *m/e* 430 (M^+).

*12,15-Dimethyl[2.2]paracyclo(4,6)[2.2]metaparacyclophane (**31**) and 21,24-Dimethyl-18-thia[3.2]paracyclo(4,6)[2.2]metaparacyclophane (**32**).* A suspension of the above dithiacyclophane **30** (100 mg, 0.2 mmol) in 14 ml of purified triethyl phosphite was externally irradiated in a quartz tube under bubbling of nitrogen at room temp for 8.5 h. The solvent was evaporated and the residue was chromatographed over silica gel (20 g, Merck act. II) with hexane–benzene (4 : 1). The initial eluate gave the desired product **31** (55 mg, 63%), colorless fine crystals from toluene, mp 192—193 °C.

6) a) T. Otsubo, S. Mizogami, I. Otsubo, Z. Tozuka, A. Sakagami, Y. Sakata, and S. Misumi, *Bull. Chem. Soc. Jpn.*, **46**, 3519 (1973); b) T. Umemoto, T. Otsubo, Y. Sakata, and S. Misumi, *Tetrahedron Lett.*, **1973**, 593.

7) For preliminary publication of this work, see N. Kannen, T. Umemoto, T. Otsubo, and S. Misumi, *Tetrahedron Lett.*, **1973**, 4537.

8) K. Hirayama, *Tetrahedron Lett.*, **1972**, 2109.

9) T. Hylton and V. Boekelheide, *J. Am. Chem. Soc.*, **90**, 6887 (1968); V. Boekelheide and P. H. Anderson, *Tetrahedron Lett.*, **1970**, 1207; V. Boekelheide, P. H. Anderson, and T. A. Hylton, *J. Am. Chem. Soc.*, **96**, 1558 (1974).

10) J. Bruhin, W. Kneubühler, and W. Jenny, *Chimia*, **27**, 277 (1973); J. Bruhin and W. Jenny, *Tetrahedron Lett.*, **1973**, 1215.

11) R. F. Borch, *J. Org. Chem.*, **34**, 627 (1969).

Heterocycles by Cycloaddition. IV.[1] Cycloaddition Reactions of Mesoionic Compounds with a 7-Azabicyclo[2.2.1]heptadiene, and Double Fragmentation of the Adducts

Hiroshi MATSUKUBO* and Hiroshi KATO

Department of Chemistry, Faculty of Science, Shinshu University, Asahi, Matsumoto 390

(Received May 29, 1976)

Cycloaddition of some five-membered mesoionic compounds with dimethyl 7-tosyl-7-azabicyclo[2.2.1]-hepta-2,5-diene-2,3-dicarboxylate occurs only across the unsubstituted double bond. Pyrolysis of the adducts resulted in a double fragmentation reaction to give two five-membered aromatic heterocycles. A dithiolone adduct gave the *S*-oxide, which was pyrolyzed to the corresponding thiopyran-2-one.

In an effort to extend the synthetic value of mesoionic compounds, we have reported that the cycloaddition-double fragmentation reactions of mesoionic compounds (**1**) with a 7-oxabicyclo[2.2.1]heptadiene (**2**) provides an attractive route for the preparation of many five- and six-membered aromatic heterocycles.[2] In these reactions, some mesoionic compounds gave adducts (or fragmentation products) with a high periselectivity, while others gave products resulting from cycloaddition across both the two double bonds of **2**. Since it was established that the approach of mesoionic compounds to **2** occurs from above the surface of the oxygen bridge,[2-4] a bulky substituent at the 7-position may be expected to cause a higher periselectivity than with **2** due to the steric effect of the substituent. With this in mind, we studied the reactions of mesoionic compounds with dimethyl 7-*p*-toluenesulfonyl-7-azabicyclo[2.2.1]hepta-2,5-diene-2,3-dicarboxylate (**3**), and report here the results.

The reaction of mesoionic 3-methyl-2,4-diphenyl-5-oxazolone (**4**) with the azabicycloheptadiene **3** proceeded at a slower rate than with the oxabicycloheptadiene **2**, and gave 1-methyl-2,5-diphenylpyrrole (**6**) and dimethyl 1-(*p*-toluenesulfonyl)pyrrole-3,4-dicarboxylate (**7**). This result shows that the cycloaddition of the oxazolone **4** took place selectively across the unsubstituted double bond to give an intermediate adduct (**5**), which spontaneously underwent double fragmentation under the reaction conditions to carbon dioxide, **6**, and **7**. This behavior is in contrast to the reaction of **4** with the oxa analog **2**, which afforded products resulting from addition of **4** on both the substituted and the unsubstituted double bonds.

The reaction of mesoionic 2,5-diphenyl-1,3-dithiol-4-one (**8a**) with **3** in benzene under reflux gave the 1 : 1 adduct, dimethyl 9-oxo-1,8-diphenyl-12-*p*-toluenesulfonyl-12-aza-10,11-dithiatetracyclo-[6.2.1.1.^{3,6}-0^{2,7}]dodec-4-ene-4,5-dicarboxylate (**9a**). The base peak of the mass spectrum of the adduct at *m/e* 236, and the lack of NMR signal assignable to olefinic protons show that the addition took place across the unsubstituted double bond of **3**. Assignment of the *exo*, *exo* configuration among the four possible stereoisomers (**9a** and **ixa--ixc**) is based on the NMR spectrum: the lack of coupling between the bridgehead and the angular protons (H_a and H_c; H_b and H_d) eliminates structures **ixb** and **ixc**, and small or no chemical shift difference of the two methoxycarbonyl (0.03 ppm) and two bridgehead protons (H_a and H_b; 0 ppm) as well as a considerable one between the two angular protons (H_c and H_d; 0.45 ppm) are compatible only with the *exo*, *exo* configuration **9a**. A larger chemical shift difference of the two bridgehead protons than that of the two angular methine protons would be expected for configuration **ixa**. Pyrolysis of the adduct **9a** in toluene under reflux afforded 2,5-diphenylthiophene (**10**) and the pyrrole **7**. The treatment of the dithiolone adduct **9** with *m*-chloroperbenzoic acid gave the corresponding *S*-oxide (**11a**). The oxide oxygen was probably introduced anti to the aza bridge because it exerted only a small effect on the chemical shift values of the angular and the bridgehead protons. The *S*-oxide was fairly stable thermally, but was pyrolyzed in refluxing diethylbenzene with an extrusion of SO to give 3,6-diphenylthiopyran-2-one (**12a**) and the pyrrole **7**. The *S*-oxide **11a** was only partly decomposed after refluxing in xylene for a long time though the yield of the thiopyranone **12a** was higher (70%) than that in diethylbenzene (29%) when based on con-

* Present Address: Okaya Works, Kyorin Pharmaceutical Co., Kohan, Okaya 394.

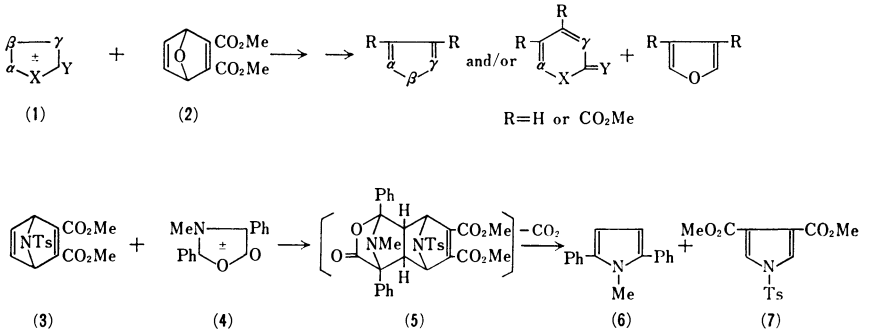

Scheme 1.

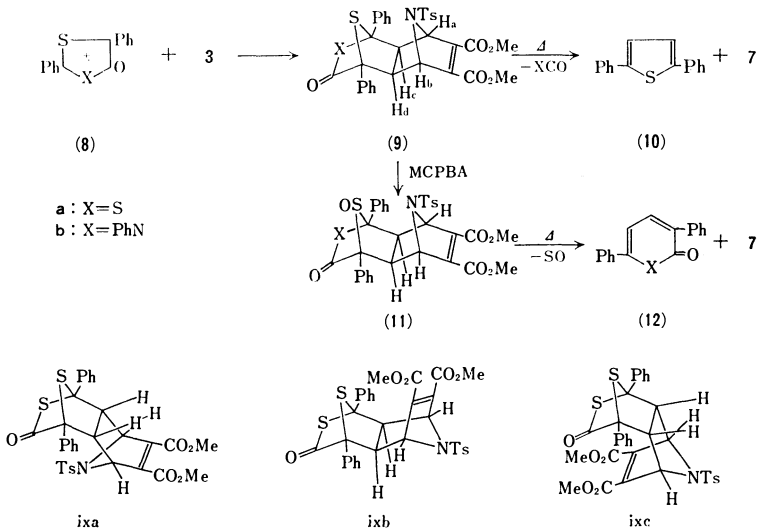

Scheme 2.

sumed *S*-oxide.

As previously reported,[2] the reaction of mesoionic 2,3,5-triphenyl-4-thiazolone (**8b**) with the oxabicycloheptadiene **2** gave adducts resulting from addition across both the substituted and the unsubstituted double bonds as well as other minor products. The reaction of **8a** with the aza analog **3** proceeded sluggishly in benzene under reflux, but afforded the cycloadduct, dimethyl *exo,exo*-9-oxo-1,8,10-triphenyl-12-*p*-toluenesulfonyl-10,12-diaza-11-thiatetracyclo[6.2.1.1.^{3,6}0^{2,7}]-dodec-4-ene-4,5-dicarboxylate (**9b**) resulting from the addition only on the unsubstituted double bond. The proposed structure and configuration of **9a** are based on spectral data (See Experimental). When the thiazolone adduct **9b** was pyrolyzed in diphenyl ether under reflux, the thiophene **10** and the pyrrole **7** were formed. The thiazolone adduct **9b** gave the corresponding (*anti*-) *S*-oxide (**11b**) on treatment with *m*-chloroperbenzoic acid. The mass spectrum of **11b** was rather complex although it showed weak peaks expected for double fragmentation products (*m/e* 337 and 323). The pyrolysis of **11b** in xylene under reflux gave complex products, from which neither the expected pyridone (**12b**) nor the pyrrole **7** could be isolated.

The above survey shows that the periselectivity of the mesoionic compounds to a bicycloheptadiene system is improved as expected by introducing a bulky substituent into the 7-position. At the outset of the present work, it was also anticipated that the double fragmentation of the adduct with **3** might be more facilitated than that of the adduct with **2** due to the pronounced aromaticity of the pyrrole ring and to the repulsive acceleration between the two bridge groups.[5] This expectation was not realized. This is probably due to the fact that the double fragmentation steps are not concerted but rather are two consecutive processes consisting of the initial extrusion of X=C=O or SO to give an unstable intermediate ylide, and its fragmentation to stable products.[6] Since the main purpose of the present work was improvement of the periselectivity, reaction conditions were not optimized. However, the high yields of products based on consumed starting materials suggest that this cycloaddition-double fragmentation reaction should constitute an attractive synthetic method of many heterocycles by appropriate selection of reaction partners.

Experimental

Mps were determined on a hot stage and are not corrected. UV and IR (KBr) spectra were recorded on a Hitachi EPS-3T and a Hitachi EPI-G3 spectrophotometer. PMR ($CDCl_3$, TMS internal standard) and mass (70 eV, direct inlet) spectra were measured with a JEOL JNM-4H-100 (100 MHz) and a Hitachi RMU-6 spectrometer. Solvents were concentrated *in vacuo*. The identity of a compound was established on the basis of mp, mixed mp, and IR and NMR spectral determinations.

*Reaction of the Oxazolone **4** with the Diene **3**.* A mixture of the diene **3**[7] (1.4 mmol) and the oxazolone **4**[8] (1.4 mmol) in benzene (50 cm^3) was stirred at 40 °C under a nitrogen atmosphere for 28 h. The solvent was concd and the residue was chromatographed (silica gel/$CHCl_3$) to give, besides the unreacted diene **3** (27%), 1-methyl-2,5-diphenylpyrrole **6** (55%), mp 206—207 °C, lit,[9] 204—205 °C, identical with an authentic specimen,[2] and dimethyl 1-tosylpyrrole-3,4-dicarboxylate **7** (56%), mp 116.5—117.5 °C; UV_{max} (MeOH) 237 (log ε 4.35) and 275^{sh} nm (2.98); IR 1747, 1730, 1720, 1709, 1378, 1275, 1192, 1176, and 1160 cm^{-1}; PMR δ=7.74 and 7.27 (AA'BB', each 2, J=8 Hz, ArH), 7.58 (s, 2, =CH), 3.80 (s, 6, OMe), and 2.41 ppm (s, 3, CMe); MS *m/e* (rel intensity), 337 (38, M$^+$), 306 (23, M$^+$—OMe), 155 (68, Ts$^+$), 151 (25, M$^+$—Ts—OMe), and 91 (100, $MeC_6H_4^+$). Found: C, 53.50; H, 4.46; N, 4.00%. Calcd for $C_{15}H_{15}NO_6S$: C, 53.41; H, 4.48; N, 4.15%.

*Adduct (**9a**) of the Dithiolone **8a** and the Diene **3**.* A soln of the diene **3** (1.1 mmol) and the dithiolone **8a**[10] (1.1 mmol) in benzene (50 cm^3) was refluxed under nitrogen for 11 h. The solvent was concd and the residue was recrystd (MeOH) to give needles of the adduct **9a** (95%), mp 154—155 °C (dec); UV (MeOH) end absorption; IR 1748, 1714, 1350, and 1165 cm^{-1}; PMR δ=7.52—7.14 (m, 14, ArH), 4.67 (s, 2, bridgehead H), 3.76 and 3.73 (s, each 3, OMe), 3.66 and 3.21 (d, each 1, J=6.5 Hz, angular H), and 2.41 ppm (s, 3, CMe); MS *m/e* (rel intensity) 337 (12, **7**$^+$), 236

(100, **10**$^+$), 155 (23, Ts$^+$), 121 (22, PhCS$^+$), 91 (48, $MeC_6H_4^+$), and 60 (37, COS$^+$). Found: C, 60.54; H, 4.21; N, 2.14%. Calcd for $C_{32}H_{27}NO_7S_3$: C, 60.65; H, 4.29; N, 2.21%.

Pyrolysis of the Adduct ***9a***. A suspension of the adduct **9a** (160 mg) in toluene (25 cm^3) was heated under reflux for 100 h. The soln was concd and the residue was chromatographed (silica gel/acetone : cyclohexane : ligroin = 1 : 3 : 6) to give 2,5-diphenylthiophene (**10**)[2] (67%), mp 154—155 °C, lit,[11] 152—153 °C, the pyrrole **7** (64%), and unchanged adduct **9a** (31%), all identical with authentic specimens.

S-*Oxide* (***11a***). A soln of the adduct **9a** (0.28 mmol) and *m*-chloroperbenzoic acid (80% purity, 0.32 mmol) in dichloromethane (20 cm^3) was stirred at room temp for 23 h. The soln was washed (aq NaOH; water), dried (Na_2SO_4), and concd, and the residue was recrystd ($CHCl_3$-Et_2O) to give prisms of the *S*-oxide **11a** (87%), mp 238—239 °C (dec); UV (MeOH) end absorption; IR 1750^{sh}, 1716, 1706^{sh}, 1350, 1164, and 1086 cm^{-1}; PMR δ=7.70—7.38 (m, 12, ArH), 7.25 (AA′ part of AA′BB′, 2, J=8 Hz, ArH), 4.78 and 4.57 (d, each 1, J=1.7 Hz, bridgehead H), 3.72 (s, 6, OMe), 3.65 and 3.05 (d, each 1, J=8 Hz, angular H), and 2.42 ppm (s, 3, CMe); MS *m/e* (rel intensity) 337 (19, **7**$^+$), 264 (27, **12a**$^+$), 236 (100, **10**$^+$), 155 (36, Ts$^+$), 121 (19, PhCS$^+$), and 91 (81, $MeC_6H_4^+$). Found: C, 59.19; H, 4.13; N, 2.03%. Calcd for $C_{32}H_{27}NO_8S_3$: C, 59.15; H, 4.19; N, 2.16%.

Pyrolysis of the S-*Oxide* ***11a***. The *S*-oxide **11a** (85 mg) was heated in diethylbenzene (10 cm^3) under reflux for 10 h. The soln was concd, and the residue was chromatographed (silica gel/$CHCl_3$) to give 3,6-diphenylthiopyran-2-one (**12a**)[2] (29%), mp 187—187.5 °C, lit,[12] 183.5—184 °C, the pyrrole **7** (23%), and unchanged **11a** (24%), all identical with authentic specimens. When the *S*-oxide **11a** was heated in xylene under reflux for 95 h, **12a** (18%), **7** (4%), and **11a** (75%) were isolated.

Adduct (***9b***) *of the Thiazolone* ***8b*** *and the Diene* ***3***. A soln of the thiazolone **8b**[13] (1.1 mmol) and the diene **3** (1.1 mmol) in benzene (50 cm^3) was refluxed for 98 h. The soln was concd and the residue was recrystd (PhH-hexane) to give prisms of **9b** (52%), mp 215—216 °C; UV (MeOH) end absorption; IR 1737, 1715, 1699^{sh}, 1350, and 1166 cm^{-1}; PMR δ=7.58—7.03 (m, 17, ArH), 6.82—6.65 (m, 2, ArH), 4.95 and 4.67 (d, each 1, J=1.7 Hz, bridgehead H), 3.81 and 3.76 (s, each 3, OMe), 3.66 and 3.16 (d, each 1, J=7 Hz, angular H), and 2.40 ppm (s, 3, CMe); MS *m/e* (rel intensity) 355 (8, M$^+$—**7**), 337 (27, **7**$^+$), 263 (23, M$^+$—**7**—PhNH), 236 (92, **10**$^+$), 155 (49, Ts$^+$), 121 (19, PhCS$^+$) 119 (47, PhNCO$^+$), and 91 (100, $MeC_6H_4^+$). Found: C, 67.50; H, 4.63; N, 3.62%. Calcd for $C_{41}H_{35}N_2O_7S_2$ (**9b**+1/2 PhH): C, 67.28; H, 4.82; N, 3.83%. Found (after prolonged heating *in vacuo*): C, 66.45; H, 4.60; N, 3.77%. Calcd for $C_{38}H_{32}N_2O_7S_2$: C, 65.88; H, 4.66; N, 4.04%.[14] From the mother liquor of recrystallization, the unchanged diene **3** (35%) was recovered.

Pyrolysis of the Adduct ***9b***. A suspension of the adduct **9b** (0.1 g) in diphenyl ether (20 cm^3) was heated under reflux for 30 min. The solvent was removed and the residue was chromatographed (silica gel/$CHCl_3$) to give the thiophene **10** (88%) and the pyrrole **7** (82%), both identical with authentic specimens.

S-*Oxide* (***11b***). A soln of the adduct **9b** (0.29 mmol) and *m*-chloroperbenzoic acid (0.32 mmol) in dichloromethane (10 cm^3) was stirred overnight at room temp. The soln was washed (aq NaOH; water), dried (Na_2SO_4), concd, and the residue was recrystd ($CHCl_3$-Et_2O) to give the *S*-oxide **11b** (83%) as prisms, mp 182—184 °C (dec); UV (MeOH) 225 nm^{sh} (log ε 4.505); IR 1722, 1713^{sh}, 1350, 1166, and 1087 cm^{-1}; PMR δ=7.68—6.92 (m, 19, ArH), 4.98 and 4.65 (d, each 1, J=1.7 Hz, bridgehead H), 3.80 and 3.72 (s, each 3, OMe), 3.67 and 3.15 (d, each 1, J=8 Hz, angular H), and 2.41 ppm (s, 3, CMe); MS *m/e* (rel intensity) 506 (21), 431 (16), 337 (7, **7**$^+$), 323 (13, **12b**$^+$), 180 (21, PhCNPh$^+$), 155 (34, Ts$^+$), 119 (12, PhNCO$^+$), 91 (100, $MeC_6H_4^+$), and 77 (43, Ph$^+$). Found: C, 64.20; H, 4.49; N, 3.73%. Calcd for $C_{38}H_{32}N_2O_8S_2$: C, 64.39; H, 4.55; N, 3.95%.

We are indebted to Kyorin Chemical Laboratories for elemental analyses and mass spectral measurements, and to Mr. Naomi Takagi for experimental assistance.

References

1) Part III, H. Matsukubo and H. Kato, *Bull. Chem. Soc. Jpn.*, **49**, 3333 (1976).
2) H. Matsukubo and H. Kato, *J. Chem. Soc., Chem. Commun.*, **1975**, 840.
3) H. Matsukubo and H. Kato, unpublished results.
4) Cycloadditions to norbornadiene derivatives occur generally from above the surface of the bridge: R. Huisgen, M. Seidl, G. Wallbillich, and H. Knupper, *Tetrahedron*, **17**, 3 (1962); R. Huisgen, R. Grashey, H. Hauck, and H. Seidl, *Chem. Ber.*, **101**, 2043 (1968); W. S. Wilson and R. N. Warrener, *Tetrahedron Lett.*, **1970**, 5203; D. Wege, *ibid.*, **1971**, 2337; S. Inagaki and K. Fukui, *Chem. Lett.*, **1974**, 509; and Refs. 5 and 10a.
5) R. McCulloch, R. R. Rye, and D. Wege, *Tetrahedron Lett.*, **1969**, 5231.
6) Such an intermediate ylide from a related system was trapped recently: H. Kato, M. Nishiwaki, and H. Matsukubo, unpublished results.
7) R. Kitzing, R. Fuchs, M. Joyeux, and H. Prinzbach, *Helv. Chim. Acta*, **51**, 888 (1968).
8) H. O. Bayer, R. Huisgen, R. Knorr, and F. C. Schaefer, *Chem. Ber.*, **103**, 2581 (1970).
9) R. Huisgen, H. Gotthardt, H. O. Bayer, and F. C. Schaefer, *Chem. Ber.*, **103**, 2611 (1970).
10) (a) H. Gotthardt and B. Christl, *Tetrahedron Lett.*, **1968**, 4743; (b) H. Gotthardt, M. C. Weisshuhn, and B. Christl, *Chem. Ber.*, **109**, 740 (1976).
11) E. Baumann and E. Fromm, *Ber.*, **28**, 890 (1895).
12) G. Laban and R. Meyer, *Z. Chem.*, **7**, 227 (1967); *Chem. Abstr.*, **67**, 64184 (1967).
13) M. Ohta, H. Chosho, C. Shin, and K. Ichimura, *Nippon Kagaku Zasshi*, **85**, 440 (1964).
14) Repeated analyses gave poor agreement with the calculated value. PMR measurement showed that many cycloadducts of thiazolone **8b** strongly hold solvents of crystallization (benzene, ether, *etc.*), which are liberated only after prolonged heating *in vacuo*.[2] The adduct **9b** could not be completely freed of solvent by heating below its dec p.

NOTES

BULLETIN OF THE CHEMICAL SOCIETY OF JAPAN, VOL. 49 (11), 3317—3318 (1976)

Determination of the Solubility of Oxygen in Copper by the Coulometric Method

Tetsuya WADA, Kazuo FUEKI,* and Takashi MUKAIBO

Department of Industrial Chemistry, Faculty of Engineering, The University of Tokyo, Bunkyo-ku, Tokyo 113

** Department of Synthetic Chemistry, Faculty of Engineering, The University of Tokyo, Bunkyo-ku, Tokyo 113*

(Received February 6, 1976)

Synopsis. The solubility of oxygen in copper was determined at 800—1000 °C by means of the coulometric method. The data obtained is represented by the following equation: $\log N(\text{atom fraction}) = -2.164 - 1820/T$

At high temperatures, the oxidation rate of alloys is significantly affected by the formation of an internal oxidation layer. Since this internal oxidation is a phenomenon of oxygen diffusion into the alloy from the oxide-alloy interface, resulting in the formation of an oxide with the less noble constituent, the data of solubilities and diffusion coefficients of oxygen in the alloy are required in order to analyze the rate of alloy oxidation. The solubility of oxygen can be determined directly by the vacuum fusion method, the inert gas fusion method, the method of reduction of a metal saturated with oxygen, and the neutron or proton activation analysis. The solubility can also be determined indirectly by electric resistance measurements, lattice parameter measurements, and E. M. F. measurements by means of solid electrolytes. On the whole the direct methods are rather complicated. Since the coulometric method allows the precise determination of the thickness of thin oxide films, such as passive films, it can be applied to the estimation of the solubility of oxygen in metals and alloys. The purpose of this note is to report the determination of the oxygen solubility in copper by means of coulometric analysis.

Experimental

Rectangular slices, 20 mm × 7 mm in area and 0.2—0.8 mm in thickness, were cut from an ingot of electrolytic copper, 99.999% pure; they were polished with alumina powders, washed with soap and water, and dried in a desiccator. The polished specimens were treated in a pure hydrogen gas flow at 500 °C for 3 h to remove strains and surface oxides. Spectroscopic analysis revealed that the copper specimen contained Pb, As, Sb, Fe, and Ni, 1 ppm each, and 6 ppm of S as impurities.

Two specimens were oxidized simultaneously at 200—240 °C in air for a definite time to obtain copper(I) oxide films, 1500—2500 Å thick. One of these two specimens was used to determine the oxide film thickness by the coulometric method. It was placed in a cell as a cathode and two platinum anodes were placed to face either side of the cathodic plate. An aqueous solution of 0.1 M KCl was used as an electrolytic solution and a saturated calomel electrode as a reference electrode. Nitrogen gas was bubbled through the solution for 20 min to remove the dissolved oxygen; then the electrolysis was carried out with a current density of 67 $\mu A/cm^2$. The time variation of the potential difference between the cathode and the reference electrode was recorded. The oxide film thickness was calculated from the total amount of charge passed.[1,2]

The second specimen was sealed in a 10 mmϕ Vycor tube *in vacuo*, annealed in an electric furnace kept at each desired temperature within ±1 °C, and quenched as soon as possible after the annealing. The thickness of the remaining oxide film was then determined by the coulometric method. During the annealing, surface copper(I) oxide decomposes into copper and oxygen at the metal-oxide interface, and the oxygen diffuses inward. Therefore, the amount of dissolved oxygen was calculated from the decrease in the oxide film thickness. The amount of dissolved oxygen was plotted against t/l,[2] where t is the annealing time and $2l$ is the thickness of the copper specimen. The solubility of oxygen was determind from the saturated value.

Results and Discussion

Preliminary experiments showed that a faint red-colored deposit of copper(I) oxide appeared on the inner wall of the Vycor tube in the case of prolonged annealing. Therefore, sufficiently thin copper specimens were used so that the saturation could be completed in a short annealing period.

Table 1 gives the oxygen solubility, N, expressed in terms of atomic fraction. The standard deviation of N was less than 34%. Figure 1 gives the temperature dependence of the averaged N as a plot of log N *vs.*

TABLE 1. SOLUBILITY OF OXYGEN IN COPPER

Temp T(°C)	Thickness of Cu specimen $2l \times 10^2$(cm)	Annealing time t(min)	$t/l^2 \times 10^{-6}$ (s/cm²)	Solubility of oxygen (ppm)
1000	2.49	10.0	3.84	273
1000	2.52	15.0	5.67	245
950	5.01	30.0	2.86	229
950	3.18	20.0	4.75	198
900	3.20	30.0	7.06	203
900	3.32	30.0	6.51	187
850	4.47	30.0	3.57	160
850	2.94	35.0	9.72	142
800	4.45	30.0	3.62	115
800	5.15	30.0	2.70	164
800	7.13	35.0	1.65	166

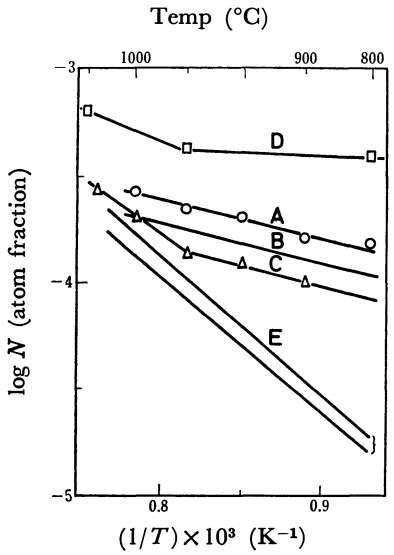

Fig. 1. Solubility of oxygen in copper.
(A) Present work, (B) Bouillon, (C) Phillips, (D) Rhines, (E) Pastrek.

$1/T$. The relationship is represented by the equation:

$$\log N = -2.164 - 1820/T \quad (1)$$

The data obtained by the previous investigators are also plotted in the same figure. Rhines and Mathewson[3] and Phillips and Skinner[4] determined the solubility from the weight decrease of copper saturated with oxygen by reduction. Bouillon and Orszagh[5] used the mass spectroscopic analysis coupled with the vacuum fusion technique. Pastrek and Rapp[6] studied the solubility using a solid electrolyte cell. The data of the present work agree well with those from Phillips and Bouillon.

From Eq. 1, the enthalpy change, the entropy change and the free energy change for the dissolution of oxygen in copper can be derived . They are

$$\Delta H = 8330 \text{ cal/mol},$$
$$\Delta S = -9.90 \text{ cal/mol deg},$$
$$\Delta F = 8330 + 9.90\,T \text{ cal/mol}$$

respectively.

References

1) H. A. Miley, *J. Am. Chem. Soc.*, **59**, 2626 (1937).
2) W. E. Campbell and U. V. Thomas, *Trans. Electrochem. Soc.*, **76**, 303 (1939).
3) F. N. Rhines and C. H. Mathewson, *Trans. Metal. Soc. AIME*, **111**, 337 (1934).
4) A. Phillips and E. N. Skinner, *Trans. Metal. Soc. AIME*, **143**, 301 (1941).
5) F. Bouillon and J. Orszagh, *J. Phys. Chem. Solids*, **33**, 1533 (1972).
6) R. F. Pastrek and R. A. Rapp, *Trans. Metal. Soc. AIME*, **245**, 1711 (1969).

BULLETIN OF THE CHEMICAL SOCIETY OF JAPAN, VOL. 49 (11), 3319—3320 (1976)

X-Ray Photoelectron Spectroscopy of Aminobenzoic Acids and Anthranilic Acid Chelates

Tooru YOSHIDA and Shigemasa SAWADA

Osaka Prefectural Industrial Research Institute, Enokojima, Nishi-ku, Osaka 550

(Received September 30, 1975)

Synopsis. Photoelectron spectra of three isomers of aminobenzoic acid and several metal chelates of *o*-isomer were measured. It was confirmed that *o*- and *p*-isomers exist in the non-polar form and *m*-isomer in the dipolar. In the chelates the trend was for the N(1s) chemical shifts to increase in parallel with the metal electronegativities.

It has been derived[1] from IR spectroscopy that *m*-amino-benzoic acid in the solid state exists in the dipolar form, while *o*- and *p*-isomers exist in the non-polar form. The *o*-isomer(anthranilic acid) exhibits a polymorphic transition;[2] its crystal structure for the form stable at room temperature has been determined from the X-ray diffraction data. It was found that there are two non-equivalent molecules per unit cell in the space group $P2_1cn$.[3]

Khan and Srivastava[4] deduced from X-ray and IR studies of the molecular stucture of *o*-isomer that the unit cell contains two equivalent molecules.

The purpose of this paper is to report the results by X-ray photoelectron spectroscopy (XPS) for the molecular structure of *o*-, *m*-, and *p*-isomers and for the chemical shift, the change in the N(1s) electron binding energy of anthranilic acid on complex formation.

The X-ray photoelectron spectra were measured on an AEI ES200 spectrometer. Al $K\alpha$ (1486.6 eV) X-ray radiation was used as the excitation source. The samples were ground to powder and then dusted onto a double-backed adhesive tape. The measurements were run at room temperature under a vacuum of about 10^{-7} Torr. The binding energy of the C(1s) peak was used as the energy standard throughout the present experiments; it was taken to be 285.0 eV. All the compounds measured are given in Table 1. Three isomers of aminobenzoic acid of an analytical grade were used after recrystallization from ethanol, and in the case of *o*-isomer after recrystallization from acetic acid,[2] which was employed to obtain the form stable at room temperature. All the anthranilic acid chelates with a ligand–metal ratio of 2 : 1 were prepared based upon the literature methods.[5]

The O(1s), N(1s), and C(1s) electron spectra of *o*-, *m*-, and *p*-aminobenzoic acids are shown in Fig. 1; their measured binding energies are given in Table 1. Two peaks were observed in the C(1s) electron spectra for all the isomers. It was determined that the one with higher binding energy corresponds to the carbon of the substituent group, and the other to the carbon of the benzene ring. The N(1s) electron binding energies of *o*- and *p*-isomers were about 2 eV lower than that of *m*-isomer. The O(1s) electron peak of *m*-isomer was narrower in full-width at half-maximum height (FWHM) and about 1—2 eV lower in binding energy, compared with those of *o*- and *p*-isomers. The O(1s) spectra of *o*- and *p*-isomers both have a broad peak, which suggests the presence of at least two kinds of oxygen atoms. The two peaks, a and b, with the different binding energies shown by the broken lines in the figure, were obtained by a graphical resolution of the peak of *p*-isomer.

In view of the stuctures[4,6] of *o*- and *p*-isomers determined from X-ray and IR analyses, it seems that the two peaks, a and b, in Fig. 1 correspond to the oxygen atoms of C–OH and C=O, respectively.

The FWHMs (2.9—3.1 eV) of the O(1s) peaks of *o*- and *p*-isomers are larger than that(2.7 eV) of benzoic acid, which is the same value as acetic acid[7] in the solid state. Such an increase of the FWHM in *o*- and *p*-isomers may be attributable to the contribution of a resonance structure, as shown below: This con-

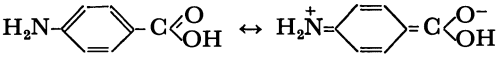

and

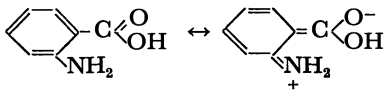

tribution has the possibility of increasing the difference between the electron densities on the two oxygens of the carboxylate group, which would give rise to the broadening of the O(1s) peak. Benzoic acid can not reasonably have the above resonance. That the FWHM of *o*-isomer is about 0.2 eV smaller than that of *p*-isomer may be attributable to the decrease of such resonance due to steric hindrance in the former, which has been suggested from IR.[8]

In the zwitterion structure of *m*-isomer,[1] the N(1s) and O(1s) peaks may correspond to the positively charged nitrogen atom and the negatively charged oxygen atoms of the carboxylate group. The C(1s) binding energy of the carboxylate group of the *m*-isomer is about 1 eV lower than those of the other two isomers. This can be explained by arguing that the electron density on the carbon atom of the carboxylate group in the former becomes larger than those of the carboxyl group in the latter, because of the delocalization of a unit negative charge within a carboxylate group.

Although *o*-isomer crystallized from acetic acid has been reported to have in part a zwitterion structure,[3] this was not confirmed by this XPS study at all.

The N(1s) and O(1s) electron spectra of all the anthranilic acid metal chelates and sodium salt were single peaks with the FWHMs of 1.6—1.8 eV and 1.7—1.9 eV, respectively, except that the FWHMs of the O(1s) peaks of Pd and Pt chelates were 2.1—2.2 eV.

In the charge-potential model,[6] the chemical shift can be expressed in terms of the charge on the atom

Table 1. Measured binding energies and frequencies

Samples		Binding energy (eV)[a] C(1s)[b]	N(1s)	ΔE[c]	O(1s)	χ[d]	ν_{N-H}[e]	ν_{COO^-}[f]
Aminobenzoic acids	*o*-	289.0	399.6		533.1(2.9) (533.8, 532.4)[g]		3450	
	m-	288.3	401.6		531.5(1.8)			
	p-	289.0	399.7		533.1(3.1) (533.9, 532.4)[g]			
Benzoic acid		289.1			533.0(2.7)			
Sodium salt of anthranilic acid		288.4	399.3		531.3(1.7)		3400	1510
Anthranilic acid chelates	Pt	288.4	400.5	0.9	531.6(2.1)	2.2	3140	1555
	Pd	288.3	400.3	0.7	531.6(2.2)	2.2	3150	1550
	Cu	288.4	399.9	0.3	531.4(1.9)	1.9	3260	1543
	Ni	288.6	399.9	0.3	531.4(1.9)	1.8	3280	1535
	Mn	288.5	399.7	0.1	531.5(1.9)	1.5	3290	1535
	Hg	288.3	400.1	0.5	531.3(1.8)	1.9	3250	1540
	Cd	288.6	399.8	0.2	531.5(1.8)	1.7	3280	1530
	Zn	288.6	399.8	0.2	531.4(1.9)	1.6	3280	1535

The numbers in parentheses indicate the full-width at half-maximum height. a) Uncertainties are less than or equal to ±0.1 eV. b) The C(1s) electron binding energy of a substituent group. c) The N(1s) chemical shift. d) Pauling electronegativity of the metal. e, f) The N-H stretching and the COO^- antisymmetrical vibration frequencies (cm^{-1}), respectively, determined in Nujol mull on a IR spectrometer, model IR-G, of Japan Spectroscopic Co., Ltd. g) The values obtained by a graphical resolution.

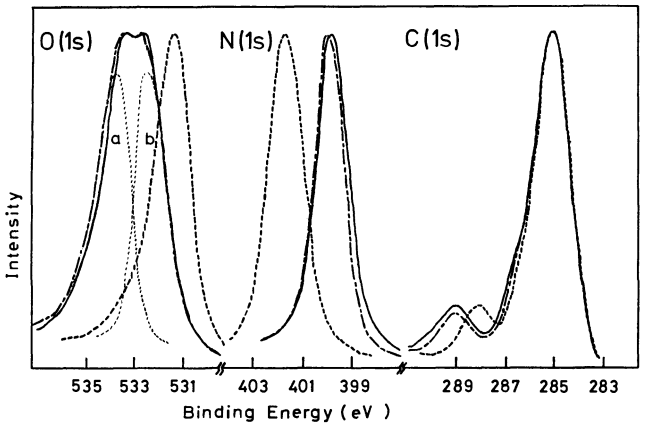

Fig. 1. O(1s), N(1s), and C(1s) photoelectron spectra of aminobenzoic acids.
——: *o*-Isomer, ------: *m*-isomer, -·-·-: *p*-isomer.

and the Coulomb potential energy of an electron due to the other atoms in the molecule. In this study, however, it was assumed that the chemical shift is dominated by the charge on the atom concerned, since the compounds studied here are covalent and their structures are similar. Therefore, the N(1s) chemical shifts in all the chelates are considered to be due to the decrease in the electron density on the nitrogen atoms caused by the coordination of lone-pair electrons of the nitrogen atoms to the metal.

The N(1s) chemical shifts tended to increase in parallel with the metal electronegativities. This can be explained by arguing that the covalent character of the bonds between the metal ions and the ligand increases with the metal electronegativity. A more covalent coordinate bond is considered to decrease the electron density on the donor atoms, which would appear in the increase of the binding energies.

It has previously been demonstrated by IR that the coordination of amino groups to metals results in appreciable decreases in the frequencies of the N–H stretching vibrations. These changes become larger with increasing covalent character of the N–M bonds.[9] There seems to be a certain reasonable relation between the N(1s) chemical shift and the N–H frequency, the N(1s) chemical shift increasing with decreasing N–H frequency.

All the binding energies and the FWHMs of the O(1s) peaks of the metal chelates were similar to those of sodium salt rather than those of free anthranilic acid. The C(1s) binding energies of the carboxylate group for the chelates (288.3—288.6 eV) were also similar to that of sodium salt (288.4 eV).

It has been concluded from the IR study that as the bonding of the carboxylate groups with a metal atom becomes more covalent the absorption peak for the antisymmetrical vibration of the COO^- groups shifts to higher frequencies.[10] All the frequencies of the chelates are larger than that of sodium salt, as shown in Table 1. Furthermore, the O(1s) binding energies of almost all chelates are slightly larger than that of sodium salt.

These results suggest that the COO^-–M^{2+} bonds in anthranilic acid chelates are not so essentially ionic as in the case of sodium salt.

Sandhu *et al.*[11] have proposed a polymeric structure for the anthranilic acid metal chelates from IR and magnetic susceptibility measurements, and suggested that the stereochemistry around the metal ion is that of a distorted octahedron, with both oxygens of carboxylate bonded to two different metal atoms, though unequally. This inequality of the two oxygens of carboxylate may be associated with the present result that the FWHMs of the O(1s) peaks of the chelates are 0.1—0.5 eV larger than that of the sodium salt, as is shown in Table 1.

References

1) L. Gopal, C. I. Jose, and A. B. Biswas, *Spectrochim. Acta, Part A*, **23**, 513 (1967).
2) A. F. Wells, *Phil. Mag.*, **37**, 184 (1946).
3) C. J. Brown, *Proc. R. Soc. London, Ser. A.*, **302**, 185 (1968).
4) M. Y. Khan and P. Srivastava, *Indian J. Pure Appl. Phys.*, **6**, 166 (1968).
5) A. G. Hill and B. C. Curran, *J. Phys. Chem.*, **64**, 1519 (1960).
6) T. F. Lai and R. E. Marsh, *Acta Crystallogr.*, **22**, 885 (1967).
7) K. Siegbahn, C. Nordling, G. Johansson, J. Hedman, P. F. Heden, K. Hamrin, U. Gelius, T. Bergmark, L. O. Werme, R. Manne, and Y. Baer, "ESCA Applied to Free Molecules," North-Holland, Amsterdam (1969).
8) T. Inomata and T. Moriwaki, *Nippon Kagaku Zasshi*, **91**, 819 (1970).
9) G. F. Svatos, C. Curran, and J. V. Quagliano, *J. Am. Chem. Soc.*, **77**, 6159 (1955).
10) P. T. Sawayer and J. M. Mckinnie, *J. Am. Chem. Soc.*, **82**, 4191 (1960).
11) S. S. Sandhu, B. S. Manhas, M. R. Mittal, and S. S. Parmar, *Indian J. Chem.*, **7**, 286 (1969).

BULLETIN OF THE CHEMICAL SOCIETY OF JAPAN, VOL. 49 (11), 3321—3322 (1976)

An MO-theoretical Study on the Hydration of Simple Olefins

Ichiro HIRONO, Osamu KIKUCHI, and Keizo SUZUKI

Department of Chemistry, The University of Tsukuba, Sakura-mura, Ibaraki 300-31

(Received February 21, 1976)

Synopsis. The acid-catalyzed hydration of simple olefins was studied on the basis of a semi-empirical SCF NDDO method. The substituent effect on the activation energy agreed well with experimental result.

Olefins can be hydrated by treatment with water and an acid catalyst. Though several mechanisms[1-3] have been proposed for the acid-catalyzed hydration of olefins, they may be written simply as:

$$CH_2{=}CH_2 + H_3O^+ \xrightarrow{\text{slow}} CH_3{-}\overset{+}{C}H_2 \xrightarrow{\text{fast}} CH_3{-}CH_2OH + H_3O$$

The rate-determining step, which is the first step, is slow proton transfer from H_3O^+ to the olefin, *via* I. This step is followed by the rapid addition of water.[1,2]

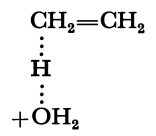

I

The hydration of simple olefins is a simple example of a catalytic reaction and a fundamental process for the preparation of alcohol from petroleum by-products. This note reports the results of an MO-theoretical study of this reaction mechanism and the substituent effect on the activation energy of the reaction. The MO method employed here is a semi-empirical NDDO method[4] which gives well-balanced molecular geometries and reaction energies.

Though the solvent effect must be considered in this reaction, it is difficult to introduce it in a precise form since this effect has very complex aspects. Here the solvent effect was introduced simply by adding one more water molecule to the system. It is assumed that

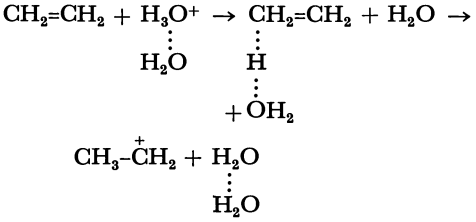

the solvent water molecule, which bonds weakly to H_3O^+, leaves the H_3O^+ ion when a new bond is formed between the H_3O^+ and an olefin. The interaction energies for II and III, where each H···O distance was optimized, are 1.79 and 0.50 eV, respectively.

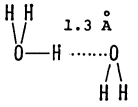

II

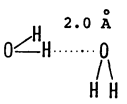

III

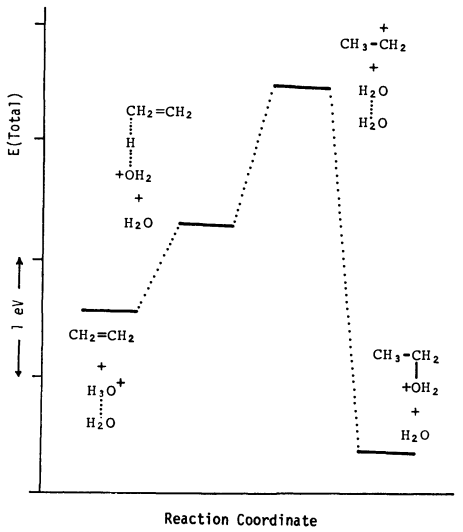

Fig. 1. Energy variation along the hydration of ethylene.

The energy diagram for this process is shown in Fig. 1. In Fig. 1, the energy of the carbonium ion, which is considered to be an intermediate of the process, is higher than that of I. In an actual water medium, the carbonium ion is stabilized by the solvent. This effect, however, is not considered in Fig. 1. The detailed calculation on the attack of H_3O^+ on ethylene from the direction shown in IV[5] was performed to examine the most favorable path for the above process.

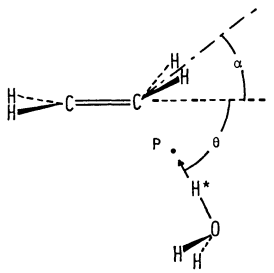

IV

The energy map of this process for $\theta=45°$ is shown in Fig. 2. It was found from Fig. 2 and from the calculated results that (1) H_3O^+ approaches the point P (the position of the H atom in the tetrahedral $-CH_3$ group) without any appreciable change in the H*–O bond length until the P–O distance becomes 1.5 Å, (2) the geometry of ethylene at P–O=1.5 Å is: C–C =1.30 Å, and $\alpha=10°$, (3) after the proton transfer from H_3O^+ to ethylene, H_2O leaves the carbonium ion, and (4) no appreciable change was observed in the energy maps for $45° < \theta < 90°$. In the calculation of the energy maps, the solvent effects of II and III

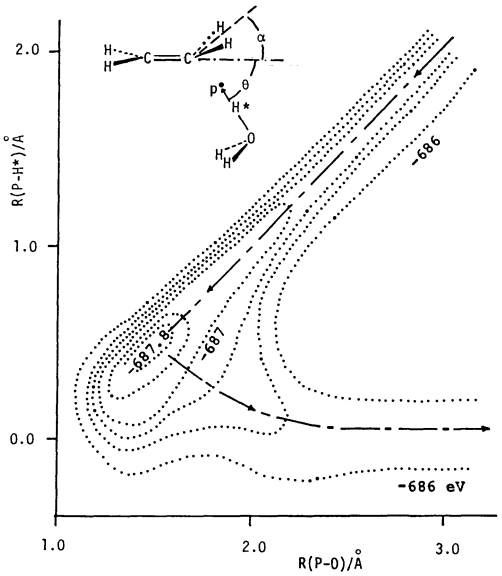

Fig. 2. Energy contours for the ethylene-H_3O^+ system. The C-C bond length and the angle α were optimized in the calculation.

were excluded. This is the reason why I is stable in Fig. 2.

The formation of the carbonium ion is followed by the rapid addition of water producing an oxonium ion (Fig. 1), and the carbonium ion does not correspond to the transition state. Nevertheless, it is expected that the transition state resembles the carbonium ion and I, and that the activation energy of the present process correlates with the difference between the energy of the carbonium ion and that of the initial state. The activation energies estimated under this assumption are listed in Table 1 as well as available experimental values.[1] The discrepancy between the calculated and experimetal activation energies is 20—30%. The activation energy for isobutene is very large, because the geometries of substituted carbonium ions were estimated from that of $CH_3-\overset{+}{C}H_2$ and this value reflects the overestimation of the steric interaction between the two CH_3 groups. The calculated values reproduce satisfactory the experimentally observed

Table 1. Activation energies for the hydration of simple olefins

Olefins[a]	E_a (kcal/mol)	
	Calcd	Exptl[1]
$CH_2=\overset{*}{C}H_2$	44.5	32.4
$CH_2=\overset{*}{C}H-Me$	35.1	26.4
$Me-CH=\overset{*}{C}H_2$	63.4	—
$CH_2=\overset{*}{C}(Me)_2$	25.7	21.1
$(Me)_2C=\overset{*}{C}H_2$	169.8	—
$Me-CH=\overset{*}{C}H-Me$	48.4	—
$CH_2=\overset{*}{C}H-Et$	34.6	—
$Et-CH=\overset{*}{C}H_2$	45.0	—

a) The asterisk indicates the carbon atom which is attacked by the hydroxyl group.

substituent effect on the activation energy. The Markownikoff rule is also reflected in the olefins listed in Table 1. The present authors thus feel that the present treatment correctly describes the reaction to some extent.

References

1) B. T. Baliga and E. W. Walley, *Can. J. Chem.*, **42**, 1019 (1964); *ibid.*, **43**, 2453 (1965).

2) W. M. Schubert, Bo Lamm, and J. R. Keeffe, *J. Am. Chem. Soc.*, **86**, 4727 (1964); W. M. Schubert and J. R. Keeffe, *ibid.*, **94**, 559 (1972); N. C. Deno, F. A. Kish, and H. J. Peterson, *ibid.*, **87**, 2157 (1965); A. J. Kresge, Y. Chiang, P. H. Fitzgerad, R. S. McDonald, and G. H. Schmid, *ibid.*, **93**, 4907 (1971).

3) R. H. Boyd, R. W. Taft, Jr., A. P. Wolf, and D. R. Christman, *J. Am. Chem. Soc.*, **82**, 4729 (1960); J. L. Jensen, *Tetrahedron Lett.*, **1971**, 7.

4) O. Kikuchi, to be published.

5) In a preliminary calculation, several interacting patterns for the H_3O^+-ethylene system were examined. The orientation of IV was the most favorable one.

BULLETIN OF THE CHEMICAL SOCIETY OF JAPAN, VOL. 49 (11), 3323—3324 (1976)

Infrared Spectra of Tribromochloro-*p*-benzoquinone and Its Anion Radical

Yôichi IIDA

Department of Chemistry, Faculty of Science, Hokkaido University, Sapporo 060

(Received May 4, 1976)

Synopsis. A chemically-stable anion radical salt of tribromochloro-*p*-benzoquinone was synthesized. The infrared spectrum of the anion radical was examined together with its neutral molecule.

The vibrational spectrum of an ion radical is known to differ distinctly from that of its neutral molecule.[1-8] So far, few quantitative studies have been made on such a difference. The infrared spectra of *p*-chloranil (*p*-QCl_4), *p*-bromanil (*p*-QBr_4), 2,5-dibromo-3,6-dichloro-*p*-benzoquinone (*p*-QBr_2Cl_2) and their corresponding anion radicals were previously examined.[3-6] In order to explain the frequency difference in fundamental vibration between the neutral molecule and its anion radical, the fundamental frequencies were assigned, and the simple Urey-Bradley force fields were determined for both the neutral and anion radical molecules. We are able to understand these frequency differences on the basis of the difference in the intramolecular force fields of the two molecules. It was found that the force constants of *p*-QBr_2Cl_2 and its anion radical can be transferred from those of *p*-QX_4, (X= Cl or Br), and its anion radical, respectively.[6] Measurements of the infrared spectra (400—4000 cm^{-1}) of tribromochloro-*p*-benzoquinone (*p*-QBr_3Cl) and its anion radical have been carried out in order to observe the difference in the spectra of these neutral and anion radical molecules. The fundamental vibrations were assigned by comparison with those of *p*-QX_4, (X=Cl or Br), *p*-QBr_2Cl_2 and their anion radicals.

The neutral *p*-QBr_3Cl was prepared by the oxidation of tribromochlorohydroquinone and purified by recrystallization from benzene or gracial acetic acid. The anion radical salt with the potassium cation (K^+ *p*-$QBr_3Cl^{\cdot-}$), which is stable at room temperature, was synthesized by the method of Torrey and Hunter.[9] The infrared spectra of these solid compounds were measured as Nujol mulls in the range 400—4000 cm^{-1} with an IR-G infrared spectrophotometer (Japan Spectroscopic Co., Ltd.). The infrared spectra in the regions where the absorption due to Nujol appears were measured using hexachlorobutadiene mulls.

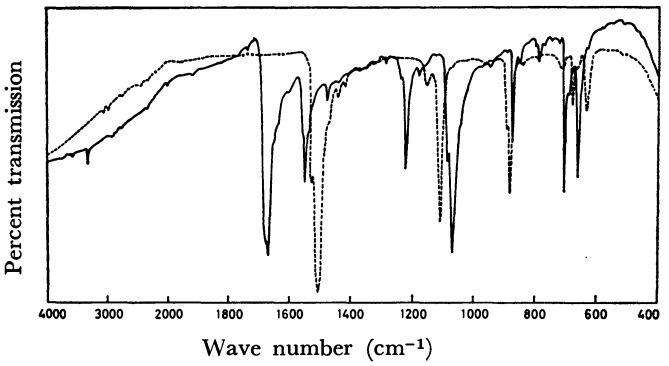

Fig. 1. The infrared spectra of neutral tribromochloro-*p*-benzoquinone (*p*-QBr_3Cl, ——) and its anion radical salt with the potassium cation (K^+ *p*-$QBr_3Cl^{\cdot-}$, ----).

The spectra obtained for these compounds are reproduced in Fig. 1. Since the counter cation of the anion radical salt is a simple alkali metal cation, the observed spectrum of K^+ *p*-$QBr_3Cl^{\cdot-}$ in the region under investigation would be due to that of the *p*-QBr_3Cl anion radical itself. In the infrared spectra of the neutral *p*-QBr_3Cl and its anion radical, we can also observe appreciable frequency shifts between their corresponding bands. Although the point groups of these molecules are degraded into C_s, their spectroscopic features are found to be close to those of *p*-QX_4, (X=Cl or Br), *p*-QBr_2Cl_2 and their anion radicals,[3-6] where *p*-QX_4 and *p*-QBr_2Cl_2 have D_{2h} and C_{2h} point groups, respectively. Thus, the assignments of the fundamental vibrations of *p*-QBr_3Cl and its anion radical were made in comparison with those of symmetrical *p*-benzoquinones.

For the neutral *p*-QBr_3Cl, two strong absorptions at 1678 and 1671 cm^{-1} can definitely be assigned to the C=O bond stretching modes. For the anion radical, however, we could observe only one fundamental absorption due to the C=O mode at 1509 cm^{-1}, although there may appear two fundamentals from the symmetry property of the molecule. We note a remarkable red shift of 166 cm^{-1} upon introduction of an extra electron to the neutral *p*-QBr_3Cl. Such a large red shift has also been found in the cases of *p*-QX_4, (X=Cl or Br), *p*-QBr_2Cl_2 and their corresponding anion radicals.[3-6]

The strong absorption at 1551 cm^{-1} with shoulders for the neutral *p*-QBr_3Cl arises from the C=C bond stretching mode, the corresponding band for the anion radical being found at 1530 cm^{-1}. Thus, the fundamental absorption due to the C=C mode is red-shifted by 21 cm^{-1} when the neutral *p*-QBr_3Cl changes into its anion radical. On the other hand, the absorption at 1222 cm^{-1} of the neutral *p*-QBr_3Cl is attributable to the C–C bond stretching mode. The band at 1069 cm^{-1} with a shoulder at 1085 cm^{-1} of the same molecule may arise from the major contribution of the C–C bond stretching mode and the minor contribution of the C–Cl bond stretching mode. In comparison with the spectroscopic data of *p*-QX_4 (X=Cl or Br),[4,5] the bands at 1222 and 1069 cm^{-1} come mostly from the B_{3u} and B_{2u} modes of *p*-QX_4, respectively. This also implies the similarity of the spectroscopic features of *p*-QBr_3Cl and *p*-QX_4 (X=Cl or Br). As regards the corresponding absorption of the *p*-QBr_3Cl anion radical, only one fundamental absorption was observed at 1109 cm^{-1}. The band is attributable to a shifted band of 1069 cm^{-1} of the neutral *p*-QBr_3Cl, indicating an

appreciable blue shift by 40 cm^{-1} upon introduction of the extra electron to the neutral *p*-QBr_3Cl. According to previous experimental and theoretical investigations,[3-6] the C=C bond-stretching force constant decreases, while the C-C bond-stretching force constant increases, in going from the neutral *p*-QX_4 (X=Cl or Br) and *p*-QBr_2Cl_2 to their corresponding anion radicals. Such an increase of the C–C bond-stretching force constant leads to the blue shift of the 1109 cm^{-1} band of the *p*-QBr_3Cl anion radical. Although the 1222 cm^{-1} band of the neutral *p*-QBr_3Cl can also be expected to shift to higher energy region in its anion radical, no such absorption was observed in the anion radical presumably because of its weak intensity. The lack of this absorption of the C–C stretching mode has also been found in the series of the *p*-QX_4 (X=Cl or Br) and *p*-QBr_2Cl_2 anion radicals.[3-6]

In the wave number region 1000—400 cm^{-1}, the spectrum of the neutral *p*-QBr_3Cl has three strong absorptions at 876, 706, and 660 cm^{-1}, respectively. By referring to the assignments of *p*-QBr_4 and *p*-QBr_2Cl_2,[5,6] the 876 cm^{-1} band seems to arise from the mixing of the C–C, C–Cl, and C–Br bond-stretching modes, and the 660 cm^{-1} band from the mixing of the C–Cl and C–Br stretching modes.[10] On the other hand, the spectrum of the *p*-QBr_3Cl anion radical has three corresponding absorptions at 881 cm^{-1} with a shoulder around 891, at 682 and at 638, respectively.[10] The 881 cm^{-1} band shows a slight blue-shift, and the 638 cm^{-1} band a red-shift as compared to the corresponding 876 and 660 cm^{-1} absorptions of the neutral molecule. The C–Cl and C–Br bond-stretching force constants are known to be weakened by the formation of the anion radicals,[5,6] so that the appreciable red-shift of the 638 cm^{-1} band can be explained in terms of the mixing of the C–Cl and C–Br stretching modes. The reason for the slight blue-shift of the 881 cm^{-1} band is that it arises from the mixing of the C–C, C–Cl and C–Br stretching modes, and the C–C stretching force constant is strengthened by forming the anion radical.

In view of these results, although the molecular symmetries of the neutral *p*-QBr_3Cl and its anion radical are degraded from those symmetrical *p*-QX_4 (X=Cl or Br), *p*-QBr_2Cl_2 and their anion radicals, the spectroscopic features of *p*-QBr_3Cl and its anion radical can be understood on the basis of the infrared spectra reported on the symmetrical *p*-benzoquinones and their anion radicals.[3-6]

References

1) J. Stanley, D. Smith, B. Latimer, and J. P. Devlin, *J. Phys. Chem.*, **70**, 2011 (1966).
2) Y. Matsunaga, *Nippon Kagaku Zasshi*, **89**, 905 (1968), and the references cited therein.
3) Y. Iida, *J. Phys. Soc. Jpn.*, **27**, 1371 (1969).
4) Y. Iida, *Bull. Chem. Soc. Jpn.*, **43**, 345 (1970).
5) Y. Iida, *Bull. Chem. Soc. Jpn.*, **46**, 2955 (1973).
6) Y. Iida, *Bull. Chem. Soc. Jpn.*, **47**, 99 (1974).
7) Y. Iida, *Bull. Chem. Soc. Jpn.*, **46**, 423 (1973).
8) J. J. Hinkel and J. P. Devlin, *J. Chem. Phys.*, **58**, 4750 (1973).
9) H. A. Torrey and W. H. Hunter, *J. Am. Chem. Soc.*, **34**, 702 (1912).
10) The 876 and 660 cm^{-1} bands of the neutral *p*-QBr_3Cl shift to the 869 and 650 cm^{-1} bands in the neutral *p*-QBr_4, respectively, while the 706 cm^{-1} band shows no such shift when the neutral *p*-QBr_3Cl changes into the neutral *p*-QBr_4. The absorptions at 881 cm^{-1} with a shoulder around 891 and at 638 of the *p*-QBr_3Cl anion radical shift to those at 879 and 618 cm^{-1} in the *p*-QBr_4 anion radical, respectively, while the 682 cm^{-1} band shows no such shift when the *p*-QBr_3Cl anion radical changes into the *p*-QBr_4 anion radical (see Ref. 5).

BULLETIN OF THE CHEMICAL SOCIETY OF JAPAN, VOL. 49 (11), 3325—3326 (1976)

NMR Studies of the Pyridine Exchange Reaction in the Pyridine Adduct of Bis(salicylaldehydato)nickel(II)

Masamoto IWAIZUMI, Kouto MIGITA, and Taro ISOBE
Chemical Research Institute of Non-Aqueous Solutions, Tohoku University, Sendai 980
(Received March 8, 1976)

Synopsis. The pyridine exchange reaction in the pyridine adduct of bis(salicylaldehydato)nickel(II) becomes appreciably slower and its activation energy increases with the decrease of the electron donor properties of the in-plane ligand. However, changes in the spin delocalization onto the coordinated pyridine by the in-plane ligand appear small.

Spin delocalization onto bases interacting with bis(acetylacetonato)nickel(II), $Ni(acac)_2$, has been one of the subjects investigated in great detail through isotropic paramagnetic shifts in NMR.[1] In this system the spin distributions in the bases are directly evaluated from the observed isotropic shifts, since the pseudocontact interaction is negligible and the exchange reaction of the bases which coordinate to $Ni(acac)_2$ is in the limit of the fast exchange rate region. However, whether or not the exchange reaction is in the fast rate region seems to have a critical dependence on the ligands already bound to the nickel. We observed that when bis(salicylaldehydato)nickel(II), $Ni(sal)_2$, is used in place of $Ni(acac)_2$, the relative ratio of contact shifts for the α, β, and γ protons in pyridine appreciably differs from that in the $Ni(acac)_2$ system. This deviation becomes much larger when the nitro derivative of salicylaldehydate ion is used as an in-plane ligand.[2] As is shown later, these changes can be related to the fact that the pyridine exchange reactions in $Ni(sal)_2$ and its derivatives are not in the fast exchange rate region at the measurement temperature, and the observed shifts are not exactly the weighted average between the free and associated forms of pyridine. The main purpose of this note is to show how the exchange reaction of pyridine at the apical position in six-coordinated nickel complexes is affected by the in-plane ligands already bound to the nickel.

Experimental

The nickel(II) complexes used were those with salicylaldehyde and its 5-methyl, 5-chloro, 5-bromo, and 5-nitro derivatives [$Ni(sal)_2$ and $Ni(5X\text{-}sal)_2$, X=Me, Cl, Br, and NO_2]. These complexes were dried at 110°C *in vacuo* before use. NMR spectra of the bulk solvent protons in pyridine solutions of these complexes were measured with a Jeol JNM PS 100 NMR spectrometer at various temperatures.

The magnetic susceptibilities of the complexes in pyridine were determined by the Evans method,[3] using TMS for a reference signal.

Results and Discussion

It was observed that the isotropic shifts and the line widths of pyridine protons change markedly with temperature. Though the ratio of the isotropic shifts of α, β, and γ protons for each nickel complex system at an ambient temperature differs, each approaches the ratio observed for pyridine interacting with $Ni(acac)_2$[1a] and all become the same as the temperature increases. The features of the changes in the line width and in the isotropic shifts are those seen typically in exchanging ligands of transition metal complex solutions.[4] In Fig. 1, the line width changes are shown by the plot of the observed transverse relaxation rates *vs.* $1/T$. It is seen that the pyridine exchange reaction is appreciably affected by the in-plane ligands, and at the ambient temperature ($1/T \approx 3.3 \times 10^{-3}$) the pyridine exchange reaction is in the slow exchange rate region. To consider quantitatively the line width changes in the present system, one needs to take into account effects of spin-spin decoupling as well as effects of changes in the quadrupole relaxation of nitrogen caused by paramagnetic

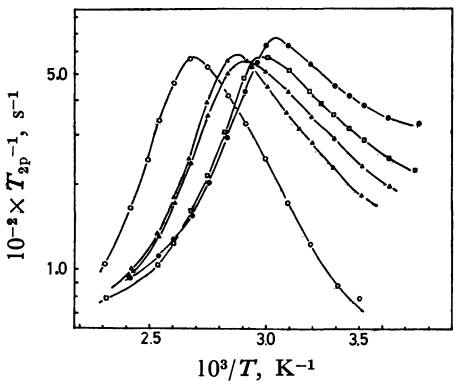

Fig. 1. Temperature dependence of $1/T_2$ for the bulk solvent α proton in the pyridine solutions of the nickel(II) complexes at 0.15 M and at 100 MHz.
—●—: $Ni(5\ Me\text{-}sal)_2$, —□—: $Ni(sal)_2$, —▲—: $Ni(5Cl\text{-}sal)_2$, —△—: $Ni(5Br\text{-}sal)_2$, —○—: $Ni(5NO_2\text{-}sal)_2$.

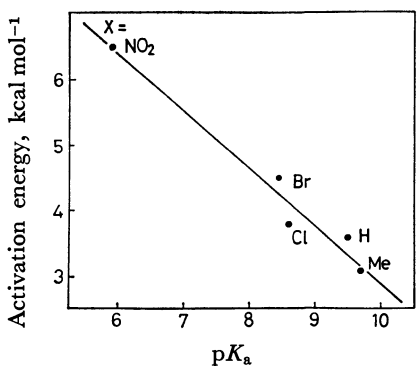

Fig. 2. Relation between the Arrhenius activation energies of pyridine exchange reaction and pK_a values of the in-plane ligands of $Ni(5X\text{-}sal)_2$.

pulses due to the presence of the nickel complexes. We assume here that the spin-spin interaction is completely decoupled and the broadening due to the quadrupole relaxation of nitrogen does not contribute any more. As a crude approximation, we further regard the observed line width as arising from only the pyridine exchange reaction.[5] The observed relaxation rate, $1/T_2$ for the case satisfying the condition $\Delta\omega_M^2 \gg (1/T_{2M})^2$ or $(1/\tau_M)^2$, is hence put equal to P_M/τ_M,[4,6] where $\Delta\omega_M$ and $1/T_{2M}$ are the chemical shift and the transverse relaxation rate of the proton in the coordinating pyridine, P_M is the ratio of the solvent bound to the Ni(II) complexes to the free-solvent concentration, and $1/\tau_M$ is the pyridine exchange rate. In Fig. 1 the region where the plots show negative slope satisfies the above rate condition. By the Arrhenius relation, these negative slopes are proportional to the activation energies of the pyridine exchange reactions. The slopes show that the activation energies increase in the order of Ni(5Me-sal)$_2$, Ni(sal)$_2$, Ni(5Cl-sal)$_2$, Ni(5Br-sal)$_2$, and Ni(5NO$_2$-sal)$_2$; their reaction rates at a given temperature also decrease in this order of the complexes. Figure 2 shows that there is a good correlation between the activation energies of the pyridine exchange reactions and the pK_a values[7] of the in-plane ligands. Here, the activation energies were evaluated from the slopes of the curves in the slow exchange rate region in Fig. 1, with the approximation $1/T_2 \approx P_M/\tau_M$.[5] The results of Fig. 2 suggest that the activation energy of the pyridine exchange reaction decreases with the increase of the electron donor property of the in-plane ligands, since pK_a values may be regarded as a measure of the electron donor properties.

In view of the above result and the fact that acetylacetone has a pK_a value, 9.50,[7] larger than salicylaldehyde and its derivatives, it can be understood that the pyridine exchange reaction in the Ni(acac)$_2$ system is much faster than the Ni(sal)$_2$ system.

The hyperfine coupling constants of pyridine protons, $A_H/\hbar$, are obtained from the isotropic shifts in the fast exchange rate region by the relation:

$$\frac{\Delta\omega_{obsd}}{P_M} = -\left(\frac{A_H}{\hbar}\right)\frac{\omega_0\mu_e\beta\sqrt{S(S+1)}}{3kT\gamma_H}$$

where $\Delta\omega_{obsd}$ is the observed isotropic shift, ω_0 is the resonant frequency, and μ_e is the effective magnetic moment of nickel in the complexes. The values obtained for the α proton are 10.1 ± 0.5 rad s^{-1} (μ_e=3.1 BM), 9.0 ± 0.5 rad s^{-1} (3.0 BM), 10.1 ± 0.5 rad s^{-1} (2.9 BM), 10.1 ± 0.5 rad s^{-1} (2.8 BM), and 9.7 ± 0.5 rad s^{-1} (2.8BM) for Ni(5Me-sal)$_2$, Ni(sal)$_2$, Ni(5Cl-sal)$_2$, Ni(5Br-sal)$_2$, and Ni(5NO$_2$-sal)$_2$, respectively. Significant changes could not be detected in the hyperfine coupling constants of these complex systems. However, it may be worth noting that the delocalized spin densities on the coordinated pyridine were estimated to be about 0.03 from the comparison with the spin density distribution estimated by the INDO calculation using a phenyl radical as a model compound for pyridine coordinated to nickel.[1d]

References

1) For examples: a) J. A. Happe and R. L. Ward, *J. Chem. Phys.*, **39**, 1211 (1963); b) R. W. Kluiber and W. DeW. Horrocks, Jr., *J. Am. Chem. Soc.*, **88**, 1399 (1966); c) I. Morishima, T. Yonezawa, and K. Goto, *ibid.*, **92**, 6651 (1970); d) W. DeW. Horrocks, Jr., and D. L. Johnston, *Inorg. Chem.* ,**10**, 1835 (1971).

2) The relative ratio of the isotropic shifts for α, β, and γ protons of pyridine was 10 : 4.8 : 1.2 in the system of Ni(sal)$_2$-pyridine at 30°C, but the ratio for the α and β protons in the Ni(5NO$_2$-sal)$_2$-pyridine system was 10 : 19. In the latter case, the isotropic shift of γ proton could not be determined with confidence because of the overlap of its signal with that of the β proton. The ratio reported for the Ni(acac)$_2$-pyridine system is 10.0 : 2.94 : 0.77.[1a]

3) D. F. Evans, *J. Chem. Soc.*, **1959**, 2003.

4) T. J. Swift, "NMR of Paramagnetic Molecules, Principle and Appricatons" ed. by G. N. LaMar, W. DeW. Horrocks, Jr., and R. H. Holm, Academic Press, New York (1973), Chap. 2.

5) Since the line broadening due to the pyridine exchange rection is much larger than the original line width of pyridine or other effects on the line width broadening, the conclusion obtained here is reliable enough in its qualitative meaning, even though the error is estimated to be about 15 — 25% at the maximum in the evaluation of the activation energies for the pyridine exchange reactions.

6) T. J. Swift and R. E. Connick, *J. Chem. Phys.*, **37**, 307 (1962).

7) This value is for 50% dioxan solution and is taken from "Stabilitiy Constants of Metal-Ion Complexes," compiled by L. G. Sillén and A. E. Martell, The Chemical Society, London, Section II (1964), and its supplent No. 1 (1971).

BULLETIN OF THE CHEMICAL SOCIETY OF JAPAN, VOL. 49 (11), 3327—3328 (1976)

Reaction of Mercury(II)–Ethylenediaminetetraacetate–Capriquat Complex with Potassium Iodide in 1,2-Dichloroethane and Its Application to the Spectrophotometric Determination of Mercury(II)

Akira SHIMAZAKI, Masao SUGAWARA, and Tomihito KAMBARA

Department of Chemistry, Faculty of Science, Hokkaido University, Sapporo 060

(Received March 12, 1976)

Synopsis. A mercury(II)–ethylenediaminetetraacetate–methyltrioctylammonium chloride (Capriquat) complex in 1,2-dichloroethane reacts quantitatively with potassium iodide and forms an ion-pair of tetraiodomercurate(II) with a capriquat cation. The composition of the extracted species was determined to be $[Hg(edta)(Cq)_2]$. The reaction was applied to the spectrophotometric determination of mercury(II).

Irving and Al-Jarrah[1] have developed a useful method for separating mercury(II) from many metal ions, based on the extraction of several edta complexes with a methyltrioctylammonium chloride (Aliquat 336) solution in 1,2-dichloroethane.

The spectrophotometric determination of mercury(II) as a tetraiodo complex has been carried out by several authors.[2-4]

In the present work, it is reported that the mercury(II)–edta–methyltrioctylammonium chloride (Capriquat, abbreviated Cq^+Cl^-) complex in the dichloroethane extract reacts quantitatively with potassium iodide forming an ion-pair consisting of a tetraiodomer-curate(II) and a capriquat cation. The present methodhas the advantage that the determination is possible with a part of the extract needed.

Experimental

Reagents. A capriquat solution (0.1 mol dm^{-3}) was prepared by dissolving 12.5 g of capriquat (Dojindo Pharmaceutical Co.) in 250 cm^3 of 1,2-dichloroethane. All other chemicals used were of analytical reagent grade. A stock solution of mercury(II) was prepared from mercury(II) nitrate (Wako Chemicals Co.) and standardized volumetrically.[5] A stock solution of ethylenediaminetetraacetic acid (H_4edta) was prepared from its disodium salts.

A stock solution of potassium iodide (Wako Chemicals Co.) was prepared and stored in a subdued light environment.

Deionized water was used.

Apparatus. A Hitachi 356 two-wavelength and double-beam spectrophotometer and a Shimadzu QV-50 spectrophotometer with 10-mm quartz cells were used for the absorptiometric measurements. An Iwaki Shaker, model KM, was used for the extraction.

Established Procedure. Into a 100-cm^3 separatory funnel were placed an aliquot of a mercury(II) solution containing less than 80 μg, 0.4 cm^3 of a 0.01 mol dm^{-3} Na_2H_2-edta solution and 10 cm^3 of a phosphate buffer solution (pH 7.0) in the sequence. The mixture was diluted to 30 cm^3 with water. After the addition of 20 cm^3 of a 0.01 mol dm^{-3} capriquat solution, two layers were shaken for 10 min and allowed to stand for 10 min. The organic layer was drained into a beaker containing anhydrous sodium sulfate and dehydrated. A 10-cm^3 portion of the extract was placed into another separatory funnel and shaken with 10 cm^3 of a 0.03 mol dm^{-3} potassium iodide solution. The organic layer was transferred into a beaker, dehydrated as above and then subjected to optical measurements.

Results and Discussion

Extraction of the Mercury(II)–edta Complex with a Capriquat Solution. As shown by Irving and Al-Jarrah,[1] the mercury(II)–edta complex in the presence of a 10% excess of Na_2H_2edta is quantitatively extractable in the pH range from 3.5 to 11 by an equal volume of a 0.2 mol dm^{-3} Aliquat 336 solution in dichloroethane.

The results of present investigation, in which the extractability of mercury(II) was determined from the absorbance measurements according to the above procedure, were almost in accordance with those of Irving and Al-Jarrah. However, it is important to note that when the Na_2H_2edta concentration was increased above 0.01 mol dm^{-3}, a decrease in extractability of mercury(II) was observed, probably because of a competitive reaction between the $Hg(edta)^{2-}$ complex and the H_2edta^{2-} ions with the capriquat cations.

The extractability of mercury(II), as determined by repeatedly shaking the separated aqueous layer with a fresh capriquat solution in dichloroethane was found to be 93.3% for a single extraction at as aqueous-to-organic volume ratio of 3 : 2. At volume ratios higher than twice the aqueous layer up to the ratio of the organic layer, the extractability decreased.

Composition of Extracted Species. The distribution ratio D is evaluated to be

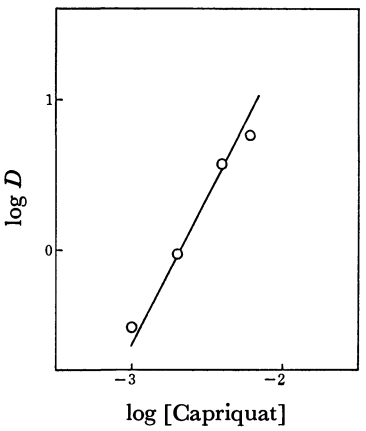

Fig. 1. A plot of log D *vs.* log [Capriquat] at pH 7.01 in the presence of 15 μmol dm^{-3} mercury(II) and 0.13 mmol dm^{-3} Na_2H_2edta.
The straight line was drawn based on the results of the method of least squares.

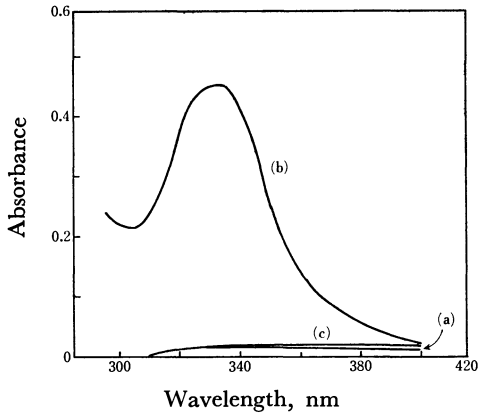

Fig. 2. Absorption spectra of dichloroethane extracts obtained from aqueous media buffered at pH 7.0 and containing 15 μmol dm^{-3} mercury(II) and 0.13 mmol dm^{-3} Na_2H_2edta.
Capriquat concentration in dichloroethane: 0.01 mol dm^{-3}.
a) $(Cq^+)_2[Hg(edta)^{2-}]$ ion-pair *vs.* dichloroethane, b) $(Cq^+)_2(HgI_4^{2-})$ ion-pair obtained by shaking with 0.03 mol dm^{-3} potassium iodide solution *vs.* dichloroethane, c) the reagent blank corresponding to curve (b).

$$D = \frac{(A/\varepsilon)}{C_1 - (A/\varepsilon)} \quad (1)$$

where C_1 is the initial concentration of $Hg(edta)^{2-}$ in the aqueous phase and ε is the molar absorption coefficient of the capriquat tetraiodomercurate(II) ion-pair. In an aqueous medium of pH 7.0 containing a large excess of Na_2H_2edta, mercury(II) exists in the form of $Hg(edta)^{2-}$. Hence, the slope of the plot of log D *vs.* log [Capriquat] should correspond to the molar ratio of the capriquat cation to the $Hg(edta)^{2-}$ anion. As is shown in Fig. 1, the plot has a slope of 1.99, clearly indicating that the composition of the extracted species *is estimated to be* $[Hg(edta)^{2-}(Cq^+)_2]$.

Absorption Spectra of Mercury(II) Complexes. The absorption spectra of the extract obtained according to the above procedure are given in Fig. 2. The ternary complex has an absorption maximum at 333 nm.

Effect of Potassium Iodide Concentration. A 10-cm^3 portion of the separated extract was shaken with an equal volume of an aqueous potassium iodide solution. It was found that a constant and maximum absorbance was obtained for potassium iodide concentration above 0.01 mol dm^{-3}. With various volumes of the potassium iodide solution, it was found that the maximum absorbance was obtained with 5—20 cm^3 of the 0.03 mol dm^{-3} potassium iodide solution.

Calibration Curve. Beer's law was obeyed in the concentration range from 1.1 to 8.8 μg cm^{-3} of Hg(II) in the extract. The molar absorption coefficient is 2.12×10^4 cm^{-1} mol^{-1} dm^3 and the Sandell sensitivity is 9.28×10^{-3} μg Hg(II) per cm^2.

Effect of Diverse Ions. The interference of diverse ions was investigated. Setting the tolerance limit for interfering ions causing an error at ±2.5% for mercury(II) recovery, the results summarized in Table 1 were found.

Table 1. Effect of diverse ions

Mercury(II) taken: 88.8 μg

Interfering ion added	Tolerance limit, mg
Mg(II), Zn(II), NO_3^-, SO_4^{2-}	10
Al(III),[a] Cd(II), Co(II), Fe(II),[a] Mn(II), Pb(II), F^-,[c]	2
Sr(II)	1
Bi(III), Ca(II), Cr(III), Cu(II), Ni(II), Cl^-,[d]	0.5
Ag(I), Sn(II),[b]	0.1

a) Added as alum. b) Added as chloride. c) Added as ammonium salt. d) Added as potassium salt. Other metal ions were added as nitrates and anions as sodium salts.

References

1) H. M. N. H. Irving and R. H. Al-Jarrah, *Anal. Chim. Acta*, **74**, 321 (1975).
2) A. J. Pappas and H. B. Powell, *Anal. Chem.*, **39**, 579 (1967).
3) I. Kressin, *Talanta*, **19**, 197 (1972).
4) C. Merrit, Jr., H. M. Hershenson, and L. B. Rogers, *Anal. Chem.*, **25**, 572 (1953).
5) K. Ueno, "Kirêto Tekiteihô," Nankodo, Tokyo (1960), p. 328.

BULLETIN OF THE CHEMICAL SOCIETY OF JAPAN, VOL. 49 (11), 3329—3330 (1976)

Preparation and Circular Dichroism of Cyanoamminebis[(R)-propylenediamine]cobalt(III) Complexes

Kazuo KASHIWABARA* and Shoichi SUZUKI

Department of Chemistry, Faculty of Science, Tohoku Universisy, Aramaki, Sendai 980

(Received June 7, 1976)

Synopsis. Three new complexes, *trans*-, *cis*-Λ-, and *cis*-Λ-$[Co(CN)(NH_3)(R\text{-}pn)_2]^{2+}$(pn=propylenediamine) were prepared. The geometrical structure was determined on the basis of ^1H NMR spectra. The optical isomers were characterized from the circular dichroism spectra.

The normal character of cyanide as a ligand has been reported in the splitting of the first and second absorption bands of cobalt(III) complexes.[1] A different case was reported [2] in which the splitting of the first absorption band in *trans*-$[Co(CN)_2(NH_3)_4]^+$ is small for the one expected from Yamatera's theory.[3] This indicates that more spectral data are necessary for cyanide complexes.

The circular dichroism (CD) spectra of dicyanobis(diamine)cobalt(III) complexes were discussed in a previous paper.[4] The CD spectra of $[Co(CN)(NH_3)(R\text{-}pn)_2]^{2+}$ complexes are discussed herewith.

Experimental

Preparation and Separation of the Isomers. $[Co(CN)(NH_3)_5]Cl_2$[5] (2g, 8.3mmol) was dissolved in a 50 cm^3 aqueous solution of R-pn(27mmol). The solution was kept at 60—70°C for 3 h with active charcoal (0.5 g). The orange red solution was filtered. The filtrate was cooled to room temperature and poured into a column (2.5 × 50 cm) of a Dowex 50W-X8 (200—400 mesh) ion exchange resin of sodium form. After the column had been washed with water, the adsorbed band was eluted with a 1M aqueous sodium chloride solution at a 15 cm^3/h rate. A small amount of the first light yellow eluate was found to be *cis*-$[Co(CN)_2(R\text{-}pn)_2]^+$ from the visible and ultraviolet absorption spectra.[4] The second orange yellow eluate was concentrated to a small volume at 40°C in a rotary evaporator under reduced pressure. Ethanol was added to the concentrate to precipitate sodium chloride. This was repeated several times in order to remove sodium chloride as far as possible. Finally, the filtrate was passed through a column (2.5×50 cm) of Sephadex LH-20 with an eluent of ethanol-water (4 : 1) for complete removal of the sodium choride. The eluate evaporated to dryness to afford an orange yellow product which was obtained in a *ca.* 100 mg yield. The product (FI) is very soluble in water, but not in organic solvents. Found : C, 22.99 ; H, 7.47 ; N, 24.00%. Calcd for $[Co(CN)(NH_3)(R\text{-}pn)_2]Cl_2\cdot 2H_2O$:C, 23.54; H, 7.62; N, 23.53%.

The third and fourth orange yellow eluates from the Dowex 50W-X8 column were treated in the same way as for the first eluate, orange yellow products FII and FIII, respectively, being obtained. The products are very soluble in water, but not in organic solvents. Yield, *ca.* 150 mg for FII and *ca.* 250 mg for FIII. Found for FII: C, 25.19; H, 7.60; N, 24.35%. Calcd for $[Co(CN)(NH_3)(R\text{-}pn)_2]Cl_2\cdot H_2O$: C, 24.79; H, 7.43; N, 24.78%. Found for FIII: C, 23.67; H, 7.47; N, 24.08%. Calcd for $[Co(CN)(NH_3)(R\text{-}pn)_2]Cl_2\cdot 2H_2O$: C, 23.54; H, 7.62; N, 23.53%.

Another orange band was observed near the top of the column, but was not characterized.

Measurements. The electronic absorption spectra were obtained with a Hitachi 323 recording spectrophotometer. The CD spectra were recorded on a Jasco Model ORD/UV-5 spectropolarimeter and the ^1H NMR spectra on a Varian A-60 spectrometer in deuterium oxide using sodium trimethylsilylpropanesulfonate (DSS) as an internal standard.

Results and Discussion

Three isomers, *trans*(CN-NH_3) and two *cis*(CN-NH_3), are possible for $[Co(CN)(NH_3)(R\text{-}pn)_2]^{2+}$ if the location of the methyl group in the pn chelate is not considered. They were isolated with a Dowex 50W-X8 ion exchange resin. No more isomers due to the location of the methyl group were obtained.

The ^1H NMR spectra of FI exhibits a doublet (J= 5.8 Hz) due to a CH_3 group of R-pn at 1.31 ppm. FII and FIII isomers showed two doublets with J=5.9 Hz and 6.3 Hz at 1.32 and 1.46 ppm, respectively. Thus, we have assigned FI to the *trans*(CN-NH_3) isomer and FII and FIII to the *cis*(CN-NH_3) isomer.

The visible and ultraviolet absorption spectra of FI, FII, and FIII are almost the same as each other and are very similar to the spectrum of $[Co(CN)(NH_3)_5]^{2+}$. The absorption data in the d-d transition region are shown in the Table together with the CD data.

Figure 1 shows the CD spectra of *trans*-$[Co(CN)(NH_3)(R\text{-}pn)_2]^{2+}$ and *trans*-$[Co(CN)_2(R\text{-}pn)_2]^+$ in water. If the electronic state in the complex *trans*-$[Co(CN)(NH_3)(R\text{-}pn)_2]^{2+}$ can be approximated to the C_{4v} form, the two CD peaks in the first absorption band might be assigned to the A_2 and E components. The apparent energy difference of these two peaks (2.9×10^3 cm^{-1}) is smaller than that (3.7×10^3 cm^{-1}) of *trans*-

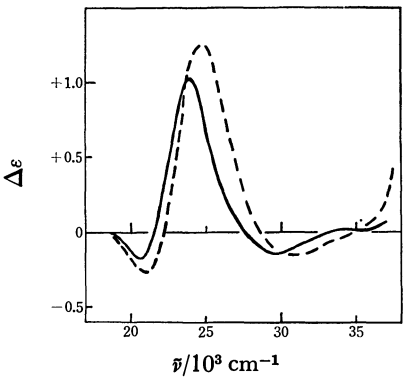

Fig. 1. CD spectra of *trans*-$[Co(CN)(NH_3)(R\text{-}pn)_2]^{2+}$ (——) and *trans*-$[Co(CN)_2(R\text{-}pn)_2]^+$(---) in water.

* Present address: Department of Chemistry, Faculty of Science, Nagoya University, Chikusa, Nagoya 464.

Table 1. Absorption and CD spectral data for $[Co(CN)(NH_3)(R\text{-}pn)_2]^{2+}$ ($\tilde{\nu}$ in 10^3 cm^{-1})

Complex	I Band		II Band	
	$\tilde{\nu}_{max}$ (log ε)	$\tilde{\nu}^{cd}_{ext}$ ($\Delta\varepsilon_{ext}$)	$\tilde{\nu}_{max}$ (log ε)	$\tilde{\nu}^{cd}_{ext}$ ($\Delta\varepsilon_{ext}$)
FI	23.09(1.88)	20.62(−0.19)	31.10(1.90)	29.41(−0.14)
		23.53(+1.05)		
FII	23.04(1.88)	22.99(+1.11)	30.91(1.90)	29.50(−0.08)
FIII	22.94(1.94)	20.83(−0.67)	30.77(1.97)	30.30(−0.11)
		23.64(+0.69)		

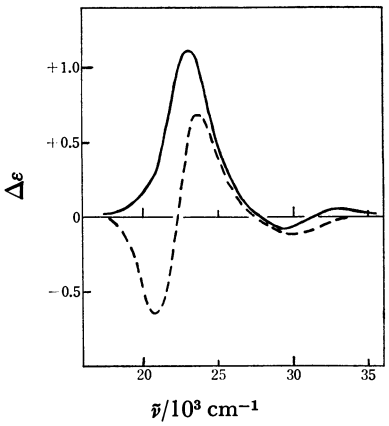

Fig. 2 CD spectra of *cis*-$[Co(CN)(NH_3)(R\text{-}pn)_2]^{2+}$ in water, FII (——) and FIII(- - - -).

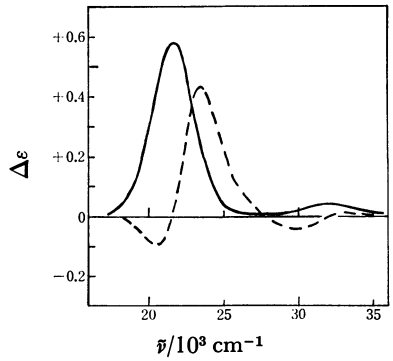

Fig. 3 Calculated configurational (——) and vicinal (- - - -) CD curves of *cis*-$[Co(CN)(NH_3)(R\text{-}pn)_2]^{2+}$.

$[Co(CN)_2(R\text{-}pn)_2]^+$ as expected from Yamatera's theory.

Figure 2 shows the CD spectra of FII and FIII. The CD spectrum of FII gives a very strong positive band in the first absorption band region, suggesting a *Λ* configuration on the basis of the empirical rule.[6] FIII can be assigned to *Δ* isomer although the spectrum shows a negative and a positive band, since the CD spectral patterns of *cis*-$[Co(CN)(NH_3)(R\text{-}pn)_2]^{2+}$ correspond to those of *cis*-*Λ*-$[Co(CN)_2(R\text{-}pn)_2]^+$.[4]

Figure 3 shows the configurational and vicinal curves of *cis*-$[Co(CN)(NH_3)(R\text{-}pn)_2]^{2+}$ which were derived by the method reported previously.[4] The pattern of the derived vicinal CD curves is similar to the observed CD spectrum of FI. The configurational CD curve of FII confirms a *Λ* configuration for the isomer. The spectral pattern of the configurational effect is similar to that of *cis*-$[Co(CN)(NH_3)(en)_2]Br_2$,[7] indicating the validity of the additivity of CD to these complexes.

The encouragement and helpful discussions of Professor Kazuo Saito are gratefully acknowledged.

References

1) K. Ohkawa, J. Hidaka, and Y. Shimura, *Bull. Chem. Soc. Jpn.*, **39**, 1715 (1966).
2) K. Konya, H. Nishikawa, and M. Shibata, *Inorg. Chem.*, **7**, 1165 (1968).
3) H. Yamatera, *Bull. Chem. Soc. Jpn.*, **31**, 95 (1958).
4) K. Kashiwabara, T. Yamanaka, K. Saito, N. Komatsu, N. Harada, H. Nishikawa, and M. Shibata, *Bull. Chem. Soc. Jpn.*, **48**, 3631 (1975).
5) H. Siebert, *Z. Anorg. Allg. Chem.*, **327**, 63 (1964).
6) C. J. Hawkins, "Absolute Configuration of Metal Complexes," Interscience, New York (1971), Chap. 5.
7) K. Ohkawa, J. Hidaka, and Y. Shimura, *Bull. Chem. Soc. Jpn.*, **40**, 2830 (1967).

BULLETIN OF THE CHEMICAL SOCIETY OF JAPAN, VOL. 49 (11), 3331—3332 (1976)

Asymmetric Oxidation of Benzyl *p*-Tolyl Sulfide with Active Halogeno Compounds in the Presence of Optically-Active Alcohols

Yoshiyasu SATO, Norio KUNIEDA, and Masayoshi KINOSHITA

Department of Applied Chemistry, Faculty of Engineering, Osaka City University, Sumiyoshi-ku, Osaka 558

(Received April 12, 1976)

Synopsis. The oxidation of benzyl *p*-tolyl sulfide with active halogeno compounds such as *N*-bromosuccinimide, *N*-chlorosuccinimide and *t*-butyl hypochlorite, affords optically-active benzyl *p*-tolyl sulfoxide. The absolute configuration of the sulfoxide obtained depends on the chirality of the alcohols used.

In previous papers,[1,2] the authors have reported that *N*-bromo-ε-caprolactam (NBC) or *N*-chloro-nylon-66 (NCN-66) oxidizes sulfides to the corresponding sulfoxides in the presence of water or alcohols. During the course of the study of the oxidation, a novel asymmetric induction was found in the presence of optically-active alcohols.[3,4] But the dependence of the absolute configuration of the sulfoxides on the chirality of alcohols used is different for NBC and for NCN-66. Accordingly, in the present note, the asymmetric oxidation of benzyl *p*-tolyl sulfide (I) with various other reagents in the presence of optically-active alcohols is reported.

Experimental

The chemical reagents and procedure are essentially the same as those described previously.[3]

The assignments of the reaction products were performed on the basis of NMR and IR spectra and elemental analysis.

The optical purity of the benzyl *p*-tolyl sulfoxide obtained was calculated from published data: (*R*)-(+)-benzyl *p*-tolyl sulfoxide, $[\alpha]_D$ +252° (acetone).[5]

Results and Discussion

Optically-active benzyl *p*-tolyl sulfoxide was formed by all the active halogeno compounds used in the presence of optically-active alcohols.

In the case of alcohols listed in Table 1, the absolute configuration of I obtained depends on the chirality of the alcohols used.

It is generally assumed that the oxidation of sulfides with active halogeno compounds in the presnece of alcohols results in the formation of alkoxysulfonium salts.[6] And the alkoxysulfonium salts can either form sulfoxides by the elimination of alkyl halides, followed by the retention of the configuration at the sulfur atom,[7] or yield sulfoxides by hydrolysis, followed by an inversion of the configuration.[8]

Thus, the oxidation of I with NBC in the presence of an (*R*)-alcohol forms more of the (*S*)-alkoxysulfonium salt than the (*R*)-alkoxysulfonium salt, and the hydrolysis of a mixture of the salts leads to larger amounts of the corresponding (*R*)-sulfoxide than that of the (*S*)-sulfoxide.

In the case of other oxidation reagents, the predominantly formed (*S*)-alkoxysulfonium salt leads to the corresponding (*S*)-sulfoxide with the elimination of an alkyl halide.

On the other hand, the results using (—)-menthol as the alcohol differ from those described above. As shown in Table 2, the oxidation of I with *N*-halogeno compounds in the presence of (—)-menthol preferentially produces the corresponding (*R*)-sulfoxide, but the oxidation of I with *t*-butyl hypochlorite gives the (*S*)-sulfoxide dominantly. Accordingly, the mechanism for the oxidation of I with *t*-butyl hypochlorite differs from that for the oxidation with *N*-halogeno compounds.

On the basis of these results, it is postulated that the

TABLE 1. ASYMMETRIC OXIDATION OF BENZYL *p*-TOLYL SULFIDE WITH ACTIVE HALOGENO COMPOUNDS IN THE PRESENCE OF OPTICALLY-ACTIVE ALCOHOLS AT −20 °C

Halogeno compound	Alcohol	Solvent	Time (h)	Sulfoxide			
				Yield (%)	$[\alpha]_D$[e] (°)	Opt. yield (%)	Abs. config.
NBC[a]	(*R*)-(−)-2-Octanol	CH_2Cl_2	70	28.0	+1.21	0.48	R
	(*S*)-(+)-2-Octanol	CH_2Cl_2	72	67.4	−0.31	0.12	S
NCN-66[b]	(*R*)-(−)-2-Octanol	Toluene	20	15.4	−2.65	1.05	S
	(*S*)-(+)-2-Octanol	Toluene	20	16.6	+2.98	1.22	R
NCS[c]	(*R*)-(−)-2-Octanol	CH_2Cl_2	20	9.6	−26.18	10.41	S
	(*R*)-(−)-2-Octanol	Toluene	20	8.7	−5.88	2.33	S
	(*S*)-(+)-2-Octanol	CH_2Cl_2	20	14.3	+13.06	5.18	R
	(*S*)-(+)-2-Octanol	Toluene	20	27.9	+0.98	0.39	R
t-BuOCl[d]	(*R*)-(−)-2-Octanol	Toluene	10	14.0	−1.45	0.58	S
	(*S*)-(+)-2-Octanol	Toluene	10	16.2	+1.06	0.42	R
	(*R*)-(−)-Borneol	Toluene	10	5.3	−0.73	0.29	S

a) *N*-Bromo-ε-caprolactam. b) *N*-Chloro-nylon-66. c) *N*-Chlorosuccinimide. d) *t*-Butyl hypochlorite. e) Determined in acetone.

Table 2. Asymmetric oxidation of benzyl *p*-tolyl sulfide in the presence of (*R*)-(−)-menthol at −20 °C

Halogeno compound	Solvent	Time (h)	Sulfoxide			
			Yield (%)	$[\alpha]_D$[c] (°)	Opt. yield (%)	Abs. config.
NBC	CH_2Cl_2[a]	70	47.0	+1.90	0.80	R
	CH_2Cl_2[b]	70	10.6	+0.42	0.17	R
	Toluene[a]	70	5.0	+102.00	41.00	R
	Toluene[b]	70	5.2	+1.43	0.57	R
NCN-66	Toluene[b]	20	20.9	+2.10	0.83	R
NBS	Toluene[b]	20	1.4	+7.57	3.00	R
NCS	Toluene[b]	20	4.6	+1.16	0.46	R
t-BuOCl	Toluene[b]	10	37.6	−2.24	0.89	S

a) Kept at −78 °C before the addition of (*R*)-(−)-menthol. b) Kept at −20 °C before the addition of (*R*)-(−)-menthol. c) Determined in acetone.

oxidation of sulfides with active halogeno compounds in the presence of potically-active alcohols affords the corresponding optically-active sulfoxides. The absolute configuration of the sulfoxides obtained depends on the chirality of the alcohols used, and the oxidation reagents affect the route of oxidation of the sulfides.

References

1) Y. Sato, N. Kunieda, and M. Kinoshita, *Memo. Fac. Eng., Osaka City Univ.*, **15**, 101 (1974).
2) Y. Sato, N. Kunieda, and M. Kinoshita, *Chem. Lett.*, **1972**, 1023.
3) M. Kinoshita, Y. Sato, and N. Kunieda, *Chem. Lett.*, **1974**, 377.
4) Y. Sato, N. Kunieda, and M. Kinoshita, *Makromol. Chem.*, in press.
5) C. J. M. Stirling, *J. Chem. Soc.*, **1963**, 5741.
6) C. R. Johnson, C. C. Bacon, and W. D. Kingsbury, *Tetrahedron Lett.*, **1972**, 501.
7) E. D. Corey, C. U. Kim, and M. Takeda, *Tetrahedron Lett.*, **1972**, 4339.
8) C. R. Johnson and D. McCants, Jr., *J. Am. Chem. Soc.*, **87**, 5404 (1965); C. R. Johnson, *ibid.*, **85**, 1020 (1963); N. J. Leonard and C. R. Johnson, *ibid.*, **84**, 3701 (1962).

BULLETIN OF THE CHEMICAL SOCIETY OF JAPAN, VOL. 49 (11), 3333—3334 (1976)

Heterocycles by Cycloaddition. III.[1] Dihydroisoindolequinone, the Correct Structure of the Proposed Azatetracyclononanedione

Hiroshi MATSUKUBO* and Hiroshi KATO**

Department of Chemistry, Faculty of Science, Shinshu University, Asahi, Matsumoto 390

(Received May 6, 1976)

Synopsis. Pyrolysis of a cyclopentadienequinone–oxazolone adduct (**3**) gives a 5,6-dihydro-4,7-isoindolequinone (**7**) and not an azatetracyclic cage compound (**4**). The dihydroquinone (**7**) was dehydrogenated to the corresponding isoindolequinone (**9**), which was synthesized *via* alternative routes.

The cycloaddition–extrusion of five-membered mesoionic compounds has been utilized for the preparation of a wide variety of heterocyclic systems.[2] The reaction with an olefin usually gives a dihydro heterocyclic compound by migration of a substituent, but with some dipolarophiles, the transient ylide formed by the cycloaddition–extrusion reaction, is trapped by the dipolarophile to give a 1 : 2 adduct.[3] When a dipolarophile has two double bonds within the molecule with a suitable framework, the initially formed ylide can be trapped intramolecularly to give a cage compound. Such cage compounds have been prepared by the reactions of a sydnone with cyclooctadiene[4] and butadienes.[5]

As an extreme case of such a double intramolecular cycloaddition, Myers *et al.*[6] recently claimed the formation of 8-aza-7,9-diphenyl-8-methyltetracyclo-[4.3.0.^{3,9}0^{4,7}]nonane-2,5-dione (**4**) by pyrolysis of 1,3,3a,4,4a,5,8,8a,9,9a-decahydro-5,8-methano-2-methyl-4,9-dioxo-1,3-diphenyl-2*H*-benz[*f*]isoindole-1,3-carbolactone (**3**),[7] the adduct of the mesoionic 3-methyl-2,4-diphenyl-5-oxazolone (**1**) and cyclopentadienequinone (**2**).

The spectral data of the product (**A**), however, do not appear to be in agreement with the proposed structure **4**. For example, the reported infrared carbonyl band of **A** at 1665 cm^{-1} is too low for a strained cyclobutanone system,[8] and the ultraviolet absorption maximum at 308 nm suggests an aromatic or a conjugated chromophor. We thought that these data are more compatible with 5,6-dihydro-2-methyl-1,3-diphenyl-4,7-isoindolequinone (**7**) than with **4**. It was found that the NMR singlet at δ 2.88 disappeared by base-catalyzed treatment of **A** with deuterium oxide. This shows that the carbonyl group of the product **A** is enolizable, and it cannot reconcile with the proposed structure **4**. Dehydrogenation of the product **A** with chloranil gave 2-methyl-1,3-diphenyl-4,7-isoindolequinone (**9**). The structure of the quinone **9** was established by an independent synthesis by pyrolysis of 4,4a,5,8,8a,9-hexahydro-5,8-methano-2-methyl-1,3-diphenyl-2*H*-benz[*f*]isoindole-4,9-dione (**8**),[6] or alternatively, by the cycloaddition–extrusion–dehydrogenation reaction of the mesoionic oxazolone **1** with

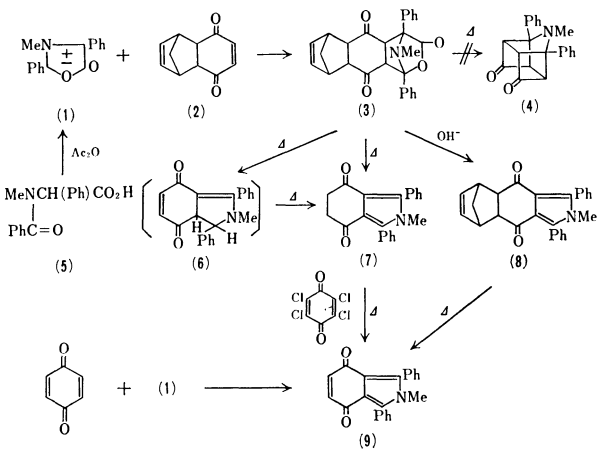

p-benzoquinone.[9]

The above results show that the pyrolysis of the adduct **3** proceeds normally to give the dihydroisoindolequinone (**6**) by extrusion of carbon dioxide and cyclopentadiene, which isomerizes under the reaction conditions to **7** with an aromatic pyrrole ring. The ease and high yields of those reactions, however, should be considered as an indirect and yet an attractive synthetic method of many benzoquinones condensed with a heterocyclic ring, and their dihydro derivatives; because it has been known that the reactions of quinones and five-membered mesoionic compounds always give fully unsaturated systems by dehydrogenation with the quinones present in the reaction system,[9,10] and that the yields of such adducts are sometimes low due to the formation of by-products including the 1 : 2 adduct of benzoquinone and a mesoionic compound. Thus, we isolated **9** only in 8% yield by the reaction of benzoquinone with the mesoionic oxazolone **1**, and the formation in 17% yield of **9** by the same reaction under slightly different (*in situ*?) conditions is reported.[9]

Experimental

Mps were determined on a Yanagimoto hot-stage apparatus and are not corrected. UV and IR spectra were recorded on Hitachi EPS-3T and Hitachi EPI-G3 spectrophotometers. NMR and mass spectra were measured with JEOL JNM-4H-100 (100 MHz) and Hitachi RMU-6 spectrometers.

Cyclopentadienequinone–Oxazolone Adduct (3). This could conveniently be prepared by the *in situ* reaction: A soln of cyclopentadienequinone **2** (10 mmol) and 2-(*N*-methylbenzamido)-2-phenylacetic acid (**5**) (10 mmol) in acetic anhydride (30 ml) was stirred at 55—60 °C for 2 h under nitrogen. The crystals which separated out were collected and washed with benzene to give pure **3** (92%), mp 160—

* Present Address: Okaya Works, Kyorin Pharmaceutical Co., Kohan, Okaya 394.

** To whom inquiries should be addressed.

161 °C (dec) (lit,[6] 158—160 °C). Spectral data were identical with those reported.

Base-Catalyzed Deuteration of Dihydroisoindolequinone (7). A soln of **7** and a small amount of anhyd potassium carbonate in a mixture of dioxane and deuterium oxide was heated under reflux for 1 h. The soln was concd *in vacuo*, the residue was extracted with deuteriochloroform, and the extract was dried ($MgSO_4$) and was used for NMR measurement. The spectral pattern was identical with **7** except that the singlet peak at δ 2.88 disappeared completely.

2-Methyl-1,3-diphenyl-4,7-isoindolequinone (9). *(a)* A soln of **7** (0.2 g; 0.64 mmol) and chloranil (0.19 g; 0.78 mmol) in xylene (10 ml) was refluxed for 4 h. The solvent was removed *in vacuo*, the residue was extracted with chloroform, and the extract was washed with aq sodium hydroxide and water, dried ($MgSO_4$), and concd. The residue was recrystd from methanol to give orange prisms of **9** (0.2 g, 100%), mp 186—187 °C. UV_{max} (MeOH) 229 (log ε 4.42), 276 (4.13), and 418 nm (3.64); IR (KBr) 1655^{sh} and 1646 cm^{-1} (C=O); NMR ($CDCl_3$; TMS) 3.27 (s, 3, Me), 6.50 (s, 2, CH=), and 7.40 ppm (br s, 10, Ph); MS (70 eV; direct inlet) *m/e* (rel intensity) 313 (M^+, 100), 312 (69), and 118 (31). Found: C, 80.22; H, 4.65; N, 4.37%. Calcd for $C_{21}H_{15}NO_2$: C, 80.50; H, 4.83; N, 4.47%.

(b) A suspension of the methanobenz[*f*]isoindoledione **8**[6] (75 mg) in xylene (10 ml) was refluxed for 18 h. The solvent was removed *in vacuo* and the residue was chromatographed (silica gel/chloroform) and recrystd from methanol to give **9** (50 mg, 81%), identical with the specimen prepared by procedure (a).

(c) A soln of *p*-benzoquinone (0.43 g; 4 mmol) and the oxazolone **1** (0.5 g; 2 mmol) in benzene (20 ml) was stirred at room temperature for 3 h under nitrogen, and was then warmed for 3 h at 60 °C. The benzene extract of the reaction mixture was chromatographed (silica gel/chloroform) to give **9** (50 mg, 8%), identical with the specimen prepared by procedure (a).

We are indebted to Kyorin Chemical Laboratories for elemental and mass spectral analyses.

References

1) Part II, H. Kato, S. Nakazawa, T. Kiyosawa, and K. Hirakawa, *J. Chem. Soc., Perkin Trans. I*, **1976**, 672.

2) M. Ohta and H. Kato, "Nonbenzenoid Aromatics," Ed. J. P. Snyder, Academic Press, Vol. 1, New York (1969), p. 117.

3) H. Gotthardt and R. Huisgen, *Chem. Ber.*, **101**, 552 (1968); **103**, 2625 (1970); R. Huisgen, H. Gotthardt, and H. O. Bayer, *ibid.*, **103**, 2368 (1970).

4) P. M. Weintraub, *J. Chem. Soc., Chem. Commun.*, **1970**, 760.

5) A. Haneda, T. Imagawa, and M. Kawanishi, *Bull. Chem. Soc. Jpn.*, **49**, 748 (1976).

6) J. A. Myers, W. W. Wilkerson, and S. L. Council, *J. Org. Chem.*, **40**, 2875 (1975).

7) This is not the first example of cycloadduct of mesoionic 5-oxazolone retaining the lactone moiety as claimed by the authors.[6] For an earlier example, see: T. Shiba and H. Kato, *Bull. Chem. Soc. Jpn.*, **43**, 3941 (1970).

8) *Cf.* the carbonyl absorption of cyclobutanone at 1786 cm^{-1}: C. J. Pouchert, "The Aldrich Library of Infrared Spectra," Aldrich Chemical Co., Milwaukee (1970), p. 197.

9) H. Nagahiro, M. Hamaguchi, and T. Ibata, Abstr. 32nd National Meeting of the Chemical Society of Japan, Tokyo, April 1975, p. 1643.

10) D. L. Hammick and D. J. Voaden, *J. Chem. Soc.*, **1965**, 5871; *Chem. Ind. (London)*, **1956**, 739; H, Brockmann and T. Reschke, *Tetrahedron Lett.*, **1965**, 4593.

BULLETIN OF THE CHEMICAL SOCIETY OF JAPAN, VOL. 49 (11), 3335—3336 (1976)

Carbonylation of Saturated Hydrocarbons Catalyzed by Copper(I) Carbonyls in FSO_3H–Sb_5F

Yoshie Souma and Hiroshi Sano

Government Industrial Research Institute, Osaka Midorigaoka, Ikeda, Osaka 563

(Received May 4, 1976)

Synopsis. Saturated hydrocarbons react with carbon monoxide in the presence of copper(I) carbonyl catalysts in FSO_3H–SbF_5. Tertiary-carboxylic acid and secondary-carboxylic acid were obtained in high yields at −2 to +2 °C and at 1 atm of carbon monoxide. For the isomerization process of intermediate carbonium ions, the cleavage of the C–C bond was recognized, and stable *t*-butyl cations were formed.

Several results on carbonylation catalyzed by copper(I) carbonyl ions have been described in previous papers.[1-5] The copper(I) carbonyl ions play an important role enriching the carbon monoxide concentration in strong acid solutions, and promotes the carbonylation rate to give tertiary-carboxylic acid in a high yield.

Olah has investigated the formation of alkyl cations from alkanes *via* hydride abstraction in FSO_3H–SbF_5, and presented the following equation.[6,7]

$$R_3CH \xrightarrow{FSO_3H\text{-}SbF_5} R_3C^+SbF_5FSO_3^- + H_2$$

Olah has reported that the alkyl cations rearranged to tertiary carbonium ions, and furthermore, stable *t*-butyl cations were formed from hydrocarbons of C_5—C_{16} by the cleavage of the C–C bond.

Paatz has studied the carbonylation of saturated hydrocarbons in HF–SbF_5 solutions, and obtained carboxylic acids and ketones.[8] However, the conversion of saturated hydrocarbons to carbonyl compounds was less than 30%, due to the low solubility of carbon monoxide in strong acids. Suzuki has also studied the carbonylation of 2,2,4-trimethylpentane and alcohol in HF–SbF_5 and obtained carboxylic acid.[9,10]

In this paper, the carbonylation of saturated hydrocarbons catalyzed by copper(I) carbonyl ions to give secondary-carboxylic acids and tertiary-carboxylic acids in high yields is described.

Table 1. The amount of carbon monoxide absorbed by Cu^+ in FSO_3H–SbF_5[a]

Temp °C	Absorbed CO n in $Cu(CO)_n^+$
−45	4.0
−30	4.0
−20	4.0
−10	3.95
0	3.80
10	3.60
20	3.50
30	3.35

a) The amount of absorbed carbon monoxide was measured using 0.858 g of Cu_2O, 20 ml of FSO_3H and 10 ml of SbF_5.

Results and Discussion

Cuprous oxide absorbs carbon monoxide in FSO_3H–SbF_5 solutions to form a homogeneous catalyst solution containing copper(I) carbonyl ions. The amount of absorbed carbon monoxide increases when the temperature is lowered, as is shown in Table 1. In FSO_3H–SbF_5 solutions, $Cu(CO)_4^+$ exists in a mixture in equilibrium with $Cu(CO)^+$. The $\nu_{C=O}$ absorptions of $Cu(CO)_4^+$ and $Cu(CO)^+$ in FSO_3H–SbF_5 solutions were observed at 2183 and 2152 cm^{-1} respectively on the other hand, that of gaseous carbon monoxide occured at 2143 cm^{-1}.[11,12] The $\nu_{C=O}$ absorptions for $Cu(CO)_4^+$ and $Cu(CO)^+$ increased more than that for gaseous carbon monoxide. This indicates that the C–O bonding order becomes higher when the carbon monoxide coordinates to the cuprous ion.

Table 2. Carbonylation of saturated hydrocarbons[a]

Substrate	Product	Yield %
Methylcyclopentane	1-Methylcyclopentanecarboxylic acid	45
	Cyclohexanecarboxylic acid	40
Methylcyclohexane	1-Methylcyclohexanecarboxylic acid	5
	Mixture of methylcyclohexanecarboxylic acid and ethylcyclopentanecarboxylic acid	90
Cyclohexane	Cyclohexanecarboxylic acid	45
Hexane	2,2-Dimethylpentanoic acid	55
	2-Methyl-2-ethylbutanoic acid	35
	2,2-Dimethylbutanoic acid	11
	2,2-Dimethylpropionic acid	17
	Cyclohexanecarboxylic acid	25
2-Methylpentane	2,2-Dimethylpentanoic acid	45
	2-Methyl-2-ethylbutanoic acid	30
2-Methylbutane	2,2-Dimethylbutanoic acid	20
	Mixture of 2,3-dimethylbutanoic acid and 4-methylpentanoic acid	40
Octane	2,2-Dimethylpropionic acid	195
Decane	2,2-Dimethylpropionic acid	102
	2,2-Dimethylbutanoic acid	20
	Mixture of 2-pentanecarboxylic acid and 3-pentanecarboxylic acid	30
	2,2-Dimethylpentanoic acid	30
	2-Methyl-2-ethylbutanoic acid	10

a) The reaction was carried out using 20 ml of FSO_3H, 10 ml of SbF_5, 0.858 g of Cu_2O and 30 mmol of saturated hydrocarbons at −2 to 2 °C for 2 h at 1 atm of CO.

In addition, ^{13}C NMR chemical shifts of $Cu(CO)_4^+$, $Cu(CO)^+$, and CO were observed at 171.1, 169.2, and 181.5 ppm, respectively.[12] The absorptions of $Cu(CO)_4^+$ and $Cu(CO)^+$ were chemically shifted to fields higher than that of gaseous carbon monoxide.

The significance of employing the copper(I) carbonyl catalysts in carbonylation reactions in FSO_3H–SbF_5 is the promotion of the rate of carbonylation, and at the same time, the increase in the yield of carbonylated products. The results are shown in Table 2. The reaction proceeded rapidly for temperatures −2 to 2 °C. Olah has stated that hydride abstraction tends to proceed in the order: primary hydrogen<secondary hydrogen<tertiary hydrogen.[7] The same tendency was observed for the carbonylation listed in Table 2.

Methylcyclopentane gave methylcyclopentanecarboxylic acid and cyclohexanecarboxylic acid.

From hexane, C_5 and C_6 carboxylic acids such as 2,2-dimethylpropionic acid and 2,2-dimethylbutanoic acid were obtained together with C_7 carboxylic acids. This may be due to the formation of tertiary-butyl cations and tertiary pentyl cations by the β-scission of C_6 tertiary carbonium ions.

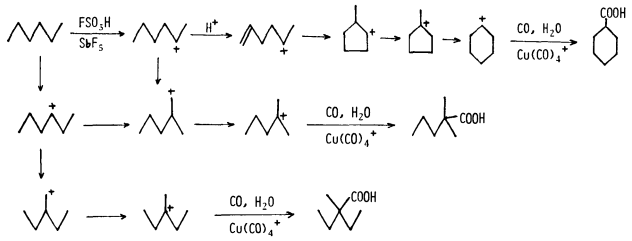

Octane gave only C_5 tertiary carboxylic acid, *i.e.*, 2,2-dimethylpropionic acid. It means that two *t*-butyl cations were formed by the cleavage of a C–C bond of octane.

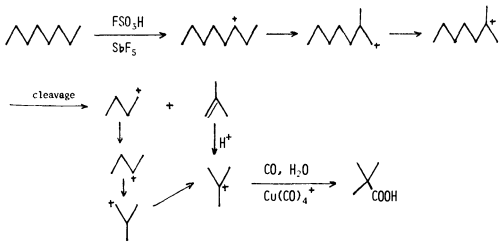

Decane gave 2,2-dimethylpropionic acid as the main product, and at the same time, C_6 tertiary and C_7 tertiary carboxylic acids were obtained. A complicated cleavage of C–C bond appears to occur.

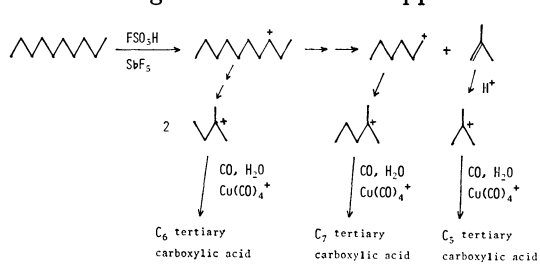

Experimental

The products were separated by preparative GLPC and analyzed by ^1H NMR, ^{13}C NMR, and IR spectroscopy, as described in a previous paper.[1] FSO_3H and SbF_5 were obtained from the Cationic Co.

Preparation of Copper(I) Carbonyl Catalysts. In a 300 ml three-necked flask equipped with a thermometer and a carbon monoxide gas burette, 0.858 g of Cu_2O was placed. The apparatus was evacuated using a rotary pump, and carbon monoxide was introduced from the gas burette. The mixture was stirred vigorously after 20 ml of FSO_3H and 10 ml of SbF_5 had been added. A colorless copper(I) carbonyl solution was formed by the absorption of carbon monoxide by Cu_2O.

Carbonylation of Saturated Hydrocarbons. From a syringe, 30 mmol of saturated hydrocarbons were added dropwise to the catalyst solution at −2 to 2 °C. Immediately carbon monoxide was absorbed. After the reaction was completed, the mixture was poured over ice. The mixture was shaken with hexane, and the total yield of carboxylic acids was determined by titrating the hexane extract with a 1/10 M NaOH ethanol solution. Each product was identified using authetic samples.[1]

References

1) Y. Souma, H. Sano, and J. Iyoda, *J. Org. Chem.*, **38**, 2016 (1973).
2) Y. Souma and H. Sano, *Bull. Chem. Soc. Jpn.*, **46**, 3237 (1973).
3) Y. Souma and H. Sano, *J. Org. Chem.*, **38**, 3633 (1973).
4) Y. Souma and H. Sano, *Bull. Chem. Soc. Jpn.*, **47**, 1717 (1974).
5) N. Yoneda, T. Fukuhara, Y. Takahashi, and A. Suzuki, *Chem. Lett.*, **1974**, 607.
6) G. A. Olah and J. Lukas, *J. Am. Chem. Soc.*, **90**, 933 (1968).
7) G. A. Olah and J. Lukas, *J. Am. Chem. Soc.*, **89**, 4739 (1967).
8) R. Paatz and G. Weisgerber, *Chem. Ber.*, **100**, 984 (1967).
9) Y. Takahashi, N, Tomita, N. Yoneda, and A. Suzuki, presented at the 32nd Annual Meeting of the Chemical, Society of Japan, April 2, 1975, Abstract, p. 1818.
10) Y. Takahashi, N. Tomita, N. Yoneda, and A. Suzuki, presented at the 34th Annual Meeting of the Chemical Society of Japan, April 2, 1976, Abstract, p. 611.
11) K. Nakamoto, "Infrared Spectra of Inorganic and Coordination Compounds," Wiley, New York (1963), p. 72.
12) Y. Souma, J. Iyoda, and H. Sano, *Inorg. Chem.*, **15**, 968 (1976).

BULLETIN OF THE CHEMICAL SOCIETY OF JAPAN, VOL. 49 (11), 3337—3338 (1976)

The ^{13}C NMR Spectra of Several 4-Amino-3-penten-2-ones and Their Palladium Complexes

Yasuhisa SENDA, Akira KASAHARA,* Akio SUZUKI,* and Taeko IZUMI*

Department of Applied Science, Faculty of Engineering, Tohoku University, Aoba, Sendai 980

** Department of Applied Chemistry, Faculty of Engineering, Yamagata University, Yonezawa 992*

(Received May 13, 1976)

Synopsis. A ^{13}C NMR study of several 4-amino-3-penten-2-ones and their palladium chelate complexes is presented. The resonances of the carbonyl carbons of these complexed molecules moved upfield by about 20 ppm relative to the free ligands, while no significant shifts were observed for those of carbons bearing the amino groups.

Three kinds of structures—I, II, and III—are possible for α,β-unsaturated β-amino ketones. In an infrared study a tautomeric equilibrium has been reported to exist between those corresponding to I and II, with the III structure ruled out.[1] Cromwell *et al.*[2] have presented convincing evidence for the II structure in the infrared study of various α,β-unsaturated β-amino ketones. It was also indicated in the ^1H NMR spectra that these tautomers are present predominantly in the II form.[3] We wish to report here a ^{13}C NMR study of several 4-amino-3-penten-2-ones and their palladium chelate complexes.

The natural-abundance 25.15 MHz ^{13}C FT-NMR spectra were obtained using the ^1H noise-decoupling technique. The assignment of the resonances to the specific carbon atoms was made with the aid of ^1H off-resonance experiments. The chemical shifts thus obtained are listed in Tables 1 and 2.

The chemical shifts for the carbonyl carbons of alkyl methyl ketones are usually more than δ; 200.[4] The resonances for the α,β-unsaturated carbonyl carbons move upfield at around δ; 190,[5] while the imino carbons in the II structure are supposed to appear at less than δ; 170.[6] The resonances around δ; 190 are, therefore, assigned to the carbonyl carbons (C-2). The signal at δ; 95.13, which is assigned to the sp^2 hybridized carbon (C-3) of 4-methylamino-3-penten-2-one is split into a doublet in the off-resonance spectra. This evidence suggests that significant portions of these compounds are present in the α,β-unsaturated amino ketone structure, II. The methyl carbon signals (C-1 and C-5) appear separately depending on the structural environments. It has been reported that the methyl carbon resonances of the alkyl methyl ketones usually appear around δ; 28—30,[7] while those of the enol ethers appear around δ; 20.[8] Consequently, the methyl carbon signals at δ; 28.63—29.60 and δ; 18.56—21.90 may correspond to C-1 and C-5 respectively. These assignments are supported by the findings that the signals which are provided by C-5 experience a large upfield shift when the hydrogen on the nitrogen atom is replaced by the methyl group. This shift may be due to the γ-effect between C-5 and the *N*-methyl group. The resonances of the carbonyl carbons of acetylacetone, which is a fifty-fifty mixture of the I and II structures, appear at a field slightly higher than those of the α,β-unsaturated β-amino ketones.

The structures of the palladium complexes are represented as IV or V and VI. The carbonyl carbon resonances of the palladium complexes appear at around δ; 170, at a field about 20 ppm higher than those of the free ligands. The resonances for the methyl carbon next to the carbonyl carbon (C-1) also move upfield, whereas the C-5 resonances move downfield compared with those of the corresponding free ligands. These results indicate the increasing contribution to the enol imine form, V, by the chelate com-

TABLE 1. ^{13}C CHEMICAL SHIFTS OF 4-AMINO-3-PENTEN-2-ONES(δ)[a]

No.	$CH_3\overset{\overset{O}{\|}}{C}CH=\overset{\overset{R}{\|}}{C}CH_3$ (NHR)	C-1	C-2	C-3	C-4	C-5	*N*-substituent
1	H	28.75	196.02	95.37	163.02	21.90	
2	CH_3	28.63	194.26	95.13	164.11	18.56	29.36
3	C_6H_5	29.06	195.84	97.74	159.86	19.65	Subst.-C; 139.05 *o*-C ;(124.67) *m*-C ;(129.10) *p*-C ; 125.46
4	*p*-$NO_2C_6H_4$	29.60	197.84	101.26	157.13	20.56	Subst.-C;(145.36) *o*-C ;(125.16) *m*-C ;(121.76) *p*-C ;(143.38)
5	$CH_3\overset{\overset{O}{\|}}{C}CH_2\overset{\overset{O}{\|}}{C}CH_3$	24.69	191.41	100.53			
		23.7	*191.6*	*100.3*			

a) The values in italics are taken from J. C. Hammel and J. A. S. Smith, *J. Chem. Soc. A*, **1969**, 2883. The values in parentheses may be interchanged.

Table 2. ^{13}C chemical shifts of Pd-complexes of 4-amino-3-penten-2-ones(δ)[a]

No.	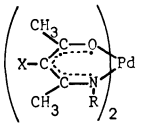 R	X	C-1	C-2	C-3	C-4	C-5	*N*-Substituent
6	H	H	25.66	176.49	96.89	164.84	24.81	
7	H	Cl	27.78	174.36	103.26	164.47	25.84	
8	H	Br	30.76	174.51	103.29	164.34	28.75	
9	CH_3	H	24.14	173.39	99.01	164.17	22.14	36.64
10	$-CH_2$	H	25.29	177.28	98.95	161.74	20.56	55.87
11	$-CH_2$	Cl	27.24	175.32	104.46	162.02	19.77	57.03
12	$-CH_2$	Br	27.82	175.84	103.37	162.10	22.81	57.63
13	C_6H_5	H	23.78	176.18	97.80	162.71	23.47	Subst.-C; 148.70 *o*-C ;(126.07) *m*-C ;(127.77) *p*-C ; 124.55
14	$Pd(acac)_2$		25.29	187.17	101.44			
15	$Rh(acac)_3$		26.57	188.68	99.25			

a) The values in parentheses may be interchanged.

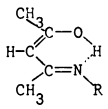

(I)

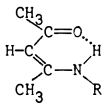

(II)

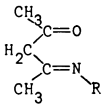

(III)

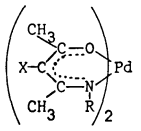

(IV)

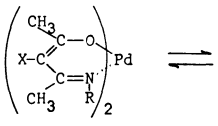

(V) (VI)

plex formation. Similarly to the case of α,β-unsaturated β-amino ketones, the upfield shift of the C-5 resonances was observed upon the replacement of the hydrogen on the nitrogen atom with the methyl, the methylene, or the phenyl groups. When the hydrogen of C-3 is replaced by the halogen, the carbon resonances of the substituents on the nitrogen atoms as well as those of the skeletal carbons usually move downfield, with the exception of those of C-2, which reveal the opposite trend.

Experimental

NMR Spectra. The ^{13}C FT-NMR spectra were obtained at 25.15 MHz with a JEOL JNM-MH-100 instrument equipped with a JNM-MFT-100 Fourier transform accessory; the instrument was controlled with a JEC-6 spectrum computer. Samples were observed in 5-mm spinning tubes at 15±5% solutions in $CDCl_3$ at 28 °C. The solvent provided the internal lock signal. The measurement conditions were as follows: pulse width, 27.5 μs (*ca.* 45°); repetition time, 4 s; spectral width, 6.25 kHz; data point, 8192; acquisition time, 0.65 s. Noise modulated proton decoupling was carried out at a nominal power of 20 W. All the chemical shifts are expressed in δ (ppm downfield from internal Me_4Si). Each observed chemical shift is estimated to be accurate to δ ±0.06.

Materials. The compounds employed in this work have been previously prepared except **5**, which was commercially available; **1**,[9] **2**,[1]**3**,[10]**4**,[10]**6**—**13**,[11] **14**,[12] and **15**.[13]

References

1) H. F. Holtzclaw, J. P. Collman, and R. M. Alire, *J. Am. Chem. Soc.*, **80**, 1100 (1958).
2) N. H. Cromwell, F. A. Miller, A. R. Johnson, R. L. Frank, and D. J. Wallace, *J. Am. Chem. Soc.*, **71**, 3337 (1949).
3) G. O. Dudek and R. H. Holm, *J. Am. Chem. Soc.*, **83**, 2099 (1961).
4) J. B. Stothers and P. C. Lauterbur, *Can. J. Chem.*, **42**, 1563 (1964).
5) D. H. Marr and J. B. Stothers, *Can. J. Chem.*, **43**, 596 (1965); Gurudata and J. B. Stothers, *ibid.*, **47**, 3601 (1969).
6) N. Naulet, M. L. Filleux and G. J. Martin, *Org. Magn. Reson.*, **7**, 326 (1975).
7) L. M. Jackman and D. P. Kelly, *J. Chem. Soc., B*, **1970**, 102.
8) A. C. Rojas and J. K. Crandall, *J. Org. Chem.*, **40**, 2225 (1975).
9) A. Combes and C. Combes, *Bull. Soc. Chim. Fr.*, **7**, 778 (1892).
10) J. P. Collman and E. T. Kittleman, *Inorg. Chem.*, **1**, 499 (1962).
11) A. Kasahara, T. Izumi, K. Sato, and K. Furukawa, *Bull. Yamagata Univ. (Natural Science)*, **8**, 179 (1973).
12) A. A. Grinberg and I. Simonova, *Zhur. Priklad. Khim.*, **26**, 880 (1953).
13) E. P. Dwyer and A. M. Sargeson, *J. Am. Chem. Soc.*, **75**, 984 (1953).

BULLETIN OF THE CHEMICAL SOCIETY OF JAPAN, VOL. 49 (11), 3339—3340 (1976)

Studies on Heterocyclic Chemistry. XX.[1] Photo-reactions of 5-Benzylideneamino-3-arylisoxazoles in Trialkylamine

Tarozaemon NISHIWAKI

Department of Chemistry, Yamaguchi University, Yamaguchi 753

(Received May 31, 1976)

Synopsis. Irradiation of 5-benzylideneamino-3-arylisoxazoles at 254 nm in a mixture of trialkylamine and nitrile gives diaminoethanes (reduction), benzamides (oxidation), and isoxazolo[5,4-*b*]pyridine (cyclization).

From a growing interest in the photo-reactions of organic compounds in amines,[2] studies were carried out on 5-benzylideneamino-3-arylisoxazoles (**1**) which undergo photo-reduction, photo-oxidation, and photo-cyclization in trialkylamine.

Irradiation of **1a** in a mixture of triethylamine and benzonitrile (2:13) at 254 nm afforded *N*,*N*′-bis-(3-phenyl-5-isoxazolyl)-1,2-*p*-anisyl-1,2-ethanediamine (**2a**) and 3-phenyl-6-*p*-anisylisoxazolo[5,4-*b*]pyridine (**3a**) in low yields. The structure of **2a** was confirmed by synthesis, and that of **3a** rests on its spectral data. The high resolution mass spectrum displays M^+ as the base peak and the NMR spectrum two sets of one-proton doublets at δ 8.10 (J=8 Hz) and 8.67 ppm (J=8 Hz) besides methyl and phenyl protons. The β,γ-unsubstituted pyridine structure is established from their J value,[3] the lower-field doublet being assigned to the γ-proton by virtue of its remarkable downfield shift (0.46 ppm) in deuteriotrifluoroacetic acid. Absence of a benzoyl ion in its mass spectrum[4] rules out the corresponding oxazolo[5,4-*b*]pyridine structure. Photolysis of **1b** likewise produced the corresponding **2b** and **3b** in low yields.

Acetonitrile may be used as a solvent, but the reaction is far less clean. Thus, **1a** afforded 3-benzoylamino-6-*p*-anisyl-5,6-dihydro-2(1*H*)-pyridone (**4a**), *N*-(3-phenyl-5-isoxazolyl)-*p*-anisamide (**5a**), *p*-methoxybenzyl alcohol,[5] and 5-amino-3-phenylisoxazole in addition to **2a** and **3a**. The NMR spectrum (see Experimental) and mass spectral fragmentations [major ions: M^+, $Ar^2CH{=}NH_2^+$ (base peak), $Ar^1C{\equiv}O^+$, $(M\text{-}Ar^1CO)^+$, and $(M\text{-}Ar^2CH{=}NH)^+$] of **4a** are consistent with the assigned structure, whereas the structure of **5a** was confirmed by synthesis.

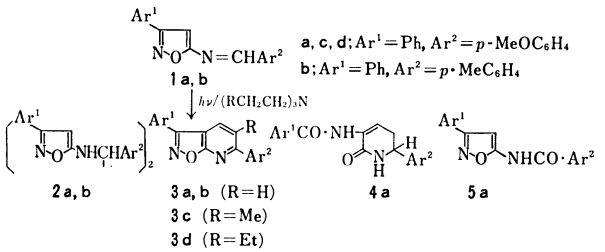

The two carbon fragment at positions 4 and 5 of the isoxazolopyridine ring arises from the amine, as supported by the regioselective formation of the 5-methyl and 5-ethyl derivatives (**3c**) and (**3d**) when **1a** was photolyzed in tripropylamine and tributyamine, respectively. It was found that **3c** and **3d** are obtained again in low yields by photolyzing **1a** in triethylamine in the presence of propionaldehyde and butyraldehyde, respectively.[6] This suggests the intermediacy of an aldehyde in the cyclization step leading to **3**, which may be formed by the photo-oxidation of the amine.[7] Isolation of butyric acid from the photolyzate in tributylamine supports the occurrence of the oxidation of amine.

Besides the occurrence of photo-reduction to **2** and photo-oxidation to **5**, photo-cyclization of **1** to **3**, which bears a marked resemblance to the photo-cyclization of some of the Schiff bases with ethanol,[8,9] is interesting because the related systems (*e.g.*, 5-benzylideneaminopyrazoles and *N*-benzylideneanilines) were photo-unreactive in amine[10] and relatively few studies[11] have been made on the isoxazolo[5,4-*b*] pyridine ring system. Attempts to obtain **3** in a moderate yield were unsuccessful. It may be relevant, however, to note some findings on the conditions to give **3**. Photolysis of a $(2\text{—}3)\times10^{-2}$ mol l^{-1} solution of **1** in a nitrile in the presence of *ca.* 50 molar excess of the amine was found to give **3** in 2—7% yield. Use of a solvent other than a nitrile (*e.g.*, ethanol and tetrahydrofuran) and >300 nm light was ineffective and use of dialkylamine (*e.g.*, diethylamine) slowed down the reaction

Experimental

NMR spectra were measured at 100 MHz using a Varian HA-100 spectrometer. The assignments were confirmed by decoupling techniques when necessary. The light source was a Riko low pressure mercury lamp (30 W) immersed in a quartz well.

*N,N′-Bis(3-aryl-5-isoxazolyl)-1,2-diaryl-1,2-ethanediamines (**2**).* The compounds were prepared in 20—48% yield as described[12] using wet tetrahydrofuran and crystallized from ethanol, for which satisfactory spectral data have been obtained. **2a**: mp 237—238 °C (dec). Found: C, 72.88; H, 5.13; N, 9.87%. Calcd for $C_{34}H_{30}N_4O_4$: C, 73.10; H, 5.41; N, 10.03%. **2b**: mp 260 °C (dec). Found: C, 77.34; H, 6.01; N, 10.75%. Calcd for $C_{34}H_{30}N_4O_2$: C, 77.54; H, 5.74; N, 10.64%.

*N-(3-Phenyl-5-isoxazolyl)-p-anisamide (**5a**).* The compound was prepared in 75% yield by the Schotten-Baumann procedure and crystallized from ethanol, mp 186—187 °C. Found: C, 69.20; H, 4.82%. Calcd for $C_{17}H_{14}N_2O_3$: C, 69.37; H, 4.80%.

Photolysis in Benzonitrile. A mixture of **1**, triethylamine (20 ml), and benzonitrile (130 ml) was irradiated under the conditions given in Table 1. Evaporation *in vacuo* and chromatography[5] of the residue with ether gave **3**, which crystallized from ethanol. **3a**: mp 170—171 °C, NMR (DMSO-d_6): δ 3.88 (s, 3H), 7.10 (d, J=9, 2H), 7.64 (m, 3H), 8.07 (m, 2H), 8.10 (d, J=8, 1H), 8.22 (d, J=9, 2H), 8.67 ppm (d, J=8, 1H); UV (EtOH) λ_{max} (log ε): 243 nm (4.12), 332

(4.43). Found: C, 75.75; H, 4.73; N, 9.42%. Calcd for $C_{19}H_{14}N_2O_2$: C, 75.48; H, 4.67; N, 9.27%. **3b**: mp 170—171 °C, NMR: δ 2.38 (s, 3H), 7.32 (d, J=9, 2H), 7.60 (m, 3H), 8.08 (m, 5H), 8.67 ppm (d, J=8, 1H); UV (EtOH) λ_{max} (log ε): 247 nm (3.96), 320 (4.12). Found: C, 79.56; H, 5.10; N, 9.64%. Calcd for $C_{19}H_{14}N_2O$: C, 79.70; H, 4.93; N, 9.78%. Elution with acetone gave **2**, identical with authentic specimens.

Table 1. Photolysis of **1** in benzonitrile

Compound	Irradiation time: Weight (g)	Irradiation time: h	Products Weights (g)
1a	(0.83)	20	**2a** (0.04) + **3a** (0.02)
2b	(1.00)	7	**2b** (0.12) + **3b** (0.01)

Photolysis in Acetonitrile. (a) A mixture of **1a** (2.78 g), triethylamine (40 ml), and acetonitrile (260 ml) was irradiated for 20 h. Evaporation *in vacuo* and chromatography of the residue with chloroform gave the starting material (0.57 g) and **3a** (0.01 g). GLC of the filtrate revealed the presence of *p*-methoxybenzyl alcohol. Elution with ether–ethyl acetate (5 : 1) gave an oil, which was triturated with ethanol to give an additional amount of **3a** (0.06 g). Evaporation of its filtrate and re-chromatography of the residue with ether–ethyl acetate (5 : 1) gave 5-amino-3-phenylisoxazole (0.10 g) and **5a** (0.10 g), identical with an authentic specimen. Elution with acetone gave **4a** (0.009 g), which was crystallized from ethanol, mp 199—200 °C, NMR: δ 2.70 (m, 2H), 3.72 (s, 3H), 4.64 (t, J=7, 1H), 6.88 (d, J=9, 2H), 7.11 (t, J=4, 1H), 7.28 (d, J=9, 2H), 7.52 (m, 3H), 7.81 (m, 2H), 8.28 (s, exchangeable, 1H), 9.04 ppm (s, exchangeable, 1H). Found: C, 70.97, H, 5.70; N, 8.76%. Calcd for $C_{19}H_{18}N_2O_3$: C, 70.79; H, 5.63; N, 8.69%. TLC of its filtrate revealed the presence of **2a**. (b) A mixture of **1a** (1.00 g), tripropylamine (or tributylamine) (20 ml), and acetonitrile (130 ml) was irradiated for 20 h and worked up as before. Elution with ether gave the corresponding 5-alkylisoxazolopyridines, which crystallized from ethanol. **3c**: mp 192—193 °C, NMR: δ 2.50 (s, 3H), 3.83 (s, 3H), 7.04 (d, J=9, 2H), 7.64 (m, 5H), 8.09 (m, 2H), 8.58 (s, 1H): UV (EtOH) λ_{max} (log ε): 236 nm (4.19), 321 (4.15). Found: C, 76.17; H, 4.96; N, 8.81%. Calcd for $C_{20}H_{16}N_2O_2$: C, 75.93; H, 5.10; N, 8.86%. **3d**: mp 144—145 °C, NMR: δ 1.16 (t, 3H), 2.84 (q, 2H), 3.83 (s, 3H), 7.04 (d, J=9, 2H), 7.53 (d, J=9, 2H), 7.62 (m, 3H), 8.08 (m, 2H), 8.57 ppm (s, 1H); UV (EtOH) λ_{max} (log ε) 234 nm (4.19), 318 (4.08). Found: C, 76.05; H, 5.51; N, 8.66%. Calcd for $C_{21}H_{18}N_2O_2$: C, 76.34; H, 5.49; N, 8.48%. (c) A mixture of **1a** (1.00 g), propionaldehyde (or butyraldehyde) (10 ml), triethylamine (10 ml), and acetonitrile (150 ml) was irradiated for 20 h. Work-up gave the corresponding 5-alkylisoxazolopyridines [**3c** (0.025 g); **3d** (0.046 g)].

References

1) Part XIX of this series: T. Nishiwaki, F. Fujiyama, and E. Minamisono, *J. Chem. Soc., Perkin Trans. 1*, **1974**, 1871.

2) J. A. Barltrop, *Pure Appl. Chem.*, **33**, 179 (1973); S. G. Cohen, A. Parola, and G. H. Parson, *Chem. Rev.*, **73**, 141 (1973).

3) T. J. Batterham, "NMR Spectra of Simple Heterocycles," Wiley, New York (1973), p. 8.

4) J. H. Bowie, P. F. Donaghue, H. J. Rodda, R. Cooks, and D. H. Williams, *Org. Mass Spectrom.*, **1**, 13 (1968).

5) *p*-Anisaldehyde, a photochemical hydrolysis product (*cf.* R. F. Furey and R. O. Kan, *Tetrahedron*, **24**, 3085 (1968)), remained intact during irradiation, but it underwent the Cannizzaro reaction during alumina chromatography (Commercial alumina was used without neutralization throughout this work).

6) Irradiation of **1a** in isobutyraldehyde gave **3a**.

7) R. F. Bartholomew and R. S. Davidson, *J. Chem. Soc., C*, **1971**, 2342.

8) Irradiation of **1** in ethanol or in a mixture of ethanol and acetonitrile gave photochemical hydrolysis products only.

9) P. J. Collin, J. S. Shannon, H. Silberman, S. Sternhell, and G. Sugowdz, *Tetrahedron*, **24**, 3096 (1968).

10) Unpublished work of this Laboratory.

11) T. Denzel and H. Hoehn, *Arch. Pharm. (Weinheim, Ger.)*, **305**, 833 (1972).

12) R. Jaunin, *Helv. Chim. Acta*, **39**, 111 (1956).

BULLETIN OF THE CHEMICAL SOCIETY OF JAPAN, VOL. 49 (11), 3341—3342 (1976)

Sulfoxonium Ylide Chemistry. VI.[1] A Convenient Method for Synthesizing 1-Substituted 4-Phenyl-3-pyrrolin-2-ones

Junya IDE and Yasuo YURA
Central Research Laboratories, Sankyo Co., Ltd., Hiromachi, Shinagawa-ku, Tokyo 140

(Received June 6, 1976)

Synopsis. Synthesis of 1-substituted 4-phenyl-3-pyrrolin-2-ones (**2**) from dimethylsulfoxonium 3-ethoxycarbonyl-2-phenylallylide (**1**) and various primary amines is described.

In the continuation of our studies on sulfoxonium ylide chemistry, we have found a convenient method for synthesizing 1-substituted 4-phenyl-3-pyrrolin-2-ones from dimethylsulfoxonium 3-ethoxycarbonyl-2-phenylallylide (**1**)[2] and primary amines in fairly good yield. There have been only a few reports on the synthesis of substituted 3-pyrrolin-2-ones.[3]

Treatment of ylide **1** with aniline in tetrahydrofuran containing a small amount of 10% HCl under reflux for 3.5 h afforded 1,4-diphenyl-3-pyrrolin-2-one (**2a**) in 75% yield. The structure of **2a** was confirmed with the spectral and elemental analysis data. Its IR spectrum showed bands at 1686, 1629, and 1608 cm^{-1} due to the α,β-unsaturated lactam. In the NMR spectrum of **2a** in $CDCl_3$, methylene protons appeared at δ 4.72 (doublet, J=2 Hz), a vinyl proton at 6.48 (triplet, J=2 Hz) and aromatic protons at 7.5 ppm (multiplet).

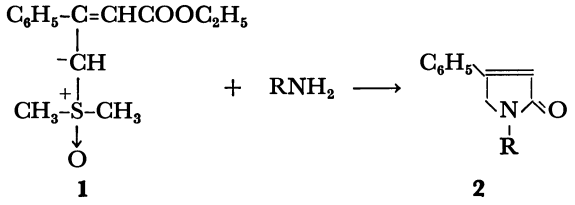

1 **2**

Speckamp *et al.*[3c] reported 1-methyl-4-phenyl-3-pyrrolin-2-one (**3**) and 1-methyl-3-phenyl-3-pyrrolin-2-one (**4**) in which vinyl protons appeared at δ 6.45 and 7.17 ppm, respectively. These data also could support the structure of **2**.

3 **4**

The 1-substituted 4-phenyl-3-pyrrolin-2-ones (**2**) prepared by this method using various primary amines are listed in Table 1.

Experimental

All the melting points are uncorrected. The NMR spectra were recorded on a Varian A-60 instrument, using TMS as the internal standard. The IR spectra were obtained on a Hitachi EPI-G3 spectrophotometer.

General Procedure for Synthesis of 1-Substituted 4-Phenyl-3-pyrrolin-2-one (2). A solution of **1** (5 mmol) and an amine (15 mmol) in 10% HCl (1.6 ml) and THF (20 ml) was heated under reflux for 2—4 h. The reaction mixture was diluted with ether and washed successively with 2% HCl solution, H_2O and sat. NaCl solution, and dried over Na_2SO_4. Evaporation of the solvent *in vacuo* gave a crude product, which was purified by column chromatography on silica gel or recrystallization from ethanol.

1-n-Butyl-4-phenyl-3-pyrrolin-2-one (2h). A solution of **1** (1.33 g) and butylamine (1.09 g) in 10% HCl (1.6 ml) and THF (20 ml) was heated under reflux for 3.5 h. The reaction mixture was diluted with ether (100 ml) and successively washed with 2% HCl solution, H_2O and sat. NaCl solution, and dried over Na_2SO_4. Evaporation of the solvent gave 1.19 g of an oily residue, which was chromatographed on silica gel (10 g) to afford 380 mg of **2h** (35% yield) by eluting with benzene.

1-Allyl-4-phenyl-3-pyrrolin-2-one (2j). A solution of **1** (1.33 g) and allylamine (855 mg) in 10% HCl (1.6 ml) and THF (20 ml) was heated under reflux for 3.5 h. The reaction mixture was treated as described above to give 1.02 g of an

TABLE 1. 1-SUBSTITUTED 4-PHENYL-3-PYRROLIN-2-ONE (**2**)

R	NMR (δ)[a]		IR[b] (cm^{-1})	Mp (°C)	Yield[c] (%)	Obsd (%)			Calcd (%)		
	3H	4H				C	H	N	C	H	N
2a; C_6H_5	6.48	4.72	1684	168—169	85	81.45	5.50	5.98	81.68	5.57	5.95
2b; *p*-$CH_3C_6H_4$	6.48	4.64	1667	156—157	90	82.11	6.31	5.47	81.90	6.06	5.62
2c; *p*-$CH_3OC_6H_4$	6.51	4.72	1670	153—154	75	77.01	5.80	5.29	76.96	5.70	5.28
2d; *p*-ClC_6H_4	6.51	4.73	1672	191—192	67	71.18	4.45	5.23	71.24	4.49	5.19
2e; *p*-BrC_6H_4	6.50	4.47	1672	202—203	70	61.19	3.71	4.51	61.16	3.85	4.46
2f; *m*-$CF_3C_6H_4$	6.52	4.78	1698	152—153	73	67.51	4.01	4.59	67.32	3.99	4.62
2g; $C_6H_5CH_2$	6.46	4.22	1670	158—159	58	81.83	6.02	5.81	81.90	6.06	5.62
2h; *n*-C_4H_9	6.43	4.34	1680	oil	35	78.21	7.90	6.60	78.10	7.96	6.51
2i; Cyclohexyl	6.42	4.30	1664	95— 96	50	79.48	7.89	5.98	79.63	7.94	5.80
2j; CH_2=$CHCH_2$	6.45	4.32	1680	oil	39	78.51	6.49	7.00	78.36	6.58	7.03

a) In deuteriochloroform. b) In Nujol for crystals and in liquid film for oils. c) Not optimized.

oily residue, which was chromatographed on silica gel (10 g) to afford 390 mg of **2j** (39% yield).

The authors thank Director Dr. K. Arima, Assistant Director Dr. Y. Kishida and former Assistant Director Dr. K. Tanabe of this Laboratories for their valuable help and advice.

References

1) Sulfoxonium Ylide Chemistry. V: J. Ide, and Y. Yura, *Tetrahedron Lett.*, **1968**, 3491.

2) a) J. Ide, and Y. Kishida, *Tetrahedron Lett.*, **1966**, 1787; b) J. Ide and Y. Kishida, *Chem. Pharm. Bull.*, **16**, 784 (1968).

3) a) Von H. Plieninger and M. Decker, *Ann.*, **598**, 198 (1956); b) Von H. Plieninger and J. Kurze, *ibid.*, **680**, 60 (1964); c) J. B. Wijnberg, W. N. Speckamp, and H. E. Schoemaker, *Tetrahedron Lett.*, **1974**, 4073; d) R. Sarges and J. R. Treffer, *J. Org. Chem.*, **39**, 1710 (1974); e) G. Stork and R. Mattews, *Chem. Commun.*, **1970**, 445.

BULLETIN OF THE CHEMICAL SOCIETY OF JAPAN, VOL. 49 (11), 3343—3344 (1976)

Luminescence of Pyridinols and Related Molecules

Ko KIMURA and Ryo NAGAI

Department of Chemistry, Faculty of Science, Osaka City University, Sumiyoshi-ku, Osaka 558

(Received March 24, 1976)

Synopsis. Quantum yields of fluorescence and phosphorescence together with lifetimes at 77 K suggest that 2-pyridinol exists in the keto form in the excited states as well as in the ground state, and the lowest excited singlet and triplet states for 2-, 3-pyridinol, 2-methoxypyridine, and *N*-methyl-2-pyridone are ($\pi\pi^*$) states. The lowest triplet state for 4-pyridinol takes the keto form, and is assigned to ($\pi\pi^*$).

Studies on tautomerism of pyridinols in the ground state carried out by Mason and others[1] show that 2- and 4-pyridinol exist as the tautomeric pyridones in aqueous solutions, whereas 3-pyridinol exists as an equilibrium mixture of the enol and keto form in the same solvent. Closely related compounds such as 2-methoxypyridine and *N*-methyl-2-pyridone correspond to the enol and keto forms of 2-pyridinol, respectively. Quantum yields of fluorescence Φ_f and phosphorescence Φ_p for these compounds in an alcohol (ethanol containing 10% methanol) mixture (A), an acidic (1 N sulfuric acid) alcohol mixture (H^+), and an alcohol mixture containing 0.1 N sodium hydroxide (B) at 77 K and at 300 K are given in Table 1, together with lifetimes of fluorescence τ_f and phosphorescence τ_p. Temperature dependence and/or protonation effect of Φ_f's, which are characteristic of some nitrogen heterocyclics, clearly show the contribution of the close $^1(n\pi^*)$ or $^3(n\pi^*)$ state in energy[2] to radiative and/or radiationless transitions from the lowest excited singlet state. The lowest excited singlet and triplet states for 2-pyridinol and its derivatives in protic solvents are assigned to ($\pi\pi^*$) from ϕ_f's and τ_p's. Fluorescence spectra of 2-pyridinol do not resemble those of 2-methoxypyridine. From a comparison of these spectra and quantum yields it is evident that 2-pyridinol takes the keto form (pyridone) even in the excited state just as in the ground state.

The temperature dependence and protonation effect of Φ_f's and Φ_p's for 3-pyridinol closely resemble those for 2-methoxypyridine. In solvent (B), the formation of the 3-pyridinolate anion[3] may partly be responsible for the temperature independence of Φ_f's. These observations together with τ_p's suggest that 3-pyridinol takes the enol form in the excited state in the solvents

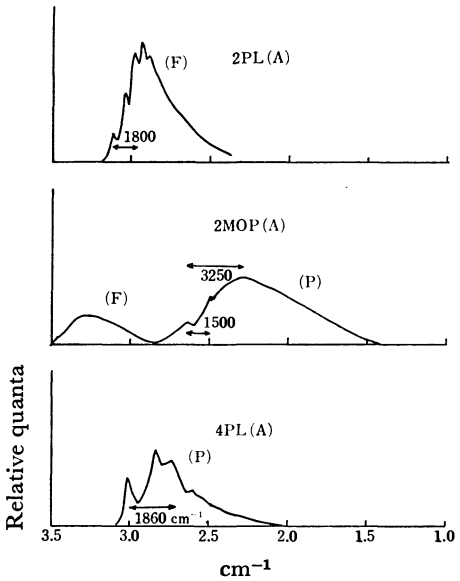

Fig. 1. Fluorescence (F) and phosphorescence (P) spectra at 77 K.

TABLE 1. QUANTUM YIELDS AND LIFETIMES OF FLUORESCENCE AND PHOSPHORESCENCE FOR PYRIDINOLS AND RELATED MOLECULES

	300 K		77 K							
	$\lambda_{f\,max}$ (nm)	Φ_f	$\lambda_{f\,max}$ (nm)	Φ_f	τ_f (ns)	$\lambda_{p\,max}$ (nm)	Φ_p	τ_p (s)	$k_f\times10^{-7}$ (s^{-1})	$k_{nr}\times10^{-7}$ (s^{-1})
2PL(H^+)	364	0.014	337	0.33	5.6	449	0.05	1.29	5.9	12
(A)	365	0.009	344	0.54	8.5	476	<0.005	0.39	6.4	5.4
(B)	351	0.10	328	0.16	4.9	444	0.26	0.91	3.3	17
2MOP(H^+)	317	0.008	309	0.14	1.3*	417	0.19	2.65		
(A)	303	0.014	295	0.06	0.9*	430	0.17	1.34		
NM2P(H^+)	357	0.009	335	0.31	8.4	444	0.08	1.44	3.7	8.2
(A)	364	0.006	342	0.53	10.6	476	<0.005	0.6	5.0	4.4
3PL(H^+)			317	0.18	9.1	476	0.04	0.84	2.0	9.0
(A)	306	0.009	306	0.06	1.1*	417	0.22	1.68		
(B)	357	0.06	326	0.06	1.2*	449	0.34	0.92		

2PL, 2MOP, NM2P, and 3PL are abbreviations for 2-pyridinol, 2-methoxypyridine, *N*-methyl-2-pyridone, and 3-pyridinol, respectively. The symbol * means the calculated lifetimes obtained from integrations of absorption and fluorescence spectra together with the observed Φ_f's.[8]

The character k_f and k_{nr} are transition rates of fluorescence and radiationless processes from the lowest excited singlet state, respectively.

used in this work, and that the lowest excited singlet and triplet states are assigned to ($\pi\pi^*$).

Φ_f's and Φ_p's for 4-pyridinol at 77 K are smaller than 0.01 irrespective of solvents, except Φ_p in solvent (A), in which Φ_p is 0.15. τ_p's for 4-pyridinol at 77 K vary from 0.3 to 1 s, depending on solvents. The phosphorescence spectra for 4-pyridinol in solvent (A) show the well defined vibrational structure, in which a characteristic vibration indicative of the keto form may be found,[4] as in the fluorescence spectra for 2-pyridinol in the same solvent. These observations lead to the conclusion that 4-pyridinol takes the keto form in the lowest triplet state which is assigned to ($\pi\pi^*$). Calculations[2] suggest the ($n\pi^*$) assignment for the lowest excited singlet state of 4-pyridinol in the keto and enol forms, but it is difficult to make conclusive assignment from observation of the small Φ_f values only.

Experimental

2-, 3-, and 4-pyridinol were recrystallized five times from ethanol and/or acetone, then purified by zone melting, and finally sublimed *in vacuo*. 2-methoxypyridine and *N*-methyl-2-pyridone were distilled through a spinning band column at reduced pressure, then purified through a basic alumina column, and finally distilled *in vacuo*. Ethanol (Wako pure chemicals, analytical grade) was refluxed over silver nitrate and potassium hydroxide, and then distilled through a glass packed column. Methanol (Wako pure chemicals, analytical grade) was distilled through a glass packed column. Sulfuric acid and sodium hydroxide were of analytical grade (Wako pure chemicals and Yashima chemicals, respectively).

Φ_f's and/or Φ_p's for luminescence were determined by comparison with those of quinine hydrogensulfate (5×10^{-3} M, $\Phi_f=0.51$ at 300 K),[5] and not corrected for change in refractive indices of solvents. The optical arrangement used in measurements of Φ_f's and Φ_p's was of surface type, which allows for the exciting light to be absorbed completely through the first 1—2 mm optical path (concentration 10^{-2}—5×10^{-4} M). The concentration quenching was negligibly small for these molecules, as is estimated by Stern-Volmer's plot (not given). The sensitivity correction of the combination of monochromator with photomultiplier was made with the use of a standard lamp.[6] The lifetime measurements for fluorescence were carried out by the stroboscopic technique,[7] and those for phosphorescence with a Tektronix 454A oscilloscope with manually operated shutter. Concentrations used in lifetime measurements were 10^{-4}—10^{-5} M. All the samples were evacuated by repeated cycles of freezing, pumping, and thawing. The sample cells were then sealed off from the evacuation system.

References

1) S. F. Mason, *J. Chem. Soc.*, **1958**, 674; H. Specker and H. Gawrosch, *Ber.*, **75**, 1338 (1942).
2) R. Nagai and K. Kimura, unpublished work of CNDO/S calculations for substituted pyridines.
3) E. Spinner, *J. Chem. Soc.*, **1960**, 1232.
4) J. A. Gibson, W. Kynaston, and A. S. Lindsey, *J. Chem. Soc.*, **1955**, 4340; F. Ramirez and A. P. Paul, *J. Am. Chem. Soc.*, **77**, 1035 (1955).
5) W. H. Melhuish, *J. Phys. Chem.*, **64**, 762 (1960); **65**, 229 (1961).
6) R. Stair, W. E. Schneider, and J. K. Jackson, *Appl. Opt.*, **2**, 1151 (1963).
7) R. G. Bennett, *Rev. Sci. Instrum.*, **31**, 1275 (1960).
8) S. J. Strickler and R. A. Berg, *J. Chem. Phys.*, **37**, 814 (1962).

BULLETIN OF THE CHEMICAL SOCIETY OF JAPAN, VOL. 49 (11), 3345—3346 (1976)

Phase Diagram of the Pyrene-Picryl Chloride System

Masaki BANDO and Yoshio MATSUNAGA*

Department of Chemistry, Faculty of Science, Hokkaido University, Sapporo 060

(Received June 19, 1976)

Synopsis. A differential scanning calorimetric study of the pyrene–picryl chloride system has revealed five molecular compounds with mole ratios of 1: 1, 4: 3, 2: 1, 3: 1, and 4: 1 respectively.

Most molecular compounds are equimolar in composition. Therefore, the phase diagrams of organic binary systems are generally simple. The pyrene-pyromellitic dianhydride system which forms three molecular compounds with ratios of 3: 1 or 2: 1, 1: 1, and 1: 3 respectively is known to be rather exceptional.[1] Such simplicity may be characteristic of organic systems but may be, at least in part, connected with the thaw-point-melting-point method employed in the determination of phase diagrams.[2] While solid–liquid equilibria give valuable information regarding the state of a system within the temperature limits of the diagram, the information obtained does not necessarily remain valid at lower temperatures. When solid-solid transitions, if any, are included in the examinations, the phase relations might be more complicated than previously reported. Studies of the anthracene–carbazole and naphthalene–2-naphthol systems made by Robinson and Scott seem to support such a postulate; however, neither of the systems gives a molecular compound.[3,4] The pyrene–picryl chloride system, which has been reported to form only an equimolar compound,[5] has been studied as our first choice along this line because of the following reasons. First, a solid-solid transition is known to occur in the molecular compound near 80 °C.[6] Secondly, the closely-related pyrene-picryl bromide system has been found to form two compounds with ratios of 1: 1 and 3: 2 respectively.[7]

Samples were prepared by melting mixtures with known ratios of the parent compounds. The composition is quoted in the mole percentage of the hydrocarbon. The melting points and transition temperatures were determined using a Rigaku Denki differential scanning calorimeter, Model 8001 SL/C. X-Ray measurements on powdered samples were made at room temperature with a Toshiba recording diffractometer, Model ADG-301, using filtered copper radiation.

As is shown in Fig. 1, the phase relations in the region from 0 to 50 mol % are simple. A eutectic occurs at 12 mol % and 75 °C; these values are to be compared with 8 mol % and 73.5 °C reported by Shinomiya.[5] All the samples in the region from this point to 50 mol % show an endothermic peak due to the appearance of the liquid phase and also one at 81 °C due to a solid-solid transition in the equimolar molecular compound. Four more distinct compounds are formed in the region from 50 to 80 mol %. If the 1: 1 molecular compound melting at 154 °C were the only compound formed in this system, the endothermic peak due to the transition should be observed in the entire region from 50 to 100 mol %. As a matter of fact, the peak is observable only up to 57 mol %. Between 58 and 75 mol %, a new endothermic peak appears at 82—83 °C. Above 67 mol % an additional peak is found at 77 °C. This disappears by 80 mol %. These observations lead to the conclusion that the peak at 82—83 °C is due to a solid-solid transition in the 2: 1 compound (66.7 mol %) and that at 77 °C is due to a solid-solid transition in the 3: 1 compound (75 mol %). Two more phase boundaries are located at 57—58 mol % and at 80 mol % respectively, on the basis of the discontinuity of the transitions. These compositions correspond to molecular compounds with ratios of 4: 3 and 4: 1. Neither of them show solid-solid transitions near 80 °C.

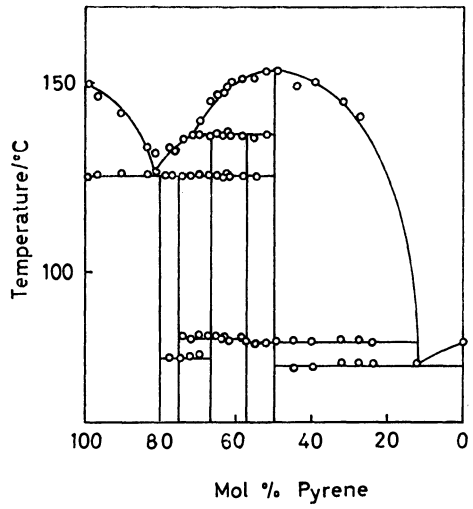

Fig. 1. The pyrene–picryl chloride phase diagram.

Turning to the solid-liquid equilibria in the region from 50 to 100 mol %, we see that only the equimolar molecular compound melts congruently. All the other four cease to be stable before their congruent melting points are reached. In the equilibrium diagram a eutectic point is cleary observed at about 81 mol % and 126 °C, and a peritectic point at about 71 mol % and 136 °C. It is evident that a eutectic conglomerate of pyrene and the 4: 1 molecular compound coexist in contact with the liquid at the former point. Shinomiya has assumed the eutectic point to be at 77 mol % and 125 °C.[5] Because of the formation of the 4: 1 compound this point cannot be at such a low percentage of the hydrocarbon. By visual examination, the thaw point in the region from 58 to 66 mol % was located not at 126 °C but at 136 °C; therefore, the molecular compound which undergoes decomposition into another compound and the liquid at the latter point was identified as the 2: 1 compound. The incongruent melting

* To whom inquiries may be addressed.

points of the 4: 1 and 3: 1 compounds are supposed to be slightly higher than the eutectic, but they are practically not distinguishable from each other. The endothermic peak observed at about 126 °C in the region from 50 to 66 mol % is nearly at the eutectic temperature. However, this must be attributed to a solid-solid transition in the 4: 3 compound, since the peak is not accompanied with liquefaction. This molecular compound also melts incongruently. Its peritectic point is located presumably very close to that of the 2: 1 compound. This conclusion is in accordance with Shinomiya's finding that the formation of liquid occurred at 135 °C in his 57.4 mol % sample.[5] If this observation was seriously taken into consideration, he could easily find the peritectic point in this system. Nevertheless, it should be emphasized that only two molecular compounds among the five may be found using the thaw-point-melting-point method.

The differences in the X-ray diffraction patterns between the equimolar molecular compound and the other four are appreciable. The crystal data of the 1: 1 compound have been determined by Herbstein and Kaftory.[8] The peak with a spacing of $a \sin\beta = 17.13$ Å is seen only in this compound. On the other hand, a spacing of about 10.6 Å, which is absent in the 1: 1 compound, is the longest in all the other compounds. The patterns of the compounds with stoichiometries other than 1: 1 are not very different from each other; however, the observed minor but definite difference is consistent with the existence of distinct compounds. The crystal structure of the stable red prisms of 3 pyrene: 2 picryl bromide has been described in terms of equimolar mixed stacks with alternating pyrene and picryl bromide molecules and interstial pyrene molecules steeply inclined to the stack axis.[7] It is likely that the hydrocarbon in the new phases of the present system also fills two different structural roles.

The authors wish to express their thanks to Professor Toshio Yokokawa for letting them use the X-ray diffractometer.

References

1) F. H. Herbstein and J. A. Snyman, *Phil. Trans. Roy. Soc. London*, **A 264**, 635 (1969).
2) H. Rheinboldt, *J. Prakt. Chem.* (2), **111**, 242 (1925).
3) P. M. Robinson and H. G. Scott, *Mol. Cryst. Liq. Cryst.*, **5**, 387 (1969).
4) P. M. Robinson and H. G. Scott, *Mol. Cryst. Liq. Cryst.*, **18**, 143 (1972).
5) C. Shinomiya, *Bull. Chem. Soc. Jpn.*, **15**, 259 (1940).
6) N. Inoue and Y. Matsunaga, unpublished work.
7) F. H. Herbstein and M. Kaftory, *Acta Crystallogr.*, **B 31**, 45 (1975).
8) F. H. Herbstein and M. Kaftory, *Acta Crystallogr.*, **B 31**, 60 (1975).

BULLETIN OF THE CHEMICAL SOCIETY OF JAPAN, VOL. 49 (11), 3347—3348 (1976)

Charge-carrier Drift Mobility in Pyrene Single Crystals

Akira SUZUKI, Hiroo INOKUCHI,* and Yusei MARUYAMA**

The Institute for Solid State Physics, The University of Tokyo, Roppongi, Minato-ku, Tokyo 106
***Department of Chemistry, Ochanomizu University, Otsuka, Bunkyo-ku, Tokyo 112*

(Received July 12, 1976)

Synopsis. The charge-carrier drift mobility in highly pure pyrene single crystals was measured. Observed values were $(3.8\pm0.1)\times10^{-3}$ cm^2 V^{-1} s^{-1} for electrons and $(3.3\pm0.4)\times10^{-3}$ cm^2 V^{-1} s^{-1} for holes at 345 K. The mobilities increased with the temperature between 333—374 K with an activation energy of 0.43 ± 0.01 eV for electrons.

Measurements of charge-carrier drift mobility in organic crystals have given the most important information in the studies of their electrical conduction processes. A few years ago, we observed rather small carrier mobilities in perylene single crystals and analyzed the obtained results taking the excimer-like excess electron state into consideration.[1)]

In this note, we will report the behavior of carrier drift mobility in pyrene single crystals in which the "dimeric structure" in an unit cell is also realized and in which its effect results in a pronounced excimer emission. In order to confirm the hypothetical transport model based on the "dimeric structure" in a perylene crystal,[1)] a similar type of measurement should be done using a dimeric pyrene crystal.

Highly pure pyrene was obtained by a careful zone-refining technique after conventional chemical and physical treatments. A single crystal ingot was grown using a pulling-down method in a Bridgman furnace from which disk-like, single crystals were carefully cleavaged out in a size of ≈10 mm $\times10$ mm $\times0.5$ mm (in thickness). Electron and hole drift mobility in the c'-direction were measured using the previously reported measuring system,[1)] but with the air-gap-discharge light pulser replaced by a xenon flash tube (Ushio Denki) as an exciting light source. Since the photocurrent sensitivity was not high enough at room temperature, the drift mobilities were observed in the temperature range of 333—374 K.

The typical photocurrent pulses observed are shown in Fig. 1 under the conditions specified in the caption. The observed electron or hole mobility was almost independent of the electric field between 1×10^4—2×10^4 V cm^{-1}, the mean value in the c'-direction was $(3.8\pm0.1)\times10^{-3}$ cm^2 V^{-1} s^{-1} for electrons and $(3.3\pm0.4)\times10^{-3}$ cm^2 V^{-1} s^{-1} for holes at 345 K. These

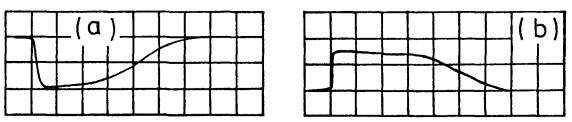

Fig. 1. Typical photocurrent *vs.* time curves.
(a) Electron current, (b) hole current, at 345 K, 0.2 ms/division (abscissa).

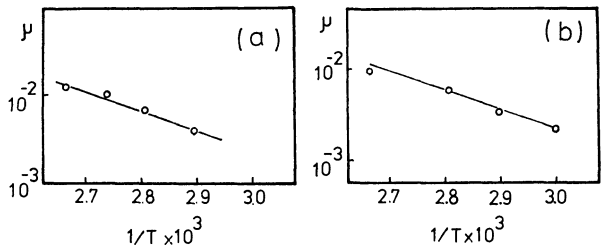

Fig. 2. Temperature dependence of drift mobility.
(a) Electron, (b) hole.

values are smaller by about one order than those in a perylene crystal.[1)] The electron mobility increased with the temperature between 345—374 K. Plots of the logarithm of the mobility *vs.* T^{-1} in Fig. 2 show an almost straight line of 0.4 eV in this temperature range. The hole mobility also showed a similar temperature dependence.

In order to elucidate the experimentally obtained characteristic of the electron drift mobility in the c'-direction, we display the relevant transfer integral values in Table 2, comparing them with the corresponding ones in a perylene crystal[1)] and an anthracene crystal.[3)]

TABLE 2. A COMPARISON OF THE ELECTRON-TRANSFER INTEGRALS IN THE c'-DIRECTION IN A PYRENE CRYSTAL WITH THOSE IN A PERYLENE OR AN ANTHRACENE CRYSTAL IN UNITS OF 10^{-4} eV

Molecule-pairs	Pyrene	Perylene	Anthracene
1— 8	74.3	3.57	0.38
1—11	— 0.60	0.84	0.67
1—13	—13.4	0.13	0.38

The physical situation in a pyrene crystal seems to be qualitatively similar to the case of perylene when we compare the values indicatied in Table 2 with the observed mobility. In the pyrene crystal, an excess electron on a dimeric point may be somewhile localized. through the formation of an excimer-like electronic state between two molecules. The excimer state in pyrene crystals is known to be located 0.4 eV below the mutually independent molecular lowest excited state.[4)] The relative displacement between dimeric molecules due to an excimer formation was estimated by Birks to be ~0.2 A.[4)] These two effects may cause the fluctuation in the transfer integrals and also the activation process in the electron-transport procedure. This type of fluctuation should be significant in determining the drift mobility value in this case.

The drift behavior of the charge carriers in organic

* Present address: Institute for Molecular Science, Okazaki-shi, Aichi 444.

molecular crystals may be determined mainly by means of the intermolecular resonance integrals or transfer integrals, which can be evaluated from the molecular wavefunctions, taking the crystal structure into consideration. The crystal structure of pyrene was analyzed by Robertson and White.[2]

The transfer integrals for each pair of molecules in a pyrene crystal were calculated using Hückel-type molecular orbitals, in which a single Slater orbital exponent, 3.08×10^8 cm^{-1}, was employed. Only the two center integrals were considered, the other procedures in the calculation were almost the same as those reported by Katz *et al.*[3]

In Table 1 we display the transfer integrals calculated between the molecule at Position 1 and the several neighboring molecules, the numbering of which is shown in Fig. 3. The same formalism as that shown in Ref. 1 will lead to the drift mobility in the c'-direction, 1.4×10^{-4} cm^2 V^{-1} s^{-1} at 345 K, using the formulae deduced by Gosar and Choi[5] and the activation energy of 0.44 eV.

Although the agreement between the calculated value, 1.4×10^{-4} cm^2 V^{-1} s^{-1}, and the observed value, 3.9×10^{-3} cm^2 V^{-1} s^{-1}, at 345 K is not so good as in the perylene crystal (0.015 cm^2 V^{-1} s^{-1} and 0.017 cm^2 V^{-1} s^{-1} respectively), the validity of the proposed electron-transfer mechanism may seem to be confirmed.

Table 1. Intermolecule transfer integrals in units of 10^{-4} eV

Molecule number	Electron	Hole
2	99.5	76.7
3	−13.5	38.1
4	− 4.07	1.06
5	−13.5	38.1
6	3.58	14.2
7	− 4.07	1.06
8	74.3	−79.6
9	0.30	0.0
10	− 0.31	0.33
11	− 0.60	−1.03
12	74.3	0.16
13	−13.4	0.14

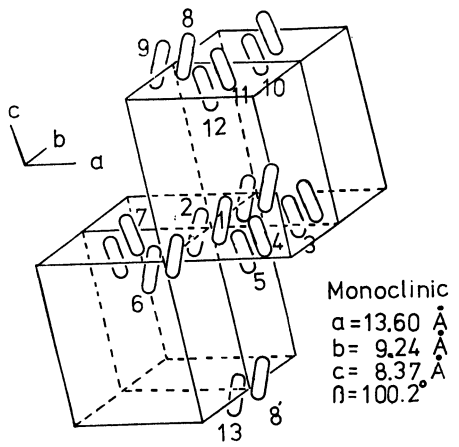

Fig. 3. Schematic representation of the pyrene unit cells, showing the numbering of the molecules used in this paper.

The large discrepancy between the previously reported value[6] and the present one may be partly due to the difference in the purity of the specimen and also partly to that in the crystal growth method. The former crystals were grown from a solution.

We wish greatly to acknowledge Professor Takaaki Danno's kind cooperation in the crystal-growth procedure.

References

1) Y. Maruyama, T. Kobayashi, H. Inokuchi, and S. Iwashima, *Mol. Cryst. Liq. Cryst.*, **20**, 373 (1973).
2) J. M. Robertson, J. G. White, and J. Jortner, *J. Chem. Soc.*, **1947**, 358.
3) J. L. Katz, S. A. Rice, S. -i. Choi, and J. Jortner, *J. Chem. Phys.*, **49**, 1683 (1963).
4) J. B. Birks, "Photophysics of Aromatic Molecules," Wiley Interscience, London (1970), p. 331.
5) P. Gosar and S. -i. Choi, *Phys. Rev.*, **150**, 529 (1966).
6) K. Ohki, H. Inokuchi, and Y. Maruyama, *Bull. Chem. Soc. Jpn.*, **36**, 1512 (1963).

BULLETIN OF THE CHEMICAL SOCIETY OF JAPAN, VOL. 49 (11), 3349—3350 (1976)

Observation of the Scale Formed on Nickel in Nitrogen Oxide

Yoshio TAKASU, Shun-ichi MARU, and Yoshiharu MATSUDA

Department of Industrial Chemistry, Faculty of Engineering, Yamaguchi University, Tokiwadai, Ube, Yamaguchi 755

(Received May 4, 1976)

Synopsis. The state of the scale formed on nickel in nitrogen oxide was examined. Its characteristics are summarized as follows: (1) remarkable oxidation of the grain boundary, (2) the formation of a large amount of lattice defects, and (3) unequal oxidation behaviors for the various crystal planes.

Concerning reactions of metals with nitrogen oxide, some previous work has been reported.[1,2] Recently, the oxidation of nickel in nitrogen oxide has been found to obey the linear rate law with a faster reaction rate than that in oxygen.[3] In this study, the state of these scales was observed.

Measurements of oxidation rates or sample preparation were carried out with a high vacuum apparatus. Nitrogen oxide of a high purity in a glass cylinder from the *Takachiho Co.* was used without further purification. The oxygen was prepared by bulb-to-bulb distillation from a commercial cylinder at liquid nitrogen temperature. Test sample (99.98% Ni) were 1.0×1.0 cm^2 in area and have a thickness of 0.0050 cm. They were annealed *in vacuo* at 800 °C for 2 h, electropolished in a mixed acid (H_2SO_4–H_3PO_4–H_2O),[4] and rinsed in distilled water. The mean size of the grains was 20 μm.

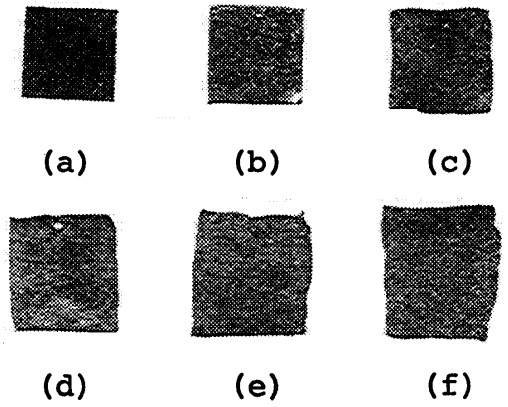

Fig. 1. Photographs of the specimens oxidized in nitrogen oxide,
where, (a): non-oxidized (electropolished), (b), (c), (d), (e), and (f): oxidized in 10 Torr of NO at 700 °C for 5, 10, 25, 40, and 90 min, respectively.

Figure 1 shows the size and shape of the specimens oxidized in nitrogen oxide, where (a) is a non-oxidized specimen and (b), (c), (d), (e), and (f) are specimens oxidized in 10 Torr of nitrogen oxide at 700 °C for 5, 10, 25, 40, and 90 min, respectively. As shown in this figure, the specimen increased in size and changed shape during the oxidation. The relation between the size of the specimen and the oxidation time was shown in Fig. 2. Since the specimens were curled or warped a little by the oxidation, the value r, the ratio of the mean length of each side of the specimen to that of a non-oxidized one, contained a noticeable error. Obviously, the r value increased rapidly during the oxidation. That is, the specimen oxidized in nitrogen oxide was very coarse and bulky. Moreover, even specimens oxidized to about 14 percent (P_{NO}=10 Torr, 700 °C, 10 min) at the early stage of the oxidation process were very brittle. These findings should suggest that preferential oxidation occured along grain boundary and the entire grain boundary was oxidized within less than 10 min. Then, all the scales oxidized in nitrogen oxide in this study were identified to be NiO using X-ray diffractometry. No nitrogen peak was found in the IMA (Ion-Micro-Analysis) spectra of these scales.[3] However, their color was grayish black, so that a large quantity of lattice defects, probably cation vacancies,[5] should be present in them. On the other hand, the scale formed in an oxygen atmosphere was greenish and dense. For example, even specimens oxidized at about 14 percent (P_{O_2}=10 Torr, 700 °C, 180 min) were not brittle and their size did not change in comparison with that prior to oxidation.

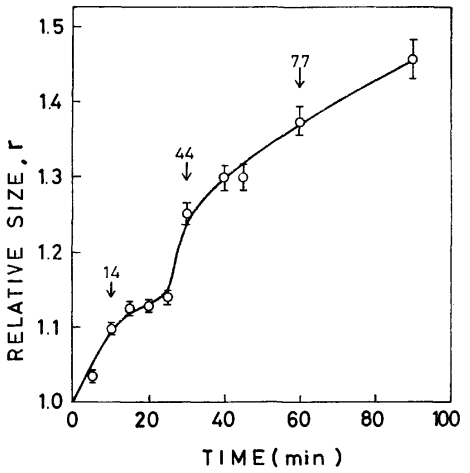

Fig. 2. Relation between the size of specimen and oxidation time.
The numerical values shown in this figure signify the percent of nickel oxidized.

Figure 3 represents the optical metallographs of scales formed in nitrogen oxide and oxygen, where (a) is a non-oxidized specimen, (b) is a specimen oxidized in 10 Torr of oxygen at 700 °C for 180 min, and (c), (d), and (e) are specimens oxidized in 10 Toor of nitrogen oxide at 700 °C for 5, 10, and 40 min, respectively. The surface oxidized in oxygen, (b), was relatively uniform in this photograph, while those in nitrogen oxide (c, d, and e) were not uniform. Namely, in the latter case, the grain boundaries were extremely swollen

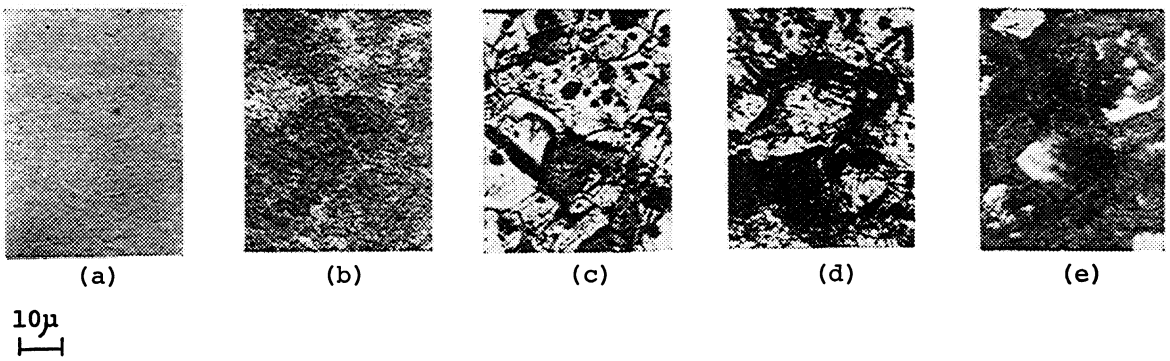

Fig. 3. Optical metallographs of the specimen oxidized in nitrogen oxide or oxygen, where, (a): non-oxidized (electropolished),
(b): oxidized in 10 Torr of O_2 at 700 °C for 180 min,
(c), (d), (e), and (f): oxidized in 10 Torr of NO at 700 °C for 5, 10, and 40 min, respectively.

during the oxidation. Moreover, the state of a few grains became very coarse (black in the photograph), while others did not. As described above, the main characteristics of the state of the scale formed on nickel in nitrogen oxide can be summarized as follows: (1) remarkable oxidation of the grain boundary, which caused the specimen to become coarse, bulky, and brittle, (2) the formation of a large amount of lattice defects, and (3) unequal oxidation behavior among the various crystal planes.

These findings appeared in the rapid diffusion rate of nickel ions through the bulky oxide layer with a large amount of lattice defects and, at the same time, agree with previous results and estimations[3] that the oxidation of nickel in nitrogen oxide was governed by a surface reaction in spite of its rapid oxidation obeying the linear rate law.

References

1) E. Schröder and G. Tamman, *Z. Anorg. Allg. Chem.*, **28**, 179 (1923).
2) M. Faber, A. J. Darnell, and D. M. Ehrenberg, *J. Electrochem. Soc.*, **102**, 446 (1955).
3) Y. Takasu, Y. Matsuda, S. Maru, and N. Hayashi, *Nature (London)*, **255**, 544 (1975).
4) Y. Takasu, H. Shimizu, S. Maru, M. Tomori, and Y. Matsuda, *Corros. Sci.*, **16**, 159 (1976).
5) R. Newman and R. M. Chrenko, *Phys. Rev.*, **144**, 1507 (1959).

BULLETIN OF THE CHEMICAL SOCIETY OF JAPAN, VOL. 49 (11), 3351—3352 (1976)

A New Synthesis of α-Santalol

Kikumasa SATO, Seiichi INOUE, Yoshihiro TAKAGI,* and Shigeki MORII

Department of Applied Chemistry, Faculty of Engineering, Yokohama National University, Ooka, Minami-ku, Yokohama 233

**Nippon Terpene Chemical Co., Ltd., Wakinohama-cho, Fukiai-ku, Kobe 651*

(Received February 6, 1976)

Synopsis. A new synthesis of α-santalol (**1**) is described. 1-Benzyloxy-4-bromo-2-methyl-2-butene (**6**) was converted by the reaction with nickel carbonyl to the π-allylic nickel bromide complex (**7**), which reacted with (−)-π-bromotricyclene (**8**) to afford benzyl ether (**2**). The benzyl ether (**2**) was led to (**1**) (cis: trans=40: 60) by reductive cleavage of the benzyloxy group.

α-Santalol (**1**), which is one of the main constituents of East Indian sandalwood oil, is highly prized in perfumery. Thus, many synthetic approaches have been studied.[1-7]

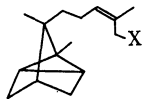

1, X=OH
2, X=OCH_2Ph
3, X=H

It is known that the π-allylnickel halide complex reacts with alkyl halides to afford allylalkanes.[8] Corey reported that α-santalene (**3**) was synthesized by the reaction of π-iodotricyclene with π-1,1-dimethylallylnickel bromide.[8] Sathe reported that the transformation of α-santalene to α-santalol was carried out by the selenium dioxide oxidation of (**3**), followed by reduction of the resulting aldehyde.[2] However, in the literature the stereochemistry of the product was not described. We reinvestigated Sathe's method and showed that the resulting alcohol was *trans*-α-santalol, isomeric to natural α-santalol, which has a *cis* configuration at the trisubstituted olefin moiety in the side chain.[9] We attempted to synthesize α-santalol by the crosscoupling reaction of a functionalized prenyl fragment with a tricyclene component.

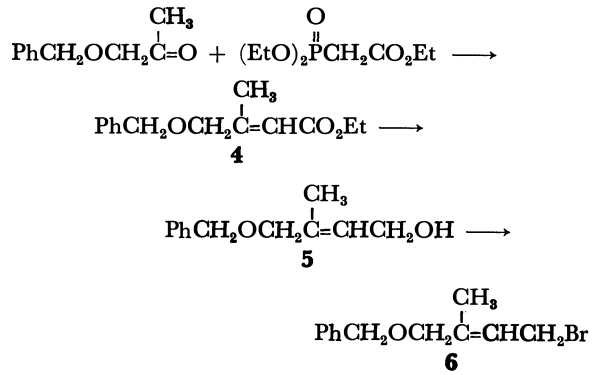

(−)-π-Bromotricyclene (**8**) was prepared by the method of Corey.[10] Ethyl 4-benzyloxy-3-methyl-2-butenoate (**4**), which was prepared by the Wittig reaction of benzyloxyacetone with diethyl (ethoxycarbonylmethyl)phosphonate, was converted to 4-benzyloxy-3-methyl-2-buten-1-ol (**5**) by lithium aluminum hydride reduction. Bromination of alcohol (**5**) was carried out by the reaction with phosphorus tribromide and pyridine in petroleum ether to give 1-benzyloxy-4-bromo-2-methyl-2-butene (**6**). Bromide (**6**) was a *cis* and *trans* mixture (32: 68). The cross-coupling reaction of π-3-(benzyloxymethyl)-2-butenylnickel bromide (**7**), which was transformed from **6** (*cis*: *trans*=32: 68) and nickel carbonyl, with (−)-π-bromotricyclene (**8**) in hexamethylphosphoric triamide (HMPT) afforded benzyl ethers of α-santalol (**2**: **9**=40: 60). The *cis* (**2**) and *trans* (**9**) mixture of benzyl ethers was led to α-santalol (**1**: **10**=40: 60) by reductive cleavage of the benzyl ether function with lithium in ethylamine at −78 °C. Efforts to increase its selectivity in dimethylformamide or *N*-methylpyrolidone were unsuccessful. Stereoisomers of α-santalol were separated by means of column chromatography over silica gel (benzene–ethyl acetate). The isolated *cis*-α-santalol (**1**) was completely identical with natural α-santalol.

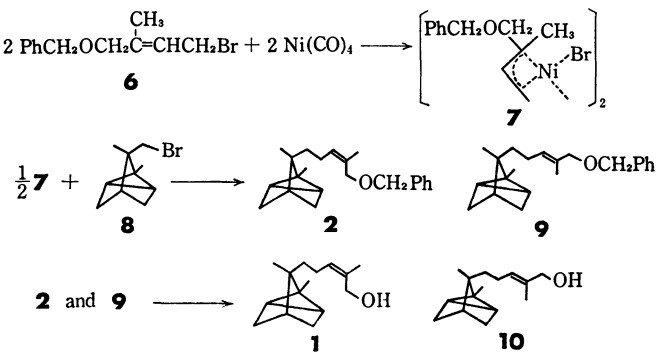

Experimental

All the boiling points are uncorrected. The IR spectra were recorded on a Hitachi Model 215 spectrophotometer. The NMR spectra were recorded on a JEOL Model C-60 spectrometer using tetramethylsilane as an internal standard.

Ethyl 4-Benzyloxy-3-methyl-2-butenoate (4). Diethyl (ethoxycarbonylmethyl)phosphonate (13.4 g) in tetrahydrofuran (THF) (20 ml) was added to sodium hydride (2.6 g) in THF (80 ml) at 22—35 °C and the mixture was stirred for 1.5 h at room temperature. Benzyloxyacetone (8.2 g) in THF (20 ml) was added dropwise to this mixture during 2.5 h at 22—35 °C with additional stirring for 1 h under reflux. After the usual work-up, distillation gave ethyl 4-benzyloxy-3-methyl-2-butenoate (**4**) (9.9 g; 74%), bp 120—129 °C/0.4 mmHg. *cis*: *trans*=37: 63. IR: 1700, 1650 cm^{-1}. NMR (CCl_4): δ 1.25 (t, 3H), 1.99 and 2.08 (*cis* and *trans* each s, 3H), 3.90 (s, 2H), 4.10 (q, 2H), 4.46 (s, 2H), 5.65 and 5.89 (*cis* and *trans* each t, 1H), 7.21 (s, 5H). Found: C, 71.80; H, 7.92%. Calcd for $C_{14}H_{18}O_3$: C, 71.77; H, 7.74%.

4-Benzyloxy-3-methyl-2-buten-1-ol (5). A solution of

ethyl 4-benzyloxy-3-methyl-2-butenoate (**4**) (18.7 g) in diethyl ether (50 ml) was added dropwise to a stirred slurry of lithium aluminum hydride (3.8 g) in diethyl ether (100 ml) for 1.5 h at 22—35 °C, and then stirred for 2 h. The mixture was neutralized with hydrochloric acid and extracted with ether. After drying over Na_2SO_4, distillation gave 4-benzyloxy-3-methyl-2-buten-1-ol(**5**) (15.3 g; quantitative), bp 125—134 °C/0.2 mmHg. *cis*: *trans*=37: 63. IR: 3350, 1070 cm^{-1}. NMR (CCl_4): δ 1.65 and 1.77 (*trans* and *cis* each s, 3H), 2.8 (br, 1H), 3.81 and 3.93 (*trans* and *cis* each s, 2H), 4.05 (d, 2H), 4.39 (s, 2H), 5.57 (t, 1H), 7.20 (s, 5H). Found: C, 74.49; H, 8.41%. Calcd for $C_{12}H_{16}O_2$: C, 74.97; H, 8.39%.

1-Benzyloxy-4-bromo-2-methyl-2-butene (6). To a solution of 4-benzyloxy-3-methyl-2-buten-1-ol (**5**) (7.0 g) and pyridine (1 ml) in petroleum ether (50 ml) was added phosphorus tribromide (4.3 g) in petroleum ether (10 ml) dropwise for 2.5 h at −15——5 °C. After the addition was complete, the reaction mixture was stirred for 1 h at −11——7 °C. After work-up, crude 1-benzyloxy-4-bromo-2-methyl-2-butene (**6**) (7.8 g; 84%) was obtained as a pale yellow oil. This bromide was used without further purification. *cis*: *trans*= 32: 68. n_D^{20} 1.5455. IR: 2850, 1660 cm^{-1}. NMR (CCl_4): δ 1.73 and 1.85 (*trans* and *cis* each s, 3H), 3.90 (s, 2H), 3.95 (d, 2H), 4.45 (s, 2H), 5.80 (s, 1H), 7.30 (s, 5H).

Benzyl Ether of α-Santalol (2 and 9). 1-Benzyloxy-4-bromo-2-methyl-2-butene (**6**) (*cis*: *trans*=32: 68, 14 g) in benzene (90 ml) was added dropwise to a solution of nickel carbonyl (14 g) in benzene (90 ml) for 1.5 h at 49—51 °C under an argon atmosphere. After the addition was complete, the reaction mixture was stirred for 3.5 h under the same conditions. Then the excess nickel carbonyl and the benzene were removed under reduced pressure, and to the residue HMPT (90 ml) was added. (−)-π-Bromotricyclene (**8**) (3.9 g) in HMPT (40 ml) was added dropwise to the solution of the nickel complex for 1 h at 40—45 °C, and stirred for 21 h. After work-up, the distillation gave benzyl ethers of α-santalol (**2** and **9**) (2.5 g; 45%), bp 138—142 °C/0.2 mmHg. *cis*: *trans*=40: 60. IR: 2920, 1080 cm^{-1}. NMR (CCl_4): δ 0.80 (s, 3H), 0.95 (s, 3H), 0.80—2.10 (m, 11H), 1.63 and 1.70 (*trans* and *cis* each s, 3H), 3.76 and 3.89 (*trans* and *cis* each s, 2H), 4.34 (d, 2H), 5.30 (m, 1H), 7.23 (s, 5H). Found: C, 85.00; H, 9.67%. Calcd for $C_{22}H_{30}O$: C, 85.11; H, 9.74%.

α-Santalol (1). Small pieces of lithium (0.3 g) were added to the stirred ethylamine (75 ml) at −10—0 °C until all the lithium was dissolved. After cooling to −78 °C, benzyl ethers of α-santalol (**2**: **9**=48: 52, 2.9 g) in petroleum ethers (10 ml) was added. After stirring for 2.5 h at −78 °C, ammonium chloride (2.0 g) was added and the ethylamine was distilled out. After work-up, the distillation gave α-santalol (**1** and **10**) (1.9 g; 90%), bp 98−102 °C/0.17 mmHg. *cis*: *trans*=48: 52. *cis*- and *trans*- α-Santalol were each isolated by means of column chromatography over silica gel (10: 1 benzene ethyl acetate as eluent). *cis*-α-Santalol (**1**): n_D^{20} 1.5018, $[\alpha]_D^{20}$ +17.20 (c=0.8, $CHCl_3$). IR: 3300, 2950, 1005 cm^{-1}. NMR ($CDCl_3$): δ 0.82 (s, 3H), 0.82—2.20 (m, 12H), 0.98 (s, 3H), 1.80 (s, 3H), 4.13 (s, 2H), 5.33 (t, 1H). *trans*-α-Santalol (**10**): n_D^{20} 1.5013, $[\alpha]_D^{20}$ +17.22 (c=1.5, $CHCl_3$). IR: 3300, 2940, 1005 cm^{-1}. NMR ($CDCl_3$): δ 0.85 (s, 3H), 0.85—2.20 (m, 12H), 1.00 (s, 3H), 1.68 (s, 3H), 3.99 (s, 2H), 5.40 (t, 1H).

References

1) J. Colonge, G. Descotes, Y. Bahurel, and A. Menet, *Bull. Soc. Chim. Fr.*, **1966**, 374.

2) V. M. Sathe, K. K. Chakravarti, M. V. Kadival, and S. C. Bhattacharyya, *Indian J. Chem.*, **4**, 393 (1966).

3) S. Y. Kamat, K. K. Chakravarti, and S. C. Bhattacharyya, *Tetrahedron*, **23**, 4487 (1967).

4) R. G. Lewis, D. H. Gustafson, and W. F. Erman, *Tetrahedron Lett.*, **1967**, 401.

5) E. J. Corey and H. Yamamoto, *J. Am. Chem. Soc.*, **92**, 226 (1970).

6) E. J. Corey, H. A. Kirst, and J. A. Katzenellenbogen, *J. Am. Chem. Soc.*, **92**, 6314 (1970).

7) M. Julia, Ger. Offen., 2341872 (1974).

8) E. J. Corey and M. F. Semmelhack, *J. Am. Chem. Soc.*, **89**, 2755 (1967).

9) We referred to Faulkner's publication in order to determine the stereochemistry by NMR data. And Bhalerao reported that the aldehyde obtained by the selenium dioxide oxidation had a *trans* configuration. D. J. Faulkner, *Synthesis*, **1971**, 175; Uday T. Bhalerao and Henry Rapoport, *J. Am. Chem. Soc.*, **93**, 4835 (1971).

10) E. J. Corey, S. W. Chow, and R. A. Scherrer, *J. Am. Chem. Soc.* **79**, 5773 (1957).

BULLETIN OF THE CHEMICAL SOCIETY OF JAPAN, VOL. 49 (11), 3353—3354 (1976)

Oxidative Ring Cleavage of 3,5-Di-*t*-butyl-catechol and -*o*-benzoquinone by Base-Catalyzed Oxygenation

Akira NISHINAGA, Toshio ITAHARA, and Teruo MATSUURA

Department of Synthetic Chemistry, Faculty of Engineering, Kyoto University, Kyoto 606

(Received May 8, 1976)

Synopsis. The oxygenation of 3,5-di-*t*-butyl-catechol and -*o*-benzoquinone in *t*-BuOH with *t*-BuOK leads to the direct oxidative cleavage of the C_1–C_2 bond affording 2,4-di-*t*-butyl-4-carboxymethyl-2-buten-4-olide, a muconic acid derivative. The reaction is rationalized by assuming the reaction of 3,5-di-*t*-butyl-*o*-benzosemiquinone with oxygen.

Oxidative ring cleavage of catechols by molecular oxygen is of interest in connection with the biological oxygenation of catechols.[1-4] It has been shown that photooxygenation[1] and oxygenation with copper(I) chloride–pyridine complex[2] lead to the direct oxidative cleavage of the C_1–C_2 bond of catechols giving rise to muconic acid derivatives. No such direct cleavage has been observed in the base-catalyzed oxygenation of 3,5-di-*t*-butylcatechol in MeOH[3] or in DMF,[4] where products were always accompained by further introduction of oxygen function to the molecules.

In the present paper it is reported that the oxygenation of 3,5-di-*t*-butylcatechol (**1**) or 3,5-di-*t*-butyl-*o*-benzoquinone (**2**) in *t*-BuOH containing *t*-BuOK causes the direct oxidative cleavage of the C_1–C_2 bond to give 2,4-di-*t*-butyl-4-carboxymethyl-2-buten-4-olide (**3**), a muconic acid derivative. When oxygen was bubbled through a solution of **1** in *t*-BuOH containing *t*-BuOK at room temperature for 8 h, compound **3**, 2,4-di-*t*-butyl-4-hydroxy-2-buten-4-olide (**4**), and 2,4-di-*t*-butyl-3-(3,5-di-*t*-butyl-2-hydroxyphenoxy)-2-buten-4-olide (**5a**) were obtained in 41, 14, and 21% yields, respectively.[5] The structure of **5a** was determined from its elemental analysis and spectral data, and also by the fact that the acetylation of **5a** gave 2,4-di-*t*-butyl-3-(2-acetoxy-3,5-di-*t*-butylphenoxy)-2-buten-4-olide (**5b**). Since compound **3** is quite stable under the reaction conditions, it should not be an intermediate for the formation of **4**. These products, therefore, must be formed *via* different reaction path.

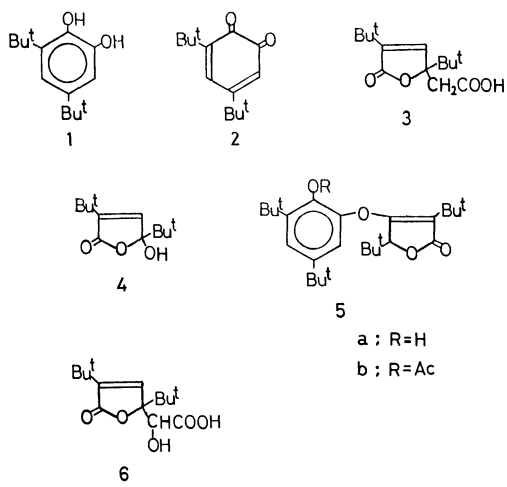

Scheme 1.

Oxygenation of 3,5-di-*t*-butyl-*o*-benzoquinone (**2**), on the other hand, in *t*-BuOH with *t*-BuOK resulted in the preferential formation of **3** (Table 1). Since the quinone **2** gave the corresponding semiquinone anion under the reaction conditions and oxygen was not significantly reduced in *t*-BuOH containing *t*-BuOK, it is believed that the formation of **3** results from the reaction of the semiquinone anion with molecular oxygen. On the other hand, 2,4-di-*t*-butyl-4-(carboxyhydroxymethyl)-2-buten-4-olide (**6**) has been found to be the sole product on the oxidation of the quinone **2** by H_2O_2[3] and compound **4** is easily obtained on the *t*-BuOK-catalyzed oxygenation of **6**.[4]

It is therefore concluded that the reaction of the *o*-benzosemiquinone with molecular oxygen leads to the direct oxidative cleavage of the C_1–C_2 bond, whereas the reaction of **2** with hydrogen peroxide or its anionic species gives rise to the formation of **4** as depicted in the following scheme.

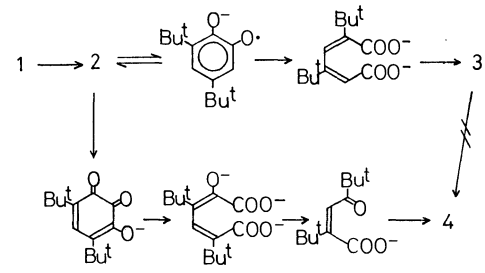

Scheme 2.

The formation of a small amount of **4** in the oxygenation of **2** may be attributed to the reduction of oxygen by an anionic species of **1** resulting from disproportionation of the semiquinone.

Table 1. Base-catalyzed oxygenation of **2** in various solvents at room tempeoature

Solvent	*t*-BuOK/2 (mol ratio)	Reaction time (h)	Conversion (%)	Product (%)[a]	
				3	**4**
MeOH	4.5	8	100	—	41
t-BuOH	4.5	8	100	64	7
$NHEt_2$	4.5	8	100	62	6
NEt_3	4.5	8	100	51	18
DMF	4.5	8	100	24	36
DMSO	4.5	8	100	35	25
HMPA	4.5	8	100	58	7
DME	4.5	8	100	62	6

a) Yields were determined by NMR.

The dimeric compound **5a** was not formed on the oxygenation of **2**, suggesting that the formation of **5a** in the oxygenation of **1** is considered to result from the combination of the phenolate anion of **1** with **2** but not from the coupling of the semiquinone with each other.

Similar results were obtained in other solvents (Table 1). Compound **3** was not isolable on the reaction in MeOH, where only **4** was isolated. In this system the reaction of **2** with H_2O_2 takes place predominantly because the quinone **2** is reduced to **1** in MeOH in the presence of base. Comparable amounts of **3** and **4** were obtained in DMF and in DMSO.[6] When luminol is added to a solution of *t*-BuOK in DMF or DMSO under O_2 bubbling, chemiluminescence is observed. This is indicative of the formation of superoxide anion.[7] Superoxide anion is well-known to form O_2 and H_2O_2 through its dismutation.[8] Therefore, the results in the oxygenation of **2** in DMF and DMSO indicate that there is a competition between the reaction of the semiquinone with O_2 and that of the quinone **2** with H_2O_2 in these solvents. A similar competition reaction has been reported for the oxidation of **1** with KO_2, where compounds **3** and **6** are main products.[9] It is suggested by Moro-oka and Foote[9] that the formation of **3** and **6** is attributed to the different type of decomposition of a common peroxide intermediate resulting from the combination of the semiquinone and superoxide anion. This mechanism is also possible for the formation of **3** and **4** in the present oxygenation.

Experimental

Oxygenation of 1 in t-*BuOH–*t-*BuOK.* Oxygen was bubbled through a soln of **1** (0.274 g) in *t*-BuOH (15 ml) containing *t*-BuOK (0.5 g) at 40 °C for 8 h. The reaction mixture was acidified with dil. HCl and extracted with ether. The extract was washed with water, dried (Na_2SO_4), and evaporated. The residue was triturated with hexane to give **3** (0.14 g, 41%), identical with the product in the photooxygenation[1] of **1** (IR, NMR, and mp). The organic soln. after removal of **3** was chromatographed on a silica gel plate (developed by $CHCl_3$) to give **4** (0.03 g, 14%), identical with the reported product[4] (IR, NMR, mp), and **5a** (0.05 g, 21%), colorless needles (hexane), mp 199—200 °C; IR (Nujol): 3380 (OH), 1715 (C=O) cm^{-1}; NMR ($CDCl_3$): δ 1.07 (*t*-Bu), 1.28 (*t*-Bu), 1.35 (*t*-Bu), 1.43 (*t*-Bu), 5.30 (1H, s, =C–CH–O), 5.74 (OH), 6.90 (1H, s, ArH), 7.21 (1H, s, ArH).

Found: C, 74.93; H, 9.58%. Calcd for $C_{26}H_{40}O_4$: C, 74.96; H, 9.68%.

Acetylation of 5a. A soln of **5a** (0.1 g) in acetic anhydride (10 ml) containing pyridine (4 ml) was allowed to stand at room temperature for 3 h. The reaction mixture was poured into a large excess of water to afford **5b** (0.11 g), colorless needles (hexane), mp 190—191 °C; IR (Nujol): 1780 (AcO), 1740 (C=O) cm^{-1}; NMR ($CDCl_3$): δ 1.07 (*t*-Bu), 1.28 (*t*-Bu), 1.38 (*t*-Bu), 1.44 (*t*-Bu), 2.35 (AcO), 5.05 (1H, s, =C–CH–O–), 6.90 (1H, d, J=2.0 Hz, ArH), 6.97 (1H, d, J=2.0 Hz, ArH).

Found: C, 73.24; H, 8.97%. Calcd for $C_{28}H_{42}O_5$: C, 73.32; H, 9.23%.

Oxygenation of 2. A procedure similar to that in the oxygenation of **1** described above was applied: **2** (1 mmol) in various solvents (15 ml). The results are summarized in Table 1.

The present work was financially supported by the Ministry of Education.

References

1) T. Matsuura, H. Matsushima, S. Kato, and I. Saito, *Tetrahedron*, **28**, 5119 (1972).

2) J. Tsuji and H. Takayanagi, *J. Am. Chem. Soc.*, **96**, 7349 (1974); *Tetrahedron Lett.*, **1975**, 1245.

3) R. R. Grinstead, *Biochemistry*, **3**, 1308 (1964).

4) A. Nishinaga, T. Itahara, and T. Matsuura, *Bull. Chem. Soc. Jpn.*, **47**, 1811 (1974).

5) A. Nishinaga, T. Itahara, and T. Matsuura, *Tetrahedron Lett.*, **1974**, 4481.

6) In a previous paper[4] only the product **4** was mentioned, but a detailed re-examination of the oxygenation in DMF or DMSO confirmed the existence of **3** in the reaction mixture.

7) A similar chemiluminescence is observed when luminol is added to a solution of KO_2 in DMF or DMSO.

8) A. U. Kahn, *Science*, **168**, 476 (1970).

9) Y. Moro-oka and C. S. Foote, *J. Am. Chem. Soc.*, **98**, 1510 (1976).

BULLETIN OF THE CHEMICAL SOCIETY OF JAPAN, VOL. 49 (11), 3355—3356 (1976)

Photoreactions of Flavanones[1]

Ruka NAKASHIMA, Kazuaki OKAMOTO, and Teruo MATSUURA

Department of Synthetic Chemistry, Faculty of Engineering, Kyoto University, Kyoto 606

(Received May 24, 1976)

Synopsis. On irradiation in benzene, 5,7-dimethyl-4′-methoxyflavanone gave a bis-flavanone V, while in 2-propanol it was largely recovered. Irradiation of 4′-methoxyflavanone in benzene and 2-propanol yielded the corresponding chalcone and pinacols, respectively. 5,7,4′-Trimethoxyflavanone was relatively inert to photolysis in benzene, but gave a complex mixture of products in 2-propanol.

In a series of our investigation on flavonoid photochemistry,[2-5] it has been found that the presence of the 5-hydroxyl group causes photo-resistance to flavonoids such as 3-methoxyflavones,[4,5] 3-hydroxyflavones,[5] and flavanones,[5] possibly due to the loss of its excitation energy. Among these flavonoids, the photoreaction of flavanones had remained unknown until Kishimoto *et al.*[6] and Mack and Pinhey[7] reported that flavanones underwent photoreduction in 2-propanol and photoisomerization to chalcones and 4-phenyl-3,4-dihydrocoumarines in benzene. These reports prompted us to communicate our independent results on the photoreactions of a few flavanone derivatives.

Irradiation of 4′-methoxyflavanone (I) with a high-pressure mercury lamp (Pyrex) in benzene and 2-propanol gave 4-methoxy-2′-hydroxychalcone (II; 14%) with the recovered I (18%) and a mixture of pinacols III[8] in 23% yield, respectively, similarly to the other flavanones.[6] In both solvents, the remaining part of products was intractable polymers. The formation of II may be recognized as a 6π-electrocyclic reaction of the enolic form of I. A similar type of photochemical electrocyclic reaction has been observed for 2*H*-pyrans.[9] The reverse reaction of 2′-hydroxychalcone to flavanone is known to occur photochemically.[10] Under similar photolysis conditions, 5,7,4′-trimethoxyflavone was largely recovered under the formation of some resinous material in benzene, while it underwent faster photodecomposition in 2-propanol to give a complex mixture of at least six products.

5,7-Dimethyl-4′-methoxyflavanone (IV), which was photochemically rather unreactive in 2-propanol underwent oxidative coupling by irradiation in benzene to give V in 8% yield. The structure of V was assigned by elemental and NMR (with decoupling) spectral analyses. On longer irradiation, V suffered further photodecomposition to give a resinous material. It may be reasonable to assume that the formation of V involves an intramolecular hydrogen abstraction of the excited IV, similar to that of *o*-alkylphenyl ketone.[11] A similar dehydrodimerization has been reported to occur in the photolysis of 5,8-dimethyltetralone.[12]

Experimental

All the melting points are uncorrected. NMR, IR, and mass spectra were measured on an NEVA T-60 or a Varian HA-100 spectrometer with TMS as the internal standard, on a Hitachi EPI-G3 spectrophotometer, and on a Hitachi RMS-4 spectrometer, respectively.

Materials. 4-Methoxy-2′-hydroxychalcone (II) was prepared from *o*-hydroxyacetophenone and *p*-anisaldehyde by the method for the preparation of chalcone.[13] The product was cyclized by refluxing in a mixture of 1: 1: 1 ethanol, acetic acid, and water for 10 h[14] to 4′-methoxyflavanone (I); mp 89—90 °C (lit,[15] mp 97 °C); NMR ($CDCl_3$), δ 2.8—3.2 (m, 2H), 3.80 (s, 3H), an ABX at 2.80, 3.18, and 5.45 (J_{AB}=17 Hz), J_{AX}=5 Hz, J_{BX}=11 Hz, $-CH_2-\underset{|}{C}H-$), 6.8—8.0 (m, 8H). 4′,5,7-Trimethoxyflavanone, mp 125—126 °C (lit,[16] mp 123 °C), was prepared by the similar method *via* 4,4′,6′-trimethoxy-2′-hydroxychalcone, mp 112.5—114 °C (lit,[17] mp 113

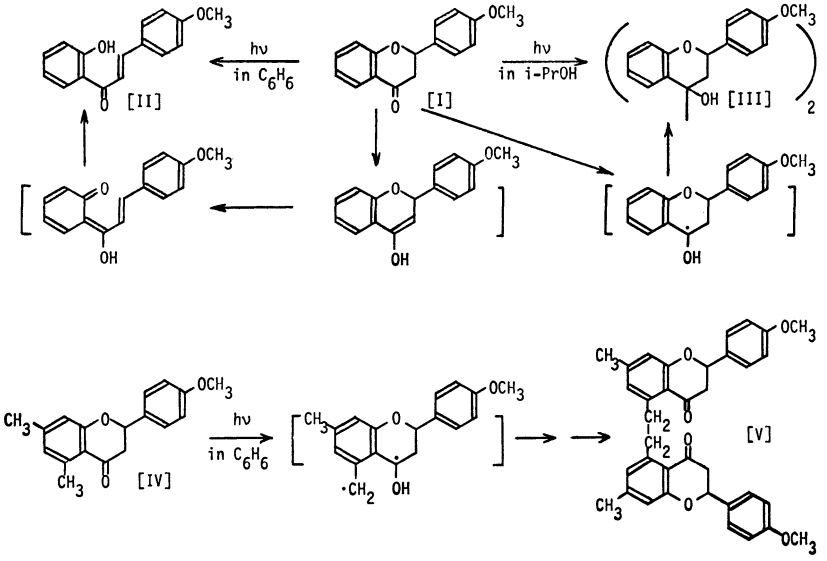

°C), which was prepared from 2-hydroxy-4,6-dimethoxyacetophenone[18] and *p*-anisaldehyde.

4′-Methoxy-5,7-dimethylflavanone (IV) was prepared by the following sequence of reactions applying the known method[14]: 3,5-xylenol→3,5-xylyl acetate→2-hydroxy-4,6-dimethylacetophenone→4-methoxy-2′-hydroxy-4′,6′-dimethylchalcone→IV. Recrystallization from ethanol gave IV as colorless crystals; mp 77—79 °C; IR (KBr), 1680, 1620, 1520 cm^{-1}; *m/e*, 282 (M^+); NMR ($CDCl_3$), δ 2.35 (s, 3H, 7-Me); 2.65 (s, 3H, 5-Me), 3.85 (s, 3H, 4′-OMe), 2.8—3.2 (m, 2H, 3-CH_2), 5.40 (dd, 1H, J=4 and 11 Hz, 2-CH), 6.30 (broad s, 1H, aromatic H), 6.36 (broad s, 1H, aromatic H), an AB at 7.00 and 7.44 (J_{AB}=9 Hz).

Found: C, 76.10; H, 6.58%. Calcd for $C_{18}H_{18}O_3$: C, 76.57; H, 6.43%.

Photolysis of 4′-Methoxyflavanone (I). *(a) In Benzene*: A solution of I (500 mg) in benzene (130 ml) was irradiated with a 100-W high-pressure mercury lamp through Pyrex glass under nitrogen for 8 h. After removal of the solvent, the residue was submitted to preparative TLC (silica gel; chloroform) to give I (90 mg) and 4-methoxy-2′-hydroxychalcone (II; 70 mg) identical with an authentic sample (IR).

(b) In 2-Propanol: A solution of I (1 g) in 2-propanol (140 ml) was irradiated for 6 h in the same manner. After removal of the solvent, the residue was crystallized four times from ethyl acetate to give a stereoisomeric mixture of 4,4-bi(4-hydroxy-4′-methoxyflavane)s (III; 230 mg) as colorless crystals; mp 229—232 °C; IR (KBr), 3500, 3440, 1620, 1520, 1480 cm^{-1}, 510 (M^+), 492, 256; NMR (DMSO-d_6), δ 1.6—2.7 (m, 2H, 3-CH_2), 3.76 (s, 3H, 4′-OMe), 5.16 (s, 1/2 H, OH), 5.21 (diffused s, 1/2H, OH), 5.8—6.2 (m, 1H, 2-CH), 6.7—7.6 (m, 8H, aromatic H).

Found: C, 74.98; H, 5.97%. Calcd for $C_{32}H_{30}O_6$: C, 75.27; H, 5.92%.

Photolysis of 4′,5,7-Trimethoxyflavanone. *(a) In Benzene*: A solution of the flavanone (800 mg) in benzene (130 ml) was irradiated in a similar manner for 5 h. TLC analysis (silica gel; ethyl acetate) of the reaction mixture showed that it consisted of the recovered starting material with a small amount of origin substances. The starting material (450 mg) was recovered by preparative TLC.

(b) In 2-Propanol: The flavanone (500 mg) in 2-propanol (140 ml) was similarly irradiated for 5 h. The reaction mixture showed a complex TLC pattern in which the presence of at least six products were observed. No pure product was isolated by preparative TLC.

Photolysis of 4′-Methoxy-5,7-dimethylflavanone (IV). *In Benzene*: A solution of IV (800 mg) in benzene (130 ml) was irradiated similarly for 2 h. After removal of the solvent, the addition of ethanol to the residue gave insoluble crystals which on two recrystallizations from chloroform yielded 1,2-[bis(4′-methoxy-7-methyl-4-oxo-5-flavanyl)]ethane (V; 60 mg) as colorless crystals; mp 221—223 °C; IR (KBr), 1680, 1620, 1520, 1470 cm^{-1}; *m/e*, 562 (M^+), 281, 267; NMR ($CDCl_3$), δ 2.35 (s, 3H, 7-Me), and ABX at 2.80, 3.10, and 5.38 (J_{AB}=9 Hz, J_{AX}=2 Hz, J_{BX}=6 Hz, $-CH_2CH-$), 3.30 (m, 2H, $-CH_2-$), 3.81 (s, 3H, 4′-OMe), AB at 6.94 and 7.39 (4H, J_{AB}=4.5 Hz, 2′,3′,5′,6′-aromatic H), 6.74 (broad s, 1H, aromatic H), 6.90 (broad s, 1H, aromatic H).

Found: C, 75.63; H, 6.42%. Calcd for $C_{36}H_{34}O_6$: C, 76.85; H, 6.09%.

(b) In 2-Propanol: A solution of IV (300 mg) in 2-propanol (140 ml) was irradiated similarly. TLC analyses of the reaction mixture after 6 and 12 h showed that it consisted mainly of the starting material and some colored polymers.

The authors express their gratitude to Dr. Tamio Ueno, Pesticide Research Institute, Faculty of Agriculture, Kyoto University for the measurement of mass spectra.

References

1) Photoinduced Reactions. XCIV.
2) T. Matsuura, H. Matsushima, and H. Sakamoto, *J. Am. Chem. Soc.*, **89**, 6370 (1967).
3) T. Matsuura, H. Matsushima, and R. Nakashima, *Tetrahedron*, **26**, 435 (1970).
4) T. Matsuura and H. Matsushima, *Tetrahedron*, **24**, 6615 (1968).
5) T. Matsuura, T. Takemoto, and R. Nakashima, *Tetrahedron*, **29**, 3337 (1973).
6) T. Kishimoto, R. Matsushima, and M. Suzuki, Abstracts of the Fall Meeting of Chubu Chemical Association, 3D19, p. 126 (1975).
7) P. O. L. Mack and J. J. Pinhey, *Chem. Commun.*, **1972**, 451.
8) The pinacol III has theoretically two *meso*-forms and four *dl*-pairs. The NMR spectrum of the pinacol product obtained appears to be a mixture of mainly two pinacols.
9) G. Büchi and N. C. Yang, *J. Am. Chem. Soc.*, **79**, 2318 (1957).
10) F. R. Stermitz, J. A. Adamovics, and J. Geigert, *Tetrahedron*, **31**, 1593 (1975).
11) N. C. Yang and C. Rivas, *J. Am. Chem. Soc.*, **83**, 2213 (1961).
12) B. J. Arnold, S. M. Mellows, P. G. Sammes, and T. W. Wallace, *J. Chem. Soc., Perkin Trans. 1*, **1974**, 401.
13) *Org. Synth.*, Coll. Vol. I, p. 78 (1943).
14) M. Taketori and S. Fujise, *Nippon Kagaku Zasshi*, **78**, 309 (1957).
15) H. Ryan and G. Cruess-Callagham, *Proc. Roy. Irish Acad.*, **39B**, 124 (1929); *Chem. Abstr.*, **24**, 4037 (1930).
16) K. Nakazawa and S. Matsuura, *Yakugaku Zasshi*, **75**, 469 (1955).
17) V. G. Bargellini, *Gazz. Chim. Ital.*, 44II, 421 (1914); *Atti Acad. Lincei*, **23II**, 135 (1914); *Chem. Abstr.*, **9**, 1042 (1915).
18) *Org. Synth.*, Coll. Vol. II, p. 522 (1943).

BULLETIN OF THE CHEMICAL SOCIETY OF JAPAN, VOL. 49 (11), 3357—3358 (1976)

Studies on Nucleosides and Nucleotides. V. Selective Aroylation of 5′-Hydroxyl Group of Uridine and Adenosine

Satoru SHIMOKAWA, Junji KIMURA, and Oyo MITSUNOBU

Department of Chemistry, College of Science and Engineering, Aoyama Gakuin University, Chitosedai, Setagaya-ku, Tokyo 157

(Received May 28, 1976)

Synopsis. When uridine was allowed to react with diethyl azodicarboxylate, triphenylphosphine and either benzoic or *p*-nitrobenzoic acid at room temperature, 5′-*O*-aroyluridines were selectively obtained in good yields. Similarly, adenosine gave 5′-*O*-aroyladenosine. In this case, however, a small amount of N^3,5′-cycloadenosine was formed.

In a previous paper, the selective acylation of the 5′-hydroxyl group of thymidine by the use of diethyl azodicarboxylate (I) and triphenylphosphine (II) was described.[1] We now report selective aroylation of 5′-hydroxyl group of uridine and adenosine with a similar system.

When 2′,3′-*O*-isopropylideneuridine was allowed to react with *p*-nitrobenzoic acid, I and II in dioxane containing a small amount of hexamethylphosphoric triamide (HMPA)[2] at room temperature overnight, 2′,3′-*O*-isopropylidene-5′-*O*-(*p*-nitrobenzoyl) uridine (IIIb) was isolated in a 65% yield. Similarly, 2′,3′-*O*-isopropylidene-5′-*O*-benzoyluridine (IIIa) and 2′,3′-*O*-isopropylidene-5′-*O*-(*p*-nitrobenzoyl) adenosine (IVb) were obtained. The 2′,3′-*O*-isopropylidene group of IIIa, IIIb and IVb was removed in the usual manner giving the corresponding 5′-*O*-aroylnucleosides (IIIc, IIId and IVd).

The reaction of uridine with I, II and either benzoic or *p*-nitrobenzoic acid under the same conditions as above also led to the formation of the corresponding 5′-*O*-aroyluridines (IIIc and IIId) in good yields. Examination of the crude reaction mixture on paper chromatography in four solvent systems revealed the presence of uridine and a nucleosidic product which have the same R_f values as the corresponding 5′-*O*-aroyluridine prepared from the 2′,3′-*O*-isopropylideneuridines. In spite of an apparently clean reaction as judged by paper chromatographical analysis (IIIc, 83%; IIId, 80%), the isolated yields of the products were about 50%. Structures of the isolated IIIc and IIId were confirmed by elemental analyses, UV spectra and positive *cis*-diol test.[3] The total analysis thus gave assurance that the reaction of uridine with I, II and either benzoic or *p*-nitrobenzoic acid brings about selective aroylation of the 5′-hydroxyl group of uridine without any accompanying 2′- and/or 3′-*O*-aroylated products.

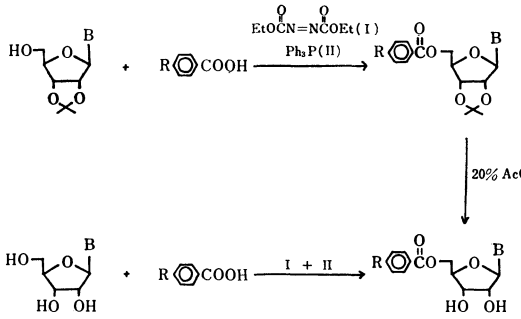

Following the method described above, 5′-*O*-(*p*-nitrobenzoyl)adenosine (IVd) was isolated in a 43% yield. The homogeneity of the isolated product was determined by paper chromatography in four solvent systems. The results are summarized in Table 1.

In the case of the aroylation of adenosine, however, the formation of a small amount of a side product was observed by examination of the reaction mixture with paper chromatography. The ultraviolet spectral characteristics of the side product indicated a chromophore similar to N^3, 5′-cycloadenosine (VI, λ_{max} 272

Table 1. Preparation of 5′-*O*-aroylnucleosides at room temperature

		B[a]	R	Yield[b] %	Mp °C	UV absorption Solvent	λ_{max} nm ($\varepsilon \times 10^{-4}$)		
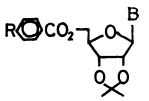	IIIa	Ur	H	43	145—146	95% EtOH	232 (1.50)	260	(1.01)
						THF		259	(1.32)
	IIIb	Ur	NO_2	65	214—215	THF		259	(2.58)
	IVb	Ad	NO_2	63	144—146	95% EtOH		259	(2.25)
						AcOH		260	(2.41)
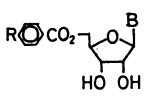	IIIc	Ur	H	56[c] (79.5) [20.2]	171—172	H_2O	234 (1.56)	263	(1.04)
	IIId	Ur	NO_2	50 (82.6) [15.2]	189—190	H_2O		262	(2.25)
	IVd	Ad	NO_2	43	229—230	THF		259.5	(2.67)

a) Ur=uracil, Ad=adenine. b) ( ): Yield estimated by paper chromatography. [ ]: Amount of recovered uridine estimated by paper chromatography. c) See Experimental.

nm, lit,[4] λ_{max} 273 nm). The formation of VI may be due to intramolecular displacement of an intermediate (V) of the present reaction.[5] When the reaction was carried out in *N,N*-dimethylformamide (DMF) at room temperature, the yield of VI was found to increase to 52% by paper chromatographical analysis.

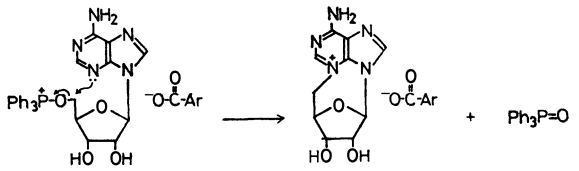

5′-*O*-Aroyluridine and 5′-*O*-aroyladenosine were treated with methanolic ammonia (saturated at room temperature) at room temperature and the reaction was monitored by paper chromatography. While *p*-nitrobenzoyl group was completely removed within 1 h, it took 8 h for the complete removal of benzoyl group.

Experimental

Method. Paper chromatography was carried out by the ascending technique using Toyo Roshi No. 51A paper. Solvent systems were A, 1-butanol: 2 M HCl (3: 1); B, ethanol: 1 M ammonium acetate (7: 3); C, 1-butanol: acetic acid: water (5: 2: 3); D, 1-butanol: water (86: 14).

Table 2. Paper chromatography of different compounds

	R_f values in solvent system			
	A	B	C	D
Uridine	0.33	0.65	0.42	0.16
5′-*O*-Benzoyluridine	0.82	0.82	0.74	0.55
5′-*O*-*p*-Nitrobenzoyluridine	0.77	0.80	0.77	0.51
Adenosine	0.10	0.57	0.42	0.19
5′-*O*-*p*-Nitrobenzoyladenosine	0.50	0.73	0.71	0.51
N^3,5′-Cycloadenosine			0.32	

5′-O-Aroyluridine. A solution of 1.5 mmol each of benzoic acid and I in dioxane (1 ml) was added to a suspension of uridine (1 mmol) and II (1.5 mmol) in dioxane (1 ml) under vigorous stirring at room temperature over a period of 1 h. In the case of *p*-nitrobenzoylation, *p*-nitrobenzoic acid and I were dissolved in a mixture of dioxane (1 ml) and HMPA (0.5 ml). The mixture became clear within 1 h. After the solution was kept stirring overnight and the solvent was removed under reduced pressure, the residue was applied to a silica gel column (Wakogel C-300, 3.2 × 100 cm). The column was eluted with ethyl acetate giving the desired product, 5′-*O*-benzoyluridine (IIIc, 291 mg, 56%) or 5′-*O*-(*p*-nitrobenzoyl)uridine (IIId, 394 mg, 50%). In a large scale reaction, the isolated yield of IIIc increased to 77%.

5′-O-(p-Nitrobenzoyl)adenosine. The reaction was carried out in the same manner as described above. After removal of the solvent, the crude product was washed with methanol, and the remaining solid was suspended in water. The suspension was heated under reflux to dissolve unchanged adenosine. 5′-*O*-(*p*-Nitrobenzoyl)adenosine was left as insoluble solid (180 mg, 43%). The product was found to be homogeneous by paper chromatography and gave satisfactory results by elemental analysis. Paper chromatography of the crude reaction mixture indicated the presence of a small amount of N^3,5′-cycloadenosine (VI).

References

1) O. Mitsunobu, J. Kimura, and Y. Fujisawa, *Bull. Chem Soc. Jpn.*, **45**, 245 (1972).

2) HMPA was used in order to dissolve *p*-nitrobenzoic acid. The benzoylation of uridine was carried out in dioxane or THF.

3) J. G. Buchanan, C. A. Dekker, and A. G. Long, *J. Chem. Soc.*, **1950**, 3162.

4) V. M. Clark, A. R. Todd, and J. Zussman, *J. Chem. Soc.*, **1951**, 2952; J. P. H. Verheyden and J. C. Moffatt, *J. Org. Chem.*, **35**, 2319 (1970).

5) O. Mitsunobu and M. Eguchi, *Bull. Chem. Soc. Jpn.*, **44**, 3427 (1971); M. Wada and O. Mitsunobu, *Tetrahedron Lett.*, **1972**, 1279.

BULLETIN OF THE CHEMICAL SOCIETY OF JAPAN, VOL. 49 (11), 3359—3360 (1976)

The Stereostructure of Acetylparabenzlactone and Its Conversion to a Lariciresinol-type Lactone

Masatake NIWA, Masanobu IGUCHI, Shosuke YAMAMURA, and Sansei NISHIBE*

Faculty of Pharmacy, Meijo University, Tenpaku-ku, Nagoya 468
**Faculty of Pharmacy, Higashi Nippon Gakuen University, Ishikari-gun, Hokkaido 061-02*

(Received June 15, 1976)

Synopsis. Acetylparabenzlactone (**1**), an acetylation product of (−)-parabenzlactone (**2**), has been newly isolated from *Parabenzoin trilobum* Nakai, and the stereostructures of these two piperolignanolides have also been elucidated. Furthermore, the chemical conversion of **1** to a lariciresinol-type lactone (**3**) has been carried out.

In the course of our search for such an epoxygermacrene as shiromodiol,[1] which has been used for a biogenetic-type reaction,[2] we have isolated a new lignanolide, named acetylparabenzlactone (**1**), from *Parabenzoin trilobum* Nakai instead of (−)-parabenzlactone (**2**),[3] whose stereostructure remains unsettled.

Fresh leaves of the same plant[4] were extracted with hot benzene. The benzene extract was repeatedly chromatographed on silica gel, and then purified by preparative TLC to give colorless needles of acetylparabenzlactone (**1**) in a 0.017% yield.

The UV and NMR spectra of **1** indicate the presence of two methylenedioxyphenyl groups [δ 5.91 (2H, s), 5.92 (2H, s) and 6.60 (6H, complex)]. Furthermore, this lignanolide is proved to have a five-membered ring lactone and a secondary acetoxyl group [δ 2.10 (3H, s) and 5.70 (1H, d, J=6.0 Hz)]. From these data, this lignanolide (**1**) must be regarded as an acetylation product of (−)-parabenzlactone (**2**), which has previously been reported by Wada and Munakata.[3] Thus, the former was readily converted to **2** on treatment with 2% methanolic KOH (room temp, 1.5 h), giving a mixture of two hydroxyl lactones (**2** and **3**) with the same molecular formula ($C_{20}H_{18}O_7$) in 65 and 21% yields respectively. One of them is completely identical with an authentic sample of (−)-parabenzlactone (**2**) (mixed mp and IR spectrum). The structure of isoparabenzlactone (**3**) was also established (see below). In addition to the two original methylenedioxyphenyl groups, this compound has a five-membered ring lactone grouping [ν_{max} 1770 cm^{-1}; δ 5.13 (1H, d, J=8.0 Hz)]. In particular, the presence of a hydroxymethyl group in **3** can be confirmed by its NMR spectrum, which has a signal at δ 3.50 (2H, complex) which is shifted to δ 3.95 on acetylation, giving the corresponding acetate (**4**). From these data, isoparabenzlactone should be a lariciresinol-type lactone (**3**), whose stereostructure is based on those of **1** and **2**.

On hydrogenolysis over a freshly prepared palladium catalyst in EtOH containing $HClO_4$, (−)-parabenzlactone (**2**) was readily converted to (−)-hinokinin (**5**) in a 71% yield (IR and CD spectra).[5] Finally, the configuration of the remaining OH group in **2** is based on the NMR signal at δ 4.60 assignable to the proton attached to the carbon atom bearing the OH group, whose coupling constant is 6.5 Hz,[6] indicating that (−)-parabenzlactone adopts the stereostructure depicted in **2**. Thus, acetylparabenzlactone also has the **1** stereostructure.

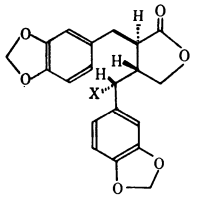

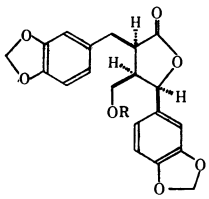

1 X=OAc
2 X=OH
5 X=H

3 X=H
4 X=Ac

Experimental

All the mps are uncorrected. The IR spectra were recorded on a Hitachi-215 spectrophotometer. The UV spectra were taken on a Hitachi-124 spectrophotometer, using MeOH as the solvent. The NMR spectra were recorded on a JEOL JNM-PS 100 NMR spectrometer, using $CDCl_3$, unless otherwise stated. The chemical shifts are given in ppm relative to the internal TMS; only prominent signals are cited (d, doublet; m, multiplet; q, quartet; s, singlet; t, triplet). The mass spectra were obtained on a Hitachi RMU-6D mass spectrometer, operating with an ionization energy of 70 eV. The optical rotation was measured on a JASCO Model DIP-SL automatic polarimeter.

Isolation of Acetylparabenzlactone (1). Fresh leaves of *Parabenzoin trilobum* Nakai (15 kg) immersed in benzene (100 l) were heated under reflux for 7 h and then filtered. The filtrates were concentrated under reduced pressure to obtain a viscous residue. After the above procedure has been repeated, the total weight of the benzene extracts thus far obtained was 430 g. The viscous residue (100 g) was chromatographed on silica gel (Mallinckrodt, 100 mesh) (900 g). After the elution of shiromodiol monoacetate[1] with hexane–AcOEt (3: 1), further elution with hexane–AcOEt (2: 1) afforded a crude oil (3.0 g), which was then rechromatographed on silica gel (Mallinckrodt, 100 mesh) (55 g) and eluted with $CHCl_3$ to give a slightly crude material (1.5 g). Further purification was carried out using preparative TLC (Kieselgel PF_{254}; $CHCl_3$) to give colorless needles of acetylparabenzlactone (**1**) (605 mg) in a pure state; mp 134—136 °C (from hexane–benzene)[7]; $[\alpha]_D^{28}$ −19.6° (c=0.82 in dioxane); λ_{max} 286 and 236 nm (ε, 7500 and 7800 respectively); ν_{max} ($CHCl_3$) 1770, 1745, 1240, and 1045 cm^{-1}; δ 2.10 (3H, s), 2.6—3.0 (4H, complex), 3.94 (2H, complex), 5.70 (1H, d, J=6.0 Hz), 5.91 (2H, s), 5.92 (2H, s), and 6.60 (6H, complex); m/e 412 (M^+), 352, 175, 151, and 135 (Found: C, 64.24; H, 4.80%. Calcd for $C_{22}H_{20}O_8$: C, 64.07; H, 4.89%).

Base-catalysed Reaction of Acetylparabenzlactone (1). A solution of **1** (150 mg) in 2% methanolic KOH (10 ml) was stirred at room temperature for 1.5 h, and then made acidic

with a dil HCl aq solution and extracted with $CHCl_3$. The extract was washed with water and then dried over anhydrous $MgSO_4$. The subsequent removal of the solvent under reduced pressure gave a pale yellow liquid, which was separated by preparative TLC (Kieselgel PF_{254}) using $CHCl_3$–Et_2O (3: 1) to give two deacetyl compounds [**2** (88 mg) and **3** (28 mg)] in a pure state. The physical data of these two compounds are shown below. Particularly, the recrystallization of the former from hexane–benzene gave (−)-parabenzlactone (**2**) with a mp of 156—158 °C (lit,[3] 159—161 °C) (mixed mp and IR spectrum); δ 1.64 (1H, br. s), 2.13 (1H, br. s, OH), 2.60 (1H, q, J=7.5 Hz), 2.95 (2H, br. s), 3.94 (2H, d, J=7.0 Hz), 4.60 (1H, d, J=6.5 Hz), 5.92 (2H, s), 5.96 (2H, s), and 6.68 (6H, complex); *m/e* 370 (M^+), 352, 175, 151, and 135 (Found: C, 65.04; H, 4.68%. Calcd for $C_{20}H_{18}O_7$: C, 64.86; H, 4.90%).

*Isoparabenzlactone (**3**) as a Colorless Viscous Liquid*: ν_{max} ($CHCl_3$) 3400 and 1770 cm^{-1}; δ 1.92 (1H, s, OH), 2.25 (1H, br. s), 3.03 (3H, complex), 3.50 (2H, complex), 5.13 (1H, d, J=8.0 Hz), 5.92 (2H, s), 5.93 (2H, s), 6.59 (1H, s), and 6.70 (5H, near s); *m/e* 370 (M^+), 178, 151, and 135 (Found: *m/e* 370.10706. Calcd for $C_{20}H_{18}O_7$: *m/e* 370.10523).

*Acetylation of (−)-Parabenzlactone (**2**).* A solution of **3** (35 mg) in Ac_2O–pyridine [1: 2 (1.5 ml)] was allowed to stand at room temperature overnight and was then diluted with $CHCl_3$ (30 ml). The chloroform solution was washed with water and then dried over anhydrous $MgSO_4$. The subsequent removal of the solvent under reduced pressure left a residue which was purified by preparative TLC (Kieselgel PF_{254}; $CHCl_3$) to give the original acetate (**1**) (33 mg) (mp, TLC and IR spectrum).[3,7]

*Acetylation of Isoparabenzlactone (**3**).* According to the same procedure as has been described above, the alcohol **3** (30 mg) was treated with Ac_2O–pyridine [1: 2 (1.5 ml)] to give a colorless viscous liquid (27 mg), which was then crystallized from hexane–benzene to afford colorless needles of acetylisoparabenzlactone (**4**); mp 56—58 °C; $[\alpha]_D^{28}$ +97.3° (*c* 1.47 in dioxane); λ_{max} 287 and 237 nm (ε, 7300 and 7700, respectively); ν_{max} ($CHCl_3$) 1770 and 1740 cm^{-1}; δ 2.00 (3H, s), 2.43 (1H, heptette, J=8.0 Hz), 2.8—3.2 (3H, complex), 3.95 (2H, m), 4.98 (1H, d, J=8.5 Hz), 5.91 (2H, s), 5.92 (2H, s), and 6.70 (6H, complex); *m/e* 412 (M^+), 220 and 135 (Found: *m/e* 412.11389. Calcd for $C_{22}H_{20}O_8$: *m/e* 412.11581).

*Hydrogenolysis of (−)-Parabenzlactone (**2**).* The catalytic hydrogenation of **2** (15 mg) in EtOH (3 ml) containing 3 drops of a 60% aq. $HClO_4$ solution was carried out over freshly prepared palladium (30 mg) at room temperature overnight. After the addition of AcOEt (20 ml), the catalyst was removed by filtration. The filtrate was washed with water and then dried over anhydrous $MgSO_4$. The subsequent removal of the solvent under reduced pressure gave a crude oil, which was purified by preparative TLC (Kieselgel PF_{254}; $CHCl_3$) to give a colorless viscous liquid (10 mg) which was completely identical with an authentic sample of (−)-hinokinin (**5**) (IR and CD spectra).

The authors wish to thank Professor Katsura Munakata and Dr. Kojiro Wada (Nagoya University) for providing them with the authentic samples of (−)-parabenzlactone and its acetate. They are also indebted to Professor Masao Noro (Meijo University) for the collection of the plant *Parabenzoin trilobum* Nakai.

References

1) K. Wada, K. Matsui, Y. Enomoto, O. Ogiso, and K. Munakata, *Agr. Biol. Chem.*, **34**, 941 (1970); K. Wada, Y. Enomoto, and K. Munakata, *ibid.*, **34**, 946 (1970).

2) M. Niwa, M. Iguchi, and S. Yamamura, *Tetrahedron Lett.*, **1975**, 3661.

3) K. Wada and K. Munakata, *Tetrahedron Lett.*, **1970**, 2017.

4) Collected at Sanage, Aichi-ken, in late October.

5) R. S. Burden, L. Crombie, and D. A. Whiting, *J. Chem. Soc., C*, **1969**, 693, and the references cited therein.

6) M. Kuhn and A. von Wartburg, *Helv. Chim. Acta*, **50**, 1546 (1967).

7) Wada and Munakata have reported that an acetylation product of (−)-parabenzlactone has a melting point (142—146 °C) different from ours. This is due to the use of different kinds of recrystallization solvents.

BULLETIN OF THE CHEMICAL SOCIETY OF JAPAN, VOL. 49 (11), 3361—3362 (1976)

The Photochemical Synthesis of 5-Aryl-7,12-benz[*a*]anthracenediones from 1,4-Naphthoquinones and 1,1-Diarylethylenes

Kazuhiro MARUYAMA, Tetsuo OTSUKI, and Kiichiro MITSUI

Department of Chemistry, Faculty of Science, Kyoto University, Kyoto 606

(Received June 23, 1976)

Synopsis. By the photolysis of the benzene solution of a variety of 2,3-disubstituted (halogeno, methoxy, and acetoxy) 1,4-naphthoquinones, **1**, and 1,1-diarylethylenes, **2**, 5-aryl-7,12-benz[*a*]anthracenediones, **3**, are obtained in fairly good yields (22—68%).

In a previous study[1] the photochemical reaction of 2-bromo-3-methoxy-1,4-naphthoquinone, **1a**, with 1,1-diphenylethylene has been found to give 5-phenyl-7,12-benz[*a*]anthracenedione, **3a**. As an extension of that work, we wish now to report a more facile and general route for the preparation of 5-aryl-7,12-benz[*a*]-anthracenediones, **3**.

In the photochemical reaction of 2-alkoxy-3-bromo-1,4-naphthoquinones, *e.g.*, **1a**, with 1,1-diphenylethylene, **2a**, the methoxyl group and the bromine atom were both found to be missing during the course of the photolysis to give 5-phenyl-7,12-benz[*a*]anthracenedione, **3a**. Although 2-alkoxy-3-bromo-1,4-naphthoquinones are good substrates for the preparation of **3a**, several steps are required to prepare them as starting materials.[2]

In this work the reactivities of other 2,3-disubstituted 1,4-naphthoquinones, such as 2,3-dichloro-1,4-naphthoquinone, **1b**, 2,3-dibromo-1,4-naphthoquinone, **1c**, and 2-acetoxy-3-bromo-1,4-naphthoquinone, **1d**, in the photolysis were investigated. Since 5-phenyl-7,12-benz[*a*]anthracenedione, **3a**, was obtained in a satisfactory yield in every case examined here (see Table 1), not only alkoxyl group but also halogen atoms were concluded to be good leaving groups in the photochemical reaction. Because of the accessibility of quinones, such as 2,3-dichloro-1,4-naphthoquinone **1b**, our photochemical reaction could provide a more facile synthetic route to 5-phenyl-7,12-benz[*a*]anthracenedione, **3a**. The use of other substituted 1,1-diphenylethylenes, **2b—e**, in the reaction opens the route to give 5-aryl-7,12-benz[*a*]anthracenediones. Every combination of a quinone, **1**, and a 1,1-diarylethylene, **2**, resulted in a similar, smooth photochemical reaction to yield 5-aryl-7,12-benz[*a*]anthracenediones, **3** (Table 1).[3] The photochemical reaction of monosubstituted 1,1-diarylethylenes, **2b—e**, with the quinone, **1**, produced two possible isomers, **3I** and **3II**; they were isolated separately in some cases. The differentiation of the two isomers, **3I** and **3II**, depends on their NMR spectra; that is, the presence or the absence of the spin-spin coupling of the aromatic proton at C-1 (δ: 9.40—9.97 ppm, characterized by its lower chemical shifts) is the indicator. The C-1 aromatic proton of the isomer, **3II**, invariably shows a doublet signal (J=8—12 Hz) due to the spin-spin coupling with the C-2 aromatic proton, while the C-1 aromatic proton of the isomer, 3I, appears as a singlet or a slightly split doublet signal (J=2 Hz) (Table 2). Thus, the isomer ratio, **3I**/**3II**, was estimated from the integration of the NMR signals of the mixture (Table 1).

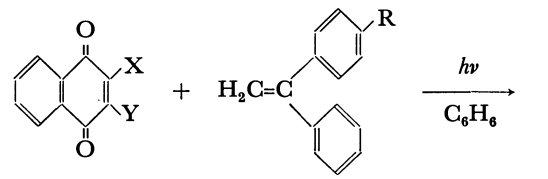

1

a: X=OCH_3, Y=Br
b: X=Y=Cl
c: X=Y=Br
d: X=O·CO·CH_3, Y=Br

2

a: R=H
b: R=CH_3
c: R=OCH_3
d: R=Cl
e: R=Br

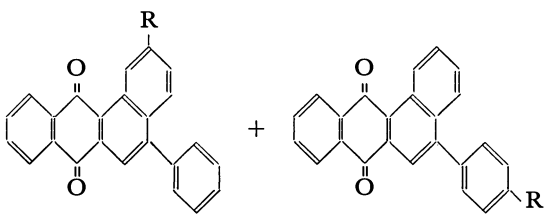

3I

a: R=H
b: R=CH_3
c: R=OCH_3
d: R=Cl
e: R=Br

3II

a: R=H(≡**3Ia**)
b: R=CH_3
c: R=OCH_3
d: R=Cl
e: R=Br

TABLE 1. THE YIELD OF 5-ARYL-7,12-BENZ[*a*]-ANTHRACENEDIONE, **3**, AND THE ISOMER RATIO (**3I**/**3II**)[a,b]

Quinone	Olefin				
	2a	**2b**	**2c**	**2d**	**2e**
1a	65%(**3a**)	50%(**3b**) (44/56)	68%(**3c**) (54/46)	61%(**3d**) (36/64)	62%(**3e**) (42/58)
1b	49%(**3a**)	28%(**3b**) (52/48)	28%(**3c**) (68/32)	34%(**3d**) (35/65)	30%(**3e**) (34/66)
1c	46%(**3a**)	29%(**3b**) (50/50)	34%(**3c**) (85/15)	22%(**3d**) (31/69)	42%(**3e**) (37/63)
1d	46%(**3a**)				

a) The yield was calculated on the basis of the quinone consumed. b) The isomer ratio was estimated from the integration of the NMR signal due to the aromatic proton at C-1.

Experimental

General Procedure. The benzene solution (20 ml) of a quinone (1 mmol) and a 1,1-diarylethylene (2 mmol) was

Table 2. Some physical and spectral properties of 5-aryl-7,12-benz[*a*]anthracenedione

	Mp	IR[a]	UV, λ_{max}[b,d] (ε)	NMR[c]	Mass (*m/e*)
3Ia	167.0—167.5 °C	1668 cm^{-1}	417nm (4.35×10^3)	7.4—8.4 ppm (13H, m)	334(M^+)
(**3IIa**)		(C=O)	368 (3.05×10^3)	9.78 (1H, C-1 CH, d, J=8.0 Hz)	
			334 (4.03×10^3)		
			291 (3.91×10^4)		
			249 (2.68×10^4)		
3Ib[d]	186 —189 °C	1666 cm^{-1}	424 (4.45×10^3)	2.60 (3H, CH_3, s)	348(M^+)
		(C=O)	371 (3.22×10^3)	7.1—8.3 (12H, m)	
			337(sh) (4.39×10^3)	9.52 (1H, C-1 CH, s)	
3IIb[d]			293 (3.63×10^4)	2.45 (3H, CH_3, s)	
			250 (2.98×10^4)	7.1—8.3 (12H, m)	
			245(sh) (2.77×10^4)	9.70 (1H, C-1 CH, d, J=10.0 Hz)	
3Ic[d]	177 —179 °C	1663 cm^{-1}	430 (5.32×10^3)	4.04 (3H, OCH_3, s)	364(M^+)
		(C=O)	293 (3.61×10^4)	7.0—8.5 (12H, m)	
			248 (3.20×10^4)	9.40 (1H, C-1 CH, d, J=2.0 Hz)	
3IIc[d]				3.93 (3H, OCH_3, s)	
				7.0—8.5 (12H, m)	
				9.84 (1H, C-1 CH, d, J=9.0 Hz)	
3Id[d]	197 —200 °C	1651 cm^{-1}	416 (2.30×10^3)	7.2—8.3 (12H, m)	370($M^+(Cl^{37})$, 38%)
		(C=O)	366 (1.62×10^3)	9.74 (1H, C-1 CH, s)	368($M^+(Cl^{35})$, 100%)
3IId[d]			290 (2.00×10^4)	7.2—8.3 (12H, m)	
			250 (1.56×10^4)	9.71 (1H, C-1 CH, d, J=12.0 Hz)	
3Ie	219.0—219.5 °C	1658 cm^{-1}	416 (4.84×10^3)	7.4—8.5 (12H, m)	414($M^+(^{81}Br)$, 100%)
		(C=O)	367 (3.42×10^3)	9.97 (1H, C-1 CH, d, J=2.0 Hz)	412($M^+(^{79}Br)$, 97%)
3IIe	231.5—233.0 °C	1663 cm^{-1}	290 (4.16×10^4)	7.4—8.5 (12H, m)	
		(C=O)	249 (3.35×10^4)	9.71 (1H, C-1 CH, d, J=8.0 Hz)	

a) The IR spectrum was measured as the state of the KBr disk. b) The UV spectrum was measured as the solution of chloroform. c) The NMR spectrum was measured as the solution of deuterated chloroform, and the chemical shifts were calibrated from TMS as the internal standard. d) The data were measured as a mixture of two isomers.

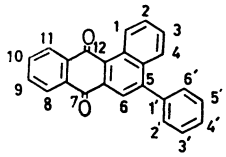

irradiated by means of a high-pressure Hg arc lamp (300 W) through a 5-cm-thick water layer at room temperature. After the complete consumption of the quinone —in general, it takes about 10 h of irradiation, the solvent was distilled off under a reduced pressure. The subsequent purification of the reaction mixture by using chromatography on silica gel gave 5-aryl-7,12-benz[*a*]anthracenediones as a mixture of two isomers; this mixture was further purified by recrystallization from benzene–hexane. The yields, the isomer ratios, and the physical properties of the products are summarized in Tables 1 and 2. The general procedures for the elucidation of the structure, **3**, were given in the previous communication.[1]

Starting Materials. 2-Bromo-3-methoxy-1,4-naphthoquinone,[2] 2,3-dibromo-1,4-naphthoquinone,[4] 2-acetoxy-3-bromo-1,4-naphthoquinone,[5] 1-(*p*-methylphenyl)-1-phenylethylene,[6] 1-(*p*-methoxyphenyl)-1-phenylethylene,[6] 1-(*p*-chlorophenyl)-1-phenylethylene,[7] and 1-(*p*-bromophenyl)-1-phenylethylene[8] were all synthesized according to the usual method; the physical and spectral data were all compatible with those described in the literature.

References

1) K. Maruyama and T. Otsuki, *Chem. Lett.*, **1975**, 87.

2) *Cf.* R. B. Woodward, F. Sondheimer, D. Taub, K. Hensler, and W. M. McLamore, *J. Am. Chem. Soc.*, **74**, 4223 (1952); L. F. Fieser and R. H. Brown, *ibid.*, **71**, 3609 (1949).

3) For the photochemical reaction of other 1,4-naphthoquinones with several olefins, see the following: K. Maruyama, T. Otsuki, A. Takuwa, and S. Kako, *Bull. Inst. Chem. Res., Kyoto Univ.*, **50**, 348 (1972); K. Maruyama, Y. Naruta, and T. Otsuki, *Bull. Chem. Soc. Jpn.*, **48**, 1553 (1975); T. Otsuki, *ibid.*, **49**, 2597 (1976).

4) Th. Zincke and M. Schmidt, *Ber.*, **27**, 2758 (1894).

5) **1d** was prepared through the acetylation of 2-bromo-3-hydroxy-1,4-naphthoquinone (O. Dimroth and E. Schultze, *Ann.*, **411**, 345 (1916)) with acetic anhydride–pyridine; mp 137.0—138.0 °C.

6) C. D. Hurd and C. N. Webb, *J. Am. Chem. Soc.*, **49**, 549 (1927).

7) E. Bergmann and A. Bondi, *Ber.*, **64**, 1455, 1468 (1931).

8) E. Bergmann, L. Engel, and H. Meyer, *Ber.*, **65**, 446, 456 (1932).

BULLETIN OF THE CHEMICAL SOCIETY OF JAPAN, VOL. 49 (11), 3363—3364 (1976)

The Structure of Hamayne, a New Alkaloid from *Crinum asiaticum* L. *var. japonicum* Baker

Masamitsu Ochi, Hitoshi Otsuki, and Kosho Nagao

Faculty of Arts and Sciences, Kochi University, Asakura, Kochi 780

(Received July 2, 1976)

Synopsis. The structure of hamayne isolated from the fruit of *Crinum asiaticum* L. *var. japonicum* Baker was established to be *O*-demethylcrinamine (IV) on the basis of spectral and chemical evidence.

Kutani and Matsumoto have reported the isolation of lycorine (I) from the fruit (or seed) of *Crinum asiaticum* L. *var. japonicum* Baker.[1] Reinvestigation of the alkaloidal components in the fruit of this plant led to the isolation of three additional alkaloids, crinamine (II), *O,N*-diacetyl-*N*-demethylgalanthamine (III),[2] and a new alkaloid. In this paper, we will deal with the structural elucidation of the new alkaloid designated as hamayne.

Hamayne (IV), $C_{16}H_{17}O_4N$, mp 79—80 °C, $[\alpha]_D^{12}$ +43° (*c* 0.1, EtOH), was obtained in a 0.002% yield from fresh fruit by partitioning and careful column chromatography. IV shows a hydroxylic absorption in the IR (KBr) spectrum at 3400 cm^{-1} and forms a diacetate (V), $C_{20}H_{21}O_6N$, mp 77.5—78 °C, the IR spectrum of which no longer exhibits a hydroxyl group. The NMR spectrum of V shows signals due to two acetyl groups at δ 2.01 and 2.07 (3H each, s), a benzyl methylene group linked to a nitrogen atom at δ 3.66 and 4.32 (1H each, AB q, J=18 Hz), a methylenedioxy group at δ 5.89 (2H, s), and two aromatic protons at δ 6.46 and 6.84 (1H each, s). In addition, the NMDR data of V indicate the presence of two groupings, $-CH(OAc)-CH_2-N<$[δ 3.40 (2H, d, J=6 Hz) and 4.95 (1H, t, J=6 Hz)] and $-CH_A=CH_B-CH_C(OAc)-$[δ_A 6.21 (1H, dd), δ_B 5.87 (1H, dd), and δ_C 5.44 (1H, m); J_{AB}=10 Hz, $J_{AC}=J_{BC}$=2 Hz]. These facts suggest that IV has a structure analogous to that of crinamine (II), in which the methoxyl group is replaced by a hydroxyl group. This was confirmed by the conversion of IV into apohaemanthamine (VI).[4] Thus, the treatment of IV with 6 M hydrochloric acid gave VI, which was also obtained by a similar treatment from II.[4] The configuration at C-3 was proven as follows. In the NMR spectrum of V, the signal due to C-1 proton appears as a doublet of doublets at δ 6.21 as a result of the coupling with the C-2 and C-3 protons, the allylic coupling constant ($J_{1,3}$=2 Hz) of which corresponds to that of C-3 equatorial (α-oriented) acetate.[5] This observation indicates that IV and II have the same configuration at C-3. Therefore, hamayne (IV) must be *O*-demethylcrinamine.

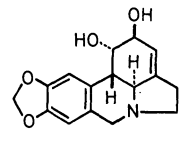

I

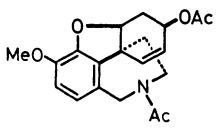

III

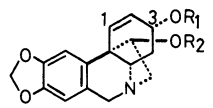

II R1 = Me, R2 = H

IV R1 = R2 = H

V R1 = R2 = Ac

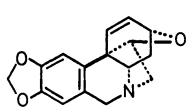

VI

Experimental

All mps are uncorrected. The IR and UV spectra were recorded on a JASCO model IR-S and a Hitachi EPS-3T spectrophotometer, respectively. The NMR spectra were determined, using a JEOL PS-100 spectrometer, in $CDCl_3$ solutions with TMS as an internal standard unless otherwise stated. A Rex Optical Works apparatus, model NEP-2, was used for the measurement of the rotations.

Isolation. Fresh fruit of *Crinum asiaticum* L. *var. japonicum* Baker (19.2 kg), collected in the garden of the Usa Marine Biological Station, Kochi University, in August 1974, were chopped up and extracted with 20 l of methanol for 2 months. The methanol extract was concentrated up to about 2 l, leaving an aqueous solution. This solution, after filtration, was basified with solid Na_2CO_3 and extracted with 3 l of chloroform. The chloroform insoluble alkaloids containing lycorine were deposited between two layers. These alkaloids (16.5 g) were collected by filtration. The chloroform layer was washed with water, dried over Na_2SO_4 and evaporated to dryness. The residue (5.08 g) was repeatedly subject to chromatography over silicic acid. Elution with $CHCl_3$–AcOEt–MeOH (5: 5: 1) gave crinamine (II) (0.684 g) (mp and IR) and the fractions eluted with $CHCl_3$–AcOEt–MeOH (5: 5: 2) yielded hamayne (IV) (0.371 g): plates from acetone; mp 79—80 °C, $[\alpha]_D^{12}$ +43° (*c* 0.1, EtOH); UV (EtOH) nm (ε) 240 (4380) and 296 (7010). Found: C, 64.42; H, 6.47; N, 4.32%. Calcd for $C_{16}H_{17}O_4N \cdot 2/3H_2O$: C, 64.20; H, 6.17; N, 4.68%.

The more polar fractions eluted with $CHCl_3$–AcOEt–MeOH (1: 1: 1) were combined and evaporated to dryness. The residue (1.07 g) was acetylated with acetic anhydride (15 ml) and pyridine (30 ml) by heating under reflux for 3 h and worked up in the usual way. The resulting precipitates were chromatographed over silicic acid, with $CHCl_3$–MeOH (99: 1) as the eluent, to give *O,N*-diacetyl-*N*-demethylgalanthamine (III) (0.784 g) (mp, IR, NMR, and chemical properties).[6]

Acetylation of IV. A solution of IV (50 mg) in acetic anhydride (1 ml) and pyridine (2 ml) was refluxed for 3 h and then worked up in the usual way to afford V (34 mg): needles from methanol; mp 77.5—78 °C; IR (Nujol) 1730 cm^{-1}. Found: C, 64.70; H, 5.70; N, 3.61%. Calcd for $C_{20}H_{21}O_6N$: C, 64.88; H, 5.70; N, 3.77%.

Formation of VI. The procedure of Fales and Wildman[4] was followed: a solution of IV (76 mg) in 2.5 ml of 6 M hydrochloric acid was heated at 100 °C for 1 h. The solution was poured into 75 ml of water, basified with aqueous ammonia

and extracted with chloroform. The chloroform layer was washed with water, dried with Na_2SO_4 and concentrated. The residual oil (69 mg) was subject to chromatography over silicic acid, and the elution with benzene–AcOEt (9: 1) gave VI (28 mg) (mp, IR, and NMR).

We are grateful to Professor T. Tokoroyama of Osaka City University for the measurement of NMR and to Professor K. Yatsuzuka of Usa Marine Biological Station, Kochi University, for the providing of the plants.

References

1) N. Kutani and Y. Matsumoto, *Yakugaku Zasshi*, **64**, 239 (1944).
2) *N*-Demethylgalanthamine may be the plant constituent. See also Ref. 6.
3) This signal was observed in C_6D_6.
4) H. M. Fales and W. C. Wildman, *J. Am. Chem. Soc.*, **82**, 197 (1960).
5) R. D. Haugwitz, P. W. Jeffs, and E. Wenkert, *J. Chem. Soc.*, **1965**, 2001.
6) S. M. Laiho and H. M. Fales, *J. Am. Chem. Soc.*, **86**, 4434 (1964).

BULLETIN OF THE CHEMICAL SOCIETY OF JAPAN, VOL. 49 (11), 3365—3366 (1976)

A General Synthetic Method for 1-Substituted 1,4-Dihydro-3(2*H*)-isoquinolinones

Hiroshi KOTAKE, Hideki KINOSHITA, Katsuhiko INOMATA, and Hiroshi MASUDA

Department of Chemistry, Faculty of Science, Kanazawa University, Kanazawa 920

(Received July 12, 1976)

Synopsis. The reaction conditions for the conversion of **3** into **4** were investigated in some detail, and it was found that the reductive amination of *o*-acylphenylacetic acid was allowed to proceed smoothly by the use of deactivated Raney nickel.

In the previous paper[1] it was shown that the reductive amination of *o*-acetylphenylacetic acid (**3a**) afforded 1-methyl-1,4-dihydro-3(2*H*)-isoquinolinone (**4a**) in the presence of Raney nickel in good yield. From this result we were interested in the investigation of the general utility of the reductive amination of this type for synthesis of 1-alkyl or 1-aryl 1,4-dihydro-3(2*H*) isoquinolinones (**4**), which may be easily converted to the corresponding tetrahydroisoquinoline by the action of $LiAlH_4$ or B_2H_6. We report here the results of a detailed study of the reductive amination of *o*-acylphenylacetic acids and provide evidence of the generality of this method.

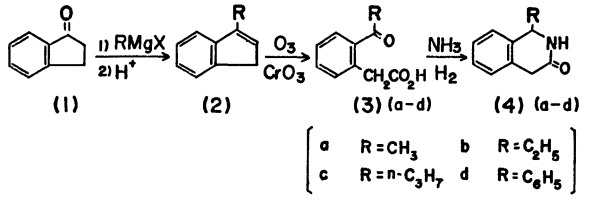

o-Acylphenylacetic acids (**3**) (**b**—**d**) were prepared easily by a Grignard reaction of indanone (**1**), followed by ozonolysis which was accompanied by oxidation with CrO_3.

Initially, the reaction condition was examined for the ring formation of *o*-propionylphenylacetic acid as a model. *o*-Propionylphenylacetic acid (**3b**) was treated with ammonia in the presence of Raney nickel in an autoclave to give a mixture of three compounds. After

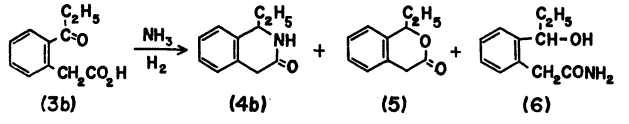

chromatographic separation, three main compounds, **4b**, **5**, and **6**, were isolated in yields of 49, 4.4, and 34%, respectively. The structures of these compounds were confirmed by means of spectroscopic evidence and elemental analysis. This result suggested that a competing reaction took place in the reductive amination reaction. This finding showed that it was necessary to reduce the activity of Raney nickel (W-5) toward the carbonyl group in order to avoid this unfavorable competing reaction. The deactivation of Raney nickel was achieved by treatment with acetone (soaking for 1.5 h at room temperature). When the reductive amination of *o*-propionylphenylacetic acid (**3b**) was carried out under the same reaction conditions using deactivated Raney nickel, 1-ethyl-1,4-dihydro-3(2*H*)-isoquinolinone (**4b**) was obtained in high yield. 1-Propyl- and 1-phenyl-1,4-dihydro-3(2*H*)isoquinolinone (**4c** and **4c**) were also obtained in high yields, as shown in the table, by the same procedure using deactivated Raney nickel.

TABLE 1. YIELDS OF **4** (**b**–**d**) FROM **3** (**b**–**d**)

R	3	4	
	Mp (°C)	Mp (°C)	Yield (%)
$-CH_2CH_3$	137 —138	107	86
$-CH_2CH_2CH_3$	115.5—116.5	97— 98	65
$-C_6H_5$	128.5—130	141.5—144	74

Experimental

All the melting points are uncorrected. The NMR and IR spectra were recorded on JEOL JNM-60 and JASCO IRA-1 spectrometers, respectively.

1-Ethyl-1,4-dihydro-3(2H)-isoquinolinone (4b). *Method A*: Raney nickel and a soln of *o*-propionylphenylacetic acid (**3b**) (300 mg) in ethanol (30 ml) previously saturated with ammonia were placed in an autoclave, and the reaction was carried out for 7 h at 110 °C in an atmosphere of hydrogen at 70 atm. After the reaction, the solvent was removed *in vacuo*, and the resulting residue was subjected to preparative TLC to give three compounds: 1-ethyl-1,4-dihydro-3(2*H*)-isoquinolinone (**4b**), lactone (**5**), and amide (**6**), in yields of 49% (134 mg), 4.4% (12 mg), and 34% (103 mg), respectively. Compound **4b**: mp 107 °C; IR (KBr): 3180, 3050, 1690 cm^{-1}; NMR ($CDCl_3$): δ 0.90 (t, 3H), 1.79 (pentuplet, 2H), 3.55 (s, 2H), 4.41 (t, 1H), 7.14 (s, 4H), 7.55—7.90 (b, 1H); Found: C, 75.67; H, 7.43; N, 8.21%. Calcd for $C_{11}H_{13}ON$: C, 75.40; H, 7.48; N, 7.99%. Compound **5**: colorless oily liquid; IR (Neat): 1740, 1235, 1150 cm^{-1}; NMR (CCl_4): δ 1.08 (t, 3H), 1.97 (dq, 2H), 3.57 (s, 2H), 5.14 (t, 1H), 7.15 (s, 4H). Compound **6**: mp 98—99.5 °C; IR (KBr): 3280, 3100, 1650, 1010 cm^{-1}; NMR ($CDCl_3$): δ 0.88 (t, 3H), 1.73 (pentuplet, 2H), 3.55 (s, 2H), 3.94 (bs, 1H), 4.66 (t, 1H), 6.06 (bs, 2H), 7.10—7.50 (m, 4H); Found: C, 68.07; H, 7.96; N, 7.27%. Calcd for $C_{11}H_{15}O_2N$: C, 68.37; H, 7.82; N, 7.25%.

Method B: Raney nickel (W-5) was soaked in acetone before use at room temperature in order to reduce the activity. When the reductive amination of **3b** was carried out under the same reaction conditions as described above using Raney nickel which was soaked in acetone for 90 min at room temperature, **4b** was obtained in an 86% yield accompanied by small amount of **6**. On the other hand, when the soaking time of the catalyst in acetone was shortened from 90 min to 40 min, the reductive amination gives rise to **4b**, **5**, and **6** in yields of 60%, 2.2%, and 15%, respectively.

1-Propyl-1,4-dihydro-3(2H)-isoquinolinone (4c). **4c** was

obtained in a 65% yield by the reductive amination of **3c** according to method B. Mp 97—98 °C; IR (KBr): 3180, 3050, 1680 cm^{-1}; NMR ($CDCl_3$): δ 0.91 (t, 3H), 1.14—1.90 (m, 4H), 3.52 (s, 2H), 4.20—4.60 (t, 1H), 6.80—7.32 (m, 5H); Found: C, 75.78; H, 8.03; N, 7.24%. Calcd for $C_{12}H_{15}ON$: C, 76.15; H, 7.99; N, 7.40%.

*1-Phenyl-1,4-dihydro-3(2H)-isoquinolinone (**4d**).* This compound was obtained in a 74% yield by the reductive amination of **3d** according to method B. mp 141.5—144 °C; IR (KBr): 3190, 3050, 1660 cm^{-1}; NMR ($CDCl_3$): δ 3.60 (s, 2H), 5.50 (s, 1H), 6.77—7.34 (m, 10H): Found: C, 80.36; H, 5.69; N, 6.31%. Calcd for $C_{15}H_{13}ON$: C, 80.69; H, 5.87; N, 6.27%.

Reference

1) H. Kotake, A. Kawashiri, S. Miyashita, and H. Kinoshita, *Nippon Kagaku Zasshi*, **92**, 878 (1971).

Nature of Oxygen Species Incorporated into Acrylaldehyde in Vapor-Phase Oxidation of Propylene over Supported Copper Catalyst

Masamichi AKIMOTO, Masao AKIYAMA, and Etsuro ECHIGOYA

Department of Chemical Engineering, Tokyo Institute of Technology, Ookayama, Meguro-ku, Tokyo 152

(Received December 11, 1975)

The oxidation of propylene with Cu_2O as active phase for acrylaldehyde formation gave no acrylaldehyde in contrast to the fully oxidized CuO–SiC. However, CuO–SiC from which adsorbed oxygen species was eliminated gave rise to the formation of a negligible amount of acrylaldehyde. The presence of molecular oxygen species adsorbed on the CuO–SiC was shown by the desorption of oxygen and the isotopic mixing reaction of ^{16}O—^{18}O. The adsorbed oxygen (possibly molecular oxygen species) seems to be necessary as oxygen incorporated into acrylaldehyde. Agreement of the ratio of $^{18}O/^{16}O$ in acrylaldehyde formed by the oxidation with oxygen containing ^{18}O over $Cu_2{}^{16}O$ with that of $^{18}O/^{16}O$ in the reaction mixture supports the role of adsorbed oxygen species. The presence of O_2^- over Cu_2O during the course of oxidation was confirmed by the formation of furan and maleic anhydride in the co-oxidation with butadiene. The results were discussed in relation to the structure of the catalyst suitable for selective oxidation, the incorporation of oxygen atom *via* electronegative oxygen species adsorbed being proposed.

The vapor-phase oxidation of propylene to acrylaldehyde over copper(I) oxide has been investigated, some of the results being summarized.[1-3] Studies were mostly focused on the determination of intermediate hydrocarbon species *via* which acrylaldehyde is formed. The initial removal of a hydrogen atom from the methyl group to form an allylic intermediate was proposed by many workers.[4-6] However, not much attention has been paid to the form of oxygen species participating in the selective oxidation of propylene to acrylaldehyde. In this selective oxidation, oxygen plays two roles, *i.e.*, abstraction of hydrogen atoms and addition to the formed intermediate hydrocarbon species.

In general, the lattice oxygen of transition metal oxides is capable of hydrogen abstraction, differing with the type of metal-oxygen bond. However, the lattice oxygen is not always incorporated into selective oxidation products, as seen in the special role of double bond type lattice oxygen in the oxidation of butadiene to maleic anhydride.[7,8] Wood and co-workers[9] assumed in their semiconductivity studies on the oxidation of propylene over Cu_2O that electronegative oxygen species sorbed on the surface is the active species for acrylaldehyde formation. On the other hand, Callahan and Grasselli[10] showed that the lattice oxygen of copper oxide catalyst is involved in acrylaldehyde formation. The form of oxygen species incorporated into acrylaldehyde has not been sufficiently clarified. We have investigated the vapor-phase oxidation of propylene over supported copper catalyst as regards the nature of oxygen species incorporated into acrylaldehyde by means of X-ray analysis, oxygen isotope (^{18}O) and co-oxidation with butadiene or furan. The results were discussed in relation to the structure of the catalyst suitable for acrylaldehyde formation.

Experimental

Vapor-phase catalytic oxidation of propylene was performed using a conventional flow microreactor and a pulse reactor under atmospheric pressure. The microreactor was a Pyrex tube of inner diam 12 mm and length 300 mm with a concentric thermowell; the pulse reactor was a 4 mm inner diam U-type Pyrex tube. Heating was carried out with a cylindrical fluidized thermal bath. The catalyst was diluted with 30—50 mesh quartz, Raschig rings (2.5 $\times$ 2.5 mm) being used as a preheating medium.

As reacting substances, air, propylene (99% up), butadiene (99% up) and reagent grade furan were used. Nitrogen, hydrogen and helium were supplied from commercial cylinders. Gaseous oxygen containing ^{18}O (Japan-Isotope Association) was used. The air was purified by passing through silica gel and a soda-lime tower in order to remove water and CO_2. Helium was used as a carrier gas for oxidation by means of pulse technique. A trace amount of impurities such as oxygen existing in helium was removed by passing through a molecular sieve 13X column (4 mm inner diam, 1 m) cooled with liquid nitrogen.

CuO–SiC catalyst was prepared as follows. SiC (60—80 mesh) was calcined at 1000 °C for 4 h in a furnace. The precipitate obtained by the addition of an aqueous solution of Na_2CO_3 to the suspension of the calcined SiC in an aqueous solution of $Cu(NO_3)_2$ was thoroughly washed with water and then dried on a water-bath. The mass obtained was then calcined at 500 °C for 5 h in the air. The amount of CuO supported is 6.2 wt%, and the surface area is about 0.3 m^2/g. The catalyst was reduced with hydrogen current at 400 °C for 1.5 h prior to the experiment. Cu_2O was prepared according to two methods: (a) by the reduction of $Cu(AcO)_2$ with 1 N hydrazine in an aqueous media[11] (denoted by Cu_2O (I)); (b) by the addition of 10% aqueous solution of glucose to an aqueous mixture of $CuSO_4$, sodium potassium tartarate and NaOH at 100 °C[12] (denoted by Cu_2O(II)). The products were found to be pure by X-ray diffraction. The reduction of CuO–SiC was carried out by immersion into an aqueous solution of hydrazine at room temperature, the amount of nitrogen evolved being measured with a capillary glass tube.

The gaseous effluent from the reactor was analyzed by gas chromatography. PEG 20 M 20 wt% on Neopak 1A (acrylaldehyde, furan, acetaldehyde) and propylene carbonate 40 wt% on Celite 545 (CO_2) were used as separating columns. Maleic anhydride formed was absorbed in water followed by boiling of the solution in order to remove dissolved CO_2 and titration with an aqueous solution of NaOH. The structure of the catalyst was investigated by X-ray diffraction using nickel-filtered Cu $K\alpha$ radiation (30 kV, 20 mA). The isotopic mixture of gaseous oxygen or acrylaldehyde was analyzed by means of mass spectroscopy. Adsorption of

oxygen on the reduced catalyst was measured with a conventional volumetric apparatus.

Results

Active Phase for the Selective Oxidation. The oxidation of propylene (C_3' 28.0 vol%, O_2 5.0 vol%, and N_2 67.0 vol%) at W/F=0.934 g-catalyst h/g-mol became observable at 320 °C. Acrylaldehyde, CO_2 and a very small amount of CH_3CHO were formed. Above 370 °C, a gradual decrease in selectivity appeared. However, change in activity and selectivity was hardly observable at 350 °C during the course of oxidation. The selectivity is independent of the contact time below W/F=0.934 g-catalyst h/g-mol at 350 °C, as shown in Fig. 1. The steady state of the catalyst during oxidation under the reaction conditions was quenched by the introduction of helium (200 NTP ml/min) for 5 min to eliminate the reactant gas followed by a rapid decrease in temperature. X-Ray diffraction of the catalyst was observed at 2θ=36.3, 42.3, 61.4 (strong), and 38.8° (weak). The catalyst is composed of Cu_2O and a very small amount of CuO.

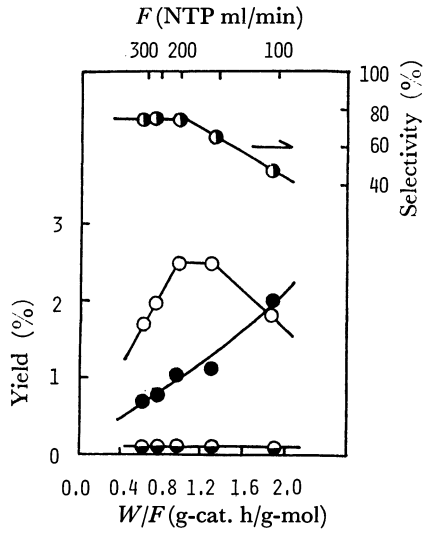

Fig. 1. Effect of the contact time on the oxidation of propylene.
Feed: C_3' 28.0 vol%, O_2 5.0 vol%, N_2 67.0 vol%.
Temp: 350 °C.
○: Yield of acrylaldehyde, ●: yield of CO_2, ◒: yield of acetaldehyde, ◑: selectivity to acrylaldehyde.

Table 1. Oxidation of propylene with various copper oxides using a pulse method[a)]

Oxidant	Pulse No.	Yield (%) Acrylaldehyde	Yield (%) CO_2	Selectivity (%) Acrylaldehyde
Cu_2O(I) 0.040 g	1	0.00	0.30	0.00
	2	0.00	0.21	0.00
	3	0.00	0.19	0.00
Cu_2O(II) 0.040 g	1	0.00	0.28	0.00
	2	0.00	0.18	0.00
	3	0.00	0.18	0.00
CuO-SiC 0.50 g	1	1.01	5.76	14.9
	2	0.11	0.86	11.3
	3	0.00	0.93	0.00
CuO-SiC 0.50 g treated with hydrazine	1	0.06	4.28	1.38
	2	0.00	0.55	0.00
	3	0.00	0.36	0.00

a) Temp: 350 °C, carrier gas: He 45 NTPml/min, pulse: C_3' 5.69 NTPml.

Oxidation of Propylene with Copper Oxides. The oxidation of propylene with various copper oxides was carried out by the pulse method. Only propylene was successively injected over the oxides (Table 1). In the case of Cu_2O (I) and Cu_2O (II), no formation of acrylaldehyde was observed even on the first injection in contrast to the case of CO_2. Use of 0.20 g Cu_2O (I) also gave the same result. In contrast, acrylaldehyde was formed in the first and second injections onto CuO–SiC which was prepared by reduction with hydrogen at 400 °C for 1.5 h followed by oxidation with air current at 350 °C. The amount of oxygen participating in acrylaldehyde formation and complete oxidation up to the second injection is 0.128 and 3.390 NTP ml/g-catalyst, respectively. However, when the CuO–SiC had been treated with 1 N NH_2–NH_2 at room temperature with evolution of 0.80 NTP ml N_2/g-catalyst, only a trace amount of acrylaldehyde was formed. X-Ray diffraction of this treated catalyst was observed at 2θ=35.7, 38.8, and 48.9° (strong). Thus the product is CuO.

Reduction of the Catalyst and Adsorption of Oxygen. Reduction of CuO–SiC with an aqueous solution of hydrazine (0.1 N) and adsorption of gaseous oxygen on the reduced one were performed in order to clarify the form of oxygen removed by treatment with the hydrazine solution. The hydrazine solution was heated at 80—90 °C for 10 min followed by cooling to room temperature. The solution was stirred for about 1 h until scarcely any evolution of nitrogen gas was observed. CuO–SiC catalyst was then introduced into the hydrazine solution and the amount of nitrogen evolved was determined (Fig. 2). CuO–SiC was prepared by the oxidation of the reduced catalyst with air current at 350 °C. An inflection point appears at 0.33 NTP ml N_2/g-catalyst (Fig. 2). No

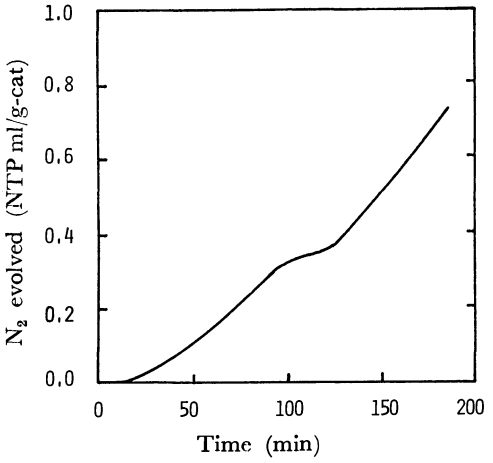

Fig. 2. Reduction of CuO–SiC catalyst with an aqueous solution of hydrazine.
CuO–SiC: 0.50 g, hydrazine: 0.1 N, temp: 18 °C.

definite inflection point was observed in the case of 1 N hydrazine. Adsorption of gaseous oxygen on the reduced catalyst was quantitatively studied. CuO–SiC reduced similarly was evacuated for 1 h at room temperature and again for 1 h at 250 °C. After determination of the dead volume of the adsorption apparatus, gaseous oxygen was introduced at room temperature and the catalyst was treated at 350 °C for 1 h. The amount of oxygen adsorbed was measured by observing the pressure drop of oxygen. When the amount of nitrogen evolved by the reduction was 0.30 or 0.60 NTP ml/g-catalyst, that of oxygen adsorbed was 0.32 or 0.63 NTP ml/g-catalyst at oxygen pressure of 137.6 or 133.6 Torr, respectively.

Isotopic Mixing Reaction of ^{18}O—^{16}O. $Cu^{16}O$–SiC was evacuated at 350 °C for 1.5 h in a vessel and then a mixture of oxygen ($^{18}O^{16}O$ 36.58, $^{16}O^{16}O$ 63.42 mol %) was introduced under 54 Torr at 20 °C. The isotopic mixing reaction was carried out at 198 °C. The gaseous oxygen was withdrawn to a small glass tube (*ca.* 1 ml) during the course of the reaction and was diluted with helium to *ca.* 5% O_2 followed by the analysis. Hardly any formation of $^{18}O^{18}O$ or change in the composition of the gaseous phase was observed (Fig. 3).

On the other hand, CuO–SiC (13.3 g) was evacuated at 525 °C under 10^{-5} Torr for 2 h. Oxygen was then adsorbed at 155 °C under $P_{O_2}=150$ Torr for 3 h. The oxygen pressure was then kept at room temperature overnight. After pumping out gaseous oxygen at room temperature, the temperature was raised and after 1 h, the amount of oxygen desorbed was determined by measuring the oxygen pressure. The amount was 0.007, 0.017, or 0.019 NTP ml/g-catalyst at 203, 350, or 448 °C, respectively.

Oxidation of Propylene with $^{18}O_2$ over $Cu_2{}^{16}O$. A pulse containing propylene and heavy oxygen was injected over $Cu_2{}^{16}O$ (I) at 350 °C and the acrylaldehyde formed was separated with a gas chromatographic column coupled with the outlet of the pulse reactor. Injection was repeated several times using new $Cu_2{}^{16}O$ (I) at each injection, and the content of ^{18}O in acrylaldehyde collected was determined (Table 2). For the sake of comparison, the result obtained by using $^{16}O_2$ is given in the Table. The relative intensity of the species was $I_{58}/I_{56}=0.213$ or $I_{57}/I_{55}=0.218$, the average being 0.215. The values were in good agreement with that of $^{18}O/^{16}O$ in the pulse.

Co-oxidation of Propylene with Furan or Butadiene over Cu_2O. In order to investigate the form of oxygen species present on Cu_2O during the course of oxidation of propylene, co-oxidation with furan or butadiene was performed with reference to the formation of maleic anhydride and furan. Oxidation of propylene was first carried out for 2 h and then furan or butadiene was supplied. The concentration of furan or butadiene in the feed was kept very low, 1.5—3.0 vol%, as com-

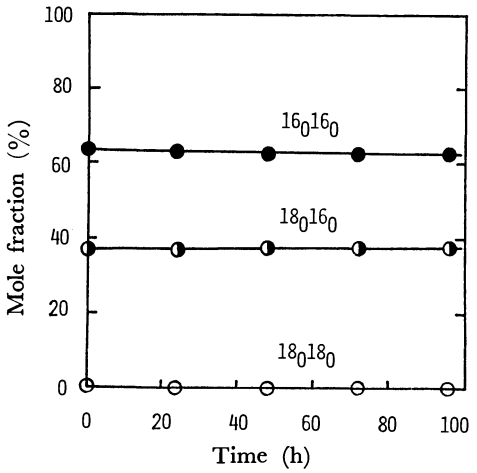

Fig. 3. Isotopic mixing reaction of ^{18}O—^{16}O over CuO–SiC catalyst.
Cat.: CuO-SiC 13.3 g, temp: 198 °C.

Table 2. Oxidation of propylene with oxygen containing ^{18}O over $Cu_2{}^{16}O$ using a pulse method[a]

m/e	Species	Intensity of mass spectra $^{16}O_2$[b]	Intensity of mass spectra $^{16}O-{}^{18}O$[c]	
55	CH_2=CH-C^{16}O	72	64	$I_{58}/I_{56}=0.213$
56	CH_2=CH-CH^{16}O	106	94	
57	CH_2=CH-C^{18}O	0	14	$I_{57}/I_{55}=0.218$
58	CH_2=CH-CH^{18}O	0	20	

a) Temp: 350 °C, carrier gas: He 45 NTPml/min, cat.: $Cu_2{}^{16}O$(I) 0.040 g, pulse: 5.69 NTPml, C_3' 28.0 vol%, O_2 5.0 vol%, N_2 67.0 vol%.
Composition of the oxygen in the pulse:
b) $^{18}O/^{16}O=0.000$. c) $^{18}O/^{16}O=0.216$.

Table 3. Co-oxidation of propylene with furan or butadiene over copper(I) oxide[a]

Temp (°C)	Furan or butadiene in feed(vol%)	Conversion of furan or butadiene(%)	Yield(%) Acrylaldehyde	CO_2	Furan	Maleic acid
352	0.00	—	1.17	0.37	0.00	0.00
352	Furan 1.55	9.38	0.35	1.01	—	0.23
375	Furan 1.55	11.7	0.47	1.75	—	0.19
378	Butadiene 3.00	5.21	1.30	1.79	0.54	0.07
400	Butadiene 3.05	6.03	1.15	2.66	0.52	0.12

a) Cat.: CuO-SiC 0.51 g, feed: C_3' 28.0 vol%, O_2 5.0 vol%, diluent N_2, $W/F=0.951$ g-catlyst h/g-mol, yield of CO_2 was calculated by propylene base.

pared with that of propylene, so that the catalyst would not change structurally. The formation of maleic anhydride or of furan and maleic anhydride in the cooxidation with furan or butadiene, respectively, is given in Table 3. The selectivity for maleic anhydride or furan and maleic anhydride formation was 1.6—2.5 or 10.6—11.7%, respectively.

Discussion

The catalyst consists of Cu_2O and a very small amount of CuO during the oxidation of propylene. Thus, Cu_2O is the active phase for acrylaldehyde formation in line with the results reported.[9,13,14] However, the oxidation of propylene with Cu_2O gave no acrylaldehyde in accordance with the result for the CuO–SiC reduced with hydrazine (Table 1). This supports strongly the view that the lattice oxygen of Cu_2O and CuO is not incorporated into acrylaldehyde though it can abstract hydrogen atom from propylene. In contrast, the formation of acrylaldehyde in the oxidation with fully oxidized CuO–SiC suggests an important role of oxygen species adsorbed on the catalyst in acrylaldehyde formation. However, if the lattice oxygen existing on the surface of CuO could be eliminated by treatment with the hydrazine solution, the important role of the lattice oxygen can not be denied.

An inflection point appears at 0.33 NTP ml N_2/g-catalyst in the reduction of CuO–SiC with an aqueous solution of hydrazine (Fig. 2). The amount of nitrogen evolved up to this point might be equivalent to that of oxygen adsorbed on the surface, and nitrogen evolved beyond this point is due to the reduction of lattice oxygen with hydrazine and the decomposition of hydrazine by contact with copper ions. Reliability of the reduction is strongly supported by the good agreement of the amount of nitrogen evolved in the reduction of CuO–SiC with hydrazine with that of oxygen adsorbed on the reduced catalysts at $P_{O_2}=134$—138 Torr. Thus, the amount of oxygen adsorbed on the surface of CuO–SiC is 0.33 NTP ml O_2/g-catalyst or 5.32 NTP ml/g-CuO. The fact that the amount of oxygen consumed for acrylaldehyde formation up to the second injection is 0.128 NTP ml/g-catalyst or 2.065 NTP ml/g-CuO and that only a trace of acrylaldehyde was formed by the oxidation with the CuO–SiC which had been treated with the hydrazine solution (N_2 0.80 NTP ml/g-catalyst evolved) offer further evidence for the very important role of the adsorbed oxygen species or the surface lattice oxygen in the selective oxidation. As lattice oxygen of metal oxide is expected to play the role of hydrogen abstraction,[15–17] the adsorbed oxygen species or the surface lattice oxygen might be necessary for acrylaldehyde formation as the oxygen species incorporated rather than that abstracting the hydrogen atom from hydrocarbon species.

Callahan and Grasselli[10] found the formation of acrylaldehyde in the oxidation of propylene with fully oxidized CuO–SiC (0.4 wt% as CuO) at 300 °C by means of a pulse method and concluded that lattice oxygen is involved in the selective oxidation. According to our calculations based on the assumption that the volume of propylene was measured at 20 °C and 1 atm, only CO_2 and H_2O being formed by unselective oxidation, the amount of oxygen used for acrylaldehyde formation is 0.01 NTP ml/g-catalyst or 2.58 NTP ml/g-CuO. The latter value is comparable to the value previously obtained 2.065 NTP ml/g-CuO and is less than the amount of adsorbed oxygen species 5.32 NTP ml/g-CuO. Even taking account of the differences in the reaction temperature and the content of CuO supported, their result is explained by assuming the very important role of adsorbed oxygen species in acrylaldehyde formation.

Formation of acrylaldehyde in the reduction of metal oxide with propylene also takes place in the case of SnO_2, Sb_2O_4, Fe_2O_3–Sb_2O_4,[16,17] MoO_3, and bismuth molybdates.[17,18] Double bond type lattice oxygen Mo=O of MoO_3 is incorporated into furan and maleic anhydride formed in the oxidation of butadiene.[8] Incorporation of the lattice oxygen into acrylaldehyde in the oxidation of propylene over the catalysts containing MoO_3 is very likely to occur. This is supported by the formation of MoO_2 in the reduction of the catalysts with propylene.[17,18] In the case of other oxides which have no double bond type lattice oxygen, formation of acrylaldehyde might be attributed to the presence of adsorbed oxygen species or to the higher positive charge of the adsorbed hydrocarbon species. Formation of acrylaldehyde appeared with a rise in the acidity of Bi_2O_3 and SnO_2 catalysts by addition of P_2O_5.[19] However, this is not the case of the selective oxidation over Cu_2O since the amount of CuO was very small.

The form of oxygen species adsorbed on the CuO–SiC is discussed in the following. The fact that no change in the composition of gaseous oxygen was observed in the isotopic mixing reaction over the catalyst suggests non-dissociative adsorption of oxygen molecule on the surface (Fig. 3). The desorption of oxygen from the CuO–SiC with a rise in temperature provides further evidence for the existence of adsorbed oxygen species and the reversibility of some portion of oxygen adsorption. A part of adsorbed oxygen species seems to be present as diatomic species. Incorporation of the adsorbed oxygen species into acrylaldehyde was also supported in accordance with $^{18}O/^{16}O$ ratio in the formed acrylaldehyde with that in the pulse (Table 2). Oxygen species adsorbed on Cu_2O are negatively charged.[20,21] This strongly suggests formation of various oxygen species over Cu_2O during the course of oxidation of propylene as follows: O_2-(gas)$\rightarrow O_2^-\rightarrow O^-\rightarrow O^{2-}$ (lattice). We showed in our studies on the oxidation of butadiene[8] and furan[22] over supported molybdena and promoted anatase-type titania catalysts that oxygen atom of O_2^- is incorporated into maleic anhydride. Furan is an intermediate of maleic anhydride from butadiene.[23] Thus, formation of furan and maleic anhydride in the cooxidations (Table 3) gives strong evidence to the formation of O_2^- over Cu_2O during the course of oxidation of propylene. Enikeev *et al.*[21] proposed in their studies on the work function of Cu_2O upon the adsorption that adsorbed propylene and various products

have a partial positive charge in contrast with adsorbed oxygen species. Even if this positively charged hydrocarbon intermediate reacts with electronegative oxygen species such as O_2^-, there appears no special difficulty in these addition reactions.

The result given in Table 1 can not clarify whether lattice oxygen on the surface of CuO is incorporated into acrylaldehyde or not. However, the fact that CuO is not a selective phase in contrast with Cu_2O during the course of oxidation and that the catalyst consists of Cu_2O and a very small amount of CuO at the steady state suggests the incorporation of the adsorbed oxygen species rather than the surface lattice oxygen during the course of steady state oxidation. Formation of the electronegative oxygen species on CuO is very difficult in contrast with that on Cu_2O[9]. This possibly accounts for the great difference in selectivity during the oxidation of propylene over these copper oxides rather than the ability to perform hydrogen abstraction. Charge of the adsorbed oxygen species existing on the surface of CuO–SiC was not clarified. It is apparent that the oxygen species adsorbed on the surface acts as oxygen incorporated into acrylaldehyde in the pulse experiment. The results provide one possibility that acrylaldehyde can be formed even over CuO if lattice oxygen of this oxide could abstract hydrogen from propylene and electronegative oxygen species adsorbed could be present. This is the case of acrylaldehyde formation in the pulse experiment.

We have no experimental result showing which electronegative oxygen species of O_2^- or O^- is incorporated. No attention was paid to the direct incorporation of gaseous oxygen into acrylaldehyde since this mechanism could not explain the difference in selectivity during the course of oxidation over Cu_2O and CuO. Kugler and Kokes[24] presumed from IR that acrylaldehyde is formed by the reaction of O_2^- with the π-allyl. Cant and Hall[25] also proposed a very important role of diatomic oxygen species in the oxidation of propylene to acrylaldehyde over Rh or Ru–α-Al_2O_3. These observations are in line with ours and offer a greater possibility for preferential incorporation of the electronegative molecular oxygen species during the course of selective oxidation over Cu_2O. This is consistent with the fact that the amount of oxygen consumed for acrylaldehyde formation, which is equal to that of the adsorbed molecular oxygen used for the incorporation, is less than that of the adsorbed oxygen species (Table 1 and Fig. 2).

References

1) T. J. Jennings and F. S. Stone, "Advances in Catalysis," Vol. 9, Academic Press, New York (1957), p. 441.
2) L. Ya. Margolis, "Advances in Catalysis," Vol. 14, Academic Press, New York (1963), p. 429.
3) H. H. Voge and C. R. Adams, "Advances in Catalysis," Vol. 17, Academic Press, New York (1967), p. 151.
4) H. H. Voge, C. D. Wagner, and D. D. Stevenson, *J. Catal.*, **2**, 58 (1963).
5) C. R. Adams and T. J. Jennings, *J. Catal.*, **2**, 63 (1963).
6) C. R. Adams and T. J. Jennings, *J. Catal.*, **3**, 549 (1964).
7) M. Akimoto and E. Echigoya, *J. Catal.*, **29**, 191 (1973).
8) M. Akimoto and E. Echigoya, *J. Catal.*, **31**, 278 (1973).
9) B. J. Wood, H. Wise, and R. S. Yolles, *J. Catal.*, **15**, 355 (1969).
10) J. L. Callahan and R. K. Grasselli, *AIChE J.*, **9**, 755 (1963).
11) G. Brauer, "Handbuch der Präparativen Anorganischen Chemie," Ferdinand Enke Verlag, Stuttgart (1954), p. 755.
12) W. M. Latimer and J. H. Hildebrand, "Reference Book of Inorganic Chemistry," 3rd ed., The Macmillan Company, New York (1951), p. 108.
13) O. V. Isaev, M. Ya. Kushnerev, and L. Ya. Margolis, *Proc. Acad. Sci. USSR, Phys. Chem. Sect. (Engl. Transl.)*, **119**, 129 (1958).
14) Y. B. Gorokhovatskii, I. I. Vovyanko, and M. Y. Rubanik, *Kinet. Catal. (Engl. Transl.)*, **7**, 65 (1966).
15) H. E. Swift, J. E. Bozik, and J. A. Ondrey, *J. Catal.*, **21**, 212 (1971).
16) V. Fattore, Z. A. Fuhrman, G. Manaro, and B. Notari, *J. Catal.*, **37**, 215 (1975).
17) V. Fattore, Z. A. Fuhrman, G. Manaro, and B. Notari, *J. Catal.*, **37**, 223 (1975).
18) M. Egashira, H. Sumie, T. Sakamoto, and T. Seiyama, *Kogyo Kagaku Zasshi*, **73**, 860 (1970).
19) T. Seiyama, M. Egashira, T. Sakamoto, and I. Aso, *J. Catal.*, **24**, 76 (1972).
20) W. E. Garner, T. J. Gray, and F. S. Stone, *Proc. R. Soc. London, Ser. A*, **197**, 294 (1949).
21) E. Kh. Enikeev, O. V. Isaev., and L. Ya. Margolis, *Kinet. Katal.* **1**, 431 (1960).
22) M. Akimoto and and E. Echigoya, *Trans. Faraday Soc.*, in press.
23) M. Akimoto and E. Echigoya, *Bull Chem. Soc. Jpn.*, **48**, 3518 (1975).
24) B. L. Kugler and R. J. Kokes, *J. Catal.*, **32**, 170 (1974).
25) N. W. Cant and W. K. Hall, *J. Catal.*, **22**, 310 (1971).

Modification of the Packed-bed Electrode and Its Potential Distribution

Shiro YOSHIZAWA, Zenichiro TAKEHARA, and Zempachi OGUMI

Department of Industrial Chemistry, Faculty of Engineering, Kyoto University, Yoshida, Sakyo-ku, Kyoto 606

(Received February 2, 1976)

The packed-bed electrode has been investigated in order to scale up the cell capacity by introducing three-dimensional electrode. The reactions of aniline formation by cathodic reduction of nitrobenzene and Fe(II) ion formation by cathodic reduction of Fe(III) ion were studied. When bed particles with high electric conductivity were used, the effective depth of the packed-bed where the electrode reaction took place was very small. However, when particles with moderate resistance were used, the effective depth increased. This is because the potential distribution in the bed material is the same as that in the electrolyte in the bed, the potential difference between particles and electrolyte thus being maintained constant at any position in the bed. From the standpoint of scaling up the cell capacity, this type of electrode can be effectively applied.

Application of a packed-bed or porous electrode[1,2] has been investigated by many workers, in order to scale up the cell capacity by introducing three-dimensional electrode. The packed-bed electrode was also recently studied as regards application to the treatment of waste water.[3,4] The increase in cell current was not large since the effective depth of packed-bed or porous electrode where the electrode reaction took place was very small. This is ascribed to the high electronic conductivity of bed material or porous material and to the apparent low conductivity of electrolyte in the bed which is caused by small void between particles in the bed. Under these conditions, the potential of solution in the bed and that of bed particles are distributed as represented by curves $\varphi_s(P)$ and $\varphi_m(P)$. Thus the potential difference between particles and electrolyte changes in the bed (curve $\Delta\varphi(P)$, Fig. 1).[5] This shows that the potential difference between particles and electrolyte enough for an electrode reaction to proceed exists only at the part of bed nearest to the counter electrode.

Fleischman *et al.*, [5] Hiddleston and Douglas[6] and Janssen[7] introduced a fluidized-bed electrode. The apparent resistance of bed material in the bed which changes with the expansion of bed causes a potential distribution in the bed (curve $\varphi_m(f)$, Fig. 1).[5] The potential distribution of solution in the bed also changes at the same time as the change of expansion (curve $\varphi_s(f)$). The potential distribution formed thus in both sides of the solution in the bed and bed particle causes an adequate potential difference between particles and electrolyte for an electrode reaction at any position in the bed as shown by curve $\Delta\varphi(f)$. Accordingly the effective depth of bed electrode where the electrode reaction took place could be expected to become large.

If particles with moderate resistance are used as bed material of a packed-bed electrode, the same potential distribution in a packed-bed electrode as in a fluidized-bed electrode can be expected. We have examined the potential profile in a packed-bed constructed with particles having a moderate resistance and also the increase of effective depth of this type of electrode.

Experimental

Carbon particles (14—20 mesh) partly graphitized were used as bed material. The resistance of the particles was about 3.4 Ωcm. Two other kinds of particle were also used, a glass bead (1—2 mm diam) chemically plated with copper, and a carbon particle (about 0.5 mm diam), also chemically plated with copper because of high resistance. Copper deposition of the particles was carried out by the same technique as that given in a previous paper.[2]

The electrolysis cell (Fig. 2) was made of polyvinyl chrolide. The bed size was 3 cm in width and 1.5 cm in thickness. The bed depth was changeable. The bed was supported on a glass filter through which electrolyte was distributed. The bed was also covered with a glass filter. A graphite plate

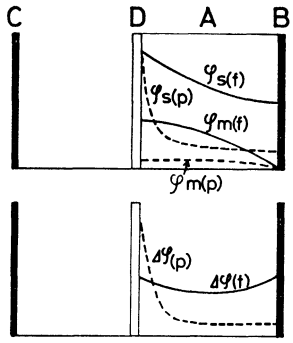

Fig. 1. Potential profiles in packed-bed and fluidized-bed electrodes.
A: Bed electrode. B: Feeder electrode. C: Counter electrode. D: Diaphragm. φ_s: Solution potential. φ_m: Particle potential. $\Delta\varphi$: Potential difference between φ_s and φ_m. Suffix f and p means fluidized-bed and packed-bed, respectively.)

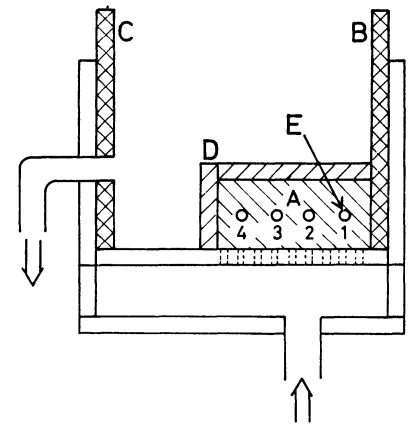

Fig. 2. A packed-bed cell.
A: Packed-bed. B: Feeder electrode. C: Counter electrode. D: Diaphragm. E: Luggin capillaries and probes.

was used as a counter electrode. A graphite or copper plate was used as a feeder electrode which was set at the opposite end of the bed from the counter electrode. Both electrodes were positioned parallel to each other. The electrolyte fed into the cell flowed across the bed.

Three kinds of electrolyte were used: 1 M HCl saturated with nitrobenzene, 0.02 M $FeCl_3$+1 M HCl and 0.5 M $FeCl_3$+1 M HCl.

Four graphite rods or four copper wires were inserted into the bed from one side for use as probes, with which the potential of the bed particle at each position was measured. Four glass capillaries were inserted into the bed from the other side for use as Luggin capillaries, with which the solution potential in the bed was measured. Potential distributions in the direction of depth in the bed* were measured. Two saturated calomel electrodes (SCE) were used for measuring the potential distribution in the solution. Electrolysis was carried out at room temperature.

Results and Discussion

Dissolution of copper occurred when glass beads or carbon particles plated with copper were used as bed material. This may be ascribed to the high conductivity of the bed material. In this case, most of the cell current came from the part of the bed electrode nearest to the counter electrode. The potential of the particle at a part farther from the counter electrode can become so positive to the solution potential at the same position as to make the dissolution of copper possible. These two kinds of particle are not suitable as bed material. In most of the experiments a third material, 14—20 mesh carbon particles, was used.

Reduction of Nitrobenzene. A nitrobenzene solution was reduced to aniline by a bed electrode constructed with carbon particles. A feeder electrode and probes were made of copper. Potential distribution was measured by constant current electrolysis at 500 mA/cm² (Fig. 3). A distribution of particle potential took place in the bed as expected. $\Delta\varphi$, the difference between particle potential and solution potential at the same position in the bed, becomes large near a feeder electrode, hydrogen evolution being observed in this region. The reduction of nitrobenzene takes place at fairly negative potential. On the other hand, hydrogen overvoltage of carbon is not so high. The potential region where the reduction of nitrobenzene occurs predominantly is narrow. The reduction of nitrobenzene to aniline is accompanied by many side reactions. $\Delta\varphi$ can not be set at a given potential throughout the bed (Fig. 3); we can not accurately control $\Delta\varphi$ throughout the bed. This causes the reduction of current efficiency of aniline formation, as confirmed experimentally. The current efficiency became less than 50%.

Reduction of Iron(III) Ion. The reduction of iron(III) ion was examined as an example of the reaction with a low overvoltage. The feeder electrode and probes consist of graphite. The potential distribution was measured at a high concentration of iron(III) ion, 0.5M in 1M HCl, under conditions of constant current electrolysis (Figs. 4 and 5). The solution potential, φ_s was referred to that at a position just next to the diaphragm on the side of the counter electrode. The particle potential, φ_m, was referred to the potential of feeder electrode. The value of φ_m at zero position was due to the contact

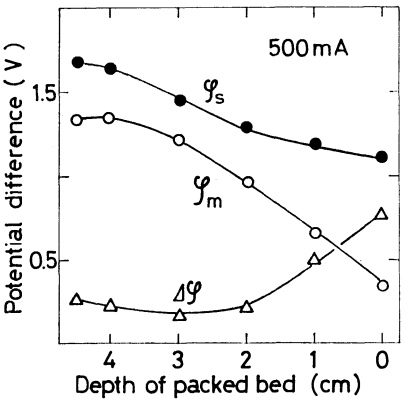

Fig. 3. Potential profiles at the reduction of nitrobenzene in 1 M HCl saturated with nitrobenzene.
Total current: 500 mA.

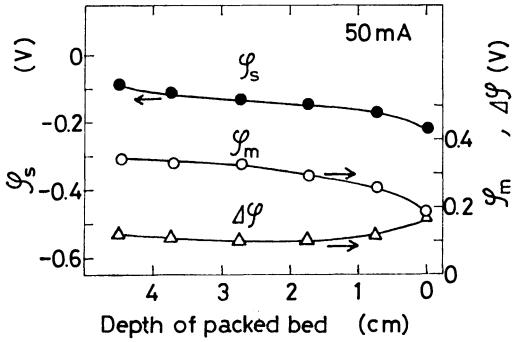

Fig. 4. Potential profiles at the reduction of Fe(III) ion in 0.5 M $FeCl_3$+1 M HCl.
Total current: 50 mA.

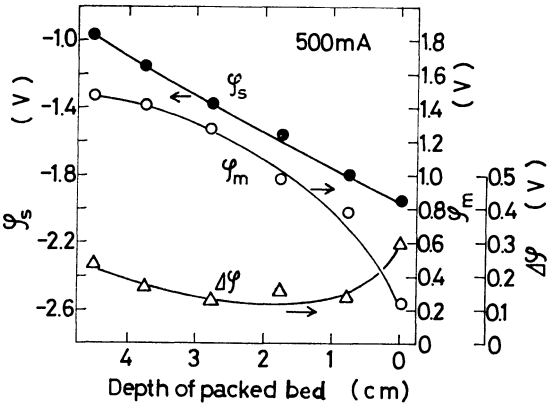

Fig. 5. Potential profiles at the reduction of Fe(III) ion in 0.5 M $FeCl_3$+1 M HCl.
Total current: 500 mA.

* A small moving Luggin capillary and a small probe made from graphite rod or copper wire were also used, for measuring the potential distribution of solution in bed and that of bed particles in the directions of width and thickness in the bed. In these directions, uniform potential distributions were observed.

resistance between particles and the feeder electrode.** $\Delta\varphi$ corresponds to the potential difference at each position in the bed from an equilibrium potential 650 mV (*vs.* SCE).

The fact that the change of $\Delta\varphi$ along the depth was not so large at the small cell current (Fig. 4) indicates that the packed-bed is active throughout. On the other hand, Fig. 5 shows that at a large cell current, $\Delta\varphi$ becomes larger near both ends than at the center. This means that a larger part of the cell current comes from the parts near both ends and that all the packed-bed is not used equally. However, the effective depth was remarkably improved as compared with the usual packed-bed.[8]

The packed-bed electrode was applied to the reduction of iron(III) ion under conditions of limiting current by mass transfer in a solution of 0.02M $FeCl_3$ in 1M HCl. The dependence of total cell current on the potential of probe No. 1 (*vs.* SCE) was examined at different flow rates by using packed-bed electrode of 1.5 cm depth constructed with 14—20 mesh carbon particles (Fig. 6). The cell current depending on flow rate was much larger than that at feeder electrode only. The limiting current appeared clearly at a lower flow rate at more negative potential than 0.3 V. But this became ambiguous with an increase in flow rate. This may be ascribed to the disturbance of flow path in the bed and to the change of potential distribution in the bed due to the increase in cell current. The total cell current is expected to increase when the flow rate becomes large. This was examined at different bed depths (Fig. 6). The total cell current

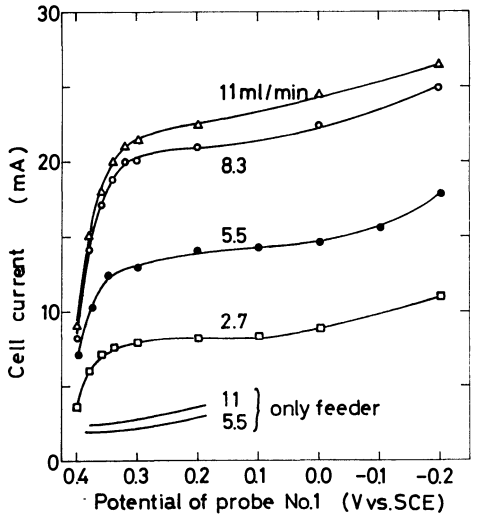

Fig. 6. Current potential relationships on a packed-bed electrode of 1.5 cm depth in 0.02 M $FeCl_3$+1 M HCl at different flow rate.
Potential of probe No. 1 was set *vs.* SCE.

** This value should be proportional to the current. However, we could not observe the proportionality and a reproducible result according to φ_m at zero position. This may be due to the small change in the surface roughness of the feeder electrode and that of film thickness of penetrated electrolyte between feeder electrode and particles.

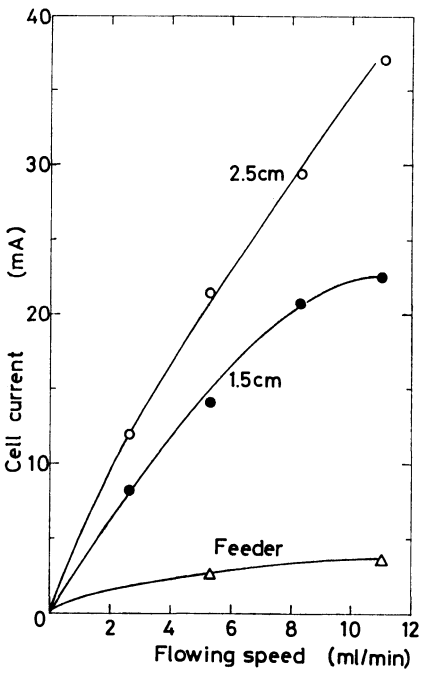

Fig. 7. The dependence of total current on flow rate in 0.02 M $FeCl_3$+1 M HCl.
Potential of probe No. 1 was set at 0.2 V (*vs.* SCE).
Bed depth, —●—: 1.5 cm, —○—: 2.5 cm, —△—: feeder electrode only.

increased with flow rate (Fig. 7). A linear relationship is expected between total cell current and flow rate under conditions of limiting mass transfer from the theory of mass or heat transfer in a packed-bed reactor.[9] However, this was not the case as shown in Fig. 7. This may also be ascribed to the disturbance of flow path in the packed-bed because of its construction.

The profile of $\Delta\varphi$ was examined under conditions of potentiostatic electrolysis where the potential of probe No.1 was set *vs.* SCE. $\Delta\varphi$ was larger than 0.4 V (Fig. 8), indicating that the particle potential throughout the bed was negative as conditions of limiting current

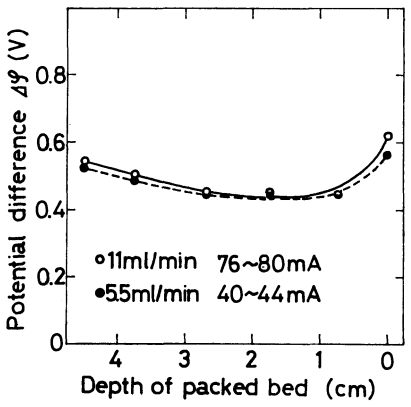

Fig. 8. The change of $\Delta\varphi$ along the bed depth in 0.02 M $FeCl_3$+1 M HCl. The potential of probe No. 1 was set at 0.2 V (*vs.* SCE).
—○—: 11 ml/min, total current 76—80 mA.
—●—: 5.5 ml/min, total current 40—44 mA.

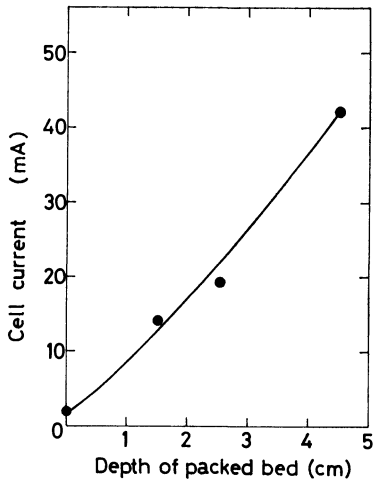

Fig. 9. Dependence of total cell current on bed depth in 0.02 M $FeCl_3$+1 M HCl at flow rate 5.5 ml/min. Potential of probe No. 1 was set at 0.2 V (*vs.* SCE).

were attained. The electrode reaction occurred almost at the same rate in the whole part of packed-bed. All the particles in the packed-bed were used effectively. This was confirmed by an experiment in which the relationship between total cell current and bed depth was examined. Total cell current increases with the bed depth (Fig. 9). The increase of cell current thus can be attained by the increase in bed depth.

The reaction ratio of reactant was small even at a low concentration because of the thinness of the bed. The reaction ratio would increase by using a thicker bed. In this case the potential distribution along the thickness might be taken into consideration. Use of this thicker bed will make this type of electrode more effective for the treatment of waste water containing harmful components in a low concentration. It is easier to control an electrode of this type than a fluidized-bed electrode.

Conclusion

The distribution of particle potential appears in the bed in a packed-bed electrode constructed with particles of moderate resistance. The distribution enables the packed-bed electrode to act in the same manner as the fluidized-bed electrode. The effective depth in the former could be improved as in the latter. As the potential in a bed can not be accurately controlled, the potential region of the desired reaction should be made wide. The electrode can be effectively applied to the solution of a low reactant concentration such as waste water.

The authors wish to thank the staff of the Asahi Glass Foundation for Contribution to Industrial Technology for their support of this work.

References

1) R. W. Houghton and A. T. Kuhn, *J. Appl. Electrochem.*, **4**, 173 (1974).
2) S. Yoshizawa, Z. Takehara, Z. Ogumi, and T. Tsuji, *Bull. Chem. Soc. Jpn.*, **49**, 2889 (1976).
3) D. N. Bennion and J. Newman, *J. Appl. Electrochem.*, **2**, 113 (1972).
4) A. K. P. Chu, M. Fleischmann, and G. J. Hills, *J. Appl. Electrochem.*, **4**, 323 (1974).
5) M. Fleischmann, J. W. Oldfield and L. Tennakoon, *J. Appl. Electrochem.*, **1**, 103 (1971).
M. Fleischmann and J. W. Oldfield, *J. Electroanal. Chem.*, **29**, 211, 231, 241 (1971).
6) J. N. Hiddleston and A. F. Douglas, *Electrochim. Acta*, **15**, 431 (1970).
7) L. J. J. Janssen, *Electrochim. Acta*, **16**, 151 (1971).
8) F. Goodridge and B. M. Ismail, "Symposium on Electrochemical Engineering," ed. by J. D. Thornton, Vol. 1, (1971), pp. 1—29.
9) R. B. Bird, W. E. Stewart, and E. N. Lightfoot, "Transport Phenomena," Wiley International (1960), p. 411.

ENDOR Studies of the Hyperfine Interaction of Phenylgalvinoxyl Radicals in Solution

Kazuo MUKAI, Takashi KAMATA, Toshiko TAMAKI, and Kazuhiko ISHIZU
Department of Chemistry, Faculty of Science, Ehime University, Matsuyama 790
(Received February 12, 1976)

The ENDOR spectra of ten kinds of phenylgalvinoxyl derivatives in solution have been observed, and the hyperfine splitting constants have been determined. The formally equivalent four meta ring protons of the galvinoxyl skeleton in the phenylgalvinoxyl radical become magnetically nonequivalent in two groups of two. This behavior may be explained by assuming that splittings arising through pure spin polarization, or through mixed hyperconjugation and spin polarization, are different for *syn* and *anti* meta ring protons of the phenylgalvinoxyl radical. A similar effect has been observed in the ENDOR spectra of other phenylgalvinoxyl derivatives. In radicals with a large substitution group at the meta or para position of the phenyl ring, the galvinoxyl skeleton twists unsymmetrically on either side; thus, all or three among the four meta ring protons become magnetically nonequivalent. The solvent dependence of the ENDOR spectra of the phenylgalvinoxyl radicals constituted strong evidence for the importance of the solvent in fixing the conformation and symmetric property of the radical molecules. The proposed analyses of the ENDOR spectra were also supported by the McLachlan Molecular Orbital calculations.

The galvinoxyl radical (I) (see Fig. 1) is well known as a very stable neutral radical.[1,2] The magnetic properties of galvinoxyl in solution and in the solid state have been extensively studied using several physical methods, such as ESR,[3] NMR,[4] ENDOR,[5] magnetic susceptibility,[6] and specific heat.[7] The quinone methide radicals obtained by the replacement of *t*-butyl groups by methoxyl or methyl groups have also been studied by means of ESR and ENDOR, showing some interesting aspects of the electronic structures of these radicals.[8]

The phenylgalvinoxyl radical (II) (see Fig. 1) has an electronic structure similar to galvinoxyl, and exhibits a stability approaching that of galvinoxyl.[9] Recent studies of the magnetic susceptibility of phenylgalvinoxyl (II) and some of its derivatives (IV)—(VIII) have clarified some interesting magnetic properties in the solid state, suggesting intermolecular ferromagnetic exchange interaction in some of these radicals.[10] The magnetic property is very sensitive to both the packing of the radical molecules in the crystal and the distribution of the unpaired electron on the radical. ESR is a frequently used method for determining the distribution of the unpaired electron on radical molecules. However, the ESR spectra of the above phenylgalvinoxyl radicals are usually resolved, showing only five line-splittings ($a_m^H = 1.32$—1.35 G) due to the four meta ring protons in the galvinoxyl skeleton of the phenylgalvinoxyl radicals.[10-12] Therefore, it is not clear whether an unpaired electron spreads all over the molecular frame, since detailed analyses of the hyperfine splitting constants have never been attempted for these radicals.

Electron nuclear double resonance (ENDOR) spectroscopy is a valuable method for the determination of the proton isotropic hyperfine couplings of organic radicals in solution, since the effective resolution is much higher than for ESR. In the preliminary ENDOR experiment on phenylgalvinoxyl (II), the ENDOR line from the four meta ring protons was observed to be split, suggesting that there are two pairs of equivalent ring protons.[13] In the work, this splitting was tentatively ascribed to a restricted rotation with molecular asymmetry. On the other hand, all four meta ring protons of galvinoxyl are equivalent within the resolution of the ENDOR experiments.[5]

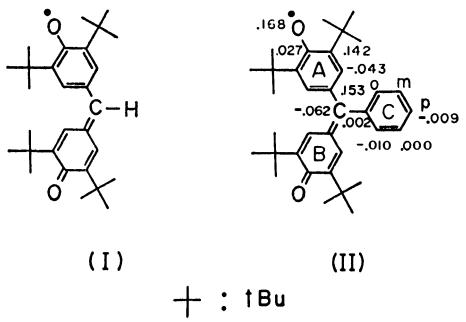

Fig. 1. Chemical structures of galvinoxyl (I) and phenylgalvinoxyl (II), showing numbering system and McLachlan unpaired spin densities.

In the present paper, proton hyperfine splitting constants measured from the solution ENDOR spectra of ten kinds of phenylgalvinoxyl radicals in toluene and, in some cases, in 2-methyltetrahydrofuran (2-MTHF) will be reported, in order to present fundamental data which are essential for a more detailed understanding of the magnetic properties of these radicals in the solid state. Even though these radicals show simple quintet ESR absorption spectra, the ENDOR experiments have yielded several notable results which, we think, could not have been obtained from the ESR spectra. Based on the ENDOR data, interesting conformational changes due to steric interactions and solvent effects for these radicals will be discussed.

Experimental

The galvinoxyl radical (I) was synthesized following the method of Kharash and Joshi[1] or Coppinger.[2] The syntheses and physical properties of the phenol precursors (P-II)—(P-X), except for the phenol (P-III), of the phenylgalvinoxyl radicals (II)—(X) (see Figs. 1 and 2) were reported previously.[10,12] The phenol (P-III) was prepared according to the method of Coffield *et al.*[14] After the condensation of 2,6-di-*t*-butylphenol with benzaldehyde-d_5 (E. Merck AG. 99%), the deuterated bisphenol (P-III) was synthesized; thereafter

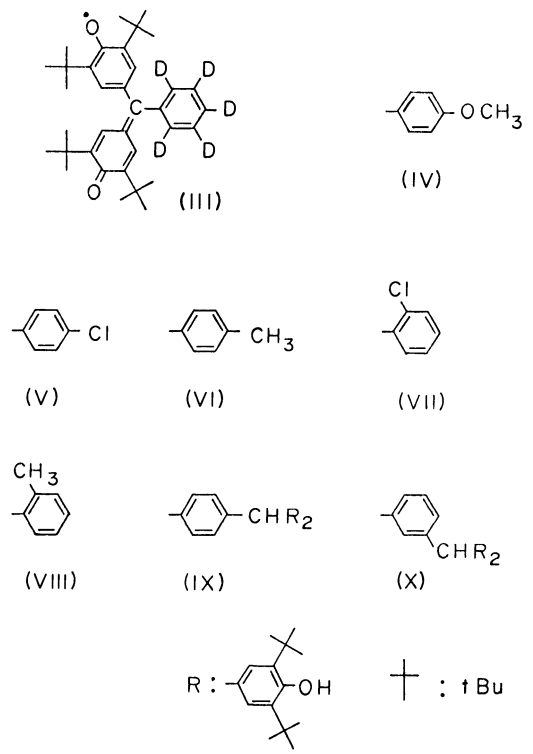

Fig. 2. Chemical structures of phenylgalvinoxyl derivatives (III)—(X).

it was recrystallized twice from ethanol. Mp 162.5—163.5 °C. Found: C, 83.44; H and D, 10.15%. Calcd for $C_{35}H_{43}D_5O_2$; C, 83.11; H and D, 10.56%. The ultraviolet absorption spectrum in ethanol with λ_{max}=279 nm (log ε=3.65) and the proton NMR spectrum in CCl_4 with $\delta_{t\text{-Bu}}$=1.38, δ_{OH}=4.92, δ_{CH}=5.28, and $\delta_{m\ H}$=6.82 ppm (TMS as the standard) are in good agreement with those of the corresponding bisphenol, except for the disappearance of the proton NMR absorption due to five phenyl protons of the undeuterated bisphenol.

The phenylgalvinoxyl radicals (II)—(X) were prepared by the oxidation of the phenols with PbO_2 in toluene or 2-MTHF under a vacuum. The initial ESR spectra resulting from the slight oxidation of the phenols with PbO_2 were a doublet of triplets.[12] After further oxidation, the phenylgalvinoxyl radical, which has the structure shown in Fig. 1, and its derivatives were formed. The ESR spectra of these phenylgalvinoxyls show five line splitting with intensities of 1 : 4 : 6 : 4 : 1.

The ENDOR spectra were recorded by means of a JEOL-type ES-EDX-1 spectrometer, operated with 80 Hz magnetic field modulation.[15] About 150 watts of the continuous radio wave frequency modulated at 6.5 kHz were running inside of the cavity for NMR excitation. The ESR measurements were carried out using a JES-ME-3X spectrometer.

Results and Discussion

The ESR spectra of the phenylgalvinoxyl (II) and some of its derivatives (III)—(X) (see Figs. 1 and 2) show only five line splittings due to four meta ring protons of the quinone methide skeleton; we were unable to resolve the splittings from the other protons. The meta ring proton hyperfine splittings, a_m^H, observed in toluene at room temperature are listed in the first column of Table 1. Figures 3 and 4 show several typical ENDOR spectra of the phenylgalvinoxyl and some of its derivatives in toluene. The ENDOR spectra of these radicals were also measured in the 2-MTHF solvent. The results of the analyses of these spectra are also tabulated in Table 1, together with the data of the galvinoxyl radical used as reference. The temperatures (T) at which the best resolved ENDOR spectra were obtained are listed in Table 1.

ENDOR Spectra of Galvinoxyl (I), Phenylgalvinoxyl (II), and Phenyl-d_5-galvinoxyl (III). The ENDOR spectrum of galvinoxyl (I) in toluene (see Fig. 3(a)) shows three different proton hyperfine splittings (5.77_4, 1.36_6, and 0.05_5 G), which are attributable, respectively, to a methide proton, four ring protons, and the 36 tertiary butyl protons. On the other hand, the ENDOR spectrum of phenylgalvinoxyl (II) in toluene (see Fig. 3(b)) clearly exhibits four different proton hyperfine splittings (1.34_7, 1.27_2, 0.20_7, and 0.05_8 G). The larger two hyperfine splittings (1.34_7 and 1.27_2 G) are easily assigned to the four meta ring protons of phenoxyl groups, taking their ESR hyperfine coupling constants (a_m^H=1.32 G) into account. This assignment

Table 1. Hyperfine splitting constants of phenoxyl radicals (in Gauss)

Radical	In toluene						In 2-MTHF					
	ESR	ENDOR					ESR	ENDOR				
	a_m^H	a_m^H		$a_{ring\ C}^{o\text{-},p\text{-}H}$	$a_{t\text{Bu}}^H$	T(°C)	a_m^H	a_m^H		$a_{ring\ C}^{o\text{-},p\text{-}H}$	$a_{t\text{Bu}}^H$	T(°C)
(I)	1.42	1.36_6		—	0.05_5	−75						
(II)	1.32	1.34_7,	1.27_2	0.20_7	0.05_8	−60	1.33	1.32_8,	1.25_8	0.20_7	0.06_1	−63
(III)	1.32	1.34_1,	1.27_6	—	0.04_9	−68						
(IV)	1.34	1.30_8,	1.25_6	0.21_4	0.04_9	−80						
(V)	1.33	1.34_8,	1.28_1	0.20_2	0.05_5	−75						
(VI)	1.35	1.33_0,	1.27_8	0.13_5	0.04_9	−80						
(VII)	1.33	1.35_8,	1.29_1	0.11_6	0.05_1	−61	1.33	1.35_4,	1.28_7	0.11_7	0.04_7	−66
(VIII)	1.34	1.31_5,	1.24_9	0.12_6	0.04_9	−70	1.33	1.33_0,	1.26_8	0.12_7	0.05_8	−80
(IX)	1.30	1.40_7,	1.35_7	0.28_9	0.05_9	−45	1.34	1.37_0,	1.30_5	0.20_2	0.06_3	−65
		1.26_0,	1.20_7	0.18_3				1.26_0				
(X)	1.33	1.37_1,	1.32_1	0.18_1	0.05_7	−73	1.33	1.34_7,	1.27_4	0.18_9	0.06_1	−54
		1.26_8										

is also consistent with the known assignments for galvinoxyl (I).[3] Since, at the temperatures at which we measured the ENDOR signal, the intensities of the ENDOR transitions corresponding to the hyperfine couplings, 1.34_7 and 1.27_2 G, are equal, the four protons must be equivalent in two groups of two protons. Here, the splitting of the meta ring proton ENDOR signal at a low temperature is independent of both the microwave and radio frequency power,[5] and we are confident that it reflects a real difference in hyperfine coupling. Similar splittings are also observed in all the other radicals investigated, except for the (IX) and (X) radicals, as is shown in Figs. 3 and 4. Comparing the ENDOR spectrum of phenylgalvinoxyl with that of galvinoxyl, the hyperfine splitting of 0.20_7 G of the former, which has never been observed in the latter, can clearly be identified as the proton hyperfine splitting in the substituted phenyl ring. We confirmed that the splitting of 0.20_7 G can be assigned to the ring protons in the substituted phenyl, because it is lost in phenyl-d_5-galvinoxyl (see Fig. 3(c)). Thus, the smallest splitting of 0.05_8 G is attributable to that of tertiary butyl protons. This fact indicates that the unpaired electron spreads over the substituted phenyl ring, C, although the magnitude of the electron density is very small. Anticipating the results of the McLachlan Molecular Orbital calculations to be described later (see Fig. 1), the 0.20_7 G splitting will be assigned to the ortho and para ring protons of the substituted phenyl ring, C, in which the unpaired spin densities on meta ring carbon atoms are too small to explain the 0.20_7 G splitting or even the 0.05_8 G splitting.

As has been discussed above, the ENDOR results indicate that the four meta ring protons must be equivalent magnetically in two groups of two protons. In support of the present assumptions, one may refer to the accurate ESR and/or ENDOR data on the allyl radical[16] and 2-methylgalvinoxyl[8] (see the structure in Ref. 8), because both radicals have electronic structures (allyl skeletons) similar to that of phenylgalvinoxyl.

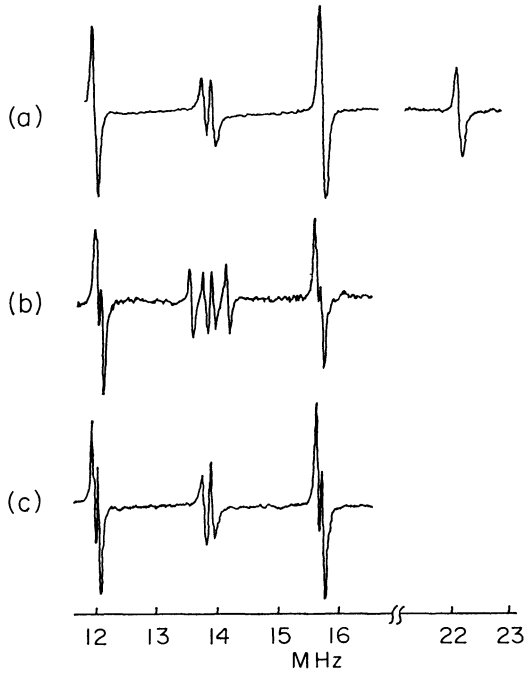

Fig. 3. ENDOR spectra of (a) galvinoxyl (I) (at −75 °C), (b) phenylgalvinoxyl (II) (at −60 °C), and (c) phenyl-d_5-galvinoxyl (III) (at −68 °C) in toluene.

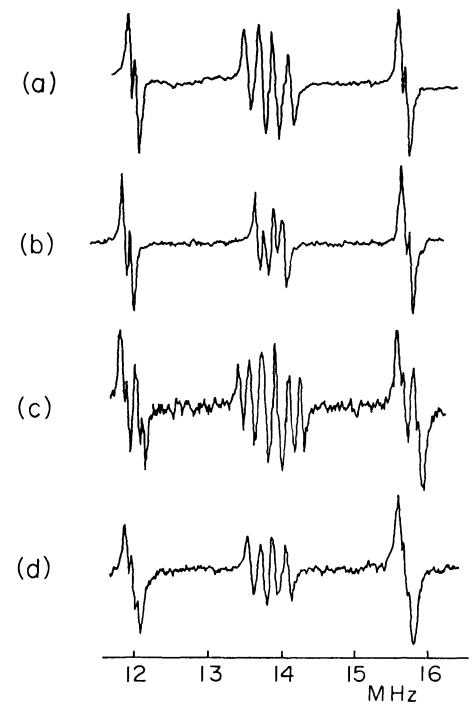

Fig. 4. ENDOR spectra of (a) radical (IV) (at −80 °C), (b) radical (VII) (at −61 °C), (c) radical (IX) (at −45 °C), and (d) radical (X) (at −73 °C) in toluene.

The low-temperature ESR spectrum of the allyl radical reveals two pairs of magnetically inequivalent *syn* and *anti* terminal protons (13.90 and 14.81 G), which give rise to a triplet-of-triplets hyperfine structure further split into doublets by the proton in the 2 position (4.06 G). The different splittings which are observed for formally equivalent methylene protons in allyl could be understood because the splitting arising through pure spin polarization, or through mixed hyperconjugation and spin polarization, is expected to be different for *syn* and *anti* terminal protons. A similar situation may be expected to explain the observed inequivalence of meta ring protons of phenylgalvinoxyl.

The non-equivalence of the methyl proton splitting has been observed in the ENDOR spectra at low temperatures of the 2-methyl-derivative of galvinoxyl by Steelink *et al.*[8] When the two *t*-butyl groups on one of the two phenyl rings of galvinoxyl are replaced by methyl groups, the two methyl groups are inequivalent, showing a splitting of the methyl proton ENDOR line. However, in this case, all four ring protons of 2-methylgalvinoxyl are equivalent within the resolution of the ENDOR experiments. The molecular structure and packing in crystalline galvinoxyl have been determined by X-ray diffraction.[17] The observed bond angle at methine carbon is 134 degrees, and the phenyl

groups are twisted by 12 degrees. On the other hand, the phenylgalvinoxyl radical may be considered rather as triphenylmethyl derivatives. The Stuart molecular model indicates that the main steric interaction in phenylgalvinoxyl works between the ring protons, although weak interactions can be seen between the substituted *t*-butyl groups. Thus, the radical most probably adopts a propeller configuration, with a bond angle of about 120° at the centered carbon and a twist angle of about 30°.[18] Therefore, the decrease in the bond angle at the centered carbon and the increase in the twist angle in phenylgalvinoxyl compared to those of galvinoxyl will induce the difference in the hyperfine splitting constants of two meta ring protons in each of two phenyl rings, A and B.

ENDOR Spectra of IV, V, and VI Radicals. The para-derivatives, (IV), (V), and (VI) (see Fig. 2), of phenylgalvinoxyl show spectra similar to that of phenylgalvinoxyl. For example, the spectrum of the IV radical clearly exhibits four different proton hyperfine splittings, as is shown in Fig. 4(a). The value of each hyperfine splitting is very close to the corresponding value of phenylgalvinoxyl. This indicates that the effects of the para-substitution of the phenyl ring C by CH_3O-, Cl-, and CH_3- groups are too small to induce any change in the unpaired spin distribution or molecular structure. The hyperfine splittings for the IV, V, and VI radicals are listed in Table 1.

ENDOR Spectra of VII and VIII Radicals. The effect of the ortho-substitution of the phenyl ring, C, by Cl- and CH_3- groups has been studied (see Fig. 2, (P-VII) and (P-VIII)). The ENDOR spectrum of the VII radical (ortho-Cl-derivative) in toluene is shown in Fig. 4(b), indicating again four different proton hyperfine splittings (1.35_8, 1.29_1, 0.11_6, and 0.05_1 G). The obvious assignments of the 1.35_8 and 1.29_1 G to two pairs of ring protons, the 0.11_6 G to the ortho and para protons of the phenyl ring, C, and the 0.05_1 G to the tertiary butyl protons, are consistent with the results for the II—VI radicals. A similar spectrum is obtained for the VIII radical (ortho-CH_3-derivative), and the hyperfine splittings observed are listed in Table 1.

As has been reported for the tris(*p*-nitrophenyl)-methyl radical from the results of X-ray analysis, three phenyl rings, A, B, and C, of the phenylgalvinoxyl are considered to be twisted with an equivalent angle, 30°. Ortho-substitution induces a strong interaction between the pendent group and the ring adjacent to the pendent group. Therefore, we can expect that the two rings, A and B, of the quinone methide skeleton will be distorted by different angles, θ_A and θ_B, respectively. If this effect is large, we can expect four kinds of ring-proton hyperfine splittings for these radicals. However, the VII and VIII radicals show two kinds of hyperfine splittings due to four meta ring protons, with values similar to that of phenylgalvinoxyl. On the other hand, the hyperfine splittings of the phenyl ring, C, are reduced to almost half of that of phenylgalvinoxyl.

Since the ring protons in the rings A and B are believed to be inequivalent, even if the steric effect by ortho-substitution is small, this perturbation might make some contribution to the width and shape of the meta ring proton absorption lines. In addition, since the steric effect of the ortho-CH_3-derivative (VIII) must, in principle, be different from that of the ortho-Cl-derivative (VII), this would also induce a difference in the width and shape of the absorption lines of these two ortho-derivatives. The surprising thing is that all of these effects are so small. These results can be understood, however, by assuming that the ring C, to which the pendent groups are attached, is twisted more than the other rings, A and B, and that the twisting angles, θ_A and θ_B, are nearly equal to each other, that is, $\theta_C > \theta_A \approx \theta_B$.

ENDOR Spectra of IX and X Radicals. The ENDOR spectrum of the IX and X radicals (see Fig. 2) in toluene at −45 and −73 °C are shown in Fig. 4(c) and (d) respectively. The spectrum of the IX radical consists of 14 lines symmetrically disposed on both sides of the free proton NMR frequency. This spectrum is very different from those of other phenylgalvinoxyls. A comparison of the present ENDOR results on IX with those of an earlier work on II suggests that one group of splittings (1.40_7, 1.35_7, 1.26_0, 1.20_7 G) should be assigned to the four meta ring protons, and the (0.05_0 G) splitting, to the *t*-butyl protons. Similarly, the (0.18_3 G) splitting is assigned to the two ortho protons, and that of 0.28_9 G, to the one remaining para-methylene proton of the phenyl ring, C. This result indicates that the galvinoxyl skeleton twists unsymmetrically on either side; thus, all four meta ring protons are magnetically inequivalent. The differences (0.05_0 and 0.05_3 G) between the two larger splittings (1.40_7, 1.35_7 G) and the two smaller splittings (1.26_0, 1.20_7 G) are similar to each other and are comparable with those of other phenylgalvinoxyls. Therefore, assuming the twist angles ($\theta_A < \theta_B$), the two larger splittings and the two smaller splittings are attributable to the two meta ring protons of the ring A and the ring B respectively of the galvinoxyl skeleton.

Figure 4(d) shows the ENDOR spectrum of the X radical in toluene at −73 °C, indicating five different hyperfine splittings. Similarly, the splitting of 0.18_1 G may be assigned to ortho and para protons of the phenyl ring C, and that of 0.05_8 G, to the *t*-butyl protons. Clearly the splittings of 1.37_1, 1.32_1, and 1.26_8 G are to be assigned to the four magnetically inequivalent meta ring protons. Again, the data may be explained tentatively by keeping in mind the fact that the galvinoxyl skeleton twists unsymmetrically on either side, but the difference in the twist angles is smaller than that in the IX radical, and thus the intermediate two splittings coincide with each other. The cause of such molecular asymmetry is steric interaction between the galvinoxyl skeleton ring and the large group substituted to the ring C. The Stuart molecular model supports the idea that such steric interaction is possible for these radicals, (IX) and (X).

Solvent Effect. The solvent dependences of the ENDOR spectra of the II, VII, VIII, IX, and X radicals were also examined. In the II, VII, and VIII radicals, the ENDOR spectra in toluene and in 2-MTHF are similar to each other, and the observed values of the hyperfine splittings show a good accordance, within

the limits of experimental error, as is shown in Table 1. On the other hand, notable solvent dependences were observed in the ENDOR spectra of the IX and X radicals. The ENDOR spectrum of the IX radical in toluene at −40°——60 °C (see Fig. 4(c)) consists of 14 lines symmetrically disposed on both sides of the free proton NMR frequency. On the other hand, the ENDOR spectrum in 2-MTHF of the same radical (IX) at −50°——70 °C consists of 10 lines. This spectrum is quite similar to that of the X radical in toluene, shown in Fig. 4(d). Clearly, in 2-MTHF, the meta ring protons show three kinds of hyperfine splittings. This result may be explained by assuming that the degree of molecular asymmetry, that is, the difference in the twist angles, θ_A and θ_B, observed for the IX radical in toluene, was decreased in 2-MTHF. The splitting of 0.28_9 G due to the para methylene proton of the phenyl ring C, also disappeared in 2-MTHF. This must be due to the change in the dihedral angle of the CH bond to the $2p_z$ orbital of the ring C. Similar solvent effects were observed for the X radical. The ENDOR spectrum of the X radical in 2-MTHF at −54 °C shows four kinds of splittings, 1.34_7 and 1.27_4 G due to meta ring protons, 0.18_9 G due to phenyl ring C protons, and 0.06_1 G due to *t*-butyl protons. This result differs from the five kinds of splittings of the same radical seen in toluene at −40°——75 °C; it implies that the molecular asymmetry of the X radical observed in toluene is eliminated in 2-MTHF.

Many investigations of the solvent effect of free radicals, including phenoxyl radicals, have been reported.[19] The effect has been explained as a redistribution of the π-electron spin density in a radical molecule induced by the electrostatic interaction and/or the hydrogen bond formation between the radical and the solvent molecules. However, in all the phenoxyl radicals studied in the present work, the variation in the hyperfine splitting constants, and thus the π-electron spin density induced by these effects, are both thought to be small because of the steric effect of tertiary butyl groups in these molecules. In fact, the observed change in the hyperfine splittings of the II, VI, and VIII radicals in toluene and 2-MTHF is negligible, as is shown in Table 1. On the other hand, the notable solvent effect in the hyperfine splitting of the IX and X radicals observed here may be explained by assuming a change in the steric structure of the radical molecules due to the solvents. Therefore, in other words, the present solvent dependences observed for the phenylgalvinoxyls serve as evidence that solvent molecules play an important role in fixing the conformations and symmetric properties of the radical molecules.

MO Calculations. Using the same parameters for the oxygen atom as those used for the galvinoxyl radical by Luckhurst,[20] the McLachlan spin density of the phenylgalvinoxyl radical was calculated. In this calculation all three phenyl groups were assumed to be twisted by 30° about the methyl carbon bonds. The choice of 30° was made on the basis of the results of the X-ray analysis of the tris(*p*-nitrophenyl)methyl radical,[18] because steric hindrance between substituted *t*-butyl groups in the phenylgalvinoxyl radical is considered to be small from the Stuart molecular model; thus, the structure of the phenylgalvinoxyl mainly depends on that of the triphenylmethyl skeleton. Spin densities are not very sensitive to the choice of this angle as long as it is small, since the resonance integral between the methyl carbon and the attached phenyl carbon varies as $\beta=\beta_0\cos\theta$. The results are given in Fig. 1. They can explain the qualitative ENDOR spectrum of phenylgalvinoxyl, assuming the Q values of 23 G for ring protons and 0.28 G[19] for tertiary butyl protons. The orbitals containing an unpaired electron of the phenylgalvinoxyls have, at least in the Hückel approximation, a node in the centered phenyl ring, C, and a carbon atom connected to the phenyl ring, giving a zero spin density on the phenyl ring. In the McLachlan approximation, the orbitals are spin-polarized so as to yield nonvanishing spin densities in the phenyl ring C of the radical. These spin densities are $\rho_{ortho}=-0.010$ and $\rho_{para}=-0.009$, and the hyperfine splitting constant ($a^H=0.20_7$ G) may be assigned to the ortho and para ring protons of the phenyl ring C. The unpaired spin densities ($\rho_{meta}=0.000$) on the meta carbon atoms are negligibly small.

Recent studies of the magnetic susceptibilities of phenylgalvinoxyl (II) and some of its derivatives (IV)—(VIII) have clarified some interesting magnetic properties in the solid states, suggesting intermolecular ferromagnetic exchange interaction in some of these radicals.[10] The sign and magnitude of the exchange interaction between the π-electron spins may depend on both the spin densities and the molecular packing.[21,22] The results of ENDOR measurements and McLachlan Molecular Orbital calculation show that there are large positive and negative atomic π-spin densities in these radicals, and it is quite possible that, in special cases, these radicals may pancake on top of one another in the crystal lattice so that atoms of a positive spin density are exchange-coupled most strongly to atoms of a negative spin density in neighboring molecules. In such a case, the apparent exchange interaction is ferromagnetic, corresponding to the results verified experimentally by magnetic susceptibility measurements.[6,10,22]

We wish to thank Professor Yasuo Deguchi and Mr. Fujito Nemoto for their helpful discussions. We also wish to express our gratitude to Drs. Osamu Takizawa and Kohji Watanabe for their McLachlan Molecular Orbital calculations. We are grateful to Messrs. Masahiro Kohno and Takamitsu Yamamoto for their kind advice on the measurements of the ENDOR spectra. We are also grateful to Mr. Taizi Itoh for his kind help in the syntheses of phenols (*p*-IX) and (*p*-X).

References

1) M. S. Kharasch and B. S. Joshi, *J. Org. Chem.*, **22**, 1435 (1957).
2) G. M. Coppinger, *J. Am. Chem. Soc.*, **79**, 501 (1957).
3) J. K. Becconsall, S. Clough, and G. Scott, *Trans. Faraday Soc.*, **56**, 459 (1960).
4) H. H. Hausser, H. Brunner, and J. C. Jochims, *Mol. Phys.*, **10**, 253 (1966); R. W. Kreilick, *ibid.*, **14**, 495 (1968).

5) J. S. Hyde, *J. Chem. Phys.*, **43**, 1806 (1965); J. H. Freed, D. S. Leniart, and J. S. Hyde, *J. Chem. Phys.*, **47**, 2762 (1967).
6) K. Mukai, *Bull. Chem. Soc. Jpn.* **42**, 40 (1969).
7) K. Kosaki, H. Suga, S. Seki, K. Mukai, and Y. Deguchi, *Bull. Chem. Soc. Jpn.*, **42**, 1525 (1969).
8) C. Steelink, J. D. Fitzpatrick, L. D. Kispert, and J. S. Hyde, *J. Am. Chem. Soc.*, **90**, 4354 (1968).
9) K. Ley, E. Müller, and K. Scheffler, *Angew. Chem.*, **70**, 74 (1958).
10) K. Mukai and T. Tamaki, *Bull. Chem. Soc. Jpn.*, to be published.
11) E. Müller, K. Ley, K. Scheffler, and R. Mayer, *Chem. Ber.*, **91**, 2682 (1958).
12) K. Mukai, *Bull. Chem. Soc. Jpn.* **48**, 2405 (1975).
13) T. Yamamoto, M. Kohno, T. Miyamae, K. Mukai, and K. Ishizu, *Chem. Lett.*, **1972**, 681.
14) T. H. Coffield, A. H. Filbey, G. G. Ecke, and A. J. Kolka, *J. Am. Chem. Soc.*, **79**, 5019 (1957).
15) T. Yamamoto, K. Sato, and T. Miyamae, *J. Appl. Phys.*, **11**, 1508 (1972).
16) R. W. Fessenden and R. H. Schuler, *J. Chem. Phys.*, **39**, 2147 (1963); J. K. Kochi and P. J. Krusic, *J. Am. Chem. Soc.*, **90**, 7157 (1968).
17) D. E. Williams, *Mol. Phys.*, **16**, 145 (1969).
18) P. Andersen and B. Klewe, *Acta Chem. Scand.*, **16**, 1817 (1962).
19) K. Mukai, H. Nishiguchi, K. Ishizu, Y. Deguchi, and H. Takaki, *Bull. Chem. Soc. Jpn.*, **40**, 2731 (1967). The other references are therein.
20) G. R. Luckhurst, *Mol. Phys.*, **11**, 205 (1966).
21) H. M. McConnell, *J. Chem. Phys.*, **39**, 1910 (1963).
22) N. Azuma, J. Yamauchi, K. Mukai, H. Ohya-Nishiguchi, and Y. Deguchi, *Bull. Chem. Soc. Jpn.*, **46**, 2728 (1973).

Electronic States of Fluorene, Carbazole and Dibenzofuran

Masashi TANAKA

Department of Chemistry, Faculty of Science, Nagoya University, Chikusa, Nagoya 464

(Received March 8, 1976)

The polarized reflection spectra of the fluorene, carbazole, and dibenzofuran crystals have been measured from 30000 to 53000 cm^{-1} and the absolute intensity of the absorption parallel to the a, b, and c axes of these crystals has been obtained by the Kramers-Kronig transformation; these data allowed an interpretation to be made for the solution spectra. Furthermore, the influence of the intermolecular interaction on each level has been examined. This analysis shows that the lowest excited state of the fluorene molecule is the B_2 state, while those of the carbazole and dibenzofuran are the A_1 states. In fluorene, the sum of the oscillator strengths of the transition to two lower excited states (α and α^* states) is 0.39 in the molecule and 0.61 in the crystal. Such hyperchromism is also observed in the α, p, and β states of carbazole and the β state of dibenzofuran. On the other hand, the α^* state of dibenzofuran is hypochromic and the oscillator strengths in the molecule (0.87) decrease to 0.36 in the crystal. However, the factor group splitting and the crystal field shift are small and a one to one correspondence can easily be obtained between the solution and crystalline spectra.

The electronic spectra of fluorene, carbazole, and dibenzofuran are of interest because of the physical and chemical properties of five-membered heterocycles; many papers concerned with an experimental or theoretical analysis of their UV spectra have been reported.

These molecules have the symmetry of point group C_{2v} and the A_1 (polarized to the short axis) and B_2 (polarized to the long axis) states can be observed in the UV measurement. According to the vapor spectra observed by Pinkham and Wait,[1] the lowest energy $\pi\rightarrow\pi^*$ transition of fluorene vapor has its origin at 33773 cm^{-1} and was assigned to $A_1\rightarrow A_1$. Two $\pi\rightarrow\pi^*$ transitions were observed for dibenzofuran vapor. The one with the origin at 31488 cm^{-1} was assigned to an $A_1\rightarrow A_1$ transition, while the one which originates at 33647 cm^{-1} was assigned to $A_1\rightarrow B_2$. The strong $\pi\rightarrow\pi^*$ transition of carbazole which originates at 36346 cm^{-1} was assigned to $A_1\rightarrow B_2$. The weaker $\pi\rightarrow\pi^*$ band system, originating at 30694 cm^{-1}, was assigned to $A_1\rightarrow A_1$.

Solution studies have been made of the absorption, fluorescence, and phosphorescence. Kanda *et al.*[2] measured the phosphorescence of fluorene and dibenzofuran in cyclohexane at 90 K. Mataga, Torihashi, and Ezumi[3] studied the solvent effects upon the fluorescence and absorption spectra of carbazole. As is cited in the paper by Dörr and Gropper,[4] Joop[5] appears to have obtained the polarization of the fluorescence excitation spectrum of fluorene and found that the *p*-values for fluorescence are positive when excitation is made to the first and second absorption bands. Schütt and Zimmerman[6] reported the fluorescence, phosphorescence, and absorption polarization ratio of carbazole and found that the *p*-values are positive for the first band at 29500 cm^{-1} and negative for the second band at 34000 cm^{-1}, Lace *et al.*[7] measured the polarized absorption of dibenzofuran in 1,2,4,5-tetramethylbenzene host and decided that the 3000 Å transition should be assigned to $A_1\rightarrow B_2$. Siegel and Judeikis[8] determined the polarization by the method of magnetophotoselection and they also demonstrated that the lowest state of fluorene has a B_2 symmetry and those of carbazole and dibenzofuran have A_1 symmetries.

In the crystal of these compounds, there are four molecules in an orthorhombic unit cell;[9-11] the long axis of the molecule lies exactly parallel to one of the crystalline axes and the short axis is perpendicular to it. Accordingly, it is possible to assign the transitions to the A_1 and B_2 states distinctly by using the polarization technique. The polarized crystalline absorption spectra were measured by the group of Bree.[12-14] The a and b axes polarized spectra of a fluorene crystal showed that the 33000 cm^{-1} system is the B_2 state, while the a and c axes spectra of a dibenzofuran crystal showed that the first band is the A_1 state. The polarized absorption spectra of carbazole in a fluorene matrix were measured by Bree and his coworkers; they made the assignment that the 30000 cm^{-1} system is the A_1 state.

The author measured the polarized reflection spectra of titled crystals with several crystalline faces and attempted to give better assignments of absorption bands for a wide spectral range. Furthermore, the influence of the intermolecular interaction on the band position and intensity of each level was examined and compared with the results calculated by the SCF-RPA exciton method.[15] This method, which takes into account the double excitation configuration, is very usefull for studying the intermolecular interaction, because the double excitation has a large effect on the hypochromism, as was shown by Tinoco[16] and Rhodes.[17]

Experimental

Single crystals of fluorene, carbazole, and dibenzofuran were grown by slow evaporation of the ethanol solution after purifying the material by column chromatography. The crystal showed well developed (001) or (010) faces.

Reflection spectra at the normal incidence have been measured over a range of 20000—53000 cm^{-1} with a reflection spectrophotometer made in our laboratory and the absorption spectra have been obtained by the Kramers-Kronig transformation.[18] The oscillator strength along the α axis of the crystal may be evaluated by using the following equation:[19]

$$f^{\alpha} = 4.32\times10^{-9} \int n_{\alpha}(\sigma)\,\varepsilon_{\alpha}(\sigma)\,d\sigma$$

where the integration is calculated over the whole band, σ is the wave number, and n_{α} and ε_{α} are the α component of the refractive index and the molar extinction coefficient.

Oscillator strengths for the three orthogonal axes in the orthorhombic crystal should be compared with that in solution:

$$f^{a} + f^{b} + f^{c} = 3f^{\text{solution}}$$

where the suffixes a, b, and c correspond to the crystal axes.

Thoeretical

The electronic states of the molecules are calculated by the RPA method.[20] This method is formulated as an eigenvalue problem for the singlet energies ΔE of a many-electron system as follows:

$$\begin{pmatrix} A & B \\ B & A \end{pmatrix}\begin{pmatrix} X \\ Y \end{pmatrix} = \Delta E \begin{pmatrix} X \\ -Y \end{pmatrix}$$

where

$$A_{ij,kl} = (\varepsilon_j - \varepsilon_i)\delta_{ik}\delta_{jl} + 2(ij|kl) - (ik|jl)$$

and

$$B_{ij,kl} = 2(ij|kl) - (il|jk)$$

The indices i, k refer to the HF orbitals occupied in the ground configuration Φ_0 and the indices j, l refer to the virtual orbitals of the HF eigenvalue problem

$$F\phi_i = \varepsilon_i\phi_i.$$

The two-electron integrals are defined by

$$(ij|kl) = \int \phi_i^*(1)\,\phi_j(1)\frac{1}{r_{12}}\phi_k^*(2)\,\phi_l(2)\,d\tau_1\,d\tau_2.$$

Then the above-mentioned equations can be evaluated with the approximations of the neglect of differential overlap[21] and of the use of two-center coulomb integrals γ_{pq} estimated by Nishimoto-Mataga's method.[22] The one-center core coulomb integrals α_p and the two-center resonance integrals β_{pq} are approximated in the following equations:

$$\alpha_p = -I_p - (n_p - 1)\gamma_{pp} - \sum_{r \neq p} n_r\gamma_{pr}$$

$$\beta_{pq} = -K(I_p + I_q)S_{pq}$$

where the constant K is taken to be 0.29. The overlap integrals S_{pq} are calculated between the nearest neighbor atoms by using the SCF-AO's[23] and neglected in other cases. The values of the ionization potentials I_p are taken from Pilcher and Skinner's table[24] and the one-center integrals γ_{pp} are estimated by the Pariser-Parr approximation.[25]

In theoretical studies of the ultraviolet spectra of five-membered rings, Momicchioli and Rasteli[26] showed that the lower excited states of these molecules have the α, α^*, p, β, β^*, and β' characters in Clar's notation, where α and β characters mean that the excited states derive mainly from the mixing of Φ (A→B′) and Φ (B→A′) configurations, and similarly α^* and β^* characters from Φ (A→C′) and Φ (C→A′) and p and β' from Φ (A→A′), Φ (B→B′), and Φ (C→C′). The letters ···C,B,A,A′,B′,C′··· are the molecular orbitals denoted according to increasing energy. In these compounds of point group C_{2v}, the molecular orbitals C, A, B′, and D′ span the a_1 representation and D, B, A′, and C′ the b_2, respectively. Therefore, the α and β states belong to the A_1 symmetry and are the short axis polarized states, and the α^*, p, β^*, and β' states belonging to the B_2 symmetry are the long axis polarized states. In addition to the above-mentioned states, two other bands can be observed in the higher energy range and may be noted as the γ and δ states of the A_1 symmetry. The γ state has the large contribution from four configurations of Φ (B→C′), Φ (C→B′), Φ (A→B′), and Φ (B→A′), and the δ state from Φ (D→C′) and Φ (C→D′).

The exciton states of the crystal are calculated according to the RPA exciton method.[15] This method takes into account the effect of the doubly excited configurations in addition to the mixing between the singly excited configurations.

All of the above-mentioned computations were carried out on a FACOM 230—60 computer at the Nagoya University computation center.

Results and Discussion

Fluorene. The solution spectrum is described in Fig. 1 and the theoretically calculated results of the molecule are given in Table 1, together with the assignment of the observed states. The first band in the region of 3000 Å has structure and consists of two electronic states. The lowest state at 33200 cm^{-1} is the long axis polarized state of B_2 symmetry (α^* state) and the short axis state (α state) is covered by the α^* state, as shown below. The third state (p state) also has structure; its origin is at 35900 cm^{-1} and other vibronic levels appear at 36900, 38100, 39200, and 40400 cm^{-1}. This state is assigned to the B_2 state. There are many other states in the higher energy region: two shoulders at 44300 cm^{-1} (β^* state) and 45500 cm^{-1} (β' state) and a stronger system (β state) beginning near 48000 cm^{-1}.

Fluorene forms orthorhombic crystals of space group Pnam (D_{2h}^{16}) having four molecules in a unit cell.[9] Projections onto the (010) and (001) faces are shown in Fig. 2. Beacuse of site symmetry (C_s), the long axis of the molecule lies exactly parallel to the c crystalline axis and the short in-plane axis is in

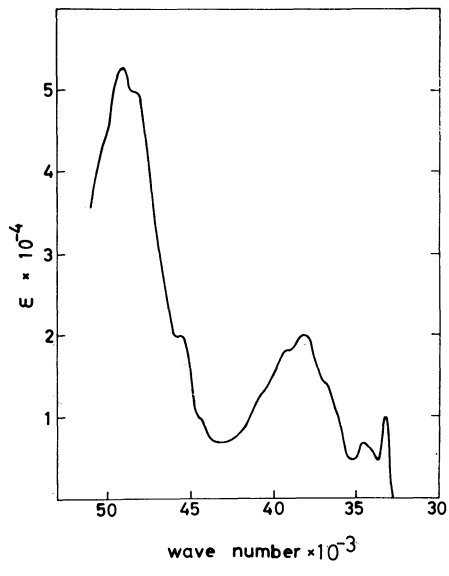

Fig. 1. The spectrum in isooctane of the fluorene molecule.

TABLE 1. THE LOWER EXCITED STATES OF THE FLUORENE MOLECULE, CALCULATED BY THE RPA METHOD
(All energy values are given in the units of $10^3\,cm^{-1}$.)

State		Obsd		Calculated Values		
		E	(f)	E	(f)	Wavefunction
A_1	α	>33.2	(0.13)	32.9	(0.00)	$0.6482\,\Phi(6\to8)-0.6482\,\Phi(5\to7)+\cdots$
B_2	α^*	33.2		33.4	(0.00)	$0.6424\,\Phi(6\to9)-0.6424\,\Phi(4\to7)+\cdots$
B_2	p	35.9	(0.43)	36.2	(0.55)	$0.9964\,\Phi(6\to7)+\cdots$
B_2	β^*	44.3	(0.04)	43.3	(0.12)	$0.7008\,\Phi(6\to9)+0.7008\,\Phi(4\to7)+\cdots$
B_2	β'	45.5	(0.13)	45.1	(0.77)	$0.7602\,\Phi(5\to8)+0.6511\,\Phi(4\to9)+\cdots$
A_1	β	48.2	(1.08)	45.5	(0.70)	$0.6970\,\Phi(6\to8)+0.6970\,\Phi(5\to7)+\cdots$
A_1	δ			55.5	(0.59)	$0.7107\,\Phi(4\to10)+0.7107\,\Phi(3\to9)+\cdots$

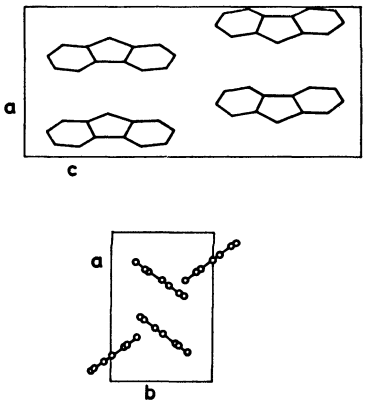

Fig. 2. Projection of fluorene onto the (010) and (001) planes.

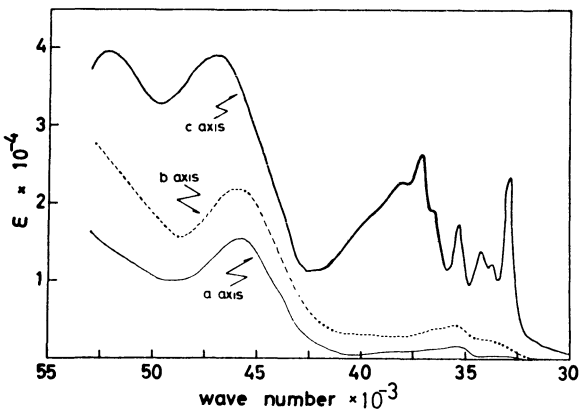

Fig. 3. The polarized absorption spectra of the fluorene crystal obtained by the K-K transformation of the reflection spectra.

the (001) plane. Thus, a long axis transition in the isolated molecule may not be observed in the (001) cleavage plane; only the short axis transition is allowed and is assigned to the $A_1\to A_1$ transition. The c axis spectrum is of the B_2 states allowed for the polarized light parallel to the long axis in the molecule. It will be expected that the A_1 and B_2 excited states can be separately measured and the absorption spectra for these crystalline axes can be obtained from the reflection spectra, as shown in Fig. 3.

In the crystalline c-axes spectrum, four transitions of α^*, p, β^*, and β' were observed at 32900, 35300, 47400, and 52600 cm^{-1}; these were assigned to the transition to the B_2 state. The a and b axes spectra have three bands (α, β, and δ) at 33500, 46000, and about 54000 cm^{-1}, which correspond to the short axis polarized bands of the molecule and are assigned to the A_1 state. The theoretical studies shown in Table 1 predict two transitions (one long and one short axis polarized) followed by a strong long axis transition. This experiment shows that the lowest excited state is the α^* state at 32900 cm^{-1} and the second state is the α state at 33500 cm^{-1}, although the first and second states obtained theoretically are reversed in order. Bree and Zwarich[12] found that 32818 cm^{-1} in fluorescence and 32910 cm^{-1} in the c axis-polarized absorption may both connect the same lowest electronic levels (B_2 state) in the crystal. Our experimental result is in good agreement with their measurement. The successive levels of the lowest α^* state are located at 33700 and 34300 cm^{-1} in the crystalline spectrum and at 34000 and 34700 cm^{-1} in the solution spectrum. The origin of the p state is assigned to the peak at 35300 cm^{-1} and higher vibronic levels appear at 36400, 37100, and 38100 cm^{-1}. The comparison of the vibronic levels between the solution and the crystalline spectra is shown in Table 2.

The excitation energies and oscillator strengths of the crystal were calculated by the RPA exciton me-

TABLE 2. VIBRONIC LEVELS FOR THE LOWER EXCITED STATES OF FLUORENE
(All energy values are given in the units of cm^{-1}.)

State	Solution		Crystal	
α^*	33200		32900	
		(800)		(800)
	34000		33700	
		(700)		(600)
	34700		34300	
α			33500	
				(1900)
			35400	
p	35900		35300	
		(1000)		(1100)
	36900		36400	
		(1200)		(700)
	38100		37100	
		(1100)		(1000)
	39200		38100	
		(1200)		
	40400			

Table 3. The calculated and observed values of the transition energies (E in 10^3 cm^{-1}) and oscillator strengths of the fluorene crystal

State		Obsd E	Obsd (f)	Calcd E	Calcd (f)
B_{3u}	α	33.5	(0.05)	33.0	(0.00)
(a axis)	β	45.7	(0.60)	44.3	(0.70)
	δ	≈54	(0.91)	54.4	(0.46)
B_{2u}	α	33.5	(0.13)	33.0	(0.00)
(b axis)	β	46.2	(0.86)	47.0	(1.04)
	δ	≈54	(1.12)	56.5	(1.65)
B_{1u}	α^*	32.9	(0.43)	33.5	(0.00)
(c axis)	p	35.3	(1.18)	33.7	(2.35)
	β^*	47.4	(1.50)	42.5	(0.55)
	β'	52.6	(1.00)	44.3	(1.42)

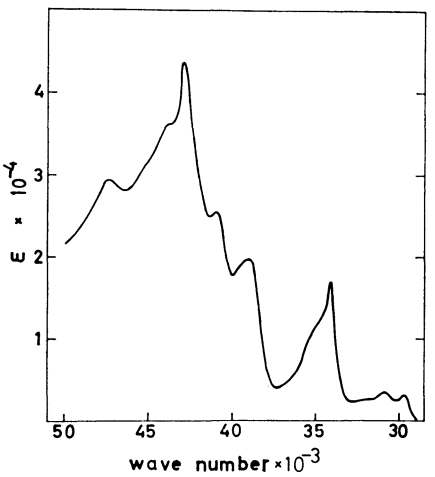

Fig. 4. The spectrum in ethanol of the carbazole molecule.

thod.[15] The results are shown in Table 3, in which the intermolecular interactions for the inner zone were calculated to 50 Å. As shown in Tables 1 and 3, the comparison between the oscillator strengths of the molecule and the crystal show that the sum of the oscillator strengths of two states (α and α^* states) is 0.39 (3 f^{solution}) in the molecule and 0.61 ($f^a+f^b+f^c$) in the crystal. In the intense p band, the absorption intensity in the molecule (3 $f^{\text{solution}}=1.29$) is comparable with 1.18 (f^c) in the crystal. The dichroic ratio($f^a/f^b=2.6$) of the α band is slightly larger than the oriented gas polarization ratio of 2.1. However, those of the higher states deviate from the values expected from the oriented gas model and can be explained by the intermolecular interaction.

Carbazole. The solution spectrum is described in Fig. 4 and the theoretically calculated results of the molecule are given in Table 4, together with the assignment of the observed states. The first band in the region of 30000 cm^{-1} has structure; the origin is located at 29700 cm^{-1} and other vibronic levels appear at 30900 and 32100 cm^{-1}. This state is assigned to the short axis polarized state of A_1 symmetry (α band). The second α^* band originating at 34100 cm^{-1} is of B_2 symmetry and a successive vibronic level appears as the shoulder at 35300 cm^{-1}. Band positions of the α and α^* states are summarized in Table 5. There are many other states in the higher energy region, the p band at 39000 cm^{-1} and a stronger and more complex system which probably contains four separate electronic transitions at 41000 cm^{-1} (β state), 43000 cm^{-1} (β' state), 45000 cm^{-1} (β^* state), and 47400 cm^{-1} (γ state).

Carbazole forms orthorhombic crystals of space group Pnma (D_{2h}^{16}) with four molecules, as shown in Fig. 5.[10] The crystal structure of carbazole resembles that of fluorene having the same space group (although the axes b and c have been interchanged) and has similar unit cell dimensions and molecular orientations. The polarized absorption spectra along three crystalline axes are obtained from the reflection spectra by the K-K transformation and are shown in Fig. 6. The excitation energies and oscillator strengths of the crystal were calculated by the SCF-RPA exciton method; the results are shown in Table 6 together with the observed values.

In the crystalline b axis spectrum, four transitions (α^*, p, β', and β^*) at 33900, 40300, 42000, and 45600 cm^{-1} must be assigned to the B_2 state. The a and c axes spectra have four bands (α, β, γ, and δ) at 29400, ≈40000, ≈44000, and 53000 cm^{-1} which should be assigned to the A_1 state. Band positions of the vibronic levels of the α and α^* states can be compared with those in the solution spectrum, as shown in Table 5. The factor group splitting and the crystal field shift are negligibly small in the a and c axes spectra,

Table 4. The lower excited states of the carbazole molecule, calculated by the RPA method
(All energy values are given in the units of 10^3 cm^{-1}.)

State		Obsd E	Obsd (f)	Calculated values E	Calculated values (f)	Wavefunction
A_1	α	29.7	(0.04)	31.9	(0.01)	$0.7390\,\Phi(6\to8)-0.5828\,\Phi(7\to9)+\cdots$
B_2	α^*	34.1	(0.16)	35.0	(0.05)	$0.5905\,\Phi(5\to8)+0.5447\,\Phi(7\to10)+\cdots$
B_2	p	39.0	(0.17)	37.7	(0.33)	$0.9095\,\Phi(7\to8)+0.2640\,\Phi(6\to9)+\cdots$
B_2	β'	43.0	(0.82)	42.0	(1.04)	$0.9351\,\Phi(6\to9)-0.2566\,\Phi(7\to8)+\cdots$
A_1	β	41.0	(0.18)	43.5	(0.46)	$0.6291\,\Phi(7\to9)+0.5614\,\Phi(6\to8)+\cdots$
A_1	γ	47.4	(0.25)	44.6	(0.26)	$0.6634\,\Phi(6\to10)+0.4311\,\Phi(7\to9)+\cdots$
B_2	β^*	45.0	(0.1)	45.6	(0.00)	$0.7252\,\Phi(7\to10)-0.6645\,\Phi(5\to8)+\cdots$
A_1	δ			57.0	(0.60)	$0.8067\,\Phi(4\to10)-0.5936\,\Phi(5\to11)+\cdots$

TABLE 5. VIBRONIC LEVELS FOR THE LOWER EXCITED STATES OF CARBAZOLE
(All energy values are given in the units of cm^{-1}.)

State	Solution		Crystal	
α	29700		29400	
		(1200)		(1300)
	30900		30700	
		(1200)		(1300)
	32100		32000	
α^*	34100		33900	
		(800)		(800)
	35300		34700	

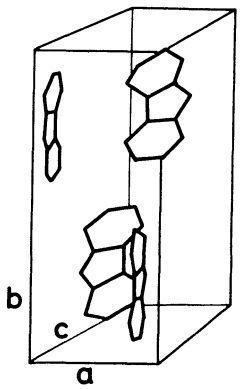

Fig. 5. The unit cell of the carbazole crystal.

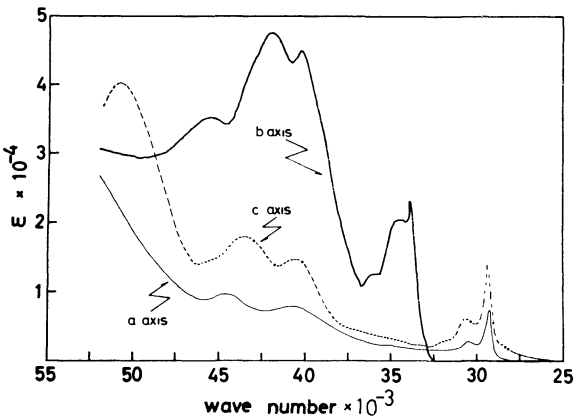

Fig. 6. The polarized absorption spectra of the carbazole crystal obtained by the K-K transformation of the reflection spectra.

although large shifts are observed in the b axis spectrum. Tables 4 and 6 show that the oscillator strength of the α state is 0.12 ($3\,f^{\text{solution}}$) in the molecule and 0.29 (f^a+f^c) in the crystal and the hyperchromism is observed. In the α^* state, the intensity of the molecule ($3\,f^{\text{solution}}=0.48$) is comparable with that of the crystal ($f^b=0.54$). The p and β states are hyperchromic and the intensities of the molecule increase in the crystal. The observed dichroic ratios (f^b/f^c) of the α and γ states are about 2.6, while the oriented gas polarization ratio is 3.2. Those of the other states (β and δ) deviate from the values expected from the oriented gas model and may be explained by the intermolecular interaction.

TABLE 6. THE CALCULATED AND OBSERVED VALUES OF THE TRANSITION ENERGIES (E IN $10^3\,cm^{-1}$) AND OSCILLATOR STRENGTHS OF THE CARBAZOLE CRYSTAL

State		Obsd		Calcd	
		E	(f)	E	(f)
B_{3u}	α	29.3	(0.08)	32.0	(0.01)
(a axis)	β	40.8	(0.34)	41.9	(0.29)
	γ	44.5	(0.21)	44.4	(0.27)
	δ	≈53	(1.04)	56.6	(0.38)
B_{1u}	α	29.4	(0.21)	32.1	(0.02)
(c axis)	β	4.04	(0.50)	41.1	(0.001)
	γ	43.5	(0.52)	44.8	(1.16)
	δ	≈50	(1.43)	58.1	(1.79)
B_{2u}	α^*	33.9	(0.54)	34.1	(1.39)
(b axis)	p	40.3	(0.90)	36.0	(0.90)
	β'	42.0	(2.00)	40.7	(2.06)
	β^*	45.6	(0.60)	49.8	(0.17)

Dibenzofuran. The solution spectrum is depicted in Fig. 7 and the theoretically calculated results of the molecule are given in Table 7 together with the assignment of the observed states. The first band, extending from about 33000 to 40000 cm^{-1}, has structure and consists of both the short axis polarized state (α state) and the long axis polarized state (α^* state). The α state in the region of the lowest energy originates at 33100 cm^{-1} and the successive vibronic levels occur as the shoulders at 34600 and 36100 cm^{-1}. The α^* state is observed as sharp peaks; the principal origin is at 33600 cm^{-1} and the higher levels are located at 34800 and 35600 cm^{-1}. The assignment for these two bands is supported by comparison with the crystalline spectra, as shown below. The third state (p state) also has structure; the origin is observed at 40100 cm^{-1} and other levels appear at 40900 and 41400 cm^{-1}. This band is assigned to the B_2 state. There are many other states in the higher energy region: two shoulders at 43900 cm^{-1} (β state) and 47200 cm^{-1} (β^* state) and two intense bands at 45800 cm^{-1} (β' state) and

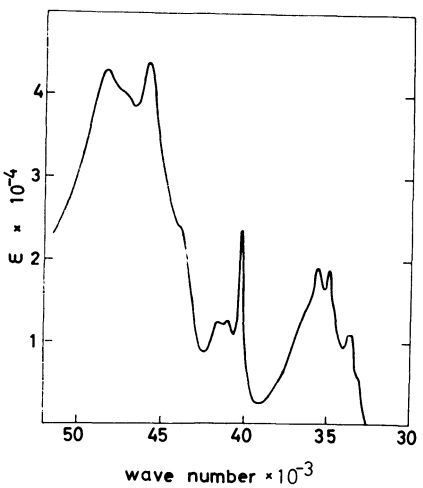

Fig. 7. The spectrum in light petroleum of the dibenzofuran molecule.

TABLE 7. THE LOWER EXCITED STATES OF THE DIBENZOFURAN MOLECULE, CALCULATED BY THE RPA METHOD
(All energy values are given in the units of $10^3\,cm^{-1}$.)

State		Obsd		Calculated values		
		E	(f)	E	(f)	Wave function
A_1	α	33.1	(0.04)	33.7	(0.003)	$0.6877\,\Phi(6\to8)-0.6186\,\Phi(7\to9)+\cdots$
B_2	α^*	33.6	(0.29)	35.5	(0.02)	$0.6252\,\Phi(5\to8)-0.5890\,\Phi(7\to10)+\cdots$
B_2	p	40.1	(0.15)	38.0	(0.55)	$0.9680\,\Phi(7\to8)+\cdots$
A_1	β	43.9	(0.17)	45.4	(0.42)	$0.5437\,\Phi(7\to9)+0.5244\,\Phi(6\to8)+\cdots$
B_2	β'	45.8	(0.54)	45.7	(0.86)	$0.8804\,\Phi(6\to9)+0.4016\,\Phi(5\to10)+\cdots$
B_2	β^*	47.2	(0.25)	45.9	(0.01)	$0.6966\,\Phi(7\to10)+0.6671\,\Phi(5\to8)+\cdots$
A_1	γ	48.3	(0.67)	46.4	(0.35)	$0.4943\,\Phi(7\to9)+0.4762\,\Phi(6\to10)$ $+0.4467\,\Phi(6\to8)+0.3957\,\Phi(5\to9)+\cdots$
A_1	δ			57.5	(0.59)	$0.7728\,\Phi(4\to10)+0.6390\,\Phi(5\to11)+\cdots$

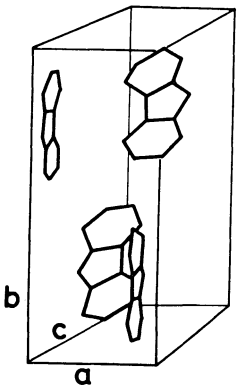

Fig. 8. The unit cell of dibenzofuran crystal.

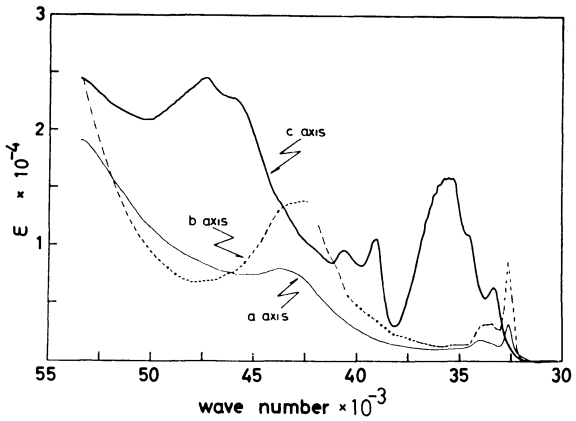

Fig. 9. The ploarized absorption spectra of the dibenzofuran crystal obtained by the K-K transformation of the reflection spectra.

48300 cm^{-1} (γ state).

Dibenzofuran crystallizes with four molecules in an orthorhombic unit cell having space group Pnam (D_{2h}^{16}).[14] Each molecule is held in the lattice with the long axis exactly parallel to the c crystal axis and with the short in-plane axis in the ab plane. The dispositions of the four molecules in the unit cell are shown clearly in Fig. 8. The polarized absorption spectra along these crystal axes are given from the reflection spectra by the K-K transformation, as shown in Fig. 9.

TABLE 8. VIBRONIC LEVELS FOR THE LOWER EXCITED STATES OF DIBENZOFURAN
(All enengy values are given in the units of cm^{-1}.)

State	Solution		Crystal	
α	33100		32600	
		(1500)		(1400)
	34600		34000	
		(1500)		(1400)
	36100		35400	
α^*	33600		33300	
		(1200)		(1200)
	34800		34500	
		(800)		(800)
	35600		35300	
p	40100		39100	
		(800)		
	40900			(1500)
		(500)		
	41400		40600	

TABLE 9. THE CALCULATED AND OBSERVED VALUES OF THE TRANSITION ENERGIES (E IN $10^3\,cm^{-1}$) AND OSCILLATOR STRENGTHS OF THE DIBENZOFURAN CRYSTAL

State		Obsd		Calcd	
		E	(f)	E	(f)
B_{3u}	α	32.6	(0.02)	33.8	(0.003)
(a axis)	β	43.5	(0.14)	44.9	(0.50)
	γ			49.6	(0.02)
	δ	≈55	(0.65)	56.9	(0.37)
B_{2u}	α	32.6	(0.06)	33.8	(0.004)
(b axis)	β	42.5	(0.60)	46.0	(0.99)
	γ			49.0	(0.04)
	δ	≈53.5	(0.76)	50.5	(0.39)
B_{1u}	α^*	33.3	(0.36)	34.8	(1.55)
(c axis)	p	39.1	(0.20)	36.0	(0.92)
	β'	≈46	(1.30)	44.4	(1.95)
	β	≈53.5	(0.27)	52.1	(0.10)

In the crystalline c axis spectrum, four transitions (α^*, p, β', and β^*) observed at 33300, 39100, 46000, and 53500 cm^{-1} must be polarized along the long axis of the molecule and may be assigned to the B_2 state. The α^* state is located at 33300 cm^{-1} and the following

levels are observed at 34500 and 35300 cm^{-1}. The p state originates at 39100 cm^{-1} and the higher level appears at 40600 cm^{-1}, while the second level at 40900 cm^{-1} in the solution spectrum can not be observed. The a and b axes spectra have three bands (α, β, and δ states) at 32600, about 43000, and 55000 cm^{-1}, corresponding to the short axis polarized band of the molecule, and can be assigned to the A_1 state. The α state has its origin at 32600 cm^{-1} and the higher successive levels are observed at 34000 and 35400 cm^{-1}.

The excitation energies and oscillator strengths of the crystal were calculated by the SCF-RPA exciton method; the results are shown in Table 9, in which the intermolecular interactions for the inner zone were calculated to be 50 Å. The factor group splitting is slightly observed for the β and δ states. However, many transitions in the crystal are red-shifted by the crystal force compared with the transitions in solution. The comparison between the observed oscillator strengths of the molecule and crystal shows that the oscillator strength of the β band is 0.51 ($3\,f^{\text{solution}}$) in the molecule and 0.74 ($f^{a}+f^{b}$) in the crystal and the hyperchromism is observed in the range of 44000 cm^{-1}. On the other hand, the α^* state is hypochromic and the intensity of the molecule ($3\,f^{\text{solution}}=0.87$) decreases to 0.36 ($f^{c}$) in the crystal. Such decreases of the intensity are also observed in all other state regions. The observed dichroic ratios (f^{b}/f^{a}) of the α and β states are 3.0 and 3.6, respectively. These values are comparable with the oriented gas polarization ratio of 3.6. However, that of the β state deviates from the values expected from the oriented gas model.

The author would like to express his deep gratitude to Professor Jiro Tanaka of this university for his kind encouragement and critical reading of the manuscript.

References

1) C. A. Pinkham and S. C. Wait, Jr., *J. Mol. Spectrosc.*, **27**, 326(1968).
2) Y. Kanda, R. Shimada, K. Hanada, and S. Kajigaeshi, *Spectrochim. Acta*, **17**, 1268 (1961).
3) N. Mataga, Y. Torihashi, and K. Ezumi, *Theor. Chem. Acta.* **2**, 158(1964).
4) F. Dörr and H. Gropper, *Ber. Bunsenges. Phys. Chem.*, **67**, 193 (1963).
5) N. Joop, *Diplom-Arbeit THMünchen*, 1960.
6) H. Schütt and H. Zimmerman, *Ber. Bunsenges. Phys. Chem.*, **67**, 55 (1963).
7) A. R. Lacey, A. E. W. Knight, and I. G. Ross, *J. Mol. Spectrosc.*, **47**, 307 (1973).
8) S. Siegel and H. S. Judeikis, *J. Phys. Chem.*, **70**, 2207 (1966).
9) D. M. Durns and J. Iball, *Proc. R. Soc. London, Ser. A*, **227**, 200 (1955).
10) M. Kurahashi, M. Fukuyo, and A. Shimada, *Bull. Chem. Soc. Jpn.*, **42**, 2174 (1969).
11) O. Dindenberg, L. Dupont, and J. M. Andrè, *Acta Crystallogr., Sect. B*, **28**, 1002 (1972).
12) A. Bree and R. Zwarich, *J. Chem. Phys.*, **51**, 903 (1969).
13) A. Bree and R. Zwarich, *J. Chem. Phys.*, **49**, 3355 (1968).
14) A. Bree, V. V. B. Vilkos, and R. Zwarich, *J. Mol. Spectrosc.*, **48**, 135 (1973).
15) M. Tanaka and J. Tanaka, *Theor. Chim. Acta*, **30**, 81 (1973).
16) I. Tinoco, Jr., *J. Chem. Phys.*, **33**, 1332 (1960), **34**, 1067 (1961).
17) W. Rhodes, *J. Am. Chem. Soc.*, **83**, 3609 (1961).
18) H. J. Bowlden and J. K. Wilmshurst, *J. Opt. Soc. Am.*, **53**, 1073 (1963).
19) A. Matsui and Y. Ishii, *J. Phys. Soc. Jpn.*, **23**, 581 (1967).
20) T. H. Dunning and V. McKoy, *J. Chem. Phys.*, **47**, 1735 (1967).
21) R. G. Parr, *J. Chem. Phys.*, **20**, 1499 (1952).
22) K. Nishimoto and N. Mataga, *Z. Phys. Chem.(NF).*, **12**, 335 (1957).
23) E. Clementi, C. C. J. Roothaan, and M. Yoshimine, *Phys. Rev.*, **127**, 1618 (1962).
24) G. Pilcher and H. A. Skinner, *J. Inorg. Nucl. Chem.*, **24**, 937 (1962).
25) R. Pariser and R. G. Parr, *J. Chem. Phys.*, **21**, 767 (1953).
26) F. Momicchioli and A. Rastelli, *J. Mol. Spectrosc.*, **22**, 310 (1967); *J. Chem. Soc., B*, **1970**, 1354.

The Alkoxylation of Aerosil Silica with C_1–C_4 Alcohols

Shigeto KITAHARA

Fukuoka University of Education, Akama, Munakata, Fukuoka 811-41

(Received March 8, 1976)

The Aerosil surface was treated with C_1–C_4 alcohols under both high-pressure and low-pressure conditions. The high-pressure treatment was carried out at various temperatures up to 250 °C using an autoclave, while the low-pressure treatment was done at 280 °C under vapor pressure at room temperature. The surface changes were followed by IR spectroscopy, and the carbon content was determined. The degrees of alkoxylation (OR groups/100 Å^2) of the Aerosils treated sufficiently under low pressures were 1.3—1.6, approximately equal to the amount of OH isolated before the treatment, while the values under high pressures reached 2.3—3.4, equal or near to the amount of the total OH. The values for methoxylation were particularly higher, while those for *t*-butoxylation were quite low. These results, in addition to the observation of the IR spectra, indicate that the isolated OH groups are predominantly esterified under low pressures, while under high pressures the vicinal OH groups are esterified as well, and the opening of the siloxane bonds occurs easily in the case of methoxylation. The stability of the alkyl groups on the Aerosil against heating decreased in the order of: primary>secondary>tertiary.

It is well known that a silica gel surface is alkoxylated with alcohols and that the resulting surface is hydrophobic. It is considered[1-3] that the alkoxylation occurs through the esterification of surface hydroxyl groups and the opening of surface siloxane bonds. The surface hydroxyls consist of the isolated OH, the single OH, the vicinal OH, and the hydrogen-bonded OH.

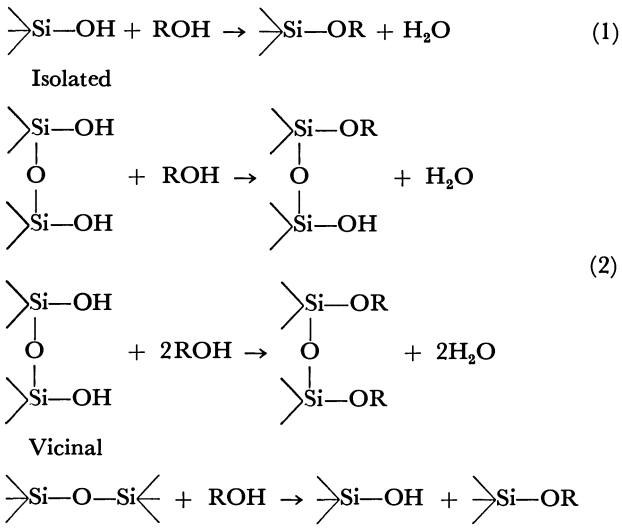

The reaction has been studied by several workers[1-17] under both high- and low-pressure conditions; however, the investigations under the two conditions have been carried out separately by different workers. Regarding a comparison in the alkoxylations under the two conditions, only Stöber *et al.*[4] have reported comparatively the degrees of alkoxylation under the two conditions. From the values, a satisfactory discussion is impossible because of the differences in the experimental conditions other than the pressure.

In the present study, including the differences in the alkoxylations under the two conditions, the effects of the kinds of alcohols and the experimental conditions on the reaction were systematically examined by means of C_1–C_4 alcohols. The conditions under which Reactions 1, 2, and 3 take place were discussed on the base of the results. In addition, the stability against the heating of the alkoxyl groups on the Aerosil surface was examined.

Aerosil-200 (Japan Aerosil Co., Ltd.) was chosen as the sample, because the Aerosil powder was adequate for the production of a transparent disc, and the same kinds of silica have been used by many workers. The reaction was mainly carried out under high pressures using an autoclave. Some runs were carried out under low pressures, though, that is, under vapor pressures of the alcohols at room temperature. The surface changes upon the treatments were followed by infrared spectroscopy, and the carbon content was determined.

Experimental

Materials. The Aerosil powder was pressed into discs 10 mm in diameter, each weighing about 10 mg, at a pressure of about 5 ton/cm^2. All the alcohols used were the purest commercially available reagents.

The surface area of the Aerosil was determined by means of the BET method, and the cross-sectional area of nitrogen was assumed to be 16.2 Å^2. The surface area of the disc before the treatment was 217 m^2/g, while those of the discs alkoxylated sufficiently were 176—188 m^2/g.

The content of the total hydroxyl groups of the Aerosil was determined from the weight loss induced by heating the Aerosil, previously dried to a constant weight at 110 °C, for 4 h at 1100 °C. The content of the isolated hydroxyl groups was determined from the chlorine content on the surface of Aerosil allowed to react with dichlorodimethylsilane, according to the procedures reported by Armistead *et al.*[18] The chlorine content was determined as follows: the chlorine on the Aerosil was extracted with a 0.1 M-NaOH solution, and then the amount of chlorine in the solution was titrated with a 0.0141 M-$Hg(NO_3)_2$ solution according to the procedures described in JIS-K0101 of the Industrial Analysis. The amount of the total OH groups and that of the isolated OH on the surface were 2.7 and 1.5 groups per 100Å^2 respectively. The former agreed with the value of 3.0±0.3 reported by the manufacturer of the Aerosil. The latter is considered to be reasonable by comparison with the following values obtained for the Aerosils: 1.4—1.5 by Hair *et al.*,[19] 1.4±0.1 by Armistead *et al.*,[20] 1.4±0.3 by Colin *et al.*,[21] and 1.4 by Tsutsumi *et al.*[12]

Alkoxylation Processes. The autoclave used was made of stainless steel and had a volume of about 30 ml. Several discs were placed in the upper part within the autoclave,

supported with a holder and above the liquid phase of 15 ml of alcohol brought into the autoclave. Prior to use, some discs were heated for 3 h at constant temperatures over the range of 550 to 900 °C in the air. The autoclave was heated in an electric oven and was kept at a constant temperature. The reaction was carried out at temperatures over the range of 30—250 °C. The autoclave was quenched with running water immediately after it was taken out of the oven.

In the case of low-pressure treatment, the discs were allowed to stand in contact with alcohol vapor at 280 °C in a glass apparatus. Prior to use, the discs were out-gassed in the same apparatus for 3 h at 280 and 570 °C under a residual pressure of about 10^{-5} Torr.

Infrared Spectroscopy. The spectrometer used was a Hitachi EPI-G Spectrophotometer. The discs were taken out into the atmosphere after they had been out-gassed; then they were immediately subjected to the infrared measurement. The moisture in the atmosphere will have little effect on them, since the discs alkoxylated have hydrophobic surfaces.

Determination of the Alkoxyl Group Concentration on the surface. The carbon content of the discs was measured by the usual combustion method. The amount of the alkoxyl groups (mol/g) was calculated from the carbon content. The degree of alkoxylation, the surface concentration of alkoxyl groups per 100Å^2, was determined from the amount of the alkoxyl groups and the surface area of the disc. The relative amount of the alkoxyl groups was also determined by the spectroscopic method.

Results and Discussion

Effect of Reaction Temperature on the Alkoxylation. It took a few hours for the autoclave to be heated to 250 °C. In order to follow the change in the Aerosil surface during that period, the infrared spectra of the Aerosil were observed at several stages during the course of heating. Those for *n*-BuOH are illustrated in Fig. 1. The increase in the bands at 2800—3200 cm^{-1} due to butyl groups corresponding to the decrease in the band at 3750 cm^{-1} due to the isolated OH groups indicates that the isolated OH groups were esterified with *n*-BuOH.

The discs were treated with the alcohols in the autoclave for 20 h at the given temperatures. The infrared spectra of the resulting discs were then observed. The spectral changes with an increase in the reaction temperature were similar to those shown in Fig. 1. The changes were quantitatively followed by means of both the optical density for the 3750 cm^{-1} band and that for the 2960 or 2970 cm^{-1} band assigned to CH stretching. Figure 2 illustrates the results obtained for the Aerosils treated with MeOH and *n*-PrOH. In Fig. 2, the increase in the optical density of the 2960 or 2970 cm^{-1} band is attended by the decrease in that of the 3750 cm^{-1} band. This relation clearly indicates that the isolated OH groups are increasingly esterified with an increase in the reaction temperature.

Figure 3 shows the amounts of alkoxyl groups obtained from the carbon content as a function of the reaction temperature. The amounts of every alkoxyl group increased with an increase in the temperature, and each arrived at its highest value at 200—250 °C. This change corresponds to the change in the optical densities of the bands due to alkyl groups in Fig. 2.

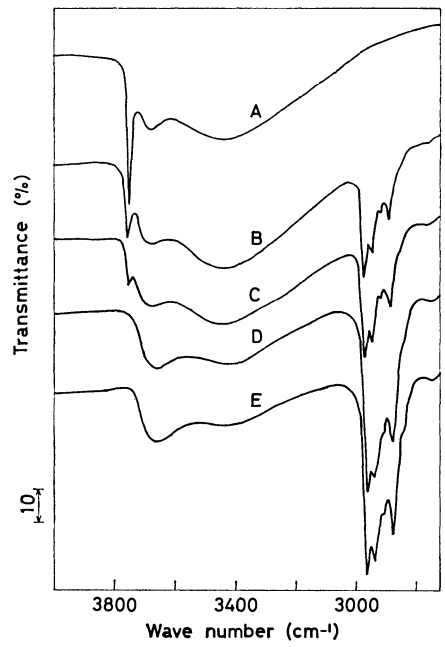

Fig. 1. Change of infrared spectra of Aerosil treated with 1-butanol during the course of reaction.
A: Original Aerosil, B: 100 °C, C: 160 °C, D: 200 °C, E: 240 °C (The numerical values indicate the temperatures at each stage during the course of heating up to 250 °C).

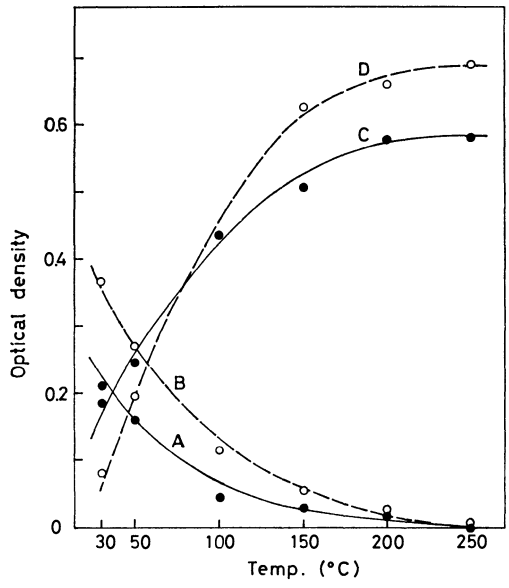

Fig. 2. Optical density for the isolated silanol band and that for the alkyl band as a function of reaction temperature.
A: OH band at 3750 cm^{-1} for the Aerosils treated with methanol, B: OH band at 3750 cm^{-1} for the Aerosils treated with 1-propanol, C: CH_3 band at 2960 cm^{-1} for the Aerosils corresponding to A, D: n-C_3H_7 band at 2970 cm^{-1} for the Aerosil corresponding to B.

The Aerosil treated with methanol had the highest values among all the alkoxylated Aerosils throughout the temperature range, the values decreased in the

order of: MeOH > EtOH > *n*-BuOH > *i*-BuOH > *s*-BuOH. The values for *n*-PrOH and *i*-PrOH are similar to those for *n*-BuOH and *i*-BuOH respectively; therefore, those values are omitted in Fig. 3.

It has previously been reported[1,9] that *t*-BuOH did not react easily with silica gel. It was found from the characteristic adsorption bands due to the *t*-butyl groups, however, that the alkoxylation was effectively carried out for 3 h at 200—240 °C. The bands were intense, but small in comparison with those due to the other alkyls, and the band at 3750 cm^{-1} still remained to a considerable extent.

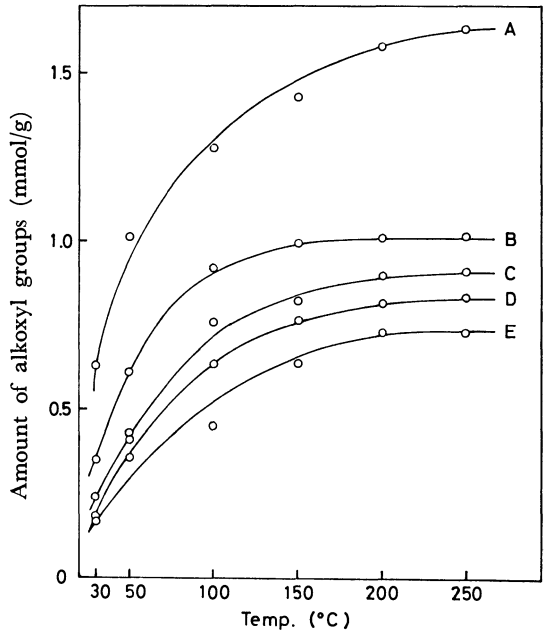

Fig. 3. Amount of alkoxyl groups as a function of reaction temperature.
A: Methoxyl, B: ethoxyl, C: butoxyl, D: isobutoxyl, E: secondary butoxyl.

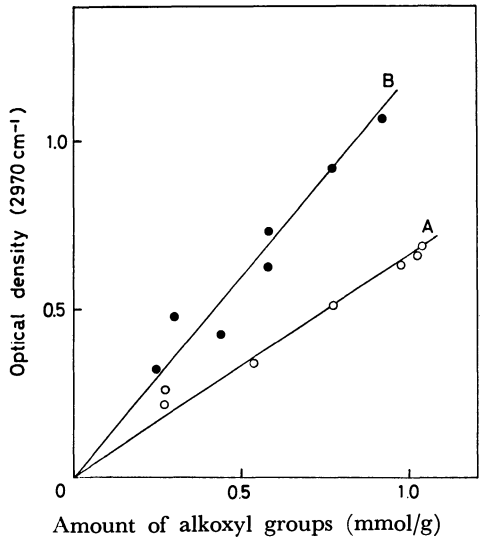

Fig. 4. Relation between amount of alkoxyl groups obtained from carbon content and optical density for the alkyl groups.
A: Ethoxyl, B: butoxyl.

The amounts of alkoxyl groups obtained by means of the carbon content were checked by means of the optical densities of the absorption bands due to the alkyl groups. Figure 4 illustrates the results for the ethoxyl and butoxyl groups. The two values bear a nearly linear relationship to each other.

Effect of Thermal Pretreatment on the Alkoxylation. The Aerosil discs were heated prior to the reaction at temperatures of 550, 700, 800, and 900 °C for 3 h in the air. The surface areas of the resulting discs corresponding to these temperatures, were 209, 167, 146, and 76 m^2/g respectively. The discs were treated with alcohols at 250 °C for 20 h in the autoclave immediately after the thermal pretreatment. Figure 5 shows the amounts of alkoxyl groups in the discs as a function of the thermal pretreatment temperature. The decrease in the amounts with the increase in the temperature must result from the decrease in both the surface area and the hydroxyl groups induced by the thermal pretreatment. The values for methoxyl were higher than those for the other alkoxyls at all pretreatment temperatures, as in the case of non-pretreatment. The infrared spectra of the Aerosils which were heated at 700, 800, and 900 °C prior to the reaction and then treated with methanol are shown in Fig. 6. The bands due to methyl groups decreased in intensity as the bands due to the isolated OH groups decreased with an increase in the pretreatment temperature.

Comparison of the Reactions under Low Pressures with Those under High Pressures. The infrared spectra of the Aerosils treated under low pressures were compared with those of the Aerosils treated under high pressures. The isolated hydroxyl band at 3750 cm^{-1} vanished almost entirely even upon the low-pressure treatment, not to mention the high-pressure treatment; however, the alkoxyl bands at 2800—3200 cm^{-1} ap-

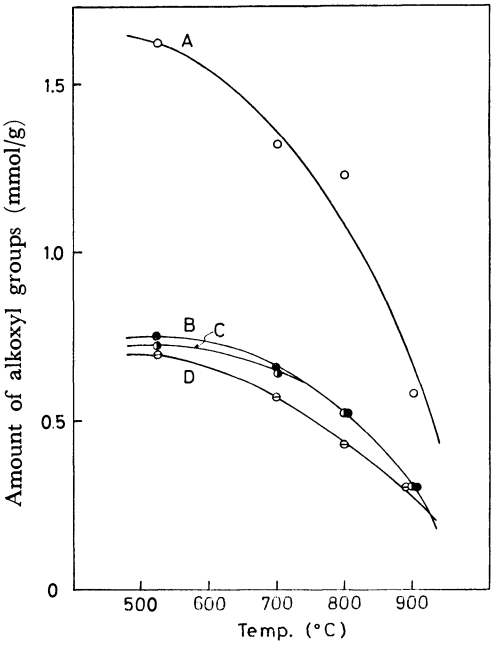

Fig. 5. Amount of alkoxyl groups as a function of thermal pretreatment temperature.
A: Methoxyl, B: ethoxyl, C: propoxyl, D: butoxyl.

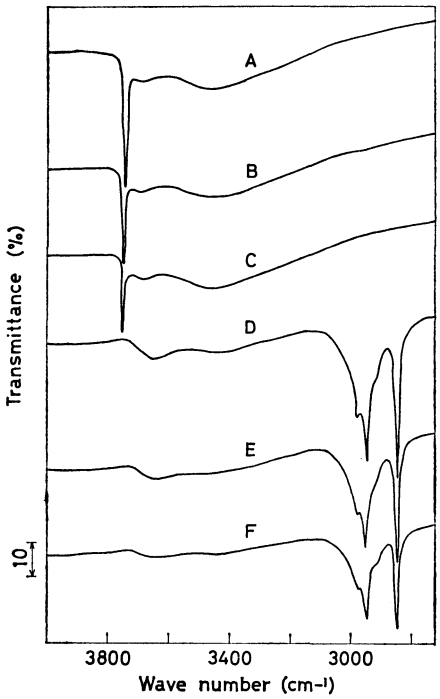

Fig. 6. Infrared spectra of the Aerosils treated with methanol after thermal pretreatment.
A: Aerosil heated for 3h at 700°C, B: Aerosil heated for 3h at 800°C, C: Aerosil heated for 3h at 900°C, D: Aerosil obtained by treatment of A, E: Aerosil obtained by treatment of B, F: Aerosil obtained by treatment of C.

peared with a stronger intensity in the case of the high-pressure treatment. The preliminary observations indicate that the isolated hydroxyl groups were almost completely esterified, even under low pressures, if sufficient time was available, while under high-pressures reactions other than the esterification of the isolated hydroxyl groups may have occurred simultaneously.

In order to obtain further information about the mode of the alkoxylation, the quantitative relations of the isolated OH and the alkoxyl groups on the Aerosils alkoxylated in varying degrees were examined by means of the optical densities of the two groups. The degrees of the alkoxylation were made to vary by a change in the reaction time under low-pressure conditions and by a change in the reaction temperature under high-pressure conditions. The optical densities for the methyl and propyl bands are plotted against those for the isolated OH band, in Fig. 7. The values bear a linear relationship to each other about the Aerosils with low optical densities of the alkyl bands; however, about those with higher optical densities upward deviations from the linearity were observed. These results show that the alkoxylation under low-pressure conditions is due only to the esterification of the isolated OH groups and support the above consideration that the alkoxylation under high-pressure conditions involves reactions other than esterification.

Comparison of the Degrees of Alkoxylation. Table 1 shows the degrees of alkoxylation for the completely

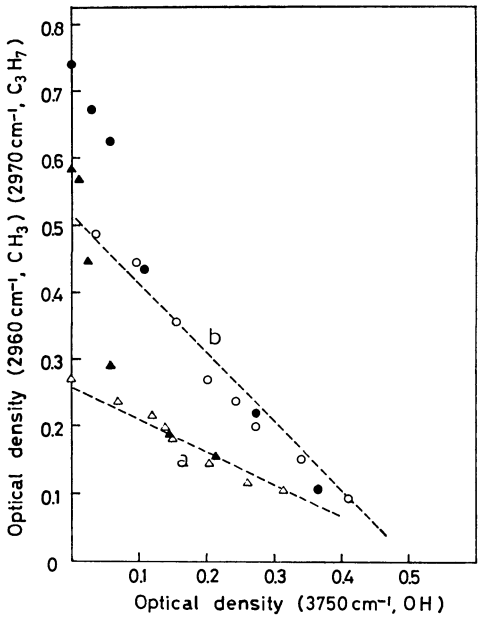

Fig. 7. Relation between optical density for the isolated silanol and that for the alkyl groups.
a △, ▲: Aerosil treated with methanol, b ○, ●: Aerosil treated with 1-propanol, △, ○: low-pressure treatment; ▲, ●: high-pressure treatment.

alkoxylated Aerosils. The values in the case of the low-pressure treatment were lower than those in the case of the high-pressure treatment. The former were approximately equal to the surface concentration of the isolated OH groups, 1.5 groups/100 Å², although the values for methoxyl groups were a little higher. The latter were in the range of 2.3—3.4 groups/100 Å², except for the much higher value for methoxyl, and were equal or near to the surface concentration of the total OH groups, 3.0 groups/100 Å². These facts indicate that, under low pressures, the alcohols react in a 1 : 1 ratio with the isolated OH groups, while under high pressures they react in a 1 : 1 with the total OH groups. However, the branched-chain alcohols can not react with all the OH groups completely because of their larger cross-sectional molecular areas. The degree of alkoxylation in the case of the high-pressure treatment decreased in the following order:

Table 1. Degrees of alkoxylation
(Alkoxyl groups/100 Å²)

Alcohols	Low-pressure		High-pressure	
	Thermal pretreatment at 280 °C	Thermal pretreatment at 570 °C	Non	Thermal pretreatment at 550 °C
MeOH	1.8	1.9	5.5	5.5
EtOH	1.6	1.8	3.4	2.5
n-PrOH	1.4	1.6	3.2	2.4
i-PrOH	1.4		2.7	
n-BuOH	1.3	1.7	3.2	2.4
i-BuOH	1.3		2.7	
s-BuOH	1.3		2.3	
t-BuOH	0.4		0.7	

MeOH> EtOH> *n*-BuOH> *i*-PrOH, *i*-BuOH> *s*-BuOH >*t*-BuOH. This order was the same as that of the amount of alkoxyl groups, since there was no considerable difference in the surface area of the alkoxylated Aerosils. Lambert *et al.*[16] have reported the same tendency for the pentanol isomers under low pressures. As they have explained, the steric factors must play an important part. That the degree of methoxylation was much larger than the concentration of the total OH groups indicates that, in addition to Reactions 1 and 2, Reaction 3 contributes in no small measure to the methoxylation. It has been concluded in a previous paper,[22] from the dissolution of silica gel in methanol methanol can easily open the siloxane bond at high temperatures and high pressures. The higher degree for the methoxylation is perhaps based on this function of methanol, in addition to the small cross sectional area of a methoxyl group.

The thermal pretreatment had an effect on the alkoxylation under low-pressure conditions, as is well known, but it was somewhat inhibitory of the alkoxylation under high-pressure conditions, as shown in Table 1. Only the methoxylation was not affected by the thermal pretreatment. In the runs under high pressures, the discs were heated in the air and then subjected to room temperature, if only for a moment, before they were sealed with an alcohol in the autoclave. During this procedure, not only the strained siloxane[2,22,23] but also the stable siloxane are caused by the dehydration of the vicinal OH groups. The stable siloxane can not easily be opened with methanol. The lowering of the degrees of alkoxylation by thermal pretreatment may be attributed to the alteration of the vicinal OH groups into the stable siloxane bonds.

Stability of Alkoxyl Groups on the Aerosil Surface against Heating. The Aerosils alkoxylated were heated at various temperatures in a vacuum of about 10^{-5} Torr, and their changes were observed by means of the infrared spectra. Morterra *et al.*[24] have observed the change about the methyl group, and Raymond *et al.*[15] have observed that about the butyl and secondary butyl groups; however, no systematic observation through various kinds of alkyls has yet been carried out. A remarkable removal of the alkyl groups occurred at the following temperatures for each alkyl group: Me: 650—750 °C, Et, *n*-Pr, *n*-Bu, *i*-Bu: 500—550 °C, *i*-Pr, *s*-Bu: 420—470 °C, *t*-Bu: about 400 °C. Methyl groups were particularly stable, and the infrared observations suggested that the removal reaction of the methyl groups is different from that of the other alkyl groups. It was found from the above results that the stability decreases in this order; primary> secondary> tertiary and that it is independent of the number of the carbon.

The author is indebted to Miss Mayumi Fukui for obtaining the IR spectra and for her carbon-content determinations.

References

1) C. C. Ballard, E. C. Broge, R. K. Iler, D. S. St. John, and J. R. McWhorter, *J. Phys. Chem.*, **65**, 20 (1961).
2) E. Borello, A. Zecchina, and C. Morterra, *J. Phys. Chem.*, **71**, 2938 (1967).
3) G. Mertens and J. J. Fripiat, *J. Colloid Interface Sci.*, **42**, 169 (1973).
4) W. Stöber, G. Bauer, and K. Thomas, *Ann. Chem.*, **604**, 104 (1957).
5) H. Akabayashi, A. Yoshida, and Y. Otsubo, *Kogyo Kagaku Zasshi*, **68**, 429 (1965).
6) H. P. Boehm, *Adv. Catal.*, **16**, 179 (1966).
7) K. R. Lange, *Chem. Ind.*, 1273 (1969).
8) T. Asano and S. Kitahara, *Nippon Kagaku Zasshi*, **91**, 109 (1970).
9) H. Utsugi, A. Watanabe, K. Ito, and S. Nishimura, *Nippon Kagaku Zasshi*, **91**, 431 (1970).
10) S. Kitahara, T. Asano, and T. Hirowatari, *Nippon Kagaku Zasshi*, **92**, 377 (1971).
11) H. Utsugi, S. Nishimura, and T. Kato, *Nippon Kagaku Kaishi*, **1972**, 1557.
12) K. Tsutsumi and H. Takahashi, *Nippon Kagaku Kaishsi*, **1972**, 1800.
13) H. Utsugi, S. Nishimura, and H. Horigoshi, *Zairyo*, **22**, 673 (1973).
14) H. Utsugi, *Hyomen*, **11**, 591, 654 (1973).
15) R. G. Azrak and C. L. Angel, *J. Pyhs. Chem.*, **77**, 3048 (1973).
16) R. Lambert and N. Singer, *J. Colloid Interface Sci.*, **45**, 440 (1973).
17) H. Utsugi, H. Horikoshi, and T. Matsuzawa, *J. Colloid Interface Sci.*, **50**, 154 (1974).
18) C. G. Armistead and J. A. Hockey, *Trans. Faraday Soc.*, **63**, 2549 (1967).
19) M. L. Hair and W. Hertl, *J. Phys. Chem.*, **73**, 2372 (1969).
20) C. G. Armistead, A. J. Tyler, F. H. Hambleton, S. A. Mitchell, and J. A. Hockey, *J. Phys. Chem.*, **73**, 3947 (1969).
21) C. Clark-Monks and B. Ellis, *J. Colloid Interface Sci.*, **44**, 37 (1973).
22) S. Kitahara, *Nippon Kagaku Zasshi*, **90**, 237 (1969).
23) K. Tarama, S. Yoshida, K. Taniguchi, and S. Osaka, *Nippon Kagaku Zasshi*, **89**, 474 (1968).
24) Claudio Morterr and M. J. D. Low, *J. Phys. Chem.*, **73**, 321 (1969).

The Photoelectrolytic Reaction of Chlorophyll–β-Carotene–Quinone Electrodes

Fujio TAKAHASHI and Ryoichi KIKUCHI

Research Laboratory of Resources Utilization, Tokyo Institute of Technology, Meguro-ku, Tokyo 152

(Received April 7, 1976)

The NAD^+ (nicotinamide adenine dinucleotide) reduction was carried out under illumination by using a platinum electrode coated with chlorophyll and quinone. Various quinones and β-carotene were used as components of the cathode layer to obtain a higher current density. The highest current density, 13 $\mu A/cm^2$, was obtained in the case in which the cathode layer contained 0.01 $\mu mol/cm^2$ of chlorophyll and the molar ratio of chlorophyll: chloranil : β-carotene was 1 : 1 : 2. The role of quinone and β-carotene in the cathode layer was discussed.

Since the photochemical reaction in chloroplasts can be compared with an electrochemical reaction, Photosystem I and Photosystem II can be regarded as a cathode and an anode, respectively. It was reported that the photoelectrolysis was carried out by the system connecting the chlorophyll-1,4-naphthoquinone electrode and the chlorophyll-9,10-anthracenediol electrode under illumination.[1] The photoexcited chlorophyll-1,4-naphthoquinone electrode and chlorophyll-9,10-anthracenediol electrode behaved as a cathode to reduce NAD^+ (nicotinamide adenine dinucleotide) and as an anode to oxidize hexacyanoferrate(II) (The expression "chlorophyll-redox compound electrode" is used for an electrode lined with a chlorophyll/redox compound mixture. Similar expressions are used where a different compound is specified.)

The redox potentials of plastocyanin and cytochrome f in Photosystem I (+0.37 V)[2] are more positive than that of plastoquinone in Photosystem II (*ca.* 0 V).[2] Therefore, plastocyanin and cytochrome f in Photosystem I are able to oxidize the reduced plastoquinone in Photosystem II. In turn, the reduced plastocyanin and cytochrome f transfer the electron to the chlorophyll cation in Photosystem I, and plastoquinone gains the electron from the photoexcited chlorophyll in Photosystem II. It was assumed that the electron transfer from Photosystem II to Photosystem I might occur with the driving force caused by the difference of redox potentials of the redox compounds in the photosystems. Therefore it was expected that a higher potential difference between two chlorophyll electrodes could be obtained under illumination if a redox compound which exhibited a more positive redox potential than 1,4-naphthoquinone was used as a component in the cathode layer.

β-Carotene, one of carotenoids in the photosystems, is known to exhibit a photoconductive property[3] and to be utilized in the mixture of chlorophyll, albumin, and 2-methyl-1,4-naphthoquinone to make an electron transfer easier under illumination.[4] An energy transfer from β-carotene to chlorophyll is known from a study of photoexcitation with a black lipid membrane containing chlorophyll and β-carotene.[5] From these facts it was thought that the addition of β-carotene as one of components in the electrode layer might make the current density higher.

This paper will present some recent results on the photoelectrolysis by using chlorophyll electrodes and the speculation on the role of quinone and β-carotene in the electrode layer under illumination.

Experimental

Chlorophyll, which was a mixture of type a and b, was prepared from spinach leaves by the method of Jacobs *et al.*[6] Various quinones were purified by sublimation. NAD^+ used was made by the Oriental Yeast Co. The other chemicals, including β-carotene, were of reagent grade or the best commercially available grade. The conducting adhesive used was Fujikura-kasei Dotite D-362.

Catholyte (anolyte): 5 mM NAD^+ (5 mM potassium hexacyanoferrate(II) in M/30 phosphate buffer (pH 6.9).* For the photoelectrolysis 60 ml of catholyte and anolyte were used.

Chlorophyll-redox compound electrodes were prepared by the method described in the previous paper:[1] The cathode layer on a platinum plate (2 cm × 4 cm) consisted of 2.5 μmol of chlorophyll, 2.5 μmol of one of the quinones, and 0.1 g of conducting adhesive. The anode layer was prepared in the same manner as the cathode, except that 2.5 μmol of 9,10-anthracenediol was added in place of the quinone. Two-layer electrodes:** A platinum wire (1 cm long with a diameter of 0.1 cm) connected with a sealed wire was used as an electrode. Two drops (0.1 ml) of 5 mM chlorophyll solution in hexane spread on the water surface. A thin layer of chlorophyll remained after evaporation of the hexane on the water surface. The thickness of the chlorophyll layer was estimated to be *ca.* 0.05 μm because the diameter of the chlorophyll layer which remained on the water surface was about 5 cm. Two grams of conducting adhesive and 10 mg of chloranil were added into 50 ml of hexane to make a suspensoid. Two drops of the suspensoid were spread on the water surface in another beaker to make a layer containing conducting adhesive and chloranil. A two-layer electrode was prepared by the following method: The platinum wire was dipped into the chlorophyll layer spread on the water surface very quietly and then pulled up. The platinum wire was thus covered by a chlorophyll layer. In turn the platinum wire coated by the chlorophyll layer was dipped into the chloroanil layer spread on the water surface. Thus the chloranil layer was coated on the chlorophyll layer. The electrode coated with chloranil first and then with a chlorophyll layer was prepared in the same manner.

The same electric cell as reported in the previous paper was used for all the experiments. The photoelectrolytic reaction was carried out under illumination (1×10^4 lx) through a heat absorber with a photoreflector lamp (100 V, 500 W). The entire electric cell including the calomel electrode was placed in a thermostat and was controlled at 20 °C. Nitrogen gas was bubbling into the electrolyte during the

* $M = 1$ mol dm^{-3}.

** We defined "two-layer" as putting one layer upon another.

experiments.

The measurements of potential and current, and the determination of NAD^+ and hexacyanoferrate(II) were carried out in the same manner as described in the previous paper.[1)]

Results and Discussion

Various Chlorophyll–Quinone Electrodes. To make the current density of the photoelectric reaction increase, various quinones were used as a component of one layer of the chlorophyll–quinone electrode.

The photoelectrolytic reaction was carried out with the systems of chlorophyll–quinone electrode in NAD^+ solution and chlorophyll–9,10-anthracenediol electrode in hexacyanoferrate (II) solution. The photovoltage and photocurrent were determined when both electrodes were illuminated at 1×10^4 lx. The photovoltage was found to increase with quinones exhibiting a more positive redox potential, as shown in Fig. 1 (above). The cathodic potential and current were observed at the chlorophyll–quinone electrode under illumination. When the light was turned off, the chlorophyll–quinone electrode became a nanode and the chlorophyll–9,10-anthracenediol electrode became a cathode. The potential difference of the chlorophyll–quinone *vs.* the chlorophyll–9,10-anthracenediol electrode in the dark increased with a positive shift of the redox potential of quinone as shown in Fig. 1 (below). The electrode potentials of the chlorophyll–1,4-naphthoquinone electrode and the chlorophyll–chloranil electrode *vs.* calomel electrode were obtained to be +80 and +90 mV in the dark, and −46 and −93 mV under illumination.

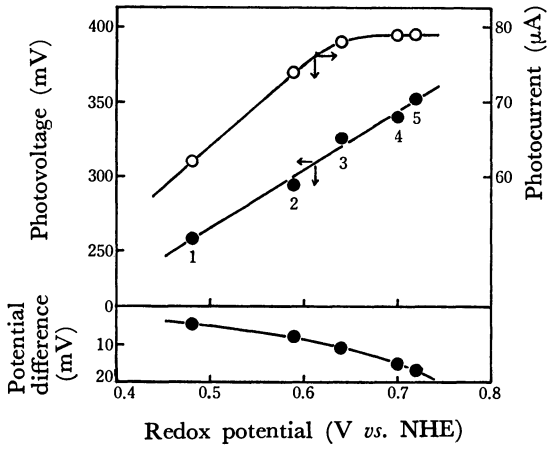

Fig. 1. Various chlorophyll–quinone electrodes.
1: 1,4-Naphthoquinone, 2: dimethyl-*p*-benzoquinone, 3: *p*-toluquinone, 4: chloranil, 5: 2,5-dichloro-*p*-benzoquinone. The values of redox potential of various quinones were cited from Ref. 7.

The value of the photocurrent reached a plateau in the case that chloranil and 2,5-dichloro-*p*-benzoquinone were used as components of the cathode layer.

The Effect of β-Carotene. To make the electric resistance of the chlorophyll electrode lower under illumination, β-carotene was added as a component of both anode and cathode layers. The chlorophyll-

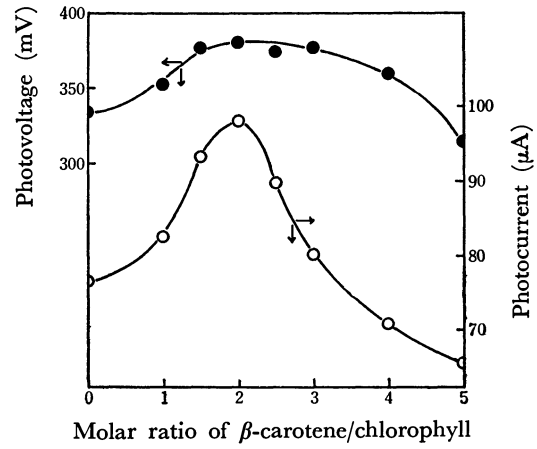

Fig. 2. The effect of β-carotene.

chloranil electrode was used as a cathode. The quantity of chlorophyll and chloranil (9,10-anthracenediol) of the electrode layer was the same as in the previous section, except for the addition of 0—12.5 μmol of β-carotene.

By using the chlorophyll–chloranil–β-carotene electrode as a cathode and the chlorophyll–9,10-anthracenediol–β-carotene electrode as an anode, the photocurrent was measured as shown in Fig. 2. The maximum photocurrent was obtained at the molar ratio of chlorophyll : chloranil (9,10-anthracenediol) : β-carotene = 1 : 1 : 2. The maximum photovoltage was about 50 mV higher than in the case where β-carotene was not included as a component of the electrode layers.

It is plausible that in the electrode layer chlorophyll, chloranil, and β-carotene may form a ternary complex which might exhibit a photoconductive property.

The Thickness of the Electrode Layer. The thickness of the electrode layer had to be considered as one of the factors which influences the electric resistance of the electrode. It was expected to obtain larger potential differences and current densities by reducing the thickness of the electrode layer.

The chlorophyll electrodes which were coated by different quantities of electrode layers were prepared with a mixture of chlorophyll, chloranil (9,10-anthracenediol), β-carotene (molar ratio of 1 : 1 : 2),

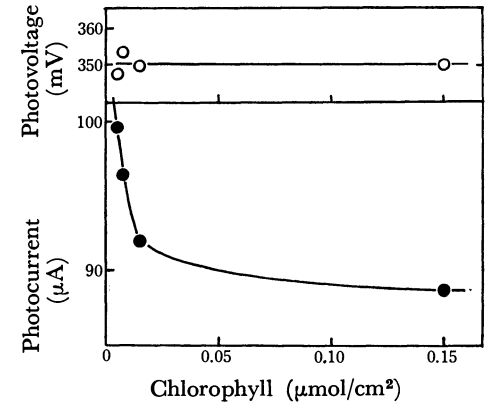

Fig. 3. The thickness of electrode layer.

and conducting adhesive (the mixing ratio: 0.1 g of conducting adhesive/2.5 μmol of chlorophyll).

The photocurrent density was found to increase by decreasing the quantity of the electrode layer from 0.16 to 0.005 μmol of chlorophyll/cm² (Fig. 3). A constant photocurrent could not be produced below 0.005 μmol/cm². The optimum thickness of the electrode layer was found to be about 0.01 μmol of chlorophyll/cm² (Fig. 3).

Photoelectrolysis. The photoelectrolysis was carried out by using the electrodes which were prepared with the optimum conditions of quantity (0.01 μmol/cm² of chlorophyll) and mixing ratio as in the previous section. The potential-time curves and the photocurrent-time curve are shown in Fig. 4. The potential difference and the current density were found to be 0.35 V and 13 μA/cm² under illumination. These values are higher than those in the case of the chlorophyll–1,4-naphthoquinone electrode (0.25 V, 8 μA/cm²) in the previous paper.[1] The quantity of electricity amounted to 5.29 C (corresponding to 54.8×10^{-6} F where F is the Faraday constant) after 12 h. This is much greater than the quantity of electricity passed for the reduction (oxidation) of chloranil (9,10-anthracenediol) in the electrode layer which contained 0.13 μmol of chloranil (9,10-anthracenediol). Meanwhile 7.4% NAD^+ was reduced and 14.2% hexacyanoferrate(II) was oxidized. The current efficiencies were 72% and 71%, respectively. When the light was turned off while the external circuit was kept closed, the reverse potential and the reverse current were observed to be 0.11 V and 10 μA/cm². The current decreased with time.

From the potential-current curves of the chlorophyll–chloranil electrode and the chlorophyll–chloranil-β-carotene electrode (Fig. 5), two reduction waves were observed, at −0.2 and −0.8 V *vs.* SCE; these were assigned to chloranil and NAD^+. The cathode potential in Fig. 4 (−0.1 V *vs.* SCE) was more positive than that obtained in Fig. 5. These results suggest that chloranil in the cathode layer could not be reduced during photoelectrolysis.

Two-layer Electrodes. To clarify the process of electron transfer on the cathode, the photoelectrolytic reaction was carried out with two-layer electrodes. The two-layer electrodes used were prepared as described in the experimental section. As the counter electrode a platinum electrode (2 cm×4 cm) was used.

In the case of the two-layer electrode coated with chloranil on a chlorophyll layer, very little current was produced, as shown in Fig. 6 (curve D). A higher current production by the two-layer electrode coated with chlorophyll on a chloranil layer in curve B was observed, as compared with curve D and with curve C, which was obtained by the single layer electrode coated with chloranil only.

It is deduced that the photoexcited chlorophyll can not, but chloranil can gain an electron from the counter electrode. It seems that the electron may

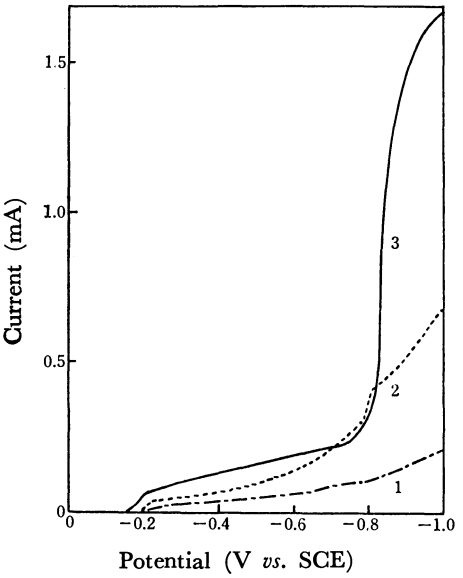

Fig. 5. The potential-current curves.
1: Chlorophyll–chloranil electrode (molar ratio of 1 : 1) in buffer solution. 2: the same electrode as 1 in NAD^+ solution, 3: chlorophyll–chloranil–β-carotene electrode (molar ratio of 1 : 1 : 2) in NAD^+ solution. A platinum plate (2 cm×4 cm) was used for the counter electrode. The potential-current curves were measured in the dark.

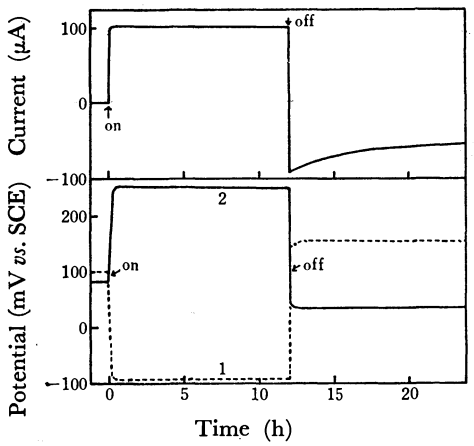

Fig. 4. The photoelectrolysis.
1: Chlorophyll–chloranil–β-carotene electrode, 2: chlorophyll–9,10-anthracenediol–β-carotene electrode.

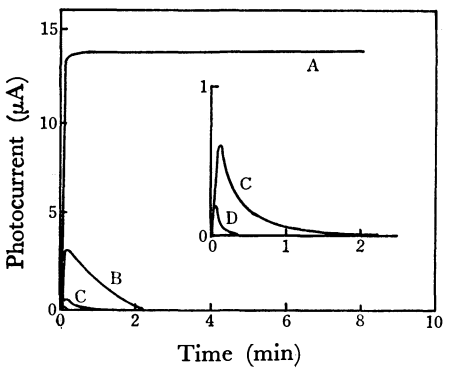

Fig. 6. Two layer electrodes.
A: Mixture of chlorophyll and chloranil on Pt, B: chlorophyll on chloranil layer on Pt, C: chloranil on Pt, D: chloranil on chlorophyll layer on Pt.

transfer from the reduced chloranil to the photoexcited chlorophyll. However, the reduced chloranil can not release an electron to NAD^+. On the other hand, the single layer electrode prepared from the mixture of chlorophyll and chloranil was able to keep producing much higher and constant current during the time tested (curve A).

The Process of Electron Transfer. It is known that the reduced plastocyanin and the reduced cytochrome f can reduce P700 under illumination.[8,9] It has been reported that a semiconductor electrode prepared by depositing chlorophyll on a single crystal of zinc oxide can exhibit an anodic behavior under illumination to transfer an electron from hydroquinone in electrolyte to zinc oxide through chlorophyll.[10] On the contrary it seems that an electron may not transfer in the order platinum, chloranil, chlorophyll, and NAD^+ in the case of a two-layer electrode. As a probable speculation, chlorophyll was thought to form a complex with chloranil in the cathode layer under illumination, and a transient state of the complex might drive the electron transfer from the layer of chlorophyll–9,10-anthracenediol in the anode to that of chlorophyll–chroanil in the cathode through platinum. A contact potential barrier, which was known to exist at the chlorophyll–metal contact,[11] might not influence the direction of current flow in the case of our chlorophyll electrodes. Because both cathode and anode were prepared in the same condition on a platinum plate, the contact potential barrier between chlorophyll and platinum at the cathode would offset that at the anode. The process of electron transfer can be expressed as the following: where Chl·TCQ and Chl·AHQ respectively represent the chlorophyll complexes of chloranil and 9,10-anthracenediol, and $Chl^+ \cdot TCQ$ and $Chl^+ \cdot AHQ$ mean the cations of these chlorophyll complexes The driving force of electron transfer from anode to cathode through the external circuit was found to increase as the redox potential of quinone in the cathode was made more positive, using the results in Fig. 1. The mechanism of electron transfer from the cathode to the catholyte will be discussed in another paper.

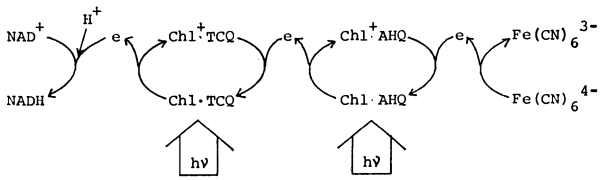

The authors express their sincere thanks to Professor Shuichi Suzuki of the Tokyo Institute of Technology for his encouragement.

References

1) F. Takahashi and R. Kikuchi, *Biochim. Biophys. Acta*, **430**, 490 (1976).
2) H. Fujishige, "Ko-gosei," Shoka-bo, Tokyo (1973), p. 134.
3) R. J. Cherry and D. Chapman, *Mol. Crystals*, **3**, 251 (1967).
4) D. D. Eley and R. S. Snart, *Biochim. Biophys. Acta*, **102**, 379 (1965).
5) G. Strauss and H. T. Tien, *Photochem. Photobiol.*, **17**, 425 (1973).
6) E. E. Jacobs, A. E. Vatter, and A. S. Jolt, *Arch. Biochem. Biophys.*, **53**, 228 (1954).
7) W. M. Clark, "Oxidation Reduction Potentials of Organic Systems," The Williams & Wilkins Company, Baltimore (1960), pp. 368, 370, 375.
8) P. M. Wood and D. S. Bendall, *Biochim. Biophys. Acta*, **387**, 115 (1975).
9) D. C. Fork and N. Murata, *Photochem. Photobiol.*, **13**, 33 (1971).
10) H. Tributsch and M. Calvin, *Photochem. Photobiol.*, **14**, 95 (1971).
11) C. W. Tang and A. C. Albrecht, *J. Chem. Phys.*, **63**, 953 (1975).

Hydrogen Atom Transfer in the Quenching of Pyrene Fluorescence by Amines

Tadashi OKADA, Takeshi MORI, and Noboru MATAGA

Department of Chemistry, Faculty of Engineering Science, Osaka University, Toyonaka, Osaka 560

(Received April 14, 1976)

The mechanism of the quenching of pyrene fluorescence by primary and secondary amines has been studied by means of fluorescence measurements and transient absorption measurements with the use of laser photolysis as well as conventional flash photolysis methods. It has been confirmed that 1-hydro-1-pyrenyl radicals and amino radicals are produced in the course of the fluorescence quenching reaction. The relative yields of 1-hydro-1-pyrenyl radicals for various amine quenchers were estimated.

It is well known that excited pyrene forms heteroexcimers with *N,N*-dimethylaniline (DMA) and *N,N*-dimethylnaphthylamines. However, when aniline, *N*-methylaniline and naphthylamines are used as electron donors for the heteroexcimer formation with excited aromatic hydrocarbons in solution at room temperature, no heteroexcimer fluorescence can be observed, quenching of the fluorescence of aromatic hydrocarbon occurring even in nonpolar solvents.[1,2] It seems plausible that the charge transfer interaction in the encounter complex followed by some efficient radiationless processes plays an important role in the case of the quenching by primary or secondary amines.

A possible mechanism for this fluorescence quenching by amines with free N–H group might be the charge transfer followed by a rapid proton transfer from the amine to the aromatic hydrocarbon in the encounter complex. In the case of hydrogen abstraction by excited ketones, especially for the ketone–amine systems, it is frequently assumed that the photoreduction proceeds *via* the charge transfer from the amine to the triplet ketone followed by proton transfer.[3,4] In contrast to the case of carbonyl compounds, only a few studies have been carried out concerning the hydrogen abstraction reaction of excited aromatic hydrocarbons. No attempt seems to have been made dealing with direct measurements on the hydrogen abstraction process of excited hydrocarbons.

In order to elucidate the mechanism of the quenching of the aromatic hydrocarbon fluorescence by amines with free N–H group, we have made detailed studies on excited pyrene–amine systems by means of fluorescence measurements as well as transient absorption measurements.

Exprimental

Fluorescence spectra were measured with an Aminco-Bowman spectrophotofluorometer equipped with an HTV-R446S photomultiplier. An ordinary flash photolysis apparatus with photoelectric detection of the transient absorption spectrum was used. A small computer (1K) was used to analyze the time dependence of transient species. The nanosecond laser photolysis method was the same as reported elsewhere.[5]

GR-grade *N*-methylaniline (NMA), *N*-ethylaniline (NEA), *N*-butylaniline (NBA), dibutylamine (DBAm), butylamine (BAm), and diethylamine (DEAm) were carefully distilled and stored in a vacuum. GR-grade aniline (AN) was steam-distilled, dried over potassium hydroxide, distilled under reduced pressure and stored in a vacuum. GR-grade diisobutylamine (DIBAm) was distilled in a vacuum and stored. Diphenylamine (DPA) was recrystallized from ethanol and sublimed. Spectro-grade hexane was distilled over metallic sodium.

All solutions for the measurement were deaerated by freeze-pump-thaw cycles, amines being added by the method of vacuum distillation to the solution for the measurements. The concentration of pyrene was 2×10^{-5} M. A cylindrical quartz cell (10 cm long, 1 cm i. d.) was used for the flash photolysis.

Results and Discussion

Quenching Rate Constant. The fluorescence quenching rate constants, k_q, for pyrene–amine–hexane systems at room temperature were determined. The plot of $\log k_q$ *vs.* ionization potential I_p of amines is given in Fig. 1. The values of the quenching rate constant for aliphatic amine systems are considerably smaller as compared with those of aromatic ones. This seems to indicate that an additional activation energy over that for the aromatic amine system is necessary for the quenching processes in the pyrene–aliphatic amine systems. The difference in the quenching rate constant of aromatic and aliphatic amines was also observed in the case of the heteroexcimer formation of such systems as pyrene–DMA and pyrene–tributylamine (TBA) studied by Nakashima *et al.*[6] According to them, additional activation energy is necessary for the change of the structure of TBA from a pyramidal one to a planar one in the course of the electron transfer. Such a structural change may occur also in the case of the present systems.

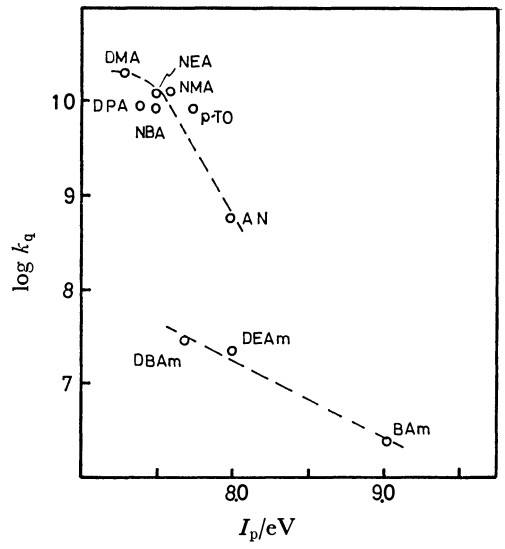

Fig. 1. Plot of $\log k_q$ *vs.* I_p for pyrene–amine–hexane systems at room temperature.

The relation between log k_q and I_p (Fig. 1) suggests that the mechanism of the quenching of the pyrene fluorescence may be charge transfer interaction in the encounter complex between excited pyrene and amine. The k_q for DMA is close to the rate constant of the diffusion-controlled reaction. Although k_q and I_p values of NMA or NEA are rather close to those of DMA, the heteroexcimer fluorescence can be observed only in the case of DMA. In view of this fact, we assume the following mechanism for the quenching by the primary or secondary amines:

$$\begin{array}{ccccccc} A^* + HD & \xrightarrow{k_q} & (A^- \cdots HD^+) & \xrightarrow{k_p} & (\dot{A}H \cdots \dot{D}) & \xrightarrow{k_d} & \dot{A}H + \dot{D} \\ & {\scriptstyle k_f'}\downarrow\ \ \downarrow{\scriptstyle k_1'} & & & \downarrow{\scriptstyle k_1''} & & \end{array} \quad (1)$$

If one assumes that the rate constants of radiative (k_f') and radiationless (k_1') transitions of the charge transfer state ($A^- \cdots HD^+$) are equal to those of the pyrene–DMA heteroexcimer in hexane, respectively, one can estimate the order of magnitude of the rate constant k_p in Eq. 1 by means of the following quantities.

$$\Phi'_{DMA} = \tau_f' k_f' = 0.66$$

$$\Phi'_{NEA} = \frac{k_f'}{k_f' + k_1' + k_p} \lesssim 10^{-4} \text{ (limit of the detection system)}$$

$$1/\tau_f' = 2.6 \times 10^6\ s^{-1}$$

where Φ'_{DMA} and Φ'_{NEA} are the fluorescence quantum yields of pyrene–DMA and pyrene–NEA heteroexcimers, respectively, and τ_f' is the lifetime of pyrene–DMA heteroexcimer. Thus, $k_p + k_1' \sim k_p \gtrsim 2 \times 10^{10}\ s^{-1}$.

A reaction mechanism similar to the above was also assumed by Yang and Libman for the primary process in photochemical addition of secondary amines to anthracene.[7]

Transient Absorption Spectra. If the reaction mechanism described above is valid, the transiently produced radicals may be detected by means of laser photolysis or conventional flash photolysis. The results of measurements for pyrene–NMA–hexane and pyrene–DBAm–hexane systems are given in Figs. 2 and 3, respectively. Absorption bands were observed in the 380—430 nm region, which could be explained as a superposition of absorption bands of pyrene triplet state and some unknown transient species. At the delay time of 50 μs, the T-T absorption band becomes much weaker while another absorption band remains fairly strong. Similar spectra were observed for all the systems of pyrene–primary and secondary amines. As an example, the transient spectra of pyrene–aniline–cyclohexane system obtained by means of the conventional flash photolysis method are shown in Fig. 4.

In order to identify the long lived transient species, 1,2-dihydropyrene in methylcyclohexane–isopentane (3 : 1) mixture was irradiated with a low pressure mercury lamp, and absorption spectra of photoproduct were measured. The spectrum obtained (Fig. 5a) might be assigned to the photoproduct radical (1-hydro-1-pyrenyl radical), being similar to the spectra shown in Figs. 2—4. As regards these results, we

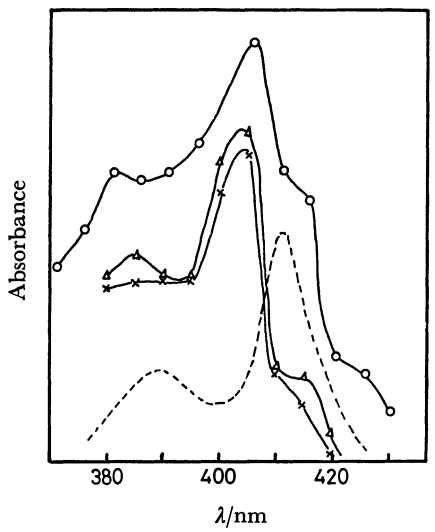

Fig. 2. Transient absorption spectra of pyrene-NMA-hexane system at room temperature.
—○—: 500 ns after laser oscillation, —△—: 50 μs after flash excitation, —×—: 200 μs after flash excitation, ----: T-T absorption spectrum of pyrene.

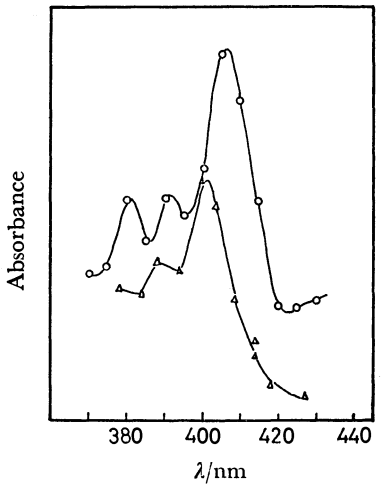

Fig. 3. Transient absorption spectra of pyrene-DBAm-hexane system at room temperature.
—○—: 1 μs after laser oscillation, —△—: 50 μs after flash excitation.

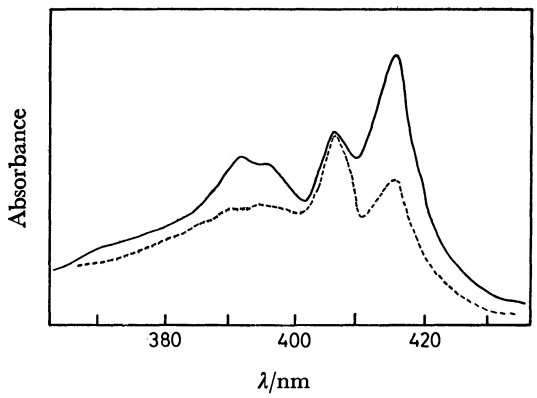

Fig. 4. Transient absorption spectra of pyrene-AN-cyclohexane system at room temperature obtained with conventional flash photolysis. Delay time from flash excitation, ——: 0 μs, ----: 50 μs.

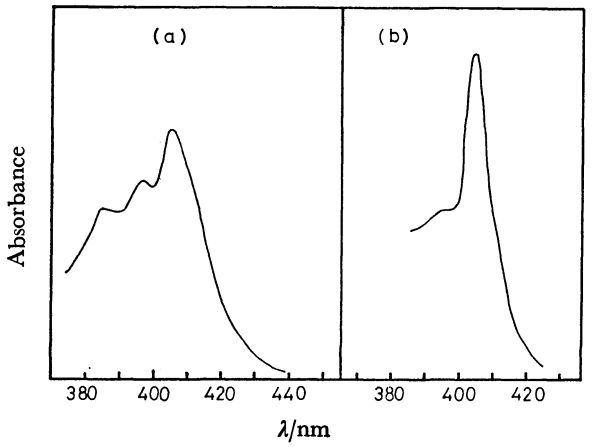

Fig. 5. (a) Absorption spectrum obtained by photolyzing 1,2-dihydropyrene at 77 K.
(b) Transient spectrum obtained by pulse radiolysis of ethanol solution of pyrene containing 1 vol% sulfuric acid.

made a semi-empirical open shell SCFMO calculation on the π-electronic state of the odd alternant hydrocarbon (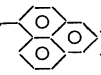).[8] The result indicates strong absorption bands at 3.7 and 4.9 eV, respectively, of which the lower energy one might be identified with the spectrum observed by means of the low temperature photolysis of 1,2-dihydropyrene and of the flash photolysis of the pyrene–amine systems.

On the other hand, pulse radiolysis studies on pyrene in ethanol containing 1 vol % sulfuric acid were made by Kira.[9] The reaction scheme of this system may be written as follows:

$$C_2H_5OH \rightsquigarrow e^-_{sol},\ \dot{H},\ C_2H_5OH_2^+,\ C_2H_5\dot{O},\ \text{and other neutral radicals}$$

$$e^-_{sol} + H^+ \longrightarrow \dot{H}$$

$$\dot{H} + P_y \longrightarrow P_y\dot{H}$$

where P_y and $P_y\dot{H}$ are pyrene and 1-hydro-1-pyrenyl radical, respectively. The spectrum obtained by Kira is given in Fig. 5b. The spectrum shows peaks at 405 nm and 395 nm, being essentially the same as the spectrum obtained by subtracting the T-T ab sorption band of pyrene from the transient spectra observed in pyrene–amine systems.

Since the absorption spectra of anilino radicals were observed in the wavelength region of *ca.* 400 nm and their intensities are rather weak,[10,11] we cannot distinguish these bands from the observed spectra. However, in the case of pyrene–DPA–hexane system, the absorption spectrum of the diphenylamino radical with maximum at *ca.* 770 nm[12] was observed clearly by means of flash photolysis (Fig. 6). Thus, the formation of both kinds of radicals has been confirmed exprimentally.

The decay processes of transient species were examined by analyzing precisely the time dependence of the transient absorption intensity at several wavelengths. It was found that the pyrene triplet state shows a single

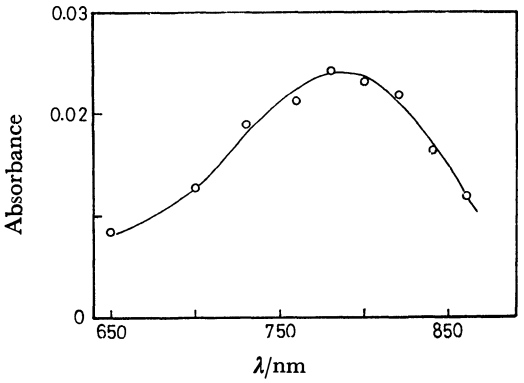

Fig. 6. Transient absorption spectrum of pyrene–DPA–hexane system at 200 μs after flash excitation. [Pyrene]$=2\times10^{-4}$ M, [DPA]$=1\times10^{-2}$ M.

exponential decay with a lifetime of *ca.* 30 μs in the case of pyrene–aniline system and that the decay of diphenylamino radical monitored at 780 nm is due to the bimolecular reaction. In contrast to the results of amino radical and pyrene triplet state, the decay process of 1-hydro-1-pyrenyl radical detected at 400 nm is rather complex. Namely, it shows an exponential decay at first over several hundred μs followed by a bimolecular decay. The two component decays in the wavelength region of the absorption band of 1-hydro-1-pyrenyl radical was observed for all pyrene-amine systems studied here. By analyzing the decay curves and time dependences of the spectra, it was established that the transient species which shows the bimolecular decay is formed from the 1-hydro-1-pyrenyl radical decaying unimolecularly. The mechanism of this two component decay process is not very clear at the present stage of investigation.

For interpretation of the fluorescence quenching mechanism in terms of the hydrogen atom transfer reaction, we assume that the reaction occurs in the singlet excited state. There is a possibility that the radicals are formed by the reaction in the triplet state. It is rather difficult to confirm this possibility since the absorption bands of the pyrene triplet state are overlapped with those of the radical. We have examined the problem by using the dilute solution of anthracene–DPA–hexane system with [anthracene]$=1\times10^{-4}$ M and [DPA]$=1\times10^{-3}$ M, since the T-T spectrum of anthracene is not overlapped with that of the hydrated radical as those of pyrene. The results of measurements by flash photolysis clearly show that no hydrogen atom transfer reaction occurs in the triplet state since no absorption of the diphenylamino radical is detected by the addition of DPA.

In order to evaluate the relative yield of 1-hydro-1-pyrenyl radical, the transient absorption due to the triplet state of the equimolar pyrene solution without amine was used as a standard. The relative yield was estimated by OD_R/OD_T, where OD_R and OD_T are absorbance extrapolated to $t=0$ of the 1-hydro-1-pyrenyl radical observed at 400 nm and that of pyrene triplet state of the standard solution observed at 415 nm, respectively. The values of OD_R/OD_T for various amines are summarized in Table 1, together with the

TABLE 1. VALUES OF OD_R/OD_T FOR THE PYRENE-AMINE-HEXANE SYSTEMS AT ROOM TEMPERATURE

Amines	OD_R/OD_T	I_p (eV)
Aniline (AN)	0.28	7.95[a]
N-Methylaniline (NMA)	0.78	7.6[a]
N-Ethylaniline (NEA)	0.87	7.5[a]
N-Butylaniline (NBA)	0.52	7.5[a]
Diphenylamine (DPA)	0.82	7.4[a]
Butylamine (BAm)	0.13	9.2[b]
Diethylamine (DEAm)	0.12	8.0[c]
Dibutylamine (DBAm)	0.52	7.7[c]
Diisobutylamine (DIBAm)	0.62	—

a) G. Briegleb and J. Czekalla, *Z. Electrochem.*, **63**, 6 (1959). b) J. D. Morrison and A. J. Nicholson, *J. Chem. Phys.*, **20**, 1021 (1952). c) K. Watanabe and J. R. Mottl, *J. Chem. Phys.*, **26**, 1773 (1957).

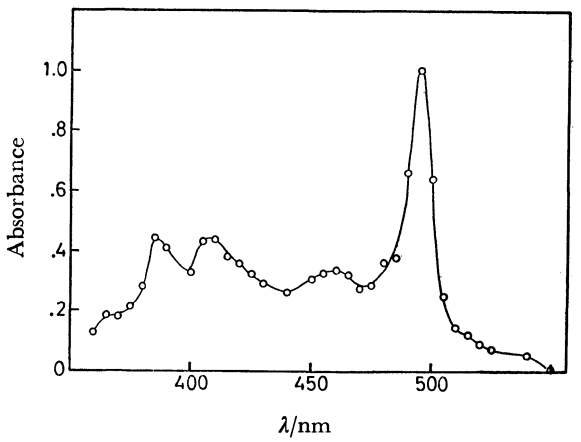

Fig. 7. Transient absorption spectra of pyrene-AN-acetonitrile system obtained by laser photolysis. [Pyrene]$=2\times10^{-4}$ M, [AN]$=1$ M.

values of I_p of amines. Since the k_q values for an amine differ, we should make correction for the difference by changing the concentrations of amines so that the extent of fluorescence quenching by various amines is equal. However, because of the large difference between the k_q values of the aromatic and aliphatic amines, it is difficult to adjust the quenching degree to the same extent. Thus, the fluorescence of pyrene in solutions examined here was quenched more than 99% in the case of aromatic amines and 90% in the case of aliphatic amines.

We see from Table 1 that OD_R/OD_T values for AN, BAm and DEAm are small as compared with the values for the other amines though the fluorescence of pyrene is quenched almost completely. The result suggests that in the case of these amines a process of returning to the ground state from radical pair $\dot{A}H....\dot{D}$ is predominant.

The quenching process of triplet benzophenone by amine has been directly demonstrated with the laser photolysis method by Arimitsu *et al.*[4,13] It has been found that no ketyl radical formation but ionic photodissociation to benzophenone anion and amine cation occurs in a strongly polar solvent such as acetonitrile, while photoreduction due to the hydrogen atom transfer from amine to ketone occurs efficiently in a nonpolar solvent, and these processes compete with each other, depending upon the solvent polarity.

In the present system, analogous solvent effects upon the transient absorption spectra as well as those upon the quenching rate constant have been observed. The k_q values for pyrene–AN, pyrene–DEAm and pyrene–DBAm systems in various solvents of different polarity are given in Table 2. We see that k_q increases with an increase in solvent polarity. The transient spectra of pyrene–AN–acetonitrile system show strong absorption bands of solvated radical ions (Fig. 7).

The k_q values for the pyrene–aniline system are much smaller than those of the other pyrene-aromatic amine systems. This seems to indicate that a considerable additional activation energy over that for the diffusional motion is necessary not only in the case of the pyrene–aliphatic amine systems but also for the quenching process in the pyrene–aniline system. The additional activation energy necessary for the charge transfer in the encounter complex becomes smaller with a decrease in the I_p values of amines. The result for the solvent effect upon the k_q value indicates that not only the I_p value of the quencher but also the solvent polarity affect the additional activation energy. Namely, it decreases with an increase in the solvent polarity, and the k_q value in polar solvents involves both hydrogen atom transfer and ionic dissociation. These two processes compete with each other, the ionic dissociation being predominant in a strongly polar solvent such as acetonitrile.

Since the $(A^-...HD^+)$ state is stabilized in polar solvents while the energy of $(\dot{A}H\cdots\dot{D})$ is independent of solvent polarity, the heteroexcimer fluorescence may be detected in slightly polar solvents, where the ionic dissociation is not predominant.

The authors are grateful to Professor S. Kato and his co-workers for use of the apparatus for flash photolysis, and for their valuable discussions concerning the experimental technique. The authors express their

TABLE 2. SOLVENT EFFECTS UPON k_q VALUES OF PYRENE-AMINE SYSTEMS AT ROOM TEMPERATURE

Solvent	AN	NMA	DEAm	DBAm
Hexane	5.7×10^8 $M^{-1}s^{-1}$	1.0×10^{10} $M^{-1}s^{-1}$	2.7×10^7 $M^{-1}s^{-1}$	3.0×10^7 $M^{-1}s^{-1}$
Diethyl ether			1.7×10^8	2.0×10^8
2-Propanol	2.6×10^9			
Acetone			3.8×10^8	8.4×10^8
Methanol		9.0×10^9		
Acetonitrile	5.3×10^9	1.5×10^{10}	2.7×10^8	8.7×10^8

cordial thanks to Dr. A. Kira of the Institute of Physical and Chemical Research for the measurement of the absorption spectrum of 1-hydro-1-pyrenyl radical by means of pulse radiolysis. The authors' thanks are also due to Mr. Y. Fujiwara and Mr. K. Mochizuki for their assistance.

References

1) N. Mataga, T. Okada, and H. Oohari, *Bull. Chem. Soc. Jpn.*, **39**, 2563 (1966).
2) N. Mataga and K. Ezumi, *Bull. Chem. Soc. Jpn.*, **40**, 1355 (1967).
3) S. G. Cohen, A. Parola, and G. H. Parsons, Jr., *Chem. Rev.*, **73**, 141 (1973).
4) S. Arimitsu, H. Masuhara, N. Mataga, and H. Tsubomura, *J. Phys. Chem.*, **79**, 1255 (1975).
5) H. Masuhara, M. Shimada, N. Tsujino, and N. Mataga, *Bull. Chem. Soc. Jpn.*, **44**, 3310 (1970).
6) N. Nakashima, N. Mataga, and C. Yamanaka, *Int. J. Chem. Kinet.*, **5**, 833 (1973).
7) N. C. Yang and J. Libman, *J. Am. Chem. Soc.*, **95**, 5783 (1973).
8) The calculation was made by using a program of Dr. Masuhara of this University.
9) A. Kira, private communication.
10) S. Arimitsu, K. Kimura, and H. Tsubomura, *Bull. Chem. Soc. Jpn.*, **42**, 1858 (1969).
11) E. J. Land and G. Porter, *Trans. Faraday Soc.*, **59**, 2027 (1963).
12) T. Shida and A. Kira, *J. Phys. Chem.*, **73**, 4315 (1969).
13) S. Arimitsu and H. Masuhara, *Chem. Phys. Lett.*, **22**, 543 (1973).

Radiotracer Studies of the Adsorption of Surface Active Substances at Aqueous Surfaces. VI. Urea Adsorption on an Adsorbed Monolayer of a Nonionic Surfactant

Kazuo TAJIMA

Department of Chemistry, Faculty of Science, Tokyo Metropolitan University, Setagaya, Tokyo 158

(Received May 1, 1976)

The surface tension and adsorption were observed by the Wilhelmy plate and radiotracer methods at the air-solution interface of an aqueous solution of urea and α-dodecyl-ω-hydroxyhexa(oxyethylene) ($D(EO)_6$). The adsorption of $D(EO)_6$ was dependent on the concentration of urea below the CMC values, but above the values it was independent of the concentration. Urea adsorption occurs positively for low-surface packing of the poly(oxyethylene) group of $D(EO)_6$, but negatively for the closest packing of the group and high concentrations of urea. It was confirmed that $D(EO)_6$ adsorption took place at the solution surface according to the Gibbs adsorption isotherm, which was taken into account as an activity coefficient in an empirical equation for the interactions of $D(EO)_6$ and urea in solution. Urea adsorption for the adsorbed monolayer of $D(EO)_6$ above the CMC value was interpreted assuming that urea, as for the nonionic micelle, was non-penetrating, which was examined by gel permeation.

The surface tension of the aqueous urea solution is almost invariant or is slightly increased with increasing urea concentration at the air-solution interface.[1,2] When covered with stearic acid[2] or protein[3] monolayers on the urea solution, urea adsorption occurs at the monolayers due to the dipole-dipole interactions of the urea and film substances, but not at the ionic monolayer of the stearate.[4] However, the micelle formation in the aqueous solution of ionic and nonionic surfactants is markedly affected by urea present in the solution, and the CMC value is shifted to higher surfactant concentrations.[5] Also, urea decreases the surface tension lowering of the surfactant solution, and causes a change in the activity of the surfactant in the solution due not only to a reduction of the dielectric constant of water, but also to a direct interaction with the surfactant.[6]

If the activity for each kinetic unit in the urea–surfactant solution is undeterminable, the Gibbs adsorption of solutes cannot be calculated from only the relationship between the surface tension and the apparent concentration of solutes in the solution,[7] without additional experimental information about the surface adsorption. In a previous paper,[1] the surface adsorption of a nonionic surfactant at constant concentration was measured as a function of the concentration of various additives, but no additive adsorption was obtained. The surface compositions of adsorbed mixed monolayers are not easily determined in comparison with the case of insoluble monolayers.

The present report is concerned with the elucidation of urea adsorption for the adsorbed monolayer by measuring the adsorption of nonionic surfactant at the air–solution interface. Further, the micelle size will be examined by the gel permeation of the urea–surfactant solution in order to check whether or not urea has penetrated into the micelle.

Experimental

Materials. α-Dodecyl-ω-hydroxyhexa(oxyethylene) ($D(EO)_6$), α-dodecyl-2,3-$^3H_2$-ω-hydroxyhexa(oxyethylene), and urea (EP. grade, purified by recrystallization with water) were the same as those used in previous experiments.[1] The water used was distilled three times after refluxing with alkali-permanganate overnight. The experimental temperature was maintained at 30.0±0.5 °C.

Measurements of Surface Tension and Adsorption. The surface tensions of surfactant solutions with and without urea were measured by the Wilhelmy plate method. The surface tension at equilibrium was taken to be those values which no longer changed with time (usually equilibrium was established after several hours). The amount of nonionic surfactant adsorption was measured by the radiotracer method using a tritiated compound. Details of the equipment and of the experimental procedure have been presented previously.[8,9]

Gel Permeation. The apparatus and procedure used for the gel permeation of a urea–nonionic surfactant solution, are almost the same as those used by Suzuki and Sasaki.[10] The gel (Sephadex G75) was embedded in a column (diameter 1.2 cm and gel height 15.0 cm) after swelling in a urea solution of the same concentration as was eluted in the gel permeation. The nonionic surfactant in the each fraction (1 ml) was analyzed by the iodine turbidity method.[11] Constant amounts of iodine (10^{-2} M, 0.3 ml) in excess of the requirement for forming the iodine–nonionic complex, and then hydrochloric acid (1 M, 0.4 mol), were added to each fraction. After shaking the mixture for about 30 min, the turbidity of the solutions was measured at 660 mμ using a Shimadzu spectrophotometer (Spectronic 20).

Results and Discussion

The surface tensions of the $D(EO)_6$ solution with and without urea are shown in Fig. 1. Surface tension lowering is markedly dependent on the urea concentration, but independent above the CMC value to within experimental error. Quite similar observations above the CMC value have been reported by Schwuger,[12] who has measured the surface tension of a urea(3 M)–$D(EO)_6$ solution by the ring method. A weak break point is observed on each curve in Fig. 1 at some solution concentration below the CMC value. This phenomenon appears to give the possibility of a change in the solubility state of the solutes in the solution, as is discussed in detail below.

Figure 2 shows the adsorption isotherms of $D(EO)_6$ at various urea concentrations. These isotherms are

nonionic adsorbed monolayer may be expected from the isotherms in Fig. 2. Sears has reported[2] that urea adsorption for a constant molecular area of a stearic acid monolayer occurs roughly in proportion to the concentration of urea in the solution. In the case of an adsorbed monolayer, the constant molecular area (constant $D(EO)_6$ density on the surface) corresponds to a constant value of Γ_1 in Fig. 2, because of the very dilute solution for C_1. Therefore, urea adsorption in the adsorbed monolayer may be estimated using a relationship between the surface tension and bulk concentrations of urea and $D(EO)_6$ such that a constant value of Γ_1 is maintained. Differentiating Eq. 1 applied to this system with respect to the logarithmic concentration of urea, we have at constant Γ_1,

$$-\left(\frac{\partial\gamma}{RT\partial\ln C_2}\right)_{\Gamma_1} = \left\{\left(\frac{\partial\ln f_1}{\partial\ln C_2}\right)_{\Gamma_1} + \left(\frac{\partial\ln C_1}{\partial\ln C_2}\right)_{\Gamma_1}\right\}\Gamma_1 + \left\{1+\left(\frac{\partial\ln f_2}{\partial\ln C_2}\right)_{\Gamma_1}\right\}\Gamma_2. \quad (7)$$

Since $C_1/C_2 \ll 1$, $(\partial \ln f_2/\partial \ln C_2)_{\Gamma_1}$ may be replaced by that for a simple aqueous solution of urea. From the empirical data for the osmotic coefficient of a urea solution[14] and Bjerrum's equation,[15] we have

$$\frac{\partial\ln f_2}{\partial\ln C_2} = -0.046C_2.$$

Also, from the Gibbs-Duhem equation for the solutes in the bulk solution and assuming Eq. 3, we have

$$\left(\frac{\partial\ln f_1}{\partial\ln C_2}\right)_{\Gamma_1} = \left\{1-\left(\frac{\partial\ln C_1}{\partial\ln C_2}\right)_{\Gamma_1}\right\}\left(\frac{\partial\ln f_1}{\partial\ln C_2}\right)_1. \quad (9)$$

Combining Eqs. 5, 7, 8 and 9, we have

$$\Gamma_2 = \frac{1}{1-0.046C_2}\left[-\left(\frac{\partial\gamma}{RT\partial\ln C_2}\right)_{\Gamma_1} + \delta\left\{1-\left(\frac{\partial\ln C_1}{\partial\ln C_2}\right)_{\Gamma_1}\right\} - \Gamma_1\left(\frac{\partial\ln C_1}{\partial\ln C_2}\right)_{\Gamma_1}\right] \quad (10)$$

where

$$\delta = 4.5\times10^{-11}C_2^{0.15}. \quad (10')$$

The relations between the surface tension and urea concentration, and C_2 *vs.* C_1 at constant Γ_1 are shown in a and b of Fig. 3. The amount of urea adsorbed, Γ_2, calculated using Eq. 10 with 1.4×10^{-10} mol/cm^2 for Γ_1 is shown in Table 2.

The increasing urea concentration in the solution enhances the urea adsorption at the adsorbed monolayer of a nonionic surfactant, the same as in the case of a stearic acid monolayer.[2] However, there are some essential differences pertinent to urea adsorption in these monolayers. The amount of adsorbed urea for an insoluble monolayer may be the absolute amount, but this is not the case for adsorbed monolayers, as expressed by Eq. 10. Namely, the last term in Eq. 10 represents the amount of urea accompanying the Γ_1 amount in proportion to the composition ratio of solutes in the bulk phase (here $\partial C_1/\partial C_2$ is almost constant), which is similar to the concept for the Gibbs adsorption.[7] Since urea itself is a surface inactive substance, it is easily deduced that Γ_2 is the difference in amounts of urea accumulated in the poly(oxyethylene) chain of the nonionic surfactant on the surface and in the bulk phases.

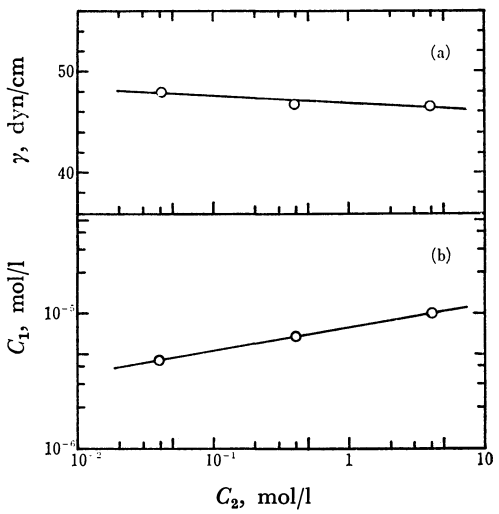

Fig. 3. Surface tension and bulk concentrations of solutes so as to maintain a constant adsorption of $D(EO)_6$ (1.4×10^{-10} mol/cm^2).
(a): Surface tension *vs.* concentration curve of $D(EO)_6$.
(b): Relationship of C_1 and C_2.

TABLE 2. ADSORPTION OF UREA ONTO THE ADSORBED $D(EO)_6$ MONOLAYER UNDER VARIOUS CONDITIONS

C_1 mol/l$\times10^5$	C_2 mol/l	Area of $D(EO)_6$ A^2/molecule	Urea adsorption mol/cm^2 $\times10^{10}$
0.45	0.040	118.6	0.90
0.70	0.40	118.6	1.01
1.0	4.0	118.6	1.39
4.0	0.040	38.9	0.06
4.0	0.40	79.4	0.06
4.0	4.0	105.7	−0.61

The Γ_2 value at the saturated adsorption region of $D(EO)_6$ (C_1 is maintained constant at 4.0×10^{-5} mol/l) at various urea concentrations is cited in Table 2. The calculation of Γ_2 in this case were performed using Eq. 11, which was derived in the same manner as in a previous paper,[16] assuming $C_1/C_2 \ll 1$ and $(\partial \ln f_1/\partial \ln C_1)_2 \approx 0$, as

$$\Gamma_2 = \left(-\frac{\partial\gamma}{RT\partial\ln C_2}\right)_1 - \left(\frac{\partial\ln f_1}{\partial\ln C_2}\right)_1\left(-\frac{\partial\gamma}{RT\partial\ln C_1}\right)_2 \quad (11)$$

where $(\partial \ln f_1/\partial \ln C_2)_1$ was deduced from Eq. 5, and the value of $(\partial\gamma/\partial \log C_2)_1$ was obtained from the curve in Fig. 4. The value of Γ_2 in the saturated adsorption region is almost zero at low urea concentrations, but is negative in 4.0 mol/l urea solutions. This property of urea adsorption can be explained by that at low urea concentrations, the accumulation of urea at the poly(oxyethylene) group of adsorbed nonionic surfactant is almost the same as that in the bulk phase, however, at high urea concentrations, it decreases in comparison with that of urea in the bulk solution owing to a squeezing from the poly(oxyethylene) group with the lateral cohesive force of hydrocarbon chains of adsorbed molecules at the surface. A similar phenomenon, which occurs when the surface density of a surface active material increases at constant urea concentration, is

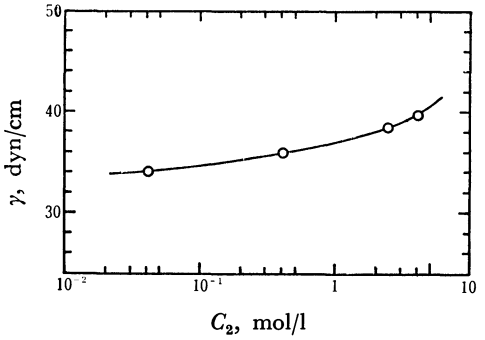

Fig. 4. Surface tension *vs.* concetration curve of urea at constant concentration of $D(EO)_6$ (4.0×10^{-5} mol/l).

observed not only in stearic acid monolayers,[2] but also in adsorbed monolayers at concentrations above the CMC value as described in the following section.

The Effect of Urea on Micelle. In the preceding section it was stated that urea adsorption occurs at adsorbed monolayers of $D(EO)_6$. However, above the CMC(0) value in the surface phase, urea appears to be forced out from inter-poly(oxyethylene) chains to below the $D(EO)_6$ monolayer as expected from the findings shown in Fig. 2. The micelle in the bulk solution is generally considered to attain the following equilibrium relation with the single species:[17]

$$\underset{\text{(single)}}{nA} \rightleftharpoons \underset{\text{(micelle)}}{A_n^M},$$

where n is the micelle aggregation number, A the single molecule and the superscript M denotes the micelle. In urea–nonionic solutions, the following processes for micellization are proposed:

$$nA + n\cdot mU \rightleftharpoons n(AUm) \rightleftharpoons [(AUm)_n^M] \rightleftharpoons A_n^M + n\cdot mU,$$

where m is conventionally constant, AUm the single molecule of nonionic surfactant ureanized, and $(AUm)_n^M$ the urea-penetrated micelle. If bound urea is squeezed out from the interior of micelle toward the outside, it may be considered to be almost the same as the $D(EO)_6$ micelle in the absence of urea. The micelle penetrated urea, which would be enclosed in either the hydrocarbon moiety and poly(oxyethylene) group or only the head group, is likely, if present, to be unstable due to the occurence of weak break points on the surface tension *vs.* concentration curves in Fig. 1 and also from the peculiar isotherms in Fig. 2. Schick *et al.*[18] have observed that the aggregation number of α-(*p*-nonylphenyl) - ω - hydroxypentadeca(oxyethylene) micelle slightly increases with the presence of urea in the solution, and suggested that the marked increments in the CMC values of α-alkyl-ω-hydroxypoly(oxyethylene) solutions are caused by a decrease in the cooperative structure of water.[5] According to Schik's suggestion, Hammes and Schimmel[6] predicted, from the results of the ultrasonic attenuation measurements in aqueous urea–poly(oxyethylene) glycol solutions, that the change in local solvent structure could involve a cooperative binding of urea to the poly(oxyethylene) group in solution. To elucidate this possibility of urea behavior in the micelle solution, the elusion volume of micelle, which is closely dependent on the micelle size,[19] was measured from the gel permeations of the micelle solution with and without urea. The results obtained are cited in Table 3. No large difference in elusion volume was observed at a urea concentration of 2.5 mol/l. Consequently, it is considered that the micelle size is not affected by the presence of urea.

TABLE 3. ELUSION VOLUMES OF MICELLE AND SINGLE SPECIES OF $D(EO)_6$ SOLUTIONS WITH AND WITHOUT UREA

(A) Water			(B) 2.5 M of urea		
C_1 mol/l $\times10^5$	Micelle ml	Single species ml	C_1 mol/l $\times10^5$	Micelle ml	Single species ml
4.4	—	17.0	4.4	—	17.0
6.6	—	17.0	6.6	—	16.6
7.7	5.5	17.0	7.7	—	17.5
8.25	5.2	17.5	8.25	—	17.0
9.9	5.5	17.3	11.0	—	16.8
11.0	5.2	17.2	15.4	5.4	17.0
13.2	5.3	17.0	18.7	5.6	17.0
			20.6	5.5	17.2
			22.0	6.0	17.5

Muller *et al.*, who studied the effects of additives on aqueous sodium ω,ω,ω-trifluorododecyl sulfate (F_3-SDS)[20] and α-(ω,ω,ω-trifluorododecyl)-ω-hydroxyhexa(oxyethylene)[21] solutions by the fluorine NMR method, have reported that the micelle chemical shifts with the presence and absence of urea in the solutions are about half (the R value in Ref. 20 is about 0.5), in comparison with those for single molecules. Though the aggregation number of nonionic micelle could not be determined and that of F_3SDS micelle was rather reduced with the presence of urea, they maintain that the urea, glycerol and glycine additives should be nonpenetrating in nonionic micelle. These results are in good agreement with the result for gel permeation and support the proposed mechanisms for micellization in urea–nonionic solutions.

The findings of the present studies and FNMR spectra may lead to the conclusion that the micelle of $D(EO)_6$ solutions with urea is almost the same as that of solutions without urea. If no urea entered into the micelle entity, none could be incorporated in the adsorbed monolayer, thermodynamically equilibrated with the micelle in bulk solution.

References

1) K. Tajima and M. Iwahashi, *Bull. Chem. Soc. Jpn.*, **46**, 3370 (1973).
2) D. F. Sears, *J. Colloid Interface Sci.*, **29**, 288 (1969).
3) S. Lewin, *Nature, (London), New Biol.*, **231**, 80 (1971).
4) D. F. Sears and J. H. Schulman, *J. Phys. Chem.*, **68**, 3529 (1964).
5) M. J. Schick, *J. Phys. Chem.*, **68**, 3585 (1964); W. U. Malik and O. P. Jhamb, *Kolloid Z. Z. Polym*, **242**, 1209 (1970).
6) G. G. Hammes and P. R. Schimmel, *J. Am. Chem. Soc.*, **89**, 442 (1967).
7) R. Defay, I. Prigogine, A. Bellemans, and D. H. Everett, "Surface Tension and Adsorption," Longmans, London (1966), p. 85.
8) K. Tajima, M. Muramatsu, and T. Sasaki, *Bull. Chem. Soc. Jpn.*, **43**, 1991 (1970).

9) K. Tajima, M. Iwahashi, and T. Sasaki, *Bull. Chem. Soc. Jpn.*, **44**, 3251 (1971).
10) H. Suzuki and T. Sasaki, *Bull. Chem. Soc. Jpn.*, **44**, 2630 (1971).
11) K. Tajima and A. Nakamura, to be published for further details.
12) M. J. Schwuger, *Kolloid Z. Z. Polym.*, **232**, 775 (1968).
13) R. A. Robinson and R. H. Stokes, "Electrolyte Solutions," 2nd ed., Butterworths, London (1959), p. 558; V. E. Bower and R. A. Robinson, *J. Phys. Chem.*, **67**, 1524 (1963).
14) F. T. Gucher, Jr. and H. B. Pickard, *J. Am. Chem. Soc.*, **62**, 1464 (1940); R. H. Stokes, *J. Phys. Chem.*, **70**, 1199 (1966).
15) I. Prigogine and R. Defay, "Chemical Thermodynamics," trans. D. E. Everett, Longmans, N. Y. (1954), p. 323.
16) K. Tajima, *Bull. Chem. Soc. Jpn.*, **44**, 1767 (1971).
17) K. Shinoda, T. Nakagawa, B. Tamamushi, and T. Isemura, "Colloidal Surfactants," Academic Press, N. Y. (1963), p. 27.
18) M. J. Schick, S. M. Atlas, and F. R. Eirich, *J. Phys. Chem.*, **66**, 1326 (1962).
19) K. S. Birdi, *Colloid Polym. Sci.*, **252**, 551 (1974).
20) N. Muller and T. W. Johnson, *J. Phys. Chem.*, **73**, 2042 (1969).
21) N. Muller and F. E. Platko, *J. Phys. Chem.*, **75**, 547 (1971).

Studies of MoO_3–Al_2O_3 Catalysts in Ethylene Polymerization. IV. Kinetics and Stoichiometry of the Reduction

Keizi HASHIMOTO, Shozi WATANABE, and Kimio TARAMA*

The Osaka Municipal Technical Research Institute, Ogimati, Kita-ku, Osaka 530

* *Department of Hydrocarbon Chemistry, Faculty of Engineering, Kyoto University, Yoshida, Sakyo-ku, Kyoto 606*

(Received May 24, 1976)

In order to reveal the formation mechanism of the active species in ethylene polymerization, the reduction of three kinds of molybdenum oxides, I, II, and III, which are insoluble in aq 10 M-NH_3, soluble in aq NH_3 but insoluble in water, and soluble in water respectively, was studied under a hydrogen pressure of 170 Torr over the temperature range 350—450 °C. The reduction rate of oxides I and II followed Elovich kinetics with a variable activation energy which increased with the progress of reduction, while that of III followed Elovich kinetics in the multiple kinetic stages and the minimum in apparent activation energy for the reduction lies at the reduction extent of $MoO_{2.7-2.6}$. The final states of reduction of I, II, and III were $MoO_{2.8-2.6}$, $MoO_{2.0}$ and $MoO_{2.2-2.1}$, respectively. The amount of Mo(V) in each oxide was determined by ESR measurements. The results indicate that Mo(V) in the II is related to the decrease of the apparent activation energy on reduction of III through their mutual interaction. A formation mechanism of the active species, Mo(V) in III, was proposed.

The polymerization over MoO_3–Al_2O_3 catalysts has been studied. The activity of the catalysts and the kinetics of the polymerization were reported.[1] The relation between the activity and chemical states in the supported molybdenum oxides, I, II and III, which are insoluble in aq 10 M-NH_3, soluble in aq NH_3 but insoluble in water, and soluble in water respectively, was reported.[2] The activity was found to be attributable to molybdenum(V) in III, $[Mo^{5+}]_w$.[3]

We have investigated the reduction mechanism of each oxide and the formation mechanism of the active species in order to clarify why the amount of $[Mo^{5+}]_w$ on alumina is greater than that on other carriers.

It is well known that in a hydro-cracking reaction[4,5] and an equilibrium reaction of H_2–D_2[6] carried out over MoO_3–Al_2O_3 catalysts, the activity is related to the chemical states of the molybdena besides polymerization. Our results might be useful for understanding the formation mechanism of the active species in the reactions.

Sontag *et al.*[7] were the first to note the extreme difficulty of reducing molybdena supported on alumina in hydrogen as compared with bulk MoO_3. They attributed this to an inhibition effect by water adsorbed on the alumina surface, which seems to raise from a localized surface equilibrium unfavorable to reduction. Kabe *et al.*[8] and Massoth[9] reported on the kinetics of reduction of MoO_3–Al_2O_3 catalysts and showed that the reduction followed the Elovich-type equation with a variable activation energy which increased with the progress of reduction. However, thier results differ as regards the final state and activation energy of the reduction. It may be pointed out that their catalysts were reduced under different conditions and that the proportion of molybdenum oxide in the three chemical states differed owing to the different conditions for the preparation of the catalysts.

Catalysts reduced under a hydrogen pressure of 170 Torr over the temperature range 350—450 °C are very active for polymerization. The kinetics of reduction of the oxide in each chemical state was studied under the same conditions. The molybdenum(V) contents were determined by ESR measurements.

The results elucidate some relations between the formation of molybdenum(V) in II and that in III. A formation mechanism of the active species, $[Mo^{5+}]_w$, is proposed.

Exprimental

Materials. Commercial hydrogen and oxygen (> 99.9%) were used without further purification. MoO_3–Al_2O_3 catalysts were prepared according to the procedure described previously.[1] Samples contained MoO_3 between 0 and 16.7 wt%. Data for the catalysts were given previously.[2] The support used was gamma alumina. X-Ray analysis gave no lines attributable to MoO_3 except for 16.7 wt% MoO_3–Al_2O_3.

Reduction of Catalysts. The apparatus was simply a closed system consisting of a furnace containing a reactor for the catalyst and a manometer made of 6-mm ID capillary tubing for measuring pressure. The system had about 160 ml capacity. Catalyst charges of 300—1000 mg were used. The catalyst was evacuated for an hour under a pressure of 10^{-3} Torr at 200 °C and then at 400 °C. The catalyst was reduced under a hydrogen pressure of 170 Torr over the temperature range 350—450 °C. The reduction was carried out in a batch system. One cycle consisted of a hydrogen reduction for a given period of 3—5, 1—2, and 1—2 min at 350, 400, and 450 °C, respectively and of an evacuation for 5 min.

The extent of reduction was determined from the amount of oxygen completely reoxidizing the catalyst. The extent shows the conversion ratio of MoO_3 to MoO_2.

ESR Measurement. The measurement was carried out as described previously.[3]

Results and Discussion

Activation Energy. The reduction of the molybdenum oxides, I, II and III, was studied in order to determine the activation energy. Since II and III can not be isolated, the following catalysts were used. (A), 16.7wt% MoO_3–Al_2O_3 consisting of I, II, and III; (B), prepared by the removal of III from (A) with water; (C), prepared by the removal of both II and III with aq 10 M-NH_3.

The reduction extent of the catalyst, θ, is given by

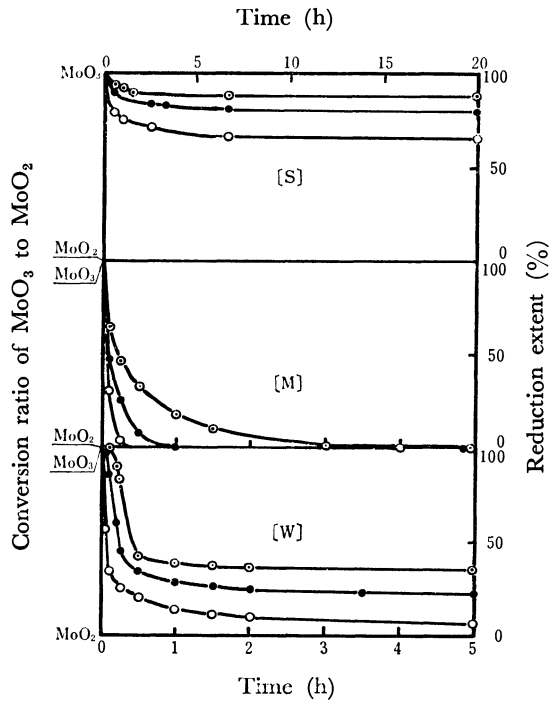

Fig. 1. Variation of the reduction extent of the oxide I, the oxide II and the oxide III with time.
⊙: 350 °C, ●: 400 °C, ○: 450 °C.

$$\theta = \frac{\theta_S[S] + \theta_M[M] + \theta_W[W]}{[S] + [M] + [W]} \quad (1)$$

where θ_S, θ_M, and θ_W denote the reduction extent of I, II, and III for given time, respectively, and [S], [M], and [W] the concentration, respectively. The reduction extent of each oxide can be determined by Eq. 1 on the basis of the reduction extents of catalysts (A), (B), and (C).

The reduction extents of the catalysts were measured at 350, 400, and 450 °C, and were evaluated as shown in Fig. 1. Catalyst(A) is the most active for the polymerization over the molybdena-content range 0—16.7 wt%. At 450 °C, I is reduced to $MoO_{2.6}$ in *ca.* 20 h and II

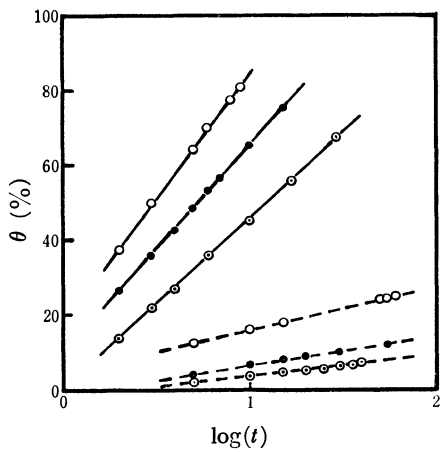

Fig. 2. Elovich plots for reduction of the oxide I and the oxide II at various temperature and 170-Torr H_2.
----: The oxide I, ——: the oxide II, ⊙: 350 °C, ●: 400 °C, ○: 450 °C.

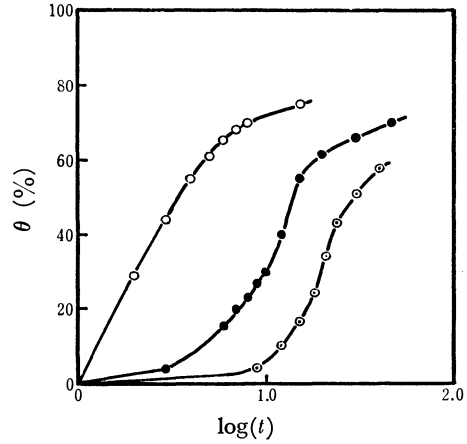

Fig. 3. Plot of reduction extent, θ, *vs.* log t for the reduction of the oxide III at various temperature and 170-Torr H_2.
⊙: 350 °C, ●: 400 °C, ○:450 °C.

to $MoO_{2.0}$ in *ca.* half an hour and III to $MoO_{2.1}$ in *ca.* 5 h. These final states in each oxide varied little with further reduction. Thus the increasing order of reduction rates is: I, III, and II.

With catalysts(A), (B), and (C) reduced under the same conditions, no signal was observed except for one of molybdenum(V) by ESR measurements. In X-ray analysis, diffraction of MoO_2 was observed but not of $MoO_{1.5}$. These indicate that I, II and III are reduced to molybdenum(IV).

The reduction extents of I and II are plotted against logarithmic time in Fig. 2 on the basis of the results in Fig. 1. θ shows a linear relation with logarithmic time. Thus, the reduction follows an Elovich-type equation.[10,11]

$$\frac{d\theta}{dt} = a \cdot \exp(-b\theta) \quad (2)$$

where a and b are constants of the extent of reduction.

Figure 3 was obtained in a similar manner for the θ of III. The values of the θ show a curve with logarithmic time. The curve indicates that the reduction follows an Elovich-type equation in multiple kinetic stages.[11,12]

When the reduction follows an Elovich-type equation, the activation energy, $E(\theta)$, is expressed by an extension of Eq. 2 as follows:[8,9]

$$\frac{d\theta}{dt} = a \cdot \exp(-b\theta) = A \cdot \exp[-E(\theta)/RT] \quad (3)$$

where A is constant. Transforming Eq. 3 into logarithmic form, we obtain

$$\ln\left(\frac{d\theta}{dt}\right) = \ln(A) - E(\theta)/RT \quad (4)$$

The rates of reduction at a discrete value of θ are obtained from the slopes of θ-time recorder tracing in Fig. 1. Therefore, the activation energies at a discrete value of θ in both I and II are calculated on the basis of the plot of the rates against θ by Eq. 4. The results are shown in Fig. 4. The energy only at the θ value 10% was calculated for I owing to the difficulty of reducing I in hydrogen in the temperature range 350—450 °C. The result: $E(\theta=10\%)=42.5$ kcal/mol. This

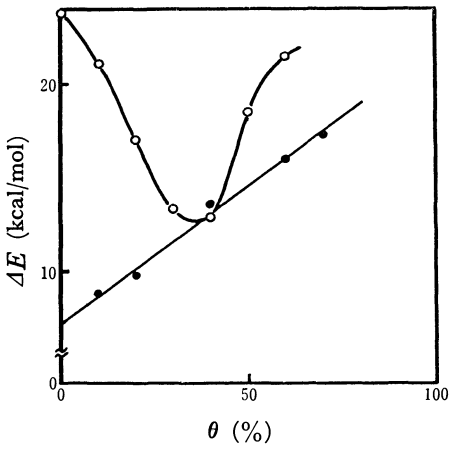

Fig. 4. Effect of reduction extent on activation energy.
●: The oxide II, ○: the oxide III.

is nearly equal to the value, $E(\theta)=30+52\theta$, reported by Kabe *et al.*[8] We see from Fig. 1. that the value of $E(\theta)$ in II is determined by

$$E(\theta) = 7.2 + 14.4\theta_M \quad (0<\theta_M<70\%) \qquad (5)$$

The value of $E(\theta)$ in II varies only 10 kcal/mol in the θ range 0—70%. This variation is smaller than that in I. This supports the conclusion[2] that as regards the strength of the interaction with alumina, the distribution in II is narrower than that in I. Extrapolation to $\theta=0$ gives $E_0=7.2$ kcal/mol. The value is smaller than 30 kcal/mol reported by Kabe *et al.*[8] and Sukeno *et al.*[13] and 9.8 kcal/mol by Massoth[9] and 27 kcal/mol for crystal MoO_3 by Kennedy *et al.*[14] The explanation for the difference is that the $E(\theta)$ in II could not be measured due to the rapid reduction of II.

The apparent activation energy of reduction in III is determined from the Arrhenius plots of the reduction rates. The results are given in Fig. 4. We see that the energy in III is minimum, 13 kcal/mol, in the θ range 30—40%, no reduction of bulk MoO_3 being observed under the present experimental conditions. MoO_3–SiO_2 catalysts (650 m^2/g) in which molybdena hardly intracts with silica support, could be reduced under a hydrogen pressure of 170 mmHg in the temperature range 400—450 °C and the apparent activation energy of reduction was determined to be constant, 39 kcal/mol, in the θ range 0—50%. These results indicate that III is reduced much more easily than the bulk MoO_3 and the MoO_3–SiO_2 catalysts.

Formation Mechanism of Active Species. MoO_3–Al_2O_3 catalysts were reduced from Mo(VI) to Mo(IV). The intermediate Mo(V) is supposed to be formed in the reduction process. In order to reveal the reduction mechanism of MoO_3–Al_2O_3 catalysts, the variation of the amount of Mo(V) in each oxide with reduction time was measured by ESR. The relation between the apparent $g'_{//}$-value and the Mo(V) content is expressed as follows.[3]

$$g'_{//} = \frac{1.9140[Mo^{5+}]_S + 1.9086[Mo^{5+}]_M + 1.8960[Mo^{5+}]_W}{[Mo^{5+}]_{total}} \qquad (6)$$

where $[Mo^{5+}]$ is a concentration of Mo(V), and S, M, and W subscripts refer to I, II, and III, respectively. The total amount of Mo(V) in the catalysts, $[Mo^{5+}]_{total}$, are expressed as follows.[3]

$$[Mo^{5+}]_{total} = [Mo^{5+}]_S + [Mo^{5+}]_M + [Mo^{5+}]_W \qquad (7)$$

In order to determine the Mo(V) content in each oxide, $[Mo^{5+}]_{total}$ and the apparent $g'_{//}$-values in catalyst(A), (B), and (C) were measured by ESR (Fig. 5). We see that $[Mo^{5+}]_{total}$ decreases within a reduction period of 50 min in the order (B)>(A)>(C). The apparent $g'_{//}$-value in (A) shows a minimum value for a reduction period of 7—10 min and that in (B) shows a nearly constant value.

$[Mo^{5+}]_M$ and $[Mo^{5+}]_S$ in (B) were calculated by substituting the apparent $g'_{//}$-values and $[Mo^{5+}]_{total}$ (Fig. 5) into Eqs. 6 and 7. The results are shown in Fig. 6. The behavior of $[Mo^{5+}]_S$ is in fair agreement with that of $[Mo^{5+}]_S$ (Fig. 5). The agreement indicates that I hardly interacts with II. $[Mo^{5+}]_M$ shows a constant value of 1.5×10^{19} spin/g-cat in the θ range 40—90%. The result supports the view that II exists in fine dispersion on the alumina surface[2] and that I

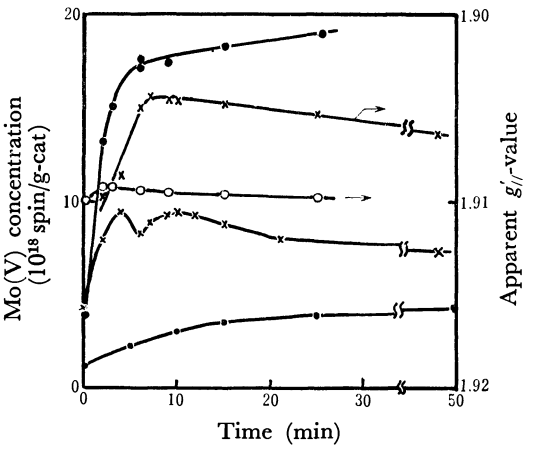

Fig. 5. Variation of Mo(V) concentration and the apparent $g'_{//}$-value in each oxide with reduction time.
×: Catalyst(A), ○: catalyst(B), ●: catalyst(C).

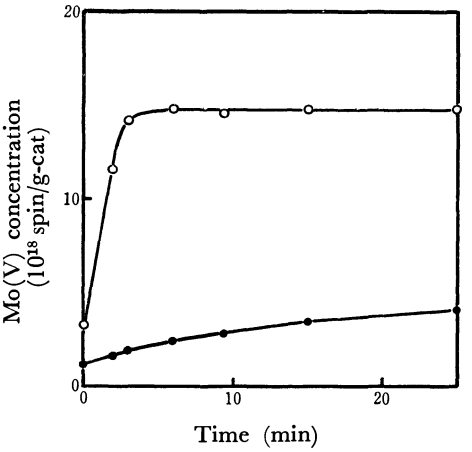

Fig. 6. Variation of Mo(V) concentration in the oxide I and the oxide II of the catalyst(B) with time.
●: The oxide I, ○: the oxide II.

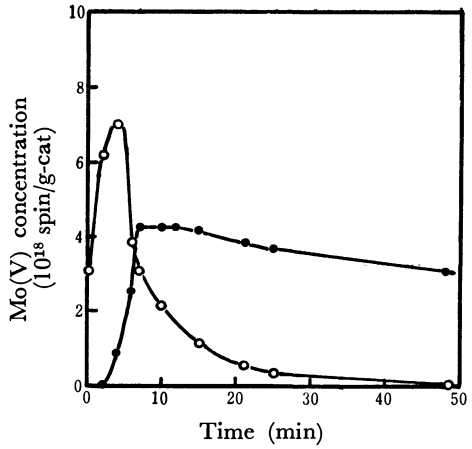

Fig. 7. Variation of Mo(V) concentration in the oxide II and the oxide III of the catalyst(A) with time.
○: The oxide II, ●: the oxide III.

and II exist separately.

$[Mo^{5+}]_M$ and $[Mo^{5+}]_w$ in (A) were calculated by substituting $[Mo^{5+}]_{total}$, the apparent $g'_{//}$-value and $[Mo^{5+}]_s$ (Fig. 5), into Eqs. 6 and 7. The results are shown in Fig. 7. $[Mo^{5+}]_M$ in (A) increases remarkably within a reduction period of 4 min and decreases rapidly during further reduction time. The behavior of $[Mo^{5+}]_M$ differs from that in (B). $[Mo^{5+}]_w$ begins to form after a remarkable increase in $[Mo^{5+}]_M$, the behavior being in contrast to that of $[Mo^{5+}]_M$ (Fig. 7). This indicates that II interacts with III. The increase and decrease of $[Mo^{5+}]_M$ in Fig. 7 correspond to the decrease and increase, respectively, of activation energy for reducing III. Recently, it has been reported that the bulk MoO_3 is easily reduced in hydrogen at a lower temperature in the presence of 0.1—0.01 mol% of Pd or Ni.[15-19] The Pd- and Ni-catalyzed reduction was explained in terms of the transfer of hydrogen chemisorbed on Pd and Ni. This supports the view that $[Mo^{5+}]_M$ catalyzes the reduction of III. This is also supported by the following : As compared with III, it is difficult to reduce the bulk MoO_3 and the MoO_3–SiO_2 catalysts, in which $[Mo^{5+}]_M$ is absent. No relation between the amount of adsorbed hydrogen and the total amount of Mo(V) was observed. We reported that the amount of chemisorbed hydrogen agrees with the concentration of $[Mo^{5+}]_w$.[3] Hydrogen is chemisorbed on Mo(V) in MoO_3–Al_2O_3 catalysts[20] and the reduction of bulk MoO_3 is auto-catalytic in hydrogen.[19] In view of these facts, the formation mechanism of active species Mo(V) in III is proposed as follows: First, II is reduced in the MoO_3–Al_2O_3 catalysts and the $[Mo^{5+}]_M$ is formed and then the hydrogen to be chemisorbed on the $[Mo^{5+}]_M$ promotes the reduction of III from Mo(VI) to Mo(V); second, the hydrogen is chemisorbed on the formed $[Mo^{5+}]_w$ which also promotes the reduction of III from Mo(VI) to Mo(V). Therefore, more $[Mo^{5+}]_w$ is formed in the MoO_3–Al_2O_3 catalysts than in the MoO_3–SiO_2 catalysts and in the bulk MoO_3.

Structure of Molybdena on Alumina. The properties of molybdena supported on alumina in the content range of 0—16.7wt% and calcined over the temperature range 400—550 °C were explained in terms of a distorted octahedral structure.[3] Concerning the structure of I, we see that I interacts strongly with alumina but hardly interacts at all with II to exist on the alumina surface[2] and the crystal field is the strongest of the three oxides;[3] I is reduced only to $MoO_{2.8-2.6}$ in the temperature range 350—450 °C, the activation energy of reduction being greater than 42.5 kcal/mol. Thus, it is concluded that Mo atom of I has 6 Mo–O bondings which are nearly equal in strength and probably located inside the alumina lattice (Fig. 8).

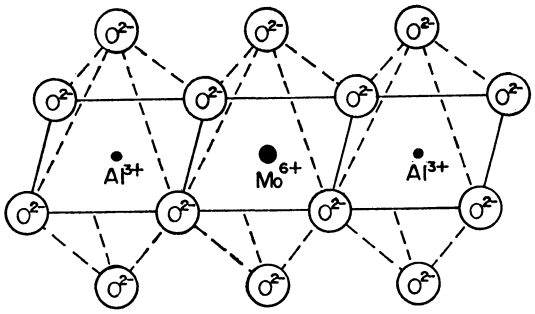

Fig. 8. Model of the oxide I.

Concerning the structures of II and III, we see that: II interacts with alumina, the interaction being weaker than that of I; the diffraction of a crystal MoO_3 is observed in the molybdena content 16.7wt%[2] II is reduced easily to MoO_2, interacts with III and promotes the reduction of III. These facts support the view that Mo atom of II has 6 Mo–O bondings, two bondings of which are weaker than the other four bondings, and that a part of III forms a crystal MoO_3 with an increase of III.

References

1) K. Hashimoto, S. Watanabe, and K. Tarama, *Nippon Kagaku Kaishi*, **1974**, 409.
2) K. Hashimoto, S. Watanabe, and K. Tarama, *Nippon Kagaku Kaishi*, **1975**, 591.
3) K. Hashimoto, S. Watanabe, and K. Tarama, *Bull. Chem. Soc. Jpn.*, **49**, 12 (1976).
4) T. Shirasaki, O. Shin, M. Kato, and K. Morikawa, *Shokubai*, **4**, 337 (1962).
5) Y. Miki, T. Kabe, S. Yamadaya, M. Oba, and Y. Kodera, *Shokubai*, **12**, 63 (1970).
6) G. S. John, M. J. D. Herber, R. J. Mikovsky, and R. F. Water, *Adv. Catal.*, **9**, 252 (1957).
7) P. Sontag, D. Q. Kim, and F. Marion, *C. R. Acad. Sci., Ser. C*, **259**, 4704 (1964).
8) T. Kabe, S. Yamadaya, M. Oba, and Y. Miki, *Int. Chem. Eng.*, **12**, 366 (1972); *Kogyo Kagaku Zasshi*, **74**, 1566 (1971).
9) F. E. Massoth, *J. Catal.*, **30**, 204 (1973).
10) M. J. D. Low, *Chem. Rev.*, **60**, 267 (1960).
11) G. Aharoni and F. C. Tomkins, *Adv. Catal. Relat. Subj.*, **20**, 1 (1970).
12) N. H. Turner, *J. Catal.*, **36**, 262 (1975).
13) T. Sukeno, M. Mimura, and H. Nomura, *Kogyo Kagaku Zasshi*, **68**, 1838 (1965).
14) M. J. Kennedy and S. C. Bevan, 1st. International

Conference on the Chemistry and Uses of Molybdenum, 11 (1973).
15) G. C. Bond and J. B. P. Tripathi, 1st. International Conference on the Chemistry and Uses of Molybdenum, 17 (1973).
16) Sancier and M. Kenneth, *J. Catal.*, **23**, 298 (1971).
17) D. K. Lambiev, T. T. Tomova, and G. V. Samsonov, *Powder Met. Int. (Bulg.)*, **4**, 17—20 (1972) (Eng).
18) I. V. Urarova, V. V. Panichkina, and L. D. Konchakovskaya, *Izv. Akad. Nauk SSSR, Metal*, **1972** (4), 86—91.
19) I. V. Urarova, V. V. Panichkina, V. V. Skorokhod, and V. V. Sukhozhak, *Konf. Met. Proszkow Rev., 3rd 1971*, **1**, 35—42 (Russ).
20) Y. Ishii and I. Matsuura, *Nippon Kagaku Zasshi*, **88**, 497 (1967).

Equilibrium Spreading Pressure of the Mixed System of Normal Long Chain Fatty Acids

Kozo Fujii, Seiji Yoshino, Kinsi Motomura, Makoto Nakamura, and Ryohei Matuura

Department of Chemistry, Faculty of Science, Kyushu University, Fukuoka 812

(Received May 24, 1976)

Equilibrium spreading pressure were measured at various compositions and temperatures for mixed systems of tridecanoic acid-myristic acid, myristic acid-pentadecanoic acid, and pentadecanoic acid-palmitic acid, and thermodynamical treatment of these data with respect to the equilibrium between crystal and monolayer was performed. By evaluating the equilibrium composition of monolayer phase from the measured curve of equilibrium spreading pressure *vs.* composition of solid phase, the phase diagram was constructed. It was found that the equilibrium curve has a maximum point where the solid and monolayer phases have the same composition and a point where the solid phase is in equilibrium with two monolayer phases. The partial molar enthalpy change accompanied by the phase transition from solid to monolayer were found to be dependent on the composition.

It is interesting to clarify the behavior and aspect of the spreading from solid to monolayer. The equilibrium spreading pressure is related to the state of the crystal and the monolayer in equilibrium with the crystal.

Indeed the equilibrium spreading pressure (ESP) of a single component has been studied by many investigators,[1-3] but there have been much less reports about equilibrium spreading pressure of mixtures dealing with the equilibrium between the two states, namely the monolayer state and the crystal state of the mixture.[4-6]

In the present paper we intended to study the ESP of the system of tridecanoic acid-myristic acid (C_{13}–C_{14} acid system), myristic acid-pentadecanoic acid (C_{14}–C_{15} acid system), and pentadecanoic acid-palmitic acid (C_{15}–C_{16} acid system). The ESP's were measured at various compositions and temperatures, and thermodynamic treatment of the data was performed in which both the three-dimensional solid state and the two-dimensional monolayer state were taken into account on the basis of the theory in the previous paper.[7]

Experimental

Materials. The fatty acids used in the present study were purified by a fractional distillation at reduced pressure. Then they were recrystallized from petroleum ether and dried for about 24 h at room temperature under reduced pressure.

The purity was checked by differential thermal analysis (DTA), X-ray diffraction, and gas-chromatography.

Method of Measurements. A) The Measurements of Three-dimensional Solid State: Samples were prepared by melting the mixture of two acids at about 100 °C for 30 min and cooling to room temperature in a thermos bottle. Before the measurement those samples were ground in a mortor. The melting points and the transition points were measured by DTA. Long spacings of the crystal were measured by X-ray diffractometer. The details of the apparatus and method of measurements were previously described.[8]

B) The Measurements of Two-dimensional Monolayer State: Surface pressure-area measurements were performed by using a modified Wilhelmy type surface balance.

Benzene, spreading solvent, was shaken with concentrated sulfuric acid. After being washed with water to be neutral, it was refluxed with metal sodium and then carefully distilled.

The underlying solution, 0.001 M HCl, was prepared by using twice distilled water. The surface of the solution was cleaned by glass barriers coated with paraffine. The monolayer spread from benzene solution was left to stand for 10 min and then compressed continuously with a constant velocity.

C) The Measurements of ESP: Equilibrium spreading pressure measurements were performed by using an automatically recording Wilhelmy type surface balance.

Solid samples used here were the same as those described in the previous section A. After the surface of the solution was cleaned and the surface tension was held constant for more than two hours, an amount of powdered sample was deposited on it.

The pressure increased as time passed and reached a value which was held constatnt within ± 0.2 dyn/cm per hour. We took it as the ESP.

Results and Discussion

Three-dimensional Solid State. The melting points, the transition points, and the freezing points measured by DTA, and the long spacings measured by X-ray diffraction for the C_{13}–C_{14} system are plotted against the composition in Figs. 1 and 2, respectively. Similar results were also obtained for the C_{14}–C_{15} and C_{15}–C_{16} systems. From these results we assume that the solid

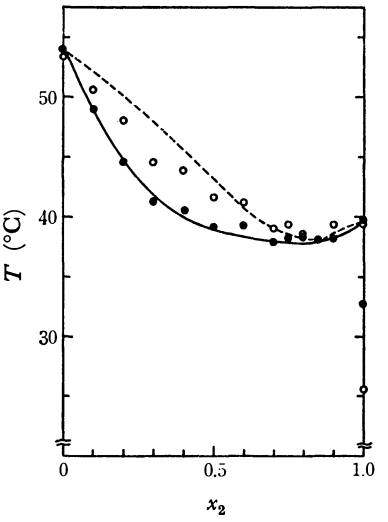

Fig. 1. Melting point, transition point, and freezing point *vs.* mole fraction of tridecanoic acid curves of the C_{13}–C_{14} system : ●, heating; ○, cooling; ——, solidus curve given by Eq. 4 ; ----, liquidus curve given by Eq. 5.

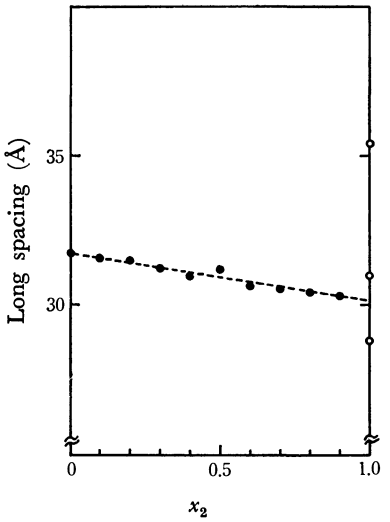

Fig. 2. Long spacing *vs.* mole fraction of tridecanoic acid curve of the C_{13}–C_{14} the system.

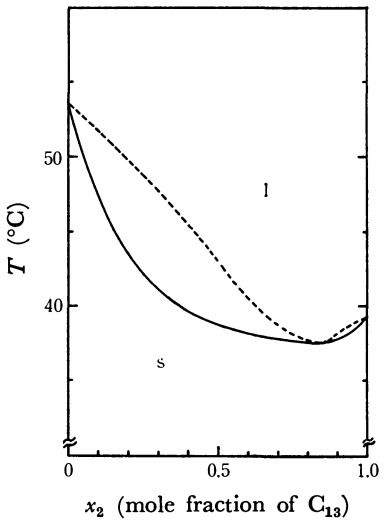

Fig. 3. Three-dimensional phase diagram of the C_{13}–C_{14} system : l, region of liquid solution; s, region of solid solution.

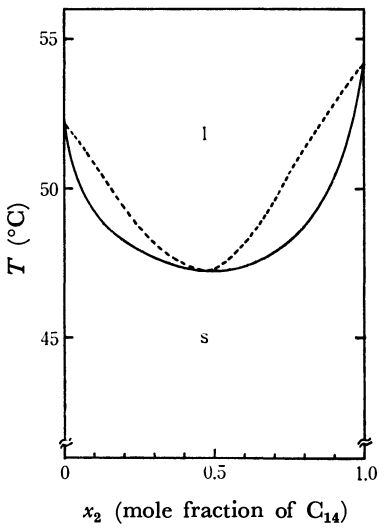

Fig. 4. Three-dimentional phase diagram of the C_{14}–C_{15} system : l, region of liquid solution; s, region of solid solution.

state is the regular solution, because the solid state deviates from ideal in such an extent that the curve representing the equilibrium between solid and liquid phases has a small minimum. And the liquid phase is assumed to be an ideal solution. Then we apply an equation similar to that for azeotropic mixture of liquid-vapor system. We have the following equations[9]

$$(\omega/RT_A)(x^s_{2,A})^2 = (\Delta h^0_1/R)(1/T_A - 1/T^0_1) \quad (1)$$

and

$$(\omega/RT_A)(x^s_{1,A})^2 = (\Delta h^0_2/R)(1/T_A - 1/T^0_2) \quad (2)$$

where Δh^0_i is the heat of fusion, T^0_i is the melting point, T_A is the temperature of minimum point, $x^s_{i,A}$, is the mole fraction of ith component at the minimum point, ω is a constant relating to the interaction energy, the superscript s denotes solid phase, and the subscripts 1 and 2 denote the fatty acids of larger and smaller carbon number, respectively. From Eqs. 1 and 2, we obtain

$$\omega = \{[\Delta h^0_1(T^0_1 - T_A)/T^0_1]^{1/2} + [\Delta h^0_2(T^0_2 - T_A)/T^0_2]^{1/2}\}^2 \quad (3)$$

The values of Δh^0_i, T^0_i, T_A, and ω for each system are listed in Table 1. Then, we can calculate the solidus and liquidus curves from the following equations;

$$x^s_2 = \{\exp[\omega(x^{s2}_2/RT) - \lambda_1] - 1\}/\{\exp[\omega(x^{s2}_2/RT) - \lambda_1] - \exp[\omega(x^{s2}_1/RT) - \lambda_2]\} \quad (4)$$

and

$$x^l_2 = \{\exp[\omega((x^{s2}_1 + x^{s2}_2)/RT) - \lambda_1 - \lambda_2] - \exp(-\lambda_2)\} / \{\exp[\omega(x^{s2}_2/RT) - \lambda_1] - \exp[\omega(x^{s2}_1/RT) - \lambda_2]\} \quad (5)$$

where

$$\lambda_1 = (\Delta h^0_1/R)(1/T - 1/T^0_1) \quad (6)$$

and

$$\lambda_2 = (\Delta h^0_2/R)(1/T^0_2 - 1/T). \quad (7)$$

So, we can depict the phase diagram, which is shown in Figs. 3 to 5 for the C_{13}–C_{14}, C_{14}–C_{15}, and C_{15}–C_{16} systems, respectively. These systems show minimum points, but there are small differences between the values of mole fraction of minimum point. It is concluded that in binary solid mixtures the different behavior is arisen from the difference in the crystalline state between an odd-numbered acid and an even-numbered acid.

Two-dimensional Monolayer State. It is impossible to perform thermodynamic analysis with respect to the ESP if we do not have information of the state of monolayer. So the surface pressure-mean molecular area (π-A) curve was measured at various compositions and temperatures. It was found that in each system the transition pressure from expanded to condensed state, π^{eq}, varied somewhat linearly with the mole fraction of component 2 referred to the fatty acids, x^π_2, over the whole range of composition.

The composition of the condensed film (c) coexisting with the expanded film (e) is calculated by using the equation [7,11]

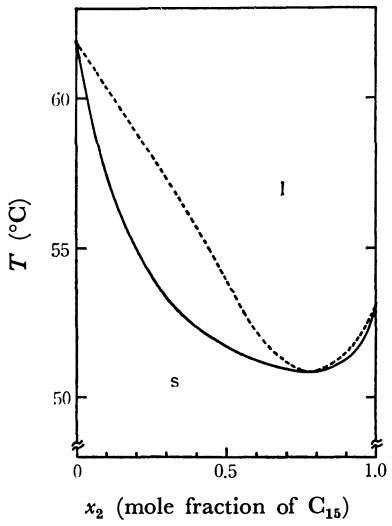

Fig. 5. Three-dimensional phase diagram of the C_{15}–C_{16} system : l, region of liquid solution; s, region of solid solution.

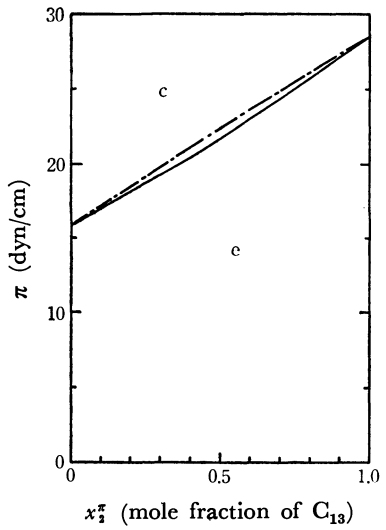

Fig. 6. Two-dimensional phase diagram of the C_{13}–C_{14} system at 20 °C : c, region of condensed monolayer; e, region of expanded monolayer.

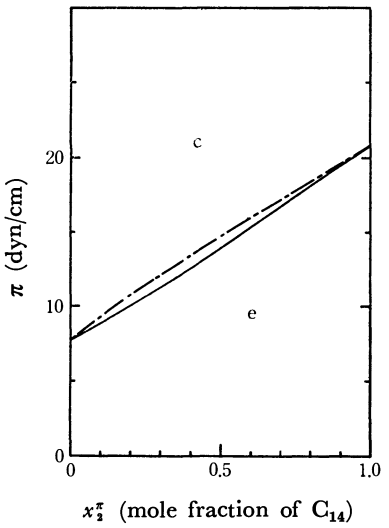

Fig. 7. Two-dimensional phase diagram of the C_{14}–C_{15} system at 25 °C : c, region of condensed monolayer; e, region of expanded monolayer.

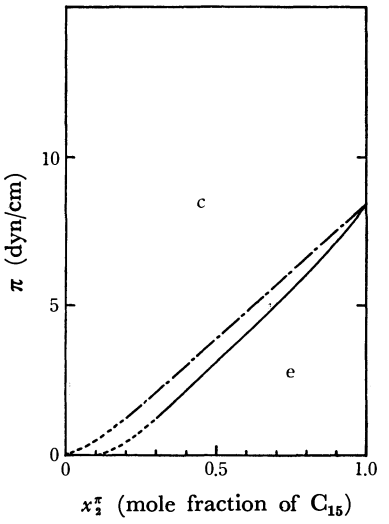

Fig. 8. Two-dimensional phase diagram of the C_{15}–C_{16} system at 25 °C : c, region of condensed monolayer; e, region of expanded monolayer.

$$x_1^{\pi,c} = x_1^{\pi,e} + [(A^c - A^e)x_1^{\pi,e}x_2^{\pi,e}/kT](\partial\pi^{eq}/\partial x_2^{\pi,e})_{p,T} \quad (8)$$

By a procedure similar to that in the previous paper,[11,12] the phase diagrams of two-dimensional monolayer state were depicted for each system in Figs. 6 to 8. The aspect of these phase diagrams is quite identical. After all, it is concluded that the two-component fatty acid system in which the number of carbon atoms is different by only one gives almost ideal mixture in monolayer state.

Equilibrium between Solid State and Monolayer State.

When a sample of fatty acid mixture is placed on the surface of water, the surface pressure increases with time as it spreads on the surface. The surface pressure-time curve is shown in Fig. 9 for the C_{14}–C_{15} system as an example.

The break point is detected at $x_2^s = 0.75$ and 0.10, but not at 0.90. The surface pressure at the break point is almost equal to that of transition from the expanded to the condensed film. So it is expected that the phase transition occurs at the break point and therefore the monolayer in equilibrium with the bulk solid forms a condensed film. Consequently it is concluded that the break point is observed if bulk solid is in equilibrium with the condensed film, but not observed if bulk solid is in equilibrium with the expanded film.

The values of ESP measured at various compositions and temperatures are plotted against the compositions of the bulk solid for the C_{14}–C_{15} system in Fig. 10. The similar curves were also obtained for other two systems. Comparing the ESP curves with the solidus curve in Fig. 4, it seems likely that the higher the melting points, the lower the ESP, and *vice versa*. We may say that the solid sample having the higher melting point is more difficult to spread because of its stronger molecular

Table 1. The calculated values of ω for each system

Fatty acid	Heat of fusion[10] (kcal/mol)	Mixture	Minimum point (°C)	ω (cal/mol)
Tridecanoic acid (C_{13})	8.02			
		C_{13}–C_{14} system	311.1	835.0
Myristic acid (C_{14})	10.74			
		C_{14}–C_{15} system	320.2	756.9
Pentadecanoic acid (C_{15})	10.30			
		C_{15}–C_{16} system	323.9	708.5
Palmitic acid (C_{16})	12.98			

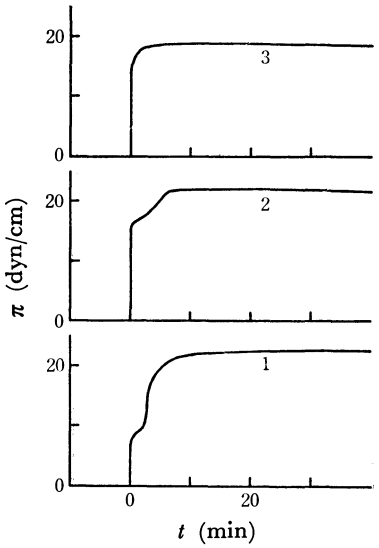

Fig. 9. Spreading pressure *vs.* time curve of the C_{14}–C_{15} system at 25 °C : 1, x_2^s=0.10; 2, 0.75; 3, 0.90.

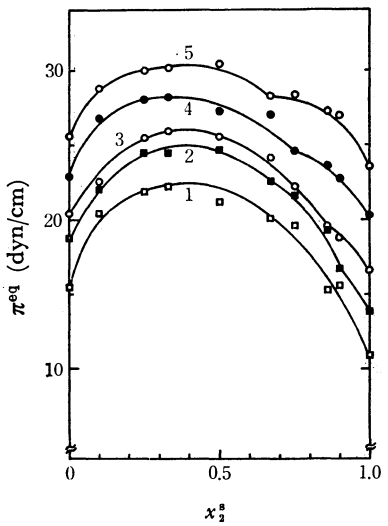

Fig. 10. Equilibrium spreading pressure *vs.* mole fraction of myristic acid curves of C_{14}–C_{15} system : 1, 15 °C; 2, 20 °C; 3, 25 °C; 4, 30 °C; 5, 35 °C.

interaction.

In Fig. 10 the break points are observed on ESP curves at 20, 25, 30, and 35 °C. For the C_{13}–C_{14} acid system the break points were observed at 25 and 30 °C, while for the C_{15}–C_{16} system the break point was not observed in the range of experimented temperatures. It might be presumed that at this break point two monolayer phases are formed by spreading from the crystal. This is understood from the fact that the curve 3 in Fig. 10 and the curves in Fig. 7 intersect in the neighborhood of that break point.

We shall consider thermodynamically the behavior of the variation of ESP with the composition shown in Fig. 10. Choosing the mole fraction x_2^s as a free variable, the variation of the ESP, π^{eq}, with x_2^s can be written in the following form[7,11]

$$(\partial\pi^{eq}/\partial x_2^s)_{T,p} = [(\partial\mu_1^s/\partial x_2^s)(\partial\mu_2^m/\partial x_2^\pi) - (\partial\mu_2^s/\partial x_2^s)(\partial\mu_1^m/\partial x_2^\pi)] / [\bar{a}_1^\pi(\partial\mu_2^m/\partial x_2^\pi) - \bar{a}_2^\pi(\partial\mu_1^m/\partial x_2^\pi)] \quad (9)$$

In Eq. 9, $\bar{a}_i^\pi$ is the apparent partial molar area related to the mean molar area, a, as

$$\bar{a}_1^\pi = a - x_2^\pi(\partial a/\partial x_2^\pi) \quad (10)$$

$$\bar{a}_2^\pi = a + x_1^\pi(\partial a/\partial x_2^\pi) \quad (11)$$

From the Gibbs-Duhem equation in the bulk phase, we have

$$x_1^s(\partial\mu_1^s/\partial x_2^s) + x_2^s(\partial\mu_2^s/\partial x_2^s) = 0 \quad (12)$$

and in the monolayer phase, we have

$$x_1^\pi(\partial\mu_1^m/\partial x_2^\pi) + x_2^\pi(\partial\mu_2^m/\partial x_2^\pi) = 0 \quad (13)$$

Substituting Eqs. 10 to 13 into Eq. 9;

$$(\partial\pi^{eq}/\partial x_2^s)_{T,p} = [(x_2^\pi - x_2^s)/x_1^s a](\partial\mu_2^s/\partial x_2^s)_{T,p} \quad (14)$$

If $(\partial\mu_2^s/\partial x_2^s)_{T,p}$ is known, the mole fraction of the equilibrium monolayer coexisting with crystal, x_2^π, can be calculated. In the previous section we have assumed the solid solution as the regular solution; *i.e.*,

$$RT\ln\gamma_1^s = \omega(x_2^s)^2 \quad (15)$$

and

$$RT\ln\gamma_2^s = \omega(x_1^s)^2 \quad (16)$$

where γ_i^s is the activity coefficient in bulk solid. The chemical potential in the bulk solid is expressed in terms of the composition as

$$\mu_2^s = \mu_2^{0,s} + RT\ln x_2^s + \omega(x_1^s)^2 \quad (17)$$

Differentiating the above equation with respect to x_2^s at constant T and p and substituting it into Eq. 14, we obtain the equation for calculating x_2^π:

$$x_2^\pi = x_2^s + [ax_1^s x_2^s/(RT - 2\omega x_1^s x_2^s)](\partial\pi^{eq}/\partial x_2^s)_{T,p} \quad (18)$$

Since it has been established that the mixed monolayers of long chain n-fatty acids have the same molar area, irrespective of the chain length, if they are in the same monolayer state, [11–13] the values of a were determined from the π-A curve of C_{14} acid when the equilibrium monolayer is the expanded film and that of C_{18} acid when the equilibrium monolayer is the condensed film.

It is now possible to make up the phase diagram of

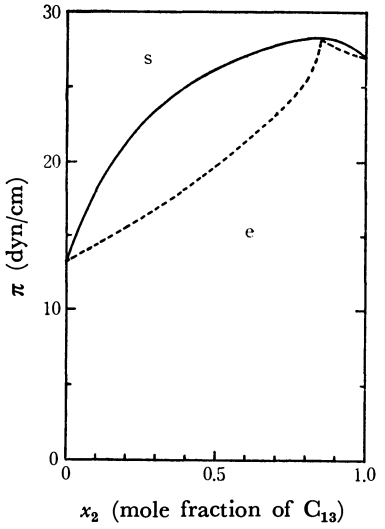

Fig. 11. Phase diagram of the C_{13}–C_{14} system at 20 °C : s, region of solid solution; e, region of expanded monolayer.

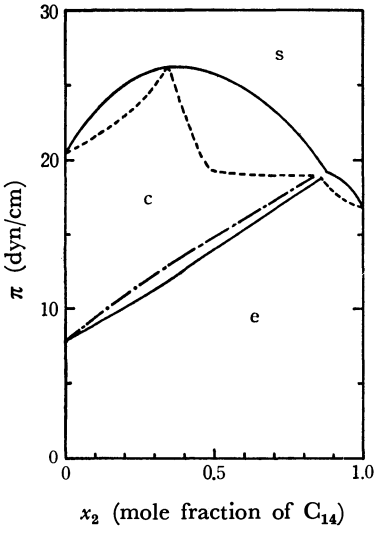

Fig. 12. Phase diagram of the C_{14}–C_{15} system at 25 °C : s, region of solid solution; c, region of condensed monolayer; e, region of expanded monolayer.

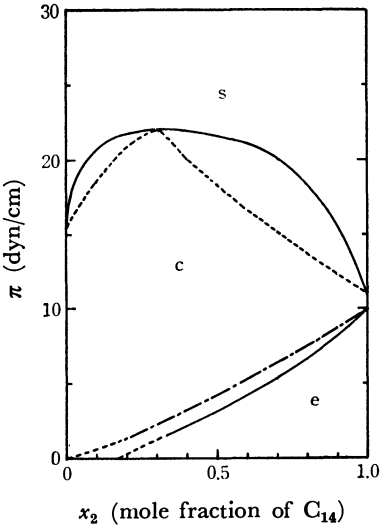

Fig. 13. Phase diagram of the C_{14}–C_{15} system at 15 °C: s, region of solid solution; c, region of condensed monolayer; e, region of expanded monolayer.

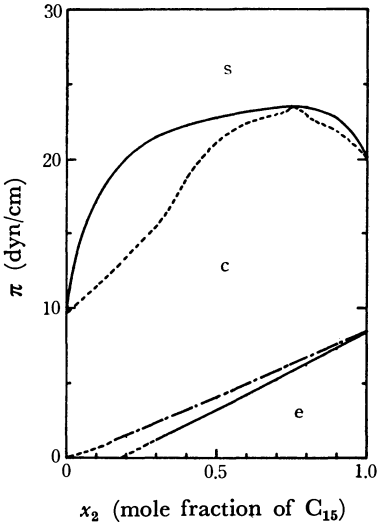

Fig. 14. Phase diagram of the C_{15}–C_{16} system at 25 °C: s, region of solid solution; c, region of condensed monolayer; e, region of expanded monolayer.

the mixed system of fatty acids representing the condition of equilibrium between phases of solid and monolayer, which is illustrated in Figs. 11 to 14 for the present three systems at different temperatures. In Fig. 11 of the C_{13}–C_{14} system it is shown that the bulk solid is in equilibrium with the expanded film at any composition, but in Fig. 14 of the C_{15}–C_{16} system the bulk solid is in equilibrium with the condensed film. In the case of the C_{14}–C_{15} system, the phase diagram at 15 °C drawn in Fig. 13 is similar to that of the C_{15}–C_{16} system. However, the phase diagram at 25 °C drawn in Fig. 12 is different from the above ones in that the bulk solid is in equilibrium with the condensed film in the portion of mole fraction from $x_2^\pi=0$ to 0.85, but in the portion of mole fraction from $x_2^\pi=0.85$ to 1.0 the bulk solid is in equilibrium with the expanded film. At this point, that is, at the mole fraction of $x_2^\pi=0.85$, the bulk solid, the condensed film, and the expanded film coexist. This is the triple point. As seen in Fig. 10, this point shifts to a higher value of x_2^s with decreasing temperature. This triple point disappears at 15 °C in the C_{14}–C_{15} system. Though there is a possibility of appearance of the triple point in the C_{15}–C_{16} system if the temperature is raised, we can not experiment at the higher temperature because of several restrictions.

Entropy and Enthalpy Changes Accompanied by the Phase Transition from Bulk Solid to Equilibrium Monolayer.

Now, from the variation of the transition pressure with temperature, the entropy changes accompanied by the phase transition from solid state to monolayer state can be calculated by using equation [7,11]

$$(\partial\pi^{eq}/\partial T)_{p,x_2^s} = [(\bar{s}_1^\pi-\bar{s}_1^s)(\partial\mu_2^m/\partial x_2^\pi) - (\bar{s}_2^\pi-\bar{s}_2^s)(\partial\mu_1^m/\partial x_2^\pi)] / [\bar{a}_1^\pi(\partial\mu_2^m/\partial x_2^\pi)-\bar{a}_2^\pi(\partial\mu_1^m/\partial x_2^\pi)] \quad (19)$$

Substituting Eqs. 10, 11, and 13 into Eq. 19, we obtain the following equation

$$a(\partial\pi^{eq}/\partial T)_{p,x_2^s} = x_1^\pi(\bar{s}_1^\pi - \bar{s}_1^s) + x_2^\pi(\bar{s}_2^\pi - \bar{s}_2^s) \quad (20)$$

The calculation of the apparent mean molar entropy change of the C_{14}–C_{15} system was carried out at 20 °C by making use of the values of $(\partial\pi^{eq}/\partial T)_{p,x_2^s}$ estimated from Fig. 10. The entropy changes plotted against the composition of the equilibrium monolayer, x_2^π, are shown in Fig. 15. It exhibits a remarkable discontinuity at the mole fraction of $x_2^\pi \approx 0.9$, and separates into two parts. It seems to be the reason for the discontinuity that the entropy of spreading to expanded film differs considerably from that to condensed film. The magnitude of this gap is fairly good agreement with the value taken at the corresponding mole fraction from Fig. 16 where the apparent mean molar entropy change, $[x_1^{\pi,c}(\bar{s}_1^{\pi,c} - \bar{s}_1^{\pi,e}) + x_2^{\pi,c}(\bar{s}_2^{\pi,c} - \bar{s}_2^{\pi,e})]$, associated with the transition from expanded to condensed monolayer is plotted against the mole fraction of the expanded monolayer, $x_2^{\pi,e}$. For the C_{15}–C_{16} system the entropy change calculated similarly indicated that the phase transition occurs from solid state to condensed film over the whole range of the composition.

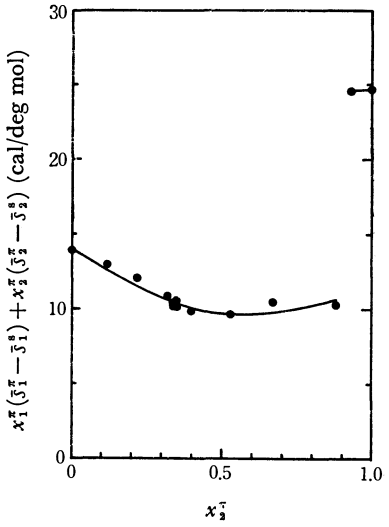

Fig. 15. Apparent mean molar entropy change *vs.* mole fraction of myristic acid curve of the C_{14}–C_{15} system at 20 °C.

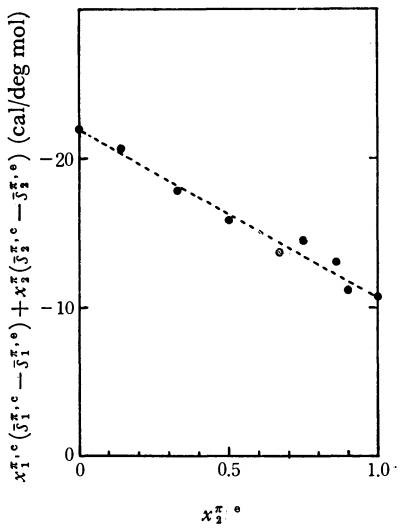

Fig. 16. Apparent mean molar entropy change *vs.* mole fraction of myristic acid curve of the C_{14}–C_{15} system at 20 °C.

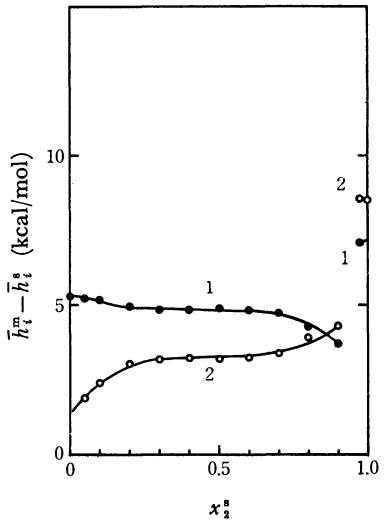

Fig. 17. Partial molar enthalpy change *vs.* mole fraction of myristic acid curve of the C_{14}–C_{15} system at 20 °C : 1, pentadecanoic acid; 2, myristic acid.

Each term of the right-hand side of Eq. 20 is the apparent partial molar entropy change of the respective component and is connected with the partial molar entropy change at the phase transition from the solid to the monolayer state, $\bar{s}_i^m - \bar{s}_i^s$, by

$$\bar{s}_1^m - \bar{s}_1^s = (\bar{s}_1^\pi - \bar{s}_1^s) - [a - x_2^\pi(\partial a/\partial x_2^\pi) - \bar{a}_1](\partial\pi/\partial T)_{p,x_w^m,x_2^\pi} - \bar{a}_1(\partial\gamma^0/\partial T)_p \quad (21)$$

and

$$\bar{s}_2^m - \bar{s}_2^s = (\bar{s}_2^\pi - \bar{s}_2^s) - [a + x_2^\pi(\partial a/\partial x_2^\pi) - \bar{a}_2](\partial\pi/\partial T)_{p,x_w^m,x_2^\pi} - \bar{a}_2(\partial\gamma^0/\partial T)_p \quad (22)$$

where $\bar{s}_i$ is partial molar entropy, $\bar{a}_i$ is the partial molar area, x_w^m is the mole fraction of water in the monolayer and γ^0 is the surface tension of pure water.[7,11] Further we can calculate the partial molar enthalpy change by

$$\bar{h}_1^m - \bar{h}_1^s = T(\bar{s}_1^m - \bar{s}_1^s) \quad (23)$$

and

$$\bar{h}_2^m - \bar{h}_2^s = T(\bar{s}_2^m - \bar{s}_2^s), \quad (24)$$

where $\mu_i^m = \mu_i^s$ has been used.

The results are shown in Fig. 17 for the C_{14}–C_{15} system at 20 °C where we have plotted it against the composition of solid state. From this figure the partial molar enthalpy change may be said to be dependent on the composition. On the other hand, the partial molar enthalpy change from expanded to condensed film, $\bar{h}_i^e - \bar{h}_i^s$, is almost independent of the composition.[12] This difference in the composition dependence of the partial molar enthalpy change seems to result from the non-ideal behavior in solid solution or from the fact that the ESP changes with the size of solid grain which is spread.[14]

References

1) W. D. Harkins and G. C. Nutting, *J. Am. Chem. Soc.*, **61**, 1702 (1939).
2) W. D. Harkins, T. F. Young, and G. E. Boyd, *J. Chem. Phys.*, **8**, 954 (1940).
3) G. E. Boyd, *J. Phys. Chem.*, **62**, 536 (1958).
4) M. Nakagaki and N. Funasaki, *Bull. Chem. Soc. Jpn.*, **47**, 2094 (1974).
5) M. Nakagaki and N. Funasaki, *Bull. Chem. Soc. Jpn.*, **47**, 2482 (1974).
6) P. Joos, *J. Colloid Interface Sci.*, **35**, 215 (1971).
7) K. Motomura, *J. Colloid Interface Sci.*, **48**, 307 (1974).
8) Y. Moroi, T. Hiraharu, S. Yoshino, and R. Matuura, *Mem. Fac. Sci. Kyushu Univ.*, **C8**, 43 (1972).
9) I. Prigogine and R. Defay, "Chemical Thermodynamics," Longmans, Green & Co. Ltd., London (1954), p. 450.
10) W. E. Garner and A. M. King, *J. Chem. Soc.*, **1926**, 2491; *ibid*, **1929** 1894.
11) K. Motomura, K, Sekita, and R. Matuura, *J. Colloid Interface Sci.*, **48**, 319 (1974).
12) K. Sekita, M. Nakamura, K. Motomura, and R. Matuura, *Mem. Fac. Sci. Kyushu Univ.*, **C10**, 51 (1976).
13) N. Kuramoto, K. Sekita, K. Motomura, M. Nakamura, and R. Matuura, *Mem. Fac. Sci. Kyushu Univ.*, **C8**, 67 (1972).
14) K. Motomura, *J. Colloid Interface Sci.*, **23**, 313 (1967).

Microwave Spectrum, Structure, Dipole Moment and Internal Rotation of Ethanethiol. II. *Gauche* Isomer

Jun NAKAGAWA, Kazunori KUWADA, and Michiro HAYASHI

Department of Chemistry, Faculty of Science, Hiroshima University, Higashi-sendamachi, Hiroshima 730

(Received June 2, 1976)

The microwave spectra of *gauche*-ethanethiol and its isotopic species were studied. Most of the observed spectra for the species having the plane of symmetry exhibited doublet structures with large spacings due to the internal rotation of the mercapto group. The r_s structure of the *gauche* isomer was determined from the observed moments of inertia. The *gauche* isomer whose dihedral angle τ(CCSH) is 61°45′±58′ has structural parameters close to those for the *trans* isomer except the angles around the carbon atom in the methylene group. The difference in angle values around the carbon atom in the methylene group between the *trans* and *gauche* isomers can be explained by the 3°7′ tilt of the methylene group towards the lone pair electrons on the sulfur atom. The direction of the dipole moment in the molecule was discussed on the basis of data given by Schmidt and Quade. The potential barrier of the mercapto internal rotation was obtained from splittings of the observed spectra. The Fourier coefficients of this barrier are $V_1=-207\pm67$, $V_2=-386\pm27$, and $V_3=1305\pm20$ cal/mol. The spectra due to the excited methyl and mercapto torsional states were also measured for the *trans* and *gauche* isomers. The potential barrier of the methyl internal rotation for the *trans* isomer was found to be 3260±30 cal/mol from splittings of the spectra due to the first excited methyl torsional state.

In previous paper,[1,2] (referred to as I) reports were given on the microwave spectrum of *trans*-ethanethiol in relation to the r_s structure, dipole moment and the observed microwave spectra of *gauche*-ethanethiol. In the present paper, we deal with the microwave spectrum, r_s structure, and internal rotation of both the mercapto and methyl groups of *gauche*-ethanethiol.

After publication of our papers on the *trans* isomer and rough descriptions of the spectra for the *gauche* isomer, Schmidt and Quade[3] reported an independent study on the microwave spectra of *gauche*-ethanethiol and its four deuterated species. They carried out the analysis of the internal rotation of the mercapto group and the dipole moment assuming a certain structure.

We were working on the same subject for the *gauche* isomer as theirs as a continuation of our work on *trans*-ethanethiol. However, publication of our experimental results was deliberately delayed in order to determine a reliable molecular structure[4] for the *gauche* isomer as well as that for the *trans* isomer and to find the spectra in the excited methyl torsional states both for the *trans* and *gauche* isomers. Wherever their measurements overlap ours, the agreement is very good.

Exprimental

Normal and deuterated species of ethanethiol were prepared and purified in the same manner as described in I. Two ^{13}C species were prepared from the corresponding ^{13}C enriched ethyl iodides (90 atom% ^{13}C, Merck Sharp & Dohme, Canada) by the standard method.[5] The spectra of ^{34}S species were measured with a sample containing this species in natural isotopic abundance. Measurements were carried out by the same apparatus and under the same conditions as those in I.

Microwave Spectra of *Gauche* Isomer

gauche-Ethanethiol is a slightly asymmetric prolate top molecule as is *trans*-ethanethiol. Though *a*-, *b*-, and *c*-type transitions are expected for the microwave spectra, *b*-type transitions are actually very weak.

Microwave spectra of *a*- and *c*-types belonging to the *gauche* isomer in the ground state were measured and assignments made for the normal and nine isotopically substituted species of ethanethiol. Observed frequencies with $J\leqq7$ are given in Tables 1 and 2. *s*- and *a*- (*e.g.* *s*-CH_2DCH_2SH) stand for the species whose deuterium atoms are situated in the CCS plane and out of the CCS plane, respectively, and -1 and -2 (*e.g.* *a*-CH_2DCH_2SH-2) stand for the species whose deuterium atoms are situated on the opposite side and the same side of the CCS plane as the hydrogen atom in the mercapto group, respectively.

The observed spectra for some of the species exhibit doublet structures whose components have identical Stark effects.[1,2]

The normal and nine isotopic species of *gauche*-ethanethiol can be classified into three groups by means of the fine structures of the spectra. Group I(CH_3CH_2SH, $CH_3CH_2{}^{34}SH$, $^{13}CH_3CH_2SH$, $CH_3{}^{13}CH_2SH$, and *s*-CH_2DCH_2SH) consists of the species which have the symmetry plane in the CH_3CH_2S part of the molecule. For Group I, observed *c*-type spectra are doublets with spacings of about 3500 MHz, *a*-type spectra with $K_{-1}=1$ are doublets with spacings of several MHz, and *a*-type spectra with $K_{-1}\neq1$ are singlets. For the CH_3CH_2-SD species (Group II), *c*-type spectra are doublets with spacings of about 140 MHz, while *a*-type spectra are singlets. For Group III, in which each species has an isotopically substituted atom situated out of the CCS plane, (*a*-CH_2DCH_2SH-1, *a*-CH_2DCH_2SH-2, CH_3CHDSH-1, and CH_3CHDSH-2), spectra are singlets.

For the species belonging to Groups I and II, tunnelling effect between two equivalent *gauche* minima in the internal rotation potential function of the mercapto group produces two different energy states (referred to as the + and − states). The + and − states indicate the symmetric and antisymmetric states with respect to the mercapto internal rotation angle, respectively. The energy difference between the + and − states for the SH group is greater than that for the SD group since the reduced moment of inertia around the internal rotation axis for the SD group is greater

TABLE 1. OBSERVED FREQUENCIES OF GROUP I AND II SPECIES OF *gauche*-ETHANETHIOL[a] (MHz)

Transition[b]	CH_3CH_2SH	CH_3CH_2SD	*s*-CH_2DCH_2SH	$CH_3CH_2{}^{34}SH$	$^{13}CH_3CH_2SH$	$CH_3{}^{13}CH_2SH$
$1_{01}\leftarrow 0_{00}{}^{++}_{--}$	10141.07(10)	9958.84(16)	9489.97(13)	9920.24(6)	9844.82(−4)	10087.97(6)
$2_{02}\leftarrow 1_{01}{}^{++}_{--}$	20275.47(−7)	19911.04(−1)	18914.87(−2)	19834.47(−2)	19683.78(−8)	20168.67(−10)
$2_{12}\leftarrow 1_{11}{}^{++}_{--}$	19832.99(3) 19836.33(−27)	19496.00(4)	18528.69(17) 18530.38(−5)	19409.88(11) 19412.97(−1)	19260.50(−2) 19263.38(−18)	19710.80(−8) 19715.72(−22)
$2_{11}\leftarrow 1_{10}{}^{++}_{--}$	20727.77(50) 20730.83(−8)	20338.84(7)	19309.39(44) 19310.84(−1)	20267.93(21) 20270.63(−31)	20116.28(41) 20118.90(−1)	20636.00(30) 20640.61(−15)
$3_{03}\leftarrow 2_{02}{}^{++}_{--}$	30396.99(−43)	29850.64(−15)	28359.91(−45)	——[c]	29511.19(4)	30235.33(−23)
$3_{13}\leftarrow 2_{12}{}^{++}_{--}$	29745.06(−17) 29736.75(−1)	29239.96(−6)	27789.32(−28) 27781.13(−3)	29110.56(−22) 29102.16(−31)	28886.65(−27) 28878.63(−14)	30966.87(7) 30956.66(−30)
$3_{12}\leftarrow 2_{11}{}^{++}_{--}$	31101.19(14) 31092.52(−5)	30504.02(−16)	28971.99(8) 28963.54(7)	30411.19(−7) 30402.44(−51)	30183.09(3) 30174.59(−32)	29561.49(−21) 29551.76(−10)
$3_{22}\leftarrow 2_{21}{}^{++}_{--}$	30423.63(65)	29876.33(28)	28379.94(35)	29761.26(66)	29535.10(45)	30264.28(45)
$3_{21}\leftarrow 2_{20}{}^{++}_{--}$	30448.16(−23)	29901.17(−13)	28398.62(−2)	29783.78(−12)	29557.77(−15)	30291.72(−9)
$1_{10}\leftarrow 0_{00}{}^{+-}_{-+}$	32287.96(4) ——[c]	31184.15(46) 31324.48(14)				
$1_{11}\leftarrow 1_{01}{}^{+-}_{-+}$	21697.94(−46) 25206.36(9)	20803.25(−35) 20944.11(−14)	21989.18(−31) 25569.18(10)	21804.58(87) 25264.92(−2)	21660.58(−30) 25146.83(19)	21086.01(−22) 24534.46(18)
$2_{12}\leftarrow 2_{02}{}^{+-}_{-+}$	21255.73(−9) 24767.49(16)	20388.32(−19) 20529.11(−6)	21602.99(−13) 25184.58(−3)	21378.33(−65) 24843.29(−13)	21237.38(−16) 24726.32(−2)	20628.15(−19) 24081.47(2)
$3_{13}\leftarrow 3_{03}{}^{+-}_{-+}$	20603.87(15) 24106.74(−2)	19777.71(−3) 19918.41(1)	21032.42(6) 24605.51(10)	20752.16(−52) 24208.97(15)	20613.44(13) 24094.01(5)	19954.55(7) 23397.74(0)
$4_{14}\leftarrow 4_{04}{}^{+-}_{-+}$	19756.94(40) 23260.82(−23)	18985.68(12) 19126.26(5)	20288.39(37) 23863.88(−17)	19938.35(31) 23395.86(2)	19801.74(33) 23283.55(−22)	19080.91(34) 22524.90(−21)

Additional Observed Frequencies of the Normal Species (CH_3CH_2SH).

$4_{04}\leftarrow 3_{03}{}^{++}_{--}$	40499.40(−60)	$4_{13}\leftarrow 3_{12}{}^{++}_{--}$	41448.46(61) 41449.06(−27)	$4_{22}\leftarrow 3_{21}{}^{++}_{--}$	40622.43(12)
$4_{14}\leftarrow 3_{13}{}^{++}_{--}$	39652.32(−51) 39653.65(−65)	$4_{23}\leftarrow 3_{22}{}^{++}_{--}$	40559.34(25)	$4_{32}\leftarrow 3_{31}{}^{++}_{--}$ $4_{31}\leftarrow 3_{30}{}^{++}_{--}$	40576.67 (18) (−16)

a) Observed frequencies of the species whose CH_3CH_2S part of the molecule has the plane of symmetry. Figures in parentheses indicate the differences between the observed and calculated frequencies.
b) − + indicates the transition from the + state to the − state and so on.
c) Overlapped with the other spectra.

TABLE 2. OBSERVED FREQUENCIES OF GROUP III SPECIES OF *gauche*-ETHANETHIOL[a] (MHz)

Transition	*a*-CH_2DCH_2SH-1	*a*-CH_2DCH_2SH-2	CH_3CHDSH-1	CH_3CHDSH-2
$1_{01}\leftarrow 0_{00}$	9787.90(6)	9779.36(12)	9988.38(−3)	9979.41(−5)
$2_{02}\leftarrow 1_{01}$	19569.18(0)	19551.40(−2)	19967.48(7)	19950.22(−7)
$2_{12}\leftarrow 1_{11}$	19148.99(−5)	19112.53(−14)	19473.71(−23)	19479.10(−9)
$2_{11}\leftarrow 1_{10}$	20002.16(1)	20004.21(7)	20479.63(9)	20438.54(11)
$3_{03}\leftarrow 2_{02}$	29337.30(−23)	29309.35(−14)	29927.47(−12)	29903.64(−24)
$3_{13}\leftarrow 2_{12}$	28719.12(−24)	28664.52(2)	29204.65(−26)	29213.13(−10)
$3_{12}\leftarrow 2_{11}$	29999.02(6)	30001.74(11)	30713.33(12)	30652.19(21)
$3_{22}\leftarrow 2_{21}$	29363.35(18)	29337.30(−13)	29965.14(25)	29938.15(22)
$3_{21}\leftarrow 2_{20}$	29389.07(25)	29365.54(16)	30002.22(3)	29971.89(−9)
$1_{10}\leftarrow 0_{00}$	31276.34(8)	31321.32(4)	30559.62(12)	30473.37(12)
$1_{11}\leftarrow 1_{01}$	21061.92(6)	21096.25(−5)	20068.25(−4)	20014.31(14)
$2_{12}\leftarrow 2_{02}$	20641.66(−6)	20657.59(4)	19574.79(−2)	19543.03(−4)
$3_{13}\leftarrow 3_{03}$	20023.45(−10)	20012.48(−8)	18851.99(−14)	18852.25(−17)
$4_{14}\leftarrow 4_{04}$	19221.73(−12)	19177.13(3)	17921.33(4)	17961.37(−8)
$5_{15}\leftarrow 5_{05}$	18256.09(22)	18172.23(7)	16809.99(−23)	16895.38(−28)
$6_{16}\leftarrow 6_{06}$			15553.26(5)	15686.46(1)
$7_{17}\leftarrow 7_{07}$			14190.08(21)	14370.55(32)

a) Observed frequencies of the species whose CH_3CH_2S part of the molecule has no plane of symmetry. Figures in parentheses indicate the difference between the observed and calculated frequencies.

TABLE 3. OBSERVED ROTATIONAL CONSTANTS (MHz) OF *gauche*-ETHANETHIOL[a)]

Species	A	B	C	$D_J \times 10^{3}$ [b)]	$\Delta\nu$[c)]	$D_{\pm}$[d)]
CH_3CH_2SH	28747.09(50)	5294.78(12)	4846.18(12)	——	1753.84(29)	12.43(37)
CH_3CH_2SD	26063.97(21)	5190.04(5)	4768.64(5)	——	70.33(14)	——
$CH_3CH_2{}^{34}SH$	28709.50(62)	5175.20(15)	4744.98(15)	——	1730.53(35)	12.07(46)
$^{13}CH_3CH_2SH$	28540.59(36)	5136.85(9)	4708.01(9)	——	1742.79(21)	11.93(28)
$CH_3{}^{13}CH_2SH$	28056.43(36)	5276.21(9)	4811.70(9)	——	1723.91(21)	13.32(24)
s-CH_2DCH_2SH	28704.62(38)	4925.35(9)	4534.49(9)	——	1789.73(23)	10.76(27)
a-CH_2DCH_2SH-1	26169.06(72)	5107.21(13)	4680.65(14)	3.7(65)	——	——
a-CH_2DCH_2SH-2	26208.79(48)	5112.49(9)	4666.76(10)	3.0(43)	——	——
CH_3CHDSH-1	25313.90(54)	5245.62(8)	4742.81(9)	3.6(60)	——	——
CH_3CHDSH-2	25243.72(60)	5229.55(9)	4749.93(10)	4.8(68)	——	——

a) Figures in parentheses indicate the uncertainty attached to the last significant figures calculated from 2.5 times the standard deviations. b) 10^3 times the coefficient of the $[J(J+1)]^2$ term in the centrifugal distortion formula in MHz. For the first six species, this term is neglected in the determination of the rotational constants. In Table 2 of the previous paper on the *trans* isomer (Ref. 2), signs of the corresponding D_J values were mistyped, that is, -4.68 in that table should read 4.68 and so on. c) Energy difference between the + and − states. d) Coefficient of $(P_xP_y+P_yP_x)$ term in Eq. 3c.

than for the SH group.

From group-theoretical considerations, the selection rules governing transitions between the rotational energy levels belonging to the + and − states are + ↔ + and − ↔ − for *a*-type transitions and + ↔ − for *c*-type transitions.

In order to obtain the rotational constants from the observed frequencies for the species belonging to Groups I and II, we must consider the effective Hamiltonian which includes not only the rigid rotor terms of the + and − states but also cross terms between the + and − states. The rotational constants obtained are given in Table 3. It is found that the rotational constants of the + and − states are essentially equal within experimental error for the species belonging to Groups I and II.

For the species belonging to Group III, splittings of the + and − states cannot occur because there are no equivalent *gauche* forms. Although the *a*-CH_2D-CH_2SH species has two equivalent *gauche* forms, tunnelling effect between these two conformers occurs through the internal rotation potential of not only the mercapto group but also the methyl group. Splittings of the + and − states are negligibly small. The rotational constatnts were obtained by a least squares analysis from all the observed frequencies so as to fit in with a modified rigid rotor expression which includes only the $D_J[J(J+1)]^2$ term of the centrifugal distortion formula. The rotational constants are given in Table 3.

Analysis of Doublet Structures of the Observed Spectra for the *Gauche* Isomer

Analysis of doublet structures of the observed spectra is necessary for the species belonging to Groups I and II. In order to derive the Hamiltonian for the coupling problem of overall rotation and internal rotation of the mercapto group, the coordinate system for the species belonging to Groups I and II is so chosen that the z-axis is parallel to the mercapto internal rotation axis, the y-axis is in the symmetry plane, and the x-axis is perpendicular to the symmetry plane. The Hamiltonian concerning overall and internal rotation is then written as the sum of the overall rotation, internal rotation, and overall-internal rotation interaction terms:[6)]

$$H = H_{\text{rot}} + H_{\text{int}} + H_{\text{rot-int}}, \tag{1}$$

$$\begin{aligned} H_{\text{rot}} = {} & \sum \mu_{xx}^{(n)} \cos n\alpha \cdot P_x^2 + \sum \mu_{yy}^{(n)} \cos n\alpha \cdot P_y^2 \\ & + \sum \mu_{zz}^{(n)} \cos n\alpha \cdot P_z^2 + \sum \mu_{yz}^{(n)} \cos n\alpha \cdot (P_yP_z + P_zP_y) \\ & + \sum \mu_{xz}^{(n)} \sin n\alpha \cdot (P_xP_z + P_zP_x) \\ & + \sum \mu_{xy}^{(n)} \sin n\alpha \cdot (P_xP_y + P_yP_x), \end{aligned} \tag{1a}$$

$$\begin{aligned} H_{\text{int}} = {} & \sum \mu_{\alpha}^{(n)} (p_\alpha^2 \cos n\alpha + \cos n\alpha \cdot p_\alpha^2) \\ & + \sum \frac{V_n}{2} (1 - \cos n\alpha), \end{aligned} \tag{1b}$$

$$\begin{aligned} H_{\text{rot-int}} = {} & \sum \mu_{\alpha x}^{(n)} (p_\alpha \sin n\alpha + \sin n\alpha \cdot p_\alpha) P_x \\ & + \sum \mu_{\alpha y}^{(n)} (p_\alpha \cos n\alpha + \cos n\alpha \cdot p_\alpha) P_y \\ & + \sum \mu_{\alpha z}^{(n)} (p_\alpha \cos n\alpha + \cos n\alpha \cdot p_\alpha) P_z, \end{aligned} \tag{1c}$$

where $\mu_{gg'}^{(n)}$, represents the n-th Fourier coefficient of the g,g'-th element of the reciprocal inertia tensor, α denotes the mercapto internal rotation angle, and P_x, P_y, P_z, and p_α represent x, y, and z components of the total angular momentum and the mercapto internal rotational angular momentum, respectively.

Assuming that the wave functions for the Hamiltonian (1) can be written as the products of overall and internal rotation wave functions and that internal rotation wave functions are obtained as the eigenfunctions of Eq. 1b, the effective Hamiltonian for the overall rotation is reduced to the following formulas.

$$\begin{aligned} \langle + |H| + \rangle = {} & A'_+P_z^2 + B'_+P_y^2 + C'_+P_x^2 + F'_+(P_yP_z + P_zP_y) \\ & + M'_+P_x, \end{aligned} \tag{2a}$$

$$\begin{aligned} \langle - |H| - \rangle = {} & A'_-P_z^2 + B'_-P_y^2 + C'_-P_x^2 + F'_-(P_yP_z + P_zP_y) \\ & + M'_+P_x + \Delta\nu, \end{aligned} \tag{2b}$$

$$\begin{aligned} \langle + |H| - \rangle = {} & D'_{\pm}(P_xP_y + P_yP_x) + E'_{\pm}(P_xP_z + P_zP_x) \\ & + N'_{\pm}P_y + Q'_{\pm}P_z, \end{aligned} \tag{2c}$$

where $\Delta\nu$ denotes the pure internal rotational energy difference between the + and − states. Coefficients A'_+, *etc.* are obtained as the matrix elements of the cor-

responding operators between the wave functions of + and +, or − and −, or + and − states. The cross term in Eq. 2c occurs from the odd functions of α, $\sin n\alpha$ and $(p_\alpha \cdot \cos n\alpha + \cos n\alpha \cdot p_\alpha)$, in Eq. 1.

After a suitable rotation about the x-axis is carried out, it is possible that Eqs. 2a and 2b are reduced to formulas containing no $(P_yP_z+P_zP_y)$ term. Furthermore, the P_x terms in Eqs. 2a and 2b can be neglected, since these terms contribute to the off-diagonal matrix elements, whose K_{-1} values are not equal. Thus the effective Hamiltonians are written as

$$\langle +|H|+\rangle = A_+P_x^2 + B_+P_y^2 + C_+P_z^2, \quad (3a)$$

$$\langle -|H|-\rangle = A_-P_x^2 + B_-P_y^2 + C_-P_z^2 + \Delta\nu \quad (3b)$$

$$\langle +|H|-\rangle = D_\pm(P_xP_y+P_yP_x) + E_\pm(P_xP_z+P_zP_x) + N_\pm P_y + Q_\pm P_z \quad (3c)$$

Taking account of the selection rules of *a*- and *c*-type transitions, it can be concluded that doublet structures of *a*-type transitions are due to the difference in the rotational constants of the + and − states or/and the cross terms of Eq. 3c, while doublet structures of *c*-type transitions arise mainly from the energy difference $\Delta\nu$ between the + and − states.

Group I. Since observed *a*-type transitions are singlets except $K_{-1}=1$ transitions, the rotational constants of the + and − states are regarded to be approximately equal to each other. Doublet structures of $K_{-1}=1$ transitions are due to the cross terms in Eq. 3c.

For the normal species, *a*-type $J=2\rightarrow3$ transitions with $K_{-1}=1$ have the largest splittings of all the *a*-type transitions.

This is understandable if the 2_{11} level of the + state is accidentally degenerate with the 2_{12} level of the − state (referred to as 2_{11}^+ and 2_{12}^-). Furthermore, the fact that the splittings of $J=1\rightarrow2$ transitions are greater than those of $J=3\rightarrow4$ transitions indicates that the

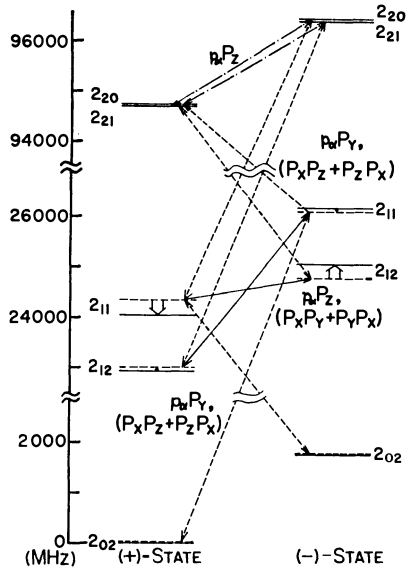

Fig. 1. The interaction scheme between the + and − states for $J=2$ levels of the normal species. Solid and dotted lines indicate perturbed and unperturbed levels, respectively.

2_{11}^+ level is slightly lower than the 2_{12}^- level.

The interaction scheme of the cross terms are shown for the normal species in Fig. 1. Since the molecule is a nearly prolate symmetric top, the P_z term connects two levels with the same K_{-1}, while the $(P_xP_y+P_yP_x)$ term connects two levels whose K_{-1} values differ by 2 from each other except $K_{-1}=1$ levels. However, the observed spectra show doublet structures only in the case of $K_{-1}=1$ transitions. Thus we cannot determine the contributions due to the P_z and $(P_xP_y+P_yP_x)$ terms independently. The determination might be possible if the transitions with $J=8$ or 9 are available, since the levels with $J=8$ or 9 would exhibit the degeneracy for $K_{-1}=2$ levels which is affected by the P_z term most sensitively. However, the corresponding transitions are expected out of our observable frequency region.

The $(P_xP_z+P_zP_x)$ and P_y terms affect the splittings only by a small amount, since the energy difference of the levels which perturb each other through these terms is ten times larger than those in the case of P_z connections so that the corresponding levels of the + and − states are equally pushed up or down. Schmidt and Quade[3] determined the coefficient of the $(P_xP_z+P_zP_x)$ term neglecting the P_y term but the error of this coefficient would be fairly large. We have analyzed the doublet structures by taking account of only the $(P_xP_y+P_yP_x)$ term of Eq. 3c.

For the *c*-type transitions, splittings are about twice the energy difference between the + and − states, *i.e.*, $2\Delta\nu$. The assignments of the *c*-type *Q* branch transitions were made taking account of the roughly estimated value of $\Delta\nu$ from the *a*-type transitions. A least squares analysis was carried out using rotational constants *A*, *B*, *C*, energy difference $\Delta\nu$, and the coefficient of the cross term $D_\pm$, as parameters. Centrifugal distortion effect was neglected since relatively low *J* transitions were used.

As is shown in Table 8 for the normal species, if a suitable choice of the components of the doublets is made, the observed *a*-type transition frequencies can be fitted with the rigid rotor expression giving the rotational constants *B* and *C* which are equal to the rotational constants obtained by the above procedures within the experimental error. This is explained as follows.

Since the rotational constants for the + and − states are approximately equal to each other, the frequencies of a given *a*-type transition for the + and − states are equal to each other if all the coupling terms are negligible. However, for the transitions with $K_{-1}=1$, the energy difference between the + and − states makes pairs of energy levels such as $(1_{10}^+, 1_{11}^-)$, $(2_{11}^+, 2_{12}^-)$, and $(3_{12}^+, 3_{13}^-)$ to be in an accidental degeneracy and the coupling term $(P_xP_y+P_yP_x)$ makes a level in a pair shift to the upper side and the other to the lower side. The frequencies of the transitions containing these levels shift from the original values. On the other hand, the coupling term makes little influence on pairs of energy levels such as $(1_{10}^-, 1_{11}^+)$, $(2_{11}^-, 2_{12}^+)$, and $(3_{12}^-, 3_{13}^+)$ which are not in degeneracy. The frequencies of the transitions containing these levels remain unchanged and they can be fitted with the rigid rotor expression as well as those of the transitions with $K_{-1}=0$ or 2.

Group II. For this group, there are no splittings for the *a*-type transitions, all the observed *c*-type transitions having splittings of about 140 MHz. The analysis of the observed spectra was carried out by a least squares technique using rotational constants and energy difference Δv as parameters neglecting centrifugal distortion contributions.

r_s Structure

Our present data are sufficient to determine the r_s structure for the *gauche* isomer by the substitutuion method. However, there are several atoms situated close to one of the principal axes for the *gauche* isomer. Solutions of the Kraitchman equations are not reliable for the coordinates having small absolute values for these atoms. These "bad" coordinates must be calculated from other reliable coordinates either with the aid of the first moment equations or by some assumptions on the structure.

There are five so-called "bad" coordinates for the *gauche* isomer: 1) x_c coodinates of the carbon atoms in the methylene and methyl groups, 2) x_b and x_c coordinates of the hydrogen atom labeled by H_s in the methyl group, and 3) x_c coodinate of the sulfur atom.

We have three first moment equations and three inertia products which should be zero in the principal axis system. Then, if desirable, some of the five "bad" coordinates can be obtained from these six relations. However, use of the inertia products makes the error of the calculated coordinates greater in general and some of three first moment equations will be useful for confirmation of the results. The following assumptions on the structure were made for the calculation of the "bad" coordinates.

The most reasonable assumptions for x_c coordinates of the carbon atoms in the methylene and methyl groups are probably $r(CH^1)=r(CH^2)$ and $r(CH_a^1)=r(CH_a^2)$, since these bond lengths are equal to each other from the symmetry for the *trans* isomer. For x_b and x_c coordinates of the H_s atom in the methyl group, assumptions $r(CH_s)=r(CH_a^1)=r(CH_a^2)$ and $r(H_sH_a^1)=r(H_sH_a^2)$ are acceptable, since $r(CH_s)$ and $r(CH_a)$ for the *trans* isomer are essentially equal to each other within experimental error. The name of each atom is shown in Fig. 2.

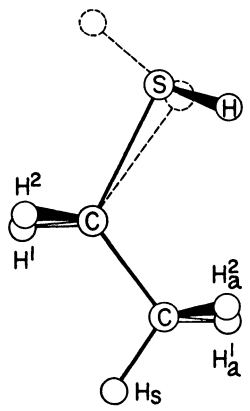

Fig. 2. Symbols of atoms in *gauche*-ethanethiol.

The x_c coordinate of the sulfur atom was solved by use of the first moment equation. The coordinates obtained are given in Table 5 where the calculated two first moments and three inertia products are also given for confirmation of the adequacy of the assumptions. Deviations of the calculated moments of inertia from the observed are also given in Table 4, for all the species. The root mean square deviation for thirty moments of inertia is 0.3938 amu Å which is satisfactorily small.

Structural parameters calculated from atom coordinates are given in Table 6, in comparison with those for the *trans* isomer.[2]

Despite many "bad" coordinates, the structural parameters for the *gauche* isomer are reliable in a similar extent to those for the *trans* isomer. Structural parameters of the CSH and CH_3C parts of the *gauche* isomer are essentially equal to those of the *trans* isomer, except slightly longer r(SH) and shorter r(CS) values (Table 6). The dihedral angle τ(CCSH) for the *gauche* isomer can also be determined satisfactorily.

Significant discrepancies are found in the six angles around the carbon atom in the methylene group. This was expected in I from the anomalous smallness of α(CCS) in the *trans* isomer. This was explained by considering the tilt of the ethyl group towards the lone pair electrons on the sulfur atom in a similar manner to the case of the methyl group in methanethiol. The

TABLE 4. MOMENTS OF INERTIA (amu Å^2)[a]

Species	I_a	δI_a[b]	I_b	δI_b[b]	I_c	δI_c[b]	P_c[c]	ΔP_c[d]
CH_3CH_2SH	17.5801 (3)	0.0627	95.4480 (22)	0.4812	104.2834 (26)	0.4831	4.3723 (17)	——
CH_3CH_2SD	19.3898 (2)	0.0667	97.3742 (9)	0.4910	105.9791 (11)	0.4809	5.3925 (7)	1.0202 (18)
$CH_3CH_2{}^{34}SH$	17.6031 (4)	0.0624	97.6534 (28)	0.4870	106.5075 (34)	0.4907	4.3745 (22)	0.0022 (28)
$^{13}CH_3CH_2SH$	17.7073 (2)	0.0630	98.3825 (17)	0.4756	107.3439 (21)	0.4786	4.3729 (13)	0.0006 (22)
$CH_3{}^{13}CH_2SH$	17.9936 (2)	0.0595	95.7839 (16)	0.4771	105.0307 (20)	0.4793	4.3734 (13)	0.0011 (21)
s-CH_2DCH_2SH	17.6061 (2)	0.0692	102.6071 (19)	0.4806	111.4516 (22)	0.4727	4.3808 (15)	0.0085 (22)
a-CH_2DCH_2SH-1	19.3119 (4)	0.0653	98.9531 (23)	0.4694	107.9718 (30)	0.4876	5.1466 (19)	0.7743 (26)
a-CH_2DCH_2SH-2	19.2827 (3)	0.0642	98.8509 (19)	0.4838	108.2929 (26)	0.4747	4.9203 (16)	0.5480 (23)
CH_3CHDSH-1	19.9644 (4)	0.0596	96.3425 (15)	0.4862	106.5562 (20)	0.4684	4.8753 (13)	0.5030 (21)
CH_3CHDSH-2	20.0199 (5)	0.0593	96.6385 (17)	0.4690	106.3965 (22)	0.4862	5.1309 (14)	0.7586 (22)

a) Figures in parentheses indicate the uncertainty attached to the last significant figures calculated from 2.5 times the standard deviations. b) $I_{obsd}-I_{calcd}$. I_{calcd} is calculated from the coordinates listed in Table 5. c) $P_c=(I_a+I_b-I_c)/2$. d) $\Delta P_c=P_c$(isotopic)$-P_c$(parent).

Table 5. Atom coordinates[a] and check calculations of *gauche*-ethanethiol

Atom	Group	x_a	x_b	x_c	Assumption used
Atom Coordinates (Å)					
H	SH	−0.9460(24)	−0.8446(25)	1.0647(24)	
S		−1.0672(17)	−0.1053(176)	−0.0414(17)	x_c from $\sum_i m_i(x_c)_i=0$
C	CH_2	0.5807(46)	0.6476(42)	0.0519(29)	x_c from $r(CH^1)=r(CH^2)$
H^1	CH_2	0.6193(42)	1.3417(19)	−0.7866(41)	
H^2	CH_2	0.6503(42)	1.2491(21)	0.9572(35)	
C	CH_3	1.7221(16)	−0.3647(78)	−0.0317(33)	x_c from $r(CH_a^1)=r(CH_a^2)$
H_s	CH_3	2.6864(11)	0.1450(128)	−0.0201(35)	x_b, x_c from $r(CH_s)=r(CH_a)$, $r(H_sH_a^1)=r(H_sH_a^2)$
H_a^1	CH_3	1.6428(19)	−0.9555(32)	−0.9453(39)	
H_a^2	CH_3	1.6798(17)	−1.0647(27)	0.8038(43)	

Inertia tensor for the normal species

$\sum m_i(x_g)_i$(amu Å)	g = a	b	c
	−0.1035	−0.1012	0 (assumed)

(amu Å²)	I_a	I_b	I_c	I_{ab}	I_{bc}	I_{ac}
Obsd	17.5801	95.4480	104.2834	0	0	0
Calctd	17.5174	94.9668	103.8003	−0.0375	0.0195	0.0389

RMS[b] for ten isotopic species used……0.3938 (amu Å²)

a) Figures in parentheses indicate 99% reliability intervals attached to the last significant figures. b) Root mean square deviation of the observed-calculated moments of inertia for all the isotopic species used.

Table 6. Structural parameters of ethanethiol

Group	Parameter	By the present authors[a]		By Schmidt *et al.*[c]	
		gauche	*trans*[b]	*gauche*	*trans*
CSH	r(SH) Å	1.336(0.010)	1.322(0.006)	1.328	1.328
	r(SC) Å	1.814(0.009)	1.820(0.005)	1.829	1.829
	α(HSC)	96°(34′)	96°13′(23′)	95°14′	95°14′
CCH_2S	r(CH) Å	1.089(0.005)	1.090(0.003)	1.088	1.088
	r(CC) Å	1.528(0.007)	1.529(0.006)	1.530	1.530
	α(CCS)	113°37′ (29′)	108°34′ (19′)	(113°16′)	(108°33′)
	α(HCH)	106°35′ (36′)	108°54′ (22′)	(107°19′)	(107°14′)
	$\alpha(H^1CC)$	110°42′ (43′)	110°14′ (33′)	109°34′	109°34′
	$\alpha(H^2CC)$	111°19′ (42′)			
	$\alpha(H^1CS)$	104°53′ (57′)	109°26′ (30′)	(106° 7′) (110°48′)	(110°55′)
	$\alpha(H^2CS)$	109°16′ (56′)			
CH_3C	$r(CH_s)$ Å	1.091(0.007)	1.095(0.006)	1.093	1.093
	$r(CH_a)$ Å		1.092(0.006)		
	$\alpha(CCH_s)$	110°30′ (40′)	109°40′ (34′)	109°42′	109°42′
	$\alpha(CCH_a)$	110°37′ (38′)	110°35′ (29′)		
	$\alpha(H_sCH_a)$	109° 2′ (60′)	108°35′ (49′)	(109°14′)	(109°14′)
	$\alpha(H_aCH_a)$	106°55′ (43′)	108° 7′ (33′)		
Dihedral angle	τ(CCSH)	61°45′ (58′)	180°	(60°)	180°
Unperturbed	α(CCS)[d]	111°55′		111°43′	
Tilt angle for the CH_2 group[d]		3° 7′		3°10′	

a) Figures in parentheses indicate 99% reliability intervals. Structural parameters for the *gauche* isomer were obtained by the following assumptions. $r(CH^1)=r(CH^2)$ for CH_2; $r(CH_a^1)=r(CH_a^2)=r(CH_s)$, $\alpha(CCH_a^1)=\alpha(CCH_a^2)$, $\alpha(H_sCH_a^1)=\alpha(H_sCH_a^2)$ for CH_3. b) Quoted from (Ref. 2). c) The proposed structure by Schmidt and Quade (Ref. 3). Figures in parentheses indicate the parameters derived from their parameters. The dihedral angle for the *gauche* isomer is defined as the dihedral angle around the internal rotation axis of the SH group and is not equal to our definition. d) See text.

present structural data for the *gauche* isomer are useful for the explanation.

Let us assume that 1) the methylene group is tilted $\delta°$ towords lone pair electrons on the sulfur atom, 2) the internal rotation axis of the mercapto group does not always coincide with the CS bond, 3) the dihedral angle is defined as that around the internal rotation axis of the mercapto group and is 180° for the *trans* isomer and $\tau°$ for the *gauche* isomer, and 4) α(HCH) and α(HCC) angles remain unchanged between the *trans* and the *gauche* isomers.

From these assumptions, the following relations can be derived approximately.

For the *trans* isomer,

$$\alpha(\mathrm{CCS})_{trans} = \beta - \gamma \quad (4)$$

$$\alpha(\mathrm{SCH})_{trans} = \gamma + \delta\cos\omega \quad (5)$$

For the *gauche* isomer,

$$\alpha(\mathrm{CCS})_{gauche} = \beta + \delta\cos\tau \quad (6)$$

$$\alpha(\mathrm{SCH}^1)_{gauche} = \gamma - \delta\cos(\tau-\omega) \quad (7)$$

$$\alpha(\mathrm{SCH}^2)_{gauche} = \gamma - \delta\cos(\tau+\omega) \quad (8)$$

where ω is the dihedral angle between the symmetry plane and the plane containing the CH bond and the internal rotation axis, and β and γ indicate the angles made by r(CC) and r(CH) against the internal rotation axis, respectively, *viz.*, the hypothetical unperturbed α(CCS) and α(SCH) angles which are free from the influence of the tilt and are common to the *trans* and *gauche* isomers.

In order to evaluate δ, β, and γ values from the relations (4)—(8), we must know the values of τ and ω, where ω is a function of α(HCH) and γ. Since the values of τ and ω are not far from 60°, it is reasonable as a first approximation to calculate the γ value with 60° for both the τ and δ values. The value γ=107°52′ is obtained. Though α(HCH) values for the *trans* and *gauche* isomers are not equal to each other beyond experimental error in contrast with the assumption 4), the average (107°45′) of the observed α(HCH) values for the two isomers is taken as the value in the evaluation of the ω angle. ω=57°57′ is obtained using γ=107°52′ and α(HCH)=107°45′. Though the experimentally obtained dihedral angle (61°45′) is actually the one defined around the CS bond, the value is taken as the τ value in the above relations as an approximation. In the calculation, because of experimental error, choice of three relations from the five gives slightly different values of δ, β, and γ. The average values for the different choices are δ=3°7′, β=111°55′, and γ=107°50′.

The α(HCC) value 110°45′ was obtained, which is in good agreement with the average (110°37′) of the experimentally obtained α(HCC) values for the two isomers.

It is interesting that the hypothetical unperturbed α(CCS) (=β) is close to α(CCC) in propane (112°24′)[7] and the tilt angle (=δ) is slightly larger than that of the methyl groups in methanethiol[8] and dimethyl sulfide[9] (2°30′). The tilt of the methylene group indicates that the internal rotation axis of the mercapto group does not coincide with the CS bond, a line from the carbon atom in the methylene group to the mercapto group making an angle of 3°7′ with the CS bond.

Schmidt and Quade[3] proposed a structure for ethanethiol. It was obtained so as to fit the calculated moments of inertia with those observed for four species of the *trans* isomer and five species of the *gauche* isomer.

For the structures of the two isomers, they took thirteen structural parameters, some of which have different definitions from ours. They assumed that 1) change in the structure from the *trans* to the *gauche* isomer has been explained solely in terms of the orientation of the mercapto group, 2) the internal rotation axis of the mercapto group does not always coincide with the CS bond, 3) the dihedral angle of the mercapto group is defined around the internal rotation axis, this being 180° for the *trans* isomer and 60° for the *gauche* isomer, respectively, and 4) the methyl group is axially symmetric.

From the assumptions, the following parameters are common to the *trans* and *gauche* isomers; for the skeleton, r(CC), r(CS), for the mercapto group, r(SH), α(CSH), for the methyl group, $r(\mathrm{CH_s})=r(\mathrm{CH_a})$, α(CCH), for the methylene group, r(CH), α(CCH) and the dihedral angle between the CCH and CCS planes.

They used the tilt angle of the methylene group and the angle between the CC bond and the internal rotation axis which is identical with our unperturbed α(CCS). Their proposed structure is given in Table 6, where some of the parameter values were converted from their parameter definitions into ours. For the dihedral angle of the mercapto group for the *gauche* isomer, their value is approximately comparable to ours since the definitions are different.

We see that the proposed structure is regarded as a fairly good approximate structure for ethanethiol. In particular, the agreement for the unperturbed α(CCS) and the tilt angle for the methylene group is surprisingly good. When the averages of our parameters for two isomers are taken, their other parameter values are in good agreement with ours within experimental error. However, they took r(CS) longer by *ca.* 0.01Å and α(CSH) smaller by *ca.* 1° than our r_s structural parameters.

Dipole Moment

The dipole moment of the *trans* isomer obtained by Stark effect measurements was reported in I, discussion being given on its direction in the molecule. Schmidt and Quade[3] also reported the dipole moments both for the *trans* and *gauche* isomers. Their values of the dipole moment and its component for the *trans* isomer are in good agreement with ours. We have not carried out measurements of the dipole moment for the *gauche* isomer. However, the direction of the dipole moment can be discussed from their reported values of the dipole moment, its components, and our r_s structure.

Schmidt and Quade extended their measurements of the dipole moments to the normal and four deuterated species. However, change in the dipole moment and its components by isotopic substitutions was negligible within experimental error.

They reported μ_a=1.49±0.02, μ_b=0.19±0.10, μ_c=0.59±0.02 and μ_{total}=1.61±0.05 *D* for the normal

species. It was found that the dipole moment exists along the line which makes angles of 22°35′, 83°14′, and 68°33′ with the *a*-, *b*-, and *c*-inertial axes, respectively.

From the structure, the dipole moment makes angles of 25° and 23°27′ with the CS bond and the bisector of the CSH angle, respectively. As we described in I, the dipole moments of *trans*-ethanethiol (1.560 *D*) and methanethiol (1.532 *D*) exist along lines which make angles of 28°46′ and 18°30′ with the bisector of the CSH angle in the symmetry plane inclining towards the ethyl and methyl groups, respectively. The difference in direction of the two molecules can be explained by an induced moment whose direction is from the methyl to the methylene groups in the ethyl group. When the group moment of the CH_2SH part of *trans*-ethanethiol is regarded to be equal to the dipole moment of methanethiol whose direction is from the inside of the CSH angle to the apex, the induced moment of the ethyl group is found to be 0.36 *D*. The dipole moment of *gauche*-ethanethiol is calculated to be 1.77 *D* whose direction is along the line making angles of 24°4′, 82°22′, and 67°20′ with the *a*-, *b*-, and *c*-inertial axes, respectively. Though the magnitude of the calculated dipole moment is larger than the observed by about 10%, the calculated direction is in good agreement with the observed one.

Microwave Spectra in the Excited States for *Trans* and *Gauche* Isomers

Several groups of weak spectra attributed to the excited vibrational states exist around the spectra due to the ground states of both the *trans* and *gauche* isomers.

For the *trans* isomer of the normal species, there are at least two groups of spectra whose $1_{10}\leftarrow1_{01}$ transitions are found at frequencies lower than the ground state spectra by about 410 and 480 MHz. The group of spectra whose $1_{10}\leftarrow1_{01}$ is found at 23053.85 MHz are much weaker than the other group whose $1_{10}\leftarrow1_{01}$

Table 7. Observed frequencies of *trans*-ethanethiol in excited torsional states[a] (MHz)

Transition	SH Torsional state ν	CH_3 Torsional state		
		ν[b]	$\Delta\nu$[c]	
$1_{10}\leftarrow1_{01}$	23124.59(−107)	23053.85(−128)	−1.72(−1)	
$2_{11}\leftarrow2_{02}$	23692.26(−51)	23658.82(−81)	−1.75(−4)	
$3_{12}\leftarrow3_{03}$	24562.63(19)	24587.58(−40)	−1.72(6)	
$4_{13}\leftarrow4_{04}$	25758.04(86)	25865.91(14)	−1.88(2)	
$5_{14}\leftarrow5_{05}$	27307.60(128)	27526.74(55)	−2.10(−5)	
$6_{15}\leftarrow6_{06}$	29245.69(71)	29609.34(49)	−2.27(3)	
$7_{16}\leftarrow7_{07}$	31611.20(−125)	32157.45(−12)	−2.40(8)	
$1_{11}\leftarrow0_{00}$	32865.88(−92)			
$2_{12}\leftarrow1_{01}$		42548.71(−24)	——[d]	
$3_{03}\leftarrow2_{12}$	8830.71(−70)	9089.97(−90)	1.37(3)	
$4_{04}\leftarrow3_{13}$		20207.70(−94)	1.33(10)	
$5_{05}\leftarrow4_{14}$		31521.62(15)[e]	1.09(1)	
$1_{01}\leftarrow0_{00}$	10297.88(−20)	10339.36(−73)		
$2_{02}\leftarrow1_{01}$	20585.80(−14)	20667.26(−79)		
$2_{12}\leftarrow1_{11}$	20039.98(79)	20087.45(73)		
$2_{11}\leftarrow1_{10}$	21153.29(24)	21271.97(−57)		
$3_{03}\leftarrow2_{02}$	30852.79(−60)	30971.72(−5)		
$3_{13}\leftarrow2_{12}$	30053.26(87)	30123.75(221)		
$3_{12}\leftarrow2_{11}$	31723.27(21)	31900.71(58)		
A	27996.23(293)	27928.77(300)	I_α(amu Å^2)[h]	3.1773
B	5427.51(36)	5466.55(36)	(λ, μ, ν)[i]	(0.7328, 0.6805, 0)
C	4870.58(34)	4873.64(37)	F(GHz)[j]	178.75
$D_J\times10^2$ [f]	0.14 (390)	2.28 (162)	s[k]	85.01
P_c (amu Å^2)[g]	3.7022	3.4241	V_3(cal/mol)	3260±30
RMS[l]	0.87	0.93		

a) Figures in parentheses indicate the difference between the observed and calculated frequencies. b) For *b*-type transitions, A component frequencies are shown. c) $\Delta\nu$ indicates the difference between A and E component frequencies. Figures in parentheses indicate differences of the observed splittings from the calculated which were computed using the listed parameters in the table. d) E component of the doublet is hidden under a strong line. e) Overlapping with a strong line with slow Stark lobes and the frequencies were obtained by measuring the Stark lobes with sine-wave Stark modulation and D. C. bias. f) Coefficient of the $[J(J+1)]^2$ term of the centrifugal distortion. g) $P_c=(I_a+I_b-I_c)/2$. For the ground state, $P_c=3.1946$ amu Å^2. h) Moment of intertia of the CH_3 group around the internal rotation axis. i) Direction cosines of the internal rotation axis in the principal inertial axes. j) $\hbar^2/2rI_\alpha$, $r=1-\lambda^2I_\alpha/I_a-\mu^2I_\alpha/I_b$. k) Reduced barrier. l) Root mean square deviation of the observed frequencies from the calculated. For the ground state, $A=28416.89(74)$, $B=5485.77(9)$, $C=4881.92(10)$, $D_J\times10^2=0.47(41)$ and RMS=0.22 MHz.

is found at 23124.59 MHz. This group of spectra exhibits doublet structures, while the other group of spectra is singlets.

Schmidt and Quade[3] also observed the spectra belonging to the stronger group and assigned them to the spectra due to the first excited mercapto torsional state. They found no spectra belonging to the weaker group. Spectra of these two groups cannot be predicted by a modified rigid rotor expression which is applied to those for the ground state. The root mean square deviations of the observed frequencies from the calculated are 0.87 and 0.93 MHz for the stronger and weaker group, respectively, while it is 0.22 MHz for the ground state. Centrifugal distortion contributions seem to be much larger for the spectra of these two groups than for those of the ground state, though the contributions cannot be determined explicitly at present because of the lack of sufficient data of the observed frequencies with different K_{-1} values. Observed frequencies of the spectra are given in Table 7.

Quantities $P_c(=(I_a+I_b-I_c)/2)$ calculated from the observed rotational constants for the ground state and the two groups of the spectra are 3.1946, 3.7022, and 3.4241 amu Å^2, respectively. The difference in the values of the two groups and the value of the ground state $\Delta P_c(=(P_c)_{excited}-(P_c)_{ground})$ (0.5076 and 0.2295 amu Å^2) indicates that these groups are due to the excited states of out of plane vibrations.[10]

Schmidt and Quade measured the intensities of the stronger group spectra relative to those of the corresponding ground state spectra and concluded that the stronger group is due to the first excited state of an out of plane vibration having the frequency of 154±18 cm^{-1}. They presumed this vibration to be the mercapto torsion for the *trans* isomer.

For the *gauche* isomer of the normal species, two groups of weak *a*-type *R* branch spectra are also observed. Spectra of these two groups exhibit doublet structures in a similar manner to those in the ground state of the *gauche* isomer. Some of the transitions with $K_{-1}=0$ also exhibit doublet structures while the corresponding transitions in the ground state are singlets. Search for *c*-type transitions of these two groups has been unsuccessful so far. The observed frequencies are given in Table 8.

Schmidt and Quade also measured the spectra of the stronger group whose relative intensities indicate that the group is due to the excited state of a vibration having the frequency of 192±20 cm^{-1}. They presumed this vibration to be the mercapto torsion for the *gauche* isomer.

There are only two out of plane vibrations expected below 400 cm^{-1} for each of the *trans* and *gauche* isomers, the mercapto torsion around 170 cm^{-1} and the methyl torsion around 250 cm^{-1}. Inagaki *et al.*[11] and Manocha *et al.*[12] reported the far-infrared spectra of ethanethiol. For the mercapto torsion, they assigned a band at 158.0 cm^{-1} to the 0→1 transition of the *trans* isomer and the bands at 193.0 and 191.8 cm^{-1} to the $0_+\rightarrow 1_-$ and $0_-\rightarrow 1_+$ transitions, respectively, of the *gauche* isomer. The frequencies are in good agreement with those obtained from the relative intensity measurements of the microwave spectra by Schmidt and Quade for the stronger groups of the *trans* and *gauche* isomers.

For the methyl torsion, they reported only a series of bands at 247.5, 233.5, and 220.5 cm^{-1} and assigned them to $v=0\rightarrow 1$, $1\rightarrow 2$, and $2\rightarrow 3$ bands of the methyl torsion, respectively.

TABLE 8. OBSERVED FREQUENCIES OF *a*-TYPE *R* BRANCH TRANSITIONS OF THE *gauche* ISOMER IN THE GROUND AND FIRST EXCITED TORSIONAL STATES[a] (MHz)

Transition[b]	Ground state	SH excited state	CH_3 excited state
$1_{01}\leftarrow 0_{00}{}^{++}_{--}$	10141.07(11)	10133.84(201)	10116.10(11)
$2_{02}\leftarrow 1_{01}{}^{++}_{--}$	20275.47(5)	20260.60(166) 20261.70	20225.79(2)
$2_{12}\leftarrow 1_{11}{}^{++}_{--}$	19832.99(17) 19836.33	19812.60(189) 19809.92	19790.24(24) 19784.31
$2_{11}\leftarrow 1_{10}{}^{++}_{--}$	20727.77 20730.83(−18)	20718.60 20714.08(−254)	20679.91 20674.00(4)
$3_{03}\leftarrow 2_{02}{}^{++}_{--}$	30396.99(0)	30376.34(−25) 30374.29	30323.17(4) 30322.86
$3_{13}\leftarrow 2_{12}{}^{++}_{--}$	29745.06(−14) 29736.75	29711.10(−203) 29714.60	29680.95(−20) 29685.13
$3_{12}\leftarrow 2_{11}{}^{++}_{--}$	31101.19 31092.82(9)	31067.98 31072.88(93)	31002.77 31006.96(−7)
B[c]	5295.03(16)	5292.39(228)	5278.99(17)
C[c]	4845.93(16)	4839.44(225)	4837.01(16)
RMS[d]	0.16	2.34	0.17

a) Figures in parentheses indicate the differences between the observed and calculated frequencies. b) ++ indicates the transition from the + state to the + state. For the first excited SH torsional state, tentative assignments are given in the table for the ++ and −− components of the doublets. c) Since the *gauche* isomer is very close to the prolate symmetric top, *a*-type transition frequencies can be expressed only by *B* and *C* rotational constants. Figures in parentheses indicate 99% reliability intervals calculated from 2.5 times the standard deviation. d) Root mean square deviation of the observed frequencies from the calculated. For the SH and CH_3 excited torsional states, RMS is 3.01 and 5.04 MHz, respectively if the choice of the components of the observed frequencies is reverse.

The doublet structures observed for the spectra belonging to the weaker group of the *trans* isomer indicate that the group is due to the first excited state of the methyl torsion. For the *gauche* isomer, the weaker group of the spectra may also be due to the first excited methyl torsional state, though there is no definite evidence for the assignment of the group.

For the methyl excited torsional state for the *gauche* isomer, components of doublets predictable by a rigid rotor expression are reverse in frequency to those for the ground state (Table 8). This is understood qualitatively as follows.

For the methyl excited torsional state, smallness of the splittings of the transitions with $K_{-1}=0$ indicates that the rotational constants of the + and − states are nearly equal in a similar manner to the ground state. However, the energy difference of the + and − states (estimated to be about 1300 MHz) seems to be much smaller than that for the ground state (determined to be 1750 MHz). This is obvious from the fact that the splittings of $J=1\rightarrow2$ are larger than those of $J=2\rightarrow3$, the reverse of the case for the ground state.

Schematic energy and transition diagrams for cases of no interactions, and ground and methyl excited torsional states are shown in Fig. 3. If there are no interactions between the + and − states, *a*-type transitions of both states have the same frequencies. For the ground state the interaction occurs strongly between the accidentally degenerate levels which are $K_{-1}=1$ levels for low J. Since the 2_{11}^{+} level is lower than the 2_{12}^{-} level, both levels are pushed down and up, respectively, by an amount of $\Delta\nu_2$. For the degenerate case of $(1_{10}^{+}, 1_{11}^{-})$ and $(3_{12}^{+}, 3_{13}^{-})$, 1_{10}^{+} and 1_{11}^{-} levels shift to lower and higher energy by an amount of $\Delta\nu_1$, and 3_{12}^{+} and 3_{13}^{-} levels are pushed up and down by an amount of $\Delta\nu_3$, respectively, since 1_{10}^{+} and 3_{13}^{-} levels are lower than the 1_{11}^{-} and 3_{12}^{+} levels, respectively. Thus the frequencies of the transitions concerned with $K_{-1}=1$ levels are

$$\left.\begin{aligned}
\nu(1_{10}^{+}\rightarrow2_{11}^{+}) &= \nu_2 + \Delta\nu_1 - \Delta\nu_2,\\
\nu(1_{11}^{-}\rightarrow2_{12}^{-}) &= \nu_1 - \Delta\nu_1 + \Delta\nu_2,\\
\nu(2_{11}^{+}\rightarrow3_{12}^{+}) &= \nu_4 + \Delta\nu_2 + \Delta\nu_3,\\
\nu(2_{12}^{-}\rightarrow3_{13}^{-}) &= \nu_3 - \Delta\nu_2 - \Delta\nu_3,
\end{aligned}\right\} \quad (9)$$

where ν_1, ν_2, ν_3, and ν_4 indicate the unperturbed frequencies of the corresponding transitions, whereas $\nu(1_{11}^{+}\rightarrow2_{12}^{+})$, $\nu(1_{10}^{-}\rightarrow2_{11}^{-})$, $\nu(2_{12}^{+}\rightarrow3_{13}^{+})$, and $\nu(2_{11}^{-}\rightarrow3_{12}^{-})$ are nearly unperturbed frequencies, since the levels are not in degeneracy.

On the other hand, for the methyl excited torsional state, since the 2_{11}^{+} level is higher than the 2_{12}^{-} level, the 2_{11}^{+} and 2_{12}^{-} levels are pushed up and down by an amount of $\Delta\nu_2$ as shown in Fig. 3(C). The directions of these shifts are the reverse of those for the case of the ground state. The frequencies of the transitions which are strongly affected by the interactions are

$$\left.\begin{aligned}
\nu(1_{10}^{+}\rightarrow2_{11}^{+}) &= \nu_2 + \Delta\nu_1 + \Delta\nu_2,\\
\nu(1_{11}^{-}\rightarrow2_{12}^{-}) &= \nu_1 - \Delta\nu_1 - \Delta\nu_2,\\
\nu(2_{11}^{+}\rightarrow3_{12}^{+}) &= \nu_4 - \Delta\nu_2 + \Delta\nu_3,\\
\nu(2_{12}^{-}\rightarrow3_{13}^{-}) &= \nu_3 + \Delta\nu_2 - \Delta\nu_3.
\end{aligned}\right\} \quad (10)$$

Since the $(2_{11}^{+}, 2_{12}^{-})$ couple is more degenerate than the $(3_{12}^{+}, 3_{13}^{-})$ couple, $\Delta\nu_2>\Delta\nu_3$, and then $\nu(2_{11}^{+}\rightarrow3_{12}^{+})$ is lower than $\nu(2_{11}^{-}\rightarrow3_{12}^{-})$ which is nearly equal to ν_4.

For the mercapto excited torsional state, splittings of the transitions with $K_{-1}=0$ are not small and the differences in the rotational constants of the + and − states are not negligible (Table 8).

According to the theoretical calculation, the rotational constants of the + and − states are nearly equal to each other within 0.1 MHz for the ground state, while they differ by *ca.* 5 MHz for the first excited mercapto torsional state. The observed results are in line with the calculated results. Though the coefficients of the cross terms $D_{\pm}$ and $E_{\pm}$ remain nearly unchanged between the ground and excited states, coefficients N and Q which correspond to the so-called Coriolis terms become about 25 times larger for the excited state than those for the ground state.

We see from Table 8 that the observed frequencies of *a*-type transitions for the mercapto excited torsional state cannot be fitted satisfactorily with a rigid rotor expression whatever choice of components of the doublets is used. This might be explained by the above results of the theoretical calculation.

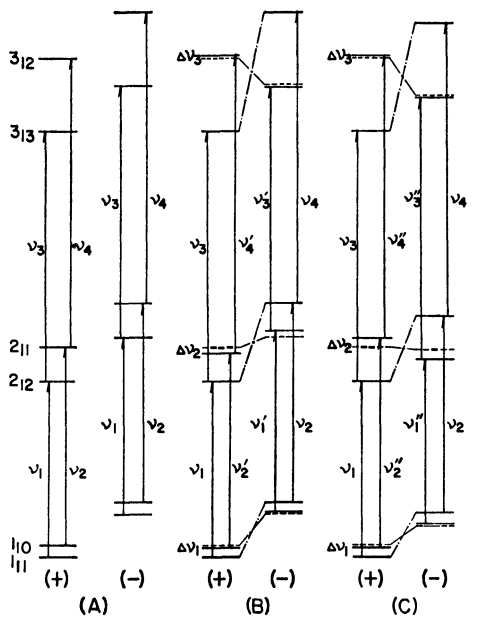

Fig. 3. Schematic energy and transition diagrams for the cases of (A) no interactions, (B) ground state and (C) methyl excited torsional state for the normal species.
Solid and dotted lines indicate perturbed and unperturbed levels, respectively.
For (B), $\nu_1'=\nu_1-\Delta\nu_1+\Delta\nu_2$, $\nu_2'=\nu_2+\Delta\nu_1-\Delta\nu_2$, $\nu_3'=\nu_3-\Delta\nu_2-\Delta\nu_3$, and $\nu_4'=\nu_4+\Delta\nu_2+\Delta\nu_3$, for (C), $\nu_1''=\nu_1-\Delta\nu_1-\Delta\nu_2$, $\nu_2''=\nu_2+\Delta\nu_1+\Delta\nu_2$, $\nu_3''=\nu_3+\Delta\nu_2-\Delta\nu_3$, and $\nu_4''=\nu_4-\Delta\nu_2+\Delta\nu_3$. See text.

Internal Rotation of the Methyl Group

As is shown in Table 7, from the observed splittings of the spectra attributed to the first excited methyl torsional state of the *trans* isomer, the barrier to internal rotation of the methyl group was determined to be $V_3=3260\pm30$ cal/mol by the principal axis method

neglecting the coupling effect of the mercapto internal rotation.

Schmidt and Quade[3] also reported the V_3 value as 3306±86 cal/mol which was obtained from very small splittings of high J, high K_{-1} transitions found in the ground state of the *trans* isomer. Their value is essentially identical with ours within experimental error.

Manocha *et al.*[12] observed only one weak series of far-infrared bands at the higher frequency wing of the strong mercapto torsion band due to the *gauche* isomer. They assigned them to the $v=0\rightarrow1$, $1\rightarrow2$, and $2\rightarrow3$ bands of the methyl torsion, though they did not confirm to which isomer these bands belong. From these bands, the barrier was calculated to be $V_3=3886\pm60$ and $V_6=-69\pm23$ cal/mol.

According to the relative intensity measurements of the microwave spectra by Schmidt and Quade, the *gauche* isomer is more stable by 406±43 cal/mol than the *trans* isomer so that populations of the *trans* and *gauche* isomers are in the ratio of *ca.* 1 : 4 at room temperature where the far-infrared spectra were observed. The barrier obtained from the far-infrared data probably belongs to the *gauche* isomer. The barrier of the methyl internal rotation for the *trans* isomer is lower by *ca.* 630 cal/mol than that for the *gauche* isomer.

Hirota[13] reported the barriers for the *trans* and *gauche* isomers of propyl fluoride which are 2690 and 2865 cal/mol, respectively. For this molecule, the barrier for the *trans* isomer is also lower by 175 cal/mol than that for the *gauche* isomer but change of the barrier is not so prominent as for ethanethiol.

Barriers to internal rotation of the CH_3–C group for a series of molecules; ethyl chloride,[14] ethyl bromide,[15] ethyl fluoride,[16] propane,[17] *trans*-ethyl methyl ether,[18] and *trans*-ethanol,[19] were reported to be 3685, 3684, 3330, 3325, 3300, and 3323 cal/mol, respectively. The barrier of *gauche*-ethanethiol is the highest among these molecules, while that of *trans*-ethanethiol is the lowest.

Internal Rotation of the Mercapto Group

The barrier to the mercapto internal rotation was determined using the Hamiltonian (1b) with the first three terms with the coefficients V_1, V_2, and V_3 of the potential function. Coefficients $\mu_\alpha^{(n)}$ of the kinetic terms were calculated on the basis of the r_s structure including the tilt angle. The first three terms of the kinetic terms were taken into consideration, though the coefficients $\mu_\alpha^{(1)}$ and $\mu_\alpha^{(3)}$ of the second and third terms were much smaller than that of the first term, $\mu_\alpha^{(0)}$.

The energy matrix was constructed from the Hamiltonian (1b) and the basis functions were chosen as $\{(1/\sqrt{2\pi}), (1/\sqrt{\pi})\cos\alpha,\cdots, (1/\sqrt{\pi})\cos 30\alpha\}$ for the symmetric states and $\{(1/\sqrt{\pi})\sin\alpha,\cdots, (1/\sqrt{\pi})\sin 30\alpha\}$ for the antisymmetric states. The torsional energy levels were obtained by a direct diagonalization of the energy matrix. A least squares analysis was carried out taking V_1, V_2, and V_3 as parameters in order to reproduce the energy differences of the + and − states of the *gauche* isomer obtained from the microwave spectra and those obtained from seven observed mercapto torsional frequencies of the *trans* and the *gauche* isomers reported

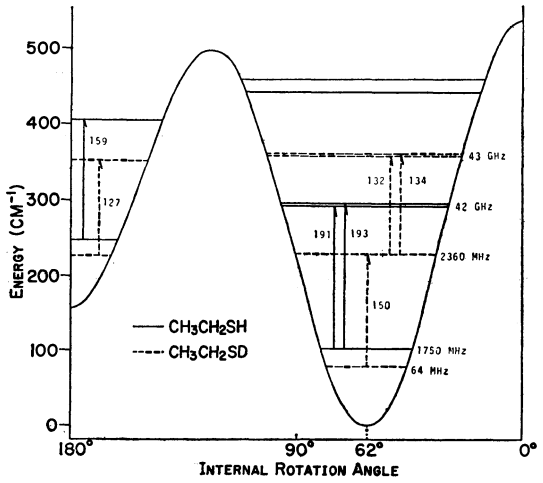

Fig. 4. Potential curve, energy levels and transition frequencies of mercapto internal rotation.

by Manocha *et al.*[12] both for the normal and CH_3CH_2SD species. The results are given in Table 9 and the resulting potential curve together with the energy levels in Fig. 4. The results reported by Schmidt and Quade and by Manocha *et al.* are also given in Table 9 for the sake of comparison.

Since the assumed structure used by Schmidt and Quade is close to our r_s structrue, the $\mu_\alpha^{(n)}$ values do not differ much between their calculation and ours. However, they disregarded the $\mu_\alpha^{(1)}$ and $\mu_\alpha^{(2)}$ terms since they were much smaller than the $\mu_\alpha^{(0)}$ term, while we included these terms in our calculation.

In order to know the influence of these terms, a calculation was made using our data neglecting these terms. It was found that the influence is negligible for the barrier values. The differences in the barrier values in our results and those by Schmidt and Quade are considered to be due to the data used in the calculations. Since their data obtained mainly from the intensity measurements have relatively large uncertainties, our results may be more reliable.

The energy differences used by us and by Manocha *et al.* are the same except for those of $g^0_+-g^0_-$ which were added to the data in our calculation. On the other hand, their assumed structure differs a great deal from our r_s structure. Actually, they used the $\mu_\alpha^{(n)}$ values calculated by Inagaki *et al.*[11] who obtained these coefficient values from a model structure. The structure is; $r(CS)=1.81$, $r(CC)=1.53$, $r(CH)=1.095$, and $r(SH)=1.329$ Å, $\alpha(CSH)=100°18'$ and other angles =tetrahedral. Not only do their structural parameters differ a great deal from the r_s structural parameters but the tilt angle was not taken into consideration. The $\mu_\alpha^{(n)}$ values of their calculations and ours greatly differ. The $\mu_\alpha^{(1)}$ and $\mu_\alpha^{(2)}$ values are much larger than ours. Furthermore, using four energy differences for the CH_3CH_2SD species, they could determine not only the V_1, V_2, and V_3 values but also the V_6 value which was neglected in our calculation.

For a comparison of our results with theirs, trial calculations were carried out with several different choices of $\mu_\alpha^{(n)}$ values and the data. It can be concluded

that 1) discrepancies found in the barrier values obtained by the present authors and by Manocha *et al.* arise form the structure used in the calculations and 2) the V_6 value cannot be determined in sufficient accuracy if the $\mu_\alpha^{(n)}$ values based on the r_s structure are used in the calculation.

References

1) M. Hayashi, H. Imaishi, K. Ohno, and H. Murata, *Bull. Chem. Soc. Jpn.*, **44**, 872 (1971).
2) M. Hayashi, H. Imaishi, and K. Kuwada, *Bull. Chem. Soc. Jpn.*, **47**, 2382 (1974).
3) R. E. Schmidt and C. R. Quade, *J. Chem. Phys.*, **62**, 2864 (1975).
4) See also, M. Hayashi, J. Nakagawa, and K. Kuwada, *Chem. Lett.*, **1975**, 1267.
5) A. Murray, III. and D. L. Williams, "Organic Syntheses with Isotopes," Part II, Interscience, New York (1958), pp. 1340, 1341.
6) C. R. Quade and C. C. Lin, *J. Chem. Phys.*, **38**, 540 (1963); J. V. Knopp and C. R. Quade, *ibid.*, **48**, 3317 (1968).
7) D. R. Lide, Jr., *J. Chem. Phys.*, **33**, 1514 (1961).
8) T. Kojima and T. Nishikawa, *J. Phys. Soc. Jpn.*, **12**, 680 (1957); T. Kojima, *ibid.*, **15**, 1284 (1960).
9) L. Pierce and M. Hayashi, *J. Chem. Phys.*, **35**, 479 (1961).
10) D. R. Herschbach and V. W. Laurie, *J. Chem. Phys.*, **40**, 3142 (1964).
11) F. Inagaki, I. Harada, and T. Shimanouchi, *J. Mol. Spectrosc.*, **46**, 381 (1973).
12) A. S. Manocha, W. G. Fateley, and T. Shimanouchi, *J. Phys. Chem.*, **77**, 1977 (1973).
13) E. Hirota, *J. Chem. Phys.*, **37**, 283 (1962).
14) R. H. Schwendeman and G. D. Jacobs, *J. Chem. Phys.*, **36**, 1245 (1962).
15) C. Flanagan and L. Pierce, *J. Chem. Phys.*, **38**, 2963 (1963).
16) B. Bak, S. Detoni, L. Hansen-Nygaard, J. Tormod Nielsen, and J. Rastrup-Andersen, *Spectrochim. Acta*, **16**, 376 (1960).
17) E. Hirota, C. Matsumura, and Y. Morino, *Bull. Chem. Soc. Jpn.*, **40**, 1124 (1967).
18) M. Hayashi and K. Kuwada, *J. Mol. Struct.*, **28**, 147 (1975).
19) J. P. Culot, Austin Symp. Gas Phase Mol. Struct., (1972), T8.

Catalytic Isotope Exchange Reaction between Deuterium Gas and Water Pre-Adsorbed on Platinum/Alumina

Itsuo IIDA, Junko KATO, and Kenzi TAMARU*

Sagami Chemical Research Center, Nishi-Ohnuma, Sagamihara, Kanagawa 229

**Department of Chemistry, Faculty of Sciense, University of Tokyo, Hongo, Tokyo 113*

(Received June 10, 1976)

The catalytic isotope exchange reaction between deuterium gas and the water pre-adsorbed on Pt/Al_2O_3 was studied. At reaction temperatures above 273 K, the exchange rate was proportional to the deuterium pressure and independent of the amount of adsorbed water, which suggests that the rate determining step is the supply of deuterium from the gas phase. Its apparent activation energy was 38 kJ mol^{-1}. Below freezing point of water, the kinetic behaviour was different from that above freezing point. At higher deuterium pressures the rate dropped abruptly at 273 K. Below the temperature the apparent activation energy was 54 kJ mol^{-1} and the exchange rate depended not on the deuterium pressure but on the amount of the pre-adsorbed water. At lower pressures, however, the kinetic behaviour was the same as that above 273 K, till the rate of the supply of deuterium from the gas phase exceeded the supply of hydrogen from adsorbed water to platinum surface.

These results suggest that below 273 K the supply of hydrogen is markedly retarded, the state of the adsorbed water differing from that above 273 K. It was also demonstrated that when the adsorbed water is in the state of capillary condensation, the exchange rate becomes very small.

The isotope exchange reaction between hydrogen and water is considered to be important in nuclear industry as a means of obtaining enriched deuterium, and the success of this process depends to a large extent upon the rate of isotope transfer between the two chemical species. The isotope separation is possible because the equilibrium constant K of the reaction, $HDO+H_2 \rightleftarrows H_2O+HD$, or the ratio of the isotope concentration in the reactants, is not equal to unity exactly, and the value of K depends upon the temperatures where equilibrium attained. In enriching the deuterium, different equilibration at different temperatures is employed. In principle, it is more effective if the temperature of the cold reactor is as low as possible, since the isotope effect is greater at lower temperatures.

Although platinum on an activated charcoal and nickel on chromium oxide were reported to be efficient catalysts for the vapour phase reaction, both catalysts lose their catalytic activities when condensed water film covers the catalyst surface at lower temperatutres,[1,2] which prevents these catalysts from being used in the lower temperature range.

The mechanism of the hydrogen exchange reaction catalyzed by transition metals at temperatures above the boiling point of water has been extensively studied.[3-5] Recently, Rolston and Goodale [6] studied the mechanism of this exchange reaction catalyzed by platinum supported on alumina and proposed that the rate determining step of the exchange reaction in the vapour phase consists of the hydrogen atom switch between chemisorbed hydrogen on platinum and physisorbed water on alumina. Sagert and Pouteau[7-9] also studied this reaction over various noble metals and reported that the exchange rate depended not on the hydrogen gas pressure but on the pressure of water vapour on platinum catalyst. They also supported the hydrogen switching mechanism proposed by Rolston and Goodale.

On the other hand, when the reaction takes place between liquid water and hydrogen gas bubble over suspended platinum charcoal catalyst at around room temperature, it was shown that the rate increases with stirring rate, which implies that the rate determining step consists of the hydrogen gas diffusion through the water to contact with the catalyst surface.[10] Since little is known of the chemical kinetic behaviour of this exchange reaction below room temperature, it is significant to examine the behaviour of each elementary step of the exchange reaction on the catalyst surface.

Experimental

The rate of exchange reaction between deuterium gas and the water adsorbed on platinum/alumina catalyst was measured in a closed circulation system, volume 340 cm^3, changing the amount of water adsorbed on the catalyst. The isotope abundance in the gas phase was determined by gas chromatography using 5% manganese chloride on an alumina column at 77 K. Prior to the measurements, the catalyst was subjected to heat-treatment *in vacuo* at 423 K, then cooled down to room temperature. The catalyst was 0.5% platinum supported on an alumina pellet (Lot No. 48-1-1 Nippon Engelhard Co., Ltd.,). Initial pretreatment of the catalyst consisted of evacuation at room temperature for 30 min, and at 398 K for 30 min. The sample was then treated with hydrogen at 623 K overnight and evacuated at the same temperature overnight. The surface area measured by the BET method was 92 m^2/g, the amount of the catalyst being 2.13 g. The adsorption isotherm of water on the catalyst in the temperature range 229—296.5 K was measured. Since the equilibrium pressure of the water at low coverage was very low, the pressure was measured with a Pirani gauge which was calibrated by a MacLeod gauge.

Results and Discussion

The adsorption isotherm of water on the catalyst at 296.5 K is shown in Fig. 1. If the area occupied by a water molecule is $1.06 \times 10^{-19} m^2$,[11] the monomolecular adsorption of water on the catalyst surface area corresponds to 0.054 g of water. In the standard run, the amount of pre-adsorbed water was fixed to 0.025 g and the pressures of the water vapour which were in equilibrium with the adsorbed water were below 40 Pa even at room temperature as given in Fig. 1. From the adsorption isotherm, the capillary condensation is considered to take place when the amount of adsorbed

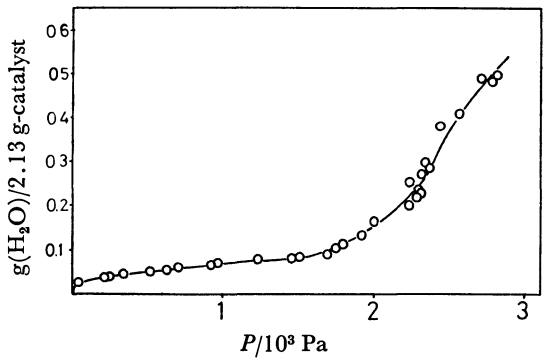

Fig. 1. Adsorption isotherm of water on 2.13 g of platinum/alumina at 296.5 K.

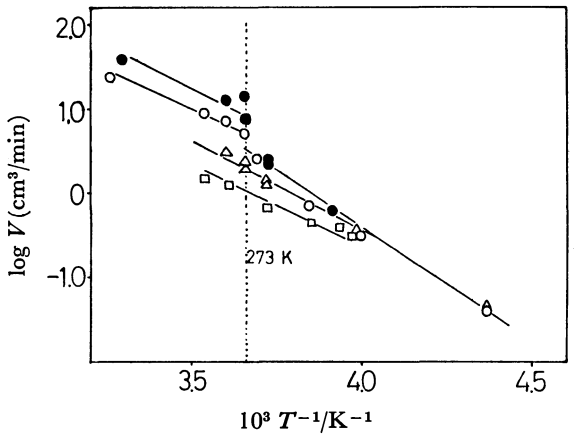

Fig. 2. Arrhenius plots for the exchange reaction between deuterium and water pre-asdorbed on platinum/alumina.
—●—; P_{D_2}=55 kPa, —○—; P_{D_2}=27 kPa, —△—; P_{D_2}=15 kPa, —□—; P_{D_2}=9.3 kPa, $H_2O(a)$=0.025 g.

water exceeds about 0.14 g.

The temperature dependence of the exchange rate between deuterium gas and the adsorbed water is given in Fig. 2 for several deuterium pressures in the Arrhenius form. Under deuterium pressures of 55 kPa and 27 kPa, the exchange rates dropped abruptly at 273 K, below which they fell to another temperature dependency. The apparent activation energies above and below 273 K correspond to 38 and 54 kJ mol^{-1}, respectively, which suggests not only an appreciable change in the rate determining step of the reaction at 273 K but also the possibility that the transport phenomena might be involved in a rate determining step which is markedly influenced by freezing the adsorbed water.

Under lower deuterium pressures such as 15 and 9.3 kPa, the Arrhenius plots exhibited no discontinuity at 273 K and the apparent activation energy was the same with 38 kJ mol^{-1}.

Consequently, the temperature dependence of the reaction rate revealed at higher deuterium pressures such as 55 and 27 kPa, the abrupt drop of exchange rate and the activation energy change could be observed, but at lower pressures such as 15 kPa and 9.3 kPa, the change of activation energy takes the form of a bent in the Arrhenius plots.

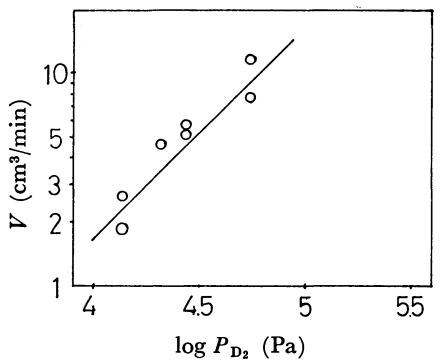

Fig. 3. Dependence of the exchange rate on D_2 pressure at 273 K.
$H_2O(a)$=0.025 g.

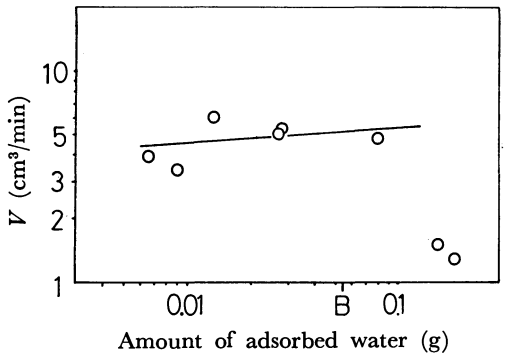

Fig. 4. Dependence of the exchange rate on the amount of adsorbed water at 273 K.
P_{D_2}=27 kPa.

The variation of the rate with deuterium pressure at 273 K is shown in Fig. 3. The reaction order with respect to deuterium pressure, given by the slope of line, is 0.9. The dependence of rate on the amount of the adsorbed water at 273 K is shown in Fig. 4. The amount of adsorbed water corresponding to that of monolayer full coverage is denoted by B. The results (Fig. 4) demonstrate that when the amount of adsorbed water does not much exceed point B, the reaction order with respect to the amount of the adsorbed water is zero. However, when the amount of the adsorbed water exceeds point B, the exchange rates decrease considerably. Judging from the results in Fig. 1, the amounts of adsorbed water in the range correspond to capillary condensation. It was accordingly suggested that when the adsorbed water is condensed in the pores of the catalyst, the diffusion of deuterium gas through the condensed water becomes the rate determining step.

The exchange rate is nearly proportional to the deuterium pressure, and is independent of the amount of the adsorbed water provided that the adsorbed water is not in the state of capillary condensation. It was suggested that the rate determining step of this exchange reaction above 273 K is the supply of deuterium from the gas phase to the active sites in the platinum surface.

In contrast to the kinetic behaviour above 273 K, the kinetic behabiour below 273 K is rather complicated. At 269 K, the order of the reaction with respect

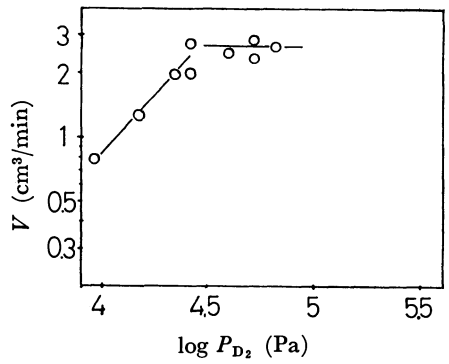

Fig. 5. Dependence of the exchange rate on D_2 pressure at 269 K.
$H_2O(a)=0.025$ g.

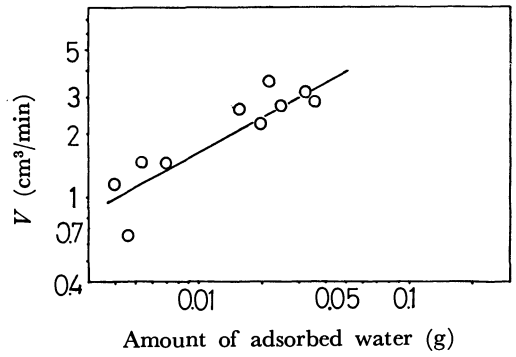

Fig. 6. Dependence of the exchange rate on the amount of adsorbed water.
$P_{D_2}=55$ kPa.

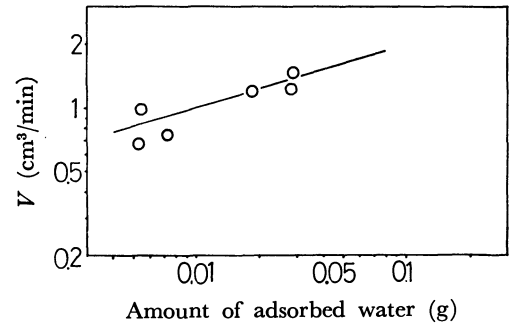

Fig. 7. Dependence of the exchange rate on the amount of adsorbed water.
$P_{D_2}=15$ kPa.

to deuterium pressure is 1.1 under lower deuterium pressures below 27 kPa, whereas at higher pressures the rate is independent of the deuterium pressure (Fig. 5). The dependence of the rates upon the amount of adsorbed water was measured under deuterium pressures of 55 and 15 kPa at 269 K (Figs. 6 and 7, respectively). The reaction order with respect to the amount of the adsorbed water is 0.5—0.6 under the deuterium pressure of 55 kPa, and 0.2 under the deuterium pressure of 15 kPa. When the exchange rates are nearly proportional to the pressure of deuterium gas, the reaction order with respect to the amount of the adsorbed water is as low as 0.2 and when the exchange rates are independent of the pressure of deuterium gas,

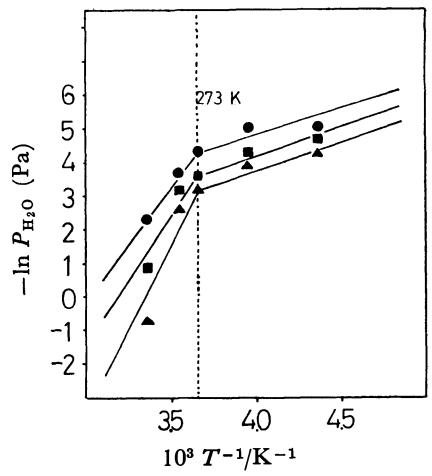

Fig. 8. Adsorption isoster of water on 9.44 g of platinum/alumina.
—●—; $H_2O(a)=4$ mmol, —■—; $H_2O(a)=5$ mmol, —▲—; $H_2O(a)=6$ mmol.

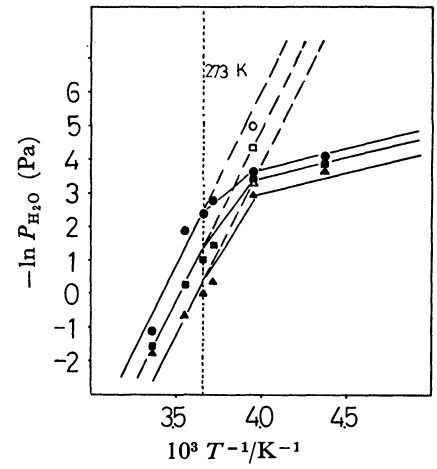

Fig. 9. Adsorption isoster of water on 9.44 g of platinum/alumina.
—●—; $H_2O(a)=7$ mmol, —■—; $H_2O(a)=8$ mmol, —▲—; $H_2O(a)=9$ mmol, --○--; $H_2O(a)=7$ mmol, --□--; $H_2O(a)=8$ mmol, --△--; $H_2O(a)=9$ mmol. Broken lines are the plots for the second adsorption after the adsorption temperature was once raised.

the order is 0.5—0.6.

Consequently, the rate determining step at 269 K shifts from the supply of deuterium from the gas phase to that of hydrogen from the adsorbed water as the pressure of the deuterium gas increases.

The adsorption isosters of water over the platinum/alumina at lower and higher coverages are shown in Fig. 8 and Fig. 9, respectively, the slope of which is proportional to the heat of adsorption. We see that the adsorption isoster bent at 273 K.

Since the phase change of the adsorbed water from liquid to solid should cause an increase in the heat of adsorption below 273 K, it was interpreted that the equilibration of the adsorption of the water below 273 K is nearly apparent. In the experiments of water adsorption below 273 K, after the apparent equilibrium, the temperature of the adsorbate rose to room tem-

perature, and after 12 h the temperature was lowered again. It was found that the additional adsorption (Fig. 9) and the plots of the equilibrium pressure of the water below 273 K come of the same line of the adsorption isoster above 273 K. The heat of adsorption of water on platinum/alumina was found to be 84 kJ mol^{-1}.

Thus, though the heat of adsorption of water on platinum/alumina is much greater than the heat of fusion of the water, the water cannot spread over the adsorbate easily and crystallizes on the surface of platinum/alumina.

Considering the results of the adsorption of water on the catalyst, it was concluded that the change in the kinetic behaviour at 273 K is due to the retardation of the supply of hydrogen from the frozen water. The apparent activation energy of the exchange reaction between deuterium and water below 273 K would be that for the transfer of adsorbed water. This activation energy might be measured above 273 K if the water coverage was very low. However, in such a case, the increase in the HD content of deuterium gas is not measurable.

This work was performed under the auspices of Power Reactor and Nuclear Fuel Development Corporation (Japan).

References

1) H. S. Taylor, U. S. Patent 2690380 (1954).
2) H. C. Urey, U. S. Patent 2690379 (1954).
3) A. Farkas, *Trans. Faraday Soc.*, **32**, 922 (1936).
4) A. Farkas and L. Farkas, *Trans. Faraday Soc.*, **33**, 678 (1937).
5) E. Hallaba and E. M. Abdel-Wahab, *Z, Anorg. Allg. Chem.*, **388**, 169 (1972).
6) J. H. Rolston and J. W. Goodale, *Can. J. Chem.*, **50**, 1900 (1972).
7) N. H. Sagert and R. M. L. Pouteau, *Can. J. Chem.*, **50**, 3686 (1972).
8) N. H. Sagert and R. M. L. Pouteau, *Can. J. Chem.*, **51**, 4031 (1973).
9) N. H. Sagert and R. M. L. Pouteau, *Can. J. Chem.*, **52**, 2960 (1974).
10) H. Saito, T. Morita, and O. Sataka, *Kagaku Kogaku*, **23**, 450 (1959).
11) S. T. Gregg and K. W. W. Sing, "Adsorption, Surface Area, and Porosity," Academic Press, London (1967) p.82.

Stereochemical Studies of Elimination Reactions of 2-Bromobutane and 2,3-Dibromobutane over Bivalent-Ion Exchanged Silica Gels

Yukio Aoki,* Makoto Misono, and Yukio Yoneda

Department of Synthetic Chemistry, Faculty of Engineering, The University of Tokyo, Hongo, Bunkyo-ku, Tokyo 113

(Received June 17, 1976)

Elimination reactions of 2-bromobutane and 2,3-dibromobutane over silica gels in which silanol protons on the surface were exchanged with bivalent ions such as Ba(II), Ca(II), Mg(II), and Ni(II) have been investigated. Dehydrobromination of 2-bromobutane was found to proceed mainly with *syn* elimination. Debromination by *anti* mode and non-stereospecific dehydrobromination were observed for 2,3-dibromobutane. The catalytic activities of these silica gels exhibit reversed volcano-type patterns when they are plotted against the electronegativity of metal ion together with those of alkali-ion exchanged silica gels. Reaction intermediates consistent with the stereochemistry observed are a *s*-butyl cation and a bromonium ion, respectively for 2-bromobutane and 2,3-dibromobutane.

In the previous paper, we reported a remarkable effect of alkali ion exchange of silica gel on the acid-base properties and the stereochemistry of the title reactions.[1] The reactions proceeded with *anti* elimination over Cs- and K-exchanged silica gels in which basic sites play a primarily important role. However, the reaction of 2-bromobutane proceeded with *syn* mode over silica gel and Na- or Li-exchanged silica gel, all of which are weakly acidic. It was demonstrated that the acid-base properties are the prime factor determining the stereochemistry.[2] The observed dependence of the steric course of reaction on the acid-base properties was explained by the variation of the reaction mechanism from a concerted elimination over basic surfaces to a carbonium-ion like mechanism over acidic surfaces.

In the present work, we have extended the study to silica gels exchanged with bivalent metal ions which are expected to be more strongly acidic, with the aim of clarifying how the reaction rate, stereochemistry, and orientation of olefin formation vary with the acid strength of the catalyst surface. Acidic properties and catalytic activities have already been investigated for the metal ion-exchanged silica or porous glass.[3,4] The metal ion loaded on oxide surface may be regarded as a model of Lewis acid sites having a series of various acid strengths.

Experimental

Apparatus and Procedure. The procedure for the reaction study (pulse technique) and the analyses of products are the same as reported.[1] 10—50 mg of catalyst was used for the reaction of 2-bromobutane and 100—200 mg for that of 2,3-dibromobutane. Effect of pyridine adsorption on the catalytic activity was studied as follows. After ordinary pretreatment of the catalysts at 300 °C in a stream of helium, 10 μl of pyridine injected into the helium stream was passed through the catalyst bed at 150 or 160 °C. The temperature was then raised at a rate of 5 °C/min to the predetermined temprature. The reaction of 2-bromobutane was examined after the temperature had been lowered to 150 or 160 °C.

Catalysts and Reagents. The same silica gels as reported[1] were used as starting material. Ion-exchange was performed by impregnating the silica gel in aqueous solutions of metal chlorides followed by washing with water and drying at 110 °C overnight. The pH (5—7) of the solution was not intentionally controlled, a small amount of metal carbonate being added in some cases. The amount of loaded metal ion was as low as *ca.* 5 μg-ion/g. The surface area was *ca.* 500 m^2/g. The reagents used for the reactions were the same as reported.[1]

Results

Dehydrobromination of 2-Bromobutane. All the silica gels exchanged with bivalent metal ions (Mg(II), Ca(II), Ba(II), and Ni(II)) exhibited much higher activity for the dehydrobromination of 2-bromobutane than the alkali-ion exchanged silica gels.[1] Decrease in activity and change in butene composition were small during the repeated pulses. Although butene injected separately did not isomerize over these catalysts under the reaction conditions, 1-pentene pulsed together with 2-bromobutane isomerized in some cases to a small extent (*ca.* 5—10%). Hydrogen bromide formed from 2-bromobutane seemed to act as a temporary catalyst for the isomerization. The butene composition observed was probably affected by the secondary isomerization, but this influence should be small, since pentenes which are more reactive than butenes[2] did not isomerize to a great extent.

Butene compositions formed from 2-bromobutane-d_0 and the contents of d_1 species in each butene isomer formed from 2-bromobutane-3-d_1 (*erythro*: *threo*: d_0=77: 17: 6)[1] are given in Table 1. The ratios, $(trans/cis)_0/(trans/cis)_1$,[5] were 0.86—0.91, indicating that *syn* elimination was the major process over these four silica gels. The d_1 content of 1-butene which should agree with that of the starting 2-bromobutane-3-d_1 (94%) was low in some cases. This seems due partly to the secondary isomerization which may cause H–D exchange and partly to experimental error because of the small amount of 1-butene formed.

Under the same assumptions that the isotope effect and % *anti* (the fraction of reaction which proceeded by *anti* mode) are the same for *trans*- and *cis*-2-butene formation,[1] % *anti* was calculated to be *ca.* 20—30% (% *syn*: 70—80%) for these silica gels (Table 1). The elimination reaction may actually be more stereospecific than the values thus determined. Hydrogen shift in an alkyl cation intermediate was found to take place during the course of reactions of alkyl halides over solid acids.[6] This hydrogen shift as well as the H–D exchange by secondary isomerization should diminish the difference in d_1 content between

* Present address: Japan Catalytic Chemical Industry Co., Ltd., Suita, Osaka.

Table 1. Dehydrobromination of 2-bromobutane over bivalent ion-exchanged silica gels

Metal ion	Relative[a] activity	Butene composition[b] (% d_1 in parentheses)			Stereochemistry % *anti*
		1-	*trans-*	*cis-*	
Mg(II)	42	1.0(88)	3.4(73)	3.2(56)	33
Ca(II)	47	1.0(91)	3.4(77)	3.3(51)	25
Ba(II)	38	1.0(93)	3.5(80)	3.5(42)	14
Ni(II)	148	1.0(88)	4.8(76)	4.3(51)	25
SiO_2[c]	3—8	1.0	2.6—3.2	2.5—3.2	*syn*

a) Conversion (%) at 160°C normalized to that over 100 mg catalyst. b) Butene composition from 2-bromobutane-d_0 and content (%) of d_1 species in each butene from 2-bromobutane-d_1 (*erythro* : *threo* : d_0 = 77 : 17 : 6). c) Ref. 1.

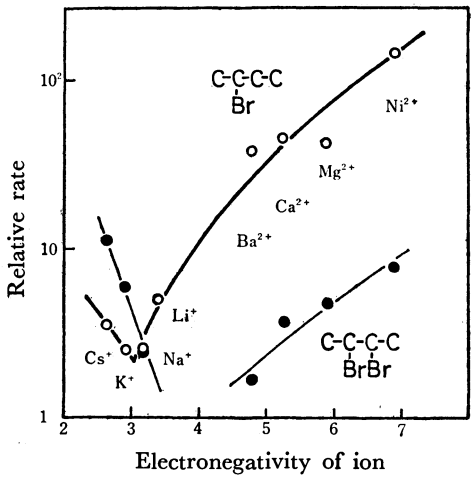

Fig. 1. Rates of elimination reactions of 2-bromobutane (○) and 2,3-dibromobutane (●) over metal-ion exchanged silica gels at 160 °C.

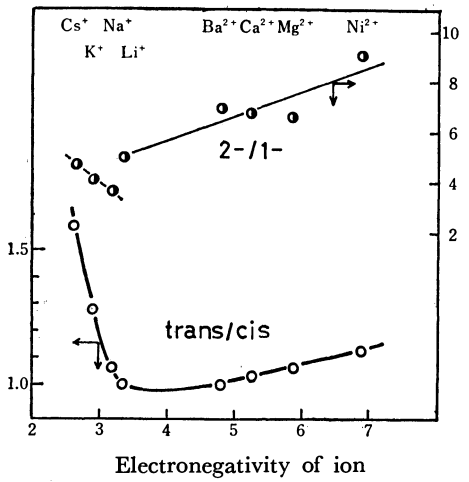

Fig. 2. Compositions of butenes formed from dehydrobromination of 2-bromobutane over metal-ion exchanged silica gels at 160 °C.

trans- and *cis*-2-butene. Thus the apparent % *anti* becomes closer to 50%.

Figure 1 shows how the catalytic activity changes with the electronegativity of metal ion[7] loaded. The results of alkali ion[1] are also given. Although the amount of metal ion loaded differs between mono- and bivalent ions, it is obvious that the activity increases from Na(I) to Ni(II) with increasing electronegativity. Since the activity increases with decreasing electronegatively from K(I) to Cs(I), a reversed volcano-type pattern exists in the activity-electronegativity correlation.

Positional and geometrical orientation of butene formation over these silica gels is shown in Fig. 2. The higher 2-/1-butene ratio (Saytzeff orientation) and the *trans*/*cis* ratio close to unity, together with the predominant *syn* elimination, are characteristic of bivalent-ion exchanged silica gels. This is in line with the view that these silica gels behave as acids like Li–SiO_2 but have much stronger acid strength. Figure 3 shows the effect of pyridine on the catalytic activity. Active sites of silica gel poisoned by pyridine were mostly regenerated at 150 °C 20 min after the addition, while only about a half was recovered in the case of Ni–SiO_2 even at 300—350 °C in a helium stream. It is seen that the strength of pyridine adsorption to active sites, which should reflect the acid strength, increases in the order Ca(II)<Mg(II)<

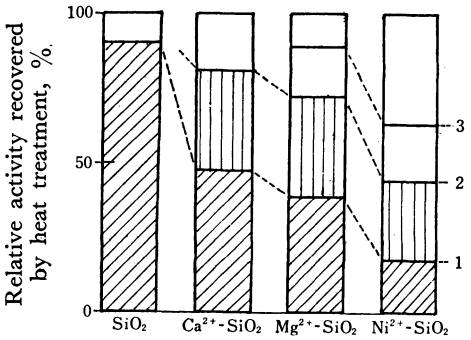

Fig. 3. Relative activity of silica gels poisoned by pyridine for dehydrobromination of 2-bromobutane. Reaction temp. : 150 °C (160 °C for Ca–SiO_2)
1: After heat treatment at the reaction temperature.
2: After heat treatment at 300 °C.
3: After heat treatment at 350 °C.

Ni(II) in accordance with electronegativity. The apparent energy of activation obtained at the state of stationary activity was 11.2 kcal/mol for Ca–SiO_2. The value is closer to that of Li–SiO_2 (9 kcal/mol) than to that Cs–SiO_2 (4—5 kcal/mol).[1] The activation energy for *trans-* and *cis*-2-butene formation was respectively 2.1 and 2.4 kcal/mol lower than that for 1-butene formation.

Reactions of 2,3-Dibromobutane. 2,3-Dibromobutane was less reactive than 2-bromobutane over bivalent-ion exchanged silica gels. Butadiene formation by the elimation of two molecules of hydrogen bromide and debromination to form 2-butene (*anti* elimination) were the major reactions. Minor reaction of dehydrobromination to form 2-bromo-2-butene was not stereospecific. No apparent difference in selectivity for these elimination reactions was observed among the bivalent ions, the fraction of debromination being 50—60% of total reactions. These elimination reactions also show a reversed volcano-type pattern when plotted against electronegativity (Fig. 1). It is to be noted that 2,3-dibromobutane is more reactive than 2-bromobutane (both with *anti* elimination) on the left branch, while the relative reactivity is the reverse on the right branch.

Discussion

Bivalent metal ions undergo exchange with two silanol groups over the surface of silica gel when the extent of exchange is low.[3]

$$M^{2+} + 2{\equiv}Si\text{-}OH \rightarrow {\equiv}Si\text{-}O\diagdown\ \diagup M + 2H^+ \quad {\equiv}Si\text{-}O\diagup$$

The acidic sites increase in number with the amount of metal ion loaded at least at low extent of exchange, and Lewis acid sites which were proposed to be active for dehydrochlorination of isopropyl chloride are predominant after evacuation above 300 °C.[3]

The relative catalytic activity, (Ni(II)>Ca(II)≈Mg(II)≈Ba(II)≫Li(I)≈Na(I))(Fig. 1), parallels the acid strength of catalysts which can be estimated from the electronegativity of metal ion and the effect of pyridine adsorption on activity (Fig. 3). We proposed that the reaction intermediate or the transition state resembles a carbonium ion more over Li–SiO_2 than over Cs–SiO_2, since the stronger acidity of the former makes the C–Br bond breaking easier. This explanation can be applied to the present results. As the acid strength increases further by the exchange with bivalent ion, the C–Br bond breaks more readily and the rate of reaction *via* a carbonium ion will increase. Thus, the activity for elimination over metal-ion exchanged silica gels shows a reversed volcano-type pattern (Fig. 1), when the results of Cs- and K–SiO_2 are included, where the activity increases with base strength.[1]

The favored steric course over basic surface was *anti* mode.[1] On the other hand, over acidic surface *syn* elimintion is favored in the case of 2-bromobutane. 2,3-Dibromobutane is likely to form a bromine-bridged intermediate after heterolytic C–Br bond breaking. The intermediate decomposes to butene (*anti* elimination), 2-bromo-2-butene (non-stereospecific) and butadiene (−2HBr *via* CH_2=CH–CHBr–CH_3).[2b,8] Although the ionic radii are similar for Ba(II) (1.50Å) and K(I)(1.52Å),[9] the preferred steric mode of the dehydrobromination of 2-bromobutane was opposite. This suggests that the ionic radius by itself is not the prime factor determining the stereochemistry of elimination. A trend of % *syn* elimination of 2-bromobutane as Ba(II) (86%)>Ca(II) (75%)>Mg(II) (67%) was found for alkali-earth metal ions. This may be a reflection of acid strength, but factors such as the difference in metal content and the secondary isomerization (or hydrogen shift during reaction) as well as experimental error should be considered before coming to such a conclusion. However, it seems remarkable that considerable stereospecificity (*syn*>75%) was observed in case that the carbonium-ion mechanism is most probable. In order to complete dehydrobromination by *syn* mode, a proton must be transferred from *s*-butyl cation toward the direction to which a bromide ion is released, possibly by a model as proposed previously,[2a] before the "roll-over" of or the hydrogen shift in the intermediate completely takes place.

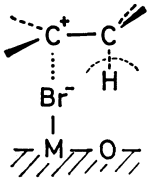

Correlations of the catalytic activity, the orientation of olefin formation, and the stereochemistry with the acid-base properties of catalyst are summarized in Table 2. We see that the stereochemistry of reaction which reflects the reaction mechanism differs for acidic and basic catalysts, their activity and selectivity definitely exhibiting different dependency on the acid–base properties. Similar changes in activity or reaction mechanism with the acid-base properties have been discussed by Noller *et al.*[10] and Mochida *et al.*[11] Trends as shown in Figs. 1 and 2 were also found in the case of metal chlorides supported on silica gel.[12] Lewis acid sites were considered to be the active sites in these catalysts. For example, they were as active as metal sulfates for dehydrobromination, but were much less active for olefin isomerization. Although the acid strength of protonic sites can increase with electroneg-

Table 2. Summary of dehydrobromination of 2-bromobutane over metal-ion exchanged silica gels

Metal ions	Cs(I), K(I)	Ca(II), Ni(II)
Electronegativity	Low	High
Surface	Basic	Acidic
Easiness of bond-breaking	C-Br≈C-H	C-Br>C-H
Activity increases with	Base strength	Acid strength
Butene composition		
2-/1-	4—5	6—9
trans/*cis*	>1	≈1
Stereochemistry	*anti*	*syn*
Mechanism[a]	Concerted	*s*-Butyl cation (ion pair)

a) Reaction mechanism for 2,3-dibromobutane seems to be a concerted elimination over a basic surface as for 2-bromobutane, but a bromine-bridged bromonium ion is the intermediate in the case of acidic surface.

ativity as in the case of butene isomerization catalyzed by metal sulfates,[13] it is most likely that metal ion itself acts as a Lewis acid in the present system.

Assistance in experiments by Messrs. N. Funamoto and T. Takizawa is gratefully acknowledged.

References

1) M. Misono, Y. Aoki, and Y. Yoneda, *Bull. Chem. Soc. Jpn.*, **49**, 627 (1976).

2) a) M. Misono, *J. Catal.*, **30**, 226 (1973); b) M. Misono and Y. Yoneda, *ibid*, **33**, 474 (1974).

3) K. Taniguchi, M. Nakajima, S. Yoshida, and K. Tarama, *Nippon Kagaku Zasshi*, **91**, 525, 529, 612(1970).

4) T. Imanaka, Y. Hayashi, and S. Teranishi, *Nippon Kagaku Kaishi*, **1973**, 889.

5) This is the ratio of *trans*-/*cis*-2-butene ratio from 2-bromobutane-d_0 to that from 2-bromobutane-3-d_1(*erythro* rich). The ratio is larger than unity for *anti* elimination and smaller than unity for *syn* elimination, owing to the deuterium isotope effect.[1]

6) 2-Bromobutane-2-d_1 was formed from the reaction of 2-bromobutane-3-d_1, and 2-bromopentane from 3-bromopentane over $CaCl_2$, $CuCl_2$, and Ba-SiO_2(M. Ishikawa, M. Misono, and Y. Yoneda, 34th Annual Meeting of the Chemical Society of Japan, 1J36, Hiratsuka, April, 1976).

7) M. Misono, E. Ochiai, Y. Saito, and Y. Yoneda, *J. Inorg Nucl. Chem.*, **29**, 2685 (1967).

8) M. Misono, M. Ishikawa, and Y. Yoneda, *Chem. Lett.*, **1976**, 69.

9) R. D. Shannon and C. T. Prewitt, *Acta. Cryst.*, **B25**, 925 (1969); Nippon Kagaku Kai, "Kagaku Binran," 2nd ed., Maruzen, Tokyo (1975), p. 1407.

10) H. Noller, P. Andreu, and M. Hunger, *Angew. Chem. Intern. Ed. Engl.*, **10**, 172 (1971).

11) I. Mochida, Y. Anju, H. Yamamoto, A. Kato, and T. Seiyama, *Bull. Chem. Soc. Jpn.*, **44**, 3305 (1971).

12) M. Misono and Y. Yoneda, Presented at the 31th Annual Meeting of the Chemical Society, 3T09, Sendai, Oct., 1974.

13) M. Misono, Y. Saito, and Y. Yoneda, *J. Catal.*, **9**, 135 (1967); M. Misono and Y. Yoneda, *J. Phys. Chem.*, **76**, 44 (1972).

Microwave Spectrum of (Chloromethyl)germane

Jun NAKAGAWA and Michiro HAYASHI

Department of Chemistry, Faculty of Science, Hiroshima University, Higashi-sendamachi, Hiroshima 730

(Received June 18, 1976)

In order to determine the molecular structure and barrier to internal rotation of the GeH_3 group, the microwave spectra of (chloromethyl)germane and its deuterated species $ClCH_2GeD_3$ have been investigated. From splittings of the spectra due to the first excited GeH_3 torsional state, the barrier to internal rotation was determined to be 1740±30 cal/mol. Assuming the cylindrical symmetry of the C–Cl bond, the quadrupole coupling constant was determined to be $\chi_{zz}=-74.7$ MHz for the $^{35}ClCH_2{}^{74}GeH_3$ species.

Several papers have been published on a series of molecules containing germanium atom. In particular, the papers on (fluoromethyl)germane by Krisher *et al.*[1] and on fluoromethylgermane by Roberts[2] called our attention because of the remarkable difference of barrier heights to internal rotation between these molecules. For a comparison of the results, we dealt with (chloromethyl)germane and chloromethylgermane, two chlorine-substituted molecules of (fluoromethyl)germane and fluoromethylgermane. In the present paper, we report the results of (chloromethyl)-germane obtained by microwave spectroscopy.

Experimental

Samples of (chloromethyl)germane and its deuterated species $ClCH_2GeD_3$ were prepared by the reaction of germanium tetrachloride with diazomethane in diethyl ether and by reducing the resulting $ClCH_2GeCl_3$ with $LiAlH_4$ or $LiAlD_4$ in dibutyl ether.[3]

The sample contained ^{74}Ge, ^{72}Ge and ^{70}Ge nuclei (37, 27 and 21%) and ^{35}Cl and ^{37}Cl nuclei (75 and 25%) in natural isotopic abundance ratio.

Microwave spectra were measured with a conventional 100 kHz Stark modulation spectrometer at the National Chemical Loboratory for Industry, Tokyo. All the spectra were measured at dry ice temperature on a recording chart. The spectra of five different isotopic species could be assinged. For the sake of simplicity, we denote the species by symbols such as (35, 74)-H_3 and (35, 74)-D_3, *etc.* for $^{35}ClCH_2{}^{74}GeH_3$ and $^{35}ClCH_2{}^{74}GeD_3$, *etc.*

Microwave Spectra

(Chloromethyl)germane has a form of a nearly prolate symmetric top with an asymmetry parameter κ of about −0.987. Both *a*- and *b*-type transitions were observed. Due to the quadrupolar coupling effect, the spectra exhibit multiplet structures which can be predicted by the first order perturbation theory. Measurements of the spectra were carried out for comparatively intense hyperfine components which satisfy the relation $\Delta F=\Delta J$. The assignment was made by first considering the hyperfine splitting pattern and finally confirming it by the double resonance technique using $7_{07}\leftarrow 6_{16}$ and $7_{07}\leftarrow 6_{06}$ transitions as pumping and signal transitions, respectively. The frequencies observed are given in Table 1.

First, the quadrupole coupling constants χ_{aa} and $\eta_a\chi_{aa}$ and rough values of the rotational constants were determined by a least squares technique from several low J transitions with relatively large splittings. Frequencies of transitions were then calculated with use of the values of the quadrupole coupling constants and rotational constants. Since the observed quadrupolar splittings were predicted by these calculations (Table 2), the hypothetical unsplit frequencies were determined by comparing the observed and calculated frequencies. From the hypothetical unsplit frequencies (Table 3), the accurate rotational constants were determined by a least squares analysis so as to fit in with a modified rigid rotor expression including only the $D_J[J(J+1)]^2$ term of the centrifugal distortion formula. The rotational constants and the quadrupole coupling constants are given in Table 4.

Molecular Structure

The data of the present work are not sufficient to determine the r_s structural parameters of (chloromethyl)germane by the substitution method. For this molecule, if C_3 symmetry of the GeH_3 group around the C–Ge bond is assumed, there are eight independent structural parameters, four of which are related to the $ClCH_2$ part of the molecule and independent of the germanium atom. Schwendeman and Jacobs[4] reported the r_s structure of (chloromethyl)-silane. Thus four parameters related to the $ClCH_2$ part were assumed to be identical to those of (chloromethyl)silane. The other four parameters were so determined as to reproduce fifteen observed rotational constants by a least squares technique. The differences between the observed and calculated rotational constants are given in Table 4. The root mean square deviation of fifteen rotational constants is smaller than 0.03 %.

The atom coordinates for the chlorine and germanium atoms can be obtained by solving the Kraitchman equations with the data for suitable pairs of the species. The x_c coordinate of the out of plane hydrogen atom in the GeH_3 group can also be obtained from the data for the (35, 74)-H_3 and (35, 74)-D_3 species. The coordinates solved are given in Table 4 with the differences from the calculated coordinates from the structural parameters adjusted. The agreement between these two coordinate values is satisfactory. The structural parameters (Table 5) are compared with the reported parameters of similar molecules such as $ClCH_2SiH_3$, CH_3SiH_3[5] and CH_3GeH_3[6]. A comparison of the adjusted structural parameters of (chloromethyl)germane with those of similar molecules indicates several interesting facts.

r(CX), (X=Si or Ge) becomes longer by replacing a hydrogen atom in the methyl group with a chlorine atom, while r(XH) becomes shorter and α(HXC)

TABLE 1. OBSERVED FREQUENCIES OF (CHLOROMETHYL)GERMANE (MHz)[a)]

	F	(35, 74)-H_3	(35, 72)-H_3	(35, 70)-H_3	(37, 74)-H_3	(35, 74)-D_3
$3_{03} \leftarrow 2_{02}$	7/2, 5/2	12149.48	12255.88	12367.66	11762.17	11693.63
	3/2, 1/2	12147.70	12254.07	12365.84	11760.73	11691.79
$3_{12} \leftarrow 2_{12}$	7/2	11968.68	12072.04	12180.64	11591.44	11532.37
	5/2	11966.80	12070.14	12178.75	11589.96	11530.59
	3/2	11965.37	12068.74	12177.36	11588.94	11529.14
	1/2	11967.12	12070.50	12179.28	—	11531.00
$3_{12} \leftarrow 2_{11}$	7/2	12335.48			11937.46	11859.77
	5/2	12333.55			11935.87	11857.90
	3/2	12334.92			11937.07	—
	1/2	12336.63			11938.57	11861.19
$4_{04} \leftarrow 3_{03}$	9/2, 7/2	16196.12	16337.89	16486.75	15680.06	15588.50
	5/2, 3/2	16195.23	16336.97	16485.89	15679.39	15587.63
$4_{14} \leftarrow 3_{13}$	9/2	15956.55	16094.30	16239.07	15453.89	
	7/2	15955.77	16093.50	16238.22	15453.26	
	5/2	15954.73	16092.53	16237.28	15452.41	
	3/2	15955.55	16093.29	16238.00	15453.00	
$4_{13} \leftarrow 3_{12}$	9/2	16445.94	16592.01	16745.44	15915.30	—
	7/2, 5/2	16445.34	16591.37	16744.81	15914.75	15811.44
	3/2	16446.35	16592.33	16745.81	15915.30	—
$5_{05} \leftarrow 4_{04}$	11/2, 9/2	20240.43	20417.58	20603.52	19595.96	19480.66
	7/2, 5/2	20239.91	20416.98	20602.93	19595.52	19480.00
$5_{15} \leftarrow 4_{14}$	11/2	19944.10	20116.34	20297.22		19217.03
	9/2	19943.74	20115.95	20296.86		19216.62
	7/2	19942.98	20115.24	20296.15		19215.93
	5/2	19943.39	20115.61	20296.56		19216.31
$5_{14} \leftarrow 4_{13}$	11/2	20556.21	20738.74	20930.17		19763.70
	9/2, 7/2	20555.82	20738.40	—		19763.32
	5/2	20556.21	20738.74	20930.17		19763.70
$5_{24} \leftarrow 4_{23}$	11/2	20252.38	20429.84	20616.17	19606.59	
	9/2, 7/2	20250.88	20428.26	20614.64	19605.35	
	5/2	20252.38	20429.84	20616.17	19606.59	
$5_{23} \leftarrow 4_{22}$	11/2	20264.22	20442.24	20628.89	19617.18	
	9/2, 7/2	20262.84	20440.83	20627.53	19616.09	
	5/2	20264.22	20442.24	20628.89	19617.18	
$6_{06} \leftarrow 5_{05}$	13/2, 11/2	24281.40	24493.62	24716.65	23508.53	23369.80
	9/2, 7/2	24281.12	24493.36	24716.36		23369.48
$1_{11} \leftarrow 0_{00}$	5/2—3/2	22619.82	22646.74			
	3/2—3/2	22618.15	22644.88			
	1/2—3/2	22621.37	22648.50			
$2_{12} \leftarrow 1_{01}$	5/2					22389.94
	3/2					22388.02
$3_{13} \leftarrow 2_{02}$	7/2	30416.40				
	5/2, 3/2	30412.66				
	1/2	30416.40				
$4_{14} \leftarrow 3_{03}$	9/2	34223.46				
	7/2	34219.04				
	5/2	34219.70				
	3/2	34224.20				
$2_{11} \leftarrow 2_{02}$	7/2	18812.22	18807.45	18802.97		
	5/2	18821.64	18816.56	18812.22		
$3_{12} \leftarrow 3_{03}$	9/2	18998.04	18996.69	18995.16		15084.02
	7/2	19005.56	19004.32	19003.01		15091.79
	5/2	19002.10	19000.75	18999.43		15088.12
	3/2	18994.50	18993.22	18991.90		15080.77

TABLE 1. (Continued)

	F	(35, 74)-H_3	(35, 72)-H_3	(35, 70)-H_3	(37, 74)-H_3	(35, 74)-D_3
$4_{13} \leftarrow 4_{04}$	11/2	19247.88	19250.85	19254.06		
	9/2	19254.93	19257.85	19260.92		
	7/2	19252.27	19255.24	19258.49		
	5/2	19245.68	19248.62	—		
$5_{14} \leftarrow 5_{05}$	13/2	19563.65	19572.05	19581.04	19499.80	15590.95
	11/2	19570.06	19578.58	19587.58	19504.79	15597.46
	9/2	19568.31	19576.78	19585.80	19503.50	15595.62
	7/2	19561.70	19570.06	19579.03	19498.18	15589.00
$6_{15} \leftarrow 6_{06}$	15/2	19947.32	19962.55	19978.61	19860.88	15935.41
	13/2	19953.80	19968.99	19985.02	19865.84	15941.89
	11/2	19952.30	19967.43	19983.53	19864.60	15940.22
	9/2	19945.91	19961.04	19977.10	19859.70	15933.80
$7_{16} \leftarrow 7_{07}$	17/2	20401.90	20425.09	20449.77	20288.00	16344.21
	15/2	20408.31	20431.45	20456.13	20293.08	16350.62
	13/2	20407.00	20430.09	20454.76	20292.02	16349.32
	11/2	20400.57	20423.74	20448.37	20287.00	16342.84
$8_{17} \leftarrow 8_{08}$	19/2	20930.17			20783.97	16820.29
	17/2	20936.57			20789.00	16826.74
	15/2	20935.40			20788.12	16825.61
	13/2	20928.91			20783.06	16819.12
$9_{18} \leftarrow 9_{09}$	21/2	21535.64			21352.03	
	19/2	21542.14			21357.07	
	17/2	21541.08			21356.22	
	15/2	21534.58			21351.23	

a) Since the measured components of the multiplets satisfy the rule of $\Delta F = \Delta J$, they can be labeled by the F quantum number of the lower level of the transitions shown in the table except for the components of the $1_{11} \leftarrow 0_{00}$ transitions. For the symbols for the species, see the text.

TABLE 2. OBSERVED QUADRUPOLAR SPLITTINGS OF TRANSITIONS FROM HYPOTHETICAL UNSPLIT FREQUENCIES (MHz)[a)]

	F	(35, 74)-H_3	(35, 72)-H_3	(35, 70)-H_3	(37, 74)-H_3	(35, 74)-D_3
$3_{03} \leftarrow 2_{02}$	7/2	0.32 (−5)	0.34 (−3)	0.34 (−3)	0.27 (−2)	0.35 (−3)
	5/2	(0)	(3)	(3)	(2)	(4)
	3/2	−1.46 (4)	−1.47 (1)	−1.48 (0)	−1.17 (2)	−1.49 (2)
	1/2	(−1)	(−4)	(−6)	(−2)	(−4)
$3_{13} \leftarrow 2_{12}$	7/2	1.07 (0)	1.08 (2)	1.07 (1)	0.82 (−2)	1.02 (−5)
	5/2	−0.81 (−1)	−0.82 (−4)	−0.82 (−4)	−0.66 (−2)	−0.76 (4)
	3/2	−2.24 (0)	−2.22 (0)	−2.21 (2)	−1.68 (8)	−2.21 (3)
	1/2	−0.49 (−11)	−0.46 (−7)	−0.29 (10)	—	−0.35 (2)
$3_{12} \leftarrow 2_{11}$	7/2	0.58 (5)			0.45 (2)	0.51 (−2)
	5/2	−1.35 (−1)			−1.14 (−9)	−1.36 (−2)
	3/2	0.02 (1)			0.06 (7)	—
	1/2	1.73 (14)			1.56 (9)	1.93 (5)
$4_{04} \leftarrow 3_{03}$	9/2	0.24 (−1)	0.25 (0)	0.23 (−2)	0.17 (−3)	0.23 (−3)
	7/2	(6)	(7)	(5)	(2)	(5)
	5/2	−0.65 (2)	−0.67 (−1)	−0.63 (2)	−0.50 (2)	−0.64 (3)
	3/2	(−6)	(−8)	(−5)	(−3)	(−5)
$4_{14} \leftarrow 3_{13}$	9/2	0.63 (1)	0.62 (1)	0.65 (4)	0.51 (3)	
	7/2	−0.15 (0)	−0.18 (−4)	−0.20 (−6)	−0.12 (0)	
	5/2	−1.19 (−1)	−1.15 (2)	−1.14 (3)	−0.97 (−4)	
	3/2	−0.37 (5)	−0.39 (3)	−0.42 (0)	−0.38 (−6)	
$4_{13} \leftarrow 3_{12}$	9/2	0.26 (−2)	0.29 (2)	0.28 (1)	0.30 (8)	—
	7/2	−0.34 (14)	−0.35 (13)	−0.35 (13)	−0.25 (13)	−0.35 (13)
	5/2	(−12)	(−15)	(−15)	(−8)	(−13)
	3/2	0.67 (−12)	0.61 (6)	0.65 (10)	0.30 (−13)	—
$5_{05} \leftarrow 4_{04}$	11/2	0.16 (−4)	0.20 (1)	0.20 (1)	0.14 (−1)	0.28 (8)
	9/2	(6)	(10)	(10)	(6)	(18)
	7/2	−0.36 (3)	−0.40 (−1)	−0.39 (1)	−0.30 (1)	−0.38 (2)
	5/2	(−6)	(−11)	(−10)	(−6)	(−9)
$5_{15} \leftarrow 4_{14}$	11/2	0.40 (0)	0.40 (0)	0.37 (−3)		0.41 (1)
	9/2	0.04 (3)	0.01 (0)	0.01 (0)		0.00 (−1)
	7/2	−0.72 (−2)	−0.70 (0)	−0.70 (0)		−0.69 (1)
	5/2	−0.31 (0)	−0.33 (−2)	−0.29 (2)		−0.31 (0)

TABLE 2. (Continued)

	F	(35, 74)-H_3	(35, 72)-H_3	(35, 70)-H_3	(37, 74)-H_3	(35, 74)-D_3
$5_{14} \leftarrow 4_{13}$	11/2	0.19(2)	0.17(1)			0.19(2)
	9/2	−0.20(3)	−0.17(5)			−0.19(3)
	7/2	(−3)	(−1)			(−2)
	5/2	0.19(−3)	0.17(−6)			0.19(−4)
$5_{24} \leftarrow 4_{23}$	11/2	0.76(12)	0.79(15)	0.77(13)	0.62(11)	
	9/2	−0.74(−11)	−0.79(−16)	−0.76(−13)	−0.62(6)	
	7/2	(10)	(5)	(8)	(−11)	
	5/2	0.67(−10)	0.79(−7)	0.77(−9)	0.62(−5)	
$5_{23} \leftarrow 4_{22}$	11/2	0.69(9)	0.70(10)	0.68(8)	0.55(8)	
	9/2	−0.69(10)	−0.71(8)	−0.68(11)	−0.54(9)	
	7/2	(−9)	(−11)	(−8)	(−7)	
	5/2	0.69(−10)	0.70(−9)	0.68(−11)	0.55(−8)	
$6_{06} \leftarrow 5_{05}$	13/2	0.08(−8)	0.07(−9)	0.09(−7)		0.10(−6)
	11/2	(3)	(2)	(4)		(6)
	9/2	−0.20(7)	−0.19(8)	−0.20(7)		−0.22(6)
	7/2	(−4)	(−3)	(−4)		(−6)
$1_{11} \leftarrow 0_{00}$	5/2—3/2	0.30(−8)	0.29(−10)			
	3/2—3/2	−1.37(15)	−1.57(1)			
	1/2—3/2	1.85(−5)	2.05(7)			
$2_{12} \leftarrow 1_{01}$	5/2					1.18(0)
	3/2					−0.74(−2)
$3_{13} \leftarrow 2_{02}$	7/2	1.58(−2)				
	5/2	−2.16(−3)				
	3/2	(8)				
	1/2	1.58(8)				
$4_{14} \leftarrow 3_{03}$	9/2	1.82(−2)				
	7/2	−2.60(0)				
	5/2	−1.94(−3)				
	3/2	2.56(3)				
$2_{11} \leftarrow 2_{02}$	7/2	−2.70(−2)	−2.55(11)	−2.61(6)		
	5/2	6.72(3)	6.56(−9)	6.64(−4)		
$3_{12} \leftarrow 3_{03}$	9/2	−2.52(0)	−2.56(−5)	−2.79(−26)		−2.65(−13)
	7/2	5.00(−4)	5.07(4)	5.06(1)		5.12(8)
	5/2	1.54(3)	1.50(−1)	1.48(−3)		1.45(−6)
	3/2	−6.06(−1)	−6.03(0)	−6.05(1)		−5.90(14)
$4_{13} \leftarrow 4_{04}$	11/2	−2.56(−6)	−2.56(−6)	−2.48(3)		
	9/2	4.49(12)	4.44(7)	4.38(−2)		
	7/2	1.83(−13)	1.83(−13)	1.95(−2)		
	5/2	−4.76(14)	−4.79(11)	—		
$5_{14} \leftarrow 5_{05}$	13/2	−2.45(7)	−2.52(1)	−2.53(1)	−1.91(6)	−2.48(5)
	11/2	3.96(−8)	4.01(−4)	4.01(−6)	3.08(−6)	4.03(−2)
	9/2	2.21(2)	2.21(2)	2.23(2)	1.79(8)	2.19(−1)
	7/2	−4.40(−2)	−4.51(−13)	−4.54(−13)	−3.53(−12)	−4.43(−4)
$6_{15} \leftarrow 6_{06}$	15/2	−2.63(−5)	−2.57(1)	−2.57(3)	−1.97(3)	−2.54(5)
	13/2	3.85(1)	3.87(0)	3.84(−6)	2.99(−1)	3.94(6)
	11/2	2.35(1)	2.31(−4)	2.35(−1)	1.75(−7)	2.27(−8)
	9/2	−4.04(6)	−4.08(2)	−4.08(5)	−3.15(4)	−4.15(−4)
$7_{16} \leftarrow 7_{07}$	17/2	−2.63(0)	−2.59(5)	−2.57(9)	−2.09(−4)	−2.62(3)
	15/2	3.78(1)	3.77(0)	3.79(−1)	2.99(6)	3.79(0)
	13/2	2.47(1)	2.41(−6)	2.42(−6)	1.93(2)	2.49(1)
	11/2	−3.96(−2)	−3.94(1)	−3.97(1)	−3.09(−3)	−3.99(−3)
$8_{17} \leftarrow 8_{08}$	19/2	−2.64(−6)			−2.12(−2)	−2.72(0)
	17/2	3.76(4)			2.91(3)	3.73(−2)
	15/2	2.59(2)			2.03(4)	2.60(1)
	13/2	−3.90(−5)			−3.03(−4)	−3.89(0)
$9_{18} \leftarrow 9_{09}$	21/2	−2.78(0)			−2.15(0)	
	19/2	3.72(2)			2.89(2)	
	17/2	2.66(1)			2.04(−3)	
	15/2	−3.84(−3)			−2.95(0)	

a) Figures in parentheses indicate the difference between observed and calculated values.

Table 3. Hypothetical unsplit frequencies of (chloromethyl)germane (MHz)[a]

Species	(35, 74)-H_3	(35, 72)-H_3	(35, 70)-H_3	(37, 74)-H_3	(35, 74)-D_3
$3_{03} \leftarrow 2_{02}$	12149.16(−5)	12255.54(−6)	12367.32(−3)	11761.90(−5)	11693.28(0)
$3_{13} \leftarrow 2_{12}$	11967.61(12)	12070.96(−11)	12179.57(14)	11590.62(11)	11531.35(13)
$3_{12} \leftarrow 2_{11}$	12334.90(−11)			11937.01(0)	11859.26(−20)
$4_{04} \leftarrow 3_{03}$	16195.88(−13)	16337.64(−13)	16486.52(−15)	15679.89(−6)	15588.27(13)
$4_{14} \leftarrow 3_{13}$	15955.92(9)	16093.68(6)	16238.42(4)	15453.38(13)	
$4_{13} \leftarrow 3_{12}$	16445.68(−17)	16591.72(−20)	16745.16(−16)	15915.00(−24)	15811.79(−3)
$5_{05} \leftarrow 4_{04}$	20240.27(−3)	20417.38(4)	20603.32(0)	19595.82(14)	19480.38(−11)
$4_{15} \leftarrow 4_{14}$	19943.70(21)	20115.94(26)	20296.85(24)		19216.62(14)
$5_{14} \leftarrow 4_{13}$	20556.02(4)	20738.57(4)			19763.51(0)
$6_{06} \leftarrow 5_{05}$	24281.32(−13)	24493.55(−12)	24716.56(−7)	23508.53(−4)	23369.70(−4)
$2_{11} \leftarrow 2_{22}$	18814.92(8)	18810.00(−20)	18805.58(−8)		
$3_{12} \leftarrow 3_{03}$	19000.56(−8)	18999.25(7)	18997.95(0)		15086.67(0)
$4_{13} \leftarrow 4_{04}$	19250.44(−4)	19253.41(8)	19256.54(−6)		—
$5_{14} \leftarrow 5_{05}$	19566.10(−6)	19574.57(5)	19583.57(4)	19501.71(−15)	15593.43(5)
$6_{15} \leftarrow 6_{06}$	19949.95(2)	19965.12(7)	19981.18(4)	19862.85(3)	15937.95(−2)
$7_{16} \leftarrow 7_{07}$	20404.53(9)	20427.68(−2)	20452.34(5)	20290.09(12)	16346.83(2)
$8_{17} \leftarrow 8_{08}$	20932.81(4)			20786.09(2)	16823.01(2)
$9_{18} \leftarrow 9_{09}$	21538.42(3)			21354.18(−2)	
$1_{11} \leftarrow 0_{00}$	22619.52(−28)	22646.45(−4)			
$2_{12} \leftarrow 1_{01}$					22388.76(−6)
$3_{13} \leftarrow 2_{02}$	30414.82(1)				
$4_{14} \leftarrow 3_{03}$	34221.64(20)				

a) Figures in parentheses indicate the difference between observed and calculated values.

Table 4. Rotational constants (MHz), quadrupole coupling constants (MHz) and atom coordinates (Å)

	(35, 74)-H_3	(35, 72)-H_3	(35, 70)-H_3	(37, 74)-H_3	(35, 74)-D_3
A[a]	20655.77(46)	20665.75(52)	20676.58(47)	20581.30(53)	16705.07(41)
B[a]	2086.54(4)	2105.33(6)	2125.04(5)	2018.46(3)	2004.01(3)
C[a]	1964.04(4)	1980.75(5)	1998.30(4)	1902.96(3)	1894.59(3)
D_J[a]	0.0010(11)	0.0010(10)	0.0009(9)	0.0013(10)	0.0007(8)
ΔA[b]	2.22(0.01)	1.80(0.01)	1.68(0.01)	1.09(0.01)	−2.51(−0.02)
ΔB[b]	0.39(0.02)	0.36(0.02)	0.31(0.02)	0.51(0.03)	0.52(0.03)
ΔC[b]	−0.44(−0.02)	−0.50(−0.03)	−0.54(−0.03)	−0.30(−0.02)	−0.14(−0.01)
χ_{aa}[c]	−29.7(4)	−29.2(5)	−29.2(5)	−23.5(6)	−29.7(7)
$\eta_a\chi_{aa}$[c]	−45.0(4)	−45.1(4)	−45.3(5)	−35.0(4)	−44.9(4)
χ_{zz}[d]	−74.5	−72.0	−71.1	−57.7	−74.4
$\eta_z\chi_{zz}$[d]	−0.2	−2.2	−3.4	−0.9	−0.2
χ_{zz}[e]	−74.7(6)	−74.3(6)	−74.5(7)	−58.5(7)	−74.6(8)
θ_{za}(st.)[f]	39°18′	39°15′	39°12′	39° 5′	39°17′
$\theta_{za}(\chi)$[f]	39°19′	39°28′	39°34′	39°11′	39°17′

Atom coordinate (Å)[g]

Atom	Used species	$\lvert x_a \rvert$	$\lvert x_b \rvert$	$\lvert x_c \rvert$
Cl	(35, 74)-H_3, (37, 74)-H_3	2.0382(−21)	0.2161(16)	0
Ge	(35, 74)-H_3, (35, 72)-H_3	1.0313	0.0758	0
	(35, 74)-H_3, (35, 70)-H_3	1.0311	0.0784	0
	average	1.0312(−11)	0.0771(−3)	0
H_a(Ge)	(35, 74)-H_3, (35, 74)-D_3	—	—	1.2540(34)

a) Figures in parentheses indicate the uncertainties calculated from 2.5 times the standard deviation attached to the last significant figures. b) These indicate the difference in the observed and calculated rotational constants. Figures in parentheses indicate quantities such as $100\times\Delta A/A$. c) Figures in parentheses indicate the experimental uncertainties attached to the last significant figures. d) Calculated from χ_{aa} and $\eta_a\chi_{aa}$ under the assumption of the coincidence of the z-axis and the C-Cl bond. e) Calculated from χ_{aa} and $\eta_a\chi_{aa}$ under the assumption of the cylindrical symmetry of the tensor ($\eta_z=0$). f) θ_{za}(st.), the angle between the z- and a-axis obtained from the structure. $\theta_{za}(\chi)$, the θ_{za} angle obtained from the χ values. g) Figures in parentheses indicate the difference of the values obtained from the solution of the Kraitchman equations and from the structure.

becomes smaller. The ratio of the changes of the parameters from CH_3XH_3 to $ClCH_2XH_3$ is close to each other for organosilane and germane. On the other hand, for α(XCCl) the germane has a larger value than the silane.

Quadrupole Coupling Constants

The principal value χ_{zz} and the asymmetry parameter $\eta_z(=\chi_{xx}-\chi_{yy})/\chi_{zz})$ of the quadrupole coupling tensor can be obtained if both the diagonal and off-diagonal values of the tensor in the principal inertial axis system are available. However, because of the lack of off-diagonal values, χ_{zz} and η_z values were calculated under an assumption of either 1) the coincidence of the z-axis and C–Cl bond or 2) the cylindrical symmetry of the tensor along the z-axis. In the former case, the angle θ_{za} between the z- and a-axes was taken as that from the structure described in the preceding section. The asymmetry parameter η_z was found to be fairly small for every species (Table 4). In the latter case where $\eta_z=0$, the angle θ_{za} can be calculated from the χ values. The calculated θ_{za} is in good agreement with that from the structure. This indicates that the structure given in the preceding section is a plausible one and the electric charge distribution around the Cl nucleus has nearly cylindrical symmetry along the C–Cl bond.

Table 5. Structural parameters

X=Si, Ge	$ClCH_2GeH_3$[a]	CH_3GeH_3[b]	$ClCH_2SiH_3$[c]	CH_3SiH_3[d]
r(CX) Å	1.961	1.945	1.889	1.867
r(XH) Å	1.517	1.529	1.477	1.485
α(HXC)	107°43′	109°41′	108°20′	110°41′
α(XCCl)	110°11′	—	109°18′	—
r(CCl) Å	1.788 (assumed)	—	1.788	—
r(CH) Å	1.096 (assumed)	1.083	1.096	1.093
α(HCH)	107°30′ (assumed)	108°25′	107°30′	107°40′
α(HCX)	109°18′ (assumed)	110°31′	109°18′	111°16′

a) This work. b) Ref. 6. c) Ref. 4. d) Ref. 5.

Table 6. Observed and hypothetical unsplit frequencies of the (35, 74)-H_3 and (35, 72)-H_3 species of (chloromethyl)germane in the excited torsional state (MHz)[a]

		(35, 74)-H_3 Species					
	F =	$J+3/2$	$J+1/2$	$J-1/2$	$J-3/2$	ν_0[b]	$\Delta\nu$[c]
$3_{13} \leftarrow 2_{12}$	A	11932.10	11930.23	11928.83	11930.64	11931.04(20)	
	E						
$4_{04} \leftarrow 3_{03}$	A	16141.86			16140.97	16141.62(−10)	
	E						
$4_{14} \leftarrow 3_{13}$	A	15907.82	15906.97	15905.97	—	15907.15(5)	
	E						
$5_{13} \leftarrow 3_{12}$	A	16385.69	16385.09		16386.08	16385.43(−14)	
	E						
$5_{05} \leftarrow 4_{04}$	A	20172.91			20172.37	20172.74(−5)	
	E						
$5_{15} \leftarrow 4_{14}$	A	19883.20	19882.86	19882.14	19882.56	19882.84(7)	
	E						
$5_{14} \leftarrow 4_{13}$	A	20481.06			20480.70	20480.88(5)	
	E						
$3_{13} \leftarrow 2_{02}$	A	30369.81	30366.03		30369.81	30368.21(−5)	
	E	30373.40	30369.81		30373.40		−3.69(−5)
$4_{14} \leftarrow 3_{03}$	A	34168.89	34164.53	34165.08	34169.46	34167.02(−1)	
	E	34172.57	34168.25	—	34173.25		−3.74(−4)
$5_{14} \leftarrow 5_{05}$	A	19526.89	19533.43	19531.41	19524.96	19529.34(−19)	
	E	19530.97	19537.44	19535.52	19528.87		−4.03(4)
$6_{15} \leftarrow 6_{06}$	A	19901.43	19907.77	19906.30	19899.86	19903.96(7)	
	E	19905.48	19911.88	19910.38	19903.92		−4.07(6)
$7_{16} \leftarrow 7_{07}$	A	20344.67	20351.00	—	20343.36	20347.28(16)	
	E	20348.85	20355.05	20353.76	20347.44		−4.07(1)
$8_{17} \leftarrow 8_{08}$	A	20859.67	20865.92	20864.76	20858.45	20862.29(13)	
	E	20863.74	20870.04	20868.96	20862.59		−4.13(3)
$9_{18} \leftarrow 9_{09}$	A	21449.57	21455.96	—	21448.60	21452.34(2)	
	E	—	21460.19	21459.15	21452.79		−4.18(1)
$10_{19} \leftarrow 10_{010}$	A	22118.33	22124.78	22123.82	22117.36	22121.12(−13)	
	E	22122.57	22128.96	22128.05	22121.60		−4.22(−1)
$11_{110} \leftarrow 11_{011}$	A	22869.53	22876.13	22875.27	22868.68	22872.44(−19)	
	E	22873.80	22880.39	22879.48	22872.96		−4.26(−5)

TABLE 6. (Continued)

				(35, 72)-H_3 Species			
$4_{04} \leftarrow 3_{03}$	A	16283.21		16282.27		16282.94(0)	
	E						
$5_{15} \leftarrow 4_{14}$	A	20054.96	20054.50	20053.81	20054.29	20054.52(−8)	
	E						
$5_{14} \leftarrow 4_{13}$	A	20662.73		20662.47		20662.60(8)	
	E						
$8_{17} \leftarrow 8_{08}$	A	20891.86	20898.17	20897.05	20890.69	20894.51(−12)	
	E	20896.00	20902.31	20901.18	20894.85		−4.14(4)
$9_{18} \leftarrow 9_{09}$	A	21492.68	21499.06	21498.03	21491.70	21495.42(3)	
	E	21496.88	21503.21	21502.20	21495.89		−4.18(3)
$10_{19} \leftarrow 10_{010}$	A	22173.89	22180.32	22179.38	22172.97	22176.69(16)	
	E	22178.11	22184.49	22183.68	22177.23		−4.24(2)
$11_{110} \leftarrow 11_{011}$	A	22939.30	22945.80	22944.94	22938.46	22942.17(6)	
	E	22943.58	22950.10	22949.27	22942.73		−4.29(−1)
$12_{111} \leftarrow 12_{012}$	A	23793.36	23800.02	23799.29	23792.54	23796.34(−14)	
	E	—	23804.36	23803.58	23796.91		−4.33(−5)

a) Components of the quadrupolar multiplets are labeled F quantum number of the lower level; components of the internal rotation doublet are labeled A or E. b) Hypothetical unsplit frequencies. Figures in parentheses indicate the difference between the observed and calculated frequencies. c) Spacing of the internal rotation doublet, $\nu_A - \nu_E$. Figures in parentheses indicate the difference between the observed and calculated values.

χ_{zz} values obtained from the above two cases are nearly equal to each other. They are -74.7 ± 0.6 and -58.5 ± 0.7 MHz, for the $^{35}ClCH_2{}^{74}GeH_3$ and $^{37}ClCH_2{}^{74}GeH_3$ species, respectively, when $\eta_z=0$ is assumed and the ratio between the ^{35}Cl and ^{37}Cl species is 1.28 which is close to the ratio of quadrupole moments of the ^{35}Cl and ^{37}Cl nuclei (1.2688).[7]

The χ_{zz} values for ethyl chloride ($^{35}ClCH_2CH_3$) and (chloromethyl)silane ($^{35}ClCH_2SiH_3$) were reported by Schwendeman and Jacobs,[4,8] to be -71.24 ± 0.19 and -72.0 ± 0.6 MHz under the same assumption as in the present work. It should be noted that the χ_{zz} value for (chloromethyl)germane is about 4% larger than that of ethyl chloride and (chloromethyl)-silane beyond experimental error.

Internal Rotation of the GeH_3 Group

Weak spectra attributed to the excited vibrational state exist around the ground state spectra. Some of them exhibit doublet structures besides the hyperfine structures due to the quadrupolar coupling effect. The assignments of the excited state spectra were made for the (34, 74)-H_3 and (35, 72)-H_3 species. They are presumably the spectra due to the first excited GeH_3 torsional state from the spacings of the doublet structures found for the b-type transitions. The observed frequencies of these spectra are given in Table 6. The χ_{aa} and $\eta_a\chi_{aa}$ values for the excited state are essentially equal to those for the ground state (Table 7).

From the splittings of the doublet structures, the barrier to internal rotation of the GeH_3 group was calculated by the principal axis method using the structure given in the preceding section. The barrier height is $V_3=1740\ \pm30$ cal/mol[10] which is much higher than that for (fluoromethyl)germane (1390 ± 40),[1] fluoromethylgermane (941 ± 5)[2] and methylgermane (1239 ± 25).[6] The ratio of the barriers for (chloromethyl)germane and (fluoromethyl)germane is calculated to be 1.25, while that for ethyl chloride (3685 ± 12)[8] and ethyl fluoride (3306 ± 100)[9] is 1.11. The increase in the barrier from the fluoride to the chloride for the germane is much larger than for the ethyl halides.

TABLE 7. TORSIONAL EXCITED STATE AND INTERNAL ROTATION BARRIER OF THE GeH_3 GROUP[a,b]

	(35, 74)-H_3	(35, 72)-H_3
A (MHz)	20634.71(46)	20646.26(45)
B (MHz)	2078.25(2)	2096.90(1)
C (MHz)	1958.63(2)	1975.31(1)
D_J (MHz)	0.0003(12)	−0.0002(13)
χ_{aa} (MHz)	−29.7(15)	−29.7(20)
$\eta_a\chi_{aa}$ (MHz)	−44.3(8)	−44.2(10)
I_α amu Å^2	6.3133	6.3133
F (GHz)	99.819	99.820
λ_a	0.86162	0.86123
λ_b	0.50759	0.50821
s	81.255	81.301
V_3 (cal/mol)	1740(30)	1741(30)

a) Figures in parentheses indicate the uncertainties calculated from 2.5 times the standard deviation attached to the last significant figures. b) I_α; Moment of inertia of the GeH_3 group about the internal rotation axis, λ_a and λ_b; direction cosine of the internal rotation axis against the a- and b-inertial axes, F; $\hbar/2rI_\alpha$, $r=1-\lambda_a{}^2I_\alpha/I_a-\lambda_b{}^2I_\alpha/I_b$, s; Reduced barrier.

The authors wish to express their thanks to Dr. C. Matsumura and Dr. H. Takeo, National Chemical Laboratory for Industry, Tokyo for their helpful discussions and use of the spectrometer.

References

1) L. C. Krisher, W. A. Watson, and J. A. Morrison, *J. Chem. Phys.*, **60**, 3417 (1974).
2) R. F. Roberts, Thesis, New York University (1972).

3) D. Seyferth and E. G. Rochow, *J. Am. Chem. Soc.*, **77**, 907 (1955).
4) R. H. Schwendeman and G. D. Jacobs, *J. Chem. Phys.*, **36**, 1251 (1962).
5) R. W. Kilb and L. Pierce, *J. Chem. Phys.*, **27**, 108 (1957).
6) V. W. Laurie, *J. Chem. Phys.*, **30**, 1210 (1959).
7) C. H. Townes and A. L. Schawlow, "Microwave Spectroscopy," McGraw-Hill, New York (1955), Appendix VII.
8) R. H. Schwendeman and G. D. Jacobs, *J. Chem. Phys.*, **36**, 1245 (1962).
9) D. R. Herschbach, *J. Chem. Phys.*, **25**, 358 (1956).
10) The barrier height slightly differs from the one reported but is essentially equal within experimental error. (J. Nakagawa and M. Hayashi; *Chem. Lett.*, **1974**, 1379).

Measurements of the Interactions between Polyethylene Glycol and Organic Compounds by Gas Chromatographic Technique*

Mitsuyasu KAWAKAMI, Makoto EGASHIRA,** and Shuichi KAGAWA

Department of Industrial Chemistry, Faculty of Engineering, Nagasaki University, Nagasaki 852

(Received June 21, 1976)

A gas-liquid chromatographic technique was employed to measure the thermodynamic properties of the solutions consisting of polyethylene glycol (PEG) and some organic compounds. Three kinds of PEG with different molecular weights were used as a stationary liquid, and six kinds of organic compounds as a solute. For most of the compounds examined, the retention volume varied with the sample size injected. By using the retention volume at an infinitesimal sample size, thermodynamic properties of organic compounds at infinite dilution in PEG, such as the activity coefficient based on weight fraction, Henry coefficient based on weight fraction, and the partial molar excess enthalpy, were determined. From the results it was found that the particular interactions between organic compounds and PEG such as the hydrogen bond formation is not significant, and the solutions can be regarded as a regular solution. The solubility parameters of PEG-600, -1000, and -4000 at 67.3 °C were found to be 10.0, 9.8, and 9.5, respectively.

Many investigations[1] have been carried out to measure thermodynamic properties of solution with gas-liquid chromatography (GLC). As an example, Everett and Stoddart[2] measured the infinite dilution activity coefficients of a series of hydrocarbons in dinonyl phthalate by GLC and obtained results in good agreement with those by a static method. However, the technique was not applied to the polymer–organic compound systems until quite recently. Since there exists a distribution of molecular weights in polymer, the activity coefficient based on mole fraction is not adequate for such a system.

Recently the activity coefficients based on weight fraction and molality were proposed for a polymer–organic compound system by Patterson *et al.*,[3] and Fritz and Kovats,[4] respectively. On the other hand, Newman and Prausnitz[5] used the GLC technique to obtain the volatility (based on weight fraction) of solvents in polymer coatings.

In the present work, the measurement of thermodynamic properties based on weight fraction by GLC technique was carried out for the system of polyethylene glycol (PEG) and some organic compounds. PEG is a popular column packing material in gas chromatography, several investigations having been made on its gas chromatographic properties. Adlard[6] found that the retention volume of alcohol decreases with increase in the molecular weight of PEG. The behavior of alcohol, which is opposite to that of other organic compounds, was considered to be due to hydrogen bond with PEG. Watanabe *et al.*,[7] and Yamao[8] independently found a similar behavior for formaldehyde. However, no thermodynamic properties were determined for the reason described above. In this work, the activity coefficient based on weight fraction at infinite dilution, Henry coefficient based on weight fraction, and the partial molar excess enthalpy of mixing were determined for several organic compounds. The solubility parameters of PEG were determined by the method of Takamiya *et al.*[9] The peculiar behavior of alcohol as regards the retention volume on the molecular weight of PEG could be interpreted by the solubility parameter.

Theoretical

The net retention volume V_N can be related to the partition coefficient K_d for GLC by

$$V_N = K_d V_2 \tag{1}$$

where V_2 is the total volume of stationary liquid in the column. The corrected retention volume divided by the weight of stationary liquid w_2 and converted into 0 °C is called the specific retention volume V_g, which is related to V_N by

$$V_g = \frac{V_N}{w_2}\frac{273}{T_c} \tag{2}$$

where T_c is the column temperature. From Eqs. 1 and 2 we obtain

$$K_d = V_g \frac{w_2}{V_2}\frac{T_c}{273} = V_g \rho_2 \frac{T_c}{273} \tag{3}$$

where ρ_2 is the density of stationary liquid. The value of V_g can be obtained experimentally by means of the equation

$$V_g = \frac{3}{2}\left\{\frac{(p_i/p_o)^2-1}{(p_i/p_o)^3-1}\right\}\frac{273}{T_r}\frac{1}{w_2}t_R F \tag{4}$$

where p_i and p_o are the pressures at inlet and outlet, respectively, t_R is the peak maximum retention time, and F is the flow rate of carrier gas at room temperature T_r.

If the temperature dependence of ρ_2 can be neglected, the differentiation of Eq. 3 by $1/T_c$ gives

$$\frac{d \ln K_d}{d(1/T_c)} = -\frac{\Delta H_s}{R} = \frac{d \ln V_g}{d(1/T_c)} - T_c \tag{5}$$

where ΔH_s is the heat of solution. Thus the value of ΔH_s can be determined from the temperature dependence of V_g.

Following Patterson *et al.*,[3] the infinite dilution activity coefficient $\gamma_1^\infty(w)$ based on weight fraction is expressed as

$$\ln \gamma_1^\infty(w) = \ln \frac{273R}{M_1 p_1^\circ V_g} - \frac{B_{11}-v_1^\circ}{RT_c}p_1^\circ \tag{6}$$

* A preliminary report of this work was presented at the 33rd National Meeting of the Chemical Society of Japan, Fukuoka, October 1975.

** Department of Materials Science and Engineering, Faculty of Engineering, Nagasaki University, Nagasaki 852.

TABLE 1. SECOND VIRIAL COEFFICIENTS, VAPOR PRESSURES, AND MOLAR VOLUMES OF SOLUTES AT 67.3 °C

Solute	$-B_{11}$ / ml mol^{-1}	p_1° / Torr	v_1° / ml mol^{-1}
Ethanol	604	486	62.3
Methanol	475	839	43.4
Ethyl acetate	1052	549	104.3
Dichloromethane	611	1852	68.1
Benzene	1041	500	94.1
Hexane	1209	728	140.1

where the subscript 1 denotes the solute. The second term of the right side is a correction for the nonideality of gas phase. B_{11} is the second virial coefficient of pure solute, p_1° the saturated vapor pressure, v_1° the molar volume at column temperature, and M_1 the molecular weight. When B_{11}, p_1°, and v_1° are known, $\gamma_1^\infty(w)$ can be calculated from V_g. In the present work, B_{11} and p_1° were evaluated by the Berthelot relation and the Antoine equation, respectively, the value of v_1° being estimated from the density by using the expansion factor proposed by Watson. These values are given in Table 1.

From the temperature dependence of activity coefficient, the partial molar excess enthalpy of mixing at infinite dilution $\Delta\bar{H}_1^{E\infty}$ can be evaluated by the equation

$$\frac{d \ln \gamma_1^\infty(w)}{d(1/T_c)} = \frac{\Delta\bar{H}_1^{E\infty}}{R}, \tag{7}$$

and the Henry coefficient based on weight fraction $H_1(w)$ can be evaluated by the equation

$$H_1(w) = p_1^\circ \gamma_1^\infty(w). \tag{8}$$

The solubility parameter of stationary liquid can be determined as follows.

If the temperature dependence of gas phase imperfection term (the second term of right side of Eq. 6) can be neglected, differentiating Eq. 6 by $1/T_c$, and using the relations of Eqs. 5 and 7 and the Clausius-Clapeyron equation, $-d\ln p_1^\circ/d(1/T) = \Delta H_1^v/R$, we obtain[10]

$$-\Delta H_s = \Delta H_1^v - RT_c - \Delta\bar{H}_1^{E\infty} \tag{9}$$

where ΔH_1^v is the heat of vaporization.

The partial molar excess enthalpy in an infinitely dilute regular solution is expressed as

$$\Delta\bar{H}_1^{E\infty} = v_1^\circ(\delta_1 - \delta_2)^2 \tag{10}$$

where δ_1 and δ_2 are the solubility parameter of solute and solvent (stationary liquid), respectively. The solubility parameter of solute can be estimated by the equation

$$\delta_1 = \left(\frac{\Delta H_1^v - RT}{v_1^\circ}\right)^{1/2}. \tag{11}$$

Substitution of Eqs. 10 and 11 into Eq. 9 gives

$$-\Delta H_s/v_1^\circ = 2\delta_1\delta_2 - \delta_2^2 \tag{12}$$

which shows that there is a linear relationship between $-\Delta H_s/v_1^\circ$ and δ_1. Hence, if the plot of $-\Delta H_s/v_1^\circ$ against δ_1 is linear, the system can be regarded as a regular solution and δ_2 can be obtained from the slope and also from the intercept, independently.[9] In the present work, ΔH_1^v was estimated from the slope of the Othmer chart drawn by the vapor pressure data, and δ_1 was calculated from Eq. 11.

Experimental

Apparatus. A Yanagimoto G-80 gas chromatograph was used. The column was a copper tube of 3 mm i.d. and 2 m in length. The measurements were carried out in the range 56.5—77.1 °C. Helium was used as carrier gas. The flow rate was measured at the outlet by soap-film flowmeter and corrected for a vapor pressure of water. The flow rate was kept at 20 ml/min. The sample was injected with a 1-μl micrometer syringe and the sample size was varied below 0.1 μl. The accurate sample size was determined from the peak area in chromatogram.

Stationary Phase and Column Preparation. PEG-600, -1000, and -4000 (Gasukuro Kogyo Co.) were coated on the solid support, 60—80 mesh of Uniport B (Gasukuro Kogyo Co.) in the range of coverage ratio 0.1—0.3. The coverage ratio which was measured with the Soxhlet extractor did not change throughout the measurement.

The properties of PEG used are given in Table 2. The melting range was determined by DSC and the concentration of end hydroxyl group C_{OH} was measured by titration. The average molecular weight M_n was calculated from C_{OH}.

TABLE 2. PROPERTIES OF PEG USED

	C_{OH} / mmol g-packing^{-1}	M_n	melt. range / °C
PEG-600	3.18	670	−4—17
PEG-1000	1.52	1400	22—48
PEG-4000	0.61	3400	50—59

Solute. The following compounds were used as a solute: ethanol, methanol, ethyl acetate, dichloromethane, benzene, and hexane. They were of reagent grade and used without further treatment.

Preliminary Experiments

Effect of Sample Size on Retention Volume. For most of the solutes, especially for methanol and hexane, the specific retention volume increased with a decrease in the sample size injected. An illustration is given in Fig. 1. The retention volume at the infinitesimal sample size obtained by extrapolation was used for calculation below.

Effect of Coverage Ratio on Retention Volume. In some GLC systems, surface adsorption occurs in addition to absorption. Martin[11] proposed that the retention volume observed would be presented by the sum of two terms,

$$V_R = K_d V_2 + K_a A$$

where K_a is the adsorption coefficient and A is the surface area of stationary liquid. Assuming that A is independent of coverage ratio α and equal to the surface area of solid support, and using V_g instead of V_R, we obtain

$$V_g = \frac{273}{T_c}\frac{1}{\rho_2}K_d + \frac{273}{T_c}s\frac{1-\alpha}{\alpha}K_a$$

where s is the specific surface area of support. Therefore, when there exists a contribution of surface adsorption, V_g should vary with α.

The retention volumes were measured by varying the coverage ratio from 0.1 to 0.3. The result is shown in Fig. 2.

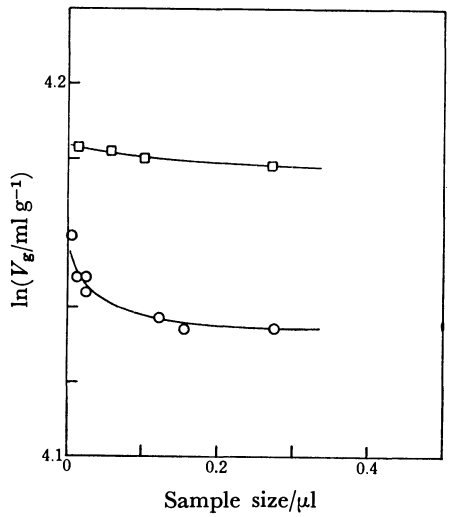

Fig. 1. An example of the variation of specific retention volumes with sample size.
□: Ethyl acetate–PEG-600 at 67.3 °C
○: Methanol–PEG-1000 at 77.1 °C

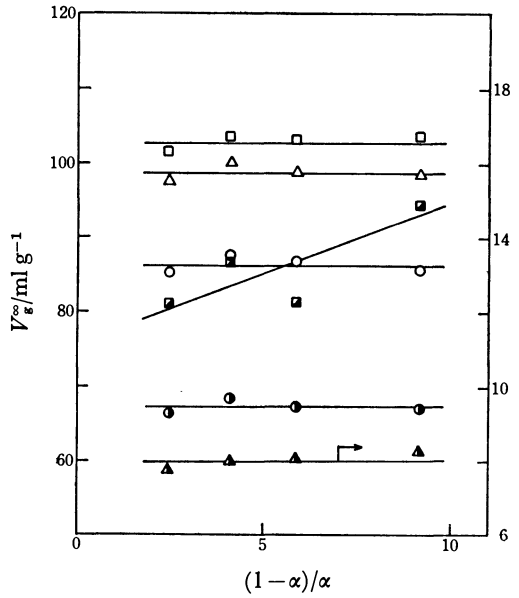

Fig. 2. The plots of V_g^∞ at 67.3 °C *vs.* $(1-\alpha)/\alpha$.
□: Ethanol, ◪: methanol, ◑: ethyl acetate, ○: dichloromethane, △: benzene, ▲: hexane.
The measure of right side is for hexane and the left for others.

Clearly the specific retention volumes are almost constant for more than 0.15 of α except for methanol. Thus the coverage ratio was kept 0.15 for each PEG, and methanol was removed from the discussion below.

Results

Thermodynamic Properties. The infinite dilution activity coefficients and Henry coefficients based on weight fraction are given in Table 3.

The partial molar heats of mixing at infinite dilution were evaluated from the slope of the plot of $\ln\gamma_1^\infty(w)$ against $1/T_c$ according to Eq. 7. An example is shown in Fig. 3.

Variations of Henry coefficients and the partial molar excess enthalpies with the concentration of hydroxyl group of PEG are shown in Figs. 4 and 5, respectively. We see that $\Delta\bar{H}_1^{E\infty}$ and $H_1(w)$ for hexane is much larger than that of other solutes. In the case of ethanol, on the other hand, the dependence of $\Delta\bar{H}_1^{E\infty}$ and $H_1(w)$ on C_{OH} is opposite that of other solutes in agreement with the result of Adlard.

Solubility Parameter of PEG. Adaptability of the thermodynamic properties we obtained to the regular solution theory will be examined. Figure

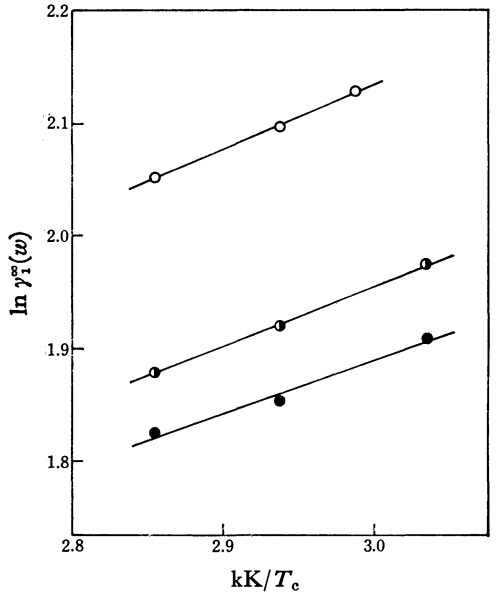

Fig. 3. An example of the plot of $\ln\gamma_1^\infty(w)$ *vs.* $1/T_c$ (sample: ethanol)
●: PEG-600, ◑: PEG-1000, ○: PEG-4000.

Table 3. Infinite dilution activity coefficients and Henry coefficients based on weight fraction at 67.3 °C

Solute	$\gamma_1^\infty(w)$ PEG			$H_1(w)$/kg atm mol^{-1} PEG		
	-600	-1000	-4000	-600	-1000	-4000
Ethanol	6.39	7.48	8.16	4.09	4.79	5.21
Ethyl acetate	5.53	5.41	5.20	3.99	3.90	3.76
Dichloromethane	1.46	1.33	1.23	3.56	3.23	3.01
Benzene	5.08	4.54	4.24	3.34	2.99	2.79
Hexane	40.1	35.3	32.7	38.4	33.8	31.3

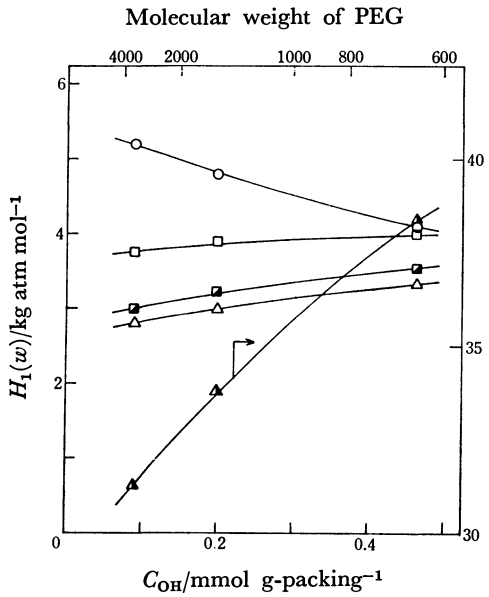

Fig. 4. The effect of end OH group of PEG on Henry coefficient at 67.3 °C.
○: Ethanol, □: ethyl acetate, △: benzene, ◪: dichloromethane, ▲: hexane.
The measure of right side is for hexane and the left for others.

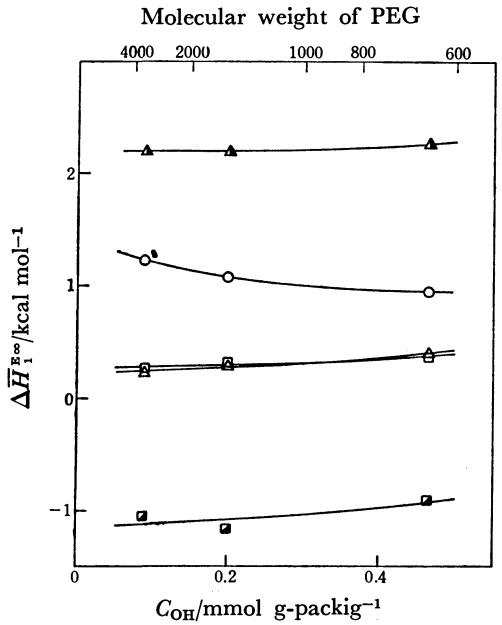

Fig. 5. The effect of end OH group of PEG on partial molar excess enthalpy.
○: Ethanol, □: ethyl acetate, △: benzene, ◪: dichloromethane, ▲: hexane.

6 shows the plot of Eq. 12. There seems to be an excellently linear relationship. The straight lines are computed by least squares treatment of data of all solutes except for the one of dichloromethane which deviates a great deal. The partial molar enthalpy of dichloromethane is negative (exothermic). This is inconsistent with Eq. 10, which shows that $\Delta\bar{H}_1^{E\infty}$ is never negative in a regular solution. Since dichloromethane is electron attractive, this seems to be due to an interaction of charge-transfer type. Therefore,

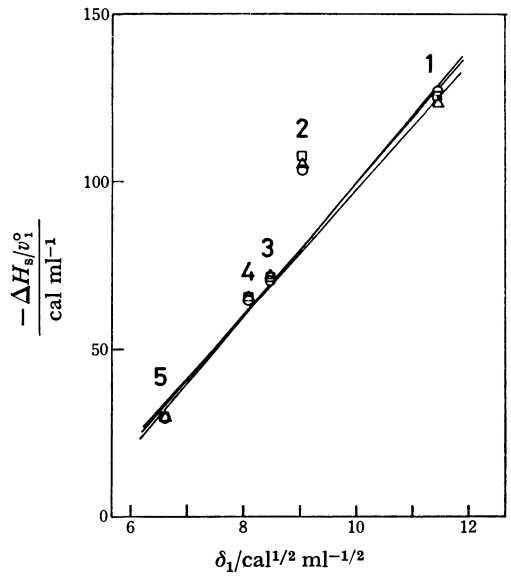

Fig. 6. The plots of $-\Delta H_s/v_1^\circ$ *vs.* δ_1.
○: PEG-600, □: PEG-1000, △: PEG-4000.
Solute 1: ethanol, 2: dichloromethane, 3: benzene, 4: ethyl acetate, 5: hexane.

the system would not show the behavior of a regular solution.

Solubility parameters of PEG calculated from the plot of Fig. 6 are given in Table 4. The values from the slope and intercept, obtained independently, show good agreement with each other. The solubility parameter decreases with increase in the molecular weight. The value calculated by Small's method[12] is about 9.1 at 25 °C, which may be more small at the measurement temperature. This method, however, refers to high molecular weight polymer in which the contribution of the end group can be neglected.

TABLE 4. SOLUBILITY PARAMETERS OF PEG AT 67.3 °C

	PEG		
	-600	-1000	-4000
From the slope	10.0	9.7	9.4
From the intercept	10.0	9.8	9.5

The hydroxylic compounds usually have high δ values due to self-association. Thus, the values obtained experimentally seem to be reasonable by taking account of the relatively low molecular weight of 600—4000 and of the appreciable contribution of the end hydroxyl group. The order of magnitude of δ is considered to be appropriate since the effect of the hydroxyl group will decrease with increase in molecular weight.

Takamiya *et al.*[9] obtained values of 8.8 and 10.0 for δ of PEG-400 and -1500, respectively, at 100 °C. While the values are close to our results, δ increases with the molecular weight of PEG. The difference may arise from the error due to a large sample size injected or from the difference in organic compounds used as solutes.

Discussion

Organic solvents can be classified on the basis of potentialities for forming hydrogen bonds.[13] For example, ethanol and methanol belong to the class containing both active donor and acceptor atoms. Benzene is known to be electron donative. Of all the solvents used here only hexane has no active atoms.

On the other hand, PEG has ether groups and end hydroxyl groups. As the molecular weight of PEG becomes larger, its nature as an ether will become dominant. PEG is known to be a polar liquid, and the interaction between PEG and polar solvent is expected to be complicated.

Adlard[6] considered that the different behavior of alcohol from other compounds in the dependence of retention volumes on molecular weight of PEG may arise from the formation of hydrogen bond between alcohols and PEG. It seems to be necessary, however, to take account of the effect of self-association in the case of hydroxylic compounds. We see that $\Delta H_1^{E\infty}$ for ethanol is endothermic (Fig. 5). This suggests that the rupture of self-association of alcohol at infinite dilution will play an important roll as well as the formation of hydrogen bond between PEG and alcohol. These phenomena contribute to the heat of mixing conversely each other. Consequently, the influence of the hydrogen bond on $\Delta H_1^{H\infty}$ will not appear apparently. For other polar compounds except for dichloromethane, no particular interaction is observed.

The system might be treated as a regular solution provided that the influence of a particular interaction such as hydrogen bond would be negligible. In the regular solution theory the heat of mixing is proportional to the difference in solubility parameters between solute and solvent as shown by Eq. 10. The solubility parameter of PEG decreases with increase in its molecular weight. Therefore, the solubility of a compound whose solubility parameter is smaller than that of PEG will increase with the molecular weight of PEG, and a compound of larger parameter than PEG will show the opposite tendency. Among the compounds examined here, only ethanol takes a larger value of solubility parameter than PEG. Thus the peculiar behavior of ethanol against the molecular weight of PEG could be explained in terms of solubility parameter. While particular interactions such as hydrogen bond between PEG and organic compound were expected to exist, the influence of such interactions was negligibly small except for dichloromethane and the solution could be treated as a regular solution.

References

1) C. L. Young, *Chromatogr. Rev.*, **10**, 129 (1968)
2) D. H. Everett and C. T. H. Stoddart, *Trans. Faraday Soc.*, **57**, 746 (1961)
3) D. Patterson, Y. B. Tewari, H. P. Schreiber, and J. E. Guillet, *Macromolecules*, **4**, 356 (1971)
4) D. F. Fritz and E. sz. Kovats, *Anal. Chem.*, **45**, 1175 (1973)
5) R. D. Newman and J. M. Prausnitz, *J. Paint Tech.*, **45**, 33 (1973).
6) E. R. Adlard, "Vapor Phase Chromatography," ed. D. H. Desty, Butterworths, London (1956), p. 98.
7) Y. Watanabe, K. Isomura, and Y. Tomari, *Kogyo Kagaku Zasshi*, **70**, 41 (1967)
8) M. Yamao, *Bunseki Kagaku*, **14**, 926 (1965).
9) N. Takamiya, J. Kojima, and Y. Tomari, *Kogyo Kagaku Zasshi*, **62**, 1371 (1959)
10) P. E. Porter, C. H. Deal, and F. H. Stross, *J. Am. Chem. Soc.*, **78**, 2999 (1956)
11) R. L. Martin, *Anal. Chem.*, **33**, 347 (1961); J. R. Conder, *ibid.*, **43**, 367 (1971)
12) P. A. Small, *J. Appl. Chem.*, **3**, 71 (1953).
13) R. H. Ewell, J. M. Harrison, and L. Berg, *Ind. Eng. Chem.*, **36**, 871 (1944).

The Crystal and Molecular Structure of Naphthanthrone

Shoji FUJISAWA, Isao OONISHI, Junji AOKI, and Satoshi IWASHIMA*

Department of Chemistry, Faculty of Science, Toho University, Funabashi-shi, Chiba 274

**Department of Chemistry, Faculty of Science and Technology, Meisei University, Hino-shi, Tokyo 191*

(Received July 5, 1976)

The crystals of naphthanthrone($C_{19}H_{10}O$) are orthorhombic, with the $P2_12_12_1$ space group and these lattice constants: $a=17.345(17)$, $b=3.973(13)$, $c=17.392(14)$ Å, and $Z=4$. The structure was solved by the Patterson method and refined by a block-diagonal least-squares program to give an R-value of 0.085 on the basis of the 897 observed reflections collected by Weissenberg photographs. The molecule is planar within the limits of experimental error and has an approximate symmetry of mm. The molecules are stacked face-to-face by van der Waals forces along the b-axis. The interplanar spacing is 3.50 Å.

The bimolecular condensation of benzanthrone (7*H*-benz[*de*]anthracen-7-one) affords condensation products with nine benzene rings. Similarly, naphthanthrone (6*H*-benzo[*cd*]pyren-6-one) gives products with eleven benzene rings. They are useful and interesting materials in the field of organic semiconductors. It is, therefore, desirable to know the crystal structures of these products and also those of the starting materials in order to study the intrinsic behavior of their electrical conduction. It may be suggested that symmetric naphthanthrone molecules are probably more closely packed in the crystal, since its melting point is 252 °C and far higher than that of benzanthrone (169 °C), in spite of the fact that the former molecule is larger than the latter one by only one additional benzene ring. From these points of view, the present investigation was carried out.

Experimental

The naphthanthrone was prepared by the condensation of pyrene and glycerol in sulfuric acid.[1] The crude product was dissolved in toluene and passed through a column of alumina to obtain the purified crystals. The crystals thus obtained were recrystallized from toluene. After several repetitions of this purification process, crystals suitable for X-ray work were selected.

The unit-cell dimensions were determined from the higher-order reflections on Weissenberg photographs calibrated by reflections from a Cu wire. The systematic absences were: $h00$ for h odd, $0k0$ for k odd and $00l$ for l odd.

Crystal data

$C_{19}H_{10}O$, $M=254.29$, mp 252 °C, Space Group: $P2_12_12_1$, $Z=4$; $a=17.345(17)$, $b=3.973(13)$, $c=17.392(14)$ Å, $U=1199$ Å^3; $D_x=1.409$, $D_m=1.42$ g cm^{-3}, $F(000)=528$, μ(Cu $K\alpha$)$=7.1$ cm^{-1}

The crystal used for X-ray work had dimensions of approximately $0.1\times0.1\times0.8$ mm. Sets of multiple-film equi-inclination Weissenberg photographs were taken about the b-axis (0th to 3rd layers) and about the c-axis (0th to 3rd layers). Cu $K\alpha$ radiation was employed throughout. The intensities were estimated by means of a Rigaku photometer MP3. Weak intensities were visually estimated with standard film strip. They were corrected for Lorentz and polarization factors, but no absorption correction was applied. The range of relative intensities was from 1 to 50000. 897 independent reflections fell within this range, whereas 429 others were too weak to be observed.

Structure Determination and Refinement

The orientation of the molecule was easily deduced from the three-dimensional Patterson maps, but the position of the center of gravity could not be fixed. Therefore, some two-dimensional models were assumed. One of them gave an R_{h0l}-value of 0.45. After two cycles of calculations of the structure factors and the electron densities $\rho(xz)$, the R_{h0l}-value dropped to 0.20. At this stage, the y coordinates of the molecule were calculated, taking the tilt and the packing into account. Structure factor calculations gave the R-value of 0.25.

The structure was refined by a block-diagonal least-squares method with a HBLS4 program written by Dr. Tamaichi Ashida. After six cycles of refinements, the R-value dropped to 0.15. Three more cycles of refinements with anisotropic temperature factors gave the R-value of 0.12. At this stage, the difference synthesis revealed all the hydrogen atoms. Further refinement cycles with isotropic temperature factors for hydrogen atoms reduced R to 0.085. The following weighting scheme was employed: $w=0.4$ if $F_0<F_{min}(=4.0)$, otherwise $w=1.0$. The atomic scattering factors were taken from "*International Table for X-Ray Crystallography*" (1962).[2] The observed and calculated structure factors are listed in Table 1.** The final atomic parameters and their estimated standard deviations are summarized in Table 2.

Description of the Structure and Discussion

Figure 1 illustrates the structure projected along the b-axis. The molecules are stacked face-to-face by van der Waals forces along the b-axis. The interplanar spacing is 3.50 Å. It is slightly greater than the 3.44 and 3.45 Å of violanthrone[3] and the 3.42 Å of isoviolanthrone.[4] Figure 2 shows the superposition of the molecules.

The closest approach between the molecules occurs between O and C(11)$(1-x, 1/2+y, 1/2-z)$, the distance being 3.355 Å. Such short contacts between an oxygen atom and a carbon atom have been found in the crystals of the quinones observed hitherto.[3,5-7]

The bond lengths and angles in the molecule are shown in Figs. 3 and 4, together with estimated standard deviations. The average C–C bond length, 1.408 Å, is comparable to the value, 1.409 Å, of tetrabenzo-[*a*, *cd*, *j*, *lm*]perylene.[8] The bond lengths of C(17)–

** Table 1 has been deposited with the office of the Chemical Socity of Japan, 1-5 Kanda-Surugadai, Chiyoda-ku, Tokyo 113 (Document No. 7634).

TABLE 2. ATOMIC PARAMETERS

(a) Positional and thermal parameters for non-hydrogen atoms ($\times 10^4$), with e. s. d.'s in parentheses. The β_{ij}'s are defined by $\exp[-(h^2\beta_{11}+k^2\beta_{22}+l^2\beta_{33}+2hk\beta_{12}+2hl\beta_{13}+2kl\beta_{23})]$.

	x	y	z	β_{11}	β_{22}	β_{33}	β_{12}	β_{13}	β_{23}
C(1)	1198(5)	1860(26)	4791(5)	54(4)	950(93)	53(4)	83(19)	25(4)	49(18)
C(2)	827(5)	3570(29)	4200(5)	45(4)	1066(97)	64(4)	−47(20)	3(4)	−24(22)
C(3)	1226(5)	4274(24)	3511(5)	45(4)	574(72)	49(4)	−35(15)	1(3)	−14(15)
C(4)	848(5)	5966(28)	2901(5)	46(4)	1060(97)	63(4)	23(21)	−2(4)	−23(21)
C(5)	1253(5)	7754(27)	2242(5)	62(5)	867(93)	57(4)	15(20)	−18(4)	−36(19)
C(6)	2032(5)	5757(25)	2153(4)	51(4)	807(82)	41(3)	6(17)	−7(3)	−58(16)
C(7)	2393(4)	4104(23)	2751(4)	40(3)	733(77)	31(3)	8(15)	−2(3)	−38(14)
C(8)	3194(5)	3181(24)	2646(4)	49(4)	813(82)	31(3)	−48(16)	1(3)	−31(14)
C(9)	3584(4)	1342(24)	3301(4)	33(3)	774(73)	33(3)	−37(15)	−2(3)	−25(14)
C(10)	4343(5)	430(24)	3226(5)	43(4)	813(83)	44(3)	−6(16)	−2(3)	−14(16)
C(11)	4720(5)	−1170(26)	3831(5)	40(4)	789(80)	55(4)	15(17)	−4(3)	−67(17)
C(12)	4323(5)	−1944(25)	4501(5)	45(4)	862(86)	49(4)	20(17)	−10(3)	−34(17)
C(13)	3545(5)	−936(25)	4591(4)	52(4)	921(81)	31(3)	−51(18)	−5(3)	−37(15)
C(14)	3175(4)	728(22)	3979(4)	38(3)	557(65)	30(3)	−23(14)	0(3)	−46(12)
C(15)	2388(4)	1649(22)	4055(4)	42(3)	643(73)	35(3)	−20(14)	4(3)	−31(14)
C(16)	2001(4)	3343(23)	3429(4)	49(3)	813(71)	31(3)	−48(13)	1(3)	−31(14)
C(17)	3117(5)	−1567(26)	5272(5)	64(5)	816(85)	41(3)	−43(18)	−6(4)	−33(16)
C(18)	2380(5)	−678(26)	5342(4)	59(4)	955(88)	34(3)	−40(18)	4(3)	23(16)
C(19)	1979(5)	926(25)	4733(4)	47(4)	777(77)	41(3)	−39(17)	6(3)	−22(16)
O	3553(3)	3753(19)	2036(3)	56(3)	1172(66)	43(2)	17(14)	7(3)	−9(13)

(b) Positional parameters for the hydrogen atoms ($\times 10^3$).
The mean isotropic temperature factor for the hydrogen atoms is 4.7(2.3) Å^2.

	x	y	z		x	y	z
H(C1)	85(5)	95(25)	526(4)	H(C10)	470(4)	95(22)	271(4)
H(C2)	19(4)	365(26)	421(4)	H(C11)	530(4)	−206(25)	381(4)
H(C4)	25(4)	644(22)	300(4)	H(C12)	467(5)	−344(26)	497(5)
H(C5)	101(4)	788(23)	179(4)	H(C17)	345(5)	−249(26)	564(5)
H(C6)	243(4)	609(20)	164(4)	H(C18)	198(4)	−131(24)	576(4)

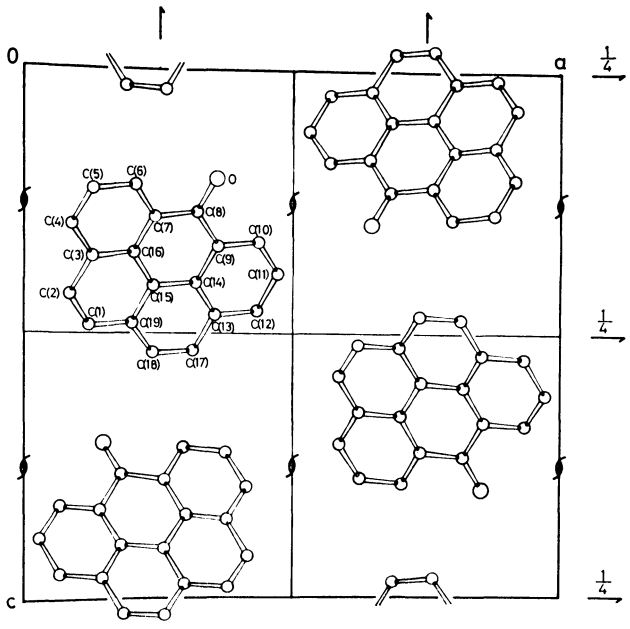

Fig. 1. A projection of the structure along the b-axis.

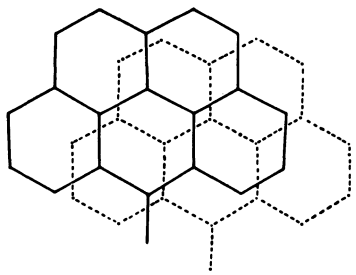

Fig. 2 Superposition of the naphthanthrone molecules.

C(18), C(14)–C(15), and C(8)–C(7) increase in that order (1.333→1.419→1.448 Å). The C(1)–C(2), C(15)–C(16), and C(8)–C(9) bonds also show a similar tendency, their bond lengths are 1.390, 1.445, and 1.513 Å respectively. Similarly, such tendencies have been observed in dinaphthperopyrene (1.387→1.423→1.472 Å)[9] and tetrabenzo[*a*, *cd*, *j*, *lm*]perylene (1.348→1.418→1.474 Å).[8] The C–C–C angles range from 117.2° to 122.5°, and the three bonds around each carbon are coplanar within the limits of experimental error. Figure 5 shows the deviation of each atom from the mean plane of the molecule. The equation of the mean molecular plane is: $-0.2831x-$

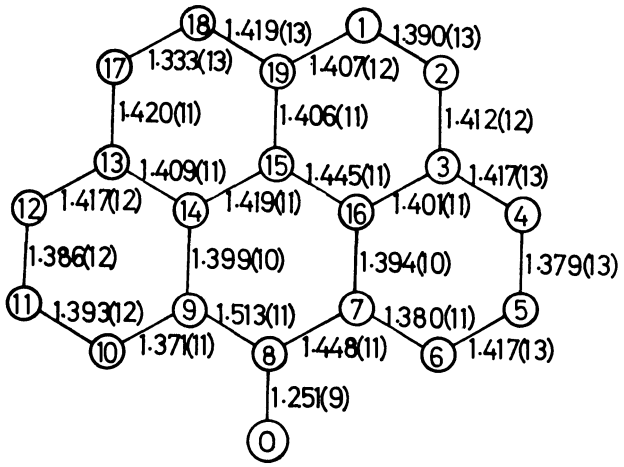

Fig. 3. Bond lengths (l/Å) with their estimated standard deviations.

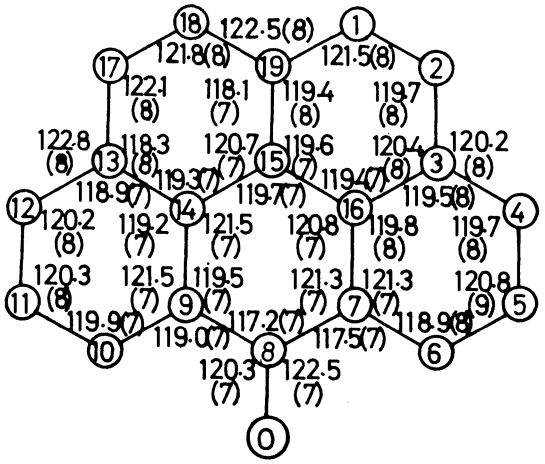

Fig. 4. Bond angles (φ/°) with their estimated standard deviations.

$0.8813y-0.3783z+4.421=0.0$, where x, y, and z are coordinates in Å units referred to the crystal axes, a, b, and c respectively.

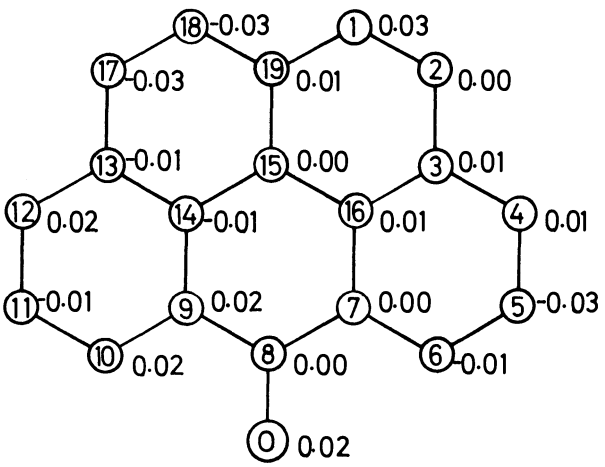

Fig. 5. Distances (l/Å) of atoms from the mean molecular plane.

All the calculations were carried out on a HITAC 8700/8800 at the Computer Center of University of Tokyo with a local version of the Universal Crystallographic Computation Program System, UNICS (1967).

References

1) W. Bradley and F. K. Sutcliffe, *J. Chem. Soc.*, **1951**, 2118.
2) "International Tables for X-Ray Crystallography," Vol. III, Birmingham, Kynoch Press (1962).
3) W. Bolten and H. P. Stadler, *Acta Crystallogr.*, **17**, 1015 (1964).
4) W. Bolten, *Acta Crystallogr.*, **17**, 1020 (1964).
5) I. A. S. Edwards and H. P. Stadler, *Acta Crystallogr.*, **B27**, 946 (1971).
6) H. P. Stadler, Solid State Physics, *Bussei*, **5**, 659 (1964).
7) H. P. Stadler, *Acta Crystallogr.*, **6**, 540 (1953).
8) Y. Kohno, M. Konno, Y. Saito, and H. Inokuchi, *Acta Crystallogr.*, **B31**, 2076 (1975).
9) J. M. Robertson and J. Trotter, *J. Chem. Soc.*, **1959**, 2614.

A pH and pNa Study of Aqueous Solutions of Sodium Deoxycholate

Gohsuke SUGIHARA and Mitsuru TANAKA

Department of Chemistry, Faculty of Science, Fukuoka University, Nishi-ku, Fukuoka 814

(Received July 7, 1976)

The pH and pNa of aqueous solutions of sodium deoxycholate (SDC) were measured at various temperatures. The critical micelle concentrations (CMC) were determined by means of the crooked points on the plot of pH or pNa *vs.* the SDC concentration. The data obtained were interpreted thermodynamically, and changes in the enthalpy and entropy of micellization were evaluated, from which it was concluded that the hydrogen bond plays a very important role in the micelle formation.

Sodium deoxycholate (SDC), a bile salt, shows unique properties in its physicochemical and biological aspects, and SDC behaves as a surfactant. Although the micellar behavior in an aqueous solution of SDC has been studied in connection with various physicochemical properties,[1-9] the peculiarity with respect to pH and pNa has not been examined sufficiently.

As SDC is a salt of the "weak acid-strong base" type, the solution is basic due to hydrolysis. Though fatty acid soaps are also salts of the "weak acid-strong base" type, they are different from SDC in terms of the architecture of the hydrophobic part of the molecule, the balance of hydrophilicity and lyophilicity, and especially the ability to form intermolecular hydrogen bonding. In this paper the unique behavior of the hydrogen-ion and sodium-ion activity in an aqueous solution of SDC will be examined and discussed.

Experimental

Materials. SDC (Merck Co.) was recrystallized several times from a mixed solution of methanol and ethanol and then dried *in vacuo* at 110 °C. Sodium chloride, of a guaranteed reagent grade, was recrystallized from thrice-distilled water and dried *in vacuo*. The distilled water used for the preparation of solutions was previously freed from CO_2 by passing sufficient CO_2 free air through a soda lime column.

Apparatus and Procedure. a) *pH Measurement*: pH measurements were performed for the determination of the CMC, which was given by the break in the SDC concentration *vs.* pH curve at each temperature. The measurements were carried out using a Hitachi-Horiba pH meter, model F-7. The influence of CO_2 during the measurements was avoided by using an air current freed from CO_2 by means of a soda lime column. The solution to be measured was stirred by means of a magnetic stirrer (Acrobat Stirrer, made by the MS-Kiki Co.) which could be immersed in a water bath. The hydrolysis equilibrium was checked by means of the curve on the recorder for each measurement. The apparatus is shown schematically in Fig. 1.

b) *Activity Measurement of the Sodium Ion*: The measurements were carried out using a Hitachi-Horiba pNa meter, model N-5. The apparatus was almost the same as that of the pH measurements. The calibration curve was made by correlating the observed value with the literature value[10] for the activity of sodium ions in an aqueous solution of NaCl.

Results and Discussion

The pH change with the SDC concentration at various temperatures is shown in Fig. 2, while the relations of the sodium-ion activity *vs.* the SDC concentration are shown in Fig. 3. Every curve in both figures shows a break in its trend at the same concentration at the same temperature. These significant points correspond to the CMC values reported in other papers.[1-7] Accordingly, these methods can be used for the determination of the CMC of SDC. Table 1 lists the values of CMC obtained by both methods at each temperature.

In the concentration range of single dispersion, SDC molecules will dissociate almost perfectly, and

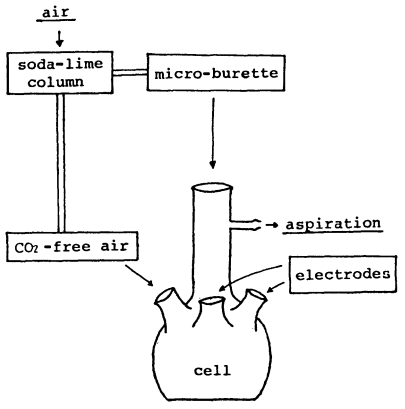

Fig. 1. The apparatus of measurement for the relation of SDC concentration *vs.* pH.

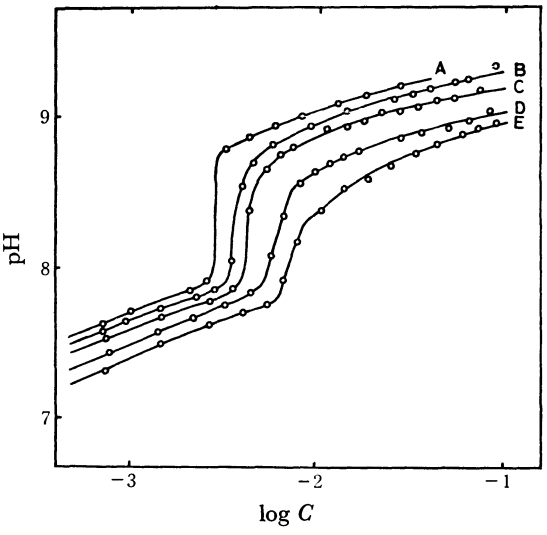

Fig. 2. Hydrolysis curves of SDC solution at various temperatures.
Key A: 10 °C, B: 15 °C, C: 20 °C, D: 30 °C, E: 40 °C.

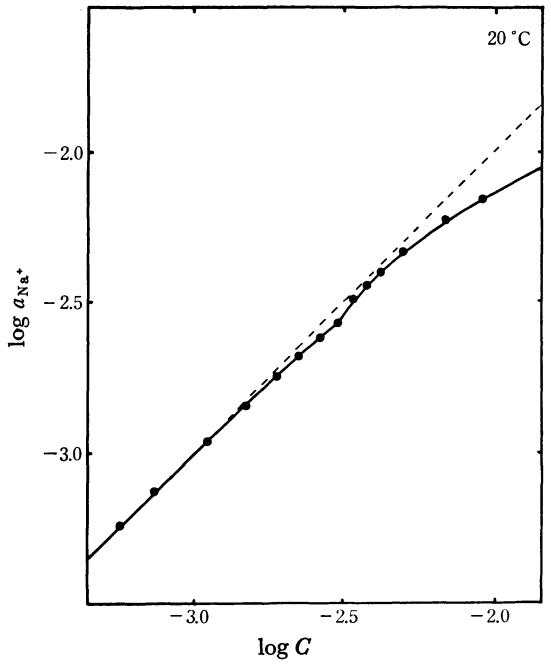

Fig. 3(a).

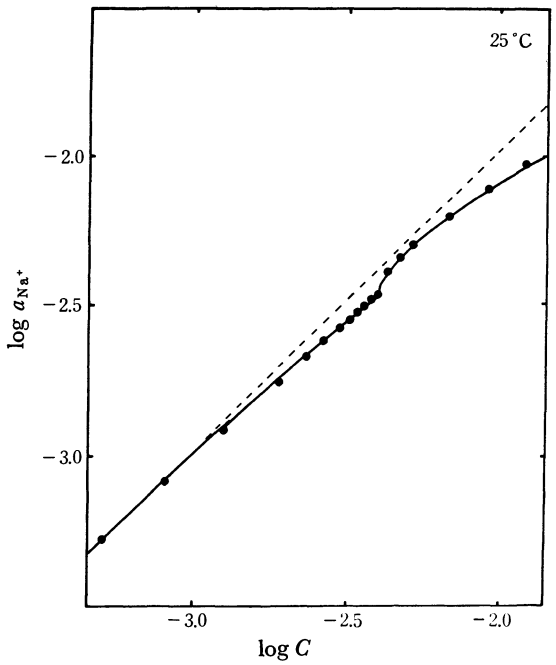

Fig. 3(b).

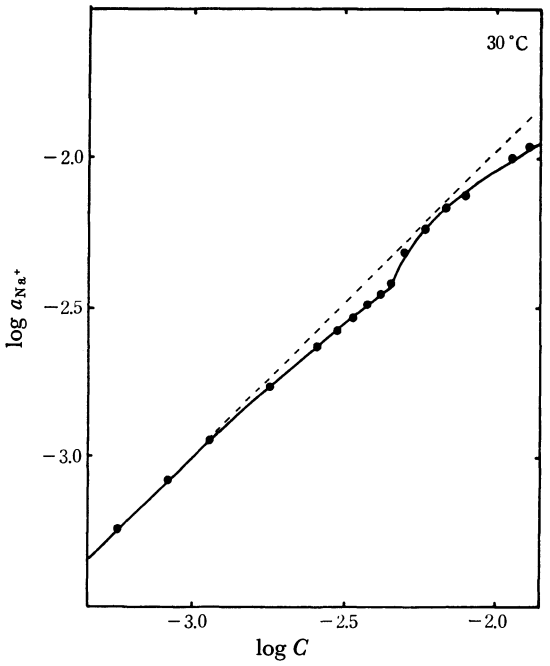

Fig. 3(c).

Fig. 3. The plot of SDC concentration *vs.* logarithm of sodium ion activity.
(a) 20 °C, (b) 25 °C, (c) 30 °C.

a hydrolysis equilibrium will be established. The concentrations of the undissociated species, sodium deoxycholate (NaDC), and the hydrolyzed species, deoxycholic acid (HDC), will increase with an increase in the SDC concentration. The associations of NaDC and HDC are expected to be easier than that of deoxycholate ions (DC^-) because of the smaller coulombic repulsion among them. Especially, HDC molecules are likely to form stable associates by hydrogen bonding. The micellization will be initiated with the association of HDC, and then accompanied by the participation of NaDC and DC^-. As soon as the micelles are formed, a new reaction of hydrolysis will begin abruptly on the surface of the micelles and a new equilibrium of hydrolysis will be established. Figure 2 shows that the pH increases abruptly from the CMC with an increase in the SDC concentration. This means that the degree of hydrolysis of DC^- in micelles is larger than that in single dispersion.

It can be seen from Fig. 3 that SDC dissociates perfectly in the dilute range of concentration below CMC as a 1-1 electrolyte, and that the degree of dissociation seems to decrease gradually up to the CMC as the concentration increases. Above the CMC the curve shows an abrupt increase in the activity coefficient. This behavior is different from that of sodium dodecylsulfate or sodium tetradecylsulfate.[11] Figures 2 and 3 tell us that the change in the sodium-ion activity in the vicinity of the CMC with an increase in the SDC concentration is contrary to that of the hydrogen-ion activity. This can be interpreted by thermodynamic considerations as follows.

We assume that the composition of the micelles is $DC^-\cdot\alpha H^+\cdot\beta Na^+$, where α and β are the numbers of the H^+ ion and the Na^+ ion respectively, per DC^- ion in the micelle.

Then, the equilibrium of micelle formation is expressed as follows:

$$DC^- + \alpha H^+ + \beta Na^+ \rightleftharpoons DC^-\cdot\alpha H^+\cdot\beta Na^+ \quad (1)$$

The chemical potentials of the components in the solution are, respectively:

$$\mu_{DC^-} = \mu^0_{DC^-} + RT \ln a_{DC^-} \quad (2)$$

$$\mu_{H^+} = \mu^0_{H^+} + RT \ln a_{H^+} \quad (3)$$

$$\mu_{Na^+} = \mu^0_{Na^+} + RT \ln a_{Na^+} \quad (4)$$

The chemical potential of the micelle-forming species ($DC^-\cdot\alpha H^+\cdot\beta Na^+$) in the micelle can be expressed by the following equation, if the micelle is regarded

Table 1. The CMC values determined by pH and pNa measurements

Temperature (°C)	CMC (mol/l) × 10^3	
	by pH measurement	by pNa measurement
10	2.95	
15	3.35	3.24
20	3.55	3.47
25	4.01	4.05
30	4.80	4.57
35	5.35	5.19
40	6.10	

as a pseudo phase:

$$\mu_m = \mu_m^0 (T, P) \tag{5}$$

From Eqs. 2—5 we obtain the free energy change of micelle formation per mole of the micelle-forming species, $\Delta\overline{G}_m$:

$$\Delta\overline{G}_m = \mu_m - \mu_{DC^-} - \alpha\mu_{H^+} - \beta\mu_{Na^+}$$
$$= \Delta\overline{G}_m^0 - RT \ln a_{DC^-} - \alpha RT \ln a_{H^+} - \beta RT \ln a_{Na^+} \tag{6}$$

where

$$\Delta\overline{G}_m^0 = \mu_m^0 - \mu_{DC^-}^0 - \alpha\mu_{H^+}^0 - \beta\mu_{Na^+}^0 = \text{const } (T, P).$$

As $\Delta\overline{G}_m$ is equal to zero at equilibrium, Eqs. 7—9 hold:

$$\ln a_{DC^-} = \text{const}(T, P) - \alpha \ln a_{H^+} - \beta \ln a_{Na^+} \tag{7}$$

Especially, at the CMC

$$\ln \text{CMC} = \text{const}(T, P) - \alpha \ln a_{H^+} - \beta \ln a_{Na^+} \tag{8}$$

and

$$\log a_{Na^+} = \text{const } (T, P) - \frac{1}{\beta} \log a_{DC^-} + \frac{\alpha}{\beta}\text{pH} \tag{9}$$

This equation tells us that $\log a_{Na^+}$ increases with the pH and α, and varies inversely with the β. The rise in $\log a_{Na^+}$ with the concentration above the CMC just corresponds to the rise in pH, and the decreasing tendency of the increase in a_{Na^+} at higher concentrations may be ascribed to the negative sign of the log a_{DC^-} term.

Since $\Delta\overline{G}_m$ can be regarded as a function of T, P a_{DC^-}, a_{Na^+} and a_{H^+}, the following equation holds for the perfect differential of $\Delta\overline{G}_m$:

$$d(\Delta\overline{G}_m) = -\Delta\overline{S}_m dT + \Delta\overline{V}_m dP + \left(\frac{\partial\Delta\overline{G}_m}{\partial \ln a_{DC^-}}\right) d \ln a_{DC^-}$$
$$+ \left(\frac{\partial\Delta\overline{G}_m}{\partial \ln a_{H^+}}\right) d \ln a_{H^+} + \left(\frac{\partial\Delta\overline{G}_m}{\partial \ln a_{Na^+}}\right) d \ln a_{Na^+} \tag{10}$$

The differential coefficients of the third, fourth, and fifth terms in Eq. 10 are obtained from Eq. 6 as $-RT$, $-\alpha RT$, and $-\beta RT$ respectively. Hence, Eq. 11 is derived from Eq. 10;

$$d(\Delta\overline{G}_m) = -\Delta\overline{S}_m dT + \Delta\overline{V}_m dP - RT d\ln a_{DC^-}$$
$$- \alpha RT d \ln a_{H^+} - \beta RT d \ln a_{Na^+} \tag{11}$$

For the reversible micelle formation at a constant pressure, we obtain the following relation:

$$\Delta\overline{S}_m = \frac{\Delta\overline{H}_m}{T} = -RT\left(\frac{\partial \ln a_{DC^-}}{\partial T}\right)_P$$
$$-\alpha RT\left(\frac{\partial \ln a_{H^+}}{\partial T}\right)_p - \beta RT\left(\frac{\partial \ln a_{Na^+}}{\partial T}\right)_P \tag{12}$$

Here, Eq. 12 may be rewritten as follows, assuming the temperature dependency of the activity coefficient of the SDC micelle is negligible:

$$\Delta\overline{S}_m = -2.303\, RT\left\{\left(\frac{\partial \log \text{CMC}}{\partial T}\right)_P - \alpha\left(\frac{\partial \text{pH}}{\partial T}\right)_P - \beta\left(\frac{\partial \text{pNa}}{\partial T}\right)_P\right\} \tag{13}$$

According to the results shown in Figs. 2 and 3, the plot of the pH value at the CMC *vs.* T affords a linear relation with a slope of -5.0×10^{-3}. The plot of the pNa value at the CMC *vs.* T similarly affords a linear relation with a slope of -1.0×10^{-2}. From Table 1, $(\partial \log \text{CMC}/\partial T)_P$ is roughly given as $+1.0\times10^{-2}$ at 20 °C. The α and β are not obtained from our experiment, but the data of Vochten and Joos[12] can be used to determine them approximately. Using Corrin's equation, they estimated β(their notation is K) as 2.0 and 2.5 under the conditions of constant pH values of 7 and 9 respectively at 20 °C. Here, it should be noted that the value of β obtained using Corrin's equation does not account for the contribution of H^+ to the micelle formation, and that β is related only to Na^+. Their data show that the CMC depends strikingly on the pH. The estimation of the α value is possible from the thermodynamic treatment of their data concerning the dependence on pH. Equation 8 is rewritten as follows:

$$\log \text{CMC} = \text{const } (T, P) + \alpha \text{ pH} + \beta \text{ pNa} \tag{14}$$

From Fig. 7 in their paper, α or $\Delta\log \text{CMC}/\Delta\text{pH}$ at a constant sodium-ion concentration is calculated to be about 0.8, independent of the value of the sodium-ion concentration. Using these values, $\Delta\overline{H}_m$ and $\Delta\overline{S}_m$ are evaluated as -6 kcal and -20 e.u. respectively from Eq. 13. On the other hand, the change in the partial molal volume of SDC on micellization, $\Delta\overline{V}_m$, has been obtained as -11 ml/mol at 30 °C from densitometry.[14] $\Delta\overline{H}$, $\Delta\overline{S}$, and $\Delta\overline{V}$ for the gelation of SDC solution all have negative signs which are characteristic of hydrogen-bond formation.[15] It is, then, reasonable to consider from these data that the micelle formation of SDC is mainly caused by hydrogen bonding, such as that between a hydroxyl group of one molecule and a carboxyl group of the other. This is in contrast to the micelle formation of other surfactants, *e.g.*, sodium dodecylsulfate and sodium tetradecylsulfate, which is mainly caused by hydrophobic interaction. It should be noted that $\alpha+\beta$ is nearly equal to unity, which means that micelles of SDC are electrically neutral. As an SDC molecule has two hydroxyl groups, SDC micelles may exist stably in the solution due to their hydrophilicity, which arises from the hydrogen-bond formation between water molecules and the remaining hydroxyl groups that have not been used for the micelle formation and so are able to contribute to the further association of the micelles.

This interpretation supports the helical structure model proposed by Rich and Blow.[8,9]

We would like to acknowledge the valuable discussions and suggestions by Prof. Dr. Ryohei Matuura, Kyushu University, and Prof. Dr. Iwao Satake, Kagoshima University. We are indebted to Miss Noriko Seike, Miss Mariko Ikeda, and Miss Kazuko Matsuo, Fukuoka University, for their technical assistance.

References

1) P. Ekwall, *J. Colloid Sci. Suppl. I*, **1944**, 66.
2) S. A. Johnston and J. W. McBain, *Proc. R. Soc. London, Ser. A*, **181**, 119 (1943).
3) T. Furusawa, *Fukuoka Acta Medica*, **53**, 124 (1962).
4) K. Fontell, *Kolloid Z. Z. Polym.*, **244**, 246 (1971).
5) K. Fontell, *Kolloid Z. Z. Polym.*, **244**, 253 (1971).
6) K. Fontell, *Kolloid Z. Z. Polym.*, **246**, 614 (1971).
7) K. Fontell, *Kolloid Z. Z. Polym.*, **246**, 710 (1971).
8) A. Rich and D. M. Blow, *Nature*, **182**, 423 (1958).
9) D. M. Blow and A. Rich, *J. Am. Chem. Soc.*, **82**, 3566 (1960).
10) G. J. Janz and A. R. Gordon, *J. Am. Chem. Soc.*, **65**, 218 (1943).
11) I. Satake, T. Tahara, and R. Matuura, *Bull. Chem. Soc. Jpn.*, **42**, 319 (1969).
12) R. Vochten and P. Joos, *J. Chem. Phys.*, **67**, 1373 (1970).
13) M. L. Corrin and W. D. Harkins, *J. Am. Chem. Soc.*, **69**, 679 (1947).
14) G. Sugihara, to be published.
15) G. Sugihara, to be published.

Theoretical Analysis of Optical Rotatory Power of Methylcyclohexanone with Treatment of Conformational Equilibria

Tomoyasu NAKAMURA and Yasumasa J. I'HAYA*

Department of Chemistry, Tokyo Kyoiku University, Otsuka, Tokyo 112

**Department of Materials Science, The University of Electro-Communications, Chofu-shi, Tokyo 182*

(Received July 14, 1976)

Optical rotational strength for the n-π^* transition of (*R*)-3-methylcyclohexanone is calculated by the CNDO/2 and INDO methods and compared with the observed values at 81 and 300 K, taking account of conformational equilibria. The conformer species are chosen so that they have minimal potential energies, the potential energy surface being estimated with a non-bonded interaction approximation. Excited state wave functions are improved by a model potential method. The ratio of the rotational strengths at 81 and 300 K, each of them being calculated as a statistical average of the rotational strengths of four conformers, is in good agreement with the corresponding observed value.

In the course of recent advances in quantum chemical approach for the prediction of optical rotatory power of optically active molecules, there have been brought forward several questions to answer; interpretation of observed circular dichroism spectra which are usually taken in solution, reasonable guess of molecular conformations, accuracy of ground and excited state functions, estimation of two-center (interatomic) matrix elements of the electric and magnetic dipole moment integrals, and so on.

Of all such problems the most important seems to be those about the first two, on which recent measurements[1] of circular dichroism spectra over a wide range of temperature have thrown the ray of hope for the settlement of the matter. That is, the rotational strengths of most optically active ketones increase as temperature goes down. Under the circumstances, one has no choice but to view that there must be several types of conformers mixed in a single solution, distributing according to the Boltzmann law, and giving one a temperature-dependent, statistically averaged rotational strength for a specific electronic transition. This view was first adopted by Moscowitz *et al.*[2] for the interpretation of thermodynamic data of (*R*)-*trans*-2-chloro-5-methylcyclohexanone, though they confined themselves only to a treatment of a two-conformer equilibrium. In the present study, we follow the above viewpoint in a comparison of experimental and theoretical optical rotatory powers of (*R*)-3-methylcyclohexanone, taking account of a multi-conformer equilibrium.

There is no definite way to guess what types of conformers effectively contribute to the mixing and what molecular geometry each conformer has. Among several procedures for conformational analysis of flexible molecules, we turn our attention to a classic model of interatomic interactions, *i.e.*, non-bonded and/or van der Waal's interactions, plus tortional interactions, which has been successfully applied to a number of saturated compounds by many authors.[3,4] Though the model is too simple to predict the precise temperature-dependent rotational strength of (*R*)-3-methylcyclohexanone, we have found after trying several other means that it is the only reliable way to guess the conformational (potential) energy surface of conformers.

As for the absolute magnitudes of rotational strengths of free molecules, there have been reported a good number of molecular orbital calculations, in particular cyclohexanone methyl derivatives have been most carefully investigated.[5] Good excited state wave functions are required in a calculation of rotational strength, and a usual procedure for improving approximate state functions is to invoke a configuration interaction (CI). Since the practical CI procedure for the calculation of matrix elements of the electric and magnetic dipole moments is rather complicated and troublesome, we shall adopt a model potential method in order to improve virtual orbitals to be used in a single-determinantal excited state functions.

Methods of Calculation

As mentioned above, we start from the viewpoint that the proper method for comparison of experimental and theoretical results would be to use a Boltzmann distribution among non-interacting conformers in order to obtain an average value for the rotational strength of the electronic transition under consideration at temperature T:

$$[R^l]^T_{\mathrm{av}} = \frac{\sum_i [\mathrm{R}^l_i]\exp(-E_i/kT)}{\sum_i \exp(-E_i/kT)} \tag{1}$$

where $[R^l_i]$ is the reduced rotational strength in the lth transition of conformer i and has the form

$$[R^l_i] = 1.08 \times 10^{40}\,\mathrm{Im}(\boldsymbol{\mu}^l \cdot \boldsymbol{m}^l), \tag{2}$$

$\boldsymbol{\mu}^l$ and $\boldsymbol{m}^l$ being the electric and magnetic dipole moments associated with transition l, and E_i is the conformational energy of conformer i measured from that of the most stable conformer.

An estimation of the value E_i is most difficult. An *ab initio* calculation of a precise potential curve associated with a conformational change is laborious, whereas a semi-empirical molecular orbital method seems no good to the estimation of such small energy differences as several kcal/mol among conformers. We therefore adopted as a measure of E_i the potential energies due to a non-bonded interaction between atoms and an internal rotation about a single bond. The former is represented by the Lennard-Jones "6—12" potential

$$U_{ij} = \frac{d_{ij}}{r_{ij}^{12}} - \frac{e_{ij}}{r_{ij}^{6}} \tag{3}$$

where d_{ij} and e_{ij} are the constants specific for atoms and assume to take the values given by Scott and Scheraga,[6] r_{ij} being the non-bonded interatomic distance in Å. The potential energy for a single internal rotation is given by

$$U_{\text{rot}} = \frac{1}{2}C(1-\cos 3\phi) \tag{4}$$

where C is the height of the potential peaks above the potential valleys and takes the values determined by Scott and Scheraga. We shall calculate U_{rot} for all the possible internal rotation arising from the change of the dihedral angles $\phi(3)$ and $\phi(5)$ (*vide infra*). An electrostatic (coulomb) interaction is neglected since there is only one polar bond in the molecule under consideration and such an interaction is very small.

The molecular orbitals used for the calculation of $[R_i^i]$ are obtained from the CNDO/2 and INDO methods. All the parameters involved are the same as those proposed by the original authors.[7] In order to obtain better excited state wave functions, we adopted Huzinaga and Arnau's model potential method.[8] The method uses the following Hartree-Fock operator[9] for a "singlet" excitation of one electron from the ith orbital

$$F_i = H + \sum_{j\neq i}(2J_j - K_j) - J_i + 2K_i \tag{5}$$

where J and K are the usual coulomb and exchange operators respectively, and $-J_i+2K_i$ is a pseudopotential which plays a significant part to improve virtual orbitals. The method has been shown to have the advantage of making an excited state calculation easier than the usual CI procedure.

The two-center (interatomic) terms of the electric and magnetic dipole moments are included in calculations of $[R_i^i]$ together with the one-center terms.[10] The dipole velocity formulation is adopted instead of the dipole length formulation. As pointed out by several writers,[11,12] the inclusion of the two-center terms in CNDO and INDO-type calculations is incompatible with the use of the zero differential overlap approximation. Therefore, CNDO and/or INDO basis sets should be transformed into deorthogonalized basis sets under the assumption that the CNDO and INDO basis are represented by Löwdin's orthogonalized atomic orbitals. We follow the recipe for deorthogonalization given by Imamura *et al.*[12]

In short, the molecular orbitals used for the purpose of comparison are divided into the following four:

Method I: CNDO/2 and/or INDO MO's without any modification.

Method II: MO's deorthogonalized.

Method III: MO's improved by the model potential method.

Method IV: MO's improved by the model potential method and deorthogonalized.

Results and Discussion

Figure 1 shows the molecular geometry of (*R*)-3-methylcyclohexanone proposed by Pao and Santry.[13] We first constructed a large number (about 200) of conformers by changing the dihedral angles $\phi(3)$ and $\phi(5)$ shown in Fig. 2, all the CCC angles being fixed

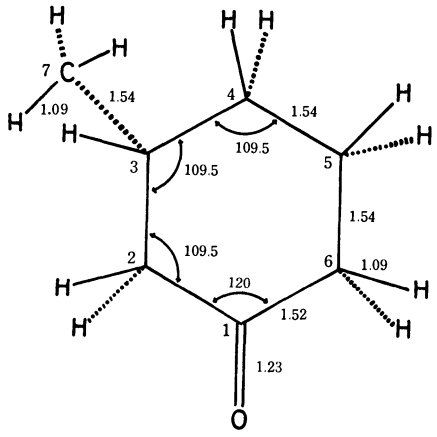

Fig. 1. Molecular geometry of (*R*)-3-methylcyclohexanone; bond lengths are given in Å and angles in degrees.

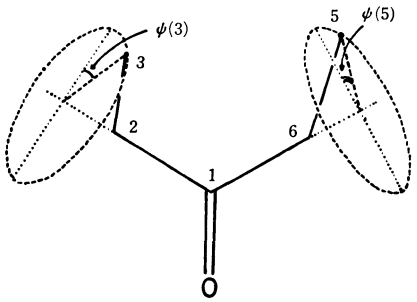

Fig. 2. Dihedral angles $\phi(3)$ and $\phi(5)$ in (*R*)-3-methylcyclohexanone.

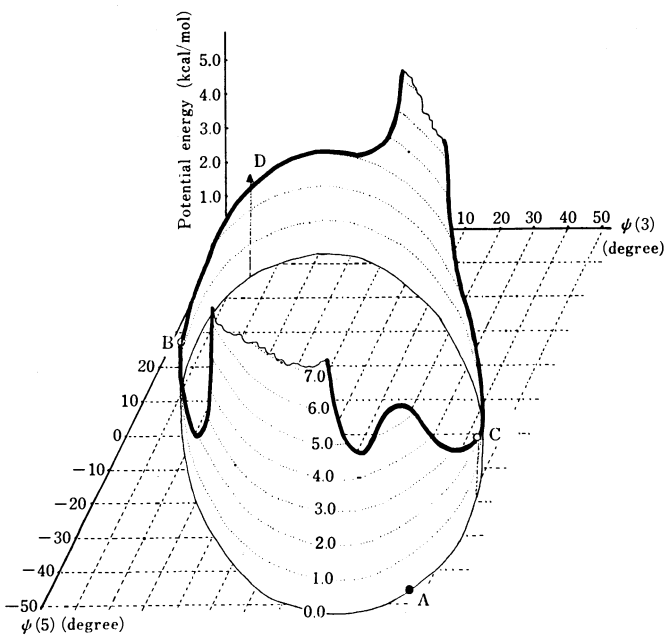

Fig. 3. Bird's-eye view of the potential surface for (*R*)-3-methylcyclohexanone.
A: Chair form with equatrial methyl; D: chair form with axial methyl; B, C: conformers corresponding to two minima of the surface.

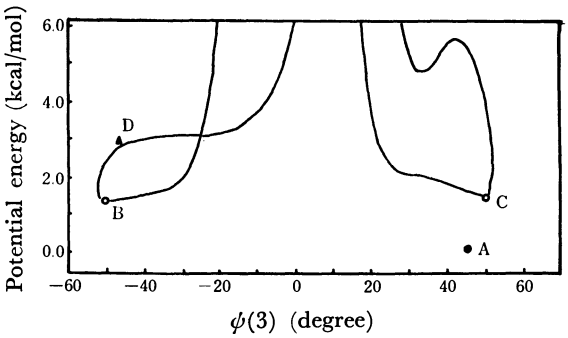

Fig. 4. Projection of the potential surface onto the $\psi(3)$-energy plane. A, B, C, and D are the same as in Fig. 3.

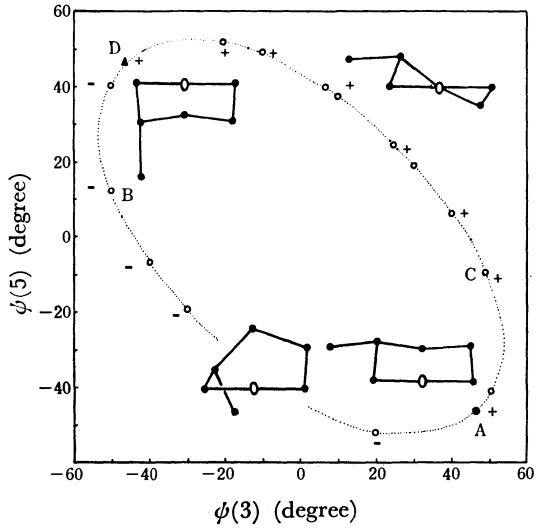

Fig. 5. Projection of the potential surface onto the plane of two dihedral angles, $\psi(3)$ and $\psi(5)$. + and − denote sings of rotational strength and A, B, C, and D are the same as in Fig. 3.

as in Fig. 1, and calculated the total non-bonded potential energies $\Sigma(U_{ij}+U_{rot})$ as a function of $\psi(3)$ and $\psi(5)$. Let the value of $\psi(3)$ be zero when atom C_3 is in the *trans* position with respect to the C=O bond and positive for the counter-clockwise rotation of the C_2–C_3 bond.

The results are illustrated in Fig. 3, where the potential energy is measured from that for the regular chair-form conformer with the equatrial methyl group (A in the figure). No conformer was found to have a lower potential energy than A, which then corresponds to a singular point in the potential energy surface. Thus, the regular chair-form conformer having the equatrial methyl group is computed out to be most stable, as might be expected. On the other hand, the potential energy of the regular chair-form conformer having the axial methyl group, D, comes to the neighborhood of the potential surface of the boat-forms. Figure 4 is a projection of the potential surface onto the $\psi(3)$-energy plane. There are found two potential minima, the corresponding conformers being called B and C.

The projection of the potential surface onto the plane of two dihedral angles $\psi(3)$ and $\psi(5)$ is illustrated in Fig. 5 which shows a correlation between signs of the calculated rotational strengths and the species of conformers. Each open circle corresponds to a selected conformer for which the rotational strength has been calculated and its sign is marked as plus or minus. For reference, some representative conformers are illustrated roughly at their proper positions. These calculated signs of rotational strength agree with those predicted by the octant rule, if it assumes to be applied even for a boat and/or twist boat-form conformer. However, in conflict with the octant rule, the calculated rotational strength for the regular chair-form conformer with the axial methyl group has a positive sign.

In Table 1 is listed a part of the calculated results for rotational strength for the n-π^* transition of (*R*)-3-methylcyclohexanone. Conformers B and C are chosen because they have the potential energies that correspond to minima of the potential surface (*vide supra*). The results for some other conformers of boat-form are also listed for reference.

With these calculated rotational strengths and potential energies of conformers A, B, C, and D, we calculate from Eq. 1 the statistical average of the rotational strength for the n-π^* transition of (*R*)-3-methylcyclohexanone at 300 and 81 K. The results are shown in Tables 2 together with the values Δ defined by

$$\Delta = \frac{[R]_{av}^{81} - [R]_{av}^{300}}{[R]_{av}^{300}} \times 100. \quad (6)$$

There can be seen in Table 2 a quite good agreement between the calculated and observed Δ values, though the absolute values of the predicted rotational strengths

Table 1. Calculated rotational strengths of conformers of (*R*)-3-methylcyclohexanone[a)]

Conformer	Angle (degree)		CNDO/2				INDO			
	$\psi(3)$	$\psi(5)$	I	II	III	IV	I	II	III	IV
A	46.02	−46.02	9.118	15.809	8.133	12.410	10.927	20.539	9.168	13.734
B	−50.00	12.49	−74.396	−100.294	−51.709	−56.239	−56.230	−75.654	−35.010	−34.204
C	48.50	−8.66	71.583	97.313	53.000	58.115	55.806	77.422	36.852	38.274
D	−46.02	46.02	16.462	20.585	13.538	15.094	9.430	10.453	7.959	8.224
Boat axial	46.02	−46.02	7.223	9.093	6.084	7.020	6.448	9.060	4.794	5.734
Boat equatrial	−46.02	46.02	−17.216	−25.673	−12.241	−14.833	−14.993	−23.582	−10.130	−11.915
Twist boat	24.67	24.67	41.126	43.017	41.855	39.601	34.151	36.826	29.937	24.600

a) Observed rotational strengths are +1.78 and +2.34 at 300 and 81 K, respectively.

TABLE 2. TEMPERATURE-DEPENDENT ROTATIONAL STRENGTHS OF (*R*)-3-METHYLCYCLOHEXANONE CALCULATED WITH NON-BONDED INTERACTION ENERGY AS CONFORMATIONAL ENERGY

Temperature	CNDO/2				INDO				Exptl.[a]
	I	II	III	IV	I	II	III	IV	
300 K	5.505	10.226	5.482	8.766	7.416	14.683	6.620	10.351	1.78
81 K	9.118	15.809	8.152	12.410	10.927	20.539	9.168	13.734	2.34
$\Delta(\%)$[b]	65.64	54.59	48.71	41.58	47.34	39.88	30.01	32.68	31.5

a) Ref. 1. b) Defined by Eq. 6 of the text.

are considerably larger than the observed value (see Table 1 also). Methods III and IV with INDO yield better results, so that an improvement of virtual orbitals such as the present one seems to be prerequisite for calculations of this type. However, we cannot say for certain about the importance of the effect of deorthogonalization which has been demonstrated by other investigators.[12] We shall report elsewhere that a calculation without deorthogonalization leads to incorrect results with respect to a sign of the rotatory strength of (*R*)-3-methylcyclohexylidene-malononitrile.[14] The calculated weights of conformers A, B, C, and D are 82.91, 9.30, 7.11, 0.68%, respectively, at 300 K with Method IV. At 81 K with the same method, the weight of conformer A is 100%.

The above-mentioned calculations are based on the assumption that the potential surface obtained from the consideration of non-bonded interactions can well describe the internal energy profile of the system. What about a situation, if we use as E_i the sum of the electronic energy calculated by the molecular orbital methods and the potential energy due to the non-bonded interactions? As can be seen in Table 3, the results obtained are rather unsatisfactory. This may partly be attributed to the present inconsistent procedure which uses the same conformers as in the previous case (A, B, C, and D). The reason why proper conformers are not used is simply because minima of the energy surface in this case have hardly been found.

Lastly, there still remains a question: Is the sign of the rotational strength of conformer D definitely positive? There has been no calculation reported that conformer D has a negative sign in accordance with the ketone octant rule. We have no mind to challenge the octant rule and simply want to find out a relationship between a sign of rotatory strength and a molecular conformation. We have found that the

TABLE 3. TEMPERATURE-DEPENDENT ROTATIONAL STRENGTHS OF (*R*)-3-METHYLCYCLOHEXANONE CALCULATED WITH THE SUM OF ELECTRONIC ENERGY AND NON-BONDED INTERACTION ENERGY AS CONFORMATIONAL ENERGY

Temperature	INDO			
	I	II	III	IV
300 K	10.885	20.473	9.140	13.695
81 K	10.904	20.505	9.151	13.711
$\Delta(\%)$[a]	0.17	0.16	0.12	0.12

a) Defined by Eq. 6.

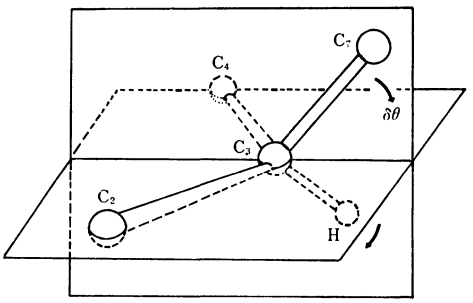

Fig. 6. Inclination angle of the methyl group, $\delta\theta$.

TABLE 4. EFFECT OF INCLINATION ANGLE ($\delta\theta$) OF METHYL GROUP ON ROTATIONAL STRENGTH OF CHAIR-FORM (*R*)-3-METHYLCYCLOHEXANONE WITH AXIAL METHYL (CONFORMER D)

$\delta\theta$[a] (degree)	INDO				Total energy (eV)
	I	II	III	IV	
0.0	9.430	10.453	7.959	8.224	−2039.219
5.0	7.594	7.539	7.764	8.073	−2039.332
10.0	4.771	2.769	7.002	7.004	−2039.282
20.0	−2.530	−10.430	4.413	2.747	−2038.996
30.0	−10.092	−25.710	0.786	−4.561	−2038.480

a) Clockwise rotation of bond C_3–C_7 in the plane which contains bond C_3–C_7 and is perpendicular to the $C_2C_3C_4$ plane. $\delta\theta$ is taken to the zero at the axial position of bond C_3–C_7 with respect to bond C_1–C_2.

rotational strength gradually decreases as the C_3–C_7 bond rotates in the plane which contains the C_3–C_7 bond and is perpendicular to the $C_2C_3C_4$ plane (Fig. 6). The numerical values obtained are listed in Table 4, where $\delta\theta$ denotes the deviation of the dihedral angle defined above, $\delta\theta=0$ being the axial position of bond C_3–C_7 with respect to bond C_1–C_2 in conformer D. In order to get the sign to be negative, the axial methyl group must rotate by about 20 degrees. This request, on the other hand, inflicts an energy loss of about 0.2 eV (see the last column of Table 4) and is rather unlikely. Thus, in so far as the above estimation is correct, a sign of the rotational strength of conformer D will probably be positive as the present and some other authors predict. It should be noted that the conclusion here is only tentative since we cannot say definitely about the accuracy of the total energies of conformers under consideration. There may be cases that a total energy favors reorientation of axial

methyl groups in some alicyclic ketones. The ketone octant rule will hold properly for such molecules.

In order to see what happens if we start from somewhat different molecular geometry, we have carried out a copy of the above calculation with the geometry of (*R*)-3-methylcyclohexanone proposed by Moffitt *et al.*[15] The overall results however were not very good; *e.g.*, the value of Δ was computed to be about 13.

It is concluded that consideration of the statistical population of conformers is indispensable for accurate understanding of rotational strength data of flexible optically active molecules.

One of us (T. N.) wishes to thank Dr. Yoshiro Nakata of Gumma University for a number of discussions and suggestions concerning the conformational equilibria.

References

1) K. M. Wellman, E. Bunnenberg, and C. Djerassi, *J. Am. Chem. Soc.*, **85**, 1870 (1963).
2) A. Moscowitz, K. Wellman, and C. Djerassi, *J. Am. Chem. Soc.*, **85**, 3516 (1963).
3) N. L. Allinger, J. Allinger, L. A. Freiberg, R. Czaja, and N. A. LeBel, *J. Am. Chem. Soc.*, **82**, 5876 (1960).
4) J. W. Snow and T. M. Hooker, Jr., *J. Am. Chem. Soc.*, **96**, 7800 (1974) and references cited in.
5) A. Imamura, T. Hirano, C. Nagata, T. Tsuruta, and K. Kuriyama, *J. Am. Chem. Soc.*, **95**, 8621 (1973) and references cited in.
6) R. A. Scott and H. A. Scheraga, *J. Chem. Phys.*, **45**, 2091 (1966).
7) J. A. Pople and G. A. Segal, *J. Chem. Phys.*, **44**, 3289 (1966); J. A. Pople, D. Beveridge and P. Dobosh, *J. Chem. Phys.*, **47**, 2026 (1967).
8) S. Huzinaga and C. Arnau, *J. Chem. Phys.*, **54**, 1948 (1971).
9) W. J. Hunt and W. A. Goddard, III, *Chem. Phys. Lett.*, **3**, 414 (1969).
10) W. Hug and G. Wagniere, *Theor. Chim. Acta*, **18**, 57 (1970).
11) F. S. Richardson, P. D. Shillady, and J. E. Bloor, *J. Phys. Chem.*, **75**, 2466 (1971); F. R. Richardson and W. Pitts, *Biopolymers*, **13**, 703 (1974).
12) A. Imamura, T. Hirano, C. Nagata, and T. Tsuruta, *Bull. Chem. Soc. Jpn.*, **45**, 396 (1972).
13) Y. -H. Pao and D. P. Santry, *J. Am. Chem. Soc.*, **88**, 4157 (1961).
14) T. Nakamura and Y. J. I'Haya, to be published.
15) W. Moffitt, R. B. Woodward, A. Moscowitz, W. Klyne, and C. Djerassi, *J. Am. Chem. Soc.*, **83**, 4013 (1961).

The Approximate Self-Consistent Renormalized RPA: The Electronic Excited States of DNA Bases in the CNDO/S Method

Hirotoshi Ito and Yasumasa J. I'Haya

Department of Materials Science, The University of Electro-Communications, Chofu-shi, Tokyo 182

(Received August 12, 1976)

Comments are given upon the *approximate* self-consistent renormalized RPA(SCrRPA) presented in our previous papar which assumes the correlated ground state wavefunction to be the linear combination of the Hartree-Fock ground state and doubly excited states, in the CI language. The rationalization of the approximate SCrRPA is made from the results computed by the *complete* SCrRPA, whose recipe is simply made. Finally, a numerical comparison of the several RPA methods is made as to the electronic spectra of four DNA bases by using the CNDO/S method.

In the pi-electron semiempirical theories like the Pariser-Parr-Pople model[1] and the valence electron theories such as the CNDO/S[2,3] and the INDO/S[4] methods, the configuration interaction (CI) method has been conventionally used to determine the excitation energies of molecules. On the other side, the random-phase approximation (RPA) has conceptually advantages over the CI method. The latter, when only all the singly excited configurations are included, is actually the same as the Tamm-Dancoff approximation (TDA) which is the lowest order approximation of the equations-of-motion method. For instance, in the CI language, the RPA can include certain *doubly* excited configurations (Z-terms; vide post), in addition to all the *singly* excited configurations (Y-terms). However, the standard RPA often gives the inconsistent solution such as the triplet instability on account of Eq. 3b (vide post). In this respect, the normal RPA (nRPA) is not necessarily superior to the TDA.

This deficiency of the nRPA can be overcome not only by the modification of the HF bases but also by introducing the correlated ground state, instead of the HF ground state, as a reference state.[5] The latter RPA is referred to as a higher RPA. On the basis of the correlated ground state assumed, several modifications to the nRPA have been proposed. The higher RPA derived by Shibuya and McKoy[6] and the self-consistent RPA presented by Ostlund and Karplus[7] are in these streams. The self-consistent polarization propagator approximation (SPPA)[8] is a similar approach. Previously, we also have applied the renormalized higher RPA(rRPA) in Rowe-Simons' formalism[9,10] to the various conjugated molecules.[5]

The rRPA method is based upon the assumption of the correlated ground state which involves the corrections of electron correlation introduced for the Hartree-Fock ground state. Previously, we calculated the non-integral occupation number, *i.e.*, the charge densities from the coefficients of the correlated ground state wavefunction (HF+doubly excited CI's) determined by admixing the Hartree-Fock ground state with various doubly excited configurations using the perturbation theory. In the present paper, we compute the correlated charge densities from the RPA ground state determined by Sanderson and da Providência's recipe.[11,12] As will be mentioned below, the correlated ground state is determined by the self-consistent solution of the rRPA equation (SCrRPA) in an iterative way.

In this case, a trial well correlated ground state may yield approximately a self-consistent solution at several rounds of iterative calculations. In fact, it is demonstrated that the correlated ground state wavefunction in our previous works[5,14] gives an approximate solution of the SCrRPA. The central concern of the present paper is therefore focussed upon the rationalization of the *approximate* SCrRPA in our previous treatment rather than the *complete* SCrRPA. The detailed report of the latter will be presented elsewhere.[13] In the following, we outline the rRPA method, then give some comments upon these two assumptions of the correlated ground state, and finally present some numerical results for DNA bases.

Renormalized Higher RPA

The rRPA equation which was originally given by Rowe[9] and later reformulated by Simons[10] explicitly for the singlet and triplet states is written down for the real basis in the following matrix form

$$\begin{pmatrix} \tilde{A}(S) & \tilde{B}(S) \\ -\tilde{B}^*(S) & -\tilde{A}^*(S) \end{pmatrix} \begin{pmatrix} \tilde{Y}(\lambda S) \\ \tilde{Z}(\lambda S) \end{pmatrix} = \omega_\lambda \begin{pmatrix} \tilde{Y}(\lambda S) \\ \tilde{Z}(\lambda S) \end{pmatrix} \qquad (1)$$

with

$$\tilde{A}_{\mathrm{ph,vf}}(S) = \delta_{\mathrm{pv}}\delta_{\mathrm{hf}}(E_{\mathrm{p}}-E_{\mathrm{h}}) + (2)^{-1}(\rho_{\mathrm{h}}-\rho_{\mathrm{p}})^{1/2}(\rho_{\mathrm{f}}-\rho_{\mathrm{v}})^{1/2} \times (\langle \mathrm{pf}|\mathrm{hv}\rangle + (-)^S\langle \mathrm{pf}|\mathrm{hv}\rangle - \langle \mathrm{pf}|\mathrm{vh}\rangle)$$

$$\tilde{B}_{\mathrm{ph,vf}}(S) = (2)^{-1}(\rho_{\mathrm{h}}-\rho_{\mathrm{p}})^{1/2}(\rho_{\mathrm{f}}-\rho_{\mathrm{v}})^{1/2} \times (\langle \mathrm{pv}|\mathrm{hf}\rangle + (-)^S\langle \mathrm{pv}|\mathrm{hf}\rangle - \langle \mathrm{pv}|\mathrm{fh}\rangle)$$

$$\langle ij|kl\rangle = \langle i(1)j(2)|1/r_{12}|k(1)l(2)\rangle$$

$$\tilde{Y}_{\mathrm{ph}}(\lambda S) = (2)^{-1/2}(\rho_{\mathrm{h}}-\rho_{\mathrm{p}})^{1/2}Y_{\mathrm{ph}}(\lambda S)$$

$$\tilde{Z}_{\mathrm{ph}}(\lambda S) = (2)^{-1/2}(\rho_{\mathrm{h}}-\rho_{\mathrm{p}})^{1/2}Z_{\mathrm{ph}}(\lambda S)$$

from which the TDA and the nRPA are derived as special case. E_i is an orbital energy for the ith Hartree-Fock molecular orbital (MO) ϕ_i. Subscripts ph and vf are used to label the *p*article-*h*ole pair and the *v*acant-*f*illed molecular orbital pair states, respectively. $Y_{\mathrm{ph}}(\lambda S)$ and $Z_{\mathrm{ph}}(\lambda S)$ without tildes are the unrenormalized amplitudes for the singly excited creation operator $0^+_{\lambda SM}$

$$0^+_{\lambda SM} = \sum_{\mathrm{ph}} (Y_{\mathrm{ph}}(\lambda S)C^+_{\mathrm{ph}}(SM) - Z_{\mathrm{ph}}(\lambda S)C_{\mathrm{ph}}(\overline{SM})) \qquad (2)$$

which produces the λth excited state $|\lambda SM>$ when operating on the correlated ground state $|0>$:

$$0^{+}_{\lambda SM}|0> = |\lambda SM> \quad (3a)$$

$$0_{\lambda SM}|0> = 0 \quad (\text{all } \lambda SM) \quad (3b)$$

Here $C^{+}_{\rm ph}(\rm SM)$ and $C_{\rm ph}(\overline{\rm SM})$ are the particle-hole pair creation and annihilation operators, respectively, in the same notation of Ref. 6, S and M being the total spin angular momentum and its z-projection, respectively. ρ_i represents the correlated charge density, *i.e.*, the non-integral occupation number of the ith orbital in the correlated ground state, defined by

$$\rho_i = (2)^{1/2}<0|(2)^{-1/2}(a^{+}_{i\alpha}a_{i\alpha}+a^{+}_{i\alpha}a_{i\beta})|0> = (2)^{1/2}<0|C^{+}_{ii}(00)|0> \quad (4)$$

where $a^{+}_{i\sigma}$ and $a_{i\sigma}$ are the Fermion creation and annihilation operators, respectively, for the ith spin-orbital $\phi_i\sigma_i$.

The correlated RPA ground state is usually assumed to be as follows

$$|0> = N_0 e^{U}|HF> \quad (5)$$

with

$$U = (1/2)\sum_{S=0,1}\sum_{i}\sum_{\rm ph\in\Gamma_i}\sum_{\rm vf\in\Gamma_i} C_{\rm ph,vf}(S)C^{+}_{\rm ph}(\overline{S0})C^{+}_{\rm vf}(S0) \quad (6a)$$

$$\Gamma_i \times \Gamma_i \in \Gamma_{\rm HF}. \quad (6b)$$

Here N_0 is the normalization constant

$$N_0^{-2} = 1 + <HF|U^{\dagger}U|HF> \quad (7)$$

and Γ denotes the irreducible representation of a certain set of excited states under consideration.

Equations 3a and 3b should be a simultaneous solution of Eq. 1, which is therefore iteratively solved in the self-consistent manner. Thus the coefficients $C_{\rm ph,vf}(S)$ can be given by a solution of Eq. 3b. However, it is known that we can safely bypass the problem of solving Eq. 3b by indirectly guessing a good starting ground state.[5,6,14,15] If we know the coefficients $C_{\rm ph,vf}(S)$ of such starting ground state, the charge densities can be calculated. Invoking the identity, Operator $\times e^{U}$, one obtaines

$$\begin{aligned}\rho_{\rm u} &= (2)^{1/2}<0|C^{+}_{\rm uu}(00)|0> \\ &= (2)^{1/2}N_0<0|e^{U}\{C^{+}_{\rm uu}(00) + [C^{+}_{\rm uu}(00),U] \\ &\qquad - (2!)^{-1}[U,[C^{+}_{\rm uu}(00),U]]+\cdots\}|HF> \\ &= (2)^{-1}\sum_{S}\sum_{\rm h}\sum_{\rm vf}|C_{\rm uh,vf}(S)|^2 \quad (\text{for all } \Gamma_i)\end{aligned} \quad (8)$$

where we use the normalization condition of Eq. 7 and assume the orthogonality condition:

$$\ll C^{+}_{\rm uo}(S0)C^{+}_{\rm eg}(\overline{S0})|HF>|C^{+}_{\rm ph}(S0)C^{+}_{\rm vf}(\overline{S0})|HF\gg = <\Psi_{\rm uo,eg}(S)|\Psi_{\rm ph,vf}(S)> = \delta_{\rm uo,ph}\delta_{\rm eg,vf} \quad (9)$$

We have used the notation uo and eg for the *u*noccupied-*o*ccupied and *e*xcited *g*round state molecular orbital pairs. In the braces of the second line of Eq. 8 the terms higher than the second term vanish, formally, under the assumption of Eq. 6.

$$\begin{aligned}\rho_{\rm o} &= 2^{1/2}<0|C^{+}_{\rm oo}(00)|0> \\ &= 2 - (1/2)\sum_{S}\sum_{\rm p}\sum_{\rm vf}|C_{\rm po,vf}(S)|^2 \quad (\text{for all } \Gamma_i)\end{aligned} \quad (10)$$

In the present paper, the starting charge densities ρ_i's are computed by using Eqs. 5, 8, and 10 together with the relationship such as suggested by Shibuya and McKoy:[15]

$$C^{\rm trial}_{\rm ph,vf}(S) \approx (E_{\rm p}+E_{\rm v}-E_{\rm h}-E_{\rm f})^{-1}B^{\rm nRPA}_{\rm ph,vf}(S) \quad (11)$$

As a matter of course, these coefficients are computed for all the particle-hole pair (ph, vf) configurations in the RPA equation. A trial correlated ground state may also be obtained either by solving the CI secular equation constructed by admixing the Hartree-Fock ground state with the doubly excited singlet configurational state, or by the corresponding perturbation treatment.[5,14] From the case when we use Eq. 11 to compute ρ_i, we should not conclude that in the CI method (*cf.* Eq. 16 below) the triplet correlation effect is formally unable to be taken into account because of the spin-orthogonality between the ground and triplet configurational state functions. As will be discussed in the next section, it should be considered that in the CI method the triplet correlation effect is implicitly included as an average of spin-flips through the $\boldsymbol{B}(S)$ matrix of the RPA equation.

If we follow Sanderson and da Providência,[11,12] we can determine a solution of Eq. 3b for the trial rRPA equation, whose matrix elements are computed by the coefficients $C_{\rm ph,vf}(S)$ assumed initially in accordance with Eq. 11. Then, we can newly determine the coefficients as

$$\boldsymbol{C}^{\rm new} = (\tilde{\boldsymbol{Y}}^{-1}\tilde{\boldsymbol{Z}})^{\rm trial} = (\tilde{\boldsymbol{Z}}\tilde{\boldsymbol{Y}}^{-1})^{\rm trial} \quad (12)$$

which gives the new correlated charge densities. Thus, the self-consistent solution of the rRPA equation, that is SCrRPA, may be obtained iteratively. The convergence criterion used is that $|\rho_i(\text{new})-\rho_i(\text{old})| \leqq 10^{-5}$ for all the MO's.

The oscillator strength $f_{\lambda 0}$ for the λth renormalized states is computed by

$$f_{\lambda 0} = (2/3)\omega_\lambda|\boldsymbol{D}_{\lambda 0}|^2 \quad (\omega_\lambda, \boldsymbol{D}_{\lambda 0} \text{ in a.u.}) \quad (13)$$

with

$$\boldsymbol{D}_{\lambda 0} = -\sum(\tilde{Y}^{*}_{\rm ph}(\lambda 0)+\tilde{Z}^{*}_{\rm ph}(\lambda 0))\tilde{\boldsymbol{d}}_{\rm ph} \quad (14)$$

and

$$\tilde{\boldsymbol{d}}_{\rm ph} = (\rho_{\rm h}-\rho_{\rm p})^{1/2}\boldsymbol{d}_{\rm ph} = (\rho_{\rm h}-\rho_{\rm p})^{1/2}<\phi_{\rm p}(1)|\boldsymbol{r}(1)|\phi_{\rm h}(1)> \quad (15)$$

Comments on the Approximately Self-Consistent Ground-State Correlation Amplitude: $C_{\rm ph,vf}(S)$

For the assumption of Eq. 5 together with those of Eq. 11 and/or Eq. 12, we can also assume the following familiar perturbation expansion, Eq. 16, in the CI method. By using the former assumption, we compute the starting correlated charge densities and perform the SCrRPA calculations in order to compare with our previous work based upon the latter assumption.

The criterion for determining the configurational functions to be chosen in Eq. 16 was set up within 10^{-3} in the absolute values of their coefficients. We broke off the CI calculation at the stage that the number of configurations amounted to fifty and computed the

charge densities. We thus truncated the configurations adopted in the RPA equation. In this section, we shall clarify the similarity and the dissimilarity of these two methods for the RPA ground state, and further elucidate the meaning of the CI (TDA) method for the $B(S)$ matrix of the RPA equation.

In the CI language, the correlated ground state may be described by

$$|0\rangle = N_0\Big\{|HF\rangle - \sum_{ij}\sum_{kl}\frac{\langle\Phi_{ij}^{kl}(00)|\mathscr{H}|HF\rangle}{\Delta^1 E_{ij}^{kl}}|\Phi_{ij}^{kl}(00)\rangle + \sum_{mn}\sum_{st}\sum_{ij}\sum_{kl}\frac{\langle\Phi_{mn}^{st}(00)|\mathscr{H}|\Phi_{ij}^{kl}(00)\rangle\langle\Phi_{ij}^{kl}(00)|\mathscr{H}|HF\rangle}{\Delta^1 E_{mn}^{st}\qquad\Delta^1 E_{ij}^{kl}} \times |\Phi_{mn}^{st}(00)\rangle + \cdots\Big\}$$
$$= N_0(|HF\rangle + \sum_{ij}\sum_{kl} C_{ij}^{kl}|\Phi_{ij}^{kl}(00)\rangle + 0(\text{2nd order})) \tag{16}$$

with

$$\Delta^1 E_{ij}^{kl} = \langle\Phi_{ij}^{kl}(00)|\mathscr{H}|\Phi_{ij}^{kl}(00)\rangle - \langle HF|\mathscr{H}|HF\rangle.$$

The HF ground-state and the five types of doubly excited configurational wavefunction $\Phi_{ij}^{kl}(SM)$ are given in terms of the following Slater determinants:[16]

$$|HF\rangle = |1\bar{1}2\bar{2}...f\bar{f}...k\bar{k}...o\bar{o}...g\bar{g}...| \tag{17}$$

$$\Phi_{hh}^{pp}(00) = a_{p\alpha}^{+}a_{p\beta}^{+}a_{h\beta}a_{h\alpha}|HF\rangle = |f\bar{f}p\bar{p}| = C_{ph}^{+}(00)C_{ph}^{+}(00)|HF\rangle \tag{18}$$

$$\Phi_{hh}^{pv}(00) = (2)^{-1/2}(a_{p\alpha}^{+}a_{v\beta}^{+}+a_{v\alpha}^{+}a_{p\beta}^{+})a_{h\beta}a_{h\alpha}|HF\rangle = (2)^{-1/2}(|p\bar{v}|+|v\bar{p}|) = (2)^{1/2}C_{ph}^{+}(00)C_{vh}^{+}(00)|HF\rangle \quad (p\neq v) \tag{19}$$

$$\Phi_{fh}^{pp}(00) = (2)^{-1/2}a_{p\alpha}^{+}a_{p\beta}^{+}(a_{h\beta}a_{f\alpha}+a_{f\beta}a_{h\alpha})|HF\rangle = (2)^{-1/2}(|f\bar{h}p\bar{p}|+|h\bar{f}p\bar{p}|) = (2)^{1/2}C_{pf}^{+}(00)C_{ph}^{+}(00)|HF\rangle \quad (f\neq h) \tag{20}$$

$$\Phi_{fh}^{pv}(I)(00) = (2)^{-1}(a_{p\alpha}^{+}a_{v\beta}^{+}+a_{v\alpha}^{+}a_{p\beta}^{+})(a_{h\beta}a_{f\alpha}+a_{f\beta}a_{h\alpha})|HF\rangle = (2)^{-1}(|f\bar{h}p\bar{v}|+|\bar{f}h\bar{p}v|-|\bar{h}fp\bar{v}|-|h\bar{f}\bar{p}v|) = (2)^{-1}(C_{pf}^{+}(00)C_{vh}^{+}(00) + C_{ph}^{+}(00)C_{vf}^{+}(00))|HF\rangle \quad (p\neq v, f\neq h) \tag{21}$$

$$\Phi_{fh}^{pv}(II)(00) = (2\sqrt{3})^{-1}\{2(a_{p\alpha}^{+}a_{v\alpha}^{+}a_{h\alpha}a_{f\alpha}+a_{p\beta}^{+}a_{v\beta}^{+}a_{h\beta}a_{f\beta}) + (a_{p\alpha}^{+}a_{v\beta}^{+}-a_{v\alpha}^{+}a_{p\beta}^{+})(a_{h\beta}a_{f\alpha}-a_{f\beta}a_{h\alpha})\}|HF\rangle = (2\sqrt{3})^{-1}\{2(|fh\bar{p}\bar{v}|+|\bar{f}\bar{h}pv|) - |fh\bar{p}\bar{v}|-|\bar{f}hp\bar{v}|-|fhp\bar{v}|-|f\bar{h}\bar{p}v|\} = (3)^{-1/2}(C_{pf}^{+}(00)C_{vh}^{+}(00) - C_{ph}^{+}(00)C_{vf}^{+}(00))|HF\rangle \quad (p\neq v, f\neq h) \tag{22}$$

Following Murrell and McEwen,[16] the matrix element between $\Phi_{ij}^{kl}(00)$ and $|HF\rangle$ are easily written down in terms of the matrix elements of $B(S)$ in the RPA equation as

$$\langle\Phi_{hh}^{pp}(00)|\mathscr{H}|HF\rangle = B_{ph,ph}(0) = -B_{ph,ph}(1) \tag{23}$$

$$\langle\Phi_{hh}^{pv}(00)|\mathscr{H}|HF\rangle = (2)^{1/2}B_{ph,vh}(0) = -(2)^{1/2}B_{ph,vh}(1) \tag{24}$$

$$\langle\Phi_{fh}^{pp}(00)|\mathscr{H}|HF\rangle = (2)^{1/2}B_{ph,pf}(1) \tag{25}$$

$$\langle\Phi_{fh}^{pv}(I)(00)|\mathscr{H}|HF\rangle = -\langle pv|fh\rangle - \langle pv|hf\rangle = (2)^{-1}(3B_{ph,vf}(1) - B_{ph,vf}(0)) \tag{26}$$

$$\langle\Phi_{fh}^{pv}(II)(00)|\mathscr{H}|HF\rangle = (3)^{1/2}(\langle pv|hf\rangle - \langle pv|fh\rangle) = (\sqrt{3}/2)(B_{ph,vf}(1)+B_{ph,vf}(0)) \tag{27}$$

which indicate that the ground-state correlation amplitude in this scheme is also determined by the singlet and triplet $B(S)$ matrices just as in Eq. 11.

The derivation of Eqs. 26 and 27 is not straightforward. Nakayama and I'Haya[17] adopted the four-electron spin-functions which are different from Eqs. 21 and 22:

$$\Psi_{fh}^{pv}(I)(00) = (2\sqrt{3})^{-1}\{2(|f\bar{h}\bar{p}v|+|\bar{f}hp\bar{v}|) - |f\bar{h}p\bar{v}|-|\bar{f}hpv|-|\bar{f}\bar{h}pv|-|fhp\bar{v}|\} \tag{28}$$

$$\Psi_{fh}^{pv}(II)(00) = (2)^{-1}\{|f\bar{h}p\bar{v}|+|\bar{f}hpv|-|\bar{f}\bar{h}pv|-|fhp\bar{v}|\}, \tag{29}$$

and obtained the corresponding matrix elements

$$\langle\Psi_{fh}^{pv}(I)(00)|\mathscr{H}|HF\rangle = (3)^{1/2}B_{ph,vf}(1) \tag{30}$$

$$\langle\Psi_{fh}^{pv}(II)(00)|\mathscr{H}|HF\rangle = -B_{ph,vf}(0). \tag{31}$$

It has been pointed out by Anno and Teruya[18] that a set of Eqs. 21 and 22 is transformed into that of Eqs. 28 and 29, and that any unitary transformation of a set of spin-functions given in Eqs. 21 and 22 may be adopted as the configurational basis functions. This implies that an arbitrary degree of freedom of spin-flips is endowed for the four-electron spin-functions. Such an inverse transformation gives

$$\begin{pmatrix}\Phi_{fh}^{pv}(I)\\ \Phi_{fh}^{pv}(II)\end{pmatrix} = \begin{pmatrix}\cos 150^\circ & \sin 150^\circ\\ -\sin 150^\circ & \cos 150^\circ\end{pmatrix}\begin{pmatrix}\Psi_{fh}^{pv}(I)\\ \Psi_{fh}^{pv}(II)\end{pmatrix} \tag{32}$$

from which we can obtain Eqs. 26 and 27 by using Eqs. 30 and 31.

From Eq. 16, the correlated charge densities are written down as (i, j: holes and k, l: particles)

$$\rho_j = 2 - N_0^2\sum_{i}\sum_{kl}|C_{ij}^{kl}|^2(1+\delta_{ij}) \tag{33a}$$

$$\rho_k = N_0^2\sum_{ij}\sum_{l}|C_{ij}^{kl}|^2(1+\delta_{lk}) \tag{34a}$$

which are easily derived in the following way by introducing the one-electron operator in the first quantization, for which we set $e_\nu=1$ after integration:

$$\rho_j = \langle 0|\sum_\nu e_\nu\delta_{\nu j}|0\rangle = N_0^2(1+\sum_{ij'}\sum_{kl}|C_{ij'}^{kl}|^2+\cdots)\langle HF|\sum_\nu e_\nu\delta_{\nu j}|HF\rangle + N_0^2\sum_{ij'}\sum_{kl}|C_{ij'}^{kl}|^2[\langle\Phi_{ij'}^{kl}|\sum_\nu e_\nu\delta_{\nu j}|\Phi_{ij'}^{kl}\rangle - \langle HF|\sum_\nu e_\nu\delta_{\nu j}|HF\rangle]+\cdots = 2 + N_0^2\sum_{ij'}\sum_{kl}|C_{ij'}^{kl}|^2(e_k\delta_{kj}+e_l\delta_{lj} - e_i\delta_{ij}-e_{j'}\delta_{j'j})+\cdots \tag{33b}$$

and similarly

$$\rho_k = \langle 0|\sum_\nu e_\nu\delta_{\nu k}|0\rangle, \tag{34b}$$

δ_{ij} being the Kronecker delta. Note that Eqs. 33a, b and 34a, b correspond to Eqs. 8 and 10 respectively.

TABLE 1. EXCITATION ENERGIES (ω, in eV), OSCILLATOR STRENGTHS (f), AND THE DIRECTIONS OF POLARIZATION(θ) FOR FOUR DNA BASES (ω, in eV)[a]

Molecule		SCrRPA			rRPA[b]			TDA[b]			nRPA[b]			Exptl[c]		
		ω	f	θ	ω	f	θ	ω	f	θ	ω	f	θ	ω	f	θ
Adenine	Singlet															
	$n\pi^*$	4.47	0.0004		4.42	0.0004		4.36	0.0004		4.36	0.0004		4.6	0.049	
	$\pi\pi^*$	4.68	0.096	8°	4.63	0.101	12°	4.58	0.100	2°	4.50	0.098	9°	4.758	0.249	−3°
	$n\pi^*$	4.79	0.001		4.75	0.001		4.70	0.001		4.70	0.001				
	$\pi\pi^*$	4.85	0.286	69°	4.80	0.279	70°	4.74	0.354	67°	4.67	0.284	69°	5.988	0.529	92°
	$n\pi^*$	5.08	0.013		5.02	0.014		4.96	0.013		4.96	0.013				
	$\pi\pi^*$	5.684	0.011	−13°	5.63	0.011	−10°	5.59	0.013	−31°	5.51	0.010	−8°			
	$n\pi^*$	5.683	0.001		5.66	0.0009		5.60	0.001		5.60	0.009				
	$\pi\pi^*$	6.40	0.580		6.36	0.580		6.43($n\pi^*$)	0.005		6.27	0.582				
	Triplet															
	$\pi\pi^*$	2.62			2.50			2.73			2.28			3.06[d]		
	$\pi\pi^*$	3.46			3.37			3.46			3.18					
Thymine	Singlet															
	$n\pi^*$	3.95	0.001		4.09	0.001		3.95	0.001		3.95	0.001				
	$n\pi^*$	4.84	0.000		4.88	0.000		4.84	0.000		4.84	0.000				
	$\pi\pi^*$	5.23	0.388	−4°	5.17	0.387	−4°	5.12	0.509	−4°	4.93	0.388	−4°	4.686	0.183	
	$\pi\pi^*$	6.41	0.154	96°	6.37	0.155	96°	6.26	0.176	96°	6.23	0.156	96°	6.046	0.314	
	$n\pi^*$	6.79	0.003		6.87	0.003		6.79	0.003		6.78	0.003				
	Triplet															
	$\pi\pi^*$	2.10			1.97			2.24			1.27			2.79[d]		
	$n\pi^*$	3.95			4.09			3.95			3.95					
Guanine	Singlet															
	$\pi\pi^*$	3.99	0.299	−68°	3.93	0.298	−68°	3.87	0.375	−68°	3.80	0.294	−68°			
	$n\pi^*$	4.13	0.003		4.10	0.003		4.02	0.002		4.02	0.003				
	$\pi\pi^*$	4.87	0.200	42°	4.83	0.197	42°	4.78	0.249	43°	4.67	0.198	42°	4.507	0.123	
	$n\pi^*$	4.94	0.004		4.88	0.004		4.84	0.004		4.84	0.004				
	$\pi\pi^*$	5.18	0.093	15°	5.14	0.093	15°	5.08	0.105	16°	4.99	0.096	14°	5.039	0.236	
	$n\pi^*$	5.20	0.013		5.17	0.013		5.09	0.013		5.09	0.013				
	$n\pi^*$	5.70	0.002		5.67	0.002		5.61	0.002		5.61	0.002				
	$\pi\pi^*$	6.53	0.114		6.50	0.116		6.40	0.128		6.37	0.106		6.324	0.564	
	Triplet															
	$\pi\pi^*$	2.22			2.13			2.27			1.88			3.05[d]		
	$\pi\pi^*$	2.77			2.70			2.77			2.43					
Cytosine	Singlet															
	$n\pi^*$	4.50	0.0001		4.46	0.0001		4.39	0.0001		4.38	0.0001				
	$\pi\pi^*$	4.61	0.158	45°	4.55	0.157	45°	4.52	0.196	46°	4.41	0.156	45°	4.64	0.116	9°
	$n\pi^*$	4.74	0.002		4.70	0.002		4.64	0.002		4.64	0.002				
	$\pi\pi^*$	6.02	0.173	−13°	5.99	0.169	−9°	5.93	0.130	−8°	5.89	0.161	−12°	6.308	0.698	10.5°
	$n\pi^*$	6.36	0.006		6.32	0.006		6.27	0.006		6.27	0.006				
	$\pi\pi^*$	6.45	0.712	137°	6.41	0.716	137°	6.48	1.013	138°	6.30	0.725	138°			104°
	$n\pi^*$	7.15	0.0001		7.12	0.0001		7.07	0.0001		7.07	0.0001				
	Triplet															
	$\pi\pi^*$	2.48			2.38			2.61			2.12			3.02[d]		
	$\pi\pi^*$	4.12			4.06			4.04			3.90					

a) 40 particle-hole pairs=5(unocc.)×8(occ.) are taken into account. For molecular geometries, see Ref. 21. $n\pi^*$ denotes the σ-π^* and π-σ^* transitions. As for definition of the transition moment directions, θ, see Ref. 22. b) Taken from our previous paper, Ref. 14, with some numerical revision. c) From Refs. 23 and 24. d) K. Imakubo, T. Higashimura, and T. Sidei, *J. Phys. Soc. Jpn.*, **22**, 339 (1967).

It is thus found that the use of Eq. 16 is one of ways to compute the approximately self-consistent charge density ρ_i and is quite similar to the use of Eq. 11. It is also clear that not only the singlet but also the triplet correlation effects are effectively included in Eq. 16 through the $B(S)$ matrix as in Eq. 11.

Numerical Results and Discussion

In the computation, we consider the 40 particle-hole pair configurations obtained by raising an electron from the *eight* highest occupied molecular orbitals to one of the *five* lowest vacant molecular orbitals. The computed results are listed in the first column of Table 1, and compared with the results of our previous work[14] and the experimental values. It is observed that the lowest triplet levels obtained by the SCrRPA are very much refined compared with those calculated with the rRPA. The computed oscillator strengths and the directions of polarizations are almost the same in these RPA's. Table 1 shows that the relationship ω(SCγ-RPA)$>\omega$(rRPA; Eq. 16)$>\omega$(TDA)$>\omega$(nRPA) holds for most cases. More detailedly, the following relationship holds for the four DNA bases:

$$\omega(\text{SCrRPA})>\omega(\text{rRPA; Eq. 16})>\omega(\text{rRPA; Eq. 11})>\omega(\text{TDA})>\omega(\text{nRPA}) \quad (35)$$

After all, the starting correlated RPA ground state obtained with Eq. 11 needs some more iteration steps to attain to a self-consistent renormalized solution, under the constraint of Eq. 12. It can be safely said that the correlated ground state (HF+doubly excited CI's) based upon Eq. 16 in the above treatment yields a satisfactorily approximate SCrRPA solution. The sequence of Eq. 35 indicates that the SCrRPA produces the upper bounds for the energy levels, while the nRPA yields the lower bounds.

The self-consistency was attained after nine iterations for adenine, guanine and cytosine, whereas thymine could not reach self-consistency even after thirteen iterations. We fixed the correlated charge densities as $\rho(\text{new}')=(1/2)\{\rho(\text{new})+\rho(\text{old})\}$ at every iteration step to get a quick convergence. In order to carry out the

Table 2. Pure $\pi\pi^*$ excitation energies (ω, in eV) and oscillator strengths (f) of four DNA bases, for which all the possible $\pi\pi^*$ configurations are taken from the CNDO/S basis MO's

Molecule	SCrRPA		rRPA		TDA		nRPA	
	ω	f	ω	f	ω	f	ω	f
Adenine	Singlet							
	4.71	0.10	4.62	0.10	4.55	0.10	4.46	0.10
	4.88	0.27	4.79	0.27	4.73	0.34	4.64	0.27
	5.71	0.01	5.61	0.01	5.57	0.01	5.48	0.01
	6.46	0.60	6.38	0.60	6.46	0.75	6.28	0.60
	Triplet							
	2.37		2.15		2.57		1.84	
	3.24		3.07		3.34		2.83	
Thymine	Singlet							
	5.36	0.41	5.29	0.41	5.20	0.54	5.02	0.41
	6.46	0.16	6.40	0.16	6.26	0.18	6.23	0.16
	7.40	0.12	7.35	0.12	7.24	0.16	7.18	0.10
	7.47	0.02	7.41	0.02	7.32	0.02	7.23	0.04
	Triplet							
	1.96		1.76		2.13		0.76	
	4.57		4.47		4.59		4.20	
Guanine	Singlet							
	4.04	0.30	3.94	0.30	3.87	0.38	3.78	0.30
	4.92	0.19	4.82	0.19	4.76	0.24	4.64	0.19
	5.20	0.08	5.11	0.08	5.05	0.09	4.95	0.08
	6.57	0.11	6.49	0.11	6.39	0.13	6.35	0.10
	Triplet							
	2.02		1.81		2.13		1.46	
	2.64		2.45		2.63		2.12	
Cytosine	Singlet							
	4.66	0.17	4.62	0.17	4.54	0.20	4.45	0.16
	6.06	0.15	6.03	0.15	5.94	0.11	5.90	0.13
	6.54	0.81	6.52	0.81	6.55	1.12	6.37	0.82
	7.48	0.11	7.46	0.11	7.40	0.11	7.36	0.11
	Triplet							
	2.38		2.30		2.55		1.94	
	4.02		3.97		3.95		3.74	

self-consistent calculation of thymine within the limited time (10 min), we therefore had to divide the 80×80 RPA matrix into the two matrices for the $(\pi\pi^*+\sigma\sigma^*)$ elements and the $(\sigma\pi^*+\pi\sigma^*)$ elements. As immediately understood from Eq. 6, such division of the matrix truncates, to some extent, the correlation effect arising from the other symmetry group, but this error seems to be not very large. Perhaps, some other suitable molecular geometries of thymine may give a self-consistent solution for the 40 particle-hole pairs after 9—10 iterations, without dividing the matrix. In fact, for the molecular geometry of thymine given in Ref. 20 we obtain the self-consistency after seven iterations. The results of the SCrRPA are as follows; 3.34 eV ($n\pi^*$, $f=0.018$), 4.36 ($n\pi^*$, $f=0.012$), 5.63 ($\pi\pi^*$, $f=0.019$, $\theta=-2°$), 6.97 ($\pi\pi^*$, $f=0.301$, $\theta=60°$), 7.02 ($n\pi^*$, $f=0.002$)eV for the singlets, and 2.08 ($n\pi^*$), 4.00 ($n\pi^*$)eV for the triplets. These results are somewhat different from those of Table 1.

We also carried out the SCrRPA calculation for all the possible pure $\pi\pi^*$ particle-hole pair configurations taken from the CNDO/S basis molecular orbitals, and found that Eq. 35 holds for the four bases of DNA as shown in Table 2. In particular, it should be noted that the pure $\pi\pi^*$ triplet levels are worse than those of Table 1 obtained from the RPA equations for the 40 particle-hole pair configurations involved the $\pi\pi^*$, $\sigma\sigma^*$, $\sigma\pi^*$, and $\pi\sigma^*$-transitions explicitly. Clearly, comparison of the results in Tables 1 and 2 suggests the great importance of the effect of σ-electron clouds to the refinement of the pure $\pi\pi^*$ triplet levels, which corresponds to the involvement of the dynamical screening by σ-electrons in π-electron transitions as mentioned by Shibuya, I'Haya, and McKoy.[19]

Finally, it should be mentioned that putting aside the problem how to include the electron correlation effect, re-parametrization of CNDO/S method is needed to refine the present results numerically. Especially, the lowest triplet levels of these DNA bases do not agree well with the experimental values. Such disagreement comes from the fact that the Nishimoto-Mataga approximation in the CNDO/S method reproduces the singlet levels well, but makes the triplet levels relatively low. Perhaps, the use of the INDO/S method[4,13] in the SCrRPA may be one of ways for taking steps.

References

1) R. G. Parr, "Quantum Theory of Molecular Electronic Structure," Benjamin, New York, N. Y. (1963).
2) J. Del Bene and H. H. Jaffé, *J. Chem. Phys.*, **48**, 1807 (1968).
3) R. L. Ellis, G. Kuehnlenz, and H. H. Jaffé, *Theor. Chim. Acta*, **26**, 131 (1972).
4) H. Ito and Y. J. I'Haya, *Bull. Chem. Soc. Jpn.*, **49**, 940 (1976).
5) O. Matsuoka and H. Ito, *Theor. Chim. Acta*, **39**, 111 (1975).
6) T. Shibuya and V. McKoy, *Phys. Rev.*, **A2**, 2208 (1970).
7) N. Ostlund and M. Karplus, *Chem. Phys. Lett.*, **11**, 450 (1971).
8) P. Jørgensen, J. Oddershede, and M. Ratner, *J. Chem. Phys.*, **61**, 710 (1974).
9) D. J. Rowe, *Rev. Mod. Phys.*, **40**, 153 (1968).
10) J. Simons, *J. Chem. Phys.*, **55**, 1218 (1971).
11) E. A. Sanderson, *Phys. Lett.*, **19**, 141 (1965).
12) J. da Providência, *Phys. Lett.*, **21**, 668 (1966).
13) H. Ito and Y. J. I'Haya, submitted for publication.
14) H. Ito and Y. J. I'Haya, *Chem. Phys. Lett.*, **38**, 271 (1976).
15) T. Shibuya and V. McKoy, *J. Chem. Phys.*, **54**, 1738 (1971).
16) J. N. Murrell and K. L. McEwen, *J. Chem. Phys.*, **25**, 1143 (1956).
17) N. Nakayama and Y. J. I'Haya, *Rept. Univ. Electro-Commun.*, **22**, 73 (1971).
18) T. Anno and H. Teruya, *Mem. Fac. Sci. Kyushu Univ., Ser. C*, **8**, 131 (1972).
19) T. Shibuya, Y. J. I'Haya, and V. McKoy, *Int. J. Quantum Chem.*, **9**, 505 (1975).
20) R. Gerdil, *Acta Crystallogr.*, **14**, 333 (1961).
21) R. Rein, *Adv. Quantum Chem.*, **7**, 335 (1973).
22) H. DeVoe and I. Tinoco, *J. Mol. Biol.*, **4**, 518 (1962).
23) A. F. Fucaloro and L. S. Forster, *J. Am. Chem. Soc.*, **93**, 6433 (1971).
24) P. Voet, W. B. Greatzer, R. A. Cox, and P. Doty, *Biopolymers*, **1**, 193 (1963).

The Crystal and Molecular Structures of Dichloro-1,2-bis(di-*t*-butylphosphino)-ethaneplatinum(II) and its Chlorobenzene Solvate

Masahiro HARADA, Yasushi KAI, Noritake YASUOKA, and Nobutami KASAI

Department of Applied Chemistry, Faculty of Engineering, Osaka University, Yamadakami, Suita, Osaka 565

(Received July 23, 1976)

X-Ray crystal structure analyses of $[PtCl_2\{(t\text{-}Bu)_2P(CH_2)_2P(t\text{-}Bu)_2\}]$ (I) and $[PtCl_2\{(t\text{-}Bu)_2P(CH_2)_2P(t\text{-}Bu)_2\}, C_6H_5Cl]$ (II) have been carried out. Crystals of I belong to monoclinic system: $a=20.595(3)$, $b=7.917(3)$, $c=14.885(2)$ Å, $\beta=109.03(1)°$, space group $P2_1/c$ with $Z=4$. II forms monoclinic crystals, $P2_1/c$: $a=14.873(2)$, $b=13.193(2)$, $c=15.314(2)$ Å, $\beta=98.75(1)°$, $Z=4$. Both structures, solved by the heavy-atom method, have been refined anisotropically by least-squares procedure to $R=0.067$ and 0.078 for I and II respectively. There is no essential difference between the structures of $[PtCl_2\{(t\text{-}Bu)_2P(CH_2)_2P(t\text{-}Bu)_2\}]$ molecules in I and II. The coordination around the platinum atom is square-planar; Pt–P=2.262(3) and 2.265(3) Å and Pt–Cl=2.374(4) and 2.365(4) Å. The molecule has a pseudo-C_2 symmetry: the platinum atom and the center of the C–C bond in the P–C–C–P lie on this pseudo-C_2 axis.

Recently, Otsuka and his co-workers have made studies of a series of bis(di-substituted phosphino)-alkaneplatinum complexes. In co-operation with them we have carried out the molecular structure determination of these complexes by means of X-ray diffraction. This paper describes the crystal structure analyses of dichloro-1,2-bis(di-*t*-butylphosphino)ethaneplatinum(II) $[PtCl_2\{(t\text{-}Bu)_2P(CH_2)_2P(t\text{-}Bu)_2\}]$ and its chlorobenzene solvate.

Experimental

Crystals of $[PtCl_2\{(t\text{-}Bu)_2P(CH_2)_2P(t\text{-}Bu)_2\}$ (I) were kindly provided by Professor Sei Otsuka and co-workers. Depending upon the recrystallization conditions two kinds of crystals were obtained. Preliminary Weissenberg photographs (Cu-$K\alpha$) showed that both crystals belong to the monoclinic system, and their corresponding space groups are both $P2_1/c$ (No. 14; absent reflections, $h0l$, $l=2n+1$ and $0k0$, $k=2n+1$). Crystals with approximate dimensions of (I) $0.15\times0.17\times0.25$ and (II) $0.27\times0.45\times0.60$ mm were carefully centered on a Rigaku automated, four-circle single-crystal diffractometer. It was necessary to seal the latter crystal in a thin-walled glass capillary tube with a small amount of chlorobenzene in order to prevent decomposition during the experiment.

The unit-cell parameters of both crystals were determined at 20 °C by least-squares fits using 23 and 45 high-angle reflections, respectively. The crystal data are given in Table 1.

Intensity data of both crystals were collected at 20 °C on the Rigaku diffractometer. Graphite-monochromatized Mo$K\alpha$ radiation was used. All data within a 2θ sphere of 54° were measured using the θ-2θ scan technique. The asymmetric scan width $\Delta(2\theta)$ of each reflection was calculated by the equation: $\Delta(2\theta)=(A+B\tan\theta_c)°$, where θ_c is the calculated value of the Bragg angle using $\lambda(MoK\alpha_1)$ (= 0.70926 Å) and $A=2.0$, $B=0.69$ for I and $A=2.4$, $B=0.69$ for II. The starting angle of the scan was $(2\theta_c-A/2)°$, and the scanning speed was 4.0° min^{-1}. The background count was obtained by averaging the two values measured, for 6 and 5 s respectively for I and II, at both ends of a scan. Corrections for background scattering and the usual Lorentz and polarization effects were applied. No absorption correction was employed. For weak reflections of $|F|<3\sigma(F)$ the peak scan was repeated twice. Four standard reflections (10,0,0, 006, 440, 42$\bar{9}$) were measured after every 60 reflections; these remained constant within the error limits, throughout the data collections. Totals of 5035 (4350 non-zero ($|F|\geqq3\sigma(F)$)) and 6504 (5437 non-zero) reflections were collected for I and II, respectively.

TABLE 1. CRYSTAL DATA OF $[PtCl_2\{(t\text{-}Bu)_2P(CH_2)_2P(t\text{-}Bu)_2\}]$ (I) AND ITS C_6H_5Cl SOLVATE (II)

	I	II
F. W.	584.46	697.02
Crystal system	monoclinic	monoclinic
Space group	$P2_1/c$	$P2_1/c$
a[Å]	20.595(3)	14.873(2)
b[Å]	7.917(3)	13.193(2)
c[Å]	14.885(2)	15.314(2)
β[°]	109.03(1)	98.75(1)
U[Å^3]	2294.4(11)	2970.0(8)
D_m[g cm^{-3}]	1.70[a]	
Z	4	4
D_c[g cm^{-3}]	1.692	1.559
μ(Mo$K\alpha$)[cm^{-1}]	68.0	53.5

a) Flotation in tribromomethane–carbon tetrachloride solution at 20 °C.

Solution and Refinement of Structures

Each of the structures of I and II was solved by the heavy atom method. The platinum atom was located from a three-dimensional Patterson map. All the non-hydrogen atoms were revealed from the subsequent Fourier syntheses. Refinement of the atomic positional and thermal parameters was carried out by the block-diagonal least-squares procedure. The HBLS V program[1] was used.

Final reliability factors are: I, $R=0.088$(0.067 for non-zero reflections); II, $R=0.105$ (0.078). The weighting scheme used was $w=\{\sigma(F)^2+a|F_o|+b|F_o|^2\}^{-1}$ for $|F_o|>0$ and $w=FWT$ for $|F_o|=0$, where $a=0.10071$, $b=0.00007$, and $FWT=0.05613$ for I and $a=0.0365$, $b=0.0039$, and $FWT=0.04715$ for II. A difference synthesis, based on the final atomic parameters, did not reveal the positions of hydrogen atoms nor any other significant features. The final positional and thermal parameters are given in Table 2.*

* The Tables of structure factors are kept as Document No. 7636 and 7637 at the Chemical Society of Japan.

TABLE 2a. ATOMIC FRACTIONAL COORDINATES ALONG WITH THEIR ESTIMATED STANDARD DEVIATIONS IN PARENTHESES

Atom	x	y	z
	$[PtCl_2\{(t\text{-}Bu)_2P(CH_2)_2P(t\text{-}Bu)_2\}]$		
Pt	0.25246(2)	0.10719(6)	0.15184(3)
Cl(1)	0.1767(2)	0.0411(5)	−0.0014(2)
Cl(2)	0.3294(2)	−0.0888(5)	0.1198(3)
P(1)	0.17675(14)	0.2917(4)	0.1782(2)
P(2)	0.32715(14)	0.1669(4)	0.2978(2)
C(1)	0.2249(6)	0.406(2)	0.2890(8)
C(2)	0.2793(6)	0.298(2)	0.3591(7)
C(10)	0.1473(7)	0.470(2)	0.0899(8)
C(11)	0.1263(8)	0.630(2)	0.1333(11)
C(12)	0.2088(8)	0.520(2)	0.0559(10)
C(13)	0.0859(7)	0.419(2)	0.0015(11)
C(20)	0.1004(5)	0.187(2)	0.1991(7)
C(21)	0.0543(6)	0.315(2)	0.2289(10)
C(22)	0.1304(8)	0.061(2)	0.2818(10)
C(23)	0.0552(7)	0.085(2)	0.1142(11)
C(30)	0.3562(6)	−0.019(2)	0.3808(8)
C(31)	0.3747(7)	0.035(2)	0.4877(10)
C(32)	0.2966(7)	−0.144(2)	0.3622(11)
C(33)	0.4186(6)	−0.113(2)	0.3674(10)
C(40)	0.4041(6)	0.297(2)	0.2970(9)
C(41)	0.4518(8)	0.337(3)	0.3956(11)
C(42)	0.3751(7)	0.468(2)	0.2461(11)
C(43)	0.4436(8)	0.214(2)	0.2381(13)
	$[PtCl_2\{(t\text{-}Bu)_2P(CH_2)_2P(t\text{-}Bu)_2\}, C_6H_5Cl]$		
Pt	0.25144(3)	0.20667(3)	0.21163(2)
Cl(1)	0.1546(3)	0.1512(3)	0.3111(2)
Cl(2)	0.3692(2)	0.1178(3)	0.3013(2)
P(1)	0.1363(2)	0.2914(2)	0.1297(2)
P(2)	0.3454(2)	0.2561(2)	0.1165(2)
C(1)	0.1874(9)	0.3640(9)	0.0486(7)
C(2)	0.2727(7)	0.3108(9)	0.0217(8)
C(10)	0.0803(10)	0.3919(10)	0.1914(9)
C(11)	0.0435(15)	0.4799(14)	0.1283(13)
C(12)	0.1518(11)	0.4353(11)	0.2632(9)
C(13)	0.0002(10)	0.3477(14)	0.2369(11)
C(20)	0.0485(11)	0.2092(11)	0.0620(9)
C(21)	−0.0290(11)	0.2736(15)	0.0073(13)
C(22)	0.0988(12)	0.1432(13)	−0.0017(10)
C(23)	0.0031(12)	0.1343(14)	0.1185(10)
C(30)	0.4014(11)	0.1471(11)	0.0626(9)
C(31)	0.4247(14)	0.179(2)	−0.0293(12)
C(32)	0.335(2)	0.0568(13)	0.0544(13)
C(33)	0.4939(13)	0.1149(15)	0.1234(12)
C(40)	0.4295(9)	0.3566(11)	0.1594(9)
C(41)	0.4890(13)	0.3861(14)	0.0853(12)
C(42)	0.3777(12)	0.4491(6)	0.1804(14)
C(43)	0.4956(11)	0.325(2)	0.2432(11)
Cl(5)	0.7707(11)	0.239(2)	0.2898(10)
C(51)	0.749(2)	0.261(3)	0.179(2)
C(52)	0.7345(15)	0.197(2)	0.115(2)
C(53)	0.716(2)	0.236(2)	0.020(2)
C(54)	0.714(2)	0.327(2)	0.005(2)
C(55)	0.735(2)	0.400(2)	0.073(4)
C(56)	0.7510(15)	0.376(2)	0.174(3)

TABLE 2b. TEMPERATURE FACTORS ALONG WITH THEIR ESTIMATED STANDARD DEVIATIONS IN PARENTHESES ($\times 10^3$)
Anisotropic temperature factors are expressed in the form: $\exp[-(\beta_{11}h^2+\beta_{22}k^2+\beta_{33}l^2+\beta_{12}hk+\beta_{13}hl+\beta_{23}kl)]$.

Atom	β_{11}	β_{22}	β_{33}	β_{12}	β_{13}	β_{23}
		[$PtCl_2\{(t\text{-Bu})_2P(CH_2)_2P(t\text{-Bu})_2\}$]				
Pt	1.655(10)	14.65(7)	2.83(2)	1.25(5)	1.50(2)	−0.45(6)
Cl(1)	2.68(9)	25.0(7)	2.81(13)	1.7(4)	1.0(2)	−2.8(5)
Cl(2)	2.84(10)	24.0(8)	5.8(2)	5.9(5)	2.1(2)	−5.9(6)
P(1)	1.70(7)	14.5(5)	2.90(13)	1.3(3)	1.5(2)	0.5(4)
P(2)	1.50(7)	15.1(5)	3.40(14)	0.4(3)	1.0(2)	−1.3(5)
C(1)	2.0(3)	17(2)	4.2(6)	0.8(13)	1.9(7)	−11(2)
C(2)	1.7(3)	21(3)	2.9(5)	0.3(14)	0.2(6)	−6(2)
C(10)	2.8(4)	18(2)	3.8(6)	7(2)	2.0(6)	5(2)
C(11)	3.9(5)	19(3)	6.8(10)	5(2)	3.3(12)	4(3)
C(12)	3.6(5)	28(4)	5.7(8)	1(2)	4.7(11)	11(3)
C(13)	1.9(4)	35(4)	5.8(9)	2(2)	−0.3(9)	1(3)
C(20)	1.7(3)	16(2)	3.3(5)	−0.6(13)	1.3(6)	1(2)
C(21)	2.0(3)	27(3)	6.6(9)	3(2)	3.7(9)	−4(3)
C(22)	3.2(5)	29(4)	5.3(8)	−1(2)	3.6(10)	8(3)
C(23)	2.8(4)	24(3)	5.8(8)	−3(2)	2.0(10)	−5(3)
C(30)	1.6(3)	18(2)	4.2(6)	0.8(14)	0.0(7)	1(2)
C(31)	2.9(4)	26(3)	4.5(7)	2(2)	0.4(9)	2(3)
C(32)	2.6(4)	20(3)	7.1(9)	−2(2)	1.8(10)	5(3)
C(33)	1.9(3)	25(3)	5.3(7)	4(2)	1.3(8)	3(2)
C(40)	1.6(3)	16(2)	5.2(7)	−4.0(13)	2.4(7)	−0(2)
C(41)	2.7(4)	34(4)	5.9(9)	−4(2)	−0.7(10)	−6(3)
C(42)	2.9(4)	17(3)	7.2(9)	0(2)	3.5(10)	5(3)
C(43)	2.9(4)	28(4)	9.9(12)	−0(2)	7.4(13)	−1(4)
		[$PtCl_2\{(t\text{-Bu})_2P(CH_2)_2P(t\text{-Bu})_2\}$, C_6H_5Cl]				
Pt	3.90(2)	4.76(2)	2.09(2)	0.43(4)	1.50(3)	0.47(3)
Cl(1)	5.5(2)	9.1(3)	3.02(12)	−0.8(3)	3.2(2)	3.0(3)
Cl(2)	5.7(2)	9.0(3)	4.1(1)	3.7(4)	1.1(3)	4.2(3)
P(1)	3.72(13)	5.4(2)	2.25(11)	−0.3(2)	1.3(2)	0.1(2)
P(2)	3.98(14)	5.3(2)	2.68(12)	0.4(3)	2.2(2)	−0.5(2)
C(1)	6.0(7)	5.1(7)	2.8(5)	1.3(11)	3.2(9)	1.8(10)
C(2)	3.3(5)	5.0(7)	3.2(5)	0.2(13)	3.4(8)	2.0(10)
C(10)	5.6(7)	5.8(8)	5.0(7)	2.7(13)	2.9(11)	−0.9(12)
C(11)	10.9(14)	8.0(12)	7.7(11)	9(2)	6(2)	1(2)
C(12)	7.1(9)	6.5(9)	4.3(7)	−0.7(14)	2.1(12)	−0.3(13)
C(13)	5.3(8)	10.4(13)	6.3(9)	2(2)	5.0(13)	−1(2)
C(20)	6.1(8)	8.2(11)	3.2(6)	−5.5(14)	0.7(11)	−1.0(12)
C(21)	5.2(8)	12(2)	6.6(10)	1(2)	−5(2)	2(2)
C(22)	8.8(11)	10.0(13)	4.2(7)	−6(2)	3.2(14)	−9(2)
C(23)	7.7(10)	10.2(13)	4.7(7)	−7(2)	1.4(14)	3(2)
C(30)	7.7(9)	7.4(10)	4.0(6)	2(2)	5.4(13)	0.7(13)
C(31)	10.1(13)	13(2)	5.4(9)	8(2)	10(2)	2(2)
C(32)	15(2)	7.9(12)	7.3(11)	−9(2)	12(2)	−9(2)
C(33)	8.1(11)	12(2)	7(2)	11(2)	3(2)	−3(2)
C(40)	4.2(6)	8.7(11)	4.2(6)	−2.5(13)	1.0(10)	1.4(13)
C(41)	8.9(12)	10.7(14)	6.6(9)	−9(2)	7(2)	3(2)
C(42)	6.8(10)	7.8(12)	10.4(14)	−0(2)	0(2)	−5(2)
C(43)	5.5(8)	13(2)	4.8(8)	−3(2)	−0.8(13)	−0(2)
Cl(5)	19.4(13)	61(3)	16.7(14)	2(3)	3(2)	18(3)
C(51)	6.0(14)	24(3)	12(2)	2(3)	3(2)	4(5)
C(52)	5.5(11)	15(2)	20(3)	−1(2)	5(3)	−12(4)
C(53)	10(2)	15(2)	15(2)	−3(3)	13(3)	−3(4)
C(54)	9(2)	12(2)	20(3)	−4(3)	13(4)	12(4)
C(55)	12(2)	5.2(13)	64(9)	6(3)	20(7)	30(6)
C(56)	6.6(12)	10(2)	33(4)	5(2)	13(4)	11(5)

Throughout the calculation the atomic scattering factors used were those of neutral atoms given in International Tables for X-ray Crystallography, Vol. IV.[2] For I, the effects of the anomalous dispersion of Pt, Cl, P, and C atoms were included in the calculation; the values of $\Delta f'$ and $\Delta f''$ were also taken from the International Tables for X-Ray Crystallography.[3]

Results and Discussion

Molecular Structure. Figure 1 gives a stereoscopic drawing of the molecule in I. Bond lengths and bond angles are listed in Table 3. Selected bond lengths and bond angles of the molecule in II are given in Fig. 2 with the numbering scheme of the atoms. Figure 3 shows a comparison of selected bond lengths and bond angles between I and II, in which chemically equivalent bond lengths and bond angles have been averaged. This result clearly shows that there is no essential difference between the molecular structures in I and II, in spite of the different molecular packings. Therefore, from now on we will discuss only the molecular structure of I, the more accurate one of the two, except for the case of crystalline chlorobenzene.

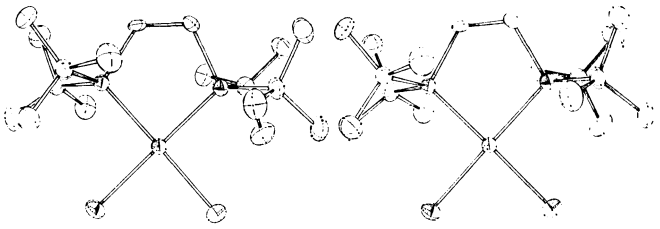

Fig. 1. A stereoscopic drawing of $[PtCl_2\{(t\text{-}Bu)_2P(CH_2)_2P(t\text{-}Bu)_2\}]$ molecule in I. Thermal ellipsoids are drawn at 30% probability level.

The co-ordination around the platinum atom is square-planar: Pt, P, and two Cl atoms are coplanar within 0.004 Å. The molecule has a pseudo C_2 symmetry. The platinum atom lies on the pseudo C_2 axis, which also passes through the center of the C(1)–C(2) bond in $\{(t\text{-}Bu)_2P(CH_2)_2P(t\text{-}Bu)_2\}$ ligand. The P–C–C–P moiety, as a bidentate chelating ligand,

Table 3. Bond lengths and bond angles in $[PtCl_2\{(t\text{-}Bu)_2P(CH_2)_2P(t\text{-}Bu)_2\}]$

Bond lengths (l/Å)			
Pt-P(1)	2.262(3)	C(10)-C(11)	1.55(2)
Pt-P(2)	2.265(3)	C(10)-C(12)	1.56(2)
Pt-Cl(1)	2.365(4)	C(10)-C(13)	1.55(2)
Pt-Cl(2)	2.374(4)	C(20)-C(21)	1.55(2)
		C(20)-C(22)	1.55(2)
P(1)-C(1)	1.859(13)	C(20)-C(23)	1.53(2)
P(2)-C(2)	1.864(14)	C(30)-C(31)	1.57(2)
P(1)-C(10)	1.886(14)	C(30)-C(32)	1.53(2)
P(1)-C(20)	1.892(13)	C(30)-C(33)	1.55(2)
P(2)-C(30)	1.889(14)	C(40)-C(41)	1.51(2)
P(2)-C(40)	1.893(13)	C(40)-C(42)	1.57(2)
		C(40)-C(43)	1.53(2)
C(1)-C(2)	1.52(2)		
Bond angles (ϕ/°)			
P(1)-Pt-P(2)	89.42(12)	Pt-P(1)-C(1)	105.7(4)
P(1)-Pt-Cl(1)	91.98(12)	Pt-P(2)-C(2)	106.5(5)
P(2)-Pt-Cl(2)	92.30(13)	Pt-P(1)-C(10)	116.4(4)
P(1)-Pt-Cl(2)	178.27(13)	Pt-P(1)-C(20)	113.7(4)
P(2)-Pt-Cl(1)	178.57(13)	Pt-P(2)-C(30)	115.8(4)
Cl(1)-Pt-Cl(2)	86.29(13)	Pt-P(2)-C(40)	114.5(4)
C(1)-P(1)-C(10)	102.3(6)	C(2)-P(2)-C(30)	102.7(6)
C(1)-P(1)-C(20)	107.3(6)	C(2)-P(2)-C(40)	106.1(6)
C(10)-P(1)-C(20)	110.3(6)	C(30)-P(2)-C(40)	109.9(6)
P(1)-C(1)-C(2)	113.4(9)	P(2)-C(2)-C(1)	111.5(9)
P(1)-C(10)-C(11)	113.1(10)	P(2)-C(30)-C(31)	111.8(10)
P(1)-C(10)-C(12)	107.8(10)	P(2)-C(30)-C(32)	108.8(10)
P(1)-C(10)-C(13)	112.8(10)	P(2)-C(30)-C(33)	113.0(10)
P(1)-C(20)-C(21)	112.4(10)	P(2)-C(40)-C(41)	112.8(11)
P(1)-C(20)-C(22)	106.0(10)	P(2)-C(40)-C(42)	106.5(9)
P(1)-C(20)-C(23)	114.1(9)	P(2)-C(40)-C(43)	111.9(10)
C(11)-C(10)-C(12)	107.1(12)	C(31)-C(30)-C(32)	106.0(12)
C(11)-C(10)-C(13)	107.7(12)	C(31)-C(30)-C(33)	108.8(12)
C(12)-C(10)-C(13)	108.3(12)	C(32)-C(30)-C(33)	108.3(12)
C(21)-C(20)-C(22)	108.5(12)	C(41)-C(40)-C(42)	108.2(12)
C(21)-C(20)-C(23)	108.4(12)	C(41)-C(40)-C(43)	110.5(13)
C(22)-C(20)-C(23)	107.1(12)	C(42)-C(40)-C(43)	106.6(12)

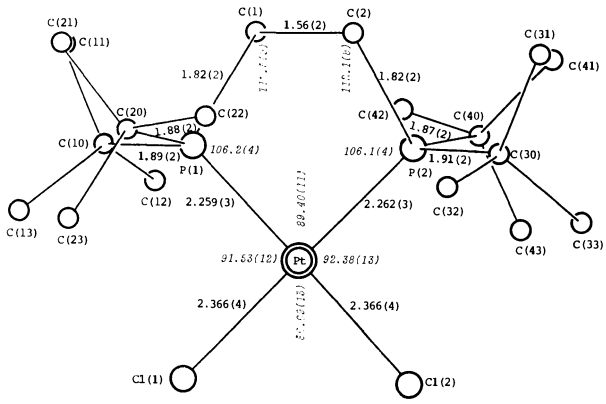

Fig. 2. Selected bond lengths (l/Å) and bond angles (ϕ/°) of the molecule in II.

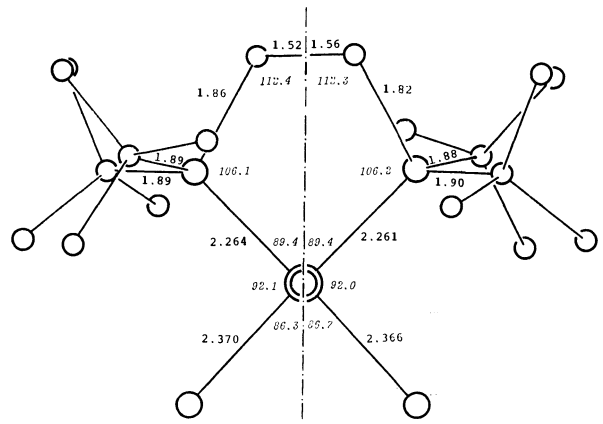

Fig. 3. Comparison of the selected bond lengths (l/Å) and bond angles (ϕ/°) of the molecule in I(left) and II(right).

is puckered in a manner similar to that observed in co-ordinated ethylenediamine rings. The methylene carbon atoms are displaced, by 0.30 and 0.28 Å, to the opposite sides of the co-ordination plane.

The Pt–P bond lengths [2.262(3) and 2.265(3) Å] are as much as 0.14 Å shorter than the sum of the covalent radii [2.41 Å].[4] On the other hand, the Pt–Cl bond lengths [2.374(4), 2.365(4) Å] are significantly longer than the sum of the covalent radii [2.30 Å].

The P–C(bridge) bond lengths [both 1.86(2) Å] are close to the sum of the covalent radii [1.87 Å], and are slightly shorter than the P–C(*t*-Bu) bonds [all 1.89(2) Å]. The two *t*-butyl groups attached to the same phosphorus atom are in a staggered position.

Solvated Chlorobenzene Molecule. Crystals of II contain solvated chlorobenzene molecules. The electron-density map calculated on the mean plane of chlorobenzene does not show a normal distribution with respect to magnitude and anisotropy. The rather low peak heights suggest that the occupancy of chlorobenzene is less than unity and/or that their positional fluctuations in the crystal are fairly large. Consequently, the bond lengths and bond angles are not satisfactory ones.

Crystal Structure. A stereoscopic drawing of the molecular packings of I and II are given in Figs. 4 and 5. Figure 6 illustrates the crystal structure of II projected along the c axis. The $[PtCl_2\{(t\text{-}Bu)_2P(CH_2)_2P(t\text{-}Bu)_2\}]$ molecules are piled up in columns along the c axis, and the chlorobenzene molecules are packed in voids between these columns with rather loose molecular contacts.

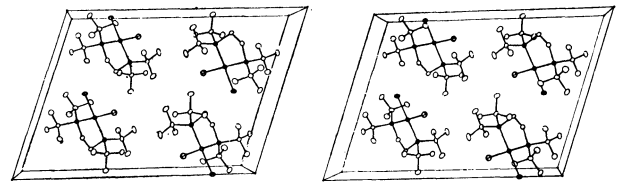

Fig. 4. A stereoscopic drawing of the molecular packing in I.

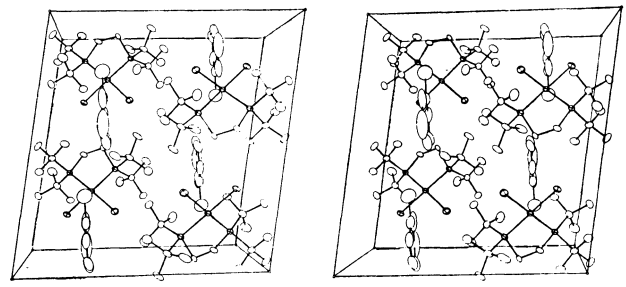

Fig. 5. A stereoscopic drawing of the molecular packing in II.

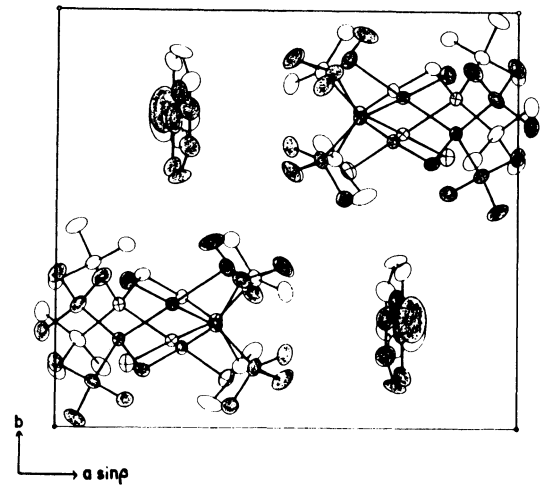

Fig. 6. Crystal structure of II projected along the c axis.

All intermolecular atomic contacts in I and II are considered to be at the usual van der Waals distances.

Computations throughout the present study were carried out on a NEAC 2200-700 computer at Osaka University. Figures 1, 4, and 6 were drawn on the NUMERICON 7000 system at Osaka University with a local version of ORTEP.[5]

The authors wish to express their thanks to Professor Sei Otsuka and his co-workers for the crystals and their helpful discussions.

References

1) T. Ashida, The Universal Crystallographic Computing System-Osaka, The Computation Center, Osaka University (1973), p. 55.

2) International Tables for X-Ray Crystallography, Vol. IV, The Kynoch Press, Birmingham (1974), p. 71.

3) International Tables for X-Ray Crystallography, Vol. IV, The Kynoch Press, Birmingham (1974), p. 148.

4) L. Pauling, "The Nature of the Chemical Bond," 3rd. ed., Cornell University Press, Ithaca, N. Y. (1960), p. 246.

5) C. K. Johnson, ORTEP, Report ORNL-3791, Oak Ridge National Laboratory, Tennessee (1965).

Carbon-13 and Proton Nuclear Magnetic Resonance Spectra of Methylmercury Nitrate in Strong Acids

Yoshikane KAWASAKI,* Mitsutoshi ARITOMI, and Jun IYODA**

Department of Petroleum Chemistry, Osaka University, Yamadakami, Suita, Osaka 565

***Government Industrial Research Institute, Midoriga-Oka, Ikeda, Osaka 566*

(Received July 24, 1976)

Proton and carbon-13 nuclear magnetic resonance spectra and Raman spectra of some methylmercury compounds, CH_3HgX, were measured. The spin-spin coupling constants, $^2J(^{199}Hg-H)$ and $^1J(^{13}C-H)$ of methylmercury nitrate in some strong acids were found to increase when the proton resonance of the methyl group attached to the mercury shifts to lower magnetic field. It was also found that the C-H stretching bands of the methyl group shift to higher frequency in the strong acids. The results are explained by an increase of the effective positive charge on the mercury. As has been observed in other alkylmercury compounds, the spin-spin coupling constant between directly bonded mercury and carbon nuclei, $^1J(^{199}Hg-^{13}C)$, of some methylmercury compounds in organic solvents increased with the geminal spin-spin coupling constant, $^2J(^{199}Hg-H)$. The $^1J(^{199}Hg-^{13}C)$ value of methylmercury nitrate in strong acids was found to decrease, whereas the $^2J(^{199}Hg-H)$ values increased in these media. The lowering of the mercury-carbon bond strengths in the strong acids, which was revealed from the mercury-carbon stretching frequency in the Raman spectra, is considered one possible reason for the decrease of the $^1J(^{199}Hg-^{13}C)$ value.

In recent years a great deal of information on heavy atom–proton and –carbon-13 spin-spin couplings has accumulated, particularly for the mercury system. Hatton, Schneider, and Siebrand[1] have shown that in a series of methylmercury compounds, CH_3HgX, the geminal spin-spin coupling constant, $^2J(^{199}Hg-H)$, is approximately accounted for by the Fermi contact mechanism. Henneike[2] has also shown from a semi-empirical molecular orbital study of a number of methylmercury compounds that the orbital contraction for the mercury 6S orbital with increasing electronegativity of the substituent, X, is an important contributing factor to the spin-spin coupling constant. Singh[3] and Ibusuki and Saito[4] have indicated that the Fermi contanct interaction is predominant in the mercury–proton and –carbon-13 spin-spin coupling constants by showing linear relationships between the spin-spin coupling constants $^1J(^{199}Hg-^{13}C)$ and $^2J(^{199}Hg-H)$ which pass almost through the origin for neopentylmercury compounds, $(CH_3)_3CCH_2HgX$, and 2-methoxy-2-methylpropylmercury compounds, $(CH_3)_2C(OCH_3)CH_2HgX$, respectively.

In parallel with these studies, the proton and carbon-13 nuclear magnetic resonance spectra of a variety of organomercury compounds have been used for structural and bonding studies,[5-26] because the $^1J(^{199}Hg-^{13}C)$ and $^2J(^{199}Hg-H)$ values are influenced markedly by substituents at the mercury.

In the present paper, the proton and carbon-13 nuclear magnetic resonance spectra of methylmercury nitrate, CH_3HgNO_3, in some strong acids were studied to find out the effect of the effective positive charge on the mercury on the spin-spin coupling constants, $^1J(^{199}Hg-^{13}C)$, $^2J(^{199}Hg-H)$, and $^1J(^{13}C-H)$. The Raman spectra of methylmercury nitrate were also measured in the strong acids; the results are discussed with the nuclear magnetic resonance spectral date.

Experimental

Preparation of Compounds. Methylmercury bromide was prepared by Grignard reaction of methylmagnesium bromide and mercury dibromide in ether and purified by recrystallization from methanol. Methylmercury cyanide and nitrate were obtained by stirring a mixtures of methylmercury bromide and appropriate silver salts in methanol for 5 h at ambient temperature. After filtering off the silver bromide, concentration of the filtrate at reduced pressure yielded crystalline compounds. The compounds were dried *in vaccuo* and were stored in a desiccator.

NMR Spectra. The Proton magnetic resonance spectra were measured on a JEOL model JNM-PS-100 spectrometer operating at 100 MHz. The chemical shifts were measured relative to internal tetramethylsilane and sodium 2,2-dimethyl-2-silapentane-5-sulfonate, DSS. The spin-spin coupling constants, $^1J(^{13}C-H)$ and $^2J(^{199}Hg-H)$, and the chemical shift of the methyl group, $\delta(Hg-C\underline{H}_3)$, obtained for methylmercury compounds in about 10 wt% solution are shown in Table 1. The values of dimethylmercury[16] and methylmercury ion[21] also appear in Table 1.

The carbon-13 nuclear magnetic resonance spectra were run on a JEOL model JNM-PFT-100 pulse Fourier transform spectrometer operating at 25.14 MHz. Broad band proton noise decoupling was employed to eliminate the spin-spin coupling with the protons and to enhance the signal-to-noise ratio. $(CD_3)_2CO$ was used as a lock signal. Good spectra were obtained generally by scanning 1500—2000 times. The spin-spin coupling constant, $^1J(^{199}Hg-^{13}C)$, for some methylmercury compounds in about 20 wt% solution is shown in Table 1.

Raman Spectra. The Raman spectra were recorded on a JEOL model JRS-02AS spectrometer using laser light of 4880 A. The mercury-carbon and carbon-hydrogen stretching frequencies of methylmercury nitrate in some strong acids are shown in Table 2. The concentration of the compounds was about 20 wt%. The data of some other methylmercury compounds[27-29] are also added for comparison.

Solvents. The organic solvents dried over a desiccant were purified by distillation. Inorganic acids obtained from commercial sources were used without further purification.

Results and Discussion

The proton magnetic resonance data of methylmercury nitrate in Table 1 show that the chemi-

* To whom correspondence should be addressed.

Table 1. Proton and carbon-13 NMR data of some methylmercury compounds, CH_3HgX, in several solvents

X	Solvent	$^1J(^{13}C\text{-}H)$ (Hz)	$^2J(^{199}Hg\text{-}H)$ (Hz)	$^1J(^{199}Hg\text{-}^{13}C)$ (Hz)	$\delta(C\underline{H}_3)$ (ppm)	$\delta(\underline{C}H_3)$ (ppm)
CH_3		129.6[a]	104.3[b]	690[a]		
CN	Pyridine	132.0	177.6	1235	0.69	6.0[c]
Br	Pyridine	135.6	214.5	1530	0.98	1.1[c]
Br	DMSO	138.5	221.5	d)	0.87	d)
NO_3	CH_3OH	139.2	251.3	1793	1.08	−3.7[c]
NO_3	H_2O	141.0	256.5	1785	1.06	−1.2[e]
NO_3	DMSO	139.0	260.3	1954	0.88	−0.9[c]
NO_3	HNO_3(60%)	142.9	257.4	1691	1.31	−1.1[e]
NO_3	$HClO_4$(10%)	142.2	262.0	d)	1.13	d)
NO_3	$HClO_4$(20%)	142.5	262.8	1761	1.20	−0.1[e]
NO_3	$HClO_4$(40%)	142.5	263.8	d)	1.25	d)
NO_3	$HClO_4$(50%)	142.8	265.8	d)	1.29	d)
NO_3	$HClO_4$(60%)	143.9	270.6	1732	1.39	1.3[e]
NO_3	$HClO_4$(70%)	144.3	273.9	1711	1.42	3.8[e]
NO_3	H_2SO_4(95%)	145.3	274.0	1654	f)	4.0[e]
NO_3	CF_3SO_3H	146.4	280.6	1667	f)	3.7[e]
FSO_3[g]	$FSO_3H\text{-}SO_2$		246		1.54	
[g]	$FSO_3H\text{-}SO_2$		240		1.46	

a) Ref. 12. b) Ref. 16. c) Internal TMS. d) Not measured. e) External TMS. f) DSS was decomposed. g) Ref. 21.

Table 2. The C-H and Hg-C stretching frequencies of some methylmercury compounds, CH_3HgX (in cm^{-1})

X	Solvent	$\nu_{asym}(C\text{-}H)$	$\nu_{sym}(C\text{-}H)$	$\nu(Hg\text{-}C)$
CH_3[a]	Neat	2965	2909	514
CN[b]	H_2O	3008	2931	564
NO_3[c]	H_2O	3025	2941	566
ClO_4[c]	H_2O	3027	2941	569
NO_3	$HClO_4$(70%)	3048 br	2945	569
NO_3	H_2SO_4(95%)	3045 br	2946	562
NO_3	CF_3SO_3H	d)	d)	561

a) Ref. 27. b) Ref. 28. c) Ref. 29. d) Could not be observed because of strong background.

cal shift of the methyl group, $\delta(Hg\text{-}C\underline{H}_3)$, shifts to lower magnetic field and concomitantly the geminal spin-spin coupling constant, $^2J(^{199}Hg\text{-}H)$, increases as the acid strength becomes large or the concentration of the acid increases. The chemical shift of the methyl proton, $\delta(Hg\text{-}C\underline{H}_3)$, of methylmercury nitrate in the strong acids is comparable to that of the methylmercury ion measured by Olah and Clifford[21] in a mixed solvent system, $FSO_3H\text{-}SO_2$, but the geminal spin-spin coupling constant, $^2J(^{199}Hg\text{-}H)$, of methylmercury nitrate is much larger than that of the methylmercury ion. The small $^2J(^{199}Hg\text{-}H)$ value of the naked methylmercury ion was predicted from the semiempirical molecular orbital calculation by Henneike.[2]

A fairly linear relation between the chemical shift of the methyl proton, $\delta(Hg\text{-}C\underline{H}_3)$, and the geminal spin-spin coupling constant, $^2J(^{199}Hg\text{-}H)$, is shown in Fig. 1. The relation is quite similar to that obtained for other series of methylmercury compounds, *i.e.*, increase of the geminal coupling constants, $^2J(^{199}Hg\text{-}H)$, is followed by increase of the electronegativity of

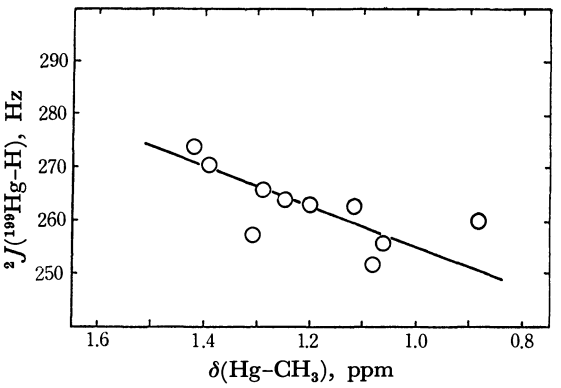

Fig. 1. Correlation between $\delta(Hg\text{-}CH_3)$ and $^2J(^{199}Hg\text{-}H)$ for methylmercury nitrate.

the substituents[10] or by decrease of the pK_a values of carboxylic acids.[15] But the relation is quite different from the relations obtained for dimethyllead dinitrate, dimethyltin oxide, and dimethylthallium nitrate in strong acids,[30] in which the geminal spin-spin coupling constants, $^2J(M\text{-}H)$(M=Sn, Pb, and Tl), decrease as the acid strength or the concentration of the acids increase.

Woodward and co-worker[29,31] have shown that there is the following equilibrium in an aqueous solution of methylmercury nitrate. Since the function of strong acids is to reduce the water activity below that necessary

$$CH_3HgONO_2 + H_2O \rightleftharpoons [CH_3HgOH_2]^+ + NO_3^-$$

to hydrate the cation fully, the equilibrium shown below may shift to the right in strong acids, where

$$[CH_3HgOH_2]^+ + Y^- + H^+ \rightleftharpoons [CH_3Hg^+\cdots Y^-] + H_3O^+$$

Y^- is the acid residue. In the $[CH_3Hg^+\cdots Y^-]$ species, the acid residue may coordinate weakly to mercury from the backside of the C–Hg bond. The effective positive charge, and therefore the orbital contraction of the mercury 6S orbital in the species, $[CH_3Hg^+\cdots Y^-]$, is probably larger than that of the hydrated species, $[CH_3HgOH_2]^+$, because the electron donating ability of the acid residue, Y^-, is considered to be smaller than water. The down field shift of the methyl proton, $\delta(Hg-C\underline{H}_3)$, and increase of the geminal spin-spin coupling constant, $^2J(^{199}Hg-H)$, in strong acids, therefore, may be due to an increase of the species $[CH_3Hg^+\cdots Y^-]$ in these media.

As can be seen from Table 1, the $^1J(^{13}C-H)$ value of the methyl group of the methylmercury nitrate increases when the acid strength or the concentration of the acids increases, although Henneike[2] obtained little variation of the $^1J(^{13}C-H)$ value for methylmercury compounds. Figure 2 gives a linear relation between the $^1J(^{13}C-H)$ and $\delta(Hg-C\underline{H}_3)$ values, which is expressed by the following equation, where the values in parentheses are the errors estimated at the 95% confidence level and the r is the correlation coefficient. The result is quite similar to that obtained for

$$^1J(^{13}C-H) = 9.8(\pm2.7)\delta(Hg-C\underline{H}_3) + 130.4(\pm3.1)\quad r=0.955$$

dimethyltin oxide in strong acids.[30] The dependence

$$^1J(^{13}C-H) = 5.6(\pm1.6)\delta(Sn-C\underline{H}_3) + 130.4(\pm2.1)\quad r=0.933$$

of the $^1J(^{13}C-H)$ value on the chemical shift of the methyl protons is much more acute in the case of methylmercury nitrate. A linear relation is also obtained between the $^1J(^{13}C-H)$ and $^2J(^{199}Hg-H)$ values for methylmercury nitrate in strong acids(see Fig. 2), which is represented by the following equation:

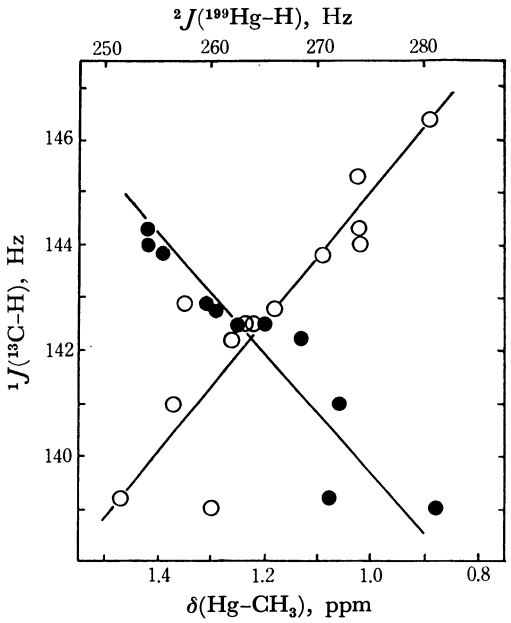

Fig. 2. Correlation between $^1J(^{13}C-H)$ and $\delta(Hg-CH_3)$ (—●—) and $^2J(^{199}Hg-H)$ (—○—) for methylmercury nitrate.

$$^1J(^{13}C-H) = 0.22(\pm0.11)^2J(^{199}Hg-H) + 84(\pm22)\quad r=0.879$$

The C–H symmetric and asymmetric stretching bands shown in Table 2 shift to higher frequencies in strong acids. The values are rather larger than those of dimethylmercury.[27] High C–H stretching freqeuencies of the methyl group of dimethyllead diperchlorate[32] and dimethyltin diperchlorate[33] in aqueous solutions relative to those of tetramethyl-lead and -tin,[34] respectively, have been reported. Brown and Puckett[35] have shown that in a variety of methyl compounds the spin-spin coupling constant, $^1J(^{13}C-H)$, of the methyl group increases linearly with increasing C–H symmetric and asymmetric stretching frequencies and therefore with the C–H stretching force constant. By using the present values for methylmercury nitrate and the reported values of the $^1J(^{13}C-H)$ and ν_{asym}-(C–H) values of 32 methyl compounds, we obtained the following equation relating these quantities:

$$^1J(^{13}C-H) = 0.237(\pm0.034)\nu_{asym}(C-H) - 576(\pm102)\quad r = 0.933$$

They[35] have shown theoretically that the C–H stretching force constant of these methyl compounds should depend on the C–H bond polarity, which will in turn depend on the electronegativity of the group attached to the methyl group. They concluded from these results that changes in the effective nuclear charge of carbon experienced by the electron in the C–H bonds can account for the principal variation in the $^1J(^{13}C-H)$ value of the methyl groups[36] and the assuming of a very large change in the hybridization parameter of carbon to fit the experimental value is not necessary. The increase of the $^1J(^{13}C-H)$ value of methylmercury nitrate in strong acids, therefore, may be accounted for by the same principle. The result is in accordance with the increase of the species $[CH_3Hg^+\cdots Y^-]$ in strong acids, since in this species the effective positive charge on the mercury and therefore the electronegativity of the mercury, is considered to be large.

Table 1 gives the spin-spin coupling constant, $^1J(^{199}Hg-^{13}C)$, of some methylmercury compounds. The value increases when the electron-withdrawing property of the substituent becomes large. A linear relation between the $^1J(^{199}Hg-^{13}C)$ and $^2J(^{199}Hg-H)$ values of these compounds in organic solvents and in water is shown in Fig. 3. The regression analysis for this relation gives the following equation:

$$^1J(^{199}Hg-^{13}C) = 7.65(\pm0.80)^2J(^{199}Hg-H) - 144(\pm173)\quad r = 0.997$$

Similar linear relations have been reported for 2-methoxy-2-methyl-propylmercury derivatives, $(CH_3)_2C(OCH_3)CH_2HgX$,[4] and for neopentylmercury compounds, $(CH_3)_3CCH_2HgX$.[3] The numerical values

$$^1J(^{199}Hg-^{13}C) = 8.47(\pm2.32)^2J(^{199}Hg-H) - 98(\pm140)\quad r=0.981***$$

$$^1J(^{199}Hg-^{13}C) = 7.8^2J(^{199}Hg-H) - 59$$

*** The regression analysis was made by using the reported values.[4]

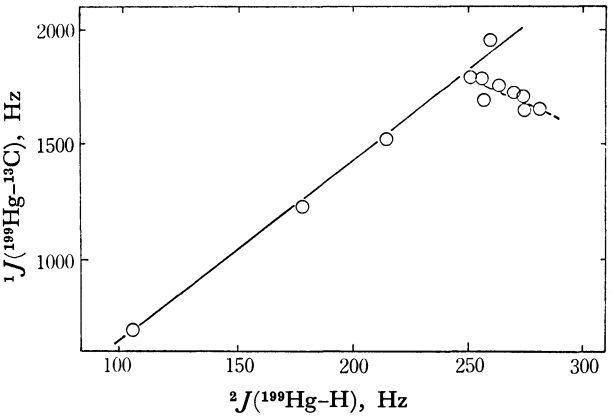

Fig. 3. Correlation between $^1J(^{199}Hg-^{13}C)$ and $^2J(^{199}Hg-H)$ for methylmercury compounds.

of these three equations are very similar. Although the lines do not pass exactly through the origin, the relations indicate that the Fermi contact term is mainly responsible for the spin-spin coupling constants, $^1J(^{199}Hg-^{13}C)$ and $^2J(^{199}Hg-H)$, in these cases. On the other hand, as can be seen from Table 1, the $^1J(^{199}Hg-^{13}C)$ value of methylmercury nitrate decreases when the acid strength increases, whereas the $^2J(^{199}Hg-H)$ value continues to incresae. These results cannot be explained by the simple assumption that the Fermi contact term plays a dominant role in the spin-spin coupling constant, $^1J(^{199}Hg-^{13}C)$.

According to the theory of spin-spin interaction developed by Ramsey,[37] the nuclear spin-spin coupling constant is, in addition to the Fermi contact interaction, affected by the following terms: 1) an orbital-dipole interaction between the magnitic field due to the orbital motion of the electron and the nuclear magnetic dipole (J_{orb}) and 2) a magnetic dipole-dipole interaction between the magnetic dipole of the spinning electron and the nuclear spin(J_{dipole}). Of these three basic interactions, the contact interaction is the main determinant of the nuclear spin-spin coupling constant, especially for H_2.[38] However, the J_{orb} and J_{dipole} terms have been found to be very important when one or both of the nuclei is electronegative, such as in the spin-spin coupling constant, $^1J(^{12}C-^{19}F)$ and $^{2,3}J(^{19}F-^{19}F)$.[39] In the spin-spin coupling constants, $^1J(^{13}C-^{13}C)$, the J_{dipole} term has been found to play a significant role.[39,40] Therefore, the contribution of the J_{orb} and J_{dipole} terms may be one reason for the decrease of the spin-spin coupling constant, $^1J(^{199}Hg-^{13}C)$, of methylmercury nitrate in strong acids. As can be seen from Table 2, the value of the mercury–carbon stretching frequency for methylmercury nitrate has a tendency to decrease in strong acids. The weakening of the mercury–carbon bond, therefore, may also be an another factor leading to a reduction of the $^1J(^{199}Hg-^{13}C)$ value. In an overlap population analysis of the molecular orbitals of the methylmercury compounds,[2] the overlap population between the mercury–carbon bond increases when the electronegativity of the substituent becomes large. The value of the overlap population of the hydrate species $[CH_3HgOH_2]^+$ is the largest among the methylmercury compounds. But the value of the naked methylmercury ion, CH_3Hg^+, is the smallest. Therefore, the bond properties for the mercury–carbon bond of the species $[CH_3Hg^+\cdots Y^-]$, which has been shown to be the predominant species of methylmercury nitrate in strong acids, may be in between those of the ions $[CH_3HgOH_2]^+$ and CH_3Hg^+.

We wish to express our hearty thanks to Professor Rokuro Okawara of Osaka University for his continuous encouragement throughout this study. We are also grateful to Dr. Teizo Kitagawa of the Protein Institute of Osaka University for the measurements of Raman spectra.

References

1) J. V. Hatton, W. G. Schneider, and W. Siebrand, *J. Chem. Phys.*, **39**, 1330 (1963).
2) H. F. Henneike, *J. Am. Chem. Soc.*, **94**, 5945 (1972).
3) G. Singh, *J. Organomet. Chem.*, **99**, 251 (1975).
4) T. Ibusuki and Y. Saito, *Chem. Lett.*, **1974**, 311.
5) F. A. Cotton and J. R. Leto, *J. Am. Chem. Soc.*, **80**, 4823 (1958).
6) R. E. Dessy, T. J. Flaut, H. H. Jaffé, and G. F. Reynolds, *J. Chem. Phys.*, **30**, 1422 (1959).
7) S. Brownstein, *Discuss. Faraday Soc.*, **34**, 25 (1962).
8) P. R. Wells and W. Kitching, *Tetrahedron Lett.*, **1963**, 1531.
9) M. M. Kreevoy and J. F. Schaeffer, *J. Organomet. Chem.*, **6**, 589 (1966).
10) W. Kitching, J. A. Smith, and P. R. Wells, *Chem. Commun.*, **1968**, 390
11) A. N. Nesmeyanov, L. A. Fedorov, R. B. Materikova, E. I. Fedlin, and N. S. Kochetkova, *Tetrahedron Lett.*, **1968**, 3753.
12) F. J. Weigert, M. Winkur, and J. D. Roberts, *J. Am. Chem. Soc.*, **90**, 1566 (1968).
13) E. F. Kiefer, W. L. Waters, and D. A. Carlson, *J. Am. Chem. Soc.*, **90**, 5127 (1968).
14) E. F. Kiefer and W. Gericke, *J. Am. Chem. Soc.*, **90**, 5131 (1968).
15) D. F. Evans, P. M. Ridout, and I. Wharf, *J. Chem. Soc., A*, **1968**, 2127.
16) R. Schefford, *Helv. Chim. Acta*, **52**, 56 (1969).
17) L. Lunazzi, M. Tiecoo, C. A. Boicelli, and F. Taddei, *J. Mol. Spectrosc.*, **35**, 190 (1970).
18) W. Kitching, B. F. Hegarty, and D. Doddrell, *J. Organomet. Chem.*, **21**, 29 (1970).
19) G. M. Cree, *J. Organomet. Chem.*, **27**, 1 (1971).
20) G. A. Olah and P. R. Clifford, *J. Am. Chem. Soc.*, **93**, 1262 (1971).
21) G. A. Olah and P. R. Clifford, *J. Am. Chem. Soc.*, **95**, 6067 (1973).
22) G. Singh and G. S. Reddy, *J. Organomet. Chem.*, **42**, 267 (1972).
23) R. A. Scherr and J. P. Oliver, *J. Am. Chem. Soc.*, **94**, 9026 (1972).
24) F. J. Weigert and J. D. Roberts, *Inorg. Chem.*, **12**, 313 (1973).
25) W. Adcock, B. D. Gupta, W. Kitching, D. Doddrell, and M. Geckle, *J. Am. Chem. Soc.*, **96**, 7360 (1974).
26) W. Adcock, B. D. Gupta, W. Kitching, and D. Doddrell, *J. Organomet. Chem.*, **102**, 297 (1975).
27) P. L. Goggin and L. A. Woodward, *Trans. Faraday Soc.*, **56**, 1591 (1960).

28) P. L. Goggin and L. A. Woodward, *Trans. Faraday Soc.*, **58**, 1495 (1962).
29) P. L. Goggin and L. A. Woodward, *Trans. Faraday Soc.*, **62**, 1423 (1966).
30) Y. Kawasaki and M. Aritomi, *J. Organomet. Chem.*, **104**, 39 (1976).
31) J. H. R. Clarke and L. A. Woodward, *Trans. Faraday Soc.*, **62**, 3022 (1966).
32) C. E. Fedline and R. S. Tobias, *Inorg. Chem.*, **5**, 354 (1966).
33) M. M. McGrady and R. S. Tobias, *Inorg. Chem.*, **3**, 1157 (1964).
34) E. R. Lippincott and M. C. Tobin, *J. Am. Chem. Soc.*, **75**, 4141 (1953).
35) T. L. Brown and L. C. Puckett, *J. Chem. Phys.*, **44**, 2238 (1966).
36) D. M. Grant and W. M. Litchiman, *J. Am. Chem. Soc.*, **87**, 3994 (1965).
37) N. F. Ramsey, *Phys. Rev.*, **91**, 303 (1953).
38) A. Carrington and A. D. McLachlan, "Introduction to Magnetic Resonance," Harper and Row, New York, N. Y. (1967).
39) A. C. Blizzard and D. P. Santry, *J. Chem. Phys.*, **55**, 950 (1971).
40) J. M. Schulman and M. D. Newton, *J. Am. Chem. Soc.*, **96**, 6295 (1974).

Crystal Vibrations and Intermolecular Interactions of CH_3X and CD_3X (X=Cl, Br, and I)

Hideo TAKEUCHI,* Jean-Luc BRIBES,** Issei HARADA, and Takehiko SHIMANOUCHI
Department of Chemistry, Faculty of Science, The University of Tokyo, Hongo, Bunkyo-ku, Tokyo 113
(Received August 11, 1976)

Normal coordinate treatments of the crystal vibrations of methyl chloride, methyl bromide, methyl iodide, and their perdeuterated analogs have been made. The values of force constants of non-bonded atom interactions have been determined so as to give the best fit to the lattice frequencies and the splitting frequencies of the intramolecular vibrations. It has been found that the dipole-dipole interactions are essential to account for the splittings of some internal modes, but their effects on lattice frequencies are negligible.

Methyl halides are fundamental polar molecules, for which the vibrational spectra in the crystalline state have been investigated extensively. Dows[1] observed the infrared spectra of methyl chloride, methyl bromide, and methyl iodide. He[2] discussed the splittings of intramolecular vibrations of methyl chloride on the basis of the crystal structure[3] and the dipole-dipole and atom-atom interactions. Hexter,[4] Jacox and Hexter,[5] and Kopelman[6] tried to interpret the splittings of the infrared absorptions of methyl halides by considering only the dipole-dipole interaction. Harada[7] also treated the splittings and lattice vibrations of methyl chloride. However, the crystal vibrations of methyl halides have not been fully explored yet, because there has been the lack of the data on the crystal structures of CH_3Br and CH_3I and on most of the lattice vibrations.

Recently, the crystal structures of CH_3Br and CH_3I have been determined.[8] The present authors have measured the Raman spectra of crystalline CH_3X and CD_3X (X=Cl, Br, and I) and interpreted the data on the basis of the crystal structures.[9] It is now possible to investigate the intermolecular interactions in the crystals of methyl halides in detail.

In this paper, we report the results of normal coordinate analysis of the optically active crystal vibrations of methyl halides, and discuss the intermolecular interactions. The observed far-infrared spectra of the crystals are also presented, which adds to the results of an earlier study by Lafferty and Robinson.[10]

Experimental

The far-infrared spectra were measured down to 60 cm^{-1} at liquid nitrogen temperature with a Hitachi FIS-1 far-infrared spectrometer after a similar procedure as described previously.[11] The samples were of the same origins as those used for the measurements of the Raman spectra.[9] The spectra are shown in Fig. 1.

Summary of the Experimental Results

Lattice Vibrations. Assignment to a translational or a rotational lattice mode is made on the basis of the frequency shift on deuteration: The frequency shifts

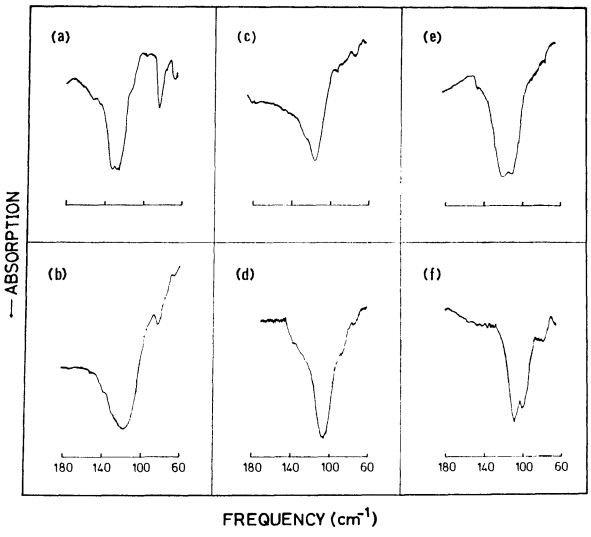

Fig. 1. Far-infrared spectra of methyl halides. (a) CH_3Cl, (b) CD_3Cl, (c) CH_3Br, (d) CD_3Br, (e) CH_3I, (f) CD_3I.

are expected to be about 30% for the rotational modes around the molecular symmetry axis and about 10% for those around the axes perpendicular to it, respectively, whereas the translational modes are expected to show no appreciable shift. Observed lattice frequencies and the assignments are summarized in Table 1.

For methyl chlorides, all the translational lattice vibrations are observed in the Raman spectra. The highest-frequency translational mode is observed also in the far-infrared spectra and therefore is assigned to either A_1 or B_2 species (see Table 2.).

Intramolecular Vibrations. Frequency splittings in the infrared spectra were observed by Dows[1] and Jacox and Hexter.[5] Frequency splittings in the Raman spectra were observed by Ito,[12] Brown and Lippincott,[13] and the present authors.[9]

The following modes are known to be perturbed by the Fermi resonance:[14] ν_1 and ν_4 of CH_3Cl, ν_1 of CH_3Br, ν_1 and ν_5 of CH_3I, and ν_1 of CD_3I.

Anomaly observed in the patterns of splitting and intensity of ν_3 mode for CH_3Cl and CD_3Cl has been ascribed to the coexistence of the chlorine isotopic (^{35}Cl and ^{37}Cl) molecules.[15]

Normal Coordinate Calculations

The calculations of the vibrational frequencies of the crystals have been performed by the use of the

* Present address: Department of Chemical Engineering and Chemical Technology, Imperial College, London SW7 2BY, England.
** Present address: Laboratoire de Spectroscopie Moléculaire, U. S. T. L. 34060, Montpellier-Cédex, France.

Table 1. Observed lattice frequencies (in cm^{-1}) of methyl halides

		CH_3Cl	CD_3Cl	CH_3Br	CD_3Br	CH_3I	CD_3I
Raman[a]							
rotational[b]	R_z	156 W	(108)				
	R_x, R_y	135 sh	124 W	119 S	106 S	113 S	100 S
		121 S	108 S	110 S	98 S	105 M	94 M
translational[c]	T_a, T_b, T_c	84 W	83 W	67 W	66 W	60 M	59 M
		71 W	68 W	60 M	60 M	49 S	48 S
		60 W	59 W	57 W	56 W		
				44 M	44 M	32 W	32 W
				39 W	38 W	28 M	27 M
Far-infrared							
rotational[b]	R_z						
	R_x, R_y	125 S, b	114 S, b	114 S, b	106 S, b	120 S	108 S
						112 S	100 S
translational[c]	T_a, T_b, T_c	82 M	82 W			55 M[d]	54 M[d]
		(41 W)[d,e]	(42 W)[d,e]	41 W[d]	41 W[d]	36 W[d]	35 W[d]

a) Ref. 9. b) R_z denotes the rotational mode about the molecular symmetry axis and R_y and R_z those about the axes perpendicular to it. c) T_a, T_b, and T_c denote the translational modes along the crystal a, b, and c axes, respectively. d) Ref. 10. e) This band may be attributed to the second-order diffraction light of 82 cm^{-1} band, since no Raman band is observed around this frequency.

Table 2. Results of factor group analysis for methyl halides

		CH_3Cl[a]	CH_3Br and CH_3I[b]
Lattice mode	translational	$A_1+A_2+B_2$	$2A_g+B_{1g}+2B_{2g}+B_{3g}+A_u+B_{1u}+B_{3u}$
	rotational	$A_1+2A_2+2B_1+B_2$	$A_g+2B_{1g}+B_{2g}+2B_{3g}+2A_u+B_{1u}+2B_{2u}+B_{3u}$
Intramolecular mode	symmetric (ν_1, ν_2, ν_3)	A_1+B_2	$A_g+B_{2g}+B_{1u}+B_{3u}$
	degenerate (ν_4, ν_5, ν_6)	$A_1+A_2+B_1+B_2$	$A_g+B_{1g}+B_{2g}+B_{3g}+A_u+B_{1u}+B_{2u}+B_{3u}$

a) Crystal structure is $Cmc2_1$ (C_{2v}^{12}), $Z=2$. A_2 mode is infrared inactive.
b) Crystal structures are isomorphous; Pnma (D_{2h}^{16}), $Z=4$. A_u mode is infrared and Raman inactive.

Table 3. Computer program CVOA for treating optically active crystal vibrations

Input
- (a) Structure data
  - (1) Unit cell dimension and atomic positions (of one molecule) in the unit-cell coordinate system, or
  - (2) Unit cell dimension and atomic positions (of one molecule) in the Cartesian coordinate system
- (b) Symmetry relationship among molecules in a unit cell
  - Matrices for rotational operations
  - Vectors for translational operations
- (c) Intramolecular coordinates and force field
  - (1) Local symmetry coordinates plus intramolecular force field, or
  - (2) Normal coordinates and normal frequencies of a free molecule
- (d) Intermolecular force field
  - (1) Functional forms of atom-atom interactions, and/or
  - (2) Force constants relating to intermolecular or inter-unit bonding (*e. g.*, hydrogen bond, bond between adjacent units in a polymer chain, *etc.*)

Output
- (a) Frequencies of intramolecular and lattice modes
- (b) Eigenvectors and Cartesian displacements
- (c) Potential energy distributions
- (d) Jacobian

GF matrix method.[16] Computer programs have been developed and the input and output of these programs are outlined in Table 3.

Positions of Atoms. The positions of heavier atoms in the crystals are taken from the data of X-ray analyses[3,8] except for that of the carbon atom of methyl iodide. The structures of methyl groups were assumed to be the same as those in the gaseous state[17] due to the lack of data on the coordinates of hydrogen atoms.

There are two possible orientations of the methyl group. We adopted the one that was preferred in the original X-ray studies[3,8] on consideration of atom-atom contacts. For methyl iodide, after a preliminary calculation the positional parameters of the carbon atom were altered from the original X-ray values (0.3144, 0.25, −0.1039) to (0.3350, 0.25, −0.1003) within the experimental errors of the X-ray analysis. This configuration gives the value (3.29 Å) of the shortest intra-layer H···I distance (in the ac plane, see Fig. 3) nearly equal to that (3.27 Å) of the shortest inter-layer one, which is consistent with the case of methyl bromide (3.02 and 3.00 Å, respectively).

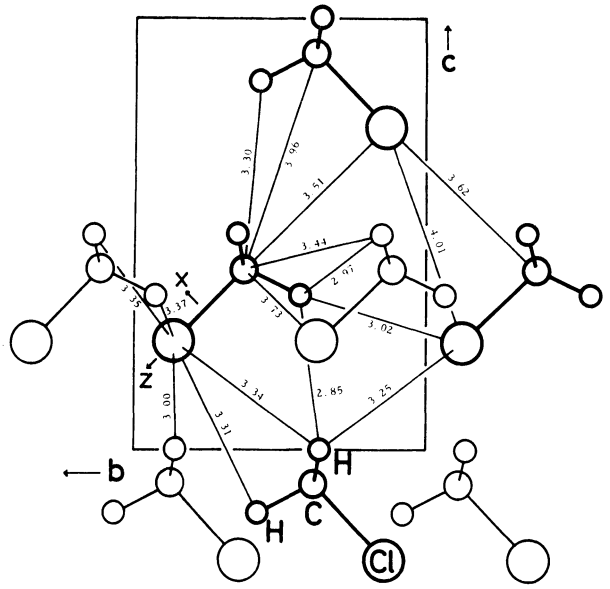

Fig. 2. Crystal structure of methyl chloride.
Interatomic distances (in Å) are indicated.

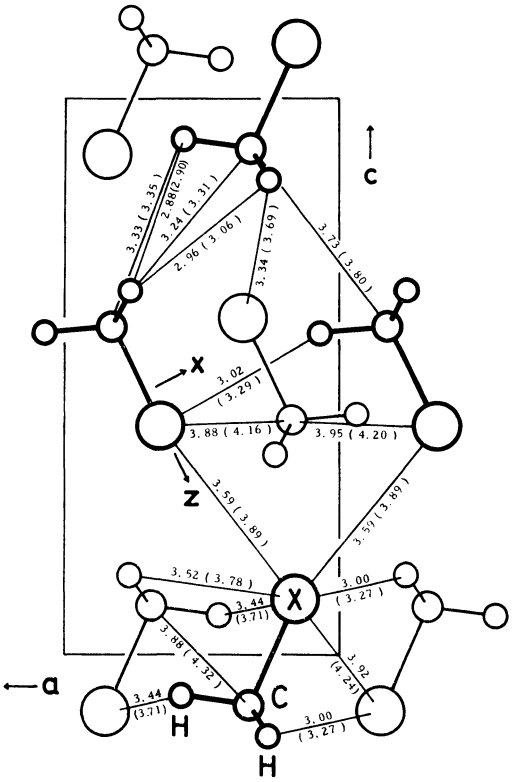

Fig. 3. Crystal structure of methyl bromide or methyl iodide.
Interatomic distances (in Å) are indicated. The values in parentheses are those for methyl iodide.

Figures 2 and 3 show the structures assumed in the calculations.

Intramolecular Potentials. The intramolecular force fields of methyl halides in the free state have been well established.[18,19] In the present calculations, the local symmetry force fields by Shimanouchi[19] are used without modification.

Intermolecular Potentials. Two sets of intermolecular potentials are assumed in the calculations. *Calculation I*: Atom-atom interaction potentials in the form,

$$V(r) = A \exp(-Br) - Cr^{-6}$$

were adopted. As for the constants A, B, and C, the

Table 4. Parameters for the atom-atom potentials

	A (mdyn Å)	B (Å^{-1})	C (mdyn Å^7)	Ref.
H···H	18.45	3.74	0.190	20
C···H	60.93	3.67	0.869	20
C···C	581.3	3.60	3.95	20
Cl···H	171.4	3.63	1.96	
Cl···C	962.0	3.56	8.92	
Cl···Cl	1592	3.513	20.2	21
Br···H	144.1	3.50	2.07	
Br···C	809.1	3.43	9.44	
Br···Br	1126	3.250	22.6	21
I···H	176.2	3.38	3.14	
I···C	988.9	3.31	14.3	
I···I	1682	3.023	51.9	21

values given by Williams(Set IV)[20] are used for H···H, H···C, and C···C pairs and those given by Dashevsky[21] are used for halogen···halogen pairs. For a pair of hydrogen···halogen or carbon···halogen type the values of potential parameters A and C are taken as the geometric means and the parameter B as the arithmetic mean of the corresponding values for the homonuclear pairs. The values of the parameters are listed in Table 4.

All the atom pairs with a distance shorter than 6.0 Å are taken into account. The second derivatives of $V(r)$'s with respect to the interatomic distances are used as the force constants.

Calculation II: Both the atom-atom interaction potential and the dipole-dipole interaction potential are taken into account.

As for the atom-atom interaction, only the short-distance pairs that are indicated in Figs. 2 and 3 are considered and the corresponding force constants are adjusted to give the best fit to the lattice and the band splitting frequencies.

The method of calculation of the force constants due to the dipole-dipole interaction is described in Appendix. The values of dipole moment derivatives with respect to the internal symmetry coordinates are calculated from the infrared intensities in the gaseous state[22] and are not varied throughout the calculations. The radius of the dipole sum sphere is set equal to 100 Å, which is found to give sufficiently converged values for the force constants.

Results

The resuts of calculations are summarized in Tables

Table 5. Calculated and observed lattice frequencies (in cm^{-1}) of CH_3Cl and CD_3Cl

Species	CH_3Cl				CD_3Cl				Mode
	Obsd	Calcd I	Calcd II	Dip.[a]	Obsd	Calcd I	Calcd II	Dip.[a]	
A_1	121	109.2	112.0	−3.6	108	97.6	99.8	−3.3	R_y
	71	75.9	72.7	−2.6	68	74.7	71.7	−2.4	T_b
A_2	156	175.2	160.7	0.0	—	124.6	115.3	−0.2	R_z
	—	96.3	108.4	−4.3	—	85.1	95.1	−3.8	R_x
	60	62.2	61.5	0.2	59	61.2	60.8	0.2	T_a
B_1	—	185.3	190.8	0.0	—	131.5	136.0	−0.2	R_z
	121	109.5	110.2	−5.0	108	98.7	98.9	−4.4	R_x
B_2	135	124.4	145.2	0.5	124	109.9	130.4	0.2	R_y
	84	85.4	83.8	−1.2	83	83.6	82.4	−0.9	T_c

a) Contributions of dipole interactions in Calculation II (see text).

Table 6. Calculated and observed lattice frequencies (in cm^{-1}) of CH_3Br and CD_3Br

Species	CH_3Br				CD_3Br				Mode
	Obsd	Calcd I	Calcd II	Dip.[a]	Obsd	Calcd I	Calcd II	Dip.[a]	
A_g	110	114.5	108.3	−1.8	98	101.6	96.3	−1.6	R_y
	67	67.1	66.2	0.1	66	66.1	65.2	0.1	T_c
	44	46.5	49.0	−0.1	44	46.3	48.7	−0.1	T_a
B_{1g}	—	138.7	134.0	0.5	—	95.2	89.4	0.2	R_z
	119	124.0	117.1	1.5	106	115.1	112.4	1.5	R_x
	57	39.1	58.2	3.7	56	39.0	56.7	2.9	T_b
B_{2g}	110	120.8	112.2	−1.4	98	107.5	99.9	−1.3	R_y
	60	65.1	64.6	−1.6	60	64.8	64.5	−1.5	T_a
	39	32.4	40.8	0.4	38	31.8	40.0	0.4	T_c
B_{3g}	—	137.6	130.8	0.6	—	94.7	88.4	0.2	R_z
	119	126.9	118.2	1.3	106	116.8	111.5	1.5	R_x
	57	40.5	58.9	3.1	56	39.2	57.7	3.6	T_b
A_u		147.5	130.6	−1.1		102.2	87.7	−0.5	R_z
		125.1	114.0	−3.7		114.8	107.8	−3.8	R_x
		25.1	31.7	3.4		24.7	31.2	3.3	T_b
B_{1u}	114	123.3	115.3	−2.9	106	110.5	103.6	−2.5	R_y
	41	49.7	43.4	−2.4	41	49.0	42.7	−2.4	T_a
B_{2u}	—	147.8	133.5	−0.5	—	102.9	89.1	−0.2	R_z
	114	123.6	115.3	−1.8	106	112.8	109.9	−1.8	R_x
B_{3u}	114	118.7	113.9	−1.8	106	106.4	102.2	−1.6	R_y
	—	67.3	64.5	−1.3	—	66.4	63.5	−1.3	T_c

a) Contributions of dipole interactions in Calculation II (see text).

TABLE 7. CALCULATED AND OBSERVED LATTICE FREQUENCIES (IN cm^{-1}) OF CH_3I AND CD_3I

Species	CH_3I				CD_3I				Mode
	Obsd	Calcd I	Calcd II	Dip.[a]	Obsd	Calcd I	Calcd II	Dip.[a]	
A_g	105	82.0	100.3	−1.3	94	73.9	89.5	−1.1	R_y
	60	55.8	58.9	−0.9	59	56.3	58.3	−0.9	T_c
	32	28.7	37.7	0.0	32	28.6	37.3	0.0	T_a
B_{1g}	—	104.1	151.6	0.0	—	79.3	107.6	0.2	R_z
	113	86.8	116.2	1.5	100	72.6	104.7	1.1	R_x
	49	28.5	48.5	2.1	48	28.0	47.7	2.1	T_b
B_{2g}	105	88.2	104.6	−1.0	94	78.7	93.4	−0.9	R_y
	49	46.9	52.1	−1.0	48	46.6	52.1	−0.9	T_a
	28	18.4	31.1	−0.3	27	18.1	30.8	−0.3	T_c
B_{3g}	—	99.7	147.2	0.0	—	70.4	104.1	0.0	R_z
	113	90.2	117.4	0.7	100	81.4	105.7	0.5	R_x
	49	29.2	49.4	1.2	48	28.8	48.8	1.1	T_b
A_u		100.9	147.2	0.0		71.8	103.9	−0.4	R_z
		94.3	117.0	−1.9		84.3	105.4	−1.3	R_x
		12.9	22.7	2.2		12.9	22.5	2.1	T_b
B_{1u}	112	91.4	107.5	−1.6	100	80.6	96.6	−1.4	R_y
	36	39.0	36.9	−1.4	35	38.6	36.5	−1.4	T_a
B_{2u}		105.3	151.6	0.0		80.1	107.4	−0.1	R_z
	120	90.6	115.4	−1.5	108	75.8	103.6	−1.3	R_x
B_{3u}	112	87.8	104.9	−1.4	100	78.8	94.3	−1.3	R_y
	55	54.6	55.7	−1.4	54	54.2	55.2	−1.4	T_c

a) Contributions of dipole interactions in Calculation II (see text).

TABLE 8. CALCULATED AND OBSERVED SPLITTINGS (IN cm^{-1}) OF CH_3Cl AND CD_3Cl[a]

Mode	CH_3Cl					CD_3Cl				
	Obsd		Calcd I	Calcd II		Obsd		Calcd I	Calcd II	
	Infrared[b]	Raman	$\Delta\nu$	$\Delta\nu$	Dip.[c]	Infrared[b]	Raman	$\Delta\nu$	$\Delta\nu$	Dip.[c]
ν_1	—	—	0.6(A_1)	0.1(B_2)	0.5	—	—	0.3(A_1)	0.3(B_2)	0.4
			0.0(B_2)	0.0(A_1)	−0.9			0.0(B_2)	0.0(A_1)	−0.8
ν_2	10.4	—	3.3(B_2)	10.7(B_2)	0.3	7	6.3	1.5(B_2)	6.6(B_2)	0.4
			0.0(A_1)	0.0(A_1)	−0.6			0.0(A_1)	0.0(A_1)	−1.2
ν_3[d]		17.3	0.1(B_2)	6.7(B_2)	1.9		13.6	0.4(B_2)	6.5(B_2)	1.5
	8.9	9.5	0.0(A_1)	0.0(A_1)	−3.5		10.2	0.0(A_1)	0.0(A_1)	−2.7
	4.6	4.6				5.5	5.3			
ν_4	4.9	4.3	0.3(B_2)	1.8(B_2)	0.1		3.5	0.2(B_2)	1.3(B_2)	0.1
			0.2(B_1)	0.4(A_1)	−0.3			0.1(B_1)	0.3(A_1)	−0.2
			0.1(A_2)	0.0(A_2)	−0.3			0.1(A_2)	0.0(A_2)	−0.3
			0.0(A_1)	0.0(B_1)	−0.4			0.0(A_1)	0.0(B_1)	−0.3
ν_5	7.6		2.3(A_1)	7.6(A_1)	−0.6	3.2	5.0	1.4(A_1)	4.8(A_1)	−0.5
		5.9	1.1(A_2)	2.1(B_2)	0.3			0.5(A_2)	1.8(B_2)	0.3
	4.2	4.0	0.7(B_1)	1.1(A_2)	−0.6			0.1(B_1)	1.2(A_2)	−0.5
			0.0(B_2)	0.0(B_1)	−0.6			0.0(B_2)	0.0(B_1)	−0.5
ν_6	—	—	3.1(A_1)	7.3(A_1)	−0.2	—	—	2.7(A_1)	6.9(A_1)	−0.1
			1.6(A_2)	3.2(A_2)	−0.3			1.7(A_2)	0.8(A_2)	−0.1
			1.1(B_1)	1.2(B_1)	−0.3			1.0(B_1)	0.7(B_1)	−0.2
			0.0(B_2)	0.0(B_2)	0.1			0.0(B_2)	0.0(B_2)	0.0

a) Splittings are referred to the lowest-frequency component of each band. ν_1 and ν_4 of CH_3Cl are in Fermi resonance with $2\nu_5$ and $3\nu_6$, respectively. b) Ref. 1. c) Contributions of dipole interactions. d) The anomalous splittings of ν_3 are due to the chlorine isotopic compounds. See text and Ref. 15 for details.

Table 9. Calculated and observed splittings (in cm^{-1}) of CH_3Br and CD_3Br[a]

Mode		CH_3Br				CD_3Br			
			Calcd I	Calcd II			Calcd I	Calcd II	
		Obsd[b]	$\Delta\nu$	$\Delta\nu$	Dip.[c]	Obsd[b]	$\Delta\nu$	$\Delta\nu$	Dip.[c]
ν_1	IR	—	0.1	1.8	1.8	—	0.1	1.5	1.5
	R	—	0.1	0.3	0.3	—	0.2	0.2	0.2
ν_2	IR	3.1	3.2	4.3	2.8	1.9	1.4	4.3	3.7
	R	2.4	3.3	2.0	0.4	1.3	1.4	1.2	0.6
ν_3	IR	6	3.1	6.5	4.5	5.1	3.5	5.2	3.0
	R	2.5	4.2	3.6	0.7	1.7	4.5	3.6	0.5
ν_4	IR	—	0.5	0.1	0.1	—	0.3	0.3	0.1
	R	2.2	0.7	0.1	−0.3	0.8	0.5	0.1	−0.2
ν_5	IR	14.5	2.4	2.1	−0.2	11.9	1.2	1.0	−0.2
	R	5.2	3.7	3.7	0.7	5.1	2.2	2.2	0.5
ν_6	IR	5.0	6.1	5.8	−0.2	5.7	4.2	4.4	−0.1
	R	7.3	6.8	7.1	0.8	7.3	5.7	4.9	0.5

a) Absolute values are given for ν_1, ν_2, and ν_3. For ν_4, ν_5, and ν_6 maximum values are listed. The ν_1 mode of CH_3Br is in Fermi resonance with $2\nu_5$. b) The infrared data are taken from Ref. 1. c) Contributions of dipole interactions.

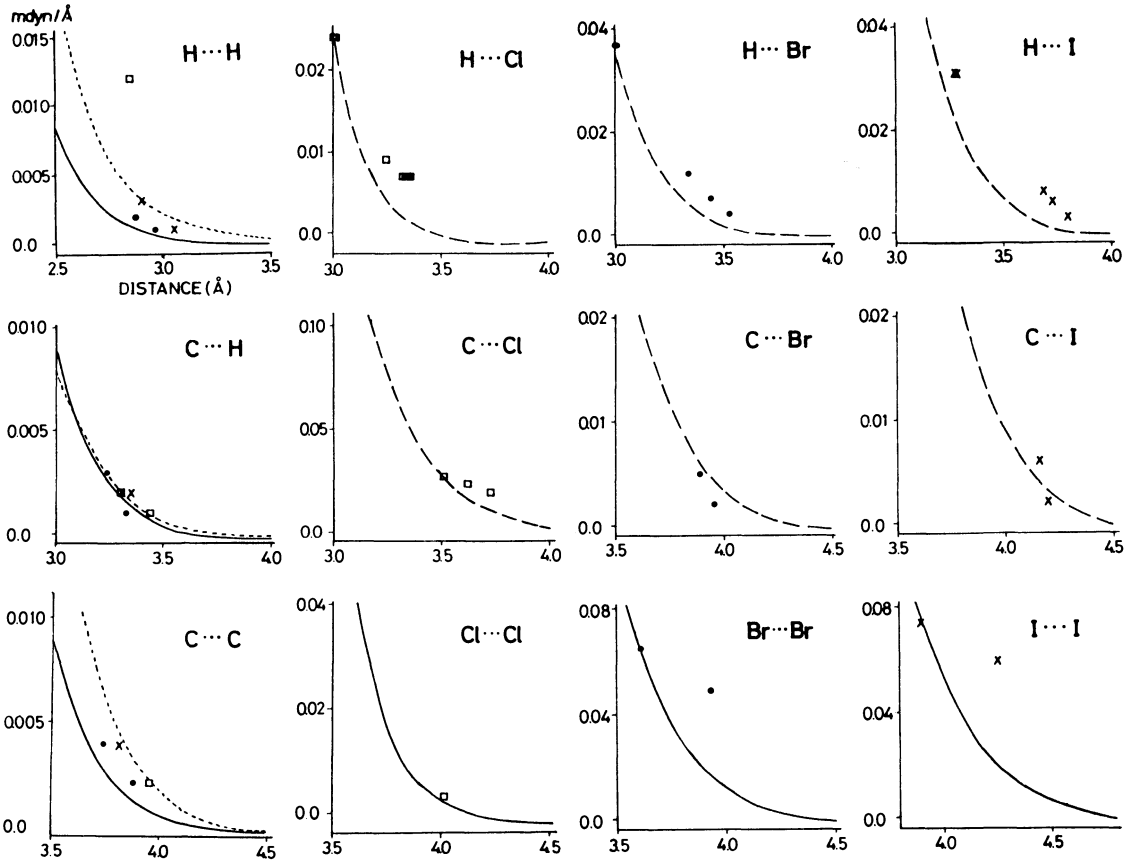

Fig. 4. Interatomic forces.
□: Methyl chloride, ●: methyl bromide, ×: methyl iodide, ——: second derivative curves of the Dashevsky potentials, ·····: second derivative curves of the Williams (Set IV) potentials, ——: second derivative curves of the hybrid potentials (see text).

TABLE 10. CALCULATED AND OBSERVED SPLITTINGS (IN cm^{-1}) OF CH_3I AND CD_3I[a]

Mode		CH_3I				CD_3I			
			Calcd I	Calcd II			Calcd I	Calcd II	
		Obsd[b]	$\Delta\nu$	$\Delta\nu$	Dip.[c]	Obsd[d]	$\Delta\nu$	$\Delta\nu$	Dip.[c]
ν_1	IR	—	0.2	1.1	1.0	—	0.1	0.7	0.7
	R	—	0.1	0.3	0.2	—	0.2	0.1	0.1
ν_2	IR	4.8	3.5	6.4	3.5	2.5	1.5	4.2	3.0
	R	2.2	3.4	3.5	0.6	1.9	1.6	1.8	0.5
ν_3	IR	4	3.5	3.7	0.6	—	3.7	3.7	0.4
	R	3.1	3.7	3.8	0.1	2.2	3.9	4.0	0.1
ν_4	IR	—	0.3	0.3	0.0	—	0.1	0.2	0.0
	R	2.8	0.1	0.4	0.1	1.3	0.1	0.3	0.1
ν_5	IR	5.9	2.2	0.5	−0.1	10.0	0.4	1.5	0.8
	R	4.7	1.9	3.0	0.3	7.1	0.1	1.8	0.5
ν_6	IR	7	3.6	3.4	0.0	7.5	3.1	3.0	0.0
	R	11.0	2.4	3.9	1.3	9.3	3.2	3.1	0.1

a) Absolute values are given for ν_1, ν_2, and ν_3. For ν_4, ν_5, and ν_6 maximum values are listed. The ν_1 and ν_5 modes of CH_3I and the ν_1 mode of CD_3I are in Fermi resonance with $2\nu_5$, $\nu_3+\nu_6$, and $2\nu_5$, respectively. b) The infrared data are taken from Ref. 1. c) Contributions of dipole interactions. d) The infrared data are taken from Ref. 5.

5—10. The values of force constants obtained in Calculation II are listed in Table 11. They are compared with the second-derivative curves of the Dashevsky and the Williams potentials in Fig. 4. Observed and calculated splittings for ν_2 and ν_3 of CH_3Br and CH_3I are compared in Fig. 5.

It is seen from the Tables 5—10 that Calculation I gives values in poor agreement with the observed except for the lattice frequencies of CH_3Cl and CD_3Cl. Especially, Calculation I fails to explain the difference in the Raman and infrared frequency splittings of ν_2 and ν_3 of CH_3Br and CH_3I. On the other hand, the lattice frequencies and frequency splittings of symmetric vibrations in Calculation II agree well with the observed except for ν_3 of methyl chlorides. The observed splittings of most of the degenerate vibrations can not be explained by either calculation. This point will be discussed in a later section.

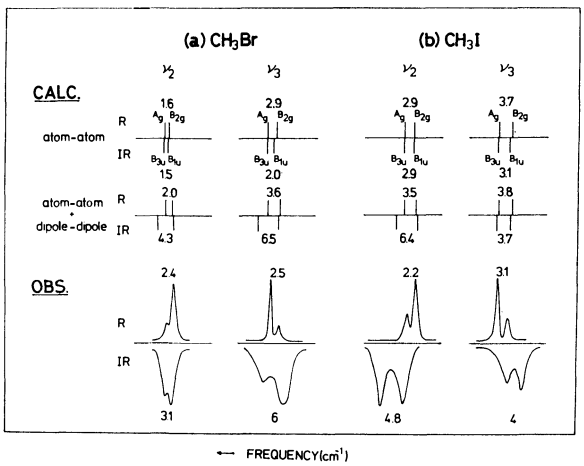

Fig. 5. Comparison of the observed and calculated splittings of ν_2 and ν_3.
(a) CH_3Br, (b)CH_3I. The values in parentheses are the splittings in cm^{-1}.

Some of the results of Calculation II are described below.

Methyl Chlorides. The vibration around 84 cm^{-1} observed in the Raman and far-infrared spectra is assigned to the translational mode along the crystal c axis (T_c) in B_2 symmetry species.

The maximum contribution of the dipole-dipole interaction to the lattice frequencies is evaluated as 5 cm^{-1}.

The splitting of ν_2 and maximum splitting of ν_5 are mainly due to the force between the hydrogen atoms at the shortest distance (2.85 Å, see Fig. 2). Therefore, the value of this force constant can be determined by fitting the calculated to the observed splittings of ν_2 and ν_5. The value thus obtained is 0.012 mdyn/Å, which corresponds to that for a distance of 2.60 Å in the Williams potential.

Although the calculated maximum splitting of ν_6 is about 7 cm^{-1}, only one band appears in each of the infrared and Raman spectra. It may be possible that the factor group components are not resolved because of their comparatively large halfwidths.

The observed splitting pattern of ν_3 is complicated by the coexistence of the chlorine isotopic molecules and simple one-to-one correspondence between the observed and calculated frequencies must be avoided. A quantitative analysis of the ν_3 splitting based on a theory of mixed crystals has shown that the calculated factor group splitting, 6.7 cm^{-1} arising mainly from the dipole-dipole interaction, accounts for the observed splitting in the Raman spectrum.[15]

The dipole-dipole interaction affects the splittings of the other modes only slightly as Dows[2] has already pointed out.

Methyl Bromides and Methyl Iodides. Calculations indicate that the frequencies of T_a mode in B_{1u} species of these molecules are mainly due to the intra-layer Br···Br or I···I interaction force. Accordingly, the values of the force constants for the intra-layer Br···

TABLE 11. INTERATOMIC FORCE CONSTANTS

Molecule	Atom pair	Distance (Å)	Force constant (mdyn/Å)
Methyl chloride	H···H	2.85	0.012
		2.97	0.0
	C···H	3.30	0.002
		3.44	0.001
	C···C	3.96	0.002
	Cl···H	3.00, 3.02	0.024
		3.25	0.009
		3.31, 3.34, 3.35, 3.37	0.007
	Cl···C	3.51	0.027
		3.62	0.023
	Cl···Cl	4.01	0.003
Methyl bromide	H···H	2.88	0.002
		2.96	0.001
	C···H	3.24	0.003
		3.33	0.001
		3.40	0.0
	C···C	3.73	0.004
		3.88	0.002
	Br···H	3.00, 3.02	0.037
		3.34	0.012
		3.44	0.007
		3.52	0.004
	Br···C	3.88	0.005
		3.94	0.002
	Br···Br	3.59	0.061
		3.92	0.049
Methyl iodide	H···H	2.90	0.003
		3.06	0.001
	C···H	3.31, 3.35	0.002
	C···C	3.80	0.004
		4.32	0.0
	I···H	3.27, 3.29	0.031
		3.69, 3.71	0.009
		3.78	0.008
	I···C	4.16	0.006
		4.20	0.002
	I···I	3.89	0.073
		4.24	0.059

Br and I···I pairs with the distances of 3.59 and 3.89 Å, respectively, are determined definitely to be 0.061 and 0.073 mdyn/Å. These values agree with those expected from the Dashevsky potential. The contributions of the inter-layer Br···Br(3.92 Å) or I···I(4.24 Å) interaction force to the calculated frequencies of T_b modes in B_{1g} and B_{3g} species are about 60% and the interaction force constant is determined to be 0.049 or 0.059 mdyn/Å, respectively. These values correspond to those for distances of 3.68 and 3.97 Å in the Dashevsky potential. The calculated frequencies of the rotational vibrations, R_x and R_y, are dominated by H···H and H···X interaction forces.

The frequency splittings of ν_2 and ν_3 modes in the infrared spectra of these molecules are greater than those in the Raman spectra. The calculated frequency splittings for ν_2 and ν_3 of CH_3Br and CH_3I are in good agreement with the observed (see Fig. 5). This is because Calculation II includes the dipole-dipole interactions and the contributions from the interactions to the infrared splittings are much greater than those to the Raman splittings.

Discussion

The lack of the knowledge on the exact positions of hydrogen atoms and of the vibrational data on single crystals prevents us from discussing the results of calculation in detail. However, it may be of use to clarify the significance of factors which are assumed or disregarded in the present calculations.

First Derivative Terms. In the case of methyl chlorides, Calculation I reproduces the observed lattice frequencies well and we have examined the effects of the first derivative terms $\partial V(r)/\partial r$ of the potentials on the crystal vibration frequencies. It has been found that these terms affect the splittings negligibly as in the case of benzene,[23] while all of the lattice fre-

quencies decrease on inclusion of the terms (8% at maximum). Since the atom-atom interaction force constant is assumed independently for each atom pair in Calculation II, the corresponding linear term may also be included as an independent parameter. The linear terms may be used to lower the lattice frequencies keeping the splittings constant. Evaluation of these terms, however, is only meaningful in the case where the crystal structure and vibrational assingment are solidly established.

Splitting of the Degenerate Modes. As is described above, the agreement between the observed and the calculated splittings of degenerate vibrations in methyl bromide and methyl iodide is poor in either calculation, while the lattice frequencies and splittings of symmetric vibrations are explained by Calculation II. The situation can not be improved by simple modification of the interaction forces. One possible explanation of the large splittings of the degenerate vibrations is that the geometry and the potential of the methyl group are distorted considerably in the crystalline state. In such case, the site group splitting is expected to be far greater than the factor group splitting. In the Raman spectrum of a mixed crystal of CD_3I and CH_3I in the ratio of one to five, ν_4 and ν_5 bands of CD_3I are observed to split into doublets with the separations of 1.5 and 5.0 cm^{-1}, respectively (Fig. 6). These are assigned to the site group splittings, since no splitting is observed at this concentration for ν_3 band for which only the factor group splitting is expected to occur. Hence, it is seen that the site group splitting of ν_5 is mainly responsible for the observed splitting in pure CD_3I and that the splitting of ν_4 observed in pure CD_3I is the site group splitting. On the other hand, the calculated site-group and factor-group splittings are of the same order (2 cm^{-1} each in the case of ν_5). According to a calculation, a change of 1° in the ∠DCD angle causes 1—4 cm^{-1} splittings between $\nu_{\text{in-plane}}$ and $\nu_{\text{out-of-plane}}$ of degenerate vibrations. A slight distortion of the intramolecular potential will give similar effects. It is probable that the cooperative effects of these distortions are observed in the large splittings of the degenerate vibrations. However, these distortions of methyl group give negligible effects to the factor group splittings and lattice frequencies since the accompanying changes in the directions and distances of the atom-atom pairs are not significant.

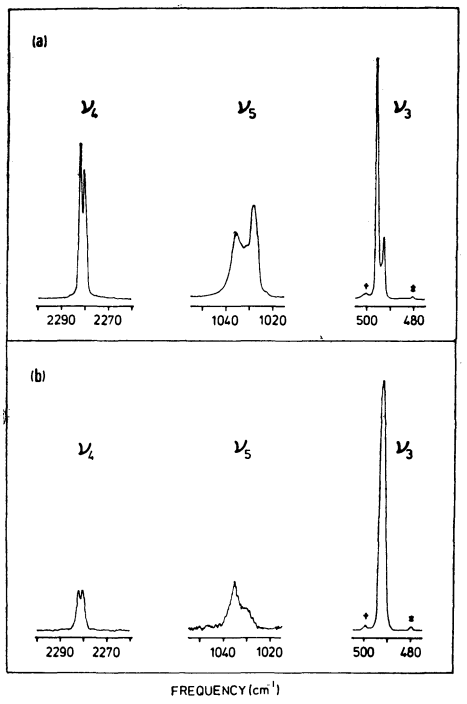

Fig. 6. Parts of the Raman spectra of methyl iodides. (a) CH_3I, (b) mixed crystal of CD_3I and CH_3I in the ratio of one to five. †: ν_3 of $^{12}CHD_2I$, *: ν_3 of $^{13}CD_3I$.

Temperature. The lattice frequencies and frequency splittings have been observed at liquid nitrogen temperature, so that we may observe the lattice vibrational bands and the band splittings as many as possible. On the other hand, the X-ray diffraction measurements have to be made at higher temperatures to avoid cracking of the crystals. The difference in temperature between two observations must also be taken into account. For this reason, Calculation I can not be simply ruled out. However, the difference in the frequency splittings of ν_2 and ν_3 in the infrared and Raman spectra in methyl bromide and methyl iodide may only be explained by taking into account the dipole-dipole interactions.

Appendix

The electrostatic interaction energy between a reference dipole and all the dipoles belonging to a sublattice β of the crystal is expressed in the tensor form

$$V = \boldsymbol{\mu}_\alpha \cdot [\sum_l (\boldsymbol{I}/r_{l\beta}^3 - 3\boldsymbol{r}_{l\beta}\boldsymbol{r}_{l\beta}/r_{l\beta}^5)\exp(-\boldsymbol{k}\cdot\boldsymbol{r}_{l\beta})] \cdot \boldsymbol{\mu}_\beta \quad \text{(A-1)}$$

where $\boldsymbol{r}_{l\beta}$ is the position vector from the reference dipole $\boldsymbol{\mu}_\alpha$ to the dipole $\boldsymbol{\mu}_{l\beta}(=\boldsymbol{\mu}_\beta)$ at the βth site in the lth unit cell and $r_{l\beta}=|\boldsymbol{r}_{l\beta}|$. $\boldsymbol{I}$ represents the identity tensor. The exponential term is the phase factor for a vibrational mode with a wave vector $\boldsymbol{k}$. The summation in the bracket of the above equation is conditionally convergent because of the long-range nature of the dipole-dipole interaction. For a slub-shaped crystal some convergent summation procedures have been developed.[24-28] For crystals of arbitrary shapes, the following approximation after the treatment of static dipole sums by Lorentz[20] will serve to avoid the troublesome convergence problem.

The sum in Eq. A-1 (hereafter signified by $\boldsymbol{T}_{\alpha\beta}$) is divided into three parts:

$$\boldsymbol{T}_{\alpha\beta} = \sum_{r_{l\beta}<R} (\boldsymbol{I}/r_{l\beta}^3 - 3\boldsymbol{r}_{l\beta}\boldsymbol{r}_{l\beta}/r_{l\beta}^5)\exp(-\boldsymbol{k}\cdot\boldsymbol{r}_{l\beta}) + \boldsymbol{T}_L + \boldsymbol{T}_S \quad \text{(A-2)}$$

The first term of this equation expresses the contribution of the dipoles inside the Lorentz sphere of radius R. $\boldsymbol{T}_L$ and $\boldsymbol{T}_S$ arise from the polarization charges on the surface of the Lorentz sphere and on the exterior surface of the crystal, respectively. The latter two influence the frequencies of infrared-active modes.

When $\boldsymbol{k}\approx 0$ (optically active modes), $\boldsymbol{T}_L$ represents the Lorentz field, $\boldsymbol{T}_L = -4\pi\boldsymbol{I}/(3V_c)$ (where V_c is the unit cell volume), and therefore Eq. A-2 leads to

$$\boldsymbol{T}_{\alpha\beta} = \sum_{r_{l\beta}<R} (\boldsymbol{I}/r_{l\beta}{}^3 - 3\boldsymbol{r}_{l\beta}\boldsymbol{r}_{l\beta}/r_{l\beta}{}^5) - 4\pi\boldsymbol{I}/(3V_c) + \boldsymbol{T}_S$$
$$= \boldsymbol{D}_{\alpha\beta} + \boldsymbol{T}_S \qquad \text{(A-3)}$$

This equation defines $\boldsymbol{D}_{\alpha\beta}$ that depends on the crystal structure but not on the shape of the crystal. On the contrary, $\boldsymbol{T}_S$ depends on the shape only.

In the spectrum of polycrystalline sample, $\boldsymbol{T}_S$ affects the band widths, since its contribution depends on the shape and orientation of each crystallite. The widths of most bands of such molecular crystals as are treated in this paper are narrow enough to show up separate band structures even in the polycrystalline state. Consequently, we may neglect the shape-dependent term $\boldsymbol{T}_S$. In this approximation, Eq. A-1 reduces to

$$V = \boldsymbol{\mu}_\alpha \boldsymbol{D}_{\alpha\beta}\boldsymbol{\mu}_\beta \qquad \text{(A-4)}$$

This expression is equivalent to that for the transverse mode in the infinite crystal.[30]

The dipole moment of a unit molecule in the crystal is expanded in powers of displacement coordinates $\boldsymbol{S}$:

$$\boldsymbol{\mu} = \boldsymbol{\mu}^\circ + \sum_i \frac{\partial \boldsymbol{\mu}}{\partial S_i} S_i + \frac{1}{2}\sum_{i,j} \frac{\partial^2 \boldsymbol{\mu}}{\partial S_i \partial S_j} S_i S_j + \cdots \qquad \text{(A-5)}$$

where $\boldsymbol{\mu}^\circ$ is the permanent dipole moment. It may be reasonable to assume that the dipole is located at the center of gravity of the molecule. Substituting Eq. A-5 into Eq. A-4, we obtain the optically-active potential energy matrix element $f_{\alpha\beta}^{ij}$ due to the dipole-dipole interaction:

$$f_{\alpha\beta}^{ij} = \frac{\partial \boldsymbol{\mu}_\alpha}{\partial S_i} \cdot \boldsymbol{D}_{\alpha\beta} \cdot \frac{\partial \boldsymbol{\mu}_\beta}{\partial S_j} \qquad \text{(A-6)}$$

$$f_{\alpha\alpha}^{ij} = \frac{\partial^2 \boldsymbol{\mu}_\alpha}{\partial S_i \partial S_j} \boldsymbol{D}_{\alpha\alpha}\boldsymbol{\mu}_\alpha \qquad \text{(A-7)}$$

The intermode coupling terms $f_{\alpha\beta}^{ij}(i \neq j)$ may be neglected in first order approximation.

For intramolecular modes the value of $\partial\boldsymbol{\mu}/\partial S_i$ is calculated from the infrared absorption intensity in the gaseous state (the oriented gas model), whereas $\partial^2\boldsymbol{\mu}/\partial S_i{}^2$ is not available at the present stage. The force constant $f_{\alpha\alpha}^{ii}$ arising from $\partial^2\boldsymbol{\mu}/\partial S_i{}^2$ contributes to the band shift alone. Therefore we can neglect it in treating only the splittings of internal modes.

For a rotational lattice mode, both of $\partial\boldsymbol{\mu}/\partial S_i$ and $\partial^2\boldsymbol{\mu}/\partial S_i{}^2$ are evaluated analytically by differentiating the permanent dipole with respect to the rotational coordinate. The forces associated with translational motions can be obtained from Eq. A-4 by numerical differentiation.

References

1) D. A. Dows, *J. Chem. Phys.*, **29**, 484 (1958); *ibid.*, **33**, 1743 (1960).
2) D. A. Dows, *J. Chem. Phys.*, **32**, 1342 (1960); *ibid.*, **35**, 282 (1962).
3) R. D. Burbank, *J. Am. Chem. Soc.*, **75**, 1211 (1953).
4) R. M. Hexter, *J. Chem. Phys.*, **33**, 1833 (1960).
5) M. E. Jacox and R. M. Hexter, *J. Chem. Phys.*, **35**, 183 (1961).
6) R. Kopelman, *J. Chem. Phys.*, **44**, 3547 (1966).
7) I. Harada, Ph. D. Thesis, The University of Tokyo, Tokyo, 1967.
8) T. Kawaguchi, M. Hijikigawa, Y. Hayafuji, M. Ikeda, R. Fukushima, and Y. Tomiie, *Bull. Chem. Soc. Jpn.*, **46**, 53 (1973).
9) H. Takeuchi, J. -L. Bribes, I. Harada, and T. Shimanouchi, *J. Raman Spectrosc.*, **4**, 235 (1976).
10) W. L. Lafferty and D. W. Robinson, *J. Chem. Phys.*, **36**, 83 (1962).
11) I. Harada and T. Shimanouchi, *J. Chem. Phys.*, **46**, 2708 (1967).
12) M. Ito, *J. Chem. Phys.*, **40**, 3128 (1964); *ibid.*, **41**, 2842 (1964).
13) C. W. Brown and E. R. Lippincott, *J. Chem. Phys.*, **52**, 786 (1970).
14) T. Shimanouchi, "Tables of Molecular Vibrational Frequencies," Consolidated Vol. 1, Nat. Stand. Ref. Data Ser., Nat. Bur. Stand. (U. S.), 39, U. S. Gov. Printing Office, Washington, D. C. (1972).
15) H. Takeuchi, I. Harada, and T. Shimanouchi, *Chem. Phys. Lett.*, **43**, 516 (1976).
16) T. Shimanouchi, M. Tsuboi, and T. Miyazawa, *J. Chem. Phys.*, **35**, 1597 (1961).
17) J. L. Duncan, *J. Mol. Struct.*, **6**, 447 (1970).
18) J. L. Duncan, A. Allan, and D. C. Mckean, *Mol. Phys.*, **18**, 289 (1970).
19) T. Shimanouchi, "Physical Chemistry," Vol. 4, H. Eyring, D. Henderson, and W. Jost, ed, Academic Press (1970), Chap. 6.
20) D. E. Williams, *J. Chem. Phys.*, **46**, 4680 (1967).
21) B. G. Dashevsky, *Zh. Strukt. Khim.*, **11**, 912 (1970).
22) A. D. Dickson, I. M. Mills, and B. Crawford, Jr., *J. Chem. Phys.*, **27**, 445 (1957).
23) G. Taddei, H. Bonadeo, M. P. Mazocchi, and S. Califano, *J. Chem. Phys.*, **58**, 966 (1973).
24) B. R. A. Nijboer and F. W. de Wette, *Physica*, **23**, 309 (1957)
25) F. W. de Wette and G. E. Schacher, *Phys. Rev.*, **137A**, 78 (1965).
26) P. P. Ewald, *Ann. Phys.*, **64**, 253 (1921).
27) H. Kornfeld, *Z. Phys.*, **22**, 27 (1924).
28) M. H. Cohen and F. Keffer, *Phys. Rev.*, **99**, 1128 (1955).
29) H. A. Lorentz, "The Theory of Electrons and Its Application to the Phenomena of Light and Radiant Heat," Dover, New York (1952).
30) J. C. Decius, *J. Chem. Phys.*, **49**, 1387 (1968).

Complexes between Nucleotide Base and Amino Acid. II. Crystal Structure of 5-Bromocytosine : *N*-Tosyl-L-glutamic Acid

Minoru OHKI, Akio TAKENAKA, Hirotaka SHIMANOUCHI, and Yoshio SASADA

Laboratory of Chemistry for Natural Products, Tokyo Institute of Technology, Ookayama, Meguro-ku, Tokyo 152

(Received August 16, 1976)

The complex crystals of 5-bromocytosine and *N*-tosyl-L-glutamic acid were obtained from their aqueous solution. The space group is P1 with dimensions of $a=10.843(1)$, $b=11.690(2)$, $c=10.879(2)$ Å, $\alpha=122.15(1)$, $\beta=121.38(1)$, $\gamma=69.93(1)°$, and $Z=2$. The structure was solved by the heavy atom method and refined by a block-diagonal least-squares method. The undissociated γ-carboxyl group of glutamic acid is bound with O(2) and N(4) of 5-bromocytosine through hydrogen bonds. This interaction mode is different from those found in some cytosine : glycine complexes and cytidine : *N*-benzyloxycarbonyl-L-glutamic acid complex dihydrate in which the dissociated α-carboxyl group plays a role. This is the first example of interaction between cytosine and the acidic side group of amino acid.

Interactions between nucleic acids and proteins take an important part in several biological processes, though the precise molecular mechanism is still unknown. We have been engaged in preparing complexes of nucleotide base and amino acid followed by X-ray crystallographic studies, which will provide stereochemical basis for the mutual recognition between nucleic acid and protein.

One interaction mode is hydrogen bonds between the dissociated α-carboxyl group of amino acid and protonated N(3) and amino group of cytosine, as found in cytosine : glycine dreivatives[1,2] and in cytidine: *N*-benzyloxycarbonyl-L-glutamic acid complex.[3] We have revealed another type of interaction between γ-carboxyl group of glutamic acid and cytosine in the complex of 5-bromocytosine : *N*-tosyl-L-glutamic acid,[4] and the present paper is a full account of its crystal structure.

Experimental

Prismatic crystals were obtained from an aqueous solution containing equimolar 5-bromocytosine and *N*-tosyl-L-glutamic acid. The complex formation was confirmed by IR spectroscopy and an elementary analysis of these crystals. Found: C, 39.06; H, 3.96; N, 11.15%. Calcd for $C_4H_4N_3OBr \cdot C_{12}H_{15}NO_6S$: C, 39.11; H, 3.91; N, 11.41%. Diffraction pattern of the crystal indicated the crystal system to be triclinic. As the amino acid is L-form, the space group should be P1. The unit-cell dimensions were determined by least-squares calculations with 113 spacings from equator Weissenberg photographs about three different axes, calibration being made with superposed silicon lines ($a=5.43075$ Å). The density measured by flotation in a $CHBr_3$–CCl_4 mixture indicated that there are two 1 : 1 molecular complexes in the unit cell. Crystal data are given in Table 1.

TABLE 1. CRYSTAL DATA

5-Bromocytosine : *N*-tosyl-L-glutamic acid		
$C_4H_4N_3OBr$: $C_{12}H_{15}NO_6S$ F. W.=491.35		
Crystal system: triclinic		
Space group: P1		
$a=10.843(1)$ Å	$b=11.690(2)$ Å	$c=10.879(2)$ Å
$\alpha=122.15(1)°$	$\beta=121.38(1)°$	$\gamma=69.93(1)°$
$U=992.6(2)$ Å^3	$Z=2$	
$D_x=1.644$ g cm^{-3}	$D_m=1.66$ g cm^{-3}	
μ(Cu $K\alpha$) = 45.56 cm^{-1}		

Diffraction data were collected on equi-inclination Weissenberg photographs (0*kl*-8*kl* and *h*0*l*-*h*8*l*) using Ni-filtered Cu $K\alpha$ radiation and the intensities were measured by a TV densitometer.[5] The crystal used for the a- and b-axis rotations were $0.22\times0.20\times0.43$ mm and $0.20\times0.30\times0.40$ mm, respectively. Corrections were made for Lorentz and polarization effects and spot size, but not for absorption. A total of 4259 independent reflexions were obtained, of which zero-reflexions numbered 803. The $N(z)$ test[6] was consistent with non-centrosymmetric space group.

Structure Determination and Refinement

The approximate structure was obtained by the usual heavy atom method. The structure was refined by a block-diagonal least-squares methos; the minimized function was $\sum w\Delta F^2$, where $\Delta F=|F_o|-|F_c|$. In this refinement, the zero-reflexions were assumed to have the value of $|F_o|_{min}(=1.55)$. The zero-reflexions, for which $|F_c|$ values at each cycle were smaller than $|F_o|_{min}$, were omitted from the refinement. The weight function used was as follows: $w=\exp(-as^2-bt^2-cst-ds-et-f)$ for $|F_o|>|F_o|_{min}$, where $s=|F_o|$ and $t=\sin\theta/\lambda$; $w=1/\langle\Delta F^2\rangle$ for $|F_o|=|F_o|_{min}$. The coefficients, *a*, *b*, *c*, *d*, *e*, and *f*, were evaluated by least-squares at each cycle of the structure refinement so that $\langle w\Delta F^2\rangle=1$. The convergence was slow owing to quasi-centrosymmetric structure of the crystal. The refinement was terminated when the maximum shifts of positional and thermal parameters were less than 0.15σ and 0.25σ, respectively. At the final cycle, the coefficients of weight function were −0.0001747, 36.59, 0.03631, 0.05322, −36.13, and 7.320, respectively, and weight for $|F_o|_{min}$ was 0.609. The final value of *R* factor is 0.082 ($R_w=0.080$), and the *R* for reflexions of $|F_o|>3\sigma$ ($\sigma=1/\sqrt{w}$) is 0.065. The comparison between observed and calculated structure factors is given in Table 2.[7] Atomic scattering factors used were taken from "International Tables for X-Ray Crystallography."[8] The positional and thermal parameters are given in Table 3.

Results and Discussion

Bond lengths and angles of the two independent molecules are listed in Table 4. For a few pairs, discrepancy between the lengths of corresponding bonds looks significant; however, this may be attributable to

Table 3. Final positional and thermal parameters

Standard deviations are given in parentheses. The temperature factor has the form, $\exp[-(\beta_{11}h^2+\beta_{22}k^2+\beta_{33}l^2+\beta_{12}hk+\beta_{13}hl+\beta_{23}kl)]$. All parameters have been multiplied by 10^4.

Atom	x	y	z	β_{11}	β_{22}	β_{33}	β_{12}	β_{13}	β_{23}
N(1A)	−1360(7)	−533(8)	176(7)	116(7)	152(8)	105(7)	−71(13)	77(12)	128(13)
C(2A)	−264(8)	−196(7)	1685(7)	108(8)	102(7)	96(8)	−53(12)	76(13)	85(12)
N(3A)	−432(8)	−194(7)	2828(7)	130(8)	141(8)	112(8)	−100(13)	100(13)	103(12)
C(4A)	−1644(7)	−583(8)	2453(8)	88(7)	110(7)	110(8)	−51(12)	46(13)	114(13)
C(5A)	−2752(8)	−1068(9)	833(9)	104(8)	134(9)	112(9)	−86(14)	13(14)	120(14)
C(6A)	−2572(8)	−991(9)	−247(8)	105(8)	143(9)	95(8)	−89(14)	27(13)	106(14)
O(2A)	885(6)	106(7)	1948(6)	106(6)	182(8)	117(7)	−129(12)	45(10)	141(12)
N(4A)	−1822(8)	−529(9)	3607(8)	126(8)	168(9)	147(10)	−76(15)	98(15)	161(16)
Br(5A)	−4420(1)	−1712(1)	273(1)	118(1)	217(1)	186(1)	−139(2)	64(2)	200(2)
N(1B)	1282(7)	678(7)	9866(7)	92(6)	125(7)	106(7)	−85(11)	29(11)	113(12)
C(2B)	214(8)	256(8)	8317(8)	100(7)	111(7)	115(9)	−69(12)	50(13)	109(13)
N(3B)	414(6)	204(6)	7178(6)	97(6)	110(6)	92(7)	−63(10)	35(11)	91(11)
C(4B)	1638(8)	571(8)	7524(9)	116(8)	100(7)	138(9)	−31(13)	98(15)	123(13)
C(5B)	2743(9)	1056(8)	9135(10)	143(10)	109(8)	154(11)	−23(14)	166(18)	121(15)
C(6B)	2535(8)	1090(8)	10284(9)	98(8)	120(8)	141(10)	−57(13)	64(14)	129(15)
O(2B)	−919(6)	−73(6)	8065(6)	102(6)	140(7)	128(7)	−86(10)	56(10)	123(11)
N(4B)	1830(8)	479(9)	6366(8)	140(9)	180(10)	118(8)	−127(16)	77(14)	137(15)
Br(5B)	4449(1)	1665(1)	9714(1)	111(1)	183(1)	172(1)	−109(2)	77(2)	166(2)
O(3A)	−9550(7)	−3524(7)	531(8)	112(7)	128(7)	213(10)	−42(11)	126(14)	147(14)
O(4A)	−7997(8)	−5323(8)	728(12)	130(8)	144(8)	359(18)	−7(13)	199(20)	285(20)
C(7A)	−8319(9)	−4129(9)	794(9)	120(9)	138(10)	127(10)	−80(16)	64(16)	122(16)
C(8A)	−7072(8)	−3517(9)	1182(9)	100(8)	126(9)	150(11)	−79(14)	84(15)	114(15)
C(9A)	−6300(9)	−2650(9)	2970(8)	124(9)	153(10)	96(8)	−113(16)	53(14)	95(15)
C(10A)	−5116(8)	−1992(8)	3304(8)	109(8)	127(9)	99(8)	−90(14)	54(14)	74(13)
C(11A)	−3999(9)	−1414(8)	5036(8)	117(9)	111(8)	118(9)	−54(14)	80(15)	90(14)
O(5A)	−2965(7)	−936(8)	5201(7)	131(7)	202(9)	126(7)	−191(14)	20(12)	147(13)
O(6A)	−4047(8)	−1406(9)	6123(7)	174(9)	215(10)	122(8)	−146(16)	80(14)	171(14)
N(5A)	−7533(7)	−2712(7)	310(7)	112(7)	113(7)	121(8)	−82(12)	64(13)	92(12)
S(1A)	−7740(2)	−3465(2)	−1535(2)	112(2)	118(2)	117(2)	−55(3)	90(3)	93(3)
O(7A)	−8034(8)	−2377(6)	−1917(7)	192(10)	117(6)	155(8)	−97(13)	141(15)	112(11)
O(8A)	−6492(6)	−4397(7)	−1602(7)	105(6)	157(8)	153(8)	−35(11)	107(12)	121(13)
C(12A)	−9264(9)	−4372(8)	−2711(9)	137(10)	89(7)	127(10)	−30(13)	107(16)	74(13)
C(13A)	−9082(12)	−5785(10)	−3193(12)	161(13)	123(10)	190(14)	−50(18)	127(22)	108(19)
C(14A)	−10311(14)	−6458(11)	−4070(14)	194(15)	117(10)	210(16)	−55(19)	150(26)	126(20)
C(15A)	−11670(11)	−5809(10)	−4460(9)	169(12)	158(11)	117(10)	−140(19)	84(18)	103(17)
C(16A)	−11827(10)	−4433(11)	−3962(11)	120(10)	172(12)	147(12)	−124(18)	36(17)	130(19)
C(17A)	−10619(9)	−3728(10)	−3121(10)	118(9)	136(10)	130(10)	−68(15)	55(16)	104(16)
C(18A)	−13018(16)	−6587(16)	−5465(16)	214(18)	225(18)	219(18)	−236(32)	81(29)	202(29)
O(3B)	9703(7)	3379(7)	9303(11)	121(7)	138(7)	322(16)	−30(12)	206(18)	217(18)
O(4B)	8165(8)	5204(8)	9396(13)	142(9)	137(8)	349(18)	−51(14)	168(20)	236(19)
C(7B)	8505(9)	3989(9)	9201(10)	108(9)	106(8)	151(11)	−54(13)	74(16)	100(14)
C(8B)	7312(8)	3291(8)	8826(9)	109(8)	127(9)	122(9)	−55(14)	71(14)	119(15)
C(9B)	6179(9)	2868(9)	7096(10)	115(9)	142(10)	164(12)	−71(16)	116(17)	138(17)
C(10B)	5017(10)	2165(11)	6766(10)	142(10)	170(11)	130(10)	−163(19)	72(17)	110(17)
C(11B)	3950(9)	1594(8)	5068(9)	121(9)	112(8)	126(9)	−66(14)	86(15)	103(14)
O(5B)	2897(7)	1110(8)	4878(6)	132(7)	199(9)	112(7)	−158(14)	52(11)	131(12)
O(6B)	4009(8)	1528(8)	3943(7)	161(8)	182(9)	130(8)	−143(14)	89(13)	129(13)
N(5B)	6632(7)	4131(8)	9910(8)	109(7)	142(8)	121(8)	−77(13)	68(13)	106(13)
S(1B)	7310(2)	4083(2)	11625(2)	111(2)	124(2)	127(2)	−64(3)	84(4)	107(3)
O(7B)	6370(7)	5036(8)	12371(8)	141(8)	171(8)	155(9)	−32(13)	155(14)	111(14)
O(8B)	7513(9)	2729(8)	11332(9)	186(10)	170(9)	189(10)	−157(16)	54(17)	198(16)
C(12B)	9047(9)	4724(8)	12783(9)	126(9)	103(7)	122(9)	−34(14)	83(15)	98(13)
C(13B)	9139(10)	6040(12)	13329(13)	114(10)	164(12)	200(15)	−62(18)	71(20)	156(22)
C(14B)	10505(12)	6514(11)	14152(12)	145(12)	148(11)	184(14)	−126(19)	33(21)	127(20)
C(15B)	11751(9)	5657(11)	14380(11)	101(9)	193(13)	160(12)	−56(17)	59(17)	210(21)
C(16B)	11586(11)	4296(13)	13765(14)	120(11)	191(14)	206(16)	12(20)	97(21)	227(25)
C(17B)	10259(12)	3807(11)	12958(13)	161(12)	134(10)	198(15)	1(18)	128(22)	178(21)
C(18B)	13186(13)	6175(19)	15287(14)	150(13)	331(26)	171(15)	−216(31)	39(23)	249(32)

TABLE 4. BOND LENGTHS AND ANGLES OF THE TWO INDEPENDENT MOLECULES
Standard deviations are given in parentheses.

	Molecule A	Molecule B
Bond lengths (l/Å)		
N(1)-C(2)	1.37(1)	1.38(1)
N(3)-C(4)	1.33(1)	1.34(1)
C(5)-C(6)	1.34(1)	1.36(1)
C(2)-O(2)	1.26(1)	1.26(1)
C(5)-Br(5)	1.87(1)	1.88(1)
C(2)-N(3)	1.35(1)	1.33(1)
C(4)-C(5)	1.44(1)	1.43(1)
C(6)-N(1)	1.35(1)	1.36(1)
C(4)-N(4)	1.33(1)	1.33(1)
C(7)-O(3)	1.24(1)	1.23(1)
C(7)-C(8)	1.51(1)	1.53(1)
C(8)-C(9)	1.52(1)	1.52(1)
C(10)-C(11)	1.52(1)	1.48(2)
C(11)-O(6)	1.21(1)	1.22(1)
C(7)-O(4)	1.29(1)	1.26(1)
C(8)-N(5)	1.47(1)	1.44(1)
C(9)-C(10)	1.51(1)	1.52(1)
C(11)-O(5)	1.31(1)	1.32(1)
N(5)-S(1)	1.63(1)	1.64(1)
S(1)-O(8)	1.43(1)	1.40(1)
C(12)-C(13)	1.42(2)	1.34(2)
C(14)-C(15)	1.36(2)	1.37(2)
C(16)-C(17)	1.39(2)	1.37(2)
C(15)-C(18)	1.53(2)	1.47(2)
S(1)-O(7)	1.43(1)	1.44(1)
S(1)-C(12)	1.75(1)	1.79(1)
C(13)-C(14)	1.38(2)	1.40(2)
C(15)-C(16)	1.38(2)	1.40(2)
C(17)-C(12)	1.36(1)	1.38(2)
Bond angles (ϕ/°)		
C(2)-N(1)-C(6)	121.1(8)	121.5(8)
N(1)-C(2)-O(2)	117.4(8)	116.4(8)
N(1)-C(2)-N(3)	120.3(8)	120.0(8)
O(2)-C(2)-N(3)	122.3(8)	123.6(8)
C(2)-N(3)-C(4)	119.3(8)	120.6(8)
N(3)-C(4)-C(5)	121.2(8)	120.4(8)
N(3)-C(4)-N(4)	118.7(8)	119.7(9)
C(5)-C(4)-N(4)	120.0(8)	119.9(9)
C(4)-C(5)-C(6)	117.4(9)	118.4(9)
C(4)-C(5)-Br(5)	121.4(7)	122.4(7)
C(6)-C(5)-Br(5)	121.2(7)	119.2(8)
C(5)-C(6)-N(1)	120.3(9)	119.0(9)
O(3)-C(7)-O(4)	124.0(10)	124.1(11)
O(3)-C(7)-C(8)	121.5(9)	120.4(9)
O(4)-C(7)-C(8)	114.5(9)	115.5(9)
C(7)-C(8)-N(5)	112.2(8)	111.5(8)
C(7)-C(8)-C(9)	111.4(8)	112.1(8)
N(5)-C(8)-C(9)	109.8(8)	110.3(8)
C(8)-C(9)-C(10)	109.9(8)	110.5(9)
C(9)-C(10)-C(11)	115.5(8)	114.2(9)
C(10)-C(11)-O(5)	111.5(8)	111.5(9)
C(10)-C(11)-O(6)	124.5(9)	126.3(9)
O(5)-C(11)-O(6)	124.1(9)	122.2(9)
C(8)-N(5)-S(1)	119.9(6)	120.3(7)
N(5)-S(1)-O(7)	104.1(5)	104.8(5)
N(5)-S(1)-O(8)	107.2(4)	108.4(5)
N(5)-S(1)-C(12)	107.3(4)	106.4(5)
O(7)-S(1)-O(8)	119.0(5)	119.9(6)
O(7)-S(1)-C(12)	109.6(5)	108.3(5)
O(8)-S(1)-C(12)	108.9(5)	108.3(5)
S(1)-C(12)-C(13)	119.6(8)	119.9(8)
S(1)-C(12)-C(17)	120.6(8)	117.8(8)
C(13)-C(12)-C(17)	119.8(10)	122.1(11)
C(12)-C(13)-C(14)	117.9(11)	119.4(12)
C(13)-C(14)-C(15)	122.4(13)	121.4(12)
C(14)-C(15)-C(16)	118.9(11)	116.6(11)
C(14)-C(15)-C(18)	121.3(12)	120.9(12)
C(16)-C(15)-C(18)	119.8(11)	122.5(12)
C(15)-C(16)-C(17)	120.4(11)	123.1(13)
C(16)-C(17)-C(12)	120.5(10)	117.4(12)

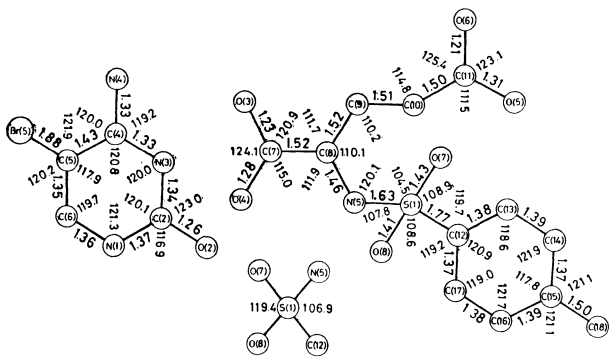

Fig. 1. Average bond lengths and angles of the two independent 5-bromocytosine and *N*-tosyl-L-glutamic acid molecules.

the difficulty in convergence due to pseudo symmetry of the crystal. Their averaged values shown in Fig. 1 are close to authentic ones.

The crystal structure is shown in Fig. 2. The molecules are arranged in layers parallel to the $(1\bar{2}0)$ plane. The complexes are formed by hydrogen bonds in the layer and come in van der Waals contancts with those in adjacent layers. The hydrogen bond scheme in the layer is illustrated in Fig. 3, relevant distances and angles being listed in Table 5. The 5-bromocytosine molecules form a ribbon elongated along [001], by the hydrogen bonds, N(1A)H···O(2B), N(1B)H···O(2A), N(4A)H···N(3B), and N(4B)H···N(3A), the former two and the latter two being related around each of pseudo-center of symmetry. The dihedral angle between the mean planes of cytosines A and B

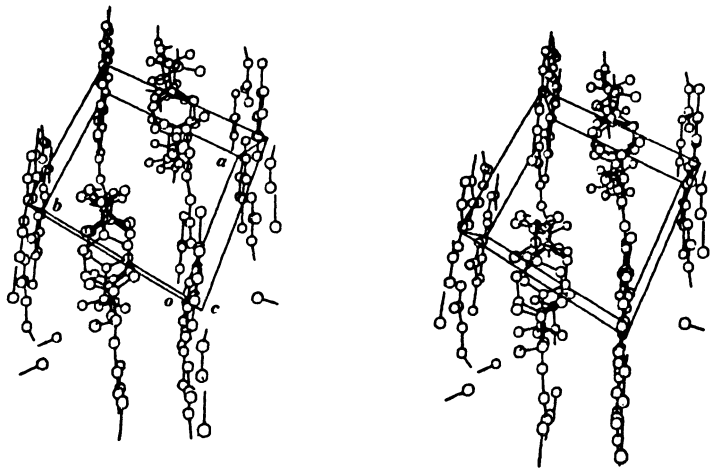

Fig. 2. A stereoscopic view of the crystal structure.

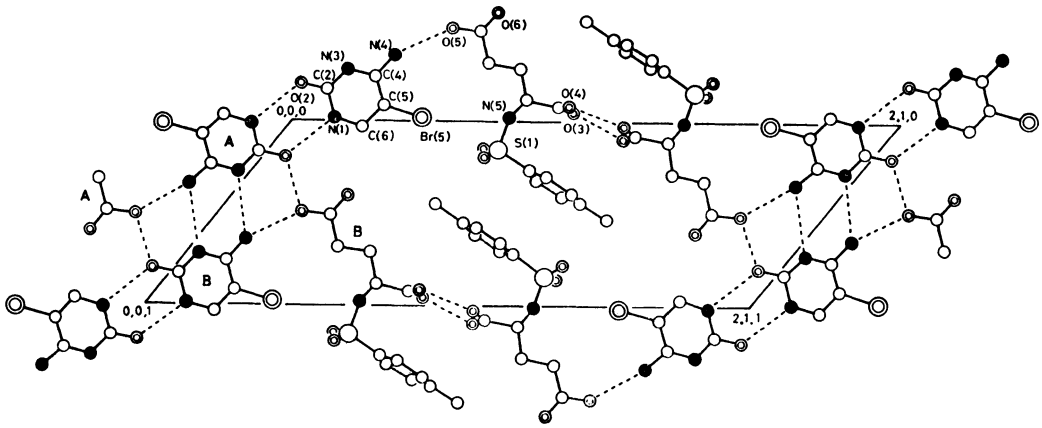

Fig. 3. The hydrogen bond scheme in the 5-bromocytosine : *N*-tosyl-L-glutamic acid. Crystallographically independent molecules are indicated as A and B. These are related to each other by pseudo-inversions.

Table 5. Distances and angles of hydrogen bonds
CH···O contacts are also listed in this table.

Distance (l/Å)					
N(1A)···O(2B)[a]	2.90	N(1B)···O(2A)[b]	2.93	N(4A)···N(3B)[c]	3.13
N(4B)···N(3A)[c]	3.12	N(4A)···O(5A)[c]	2.88	N(4B)···O(5B)[c]	2.88
O(5A)···O(2B)[c]	2.58	O(5B)···O(2A)[c]	2.61	O(4A)···O(3B)[d]	2.65
O(4B)···O(3A)[e]	2.70	C(6A)···O(6A)[a]	3.21	C(6B)···O(6B)[b]	3.23
Angle (ϕ/°)					
N(1A)···O(2B)[a]-C(2B)[a]	127.8	C(2A)-N(1A)···O(2B)[a]	115.1	C(6A)-N(1A)···O(2B)[a]	123.7
N(1B)···O(2A)[b]-C(2A)[b]	126.5	C(2B)-N(1B)···O(2A)[b]	114.4	C(6B)-N(1B)···O(2A)[b]	123.1
N(4A)···N(3B)[c]-C(2B)[c]	127.0	N(4A)···N(3B)[c]-C(4B)[c]	112.2	C(4A)-N(4A)···N(3B)[c]	128.0
N(4B)···N(3A)[c]-C(2A)[c]	127.3	N(4B)···N(3A)[c]-C(4A)[c]	113.3	C(4B)-N(4B)···N(3A)[c]	127.5
N(4A)···O(5A)[c]-C(11A)[c]	146.1	N(4A)···O(5A)[c]···O(2B)[c]	99.7	C(4A)-N(4A)···O(5A)[c]	161.2
N(4B)···O(5B)[c]-C(11B)[c]	146.2	N(4B)···O(5B)[c]···O(2A)[c]	98.2	C(4B)-N(4B)···O(5B)[c]	158.2
O(5A)···O(2B)[c]-C(2B)[c]	119.3	O(5A)···N(4A)[c]···N(3B)[c]	70.0	O(5A)···O(2B)[c]···N(1A)[b]	127.5
C(11A)-O(5A)···O(2B)[c]	114.1	O(5B)···O(2B)[c]-C(2B)[c]	119.9	O(5B)···N(4B)[c]···N(3A)[c]	70.8
O(5B)···O(2A)[c]···N(1B)[a]	110.5	C(11B)-O(5B)···O(2A)[c]	115.4	O(4A)···O(3B)[d]-C(7B)[d]	121.6
C(7A)-O(4A)···O(3B)[d]	113.3	O(4B)···O(3A)[e]-C(7A)[e]	120.6	C(7B)-O(4B)···O(3A)[e]	113.2
C(6A)···O(6A)[a]-C(11A)[a]	151.0	N(1A)-C(6A)···O(6A)[a]	94.8	C(5A)-C(6A)···O(6A)[a]	144.9
C(6B)···O(6B)[b]-C(11B)[b]	151.5	N(1B)-C(6B)···O(6B)[b]	95.1	C(5B)-C(6B)···O(6B)[b]	145.5

a) At x, y, $-1+z$. b) At x, y, $1+z$. c) At x, y, z. d) At $-2+x$, $-1+y$, $-1+z$. e) At $2+x$, $1+y$, $1+z$.

is 3.5°. On the other hand, the two independent *N*-tosyl-L-glutamic acid molecules are associated by the two hydrogen bonds between the α-carboxyl groups, O(4A)H···O(3B) and O(4B)H···O(3A), related by a pseudo-inversion. These dimers are stacked, by overlapping the tosyl groups, in the same direction as the ribbon. The two independent phenyl planes are almost parallel to each other; the dihedral angle between them is 1.7°, and its spacing is 3.59 Å.

The cytosine ribbons and glutamic acid stacks are linked by the other hydrogen bonds in which the side group of the glutamic acid participates. The O(5) atom is the donor to O(2) of 5-bromocytosine and at the same time the acceptor from N(4) of the neighboring base. In addition, the O(6) atom seems to make a CH···O type interaction with C(6) of the third base. Similar C(6)H···O contact is also observed in crystals of the two forms of cytidylic acid,[9,10] 1-methylcytosine hydrochloride,[11] and 1-(β-D-arabinofuranosyl)cytosine hydrochloride.[12]

The hydrogen bond scheme suggests that the protonation to N(3) of cytosine by the carboxyl group does not occur in the present complex. This is supported by the bond lengths and angles of cytosine molecule (Fig. 3); the C(2)–N(3)–C(4) bond angle 120.0° is close to unprotonated form, and the dimensions of α- and γ- carboxyl groups indicate that their hydrogen atoms are bonded to O(4) atom in α-carboxyl group and O(5) atom in γ-carboxyl group.

In the tosyl groups S(1)–O(8) bonds are *cis* to N(5)–C(8) bonds, and the N(5)–S(1)–O(8) bond angles are larger than N(5)–S(1)–O(7).

The conformations of the two independent glutamic acids are extended ones; the relevant torsion angles are given in Table 6. Atoms in the side group of the amino acid are coplanar; the largest deviation of atoms from the mean plane is 0.14 Å at C(8A) and 0.10 Å at C(9B), and the largest deviation in torsion angle from the *trans* conformation arises around C_β–C_γ bond in both A and B molecules; 15.9° and 6.0°, respectively. The α-carboxyl group makes an angle of 80.9° in A and 84.5° in B with the side group mean plane.

In summary, the present complex formation is due to the undissociated γ-carboxyl group of glutamic acid bound with O(2) and N(4) of 5-bromocytosine through hydrogen bonds. It is quite different from those found in cytosine : *N*-benzoylglycine complex monohydrate,[1] cytosine : *N*-formylglycine complex,[2] and cytidine : *N*-benzyloxycarbonyl-L-glutamic acid complex dihydrate,[3] where the dissociated α-carboxyl group plays a role. The present crystal provides the first example of interaction mode between cytosine and acidic side group of amino acid.

Table 6. Torsion angles of the glutamic acids

	Molecule A	Molecule B
O(4)-C(7)-C(8)-N(5)	143.5°	−47.9°
O(3)-C(7)-C(8)-N(5)	−35.0	131.8
C(7)-C(8)-N(5)-S(1)	−81.7	−87.1
C(9)-C(8)-N(5)-S(1)	153.8	147.6
O(4)-C(7)-C(8)-C(9)	−93.0	76.4
O(3)-C(7)-C(8)-C(9)	88.5	−103.9
N(5)-C(8)-C(9)-C(10)	−51.9	−55.6
C(7)-C(8)-C(9)-C(10)	−176.8	179.5
C(8)-C(9)-C(10)-C(11)	−164.1	174.0
C(9)-C(10)-C(11)-O(5)	176.2	−174.2
C(9)-C(10)-C(11)-O(6)	−3.2	7.5

References

1) C. Tamura, T. Hata, S. Sato, and N. Sakurai, *Bull. Chem. Soc. Jpn.*, **44**, 1473 (1971).
2) M. Ohki, A. Takenaka, H. Shimanouchi, and Y. Sasada, *Bull. Chem. Soc. Jpn.*, **48**, 848 (1975).
3) T. Hata, M. Yoshikawa, S. Sato, and C. Tamura, *Acta Crystallogr.*, **B31**, 312 (1975).
4) M. Ohki, A. Takenaka, H. Shimanouchi, and Y. Sasada, *Chem. Lett.*, **1974**, 551.
5) T. Izumi, *Jpn. J. Appl. Phys.*, **10**, 1724 (1971).
6) E. R. Howells, D. C. Phillips, and D. Rogers, *Acta Crystallogr.*, **3**, 210 (1950).
7) Table 2 has been deposited at the Chemical Society of Japan (Document No. 7638).
8) "International Tables for X-Ray Crystallography," Vol. III, Kynoch Press, Birmingham (1962), p. 201.
9) M. Sundaralingam and L. H. Jensen, *J. Mol. Biol.*, **13**, 914 (1965).
10) C. E. Bugg and R. E. Marsh, *J. Mol. Biol.*, **25**, 67 (1967).
11) B. L. Trus and R. E. Marsh, *Acta Crystallogr.*, **B28**, 1834 (1972).
12) J. S. Sherfinski and R. E. Marsh, *Acta Crystallogr.*, **B29**, 192 (1973).

Complex Formation of Crosslinked Poly(4-vinylpyridine) Resins with Copper(II)

Hiroyuki NISHIDE, Jichio DEGUCHI, and Eishun TSUCHIDA

Department of Polymer Chemistry, Waseda University, Tokyo 160

(Received March 12, 1976)

Poly(4-vinylpyridine) was crosslinked with 1,4-dibromobutane. The obtained resin(DBQP) formed a stable complex with Cu^{2+}, and the adsorption capacity of DBQP varied with the degree of crosslinking. The complex formation of DBQP with Cu^{2+} was studied by examining the adsorption equilibrium and the spectroscopic measurement. The resin complex seems to be formed *via* no step-by-step mechanism, and the stability constant was appreciably large in comparison with those of non-crosslinked polymers and of a monomeric analogue. In the highly crosslinked resins, the ligand-field is relatively weak and the stability of the Cu^{2+} complex is decreased.

Poly(4-vinylpyridine) (PVP) forms a stable intrapolymer chelate with copper ions, in which the PVP-chain is markedly contracted.[1-3] Thus, if one makes the PVP-ligand crosslinked and the polymer chain is previously contracted, it is expected that the obtained PVP resin will form the stable complex with Cu^{2+}.

In the present paper, PVP was crosslinked with 1,4-dibromobutane to yield the insoluble PVP resin-(DBQP, I), of which free and unquaternized pyridine groups were utilized to coordinate with a metal ion.

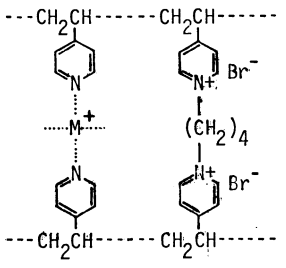

I

The complex formation of this DBQP resin with Cu^{2+} was studied by the adsorption equilibrium and the spectroscopic measurement. The effects of the crosslinking on the stability and structure of the resin complex were discussed.

Experimental

Materials. PVP was prepared by radical polymerization of 4-vinylpyridine, and was purified twice by reprecipitation. The average degree of polymerization of PVP used in this experiment was 122 as measured by vapor pressure osmometry. Analytical grade reagents of 1,4-dibromobutane, pyridine (Py), and copper(II) chloride were used. All solutions were prepared with deionized water.

Preparation of DBQP Resins. The crosslinking reagent, 1,4-dibromobutane, of prescribed concentration [0.025 M (DBQP(1)), 0.1 M (DBQP(2)), 0.3 M(DBQP(3)), or 0.5 M (DBQP (4))] was added to the methanol solution of PVP (1 M). The mixture was vigorously stirred at 65 °C for 5 days. The resin was filtered off, washed with methanol repeatedly, and dried *in vacuo*. The dried resin was ground and the portion of 100—150 mesh size was used in all the experiments presented. The elemental analyses of the resins are shown in Table 1. The total Br content was determined by the Volhard method and the free Br ion in the resin was titrated after the resin was soaked into water. The percentages of crosslinking and of quaternization were calculated by using the C/N ratio, the free Br ion, and the total Br content. The percentage of quaternization was also deduced from the ratio of absorption at 1600 cm^{-1} (due to pyridine group) to the absorption at 1640 cm^{-1} (due to quaternized pyridine group) of IR spectra, and this value was nearly equal to the value which was determined

TABLE 1. ELEMENTAL ANALYSES OF PVP WITH 1,4-DIBROMOBUTANE

Resin	Found(Calcd)				Crosslinking %[a]	Quaternization %[b]	Quaternization %[c]
	C%	N%	Br ion %	Br total %			
DBQP (1)	75.7 (75.5)	12.3 (12.3)	5.77 (5.76)	5.78 (5.76)	4.1	8.2	10
DBQP (2)	68.7 (68.6)	10.6 (10.7)	14.6 (14.7)	14.6 (14.7)	12	24	22
DBQP (3)	60.3 (59.9)	8.65 (8.69)	25.3 (25.3)	26.0 (25.8)	25	51	53
DBQP (4)	57.9 (57.1)	8.02 (8.04)	29.0 (29.0)	29.6 (29.4)	31	63	68

a) Percentage of bridged dibromobutane per pyridine groups of PVP=$y/2$(If all pyridine groups of PVP are crosslinked by dibromobutane, crosslinking % is 50). b) Percentage of quaternized pyridine groups per pyridine groups of PVP=$(y+z)$. c) Percentage of quaternized pyridine groups per pyridine groups of PVP determined by IR spectra.

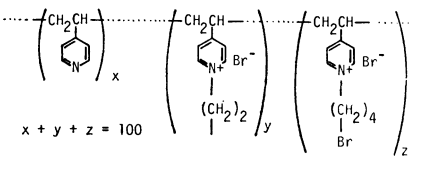

by the elemental analyses (Table 1). The z term given in the footnote of Table 1 was extremely small, and almost all 1,4-dibromobutane molecules built bridges between two vinylpyridine groups.

Partially-quaternized PVP (QPVP) was prepared by quaternization of PVP with ethylbromide, and the percentage of quaternization was 45.

Adsorption of Cu^{2+} on the DBQP Resin. A batch type equilibration procedure was used to determine the Cu^{2+} uptaken from solution by the resin. The pH value of the system was kept constant by a 0.1 M CH_3COOH-CH_3COONa buffer. The two phases were shaken on a mechanical shaker at room temperature for 5 h. After shaking, the two phases were separated, and the supernatant solution was then analyzed for Cu^{2+} using atomic absorption spectrophotometry (JEOL JAA-7000). The amount of Cu^{2+} in the supernatant subtracted from the amount initially added gave the amount of Cu^{2+} adsorbed on the resin. Cu^{2+} adsorbed on QPVP and PVP were determined by dialysis equilibrium.

Measurements. The visible absorption spectra of the Cu^{2+} complexes of the fine powdered DBQP resin were measured in a Nujol mull or in suspension with a high sensitive spectrophotometer (Union Giken SM-401).

The apparent dissociation rate constant of Cu^{2+} from the Cu^{2+}-resin complex was determined as follows; the Cu^{2+}-resin complex was soaked into 0.1 M EDTA solution, and the increase in the spectra of the Cu^{2+}-EDTA (λ_{max}: 745 nm) formed in the supernatant solution was continuously measured.

Magnetic susceptibility measurements were carried out by Gouy method.

Results and Discussion

When the DBQP resin is added to the Cu^{2+} aqueous solution, the Cu^{2+}–resin complex is easily formed. As seen in Fig. 1, the adsorption equilibrium was attained within 1 h. It was shown in Figs. 1 and 2 that the adsorption of Cu^{2+} on the DBQP resins varied with the degree of crosslinking. Here the concentration of the unquaternized pyridine groups in the resin was kept constant for each resin. The adsorption capacity of Cu^{2+}, *i.e.*, the value of ordinate in Fig. 2 was changed with the degree of crosslinking. The effect of the crosslinking on the Cu^{2+}-resin complexes

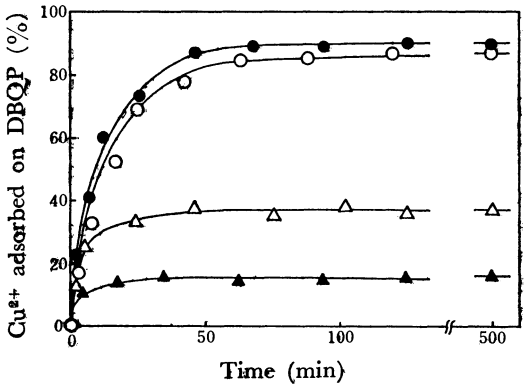

Fig. 1. Complexation between DBQP and Cu^{2+}. [Cu]=0.001 M, $[\bar{N}]/[Cu]=10$, $\mu=0.1$, pH 5.5, ○: DBQP(1), ●: DBQP(2), △: DBQP(3), ▲: DBQP(4), where $\bar{N}$ is the unquaternized and coordinable vinylpyridine group in the resin. DBQP(1)—(4) are shown in Table 1.

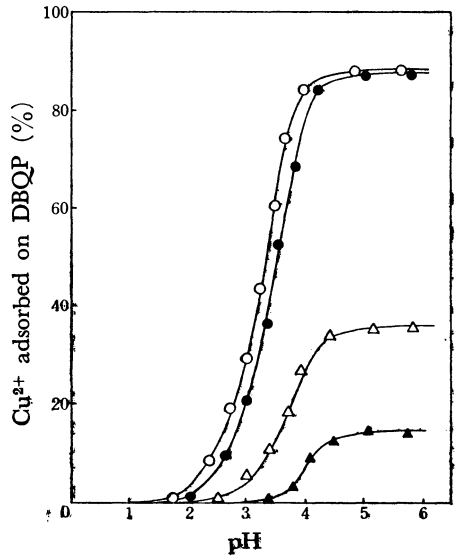

Fig. 2. Effect of crosslinking on Cu^{2+} adsorption. $[\bar{N}]=0.01$ M, $[\bar{N}]/[Cu]=4$, $\mu=0.1$, ○: DBQP(1), ●: DBQP(2), △: DBQP(3), ▲: DBQP(4).

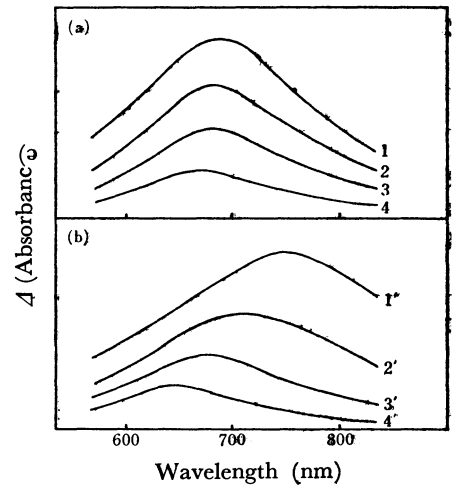

Fig. 3. Visible spectra of Cu^{2+}-DBQP(a) and Cu^{2+}-Py complexes(b). $[\bar{N}]=[Py]=0.05$ M, $\mu=0.1$, pH 5.5, $[\bar{N}]$ or $[Py]/[Cu]=1(1, 1'), 2.5(2, 2'), 5(3, 3'), 20(4), 100(4')$.

were studied from the complex formation equilibrium and the structure of the Cu^{2+} complex.

The visible spectra of the Cu^{2+} complexes with the resin and with Py were measured. As seen in Fig. 3(b), the absorption maximum of the Cu^{2+} complex shifted progressively to shorter wave length as the concentration of Cu^{2+} decreased. This suggests the stepwise formation of Cu^{2+}–Py complexes. On the contrary, the absorption maximum of the Cu^{2+} complex with the resin hardly shifted in Fig. 3 (a). It means that the complex formation between Cu^{2+} and the resin does not proceed *via* step-by-step mechanism and the composition of the Cu^{2+} complex in the resin remains constant throughout the experimental conditions.

The successive stepwise formation constants are represented in Eq. 1 and were calculated by Eq. 2 as follows:

$$\left.\begin{aligned} &Cu + L \overset{\kappa_1}{\rightleftharpoons} CuL_1 \\ &CuL_1 + L \overset{\kappa_2}{\rightleftharpoons} CuL_2 \\ &CuL_2 + L \overset{\kappa_3}{\rightleftharpoons} CuL_3 \\ &CuL_3 + L \overset{\kappa_4}{\rightleftharpoons} CuL_4 \end{aligned}\right\} \quad (1)$$

$$\frac{[Cu]_t}{[Cu]} = 1 + \sum_{n=1}^{4}\left(\prod_{n=1}^{n}\kappa_n\right)[L]^n \quad (2)$$

(L is a pyridine group in the resin and $[Cu]_t$ is the total concentration of Cu)

The concentrations of Cu^{2+} in the supernatant were measured as changing the amount of the resin ($[Cu]_t = 1\times10^{-5}$ M=const, $[L] \gg [Cu]_t$, $[\bar{N}] = 2\times10^{-3}$—$5\times10^{-4}$ M).* As shown in Table 2, the constants increased from κ_1 to κ_4 in the resin system in contrast to the monomeric Py system. This result also supports that the composition of the Cu^{2+} complex is almost CuL_4 where four pyridine groups in the resin coordinate to the Cu^{2+} ion, although the experimental conditions of Table 2 are not the same as the others.

TABLE 2. STEPWISE FORMATION CONSTANTS (κ l/mol) OF Cu^{2+}-DBQP COMPLEXES

Ligand	$\log \kappa_1$	$\log \kappa_2$	$\log \kappa_3$	$\log \kappa_4$
DBQP (1)	2.4	2.8	3.3	3.8
DBQP (2)	2.3	2.7	3.2	3.7
DBQP (3)	2.2	2.4	3.1	3.3
DBQP (4)	1.9	2.3	3.0	3.1
Py[2]	2.5	1.9	1.3	0.8

$[Cu]_t = 1\times10^{-5}$ M, $[\bar{N}] = 2\times10^{-3}$—$5\times10^{-4}$ M, $\mu = 0.10$, pH 5.5.

From the results, the above equations can be also represented by the following.

$$Cu + L' \overset{K}{\rightleftharpoons} CuL' \quad (3)$$

(L' is four pyridine groups in the resin)

The adsorption curves given in Fig. 4 appeared to be a Langmuir type and the stability constant K of the Cu^{2+} complex and the saturated adsorption amount of Cu^{2+} were evaluated by fitting Langmuir's Eq. 4;

$$\frac{c}{a} = \frac{1}{K\cdot A_s} + \frac{1}{A_s}c \quad (4)$$

where A_s is a constant value which corresponds to the saturated adsorption amount, c is the concentration of Cu^{2+}, K is the stability constant, and a is the quantity of adsorption. They are summarized in Table 3 with those of the Cu^{2+} complexes of Py, PVP, and QPVP.

The stability constant K of the Cu^{2+}–PVP complex was about forty times as large as that of the Cu^{2+}–Py complex. Furthermore, the K values in the Cu^{2+}–DBQP system were about one order of magnitude greater than in the non-crosslinked PVP system, which indicates that the DBQP resin uptakes Cu^{2+} from solution in a high efficiency. This phenomenon appears to be general with the polymer complex system,[2,3] and can be explained by the assumption that the concentration of ligand is higher in the polymer domain, especially in the domain for the crosslinked resin system. So that, once the metal ion is attached to one ligand group of the polymer chain, other ligands coordinate more readily.

K and A_s for DBQP decreased largely according to an increase in the number of the crosslinking points. This seems to be caused by the steric hindrance of the crosslinking agent and of the contracted polymer chain, and caused by the electrostatic repulsion among the coordinating Cu^{2+} and the pyridinium ions on the polymer chain as the K value of QPVP is smaller than that of PVP.

Apparent rate constant k_f' of the complex formation given in Eq. 5 was determined. The stability constant of Cu^{2+}–EDTA complex is moderately larger than that of Cu^{2+}–DBQP, and we estimated the apparent

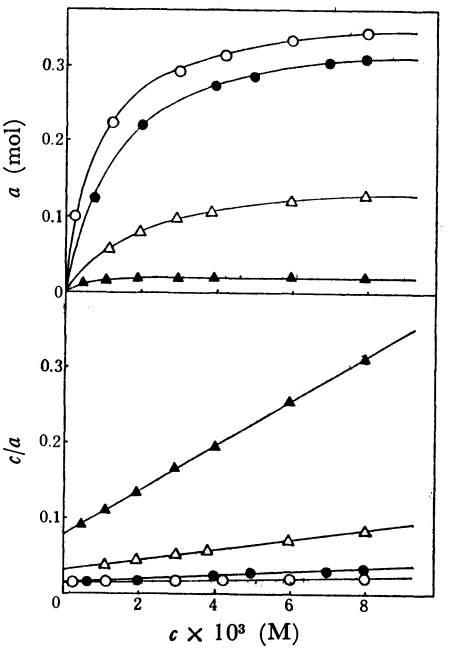

Fig. 4. Adsorption behavior of Cu^{2+} on DBQP resins. $[\bar{N}] = 0.01$ M const., $\mu = 0.1$, pH 5.5, ○: DBQP(1), ●: DBQP(2), △: DBQP(3), ▲: DBQP(4), a is $[Cu^{2+}]$ in solution(M), c is Cu^{2+} adsorbed on DBQP(mol).

TABLE 3. K AND A_s OF Cu^{2+} COMPLEXES

Ligand	K(l/mol)	A_s(mol/unit mol)
DBQP (1)	2810	0.32
DBQP (2)	2370	0.30
DBQP (3)	630	0.12
DBQP (4)	540	0.03
PVP	124	0.45
QPVP	97	0.48
Py[2]	3.2	—

$[\bar{N}]$ in DBQP, QPVP $\doteqdot 0.01$ M, $\mu = 0.10$, pH 5.5.

* Although the κ values in Table 2 are valid under the conditions given in the footnote in Table 2, they may not be adequate under the other conditions (*e. g.* in Fig. 1).

dissociation rate constant k_b' for the reaction in which

$$Cu^{2+} + DBQP \underset{}{\overset{k_f'}{\rightleftharpoons}} Cu^{2+}\text{-}DBQP \quad (5)$$

$$Cu^{2+}\text{-}DBQP + EDTA \underset{}{\overset{k_b'}{\rightleftharpoons}} Cu^{2+}\text{-}EDTA + DBQP \quad (6)$$

EDTA took Cu^{2+} from the stable resin complex, as represented by Eq. 6. In Fig. 5, k_f' and k_b' were plotted against the degree of crosslinking. The k_b' value increased with the stability constant, *i.e.*, Cu^{2+} is more easily dissociated in the highly crosslinked resin, because of the instability of the complex.

The structure of Cu^{2+} complexes involving the resin was deduced from the measurements of visible spectra and magnetic susceptibility of the fine powdered resin complex (Table 4). The effective magnetic moments of the Cu^{2+}–DBQP complexes were about 1.7 B. M. and approximately equal to the value for the mononuclear Cu^{2+} complex. The d-d absorption maxima for the highly crosslinked resins were located at longer wave length and this suggests the relatively weak ligand-field of the highly crosslinked resins.

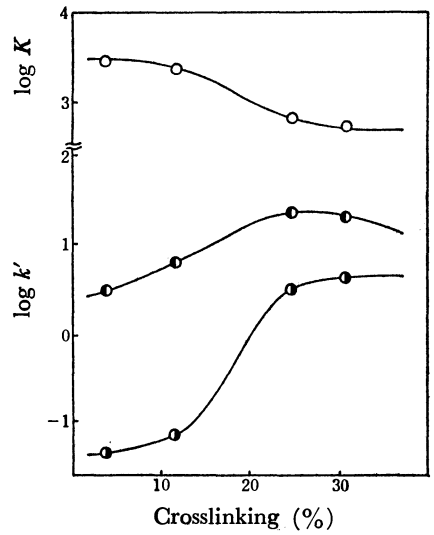

Fig. 5. Effect of crosslinking on k_f' and k_b'.
◐: k_f', ◑: k_b', ○: K value being in Table 3.

Table 4. D-d Absorption maximum and magnetic susceptibility of Cu^{2+}-DBQP complexes

Ligand	λ_{max}(nm)	Magnetic Moment (B.M.)
DBQP (1)	668	1.6
DBQP (2)	658	1.8
DBQP (3)	700 (broad)	1.6
DBQP (4)	700 (broad)	1.4
QPVP	692	1.7

a) $[\overline{N}]$ in DBQP=0.05 M, $[\overline{N}]/[Cu]=5$, $\mu=0.1$, pH 5.5. b) Gouy method: 20 °C, 7000 G.

The authors wish to thank the Ministry of Education, Japan, for a Grant-in-Aid(No. 011011).

References

1) E. Tsuchida, H. Nishide, and T. Nishiyama, *J. Polym. Sci., Polym. Symp.*, **47**, 35 (1974).
2) H. Nishikawa and E. Tsuchida, *J. Phys. Chem.*, **79**, 2072 (1975).
3) Yu. E. Kirsh, V. Ya. Kovner, A. I. Kokorin, K. I. Zanaraev, V. Ya. Chernyak, and V. A. Kabanov, *Eur. Polym. J.*, **10**, 671 (1974).

Crystal Structures of Bis[*N*-(3-methoxysalicylidene)isopropylaminato]nickel(II) (Brown Room Temperature Phase) and -cobalt(II)

Tamaichi ASHIDA, Suteo IWATA, Takashi YAMANE, Masao KAKUDO,*
Akira TAKEUCHI,** and Shoichiro YAMADA**

Department of Applied Chemistry, Faculty of Engineering, Nagoya University, Chikusa-ku, Nagoya 464
**Institute for Protein Research, Osaka University, Suita, Osaka 565*
***Institute of Chemistry, College of General Education, Osaka University, Toyonaka, Osaka 560*

(Received April 22, 1976)

The crystal structures of two Schiff base complexes, bis[*N*-(3-methoxysalicylidene)isopropylaminato]nickel (II) and -cobalt(II), have been determined. Ni complex: brown, room temperature phase, monoclinic, $P2_1/c$, $a=21.089$, $b=7.254$, $c=14.386$ Å, $\beta=98.40°$, $Z=4$, final $R=0.076$. Co complex: red, triclinic, $P\bar{1}$, $a=22.699$, $b=7.395$, $c=14.099$ Å, $\alpha=107.78$, $\beta=99.03$, $\gamma=93.75°$, $Z=4$, final $R=0.13$. In both crystals the metal ions have distorted tetrahedral coordinations. The two crystals are roughly isostructural, although appreciable differences exist in both of the molecular and crystal structures. The Co complex gives a unique example of the methoxy group which sticks out nearly perpendicularly from the phenyl plane.

Recently Takeuchi and Yamada[1] isolated two stereochemical isomers of bis[*N*-(3-methoxysalicylidene) isopropylaminato]nickel(II). Brown and green crystals were obtained from methanol and ethylether solutions, respectively. In addition to these two crystalline forms, two other new high temperature forms, again brown and green ones, were found by Arai *et al.*[2] in their detailed studies on the thermal and magnetic properties of this complex. The spectroscopic and magnetic studies revealed that in both of the brown forms, room and high temperature ones, the molecular structures are almost the same and the central Ni ions are coordinated tetrahedrally, while in the two green forms the molecules have a square-planar coordination of Ni.[1,2]

The cobalt(II) complex of the same ligand was also prepared, and the Co ion was shown to have a tetrahedral coordination.[3] The unit cell dimension of the crystal is not so far from that of the brown Ni complex in the room temperature form. Thus it may be expected that these two crystals are isostructural with each other, although they are different in symmetry.

In this work, the crystal structures of the brown Ni complex in the room temperature form and of the Co complex were studied.

TABLE 1. CRYSTALLOGRAPHIC DATA OF (3-CH_3O-SAL·i-C_3H_7)$_2$M(II)

	Ni complex	Co complex	Cu complex
Color	Brown	Red	Red brown
Crystal system	Monoclinic	Triclinic	Monoclinic
Space group	$P2_1/c$	$P\bar{1}$	$P2_1/n$
a (Å)	21.089(2)	22.699(3)	10.329(1)
b	7.254(1)	7.395(2)	23.155(2)
c	14.386(1)	14.099(3)	9.188(1)
α (°)		107.78(2)	
β	98.40(1)	99.93(2)	96.04(1)
γ		93.75(2)	
V (Å^3)	2177.2	2202.2	2185.3
D_m (g/cm^3)	1.352	1.350	1.354
D_x	1.350	1.336	1.356
Z	4	4	4

Experimental

The crystallographic data of the brown room temperature form of bis[*N*-(3-methoxysalicylidene)isopropylaminato]-nickel(II) and those of the red Co complex are listed in Table 1. The data of the red brown crystal of the Cu complex with the same ligand[4] are also listed for comparison.

The X-ray intensity data were obtained on a four-circle diffractometer (Rigaku) with Zr-filtered Mo$K\alpha$ radiation. The 2θ-ω scan method was used, and the background counts were made at both scan limits. The maximum 2θ measured and numbers of non-zero reflections collected and used in the structure determinations are: 55° and 3845 for the Ni complex, and 45° and 3676 for the Co complex, respectively. The intensities were corrected for only Lp factors. The sizes of the crystals used were $0.5\times0.4\times0.2$ mm for the Ni complex, and $0.1\times0.1\times0.3$ mm for the Co complex.

Structure Determination

The structures were determined by the heavy atom Fourier method. The refinements were made by a block-diagonal least-squares calculations.[5] Unit weight was assigned for all the non-zero reflections. All the atomic scattering factors were taken from International Tables for X-Ray Crystallography, Vol. III.[6] For the metal ions the scattering factors of the univalent cations Co^+ and Ni^+ were used in consideration of the electroneutrality principle.[7] The computations were done on a NEAC 2200-700 of Osaka University and a FACOM 230-60 of Nagoya University.

Ni Complex: All the hydrogen atoms were included in the refinement. The final R is 0.076 for non-zero reflections.[8] The final parameters are listed in Tables 2 and 3. The bond distances and angles are shown in Fig. 1. The e.s.d.'s of the distances and angles among the non-hydrogen atoms are 0.004—0.014 Å and 0.2—0.8°, respectively. The ORTEP drawing[9] is shown in Fig. 2.

Co Complex: Two crystallographically independent molecules exist in the crystal. Anisotropic temperature factors were assigned to the Co atoms only, and the C, N and O atoms were refined with isotropic temperature factors. No hydrogen atoms were included in the calculation. The final R is 0.128.[8] No further

TABLE 2. Ni(3-CH_3O-SAL·*i*-C_3H_7)$_2$: THE ATOMIC PARAMETERS AND THEIR ESTIMATED STANDARD DEVIATIONS ($\times 10^4$)
Thermal parameters are in the form: $\exp[-(\beta_{11}h^2+\beta_{22}k^2+\beta_{33}l^2+\beta_{12}hk+\beta_{13}hl+\beta_{23}kl)]$.

	x	y	z	β_{11}	β_{22}	β_{33}	β_{12}	β_{13}	β_{23}
Ni	2371(0)	6749(1)	1336(1)	16(0)	136(1)	46(0)	−9(1)	9(0)	−6(1)
C(1)	3721(3)	8639(7)	926(4)	19(1)	122(10)	47(3)	3(6)	14(3)	12(9)
C(2)	3593(2)	8549(7)	1860(4)	17(1)	104(10)	49(3)	3(5)	15(3)	0(9)
C(3)	4090(3)	9126(8)	2572(4)	19(1)	173(12)	48(3)	−9(7)	9(3)	16(10)
C(4)	4677(3)	9728(10)	2369(5)	19(1)	214(15)	67(4)	−18(8)	11(4)	6(13)
C(5)	4786(3)	9821(10)	1438(5)	20(1)	220(15)	78(5)	−3(8)	33(4)	24(14)
C(6)	4327(3)	9284(9)	739(5)	22(1)	204(14)	59(4)	6(7)	31(4)	12(12)
C(7)	3248(3)	8144(9)	132(4)	20(1)	212(13)	45(3)	11(8)	14(3)	36(11)
C(8)	2293(3)	7131(13)	−772(5)	28(1)	398(24)	46(4)	4(11)	−2(4)	−15(16)
C(9)	1752(4)	8534(16)	−902(6)	33(2)	521(34)	82(6)	26(15)	−10(6)	89(24)
C(10)	2028(4)	5172(15)	−834(6)	42(3)	494(32)	68(5)	−50(16)	−19(6)	−164(22)
C(11)	4391(4)	9729(12)	4200(5)	31(2)	327(21)	61(4)	−79(11)	−4(5)	−18(16)
N(1)	2695(2)	7420(7)	161(3)	22(1)	210(11)	43(3)	18(6)	10(3)	−7(9)
O(1)	3050(2)	7986(5)	2101(3)	17(1)	182(9)	42(2)	−25(5)	11(2)	−12(7)
O(2)	3931(2)	9040(7)	3463(3)	27(1)	298(12)	42(2)	−63(6)	5(3)	11(9)
C(21)	1231(3)	3822(8)	1609(4)	22(1)	178(12)	45(3)	−21(7)	13(3)	−7(10)
C(22)	1066(3)	5683(8)	1385(4)	17(1)	193(13)	38(3)	−23(6)	9(3)	−31(10)
C(23)	400(3)	6142(9)	1241(4)	20(1)	209(13)	42(3)	−24(7)	15(3)	−25(10)
C(24)	−53(3)	4825(10)	1372(5)	20(1)	282(18)	58(4)	−37(8)	8(4)	−39(14)
C(25)	120(3)	2999(10)	1610(5)	27(2)	258(17)	61(4)	−70(9)	19(4)	11(14)
C(26)	751(3)	2505(9)	1712(5)	27(2)	208(14)	51(4)	−38(8)	6(4)	21(12)
C(27)	1882(3)	3205(9)	1746(4)	26(2)	161(12)	50(3)	−2(8)	7(4)	−8(11)
C(28)	3008(3)	3120(9)	1932(5)	24(2)	146(12)	87(5)	33(8)	11(4)	17(13)
C(29)	3449(4)	3500(11)	1221(6)	28(2)	256(19)	114(7)	49(10)	33(6)	11(19)
C(30)	3314(4)	3651(13)	2905(6)	31(2)	335(24)	91(6)	58(12)	−19(6)	27(19)
C(31)	−402(3)	8408(12)	757(5)	21(2)	321(20)	67(4)	31(10)	13(4)	38(16)
N(2)	2396(2)	4115(7)	1685(4)	19(1)	158(10)	57(3)	7(6)	9(3)	−6(9)
O(3)	1481(2)	6980(6)	1296(3)	18(1)	167(9)	62(2)	17(5)	17(2)	4(8)
O(4)	265(2)	7920(6)	993(3)	19(1)	225(11)	76(3)	17(5)	12(3)	13(9)

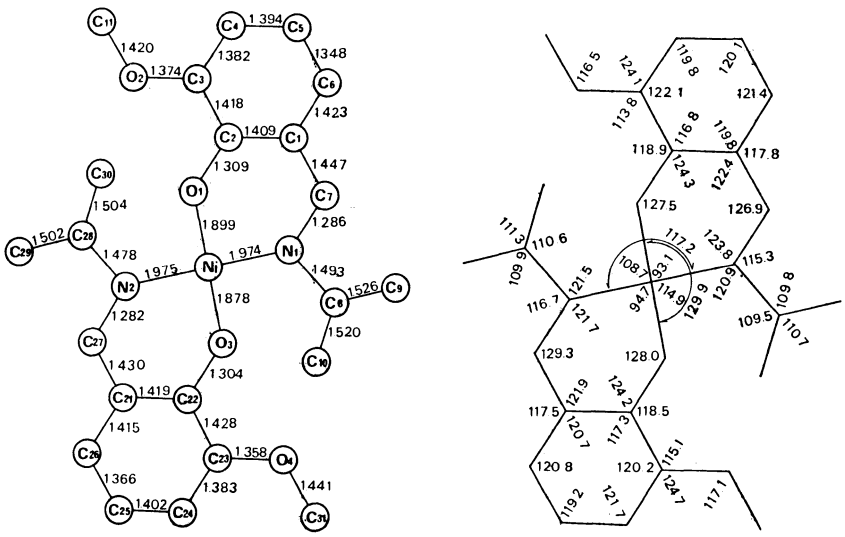

Fig. 1. Ni(3-CH_3O-SAL·*i*-C_3H_7)$_2$: bond distances and angles. The e.s.d.'s of the distances and angles among C, N, and O are 0.004—0.014 Å, and 0.2—0.8°, respectively.

refinements were attempted, because too much CPU time was needed, and also the higher accuracies seemed to be of less importance for this crystal. The parameters are listed in Table 4. The e.s.d.'s of the distances and angles are 0.01—0.035 Å and 0.5—2°, respectively. Only the mean values of the distances and angles of the chemically equivalent bonds are shown in Fig. 3. The ORTEP drawing is shown in Fig. 4.

Table 3. Ni(3-CH_3O-SAL·*i*-$C_3H_7)_2$: the positional parameters of the hydrogen atoms ($\times 10^3$)

	x	*y*	*z*		*x*	*y*	*z*
H(1)	500	1028	287	H(21)	−50	515	123
H(2)	523	1032	133	H(22)	−27	217	169
H(3)	435	934	0	H(23)	90	132	194
H(4)	340	839	−51	H(24)	192	190	188
H(5)	259	723	−134	H(25)	284	170	184
H(6)	145	837	−167	H(26)	321	316	61
H(7)	147	821	−34	H(27)	359	490	123
H(8)	193	973	−88	H(28)	380	277	130
H(9)	183	497	−141	H(29)	297	354	333
H(10)	246	435	−67	H(30)	336	479	302
H(11)	165	501	−19	H(31)	376	322	305
H(12)	452	1110	406	H(32)	−67	739	19
H(13)	417	967	479	H(33)	−63	826	130
H(14)	482	882	422	H(34)	−42	973	51

The average e. s. d. of the parameters is 0.075 Å.

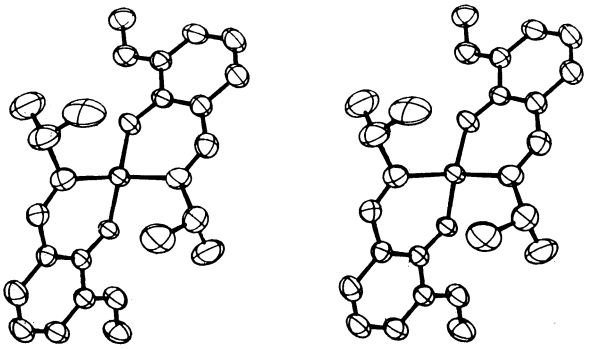

Fig. 2. Ni(3-CH_3O-SAL·*iso*-$C_3H_7)_2$: ORTEP drawing of a molecule, thermal ellipsoids are drawn at 50% probability level.

Table 4. Co(3-CH_3O-SAL·*i*-$C_3H_7)_2$: the atomic coordinates ($\times 10^4$), isotropic temperature factors (Å$^2\times 10$) and their e. s. d.

	x	*y*	*z*	*B*		*x*	*y*	*z*	*B*
Molecule A					Molecule B				
Co(A)	1863(1)	223(3)	1253(2)	*	Co(B)	3289(1)	2246(3)	6510(2)	*
N(1A)	1628(5)	−1681(17)	−102(9)	37(3)	N(1B)	3533(6)	1783(18)	5190(10)	45(3)
O(1A)	2685(4)	−185(14)	1513(7)	40(2)	O(1B)	4028(5)	3767(14)	7296(8)	44(2)
O(2A)	3837(5)	−89(16)	2070(9)	54(3)	O(2B)	4964(6)	5633(18)	8654(10)	66(3)
C(1A)	2683(6)	−2305(21)	−176(11)	35(3)	C(1B)	4561(7)	3087(24)	5942(13)	48(4)
C(2A)	2974(6)	−1195(18)	815(10)	26(3)	C(2B)	4525(7)	3890(22)	6956(12)	41(3)
C(3A)	3593(7)	−1219(21)	1110(11)	37(3)	C(3B)	5052(7)	4915(23)	7673(12)	44(3)
C(4A)	3911(7)	−2217(23)	406(12)	44(3)	C(4B)	5614(9)	5105(30)	7388(16)	71(5)
C(5A)	3616(8)	−3372(24)	−562(13)	51(4)	C(5B)	5651(10)	4298(32)	6404(17)	76(5)
C(6A)	3006(7)	−3456(23)	−853(12)	43(3)	C(6B)	5147(10)	3257(32)	5643(17)	78(6)
C(7A)	2024(7)	−2533(22)	−571(12)	41(3)	C(7B)	4077(8)	2194(26)	5122(14)	57(4)
C(8A)	973(7)	−2270(24)	−699(13)	48(4)	C(8B)	3082(9)	1050(29)	4170(16)	68(5)
C(9A)	666(8)	−470(26)	−584(14)	55(4)	C(9B)	2648(12)	−574(39)	4197(21)	101(7)
C(10A)	668(11)	−3676(34)	−257(18)	83(6)	C(10B)	2727(10)	2647(31)	4058(17)	74(5)
C(11A)	4506(9)	32(28)	2401(15)	65(5)	C(11B)	5467(10)	6748(32)	9461(17)	77(5)
N(2A)	1770(5)	2986(17)	1412(9)	38(3)	N(2B)	3030(5)	102(17)	6949(9)	38(3)
O(3A)	1363(4)	9(14)	2186(7)	38(2)	O(3B)	2567(4)	3445(14)	6626(7)	39(2)
O(4A)	741(5)	−754(17)	3452(9)	59(3)	O(4B)	1613(5)	5539(16)	6683(8)	51(2)
C(21A)	998(6)	3100(20)	2430(11)	33(3)	C(21B)	2018(6)	1017(21)	7068(11)	36(3)
C(22A)	1027(6)	1305(20)	2594(11)	32(3)	C(22B)	2079(7)	2716(21)	6823(11)	37(3)
C(23A)	680(7)	949(23)	3258(12)	44(3)	C(23B)	1564(7)	3766(23)	6852(12)	46(4)
C(24A)	296(8)	2173(24)	3704(13)	50(4)	C(24B)	1036(8)	3125(25)	7066(13)	51(4)
C(25A)	257(8)	3890(27)	3482(14)	58(4)	C(25B)	999(8)	1430(25)	7295(13)	54(4)
C(26A)	597(7)	4359(23)	2875(12)	44(3)	C(26B)	1481(7)	393(24)	7282(13)	48(4)
C(27A)	1384(7)	3848(21)	1904(11)	36(3)	C(27B)	2510(6)	−157(20)	7157(11)	33(3)
C(28A)	2158(7)	4111(23)	1008(13)	47(4)	C(28B)	3450(8)	−1270(26)	7196(14)	54(4)
C(29A)	2229(9)	2898(30)	−67(16)	70(5)	C(29B)	3756(10)	−2007(32)	6288(17)	77(5)
C(30A)	2801(8)	4731(27)	1752(14)	59(4)	C(30B)	3927(10)	−142(31)	8156(16)	73(5)
C(31A)	774(12)	−838(39)	4430(21)	100(7)	C(31B)	1622(10)	5465(33)	5685(18)	81(6)

*Anisotropic temperature factors of Co ($\times 10^4$) in $\exp[-(\beta_{11}h^2+\beta_{22}k^2+\beta_{33}l^2+\beta_{12}hk+\beta_{13}hl+\beta_{23}kl)]$

	β_{11}	β_{22}	β_{33}	β_{12}	β_{13}	β_{23}
Co(A)	18(0)	184(5)	52(1)	20(3)	14(1)	50(4)
Co(B)	19(1)	200(5)	49(1)	11(3)	13(1)	47(4)

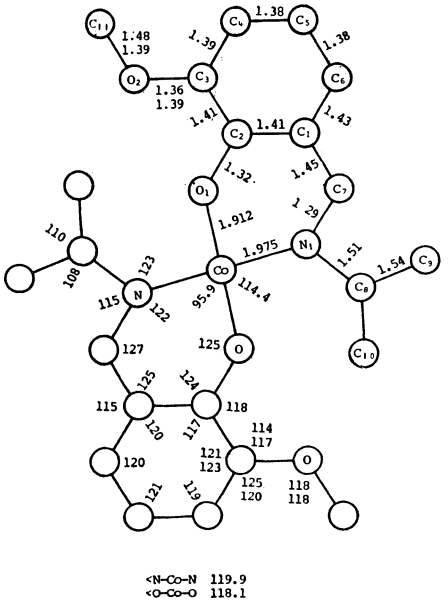

Fig. 3. Co(3-CH_3O-SAL·*i*-C_3H_7)$_2$: bond distances and angles. The mean values of the chemically equivalent bonds are shown. For the methoxy groups, the mean values in the planar methoxyphenyl groups (upper) and in the non-planar groups(lower) are shown.

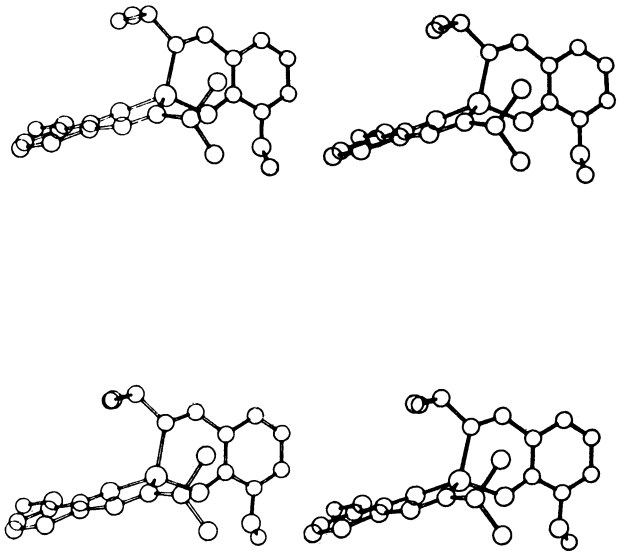

Fig. 4. Co(3-CH_3O-SAL·*i*-C_3H_7)$_2$: ORTEP drawing of molecules A (top) and B (bottom).

Molecular Structure

The molecular stucture of the present Ni complex, except for the methoxy group, is nearly identical with that of bis[*N*-isopropylsalicylaldiminato]nickel(II),[10] and no appreciable difference in the shapes and sizes is found between the two complexes. In the crystal of the Co complex two crystallographically independent molecules, A and B, have almost the same stucture, which bears also close resemblance to those of the two Ni complexes.

The tetrahedral coordination of the Ni(II) and Co(II) ions is thus confirmed. Although the distortions from the ideal tetrahedral form are large owing to the formations of the chelate rings, the distortion in the Co complex is a little smaller than that in the Ni complex. This finding agrees with the expectation of the simple crystal field theory.

Each molecule is characterized by several planar groups, of which details are listed in Tables 5 and 6. In any molecule two salicylideneamine planes intersect nearly at right angle with each other, the dihedral angles being 87, 87, and 79° for the Co(A), Co(B), and Ni complexes, respectively. The angle in bis-[*N*-isopropylsalicylaldiminato]nickel(II) is 82°.[10] The variation in the dihedral angles reflects the magnitudes of the distortions from the ideal tetrahedral coordi-

Table 5. Ni(3-CH_3O-SAL·*i*-C_3H_7)$_2$: Best planes
Planes I and II: each half of the molecule.
Planes III and IV: isopropyl groups.

(a) Equations* $lX+mY+nZ=p$

	l	m	n	p
I	0.3658	−0.9287	0.0610	−2.9432
II	0.0692	−0.2393	−0.9685	−2.7385
III	−0.1626	0.0013	0.9867	−1.8904
IV	−0.3664	0.9199	−0.1400	−0.4790

* $X=ax+cz\cos\beta$, $Y=by$, $Z=cz\sin\beta$

(b) Dihedral angles (°)

	II	III	IV
I	79.1	90.0	4.6
II		14.7	83.7
III			85.6

(c) Displacements from planes (×10^3 Å)

Plane I		Plane II	
C (1)	3	C (21)	13
C (2)	−26	C (22)	−22
C (3)	−24	C (23)	3
C (4)	21	C (24)	−18
C (5)	33	C (25)	−7
C (6)	34	C (26)	28
C (7)	−36	C (27)	25
C (8)	−100	C (28)	−55
N (1)	25	N (2)	27
O (1)	−63	O (3)	−62
O (2)	−80	O (4)	19
Ni	239	Ni	52
C (11)*	−182	C (31)*	166

* Not included in the estimations of the equations.

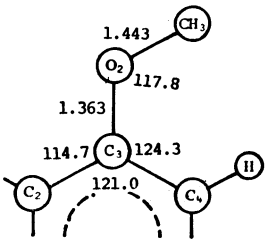

Fig. 5. The bond distances (Å) and angles (°) for the methoxy groups in the planar methoxyphenyl groups reported so far.

nation. The metal ions are slightly out of the chelate ring planes by 0.05—0.23 Å. The isopropyl group plane is nearly perpendicular to the chelate ring to which it is attached.

The phenyl groups show a common interesting feature, that is, the three C–C bonds nearest to the metal ion, C(1)–C(2), C(2)–C(3), C(1)–C(6) and their equivalents, are longer than the three farthest C–C bonds, C(3)–C(4), C(4)–C(5), C(5)–C(6) and their equivalents. This feature has been also found in several related compounds,[11] and may be explained by the presences of significant double bond characters in the exocylclic C(2)–O(1), C(1)–C(7) and their equivalents, although the shortenings of the farthest bonds may be partly due to the thermal vibration of the molecules.

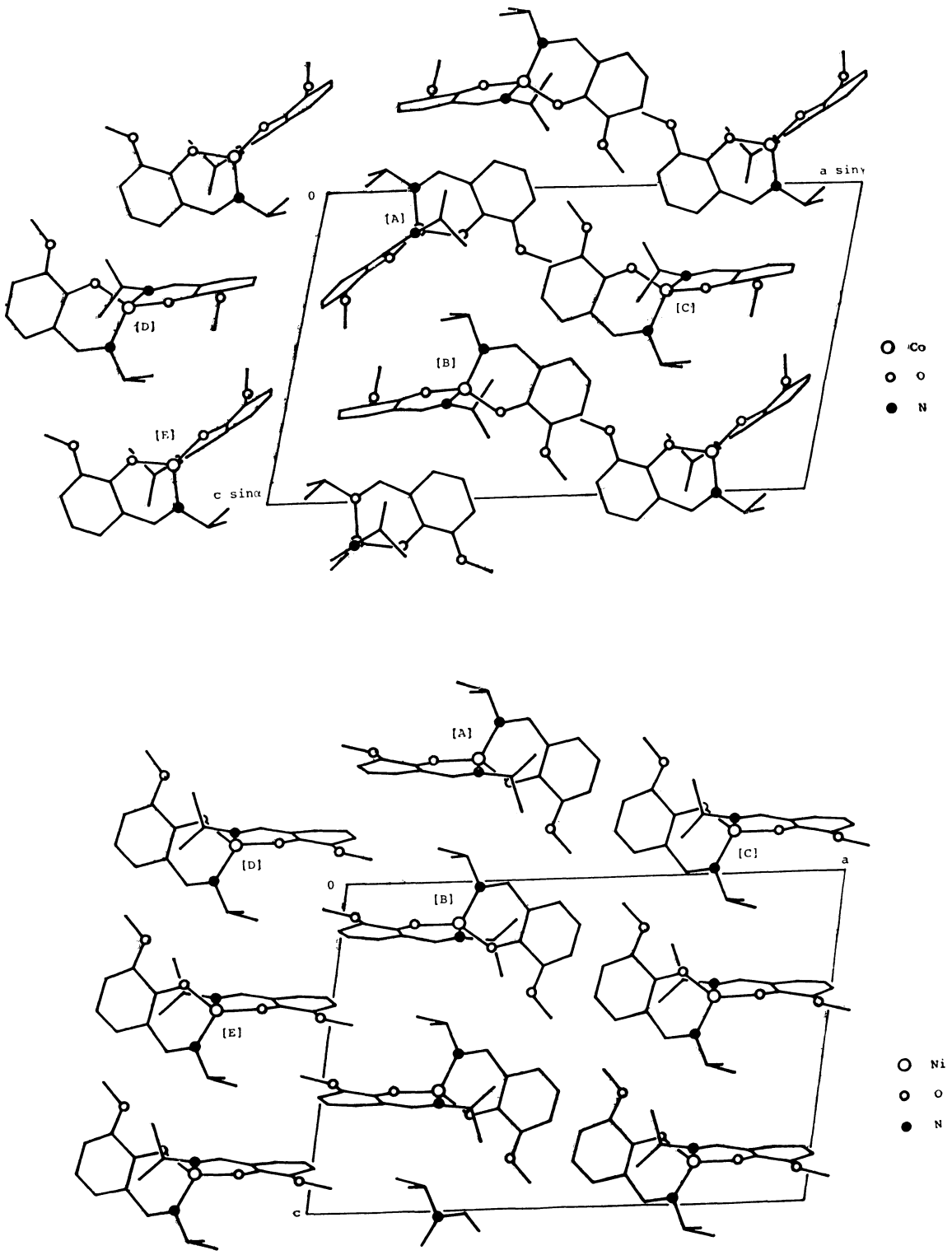

Fig. 6. The crystal structures viewed along the *b* axes; top, Co complex; bottom, Ni complex.

TABLE 6. Co(3-CH_3O-SAL·*i*-C_3H_7)$_2$: BEST PLANES
Planes I and II: each half of the molecule.
Planes III and IV: isopropyl groups.

(a) Equations* $lX+mY+nZ=p$

	l	m	n	p
Molecule A				
I	0.1557	0.9269	−0.3414	−0.5049
II	−0.5632	−0.1421	−0.8141	−3.7144
III	−0.4273	−0.1659	−0.8888	−0.0197
IV	−0.0991	−0.9634	0.2491	−2.5999
Molecule B				
I	−0.2537	0.9588	−0.1282	−3.5352
II	−0.1262	−0.2215	−0.9670	−8.8492
III	0.0620	−0.0763	−0.9952	−5.0049
IV	−0.1378	0.9654	−0.2216	−6.9555

* orthogonal coordinate system in Å unit, X along the a axis, Y in the ab plane

(b) Dihedral angles (°)

	Molecule A			Molecule B		
	II	III	IV	II	III	IV
I	86.6	85.2	6.6	86.8	87.8	8.6
II		9.0	89.4		13.8	89.0
III			88.9			82.4

(c) Displacements from planes (×10^3 Å)

Plane I			Plane II		
Molecule	A	B	Molecule	A	B
C (1)	52	−53	C (21)	84	43
C (2)	13	2	C (22)	44	38
C (3)	−50	52	C (23)	−62	−13
C (4)	−19	18	C (24)	−54	−6
C (5)	9	−57	C (25)	56	11
C (6)	−1	−109	C (26)	112	51
C (7)	22	22	C (27)	−10	−15
C (8)	−56	282	C (28)	−240	−154
N (1)	35	4	N (2)	−8	33
O (1)	−36	18	O (3)	70	9
O (2)	−66	94	O (4)	−177	−113
Co	185	−231	Co	227	122
C (11)*	−45	175	C (31)*	−1064	1035

* Not included in the estimations of the equations.

The only distinct difference in the molecular structures of the present complexes exist in the methoxy groups. In the Ni complex the methoxy group is coplanar with the phenyl plane to which it is attached. In the Co complexes, one methoxy group is coplanar with the pheny plane, but the other sticks out nearly perpendicularly from the phenyl plane. As shown in Figs. 4 and 6, the orientations of the latter methoxy groups are opposite in the two molecules, A and B.

To our knowledge, the methoxyphenyl group is usually planar, because the planar stucture with a larger conjugate system is usually more stable than the non-planar stucture with a smaller conjugate system. The present Co complex gives a unique example of the non-planar methoxyphenyl group. The bond distances and angles are affected seriously by the orientations of the methoxy groups. The mean values of the bond distances and angles in each of the planar and non-planar structures in the Co complex are shown in Fig. 3, while those for the planar structures reported so far[12] are shown in Fig. 5. In the planar structures the repulsion between the methyl group and the peri-hydrogen atom of C(4) makes the O(2)–C(3)–C(4) angle significantly larger than 120°. The inequality in two bond distances of O(2)–CH_3 and O(2)–C(3) is also characteristic of the planar stucture. The latter bond is shorter than usual O–C single bond. In the non-planar structure the O(2)–C(3)–C(4) angle decreases to the normal value, and the inequality in the two C–O bond distances disappears.

Crystal Structure

The crystal structures viewed along the b axes are compared in Fig. 6. As was expected from the similarity in the unit cell dimensions, two crystals are isostructural in a very rough comparison. The orientations of the Co complexes A and B are not so different from those of the Ni complexes A and B which are related by a c glide plane. The packing schemes in the crystals are also similar to each other. Therefore, the intermolecular potential energies due to the van der Waals forces seem to be almost equal in the two crystals. The difference, however, is singificant, and seems to be in entropy. The crystal of the Ni complex is in a highly ordered state with smaller entropy, while the crystal of the Co complex is in a less ordered state with larger entropy.

The authors express their sincere thanks to Miss Sachiko Bando and Mr. Ken-ichi Sakaguchi for their kind assistance in the experiments.

References

1) A. Takeuchi and S. Yamada, *Bull. Chem. Soc. Jpn.*, **42**, 3046 (1969).
2) N. Arai, M. Sorai, and S. Seki, *Bull. Chem. Soc. Jpn.*, **45**, 2398 (1972).
3) E. Yoshida and S. Yamada, *Bull. Chem. Soc. Jpn.*, **40**, 1395 (1967).
4) A. Takeuchi and S. Yamada, *Bull. Chem. Soc. Jpn.*, **43**, 3628 (1970).
5) All the programs used are in "UNICS-Osaka" system, The computation Center, Osaka University (1973).
6) "International Tables for X-Ray Crystallography," Vol. III, Kynoch Press, Birmingham (1962).
7) L. Pauling, "The Nature of the Chemical Bond," 3rd ed, Cornell University Press, Ithaca (1960).
8) The observed and calculated structure factors are available at the office of This Bulletin as Document No. 7635.
9) C. K. Johnson, "ORTEP," Report ORNL-3794, Oak Ridge National Laboratory, Tennessee (1965).
10) M. R. Fox, P. L. Orioli, E. C. Lingafelter, and L. Sacconi, *Acta Crystallogr.*, **17**, 1159 (1964).
11) For example, R. M. Kirchner, G. D. Andreetti, D. Barnhart, F. D. Thomas II, D. Welsh, and E. C. Lingafelter, *Inorg. Chim. Acta*, **7**, 17 (1973).
12) The mean values were obtained from the following 11 structures: present Ni complex, 2 structures; *o*-methoxybenzenediazonium chloride·ferric chloride, T. N. Polynova, N. G. Bokii, and M. A. Porai-Koshits, *Zh. Strukt. Khim.*,

6, 841 (1965); 2-(*p*-methoxyphenyl)-3,4-dibenzyl-1,3,4-thiazolidine-5-thione, I. L. Karle and J. Karle, *Acta Crystallogr.*, **19**, 92 (1965); *p*-methoxyindophenol *N*-oxide, C. Romers and B. Hesper, *ibid.*, **20**, 162 (1966); α-5-(2-chloroethoxy)-*o*-benzoquinone 2-oxime, J. W. L. van Oijen and C. Romers, *ibid.*, **20**, 169 (1966); β-5-propoxy-*o*-benzoquinone 2-oxime, C. Romers *ibid.*, **17**, 1287 (1964); diaquabis(*p*-methoxyphenoxyacetato) copper(II) dihydrate, and anhydrate, K. Prout, P. J. Grove, B. D. Harridine, and F. J. C. Rossotti, *ibid.*, **B31**, 2047 (1975); propyl *p*-(*p*-methoxybenzylideneamino)-α-methylcinnamate, M. Cotrait, D. Sy, and M. Ptak, *ibid.*, **B31**, 1869 (1975); 7-benzylideneamino-7-methoxycarbonyl-4-(*p*-methoxybenzyloxycarbonyl)-Δ^3-cephem, E. F. Paulus, *ibid.*, **B30**, 2918 (1974).

Stereochemistry and Reactivity of Metal–Schiff-base Complexes. I. Preparation and Thermodynamic Stereoselectivity of Mixed Ligand Cobalt(III) Complexes Containing *N,N'*-Ethylenebis(salicylideneamine) Dianion (sal_2en) or *N,N'*-Ethylenebis(7-methylsalicylideneamine) Dianion (7,7'-Me-sal_2en) and L-Amino Acid Anion

Yuki FUJII, Takashi ISAGO, Mitsuo SANO, Noriko YANAGIBASHI, Shigeru HIRASAWA, and Sozo TAKAHASHI*

Department of Chemistry, Faculty of Science, Ibaraki University, Bunkyo-cho, Mito, Ibaraki 310

**Department of Chemistry, Ibaraki Technical College, Nakane, Katsuta, Ibaraki 312*

(Received May 11, 1976)

Two series of new mixed ligand cobalt (III) complexes with the general formulas of [Co(sal_2en)(L-aa)] and [Co(7,7'-Me-sal_2en)(L-aa)] (where L-aa=anion of L-ala, L-val, L-leu, L-isoleu, L-met, L-thr, L-phe, L-tyr, or L-trp) have been prepared and characterized. All are labile for both isomerization and substitution reactions and each exists in an equilibrium mixture of Λ_L- and Δ_L-*cis*-β_1(fac)-isomers ($\Lambda_L > \Delta_L$) in methanol. The isomer's ratios, Λ_L/Δ_L, were estimated from their PMR spectra, and the following facts were found: The increasing order of the ratios is L-ala∼L-met∼L-leu<L-val<L-isoleu<L-thr<L-phe∼L-tyr<L-trp, and the ratios are larger in 7,7'-Me-sal_2en-complexes than in sal_2en-complexes for each amino acid.

Many studies have been undertaken about the steroselectivity in inert cobalt(III) complexes. However, it is often difficult to distinguish between kinetic and thermodynamic stereoselectivities in the inert cobalt(III) complexes.[1-9] On the other hand, it is well known that mixed ligand cobalt(III) complexes containing Schiff-bases are generally substitution labile.[10-15] Since the origin of the stereoselectivity in labile complexes is thought to be thermodynamic, a study of the stereoselectivity of the mixed ligand cobalt(III)–Schiff-base complexes is very interesting. Another interest is from the stereochemical viewpoint. That is, as shown in Fig. 1, the steric stucture of *cis*-β-[Co(sal_2en)(acac)] is extremely distorted as compared with those of the usual cobalt(III) complexes.[16-19] Especially, chelates A and C are so close that an intramolecular steric interaction is expected between them. Therefore, if an optically active bidentate ligand coordinates at the site of the chelate C, such a complex may show high stereoselectivity. In this paper, we report the preparation, the properties and the thremodynamic stereoselectivity of the mixed ligand cobalt(III) complexes containing sal_2en or 7,7'-Me-sal_2en as a Schiff-base ligand and L-amino acid anion.

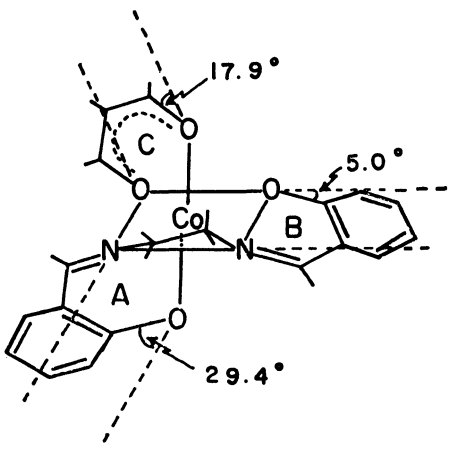

Fig. 1. The distorted chelate skeleton in [Co(sal_2en)(acac)].[17] ---- shows the normal bond direction.

Experimental

Preparation of the Complexes. All the complexes were synthesized from [Co(sal_2en)][20] or [Co(7,7'-Me-sal_2en)][21] and amino acids by air oxidation.

1) Co(III)-sal_2en Series Complexes: Amino acid (0.015 mol) partially dissolved in 25 ml of water was added to a suspension of [Co(sal_2en)] (5.0 g, 0.015 mol) in 130 ml of methanol. In the cases of L-ala, L-val, and L-asp, the amino acid solution was partially neutralized with KOH (0.2 g for L-ala and L-val, 0.5 g for L-asp). The mixture was stirred vigorously in open air at room temperature for the time periods listed in Table 1. The unreacted materials were then removed by filtration, and a brownish green solution was obtained. The methods for isolation and purification of the crude product are as follows.

i) [Co(sal_2en)(gly)], [Co(sal_2en)(L-isoleu)], [Co(sal_2en)(L-met)], [Co(sal_2en)(L-ser)], and [Co(sal_2en)(L-asp)]: The brownish green solution was concentrated to about a half volume at room temperature and to this solution was added water (100 ml). Chloroform (80 ml, twice) was then added and the complex was extracted. Concentrating the solution to a small volume (about 40 ml for gly, L-met, and L-asp) or to dryness (for L-ser and L-isoleu) at room temperature, a green product was obtained. It was recrystallized from methanol–acetone–water (10 : 2 : 1) for gly and L-isoleu or from chloroform for L-met, L-ser, and L-asp. Green crystals were obtained except for L-isoleu (powder).

ii) [Co(sal_2en) (L-ala)], [Co(sal_2en)(L-val)], and [Co(sal_2en)(L-leu)]: Upon concentrating the brownish green solution to about 30 ml under reduced pressure at room temperature, green crystals were deposited. They were recrystallized from methanol–acetone–water (10 : 2 : 1) for L-ala and L-val or from methanol containing 0.1% (gravimetric) KOH for L-leu.

iii) [Co(sal_2en) (L-thr)], [Co(sal_2en)(L-phe)], and [Co(sal_2en)(L-trp)]: Concentrating the brownish green solution to a half or one third volume at room temperature, a green product was obtained. It was recrystallized from methanol for L-thr and L-trp or from methanol–acetone–water (10 : 2 : 1) for L-phe.

iv) [Co(sal_2en) (L-tyr)]: After concentrating the brownish green solution to about a half volume, water (300 ml) and

chloroform (100 ml) were added. The water layer was concentrated to about 100 ml at 50 °C under reduced pressure. The green powder thus obtained was purified by dissolving it in chloroform, followed by filtration and concentration to dryness.

The yields are summarized in Table 1 and the analytical data are listed in Table 2.

2) Co(III)-7,7'-Me-sal$_2$en Series Complexes: Amino acid (0.017 mol) partially dissolved in 50 ml of water was added to a suspension of [Co(7,7'-Me-sal$_2$en)] (5.0 g, 0.014 mol) in 200 ml methanol. The mixture was stirred vigorously in open air for about 3 h at room temperature. In the case of L-tyr, the reaction was continued for a day. After filtration of the solution, the green solution thus obtained was concentrated to a small volume (50—100 ml). Green crystals were obtained and recrystallized from methanol. In the cases of L-leu and L-ser, their complexes were recrystallized from acetone and *N,N*-dimethylformamide, respectively. Yields, 60—90%. The anal. data are listed in Table 2.

In both series of complexes, L-ser- and L-asp-complexes are hardly soluble in methanol. Therefore, we did not measure their AB, CD, and PMR spectra. The IR spectra of all the complexes showed asym. ν(COO) at about 1625—1635 cm^{-1}.

Measurements. The electronic absorption spectra were

Table 1. Abbreviations of amino acids and preparative conditions for [Co(sal$_2$en)(L-aa)] complexes

Amino acid	Abbreviation	Reaction time[b] (h)	Solvent for recrystallization	Yield (%)
Glycine	gly	1	Methanol-acetone-water (10 : 2 : 1)	10
L-Alanine	L-ala	2.5	Methanol-acetone-water (10 : 2 : 1)	25
L-Valine	L-val	1	Methanol-acetone-water (10 : 2 : 1)	10
L-Leucine	L-leu	1	Methanol containing 0.1% KOH	10
L-Isoleucine	L-isoleu	2.5	Methanol-acetone-water (10 : 2 : 1)	10[a]
L-Methionine	L-met	0.5	Chloroform	25
L-Serine	L-ser	1	Chloroform	13
L-Threonine	L-thr	0.5	Methanol	10[a]
L-Phenylalanine	L-phe	2.5	Methanol-acetone-water (10 : 2 : 1)	20
L-Tyrosine	L-tyr	24	Chloroform	10
L-Triptophan	L-trp	0.5	Methanol	30
L-Aspartic acid	L-asp	1	Chloroform	10

a) Obtained as a powder. b) Longer reaction time produces brown complex.

Table 2. Elemental analyses data

Number	Complex	C (%)		H (%)		N (%)	
		Found	(Calcd)	Found	(Calcd)	Found	(Calcd)
1	[Co(sal$_2$en)(gly)]·2H$_2$O	50.04	(49.66)	5.17	(5.09)	9.74	(9.65)
2	[Co(sal$_2$en)(L-ala)]·3H$_2$O	48.87	(48.83)	5.50	(5.61)	9.15	(9.00)
3	[Co(sal$_2$en)(L-val)]·2H$_2$O	52.92	(52.80)	6.01	(5.91)	8.92	(8.80)
4	[Co(sal$_2$en)(L-leu)]·2.5H$_2$O	52.61	(52.80)	6.26	(6.24)	8.58	(8.40)
5	[Co(sal$_2$en)(L-isoleu)]·H$_2$O	56.03	(55.82)	6.04	(5.96)	8.78	(8.88)
6	[Co(sal$_2$en)(L-met)]·2CHCl$_3$	39.00	(38.78)	3.80	(3.68)	5.67	(5.90)
7	[Co(sal$_2$en)(L-ser)]·2CHCl$_3$	38.07	(37.78)	3.44	(3.32)	6.32	(6.29)
8	[Co(sal$_2$en)(L-thr)]·H$_2$O	52.08	(52.07)	5.42	(5.24)	9.17	(9.11)
9	[Co(sal$_2$en)(L-aspH)]	52.31	(52.53)	4.45	(4.41)	9.08	(9.19)
10	[Co(sal$_2$en)(L-phe)]·4.5H$_2$O	52.45	(52.63)	5.52	(5.83)	7.44	(7.34)
11	[Co(sal$_2$en)(L-tyr)]·CHCl$_3$	49.39	(49.19)	3.92	(4.03)	6.88	(6.73)
12	[Co(sal$_2$en)(L-trp)]·3.5H$_2$O	53.31	(53.38)	5.47	(5.31)	9.20	(9.22)
13	[Co(7,7'-Me-sal$_2$en)(gly)]·3H$_2$O	49.77	(49.90)	5.89	(5.86)	8.69	(8.73)
14	[Co(7,7'-Me-sal$_2$en)(L-ala)]	56.94	(57.15)	5.62	(5.48)	9.61	(9.52)
15	[Co(7,7'-Me-sal$_2$en)(L-val)]·2H$_2$O	54.71	(54.65)	6.27	(6.38)	8.40	(8.31)
16	[Co(7,7'-Me-sal$_2$en)(L-leu)]·2H$_2$O	55.52	(55.49)	6.53	(6.60)	8.25	(8.09)
17	[Co(7,7'-Me-sal$_2$en)(L-isoleu)]·1.5H$_2$O	56.30	(56.45)	6.77	(6.52)	8.24	(8.23)
18	[Co(7,7'-Me-sal$_2$en)(L-met)]·2H$_2$O	51.73	(51.39)	6.31	(6.00)	7.45	(7.82)
19	[Co(7,7'-Me-salen)(L-ser)]	54.98	(55.15)	5.43	(5.29)	9.11	(9.19)
20	[Co(7,7'-Me-sal$_2$en)(L-thr)]·3.5H$_2$O	49.60	(49.44)	5.89	(6.22)	7.63	(7.86)
21	[Co(7,7'-Me-sal$_2$en)(L-aspH)]·0.5H$_2$O	53.72	(53.45)	5.21	(5.10)	8.36	(8.50)
22	[Co(7'7'-Me-sal$_2$en)(L-phe)]·2.5H$_2$O	57.65	(57.65)	6.02	(5.91)	7.60	(7.47)
23	[Co(7'7'-Me-sal$_2$en)(L-tyr)]·2.5H$_2$O	56.17	(56.06)	5.78	(5.75)	7.00	(7.26)
24	[Co(7,7'-Me-sal$_2$en)(L-trp)]·2H$_2$O	57.40	(57.24)	5.34	(5.46)	9.05	(9.21)

measured with a Hitachi EPS-3 Spectrophotometer. The CD spectra were recorded with a JASCO J-20 Automatic Recording Spectropolarimeter. Optical rotations at 435 nm were recorded with a JASCO DIP-180 Automatic Polarimeter. The IR spectra were recorded with a Hitachi EPI-S2 Spectrometer in KBr pellets. The PMR spectra were measured with a Hitachi R-20 Spectrometer (60 MHz) at 35 °C in CD_3OD by using TMS as the internal reference.

Results and Discussion

Properties of the Complexes. All the complexes except for the gly-complexes **1** and **13** exhibit mutarotations in methanol; the data are summarized in Table 3. Some representative mutarotations are shown in Fig. 2. It is seen that there are two patterns of mutarotation; one is for the complexes **2**—**6**, **14**—**16**, **20**, **22**, and **23**, which show quite small rotations soon after dissolution but show large $(-)_{435}$-rotations at equilibrium conditions, The other is for the complexes **8**, **10**, **12**, **17**, **18**, and **24**, which show quite large $(-)_{435}$-rotations soon after dissolution but decrease their magnitudes at equilibrium conditions. As mentioned later, each of the complexes exists as only *cis*-β_1(fac)-geometrical isomer in methanol. Therefore, the mutarotations correspond to the isomerization reaction between $(-)_{435}$- and $(+)_{435}$-isomers. The plots of $\log(\alpha_\infty-\alpha_t)$ *vs.* time give linear relations. Accordingly, the observed isomerization rates, k_{obsd}, can be estimated as listed in Table 3. Since the following equilibrium reaction is thought to occur in solution,

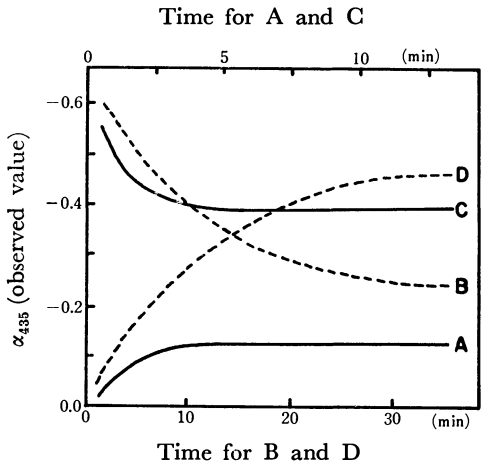

Fig. 2. The representative mutarotations of the complexes in methanol at 25 °C. A: [Co(sal$_2$en)(L-met)], B: [Co(7,7′-Me-sal$_2$en)(L-met)], C: [Co(sal$_2$en)(L-phe)], D: [Co(7,7′-Me-sal$_2$en)(L-phe)].

$(+)_{435}$-isomer $\underset{k_{-1}}{\overset{k_{+1}}{\rightleftharpoons}}$ $(-)_{435}$-isomer, the isomerization rate constants from $(+)_{435}$-isomer to $(-)_{435}$-isomer, k_{+1}, and from $(-)_{435}$-isomer to $(+)_{435}$-isomer, k_{-1}, are written by $k_{+1}=2.303[S/(S+1)]k_{obsd}$ and $k_{-1}=2.303[1/(S+1)]k_{obsd}$ respectively, where S is the stereoselectivity in each complex at the equilibrium condition, $S=(-)_{435}$-isomer/$(+)_{435}$-isomer.[22] The estimated rate constants, k_{+1} and k_{-1}, are also listed in Table 3. It is seen that the isomerization rates are fairly rapid,

Table 3. Mutarotation at 435 nm of the complexes in methanol (T=25 °C)

Amino acid and number of complex	Concentration of the soln. (mol l^{-1}) $\times10^3$	α_{435} with 1 cm cell (° cm^{-1}) (soon after dissolution)[a]	α_{435} with 1 cm cell (° cm^{-1}) (at equilibrium condition)	$[M]^{25}_{435}$ at equilibrium condition (° m^{-1} mol l^{-1})	Isomerization rate, k_{obsd} (s^{-1})	Isomerization rate constants (s^{-1}) k_{+1} ($\Delta\rightarrow\Lambda$),	k_{-1} ($\Lambda\rightarrow\Delta$)
[Cosal$_2$en)(L-Amino acid anion)] Complex							
L-ala (2)	1.70	+0.038	−0.109	−6400	1.7×10^{-2}	2.4×10^{-2}	1.6×10^{-2}
L-val (3)	1.63	+0.028	−0.110	−6700	1.3×10^{-2}	1.8×10^{-2}	1.2×10^{-2}
L-leu (4)	1.61	+0.033	−0.117	−7300	1.4×10^{-2}	1.9×10^{-2}	1.3×10^{-2}
L-isoleu (5)	1.74	−0.007	−0.140	−8000	1.1×10^{-2}	1.5×10^{-2}	1.0×10^{-2}
L-met (6)	1.24	+0.016	−0.119	−9600	1.3×10^{-2}	1.8×10^{-2}	1.2×10^{-2}
L-thr (8)	1.50	−0.736	−0.440	−29300	8.5×10^{-3}	1.6×10^{-2}	3.9×10^{-3}
L-phe (10)	1.34	−0.657	−0.375	−28000	1.4×10^{-2}	2.6×10^{-2}	6.3×10^{-3}
L-tyr (11)	1.27	−0.311[b]	−0.382	−30100	1.4×10^{-2}	2.7×10^{-2}	5.6×10^{-3}
L-trp (12)	1.28	−0.549	−0.482	−37700	8.4×10^{-3}	1.7×10^{-2}	2.1×10^{-3}
[Co(7,7′-Me-sal$_2$en)(L-Amino acid anion)] Complex							
L-ala (14)	1.68	+0.019	−0.215	−12800	1.0×10^{-3}	1.5×10^{-3}	7.5×10^{-4}
L-val (15)	1.59	+0.011	−0.335	−21100	1.7×10^{-3}	2.6×10^{-3}	1.0×10^{-3}
L-leu (16)	1.61	−0.036	−0.227	−14100	1.0×10^{-3}	1.5×10^{-3}	7.5×10^{-4}
L-isoleu (17)	1.56	−0.677	−0.313	−20100	1.6×10^{-3}	2.7×10^{-4}	9.7×10^{-4}
L-met (18)	1.56	−0.649	−0.223	−14300	1.4×10^{-3}	2.2×10^{-3}	1.1×10^{-3}
L-thr (20)	1.50	+0.033	−0.453	−30200	8.0×10^{-4}	1.5×10^{-3}	2.8×10^{-4}
L-phe (22)	1.39	+0.021	−0.445	−32000	1.6×10^{-3}	3.3×10^{-3}	3.5×10^{-4}
L-tyr (23)	1.36	+0.008	−0.515	−37900	1.5×10^{-3}	3.1×10^{-3}	3.3×10^{-4}
L-trp (24)	1.29	−0.606	−0.540	−41900	1.2×10^{-3}	2.6×10^{-3}	1.6×10^{-4}

a) Estimated value from k_{obs} by extrapolating to time=0; this value contains some error because it takes a few minutes to dissolve the complex in methanol, the + or − rotation is perhaps due to the error and/or the vicinal effect of the coordinated amino acid. b) This complex shows medium $(-)_{435}$-rotation soon after dissolution by exception.

as compared with those of the usual cobalt(III) complexes.[23] As the complexes easily isomerize to establish equilibrium conditions in methanol with $(-)_{435}$-rotations, the stereoselectivity in these complexes at equilibrium conditions is thermodynamic in origin, and $(-)_{435}$-isomers are more stable than $(+)_{435}$-isomers.

It should be noted that the complexes are labile not only for the isomerization reaction mentioned above but also for the substitution reaction of the coordinated amino acid anion. For example, the substitution rate, k_{obsd}, in the following reaction in methanol is observed to be 2.2×10^{-2} s^{-1} mol l^{-1} at 25 °C:

[Co(7,7′-Me-sal$_2$en)(L-phe)] + D-phe$^-$
$\longrightarrow$ [Co(7,7′-Me-sal$_2$en)(D-phe)] + L-phe$^-$

From the above mutarotations and the time dependnt PMR spectra mentioned later, the following facts become clear that the complexes **2**—**6**,**14**—**16**, **20**, **22**, and **23** are isolated each as an 1 : 1 mixture of $(-)_{435}$-and $(+)_{435}$-isomers, but the complexes **8**, **10**, **12**, **17**, **18**, and **24** are isolated each as a pure $(-)_{435}$-isomer. The discrepancy of the composition of the two isomers between the solid state and solution is perhaps due to the solubility of the complexes. That is, when the isomerization is rapid, only the least soluble isomer may be preferentially isolated.

Structure of the Complexes. Figure 3 shows representative AB and CD spectra of the complexes at equilibrium conditions. All the AB and CD spectral data are summarized in Tables 4 and 5.

All the complexes reveal nearly the same AB spectra and very similar CD spectra at equilibrium conditions.

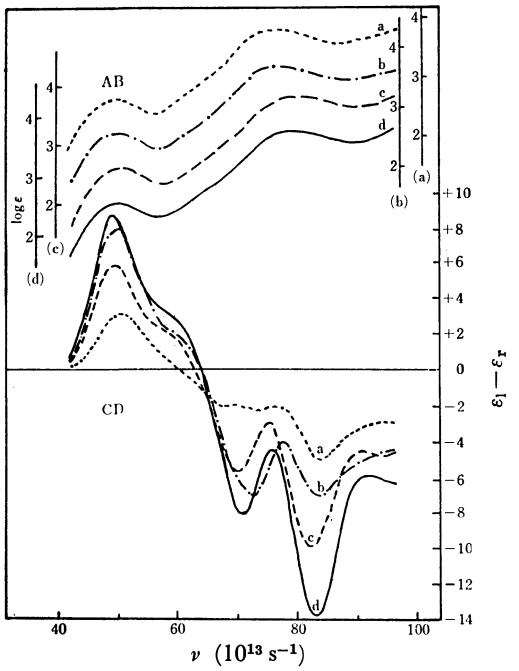

Fig. 3. The representative AB and CD spectra of the complexes in methanol at equilibrium conditions. a: [Co(sal$_2$en) (L-val)], b: [Co(sal$_2$en) (L-phe)], c: [Co(7,7′-Me-sal$_2$en) (L-val)], d: [Co(7,7′-Me-sal$_2$en) (L-phe)]. (a), (b), (c), and (d) are log ε value for the corresponding complexes.

The AB spectra soon after dissolution are also nearly the same as those at the equilibrium conditions in all the complexes. Therefore, these results suggest that 1) $(-)_{435}$- and $(+)_{435}$-isomers in each complex have the same geometrical configuration and 2) the geometrical configuration is the same for all the complexes. It is known that *cis*-α-structure is unstable in cobalt(III)–Schiff-base complexes and the existence of such a complex has not yet been found.[16,19] On the other hand, the *cis*-β-structure is well known.[16-21] Therefore, all the complexes may take either *cis*-β_1(*fac*)- or *cis*-β_2(*mer*)-structure. Another experiment[24] shows that [Co(sal$_2$-(*S*,*S*)-chxn(aa)] complex (where sal$_2$-(*S*,*S*)-chxn indicates the dianion of (1*S*,2*S*) - *N*,*N*′ - 1,2 - cyclohexylenebis (salicylideneamine) and aa, amino acid anion) takes stereoselectively the Λ-*cis*-β-structure with a large $(-)_{435}$-rotation and its AB and CD spectra are quite similar to those of $(-)_{435}$-isomers obtained here. Thus, the Λ-configuration is assigned to the $(-)_{435}$-isomers and Δ to the $(+)_{435}$-isomers. As mentioned later, the results of the stereoselectivity in the complexes show that there exists intramolecular steric repulsion between the alkyl group of the coordinated amino acid anion and H–C=N or CH_3–C=N groups of the Schiff-base ligand, and that the repulsion is stronger in $(+)_{435}$-isomer than in $(-)_{435}$-isomer. The molecular model indicates that such a steric interaction is stronger in Δ_L-configuration than Λ_L, if the complex takes the *cis*-β_1(*fac*)-structure, but is stronger in Λ_L-configuration than in Δ_L, if the complex takes the *cis*-β_2(*mer*)-structure. Therefore, all the complexes are suggested to take the *cis*-β_1(*fac*)-structure. The proposed structures are shown in Fig. 4.

Stereoselectivity. All the PMR specrtal data are summarized in Tables 6 and 7, and the representative PMR spectra are shown in Fig. 5.

In complexes **2**—**6**, **8**, and **14**—**18**, the signal of H-C=N or CH_3–C=N protons of the Schiff-base ligand shows no time dependence; the signal appears only as two peaks with equal intensity, not onoy soon after dissolution but also at the equilibrium condition. However, the signal of the coordinated amino acid anion shows a clear time dependence. For example, as shown in Figs. 5 A and A′, the L-ala-complex **2** shows two kinds of signals with equal intensity for the methyl group of the coordinated L-alanine anion soon after dissolution, but these two signals change in their intensities at the equilibrium condition. Similar behaviors are observed for the complexes **3**—**6**,

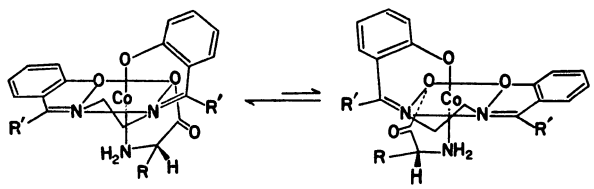

Λ_L-*cis*-β_1(fac) ($(-)_{435}$-isomer) Δ_L-*cis*-β_1(fac) ($(+)_{435}$-isomer)

Fig. 4. The proposed structure of the complexes and the equilibrium in methanol. R=H or CH_3.

TABLE 4. AB AND CD SPECTRAL DATA FOR [Co(sal$_2$en)(Amino acid anion)] IN METHANOL AT THE EQUILIBRIUM CONDITION (Wave numbers are in 10^3 cm^{-1})

Amino acid and No. of complex	AB(log ε_{max})	CD($\Delta\varepsilon_{max}$)	Amino acid and No. of complex	AB(log ε_{max})	CD($\Delta\varepsilon_{ext}$)
gly (1)	16.95(2.53)		L-met (6)	17.00(2.62)	17.00 (+2.62)
	21.23(2.74)*			21.23(2.73)*	19.61 (+0.90)
	24.39(3.57)*			24.39(3.63)*	23.81 (−2.11)
	25.98(3.78)			25.98(3.82)	25.00 (−2.55)
L-ala (2)	16.95(2.65)	17.09(+3.07)			28.57 (−3.78)
	21.23(2.73)	19.61(+0.66)	L-thr (8)	16.95(2.55)	17.00 (+8.64)
	24.39(3.56)*	23.53(−2.20)		21.23(2.74)*	20.83 (+1.32)
	25.98(3.77)	25.00(−2.36)		24.39(3.58)*	24.88 (−7.80)
		28.74(−3.53)		25.98(3.79)	28.41(−10.92)
L-val (3)	16.95(2.62)	17.18(+3.12)	L-phe (10)	16.95(2.59)	16.89 (+7.97)
	21.23(2.75)*	19.61(+0.75)		21.23(2.65)*	20.83 (+2.47)
	24.39(3.62)*	23.26(−2.18)		22.73(3.03)*	24.61 (−6.80)
	25.98(3.79)	25.00(−2.20)		24.39(3.55)*	28.17 (−7.02)
		28.49(−4.97)		25.98(3.74)	
L-leu (4)	16.95(2.62)	16.98(+2.79)	L-tyr (11)	17.04(2.64)	16.67 (+8.13)
	21.23(2.74)*	19.61(+0.60)		21.93(2.75)*	20.41 (+1.63)
	24.39(3.55)*	23.53(−2.00)		23.87(3.64)*	23.81 (−6.97)
	25.98(3.75)	25.00(−2.10)		25.97(3.84)	24.69 (−7.73)
		28.57(−3.40)			28.09(−10.46)
L-isoleu (5)	16.95(2.58)	16.95(+2.22)	L-trp (12)	16.95(2.61)	16.95(+11.03)
	21.23(2.78)*	18.52(+1.09)		21.74(2.68)*	20.83 (+2.47)
	24.39(3.58)*	23.15(−1.70)		24.69(3.66)*	24.61 (−8.94)
	25.98(3.79)	25.00(−2.05)		25.98(3.80)	28.57(−11.77)
		27.93(−3.11)			

* shoulder

TABLE 5. AB AND CD SPECTRAL DATA FOR [Co(7,7′-Me-sal$_2$en)(Amino acid anion)] IN METHANOL AT THE EQUILIBRIUM CONDITION (Wave numbers are in 10^3 cm^{-1})

Amino acid and No. of complex	AB(log ε_{max})	CD($\Delta\varepsilon_{ext}$)	Amino acid and No. of complex	AB(log ε_{max})	CD($\Delta\varepsilon_{ext}$)
gly (13)	17.09(2.46)		L-met (18)	17.24(2.57)	16.72 (+5.10)
	21.74(2.72)*			21.74(2.75)*	19.61 (+1.40)
	24.69(3.45)*			24.69(3.53)*	23.70 (−5.11)
	26.67(3.72)			26.67(3.82)	27.86 (−7.45)
L-ala (14)	17.09(2.48)	16.67 (+3.86)	L-thr (20)	17.09(2.57)	16.61 (+8.26)
	21.74(2.74)*	19.80 (+0.80)		21.74(2.73)*	19.61 (+2.69)
	24.69(3.45)*	23.64 (−3.74)		24.69(3.46)*	23.81 (−8.24)
	26.67(3.76)	27.78 (−5.85)		26.67(3.76)	28.01(−13.77)
L-val (15)	17.09(2.56)	16.67 (+5.86)	L-phe (22)	17.09(2.56)	16.61 (+8.71)
	21.74(2.73)*	19.80 (+1.98)		21.74(2.74)*	19.80 (+3.18)
	24.69(3.50)*	23.53 (−5.67)		24.69(3.48)*	23.81 (−8.05)
	26.67(3.77)	27.55 (−9.86)		26.67(3.76)	27.78(−13.77)
L-leu (16)	17.09(2.56)	16.61 (+4.38)	L-tyr (23)	17.09(2.57)	16.64(+11.14)
	21.74(2.74)*	19.61 (+1.36)		22.22(2.93)*	19.61 (+4.13)
	24.69(3.40)*	23.64 (−4.04)		25.00(3.61)*	23.92(−10.35)
	26.67(3.78)	27.78 (−6.70)		27.40(3.77)	27.93(−16.34)
L-isoleu (17)	17.09(2.55)	16.67 (+6.26)	L-trp (24)	17.09(2.56)	16.64(+12.35)
	21.74(2.73)*	19.61 (+2.28)		22.22(2.73)*	19.61 (+4.53)
	24.69(3.51)*	23.53 (−6.25)		25.00(3.57)*	23.87(−11.22)
	26.67(3.80)	27.55(−10.40)		27.40(3.84)	27.93(−16.90)

* shoulder

TABLE 7. PMR DATA FOR [Co(7,7′-Me-sal$_2$en)(Amino acid anion)] IN METHANOL (δ, ppm)

Amino acid and No. of complex	Soon after dissolution		At equilibrium condition	
	CH_3-C=N of 7,7′-Me-sal$_2$en[a]	R of amino acid	CH_3-C=N of 7,7′-Me-sal$_2$en[a]	R of amino acid
gly (13)	2.72(3) 2.84(3)	(c)	2.72(3) 2.84(3)	(c)
L-ala (14)	2.72(3) 2.84(3)	CH_3(a) {1.46(1.5) 1.58 CH_3(b) {1.26(1.5) 1.48	2.72(3) 2.84(3)	CH_3(a) {1.46(1.0) 1.58 CH_3(b) {1.26(2.0) 1.48
L-val (15)	2.72(3) 2.84(3)	CH_3(a) {0.93(3.0) 1.05 CH_3(b) {{0.65(1.5) 0.77 {0.85(1.5) 0.97	2.72(3) 2.84(3)	CH_3(a) {0.93(1.7) 1.05 CH_3(b) {{0.65(2.2) 0.77 {0.85(2.1) 0.97
L-leu (16)	2.73(3) 2.85(3)	CH_3 9.08[b]	2.73(3) 2.85(3)	CH_3 9.06[b]
L-isoleu (17)	2.72(3) 2.83(3)	CH_3(b) (0.83, 0.89, 0.92, 0.95)	2.72(3) 2.83(3)	CH_3 (0.83, 0.89, 0.92, 0.95, 1.00, 1.03)[c]
L-met (18)	2.69(3) 2.81(3)	CH_3(b) 2.00(3.0)	2.69(3) 2.81(3)	CH_3(a) 2.05(1.0) CH_3(b) 2.00(2.0)
L-thr (20)	(b) 2.67(1.5) (a) 2.69(1.5) 2.82(3.0)	CH_3(a) {1.18(1.5) 1.29 CH_3(b) {1.07(1.5) 1.18	2.67(3) 2.82(3)	CH_3(a) {1.18(0.48) 1.29 CH_3(b) {1.07(2.52) 1.18
L-phe (22)	(b) 2.40(1.5) (a) 2.72(1.5) (b) 2.81(1.5) (a) 2.84(1.5)	(c)	(b) 2.40(2.72) (a) 2.72(0.28) (b) 2.81(2.73) (a) 2.84(0.27)	(c)
L-tyr (23)	(b) 2.40(1.5) (a) 2.70(1.5) (b) 2.80(1.5) (a) 2.85(1.5)	(c)	(b) 2.40(2.74) (a) 2.70(0.26) (b) 2.80(2.74) (a) 2.85(0.26)	(c)
L-trp (24)	(b) 2.73(3) (b) 2.01(3)	(c)	(a) 2.80(0.17) (a) 2.61(0.17) (b) 2.73(2.83) (b) 2.01(2.83)	(c)

( ) represents the number of proton(s). (a), peak(s) corresponding to $(+)_{435}$-isomer. (b), peaks corresponding to $(-)_{435}$-isomer. (c), not clear due to overlap with other peaks.
a) CH_2-CH_2 signal appears at 3.4—3.6 ppm as broad multiplet and that of phenyl protons at 6.5—7.7 ppm as multiplet. b) Center of broad multiplet. c) Complicated multiplet.

4, **5**, **16**, and **17**, due to the complicated overlaps of the alkyl signals, their PMR spectra give no fine information about the isomer's ratios at equilibrium conditions. Therefore, the ratios were estimated from their rotational values at 435 nm or from their CD strengths at 589 nm. That is, the ratio in the complex **17** was estimated by using the $[M]_{435}$-value for its pure $(-)_{435}$-isomer, which was estimated from the kinetic data by extrapolating to time=0, and the $[M]_{435}$-value at the equilibrium condition. The ratio in the complex **16** was obtained by using the $[M]_{435}$-value of pure $(-)_{435}$-isomer of the complex **17** as the $[M]_{435}$-value for a pure $(-)_{435}$-isomer of the complex **16**. In these estimations, we used the following assumptions: that the $[M]_{435}$-values for $(-)_{435}$- and $(+)_{435}$-isomers are the same in each complex, except for the reversed sign, and that the values are quite similar in both L-isoleu- and L-leu-complexes, because the vicinal effect of the coordinated amino acid anion is generally very small as compared with the configurational effect of the chelated ligands.[25-27] However, recently it has been shown for the $[Co(aa)_2(en)]^+$ complex that the vicinal effect is fairly large in some kinds of amino acids.[28] Nearly the same result was also obtained for the [Co(tfac$_2$en)(L-aa)] complex (tfac$_2$en=dianion of *N*,*N*′-ethylenebis(trifluoroacetylacetoneamine)).[29] Thus, the stereoselectivity determined by using CD or ORD strengths may not be so exact as compared with that by PMR intensity. The isomer's ratios in the complexes **4** and **5** were estimated by nearly the same method as those in the complexes **16** and **17**, but by using the $\Delta\varepsilon_{589}$-values at the first absorption region for the complexes **4** and **5** and by using the $\Delta\varepsilon_{589}$-value for pure $(-)_{435}$-isomer of the complex **3**, which was calculated from the $\Delta\varepsilon_{589}$-value of the complex **3** at the equilibrium condition and its isomer's ratio at the same condition.

From the data for the isomer's ratios (Table 8), the

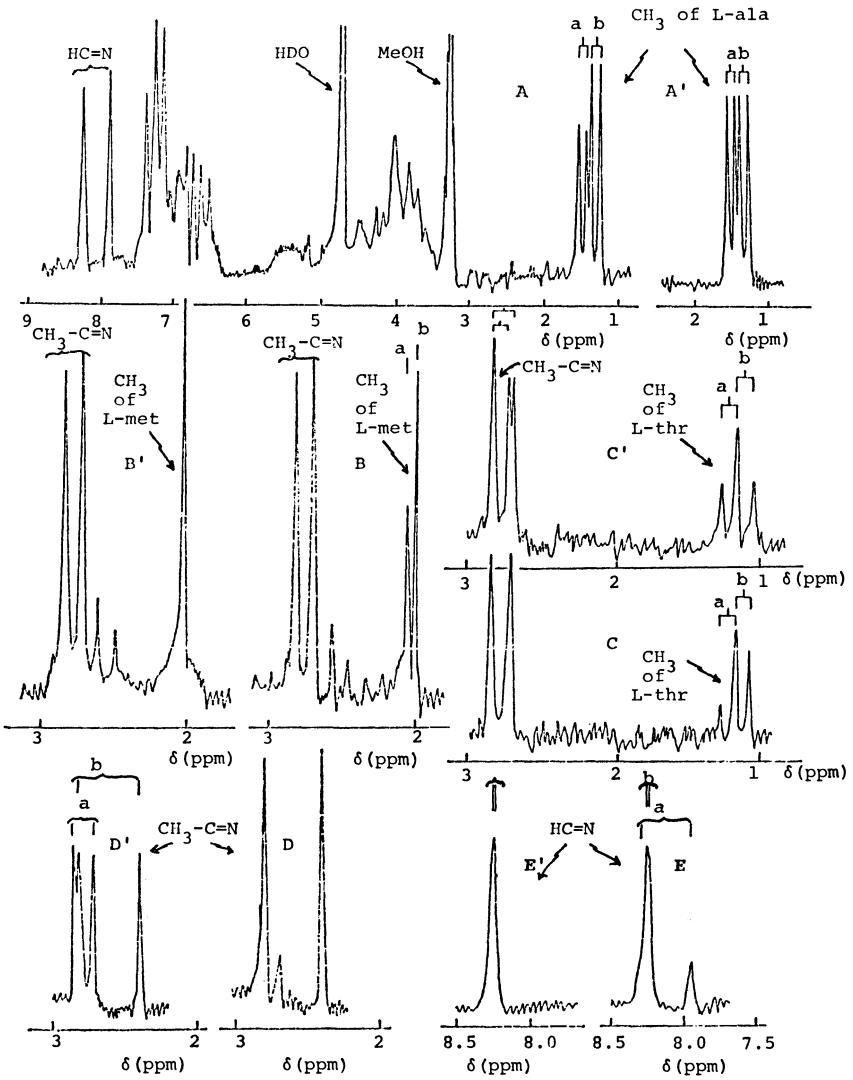

Fig. 5. The representative PMR spectra of the complexes in CD_3OD. A and A′ are PMR spectra of [Co(sal$_2$en)(L-ala)] (1) at the equilibrium condition (A) and soon after dissolution (A′). B and B′ are those of [Co(7,7′-Me-sal$_2$en)(L-met)] (18) at the equilibrium condition (B) and soon after dissolution (B′). C and C, D and D′, and E and E′ are those of [Co(7,7′-Me-sal$_2$en)(L-thr)] (20), [Co(7,7′-Me-sal$_2$en)(L-phe)] (22), and [Co(sal$_2$en)(L-phe)] (10) at the equilibrium conditions (C, D, and E) and soon after dissolution (C′, D′, and E′). The signal of a corresponds to $(+)_{435}$-isomer and that of b to $(-)_{435}$-isomer for all the PMR spectra.

Table 8. Stereoselectivity in the complexes at equilibrium conditions

Amino acid	R-Group	Isomer's ratio, sal$_2$en-complex	$(-)_{435}$-Isomer/$(+)_{435}$-isomer 7,7′-Me-sal$_2$en-complex
L-ala	$-CH_3$	1.4—1.6	1.9—2.1
L-met	$-(CH_2)_2-S-CH_3$	1.4—1.6	1.9—2.1
L-leu	$-CH_2-CH(CH_3)_2$	1.3—1.5[b]	1.9—2.1[a]
L-val	$-CH(CH_3)_2$	1.4—1.6	2.4—2.6
L-isoleu	$-CH(CH_3)(C_2H_5)$	1.2—1.4[b]	2.7—2.9[a]
L-thr	$-CH(CH_3)(OH)$	3.9—4.1	5.2—5.4
L-phe	$-CH_2-C_6H_5$	3.9—4.1	9— 10
L-tyr	$-CH_2-C_6H_4OH$	4.7—4.9	9— 10
L-trp	$-CH_2-C_8H_6N$	7.9—8.3	15— 18

a) Estimated value from α_{435}. b) Estimated value from $\Delta\varepsilon_{589}$.

following facts become clear: that 1) the ratios increase in the order of the amino acid, L-ala∼L-met∼L-leu∼L-val∼L-isoleu<L-thr∼L-phe∼L-tyr<L-trp for sal$_2$en-complexes and L-ala∼L-met∼L-leu<L-val<L-isoleu<L-thr<L-phe∼L-tyr<L-trp for 7,7′-Me-sal$_2$en-complexes; 2) the increasing order coincides with the increasing order of the steric crowding of the alkyl group of the amino acid, especially the steric crowding at the β-carbon atom; and 3) the ratio is larger in 7,7′-Me-sal$_2$en-complexes than in sal$_2$en-complexes for each amino acid. These results show that the stereoselectivity in these complexes at least depends on the intramolecular steric repulsion between the alkyl group of the amino acid anion and the hydrogen atom or methyl group at the C=N bonds of the Schiff-base ligand, and thus the steric interaction is stronger in 7,7′-Me-sal$_2$en-than in the sal$_2$en-complexes. Since the stereoselectivity in these Schiff-base complexes is thermodynamic in origin, as mentioned above, it is also shown that the steric interaction is stronger in $(+)_{435}$-isomer (unstable) than $(-)_{435}$-isomer (stable).

The authors wish to express their deep thanks to Prof. Y. Yoshino of Tokyo University and Prof.K. Sone and Dr. Y. Fukuda of Ochanomizu University for their kind assistance in the CD spectral measurement. This work was supported in part by a Science Reserch Grant from the Ministry of Education Japan (No. 154189).

References

1) J. H. Dunlop, R. D. Gillard, N. C. Payne, and G. B. Robertson, *Chem. Comm.*, **1966**, 874.
2) J. H. Dunlop, R. D. Gillard, and N. C. Payne, *J. Chem. Soc., A*, 1469 (1967).
3) R. J. Gillard, N. C. Payne, and G. B. Robertson, *J. Chem. Soc., A*, 2579 (1970).
4) R. D. Gillard, R. Maskill, and A. Parini, *J. Chem. Soc., A*, 2268 (1971).
5) L. J. Legg and J. Steele, *Inorg. Chem.*, **10**, 2177 (1971).
6) Y. Kojima and M. Shibata, *Inorg. Chem.*, **12**,1009(1973).
7) D. A. Buckingham, J. Dekkers, A. M. Sargeson, and L. G. Marzilli, *Inorg. Chem.*, **12**, 1207 (1973).
8) D. A. Buckingham, J. Dekkers, A. M. Sargeson, and M. Wein, *Inorg. Chem.*, **12**, 2019 (1973).
9) M. Saburi, M. Homma, and S. Yoshikawa, *Inorg. Chem.*, **8**, 367 (1969).
10) J. M. Pratt, *J. Chem. Soc.*, **1964**, 5154.
11) G. C. Hayward, H. A. O. Hill, J. M. Pratt, N. J. Vanston, and R. J. P. Williams, *J. Chem. Soc.*, **1965**, 6405.
12) J. M. Pratt and R. G. Thorp, *J. Chem. Soc.*, **1966**, 188.
13) G. Costa, *Coord. Chem. Rev.*, **8**, 63, (1972).
14) Y. Fujii, *Bull. Chem. Soc. Jpn.*, **45**, 3084 (1972).
15) Y. Fujii, *Bull. Chem. Soc. Jpn.*, **47**, 2856 (1974).
16) Y. Fujii, A. Osawa, Y. Furukawa, F. Ebina, and S. Takahashi, *Bull. Chem. Soc. Jpn.*, **45**, 2459 (1972).
17) M. Caligaris, G. Manzini, G. Nardin, and L. Randaccio, *J. Chem. Soc., Dalton Trans.*, **1972**, 543.
18) N. A. Bailey, B. M. Higson, and E. D. McKenzie, *J. Chem. Soc., Dalton Trans.*, **1972**, 503.
19) D. Cummins, B. M. Higson, and E. D. McKenzie, *J. Chem. Soc., Dalton Trans.*, **1973**, 1359.
20) P. Pfeiffer, E. Breith, E. Lubbe, and T. Tsumaki, *Ann. Chem.*, **503**, 84 (1933).
21) A. Bigotto, G. Costa, G. Mestroni, G. Pellizer, A. Puzeddu, E. Reicenhofer, L. Stefani, and G. Tauzer, *Inorg. Chem. Acta, Reviews*, **4**, 41 (1970).
22) The derivation of the kinetic equation and the study of the reaction mechanism will be reported elsewhere.
23) F. Basolo and R. G. Pearson, "Mechanisms of Inorganic Reactions," 2nd ed, John Wiley & Sons, New York (1967), pp. 278, 303.
24) Y. Fujii and M. Sano, *Chem. Lett.*, **1976**, 745.
25) J. Fujita and Y. Shimura, "Spectroscopy and Structure of Metal Chelate Compounds," John Wiley & Sons, New York (1968), p.197.
26) C. J. Hawkins, "Absolute Configuration of Metal Complexes," John Wiley & Sons, New York (1971), p. 185.
27) Some recent papers: a) K. Yamanari, J. Hidaka, and Y. Shimura, *Bull. Chem. Soc. Jpn.*, **48**, 1653 (1975); b) M. Takeuchi and M. Shibata, *ibid.*, **47**, 2797 (1974); c) T. Yasui, *ibid.*, **48**, 454 (1975); d) Y. Kojima and M. Shibata, *Inorg. Chem.*, **12**, 1009 (1973); e) N. Matsuoka, J. Hidaka, and Y. Shimura, *Bull. Chem. Soc. Jpn.*, **45**, 2491 (1972); f) J. P. Glusker, H. L. Carrell, R. Job, and T. C. Bruice, *J. Am. Chem. Soc.*, **96**, 5741 (1974); g) S. Yamada, J. Hidaka, and B. E. Douglas, *Inorg. Chem.*, **10**, 2187 (1971); h) G. R. Brubaker and D. P. Schaefer, *ibid.*, **10**, 2170 (1971); i) J. I. Legg and J. Steele, *ibid.*, **10**, 2177 (1971).
28) N. Matsuoka, J. Hidaka, and Y. Shimura, *Bull. Chem. Soc. Jpn.*, **48**, 458 (1975).
29) Will be reported elsewhere.

The Polarography of the Cadmium(II)–2-Carboxy-1-pyrrolidine-carbodithioate Chelate

Toyokichi KITAGAWA and Kazuo NOMURA

Department of Chemistry, Faculty of Science, Osaka City University, Sumiyoshi-ku, Osaka 558

(Received May 15, 1976)

The electrochemical behavior of the cadmium(II) ion in the presence of 2-carboxy-1-pyrrolidinecarbodithioic acid (H_2cpcd) as a chelating agent was investigated in an alkaline medium by d.c. polarography, a.c. polarography, cyclic voltammetry, and chronopotentiometry. The cadmium(II) chelate gave a reversible two-electron reduction wave at −0.86 V *vs.* SCE, with a postwave at −0.95 V. From the dependence of the total wave height on the mercury column height and from the methods of cyclic voltammetry, the electrode reduction of the cadmium(II) chelate was found to be diffusion-controlled. The diffusion current constant was 2.42 $\mu A\ mol^{-1}\ m^3\ mg^{-2/3}\ s^{1/2}$. The postwave was identified as an adsorption wave of the cadmium(II) chelate from the dependence of the postwave height on the mercury column height, the a.c. peak height, the electrocapillary curves, and the results of chronopotentiometry. The surface excess of cadmium(II) chelate adsorbed on the mercury electrode was evaluated by means of three different electrochemical techniques. The composition of the cadmium(II)–cpcd chelate in the presence of excess H_2cpcd was $Cd(cpcd)_2^{2-}$, and the overall stability constant was estimated to be 8.0×10^{12} at 25.0 °C and $\mu=1.5$.

1-Pyrrolidinecarbodithioic acid (Hpcd) [I] is more stable to an acidic solution than 1,1-diethyldithiocarbamic acid, and it forms insoluble complexes with various metal ions. The [I] reagent has been used for the colorimetric determinations and atomic absorption spectrophotometric determinations of metal ions after solvent extraction,[1-3] X-ray analysis of the mercury complex[4] and electrochemical studies of the manganese complex.[5]

The reagent synthesized by the introduction of a carboxyl group at the 2-position of [I], 2-carboxy-1-pyrrolidinecarbdithioic acid (H_2cpcd)[II], has been recently found to form soluble complexes with metal ions in an aqueous solution,[6] and it may be that [II] can be used as an analytical reagent, much like other dithiocarbamic acids.

In a previous paper,[7] the polarographic behavior of [I] and [II], particularly the characteristics of the adsorption prewave, was investigated. Few of polarographic studies of the adsorption postwave has been presented than those of the prewave.[8-10] This paper will deal with the polarographic behavior of the cadmium(II) ion in the presence of H_2cpcd, and particularly with the characteristics of the adsorption postwave.

The structural formulas of [I] and [II] are as follows:

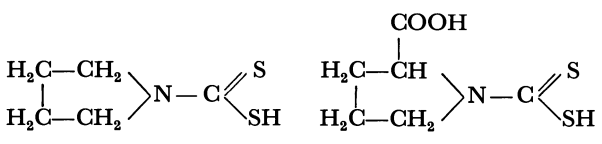

[I] [II]

Experimental

Reagents. Ammonium salt of [II] was prepared by the following procedure. L-Proline (11.5 g) was dissolved in a minimum amount of methanol, and then carbon disulfide (6 ml) was added. The solution was saturated with ammonia gas at 0 °C. The product was filtered off, recrystallized a few times by dissolving it in methanol and precipitating with ethyl ether, and dried under a vacuum for 24 h. Found: C, 32.07; H, 6.64; N, 18.56%. Calcd for $C_6H_{15}O_2N_3S_2$: C, 31.98; H, 6.71; N, 18.65%.

The cadmium(II) sulfate solution was standardized by chelatometric titration, with EDTA as the titrant. All chemicals were of an analytical reagent grade and were used without further purification.

Apparatus. The d.c. and a.c. polarograms were recorded with a Yanagimoto PA-102 polarograph connected to a conventional H-type cell, which was used in conjunction with a saturated calomel electrode (SCE) as a reference electrode and, if necessary, a coiled platinum wire electrode as a counter electrode. The dropping mercury electrode (DME) had the following characteristics: mercury flow-rate $m=0.499$ mg s^{-1} and drop time $t=5.24$ s in a 0.5 mol dm^{-3} sodium sulfate solution at an open circuit and at a mercury column height $h=60$ cm. The AC current was by-passed by the use of a 200 μF capacitor between the coiled platinum wire electrode and SCE. Cyclic voltammograms were recorded with Riken Denshi F-32 or F-43 X-Y recorders in conjunction with the polarograph, using a hanging mercury drop electrode (HMDE). Chronopotentiograms were also recorded with X-Y recorder in conjunction with a Riken Denshi transient time converter TCA-200 using a slow dropping mercury electrode, where $m=0.0349$ mg s^{-1} and $t=208.2$ s. A constant current for the chronopotentiometric measurements was obtained using a dry cell of 200 V and appropriate resistors. The pH of a sample solution was measured with a Toa Denpa HM-5A pH meter.

Procedure. To a freshly prepared sample solution containing 0.5 mol dm^{-3} sodium sulfate as a supporting electrolyte, a 0.02 mol dm^{-3} sodium borate–sodium hydroxide buffer was added to prevent the sample from decomposition because of the poor stability of H_2cpcd in an acidic solution.[11] Solutions were de-aerated with highly purified nitrogen gas for 15 min before recording the polarograms. The cell was immersed in a water thermostat controlled at 25±0.1 °C, and measurements were carried out under a nitrogen atmosphere. Electrocapillary curves were obtained by converting the drop times into the interfacial tension in the potential range from 1.0—1.8 V.

Results and Discussion

D.c. and a.c. Polarography. Figure 1 shows, the d.c. and a.c. polarograms of the cadmium(II) ion in an alkaline solution containing excess H_2cpcd. At the concentrations of 2×10^{-4} mol·dm^{-3} cadmium(II) and 1×10^{-2} mol dm^{-3} H_2cpcd, the d.c. polarogram gives the main wave A at −0.86 V and a postwave, B,

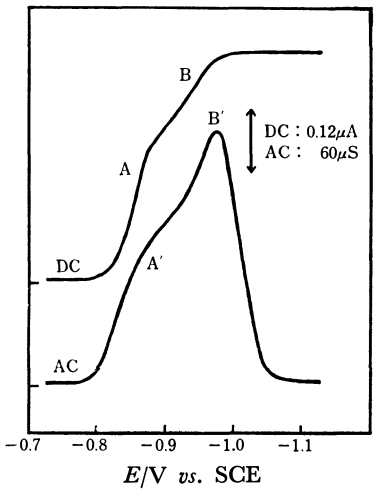

Fig. 1. Polarograms of cadmium(II)-cpcd chelate. [Cd(II)]=2×10^{-4} mol dm^{-3}, [cpcd]=1×10^{-2} mol dm^{-3}, pH 9.4.

at −0.95 V. Two peaks, A′ and B′ of the a.c. polarogram correspond to the d.c. waves. The wave heights are almost constant in the pH range from 4.5 to 11.0 and decrease below pH 4.5. The reversibility of the electrode reactions has been introduced by Senda *et al.* and the reversibility constant is expressed as $K=Y_p\, i_l^{-1}\, n^{-1}\, t^{-1/2}$ where Y_p is the peak admittance of the a.c. wave. The K values for the electrode processes of the two reduction waves are 70.4 and 439.9 S A^{-1} s$^{-1/2}$ respectively. The latter value is much greater than the former, which shows a reversible process. These values suggest that the electrode reaction accompanies a specific adsorption. The adsorption of the reactant and/or product will affect the observed electrochemical behavior. Brdička has shown that, on d.c. polarography, adsorption of the product should manifest itself as an adsorption-controlled prewave, while, the adsorption of the reactant should appear as a postwave.[12]

As Fig. 2 shows, the height of the B postwave is independent of the concentration of the cadmium(II)

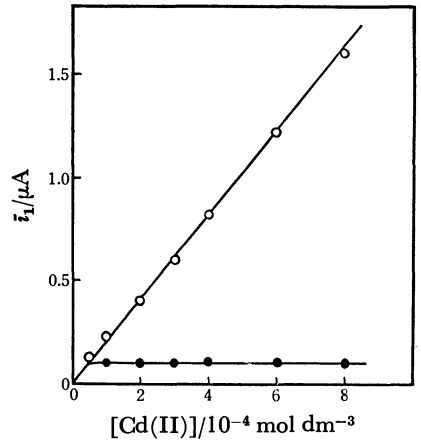

Fig. 2. Dependence of the limiting currents on the concentration of cadmium(II) ion. [cpcd]=1×10^{-2} mol dm^{-3}, pH 9.4, ○: total wasve (A+B), ●: postwave(B).

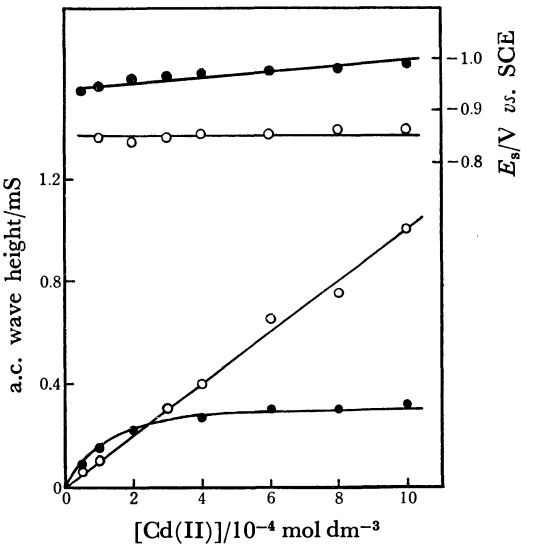

Fig. 3. Dependence of the summit potentials and a.c. wave heights on the concentration of cadmium(II) ion. [cpcd]=1×10^{-2} mol dm^{-3}, pH 9.4, ○: 1st wave(A′), ●: 2nd wave(B′).

ion in the range over 1×10^{-4} mol dm^{-3}, while that of the total wave (A+B) is proportional to the concentration in the range less than 1×10^{-3} mol dm^{-3}. Therefore, the postwave may be considered to be an adsorption wave of the reactant. Figure 3 shows the dependence of the a.c. peak height and the summit potential on the concentration of the cadmium(II) ion. The height of the second peak, B′, increases nonlinearly with an increase in the concentration and approaches a limiting value, while that of the first peak, A′, is approximately proportional to the concentration. The summit potential of B′ shifts to a more negative potential with an increase in the concentration, while that of A′ is independent of the concentration. From these results, the second a.c. wave seems to be a tensammetric desorption wave.[13,14]

The plot of $\log(i/(i_d-i))$ *vs.* E gives a straight line with a reciprocal slope of 30 mV, although the plot displays a downward curvature near the potential corresponding to the postwave. The electrode process of the cadmium(II) chelate is found to be a reversible two-electron reduction.

Electrocapillary Curves. The electrocapillary curves of the cadmium(II) ion in the presence of excess H_2cpcd are shown in Fig. 4. In the presence of H_2cpcd alone a marked depression of the interfacial tension of mercury is observed in the potential range from 0 to −0.85 V. At more negative potentials than about 0.85 V, the interfacial tension of mercury in the presence of H_2cpcd is almost identical to that in its absence. As has been reported previously,[7] cpcd^{2-} itself adsorbs strongly on the surface of the DME in the above potential range. On the addition of the cadmium(II) ion to the H_2cpcd solution, the interfacial tension is depressed much more than in the presence of H_2cpcd only, and the potentials of the desorption shift to more negative values as the concentration of

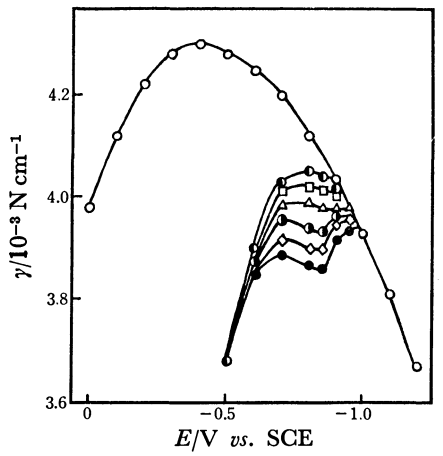

Fig. 4. Electrocapillary curves of cadmium(II)-cpcd chelate.
[cpcd]$=1\times10^{-2}$ mol dm^{-3}, [Cd(II)]=◐: 0, □: 1×10^{-5}, △: 2×10^{-5}, ◑: 4×10^{-5}, ◇: 8×10^{-5}, ●: 2×10^{-4} mol dm^{-3}, ○: base solution.

the cadmium(II) ion increases. At 2×10^{-4} mol dm^{-3} cadmium(II), the interfacial tension is depressed in the potential range from 0 to −0.95 V and reaches its lower limit. This behavior corresponds to the saturation of the adsorbate on the electrode surface. The potential slightly more positive than that of the desorption corresponds to be the potential of the postwave on the d.c. polarogram. Therefore, the postwave is also assigned to the adsorption wave of the cadmium(II) chelate. The minimum of the interfacial tension on the electrocapillary curves for the cadmium(II) chelate appears at the potential of −0.85 V, which corresponds to the initial rise in the polarogram.

Effect of the Mercury Column Height. Table 1 shows the dependence of the wave heights on the mercury column height. The limiting current of the total wave (A+B) is proprotional to $h^{1/2}$; hence, the electrode process is diffusion-controlled. According to the Ilkovič equation, the diffusion current constant, I_d, and the diffusion coefficient, D, of the cadmium chelate can be calculated: $I_d=2.42$ μA mol^{-1} m^3 mg$^{-2/3}$ s$^{1/2}$ and $D=3.97\times10^{-6}$ cm^2 s^{-1} where $n=2$. From the equation of the mean adsorption current, i_a, gives below, i_a should be proportional to h, because m is proportional to h and t to h^{-1}. The limiting current of the B postwave is proportional to h, and the postwave is reassigned to the adsorption wave of cadmium(II) chelate.

Table 1. Dependence of the limiting currents on the mercury column height

h / cm	$\bar{i}_{post}$ / nA	$\bar{i}_{total}$ / nA	$\bar{i}_{post}/h$ / nA·cm^{-1}	$\bar{i}_{total}/h^{1/2}$ / nA·cm$^{-1/2}$
55.0	116	388	2.1	52.3
60.0	128	401	2.2	51.8
65.0	140	422	2.2	52.3
70.0	152	432	2.2	51.6
75.0	165	449	2.2	51.8

[Cd(II)]$=2\times10^{-4}$ mol dm^{-3}, [cpcd]$=1\times10^{-2}$ mol dm^{-3}, pH 9.4.

Cyclic Voltammerty. A cyclic voltammogram obtained under the same conditions is shown in Fig. 5. An exceptionally steep rise of the current is observed in the reduction step and is considered to be due to the adsorption of the cadmium(II) chelate. The peak current which is obtained by subtracting the current of the steep rise is proportional to the squareroot of the sweep rate. Consequently, the electrode process is the diffusion-controlled process acompanying the adsorption of the reactant.

Chronopotentiometry, Chronopotentiometry has often been used for the investigation of the adsorption of reactants.[15-17] Figure 6 shows a characteristic potential-time curve of the cadmium(II) chelat. The transition time constant, T, in chronopotentiometry has been revealed by Sand to be as follows; it is constant when the electrode process is diffusion-controlled:

$$T=\frac{i_A\tau^{1/2}}{C}=\frac{1}{2}\pi^{1/2}nFD^{1/2}$$

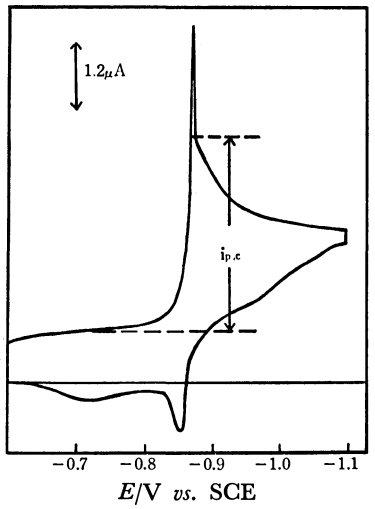

Fig. 5. Cyclic voltammogram of cadmium(II)-cpcd chelate at HMDE.
[Cd(II)]$=2\times10^{-4}$ mol dm^{-3}, [cpcd]$=1\times10^{-2}$ mol dm^{-3}, pH 9.4, sweep rate=30 mV s^{-1}.

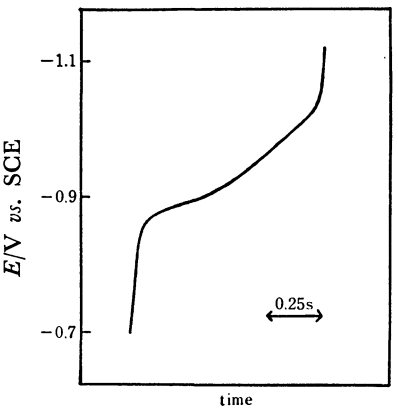

Fig. 6. Chronopotentiogram for the reduction of cadmium(II)-cpcd chelate at HMDE.
[Cd(II)]$=2\times10^{-4}$ mol dm^{-3}, [cpcd]$=1\times10^{-2}$ mol dm^{-3}, pH 9.4. $i_A=1.66\times10^{-5}$ A cm^{-2}.

Table 2. Chronopotentiometric data for the reduction of $Cd(cpcd)_2^{2-}$

i_A / 10^{-4} A·cm^{-2}	τ / s	$i_A\tau^{1/2}/C$ / 10^2 A·cm·s$^{1/2}$·mol^{-1}
1.01	1.49	6.16
1.19	1.12	6.31
1.46	0.798	6.52
1.85	0.558	6.91
2.57	0.341	7.50
3.78	0.203	8.52
5.32	0.136	9.82
7.68	0.0854	11.2

$[Cd(II)]=2\times10^{-4}$mol dm^{-3}, $[cpcd]=1\times10^{-2}$ mol dm^{-3}, pH 9.4.

where i_A is the applied current density, τ is the transition time, and F is the Faraday constant. The results for the reduction of the cadmium(II) chelate which are summarized in Table 2 show that T tends to increase with an increase in i_A. This behavior is indicative of the adsorption of the electroactive reactant on the surface of the mercury drop electrode.

Surface Excess. Γ_m was calculated by the quantitative treatment of the limiting current caused by the formation of a monolayer of the reactant on the surface of the dropping mercury electrode.[12] Provided the quantity of electricity, Q, is based on the formation of a monolayer until the final time of drop-growth, Q is expressed as Eq. 1:

$$Q = n\,F\,A_t\,\Gamma_m \tag{1}$$

Where Γ_m is the number of moles of a monolayer in a unit area, *i.e.*, the surface excess, A_t is the srea of a mercury drop after t seconds, and n is the number of electrons per mole of a monolayer. Therefore, the net current until the final time of drop-growth is given as:

$$i_a = \frac{\partial Q}{\partial t} = n\,F\,\Gamma_m\left(\frac{\partial A_t}{\partial t}\right) \tag{2}$$

Provided a mercury drop is a complete sphere, the following equation is given:

$$A_t = \left(\frac{3mt}{4\pi d}\right)^{2/3} = 0.848\,m^{2/3}\,t^{2/3} \tag{3}$$

where m is expressed in g s^{-1} and where d is the density of mercury (13.6 g cm^{-3}). The net current introduced from Eq. 2 is:

$$i_a = 5.47\times10^4\,n\,m^{2/3}\,t^{-1/3}\,\Gamma_m \tag{4}$$

and from Eq. 4 the mean adsorption current is:

$$\bar{i}_a = \frac{1}{t_m}\int_0^{t_m} i_a\,dt = 8.17\times10^8\,n\,m^{2/3}\,t_m^{-1/3}\,\Gamma m \tag{5}$$

where m is expressed in mg s^{-1} and $\bar{i}_a$ in μA.

The surface excess of the cadmium(II) chelate can be calculated by the following three methods. The first method[12] is based upon the mean adsorption current of the d.c. polarogram, using Eq. 5. On substituting 0.114 μA for $\bar{i}_a$, Γ_m is 1.93×10^{-10} mol cm^{-2}.

The area occupied by one molecule of an adsorption monolayer can be calculated as follows. The maximum area of a mercury drop, A_m is obtained by the substitution of t for t_m in Eq. 3. $\bar{i}_a t_m/A_m$ is the quantity of electricity per area at the last moment of drop-growth. The quantity of electricity required to form a monolayer according to a two-electron process is:

$$\frac{n\,F}{\text{Avogadro number}} = 3.20\times10^{-19}\text{ C molecule}^{-1}$$

Therefore, the area per molecule of a monolayer, A, is obtained by means of the following equation:

$$\bar{A} = \frac{3.20\times10^{-19}\,A_m}{\bar{i}_a t_m}$$

$\bar{A}$ is 85.8×10^{-16} cm^2 molecule^{-1}.

The second method is a calcualtion from the interfacial tensions at the constant potential, E, using the following equations:[18]

$$\Gamma_s = -\frac{1}{RT}\left(\frac{\partial\gamma}{\partial\ln C}\right)_E \tag{6}$$

where γ is the interfacial tension. Figure 7 shows the variation in the γ of the electrocapillary curves with the concentration of cadmium(II) ion at the potential, E. Γ_s is calculated to be 2.15×10^{-10} mol cm^{-2}.

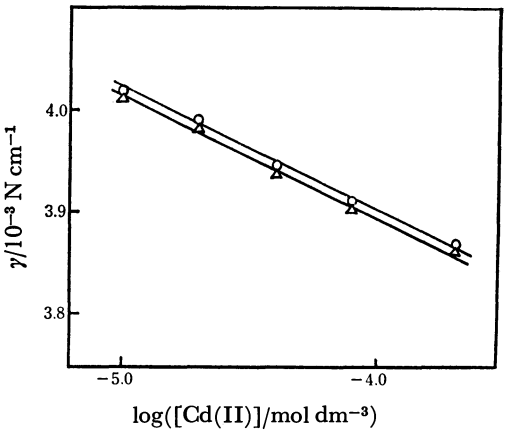

Fig. 7. Dependence of the interfacial tention on the concentration of cadmium(II) ion.
E ○: −0.80 V, △: −0.85 V.

The third methcd is a calculation from the variation in $i_A\tau^{1/2}/C$ with the τ through chronopotentiometry, using various theoretical models of adsorption. Lorenz[19] proposed four theoretical models for chronopotentiomety involving the adsorption of electroactive species. These can be denoted as the ARSR, SAR, SRAR, and equilibrium cases.[17,20] The ARSR model assumes that the adsorbed reactant, AR, is coulometrically depleted prior to the reduction of the solution reactant, SR, and that τ is the sum of the transition times of the AR and SR species. The mathematical relation is:

$$i_A\tau = n\,F\,\Gamma_c + \frac{\pi D(n\,F\,C)^2}{4\,i_A} \tag{7}$$

The SAR model assumes that the SR and AR species react and are depleted simultaneously, that a fixed fraction of the applied current goes to each phase during the entire electrolysis, and that the relation is:

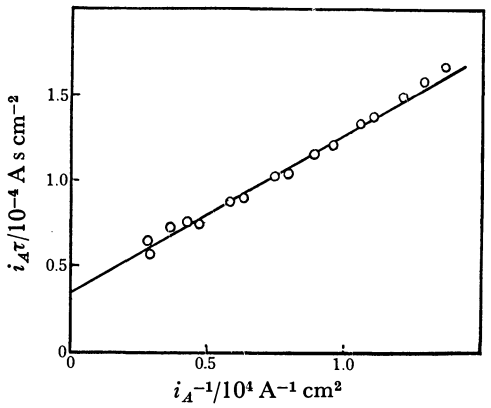

Fig. 8. The plot of $i_A\tau$ *vs.* i_A^{-1}.

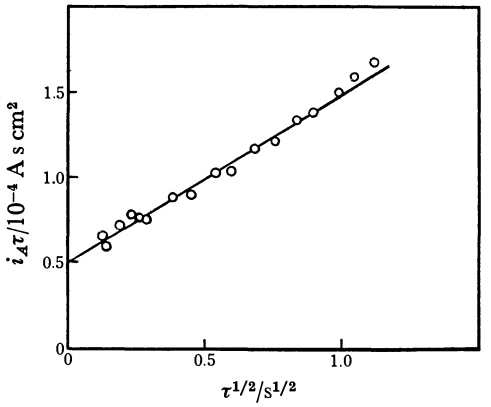

Fig. 9. The plot of $i_A\tau$ *vs.* $\tau^{1/2}$.

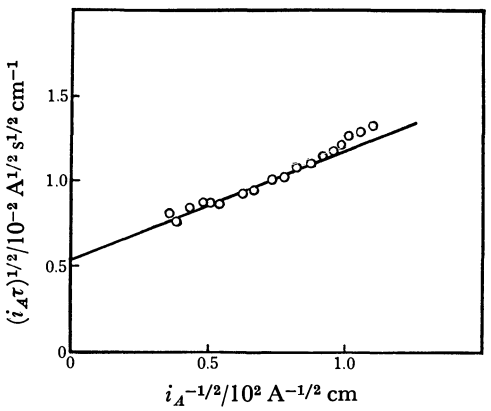

Fig. 10. The plot of $(i_A\tau)^{1/2}$ *vs.* $i_A^{-1/2}$.

$$i_A\tau = n\,F\,\Gamma_c + \frac{n\,F\,C(\pi D\tau)^{1/2}}{2} \tag{8}$$

The SRAR model is the reverse of the ARSR model and assumes that the SR species is coulometrically depleted prior to the reduction of the AR species and that the relation is:

$$(i_A\tau)^{1/2} = (n\,F\,\Gamma_c)^{1/2} + \frac{n\,F\,C(\pi D)^{1/2}}{2\,i_A^{1/2}} \tag{9}$$

The equlibrium model assumes that the species are coupled by a rapid equilibration process accroding to a linear adsorption isotherm, that they are simultaneously depleted at the total transition time, and that the relation is:

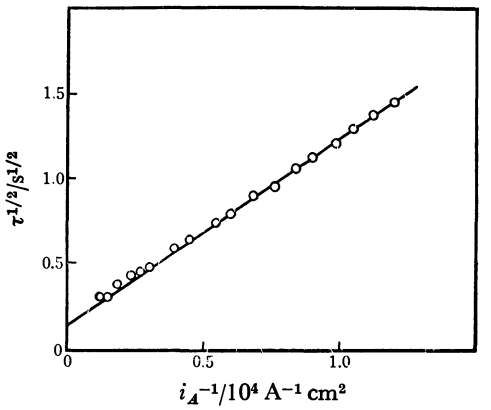

Fig. 11. The plot of $\tau^{1/2}$ *vs.* i_A^{-1}.

$$\tau^{1/2} = \frac{n\,F\,C(\pi D)^{1/2}}{2\,i_A} + \frac{\pi^{1/2}\,\Gamma_c}{2\,D^{1/2}\,C} \tag{10}$$

Figures 8 to 11 show the plots of the four models. Each of them gives a straight line, and the diffusion coefficient, D, can be obtained from the intercept, and Γ_c from the slope; those values are summarized in Table 3. Although it is not possible to make a clear choice between the models on the basis of only these results, the adsorption behavior may be an equilibrium case because of the excellent linearity of the plot according to Eq. 10.

The values of the surface excess obtained from the three methods closely agree with one another. The area per molecule of a monolayer of the complex is about 80×10^{-16} cm^2. The surface excess of $Cd(cpcd)_2^{2-}$ is shown in Table 4, together with $Hg(cpcd)_2^{2-}$ and $Hg(pcd)_2$, which are the oxidationproducts at the DME. On applying either method, the order of the magnitude of the surface excess on the mercury drop is $Hg(pcd)_2 > Hg(cpcd)_2^{2-} > Cd(cpcd)_2^{2-}$. This order may be due to the steric hindrance of the carboxyl group and the spcific interaction between the mercury and the sulfur atoms.

Effect of the Ligand Concentration. By means of the variation in the concentration of H_2cpcd in the presence of the cadmium (II) ion, the stability constants of the

Table 3. Surface excess and diffusion coefficient obtained by four theoretical models for chronopotentiometry

Model	$\Gamma/10^{-10}$ mol cm^{-2}	$D/10^{-6}$ cm^2 s^{-1}
ARSR	2.60	8.16
SAR	1.84	6.96
SRAR	1.59	3.36
Equilibrium	1.10	9.86

Table 4. Surface excess of carbodithioates

Substance	$\Gamma/10^{-10}$ mol cm^{-2}			Reference
$Cd(cpcd)_2^{2-}$	1.9[a]	2.1[b]	1.1[c]	this work
$Hg(cpcd)_2^{2-}$	4.8	2.6	—	Ref. 7
$Hg(pcd)_2$	6.9	5.8	—	Ref. 7

a) D.c. polarography. b) Electrocapillary curve.
c) Chronopotentiometry.

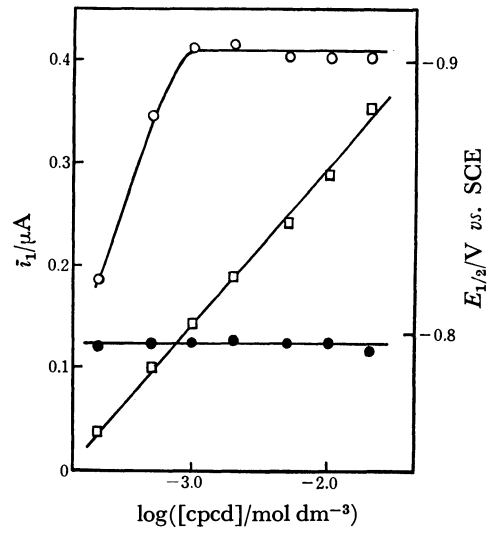

Fig. 12. Dependence of the limiting currents and the halfwave potential on the ligand concetration. [Cd(II)]=2×10^{-4} mol dm^{-3}. ○: total wave(A+B), ●: postwave(B), □: $E_{1/2}$ of the main wave.

cadmium (II)-cpcd chelate can be determined. Figure 12 shows the dependence of these wave heiths and half-wave potentials on the concentartion of H_2cpcd. The limiting current of the total wave (A+B) is nearly constant in concentrations more than 10^{-3} mol dm^{-3}. That of the postwave B is independent of the concentration. The half-wave potential of the main wave, A, shifts linearly to a more negative potential as the concentration of the ligand increases. The slope of the $E_{1/2}$ *vs.* log[cpcd]plot is 57 mV, which corresponds the formation of the 1 : 2 complex. The overall stability costant of the chelate, β_2, is calculated by the Lingane method[21]; it is 5.1×10^{12} at 25 °C and μ= 1.5. The relationship between $E_{1/2}$ and the ligand concentration can slao be analyzed by the method of DeFord and Hume[22]; the value of β_1 and β_2 are 5.5×10^{8} and 8.0×10^{12} respectively.

The electrode reactions for the cadmium(II) chelate are inferred to proceed according to the following four steps:

(1) The $Cd(cpcd)_2^{2-}$ reactant diffuses toward the DME, and then the reactant is completely adsorbed on the surface. The adsorbed molecules are stabilized because of the adsorption energy; hence, the reduction of the adsorbed reactant require a much higher enregy than that of the solute reactant.

$$Cd(cpcd)_2^{2-} \rightleftharpoons Cd(cdcd)_2^{2-}{}_{ads.}$$

(2) The $Cd(cpcd)_2^{2-}$ species, which diffuses from the bulk of the solution, is reduced at first.

$$Cd(cpcd)_2^{2-} + 2e \rightleftharpoons Cd(Hg) + 2\,cpcd^{2-} \text{ (main wave)}$$

(3) The reduction of $Cd(cpcd)_2^{2-}{}_{ads.}$, which was stabilized by adsorption, requires a high energy, and then the wave appears at amore negative potential.

(4) The $Cd(cpcd)_2^{2-}$, which diffuses from the bulk of the solution, is directly reduced.

The authors wish to thank Mr. A. Ichimura for his valuable suggestions and discussions in the course of this work.

References

1) R. R. Brooks, B. J. Presley, and I. R. Kaplan, *Talanta*, **14**, 809 (1967).
2) W. Likussar and D. F. Boltz, *Anal. Chem.*, **43**, 1273 (1971).
3) R. W. Looyenga and D. F. Boltz, *Talanta*, **19**, 82 (1972).
4) A. H. White and A. C. Willis, *J. Chem. Soc., Dalton Trans.*, **1974**, 2341.
5) A. R. Hendrickson, R. L. Martin, and N. M. Rohde, *Inorg. Chem.*, **13**, 1933 (1974).
6) To be published.
7) T. Kitagawa and K. Taku, *Bull. Chem. Soc. Jpn.*, **46**, 2151 (1973).
8) I. M. Kolthoff and Y. Okinaka, *J. Am. Chem. Soc.*, **82**, 3528 (1960).
9) E. C. Gregg and W. P. Tyler, *J. Am. Chem. Soc.*, **72**, 4561 (1950).
10) M. Heyrovsky, S. Vavricka, and R. Heyrovska, *J. Electroanal. Chem.*, **46**, 391 (1973).
11) R. R. Scharfe, V. S. Sastri, and C. L. Chakrabarti, *Anal. Chem.*, **45**, 413 (1973).
12) K. Hasebe and T. Kambara, *Rev. Polarog.(Kyoto)*, **15**, 37 (1968).
13) B. Breyer and H. H. Bauer, "Alternating Current Polarography and Tensammetry," Chemical Analysis, Vol. 13, Interscience publishers, New York (1963), p.19.
14) T. Kakutani, S. Totsuka, and M. Senda, *Bull. Chem. Soc. Jpn.*, **46**, 3652 (1973).
15) S. V. Tatwawadi and A. J. Bard, *Anal. Chem.*, **36**, 2 (1964).
16) H. A. Laitinen and L. M. Chambers, *Anal. Chem.*, **36**, 5 (1964).
17) R. W. Murray and D. J. Gross, *Anal. Chem.*, **38**, 392 (1966).
18) B. B. Damaskin, O. A. Petrii, and V. V. Batrakov, "Adsorption of Organic Compounds on Electrodes," Plenum Press, New York (1972), p.22.
19) W. Lorenz, *Z. Electrochem.*, **59**, 730 (1955).
20) R. W. Murray, *J. Electroanal. Chem.*, **7**, 242 (1964).
21) D. R. Crow, "Polarography of Metal Complexes," Academic Press, London (1969), p.59.
22) D. D. DeFord and D. N. Hume, *J. Am. Chem. Soc.*, **73**, 5321 (1951).

Studies of Nitrogen–Phosphorus Compound. XXVII.[1] Synthesis of $N_4P_4(NH_2)_8$ and Its Hydrolysis

Etsuro KOBAYASHI

National Chemical Laboratory for Industry, Hon-machi, Shibuya-ku, Tokyo 151

(Received May 20, 1976)

The method for synthesis of $N_4P_4(NH_2)_8$ by the reaction between $(NPCl_2)_4$ and ammonia and its hydrolysis behavior were investigated. The reaction of $(NPCl_2)_4$ with liquid ammonia took place violently at first, and the resulting product contained more than several percents of an insoluble material. The extract from this product had a rather low yield, about 20—25%. However, such a drastic reaction could be avoided by the addition of a small amount of dioxane to the reaction system; then the insoluble material did not form, and the yield increased to 55—66%. The final product contained P 37—38% and N 50—51%; thus the mole ratio of N to P was exactly 3 : 1 and the composition agreed with that of $N_4P_4(NH_2)_8 \cdot H_2O$. When an aqueous solution of $N_4P_4(NH_2)_8$ was refluxed at 100 °C, the compound was initially hydrolyzed to $PO(NH_2)_3$ and $P_2O_2NH(NH_3)_4$, these being converted into $PO(ONa)(NH_2)_2$. At room temperature, the rate of hydrolysis was quite slow, but the composition of the hydrolysis products was similar to that at 100 °C. In a sodium hydroxide solution, $N_4P_4(NH_2)_8$ was converted directly into $PO(ONa)(NH_2)_2$ at an elevated temperature. The rate of the alkali hydrolysis obeyed a first-order equation, with the rate constants of 1.0×10^{-3}, 2.5×10^{-3}, 1.9×10^{-2}, and 4.2×10^{-2} at 50, 60, 80, and 90 °C, respectively. These values were about 2.7 times that of $N_3P_3(NH_2)_6$. The activation energy of the reaction was 20.8 kcal/mol. The acid hydrolysis behavior resembled that in the neutral hydrolysis, but the reaction was accelerated with acid strength. The formation of tetrametaphosphimate by the hydrolysis of $N_4P_4(NH_2)_8$, that had previously been claimed, could not be reproduced in this study.

The amidated derivatives of the lower polymers of phosphorus dichloride nitride are of interest as fireproof materials[2,3] and fertilizers.[4,5] The completely ammonated products, $N_3P_3(NH_2)_6$ and $N_4P_4(NH_2)_8$, were synthesized by the reactions between $(NPCl_2)_3$ or $(NPCl_2)_4$ and liquid ammonia.[6] The present author previously reported the synthesis of $N_3P_3(NH_2)_6$[7] and the formation of $PO(ONa)(NH_2)_2$ by the alkali hydrolysis of the trimeric variety.[8] In this work, the hydrolysis of $N_4P_4(NH_2)_8$ in neutral, alkali, and acid solutions was investigated. The experimental results partially differ from the previous explanations.[9,10] Thus an improvement in the synthesis of $N_4P_4(NH_2)_8$ and its hydrolysis behaviors will be described.

Experimental

Preparation of $N_4P_4(NH_2)_8$. $(NPCl_2)_4$ (mp 123.0—123.7 °C) used as the raw material was obtained by fractional sublimation under a vacuum from $(NPCl_2)_n$ (n=3—7), which was synthesized by the reaction between phosphorus pentachloride and ammonium chloride. $(NPCl_2)_4$ was treated with liquid ammonia in the presence of a small amount of dioxane. The resulting product was dissolved in water, and the addition of ethanol into the solution gave rise to the precipitate of $N_4P_4(NH_2)_8 \cdot H_2O$, which was separated by filtration from the mother liquor and finally vacuum-dried over over phosphorus pentoxide.

Preparation of Alkali-hydrolysis Product. A 1.00 g portion of $N_4P_4(NH_2)_8 \cdot H_2O$ was refluxed with 100 ml of 0.65 M NaOH in a stainless steel flask for 3 h. The product was precipitated by the addition of excess ethanol into the solution, purified by recrystallization using ethanol, and finally vacuum dried over phosphorus pentoxide for 24 h.

Hydrolysis. For the neutral hydrolysis, a solution of 0.05 M $N_4P_4(NH_2)_8$ (or 0.05 M $N_3P_3(NH_2)_6$) was refluxed at 100 °C. Parts of the solution were taken out at proper time intervals, and these were supplied as the samples for the analysis. Hydrolysis was also carried out at room temperature for 3 weeks. For the alkali hydrolysis, a solution containing 0.05 M $N_4P_4(NH_2)_8$ in 1 M NaOH was prepared, and divided into several test tubes. The tubes were immersed in a bath regulated to a certain temperature. They were then successively withdrawn from the bath at proper time intervals. Both $N_4P_4(NH_2)_8$ and the $PO(ONa)(NH_2)_2$ formed were determined by means of ion-exchange chromatography. The rate of alkali hydrolysis and its activation energy were calculated. For the acid hydrolysis, a solution containing 0.05 M $N_4P_4(NH_2)_8$ in 0.25 M HCl was used. The acid hydrolysis was carried out in the same way as that for the neutral hydrolysis.

Analysis. The phosphorus content was determined gravimetrically as magnesium pyrophosphate. The total nitrogen content was determined by Kjeldahl's method. The sodium content was determined by using a flame photometer. The species of phosphorus amide-compounds were analyzed by ion-exchange chromatography,[8] and distinguished by paper chromatography using an alkalisolvent.[11]

Results and Discussion

Synthesis of $N_4P_4(NH_2)_8$. The synthesizing conditions of tetrameric phosphours diamide nitride and its analytical results are summarized in Table 1.

Formation of Insoluble Material: Generally, the reaction between a low polymer of phosphorus dichloride nitride and liquid ammonia is vigorously carried out, and some partially substituted products represented by $N_nP_nCl_{2n-x}(NH_2)_x$ (n=3,4) form; these are then gradually converted into the completely substituted products. The reactions are as follows:

$$(NPCl_2)_3 + 12NH_3 \rightarrow N_3P_3(NH_2)_6 + 6NH_4Cl \quad (1)$$

$$(NPCl_2)_4 + 16\,NH_3 \rightarrow N_4P_4(NH_2)_8 + 8NH_4Cl \quad (2)$$

The composition of the reaction product in (1) agreed fairly well with the calculated values as the sum of $N_3P_3(NH_2)_6$ and 6 NH_4Cl.[7] However, in the product of Eq. 2, the nitrogen content was less than that of its calculated value, the phosphorus and chlorine contents were conversely greater, and there was a considerable amount of an insoluble material as a by-product. The relations of the content of the insoluble material to the reaction time are shown in Fig. 1.

Table 1. Synthesis and analysis of tetrameric phosphorus nitride diamide

No.	Reaction conditions					Reaction products	Reaction products			
	$(NPCl_2)_4$ (g)	NH_3 (ml)	Solvent (ml)	Temp (°C)	Time (h)	Reaction products (g)	$N_4P_4(NH_2)_8$ (g)	P (%)	N (%)	Atomic ratio (P : N)
1	10.0	100	—	16—20	24	14.90	1.35	38.1	49.4	4.0 : 11.5
2	10.0	100	—	5—10	20	15.00	1.97	37.6	50.1	4.0 : 11.8
3	2.5	25	—	20—25	1	3.60	0.38	38.7	51.7	4.0 : 11.8
4	2.5	25	—	20—25	3	3.70	0.71	37.3	50.9	4.0 : 12.1
5	2.5	25	—	20—25	5	3.80	0.80	37.4	51.1	4.0 : 12.1
6	2.5	25	—	20—20	24	3.70	0.66	37.8	52.4	4.0 : 12.3
7	2.5	25	0.8	20—25	1	3.54	0.87	37.7	50.2	4.9 : 11.8
8	2.5	25	1.2	20—25	1	3.55	1.01	37.5	50.3	4.0 : 11.9
9	2.5	25	5.0	20—25	1	3.57	0.92	36.8	50.6	4.0 : 12.2
10	2.5	25	10.0	20—25	1	3.62	0.97	37.2	49.8	4.0 : 11.9
11	9.6	100	50.0	18—23	24	14.50	3.47	37.9	49.9	4.0 : 11.6
Composition of $N_4P_4(NH_2)_7.H_2O$ (Calcd values)							P : 37.99%		N : 51.54%	
Composition of $N_4P_4(NH_2)_8$ (Calcd values)							P : 40.22%		N : 54.55%	

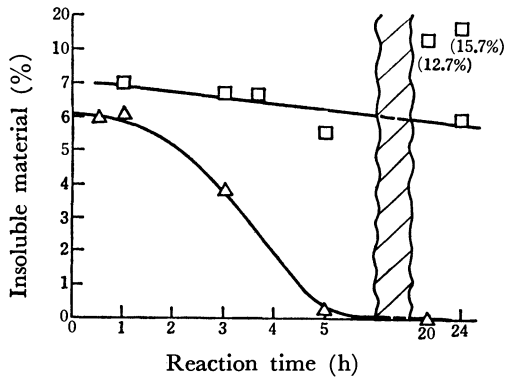

Fig. 1. Weight percent of insoluble material to reaction time.
△ : In the synthesis of $N_3P_3(NH_2)_6$.
□ : In the synthesis of $N_4P_4(NH_2)_8$.

In the formation of $N_3P_3(NH_2)_6$, the insoluble material disappeared in the reaction which lasted for about 5 h. Consequently, all the chloride atoms in $(NPCl_2)_3$ could be completely substituted by the amido groups. In the formation of $N_4P_4(NH_2)_8$, the insoluble material formed did not decrease so much in the course of time. For Nos. 3—6, which use a small amount of chloride, the insoluble material content was 5—6%, while for Nos. 1 and 2, which use a great amount of chloride, it was about 15%. In these cases, no homogeneous reaction between the liquid and solid phases evidently took place. Thus the insoluble material had not disappeared even in a reaction over a long period of time such as 24 h. It was therefore not the partially substituted product designated by $N_4P_4Cl_{8-x}(NH_2)_x$, but possibly a condensed product formed by the deammonation between the amide-phosphorus compounds as the intermediates. In order for the reaction to take place smoothly, the addition of dioxane in the reaction system of $(NPCl_2)_3$ with liquid ammonia has been proposed.[7] Thus in the reaction system of $(NPCl_2)_4$ with liquid ammonia, dioxane was added which resulted in no drastic reaction and very little insoluble material being formed. When no dioxane was added, the reaction product contained more than several% of the insoluble material, and the tetrameric variety extracted from the product showed a lower yield. The yields were remarkably increased by the addition of dioxane as shown in Table 1. The yields of the tetrameric variety were also calculated as 23 (non-addition), 53, 61, 55, and 59% in Nos. 3, 7, 9, and 10, respectively. The effect of dioxane as a medium in this reaction was evident.

Composition of The Product: The tetrameric phosphorus diamide nitride, which separates ammonium chloride as the by product from the reaction product by using liquid ammonia, is an anhydrous product. However, the composition of the material crystallized from an aqueous solution of the reaction product is not yet known. For the products obtained in this work, P content was 37—38%, N content was 50—51%, and the mole ratio of P to N was exactly 1 : 3. From these results, the expected composition was given by the formula $N_4P_4(NH_2)_8 \cdot H_2O$. The X-ray diffraction values of tetrameric phosphorus diamide nitride have not yet been registered on the ASTM X-ray data cards. An X-ray diffraction data of $N_4P_4(NH_2)_8 \cdot H_2O$ is shown in Table 2.

Hydrolysis of $N_4P_4(NH_2)_8$. Neutral Hydrolysis: After refluxing of an aqueous solution of $N_4P_4(NH_2)_8$ at 100 °C, the hydrolysis products were determined by means of ion-exchange chromatography. The results are given in Fig. 2.

Chromatogram I shows the elution for a mixture of various standard materials, while II, III, IV, V, and VI show elutions for some hydrolysis products over the course of time. The hydrolysis of $N_4P_4(NH_2)_8$ (A) was recognized by refluxing for 30 min. A considerable amount of $P_2O_2NH(NH_2)_4$ (C) and $PO(OH)(NH_2)_2$ (D) were formed after 60 min. Form the expected hydrolysis mode shown in Fig. 7, it can be considered that $PO(NH_2)_3$ and $P_2O_2NH(NH_2)_4$ are simultaneously formed. Both $N_4P_4(NH_2)_8$ and $PO(NH_2)_3$ are typical non-electrolytes. They were therefore eluted

TABLE 2. X-RAY DIFFRACTION DATA FOR $N_4P_4(NH_2)_8 \cdot H_2O$, ITS ALKALI HYDROLYSIS PRODUCT AND $PO(ONa) \cdot (NH_2)_2$

$N_4P_4(NH_2)_8 \cdot H_2O$	Alkali-hydrolysis product	$PO(ONa) \cdot (NH_2)_2$
α, Å I	α, Å I	α, Å I
8.40 M		
7.69 W		
7.19 W		
6.68 W		
6.65 W		
6.06 S	5.21 S	5.21 S
5.06 S	5.01 W	5.01 W
	4.67 M	4.67 W
		4.57 W
	4.48 M	4.48 W
	3.90 S	3.90 M
3.81 W		
	3.75 W	3.75 S
3.67 S		
3.59 M		
3.50 W		3.53 M
3.45 W		
3.34 S		
3.26 W		
	3.13 M	3.13 M
	3.00 M	3.00 S
2.92 W	2.91 W	
2.65 W	2.67 S	2.67 M
	2.60 M	2.59 M
	2.50 W	2.50 W

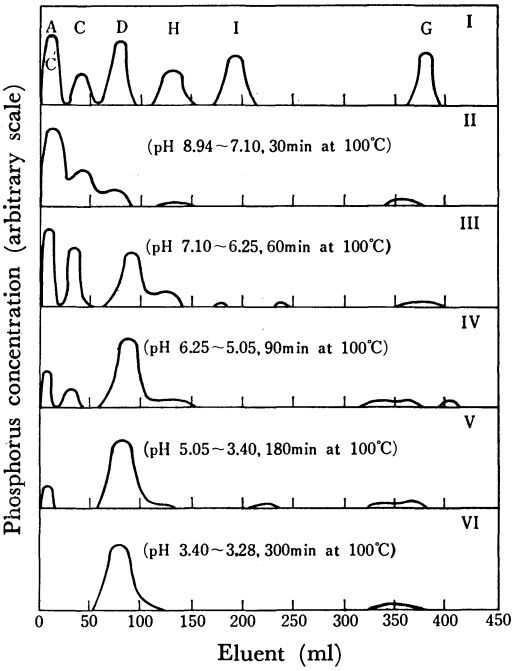

Fig. 2. Gradient elution analysis of various phosphorus compounds and hydrolysis products of $N_4P_4(NH_2)_8$.
Eluent: 1 l H_2O in mixing bottle, 400 ml 0.8 mol/l KCl in stock bottle.
I: Mixture of amide phosphorus compounds and phosphates [A: $N_4P_4(NH_2)_8$, C: $P_2O_2(NH)(NH_2)_4$, C': $PO(NH_2)_3$, D: $PO(ONa)(NH_2)_2$, H: $PO(ONa)_2NH_2$, I: Na_2HPO_4, G: $Na_4P_2O_7$].
II—VI: Hydrolysis products of $N_4P_4(NH_2)_8$.

at the same position on the ion-exchange chromatogram, as is shown in Fig. 3. However, in paper chromatography, R_f 0.27 $N_4P_4(NH_2)_8$ can be clearly distinguished from R_f 0.67 $PO(NH_2)_3$. In fact, it was seen that both components exist in the solution refluxed for 60 min. The pH of the solution was gradually lowered in the course of the refluxing time. $N_4P_4(NH_2)_8$, $PO(NH_2)_3$, and $P_2O_2NH(NH_2)_4$ then decreased, and $PO(OH)(NH_2)_2$ increased as the main hydrolysis product. A part of the formed diamidophosphate gradually decomposed to monoamidophosphate (H) and some orthophosphate (I). The hydrolysis behavior of $N_3P_3(NH_2)_6$ at 100 °C had also been recognized as analogous to that of $N_4P_4(NH_2)_8$.

Hydrolysis of $N_4P_4(NH_2)_8$ and $(NPCl_2)_8$ at Room Temperature: The elution chromatograms of a mixture of standard materials and hydrolysis products of $N_4P_4(NH_2)_8$ and $(NPCl_2)_4$ are shown in Fig. 3.

In an aqueous solution, $N_4P_4(NH_2)_8$ was stable for about 3 days at room temperature, after which it graudually hydrolyzed. Chromatogram II shows an elution curve for the hydrolysis product of $N_4P_4(NH_2)_8$ after 20 days. The rate of hydrolysis was remarkably slow, the composition of the hydrolysis products being similar to that at 100 °C. Chromatogram III shows the elution for the hydrolysis product of $(NPCl_2)_4$ (0.5 g) in an ether (7.5 ml)–aqueous ammonia (3 M, 8 ml) solution. $(NPCl_2)_4$ was partly converted into $N_4P_4(NH_2)_8$ in spite of the presence of water. The other products were some phosphoryl triamide, tetramidoimdodiphosphate, orthophosphate, and imidodiphosphate. $(NPCl_2)_4$ (0.5 g) was also hydrolyzed in an ether (15 ml)–water (5 ml) solution. The product was neutralized by employing aqueous ammonia, and analyzed by means of ion-exchange chromatography. The result is shown as chromatogram IV. In this hydrolysis, $(NPCl_2)_4$ was converted simultaneously into a cyclic tetrametaphosphimate which gradually hydrolyzed into imidotetraphosphate, imidotriphosphate, imidodiphosphate, and some amidophosphate.

Moureu and Rocquet[9] observed by microscopic examination that the hydrolysis product of $N_4P_4(NH_2)_8$ closely resembles $P_4N_4O_4H_4(ONH_4)_4 \cdot 4H_2O$ which[12] was obtained by the hydrolysis of $(NPCl_2)_4$. It was concluded that the hydrolysis product of $N_4P_4(NH_2)_8$ is the same compound as $P_4N_4O_6H_6(ONH_4)_2$. However, the components were not examined by other analytical techniques. Their result was referred to in a science text.[13] To confirm the validity of their result, the present author has investigated the hydrolysis behavior of $(NPCl_2)_4$ and $N_4P_4(NH_2)_8$. The cyclic tetrametaphosphimate was obviously formed by the hydrolysis of $(NPCl_2)_4$, but the formation of tetrametaphosphimate by the hydrolysis of $N_4P_4(NH_2)_8$ could not be recognized.

Alkali Hydrolysis: The results of alkali and ammoniacal hydrolysis are shown in Fig. 4.

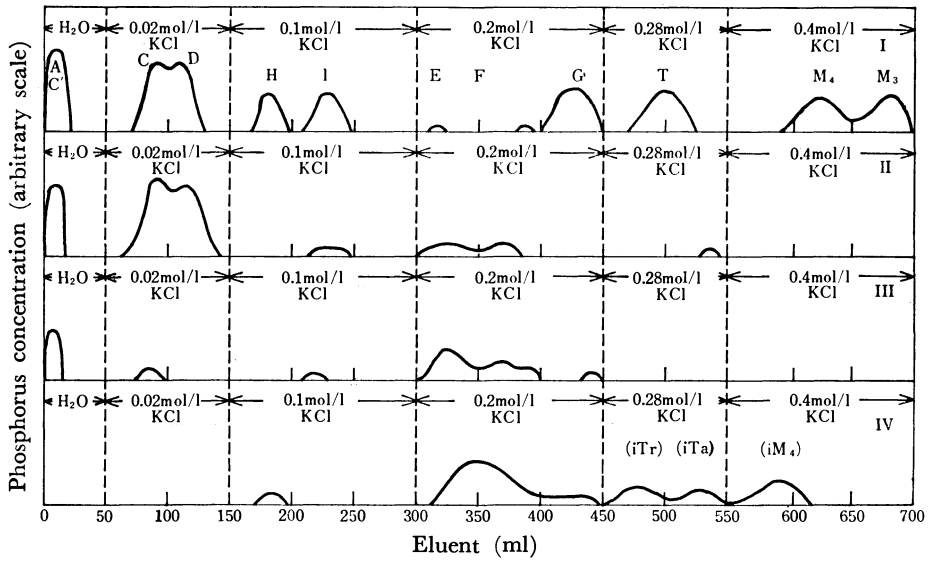

Fig. 3. Chromatographic analysis of hydrolysis products of $N_4P_4(NH_2)_8$ and $(NPCl_2)_4$ at room temperature.
I: Mixture of standard materials [A: $N_4P_4(NH_2)_8$, C: $P_2O_2(NH)(NH_2)_4$, C': $PO(NH_2)_3$, D: $PO(ONa)(NH_2)_2$, G: $Na_4P_2O_7$, H: $PO(ONa)_2NH_2$, I: Na_2HPO_4, T: $Na_5P_3O_{10}$, M_3: $(NaPO_3)_3$, M_4: $(NaPO_3)_4$]
II: Hydrolysis product of $N_4P_4(NH_2)_8$ for 20 day.
III: Hydrolysis product of $(NPCl_2)_4$ in ether-aqueous ammonia solution for 1 h.
IV: Hydrolysis product of $(NPCl_2)_4$ in ether-water solution for 2 h.
Estimated compounds: [E: $P_2O_2(NH)(NH_2)_2$, F: $P_2O_2(NH)(OH)_4$, iTr: $P_3O_3(NH)_2(OH)_5$, iTa: $P_4O_4(NH)_3(OH)_6$, iM_4: $P_4N_4O_4H_4(OH)_4$].

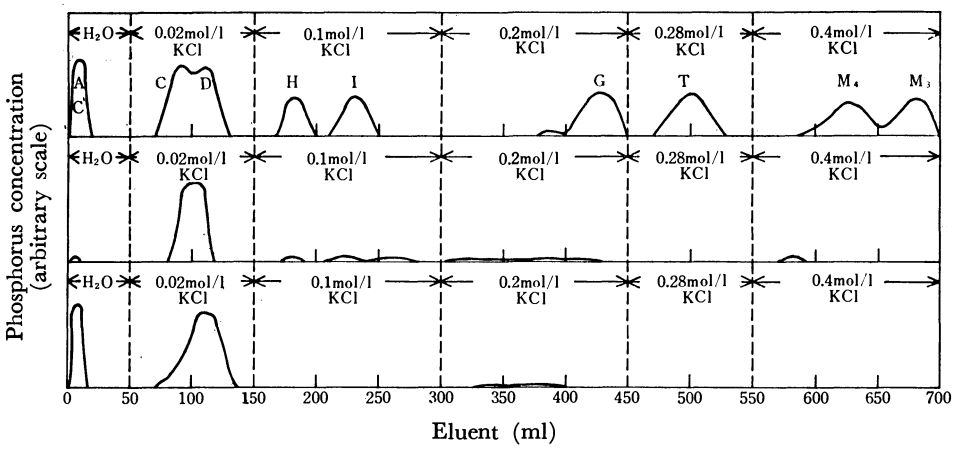

Fig. 4. Chromatographic analysis of various phosphorus compounds and hydrolysis products of $N_4P_4(NH_2)_8$ in alkali solution.
I: Mixture of standard materials [A: $N_4P_4(NH_2)_8$, C: $P_2O_2(NH)(NH_2)_4$, C': $PO(NH_2)_3$, D: $PO(ONa)(NH_2)_2$, G: $Na_4P_2O_7$, H: $PO(ONa)_2NH_2$, I: Na_2HPO_4, T: $Na_5P_3O_{10}$, M_3: $(NaPO_3)_3$, M_4: $(NaPO_3)_4$].
II: Hydrolysis product of $N_4P_4(NH_2)_8$ in 0.65 M NaOH for 3 h at 100 °C.
III: Hydrolysis product of $N_4P_4(NH_2)_8$ in 3 M NH_4OH for 3 h at 100 °C.

Chromatogram I shows the elution for a mixture of the standard materials. Chromatogram II, shows that $N_4P_4(NH_2)_8$ was converted directly into diamidophosphate. On the paper chromatogram for a certain sample of the alkali hydrolysis, only the spots of R_f 0.27 $N_4P_4(NH_2)_8$ and R_f 0.52 $PO(ONa)(NH_2)_2$ appeared. Thus the alkali hydrolysis behavior of $N_4P_4(NH_2)_8$ is much the same as that of $N_3P_3(NH_2)_6$[8]. Chromatogram III shows the elution for an ammoniacal hydrolysis product. The rate of ammoniacal hydrolysis was slower than that of alkali hydrolysis even using the highly concentrated aqueous ammonia; even then $N_4P_4(NH_2)_8$ could not be completely converted into diamidophosphate.

Composition of the Alkali Hydrolysis Product: The formation of the alkali hydrolysis products and diamidophosphate and their analyses are summarized in Table 3.

The phosphorus and nitrogen contents of the hydrolysis products were less than that of $PO(ONa)(NH_2)_2$ obtained by Stokes' method,[14] but the mole ratio of N to P was close to 2 : 1, while the sodium content was greater than the expected value. The previous report[8] gave details of this reasoning. Its

TABLE 3. FORMATION AND ANALYSIS OF DIAMIDOPHOSPHATES

No.	Method	Reaction conditions: Sample (g)	NaOH (g)	Time (min)	Recrystallization	Dry agent	Reaction products: Yield (g)	P (%)	N (%)	Na (%)	P : N : Na (Atomic ratio)
1	Hydrolysis of $N_3P_3(NH_2)_6$ with NaOH solution	2.00	3.2	120	3	Phosphorus pentoxide	2.27	16.4	14.2	23.4	1 : 1.92 : 1.92
2	Hydrolysis of $N_4P_4(NH_2)_8$ with NaOH solution	1.00	2.5	150	3	Phosphorus pentoxide	1.30	15.7	13.6	24.9	1 : 1.92 : 2.14
3	Saponification of $PO(OC_6H_5)(NH_2)_2$ with NaOH solution (Stokes' method)	3.40	0.85	5	4	Phosphorus pentoxide	1.02	25.6	23.3	19.6	1 : 2.01 : 1.03

outline is explained as follows. When an oily diamidophosphate is deposited from its aqueous solution by the addition of ethanol, the salt has a character including an excess of sodium hydroxide. However, the X-ray diffraction of the alkali hydrolysis product of N_4P_4 $(NH_2)_8$ roughly agreed with that of $PO(ONa)(NH_2)_2$ as shown in Table 2, and these values also agreed with those of ASTM X-ray powder data cards. Thus the alkali hydrolysis product is obviously identical with diamidophsphate.

Rate Constants and Activation Energy of the Reaction: Both $N_4P_4(NH_2)_8$ and $PO(ONa)(NH_2)_2$ contained in an aqueous solution of the alkali hydrolysis were studied by means of ion-exchange chromatography. The percentages of $N_4P_4(NH_2)_8$ which remained in the hydrolysis are shown in Fig. 5.

The rate of the hydrolysis increased with the increase of the reaction temperature, obeying a first-order equation, with the rate constants (k) 1.0×10^{-3}, 2.5×10^{-3}, 1.9×10^{-2}, and 4.2×10^{-2} at 50, 60, 80, and 90 °C, respectively. These values are about 2.7 times the value of the alkali hydrolysis of $N_3P_3(NH_2)_6$. The activation energy, obtained from the relation of log k with the reciprocal of the reaction temperature, was 20.8 kcal/mol. This value agrees nearly with 20 kcal/mol for $N_3P_2(NH_2)_6$.[8]

Acid Hydrolysis: The results of the acid hydrolysis are shown in Fig. 6.

The acid hydrolysis behavior resembles that of neutral hydrolysis. However, when the reaction was

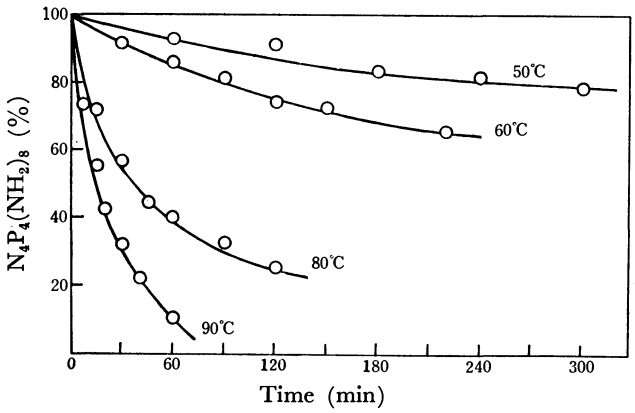

Fig. 5. Hydrolysis of tetrameric phosphorus diamide nitride in 1 M sodium hydroxide solution.

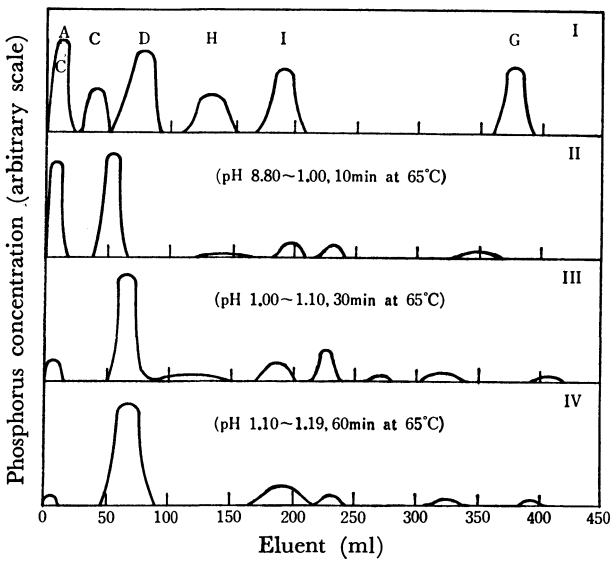

Fig. 6. Gradient elution analysis of various phosphorus compounds and hydrolysis products of $N_4P_4(NH_2)_8$ in acid solution.
Eluent: 1 l H_2O in mixing bottle, 400 ml 0.8 mol/l KCl in stock bottle.
I: Mixture of amide phosphorus compounds and phosphates [A: $N_4P_4(NH_2)_8$, C: $P_2O_2(NH)(NH_2)_4$, C': $PO(NH_2)_3$, D: $PO(ONa)(NH_2)_2$, H: $PO(ONa)_2NH_2$, I: Na_2HPO_4, G: $Na_4P_2O_7$].
II—IV: Hydroysis products of $N_4P_4(NH_2)_8$.

accelerated with an acid strength such as pH 1.0, the existence of $PO(NH_2)_3$ and $P_2O_2NH(NH_2)_4$ which are unstable in an acid solution could not be recognized. In this case, $N_4P_4(NH_2)_8$ was hydrolyzed up to the formation of orthophosphates and diphosphates.

Process of Hydrolysis: The process of the neutral or acid hydrolysis is shown in Fig. 7.

A proton from water coordinates to an N atom on the ring of $N_4P_4(NH_2)_8$, one in a double bond between the N and P atoms is cut off, and then the P atom has a positive charge. This coordinates to an OH group, and then the ring is opened. An intermediate (B), which has an asymmetrical structure and is unstable, is formed. It immediately decomposes into unknown compounds (B' and B''), tetramidoimidodiphosphate (C), and phosphoryl triamide (C'). The arrows shown in Fig. 7 denote the course of the hydrolysis. The hy-

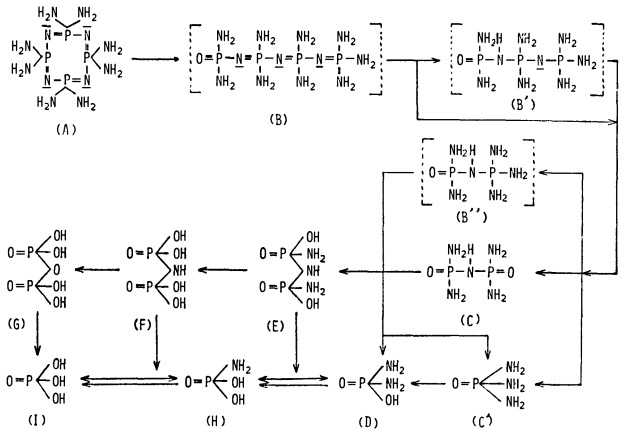

Fig. 7. Hydrolysis of $N_4P_4(NH_2)_8$ in neutral or acid solution.

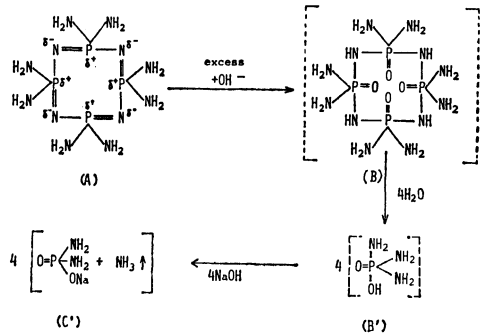

Fig. 8. Hydrolysis of $N_4P_4(NH_2)_8$ in alkali solution.

drolysis of $N_4P_4(NH_2)_8$ roughly progresses up to the formation of diamidophosphate in the neutral solution.

The alkali hydrolysis of $N_4P_4(NH_2)_8$ can be expressed as follows:

$$N_4P_4(NH_2) + 4H_2O + 4NaOH \rightarrow 4PO(ONa)(NH_2) + 4NH_3 \quad (3)$$

The process of the reaction is shown in Fig. 8.

In the P–N ring of $N_4P_4(NH_2)_8$, the electronegativity of phosphorus (2.1) is less than that of nitrogen (3.0). Thus there is the possibility of a polarization such as $N^{\delta-}$–$P^{\delta+}$. In an alkali aqueous solution, the ionic strength of OH^- is large, and this OH group coordinates to the $P^{\delta+}$ atom. Consequently, the double bond between the P and N atoms is cut off and a single bond forms simultaneuously, since the N atom has an electron. At the same time, the P atom is combined by a co-coordinate bond to the O atom in the previously coordinated OH group, and the H in the OH group is separated as an ion; it reacts with the N atom in the P–N ring and then an imido group is formed. This state can be represented as an unknown compound (B). Further, (B) is immediately hydrolyzed into an unknown compound (B'). (B') separates ammonia by the reaction with sodium hydroxide, and is converted directly into diamido phosphate, which is of a stable structure of the sp^3 hybridization.

References

1) a) The paper was presented at the 33th Annual Meeting of the Chemical Society of Japan, Fukuoka, October, 1975. A part of this report was published in *Chem. Lett.*, **1976**, 479; b) Part XXVI of this series: E. Kobayashi and S. Kamagami, *Nippon Kagaku Kaishi*, **1975**, 2098.

2) C. A. Redfarn and H. Coates (Albright & Wilson Ltd.), Brit. 788785 (1958).

3) Erik R. Nielsen and William L. Stepp, U.S. Patent 3348926 (1967).

4) T. Z. Wakefield, E. S. Allen, F. J. McCullough, C. R. Sheridan, and J. J Kohlen, *J. Agr. Food. Chem.*, **19**, 99 (1971).

5) W. Wanek, L. Ondracek, and J. Hampl, *Z. Pflanzenernaehr. Bodenkd.*, **128**, 169 (1971); *Agrokhimiya*, **11**, (6) 177 (1971).

6) L. F. Audrieth, R. Steinman, and A. D. F. Toy, *Chem. Rev.* **32**, 99 (1943).

7) E. Kobayashi, *Nippon Kagaku Kaishi*, **1972**, 38; *Tokyo Kogyo Shikensho Hokoku*, **68**, 19 (1973).

8) E. Kobayashi, *Nippon Kagaku Kaishi*, **1973**, 1437; *Tokyo Kogyo Shikensho Hokoku*, **69**, 470 (1974).

9) H. Moureu and P. Rocquet, *Bull. Soc. Chim. Fr.*, **1936** 829.

10) K. Dostal, M. Kouril, and J. Novak, *Z. Chem.*, **4**, 353 (1964); *Chem. Abstr.*, **62**, 4670 (1965).

11) G. Biberacher, *Z. Anorg. Allg. Chem.*, **285**, 86 (1956).

12) H. N. Stokes, *Am. Chem. J.*, **18**, 780 (1896).

13) Charles B. Colburn, "Developments in Inorganic Nitrogen Chemistry I," Elsevier, Amsterdam (1966), p.356.

14) H. N. Stokes, *Am. Chem. J.*, **16**, 123 (1894).

Structure of Ziegler-Natta Catalysts for the Polymerization of Isoprene

Masao UETSUKI and Yuzuru FUJIWARA

Central Research Laboratories, Kuraray Co, Ltd., Sakazu 2045, *Kurashiki 710*

(Received June 17, 1976)

Structural investigation was carried out by means of ^{1}H-NMR, ESR, and chemical ionization mass spectrometry on the complexes formed by the reaction of alkylaluminum with titanium(IV) *t*-butoxide or vanadium(IV) *t*-butoxide as a catalyst for polymerization of isoprene. The *t*-butoxide was monomeric in benzene, and reduced to form a bivalent complex *via* trivalent ones on addition of the alkylaluminum to the solution followed by the formation of two kinds of binuclear aluminum complexes. In the trivalent state the complexes caused polymerization of isoprene to form five kinds of polymers, 1,4-polymerization of isoprene being likely caused by tris[di-μ-t-butoxo-dialkyltitanium(III)]aluminum, or the corresponding vanadium(III) complex. The final product of the reduction of vanadium(IV) *t*-butoxide was bis(di-μ-alkyl-dialkylaluminum)vanadium(II), which exhibits no catalytic activity.

It is well-known that polymerization of isoprene is caused either by Ziegler-Natta catalysts or by organolithiums. Significant characteristics of the Ziegler-Natta catalysts lie in their ability to form stereoregular polymers, the chemical nature of the catalysts being ascribed to structure and electronic state of the complex composed of aluminum and one of transition elements. Since the pioneer work of Natta *et al.*[1] a number of investigations have been made in this field, but the stucture of the catalysts is not clear so that the mechanism of the catalytic reaction is still ambiguous. The original Ziegler-Natta catalysts, prepared by the reaction of alkylalumium with chloride of titanium or other transition elements, formed a heterogeneous system, which resulted in difficulty in structural study of the catalysts. The polymerization mechanism of isoprene with the catalyst of organolithiums, however, was studied in detail by Morton *et al.*,[2] who examined the propagating chain end of polyisoprene by means of ^{1}H NMR.

Alkylaluminums react with alkoxides of titanium(IV) or vanadium(IV) to form a homogeneous system.[3-6] Natta *et al.*[3] examined polymerization of butadiene and isoprene with the catalysts prepared by the reaction of the alkylaluminums with the titanium(IV) alkoxides by measuring the infranred absorption and X-ray diffraction of the reaction products, and by determining the structures of the 1,2- and the 3,4-polymers. Angelscu *et al.*[4] measured the ESR spectra of the reaction mixture of triethylaluminum and titanium(IV) *t*-butoxide to detect a titanium(III) complex containing two aluminum nuclei. Hirai *et al.*[5,6] also studied the ESR spectra of the reaction mixture of triethylalumium and titanium(IV) butoxide as a catalyst for the polymerization of butadiene, penta-1,3-diene and isoprene to determine the molar ratio of aluminum and titanium in the resulting polynuclear complexes. However, they could not throughly correlate the structure of the Ziegler-Natta catalyst to the reaction mechanism.

We have tried to determine the structure and electronic state of the Ziegler-Natta catalysts prepared by the reaction of trimethyl-, triethyl- or triisobutylaluminum with titanium(IV)- or vanadium(IV) *t*-butoxide as a catalyst for the polymerization of isoprene. The paramagnetic and the diamagnetic species were examined by means of ESR and ^{1}H-NMR, respectively. The evaluation of the *g* factor was performed on the basis of the ligand field theory. Chemical ionization mass spectrometry was utilized in dtermination of the molecular weight of the catalytic complexes.

Experimental

Reagents. Trimethyl-, triethyl-, and triisobutylaluminum were obtained from Ethyl Co. Titanium(IV) chloride was manufactured by Kishida Chemical Co., vanadium(IV) chloride by Wako Pure Chemical Industries, Ltd., and butyllithium by Mitsuwa Chemical Co. These reagents were used without further purification. Aluminum chloride (Kanto Chemical Co.) was ground into powder, and dried *in vacuo* at 25 °C for 20 h. Organic reagents were purified by using dehydration reagents as the occasion demanded. Aluminum-, titanium(IV)- and vanadium(IV) *t*-butoxides were synthesized in diisopropyl ether according to the following reactions,[7,8] and purified by distillation under reduced pressure.

$$\mathrm{LiBu} + \mathrm{HNEt_2} \rightarrow \mathrm{LiNEt_2} + \mathrm{BuH}$$

$$\mathrm{MCl}_n + n\mathrm{LiNEt_2} \rightarrow \mathrm{M(NEt_2)}_n + n\mathrm{LiCl}$$

$$\mathrm{M(NEt_2)}_n + n\textit{t}\text{-BuOH} \rightarrow \mathrm{M}(\textit{t}\text{-BuO})_n + n\mathrm{HNEt_2}$$

where M denotes aluminum, titanium or vanadium.

Preparation of Samples. Samples were prepared under nitrogen atmosphere. The alkylaluminum and the metal alkoxide were separately dissolved in benzene or toluene, and the solutions were mixed to form the catalyst. Aging of the catalyst and polymerization of isoprene were carried out in a reaction tube made of stainless steel for 0.5 and 20 h, respectively. Molar ratios of the transition elements, isoprene and the solvent were fixed at 1.00 : 100 : 300.

Spectral Measurements. ^{1}H-NMR spectra were measured with a Varian Associates HA-100 high resolution spectrometer operating at 100 MHz. ESR spectra were taken on a Japan Electron Optics Laboratory JES-ME3 spectrometer operating in the X-band with 100 KHz modulation. *g*-Values and hyperfine coupling constants were determined by using the ESR signal of manganese dioxide as a standard. Liquid nitrogen was used to measure the ESR spectra at −196 °C. Mass spectra were recorded on a Finnigan 3300F quadrupole spectrometer equipped with a chemical ionization system. Isobutane was used as a reactant gas for the chemical ionization.

Results and Discussion

Polymerization of Isoprene. Experiments of isoprene polymerization were performed in benzene at

80—140 °C with the catalysts prepared by the reaction of trimethyl-, triethyl- or triisobutylaluminum with titanium(IV)- or vanadium(IV) *t*-butoxide. Structure of the reaction products was studied by ^{1}H-NMR spectra. It was found that five types of reactions take place to form 1,4-polyisoprene, 3,4-polyisoprene, 2,6-dimethyl-1,3,6-octatriene, 1-methyl-4-isopropenyl-1-cyclohexene, or 2-methyl-4-isopropenyl-1-cyclohexene. The molar ratio of *cis*- and *trans*-1,4 bonds in 1,4-polyisoprene was *ca.* 1 : 2 showing dependence neither upon the species of the transition element nor upon the present reaction conditions. Three kinds of isoprene dimers, 2,6-dimethyl-1,3,6-octatriene, and 1- and 2-methyl-4-isopropenyl-1-cyclohexenes, could be distilled out from the reaction mixture under reduced pressure, but it was difficuot to separate the two high polymers, 1,4- and 3,4-polyisoprenes, from each other. For convenience, the symbol A is used to show the added molar ratio of the alkylaluminum and titanium-(IV)- or vanadium(IV) *t*-butoxide.

Aging of the catalytic system at 100—140 °C for 20—30 min was required to reproduce the reactions. Yield of the reaction products varied in accordance with the value of A, and the catalytic reaction system containing vanadium was higher in conversion of isoprene as well as in selectivity of the reactions than the system containing titanium. Experimental data with the catalysts composed of trimethylaluminum and titanium(IV)- or vanadium(IV) *t*-butoxide are shown in Figs. 1 and 2, respectively. All the reactions took place mainly in the region $A=1$—7. This suggests that the transition element of the catalytic complex is active at the trivalent state, but not at the tetra- or the bivalent state. Titanium and vanadium are supposed to produce the active complexes with a similar stucture, though their amounts are not equal to each other depending upon the relative stability of the trivalent state.

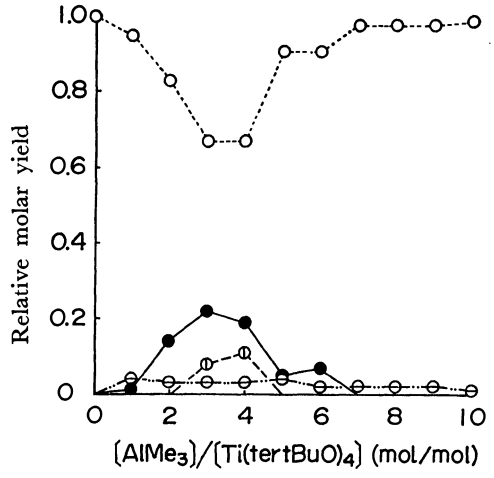

Fig. 1. Yield of the reaction products of isoprene in the catalytic system prepared by trimethylaluminum and titanium(IV) *t*-butoxide. Reaction was performed in benzene at 100 °C for 20 h after aging the catalyst at 140 °C for 30 min. ○, ⦶, ⊖, and ● show isoprene, 2,6-dimethyl-1,3,6,-octatriene, 1-methyl-4-isopropenyl-1-cyclohexene, and 1,4-polyisoprene, respectively.

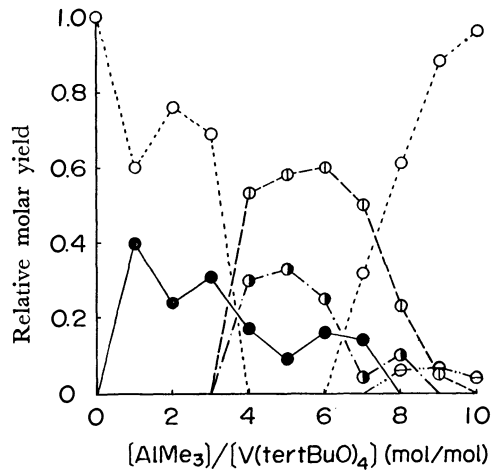

Fig. 2. Yield of the reaction products of isoprene in the catalytic system prepared by trimethylaluminum and vanadium(IV) *t*-butoxide. Reaction was performed in benzene at 100 °C for 20 h after aging the catalyst at 100 °C for 30 min. ◑ show 3,4-polyisoprene, and other circles are the same as in Fig. 1.

When the reaction of isoprene was performed at 100 °C, 1,4-polyisoprene showed the maximum yield at $A=2$—4 and 1—3 with the catalysts containing titanium and vanadium, respectively, and the highest selectivity at $A=1$—2. Both 3,4-polyisoprene and 2,6-dimethyl-1,3,6-octatriene were produced at $A=$ 3—5 and 4—7 with the catalysts containing titanium and vanadium, respectively. 1-Methyl-4-isopropenyl-1-cyclohexene was observed in the whole region of A, and its yield decreased when the catalytic system was aged at relatively low temperature. A similar result was obtained by using triethyl- or triisobutyl-aluminum instead of trimethylaluminum. However, the catalytic system prepared from triisobutylaluminum caused formation of 2-methyl-4-isopropenyl-1-cyclohexene, the yield of which increased with increase in the A value. Thermal reactions of isoprene[9] took place above 140 °C to produce 1- and 2-methyl-4-isopropenyl-1-cyclohexenes.

^{1}H-NMR Spectra. Trivalent aluminum complexes are diamagnetic, their valence state being stable. Trimethylaluminum reacts with aluminum isopropoxide to form three kinds of tetranuclear and two kinds of binuclear complexes, structures of which were determined by means of ^{1}H-NMR in benzene.[10] Similar complexes were observed with the ^{1}H-NMR spectra when aluminum *t*-butoxide was used instead of isopropoxide. Titanium(IV) is also diamagnetic, while the complexes of titanium(III) or vanadium(IV) are paramagnetic because of the electronic configuration of $3d^1$. The diamagnetic complexes showed ^{1}H-NMR signals with high resolution even when a considerable amount of paramagnetic complexes coexisted, though the latter displayed either broad or no signals.

^{1}H-NMR spectra (Fig. 3) were measured with a mixture of trimethylaluminum and titanium(IV) *t*-butoxide at 30 °C after being heated in benzene at 140 °C for 30 min. Bradley *et al.*[11] measured volatility

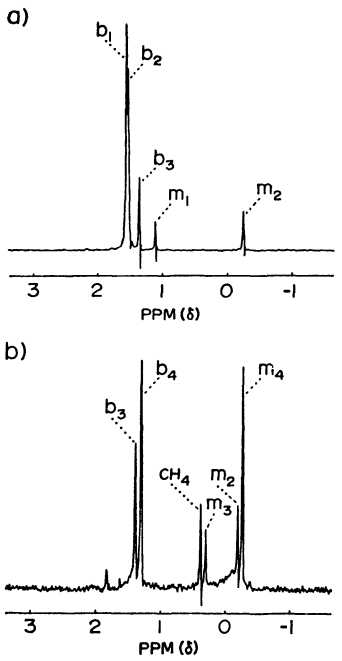

Fig. 3. ^{1}H NMR spectra of the mixture of trimethylaluminum and titanium(IV) *t*-butoxide in benzene at 30 °C after heating at 140 °C for 30 min. The prepared molar ratio of trimethylaluminum and titanium(IV) *t*-butoxide is a) 0.40 : 0.60, and b) 0.90 : 0.10.

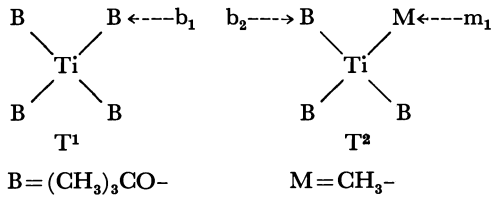

of titanium(IV) *t*-butoxide in order to determine a monomeric stucture of T^1. The monomeric structure was reconfirmed by the fact that titanium(IV) *t*-butoxide shows a ^{1}H-NMR signal, b_1, alone, which represents no splitting attributable to two or more kinds of coordination states of the ligands in toluene even below −50 °C. A pair of signals, b_2 and m_1, with a molar ratio of 3 : 1 are assigned to the *t*-butoxyl and the methyl groups, respectively, of methyl-tri-*t*-butoxotitanium(IV), T^2. Signals of b_3, b_4, m_2, m_3, and m_4, which increased in intensity with increase in the amount of added trimethylaluminum, are assigned to the ligands of binuclear aluminum complexes, A^1 and A^2, from the result of the ^{1}H-NMR measurements of the reaction mixture of trimethylaluminum and aluminum *t*-butoxide.

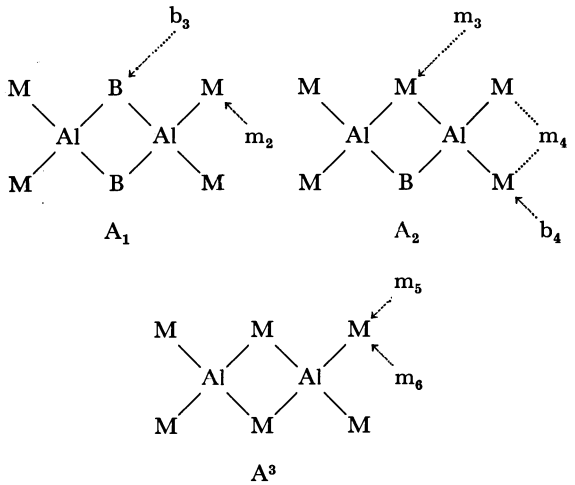

Hoffmann,[12] and Haaland *et al.*[13] determined the structure of A^1 by use of ^{1}H-NMR and electron diffraction, respectively. A dimeric stucture of trimethylaluminum, A^3, is well-known. The NMR assignment was performed by Muller *et al.*[14]

Vanadium(IV) *t*-butoxide displayed a ^{1}H-NMR signal with a half-height width of 147 Hz at τ=6.82 in benzene at 30 °C, though the line broadening caused by the paramagnetic effect of vanadium(IV) prevented structural examination. On addition of trimethylaluminum to the solution, NMR signals of the binuclear aluminum complexes appeared but none of vanadium(III) and vanadium(II) complexes.

ESR Spectra of Vanadium Complexes. On the basis of volatility measurements, Bradley *et al.*[8] found that vanadium(IV) *t*-butoxide as well as other tertiary alkoxides are monomeric so that the question is the coordination symmetry of the complex. If vanadium(IV) *t*-butoxide takes Td symmetry, the 3d orbitals split into two levels, lower and upper ones of which are degenerate 2-fold with E symmetry and 3-fold with T_2 symmetry, respectively. Taking the spin-orbit interaction as a first-order perturbation to the ligand field splitting, principal values of the *g*-tensor of the tetrahedral complex are represented by

$$\begin{aligned} g_x &= g_e - 2\rho^2\zeta\varepsilon[\sin(\theta/2) - 3\cos(\theta/2)]^2 \\ g_y &= g_e - 2\rho^2\zeta\varepsilon[\sin(\theta/2) + 3\cos(\theta/2)]^2 \\ g_z &= g_e - 2\rho^2\zeta\varepsilon[2\sin(\theta/2)]^2 \end{aligned} \quad (1)$$

where g_e, ρ, and ζ are the *g*-factor for a free electron, an orbital reduction factor, and a spin-orbit coupling constant, respectively. θ is a tortion angle of the ligand about a coordination bond caused by the Jahn-Teller effect.[15] ε denotes the reciprocal of the energy difference between the orbitals with E and T_2 symmetries.

As shown in Fig. 4 the ESR spectrum of vanadium(IV) *t*-butoxide, which was measured in toluene at −196 °C, represents a double octet pattern with an axial symmetry. Anisotropic *g*-values obtained are $g_{//}=1.9395\pm0.0005$ and $g_\perp=1.9870\pm0.0005$, and anisotropic hyperfine coupling constants $A_{//}=1.46\times10^{-2}$ cm^{-1} and $A_\perp=2.13\times10^{-3}$ cm^{-1}. When θ is π in Eq. 1, g_x and g_y become equivalent resulting in the axial symmetry of the complex, *i.e.* $g_{//}=g_z$ and $g_\perp=g_x=g_y$. Thus the axial symmetry of the experimental *g*-values can be interpreted to support the view that vanadium(IV) *t*-butoxide takes the tetrahedral structure. The condition, $\theta=\pi$, indicates that the tetrahedral structure is compressed along one of the 3-fold improper axes.[15]

The magnitude of the spin-orbit coupling constant is estimated from the atomic spectrum as ζ=248 cm^{-1} for the vanadium(IV) ion.[16] The ligand field splitting of the 3d orbitals of vanadium(IV) *t*-butoxide was determined from the near-infrared absorption

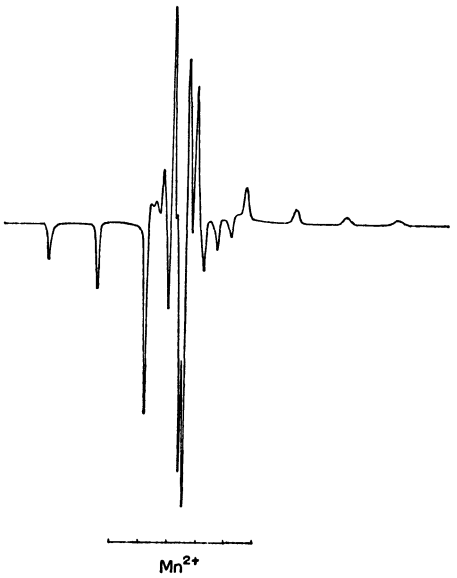

Fig. 4. ESR spectrum of vanadium(IV) *t*-butoxide in toluene at −196 °C.

spectrum in benzene as $\varepsilon^{-1}=1.45\times10^{4}\,cm^{-1}$, a little larger than that obtained by Kokoszka *et al.*[17] The orbital reduction factor of the complex was determined to be $\rho=0.67$ by comparing the calculated values of $g_{//}$ and $g_{\perp}$ with observed values. The anisortopic *g*-values are averaged to be $\bar{g}=1.9712$, which agrees closely with the observed value at 25 °C.

A mixture of trimethylaluminum and vanadium(IV) *t*-butoxide exhibited ESR signals from two kinds of vanadium(IV) complexes besides the signal of vanadium(IV) *t*-butoxide at −196 °C immediately after mixing in toluene at 25 °C. However, partial overlapping of the signals made it difficult to determine both the values of the *g*-factor and the hyperfine coupling constant of the complexes. After the mixture of trimethylaluminum and vanadium(IV) *t*-butoxide was allowed to stand for 1 h at 25 °C ,the signal of vanadium-(IV) *t*-butoxide vanished, and the remaining signals varied with the *A* value as follows: signals of the two kinds of vanadium(IV) complexes were observed at $A<6$, a singlet signal with a maximum slope width of 280—300 Gauss at $6\leq A<8$, an octet signal with a super hyperfine structure, which displayed a coupling with two aluminum nuclei, at $A\geq9$, and the latter two signals at $8\leq A<9$. Since the broad signal observed at $6\leq A<9$ become wider and disappeared with increasing *A* value, it is suggested that the 3d electron of the complex moves between the nuclei of vanadium(IV) and vanadium(III) in the stationary state.

After the disappearance of the signals of vanadium-(IV) complexes at $A=9$ (Fig. 5), the octet signal (Fig. 6) became large in intensity, attaining maximum intensity in 3 h. The signal is, therefore, attributed to a vanadium(II) complex, which takes an electron configuration of $3d^3$. Each peak of the octet signal is composed of eleven consitituent lines to represent the super hyperfine coupling with the spins of a pair of aluminum nuclei. ESR measurements were carried

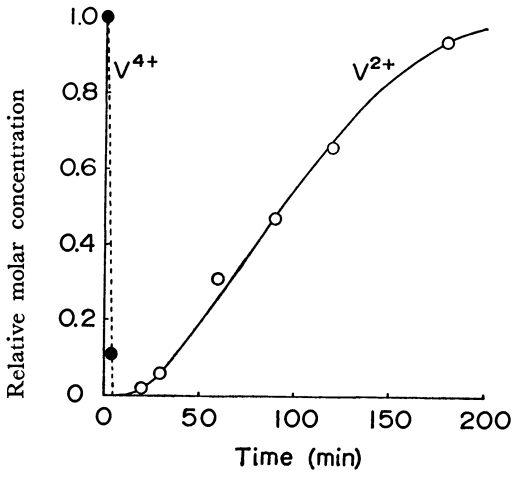

Fig. 5. Concentration of the paramagnetic species measured by the ESR spectrum of the mixture of trimethylaluminum and vanadium(IV) *t*-butoxide in toluene at 25 °C. The prepared molar ratio of trimethylaluminum and vanadium(IV) *t*-butoxide is 0.90 : 0.10.

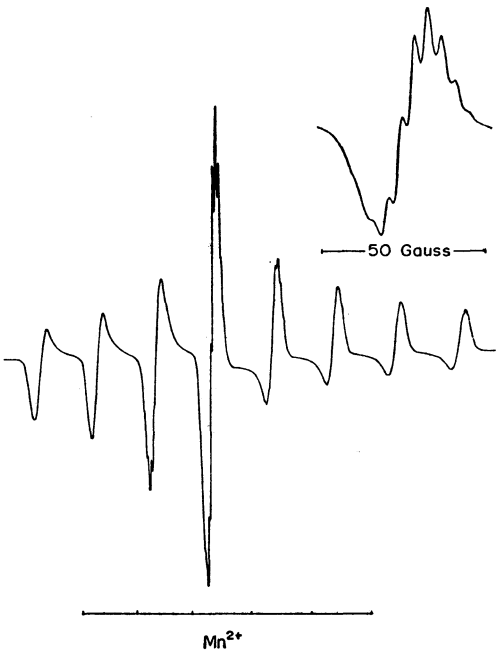

Fig. 6. ESR spectrum of the mixture of trimethylaluminum and vanadium(IV) *t*-butoxide in toluene at −196 °C. The prepared molar ratio of trimethylaluminum and vanadium(IV) *t*-butoxide is 0.90 : 0.10.

on 21 combinations of alkylaluminums and vanadium-(IV) alkoxides in toluene at −196 °C, the values of the ESR parameters being almost invariant with changes in the alkyl groups, *i.e.* methyl, ethyl and isobutyl, or the alkoxyl groups, *i.e.* methyl, ethyl and isobutyl, or the alkoxyl groups, *i.e.* methoxyl, ethoxyl, propxyl, isopropoxyl, butoxyl, isobutoxyl, and *t*-butoxyl. Each combination resulted in an almost isotropic *g*-value, 1.9835±0.0004, and almost isotropic values of hyperfine and super hyperfine coupling constants,

Table 1. Observed values of $\bar{g}$-factor, hyperfine coupling constant, $\bar{A}$, and super hyperfine coupling constant, $\bar{B}$, of vanadium(II) complexes[a)]

Alkyl group[b)]	Alkoxyl group[c)]	$\bar{g}$-Value	$\bar{A}$ (10^{-3} cm^{-1})	$\bar{B}$ (10^{-4} cm^{-1})
CH_3-	CH_3O-	1.9836	8.23	3.8
	CH_3CH_2O-	1.9336	8.18	3.7
	$CH_3(CH_2)_2O$-	1.9839	8.22	3.7
	$(CH_3)_2CHO$-	1.9833	8.21	3.7
	$CH_3(CH_2)_3O$-	1.9833	8.21	3.8
	$(CH_2)CHCH_2O$-	1.9835	8.26	3.7
	$(CH_3)_3CO$-	1.9835	8.25	3.7
CH_3CH_2-	CH_3O-	1.9835	8.18	3.7
	CH_3CH_2O-	1.9831	8.22	3.7
	$CH_3(CH_2)_2O$-	1.9833	8.26	3.6
	$(CH_3)_2CHO$-	1.9834	8.16	3.7
	$CH_3(CH)_3O$-	1.9836	8.26	3.6
	$(CH_3)_2CHCH_2O$-	1.9833	8.21	3.6
	$(CH_3)_3CO$-	1.9833	8.20	3.6
$(CH_3)_2CHCH_2$-	CH_3O-	1.9835	8.17	3.7
	CH_3CH_2O-	1.9836	8.16	3.7
	$CH_3(CH_2)_2O$-	1.9833	8.25	3.7
	$(CH_3)_2CHO$-	1.9836	8.23	3.7
	$CH_3(CH_2)_3O$-	1.9835	8.22	3.8
	$(CH_3)_2CHCH_2O$-	1.9835	8.25	3.7
	$(CH_3)_3CO$-	1.9835	8.26	3.8

a) The complex was obtained by the reaction of alkylaluminum with vanadium(IV) alkoxide in toluene at 25 °C, and the ESR spectrum was measured at −196 °C. b) Alkyl group of alkylaluminum. c) Alkoxyl group of vanadium(IV) alkoxide.

$(8.21\pm0.05)\times10^{-3}$ and $(3.7\pm0.1)\times10^{-4}$ cm^{-1}, respectively, as listed in Table 1.

It is difficult to determine the structure of the vanadium(II) complexes from the g-value and the hyperfine and the super hyperfine coupling constants. However, the dependence of the signal intensity upon the A value indicates that they are possibly bis(di-μ-alkyldialkylaluminum)vanadium(II), which is regarded as the final product of a series of reductions of the vanadium(IV) alkoxides with the alkylaluminums as follows. The reactions are summarized as

$$(A/2)(AlR_3)_2 + V(R'O)_4 \rightarrow V(R_2AlR_2)_2 + (A-6)R_2Al(R'O)_2AlR_2 + (1/2)(10-A)R_2AlR(R'O)AlR_2 + R_2 \quad (2)$$

where R and R'O denote the alkyl and the alkoxyl groups, respectively. The condition $6\leq A\leq10$, which is required in Eq. 2, agrees with the result of ESR measurements. The vanadium(II) complexes and the vanadium(IV) alkoxides caused none of the reactions of isoprene.

ESR Spectra of Titanium Complexes. The catalytic reactions of isoprene took place in the region of A in which the transition element assumed a trivalent state. The structures of the catalytic complexes were studied from the ESR spectra of titanium(III) complexes. The ESR spectra of the catalytic system prepared from trimethylaluminum and titanium(IV) t-butoxide are shown in Fig. 7. They were measured in benzene at 25 °C after aging at 140 °C for 30 min, and showed little change through the reactions of isoprene at 100 °C for 20 h.

The ESR signal with $\bar{g}=1.963$ observed at $A=2$—4

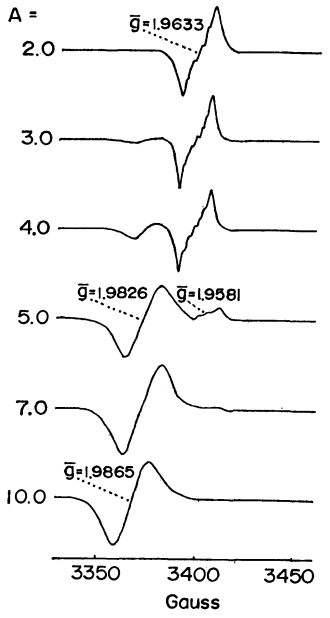

Fig. 7. ESR spectra of titanium(III) complexes of the catalytic system at 25 °C after aging at 140 °C for 30 min. Trimethylaluminum and titanium(IV) t-butoxide were mixed in benzene at the molar ratio, A.

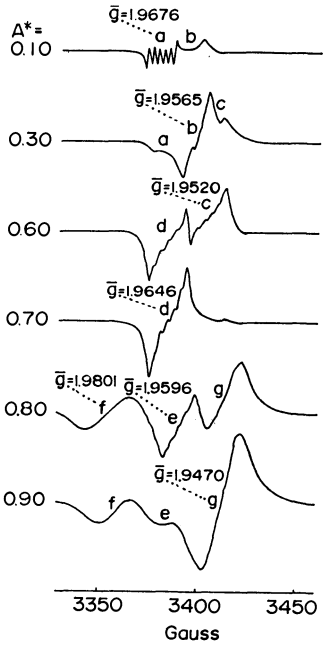

Fig. 8. ESR spectra of titanium(III) complexes at 25 °C immediately after mixing trimethylaluminum and titanium(IV) *t*-butoxide in benzene.
A* designates the prepared molar fraction of trimethylaluminum.

is attributed to the catalyst which caused 1,4-polymerization of isoprene. The signal exhibited a super hyperfine structure bearing six constituent lines to show coupling with an aluminum nucleus, and was affected little by the reactions of isoprene. Some of the other signals might correspond to the titanium(III) complexes, which caused reactions of isoprene other than 1,4-polymerization. Similar results were obtained by using triethylaluminum instead of trimethylaluminum. However, when triisobutylaluminum was used, the signal with $\bar{g}=1.963$ virtually disappeared during the course of reaction of isoprene and turned into signals of other titanium(III) complexes. Before aging the catalyst, seven kinds of signals, denoted by a, b, c, d, e, f, and g in order of appearance with increase in the amount of trimeth ylaluminum, were observed in the mixed solution of trimethylaluminum and titanium(IV) *t*-butoxide at 25 °C as shown in Fig. 8. The signals a, b, c, d, and g displayed a super hyperfine structure owing to coupling with an aluminum nucleus, and the signal e showed coupling with two aluminum nuclei. When trimethylaluminum was added at the molar fraction of 0.10—0.70 in the solution, only the signal d with $\bar{g}=1.965$ remained after aging at 140 °C for 30 min. The signal is attributed to the catalyst for 1,4-polymerization of isoprene.

The molecular structures of the titanium(III) complexes were determined by caluclating the *g*-values with use of models of the coordination structures. The model structures are shown in Fig. 9, where the titanium(III) nucleus is situated in the origin of the Cartesian coordinates. The dashed line designates chelation formed by a pair of ligands between titanium-

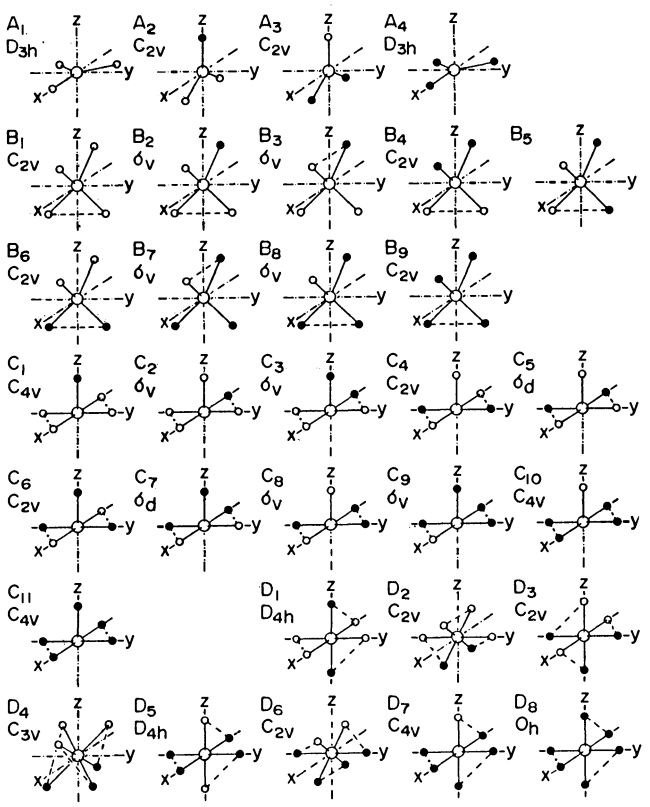

Fig. 9. Model structures of titanium(III) complexes. The titanium(III) nucleus is located at the origin. Dashed line shows chelation formed by a pair of ligands between aluminum and titanium(III) nuclei. The alkoxy and the alkyl groups are shown by ○ and ●, respectively.

(III) and aluminum nuclei. The structures are classified into four groups, A, B, C, and D, in accordance with the number of aluminum nuclei combined with a titanium(III) nucleus, zero, unity, two and three, respectively, which have four, nine, eleven an eight kinds of stuctures, respectively. The structural symmetry of each is designated by the ordinary symbols except the structure, B_5, which has no center of symmetry.

The wave function of the 3d orbital of the titanium(III) complexes, φ_i, is given by a linear combination of d functions, d_0, $d_{\pm1}$ and $d_{\pm2}$, which are classified into six groups (Table 2). In groups 1, 2, 3, and 4 the Jahn-Teller distortion resolves orbital degeneracy of the ground level changing φ_i to φ_i' or φ_i'', while the ground level takes none of the degenerate orbitals in groups 5 and 6. On the basis of the ligand field theory, energy of the orbital, φ_i, is expressed as

$$E_i = Ze^2 \sum_j (\alpha \bar{r^2} \gamma_j R_j^{-3} + \beta \bar{r^4} \delta_j R_j^{-5}) \qquad (3)$$

where the subscript j denotes the coordination electron of the ligand, e the charge of an electron, and *Ze* the effective nuclear charge of the transition element. The charge of a coordination electron is estimated to be *e* and *e*/2 at the terminal and the bridging ligands, respectively, and *r* and *R* designate the radius of the 3d electron and the distance between the coordination

Table 2. Wave functions of 3d orbitals of titanium(III) complexes[a]

Structures A_1 and A_4.[b] (E_3, $E_4 \neq E_{min}$)

i	$\varphi_i(E_5=E_{min})$	φ_i' $(E_1=E_2=E_{min})$
1	$(1/\sqrt{2})(d_1-d_{-1})$	$\varphi_1\cos(\theta/2)-\varphi_2\sin(\theta/2)$
2	$(1/\sqrt{2})(d_1+d_{-1})$	$\varphi_1\sin(\theta/2)+\varphi_2\cos(\theta/2)$
3	$(1/\sqrt{2})(d_2-d_{-2})$	φ_3
4	$(1/\sqrt{2})(d_2+d_{-2})$	φ_4
5	d_0	φ_5

Structures C_1, C_5, C_7, C_{10}, C_{11}, D_1, D_5, and D_7. ($E_4 \neq E_{min}$)

i	$\varphi_i(E_3$ or $E_5=E_{min})$	$\varphi_i'(E_1=E_2=E_{min})$	$\varphi_i''(E_1=E_2=E_{min})$
1	$(1/\sqrt{2})(d_1-d_{-1})$	φ_1	$(1/\sqrt{2})(\varphi_1+\varphi_2)$
2	$(1/\sqrt{2})(d_1+d_{-1})$	φ_2	$(1/\sqrt{2})(\varphi_1-\varphi_2)$
3	$(1/\sqrt{2})(d_2-d_{-2})$	φ_3	φ_3
4	$(1/\sqrt{2})(d_2+d_{-2})$	φ_4	φ_4
5	d_0	φ_5	φ_5

Structure D_8. (E_4, $E_5 \neq E_{min}$)

i	φ_i	$\varphi_i'(E_1=E_2=E_3=E_{min})$	$\varphi_i''(E_1=E_2=E_3=E_{min})$
1	$(1/\sqrt{2})(d_1-d_{-1})$	φ_1	$(1/\sqrt{3})(\varphi_1+\varphi_2+\varphi_3)$
2	$(1/\sqrt{2})(d_1+d_{-1})$	φ_2	$(1/\sqrt{6})(\varphi_1+\varphi_2-2\varphi_3)$
3	$(1/\sqrt{2})(d_2-d_{-2})$	φ_3	$(1/\sqrt{2})(\varphi_1-\varphi_2)$
4	$(1/\sqrt{2})(d_2+d_{-2})$	φ_4	φ_4
5	d_0	φ_5	φ_5

Structure D_4. (E_2, $E_4 \neq E_{min}$)

i	φ_i	$\varphi_i'(E_1=E_3=E_5=E_{min})$
1	$(1/\sqrt{6})[\sqrt{2}(d_1-d_{-1})-(d_2+d_{-2})]$	$(1/\sqrt{10})(\varphi_1\sqrt{5+\sqrt{5}}+\varphi_5\sqrt{5-\sqrt{5}})$
2	$(1/\sqrt{6})[d_1-d_{-1}+\sqrt{2}(d_2+d_{-2})]$	$(1/\sqrt{10})(\varphi_1\sqrt{5-\sqrt{5}}-\varphi_5\sqrt{5+\sqrt{5}})$
3	$(1/\sqrt{6})[\sqrt{2}(d_1+d_{-1})+d_2-d_{-2}]$	φ_3
4	$(1/\sqrt{6})[-(d_1+d_{-1})+\sqrt{2}(d_2-d_{-2})]$	φ_2
5	d_0	φ_4

Structures A_2, A_3, B_1, B_4, B_6, B_9, C_2, C_3, C_4, C_6, C_8, C_9, D_2, D_3, and D_6.[c] ($E_4 \neq E_{min}$)

i	$\varphi_i(E_1$, E_2, E_3 or $E_5=E_{min})$
1	$(1/\sqrt{2})(d_1-d_{-1})$
2	$(1/\sqrt{2})(d_1+d_{-1})$
3	$(1/\sqrt{2})(d_2-d_{-2})$
4	$(1/\sqrt{2})C_{44}(d_2+d_{-2})+C_{45}d_0$
5	$(1/\sqrt{2})C_{55}(d_2+d_{-2})+C_{55}d_0$

Structures B_2, B_3, B_7, and B_8.[c] ($E_1 \neq E_{min}$)

i	φ_i (E_2, E_3, E_4 or $E_5=E_{min}$)
1	$(1/\sqrt{2})[C_{11}(d_1+d_{-1})+C_{12}(d_2-d_{-2})]$
2	$(1/\sqrt{2})[C_{21}(d_1+d_{-1})+C_{22}(d_2-d_{-2})]$
3	$(1/\sqrt{2})[C_{33}(d_1-d_{-1})+C_{34}(d_2+d_{-2})]+C_{35}d_0$
4	$(1/\sqrt{2})[C_{43}(d_1-d_{-1})+C_{44}(d_2+d_{-2})]+C_{45}d_0$
5	$(1/\sqrt{2})[C_{53}(d_1-d_{-1})+C_{54}(d_2+d_{-2})]+C_{55}d_0$

a) Wave function is designated by φ_i when the ground level is not degenerate, and by φ_i' or φ_i'' when the ground level is degenerate. b) θ shows magnitude of the Jahn-Teller distortion. c) C_{ij} is a constant characteristic of the coordination structure.

electron and the center of the transition elements, respectively. α, β, γ_j, and δ_j are variables characteristic of the symmetry of the coordination stucture about the transition element.

If we assume that the 3d electron is distributed spherically around the transition element, $\bar{r}^2$ and $\bar{r}^4$ are substituted by r^2 and r^4, respectively, and r is supposed to be equivalent to the ionic radius, the magnitude of which is known to be 0.76 and 0.60 Å for titanium(III) and vanadium(IV), respectively.[18] Crystallographic data suggest that the length of the coordination bond, L_j, is little affected by the species of the metal atom as well as the saturated alkyl group of the ligand as far as the present compounds are concerned.[19-23] Magnitude of L_j is 1.78 and 2.01 Å for the terminal and the bridging alkoxyl groups, respectively which were determined from the results of studies on titamium(IV) methoxide,[19] titanium(IV) ethoxide,[20] bis[2-methylpentane-2,4-dioxydimethyltitanium(IV)],[21] and oxyvanadium(V) methoxide,[22] and 2.15 and 2.34 Å for

the terminal and the bridging methyl groups, respectively, from the data of trimethylaluminum.[23] A symbol, f_j, is employed to define an attraction rate of the coordination electron toward the transition element on the coordination bond. Then R_j is replaced by $L_j(1-f_j)$. For the sake of simplicity f_j's of the alkyl and the alkoxyl groups are denoted by f_R and f_{RO}, respectively. The value of $G=Ze^2(\rho^2\zeta)^{-1}(g_e-g)$ is then calculated by means of the model structures except B_5 of the titanium(III) complexes, as a function of f_R and f_{RO}.

Numerical calculation was performed with the model structures of group B to obtain a set of values of f_R and f_{RO} so that a linear relation holds between the value of $\bar{G}=(1/3)(G_x+G_y+G_z)$ and the observed value of $g_e-\bar{g}$. The condition $f_R>f_{RO}$ was assumed based on the empirical fact that the alkyl group is stronger in reducing power than the alkoxyl group. The molar ratio of the methyl and the *t*-butoxyl groups of the titanium(III) complexes was assumed to increase with increase in the amount of trimethylalumiunm. Under the conditions that $f_R/f_{RO}=1.4$ and $f_{RO}=0.14$, a linear relation was ontained by choosing pairs of the model structures and the ESR signals as B_1 and a, B_2 and b, B_3 and c, B_4 and d, and B_7 and g as shown in Fig. 10. No other values of f_R and f_{RO} gave such a linear relation. The numerical calculation was also carried out with groups A, C and D to find the linear relation for the pairs of C_6 and e, and D_5 and f. The values of $\bar{G}$ and $g_e-\bar{g}$ are plotted in Fig. 11, where the slope of the straight line yields $\rho^2\zeta(Ze^2)^{-1}=5.0\times10^{-3}$. The $\bar{g}$-values of the model structures thus calculated are given in Table 3. The structures having the degenerate ground level would not exhibit the ESR signal because of molecular vibration.

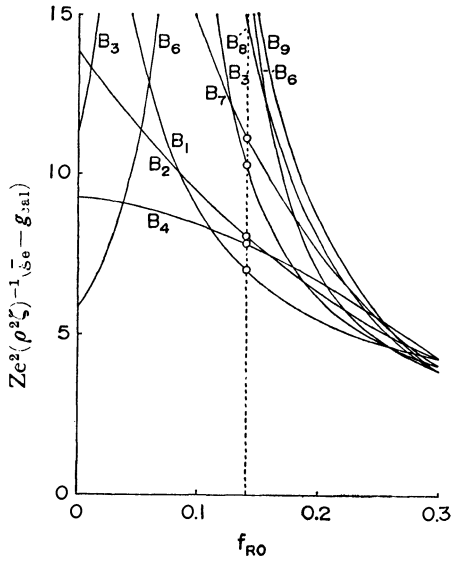

Fig. 10. Variation of calculated $\bar{g}$-value with attraction rate of the coordination electron toward the titanium(III) nucleus at $f_R/f_{RO}=1.4$.

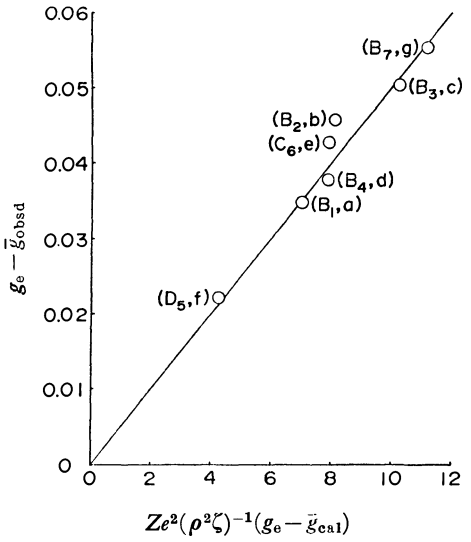

Fig. 11. Calculated and observed $\bar{g}$-values of titanium(III) complexes prepared by trimethylaluminum and titanium(IV) *t*-butoxide.

It is known that the magnitude of ζ of the titanium(III) ion is 154 cm^{-1},[16] and that the ratio of the effective nuclear charge of titanium(III) and that of vanadium(IV) is 3 : 4.[24] Hence the orbital reduction factor of the titanium(III) complex is estimated to be $\rho=0.59$ by using the experimental value of the orbital splitting energy of vanadium(IV) *t*-butoxide. The ρ value suggests that the titanium(III) complexes are larger in covalency of the coordination bond than vanadium(IV) *t*-butoxide. It can be seen from the coordination structure and the electronic state of the titanium(III) complex of B_4 that one of three molecular structures designated by AT^1, AT^2, and AT^3 is

Table 3. $\bar{g}$-vales of titanium(III) complexes

Structure	$\bar{g}$-Value		Structure	$\bar{g}$-Value	
	Calcd[a]	Obsd[b]		Calcd[a]	Obsd[b]
A_1	1.985		C_4	1.987	
A_2	1.978		C_5	1.989	
A_3	1.977		C_6	1.963	1.960
A_4	1.984		C_7	1.975	
			C_8	1.987	
B_1	1.967	1.968	C_9	1.978	
B_2	1.962	1.957	C_{10}	1.986	
B_3	1.951	1.952	C_{11}	1.981	
B_4	1.963	1.965			
B_6	1.917		D_1	(1.986)	
B_7	1.946	1.947	D_2	1.970	
B_8	1.928		D_3	1.965	
B_9	1.916		D_4	(1.994)	
			D_5	1.981	1.980
C_1	(1.994)		D_6	1.958	
C_2	1.989		D_7	1.972	
C_3	1.939		D_8	(1.989)	

a) $\bar{g}$-values given in parentheses indicate that the complex will not show the ESR signal as a result of degeneracy of the ground level. b) The complex was obtained by the reaction of trimethylaluminum with titanium(IV) *t*-butoxide in toluene, and ESR spectrum was measured at 25 °C.

possible as the catalyst for 1,4-polymerization of isoprene.

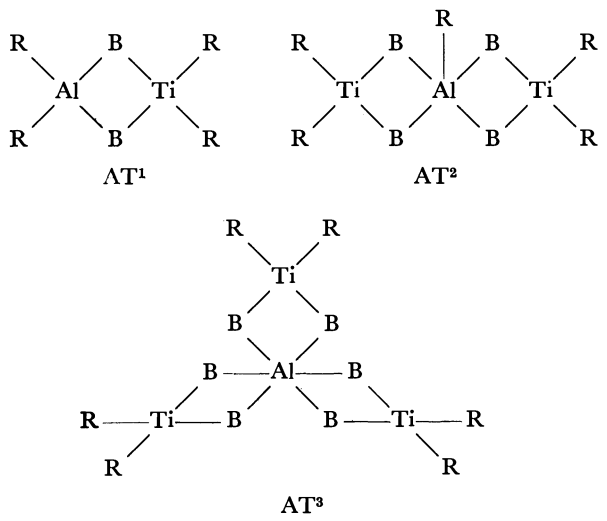

R=CH_3-, CH_3CH_2-, or $(CH_3)_2CHCH_2$-

Chemical Ionization Mass Spectra. Measurement of molecular weight is useful for determination of the molecular structure of the catalyst for 1,4-polymerization of isoprene. However, the titanium(III) complex is unstable in the air and its isolation is very difficult, so that ordinary techniques for molecular weight measurements are not available. Chemical ionization mass spectrometry is a useful means for the determination of the molecular weight of such a compound since ions are produced under mild conditions as compared with electron impact mass spectrometry.

The chemical ionization mass spectrum of the reaction mixture of trimethylaluminum and titanium(IV) *t*-butoxide at the molar ratio of 0.60 : 0.40, prepared in benzene followed by aging at 140 °C for 30 min to exhibit the ESR signal of d alone, is shown in Fig. 12. M and B denote the methyl and the *t*-butoxyl groups, respectively. None of the mass peaks observed are from a tetranuclear ion bearing an aluminum nucleus and three titanium nuclei. Peaks at *m/e* 550, 506 and 477 are assigned to ions containing an aluminum nucleus and two tiatnium(III) nuclei, $[AlTi_2M_4B_5H]^+$, $[AlTi_2M_6B_4]^+$ and $[AlTi_2M_4B_4H_2]^+$, respectively, and peaks at *m/e* 492 and 434 to ions having the nuclei of an aluminum, a titanium(III) and a titanium(IV), $[AlTi_2M_5B_4H_2]^+$ and $[AlTi_2M_6B_3H_2]^+$, respectively. On the other hand, the ESR spectrum of this sample showed a single species of the titanium(III) complex, and therefore AT^1 can not exist. If the catalyst is AT^2, the peak at *m/e* 506 should not be observed. An adequate explanation of the mass pattern is that fragments from a tatranuclear complex displayed the mass peaks of the trinuclear ions. Hence AT^3 is the molecular structure of the catalyst for 1,4-polymerization of isoprene.

The catalytic complex, AT^3, is named tris[di-μ-*t*-butoxo-dialkyltitanium(III)]aluminum. The aluminum nucleus is located at the center of the tetranuclear complex with the coordination number of six, while the titanium(III) nuclei occupy the outer three positions at a distance suitable for bidentate coordination of isoprene. Three pairs of the *t*-butoxyl groups combine three titanium(III) nuclei with an aluminum nucleus to support the tetranuclear structure. The alkyl group takes the terminal positions of the titanium(III) nuclei, and may participate directly in the reaction of isoprene.

A proposal is made to interpret the mechanism of 1,4-polymerization of isoprene as follows. Three molecules of isoprene can form bidentate coordi-

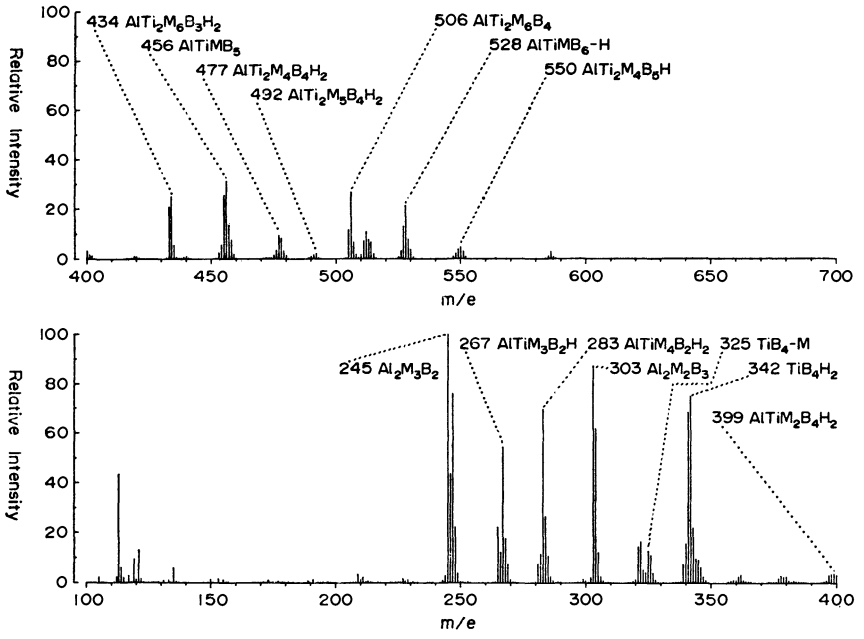

Fig. 12. Chemical ionization mass spectrum of the mixture of trimethylaluminum and titanium(IV) *t*-butoxide at the molar ratio of 0.60 : 0.40 after heating in benzene 140 °C for 30 min.

nation to a catalyst molecule at the same time. As soon as an alkyl group of the catalyst activates one of the terminal carbons of isoprene on the catalyst, another terminal carbon attacks the end of the neighboring isoprene releasing the coordination bond. A new isoprene molecule then takes the unoccupied sites of the catalyst. Thus, 1,4-polyisoprene is produced through the successive coordination of isoprene followed by formation of new carbon-carbon bonds, although the mechanism can not explain regular head to tail polymerization of isoprene and its *cis-trans* selectivity.

Conclusion

Structures of the Ziegler-Natta catalysts for the polymerization of isoprene were studied by means of ^{1}H-NMR, ESR and chemical ionization mass spectrometry. The catalyst was prepared in benzene or toluene by the reaction of alkylaluminum with titanium(IV)- or vanadium(IV) *t*-butoxide. The experiment of polymerization was carried out at 80—140 °C for 20 h after heating the catalyst.

The alkoxide was monomeric in the solution, and reduced by the alkylaluminum to produce a bivalant complex *via* trivalent complexes. The final product of the reduction of vanadium(IV) *t*-butoxide was bis(di-μ-alkyl-dialkylaluminum)vanadium(II). When the transition element took the trivalent state, the catalytic system caused five kinds of polymerization of isoprene.

Coordination structure of seven kinds of titanium(III) complexes was determined by comparing the observed *g*-values with the calculated ones, three kinds of molecular structures remaining as the catalyst for 1,4-polymerization of isoprene. As a result of molecular weight determination it was found that the catalytic complex was tris[di-μ-*t*-butoxo-dialkyltitanium(III)]aluminum.

The catalyst has a tetranuclear stucture suitable for bidentate coordination of isoprene. A proposal was made to interpret the reaction mechanism: the 1,4-polymerization takes place through succssive coordination of isoprene to the catalyst followed by bond formation between a terminal carbon of isoprene and a propagating chain end of polyisoprene, both of which occupy adjacent positions on the catalyst.

References

1) G. Natta and I. Pasquon, *Adv. Catal.*, **11**, 1 (1959).
2) M. Morton, R. D. Sanderson, R. Sakata, and L. A. Falvo, *Macromolecules*, **6**, 186 (1973).
3) G. Natta, L. Porri, and A. Carbonaro, *Makromol. Chem.*, **77**, 126 (1964).
4) E. Angelscu, C. Nicolau, and Z. Simon, *J. Am. Chem. Soc.*, **88**, 3910 (1966).
5) H. Hirai, K. Hiraki, I. Noguchi, and S. Makishima, *J. Polymer Sci., Part A-1*, **8**, 147 (1970).
6) H. Hirai, K. Hiraki, I. Noguchi, T. Inoue, and S. Makishima, *J. Polymer Sci., Part A-1*, **8**, 2393 (1970).
7) M. Thomas, *Can. J. Chem.*, **39**, 1386 (1961).
8) D. C. Bradley and M. L. Mehta, *Can. J. Chem.*, **40**, 1183 (1962).
9) C. Walling and J. Reisach, *J. Am. Chem. Soc.*, **80**, 5819 (1958).
10) M. Uetsuki and Y. Fujiwara, *J. Am. Chem. Soc.*, **95**, 4142 (1973).
11) D. C. Bradley, R. C. Mehrotra, and W. Wardlaw, *J. Chem. Soc.*, **1952**, 4204.
12) E. G. Hoffmann, *Trans. Faraday Soc.*, **58**, 642 (1962).
13) A. Haaland and O. Stokkeland, *J. Organomet. Chem.*, **94**, 345 (1975).
14) N. Muller and D. E. Pritchard, *J. Am. Chem. Soc.*, **82**, 248 (1960).
15) C. J. Ballhausen, "Introduction to Ligand Field Theory," McGraw-Hill, New York, N. Y. (1962), p.198.
16) J. S. Griffith, "The Theory of Transition Metal Ions," Cambridge Univ. Press, London (1961), p. 437.
17) G. F. Kokoszka, H. C. Allen, Jr., and G. Gordon, *Inorg. Chem.*, **5**, 91 (1966).
18) L. Pauling, "The Nature of the Chemical Bond," Cornell Univ. Press, New York, N. Y. (1960).
19) D. A. Wright and D. A. Williams, *Acta Crystallogr., Sect. B*, **24**, 1107 (1968).
20) J. A. Ibers, *Nature*, **197**, 686 (1963).
21) A. Yoshino, Y. Shuto, and T. Iitaka, *Acta Crystallogr., Sect. B*, **26**, 744 (1970).
22) C. N. Caughlan, H. M. Smith, and K. Watenpaugh, *Inorg. Chem.*, **5**, 2131 (1966).
23) R. G. Vranka and E. L. Amma, *J. Am. Chem. Soc.*, **89**, 3121 (1967).
24) C. A. Coulson, "Valence," Oxford Univ. Press, London (1961), p. 40.

The Preparation and Characterization of Isomers of (Amino acidato)-(iminodiacetato)nitrocobaltate(III)(1−) Complexes

Yukihiro YAMAMOTO, Sumio KAIZAKI, and Yoichi SHIMURA

Department of Chemistry, Faculty of Science, Osaka University, Toyonaka, Osaka 560

(Received July 1, 1976)

Three geometrical isomers of *fac(ida)*-$[Co(NO_2)(gly)(ida)]^-$ have been prepared and optically resolved (gly=glycinato(1−) and ida=iminodiacetato(2−) ligand), and their configurations were determined from the visible and ultraviolet absorption, and circular dichroism spectra. A diastereomeric pair was obtained for the corresponding L-alaninato, L-serinato, or L-prolinato complex.

There have been studied several types of cobalt(III) complexes with each one of uni-, bi-, and linear terdentate ligand. Those prepared previously include $[CoX(N-N)(N-N-N)]$,[1] $[CoX(N-N)(O-N-O)]$,[2] $[CoX(N-O)(N-N-N)]$,[3] $[CoX(O-O)(N-N-N)]$,[2,4] and $[CoX(O-O)(O-N-O)]$[4] types: X=unidentate ligand, N-N and N-O=bidentate ligands, N-N-N and O-N-O=linear terdentate ligands, where N and O denote the coordinating atoms. In the present paper, the $[Co(NO_2)(am)(ida)]^-$ complexes belonging to a new type, $[CoX(N-O)(O-N-O)]$, will be reported, where am stands for an amino acidato(1−) ligand such as gly (glycinato), L-ala (L-alaninato), L-ser (L-serinato), or L-pro (L-prolinato), and ida an iminodiacetato(2−) ligand.

Experimental

Preparation and Resolution. 1) Isomers of Na[Co(NO$_2$)(gly)(ida)]: Three grams (0.04 mol) of glycine and 6.80 g of potassium nitrite were dissolved in an aqueous solution (60 cm^3) containing 4.48 g (0.08 mol) of potassium hydroxide and 5.32 g (0.04 mol) of H_2ida. To this mixture was added 9.52 g (0.04 mol) of cobalt(II) chloride hexahydrate in 20 cm^3 of water at 45 °C. The dark red solution resulted was oxidized by adding 5.0 g of 30% hydrogen peroxide and stirring mechanically for about two hours. The deep red reaction mixture was poured into a column (45×750 mm) of a strong base anion-exchange resin (Dowex 1-X8, 200—400 mesh, chloride form). A reddish violet solution was swept out with water. The adsorbed band was eluted with a 0.07 M aqueous solution of sodium chloride. Five colored bands, a red one (i), a violet one (ii), a pinkish red one (iii), and two yellow ones (iv), (v) were eluted in this order. The amounts of the eluates (i) and (iii) were much larger than those of the (ii), (iv) and (v) eluates. The eluate (i) was condensed to a small volume with a vacuum rotary evaporator below 40 °C and the sodium chloride deposited was removed. To the filtrate a small amount of methanol was added and the sodium chloride deposited was removed again. After repeating this procedure, the filtrate was allowed to stand overnight in a refrigerator. Deep red prismatic crystals (isomer A) were obtained. They were filtered and washed with methanol-water(1:1), methanol and ether and then air-dried. Recrystallization was carried out from warm water.

The isolation of crystals from the eluate(iii) was performed by the same method; then violet prismatic fine crystals (isomer B) were obtained and recrystallized from warm water.

To the filtrate from the isomer B were added a mixture of water, methanol, ethanol and acetone (1:1:1:1). After allowing to stand for a long period at room temperature, a mixture of the violet and pinkish red crystals was obtained. The two kinds of crystals were separated by hand. The violet crystals were confirmed to be isomer B, while the pinkish red ones were found to be a new isomer (isomer C).

The eluate (ii) was confirmed to be *cis(N)*-$[Co(ida)_2]^-$ by the measurement of visible to near ultraviolet absorption spectra and elemental analysis. The absorption spectra of the eluate (iv) showed peaks at 21050 and 30030 cm^{-1} and that of the eluate (v) at 21370 and 30030 cm^{-1}. By comparing the absorption data with those reported by Ćelap *et al.*[5], these two complexes seem to correspond to the isomers of $[Co(NO_2)_2(gly)_2]^-$. The elemental analysis of crystals from the eluate (iv) showed the chemical composition of $Na[Co(NO_2)_2(gly)_2]\cdot 1.5H_2O$, but pure crystals were not obtained from the eluate (v).

2) Optical Resolution of the Isomers A, B and C: A suspension of 0.3 g of $(+)_{589}$-$[Co(ox)(en)_2]I$ and 0.13 g of silver acetate in 5 cm^3 of water was ground in a mortar for about 5 minutes. The silver iodide precipitated was filtered off and washed with a small amount of water. To the combined filtrate and washings was added 0.56 g of isomer A. The solution was kept in a refrigerator for a week; then the deep red diastereomer deposited was filtered. The less soluble diastereomer was recrystallized several times to show constant rotation ($[\alpha]_{589}=775°$) from warm water. The diastereomer was converted to the sodium salt by using a cation exchange resin of sodium form (Dowex 50W-X8, 200—400 mesh): $[\alpha]_{589}=-791°$.

The optical resolution of the isomers B and C was carried out by the same method as that of the isomer A: $[\alpha]_{589}=611°$ and 397° for the less soluble diastereomers of the isomers B and C, respectively; $[\alpha]_{589}=194°$ and $-142°$ for the sodium salts, respectively.

3) L-Amino Acidato Complexes: The complex with an L-alaninato, L-serinato, or L-prolinato ligand was prepared by the same method as that of the glycinato complex. In these cases, only one diastereomeric pair (corresponding to the isomer A) was isolated. On the column chromatography (Dowex 1-X8, 200—400 mesh, chloride form, eluting by 0.07 M KCl aqueous solution) of the L-alaninato or L-prolinato complex, two earlier eluted red bands showed the similar absorption bands to the isomer A of glycinato complex. The major CD bands of the two eluates had the opposite signs in the first d-d absorption band region, *i, e.*, (−) for the first eluate (A-1) and (+) for the second eluate (A-2). In the case of L-serinato complex, the separation of isomers on the column chromatography was poor, and these were separated into two parts with opposite rotations at 589 nm by using a fraction collector. The major CD band of the faster eluting part (A-1) had (−) sign and that of the later one (A-2) (+) sign. The crystallizations of these red isomers were made by the same method as that for glycinato isomers. The faster eluted isomer of the L-alaninato complex was not obtained in pure solid. Thus, the absorption and CD measurements of this isomer (A-1) were made in an aqueous

eluate purified on a QAE-sephadex column chromatography; the molar absorptivity is assumed to be the same as that of the isomer A-2.

4) Other Complexes: The complex $Na_2[Co(NO_2)(edta)]\cdot 3H_2O$ was prepared and resolved following the directions of Dwyer and Garvan[6] (edta=ethylenediaminetetraacetato (4−)). The complex $Na[Co(NO_2)(ed3a)]\cdot H_2O$ was prepared by the method of Blackmer *et al.*[7] and resolved by the method of Maricondi and Maricondi[8] (ed3a=ethylenediaminetriacetato(3−)).

Measurements. The visible and ultraviolet absorption spectra were obtained with a Shimadzu UV-200 spectrophotometer. The CD spectra were recorded on a Jasco MOE-1 spectropolarimeter. A Jasco DIP-4 digital polarimeter was used to check optical rotations. Proton magnetic resonance spectra were recorded on a Varian XL-100 spectrometer at about 36 °C, the internal temperature of the probe. A granule of DSS (sodium 2,2-dimethyl-2-silapentane-5-sulfonate) was added to serve as an internal reference. Two drops of 1M-DCl was added to the solvent, D_2O.

Results and Discussion

The analytical data of the complexes obtained are presented in Table 1. For the complex $[Co(NO_2)(gly)(ida)]^-$ five geometrical isomers are possible as is shown in Fig. 1. Three of them (I, II, and III) have a facially coordinating ida ligand and are optically resolvable, while the other two (IV and V) have a meridionally coordinating ida ligand and are optically unresolvable. In the glycinato complex, three optically resolvable geometrical isomers were obtained; thus they should take *fac(ida)* structures, I, II, and III. The fact that the remaining two *mer(ida)* isomers were not obtained is compatible with the previous recognition that the ida ligand can take a *meridional* coordination only with much difficulty.[9] The visible and ultraviolet absorption spectra of the three isomers are shown in Fig. 2. The absorption spectra resemble each other in the charge transfer region, while they are distinguished in the first d-d absorption band region. The three

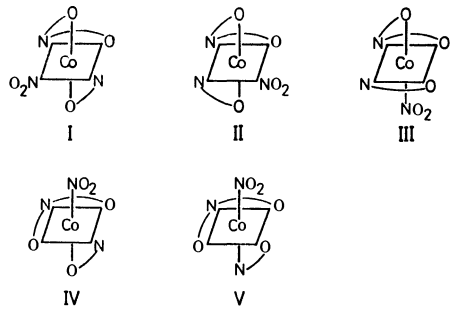

Fig. 1. Five possible geometrical isomers of $[Co(NO_2)(gly)(ida)]^-$. Upper three: *fac(ida)* type; (I) *mer(O)trans(N)*, (II) *mer(O)cis(N)*, and (III) *fac(O)*. Lower two: *mer(ida)* type; (IV) *mer(O)trans(N)* and (V) *mer(O)cis(N)*.

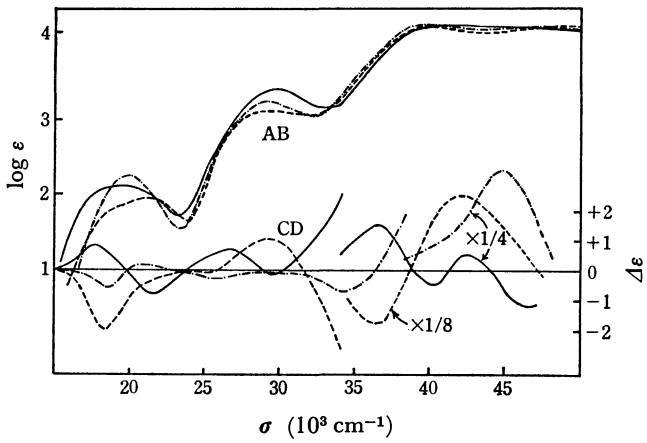

Fig. 2. Absorption (AB) and CD curves of three isomers of *fac(ida)*-$[Co(NO_2)(gly)(ida)]^-$: (----), $(-)_{589}$-A (I); (——) $(+)_{589}$-B (II); (-·-·-), $(-)_{589}$-C (III).

fac(ida) isomers belong to a CoN_3O_3 chromophore, and are classified into the *mer(O)* (I and II) and the

Table 1. Analytical data of the complexes (%)

Label	Complex	C Found	C Calcd	H Found	H Calcd	N Found	N Calcd
Gly (unresolved)							
A	$Na[Co(NO_2)(gly)(ida)]\cdot 2H_2O$	19.24	19.52	3.57	3.56	11.52	11.39
B	$Na[Co(NO_2)(gly)(ida)]\cdot 2H_2O$	19.59	19.52	3.50	3.56	11.79	11.39
C	$Na[Co(NO_2)(gly)(ida)]\cdot H_2O$	20.12	20.52	3.28	3.16	12.02	11.97
Gly (resolved)							
A	$(-)$-$Na[Co(NO_2)(gly)(ida)]\cdot 2H_2O$	19.69	19.52	3.74	3.56	11.67	11.39
B	$(+)$-$Na[Co(NO_2)(gly)(ida)]\cdot 2H_2O$	19.28	19.52	3.61	3.56	11.08	11.39
C	$(-)$-$Na[Co(NO_2)(gly)(ida)]\cdot 2H_2O$	19.27	19.52	3.52	3.56	11.66	11.39
L-Ser							
A-1	$(-)$-$Na[Co(NO_2)(L\text{-ser})(ida)]\cdot 3H_2O$	19.87	20.15	3.96	4.11	10.05	10.07
A-2	$(+)$-$Na[Co(NO_2)(L\text{-ser})(ida)]$	23.00	23.16	3.14	3.05	11.31	11.57
L-Pro							
A-1	$(-)$-$K[Co(NO_2)(L\text{-pro})(ida)]\cdot 1.5H_2O$	25.84	25.96	3.91	3.88	10.20	10.10
A-2	$(+)$-$K[Co(NO_2)(L\text{-pro})(ida)]\cdot 1.5H_2O\cdot 0.2KCl$	24.64	25.07	3.82	3.75	9.90	9.75
L-Ala							
A-2	$(+)$-$K[Co(NO_2)(L\text{-ala})(ida)]\cdot 2H_2O$	20.94	21.06	3.78	3.79	10.64	10.53

The signs of the optical rotation, (+) or (−), at 589 nm are shown.

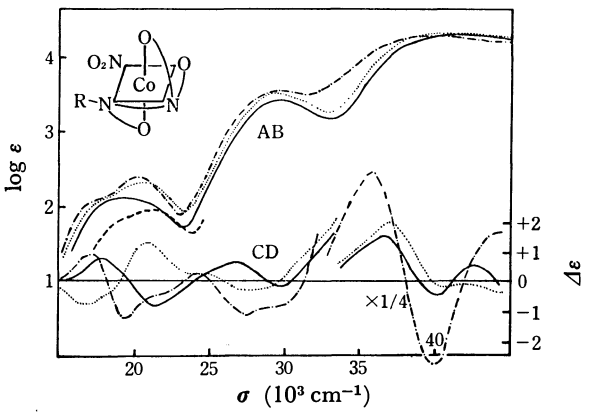

Fig. 3. Absorption (AB) and CD curves of (——), $(+)_{589}$-B; (-·-·-), $(-)_{546}$-$[Co(NO_2)(edta)]^{2-}$; (····), $(+)_{546}$-$[Co(NO_2)(ed3a)]^-$; and absorption curve of (----) the isomer A. The absolute configuration of $(-)_{546}$-$[Co(NO_2)(edta)]^{2-}$ (R=CH_2COO^-) and $(+)_{546}$-$[Co(NO_2)(ed3a)]^-$ (R=H), is shown in the left upper corner.

fac(O) (III) types. The first d-d absorption bands of isomers A and B are broad and that of isomer C sharp as in Fig. 2. According to a semi-empirical rule,[10,11] the former two are assigned to the *mer(O)* configuration and the latter to the *fac(O)*. The geometrical configuration II of the *mer(O)* is similar to that of the $[Co(NO_2)(edta)]^{2-}$ [12] and $[Co(NO_2)(ed3a)]^-$ [7] complexes, except for the chelate ring connecting two donor nitrogens in the latter two complexes. As is shown in Fig. 3, the first absorption band of the isomer B is closer to those of the $[Co(NO_2)(edta)]^{2-}$ and $[Co(NO_2)(ed3a)]^-$ complexes. Moreover, Yamatera's rule[11] predicts, by taking a zero point at the first band position of $[Co(en)_3]^{3+}$ and using parameter values, $\delta(N)=0$, $\delta(O)=-4730\ cm^{-1}$ (estimated from $[Co(ox)_3]^{3-}$), and $\delta(NO_2)=4000\ cm^{-1}$ (estimated from *mer*-$[Co(NH_3)_3(NO_2)_3]$ and *cis*-$[Co(NH_3)_4(NO_2)_2]^{+}$[13]), that the first band splitting components locate at 18700, 18900, and 21100 cm^{-1} for the structure I, 17760, 19920, and 21100 cm^{-1} for II, and 18900, 19920, and 19920 cm^{-1} for III. The lowest energy component of the structure II is expected to lie at lower energy side than that of the structure I, and this is in accord with the observation that the first absorption band of the isomer B extends to the lower energy side. Thus the isomers A, B, and C are assigned to the structure I (*mer(O)trans(N)*), II (*mer(O)cis(N)*), and III (*fac(O)*), respectively.

The CD curves of $(+)_{589}$-B isomer, $(+)_{546}$-$[Co(NO_2)(ed3a)]^-$ and $(-)_{546}$-$[Co(NO_2)(edta)]^{2-}$ are shown in Fig. 3. It has been determined that the latter two complexes take the absolute configuration shown in Fig. 3 on the comparison of their CD spectra with those of the stereospecifically formed $(+)_{546}$-$[Co(NO_2)((R)\text{-pdta})]^{2-}$ [14] and $(-)_{546}$-$[Co(NO_2)((R)\text{-pd3a})]^-$,[15] respectively. Three complexes in Fig. 3 give the resembling CD pattern in the charge transfer band region; *i.e.*, (+) at about 36000 cm^{-1} and (−) at about 40000 cm^{-1}. Therefore, it may be concluded that the $(+)_{589}$-B isomer has the same absolute configuration of the arrangement of donor atoms as the $(+)_{546}$-$[Co(NO_2)(ed3a)]^-$ and $(-)_{546}$-$[Co(NO_2)(edta)]^{2-}$ complexes. The fact that the CD curves of the $(+)_{589}$-B isomer and $(+)_{546}$-$[Co(NO_2)(ed3a)]^-$ are enantiomeric to each other in the first d-d absorption band region suggests that the vicinal effect due to the asymmetric nitrogen atom of $(+)_{546}$-$[Co(NO_2)(ed3a)]^-$ is large enough to invert the CD sign as pointed out by Maricondi and Maricondi.[8] It seems that the CD in the charge transfer region is ascribed mainly to the configurational chirality due to the arrangement of donor atoms. The absolute configuration of the isomer B cannot be named by the current IUPAC rule,[16] because two chiralities due to the arrangement of chelate rings are cancelled by each other such as *ΔΔ*. On the other hand, the IUPAC rule is applicable to the other two isomers, A and C.

The $(-)_{589}$-A and $(-)_{589}$-C isomers give a negative major CD band in the first d-d absorption band region. Thus, the $(-)_{589}$-A and $(-)_{589}$-C isomers may be assigned tentatively to the *Δ* configurations. These two complexes show the similar CD pattern in the charge transfer region also as in Fig. 2.

By applying the additivity rule[17] of the configurational and vicinal effects to the CD curves of A-1 and A-2 diastereomeric isomers with L-ala, L-ser or L-pro, the configurational and vicinal CD contributions can be separated. All the calculated configurational CD curves of the A-1 isomers agree with the observed CD curve of the $(-)_{589}$-A isomer of glycinato complex as in Fig. 4. It was concluded, therefore, that the first eluted A-1 diastereomers with L-amino acidato ligand take the absolute configuration *Δ* same as the $(-)_{589}$-A glycinato complex. The vicinal CD curves of these isomers are different from each other as in Fig. 4.

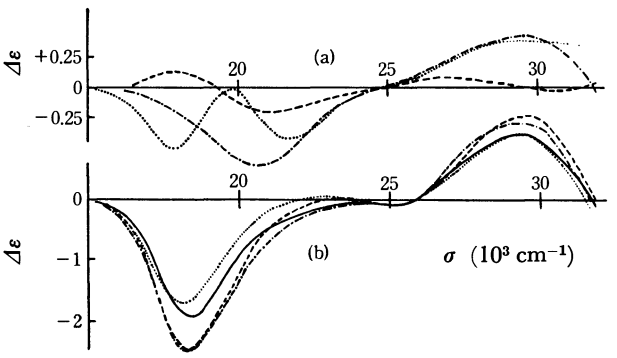

Fig. 4. Calculated vicinal effect (2L) curves (a) and caluculated configurational effect curves (b) of (----), L-alaninato; (-·-·-), L-serinato; and (····), L-prolinato complexes (A-1 series). Observed CD curve of $(-)_{589}$-A glycinato isomer (——) is also shown in (b).

In the pmr spectra of the L-prolinato diastereomers, it is predicted that the magnetic anisotropy of two carbon-oxygen single bonds[18] of the ida ligand plays the most influensive part for the NH proton chemical shift of the coordinated prolinato ligand, and that the NH proton of the *Δ* isomer resonates at the higher magnetic field than that of the *Λ* isomer. In fact, the isomer A-1 resonated at 7.19 ppm and the A-2 at 7.41

ppm. Thus it is confirmed that the A-1 series has the *Δ* absolute configuration and the A-2 *Λ*, and hence that the $(-)_{589}$-A isomer of glycinato complex has the *Δ* absolute configuration.

References

1) A. R. Gainsford and D. A. House, *Inorg. Chim. Acta*, **6**, 227 (1972).
2) K. Kobayashi and M. Shibata, *Bull. Chem. Soc. Jpn.*, **48**, 2561 (1975).
3) K. Ohkawa, J. Fujita, and Y. Shimura, *Bull. Chem. Soc. Jpn.*, **45**, 161 (1972).
4) S. Nakashima and M. Shibata, *Bull. Chem. Soc. Jpn.*, **48**, 3128 (1975).
5) M. B. Ćelap, D. J. Radanović, T. I. Nikolić, and T. J. Janjić, *Inorg. Chim. Acta*, **2**, 52 (1968).
6) F. P. Dwyer and F. L. Garvan, *J. Am. Chem. Soc.*, **80**, 4480 (1958).
7) G. L. Blackmer, R. E. Hamm, and J. I. Legg, *J. Am. Chem. Soc.*, **91**, 6632 (1969).
8) C. W. Maricondi and C. Maricondi, *Inorg. Chem.*, **12**, 1524 (1973).
9) J. I. Legg and D. W. Cooke, *Inorg. Chem.*, **5**, 594 (1966); J. Hidaka, Y. Shimura, and R. Tsuchida, *Bull. Chem. Soc. Jpn.*, **35**, 567 (1962).
10) Y. Shimura, *Bull. Chem. Soc. Jpn.*, **31**, 173 (1958).
11) H. Yamatera, *Bull. Chem. Soc. Jpn.*, **31**, 95 (1958).
12) G. L. Blackmer and J. L. Sudmeier, *Inorg. Chem.*, **10**, 2019 (1971).
13) M. Linhard and M. Weigel, *Z. Anorg. Chem.*, **269**, 113 (1951).
14) F. P. Dwyer and F. L. Garvan, *J. Am. Chem. Soc.*, **83**, 2610 (1961).
15) C. W. Maricondi and C. Maricondi, *Inorg. Chem.*, **13**, 1110 (1974).
16) IUPAC, "Nomenclature of Inorganic Chemistry, 1970," Butterworths, pp. 75—83.
17) C. T. Liu and B. E. Douglas, *Inorg. Chem.*, **3**, 1356 (1964); N. Matsuoka, J. Hidaka, and Y. Shimura, *Inorg. Chem.*, **9**, 719 (1970); *Bull. Chem. Soc. Jpn.*, **48**, 458 (1975).
18) E. A. Berends and J. G. Brushmiller, *Inorg. Nucl. Chem. Lett.*, **6**, 847 (1970).

XPS Study on the Charge Distribution in Chromium(0) Complexes

Fumio KINOMURA, Tadashi TAMURA, Iwao WATANABE, Yu YOKOYAMA, and Shigero IKEDA

Department of Chemistry, Faculty of Science, Osaka University, Toyonaka, Osaka 560

(Received July 5, 1976)

Binding energies of core electrons in $Cr(C_6H_6)_2$, $Cr(C_6H_6)(CO)_3$, and $Cr(CO)_6$ were measured by means of X-ray photoelectron spectroscopic method in solid phase. By comparison with their UPS spectra observed in gasous phase, binding energies referred to vacuum level can be obtained. On the basis of this result, charge distribution in these complexes are estimated. The intramolecular relaxation energy of $Cr(C_6H_6)_2$ is also discussed.

The study of X-ray photoelectron spectroscopic, (XPS), spectra of solid material reveals that the observed binding energy of a core electron is a function of not only the charge density on an atom but also the matrix effects such as Madelung energy, polarization energy, and work function.[1] Therefore, the evalutaion of the matrix effects is required so as to elucidate the charge density on atom from the observed binding energy by XPS method.

In this paper, results of XPS measurements of bis-(benzene) chromiun, chromium benzene tricarbonyl, and chromium hexacarbonyl in solid phase are reported. The matrix effects on observed binding energy were calibrated by comparing the observed valence bands of these compounds to their UPS spectra in gasous phase. This correction made it possible to estimate the effective charge on each atom except for hydrogen atom. Finally, these resullts were examined by comparison of the predicted chemical shift in binding energy of Cr 3p electrons with that of the observed energy. Estimation of the difference of relaxation energies of C ls electrons between benzene and bis-benzene chromium was also attempted.

Exprimental

Bisbenzene chromium[2] and chromium benzene tricarbonyl[3] were prepared, and identified by the elemental analysis and mass spectrometric analysis. Those were stored in sealed samples. Chromium hexacarbonyl was of commercial source (Sterm Chemicals Inc.) and used without any further purification. Thin film of samples was prepared by condensing the sublimated compounds under a vacuum of 10^{-2} Pa on the sample-holder. The surface of the sample-holder was covered with vacuum deposited gold and kept at a temperature of 200 K during XPS measurement.

All of the XPS spectra were recorded by means of an AEI ES 200 type photoelectron spectrometer with aluminium target as an X-ray source. During measurements of XPS spectra the spectrometer was kept at the pressure lower than 10^{-5} Pa. An Au $4f_{7/2}$ peak (83.8 eV), which came from the surface of the sample-holder, was measured simultaneously with XPS spectra of sample and used as a reference of bending energy.

Results and Discussion

The compounds investigated have sufficient vapor pressure to measure XPS spectra in gaseous phase at the moderately elevated temperature. However, the partial decomposition of the sample by heat and/or X-ray irradiation and deposition of thin layer of metallic chromium of non-volatile compounds on aluminum X-ray window was observed. This not only gave the unreliable XPS data but also caused serious damage to XPS spectrometer preventing a prolonged XPS measurement. The XPS measurement in solid phase at low temperature did not cause any trouble and the surface of samples was continuously renewed by the slight evaporation of samples.

The valence region of XPS spectra of these compounds are shown in Fig. 1. The energy level diagrams thus obtained are illustrated in Fig. 2, together with results of UPS spectra in gaseous phase.[4,5] In UPS spectra, chromium benzenene tricarbonyl and hexacarbonyl give the well difined first band separating from the succeeding bands, but the first and second bands in UPS spectrum of bis-benzene chromium close to each other and are observed as a single peak in its XPS spectrum.

When compounds form molecular crystals and the interaction beween molecules in crystal is very weak, their MO's would not encounter with serious perturbation and ionization potentials or binding energies in both solid and gaseous phase would be coincident with each other. Then, the difference of binding energies between gaseous and solid phase should be brought solely by the matrix effects. Of these effects, Madelung energy must be so small that it might be disregarded. Seki *et al.*[6] show that the polarization energy in molecular crystals of some aromatic compounds lies around 1.1 eV within the range of 0.2 eV. Very similar results were obtained by Lyons and Mackie.[7] Therefore the main part of the observed difference of binding energies between gaseous and solid phase is considered to come from the work function.

When the weighted mean values of binding energies of the very closed orbitals observed by He(II) or He(I) UPS were compared with the binding energies of the corresponding bands in XPS spectra, the shifts are paralled and the difference falled within ± 0.2 eV. In Fig. 2, the calibrated binding energies of XPS data were given by broken lines. In the case of bis-benzene chromium, the binding energy of the first band in XPS spectra was set equal to the weighted average of those of the first and second bands in He(II) UPS spectrum. The calibrated binding energies agree well with the binding energies of the corresponding bands in UPS spectra. According to Guest *et al.*[4] the first band of $Cr(C_6H_6)_2$ should be assigned to t_{2g} orbital mainly localized on a chromium atom and the bands below the third bands come from MO's on ligands. A similar assignments were made for $Cr(C_6H_6)(CO)_3$[4] and $Cr(CO)_6$.[5]

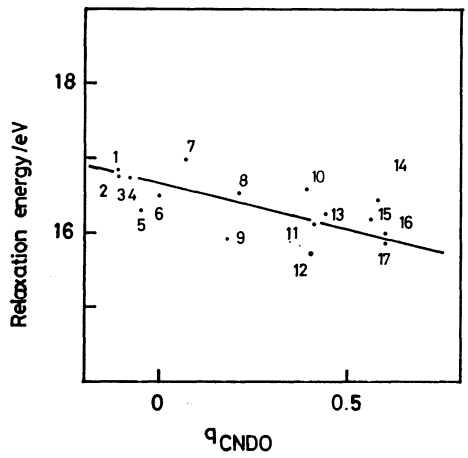

Fig. 3. The correlation between the relaxation energy and the charge density on carbon atom of the compounds : 1) $C^*H_2CF_2$; 2) $C^*H_3CF_3$; 3) $C^*H_3CHF_2$; 4) $C^*H_3CHF_2$; 5) $CH_3C^*H_2F$; 6) C_2H_6; 7) $C^*HF=CF_2$; 8) $CH_2=C^*HF$; 9) CH_3F; 10) $CHF=C^*F_2$; 11) $CH_3C^*HF_2$; 12) CH_2F_2; 13) $CH_2=C^*F_2$; 14) $C^*F_3CF_2CF_3$; 15) CF_3CF_3; 16) $C^*F_3CH_2NH_2$; 17) $CH_3C^*F_3$: [after Ref. 11].

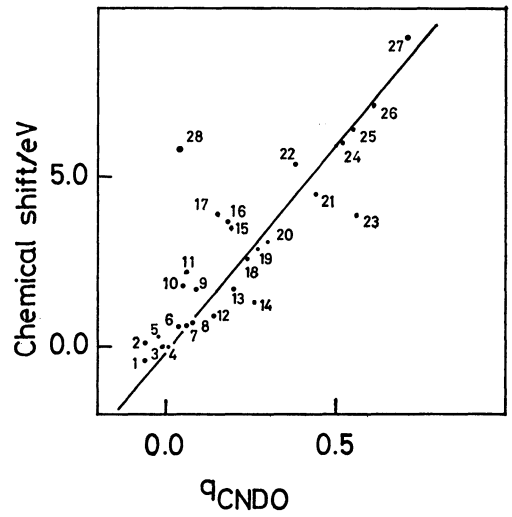

Fig. 4. The correlation between chage density on carbon atom calculated by CNDO/2 method and chemical shift in C 1s binding energy relative to that of benzene: 1)pyrrole, (β-carbon); 2) furan, (β-carbon); 3) thiophene, (β-carbon) ; 5) thiophene, (α-carbon) ; 14) furan, (α-carbon); 23) pyrrole, (α-carbon): [after Ref. 18]; 4) benzene; 6) toluene, (α-carbon); 8) $C_6H_5C^*N$; 9) chlorobenzene, (α-carbon); 12) aniline, (α-carbon); 13) phenol, (α-carbon); 18) fluorobenzene, (α-carbon): [after Ref. 17]; 15) C_6O_6; 16) $CF_3C^*OCH_3$; 17) C_6F_6; 19) H_2C^*O; 20) $(CH_3)_2C^*O$; 21) CH_3C^*OOH; 23) $(NH_2)_2C^*O$; 24) $C_2H_5OC^*OCl$; 25) $(CH_3O)_2C^*O$; 26) CO_2; 27) F_2CO: [after Ref. 13]; 28) CO: [after Ref. 11].

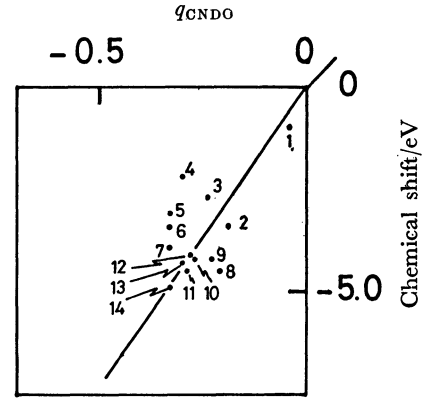

Fig. 5. The correlation between charge density on oxygen atom calculated by CNDO/2 method and chemical shift in O 1s binding energy relative to that of O_2 : 1) CO; 2) NNO; 4) CO_2 ; 5) CH_3CO^*OH 6) H_2O; 10) CH_3OH; 11) C_2H_5OH; 12) $(CH_3)_2CO$; 14) CH_3COO^*H: [after Ref. 19]; 3) $HCOO^*H$; 7) CH_3NO_2; 8) C_2H_4O; 9) $(C_2H_5)_2O$; 13) HCO^*OH : [after Ref. 11].

C 1s bind eningergies could be given by the sum of group shifts.[13] This reflects that the σ-bond is strongly localized, and leads to the conclusion that most of Δq come from the substituent X, and that the charge distribution on both the substituent and residual groups remains almost constant. Most of the second row elements attach to a carbon atom with the bond length ranging from 1.1 Å to 1.5 Å. Then, in the case where molecules have a similar skeletal structure and do not have polar bonds, it might be expected that the change in V of Eq. 1 can be given as a linear function of the charge density on the carbon atom concerned. Under such circumstances, Eq. 1 can be rewritten as follows:

$$BE = k' \cdot q_C + l' \qquad (2)$$

as has been given by K. Siehgbahn *et al.* in the XPS study of free molecules.[14] For the present purposes, we selected the observed C 1s binding energies for the sp^2 carbon taken from the reliable data and reproduced in the plots of *BE vs.* q_C (Fig. 4.), (the same plot for O 1s binding energies was also given in Fig. 5).

Equation 2 may be used to get the charge distribution in the present compounds from binding energies given in Table 1. Some objection may exist to the utility of Eq. 2 for those compounds owing to 1) the difference of the skeletal structure of bisbenzene chromium from that of the compounds used to induce Eq. 2, and 2) smaller relaxation energy for a C 1s electron in free CO. Bis-benzene chromium forms a π-complex with the separation of 2.19 Å between carbon and chromium atoms. However, in the case of bis-benzene chromium, positive potential at ionized carbon caused by a chromium atom is reduced by negative potential caused by other eleven carbon atoms. This makes the situation simply as the substitution by the twelfth part of chromium with a bond length of 0.8 Å.

The binding energy of a C 1s electron in free CO lies significantly far from the relation given by Eq. 2 as clearly seen from Fig. 4. Davis and Shirley[11] have shown that the relaxation energy of a C 1s electron in CO is the smallest of the compounds of all they studied. According to their results, the relaxation energy of a C 1s electron in CO is smaller than the average of relaxation energies calculated for C 1s electrons in various compounds by amounts of 4.8 eV.

On the other hand, Baerends and Ros[15] showed in the study of metal carbonyls by DVM Xα-SCF MO calculation that the relaxation energy for a C 1s electron in $Cr(CO)_6$ is larger than that in free CO by amounts of 4.0 eV. Therefore, it might be said that the relaxation energy for C 1s electron in $Cr(CO)_6$ is comparable to that found in molecules used to decide Eq. 2.

The Estimation of Chemical Shifts in Cr 3p Binding Energies. The charge distribution in $Cr(CO)_6$, $Cr(C_6H_6)(CO)_3$, and $Cr(C_6H_6)_2$ are given in Table 2. It is presumed that the charge density on a hydrogen atom in benzene remains constant before and after the formation of a complex because a benzene molecule attached to a chromium atom through its π-orbital. Standing on this assumption we determined the charge density on a chromium atom. Assuming that the relaxation energy of 3p electron in these compounds is constant, chemical shifts in Cr 3p binding energy relative to bis-benzene chromium may be obtained to substitute the above obtained charge densities into the equation similar to the Eq. 1. The *k*-value for Cr 3p electron is decided to be 22 eV/unit charge calculating the Coulomb integral between Cr 3p and 3d electrons with Slater orbitals. The calculated chemical shifts are given in Table 3. It should be noted that the binding energy of Cr 3p electron in $Cr(CO)_6$ is larger than that in $Cr(C_6H_6)(CO)_3$, whereas the charge density on chromium atom in $Cr(CO)_6$ is smaller than in $Cr(C_6H_6)(CO)_3$, that is, the later is more positive than the former. The observed chemical shifts agreed well with the calculated chemical shifts. In other words, the relation given by Eq. 2 is no longer applied to the chemical shift in Cr 3p electrons. Evidently, this is due to the difference in molecular structure. CO coordinated through the carbon atom which is more positive than that in benzene. Furthermore, the distance between Cr and C for benzene is larger than that between Cr and C for CO. Therefore, electrostatic potential felt by a chromium atom in $Cr(CO)_6$ is more positive than that in $Cr(C_6H_6)(CO)_3$.

The Relaxation Energy for C 1s Electron in $Cr(C_6H_6)_2$. The difference between the relaxation energies in free and coordinated benzenes, ΔE_R, was obtained to be 0.4 eV to substitute above obtained charge distribution in bis-benzene chromium into Eq. 1. The relaxation energy is given by the equation[11]

$$E_R = \frac{1}{2}(V^* - V)$$

where V^* and V are respectively, the electrostatic potential at ionized carbon in the relaxed hole state and in the ground state. The hole state was expressed by equivalent core model. V^* and V caused by surrounding atoms were calculated on the basis of the potential model. For the atom which has a 1s hole, $1/2(V^* - V)$ was calculated by using the equation given by Basch.[16] The results of these calculation predict that $\Delta E_R = -0.9$ eV. ΔE_R can be estimated also from Fig. 3, which gives $\Delta E_R = -0.1$ eV. The values of ΔE_R obtained by each method may be considered to show a rather agreement with each other.

Table 2. The charge density on atoms estimated from XPS data, (in unit of |e|)

Compound	q_C	q_O	q_{Cr}
$Cr(CO)_6$	0.23	−0.24	0.06
$Cr(C_6H_6)(CO)_3$	0.15	−0.29	0.54
	−0.02[a]		
$Cr(C_6H_6)_2$	−0.05	—	0.60

a) The charge density on carbon atom in benzene.

Table 3. Comparison of the estimated chemical shift in Cr 3p electron with that of observed, (in unit of eV).

Compound	Calcd	Obsd
$Cr(C_6H_6)_2$	0.0	0.0
$Cr(C_6H_6)(CO_3)$	1.1	1.9
$Cr(CO)_6$	2.7	2.9

Conclusion

We could obtain the binding energy of a core electron referred to vacuum level by calibrating the binding energy of a valence band observed in solid phase with that in gaseous phase. Within certain selected molecules, the change in binding energy can be directly correlated to the change in charge density. This relation could be applied to the results of XPS measurements of the present compounds for the estimation of charge distribution in these compounds.

This work was achieved by the financial support by TORAY SCIENCE FOUNDATION.

References

1) a) P. H. Citrin and T. D. Thomas, *J. Chem. Phys.*, **57**, 4446 (1972); b) P. H. Citrin and D. R. Hamann, *Chem. Phys. Lett.*, **22**, 301 (1973); c) K. S. Kim and N. Winograd, *Chem. Pyhs. Lett.*, **30**, 91 (1975).
2) E. O. Fischer, *Inorg. Synth.*, **6**, 132 (1960).
3) M. C. Whiting, Brit. 941061 (Cl. CO7f), Nov. 6, 1963.
4) M. F. Guest, I. H. Hillier, B. R. Higginson, and D. R. Lloyd, *Mol. Phys.*, **29**, 113 (1975).
5) B. R. Higginson. D. R. Lloyd, P. Burroughs, D. M. Gibson, and A. F. Orchard, *J. Chem. Soc., Faraday Trans. 2*, **69**, 1659 (1973).
6) K. Seki, H. Inokuchi, and Y. Harada, *Chem. Phys. Lett.*, **20**, 197 (1973).
7) L. E. Lyons and J. C. Mackie, *Proc. Chem. Soc.*, **1962**, 71.
8) K. Siegbahn *et al.*, "ESCA Applied to Free Molecules," North-Holland Publ. Co., Amsterdam (1969), p. 108.
9) L. C. Snyder, *J. Chem. Phys.*, **55**, 95 (1971).
10) U. Gelius, *Physica Scripta*, **9**, 133 (1974).
11) D. W. Davis and D. A. Shirley, *J. Electron Spectrosc.*, **3**, 137 (1974).
12) H. Siegbahn, R. Medeiros, and O. Goscinski, *J. Electron Spectrosc.*, **8**, 149 (1976).
13) U. Gelius, P. F. Hedén, J. Hedman, B. J. Lindberg, R. Manne, R. Nordberg, C. Nordling, and K. Siegbahn, *Physica Scripta*, **2**, 70 (1970).
14) Ref. 8, p. 117.
15) E. J. Baerends and P. Ros, *J. Electron Spectrosc.*, **7**, 69 (1975).
16) H. Basch, *J. Electron Spectrosc.*, **5**, 463 (1974).
17) T. Ohta, T. Fujikawa, and H. Kuroda, *Bull. Chem. Soc. Jpn.*, **48**, 2017 (1975).
18) U. Gelius, C. J. Allan, G. Johansson, H. Siegbahn, D. A. Allison and K. Siegbahn, *Physica Scripta*, **3**, 237 (1971).
19) Ref. 8, p. 126.

Hydrothermal Synthesis of Some Varieties of Zircon

Izumi NAKAI, Tetsuo SHIMA, Mihoko IZAWA, and Kozo NAGASHIMA

Department of Chemistry, Faculty of Science, Tokyo University of Education, Otsuka, Bunkyo-ku, Tokyo 112

(Received July 10, 1976)

Some varieties of zircon which contain yttrium, niobium, and phosphorus in solid solution have been synthesized at temperatures 500—550 °C and under pressures 700—1000 kg/cm². In zircon containing yttrium, the unit cell constants *a* and *c* increase with increase in yttrium content up to 70 mol%. From IR and TGA studies, a valence compensation accompanying the substitution of yttrium is assumed to be effected by a concomitant substitution of OH for O sites, and the variety is represented by a formula $(Zr,Y)Si(O,OH)_4$. On the other hand, the substitution of Nb^{5+} for Zr^{4+} is followed by a decrease in the cell constants. Zircon phase did not form from starting materials with more than 20 mol% of niobium content. From the syntheses of zircon containing both yttrium and niobium, the formula $(Zr,Y,Nb)\ Si(O,OH)_4$ is found to be appropriate for naegite. An attempt was made to synthesize some solid solutions between zircon and xenotime. The unit cell constant *c* of the products is found to decrease with the substitution of PO_4 for SiO_4.

Zircon, $ZrSiO_4$, a widely distributed accessory mineral in igneous rocks, is known to have many varieties such as cyrtolite (water, yttrium rich zircon), naegite (yttrium, niobium rich zircon) and yamaguchilite (yttrium, phosphorus rich zircon).[1] Since the varieties of zircon usually occur in metamict state due to radioactive elements such as uranium and thorium, the properties of the varieties and the mechanisms of the substitutions are not well-known.

In zircon, each silicon atom is surrounded by a tetrahedral group of four oxygen atoms at a distance of 1.61 Å, while each zirconium atom lies between four oxygen atoms at 2.15 Å and a further four at 2.29 Å. These Zr–O distances lie between the limits of 8- and 6-fold coordination.[2] We have studied the isomorphous substitutions of Y^{3+}, Nb^{5+}, and P^{5+} for Zr^{4+} and Si^{4+} sites in zircon. From the relative sizes of the ions involved, it is expected that Zr^{4+} is substituted by Y^{3+} and Nb^{5+}, and Si^{4+} by P^{5+}. This is found to be true in the present work.

Frondel and Collette carried out the hydrothermal synthesis of zircon over the range 150 °C and 4.8 bars to 700 °C and 3100 bars by heating admixed ZrO_2 and SiO_2 gels with water in steel bombs.[3] Single crystal of zircon was also obtained by hydrothermal method.[4,5] In our study, the syntheses of some varieties were carried out by the hydrothermal crystallization of precipitated gels of stoichiometric composition, and the mechanisms of the substitutions and the variations of cell constants were studied.

Experimental

The reagents employed were dilute HNO_3 solutions of $ZrO(NO_3)_2 \cdot 2H_2O$ (EP-grade) and Y_2O_3 (99.99% pure), dilute H_2SO_4 solution of Nb_2O_5(99.9% pure) and aqueous solutions of Na_2SiO_3 (CP-grade, standardized by gravimetric analysis) and $(NH_4)_2HPO_4$ (EP-grade). The starting gels were prepared by mixing each solution to the desired composition. The mixed solutions were adjusted to pH 10 with dilute ammonia. The resulting precipitates were centrifuged, washed with dilute ammonia, dried at 130 °C in an oven and finely ground. The gels were sealed with 0.05 ml water in Ag capsules, inner diameter 3 mm and length 35 mm. The hydrothermal synthesis was carried out in a 150 ml cold seal rene bomb.

All the products were examined by the X-ray powder diffraction method using CuK_α radiation and internal silicon standard. The composition of synthesized zircon is assumed to have a composition corresponding to the initial gel when it appears in a single phase in the product. Unit cell constants were calculated according to the known space group. Some of the products were examined by infrared spectroscopy by the KBr disk method and TGA.

Results and Discussion

Isomorphous Substitution of Yttrium in Zircon. Syntheses of zircon which contains various amounts of yttrium were carried out with gels which have the composition $ZrO_2 : Y_2O_3 : SiO_2 = 1-x : x/2 : 1$, where x varied from 0 to 1. The runs were made under the conditions 530 °C, and 700 kg/cm² for 55 h. The products were white and microcrystalline. The calculated unit cell constants plotted against the initial gel composition are given in Fig. 1. The cell constants *a* and *c* increase linearly as a function of the composition up to about 70 mol% of yttrium content. The significant increase in the cell constants seems to indicate the continuous substitution of large Y^{3+} ion for Zr^{4+} ion. The limit of the substitution is about 70 mol% under our experimental conditions. The product is no longer present in a single phase beyond 70 mol% of yttrium content, and β-yttrialite $Y_2Si_2O_7$ phase and a small amount of an unidentified phase appear besides the zircon phase. Therefore, zircon with high yttrium content (more than 70 mol%) is presumed to be unstable and stabilized by forming

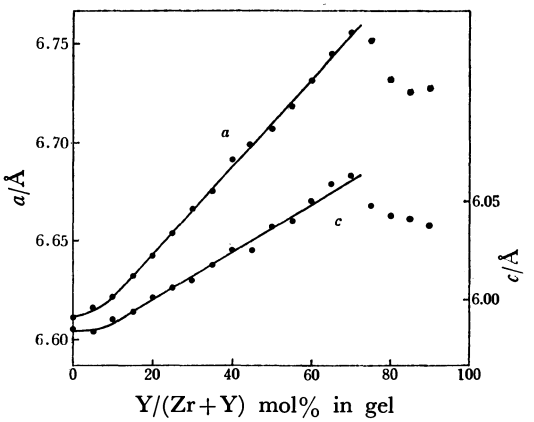

Fig. 1. Unit cell constants *a* and *c* of zircon containing Y.

β-yttrialite and zircon with low yttrium content.

The substitution of trivalent yttrium for quadrivalent zirconium requires some valence compensations in the zircon structure. From an EPR study of natural zircon, Bershov found that when two Y^{3+} ions enter simultaneously into two neighboring zirconium sites the structure is stabilized by the formation of O^- center.[6] The valence compensation of this type, however, seems to be possible only when yttrium is present in zircon in a low concentration less than a few per cent. It should be noted that some varieties of zircon often contain significant amount of water up to 10%. Frondel postulated that some of the water characteristically present in metamict zircon should be regarded as essential and required for the valence compensation in the structure.[7] He suggested a substitution of OH for O in SiO_4 tetrahedra as the valence compensation on the basis of the chemical analysis and thermal study of a natural sample by Kostyleva.[8] This mechanism is adopted here to explain the valence compensation in synthesized zircon. In order to determine the presence of OH, infrared measurements were made on a number of the products which had been dried at 130 °C before measurements. Figure 2 shows IR spectra of pure zircon and zircons containing niobium (16 mol%), yttrium (34 mol%) and yttrium (32 mol%) which was heated at 350 °C for 40 min in advance. Figure 3 shows IR spectra in the 2500—4000 cm^{-1} region of zircon with 5, 25, 45, and 65 mol% yttrium content and zircon with 60 mol% yttrium content which was heated at 1100 °C for 2 h in advance. Zircon containing yttrium gives weak infrared OH absorptions at about 3400, 3200, and 1600 cm^{-1}. Since the absorption at about 3200 cm^{-1} remained after the sample had been dried at 350 °C but disappeared when it had been heated to 1100 °C, the absorption

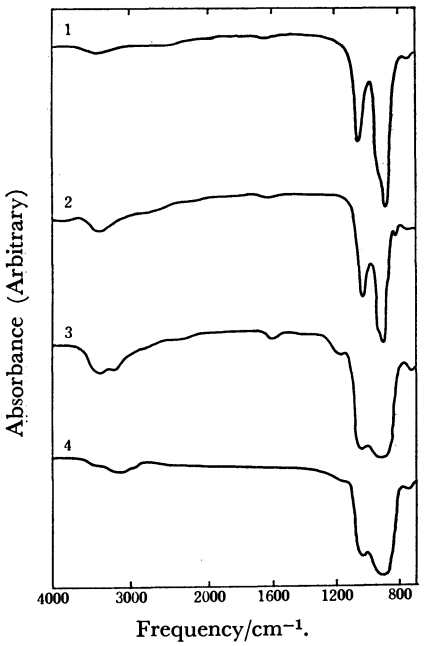

Fig. 2. IR spectra of zircon.
1: Pure, 2: containing 16 mol% Nb, 3: containing 34 mol% Y, 4: containing 32 mol% Y, heated at 350 °C for 40 min.

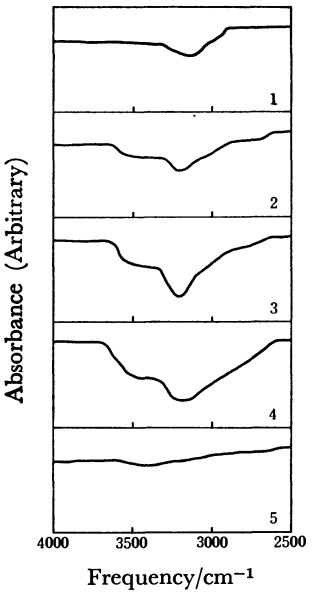

Fig. 3. IR spectra of zircon with Y content of 1 : 5 mol%, 2 : 25 mol%, 3 : 45 mol%, 4 : 65 mol%, 5 : 60 mol%, heated at 1100 °C for 2 h.

is assumed to be due to OH substituting for O in the SiO_4 tetrahedra. The absorptions at about 3400 and 1600 cm^{-1} disappeared when the sample had been dried at 350 °C. These absorptions are assigned to molecular water and OH in the hydrogen bond. The relative intensity of the peak at about 3200 cm^{-1} increases with an increase in yttrium content (Fig. 3). The result seems to support the view that the absorption is due to OH substituting for O in the SiO_4 tetrahedra. The doublet absorption band centered at about 1000 cm^{-1} has been assigned to the Si–O bonds. We see from Fig. 2 that the doublet structure of the absorption band is very indistinct in zircon containing yttrium as compared with that of the band in pure zircon and zircon containing niobium. The indistinctness for the former is probably due to the non-uniformity of the strength of the Si–O bonds in zircon containing yttrium because it has two kinds of Si–O bond, *viz.* Si–O and Si–OH.

TGA study was carried out for the sample containing 40 mol% of yttrium. The result is given in Fig. 4. The TGA curve shows a gradual loss of H_2O up to 0.85% at 350 °C, and a gradual loss of 2.0% H_2O

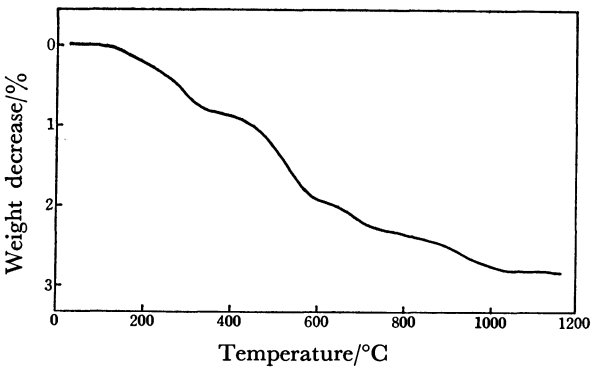

Fig. 4. TGA curve for zircon containing 40 mol% Y.

from 350 to 1000 °C. The former seems to be caused by the dehydration of molecular water and the latter by that of OH substituting for the O sites. The latter 2.0% loss agrees with the calculated value 1.97% evaluated by assuming that the concentration of OH substituting for the O sites in zircon is equal to that of yttrium. The above observations suggest that the following formula is appropriate for the synthesized zircon : $(Zr,Y)Si(O,OH)_4$.

X-Ray diffraction powder pattern for the product heated at 1100 °C for 2 h shows the presence of β-yttrialite as well as zircon. This indicates that $(Zr,Y)Si(O,OH)_4$ decomposes to $ZrSiO_4$, $Y_2Si_2O_7$, and H_2O.

Study on Naegite by Means of Synthesis. One variety of zircon which mainly contains yttrium and niobium is called naegite* and usually written as $(Zr,Y)(Si,Nb)O_4$. The site occupancy of niobium in zircon is of interest. In order to confirm the assumption that Nb^{5+} does not substitute for Si^{4+}, attempts were made to obtain zircon containing niobium from gels having the composition $ZrO_2 : Nb_2O_5 : SiO_2 = 1-x : x/2 : 1$, where x varies from 0 to 1. The syntheses were carried out under the conditions 530 °C and 700 kg/cm² for 55 h. Attempts to prepare zircon containing over 20 mol% niobium were not successful, resulting in mixed phases of ZrO_2, SiO_2 and unknown substances which gave very diffuse X-ray powder patterns. The zircon phase is found to form only when niobium is less than about 15 mol% in the gel composition. A plot of the unit cell constants of the synthesized zircon *versus* the composition is given in Fig. 5. The cell constants decrease slightly with increase in niobium content up to 10 mol% but remain nearly constant above 10 mol%. In view of the relative size of ions, it seems reasonable to consider that the observed decrease in the cell constants results from the substitution of Nb^{5+} for Zr^{4+} and not for Si^{4+}. The substitution of Nb^{5+} for Zr^{4+} requires valence compensation. There are two explanations: (1) It is achieved by cation deficiency. When the concentration of the deficiency is high, cation deficient zircon becomes unstable. This

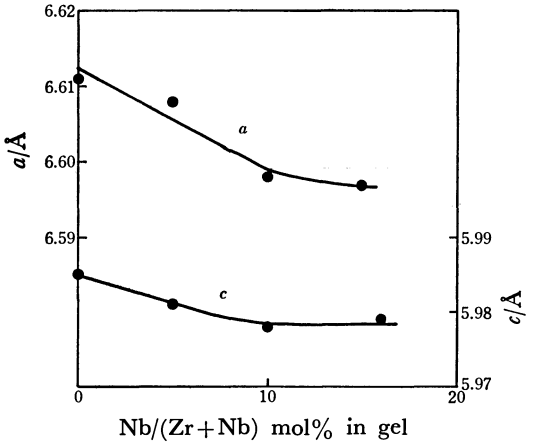

Fig. 5. Unit cell constants a and c of zircon containing Nb.

* A name proposed by T. Wada (1904).

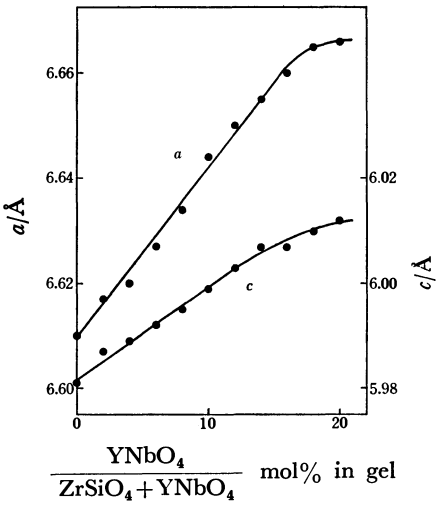

Fig. 6. Unit cell constants a and c of zircon containing Y and Nb.

corresponds to the fact that zircon with high niobium content is not obtained in our syntheses. (2) Niobium exists in zircon in the quadrivalent state but not in the quinquevalent state. The possibility of its presence was reported by Matkovich and Corbett.[9] They heated equimolar amounts of ZrO_2 and SiO_2 in the presence of Nb_2O_5 at 1000 °C in an electric furnace and obtained zircon with cell constants slightly smaller than that of pure zircon. They also heated equimolar amounts of ZrO_2 and SiO_2 in the presence of V_2O_5 and obtained light blue zircon. The color implies the presence of quadrivalent vanadium in zircon. By analogy with vanadium in zircon, they inferred the presence of quadrivalent niobium in zircon. There is, however, no direct evidence of quadrivalent niobium and its presence remains to be clarified.

The syntheses of naegite were carried out under the conditions 530 °C, and 1000 kg/cm² for 81 h. The initial gels had the composition $(Zr_{1-x},Y_x)(Si_{1-x},Nb_x)O_4$, x varying from 0 to 0.2. A plot of the cell constants of the products against the composition is shown in Fig. 6. If we compare the curves in Fig. 1

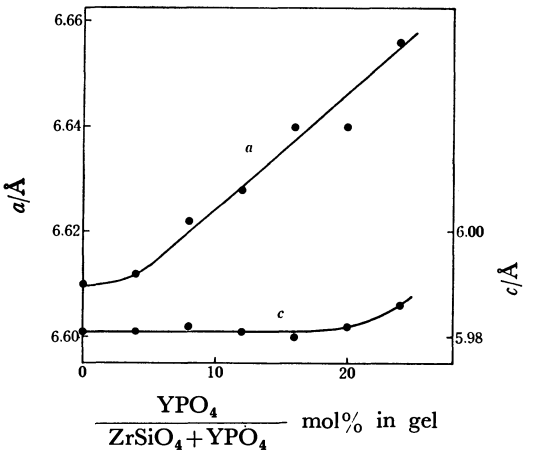

Fig. 7. Unit cell constants a and c of zircon containing Y and P.

and Fig. 6, we see that their shapes resemble each other. Since zircon does not contain niobium in high concentration, the variation in the cell constants seems to be mainly due to the yttrium concentration in synthesized naegite. This corresponds to the fact that yttrium is present in much higher concentration than niobium in natural naegite. Substitution of OH for O sites seems to occur in naegite for valence compensation. Thus the formula $(Zr, Y, Nb)Si(O, OH)_4$ might be appropriate for naegite. The phase $(Zr, Y, Nb)Si(O, OH)_4$ was no longer present in a single phase under the hydrothermal conditions 700 °C and 1000 kg/cm^2, decomposing into fergusonite $YNbO_4$ and zircon phases.

An Attempt to Synthesize Yamaguchilite $(Zr,Y)(Si,P)O_4$. The syntheses of yamaguchilite,* solid solutions of zircon and xenotime (YPO_4), were carried out under the conditions 530 °C and 1000 kg/cm^2 for 81 h. The cell constants of synthesized $(Zr,Y)(Si,P)O_4$ *versus* initial gel composition are plotted in Fig. 7. Although there is no direct evidence of the $ZrSiO_4 : YPO_4$ ratio in the products, there is a significant difference in the variation of the cell constant c between the curves in Figs. 1 and 7: in $(Zr,Y)(Si,P)O_4$, c remains nearly constant up to 20 mol% of the yttrium content. Therefore the substitution of PO_4 for SiO_4 is found to cause a relative decrease in c dimension, not a dimension.

* A name proposed by K. Kimura and Y. Hironaka[1] (1936).

The authors wish to express their thanks to Dr. Yoshinori Fujiki, Mr. Isamu Shindo, Dr. Mamoru Watanabe and Mr. Fujio Izumi of National Institute for Researches in Inorganic Materials for their technical assistance. The authors also wish to thank Dr. Yoshinori Sugitani, Tokyo University of Education, for critical reading of the manuscript. The present work was partially supported by a Grant-in Aid for Scientific Research from the Ministry of Education.

References

1) K. Kimura and Y. Hironaka, *Nippon Kagaku Kaishi*, **57**, 1195 (1936).
2) W. A. Deer, R. A. Howie, and J. Zussman, "Rock-Forming Minerals," 5th ed., Longmans Green & Co., Vol. 1, London (1967), p. 59.
3) C. Frondel and R. L. Collette, *Am. Mineral.*, **42**, 759 (1957).
4) R. Dharmarajan, R. F. Belt, and R. C. Puttbach, *J. Cryst. Growth*, **13/14**, 535 (1972).
5) R. Uhrin, R. F. Belt, and R. C. Puttbach, *J. Cryst. Growth*, **21**, 65 (1974).
6) L. V. Bershov, *Geokhimiya*, **1971**, 48.
7) C. Frondel, *Am. Mineral.*, **38**, 1007 (1953).
8) E. E. Kostyleva, *Dokl. Akad, Nauk SSSR*, Fresman Memorial Volume, 27 (1946).
9) V. I. Matkovich and P. M. Corbett, *J. Am. Ceram. Soc.*, **44**, 128 (1961).

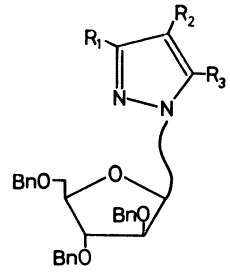

5α, R_1=CO_2Et, R_2=R_3=H
5β, R_1=CO_2Et, R_2=R_3=H
6α, R_3=CO_2Et, R_1=R_2=H
7 (Anomeric mixture)
R_1=R_3=CO_2Et, R_2=H
8α, R_1=R_3=CO_2Et, R_2=NO_2
8β, R_1=R_3=CO_2Et, R_2=NO_2

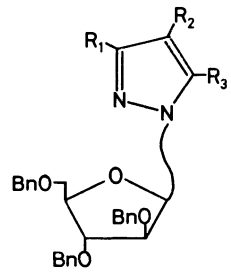

9α, R_1=$CONH_2$, R_2=R_3=H
9β, R_1=$CONH_2$, R_2=R_3=H
10α, R_3=$CONH_2$, R_1=R_2=H
11α, R_1=R_3=$CONH_2$, R_2=H
11β, R_1=R_3=$CONH_2$, R_2=H
12α, R_1=R_3=$CONH_2$, R_2=NO_2
12β, R_1=R_3=$CONH_2$, R_2=NO_2

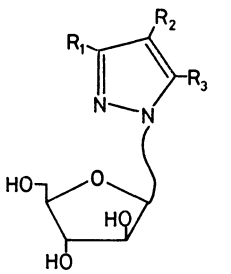

13α, R_1=$CONH_2$, R_2=R_3=H
13β, R_1=$CONH_2$, R_2=R_3=H
14α, R_3=$CONH_2$, R_1=R_2=H
15α, R_1=R_3=$CONH_2$, R_2=H
16α, R_1=R_3=$CONH_2$, R_2=NH_2

Chart 2

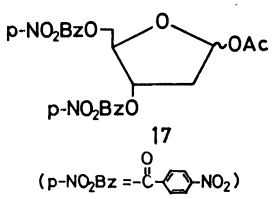

17

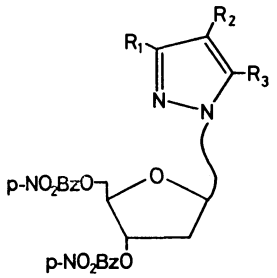

18α, R_1=CO_2Et, R_2=R_3=H
18β, R_1=CO_2Et, R_2=R_3=H
19α, R_3=CO_2Et, R_1=R_2=H
19β, R_3=CO_2Et, R_1=R_2=H
20 (Anomeric mixture)
R_1=R_3=CO_2Et, R_2=H
21 (Anomeric mixture)
R_1=R_3=CO_2Et, R_2=NO_2

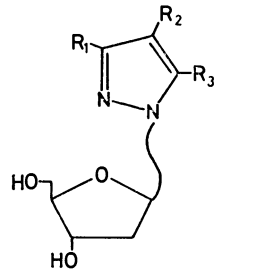

22α, R_1=$CONH_2$, R_2=R_3=H
22β, R_1=$CONH_2$, R_2=R_3=H
23α, R_3=$CONH_2$, R_1=R_2=H
23β, R_3=$CONH_2$, R_1=R_2=H
24 (Anomeric mixture)
R_1=R_3=$CONH_2$, R_2=H
25 (Anomeric mixture)
R_1=R_3=$CONH_2$, R_2=NO_2

Chart 3

benzoyl)-D-*erythro*-pentofuranoside[8] by acetolysis. The fusion reaction of **17** with **2** gave a mixture of blocked nucleosides, which was subjected to the chromatographic separation on silica gel to give the α- and β-anomers of 1-glycosylpyrazole-3-carboxylate (**18**α, **18**β) and 1-glycosylpyrazole-5-carboxylate (**19**α, **19**β) in yield of 27.4, 20.0, 3.3, and 4.9%, respectively, as crystalline products except for **19**α. It may be noted, in this reaction, that the 3-substituted 1-glycosylpyrazoles (**18**α, **18**β) were formed as major products in accord with the cases of the ribonucleosides[1] and the arabinonucleosides (**5**α, **5**β) syntheses under similar conditions.

Treatment of **18**α, **18**β, **19**α, and **19**β with methanolic ammonia gave 1-(2-deoxy-α-D-*erythro*-pentofuranosyl)-pyrazole-3-carboxamide (**22**α), its β-anomer (**22**β), 1-(2-deoxy-α-D-*erythro*-pentofuranosyl)pyrazole-5-carboxamide (**23**α), and its β-anomer (**23**β), respectively. The chemical shifts for the *H*-5 proton signals of **22**α and **22**β are in agreement with those of the arabinonucleosides **13**α and **13**β, and the chemical shifts for the *H*-3 protons of **23**α and **23**β are comparable with those for **14**α and 1-(β-D-ribofuranosyl)pyrazole-5-carboxamide.[1] Thus, **22**α and **22**β were established as 1-glycosylpyrazole-3-carboxamides, and **23**α and **23**β were as the corresponding 5-carboxamides, respectively. Inspection of the PMR spectra of **22**β and **23**β also revealed that the β-anomers are characterized by each triplet of their anomeric proton signals with a peak width of 12 Hz which is consistent with the β-configuration, and, a quartet with a peak width of 10.7 Hz was observed for the anomeric proton of **23**α. These data were consistent with those reported for 2'-deoxyribonucleosides by Robins and Robins[9], and Witkowski *et al.*[10]

The ultraviolet spectra of the 3-carboxamides (**13**α, **13**β, **22**α, and **22**β) and 5-carboxamides (**14**α, **23**α, and **23**β) showed a characteristic difference each other similar to that reported with respect to the corresponding D-ribofuranosyl derivatives.[1]

Similar fusion of **17** with diethyl pyrazole-3,5-dicarboxylate (**3**) afforded blocked nucleosides (**20**),

which, by treatment with methanolic ammonia, led to an anomeric mixture of 1-(2-deoxy-D-*erythro*-pentofuranosyl)pyrazole-3,5-dicarboxamides (**24**).

Further we similarly synthesized its 2'-deoxy analogue (**25**) as an anomeric mixture since 1-(β-D-ribofuranosyl)-4-nitropyrazole-3,5-dicarboxamide[1] was found cytotoxic.[11]

The downfield shifts of the anomeric proton signals of **24** and **25** were also observed.

Preliminary accounts for structure-activity relationships of the above nucleosides as antiviral agents have already been reported.[11]

Experimental

Melting points were determined on a micro hot stage and were uncorrected. Thin layer chromatography (TLC) was conducted by the use of Wakogel B-5. Silica gel column chromatography was performed by using Wakogel G-200. UV-spectra were taken with a Hitachi Perkin-Elmer UV-VIS spectrometer 139. The PMR spectra were recorded with a Varian A-60D spectrometer (TMS as an internal standard).

*1-O-Acetyl-2,3,5-tri-O-benzyl-D-arabinofuranose (**1**).* 2,3,5-Tri-O-benzyl-D-arabinofuranose (10.0 g, 23.8 mmol) was dissolved in anhydrous pyridine (50 ml), to which was added acetic anhydride (50 ml) under ice-cooling. The mixture was stirred at room temperature for 12 h. After removal of the solvent by evaporation, the resulting syrup was dissolved in ethyl acetate (10 ml) and chromatographed on a silica gel column (400 g, 5×100 cm, packed with benzene). Elution with 20 : 1 benzene–ethyl acetate afforded a syrup of **1**, 9.48 g (86.4%); PMR ($CDCl_3$) : δ 7.40 (s, 15H, Ar), 6.40 (br s, 1H, H-1'), 4.75—3.95 (m, 9H, CH_2–Ar, H-2', H-3', H-4'), 3.65 (d, 2H, H-5', 5''), 2.00 (s, 2.1H, CH_3), 1.95 (s, 0.9H, CH_3), *ca.* 21 : 9 mixture of α and β. Found: C, 72.49; H, 6.36%. Calcd for $C_{28}H_{30}O_6$: C, 72.71; H, 6.54%.

*Ethyl 1-(2,3,5-Tri-O-benzyl-β-D-arabinofuranosyl)pyrazole-3-carboxylate (**5β**), Its α-Anomer (**5α**), and Ethyl 1-(2,3,5-Tri-O-benzyl-α-D-arabinofuranosyl)pyrazole-5-carboxylate (**6α**).* A mixture of ethyl pyrazole-3-carboxylate[5] (**2**, 550 mg, 3.93 mmol) and 1-*O*-acetyl-2,3,5-tri-*O*-benzyl-D-arabinose **1**, 1.70 g, 3.68 mmol) was heated at 140 °C to a melt, to which bis(*p*-nitrophenyl) hydrogenphosphate (3 mg) was added, and the mixture was heated at 140 °C under reduced pressure for 8 min until the evolution of acetic acid ceased. The resulting gum was dissolved in ethyl acetate (5 ml), silica gel (2.5 g) was added, and the resulting suspension was evaporated to dryness. The residue was placed on a column of silica gel (110 g, 2.8×45 cm, packed with 1 : 1 hexane–diisopropyl ether) and eluted with the same solvent system. The effluent was fractionated into 11 mls.

Fraction Nos. 31—38 gave **6α**, a colorless syrup, 165 mg (8.3%). $[\alpha]_D^{25}$+55.3° (*c* 0.77, chloroform). PMR ($CDCl_3$): δ 7.79 (d, 1H, H-3), 7.40 (d, 15H, Ar), 7.10 (d, 1H, $J_{1',2'}$= 3.8 Hz, H-1'), 7.04 (d, 1H, H-4), 5.23 (dq, 1H, H-2'), 4.80—4.20 (m, 10H, CH_2–Ar, H-3', H-4', CH_2–ester), 3.72 (d, 2H, H-5',5''), 1.40 (t, 3H, CH_3–ester). Found: C, 70.85; H, 6.52; N, 4.88%. Calcd for $C_{32}H_{34}O_6N_2$: C, 70.83; H, 6.32; N, 5.16%. Fraction Nos. 63—79 gave **5α**, a colorless syrup, 605 mg (30.4%); $[\alpha]_D^{25}$+35.0° (*c* 1.0, chloroform). PMR ($CDCl_3$): δ 7.80 (d, 1H, H-5), 7.40 (s, 15H, Ar), 6.90 (d, 1H, H-4), 6.18 (d, 1H, $J_{2',1'}$=2.2 Hz, H-1'), 4.80—4.18 (m, 11H, CH_2–Ar, H-2', H-3', N-4', CH_2–ester), 3.70 (d, 2H, H-5', 5''), 1.42 (t, 3H, CH_3–ester). Found: C, 70.53; H, 6.19; N, 4.83%. Calcd for $C_{32}H_{34}O_6N_2$: C, 70.83; H, 6.32; N, 5.16%.

Fraction Nos. 87—102 gave **5β**, a colorless syrup, 957 mg (48.2%); $[\alpha]_D^{25}$+15.0° (*c* 0.50, chloroform). PMR ($CDCl_3$): δ 7.95 (d, 1H, H-5), 7.40 (s, 15H, Ar), 6.88 (d, 1H, H-4), 6.40 (d, 1H, $J_{1',2'}$=4.5 Hz, H-1'), 4.65—4.20 (m, 11H, CH_2–Ar, H-2', H-3', H-4', CH_2–ester), 3.75 (d, 2H, H-5', 5''), 1.38 (t, 3H, CH_3–ester). Found: C, 71.01; H, 6.33; N, 5.07%. Calcd for $C_{32}H_{34}O_6N_2$: C, 70.83; H, 6.32; N, 5.16%.

*Diethyl 1-(2,3,5-Tri-O-benzyl-D-arabinofuranosyl)pyrazole-3,5-dicarboxylate (**7**).* By a method similar to that described above, diethyl pyrazole-3,5-dicarboxylate (**3**) (152 mg, 0.715 mmol) was allowed to react with **1** (330 mg, 0.715 mmol) to afford a gum, which was dissolved in ethyl acetate and chromatographed on a column of silica gel (20 g, 1×20 cm, packed with 20 : 1 benzene–ethyl acetate). Elution with the same solvent afforded **7** as a syrup of an anomeric mixture, 334 mg (76%); PMR ($CDCl_3$) : δ 7.38 (d, 16H, Ar, H-4), 7.10 (d, 0.2H, $J_{1',2'}$=5.0 Hz, H-1') 7.08 (d, 0.8H, $J_{1',2'}$=3.7 Hz, H-1'), 5.25 (dq, 1H, H-2'), 4.75—4.17 (m, 12H, CH_2–Ar, CH_2–ester, H-3', N-4'), 3.68 (d, 2H, H-5', 5''), 1.34 (tt, 6H, CH_3–ester). Found: C, 68.10; H, 6.12; N, 4.27%. Calcd for $C_{35}H_{38}O_8N_2$: C, 68.39; H, 6.23; N, 4.56%.

*Diethyl 1-(2,3,5-Tri-O-benzyl-α-D-arabinofuranosyl)-4-nitropyrazole-3,5-dicarboxylate (**8α**) and Its β-Amoner (**8β**).* By a method similar to that described above, diethyl 4-nitropyrazole 3,5-dicarboxylate[1] (**4**) (355 mg, 1.30 mmol) was allowed to react with **1** (600 mg, 1.30 mmol) to give a gum, which was dissolved in ethyl acetate (1 ml), placed on a column of silica gel (70 g, 2.5×40 cm, packed with 2 : 1 hexane–diisopropyl ether) and eluted successively with 2 : 1 (80 ml) and 1 : 1 hexane–diisopropyl ether. The effluent was fractionated into 7.5 mls.

Fraction Nos. 17—26 gave **8α**, a colorless oil, 464 mg (54.2%); $[\alpha]_D^{25}$+129.5° (*c* 1.0, chloroform). PMR ($CDCl_3$): δ 7.41 (d, 15H, Ar), 6.69 (d, 1H, $J_{1',2'}$=3.4 Hz, H-1'), 5.19 (dt, 1H, H-2'), 4.72—4.25 (m, 12H, CH_2–Ar, CH_2–ester, H-3', H-4'), 3.70 (d, 2H, H-5',5''), 1.33 (tt, 6H, CH_3–ester). Found: C, 64.01; H, 5.81; N, 6.11%. Calcd for $C_{35}H_{37}O_{10}N_3$: C, 63.72; H, 5.65; N, 6.37%.

Fraction Nos. 32—41 gave **8β**, a colorless oil, 124mg (14.5%); $[\alpha]_D^{25}$−75.0° (*c* 1.0, chloroform). PMR ($CDCl_3$): δ 7.40 (d, 15H, Ar), 7.31 (d, 1H, $J_{1',2'}$=5.8 Hz, H-1'), 4.7—3.85 (m, 15H, CH_2–Ar, CH_2–ester, H-2', H-3', H-4', H-5',5''), 1.39 (tt, 6H, CH_3–ester). Found: C, 63.92; H, 5.62; N, 6.19%. Calcd for $C_{35}H_{37}O_{10}N_3$: C, 63.72; H, 5.65; N, 6.37%.

*1-(2,3,5-Tri-O-benzyl-α-D-arabinofuranosyl)pyrazole-3-carboxamide (**9α**).* A solution of **5α** (550 mg, 1.01 mmol) in absolute methanol (15 ml) saturated with ammonia at 0 °C was kept at room temperature for 24 h and evaporated. The residual syrup was washed with hexane and dried at 80 °C *in vacuo* for 10 h to give a colorless syrup of **9α**, 415 mg (80%); $[\alpha]_D^{25}$+39.6° (*c* 1.70, chloroform). PMR ($CDCl_3$): δ 7.71 (d, 1H, H-5), 7.38 (d, 15H, Ar), 7.20 (d, 1H, $J_{1',2'}$= 4.0 Hz, H-1'), 6.97 (d, 1H, H-4), 5.13 (dq, 1H, H-2'), 4.8—4.16 (m, 8H, CH_2–Ar, H-3', H-4'), 3.63 (m, 2H, H-5, 5''). Found: C, 70.14; H, 6.15; N, 8.11%. Calcd for $C_{30}H_{31}O_5N_3$: C, 70.16; H, 6.08; N, 8.18%.

*1-(2,3,5-Tri-O-benzyl-β-D-arabinofuranosyl)pyrazole-3-carboxamide (**9β**).* By the same procedure as that for **9α**, **5β** (800 mg, 1.47 mmol) gave **9β**, 635 mg (84%), as a colorless syrup; $[\alpha]_D^{25}$+19.4° (*c* 1.0 chloroform). PMR ($CDCl_3$): δ 7.89 (d, 1H, H-5), 7.42 (m, 15H, Ar), 6.91 (d, 1H, H-4), 6.50 (br d, 2H, $CONH_2$), 6.22 (d, 1H, $J_{1',2'}$=4.5 Hz, H-1'), 4.7—4.2 (m, 9H, CH_2–Ar, H-2', H-3', H-4'), 3.77 (d, 2H, H-5',5''). Found: C, 70.14; H, 6.15; N, 8.07%. Calcd for

pressure gave a syrup, which was dissolved in 20 : 1 benzene–ethyl acetate and chromatographed on a silica gel column (80 g, 2.5×50 cm, packed with the same solvent system). Elution with the same solvent system afforded a pale-yellow glass of **17**, 4.2 g (88%); PMR ($CDCl_3$): δ 8.32 (s, 8H, Ar), 6.60 (m, 1H, H-1), 5.70 (m, 1H, H-3), 4.70 (br s, 3H H-4, H-5,5′), 2.52 (m, 2H, H-2,2′), 2.13 (d, 3H, CH_3). Found: C, 52.89; H, 3.70; N, 5.68%. Calcd for $C_{21}H_{18}O_{11}N_2$: C, 53.17; H, 3.82; N, 5.91%.

*Ethyl 1-(2-Deoxy-3,5-di-*O*-p-nitrobenzoyl-β-*D*-*erythro*-pentofuranosyl)pyrazole-3-carboxylate (**18β**), Its α-Amoner (**18α**), Ethyl 1-(2-Deoxy-3,5-di-*O*-p-nitrobenzoyl-β-*D*-erythro-pentofuranosyl)pyrazole-5-carboxylate (**19β**) and Its α-Anomer (**19α**).* To a mixture of ethyl pyrazole-3-carboxylate (**2**, 539 mg, 4.24 mmol) and 1-*O*-acetyl-2-deoxy-3,5-di-*O*-*p*-nitorobenzoyl-D-*erythro*-pentofuranose (**17**, 1.6 g, 3.38 mmol) heated at 136 °C to a melt, a catalytic amount of bis(*p*-nitrophenyl) hydrogenphosphate (1 mg) was added and the mixture was kept at 136 °C for 3 min under reduced pressure until the evolution of acetic acid ceased. The resulting mixture was triturated with ethyl acetate (5 ml) and chloroform (20 ml). The chloroform solution was evaporated to dryness and the solid was recrystallized from ethyl acetate to give **18α**, 420 mg (22.6%). The mother liquor and the above ethyl acetate layer were combined, and concetrated to about 2 ml. This was chromatographed on a silica gel column (90 g, 2.5×50 cm, packed with 20 : 1 benzene–ethyl acetate) with the same solvent system. The effluent was fractionated into 9 mls.

Fraction Nos. 34—38 gave colorless crystals of **19β**. Recrystallization from benzene and hexane, 94 mg (4.9%); mp 145.5—146.5 °C. $[\alpha]_D^{25}$ −48.0° (*c* 1.0, chloroform). PMR ($CDCl_3$): δ 8.34 (d, 8H, Ar), 7.68 (d, 1H, H-3), 7.41 (q, 1H, H-1′), 6.98 (d, 1H, H-4), 6.00 (br t, 1H, H-3′), 4.86 (br s, 3H, H-4′, H-5′,5″), 4.42 (q, 2H, CH_2-ester), 3.75—2.40 (m, 2H, H-2′,2″), 1.40 (t, 3H, CH_3-ester). Found: C, 54.00; H, 4.20; N, 10.16%. Calcd for $C_{25}H_{22}O_{11}N_4$: C, 54.15; H, 4.00; N, 10.10%.

Fraction Nos. 39—42 gave a mixture of **19β** and **19α**, 25.9 mg (1.4%), *ca.* 5 : 8 mixture of **19β** and **19α**, by PMR.

Fraction Nos. 41—44 gave **19α**, a colorless syrup, 62 mg (3.3%); $[\alpha]_D^{25}$ +29.5° (*c* 1.0, chloroform). PMR ($CDCl_3$): δ 8.35 (s, 8H, Ar), 7.69 (d, 1H, H-3), 7.32 (q, 1H, H-1′), 7.00 (d, 1H, H-4), 5.70 (q, 1H, H-3′), 5.04—4.60 (m, 3H, H-4′, H-5′,5″), 4.43 (q, 2H, CH_2-ester), 3.11 (t, 2H, H-2′,2″), 1.40 (t, 3H, CH_3-ester). Found: C, 54.73; H, 4.01; N, 9.90%. Calcd for $C_{25}H_{22}O_{11}N_4$: C, 54.15; H, 4.00; N, 10.00%.

Fraction Nos. 64—73 gave colorless crystals of **18β**. Recrystallization of **18β** from ethyl acetate gave a pure sample, 372 mg (20.0%); mp 138—140 °C. $[\alpha]_D^{25}$ −22.5° (*c* 1.0, chloroform). PMR ($CDCl_3$): δ 8.38 (s, 8H, Ar), 7.82 (d, 1H, H-5), 6.90 (d, 1H, H-4), 6.43 (t, 1H, H-1′), 5.98 (br t, 1H, H-3′), 4.72 (br s, 3H, H-4′, H-5′,5″), 4.45 (q, 2H, CH_2-ester), 3.72—2.65 (m, 2H, H-2′,2″), 1.39 (t, 3H, CH_3-ester). Found: C, 54.39; H, 4.22; N, 9.95%. Calcd for $C_{25}H_{22}O_{11}N_4$: C, 54.15; H, 4.00; N, 10.10%.

Fraction Nos. 74—77 gave a mixture of **18β** and **18α**, 120 mg (6.7%), *ca.* 1 : 3 mixture of **18β** and **18α**, by PMR.

Fraction Nos. 78—95 gave crystals of **18α**. Recrystallization of **18α** from ethyl acetate gave a pure sample, 90.9 mg (4.8%); mp 183.5—184.5 °C. $[\alpha]_D^{25}$ −6.0° (*c* 1.0, chloroform). PMR ($CDCl_3$): δ 8.25 (m, 8H, Ar), 7.90 (d, 1H, H-5), 6.97 (d, 1H, H-4), 6.45 (q, 1H, H-1′), 5.77 (m, 1H, H-3′), 4.75 (m, 3H, H-4′, H-5′,5″), 4.48 (q, 2H, CH_2-ester), 3.57—2.62 (m, 2H, H-2′,2″), 1.40 (t, 3H, CH_3-ester). Found: C, 54.28; H, 4.03; N, 10.14%. Calcd for $C_{25}H_{22}O_{11}N_4$: C, 54.15; H, 4.00 N, 10.10%.

*Diethyl 1-(2-Deoxy-3,5-di-*O*-p-nitrobenzoyl-*D*-erythro-pentofuranosyl)pyrazole-3,5-dicarboxamide (**20**).* The reaction of diethyl pyrazole-3,5-dicarboxylate (**3**, 630 mg, 2.96 mmol) with **17** (1.4 g, 2.96 mmol) was carried out in a manner similar to that described above. To a solution of the resulting mixture in acetone (5 ml) silica gel (2.2 g) was added and the mixture was evaporated. The residue was chromatographed on a column of silica gel (100 g) packed with 20 : 1 benzene–ethyl acetate. Elution with benzene–ethyl acetate (10 : 1) afforded **20** as an anomeric mixture, 1.18 g (64%); PMR ($CDCl_3$): δ 8.41 (s, 8H, Ar), 7.50 (m, 2H, H-1′, H-4), 6.2—5.5 (m, 1H, H-3′), 4.75 (m, 3H, H-4′, H-5′,5″), 4.50 (q, 4H, CH_2-ester), 3.6—2.1 (m, 2H, H-2′,2″), 1.40 (t, 6H, CH_3-ester). Found: C, 53.39; H, 4.26; N, 9.01%. Calcd for $C_{28}H_{26}O_{13}N_4$: C, 53.67; H, 4.18; N, 8.94%.

*Diethyl 1-(2-Deoxy-3,5-di-*O*-p-nitrobenzoyl-*D*-erythro-pentofuranosyl)-4-nitropyrazole-3,5-dicarboxylate (**21**).* The reaction of diethyl 4-nitropyrazole-3,5-dicarboxylate (**4**) (590 mg, 2.39 mmol) with **17** (1.13 g, 2.39 mmol) was carried out in the similar manner as described above. The resulting mixture was dissolved in ethyl acetate (5 ml), silica gel (1.8 g) was added and the mixture was evaporated to dryness. The residue was placed on a column of silica gel (80 g, 3×60 cm, packed with 1 : 1 hexane–diisopropyl ether) and eluted by the same solvent system. The effluent was fractionated into 8 mls. Fraction Nos. 21—57 gave a colorless syrup of **21**, 664 mg (42%), as an anomeric mixture; PMR ($CDCl_3$): δ 8.40 (s, 8H, Ar), 7.30 (m, 1H, H-1′), 6.2—5.8 (m, 1H, H-3′), 4.75 (m, 3H, H-4′, H-5′,5″), 4.52 (qq, 4H, CH_2-ester), 3.5—2.5 (m, 2H, H-2′, 2″), 1.45 (tt, 6H, CH_3-ester). Found: C, 49.89; H, 3.60; N, 10.18%. Calcd for $C_{28}H_{25}O_{15}N_5$: C, 50.08; H, 3.75; N, 10.43%.

*1-(2-Deoxy-β-*D*-erythro-pentofuranosyl)pyrazole-3-carboxamide (**22β**)* A solution of **18β** (380 mg, 0.686 mmol) in absolute methanol (10 ml) saturated with ammonia at 0 °C was kept at room temperature for 3 days and evaporated. The residual oil was dissolved in water (10 ml) and the solution was extracted with ethyl acetate (3 ml×4). The aqueous layer was evaporated and the residue was chromatographed on a silica gel column (4 g, 0.8×20 cm) packed with 4 : 1 chloroform–methanol. Elution with the same solvent system afforded a glass of **22β**, 129 mg (83%); $[\alpha]_D^{25}$ −17.5° (*c* 1.0, methanol). PMR (CD_3OD): δ 8.09 (d, 1H, H-5), 6.92 (d, 1H, H-4), 6.35 (t, 1H, H-1′), 4.68 (m, 1H, H-3′), 4.11 (m, 1H, H-4′), 3.78 (m, 2H, H-5′,5″), 2.67 (m, 2H, H-2′,2″). UV: λ_{max}^{water} 213 (ε 11900), λ_{max}^{pH1} 198 (ε 12000), λ_{max}^{pH13} 218 nm (ε 11500). Found: C, 47.27; H, 5.90; N, 18.20%. Calcd for $C_9H_{13}O_4N_3$: C, 47.57; H, 5.77; N, 18.49%.

*1-(2-Deoxy-α-*D*-erythro-pentofuranosyl)pyrazole-3-carboxamide (**22α**).* By a procedure similar to that described above, **18α** (580 mg, 1.05 mmol) gave **22α**, 188 mg (79%), as a colorless syrup; $[\alpha]_D^{25}$ +32.5° (*c* 1.0, methanol). PMR (CD_3OD): δ 8.17 (d, 1H, H-5), 6.96 (d, 1H, H-4), 6.32 (q, 1H, H-1′), 4.39 (m, 2H, H-3′, H-4′), 3.72 (m, 2H, H-5′,5″), 3.12—2.34 (m, 2H, H-2′,2″). UV: λ_{max}^{water} 212 nm (ε 12800), λ_{max}^{pH1} 198 nm (ε 12500), λ_{max}^{pH13} 218 nm (ε 11800). Found: 47.26; H, 5.95; N, 18.19%. Calcd for $C_9H_{13}O_4N_3$: C, 47.57; H, 5.77; N, 18.49%.

*1-(2-Deoxy-β-*D*-erythro-pentofuranosyl)pyrazole-5-carboxamide (**23β**).* By a procedure similar to that described above, **19β** (102 mg, 0.546 mmol) gave **23β**, a colorless glass, 36 mg (82%); $[\alpha]_D^{25}$ −69.5° (*c* 1.0, methanol). PMR (CD_3OD): δ 7.82 (d, 1H, H-3) 7.33 (t, 1H, H-1′), 7.03 (d, 1H, H-4), 4.7—4.18 (m, 2H, H-3′, H-4′), 3.90 (m, 2H, H-5′, 5″), 3.23—2.30 (m, 2H, H-2′,2″). UV: λ_{max}^{water} 220 (ε 12800), λ_{max}^{pH1} 198 (ε 13000), λ_{max}^{pH13} 220 nm (ε 11000).

Found: C, 47.45; H, 5.80; N, 18.64%. Calcd for $C_9H_{13}O_4N_3$: C, 47.57; H, 5.77; N, 18.49%.

*1-(2-Deoxy-α-*D*-erythro-pentofuranosyl)pyrazole-5-carboxamide (**23α**).* By a procedure similar to that described above, **19α** (68 mg, 0.123 mmol) gave **23α**, 21.2 mg (76%), as a colorless glass; $[\alpha]_D^{25}$ +18.3° (*c* 1.0, methanol). PMR (CD_3OD): δ 7.80 (d, 1H, H-3), 7.29 (q, 1H, H-1′), 7.00 (d, 1H, H-4), 4.7—4.2 (m, 2H, H-3′, H-4′), 3.85 (m, 2H, H-5′,5″), 3.20—2.25 (m, 2H, H-2′,2″). UV: λ_{max}^{water} 219 (ε 8300), λ_{max}^{pH1} 200 (ε 8100), λ_{max}^{pH13} 220 nm (ε 9000). Found: C, 47.38; H, 5.85; N, 18.60%. Calcd for $C_9H_{13}O_4N_3$: C, 47.57; H, 5.77; N, 18.49%.

*1-(2-Deoxy-*D*-erythro-pentofuranosyl)pyrazole-3,5-dicarboxamide (**24**).* A solution of **20** (800 mg, 1.28 mmol) in absolute methanol (120 ml) saturated with ammonia at 0 °C was kept at room temperatuer for 12 h, and then heated at 90 °C for 30 h in a sealed tube. The solution was evaporated and the resultant syrup was chromatographed on a silica gel column (40 g, 2×30 cm, packed with 4 : 1 chloroform–methanol): Elution by the same solvent system afforded a syrup of **24**, 218 mg (63%); PMR (DMSO-d_6): δ 7.30 (d, 1H, H-4), 7.00 (tq, 1H, H-1′), 4.8—4.2 (m, 2H, H-3′, H-4′), 3.80 (m, 2H, H-5′,5″), 2.80 (m, 2H, H-2′,2″). Found: C, 44.19; H, 5.18; N, 20.61%. Calcd for $C_{10}H_{14}O_5N_4$: C, 44.44; H, 5.22; N, 20.73%.

*1-(2-Deoxy-*D*-erythro-pentofuranosyl)-4-nitropyrazole-3,5-dicarboxamide (**25**).* By a procedure similar to that described above, **21** (600 mg, 0.91 mmol) gave **25** as an anomeric mixture, 179 mg (61%); PMR (CD_3OD): δ 6.40 (tq, 1H, H-1′), 4.40 (m, 2H, H-3′, H-4′), 3.78 (m, 2H, H-5′,5″), 2.80 (m, 2H, H-2′,2″). Found: C, 38.01; H, 4.00; N, 22.09%. Calcd for $C_{10}H_{13}O_7N_5$: C, 38.10; H, 4.16;N, 22.22%.

The authors wish to thank Mr. Saburo Nakada, Department of Chemistry, Keio University, for microanalysis. This research was supported in part by a grant for cancer research, Ministry of Education, Science and Culture.

References

1) O. Makabe, M. Nakamura, and S. Umezawa, *Bull. Chem. Soc. Jpn.*, **48**, 3210 (1975).
2) K. Gerzon, R. H. Williams, M. Hoehn, M. Gorman, and D. C. DeLong, 2nd Intern. Cong. Heterocyclic Chem., Montpellier, France, July 10 (1969), Abstr. C-30.
3) L. T. Chien, F. M. Schabel Jr., and C. A. Alford Jr., "Arabinosyl Nucleosides and Nucleotides," in "Selective Inhibitors of Viral Functions," W. A. Carter, Ed., CRC Press, Cleaveland, Ohio (1973), p. 213.
4) C. P. J. Glaudemans and H. G. Fletcher, Jr., in "Synthetic Procedures in Nucleic Acid Chemistry," W. W. Zorbach and R. S. Tipson, Ed., Vol. 1, Wiley-Interscience, New York. N. Y. (1968), p. 126.
5) K. V. Auwers and F. Cauer, *Ann.*, **470**, 287 (1927).
6) T. Hashizume and H. Iwamura, *Tetrahedron Lett.*, **1965**, 3095.
7) L. B. Townsend, in "Synthetic Procedures in Nucleic Acid Chemistry," W. W. Zorbach and R. S. Tipson, ed., Vol. 2, Wiley-Interscience, New York. N. Y. (1973), p. 331.
8) M. Hoffer, *Chem. Ber.*, **93**, 2777 (1960).
9) M. J. Robins and R. K. Robins, *J. Amer. Chem. Soc.*, **87**, 4934 (1965).
10) J. T. Witkowski, M. Fuertes, P. D. Cook, and R. K. Robins, *J. Carbohyd. Nucleosides Nucleotides*, **2**, 1 (1975).
11) O. Makabe, S. Umezawa, and T. Aota, *Saishin Igaku*, **30**, 1056 (1975).

Steric Control in the Diels-Alder Reaction[1]

Kazuyoshi SEGUCHI,* Akira SERA,** and Kazuhiro MARUYAMA
Department of Chemistry, Faculty of Science, Kyoto University, Sakyo-ku, Kyoto 606
(Received January 24, 1976)

The Diels-Alder reactions of polychlorocyclopentadienes with substituted ethylenes were investigated, and the rates of the reaction and the *endo* : *exo* adduct distributions were determined. The introduction of a chlorine atom at the C_5 position of cyclopentadiene resulted in an enhanced *endo* preference for substituents in the adducts, despite the depressed reactivity of the diene. This is contrary to what is to be expected from the so-called "selectivity-reactivity relationship in the Diels-Alder reaction." The results in this work were explained in terms of steric interaction between the C_5-chlorine atom of the diene and the substituent of dienophiles.

Many investigators have been interested in *endo* selectivity in the Diels-Alder reaction from both experimental and theoretical points of view. Many factors have been considered to be responsible for the stereochemistry of the reaction.[2-7] However, the elucidation of the steric factor seems to remain incomplete. Early, Martin, and Hill[3] ascribed the deviation from the *endo* rule[2a,3] mainly to a repulsive interaction between the methylene group of cyclopentadiene and substituent(s) of dienophile. This concept has also been employed widely in other reactions.[4] Kobuke *et al.*[6] pointed out the importance of the dispersion force rather than the steric factor in the same reaction.

In the course of our investigation of the correlation between the selectivity and the reactivity in the Diels-Alder reaction,[7] we found a significant deviation when hexachlorocyclopentadiene was employed as a diene. The reaction was found to give *endo* adducts preferentially, although low *endo* adduct distributions were predicted from the correlation.[7] This paper will be concerned with the enhanced *endo* epimer preference of the Diels-Alder reaction of polychlorocyclopentadienes. The role of steric interaction will be discussed in connection with the selectivity-reactivity correlation in the Diels-Alder reaction.

Results and Discussion

The rates and the epimer distributions in the Diels-Alder reactions of 1,2,3,4-tetrachloro- (**1a**) and hexachlorocyclopentadiene (**1c**) with methyl acrylate and styrene were examined by means of GLC. The results are tabulated in Table 1. We already pointed out in the previous paper[7] that the more reactive addenda there are, the more selective the Diels-Alder reaction, where secondary orbital interaction plays an important role. However, Reactions 2 and 3 in Table 1 gave rather high *endo* epimer distributions in spite of the lower reactivity of the substrates. This anormalous behavior is shown definitely in Fig. 1 as a significant deviation from the selectivity-reactivity correlation (Points 2 and 3), while no such deviation was observed in the reaction of tetrachlorocyclopentadiene (Point 1). These facts are likely to indicate the relative importance of steric interaction between the chloromethylene group of **1c** and the substituent of a dienophile; the electronic effect or the secondary orbital interaction plays a subordinate role. Accordingly, we examined more systematically the steric control for the *endo*

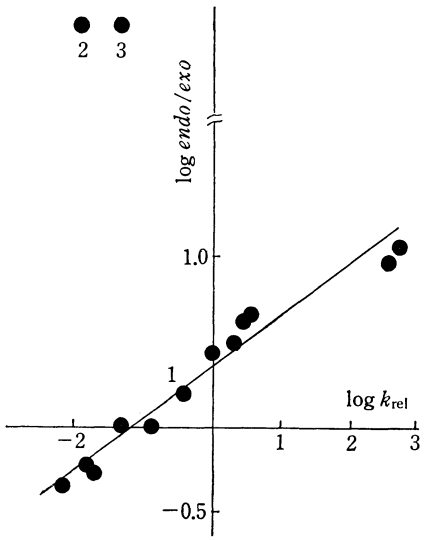

Fig. 1. A correlation of selectivity (log *endo*/*exo*) and reactivity (log k_{rel}) in the Diels-Alder reaction. Numerals denote the reaction numbers cited in Table 1; for the other points (not numbered), see Ref. 7.

TABLE 1. RATES AND *endo* SELECTIVITIES FOR THE REACTION OF **1a** AND **1c** WITH METHYL ACRYLATE AND STYRENE AT 40 °C

Reaction No.	Diene	Dienophile	Rate const[a] (l/mol, s)	k_{rel}[b]	*endo* Selectivity[a] (%)
1	**1a**	Methyl acrylate	1.89×10^{-5}	3.57×10^{-1}	60.1
2	**1c**	Methyl acrylate	6.04×10^{-7}	1.14×10^{-2}	100
3	**1c**	Styrene	2.12×10^{-6}	4.00×10^{-2}	100

a) Determined by means of GLC. b) Relative rates to the reaction of cyclopentadiene with methyl acrylate; see Ref. 7.

* Present address: Faculty of Home Economics, Mukogawa Women's University, Nishinomiya 663.

** Present address: Department of Chemistry, Faculty of Science, Kobe University, Nada-ku, Kobe 657.

selectivity in the Diels-Alder reaction.

The following sets of reactions were carried out in *p*-xylene at 90 °C: diene; **1a** and **1c**: dienophile; monosubstituted ethylenes (methyl acrylate, acrylic acid, acrylonitrile, vinyl acetate, and styrene) and 1,1-disubstituted ethylenes (corresponding alkyl-substituted derivatives). The reactions proceeded smoothly when monosubstituted ethylenes were employed as dienophiles. However, the reactions of **1c** with 1,1-disubstituted ethylenes were not very fast; even after fifteen days at 90 °C the yields of the products were about 30% (the starting materials were recovered). In all the case, the reaction mixtures were readily separated to the *exo* and *endo* isomers by means of GLC. The *endo* isomer distribution was determined by means of GLC or NMR. The *endo* : *exo* isomer ratio was almost independent of the reaction times. The results are tabulated in Table 2, together with the reported data of the reactions of 1,2,3,4,5-pentachlorocyclopentadiene (**1b**).[8] Since the reaction of **1b** gave a mixture of *anti-endo*, *syn-endo*, and *syn-exo* isomers, the 7-*syn*-chloro-*endo*/7-*syn*-chloro-*exo* ratios are also given in Table 2.

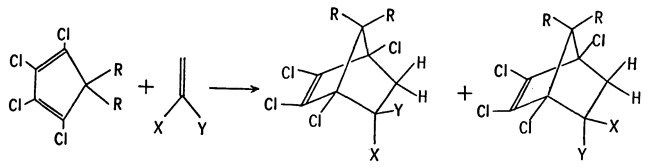

Diene Dienophile *exo*- (**x**) *endo*- (**n**)
(**1a**) R=H X=H, Me, Bu
(**1b**) R=H, Cl Y=CO_2Me, CO_2H, CN,
(**1c**) R=Cl OAc, Ph

Scheme 1.

The configuration of the isomeric adducts was deduced by means of NMR analysis, taking into account the following characteristic signals of norbornene derivatives. The shielding effect of the double bond in 5-substituted 2-norbornene leads the proton signals

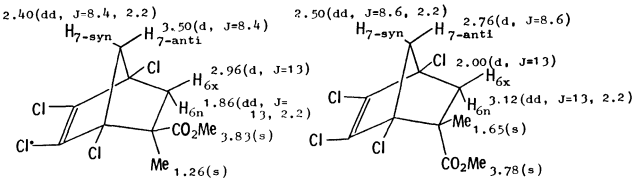

Scheme 2. Chemical shift in ppm, coupling constant in Hz.

of the 5-*endo* substituents to a higher field than those of the corresponding *exo* substituents. A long-range coupling over the planar W-letter configuration is present between H_{7-syn} and $H_{5n,6n}$. An *exo*-oriented Y makes the difference in the chemical shift between H_{7-syn} and H_{7-anti} larger than an *endo*-oriented Y does. A typical example is shown in Scheme 2 for the adducts of **1a** with methyl methacrylate (**2x** and **2n**).

5-*endo*-Methyl protons in **2x** and *endo*-5-methoxycarbonyl methyl protons in **2n** absorb at a higher field than the corresponding protons of their isomers. The signal of H_{6n} is split into a double doublet by the long-range coupling with H_{7-syn} (J=2.2 Hz) as well as by the coupling with H_{6x}. The configurations of the isomers of the other Diels-Alder adducts were similarly analyzed. The chemical shift and the splitting pattern of these compounds were similar to those of

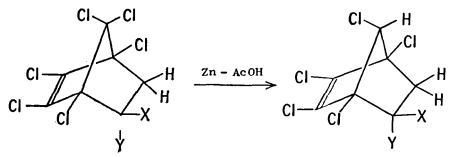

3n X=H, Y=CO_2Me **9n** X=H, Y=CO_2Me
4n X=H, Y=CO_2H **10n** X=H, Y=OAc
5n X=H, Y=OAc **11n** X=H, Y=Ph
6n X=H, Y=Ph **12n** X=Me, Y=OAc
7n X=Me, Y=OAc **13n** X=Me, Y=CN
8n X=Me, Y=CN

Scheme 3.

Table 2. *endo* Selectivity in the Diels-Alder reactions of polychlorocyclopentadienes with various dienophiles

Dienophile		Diene				
		(**1a**)[a]		(**1b**)[a]	(**1c**)[a]	
X[a]	**Y**[a]	Yield of adduct (%) [reaction time, h]	*endo* Selectivity (%)	*endo* Selectivity (%)[b]	Yield of adduct (%) [reaction time, h]	*endo* Selectivity (%)
H	OAc	56 [24]	75.5 (3.08)[c]	92.8 (6.28)[d]	72 [40]	100
H	CO_2CH_3	75 [15]	60.7 (1.54)[c]	89.8 (3.59)[d]	72 [54]	100
H	CO_2H	86 [24]	66.7 (2.00)[c]	—	85 [40]	100
H	CN	61 [24]	53.7 (1.16)[c]	86.8 (1.14)[d]	65 [40]	94.2
H	Ph	59 [60]	78.8 (3.72)[c]	100 (2.92)[d]	95 [40]	100
Me	OAc	17 [40]	57.1	—	15 [240]	100
Me	CO_2CH_3	80 [40]	41.8	—	10 [240]	95
Bu	CO_2CH_3	57 [40]	33.9	—	37 [300]	87
Me	CN	83 [40]	23.0	—	25 [240]	18.3
Me	Ph	64 [70]	64.3	—	22 [240]	94.2

a) See Scheme 1. b) Ref. 8. c) *endo*/*exo* Ratios. d) 7-*syn*-Chloro-*endo*/7-*syn*-chloro-*exo* isomer ratios.

the reported compounds.[8-11]

On the other hand, in the reactions of **1c** with methyl acrylate, acrylic acid, vinyl acetate, styrene, and isopropenyl acetate, only ones (**3n**—**7n**) of the epimeric adducts were produced (Scheme 3). The configurations of these adducts were determined by zinc–acetic acid reduction.[12] The procedure is known to give the corresponding 1,2,3,4-*syn*-7-pentachloronorbornene derivatives stereoselectively. The reduction products, **9n**—**11n**, were proved to be identical with the respective known compounds by a comparison with their NMR spectra.[8] That is, all of the adducts, **3n**—**6n**, were found to have the *endo* configuration. The configuration of **4n** was determined after it had been converted into **3n** by diazomethane.

The configuration of **12n** was deduced on the basis of the following NMR spectral evidence. The replacement of a 7-*anti*-chlorine atom by a hydrogen atom must affect the chemical shift of 5-*exo*-methyl protons more markedly than that of 5-*endo*-methyl protons. This concept was exemplified by the fact that, of the two epimeric adducts of **1c** with methacrylonitrile, the 5-*endo*-cyano-5-*exo*-methyl epimer (**8n**) revealed its methyl signal at δ 1.98, while the 5-*endo*-methyl-5-*exo*-cyano epimer (**8x**) did so at δ 1.47. Upon the above-cited reduction, **8n** gave **13n**, in which the methyl group resonated at δ 1.71. Similarly, **8x** gave **13x**, with its methyl signal at δ 1.42. That is, the replacement of a 7-*anti*-chlorine atom by a hydrogen atom led the 5-*exo*-methyl signal to a field higher by 0.27 ppm, but had little effect on the 5-*endo*-methyl signal. The chemical-shift difference of the methyl signal of **7n** (δ 2.00) and that of **12n** (δ 1.80) manifested an *exo* configuration for these methyl groups. Accordingly, **7n** was determined to be the 5-*endo*-acetoxy-5-*exo*-methyl epimer.

As is shown in Table 2, the introduction of succesive chlorine atoms at the C_5 position of cyclopentadiene resulted in enhanced *endo* adduct distributions for the reactions of polychlorocyclopentadienes with monosubstituted ethylenes. According to the "Diels-Alder selectivity-reactivity relationship,"[7] the less reactive diene, **1c**, may be anticipated to reveal a lower *endo* selectivity than **1a**. However, this was not the case. The *endo* selectivity for the Diels-Alder reactions of cyclopentadiene has been thought, in general, to be caused by dipole-dipole interaction, attractive force, and other ineractions. However, in the present case, the dienes have chlorine atoms at the C_5 position, so the steric situation should be some what different from the usual Diels-Alder reactions. That is, *exo*-orienting substituent in a transition state should experience rather strong steric crowding. The high *endo* epimer distributions observed for the reactions of **1b** and **1c** suggest that the substituents of the dienophiles are forced to occupy the sterically less hindered *endo* position. In addition, the *endo* : *exo* ratios for **1a** and the 7-*syn*-chloro-*endo* : 7-*syn*-chloro-*exo* ratios for **1b** change almost in parallel with the change in the substituent of dienophiles. Furthermore, no 7-*anti*-chloro-*exo* isomers were found in the adducts of **1b** with monosubstituted ethylenes.[8] These facts clearly indicate the existence of steric repulsion between the *anti* chlorine atom and the *exo* substituent in the transition state. This can be further explained by inspecting the results obtained from the reactions of **1a** and **1c** with 1,1-disubstituted ethylenes. Here, two substituents, X and Y, occupy competitively the *endo* position in the transition state. Table 2 shows that the amounts of the *endo* adducts increase remarkably when the methylene hydrogen atoms of **1a** are replaced by chlorine atoms. Methacrylonitrile reveals a lower *endo*-CN preference in the reaction with **1c**. This is in good accord with Mark's consideration that the sterically least demanding cyano group is forced to the rather unfavored *exo* position when it is in competition with a bulkier group.[13] In addition, such steric crowding in the transition state will be responsible for the lower reactivity of **1c** toward 1,1-disubstituted ethylenes, as is shown in Table 2.

In conclusion, in the Diels-Alder reactions of polychlorocyclopentadienes with substituted ethylenes the steric requirement of bulkier substituents should be considered as one of the predominant factors in determining the *endo* selectivity and should cause the deviation from the selectivity-reactivity relationship.

Experimental

The NMR spectra were recorded on a JEOL PS-100 spectrometer, using TMS as the internal standard. The analytical determination by GLC was performed on a JEOL 20 K gas chromatograph.

Materials. Hexachlorocyclopentadiene (**1c**) was commercially obtained and was distilled; bp 116 °C/17 Torr. The preparation and purification of other diene and dienophiles were reported previously.[7]

The Diels-Alder Reaction and Analytical Procedure. In a typical run, a mixture of 7.3×10^{-3} M of a dienophile, 2.8×10^{-2} M of a diene, and 2 ml of *p*-xylene was sealed in a glass ampoule maintained at 90±0.1 °C. The reaction time was changed from 15 to 72 h for the reactions with 1,2,3,4-tetrachlorocyclopentadiene (**1a**) and from 40 to 300 h for the reactions of hexachlorocyclopentadiene (**1c**) according to the reactivity of the dienophiles. The Diels-Alder adducts were analyzed by means of GLC and NMR, after passage to a bed of silica gel, if neccesary. Stainless steel columns (2 m) packed with 7% Silicon QF-1 (Column A), 5% PEG 20 M (Column B), and 5% Silicon DC550 (Column C) on a Diasolid L were used. For the adducts of **1a**, *endo* isomers showed longer retention times, while for the adducts of **1c** they showed shorter retention times.

Kinetics. Stock solutions of a diene and a dienophile in butyl chloride were prepared and stored in a freezer. Aliquots were taken from the stock solutions and mixed for

Table 3. Data for kinetic measurements

Reaction No.[a]	Initial concentration (×10 M)		GLC column[b]	GLC internal standard
	Diene	Dienophile		
1	2.33	2.20	D	**12n**
2	0.890—2.15	1.64—32.8	E	*o*-Terphenyl
3	0.890—2.15	3.22—16.8	E	*o*-Terphenyl

a) Reaction numbers cited correspond to those in Table 1. b) D, 1 m PEG 20 M (1%); E, 1 m Apiezone Grease L (5%).

each kinetic run. Analysis was done by means of GLC. The initial concentrations of the diene and the dienophile, the column specifications, and the internal standards for quantitative GLC analyses are shown in Table 3. All the reactions studied were clearly second-order and gave a single product or a mixture of *endo* and *exo* isomeric products.

Reaction of **1a** *with Methyl Acrylate.* The Diels-Alder adducts, 1,2,3,4-tetrachloro-5-*endo*-methoxycarbonylbicyclo-[2.2.1]hept-2-ene (**14n**) and its 5-*exo* isomer (**14x**), were separated by the use of Column A at 160 °C (retention times: **14n**, 8.5 min; **14x**, 6.3 min). Mp: **14n**, 86—87 °C; **14x**, 61.5—62.5 °C. NMR (δ): **14n**, 3.78 (3H, s, CO_2CH_3), 3.40 (1H, dd, J=4 and 8 Hz, 5-*exo*-H), 2.52 (2H, bs, 7-*syn*-H and 7-*anti*-H), 2.40—2.50 (2H, m, 6-*endo*-H and 6-*exo*-H); **14x**, 3.83 (3H, s, CO_2CH_3), 2.92 (1H, m, J=2, 4, and 8 Hz, 5-*endo*-H), 3.32 (1H, d, J=8 Hz, 7-*anti*-H), 2.58 (1H, dd, J=4 and 12 Hz, 6-*exo*-H), 2.24—2.32 (2H, m, 6-*endo*-H and 7-*syn*-H). Found: **14n**, C, 36.89; H, 2.79; Cl, 49.05%; **14x**, C, 37.29; H, 2.69; Cl, 48.88%. Calcd for $C_9H_8O_2Cl_4$: C, 37.27; H, 2.78; Cl, 48.99%.

Reaction of **1a** *with Acrylic Acid.* The isomeric distribution was determined by means of the NMR spectra. The Diels-Alder adducts, 1,2,3,4-tetrachloro-5-*endo*-carboxybicyclo-[2.2.1]hept-2-ene (**15n**) and its 5-*exo* isomer (**15x**), were fractionated by recrystallization from benzene–hexane. They were then esterified by diazomethane, and the products were identified by means of GLC with **14n** and **14x** respectively. Mp: **15n**, 161 °C; **15x**, 127—129 °C. NMR (δ): **15n**, 9.30 (1H, s, CO_2H), 3.44 (1H, dd, J=4 and 8 Hz, 5-*exo*-H), 2.41—2.48 (4H, m, other protons); **15x**, 10.45 (1H, s, CO_2H), 3.12 (1H, d, J=8 Hz, 7-*anti*-H), 2.92 (1H, m, J=1, 4, and 8 Hz, 5-*endo*-H), 2.26—2.60 (3H, m, other protons). Found: **15n**, C, 34.57; H, 1.94; Cl, 51.20%; **15x**, C, 35.00; H, 2.18; Cl, 51.22%. Calcd for $C_8H_6O_2Cl_4$: C, 34.82; H, 2.19; Cl, 51.40%.

Reaction of **1a** *with Vinyl Acetate.* The Diels-Alder adducts, 1,2,3,4-tetrachloro-5-*endo*-acetoxybicyclo[2.2.1]hept-2-ene (**16n**) and its 5-*exo* isomer (**16x**), were separated by the use of Column B at 150 °C (retention times: **16n**, 16.3 min; **16x**, 14.1 min). Mp: **16n**, 52—53 °C; **16x**, colorless liquid. NMR (δ): **16n**, 5.54 (1H, dd, J=2 and 8 Hz, 5-*exo*-H), 2.78 (1H, dd, J=8 and 12 Hz, 6-*exo*-H), 2.50—2.58 (2H, bs, 7-*syn*-H and 7-*anti*-H), 2.10 (3H, s, $OCOCH_3$), 1.84 (1H, dd, J=3 and 12 Hz, 6-*endo*-H); **16x**, 5.02 (1H, m, J=1, 3, and 8 Hz, 5-*endo*-H), 2.87 (1H, d, J=8 Hz, 7-*anti*-H), 2.56—2.66 (2H, m, 6-*exo*-H and 7-*syn*-H), 2.17 (3H, s, $OCOCH_3$), 2.02 (1H, dd, J=3 and 12 Hz, 6-*endo*-H). Found: **16n**, C, 37.43; H, 3.05%; **16x**, C, 37.08; H, 2.66%. Calcd for $C_9H_8O_2Cl_4$: C, 37.27; H, 2.78%.

Reaction of **1a** *with Acrylonitrile.* The Diels-Alder adducts, 1,2,3,4-tetrachloro-5-*endo*-cyanobicyclo[2.2.1]hept-2-ene (**17n**) and its 5-*exo* isomer (**17x**), were separated by the use of Column A at 160 °C (retention times: **17n**, 13.5 min; **17x**, 9.7 min). Mp: **17n**, 75—76 °C; **17x**, 92—93 °C. NMR (δ): **17n**, 3.50 (1H, dd, J=4 and 10 Hz, 5-*exo*-H), 2.74 (1H, dd, J=10 and 12 Hz, 6-*exo*-H), 1.50 (2H, bs, 7-*syn*-H and 7-*anti*-H), 1.34 (1H, dd, J=4 and 12 Hz, 6-*endo*-H); **17x**, 3.02 (1H, m, J=2, 5, and 9 Hz, 5-*endo*-H), 2.86 (1H, d, J=8 Hz, 7-*anti*-H), 2.53—2.74 (3H, m, 7-*syn*-H, 6-*endo*-H, and 6-*exo*-H). Found: **17n**, C, 37.58; H, 1.71; Cl, 55.53%; **17x**, C, 37.37; H, 1.71; Cl, 55.18%. Calcd for $C_8H_5NCl_4$: C, 37.44; H, 1.98; Cl, 55.20%.

Reaction of **1a** *with Styrene.* The Diels-Alder adducts, 1,2,3,4-tetrachloro-5-*endo*-phenylbicyclo[2.2.1]hept-2-ene (**18n**) and its 5-*exo* isomer (**18x**), were separated by the use of Column A at 180 °C (retention times: **18n**, 10.2 min; **18x**, 9.1 min). Mp: **18n**, 64—65 °C; **18x**, colorless liquid. NMR (δ): 6.96—7.28 (5H, m, Ph), 3.64 (1H, dd, J=4 and 8 Hz, 5-*exo*-H), 2.32—2.76 (4H, m, other protons); **18x**, 7.30 (5H, s, Ph), 3.10 (1H, m, J=1, 5, and 8 Hz, 5-*endo*-H), 2.80 (1H, d, J=8 Hz, 7-*anti*-H), 2.40—2.76 (3H, m, other protons). Found: **18n**, C, 50.84; H, 3.31%; **18x**, C, 50.85; H, 2.95%. Calcd for $C_{13}H_{10}Cl_4$: C, 50.68; H, 3.27%.

Reaction of **1a** *with Methyl Methacrylate.* The Diels-Alder adducts, 1,2,3,4-tetrachloro-5-*endo*-methoxycarbonyl-5-*exo*-methylbicyclo[2.2.1]hept-2-ene (**2n**) and its 5-*exo*-methoxycarbonyl-5-*endo*-methyl isomer (**2x**), were separated by the use of Column A at 160 °C (retention times: **2n**, 8.7 min; **2x**, 7.0 min) after passage through a bed of silica gel (using benzene–hexane as the eluent). Mp: **2n**, 58.5—59.5 °C; **2x**, 64.5—65.5 °C. The NMR data of these compounds are shown in Scheme 2. Found: **2n**, C, 39.41; H, 3.19%; **2x**, C, 39.23; H, 3.17%. Calcd for $C_{10}H_{10}O_2Cl_4$: C, 39.51; H, 3.32%.

Reaction of **1a** *with Methyl 2-Butylacrylate.* The Diels-Alder adducts, 1,2,3,4-tetrachloro-5-*endo*-methoxycarbonyl-5-*exo*-butylbicyclo[2.2.1]hept-2-ene (**19n**) and its 5-*exo*-methoxycarbonyl-5-*endo*-butyl isomer (**19x**), were separated by the use of Column A at 180 °C (retention times; **19n**; 21.1 min; **19x**, 13.8 min). Mp: **19n**, 77—80 °C; **19x**, colorless liquid. NMR (δ): **19n**, 3.78 (3H, s, CO_2CH_3), 3.02 (1H, dd, J=2 and 12 Hz, 6-*endo*-H), 2.72 (1H, d, J=8 Hz, 7-*anti*-H), 2.46 (1H, dd, J=2 and 8 Hz, 7-*syn*-H), 1.98 (1H, d, J=12 Hz, 6-*exo*-H), 0.96—1.60 (9H, m, Bu); **19x**, 3.87 (3H, s, CO_2CH_3), 3.17 (1H, d, J=8 Hz, 7-*anti*-H), 2.98 (1H, d, J=12 Hz, 6-*exo*-H), 2.34 (1H, dd, J=2 and 12 Hz, 7-*syn*-H), 1.90 (1H, dd, J=2 and 12 Hz, 6-*endo*-H), 0.92—1.55 (9H, m, Bu). Found: **19n**, C, 44.95; H, 4.63%; **19x**, 45.28; H, 4.63%. Calcd for $C_{13}H_{16}O_2Cl_4$: C, 45.11; H, 4.66%.

Reaction of **1a** *with Isopropenyl Acetate.* The isomer distribution was determined by means of GLC using Column A (retention times: 1,2,3,4-tetrachloro-5-*endo*-acetoxy-5-*exo*-methylbicyclo[2.2.1]hept-2-ene (**20n**), 8.2 min; and its 5-*exo*-acetoxy-5-*endo*-methyl isomer (**20x**), 7.2 min). However, the pure isomers could not be obtained because their retention times were too close to each other. NMR (δ, characteristic signals): **20n**, 1.76 (s, 5-CH_3), 1.92 (s, $OCOCH_3$); **20x**, 1.44 (s, 5-CH_3), 2.04 (s, $OCOCH_3$). For the isomer mixture, Found: C, 39.57; H, 3.26%. Calcd for $C_9H_8O_2Cl_4$: C, 39.51; H, 3.32%.

Reaction of **1a** *with Methacrylonitrile.* The Diels-Alder adducts, 1,2,3,4-tetrachloro-5-*endo*-cyano-5-*exo*-methylbicyclo-[2.2.1]hept-2-ene (**21n**) and its 5-*exo*-cyano-5-*endo*-methyl isomer (**21x**), were separated by the use of Column A at 155 °C (retention times: **21n**, 12.0 min; **21x**, 7.7 min). Mp: **21n**, 99—100 °C; **21x**, colorless liquid. NMR (δ): **21n**, 2.70 (1H, dd, J=2 and 12 Hz, 6-*endo*-H), 2.60 (2H, m, 7-*syn*-H and 7-*anti*-H), 2.27 (1H, d, J=12 Hz, 6-*exo*-H), 1.75 (3H, s, CH_3); **21x**, 3.01 (1H, d, J=10 Hz, 7-*anti*-H), 2.86 (1H, d, J=13 Hz, 6-*exo*-H), 2.64 (1H, dd, J=3 and 10 Hz, 7-*syn*-H), 2.10 (1H, dd, J=3 and 13 Hz, 6-*endo*-H), 1.42 (3H, s, CH_3). Found: **21n**, C, 39.89; H, 2.55%; **21x**, C, 39.76; H, 2.49%. Calcd for $C_9H_7NCl_4$: C, 39.89; H, 2.60%.

Reaction of **1a** *with* α*-Methylstyrene.* The isomeric distribution was determined by means of GLC using Column A at 180 °C (retention times: 1,2,3,4-tetrachloro-5-*endo*-phenyl-5-*exo*-methylbicyclo[2.2.1]hept-2-ene (**22n**), 8.8 min and its 5-*exo*-phenyl-5-*endo*-methyl isomer (**22x**), 7.8 min). However, the pure isomers could not be obtained because their retention times were too close to each other. NMR (δ, characteristic signals): **22n**, 1.76 (s, CH_3); **22x**, 1.45

(s, CH_3). For the isomer mixture, Found: C, 52.75; H, 3.81%. Calcd for $C_{14}H_{10}Cl_4$: C, 52.21; H, 3.76%.

Reaction of ***1c*** *with Methyl Acrylate.* The GLC, TLC, and NMR all indicated the presence of a single product, 1,2,3,4,7,7-hexachloro-5-*endo*-methoxycarbonylbicyclo[2.2.1]-hept-2-ene (**3n**); bp 140—145 °C/7 Torr. NMR (δ): 3.65 (1H, dd, J=4 and 7 Hz, 5-*exo*-H), 2.60—2.76 (2H, m, 6-*endo*-H and 6-*exo*-H), 3.82 (3H, s, CO_2CH_3). Found: C, 30.13; H, 1.91; Cl, 59.55%. Calcd for $C_9H_6O_2Cl_6$: C, 30.12; H, 1.69; Cl, 59.28%.

Reaction of ***1c*** *with Acrylic Acid.* The NMR indicated the presence of a single product, 1,2,3,4,7,7-hexachloro-5-*endo*-carboxybicyclo[2.2.1]hept-2-ene (**4n**); mp 142—145 °C. This product was esterified to **3n** by diazomethane. NMR (δ): 11.36 (1H, s, CO_2H), 3.70 (1H, dd, J=4 and 8 Hz, 5-*exo*-H), 2.78 (1H, dd, J=8 and 12 Hz, 6-*exo*-H), 2.62 (1H, dd, J=4 and 12 Hz, 6-*endo*-H). Found: C, 27.84; H, 1.08; Cl, 61.58%. Calcd for $C_8H_4O_2Cl_6$: C, 27.86; H, 1.17; Cl, 61.69%.

Reaction of ***1c*** *with Vinyl Acetate.* The GLC, TLC, and NMR all indicated the presence of a single product, 1,2,3,4,7,7-hexachloro-5-*endo*-acetoxybicyclo[2.2.1]hept-2-ene (**5n**); mp 42.5—43.0 °C. NMR (δ): 5.64 (1H, dd, J=3 and 8 Hz, 5-*exo*-H), 3.10 (1H, dd, J=8 and 13 Hz, 6-*exo*-H), 2.05 (3H, s, $OCOCH_3$), 1.95 (1H, dd, J=3 and 13 Hz, 6-*endo*-H). Found: C, 29.89; H, 1.55; Cl, 59.49%. Calcd for $C_9H_6O_2Cl_6$: C, 30.12; H, 1.69; Cl, 59.28%.

Reaction of ***1c*** *with Styrene.* The GLC, TLC, and NMR all indicated the presence of a single product, 1,2,3,4,7,7-hexachloro-5-*endo*-phenylbicyclo[2.2.1]hept-2-ene (**6n**); mp 74—75 °C. NMR (δ): 6.96—7.40 (5H, m, Ph), 3.90 (1H, dd, J=4 and 12 Hz, 5-*exo*-H), 2.84 (1H, dd, J=8 and 12 Hz, 6-*exo*-H), 2.42 (1H, dd, J=4 and 12 Hz, 6-*endo*-H). Found: C, 41.53; H, 1.92; Cl, 56.17%. Calcd for $C_{13}H_8Cl_6$: C, 41.42; H, 2.14; Cl, 56.44%.

Reaction of ***1c*** *with Acrylonitrile.* The Diels-Alder adducts, 1,2,3,4,7,7-hexachloro-5-*endo*-cyanobicyclo[2.2.1]-hept-2-ene (**23n**) and its 5-*exo*-isomer (**23x**), were separated by the use of Column A at 165 °C (retention times: **23n**, 9.8 min; **23x**, 15.7 min). Mp: **23n**, 141—143 °C; **23x**, 72—75 °C. NMR (δ): **23n**, 3.62 (1H, dd, J=4 and 8 Hz, 5-*exo*-H), 2.86 (1H, dd, J=8 and 12 Hz, 6-*exo*-H), 2.32 (1H, dd, J=4 and 12 Hz, 6-*endo*-H); **23x**, 3.06 (1H, dd, J=4 and 8 Hz, 5-*endo*-H), 2.76 (1H, dd, J=4 and 12 Hz, 6-*exo*-H), 2.42 (1H, dd, J=8 and 12 Hz, 6-*endo*-H). Found: **23n**, C, 29.49; H, 0.86; Cl, 64.84%; **23x**, C, 30.35; H, 0.98; Cl, 63.92;. Calcd for $C_9H_3NCl_6$: C, 29.49,; H, 0.93; Cl, 65.29%.

Reaction of ***1c*** *with Methyl Methacrylate.* Since the GLC peaks of the Diels-Alder adducts, 1,2,3,4,7,7-hexachloro-5-*endo*-methoxycarbonyl-5-*exo*-methylbicyclo[2.2.1]hept-2-ene (**24n**) and its 5-*exo*-methoxycarbonyl-5-*endo*-methyl isomer (**24x**), did not resolve satisfactorily, the isomer distribution was determined by the integration of the NMR spectra. A mixture of **24n** and **24x**; mp 68—70 °C. NMR (δ, characteristic signals): **24n**, 3.79 (s, CO_2CH_3), 1.80 (s, 5-CH_3); **24x**, 3.85 (s, CO_2CH_3), 1.38 (s, 5-CH_3). For the same mixture, Found: C, 32.82; H, 2.17%. Calcd for $C_{10}H_8O_2Cl_6$: C, 32.21; H, 2.16%.

Reaction of ***1c*** *with Methyl 2-Butylacrylate.* Since the GLC peaks of the Diels-Alder adducts, 1,2,3,4,7,7-hexachloro-5-*endo*-methoxycarbonyl-5-*exo*-butylbicyclo[2.2.1]hept-2-ene (**25n**) and its 5-*exo*-methoxycarbonyl-5-*endo*-butyl isomer (**25x**), did not resolve satisfactorily, the isomer distribution was determined by the integration of the NMR spectra. NMR (δ, characteristic signals): **25n**, 3.78 (s, CO_2CH_3), 3.18 (d, J=12 Hz, 6-*endo*-H), 2.44 (d, J=12 Hz, 6-*exo*-H); **25x**, 3.96 (s, CO_2CH_3), 3.39 (d, J=12 Hz, 6-*exo*-H), 1.95 (d, J=12 Hz, 6-*endo*-H). Found: C, 37.62; H, 3.11; Cl, 51.53%. Calcd for $C_{13}H_{14}O_2Cl_6$: C, 37.62; H, 3.40; Cl, 51.27%.

Reaction of ***1c*** *with Isopropenyl Acetate.* The GLC and NMR indicated the presence of a single product, 1,2,3,4,7,-7-hexachloro-5-*endo*-acetoxy-5-*exo*-methylbicyclo[2.2.1]hept-2-ene (**7n**); colorless liquid. NMR (δ): 2.85 (2H, s, 6-*endo*-H and 6-*exo*-H), 2.02 (3H, s, $OCOCH_3$), 2.00 (3H, s, CH_3). Found: C, 32.51; H, 2.17; Cl, 57.11%. Calcd for $C_{10}H_8O_2Cl_6$: C, 32.21; H, 2.16; Cl, 57.05%.

Reaction of ***1c*** *with Methacrylonitrile.* The Diels-Alder adducts, 1,2,3,4,7,7-hexachloro-5-*endo*-cyano-5-*exo*-methylbicyclo[2.2.1]hept-2-ene (**8n**) and its 5-*exo*-cyano-5-*endo*-methyl isomer (**8x**), were separated by the use of Column A at 180 °C (retention times: **8n**, 7.0 min; **8x**, 8.7 min). Mp: **8n**, 185—188 °C; **8x**, 144—145 °C. NMR (δ): **8n**, 2.80 (2H, s, 6-*endo*-H and 6-*exo*-H), 1.98 (3H, s, CH_3); **8x**, 3.12 (1H, d, J=12 Hz, 6-*exo*-H), 2.12 (1H, d, J=12 Hz, 6-*endo*-H), 1.47 (3H, s, CH_3). Found: **8n**, C, 31.84; H, 1.36; Cl, 62.49%; **8x**, C, 32.00; H, 1.40; Cl, 62.42%. Calcd for $C_9H_5NCl_6$: C, 31.80; H, 1.48; Cl, 62.59%.

Reaction of ***1c*** *with α-Methylstyrene.* The Diels-Alder adducts, 1,2,3,4,7,7-hexachloro-5-*endo*-phenyl-5-*exo*-methylbicyclo[2.2.1]hept-2-ene (**26n**) and its 5-*exo*-phenyl-5-*endo*-methyl isomer (**26x**), were separated by the use of Column A at 180 °C (retention times: **26n**, 19.0 min; **26x**, 21.5 min). Mp: **26n**, 67—68 °C; **26x**, colorless liquid. NMR (δ): **26n**, 7.22 (5H, s, Ph), 3.12 (1H, d, J=14 Hz, 6-*exo*-H), 2.64 (1H, d, J=14 Hz, 6-*endo*-H), 1.90 (3H, s, CH_3); **26x**, 7.20—7.80 (5H, m, Ph), 3.50 (1H, d, J=13 Hz, 6-*exo*-H), 2.10 (1H, d, J=13 Hz, 6-*endo*-H), 1.38 (3H, s, CH_3). Found: **26n**, C, 42.92; H, 2.46; Cl, 54.11%; **26x**, C, 43.01; H, 2.71; Cl, 54.64%. Calcd for $C_{14}H_{10}Cl_6$: C, 43.21; H, 2.58, Cl, 54.48%.

Zinc-Acetic Acid Reductions of ***3n—8n.*** Williamson's procedure[12] was used, and the main products were collected by preparative gas chromatography (Column C at 170 °C). 1,2,3,4-*syn*-7-Pentachloro-5-*endo*-methoxycarbonylbicyclo-[2.2.1]hept-2-ene (**9n**), mp 58—59 °C (yield, 66%); lit,[8] 59—60 °C. 1,2,3,4-*syn*-7-Pentachloro-5-*endo*-acetoxybicyclo-[2.2.1]hept-2-ene (**10n**), mp 82—84 °C (yield, 57%); lit,[8] 83.5—84 °C. 1,2,3,4-*syn*-7-Pentachloro-5-*endo*-phenylbicyclo[2.2.1]hept-2-ene (**11n**), mp 61—63 °C (yield, 40%); lit,[8] 62—66 °C. 1,2,3,4-*syn*-7-Pentachloro-5-*endo*-cyano-5-*exo*-methylbicyclo[2.2.1]hept-2-ene (**13n**), mp 101—102 °C (yield, 91%). NMR (δ): 4.37 (1H, s, 7-*anti*-H), 2.78 (1H, d, J=13 Hz, 6-*endo*-H), 2.27 (1H, d, J=13 Hz, 6-*exo*-H), 1.71 (3H, s, CH_3). 1,2,3,4-*syn*-7-Pentachloro-5-*exo*-cyano-5-*endo*-methylbicyclo[2.2.1]hept-2-ene (**13x**), mp 112—114 °C (yield, 81%). NMR (δ): 4.66 (1H, s, 7-*anti*-H), 2.90 (1H, d, J=12 Hz, 6-*exo*-H), 2.17 (1H, d, J=12 Hz, 6-*endo*-H), 1.42 (3H, s, CH_3). Found: **13n**, C, 35.67; H, 2.06%; **13x**, C, 35.55; H, 2.11%. Calcd for $C_9H_6NCl_5$: C, 35.39; H, 1.98%. 1,2,3,4-*syn*-7-Pentachloro-5-*endo*-acetoxy-5-*exo*-methylbicyclo[2.2.1]hept-2-ene (**12n**), mp 74—75 °C (yield, 30%). NMR (δ): 4.30 (1H, s, 7-*anti*-H), 2.72 (1H, d, J=13 Hz, 6-*exo*-H), 2.42 (1H, d, J=13 Hz, 6-*endo*-H), 1.98 (3H, s, $OCOCH_3$), 1.80 (3H, s, CH_3). Found: C, 35.74; H, 2.85%. Calcd for $C_{10}H_9O_2Cl_5$: C, 35.48; H, 2.68%.

References

1) Presented at the 30th Annual Meeting of the Chemical Society of Japan, Osaka (1974). Abstract Papers, III, p. 1186.

2) a) J. Sauer, *Angew. Chem.*, **79**, 76 (1967); b) W. C. Herndon and L. H. Hall, *Tetrahedron Lett.*, **1967**, 3095; c) J. A. Benson, Z. Hamlet, and W. A. Mueller, *J. Am. Chem. Soc.*, **84**, 297 (1962); d) R. B. Woodward and R. H. Hoffmann, "The Conservation of Orbital Symmetry," Academic Press, New York (1970), p. 145.

3) J. G. Martin and R. K. Hill, *Chem. Rev.*, **61**, 637 (1961).

4) K. N. Houk, *Tetrahedron Lett.*, **1970**, 2621; K. N. Houk and L. J. Luskus, *J. Am. Chem. Soc.*, **93**, 4606 (1971).

5) B. C. C. Cantello, J. Mellor, and C. F. Webb, *J. Chem. Soc., Perkin Trans.* 2, **1974**, 22, 26.

6) Y. Kobuke, T. Fueno, and J. Furukawa, *J. Am. Chem. Soc.*, **94**, 6548 (1972).

7) K. Seguchi, A. Sera, Y. Otsuki, and K. Maruyama, *Bull. Chem. Soc. Jpn.*, **48**, 3641 (1975).

8) K. L. Williamson, Y-F. Li Hsu, R. Lacko, and C. H. Youn, *J. Am. Chem. Soc.*, **91**, 6129 (1969).

9) K. L. Williamson, *J. Am. Chem. Soc.*, **85**, 516 (1963).

10) R. G. Pew, C. W. Roberts, and C. R. Hand, *Tetrahedron*, **26**, 1711 (1970).

11) C. M. Anderson, I. W. McCay, and R. W. Warrender, *Tetrahedron Lett.*, **1970**, 2735.

12) K. L. Williamson, Y-F. Li Hsu, and E. Young, *Tetrahedron*, **24**, 6007 (1968).

13) V. Mark, *J. Org. Chem.*, **37**, 3181 (1974).

Studies on Lignoids in *Lauraceae*. II.[1] Studies on Lignans in the Leaves of *Machilus Japonica* Sieb. et Zucc.

Daisuke TAKAOKA, Keiko WATANABE, and Mitsuru HIROI

Department of Chemistry, Faculty of Science, Ehime University, Bunkyo-cho, Matsuyama 790

(Received February 2, 1976)

From the leaves of *Machilus japonica* Sieb. et Zucc., four lignans were isolated; they have been found to be (+)-galbacin [**1**], (+)-galbelgin [**2**], (−)-licarin-B [**4**], and a new lignan, machilusin, whose structure can be described as [**3a**] or [**3b**].

The leaves of most species of *Lauraceae* are known to contain the characteristic essential oil, but the systematic studies of the non-volatile components have been few. We planned such systematic studies of the lignans of *Lauraceae* and have already reported the isolation and characterization of several lignans from the leaves of *Cinnamomum Camphora* (Camphor tree).[1]

In this paper, we wish to report some lignans contained in the leaves of *Machilus japonica* Sieb. et Zucc.

Results

From an acetone extract of fresh leaves of *Machilus japonica* Sieb. et Zucc. (Japanese name: "Hosobatabu"), four lignans were isolated; they have been found to be enantiomers of (−)-galbacin[2] isolated from *Himantandra baccata* Bail (syn. *Galbulimima baccata*), of (−)-galbelgin[3] isolated from *Himantandra belgraveana* F. V. Mull., (−)-licarin-B[4] isolated from *Licaria aritu* Ducke (*Lauraceae*), and a new lignan, machilusin.

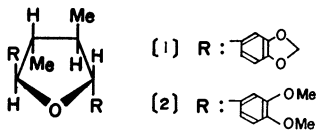

[1] R:

[2] R:

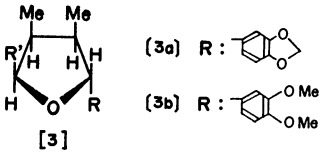

[3]

[3a] R: , R': 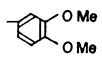

[3b] R:

, R':

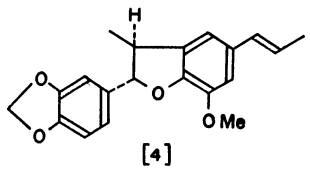

[4]

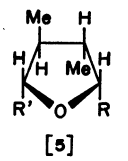

[5]

[5a] R:

, R':

[5b] R, R': 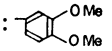

(+)-Galbacin [*1*]. Oxidation with potassium permanganate affords piperonylic acid. NMR and mass spectra show that this compound is a 2,5-diaryl-3,4-dimethyltetrahydrofuran. Furthermore, the chemical shift of the protons of the two methyl groups in the NMR spectrum indicates that each methyl group is located in *trans* relation to the vicinal aryl group.[5] From this fact, along with the optical activity (dextro), we conclude that this compound is (+)-galbacin [**1**]. The almost identical mp, the absolute value of $[\alpha]_D$, and the mass spectrum[6] confirm this conclusion.

(+)-Galbelgin [*2*]. Oxidation with potassium permanganate affords veratric acid. Mass and NMR spectra and optical activity (dextro) show that this lignan must be the enantiomer of (−)-gabelgin, as in the case of (+)-galbacin. This conclusion is confirmed by the NMR[5] and mass spectra,[6] which are almost identical with those of (−)-galbelgin. The reason why the mp is higher and the absolute value of $[\alpha]_D$ is larger than those reported for (−)-galbelgin is obscure, but we think that the latter might be contaminated with the optically inactive mesoisomer, galgravin, since (−)-galbelgin was isolated along with a very large amount of galgravin from *Himantandra belgrbeana* F. V. Mull.,[3] while we could not find any galgravin in *Machilus japonica* Sieb. et Zucc.

(−)-Machilusin [*3*]. This compound is a new lignan. Oxidation with potassium permanganate affords piperonylic acid and veratric acid (1 : 1). NMR and mass spectra indicate that this compoud is a 2,5-diaryl-3,4-dimethylterahydrofuran.

All of the major peaks of galbacin and galbelgin in the mass spectra have been well established;[6] in the same manner, the fragmentation of machilusin can be explained as represented in Scheme 1.

From the chemical shift of methyl protons in NMR spectrum, it is found that one of the methyl groups is located in *cis* relation and the other in *trans* relation to the vicinal aryl group.[5] Then the relative configuration of this compound can be represented as **3** or **5**.

(+)-Calopeptin[7] and (+)-veraguensin[5] have been reported to have the absolute configurations [**5a**] and [**5b**] respectively. The difference of $[\alpha]_D$ between them is relatively small, and the signals of CH_3CH– in their NMR spectra apear over a relatively wide range, *viz.* from δ 1.5 to 2.5 ppm.[7]

Machilusin is levorotatory and the absolute value of $[\alpha]_D$ differs considerably from the values for calopeptin and veraguensin. The signals of CH_3CH– in the NMR specrum appear in a narrow range, centered at δ 2.4 ppm. These facts indicate that the relative configuration of machilusin must be represented as **3**, *i.e. cis, cis, trans* configuration, not as **5**. In fact, the construction of a molecular model for **3** shows that the two CH_3CH– are so equivalent to each other

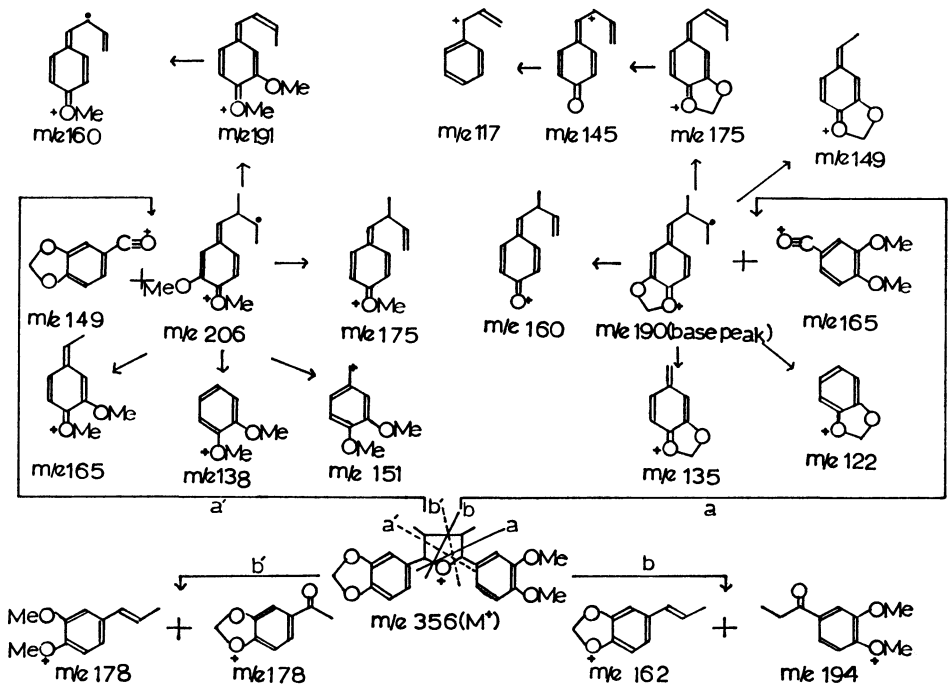

Scheme 1.

in the preferential conformation that they would appear in a narrow range in a NMR spectrum.

Then machilusin has either the configuration **3a** or **3b**. **3a** is supposed to be more rational from the viewpoint of the base peak (*m/e* 190) in the mass spectrum, because the bond between C2 and C3 (2,3-bond), bearing two *cis* substituents, may be considered to be cleaved more easily than the 4,5-bond bearing *trans* substituents. A lack of specimen prevented us from performing further studies

Licarin-B [*4*]. The 4th lignan was identified as licarin-B[4] isolated from *Licaria aritu* Ducke, by mp, $[\alpha]_D$ and spectral data.

Experimental

Instruments. $[\alpha]_D$ was measured by the use of Yanako OR-50 (Yanagimoto) and elemental analyses were carried out by CHN Corder MT-2 (Yanagimoto). IR, NMR, and mass spectra were obtained by using IR-400 (Shimadzu), JNM-4H-100 (JEOL), and JMS-01SG-2 (JEOL) respectively.

Isolation of Lignans. Fresh leaves of *Machilus japonica* Sieb. et Zucc., collected at Okitsu, Kochi prefecture, were extracted with acetone; the acetone solution was concentrated and the residue was extracted with hexane. The hexane solution, after concentration, was steam distilled to remove the volatile components and the residue was extracted with hexane. The resulting hexane solution was dried over anhydrous sodium sulfate and, after concentration, was chromatographed on a neutral alumina column (solvent: hexane–ethyl acetate, 95 : 5 to 50 : 50) into 14 fractions.

From the 4th and the 5th fractions, (+)-galbacin, the major lignan, was crystallized in mass, then recrystallized from ethyl acetate (yield: 0.3%).

From the 8th fraction, a white precipitate was filtered and recrystallized from ethyl acetate. The resulting crystals in rod form and the amorphous ones were separated from each other by handpicking. The former were recrystallized from ethyl acetate into pure (+)-gabelgin (yield: 0.005%).

The mother liquid of crude (+)-galbacin, obtained from the 5th fraction, was rechromatographed on a silica gel column (solvent: hexane–ethyl acetate, 95 : 5 to 50 : 50) into 21 fractions. Machilusin was obtained from the 18th fraction by preparative TLC (solvent : hexane–ethyl acetate, 80 : 20) as colorless flat plates (yield: 0.01%).

The 3rd fraction in the first chromatography was rechromatographed on a silica gel column (solvent: hexane–ethyl acetate, 100 : 0 to 60 : 40) into 25 fractions. From the 21st fraction, a pale yellow oil was obtained by means of preparative TLC (solvent: hexane containing 10% ethyl acetate), and this oil was dissolved in a minute amount of hot hexane. On cooling, licarin-B was deposited in white needle-like crystals (a minute amount).

(+)-Galbacin (1). The major lignan, mp 115.5—116 °C, $[\alpha]_D=+117.0°$ (in $CHCl_3$). Found: C, 70.63; H, 5.76%. Calcd for $C_{20}H_{20}O_5$: C, 70.59; H, 5.88%. NMR (δ ppm in $CDCl_3$): 1.03 (6H, d, $J=7$ Hz; CH_3), 1.75 (2H, m; H3, H4), 4.63 (2H, d, $J=9.5$ Hz; H2, H5), 5.97 (4H, s; OCH_2O), 6.75—7.0 (6H; aromatic H).

(+)-Galbelgin (2). Mp 142—142.5 °C, $[\alpha]_D=+129.0°$ (in $CHCl_3$). Found: C, 70.98; H, 7.46%. Calcd for $C_{22}H_{28}O_5$: C, 70.91; H, 7.53%. NMR (δ ppm in $CDCl_3$): 1.07 (6H, d, $J=6$ Hz; CH_3), 1.82 (2H, m; H3, H4), 3.90 (6H, s; CH_3O), 3.94 (6H, s; CH_3O), 4.69 (2H, d, $J=9$ Hz; H2, H5), 6.80—7.05 (6H; aromatic H). MS: *m/e* 372 (M^+), 206 (base peak), 194, 191, 178, 175, 165, 138.

(−)-Machilusin (3). Mp 121—122.0 °C, $[\alpha]_D=-130.6°$ (in $CHCl_3$). Found: C, 70.81; H, 6.68%. Calcd for $C_{21}H_{24}O_5$: C, 70.79; H, 6.74%. NMR (δ ppm in $CDCl_3$): 0.62 (3H, d, $J=7$ Hz; CH_3), 1.01 (3H, d, $J=6.5$ Hz; CH_3), 2.45 (2H, m; H3, H4), 3.90 (6H, s; CH_3O), 4.65 (1H, d, $J=9$ Hz; H2 or H5), 5.47 (1H, d, $J=4$ Hz; H2 or H5), 5.95 (2H, s; OCH_2O), 6.80—7.0 (6H; aromatic H). IR (cm^{-1}, KBr): 1603, 1590, 1510, 1500, 1482, 1463, 1458, 1438, 1418, 1380, 1360, 1344, 1313, 1286, 1262, 1240, 1235, 1220, 1190, 1180, 1152, 1140, 1125, 1090, 1060, 1030, 1020, 1005, 995, 970, 960, 940, 925, 895, 860, 850,

810, 798, 780, 770, 750, 725, 720, 705.

(−)-Licarin-B (4). Mp 86.5—88.0 °C, $[\alpha]_D = -45.4°$ (in $CHCl_3$).

Oxidation of Machilusin (3), Galbacin (1), and Galbelgin (2). To a boiling solution of 50 mg of **3** in 10 ml of acetone, 350 mg of a mixture of potassium permanganate and magnesium sulfate (6 : 5) were added little by little over 30 min and the reaction mixture was refluxed for 6 h. Then it was made alkaline with aq. sodium hydroxide and was filtered. The precipitate was washed with hot water, and the combined washing and filtrate were concentrated *in vacuo* to remove acetone and were washed with ether. The aqueous layer was acidified with dil. sulfuric acid and was extracted with ether. The ether solution was dried over anhydrous sodium sulfate and an excess amount of ether solution of diazomethane was added to this solution. The resulting solution, after being concentrated *in vacuo* to remove unreacted diazomethane, was subjected to gas chromatography (SE 30-golay column, at 150 °C). The product was shown to be a mixture of methyl piperonylate and methyl veratrate (1 : 1) by comparing their R_ts with those of the authentic samples.

In the same manner, galbacin and galbelgin gave methyl piperonylate and methyl veratrate respectively.

The authors wish to express their gratitude to Professor Masahide Kurita, Department of Biology, Ehime University, for his valuable advice in the identification of the species of the material tree, and also to Mr. Muneki Ohuchi, Japan Electon Optics Laboratory Co., LTD., for carrying out some parts of the spin-decoupling experiment.

References

1) Previous report: D. Takaoka, N. Takamatsu, Y. Saeki, K. Kono, C. Nakaoka, and M. Hiroi, *Nippon Kagaku Kaishi*, **1975**, 2192.

2) G. K. Hughes and E. Ritchie, *Aust. J. Chem.*, **7**, 104 (1954).

3) J. Birch, B. Milligan, E. Smith, and R. N. Speake, *J. Chem. Soc.*, **1958**, 4471.

4) C. J. Aiba, R. G. C. Correa, and O. R. Gottlieb, *Phytochemistry*, **12**, 1163 (1973).

5) J. B. McAlpine, N. V. Riggs, and P. G. Gordon, *Aust. J. Chem.*, **21**, 1095 (1968).

6) A. Pelter, A. P. Stainton, and M. Barber, *J. Heterocycl. Chem.*, **3**, 191 (1966).

7) N. V. Riggs and J. D. Stevens, *Aust. J. Chem.*, **15**, 305 (1962).

1,3-Benzodithiolylium Salts. Synthesis and Reactions with Nucleophilic Reagents

Jyuzo NAKAYAMA, Kazuo FUJIWARA, and Masamatsu HOSHINO

Department of Chemistry, Faculty of Science, Saitama University, Urawa, Saitama 338

(Received March 15, 1976)

Various salts of 1,3-benzodithiolylium ion were prepared in excellent yields on treatment of 2-alkoxy- and 2-alkylthio-1,3-benzodithioles with acids in acetic anhydride. The reactions of 1,3-benzodithiolylium tetrafluoroborate (**1a**) with a wide variety of nucleophilic reagents (alcohols, water, thiols, hydrogen sulfide, primary, secondary, and tertiary amines, ammonia, *N,N*-dimethylformamide, electron-rich aromatic compounds, active methylene compounds, tropilidene, and sodium borohydride) were studied. In all cases examined, **1a** reacted with nucleophilic reagents at the 2-position to give the corresponding 1,3-benzodithioles in good yields, excepting the reactions with tertiary amines and *N,N*-dimethylformamide which resulted in the formation of dibenzotetrathiafulvalene. Salt **1a** was also prepared from 1,3-benzodithiole and trityl tetrafluoroborate.

Like 1,2-dithiolylium ion, 1,3-dithiolylium ion possesses a potential aromatic sextet, its aromaticity being the subject of controversy. Recently the synthesis, reactivity, and spectral properties of 1,3-dithiolylium compounds have been intensively studied in efforts to find relationships between their structure and thier chemical and physical properties.[1–3] In a preliminary report we briefly described a convenient synthesis of 1,3-benzodithiolylium tetrafluoroborate (**1a**).[4] We now report the synthesis of various salts of 1,3-benzodithiolylium ion and the reactions of the fluoroborate salt **1a** with a wide variety of nucleophilic reagents.

Results and Discussion

Synthesis of 1,3-Benzodithiolylium Salts. We recently reported a one-step synthesis of 2-alkoxy-1,3-benzodithioles (**2**) on a preparative scale which involves addition of alcohols to the carbene (1,3-benzodithiol-2-ylidene) produced from carbon disulfide and benzyne generated by aprotic diazotization of anthranilic acid.[5] Treatment of a solution of 2-isopentyloxy-1,3-benzodithiole (**2c**) in acetic anhydride with tetrafluoroboric acid at 0 °C gave 1,3-benzodithiolylium tetrafluoroborate (**1a**) in 96% yield. The structure of **1a** was determined on the basis of spectral data and elemental analysis. Benzodithioles **2a** and **2b** gave the fluoroborate salt **1a** in 94 and 88% yields, respectively. Other slats of 1,3-benzodithiolylium ion could also be prepared in a similar way; sulfuric, perchloric, hydriodic, and hydrobromic acids reacted with the benzodithiole **2c** in acetic anhydride to give the hydrogen sulfate **1b** (81%), perchlorate **1c** (94%), iodide **1d** (81%), and bromide **1e** (95%), respectively. The chloride salt **1f**, soluble in the reaction medium when prepared from **2c** and concentrated hydrochloric acid in acetic anhydride, could not be isolated, but its zinc chloride double salt **1g** was obtained in 96% yield by treating the mixture with zinc chloride.

2-Alkylthio-1,3-benzodithioles (**3**) have been easily synthesized in good yields by treatment of the benzodithiole **2c** with thiols in acetic acid.[6] Treatment of compounds **3a**—**c** with tetrafluoroboric acid also yielded the fluoroborate salt **1a** in a respective yield of 86, 90, and 92%.

The only synthetic method for preparing 1,3-benzodithiolylium salts involves the condensation of 1,2-benzenedithiol with formic acid or triethyl orthoformate in the presence of acids.[7] However, the synthesis of 1,2-benzenedithiol is laborious.[8] The present reaction provides the most straightforward synthetic method of salts **1** since the starting material can be obtained on a preparative scale by one-step synthesis. The formation of 1,3-dithiolylium salts from 2-methoxy- and 2-methylthio-1,3-dithioles has been reported.[3b,9]

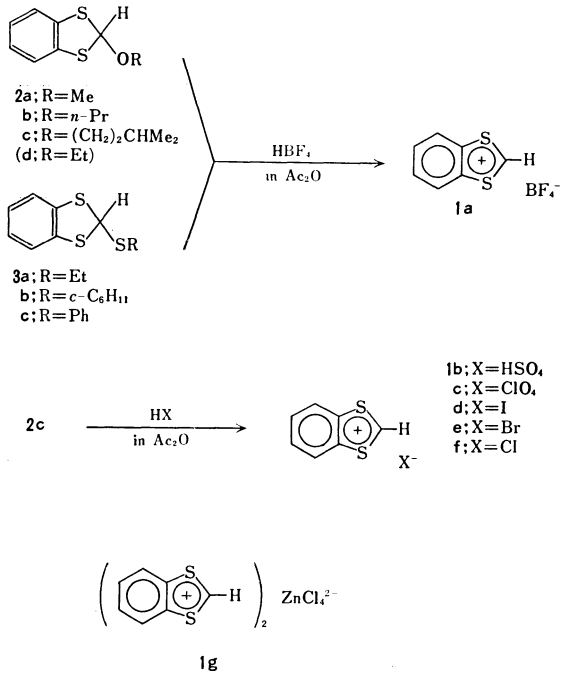

Scheme 1.

The fluoroborate salt **1a** is stable at room temperature and soluble in polar solvents; it was used to investigate the reactivity of 1,3-benzodithiolylium ion toward a wide variety of nucleophilic reagents.

*Reactions of 1,3-Benzodithiolylium Tetrafluoroborate (**1a**) with Nucleophilic Reagents.* Standing the fluoroborate salt **1a** in methanol for 1 h at room temperature gave rise to 2-methoxy-1,3-benzodithiole (**2a**) in 87% yield. Similar treatment of **1a** with ethanol and 1-propanol gave benzodithioles **2d** (75%) and **2b** (94%), respectively. The formation of 2-alkoxy-1,3-dithioles from 1,3-dithiolylium perchlorates and alcohols

in the presence of base has been reported.[3b,7e,10]

Buza *et al.* reported that the perchlorate salt **1c**, on treatment with triethylamine in an aqueous acetonitrile or *N,N*-dimethylformamide, gives compound **4** by partial hydrolysis.[7c] The fluoroborate salt **1a**, when allowed to stand in an aqueous acetonitrile at room temperature for a long period, gave compound **4** in 88% yield. The mechanism of the formation of **4** probably involves the tautomerization of the 2-hydroxy compound **6** to the open chain compound **7** as an initial process as postulated. A similar reaction has been observed with the benzodithiole **2c** in acetic acid.[11]

A solution of the salt **1a** in ethanol was allowed to stand at room temperature for 1 h and then 4 molar amounts of ethanethiol was added. Standing the resulting mixture for another 1 h gave rise to 2-ethylthio-1,3-benzodithiole (**3a**) in 81% yield. This suggests that in ethanol the equilibrium between 1,3-benzodithiolylium ion and 2-ethoxy-1,3-benzodithiole (**2d**), which lies far to **2d**, takes place and that **2d** is converted into the final product **3a** *via* 1,3-benzodithiolylium ion on addition of ethanethiol. Thus, upon standing **1a** in ethanol containing 4 molar amounts of ethanethiol, compound **3a** was obtained in 80% yield; ^{1}H NMR analysis indicated no formation of **2d**. Similarly, **1a** and ethanethiol in methanol gave **3a** in 81% yield.

Sodium sulfide reacted with the salt **1a** in methanol to give the sulfide **5** (15%) and the benzodithiole **2a** (69%). The reaction of sodium hydrogensulfide with **1a** in methanol also yielded compounds **5** (33%)

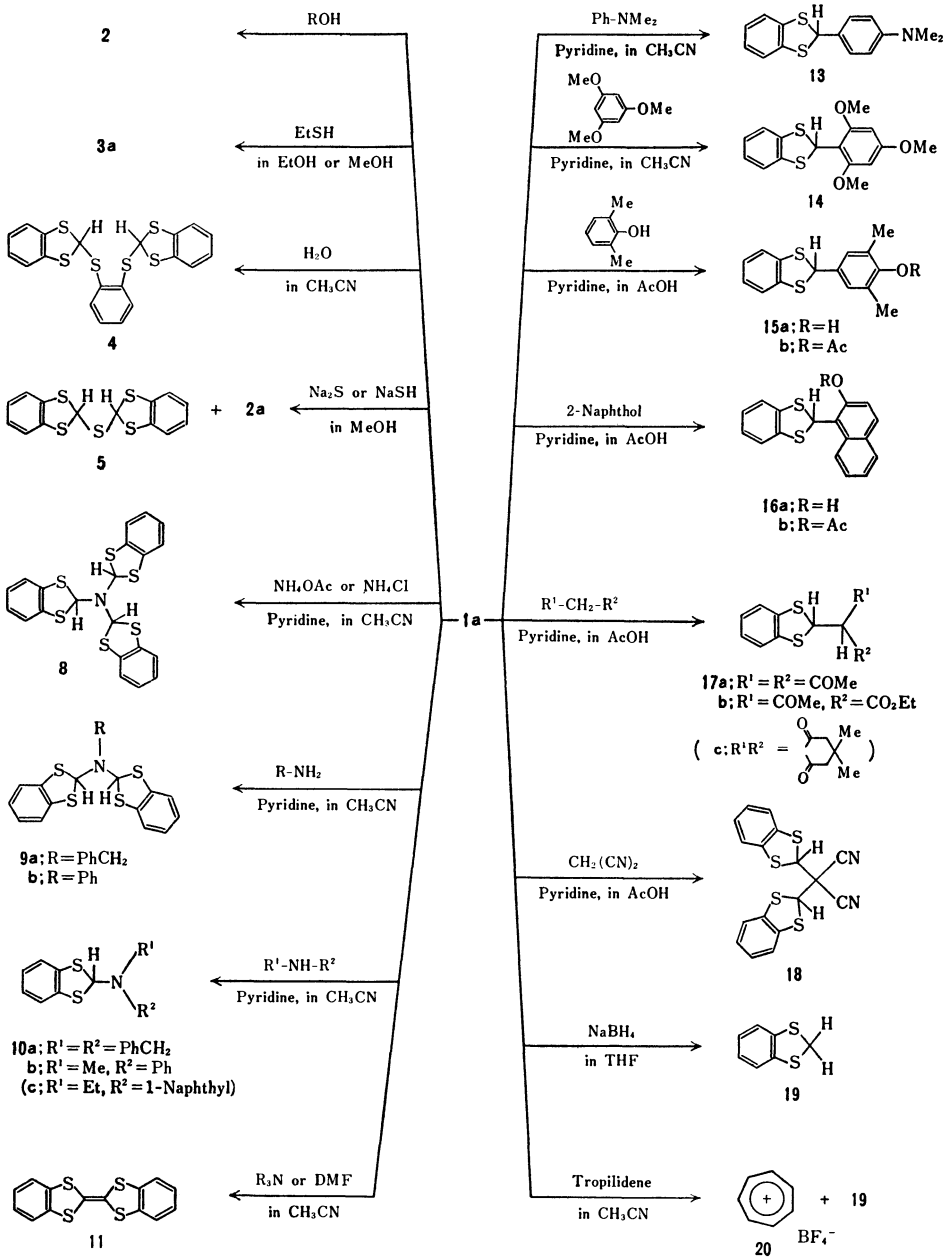

Scheme 2.

and **2a** (54%). The tropylium ion reacts in a similar way with hydrogen sulfide to give ditropyl sulfide.[12] It is of interest that the reaction of 2,4,5-triphenyl-1,3-dithiolylium perchlorate with sodium hydrogensulfide in methanol gives 2,4,5-triphenyl-1,3-dithiole in good yield.[10] In our case no such reduction product was formed.

The reactions of some 1,3-dithiolylium salts with ammonia have been examined,[10,13] a 2-aminodithiole adduct being isolated in one instance.[10] The reaction of ammonium acetate with 3 molar amounts of the salt **1a** in the presence of pyridine in acetonitrile at room temperature gave tris(1,3-benzodithiol-2-yl)amine (**8**) in 86% yield. Neither (1,3-benzodithiol-2-yl)-amine nor bis(1,3-benzodithiol-2-yl)amine was isolated. The strongest support for structure of **8** was provided by ^{1}H NMR spectrum: δ (CS_2) 6.30 (3H, s, methine) and 6.90—7.25 (12H, A_2B_2m, aromatic). Under the same conditions, ammonium chloride and 3 molar amounts of **1a** also gave the amine **8** in 50% yield.

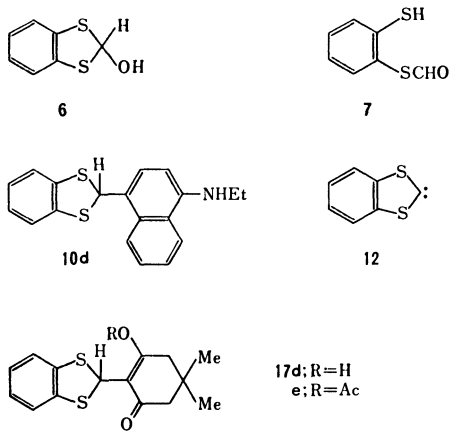

Scheme 3.

Benzylamine reacted with 2 molar amounts of the salt **1a** in the presence of pyridine in acetonitrile at room temperature to give *N*,*N*-bis(1,3-benzodithiol-2-yl)benzylamine (**9a**) in 86% yield. Similarly, aniline and **1a** gave the amine **9b** in 79% yield. Thus, evidently all the amino hydrogens of ammonia and primary amines are replaceable by 1,3-benzodithiol-2-yl groups by **1a**, whereas the reactions of 2-methylthio-1,3-dithiolylium salts with primary amines give either 2-imino-1,3-dithioles or 2-amino-1,3-dithiolylium salts with evolution of methanethiol, depending upon the number of moles of amines employed.[13a,14]

Secondary amines such as dibenzylamine and *N*-methylaniline reacted with the salt **1a** in the presence of pyridine in acetonitrile to give compounds **1a** (90%) and **10b** (92%), products of *N*-alkylation, respectively. With *N*-ethyl-1-naphthylamine, unexpectedly, 4-(1,3-benzodithiol-2-yl)-*N*-ethyl-1-naphthylamine (**10d**) was obtained nearly quantitatively. The formation of **10d** can be explained either by direct electrophilic attack of **1a** on the 4-position of the naphthalene ring of the substrate or by the rearrangement of the primary product **10c** under the conditions employed. In either case, the steric hindrance caused by the *peri*-hydrogen may be responsible for the formation of the product.[15] In this connection it is of interest that the reaction of 2-methylthio-4-phenyl-1,3-dithiolylium perchlorate with *N*-methylaniline gives 2-(*N*-methylanilino)-4-phenyl-1,3-dithiolylium perchlorate with loss of methanethiol, whereas the reaction with diphenylamine yields 2-(*p*-anilinophenyl)-4-phenyl-1,3-dithiolylium perchlorate.[16]

Treatment of the salt **1a** with triethylamine in acetonitrile gave dibenzotetrathiafulvalene **11** in 81% yield in accord with the findings with the perchlorate salt **1c**.[7c-e] Treatment of **1a** with tripropylamine also gave **11** in 84% yield. The formation of **11** can be readily explained by base-catalyzed deprotonation of **1a** and subsequent reaction of the resulting carbene **12** with **1a** followed by deprotonation. Standing **1a** in *N*,*N*-dimethylformamide for 1.5 h at room temperature resulted in the formation of **11** in 80% yield. In connection with the recent discovery of the highly conducting charge transfer salts of tetrathiafulvalenes with 7,7,8,8-tetracyanoquinonedimethane,[17] many derivatives of tetrathiafulvalene have been prepared by treatment of 1,3-dithiolylium salts with base. We believe that *N*,*N*-dimethylformamide serves as a useful base for this conversion, although only tertiary amines have been so far employed.[3b,7c-e,9,18]

Like other 1,3-dithiolylium ions,[16,19] 1,3-benzodithiolylium ion undergoes electrophilic substitution with electron-rich aromatic compounds; *N*,*N*-dimethylaniline and 1,3,5-trimethoxybenzene reacted with the salt **1a** to give compounds **13** (89%) and **14** (98%), respectively. Although the reaction of **1a** with phenol in the presence of pyridine in acetic acid at 60—70 °C for 3 h gave unidentified oils and intractable tars, 2,6-dimethylphenol and 2-naphthol reacted with **1a** to give **15b** (68%) and **16b** (97%), respectively. In these cases, primary products **15a** and **16a** must be acetylated under the conditions employed to give the final products **15b** and **16b**, respectivley.

Reaction of 1,3-dithiolylium salts with active methylene compounds leading to 1,3-dithiol-2-ylidene derivatives have been extensively studied.[3e,14,19c,20] The reaction of **1a** with acetylacetone and ethyl acetoacetate in the presence of pyridine in acetic acid afforded **17a** (92%) and **17b** (89%), respectively. Under the same conditions, dimedone and **1a** gave the acetate **17e** in 76% yield; the primary product **17c**, which exists in the enol form **17d**[21] must be acetylated to give **17e** as observed with 2,6-dimethylphenol and 2-naphthol. The reaction of **1a** with malononitrile, in striking contrast to the foregoing results, gave bis-(1,3-benzodithiol-2-yl)malononitrile (**18**) in 86% yield, although a slight excess of malononitrile was employed. Similar reactions have been observed with benzodithioles **2** and active methylene compounds in acetic acid.[21]

Reduction of the salt **1a** with sodium borohydride in tetrahydrofuran afforded 1,3-benzodithiole (**19**) in 81% yield. The reaction of **1a** with a slight excess of tropilidene in acetonitrile at 0 °C gave tropylium tetrafluoroborate (**20**) and the benzodithiole **19** in a respective yield of 90 and 65%. Hirai has reported

that the reaction of 4-phenyl-1,3-dithiolylium perchlorate with a slight excess of tropilidene in acetic acid at 80 °C gives a mixture of tropylium perchlorate and the starting perchlorate.[3d] These results lead to the conclusion that 1,3-benzodithiolylium ion surpasses 4-phenyl-1,3-dithiolylium ion in ability to accept a hydride, thus suggesting that the positive charge of the former ion is more localized on the 2-position as compared with that of the parent 1,3-dithiolylium ion by the influence of the fused benzene ring.

The benzodithiole **19**, when allowed to react with trityl tetrafluoroborate in acetonitrile, gave rise to the salt **1a** (75%) and triphenylmethane (75%). The reaction provides another new synthetic way to **1a** since **19** can be also synthesized by the literature method.[22]

$$\mathbf{19} + Ph_3C^+BF_4^- \longrightarrow \mathbf{1a} + Ph_3CH$$

Scheme 4.

Finally, it is concluded that 1,3-benzodithiolylium ion reacts exclusively at the 2-position with nucleophilic reagents in agreement with the results by molecular orbital calculations.[23]

Experimental

2-Alkoxy- and 2-alkylthio-1,3-benzodithioles (**2** and **3**) were prepared by the methods described.[5,6] Acetic acid and acetonitrile were distilled over phosphorus pentoxide before use. Other commercial materials were used without further purification, unless otherwise stated. ^1H NMR spectra were determined at 100 MHz with tetramethylsilane as internal reference. IR spectra of solids were taken for Nujol mulls, and those of liquids for films. All melting points are uncorrected.

*1,3-Benzodithiolylium Salts (**1**) from 2-Alkoxy-1,3-benzodithioles (**2**). a) 1,3-Benzodithiolylium Tetrafluoroborate (**1a**)*: To a stirred and ice-cooled solution of 2-isopentyloxy-1,3-benzodithiole (**2c**) (24.0 g, 0.1 mol) in acetic anhydride (300 ml) was added dropwise 42% tetrafluoroboric acid (42 g, 0.2 mol) over a period of 0.5 h. After 0.5 h of stirring at 0 °C, ether (400 ml) was added to precipitate the product completely. Filtration and washing with anhydrous ether (150 ml) gave **1a** as near-white crystals, 23.0 g (96%), mp 149—150 °C (dec). The salt thus obtained gave satisfactory result of elemental analysis and was used for investigation of the reactions with nucleophilic reagents. Recrystallization from anhydrous acetic acid gives a more pure specimen, mp 150—150.5 °C (dec).

ν_{max} 1000—1120 cm^{-1} (BF_4^-); δ (CF_3CO_2D) 8.06—8.26 and 8.66—8.86 (4H, m, aromatic) and 11.50 (1H, s, methine).

Found: C, 35.25; H, 2.11%. Calcd for $C_7H_5BF_4S_2$: C, 35.02; H, 2.10%.

In a similar way, **1a** was prepared from **2a** and **2b** in a respective yield of 94 and 88%.

*b) 1,3-Benzodithiolylium Hydrogen Sulfate (**1b**)*: This salt was prepared from **2c** (0.72 g, 3 mmol) and concentrated sulfuric acid (1.2 g, 12 mmol) in acetic anhydride (15 ml) in 81% yield (0.61 g) as white crystals. It showed no difinite melting point and decomposed gradually from 130 °C. It turned violet even when kept in refrigerator.

Found: C, 33.29; H, 2.46; S, 37.62%. Calcd for $C_7H_6O_4S_3$: C, 33.59; H, 2.42; S, 38.43%.

*c) 1,3-Benzodithiolium Perchlorate (**1c**)*: This salt was prepared from **2c** (0.72 g, 3 mmol) and 60% perchloric acid (1.0 g, 6 mmol) in acetic anhydride (15 ml) in 94% yield (0.71 g) as white crystals. It exploded violetly at 185 °C in agreement with the findings of the previous workers.[7c-e]

*d) 1,3-Benzodithiolylium Iodide (**1d**)*: This salt was prepared from **2c** (0.72 g, 3 mmol) and 57% hydriodic acid (1.35 g, 6 mmol) in acetic anhydride (15 ml) in 81% yield (0.68 g) as orange crystals, mp 101—103 °C (dec).

Found: C, 29.93; H, 1.79; I, 45.25; S, 22.84%. Calcd for $C_7H_5IS_2$: C, 30.00; H, 1.80; I, 45.30; S, 22.89%.

*e) 1,3-Benzodithiolylium Bromide (**1e**)*: This salt was prepared from **2c** (0.72 g, 3 mmol) and 47% hydrobromic acid (1.03 g, 6 mmol) in acetic anhydride (15 ml) in 95% yield (0.66 g) as white crystals, mp 169—170 °C (dec).

Found: C, 36.04; H, 2.14; Br, 34.14; S, 27.51%. Calcd for $C_7H_5BrS_2$: C, 36.06; H, 2.16; Br, 34.28; S, 27.51%.

*f) Bis(1,3-benzodithiolylium) Zinc Tetrachloride (**1g**)*: To a stirred and ice-cooled solution of **2c** (0.72 g, 3 mmol) in acetic anhydride (15 ml) was slowly added concentrated hydrochloric acid (0.61 g, 6 mmol) at 0 °C. After being stirred for 0.5 h, zinc chloride (0.20 g, 1.5 mmol) was added and the mixture was stirred at 0 °C for another 0.5 h. The resulting precipitate was collected and washed with acetonitrile (10 ml) to give 0.74 g (96%) of **1g**. Hurtley and Smiles[7a] reported this salt as orange needles with a red tint of varying depth. However, our product freshly prepared was a white solid, scarcely soluble in organic solvents, darkening from 180 °C and melting at 201—202°C accompanied by decomposition. Its IR spectrum was essentially the same as those of **1a—e.**

Found: C, 32.68; H, 1.96; S, 25.06%. Calcd for $C_{14}H_{10}Cl_4S_4Zn$: C, 32.73; H, 1.96; S, 24.97%.

*Fluoroborate Salt **1a** from 2-Alkylthio-1,3-benzodithioles (**3**).* **1a** was prepared from benzodithioles **3a**, **3b**, and **3c** in a respective yield of 86, 90, and 92% by treatment with tetrafluoroboric acid in the manner described above except that the reaction with **3b** (insoluble in acetic anhydride) was carried out in a mixture of ether and acetic anhydride.

*Reaction of the Salt **1a** with Alcohols.* **1a** (3.60 g, 15 mmol) was dissolved in alcohols (50 ml) and left to stand at room temperature for 1 h. The mixture was poured into water (150 ml) and extracted with ether (150 ml). The ether extract was washed with water, dried over sodium sulfate, and evaporated. The oily residue was purified by distillation.

2-Methoxy-1,3-benzodithiole (**2a**), 87%, colorless oil (solidified in a refrigerator), bp 80 °C/0.5 Torr (lit,[5b] bp 105—106 °C/2 Torr).

2-Ethoxy-1,3-benzodithiole (**2d**), 75%, colorless oil, bp 92—93 °C/1.5 Torr, ν_{max} 1050 cm^{-1} (C–O), δ (CCl_4) 1.12 (3H, t, methyl), 3.43 (2H, q, methylene), 6.80 (1H, s, methine), and 6.9—7.5 (4H, m, aromatic).

Found: C, 54.63; H, 5.14; S, 32.19%. Calcd for $C_9H_{10}OS_2$: C, 54.54; H, 5.09; S, 32.29%.

2-Propoxy-1,3-benzodithiole (**2b**), 94%, colorless oil, bp 86—88 °C/0.5 Torr (lit,[5a] bp 104—105 °C/0.1 Torr).

*Reaction of **1a** with Water.* **1a** (1.20 g, 5 mmol) was dissolved in 4:1 acetonitrile-water (25 ml) and left to stand at room temperature. After several hours colorless needles began to precipitate. The mixture was allowed to stand at room temperature until the needles no longer precipitated (one week). Filtration and wahsing with methanol (10 ml) gave 2,2'-(*o*-phenylenedithio)bis(1,3-benzodithiole), (**4**), 0.66 g (88%), mp 129—131 °C, undepressed on admixture with the authentic specimen.[11]

*Reaction of **1a** with Ethanethiol.* A solution of **1a** (1.20 g, 5 mmol) in ethanol (25 ml) was left at room temperature for 1 h, and then ethanethiol (1.24 g, 20 mmol) was added. After

being left to stand 1 h at room temperature, the mixture was poured into water and extracted with ether. The extract was washed successively with water, 2 M sodium hydroxide, and water, and dried over sodium slfate. The ether was evaporated and the crystalline residue was washed with cold methanol to give 2-ethylthio-1,3-benzodithiole (**3a**), 0.87 g (81%), mp 49—51 °C, undepressed on admixture with the authentic specimen.[6]

When **1a** (1.20 g, 5 mmol) was dissolved in a mixture of ethanethiol (1.24 g, 20 mmol) and ethanol (25 ml) and left to stand at room temperature for 1 h, **3a**, mp 51—51.5 °C, was obtained in 80% yield. ^{1}H NMR analysis of the crude product indicated no formation of **2d**.

*Reaction of **1a** with Sodium Sulfide and Sodium Hydrogensulfide.* **1a** (1.20 g, 5 mmol) was added to a stirred solution of sodium sulfide nonahydrate (1.20 g, 5 mmol) in methanol (15 ml) at room temperature and the mixture was stirred for 0.5 h. The crystalline precipitate was collected and washed with water (30 ml) and then with ethanol (10 ml) to give bis(1,3-benzodithiol-2-yl) sulfide (**5**), 0.13 g (15%), mp 145—147 °C (from $CHCl_3$/hexane), undepressed on admixture with the authentic specimen.[6] The filtrate was poured into water (50 ml) and extracted with ether (100 ml). The ether extract was washed with water, dried over sodium sulfate, and evaporated. The oily residue was distillated to give 2-methoxy-1,3-benzodithiole (**2a**), 0.63 g (69%), bp 130 °C (bath temperature) at 2 Torr.

1a (1.20 g, 5 mmol) was added with stirring to a solution of sodium hydrogensulfide (0.28 g, 5 mmol) in methanol (15 ml) at room temperature. The mixture was stirred for 2 h and worked up as described for the reaction with sodium sulfide to give the sulfide **5**, 0.28 g (33%), mp 145—147 °C and the benzodithiole **2a**, 0.49 g (54%), bp 110 °C (bath temperature) at 0.5 Torr.

*Reaction of **1a** with Ammonium Salts.* To a stirred mixture of ammonium acetate (154 mg, 2 mmol) and pyridine (0.2 ml) in acetonitrile (15 ml) was added in portions **1a** (1.44 g, 6 mmol) and the mixture was stirred at room temperature for 6 h. The crystalline precipitate was collected and washed with ethanol (10 ml) to give tris(1,3-benzodithiol-2-yl)amine (**8**), 0.81 g (86%), mp 247—248 °C (dec) (from benzene, colorless granules).

Found: C, 53.24; H, 3.33; N, 3.19; S, 40.05%. Calcd for $C_{21}H_{15}NS_6$: C, 53.28, H, 3.19; N, 2.96; S, 40.56%.

The reaction of **1a** (1.44 g 6 mmol) with ammonium chloride (105 mg, 2 mmol) in the presence of pyridine (0.2 ml) in acetonitrile (15 ml) at room temperature for 6 h gave compound **8** in 50% yield in addition to a small amount of dibenzotetrathiafulvalene **11**.

*Reaction of **1a** with Primary Amines.* To a stirred mixture of amines (2.5 mmol) and pyridine (0.5 ml) in acetonitrile (10 ml) was added dropwise a solution of **1a** (1.20 g, 5 mmol) in acetonitrile (15 ml) over a period of 5 min. After being stirred for 0.5 h at room temperature, ice water (15 ml) was added to precipitate the products. The precipitate was collected and washed with cold methanol (15 ml).

N,N-Bis(1,3-benzodithiol-2-yl)benzylamine (**9a**), 0.88 g (86%), mp 128—129 °C (from cyclohexane, colorless needles), δ ($CDCl_3$) 3.89 (2H, s, methylene), 6.37 (2H, s, methine), and 6.9—7.4 (13H, m, aromatic).

Found: C, 61.30; H, 4.26; N, 3.36; S, 30.65%. Calcd for $C_{21}H_{17}NS_4$: C, 61.31; H, 4.17; N, 3.41; S, 31.12%.

N,N-Bis(1,3-benzodithiol-2-yl)aniline (**9b**), 0.78 g (79%), mp 134—138 °C (from cyclohexane, colorless granules), δ ($CDCl_3$) 6.71 (2H, s, methine) and 6.8—7.5 (13H, m, aromatic).

Found: C, 60.43; H, 3.96; N, 3.35; S, 32.03%. Calcd for $C_{20}H_{15}NS_4$: C, 60.45; H, 3.81; N, 3.53; S, 32.22%.

*Reaction of **1a** with Secondary Amines.* **1a** (0.48 g, 2 mmol) was added in portions to a stirred mixture of amines (2 mmol) and pyridine (0.2 ml) in acetonitrile (10 ml). After 0.5 h of stirring at room temperature, ice water was added to precipitate the products completely. The precipitate was collected and washed with methanol (10 ml).

N,N-Dibenzyl-1,3-benzodithiol-2-ylamine (**10a**), 0.63 g (90%), mp 94—95 °C (from methanol, colorless needles), δ ($CDCl_3$) 3.63 (4H, methylene), 6.30 (1H, s, methine), and 6.9—7.5 (14H, m, aromatic).

Found: C, 72.14; H, 5.53; N, 4.00; S, 18.20%. Calcd for $C_{21}H_{19}NS_2$: C, 72.19; H, 5.48; N, 4.01; S, 18.32%.

N-Methyl-*N*-(1,3-benzodithiol-2-yl)aniline (**10b**), 0.48 g (92%), mp 120—121 °C (from hexane, colorless needles), δ ($CDCl_3$) 2.71 (3H, s, methyl), 7.13 (1H, s, methine), and 6.95—7.45 (9H, m, aromatic).

Found: C, 64.90; H, 5.10; N, 5.40; S, 24.70%. Calcd for $C_{14}H_{13}NS_2$: C, 64.86; H, 5.05; N, 5.40; S, 24.69%.

4-(1,3-Benzodithiol-2-yl)-*N*-ethyl-1-naphthylamine (**10d**), 0.64 g (99%), mp 97—99 °C (from cyclohexane, needles with a pink tinge), ν_{max} 3350 cm^{-1} (N–H), δ ($CDCl_3$) 1.33 (3H, t, methyl), 3.26 (2H, q, methylene), 4.34 (1H, broad s, N–H), 6.52 (1H, d, aromatic), 7.00 (1H, s, methine), 6.95—7.35 (4H, m, aromatic), *ca.* 7.5 (2H, m, aromatic), *ca.* 7.8 (1H, d/d, aromatic), 7.94 (1H, d, aromatic), and *ca.* 8.1 (1H, d/d, aromatic).

Found: C, 70.51; H, 5.33; N, 4.29; S, 19.81%. Calcd for $C_{19}H_{17}NS_2$: C, 70.57; H, 5.30; N, 4.33; S, 19.79%.

*Reaction of **1a** with Triethylamine.* To a stirred solution of **1a** (2.40 g, 10 mmol) in acetonitrile (10 ml) was added dropwise a solution of triethylamine (3 ml) in acetonitrile (15 ml) over a period of 15 min at room temperature. After being stirred for 0.5 h, the precipitate was collected and washed with benzene (15 ml) to give 1.24 g (81%) of dibenzotetrathiafulvalene **11** as yellow crystals, mp 235—237 °C, undepressed on admixture with the authentic specimen.[24]

*Reaction of **1a** with N,N-Dimethylformamide.* **1a** (2.40 g, 10 mmol) was dissolved in 20 ml of anhydrous *N,N*-dimethylformamide and left at room temperature for 1.5 h. The precipitate was collected and washed with benzene (10 ml) to give 1.21 g (80%) of **11**, mp 235—237 °C.

*Reaction of **1a** with Aromatic Compounds.* *a) With N,N-dimethylaniline and 1,3,5-Trimethoxybenzene*: To a stirred mixture of *N,N*-dimethylaniline (194 mg, 1.6 mmol) and pyridine (0.2 ml) in acetic acid (15 ml) was added **1a** (0.36 g, 1.5 mmol). After 0.5 h, the mixture was diluted with water (10 ml). Filtration of the precipitate and washing with methanol (5 ml) gave 2-[*p*-(dimethylamino)-phenyl]-1,3-benzodithiole (**13**), 0.37 g (89%), mp 119 °C (from ethanol), undepressed on admixture with the authentic specimen.[11]

The reaction of **1a** with 1,3,5-trimethoxybenzen carried out in a similar way gave 0.47 g (98%) of 2-(2,4,6-trimethoxyphenyl)-1,3-benzodithiole (**14**), mp 140—141 °C (from ethanol), undepressed on admixture with the authentic specimen.[11]

b) With 2,6-Dimethylphenol and 2-Naphthol: **1a** (0.36 g, 1.5 mmol) was added in portions to a stirred mixture of 2,6-dimethylphenol (1.6 mmol) and pyridine (0.2 ml) in acetic acid (15 ml). The mixture was heated at 60—70 °C for 3 h and cooled. Ice water (15 ml) was added to precipitate the products. The precipitate was collected and washed with ethanol (10 ml).

2-(4-Acetoxy-3,5-dimethylphenyl)-1,3-benzodithiole (**15b**), 0.32 g (68%), mp 136—137 °C (from ethanol, colorless granules), ν_{max} 1730 cm^{-1} (C=O), δ ($CDCl_3$) 2.10 (6H, s, methyl),

2.30 (3H, s, methyl), 6.18 (1H, s, methine), 6.95—7.30 (4H, m, aromatic), and 7.26 (2H, s, aromatic).

Found: C, 64.24; H, 5.11; S, 20.05%. Calcd for $C_{17}H_{16}O_2S_2$: C, 64.55; H, 5.10; S, 20.23%.

1-(1,3-Benzodithiol-2-yl)-2-acetoxynaphthalene (**16b**), 0.49 g (97%), mp 218—129 °C (from benzene, colorless needles), ν_{max} 1750 cm^{-1} (C=O), δ (DMSO-d_6, at 100 °C) 2.14 (3H, s, methyl), 7.05—7.40 (5H, m, aromatic), 7.48 (1H, s, methine), 7.5—7.6 (2H, m, aromatic), 7.9—8.1 (2H, m, aromatic), and 8.75 (1H, m, aromatic).

Found: C, 67.44; H, 3.88; S, 18.62%. Calcd for $C_{19}H_{14}O_2S_2$: C, 67.45; H, 4.17; S 18.92%.

Reaction of ***1a*** *with Active Methylene Compounds.* To a stirred mixture of active methylene compounds (1.5 mmol) and pyridine (0.2 ml) in acetic acid (10 ml) was added **1a** (0.36 g, 1.5 mmol). After being stirred for 3 h at room temperature, the mixture was diluted with ice water (10 ml). The precipitate was collected and washed with methanol (5 ml). In the reaction with malononitrile, colorless needles separated without addition of water.

3-(1,3-Benzodithiol-2-yl)-2,4-pentanedione (**17a**), 0.35 g (92%), mp 129 °C (from ethanol), undepressed on admixture with the authentic specimen.[21]

Ethyl 2-(1,3-benzodithiol-2-yl)acetoacetate (**17b**), 0.38 g (90%), mp 59—60 °C (from aqueous ethanol), undepressed on admixture with the authentic specimen.[21]

2-(1,3-Benzodithiol-2-yl)-3-acetoxy-5,5-dimethyl-2-cyclohexen-1-one (**17e**), 0.38 g (76%), mp 117—118 °C (from ethanol, colorless needles), ν_{max} 1760, 1658, and 1635 cm^{-1}, δ ($CDCl_3$) 1.07 (6H, s, methyl), 1.54 (3H, s, methyl), 2.34 (2H, s, methylene), 2.55 (2H, s, methylene), 6.38 (1H, s, methine), and 6.9—7.2 (4H, m, aromatic).

Found: C, 60.70; H, 5.20; S, 19.17%. Calcd for $C_{17}H_{18}O_3S_2$: C, 61.07; H, 5.43; S, 19.14%.

Bis(1,3-benzodithiol-2-yl)malononitrile (**18**), 0.24 g (86%), mp 220—221 °C (dec), undepressed on admixture with the authentic specimen.[21]

Reduction of ***1a*** *with Sodium Borohydride.* To a stirred mixture of sodium borohydride (0.40 g, 10 mmol) in anhydrous tetrahydrofuran (30 ml) was added in portions **1a** (2.40 g, 10 mmol) at room temperature. After being stirred for 2 h, the mixture was poured into ice water (200 ml) and extracted with ether (200 ml). The ether extract was washed with water, dried over sodium sulfate, and evaporated. The oily residue was distillated to give 1.24 g (81%) of 1,3-benzodithiole (**19**), bp 103—104 °C/3 Torr (lit,[22] bp 88 °C/0.6 Torr).

Reaction of ***1a*** *with Tropilidene.* To a stirred and ice-cooled solution of tropilidene (1.56 g, 17 mmol) in acetonitrile (10 ml) was added dropwise a solution of **1a** (3.60 g, 15 mmol) in acetonitrile (15 ml) during 20 min. After stirring for 0.5 h at 0 °C, anhydrous ether (40 ml) was added to precipitate the product. Filtration and washing with anhydrous ether (10 ml) gave tropylium tetrafluoroborate (**20**) as white crystals, 2.40 g (90%), mp>210 °C (dec) [lit,[25] mp>210 °C (dec)]. The filtrate and washings combined were washed with water and dried. The ether was evaporated and the residual oil was distillated to give the benzodithiole **19**, 1.50 g (65%), bp 83—85 °C/0.5 Torr.

Fluoroborate Salt ***1a*** *from 1,3-Benzodithiole.* To a stirred and ice-cooled solution of **19** (1.07 g, 7 mmol) in acetonitrile (10 ml) was added dropwise a solution of trityl tetrafluoroborate[25] (2.31 g, 7 mmol) in acetonitrile (15 ml) over a period of 20 min. After stirring for 20 min at 0 °C, anhydrous ether (50 ml) was added to the mixture. The resulting crystalline precipitate was collected and washed with anhydrous ether (10 ml) to give **1a**, 1.26 g (75%), mp 148—150 °C (dec). The filtrate and washings combined were washed with water, dried, and evaporated. The crystalline residue was washed with methanol (10 ml) to give triphenylmethane as white crystals, 1.29 g (75%), mp 93 °C.

References

1) H. Prinzbach and E. Futterer, "Advances in Heterocyclic Chemistry," Vol. 7, ed. by A. R. Katritzky and A. J. Boulton, Academic Press, New York (1966), p. 39.

2) E. Campaigne and R. D. Hamilton, *Quart. Reports on Sulfur Chem.*, **5**, 275 (1970).

3) a) A. Takamizawa and K. Hirai, *Chem. Pharm. Bull.*, **17**, 1924 (1969); b) A. Takamizawa and K. Hirai, *ibid.*, **17**, 1931 (1969); c) A. Takamizawa and K. Hirai, *ibid.*, **18**, 865 (1970); d) K. Hirai, *Tetrahedron*, **27**, 4003 (1971); e) K. Hirai, T. Ishiba, and H. Sugimoto, *Chem. Pharm. Bull.*, **20**, 1711 (1972).

4) J. Nakayama, K. Fujiwara, and M. Hoshino, *Chem. Lett.*, **1975**, 1099.

5) a) J. Nakayama, *Synthesis*, **1975**, 38; b) J. Nakayama, *J. Chem. Soc., Perkin Trans. 1*, **1975**, 525; c) J. Nakayama, *J. Chem. Soc. Chem. Commun.*, **1974**, 166.

6) J. Nakayama, *Synthesis*, **1975**, 436.

7) a) W. R. H. Hurtley and S. Smiles, *J. Chem. Soc.*, **1926**, 2263; b) L. Soder and R. Wizinger, *Helv. Chim. Acta*, **42**, 1733 (1959); c) D. Buza, A, Gryff-Keller, and S. Szymański, *Rocz. Chem.*, **44**, 2319 (1970); d) S. Hünig, G. Kieblich, H. Quast, and D. Scheutzow, *Ann. Chem.*, **1973**; 310; e) G. Scherowsky and J. Weiland, *ibid.*, **1974**, 403.

8) a) W. R. H. Hurtley and S. Smiles, *J. Chem. Soc.*, **1926**, 1821; b) R. Adams and A. Ferretti, *J. Am. Chem. Soc.*, **81**, 4927, 4939 (1959); c) S. Hünig and E. Fleckenstein, *Ann. Chem.*, **738**, 192 (1970).

9) F. Wudl, M. L. Kaplan, E. J. Hufnagel, and E. W. Southwick, Jr., *J. Org. Chem.*, **39**, 3608 (1974).

10) D. Leaver, D. M. McKinnon, and W. A. H., Robertoson, *J. Chem. Soc.*, **1965**, 32.

11) J. Nakayama, *Synthesis*, **1975**, 170.

12) W. von E. Doering and L. H. Knox, *J. Am. Chem. Soc.*, **79**, 352 (1957).

13) a) E. Campaigne, T. Bosin, and R. D. Hamilton, *J. Org. Chem.*, **30**, 1677 (1965); b) E. Campaigne and R. D. Hamilton, unpublished results; see Ref. 2.

14) R. Mayer and B. Gebhardt, *Chem. Ber.*, **97**, 1298 (1964).

15) Studies regarding the mechanism of this reaction are under way.

16) E. Campaigne and R. D. Hamilton, *J. Org. Chem.*, **29**, 2877 (1964).

17) A. F. Garito and A. J. Heeger, *Acc. Chem. Res.*, 7, 232 (1974).

18) a) H. Prinzbach, H. Berger, and A. Lüttringhaus, *Angew. Chem., Int. Ed. Engl.*, **4**, 435 (1965); b) C. D. Coffen, J. Q. Chambers, D. R. Williams, P. E. Garrett, and N. D. Canfield, *J. Am. Chem. Soc.*, **93**, 2258 (1971); c) J. P. Ferraris, T. O. Poehler, A. N. Bloch, and D. O. Cowan, *Tetrahedron Lett.*, **1973**, 2253; d) L. R. Melby, H. D. Hartzler, and W. A. Sheppard, *J, Org. Chem.*, **39**, 2456 (1974); e) Y. Ueno, Y. Masuyama, and M. Okawara, *Chem. Lett.*, **1975**, 603.

19) a) R. Wizinger and L. Soder, *Chimia (Switz)*, **12**, 79 (1958); b) L. Soder and R. Wizinger, *Helv. Chim. Acta*, **42**, 1779 (1959); c) E. Campaigne and R. D. Hamilton, *J. Org. Chem.*, **28**, 1711 (1964); d) R. Gompper and E. Kutter, *Chem. Ber.*, **98**, 1365 (1965); e) E. Klingsberg, *J. Am. Chem.*

Soc., **86**, 5290 (1964).
20) a) A. Lüttringhaus, E. Futterer, and E. Prinzbach, *Tetrahedron Lett.*, **1963**, 1209; b) A. Lüttringhaus, H. Berger, and H. Prinzbach, *ibid.*, **1965**, 2121; c) E. Campaigne and F. Haaf, *J. Org. Chem.*, **30**, 732 (1965).
21) J. Nakayama, *J. Chem. Soc., Perkin Trans. 1*, in press.
22) D. Seebach, K. H. Geib, A. K. Beck, B. Graf, and H. Daum, *Chem. Ber.*, **105**, 3280 (1972).
23) J. Koutecký, J. Paldus, and R. Zahradník, *Collect. Czech. Chem. Commun.*, **27**, 617 (1960).
24) J. Nakayama, *Synthesis*, **1975**, 168.
25) H. J. Dauben, Jr., L. R. Honnen, and K. N. Harmon, *J. Org. Chem.*, **25**, 1442 (1960).

Acyl Cyanide. III. Thermal and Base-Catalyzed Reactions of Phenylcarbamoyl Cyanide

Akira Oku,* Takamasa Suzuki, Hajime Koura, and Fujio Mashio
Department of Chemistry, Kyoto Institute of Technology, Matsugasaki, Sakyo-ku, Kyoto 606
(Received May 6, 1976)

Phenylcarbamoyl cyanide (**1**), under thermal conditions or base-catalysis, behaves as a source of both phenyl isocyanate and hydrogen cyanide in the syntheses of carbamates, cyanohydrins, and iminohydantoins. The reaction mechanism of **1** with methanol in the presence of tertiary amine was investigated. The following observations (i—iii) led us to deduce that phenyl isocyanate was not involved as the intermediate and that the rate-determining step involves nucleophilic displacement of **1** by the alkoxyl group, reinforced by the base: (i) the N–H exchange was too fast to be rate-determining; (ii) *d*-labelling experiments showed $k_H/k_D=1.8$—1.9 in any of the reactions, **1**-d_1+MeOH, **1**-d_0+MeOD, and **1**-d_1+MeOD, and (iii) diphenylcarbamoyl cyanide reacted only 7.2 times slower than did **1**.

Monosubstituted carbamoyl cyanides, RNHCOCN, have been known since 1905, when Dieckmann prepared 1,3-diphenyl-5-iminohydantoin from phenyl isocyanate. However, because of their low thermal stability, relatively few surveys of their chemical properties have appeared in the literature.[1,2] Through the synthesis of a series of thermostable poly(5-iminohydantoin)s from diisocyanates,[3,4] we previously found that the formation of iminohydantoins by the self-condensation of carbamoyl cyanides was facilitated by heating as well as by base catalysis. For this reaction, two mechanisms can be postulated: a) carbamoyl cyanide decomposes thermally or base-catalytically into hydrogen cyanide and isocyanate, after which the latter reacts with another cyanide to give the hydantoin, or b) carbamoyl cyanide self-condenses without forming isocyanate. Much as in the above reaction, carbamoyl cyanide was found to react easily with alcohols to give the corresponding carbamates, and two mechanisms analogous to the above can be postulated: a′) *via* isocyanate, or b′) *via* the nucleophilic displacement of carbamoyl cyanide by alcohol. In view of the paucity of information supporting either mechanism, we have now performed a kinetic study of the reaction of phenylcarbamoyl cyanide with alcohols. Also investigated in the present study is the utilization of phenylcarbamoyl cyanide as a source of isocyanate (masked isocyanate reagent) and hydrogen cyanide as well.

Results and Discussion

Thermal Decomposition of Phenylcarbamoyl Cyanide (1). Cyanide (**1**) gives 1,3-diphenyl-5-iminohydantoin (**4**) when heated in solutions or in molten states. The reaction was interpreted in terms of the thermal decomposition of **1** into hydrogen cyanide and phenyl isocyanate (**2**, not isolated); the latter then reacted further with the undecomposed **1** to give **4**. This assumption prompted the use of bifunctional carbamoyl cyanides as masked reagents of diisocyanates for the synthesis of poly(5-iminohydantoin)s.[3] Thus, we hope that monofunctional carbamoyl cyanides can be utilized as a stable source of isocyanates as well as of hydrogen cyanide in reactions requiring neutral or thermal conditions.

$$\underset{\mathbf{1}}{\mathrm{PhNHCOCN}} \xrightarrow{\text{heat}} \underset{\mathbf{2}}{\mathrm{Ph\text{-}NCO}} + \underset{\mathbf{3}}{\mathrm{HCN}} \qquad (1)$$

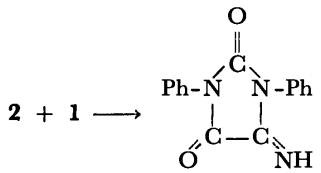

$$\mathbf{2} + \mathbf{1} \longrightarrow \mathbf{4} \qquad (2)$$

The mass spectrum of phenylcarbamoyl cyanide (**1**), even when the ionization chamber voltage was varied from 80 to 15 eV and the chamber temperature was lowered from 250 to 160 °C by both direct and indirect in-letting methods, showed no P^+ peak (*m/e* 146 for $C_8H_6N_2O$), but only those peaks ascribable to phenyl isocyanate and hydrogen cyanide. Therefore, either the decomposition of the parent molecule into isocyanate prior to the electron bombardment or the fragmentation of the parent molecular ion after the bombardment must be too fast to allow the detection of the P^+ ion. Coupled with this measurement, the pyrolysis of **1** was carried out by the thermobalance method. Under reduced pressure (20 Torr) **1** started to lose weight appreciably at 85 °C. The decomposition gas trapped in a cold vessel was proved by IR (N=C=O 2270 cm^{-1}) to consist mainly of **2**, while treatment with aniline gave *N,N′*-diphenylurea. Above 110 °C, **1** became a liquid and its decomposition as well as sublimation were considerably accelerated.

The thermal reaction of **1** in solution was then investigated. When **1** alone was heated in boiling dioxane for 60 h, 1,3-diphenyl-5-(phenylcarbamoylimino)-hydantoin (**5**) or **4** was obtained, depending on the reaction conditions (concentration, solvent, and catalyst.)[5] The IR analysis of the solution did not detect

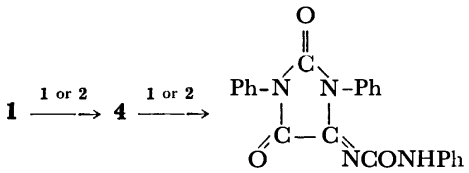

$$\mathbf{1} \xrightarrow{\text{1 or 2}} \mathbf{4} \xrightarrow{\text{1 or 2}} \qquad (3)$$

5

2 throughout the period. Similarly, when **1** was warmed with alcohols in dioxane, the corresponding phenylcarbamates were formed in high yields (Table 1) (as for the mechanism, see below). Consequently, **1** can be adopted as a *phenylcarbamoylating* reagent or, in other words, as a masking reagent of phenyl

Table 1. Reaction of PhNHCOCN (**1**) with alcohols

ROH	[ROH]/[1]	Solvent	[1]/Solvent mol/l	Temp °C	Time h	Urethane %
CH_3OH	2.5×10^5	CH_3OH	7.8×10^{-5}	30	8	45
CH_3OH	2.5×10^5	CH_3OH[b]	7.5×10^{-5}	30	4	56
CH_3OH	1×10^2	CH_3OH[c]	2.8×10^{-1}	30	0.1	*a*)
CH_3OH	2	Dioxane	7×10^{-2}	50	15	98
CH_3OH	1×10^2	*c*-C_6H_{12}	7×10^{-2}	50	25	3
C_2H_5OH	2	Dioxane	7×10^{-2}	100	68	95
$PhCH_2OH$	2	Dioxane	7×10^{-1}	100	25	65

a) Iminohydantoin 90%. b) Et_3N 7×10^{-7} mol/l added. c) Et_3N 2.8×10^{-3} mol/l added.

Table 2. Reaction of PhNHCOCN (**1**) with cyclohexanone (**8**)

Run	[1]/[8] mol ratio	8 (g)	Additive (g)[b] H_2O	AcOH	NaCN	Temp (°C)	Time (h)	Cyanohydrin (%)
1	0.12	14.1	—	—	—	150	2	—
2	0.12	13.5	0.6	—	—	80	24	—[a]
3	0.15	14.1	0.5	1.5	—	80	20	29
4	0.15	14.1	0.5	1.5	0.001	80	20	49
5	0.20	9.5	1.0	1.0	—	80	20	36
6	0.20	9.5	1.0	1.0	0.001	67	17	98
7	0.15	14.1	0.5	—	—[c]	25	1	—[d]

a) A trace amount. b) AcONa was added in Runs 5 and 6. c) Et_3N(0.1 g) was added instead of NaCN. d) The main product was 1,3-diphenyl-5-iminohydantoin.

$$\underset{\mathbf{6}}{\mathbf{1}} + \text{R-OH} \longrightarrow \underset{\mathbf{7}}{\text{PhNHCOOR}} + \text{HCN} \qquad (4)$$

isocyanate in some thermal reactions (or in low-temperature reactions with the aid of bases). Analogously, though less effectively, compound **5** yielded a trace amount of benzyl phenylcarbamate (2%) when treated with benzyl alcohol in boiling dioxane for 30 h, whereas **4** did not.

Generally, investigators are nervous handling hydrogen cyanide in the laboratory. Carbamoyl cyanide, *e.g.*, **1**, can be handled in solid states, being soluble in many organic solvents, and is a safer HCN source. In order to estimate this utilizability, the reaction of **1** with cyclohexanone (**8**) was chosen as the model. The reaction was carried out in the presence of water in order to remove the simultaneously formed isocyanate, **2**, from the reaction system by forming diphenylurea (**10**), because **2** will react further with cyanohydrin,

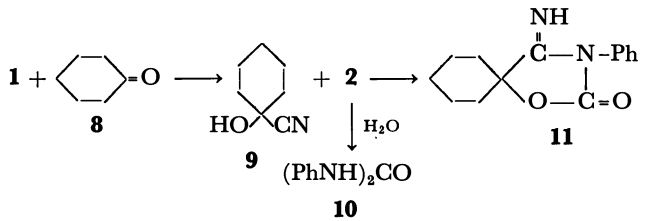

9, to give cyclic urethane, **11**.[6] The results are shown in Table 2, in which the same salt effect as has been known for the general cyanohydrin synthesis[7] is indicated: *i.e.*, catalysis by a trace amount of the cyanide anion and a buffer effect of sodium acetate in acetic acid.[8] These basic additives also seem to facilitate the decomposition of **1** to generate HCN. Thus, the optimum yield of cyanohydrin **9** was attained almost quantitatively under the conditions of Run 6.

*Base-Catalyzed Reaction of Phenylcarbamoyl Cyanide (**1**) with Methanol.* The formation of carbamates as well as of 5-iminohydantoins from **1** has been known to be facilitated significantly by bases, such as tertiary amines and basic solvents.[3] In order not only to clarify the characteristics of this catalysis, but also to make a rational choice between the two reaction mechanisms, a') and b') (see the Introduction), the rate of the reaction of **1** with methanol was measured under various conditions of base-catalysts, solvents, and isotope-labelling.

Table 3, showing the rate constants as measured by a UV spectroscopic method, indicates that the catalysis of weak bases, such as pyridine or *N,N*-dimethylaniline, is not appreciable, while strong bases such as triethylamine exhibit an apparent rate enhancement even in diluted solutions (10^{-4}—10^{-6} mol/l for base). The

Table 3. Rates of reaction of PhNHCOCN (**1**) with methanol (31±0.5 °C in MeOH)[a]

Base	$[Base]/[1]_0$	$k_1\times10^4$ s^{-1}
—	—	4.2
Me_2N-Ph	0.025	3.8
Pyridine	0.040	4.2
Pyridine	0.40	3.8
Et_3N	0.002	4.1
Et_3N	0.020	6.6
Et_3N	0.048	10.0
Et_3N	0.23	37.7
Imidazole	0.021	4.6

a) $[1]_0$: 8.7×10^{-5} mol/l.

Table 4. Rates of reaction of PhNHCOCN (**1**) with methanol in solvents other than methanol (at 31±0.5 °C)

Solvent	Substrate ratio (10^{-5} mol/l)			$k_2\times10$ (l/mol s)
	1	MeOH	Et_3N	
Dioxane	1	1	1	7.83
Dioxane	1	5	1	7.75
Dioxane	1	1	5	28
c-C_6H_{12}	1	1	1	$<10^{-1}$

Table 5. Rates of reaction of PhNDCOCN (**1**-d_1) with methanol-d_1 in dioxane (at 31±0.5 °C)

Run	Reactant[a,b]	$k_2\times10$ (l/mol s)	k_H/k_D[c]
1	**1**-d_0+MeOH	7.8	—
2	**1**-d_1(20%)+MeOH	7.0	1.11
3	**1**-d_1(85%)+MeOH	4.6	1.70
4	**1**-d_0+MeOD	4.2	1.85
5	**1**-d_1(85%)+MeOD	4.0	1.95

a) The d-content was roughly determined by IR and MS. b) Et_3N was added; substrate ratio [**1**]:[MeOH]:[Et_3N]=1:1:1. c) Uncorrected for **1**-d_1(100%)

solvent effect is also significant (see Table 4). For example, in dioxane the rate is only 9 times as slow as in methanol, while in cyclohexane it is more than 10^2 times as slow as in dioxane. From these results, we presumed that either of the following two transitions constitutes the rate-determining step: a'') proton abstraction from **1** by a base, or the elimination of cyanide anion from the conjugate base, or b'') the nucleophilic displacement of the cyano group by a base-reinforced methoxyl group.[9]

Mechanism b'') was preferred to a'') by characterizing the deuterium-labelling effect on the rate of the reaction system, Ph–ND (or H)–CO–CN+MeOD(or H) (Table 5). First of all, it was noted that, when **1**-d_1 was prepared by shaking a warm $CDCl_3$ solution of **1**-d_0 with D_2O, the H–D exchange was completed rapidly, without forming either diphenylurea (**10**) or phenyloxamide. This indicates that the N–H abstraction, followed by the rapid elimination of the cyanide anion to give **2**, does not constitute the rate-determining step. In addition, the observed isotope effect, k_H/k_D=1.8—1.95, though not large enough to be the primary kinetic isotope effect, indicates that the elimination of the CN^- group can not be the single step constituting the transition state. The almost equal isotope effects in Runs 3 and 4 (Table 5) may be attributed to the rapid H–D exchange between **1** and methanol prior to the substitution in both runs, and the same equilibrium mixture, in which deuterium incorporates largely into methanol, is formed. This assumption is supported by Run 5, where k_H/k_D is about the same as in Runs 3 and 4.

Consequently, the observed isotope effect can be most rationally interpreted by means of the following tentative model, **12**, for the transition state where the bond fission of MeO–H(D), but not of N–H(D), is involved and where the proton must be almost completely transferred to the base, as is indicated by the small value of the isotope effect. In this mechanism,

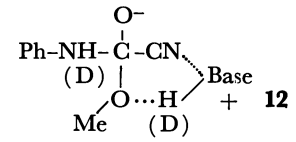

+ **12**

the presence of hydrogen on the amide nitrogen must be unimportant in effecting the rate.[10] In fact, the rate of the reaction of diphenylcarbamoyl cyanide (**13**)[11] with methanol, as measured under the same conditions as were set for **1** was only slightly slower than that of **1** ($k_{13}=6.5\times10^{-5}$ s^{-1}, $k_1/k_{13}=7.2$).[12]

$$(Ph)_2NCOCN + MeOH \longrightarrow (Ph)_2NCOOMe \quad (6)$$

13 **14**

A disproof of Mechanism a'') can also be deduced from the results of Hutchins and his co-workers,[13] who observed a 10^4-fold faster rate of the base-catalyzed intramolecular cyclization of **15** than that of **16**. They elucidated how the reaction of **15** proceeds *via* an isocyanate intermediate, followed by a fast addition of the benzyloxy group, whereas in **16** only a slow displacement by the benzyloxy group is possible. Although this interpretation seems quite similar to Mechanism a''), the k_1/k_{13} ratio of 7.2 seems too small to be accounted for analogously.[14]

In conclusion, though some ambiguity still remains with regard to its details, Mechanism b''), where the RO–H bond fission and the nucleophilic attack of the resulting alkoxyl group are simultaneously involved in the rate-determining transition state, seems most plausible for the reaction of carbamoyl cyanide with alcohols.

15

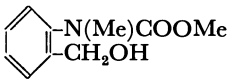

16

Experimental

Reagents. Phenylcarbamoyl cyanide (**1**) was synthesized from Ph–NCO and HCN according to the method reported for diisocyanates in our previous study.[3] Recrystallization from alcohol-free $CHCl_3$ or Et_2O yielded colorless flakes of **1** (>90%): mp 116—117 °C; $UV_{max}^{cyclohexane}$ 267 nm (ε 10050). Diphenylcarbamoyl cyanide (**13**) was prepared by the reaction of the corresponding chloride with NaCN in MeCN.[11] Recrystallization from a cyclohexane–benzene mixture afforded slightly yellow solids of **13** (65%): mp 130—132 °C; $UV_{max}^{dioxane}$ 262 nm (ε 5000).

Preparation of Phenylcarbamoyl Cyanide-d_1 (*1*-d_1). Deuterated cyanide was prepared by two methods: (i) the reaction of Ph–NCO with DCN, which had been generated from D_2SO_4–D_2O and anhydrous NaCN; (ii) shaking a warm $CDCl_3$ (99.8% d-content) solution of **1** with excess D_2O (99.8% d_2). For recrystallization, $CDCl_3$ was used; otherwise, D–H exchange took place. Also, care was taken not to heat the solution longer than 30 min.

Kinetics. S.P.-Reagent-grade methanol, dioxane, and cyclohexane, available from the Nakarai Chemicals Co., were used in all the measurements. The rates of the reactions of **1** and **13** with methanol were obtained by measuring the change in the absorbance in diluted dioxane solutions (*ca.*

6—8.8×10^{-5} mol/l), where the validity of Beer's rule has preliminarily been confirmed. A Hitachi Model-124 spectrophotometer was used. The analyzing UV bands were: **1** 267 nm (ε 10050), **13** 262 (5000), **7** (R=Me) 236 (15070).

*Pyrolysis of **1**.* A 0.194-g portion of finely pulverized powder of **1** was placed in a platinum basket of a thermobalance (Shimadzu Thermobalance for 2000 mg), whose evacuating outlet was connected to a cold trap cooled at −78 °C. The apparatus was then evacuated to a reduced pressure (20 Torr), and the temperature was raised at a programming rate of 0.7 °C/min from 21 to 74 °C, at a rate of 0.5 °C/min from 74 to 94 °C, and at a rate of 0.2 °C/min from 94 to 103 °C; the weight loss *vs.* time was plotted. The weight loss was observed from 80 °C and was remarkable above 90 °C. Above 110 °C, however, a considerable amount of **1** was sublimed and deposited on the wall of the glass ware; the net loss by the pyrolysis was 46% of the gross loss after 2 h. The trapped liquid (*ca.* 40 mg) showed its ν(NCO) at 2270 cm^{-1} (taken by JASCO IRA-1). An ethereal solution of the trapped liquid gave diphenylurea (65 mg) upon treatment with a few drops of aniline. The remaining solid (88 mg) in the basket was analyzed by TLC (silica gel, $CHCl_3$). Two spots appeared; they were identified with 1,3-diphenyl-5-(phenylcarbamoylimino)hydantoin (**5**, mp 223—225 °C) and unreacted **1** by comparing the R_f values. The mass spectrum of **1** was taken by means of a Hitachi Model RMU-6L by both indirect and direct inletting methods. The spectrum taken at 160 °C and 30 eV showed ion peaks at (*m/e*) 119(Ph-NCO$^+$), 91(PhN$^+$), 64, and 27(HCN$^+$).

*Decomposition of **1** in Cyclohexanone.* To a mixture of **1** (2.6 g, 0.018 mol) and cyclohexanone (9.5 g), we added a solution (2 g) of AcONa saturated in a 1 : 1 mixture of H_2O and AcOH. A catalytic amount of aq NaCN (10 µl of 10% aq solution) was then added, and the total mixture was heated at 67 °C for 17 h. The reaction mixture, without working-up, was directly analyzed by GLC (Apiezon L, 10%, 3 mm×2 m) at 160 °C (below this temperature decomposition of the cyanohydrin was negligible) to find that it consisted of cyclohexanone cyanohydrin (**9**, 98%) and *N,N'*-diphenylurea (**10**). For other runs, see the details in Table 2.

*Thermal Reaction of **1** with Alcohols.* A dioxane solution of **1** and an alcohol were mixed, and the mixture was warmed under the conditions cited in Table 1. After removing the solvent *in vacuo*, the residue was chromatographed (silica gel, $CHCl_3$). The phenylcarbamates thus obtained were all identical with those synthesized independently from Ph-NCO and the corresponding alcohols as for mp and spectroscopic data.

*Reaction of Diphenylcarbamoyl Cyanide (**13**) with Methanol.* Methyl diphenylcarbamate (**14**) was obtained by heating a methanol solution of **13** with a trace amount of triethylamine over 18 h; 100%; mp 84—86 °C.

The authors wish to express their thanks to Mr. Shigeru Fukumori and Mr. Hiroyuki Ueda for their assistance in this study.

References

1) W. Dieckmann and H. Kammerer, *Ber.*, **38**, 2977 (1905).
2) a) W. Dieckmann and H. Kammerer, *Ber.*, **40**, 3737 (1907); b) Schulz, Rhode, and Herzog, *J. Prakt. Chem.* (2), **74**, 86.
3) A. Oku, M. Okano, and R. Oda, *Makromol. Chem.*, **78**, 186 (1964).
4) A. Oku, T. Shono, and R. Oda, *Makromol. Chem.*, **100**, 224 (1967).
5) W. Dieckmann and H. Kammerer, *Ber.*, **40**, 3742 (1907).
6) T. L. Patton, *J. Org. Chem.*, **32**, 383 (1967).
7) H. A. Piggott, *J. Chem. Soc.*, **1955**, 425.
8) a) R. L. Frank, R. E. Berry, and O. L. Shotwell, *J. Am. Chem. Soc.*, **71**, 3889 (1949); b) W. D. Emmons and J. P. Freeman, *ibid.*, **77**, 4387 (1955).
9) An analogous displacement has been reported for the hydrolysis of acyl cyanides: a) F. Hibbert and D. P. N. Satchell, *J. Chem. Soc., B*, **1967**, 653; b) A. Dornow and H. Theidel, *Angew. Chem.*, **66**, 605 (1954); c) J. Thesing and D. Witzel, *ibid.*, **68**, 432 (1956).
10) The hyperconjugative secondary isotope effect of the N-H(D) bond, if any, may be comparable to the k_H/k_D value of 1.2 that was observed for the C-H(D) bond: see A. Streitwieser, Jr., R. H. Jagow, R. C. Fahey, and S. Suzuki, *J. Am. Chem. Soc.*, **80**, 2367 (1958).
11) R. G. Hisky and F. I. Carroll, *J. Am. Chem. Soc.*, **83**, 4644 (1961).
12) The small difference observed in the rates (k_1/k_{13}= 7.2) seems ascribable to the steric hindrance in **13** or to the difference in the carbonyl polarization, that might be greater in **1** ($\nu_{C=O}$ 1670 cm^{-1}) than in **13** (1680).
13) J. E. C. Hutchins and T. H. Tafe, *J. Am. Chem. Soc.*, **95**, 3786 (1973).
14) In other words, if Mechanism a'') is correct, the k_1/k_{13} ratio should have been more than 10^4 because the acidity of the N-H in **1** is greater than in **15** due to the conjugation in the conjugate base, Ph-N=C(-O$^-$)-C≡N.

The Solution Photodimerization of (*E*)-*p*-Nitrocinnamates

Tatsuzo Ishigami, Tomoji Murata, and Tadashi Endo

Department of Chemistry, College of Science and Engineering, Aoyama Gakuin University, Chitosedai, Setagaya-ku, Tokyo 157

(Received May 12, 1976)

The solution photodimerization of methyl (*E*)-*p*-nitrocinnamate has been studied under various conditions. *Cis* and *trans* dimers of head-to-head configuration were formed predominantly, the ratio of the dimers being highly dependent on the concentration and the solvent. The sensitization, the quenching phenomena, and the external heavy-atom effect were observed in this photodimerization. It appears likely that the excited multiplicity responsible for the formation of the *trans*-dimer is the triplet π,π^* state and that both the singlet and the triplet π,π^* states contribute to the production of the *cis*-dimer.

The formation of four-membered rings through the irradiation of olefins, especially of the α,β-unsaturated carbonyl compounds, is one of the oldest photoreactions in organic chemistry. The photocyclodimerization of the *crystalline* cinnamic acids is a classic illustration of this type of reaction.[1] The crystallographically different α- and β-forms of (*E*)-cinnamic acid exclusively give α-truxillic acid (head-to-tail dimer) and β-truxinic acid (heat-to-head dimer), respectively. The stereospecificity of this cycloaddition is shown to depend mainly upon the packing arrangement of the nearest neighbours in the monomer lattice. Further, cyrstallographic studies have made it clear that, in order for dimerization to occur in either crystal form, the reacting centers must be separated by no more than 4 Å.[1] On the other hand, in *solution* or in the *liquid* state of cinnamic acid, ultraviolet light merely causes an equilibration between the *Z* and *E* isomers.[2] The absence of photodimerization in solution is attributable to the lack of a situation in which the intermolecular carbon-carbon double bonds lie close together, *e.g.*, within 4 Å.

As a fundamental study on the control of photoreactions, this paper deals with the solution photodimerization of (*E*)-*p*-nitrocinnamates giving the two head-to-head photocyclodimers whose ratios vary largely, depending on the irradiation conditions, and also with the mechanistic aspects of this photodimerization.

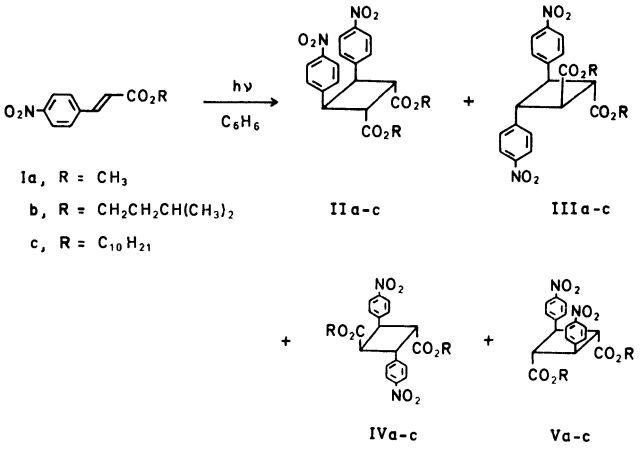

Results

Photodimerization of Substituted (E)-Cinnamates in Benzene. An argon-saturated benzene solution (0.05 mol dm^{-3}) of methyl (*E*)-*p*-nitrocinnamate (Ia) was externally irradiated with a 450-watt high-pressure mercury arc for 3 h at 10 °C. The resulting solution was subjected to TLC to give the *cis*- (IIa, 14%) and *trans*-head-to-head cyclodimers (IIIa, 29%), together with only a trace amount (1%>) of the *cis*- (IVa) and *trans*-head-to-tail cyclodimers (Va). When the irradiation was effected by the Pyrex-filtered light, the yields of IIa and IIIa were 13 and 36%, respectively. The structures of these cyclobutane derivatives were established by an examination of their NMR and mass spectra.[3] It was also confirmed that both IIa and IIIa are extremely stable under all the irradiation conditions employed.

The *Z*, *E* isomerization of the carbon-carbon double bond generally competes with photodimerization. In the above photoreaction, the rapid equilibration between Ia and its *Z* isomer (VIa) was confirmed by the gas-chromatographic analysis of the reaction mixture; the ratio of Ia to VIa was 0.94 when Ia was irradiated for 10 min and 1.13 under a 3-h irradiation.

In contrast, methyl (*E*)-cinnamate and its derivatives possessing the *p*-chloro, *p*-methoxyl, *p*-methyl, *p*-isopropyl, and *p*-dimethylamino groups underwent only *Z*, *E* isomerization and gave no cyclodimers when irradiated under the conditions described above. However, the prolonged irradiation (65 h) of a more concentrated solution (0.5 mol dm^{-3}) of methyl (*E*)-cinnamate gave the corresponding *cis*- and *trans*-head-to-head cyclodimers in 16 and 37% yields, respectively.

When the bulky isopentyl (Ib) or decyl group (Ic) is the ester moiety, the ratio of the corresponding two cyclodimers (II/III) was found to be 0.26 or 0.20, respectively (Table 1). This can be explained by the greater steric repulsion between the two alkyl groups in II than that in III.

Solvent Effect on the Photodimerization of Ia. The data in Table 2 indicate the dependence of the product distribution on the solvent polarity. The amount of IIa proved to increase with an increase in the dielectric constants[4] or dipole moments[5] of the solvents employed.[6] No relationship existed between the selectivity in this photodimerization and the coefficients of the viscosity[5] of the solvents or the reaction temperature.[7] The use of the polar solvents such as pyridine, acetone, and acetonitrile, raised the yields of the head-to-tail cyclodimers (IVa and Va) considerably in comparison with the use of the nonpolar solvents.

Table 1. Photodimerization of I[a]

Compound	Filter	Conversion (%)	Yield (%)[b]			II/III
			II	III	IV, V	
Ia	Quartz	54	14	29	1	0.48
Ia	Pyrex	62	13	36	2	0.36
Ib	Quartz	55	6	23	1>	0.26
Ic	Quartz	65	8	40	1	0.20

a) Irradiated in a benzene solution (0.05 mol dm^{-3}) under an argon atmosphere with a 450-watt high-pressure mercury lamp for 3 h. b) Based on I employed.

Table 2. Solvent effects on the photodimerization of Ia[a]

Solvent	ε[b]	μ[c]	Conversion (%)	Yield (%)[d]			IIa/IIIa
				IIa	IIIa	IVa, Va	
1,4-Dioxane	2.21	0.45	58	8	16	2	0.50
C_6H_6	2.28	0	54	14	29	1	0.48
$CH_3CO_2C_2H_5$	6.02	1.88	55	15	26	2	0.58
Pyridine	12.4	2.37	64	19	24	5	0.79
CH_3COCH_3	20.7	2.69	63	21	22	8	0.95
CH_3CN	37.5	3.44	82	27	26	8	1.04
CH_2Cl_2	8.93	1.14	49	3	26	1	0.12
$CHCl_3$	4.81	1.15	48	2	25	1	0.08
CH_2Br_2	4.78	1.23	59	1	30	1	0.03

a) Irradiated under the same conditions as in the case of Table 1. b) Dielectric constant at 20 °C. c) Dipole moment at 25 °C. d) Based on Ia employed.

Table 3. Concentration effects and solid-state irradiation

Solvent[a]	Concn. (mol dm^{-3})	Conversion (%)	Yield (%)[b]		IIa/IIIa
			IIa	IIIa	
Solid-state	—	100	95	0	—
C_6H_6	1×10^{-1}	73	41	16	2.56
C_6H_6	5×10^{-2}	69	15	22	0.68
C_6H_6	5×10^{-3}	69	2	6	0.33

a) Irradiated under an oxygen atmosphere with a 450-watt high-pressure mercury lamp for 3 h. b) Based on Ia employed.

The irradiation of Ia in the halogenated hydrocarbons resulted in the predominant formation of the *trans*-cyclodimer (IIIa) probably by means of the external heavy-atom effect.[8] In the case of dibromomethane, the heavy-atom effect was remarkable, the IIa/IIIa value being 0.03. However, at a lower concentration (5 mol% dibromomethane in benzene) the halogen-containing compounds showed no significant effect.

Effect of Concentration. As is shown in Table 3, the concentration of the reactant (Ia) proved to influence the ratio of the photodimers remarkably. The IIa/IIIa value increased from 0.68 to 2.56 with an increase in the concentration of benzene solution under an oxygen atmosphere. In the case of a dilute solution (5×10^{-3} mol dm^{-3}), polymerization prevailed. These results led us to investigate the solid-state photodimerization. The irradiation of crystalline Ia afforded a single topochemical *cis*-head-to-head cyclodimer (IIa) almost quantitatively. On the other hand, the *trans*-head-to-head cyclodimer was formed as the sole product in only a 7% yield on the irradiation of crystalline methyl (*E*)-*p*-methoxycinnamate. The formation of this "nontopochemical product"[9] might be explained in terms of local melting and the disruption of the lattice control.

Quenching and Sensitization Experiments. The quenching effects of oxygen, azulene, ferrocene, and hydroquinone were also examined (Table 4). In the presence of oxygen, the formation of IIIa was suppressed considerably, the yield of IIa being unaffected. When an argon-saturated 0.05 mol dm^{-3} benzene solution of Ia was irradiated in the presence of azulene (10 mol%, E_T=30.9 kcal/mol[10]), an efficient triplet quencher, the yield of IIIa (10%) turned out to be about one-third that (29%) in the non-quenching solution, the yield of IIa being less affected.

To elucidate the nature of the excited state involved in the formation of IIa and IIIa, the ferrocene quenching[11] was studied in detail. Figures 1 and 2 illustrate the Stern-Volmer plots of the Φ^0/Φ values against the ferrocene concentration for two cyclodimers IIIa and IIa, respectively. With low concentrations of ferrocene ([FcH]$<2.5\times10^{-2}$ mol dm^{-3}) the plot in Fig. 1 is approximately linear, but with higher concentrations ([FcH]$>3.5\times10^{-2}$ mol dm^{-3}) the plot showed an extreme curvature. On the contrary, the relationship between Φ^0_{IIa}/Φ_{IIa} and the ferrocene concentration shown in Fig. 2 is quite different from that of $\Phi^0_{IIIa}/\Phi_{IIIa}$. The quenching plot leveled off once (Φ^0_{IIa}/Φ_{IIa}=1.43) at the concentrations of ferrocene between 5.0×10^{-3} and 3.5×10^{-2} mol dm^{-3}, and again showed a linear increment at higher concentrations.

Table 4. Results of quenching experiments[a]

Solvent	Additive (mol/mol)	Filter[b]	Ia/VIa after[c] irradiation	Yield (%)[d]			IIa/IIIa
				IIa	IIIa	IVa, Va	
C_6H_6	None	Q	1.13	14	29	1	0.48
C_6H_6	O_2[e]	Q	1.06	15	22	1>	0.68
C_6H_6	Az(0.1)[f]	Q	0.57	10	10	1>	1.00
CH_3CN	None	P	1.59	40	26	7	1.54
CH_3CN	FcH(0.1)[g]	P	0.50	32	7	2	4.57
CH_3CN	FcH(0.7)	P	0.19	28	1	1>	28.0
CH_3CN	None	Q	1.44	27	26	8	1.04
CH_3CN	HQ(1.0)[h]	Q	0.48	23	8	0	2.88

a) Irradiated under the same conditions as in the case of Table 1. b) Q=quartz and P=Pyrex. c) Determined by GLPC. d) Isolation yield based on Ia employed. e) Saturated with oxygen. f) Azulene. g) Ferrocene. h) Hydroquinone.

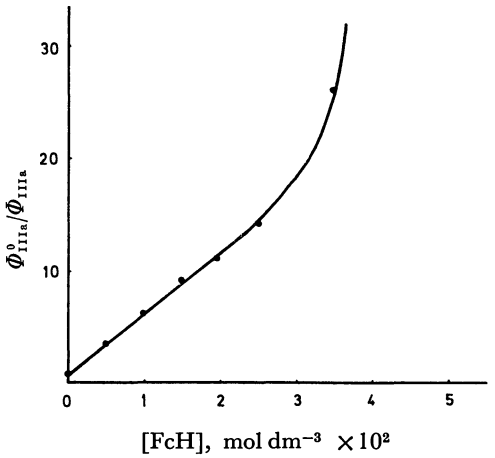

Fig. 1. A Stern-Volmer plot of the IIIa formation as a function of the ferrocene concentration in acetonitrile.

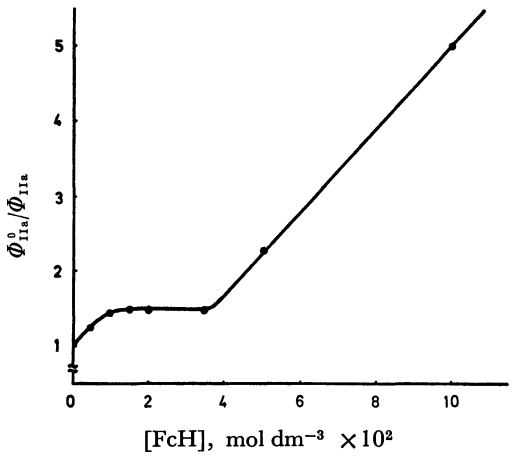

Fig. 2. A Stern-Volmer plot of the IIa formation as a function of the ferrocene concentration in acetonitrile.

The irradiation of Ia in acetonitrile in the presence of an equimolar amount of hydroquinone (an excellent radical scavenger) caused a drastical reduction in the yield of IIIa, along with a slight decline in IIa. It was found that the formation of the head-to-tail cyclodimers (IVa and Va) was suppressed completely by the addition of such a radical scavenger. Further, the rate of the *Z,E* isomerization of Ia was lowered significantly by both the quenchers.

In relation to the possibility of excimer formation in this dimerization, the luminescence of Ia was investigated. No fluorescence from Ia could be observed in benzene at room temperature, probably because of the self-quenching by the methoxycarbonyl or nitro group.[12] The triplet energy of Ia was estimated to be *ca.* 54 kcal/mol based on the phosphorescence measurement of Ia in EPA glass at 77 K. This E_T value suggests that 2,3-butanedione (E_T=56.3 kcal/mol)[13] or 4,4'-bis(dimethylamino)benzophenone (Michler's ketone, E_T=62 kcal/mol)[14] may be an efficient sensitizer. When a benzene solution of Ia (0.05 mol dm^{-3}) and 2,3-butanedione (1.0 mol dm^{-3}) was irradiated (λ>430 nm) for 8 h, the triplet sensitization was observed and the yields of IIa and IIIa were 2 and 17%, respectively. Contrary to our expectations, neither photodimerization nor *Z,E* isomerization of Ia was observed in the Michler's ketone sensitized irradiation (λ>330 nm). This was also the case with the use of dimethylaniline (E_T=76 kcal/mol)[15] in place of Michler's ketone. The quenching by these dimethylamino-containing compounds can be explained by the assumption that the short-lived singlet or triplet exciplex is formed between the nitrophenyl and dimethylaminophenyl moieties and that the excited π-complex consequently undergoes a radiative or radiationless decay to the ground state before the reaction takes place.

Discussion

Increasing solvent polarity favored *cis*-head-to-head cyclodimer formation, while decreasing solvent polarity favored *trans*-head-to-head dimerization. Although neither fluorescence nor triplet excimer[16] phosphorescence from Ia could be observed, it seems probable that this predominant formation of the *cis*-cyclodimer can be interpreted by the hypothesis[17,18] that polar solvents and a concentrated solution generally aid a ground- or excited-state aggregation, leading to a singlet excimer. However, monomer association was not detected in any of the UV spectra at various concentrations (1.0×10^{-5} to 1.0×10^{-1} mol dm^{-3}) in benzene and acetoni-

trile.

Another possible explanation of these observations is the following.[19] Since *cis*-head-to-head dimerization is accompanied by a net increase in the dipole moment, and since *trans* dimerization proceeds with its reduction, solvents of appreciable dipole moments stabilize the transition state[20] (a 1,4-biradical intermediate or weak association between two Ia molecules of the *cis*-head-to-head type orientation), leading to the polar dimer (IIa). This explanation is consistent with the concentration dependence of the *cis* dimerization described before. Concerning the relationship between the concentration and the solvent polarity, Ruhlen and Leermakers have reported that "macroscopic" and "microscopic" polarity decreases as the concentration is reduced.[21] As is shown in Table 2, the effectiveness of *trans* cyclodimerization varied little with the solvents. For *cis* dimerization, however, a change in the solvent from benzene to acetonitrile caused a remarkable two-fold rate acceleration.

The excited-state multiplicities and reaction pathways in this cyclodimerization were studied through sensitization and quenching experiments. The 2,3-butanedione-sensitized irradiation afforded IIIa (IIa/IIIa=0.12) mainly. In the presence of azulene or hydroquinone, the quenching against the IIIa formation is larger than that against the IIa (Table 4). The dissolved oxygen only suppressed the production of IIIa; it had no effect on the yield of IIa.[22] These sensitization and qualitative quenching data suggest that IIIa is formed exclusively from a 1,4-biradical intermediate *via* triplet-excited Ia and IIa mainly from the less-quenchable singlet state with a partial contribution of the triplet-excited state. The linearity of the Stern-Volmer plot for IIIa is a further indication that only one excited state (the triplet state) is involved in the IIIa formation. At the point of $[FcH]=3.5\times10^{-2}$ mol dm^{-3}, the IIIa formation ($\Phi^0_{IIIa}/\Phi_{IIIa}=25.8$) and the *Z*,*E* isomerization of Ia (Ia/VIa=0.188) are quenched almost completely. For IIa, the quenching plot of Φ^0_{IIa}/Φ_{IIa} is once leveled off at the ferrocene concentrations between 5.0×10^{-3} and 3.5×10^{-2} mol dm^{-3}, then it shows a linear increment. The former quenching effect is probably based on the quenching of the triplet state of Ia, and the latter on the singlet quenching (Fig. 2). From the Stern-Volmer plot shown in Fig. 2, the contribution of the triplet state to the IIa formation can be estimated to be 30%; therefore, 70% of the IIa may be formed *via* a singlet state of Ia.

Moreover, the formation of the singlet-derived dimer (IIa) was found to be enormously suppressed in dichloromethane, chloroform, and dibromomethane. This can be ascribed to the heavy-atom solvent, which promotes intersystem crossing, hence providing a higher steady-state concentration of the Ia triplet and resulting in a low efficiency of dimerization from the singlet state (external heavy-atom effect).[23] Considering the heavy-atom effect, which is known to promote the S-$T_{\pi,\pi}$ transition, but not the S-$T_{n,\pi}$ transition,[24] it is likely that the $^3\pi,\pi^*$ state participates in the photodimerization of the aromatic nitro compound Ia to IIa and IIIa. Recent study has shown that the liquid state dimerization of ethyl cinnamate is photosensitized by picramide and *p*-nitroaniline,[25] each of which has a nitro group on its benzene ring. In addition to this fact, our observation described above on the extremely facile photodimerization of Ia should be noted in comparison with methyl (*E*)-cinnamates, which have no nitro group. One possible explanation for these phenomena is that the nitro group in Ia acts as a built-in photosensitizer.

The rapid *Z*,*E* isomerization of Ia competes with its photodimerization, and the photo-stationary value (Ia/VIa) is 1.35 in benzene. Accordingly, there is a very fair possibility that IIa and IIIa might be produced by the turn-over[26] of the VIa-derived intermediate biradicals with the alleviation of the steric intricacy.

In conclusion, we propose the following multipathway mechanism, which is consistent with all of the experimental observations:[27,28] where S=Ia, ^{1}(S···S)=singlet excimer, D=dimers (IIa and IIIa), HA=halo-solvent, Sens=2,3-butanedione, and Q=quencher.

$$S + h\nu \rightarrow {}^1S$$
$${}^1S + S \rightarrow {}^1(S\cdots S)$$
$${}^1(S\cdots S) \rightarrow D\ (IIa)$$
$${}^1S + S \rightarrow D\ (IIa)$$
$${}^1S \rightarrow {}^3S$$
$$S + {}^3Sens \rightarrow {}^3S + Sens$$
$${}^1S + HA \rightarrow {}^3S + HA$$
$${}^3S + S \rightarrow D\ (IIa\ and\ IIIa)$$
$${}^3S + Q \rightarrow S + {}^3Q$$
$${}^3S \rightarrow VIa$$
$$VIa + h\nu \rightarrow {}^1VIa$$
$${}^1VIa \rightarrow S$$

It appears most likely that the IIIa formation proceeds through a biradical intermediate derived from the triplet state (π,π^*) of Ia. In contrast, two different mechanisms are probably concerned with the IIa formation. The major possible pathway is the contribution of a concerted [$_\pi2_s+{}_\pi2_s$] transition state or the geminate reaction of the 1,4-biradical intermediate stabilized in the solvent cage,[29] which is known not to be quenched by a radical scavenger, *via* the singlet excimer of Ia; the minor pathway being the ring closure of the intermediary 1,4-biradical by way of the triplet state (π,π^*) of Ia.

Experimental

General. (*E*)-*p*-Nitrocinnamic acid was prepared from *p*-nitrobenzaldehyde[30] and malonic acid by the method of Wiley and Smith.[31] The following (*E*)-cinnamic acid derivatives were prepared according to the known procedures: *p*-methoxy-,[32] *p*-methyl-,[33] *p*-isopropyl-,[33] *p*-chloro-,[32] and *p*-dimethylamino-(*E*)-cinnamic acid.[34] The esterification of each acid was performed in the presence of sulfuric acid.[35] Acetonitrile was purified in the usual manner.[36] Benzene was purified by two successive distillations. The other reagents were obtained commercially, the liquids were distilled, and the solids were recrystallized, before use. The NMR spectra were taken with a Hitachi R-20 spectrometer in a $CDCl_3$ solution with tetramethylsilane as the internal standard. The mass spectra were made on a Hitachi RMU-

6M mass spectrometer at 70 eV using a heating inlet system. Analytical GLPC chromatography was performed on a Hitachi Model 063 instrument with a flame-ionizaion detector and nitrogen as the carrier gas. The column (3-mm × 1-m) used was 10% silicone SE-30 on Chromosorb W. Analytical and preparative thin layer chromatography (TLC) was carried out on silica gel plates (Merck silica gel 60 F_{254} pre-coated plates).

Irradiation Procedure. All irradiations of solutions were conducted in a 20-ml syrindrical quartz vessel with a neck to accommodate a three-way stopcock. Stirring was effected magnetically. For irradiation with or without a Pyrex filter, a reaction vessel was placed 5 cm away from a light source (Ushio 450 watt UM-452 high-pressure mercury lamp) placed in a water bucket for cooling. In the case of the 313 nm light, the sample solution was irradiated through a Pyrex filter sleeve and a 1-cm path of a 2.0×10^{-3} mol dm^{-3} potassium chromate solution filter.[37] A Toshiba filter V-Y45 was used for the 2,3-butanedione sensitization. The solids were irradiated on Pyrex glass plates at a distance of *ca.* 15 cm at 20 °C.

Irradiation of Ia in Solution. The general execution of the present photodimerization is typically illustrated by the procedure for the conversion of Ia to IIa and IIIa. A benzene solution (20 cm^3) of Ia (207 mg, 1.0 mmol) was saturated with argon after evacuation and then irradiated for 3 h. A quantitative determination by GLPC indicated the recovery of Ia and the yield of VIa to be 23 and 24%, respectively. The reaction mixture was concentrated *in vacuo*, and the residue was subjected to preparative tlc with hexane–ethyl acetate (5:1 v/v) as the eluent to give pure IIa (14%) and IIIa (27%). The identification of IIa and IIIa was made on the basis of the following NMR and mass spectral data by the method given in the literature.[3]

Compound IIa: NMR (60 MHz, $CDCl_3$) δ 3.80 (s, 6H, CH_3), 3.80—4.75 (AA'BB', 4H, cyclobutane ring), 7.24 ($d_{J=9.0\,Hz}$, 2H, aromatic ring), and 8.03 ($d_{J=9.0\,Hz}$, 2H, aromatic ring); mass *m/e* (rel. intensity) 414 (6.8, M^+, $C_{20}H_{18}O_8N_2$), 270 (5.3, $C_{14}H_{10}O_4N_2$), and 207 (100, M/2, $C_{10}H_9O_4N$).

Found: C, 57.88; H, 4.46; N, 6.53%. Calcd for $C_{20}H_{18}O_8N_2$: C, 57.97; H, 4.38; N, 6.76%.

Compound IIIa: NMR (60 MHz, $CDCl_3$) δ 3.82 (s, 6H, CH_3), 3.40—4.10 (AA'BB', 4H, cyclobutane ring), 7.60 ($d_{J=9.0\,Hz}$, 2H, aromatic ring), and 8.20 ($d_{J=9.0\,Hz}$, 2H, aromatic ring); mass *m/e* (rel. intensity) 414 (4.2, M^+, $C_{20}H_{18}O_8N_2$), 270 (12.7, $C_{14}H_{10}O_4N_2$), and 207 (100, M/2, $C_{10}H_9O_4N$).

Found: C, 58.15; H, 4.35; N, 6.88%. Calcd for $C_{20}H_{18}O_8N_2$: C, 57.97; H, 4.38; N, 6.76%.

Despite all our efforts to separate the mixture of IVa and Va, we could not isolate the two isomers in a pure form. Therefore, the structures of IVa and Va were determined by means of the NMR and mass spectra of the mixture. The quantitative analysis of Ia and VIa was performed by the cut-and-weigh integration of GLPC traces using a known amount of benzophenone as the external standard for the correction of the detector response differences.

Actinometry. A conventional method of actinometry was employed; it eliminated errors due to light fluctuations and may inherently give good quantum yield ratios for the Stern-Volmer plot. The actinometer solution, which contained 0.05 mol dm^{-3} Ia in acetonitrile, was photolyzed simultaneously with sample solutions containing 0.05 mol dm^{-3} Ia and varying concentrations of ferrocene. No quantum-yield value was assumed for the actinometer solution. Instead, the ratio (Y^0/Y) of the yields of the dimer in the actinometer and in the sample solutions was used directly. The light absorbed and the time of photolysis were the same for both solutions, so the Y^0/Y value should be equal to the ratio of the quantum yields (Φ^0/Φ).

The support of this work by the Matsunaga Science Foundation is gratefully acknowledged.

References

1) M. D. Cohen, G. M. J. Schmidt, and F. I. Sonntag, *J. Chem. Soc.*, **1964**, 2000; J. Bregman, K. Osaki, G. M. J. Schmidt, and F. I. Sonntag, *ibid.*, **1964**, 2021.

2) M. Freedman, Y. Mohadger, J. Rennert, S. Soloway, and I. Waltcher, *Org. Prep. Proc. Int.*, **1**, 267 (1969).

3) D. A. Ben-Efraim and B. S. Green, *Tetrahedron*, **30**, 2357 (1974); B. S. Green and L. Heller, *J. Org. Chem.*, **39**, 196 (1974).

4) S. L. Murov, "Handbook of Photochemistry," Dekker, New York, N. Y. (1973), p. 85.

5) J. A. Riddick and W. B. Bunger, "Techniques of Chemistry," Vol. II, ed. by A. Weissberger, Wiley, New York, N. Y. (1970), p. 61.

6) Irradiation in dimethylformamide resulted in the complete polymerization of Ia.

7) For the temperature dependence of olefin photodimerization, see R. Livingston and K. S. Wei, *J. Phys. Chem.*, **71**, 541 (1967).

8) M. A. El-Sayed, *Acc. Chem. Res.*, **1**, 8 (1968); S. K. Lower and M. A. El-Sayed, *Chem. Rev.*, **66**, 199 (1966).

9) M. D. Cohen, *Angew. Chem., Int. Ed. Engl.*, **14**, 386 (1975).

10) P. M. Rentzepis, *Chem. Phys. Lett.*, **3**, 715 (1969).

11) More than 98% of the incident light is absorbed by Ia throughout the wavelength range irradiated.

12) No fluorescence could be detected in the case of the other *p*-substituted (*E*)-cinnamates, either.

13) R. R. Callis and R. W. Wilson, *Chem. Phys. Lett.*, **13**, 416 (1972).

14) G. N. Lewis and M. Kasha, *J. Am. Chem. Soc.*, **66**, 2100 (1944). Another E_T value of 65.7 kcal/mol has been reported; G. Porter and P. Suppan, *Trans. Faraday Soc.*, **61**, 1664 (1965).

15) D. S. McClare, *J. Chem. Phys.*, **17**, 903 (1949).

16) M. Aikawa, T. Takemura, and H. Baba, *Bull. Chem. Soc. Jpn.*, **49**, 437 (1976).

17) C. H. Krauch, S. Farid, and G. O. Schenck, *Chem. Ber.*, **99**, 625 (1966).

18) H. Morrison, H. Curtis, and T. McDowell, *J. Am. Chem. Soc.*, **88**, 5415 (1966).

19) A similar conclusion was reported by O. L. Chapman, H. G. Smith, and F. W. King, *J. Am. Chem. Soc.*, **85**, 806 (1963), and the references cited therein; T. Mukai and T. Shishido, *J. Org. Chem.*, **32**, 2744 (1967).

20) E. Y. Lam, D. Valentine, and G. S. Hammond, *J. Am. Chem. Soc.*, **89**, 3482 (1967).

21) J. L. Ruhlen and P. A. Leermakers, *J. Am. Chem. Soc.*, **89**, 4944 (1967).

22) Oxygen is known to act as either a triplet quencher or a radical scavenger.

23) For example, the influence of a heavy-atom solvent on photodimerization has been reported for acenaphthylene; see, I. M. Hartmann, W. Hartmann, and G. O. Schenck, *Chem. Ber.*, **100**, 3146 (1967).

24) D. R. Kearns and W. A. Case, *J. Am. Chem. Soc.*, **88**, 5087 (1966); P. J. Wagner, *J. Chem. Phys.*, **45**, 2335 (1966).

25) H. G. Curme, C. C. Natale, and D. J. Kelley, *J.*

Phys. Chem., **71**, 767 (1967).
26) The phenomenon of "turn over" is known (Ref. 1) even in the solid state: the crystalline (*Z*)-cinnamic acid photodimerizes only after photochemical isomerization to (*E*)-cinnamic acid *via* a metastable complex between an excited monomer and its nearest neighbor.
27) The deactivation processes from excited states are omitted in this scheme.
28) The isomerization of Ia to VIa proceeds *via* a triplet state and that of VIa to Ia *via* a singlet state; T. Ishigami, T. Murata, M. Uehara, and T. Endo, unpublished result.
29) T. Koenig and H. Fischer, "Free Radicals," Vol. 1, ed by J. K. Kochi, Wiley, New York, N. Y. (1973), p. 157.
30) S. V. Lieberman and R. Connor, *Org. Synth.*, Coll. Vol. 2, 441 (1943).
31) R. H. Wiley and N. R. Smith, *J. Am. Chem. Soc.*, **72**, 5198 (1950).
32) C. Walling and K. B. Wolfstirn, *J. Am. Chem. Soc.*, **69**, 852 (1947).
33) K. H. Slotta and H. Heller, *Ber.*, **63**, 3029 (1930).
34) C. W. Shoppee, *J. Chem. Soc.*, **1930**, 968.
35) A. Weissberger and C. J. Kibler, *Org. Synth.*, Coll. Vol. III, 610 (1955).
36) S. Wawzonek and M. E. Runner, *J. Electrochem. Soc.*, **99**, 457 (1952).
37) J. G. Calvert and J. N. Pitts, Jr., "Photochemistry," Wiley, New York, N. Y. (1966), p. 728.

pH Effects on the Radical Addition of Hydrogensulfite Ion to Olefins

Akihisa SAKUMOTO, Teijiro MIYATA, and Masamitsu WASHINO

Japan Atomic Energy Research Institute, Takasaki, Gunma 370-12

(Received May 20, 1976)

The competitive addition of sodium hydrogensulfite to allyl and 2-methylallyl alcohols was investigated at the pH range from 3 to 5. The relative reactivity of allyl alcohol to 2-methylallyl alcohol decreased with increasing pH. Sulfite radical ion was mainly participating in the addition at pH 5, and hydrogensulfite radical at pH 3. From the kinetic analysis of the pH dependence, the ratio of reactivities of allyl alcohol and 2-methylallyl alcohol toward sulfite radical ion was 0.213, and the same ratio toward hydrogensulfite radical was 0.305. Further, the ratio of reactivities of hydrogensulfite radical and sulfite radical ion toward allyl alcohol was 1.32, and the same ratio toward 2-methylallyl alcohol was 0.927. The dissociation constant of hydrogensulfite radical was the order of 3×10^{-5} ($pK_a=4.5$).

It is well known that the addition reaction of hydrogensulfite ion on α,β-unsaturated bonds conjugated with a functional group such as carbonyl, cyano or nitro group proceeds with an ionic mechanism and produces 1-alkanesulfonates in accord with a simple Michael addition product.[1,2] In the ionic addition, the kinetics and the pH dependence have been extensively investigated.[3,4]

On the other hand, the addition reaction of hydrogensulfite ion to non-conjugated α,β-unsaturated bonds is known to proceed with a radical mechanism and to give products of the anti-Markownikoff character as a main product.[5] Since 1-alkanesulfonates have good surfactant properties and excellent biodegradability,[6] the synthetic reaction initiated by dissolved oxygen,[7] by added free radical agents[8] or by ultraviolet light[9] has been extensively studied, though the kinetics and the adding species are still insufficiently investgated.

In general, sulfite radical ion has been postulated to be the adding species as a chain carrier,[5] but the eleectrically neutral hydrogensulfite radical[10] must be taken into account as the acidity of the solution is increased.

In previous papers, we investigated the kinetics and the hydrogen isotope effect on the radiation-induced addition of sodium hydrogensulfite to allyl alcohol[11,12] and 1-dodecene,[13] in which the sulfite radical ion was postulated as an adding species, but the exact nature of the adding species was not established.

In the present work, allyl and 2-methylallyl alcohols were employed as water soluble olefins for the competitive addition of sodium hydrogensulfite by the photolysis, and the effects of pH and sodium chloride were investigated. From comparison of the ratio of the reactivities of these olefins, some information on the adding species was obtained.

Experimental

Materials. Hydroquinone, sodium hydrogensulfite, and sodium chloride were of GR grade, and no further purification was made. Allyl and 2-methylallyl alcohols of GR grade were refluxed with 2,4-dinitrophenylhydrazine for a few hours and then distilled twice under atmospheric pressure. The purification of water used was performed by distillation.[11]

Preparations of Solutions. Allyl and 2-methylallyl alcohols, and sodium hydrogensulfite were dissolved in the Sörensen solution. Concentrations of allyl and 2-methylallyl alcohols, and sodium hydrogensulfite were 0.439, 0.355, and 0.384—0.480 mol/l, respectively. The ionic strength of the solutions was 1.22 except the case of the solutions including sodium chloride.

pH Range. Figure 1 shows the distribution of ion species of sulfite-hydrogensulfite reagent, which was calculated from the dissociation constant of sulfurous acid.[14] In this work, the pH of the solutions was varied from 3 to 5. The pH value was measured with a TOA HM-18B Digital pH meter.

Irradiation. The reaction vessel was a cylindrical quartz flask fitted with a gas delivery tube which nearly reached to the bottom of the vessel, through which a fairly slow stream of oxygen was supplied during the irradiation. A 30 watt low pressure mercury lamp employed (Rikō-Kagaku UVL-30 LQ) was centered in the reaction vessel. The solution was irradiated at 25 °C for 20 min.

Identification. Allyl and 2-methylallyl alcohols remained in the solution were determined by using a gas chromatograph (Yanagimoto Model G-80) equipped with a flame ionization detector, a thermal conductivity detector, and a 2 m glass column packed with 60—80 mesh Celite 545 coated with 30% Silicone DC 550. 2-Chloroethanol was used as an internal standard.

Conversions of Olefins. The sample solution was irradiated such that from 10 to 40% of 2-methylallyl alcohol was consumed at pH 3.50. In this case, the ratio of conversions of allyl and 2-methylallyl alcohols was independent of the per cent of these olefins consumed. Thus, in this work, about 9% of allyl alcohol and 34% of 2-methylallyl alcohol were consumed.

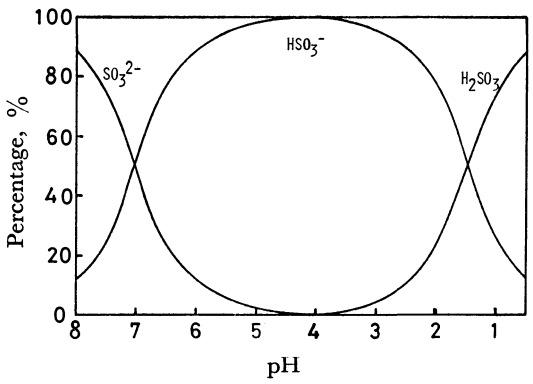

Fig. 1. The ion species distribution of sulfite-hydrogensulfite reagent at 18 °C, which was calculated from the dissociation constant of sulfurous acid.

Results

Competitive additions were performed with runs in duplicate at least. The extent of reaction, that is, the per cent of olefins consumed during a given time of irradiation was not a quite reproducible quantity. It is presumably ascribable to that the chain process by which hydrogensulfite ion adds to olefins is quite susceptible to irradiation time and to trace impurities which can serve as initiators or retardants. However, the ratio of conversions of allyl and 2-methylallyl alcohols was a reproducible quantity at any pH.

The relative reactivity of allyl alcohol (I) to 2-methylallyl alcohol(II) was calculated from the following expression:

$$\text{Relative reactivity} = \frac{(\text{moles of I consumed})/(\text{moles of I initially})}{(\text{moles of II consumed})/(\text{moles of II initially})}$$

The quantity of the relative reactivity was independent of the change from 1.2 to 2.3 in the ratio of the initial concentrations of allyl and 2-methylallyl alcohols.

A plot of the relative reactivity to pH is shown in Fig. 2. As pH was increased, the relative reactivity which remained constant up to about pH 3 decreased gradually and then reached a limiting value above pH 5. The sum of conversions of allyl and 2-methylallyl alcohols at pH 3.07 was 0.162 mol/l and that at pH 4.92 was 0.160 mol/l (Table 1).

Plots of the relative reactivity against the concentration of sodium chloride are shown in Fig. 3. No change of the relative reactivity was observed at pH 2.90. However, the relative reactivity decreased from 0.269 to 0.193 with increasing sodium chloride at pH 4.54. In this case, conversion of 2-methylallyl alcohol increased with increasing sodium chloride; on the other hand, conversion of allyl alcohol remained constant.

Table 1 shows the effect of hydroquinone on conversions of allyl and 2-methylallyl alcohols at pH's 2.90 and 4.54. The solution was added with 2.70×10^{-2} mol/l of hydroquinone and irradiated for 120 min. No consumptions of allyl and 2-methylallyl alcohols were observed in the presence of hydroquinone regardless of the change of pH. Table 1 also shows that the variation of pH in the solution is slight during the irradiation.

Discussion

There is the possibility of the reactions between allyl alcohol and the species $HOCH_2\dot{C}(CH_3)CH_2SO_3^-$ or between 2-methylallyl alcohol and the species $HOCH_2\dot{C}HCH_2SO_3^-$ in the competitive addition because the termination step in the radiation-induced addition of hydrogensulfite ion to allyl alcohol was the reaction between allyl alcohol and the radical $HOCH_2\dot{C}HCH_2SO_3^-$ which was produced by the addition of sulfite radical ion to allyl alcohol.[11]

The kinetic chain length defined as the number of propagation steps per radical of initiator starting chains was 344 in the radiation-induced addition.[11] Since the rate of the termination step is governed by the lability of the hydrogen atom abstracted in olefin, it is assumed that the chain length in the competitive addition is in the same order of magnitude as compared with that in the radiation-induced addition. In other words, the conversions of allyl and 2-methylallyl alcohols by the termination step may be neglected in comparison with the total conversions of these olefins.

In the competitive addition of hydrogensulfite ion to allyl and 2-methylallyl alcohols in the presence of oxygen, it is deduced from the previous paper[11] to produce 3-hydroxypropane-1-sulfonate and 3-hydroxy-2-methylpropane-1-sulfonate with the corresponding 2-hydroxy-1-alkanesulfonates. The formation of these 2-hydroxy-1-alkanesulfonates, however, does not affect conversions of allyl and 2-mehtylallyl alcohols by the reaction of the adding species with these olefins. Therefore, conversions of allyl and 2-methylallyl alcohols in the competitive addition may be regarded as a measure of the reactivities of the corresponding olefins.

Adding Species. The optimum pH for the reaction process was reported to be near 7 by Adams *et al.*[15] or 5—7 by Norton *et al.*[4] This was partly due to a good proportion of hydrogensufite and sulfite ions involved in the propagation during the initial state of the reaction and partly due to decrease in the acidity of the solution causes the undesired side reaction such as the two-electron oxidation of hydrogensulfite ion to hydrogensulfate ion.[4] In this work, the pH range of 3 to 5 was used where nearly 100% of sodium hydrogensulfite dissociated to hydrogensulfite ion.

It is assumed that the species such as SO_2^-, SO_4^- or SO_5^-, produced by the flash photolysis or the pulse radiolysis of sulfite–hydrogensulfite–disulfite ion system,[16] may add to various olefins. Such species, however, should be excluded from the adding species as chain carriers because it is difficult to imagine they can sustain the chain reaction.

Sulfite radical ion, which is proposed as an adding species in the radical addition of hydrogensulfite ion to olefins,[17] possibly exists in equilibrium with hydrogensulfite radical as follows:

$$HSO_3\cdot \rightleftharpoons \cdot SO_3^- + H^+$$

Hydrogensulfite radical, an acidic form of sulfite radical ion, may add to allyl and 2-methylallyl alcohols. Furthermore, this radical in addition to sulfite radical ion had been postulated as one of chain carriers in the autoxidation of sulfite and hydrogensulfite ions, which is one of the most well konwn chain reaction in solution.[18] Therefore, the hydrogensulfite radical is deduced to be one of the adding species in the addition reaction of hydrogensulfite ion.

Addition of hydroquinone suppressed the addition reaction of hydrogensulfite ion as shown in Table 1. Since hydroquinone is an efficient radical scavenger, this observation suggests that the addition reaction proceeds with a radical mechanism over the whole pH range studied.

The effect of hydrogen ion on the relative reactivity was studied. It is well known that when reactions

Table 1. Effect of hydroquinone on conversions of allyl and 2-methylallyl alcohols, and the pH change during the irradiation

Initial concentrations of allyl and 2-methylallyl alcohols are 0.439 and 0.355 mol/l, respectively.

Run	[NaCl][c]	pH		Concentration[d]	
		Initial	Final	Allyl alcohol	2-Methyl-allyl alcohol
1[a]	0.835	4.41		0.434	0.350
2[a]	0.835	2.90		0.436	0.351
3[a]	0	2.95		0.435	0.351
4[b]	0	3.07	3.02	0.395	0.237
5[b]	0	4.92	4.84	0.403	0.231

a) [Hydroquinone] = 2.70×10^{-2} mol/l; irradiation time, 120 min. b) Irradiation time, 20 min. c) mol/l. d) mol/l, after irradiation.

between dipolar molecules or between ions and dipolar molecules occur in solution, there are dipole-dipole interactions between such molecules which promote chemical changes. These interactions are modified by the solvent through its dielectric constant and polar properties.[19] However, the effects of the solvent on such reactions are very small in comparison with the effects on the reactions between ions,[19] as shown in the solvent effects on diazo-coupling reactions.[20,21] Since both allyl and 2-methylallyl alcohols are neutral molecules, the effect of the solvent through the pH change appears to be small. In addition, the extent of the solvent effect tends to cancel in the ratio of the rate constants. Then, if sulfite adical ion is the adding species over the whole pH range studied, the relative reactivity in the competitive addition should be fairly constant, despite change in pH.

The relative reactivity decreased with pH as shown in Fig. 2. Taking account of the equilibrium of sulfite radical ion, it is deduced that hydrogensulfite radical mainly participates in the addition reaction at pH 3 and sulfite radical ion at pH 5. The electronegativity of hydrogensulfite radical is assumed to be different from that of sulfite radical ion. Therefore, decrease of the relative reactivity may be explained by the difference in reactivities of hydrogensulfite radical and sulfite radical ion toward allyl alcohol, and toward 2-methylallyl alcohol.

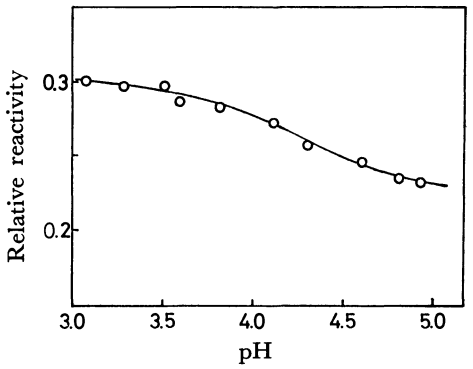

Fig. 2. Variation of the relative reactivity of allyl alcohol to 2-methylallyl alcohol as a function of pH.

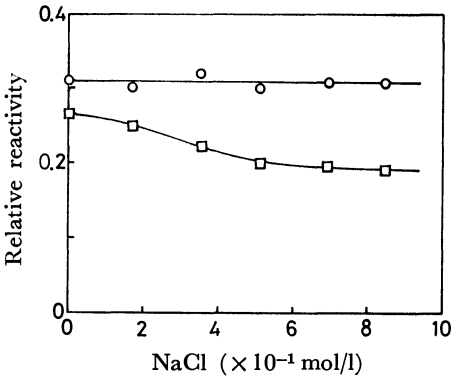

Fig. 3. Effect of sodium chloride on the relative reactivity.
—○— : pH 2.90, —□— : pH 4.54.

In reactions involving neutral molecules or ions and neutral molecules, the influence of the ionic strength on the rate constants is small.[22] The influence of the ionic strength on the relative reactivity in the competitive addition was observed. Namely, the relative reactivity at pH 4.54 decreased with increasing sodium chloride as shown in Fig. 3. In this case, conversion of allyl alcohol remained constant regardless of sodium chloride, while conversion of 2-methylallyl alcohol increased. This observation can also be explained by postulating hydrogensulfite radical and sulfite radical ion as adding species. Hydrogensulfite radical was deduced to be the main adding species at pH 2.90 and sulfite radical ion at pH 4.54. Hence, it is evident that there is the influence of the ionic strength in the reaction between sulfite radical ion and 2-mehtylallyl alcohol.

The methyl group on β-position of 2-methylallyl alcohol is deficient in the electron density because of a electron-donating group. On this basis it is considered that there is the interaction between the negative charge on sulfite radical ion and the methyl group in 2-methylallyl alcohol. Therefore, the influence of the ionic strength is attributable to the difference in the interactions of sulfite radical ion and hydrogensulfite radical toward the methyl group in 2-methylallyl alcohol as follows:

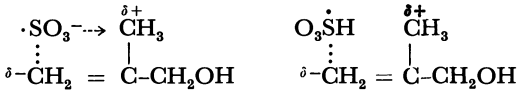

At present, however, no explanation is available to explain the influence of the ionic strength on increase in conversion of 2-methylallyl alcohol.

Dissociation Constant of Hydrogensulfite Radical. The dissociation constant of hydrogensulfite radical, K, was evaluated from the relative reactivity.

Rate constants of reactions between two olefins, allyl and 2-methylallyl alcohols, and the adding species, hydrogensulfite radical and sulfite radical ion, were defined as follows:

$$CH_2{=}CHCH_2OH + \cdot SO_3^- \xrightarrow{k_1} \text{product} \qquad (1)$$

$$CH_2{=}\underset{\underset{CH_3}{|}}{C}CH_2OH + \cdot SO_3^- \xrightarrow{k_2} \text{product} \quad (2)$$

$$CH_2{=}CHCH_2OH + HSO_3\cdot \xrightarrow{k_3} \text{product} \quad (3)$$

$$CH_2{=}\underset{\underset{CH_3}{|}}{C}CH_2OH + HSO_3\cdot \xrightarrow{k_4} \text{product} \quad (4)$$

The ratio of conversion of allyl alcohol, x, to that of 2-methylallyl alcohol, y, at the initial stage of the reaction is expressed by the following equation:

$$\frac{x}{y} = \frac{x_0(k_1[\cdot SO_3^-] + k_3[HSO_3\cdot])}{y_0(k_2[\cdot SO_3^-] + k_4[HSO_3\cdot])} \quad (5)$$

where $[HSO_3\cdot]$ and $[\cdot SO_3^-]$ are concentrations of hydrogensulfite radical and sulfite radical ion, and x_0 and y_0 are initial concentrations of allyl and 2-methylallyl alcohols, respectively.

The K is expressed by the following equation:

$$K = \frac{[\cdot SO_3^-][H^+]}{[HSO_3\cdot]} \times \frac{f(\cdot SO_3^-)f(H^+)}{f(HSO_3\cdot)} \quad (6)$$

where $[H^+]$ is the concentration of hydrogen ion, and $f(HSO_3\cdot)$, $f(\cdot SO_3^-)$, and $f(H^+)$ are activity coefficients of hydrogensulfite radical, sulfite radical ion, and hydrogen ion, respectively.

Substituting Eq. 6 to Eq. 5, the equation required to calculate the K was obtained as follows:

$$\frac{f(\cdot SO_3^-)}{f(HSO_3\cdot)} \times \frac{k_4}{k_2} \times \frac{1}{K} \times [H^+]\times f(H^+) = \frac{\alpha - a}{b - \alpha} \quad (7)$$

where α, a, and b are $(x/y)(y_0/x_0)$, k_1/k_2, and k_3/k_4, respectively.

According to this equation, the term $(\alpha-a)/(b-\alpha)$ should be proportional to the activity of hydrogen ion $[H^+]\times f(H^+)$, because the term $f(\cdot SO_3^-)/f(HSO_3\cdot)\times k_4/k_2\times 1/K$ is constant with a fixed ionic strength. Therefore, the a and b to give this linear relation could be obtained by trial and error. The fitted values of a and b were 0.213 and 0.305, respectively. The solide line in Fig. 4 was drawn by substituting these values into Eq. 7, and the slope was 2.26×10^4.

The term $f(\cdot SO_3^-)/f(HSO_3\cdot)\times k_4/k_2\times 1/K$ in Eq. 7 is equivalent to the slope of the straight line in Fig. 4. Hence, the K can be evaluated by using $f(SO_3^-)$, $f(HSO_3\cdot)$, and k_4/k_2.

The $f(HSO_3\cdot)$ is assumed to be unity because hydrogensulfite radical is a non-charged species.[23] The value of $f(HSO_3^-)$ may be employed to $f(\cdot SO_3^-)$ because the effective diameter of hydrated sulfite radical ion is deduced to be close to that of hydrated hydrogensulfite ion.[24] Now, using the relation between the activity coefficient of ion and the ionic strength in water,[24] the $f(HSO_3^-)$, and hence $f(\cdot SO_3^-)$, was estimated to be 0.70 at the ionic strength 1.2.

The k_4/k_2 was estimated as follows. As shown in Fig. 1, the concentration of hydrogensulfite ion at pH 3.07 is almost equal to that at pH 4.92. Moreover, the pH of the solution hardly changed during the irradiation. Therefore, the sum of rates of hydrogensulfite radical and sulfite radical ion formed by the photolysis at pH 3.07 appears to be equal to that at pH 4.92. In addition, the sum of conversions of allyl and 2-methylallyl alcohols at pH 3.07 was almost equal to that at pH 4.92. In these cases, the irradiation time was fixed for 20 min. On the basis of these results, it is permissible to neglect the difference in the sum of rates of hydrogensulfite radical toward two olefins, allyl and 2-methylallyl alcohols, and sulfite radical ion toward same olefins. Therefore, it may be regarded that allyl and 2-methylallyl alcohols are converted by sulfite radical ion at pH 4.92 and by hydrogensulfite radical at pH 3.07.

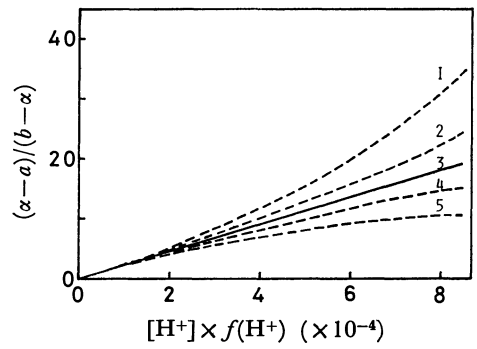

Fig. 4. Variation of $(\alpha-a)/(b-\alpha)$ as a function of the activity of hydrogen ion $[H^+]\times f(H^+)$.
(1) For $a=0.213$ and $b=0.303$, (2) for $a=0.214$ and $b=0.303$, (3) for $a=0.213$ and $b=0.305$, (4) for $a=0.217$ and $b=0.306$, (5) for $a=0.220$ and $b=0.308$.

Now, the ratio of the total amount of allyl and 2-methylallyl alcohols consumed at pH 4.92, S_1, and that at pH 3.07, S_2, at the initial stage of the reaction may be expressed by the following equation.

$$\frac{S_1}{S_2} = \frac{k_2}{k_4} \times \frac{(ax_0+y_0)}{(bx_0+y_0)} \times \frac{[\cdot SO_3^-]}{[HSO_3\cdot]} \quad (8)$$

Taking into account that the rate of the formation of sulfite radical ion at pH 4.92 is deduced to be equal to that of hydrogensulfite radical at pH 3.07 and that the sum of conversions of allyl and 2-methylallyl alcohols at pH 4.92 was almost equal to that at pH 3.07, it may be permitted to postulate $[\cdot SO_3^-]/[HSO_3\cdot]=1$. Now, substituting known values of $a=0.213$, $b=0.305$, $S_1=0.160$, $S_2=0.162$, $x_0=0.439$, and $y_0=0.355$ into Eq. 8, the k_4/k_2 was estimated to be 0.927.

Using the values of k_4/k_2, $f(HSO_3\cdot)$, and $f(\cdot SO_3^-)$, the dissociation constant K was evaluated to be the order of 3×10^{-5} ($pK_a=4.5$). This value is similar to that of $HO_2\cdot$ ($pK_a=4.8$)[25] or simple organic free radical such as $\dot{C}H(OH)CONH_2$ ($pK_a=5.5$)[26] or $CH_3\dot{C}(OH)COOH$ ($pK_a=5.3$).[27]

Apparent Dissociation Constant Obtained Graphically. Since conversion of 2-methylallyl alcohol is more remarkable than that of allyl alcohol, and there is little difference in reactivities of hydrogensulfite redical and sulfite radical ion toward 2-methylally alcohol ($k_4/k_2=0.927$), the relative reactivity-pH curve in Fig. 2 appears to be similar to the dissociation curve of hydrogensulfite radical.

The pH value for the inflection point in Fig. 2 was obtained graphically to be 4.3. Thus, from this pH value, an apparent dissociation constant of hydrogensulfite radical was calculated to be the order of

5×10^{-5} which is compared to the corrected value of 3×10^{-5}.

Reactivities of Olefins and Adding Species. Replacement of one hydrogen atom on β-position of allyl alcohol by a methyl group should donate a negative charge on the terminal methylene carbon. Hence, the electron density on the terminal carbon in 2-methylallyl alcohol is deduced to be higher than that in allyl alcohol.

As already described, k_1/k_2, the ratio of rates in the reactions of allyl and 2-methylallyl alcohols toward sulfite radical ion, was 0.213 and k_3/k_4, the same ratio toward hydrogensulfite radical, was 0.305. These results mean that the reactivity of 2-methylallyl alcohol is larger than that of allyl alcohol regardless of the adding species. This difference in the reactivities is attributed to the difference in the electron densities on the terminal methylene carbon in allyl and 2-methylallyl alcohols.

The k_4/k_2 and k_3/k_1 were used for comparison with the reactivities of hydrogensulfite radical and sulfite radical ion. Since k_4/k_2 was 0.927 as mentioned above, k_3/k_1 was estimated to be 1.32. The former is the ratio of rates in the reactions of hydrogensulfite radical and sulfite radical ion toward 2-methylallyl alcohol, and the latter is the same ratio toward allyl alcohol. Apparently, the reactivity of hydrogensulfite radical toward allyl alcohol is large as compared with that of sulfite radical ion toward same olefin, while the reactivity of hydrogensulfite radical toward 2-methylallyl alcohol is smaller than that of sulfite radical ion toward same olefin. This difference in the trend of reactivities of hydrogensulfite radical and sulfite radical ion is considered, as already described, to be due to the difference in the interactions of hydrogensulfite radical and sulfite radical ion toward the methyl group in 2-methylallyl alcohol.

The addition reaction in this work proceeded with a radical mechanism. Moreover, this addtion was governed by the electronic effect of the methyl group in 2-methylallyl alcohol. This is considered to be due to some degree of electrophilic character of hydrogensulfite radical or sulfite radical ion. No individual rate constant k was determined in this work. Further investigations with different approaches will be necessary.

References

1) R. T. E. Schenck and I. Danishefsky, *J. Org. Chem.*, **16**, 1683 (1951).
2) H. D. Finch, *J. Org. Chem.*, **27**, 649 (1962).
3) M. Morton and H. Landfield, *J. Am. Chem. Soc.*, **74**, 3523 (1952).
4) C. J. Norton, N. F. Seppi, and M. J. Reuter, *J. Org. Chem.*, **33**, 4158 (1968).
5) M. S. Kharasch, E. M. May, and F. R. Mayo, *J. Org. Chem.*, **3**, 175 (1938).
6) J. Rubinfeld and H. D. Cross, *Soap. Chem. Spec.*, **43**, 41 (1967).
7) For instance, H. Helberger, *Angew. Chem.*, **73**, 69 (1961).
8) For instance, R. J. Koshar, P. W. Trott, and J. D. LaZerte, *J. Am. Chem. Soc.*, **75**, 4595 (1953).
9) C. L. Furrow and C. E. Stoops, *Ind. Eng. Chem. Prod. Res. Develop.*, **7**, 26 (1968).
10) W. A. Waters, "The Chemistry of Free Radicals," Oxford University Press, Amen House, London (1948) p. 187.
11) T. Miyata, A. Sakumoto, M. Washino, and T. Abe, *Nippon Kagaku Kaishi*, **1976**, 15.
12) T. Miyata, A. Sakumoto, M. Washino, and T. Abe, *Chem. Lett.*, **1975**, 367.
13) A. Sakumoto, T. Miyata, and M. Washino, *Chem. Lett.*, **1975**, 563.
14) Landolt-Börstein, "Zahlenwerte und Funktionen," Springer (1960), II B. 7 teil, p. 842.
15) R. T. Admas, E. E. Johnson, and J. M. Salmela, U. S. Patent 3306931 (1967).
16) E. Hayon, A. Treinin, and J. Wilf, *J. Am. Chem. Soc.*, **94**, 47 (1972).
17) M. S. Kharasch, E. M. May, and F. R. Mayo, *Chem. Ind. (London)*, **57**, 774 (1938).
18) H. Backström, *Z. Phys. Chem.*, **B25**, 122 (1934).
19) E. S. Amis, "Solvent Effects on Reaction Rates and Mechanisms," Academic Press, New York (1966), pp. 31, 59.
20) J. R. Penton and H. Zollinger, *Helv. Chim. Acta*, **54**, 573 (1971).
21) Y. Hashida, H. Ishida, S. Sekiguchi, and K. Matsui, *Bull. Chem. Soc. Jpn.*, **47**, 1224 (1974).
22) A. A. Frost and R. G. Pearson, "Kinetics and Mechanism," John Wiley & Sons, New York (1961), p. 123.
23) W. B. Guenther, "Quantitative Chemistry, Measurement and Equilibrium," Addison-Wesley (1968).
24) J. Kielland, *J. Am. Chem. Soc.*, **59**, 1675 (1937).
25) J. Rabani and S. O. Nielsen, *J. Phys. Chem.*, **73**, 3736 (1969).
26) P. S. Rao and E. Hayon, *J. Am. Chem. Soc.*, **96**, 1287 (1974).
27) M. Simic, P. Neta, and E. Hayon, *J. Phys. Chem.*, **73**, 4214 (1969).

Synthesis of Protected Peptide Fragments Related to Porcine Motilin[1)]

Shigeru MIHARA, Fumio SHIMIZU, and Seiji MIYAMOTO

The First Research Institute, Tokushima Factory, Otsuka Pharmaceutical Co., Ltd., Kagasuno, Kawauchi-cho, Tokushima 771-01

(Received May 22, 1976)

Syntheses are described of three protected peptide fragments which correspond to positions 1—6, 7—11, and 12—22, respectively, of the entire amino acid sequence of porcine motilin, a gastric motoractivity-promoting polypeptide. Stable tosyl group was used for the protection of ε-amino group of lysine and guanidino group of arginine. These protected peptide fragments were mainly constructed in stepwise manner using benzyloxycarbonyl amino acid by mixed anhydride method in the presence of *N*-hydroxysuccinimide. For preparation of the C-terminal undecapeptide, fragment condensation method was employed using two protected tripeptide azides. The protected peptides and intermediates could be readily purified by simple procedure.

Brown *et al.*[2)] reported the determination of primary structure of porcine motilin, a gastric motoractivity-promoting polypeptide. Synthesis by Wünsch *et al.*[3)] of a norleucine analog based on that structure revealed an incorrect assingment of the amino acid at position 14, and the structure was revised at this position from Glu to Gln.[4)] Yajima *et al.*[5)] have synthesized the docosapeptide corresponding to the revised sequence of porcine motilin.

Limited availability of natural material of this hormone prompted us to prepare it in sufficient amount for further biological and immunological studies. The present paper describes the synthesis of three protected peptide fragments related to porcine motilin which may be employed for the construction of the entire molecule. These protected peptide fragments differ from those used by other investigators for synthesis, of motilin, which correspond to the sequences 1—6 7—11, and 12—22, respectively, as shown in Chart 1.

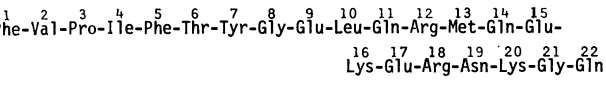

Chart 1. Primary structure of porcine motilin.

Stable tosyl group was selected for the protection of ε-amino group of lysine and guanidino group of arginine and Z-group was used for protection of α-amino group, since both of the protecting groups can be readily removed by sodium–liquid ammonia or anhydrous HF[6)] treatment at the final step in the synthesis of porcine motilin.

The route for the preparation of C-terminal protected undecapeptide (Fragment 1) (I) is shown in Scheme 1. Protected pentapeptide (IV) was prepared in stepwise manner using Z amino acids by mixed anhydride method in the presence of *N*-hydroxysuccinimide[7)] and then the chain was elongated by acylation with the azides of *N*-benzyloxycarbonyl tripeptides to give protected undecapeptide (I).

Coupling of Z–Lys(Tos)–OSu with triethylammonium salt of H–Gly–Gln–OH[8,9)] produced Z–Lys(Tos)–Gly–Gln–OH (II), which was partially deblocked by hydrogenolysis. Interaction of the resulting product with Z–Asn–OSu[10)] gave Z–Asn–Lys(Tos)–Gly–Gln–OH (III), which was hydrogenated. The partially deblocked tetrapeptide was coupled with Z–Arg(Tos)–OSu and the resulting protected pentapeptide

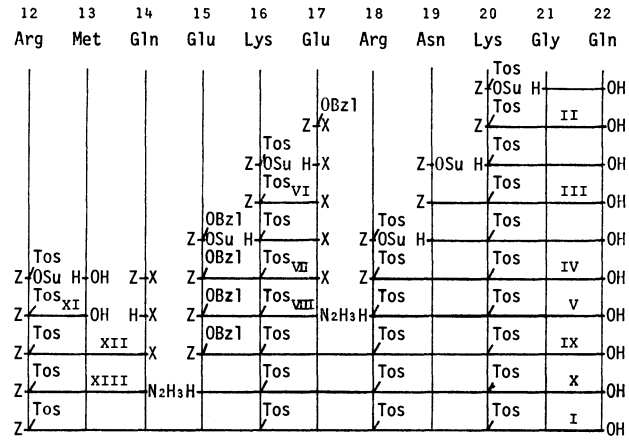

Scheme 1. Synthesis of fragment 1.
X=*t*-butoxycarbonyl hydrazide.

(IV) was subjected to hydrogenolysis to yield H–Arg(Tos)–Asn–Lys(Tos)–Gly–Gln–OH (V). Acylation of V with azide derived from Z–Glu(OBzl)–Lys(Tos)–Glu–NHNH–Boc (VII) gave Z–Glu(OBzl)–Lys(Tos)–Glu–Arg(Tos)–Asn–Lys(Tos)–Gly–Gln–OH (IX). The protected tripeptide hydrazide, VIII, was obtained by the stepwise chain elongation starting from H–Glu–NHNH–Boc derived from Z–Glu(OBzl)–NHNH–Boc.

Hydrogenolysis of IX yielded partially protected octapeptide, H–Glu–Lys(Tos)–Glu–Arg(Tos)–Asn–Lys(Tos)–Gly–Gln–OH (X). This was acylated with azide derived from Z–Arg(Tos)–Met–Gln–NHNH–Boc (XII) to give protected undecapeptide, Z–Arg(Tos)–Met–Gln–Glu–Lys(Tos)–Glu–Arg(Tos)–Asn–Lys(Tos)–Gly–Gln–OH (I). The product was purified by reprecipitation from MeOH with ethyl acetate. Preparation of the protected tripeptide hydrazide XII was accomplished by the interaction of H–Gln–NHNH–Boc[11)] with a mixed anhydride of Z–Arg(Tos)–Met–OH.[12)]

The protected pentapeptide hydrazide (Fragment 2) (XIV) was prepared by the route shown in Scheme 2. Z–Leu–Gln–NHNH–Boc (XV) was obtained by coupling of a mixed anhydride of Z–Leu–OH with H–Gln–NHNH–Boc. This compound was employed as intermediate for preparation of an LH–RH analog.[13)] Hydrogenation of XV gave H–Leu–Gln–NHNH–Boc, which was coupled with Z–Glu(OBzl)–OSu to give protected tripeptide hydrazide (XVI). Subsequent introduction of Gly and Tyr residues was also per-

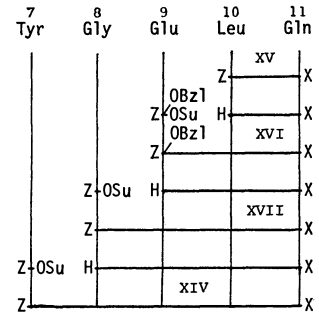

Scheme 2. Synthesis of fragment 2.

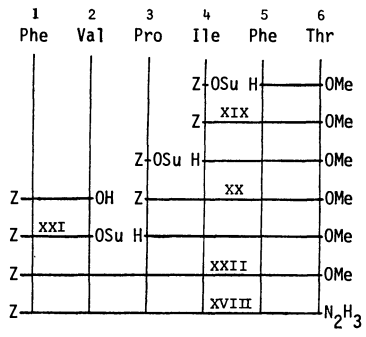

Scheme 3. Synthesis of fragment 3.

formed by active ester procedure.[7] The final product was purified by reprecipitation from MeOH with ethyl acetate to afford the protected pentapeptide hydrazide, Z–Tyr–Gly–Glu–Leu–Gln–NHNH–Boc (XIV).

The route for the preparation of the protected hexapeptide hydrazide (Fragment 3) (XVIII) is shown in Scheme 3.

Z–Phe–Thr–OMe[14] was used as the starting material and hydrogenated to give H–Phe–Thr–OMe, which was coupled with Z–Ile–OSu.[15] The resulting protected tripeptide methyl ester (XIX) was hydrogenated and then the product was acylated with Z–Pro–OSu[7] to give Z–Pro–Ile–Phe–Thr–OMe (XX). Hydrogenation of XX and then acylation with Z–Phe–Val–OSu (XXI) gave Z–Phe–Val–Pro–Ile–Phe–Thr–OMe (XXII), which was converted to the corresponding hydrazide, Z–Phe–Val–Pro–Ile–Phe–Thr–$NHNH_2$ (Fragment 3), by the action of hydrazine.

High purity of the protected peptide fragments, 1, 2, and 3, prepared in this study was proved by elemental analysis, amino acid analysis of their acid hydrolysates and thin-layer chromatography in two solvent systems. The syntheses of these protected peptide fragments proceeded smoothly and homogeneous materials were obtained by simple purification steps. The protected peptide hydrazides, which were prepared mainly by active ester method *via* mixed anhydride or azide procedure, in this study may be suitable intermediates for construction of a large quantity of porcine motilin *via* fragment condensation.[16]

Experimental

The melting points were uncorrected. Optical rotations were measured on a JASCO DIP4 Automatic Polarimeter. Analytical samples were dried *in vacuo* over P_2O_5 at 60—70 °C for 20 h. Amino acid analysis was performed with a HITACHI Model KLA-3B amino acid analyzer. Acid hydrolysis of a sample for amino acid analysis was conducted with 6M HCl at 110 °C for 24 h in a sealed tube. Designations of solvent systems for TLC on silica gel G (Merck) are : R_f^I *n*-BuOH–AcOH–H_2O (4 : 1 : 5) upper layer; R_f^{II} *n*-BuOH–pyridine–AcOH–H_2O (30 : 20 : 6 : 24). All solvents were of reagent grade and were distilled before use. Evaporations were carried out *in vacuo* at 40—45 °C in rotary evaporators.

Z–Lys(Tos)–Gly–Gln–OH (II). Z–Glu–Gln–OH[9] (3.00 g) was hydrogenated over Pd in MeOH (80 ml) containing 10% AcOH (10 ml) in the usual manner. The catalyst was removed by filtration, the filtrate was evaporated and the residue was dried *in vacuo* over P_2O_5 to give H–Gly–Gln–OH[8,9] R_f^I 0.11. To a solution of Z–Lys(Tos)–OH (3.86 g) and *N*-methylmorpholine (0.91 ml) in THF (50 ml) cooled to −15 °C, isobutyl chloroformate (1.11 ml) was added and, after 1 min, an ice-cold solution of *N*-hydroxysuccinimide (1.12 g) in THF (5 ml) was added. The mixture was kept at 0 °C for 5 min and at 20 °C for additional 15 min. The resulting active ester was combined with an ice-cold solution of the above deblocked dipeptide and TEA (1.24 ml) in H_2O (50 ml). The mixture was kept at 20 °C for 20 h, and a bulk of THF was evaporated. The residual aqueous solution was adjusted to pH 8 with TEA and washed with ethyl acetate three times. The solution was acidified with 1 N citric acid and extracted with ethyl acetate. The extracts were dried over Na_2SO_4 and evaporated to give a solid, which was collected by filtration and dried. Reprecipitation from MeOH with ethyl acetate gave II; yield, 3.90 g (70.8%); mp 147—148 °C; $[\alpha]_D^{14}$ −9.6° (*c* 0.52 MeOH); R_f^I 0.64, R_f^{II} 0.72. Found: C, 54.75; H, 6.12; N, 11.09%. Calcd for $C_{28}H_{37}O_9N_5S$: C, 54.27; H, 6.02; N, 11.30%.

Z–Asn–Lys(Tos)–Gly–Gln–OH (III). Hydrogenation of II (1.50 g) was carried out over Pd in MeOH (50 ml) and H_2O (50 ml) in the usual manner. Isolation of the product was performed in the manner as described for the hydrogenation of Z–Gly–Gln–OH, R_f^I 0.33. The hydrogenated material was acylated with the *N*-hydroxysuccinimide ester of Z-Asn-OH (0.96 g) and the product was isolated in the same manner as described for preparation of II. Reprecipitation from MeOH with ethyl acetate gave III; yield, 1.28 g (72.3%); mp 148—150 °C; $[\alpha]_D^{18}$ −27.3° (*c* 0.55 MeOH); R_f^I 0.45, R_f^{II} 0.67. Found: C, 51.76; H, 5.89; N, 13.30%. Calcd for $C_{32}H_{47}O_{11}N_7S \cdot 1/2H_2O$: C, 51.74; H, 5.97; N, 13.19%.

Z–Arg(Tos)–Asn–Lys(Tos)–Gly–Gln–OH (IV). Compound III (1.18 g) was hydrogenated over Pd in MeOH (50 ml) containing 10% AcOH (10 ml) in the usual manner, R_f^I 0.18. The hydrogenated material was acylated with the *N*-hydroxysuccinimide ester of Z–Arg(Tos)–OH (1.11 g) and the product was isolated in the same manner as described for preparation of II. Reprecipitation from MeOH with ethyl acetate gave IV; yield, 1.53 g (91.6%); mp 125—129 °C; $[\alpha]_D^{18}$ −13.0° (*c* 0.54 DMF); R_f^I 0.49, R_f^{II} 0.69. Found: C, 51.17; H, 5.93; N, 14.68%. Calcd for $C_{45}H_{61}O_{14}N_{11}S_2 \cdot H_2O$: C, 50.89; H, 5.98 N, 14.51%.

Z–Lys(Tos)–Glu–NHNH–Boc (VI). Z–Glu(OBzl)–NHNH–Boc (2.60 g) was hydrogenated over Pd in MeOH (50 ml) containing 1 M HCl (5.35 ml) in the usual manner, R_f^I 0.50. The hydrogenated material was coupled with the *N*-hydroxysuccinimide ester of Z–Lys(Tos)–OH (2.55 g) in the same manner as described for preparation of II. The solvents were evaporated. The residue was extracted with ethyl acetate, which was washed with 1 N citric acid and

saturated NaCl and dried over Na_2SO_4. The solvent was evaporated and the residue was solidified by addition of ether. The product was reprecipitated from ethyl acetate with ether; yield, 3.30 g (91.0%); mp 79 °C (dec.); $[\alpha]_D^{25}$ −28.2° (*c* 0.48 MeOH); R_f^I 0.89, R_f^{II} 0.85. Found: C, 55.25; H, 6.77; N, 9.76%. Calcd for $C_{31}H_{43}O_{10}N_5S$: C, 54.93; H, 6.39; N, 10.33%.

Z-Glu(OBzl)-Lys(Tos)-Glu-NHNH-Boc (VII). Compound VI (1.09 g) was hydrogenated over Pd in MeOH (50 ml) in the usual manner, R_f^I 0.60. The hydrogenated material was acylated with the *N*-hydroxysuccinimide ester of Z-Glu(OBzl)-OH (0.71 g) and the product was isolated in the same manner as described for preparation of VI. Reprecipitation from MeOH with ethyl acetate gave VII; yield, 1.03 g (72.0%); mp 81 °C (dec.); $[\alpha]_D^{18}$ −26.8° (*c* 0.50 DMF); R_f^I 0.90, R_f^{II} 0.88. Found: C, 55.56; H, 6.15; N, 8.78%. Calcd for $C_{43}H_{56}O_{13}N_6S\cdot 2H_2O$: C, 55.36; H, 6.48; N, 9.01%.

Z-Arg(Tos)-Met-OH[12] *(XI).* A solution of Z-Arg(Tos)-OH (2.54 g) and *N*-methylmorpholine (0.56 ml) in THF (30 ml) was cooled to −15 °C and isobutyl chloroformate (0.66 ml) was added. After 30 s, *N*-hydroxysuccinimide (0.86 g) dissolved in THF (10 ml) was added. The mixture was combined with an ice-cold solution of H-Met-OH (0.75 g) and TEA (0.70 ml) in H_2O (20 ml). The mixture was kept at 20 °C for 20 h and THF was evaporated. Isolation of the product was carried out in the manner as described for the preparation of II. The residue which was solidified on addition of ether was collected, dried, and reprecipitated from ethyl acetate with ether to give product XI; yield, 2.02 g (66.7%); mp 101—105 °C; $[\alpha]_D^{18}$ −7.4° (*c* 1.01 MeOH); R_f^I 0.83, R_f^{II} 0.80. Found: C, 52.03; H, 5.98; N, 11.54%. Calcd for $C_{26}H_{35}O_7N_5S_2\cdot 1/2H_2O$: C, 51.81; H, 6.02; N, 11.62%.

Z-Arg(Tos)-Met-Gln-NHNH-Boc (XII). Z-Gln-NHNH-Boc[11] (1.00 g) was hydrogenated over Pd in MeOH (50 ml) in the usual manner, R_f^I 0.36. A solution of XI (1.66 g) and *N*-methylmorpholine (0.28 ml) in THF (30 ml) was cooled to −15 °C and isobutyl chloroformate (0.33 ml) was added. After 1 min, the resulting mixed anhydride was combined with an ice-cold solution of the above hydrogenated material in THF (10 ml). The mixture was kept at 0 °C for 5 min and at 20 °C for additional 15 min. The solution was evaporated. The residue was dissolved in ethyl acetate, and the solution was washed successively with 1 N citric acid, saturated NaCl, saturated Na_2HCO_3 and saturated NaCl. The organic layer was dried over Na_2SO_4 and evaporated. The residue which was solidified on addition of ether was collected, dried, and recrystallized from MeOH with ether to give XII; yield, 1.29 g (60.8%); mp 182—183 °C; $[\alpha]_D^{18}$ −16.6° (*c* 0.51 DMF); R_f^I 0.80, R_f^{II} 0.81. Found: C, 51.09; H, 6.38; N, 14.95%. Calcd for $C_{36}H_{53}O_{10}N_9S_2\cdot 1/2H_2O$: C, 51.17; H, 6.44; N, 14.92%.

Z-Glu(OBzl)-Lys(Tos)-Glu-Arg(Tos)-Asn-Lys(Tos)-Gly-Gln-OH (IX). Compound IV (1.00 g) was hydrogenated over Pd in MeOH (50 ml) containing 10% AcOH (10 ml) in the usual manner to give V, R_f^I 0.27. A solution of VII (1.64 g) in TFA (5 ml) was kept at 20 °C for 20 min and addition of ether gave precipitate, which was collected by filtration and dried over KOH. This material (VIII) (1.53 g) was dissolved in DMF (20 ml), and the solution cooled at −15 °C, and 6 M HCl in dioxane (0.96 ml) and isopentyl nitrite (0.28 ml) were added. The mixture was left at −10 °C for 5 min and neutralized with TEA (0.81 ml). To the solution was added an ice-cold solution of the above hydrogenated material V and TEA (0.13 ml) in DMF (30 ml). The mixture was stirred at 4 °C for 20 h and the solvent was evaporated. The residue was extracted with five portions of *n*-BuOH which were washed with six portions of 10% AcOH. Evaporation of *n*-BuOH layers gave a viscous oil, which was solidified from MeOH with ethyl acetate, collected and reprecipitated from MeOH with ethyl acetate to give IX; yield, 1.56 g (97.0%); mp 165—166 °C; $[\alpha]_D^{18}$ −13.4° (*c* 0.52 DMF); R_f^I 0.60, R_f^{II} 0.72. Found: C, 53.36; H, 6.00; N, 12.10%. Calcd for $C_{75}H_{99}O_{23}N_{15}S_3$: C, 53.78; H, 5.96; N, 12.54%.

Z-Arg(Tos)-Met-Gln-Glu-Lys(Tos)-Glu-Arg(Tos)-Asn-Lys(Tos)-Gly-Gln-OH (I) (Fragment 1). Compound IX (0.80 g) was hydrogenated over Pd in MeOH (50 ml) and 50% AcOH (50 ml) for 40 h in the usual manner to give X, R_f^I 0.38. A solution of XII (0.80 g) in TFA (3.5 ml) was kept at 20 °C for 30 min and addition of peroxide free ether gave precipitate, which was collected by filtration and dried over KOH. This material (XIII) was dissolved in DMF (20 ml) and the solution cooled at −15 °C and 6 M HCl in dioxane (0.48 ml) and isopentyl nitrite (0.14 ml) were added. The mixture was left at −10 °C for 5 min and neutralized with TEA (0.53 ml). To the solution was added an ice-cold solution of the above hydrogenated material X and TEA (0.06 ml) in DMF (15 ml). The mixture was stirred at 4 °C for 20 h and the solvent was evaporated. The residue was extracted with five portions of *n*-BuOH which were washed with six portions of 15% AcOH. Evaporation of the *n*-BuOH layers gave an oil, which was solidified from MeOH with ethyl acetate, collected and reprecipitated from MeOH with ethyl acetate to give I; yield, 0.61 g (59.3%); mp 164—165 °C; $[\alpha]_D^{18}$ −17.0° (*c* 0.53 DMF); R_f^I 0.38, R_f^{II} 0.61; amino acid ratios in acid hydrolysate: Met, 0.84; Glu, 4.15; Asp, 0.96; Gly, 0.90; Arg(Tos) and Lys(Tos) were not determined. Found: C, 50.12; H, 6.04; N, 13.66%. Calcd for $C_{91}H_{128}O_{29}N_{22}S_5\cdot 2H_2O$: C, 49.90; H, 6.07; N, 14.07%.

Z-Leu-Gln-NHNH-Boc (XV). A solution of Z-Leu-OH (3.82 g) and *N*-methylmorpholine (1.46 ml) in THF (50 ml) was cooled to −15 °C and isobutyl chloroformate (1.74 ml) was added. After 30 s, the resulting mixed anhydride was combined with an ice-cold solution of H-Gln-NHNH-Boc, derived from Z-Gln-NHNH-Boc[11] (4.37 g), and TEA (1.68 ml) in THF (40 ml). The mixture was kept at 4 °C for 5 min and at 20 °C for further 15 min. The solvent was evaporated. Isolation of the product XV was carried out in the manner as described for the preparation of II; yield, 4.02 g (66.0%); mp 139—140 °C; $[\alpha]_D^{20}$ −44.2° (*c* 0.50 MeOH); R_f^I 0.79, R_f^{II} 0.87. Found: C, 56.47; H, 7.43; N, 13.89%. Calcd for $C_{28}H_{37}O_7N_5$: C, 56.79; H, 7.35; N, 13.80%.

Z-Glu(OBzl)-Leu-Gln-NHNH-Boc (XVI). Compound XV (2.00 g) was hydrogenated over Pd in MeOH (50 ml) containing 1 M HCl (3.9 ml) in the usual manner, R_f^I 0.48. The hydrogenated material was coupled with the *N*-hydroxysuccinimide ester of Z-Glu(OBzl)-OH (1.74 g) in the same manner as described for preparation of II. The solvent was evaporated. The residue was solidified by addition of H_2O, which was collected by filtration and dried. Reprecipitation from MeOH with ethyl acetate gave XVI; yield, 2.30 g (81.1%); mp 175—180 °C; $[\alpha]_D^{18}$ −26.6° (*c* 0.53 DMF); R_f^I 0.89, R_f^{II} 0.92. Found: C, 59.73; H, 6.93; N, 11.44%. Calcd for $C_{36}H_{50}O_{10}N_6$: C, 59.49; H, 6.93; N, 11.56%.

Z-Gly-Glu-Leu-Gln-NHNH-Boc (XVII). Compound XVI (2.20 g) was hydrogenated over Pd in MeOH (80 ml) containing 10% AcOH (10 ml) in the usual manner, R_f^I 0.38. The hydrogenated material was coupled with the *N*-hydroxysuccinimide ester of Z-Gly-OH (0.76 g) in

the same manner as described for preparation of II. The solvents were evaporated. The residue was dissolved in ethyl acetate, and the solution was washed with 1 N citric acid and H_2O and dried over Na_2SO_4. The solvent was evaporated to give solid which was collected by filtration and dried. Reprecipitation from MeOH with ethyl acetate gave XVII; yield, 1.44 g (68.6%); mp 163—166 °C; $[\alpha]_D^{20}$ −22.9° (*c* 0.50 DMF); R_f^I 0.75, R_f^{II} 0.76. Found: C, 53.38; H, 6.93; N, 14.46%. Calcd for $C_{31}H_{47}O_{11}N_7$: C, 53.67; H, 6.83; H, 14.13%.

Z–Tyr–Gly–Glu–Leu–Gln–NHNH–Boc (XIV) (Fragment 2). Compound XVII (1.41 g) was hydrogenated over Pd in MeOH (50 ml) containing 10% AcOH (5 ml) in the usual manner, R_f^I 0.35. DCC (0.50 g) was added to a solution of Z–Tyr–OH (0.77 g) and *N*-hydroxysuccinimide (0.28 g) in THF (40 ml) at 4 °C. The mixture was stirred at 4 °C for 20 h. The dicyclohexylurea was removed by filtration, and the solvent was evaporated. The residue, which was solidified on addition of ether–petroleum ether (1 : 2), was collected and dried. The resulting active ester was added to an ice-cold solution of the above hydrogenated material and TEA (0.28 ml) in DMF (20 ml). The mixture was kept at 20 °C for 20 h and DMF was evaporated. The residue was dissolved in ethyl acetate, which was washed with 1 N citric acid and H_2O and dried. The solvent was evaporated and the residue was solidified by addition of MeOH–ethyl acetate, collected, and reprecipitated from MeOH with ethyl acetate to give XIV; yield, 1.46 g (84.0%); mp 164—165 °C; $[\alpha]_D^{16}$ −46.4° (*c* 0.54 DMF); R_f^I 0.79, R_f^{II} 0.77; amino acid ratios in acid hydrolysate: Tyr, 0.89; Gly, 0.99; Glu, 2.10; Leu, 1.03. Found: C, 54.87; H, 6.62; H, 12.86%. Calcd for $C_{40}H_{56}O_{13}N_8 \cdot H_2O$: C, 54.91; H, 6.68; N, 12.81%.

Z–Ile–Phe–Thr–OMe (XIX). *Z–Phe–Thr–OMe*[14] (2.90 g) was hydrogenated over Pd in MeOH (50 ml) containing 1 M HCl (7 ml) in the usual manner, R_f^I 0.55. Z–Ile–OSu[15] (3.80 g) was added to an ice-cold solution of the above hydrogenated material and TEA (0.98 ml) in DMF (50 ml). The mixture was kept at 20 °C for 40 h and the solvent was evaporated. To the residue was added 1 N citric acid. The precipitate thus formed was collected by filtration and then washed with hot MeOH to yield XIX; yield, 3.15 g (85.4%); mp 210—211 °C; $[\alpha]_D^{20}$ −13.1° (*c* 0.50 DMSO); R_f^I 0.87, R_f^{II} 0.85. Found: C, 63.66; H, 7.11; N, 8.19%. Calcd for $C_{28}H_{37}O_7N_3$: C, 63.74; H, 7.07; N, 7.96%.

Z–Pro–Ile–Phe–Thr–OMe (XX). Compound XIX (3.00 g) was hydrogenated over Pd in MeOH (80 ml) containing 10% AcOH (10 ml) in the usual manner, R_f^I 0.52. Z–Pro–OSu[7] (2.95 g) was added to an ice-cold solution of the above hydrogenated material and TEA (0.79 ml) in DMF (50 ml). The mixture was kept at 20 °C for 20 h and the solvent was evaporated. The residue was solidified by addition of 5% AcOH, which was collected by filtration, washed with H_2O and dried. The solid was then washed with hot MeOH to give XX; yield, 3.35 g (94.4%); mp 235—236 °C; $[\alpha]_D^{20}$ −38.2° (*c* 0.50 DMSO); R_f^I 0.86, R_f^{II} 0.85. Found: C, 63.00; H, 7.02; N, 9.27%. Calcd for $C_{33}H_{44}O_8N_4$: C, 63.44; H, 7.10; N, 8.97%.

Z–Phe–Val–OSu (XXI). To an ice-cold solution of Z–Phe–Val–OH[17] (3.05 g) and *N*-hydroxysuccinimide (0.88 g) in THF (40 ml) was added DCC (1.58 g), and the mixture was stirred at 4 °C for 18 h. The suspension was filtered, and the filtrate was evaporated. The solid residue, which was obtained on addition of ether, was collected, dried, and recrystallized from EtOH; 3.25 g (85.2%); mp 156—157 °C; $[\alpha]_D^{20}$ −11.6° (*c* 2.30 dioxane); Found: C, 63.23; H, 6.14; N, 8.46%. Calcd for $C_{26}H_{29}O_7N_3$: C, 63.02; H, 5.90; N, 8.48%.

Z–Phe–Val–Pro–Ile–Phe–Thr–OMe (XXII). Compound XX (1.73 g) was hydrogenated over Pd in a mixture of MeOH (80 ml), 10% AcOH (30 ml) and *n*-BuOH (20 ml) in the usual manner, R_f^I 0.51. Z–Phe–Val–OSu (1.64 g) was added to an ice-cold solution of the above hydrogenated material and TEA (0.38 ml) in DMF (20 ml). The mixture was kept at 20 °C for 20 h and the solvent was evaporated. Isolation of the product was carried out in the manner as described for the preparation of I; yield, 0.99 g (40.3%); mp 172—174 °C; $[\alpha]_D^{16}$ −58.5° (*c* 0.51 DMF); R_f^I 0.86, R_f^{II} 0.90. Found: C, 63.31; H, 7.25; N, 9.89%. Calcd for $C_{47}H_{62}O_9N_6 \cdot H_2O$: C, 63.50; H, 7.26; H, 9.45%.

Z–Phe–Val–Pro–Ile–Phe–Thr–NHNH$_2$ (XVIII) (Fragment 3). Hydrazine hydrate (90%) (0.92 ml) was added to an ice-cold solution of XXII (0.95 g) in DMF (3 ml) and the solution was kept at 20 °C for 20 h. The solvent was evaporated and the residue was extracted with five portions of *n*-BuOH which were washed with six portions of 10% AcOH. Evaporations of the *n*-BuOH layers gave an oil which was solidified by addition of ether. The solid was collected and dried; yield, 0.58 g (60.7%); mp 209—211 °C; $[\alpha]_D^{20}$ −45.9° (*c* 0.51 DMSO); R_f^I 0.75, R_f^{II} 0.80; amino acid ratios in acid hydrolysate: Phe, 2.04; Val, 1.12; Pro, 0.93; Ile, 1.00; Thr, 0.92. Found: C, 62.64; H, 7.06; N, 12.55%. Calcd for $C_{46}H_{62}O_9N_8 \cdot H_2O$: C, 62.14; H, 7.26; N, 12.60%.

The authors are deeply indebted to Prof. Noboru Yanaihara, Shizuoka College of Pharmacy, and Mr. Akihiko Otsuka, vice president of Otsuka Pharmaceutical Co., Ltd., for their kind advice and encouragment during the course of this work.

References

1) The amino acids except glycine are of the L-configuration. Abbreviations used are: Z, benzyloxycarbonyl; OBzl, benzyl ester; OSu, *N*-hydroxysuccinimide ester; Tos, *p*-toluenesulfonyl; Boc, *t*-butoxycarbonyl; *n*-BuOH, 1-butanol; TEA, triethylamine; DMF, *N*,*N*-dimethylformamide; TFA, trifluoroacetic acid; HCl, hydrochloric acid or hydrogen chloride; DCC, dicyclohexylcarbodiimide; DMSO, dimethyl sulfoxide.

2) J. C. Brown, J. A. Cook, and J. R. Dryburge, *Can. J. Biochem.*, **51**, 533 (1973).

3) E. Wünsch, J. C. Brown, K. H. Deimer, F. Dres, E. Jaeger, J. Mousiol, R. Stocker, P. Thamm, and G. Wendlberger, *Z. Naturforsch.*, **28c**, 235 (1973).

4) H. Schubert and J. C. Brown, *Can. J. Biochem.*, **52**, 7 (1974).

5) H. Yajima, Y. Kai, and H. Kawatani, *J. Chem. Soc., Chem. Commun.*, **1975**, 159; J. Kai, H. Kawatani, H. Yajima, and Z. Itoh, *Chem. Pharm. Bull. (Tokyo)*, **23**, 2346 (1975).

6) S. Sakakibara, Y. Shimonishi, Y. Kishida, H. Okada, and H. Sugihara, *Bull. Chem. Soc. Jpn.*, **40**, 2146 (1974).

7) G. W. Anderson, J. E. Zimmerman, and F. Callahan, *J. Am. Chem. Soc.*, **86**, 1839 (1964).

8) Y. Shimonishi, S. Sakakibara, and S. Akabori, *Bull. Chem. Soc. Jpn.*, **35**, 1966 (1962).

9) Y. Kai, H. Kawatani, and H. Yajima, *Chem. Pharm. Bull.*, **23**, 2339 (1975).

10) S. Sakakibara and S. Hase, *Bull. Chem. Soc. Jpn.*, **41**, 2816 (1968).

11) J. Beacham, D. Dupuis, F. M. Finn, H. T. Storeg, C. Yanaihara, H. Yanaihara, and K. Hofmann, *J. Am.*

Chem. Soc., **93**, 5526 (1971).
12) H. Yajima, Y. Kinomura, T. Oshima, and Y. Okada, *Chem. Pharm. Bull.*, **15**, 1922 (1967).
13) N. Yanaihara, C. Yanaihara, T. Hashimoto, Y. Kenmochi, H. Oka, S. Saito, A. V. Schally, and A. Arimura, *Biochem. Biophys. Res. Commun.*, **49**, 1280 (1972).
14) A. Corbellini, F. Chillemi, and P. G. Pietta, *Gazz. Chim. Ital.*, **97**, 514 (1967).
15) H. Aoyagi, M. Ohno, N. Izumiya, and B. Witkop, *J. Org. Chem.*, **29**, 1382 (1964).
16) K. Hofmann, A. Lindermann, M. Z. Nagee, and N. H. Khan, *J. Am. Chem. Soc.*, **74**, 470 (1952).
17) E. Schnabel, H. Klostermeyer, T. Dahlmans, and H. Zahn, *Justus Liebigs Ann. Chem.*, **707**, 277 (1967).

Synthesis of Porcine Motilin by Fragment Condensation Using Three Protected Peptide Fragments[1)]

Fumio SHIMIZU,* Kenichi IMAGAWA, Shigeru MIHARA, and Noboru YANAIHARA*

The First Research Institute, Tokushima Factory, Otsuka Pharmaceutical Co., Ltd., Kagasuno, Kawauchi-cho, Tokushima 771-01

**Laboratory of Bio-organic Chemistry, Shizuoka College of Pharmacy, 2-2-1, Oshika, Shizuoka 422*

(Received May 22, 1976)

Synthesis of porcine motilin is described. Construction of the entire molecule of this hormone was carried out by the fragment condensation method in solution employing Rudinger's azide modification, and the resulting protected docosapeptide was deblocked by sodium-liquid ammonia procedure. Purification of the final product was performed by ion exchange chromatography on CM-Sephadex using ammonium acetate as eluent and gel filtration on BiO-Gel P-6. Purity of the synthetic docosapeptide was assessed by TLC in two different solvent systems and amino acid analysis. This polypeptide showed gastric motoractivity stimulating action on 30 min intravenous infusion in dogs in 5 ng/kg/min doses, which is characteristic to porcine motilin.

Porcine motilin is a single chain peptide consisting of 22 amino acid residues.[2,3)] We have described in the preceding paper[4)] synthesis of the three protected peptide fragments 1, 2, and 3 corresponding to the amino acid sequences 1—6, 7—11, and 12—22 of the porcine motilin molecule, respectively (Chart 1). Using these fragments, our continuous synthetic studies on this gastrointestinal hormone have been focussed on its total synthesis by efficient means in regard to yield and purity of the products. The details of the synthesis are described in this communication. Syntheses of porcine motilin[5,6)] and its analogs, [13-Nle, 14-Glu]-motilin,[7)] by different approaches have been reported.

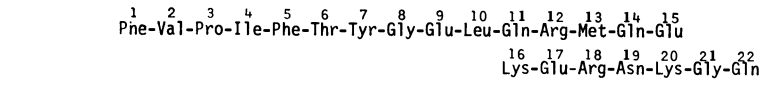

Chart 1. Primary structure of porcine motilin.

Construction of the entire molecule of porcine motilin was conducted by the fragment condensation method in solution employing Rudinger's azide modification.[8)] Scheme 1 shows the route for our synthesis of porcine motilin using the three protected peptide fragments 1, 2, and 3.

Z–Arg(Tos)–Met–Gln–Glu–Lys(Tos)–Glu–Arg(Tos)–Asn–Lys(Tos)–Gly–Gln–OH[4)] (Fragment 1) (II) was deblocked by HBr in acetic acid in the presence of anisole and ethyl methyl sulfide as scavengers. The resulting partially protected undecapeptide H–Arg(Tos)–Met–Gln–Glu–Lys(Tos)–Glu–Arg(Tos)–Asn–Lys(Tos)–Gly–Gln–OH (V) was coupled with the azide derived from Z–Tyr–Gly–Glu–Leu–Gln–NHNH–Boc[4)] (Fragment 2) (III) to give protected hexadecapeptide, Z–Tyr–Gly–Glu–Leu–Gln–Arg(Tos)–Met–Gln–Glu–Lys(Tos)–Glu–Arg(Tos)–Asn–Lys(Tos)–Gly–Gln–OH (VII). The crude product was distributed into *n*-BuOH and 10% AcOH. The *n*-BuOH layers were evaporated and the desired product was precipitated by addition of 10% AcOH. Removal of the Z-group from the protected hexadecapeptide (VII) was conducted with HBr in trifluoroacetic acid containing anisole and ethyl methyl sulfide as scavengers. The resulting partially protected hexadecapeptide hydrobromide was converted to the acetate (VIII) and coupled with the azide derived from Z–Phe–Val–Pro–Ile–Phe–Thr–$NHNH_2$[4)] (Fragment 3) (IV). The products were distributed into *n*-BuOH and 10% AcOH. Crude protected docosapeptide Z–Phe–Val–Pro–Ile–Phe–Thr–Tyr–Gly–Glu–Leu–Gln–Arg(Tos)–Met–Gln–Glu–Lys(Tos)–Glu–Arg(Tos)–Asn–Lys(Tos)–Gly–Gln–OH (IX) was obtained from the *n*-BuOH layers.

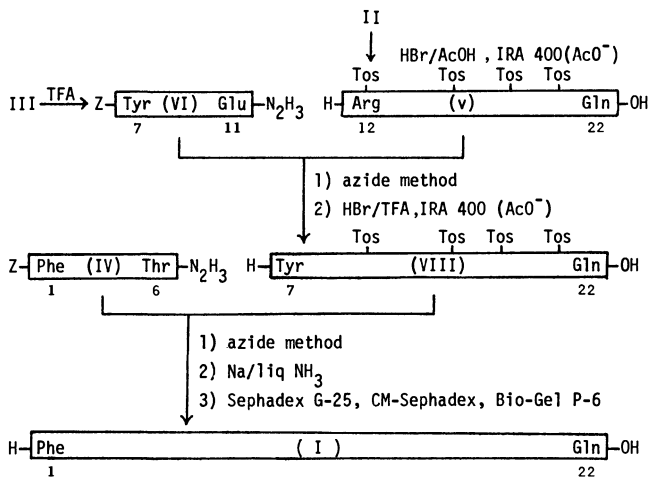

Scheme 1. Synthesis of porcine motilin.

Deblocking of this material was carried out by the treatment of sodium in liquid ammonia. The tosyl groups protecting the side chain amino function of lysine and guanidino function of arginine and the Z-group attached to the N-terminal phenylalanine were simultaneously cleaved by this process. The resulting material was subjected to gel filtration on Sephadex G-25 and then to ion exchange chromatography on CM-Sephadex using as eluate NH_4OAc buffer (pH 4.5) of linear gradient concentration. The desired product was eluated with 0.2—0.3 M NH_4OAc. The purified docosapeptide, after gel filtration on Bio-Gel P-6, gave the expected amino acid analysis with its acid hydrolysate and behaved as a single component on thin-layer chromatography in two solvent systems. Its stereohomogeneity was assessed by AP-M digestion.

This synthetic polypeptide showed gastric motoractivity stimulating action in the stomach and duodenum of dogs on 30 min intravenous infusion in 5 ng/kg/min

doses, which is characteristic to natural porcine motilin.

In the present investigation, our route for synthesis of porcine motilin using three protected peptide fragments was found to be efficient to obtain the hormone of high purity. In particular, use of sodium in liquid ammonia for deprotection of the final coupling product was effective in this synthesis.

Experimental

The melting points were uncorrected. Optical rotations were measured on a JASCO DIP4 Automatic Polarimeter. Analytical samples were dried *in vacuo* over P_2O_5 at 60—70 °C for 20 h. Amino acid analysis was performed with a HITACHI Model KLA-3B amino acid analyzer. Acid hydrolysis of a sample for amino acid analysis was conducted with 6 M HCl at 110 °C for 24 h in a sealed tube. AP-M digestion[9] (400 mU AP-M/mg sample) was carried out in 0.05 M Tris-HCl buffer (pH 7.8) at 37 °C for 24 h. Designations of solvent systems for TLC on silica gel G (Merck) are: R_f^I *n*-BuOH–AcOH–H_2O (4 : 1 : 5) upper layer; R_f^{II} *n*-BuOH–pyridine–AcOH–H_2O (30 : 20 : 6 : 24). All solvents were of reagent grade and were distilled before use. Evaporations were carried out *in vacuo* at 40—45 °C in rotary evaporaters.

Z–Tyr–Gly–Glu–Leu–Gln–Arg(Tos)–Met–Gln–Glu–Lys(Tos)–Glu–Arg(Tos)–Asn–Lys(Tos)–Gly–Gln–OH (VII). To a solution of II (0.517 g) in glacial AcOH (2 ml) was added 25% HBr solution in AcOH (3 ml) containing anisole (0.1 ml) and ethyl methyl sulfide (0.1 ml). The solution was kept at 20 °C for 1 h and peroxide-free anhydrous ether was added. The resulting precipitate was collected, washed with ether and dried over KOH. The material was dissolved in *n*-BuOH–MeOH–H_2O (1 : 1 : 1) (100 ml) and the solution was passed through IRA-400 column (acetate form). The solvents were evaporated and the residue was lyophilized to give V; yield, 0.303 g (67.2%), R_f^I 0.29.

A solution of III (0.257 g) in TFA (1 ml) was kept at 20 °C for 30 min and addition of anhydrous ether gave precipitate, which was collected by filtration and dried over KOH. This material was dissolved in DMF (3 ml), and the solution cooled at −15 °C, and 6 M HCl in dioxane (0.25 ml) and 10% isopentyl nitrite in DMF (0.44 ml) were added. The mixture was left at −10 °C for 5 min and neutralized with 10% TEA in DMF (2.50 ml). To the solution was added an ice-cold solution of V (0.303 g) in DMF (5 ml) containing TEA (0.06 ml). The mixture was stirred at 4 °C for 20 h. An additional azide prepared from III (0.257 g) was added and the reaction mixture was stirred at 4 °C for further 20 h. After evaporation of solvents, the product was distributed into *n*-BuOH and 10% AcOH in 10 separatory funnels, and the *n*-BuOH layers containing the desired material was evaporated. To the residue was added 10% AcOH to give precipitate, which was collected by filtration, washed with MeOH and dried; yield, 0.190 g (46.2%); mp 120 °C (dec); $[\alpha]_D^{18}$ −21.0° (*c* 0.50 DMF); R_f^I 0.40, R_f^{II} 0.62. Found: C, 50.18; H, 6.03; N, 13.43%. Calcd for $C_{118}H_{166}O_{38}N_{28}S_5 \cdot 4H_2O$: C, 50.30; H, 6.22; N, 13.92%.

H–Phe–Val–Pro–Ile–Phe–Thr–Tyr–Gly–Glu–Leu–Gln–Arg–Met–Gln–Glu–Lys–Glu–Arg–Asn–Lys–Gly–Gln–OH (I) (Porcine motilin). Compound VII (0.170 g) was dissolved in TFA (5 ml) containing anisole (0.1 ml) and ethyl methyl sulfide (0.1 ml), which was bubbled with HBr gas at 0 °C for 15 min and then at 20 °C for 15 min. The reaction mixture was allowed to stand at 20 °C for 30 min, and peroxide-free anhydrous ether was added. The resulting precipitate was collected by filtration and dried. The amorphous material was dissolved in *n*-BuOH–MeOH–H_2O (1 : 1 : 1) (50 ml) and the solution was passed through IRA-400 column (acetate form). The solvents were evaporated and the residue was lyophilized to yield VIII as acetate, R_f^I 0.38. A solution of IV (0.160 g) in DMF (3 ml) was cooled to −15 °C and 6 M HCl in dioxane (0.16 ml) and 10% isopentyl nitrite in DMF (0.28 ml) were added. After 1 min, the solution was neutralized with 10% TEA in DMF (1.28 ml) and mixed with an ice-cold solution of the above partially deblocked material VIII in DMF (4 ml) containing TEA (0.04 ml). The mixture was stirred at 4 °C for 20 h. An additional azide prepared from IV (0.120 g) was added and the reaction mixture was stirred at 4 °C for further 20 h. After evaporation of solvents, the product was distributed into *n*-BuOH and 10% AcOH in 5 separated funnels and the *n*-BuOH layers containing the desired material were evaporated. Ethyl acetate was added to the residual solution to give amorphous material, which was reprecipitated from MeOH with ethyl acetate to give IX.

The protected docosapeptide, IX, was dissolved in liquid ammonia (20 ml) and small pieces of Na were added until the blue color of the reaction mixture was maintained for 2 min. Ammonium chloride (1.0 g) was added and ammonia was evaporated off. The residue was dissolved in 50% AcOH and applied to a Sephadex G-25 column (3.1 × 190 cm) which was eluted with the same solvent. Fractions of 15 g each were collected. The desired material was located in the tubes No. 36—46. The solvents of these fractions were evaporated and the residue was dissolved in 0.01 M NH_4OAc (pH 4.5) (5 ml). The solutions were applied to a column of CM-Sephadex C-25 (2.0 × 5 cm) equilibrated with the buffer. The column was washed with 0.01 M NH_4OAc (pH 4.5) (200 ml) and then eluted with linear gradient of NH_4OAc (pH 4.5) from 0.01 M to 0.5 M using 0.01 M (500 ml) and 0.5 M (500 ml) of the buffer. Fractions of 10 g each were collected. Each fraction was examined by TLC in two different solvent systems and UV absorption at 278 nm. The desired material with minor contamination was eluted in the tubes No. 65—85. The eluates were collected and the solvent was evaporated. After repeated lyophilization, the product was dissolved in 50% AcOH and applied on Bio-Gel P-6 column (3.2 × 190 cm), which was eluted with the same solvent. Fractions of 10 ml each were collected. The desired peptide behaving as a single component on TLC was located in tubes No. 64—75. These were pooled and lyophilized; yield, 49 mg. $[\alpha]_D^{20}$ −53.7° (*c* 0.49 H_2O); R_f^I 0.15, R_f^{II} 0.43; amino acid ratios in acid hydrolysate: Phe, 1.87; Val, 0.96; Pro, 0.96; Ile, 1.04; Thr, 0.94; Tyr, 0.97; Gly, 2.00; Glu, 5.60; Leu, 1.07; Arg, 2.00; Met, 0.77; Lys, 2.13; Asp, 1.00 (average recovery 88%); amino acid ratios in AP-M digest[10]: Phe, 2.18; Ile, 1.22; Tyr, 0.97; Gly, 2.08; Glu, 2.90; Leu, 1.01; Arg, 1.69; Met, 0.84; Lys, 2.10 (recovery 81%) (Asn, Gln and Thr were not estimated and Val and Pro were found in trace).[11,12] Found: C, 47.45; H, 7.39: N, 15.38%. Calcd for $C_{120}H_{188}O_{35}N_{34}S \cdot CH_3COOH \cdot 18H_2O$: C, 47.52; H, 7.45; N, 15.44%.

The authors wish to express their sincere thanks to Dr. Zen Itoh, the Department of Surgery of Gunma University, for bioassay. Thanks are also due to Mr. Akihiko Otsuka, vice president of Otsuka Pharmaceutical Co., Ltd., for his support during the course of this work.

References

1) The amino acids except glycine are L-configuration.

Abbreviations used are: Z, benzyloxycarbonyl; Tos, *p*-toluenesulfonyl; HBr, hydrogen bromide; Boc, *t*-butoxycarbonyl; *n*-BuOH, 1-butanol; HCl, hydrogen chloride; TFA, trifluoroacetic acid; DMF, *N,N*-dimethylformamide; TEA, triethylamine; AP-M, aminopeptidase-M.

2) J. C. Brown, M. A. Cook, and J. R. Dryburge, *Can. J. Biochem.*, **51**, 533 (1973).

3) H. Schubert and J. C. Brown, *Can. J. Biochem.*, **52**, 7 (1974).

4) S. Mihara, F. Shimizu, and S. Miyamoto, *Bull. Chem. Soc. Jpn.*, **49**, 3589 (1976).

5) Y. Kai, H. Kawatani, and H. Yajima, *Chem. Pharm. Bull.*, **23**, 2346 (1975).

6) S. Yamada, N. Ikota, T. Shioiri, and S. Tachibana, *J. Am. Chem. Soc.*, **97**, 7174 (1975).

7) E. Wünsch, J. C. Brown, K. H. Deimer, F. Dres, E. Jaeger, J. Musiol, H. Stocker, P. Thamm, and G. Wendelberger, *Z. Naturforsch.*, **28c**, 235 (1973).

8) J. Honzl and J. Rudinger, *Collect. Czech. Chem. Commun.*, **26**, 2333 (1961).

9) AP-M was purchased from Röhm and Hass GMBH, Darmstadt. (Lot No. 2056195).

10) K. Hofmann, F. M. Finn, M. Limetti, J. Montibeller, and G. Zanetti, *J. Am. Chem. Soc.*, **88**, 3633 (1966).

11) E. C. Jorgensen, G. C. Windrige, W. Patton, and J. C. Lee, *J. Med. Chem,*. **12**, 733 (1969).

12) N. Yanaihara, C. Yanaihara, M. Sakagami, K. Tsuji, T. Hashimoto, T. Kaneko, H. Oka, A. V. Schally, A. Arimura, and T. W. Redding, *J. Med. Chem.*, **16**, 373 (1973).

The Reaction of Disodium Tetracarbonylferrate(−II) with Aldehydes[1]

Masakazu YAMASHITA, Yoshihisa WATANABE, Take-aki MITSUDO, and Yoshinobu TAKEGAMI

Department of Hydrocarbon Chemistry, Faculty of Engineering, Kyoto University, Sakyo-ku, Kyoto 606

(Received June 1, 1976)

Disodium tetracarbonylferrate (−II) is an efficient catalyst for the dismutation of aromatic aldehydes to esters, $2RCHO \rightarrow RCOOCH_2R$. Aliphatic ones give aldol-condensation products upon treatment with the ferrate. A successive reaction of the ferrate with an aldehyde, RCHO, and then with alkyl iodide, R'I, gives an ester, $R'COOCH_2R$, after protonation. The mechanisms of these reactions are discussed.

Disodium tetracarbonylferrate(−II) (**1**) is known to be a selective reagent for organic syntheses. For example, using this reagent, alkyl halides or carboxylic acid derivatives are selectively converted into aldehydes[2-5] or ketones,[6,7] and enol esters are derived from β-oxoalkyl halides.[8]

Although the reactions of alkyl halides, tosylates, or carboxylic acid derivatives with **1** have been studied hitherto, little attention has been paid to the reaction of **1** with carbonyl compounds. This report will deal with the reaction of **1** with aldehydes.

Results and Discussion

Certain aldehydes react with **1** under mild conditions to give an ester; two aldehyde groups are transformed into the corresponding alkoxyl and carboxyl functions, existing in combination as an ester. These reactions proceed by means of a catalytic amount of

$$2RCHO \xrightarrow{(1)} RCOOCH_2R$$

1. When benzaldehyde (100 mmol) was treated with **1** (3 mmol) in tetrahydrofuran at 25 °C for 40 h under an argon atmosphere, an essentially complete convertion of the aldehyde was observed and benzyl benzoate was obtained in a 95% yield. Under similar conditions, *p*-tolualdehyde, *p*-chlorobenzaldehyde, and α-naphthaldehyde gave the corresponding esters. *p*-Anisaldehyde scarcely reacted with **1** at 25 °C, but gave the *p*-methoxybenzyl *p*-methoxybenzoate ester at 60 °C. The by-products obtained in these reactions were small amounts of alcohols such as benzyl alcohol (less than 3%). Aliphatic aldehydes and furfural also reacted with **1** under identical conditions, but the corresponding esters were not obtained. Furfural gave only tarry materials upon treatment with **1**. The treatment of aliphatic aldehydes such as *n*-butyraldehyde with an equimolar amount of **1** gave aldol condensates and then hydrogenated products, such as 2-ethyl-2-hexenal and 2-ethylhexanal. The formation of these products is due to the basicity of **1**, $[Fe(CO)_4]^{2-}$[9] and the reducing ability of $[FeH(CO)_4]^-$[10] which transforms α,β-unsaturated carbonyl compounds into saturated ones.[11] The results are summarized in Table 1. The conditions were not optimized for these reactions. These reactions are scarcely affected by the atmosphere; no remarkable difference was detected in the reaction rates under a carbon monoxide atmosphere compared with that under an argon atmosphere.

In the reactions of *p*-substituted benzaldehydes with **1**, there is a remarkable influence of the substituents on the relative reaction rates. The yields of esters *vs.* time plots for the reaction of **1** with the substituted benzaldehydes are shown in Fig. 1. The apparent order of their reactivities was as follows: $p\text{-}ClC_6H_4CHO > C_6H_5CHO > p\text{-}CH_3C_6H_4CHO > p\text{-}CH_3OC_6H_4CHO$. The reactivity decreases with an increase in the electron-releasing property of the substituents. This suggests that the reaction is influenced by the electron density on the carbonyl carbon of the aldehydes which the ferrate (**1**) attacks nucleophilically.

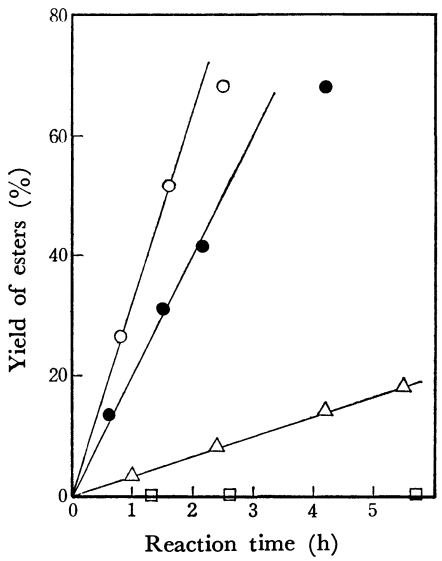

Fig. 1. Yield of ester *vs.* time plots for the reaction of $Na_2Fe(CO)_4$ with aldehydes (in THF, at 25 °C, under argon).
○ : *p*-Chlorobenzaldehyde, ● : benzaldehyde, △ : *p*-tolualdehyde, □ : *p*-anisaldehyde.

When an equimolar mixture of benzaldehyde (50 mmol) and *p*-anisaldehyde (50 mmol) was stirred with **1** (3 mmol) at 25 °C, 17 mmol of benzyl benzoate and 11 mmol of benzyl *p*-methoxybenzoate were obtained, but no *p*-methoxybenzyl *p*-methoxybenzoate and *p*-methoxybenzyl benzoate were produced. This shows that *p*-anisaldehyde can react as only an acid component even at 25 °C, though alone it scarcely reacts with **1** at this temperature (Exp. 5).

As the reaction scheme, the following one is considered (Scheme 1). First, the ferrate (**1**) attacks the carbonyl carbon of the aldehyde nucleophilically to give an adduct (**2**). The addition of the second aldehyde to **2** is followed by the loss of the ferrate

TABLE 1. REACTION OF ALDEHYDES WITH $Na_2Fe(CO)_4$

Exp. No.	Aldehyde (mmol)	$Na_2Fe(CO)_4$ (mmol)	Reaction conditions: Temp (°C)	Time (h)	Solvent	Product	Yield (%)[a]
1	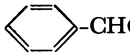 (100)	3	25	40	THF		95
2	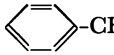 (100)	3	25	20	THF-NMP[b] 1 : 1		92
3	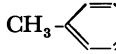 (100)	3	25	50	THF		73
4	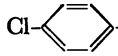 (100)	3	25	20	THF		90
5	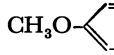 (100)	3	25	50	THF	—[c]	—
6	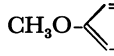 (100)	3	60	20	THF		76
7	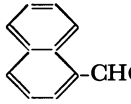 (100)	3	25	40	THF		72
8	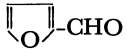 (30)	6	25	20	THF	—[d]	—
9	$CH_3CH_2CH_2CHO$ (13)	11	25	3	THF	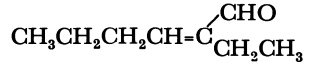	38
						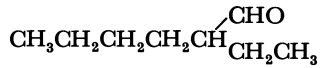	32
10	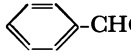 (50)	3	25	40	THF		(17 mmol)
	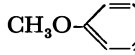 (50)					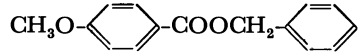	(11 mmol)

a) Based on the amount of aldehydes. b) *N*-Methylpyrrolidone. c) The remainder consisted mainly of the starting material. d) Tarry materials were obtained.

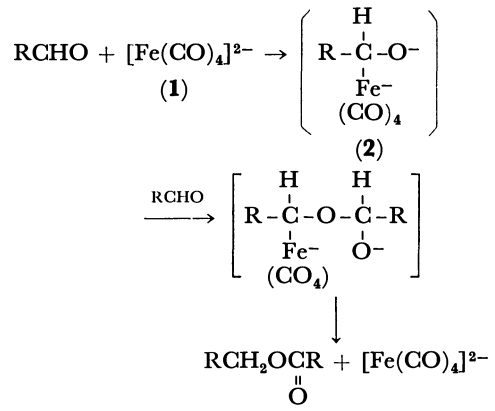

Scheme 1.

to give the esters. This scheme is roughly the same as that of the well-known variations of the base-induced dismutation of aldehydes, *e.g.*, catalyzed by the RO^- alkoxide.[12] In the base-catalysed dismutation of aldehydes, the view that the first step of the reaction proceeds by an initial coordination of the base with the aldehyde carbonyl group is supported by the investigations of the effect of substituents upon the rate of the reaction.[12]

The formation of benzyl *p*-methoxybenzoate (Exp. 10) implies that *p*-anisaldehyde is able to react with the adduct (**2**), as a second aldehyde, though it does not form an adduct (**2**) upon treatment with **1** at 25 °C.

After **1** had been stirred with an equimolar amount of an aldehyde (R^1CHO) in tetrahydrofuran at 25 °C for 5 h, an excess of alkyl iodide (R^2I) was added and the reaction mixture was stirred for an additional 5 h. After the treatment of the mixture with acetic acid and a usual workup, a second ester, $R^2COOCH_2R^1$, was obtained besides the $R^1COOCH_2R^1$ ester. The

results are listed in Table 2. The acetyl and propionyl groups of the esters ($R^2COOCH_2R^1$) appear to be from methyl or ethyl iodide, and the ferrate

Table 2. Successive reactions of $Na_2Fe(CO)_4$ with aldehyde and with alkyl iodide[a]

Exp. No.	Aldehyde (mmol)	RI (mmol)	Reaction conditions: Temp (°C)	Time (h) (A)[b]	Time (h) (B)[c]	Products	Yield[d] (%)
11	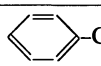 (11)	CH_3I (30)	25	5	5		75
						CH_3COOCH_2-	13
12	(11)	CH_3I (30)	25	4	5		70
						CH_3COOCH_2-	10
13	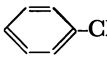 (11)	CH_3CH_2I (25)	25	5	5		70
						$CH_3CH_2COOCH_2$-	9
14	CH_3- -CHO (11)	CH_3I (30)	25	6	6	CH_3- 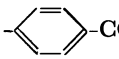 -$COOCH_2$- 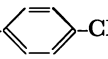 -CH_3	42
						CH_3COOCH_2- 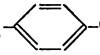 -CH_3	22

a) Eleven mmol of $Na_2Fe(CO)_4$ were used in each run. b) Prior to addition of alkyl iodide. c) After addition of alkyl iodide. d) Based on the amount of aldehydes.

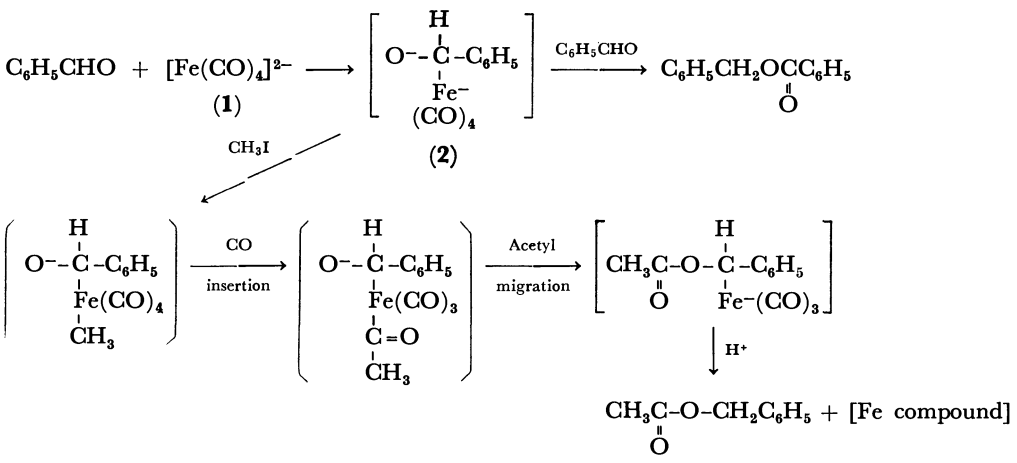

Scheme 2.

(**1**), *via* a carbonyl insertion reaction.

In these reactions, the initial adduct (**2**) (in Scheme 1) is also assumed to be an intermediate. As for the formation of benzyl acetate, the following reaction scheme is considered (Scheme 2). The adduct (**2**) is methylated at first;[13] this is followed by a carbonyl insertion reaction, the intramolecular migration of the acetyl group,[14] and protonation to give benzyl acetate. The fact that the deuteration of the reaction mixture with deuterium oxide instead of protonation gave deuterated benzyl acetate, $CH_3COOCH(D)C_6H_5$, is consistent with the scheme described above.

The effect of disodium tetracarbonylferrate (**1**) as a catalyst of the dismutation of aldehydes to the ester is assumed to be due to its high nucleophilicity. Less nucleophilic alkyl or acyl carbonylferrates(0) did not react with the aldehydes used in this reaction.

Experimental

The aldehydes were all commercial products; they were dehydrated over Drierite and distilled twice before use. The disodium tetracarbonylferrate (**1**) was prepared according to the method described in the literature.[3] The pentacarbonyliron was a commercial product and was used without further purification. The methyl iodide and ethyl iodide were also commercial products and were distilled before use. The solvent, tetrahydrofuran, was purified by distillation after being dried over lithium aluminium hydride.

Reaction of Aldehydes with ***1***. The reaction of benzaldehyde with **1** illustrates a typical procedure. Freshly distilled benzaldehyde (100 mmol) was added to a solution of 3 mmol of **1** in 25 ml of tetrahydrofuran, and the mixture was stirred at 25 °C under an argon atmosphere. After 40 h, the solvent was evaporated and the liquid thus obtained was chromatographed over alumina and then distilled to give pure benzyl benzoate(yield, 95%). The identity was established by a comparison of the spectral data(IR and NMR) and retention time of GLPC with those of an authentic sample. In the case of *p*-chlorobenzaldehyde and α-naphthaldehyde, the products were purified by recrystallization after being chromatographed.

The reaction procedure of butyraldehyde with (**1**) was as follows. To a solution of 11 mmol of (**1**) in tetrahydrofuran (40 ml), we added 0.94 g (13 mmol) of freshly distilled butyraldehyde, after which the reaction mixture was stirred at 25 °C for 3 h under an argon atmosphere. Then the mixture was poured into 50 ml of water and extracted with 50 ml of diethyl ether, after which the organic extracts were submitted to GLPC analysis. The products, 2-ethyl-2-hexenal and 2-ethylhexanal, were identified by a comparison of the retention time of the GLPC with those of authentic samples; the yields were determined using internal standards.

Successive Reaction of ***1*** *with Aldehydes and with Alkyl Iodides.* In a typical procedure, into 11 mmol of **1** in tetrahydrofuran (50 ml) we stirred 11 mmol of aldehyde in tetrahydrofuran (10 ml) at 25 °C under an argon atmosphere. A few hours later, the reaction mixture was treated with an excess of alkyl iodide and stirred for an additional 5 h. After 2 ml of water or acetic acid had then been poured into the reaction mixture, the solvent was evaporated and the residue was fractionally distilled. The esters thus obtained were identified by means of their spectral data (IR and NMR) and by a comparison of the retention time of the GLPC with those of authentic samples; the yields were determined using internal standards.

References

1) This work was presented at the 34th Annual Meeting of the Chemical Society of Japan, Hiratsuka, April, (1976).
2) M. P. Cooke, Jr., *J. Am. Chem. Soc.*, **92**, 6080 (1970).
3) Y. Watanabe, T. Mitsudo, M. Tanaka, K. Yamamoto, T. Okajima, and Y. Takegami, *Bull. Chem. Soc. Jpn.*, **44**, 2569.
4) Y. Watanabe, M. Yamashita, T. Mitsudo, M. Igami, and Y. Takegami, *Bull. Chem. Soc. Jpn.*, **48**, 2490 (1975).
5) Y. Watanabe, M. Yamashita, T. Mitsudo, M. Igami, K. Tomi, and Y. Takegami, *Tetrahedron Lett.*, **1975**, 1063.
6) J. P. Collman, S. R. Winter, and D. R. Clark, *J. Am. Chem. Soc.*, **94**, 1788 (1972).
7) J. P. Collman and N. W. Hoffman, *J. Am. Chem. Soc.*, **95**, 2689 (1973).
8) T. Mitsudo, Y. Watanabe, T. Sasaki, H. Nakanishi, M. Yamashita, and Y. Takegami, *Tetrahedron Lett.*, **1975**, 3163.
9) The basicity of $[Fe(CO)_4]^{2-}$ is estimated to be about that of the $[OH]^-$ ion; W. Hieber and W. Hubel, *Z. Electrochem.*, **57**, 235 (1953).
10) $[FeH(CO)_4]^-$ is formed from $[Fe(CO)_4]^{2-}$ and H_2O, which is itself formed from an aldol condensate.
11) R. Noyori, I. Umeda, and T. Ishigami, *J. Org. Chem.*, **37**, 1542 (1972).
12) T. A. Geissman, "Organic Reactions," Vol. 2, ed. by R. Adams, John Wiley & Sons, New York, N. Y. (1957), p. 94.
13) The alkylation of carbonylferrate complexes(0) by alkyl iodides occurs at the iron atom; see H. L. Conder and M. Y. Darensbourg, *Inorg. Chem.*, **13**, 506 (1974) and the references cited therein.
14) The intramolecular migration of an acyl group from the cobalt to the oxygen of a carbonyl group of an aldehyde has been suggested; R. F. Heck, *J. Am. Chem. Soc.*, **87**, 4727 (1965).

Formation and Reactions of Alkoxydiaminosulfonium Salts

Hiroshi MINATO,* Kentaro OKUMA, and Michio KOBAYASHI

Department of Chemistry, Tokyo Metropolitan University, Fukazawa, Setagaya, Tokyo 158

(Received June 7, 1976)

Ethoxydimorpholinosulfonium tetrafluoroborate and tetraphenylborate were prepared by ethylation of dimorpholino sulfoxide. They were readily hydrolyzed with water but did not react with methanol. In the reactions with nucleophiles, they acted as ethylating agent for β-picoline, triethylamine, diethylamine, methoxide ion, and chloride ion. When dimorpholino sulfide, 1-chlorobenzotriazole, and an alcohol were allowed to react at −80 °C, the main products were an alkyl chloride, dimorpholino sulfoxide, and morpholinium chloride. Alkoxydimorpholinosulfonium chloride was presumed to be the intermediate, which decomposed by an S_N2-type nucleophilic attack of chloride ion on the alkyl group. When (+)-2-octanol was used, the 2-chlorooctane formed was of almost completely inverted configuration (enantiomeric excess, 97%). The yield of alkyl chlorides decreased in the order of methyl (80%), isopropyl (51), and *t*-butyl (20).

Dialkoxysulfonium ions,[1-3] alkoxyaminosulfonium ions,[3,4] diaminosulfonium ions[5] were reported, but sulfonium ions possessing three hetero-substituents have not been described in the literature except a short communication from our laboratories.[6] Since alkoxydiaminosulfonium ions appear to be interesting species, we have studied their chemistry, and the results are described in this paper.

Results and Discussion

The synthesis of alkoxydiaminosulfonium ions was attempted by alkylation of diamino sulfoxides. Diamino sulfoxides were prepared by the reaction of an amine with thionyl chloride. They are readily decomposed by a trace amount of moisture, and must be handled with great care. Ethoxydimorpholinosulfonium tetrafluoroborate (**1a**) was successfully prepared by ethylation of dimorpholino sulfoxide (**2**) with triethyloxonium tetrafluoroborate (**3**) in well-dried dichloromethane in a dry box. The pale-yellow

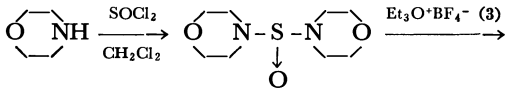

2

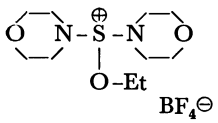

1a

crystals obtained are extremely moisture-sensitive, and all the synthetic procedure must be carried out in a dry box. They are easily decomposed by a small amount of water in solvents or in the atmosphere, and morpholinium salts are produced. However, when crude crystals of **1a** were dissolved in anhydrous methanol and recrystallized, purified crystals were obtained without decomposition or alcohol exchange. Thus, alkoxydiaminosulfonium ions are not affected by alcohols, but extremely sensitive towards water. The reaction with water produces HBF_4, which probably catalyzes the decomposition.

In an attempt to convert **1a** into crystals which can be handled more easily, crystals of **1a** were dissolved in acetone and anion exchange was attempted by addition of an acetone solution of sodium tetraphenylborate. However, such treatment simply hydrolyzed **1a**, and ethoxydimorpholinosulfonium tetraphenylborate (**1b**) was not obtained. After several attempts, crystalline **1b** was successfully prepared when sodium tetraphenylborate was added to the reaction mixture without isolating solid **1a**. In a similar manner, crystalline ethoxybis(diethylamino)sulfonium tetraphenylborate was prepared.

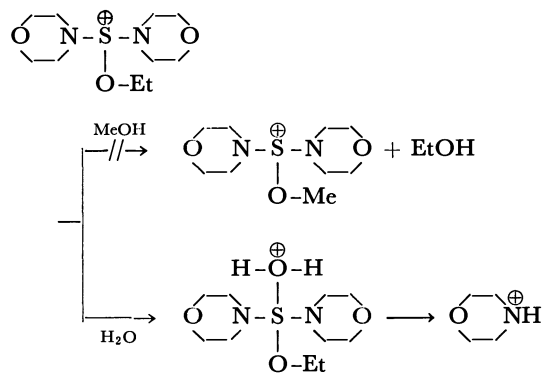

Crystalline **1b** can be handled much more easily than **1a**, and its elemental analyses gave satisfactory results. It was possible to determine its melting point too.

When the reactivity of **1b** with methanol and water was examined, it was found that an equimolar mixture of **1b** and methanol in hexadeuterioacetone did not react at all after 1 day, whereas **1b** was completely hydrolyzed when its hexadeuterioacetone solution was allowed to stand in an uncapped PMR tube for 1 day.

Such remarkable difference in reactivities of **1** with water and methanol appears to be of considerable interest, and we investigated reactions of a simpler alkoxysulfonium salt, dimethylethoxysulfonium tetrafluoroborate. When this alkoxysulfonium salt was

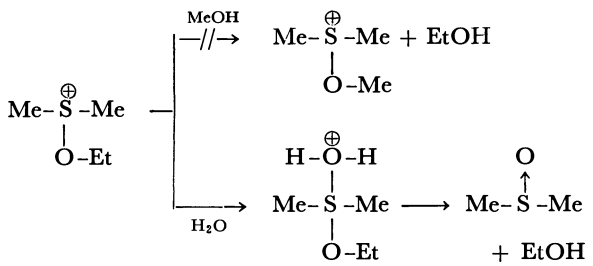

allowed to stand in methanol for 12 h, it did not react at all with methanol, whereas in a hexadeuterioacetone solution containing water (10 equiv.) 65% of the salt was hydrolyzed in 12 h.

Smith and Winstein found that dimethylbenzyloxysulfonium tosylate was not solvolyzed in absolute methanol but yielded benzyl alcohol upon addition of water.[6,7] Thus not only **1** but also dialkylalkoxysulfonium salts are very reactive with water and not reactive with alcohols.

By use of ^{18}O-enriched water[8] and an optically-active alkoxysulfonium salt,[9] Johnson and his coworkers showed that the hydrolysis of alkoxysulfonium salts proceeds by a nucleophilic displacement on sulfur with inversion of configuration of the sulfur atom. It is likely that the hydrolysis of **1** proceeds in a similar manner.

Then the reactions of **1** with nucleophiles were investigated. When **1a** was mixed with an equimolar amount of β-picoline at room temperature, **1a** acted as an ethylating agent but only in a 40% yield. The rest of the **1a** used was hydrolyzed by moisture in solvent and atmosphere, and morpholinium tetrafluoroborate was formed.

When equimolar amounts of **1b** and triethylamine were allowed to react in hexadeuterioacetone, the products showed that both ethylation of the amine (50%) and hydrolysis with moisture (50%) took place.

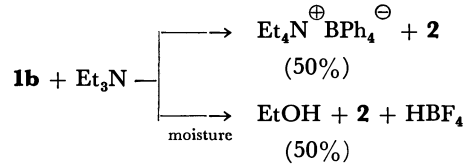

In a similar manner, the treatment of **1b** with diethylamine resulted in ethylation of the amine (40%) and hydrolysis with moisture (60%).

When **1b** was let to react with a slightly excess of potassium methoxide in hexadeuterated DMSO, **1b** ethylated the nucleophile.

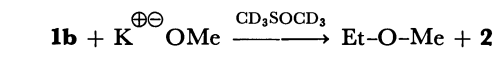

When **1b** and lithium chloride were dissolved in hexadeuterioacetone, the PMR spectrum of the solution showed that **1b** was converted to ethyl chloride and **2**.

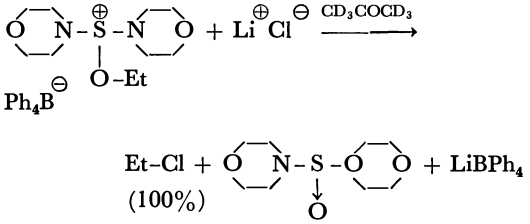

The reactivity of **1** with nucleophiles is summarized below, and compared with those of alkoxyaminosulfonium ions,[3] dialkoxysulfonium ion,[1] and alkoxysulfonium ions.[10,11] The above comparison shows that alkoxysulfonium ions possessing an amino group, two amino groups, or another alkoxy group receive the attack of nucleophiles (except water) on the carbon atom adjacent to the oxygen atom. Thus, the reactions of hetero-atom substituted alkoxysulfonium ions with nucleophiles are simpler than those of alkylaryl-alkoxysulfonium ions.[11]

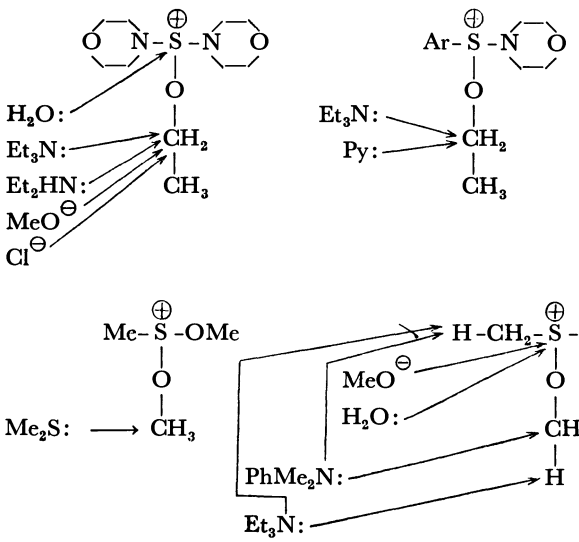

Since the main reaction of **1** with nucleophiles has been shown to be ethylation of the nucleophiles, it seems desirable to study the reactions of alkoxydiaminosulfonium salts other than **1**. However, it was not possible to prepare such sulfonium salts by the method used for the preparation of **1**, because trimethyloxonium tetrafluoroborate is not soluble in dichloromethane, and neither triisopropyl- nor tri-*t*-butyloxonium salts are available.

Therefore, preparation of alkoxydiaminosulfonium salts was attempted from other routes. Johnson *et al.*[13] prepared alkoxysulfonium salts by treating dialkyl sulfides with 1-chlorobenzotriazole, an alcohol and silver tetrafluoroborate. If diamino sulfides react in a similar manner, formation of alkoxydiaminosulfonium salts is expected. Therefore, equimolar amounts

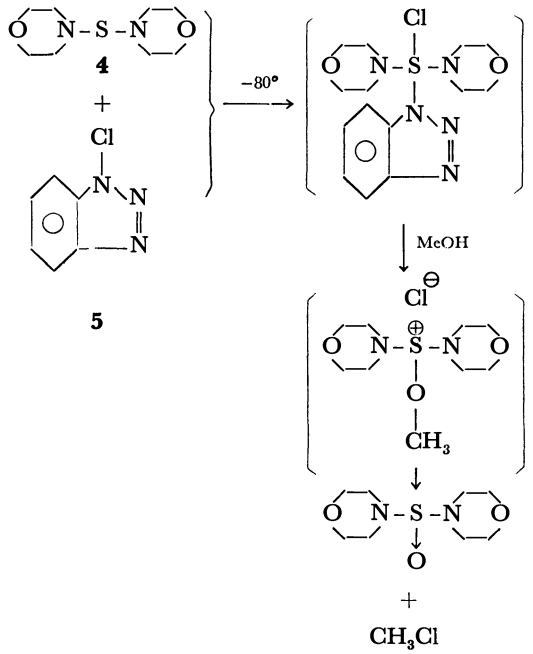

of dimorpholino sulfide (**4**) and 1-chlorobenzotriazole (**5**) were mixed in dichloromethane at −80 °C, and to the yellow solution formed (a sulfurane[13]) an equimolar amount of methanol was added. When the mixture was warmed up, its PMR spectrum suggested that the reaction shown above occurred. Methoxydimorpholinosulfonium chloride is the product expected from the results of Johnson *et al.*[13] Since we have already shown that **1b** is readily converted by chloride ion to **2** and ethyl chloride, the scheme shown above probably represents the main reactions taking place in a mixture of **4**, **5**, and an alcohol. In order to determine the stereochemistry of this nucleophilic reaction on the carbon atom adjacent to the oxygen atom, (+)-2-octanol was treated in a similar manner. The 2-chlorooctane obtained was found to be of almost completely inverted configuration (enantiomeric excess, 97%). Thus the nucleophilic attack of chloride ion on an alkoxydiaminosulfonium ion is an S_N2-type reaction with inversion of configuration.

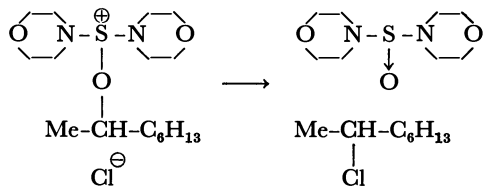

Table 1 summarizes the results of reactions of diamino sulfide (**4** or bis(dimethylamino) sulfide (**6**)) with **5** (or *N*-chlorosuccinimide (**7**)) and an alcohol (MeOH, *i*-Pr-OH, or *t*-BuOH).

As shown in Table 1, the yields of alkylation of chloride by alkoxydiaminosulfonium ions decrease in the order of Me, *i*-Pr, and *t*-Bu. This fact is probably ascribable to greater tendency for S_N1-type reaction of alkoxydiaminosulfonium ions when the alkyl group is secondary or tertiary. When **7** was used in place of **5**, yields were not improved, but when **6** was used in place of **4**, the yields were improved. Even with isopropyl alcohol, S_N2-type alkylation of chloride took place in an 85% yield.

Table 1. Products of the reaction of diamino sulfides with 5 (or 7) and alcohols

Reactants	Products (mol %)
4 + **5** + MeOH	MeCl(80), **2**(80)
4 + **5** + *i*-PrOH	*i*-PrCl(51), *i*-PrOH(21), **2**(60)
4 + **5** + *t*-BuCl(20)	*t*-BuCl(20), *t*-BuOH(10)
4 + **5** + (+)-2-octanol	(−)-octylCl (25)[a]
4 + **7** + MeOH	MeCl(45),
4 + **7** + *i*-PrOH	*i*-PrCl(47), Me_2CO(6)
4 + **7** + *t*-BuOH	*t*-BuCl(18), *t*-BuOH(16)
6 + **7** + MeOH	many products
6 + **7** + *i*-PrOH	*i*-PrCl(51), *i*-PrOH(40), Me_2CO(8.7)
6 + **7** + *t*-BuOH	*t*-BuCl(35)
6 + **5** + MeOH	MeCl(83), $(Me_2N)_2S{\rightarrow}O$ (90)
6 + **5** + *i*-PrOH	*i*-PrCl(85), $(Me_2N)_2S{\rightarrow}O$ (78)
6 + **5** + *t*-BuOH	*t*-BuCl(40)
6 + **5** + 2-octanol	2-octylCl (51),[a,b] $(Me_2N)_2S{\rightarrow}O$ (95)

a) Yield after isolated. b) By PMR, the yield was 70%.

Corey et al. treated succinimidodimethylsulfonium ion with benzyl and allyl alcohols, and obtained the corresponding chloride.[14] However, their reaction works only with benzyl and allyl alcohols, and not with ordinary primary or secondary alcohols. It is of interest that in our system a primary alcohol or a secondary alcohol is transformed into chloride in much better yield than a tertiary alcohol.

Experimental

Dimorpholino sulfide (mp 125—126°; lit,[15] 125—126 °C), and bis(dimethylamino) sulfide (bp 30—32 °C/15 Torr; lit,[15] 33.5—36 °C/14 Torr) were prepared by the methods described in the literature.[15] (+)-2-Octanol was purchased from Fluka AG; $[\alpha]_{546}^{20}=+11°$.

Dimorpholino sulfoxide was prepared from morpholine and thionyl chloride; mp 52 °C.[16] Bis(diethylamino) sulfoxide was prepared in a similar manner.

1-Chlorobenzotriazole was prepared from benzotriazole and a 10% aq NaOCl solution according to the method in the literature.[13]

*Formation of Ethoxydimorpholinosulfonium Tetrafluoroborate (**1a**).* After a dichloromethane solution of **2** (40 mmol) and **3** (42 mmol) was refluxed for 2 h, ether was added. The brown-black oil which precipitated was recrystallized from methanol in a dry box. Pale yellow crystals of **1a** were obtained (24.6%). PMR (CD_3COCD_3), δ 1.52 (t, 3, CH_3), 3.50—3.71 (m, 8, N-CH_2), 3.74—4.00 (m, 8, O-CH_2), 4.61 (q, 2, $C\underline{H}_2CH_3$). Because of its instability, it was not possible to carry out successful elemental analysis.

*Reaction between **1a** and β-Picoline.* An equimolar mixture of the reactants were allowed to stand in CD_3COCD_3 at room temperature for 2 h, and *N*-ethylpicolinium salt was found in a 40% yield (identified by comparison with an authentic sample). PMR(CD_3COCD_3), δ 1.71 (t, $C\underline{H}_3$-CH_2), 2.60 (s, CH_3-Py), 4.80 (q, $C\underline{H}_2CH_3$).

*Formation of Ethoxydimorpholinosulfonium Tetraphenylborate (**1b**).* A dichloromethane solution (30 ml) of **2** (10 mmol) and **3** (10.6 mmol) was refluxed for 2 h, and to this orange-red solution an acetone solution (25 ml) of $NaBPh_4$(9.36 mmol) was added. Addition of some ether and acetone precipitated $NaBF_4$, and further addition of ether precipitated **1b**: 3.85 g (67.7%). Repeated crystallizations from acetone–ether yielded white prisms, mp 113 °C (dec). Found: C, 71.78; H, 7.54; N, 5.02%. Calcd for $C_{34}H_{41}N_2O_3BS$: C, 71.82; H, 7.27; N, 4.93%. PMR(CD_3COCD_3) δ 1.47 (t, 3, J= 7.2 Hz, $C\underline{H}_3CH_2O$), 3.30—3.57 (m, 8, $NC\underline{H}_2$), 3.63—3.90 (m, 8, $NCH_2C\underline{H}_2O$), 4.46 (q, 2, J=7.2 Hz, $OC\underline{H}_2CH_3$), 6.82—7.53 (m, 20, C_6H_5); ^{13}CMR(CD_3COCD_3) δ 15.34 ($\underline{C}H_3CH_2O$), 47.07 ($NCH_2\underline{C}H_2O$), 66.88 ($N\underline{C}H_2$), 72.07 ($O\underline{C}H_2CH_3$).

Ethoxybis(diethylamino)sulfonium Tetraphenylborate was prepared in a similar manner; yield, 60.0%, mp 119 °C (dec). Found: C, 75.39; H, 8.85; N, 4.90%. Calcd for $C_{34}H_{55}N_2OBS$: C, 75.54; H, 8.39; N, 5.18%. PMR(CD_3COCD_3) δ 1.22 (t, 12, J=7.0 Hz, $C\underline{H}_3CH_2N$), 1.45 (t, 3, J=6.5 Hz, $C\underline{H}_3CH_2O$), 3.46 (q, 8, J=7.0 Hz, $CH_3C\underline{H}_2N$), 4.28 (q, 2, J=6.5 Hz, $CH_3C\underline{H}_2O$); ^{13}CMR(CD_3COCD_3) δ 13.72 ($\underline{C}H_3CH_2N$), 15.18 ($\underline{C}H_3CH_2O$), 42.45 ($CH_3\underline{C}H_2N$), 70.29 ($CH_3\underline{C}H_2O$).

*Decomposition of **1b** in CD_3COCD_3.* When a CD_3COCD_3 solution of **1b** was allowed to stand in an uncapped PMR

tube at room temperature for 1 day, **1b** was hydrolyzed and morpholinium tetraphenylborate precipitated, which was identified by determining its PMR spectrum in CD_3SOCD_3.

*Treatment of **1b** with Methanol in CD_3COCD_3.* When equimolar amounts of **1b** and well-dried methanol were dissolved in CD_3COCD_3 and allowed to stand in a capped PMR tube at room temperature for 1 day, no change was observed in its PMR spectrum.

Reaction between Dimethylethoxysulfonium Tetrafluoroborate and D_2O or CD_3OD. When a CD_3COCD_3 solution of the salt (1 equiv.) and D_2O (10 equiv.) was allowed to stand for 12 h at 34 °C, its PMR spectrum showed that 65% of the salt was hydrolyzed, forming CH_3SOCH_3 (δ 2.67) and EtOD (δ 1.10(t) and 3.56(q)). When a CD_3OD solution of the salt was allowed to stand for 12 h at 34 °C, no CD_3O-EtO exchange was observed and about 10% of the salt was hydrolyzed probably by the moisture in CD_3OD, forming CH_3SOCH_3 and EtOD.

*Reaction between **1b** and Triethylamine.* When equimolar amounts of **1b** and triethylamine were mixed in CD_3COCD_3 at room temperature, reaction was complete in 3 h, and tetraethylammonium tetraphenylborate precipitated. It was filtered and identified by determining its PMR spectrum in CD_3SOCD_3; δ 1.22 (t, 3, CH_3), 3.21 (q, 2, CH_2); yield, 50%. In the filtrate, ethanol (50%) and **2**(100%) (PMR-(CD_3COCD_3), δ 2.90—3.12 (NCH_2), 3.60—3.78 (OCH_2)) were found.

*Reaction between **1b** and Diethylamine.* When equimolar amounts of **1b** and diethylamine were mixed in CD_3COCD_3 at room temperature, reaction was complete in 20 min; its PMR spectrum showed complete disappearance of **1b** and formation of **2**. The precipitates formed were filtered, and their PMR spectrum in CD_3SOCD_3 showed the presence of $Et_3NH^+BPh_4^-$ (40%) (δ 1.34(t, 9, CH_3), 3.16 (q, 6, CH_2), and 6.80—7.50 (m, 20, C_6H_5)) and $Et_2NH_2^+BPh_4^-$ (60%) (δ 1.27 (t, 6, CH_3), 3.12 (q, 4, CH_2), and 6.80—7.50 (m, 20, C_6H_5)).

*Reaction between **1b** and Potassium Methoxide.* When CD_3SOCD_3 solutions of **1b** (0.53 mmol) and KOMe (0.93 mmol) were mixed at room temperature the PMR spectrum of the mixture showed that **1b** was quantitatively converted to ethyl methyl ether; δ 1.08 (t, 3, $\underline{CH_3}CH_2$), 3.18 (s, 3, CH_3O), and 3.47 (q, 2, CH_2).

*Reaction between **1b** and Chloride Ion.* When **1b** (1 equiv.) and lithium chloride (4 equiv.) were mixed in CD_3COCD_3 at room temperature, the PMR spectrum of the solution showed that **1b** was quantitatively converted to **2** and ethyl chloride (δ 1.47 (t, 3, J=7.2 Hz, CH_3), and 3.63 (q, 2, J=7.2 Hz, CH_2).

*Reaction of **4** with **5** and MeOH.* A dichloromethane solution (3 ml) of **4** (3.0 mmol) and dichloromethane solution (4 ml) of **5** (3.0 mmol) were cooled to −18 °C, and then mixed. To this yellow solution, a cooled dichloromethane solution (2 ml) of methanol (3.0 mmol) was added at −80 °C. Mixing of these three solutions must be done with exclusion of moisture either in a glass apparatus sealed from the atmosphere or in a dry box. The mixture was warmed up to room temperature. Distillation gave a distillate and a residue. The distillate contained CH_3Cl (δ 3.00; yield, 80%). The residue contained **2** [δ 3.00—3.20 (N-CH_2) and 3.60—3.80 (OCH_2); yield, 80%] and an unidentified methyl compound (δ 3.50; yield, 20%).

Reactions with other alcohols were carried out in a similar manner with equimolar mixtures.

The reaction of **6** with **5** and 2-propanol gave *i*-PrCl (δ 1.46 (d); yield 85%) and acetone (δ 2.13(s); yield 15%) in the distillate, and $(Me_2N)_2S\rightarrow O$ (δ 2.61 (s); yield 78%) and an unidentified compound (δ 2.81(s); yield 22%) in the residue.

*Reaction of **4** with **5** and (+)-2-Octanol.* An equimolar mixture (10 mmol each) of the reactants was treated as described above. 2-Chlorooctane was collected at 51—52°/14 Torr; yield, 25%. $[\alpha]_D^{23}=-34.91°$ (c 7.38, CH_2Cl_2); enantiomeric excess $\%=-34.91/-36.15^{17)}\times 100=96.6\%$.

References

1) H. Minato, K. Yamaguchi, and M. Kobayashi, *Chem. Lett.*, **1975**, 307.
2) H. Warthmann and A. Schmidt, *Chem. Ber.*, **108**, 520 (1975).
3) H. Minato, K. Yamaguchi, K. Okuma, and M. Kobayashi, *Bull. Chem. Soc. Jpn.*, **49**, 2590 (1976).
4) H. Minato, K. Yamaguchi, and M. Kobayashi, *Chem. Lett.*, **1975**, 991.
5) J. L. Richards and D. S. Tarbell, *J. Org. Chem.*, **35**, 2079 (1970).
6) H. Minato, K. Okuma, and M. Kobayashi, *J. Chem. Soc., Chem. Commun.*, **1975**, 868.
7) S. G. Smith and S. Winstein, *Tetrahedron*, **3**, 317 (1958).
8) S. G. Smith, Ph. D. Thesis, University of California, Los Angeles, Calif., 1959.
9) N. J. Leonard and C. R. Johnson, *J. Am. Chem. Soc.*, **84**, 3701 (1962).
10) C. R. Johnson and D. McCants, Jr., *J. Am. Chem. Soc.*, **87**, 5404 (1965).
11) K. Tsumori, H. Minato, and M. Kobayashi, *Bull. Chem. Soc. Jpn.*, **46**, 3503 (1973).
12) C. R. Johnson and W. G. Phillips, *Tetrahedron Lett.*, **1965**, 2101.
13) C. R. Johnson, C. C. Bacon, and W. D. Kingsbury, *Tetrahedron Lett.*, **1972**, 501.
14) E. J. Corey, C. U. Kim, and M. Takeda, *Tetrahedron Lett.*, **1972**, 4339.
15) E. S. Blake, *J. Am. Chem. Soc.*, **65**, 1267 (1943).
16) G. Zinner and W. Kollig, *Naturwissenschaften*, **46**, 354 (1959).
17) I. Heilbron and H. M. Bunberry, Ed., "Dictionary of Organic Compounds," Oxford Univ. Press, Vol. 4, New York (1953), p. 15.

Substituent Effect on the Dissociation Constants of 5-(Substituted Styryl)-2-aminotropones

Toshio KOBAYASHI, Kimiaki IMAFUKU, and Hisashi MATSUMURA

Department of Chemistry, Faculty of Science, Kumamoto University, Kurokami, Kumamoto 860

(Received June 7, 1976)

The dissociation constants of various 5-styryl-2-aminotropones were determined spectrophotometrically using 50%(v/v) aqueous methanol and correlated by the use of Hammett equation, with $\rho=0.57$.

The quantitative estimation of the transmission of electronic effects through a system of conjugated double bonds is of great theoretical importance and has attracted the attention of many chemists. The most convenient systems are aromatic compounds of the R–C_6H_4–CH=CH–G–Y type, where G is an aromatic ring, such as benzene, pyridine, and tropone. The dissociation constants of various 4-aminostilbenes (G=C_6H_4, Y=NH_2),[1] 4-hydroxystilbenes (G=C_6H_4, Y=OH),[2] and 4-styrylpyridines (G=C_5H_4N)[3] and the chemical shifts of 4-fluorostilbenes (G=C_6H_4, Y=F)[4] have been measured in the past. It has been found that the electronic effect of the substituent in one ring is transmitted through the ethylene linkage to the reaction center in another ring and correlated by the Hammett equation.

Previously, we reported the substituent effects on the dissociation constants of 4-[5] and 5-styryltropolones[6] and 4- and 6-styryl-2-aminotropones.[7] However, the substituent effect in 5-styryl-2-aminotropones has not been investigated. In the present study, the dissociation constants of several 5-styryl-2-aminotropones, shown in Fig. 1, were measured spectrophotometrically, and the electronic effects of the substituents on their dissociation constants were discussed quantitatively.

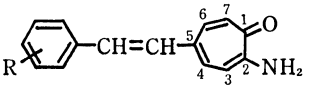

Fig. 1.

Results and Discussion

The dissociation constants of 5-(*p*-methoxystyryl)-, 5-(*p*-methylstyryl)-, 5-(*m*-methylstyryl)-, 5-styryl-, 5-(*m*-methoxystyryl)-, and 5-(*p*-chlorostyryl)-2-aminotropones were determined spectrophotometrically in 50%(v/v) aqueous methanol at 23 °C. Their pK_a values are listed in Table 1, together with their mp's. The pK_a value (2.21) of 5-styryl-2-aminotropone is smaller than those of 4- and 6-styryl-2-aminotropones (pK_a 2.54 for 4-styryl and 2.57 for 6-styryl isomers).[7] This might be mainly due to the conjugate interaction between the amino group and the styryl group in 5-styryl-2-aminotropones. Further, 5-styryl-2-aminotropones show pK_a values between 2.05 (*p*-chloro) and 2.35 (*p*-methoxy) and are less basic than *p*-(substituted styryl)anilines (*i.e.*, 3'- and 4'-substituted 4-aminostilbenes [pK_a 3.67 (*p*-chloro) to 3.86 (*p*-methoxy)]).[1] This may be attributed to the electron-withdrawing effect of the carbonyl group adjacent to the amino group in the tropone nucleus.

TABLE 1. pK_a VALUES OF 2-AMINO-5-STYRYLTROPONES IN 50%(v/v) METHANOL

No.[a]	R	Mp (°C)	$c\times10^5$ (mol/l)	λ (nm)	pK_a
1	*p*-OCH_3	244—245	1.640	290	2.35±0.05
2	*p*-CH_3	232—234	1.881	284	2.28±0.03
3	*m*-CH_3	172	1.991	282	2.24±0.04
4	H	205—206[b]	2.273	280	2.21±0.07
5	*m*-OCH_3	162	1.877	287	2.15±0.05
6	*p*-Cl	231—232	1.585	283	2.05±0.03

a) Numbers correspond to those given in Fig. 2.
b) Mp 205—206 °C (Ref. H. Matsumura, *Nippon Kagaku Zasshi*, **81**, 1763 (1960)).

When the pK_a values of 5-styryl-2-aminotropones are plotted against the Hammett substituent constants, σ,[8] of the substituent in the benzene ring, the plot gives the straight line shown in Fig. 2, and the following equation is obtained by the least-squares method:

$$pK_a = 2.20 - 0.57\,\sigma \quad (r=0.991)$$

In the case of 4- and 6-styryl-2-aminotropones, the effects of the substituents in the benzene ring are mainly transmitted to the amino group in the tropone nucleus by the inductive effect, while the styryl group in 5-styryl-2-aminotropones is located at a position where resonance interaction between the styryl group and the reaction center of tropone nucleus is possible; therefore, the transmission of the electronic effects by the fairly large resonance effect as well as by the inductive effect can be expected. The ρ values of 4-, 5-, and 6-styryl-2-aminotropones are listed in Table 2. When the 4-styryl and 6-styryl derivatives are compared

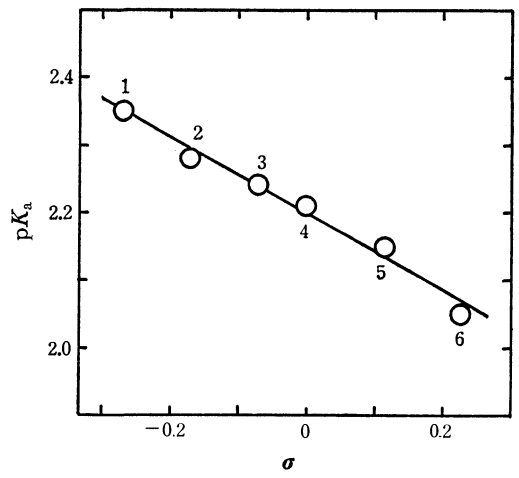

Fig. 2. The Hammett plot of pK_a's of 2-amino-5-styryltropones.

TABLE 2. THE ρ VALUES OF 4-, 5-, AND 6-STYRYL-2-AMINOTROPONES

Styryl-substituted 2-aminotropones	ρ
4-Styryl	0.59
5-Styryl	0.57
6-Styryl	0.40

with each other, the ρ value of the 4-styryl isomers is larger than that of the 6-styryl isomers because of the difference in distance between the styryl group and the amino group. On the other hand, the distance of the 5-styryl group in this work from the amino group is almost equal to that in the case of the 6-styryl derivatives. In other words, it may be assumed that the transmissibility which is caused by the inductive effect is almost equal in the 5- and 6-styryl derivatives. Thus, it is thought that a part of the ρ value of the 5-styryl isomers is due to the resonance effect mentioned above and is comparable to the difference in the ρ values based on the inductive effect, which is caused by the difference in distance from the 4- and 5-styryl groups to the amino group. Our results revealed that transmission through the styryl group varies with the position at which the styryl group is attached, the values being reduced in this order:

$$\text{4-styryl} \simeq \text{5-styryl} > \text{6-styryl}$$

Next, the dissociation constants were determined in 50%(v/v) aqueous ethanol at 25 °C. The Hammett analysis of them gave the following linear regression:

$$pK_a = 2.02 - 0.92\,\sigma \quad (r=0.992)$$

This ρ value is larger than that in 50% aqueous methanol. Such a difference is also observed[8] in the dissociation of benzoic acids, the ρ values being 1.085 in 50% aqueous methanol and 1.601 in 50% aqueous ethanol. It is thought that the difference between the two media is attributable to their polarity. Furthermore, the ρ value of 5-styryl-2-aminotropones is larger than the value for the dissociation of 4-aminostilbenes (0.42 in 50% aqueous ethanol at 20 °C).[1] This might be due to the fact that the tropone nucleus is charged slightly by the polarization of the carbonyl group. It is thought that there is some conjugate interaction between the styryl group and the carbonyl group.

Experimental

Materials. The 5-(substituted styryl)-2-aminotropones were prepared by the abnormal substitution reaction of 2-chloro-4-styryltropones, which has themselves been obtained from 4-styryltropolones in three steps. This method will be described elsewhere. Their melting points are listed in Table 1.

Measurement of Dissociation Constants. The dissociation constants of the 2-amino-5-styryltropones were measured spectrophotometrically in 50% aqueous methanol at 23 °C and in 50% aqueous ethanol at 25 °C, using the method of Albert and Serjeant.[9] The constants were obtained by using this equation:

$$pK_a = pH + \log \frac{A_B - A}{A - A_{BH^+}}$$

where A_B and A_{BH^+} are the absorbance of the base and its conjugate acid respectively. The absorption spectra were taken on a Hitachi EPS-3T spectrophotometer, while the pH values were measured by mean of Hitachi-Horiba F-7 pH meter.

References

1) H. Veschambre and A. Kergomard, *Bull. Soc. Chim. Fr.*, **1966**, 336.
2) H. Veschambre, G. Dauphin, and A. Kergomard, *Bull. Soc. Chim. Fr.*, **1967**, 2846.
3) A. Katritzky, D. J. Short, and A. J. Boulton, *J. Chem. Soc.*, **1960**, 1516.
4) R. G. Pews and N. D. Ojha, *J. Am. Chem. Soc.*, **91**, 5769 (1969).
5) K. Imafuku, S. Nakama, and H. Matsumura, *Tetrahedron*, **26**, 1821 (1970).
6) K. Hamada, S. Nakama, K. Imafuku, K. Kurosawa, and H. Matsumura, *Tetrahedron*, **27**, 337 (1971).
7) K. Imafuku and H. Matsumura, *Bull. Chem. Soc. Jpn.*, **46**, 544 (1973).
8) H. H. Jaffé, *Chem. Rev.*, **53**, 191 (1953).
9) E. Albert and E. P. Serjeant, "Ionization Constants of Acids and Bases," Methuen, London (1962), Chap. 4.

N-Halogen Compounds of Cyanamide Derivatives. VIII.[1] A Convenient Method of Preparing 1,2,4-Oxadiazoles from *N*-Haloamidino Compounds

Toshio FUCHIGAMI and Keijiro ODO

Department of Electronic Chemistry, The Graduate School, Tokyo Institute of Technology
Ookayama, Meguro-ku, Tokyo 152

(Received June 11, 1976)

A new, efficient method for the preparation of 1,2,4-oxadiazoles from *N*-benzoylamidino compounds by treatment with *t*-butyl hypochlorite and sodium hydroxide has been devised. It was supposed that the ring formation proceeds *via* a nitrene intermediate.

1,2,4-Oxadiazoles have usually been prepared by the acylation of amidoximes[2] or by the Beckmann rearrangement of glyoximes.[3] In both cases, the cyclization involves dehydration and needs vigorous reaction conditions, and these procedures have not always given satisfactory results.

In this paper, we will describe a new, convenient method of synthesizing 1,2,4-oxadiazoles from *N*-chloro-*N'*-benzoylamidino compounds (amidines, *O*-alkylisoureas, and guanidine), together with the mechanism of the ring formation.

Results and Discussion

N-Benzoyl Derivatives of Amidino Compounds (I, II, and III). *N*-Benzoylamidines (I) are usually available by the reactions of amidines with benzoic anhydride.[4] We have found that I were prepared in good yields by the reaction of amidine hydrochlorides with benzoyl chloride in the presence of two equivalents of sodium hydroxide. *N*-Benzoyl-*O*-alkylisoureas (II) and *N*-benzoyl-*N',N'*-pentamethyleneguanidine (III) were prepared by a similar method. Isoureas, II, which were solids with low melting points, could be isolated from an aqueous reaction mixture by extraction with ether.

Table 1 summarizes the results of the preparation of I, II, and III.

Preparation of 1,2,4-Oxadiazoles (IV, V, and VI). 1,2,4-Oxadiazoles were easily obtained from I, II, and III in excellent yields under mild conditions. The following procedure is a typical one. An ethanolic suspension of an amidino compound was treated with *t*-butyl hypochlorite to form *N*-chloro compound, which was then warmed with aqueous sodium hydroxide. The structures of these heterocyclic compounds were confirmed by means of elemental analysis and by studies of the IR and mass spectra.

Table 2 shows the results of the preparation of IV, V, and VI.

As is shown in Table 2, *N*-benzoylbenzamidine (Ia) was transformed to 1,2,4-oxadiazole (IVa) in a good yield. However, in the case of *N*-benzoyl-*p*-toluamidine (Ib), the yield of IVb decreased because of the formation of a by-product, *p*-tolylurea, which was due to the migration of the *p*-tolyl group to a nitrogen atom. Thus, the *p*-methyl group was found to cause the rearrangement, but the reason has not yet been clarified. Studies of the relationship between various substituents and the reactivities of *N*-chloro compounds of I are in progress.

In the case of II, 1,2,4-oxadiazoles (Va—d) were prepared in excellent yields without exception.

This new method of synthesizing 1,2,4-oxadiazoles

TABLE 1. PREPARATION OF *N*-BENZOYLAMIDINO COMPOUNDS (I, II, and III)

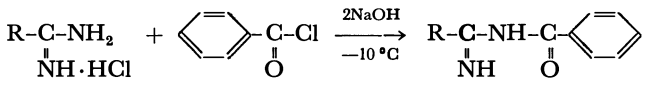

Amidino compd No.	R	Reaction time (h)	Yield (%)	Mp (°C)	Recrystn solvent	Found (calcd %) C	H	N
Ia		1.0	74	98 (98)[8]	aq MeOH	—	—	—
Ib	CH_3- 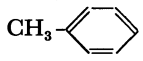	0.5	82	129—130	aq MeOH	75.79 (75.61)	5.97 (5.92)	11.67 (11.76)
IIa	CH_3O	1.0	74	77 (76.5)[9]	aq MeOH	60.83 (60.63)	5.66 (5.66)	15.60 (15.72)
IIb	EtO	1.0	77	76 (74—75)[10]	aq MeOH	62.28 (62.49)	6.50 (6.29)	14.54 (14.57)
IIc	*i*-PrO	1.0	85[a]	153—155[b]	H_2O	46.77 (46.90)[c]	4.02 (3.94)[c]	16.12 (16.09)[c]
IId	*n*-BuO	1.0	75	40.5	Ligroin	65.14 (65.43)	7.59 (7.32)	12.73 (12.72)
III		1.0	81	149—150	MeOH	67.35 (67.51)	7.62 (7.41)	17.73 (18.13)

a) Yield of crude IIc. b) Mp of the picrate; a substance free of IIc, which has a low melting point, could not be recrystallized. c) Calcd for $C_{17}H_{17}N_5O_9$.

Table 2. Preparation of 1,2,4-oxadiazoles from *N*-benzoylamidino compounds

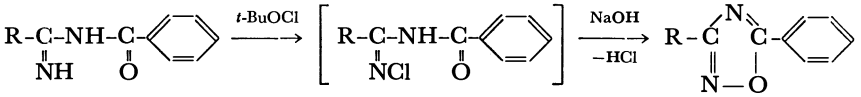

Oxadiazole No.	R	Reaction temp (°C)	Reaction time (min)	Yield (%)	Mp (bp) (°C)	Recrystn solvent	Found (calcd %) C	H	N
IVa		≈70	5	80 (74)[a]	108 (108)[11]	aq EtOH	75.74 (75.66)	4.56 (4.54)	12.67 (12.60)
IVb	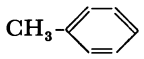	75—79	5	46 (44)[a]	103—104 (103)[12]	EtOH	76.26 (76.25)	5.02 (5.12)	11·92 (11.86)
Va	CH_3O	Room temp	60	91	57 (58—59)[13]	aq MeOH	61.33 (61.36)	4.52 (4.58)	15.94 (15.90)
Vb	EtO	Room temp	60	88	51 (49—55)[13]	aq MeOH	63.05 (63.15)	5.32 (5.30)	14.57 (14.73)
Vc	*i*-PrO	Room temp	60	96[b] (71)[c]	128—132/ 6 Torr	—	64.56 (64.70)	6.03 (5.92)	13.68 (13.72)
Vd	*n*-BuO	Room temp	60	93	36—37	MeOH	65.84 (66.04)	6.63 (6.46)	12.95 (12.83)
VI		≈15	30	58	169—170	aq EtOH	67.80 (68.10)	6.73 (6.59)	17.99 (18.33)

a) *N*-Chloro intermediate was isolated, and then 2 M sodium hydroxide was added. The yield was calculated based on the starting material, I. b) Yield of crude Vc. c) Yield of the distillate of Vc.

Table 3. Spectral data of 1,2,4-oxadiazoles

Compd No.	UV Absorption[a] λ_{max}, nm	NMR Spectra[b] δ ppm	
Vc	255 (13900)	$(CH_3)_2C$	1.46 (d, 6H)
		CH	5.00 (h, 1H)
		Ar-H (*o*-, *p*-)	7.55 (m, 3H)
		Ar-H (*m*-)	8.10 (m, 2H)
Vd	255 (15200)	CH_3	0.98 (t, 3H)
		CH_2CH_2	1.20—2.00 (m, 4H)
		CH_2O	4.38 (t, 2H)
		Ar-H (*o*-, *p*-)	7.55 (m, 3H)
		Ar-H (*m*-)	8.10 (m, 2H)
VI	234 (9700) 278 (16400)	—	— —

a) In CH_3OH. b) In $CDCl_3$. d-doublet, t-triplet, h-heptet, m-multiplet.

Table 4. Physical properties of *N*-chloro compounds

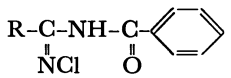

R	Mp (°C)	Appearance	Recrystn solvent	Cl Found[a] (calcd %)	Formula
	98	Needles	Acetone-P. ether	13.45 (13.70)	$C_{14}H_{11}N_2OCl$
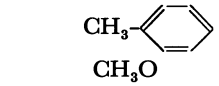	129—130	Needles	Acetone-P. ether	13.30 (13.30)	$C_{15}H_{13}N_2OCl$
CH_3O	—	Colorless oil	—	16.40 (16.67)	$C_9H_9N_2O_2Cl$
EtO	56—57	Needles	EtOH-Ether	15.40 (15.64)	$C_{10}H_{11}N_2O_2Cl$
i-PrO	62	Needles	EtOH-Ether	14.31 (14.73)	$C_{11}H_{13}N_2O_2Cl$
n-BuO	—	Colorless oil	—	13.58 (13.92)	$C_{12}H_{15}N_2O_2Cl$
	124—125	Granular form	Acetone-P. ether	13.26 (13.34)	$C_{13}H_{16}N_3OCl$

a) The active chlorine contents were iodometrically determined.

seems to be very convenient, that is, all operations are simple and the products can be obtained directly in an adequate purity.

N-Chloro compounds of I, II, and III are relatively stable; their physical properties are shown in Table 4.

Reaction Mechanism. The hydrogen atom of the NH group of a *N*-chloro compound seems to be acidic as a result of the electron-attracting effect of the chlorine atom and the benzoyl group.

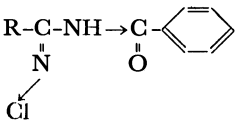

In fact, *N*-chloro compounds of I, II, and III are soluble in an alkaline solution, and the disapearance of the active chlorine takes only a short time. Therefore, this cyclization may be initiated by the removal of a proton from the NH group with a hydroxide ion. The loss of a chloride ion from the resulting anion may form a nitrene intermediate (A). The nitrene thus formed probably attacks the oxygen of the carbonyl group to give 1,2,4-oxadiazole. Such a

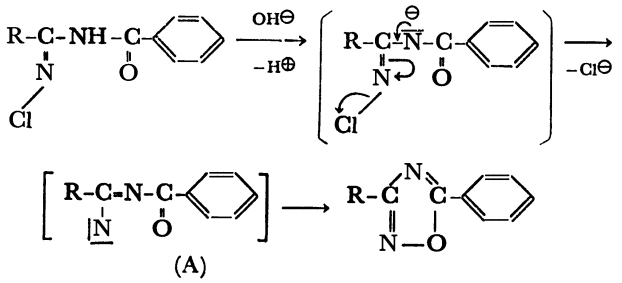

Scheme 1.

nitrene intermediate has previously been proposed by us[5] in the thermolysis of acyl derivatives of *N*-benzimidoyl-*S,S*-dimethylsulfilimine, giving 1,2,4-oxadiazoles, and by Miorana[6] in the photolysis of *β*-azidovinyl ketones, giving isoxazoles.

The by-product, *p*-tolylurea, may be formed by a mechanism similar to that mentioned in the rearrangement of *N*-alkyl-*N'*-chloroamidines.[7]

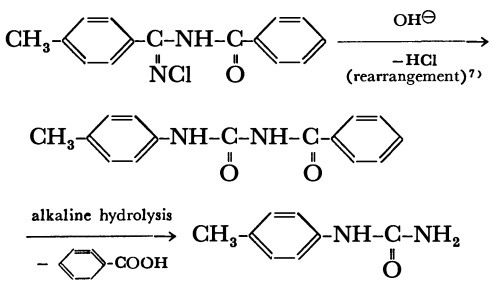

Experimental

The melting points are uncorrected. The NMR spectra were recorded at 60 MHz in $CDCl_3$, with TMS as the internal standard, using a Hitachi R-24A spectrometer. The mass spectra were taken with a JEOL JMS-D100 mass spectrometer. The UV spectra were taken with a Hitachi 624 spectrometer.

N-*Benzoylbenzamidine (Ia).* Benzamidine hydrochloride (3.85 g, 20 mmol) was dissolved in a solution of 2 M sodium hydroxide (25 ml) and acetone (5 ml) below 5 °C, and then benzoyl chloride (2.3 ml, 20 mmol) was gradually stirred in. After about 1 h of continued stirring below 10 °C, the white precipitate was filtered off and washed with water. The crude product melted at 90—92 °C; yield, 4.20 g (94%). Recrystallization from 80% aqueous methanol gave pure Ia; mp 98 °C.

N-*Benzoyl*-p-*toluamidine (Ib).* Using the same procedure, the crude product was obtained; yield, 3.50 g (82%). Recrystallization from aqueous methanol gave pure Ib; mp 129—130 °C.

N-*Benzoyl*-O-*methylisourea (IIa).* *O*-Methylisourea (5.53 g, 50 mmol) was dissolved in 70 ml of 2 M sodium hydroxide below 5 °C, and then benzoyl chloride (5.8 ml, 50 mmol) was gradually stirred in. After the addition, the reaction mixture was stirred below 10 °C for 1 h. The resulting oily material was extracted once with a 30-ml portion and twice with 10-ml portions of ether. After the combined ethereal extracts had been dried (Na_2SO_4), filtered, and concentrated under reduced pressure, colorless, needle-like crystals of *N*-benzoyl-*O*-methylisourea were obtained; yield, 6.60 g (74%); mp 76 °C. Recrystallization from aqueous methanol gave pure IIa; mp 77 °C.

The other *N*-benzoylisoureas (IIb—d) were prepared by the same procedure.

N-*Benzoyl*-N',N'-*pentamethyleneguanidine (III).* Using the same procedure but without acetone, the crude product was obtained; yield, 5.60 g (81%); mp 133—135 °C. Recrystallization from methanol gave pure III; mp 149—150 °C.

3,5-Diphenyl-1,2,4-oxadiazole (IVa). To a stirred suspension of Ia (1.12 g, 5 mmol) in ethanol (8 ml), we gradually added, drop by drop, an ethanolic solution (2 ml) of *t*-butyl hypochlorite (0.60 g, 5.5 mmol) at 0—5 °C. After the mixture had been stirred at the same temperature for 30 min, a 4-ml portion of 2 M sodium hydroxide was added. After the mixture had then been warmed at 70 °C, white needle-like crystals began to appear. After 5 min, the mixture was cooled, and then the precipitate was separated by filtration; IVa, 0.77 g; mp 108 °C. Further IVa was obtained by the addition of water (10 ml) to the filtrate; 0.11 g; mp 105—106 °C. The total yield was 80%. Recrystallization from aqueous ethanol gave a pure product; mp 108 °C; *m/e* 222 (M^+).

3-p-*Tolyl*-*5*-*phenyl*-*1,2,4*-*oxadiazole (IVb)* *and* p-*Tolylurea.* To a stirred suspension of Ib (1.36 g, 5 mmol) in ethanol (8 ml), we gradually added, drop by drop, an ethanolic solution (2 ml) of *t*-butyl hypochlorite (0.60 g, 5.5 mmol) at 0—5 °C. After the mixture had been stirred at the same temperature for 30 min, 4 ml of 2 M sodium hydroxide was added. The reaction mixture was subsequently warmed at 70—75 °C for 5 min and then cooled. The resulting needle-like precipitate was separated by filtration; IVb; yield, 0.54 g (46%). Recrystallization from aqueous ethanol gave pure IVb; mp 103—104 °C; *m/e* 236 (M^+). When the filtrate was evaporated to remove the ethanol, the precipitate, *p*-tolylurea, was filtered off and washed with a small amount of benzene. The yield was 0.16 g (21%). Recrystallization from dioxane-benzene gave a pure product; mp 176—177 °C.

3-Methoxy-5-phenyl-1,2,4-oxadiazole (Va). By the same procedure, but using ether as a solvent, a mixture of *N*-chloro compound of IIa (0.89 g, 5 mmol) and 3 ml of 2 M sodium hydroxide was stirred at room temperature for 60 min. When the reaction mixture was then evaporated under reduced pressure to remove the ether, an oily material was separated. The oily material was crystallized by rubbing with spatera and filtered off; mp 57 °C; yield 0.80 g (91%). Recrystalli-

zation from aqueous methanol gave pure Va; mp 57 °C; *m/e* 176 (M^+).

3-Ethoxy and *3-n*-butoxy-*5*-phenyl-*1,2,4*-oxadiazoles (Vb, d) were obtained by a similar method.

3-Isopropoxy-5-phenyl-1,2,4-oxadiazole (Vc). After working up the reaction mixture (10 mmol) as has been described above, the upper oily material was extracted once with a 10-ml portion and twice with 5-ml portions of dichloromethane. After the combined extracts had then been dried (Na_2SO_4), filtered, and concentrated under reduced pressure, the oily material Vc was obtained (1.95 g, 96%). Distillation under reduced pressure gave a fraction; bp 128—132 °C/6 Torr; 1.50 g (71%); *m/e* 204 (M^+).

3-Piperidino-5-phenyl-1,2,4-oxadiazole (VI). By the same procedure, 4 ml of 2 M sodium hydroxide was added to a solution of a *N*-chloro compound of III (1.16 g, 5 mmol). The mixture, which soon turned reddish yellow, was stirred below 15 °C for 30 min. An orange-yellow precipitate was then filtered off and washed with water; dp 173 °C; yield, 0.67 g (58%). Recrystallization from aqueous ethanol gave a pure product melting at 175 °C (with decomposition); *m/e* 229 (M^+).

References

1) Part 105 of "Studies of Cyanamide Derivatives;" A part of this work has been reported in our previous paper [*Chem. Lett.*, **1974**, 1139; *Yuki Gosei Kagaku Kyokai Shi*, **33**, 66 (1975)]. Part 104: T. Fuchigami, T. Nonaka, and K. Odo, *Bull. Chem. Soc. Jpn.*, **49**, 3170 (1976).
2) F. Tiemann and P. Kruger, *Ber.*, **17**, 1694 (1884).
3) E. Grunther, *Ann. Chem.*, **252**, 48 (1889).
4) A. Titherlag and E. Hughes, *J. Chem. Soc.*, **1911**, 1507.
5) T. Fuchigami and K. Odo, *Chem. Lett.*, **1974**, 247. T. Fuchigami and K. Odo, *Tetrahedron*, submitted for publication.
6) S. Maiorana, *Ann. Chim. (Rome)*, **56**, 1531 (1966).
7) T. Fuchigami, E. Ichikawa, and K. Odo, *Bull. Chem. Soc. Jpn.*, **46**, 1765 (1973).
8) D. Peak, *J. Chem. Soc.*, **1953**, 215.
9) R. Mackee, *Am. Chem. J.*, **26**, 250 (1901).
10) H. Wheeler and T. Johnson, *Am. Chem. J.*, **24**, 205 (1900).
11) E. Beckmann and K. Sandel, *Ann. Chem.*, **296**, 285 (1897).
12) L. Schubart, *Ber.*, **19**, 1490 (1886).
13) S. Yang and T. Johnson, *J. Am. Chem. Soc.*, **54**, 2066 (1932).

Synthesis of Streptolidine from D-Xylose

Shoichi KUSUMOTO, Shinichi TSUJI, Keiyuu SHIMA, and Tetsuo SHIBA

Department of Chemistry, Faculty of Science, Osaka University, Toyonaka, Osaka 560

(Received June 21, 1976)

An alternative total synthesis of streptolidine (roseonine, geamine) was achieved starting from D-xylose. Direct azidolysis of methyl 2,3,5-tri-*O*-mesyl-α-D-xylofuranoside (**6a**) afforded methyl 2,3,5-triazido-2,3,5-trideoxy-α-D-arabinofuranoside (**9a**), whereas the β-anomer of **6a** gave only 3,5-diazido-3,5-dideoxy-2-*O*-mesyl-β-D-ribofuranoside (**8b**) indicating that the glycosidic configuration in the furanoside system has a decisive influence on the reactivity of the 2-mesyloxy group. However, the β-anomer of diazide (**8b**) was anomerized to α-anomer which readily undergoes azidolysis to give the triazide (**9a**). The triazide was successively hydrogenated, benzyloxycarbonylated, and then hydrolyzed to give 2,3,5-tris(benzyloxycarbonylamino)-2,3,5-trideoxy-D-arabinofuranose, which was identical with that prepared from D-ribose. Streptolidine could be synthesized from this key intermediate.

In a previous paper,[1] a report was given on the total synthesis of streptolidine (roseonine, geamine)[2] (**1**), a component guanidino amino acid of streptothricin antibiotics, which had been performed starting from D-ribose. Fully controlled substitution of three hydroxyl group in D-ribose (**2**) *via* twelve synthetic steps involving azidolysis of an epimino ring yielded 2,3,5-tris(benzyloxycarbonylamino)-2,3,5-trideoxy-D-arabinofuranose (**3**), which was then oxidized to (2*S*, 3*S*, 4*R*)-2,3,5-triamino-4-hydroxypentanoic acid (**4**) derivative. Guanidination of δ-lactam of **4** with cyanogen bromide afforded streptolidine of the natural configuration. The above complicated synthesis can be improved if simultaneous S_N2 displacement of the three hydroxyl groups on C-2, -3, and -5 of D-xylose (**5**) with nitrogen functions would occur leading to the same key intermediate (**3**). Although a sulfonyloxy group on C-2 of a furanoside or pyranoside resists substitution with azide anion in general, some successful cases of this reaction have recently been reported.[3,4] In the present investigation on the direct azidolysis of methyl 2,3,5-tri-*O*-mesyl-D-xylofuranoside (**6**), we could obtain the compound **3** as expected, thus accomplishing a new route to the synthesis of streptolidine from D-xylose.

Results and Discussion

D-Xylose was treated with hydrogen chloride in methanol and then with mesyl chloride in pyridine to afford a mixture of tri-*O*-mesyl-α and β-D-xylofuranoside (**6a** and **6b**), in which the β-anomer (**6b**) exists predominantly. When the mixture[5] was treated with sodium azide in *N*,*N*-dimethylformamide (DMF) at 100 °C for 2 h and then at 140 °C for 2 h, four azido compounds were formed, which were isolated by column chromatography.

In the NMR spectra (100 MHz) of these compounds, most of the signals of the individual protons were well separated from each other, and could be assigned with the aid of decoupling experiments. They are given in Table 1. The data indicate the number of the remaining mesyloxy groups, the positions of substituents as well as the anomeric configuration in each compound. The main syrupy product (**7**) (37% of the starting mixture) retaining two unchanged mesyl groups was found to be 5-monoazide since only the

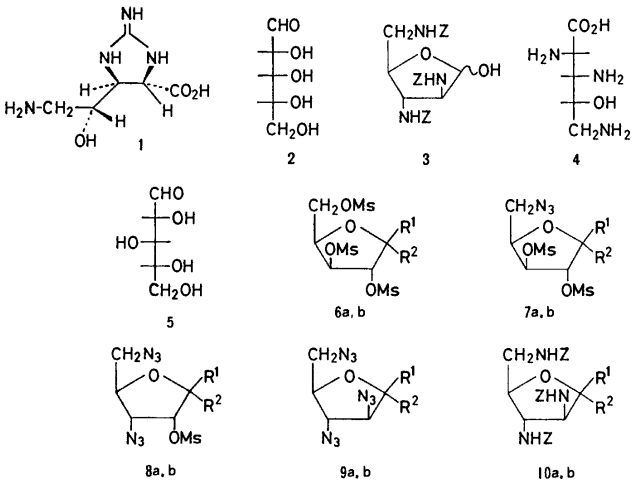

Z=$C_6H_5CH_2OCO$, Ms=CH_3SO_2

a: R^1=H, R^2=OCH_3

b: R^1=OCH_3, R^2=H

signals of C-5 protons shifted considerably into higher field. The product is probably a mixture of anomers, being rich in β-form (**7b**) contaminated with a minor amount of α-form (**7a**). The assignment of the monoazide structure was supported by the formation of monobenzamido derivative on hydrogenation of **7** followed by benzoylation. The other two products (**8a** and **8b**, 3.4 and 27%, respectively, of the starting mixture), both being diazides, were assigned to anomers of 3,5-diazide, because the chemical shift values of C-3 and C-5 protons indicate undoubtedly the location of the azide groups on these carbon atoms. The anomeric configurations were determined on the basis of coupling constants. Thus, $J_{1,2}$ value of **8a** (4.5 Hz) shows cis relation of C-1 and C-2 protons, while that of **8b** (0 Hz) shows trans relation, indicating the structure of metyl 3,5-diazido-3,5-dideoxy-2-*O*-mesyl-α- and β-D-ribofuranoside for **8a** and **8b**, respectively.

The fourth product (**9a**) obtained in only a very small amount (0.75% of starting mixture) showed no NMR signal of the mesyl group. On catalytic hydrogenation followed by benzyloxycarbonylation, it afforded tris(benzyloxycarbonylamino) derivative (**10a**) which was differentiated from methyl 2,3,5-tris(benzyloxycarbonylamino)-2,3,5-trideoxy-β-D-arabinofuranoside (**10b**) prepared from D-ribose.[1]

Table 1. Chemical shifts and coupling constants of protons in mesyl and azide derivatives[a)]

	H-1	H-2	H-3	H-4	H_2-5	OCH_3	OMs
6b	5.10	5.10 (J=2)	5.28 dd (J=2, 6)	4.74 q (J=6)	4.41 d (J=6)	3.44	3.08 (3H) 3.14 (3H) 3.16 (3H)
7		5.1——5.3		4.53	≈3.55 d	3.50	3.20 (6H)
8a	5.04 d (J=4.5)	4.90 dd (J=4.5, 7.5)	3.88 dd (J=7.5, 5)	4.05 m	3.36 dd(1H) 3.55 dd(1H)	3.38	3.10 (3H)
8b	4.96 s	4.91 d (J=4)	≈4.05	≈4.05	≈3.3 dd(1H) 3.50 dd(1H)	3.33	3.06 (3H)
9a	4.90 d (J=3)	3.93 dd (J=3, 5.5)	3.72 dd (J=5.5, 7)	4.06 m	≈3.4 dd(1H) ≈3.6 dd(1H)	3.40	—

a) Measured on Varian XL-100 spectrometer in $CDCl_3$. The chemical shifts and the coupling constants were recorded in δ values and Hz.

The coupling constant value of $J_{1,2}$=0 Hz in **10a** indicated trans relation of C-1 and C-2 protons. NMR data (Table 1) confirmed the structure of **9a** to be the triazide of the desired configuration, *i.e.*, methyl 2,3,5-triazido-2,3,5-trideoxy-α-D-arabinofuranoside.

The exclusive formation of triazide (**9a**) of α-glycoside structure may suggest that azidolysis of C-2 mesyloxy group proceeds only from the methyl α-glycoside (**6a**) but not from the β-anomer (**6b**) in the starting mixture. In fact, no trace of a triazide was detected when the pure β-glycoside of monomesyl diazide (**8b**) was treated with sodium azide in DMF or HMPA at 140 °C; whereas its α-anomer (**8a**) could be readily converted into the triazide (**9a**) in DMF at 140 °C.

Great differences in the reactivity of 2-sulfonate between both anomers have been observed by Miljković *et al.*[3)] but only in pyranoside systems. They reported that S_N2 type substitution of C-2 mesyloxy groups with a charged nucleophile occurs in methyl β-gluco- and β-mannopyranoside but not in the corresponding α-anomers. In our experiments, however, the substitution reaction of the 2-mesyloxy group occurs only in the α-furanoside. The apparent discrepancy in the reactivity of each anomer of the furanoside and the pyranoside is not surprising since steric situations in the two ring systems differ a great deal.

The exhaustive azidolysis of D-xylose derivative might be utilized as a new direct method leading to the 2,3,5-triaminopentose derivative of desired stereochemistry. Attempts were next made to anomerize the β-glycofuranosides, the main product in Fischer's glycosidation reaction of xylose, to the α-furanoside derivative which can be used as the starting material for the triazide (**9a**). When β-diazide (**8b**) was heated in methanol containing dry hydrogen chloride, anomerization took place giving 16% of α-diazide (**8a**) and 61% of unchanged **8b** which were separated from each other by column chromatography. Use of titanium tetrachloride in methylene chloride gave a similar result. On the other hand, no anomerization occurred on the β-anomer of the trimesylate (**6b**) under similar conditions.

The α-diazide (**8a**) thus obtained was converted into the triazide (**9a**) in 38% yield by heating with sodium azide in DMF at 140 °C for 4 h. This condition seemed to be optimal, since higher temperature caused decomposition of the materials resulting in loss of the yield. In order to increase the yield of triazide, effect of "crown ether"[6)] on the substitution reaction was examined. Addition of 18-crown-6 to the reaction mixture did not improve the reaction. In other solvents such as acetonitrile, benzene, dioxane, toluene, and *o*-xylene, **8a** did not react with sodium azide at all even on addition of 18-crown-6.

After the triazide (**9a**) was converted into the tris(benzyloxycarbonylamino) derivative (**10a**) as described above, the glycoside linkage was hydrolyzed with *p*-toluenesulfonic acid in aqueous dioxane. Comparison of mps, IR and NMR spectra showed that the hydrolysis product was identical with 2,3,5-tris(benzyloxycarbonylamino)-2,3,5-trideoxy-D-arabinofuranose (**3**) previously prepared from D-ribose.[1)] Since the conversion of **3** into streptolidine had been performed through oxidation, deprotection and guanidination successively,[1)] it is now established that streptolidine was formally synthesized also from D-xylose by an alternative and improved method.

Experimental

All melting points are uncorrected. Silica gel 60 (0.063—0.200mm, Merck) was used for column chromatography. TLC and preparative TLC were performed on Silica gel G and H, Merck, respectively.

*Methyl 2,3,5-Tri-O-mesyl-α- and β-D-xylofuranoside (**6a** and **6b**).* A mixture of D-xylose (20.0 g, 0.133 mol) in methanol (500 ml) containing dry HCl (0.5 wt%) was stirred at room temperature overnight. After neutralization with Ag_2CO_3, the mixture was filtered and the solvent was evaporated *in vacuo* to a syrupy residue. To an ice-cooled solution of this residue in pyridine (200 ml) was added mesyl chloride (50 ml, 0.64 mol) dropwise with stirring. The mixture was stirred in an ice bath for 5 h, allowed to stand at room temperature overnight and then evaporated *in vacuo*. The residue was taken up in CH_2Cl_2, washed with water, dried (Na_2SO_4) and evaporated *in vacuo*. Recrystallization from ethyl acetate–hexane afforded a mixture of **6a** and **6b** yield, 35.8 g (68%). The proportion of **6a** to **6b** was determined by preparative TLC on silica gel (benzene–ethyl acetate 1 : 2). From 108.0 mg of the mixture, 9.4 mg of **6a** and 96.4 mg of **6b** were obtained, indicating a ratio

of 9 : 91.

Repeated recrystallization of this mixture from ethyl acetate–benzene afforded pure **6b**; mp 111—112 °C; $[\alpha]_D^{17}$ −18.6° (*c* 1.83, ethyl acetate); NMR, see Table 1.

Found: C, 27.41; H, 4.55; S, 23.89%. Calcd for $C_9H_{18}O_{11}S_3$: C, 27.13; H, 4.55; S, 24.14%.

From the mother liquor of **6b**, the anomer **6a** was isolated by column chromatography on silica gel (benzene–ethyl acetate), and recrystallized from benzene–ethyl acetate; mp 132 °C; $[\alpha]_D^{17}$ +10.8° (*c* 1.97, ethyl acetate).

Found: C, 27.05; H, 4.59; S, 23.87%.

*Azidolysis of a Mixture of **6a** and **6b**.* A mixture of **6a** and **6b** described above (10.0 g, 25.2 mmol) was heated with NaN_3 (11.5 g, 178 mmol) in DMF (150 ml) at 100—110 °C (bath temp) for 2 h, then at 135—140 °C (bath temp) for 2 h. After the mixture had been cooled, the precipitate was filtered off and the solvent was evaporated *in vacuo*. The residue was dissolved in CH_2Cl_2, washed with water, dried ($MgSO_4$) and evaporated *in vacuo*. The residue was subjected to column chromatography on silica gel. A mixture of hexane–ethyl acetate (4 : 1) eluted **9a**, **8b**, **8a**, and **7** in this order.

i) *Methyl 5-Azido-5-deoxy-2,3-di-O-mesyl-α- and β-D-xylofuranoside (**7a** and **7b**)*: Yield, 3.19 g (37%); syrup; NMR see Table 1. This product was hydrogenated in methanol–tetrahydrofuran in the presence of HCl and Pd on charcoal, and then treated with benzoyl chloride and triethylamine to afford monobenzamido derivative; mp 146—147 °C.

Found: C, 42.06; H, 5.03; N, 3.22; S, 15.19%. Calcd for $C_{15}H_{21}O_9NS_2$: C, 42.54; H, 5.00; N, 3.31; S, 15.14%.

ii) *Methyl 3,5-Diazido-3,5-dideoxy-2-O-mesyl-α-D-ribofuranoside (**8a**)*: Yield, 250 mg (3.4% of the starting anomeric mixture, 38% of **6a**); syrup; NMR, see Table 1. This compound was characterized by conversion into crystalline dibenzamido derivative in a similar manner to that described in (i); mp 210 °C; $[\alpha]_D^{19}$ +82.4 °C (*c* 2.08, $CHCl_3$).

Found: C, 55.96; H, 5.36; N, 6.22; S, 7.18%. Calcd for $C_{21}H_{24}O_7N_2S$: C, 56.24; H, 5.39; N, 6.25; S, 7.15%.

iii) *Methyl 3,5-Diazido-3,5-dideoxy-2-O-mesyl-β-D-ribofuranoside (**8b**)*: Yield, 1.98 g (27% of the mixture, 30% of **6b**); mp 59—60 °C; $[\alpha]_D^{14}$ +72.8° (*c* 1.51, ethyl acetate); NMR, see Table 1.

Found: C, 28.75; H, 4.21; N, 28.43; S, 10.90%. Calcd for $C_7H_{12}O_5N_6S$: C, 28.77; H, 4.11; N, 28.77; S, 10.96%.

iv) *Methyl 2,3,5-Triazido-2,3,5-trideoxy-α-D-arabinofuranoside (**9a**)*: Yield, 45 mg (0.75% of the mixture, 8.4% of **6a**); syrup; $[\alpha]_D^{20}$ +195.0° (*c* 2.26, $CHCl_3$); NMR, see Table 1. This compound was hydrogenated in ethanol in the presence of Pd black and HCl. The product was treated with benzyloxycarbonyl chloride and triethylamine to afford methyl 2,3,5-tris(benzyloxycarbonylamino)-2,3,5-trideoxy-α-D-arabinofuranoside (**10a**); mp 204—205 °C; $[\alpha]_D^{21}$ +32.0° (*c* 0.75, $CHCl_3$). NMR: δ 4.78 (1H s, H-1), 5.03 (6H s, $C_6H_5CH_2$), 7.25 (15H, aromatic H).

Found: C, 63.93; H, 6.04; N, 7.50%. Calcd for $C_{30}H_{33}O_8N_3$: C, 63.93; H, 5.90; N, 7.46%.

*Attempts at Azidolysis of **8b**.* A stirred mixture of **8b** (15 mg, 0.05 mmol) and NaN_3 (16 mg, 0.25 mmol) in HMPA (3 ml) was heated and the product was tested by TLC. No reaction occurred at 145 °C (bath temp). When the mixture was heated over 155 °C (bath temp), **8b** decomposed completely, no definite spots on TLC being detected. A similar result was obtained using DMF as solvent.

*Preparation of **8a** by Anomerization of **8b**. With HCl in Methanol*: A solution of **8b** (452 mg) in methanol (50 ml) containing dry HCl (23 wt%) was heated under reflux for 6 h. After the mixture had been cooled, the solvent was evaporated *in vacuo* and the residue was chromatographed on silica gel. Elution with hexane–ethyl acetate (4 : 1) afforded **8b** (274 mg, 61%) and then **8a** (74 mg, 16%).

With $TiCl_4$ in CH_2Cl_2: To a solution of **8b** (520 mg) in CH_2Cl_2 (90 ml) was added $TiCl_4$ (0.25 ml) in CH_2Cl_2 (10 ml) and the mixture was stirred at room temperature for 1 h. On addition of ice, the mixture was stirred until the CH_2Cl_2 layer became clear. The CH_2Cl_2 layer was washed with aq $NaHCO_3$ solution and water, dried (Na_2SO_4), and evaporated *in vacuo*. The residue was chromatographed as above to give **8b** (308 mg, 59%) and **8a** (80 mg, 15%). Prolonged reaction time caused decomposition of the material.

*Triazide (**9a**) from **8a**.* A mixture of **8a** (155 mg, 0.53 mmol) and NaN_3 (240 mg, 3.7 mmol) in DMF (15 ml) was heated at 140—150 °C (bath temp) with stirring for 4 h and then treated as usual. The product (**9a**) was isolated by preparative TLC on silica gel (hexane–ethyl acetate 2 : 1); yield, 48 mg (38%).

*Examination of the Effect of 18-Crown-6 on Azidolysis of **8a**. In DMF*: A mixture of **8a** (1.0 g, 3.4 mmol), NaN_3 (0.88 g, 13.5 mmol), and 18-crown-6 (90 mg, 0.34 mmol) in DMF (100 ml) was heated at 130 °C (bath temp) with stirring for 18 h. By the usual work-up and chromatography, **9a** (0.23 g, 28%) and unchanged **8a** (0.06 g, 6%) were obtained. Without addition of 18-crown-6, but otherwise under the same conditions, the situation did not change; **9a** (0.23 g, 28%) and **8a** (0.06 g, 6%).

In Other Solvents: Mixtures of **8a** (25—50 mg) and NaN_3 (4 mol equivalent) in various solvents (acetonitrile, dioxane, benzene, toluene, or *o*-xylene) were heated under reflux in the presence of 18-crown-6 (1—2 mol equivalent). TLC examination indicated that **9a** was never formed in any of the solvents employed.

*Methyl 2,3,5-Tris(benzyloxycarbonylamino)-2,3,5-trideoxy-α-D-arabinofuranoside (**10a**).* The triazide (**9a**) (300 mg, 1.25 mmol) was dissolved in ethanol (30 ml) and hydrogenated in the presence of Pd black catalyst. After the catalyst had been removed, the mixture was cooled in an ice bath. Triethylamine (0.71 ml, 5.0 mmol) and benzyloxycarbonyl chloride (0.73 ml, 5.0 mmol) were added and the mixture was stirred overnight. Triethylamine (0.36 ml) and benzyloxycarbonyl chloride (0.37 ml) were again added and stirring was continued for further 4 h. The mixture was concentrated *in vacuo*, water was added and the crystalline substance was collected by filtration; yield, 580 mg (83%). Recrystallization was effected from $CHCl_3$; mp 171—173 °C.

Found: C, 62.63; H, 6.03; N, 7.54%. Calcd for $C_{30}H_{33}O_8N_3 \cdot 1/2H_2O$: C, 62.92; H, 5.99; N, 7.34%.

An anhydrous crystals of the same compound showed mp 204—205 °C.

*2,3,5-Tris(benzyloxycarbonylamino)-2,3,5-trideoxy-D-arabinofuranose (**3**).* To a solution of **10a** (600 mg) in dioxane (30 ml) was added 2 M aq solution of *p*-toluenesulfonic acid (30 ml). The mixture was heated under reflux for 1.5 h, concentrated *in vacuo*, and then extracted with $CHCl_3$. The $CHCl_3$ layer was washed with water, dried ($MgSO_4$) and evaporated *in vacuo*. The residue was subjected to a silica gel column. A mixture of $CHCl_3$–ethyl acetate (3 : 1) eluted first unchanged **10a** (197 mg, 30%) and then **3** (177 mg, 30%). The latter was recrystallized from $CHCl_3$; mp 208—210 °C. Its IR and NMR spectra were identical with those of the sample prepared from D-ribose.[1]

References

1) S. Kusumoto, S. Tsuji, and T. Shiba, *Tetrahedron Lett.*, **1974**, 1417; *Bull. Chem. Soc. Jpn.*, **47**, 2690 (1974). Goto

and Ohgi also reported independently a similar synthesis starting from D-ribose: T. Goto and T. Ohgi, *Tetrahedron Lett.*, **1974**, 1413.

2) Isolation: a) H. E. Carter, R. K. Clark, P. Kohn, J. M. Rothrock, W. R. Taylor, C. A. West, G. B. Whitfield, and H. G. Jackson, *J. Am. Chem. Soc.*, **76**, 566 (1954); b) K. Nakanishi, T. Ito, and Y. Hirata, *ibid.*, **76**, 2845 (1954); c) H. Brockmann and H. Musso, *Chem. Ber.*, **88**, 648 (1955); Structure determination: d) H. E. Carter, C. C. Sweeley, E. E. van Tamelen, J. R. Dyer, and H. A. Whaley, *J. Am. Chem. Soc.*, **83**, 4296 (1961); e) B. W. Bycroft and T. J. King, *J. Chem. Soc., Chem. Commun.*, **1972**, 652.

3) M. Miljkovic, M. Gligorijević, and D. Glisin, *J. Org. Chem.*, **39**, 3223 (1974).

4) M. Nakajima, H. Shibata, K. Kitahara, S. Takahashi, and A. Hasegawa, *Tetrahedron Lett.*, **1968**, 2271.

5) The ratio of α- to β-anomer was 9 : 91 (see Experimental). Although each anomer could be separated by means of column chromatography, the procedure was time-consuming and the azidolysis was thus carried out using the mixture.

6) a) C. J. Pederson, *J. Am. Chem. Soc.*, **89**, 7017 (1967); b) G. W. Gokel and H. O. Durst, *Synthesis*, **1976**, 168.

Synthesis of Corticotropin Peptides. X. The Synthesis of ACTH(1—18)-OH, ACTH(1—18)-NH_2 and ACTH(1—19)-NH_2*

Ken INOUYE, Fusako SHINOZAKI, Makoto KANAYAMA, and Hideo OTSUKA

Shionogi Research Laboratory, Shionogi & Co., Ltd., Fukushima-ku, Osaka 553

(Received June 29, 1976)

The final coupling, deprotection and purification processes for the synthesis of octadecapeptides, H-Ser-Tyr-Ser-Met-Glu-His-Phe-Arg-Trp-Gly-Lys-Pro-Val-Gly-Lys-Lys-Arg-Arg-OH(I) and H-Ser-Tyr-Ser-Met-Glu-His-Phe-Arg-Trp-Gly-Lys-Pro-Val-Gly-Lys-Lys-Arg-Arg-NH_2 (II), corresponding to the first eighteen amino acid residues of corticotropin (ACTH) are described, in which the *N*-hydroxysuccinimide ester of the N-terminal decapeptide derivative is coupled with the C-terminal octapeptide and octapeptide amide derivatives to give the two protected end products. The same decapeptide active ester is also utilized to the synthesis of a nonadecapeptide, H-Ser-Tyr-Ser-Met-Glu-His-Phe-Arg-Trp-Gly-Lys-Pro-Val-Gly-Lys-Lys-Arg-Arg-Pro-NH_2 (III), identical with the first nineteen amino acid residues of ACTH. The *in vivo* steroidogenic potencies of the synthetic peptides are compared with that of the synthetic human ACTH (α_h-ACTH) as reference to show that the relative potencies of I, II, and III *vs.* α_h-ACTH are 0.14, 0.48, and 0.47, respectively, as estimated on a molar basis.

In early 1960's considerable effort was devoted to the synthesis of peptides related to corticotropin (ACTH) to obtain a picture of the structural features essential for eliciting the adrenal-stimulating activity. Thus, ACTH(1—19)-OH,[1] ACTH(1—20)-NH_2,[2] ACTH(1—23)-OH,[3] and ACTH(1—24)-OH[4] were synthesized in three different laboratories, and their activities were found to be comparable enough to that of the native hormone. However, a heptadecapeptide ACTH(1—17)-OH[5] was only 15% as active as the nonadecapeptide ACTH(1—19)-OH. We also demonstrated that a hexadecapeptide [Gly^1, $Arg^{15,16}$]-ACTH(1—16)-OH[6] and a heptadecapeptide [Gly^1, Arg^{16}]-ACTH(1—17)-NH_2[7] were only slightly active in adrenal steroidogenesis. These observations suggested that the integrity of the unique Lys-Lys-Arg-Arg sequence in positions 15—18 of the ACTH molecule was crucial for eliciting a high degree of activity. In order to ascertain this point and to find the smallest peptide possessing a moderate adrenal-stimulating potency, we decided to synthesize an octadecapeptide, H-Ser-Tyr-Ser-Met-Glu-His-Phe-Arg-Trp-Gly-Lys-Pro-Val-Gly-Lys-Lys-Arg-Arg-OH, ACTH(1—18)-OH (I), and an octadecapeptide amide, H-Ser-Tyr-Ser-Met-Glu-His-Phe-Arg-Trp-Gly-Lys-Pro-Val-Gly-Lys-Lys-Arg-Arg-NH_2, ACTH(1—18)-NH_2 (II). A preliminary account of the synthetic and biological studies of peptides I and II has appeared.[8] The syntheses of the N-terminal decapeptide derivative, Boc-Ser-Tyr-Ser-Met-Glu(OBu^t)-His-Phe-Arg(H^+)-Trp-Gly-O^- (IV),[9] and the C-terminal octapeptide derivatives, H-Lys(Boc)-Pro-Val-Gly-Lys(Boc)-Lys(Boc)-Arg-Arg-OH (V) and H-Lys(Boc)-Pro-Val-Gly-Lys(Boc)-Lys(Boc)-Arg-Arg-NH_2 (VI),[10] have already been reported. In this paper the final coupling, deprotection and purification processes to lead to the production of peptides I and II are described in detail. In addition, the synthesis of a nonadecapeptide amide, H-Ser-Tyr-Ser-Met-Glu-His-Phe-Arg-Trp-Gly-Lys-Pro-Val-Gly-Lys-Lys-Arg-Arg-Pro-NH_2, ACTH(1—19)-NH_2 (III), is also a subject of this paper.

Synthesis of ACTH(1—18)-OH (I) and ACTH(1—18)-NH_2 (II). The final coupling reaction to produce the protected octadecapeptides was carried out by the *N*-hydroxysuccinimide (HOSu) ester method[11] in essentially the same manner as described in the synthesis of [Gly^1]-ACTH(1—18)-NH_2.[12] The protected decapeptide (IV) was converted into the hydrochloride Boc-Ser-Tyr-Ser-Met-Glu(OBu^t)-His-Phe-Arg(HCl)-Trp-Gly-OH and this was esterified with HOSu by means of dicyclohexylcarbodiimide (DCC). For the synthesis of peptide I, the resulting decapeptide active ester hydrochloride was allowed to react with the acetate salt of the N^{α}-free octapeptide derivative (V) in the presence of triethylamine to give Boc-Ser-Tyr-Ser-Met-Glu(OBu^t)-His-Phe-Arg-Trp-Gly-Lys(Boc)-Pro-Val-Gly-Lys(Boc)-Lys(Boc)-Arg-Arg-OH. The protected octadecapeptide thus obtained was treated with trifluoroacetic acid in the presence of anisole and 2-mercaptoethanol as

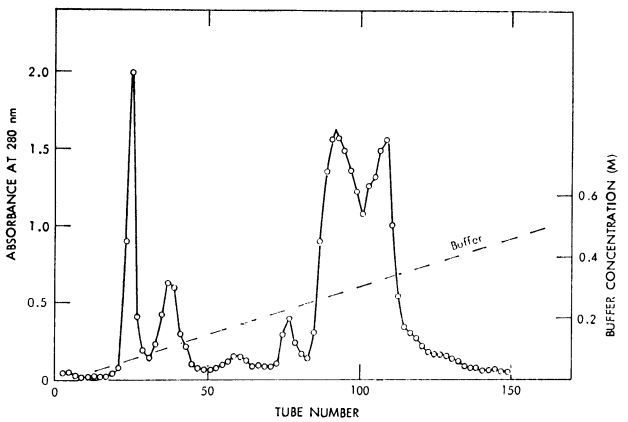

Fig. 1. Carboxymethyl cellulose column chromatography of crude synthetic ACTH(1—18)-OH: sample, 0.28 g; column, Serva, 0.7 meq/g, 1.7×21 cm; buffer, 0—0.6 M ammonium acetate (pH 6.0), 2000 ml; fractionation, 10 ml/tube.

* All the amino acid residues mentioned in this communication are of the L-configuration. Abbreviations used are those recommended by the IUPAC-IUB Commission of Biochemical Nomenclature [*Biochemistry*, **5**, 2485 (1966); *ibid.*, **6**, 362 (1967); *ibid.*, **11**, 1726 (1972)].

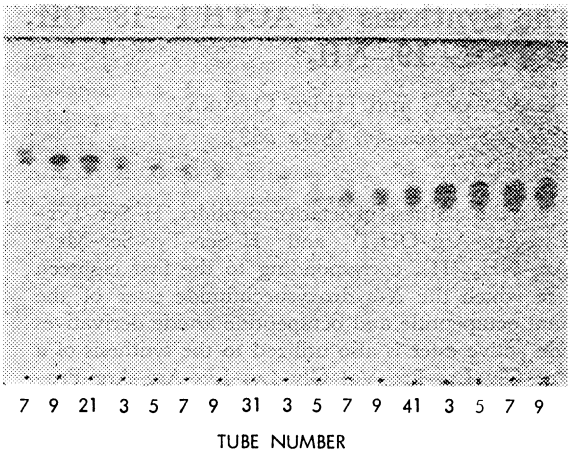

Fig. 2. Examination of fractions by TLC in the partition chromatography of partially purified ACTH(1—18)-OH. Partition chromatography: sample, 0.16 g, derived from tubes 86—115 in Fig. 1; column, Sephadex G-25 (medium), 2.2×50 cm; solvent, 1-butanol–acetic acid–pyridine–water (12:3:4:6); fractionation, 4.4 ml/tube. TLC: on a cellulose plate (precoated, Merck) with 1-butanol–acetic acid–pyridine–water (15 : 3 : 10 : 15) as solvent; detection, Ehrlich reagent.

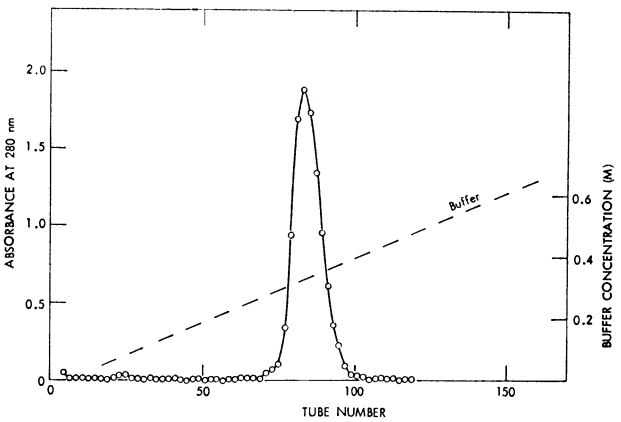

Fig. 3. Rechromatography of partially purified synthetic ACTH(1—18)-OH on a carboxymethyl cellulose column: sample, 0.11 g, fractionated by partition chromatography (Fig. 2, see Experimental for details); column, CM-52 (Whatman), 1.7×18 cm; buffer, 0—0.6 M ammonium acetate (pH 6.0), 1500 ml; fractionation, 10 ml/tube.

scavengers to liberate the desired peptide (I) in the form of trifluoroacetate. This was converted into the corresponding acetate by the treatment with Amberlite CG-400 (acetate form). The resulting crude preparation of peptide I was then purified by carboxymethyl cellulose column chromatography and by partition chromatography on a Sephadex G-25 column (Fig. 1—3). The partition chromatography was performed with a homogeneous mixture, 1-butanol–acetic acid–pyridine–water (12 : 3 : 4 : 6), as solvent[13] and the collected fractions were monitored by the Folin-Ciocalteu method[14] or by TLC more effectively (Fig. 2). The synthesis of peptide II was accomplished in the same manner as described above except that the acetate salt of VI was used as the amine component in the coupling reaction. The overall yields for the final coupling, deprotection and purification processes of peptide I and peptide II were 37 and 26%, respectively.

The synthetic octadecapeptides thus obtained were found to be homogeneous to ninhydrin and the Ehrlich reagent in TLC. Their acid hydrolysates contained the constituent amino acids in the ratios expected by theory with the exception of tryptophan. The tryptophan-tyrosine ratio in intact I and II was determined spectrophotometrically to be unity.[15]

Synthesis of ACTH(1—19)-NH_2 (III). The C-terminal tetrapeptide sequence Lys–Arg–Arg–Pro–NH_2 was synthesized by the step-by-step procedure starting with H–Pro–NH_2 derived from Z–Pro–NH_2[16] by catalytic hydrogenolysis. The two arginines were incorporated in the form of Z–Arg(NO_2) by the DCC method and by the mixed anhydride procedure, respectively, in combination with the removal of benzyloxycarbonyl (Z) group with hydrogen bromide in acetic acid. The resulting N^{α}-free tripeptide was then allowed to react with Z–Lys(Boc)–OSu[10] to afford Z–Lys(Boc)–Arg(NO_2)–Arg(NO_2)–Pro–NH_2 (IX). Compound IX was hydrogenolyzed for removal of the Z and two nitro groups and the product was coupled with Z–Lys(Boc)–Pro–Val–Gly–Lys(Boc)–N_3[10] to give a nonapeptide, Z–Lys(Boc)–Pro–Val–Gly–Lys(Boc)–Lys(Boc)–Arg–Arg–Pro–NH_2 (X), corresponding to positions 11—19 of ACTH.

Compound X was hydrogenolyzed and the resulting N^{α}-free nonapeptide was made react with the decapeptide *N*-hydroxysuccinimide ester, derived from IV, to yield Boc–Ser–Tyr–Ser–Met–Glu(OBu^t)–His–Phe–Arg–Trp–Gly–Lys(Boc)–Pro–Val–Gly–Lys(Boc)–Lys(Boc)–Arg–Arg–Pro–NH_2. This protected nonadecapeptide was treated with trifluoroacetic acid in the presence of anisole and 2-mercaptoethanol as scavengers to liberate peptide III, which was, after conversion into the acetate form, purified by partition chromatography and by ion-exchange chromatography in essentially the same manner as described for peptides I and II. The overall yield for the final coupling, deprotection and purification processes of peptide III was 38%. The purified material behaved as a single component in TLC and its acid hydrolysate contained the constituent amino acids in the ratios expected by theory with the exception of tryptophan. The tryptophan-tyrosine ratio in intact III was determined spectrophotometrically to be unity.[15]

The octadecapeptide amide (II) and the nonadecapeptide amide (III) have been synthesized by two other groups independently.[17,18] The optical rotations of our preparations of peptides II and III were found to differ significantly from those reported by Ramachandran *et al.*[17] Bajusz and Medzihradszky[18] also pointed out this lack of identity in optical rotation between their peptides and those of Ramachandran *et al.*

Biological Activity of ACTH(1—18)-OH (I), ACTH-(1—18)-NH_2 (II) and ACTH(1—19)-NH_2 (III).

TABLE 1. STEROIDOGENIC ACTIVITY OF SYNTHETIC PEPTIDES[19]

Compound	Molecular weight[a]	*In vivo* steroidogenic activity	
		units/mg[b]	units/μmol
ACTH(1—18)-OH (I)	2250	26.8	60.3
ACTH(1—18)-NH_2 (II)	2249	96.7	217
ACTH(1—19)-NH_2 (III)	2346	90.4	212
Synthetic α_h-ACTH[20]	4541	98.6	448

a) As anhydrous free base. b) Third USP Corticotropin Reference Standard was used as reference.

The synthetic peptides obtained above were assayed for the *in vivo* steroidogenic activity by a method based on the elevated levels of 11-hydroxycorticosteroids in the adrenal venous plasma of the hypophysectomized rat in response to intravenous administration of the test sample. The results are shown in Table 1,[19] in which the potencies of peptides I, II, and III are compared with that of the synthetic human hormone (α_h-ACTH).[20]

Table 1 first shows that the octadecapeptide amide (II) is three to four times more active than the corresponding peptide acid (I) in the *in vivo* adrenal steroidogenesis. The similar potentiation effect associated with the C-terminal amidation has been reported with ACTH(1—17)-NH_2 and ACTH(1—19)-NH_2.[17] Imura *et al.* has found that peptide II is inactivated more slowly than peptide I in fresh human plasma.[21] This finding would offer evidence to support the view that the observed higher potency of the peptide amide is a consequence of the increased stability in the biological systems. When the steroidogenic activity was assayed in isolated rat adrenal cells, peptide I and peptide II were found to exhibit virtually the same degree of potency.[22] This is probably due to the absence of carboxypeptidase action in the assay system employed.

Table 1 next shows that ACTH(1—18)-NH_2 (II) and ACTH(1—19)-NH_2 (III) exhibit almost the same potency and they are as active as the synthetic α_h-ACTH when compared by weight. In the table, the potencies are also expressed in terms of units per μmole to compare the synthetic fragments with α_h-ACTH taking account of their molecular weights. Thus, the relative potencies *vs.* α_h-ACTH may be calculated as 0.48 and 0.47 for II and III, respectively, indicating that these fragment peptides are nearly half as active as the intact hormone, as compared on a molar basis. Ramachandran *et al.* also demonstrated that ACTH(1—18)-NH_2 and ACTH(1—19)-NH_2 possessed almost identical potency in the *in vivo* steroidogenesis.[17] From their data the relative potencies *vs.* sheep ACTH (481 USP units/μmol)[17] of the octadecapeptide amide and the nonadecapeptide amide are estimated to be 0.62 and 0.72, respectively.

The biological data obtained above clearly indicate that all the structural features required for the manifestation of steroidogenic activity reside within the first eighteen amino acid sequence of the ACTH molecule. Since it has been reported that ACTH(1—17)-NH_2 is only 23% as active as ACTH(1—18)-NH_2,[17] the octadecapeptide should be the smallest ACTH fragment that is comparable to the intact hormone as a steroidogenic agent. As mentioned above, the C-terminal amide group in ACTH(1—18)-NH_2 appears to be effective only for the stabilization of the peptide *in vivo*. It has been shown that a natural ACTH and a synthetic 39 amino acid peptide are inactivated more slowly than the fragment peptides such as ACTH(1—18)-NH_2, ACTH(1—19)-OH and ACTH(1—26)-OH.[21] Therefore, the C-terminal portion of the ACTH molecule may not be involved in the process of adrenal stimulation, but may play a role in stabilizing the N-terminal half of the hormone in the physiological environment.

Experimental

Thin layer chromatography was (TLC) performed on precoated "silica gel" plates (Kieselgel 60 F_{254}, Merck) or precoated "cellulose" plates (Cellulose F_{254}, Merck).

H–Ser–Tyr–Ser–Met–Glu–His–Phe–Arg–Trp–Gly–Lys–Pro–Val–Gly–Lys–Lys–Arg–Arg–OH Acetate, ACTH(1—18)-OH (I).[8] To a solution of IV (0.16 g, 0.11 mmol)[9] in *N,N*-dimethylformamide (DMF, 4 ml) previously chilled in an ice-bath was added M hydrochloric acid (0.3 ml) and the solution was introduced into ice-cold ethyl acetate (50 ml). The resulting precipitates of the decapeptide hydrochloride (0.17 g) was dissolved in DMF (4 ml) together with *N*-hydroxysuccinimide (HOSu, 0.050 g, 0.44 mmol) and to this was added dicyclohexylcarbodiimide (DCC, 0.091 g, 0.44 mmol) at 0 °C. The mixture was kept at 4 °C overnight, after which it was introduced into ethly acetate-ether (1:1, 100 ml) to give the decapeptide active ester hydrochloride as amorphous precipitates (0.18 g). The active ester thus obtained was added to a solution of the octapeptide acetate [V, prepared from the N^{α}-benzyloxycarbonyl (*Z*) derivative (0.16 g, 0.1 mmol) by catalytic hydrogenolysis][10] and triethylamine (0.056 ml, 0.4 mmol) in DMF (6 ml) and the mixture was kept at 4 °C for 2 days. The product was isolated as precipitates which formed when the reaction mixture was introduced into ethyl acetate (50 ml). The crude protected octadecapeptide thus obtained (0.32 g) was mixed with anisole (0.2 ml) and 2-mercaptoethanol (0.2 ml) and chilled in an ice-bath. To this was added trifluoroacetic acid (5 ml) and the mixture was kept at room temperature for 60 min. The precipitates which formed upon addition of ether were filtered off, washed with ether and dried *in vacuo*. This was then dissolved in water and the solution was passed through a column (1.7×6 cm) of Amberlite CG-400 (acetate form) with additional portions of water. The aqueous solutions were combined and lyophilized to give the deprotected octadecapeptide (0.28 g).

For purification the crude peptide obtained above was chromatographed on a carboxymethyl cellulose column using an ammonium acetate buffer (Fig. 1). The fractions corresponding to a main peak (tubes 86—115) were pooled, evaporated *in vacuo* at a bath temperature of 50 °C and lyophilized (0.16 g). This material was then submitted to partition chromatography on a column of Sephadex G-25 (medium) with 1-butanol-acetic acid-pyridine-water (12:3:4:6) as solvent. Tubes 41—65 containing the desired peptide as a single component, as examined by means of TLC (cellulose) with 1-butanol-acetic acid-pyridine-water (15:3:10:15) as solvent and the Ehrlich reagent as reagent for locating peptide spots (Fig. 2), were combined and evaporated

in vacuo at a bath temperatuer of 45 °C and the residue was lyophilized (0.10 g). Tubes 31—40 containing a less polar impurity in addition to the desired peptide were combined and evaporated *in vacuo*. The residue was rechromatographed on a Sephadex G-25 column (1.7×30 cm) in the same manner as above to give an additional amount of the homogeneous peptide (0.01 g). These preparations were combined (0.11 g) and rechromatographed on a carboxymethyl cellulose column using an ammonium acetate buffer (Fig. 3). The fractions corresponding to a single peak (tubes 77—100) were combined, evaporated and lyophilized to afford the pure octadecapeptide (I) as colorless fluffy powder; yield 0.10 g (37%), $[\alpha]_D^{25.5}$ −61.2±1.9° (*c* 0.5, 0.1 M acetic acid). $\lambda_{max}^{0.1M\ HCl}$ 280 nm ($E_{1cm}^{1\%}$ 25.1), $\lambda_{shoulder}^{0.1M\ HCl}$ 288 nm ($E_{1cm}^{1\%}$ 19.0); $\lambda_{max}^{0.1M\ NaOH}$ 282 nm ($E_{1cm}^{1\%}$ 25.8), 289 nm ($E_{1cm}^{1\%}$ 25.1). TLC (cellulose): a single component (ninhydrin and Ehrlich reagents) in 1-butanol–acetic acid–pyridine–water (15:3:10:15). Amino acid ratios in acid hydrolysate (figures in parentheses represent theoretical values): Lys 2.94 (3), His 1.00 (1), Arg 3.00 (3), Ser 1.72 (2), Glu 1.03 (1), Pro 0.95 (1), Gly 2.00 (2), Val 1.00 (1), Met 0.98 (1), Tyr 0.98 (1), Phe 0.98 (1). The Trp/Tyr ratio in intact I was 0.98 as determined spectrophotometrically.[15]

H–Ser–Tyr–Ser–Met–Glu–His–Phe–Arg–Trp–Gly–Lys–Pro–Val–Gly–Lys–Lys–Arg–Arg–NH_2 Acetate, ACTH(1—18)–NH_2 (II).[8] To a solution of the octapeptide amide acetate [VI, prepared from the N^{α}–Z derivative (0.18 g, 0.12 mmol) by catalytic hydrogenolysis][10] and triethylamine (0.033 ml, 0.24 mmol) in DMF (5 ml) was added the decapeptide *N*-hydroxysuccinimide ester [prepared from IV (0.19 g, 0.13 mmol)[9] in exactly the same manner as described above] and the mixture was kept at 4 °C for 2 days. The crude protected octadecapeptide obtained (0.34 g) was, in the presence of anisole (0.2 ml) and 2-mercaptoethanol (0.2 ml), treated with trifluoroacetic acid (4 ml) at room temperature for 65 min to give the deblocked peptide (0.32 g).

The crude peptide (acetate form) obtained above was chromatographed on a column (1.7×20 cm) of carboxymethyl cellulose (Serva, 0.7 meq/g) using an ammonium acetate buffer (pH 6.0, 2000 ml) with a linear concentration gradient of 0—0.6 M. Ten-ml fractions were collected and their absorption at 280 nm was measured. The fractions corresponding to a main peak (tubes 96—127) were pooled, evaporated *in vacuo* at a bath temperature of 50 °C and lyophilized (0.11 g). This material was then submitted to partition chromatography on a column (2.7×24 cm) of Sephadex G-25 (medium) with 1-butanol–acetic acid–pyridine–water (12:3:4:6) as solvent and 5 ml-fractions were collected. The Folin-Ciocalteu method[14] was effected for monitoring the peptide content of the fractions. Tubes 14—45 were combined and evaporated *in vacuo* at a bath temperature of 45 °C to give a residue which was lyophilized (0.1 g). The partially purified peptide was rechromatographed on a column (1.7×20 cm) of carboxymethyl cellulose (CM-52, Whatman) using an ammonium acetate buffer (pH 6.0, 1500 ml) with a linear concentration gradient of 0—0.6 M. Ten-ml fractions were collected and those corresponding to a single peak (tubes 138—165) were combined, evaporated *in vacuo* and lyophilized to give the pure octadecapeptide amide (II) as colorless fluffy powder; yield 0.086 g (26%), $[\alpha]_D^{25}$ −61.5±2.4° (*c* 0.4, 0.1 M acetic acid). Lit, $[\alpha]_D^{25}$ −92.7° (*c* 0.1, 0.1 M acetic acid);[17] $[\alpha]_D^{20}$ −54.0° (*c* 0.1, 0.1 M acetic acid).[18] $\lambda_{max}^{0.1M\ HCl}$ 280 nm ($E_{1cm}^{1\%}$ 25.8), $\lambda_{shoulder}^{0.1M\ HCl}$ 288 nm ($E_{1cm}^{1\%}$ 19.6); $\lambda_{max}^{0.1M\ NaOH}$ 282 nm ($E_{1cm}^{1\%}$ 26.9), 289 nm ($E_{1cm}^{1\%}$ 26.0). TLC (cellulose): a single component (ninhydrin and Ehrlich reagents) in 1-butanol–acetic acid–pyridine–water (15 : 3 : 10 : 15). Amino acid ratios in acid hydrolysate: Lys 3.02 (3), His 1.04 (1), Arg 3.07 (3), Ser 1.80 (2), Glu 1.04 (1), Pro 1.04 (1) Gly 2.02 (2), Val 1.00 (1), Met 1.00 (1), Tyr 1.00 (1), Phe 0.98 (1). The Trp/Tyr ratio in intact II was 0.94 as determined spectrophotometrically.[15]

H–Ser–Tyr–Ser–Met–Glu–His–Phe–Arg–Trp–Gly–Lys–Pro–Val–Gly–Lys–Lys–Arg–Arg–Pro–NH_2 Acetate, ACTH(1—19)–NH_2 (III). Compound X (0.17 g, 0.1 mmol) was hydrogenolyzed over palladium in methanol containing acetic acid (0.5 ml) for 3 h. Removal of the solvent by evaporation *in vacuo* followed by lyophilization from acetic acid gave the N^{α}-free nonapeptide derivative (0.17 g). This was dissolved in DMF (3 ml) and triethylamine (0.042 ml, 0.3 mmol) was added. To this solution was added the decapeptide *N*-hydroxysuccinimide ester [prepared from IV (0.16 g, 0.11 mmol)[9] as described above] and the mixture was kept at 4 °C for 2 days. The crude protected nonadecapeptide obtained (0.32 g) was, in the presence of anisole (0.2 ml) and 2-mercaptoethanol (0.2 ml), treated with trifluoroacetic acid (5 ml) at room temperature for 60 min to give the deblocked peptide (0.30 g).

The crude peptide obtained above was, after treatment with Amberlite CG-400 (acetate), submitted to a column (1.7×30 cm) of carboxymethyl cellulose (Serva, 0.7 meq/g) using an ammonium acetate buffer (pH 6.0, 2000 ml) with a linear concentration gradient of 0—0.6 M. The fractions (10 ml/tube) corresponding to a main peak (tubes 106—160) were pooled and lyophilized (0.19 g). This material was chromatographed on a Sephadex G-25 column (medium, 1.7×45 cm) with 1-butanol–acetic acid–pyridine–water (12:3:4:6) as solvent and 4.5 ml-fractions were collected. The fractions containing the desired peptide as a single component (tubes 35—47), as examined by TLC, were combined (0.13 g). For final purification this was rechromatographed on a carboxymethyl cellulose column (CM-52, Whatman, 1.7×30 cm) using an ammonium acetate buffer (pH 6.0, 2000 ml) with a linear concentration gradient of 0—0.6 M. The franctions (10 ml/tube) corresponding to a single peak (tubes 158—185) were combined, evaporated and lyophilized to afford the pure nonadecapeptide (III) as colorless fluffy powder; yield 0.11 g (38%), $[\alpha]_D^{26}$ −69.4±2.1° (*c* 0.5, 0.1 M acetic acid). Lit, $[\alpha]_D^{25}$ −102.6° (*c* 0.5, 0.1 M acetic acid);[17] $[\alpha]_D^{20}$ −50.0° (*c* 0.5, 0.1M acetic acid).[18] $\lambda_{max}^{0.1M\ HCl}$ 280 nm ($E_{1cm}^{1\%}$ 23.6), $\lambda_{shoulder}^{0.1M\ HCl}$ 288 nm ($E_{1cm}^{1\%}$ 17.8); $\lambda_{max}^{0.1M\ NaOH}$ 282 nm ($E_{1cm}^{1\%}$ 24.1), 289 nm ($E_{1cm}^{1\%}$ 23.3). Tlc (cellulose): a single component (ninhydrin and Ehrlich reagents) in 1-butanol–acetic acid–pyridine–water (15:3:10:15). Amino acid ratios in acid hydrolysate: Lys 2.98 (3), His 1.00 (1), Arg 3.02 (3), Ser 1.71 (2), Glu 1.06 (1), Pro 1.91 (2), Gly 1.98 (2), Val 1.00 (1), Met 0.98 (1), Tyr 1.00 (1), Phe 0.96 (1). The Trp/Tyr ratio in intact III was 0.95 as determined spectrophotometrically.[15]

Z–Arg(NO_2)–Pro–NH_2 (VII). Z-Pro-NH_2 (3.43 g, 13.8 mmol)[16] was hydrogenolyzed over palladium in methanol for 4 h. The resulting H–Pro–NH_2 (crystalline free base) and Z–Arg(NO_2)–OH (4.42 g, 12.5 mmol) were coupled with DCC (2.58 g, 12.5 mmol) in DMF–acetonitrile (1 : 5, 48 ml) at room temperature overnight. The product was precipitated from methanol–ethyl acetate and then crystallized from methanol; yield 3.14 g (56%), mp 173—174 °C, $[\alpha]_D^{25.5}$ −19.6±0.6° (*c* 1.0, DMF).

Found: C, 49.89; H, 6.03; N, 21.69%. Calcd for $C_{19}H_{27}N_7O_6$: C, 50.77; H, 6.05; N, 21.82%.

Z–Arg(NO_2)–Arg(NO_2)–Pro–NH_2 (VIII). Compound VII (2.65 g, 5.9 mmol) was treated with 25% hydrogen bromide in acetic acid (10 ml) at room temperature for 60 min to give H–Arg(NO_2)–Pro–NH_2 hydrobromide which

was precipitated by the addition of ether (2.85 g).

A solution of Z-Arg(NO_2)-OH (1.77 g, 5 mmol) and tributylamine (1.31 ml, 5.5 mmol) in anhydrous tetrahydrofuran (20 ml) was chilled in an ice-salt bath and ethyl chloroformate (0.53 ml, 5.5 mmol) was added dropwise. The mixture was stirred at the same temperature for 5 min, after which an ice-cold solution of the dipeptide amide hydrobromide obtained above and tributylamine (3.58 ml, 15 mmol) in tetrahydrofuran-water (3 : 1, 20 ml) was introduced. The reaction mixture was stirred at −10—0 °C for 3 h followed by evaporation *in vacuo* at a bath temperature of 40 °C. The sirupy residue, dissolved in 1-butanol-ethyl acetate (1 : 3), was washed with M hydrochloric acid and M sodium hydrogencarbonate, and evaporated *in vacuo*. The crude product thus obtained was chromatographed on a column of silica gel (30 g, Kieselgel 60, Merck) with ethyl acetate-acetic acid-water (4 : 1 : 1) as solvent. The fractions containing the desired product as a major component were collected and evaporated *in vacuo* at a bath temperature of 40 °C, and the residue was precipitated from methanol-ether. The chromatography was repeated until the precipitates became completely homogeneous as examined by TLC on a silica gel plate with ethyl acetate-acetic acid-water (4:1:1) as solvent; yield 0.98 g, $[\alpha]_D^{25.5}$ −36.4±0.8° (*c*, 1.0, methanol).

Found: C, 46.18; H, 6.39; N, 23.82%. Calcd for $C_{25}H_{38}N_{12}O_9 \cdot 2CH_3OH$: C, 45.37; H, 6.49; N, 23.52%.

Z-Lys(Boc)-Arg(NO_2)-Arg(NO_2)-Pro-NH_2 (IX). Compound VIII (0.78 g, 1.2 mmol) was treated with 25% hydrogen bromide in acetic acid (10 ml) at room temperature for 90 min to give H-Arg(NO_2)-Arg(NO_2)-Pro-NH_2 hydrobromide (0.93 g). This was allowed to react with Z-Lys(Boc)-OSu (0.57 g, 1.2 mmol)[10] in DMF in the presence of triethylamine (0.56 ml, 4.0 mmol) at 4 °C overnight. The solvent was evaporated *in vacuo* and the residue dissolved in 1-butanol-ethyl acetate (1:3) was washed with ice-cold M hydrochloric acid and M sodium hydrogencarbonate and evaporated *in vacuo*. The residue was solidified by treatment with ether; yield 0.91 g (87%), $[\alpha]_D^{25}$ −38.9±0.8° (*c* 1.0, methanol). TLC (silica gel): homogeneous (sulfuric acid) in ethyl acetate-acetic acid-water (4 : 1 : 1).

Found: C, 48.76; H, 7.05, N, 21.36%. Calcd for $C_{36}H_{58}N_{14}O_{12} \cdot CH_3OH$: C, 48.78; H, 6.86; N, 21.53%.

Z-Lys(Boc)-Pro-Val-Gly-Lys(Boc)-Lys(Boc)-Arg-Arg-Pro-NH_2 Acetate (X). Compound IX (0.66 g, 0.75 mmol) was hydrogenolyzed over palladium in 20% acetic acid in methanol (10 ml) for 7 h to give the N^{α}-free tetrapeptide H-Lys(Boc)-Arg-Arg-Pro-NH_2. A 0.60 g-portion (0.65 mmol) was dissolved in tetrahydrofuran-water (5 : 2, 7 ml) and triethylamine (0.20 ml) was added. The resulting solution was combined with an ice-cold solution of Z-Lys(Boc)-Pro-Val-Gly-Lys(Boc)-N_3 [derived from the corresponding hydrazide (0.89 g, 1mmol)][10] in 90% tetrahydrofuran and the mixture was stirred at 4 °C overnight followed by evaporation *in vacuo*. To this were added ethyl acetate (15 ml) and M acetic acid (15 ml) and the mixture was shaken vigorously. The aqueous phase which separated was extracted repeatedly with ethyl acetate. The organic solutions were combined and evaporated *in vacuo*. The residue was again distributed between ethyl acetate (15 ml) and M acetic acid (15 ml), and the organic phase was extracted with M acetic acid repeatedly. The aqueous solutions were combined and evaporated *in vacuo* at a bath temperature of 45 °C. The residue was redissolved in M acetic acid (15 ml) and the solution was extracted with water-saturated 1-butanol repeatedly. The butanol extracts were combined and evaporated *in vacuo* at a bath temperature of 45 °C. The resulting sirupy residue was precipitated from methanol-ether and was then lyophilized to give X; yield 0.78 g (73%), $[\alpha]_D^{25}$ −53.5±0.9° (*c* 1.0, methanol). Tlc (silica gel): homogeneous (ninhydrin, after pretreatment with hydrochloric acid) in ethyl acetate-acetic acid-water (3 : 1 : 1).

Found: C, 51.78; H, 8.00; N, 16.08%. Calcd for $C_{70}H_{119}N_{19}O_{17} \cdot 2CH_3COOH \cdot 4H_2O$: C, 52.56; H, 8.05; N, 15.74%.

References

1) C. H. Li, J. Meienhofer, E. Schnabel, D. Chung, T-B. Lo, and J. Ramachandran, *J. Am. Chem. Soc.*, **82**, 5760 (1960); **83**, 4449 (1961).

2) K. Hofmann, H. Yajima, T-Y. Liu, N. Yanaihara, C. Yanaihara, and J. L. Humes, *J. Am. Chem. Soc.*, **84**, 1054 (1962); **84**, 4481 (1962).

3) K. Hofmann, H. Yajima, T-Y. Liu, and N. Yanaihara, *J. Am. Chem. Soc.*, **83**, 487 (1961); **84**, 4475 (1962).

4) H. Kappeler and R. Schwyzer, *Helv. Chim. Acta*, **44**, 1136 (1961); R. Schwyzer and H. Kappeler, *ibid.*, **46**, 1550 (1963).

5) C. H. Li, D. Chung, J. Ramachandran, and B. Gorup, *J. Am. Chem. Soc.*, **86**, 2703 (1964); **84**, 2460 (1962).

6) H. Otsuka, K. Inouye, M. Kanayama, and F. Shinozaki, *Bull. Chem. Soc. Jpn.*, **38**, 679 (1965).

7) H. Otsuka, K. Inouye, M. Kanayama, and F. Shinozaki, *Bull. Chem. Soc. Jpn.*, **38**, 1563 (1965).

8) H. Otsuka, K. Inouye, F. Shinozaki, and M. Kanayama, *J. Biochem.* (Tokyo), **58**, 512 (1965).

9) H. Otsuka, K. Inouye, F. Shinozaki, and M. Kanayama, *Bull. Chem. Soc. Jpn.*, **39**, 1171 (1966).

10) H. Otsuka, K. Inouye, M. Kanayama, and F. Shinozaki, *Bull. Chem. Soc. Jpn.*, **39**, 882 (1966).

11) G. W. Anderson, J. E. Zimmerman, and F. M. Callahan, *J. Am. Chem. Soc.*, **86**, 1839 (1964); **85**, 3039 (1963).

12) H. Otsuka, M. Shin, Y. Kinomura, and K. Inouye, *Bull. Chem. Soc. Jpn.*, **43**, 196 (1970).

13) An effective use of a homogeneous solvent system in partition chromatography was demonstrated previously: K. Inouye, *Bull. Chem. Soc. Jpn.*, **38**, 1148 (1965).

14) J. L. Bailey, "Techniques in Protein Chemistry," Elsevier, Amsterdam-London-New York (1967), p. 340.

15) D. H. Beaven and E. R. Holiday, *Adv. Protein Chem.*, **7**, 319 (1952); T. W. Goodwin and R. A. Morton, *Biochem. J.*, **40**, 628 (1946).

16) K. Inouye, K. Namba, and H. Otsuka, *Bull. Chem. Soc. Jpn.*, **44**, 1689 (1971).

17) J. Ramachandran, D. Chung, and C. H. Li, *J. Am. Chem. Soc.*, **87**, 2696 (1965).

18) S. Bajusz and K. Medzihradszky, "Peptides," Proceedings of the 8th European Peptide Symposium, Noordwijk, The Netherlands, 1966, H. C. Beyerman, A. van de Linde, and W. Maassen van den Brink (eds.), North-Holland, Amsterdam (1967), p. 209.

19) The assays were performed by Dr. Akira Tnaka and Mr. Kunihiro Odaguchi of this laboratory. We thank Dr. Tanaka for permission to include these data in the present communication.

20) K. Inouye, K. Watanabe, and H. Otsuka, *Bull. Chem. Soc. Jpn.*, in press.

21) H. Imura, H. Matsuyama, S. Matsukura, T. Miyake, and M. Fukase, *Endocrinol.*, **80**, 599 (1967).

22) M. Nakamura, *J. Biochem.* (Tokyo), **71**, 1029 (1972).

Synthesis of Corticotropin Peptides. XIII. The Synthesis of a Hexacosapeptide and a Heptacosapeptide Corresponding to the First Twenty-six and Twenty-seven Amino Acid Residues of Corticotropin (ACTH)*

Ken INOUYE, Yoshie SUMITOMO, and Masaru SHIN

Shionogi Research Laboratory, Shionogi & Co., Ltd., Fukushima-ku, Osaka 553

(Received June 29, 1976)

The syntheses are described of a hexacosapeptide H-Ser-Tyr-Ser-Met-Glu-His-Phe-Arg-Trp-Gly-Lys-Pro-Val-Gly-Lys-Lys-Arg-Arg-Pro-Val-Lys-Val-Tyr-Pro-Asn-Gly-OH (I) and a heptacosapeptide H-Ser-Tyr-Ser-Met-Glu-His-Phe-Arg-Trp-Gly-Lys-Pro-Val-Gly-Lys-Lys-Arg-Arg-Pro-Val-Lys-Val-Tyr-Pro-Asn-Gly-Ala-OH (II) corresponding to the first twenty-six and twenty-seven amino acid residues, respectively, of corticotropin (ACTH), in which a new protecting group 1-methylcyclohexyloxycarbonyl (Mhoc) is utilized for the temporary protection of the ε-amino function of lysines. The *in vivo* steroidogenic potencies of the synthetic peptides I and II are compared on a molar basis with those of ACTH(1—18)-NH_2 and synthetic human ACTH (α_h-ACTH) to demonstrate that the relative potencies of I and II *vs.* ACTH(1—18)-NH_2 are 2.3 and 2.3—3.8, respectively, and those *vs.* α_h-ACTH are 1.1 and 1.1—1.8, respectively.

The primary structure of porcine corticotropin (ACTH) and that of human ACTH were first proposed by Shepherd *et al.*[1] in 1956 and by Lee *et al.*[2] in 1961, respectively. The proposed structure of porcine ACTH was synthesized by Schwyzer and Sieber[3] in 1963 and that of human ACTH by Bajusz *et al.* in 1967.[4]

In a previous communication we reported the synthesis of a heptacosapeptide corresponding to the first twenty-seven amino acid residues of human ACTH.[5] In 1971, however, Gráf *et al.*[6] followed by Riniker *et al.*[7] revised the amino acid sequences of porcine and human ACTH's. In addition, the structures of bovine and ovine ACTH's have also been revised recently not only to establish the identity between these two mammalian hormones,[8,9] but also to show that the only structural differences among the human, porcine, bovine and ovine hormones are confined to the two positions 31 and 33. Thus, we have carried out the synthesis of ACTH(1—27)-OH according to the revised amino acid sequence, H-Ser-Tyr-Ser-Met-Glu-His-Phe-Arg-Trp-Gly-Lys-Pro-Val-Gly-Lys-Lys-Arg-Arg-Pro-Val-Lys-Val-Tyr-Pro-Asn-Gly-Ala-OH (II), which differs from the one previously proposed for the human hormone[2] in positions 25 through 27, Asn-Gly-Ala instead of Asp-Ala-Gly. In parallel with peptide II, a hexacosapeptide, H-Ser-Tyr-Ser-Met-Glu-His-Phe-Arg-Trp-Gly-Lys-Pro-Val-Gly-Lys-Lys-Arg-Arg-Pro-Val-Lys-Val-Tyr-Pro-Asn-Gly-OH, ACTH(1—26)-OH (I), has also been synthesized. For their size peptides I and II may be placed halfway between the nonatriacontapeptide of natural ACTH and the octadecapeptide ACTH(1—18)-NH_2 which is the smallest peptide endowed with all the structural features required for the manifestation of steroidogenic activity.[10] Comparison of I or II with these peptides for the hormonal action will, therefore, provide data important for evaluating the role of the C-terminal half of the ACTH molecule. This paper describes the details of the synthesis of

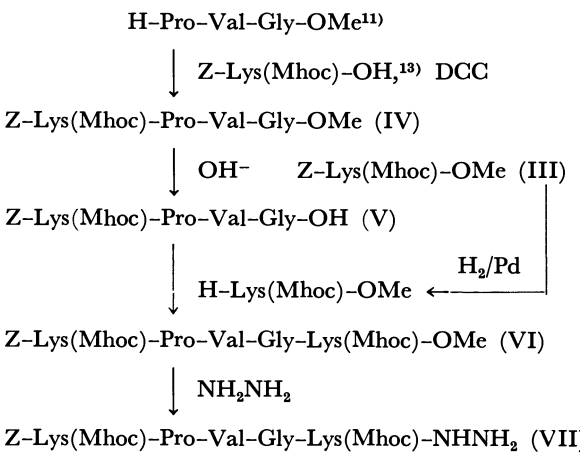

Fig. 1. Synthesis of amino acid sequence 11—15 of ACTH. Mhoc: 1-methylcyclohexyloxycarbonyl.

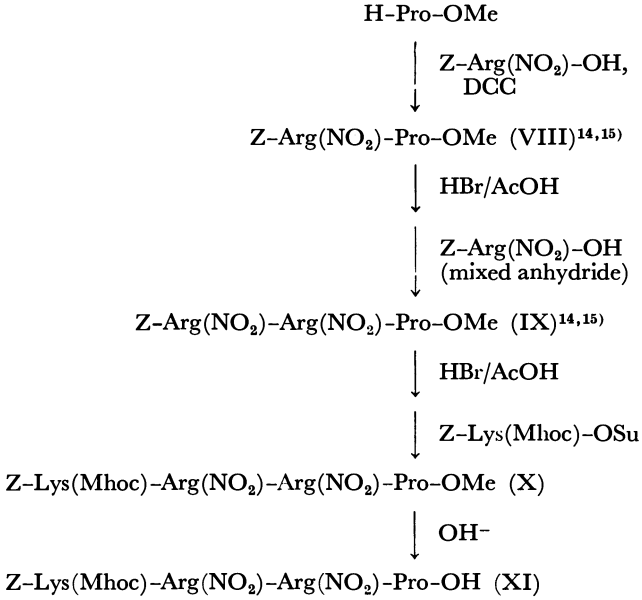

Fig. 2. Synthesis of amino acid sequence 16—19 of ACTH. Mhoc: 1-methylcyclohexyloxycarbonyl.

* All the amino acid residues mentioned in this communication are of the L-configuration. Abbreviations used are those recommended by the IUPAC-IUB Commission of Biochemical Nomenclature [*Biochemistry*, **5**, 2485 (1966); *ibid.*, **6**, 362 (1967); *ibid.*, **11**, 1726 (1972)] and include Mhoc: 1-methylcyclohexyloxycarbonyl.

peptides I and II.

The pentapeptide derivative (VII) corresponding to positions 11—15 of the ACTH molecule was synthesized according to the procedure illustrated in Fig. 1. This procedure is much the same as that employed for the synthesis of Z-Lys(Boc)-Pro-Val-Gly-Lys-(Boc)-OMe (and $-NHNH_2$)[11,12] except that the ε-amino function of lysines was blocked by the 1-methylcyclohexyloxycarbonyl (Mhoc) groups. The Mhoc group is cleavable by acidolysis in almost the same rate as the Boc group. However, a highly lipophilic nature of the new protecting group would increase the solubility of protected peptides in organic solvents, thus facilitating their chromatographic purification remarkably. A full account of the Mhoc and other new protecting groups will be given elsewhere.[13]

The amino acid sequence 16—19 was synthesized in the form of Z-Lys(Mhoc)-Arg(NO_2)-Arg(NO_2)-Pro-OH (XI) as shown in Figure 2. The two arginines were successively incorporated by the dicyclohexylcarbodiimide (DCC) method and by the mixed anhydride procedure to give IX.[14,15] Removal of the Z group with hydrogen bromide in acetic acid yielded the N^{α}-free tripeptide which was coupled with the *N*-hydroxysuccinimide (HOSu) ester of Z-Lys(Mhoc)-OH to produce X. Saponification of ester X gave the corresponding acid (XI). An alternative synthesis of XI has recently been accomplished by the use of H-Arg(NO_2)-Arg(NO_2)-Pro-OH, derived from Z-Arg(NO_2)-Arg(NO_2)-Pro-OBzl with hydrogen bromide

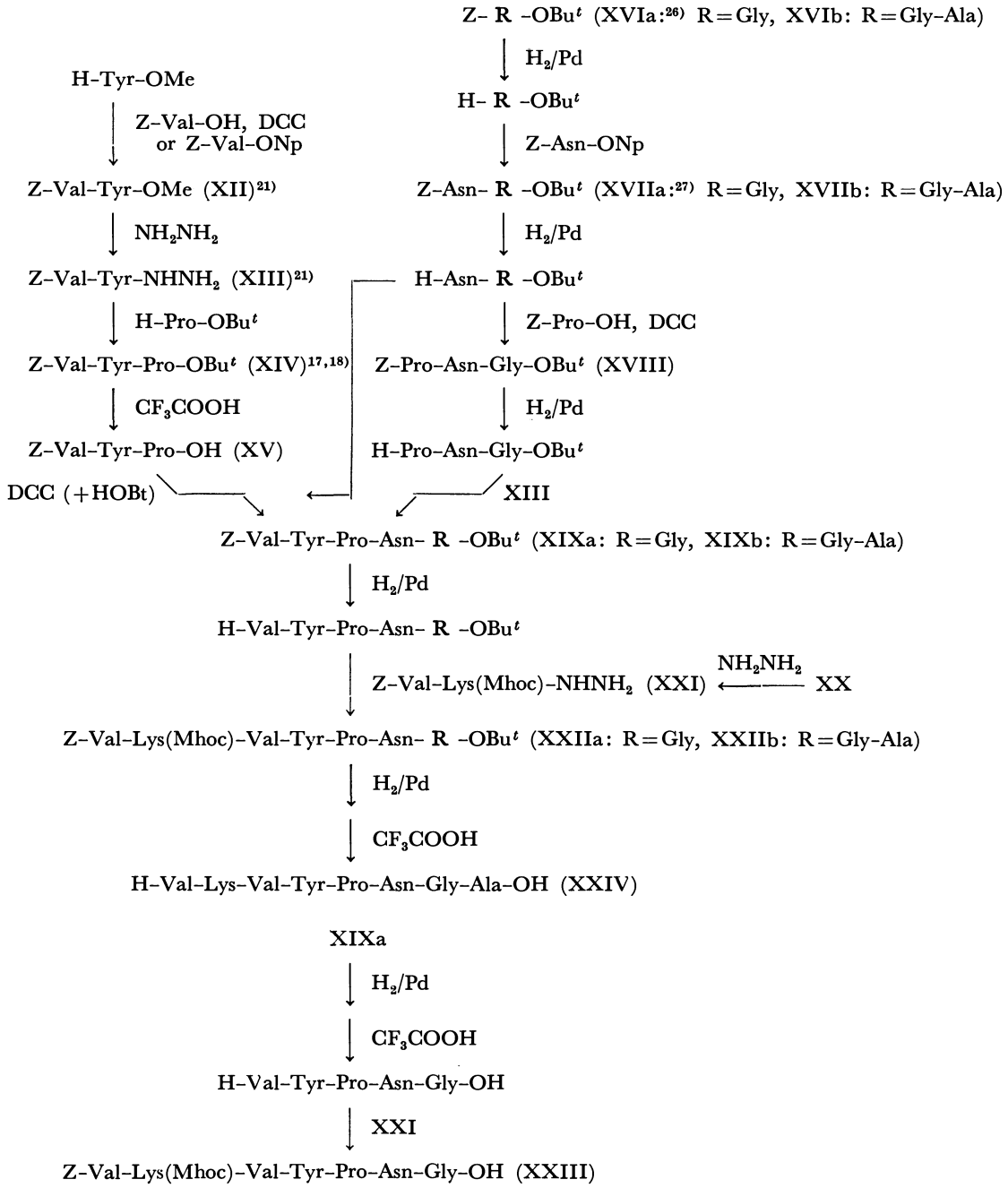

Fig. 3. Snythesis of amino acid sequences 20—26 and 20—27 of ACTH.
Mhoc: 1-methylcyclohexyloxycarbonyl.

in acetic acid, as intermediate.[16] The optical rotation of the product was identical with that of the one derived from the methyl ester. This provides a proof for the optical purity of XI.

The synthetic routes to the amino acid sequences 20—26 and 20—27 are summarized in Fig. 3. The tripeptide derivative XV corresponding to positions 22—24 was derived from the *t*-butyl ester (XIV)[17,18] by the treatment with trifluoroacetic acid. Compound XV could not be obtained from Z-Val-Tyr-Pro-OMe without any danger of racemization, because the methyl ester was remarkably resistant to the action of alkali. In contrast to the methyl ester the corresponding benzyl ester may be used as an intermediate to XV, since Ramachandran and Li have reported that Z-Val-Lys(Tos)-Val-Tyr-Pro-OBzl can be saponified to the corresponding acid in an 84% yield.[19] Coupling of XV with H-Asn-Gly-OBu^t and H-Asn-Gly-Ala-OBu^t by means of the DCC method in the presence of 1-hydroxybenzotriazole (HOBt)[20] gave crystalline compounds XIXa and XIXb, respectively, in moderate yields. Compound XIXa was also obtained by the reaction of Z-Val-Tyr-N_3, derived from the preceding hydrazide (XIII)[21] by the treatment with nitrous acid, with a crystalline tripeptide H-Pro-Asn-Gly-OBu^t (free base) in a comparable yield. Catalytic hydrogenolysis of XIXa and XIXb yielded the N^{α}-free penta- and hexapeptides, which were then acylated with Z-Val-Lys(Mhoc)-N_3, derived from the hydrazide (XXI) with nitrous acid in the usual manner, to give crystalline derivatives XXIIa and XXIIb, respectively, in excellent yields.

A portion of XXIIb was fully deblocked by catalytic hydrogenolysis and subsequent treatment with trifluoroacetic acid to afford an octapeptide (XXIV) corresponding to ACTH(20—27). The acid hydrolysate of XXIV was found to contain the constituent amino acids (and ammonia derived from Asn) in the ratios predicted by theory. Compound XIXa was deprotected in the same manner as above and the resulting pentapeptide was acylated with Z-Val-Lys-(Mhoc)-N_3 to give XXIII in a crystalline form. Compound XXIII may be used as an intermediate for the synthesis of peptides related to the C-terminal half of the ACTH molecule.

The fragment peptides obtained above were assembled as illustrated in Fig. 4, leading to the formation of a hexadecapeptide and a heptadecapeptide corresponding to ACTH(11—26) and ACTH(11—27), respectively. The N^{α}-free peptides, derived from XXIIa and XXIIb by catalytic hydrogenolysis, were coupled with XI by the DCC method in the presence of HOBt[20] to yield XXVa and XXVb, respectively, both of which were purified on silica gel columns with chloroform–methanol systems as solvent. For removal of the N^{α}-benzyloxycarbonyl (Z) group and nitro groups, XXVa and XXVb were hydrogenolyzed; the completion of reaction was checked by TLC and by the disappearance of absorption at 275 nm characteristic of the nitro group. The resulting partially protected peptides XXVIa and XXVIb were then allowed to react with the azide, derived from hydrazide VII with nitrous acid in the usual manner, to give a hexadecapeptide (XXVIIIa) and a heptadecapeptide (XXVIIIb) corresponding to ACTH(11—26) and ACTH(11—27), respectively. They were obtained in moderate yields after purification by silica gel column chromatography with chloroform–methanol systems as solvent. The acid hydrolysates of XXVIIIa and XXVIIIb were found to contain the constituent amino acids in the ratios expected by theory.

A portion of XXVIa was treated with trifluoroacetic acid in the presence of anisole and 2-mercaptoethanol as scavengers to liberate a free undecapeptide XXVIIa, that is ACTH(16—26). In the same manner a free dodecapeptide (XXVIIb) corresponding to ACTH-(16—27) was derived from XXVIb. Both XXVIIa and XXVIIb, purified on a carboxymethyl cellulose column, behaved as a single component in TLC.

The final coupling process for connecting the N-terminal decapeptide with the C-terminal hexadecapeptide and the subsequent deprotection to lead to

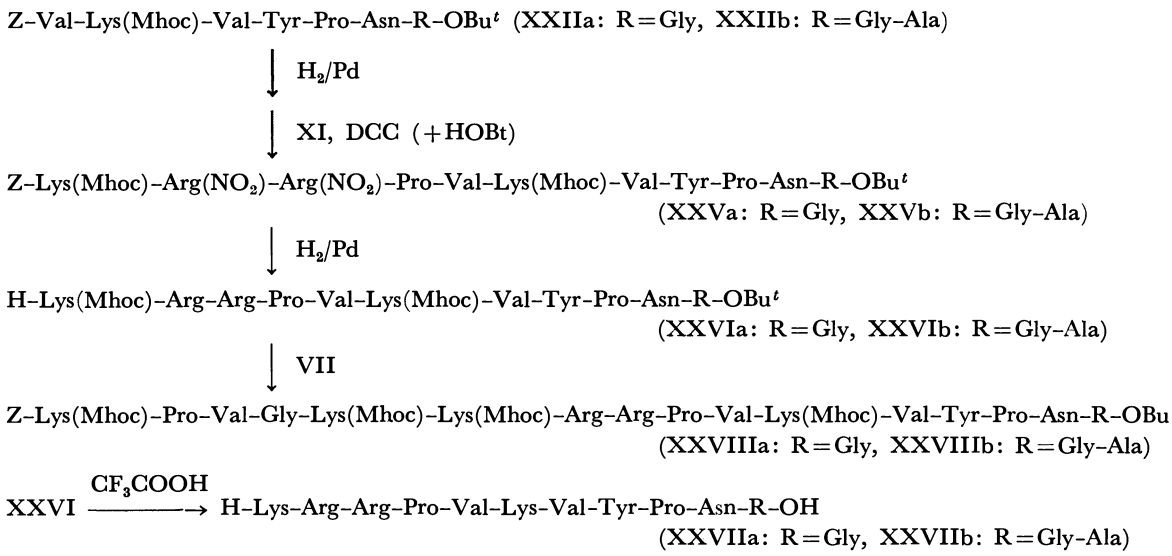

Fig. 4. Synthesis of amino acid sequences 11—26 and 11—27 of ACTH.
Mhoc: 1-methylcyclohexyloxycarbonyl.

the production of a hexacosapeptide, ACTH(1—26)-OH (I), were performed as follows. Boc-Ser-Tyr-Ser-Met-Glu(OBu^t)-His-Phe-Arg(H^+)-Trp-Gly-O^- [22] was converted into the hydrochloride Boc-Ser-Tyr-Ser-Met-Glu(OBu^t)-His-Phe-Arg(HCl)-Trp-Gly-OH and this was esterified with HOSu by the DCC method. The resulting active ester hydrochloride was coupled with the N^{α}-free hexadecapeptide, derived from XXVIIIa by catalytic hydrogenolysis, to give the protected hexacosapeptide, Boc-Ser-Tyr-Ser-Met-Glu(OBu^t)-His-Phe-Arg-Trp-Gly-Lys(Mhoc)-Pro-Val-Gly-Lys(Mhoc)-Lys(Mhoc)-Arg-Arg-Pro-Val-Lys(Mhoc)-Val-Tyr-Pro-Asn-Gly-OBu^t. Finally, this was submitted for deprotection to the trifluoroacetic acid treatment in the presence of anisole and 1,2-ethanedithiol as scavengers to liberate hexacosapeptide I as the trifluoroacetate, which was converted into the acetate by passing through a column of Amberlite CG-400 (acetate form). The heptacosapeptide ACTH(1—27)-OH (II) was obtained in exactly the same manner as described above except that the N^{α}-free heptadecapeptide, derived from XXVIIIb by catalytic hydrogenolysis, was used as the amine component in the coupling reaction. The deblocked peptides were then purified by partition chromatography on a column of Sephadex G-25 with 1-butanol-acetic acid-pyridine-water (12 : 3 : 4 : 6) as solvent[10b] and by carboxymethyl cellulose column chromatography in an ammonium acetate buffer. The overall yields of peptide I and peptide II for the final coupling, deprotection and purification processes were 26% and 27%, respectively. These preparations were found to be homogeneous in TLC, and their acid hydrolysates contained the constituent amino acids in the ratios expected by theory except for tryptophan. The Tyr/Trp ratio was 2.0 for both peptides, as determined spectrophotometrically.[23]

The synthetic peptides thus obtained were assayed for the *in vivo* steroidogenic activity by a method based on the elevated levels of 11-hydroxycorticosteroids in the adrenal venous blood of the hypophysectomized rat in response to intravenous administration of the peptide. The results are shown in Table 1,[24] in which the potencies of ACTH(1—26)-OH (I) and ACTH(1—27)-OH (II) are compared with those of ACTH(1—18)-NH_2[10b] and the synthetic human hormone (α_h-ACTH).[25] The *in vivo* steroidogenic potencies of I and II appear to be comparable, although the heptacosapeptide is rather variable and tends to give potencies somewhat higher than that of the hexacosapeptide. When compared on a molar basis, peptide I and peptide II are more than twice as active as the octadecapeptide and equal to, or even more active than, the intact hormone; the relative potencies of I and II *vs.* ACTH(1—18)-NH_2 are 2.3 and 2.3—3.8, respectively, and those *vs.* α_h-ACTH are 1.1 and 1.1—1.8, respectively, as calculated from Table 1. More of the comparative studies including a detailed examination of the time-action relations are obviously needed to evaluate the effect of chain length on biological activity. Such studies are now in progress.

Table 1. Steroidogenic activity of snythetic peptides[24]

Compound	Molecular weight[a]	*In vivo* steroidogenic activity	
		units/mg[b]	units/μmol
ACTH(1—18)-NH_2[10b]	2249	96.7	217
ACTH(1—26)-OH (I)	3105	160	497
ACTH(1—27)-OH (II)	3176	155—259	492—823
Synthetic α_h-ACTH[25]	4541	98.6	448

a) As anhydrous free base. b) The Third USP Corticotropin Reference Standard was used as reference.

Experimental

Thin layer chromatography was (TLC) performed on "silica gel" plates [Kieselgel GF_{254} or Kieselgel $60F_{254}$ (precoated), Merck] or precoated "cellulose" plates (Cellulose F, Merck), and the following solvent systems were employed: A, benzene-ethyl acetate (7 : 3); B, ethyl acetate-methanol (8 : 2); C, chloroform-methanol (9 : 1); D, chloroform-methanol (85 : 15); E, chloroform-methanol (8 : 2); F, chloroform-methanol-acetic acid (95 : 5 : 3); G, chloroform-methanol-acetic acid (90 : 10 : 3); H, chloroform-methanol-acetic acid (8 : 1 : 1); I, chloroform-methanol-acetic acid (80 : 20 : 3); J, 1-butanol-acetic acid-water (4 : 1 : 2); K, 1-butanol-acetic acid-pyridine-water (15 ; 3 : 10 : 12); L, 1-butanol-acetic acid-pyridine-water (15 : 3 : 10 : 15).

Z-Lys(Mhoc)-OMe (III). Z-Lys(Mhoc)-OH, derived from the dicyclohexylamine (DCHA) salt (12.04 g, 20 mmol)[13] by the treatment with Dowex 50W×8 (H^+ form) in 60% ethanol in the usual manner, was esterified with diazomethane to give III as amorphous solid; wt 8.38 g (96%), $[\alpha]_D^{22}$ −9.6± 0.3° (*c* 2.0, acetone). TLC (silica gel): a single component (ninhydrin, after pretreatment with hydrobromic acid) in system A and system B.

Found: C, 63.60; H, 8.07; N, 6.56%. Calcd for $C_{23}H_{34}N_2O_6$: C, 63.57; H, 7.89; N, 6.54%.

Z-Lys(Mhoc)-Pro-Val-Gly-OMe (IV). Z-Lys(Mhoc)-OH, derived from the DCHA salt (15.05 g, 25 mmol)[13] in the usual manner, and H-Pro-Val-Gly-OMe (7.13 g, 25 mmol)[11] were coupled with DCC (5.16 g, 25 mmol) in dichloromethane at 4 °C overnight. The reaction mixture was worked up in the usual manner to give the desired tetrapeptide, which was separated as gelatinous precipitates from ether; wt 11.0 g (64%), mp 71—73 °C, $[\alpha]_D^{23}$ −73.1±1.1° (*c* 1.0, methanol). TLC (silica gel): a single component (sulfuric acid) in system C and system F.

Found: C, 60.88; H, 7.70; N, 10.11%. Calcd for $C_{35}H_{53}N_5O_9$: C, 61.12; H, 7.77; N, 10.18%.

Z-Lys(Mhoc)-Pro-Val-Gly-OH (V). Compound IV (1.38 g, 2 mmol) in methanol (5 ml) was saponified with 2 M sodium hydroxide (2 ml) at 0 °C for 60 min to give V as amorphous solid; wt 1.26 g (92%), $[\alpha]_D^{23}$ −71.1±1.1° (*c* 1.0, methanol). TLC (silica gel): a single component (sulfuric acid) in system G.

Found: C, 59.97; H, 7.84; N, 9.92%. Calcd for $C_{34}H_{51}N_5O_9 \cdot 1/2H_2O$: C, 59.81; H, 7.68; N, 10.26%.

Z-Lys(Mhoc)-Pro-Val-Gly-Lys(Mhoc)-OMe (VI). Compound III (5.21 g, 12 mmol) was hydrogenolyzed over palladium in methanol in the presence of acetic acid (1 ml) for 2 h to give the acetic acid salt of H-Lys(Mhoc)-OMe as a sirupy residue. This was then treated with 50% potassium carbonate at 0 °C in the presence of dichloromethane. The resulting free base and V (6.74 g, 10 mmol) were coupled

with dicyclohexylcarbodiimide (DCC, 2.48 g, 12 mmol) in dichloromethane at 4 °C for 20 h to give VI, which was separated as gelatinous precipitates from ether. Reprecipitation from ethyl acetate–ether afforded the pure material; wt 7.51 g (79%), mp 84—85 °C, $[\alpha]_D^{23}$ −51.1±0.9° (*c* 1.0, methanol). TLC (silica gel): a single component (sulfuric acid) in system C.

Found: C, 61.84; H, 8.37; N, 10.02%. Calcd for $C_{49}H_{77}N_7O_{12}$: C, 61.55; H, 8.12; N, 10.25%.

Z-Lys(Mhoc)-Pro-Val-Gly-Lys(Mhoc)-NHNH$_2$ (VII). Compound VI (6.69 g, 7 mmol) was treated with hydrazine hydrate (3.4 ml, 70 mmol) in methanol (30 ml) at room temperature for 45 h, after which the product was separated as gelatinous precipitates by the addition of ether. Reprecipitation from methanol–ether gave VII in pure form; wt 6.50 g (97%), mp 165—166 °C, $[\alpha]_D^{22.5}$ −52.0±0.9° (*c* 1.0, methanol), −28.3±0.4° [*c* 2.0, *N,N*-dimethylformamide (DMF)]. TLC (silica gel): a single component (sulfuric acid) in system B and system C.

Found: C 60.19; H, 8.46; N, 13.21%. Calcd for $C_{48}H_{77}N_9O_{11}$: C, 60.29, H, 8.12; N, 13.18%.

Z-Lys(Mhoc)-Arg(NO$_2$)-Arg(NO$_2$)-Pro-OMe (X). Compound IX (2.00 g, 3 mmol) was treated with 25% hydrogen bromide in acetic acid (7 ml) at room temperature for 120 min to give H-Arg(NO$_2$)-Arg(NO$_2$)-Pro-OMe hydrobromide (2.44 g).

Z-Lys(Mhoc)-OH, derived from the DCHA salt (1.80 g, 3 mmol)[13] in the usual manner, and *N*-hydroxysuccinimide (HOSu, 0.35 g, 3 mmol) were coupled with DCC (0.62 g, 3 mmol) in acetonitrile at 0 °C for 3 h. The resulting active ester was allowed to react with the N^{α}-free tripeptide ester obtained above in DMF (15 ml) in the presence of triethylamine (1.7 ml, 12 mmol) at 4 °C for 2 days. The product was dissolved in 10% 1-butanol in ethyl acetate and the solution was washed with ice-cold M hydrochloric acid and M sodium hydrogencarbonate, dried over magnesium sulfate and evaporated *in vacuo*. The resulting sirupy residue was reprecipitated from methanol–ether yielded X in pure form; wt 2.40 g (86%), mp 111—119 °C, $[\alpha]_D^{24.5}$ −45.2±0.9° (*c* 1.0, methanol). TLC (silica gel): a single component (sulfuric acid) in system D.

Found: C, 50.67; H, 6.87; N, 18.81%. Calcd for $C_{40}H_{63}N_{13}O_{13}\cdot H_2O$: C, 50.46; H, 6.88; N, 19.13%.

Z-Lys(Mhoc)-Arg(NO$_2$)-Arg(NO$_2$)-Pro-OH (XI). Compound X (2.15 g, 2.3 mmol) in methanol (7 ml) was saponified with sodium hydroxide (4.6 ml) at room temperature for 2 h followed by neutralization with M hydrochloric acid (4.6 ml) at 0 °C and concentration *in vacuo* to remove methanol. The resulting aqueous mixture was extracted three times with 10% 1-butanol in ethyl acetate. The organic extracts were combined, dried over magnesium sulfate and evaporated *in vacuo*. The crude product thus obtained was purified on a silica gel column (100g, Kieselgel 60, Merck) with chloroform–methanol–acetic acid systems (90 : 10 : 3, 400 ml; 85 : 15 : 3, 500 ml; 80 : 20 : 3, 600 ml) as solvent. The fractions were examined by TLC (silica gel, in system I) and those containing the desired compound as a single component were combined and evaporated *in vacuo* to give a residue which was solidified by treatment with ether; wt 1.72 g (80%), mp 137—142 °C, $[\alpha]_D^{21}$ −36.8±0.8° (*c* 1.0, methanol).

Found: C, 50.16; H, 6.79; N, 19.25%. Calcd for $C_{39}H_{61}N_{13}O_{13}\cdot H_2O$: C, 49.94; H, 6.77; N, 19.41%.

Z-Val-Lys(Mhoc)-OMe (XX). Compound III (2.17 g, 5 mmol) was hydrogenolyzed over palladium in 10% acetic acid in methanol for 2 h. The solvent was removed by evaporation *in vacuo* to give an oily residue which was treated with aqueous potassium carbonate at 0 °C in the presence of dichloromethane. The resulting free base of H-Lys(Mhoc)-OMe and Z-Val-OH (1.26 g, 5 mmol) were coupled with DCC (1.03 g, 5 mmol) in dichloromethane at 4 °C overnight to give XX; wt 2.31 g (87%), mp 65—67 °C, $[\alpha]_D^{25}$ −18.7±0.5° (*c* 1.0, methanol). TLC (silica gel): a single component (sulfuric acid) in system G.

Found: C, 63.23; H, 8.24; N, 8.14%. Calcd for $C_{28}H_{43}N_3O_7$: C, 63.02; H, 8.12; N, 7.87%.

Z-Val-Lys(Mhoc)-NHNH$_2$ (XXI). Compound XX (1.87 g, 3.5 mmol) was treated with hydrazine hydrate (1.7 ml) in ethanol (15 ml) at room temperature overnight. The product was reprecipitated from ethanol–ether to afford XXI; wt 1.46 g (78%), mp 147—149 °C, $[\alpha]_D^{25.5}$ −25.8±0.7° (*c* 1.0, acetic acid).

Found: C, 60.80; H, 8.11; N, 13.04%. Calcd for $C_{27}H_{43}N_5O_6$: C, 60.77; H, 8.12; N, 13.12%.

Z-Pro-Asn-Gly-OBu^t (XVIII). Compound XVIIa (4.93 g, 13 mmol) was hydrogenolyzed over palladium in methanol for 4 h to give H-Asn-Gly-OBu^t (free base) as an oil. This was then coupled with Z-Pro-OH (3.24 g, 13 mmol) by means of DCC (2.68 g, 13 mmol) in dichloromethane at 4 °C overnight. The product was repeatedly recrystallized from acetonitrile; wt 4.84 g (78%), mp 146—147.5 °C, $[\alpha]_D^{23}$ −64.6±1.0° (*c* 1.0, methanol). TLC (silica gel): a single component (sulfuric acid) in system G.

Found: C, 57.52; H, 6.73; N, 11.63%. Calcd for $C_{23}H_{32}N_4O_7$: C, 57.97; H, 6.77; N, 11.76%.

Z-Val-Tyr-Pro-Asn-Gly-OBu^t (XIXa). *a)* Via *Val-Tyr-Pro + Asn-Gly.* Compound XVIIa (0.38 g, 1 mmol) was hydrogenolyzed over palladium in methanol for 4 h to give H-Asn-Gly-OBu^t (free base) as an oil.

Compound XIV (0.57 g, 1 mmol) was treated with trifluoroacetic acid (5 ml) at room temperature for 60 min. The solvent was evaporated *in vacuo* and the residue was lyophilized from acetic acid. The resulting powder was dissolved in ethyl acetate and the solution was extracted with 5% sodium hydrogencarbonate three times. The aqueous solutions combined were acidified with hydrochloric acid followed by extraction with ethyl acetate. The combined extracts were dried over magnesium sulfate and evaporated *in vacuo* to give XV as a sirupy residue. This was then coupled with the above dipeptide ester by means of DCC (0.21 g, 1 mmol) in acetonitrile in the presence of 1-hydroxybenzotriazole (HOBt, 0.14 g, 1 mmol) at 4 °C overnight. The crystalline precipitates which had formed were filtered off and recrystallized from acetonitrile (20 ml) to afford XIXa in pure form; wt 0.50 g (66%), mp 152—155 °C, $[\alpha]_D^{22}$ −33.0±2.0° (*c* 0.4, DMF). TLC (silica gel): a single component (sulfuric acid) in system H.

Found: C, 58.79; H, 6.89; N, 10.92%. Calcd for $C_{37}H_{50}N_6O_{10}\cdot H_2O$: C, 58.72; H, 6.93; N, 11.10%.

b) Via *Val-Tyr + Pro-Asn-Gly.* Compound XVIII 2.38 g, 5 mmol) was hydrogenolyzed over palladium in methanol for 4 h to give H-Pro-Asn-Gly-OBu^t (free base) in a crystalline form. This was then coupled with Z-Val-Tyr-N_3 [derived from XIII (2.14 g, 5 mmol) by the treatment with nitrous acid in the usual manner in DMF–ethyl acetate at 4 °C overnight. Evaporation of the solvent *in vacuo* gave a residue which was crystallized from acetonitrile. Recrystallization from the same solvent gave the desired XIXa; wt 2.22 g (59%), mp 154—156 °C, $[\alpha]_D^{23}$ −34.2±1.5° (*c* 0.5, DMF).

Found: C, 58.58; H, 6.84; N, 10.91%.

Z-Gly-Ala-OBu^t (XVIIb). Z-Ala-OH (11.2 g, 50 mmol) was treated with 2-methylpropene (isobutene, 50 ml) in dichloromethane in the presence of sulfuric acid (1.5 ml)

at room temperature for 3 days to give Z-Ala-OBu^t as an oily residue (13.7 g). This was hydrogenolyzed over palladium in methanol for 7 h to yield H-Ala-OBu^t (free base) as an oil (6.97 g).

The alanine ester obtained above was coupled with Z-Gly-OH (9.41 g, 45 mmol) with DCC (9.33 g, 45 mmol) in dichloromethane at 4 °C overnight to give a crude preparation of XVIb (15.9 g). A 1.06-g portion was chromatographed on a column of silica gel (20 g, Kieselgel 60, Merck) with benzene-ethyl acetate (3 : 2) as solvent. The fractions were examined by TLC (silica gel, in the same solvent as that for the column) and those containing the desired compound as a single component were combined and evaporated *in vacuo*; wt 0.95 g (94%), $[\alpha]_D^{24.5}$ $-31.5\pm0.8°$ (*c* 0.9, methanol).

Found: C, 60.77; H, 7.33; N, 8.30%. Calcd for $C_{17}H_{24}N_2O_5$: C, 60.70; H, 7.19; N, 8.33%.

Z-Asn-Gly-Ala-OBu^t (XVIIb). Compound XVIb (6.57 g, 19.5 mmol) was hydrogenolyzed over palladium in methanol for 10 h to give H-Gly-Ala-OBu^t as an oil. This was then coupled with Z-Asn-ONp (7.55 g, 19.5 mmol) in DMF at 4 °C overnight. The product was crystallized from acetonitrile. Recrystallization from the same solvent yielded XVIIb; 6.63 g (74%), mp 159—160 °C, $[\alpha]_D^{23.5}$ $-20.4\pm0.6°$ (*c* 1.0, methanol). TLC (silica gel): a single component (sulfuric acid) in system E.

Found: C, 56.19; H, 6.78; N, 12.56%. Calcd for $C_{21}H_{30}N_4O_7$: C, 55.99; H, 6.71; N, 12.44%.

Z-Val-Tyr-Pro-Asn-Gly-Ala-OBu^t (XIXb). Compound XVIIb (1.80 g, 4 mmol) was hydrogenolyzed over palladium in methanol for 3 h to give H-Asn-Gly-Ala-OBu^t as an oily residue.

Compound XIV (2.27 g, 4 mmol) was treated with trifluoroacetic acid (20 ml) at room temperature for 60 min to give XV, which was isolated in the manner described above in the synthesis of XIXa. Compound XV was coupled with the above tripeptide ester by means of DCC (0.82 g, 4 mmol) in acetonitrile in the presence of HOBt (0.54 g, 4 mmol) at 4 °C overnight. The desired XIXb was isolated in the same manner as described above for XIXa; wt 1.93 g (58%), mp (70) 140—145 °C, $[\alpha]_D^{23.5}$ $-57.2\pm0.8°$ (*c* 1.0, methanol). TLC (silica gel): a single component (sulfuric acid) in system H.

Found: C, 57.82; H, 6.98; N, 12.18%. Calcd for $C_{40}H_{55}N_7O_{11}\cdot H_2O$: C, 58.03; H, 6.94; N, 11.84%.

Z-Val-Lys(Mhoc)-Val-Tyr-Pro-Asn-Gly-OBu^t (XXIIa). Compound XIXa (2.22 g, 3 mmol) was hydrogenolyzed over palladium in acetic acid (20 ml) for 4 h to give H-Val-Tyr-Pro-Asn-Gly-OBu^t acetate as amorphous solid (1.93 g).

To a DMF solution of XXI (1.04 g, 1.95 mmol) previously chilled in an ice-bath were added ice-cold M hydrochloric acid (5 ml) and 2 M sodium nitrite (1.07 ml) and the mixture was shaken at 0 °C for 4 min. The resulting azide was extracted with ethyl acetate and the combined extracts were washed twice with M sodium hydrogencarbonate and dried over magnesium sulfate at 0 °C. This was combined with a solution of the above pentapeptide ester (0.87 g, 1.3 mmol) and triethylamine (0.28 ml, 2 mmol) in DMF and the mixture was kept at 4 °C for 2 days. The crude product was crystallized and recrystallized from methanol-ethyl acetate to afford the pure XXIIa; wt 1.21 g (84%), mp 152—155 °C, $[\alpha]_D^{25}$ $-66.9\pm2.0°$ (*c* 0.5, methanol). TLC (silica gel): a single component (ninhydrin, after preheating at 150 °C) in system H.

Found: C, 60.54; H, 7.72; N, 11.26%. Calcd for $C_{56}H_{83}N_9O_{14}$: C, 60.80; H, 7.56; N, 11.40%.

Z-Val-Lys(Mhoc)-Val-Tyr-Pro-Asn-Gly-OH (XXIII). A 0.81-g portion (1.3 mmol) of H-Val-Tyr-Pro-Asn-Gly-OBu^t acetate obtained above was treated with trifluoroacetic acid at room temperature for 30 min to give the trifluoroacetic acid salt of H-Val-Tyr-Pro-Asn-Gly-OH as amorphous solid (0.88 g).

This pentapeptide was then coupled with Z-Val-Lys-(Mhoc)-N_3 [derived from XXI (0.88 g, 1.65 mmol) in the same manner as described above] in DMF in the presence of triethylamine (0.23 ml, 1.65 mmol) at 4 °C overnight. The crude product was purified on a silica gel column (30 g, Kieselgel 60, Merck) with chloroform-methanol-acetic acid (8 : 2 : 1) as solvent. The fractions were examined by TLC (silica gel, in the same solvent as that for the column) and those containing the desired compound as a single component were combined and evaporated *in vacuo*. The resulting residue was crystallized from methanol-ether; wt 0.90 g (65%), mp 173—177 °C decomp., $[\alpha]_D^{23.5}$ $-33.5\pm1.5°$ (*c* 0.5, DMF). Amino acid ratios in acid hydrolysate (theoretical values are given in parentheses): Lys 0.97 (1), NH_3 1.22 (1), Asp 1.07 (1), Pro 1.00 (1), Gly 1.07 (1), Val 2.00 (2), Tyr 0.97 (1).

Found: C, 57.94; H, 7.31; N, 11.67%. Calcd for $C_{52}H_{75}N_9O_{14}\cdot 3/2\,H_2O$: C, 57.98; H, 7.30; N, 11.70%.

Z-Val-Lys(Mhoc)-Val-Tyr-Pro-Asn-Gly-Ala-OBu^t (XXIIb). Compound XIXb (1.62 g, 2 mmol) was hydrogenolyzed over palladium in methanol for 3.5 h to give the N^α-free hexapeptide ester as a sirupy residue. This was then coupled with Z-Val-Lys(Mhoc)-N_3 [derived from XXI (1.63 g, 3 mmol) in the usual manner as described above] in DMF at 4 °C overnight. The crude product was crystallized and recrystallized from methanol-ethyl acetate to give the pure XXIIb; wt. 2.02 g (86%), mp 214—217 °C decomp., $[\alpha]_D^{24}$ $-25.7\pm0.5°$ (*c* 1.0, DMF). TLC (silica gel): a single component (ninhydrin, after preheating at 150 °C) in system H.

Found: C, 59.89; H, 7.50; N, 11.87%. Calcd for $C_{59}H_{88}N_{10}O_{15}$: C, 60.19; H, 7.53; N, 11.90%.

H-Val-Lys-Val-Tyr-Pro-Asn-Gly-Ala-OH Acetate (XXIV). Compound XXIIb (0.15 g) was hydrogenolyzed over palladium in acetic acid for 2.5 h. The resulting N^α-free peptide was then treated with trifluoroacetic acid (2 ml) in the presence of anisole (0.1 ml) and 2-mercaptoethanol (0.1 ml) at room temperature for 30 min. The precipitates which formed upon addition of ether were filtered off, thoroughly washed with ether and dried *in vacuo*. This was dissolved in water (10 ml) and the solution was passed through a column (0.9 × 10 cm) of Amberlite CG-400 (acetate) with portions of water. The aqueous solutions were combined, concentrated *in vacuo* at a bath temperature of 50 °C and lyophilized to give XXIV; wt 0.10 g (86%), $[\alpha]_D^{26}$ $-74.3\pm2.3°$ (*c* 0.5, 0.1 M hydrochloric acid). TLC (cellulose): a single component (ninhydrin) in system J. Amino acid ratios in acid hydrolysate: Lys 1.11 (1), NH_3 1.14 (1), Asp 1.02 (1), Pro 0.99 (1), Gly 1.07 (1), Ala 1.05 (1), Val 2.00 (2), Tyr 0.95 (1).

Z-Lys(Mhoc)-Arg(NO_2)-Arg(NO_2)-Pro-Val-Lys(Mhoc)-Val-Tyr-Pro-Asn-Gly-OBu^t (XXVa). Compound XXIIa (1.11 g, 1 mmol) was hydrogenolyzed over palladium in acetic acid (10 ml) for 3 h to give the acetic acid salt of H-Val-Lys(Mhoc)-Val-Tyr-Pro-Asn-Gly-OBu^t as fluffy powder (1.15 g). A half portion of this material was dissolved in a mixture of 1-butanol (8 ml) and ethyl acetate (16 ml) and the solution was shaken with 50% potassium carbonate (5 ml) at 0 °C. The organic phase was dried over magnesium sulfate followed by evaporation *in vacuo* to give the free base which was crystallized from methanol-ether; wt 0.46 g, $[\alpha]_D^{21}$ $-36.5\pm1.5°$ (*c* 0.5, DMF).

Compound XI (0.41 g, 0.45 mmol) and the heptapeptide

ester obtained above (0.44 g, 0.45 mmol) were coupled with DCC (0.19 g, 0.9 mmol) in DMF (9 ml) in the presence of HOBt (0.12 g, 0.9 mmol) at 4 °C overnight. The crude product was submitted to chromatography on a silica gel column (100 g, Kieselgel 60, Merck) with chloroform–methanol systems (95 : 5, 500 ml; 90 : 10, 200 ml; 85 : 15, 1200 ml) as solvent. The fractions were examined by TLC (silica gel, in system D) and those containing XXVa as a single component were combined and evaporated *in vacuo* to give a residue which was precipitated from methanol–ether; wt 0.74 g (87%), mp 150—155 °C, $[\alpha]_D^{21.5}$ −78.5±2.3° (*c* 0.5, methanol).

Found: C, 55.62; H, 7.06; N, 16.35%. Calcd for $C_{87}H_{136}N_{22}O_{24}$: C, 55.75; H, 7.31; N, 16.44%.

H–Lys(Mhoc)–Arg–Arg–Pro–Val–Lys(Mhoc)–Val–Tyr–Pro–Asn–Gly–OBu^t Acetate (XXVIa). Compound XXVa (0.94 g) was hydrogenolyzed over palladium in acetic acid (15 ml) for 40 h to give XXVIa; wt 1.09 g $\lambda_{max}^{0.1M\ HCl}$ 275 nm ($E_{1cm}^{1\%}$ 6.8). TLC (cellulose): almost homogeneous in system J.

H–Lys–Arg–Arg–Pro–Val–Lys–Val–Tyr–Pro–Asn–Gly–OH Acetate (XXVIIa). Compound XXVIa (0.33 g) was treated with trifluoroacetic acid (9 ml) in the presence of anisole (0.1 ml) and 2-mercaptoethanol (0.1 ml) at room temperature for 30 min. An aqueous solution of the product was treated with Amberlite CG-400 (acetate) and lyophilized (0.23 g).

A 0.1-g portion of this product was submitted to a column (1.7×21 cm) of carboxymethyl cellulose (CM-52, Whatman) using an ammonium acetate buffer (pH 6, 1500 ml) with a linear concentration gradient of 0—0.6 M. Fractions (7 ml/tube) were collected and their absorption at 275 nm was measured. The fractions corresponding to a major peak (tubes 110—133) were pooled, evaporated *in vacuo* and lyophilized to give XXVIIa as fluffy powder; wt 82 mg, $[\alpha]_D^{23}$ −85.7±3.0° (*c* 0.5, 0.1 M hydrochloric acid). TLC (cellulose): a single component (ninhydrin) in system K. Amino acid ratios in acid hydrolysate: Lys 1.99 (2), NH_3 1.13 (1), Arg 1.92 (2), Asp 1.03 (1), Pro 1.90 (2), Gly 1.00 (1), Val 2.08 (2), Tyr 0.99 (1).

Z–Lys(Mhoc)–Arg(NO_2)–Arg(NO_2)–Pro–Val–Lys(Mhoc)–Val–Tyr–Pro–Asn–Gly–Ala–OBu^t (XXVb). Compound XXIIb (0.47 g, 0.4 mmol) was hydrogenolyzed over palladium in acetic acid for 4 h to give the acetic acid salt of N^{α}-free octapeptide ester. This was dissolved in a mixture of 1-butanol (5 ml) and ethyl acetate (5 ml) and the solution was shaken with 50% potassium carbonate (5 ml) at 0 °C. The organic phase was dried and evaporated *in vacuo* to give the crystalline free base (0.42 g).

Compound XI (0.37 g, 0.4 mmol) and the octapeptide ester obtained above (0.42 g) were coupled with DCC (0.17 g, 0.8 mmol) in DMF (4 ml) in the presence of HOBt (0.11 g, 0.8 mmol) at 4 °C for 2 days. The crude product (1.03 g) was purified on a silica gel column in the same manner as described above for XXVa; wt 0.50 g (64%), mp 150—156 °C, $[\alpha]_D^{26}$ −73.4±2.3° (*c* 0.5, methanol).

Found: C, 54.70; H, 7.31; N, 15.94%. Calcd for $C_{90}H_{141}N_{23}O_{25}\cdot 2H_2O$: C, 54.56; H, 7.38; N, 16.26%.

H–Lys(Mhoc)–Arg–Arg–Pro–Val–Lys(Mhoc)–Val–Tyr–Pro–Asn–Gly–Ala–OBu^t Acetate (XXVIb). Compound XXVb (0.39 g) was hydrogenolyzed over palladium in acetic acid (8 ml) for 21 h. The catalyst was filtered off and the filtrate was lyophilized; wt 0.51 g, $\lambda_{max}^{0.1M\ HCl}$ 275 nm ($E_{1cm}^{1\%}$ 5.0). TLC (cellulose): almost homogeneous in system J.

H–Lys–Arg–Arg–Pro–Val–Lys–Val–Tyr–Pro–Asn–Gly–Ala–OH Acetate (XXVIIb). Compound XXVIb (0.13 g) was deprotected with trifluoroacetic acid (3 ml) in the presence of anisole (0.1 ml) and 2-mercaptoethanol (0.1 ml) at room temperature for 30 min. The product was treated with Amberlite CG-400 (acetate) in the usual manner to give the crude XXVIIb. This was then purified on a carboxymethyl cellulose column in the same manner as described above for XXVIIa; wt. 81 mg, $[\alpha]_D^{23}$ −86.9±2.5° (*c* 0.5, 0.1 M hydrochloric acid). TLC (cellulose): a single component (ninhydrin) in system L. Amino acid ratios in acid hydrolysate: Lys 1.75 (2), NH_3 0.91 (1), Arg 2.04 (2), Asp 1.06 (1), Pro 1.05 (1), Gly 1.05 (1), Ala 1.05 (1), Val 2.00 (2), Tyr 0.88 (1).

Z–Lys(Mhoc)–Pro–Val–Gly–Lys(Mhoc)–Lys(Mhoc)–Arg–Arg–Pro–Val–Lys(Mhoc)–Val–Tyr–Pro–Asn–Gly–OBu^t (XXVIIIa). A solution of VII (0.29 g, 0.3 mmol) in 90% aqueous tetrahydrofuran (5 ml) was chilled in an ice-bath and to this were added ice-cold M hydrochloric acid (0.75 ml) and ice-cold 2 M sodium nitrite (0.17 ml) successively. The mixture was stirred at 0 °C for 5 min, after which triethylamine (0.27 ml, 1.9 mmol) was added. The azide solution thus obtained was combined with a solution of XXVIa (0.28 g, 0.15 mmol) in 95% aqueous DMF (8 ml) and the mixture was stirred at 4 °C overnight. The product (0.51 g) was submitted to chromatography on a silica gel column (50 g, Kieselgel 60, Merck) with chloroform–methanol systems (9 : 1, 300 ml; 8 : 2, 400 ml; 7 : 3, 400 ml) as solvent. The fractions were examined by TLC (silica gel, in system J) and those containing the desired hexadecapeptide as a single component were pooled and evaporated *in vacuo* to give a residue which was precipitated from methanol–ether; wt 0.25 g (64%), mp 170—175 °C decomp., $[\alpha]_D^{23}$ −65.0±2.0° (*c* 0.5, methanol). Amino acid ratios in acid hydrolysate: Lys 3.97 (4), NH_3 1.10 (1), Arg 2.00 (2), Asp 1.12 (1), Pro 3.25 (3), Gly 2.09 (2), Val 3.00 (3), Tyr 1.01 (1).

A sample was reprecipitated from methanol–water and lyophilized from acetic acid for elemental analysis.

Found: C, 54.45; H, 7.45; N, 13.75%. Calcd for $C_{127}H_{205}N_{27}O_{29}\cdot 2CH_3COOH\cdot 10H_2O$: C, 54.74; H, 8.17; N, 13.16%.

Z–Lys(Mhoc)–Pro–Val–Gly–Lys(Mhoc)–Lys(Mhoc)–Arg–Arg–Pro–Val–Lys(Mhoc)–Val–Tyr–Pro–Asn–Gly–Ala–OBu^t (XXVIIIb). Compound XXVIb (0.22 g, 0.1 mmol) and the azide derived from VII (0.19 g, 0.2 mmol) in the manner as described above were coupled in aqueous tetrahydrofuran–DMF in the presence of triethylamine (0.13 ml, 0.9 mmol) at 4 °C overnight. The crude product was purified on a silica gel column in the same manner as described above for XXVIIIa; wt 0.14 g (52%), $[\alpha]_D^{24}$ −64.0±2.0° (*c* 0.5, methanol). TLC (silica gel): almost homogeneous (ninhydrin, after preheating at 150 °C) in system J. Amino acid ratios in acid hydrolysate: Lys 3.72 (4), NH_3 1.17 (1), Arg 1.98 (2), Asp 1.03 (1), Pro 2.98 (3), Gly 2.10 (2), Ala 1.11 (1), Val 3.00 (3), Tyr 0.93 (1).

A sample for elemental analysis was reprecipitated from methanol–water and lyophilized from acetic acid.

Found: C, 55.02; H, 7.99; N, 13.80%. Calcd for $C_{130}H_{210}N_{28}O_{30}\cdot 2CH_3COOH\cdot 8H_2O$: C, 55.32; H, 8.11; N, 13.48%.

H–Ser–Tyr–Ser–Met–Glu–His–Phe–Arg–Trp–Gly–Lys–Pro–Val–Gly–Lys–Lys–Arg–Arg–Pro–Val–Lys–Val–Tyr–Pro–Asn–Gly–OH Acetate, ACTH(1—26)–OH (I). Compound XXVIIIa (0.14 g, 0.05 mmol) was hydrogenolyzed over palladium in methanol containing acetic acid (0.5 ml) for 5 h. Removal of the solvent by evaporation *in vacuo* followed by lyophilization from acetic acid gave the N^{α}-free hexadecapeptide derivative (0.13 g).

To a solution of Boc–Ser–Tyr–Ser–Met–Glu(OBu^t)–His–Phe–Arg–Trp–Gly–OH (0.11 g, 0.075 mmol)[22] in DMF (2 ml) previously chilled in an ice-bath was added M hydro-

chloric acid (0.15 ml) and the solution was introduced into ice-cold ethyl acetate–ether (1 : 1, 50 ml). The resulting precipitates of the decapeptide hydrochloride were dissolved in DMF (3 ml) together with *N*-hydroxysuccinimide (HOSu, 0.035 g, 0.3 mmol) and to this was added DCC (0.062 g, 0.3 mmol) at 0 °C. The mixture was kept at 4 °C overnight, after which it was introduced into ethyl acetate–ether (1 : 1, 50 ml) to give the decapeptide active ester hydrochloride as amorphous precipitates (0.12 g). The active ester thus obtained was added to a solution of the N^{α}-free hexadecapeptide obtained above and triethylamine (0.07 ml) in DMF (3 ml), and the mixture was kept at room temperature for 2 days. The product was isolated as precipitates which formed when the reaction mixture was introduced into ethyl acetate (60 ml). The crude protected hexacosapeptide thus obtained (0.24 g) was mixed with anisole (0.1 ml) and 1,2-ethanedithiol (0.1 ml) and chilled in an ice-bath. To this was added trifluoroacetic acid (5 ml) and the mixture was kept at 0 °C for 60 min. The precipitates which formed upon addition of ether were filtered off, washed with ether and dried *in vacuo*. This was then dissolved in water and the solution was passed through a column (1.1×20 cm) of Amberlite CG-400 (acetate form) with additional portions of water. The aqueous solutions were combined and lyophilized to give the deprotected hexacosapeptide (0.24 g).

The crude peptide obtained above was submitted to partition chromatography on a column (2.0×75 cm) of Sephadex G-25 (medium) with 1-butanol–acetic acid–pyridine–water (12 : 3 : 4 : 6) as solvent and 5-ml fractions were collected. The tubes (no. 25—50) containing the desired peptide as a major component, as examined by TLC (cellulose, in system L) with the ninhydrin and Ehrlich reagents as reagents for locating peptide spots, were combined and evaporated *in vacuo* at a bath temperature of 45 °C and the residue was lyophilized (0.096 g). This was then chromatographed on a column (1.7×20 cm) of carboxymethyl cellulose (CM-52, Whatman) using an ammonium acetate buffer (pH 6.0, 2000 ml) with a linear concentration gradient of 0—0.6 M. Ten-ml fractions were collected and their absorption at 280 nm was measured. The fractions corresponding to a main peak (tubes 134—159) were combined, evaporated and lyophilized (0.051 g). For final purification this was submitted to gel filtration on a column (2.0×75 cm) of Sephadex G-25 (medium) with 0.1 M acetic acid as solvent. Five-ml fractions were collected and those corresponding to a single peak (tubes 20—35), as monitored by absorption at 280 nm, were combined, lyophilized and dried over sodium hydroxide pellets and phosphorus pentoxide *in vacuo* to afford the pure hexacosapeptide (I) as colorless fluffy powder; wt 0.048 g (26%), $[\alpha]_D^{25}$ −87.6±2.5° (*c* 0.5, 0.1 M acetic acid). $\lambda_{max}^{0.1M\ HCl}$ 276.5 nm ($E_{1cm}^{1\%}$ 20.5), $\lambda_{shoulder}^{0.1M\ HCl}$ 288 nm ($E_{1cm}^{1\%}$ 13.7); $\lambda_{max}^{0.1M\ NaOH}$ 283 nm ($E_{1cm}^{1\%}$ 22.9), 289 nm ($E_{1cm}^{1\%}$ 23.5). TLC (cellulose): a single component (ninhydrin and Ehrlich reagents) in system L. Amino acid ratios in acid hydrolysate: Lys 3.80 (4), His 1.00 (1), Arg 3.08 (3), Asp 1.00 (1), Ser 1.80 (2), Glu 1.10 (1), Pro 3.02 (3), Gly 3.05 (3), Val 3.15 (3), Met 1.00 (1), Tyr 2.05 (2), Phe 1.02 (1). The Tyr/Trp ratio in intact I was 1.99 as determined spectrophotometrically.[23]

H–Ser–Tyr–Ser–Met–Glu–His–Phe–Arg–Trp–Gly–Lys–Pro–Val–Gly–Lys–Lys–Arg–Arg–Pro–Val–Lys–Val–Tyr–Pro–Asn–Gly–Ala–OH Acetate, ACTH(1—27)-OH (II). Compound XXVIIIb (0.15 g, 0.05 mmol) was hydrogenolyzed over palladium in methanol containing acetic acid (0.5 ml) for 3 h to give the N^{α}-free heptadecapeptide derivative (0.13 g). This was allowed to react with the decapeptide *N*-hydroxysuccinimide ester [prepared from Boc–Ser–Tyr–Ser–Met–Glu(OBu^t)–His–Phe–Arg–Trp–Gly–OH (0.11 g, 0.075 mmol)[22] in exactly the same manner as described above] in DMF (3 ml) in the presence of triethylamine (0.07 ml) at room temperature for 2 days. The resulting protected peptide (0.24 g) was treated with trifluoroacetic acid (5 ml) at 0 °C for 60 min in the presence of anisole (0.1 ml) and 1,2-ethanedithiol (0.1 ml). The product was then treated with Amberlite CG-400 (acetate form) to give a crude preparation of II (0.23 g).

The crude peptide obtained above was purified by partition chromatography on a column of Sephadex G-25 and by carboxymethyl cellulose column chromatography in the same manner as described above for I. The resulting material (0.054 g) was then submitted to gel filtration on a Sephadex G-25 column with 0.1 M acetic acid as solvent to give the pure heptacosapeptide (II); wt 0.050 g (27%), $[\alpha]_D^{25}$ −86.6± 2.3° (*c* 0.5, 0.1 M acetic acid). $\lambda_{max}^{0.1M\ HCl}$ 276.5 nm ($E_{1cm}^{1\%}$ 21.5), $\lambda_{shoulder}^{0.1M\ HCl}$ 288 nm ($E_{1cm}^{1\%}$ 14.5); $\lambda_{max}^{0.1M\ NaOH}$ 283 nm ($E_{1cm}^{1\%}$ 23.1), 289 nm ($E_{1cm}^{1\%}$ 23.6). TLC (cellulose): a single component (ninhydrin and Ehrlich reagents) in system L. Amino acid ratios in acid hydrolysate: Lys 4.00 (4), His 1.00 (1), Arg 3.10 (3), Asp 1.00 (1), Ser 1.85 (2), Glu 1.08 (1), Pro 3.08 (3), Gly 3.10 (3), Ala 1.08 (1), Val 3.05 (3), Met 0.98 (1), Tyr 1.93 (2), Phe 0.98 (1). The Tyr/Trp ratio in intact II was 1.98 as determined spectrophotometrically.[23]

The authors wish to thank Miss Yuriko Kawana for able technical assistance.

References

1) R. G. Shepherd, S. D. Willson, K. S. Howard, P. H. Bell, D. S. Davies, S. B. Davis, E. A. Eigner, and N. E. Shakespeare, *J. Am. Chem. Soc.*, **78**, 5067 (1956); P. H. Bell, *ibid.*, **76**, 5565 (1954).
2) T. H. Lee, A. B. Lerner, and V. Buettner-Janusch, *J. Biol. Chem.*, **236**, 2970 (1961).
3) R. Schwyzer and P. Sieber, *Helv. Chim. Acta*, **49**, 134 (1966); *Nature*, **199**, 172 (1963).
4) S. Bajusz, K. Medzihradszky, Z. Paulay, and Zs. Láng, *Acta Chim. Acad. Sci. Hung.*, **52**, 335 (1967).
5) H. Otsuka, K. Watanabe, and K. Inouye, *Bull. Chem. Soc. Jpn.*, **43**, 2278 (1970).
6) L. Gráf, S. Bajusz, A. Patthy, E. Barát, and G. Cseh, *Acta Biochim. Biophys. Acad. Sci. Hung.*, **6**, 415 (1971).
7) B. Riniker, P. Sieber, W. Rittel, and H. Zuber, *Nature New Biology*, **235**, 114 (1972); B. Riniker, in "Structure-Activity Relationships of Protein and Polypeptide Hormones," Proceedings of the 2nd International Symposium, Liège, 1971, Excerpta Medica, Amsterdam, p. 519.
8) C. H. Li, *Biochem. Biophys. Res. Commun.*, **49**, 835 (1972).
9) A. Jöhl, B. Riniker, and L. Schenkel-Hulliger, *FEBS Lett.*, **45**, 172 (1974).
10) a) H. Otsuka, K. Inouye, F. Shinozaki, and M. Kanayama, *J. Biochem. (Tokyo)*, **58**, 512 (1965); b) K. Inouye, F. Shinozaki, M. Kanayama, and H. Otsuka, *Bull. Chem. Soc. Jpn.*, **49**, 3615 (1976).
11) H. Otsuka, K. Inouye, and Y. Jono, *Bull. Chem. Soc. Jpn.*, **37**, 1471 (1964).
12) H. Otsuka, K. Inouye, M. Kanayama, and F. Shinozaki, *Bull. Chem. Soc. Jpn.*, **39**, 882 (1966).
13) K. Inouye, K. Watanabe, and K. Namba, in preparation.
14) R. Schwyzer and H. Kappeler, *Helv. Chim. Acta*, **46**, 1550 (1963).
15) M. Fujino, O. Nishimura, and C. Hatanaka, *Chem. Pharm. Bull.*, **17**, 2135 (1969).

16) K. Inouye and K. Watanabe, *Bull. Chem. Soc. Jpn.*, in press.
17) R. Schwyzer, B. Riniker, and H. Kappeler, *Helv. Chim. Acta*, **46**, 1541 (1963).
18) C. Hatanaka, O. Nishimura, and M. Fujino, *Chem. Pharm. Bull.*, **23**, 1017 (1975).
19) J. Ramachandran and C. H. Li, *J. Am. Chem. Soc.*, **87**, 2691 (1965).
20) W. König and R. Geiger, *Chem. Ber.*, **103**, 788 (1970).
21) H. Schwarz, F. M. Bumpus, and I. H. Page, *J. Am. Chem. Soc.*, **79**, 5697 (1957).
22) H. Otsuka, K. Inouye, F. Shinozaki and M. Kanayama, *Bull. Chem. Soc. Jpn.*, **39**, 1171 (1966).
23) G. H. Beaven and E. R. Holiday, *Adv. Protein Chem.*, **7**, 319 (1952); T. W. Goodwin and R. A. Morton, *Biochem. J.*, **40**, 628 (1946).
24) The assays were performed by Dr. A. Tanaka and Mr. K. Odaguchi of this laboratory. We thank Dr. Tanaka for permission to include these data in the present communication.
25) K. Inouye, K. Watanabe, and H. Otsuka, *Bull. Chem. Soc. Jpn.*, in press.
26) G. W. Anderson and F. M. Callahan, *J. Am. Chem. Soc.*, **82**, 3359 (1960).
27) O. Nishimura, C. Hatanaka, and M. Fujino, *Chem. Pharm. Bull.*, **23**, 1212 (1975).

Mechanism of the Optical Activation of α-Substituted Carbonyl Compounds *via* Optically Active Immonium Salts

Hajime MATSUSHITA, Yasuko TSUJINO, Masao NOGUCHI, and Sadao YOSHIKAWA*

Central Research Institute, The Japan Tobacco & Salt Public Corporation, 6-2 Umegaoka, Midori-ku, Yokohama, Kanagawa 227

**Department of Synthetic Chemistry, Faculty of Engineering, The University of Tokyo, Hongo, Bunkyo-ku, Tokyo 113*

(Received July 6, 1976)

The degree of the optical activations of racemic α-substituted carbonyl compounds *via* the formation of optically active immonium salts and the subsequent hydrolysis were largely affected by acids used for the hydrolysis of the enamines. The ratio of the diastereomeric immonium salts depends on the temperature. There is a relationship between the configuration of the optically activated carbonyl compounds and those of amines used. These suggest that the optical activation is due to the asymmetric transformation.

Enamines are known to be very useful starting materials for various organic syntheses.[1] Asymmetric alkylation and halogenation were reported by Yamada *et al.*[2] Optical activation of racemic α-substituted carbonyl compounds *via* enamine has been studied in our laboratory. Formation of an enamine (I) causes deprotonation from the α-carbon of the racemic α-substituted carbonyl compounds, and formation of the immonium salt (II) causes protonation to the carbon, which is the first step of hydrolysis of the enamine.[3] In an asymmetrical circumstance, it is possible that an asymmetric protonation to the enamine takes place at the step of formation of the salt. On hydrolysis of the salt, the optically active carbonyl compound can be recovered.

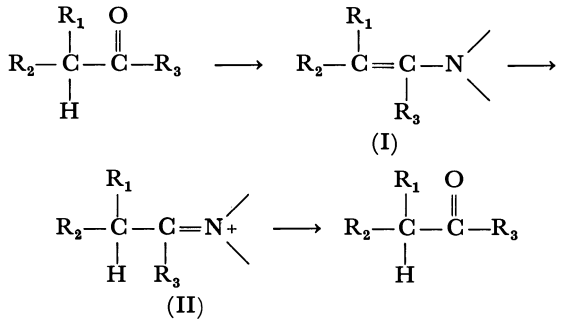

In our previous paper, optical activation of racemic α-substituted carbonyl compounds were reported.[4,5] The hydrolysis of the immonium salts consisting of the optically active amine enamine of the racemic α-substituted carbonyl compounds and achiral acid gave the optically active compounds. This paper deals with the mechanism of this optical activation.

Experimental

Optical rotations were determined with a JASCO Digital Automatic Polarimeter Model DIP 181. Gas chromatographic analyses were carried out on a 2 m column of 20% Carbowax 20 M on Cromosorb W with a Hitachi Gas Chromatograph, Model K 53. Nuclear magnetic resonance spectra were obtained with a JNM-PS-100 Spectrometer with tetramethylsilane as an internal standard.

S(+)-2-Methylpiperidine. This was obtained by the procedure described by Kostyanovsky *et al.*[6]

R(−)-2-Methylpyrrolidine. This was prepared according to the method reported in our previous paper.[5]

S(−)-Benzyloxycarbonylcysteic Acid Ethyl Ester. This was prepared by treatment of L-cysteic acid with carbobenzoxy chloride. It was purified *via* its ethyl ester sodium salt. Using 29 g (0.155 mol) of L-cysteic acid, 32.2 g (58.9%) of *S*(−)-benzyloxycarbonylcysteic acid ethyl ester sodium salt, as white needle, was obtained: mp 164—172 °C; $[\alpha]_D^{23}$ −18.4° (*c* 0.74 H_2O); IR (Nujol) 3350 cm^{-1} (ν_{NH}), 1739 cm^{-1} (ν_{CO}), 1690 cm^{-1} (ν_{CO}), 1528 cm^{-1} (δ_{NH}), 1258 cm^{-1} (ν_{CN}); NMR ($CDCl_3$) 1.16 (CH_3, t, *J* 7.2 Hz), 2.96 (S-CH_2, d, *J* 6.0 Hz), 4.13 (COOCH_2, q, *J* 7.2 Hz), 4.40 (CH-N, q), 5.04 (NH, broad), 5.11 (O-CH_2, s), 7.43 (phenyl, 5H). *S*(−)-Benzyloxycarbonylcysteic acid ethyl ester was obtained by treatment of the salt with cation exchange resin (Dowex 50 W). NMR spectrum showed that the peak at 2.96 ppm was shifted to lower field, 3.60 ppm.

Enamines. The preparation of enamines of α-phenylpropionaldehyde and 2-methylcyclohexanone were reported in our previous paper.[4,5] Enamine from piperidine and 2-methylbutanal: bp 36—38 °C (0.7 Torr); IR (film) 1655, 1665 cm^{-1} ($\nu_{C=C}$); NMR ($CDCl_3$) mixture of two geometrical isomers (8 : 3 at room temperature), major isomer, 1.00 (CH_3, t, *J* 7.7 Hz), 1.71 (CH_3, s), 1.98 (CH_2, q, *J* 7.7 Hz), 5.43 (C=CH, s), minor isomer, 1.63 (CH_3, s), 2.18 (CH_2, q, 7.9 Hz), 5.35 (C=CH, s). Enamine from 2-methylpiperidine 2-methylbutanal: Yield 89%; bp 45—46.5 °C (2.2 Torr); IR (film) 1670, 1650 cm^{-1} ($\nu_{C=C}$); NMR ($CDCl_3$) mixture of two geometrical isomers (5 : 2 at room temperature), major isomer 1.73 (CH_3, s), 5.34 (C=CH, s), minor isomer 1.64 (CH_3, s), 5.23 (C=CH, s); $[\alpha]_D^{23}$ −6.79° (neat). Enamine from *S*(+)-2-methylpiperidine and 2-(2-cyanoethyl)cyclohexanone was not isolated.

Hydrolysis. Acid (0.01 mol) was added to a benzene solution (20 ml) of the enamine (0.01 mol) and the mixture was stirred. To the solution in an ice bath, water (20 ml) was added dropwise with vigorous stirring. The reaction was continued until the completion of the hydrolysis which was confirmed gas chromatographically. The benzene layer was separated, washed with water until the amine and the acid were removed completely, and dried over anhydrous Na_2SO_4. In the case of α-phenylpropionaldehyde, it was purified by column chromatography on silica gel (benzene : hexane 1 : 1). The purity was checked by TLC on silica gel (benzene : hexane 1 : 1, R_f 0.38). Optical rotations of carbonyl compounds were measured in benzene. The recoveries were obtained with a gas chromatograph.

Optical Rotation of the α-Phenylpropionaldehyde Recovered at Regular Time Interval. To a benzene solution (50 ml) of the optically active enamine from 2-methylpiperidine and α-phenylpropionaldehyde (2.15 g, 0.01 mol) was added 1 M hydrochloric acid (15 ml, 0.015 mol) under vigorous stirring. After ten minutes, benzene layer was separated, and additional aliquot (50 ml) of benzene was immediately applied to the aqueous layer, and reaction was continued.

TABLE 1. OPTICAL ACTIVATION OF SOME CARBONYL COMPOUNDS *via* OPTICALLY ACTIVE ENAMINES

Amine component	Carbonyl component	Acid component	Recovered carbonyl compound $[\alpha]_D^{23}$ in benzene		ee	Recovery (%)	Lit.
S(+)-2-Methyl-piperidine	α-phenylpropion aldehyde	HCl	−80.8° (*c* 25.0)			91	5
		H_2SO_4	−65.2° (*c* 0.99)			67	
		p-toluene-sulfonic acid	−60.4° (*c* 1.88)			81	
		CH_3COOH	−54.5° (*c* 1.21)			62	
	2-methyl-cyclohexanone	HCl	−2.87° (*c* 42.2)	*R*	20.2[9]	77	5
		CH_3COOH	−0.92° (*c* 30.0)	*R*	6.5	61	
	2-methylbutanal	HCl	−1.82° (*c* 18.9)	*R*	5.7[10]	73	
		CH_3COOH	−0.72° (*c* 25.9)	*R*	2.2	58	
	2-(2-cyanoethyl)-cyclohexanone	HCl	−0.858° (neat)	*R*		84	
		CH_3COOH	−0.099° (neat)	*R*		78	
R(−)-2-Methyl-pyrrolidine	α-phenylpropion-aldehyde	HCl	+51·6° (*c* 8.11)			79	5
	2-methyl-cyclohexanone	HCl	+0.881° (*c* 15.5)	*S*	6.2	60	5

The same treatment was repeated four times at ten minutes intervals. Finally, the aqueous layer was refluxed, and extracted with benzene. Every benzene extract was washed with water and dried, and the optical rotation and the concentration were measured.

Results and Discussion

Optical Activation of Racemic Carbonyl Compounds via *Optically Active Immonium Salts.* Hydrolysis of immonium salts consisting of optically active amine enamines of racemic α-substituted carbonyl compounds and achiral acids gave the corresponding optically active carbonyl compounds. The results are shown in Table 1.

Strong acids were well suited for the introduction of optical activity. This tendency was observed with both six and five membered ring amines. It is known that strong acid components are preferable for the stability of immonium salts.[7] The result suggests that the stability of an immonium salt is an important factor for the introduction of optical activity. This is also supported in the case of the immonium salts consisting of pyrrolidine or piperidine enamine and chiral acids.

Table 2 shows that the degree of the optical activation and direction of the optical rotation were affected by both the structure and the strength of acidity of chiral acids. *S*(+)-Cysteic acid has an amino group, a carboxyl group and a sulfonyl group. *S*(−)-*N*-Benzyloxycarbonylcysteic acid ethyl ester has neither a free amino group nor a free carboxyl group, but a sulfonyl group. *S*(−)-*N*-Benzyloxycarbonylalanine has a carboxyl group. The direction of the optical rotation of the recovered carbonyl compounds in the case of *S*(−)-*N*-benzyloxycarbonylcysteic acid ethyl ester was opposite to that in the case of *S*(+)-cysteic acid or *S*(−)-*N*-benzyloxycarbonylalanine. This means that *S*(+)-cysteic acid has the inner salt structure, ^-O_3S–CH_2–$\underset{\displaystyle NH_3^+}{\underset{|}{CH}}$–COOH, and its carboxyl group is used to form immonium salts. The degrees of the optical rotation in Table 2 suggest that sulfonic acid

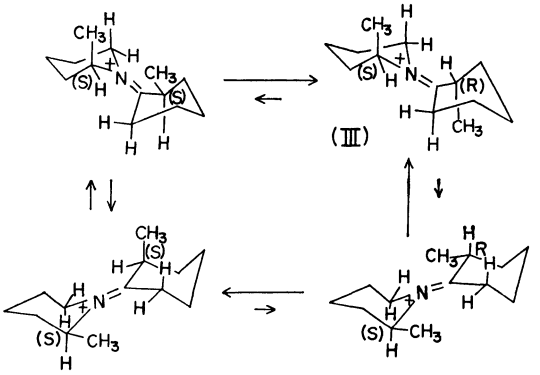

Fig. 1.

was superior to carboxylic acid, and *S*(+)-cysteic acid react with enamines as an carboxylic acid. One of the reasons of the low optical rotation of recovered α-phenylpropionaldehyde in the case of L-tartaric acid, D-camphoric acid and D-quinic acid[4] may be the weak acidity of these acids.

Table 1 also shows that carbonyl compounds with *R*-configuration was obtained by the use of *S*-amines as the amine components. In the case of 2-methylcyclohexanone, the result was interpreted by the stability of the immonium salt. As there are large interactions between the equatorial methyl group and the hydrogen on the α-methylene of the ring, the structure (III), in which two methyl groups occupies the axial positions, was most stable. When *S*-amine is used as the amine component, introduced asymmetric carbon into the enamine is an *R*-configuration. In the case of the asymmetric alkylation to cyclohexanone enamine, the same results were observed.[2]

Optical Rotation of the α-Phenylpropionaldehyde Recovered at Regular Time Intervals. Considering the mechanisms of the optical activation, there are (1) asymmetric synthesis, (2) asymmetric transformation, and (3) asymmetric destruction. It is known that the proton at the β-carbon of the enamine grouping is easily exchanged.[8] In our previous paper,[5] HCl salt of the enamine was hydrolyzed with rich D_2O

TABLE 2. OPTICAL ACTIVATION OF SOME CARBONYL COMPOUNDS FROM THE IMMONIUM SALTS CONSISTING OF CHIRAL ACIDS AS THE ACID COMPONENT

Amine component	Carbonyl component	Acid component	Recovered carbonyl compound			Lit.
			$[\alpha]_D^{23}$ in benzene		Recovery (%)	
Piperidine	α-Phenylpropion-aldehyde	D-10-Camphorsulfonic acid	+16.2° (c=3.67)		89.6	4
		S(+)-Cysteic acid	−1.06° (c=4.25)		82.0	
		S(−)-N-Benzyloxycarbonyl-cysteic acid ethylester	+2.80° (c=4.50)		80.9	
		α-Bromo-d-camphor-π-sulfonic acid	+3.67° (c=4.31)		78.1	
		S(−)-N-Benzyloxycarbonyl-alanine	−0.58° (c=10.8)		65.7	
	2-Methylcyclo-hexanone	D-10-Camphorsulfonic acid	+0.63° (c=2.30)	S	73.1	4
		S(+)-Cysteic acid	−0.03° (c=33.3)	R	86.2	
		S-(−)-N-Benzyloxycarbonyl-cysteic acid ethylester	+0.11° (c=18.2)	S	69.8	
	2-Methylbutanal	D-10-Camphorsulfonic acid	+0.000° (c=4.41)		68.0	
		S(+)-Cysteic acid	+0.000° (c=5.22)		72.0	
Pyrrolidine	α-Phenylpropion-aldehyde	D-10-Camphorsulfonic acid	+13.8° (c=7.10)		84.1	
		S(+)-Cysteic acid	−0.58° (c=6.03)		83.9	
		S(−)-N-Benzyloxycarbonyl-cysteic acid ethylester	+1.43° (c=7.57)		78.9	
		α-Bromo-d-camphor-π-sulfonic acid	+3.96° (c=3.37)		71.3	
		S(−)-N-Benzyloxycarbonyl-alanine	−0.19° (c=9.90)		67.9	
	2-Methylcyclo-hexanone	D-10-Camphorsulfonic acid	+0.39° (c=10.8)	S	88.8	4

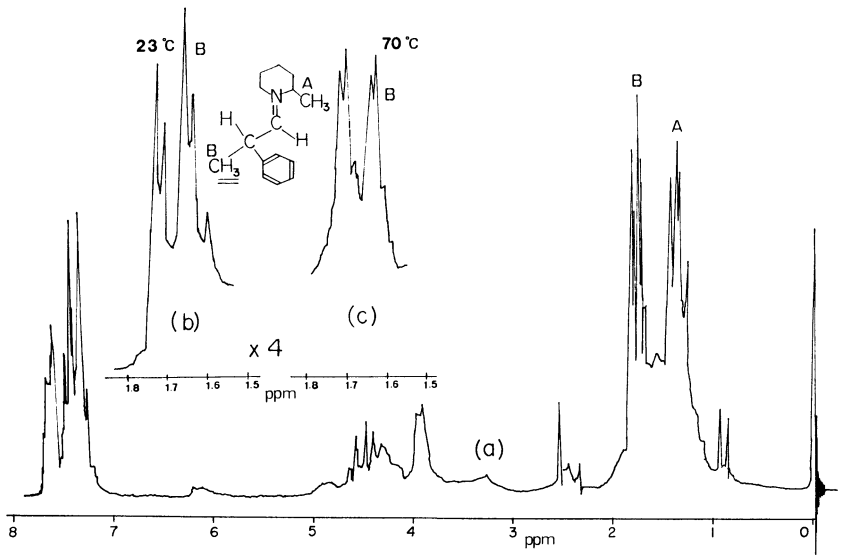

Fig. 2. (a) 100 MHz spectrum of the immonium salt, probe temperature 23 °C (in $CDCl_3$).
(b) Enlargement of the signal (B) due to the methyl group attached to the β-carbon, probe temperature 23 °C. (×4)
(c) The same part of the spectrum, probe temperature 70 °C. (×4)

and deuterated α-phenylpropionaldehyde was recovered. The isotope labeling experiment suggests that this optical activation is not due to the asymmetric synthesis. To see whether this activation is due to asymmetric destruction or not, variations in optical activity of the recovered α-phenylpropionaldehyde during the enamine hydrolysis were followed at ten minute intervals. After the reaction for 40 min, to ascertain the completion of hydrolysis, concentrated hydrochloric acid was added to the residual water phase and the solution was refluxed. Gas chromatographically, no α-phenylpropionaldehyde could be detected in the benzene extract of the solution. Total recovery of the aldehyde was 87.3%. It seems that some of the aldehyde was lost when the benzene extract was washed with water. As shown in Table 3, the directions of the optical rotation of all fractions were the same. This result clearly shows that the optical activation was not due to asymmetric destruction.

Studies of the NMR Spectra. Dry HCl gas was

Table 3.

Reaction time (min)	$[\alpha]_D^{23}$	Recovery (%)
10	+10.7°	64.2
20	+10.5°	19.4
30	+14.5°	3.7
40	(+)	trace
Recovered from aqueous layer		0
Total recovery		87.3

bubbled slowly into a $CDCl_3$ solution of optically active 2-methylpiperidine enamine of α-phenylpropionaldehyde and a slightly yellow solution of the corresponding immonium salt was obtained. NMR spectrum of the solution shows that the immonium salt was a mixture of two diastereomeric isomers (Fig. 2(a).). An increase in temperature as high as 70 °C gradually changed the region of the methyl groups (B) at the asymmetric carbon atoms in NMR spectra from (b) to (c). The major methyl proton signal at 23 °C (1.69 ppm, J 7.5 Hz) was changed to the minor one at 70 °C (1.68 ppm, J 7.3 Hz). On the contrary, the minor methyl proton signal at 23 °C (1.66 ppm, J 7.5 Hz) was changed to the major one at 70 °C (1.65 ppm, J 7.3 Hz). This result suggests that the ratio of the two diastereomers was controlled thermodynamically. Thus the mechanism of the optical activation is considered to be an asymmetric, reversible protonation to the enamine and successive hydrolysis of the immonium salt. The spectra of the D_2SO_4 salt and CD_3COOD salt were also obtained. The former has many unassignable peaks. The latter shows that the formation of immonium salt was incomplete by the addition of an equimolar CD_3COOD to the enamine. These spectra may suggest that H_2SO_4 and CH_3COOH are not so good as HCl for the optical activation.

References

1) A. G. Cook, "Enamines," Marcel Dekker, New York and London (1969), p 313.
2) S. Yamada, K. Hiroi, and K. Achiwa, *Tetrahedron Lett.*, **1969**, 4233; S. Yamada and G. Otani, *ibid.*, **1969**, 4237; K. Hiroi and S. Yamada, *Chem. Pharm. Bull.*, **21**, 54 (1973).
3) G. Stork, A. Brizzolara, H. Landesman, J. Szmuszkovicz, and R. Terrell, *J. Am. Chem. Soc.*, **85**, 207 (1963).
4) H. Matsushita, M. Noguchi, M. Saburi, and S. Yoshikawa, *Bull. Chem. Soc. Jpn.*, **48**, 3715 (1975).
5) H. Matsushita, M. Noguchi, and S. Yoshikawa, *Bull. Chem. Soc. Jpn.*, **49**, 1928 (1976).
6) R. G. Kostyanovsky, I. M. Gella, V. I. Markov, and Z. E. Samojlova, *Tetrahedron*, **30**, 39 (1974).
7) M. E. Herr, M. E. Heyl, J. C. Babcock, A. E. Fonken, J. E. Stafford, and F. W. Heyl, *J. Am. Chem. Soc.*, **78**, 430 (1956).
8) N. J. Leonard and R. R. Sauers, *J. Am. Chem. Soc.*, **79**, 6210 (1957).
9) G. A. C. Gough, H. Hunter, and Kenyon, *J. Chem. Soc.*, **1926**, 2052.
10) E. J. Badin and E. Pacsu, *J. Am. Chem. Soc.*, **67**, 1352 (1945).

A Macrocyclic Enzyme Model System. An Electrostatic-Hydrophobic Double-Field Catalysis by a [20]Paracyclophane in the Deacylation of *p*-Nitrophenyl Hexadecanoate†

Yukito MURAKAMI,* Yasuhiro AOYAMA, Kazuyuki DOBASHI, and Masaaki KIDA

Department of Organic Synthesis, Faculty of Engineering, Kyushu University, Hakozaki, Higashi-ku, Fukuoka 812

(Received July 9, 1976)

The catalytic functions of 10-oxo[20]paracyclophanyl-22(23)-methyltrimethylammonium chloride (**1**) in the hydrolysis and aminolysis reactions of *p*-nitrophenyl hexadecanoate (PNPP) were investigated in 1% (v/v) methanol–1% (v/v) dioxane–water over the pH 9—10 region at 40.0 °C and μ=0.2 (NaCl) with the initial PNPP concentration of 1.00×10^{-5} M. The paracyclophane (0.88×10^{-5} M) accelerated the hydrolysis of PNPP by one order of magnitude at pH 9.7. The presence of either ethanolamine or glycine in the **1**-catalyzed deacylation of PNPP resulted in further rate enhancement. The rate enhancement was brought about by the aminolysis reaction of PNPP with the amines as confirmed by the product analysis. The greater reactivity of glycine relative to that of ethanolamine was attributed to the electrostatic interaction between the anionic carboxylate group of glycine and the cationic ammonium group of **1**. The novel electrostatic-hydrophobic double-field catalysis was discussed for the glycinolysis reaction.

[20]Paracyclophanes have been shown to function as host molecules in aqueous media for the incorporation of *p*-nitrophenyl carboxylates bearing a sufficiently long alkyl chain *via* hydrophobic interaction.[1-6] An efficient acyl transfer from the bound substrate to either oxime[1-5] or amino group[6] placed on the paracyclophane skeleton has been observed. In the absence of an effective nucleophile on the macrocycle, the bound substrate would be susceptible to an attack by any nucleophile present in the bulk phase. In such occasions, the reactivity of the bimolecular deacylation reaction would be controlled by the geometry and spatial orientation of a bound substrate against an attacking nucleophile as well as by the approaching mechanism played by the latter species. This state of affairs should be even more pronounced when the macrocycle carries a functional group which may interact with a nucleophile. In this study, we have investigated the hydrolysis and aminolysis of *p*-nitrophenyl hexadecanoate as catalyzed by a [20]-paracyclophan-10-one carrying a quaternary ammonium group on its benzene ring (**1**). The specific catalytic function of the ammonium group is to be characterized from the kinetic viewpoints.

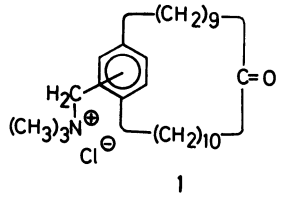

1

Experimental

Materials. 10-Oxo[20]paracyclophanyl-22(23)-methyltrimethylammonium chloride (**1**) was prepared as described previously.[4] The crude product was purified by repeated high speed liquid chromatography using a Hitachi 635 liquid chromatograph equipped with a column of Hitachi gel 3019, methanol being used as an eluant. *p*-Nitrophenyl hexadecanoate was the product of E. Merck, Darmstadt, West Germany and used after inspection of its purity by elemental analysis. Glycine obtained from commercial source was recrystallized from water. Ethanolamine was distilled *in vacuo* immediately before use.

Kinetic Measurements. Rates of *p*-nitrophenoxide liberation were measured at 400 nm. Each run was initiated by adding 30 μl of 1.0×10^{-3} M *p*-nitrophenyl hexadecanoate in dioxane to 2.97 ml of a reaction medium which was preequilibrated at 40.0±0.1 °C in a thermostatted cell set in a Hitachi 124 recording spectrophotometer. The reaction medium was prepared by mixing 30 μl of a stock solution of **1** in methanol with 2.94 ml of an aqueous buffer solution of $Na_2B_4O_7$–Na_2CO_3, or otherwise either of glycine–sodium glycinate or ethanolamine–ethanolammonium chloride. The ionic strength was maintained constant at 0.2 with sodium chloride.

pH *and* pK_a *Measurements.* pH-Values of the buffer solutions were measured at 40.0±0.1 °C with a Beckman expandomatic SS-2 pH meter equipped with a Metrohm EA-125 combined electrode after calibration with a combination of appropriate standard buffers. The potentiometric titrations were carried out at 40.0±0.1 °C and μ=0.20 (NaCl) with sodium hydroxide to determine pK_a values of glycine and ethanolamine.

Analysis of Glycinolysis Product. A solution of *p*-nitrophenyl decanoate (100 mg) and **1** (1.53×10^{-3} mmol) in a mixture of glycine buffer (pH 9.7, 1000 ml containing 0.07 mol of glycine, 0.03 mol of sodium hydroxide, and 0.07 mol of sodium chloride) and dioxane (70 ml) was stirred at room temperature for 65 h. The reaction mixture was acidified (pH 2) with hydrochloric acid and then extracted with ether (100 ml×2) and chloroform (100 ml×3). The combined extracts were extracted with 5% aqueous sodium hydroxide. The aqueous extract was acidified and extracted with ether (100 ml×3). After drying over sodium sulfate, the ether extract was evaporated to give an oil (30 mg) which was subsequently chromatographed on a column (2.4×10 cm) of silica gel (Wako gel C-100) after esterification with excess diazomethane. *p*-Nitrophenol (15 mg) and methyl decanoate (small amount) showing a C=O stretching band (neat) at 1730 cm^{-1} were eluted with benzene and benzene–chloroform (1 : 1), respectively. Further elution with chloroform afforded glycinolysis product **2** (15 mg). IR (neat): 3320

$CH_3(CH_2)_8CONHCH_2CO_2CH_3$

2

† Contribution No. 413 from this Department.

* To whom correspondence should be addressed.

Table 1. First-order rate constants for the *p*-nitrophenol release from PNPP in the presence and absence of **1** at $\mu=0.2$ (NaCl), 40.0±0.1 °C[a)]

$[\mathbf{1}]\times10^5$ (M)	pH	Buffer system[b)]	$k_{obs}\times10^4$ (s^{-1})
None	9.70	$Na_2B_4O_7$–Na_2CO_3	0.14
None	9.70	$H_2NCH_2CO_2^-$–$H_3N^+CH_2CO_2^-$	0.15
None	9.70	$H_2N(CH_2)_2OH$–$H_3N^+(CH_2)_2OH$	0.23
0.88	9.32	$Na_2B_4O_7$–Na_2CO_3	0.78
0.88	9.73		1.3
0.88	10.03		2.2
0.88	10.16		2.8
0.88	10.33		3.3
0.88	8.80	$H_2NCH_2CO_2^-$–$H_3N^+CH_2CO_2^-$	1.3
0.88	9.10		1.8
0.88	9.40		3.3
0.88	9.75		5.3
0.88	10.07		5.9
0.88	10.25		6.4
0.88	8.96	$H_2N(CH_2)_2OH$–$H_3N^+(CH_2)_2OH$	0.58
0.88	9.33		1.4
0.88	9.79		2.4
0.88	10.10		3.1

a) $[PNPP]_0=1.00\times10^{-5}$ M in 1%(v/v)methanol-1%(v/v)dioxane-water. b) The total amine concentration was kept constant at 0.05 M in the case of amine buffers. The total buffer concentration was kept constant at 0.0098 M in the case of borate-carbonate buffers.

(NH str.), 1730 (ester C=O str.), 1640 (amide C=O str., amide I band), and 1545 cm^{-1} (NH bend + CN str., amide II band). NMR ($CDCl_3$, TMS) : δ 6.02 (1H, broad s, NH), 4.09 (2H, d, $NHC\underline{H}_2$), 3.78 (3H, s, OCH_3), 2.29 (2H, t, CH_2-CO), 1.9—1.1 (14H, m, methylene), and 0.89 (3H, distorted t, $C\underline{H}_3CH_2$).

Results and Discussion

The hydrolysis of *p*-nitrophenyl hexadecanoate (PNPP) was accelerated by the ammonium salt (**1**) in reference to the spontaneous hydrolysis under the same conditions: initial PNPP concentration of 1.00×10^{-5} M, $\mu=0.2$ with NaCl, in 1%(v/v)methanol–1% (v/v)dioxane–water, at 40.0±0.1 °C. The observed rates are 1.3×10^{-4} and 0.14×10^{-4} s^{-1} for catalyzed and spontaneous reactions at pH 9.7, respectively. The rate enhancement is significant for the presence of a small amount of **1** (0.88×10^{-5} M). The catalytic effect of **1** must be developed by the quaternary ammonium group since [20]paracyclophan-10-one (**3**)

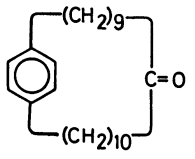

3

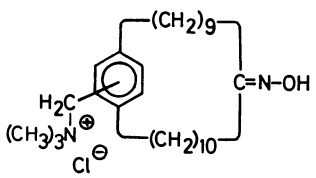

4

which lacks in a positive charge showed no acceleration effect in the PNPP hydrolysis. Two kinetically indistinguishable mechanisms can be cited for the catalytic function of **1**. The ammonium group concentrates anionic hydroxide ions around it as in cationic micelles.[7)] Alternatively, the ammonium group may serve as a super acid which neutralizes a negative charge developing at the carbonyl oxygen of bound PNPP in the transition state in a manner as predicted for the deacylation of PNPP catalyzed by 10-hydroxyimino [20] paracyclophanyl - 22 (23) - methyltrimethyl - ammonium chloride (**4**).[4)] There is a significant difference between these two mechanisms. The former involves the direct electrostatic interaction between the positive ammonium group of the catalyst and the hydroxide ion of nucleophilic nature prior to the rate-determining step while the latter does not. In order to examine this criterion, the kinetic behavior of glycine in the deacylation of PNPP was investigated in reference to that of ethanolamine which has a similar pK_a (amine) as glycine. Glycine is a nucleophile of significant choice since it contains a neutral amino nucleophile as well as an anionic carboxylate having a potentiality to interact electrostatically with the ammonium group of **1**.

A large excess of ethanolamine (0.05 M) in the absence of **1** gave out some 1.5-fold increase in the deacylation rate of PNPP at pH 9.70, whereas glycine hardly affected the reaction rate in the same concentration range. The **1**-catalyzed deacylation of PNPP, on the other hand, was enhanced with glycine (0.05 M) by a factor of 4 relative to the **1**-catalyzed alkaline hydrolysis without added glycine. Ethanolamine also showed a similar enhancement effect but to a lesser extent. The effect of pH variation in the pH range 8.8—10.4 at a constant amine concentration (0.05 M) and the effect of an amine concentration in the 0.01—0.1 M range at constant pH (9.70) on the **1**-catalyzed deacylation were investigated to go through a more critical assessment of the effects of amine bases. The observed first-order rate constants (k_{obsd}) for the deacylation of PNPP are summarized in Tables 1 and 2. The pH-rate and amine concentration-rate correla-

Table 2. Effects of concentration changes of glycine and ethanolamine on the *p*-nitrophenol release from PNPP as catalyzed by **1** at pH 9.70±0.02, μ=0.2 (NaCl), and 40.0±0.1 °C[a)]

[Glycine] (M)	$k_{obs}\times10^4$ (s^{-1})	[Ethanolamine] (M)	$k_{obs}\times10^4$ (s^{-1})
0.01	3.5	0.013	2.5
0.03	5.7	0.033	3.0
0.05	7.1	0.05	3.4
0.075	9.2	0.07	4.3
0.088	10.8	0.1	4.3
0.1	12.3		

a) $[PNPP]_0=1.00\times10^{-5}$ M, $[\mathbf{1}]=1.53\times10^{-5}$ M in 1% (v/v)methanol−1%(v/v)dioxane-water.

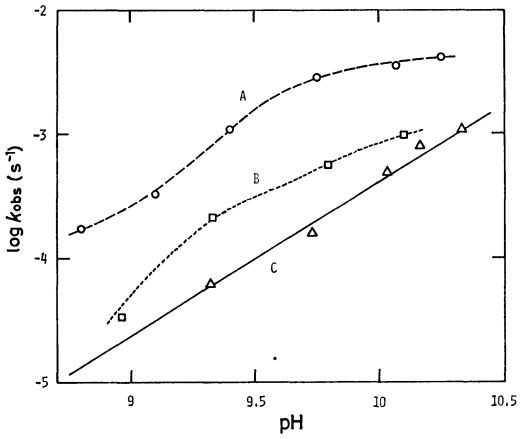

Fig. 1. pH-Rate correlation for the *p*-nitrophenol release from PNPP as catalyzed by **1** (0.88×10^{-5} M) at μ=0.2 (NaCl), and 40.0±0.1 °C: A, glycine buffer (0.05 M); B, ethanolamine buffer (0.05 M); C, borate-carbonate buffer (0.01 M).

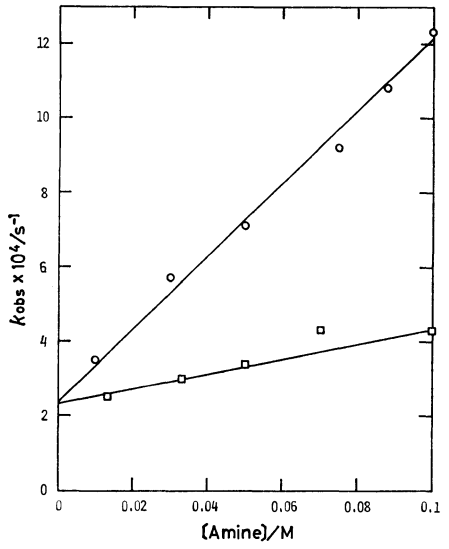

Fig. 2. Correlations between first-order rate constant for the *p*-nitrophenol release from PNPP as catalyzed by **1** (1.53×10^{-5} M) and concentrations of glycine (○) and ethanolamine (□) at pH 9.70±0.02, μ=0.2 (NaCl), and 40.0±0.1 °C.

tions are shown in Figs. 1 and 2, respectively. Aminolysis by the added amine may certainly be responsible for the rate enhancement. That the aminolysis was actually taking place was confirmed by the product analysis using *p*-nitrophenyl decanoate instead of hexadecanoate as a substrate; the decanoate ester in a glycine buffer (pH 9.7) containing a catalytic amount of **1** afforded the glycinolysis product. Judging from the nucleophilicities of glycine and hydroxide toward *p*-nitrophenyl acetate, second-order rate constants being respectively 155 and 890 $M^{-1}\,min^{-1}$ at 25 °C,[8)] the kinetic effect of glycine observed for the present system is surprisingly small. This is most likely ascribed to a steric factor pertaining to such a bulky substrate as PNPP and its complex with **1**.

At constant pH (9.70), the **1**-catalyzed deacylation rate (k_{obsd}) can be correlated linearly with the amine concentration (Fig. 2); $k_{obsd}=\kappa(OH)+k_{amine}[Amine]$ where $\kappa(OH)$[9)] represents the hydrolysis rate factor as a function of pH and k_{amine} the catalytic rate constant effected by the presence of glycine or ethanolamine. It is evident that the k_{amine} value for glycine is 5 times as large as that for ethanolamine. Thus, a novel reaction mechanism must take place in the degradation of PNPP effected by glycine in consistent with the following facts. Firstly, the basicities of glycine and ethanolamine are mutually comparable; the pK_a (amine) values determined potentiometrically under the kinetic condition are 9.4 and 9.3 for glycine and ethanolamine, respectively. The difference in nucleophilic reactivity between the two bases toward a *p*-nitrophenyl ester would be in a neighborhood of 1.2-fold judging from the rate-basicity correlation established for amine bases in the deacylation of *p*-nitrophenyl acetate.[8)] Secondly, there is a good reason to expect that a hydrophobic environment provided by the inclusion complex formed between **1** and PNPP would favor the attack of neutral ethanolamine rather than that of charged glycine. In fact the deacylation of PNPP in the absence of **1** was moderately accelerated by ethanolamine but hardly affected by glycine (*vide supra*). Furthermore, the uncharged paracyclophane (**3**) was confirmed qualitatively to show a rate enhancement effect in the aminolysis but not in the hydrolysis of PNPP; ethanolamine was found to show greater enhancement effect than glycine in the aminolysis reaction. Thirdly, steric interaction between an amine nucleophile and the inclusion complex formed between **1** and PNPP may possibly be an important factor governing the reactivity of the amine. However, it is unreasonable that ethanolamine is more bulky than glycine.[10)]

On the basis of these considerations, the enhanced reactivity of glycine should be ascribed to the favorable electrostatic interaction between the negative carboxylate group of glycine and the positive ammonium group of **1** into which PNPP is incorporated (Fig. 3). If there is no special interaction between an amine and **1**, an amine nucleophile attacks unimolecularly on the substrate and the deacylation rate (k_{obsd}) is given by $k_{obsd}=\kappa(OH)+k_{amine}[Amine]$, where $\kappa(OH)$ represents the hydrolysis rate factor[9)] and is evaluated from line C in Fig. 1. Thus, ($k_{obsd}-\kappa$-

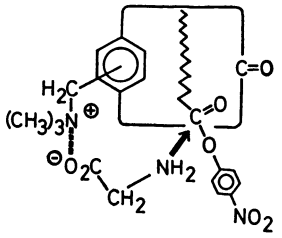

Fig. 3. A plausible reactiom mechanism for the glycinolysis of PNPP: the anionic carboxylate group of glycine is anchored on the ammonium group and the amine nucleophile attacks on PNPP which is incorporated into the hydrophobic cavity of **1**.

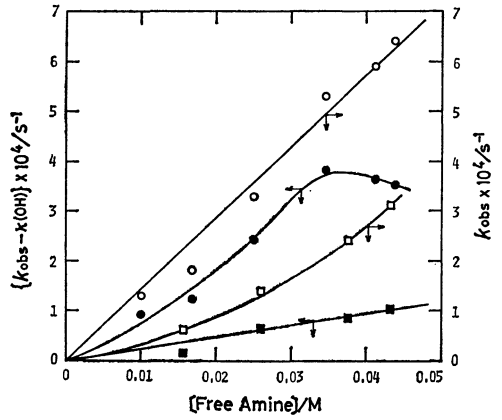

Fig. 4. Correlations between PNPP-deacylation rate and free amine concentration at constant total concentration of amine species (0.05 M) based on the data shown in Fig. 1:
(○, ●), glycine; (□, ■), ethanolamine.

(OH)) should give a linear correlation with the concentration of free amine evaluated from its pK_a value while the total concentration of amine is maintained constant. This is what is observed for the ethanolamine system (Fig. 4). Such a correlation, however, fails to be applied to the glycine system. Free glycine concentrations correlate more satisfactorily in a linear manner with k_{obsd} rather than $(k_{obsd}-\kappa(OH))$ (Fig. 4), and the $(k_{obsd}-\kappa(OH))$ curve is bent down beyond pH 9.7. These results are indicative of an important difference in kinetic behaviors of the two amines. The glycinate ion in a large excess amount seems to exclude the hydroxide ion from the vicinity of the ammonium group of **1** and the glycinolysis becomes a major reaction for the glycine system in a whole pH region studied.

The present work has made a step toward the development of an effective organic double-field catalyst (C) with which the two reacting molecules (A and B) are complexed through two different kinds of interaction forces effected by functions (C_A and C_B) placed in C (Fig. 5). The reactivity and selectivity of the bimolecular reaction of A and B would be much affected by such complexation. The present work demonstrates that the ammonium salt (**1**) should be

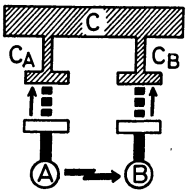

Fig. 5. Schematic representation of double-field catalysis:
A and B, reacting molecules; C, catalyst; C_A and C_B, catalytic functions of different nature provided by the catalyst.

regarded as a hydrophobic-electrostatic double-field catalyst. The hydrophobic field provided by the polymethylene chain and benzene ring incorporates the substrate (PNPP), while the electrostatic field provided by the ammonium group exhibits a kinetically significant interaction with the anionic carboxylate of the other reactant, glycine (Fig. 3). Another important role played by the hydrophobic cavity of [20]paracyclophanes is the deaggregation of carboxylic esters bearing a long alkyl chain. Such carboxylic esters are known to exist in a self-aggregated form in bulk phase.[11] The incorporation into the hydrophobic cavity tends to set the substrate more or less in an elongated form so that the site of ester bond becomes open and susceptible to the attack of nucleophile.

References

1) Y. Murakami, J. Sunamoto, and K. Kano, *Bull. Chem. Soc. Jpn.*, **47**, 1238 (1974).
2) Y. Murakami, J. Sunamoto, H. Okamoto, and K. Kawanami, *Bull. Chem. Soc. Jpn.*, **48**, 1537 (1975).
3) J. Sunamoto, H. Okamoto, H. Kondo, and Y. Murakami, *Tetrahedron Lett.*, 2761 (1975).
4) Y. Murakami, Y. Aoyama, and K. Dobashi, *J. Chem. Soc., Perkin II*, in the press.
5) Y. Murakami, Y. Aoyama, and K. Dobashi, *J. Chem. Soc., Perkin II*, in the press.
6) Y. Murakami, J. Sunamoto, H. Kondo, and H. Okamoto, *Bull. Chem. Soc., Jpn.*, submitted for publication.
7) J. H. Fendler and E. J. Fendler, "Catalysis in Micellar and Macromolecular Systems," Academic Press, New York, N. Y. (1975).
8) W. P. Jencks and J. Carriuolo, *J. Am. Chem. Soc.*, **82**, 1778 (1960).
9) $\kappa(OH)$ can not be simply correlated with spontaneous (k_0) and hydrolysis (k_{OH}) rate constants by $\kappa(OH)=k_0+k_{OH}[OH^-]$ under the present experimental conditions (refer to Fig. 1). This may be attributed to the direct electrostatic interaction of hydroxide ions with the ammonium group of **1** and to the hydrophobic effect exerted by the inclusion complex formed between **1** and PNPP.
10) E. L. Eliel, N. L. Allinger, S. L. Angyal, and G. A. Morrison, "Conformational Analysis," John Wiley & Sons, Inc., New York, N. Y. (1965), Chap. 7.
11) F. M. Menger and C. E. Portnoy, *J. Am. Chem. Soc.*, **90**, 1875 (1968).

A Study of the 1,3,5-Trialkylbenzenes with Aluminum Chloride-Hydrogen Chloride Systems

Nobuyoshi NAMBU, Nobumoto HIRAOKA, Kenji SHIGEMURA, Sawako HAMANAKA, and Masaya OGAWA

Department of Applied Chemistry, Faculty of Engineering, Kansai University, Senriyama, Suita, Osaka 564

(Received July 10, 1976)

The "red-oil" complex layers of systems of 1,3,5-trialkylbenzenes (Me_3B, Et_3B, i-Pr_3B, and s-Bu_3B) with $AlCl_3$–HCl were prepared and studied by means of ^1H NMR and ^{13}C NMR spectroscopy. The results show that the 2,4,6-trialkylbenzenium ion is evidently formed in the complex layer of the $AlCl_3$–HCl system, much as in other superacid systems, and that those ions from i-Pr_3B and s-Bu_3B are substantially stable, even at room temperature. The molar ratios of i-Pr_3B and s-Bu_3B to HAl_2Cl_7 are almost 1. On the other hand, the molar ratios of Me_3B and Et_3B to HAl_2Cl_7 are 4.5 and 1.9 respectively. These two complex layers are considered to be formed by both 1,3,5-trialkylbenzene and its protonated product, and to be in a certain equilibrium state as a result of proton exchange at room temperature.

Many investigations of benzenium ions by using NMR have been reported in recent years,[1] and most of them have been carried out in various superacids, such as HF–BF_3, HSO_3F, and HF–SbF_5, at low temperatures. In the Friedel-Crafts reaction, alkylbenzene–$AlCl_3$–HCl systems are frequently used in commercial processes. However, the structures and compositions of the above systems have not yet been ascertained. The reasons for this are that the measurement of the NMR spectrum is difficult at low temperatures because of the solidification of the system, and that it is hard to obtain at room temperature because of the disproportionation process.

In a previous paper,[2] we reported that some of the methylbenzenes are stable in the system at room temperature, and are scarcely disproportionated even at room temperature. In order to obtain further information about the structure and composition of the "red-oil" complex layer (complex layer) in the system, we will now deal with the system of 1,3,5-trialkylbenzenes with $AlCl_3$–HCl and the formation of the stable benzenium ions by using NMR.

Experimental

Materials. The mesitylene (Me_3B) was commercially available in a high purity. The 1,3,5-trialkylbenzenes were known; they were prepared from mono- or di-alkylbenzene by Friedel-Crafts type reactions. The purities of the 1,3,5-triethyl-, 1,3,5-triisopropyl-, and 1,3,5-tri-s-butylbenzenes (Et_3B, i-Pr_3B, and s-Bu_3B respectively) were 96, 100, and 98% respectively, as determined by means of VPC analysis. All the alkylbenzenes dried over metallic Na were distilled just before use.

Preparation of Complex Layers. The complex layers of the systems of 1,3,5-trialkylbenzenes with $AlCl_3$ were prepared by the method reported previously.[2] After the reaction had been completed, the complex layer was separated as a lower layer, leaving colorless hydrocarbon as an upper layer. The volumes of the two layers were almost equal. The lower layer was then pipetted out and measured. This layer is substantially stable and keeps for several days at room temperature.

Measurements. The ^{13}C NMR spectra were obtained using a JNM-PS-100/EC-100 spectrometer equipped with a Fourier transform recorder at 25.15 MHz under a complete proton decoupling. The pulse width and repetition time were 12 μs (about $\pi/4$ pulse) and 6s respectively. The spectra were observed at 6250 Hz (data point 8191) in a 10 mmϕ tube with an external lock standard contained in a 3 mmϕ tube, holding acetone-d_6 and TMS, coaxially centered. All chemical shifts are referred to this TMS standard. The ^1H NMR spectra were also obtained using a JNM-PS-100 spectrometer, with external TMS (capillary) as the reference.

Analyses of Hydrocarbons. Hydrocarbons in both the upper and lower (complex) layers were analyzed by means of VPC after each layer had been decomposed with water. The analyses were made on a Shimadzu GC-3AF apparatus, fitted with a 3 m × 3 mm column packed with Apiezon grease L 10% and with an ionization detector, at 160 and 200 °C.

Analyses of Aluminum and Chlorine.[3] The aluminum and chlorine in the complex layer were determined by the oxine and mercury-titration methods respectively.

Results and Discussion

Analyses of Complex Layers. As was described in our previous paper,[2] the formation of a reaction system, that is, a complex layer and a hydrocarbon layer, requires a limited amount of HCl evolved by moisture contained in $AlCl_3$. In this study, when suitable amounts of alkylbenzene and $AlCl_3$ were used, it was

Table 1. Disproportionated products of 1,3,5-trialkylbenzenes at 2 °C

Starting material	Layer	Products (mol%)				
		m-Di-R-C_6H_4	*p*-Di-R-C_6H_4	1,3,5-Tri-R-C_6H_3	1,2,4-Tri-R-C_6H_3	Tetra-R-C_6H_2 and unknown products
R=Me[a]	Upper	—	—	100	—	—
	Lower	—	—	100	—	—
R=Et[b]	Upper	2.7	0.7	88.5	4.8	3.3
	Lower	3.0	1.3	87.0	4.6	4.1
R=i-Pr	Upper	0.4	0.2	99.0	—	0.4
	Lower	0.6	0.3	98.5	—	0.6
R=s-Bu[c]	Upper	0.6	0.2	96.6	2.1	0.5
	Lower	0.6	0.3	96.1	2.2	0.8

a) Ref. 2. b) 1,3,5-Triethylbenzene: 1,2,4-triethylbenzene=96.0: 4.0. c) 1,3,5-Tri-s-butylbenzene: 1,2,4-tri-s-butylbenzene=98.0: 2.0.

Table 2. The constituents of the complex layers of 1,3,5-trialkylbenzenes with aluminum chloride–hydrogen chloride

Starting material 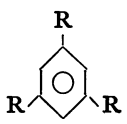	Al (wt%)	Cl (wt%)	Hydrocarbon (wt%)	Molar ratios			
				Al[a)]	Cl[a)]	1,3,5-Trialkylbenzene	Hydrocarbon
R=Me	6.4	29.7	63.9	1	3.53	2.24	2.24
R=Et	8.3	38.2	53.5	1	3.50	0.93	1.07
R=*i*-Pr	9.4	43.2	47.4	1	3.50	0.66	0.67
R=*s*-Bu	9.2	42.3	48.5	1	3.50	0.56	0.58

a) Al: ±0.3 wt%, Cl: ±1.0 wt%.

possible to obtain two layers apparently equal in volume. The data of the disproportionated products of 1,3,5-trialkylbenzene obtained in the reaction with $AlCl_3$ and HCl at 2 °C are listed in Table 1. The contents of the hydrocarbons in both upper and lower layers, that is, the hydrocarbon layer and the complex layer respectively, were separately analyzed by means of VPC.

The results indicate that the disproportionation of 1,3,5-trialkylbenzene scarcely proceeds at all. These relations held constantly up to about 30 °C. To obtain the contents of $AlCl_3$ and HCl in the complex layer, Al and Cl were analyzed and the molar ratios of Al, Cl, and alkylbenzene were estimated, as is shown in Table 2.

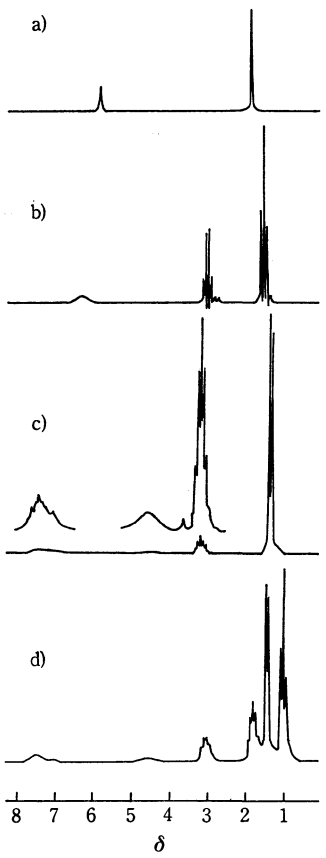

Fig. 1. 100 MHz ^1H NMR spectra of complex layers of 1,3,5-trialkylbenzenes with aluminum chloride–hydrogen chloride at 30 °C.
a) 1,3,5-Trimethylbenzene. b) 1,3,5-Triethylbenzene. c) 1,3,5-Triisopropylbenzene. d) 1,3,5-Tri-*s*-butylbenzene.

The molar ratio of Al/Cl was 1/3.5 for all the complex layers. This means that HAl_2Cl_7,[4)] made up of 2 mol of $AlCl_3$ and 1 mol of HCl, plays an important role in the formation of the complex layer. The molar ratio of 1,3,5-trialkylbenzene/HAl_2Cl_7 decreased with an increase in the alkyl carbon numbers as follows; 4.5 for Me_3B, 1.9 for Et_3B, 1.3 for *i*-Pr_3B, and 1.1 for *s*-Bu_3B. Therefore, the constituents of the complex layers are somewhat different from each other.

^1H NMR Spectra of Complex Layers. The ^1H NMR spectrum of each complex layer is shown in Fig. 1.

The ring protons of Me_3B and Et_3B exhibited considerably sharp singlet signals at δ 6.0 and 6.4 respectively, but those of *i*-Pr_3B and *s*-Bu_3B were each detected as a set of two broad signals, at about δ 7.5 and 4.6 respectively. The former is a signal of the ring protons, H_3 and H_5, of 2,4,6-trialkylbenzenium ions, while the latter is attributable to the methylene protons, H_1, of 2,4,6-trialkylbenzenium ions, which correspond to those reported by Olah *et al.* in their investigation with superacid. Therefore, the singlets of the ring protons of Me_3B and Et_3B, which unusually shifted to a high field, probably result from the fusions of the ring signals of 1,3,5-trialkylbenzene and the 2,4,6-trialkylbenzenium ion.

In the spectrum of *i*-Pr_3B, a weak singlet signal was observed at δ 3.69; it increased in intensity with the temperature. When this signal was detected somewhat intensely, 1,1-dimethyl-3-methylene-5- or -6-isopropylindan (**1**)[5)] was also found in the products. From this fact, and reference to the chemical shifts of the phenyl isopropyl cation, which were shown by Olah *et al.*[6)] and Farnum,[7)] the singlet signal is assigned to methyl protons of the 3,5-diisopropyl phenyl isopropyl cation (**2**).

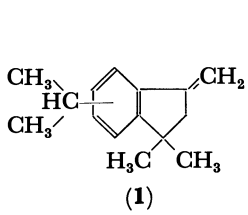

(**1**)

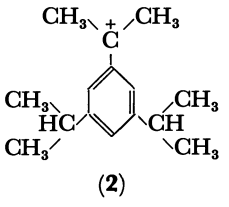

(**2**)

^{13}C NMR Spectra of Complex Layers. The ^{13}C NMR spectrum of each complex layer at 30 °C is shown in Fig. 2. In the spectrum of Et_3B, some of the sharp signals obtained at δ 146—125 and 30—16, result from

Table 3. Carbon-13 chemical shifts for 2,4,6-trialkylbenzenium ions

Ion	Carbon-13 chemical shifts[a]				
	Benzenium-ring carbons				2,4,6-Alkyl-substituent carbons
	C_1	C_2, C_6	C_3, C_5	C_4	Additional
R=Me	b) 54.5	193.3	134.8	193.3	$C_{2,6}$–CH_3, 27.3; C_4–CH_3, 29.6
	c) 51.9	194.0	133.9	194.3	$C_{2,6}$–CH_3, 25.2; C_4–CH_3, 27.6
R=Et	d) 52.9	197.8	128.6	197.8	$C_{2,4,6}$–CH_2, 32.9; $C_{2,4,6}$–CH_3, 14.8
	c) 49.8	199.2	130.8	198.3	$C_{2,6}$–CH_2, 32.1; C_4–CH_2, 34.3; $C_{2,4,6}$–CH_3, 12.1
R=*i*-Pr	e) 50.3	205.4	130.2	202.8	$C_{2,4,6}$–CH, 39.7; $C_{2,4,6}$–CH_3, 24.1
R=*s*-Bu	e) 50.6	204.6	132.0	202.0	C_α–CH, 47.0; C_β–CH_2, 32.1; $C_{\beta'}$–CH_3, 21.4; C_γ–CH_3, 13.5

a) The chemical shifts are in parts per million relative to the external (capillary) TMS. b) Data from Ref. 2; original data converted using $\delta_C^{CS_2}$ 193.7. Counter-ion, $Al_2Cl_7^-$. c) Data from Ref. 1. j) In HF–SbF_5–SO_2 at −65 °C. d) This work, at −50 °C. e) This work, at 0 °C.

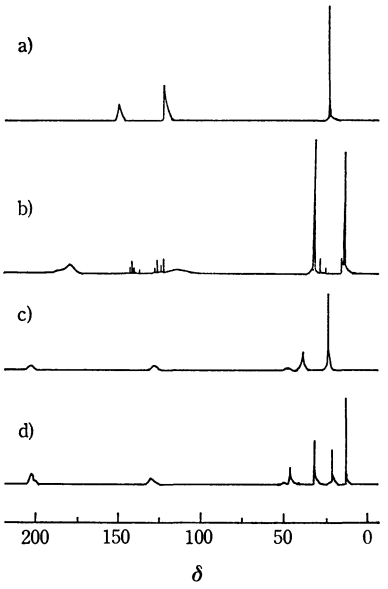

Fig. 2. ^1H decoupled ^{13}C NMR spectra of complex layers of 1,3,5-trialkylbenzenes with aluminum chloride–hydrogen chloride at 30 °C.
a) 1,3,5-Trimethylbenzene. b) 1,3,5-Triethylbenzene. c) 1,3,5-Triisopropylbenzene. d) 1,3,5-Tri-*s*-butylbenzene.

the presence of some other alkylbenzenes produced by disproportionation. The other complex layers were not contaminated by significant disproportionated products. The methylene signals of the 2,4,6-trialkylbenzenium ions were observed at about δ 50 for *i*-Pr_3B and *s*-Bu_3B, but not for Me_3B and Et_3B. The latter complex layers, which were measured at sufficiently low temperatures, apparently gave methylene signals in the spectrum. The chemical shifts of the 2,4,6-trialkylbenzenium ions are shown in Table 3, compared with those cited in the literature.

The results show that the 2,4,6-trialkylbenzenium ion is evidently formed in the complex layer of the $AlCl_3$–HCl system, much as in other superacid systems, and that those ions from *i*-Pr_3B and *s*-Bu_3B are substantially stable even at room temperature. As the molar ratios of *i*-Pr_3B and *s*-Bu_3B to HAl_2Cl_7 are almost 1 (1.3 for *i*-Pr_3B and 1.1 for *s*-Bu_3B), the complex layer may mainly consist of the following product:

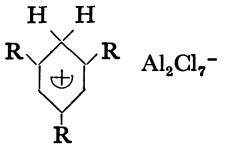

R=*i*-Pr, *s*-Bu

On the other hand, the molar ratios of 1,3,5-trialkylbenzenes to HAl_2Cl_7 in the complex layers of Me_3B and Et_3B are 4.5 and 1.9 respectively. These two complex layers are considered to be formed by both 1,3,5-trialkylbenzene and its protonated product, and to be in a certain equilibrium state by means of proton exchange as follows:

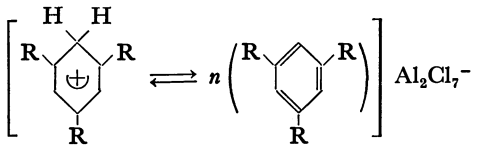

R=Me (n=3.5), Et (n=0.9)

In these states, the spectra of complex layers may exhibit fused signals between 1,3,5-trialkylbenzene and the 2,4,6-trialkylbenzenium ion. The chemical shift of the fused signal may be estimated by means of the molar ratio of two components. An example of calculation for Me_3B will be given:

	Molar ratio	Unsubstituted carbon		Me substituted carbon	
		C_1	C_3, C_5	C_2, C_6	C_4
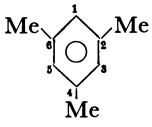	3.5	127.6		137.7	
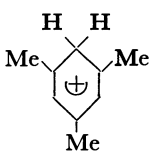	1.0	54.5	134.8	193.3	193.3
		108.0		193.3	
Fused signal (calcd)		123.3		150.1	
Fused signal (obsd)		123.3		151.6	

The calculated chemical shift of the fused signal agreed fairly well with the observed one. In the case of

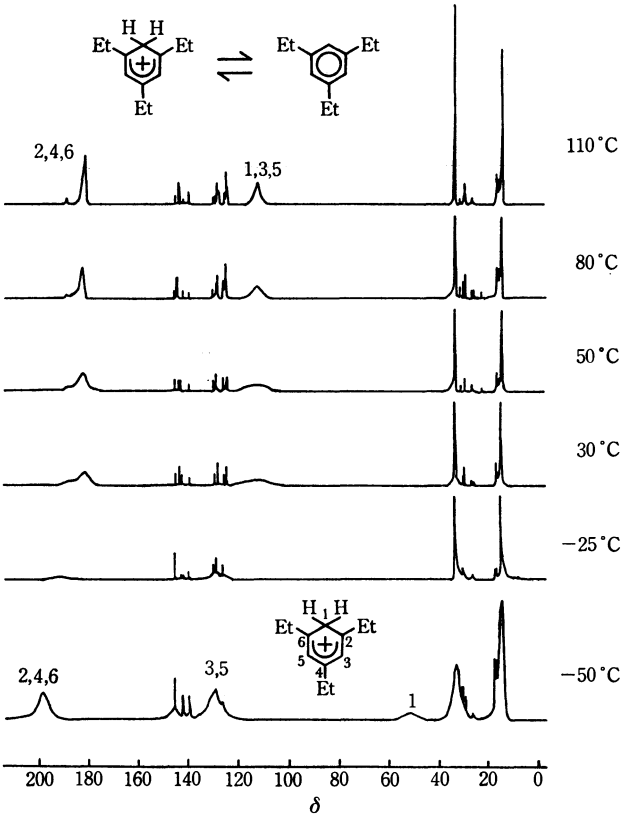

Fig. 3. Temperature-dependent ^{13}C NMR spectra of 1,3,5-triethylbenzene complex layer.

Et_3B, the calculated chemical shift of unsubstituted carbon (δ 113.8) agreed with the observed one (δ 114.0), but that of methyl-substituted carbon (δ 172.6) showed a considerable difference from the observed one (δ 182.5). This difference results from the existence of disproportionated products in the case of Et_3B.

Temperature-dependent ^{13}C NMR Spectra of the Et_3B Complex Layer. The ^{13}C NMR spectra of the Et_3B complex layer were measured in the temperature range from −50 to 110 °C; the results are shown in Fig. 3. A lot of small sharp signals observed at about δ 140 and 30 are attributable to the formation of disproportionated products. The spectrum obtained at −50 °C apparently exhibited a ring methylene signal, which indicates the presence of the 2,4,6-triethylbenzenium ion. In the spectrum at −25 °C, the weak, broad signals of ring carbons are interpreted as indicating that the life-time of the two components decreases through the critical range in the proton exchange at this temperature. At elevated temperatures the signals tend to coalesce in a singlet and to sharpen with the increase in the temperature.

All these pieces of evidence support the idea that some parts of the 1,3,5-trialkylbenzene in the complex layer are protonated by HAl_2Cl_7 and are in a certain equilibrium state with other parts by means of proton exchange.

References

1) a) W. von E. Doering, M. Saunders, H. G. Boyton, H. W. Earhart, E. F. Wadley, W. R. Edwards, and G. Laber, *Tetrahedron*, **4**, 178 (1958); b) G. Dallinga, E. L. Mackor, and A. A. Verrijn Stuart, *Mol. Phys.*, **1**, 123 (1958); c) E. L. Mackor, A. Hofstra, and J. H. van der Waals, *Trans. Faraday Soc.*, **54**, 66 (1958); d) C. MacLean and E. L. Mackor, *Mol. Phys.*, **4**, 241 (1961); *Discuss. Faraday Soc.*, **1962**, 165; e) T. Birchall and R. J. Gillespie, *Can. J. Chem.*, **42**, 502 (1964); f) G. A. Olah, *J. Am. Chem. Soc.*, **87**, 1103 (1965); g) V. Koptyug, A. Rezvukhin, E. Lippmaa, and T. Pehk, *Tetrahedron Lett.*, **1968**, 4009; h) G. A. Olah, R. H. Schlosberg, R. D. Porter, Y. K. Mo, D. P. Kelly, and G. D. Mateescu, *J. Am. Chem. Soc.*, **94**, 2034 (1972); i) G. A. Olah and Y. K. Mo, *ibid.*, **94**, 9241 (1972); *J. Org. Chem.*, **38**, 353 (1973); j) G. A. Olah, R. J. Spear, G. Messina, and P. W. Westerman, *J. Am. Chem. Soc.*, **97**, 4051 (1975).

2) Y. Okami, N. Otani, D. Katoh, S. Hamanaka, and M. Ogawa, *Bull. Chem. Soc. Jpn.*, **46**, 1860 (1973).

3) Yuki Biryo Bunseki Kenkyu Kondankai, "Yuki Biryo Teiryo Bunseki," Tokyo (1969), pp. 388, 422.

4) J. F. Norris and J. N. Ingraham, *J. Am. Chem. Soc.*, **62**, 1298 (1940); H. C. Brown and H. W. Pearsall, *ibid.*, **74**, 191 (1952).

5) In the ^1H NMR spectrum of **1**, the chemical shifts are δ 1.3 (m, CH_3), δ 2.1 (s, CH_2), δ 2.8 (m, CH), δ 5.9 (s, $=CH_2$), and δ 7.1 (m, ring H) in a ratio of 12: 2: 1: 2: 3.

6) G. A. Olah, *J. Am. Chem. Soc.*, **86**, 932 (1964); G. A. Olah and Y. K. Mo, *ibid.*, **95**, 6827 (1973).

7) D. G. Farnum, *J. Am. Chem. Soc.*, **86**, 934 (1964).

Reactions of Transition Metal Dihydrides. VII. Further Investigations on Charge-Transfer Interaction between σ-Basic Metal Hydrides and Organic π-Acceptors

Akira NAKAMURA and Sei OTSUKA

Department of Chemistry, Faculty of Engineering Science, Osaka University, Toyonaka, Osaka 560

(Received July 10, 1976)

Charge transfer (CT) absorptions between transition metal polyhydrides, *e.g.* MH_2Cp_2 ($Cp=\eta$-C_5H_5; M=Mo, W), $FeH_2(dppe)_2$, $MH_4(dppe)_2$(dppe=$Ph_2PCH_2CH_2PPh_2$; M=Mo, W), and organic π-acceptors such as maleic anhydride were measured. The position of the CT bands gave an I_p value of 6.3 eV for WH_2Cp_2. The value indicates transfer of electron from the filled non-bonding metal orbital to the acceptors. Role of the electron donor-acceptor interactions prior to insertion or substitution of transition metal hydrides is discussed.

Electron transfer reactions of transition metal complexes are receiving considerable attention in modern inorganic chemistry.[1] In many cases, the transfer of electron accompanies a change in formal oxidation state of the metal. In some cases partial transfer of an electron (electron donor accepter interaction or charge transfer) can be observed between metal compounds and organic substances. Our primary concern here is with the intermolecular charge transfer (CT) interactions. Thus, ferrocene forms a green CT-complex[2] with TCNE, whereas cobaltocene ($CoCp_2$ Cp: η-C_5H_5) and nickelocene ($NiCp_2$) give ionic salts, *e.g.* $(Cp_2M)^+(TCNE)^-$, resulting from complete electron transfer.[3] An X-ray structure of the ferrocene/TCNE adduct[4] revealed the charge transfer between the Cp ring and π-orbital of TCNE. A similar structure has been reported for CT complexes of arenechromium tricarbonyls with 1,3,5-trinitrobenzene.[5] H. Kobayashi *et al.* have proposed participation of a metal orbital in the charge transfer observed in arenechromium tricarbonyl/TCNE[6] systems. The ease of electron transfer, in principle, depends on the relative energy levels and electronic configuration of the metal orbitals of these organometallic complexes and on those of the accepting orbitals of organic molecules. This electron donor-acceptor interaction is generally an unobservable low-evergy process, occurring prior to such reactions as olefin π-complex formation and olefin insertion, both of which constitute essential steps in olefin catalysis.

We have been interested in the electron-donating property of various transition metal hydrides and phosphine complexes as they are important in olefin catalysis or organic synthesis in general. During studies on the reactivity of MH_2Cp_2 compounds (M=Mo, W; Cp=η^5-C_5H_5) we were able to observe CT interactions between these metal σ-bases and organic π-acids, and found that the interactions could be influential for the kinetic behavior observed in the subsequent olefin insertion reactions.[7] In addition, this has an important bearing on the olefin catalysis. The absence of study experimentally identifying interactions of this type prompted us to report our study which shed light on the nature of the interactions.

Results

Charge Transfer Complexes. When a concentrated solution of metallocene hydrides, MH_2Cp_2 (M=Mo and W), in toluene or acetonitrile, was mixed with π-acidic olefins such as maleic anhydride or fumaronitrile, immediate coloration, ranging blue to red, occurred. The color is due to the charge transfer absorption band as shown by a trend in the absorption maximum observed when the π-acidity is systematically varied (Table 1). It is important to exclude air from the interacting systems to successfully record the spectra. In many cases, the coloration fades on standing even under nitrogen for *ca.* 1 h. The extreme air-sensitivity of the hydrides and the weakness of the charge transfer absorption made quantitative spectral measurements very difficult. Therefore, no attempt was made to estimate the formation constants of the charge transfer complexes.

The charge transfer bands observed with *N,N*-dimethylaniline, a typical organic donor, are also listed in Table 1 to facilitate the comparison with the data of the metal σ-donor, WH_2Cp_2. An essentially constant shift ($\approx$7000 cm^{-1}) in the maxima is apparent by comparing *N,N*-dimethylaniline with WH_2Cp_2. Hence WH_2Cp_2 has a lower I_p than that of dimethylaniline. Since the I_p of the dimethylaniline is 7.1 eV,[8] the I_p value for WH_2Cp_2 will be 6.3 eV. The estimated I_p value is in good agreement with the I_p data obtained by an ESCA[9] (6.4 eV), and by an photocurrent measurement[10] (6.3 ± 0.1 eV), but different from one by a molecular orbital calculation (8.3 eV).[11]

The variation of polarity of the solvent from CH_2Cl_2 to benzene caused a moderate blue shift (20000 cm^{-1} to 19200 cm^{-1}) of the maxima of charge transfer band for the system WH_2Cp_2/citraconic anhydride. The approximate value of the extinction coefficient (ε: 5×10^3) in neat citraconic anhydride was as expected for the charge transfer absorption. These characteristics of the spectra unambiguously indicate the absorption maxima to be real charge transfer band.

Substitution with a methyl group on the Cp rings in MH_2Cp_2 molecule did not significantly affect the band. Thus, $WH_2(C_5H_4CH_3)_2$[12] exhibited a blue color (λ_{max} at 528 nm) in neat citraconic anhydride. MoH_2Cp_2 and $MoH_2(C_5H_4CH_3)_2$[12] exhibited almost the same pale blue color when mixed with phenylmaleic anhydride in toluene. The color turned to deep brown in 1 h at room temperature. In comparison with the tungsten congener, the molybdenum hydride, MoH_2Cp_2, did not show a clear absorption maximum even with maleo- or fumaronitrile in toluene. The coloration is very similar to the case with the tungsten hydride. The similarity

TABLE 1. FREQUENCIES OF CHARGE TRANSFER BANDS

Acceptor	Donor: Cp_2WH_2[a] Color	Cp_2WH_2[a] Maximum ($10^3 \times cm^{-1}$)	$PhN(CH_3)_2$ Color	$PhN(CH_3)_2$ Maximum ($10^3 \times cm^{-1}$)
Phenylmaleic anhydride	Blue	15.8	Red orange	22.6
Maleic anhydride	Bluish violet	17.5	Reddish orange	24.6
Methylmaleic anhydride (citraconic anhydride)	Purple	19.2	Orange	26.2
Dimethylmaleic anhydride	Reddish purple	20.0[b]	Orange	27.2
Nitrobenzene	Red	20.0	Yellow	—
m-Dinitrobenzene	Pale violet	17.8	Orange	23.8
1,3,5-Trinitrobenzene	Pale blue	16.8[b,c]	Red	20.6
Dimethyl maleate	Red	25.0[b]	—	—
Dimethyl fumarate	Red	22.5[b]	—	—
Fumaronitrile	Deep red	20.0[b]	Yellow	27.0
Maleonitrile	Deep red	20.0[b]	Yellow	27.0
Tetracyanoethylene	Ionized complex (Brown)		Blue	14.6

a) 0.002—0.01 mol/l for WH_2Cp_2 as donor. b) Shoulder. c) Inaccurate due to faint absorption.

indicates that the I_p value[9] for MoH_2Cp_2 is essentially identical to WH_2Cp_2. The failure to observe clear maxima for MoH_2Cp_2/π-acceptor systems may be due to the instability of the hydride $[MoH_2Cp_2]^{\delta+}$ with partial positive charge in solution. Although trihydrido cation, $[MoH_3Cp_2]^+$, is coordinatively saturated and thermally stable, the dihydrido cation, $[MoH_2Cp_2]^+$, is thermally unstable as evidenced by reaction between MoH_2Cp_2 and TCNE as described below. Generally tungsten hydride complexes are much more inert to olefins than the corresponding molybdenum hydride complexes.[12]

Although formation constants of the CT complexes of metallocene hydrides have not been measured, the intensity of the coloration implies that the values are low. Small formation constants have been recorded in systems such as polypermethylsilane/TCNE.[13] Due to the small formation constants, we could not measure the exact absorption maximum, especially with MoH_2Cp_2 as the donor. A faint coloration due to the CT absorption was observed in the following interactions: $MoH_2Cp_2/Ph_2C{=}C(CN)_2$, faint red; MoH_2Cp_2/pyromellitic dianhydride, faint blue (in CH_3CN).

$$\{MoH_2Cp_2\}^{\delta+}\{NCCH{=}CHCN\}^{\delta-} \xrightarrow{80°C} Cp_2Mo(H)(CH\text{-}CH_2CN)(CN) \quad (1)$$

$$\{MoH_2Cp_2\}^{\delta+}\{NCCH{=}CHCN\}^{\delta-} \xrightarrow{CH_2{=}CHCO_2CH_3} Cp_2Mo(H)(CH\text{-}CH_3)(CO_2CH_3) \quad (2)$$

$$Cp_2Mo(H)(CH\text{-}CH_3)(CO_2CH_3) \xleftarrow{CH_2{=}CHCO_2CH_3} MoH_2Cp_2$$

The deep red solution of the CT complex, MoH_2Cp_2/fumaronitrile, gave a hydrido-σ-alkyl complex on heating to 80 °C in toluene (Eq. 1). An attempted reaction of the CT complex with methyl acrylate did not give the acrylate insertion product which can be readily prepared by the reaction with MoH_2Cp_2 even at 0 °C (Eq. 2). Similar insertion of fumaronitrile into one of the W–H bonds in $\{WH_2Cp_2\}^{\delta+}\{NCCH{=}CHCN\}^{\delta-}$ did not occur at 80 °C.

The interaction of metallocene monoalkyl-hydrides, *e.g.* $Cp_2MoH[CH(CN)CH_2CN]$ with π-acceptors *e.g.* TCNE, did not give rise to charge transfer absorptions.

A rhenium hydride, $ReHCp_2$, also exhibited a CT maximum with trinitrobenzene at 540 nm and with citraconic anhydride at 480 nm in CH_3CN.

The interaction in mixture of MH_2Cp_2 and π-acceptors was investigated by physical methods such as the infrared and NMR spectroscopy and conductivity measurements. Thus, evaporation of a solution of an equimolar mixture of WH_2Cp_2 and maleonitrile gave a deep red solid which shows a new somewhat broad IR $\nu_{C\equiv N}$ band at 2200 cm^{-1} in addition to the bands due to the free olefin at 2237 and 2256 cm^{-1}. Similarly, evaporation of the solution containing fumaronitrile gives an orange solid which is contaminated by crystals of the starting materials and also shows a new ν_{CN} band at 2200 cm^{-1}. Conductivity measurement of the CT mixture dissolved in CH_2Cl_2 clearly shows some increase in conductivity as compared with the value of each component at the same concentration. The molar conductivity ($\Lambda = 1.0 \times 10^{-3}\ \Omega^{-1}\ cm^2\ mol^{-1}$) suggests presence of solvent-separated ions in small concentrations and yet provides firm evidence for the presence of an intimate ion pair together with the CT complex in the solution.

A similar, but weaker, red coloration was observed for systems, MoH_2Cp_2/PhCH=CHCN, or /$CH_3CH{=}CHCN$. No physical evidence has been obtained for these weakly interacting systems. The tungsten analog, WH_2Cp_2, behaves similarly to the Mo derivative, but the red coloration is still weaker. The red C_6D_6 solutions of a system, MoH_2Cp_2/maleonitrile or WH_2Cp_2/maleonitrile, were examined by ^1H NMR spectroscopy. The signals observed were almost identical to those of the each component only. These results are in agreement with the small formation constants of the CT complexes. Consistently, the IR spectrum of the concentrated solution showed only a weak peak at 2200 cm^{-1}, in addition to the ν_{CN} of unchanged maleonitrile.

Electron Transfer Complexes. Formation of the ionized species was demonstrated in the reaction of

MH_2Cp_2 with strong π-acids. Thus, tetracyanoethylylene (TCNE) was mixed, at -35 °C in toluene or in CH_2Cl_2, with dilute solutions of MH_2Cp_2 (M=Mo and W) to give deep brown precipitates, soluble only in polar, coordinating solvents. When the components are mixed in high concentrations, evolution of H_2 was observed in small amounts. The composition and the visible spectrum (in DMSO) of the product depend on the reaction conditions. Thus, elemental analysis indicated compositions, $MoH_2Cp_2\cdot(TCNE)_n$, $n=1$—1.5 and $WH_2Cp_2\cdot(TCNE)_n$, $n=1$—1.5. $ReHCp_2$ behaves similarly, and instantly gives brown precipitates from benzene solution. Infrared CN stretching frequencies (2150, 2200 cm^{-1}), visible, and conductivity data (see Experimental) suggest an ionized structure[14] analogues to the known ionic compounds, $Cr(C_6H_6)_2{}^+TCNE^-$.[3] The ^1H NMR spectrum in dimethyl-d_6 sulfoxide exhibited only a broadened signal at δ 5.5 indicating its paramagnetism, but the bulk magnetic moment was not measurable.

Tetracyanoquinodimethane (TCNQ) also gives deep brown precipitates from benzene solutions of MH_2Cp_2. In acetonitrile, the addition of MH_2Cp_2 at first gave a deep red solutions which then became deep green. The visible spectrum (in CH_3CN) indicated the presence of $TCNQ^-$.[14] The deep green powder obtained by evaporation had a composition, $[WH_2Cp_2\cdot(TCNQ)_2]$ with λ_{max} (in CH_3CN) 780, and 820 nm. 9,10-Phenanthrenequinone when mixed with MH_2Cp_2 (M=Mo, W) in benzene instantly produces deep purple precipitates which revert to the starting materials on dissolution in dimethyl sulfoxide. No coloration due to the CT interaction of WH_2Cp_2 was observed with anthraquinone, azobenzene, or succinic anhydride.

Electron Donor-Acceptor Interactions of Coordinatively Saturated Transition Metal Hydrides. Coordinatively saturated hydride complexes, *e.g.* $MH_4(dppe)_2$ (M=Mo, W, dppe=$Ph_2PCH_2CH_2PPh_2$) or $MH_2(dppe)_2$ (M=Fe, Ru), exhibit σ-basicity towards CF_3CO_2H and also an electron transfer with TCNE or TCNQ in acetonitrile, as evidenced by the visible peaks of $TCNE^-$ or $TCNQ^-$. The ratio of donor/acceptor in the interactions were investigated for the $MoH_4(dppe)_2$/TCNE system and found to be 1 : 2 by the visible spectrum. The electric conductivity in CH_3CN was found to be $\Lambda_m=64\ \Omega^{-1}\ cm^2$ at ambient temperature. The value for the $MoH_4(dppe)_2$/TCNQ was $\Lambda_m=49\ \Omega^{-1}\ cm^2$. Strong green coloration was observed when these interactions were examined in benzene or toluene. The band positions in benzene vary with the different donors; *e.g.* $MoH_4(dppe)_2$/TCNE 613 nm, $Mo(N_2)_2(dppe)_2$/TCNE 617 nm, $WH_4(dppe)_2$/TCNE 630 nm (at $-30°$ in toluene), $FeH_2(dppe)_2$/TCNE 639 nm.

The green color due to the CT band of $MoH_4(dppe)_2$/TCNE slowly changed to purple on standing for a day. A deep purple powder obtained by evaporation had a composition near $Mo(TCNE)_2(dppe)_2$ which can be separated by alumina chromatography into at least seven components differing in color. Low-valent phosphine complexes, *e.g.* $CoH(dppe)_2$, $Ni(dppe)_2$, $NiI_2(PPh_3)_2$, and $CoI_2(PPh_3)_2$, transfer an electron to TCNE when mixed in CH_3CN. No CT absorptions have been detectable even in non-polar solvents, such as benzene.

Discussion

Transition metal complexes in low-valent states are readily oxidized by electron transfer when some electron acceptors are allowed to react with it. The one- and two-electron transfer processes have long been important research fields in inorganic chemistry. However, only a few examples has been known for *charge transfer* complex formation arising from the non-bonding orbitals of low-valent transition metal compounds (metal donors) to organic acceptors. The paucity of examples for the charge transfer complexes with metal donors seems to be due to the ease of electron transfer from the non-bonding metal orbitals. For example, only very low energy barrier exists to remove one electron from octahedrally coordinated cobalt(II) ions. Our successful observation of a clear charge transfer absorption band for a system, MH_2Cp_2/π-acceptors, can be ascribed to the sufficient energy barrier of Cp_2MH_2 molcules to loose one electron. The charge transferred state is stabilized presumably due to the high potential energy of the positively charged species, $[MH_2Cp_2]^+$. Indeed, the dihydridometallocene cation, formed by addition of TCNE into a benzene solution/suspension of MH_2Cp_2, slowly decomposes with evolution of hydrogen at room temperature. A qualitative energy profile of the processes are schematically shown in Fig. 1.

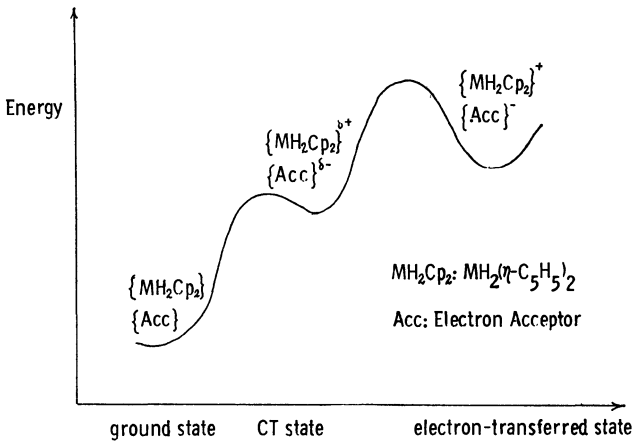

Fig. 1. A qualitative energy profile of the electron transfer process between metallocene dihydrides and electron acceptors.

The relative instability of the cationic species thus seems to be the prerequisite to observe charge transfer states. Some organic electron donors such as *N,N,N',N'*-tetramethyl-*p*-phenylenediamine and their derivatives form relatively stable cationic species through one-electron transfer. In contrast to these delocalized electron donors, aliphatic or simple aromatic monoamines do not form stable cationic species but form charge transfer complexes with relevant acceptors.[8] Metallocene hydrides thus resemble these monoamines in their ability to form charge transfer complexes. The present systems represent rare cases where the charge transfer from the essentially non-bonding metal orbital is possible.

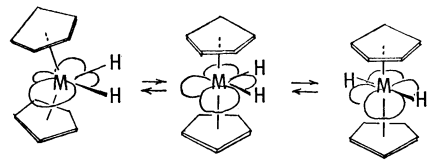

σ-basic π-basic

ground state thermally excited state

Fig. 2. Shape of an essentially non-bonding metal orbital of $MH_2(\eta\text{-}C_5H_5)_2$ molecules.

The interaction of low-valent transition metal compounds with π-acidic molecules frequently leads to π-complex formation. The propensity for the π-complex formation is especially pronounced with labile low-valent compounds of d^8- of d^{10}-metals, *e.g.* $Pt(PPh_3)_4$. Although the I_p values[15] of these compounds are in a range (6—8 eV) suitable for the charge transfer complex formation with relevant acceptors, no evidence of the charge transfer has been recorded so far. Ligand dissociation from these low-valent compounds affords a metal site of strong π-basicity which rapidly combines with the π-acceptor. Therefore unless ligand substitution process in the donor molecules is prevented either thermodynamically or kinetically, stable charge transfer complexes should not be observable.

WH_2Cp_2 molecule seems to be sufficiently inert to π-complex formation as the shape of the HOMO defines its σ-basic property at the wedged ground-state structure and the π-complex formation with π-accepting olefins is forbidden by the orbital symmetry restriction.[16] In the thermally excited parallel metallocene structure, π-basic property is expected as illustrated in Fig. 2. Thus, thermal reaction of WH_2Cp_2 with diethyl maleate gives $Cp_2W(EtO_2C\text{–}CH{=}CH\text{–}CO_2Et)$ through the initial insertion into one of the W–H bonds[17] followed by reductive elimination producing a strong metal π-base, Cp_2W. The insertion has been proposed to proceed *via* incipient π-complex formation with WH_2Cp_2 in the parallel metallocene structure.

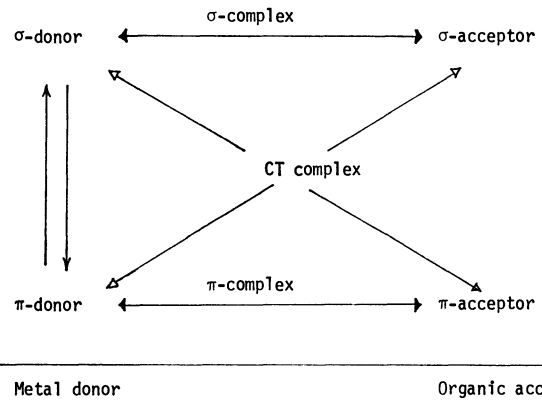

Scheme 1. Idealized schemes of interaction between metal donors and organic acceptors.

Scheme 1 shows a simplified scheme for the interactions between metal donors and organic acceptors with an emphasis on the symmetry property of interacting orbitals. It is to be noted that the symmetry properties of the metal donor orbitals will be altered by a change in the stereochemistry or coordination number. The energy barrier for the change generally increases with an increase in the strength of the metal-ligand bonding.[18] In particular, the molybdenum analog of metallocene hydrides, MoH_2Cp_2, undergoes the stereochemical change more readily than the corresponding tungsten complex.[12] In other words, MoH_2Cp_2 is stereochemically more non-rigid than WH_2Cp_2. This trend is in agreement with the general tendency in the non-rigidity of transition metal hydrides[18] and also explains the different behavior of these metallocene hydrides toward electronegative olefins. Thus, MoH_2Cp_2 readily inserts methyl acrylate into one of the Mo–H bonds at 20 °C and the CT complex, MoH_2Cp_2/fumaronitrile, is also slowly transformed to the insertion products (*cf.* Eqs. 1 and 2). By contrast, the tungsten hydride, WH_2Cp_2, forms CT complexes but no insertion products at 20 °C. Since the olefin insertion has been proposed[16] to proceed by incipient formation of a metal-olefin π-complex, the inertness of WH_2Cp_2 seems to be due to its reluctance to undergo polytopal rearrangement to give the thermally-excited π-basic form shown in Fig. 2.

Conclusions

Clear charge transfer absorption maxima were observed for the first time in the interaction of π-basic metallocene hydrides, MH_2Cp_2, with π-acidic organic molecules.[7] The *charge transfer* arises from the filled nonbonding metal orbital as indicated by the substituent effect on the Cp rings of MH_2Cp_2 and also by the I_p value calculated from the charge transfer absorption maxima. *Electron transfer* occurs between MH_2Cp_2 and strong π-acids like TCNE. The formation of charge transfer or electron transfer complexes of MH_2Cp_2 retards the olefin insertion into the M–H bonds. Hence, we feel that these electron-donor-acceptor interactions between metal σ-bases and organic π-acids are not prerequisite to π-complex formation of olefin insertion.

Experimental

Material and Apparatus. Metallocene hydrides (MH_2Cp_2, M=Mo, W and $ReHCp_2$),[19] $MH_4(dppe)_2$ (M=Mo, W),[18] and $MH_2(dppe)_2$ (M=Fe, Ru)[20] were prepared by literature methods. Maleonitrile was prepared from maleamide by dehydration with P_2O_5. The other organic acceptors are commercial products and were purified when necessary. Electronic, vibrational, and ^1H NMR spectra were measured by a Hitachi Model EPS-3T, a Hitachi-Perkin Elmer Model 225, and Jeol JMN-60HL, respectively. Electric conductivity was measured by a Yanagimoto's Conductivity Outfit MY-7 using white platinum plates as electrodes. These physical measurements with air-sensitive metal complexes were performed under pure nitrogen in solvents previously saturated with nitrogen.

Measurement of the Charge Transfer Spectra. Saturated toluene solutions of MH_2Cp_2 (M=W or Mo) were mixed with organic acceptor in question and the supernatant liquor was taken out by a syringe to a 2 mm cell for immediate examination by the visible spectra. When liquid acceptors, *e.g.* maleonitrile or citraconic anhydride, were to be examined, the measurement was also performed in neat liquids. The visible spectra of interacting CT couples, $MH_4(dppe)_2$/TCNE (M=

Mo, W) or $MH_2(dppe)_2$/TCNE (M=Fe, Ru) were recorded similarly in toluene.

Investigation of Physical Property of Interacting Mixtures of MH_2Cp_2 (M=Mo or W) with Fumaro- or Maleonitrile at Ambient Temperature. *a) Visible Spectrum*: An equimolar fresh solution of MoH_2Cp_2 and fumaro- or maleonitrile in dichloromethane (0.1 mmol/l) showed no maximum in the visible absorption. A difference spectrum revealed an increased absorption in the equimolar mixed solution (0.06 mmol/l) at 360—450 nm region without maximum. Experimental difficulty, however, precluded quantitative data. When the amount of fumaronitrile is increased to 2—4 times molar in excess, the absorption around 500 nm increased and when a more concentrated solution (0.1 mol/l) was made, the spectrum began to show a distinct shoulder at 490 nm (ε 10000). By contrast, WH_2Cp_2 showed a clear absorption maximum with many organic acceptors in toluene or in CH_3CN (*cf.* Table 1).

b) Conductivity: Conductivity was measured by a Yanagimoto MY-7 with white platinum electrodes at 1 cm apart, under nitrogen when necessary. A dichloromethane solution (0.1 mmol/l) of MoH_2Cp_2 containing 10-fold excess fumaronitrile showed low molar conductivity, $0.1\times10^{-3}\ \Omega^{-1}$ $cm^2\ mol^{-1}$ at 23 °C. Each reagent showed no conductivity in dichloromethane. The result in acetonitrile was complicated by low conductivity of each reagent, but a value $2\times10^{-3}\ \Omega^{-1}$ $cm^2\ mol^{-1}$ was found in reddish orange solution made from MoH_2Cp_2 and excess fumaronitrile.

c) ^1H NMR Spectrum: An orange equimolar mixture of MoH_2Cp_2 and fumaro- or maleonitrile freshly dissolved in C_6D_6 or in $(CD_3)_2CO$ failed to give any unambiguous evidence for the formation of an stable adduct as judged from the chemical shift values of the observed peaks, which differ only *ca.* 0.1 ppm from that of free olefins. Similar results were obtained for WH_2Cp_2 as a donor. Observed change in the value from that of the free olefins may indicate difference in extent of solvation because the solvent effect was exceptionally large in C_6D_6.[21] On standing for a few hours at room temperature, weak signals due to the hydride-alkyl complex[16] appear.

d) IR Spectrum: Solution spectra of the fresh mixture of MoH_2Cp_2 or WH_2Cp_2 and fumaronitrile (ν_{CN} at 2246 cm^{-1}) in toluene or in acetone revealed a weak new $\nu_{C\equiv N}$ band at 2200 cm^{-1}. On standing the solution of MoH_2Cp_2 containing fumaronitrile, a strong $\nu_{C\equiv N}$ band (at 2190 cm^{-1}) of the hydrido-alkyl complex appeared.[16] The hydrido-alkyl complex did not form from WH_2Cp_2 even at higher temperatures.

Interaction of MH_2Cp_2 (M=W and Mo) with Tetracyanoethylene(TCNE). Dropwise addition of a dilute TCNE solution in toluene (0.13 g in 10 ml) into WH_2Cp_2 dissolved in toluene (0.03 g in 5 ml) at −35 °C gave a deep purple floculent precipitate which changed to deep brown on further addition. It was filtered, washed, and dried to give a dark brown powder soluble in dimethyl sulfoxide (DMSO) and also in *N*-methylformamide. Attempted purification by recrystallization has been unsuccessful. Elemental analysis roughly corresponded to $WH_2(C_5H_5)_2(C_6N_4)_{1.5}$. IR (Nujol) in cm^{-1}, $\nu_{C\equiv N}$, 2200 broad, 2130 broad, 1600 broad. Visible maxima (DMSO) in nm, 398, 415, 570 shoulder. ^1H NMR spectrum (DMSO-d_6) was obscured by some paramagnetic impurities although the most part was diamagnetic as confirmed by magnetic susceptibility measured in the same solution. The solution had a weak electrolytic property ($\Lambda_m=3.6\ \Omega^{-1}\ cm^2$) in DMSO at 20 °C which somewhat increased on standing. The sample prepared by the inverse addition had similar analytical data but a different visible spectrum (λ_{max} (in nm) at 393, 420 sh, 450 sh). The corresponding reaction of MoH_2Cp_2 with TCNE evolved a small amount of hydrogen, giving a deep brown amorphous powder soluble in DMSO; $[Mo(C_5H_5)_2H_2(C_6N_4)_{1-1.5}]$, IR (Nujol) in cm^{-1}, 2200 broad, 2130 broad, 1650—1600 broad. No maximum was observed in the visible spectrum in DMSO. $\Lambda_m=6\ \Omega^{-1}\ cm^2$ in DMSO at 20 °C. The rhenium hydride, $ReHCp_2$, instantly gave brown precipitates on mixing with a TCNE solution in benzene. The IR spectrum was similar to those obtained by reaction MH_2Cp_2 with TCNE.

References

1) T. J. Meyer, *Progr. Inorg. Chem.*, **19**, 1 (1975).
2) M. Rosenblum, R. W. Fish, and C. Bennett, *J. Am. Chem. Soc.*, **86**, 5166 (1964).
3) J. W. Fitch, III and J. J. Lagowski, *Inorg. Chem.*, **4**, 864 (1965); R. L. Brandon, J. H. Osiecki, and A. Ottenberg, *J. Org. Chem.*, **31**, 1214 (1966).
4) E. Adman, M. Rosenblum, S. Sullivan, and T. N. Margulis, *J. Am. Chem. Soc.*, **89**, 4540 (1967).
5) D. M. Braitsch, *J. Chem. Soc., Chem. Commun.*, **1975**, 460; O. L. Carter, A. T. Mcphail, and G. A. Sim, *J. Chem. Soc., A*, **1966**, 822.
6) H. Kobayashi, M. Kobayashi, and Y. Kaizu, *Bull. Chem. Soc. Jpn.*, **46**, 3109 (1973); **48**, 1222 (1975).
7) A part of this paper has been communicated before; A. Nakamura and S. Otsuka, *J. Am. Chem. Soc.*, **95**, 5091 (1973).
8) R. Foster, "Organic Charge-Transfer Complexes," Academic Press, London (1969).
9) J. C. Green, S. E. Jackson, and B. Higginson, *J. Chem. Soc., Dalton Trans.*, **1975**, 403.
10) Y. Nakato, T. Chiyoda, and H. Tsubomura, *Bull. Chem. Soc. Jpn.*, **47**, 3001 (1974).
11) J. L. Petersen, D. L. Lichtenberger, R. F. Fenske, and L. F. Dahl, *J. Am. Chem. Soc.*, **97**, 6433 (1975).
12) A. Nakamura and S. Otsuka, *J. Mol. Catal.*, **1**, 285 (1976).
13) R. West and V. F. Traven, *J. Am. Chem. Soc.*, **95**, 6824 (1973); H. Sakurai, M. Kita, and T. Uchida, *ibid.*, **95**, 6826 (1973).
14) M. Itoh, *J. Am. Chem. Soc.*, **92**, 886 (1970); L. R. Melby, R. J. Harder, W. Mahler, R. E. Benson, and W. E. Mochel, *J. Am. Chem. Soc.*, **84**, 3374 (1962).
15) C. A. Tolman, *J. Am. Chem. Soc.*, **96**, 2780 (1974).
16) A. Nakamura and S. Otsuka, *J. Am. Chem. Soc.*, **95**, 7262 (1973).
17) B. R. Francis, M. L. H. Green, and G. G. Roberts, *Chem. Commun.*, **1971**, 1290.
18) P. Meakin, L. J. Guggenberger, W. G. Peet, E. L. Muetterties, and J. P. Jesson, *J. Am. Chem. Soc.*, **95**, 1467 (1973).
19) R. B. King, "Organometallic Syntheses," Vol. 1, Academic Press, New York, N. Y. (1965), p. 79.
20) D. H. Gerlach, W. G. Peet, and E. L. Muetterties, *J. Am. Chem. Soc.*, **94**, 4545 (1972).
21) R. Foster and C. A. Fyfe, "Progress in NMR Spectroscopy," ed by J. W. Emsley, J. Feeney, and L. H. Sutcliffe, Vol. 4, Pergamon Press, London (1969).

Metal-Assisted Terpenoid Synthesis. IV.[1] Nickel-Catalyzed Reactions of 1,3-Dienes with Ketones. A New Synthesis of Long Chain Tertiary Alcohols

Susumu AKUTAGAWA

Central Research Laboratory, Takasago Perfumery Co. Ltd., 31-36, 5-Chome, Kamata, Ohta-ku, Tokyo 144

(Received July 17, 1976)

Catalytic reactions of 1,3-butadiene with ketones were carried out with a nickel-ligand system to give stereoselectively tertiary alcohols having a (2*Z*, 5*E*)-2,5,7-octatrienyl- or a (2*Z*, 6*E*, 9*E*)-2,6,9,11-dodecatetraenyl chain. Similar reactions of isoprene gave a mixture of terpenic and apoterpenic alcohols. A possible reaction scheme was discussed in terms of an insertion of the carbonyl group to a σ-allyl end of octadienyl or dodecatrienyl nickel complexes.

Despite extensive studies on telomerization of conjugated dienes with various protic substances[2] including carbonyl-activated methylene compounds, no report has been given on the catalytic formation of tertiary alcohols from ketones and oligodienes. A closely related reaction may be the secondary alcohol formation in the palladium-catalyzed reactions of 1,3-butadiene with aldehydes.[3a-d] A nickel catalyst system has been found to be effective for the synthesis of tertiary alcohols of types **1** and **2**. The reaction provides a convenient synthetic route for long chain alcohols, some of which are useful for terpenoid synthesis.

The reactions of conjugated dienes with ketones were carried out at 70 °C for 10 h in the presence of a nickel catalyst (5 mol % of dienes) either prepared *in situ* by reducing an equimolar mixture of acetylacetonatonickel(II) and a ligand with triethyl aluminum or treating bis(cyclooctadienyl)nickel(0) with an equimolar amount of the ligand. The products were identified by means of VPC and IR, UV, mass and NMR spectroscopy. The physical properties of **1a—e** and **2** are summarized in Table 1. The reaction of 1,3-butadiene

Table 1. Spectral data of the products

Product	NMR[a] (δ)	IR[b] (cm^{-1})	UV[c] (nm)	Bp (°C/Torr)
1a	1.18 (6H, s), 2.15 (2H, d, J=7.0 Hz), 2.82 (2H, t, J=8.0 Hz), 3.12 (1H, s), 4.90—5.32 (3H, ABX), 5.51 (2H, q, J=7.0 Hz), 5.63—7.01 (2H, m, J=16.0 Hz)	3365, 1800, 1640, 1598, 1150, 973, 952, 900	238 (ε 18000)	72/15
1b	1.17 (6H, d), 1.18 (3H, s), 2.15 (2H, d, J=7.0 Hz), 2.82 (2H, t, J=8.0 Hz), 3.05 (1H, s), 4.90—5.32 (3H, ABX), 5.51 (2H, q, J=7.0 Hz), 5.63—7.01 (2H, m, J=16.0 Hz)	3365, 1800, 1640, 1598, 1150, 995, 973, 952, 900	231 (ε 21000)	85/3
1c	1.18 (3H, s), 2.15 (2H, d, J=7.0 Hz), 2.82 (2H, t, J=8.0 Hz), 3.45 (1H, s), 4.90—5.32 (3H, ABX), 5.51 (2H, q, J=7.0 Hz), 5.63—7.01 (2H, m, J=16.0 Hz), 7.20 (5H, s)	3365, 1800, 1640, 1598, 1150, 995, 973, 952, 900, 785	225 (ε 24000)	112/2
1d	1.19 (6H, s), 1.62 (3H, s), 1.83 (3H, s), 2.19 (2H, d, J=8.0 Hz), 2.87 (2H, d, J=7.0 Hz), 3.04 (1H, s), 4.83 (2H, s), 5.28 (1H, t), 5.53 (1H, dt, J=16.0 Hz), 6.10 (1H, d)	3490, 3081, 1780, 1601, 1145, 970, 890, 835	239 (ε 25000)	92/3
1e	1.18 (6H, s), 1.73 (3H, s), 1.80 (3H, s), 2.16 (2H, s), 2.82 (2H, t, J=7.0 Hz), 2.94 (1H, s), 4.82 (2H, s), 5.15 (1H, t, J=7.0 Hz), 5.52 (1H, dt, J=16.0 Hz), 6.10 (1H, d)	3495, 3080, 1772, 1601, 1141, 963, 886, 842	239 (ε 24900)	92/3
2	1.18 (6H, s), 2.15 (2H, d, J=2.0 Hz), 2.80—2.91 (6H, m), 3.10 (1H, s), 4.90—5.32 (3H, ABX), 5.51 (2H, q, J=7.0 Hz), 5.60—7.01 (4H, m, J=16.0 Hz)	3365, 1800, 1640, 1598, 1150, 973, 952, 900	229 (ε 85200)	103/3

a) 60 MHz, in CCl_4, s: singlet, d: doublet, t: triplet, q: quartet, m: multiplet. b) Neat. c) Measured in ethanol.

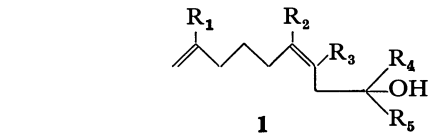

1

a: $R_1=R_2=R_3=H$, $R_4=R_5=Me$
b: $R_1=R_2=R_3=H$, $R_4=Me$, $R_5=i\text{-}C_3H_7$
c: $R_1=R_2=R_3=H$, $R_4=Me$, $R_5=C_6H_5$
d: $R_1=R_2=R_4=R_5=Me$, $R_3=H$
e: $R_1=R_3=R_4=R_5=Me$, $R_2=H$

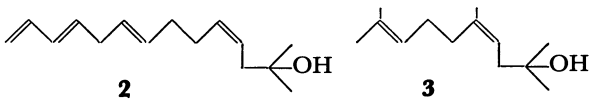

2 **3**

with acetone was effected with Ni–P (O–*o*-Me–C_6H_4)$_3$ to give a mixture of **1a** and **2** in 62 and 16% yields, respectively (based on reacted 1,3-butadiene). Similar results were obtained using other ligands, such as PPh_3 or $P(OPh)_3$. However, catalyst activity was rather low (65% conversion for PPh_3 and 70% for $P(OPh)_3$) as compared to that of P(O–*o*-Me–C_6H_4)$_3$ (81%). A small amount of 1,3-butadiene dimers and higher products[4] were also formed. The *cis*-geometry of the C4—5 and *trans* geometry of the C7—8 double bonds in **1a** can be deduced from the olefin proton coupling constants, 7, and 16 Hz, respectively. The structure of **2** was deduced from the hydrogenated product; an alkanol obtained was identical with the authentic 2-methyl-2-tetradecanol in their physical and spectral properties. The NMR spectroscopy of **2** showed the presence of two *trans*-double bonds at C8 and C11 (5.60—7.01, 4H, m, J=16.0 Hz) and a *cis*-double bond at C4 (5.51, 2H, m, J=7.0 Hz). The regioselective linear linkage of three 1,3-butadiene molecules in **2** is noteworthy in view of the unavoidable formation of branched isomers in the catalytic linear oligomerization of the diene. Similarly the reactions of methyl isopropyl ketone and acetophenone with 1,3-butadiene gave **1b** and **1c** in 55 and 52% yields, respectively. Bulkier ketones such as diisopropyl ketone gave no alcohol. No alcohol formation was observed with propionaldehyde. Typical results are given in Table 2.

The rate of reaction of isoprene with acetone was small as compared to that of the reaction of 1,3-butadiene.

Table 2. Reactions[a] of 1,3-butadiene with carbonyl compounds

No.	Carbonyl compound[b]	Conversion (%)	Dimers (%)	Alcohols (%)[c]	Higher products (%)
1.	Me_2CO	81	15	**1a**(62) **2** (16)	7
2.	$i\text{-}C_3H_7COMe$	55	21	**1b**(55)	24[d]
3.	$MeCOC_6H_5$	61	23	**1c**(52)	25[d]
4.	$(i\text{-}C_3H_7)_2CO$	12	91	—	9
5.	CH_3CH_2CHO	7	100	—	

a) Conditions: 5 mol% of Ni(acac)$_2$, P(O–*o*-Me–C_6H_4)$_3$ and $AlEt_3$ (1: 1: 5) based on 1,3-butadiene at 70 °C for 10 h. b) The ratio of 1,3-butadiene to carbonyl compounds was 4: 1. c) Based on reacted 1,3-butadiene. d) Alcohols were detected by IR and TLC.

Table 3. Reactions of isoprene with acetone[a]

No.	Ligand	Conversion (%)	Dimers (%)	Alcohols (**1d**+**1e**) (%)[b]	Higher products (%)	Ratio[c] **1d**/**1e**
1.	P(O–*o*-MeC_6H_4)$_3$	62	12	72	16	15/85
2.	P(O–C_6H_5)$_3$	57	20	61	19	21/79
3.	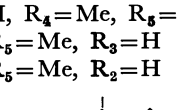	47	10	52	38	55/45
4.	$P(C_6H_5)_3$	35	37	48	15	75/25
5.	$PPh(NEt_2)_2$	35	31	45	24	59/41
6.	P(*n*-C_4H_9)$_3$	22	70	0	30	

a) Reaction conditions: Ni(COD)$_2$/ligand/isoprene/acetone 1/1/200/70 at 70 °C for 10 h. b) Based on reacted isoprene. c) Calculated by VPC.

The reaction with isoprene gave two isomeric alcohols **1d** and **1e**, together with a relatively large amount of the dimers. The structure of **1d** is related to that of terpenoids. (*Z*)-2,5,9-Trimethyl-4,8-decadien-2-ol (**3**), for example, can be readily derived from partial hydrogenation of **1d**.

The nature of the ligand affects the activity and regioselectivity. As shown in Table 3, electron-donating trialkylphosphines, like P(*n*-C_4H_9)$_3$, completely suppress the reaction, while electron-accepting phosphites facilitate the reaction. The bulkier the phosphite ligand, the higher the selectivity for **1e**.

The requirement of a phosphite ligand suggests the importance of the low valence state of nickel in the catalysis. This is in contrast to the linear trimerization of isoprene[5] where a Ni(II) species, formation of which is assisted by coordination of an electron-donating ligand, plays an important role. One conspicuous feature of the products is the *cis*-configuration of the inner double bond nearest to the alcohol carbon. This leads to a reaction scheme involving a nucleophilic

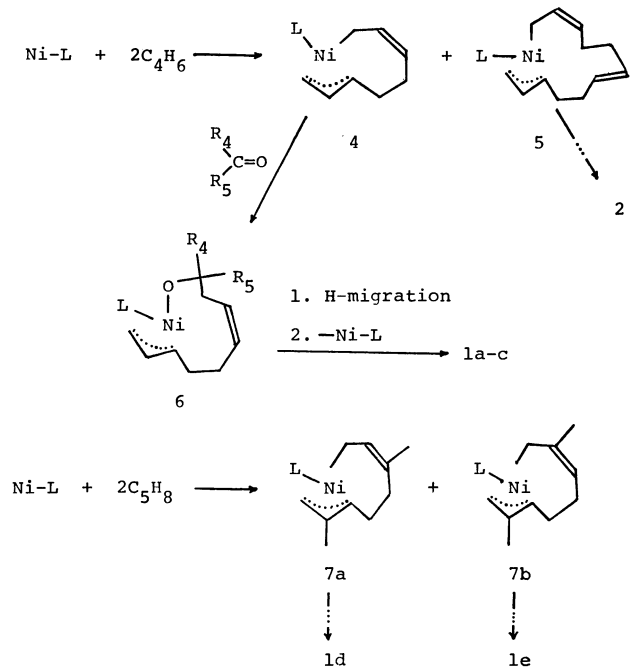

attack of the carbanionic allyl end of the dimer or the trimer ligand on the carbonyl carbon in intermedates **4**, **7a**, or **7b** and **5**. The subsequent step will be the formation of **6**, where hydrogen migration from a methylene group, adjucent to the π-allyl group, to the carbonyl oxygen atom will take place to give the alcohols and to regenerate the catalyst. Baker *et al.*[6] observed a similar insertion of an aldehydic carbonyl group into a metal–allyl bond of dodecatrienyl nickel complex in the stoichiometric reaction. However, because of hydrolysis of the product they isolated alcohols of dodecatrienyl derivatives.

The stereoselective formation of the *cis*-double bond in the alkoxy ligand of **6** is accounted for by the preferential insertion of the carbonyl group into the σ-allylic end of **4**. The *anti*-configuration of the π-allylic part in **6** appears to be responsible for the *trans* configuration of the conjugated part of the products.

Although regioselective head to tail coupling of isoprene for the linear oligomerization has been achieved with suitable ligands such as trialkylarsines or aminophosphines,[5] no such regioselectivity was achieved in this reaction (run 5, Table 3).

Experimental

Reaction of 1,3-Butadiene with Carbonyl Compounds. Typical Procedure: To a mixture of $Ni(acac)_2$ (5.0 mmol) and $P(O\text{-}o\text{-}Me\text{-}C_6H_4)_3$ (5.0 mmol) in 65 ml (*ca.* 0.8 mol) of 1,3-butadiene was added a hexane solution of $AlEt_3$ (25 mmol) at -10 °C and subsequently 0.2 mol of a carbonyl compound. After being heated at 70 °C for 10 h, the catalyst was deactivated with a small portion of methanol and the whole reaction mixture was fractionally distilled. The dimer fraction (bp 50—65 °C/30 Torr) consists of 4-vinylcyclohexene, 1,5-cyclooctadiene and 1,3,6-octatriene (VPC, capillary column, PEG 2000, 45 m×0.2 mm). The main fraction consists of **1a**—**c** and **2**. The analytical samples were obtained by preparative VPC (PEG 4000 on Chromosorb W, 3 m×2 cm).

Hydrogenation of (4Z,8E,11E)-2-Methyl-4,8,11,13-tetradecatetraen-2-ol. Catalytic hydrogenation (Pd on charcoal, 10 kg/cm², 25 °C in AcOEt) of **2** gave 2-methyl-2-tetradecanol, *m/e* 228 (2%, M^+), 210 (98%, M^+-H_2O), which was identical with an authentic sample prepared by the reaction of $n\text{-}C_{12}H_{25}MgBr$ with Me_2CO in IR and VPC (capillary column, PEG 2000, 45 m×0.2 mm).

Reaction of Isoprene with Acetone. General Procedure: To a solution of bis(cyclooctadieneyl)nickel(0) (1 mmol) and ligand (1 mmol) in 20 ml (*ca.* 0.2 mol) of isoprene was added 4 ml (*ca.* 0.08 mol) of acetone at 0 °C. The mixture was stirred at 80 °C for 10 h. After deactivation of the catalyst with methanol, the reaction products were distilled to give isoprene dimers, a mixture of C_{13} alcohols and the higher products.[4] Isoprene dimer fraction for every case consisted of dipentene, 1,5-dimethyl-5-vinyl-1-cyclohexene and 1,5- and 1,6-dimethyl-1,5-cyclooctadiene. Preparative VPC (PEG 4000 on 60—80 Chromosorb W, 3 m×2 cm) was used to separate the mixture of **1d** and **1e**.

(Z)-2,5,9-Trimethyl-4,8-decadien-2-ol (Dimethylnerylcarbinol) (3). Partial hydrogenation of 150 mg of **1d** was carried out (10 wt.% of PtO_2, 755 mmHg, 21 °C) to give **3** as an oil, bp 85 °C/5 Torr: IR (neat) cm^{-1}; 3490 and 1145 (alcohol), 842 (*cis*-C=CH-); *m/e* 196 (2%, M^+), 178 (95%, M^+-H_2O); NMR (CCl_4) δ, 1.18 (6H, s), 1.62—1.79 (6H, s), 2.19 (2H, d, J=7.0 Hz), 2.75—2.82 (4H, m), 3.45 (1H, s), 5.28 (1H, t, J=8.0 Hz) and 5.95—6.05 (1H, m). These data and the retention time of VPC (capillary column) were identical with those of the authentic sample prepared by treating (*Z*)-4,8-dimethyl-3,7-nonadienoic acid with an excess of MeMgI.

The author wishes to express his sincere thanks to Professor S. Otsuka, Osaka University, for his valuable suggestions and discussions. Thanks are also due to Mr. T. Yamamoto and Mr. K. Ueda for technical assistance.

References

1) For part III see: S. Akutagawa and S. Otsuka, *J. Am. Chem. Soc.*, in press.

2) For reviews see: a) R. Baker, *Chem. Rev.*, **73**, 487 (1973); b) G. Wilke and P. W. Jolly, "Organic Chemistry of Nickel," Vol. 2, Academic Press, New York, N. Y. (1975).

3) a) P. Haynes, *Tetrahedron Lett.*, **1970**, 3687; b) R. M. Manyik, W. E. Walker, K. E. Atkins, and E. S. Hammack, *ibid.*, **1970**, 3813; c) K. Ohno, T. Mitsuyasu, and J. Tsuji, *ibid.*, **1971**, 67; d) K. Ohno, T. Mitsuyasu, and J. Tsuji, *Tetrahedron*, **28**, 3705 (1972).

4) Full analysis of the higher products has not been carried out. However, alcohols and no hydrocarbon were detected by TLC and IR spectroscopy.

5) S. Akutagawa, T. Taketomi, and S. Otsuka, *Chem. Lett.*, **1976**, 485.

6) R. Baker, B. N. Blackett, R. C. Cookson, R. C. Cross, and D. O. Madden, *J. Chem. Soc., Chem. Commun.*, **1972**, 343.

Synthesis of 3′-Deoxykanamycin B (Tobramycin)[1]

Yasushi TAKAGI, Toshiaki MIYAKE,* Tsutomu TSUCHIYA, Sumio UMEZAWA, and Hamao UMEZAWA

Institute of Bioorganic Chemistry, 1614 Ida, Nakahara-ku, Kawasaki 211
**Department of Applied Chemistry, Faculty of Engineering, Keio University, Hiyoshi, Kohoku-ku, Yokohama 223*

(Received July 20, 1976)

3′-Deoxykanamycin B (tobramycin) was prepared from kanamycin B. 3′,4′:4″,6″-Di-*O*-cyclohexylidene derivative (**2**) of penta-*N*-ethoxycarbonylkanamycin B was 2″-*O*-benzoylated and the 3′,4′-*O*-cyclohexylidene group was selectively and quantitatively removed by treatment with 1 mol equivalent of water in *N*,*N*-dimethylformamide (DMF) to give the de-3′,4′-*O*-cyclohexylidene derivative (**4**). Regioselective tosylation in pyridine at −20 °C gave the 3′-*O*-tosyl derivative (**5**) in 70% yield. Despite the 1,3-diaxial interaction in the transition state, replacement of the tosyl group with iodide was successfully performed in high yield with NaI in DMF. Hydrogenolysis of the iodo derivative (**6**) and subsequent removal of the protecting groups gave 3′-deoxykanamycin B (**10**) in ≈25% overall yield from kanamycin B. Confirmation of the 3′-deoxy group was performed by measurement of $\Delta[M]_{TACu}$ of 3′-deoxyneamine which was obtained from **10** by hydrolysis.

In recent papers[2-7] we synthesized a number of deoxy derivatives of aminoglycoside antibiotics and were able to establish the importance of having a 3,4-dideoxy or a 3-deoxy aminohexose moiety at the C-4 of 2-deoxystreptamine portion of aminoglycoside antibiotics to overcome inactivation by phosphorylating enzymes present in resistant bacteria. The present paper lies on the same line and describes the synthesis of 3′-deoxykanamycin B (tobramycin[8]) starting from kanamycin B.

Penta-*N*-ethoxycarbonylkanamycin B[2] (**1**) was treated with 1,1-dimethoxycyclohexane in *N*,*N*-dimethylformamide (DMF) in the presence of *p*-toluenesulfonic acid to give 3′,4′:4″,6″-di-*O*-cyclohexylidene derivative (**2**). Benzoylation of **2** gave 2″-*O*-benzoyl derivative (**3**). Selective removal of the 3′,4′-*O*-cyclohexylidene group of **3** was first effected[1] by hydrolysis in methanol in the presence of catalytic amount of *p*-toluenesulfonic acid (25 °C for 24 h). In this case, a mixture of **3**, 4″,6″-*O*-cyclohexylidene (**4**), and decyclohexylidenated derivatives was obtained from which **4** was isolated in a yield of 70—80%. Further experiment showed that when a solution of **3** in DMF was treated with 1 mol equivalent of water in the presence of *p*-toluenesulfonic acid, the 3′,4′-*O*-cyclohexylidene group was selectively removed to give **4** in a yield of 96% without purification by column chromatography. Evidence for the removal of the 3′,4′-*O*-cyclohexylidene group was the fact that **4** was led to 3′-deoxykanamycin B at the end of this synthesis.

Regioselective 3′-*O*-tosylation of **4** was successfully carried out by treating **4** in cold pyridine (−20 °C) with *p*-toluenesulfonyl chloride for 9 days to give the 3′-*O*-tosyl derivative (**5**) in 70% yield.

Replacement of the tosyloxy group with iodide was carried out with 50% sodium iodide in DMF to give the 3′-iodo derivative (**6**) in 91% yield although the configuration at C-3 remains unconfirmed. Generally, the 3-sulfonyloxy group in an α-D-glucopyranoside is known to be resistant to displacement by a nucleophile owing to 1,3-diaxial type interaction[9,10] occured between axial 1-*O*-aglycon group and the nucleophile attacking the C-3 in the transition state. The successful iodination may be due to the neighboring group participation[11] of the 2-acylamino group.

The iodo derivative (**6**) was hydrogenated with Raney nickel to give 3′-deoxy derivative (**7**) quantitatively. Hydrolysis of **7** with barium hydroxide removed its benzoyl and ethoxycarbonyl groups to give 4″,6″-*O*-cyclohexylidene-3′-deoxy derivative (**8**, major) and an unidentified compound (**9**, minor) which is probably a ureido-type compound[12] formed between N-1 and N-3 of 2-deoxystreptamine moiety judging from the mobility in electrophoresis. Finally, treatment of **8** with 50% acetic acid removed the cyclohexylidene group to afford 3′-deoxykanamycin B (**10**).

TABLE 1. THE $\Delta[M]_{TACu}$ VALUES MEASURED AT 20° C

	$\Delta[M]_{TACu}$
Paromamine	−203°[14]
3′-Deoxyparomamine[15]	+988°
Neamine	−183°
3′-*O*-Methylneamine	+730°[4b]
4′-*O*-Methylneamine	−200°[4b]
3′-Deoxyneamine[8] (**11**)	+648°

In order to confirm the structure of **10**,**10** was partially hydrolyzed with 6 M hydrochloric acid. Major components of the hydrolyzate were found to be 3′-deoxyneamine (**11**) and 3-amino-3-deoxy-D-glucose, the latter being identified, on paper chromatogram, by comparison of the R_f value and coloration with those of authentic sample. The structure of **11** was proved on the basis† of $\Delta[M]_{TACu}$[13] values (Table 1). TACu can form complex with vicinal amino and hydroxyl groups when they have ≈60° dihedral angle, showing approximately $\Delta[M]$ ±900°, the sign being decided depending on counterclockwise and clockwise rotation (measured from the front to the rear) in the Newman projection of

† Regarding the $\Delta[M]_{TACu}$ values of 3′-deoxykanamycin B (**10**) and structurally related compounds, we previously reported in a short communication,[1] and the results supported the structure of **10**. The $\Delta[M]_{TACu}$ studies on **11** and related compounds described here were performed in order to confirm the previous conclusion.

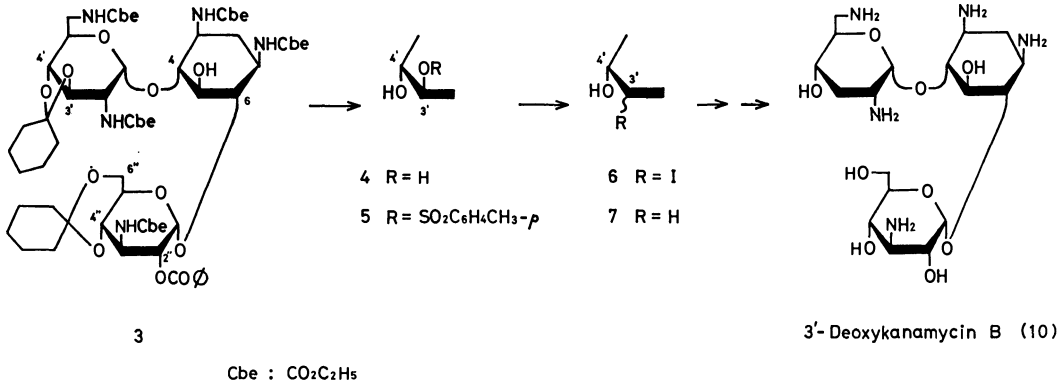

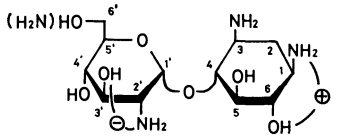

Fig. 1. The complex-forming sites and the signs for contribution to $\Delta[M]_{TACu}$ in paromamine and neamine.

$-(NH_2)CH-CH(OH)-$. TACu can not form complex with two vicinal hydroxyl groups, and, with 6-amino and 4-hydroxyl groups in a glycopyranoside structure, only small contribution in magnitude was observed.[13] As depicted in Fig. 1, paromamine or neamine can form complexes in two sites, but the two contributions are almost cancelled owing to the opposite sign of the values. In the cases of 3'-deoxyparomamine, 3'-*O*-methylneamine and 3'-deoxyneamine (**11**), the complex can be formed only at 1-NH_2 and 6-OH of the 2-deoxystreptamine portion. The value of **11** ($\Delta[M]_{TACu}$ +648°), therefore, substantiated its structure.

Antibacterial spectrum was reported[1] already with other structurally related antibiotics.

Experimental

NMR spectra were recorded at 60 and 100 MHz with Varian A-60D and HA-100 spectrometers, respectively. Infrared spectra were determined in KBr discs with Hitachi 285 grating infrared spectrophotometer. Thin-layer chromatography (TLC) was carried out on Wakogel B-5 with sulfuric acid spray for detection. For column chromatography, silica gel (Wakogel C-200) was used unless otherwise stated. Paper-chromatography (PPC) was carried out on Toyo Roshi No. 50 with 1-butanol–pyridine–water–acetic acid (6:4:3:1, Solvent A) as the developer, descending for 18 h, and colorized with 0.25% ninhydrin in pyridine. Paper electrophoresis was conducted in a Savant LT48A apparatus (Savant Instrument, Inc.) on Toyo Roshi No. 51 in formic acid–acetic acid–water (1:3:36) at 3500 V for 15 min, and after drying the paper in a hood, it was colorized as stated above.

3',4':4'',6''-Di-O-cyclohexylidene-penta-N-ethoxycarbonylkanamycin B (2). To a hot solution (≈50 °C) of **1** (522 mg) in dry DMF (2.5 ml), 1,1-dimethoxycyclohexane (0.5 ml) and anhydrous *p*-toluenesulfonic acid (26 mg) were added and the solution was heated at the temperature under reduced pressure (20—30 Torr) to remove the generated methanol by coevaporation with the solvent. After 1 h, 1,1-dimethoxycyclohexane (0.5 ml) was added and the reaction was continued for further 1 h. TLC (chloroform–ethanol 12:1) then showed two components (monocyclohexylidene derivative, R_f 0.15, minor; and **2**, R_f 0.33, major). Further reaction with additions of the above reagent did not change the ratio of the products. The solution was poured into a mixture of benzene and aqueous sodium hydrogencarbonate and the mixture was stirred vigorously for a while. After centrifugation, the powder appeared between the two layers was collected, washed with water, and dried to give a monocyclohexylidene derivative (27 mg). The benzene layer was concentrated to give a solid, which was dissolved in methanol and **2** was precipitated by addition of water, 506 mg (82%), $[\alpha]_D^{20}$ +99° (*c* 1, methanol).

Found: C, 53.50; H, 7.32; N, 6.77%. Calcd for $C_{45}H_{73}N_5O_{20}$: C, 53.83; H, 7.33; N, 6.98%.

2''-O-Benzoyl-3',4':4'',6''-di-O-cyclohexylidene-penta-N-ethoxycarbonylkanamycin B (3). A solution of **2** (4.95 g) and benzoyl chloride (3.07 g) in pyridine (60 ml) was heated at 50 °C for 1.5 h. After addition of water (0.5 g), the solution was concentrated to a half volume, and poured into aqueous sodium hydrogencarbonate. The resulting precipitate was washed with water and dried to give a solid of **3** (5.44 g, 99%), mp 152—154 °C, $[\alpha]_D^{20}$ +99° (*c* 1.4, methanol).

Found: C, 56.46; H, 6.76; N, 6.07%. Calcd for $C_{52}H_{77}N_5O_{21}$: C, 56.36; H, 7.00; N, 6.32%.

2''-O-Benzoyl-4'',6''-O-cyclohexylidene-penta-N-ethoxycarbonylkanamycin B (4). A solution of **3** (55.1 mg) in DMF (1.1 ml) containing water (0.9 mg, 1 mol equivalent for **3**) and anhydrous *p*-toluenesulfonic acid (1.9 mg, 0.2 mol equivalent for **3**) was kept at room temperature for 43 h. The solution showed on TLC with chloroform–ethanol 12:1 only one major product (R_f 0.26) (*cf.* **3**, R_f 0.45; decyclohexylidene derivative, R_f 0). After addition of 2.5% aqueous sodium hydrogencarbonate (0.1 ml) with stirring, the solution was concentrated *in vacuo* to give a solid, which was thoroughly washed with water to give a solid of **4** (49.0 mg, 96%), $[\alpha]_D^{20}$ +147° (*c* 0.6, DMF).

Found: C, 53.49; H, 6.41; N, 6.69%. Calcd for $C_{46}H_{69}N_5O_{21}$: C, 53.74; H, 6.76; N, 6.81%.

2''-O-Benzoyl-4'',6''-O-cyclohexylidene-penta-N-ethoxycarbonyl-3'-O-tosylkanamycin B (5). To a solution of **4** (106.4 mg) in dry pyridine (2 ml) at −20 °C, *p*-toluenesulfonyl chloride (99.6 mg, 5 mol equivalents for **4**) was added and the solution was kept at −20 °C for 9 days. The solution showed, on TLC (chloroform–2-propanol 10:1), three spots of R_f 0.24 (**5**, major), 0.28 (4'-*O*-tosyl isomer, trace) and 0.3 (di-*O*-tosyl isomer, trace). After addition of water (0.08 ml) followed by standing the solution at room temperature for 1 h, the solution was concentrated *in vacuo* to a syrup, which was dissolved in chloroform. The solution was washed successively with 5% aqueous potassium hydrogensulfate, water, 5% aqueous sodium hydrogencarbonate, and water, dried over $MgSO_4$,

and concentrated. The resulting solid (113.8 mg) was triturated with acetone (2 ml×2) and the acetone-soluble material (104.2 mg) was chromatographed on a column of silica gel with chloroform–2-propanol (15: 1) to give **5** (85.6 mg, 70%) and a mixture of 4′-*O*-tosyl and 3′,4′-di-*O*-tosyl isomers (18 mg). The acetone-insoluble component was found to be 4′-*O*-tosyl isomer[16] (9.6 mg). Compound **5**, mp 149—150 °C, $[\alpha]_D^{20}$ +88° (*c* 1, methanol); IR (KBr): 1720, 1530; 1175 cm^{-1} ($\nu_s SO_2$).

Found: C, 53.90; H, 6.58; N, 5.67; S, 3.00%. Calcd for $C_{53}H_{75}N_5O_{23}S$: C, 53.84; H, 6.40; N, 5.93; S, 2.71%.

NMR ($CDCl_3$) δ: 2.42 (3H, s, CH_3 of Ts).

*2″-O-Benzoyl-4″,6″-O-cyclohexylidene-3′-deoxy-penta-N-ethoxycarbonyl-3′-iodokanamycin B (**6**).* A mixture of **5** (282 mg) and sodium iodide (3 g) in DMF (6 ml) was stirred at 100 °C for 20 h. The resulting reddish brown solution, which soon solidified on cooling, was extracted with chloroform and the chloroform solution was concentrated with aid of toluene. The solid obtained was dissolved in chloroform and the solution was washed successively with saturated aqueous sodium chloride, aqueous sodium thiosulfate, and water, dried over $MgSO_4$, and concentrated to give a brown solid (247 mg, 91%). Slight impurities were removed by chromatography on a column of silica gel with chloroform–2-propanol (14: 1) to give a solid of **6** (195 mg, 72%).

Found: C, 48.75; H, 6.09; N, 6.57; I, 11.45%. Calcd for $C_{46}H_{68}N_5O_{20}I$: C, 48.55; H, 6.02; N, 6.15; I, 11.15%.

*2″-O-Benzoyl-4″,6″-O-cyclohexylidene-3′-deoxy-penta-N-ethoxycarbonylkanamycin B (**7**).* To a solution of **6** (133 mg) in dioxane (1.3 ml), Raney nickel was added and the mixture was hydrogenated (50 p.s.i.) at room temperature for 1.5 h. After filtration, the solution was treated as above with fresh Raney nickel 3 times more in every 1.5 h intervals. Concentration of the solution gave a solid of **7** (114 mg, 96%), $[\alpha]_D^{20}$ +86° (*c* 0.76, methanol).

Found: C, 54.58; H, 6.80; N, 6.84%. Calcd for $C_{46}H_{69}N_5O_{20}$: C, 54.59; H, 6.87; N, 6.92%.

*3′-Deoxykanamycin B (**10**).* A mixture of **7** (90.6 mg) and barium hydroxide ($Ba(OH)_2 \cdot 8H_2O$, 650 mg) in decarbonated water (0.7 ml) was stirred at 100 °C for 10 h. The solution showed, on PPC, two spots of R_f 0.16 (**8**, major) and 0.22 (**9**, minor), and, on paper electrophoresis, also showed two spots (R_f of **9** is 0.79 of that of **8**). After addition of 5% aqueous sulfuric acid (2.0 ml), the mixture was stirred at 50 °C for 1.5 h. Barium sulfate precipitated was removed by filtration and it was washed with hot water thoroughly. The filtrate and washings were combined, concentrated, and, to the concentrate, acetone was added to give a pale brown solid. The crude **8** (64.3 mg) was dissolved in 50% acetic acid (0.65 ml) and the solution was heated at 80 °C for 3 h. The solution was concentrated and then concentrated with additions of water to give a pale brown solid (62 mg). The aqueous solution of the solid was subjected to column chromatography of Dowex 1X2 (OH form, 1.1 ml) resin with water and from the eluate, colorless solid (free base, 37.5 mg) was obtained. The solid was chromatographed on a column of CM-Sephadex C-25 (NH_4 form) with 0—0.15 M ammonia, the concentration being linearly increased. From the faster moving fractions, an unidentified compound (9.3 mg, a ureido-type compound?) was obtained, and from the slower moving fractions, 3′-deoxykanamycin B base (**10**) was isolated as a monohydrate, 28.5 mg (65%), $[\alpha]_D^{20}$ +129° (*c* 1, water) (lit,[8] +128°). $R_{f\ \text{kanamycin B}}$ 1.25 (PPC, by solvent A).

Found: C, 44.92; H, 8.09; N, 14.61%. Calcd for $C_{18}H_{37}N_5O_9 \cdot H_2O$: C, 44.53; H, 8.10; N, 14.43%.

NMR (D_2O) δ: 1.1—2.3 (4H m, H-2 and 3′).

*3′-Deoxyneamine (**11**).* Compound **10** (100 mg as base) was dissolved in 6 M hydrochloric acid (2 ml) and the solution was heated at 100 °C for 2 h. The solution showed, on PPC, five spots of R_f 0.3 (3-amino-3-deoxy-D-glucose), 0.16 (trace, 2,6-diamino-2,3,6-trideoxy-D-ribohexose), 0.12 (trace, 2-deoxystreptamine), 0.06 (**11**), and 0.03 (trace, **10**). After concentration, the resulting syrup was chromatographed on a column of Dowex 1X2 (OH form) resin with water. The free sugars were retained in the column. The eluate was concentrated and the resulting syrup was chromatographed on a column of CM-Sephadex C-25 (NH_4 form) with 0—0.15 M ammonia, the concentration being linearly increased. 2-Deoxystreptamine (0.5 mg), **10** (6.1 mg) and **11** (54 mg, 78%) were eluted in the order of mobility. 3′-Deoxyneamine (**11**), $[\alpha]_D^{20}$ +122° (*c* 0.3, water); $[\alpha]_{436}^{20}$ +230° (*c* 0.3, water), $[\alpha]_{436}^{20}$ +430° (*c* 0.3, TACu[13]); $\Delta[M]_{TACu}$ is +648°.

Found: C, 44.39; H, 8.30; N, 17.26%. Calcd for $C_{12}H_{26}N_4O_5 \cdot H_2O$: C, 44.43; H, 8.70; N, 17.27%.

References

1) Short communication: Y. Takagi, T. Miyake, T. Tsuchiya, S. Umezawa, and H. Umezawa, *J. Antibiot.*, **26**, 403 (1973).

2) H. Umezawa, S. Umezawa, T. Tsuchiya, and Y. Okazaki, *J. Antibiot.*, **24**, 485 (1971); S. Umezawa, H. Umezawa, Y. Okazaki, and T. Tsuchiya, *Bull. Chem. Soc. Jpn.*, **45**, 3624 (1972).

3) S. Umezawa, T. Tsuchiya, R. Muto, Y. Nishimura, and H. Umezawa, *J. Antibiot.*, **24**, 274 (1971); S. Umezawa, Y. Nishimura, H. Hineno, K. Watanabe, S. Koike, T. Tsuchiya, and H. Umezawa, *Bull. Chem. Soc. Jpn.*, **45**, 2847 (1972).

4) a) S. Umezawa, T. Tsuchiya, T. Jikihara, and H. Umezawa, *J. Antibiot.*, **24**, 711 (1971). b) T. Jikihara, T. Tsuchiya, S. Umezawa, and H. Umezawa, *Bull. Chem. Soc. Jpn.*, **46**, 3507 (1973).

5) S. Umezawa, T. Tsuchiya, D. Ikeda, and H. Umezawa, *J. Antibiot.*, **25**, 613 (1972); D. Ikeda, T. Suzuki, T. Tsuchiya, S. Umezawa, and H. Umezawa, *Bull. Chem. Soc. Jpn.*, **46**, 3210 (1973).

6) H. Sano, T. Tsuchiya, S. Kobayashi, M. Hamada, S. Umezawa, and H. Umezawa, *J. Antibiot.*, **29**, 978 (1976).

7) On the survey of the inactivation mechanism of resistant bacteria and of the modification of the antibiotics to active derivatives, see a) H. Umezawa, *Adv. Carbohydr. Chem. Biochem.*, **30**, 183 (1974); b) S. Umezawa, *ibid.*, **30**, 111 (1974).

8) K. F. Koch and J. A. Rhoades, *Antimicrob. Agents Chemother.*, **1970**, 309 (1970).

9) N. A. Hughes and P. R. H. Speakman, *J. Chem. Soc.*, **1965**, 2236.

10) A. C. Richardson, *Carbohydr. Res.*, **10**, 395 (1969).

11) A. C. Richardson, *J. Chem. Soc.*, **1964**, 5364.

12) Unpublished data.

13) S. Umezawa, T. Tsuchiya, and K. Tatsuta, *Bull. Chem. Soc. Jpn.*, **39**, 1235 (1966).

14) S. Umezawa, T. Miyazawa, and T. Tsuchiya, *J. Antibiot.*, **25**, 530 (1972).

15) T. Oda, T. Mori, and Y. Kyotani, *J. Antibiot.*, **24**, 503 (1971).

16) T. Miyake, T. Tsuchiya, S. Umezawa, and H. Umezawa, The details will be reported in near future.

Coenzyme Models. VII. Micellar Catalysis of Acid-Catalyzed Hydration of 1-Dodecyl-1,4-Dihydronicotinamide*

Seiji SHINKAI, Reiko ANDO, and Toyoki KUNITAKE

Department of Organic Synthesis, Faculty of Engineering, Kyushu University, Fukuoka 812

(Received July 26, 1976)

The acid-catalyzed hydration reaction of 1-dodecyl-1,4-dihydronicotinamide was examined in cationic(CTAB) and anionic (SDS) micelles. The H_3O^+-catalysis(k_H) was negligibly small in the presence of the CTAB micelle and 225—521 M^{-1} s^{-1} in the presence of the SDS micelle, the difference being about 10^7-fold. The catalysis by carboxylic acids (k_{HA}) was considerably suppressed in the CTAB micelle, but was promoted in the SDS micelle, suggesting the development of a cationic charge on a nitrogen atom of dihydropyridine at the rate-determining step. Brönsted plots for log k_{HA} in the CTAB and SDS micelles *vs.* pK_a of carboxylic acids gave straight lines with the slope of −0.8, the line for SDS being higher by two orders of magnitude than that for CTAB. These results indicate that a cationic charge (*e.g.*, the lysine residue of alcohol dehydrogenase located very close to the bound NADH) may protect the NADH from hydration decay.

It has been established that NADH (reduced form of nicotinamide adenine dinucleotide) and its model compounds, 1,4-dihydronicotinamide derivatives rapidly decompose in aqueous acidic media.[1] The decomposition causes shifts of the characteristic UV absorption band of dihydronicotinamides in the 340—360 nm region downward to around 290 nm with isosbestic points.[1] The 290 nm-absorbing compound was later confirmed to be a 6-hydroxy-1,4,5,6-tetrahydronicotinamide by X-ray crystallography.[2] The following reaction scheme (Eq. 1 or 2) was thus suggested by Johnston and others,[1] in which the protonation of dihydronicotinamide is involved in the rate-determining step.

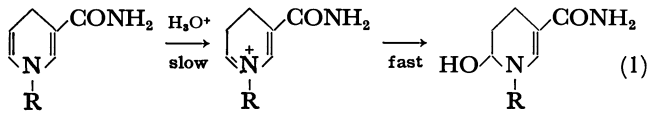

(1)

or

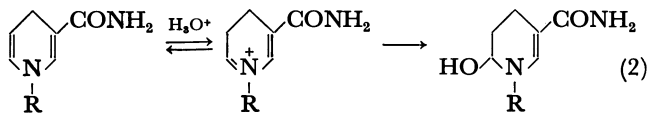

(2)

The biological importance of this reaction was pointed out by Meinhart and co-workers,[3] since NADH bound to glyceraldehyde-3-phosphate dehydrogenase is characterized by a change in the UV spectrum similar to that of the acid-catalyzed hydration of dihydronicotinamides.

In the previous paper,[4] we demonstrated a striking effect of micelles on the acid-catalyzed hydration of 1,4-dihydronicotinamide derivatives. The hydration rates were accelerated by an anionic micelle of sodium dodecylsulfate (SDS), in accord with the fact that the anionic environment would result in the acceleration of the protonation step in the hydration reaction as seen in acetal hydrolyses.[5,6] On the contrary, a cationic micelle of cetyltrimethylammonium bromide (CTAB) pronouncedly depressed the hydration rate of 1-dodecyl-1,4-dihydronicotinamide (NDNH; R=$CH_3(CH_2)_{11}$–); the rate being 414-fold slower than that in SDS. To our knowledge this was the first example that the reaction involving NADH analogs is subject to the microenvironmental effects.

* Contribution No. 394 from this Department.

In this paper, we wish to report further investigations on the micellar catalysis of the hydration reaction, which was conducted in order to evaluate the respective rate constants for three catalytic species, water, oxonium ion, and buffer acid in the presence of micelles. NDNH was employed as substrate, since it undergoes the largest micellar effect in the hydration reaction.[4] Surfactants chosen were CTAB and SDS.

Surfactants: $CH_3(CH_2)_{11}SO_4Na$ (SDS)

$CH_3(CH_2)_{15}N^+(CH_3)_3Br^-$ (CTAB)

Experimental

Materials. Surfactants were products of Wako Pure Chemical Ind. SDS (biochemical use) was used without further purification. CTAB was recrystallized from ethanol before use. Preparation of NDNH was reported previously.[4]

Kinetics. The kinetic measurements were carried out at 30±0.1 °C at a calculated ionic strength (with KCl) using a Hitachi 124 spectrophotometer. The reaction was initiated by mixing NDNH (alcohol solution) with a buffered, aqueous solution of surfactant, and the rate of hydration was estimated by monitoring the disappearance of absorbance at 357 nm, which is characteristic of 1,4-dihydronicotinamides. The pseudo-first-order rate constants (k_{obsd}) thus obtained can be satisfactorily described by Eq. 3, in which k_0 is the reaction rate with water, and k_H and k_{HA} are the catalytic constants for oxonium ion and buffer acid, respectively.

$$k_{obsd} = k_0 + k_H[H_3O^+] + k_{HA}[HA] \quad (3)$$

One can separately determine $k_0+k_H[H_3O^+]$ and k_{HA} from the slope and the intercept of k_{obsd} *vs.* [HA] plots.[1] Although it was desirable to lower the ionic strength as much as possible in order to obtain large micellar effects, the data measured in the absence of added salts did not give linear plots: the lower the buffer concentration, the faster is the rate of hydration. When ionic strength (defined here as $[A^-]$+[KCl added], the concentration of surfactants was always held constant above their CMC) was maintained constant, the plots showed excellent linear relationships ($r>0.99$). Thus, the two kinetic term could be determined by the least-squares method.

Results

Hydration Reaction in the Presence of the CTAB Micelle. In Fig. 1, pseudo-first-order rate constants (k_{obsd}) for the

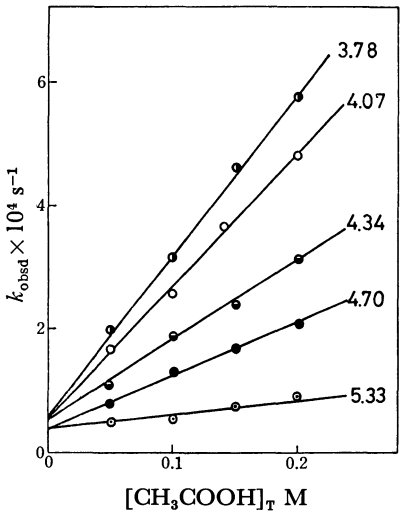

Fig. 1. Pseudo-first-order rate constants for hydration of NDNH in the presence of 1.0×10^{-3} M CTAB plotted as a function of the concentration of acetic acid. 30 °C, μ=0.2, 8.7 vol% ethanol. Numbers in Figure denote pH values.

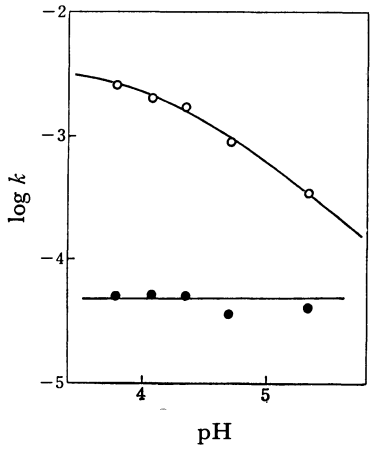

Fig. 2. pH *vs.* log $k_{HA} \cdot [CH_3COOH]_T$ (○) and log $(k_0 + k_H[H_3O^+])$ (●) for the CTAB catalysis.

hydration of NDNH in the presence of the CTAB micelle were plotted against the total concentration of acetic acid, $[CH_3COOH]_T = [CH_3COOH] + [CH_3COO^-]$. The concentration of surfactant ($[CTAB] = 1.0 \times 10^{-3}$ M) and ionic strength (μ=0.2) were kept constant. The slope, which corresponds to the buffer-catalyzed term (Eq. 3), increased with lowering pH. In contrast, the intercepts which are equal to the sum of k_0 and $k_H[H_3O^+]$ were found to be essentially independent on pH. Figure 2 gives the plots of logarithmic rate constants against pH. The apparent, buffer-catalyzed term (k_{HA}') showed a kinetic pK_a at around 4.60, which is in accord with the potentiometric pK_a value (4.62) of acetic acid. Thus, the true second-order rate constant (k_{HA}) for the undissociated species of acetic acid can be related to k_{HA}' by Eq. 4,

$$k'_{HA} = \frac{a_H}{K_a + a_H} k_{HA} \qquad (4)$$

where K_a denotes the acid dissociation constant of acetic acid. The solid curve in Fig. 2 was depicted from Eq. 4 by using pK_a=4.62 and $k_{HA} = 3.81 \times 10^{-3}\ M^{-1}\ s^{-1}$.

Since the $k_0 + k_H[H_3O^+]$ term is not dependent on pH, the k_H term must be negligibly small in the presence of the CTAB micelle, and the k_0 term is equal to $5.0 \times 10^{-5}\ s^{-1}$ under the given condition.

Hydration Reaction in the Presence of the SDS Micelle. It has been noted that the hydration rate of 1,4-dihydropyridine derivatives is conspicuously accelerated in the presence of the SDS micelle at extremely low ionic strength.[4] However, this rate acceleration by the SDS micelle is suppressed at higher ionic strengths (Fig. 3), and the hydration rate of NDNH in the SDS micelle at $([CH_3COOK] + [KCl]) > 0.01$ is not much different from that of 1-propyl-1,4-dihydronicotinamide in a non-micellar system (*vide post*).

Buffer dilution and pH change were carried out at $([CH_3COOK] + [KCl]) = 0.03$. The pH of the reaction mixture was confirmed not to vary from pH measurements before and after the reaction. At lower ionic strengths, it was extremely difficult to maintain the pH

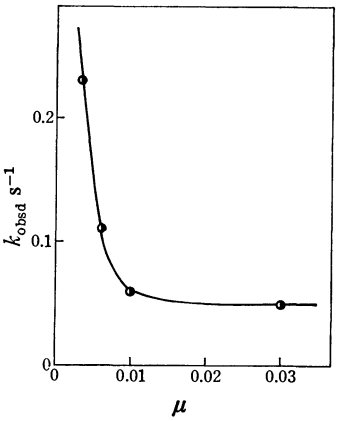

Fig. 3. Pseudo-first-order rate constants for hydration of NDNH in the presence of 5.0×10^{-2} M SDS plotted as a function of ionic strength. 30 °C, 8.7 vol% ethanol, pH 3.80.

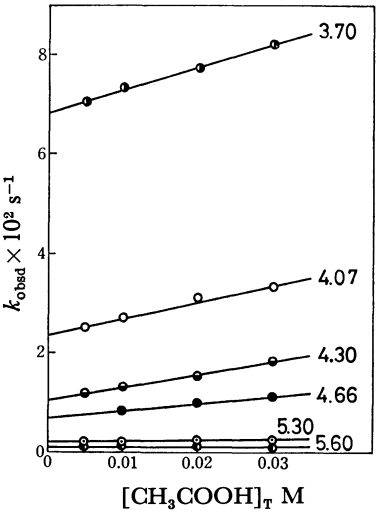

Fig. 4. Pseudo-first-order rate constants for hydration of NDNH in the presence of 5.0×10^{-2} M SDS plotted as a function of the concentration of acetic acid. 30 °C, μ=0.03, 8.7 vol% ethanol. Numbers in figure denote pH values.

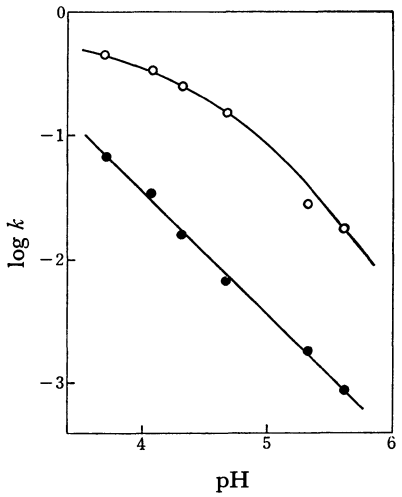

Fig. 5. pH *vs.* log $k_{HA}\cdot[CH_3COOH]_T$ (○) and log $(k_0+k_H[H_3O^+])$ (●) for the SDS catalysis.

of the reaction system constant. The results are illustrated in Fig. 4. Excellent linear correlations are demonstrated between k_{obsd} and $[HA]_T$ (correlation coefficient better than 0.99 in all cases). The hydration reaction in the presence of the SDS micelle is catalyzed by both H_3O^+ and HA, since both of the slope and the intercept increase by lowering pH of the reaction system in Fig. 4. The k_{HA}'-pH plots of Fig. 5 showed a kinetic pK_a at 4.68, which again coincides with the potentiometric pK_a of acetic acid (4.62). The theoretical curve in Fig. 5 was obtained from Eq. 4 for $k_{HA}=0.581$ M^{-1} s^{-1} and $pK_a=4.68$, which produced the best fit to the experimental plots.

Figure 5 also gives log $(k_0+k_H[H_3O^+])$ plotted against pH. The linear relation of slope of −1.0 indicates that the H_3O^+-catalysis is predominant, and the following rate constants are obtained: $k_0\approx 0$ s^{-1} (negligibly small compared with the $k_H[H_3O^+]$ term) and $k_H=341$ M^{-1} s^{-1}.

The rate constants determined by the acetate-buffer dilution and by the pH change are summarized in Table 1.

Hydration Catalyzed by Miscellaneous Carboxylic Acids. Five different carboxylic acids were examined as buffer in addition to acetic acid, *i.e.* α-chloroacetic acid, malonic acid, decanoic acid, hippuric acid, and isobutyric acid. Buffer dilutions were carried out at one pH at the constant surfactant concentration. From the slope and the intercept were determined the rate constants for each carboxylic acid, and the k_{HA} values were evaluated by using the potentiometric pK_a values. The results are recorded in Table 2. It is seen from Table 2 that the k_H terms are again suppressed by the CTAB micelle. It is also worth mentioning that the k_{HA} values in the presence of the CTAB micelle are decreased by more than 100 times as compared with those in the presence of the SDS micelle.

Table 1. Rate constants for the hydration reaction of NDNH catalyzed by acetic acid at 30 °C

Micelle	k_0 s^{-1}	k_H $M^{-1}s^{-1}$	k_{HA} $M^{-1}s^{-1}$
None[a)]	d)	260	0.15
CTAB[b)]	5×10^{-5}	$\sim0(<10^{-4})$	0.00381
SDS[c)]	d)	341	0.581

a) Determined for 1-propyl-1,4-dihydronicotinamide; 25 °C, $\mu=0.48$.[1)] b) $[CTAB]=1.0\times10^{-3}$ M, $\mu=0.2$ (KCl), 8.7 vol% ethanol. c) $[SDS]=5.0\times10^{-3}$ M, $\mu=0.03$ (KCl), 8.7 vol% ethanol. d) Too small to determine as compared with other terms.

Discussion

Since NDNH is not soluble by itself in aqueous solutions, one may assume that it is solubilized in the micellar phase. This assumption is very important in discussing the micellar catalysis, for partitioning of the substrate between the micellar phase and the bulk phase frequently gives rise to complications of the micellar systems.

Although our previous study showed that an anionic micelle accelerated the hydration reaction and that an cationic micelle decelerated,[4)] the contribution of each catalytic species, water, oxonium ion, and buffer acid, remained ambiguous. The k_0 value of 1-propyl-1,4-dihydronicotinamide in a non-micellar system was previously evaluated to be 2.6×10^{-5} s^{-1} (25 °C)** by Johnston and co-workers.[1)] This value is very close to

Table 2. Rate constants for the hydration reaction of NDNH catalyzed by various carboxylic acids at 30 °C

Carboxylic acid	pK_a[a)]	Rate Constant in SDS k_H $M^{-1}s^{-1}$	SDS k_{HA} $M^{-1}s^{-1}$	CTAB $k_0\times10^5$ s^{-1}	CTAB k_H $M^{-1}s^{-1}$	CTAB k_{HA} $M^{-1}s^{-1}$
1. $ClCH_2COOH$	2.84	521	12.3	5	~0	0.0810
2. $C_6H_5CONHCH_2COOH$	3.10	494	7.67			
3. CH_3COOH	4.62	341	0.581	5	~0	0.00381
4. $CH_3(CH_2)_8COOH$	4.82	304	0.905			
5. *iso*-C_3H_7COOH	4.86	311	0.641	5	~0	0.00203
6. $^-OOCCH_2COOH$	5.65	225	0.0368	3	~0	0.00085

a) Determined potentiometrically in the absence of micelles at 30 °C.

** Johnston *et al.*[1)] reported $k_{H_2O}=4.7\times10^{-7}$ M^{-1} s^{-1}. This value was multiplied by 55 to give $k_0(s^{-1})$.

$k_0=5.0\times10^{-5}$ s^{-1} obtained for NDNH in the presence of the CTAB micelle. Therefore, the k_0 term is little affected by the micelle. On the other hand, the results shown in Table 1 clearly demonstrate that rate suppression observed in the CTAB micelle is largely derived from the lack of the H_3O^+-catalysis. Apparently, oxonium ion cannnot catalyze the hydration reaction of 1,4-dihydronicotinamide if it is trapped in the Stern layer of the CTAB micelle ($k_H\approx0$). It has been noticed that cationic micelles have inhibitory effect upon the acid-catalyzed reactions. Typical examples are seen in the hydrolyses of orthoesters and acetals which involve proton transfer from the acid to the substrate.[7]

Table 1 shows that the k_{HA} value for acetic acid is *ca.* 40-fold smaller in the CTAB micelle than in the nonmicellar system. This term is associated with the catalysis by neutral species (undissociated acetic acid), so that it is unlikely that this rate suppression is related to the proximity effect of the micelle. Instead, this would reflect the fact that the formation of such a positively charged intermediate be destabilized by the cationic environment of the CTAB micelle.

An alternate reaction mechanism for the k_{HA} term involves a concerted catalysis.[1] Carboxylic acids can donate both a proton and an anion simultaneously as shown in Eq. 5. This possibility cannot be ruled out kinetically because it is equivalent to Eqs. 1 and 2.

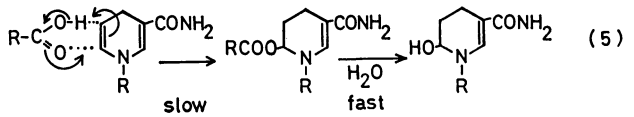

(5)

As can be seen from Eq. 5, the concerted mechanism produces a less charged intermediate. The pronounced lowering of the k_{HA} value observed in the presence of the CTAB micelle is incompatible with this supposition. Therefore, the concerted reaction is unlikely under the present condition. Johnston *et al.*[1] and Kim and Chaykin[2] are similarly against the concerted mechanism.

The SDS micelle enhanced both the k_H and k_{HA} values. Apparently, the magnitude of the rate enhancements is not very large because of the use of high ionic strength which suppresses the reaction. The high ionic strength was necessitated due to the high buffer concentration employed. As shown in Fig. 3, the k_{obsd} value rapidly increased with decreasing ionic strength. This rate variation is probably related to the change in the k_H term, for oxonium ion would be adsorbed on the SDS micelle in competition with added salts. Unfortunately, however, the k_H value at the very low ionic strength could not be evaluated (see Experimental section).

Figure 6 gives Brönsted plots for the k_{HA} term in micellar systems. Both plots gave approximately linear relations with the slope of -0.8, and the difference in the intercept between CTAB and SDS was about two orders of magnitude. The SDS micelle provides much more favorable environments for the carboxylic acid-catalyzed hydration reaction than the CTAB micelle.

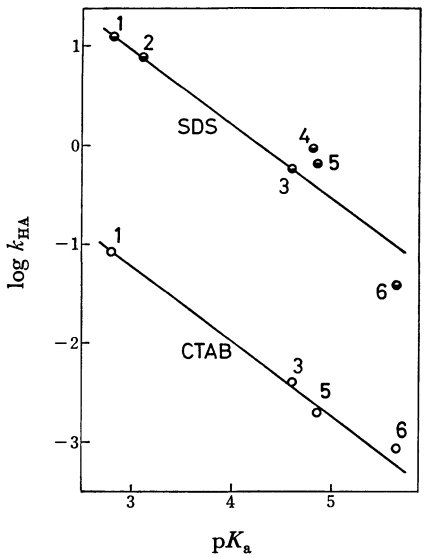

Fig. 6. Brönsted relationship. Numbers in figure correspond to carboxylic acids in Table 2.

This difference would become more conspicuous by lowering the ionic strength of the reaction system.

The plot for malonic acid (Fig. 6) was lowered by the 0.4 log unit in the relation for the SDS micelle. In contrast, the plot for malonic acid is slightly deviated to the upper part from the CTAB line, the deviation, however, being rather small. These deviations are obviously due to electrostatic repulsion and attraction, respectively.*** and would be more clearly demonstrated at the lower ionic strength.

In conclusion, the acid-catalyzed hydration reaction of 1,4-dihydronicotinamides is very sensitive to the micellar environmental effects. In particular, the k_H value in the presence of the CTAB micelle is suppressed by a factor of 10^7 as compared with the nonmicellar system. Similarly, the reactivity of NADH and its analogs must be greatly affected by the enzymatic microenvironments.

References

1) C. C. Johnston, J. L. Gardner, C. H. Suelter, and D. E. Metzler, *Biochemistry*, **2**, 689 (1963).
2) C. S. Y. Kim and S. Chaykin, *Biochemistry*, **7**, 2339 (1968).
3) J. O. Meinhart, S. Chaykin, and E. G. Krebs, *J. Biol. Chem.*, **220**, 821 (1956).
4) S. Shinkai, R. Ando, and T. Kunitake, *Bull. Chem. Soc. Jpn.*, **48**, 1914 (1975).
5) R. B. Dunlop, G. A. Ghanim, and E. H. Cordes, *J. Phys. Chem.*, **73**, 1898 (1969).
6) B. M. Dunn and T. C. Bruice, *J. Am. Chem. Soc.*, **92**, 6589 (1970).
7) E. J. Fendler and J. H. Fendler, "Advances in Physical Organic Chemistry," Vol. 8, ed. by V. Gold, Academic Press, New York, N. Y. (1970).
8) L. S. Darken, *J. Am. Chem. Soc.*, **63**, 1007 (1941).

*** $pK_{a1}=2.86$, $pK_{a2}=5.70$ at 25 °C[8]

Coenzyme Models. VIII. Reduction of the Schiff Base of Pyridoxal Analogs by 1,4-Dihydronicotinamide*

Seiji SHINKAI, Sumihiro SHIRAISHI, and Toyoki KUNITAKE

Department of Organic Synthesis, Faculty of Engineering, Kyushu University, Fukuoka, 812

(Received July 26, 1976)

Reduction of Schiff bases by 1-benzyl-1,4-dihydronicotinamide (BzlNH) was performed in refluxing methanol. Protonated imines such as *N*-(*p*-nitrobenzylidene)benzylamine hydrochloride (**1H**$^+$) and *N*-(4-nitrosalicylidene)-benzylamine hydrochloride (**1(OH)H**$^+$) were reduced to the corresponding aminomethyl derivatives. The NMR product analysis for the reaction of BzlNH and **1H**$^+$ in refluxing ethanol-*d* established that the solvent deuteron was not incorporated into the aminomethylene product. **1(OH)**, unprotonated species, was partially reducible, whereas **1** was totally unreactive. The facile reduction of **1** occurred in the presence of several amine hydrochlorides ($NEt_3 \cdot HCl$, imidazole hydrochloride, *N,N,N',N'*-tetramethylethylenediamine dihydrochloride). These results show that the *ortho* hydroxyl group of **1(OH)** facilitates imine reduction not only by polarization of the Schiff base *via* hydrogen bonding but also by proton transfer. The relative reactivity of the Schiff base to the BzlNH reduction is: **1H**$^+$, **1**$+NEt_3 \cdot HCl \geqq$**1(OH)H**$^+ >$**1(OH)**$>$**1**(unreactive) This order is similar to that found in "*trans*-Schiffization" between semicarbazide and the Schiff base of pyridoxal and its analogs, as reported by Cordes and Jencks.

The nicotinamide adenine dinucleotide and its reduced form (NAD and NADH) serve as coenzymes in a very large number of enzymatic oxidation-reduction reactions.[1] As for example, NAD-dependent dehydrogenases catalyze the stereospecific, direct transfer of a hydride ion (or its equivalent) to aldehyde substrates.[2] Steffens and Chipman[3] and Creighton *et al.*[4] proposed a kinetically detectable complex as an intermediate along the reaction path in model systems. Contrary to this proposition, Kurz and Frieden[5] concluded that the enzyme-substrate transition state is analogous to that pictured for simple S_N2 nucleophilic substitution with "hydride" ion acting as the nucleophilic agent. In any case, it is clear that substantial charge transfer from NADH to substrate occurs in the rate-determining step, and that substrates are significantly activated by electron-withdrawing substituents.

The enzymatic reduction of pyridoxal-5'-phosphate has been investigated in detail.[6,7] Recently, it was reported that the nonenzymatic reduction of pyridoxal and its analogs by 1,4-dihydropyridines did occur at ambient conditions and that the *ortho*-hydroxyl group facilitated the "hydride" acceptability of the carbonyl group.[8-10] Intrestingly, the reduction rate for the respective pyridoxal species was parallel to the rates of other reactions which were catalyzed by these pyridoxals; imine formation, general base-catalyzed *trans*-amination, *etc.*[10]

Imines show higher affinities toward the carbonyl agents than the corresponding carbonyl compounds.[11,12] A typical example would be a "*trans*-Schiffization" reaction demonstrated by Cordes and Jencks.[12] According to their detailed examination, the Schiff base is inherently more reactive than pyridoxal-5'-phosphate toward semicarbazide, and the protonated Schiff base is further activated. These results suggest that protonated imines (iminium salts) would be suitable substrates for the reduction by NADH. In fact, the enzymatic reduction of the iminium group of N^5,N^{10}-methenyl-tetrahydrofolic acid to N^5,N^{10}-methylene-tetrahydrofolic acid by NADPH,[13] and the nonenzymatic reduction of a thiazolium salt (Vitamin B_1 analogue)[14] and the iminium group of steroid derivatives to the corresponding amine[15] have been reported.

The object of the present investigation is to examine the reaction of 1-benzyl-1,4-dihydronicotinamide (BzlNH) with the Schiff base of pyridoxal analogs, *p*-nitrobenzaldehyde and 4-nitrosalicylaldehyde, and to establish the relative susceptibility of these Schiff bases toward the "hydride" reduction. In order to avoid the complication which arises from the reversible imine formation, we isolated Schiff bases, *p*-nitrobenzylidene-benzylamine (**1**), *N*-(4-nitrosalicylidene)benzylamine (**1** (**OH**)), and their hydrochlorides (**1H**$^+$ and **1(OH)H**$^+$, respectively), and carried out the reaction in refluxing anhydrous methanol.

Schiff base:

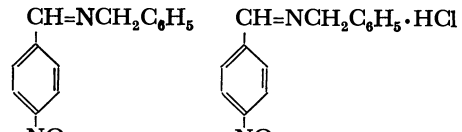

1 **1 H**$^+$

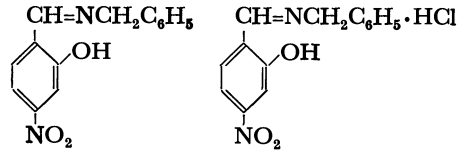

1 (OH) **1 (OH)H**$^+$

BzlNH:

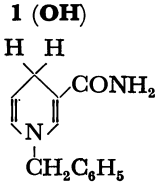

Experimental

Materials. 4-Nitrosalicylaldehyde was prepared according to the method of Tsumaki *et al.*,[16] and was identified by the NMR and IR (KBr disc) methods, and by the elemental analysis. Mp 134—135 °C (lit,[16] 133—134 °C. Found: C, 50.43; H, 3.02; N, 8.40%. Calcd for $C_7H_5O_4N$: C, 50.31; H, 3.02; N, 8.38%.

* Contribution No. 404 from this Department.

The preparation of Schiff bases was conducted according to the Matsuo's method.[17] Equimolar amounts of aldehyde and benzylamine were refluxed in anhydrous methanol for 1 h. The solvent was evaporated *in vacuo*, and the residual yellow solid was recrystallized from benzene and petroleum ether. The products were identified by NMR and IR spectroscopies and elemental analysis. Elemental analysis for **1** (**OH**), Found: C, 65.48; H, 4.70; N, 10.92%. Calcd for $C_{14}H_{12}N_2O_3$: C, 65.61; H, 4.73; N, 10.93%. Other results are summarized in Table 1.

Table 1. Characterization of Schiff bases and their hydrochloride salts

	Mp (°C)	IR (KBr) $\nu_{C=N}$ (cm^{-1})	NMR ($CDCl_3$) N-CH_2- (ppm)	NMR ($CDCl_3$) N=CH-
1	54—55	1635	4.84	8.35
1H$^+$	105—110			
1(OH)	88—89	1630	4.81	8.45
1(OH)H$^+$	176—179	1660		

The Schiff base was dissolved in anhydrous ether, and dry hydrogen chloride gas was introduced into the solution. White needles precipitated were collected, and recrystallized from anhydrous methanol. The analytical results are also recorded in Table 1.

N-Benzyl-4-nitro-2-hydroxybenzylamine hydrochloride (**2(OH)H**$^+$), the product expected for the BzlNH reduction of **1(OH)H**$^+$, was prepared by the sodium tetrahydroborate reduction of **1(OH)**. A solution of **1(OH)** (0.40 g, 1.6 mmoles) in 20 ml of methanol was stirred at 0—5 °C and a solution of sodium tetrahydroborate (0.06 g, 1.6 mmoles) in 10 ml of methanol was added from a dropping funnel. Subsequently, the reaction mixture was heated at 45 °C on a steam bath for 6.5 h. The solvent was evaporated *in vacuo*, the residual brown solid being extracted with water and ether. The ether layer was separated, and evaporated to dryness. The solid was again taken in anhydrous ether, from which (**2(OH)H**$^+$) was recovered by introducing dry hydrogen chloride gas. Recrystallization of the resulting precipitates from methanol–ether gave colorless powders; yield 21%, mp 210—213 °C. IR (KBr): 1525, 1340 cm^{-1} (nitro). NMR (Me_2SO-d_6): benzyl-CH_2, 4.13, 4.20 ppm, 4H; benzene rings, 7.3—7.8 ppm, 8H. Found: C, 56.93; H, 5.12; N, 9.43%. Calcd for $C_{14}H_{14}N_2O_3 \cdot HCl$: C, 57.05; H, 5.13; N, 9.45%.

The preparation of 1-benzyl-1,4-dihydronicotinamide (BzlNH) was described elsewhere.[18]

Reaction of Schiff Base and BzlNH. All the reactions were carried out in refluxing anhydrous methanol. A typical example for the reaction of **1H**$^+$ and BzlNH is stated below. A solution of **1H**$^+$ (0.64 g, 2.3 mmoles) and BzlNH (0.72 g, 3.4 mmol) in 20 ml of anhydrous methanol was refluxed for 9.5 h. The solvent was evaporated *in vacuo*, and residual oil was extracted with ether and water (pH 9 with *ca.* 0.05 M borate and 1 mM triethylamine hydrochloride). The ether layer was evaporated to dryness, again taken in ether, and dry hydrogen chloride gas was introduced. Recrystallization of the light yellow precipitates from methanol–ether gave almost colorless powders; yield 19%, mp 210—220 °C. The product was identified to be *N*-benzyl-*p*-nitrobenzylamine hydrochloride (**2H**$^+$). IR (KBr): 1510, 1350 cm^{-1} (nitro). NMR (Me_2SO-d_6): benzyl-CH_2, 4.17, 4.30 ppm, 4H; benzene ring, 7.3—7.6 ppm, 5H; *o*-proton of benzene ring, 7.87 ppm, 2H; *m*-proton of benzene ring, 8.25 ppm, 2H. Found: C, 59.55; H, 5.40; N, 9.78%. Calcd for $C_{14}H_{14}N_2O_2 \cdot HCl$: C, 60.33; H, 5.42; N, 10.05%.

Product Analysis. NMR was recorded by using a Varian A-60 instrument. The purity of the recovered products was examined by a Hitachi High Speed Liquid Chromatograph, Type 635 (Hitachi Gel 3018, methanol). UV absorption spectra were taken by a Hitachi 124 spectrophotometer at 30 °C.

Results

Spectral Study of the Reaction. The decrease in the absorption of BzlNH in refluxing methanol was followed at 354 nm (λ_{max} of BzlNH) in the absence and the presence of the Schiff base, **1** or **1(OH)** (Fig. 1).

Aliquots (3 ml) of the reaction mixture were withdrawn at appropriate intervals and scanned in the UV range at 30 °C. Figure 2 shows that the absorption of BzlNH decreases in the presence of **1(OH)**. In contrast, no significant spectral change was observed in the presence of **1** and in the absence of the Schiff base. The absorbance decrease at 354 nm in the presence of **1(OH)** was accompained by the increase in the absorption band at 250—280 nm and at 400—440 nm, but no significant increase occurred near 290 nm (Fig. 1). If the acid-catalyzed decomposition of 1,4-dihydronicotinamide occur, the product (1,4,5,6-tetrahydronicotinamide derivative) would give rise to a new, strong absorption at around 290 nm.[18-20] Therefore, the decrease in the BzlNH absorbance may be attributed to the disappearance of BzlNH due to the hydrogen transfer reaction. Apparently, the *ortho*-hydroxyl group facilitates the reaction, as in the pyridoxal-catalyzed reactions.

Reaction of BzlNH with Schiff Bases and Their Hydrochloride Salts. Introduction of hydrogen chloride gas to an ether solution obtained from the reaction of

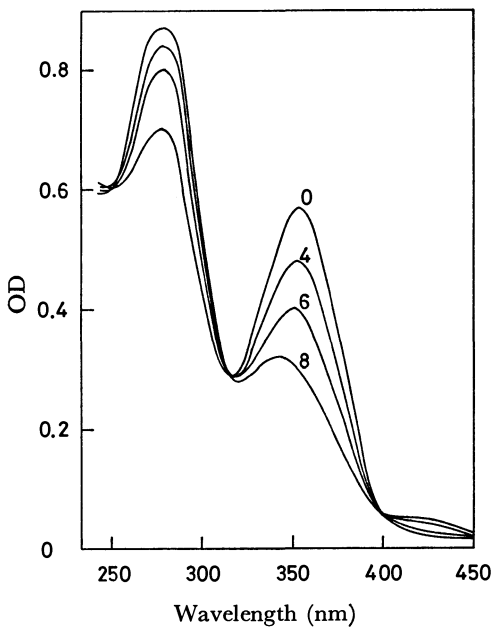

Fig. 1. Spectral changes in the reaction of 1-benzyl-1,4-dihydronicotinamide (BzlNH: 5.65×10^{-5} M) with 4-nitrosalicylidene–benzylamine (**1(OH)**: 5.34×10^{-5} M) in refluxing methanol. Numbers indicate the reaction time (h).

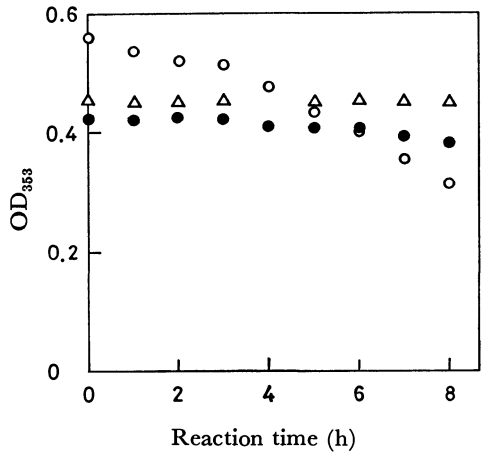

Fig. 2. Time dependence of the absorbance of BzlNH (353 nm) in the presence and the absence of the Schiff base:
○: [BzlNH]=5.65×10^{-5} M, [**1**(**OH**)]=5.34×10^{-5} M; ●: [BzlNH]=5.65×10^{-5} M, [**1**]=5.50×10^{-5} M; △: [BzlNH]=5.65×10^{-5} M.

1(**OH**) and BzlNH gave oily products. A TLC study (silica gel, ethyl acetate) showed that the oil is a mixture of *N*-benzyl-4-nitro-2-hydroxybenzylamine hydrochloride, **2**(**OH**)**H**$^+$ (R_f=0.64—0.65), **1**(**OH**)**H**$^+$ (R_f=0.40—0.42), and BzlNH or 1-benzylnicotinamide (R_f=0—0.23). The product analysis by liquid chromatograph (Table 2) established that it contained 38 mol% of **2**(**OH**)**H**$^+$ and 62 mol% of **1**(**OH**)**H**$^+$ (Table 2; the amount of BzlNH could not be determined because its retention time was too long).

On the other hand, the product obtained from the reaction of **1** and BzlNH displayed a broad melting point (135—156 °C), and was identified to be a mixture of benzylamine hydrochloride and BzlNH by liquid chromatography. These results, together with the spectral evidence, are explained by reaction schemes 1 and 2.

Table 2. Product analysis of the reaction of BzlNH and schiff bases

Schiff base	Recovered products[a] (%)				Yield of the reduced product (%)[c]
	$PhCH_2NH_2$·HCl	**2**H$^+$	**1**(**OH**)**H**$^+$	**2**(**OH**)**H**$^+$	
1	100	0			0
1+NEt_3·HCl[b]	0	100			26
1+Imidazole·HCl[b]	0	100			15
1+$(Me_2NCH_2)_2$·2HCl[b]	0	100			13
1H$^+$	0	100			19
1(**OH**)			62	38	
1(**OH**)+NEt_3·HCl[b]			79	21	
1(**OH**)**H**$^+$			7	93	8

a) Semi-quantitative analyses were performed by using high speed liquid chromatography: 260 nm for **2H**$^+$ and 280 nm for **1**(**OH**)**H**$^+$ (ε=18180) and **2**(**OH**)**H**$^+$ (ε=5980). b) [Amine hydrochloride]=*ca.* 10 [Schiff base]. c) Determined after recrystallization for **2H**$^+$. The low yields are due to the loss in the extraction with ether, products being poorly soluble in ether.

The hydrochloride of Schiff bases was more easily reduced by BzlNH. **1**(**OH**)**H**$^+$ was converted almost exclusively to **2**(**OH**)**H**$^+$ (93%, Table 2). Interestingly, **1H**$^+$ was also susceptible to the BzlNH reduction, though the free Schiff base was totally unreactive. The product showed a single spot (R_f=0.71) on TLC, and was confirmed to be pure *N*-benzyl-*p*-nitrobenzylamine hydrochloride, **2H**$^+$ (see Experimental). Thus, the role of the *ortho*-hydroxyl group becomes less important if the Schiff base is activated by protonation.

In order to prove direct hydrogen transfer from BzlNH to the Schiff base, the reaction of BzlNH and **1H**$^+$ was performed in ethanol-*d* (99%). The recovered **2H**$^+$ (24% yield, mp 207—222 °C) again showed a single spot on TLC. As described in Experimental, the NMR spectrum of **2H**$^+$ obtained in non-deuterated ethanol possessed the peaks of the methylene hydrogen at 4.17 and 4.30 ppm (δ) with 1 : 1 intensity. The NMR spectrum of **2H**$^+$ obtained in ethanol-*d* possessed similar methylene peaks. These results prove that no deuterium was incorporated to the 1-methylene group in the reaction in the deuterated medium. Therefore, the reduction of the Schiff base must occur *via* direct hydrogen transfer as in some enzymatic reductions.[2]

Reaction in the Presence of Amine Hydrochlorides. The susceptibility of the Schiff base to the BzlNH reduction was evaluated in the presence of amine hydrochlorides such as triethylamine hydrochloride. The reduction of **1**(**OH**) was hardly affected by the addition of triethylamine hydrochloride (10-fold of **1**(**OH**); Table 2). In contrast, **1** was readily converted to **2H**$^+$ in the presence of triethylamine hydrochloride in 23% yield. Other hydrochlorides similarly facilitated the reduction of **1**. Therefore, these hydrochlorides may replace the role played by the *ortho*-hydroxyl group of **1**(**OH**).

Discussion

Until recently, the nonenzymatic reduction by 1,4-dihydropyridines has been limited to highly electron-deficient carbonyl compounds such as hexachloroacetone,[21] trifluoroacetophenone,[3] chloranil,[22] thiobenzophenone,[23] *etc.* Some alcohol dehydrgenases contain Zn(II) at the active site,[24] and the chelation and hydrogen bonding with substrates facilitate the hydrogen transfer.[25] The use of these interactions to facilitate NADH-mediated oxidation-reduction reactions has largely escaped attention in model studies. More recently, however, the nonenzymatic transformation of the carbonyl group to the corresponding alcohol was found to be significantly catalyzed by Zn(II)[26] and Mg(II)[27] and by *ortho*-phenolic hydroxyl groups.[8-10] For example, *m*-nitrobenzaldehyde and 4-pyridinecarbaldehyde are not reduced by 1,4-dihydropyridines, whereas 5-nitrosalicylaldehyde and 3-hydroxy-4-pyridinecarbaldehyde serve as substrates.[8,10] These results clearly substantiate the importance of hydrogen bonding in lowering the activation energy for the reduction of the carbonyl function.

In the reaction of 1-substituted dihydronicotinamides

and carbonyl substrates, the transfer of the hydride anion or its equivalent would produce an unstable, alkoxide anion. When pK_a of this anion is considerably low due to the electron-withdrawing substituents, the reduction would be rather facile. Hexachloroacetone and trifluoroacetophenone belong to this class of the substrate. On the other hand, for the substrate with relatively high pK_a, the proton transfer to the carbonyl group prior to or at the transition state of the reaction could avoid the formation of energetically unfavorable alkoxide anions. Supposedly, the *ortho* hydroxyl groups of salicylaldehyde and 3-hydroxy-4-pyridinecarboxaldehyde can facilitate the reduction not only by polarization of the carbonyl group *via* hydrogen bonding but also by the efficient, intramolecular proton transfer (Eq. 1). This situation is similar to the ester cleavage reaction: *i.e.*, esters with good leaving groups are cleaved simply by the nucleophilic attack, while esters with poor leaving groups have to be cleaved by assistance of the general acid catalysis.[28]

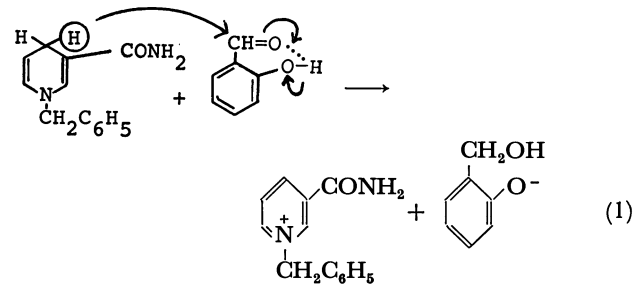

Thus, the BzlNH reduction of Schiff bases possesses a feature which is common to the amide cleavage. The simple nucleophilic cleavage of amide substrates produces the amine anion (pK_a *ca.* 27), which is so unstable that it almost certainly does not occur without the assistance of the acid catalysis.[29] Similarly, the BzlNH reduction of the Schiff base primarily produces the amine anion (Eq. 2), which would be energetically unfavorable. Therefore, appropriate proton sources are required for this reaction.

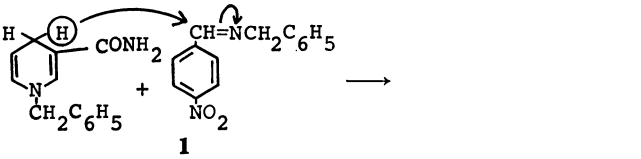

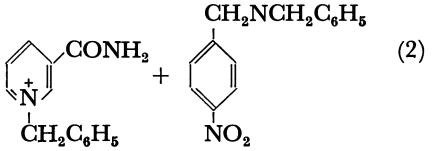

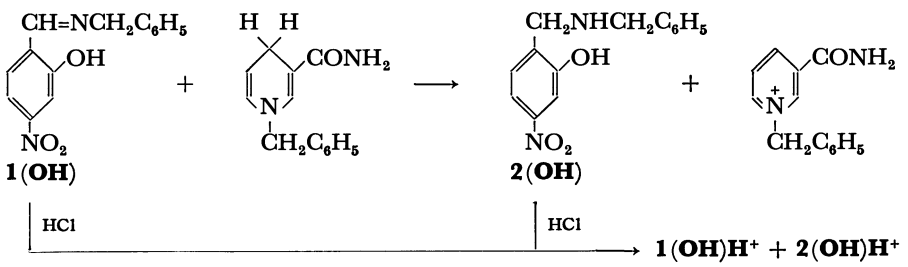

Scheme 1.

Although Schiff bases are more reactive to the nucleophilic attack than the corresponding carbonyl functions,[12] **1** did not undergo the BzlNH reduction. In contrast, **1(OH)** was reducible by BzlNH in refluxing methanol due to the presence of the *ortho* hydroxyl group as a proton source. The role of the hydroxyl group of **1(OH)** may be complicated, however. The Schiff base nitrogen is basic, so that a zwitterionic species (>C=N$^+$H–: **1(OH)-Z**) may be present in addition to the neutral species (**1(OH)-N**). Thus, two reaction paths become possible as depicted in Scheme 3; that is, one involves the concerted proton transfer from the *ortho* hydroxyl group and the other involves the preequilibrium proton transfer to the Schiff base. Fortunately, the distribution of the chemical species of pyridoxal and its Schiff base in methanol (27 °C) have been reported by Matsushima and Martell.[30] They demonstrated the presence of two species, zwitterionic (418 nm) and neutral (337 nm), for pyridoxalidenevaline. The UV spectrum of **1(OH)** recorded in dry methanol at 30 °C showed an absorption maximum at 353 nm, but not at longer wavelengths beyond 400 nm. This absorption maximum is reasonably attributed to **1(OH)-N**, and **1(OH)-Z** exists little under this condition. At refluxing temperature, however, the reaction path *via* **1(OH)-Z** may not be ruled out, since the formation of the zwitterionic form could be increased by raising the temperature. We consider both reaction paths to be plausible, though **1(OH)-N** probably being the major reacting species.

Since the reaction media were not buffered, the progress of the BzlNH reduction would produce the phenoxide anion of **2(OH)** as illustrated in Scheme 3. However, in the presence of the unreacted **1(OH)**, the prototropic equilibrium of Eq. 3 must be overwhelmingly shifted to the right because the acidity of the two phenol groups are rather different.

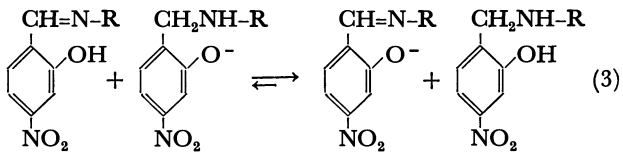

Figure 1 shows that a new, weak absorption band appears at 400—440 nm toward the end of the reaction. This peak may be ascribed to the anionic species of **1(OH)** (*cf.* λ_{max} for the 2-cyano-5-nitrophenolate anion is at 410 nm[31]). A similar spectral observation has been made for the 1,4-dihydronicotinamide reduction of 3-hydroxy-4-pyridinecarbaldehyde in refluxing methanol.[10] The anionic species of **1(OH)** will be much less

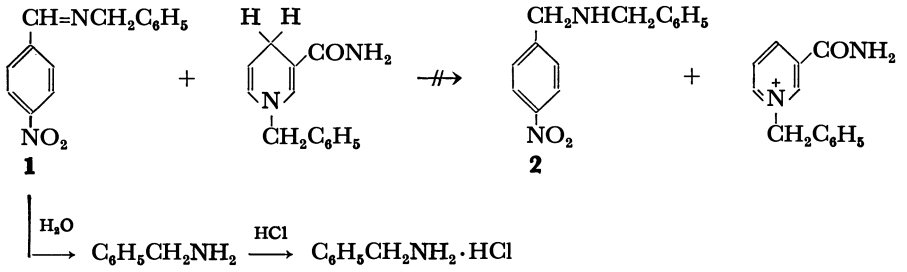

Scheme 2.

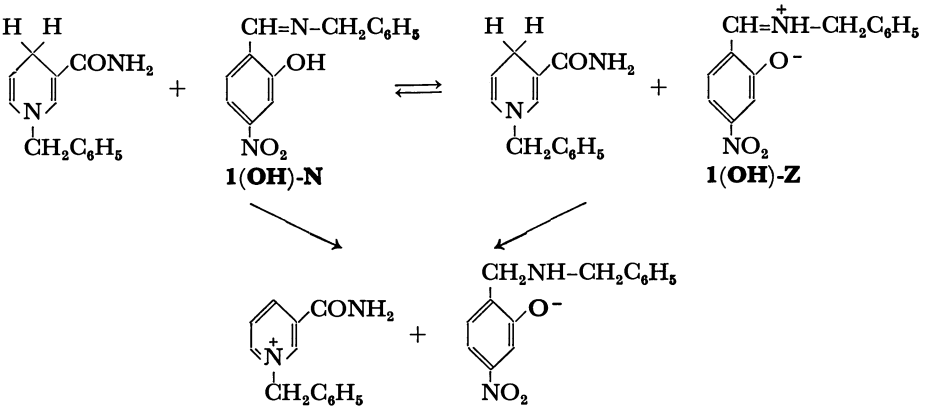

Scheme 3.

reactive in the BzlNH reduction, because of its increased electron density. This can explain why the reduction of **1**(**OH**) did not conclude even after refluxing for 9.5 h in methanol (Table 2).

The reaction of **1**(**OH**) with Hantzsch ester (HE: 2,6-dimethyl-3,5-bis(ethoxycarbonyl)-1,4-dihydropyridine) did not yield an anionic species,[32] since HE can supply two hydrogenes (presumably, one as a "hydride" and the other as a proton: Eq. 4).

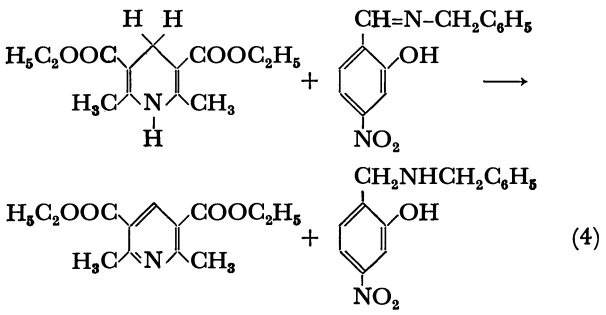

(4)

1(**OH**)**H**$^+$ was converted in 93% yield to **2**(**OH**) under the same reaction conditions (Table 2). Conceivably, **1H**$^+$ and **1**(**OH**)**H**$^+$ are quite reactive because (1) the protonated iminium group is prone to accept the "hydride" and (2) the product is not the energetically unfavorable anion.

Interestingly, addition of triethylamine hydrochloride and other amine hydrochlorides greatly improved the reactivity of **1** (Table 2). It is evident that these amine hydrochlorides act as the proton source. Here again, two proton transfer mechanisms are possible: the concerted and preequilibrium mechanisms (Eqs. 5 and 6).

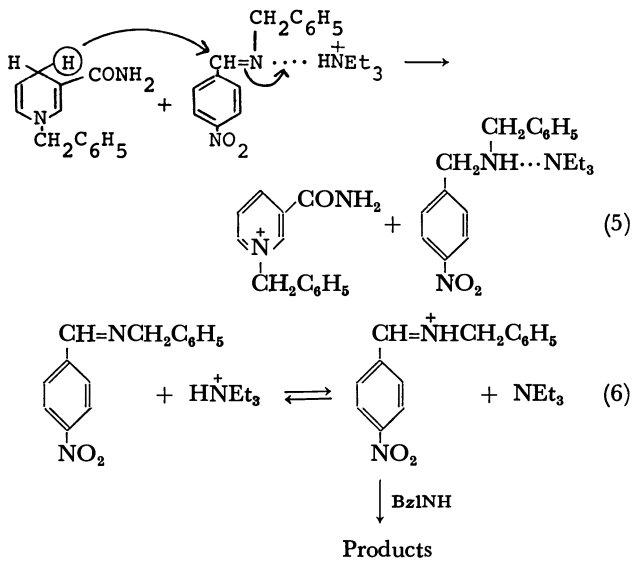

(5)

(6)

Products

Equation 5 is a termolecular reaction, and entropically unfavorable. The pK_a value of *N*-(*p*-nitrobenzylidene)-*t*-butylamine was determined by Cordes and Jencks[33] to be 5.40, and is much lower than that of triethylamine (10.65).[34] Thus, the formation of **1H**$^+$ (Eq. 6) in the presence of only 10 times excesses of triethylamine hydrochloride is considered to be insignificant. It cannot be decided at present which reaction path is preferable.

In conclusion, the present study indicates the following order of the reactivity of the Schiff base toward the BzlNH reduction.

1H$^+$, **1** + NEt_3·HCl,

$\geqq$ **1** (**OH**)**H**$^+$ > **1** (**OH**) > **1** (unreactive).

This is in good accord with that demonstrated for the "*trans*-Schiffization,"[12] and suggests that the reduction by 1,4-dihydronicotinamide has the S_N2-type nature. Also suggested is that the reduction of the Schiff base can be acid-catalyzed, though the detailed mechanism (general acid or specific acid) was not established. These results may have important bearing with the interaction between the Schiff base and NADH in biological systems.

References

1) T. C. Bruice and S. J. Benkovic, "Bioorganic Mechanism," Vol. 2, W. A. Benjamin, New York, N. Y. (1966), Chapter 9.

2) B. Vennesland and F. H. Westheimer, "The Mechanism of Enzyme Action," ed by W. D. McElroy and B. Glass, John Hopkins, Baltimore (1954), p. 357.

3) J. J. Steffens and D. M. Chipman, *J. Am. Chem. Soc.*, **93**, 6694 (1971).

4) D. J. Creighton, J. Hajdu, G. Mooser, and D. S. Sigman, *J. Am. Chem. Soc.*, **95**, 6855 (1973).

5) L. C. Kurz and C. Frieden, *J. Am. Chem. Soc.*, **97**, 677 (1975).

6) Y. Morino and Y. Sakamoto, *J. Biochem.*, **48**, 733 (1960).

7) H. Holzer and S. Schneider, *Biochim. Biophys. Acta*, **48**, 71 (1961).

8) U. K. Pandit and F. R. Mas Cabre, *Chem. Commun.*, **1971**, 552.

9) S. Shinkai and T. C. Bruice, *J. Am. Chem. Soc.*, **94**, 8258 (1972).

10) S. Shinkai and T. C. Bruice, *Biochemistry*, **12**, 1750 (1973).

11) F. H. Westheimer and H. Cohen, *J. Am. Chem. Soc.*, **60**, 90 (1938).

12) E. H. Cordes and W. P. Jencks, *Biochemistry*, **1**, 773 (1962).

13) Ref. 1), Chapter 10.

14) S. Shinkai and T. Kunitake, *Chem. Lett.*, **1974**, 1113.

15) U. K. Pandit, R. A. Gase, F. R. Mas Cabre, and M. J. Sarink, *J. Chem. Soc., Chem. Commun.*, **1975**, 211.

16) T. Tsumaki, H. Ohta, and T. Tsutsumi, *Nippon Kagaku Kaishi*, **74**, 859 (1953).

17) Y. Matsuo, *J. Am. Chem. Soc.*, **79**, 2061 (1957).

18) S. Shinkai, R. Ando, and T. Kunitake, *Bull. Chem. Soc. Jpn.*, **48**, 1914 (1975).

19) C. C. Johnston, J. L. Gardner, C. H. Suelter, and D. E. Metzler, *Biochemistry*, **2**, 689 (1963).

20) C. S. Y. Kim and S. Chaykin, *Biochemistry*, **7**, 2339 (1968).

21) D. C. Dittmer and R. A. Fouty, *J. Am. Chem. Soc.*, **86**, 91 (1964).

22) E. A. Braude, J. Hannah, and R. Linstead, *J. Chem. Soc.*, **1960**, 3249, 3257.

23) R. H. Abeles, R. F. Hutton, and F. H. Weshimer, *J. Am. Chem. Soc.*, **79**, 712 (1957).

24) G. Popjak, *Enzymes*, **2**, 134 (1970).

25) J. H. Wang, *Science*, **161**, 328 (1968).

26) D. J. Creighton and D. S. Sigman, *J. Am. Chem. Soc.*, **93**, 6314 (1971).

27) Y. Ohnishi, M. Kagami, and A. Ohno, *Tetrahedron Lett.*, **1975**, 2437.

28) T. C. Bruice and S. J. Benkovic, "Bioorganic Mechanism," Vol. 1, W. A. Benjamin, New York (1966), Chapter 1.

29) W. P. Jencks, "Catalysis in Chemistry and Enzymology," McGraw-Hill, New York, N. Y. (1969), Chapter 10.

30) Y. Matsushima and A. E. Martell, *J. Am. Chem. Soc.*, **89**, 1322 (1967).

31) C. A. Bunton, M. J. Minch, J. Hidalgo, and L. Sepulveda, *J. Am. Chem. Soc.*, **95**, 3262 (1973).

32) S. Shiraishi, Senior Research Thesis of Faculty of Engineering, Kyushu University, 1976.

33) E. H. Cordes and W. P. Jencks, *J. Am. Chem. Soc.*, **85**, 2843 (1963).

34) H. K. Hall, Jr., *J. Am. Chem. Soc.*, **79**, 5441 (1957).

Regioselectivity of Palladium(II)-Induced Intramolecular Cyclization of 2-(3-Methyl-2-butenyl)phenol

Takahiro HOSOKAWA,* Shinji YAMASHITA, Shun-Ichi MURAHASHI, and Akio SONODA

Department of Chemistry, Faculty of Engineering Science, Osaka University, Toyonaka, Osaka 560

(Received July 27, 1976)

Reaction of 2-(3-methyl-2-butenyl)phenol (**1**) with $PdCl_2$ gives 2,2-dimethylchromene (**3**) and 2,2-dimethyl-4-methoxychroman (**4**) (six-membered products) predominantly, together with trace amounts of 2-isopropylbenzofuran (**5**) and 2-isopropenyl-2,3-dihydrobenzofuran (**6**) (five-membered products). The reaction involves attack of the oxygen atom of the phenoxyl group at 2- or 3-position of the allylic side chain. Addition of various sodium carboxylates to the reaction mixture changes the regioselectivity. In the presence of sodium salts of carboxylic acids bearing electron-releasing substituents, nearly equal amounts of five and six-membered products are formed. The presence of sodium salts of carboxylic acids bearing electron-withdrawing substituents results in the predominant formation of the six-membered products. These results are discussed on the basis of alternation of reactive Pd(II) species. Results obtained from 2-(2-butenyl)phenol (**2**) are also reported.

In 1973 a synthetic process of 2-substituted benzofurans *via* palladium(II)-induced intramolecular cyclization of 2-allylphenols was reported.[1] Thereafter, the cyclization has been applied to unsaturated ketoximes[2] and alcohols[3] for synthesizing various heterocyclic compounds.[4]

During the course of investigations on the cyclization of 2-allylphenols, it has been found that the cyclization of 2-(3-methyl-2-butenyl)phenol (**1**) involves attack of the oxygen atom of the phenoxyl group on either 2- or 3-position of the allylic side chain, and that the regioselectivity depends on the ligands of palladium(II) salts. Similar results were also obtained from the cyclization of 2-(2-butenyl)phenol (**2**). In order to elucidate factors controlling the regioselectivity, the reaction of **1** with palladium(II) salts, $PdCl_2$ or $Pd(OAc)_2$, was carried out in the presence of various sodium carboxylates. In the present paper, we report the effect of sodium carboxylates on the palladium(II)-induced cyclization of **1**.

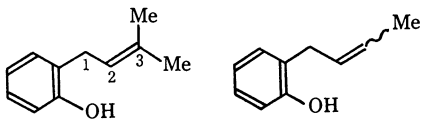

1 **2**

Results and Discussion

The reaction of **1** with $PdCl_2$ in aq methanol at 35 °C for 3 h in the air gave a 43% combined yield of six-membered products **3** and **4** (**3**: **4**=32: 11), along with

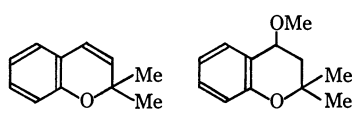

3 **4**

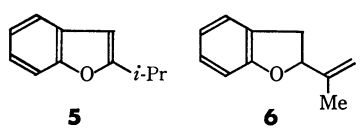

5 **6**

* To whom correspondence should be addressed.

TABLE 1. PRODUCT DISTRIBUTION IN THE REACTION OF **1** WITH $PdCl_2$ OR $Pd(OAc)_2$ IN THE PRESENCE OF NaOAc[a]

Run	Molar ratio NaOAc/ PdX_2	Cyclized products: Yield[b] (%)	Ratio **3** : **5** : **6**	Unreacted **1** (%)
	X=Cl			
1	2	20	55 : 25 : 20	63
2	6	26	54 : 23 : 23	63
3	16	34	50 : 21 : 29	52
4	30	46	48 : 17 : 35	14
5	50	61	46 : 16 : 38	5
	X=OAc			
6	0	22	41 : 5 : 54	36
7	6	49	45 : 16 : 39	9
8	30	48	44 : 17 : 39	9

a) The reaction was carried out by using 0.5 mmol of **1**, 0.25 mmol of palladium(II) salt, and the corresponding amount of NaOAc in 9.5 ml of MeOH and 0.5 ml of H_2O at 35 °C for 3 h in the air. b) Yield was determined by GLC, and based on **1** used.

trace amounts of benzofurans **5** and **6** in less than 2% yields. Addition of NaOAc to the reaction mixture or the use of $Pd(OAc)_2$ instead of $PdCl_2$ caused a change in the product distribution (Table 1); that is, substantial amounts of benzofurans **5** and **6** were formed along with chromene **3**, but no other product such as **4** was detected. The results given in Table 1 indicate the following. (1) In the $PdCl_2$ system, the total product yield increases by increasing the amount of added NaOAc, accompanied by an increase in the relative yield of **6** and a decrease in that of **5** and **3** (runs 1—5). (2) In the $Pd(OAc)_2$ system, the product distribution changes with the addition of six-fold excess of NaOAc (runs 6—7), further addition of NaOAc giving no significant effect (runs 7—8). (3) In the $PdCl_2$ system, the product distribution approaches that in the $Pd(OAc)_2$–NaOAc system by increasing the amount of added NaOAc (runs 5 and 7). The results suggest that both reaction systems involve analogous reactive Pd(II) species, and excess acetate ion must displace the chloride ligands in $PdCl_2$.[5]

Table 2. Product distribution in the reaction of **1** with $PdCl_2$ in the presence of various sodium carboxylates or sodium chloride[a)]

Run	Sodium Salts	pK_a[b)] (H_2O)	Cyclized products: Yield[c)] (%)	Ratio **3**	**4**	**5**	**6**	Unreacted **1** (%)
1	NaCl[d)]		32	89:	9:	2:	1	55
2	CF_3COONa	0.23	45	82:	10:	6:	2	36
3	$CCl_2HCOONa$	1.25	36	80:	4:	8:	8	51
4	CFH_2COONa	2.57	43	60:	2:	21:	17	42
5	CH_3COONa	4.75	34	50:	—:	21:	29	51
6	CH_3CH_2COONa	4.87	62	50:	—:	17:	33	6
7	$(CH_3)_3CCOONa$	5.05	71[e)]	51:	—:	12:	37	3

a) The reaction was performed by using 16 molar equivalents of sodium carboxylate to $PdCl_2$ under the conditions described in footnote a) in Table 1. b) A. Albert and E. P. Serjeant, "Ionization Constants of Acids and Bases," John Wiley & Son Inc., New York (1962), p. 124. c) Yield was determined by GLC, and based on charged **1**. d) 4 molar equivalents of NaCl to $PdCl_2$ was used. e) Reaction time was 1 h.

This is supported by the examination of absorption spectra of $PdCl_2$ in the presence of NaOAc. The solution of $PdCl_2$ in aq methanol showed a maximum absorption at 422 nm. Addition of NaOAc shifted the maximum to a shoulder peak around 400 nm,[6)] which is similar to a spectrum of $Pd(OAc)_2$ in the presence of NaOAc.

On the basis of these results, we have carried out the reaction of **1** with $PdCl_2$ in the presence of various sodium carboxylates (16 molar equiv to $PdCl_2$) or NaCl.[7)] The results summarized in Table **2** are as follows. (1) Formation of the six-membered products (**3** and **4**) predominates that of the five-membered products (**5** and **6**), when the reaction is performed in the presence of either sodium salts of carboxylic acids bearing electron-withdrawing group (runs 2—4) or NaCl, and the relative ratio of **3**+**4**/**5**+**6** (regioselectivity) correlates well with pK_a values of the corresponding carboxylic acids; thus, the higher ratio is observed with the lower pK_a value. (2) In the presence of sodium salts of carboxylic acids bearing electron-releasing group (runs 5—7), the amounts of six- and five-membered products formed are nearly equal, the ratio **3**/**5**+**6** not changing a great deal. These results can be ascribed to an alternation of reactive Pd(II) species through co-ordination of sodium carboxylates to $PdCl_2$, and the change in electron density of palladium appears to affect the regioselectivity. The following facts should be noted here. Firstly, in the reaction using $(CH_3)_3CCOONa$, if the total product yield is calculated on the basis of $PdCl_2$ used, it becomes 142%, suggesting that the reaction involves a catalytic process. When the reaction was carried out under an atmosphere of nitrogen or argon instead of air, the yield was reduced to ≈60% (≈30% based on charged **1**). Thus the catalytic process would be effected by oxygen in air. However, the relative ratios among the cyclized products did not change. Secondly, no double bond isomerization of **1** recovered took place.

From these results we propose the following explanation for the regioselectivity of the cyclization. The cyclization would proceed *via* co-ordination of olefin to the reactive Pd(II) species, as has been generally accepted in many organic reactions using palladium(II).[8)] On the co-ordinated olefin, an extensive positive charge may be induced by a decrease in electron density on palladium, if the reactive Pd(II) species bears electron-withdrawing ligands. Nucleophilic attack of the oxygen atom would thus occur predominantly at the 3-position of the allylic side chain, since a positive charge at this position is highly stabilized by two methyl groups. If so, one factor controlling the regioselectivity would be the electron density of palladium. This may be supported by the following results. (1) The use of $Pd(OCOCF_3)_2$ also led to a predominant formation of **3**. (2) The reaction of **1** with $Hg(OAc)_2$ (a more electrophilic reagent[9)] than palladium(II)) in aq. methanol followed by $NaBH_4$ reduction gave a six-membered product, 2,2-dimethylchroman, as the sole product.

The reaction of 2-(2-butenyl)phenol (**2**) with palladium(II) salts gave cyclized products such as **7**, **8**, **9**, **10**, and **11**. As shown in Table 3, the reaction using $PdCl_2$ alone gives six-(**7**+**8**+**9**) and five-membered product (**10**) in the ratio 89: 21. The result shows a tendency similar to the case of **1**. Addition of NaOAc to $PdCl_2$ or the use of $Pd(OAc)_2$ instead of $PdCl_2$ leads to none of the six-membered products, only the five-membered products **10** and **11** being formed. Hence, the facile formation of the six-membered product(s) from **1** would be also governed by a favorable attack of Pd(II) on a less crowded carbon (2-position) of the allylic side chain of **1**.

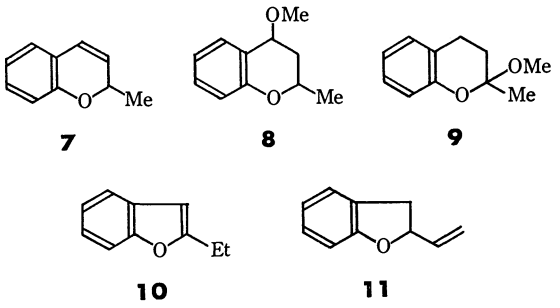

7 **8** **9** **10** **11**

Table 3. Product distribution in the reaction of **2** with palladium(II) salts[a)]

Palladium(II) salts	Cyclized products: Yield (%)	**7**	**8**	**9**	**10**	**11**
$PdCl_2$	34[b)]	50 :	11 :	18 :	21 :	—[c)]
$PdCl_2$–NaOAc[d)]	40[e)]	— :	— :	— :	52 :	58
$Pd(OAc)_2$[f)]	65	— :	— :	— :	29 :	71

a) Palladium(II) salt was reacted with two molar equivalents of **2** in aq MeOH at 35 °C for 3 h in the air. b) The yield, based on charged **2**, was estimated from a mixture of isolated products by GLC. c) The ratio was determined by GLC peak areas. d) 16 molar equivalents of NaOAc to $PdCl_2$ was used. e) The yield was determined by GLC with biphenyl as an internal standard, and based on charged **2**. f) Data from Ref. 1b.

Experimental

Materials. 2-(2-Methyl-2-butenyl)phenol (**1**) was synthesized by C-alkylation of sodium phenoxide with 4-bromo-2-methyl-2-butene[10] according to the procedure of Hurd and Hoffman.[11] 2-(2-Butenyl)phenol (**2**) was prepared as reported previously.[1b] Palladium(II) chloride was prepared from a solution of palladium metal in *aqua regia* by diluting with aq hydrogen chloride and heating to dryness. Palladium(II) acetate was prepared by the method of Wilkinson *et al.*[12]

*Reaction of **1** with Palladium(II) Salts. A) Analyses of Product Distributions*: A suspension of palladium(II) salt ($PdCl_2$ or $Pd(OAc)_2$, 0.25 mmol) and a given amount of NaOAc in MeOH (4.5 ml)–H_2O (0.5 ml) was stirred at 35 °C for 10 min in the air, and then a mixture of allylphenol **1** (0.081 g, 0.5 mmol) and appropriate amount of biphenyl (internal standard for GLC analysis) in MeOH (5 ml) was added to the suspension, stirring being continued for 3 h. Product distributions were analyzed by gas chromatography (a JEOL Model JGC-20KFP gas chromatography) equipped with a FID detector using 10% PEG-20 M Celite Column (1 m×4 mm). Peaks attributed to chromene **3**, benzofurans **5** and **6**, chroman **4**, biphenyl (internal standard), and unreacted **1** appeared with retention times of 10.0, 11.6, 14.3, 20.3, and 28.8 min, respectively, under the conditions of injection temperature 300 °C and column temperature 120 °C which was raised up at the rate of 5 °C/min after 7 min. The results are summarized in Table 1.

Analyses of product distribution in the presence of various sodium carboxylates were performed by the same procedure, the results being given in Table **2**. All the product yields are based on **1** used. Isolation, purification, and identification of cyclized products were carried out as follows.

*B) Isolation and Identification of 2,2-Dimethylchromene (**3**) and 2,2-Dimethyl-4-methoxychroman (**4**)*: For isolation of cyclized products **3** and **4**, the reaction was carried out by using a catalytic amount of $PdCl_2$. A mixture of **1** (1.620 g, 10 mmol), $PdCl_2$ (0.035 g, 0.2 mmol), and $CuCl_2$ (0.670 g, 5 mmol) in MeOH (25 ml)–H_2O (2 ml) was stirred at 65 °C under a slow stream of oxygen. After 24 h, the reaction mixture was filtered and extracted with ether. The ether extract was washed with water and dried over $MgSO_4$. The solvent was removed *in vacuo* and the residue was distilled under reduced pressure, giving 1st fraction (0.506 g) at 85—90 °C/4 mmHg and 2nd fraction (0.658 g) at 101—105 °C/4 mmHg. GLC analyses showed that the 1st fraction contained chromene **3**, chroman **4**, unreacted **1**, and an unidentified product in 55, 15, 9, and 21% on GLC peak areas, respectively, and the 2nd fraction in 27, 28, 15, and 30%. The unidentified compound is a phenolic material since it can be removed from the mixtures by treating with Claisen's alkali. Although its isolation was unsuccessful owing to decomposition during the course of preparative GLC, the compound is probably 2-(2-methoxy-3-methylbutyl)phenol. The other products were isolated by preparative GLC using 10% PEG-20 M Celite Column at 165 °C. 2,2-Dimethylchromene (**3**), NMR (CCl_4), δ 1.37 (s, 6H), 5.44 (d, J=10 Hz, 1H), 6.18 (d, J=10 Hz, 1H), and 7.1—6.4 (m, 4H). (Found: C, 82.41; H, 7.48%. Calcd for $C_{11}H_{12}O$: C, 82.46; H, 7.55%). The spectral properties of this compound were identical with those of the authentic sample prepared by the method of Campbell *et al.*[13] 2,2-Dimethyl-4-methoxychroman (**4**), NMR (CCl_4), δ 1.27 (s, 3H, Me), 1.35 (s, 3H, Me), 1.92 (d, J=7 Hz, 2H, C-3 proton), 3.32 (s, 3H, OMe), 4.27 (t, J=7 Hz, 1H, benzylic proton), and 7.2—6.2 (m, 4H); IR, cm^{-1} 1608 (m), 1580 (s), 1482 (s), 1485 (s), 1367 (m), 1258 (s), 1203 (s), 1128 (s), 1090 (s), 920 (s), 908 (m), and 748 (s); Found: C, 75.19; H, 8.53%. Calcd for $C_{12}H_{16}O_2$: C, 74.97; H, 8.39%. The position of the methoxyl group was assigned on the basis of the downfield shift of benzylic proton (δ 4.27) caused by both phenyl ring and methoxyl group. The benzylic protons of 2,2-dimethylchroman (see below) show resonance at δ 2.72 as a triplet. The assignment is also supported by comparison with the NMR spectrum of 2-methyl-4-methoxychroman (**7**).

*C) Isolation and Identification of 2-Isopropylbenzofuran (**5**) and 2-Isopropenyl-2,3-dihydrobenzofuran (**6**)*: For the isolation of **5** and **6**, allylphenol **1** (1.620 g, 10 mmol) was similarly reacted with a catalytic amount of $Pd(OAc)_2$ (0.046 g, 0.2 mmol) in the presence of $Cu(OAc)_2 \cdot H_2O$ (0.998 g, 5 mmol) for 48 h. The usual work-up followed by distillation (~105 °C/6 mmHg) gave an oil (1.260 g) which contained largely unreacted **1**. The distillate was then treated with Claisen's alkali, and the organic products were extracted with petroleum ether. The extract was washed with water and dried over $MgSO_4$. Removal of the solvent afforded colorless oil (0.358 g) which was found to contain **3**, **5**, and **6** in the ratio 47: 3: 50 on GLC peak areas. Isolation of these products was performed by preparative GLC under the same conditions as above. 2-Isopropylbenzofuran (**5**), NMR (CCl_4), δ 1.41 (d, J=7 Hz, 6H, Me) 3.06 (h, J=7 Hz, 1H), 6.31 (s, 1H, C-3 proton), 7.1—7.3 (m, 2H), and 7.3—7.5 (m, 2H): IR, cm^{-1} 1582 (s), 1592 (s), 1462 (s), 1425 (s), 1223 (s), 1158 (m), 930 (m), 783 (s) and 725 (s); Found: C, 82.45; H, 7.61%. Calcd for $C_{11}H_{12}O$: C, 82.46; H, 7.55%. 2-Isopropenyl-2,3-dihydrobenzofuran (**6**), NMR (CCl_4), δ 1.70 (broad s, 3H, Me), 2.89 (dd, J=16 and 8 Hz, 1H, C-3 proton), 3.21 (dd, J=16 and 8.5 Hz, 1H, C-3 proton), 4.74 (broad s, 1H, olefinic proton), 4.94 (broad s, 1H, olefinic proton), 4.95 (t, J=8 Hz, 1H, C-2 proton), 6.58 (2H, phenyl proton), and 6.86 (2H, phenyl proton): IR, cm^{-1} 1643 (w), 1590 (s), 1476 (s), 1458 (s), 1368 (m), 1318 (m), 1210 (s), 1160 (w), 1090 (w), 1010 (m), 950 (m), 890 (m), 850 (m), and 738 (s): Found: C, 82.31; H, 7.54%. Calcd for $C_{11}H_{12}O$: C, 82.46; H, 7.55%.

*D) Reaction of **1** with $Pd(OCOCF_3)_2$*: $Pd(OCOCF_3)_2$ was prepared by the procedure of Wilkinson *et al.*[12] $Pd(OCOCF_3)_2$ (0.083 g, 0.25 mmol) was reacted with **1** (0.081 g, 0.5 mmol) according to the same procedures as above. GLC analysis showed that **3**, **5**, and **6** were formed in 45% combined yield, based on charged **1**, in the ratio 83: 14: 3. The yield was determined with biphenyl as an internal standard.

*Reaction of **1** with $Hg(OAc)_2$.* $Hg(OAc)_2$ (0.318 g, 1 mmol) was reacted with **1** (0.162 g, 1 mmol) in MeOH (19 ml)–H_2O (1 ml) at 35 °C for 3 h. The reaction mixture was extracted with ether, washed with water, and dried over $MgSO_4$–$NaHCO_3$. After evaporation of ether, the residue was dissolved in carbon tetrachloride. Organomercurial, probably 3-acetoxymercuri-2,2-dimethylchroman, was precipitated (0.247 g, 59%) by adding petroleum ether to the solution. The mercurial (0.247 g, 0.59 mmol) was added to a solution of $NaBH_4$ (0.022 g, 0.58 mmol) in 2 M sodium hydroxide (2 ml). The reaction mixture was stirred for 45 min at 15 °C, and extracted with ether. The extract was washed with water and dried over $MgSO_4$. Removal of ether gave a colorless oil (0.079 g, 83%) which was found to contain only 2,2-dimethylchroman by GLC analysis. 2,2-Dimethylchroman, NMR (CCl_4), δ 1.28 (s, 6H, Me), 1.73 (t, 2H, J=7 Hz, C-3 proton), 2.72 (t, 2H, J=7 Hz, benzylic proton), and 7.1—6.4 (m, 4H): (Found: C, 81.58; H, 8.78%. Calcd for $C_{11}H_{14}O$: C, 81.44; H, 8.70%.). The structure was confirmed by comparison with an authentic sample prepared by hydrogenation of **3** with palladium on charcoal.

*Reaction of 2-(2-Butenyl)phenol (**2**) with $PdCl_2$.* A mix-

ture of *cis*- and *trans*-**2** (*cis*/*trans*=1/1.9) was reacted with $PdCl_2$ (0.177 g, 1 mmol) in MeOH (38 ml)–H_2O (2 ml) at 35 °C for 5 h in the air. After filtration of precipitated metallic palladium, organic products were extracted with ether in the usual way. After removal of ether, the residue was subjected to alumina column chromatography (Al_2O_3, 8 g). Elution with petroleum ether (50 ml) gave colorless oil (0.110 g) containing **7**, **8**, **9**, and **10** in the ratio 50: 11: 18: 21 on GLC peak areas and unidentified products in less than 4%. The combined yield of cyclized products was approximately 34% based on charged **2**. These products were isolated by preparative GLC using 5% PEG-20 M Celite Column at 125 °C. 2-Methylchromene (**7**), NMR (CCl_4), δ 1.32 (d, 3H, J=6.5 Hz, Me), 4.90 (ddq, 1H, J=6.5, 3, and 1.8 Hz, C-2 proton), 5.56 (dd, 1H, J=3 and 9 Hz, olefinic proton), 6.28 (dd, 1H, J=9 and 1.8 Hz, olefinic proton), and 7.5—6.7 (m, 4H); Found: C, 82.25; H, 6.82%. Calcd for $C_{10}H_{10}O$: C, 82.16; H, 6.90%. 2-Methyl-4-methoxychroman (**8**), NMR (CCl_4), δ 1.40 (d, 3H, J=6.5 Hz, Me), 1.62 (ddd, 1H, J=13, 9.5, and 3 Hz, C-3 proton), 2.05 (ddd, 1H, J=13, $\approx$1, and $\approx$2 Hz, C-3 proton), 3.33 (s, 3H, OMe), 4.10 (dd, 1H, J=3 and $\approx$2 Hz, benzylic proton), 4.32 (m, 1H, C-2 proton), 6.7—6.9 (m, 2H), and 7.0—7.3 (m, 2H). Found: C, 73.98; H, 7.75%. Calcd for $C_{11}H_{14}O_2$: C, 74.13; H, 7.92%. The assignment of structure **8** is supported by the double irradiation experiment in NMR. Double irradiation of benzylic proton (δ 4.10) simplified the signals of C-3 protons (δ 1.62 and 2.05), showing two sets of double doublet (J=13 and 9.5 Hz and J=13 and $\approx$1 Hz). The signals of C-3 protons were transformed into two sets of broad doublet by irradiating on the C-2 proton (δ 4.32). The multiplet of C-2 proton was simplified by double irradiation of the methyl signal at δ 1.04 to show a broad doublet (J=9.5 Hz). The C-2 proton signal was also simplified by double irradiation of C-3 proton at δ 1.62 and 2.05 to show a doublet of quartet, in each case, bearing coupling constants of J=6.5 and $\approx$1 Hz, and J=6.5 and 9.5 Hz, respectively. 2-Methyl-2-methoxychroman (**9**) was identified by comparison with the spectral data reported by Dolby *et al.*[14] (Found: C, 74.29; H, 7.69%. Calcd for $C_{11}H_{14}O_2$: C, 74.13; H, 7.92%). Identification of 2-ethylbenzofuran (**10**) and 2-vinyl-2,3-dihydrobenzofuran (**11**) was described previously.[2b]

Reaction of **2** *with* $PdCl_2$ *in the Presence of NaOAc.* Allylphenol **2** (0.445 g, 3 mmol) was reacted with $PdCl_2$ (0.276 g, 1.5 mmol) in the presence of NaOAc (1.968 g, 24 mmol) in MeOH (57 ml)–H_2O (3 ml) at 35 °C for 3 h in the air. GLC analysis showed that only benzofurans **5** and **6** were formed in 40% combined yield based on charged **2**, in the ratio 52: 58. The yield was determined with biphenyl as an internal standard.

References

1) a) T. Hosokawa, K. Maeda, K. Koga, and I. Moritani, *Tetrahedron Lett.*, **1973**, 739; b) T. Hosokawa, H. Ohkata, and I. Moritani, *Bull. Chem. Soc. Jpn.*, **48**, 1533 (1975).

2) a) K. Maeda, T. Hosokawa, S-I, Murahashi, and I. Moritani, *Tetrahedron Lett.*, **1973**, 5057; b) T. Hosokawa, N. Shimo, K. Maeda, A. Sonoda, and S-I. Murahashi, *ibid.*, **1976**, 383.

3) T. Hosokawa, M. Hirata, S-I. Murahashi, and A. Sonoda, *Tetrahedron Lett.*, **1976**, 1821.

4) Other workers have also succeeded in preparing some heterocyclic compounds by using cyclizations of this type; a) A. Kasahara, T. Izumi, and M. Ooshima, *Bull. Chem. Soc. Jpn.*, **47**, 2526 (1974); b) T. Izumi and A. Kasahara, *ibid.*, **48**, 1673 (1975); c) L. S. Hegedus, G. F. Allen, and E. L. Waterman, *J. Am. Chem. Soc.*, **98**, 2674 (1976).

5) In practice, several palladium(II) species such as $PdCl_{4-n}(OAc)_n^{2-}$ (n=0—4) would be in equilibrium in solution, and the extent of displacement will increase by increasing the amount of NaOAc added. In this report such palladium(II) species are referred to as Pd(II) species. The displacement of chloride ligands in $PdCl_2$ by excess NaOAc in acetic acid has been reported: *Cf.* M. Tamura and T. Yasui *Kogyo Kagaku Zasshi*, **71**, 1855 (1968). It has also been reported that palladium(II) acetate existing as trimeric form in solid reacts with excess NaOAc in acetic acid to give monomeric species such as $NaPd(OAc)_4$: *Cf.* P. M. Henry and R. N. Pandey, *Adv. Chem. Ser.*, **132**, 33 (1974) and also L. Eberson and L. Gomez-Gonzalez, *Acta Chem. Scand.*, **27**, 1162 (1973).

6) Owing to decomposition to metallic palladium under these conditions, no accurate absorption intensity could be determined. In this experiment, 2—30 fold excess of NaOAc was added to $PdCl_2$.

7) Interaction of $PdCl_2$ and NaCl in aqueous solution leads to the formation of $PdCl_4^{2-}$ as a predominant palladium(II) species existing in solution: *Cf.* A. Aguiló, *Adv. Organomet. Chem.*, **5**, 322 (1967).

8) P. M. Maitlis, "The Organic Chemistry of Palladium," Vol. 2, Academic Press, New York (1971), p. 77.

9) W. M. Scovell, *J. Am. Chem. Soc.*, **96**, 3451 (1974).

10) L. Claisen, *J. Prakt. Chem.*, **105**, 76 (1922).

11) C. D. Hurd and W. A. Hoffman, *J. Org. Chem.*, **5**, 212 (1940).

12) T. A. Stephenson, S. M. Morehouse, A. R. Powell, J. P. Heffer, and G. Wilkinson, *J. Chem. Soc.*, **1965**, 3632.

13) I. M. Campbell, C. H. Calzadilla, and N. J. McCorkindale, *Tetrahedron Lett.*, **1966**, 5107; *Cf.* also, G. Cardillo, R. Cricchio, and L. Merlini, *Tetrahedron*, **24**, 4825 (1968).

14) L. J. Dolby, C. A. Elliger, S. Esfandiari, and K. S. Marshall, *J. Org. Chem.*, **33**, 4508 (1968).

Synthesis of 1-*N*-[(*S*)-4-amino-2-hydroxybutyryl]-3′-deoxyribostamycin[1] (3′-Deoxybutirosin B)

Daishiro IKEDA,* Fumiko NAGAKI,* Tsutomu TSUCHIYA, Sumio UMEZAWA, and Hamao UMEZAWA

Institute of Bioorganic Chemistry, 1614 Ida, Nakahara-ku, Kawasaki 211
**Department of Applied Chemistry, Faculty of Engineering, Keio University, Hiyoshi, Kohoku-ku, Yokohama 223*

(Received July 28, 1976)

3′-Deoxybutirosin B (**13**) was prepared from ribostamycin by way of the following reaction sequences: 1) selective 3′-*O*-arylsulfonylation, 3′-iodination, and 3′-deoxygenation; 2) 1,6-cyclic carbamate formation,selective hydrolysis of the carbamate and acylation of the free 1-NH_2 group with an active ester of (*S*)-4-amino-2-hydroxybutyric acid. The structure of **13** was confirmed by comparison of its $\Delta[M]_{TACu}$ value with those of butirosin B and 4′-deoxybutirosin B.

As reported in a previous paper,[2] 3′-deoxyribostamycin exhibits antibacterial activity against various bacteria including those which produce kanamycin-neomycin phosphotransferase II[3] (P-ase II). 3′-Deoxyribostamycin, however, does not inhibit the growth of resistant organisms which produce kanamycin-neomycin phosphotransferase I[4] (P-ase I). On the other hand, butirosin B,[5] 1-*N*-[(*S*)-4-amino-2-hydroxybutyryl]-ribostamycin, inhibits the growth of resistant organisms producing P-ase I but not those producing P-ase II.

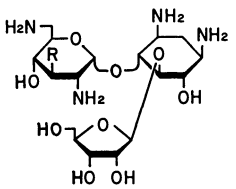

Ribostamycin R : OH
3′-Deoxyribostamycin R : H

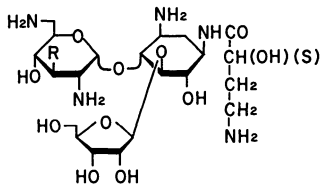

Butirosin B R : OH
3′-Deoxybutirosin B R : H

The titled compound, 3′-deoxybutirosin B is, therefore, expected to be active against both kinds of resistant bacteria.

This paper describes the synthesis of the titled compound starting from ribostamycin. This synthesis is an extension of the method[6] developed by us and involves the following reaction sequences: 1) removal of the 3′-hydroxyl group of ribostamycin by selective 3′-*O*-arylsulfonylation followed by iodination and hydrogenolysis of the iodine group in a similar fashion as reported in the synthesis[7] of tobramycin (3′-deoxykanamycin B) from kanamycin B; 2) coupling of (*S*)-4-amino-2-hydroxybutyryl group with the free 1-NH_2 group which is produced by way of 1,6-cyclic carbamate[8] formation followed by its selective cleavage.

Tetra-*N*-benzyloxycarbonyl-3′,4′:2″,3″-di-*O*-cyclohexylidene-5″-*O*-(1-methoxycyclohexyl) ribostamycin[9] (**1**) was treated with dilute acetic acid to split the acid-sensitive 5″-*O*-protecting group selectively. Treatment of the demethoxycyclohexyl derivative (**2**) with sodium hydride in *N*,*N*-dimethylformamide (DMF) gave the

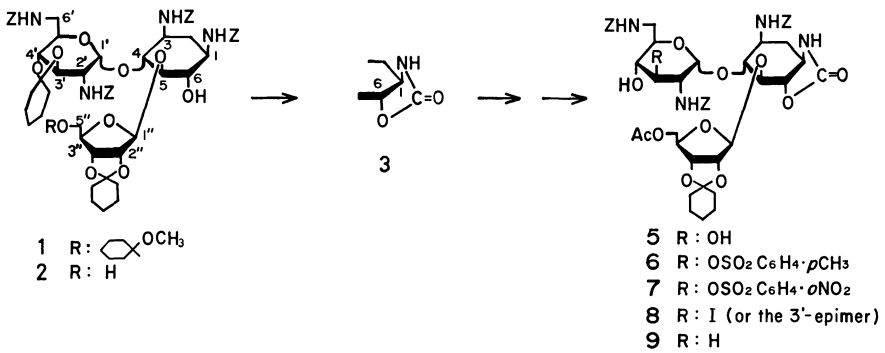

1 R:
2 R: H

3

5 R : OH
6 R : $OSO_2C_6H_4$-*p*CH_3
7 R : $OSO_2C_6H_4$-*o*NO_2
8 R : I (or the 3′-epimer)
9 R : H

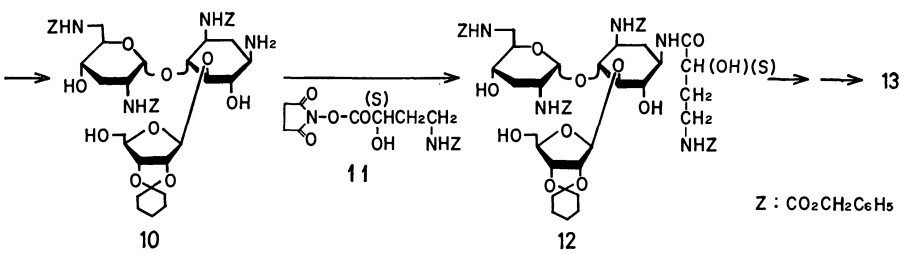

11

10

12

Z : $CO_2CH_2C_6H_5$

1,6-cyclic carbamate (**3**) as described in a previous paper.[8] Acetylation of **3** gave the 5″-*O*-acetyl derivative (**4**), from which the 3′,4′-*O*-cyclohexylidene group was selectively removed in a weakly acidic medium quantitatively.

Treatment of the partially decyclohexylidenated derivative (**5**) with *p*-toluenesulfonyl chloride or *o*-nitrobenzenesulfonyl chloride in pyridine at −37 °C successfully gave the selectively sulfonylated derivatives **6** and **7**, respectively.

Replacement of the 3′-*O*-tosyl or 3′-*O*-*o*-nitrobenzenesulfonyl group of **6** or **7** with iodide was carried out with 50% sodium iodide in DMF to give the 3′-iodo derivative (**8**). This iodination might be due to the participation by the 2′-acylamino group, as described in the preparation of tobramycin.[7] In the iodination, **7** reacted with sodium iodide more smoothly than **6**. Hydrogenation of **8** with Raney nickel in dioxane in the presence of triethylamine gave the 3′-deoxy derivative (**9**).

Selective opening of the 1,6-carbamate was successfully performed by use of a limited amount of barium hydroxide in dioxane, as reported in a previous paper,[8] to give **10**. To the free 1-NH_2 group, then, (*S*)-4-benzyloxycarbonylamino-2-hydroxybutyryl group was introduced by using an active ester (**11**)[10] prepared from (*S*)-4-benzyloxycarbonylamino-2-hydroxybutyric acid, *N*-hydroxysuccinimide, and dicyclohexylcarbodiimide. Catalytic hydrogenolysis of the *N*-benzyloxycarbonyl groups of the amide (**12**) followed by removal of the 2″,3″-*O*-cyclohexylidene group with aqueous hydrochloric acid gave 3′-deoxybutirosin B (**13**). The compound had strong antibacterial activity[1] against various strains of both usual and resistant bacteria.

To confirm the structure of **13**, its $\Delta[M]_{TACu}$ value[11] was measured, as well as those of butirosin B and 4′-deoxybutirosin B,[12] to be +410°, −398°, and −528°, respectively. The facts that butirosin B and 4′-deoxybutirosin B had similar values in sign and magnitude and that **13** had a value of +800—900° larger than that of butirosin B or 4′-deoxybutirosin B show that **13** has no 3′-hydroxyl group, which renders **13** impossible to form a Cu-complex between 2′-NH_2 and 3′-OH groups, the contribution being estimated to be $\Delta[M]_{TACu} \approx -900°$.

Experimental

NMR spectra were recorded at 60 MHz with Varian A-60D spectrometer. Infrared spectra were determined in KBr discs with Hitachi 285 grating infrared spectrophotometer. Thin-layer chromatography (TLC) was carried out on Wakogel B-5 with sulfuric acid spray for detection unless otherwise stated. For column chromatography, silica gel (Wakogel C-200) was used.

Tetra-N-*benzyloxycarbonyl-3′,4′ : 2″,3″-di*-O-*cyclohexylideneribostamycin (2).* A solution of **1**[9] (4.50 g) in a mixture of 40% acetic acid–acetone (1 : 5, 92 ml) was heated at 37 °C for 7.5 h. The solution was poured into a mixture of chloroform (400 ml) and an aqueous saturated sodium hydrogencarbonate solution (200 ml) with stirring. The organic layer separated was washed with water, dried (Na_2SO_4), and concentrated to give a solid (4.50 g). The solid contained two components, **1** (TLC, R_f 0.84 with benzene–ethyl acetate=5 : 3) and **2** (R_f 0.35). The mixture was chromatographed over silica gel firstly with benzene–ethyl acetate (5 : 3) containing 0.5% triethylamine,* and **1** (1.11 g) was eluted. The developing solvent was then changed to benzene–ethyl acetate (1 : 1) containing 0.5% triethylamine to give **2**, 2.58 g (84%), mp 103—107 °C, $[\alpha]_D^{20}$ +23° (*c* 2, $CHCl_3$).

Found: C, 63.51; H, 6.47; N, 4.85%. Calcd for $C_{61}H_{74}N_4O_{18}$: C, 63.64; H, 6.48; N, 4.87%.

3,2′,6′-Tri-N-*benzyloxycarbonyl-3′,4′ : 2″,3″-di*-O-*cyclohexylideneribostamycin 1,6-Carbamate (3).* To an ice-cold solution of **2** (0.99 g) in dry DMF (11.5 ml), 50% oily sodium hydride (86 mg) was added and the mixture was stirred for 2 h in the cold under atmosphere of nitrogen. The mixture became clear after 30 min. The solution, after neutralization with acetic acid, was poured into a mixture of chloroform-saturated sodium chloride solution (1 : 1, 200 ml) with vigorous stirring. The organic layer separated was washed with water, dried (Na_2SO_4), and concentrated to give a pale yellow syrup. It was chromatographed over silica gel with benzene–ethyl acetate (1 : 1) containing 0.1% triethylamine. From the earlier and the later fractions, **2** (0.08 g) and **3** (0.62 g, 69%) were isolated, respectively. Compound **3**: mp 115—118 °C, $[\alpha]_D^{20}$ +26° (*c* 2, $CHCl_3$); IR: 1770 (cyclic carbamate[13]), 1715 (carbamate), 1520 (amide II) cm^{-1}.

Found: C, 62.07; H, 6.44; N, 5.50%. Calcd for $C_{54}H_{66}N_4O_{17}$: C, 62.18; H, 6.38; N, 5.37%.

5″-O-Acetyl-3,2′,6′-tri-N-*benzyloxycarbonyl-3′,4′ : 2″,3″-di*-O-*cyclohexylideneribostamycin 1,6-Carbamate (4).* Compound **3** was treated with acetic anhydride and pyridine in a usual manner to give **4** (98%), mp 110—113 °C, $[\alpha]_D^{20}$ +20° (*c* 1.5, $CHCl_3$); IR: 1770, 1730 (sh), 1715, 1520 cm^{-1}; NMR ($CDCl_3$) δ: 2.05 (3H, s, Ac).

Found: C, 61.72; H, 6.28; N, 4.92%. Calcd for $C_{56}H_{68}N_4O_{18}$: C, 61.98; H, 6.32; N, 5.16%.

5″-O-Acetyl-3,2′,6′-tri-N-*benzyloxycarbonyl-2″,3″*-O-*cyclohexylideneribostamycin 1,6-Carbamate (5).* A solution of **4** (2.96 g) in a mixture of acetone–60% acetic acid (1 : 1, 120 ml) was heated at 60 °C. After 1 h, the solution contained only **5** (TLC, R_f 0.15 with benzene–ethyl acetate=1 : 2), **4** (R_f 0.6) disappearing completely. The solution was concentrated *in vacuo* and the concentrate was extracted with chloroform. The organic layer was washed successively with aqueous sodium hydrogencarbonate, water, dried (Na_2SO_4), and concentrated to give a solid of **5** (2.75 g), which was purified by reprecipitation from chloroform–hexane, 2.61 g (95%), mp 109—112 °C, $[\alpha]_D^{20}$ +11° (*c* 2, $CHCl_3$); IR: 1760 (m), 1730 (sh), 1700, 1520 cm^{-1}; NMR ($CDCl_3$) δ: 2.03 (3H, s, Ac), 1.2—1.85 (≈11H).

Found: C, 59.59; H, 6.04; N, 5.33%. Calcd for $C_{50}H_{60}N_4O_{18}$: C, 59.75; H, 6.02; N, 5.57%.

5″-O-Acetyl-3,2′,6′-tri-N-*benzyloxycarbonyl-2″,3″*-O-*cyclohexylidene-3′*-O-*tosylribostamycin 1,6-Carbamate (6).* To a solution of **5** (1.77 g) in dry pyridine (38 ml), *p*-toluenesulfonyl chloride (1.91 g, 5 mol equivalents for **5**) was added and the solution was heated at 37 °C for 18 h and then additionally at 60 °C for 1 h. The solution showed, on TLC with benzene–ethyl acetate (1 : 1), a major spot (**6**, R_f 0.4) accompanied with other two minor spots of R_f 0.06 (**5**) and 0.6 (4′-*O*-tosyl isomer ?). Water (0.3 ml) was added and the solution was concentrated to give a reddish syrup. The chloroform solution of the syrup was washed successively with aqueous potassium hydrogensulfate, aqueous sodium hydrogencarbonate, and water, dried (Na_2SO_4), and concentrated. The resulting yellow syrup was chromatographed over silica gel with benzene–ethyl acetate (1 : 1) and from the fraction containing the major component, **6** was isolated as a colorless solid, 1.55 g (76%),

* Triethylamine was added in order to prevent removal of the cyclohexylidene groups during the chromatography.

mp 110—112 °C, $[\alpha]_D^{20}$ +13° (*c* 1.7, $CHCl_3$); IR: 1770 (cyclic carbamate), 1720 (carbamate), 1740 (sh, ester), 1520 (amide II); NMR ($CDCl_3$) δ: 2.05 (3H, s, Ac), 2.38 (3H, s, CH_3(Ts)).

Found: C, 59.30; H, 5.78; N, 4.72; S, 2.66%. Calcd for $C_{57}H_{66}N_4O_{20}S$: C, 59.06; H, 5.74; N, 4.83; S, 2.77%.

*5″-O-Acetyl-3,2′,6′-tri-*N*-benzyloxycarbonyl-2″,3″-O-cyclohexylizene-3′-O-(o-nitrobenzenesulfonyl)ribostamycin 1,6-Carbamate (7).* Compound **5** was treated with *o*-nitrobenzenesulfonyl chloride in a similar manner as described for **6** to give **7** (66%), mp 114—116 °C, $[\alpha]_D^{14}$ +6.5° (*c* 2.3, $CHCl_3$); NMR ($CDCl_3$) δ: 2.02 (3H, s, Ac).

Found: C, 56.25; H, 5.40; N, 5.75; S, 2.88%. Calcd for $C_{50}H_{63}N_5O_{22}S$: C, 56.51; H, 5.34; N, 5.88; S, 2.69%.

*5″-O-Acetyl-3,2′,6′-tri-*N*-benzyloxycarbonyl-2″,3″-O-cyclohexylidene-3′-deoxy-3′-iodoribostamycin 1,6-Carbamate (8).*

A. From **6**: To a solution of **6** (0.58 g) in dry DMF (10 ml), sodium iodide (6 g, dried at 100 °C *in vacuo*) was added and the mixture was stirred at 100 °C for 10 h under the atmosphere of nitrogen. The reddish-brown solution, which soon solidified on cooling, was extracted with chloroform and the organic solution was concentrated with several additions of toluene. The resulting solid was extracted again with chloroform and the solution was washed successively with saturated sodium chloride solution, aqueous sodium thiosulfate, and water, dried (Na_2SO_4), and concentrated. The brown solid was chromatographed over silica gel with benzene–ethyl acetate (1: 1) to give a solid of **8**, 324 mg (58%), mp 108—110 °C, $[\alpha]_D^{15}$ +5° (*c* 3, $CHCl_3$); NMR ($CDCl_3$) δ: 2.1 (3H, s, Ac).

Found: C, 54.23; H, 5.49; N, 5.02; I, 11.05%. Calcd for $C_{50}H_{59}N_4O_{17}I$: C, 53.86; H, 5.34; N, 5.03; I, 11.38%.

B. From **7**: Compound **7** was treated similarly as described above except that the reaction period and the developing solvent on column chromatography were changed to 1.5 h and benzene–ethyl acetate (2: 3). Yield of **8** was 65%.

*5″-O-Acetyl-3,2′,6′-tri-*N*-benzyloxycarbonyl-2″,3″-O-cyclohexylidene-3′-deoxyribostamycin 1,6-Carbamate (9).* To a solution of **8** (310 mg) in dioxane (9 ml), triethylamine (0.04 ml) was added, and the solution was hydrogenated with Raney nickel at 80 °C for 1 h under atmospheric pressure of hydrogen. After filtration, the solution was repeatedly hydrogenated with twice additions of fresh Raney nickel and triethylamine. Concentration of the solution gave a solid, which was chromatographed over silica gel with benzene–ethyl acetate (1: 2) to give **9**, 192 mg (70%), mp 97—99 °C, $[\alpha]_D^{13}$ +5° (*c* 1, $CHCl_3$).

Found: C, 60.35; H, 6.20; N, 5.52%. Calcd for $C_{50}H_{60}N_4O_{17}$: C, 60.72; H, 6.11; N, 5.66%.

*3,2′,6′-Tri-*N*-benzyloxycarbonyl-2″,3″-O-cyclohexylidene-3′-deoxyribostamycin (10).* To a solution of **9** (156 mg) in dioxane (3 ml), 0.1 M barium hydroxide solution (2.4 ml, 1.5 mol equivalents for **9**) was added and the mixture was stirred at 60 °C for 1 h. TLC (with benzene–methanol 4: 1) showed a single spot of **10** (R_f 0.5, ninhydrin positive) and none of **9** (R_f 0.8). After introduction of carbon dioxide followed by centrifugation, the solution was concentrated to dryness. The solid was extracted with dioxane and, after centrifugation, the supernatant layer was concentrated. The resulting solid (151 mg) still contained a trace of inorganic salt, however, it was chromatographically homogeneous and was used without purification for the next step. IR: 1700 cm^{-1} (carbamate).

*3,2′,6′-Tri-*N*-benzyloxycarbonyl-1-*N*-[(S)-4-benzyloxycarbonylamino-2-hydroxybutyryl]-2″,3″-O-cyclohexylidene-3′-deoxyribostamycin (12).* To a solution of **10** (370 mg) and triethylamine (0.04 g) in THF (8 ml), the active ester[10] (**11**, 170 mg) was added and the solution was kept at room temperature overnight. The solution was concentrated and the residue was chromatographed over silica gel with chloroform–2-propanol (10: 1). The fractions containing the major component (**12**, R_f 0.42 on TLC with the above solvent system) were collected and concentrated to give a solid of **12**, 186 mg (40% based on **9**), mp 102—106 °C, $[\alpha]_D^{18}$ +2.5° (*c* 1, $CHCl_3$).

Found: C, 59.44; H, 6.21; N, 5.87%. Calcd for $C_{59}H_{73}N_5O_{19}\cdot 2H_2O$: C, 59.44; H, 6.51; N, 5.87%.

*1-*N*-[(S)-4-Amino-2-hydroxybutyryl]-3′-deoxyribostamycin (3′-Deoxybutirosin B) (13).* To a solution of **12** (178 mg) in dioxane (4.3 ml), water (1.4 ml) was added and the slight opalescent solution was hydrogenated with palladium black under atmospheric pressure of hydrogen. After 2 h, the solution showed, on TLC with a system of $CHCl_3$–CH_3OH–17% NH_4OH (2: 2: 1), two ninhydrin positive spots (R_f 0.4, major; and R_f 0.7, slight). The solution was filtered and the filtrate was concentrated to dryness. The residue was dissolved in a drop of 1 M aqueous hydrochloric acid and the solution was heated at 60 °C for 1 h. The solution then showed, on TLC with a system of $CHCl_3$–CH_3OH–17% NH_4OH (1: 4: 3) (detected by 0.2% ninhydrin in pyridine) a major spot at R_f 0.27. Addition of acetone gave precipitates, which were charged on a column of CM-Sephadex C-25 (NH_4 form) and, after washing the column with water, elution was effected with aqueous ammonia with linear increase in ammonia concentration (0.1—0.4 M). The eluate containing **13** was concentrated to give a solid, 35 mg (37%), $[\alpha]_D^{24}$ +27° (*c* 2, H_2O); IR: 1640, 1560 cm^{-1}.

Found: C, 43.44; H, 7.26; N, 11.45%. Calcd for $C_{21}H_{41}N_5O_{11}\cdot H_2CO_3$: C, 43.92; H, 7.20; N, 11.64%.

The authors wish to express their thanks to Dr. H. Kawaguchi, Director of Research Institute, Bristol Banyu Co. Ltd., for the kind supply of 4′-deoxybutirosin B.

References

1) D. Ikeda, F. Nagaki, S. Umezawa, T. Tsuchiya, and H. Umezawa, *J. Antibiot.*, **28**, 616 (1975).
2) D. Ikeda, T. Tsuchiya, S. Umezawa, and H. Umezawa, *J. Antibiot.*, **26**, 799 (1973).
3) M. Yagisawa, H. Yamamoto, H. Naganawa, S. Kondo, T. Takeuchi, and H. Umezawa, *J. Antibiot.*, **25**, 748 (1972).
4) H. Umezawa, H. Yamamoto, M. Yagisawa, S. Kondo, T. Takeuchi, and Y. A. Chabbert, *J. Antibiot.*, **26**, 407 (1973).
5) P. W. K. Woo, H. W. Dion, and Q. R. Bartz, *Tetrahedron Lett.*, **1971**, 2617; *ibid.*, **1971**, 2625.
6) S. Umezawa, *Adv. Carbohydr. Chem. Biochem.*, **30**, 111 (1974).
7) Y. Takagi, T. Miyake, T. Tsuchiya, S. Umezawa, and H. Umezawa, *J. Antibiot.*, **26**, 403 (1973); *Bull. Chem. Soc. Jpn.*, **49**, 3649 (1976).
8) D. Ikeda, T. Tsuchiya, S. Umezawa, and H. Umezawa, *Bull. Chem. Soc. Jpn.*, **47**, 3136 (1974).
9) D. Ikeda, T. Suzuki, T. Tsuchiya, S. Umezawa, and H. Umezawa, *Bull. Chem. Soc. Jpn.*, **46**, 3210 (1973).
10) H. Kawaguchi, T. Naito, S. Nakagawa, and K. Fujisawa, *J. Antibiot.*, **25**, 695 (1972).
11) S. Umezawa, T. Tsuchiya, and K. Tatsuta, *Bull. Chem. Soc. Jpn.*, **39**, 1235 (1966).
12) M. Konishi, K. Numata, K. Shimoda, H. Tsukiura, and H. Kawaguchi, *J. Antibiot.*, **27**, 471 (1974).
13) S. Umezawa, Y. Takagi, and T. Tsuchiya, *Bull. Chem. Soc. Jpn.*, **44**, 1411 (1971).

Quantitative Analysis of Organocalcium Halides by Double Titration

Nariyoshi KAWABATA,* Hisao NAKAMURA, and Shinzo YAMASHITA

Department of Chemistry, Kyoto Institute of Technology, Matsugasaki, Sakyo-ku, Kyoto 606

(Received July 30, 1976)

The principle of Gilman's double titration method for organolithium compounds was applied to the quantitative analysis of organocalcium halides. Chloroform was found to be useful as a reactive halide which completely decomposed organocalcium halides, but did not react with other alkali. The method gave satisfactory analysis for methyl-, propyl- and phenylcalcium iodides.

Simple acid titration for the quantitative analysis of organocalcium halides (RCaX) usually gives too high values.[1] The quantitative analysis of organocalcium halides based on the amount of hydrocarbon (RH) evolved by the addition of water, alcohol or carboxylic acid usually gives reliable results. However, when R is a higher alkyl or aryl group, the analytical procedure gives satisfactory results only immediately after preparation of the organocalcium halides, since they react slowly with ethereal solvents to give the same hydrocarbon (RH), which remains in the system. Quantitative analysis based on the amount of carboxylic acid produced by carboxylation of organocalcium halides is not useful when R is an alkyl group, since the carboxylation does not give the corresponding carboxylic acid quantitatively.[1,2] The present work was undertaken to establish a useful, convenient, and reliable method for the quantitative analysis of organocalcium halides by application of Gilman's double titration method to organolithium compounds.[3-5] No successful result was available in the literature on quantitative analysis of organocalcium compounds by the double titration method.

Results and Discussion

In order to obtain accurate results in the Gilman's double titration method, it is necessary to completely decompose the organolithium compounds by the addition of a reactive halide before the second titration. The halide should not react with alkali other than the organolithium compounds. Thus the first problem was to find a suitable halide which rapidly reacts with organocalcium halides but not with other alkali. Benzyl chloride is not adequate for this purpose, since it reacts very slowly with organocalcium halides.[6] Bryce-Smith and Skinner[1] reported that preliminary attempts to use benzyl chloride in a double titration procedure for organocalcium halides gave no promising results. We attempted to use a variety of organic halides which were more reactive than benzyl chloride toward organocalcium halides.

First we carried out a double titration on a supernatant layer of phenylcalcium iodide in diethyl ether using carbon tetrachloride, chloroform, dibromomethane, and 1,2-dibromoethane. These halides were allowed to react with phenylcalcium iodide for 5—10 min at room temperature before the second titration. The standard molarity was determined based on the amount of benzoic acid obtained by carboxylation. Vapor phase chromatographic analysis showed neither benzophenone nor triphenylmethanol in the products of carboxylation indicating the adequacy of the above molarity as a standard. Chloroform gave satisfactory results which are given in Table 1. Carbon tetrachloride gave a too high value, probably due to the reaction of the chloride with alkali other than phenylcalcium iodide. On the other hand, dibromomethane and 1,2-dibromoethane gave too low values, apparently due to slow reactions of these halides with phenylcalcium iodide.

Table 1. Analysis of phenylcalcium iodide solution in diethyl ether[a]

Organic halide	Molarity: Total alkali	Molarity: By double titration	Molarity: Standard[b]	Error (%)
CCl_4	0.501	0.369	0.292	+26
$CHCl_3$	0.501	0.291	0.292	0
CH_2Br_2	0.501	0.189	0.292	−35
$BrCH_2CH_2Br$	0.501	0.189	0.292	−35

a) Phenylcalcium iodide was prepared by the reaction of 5.0 mmol of iodobenzene with 6.5 mmol of calcium metal in 10 ml of diethyl ether. The analysis was carried out for a supernatant layer of phenylcalcium iodide in diethyl ether at room temperature, and the reaction with organic halides was carried out for 5—10 min at room temperature before the second titration. b) The standard molarity was determined from the amount of benzoic acid evolved by carboxylation.

The mode of titration in a uniform suspension of phenylcalcium iodide in diethyl ether was similar to that in solution (Table 2). Although excess calcium metal was used in the preparation of phenylcalcium iodide, chloroform gave satisfactory results. Probably the reaction of the halide with excess calcium metal was

Table 2. Analysis of phenylcalcium iodide suspension in diethyl ether[a]

Organic halide	Molarity: Total alkali	Molarity: By double titration	Molarity: Standard[b]	Error (%)
$CBrCl_3$	0.583	0.302	0.216	+40
CCl_4	0.583	0.276	0.216	+28
$CHCl_3$	0.583	0.227	0.216	+5
CH_2Br_2	0.583	0.151	0.216	−30

a) See footnote (a) in Table 1. b) See footnote (b) in Table 1.

* To whom correspondence should be addressed.

negligibly slow under the conditions. Thus, the double titration method can be satisfactorily applied to suspensions in diethyl ether, although experimental error would be more significant since it is not easy to take out a homogeneous sample.

Chloroform gave satisfactory results for a supernatant layer of phenylcalcium iodide in tetrahydrofuran (Table 3).

TABLE 3. ANALYSIS OF PHENYLCALCIUM IODIDE SOLUTION IN TETRAHYDROFURAN[a)]

Organic halide	Molarity			Error (%)
	Total alkali	By double titration	Standard[b)]	
$CHCl_3$	0.223	0.157	0.163	−4
$CHCl_3$	0.821	0.490	0.485	+1
CH_2I_2	0.223	0.120	0.163	−26
CH_2I_2	0.821	0.390	0.485	−20
CH_2ClI	0.223	0.105	0.163	−26
CH_2ClI	0.821	0.350	0.485	−28

a) See footnote (a) in Table 1. b) See footnote (b) in Table 1.

Two series of experiments were carried out on a uniform suspension of phenylcalcium iodide in tetrahydrofuran (Table 4). In series A, excess iodobenzene was used in the preparation of phenylcalcium iodide. Chloroform gave satisfactory results. In series B, excess calcium metal was used in the preparation of phenylcalcium iodide. Each titration gave too high values, probably due to the reaction of the halides with calcium metal which remained unchanged in the suspension of phenylcalcium iodide. Thus, the double titration method can be satisfactorily applied to suspensions in tetrahydrofuran in the absence of unchanged calcium metal.

TABLE 4. ANALYSIS OF PHENYLCALCIUM IODIDE SUSPENSION IN TETRAHYDROFURAN[a)]

Organic halide	Molarity			Error (%)
	Total alkali	By double titration	Standard[b)]	
Series A[c)]				
$CHCl_3$	0.776	0.512	0.502	+2
CH_2I_2	0.776	0.417	0.502	−17
CH_2ClI	0.776	0.379	0.502	−25
Series B[d)]				
$CHCl_3$	0.834	0.625	0.490	+28
CH_2I_2	0.834	0.614	0.490	+25
CH_2ClI	0.834	0.598	0.490	+22

a) The analysis was carried out for a uniform suspension of phenylcalcium iodide in tetrahydrofuran at room temperature, and the reaction with organic halides was carried out for 5—10 min at room temperature before the second titration. b) The standard molarity was determined from the amount of benzoic acid evolved by carboxylation. c) Phenylcalcium iodide was prepared by the reaction of 7.0 mmol of iodobenzene with 6.5 mmol of calcium metal in 10 ml of tetrahydrofuran. d) Phenylcalcium iodide was prepared by the reaction of 5.0 mmol of iodobenzene with 6.5 mmol of calcium metal in 10 ml of tetrahydrofuran.

Chloroform gave satisfactory results for suspensions of methylcalcium iodide in diethyl ether (Table 5). The standard molarity was determined from the amount of methane evolved by the addition of acetic acid. Carbon tetrachloride also showed satisfactory results in contrast to the case of phenylcalcium iodide. The reaction of carbon tetrachloride with alkali other than methylcalcium iodide seems to be insignificant. Dibromomethane and 1,2-dibromoethane gave better results when allowed to react with methylcalcium iodide at room temperature for a period of time before the second titration.

TABLE 5. ANALYSIS OF METHYLCALCIUM IODIDE SUSPENSION IN DIETHYL ETHER[a)]

Organic halide	Molarity			Error (%)
	Total alkali	By double titration[b)]	Standard[c)]	
$CBrCl_3$	0.895	>0.895(5)	0.657	>+36
CCl_4	0.895	0.611(10)	0.657	−8
CCl_4	0.659	0.482(10)	0.497	−3
$CHCl_3$	0.659	0.435(5)	0.497	−12
CH_2Br_2	0.659	0.459(45)	0.497	−8
$BrCH_2CH_2Br$	0.659	0.419(35)	0.497	−16
$BrCH_2CH_2Br$	0.453	0.097(5)	0.331	−71

a) Methylcalcium iodide was prepared by the reaction of 5.0 mmol of methyl iodide with 6.5 mmol of calcium metal in 10 ml of diethyl ether. The analysis was carried out for a uniform suspension of methylcalcium iodide in diethyl ether at room temperature. b) The number in parentheses indicates the time in min of the reaction of methylcalcium iodide with organic halides at room temperature before the second titration. c) The standard molarity was determined from the amount of methane evolved by the addition of acetic acid.

TABLE 6. ANALYSIS OF METHYLCALCIUM IODIDE SUSPENSION IN TETRAHYDROFURAN[a)]

Organic halide	Molarity			Error (%)
	Total alkali	By double titration	Standard[b)]	
$CHCl_3$	0.394	0.306	0.299	+2
$CHCl_3$[c)]	0.422	0.254	0.196	+30
CH_2I_2	0.394	0.276	0.299	−8
CH_2ClI	0.394	0.243	0.299	−19
CH_2Br_2	0.394	0.255	0.299	−15

a) Methylcalcium iodide was prepared by the reaction of 7.0 mmol of methyl iodide with 6.5 mmol of calcium metal in 10 ml of tetrahydrofuran. The analysis was carried out for a uniform suspension of methylcalcium iodide in tetrahydrofuran at room temperature, and the reaction with organic halides was carried out at room temperature for 5—10 min before the second titration. b) The standard molarity was determined from the amount of methane evolved by the addition of acetic acid. c) Methylcalcium iodide was prepared by the reaction of 5.0 mmol of methyl iodide with 6.5 mmol of calcium metal in 10 ml of tetrahydrofuran.

tion. Bromotrichloromethane gave a too high value. In this case, the reaction mixture of the halide with methylcalcium iodide was already acidic before the second titration.

Chloroform gave satisfactory results for a uniform suspension of methylcalcium iodide in tetrahydrofuran in the absence of unchanged calcium metal (Table 6).

In a double titration on a uniform suspension of propylcalcium iodide in diethyl ether, propylcalcium iodide was prepared in diethyl ether. Most of the solvent was removed by evaporation under reduced pressure at room temperature and replaced by cyclohexane. The analysis was carried out for the suspension of propylcalcium iodide. The standard molarity was determined based on the amount of propane evolved by the addition of acetic acid. The replacement of diethyl ether by cyclohexane was carried out in order to make the standard molarity more accurate by decreasing the amount of propane dissolved in the solvent and that of vaporized solvent. Cyclohexane can easily be frozen. Another aliquot of the suspension was taken out and added to diethyl ether containing reactive organic halides at room temperature. The reaction of propylcalcium iodide with the halides was carried out at room temperature for 10 min before the second titration. The results are given in Table 7. Chloroform and dibromomethane gave satisfactory results.

Chloroform gave satisfactory results for a uniform suspension of propylcalcium iodide in tetrahydrofuran (Table 8).

From the results, the reactivity of organic halides toward organocalcium halides appears to be in the order bromotrichloromethane>carbon tetrachloride>chloroform>dibromomethane>1,2-dibromoethane>benzyl chloride. Of these halides we recommend chloroform for the double titration, since it gave satisfactory results for methyl-, propyl-, and phenylcalcium iodides. Only 5—10 min was sufficient to destroy the organocalcium halides at room temperature, the coloration during the course of titration not being significant.

Table 7. Analysis of propylcalcium iodide suspension in diethyl ether[a)]

Organic halide	Molarity: Total alkali	Molarity: By double titration	Molarity: Standard	Error (%)
CCl_4	0.693	0.112	0.129	−13
$CHCl_3$	0.693	0.121	0.129	−6
CH_2Br_2	0.693	0.126	0.129	−2
$BrCH_2CH_2Br$	0.693	0.050	0.129	−61

a) Propylcalcium iodide was prepared by the reaction of 5.0 mmol of propyl iodide with 6.5 mmol of calcium metal in 10 ml of diethyl ether, most of the solvent being removed by evaporation under reduced pressure at room temperature and replaced by cyclohexane. The standard molarity was determined from the amount of propane evolved by the addition of acetic acid to the suspension. The double titration was carried out for the suspension in diethyl ether at room temperature. The reaction of propylcalcium iodide with organic halides was carried out at room temperature for 10 min before the second titration.

Table 8. Analysis of propylcalcium iodide suspension in tetrahydrofuran[a)]

Organic halide	Molarity: Total alkali	Molarity: By double titration	Molarity: Standard[b)]	Error (%)
$CHCl_3$	0.487	0.242	0.240	+1
$CHCl_3$	0.259	0.080	0.086	−7
CH_2I_2	0.487	0.229	0.240	−5
CH_2I_2	0.259	0.064	0.086	−26
CH_2ClI	0.487	0.178	0.240	−26
CH_2ClI	0.259	0.043	0.086	−50

a) Propylcalcium iodide was prepared by the reaction of 8.0 mmol of propyl iodide with 6.5 mmol of calcium metal in 10 ml of tetrahydrofuran. The analysis was carried out for a uniform suspension of propylcalcium iodide in tetrahydrofuran at room temperature, and the reaction with organic halides was carried out at room temperature for 5—10 min before the second titration. b) The standard molarity was determined from the amount of propane evolved by the addition of acetic acid.

The double titration method using chloroform as a reactive halide gave good results for a solution of phenylcalcium iodide. The method can be applied to uniform suspensions of methyl-, propyl-, and phenylcalcium iodides in tetrahydrofuran in the absence of unchanged calcium metal, and to those in diethyl ether even in the presence of some amount of unchanged calcium metal, although experimental error would be significant because of the difficulty to take out a uniform sample.

Thus, double titration using chloroform would be useful as a method for quantitative analysis for organocalcium halides, although its accuracy would compare unfavorably with the Gilman procedure for organolithium compounds, since many organocalcium halides are poorly soluble in organic solvents and we must use suspensions instead of solutions.

Experimental

Vapor phase chromatographic analysis was performed on a Shimadzu GC-4A gas chromatograph using columns of Chromosorb 101 (80—100 mesh), active charcoal (60—80 mesh) and polyethylene glycol 20 M on Celite 545 (60—80 mesh) for benzoic acid, methane and propane, and other products, respectively.

Materials. Calcium metal of higher purity (Mitsuwa Chemicals, Ltd., Osaka) was rasped in dry liquid paraffin. Particle size of the rasped calcium was 0.1—0.3 mm. Organocalcium halides were prepared in diethyl ether or in tetrahydrofuran. The organocalcium halides were immediately subjected to double titration, or left to stand at room temperature for several days before analysis. Organic halides were purified by distillation after being dried with calcium chloride or phosphorus pentoxide. Purification of diethyl ether, tetrahydrofuran, cyclohexane, and nitrogen was carried out as described.[7,8)] Carbon dioxide was dried with concentrated sulfuric acid and molecular sieves.

Analytical Procedure. A 2 or 3 ml aliquot of the solution or suspension of organocalcium halides to be analyzed was taken out with a hypodermic syringe and hydrolyzed with 30

ml of distilled water in a 100 ml beaker and acidified with excess standard 0.5 M hydrochloric acid, and titrated with standard 0.1 M sodium hydroxide solution using phenolphthalein as an indicator to give the total alkali present. A second aliquot was taken out and added to 10 ml of diethyl ether or tetrahydrofuran containing 1 ml of the organic halide in a 100 ml Erlenmeyer flask under a nitrogen atmosphere. The mixture was stirred at room temperature for the prescribed time, after which it was hydrolyzed with distilled water, acidified with excess standard 0.5 M hydrochloric acid and titrated with a standard 0.1 M sodium hydroxide solution, phenolphthalein being used as the indicator. In the second titration, the end point sometimes became obscure due to the coloration of the system, but the coloration was not significant when chloroform was used.

The standard molarity of phenylcalcium iodide was determined from the amount of benzoic acid evolved after carboxylation. Carboxylation was carried out at −30 °C for 2 h, and acidified by the addition of 6 M hydrochloric acid. The amount of evolved benzoic acid was determined by vapor phase chromatography.

The standard molarity of methylcalcium iodide and propylcalcium iodide was determined from the amount of methane and propane evolved by the addition of acetic acid at −70 and −10 °C, respectively. The total amount of evolved gas was determined by a gas burette, the gas being analyzed by vapor phase chromatography. The gas usually contained a small amount of hydrogen.

References

1) D. Bryce-Smith and A. C. Skinner, *J. Chem. Soc.*, **1963**, 577.
2) R. N. Meals, *J. Org. Chem.*, **9**, 211 (1944).
3) H. Gilman and A. H. Haubein, *J. Am. Chem. Soc.*, **66**, 1515 (1944).
4) C. W. Kamienski and D. L. Esmay, *J. Org. Chem.*, **25**, 115 (1960).
5) H. Gilman and F. K. Cartledge, *J. Organomet. Chem.*, **2**, 447 (1964).
6) N. Kawabata, H. Nakamura, and S. Yamashita, *J. Org. Chem.*, **38**, 3403 (1973).
7) N. Kawabata, A. Matsumura, and S. Yamashita, *J. Org. Chem.*, **38**, 4268 (1973).
8) N. Kawabata, A. Matsumura, and S. Yamashita, *Tetrahedron*, **29**, 1069 (1973).

Direct Observation of Dienol Intermediates in Photochemical Deconjugation of an α,β-Uusaturated Ketone. Photoisomerization of 1-Acetylcyclooctene[1]

Ryoji Noyori, Hiroshi Inoue, and Masao Katô

Department of Chemistry, Nagoya University, Chikusa, Nagoya 464

(Received August 30, 1976)

The photolysis of 1-acetylcyclooctene in acetonitrile solution leads to 3-(α-hydroxyethylidene)cyclooctene (two stereoisomers). Structures of the stable 1,3-dienols have been elucidated on the basis of their spectral data and chemical behavior. The dienols are highly air-sensitive. Upon heating, or by the action of an acid or base, they are converted to 3-acetylcyclooctene. In methanol-*O*-*d*, 3-acetylcyclooctene-3-*d* is formed. These findings provide the first, unambiguous evidence for the intervention of 1,3-dienol intermediates in photochemical deconjugation of an α,β-unsaturated ketone into the β,γ isomer.

Photo-irradiation of open-chain α,β-unsaturated ketones which bear hydrogen atom(s) at the position γ to the carbonyl function causes facile double bond migration to give the corresponding β,γ-unsaturated ketones.[2] Large-membered cyclic enones also undergo photoisomerization.[3] The deconjugation reaction is of

$$RCOCH{=}CHCH_2R' \xrightarrow{h\nu} RCOCH_2CH{=}CHR'$$

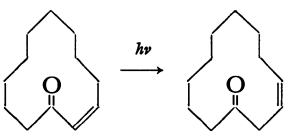

great synthetic value, because (1) the reaction proceeds under neutral and thermally moderate conditions and (2) the nonconjugated enone products are usually less stable compared with the starting conjugated enones. The reaction is considered to proceed *via* the mechanism outlined in Scheme 1, where the reaction of 5-methyl-3-hexen-2-one is exemplified. First, exposure of the α,β-unsaturated ketone leads to a photo-equilibrated mixture of the *trans* and *cis* isomers. The *cis* enone in an n, π* excited state[2] can abstract a γ-hydrogen atom to produce a 1,3-dienol, which upon ketonization results in the formation of the β,γ-isomer. The existence of the unstable dienol species has been suggested by the fact that photolysis in methanol-*O*-*d* affords 3-deuterio-5-methyl-4-hexen-2-one.[2b] However, none of these intermediates has been definitely characterized yet.[4] This paper describes direct observation of such a dienol intermediate in the photochemical deconjugation of enones, which provides unambiguous evidence for the mechanism involving dienol species.[5]

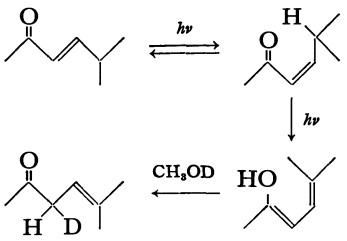

Scheme 1.

Results and Discussion

1-Acetylcyclooctene (**1**), taken as the enone substrate, was prepared by the titanium tetrachloride-catalyzed reaction of cyclooctene and acetyl chloride. The α,β-unsaturated ketone has characteristic IR bands (neat film) at 1668 (C=O) and 1638 cm^{-1} (C=C). The UV absorption maxima in acetonitrile solution occur at 233 (log ε 4.00) (π-π* band) and 319 nm (log ε 0.89) (n-π* band). All photolyses were effected in a well-deoxygenated solution placed in a Pyrex tube. A 200-W high-pressure mercury lamp was used as a light source and a 10% aq copper sulfate solution (1-cm depth) was employed as filter (<350-nm cut-off). Progress of the reaction was monitored spectroscopically.

Photolysis of the Enone **1** *in Acetonitrile.* A 5% solution of **1** in acetonitrile was placed in a Pyrex NMR tube and irradiated at room temperature under nitrogen atmosphere. The reaction was monitored by NMR. When the irradiation was continued for 10 h, the starting enone **1** was consumed completely and new alcoholic products (*vide infra*) were produced in *ca.* 80% yield. The products consisted of a 5: 1 mixture of two stereoisomers. The same ratio was obtained by GLPC analysis after conversion to the trimethylsilyl ethers by treating the reaction aliquot with *N*,*O*-bis(trimethylsilyl)acetamide. The photoreaction with more diluted solution (2.7×10^{-3} M) of **1** in acetonitrile proceeded in quantitative yield, as was indicated by monitoring the photolysis by UV spectroscopy. The absorption maximum of the enone at 233 nm was cleanly replaced by a new absorption band, λ_{max} 255 nm (log ε ≈4.0). The new products were identified as the dienols **2** and **3** on the basis of the following spectral and chemical evidence.

Infrared Spectrum of the Dienols **2** *and* **3**. Proof of the dienol structure was gained by the IR spectra shown

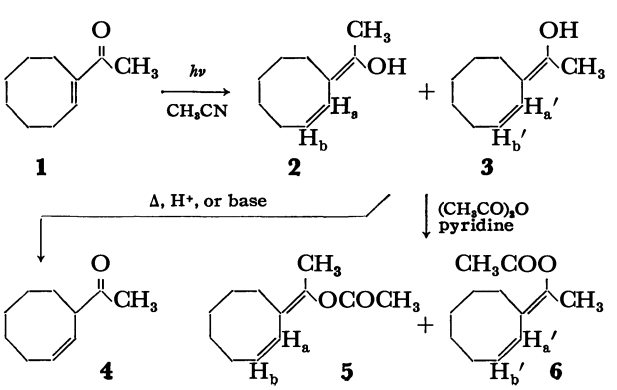

in Fig. 1. The photolysate exhibited a strong O–H strech at 3450 cm^{-1}, olefinic absorption at 1656 cm^{-1}, and C–O band at 1191 cm^{-1}, in accord with the assigned structures **2** and **3**. A carbonyl group is not present in the new products. A small absorption band was observed at $\approx$1700 cm^{-1}, but there were considerable variations in relative intensity of the band depending on the individual photolysis conditions. Therefore, apparently this is due to the presence of some impurities in the reaction mixture.

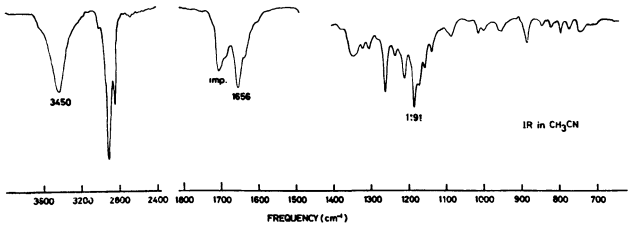

Fig. 1. Infrared spectrum of the photolysate of **1** (5% CH_3CN solution).

NMR Spectrum of the Dienols 2 and 3. Figure 2 shows the NMR signals arising from the olefinic protons of the photoproducts. The spectrum can be explained only in terms of a 5:1 mixture of the dienols **2** and **3**. The observed coupling constants were: $J_{Ha-Hb}=J_{Ha'-Hb'}=12$ Hz and $J_{Hb-CH_3}=8$ Hz. The splitting patterns bear a close resemblance to those of 3-methylenecyclooctene; the endocyclic vinylic protons (δ 5.50 (C-2) and 6.20 (C-1)) are coupled to each other with $J=12$ Hz. Occurrence of the Ha signal at a lower field, δ 6.48, than that of Ha′, δ 6.14, should be ascribed to the anisotropic effect of the enol oxygen. The spectrum at the higher field, even when taken in CD_3CN, is rather complicated by overlapping with signals of high molecular weight by-products (<20%) and CHD_2CN. However, the spectrum exhibited distinct singlets at δ 1.88 and 1.82 arising from the vinylic methyl groups of **2** and **3**, respectively. The signal assignments were further confirmed by double resonance techniques; when Hb and Hb′ were irradiated, Ha and Ha′ appeared as singlets, while irradiation of Ha changed the signal pattern of Hb into a triplet with $J=8$ Hz.

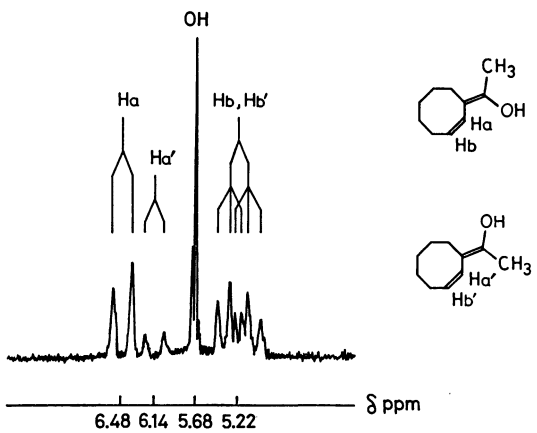

Fig. 2. NMR spectrum of the photolysate of **1** (5% CH_3CN solution, 60 MHz, tetramethylsilane as internal standard).

Intermolecular exchange of the hydroxylic protons is not rapid and hence the NMR absorption for each stereoisomer occurred separately. The chemical shift values, δ 5.68 and 5.71, are intermediate between that of ordinaryl alcoholic protons and that of phenolic protons;[6] methyl alcohol and phenol (4% acetonitrile solution, room temperature) give the OH signals at δ 2.45 (quartet) and 6.96, respectively. The low exchangeability of the OH protons should be ascribed to the moderate acidity and the intermolecular hydrogen-bonding with solvent acetonitrile. The hydroxy signals disappeared upon addition of an excess of methanol-*O-d*.

Stability of the Dienols 2 and 3. The dienols produced by photolysis of **1** were highly air-sensitive. When air was introduced to the acetonitrile solution, the dienols disappeared immediately and dimeric and polymeric substances were formed. When the acetonitrile solution was concentrated *in vacuo* at room temperature, polymerization of the products took place. The dienols, however, were quite stable in dilute acetonitrile solution covered by inert gas and remained virtually unchanged for 3 days at ambient temperature. Under forcing conditions, or with added acids or bases, the dienols were converted irreversibly to β,γ-(and α,β-)unsaturated ketones. The product ratio is dependent on the reaction conditions (Table 1). Heating at 100 °C gave an 83:17 mixture of the β,γ-unsaturated ketone **4** and the starting enone **1**. Addition of a trace amount of sulfuric acid led to a similar mixture of the enones. On the other hand, treatment with potassium *tert*-butoxide produced the β,γ isomer exclusively. When pyridine was added to the acetonitrile solution, the NMR signal due to the OH proton disappeared spontaneously but the isomerization proceeded very slowly. When the mixture stood for 4 days at 25 °C, **4** was formed as a sole product.

Table 1. Ketonization of the dienols **2** and **3**[a]

Additive	Solvent	Reaction conditions	Yield %[b]	**4**:**1** ratio[b]
None	CH_3CN	25 °C, 3 days	0	—
None	CH_3CN	100 °C, 2 h	80	83:17
None	CH_3OH	25 °C, 4 days	100	100:0
H_2SO_4[c]	CH_3CN	25 °C, <30 s	100	75:25
t-C_4H_9OK[c]/ t-C_4H_9OH	CH_3CN	25 °C, <30 s	80	100:0
$(C_2H_5)_3N$[d]	CH_3CN	25 °C, <30 s	52	100:0
Pyridine[d]	CH_3CN	0 °C, 4 days	~100	100:0

a) A 5:1 mixture of **2** and **3** in acetonitrile was used as starting material. b) Determined by NMR analysis using benzene as internal standard. c) A trace amount was used. d) Excess reagent was used.

The structure of the enone **4** was fully substantiated by the analytical and spectral data. The nonconjugated enone **4** gave an IR carbonyl band at 1710 cm^{-1}. The presence of an acetyl group and a disubstituted double bond was confirmed by the three-proton NMR singlet at δ 2.10 and two-proton multiplet at δ 5.66, respectively.

Acetylation of the Dienols. Owing to high air-sensitivity, the dienols **2** and **3** could not be isolated from the acetonitrile solution. However, the corresponding acetates were stable enough to isolated and their characteri-

zation provided further chemical evidence for the dienol structure. Thus treatment of a mixture of **2** and **3** in acetonitrile with acetic anhydride–pyridine at −20 °C furnished an 83: 17 mixture of the acetates **5** and **6** in 60% yield together with the enone **4** (40%). The acetoxy derivatives **5** and **6** separated by preparative GLPC were identical with samples which were prepared independently by the reaction of the enone **1** and acetic anhydride in the presence of *p*-toluenesulfonic acid (**5**: **6** ratio in the latter case was 24: 76). UV absorption maximum of both acetates occurred at ≈240 nm (log ε 4.0—4.1). The IR spectra exhibited characteristic bands at 1755—1753 and 1206 cm^{-1} due to the acetate moieties. The NMR spectra exhibited singlets at δ 1.87 (broad) and 2.07 (sharp), indicating the presence of vinylic and acetyl methyl groups, respectively. The signal patterns in the olefinic region are given in Figs. 3 and 4. The vinylic proton Ha (or Ha′) is coupled to Hb (or Hb′) with J=12 Hz and appeared as a doublet. The Hb (or Hb′) signal is further split by coupling with the adjacent methylene protons (J=7 Hz). The stereochemistry of these isomers could be distinguished by examining the intermolecular nuclear Overhauser effect (NOE).[7] When the vinylic methyl protons of **6** were saturated by double irradiation, the Ha′ signal showed a 19±1% increase in integrated intensity. By contrast, irradiation of the methyl group in **5** resulted in no change in the signal intensity of Ha (0±1%). These results indicate that the methyl protons and Ha′ proton in **6** are in close proximity but the methyl group and Ha proton in **5** are not.

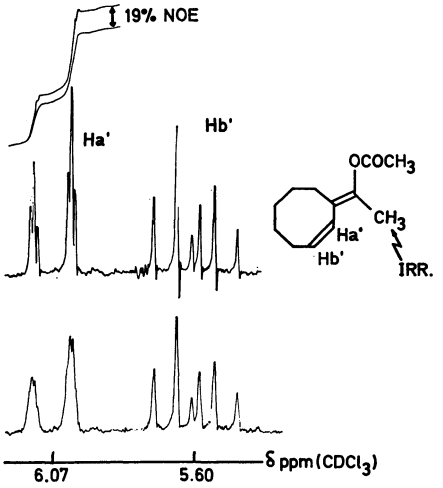

Fig. 3. Measurement of NOE in **6** (10% $CDCl_3$ solution, 100 MHz, tetramethylsilane as internal standard). Upper: spectrum taken with irradiation at the methyl group. Lower: normal spectrum.

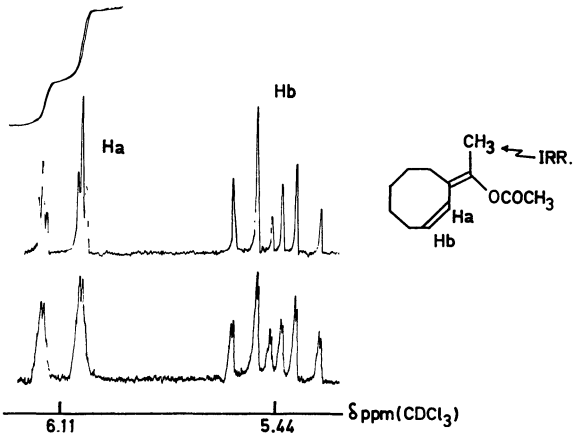

Fig. 4. Measurement of NOE in **5** (10% $CDCl_3$ solution, 100 MHz, tetramethylsilane as internal standard). Upper: spectrum taken with irradiation at the methyl group. Lower: normal spectrum.

Photolysis of the Enone 1 in Methanol. The enone **1** in methanol has in UV region a π-π* and n-π* band at 234 (log ε 4.00) and 306 nm (log ε 0.89), respectively. When the enone **1** in methanol-*O*-*d* placed in an NMR tube was exposed to light of wavelength >350 nm for 10 h, the dienols **2**-*O*-*d* and **3**-*O*-*d* were produced. These dienols are remarkably stable even in the alcoholic solvent. The NMR spectrum of the photolysate was practically the same as that obtained in the acetonitrile (Fig. 2) except for the lack of the OH signal. When stood at room temperature, the dienols were isomerized slowly. After 4 days, the deuterated β,γ enone **4**-*d* was

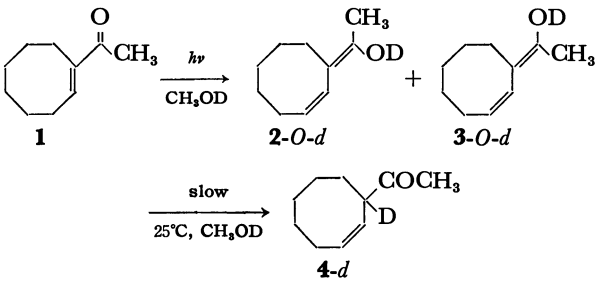

formed as a sole product. NMR analysis of the isolated product indicated the isotopic purity of *ca.* 95%; in going from **4** to the deuterated product **4**-*d*, a multiplet at δ 3.4 srising from the CHCOCH$_3$ proton vanished almost completely.

Photolysis of the Enone 1 under Other Conditions. Neither the dienols **2** and **3** nor the enone **4** was produced by the photolysis of **1** in nonpolar solvents such as benzene, cyclohexane, carbon tetrachloride, chloroform, or carbon disulfide. Irradiation of **1** in pyridine or dimethyl sulfoxide gave the deconjugation product **4**. Attempted sensitization of the photoreaction (benzophenone in acetonitrile, acetophenone in acetonitrile, or acetone as solvent) has not been successful.

Mechanism of the Dienol Formation from 1. The photochemical formation of the dienols **2** and **3** from the enone **1** is best explained by a mechanism outlined in Scheme 2. The conjugated enone **1** is known to undergo photochemical *cis-trans* isomerization, establishing an equilibrium between **1** and **7**.[8] The *trans* isomer **7** contains a torsionally strained double bond and is much less stable than the starting *cis* enone **1**. Therefore, this isomer with a short lifetime, reverting thermally to **1**, is contained in rather low concentration in the equilibrium mixture. Fortunately, however, the labile isomer **7**, owing to a reduction in the symmetry-forbiddenness of the n-π* transition, has the enhanced extinction coefficient in the >300-nm region and can absorb incident light

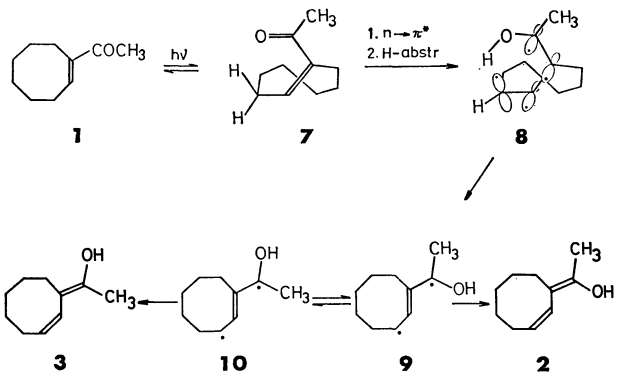

Scheme 2

more efficiently than the major *cis* isomer **1**.[8] Inspection of models indicates that the γ-hydrogen abstraction by the n, π^* carbonyl oxygen through a cyclic transition state is feasible only with such *trans* enone **7**. Although the spin multiplicity of the n, π^* state that causes this hydrogen abstraction is uncertain as yet, the observation can be simply accounted for by assuming the involvement of the triplet species.[2] Thus the twisted triplet biradical **8** initially formed from **7** is stabilized by changing the geometry to give the sterically less constrained, interconvertible biradicals **9** and **10**. Subsequent decay to the ground state affords the dienols **2** and **3**. The production of these two isomers even at an early stage of the reaction as well as the lack of noticeable time-dependency of the isomeric ratio (5: 1 by NMR analysis) is in accord with this consideration. However, the stereoisomeric biradicals **9** and **10** could also be formed *via* the possible long-lived, singlet biradical **8** arising from the excited singlet enone **7**. Finally, thermal or catalyzed ketonization of the dienol intermediates concludes the overall photo-induced deconjugation reaction of the α,β-unsaturated ketone.

Origin of the High Stability of the Dienol Species. The existence of the simple dienols **2** and **3** as long-lived species seems highly unusual.[9] Full account for this observation is open to further detailed studies. At present, the following three factors are conceived to be contributing to the stability. First, the dienols **2** and **3** have the fairly rigid *s-trans* diene structure. The restriction of conformational freedom may preserve stability through double bond conjugation. On the other hand, in the ordinary photoisomerization of α,β-unsaturated ketones, the initially formed dienols have an open-chain *s-cis* dienoid structure. The flexible dienols are liable to ketonize through conformational change accompanying loss of the conjugation (*cf.* **11**). Secondly, the dienol-enone isomerization **2**→**4** (or **3**→**4**) is accompanied by decrease in the number of sp^2-hybridized carbons in the eight-membered skeleton (three to two). The favoring of sp^2 configuration in eight-membered rings over sp^3 structure[10] may be one source of the unusual stability. Finally, the presence of strong intermolecular hydrogen bonding between the dienols and the acetonitrile solvent may be an additional stabilization factor.[11]

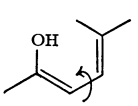

11

Experimental

General. NMR spectra were measured with a JEOL CO JMN-C-60H or C-100H spectrometer. Unless otherwise stated, tetramethylsilane was used as internal standard. IR spectra were recorded with a Japan Spectroscopic Co. DS-402G spectrometer, with a polystyrene film used for calibration. Air-sensitive solutions were transferred to a cell with a syringe which had been previously wet with nitrogen-saturated solvent to preclude air leakage along the barrel. UV spectra were taken with a Perkin-Elmer 202 spectrometer. Mass spectra were taken with a Hitachi RMU-6C spectrometer. Analytical gas-liquid partition chromatography (GLPC) was performed on a Yanagimoto Model G-8 instrument, equipped with a 2 mm×2 m column of Apiezon grease L (5%) on Chromosorb W and a flame ionization detector using nitrogen as carrier gas. The column temperature was maintained at 160 °C. In quantitative analyses, areas under the peaks in the chromatogram were measured by the cut-and-weigh method. Preparative GLPC was done on a Yanagimoto Model GCG-3D instrument using helium as carrier gas and a 4 mm×2 m column of Apiezon grease L (10%) on Chromosorb W. All irradiations were effected externally using a 200-W high-pressure mercury arc through 10% aq $CuSO_4$ filter solution (1 cm depth).

Materials. Solvents for photochemical reactions were purified by simple distillations and stored under nitrogen atmosphere. Acetonitrile was dried by distillation from P_2O_5 (four times) and anhydrous K_2CO_3. The solvent was further purified by simple distillation under nitrogen. 1-Acetylcyclooctene (**1**), bp 75—85 °C (3 mmHg), was prepared by the method of Cantrell and Shechter from cyclooctene and acetyl chloride.[12] As the Lewis acid catalyst, titanium tetrachloride was used in place of stannic chloride. Usually, the material was freshly purified by preparative GLPC before each photolytic experiment.

*Photolysis of **1** in Acetonitrile.* A 5% acetonitrile solution of **1** was placed in a Pyrex NMR tube and deoxygenated by bubbling slowly with pure nitrogen for 30 min. The solution covered by nitrogen was irradiated at room temperature. Progress of the reaction was monitored by NMR analysis. After 10-h irradiation, the starting material was consumed completely and a 5: 1 mixture of the dienols **2** and **3** was formed. Its NMR spectrum is given in Fig. 2; δ 5.22 (dt, J=12 and 8 Hz, Hb and Hb'), 5.68 (s, OH of **2**), 5.71 (s, OH of **3**), 6.14 (d, J=12 Hz, Ha'), and 6.48 (d, J=12 Hz, Ha). The OH signals disappeared upon addition of an excess of CH_3OD. Yield determined on the basis of added benzene standard was *ca.* 80%. The photolysate obtained by the reaction in CD_3CN showed NMR signals at δ 1.88 and 1.82 (singlets) due to the olefinic methyl groups of **2** and **3**. Results of the decoupling experiments were in accord with the assignments. The photolysate in an NMR tube was transferred with a syringe into an NaCl IR cell which had been flushed with nitrogen, and subjected to IR measurement (Fig. 1).

A 2.7×10^{-3} M solution of **1** in acetonitrile was deoxygenated by four freeze(−78 °C)-pump(0.008 mmHg)-thaw cycles, transferred directly to a UV cell (1 cm×1 cm), and sealed under nitrogen atmosphere. The photolysis was conducted by external irradiation (>350 nm) and the reaction course was monitored by UV analysis. The absorption of **1**, λ_{max} 233 nm, was cleanly replaced by a new band, λ_{max} 252 nm (log $\varepsilon \approx 4.0$). After a 6 h irradiation, the reaction was complete.

*Preparation of the Dienol Acetates **5** and **6**.* An acetic anhydride solution (170 ml) containing **1** (1.2 g, 80 mmol) and

p-toluenesulfonic acid (1.5 g, 80 mmol) was slowly distilled under atmospheric pressure through a short column. About 4 h were required until the final volume was reduced to 70 ml. Most of the acetic anhydride then was removed under reduced pressure. The residue was dissolved in ether, treated with ice-cooled 5% aq sodium hydroxide and then with water, and dried over $MgSO_4$. Concentration followed by distillation gave an oil (830 mg), bp 95—100 °C (3 mmHg). GLPC analysis gave three peaks at 4.7 (71%, **6**), 5.4 (22%, **5**), and 6.6 min (7%). Each component was collected by preparative GLPC. **5**, UV (95% C_2H_5OH) 241 nm (log ε 4.15); IR (neat) 1755 and 1206 cm^{-1} (acetate); NMR (CCl_4) δ 1.59 (m, 6H, CH_2), 1.87 (broad s, 3H, $=C(OCOCH_3)C\underline{H}_3$), 2.07 (sharp s, 3H, $COCH_3$), 2.2—2.6 (m, 4H, allylic CH_2), 5.44 (dt, 1H, J=12 and 7 Hz, Hb), and 6.11 (d, 1H, J=12 Hz, Ha); the exact mass spectrum *m/e* 194.1310 (calcd for $C_{12}H_{18}O_2$: 194.1307). **6**, UV (95% C_2H_5OH) 239 nm (log ε 3.98); IR (neat) 1753 and 1206 cm^{-1} (acetate); NMR (CCl_4) δ 1.55 (m, 6H, CH_2), 1.87 (broad s, 3H, $=C(OCOCH_3)C\underline{H}_3$), 2.07 (sharp s, 3H, $COCH_3$), 2.2—2.5 (m, 4H, allylic CH_2), 5.60 (dt, 1H, J=12 and 7 Hz, Hb'), and 6.07 (d, 1H, J=12 Hz, Ha'); exact mass spectrum *m/e* 194.1300 (calcd for $C_{12}H_{18}O_2$: 194.1307). The nuclear Overhauser effects in the NMR of **5** and **6** were measured in the well-deoxygenated $CDCl_3$ solutions. The results were shown in Figs. 3 and 4. The third component was produced in only a small amount and was not isolated in an analytically pure state. Based on the following spectral data, it was tentatively assigned as 1-(α-acetoxyvinyl)-cyclooctene. IR(neat) 1757 (acetate), 1635 and 1608 (C=C), 1214 and 1184 (acetate), and 871 cm^{-1} ($=CH_2$); NMR (CCl_4) δ 1.49 (m, 8H, CH_2), 2.12 (s, 3H, $COCH_3$), 2.2—2.5 (m, 4H, allylic CH_2), 4.64 and 4.93 (d, 1H each, J=2 Hz, $=CH_2$), and 5.78 (t, 1H, J=8 Hz, =CH); mass spectrum *m/e* 194 (M^+).

*Acetylation of the Dienols **2** and **3**.* *(a) Analytical Scale*: Under nitrogen atmosphere a 5-μl portion of a 5: 1 mixture of **2** and **3** in acetonitrile (photolysate of **1**) was added to a mixture of pyridine (10 μl) and acetic anhydride (5 μl) which had been cooled at −20 °C in a semimicro sampling tube. GLPC analysis of the mixture revealed the formation of **4** (42%, 2.8 min), **5** (48%, 6.6 min), and **6** (10%, 4.7 min).

(b) Preparative Scale: A solution of **1** (500 mg; 3.3 mmol) in acetonitrile (12 ml) was divided in three Pyrex tubes (0.8 cm × 4 cm), deoxygenation by bubbling with purified nitrogen for 10 min, and irradiated under the above described conditions. The photolysate obtained after 18-h irradiation was treated with a mixture of pyridine (0.2 ml) and acetic anhydride (0.3 ml) for 1 h at room temperature. The solutions were combined and concentrated *in vacuo*. The residue was dissolved in ether, washed with water, and dried over $MgSO_4$. Concentration and distillation (90—100 °C (3 mmHg)) gave an oil (256 mg). GLPC analysis of the oil afforded three peaks at 2.8 (80%, **4**), 4.7 (3%, **6**), and 6.6 min (15%, **5**). Each component was isolated by preparative GLPC and identified on the basis of its spectral properties. The dienol acetates **5** and **6** were compared with the authentic samples. Spectral characteristics of 3-acetylcyclooctene (**4**)[13] were: IR (neat) 1710 (C=O) and 1360 cm^{-1} ($COCH_3$); NMR (CCl_4) δ 1.60 (m, 8H, CH_2), 2.10 (s, 3H, $COCH_3$), 2.20 (m, 2H, allylic CH_2), 3.37 (m, 1H, $C\underline{H}COCH_3$), and 5.66 (m, 2H, =CH); mass spectrum *m/e* 152 (M^+).

Found: C, 78.95; H, 10.69%. Calcd for $C_{10}H_{16}O$: C, 78.89; H, 10.57%.

*Silylation of the Dienols **2** and **3**.* A 5-μl portion of the photolysate of **1** in acetonitrile was mixed with *N,O*-bis(trimethylsilyl)acetamide (10 μl) in a semimicro sampling tube under nitrogen atmosphere at room temperature. GLPC analysis of the mixture revealed eluates at 2.8 (28%), 7.7 (14%), and 8.8 min (60%). The first peak was due to **4**, and the latter two were assigned as the silyl ethers of **2** and **3**.

*Examination of the stability of **2** and **3**.* The stability of the dienols was examined under various conditions. When air was admitted to an acetonitrile solution of **2** and **3**, polymeric substances were formed immediately. A solid dimer was separated from the solution; mass spectrum *m/e* 302 (M^+); IR (KBr) 1656 cm^{-1} (C=O). The exact structure remains to be determined. The dienols, however, were fairly stable under inert gas atmosphere. The dienols were allowed to react in an NMR tube under conditions described in Table 1.

*Photolysis of **1** in Methanol-O-d.* The enone **1** (35 mg, 0.23 mmol) was dissolved in methanol-*O*-*d* (0.5 ml, E. Merck, deuterium content >99%) in an NMR tube, deoxygenated, and irradiated as described above. After a 10 h irradiation, **1** was consumed completely to yield the dienols **2**-*O*-*d* and **3**-*O*-*d*. NMR in the olefinic region was identical with that taken in acetonitrile except the absence of OH signals. After the solution stood at 25 °C for 4 days, the signals due to these dienols vanished completely and the peaks due to the enone **4**-*d* appeared. GLPC analysis of the aliquot exhibited a single peak with retantion time of 2.8 min (identical with that of **4**) except for the solvent peak. Concentration of the photolysate, followed by distillation (bath temp 75—85 °C (3 mmHg)) gave 3-acetylcyclooctene-3-*d* (**4**-*d*) as a colorless oil. NMR analysis (CCl_4) revealed the isotopic purity of *ca.* 95%; δ 1.60 (m, 8H, CH_2), 2.10 (s, 3H, $COCH_3$), 2.20 (m, 2H, allylic CH_2), and 5.66 (m, 2H, =CH). Mass spectrum *m/e* 153 (M^+).

We thank Professor Akira Tatematsu of Meijo University for obtaining the exact mass spectra. We are also grateful to Drs. Toshiaki Nishida and Iwao Miura of Nippon Electric-Varian for the measurement of NOE effects.

References

1) A preliminary account of this work was presented some years ago. R. Noyori, H. Inoue, and M. Katô, *J. Am. Chem. Soc.*, **92**, 6699 (1970).

2) a) M. Mousseron, *Pure Appl. Chem.*, **9**, 481 (1964); b) N. C. Yang and M. J. Jorgenson, *Tetrahedron Lett.*, **1964**, 1203; c) K. J. Crowley, R. A. Schneider, and J. Meinwald, *J. Chem. Soc. C*, **1966**, 571; d) M. J. Jorgenson and L. Gundel, *Tetrahedron Lett.*, **1968**, 4991; e) J. A. Barltrop and J. Wills, *ibid.*, **1968**, 4987. Review: N. C. Yang in "Reactivities of the Photoexcited Molecule," Interscience, New York, N. Y. (1967), p. 145.

3) H. Nozaki, T. Mori, and R. Noyori, *Tetrahedron*, **22**, 1207 (1966); A. Marchesni, G. Pagani, and U. M. Pagnomi, *Tetrahedron Lett.*, **1973**, 1041; R. G. Carlson and J. H. Bateman, *ibid.*, **1967**, 4151.

4) In the vapor-phase photolysis of crotonaldehyde, its enol form was detected by IR spectroscopy: J. W. Coomber, J. N. Pitts, Jr., and R. R. Schrock, *Chem. Commun.*, **1968**, 190.

5) After completion of this work,[1] photoenolization of β-di-alkylated α,β-unsaturated ketones *via* n, π* singlet state has been reported: M. Tada and K. Miura, *Bull. Chem. Soc. Jpn.*, **49**, 713 (1976).

6) R. M. Silverstein, G. C. Bassler, and T. C. Morrill, "Spectrometric Identification of Organic Compounds," 3rd ed., Wiley, New York, N. Y. (1974), p. 174ff.

7) F. A. L. Anet and A. J. R. Bourn, *J. Am. Chem. Soc.*, **87**, 5250 (1965). Reviews: G. E. Bachers and T. Schaefer, *Chem. Rev.*, **71**, 617 (1971); G. Moreau, *Bull. Soc. Chim. Fr.*, **1969**, 1770.

8) P. E. Eaton, *Acc. Chem. Res.*, **1**, 50 (1968).

9) Recently some stable enols and dienols have been reported: H. M. R. Hoffmann, K. E. Clemmens, E. A. Schmidt, and R. H. Smithers, *J. Am. Chem. Soc.*, **94**, 3201 (1972); E. A. Schmidt and H. M. R. Hoffmann, *ibid.*, **94**, 7832 (1972); H. M. R. Hoffmann and E. A. Schmidt, *Angew. Chem.*, **85**, 227 (1973). Highly crowded enols: J. Attenburrow, J. E. Connett, W. Graham, J. F. Oughton, A. C. Ritchie, and P. A. Wilkinson, *J. Chem. Soc.*, **1961**, 4547; P. R. Enslin, *Tetrahedron*, **27**, 1909 (1971). Phenylated enol: V. J. Shiner, Jr. and B. Martin, *J. Am. Chem. Soc.*, **84**, 4824 (1962). Special enols that are stable at low temperatures: K. R. Huffman, M. Loy, and E. F. Ullman, *J. Am. Chem. Soc.*, **87**, 5417 (1965); W. A. Henderson, Jr. and E. F. Ullman, *ibid.*, **87**, 5424 (1965). For a review on photo-enols formed from *o*-alkylated aromatic carbonyl compounds, see P. G. Sammes, *Tetrahedron*, **32**, 405 (1976).

10) E. L. Eliel, "Stereochemistry of Carbon Compounds," McGraw-Hill, New York, N. Y. (1962), p. 267ff.

11) O. L. Chapman and R. W. King, *J. Am. Chem. Soc.*, **86**, 1256 (1964); F. A. L. Anet, L. M. Sweeting, T. A. Whitney, and D. J. Cram, *Tetrahedron Lett.*, **1968**, 2617; W. H. Pirkle and S. D. Beare, *J. Am. Chem. Soc.*, **90**, 6250 (1968); G. Satzinger, *Tetrahedron*, **27**, 3739 (1971).

12) T. S. Cantrell and H. Shechter, *J. Am. Chem. Soc.*, **89**, 5868 (1967).

13) L. S. Hegedus, Ph. D. Thesis, Harvard University, Cambridge, Mass. (1970).

A Study of the Solubilization of Polar Oily Materials by Sodium Dodecyl Sulfate

Keizo OGINO, Masahiko ABE, and Nobuo TAKESITA

Faculty of Science and Engineering, Science University of Tokyo, 2641, Yamazaki, Noda, Chiba 278

(Received May 21, 1976)

The difference due to carbon-chain lengths and kinds of polar groups in the solubilizing phenomenon caused by Sodium Dodecyl Sulfate (SDS) of polar normal fatty acids and polar normal alcohols has been studied in terms of the amount of solubilization, the viscosity, and the surface tension. The amount of solubilization decreased with an increase in the number of carbon atoms in the molecules of oily materials, and it was larger for normal fatty acids than for normal higher alcohols with the same number of carbon atoms in the molecule. It was found that the oily materials of a greater amount of solubilization exhibited a small viscosity and a small rate of the reduction of surface tension.

Solubilization is a phenomenon in which a solution of a surfactant in concentrations beyond the critical micelle concentration (CMC) dissolves a variety of organic compounds to yield a transparent solution. This results from the solution of the substances into the micelles. The structure of the micelles has been described by McBain[1] and by Hartley and coworker,[2] but it is still a matter of controversy. Among the ways of incorporating the solubilizate into the micelles, which are closely related to the structure of the micelles, are (a) adsorption on the surface of the micelles; (b) deep penetration of the palisade layer and (c) dissolution in the hydrocarbon core, these methods have been described by Kolthoff,[3] Riegleman,[4] and Mulley respectively.[5]

In this study normal fatty acids and normal higher alcohols with different polarities were solubilized by SDS, and the mechanism of the solubilization was investigated by measuring the amount of solubilization, the values of the CMC, the relative viscosities, and the surface tension. We found that the amount of solubilization decreased with an increase in the number of carbon atoms in the molecules of polar oily materials, and was larger for fatty acids than for alcohols with the same number of carbon atoms in the molecule.

As regards the CMC, the smaller the number of carbon atoms in the molecules of polar oily materials, the greater the reduction in CMC compared with that of SDS alone. It has been found that the CMC of SDS solubilizing an oily material is given by:

$$\mathrm{CMC} = A\sqrt{N_c} + B$$

where A and B are experimental constants and N_c is the number of carbon atoms in the molecules of the oily materials.

The relative viscosities of SDS solutions of oily materials increased with an increase in the number of carbon atoms in the molecules of oily materials, and they were larger for normal higher alcohols than for normal fatty acids with the same number of carbon atoms in the molecules.

The rate of the reduction of surface tension increased with an increase in the number of carbon atoms in the molecules of polar oily materials; it was greater for alcohols than for fatty acids with the same number of carbon atoms in the molecules. The surface tension at the saturation of solubilization exhibited a constant value, regardless of the kinds of oily materials added.

To summarize, it was found from this experiment that the oily materials of greater amounts of solubilization exhibited a smaller viscosity and a smaller rate of reduction in the surface tension.

Experimental

Materials. *Surfactant*: Sodium Dodecyl Sulfate (SDS) of a regent grade was extracted with ether and recrystallized from ethanol.

Polar Oily Materials: The octanoic acid (C_8), decanoic acid (C_{10}), dodecanoic acid (C_{12}), and tetradecanoic acid (C_{14}) were the purest grade products of Wako-Junyaku and were more 99% pure; The octyl alcohol (C_8, bp 179.5 °C), decyl alcohol (C_{10}, bp 228—232 °C), dodecyl alcohol (C_{12}, bp 86.5 °C), tetradecyl alcohol (C_{14}, bp 255—259 °C), and hexadecyl alcohol (C_{16}, bp 190 °C) were the purest grade products of Wako-Junyaku.

Apparatus and Conditions. When polar oily materials are added to a SDS solution, beyond the saturation point they are emulsified and the solution becomes turbit. The following procedure was used for the determination of the limits of solubilization. Into several 100 ml glass-stoppered flasks, 50 ml portions of a solution of a given concentration of SDS were placed; then varying amounts of polar oily materials were added to them, and the mixtures were shaken while being stirred for 12 h in a thermostat at 40 °C, followed by setting until a solubilization equilibrium was established. After the equilibrium had been established, the turbidity of the solution was measured with an Electro photocolorimeter, Hirama 2B type, with a cell 10.0 mm in length at 655 nm. The turbidity concentration obtained was extrapolated to zero in order to obtain the amount of solubilization. The CMC of SDS was determined from the solubilities of the polar oily materials in SDS solutions of various concentrations.

The relative viscosities of the solutions solubilizing oily substances were measured at 40.0 °C$\pm$0.1 with an Ubelohde viscometer with appropriate auxiliary equipment to keep atmospheric moisture off as far as possible. The time of flow was determined with a stop watch of a 0.1 s precision; the overall fluctuations of the time measured were within$\pm$0.1 to 0.2 s. The specific gravity was determined by using a pycnometer with a capacity of about 25 ml.

The effective specific volume of 1 g of a SDS including a polar oily material was calculated from the values of the relative viscosity.[6]

The surface tensions of the solubilized solutions were measured at 40.0 °C$\pm$0.1 with a Wilhelmy tensiometer, Shimadzu ST-1 type, equipped with a glass plate.

Results and Discussion

Solubilizing Power and CMC of SDS. The difference due to the carbon-chain lengths and the kinds of polar groups in the solubilization caused by SDS solutions has been studied. Figure 1 shows the optical densities of various concentrations of SDS solutions with an increase in the amounts of dissolved octanoic acid. The rapid increase in I_0/I began when emulsion droplets first appeared. The point of the intersection of the curves representing the optical density with the horizontal axis is considered to give the solubility of octanoic acid in the SDS solution. Plots of the solubility of materials in SDS of various concentrations which were obtained in the manner described above are shown in Figs. 2 and 3. As is evident from the figures, the solubility remained constant near null until the critical concentration was reached, beyond which point it showed a sharp increase in the SDS micelles due to solubilization. The slopes of these lines and the intersections of the horizontal

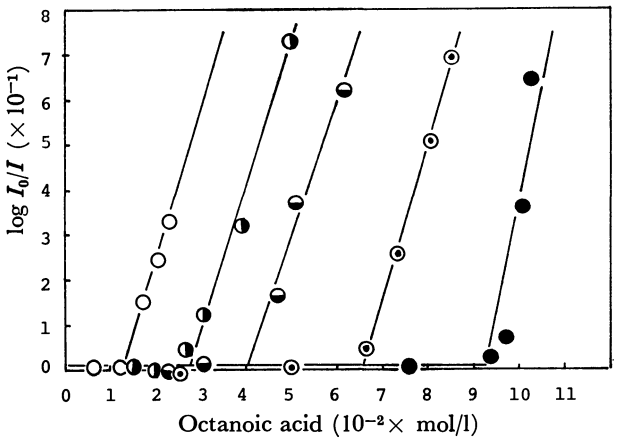

Fig. 1. Optical density of various concentrations of SDS solution with increasing amount of dissolved octanoic acid.
○=3.47×10⁻³ mol/l SDS; ◑=6.94×10⁻³ mol/l SDS; ◒=10.4×10⁻³ SDS; ⊙=17.4×10⁻³ mol/l SDS; ●=24.3×10⁻³ SDS.
I=intensity of permeable light; I_0=intensity of incident light.

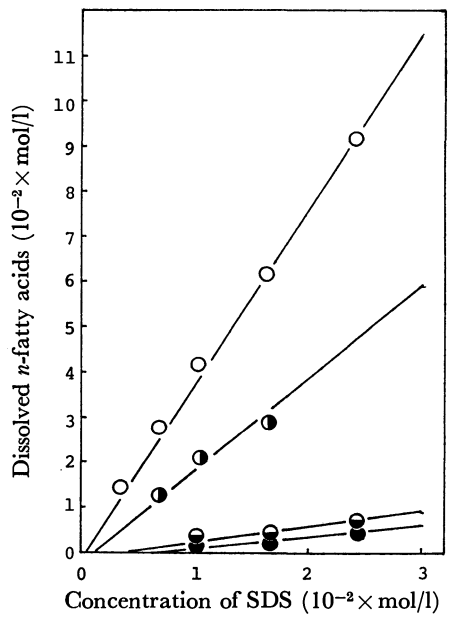

Fig. 2. Solubilizing power and critical micelle concentration of SDS.
○=Octanoic acid; ◑=decanoic acid; ◒=dodecanoic acid; ●=tetradecanoic acid.

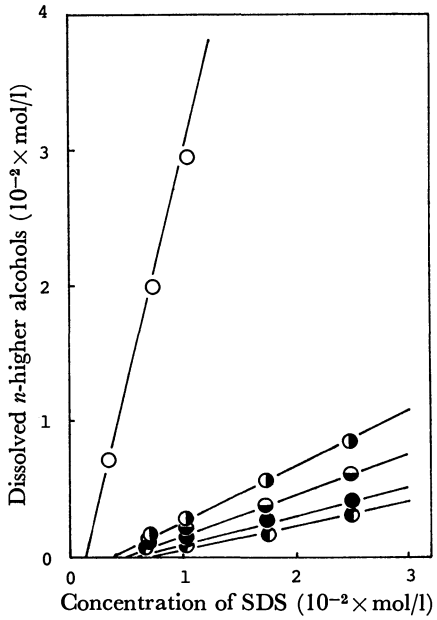

Fig. 3. Solubilizing power and critical micelle concentration of SDS.
○=Octyl alcohol; ◑=decyl alcohol; ◒=dodecyl alcohol; ●=tetradecyl alcohol; ◐=hexadecyl alcohol.

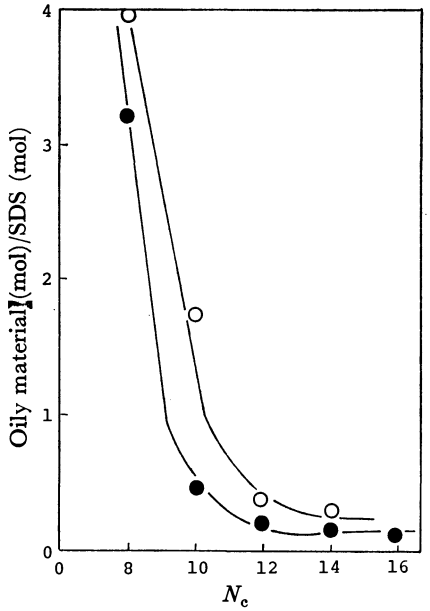

Fig. 4. The change of solubilizing power with increasing number of carbon atoms of oily materials.
N_c is the number of carbon atoms in the molecules of oily materials.
○=Normal fatty acids; ●=normal higher alcohols.

axis with these lines are the solubilizing power and the CMC respectively. Figure 4 shows the change in the solubilizing power with an increase in the number of carbon atoms in the molecules of oily materials. As is evident from Figs. 1, 2, and 3, the solubility and the solubilizing power decreased with an increase in the number of carbon atoms in the molecules of oily materials, and they were larger for normal fatty acids than for normal higher alcohols with the same number of carbon atoms in the molecule. This result is considered to be due to the decrease in the magnitude of the dipole moment with the increase in the number of carbon atoms in the molecule of the oily material and to the difference in polar groups between normal fatty acids and normal higher alcohols with the same number of carbon atoms in the molecule.[7]

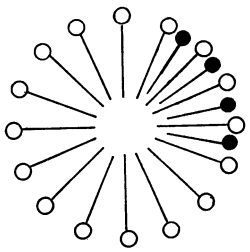

Fig. 5. Formation of palisade layer of mixing micelle between surfactant anion and polar molecule.
○——=Surfactant anion; ●——=polar molecule.

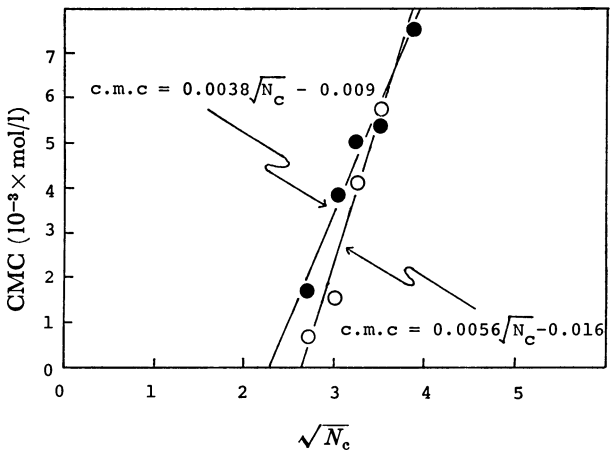

Fig. 6. Relationship between the CMC of SDS and the carbon number of oily materials.
N_c is the number of carbon atoms in the molecules of oily materials.
○=Normal fatty acids; ●=normal higher alcohols.

As is shown in Figs. 2 and 3, the CMC of SDS with oily materials was smaller than that of SDS alone (6.94×10^{-3} mol/l) and decreased with a decrease in the number of carbon atoms in the molecules of the oily materials. As may be seen from Fig. 5, this is considered to be due to the fact that the deep penetration of polar molecules into the palisade layer caused the surface charge density to decrease, leading to a reduction of the free energy of mixing.[8] Figure 6 shows the effect of oily materials added on the CMC of SDS; the following equations can be written:

for normal fatty acids,

$$\mathrm{CMC} = 0.0056\sqrt{N_c} - 0.016$$

for normal higher alcohols,

$$\mathrm{CMC} = 0.0038\sqrt{N_c} - 0.009$$

where N_c is the number of carbon atoms in the molecules of the oily materials.

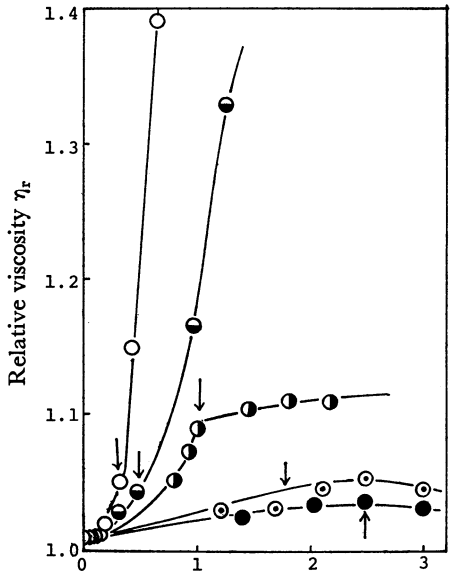

Fig. 7. The relative viscosity of the solutions which were produced by solubilizing oily materials using SDS of given concentration (6.94×10^{-3} mol/l).
●=Octanoic acid; ◑=decanoic acid; ⊙=octyl alcohol; ◒=decyl alcohol; ○=dodecyl alcohol.
Arrows show the limit of solubilization of oily materials in 6.94×10^{-3} mol/l of SDS.

Relative Viscosity and Effective Specific Volume. Figure 7 shows the relative viscosities of the solutions which were produced by solubilizing oily materials using SDS of a given concentration (6.94×10^{-3} mol/l). The arrows in the figure indicate the limits of solubilization in Figs. 2 and 3. For a given concentration of oily materials, the relative viscosity of the solution increased with an increase in the number of carbon atoms in the molecules of oily materials. For the same number of carbon atoms in the molecules of oily materials, the relative viscosity of the normal higher alcohols was larger than for normal fatty acids. Past the limit of solubilization, the relative viscosities of octanoic acid, of decanoic acid, and of octyl alcohol remained approximately constant; on the other hand, that of decyl alcohol and dodecyl alcohol continued to grow. This is considered to be because emulsification occurs and because the effect which polar materials have on relative viscosities under the states of dispersion of emulsion seems to become greater. As may be seen from Fig. 4, there are inflection points in solubilizing power: at a dodecyl alcohol for normal higher alcohols and at a dodecanoic acid for normal fatty acids. According to the study of the rolling-up phenomenon of polar oily materials in SDS solutions,[9] both octanoic acid and octyl alcohol were

immediately dissolved or solubilized by SDS solutions, a decanoic acid–SDS solution system occurred simultaneously with solubilization and molecular complex formation at the interface, and a molecular complex was formed at the decyl alcohol and dodecyl alcohol/SDS solution interface. In consideration of the above findings, there must be same changes in the properities of decyl alcohol and decanoic acid. According to Klevens,[7] when the non-polar parts of the solubilizates, polar compounds, become too large to overcome the effects of polar groups in the molecules, the solubilizates exhibit behavior resembling that of hydrocarbons, giving rise to a so-called transition solubilization phenomenon, which represents properties intermediate between polar compounds and hydrocarbons.

Based on the relative viscosity, η_r, obtained from Guth and Simha's equation,[10-13] which is a form of Einstein's equation extended to more concentrated solutions:

$$\eta_r = 1 + 2.5\phi + 14.1\phi^2$$

where ϕ is the volume fraction occupied by the spherical particles, the effective specific volume of 1 g of SDS including oily materials, V, is expressed as follows:[6,10]

$$V = \phi/C$$

where C is the concentration of the solution in g/ml. The specific volumes of octanoic acid, octyl alcohol, and decanoic acid changed at the limit of solubilization. From the standpoint of the solubilizing phenomenon, a comparison of polar oily materials based on fixed concentrations is not always appropriate. Therefore, a comparison of the relative viscosity, η_r, with the effective specific volume, V, at the saturation of an solubilized oily material is shown in Table 1. As may be seen from

Table 1. Comparison of the relative viscosity with the effective specific volume at the saturation of oily materials

	N_c	Limits of solubilization (mol/l)	η_r	V (ml/g)
Normal fatty acids	C_8	2.50×10^{-2}	1.040	2.65
	C_{10}	1.00×10^{-2}	1.094	8.58
Normal higher alcohold	C_8	1.83×10^{-2}	1.042	3.40
	C_{10}	0.13×10^{-2}	1.020	3.49
	C_{12}	0.08×10^{-2}	1.050	8.65
SDS alone				1.3

Table 1, as for the relative viscosity there was no apparent regularity, as in Fig. 7. With the effective specific volume, V, the order of increasing specific volume is; octanoic acid<octyl alcohol<decyl alcohol<decanoic acid<dodecyl alcohol; on the other hand, the order of increasing limits of solubilization is; dodecyl alcohol< decyl alcohol<decanoic acid<octyl alcohol<octanoic acid. The oily materials of a greater amount of solubilization in the SDS micelle exhibits a smaller effective specific volume. This result is considered to be due to the difference in the penetration of micelles through the palisade layer resulting from the difference in polar groups.

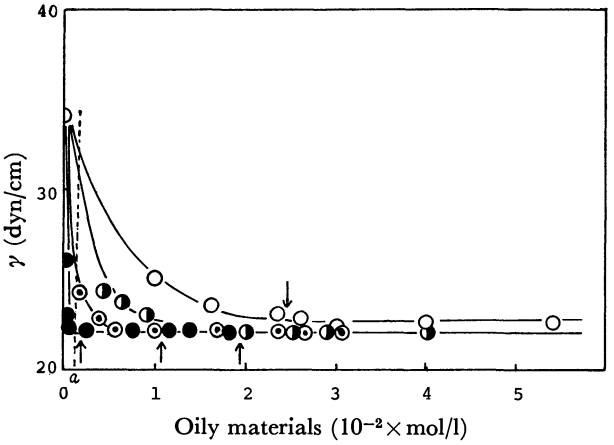

Fig. 8. Surface tension of solutions which is produced by dissolving oily materials in a given concentration of SDS (6.94×10^{-3} mol/l).
○=Octanoic acid; ⊙=decanoic acid; ◑=octyl alcohol; ●=decyl alcohol.
Arrows show the limit of solubilization of oily materials in 6.94×10^{-3} mol/l of SDS.

Surface Tension. Figure 8 shows the surface tensions of solutions which are produced by dissolving oily materials in given concentrations of SDS (6.94×10^{-3} mol/l). The rate of the reduction of the surface tension increased with an increase in the number of carbon atoms in the molecules of oily materials; it was larger for normal higher alcohols than for normal fatty acids with the same number of carbon atoms in the molecule. At the limits of solubilization (arrows in the figure), all the oily materials showed constant values of about 22 dyn/cm, this value remaining fixed even after the formation of a state of emulsion. Nakagawa and his coworkers,[14] with the aid of the electron spin resonance (ESR) spectra and the nuclear magnetic resonance (NMR) spectra, suggested that the lifetime of the benzene molecules in SDS micelles saturated with benzene was 10^{-4} s. It is considered that polar molecules adsorbed onto the air-water interface are en route to transition to polar oily molecules within the micelles or in the solution and are responsible for the reduction of the surface tension.

In connection with the difference in the reduction of the surface tension at a constant concentration of oily material (a in Fig. 8), it is generally true that normal fatty acids and normal higher alcohols with 12 or less carbon atoms form a gaseous membrane when spread over the surface of water at room temperatures. At a constant concentration of oily materials, the more hydrophobic the materials, the more tendency for the materials to reduce the surface tension by adsorbing onto the air-water interface. The fact that the surface tension shows a constant value of about 22 dyn/cm above the saturation of solubilization may be ascribed to the approximately equal contributions of polar materials to the surface tension in the emulsion state, regardless of the kinds of polar oily materials.

The changes in the amount of solubilization and in the relative viscosity, due to the difference between the carbon chain lengths and the kinds of polar groups,

result from the difference in the penetration of the palisade layer of the micelles; the difference in the surface tension results from the difference in the state of adsorption of the molecules of oily materials at the air-water interface.

References

1) J. W. McBain, "Colloid Science," D. C Heath and Co., Boston (1950).
2) G. S. Hartley, "Aqueous Solution of Paraffin Chain Salts," Hermann, Paris (1936).
3) W. D. Kolthoff and I. M. Stricks, *J. Phys. Colloid Chem.*, **52**, 915 (1948).
4) S. Riegleman, N. A. Allawala, M. K. Hrenoff, and L. A. Strait, *J. Colloid. Sci.*, **13**, 208 (1954).
5) B. A. Mulley and A. D. Metcalf, *J. Pharm. Pharmacol.*, **8**, 774 (1956).
6) Y. Iwadera and T. Suyama, *Bull. Chem. Soc. Jpn.*, **43**, 2326 (1970).
7) H. B. Klevens, *Chem. Rev.*, **47**, 1 (1950).
8) K. Shinoda, T. Nakagawa, S. Tomiyama, and T. Isemura, "Colloid Surfactant," Academic Press, New York (1963).
9) K. Ogino and K. Shigemura, *Bull. Chem. Soc. Jpn.*, **49**, 3236 (1976).
10) E. Guth and R. Simha, *Kolloid-Z.*, **74**, 266 (1936).
11) D. C. Robins and I. L. Thomas, *J. Colloid Interface Sci.*, **26**, 415 (1968).
12) T. Ito and H. Mizutani, *Yakugaku*, **17**, 246 (1968).
13) K. Shinoda, T. Nakagawa, B. Tamamushi, and T. Isemura, "Colloid Surfactants," Academic Press, New York (1963), p. 115.
14) T. Nakagawa and K. Tori, *Kolloid-Z.*, **194**, 143 (1964).

NOTES

BULLETIN OF THE CHEMICAL SOCIETY OF JAPAN, VOL. 49 (12), 3684 (1976)

Nuclear Spin-lattice Relaxation in $Sn(CH_3)_4$

Tooru HASEBE,* Gen SODA, and Hideaki CHIHARA

Department of Chemistry, Faculty of Science, Osaka University, Toyonaka 560

(Received August 6, 1976)

Synopsis. Nuclear magnetic relaxation T_1 of solid $Sn(CH_3)_4$ increased monotonously with temperature between 77 and 217 K. The activation energy for intramolecular methyl reorientation was 2.6 ± 0.3 kJ mol^{-1}. From measurements on the liquid phase, the apparent activation energy associated with the relaxation process was 8.6 kJ mol^{-1}. Differential thermal analyses revealed the existence of another unstable solid phase.

Tetramethylstannane $Sn(CH_3)_4$ was studied by nuclear magnetic resonance by Smith[1] who measured the spin-lattice relaxation time T_1 by the method of signal decay. We have re-examined the solid and the liquid phases of $Sn(CH_3)_4$ by calorimetry and NMR. This Note will describe the NMR results and point out some new features which supplement the previous studies.

Differential Thermal Analyses

Unlike its lighter homologues $C(CH_3)_4$[2] and $Si(CH_3)_4$[3], $Sn(CH_3)_4$ has no plastic crystal phase below its triple point. However, differential thermal analyses revealed that an unstable solid phase appeared when the liquid is cooled through the freezing point. This unstable phase spontaneously transforms itself to the stable phase which has the melting point at 217 K. We were not able to hold the unstable phase long enough to make NMR measurements, and it was not made certain whether it was a plastic crystal phase.

NMR Line Width

The temperature dependence of the NMR line-width was measured on a polycrystalline specimen; the width remained constant at 5.7 ± 0.6 G from 20 K to the melting point**. Corresponding to this, the second moment was 9.0 ± 1.0 G^2, which roughly agrees with 8.4 G^2 calculated on the basis of fully excited intramolecular methyl reorientation. When measured with a specimen of poorer purity (99.8 moles per cent), a narrow absorption peak was super-imposed on a broad signal, which was also reported by Smith. However, a purer specimen*** (better than 99.99 moles per cent) did not show the narrow peak.

Spin-Lattice Relaxation Time

The spin-lattice relaxation time T_1 at 10 MHz was measured between 77 K and the melting point by $\pi/2$-τ-$\pi/2$ pulse sequences and between 182 K and 244 K (undercooled and normal liquid) by π-τ-$\pi/2$ pulses. The results are shown in Fig. 1. In the solid state, the T_1 values here obtained show a monotonous increase with temperature and are shorter than the values reported by Smith by a factor of 2: There is no trend of levelling off above 160 K either. On the assumption that we are looking at extreme narrowing case, $\omega\tau_c \ll 1$, which we believe plausible, the activation energy for intra-methyl reorientation was derived as 2.6 ± 0.3 kJ mol^{-1} in comparison with Smith's value[1] 1.93 ± 0.05 kJ mol^{-1} and with Durig's value[4] 3.35 kJ mol^{-1} derived from far infrared study.

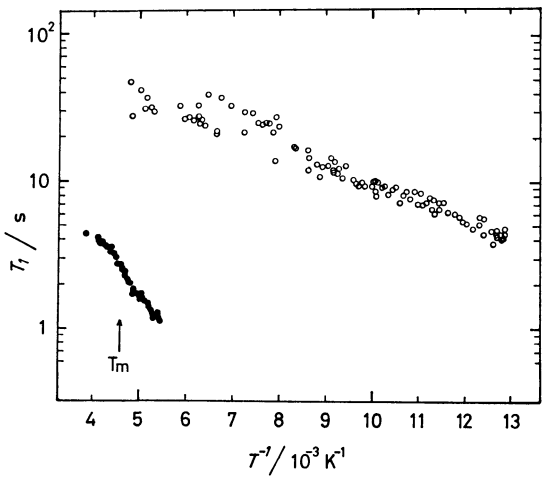

Fig. 1. A semilog plot of T_1 *vs.* the inverse temperature for $Sn(CH_3)_4$ as observed at 10 MHz. (●) liquid phase, (○) crystal phase.

From the T_1 in the liquid state, an apparent activation energy was obtained as 8.6 ± 1.0 kJ mol^{-1}. It is interesting to note that this is close to the enthalpy of fusion[5] 9.24 ± 0.05 kJ mol^{-1}. It is difficult to assess the mode or modes of motion responsible for the relaxation in this temperature region, but it is likely that self-diffusion is at least partly responsible for that.

The authors would like to express gratitude to Dr. T. Atake for purification of $Sn(CH_3)_4$.

References

1) G. W. Smith, *J. Chem. Phys.*, **42**, 4229 (1965).
2) J. G. Aston and G. H. Messerly, *J. Am. Chem. Soc.*, **58**, 2354 (1936).
3) T. Hasebe, G. Soda, and H. Chihara, *Proc. Jpn. Acad.*, **51**, 168 (1975).
4) J. R. Durig, S. M. Craven, and J. Bragin, *J. Chem. Phys.*, **52**, 2046 (1970).
5) T. Atake and H. Chihara, to be published.

* Present address: Department of Chemistry, Faculty of Education, Fukushima University, Fukushima 960.

** 1 G$=10^{-4}$ T

*** Purification was carried out by a preparative gas chromatograph. The thermodynamic properties of this purer specimen will be reported elsewhere.[5]

BULLETIN OF THE CHEMICAL SOCIETY OF JAPAN, VOL. 49 (12), 3685—3686 (1976)

Studies of the π,π^* Absorption Bands of 2,6-Dimethyl-4-pyrone

Akira KUBOYAMA, Yoshikuni SATO,[1] and Hiroshi ARANO

National Chemical Laboratory for Industry, Hon-machi, Shibuya-ku, Tokyo 151

(Received December 12, 1975)

Synopsis. The π,π^* S-S absorption spectra of 2,6-dimethyl-4-pyrone in solutions up to the vacuum UV region were obtained. Based on the results of the MO calculations, the assignment and characterization of the observed π,π^* bands were studied, together with the assignment of the π,π^* bands near 250 nm of 4-pyrone.

Previously, we have theoretically and experimentally studied the π,π^* singlet-singlet absorption bands of *p*-[2] and *o*-quinones[3] and α-santonin[4] up to the vacuum UV region. 4-Pyrone is one of the fundamental unsaturated carbonyl compounds in organic and biological chemistry. As for the π,π^* absorption spectra of 4-pyrones, heretofore, only the π,π^* bands near 250 nm have been investigated.[5] In this work, we have studied the π,π^* absorption spectrum of 2,6-dimethyl-4-pyrone (II) up to the vacuum UV region in the same manner as in the previous works. The assignment of the π,π^* bands near 250 nm of 4-pyrone (I) has also been studied.

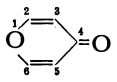

4-Pyrone (I)

The absorption spectra were measured in the same manner as in the previous works. The solvents used—heptane and 1,1,1,3,3,3-hexafluoro-2-propanol (HFP)—were the same as those used previously. Commercially available II was purified by the zone-melting method after being purified by vacuum sublimation (mp 133.6—134.5 °C).

As the electronic integral values in the Pariser-Parr-Pople method,[6] various kinds of integral values were tentatively used, based on the results obtained in the previous calculations.[2-4] Finally, the following integral values were chosen in this work. The core Coulomb integral of the carbonyl oxygen atom and the core resonance integral of the conventional C–C single bonds were taken as −14.00 and −1.50 eV, respectively. Otherwise, the intergral values used were the same as those used in the calculations of *p*-benzoquinone[2] and α-santonin.[4] For the oxygen atom of the 1-position, its core Coulomb integral, its Coulomb electron repulsion integral, and the core resonance integral of the C–O bonds were taken as −27.00, 19.46,[7] and −1.20 eV, respectively. As for the effect of methyl-group substitution, the core Coulomb integral of the substituted carbon atoms was taken as −9.00 eV, considering only the inductive effect of alkyl group, as in the previous works.[2,3] In the calculations, all the singly-excited configurations were included. As the dimention of the π-electronic system of I, that of the C_{2v} symmetry estimated by Norris *et al.*[8] from the microwave spectrum was used.

In Fig. 1, three π,π^* bands can be found, among which the strongest band is in the vacuum UV region.[9]

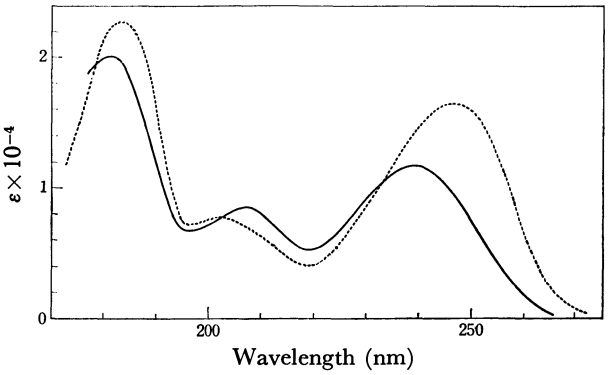

Fig. 1. Absorpion spectra of II in solutions.
——: Heptane, ------: HFP.

These three π,π^* bands are denoted as Bands A, B, and C in order of wavelength. A relatively large red-shift and a large intensity enhancement of Band A in the HFP solution in comparison with that in the heptane solution are noticeable. A strong hydrogen-bond between the oxygen atom of the 1-position of II and HFP may not be formed because of the steric hindrance caused by the two methyl groups of II. II is known to have a relatively strong basicity and this basicity is ascribed to the lone-electron-pair of the carbonyl oxygen atom.[5b,10] Therefore, the above-mentioned fact may be due to the strong hydrogen-bond formation between the carbonyl oxygen atom of II and HFP.

TABLE 1. WAVELENGTHS (λ), MOLAR ABSORPTION COEFFICIENTS (ε), AND OSCILLATOR STRENGTHS (f) OF THE ABSORPTION MAXIMA OF II

Heptane			HFP			Band name
λ(nm)	ε	f	λ(nm)	ε	f	
238.5	11800	0.25	246	16450	0.35	A
207	8550	≈0.17	202.5	7810	≈0.16	B
181	20200	0.5	183	22800	0.52	C

In Table 2, the first column denotes the numbering of the states in order of increasing excitation energies (calculated). In this table, the data on the higher excited states with small f values have been omitted. In view of the calculated results in Table 2, Band A is thought to consist of the $^1A_1$ (the No. 1 state)←$^1A_1$ and $^1B_2$ (the No. 2 state)←$^1A_1$ transition bands, but mostly of the former. On the other hand, in the spectrum of I in the hexane solution, obtained by Efimov *et al.*,[5e] the band near 250 nm corresponding to Band A has a shoulder on its long wavelength-side and the large distance (*ca.* 2800 cm^{-1}) between its peak and this shoulder shows that the main band and this shoulder belong to separate π,π^* bands. A similar spectrum for I in the

Table 2. Calculated excitation energies (E) and oscillator strengths (f) of the singlet π,π^* excited states of I and II and the corresponding observed π,π^* bands

No.	Calculated: Symmetry	Calculated: E(eV)	Calculated: f	Observed[a]: Band name	Observed[a]: E(eV)	Observed[a]: ε,f[b]
			(1) I			
1	$^1B_2$	4.306	0.055		≈4.75[5e]	3000[5e]
2	$^1A_1$	4.367	0.365		5.09[5e]	12600[5e]
3	$^1B_2$	5.445	0.056			
4	$^1A_1$	6.095	0.029			
5	$^1A_1$	6.612	0.077			
6	$^1B_2$	6.946	0.071			
7	$^1A_1$	7.422	1.157			
			(2) II			
1	$^1A_1$	4.456	0.372	A	5.20	0.25
2	$^1B_2$	4.512	0.048			
3	$^1B_2$	5.362	0.063	B	5.99	≈0.17
4	$^1A_1$	6.178	0.038			
5	$^1A_1$	6.681	0.051			
6	$^1B_2$	7.045	0.070			
7	$^1A_1$	7.438	1.180	C	6.85	0.5

a) The data for I and II are those in the hexane and heptane solutions, respectively. b) The values for I and II are molar absorption coefficient and oscillator strength, respectively.

ethanol solution has been reported by Franzosini *et al.*[5a,11] Therefore, as is shown in Table 2, the main band and the shoulder may be reasonably assigned to the $^1B_2$ (the No. 1 state)←$^1A_1$ and $^1A_1$ (the No. 2 state)← $^1A_1$ bands of I, respectively.

As for Band B, the assignment based on the calculated results is not clear. Band C may be safely assigned to the $^1A_1$ (the No. 7 state)←$^1A_1$ band, in view of the large f value of this transition, as is shown in Table 2. Therefore, it may be concluded that both Bands A and C are polarized almost along the symmetry axis of II. According to the calculated results, Band A has the character of the intermolecular charge-transfer band[12] from the oxygen atom of the 1-position to the carbonyl group, and the excited state of Band C is greatly localized in two vinyl groups, as in the case of Band D of α-santonin.[4] In the HFP solution, the strong hydrogen-bond formation between II and HFP, mentioned above, may intensify this character of Band A. So, the noticeable solvent effect for Band A in the HFP solution, mentioned above, may be reasonably explained on the basis of this characteristic of Band A.

As is seen in Table 2, the calculated excitation energy of the lowest $^1A_1$ state (the No. 1 state) of II is 0.09 eV greater than that of the corresponding state (the No. 2 state) of I. On the other hand, the corresponding state of 3,5-dialkyl-4-pyrone is 0.153 eV smaller than that of I. Based on the calculated results, therefore, the main band near 250 nm of I may be expected to be at longer wavelengths than Band A and at shorter wavelengths than the corresponding band of 3,5-dialkyl-4-pyrone, respectively. This expectation is verified in the case of Band A, as is seen in Table 2.

References

1) Permanent address: The Tokyo Metropolitan Industrial Technology Center, Kita-ku, Tokyo.

2) A. Kuboyama, S. Matsuzaki, M. Takagi, and H. Arano, *Bull. Chem. Soc. Jpn.*, **47**, 1604 (1974); *Tokyo Kogyo Shikensho Hokoku*, **69**, 492 (1974).

3) a) A. Kuboyama, F. Kobayashi, and S. Morokuma, *Bull. Chem. Soc. Jpn.*, **48**, 2145 (1975); *Tokyo Kogyo Shikensho Hokoku*, **71**, 180 (1976); b) A. Kuboyama and H. Arano, *Bull. Chem. Soc. Jpn.*, **49**, 1401 (1976).

4) A. Kuboyama, Y. Sato, and F. Kobayashi, *Bull. Chem. Soc. Jpn.*, **48**, 3381 (1975); *Tokyo Kogyo Shikensho Hokoku*, to be published.

5) a) P. Franzosini, G. Trauerso, and M. Senesi, *Ann. Chim. (Rome)*, **45**, 128 (1955); M. Rolla and P. Franzosini, *ibid.*, **46**, 582 (1956); b) H. Tsubomura, *Nippon Kagaku Zasshi*, **78**, 106 (1957); c) K. Yamada, *Bull. Chem. Soc. Jpn.*, **35**, 1323 (1962); d) R. Zahradnik, C. Parkanyi, and J. Koutecky, *Collect. Czech. Chem. Commun.*, **27**, 1242 (1962); e) A. A. Efimov, R. N. Nurmuchametov, and A. I. Tolmachev, *Opt. Spektrosk.*, **29**, 6 (1970); f) J. Gayoso, H. Bouanani, and A. Boucekkine, *Bull. Soc. Chim. Fr.*, **1974**, 553.

6) R. Pariser and R. G. Parr, *J. Chem. Phys.*, **21**, 466, 767 (1953); J. A. Pople, *Trans. Faraday Soc.*, **49**, 1375 (1953).

7) S. Nagakura, "Yuuki Denshi Riron," Baifuukan, Tokyo (1966), 283.

8) C. L. Norris, R. C. Benson, P. Beak, and W. H. Flygare, *J. Am. Chem. Soc.*, **95**, 2768 (1973).

9) The n, π^* absorption bands of I[5e] and II are found near 300 nm in the heptane solutions.

10) L. F. Cavalieri, *Chem. Rev.*, **41**, 525 (1947).

11) In Yamada's paper,[5c] the existence of two shoulders on the long wavelength-side of the main peak is described, but no data about the absorption intensity are given.

12) S. Nagakura and J. Tanaka, *J. Chem. Phys.*, **22**, 236 (1954); S. Nagakura, *Pure Appl. Chem.*, **7**, 79 (1963).

BULLETIN OF THE CHEMICAL SOCIETY OF JAPAN, VOL. 49 (12), 3687—3688 (1976)

Enthalpy-Controlling Adsorption of Hydrocarbons on 1,3,5-Trinitrobenzene as Revealed by Gas Chromatography

Masamichi AKIMOTO and Etsuro ECHIGOYA

Department of Chemical Engineering, Tokyo Institute of Technology, Ookayama, Meguro-ku, Tokyo 152

(Received June 9, 1976)

Synopsis. Equilibrium adsorption constants for a series of olefins and paraffins on 1,3,5-trinitrobenzene were enhanced upon increasing the electron-donating nature of the hydrocarbons; the trend in the adsorption constants was entirely due to variations in the enthalpy change of adsorption rather than the entropy one. These results are characteristics of the adsorption in which the donation of electrons from a hydrocarbon molecule is strongly predominant.

The importance of adsorption in heterogeneous catalysis has often been pointed out. However, it is very difficult to clarify the mechanism of electron transfer on the adsorption by means of spectroscopy. Hence, it would be very useful if the electron transfer could be estimated by measuring the effect of the enthalpy and the entropy changes on the adsorption constant. Cvetanovic and co-workers[1] showed in their gas chromatographic studies on the adsorption of olefinic hydrocarbons on 1,3,5-trinitrobenzene (TNB) that the retention time of olefins increased with the increase in their electron-donating nature. A similar trend was also observed on NiO, for which the important role of the donation of electrons from olefin molecules was discussed.[2] The present study attempted to find a correlation between the electron transfer in the adsorption of noncyclic hydrocarbons on TNB and the trends in the thermodynamic parameters of the adsorption constant by investigating the effect of hydrocarbon structure on the adsorption constant, which can be determined by means of gas chromatography. Furthermore, the enthalpy change of the adsorption observed was discussed in relation to the electron-donating nature of hydrocarbons.

Experimental

Column packing (20 wt% TNB on 60—80 mesh Chromosorb P) was prepared according to the method proposed.[1] This was packed in a stainless steel pipe (3 mm i.d., 4 m) and was pretreated with a helium current (30 NTPml/min) for 2 h at room temperature. Helium was used as a carrier gas. The mixture (olefin 10 vol%, paraffin 10 vol%, and N_2 80 vol%) was injected into the column using an U-shaped bypass injector whose volume was 0.56 NTPml. Here, the saturated hydrocarbon has the same skeletal structure as that of the olefinic one.

By means of gas chromatography, the equilibrium adsorption constant and the heat of adsorption were determined using the following equation.[3]

$$\mu/T = (R/V_g)n_m e^{\Delta S/R} e^{Q/RT}$$

where T: temperature (K); R: gas constant; V_g: void volume in the column; ΔS: entropy change of adsorption; n_m: amount of sample required for making monolayer coverage; Q: heat of adsorption, $Q=-\Delta H$; ΔH: enthalpy change of adsorption; K: equilibrium adsorption constant $K=e^{\Delta S/R}\,e^{Q/RT}$; μ: relative retention time, $\mu=(t-t_0)/t_0$; t_0 and t are the retention times of N_2 and the sample, respectively.

Results and Discussion

Figure 1 shows the linear plot of μ_{ol}/T *vs.* $1/T$ for olefin adsorption. Values of μ_{ol}/T, μ_p/T, and heats of adsorption for a series of hydrocarbons are summarized with the ionization potential of the hydrocarbons (Table 1). These values are enhanced upon decreasing the ionization potential of the hydrocarbons, *i.e.*, upon increasing their electron-donating nature, as was report-

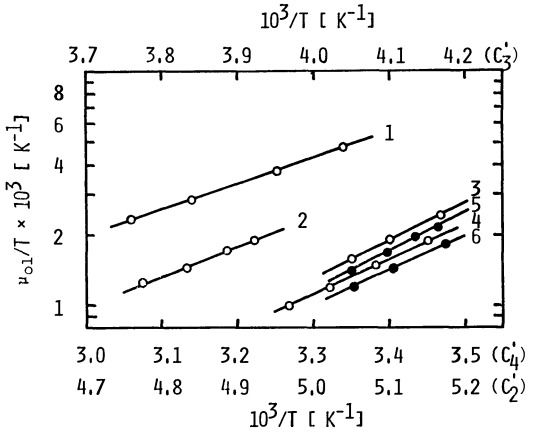

Fig. 1. Linear plot of the results obtained in olefin adsorption.
1: Ethylene, 2: propylene, 3: *cis*-2-butene, 4: 2-methylpropene, 5: *trans*-2-butene, 6: 1-butene.

TABLE 1. THERMODYNAMIC PARAMETERS OF THE EQUILIBRIUM ADSORPTION CONSTANT

Hydrocarbon	μ/T $\times 10^3$ $[K^{-1}]$[a]	$-\Delta H$ [kcal/g-mol]	$-\Delta(\Delta S)$ [cal/g-mol K]	Ionization potential[b] [eV]
Ethylene	4.29	4.93	—	10.62
Propylene	1.77	5.97	—	9.84
1-Butene	1.42	6.59	0.00	9.58
2-Methylpropene	1.61	7.06	1.35	9.23
trans-2-Butene	1.72	7.41	2.41	9.13
cis-2-Butene	1.90	7.49	2.56	9.13
Ethane	3.05	4.20	—	11.78
Propane	1.18	4.87	—	11.04
Isobutane	0.97	5.00	—	10.79
Butane	1.15	6.31	—	10.71

a) Ethane, ethylene 200 K; propane, propylene 256 K; butane, butene 294 K. b) Reference: ethylene, propylene (4); 1-butene (5); 2-butene, 2-methylpropene (6); paraffin (7).

ed earlier.[1] So long as the same column is used, V_g is constant, and n_m is expected to be constant for butene isomers. In the case of propylene and ethylene, n_m is either at least equal to that of butene or it increases with decreasing the shape of the hydrocarbon molecule. Hence, the sequence of μ/T observed agrees with that of the adsorption constants. Table 1 also shows that each trend in the adsorption constants is entirely due to variations in the heat of adsorption. Taking subscript 1 to mean the most weakly adsorbed butene (1-butene), the difference in the entropy changes for other butene isomers (subscript 2), $\Delta(\Delta S)=\Delta S_2-\Delta S_1$, was calculated (Table 1). The sequence of $\Delta(\Delta S)$ suggests that the entropy change occurs in the same order as that of the enthalpy change. Therefore, it was concluded that the increment in the adsorption constant should be attributed to that in the enthalpy change rather than the entropy one. This enthalpy-controlling nature is also the case for paraffin adsorption (Table 1). Furthermore, the enhancement in the enthalpy change upon decreasing the ionization potential shows the presence of a close relationship existing between the strength of the electron donation and the enthalpy change. TNB is a strong electron-acceptor. Hence, this can be reasonably understood by assuming that these hydrocarbons donate their electrons to TNB in proportion to their electron-donating nature.

It is also instructive to discuss the relative retention time $(t_{ol}-t_0)/(t_p-t_0)$. Since $RT\ln[(t_{ol}-t_0)/(t_p-t_0)]=RT\ln(K_{ol}/K_p)=-(\Delta G_{ol}-\Delta G_p)=-\Delta(\Delta G)$, this procedure elucidates the effect of the double bond on the adsorption constant of the olefin. Table 2 indicates that the increase in $-\Delta(\Delta G)$ by introduction of the olefinic bond is due to the rise in the relative enthalpy change $-\Delta(\Delta H)$ rather than the relative entropy one $-\Delta(\Delta S)$. This enthalpy-controlling character is also inherent to the adsorption in which the donation of electrons from an olefin to the adsorbent plays a very important role in the adsorption.

Table 2. Thermodynamic parameters of the K_{ol}/K_p

System	$-\Delta(\Delta G)$ [cal/g-mol] at 290 K	$-\Delta(\Delta H)$ [cal/g-mol]	$-\Delta(\Delta S)$ [cal/g-mol K]
Ethylene–ethane	128[a]	558	2.15
Propylene–propane	199[b]	940	2.85
1-Butene–butane	132	953	2.83
trans-2-Butene–butane	247	987	2.55
cis-2-Butene–butane	300	1124	2.84
2-Methylpropene–isobutane	328	1955	5.61

a) at 200 K. b) at 260 K.

References

1) R. J. Cvetanovic, F. J. Duncan, and W. E. Falconer, *Can. J. Chem.*, **42**, 2410 (1964).
2) Y. Moro-oka and A. Ozaki, *J. Am. Chem. Soc.*, **89**, 5124 (1967).
3) N. Hara, "Jikken Kagaku Koza, Vol. 9, Gas Chromatography," Maruzen Press, Tokyo (1965), p. 520.
4) R. E. Honig, *J. Chem. Phys.*, **16**, 105 (1948).
5) K. Watanabe, *J. Chem. Phys.*, **26**, 542 (1957).
6) J. Collin and E. P. Lossing, *J. Am. Chem. Soc.*, **81**, 2064 (1959).
7) A. Streitwieser, Jr., *J. Am. Chem. Soc.*, **82**, 4123 (1960).

BULLETIN OF THE CHEMICAL SOCIETY OF JAPAN, VOL. 49 (12), 3689—3690 (1976)

Electrical Conductivity Changes in α-FeOOH and β-FeOOH upon Surface Dehydration

Katsumi KANEKO and Katsuya INOUYE

Department of Chemistry, Faculty of Science, University of Chiba, Yayoi-cho, Chiba 280

(Received July 5, 1976)

Synopsis. The electrical conductivity of α-FeOOH and β-FeOOH, preheated at 100—140 °C *in vacuo*, was determined over the temperature range from 0 to 140 °C. The conductivity increased considerably with a rise in the preheating temperature. The increase appears to be due to Fe^{2+} ions produced by surface dehydration in the preheating.

Among the polymorphs of iron(III) hydroxide oxide (the so-called ferric oxyhydroxide), α-FeOOH, β-FeOOH, and γ-FeOOH occur naturally as minerals and as major components of the corrosion product of iron-base alloys. Each iron(III) hydroxide oxide has the characteristic structure.[1-3] It has been known that iron(III) hydroxide oxides are transformed into iron oxides (α-Fe_2O_3 or γ-Fe_2O_3) at around 300 °C in air according to this formula:

$$2\,FeOOH \longrightarrow Fe_2O_3 + H_2O.$$

However, when FeOOH crystals are heated under 10^{-5} Torr, the decomposing dehydration begins at temperatures as low as 100 °C.[4] In the preceding papers,[5,6] the present authors reported that the electrical conductivity of γ-FeOOH increases remarkably with a rise in the preheating temperature in the range of 100—140 °C under 10^{-5} Torr, and that this behavior can be explained by the formation of excess d-electrons due to dehydration. It was proposed that excess d-electrons migrate in γ-FeOOH crystals by means of the small-polaron hopping mechanism.[6]

In this work, the effect of the preheating temperature (100—140 °C) on the electrical conductivity will be examined for α-FeOOH and β-FeOOH in order to discuss the mechanism of carrier formation in comparison with the case of γ-FeOOH.

The α-FeOOH and β-FeOOH used in this study were the same samples as those examined earlier.[7] The pretreatment of the samples was also identical to that carried out for γ-FeOOH.[6] The conductivity of the compressed specimens, formed by applying a pressure of 150 kg/cm², was measured over the temperature range from 0 to 140 °C and at various frequencies (d.c., 200 Hz—10 MHz) by a method described previously.[8] The current-voltage characteristics for d.c. indicated that the contact between the specimen and an electrode was nearly ohmic.

The effect of oxygen on the dc conductivity was examined for α-FeOOH and β-FeOOH, evacuated at 10^{-5} Torr and 140 °C, by supplying oxygen of 0.1 Torr at 30 °C.

The total iron and Fe^{2+} contents were determined by conventional titration methods.[6,7]

The electrical conductivity at d.c. and in the lower-frequency range increased with the preheating temperature in the range from 100 to 140 °C. The variation in the conductivity, σ_{dc}, at 30 °C with the preheating temperature is shown in Fig. 1 (a). The Fe^{2+} concentration also increased with the preheating temperature (Fig. 1 (c)).

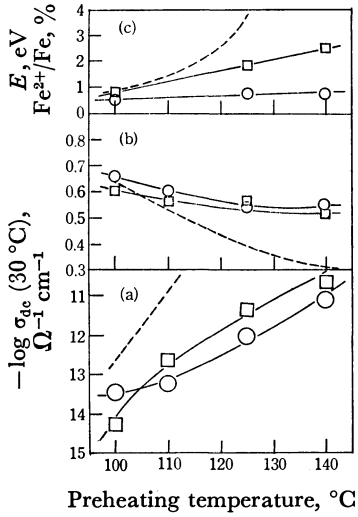

Fig. 1. Variations of (a) the logarithm of d.c. electrical conductivity at 30 °C, (b) activation energy of conductivity at d.c., and (c) Fe^{2+} concentration, with the preheating temperature for α-FeOOH (○) and β-FeOOH (□). The broken lines show the results on γ-FeOOH.[6]

It was found that logarithm of σ_{dc} is proportional to the reciprocal of the measuring temperature (0—140 °C), as is shown in Figs. 2 and 3 for α-FeOOH and β-FeOOH respectively. The notations α(β)-100, α(β)-110, α(β)-125, and α(β)-140 denote α-FeOOH or β-FeOOH samples preheated at 100, 110, 125, and 140 °C respectively. These linear relations have previously been found for γ-FeOOH.[6] The activation energy at

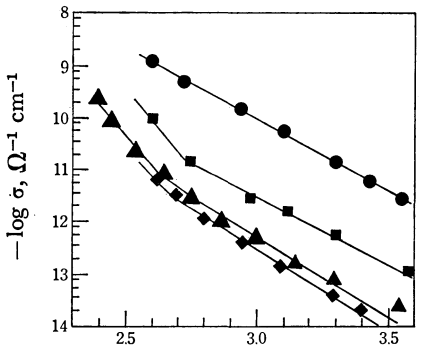

Fig. 2. The temperature dependence of electrical conductivity at d.c. for α-100 (◆), α-110 (▲), α-125 (■), and α-140 (●).

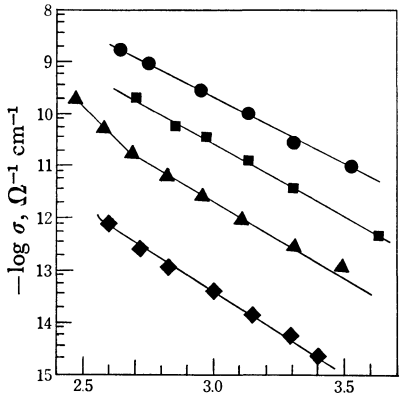

Fig. 3. The temperature dependence of electrical conductivity at d.c. for β-100 (◆), β-110 (▲), β-125 (■), and β-140 (●).

d.c., calculated from the linear relation below 100 °C, was less than 1 eV and decreased slightly with the preheating temperature, as is shown in Fig. 1 (b). The activation energy above 100 °C was 1—1.5 eV. The activation energy generally decreased with an increase in the frequency. The conductivity at higher frequencies varied slightly with the measuring temperature.

It was confirmed that the a.c. conductivity σ_{ac} ($=\sigma - \sigma_{dc}$) was proportional to f^s ($0.5<s<1$) in the frequency range of 200 Hz—1 MHz. The constant s, representing the frequency dependence of the conductivity, decreased with an increase in the measuring temperature.

The exposure to oxygen of α-FeOOH and β-FeOOH preheated at 140 °C resulted in a lowering of the electrical conductivity at d.c. to less than a half of the initial value within 2 h.

The surface property of α-FeOOH and β-FeOOH crystals is characterized by their predominant surfaces, namely, the (100) planes for both α-FeOOH and β-FeOOH. The structures of these predominant surfaces were discussed in a previous paper.[9] The OH groups aligned in the c direction on surfaces are connected with each other by hydrogen bonding. The dehydration of an OH^- pair below 150 °C *in vacuo* appears to proceed through the formation of a quasi-molecular water by means of the following mechanism:

$$2\,OH^- \longrightarrow H_2O + V_o^- + O^-,$$

where V_o^- denotes the mono-charged oxygen vacancy. The dehydration causes an increase in the Fe^{2+} concentration by providing electrons from V_o^- to Fe^{3+}, which results in an increase in the conductivity.

α-FeOOH has OH^- pairs only at the surface, whereas β-FeOOH has the pairs not only on the surface, but also in pores in parallel to the c-axis (see Ref. 9). For γ-FeOOH, on the other hand, the dehydration occurs on the surface as well as in the bulk of the crystal.[6] The increase in the Fe^{2+} concentration with the pretreating temperature, in the order γ-FeOOH>β-FeOOH>α-FeOOH (Fig. 1 (c)), is pertinent to both the ability to dehydrate by the mechanism mentioned above and the difference in the surface area for each crystal form. The BET surface areas are in the following decreasing order[7]: γ-FeOOH: 124 m²/g, α-FeOOH: 65 m²/g, and β-FeOOH: 34 m²/g.

The conductivity is assumed to follow the small-polaron hopping mechanism of excess d-electrons formed by the same surface dehydration for α-FeOOH and β-FeOOH as for γ-FeOOH. This assumption is supported by the frequency-dependence of the conductivity and the small activation energy of the conduction, and further by the fact that the mobility calculated from the conductivity and the Fe^{2+} concentration is less than 10^{-7} cm² V^{-1} s^{-1} at 30 °C. It was explained in the case of γ-FeOOH[6] that a decrease in the activation energy is due to an increase in the Fe^{2+} concentration and that the conductivity increase with the preheating temperature is caused by the increase in the interaction between Fe^{2+} ions. The same mechanism may also be applied to α-FeOOH and β-FeOOH. However, the decrease in activation energy with the preheating temperature for α-FeOOH and β-FeOOH is smaller than that for γ-FeOOH (Fig. 1 (b)). A lower interaction between Fe^{2+} ions in α-FeOOH and β-FeOOH than γ-FeOOH is presumed, because the Fe^{2+} concentration is considerably lower in α-FeOOH and β-FeOOH than in γ-FeOOH. It is noteworthy that the conductivity increase with the preheating temperature is less marked for α-FeOOH and β-FeOOH than for γ-FeOOH.

The decrease in the d.c. conductivity observed when oxygen was introduced into the evacuated sample indicates that electrons once formed by the dehydration are consumed by chemisorbed oxygen molecules at surface defects.

This research has been partially supported by the Government Science Research Grant of the Ministry of Education.

References

1) F. J. Ewing, *J. Chem. Phys.*, **3**, 203 (1935).
2) F. J. Ewing, *J. Chem. Phys.*, **3**, 420 (1935).
3) A. L. Mackay, *Mineral. Mag.*, **32**, 545 (1960).
4) T. Ishikawa and K. Inouye, *Bull. Chem. Soc. Jpn.*, **46**, 2665 (1973).
5) K. Kaneko and K. Inouye, *J. Electrochem. Soc.*, **122**, 451 (1975).
6) K. Kaneko and K. Inouye, *J. Chem. Soc., Faraday Trans. 1*, **72**, 1258 (1976).
7) K. Kaneko and K. Inouye, *Bull. Chem. Soc. Jpn.*, **47**, 1139 (1974).
8) K. Kaneko and K. Inouye, *Nippon Kagaku Kaishi*, **1973**, 1975.
9) K. Kaneko, M. Serizawa, T. Ishikawa, and K. Inouye, *Bull. Chem. Soc. Jpn.*, **48**, 1764 (1975).

BULLETIN OF THE CHEMICAL SOCIETY OF JAPAN, VOL. 49 (12), 3691—3692 (1976)

Oxidation-Reduction Potentials in the Formation of Anion Radicals

Yôichi IIDA

Department of Chemistry, Faculty of Science, Hokkaido University, Sapporo, 060

(Received May 15, 1976)

Synopsis. The oxidation-reduction potentials in the formation of anion radicals were determined by using the equilibrium constant of the preferred electron transfer reaction between anion radicals in acetonitrile solution.

The 7,7,8,8-tetracyanoquinodimethane (TCNQ), 2,3-dicyano-*p*-benzoquinone (*p*-H_2QCy_2) and 2,3-dichloro-5,6-dicyano-*p*-benzoquinone (*p*-Cl_2QCy_2) molecules are known to be strong electron acceptors and to form stable anion radical salts with some diamagnetic counter cations.[1-3]

Several years ago,[4] we reported on the preferred electron transfer reaction between anion radicals in solution. When *p*-X_2QCy_2 (X=H or Cl) was added to an acetonitrile solution of the sodium salt of the TCNQ anion radical, the oxidation-reduction reaction was found to take place simply through a one-electron transfer from the TCNQ anion radical to *p*-X_2QCy_2. This reaction was expressed by the following oxidation-reduction equilibrium:

$$TCNQ^- + p\text{-}X_2QCy_2 \rightleftarrows TCNQ + p\text{-}X_2QCy_2^-, \quad (1)$$

where X=H or Cl. It was assumed that the activity coefficients of the solutes were unity, since their concentrations were as dilute as 10^{-5} mol/l. In this case, the equilibrium constant, K, of this reaction was simply expressed by

$$K = \frac{[TCNQ][p\text{-}X_2QCy_2^-]}{[TCNQ^-][p\text{-}X_2QCy_2]}. \quad (2)$$

The value of K in acetonitrile solution at 20±1 °C was determined spectrophotometrically as $K=30$ for the case of X=H, while it was $K \geq 2 \times 10^3$ for the case of X=Cl.[4] At that time, we related the values of K to the half-wave potentials in polarography or to the electron affinities of the neutral *p*-X_2QCy_2 molecules. In the present paper, we obtained oxidation-reduction potentials in the formation of anion radicals, because attempts have scarcely been made to obtained such values.

The occurence of the equilibrium of Eq. 1 means that[5]

$$E_0(TCNQ, TCNQ^-) - \frac{RT}{F}\ln\frac{[TCNQ^-]}{[TCNQ]} = E_0(p\text{-}X_2QCy_2, p\text{-}X_2QCy_2^-) - \frac{RT}{F}\ln\frac{[p\text{-}X_2QCy_2^-]}{[p\text{-}X_2QCy_2]}, \quad (3)$$

where $E_0(TCNQ, TCNQ^-)$ and $E_0(p\text{-}X_2QCy_2, p\text{-}X_2QCy_2^-)$ represent the standard oxidation-reduction potentials of

$$TCNQ + e \rightleftarrows TCNQ^-, \quad (4)$$

$$p\text{-}X_2QCy_2 + e \rightleftarrows p\text{-}X_2QCy_2^-. \quad (5)$$

They were assumed to be reversible electrode reactions in acetonitrile solution. In Eq. 3, R, T, and F are the gas constant, the observed temperature and the Faraday constant, respectively. Eq. 3 leads to

$$E_0(p\text{-}X_2QCy_2, p\text{-}X_2QCy_2^-) - E_0(TCNQ, TCNQ^-) = \frac{RT}{F}\ln K. \quad (6)$$

When the spectrophotometrically determined values of K are put into Eq. 6, we have

$$E_0(p\text{-}H_2QCy_2, p\text{-}H_2QCy_2^-) = E_0(TCNQ, TCNQ^-) + 0.09\ V, \quad (7)$$

$$E_0(p\text{-}Cl_2QCy_2, p\text{-}Cl_2QCy_2^-) \geq E_0(TCNQ, TCNQ^-) + 0.19\ V. \quad (8)$$

The absolute values of $E_0(p\text{-}X_2QCy_2, p\text{-}X_2QCy_2^-)$, (X=H or Cl), will be determined from these relations if the value is once given for $E_0(TCNQ, TCNQ^-)$. Although no definite value has been determined for $E_0(TCNQ, TCNQ^-)$, we obtained, in a previous paper,[6] the relationship of Eq. 9 by analyzing spectrophotometrically the oxidation-reduction reaction between TCNQ and iodide ion in acetonitrile solution:

$$E_0(TCNQ, TCNQ^-) = E_0(I_2, 2I^-) + 0.045 \pm 0.004\ V, \quad (9)$$

where $E_0(I_2, 2I^-)$ represents the standard oxidation-reduction potential for the following reversible electrode reaction in acetonitrile solution:

$$I_2 + 2e \rightleftarrows 2I^-. \quad (10)$$

Therefore, by using Eqs. 7, 8, and 9, the values for $E_0(p\text{-}X_2QCy_2, p=X_2QCy_2^-)$, (X=H or Cl), versus $E_0(I_2, 2I^-)$ are obtained as is shown in Table 1.

Table 1. The data on the oxidation-reduction potentials in the formation of the TCNQ, *p*-H_2QCy_2, and *p*-Cl_2QCy_2 anion radicals in acetonitrile solution

Oxidation-reduction system	Oxidation-reduction potential, V
$I_2+2e \rightleftarrows 2I^-$	$E_0(I_2, 2I^-)$
$TCNQ+e \rightleftarrows TCNQ^-$	$E_0(I_2, 2I^-)+0.045\pm0.004$
$p\text{-}H_2QCy_2+e \rightleftarrows p\text{-}H_2QCy_2^-$	$E_0(I_2, 2I^-)+0.14$
$p\text{-}Cl_2QCy_2+e \rightleftarrows p\text{-}Cl_2QCy_2^-$	$\geq E_0(I_2, 2I^-)+0.24$

The oxidation-reduction potentials in acetonitrile solution are found to range, with increasing the electron-accepting strength, as $E_0(I_2, 2I^-) < E_0(TCNQ, TCNQ^-) < E_0(p\text{-}H_2QCy_2, p\text{-}H_2QCy_2^-) < E_0(p\text{-}Cl_2QCy_2, p\text{-}Cl_2$-

QCy_2^-). These oxidation-reduction potentials in the formation of ion radicals are important not only for the electrochemical study, but also for the investigation on the mechanism of certain chemical reactions involving ion radical molecules. The values of the oxidation-reduction potentials in the present paper were obtained by analyzing spectrophotometrically the oxidation-reduction reaction between anion radicals in solution, but an attempt is currently under way to measure those values of E_0 (TCNQ, $TCNQ^-$), E_0(p-X_2QCy_2, p-X_2-QCy_2^-), (X=H or Cl), directly by electrochemical method.

References

1) L. R. Melby, R. J. Harder, W. R. Hertler, W. Mahler, R. E. Benson, and W. E. Mochel, *J. Am. Chem. Soc.*, **84**, 3374 (1962).
2) Y. Iida, *Bull. Chem. Soc. Jpn.*, **44**, 1430 (1971).
3) Y. Iida, *Bull. Chem. Soc. Jpn.*, **44**, 1777 (1971).
4) Y. Iida and H. Akamatu, *Bull. Chem. Soc. Jpn.*, **40**, 231 (1967).
5) See, for example, I. M. Kolthoff, and E. B. Sandell, "Textbook of Quantitative Inorganic Analysis," MacMillan Co., New York (1952), p. 463.
6) Y. Iida, *Bussei*, **13**, 99 (1972), published by Maki Shoten, Tokyo, Japan.

BULLETIN OF THE CHEMICAL SOCIETY OF JAPAN, VOL. 49 (12), 3693—3694 (1976)

A Simple Method for Measuring Mass Spectra of Ions with Excess Kinetic Energy

Susumu TAJIMA,* Mitsuo NAKAMURA,* Tadashige AZAMI,* and Toshikazu TSUCHIYA

*Department of Engineering Chemistry, Gunma Technical College, Toribacho, Maebashi, Gunma 371
National Chemical Laboratory for Industry, Honmachi, Shibuya-ku, Tokyo 151

(Received March 9, 1976)

Synopsis. Mass spectra of ions with excess kinetic energy have been measured by applying a small negative voltage to the repeller electrode.

An important function of mass spectrometry is determination of the structure of organic compounds,[1] but this is not easy, since many rearrangement ions appear in an ordinary mass spectrum. Thus it is desirable to obtain mass spectra that are free of rearrangement ions and consist only of simple cleavage ions.

Recently, a method for measuring mass spectra of ions with excess kinetic energy was reported by Tsuchiya and Horii.[2] They used a modified ion source equipped with a metal gauze electrode between the exit slit and the focus slit. The electrode was kept at a potential a little higher than that of the ionization chamber. The term KE mass spectrum (kinetic energy mass spectrum) was given to the spectrum measured from the ion source. From the fact that simple cleavage ions consist of two kinds of ions, one with thermal energy only and the other with additional excess kinetic energy, and that the rearrangement ions usually have no kinetic energy with exception of a few instances,[3,4] they concluded that a large portion of the KE mass spectra consists of ions produced by simple cleavage, and that KE mass spectra might facilitate the determination of the structure of organic compounds. However, the method is not suitable for measuring both KE and ordinary mass spectra with an analytical mass spectrometer, since the ion source has to be modified in order to measure the KE mass spectra. A simple method for measuring the KE mass spectra with use of a commercial mass spectrometer is needed.

In the present note a simple method for measuring the KE mass spectra is reported. By applying a small negative voltage to the repeller electrode ($-V_r$), the KE mass spectra can be easily obtained without any modification of the ion source. However, the same KE mass spectra as those obtained by Tsuchiya and Horii[2] cannot be expected by the present method, sicnce the potential energy distribution inside the ionization chamber differs in the two methods.

Experimental

The mass spectra were obtained with a Hitachi RMU-5B mass spectrometer. A small negative voltage to the repeller electrode is supplied from the circuit (Fig. 1) by controlling the value of the 20-turn potentiometers R_r and R_r' (Sakae Tsushin Kogyo Co., Ltd.). The connections to the repeller electrode and ionization chamber are made by replacing the clips, so that the normal experimental condition can be recovered easily.

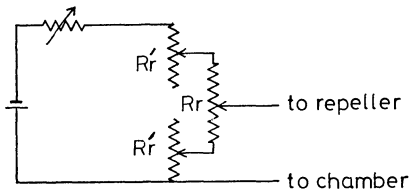

Fig. 1. Diagram of the modified electric circuit for the repeller voltage.

Other conditions of measurement were: electron accelerating voltage, 80 V; ion accelerating voltage, 2000 V; trap current, 60 μA; temperature of ion source, 250 °C; temperature of sample manifold, 20—25 °C.

The intensities of the ions in the KE mass spectra were about one-hundredth of those in ordinary mass spectra.

The samples (Kanto Kagaku Kogyo Co., Ltd.) were used without further purification.

Results and Discussion

In the usual type of mass spectrometer, a small positive voltage is applied to the repeller electrode (V_r) to draw out the ions efficiently from the ion source. Consequently, both ions with no excess kinetic energy, and those with some kinetic energy are pushed out from the ion source. However, when a small negative voltage is applied to the repeller electrode ($-V_r$), only the ions with a kinetic energy greater than half the value of the repeller voltage can emerge from the ion source. Thus it becomes possible to measure the KE mass spectra by

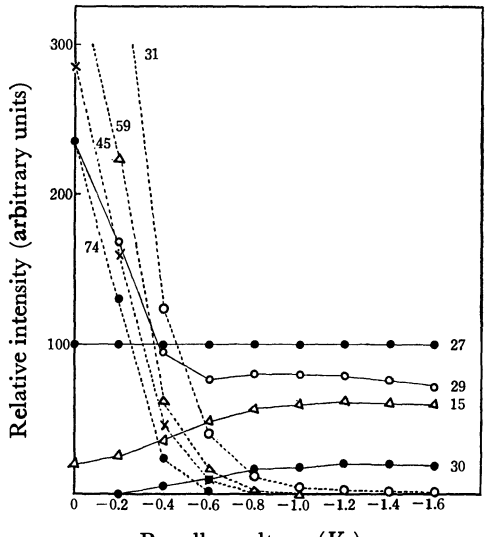

Fig. 2. Variation of the relative intensity for several intense fragment ion peaks of diethyl ether *vs.* repeller voltage.

applying an appropriate negative voltage to the repeller electrode ($-V_r$).

The intensities of several intense fragment ion peaks for diethyl ether are shown in Fig. 2 as a function of repeller voltage (V_r). The intensity of $C_2H_3^+$ (*m/e* 27) is taken as a reference. We see that the molecular ion (*m/e* 74) and the rearrangement ion (*m/e* 31), a large number of which being considered to have no excess kinetic energy, decrease rapidly with decrease in the value of V_r. While simple cleavage ions, *m/e* values of which are larger than a half of the *m/e* value of the molecular ion, *i.e.*, *m/e* 59 and *m/e* 45 ions, also decrease with the V_r value. The intensities of some simple cleavage ions (*m/e* 29, 15 *etc.*,) which are smaller in *m/e* than a half of that of the molecular ion remain approximately constant between -1.0 and -1.6 V (V_r). This implies that a reproducible KE mass spectrum can be obtained at -1.0 —— -1.6 V by our method.

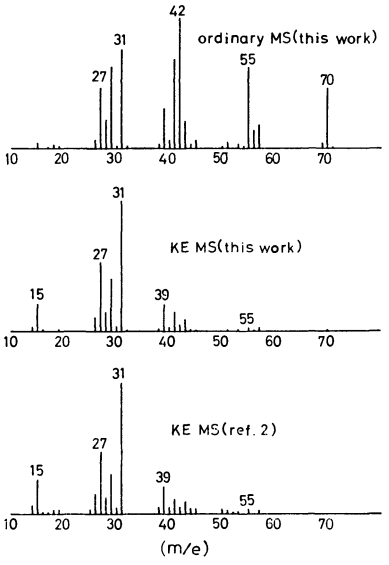

Fig. 3. KE mass spectra and ordinary mass spectrum of pentyl alcohol.

The KE mass spectrum measured at -1.5 V (V_r) and the ordinary mass spectrum (10 V (V_r)) of pentyl alcohol are shown in Fig. 3 together with the KE mass spectrum of Tsuchiya and Horii.[2] The KE mass spectrum measured by our method is close to the theirs, but differs from the ordinary one.

An analytical mass spectrometer can be used readily to measure the KE mass spectrum, since we can obtain the KE mass spectrum by this method without any modification of the ion source.

The authors wish to thank Mr. Takeshi Satō, Mr. Masanori Suzuki, and Mr. Minoru Imai of this College for their help in measuring the spectra. They are also indebted to Mr. Hirokazu Hanaoka, Gunmaken Industrial Research Laboratory, for valuable discussions.

References

1) T. Furumai, Y. Seki, K. Takeda, A. Kinumaki, and M. Suzuki, *J. Antibiot.*, **26**, 708 (1973).

2) M. Tsuchiya and Y. Horii, *Shitsuryo Bunseki*, **22**, 79 (1974).

3) J. H. Beynon, R. A. Saunders, and A. E. Williams, *Z. Naturforsch., Teil A*, **20**, 180 (1965); E. G. Jones, J. H. Beynon, and R. G. Cooks, *J. Chem. Phys.*, **57**, 2652 (1972).

4) B. Davis and D. H. Williams, *Chem. Commun.*, **1970**, 412.

BULLETIN OF THE CHEMICAL SOCIETY OF JAPAN, VOL. 49 (12), 3695—3696 (1976)

Preparation of γ-FeOOH by Aerial Oxidation of Iron(II) Chloride Solution

Shuichi HAMADA and Kenshi KUMA

Department of Chemistry, Faculty of Science, Science University of Tokyo, Kagurazaka, Shinjuku-ku, Tokyo 162

(Received May 26, 1976)

Synopsis. Detailed conditions for preparing γ-FeOOH by aerial oxidation of iron(II) chloride solution were studied. The upper limit of temperature for obtaining only the γ-FeOOH decreased with increases in the pH value and the initial concentration of Fe(II) ions. The shapes of the prepared γ-FeOOH particles were examined in connection with the oxidizing conditions.

The kind of aerial oxidation products of iron(II) salt solutions has been well known to be dependent on the preparative conditions. No detailed conditions for preparing the γ-FeOOH, one of the iron(III) hydroxide oxides, have been studied, though its formation has been reported.[1-5] In this work, such preparative conditions for γ-FeOOH as the concentration of Fe(II) ions, the reaction temperature, and the acidity were studied. Furthermore, the shapes of the prepared γ-FeOOH particles were examined in connection with the oxidizing conditions.

Experimental

The iron(II) chloride solution was used as the starting material. The dissolved oxygen was removed by passing nitrogen into the iron(II) chloride solution before the oxidation. The Fe(II) ions were oxidized at the specified temperatures and acidities by bubbling air, free from carbon dioxide, through a glass filter at a constant flow rate with vigorous stirring.

As the acidity of the solution increased with the progress of oxidation, the pH value of the reaction mixture was kept within ±0.15 of the specified acidity by using a pH-stat model HS-2A, from Toa Electronics Ltd., and aqueous ammonia, except for solutions at higher basicities. The air was bubbled for 3 h after the reaction ended under the same conditions in order to age the precipitates. The oxidation product was washed with water until chloride ions were no longer detectable, followed by air-drying for 3 weeks.

The X-ray powder diffraction patterns of the products were taken using Fe*K*α radiation with a Rigaku Denki Geigerflex, model D-3F, X-ray diffractometer. The identification of the products and the estimation of their relative amounts were carried out by using the diffraction peaks at (020) and (031) of the γ-FeOOH, that at (110) of the α-FeOOH, and those at (311) and (440) of the Fe_3O_4.

The shapes of the prepared γ-FeOOH particles were observed with the magnifications of from 10000 to 30000 times by using an electron microscope, model HU-200F, from Hitachi Seisakusho.

Results and Discussion

The final oxidation products of the iron(II) chloride solution were identified as the γ-FeOOH, the α-FeOOH, and the Fe_3O_4: the β-FeOOH was not detectable in this work, though Kiyama *et al.*[6] have reported the formation of β-FeOOH together with γ-FeOOH. In order to estimate the conditions for preparing the pure γ-FeOOH, the kind of products and their relative amounts were examined over a wide range of oxidizing conditions.

The influence of the flow rate of air on the kind of products was determined to be as follows:

Flow rate (l/min)	0.1	1.0	2.4	2.8
	α-, γ-FeOOH	γ-FeOOH	α-, γ-FeOOH	

(pH 6.5, 25°C, and 0.064 mol/l)

Though the flow rate range for preparing only the γ-FeOOH was not found at higher concentrations of Fe(II) ions under the same conditions of the pH and the temperature, the relative amount of the γ-FeOOH was large enough in the flow rate from 1.0 to 2.4 l/min even at higher concentrations. Therefore, subsequent oxidations were carried out at the constant flow rate of 2.0 l/min.

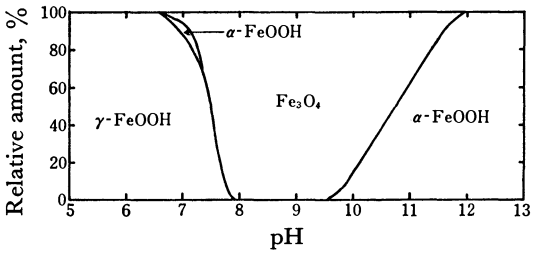

Fig. 1. Relationship between relative amounts of products and acidity.
Temp; 25 °C, init. concn; 0.064 mol/l, flow rate; 2 l/min.

Figure 1 shows the relationship between the relative amounts of the products and the acidity. Only the γ-FeOOH was obtained up to pH 6.5 by the aeration at 25 °C in the 0.064 mol/l solution, though only the Fe_3O_4 was obtained in the pH range from about 8.0 to 9.5. Misawa *et al.*[7,8] also reported the formation of Fe_3O_4 by the solid state oxidation of $Fe(OH)_2$ formed in a slightly alkaline solution of iron(II) chloride. Even if the aeration was allowed to continue, the Fe_3O_4 was no longer completely oxidizable into the γ-FeOOH. This solid state oxidation is considered to be difficult

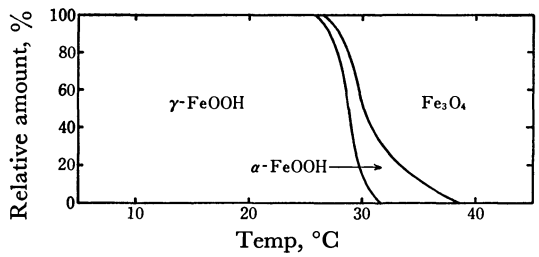

Fig. 2. Relationship between relative amounts of products and reaction temperature.
pH; 6.5, init. concn; 0.064 mol/l, flow rate; 2 l/min.

because the OH groups must be introduced into the Fe_3O_4 lattice which has a cubic close-packed structure of oxygen.[9]

Figure 2 shows the relationship between the relative amounts of the products and the reaction temperature. Only the γ-FeOOH was obtained below 25 °C, while the formations of the α-FeOOH and the Fe_3O_4 were observed at the temperatures higher than 25 °C.

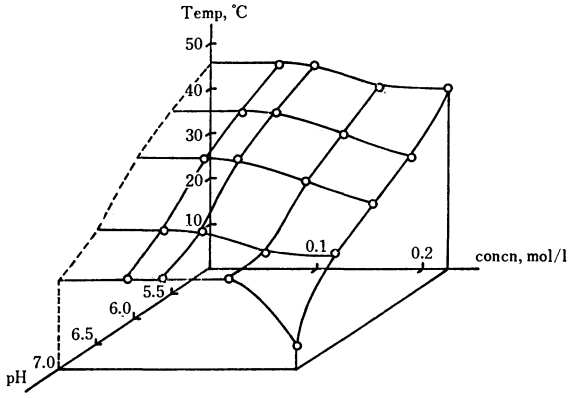

Fig. 3. Upper limit of temperature for preparing only γ-FeOOH as functions of initial concentration and acidity.
Flow rate; 2 l/min.

The critical conditions for preparing only the γ-FeOOH around neutrality varied according to changes in the temperature, the concentration of Fe(II) ions, and the acidity. A curved surface in Fig. 3 shows the upper limit of temperature for obtaining only the γ-FeOOH as the functions of the concentration and the acidity in the ranges from 0.064 to 0.224 mol/l and from pH 5.0 to 7.0 respectively. At the temperatures above this curved surface, the α-FeOOH and/or the Fe_3O_4 were precipitated with the γ-FeOOH. The upper limit of temperature for forming only the γ-FeOOH was found to decrease as both the pH value and the concentration increased, as is shown in Fig. 3. The reaction mixture showed a gradual change in color as follows:

pH 6.0 (higher temp)—7.0

light green → dark greenish blue → yellowish brown

pH 5.0—6.0 (lower temp)

faint green → reddish brown

The γ-FeOOH was formed *via* the green rust I,[1,10] its oxidation intermediate, under the former conditions, but it was formed directly from the solution without passing through the green rust I in the latter cases.[11] Bernal *et al.*[1] stated that the green rust I formed only in neutral and slightly alkaline solutions of iron(II) chloride. Misawa *et al.*[8] proposed a mechanism for direct formation of γ-FeOOH: after the $FeOH^+$ ions have been oxidized, the $Fe(OH)_2^+$ ions dimerized into $[(OH)_2Fe–O–FeOH]^+$ and then polymerized into $[n FeOOH \cdot Fe(OH)_2]^+$ by forming oxo-bridges, Fe–O–Fe, followed by precipitation of γ-FeOOH.

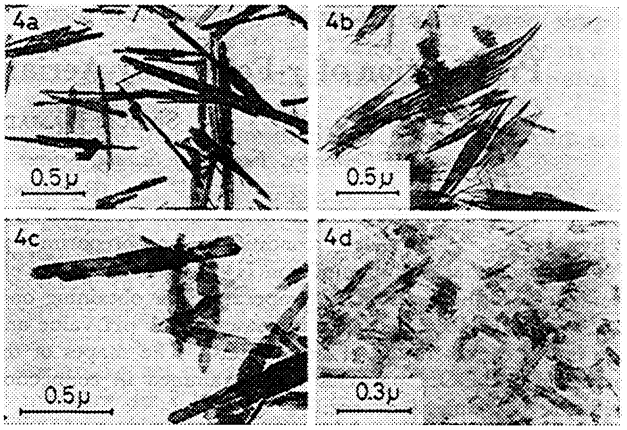

Fig. 4. Shapes and sizes of γ-FeOOH particles prepared as several conditions.
a; pH 6.0, 30 °C, 0.096 mol/l, b; pH 6.5, 15 °C, 0.224 mol/l, c; pH 6.0, 25 °C, 0.096 mol/l, d; pH 6.0, 10 °C, 0.064 mol/l.

The shape and the size of γ-FeOOH particles were extremely dependent on the preparative conditions. Needle-like particles were obtained in the oxidation just below the upper limit of temperature for preparing only the γ-FeOOH at pH 6.0—7.0, while irregularly shaped plate particles were precipitated at lower temperatures for pH 6.5—7.0, as is shown in Figs. 4a and 4b. On the contrary, elongated hexagonal plate particles were obtained at lower temperatures at pH 6.0, as is shown in Fig. 4c. When the γ-FeOOH was formed without formation of the green rust I as the intermediate, the particles lost their uniformity in shape; in particular, fine particles showing broad X-ray powder diffraction peaks were obtained at much lower temperatures, as is shown in Fig. 4d.

References

1) J. D. Bernal, D. R. Dasgupta, and A. L. Mackay, *Clay Miner. Bull.*, **4**, 15 (1959).
2) U. Schwertmann, *Z. Anorg. Allg. Chem.*, **298**, 337 (1959).
3) J. V. Schuylenborgh and P. L. Arens, *Recl. Trav. Chim., Pays-Bas*, **69**, 1557 (1950).
4) O. Glemser, *Ber.*, **70**, 2117 (1935).
5) O. Baudish and W. H. Albrecht, *J. Am. Chem. Soc.*, **54**, 943 (1932).
6) M. Kiyama, N. Jikuhara, and T. Takada, *Bull. Chem. Soc. Jpn.*, **46**, 323 (1973).
7) T. Misawa, T. Kyuno, W. Suetaka, and S. Shimodaira, *J. Jpn. Inst. Metals*, **33**, 1149 (1969).
8) T. Misawa, W. Suetaka, and S. Shimodaira, *Bull. Chem. Soc. Jpn.*, **42**, 3339 (1969).
9) T. Misawa, K. Hashimoto, and S. Shimodaira, *Corros. Sci.*, **14**, 131 (1974).
10) T. Misawa, K. Hashimoto, and S. Shimodaira, *J. Inorg. Nucl. Chem.*, **35**, 4167 (1973).
11) M. Kiyama and T. Takada, *Bull. Chem. Soc. Jpn.*, **45**, 1923 (1972).

BULLETIN OF THE CHEMICAL SOCIETY OF JAPAN, VOL. 49 (12), 3697—3698 (1976)

The Relationship between the Atmospheric Carbon Dioxide Concentration and the Carbon-14 Activity in Tokyo

Sakuji IKEDA, Hideki SHIRAKAWA, and Iwakazu HATTORI

Research Laboratory of Resources Utilization, Tokyo Institute of Technology, Meguro-ku, Tokyo 152

(Received June 4, 1976)

Synopsis. Measurements of the atmospheric CO_2 concentration and the ^{14}C activity in Tokyo were carried out. The activity of ^{14}C in the CO_2 decreased with an increase in the atmospheric CO_2 concentration, indicating that increases in the atmospheric CO_2 are caused only by the burning of fossil fuels.

Studies of atmospheric CO_2 have been carried out either by the measurement of the concentrations or by ^{14}C-activity measurement. Thus, measurable increases on a global scale have been reported for the atmospheric CO_2 concentrations at several locations; thus, the increases are not the result of local influences.[1] An alternative evidence for the global increases caused by the burning of carbonaceous fossil fuels is the Suess effect,[2] which is the decrease in atmospheric ^{14}C concentrations caused by the combustion of ^{14}C-free fossil fuels.

Since the increments in the atmospheric carbon dioxide concentration at any site reflect the emissions of CO_2 from man-made combustion sources as well as from natural sources, it is not possible to identify the type of source only by the concentration measurement; simultaneous measurements with the ^{14}C activity in the atmospheric CO_2 are necessary to identify the type of source and to quantify the fossil CO_2 in the atmosphere. The source analysis in the atmospheric CO_2 would be of value in studies not only of air pollution but also of the circulation of carbon and of climatic influence.

Toward this purpose, we have been conducting measurements of atmospheric CO_2 and ^{14}C concentrations in Tokyo since April, 1975. This note is a brief report on the atmospheric CO_2 based on one year of measurement.

Experimental

The concentration of atmospheric CO_2 was continuously recorded by means of a Shimadzu Model URA-2S nondispersive infrared CO_2 analyzer at the Ookayama campus of this Institute (35°35′54″ N, 135°42′18″ E). The sampling probe was set on the roof of the building of this Research Laboratory about 20 m above the ground. The CO_2 was collected two or three times a month. Each time about one mole of CO_2 was collected as sodium carbonate by bubbling air, at the rate of 50 l/min for 24 h, through 3 l of a carbonate-free solution containing 5 mol of sodium hydroxide. The collection was almost quantitative. The carbonate thus obtained was then converted into benzene according to the benzene-radiocarbon-dating process.[3] The samples were counted in a modified Packard Tri-Carb Model 3390 liquid scintillation spectrometer. The activity of ^{14}C was given as the disintegration per minute per gram carbon (dpm/g-C). Calibration curves for the correction of the counting efficiencies of the samples were made by the use of a series of unquenched and least-quenched 10^5 dpm standards prepared from toluene-^{14}C of $5.92\times10^5\pm3\%$ dpm/g (Packard Instrument Co., Inc.). The standard deviations quoted (1σ) describe the uncertainties associated with toluene-^{14}C, standard preparation, and measurements of the sample, the standard, and the background. The activity of the NBS oxalic acid reference standard was 14.39 ± 0.46 dpm/g-C.

Results and Discussion

Figure 1 indicates the mean monthly CO_2 concentrations from April, 1975, through March, 1976. The maximum and minimum mean hourly concentrations observed through the month are also illustrated in the figure. The seasonal variation is obvious. Since the variation is negatively correlated with the air temperature in Tokyo, since the estimated amount of total fossil fuel consumption, including mobile fuels, in Tokyo during the winter season is double that in summer, and since an extremely high concentration is observed during the winter season, especially at low wind speeds, it can be considered that the principal origin of this variation

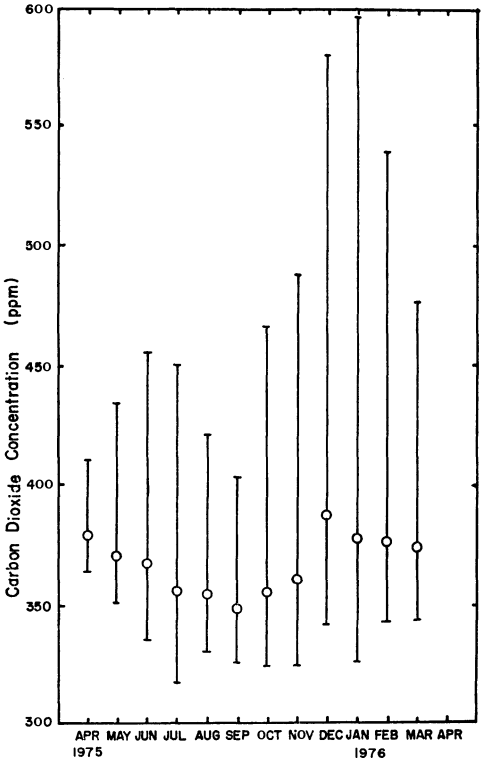

Fig. 1. Mean monthly atmospheric CO_2 concentrations in Tokyo.
Open circles represent mean monthly value. The upper and the bottom limits indicate the maximum and the minimum mean hourly values, respectively, observed through the month.

is due to the combustion of fuels for heating purposes.

The CO_2 concentrations generally decreased with an increase in the wind speed, but never fell for below the values of 317—325 ppm, which can be regarded as the background concentration in air coming into Tokyo. The atmospheric ^{14}C activities (δ ^{14}C % above the modern reference) in 1970 were reported to be 50—59% at Monaco,[4] 44.7—56.4% at Taipei, Taiwan,[5] and 50.4—53.1% at Trnava, Czechoslovakia.[6] The scattered values would appear to indicate a local Suess effect, although the investigations stated that the sampling sites were far from local pollution. Taking into consideration the recent trend of atmospheric ^{14}C activities to decrease as a result of various mixing processes of ^{14}C produced by nuclear weapons testing, coupled with the global Suess effect, the ^{14}C activity in the background CO_2 in 1975 was estimated to be 50.0% above the modern reference or 20.5 dpm/g-C.

The relationship between the atmospheric CO_2 concentrations and the ^{14}C activities is shown in Fig. 2. The smooth curve in the figure represents the calculated relationship under the assumptions that the CO_2 increments from the background concentration are caused only by the fossil CO_2, and that the background concentration and ^{14}C activity in the CO_2 are 325 ppm and 20.5 dpm/g-C respectively. The overall agreement between the observed values and the smooth curve strongly suggests that increases in the atmospheric CO_2 concentration in Tokyo are caused only by the burning of fossil fuels. In fact, the estimated amount of fossil CO_2 released into atmosphere over Tokyo in 1975 reached 7.5×10^{13} g, whereas natural emissions from green areas in Tokyo were estimated to be less than 1.8×10^{11} g/year. On the other hand, the CO_2 from human resipiration and from the decomposition of human excreta can be calculated to be 0.42×10^{13} g/year based on the population in Tokyo and the amount of food consumed. The activity of the ^{14}C in the CO_2, of course, is almost the same as that in natural CO_2.

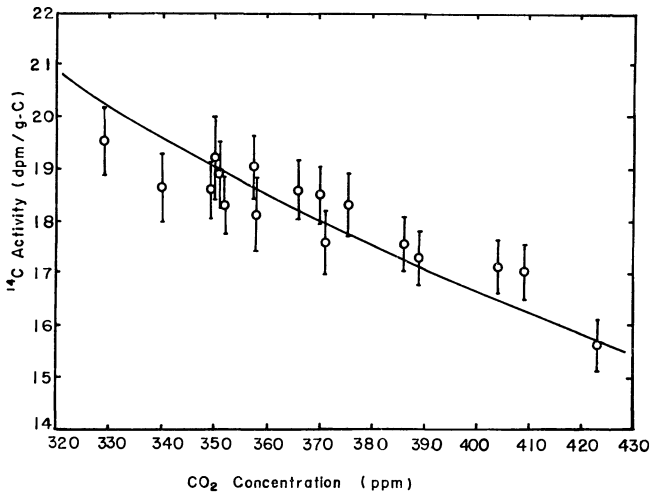

Fig. 2. Relationship between atmospheric CO_2 concentration and ^{14}C activity.
The solid curve represents the calculated relationship by the fossil CO_2.

An analysis with increased precision could be achieved by measurements of the background levels of both the atmospheric CO_2 concentration and the ^{14}C activity in air coming into the observed site, because the background concentrations of atmospheric CO_2 show seasonal variation and have increased at least 1.0 ppm per year after 1969,[1] fluctuations of atmospheric ^{14}C activity as a result of causes have also been observed.[7]

We wish to thank Miss Kyoko Hyakkoku for her assistance in the benzene synthesis and CO_2 measurement.

This work was supported in part by a grant from the Ministry of Education, No. 943015, in 1974 and 1975.

References

1) L. Machta, *Am. Meteorological Soc.*, **53**, 402 (1972).
2) H. E. Suess, *Science, N. Y.*, **122**, 415 (1955).
3) J. Noakes, S. Kim, and L. Akers, *Geochim. Cosmochim. Acta*, **31**, 1094 (1967).
4) J. Thommeret and Y. Thommeret, *Radiocarbon*, **15**, 321 (1973).
5) Y. Hsu, M. Chou, Y. Hsu, S. Lin, and S. Lu, *Radiocarbon*, **15**, 345 (1973).
6) S. Usačev, P. Povinec, M. Chudy, and Š. Šáró, *Radiocarbon*, **15**, 443 (1973).
7) M. S. Baxter and A. Walton, *Proc. R. Soc. London, Ser. A*, **321**, 105 (1971).

BULLETIN OF THE CHEMICAL SOCIETY OF JAPAN, VOL. 49 (12), 3699—3700 (1976)

Amination of Decyl Alcohol over the Binary Metal Oxide Catalysts

Yusaku TAKITA, Yasuo NISHIDA,* and Tetsuro SEIYAMA

Department of Materials Science and Technology, Faculty of Engineering, Kyushu University, Higashi-ku, Fukuoka 812
**Sumitomo Rubber Industry LTD., Fukiai-ku, Kobe 651*

(Received June 12, 1976)

Synopsis. Catalytic amination of decyl alcohol was examined over binary oxide catalysts containing molybdenum, and the selective formation of decylamine was observed over TiO_2–, SnO_2–, and Fe_2O_3–MoO_3 catalysts. The reaction was often accompanied by the formation of 1-decene. It was found that catalytic activity for the amination of aliphatic alcohol was associated with the acidic property of metal oxide catalysts.

Olefins, alcohols and carbonyl compounds can be catalytically aminated by ammonia in the heterogeneous system.

$$\text{R-CH=CH-R}' + \text{NH}_3 \longrightarrow \text{R-CH}_2\text{-CH(NH}_2\text{)-R}'$$

$$\text{R-OH} + \text{NH}_3 \longrightarrow \text{R}_n\text{NH}_{3-n} + n\text{H}_2\text{O} \quad (n=1\text{—}3)$$

$$\text{R-C(=O)-H} + \text{NH}_3 + \text{H}_2 \longrightarrow \text{RCH}_2\text{NH}_2 + \text{H}_2\text{O}$$

Since the amination of aliphatic alcohols involves intermolecular dehydration, the catalytic activity might be associated with acidic property of catalysts, as in the case of intramolecular dehydration of alcohols. In fact, most of the catalysts such as SiO_2–Al_2O_3,[1] Co_3O_4–CuO–Kieselguhr,[2] metal sulfate[3] which are claimed to be effective for the reactions show notable acidity. Since only a few studies have been carried out on the catalytic amination of aliphatic alcohols, we have examined the amination of decyl alcohol by NH_3 over the various binary oxide catalysts containing molybdenum.

$$n\text{-}C_{10}H_{21}\text{-OH} + \text{NH}_3 \longrightarrow n\text{-}C_{10}H_{21}\text{NH}_2 + \text{H}_2\text{O}$$

Experimental

SnO_2–MoO_3 catalyst was prepared by conventional methods from ammonium paramolybdate and tin(II) hydroxide precipitated from aqueous tin(II) chloride solution with ammonia. Other catalysts were prepared from respective metal nitrates and ammonium paramolybdate. The reaction was carried out in an ordinary flow reactor with a fixed catalyst bed under an atmospheric pressure at contact time of about 0.32 g s cm^{-3}. The composition of feed gas is given in Table 1. All the products were analyzed by gas chromatography except for didecylamine. The analysis of didecylamine was carried out chemically,[4] no didecylamine being detected.

Results and Discussion

The results of amination of decyl alcohol over various catalysts are given in Table 1. Decylamine was formed in a considerable yield at temperatures below 350 °C over TiO_2–, SnO_2–, Fe_2O_3–MoO_3 catalysts. A small amount of decylamine was also obtained over the Cr_2O_3–MoO_3 catalyst but no amination proceeded over the Mn_2O_3–MoO_3 catalyst. In addition to the amination reaction, 1-decene and its decomposition products such as lower olefins and their aminated compounds were formed with increasing selectivity at higher temperature. This indicates that only 1-decene is formed by the intramolecular dehydration of decyl alcohol, without any further double bond isomerization of 1-decene. It was confirmed that no amination of 1-decene with ammonia took place under similar conditions.

Table 1. Amination of decyl alcohol over the binary oxide catalysts

Catalyst	Temperature (°C)	Conversion of decyl alcohol (%)	Selectivity (%)		
			Decylamine	1-Decene	Others
TiO_2–MoO_3	260	11.2	68.7	31.3	
	300	26.6	46.6	53.4	
	340	49.2	14.5	85.5	Tr
	380	52.9	Tr	91.1	8.9
SnO_2–MoO_3	250	15.1	50.3	49.7	
	300	47.9	26.5	73.5	
	350	57.4	1.9	97.2	0.9
Fe_2O_3–MoO_3	300	13.2	37.1	62.9	
	350	37.7	10.8	79.2	10.0
Cr_2O_3–MoO_3	300	7.3	13.5	86.5	
	350	30.0	5.7	92.3	
Mn_2O_3–MoO_3	300	—	—	—	
	380	17.2	—	97.1	2.9

Catalyst; 1.20 g, Feed gas; decyl alcohol 4.2 cm^3/min, ammonia 8.4 cm^3/min, H_2 4.2 cm^3/min, N_2 2.1 cm^3/min.

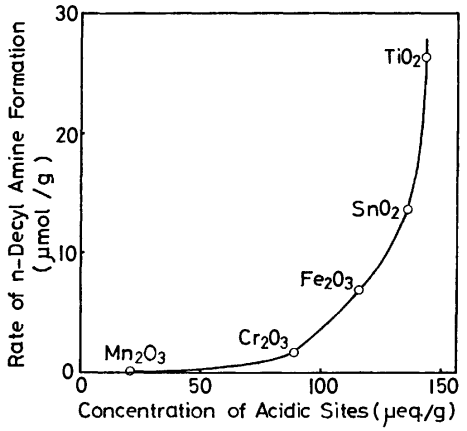

Fig. 1. Relation between activity of amination and concentration of acidic sites.
Catalyst; metal oxide–MoO_3 (9: 1).
Reaction temperature; 300 °C.

This suggests that ammonia, a stronger base than olefin, retards the adsorption of 1-decene onto acidic sites. It is unlikely that decyl cation is formed from decyl alcohol in the course of amination, although it is known that such a cation can be an intermediate in the usual isomerization of olefin over an acidic catalyst.

The acidity of the catalysts measured by butylamine titration using Dimethyl Yellow indicator ($pK_a < +3.3$) is correlated with the catalytic activity at 300 °C (Fig. 1). We see that catalytic activity increases with the acidity of catalysts, though the dependence far exceeds a linear relation. It is difficult to analyze the deviation from linearity. However, an explanation might be given by taking into account the acid strength. The acidic sites actually effective for the amination might be limited to only those with sufficient acid strength and such sites might increase with the change of catalysts more steeply than the measured total acidic sites. X-Ray diffraction patterns of these catalysts show formation of no solid solution. Appearance of $Fe_2(MoO_4)_3$ was detected only in the case of Fe_2O_3–MoO_3. However, metal oxides combined with molybdenum oxide are not considered as simple carriers, since acidic properties of catalysts were shown to be enhanced in the mixed systems. We consider from Fig. 1 that the intermolecular dehydration process involved in the amination is catalyzed by acidic sites. This is in contrast to the Ni–Al_2O_3 or Fe catalyzed amination of aliphatic alcohol by ammonia under hydrogen pressures, for which it was reported[5] that the catalysis is irrespective of acidic property of the catalyst.

References

1) N. S. Kozlov, *Uch. Zap. Perm. Gso. Pedagog. Inst.*, **32**, 27 (1965).
2) Japan Patent 85511 (1973).
3) France Patent 2168716 (1972).
4) F. Feigl and V. Anger, *Mikrochemie*, **16**, (1934).
5) T. Aonuma, *Kogyo Kagaku Zasshi*, **65**, 1819 (1962).

BULLETIN OF THE CHEMICAL SOCIETY OF JAPAN, VOL. 49 (12), 3701—3702 (1976)

Photochemical Addition Reactions of Methanol and Ethanol to 1,4-Diaminoanthraquinone

Kimiho YAMADA, Hideto SHOSENJI, Seiki FUKUNAGA,* and Kazuyoshi HIRAHARA

Department of Synthetic Chemistry, Faculty of Engineering, Kumamoto University, Kurokami, Kumamoto 860

(Received March 29, 1976)

Synopsis. Photochemical reactions of 1,4-diaminoanthraquinone in methanol and/or ethanol yielded solvent adducts, **4a** and **4b**. The reactions proceeded *via* an upper triplet state. The quantum yields were 0.013—0.019 at 280 nm.

Anthraquinone compounds undergo various photochemical reactions.[1] The photoreductions have been the most extensively studied. 9,10-Anthracenediol is, as is well known, formed on the irradiation of anthraquinone in a reducing solvent.[2]

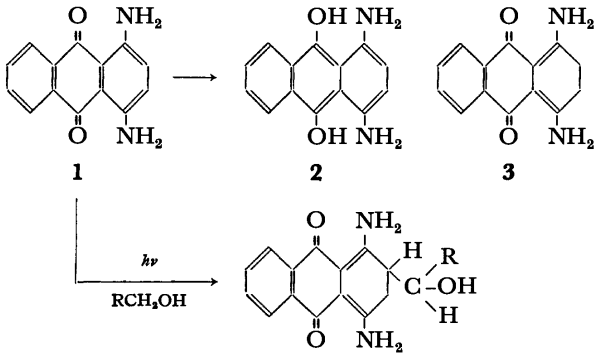

4a: R=H
4b: R=CH_3

Several works have been undertaken on the photofading reactions of 1,4-diaminoanthraquinone (**1**) and its homologues because of their industrial importance as dyestuffs. A 9,10-anthracenediol compound (**2**) or its leuco-tautomer (**3**) has been proposed as a product, by analogy with anthraquinone.[3] In the present investigation, however, we observed solvent addition reactions; that is, compounds **4a** and **4b** were obtained on the irradiation of **1** in methanol and ethanol respectively. Similar photoinduced solvent additions have been reported for unsaturated ketones,[4] lactones,[5] and acridines.[6]

Results and Discussion

The irradiation of air-free solutions of **1** yielded the solvent adducts, **4a** and **4b**. The adducts were isolated by preparative thin-layer chromatography (TLC) in 30—40% yields. Neither **2** nor **3** was detected in the reaction mixture.

The wavelength effects on the reaction were investigated by irradiation with monochromatic lights of various wavelengths. No substantial reaction was observed for the light at visible-region band which is assigned to the charge-transfer (CT) transition associated with the charge migration from the amino group to the carbonyl group.[7] The light shorter than 300 nm gave rise to the degradation of **1**. It should be noted that the sunlight still has enough intensity in this wavelength region to cause troublesome photofading of dyed fabrics. The quantum yields for the disappearance of **1** were below 0.02 and reached their maxima around 280 nm, as is shown in Fig. 1. According to Inoue *et al.*, the band at 280 nm is $\pi\pi^*$ in nature and is polarized along the axis parallel to the C=O bond.[7]

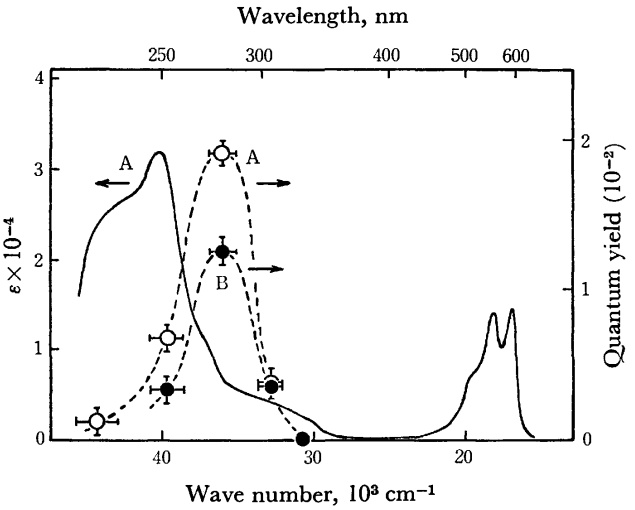

Fig. 1. Electronic spectrum of **1** and quantum yields for its disappearance. A: Ethanol solution; B: methanol solution.

The reaction undoubtedly proceeded *via* a triplet state, as is indicated by the fact that the photo-addition was sensitized by acetophenone and benzophenone[8] and quenched by piperylene. Neither phenanthrene nor biacetyl sensitized the reaction. Hence, the triplet energy for the reaction was estimated to be 62—68 kcal/mol.[9] This is close to the anthracene triplet energy of 62.7 kcal/mol.[10]

Davies *et al.* distinguished between the photoreduction in alcoholic solutions of "strong" sensitizers, such as, for example, anthraquinonesulfonates, and "weak" sensitizers, such as aminoanthraquinone.[11] The former have the lowest triplet of the $n\pi^*$ type, which abstracts hydrogen efficiently from the substrates to initiate the reaction. On the other hand, the CT triplet lies below the $n\pi^*$ triplet in the weak sensitizer. The CT state of **1** does not cause any significant reaction. Evidently the reaction is associated with the upper triplet. The participation of an upper triplet was also pointed out in the photoreduction of 1-dimethylaminoanthraquinone.[12] There still remains a question which character, $n\pi^*$ or $\pi\pi^*$, the triplet has in the present reaction.

* Present address: Nippon Kayaku Co., Ltd., Shimo, Kita-ku, Tokyo 115.

Radical-chain processes have been proposed for the photoinduced solvent-addition reactions of 2-cyclopentenone[4c] and α,β-unsaturated lactones[5] from the facts that the quantum yields exceeded unity[4c,5] and that the same adducts could be obtained in the thermal radical reactions.[5] It might seem that the low quantum yields in the present photoreactions do not afford positive support to the radical-chain mechanism. However, **4b** can be prepared by decomposing azobis(isobutyronitrile) in the ethanol solution of **1**. It can, thus, be presumed that the quantum yield for the solvent addition remains far below unity even if the mechanism involves a radical-chain processes, because **1** gives so low a quantum yield for the triplet formation,[10] and the active triplet might decay rapidly through a subsequent internal conversion to the inactive CT triplet, leaving a really small quantum yield to initiate the radical process. One cannot overlook other possibilities as well, such as a radical cage reaction or nonradical processes.

Experimental

The IR spectra were obtained on a Hitachi-Perkin-Elmer Model 125 spectrophotometer. The UV spectra were taken on a Shimadzu UV-200 or a Hitachi 101 spectrometer. The proton NMR spectra were recorded with a Hitachi R-24 spectrometer at 60 MHz, using tetramethylsilane as the internal standard.

Materials. Compounds **1** and **3** were supplied by the Nihon Kayaku Co., Ltd., and were purified by recrystallization. All the other compounds were commercially available and were recrystallized before use. The methanol and ethanol were purified by the usual methods.

Photochemical Reaction. Solutions of 100 mg of **1** in 400 ml of alcohols were irradiated under nitrogen for 10 h at room temperature using an internal 100 W high pressure mercury lamp. The reaction period could be reduced to one-tenth by sensitizing the solution with 150 mg of benzophenone, while employing Pyrex as a filter. Each reaction mixture contained one main fluorescing product, along with unreacted starting meterials and traces of unidentified by-products, as revealed by silica gel TLC with a benzene–ethyl acetate–methanol mixture (5: 5: 1) as the eluent. The R_f values were in this order: **4a**<**4b**<**3**. The adducts were isolated by preparative TLC as yellow powders in 30—40% yields. The low yields are mainly attributable to the poor recovery by the isolation. The products decomposed above 150 °C without showing definite melting points. They gave UV spectra which quite resembled that of **3**. Their structures were determined from the following data.

1,4-Diamino-2-hydroxymethyl-2,3-dihydroanthraquinone (**4a**): IR (KBr) 2925 (ν_{CH}, alkyl), 1610 ($\nu_{C=O}$) and 1055 cm^{-1} (ν_{C-O}); NMR (CF_3CO_2H) τ 1.1—1.6 (m; C^5–H and C^8–H), 1.6—2.0 (m; C^6–H and C^7–H), 5.4—5.8 (m; methylene of CH_2OH) and 5.8—6.5 (m; C^2–H and C^3–H). Found: C, 58.57; H, 5.30; N, 8.85%. Calcd for $C_{15}H_{14}N_2O_3 \cdot 2H_2O$: C, 58.82; H, 5.88; N, 9.12%.

1,4-Diamino-2-(α-hydroxyethyl)-2,3-dihydroanthraquinone (**4b**): IR (KBr) 2970 (ν_{CH}, alkyl), 1612 ($\nu_{C=O}$) and 1110 cm^{-1} (ν_{C-O}); NMR (CF_3CO_2H) τ 1.1—1.5 (m; C^5–H and C^8–H), 1.5—2.0 (m; C^6–H and C^7–H) 5.2—5.8 (m; methyne of $CHOHCH_3$), 6.1—6.5 (m; C^2–H and C^3–H) and 8.37 (d, J=6.0 Hz; methyl). In a pyridine solution the methyl signal splits into a pair of doublets, situated at τ 8.5 (J=6.0 Hz) and 8.6 (J=6.0 Hz). The splitting is considered to arise because the photoadduct is a mixture of the diastereomers. The separation of the diastereomers was attempted using TLC, but it was unsuccessful. Found: C, 60.28; H, 5.27; N, 8.98%. Calcd for $C_{16}H_{16}N_2O_3 \cdot 2H_2O$: C, 60.00; H, 6.25; N, 8.75%.

The isolated adducts were both relatively stable to air under room conditions, but they gradually oxidized on the TLC plate when exposed to air. UV, IR, and NMR analyses suggested the formation of 2-hydroxymethyl- and 2-(α-hydroxyethyl)-1,4-diaminoanthraquinone.

Quantum Yield. Degassed solutions of 2×10^{-5} mol/l in 1 cm quartz cells were irradiated at 25±1 °C with monochromatic lights of various wavelengths, using a Nihon Bunko CRM-FA Spectral Irradiator equipped with a 2-kW xenon lamp and a 105 Integrator to monitor the light quanta irradiated. Potassium tris(oxalato)ferrate(III) actinometry was employed to calibrate the integrator at each selected wavelength. The light quanta transmitted by the reaction cells were also measured with other potassium tris(oxalato)ferrate(III) actinometer placed immediately behind the cells.

Thermal Radical Reaction. A solution of 10 mg of **1** and 200 mg of azobis(isobutyronitrile) in 100 ml of ethanol was kept at 64 °C for 5 h under nitrogen. After a work-up, the TLC analysis of the reaction mixture revealed the presence of **4b**, along with recovered **1**. The IR spectrum of the isolated product was identical with that of the photochemically obtained one.

The authors wish to thank Professor J. Malcolm Bruce of Manchester University for his valuable discussions.

References

1) J. M. Bruce, *Quart. Rev.*, **21**, 405 (1967); J. M. Bruce, "The Chemistry of the Quinoid Compounds," Part 1, John Wiley & Sons, London (1974), p. 465; H. Inoue and M. Hida *Yuki Gosei Kagaku Kyokai Shi*, **32**, 348 (1974).

2) P. A. Leighton and G. S. Forbes, *J. Am. Chem. Soc.*, **51**, 3549 (1929).

3) G. S. Egerton, J. M. Gleadle, and A. G. Roach, *J. Soc. Dyers Colour.*, **82**, 369 (1966); Y. Tanaka, Y. Oki, and Y. Ishii, *Sen'i Gakkai Shi*, **24**, 132 (1968).

4) (a) P. Bladon and I. A. Williams, *J. Chem. Soc., C*, **1967**, 2032; (b) I. Moritani and N. Toshima, *Tetrahedron Lett.*, **1967**, 467; (c) P. De Mayo, J. P. Pete, and M. Tchir, *Can. J. Chem.*, **46**, 2535 (1968); (d) N. Filipescu and F. L. Minn, *J. Am. Chem. Soc.*, **90**, 1544 (1968).

5) K. Ohga and T. Matsuo, *J. Org. Chem.*, **39**, 106 (1974).

6) H. Göth, P. Cerrutti, and H. Schmid, *Helv. Chim. Acta*, **48**, 1395 (1965).

7) H. Inoue, T. Hoshi, J. Yoshino, and Y. Tanizaki, *Bull. Chem. Soc. Jpn.*, **45**, 1018 (1972).

8) No substantial degradations of the sensitizers were observed during the measurement.

9) We could not detect any phosphorescence from **1** in rigid glass at 77 K.

10) H. H. Dearman and A. Chan, *J. Chem. Phys.*, **44**, 416 (1966).

11) A. K. Davies, J. F. McKellar, and G. O. Phillips, *Proc. R. Soc., London, Ser A*, **323**, 69 (1971).

12) A. K. Davies, R. Ford, J. F. McKellar, and G. O. Phillips, *J. Chem. Soc. Perkin Trans. 2*, **1972**, 923.

BULLETIN OF THE CHEMICAL SOCIETY OF JAPAN, VOL. 49 (12), 3703—3704 (1976)

On the Mechanism of Uncatalyzed Reduction of Triphenylmethyl Chloride with Triethylgermane[1)]

Hideki SAKURAI and Kunio MOCHIDA

Department of Chemistry, Faculty of Science, Tohoku University, Sendai 980

(Received August 3, 1976)

Synopsis. Reduction of triphenylmethyl chloride with triethylgermane in benzene proceeds by a free-radical mechanism as evidenced by the observation of an ESR spectrum of the triphenylmethyl radical. However, the reduction involves apparently an ionic mechanism in a polar solvent such as dichloromethane and nitromethane.

Corey and West first reported that triphenylmethyl chloride can be reduced with hydrosilanes in high yield under moderate conditions without any added catalyst.[2)]

$$Ph_3CCl + R_3SiH \longrightarrow Ph_3CH + R_3SiCl$$

Ionic mechanisms, especially a four-centered[2,3)] and an ion-pair mechanism[4)] have been proposed to this reaction.

The fact that triphenylmethyl chloride can also be reduced with hydrogermanes without catalyst is not surprising because of the known capability of hydrogermanes to reduce organic halides.[5)] However, we report here that the reduction proceeds through a free radical mechanism in non-polar solvents such as benzene.

Reduction of triphenylmethyl chloride with triethylgermane was affected strongly by the nature of a solvent employed. Thus, in a polar solvent such as dichloromethane and nitromethane, the reduction takes place very rapidly even at room temperature.

$$Ph_3CCl + Et_3GeH \longrightarrow Ph_3CH + Et_3GeCl$$

However, in benzene it was required to raise the reaction temperature to 80 °C for completion of the reduction. Interestingly, a strong ESR signal of the triphenylmethyl radical was observed as shown in Fig. 1 after a benzene solution of triphenylmethyl chloride containing triethylgermane in an ESR tube was heated for a few seconds at 80 °C. This fact strongly indicates that the reduction with organogermane in benzene should proceed by a free-radical mechanism.

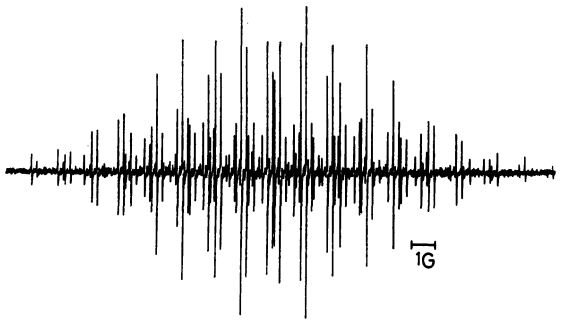

Fig. 1. ESR spectrum of the triphenylmethyl radical, a_{o-H}=2.53G, a_{m-H}=1.11G, a_{p-H}=2.77G.

$$Et_3GeH \longrightarrow Et_3Ge\cdot + (\cdot H)$$

$$Ph_3CCl + Et_3Ge\cdot \longrightarrow Ph_3C\cdot + Et_3GeCl$$

$$Ph_3C\cdot + Et_3GeH \longrightarrow Ph_3CH + Et_3Ge\cdot$$

However, when dichloromethane, nitromethane, or diethyl ether was employed as a solvent, instead of benzene, no ESR signal was observed under various conditions. When triphenylmethyl chloride was dissolved in dichloromethane or nitromethane, color of the solution immediately turned to deep yellow due to the formation of the triphenylmethyl cation. Addition of triethylgermane to the colored solution caused immediate fading with concurrent formation of both triphenylmethane and triethylchlorogermane. These facts suggest that the reduction of triphenylmethyl chloride with hydrogermane in a polar solvent proceeds by an ionic mechanism.

The nature of the initiation step is uncertain, but probably a trace amount of oxygen plays a role. Photochemical generation of the triphenylmethyl radical from triphenylmethyl chloride is known,[6)] but no free radical was detected by ESR for a solution of triphenylmethyl chloride in benzene heated at 80 °C. Therefore, thermal generation of the triphenylmethyl radical is unimportant at least under the conditions.

Incidentally, the ESR spectrum of the triphenylmethyl radical obtained in this study is extremely well-resolved compared to those reported previously.[7)] Generation of free radicals for the ESR studies by reduction with triorganosilanes is well documented,[8)] but no modification using hydrogermane has been reported. We have found recently that reduction of organic halide with hydrogermane has several advantages even for generation of very unstable radicals.[9)]

Experimental

Materials. Triethylgermane[10)] and triphenylmethyl chloride[11)] were prepared according to the literature.

Reduction of Triphenylmethyl Chloride with Triethylgermane in Dichloromethane. Triphenylmethyl chloride (0.17 g, 0.60 mmol) was added to a solution of triethylgermane (0.48 g, 3.01 mmol) in dichloromethane (2.0 ml). The mixture was kept at room temperature for 30 min. GLC analysis showed formation of triphenylmethane (0.13 g, 0.53 mmol) in 88.0% yield.

Another run with a mixture of triphenylmethyl chloride (0.030 g, 0.10 mmol) and triethylgermane (0.160 g, 1.0 mmol) in dichloromethane (0.5 ml), which was subjected to react for 5 min at room temperature, gave triphenylmethane in 46% yield.

Reaction of Triphenylmethyl Chloride with Triethylgermane in Benzene. A mixture of triphenylmethyl chloride (0.49 g, 1.74 mmol) and triethylgermane (1.40 g, 8.71 mmol) in ben-

zene (2.0 ml) was placed in an ampoule which was bubbled with dry nitrogen, sealed and immersed in a constant-temperature bath kept at 80 °C for 2 h. Triphenylmethane (0.37 g, 1.52 mmol, 87.4% yield) was identified and analyzed by GLC.

Another mixture of triphenylmethyl chloride (0.030 g, 0.1 mmol) and triethylgermane (0.160 g, 1.0 mmol) in benzene (0.5 ml) was heated at 80 °C for a few second. GLC analysis showed formation of triphenylmethane in 41% yield.

ESR Measurement. Triethylgermane (0.100 g, 0.62 mmol) was added to a solution of triphenylmethyl chloride (0.011 g, 0.045 mmol) in benzene (0.01 ml) placed in an ESR tube. The tube was bubbled with dry nitrogen and immersed in a constant-temperature bath kept at 80 °C for a few second. Then the ESR spectrum of triphenylmethyl radical was recorded with a Varian E-12 spectrometer.

References

1) Organogermanium compounds VII.
2) J. Y. Corey and R. West, *J. Am. Chem. Soc.*, **85**, 2436 (1963).
3) J. D. Austin and C. Eaborn, *J. Chem. Soc.*, **1964**, 2279.
4) L. H. Sommer and D. L. Bauman, *J. Am. Chem. Soc.*, **91**, 7076 (1969).
5) H. Sakurai, K. Mochida, A. Hosomi, and F. Mita, *J. Organomet. Chem.*, **38**, 275 (1972).
6) H. G. Lewis and E. D. Owen, *Chem. Commun.*, **1966**, 216.
7) (a) S. I. Weissman and J. C. Sowden, *J. Am. Chem. Soc.*, **75**, 503 (1953); (b) P. B. Ayscough, A. P. McCann, and R. Wilson, *Proc. Chem. Soc.*, **1961**, 16; (c) D. B. Chesnut and G. J. Sloon, *J. Chem. Phys.*, **33**, 637 (1960); (d) J. S. Hyde, *ibid.*, **43**, 1806 (1965).
8) P. J. Krusic and J. K. Kochi, *J. Am. Chem. Soc.*, **90**, 7155 (1970).
9) M. Sato, M. Kira, and H. Sakurai, the 14th ESR Symposium Oct. 10, 1975; *Abstracts*, **10**.
10) H. H. Anderson, *J. Am. Chem. Soc.*, **79**, 326 (1957).
11) W. E. Bachmann, *Org. Synth.*, Coll., Vol. III, 841 (1955).

BULLETIN OF THE CHEMICAL SOCIETY OF JAPAN, VOL. 49 (12), 3705—3706 (1976)

Reaction of Tetramethylurea with Photoexcited Carbonyl Compounds

Yuji TSUJIMOTO, Akihiro NAKAHARA, Yoshiyuki NISHIMURA, Takuji MIYAMOTO, and Yoshinobu ODAIRA

Department of Petroleum Chemistry, Faculty of Engineering, Osaka University, Suita-shi, Osaka 565

(Received May 31, 1976)

Synopsis. The photoreaction of tetramethylurea (I) with some carbonyl compounds (II) afforded in good yields the respective urea derivatives (III), which were converted into 2-oxazolidinones (IV).

Many studies have been carried out on the photochemistry of amides, and some interesting photoreactions such as photocyclization of α,β-unsaturated amides,[1] photooxidation of *N*-alkylamides,[2] and photoamidation to unsaturated systems[3] have been found. It has been reported that a new photobenzoylation of the olefin takes place preferentially in the photoreaction of *N,N*-dimethylbenzamide with 1,1-diphenylethylene.[4] On the other hand, little is known of the photoreactions of ureas except for the photolysis of tetramethylurea in vapor phase.[5] The present study was undertaken to see whether photochemical hydrogen abstraction from tetramethylurea (I) by n-π^* photoexcited carbonyl compounds (II) can occur. We wish to report that hydrogen abstraction occurs very easily to give the urea derivatives (III) in good yields, and that 2-oxazolidinones (IV) can be prepared from the obtained ureas (III). In the present study, benzophenone (II-a), acetophenone (II-b), benzaldehyde (II-c), and acetone (II-d) were used as carbonyl compounds.

Irradiation of I and II-a in acetonitrile through a Pyrex filter for 10 h afforded the urea (III-a) and 2-oxazolidinone (IV-a) in 46 and 4% yields, respectively, together with the pinacol (V-a) and the dimeric urea (VI). The photoreaction of I with II-b under the same conditions as above gave rise to the urea (III-b) and 2-oxazolidinone (IV-b) in 30 and 11% yields, respectively, along with the pinacol (V-b) and VI. Similarly, the photoreaction with II-c gave the urea (III-c) and 2-oxazolidinone (IV-c) in 26 and 11% yields, the urea (III-d) being obtained in 24% yield with II-d.

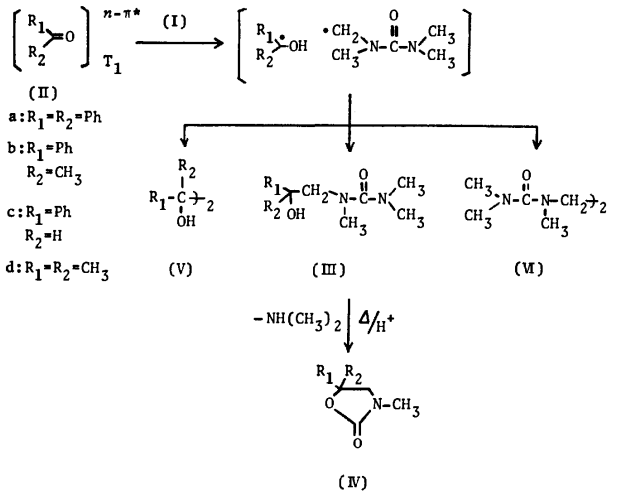

Scheme 1.

From the results, it was proved that photochemical hydrogen abstraction from I occurred very efficiently.

Concerning the formation of IV obtained as by-products, it was clarified by the following experiments that IV-a—d were derived from III-a—d. When III-a was heated in benzene for 10 h, IV-a was obtained almost quantitatively. In the above reaction, the presence of acid enhanced the rate of cyclization. Consequently, in the case of ureas (III-b—d), each cyclization was carried out with acid. The reaction is illustrated in Scheme 1.

The hydrogen abstraction from I by n-π^* triplet of II results in the formation of a carbinol radical and a ureidomethyl radical, which are precursors of three sets of the coupling products III, V, and VI. III can undergo cyclization to 2-oxazolidinones (IV), accompanied by the elimination of dimethylamine by heat or with acid.

Experimental

Material. Commercial tetramethylurea (I) and carbonyl compounds (II) were purified by the usual methods before use. Dimeric urea (VI) was prepared by the reported method.[6]

General Procedure for Photoreaction. Carbonyl compounds (II) and three molar excess of tetramethylurea (I) were dissolved in acetonitrile. After the solution was bubbled with nitrogen for 10 min, it was irradiated with a 500 W high-pressure mercury lamp through a Pyrex filter for 10 h at room temperature. After evaporation of the solvent, unreacted I was recovered *in vacuo*, and the residue was chromatographed on silica gel, except in the case of acetone (II-d). Dimeric urea (VI) was eluted with ether–benzene (4:6), and confirmed by comparison with an authentic sample.

Photoreaction of I with Benzophenone (II-a). A solution of I [7.0 g, 0.06 mol] and II-a [3.6 g, 0.02 mol] in acetonitrile (40 ml) was irradiated. The following products were isolated. Elution with benzene–petroleum ether gave benzopinacol (V-a) [527 mg, 30%], and the first elution with ether–benzene (2:8) gave 2-oxazolidinone (IV-a) [206 mg, 4%], mp 137—140 °C; Mass *m/e* 253 (M^+); IR (KBr) 1750, 740, 700 cm^{-1}; NMR (CCl_4) δ, 2.8 (s, 3H), 4.0 (s, 2H), 7.0—7.5 (m, 10H). Found: C, 75.67; H, 5.79; N, 5.47%. Calcd for $C_{16}H_{15}NO_2$: C, 75.87; H, 5.97; N, 5.53%. Next elution with ether–benzene (2:8) gave urea (III-a) [2.65 g, 46%] mp 147—148.5 °C; Mass *m/e* 298 (M^+); IR (Nujol) 3400, 1630, 750, 700 cm^{-1}; NMR (CCl_4), 2.5 (s, 3H), 2.64 (s, 6H), 4.0 (s, 2H), 5.5 (s, 1H), 7.0—7.6 (m, 10H). Found: C, 72.28; H, 7.48; N, 9.23%. Calcd for $C_{18}H_{22}N_2O_2$: C, 72.45; H, 7.43; N, 9.39%.

Photoreaction of I with Acetophenone (II-b). A solution of I [26.1 g, 0.23 mol] and II-b [8.9 g, 0.07 mol] in acetonitrile (150 ml) was irradiated. The work-up as above gave the following products: Pinacol (V-b) [3.94 g, 44%], mp 123—125 °C [lit,[7] 122 °C (racemic), 117—118 °C (meso)], urea (III-b) [5.30 g, 30%], mp 155—158 °C; Mass *m/e* 236 (M^+);

IR (Nujol) 3400, 1590, 760, 700 cm^{-1}, 2-oxazolidinone (IV-b) [1.61 g, 11%], Mass *m/e* 191 (M^+); IR (neat) 1740, 760, 690 cm^{-1}; NMR (CCl_4) δ, 1.65 (s, 3H), 2.8 (s, 3H), 3.5 (s, 2H), 7.0—7.5 (m, 5H).

Photoreaction of I with Benzaldehyde (II-c). A solution of I [20.9 g, 0.18 mol] and II-c [6.4 g, 0.06 mol] in acetonitrile (60 ml) was irradiated. The work-up as above gave the following products: Pinacol (V-c) [1.29 g, 11%], mp 137—138 °C [lit,[8] 137.5—138 °C], urea (III-c) [3.40 g, 26%], mp 88—90 °C; IR (KBr) 1600 cm^{-1}; Mass *m/e* 222 (M^+); NMR ($CDCl_3$) δ, 2.8 (s, 6H), 2.9 (s, 3H), 3.1, 3.6 (ABX *octet*, $J_{ab}=15$ Hz, $J_{ax}=9$ Hz, $J_{bx}=3$ Hz, 2H), 4.9 (ABX *q*, 1H), 5.4 (s, 1H), 7.0—7.5 (m, 5H). Found: C, 64.75; H, 8.29; N, 12.48%. Calcd for $C_{12}H_{18}N_2O_2$: C, 64.84; H, 8.16; N, 12.60%. 2-Oxazolidinone (IV-c) [1.17 g, 11%], IR (neat) 1750 cm^{-1}.

Photoreaction of I with Acetone (II-d). A solution of I [23.9 g, 0.21 mol] and II-d [4.0 g, 0.069 mol] in acetonitrile (60 ml) was irradiated. After evaporation of the solvent, unreacted I was recovered *in vacuo*. The remaining residue was distilled under reduced pressure (0.5—0.8 Torr). Besides VI, the urea (III-d) was obtained, [2.78 g, 24%], bp 86 °C (0.55 Torr); IR (neat) 1600 cm^{-1}; Mass *m/e* 174 (M^+); NMR (neat) δ, 1.25 (s, 6H), 2.8 (s, 6H), 3.0 (s, 3H), 3.3 (s, 2H), 4.7 (s, 1H).

Cyclization of III to 2-Oxazolidinones (IV). 3-Methyl-5,5-diphenyl-2-oxazolidinone (IV-a): A solution of III-a [344 mg, 1.15 mmol] in benzene (15 ml) was refluxed for 10 h. Evaporation of the solvent gave crude product (IV-a) [300 mg, 100%]. Recrystallization from benzene afforded a sample identical with the authentic sample. 3,5-Dimethyl-5-phenyl-2-oxazolidinone (IV-b): A solution of III-b [140 mg, 0.59 mmol] in chloroform (5 ml) containing a trace of sulfuric acid was stirred for 4 h at room temperature. After the mixture had been washed with water, the organic layer was dried over calcium chloride. Evaporation of the solvent gave crude product (IV-b) [96 mg, 85%]. 3-Methyl-5-phenyl-2-oxazolidinone (IV-c): A solution of III-c [98 mg, 0.44 mmol] in benzene (3 ml) with a trace of sulfuric acid was stirred for 1 h. The same work-up as above gave crude product (IV-c) [29 mg, 37%]. 3,5,5-Trimethyl-2-oxazolidinone (IV-d): A solution of III-d [90 mg, 0.51 mmol] in chloroform (5 ml) containing a trace of sulfuric acid was stirred for 4 h at room temperature. The same work-up as above gave crude product (IV-d) [54 mg, 80%]. Separation by GLC (10% FEAP) gave an analytical sample, Mass *m/e* 129 (M^+); IR (neat) 1740 cm^{-1}; NMR (CCl_4) δ, 1.4 (s, 6H), 2.75 (s, 3H), 3.15 (s, 2H).

References

1) O. L. Chapman and W. R. Adams, *J. Am. Chem. Soc.*, **89**, 4243 (1967); **90**, 2333 (1968).
2) W. H. Sharkey and W. E. Mochel, *J. Am. Chem. Soc.*, **81**, 3000 (1959).
3) D. Elad and J. Rokah, *J. Org. Chem.*, **29**, 1855 (1964).
4) Y. Katsuhara, R. Tsujii, K. Hara, Y. Shigemitsu, and Y. Odaira, *Tetrahedron Lett.*, **1974**, 453.
5) J. R. Majer, S-A. M. A. Naman, and J. C. Robb, *J. Chem. Soc., B*, **1970**, 93.
6) W. R. Boon, *J. Chem. Soc.*, **1947**, 307.
7) "Beilstein Handbuch der Organischen Chemie," Band 6, EII (1944), p. 979.
8) R. Kuhn and O. Rebel, *Chem. Ber.*, **60**, 1565 (1927).

BULLETIN OF THE CHEMICAL SOCIETY OF JAPAN, VOL. 49 (12), 3707—3708 (1976)

Substituent Effects on Photochemical Extrusion of Phosphorus Group from 3-Phospholene System

Hideo TOMIOKA, Shigehiro NAKAMURA, Tsutomu OHI, and Yasuji IZAWA*

Department of Industrial Chemistry, Faculty of Engineering, Mie University, Tsu, Mie 514

(Received June 17, 1976)

Synopsis. The rate of photo-extrusion of phenylphosphinidene oxide from 1-phenyl-3-phospholene 1-oxide was enhanced by β-methylation. It was found that the photo-extrusion can be extended to the generation of phenylphosphinidene, but attempts to generate other phosphorus intermediates *i.e.*, metaphosphite and methylphosphinidene oxide, were unsuccessful.

During the course of a study of the photochemical reactions of phosphorus heterocycles,[1] it was found[2] that 1-phenyl-3-phospholene 1-oxide upon UV irradiation efficiently cleaves to diene and phenylphosphinidene oxide (**3**) which is trapped by alcohol to give phosphinates (**4**). The reaction was shown[3] to proceed *via* excited singlet state of **1a**. In view of an increasing interest in the reactive phosphorus intermediate,[4] analog of carbene and nitrene, we have examined the substituent effects on the present reaction in an attempt to extend it to the generation of other important phosphorus intermediates, *e.g.*, metaphosphite and phosphinidenes.

Photolysis of a methanol solution of **1a** in a quartz tube was monitored by GLPC, which revealed a gradual disappearance of the starting material along with the formation of butadiene and methyl phenylphosphinate (**4**). The reaction was incomplete, more than 70% of starting material being recovered after 3 h irradiation.

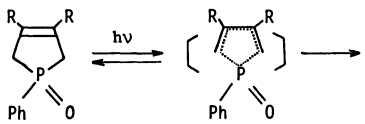

1 a R=H
b R=Me

2

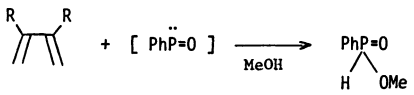

3 4

In contrast, a similar irradiation of 3,4-dimethyl derivative (**1b**) resulted in almost complete consumption of the starting material within *ca.* 1 h, being accompanied by efficient formation of 3,4-dimethylbutadiene and phosphinate (**4**) in nearly quantitative yields. Since apparent rates of disappearance are not always an indication of relative rates, the relative rates (k_r/k_{r_0}) of the photo-extrusion were calculated using quantum yields of the reaction (ϕ_r) and fluorescence (ϕ_f) and absorption spectrum according to the following equation:[5]

$$k_r/k_{r_0} = \phi_r\phi_{f_0}k_f/\phi_{r_0}\phi_f k_{f_0}$$

where k_f = rate constant for fluorescence calculated from the absorption spectrum. This gives the value k_r/k_{r_0} = 467. Alkylation in the β-position reduces the rate of thermal sulfur dioxide extrusion from sulfolene system by stabilizing the starting sulfolene.[6] Thus a large rate enhancement by β-methylation in the present photo-extrusion reaction is especially noteworthy in this connection. An explanation of the result should include, at least in part, the stabilization of incipient diene by β-methyl group in the transition state (**2**) of the cleavage.

The photo-extrusion reaction was found to occur also in 1-phenyl-3-phospholene (**5**). Thus, irradiation of **5** in methanol under nitrogen gave isoprene as the sole low-boiling product detectable with GLPC. Evidence

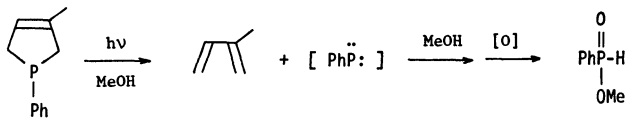

5 6 4

for the intervention of phenylphosphinidene (**6**) was provided by the formation of phosphinate (**4**) (20%) in the reaction mixture after oxidation. A possible formation of **4** should also be considered by the photolysis of phospholene 1-oxide resulting from the oxidation of **5** during the course of irradiation. However, this was ruled out since **4** could not be detected before oxidation. The reaction was much more complicated than that of the oxide, being accompanied by the formation of more than fourteen by-products which were detected by GLPC but not further characterized.

In order to examine whether the reaction can be applied to the generation of other phosphorus intermediates, the photochemical behavior of other 3-phospholene systems in alcohol was investigated. Irradiation of 1-ethoxy derivative (**7a**) in ethanol, however, gave no detectable amounts of diene and diethyl phosphite (**8a**) by GLPC. Introduction of phenyl group as a chromophor on ring carbon (**7b**) or oxygen atom (**7c**)

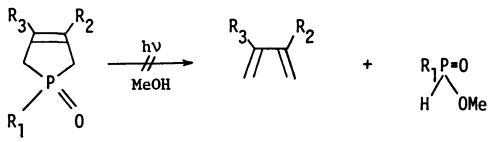

7 8

a R_1=OEt, R_2=R_3=Me
b R_1=OEt, R_2=R_3=Ph
c R_1=OPh, R_2=Me, R_3=H
d R_1=R_2=Me, R_3=H

also did not lead to the extrusion reaction, while these compounds were gradually photolyzed to give mainly intractable oil. Methyl derivative (**7d**) was recovered unchanged even after prolonged irradiation.

It can be concluded that the presence of the phenyl group on phosphorus atom is required for photochemical extrusion of the phosphorus group from the 3-phospholene system, indicating that the stabilization of incipient unshared electrons on phosphorus in the transition state of the cleavage is so stringent as to allow the present reaction to be utilized in general for the generation of phosphorus intermediates.

Experimental

GLPC analysis were performed on a Yanagimoto instrument, Model G-80. GLPC column A was prepared from 10% β,β'-dioxypropionitrile on Diasolid L (5.0 mm × 2.0 m); column B consisted of 10% SE-30 on Diasolid L (5.0 mm × 2.0 m).

H^1 NMR spectra were determined on a JEOL JNM-MH-100 NMR spectrometer. UV and fluorescence spectra were measured with Shimadzu UV 250 recording spectrometer and Hitachi MPF-2A spectrofluorometer, respectively.

Materials. All the 3-phospholene 1-oxides were prepared by cyclo-addition of dienes with phosphonous dihalides, followed by hydrolysis of the resulting adducts.[7] 3-Phospholene (**5**) was prepared[8] by trichlorosilane reduction of the corresponding phospholene 1-oxide.

Irradiations. All the irradiations were carried out using a Halos 300 W high-pressure mercury lamp unless otherwise stated. For analytical purposes, solutions (5.0 ml) of 3-phospholene 1-oxide (50 mg) in methanol were sealed in quartz tubes and irradiated at room temperature. The analyses of the reaction mixture were done by means of GLPC using column A for low-boiling products and column B for high-boiling one. Quantum yields were determined with 254 nm light from the monochrometer using potassium ferrioxalate solution as an actinometer.

Irradiation of 1-Phenyl-3-phospholene (5) in Methanol. To 250 ml of methanol which had been rigorously degassed by bubbling nitrogen was added 2.0 g of freshly distilled 3-phospholene (**5**) under nitrogen and the solution was irradiated using a water-cooled quartz immersion well under nitrogen. The reaction monitored by GLPC revealed a buildup of complex product mixtures as well as isoprene. The irradiation was interrupted when approximately 80% of the starting material had disappeared (*ca.* 6 h). No methyl phosphinate (**4**) was detected. Oxygen was bubbled through the resulting solution under vigorous stirring in the dark until all phosphines were oxidized to oxides. Evaporation of volatile components under reduced pressure at 30 °C gave viscous oil which was chromatographed on silica gel (Woelm Activity II) and eluted with ethyl ether. The foreband gave methyl phenylphosphinate (**4**) (210 mg, 20%), identical with an authentic sample as confirmed by NMR and IR.

The authors wish to thank Japan Synthetic Rubber Co. for the supply of dienes.

References

1) a) H. Tomioka and Y. Izawa, *Tetrahedron Lett.*, **1973**, 5059; b) H. Tomioka, Y. Hirano, and Y. Izawa, *ibid.*, **1974**, 4477.

2) H. Tomioka, Y. Hirano, and Y. Izawa, *Tetrahedron Lett.*, **1974**, 1865.

3) H. Tomioka and Y. Izawa, to be published.

4) For the review of phosphinidene and its oxide, see U. Schmidt, *Angew. Chem. Int. Ed. Engl.*, **14**, 523 (1975).

5) S. S. Hixon, *J. Am. Chem. Soc.*, **94**, 2507 (1972).

6) W. L. Mock, *J. Am. Chem. Soc.*, **97**, 3673 (1975).

7) L. D. Quin and T. P. Barket, *J. Am. Chem. Soc.*, **92**, 4303 (1970).

8) L. D. Quin, S. G. Borleske, and J. F. Engel, *J. Org. Chem.*, **38**, 1858 (1973).

BULLETIN OF THE CHEMICAL SOCIETY OF JAPAN, VOL. 49 (12), 3709—3710 (1976)

Synthesis of Dibenzo[*d,j*]-6,8-bisdehydro-oxa-[13]annulene

Jūro OJIMA,* Akihiko KIMURA, and Masahiko IKEGUCHI

Faculty of Literature and Science, Toyama University, Gofuku, Toyama 930

(Received July 7, 1976)

Synopsis. The title compound (VII or VIII) has been synthesized from *o*-ethynylbenzaldehyde (II) by the Wittig reaction with the salt (III) followed by the oxidative coupling. The examination of the NMR spectra suggests that both of VII and VIII are atropic molecules.

In a previous paper, we have reported a synthesis of tribenzo[*a,e,i*]-11,13-bisdehydro[14]annulene (I) by a double Wittig reaction followed by the oxidative coupling starting from *o*-ethynylbenzaldehyde (II).[1] As an extension of our work on benzofused annulenes, we attempted to synthesize a corresponding oxygen analogue, *i.e.*, dibenzo[*d,j*]-6,8-bisdehydro-oxa-[13]annulene according to the same sequence of reactions used in preparation of I.

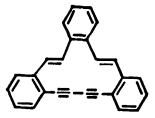

I

The synthesis of the title compound (VII or VIII) was carried out as follows.

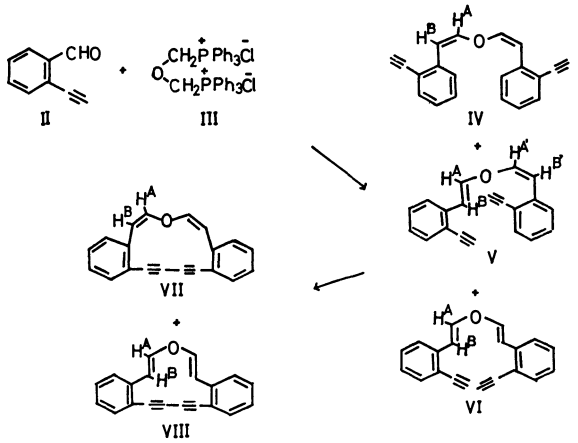

Wittig reaction of II and dimethyl ether-α,α′-bis(triphenylphosphonium chloride) (III)[2] in *N,N*-dimethylformamide by means of ethanolic lithium ethoxide at 80 °C led to, together with the recovered aldehyde, a mixture of acyclic compound in 14% yield from which IV, V, and VI were isolated in a ratio of *ca.* 3: 2: 1, respectively. Configuration of each isomer was confirmed by IR and NMR spectra. Oxidation of the mixture (IV, V, and VI) with copper(II) acetate in pyridine[3] at 60 °C afforded unstable *cis-cis* isomer (VII) and *trans-trans* isomer (VIII) in 6 and 17% yields, respectively.

Wittig reaction between *o*-ethynylcinnamaldehyde[4] and the salt (III) was also attempted to prepare a higher vinylogue of VIII. However, all attempts to obtain the corresponding acyclic compound were unsuccessful in cases using either phenyl lithium in ether or ethanolic lithium ethoxide as a base.[5]

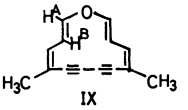

Table 1. ^{1}H-NMR data of VII-IX in $CDCl_3$ (τ-values; internal standard, TMS; *J* values in Hz in parentheses)

	VII[a]	VIII[a]	IX[b]
H^A	3.21d (8)	2.95d (13)	3.87d (13.5)
H^B	3.73d (8)	3.67d (13)[c]	5.09dd (9.5, 13.5)
benzenoid H	1.8—2.4m	2.4—2.7m	

a) At 60 MHz. b) At 100 MHz. c) We assigned the high field signal to H^B proton by reference to the chemical shifts of the related compounds.[7]

The NMR spectral data of the protons of VII and VIII together with those of IX reported by Wife and Sondheimer[7] are summarized in Table 1. The chemical shift of olefinic protons of VII or VIII, particularly of the inner protons, H^B is in normal region. Thus, it is apparent that both of VII and VIII are atropic. Support for this interpretation is given by comparison of the inner H^B proton chemical shift of VII or VIII with that of the closely related annulene IX which was shown to be weakly diatropic (Table 1). The chemical shift of H^B of VII or VIII is at lower field than that of IX.

Experimental

All melting points are not corrected. The alumina used for column chromatography is Brockmann, Act. II—III. The IR and UV spectra were taken on a Hitachi EPI-S2 and a Hitachi 124 spectrophotometers, respectively. Shoulders in UV spectra are indicated by sh. The NMR and mass spectra were taken on JEOL-MH-60 at 60 MHz and JEOL-JMS-OI-SG-2 spectrometers, respectively. The chemical shifts are given in τ-values with respect to TMS as the internal standard, and the coupling constants are given in Hz.

Dimethyl Ether-α,α′-bis(triphenylphosphonium chloride) (III).[2] Triphenylphosphine (52.4 g, 0.2 mol) and α,α′-dichlorodimethyl ether (11.2 g, 0.1 mol)[8] were heated in dry *N,N*-dimethylformamide for 7 h. The mixture was then cooled, the resulting crystals were collected and washed with ether–*N,N*-dimethylformamide. Recrystallization from chloroform and drying *in vacuo* at 80 °C afforded 43.8 g (69%) of III,[2] mp 294—296 °C.

The Isomeric Bis[2-(o-ethylphenyl)vinyl]ether (IV), (V), and (VI). Lithium ethoxide prepared from lithium (0.354 g,

* Correspondence should be addressed to this author.

0.051 g atom) in ethanol (114 ml) was added dropwise with stirring under nitrogen atmosphere at 80 °C for 1 h to *o*-ethynylbenzaldehyde (II, 5.68 g, 0.044 mol) and dimethyl ether-α,α′-bis(triphenylphosphonium chloride) (III, 14.2 g, 0.022 mol) in *N,N*-dimethylformamide (437 ml). After completion of addition, the reaction mixture was stirred for further 2 h under an atmosphere of nitrogen at 80—85 °C, and cooled. The mixture was then poured into water (1000 ml) and extracted thoroughly with ether. The ethereal extracts were washed with dilute hydrochloric acid, aqueous sodium hydrogencarbonate and saturated sodium chloride solutions successively, dried over sodium sulfate, and evaporated to give a pale yellow liquid. The oil was dissolved in ether and chromatography on alumina with light petroleum as eluent gave a mixture of acyclic compd (0.82 g, 14, 29% based on consumed II) as an oil from early fractions, Mass: *m/e* 270 (M^+, 25), 160 (100); mol. wt., 270.3. The following fractions eluted with the same solvent afforded the recovered aldehyde (II, 2.98 g). The mixture was again dissolved in ether and absorbed onto alumina (100 g). Careful elution with light petroleum resulted in separation of three isomers. Early fractions gave *cis-cis* isomer (IV) (0.26 g, 4.5%) as an unstable colorless liquid, IR (neat): 3250 (-C≡CH), 2100 (-C≡C-), 1650, 1595 (C=C), 700 cm^{-1} (*cis* C=C), UV (EtOH): λ_{max} 229 sh, 237, 243, 268 sh, 275, 285 sh, 320 sh nm, NMR ($CDCl_3$): 2.4—3.0 (m, 8H, phenyl H), 3.80 (d, $J=7$, 2H, H^A), 4.15 (d, $J=7$, 2H, H^B), 6.73 (s, 2H, -C≡CH). The next material eluted was *cis-trans* isomer (V) (0.163 g, 2.8%) as a colorless oil. IR (neat): 3300 (-C≡CH), 2090 (-C≡C-), 1640, 1595 (C=C), 940 (*trans* C=C), 700 cm^{-1} (*cis* C=C), UV (EtOH): λ_{max} 230 sh, 237, 243, 268 sh, 274, 290 sh, 320 sh nm, NMR ($CDCl_3$): 2.4—3.1 (m, 9H, phenyl H and H^A), 3.77 (d, $J=13$, 1H, H^B), 3.83 (d, $J=8$, 1H, $H^{A'}$), 4.21 (d, $J=8$, 1H, $H^{B'}$), 6.77 (s, 2H, -C≡CH). The last fractions gave *trans-trans* isomer (VI) (0.079 g, 1.34%) as a colorless liquid. IR (neat): 3250 (-C≡CH), 2100 (-C≡C-), 1640, 1600 (C=C), 1000, 940 cm^{-1} (*trans* C=C), UV (EtOH): λ_{max} 230 sh, 237, 243 sh, 273, 290 sh, 320 sh nm, NMR ($CDCl_3$): 2.4—3.1 (m, 10H, phenyl H and H^A), 3.75 (d, $J=13$, 2H, H^B), 6.67 (s, 2H, -C≡CH).

The Isomeric Dibenzo[d,j]-*6,8-bisdehydro-oxa-*[*13*]*annulene (VII), (VIII).* A soln of a mixture of IV, V, and VI (0.6 g, 0.002 mol) in pyridine (15 ml) was added dropwise to a stirred soln of copper(II) acetate monohydrate (5.1 g) in pyridine (20 ml) for 10 min at 50 °C, and the reaction mixture was stirred for further 2 h at 60—65 °C. The precipitate formed on cooling and diluting with benzene (100 ml) was washed with benzene (50 ml×2). Then the filtrate was washed with 6% hydrochloric acid until it was acid to litmus, and saturated sodium chloride solution successively, and dried over sodium sulfate. The residual dark red liquid obtained after evaporation of the solvent was chromatographed on alumina (80 g) with light petroleum as eluent. Early fractions gave *cis-cis* isomer (VII) (35 mg, 6%) as unstable white crystals (mp 104—106 °C) which turned to brownish mixtures when exposed to air and light in neat state, IR (KBr disk): 2100 (-C≡C-), 1640, 1595 (C=C), 705 cm^{-1} (*cis* C=C), UV (EtOH): λ_{max} 248, 264 sh, 275, 308, 328, 355 sh nm, NMR: see Table 1. The following fractions afforded *trans-trans* isomer (VIII) (100 mg, 17%) as relatively stable white needles (from benzene), mp 172 °C (dec), Mass: *m/e* 268 (M^+, 30), 239 (100); mol. wt., 268.3, IR (KBr disk): 2100 (-C≡C-), 1640, 1595 (C=C), 930 cm^{-1} (*trans* C=C), UV (EtOH): λ_{max} (ε) 237 (30800), 258 sh (15500), 277 (20000), 311 (5960), 352 (7250), 353 nm (6790), NMR: see Table 1.

The authors wish to thank Dr. Terry M. Cresp, University College London, for kindly providing unpublished data, and Miss Chikako Uwai for experimental help. This research was supported by a Grant-in-Aid for Scientific Research from the Ministry of Education (974151, 1974), which is gratefully acknowledged.

References

1) J. Ojima, T. Yokomachi, and A. Kimura, *Bull. Chem. Soc. Jpn.*, **49**, 2840 (1976).

2) We tried to prepare the dichloride (III) by the reported method of the corresponding bromide (Ref. 6), but we could not get a satisfactory result. This procedure was given by Dr. Terry M. Cresp.

3) G. Eglinton and A. R. Galbraith, *Chem. Ind.*, **1956**, 737; *J. Chem. Soc.*, **1959**, 889.

4) J. Ojima, A. Kimura, Y. Yokoyama, and T. Yokoyama, *Bull. Chem. Soc. Jpn.*, **48**, 367 (1975).

5) Although the cause of failure of this reaction is not established, a similar result has been reported for attempts to obtain a higher vinylogue of IX, see, R. L. Wife and F. Sondheimer, *Tetrahedron Lett.*, **1975**, 195.

6) K. Dimroth, G. Pohl, and H. Follmann, *Chem. Ber.*, **99**, 634 (1966).

7) R. L. Wife and F. Sondheimer, *J. Am. Chem. Soc.*, **97**, 640 (1975).

8) M. H. Beeby and F. G. Mann, *J. Chem. Soc.*, **1949**, 1799.

BULLETIN OF THE CHEMICAL SOCIETY OF JAPAN, VOL. 49 (12), 3711—3712 (1976)

The Reaction of Benzofuran with Manganic Acetate

Akira KASAHARA, Taeko IZUMI, Akio SUZUKI, and Toru TAKEDA

Department of Applied Chemistry, Faculty of Engineering, Yamagata University, Yonezawa 992

(Received July 20, 1976)

Synopsis. The oxidation of benzofuran with manganic acetate in a mixture of acetic acid and acetic anhydride yielded four products: 2-(acetoxymethyl)benzofuran, 3a,8b-dihydrofuro[3,2-*b*]benzofuran-2(3*H*)-one, bis(2-benzofuranyl)methane, and 2-benzofuranylacetic acid.

Previously, Heiba *et al.*[1] reported a novel one-step synthesis of γ-lactones by the reaction of olefins with manganic acetate in acetic acid; they suggested that a free radical mechanism involving the selective generation and oxidation of organic free radicals is present. The oxidation of aromatic hydrocarbons by manganic acetate was also described by the same authors.[2]

It is considered that benzofuran (I) possesses a generally aromatic character, plus some characteristics of an enol ether. The present investigation deals with the manganic acetate oxidation of I.

Results and Discussion

In a mixture of acetic acid and acetic anhydride, I and manganic acetate were heated to reflux until the dark brown color of the Mn(III) had disappeared. 2-(Acetoxymethyl)benzofuran (**A**) and 3a,8b-dihydrofuro-[3,2-*b*]benzofuran-2(3*H*)-one (**B**) were obtained as the main products and bis(2-benzofuranyl)methane (**C**) and 2-benzofuranylacetic acid (**D**) as the minor products.

In general, the thermolysis of manganic acetate leads almost exclusively to the formation of $\cdot CH_2COOH$ radical.[2,3] Spagnolo *et al.*[4] reported that, in I, the attack by the free radicals mainly occurs at the 2-position. Consequently, in the reaction of I with manganic acetate, the attack by the $\cdot CH_2COOH$ radical most likely occurs at the 2-position of I; this mechanism is shown in Scheme 1. The mechanism to account for the formation of **B** and **D** is similar to the one suggested for the olefin-manganic acetate oxidation.[1] Heiba *et al.*[2] reported that the oxidation of anisole with manganic acetate leads to the formation of a mixture of *o*-, *m*-, and *p*-methoxybenzyl acetate, and also suggested that *o*-, *m*-, and *p*-methoxyphenylacetic acid, formed primarily from the reaction of anisole with $\cdot CH_2COOH$ radicals, are the precursors of these products. Van Der Ploeg *et al.*[3] also showed that phenylacetic acid is decarboxylated by manganic acetate, leading to the formation of benzyl radicals. Therefore, the formation of **A** and **C** may well be attributed to the reaction of **D** with manganic acetate, followed by the formation of 2-benzofuranylmethyl radicals.

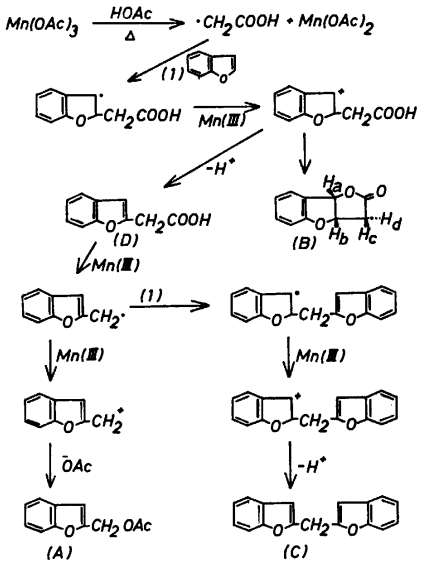

Scheme 1

Experimental

The melting and boiling points are uncorrected. The IR and mass spectra were measured using a Hitachi 215 spectrophotometer and a Model RMU-6M mass spectrometer at 70 eV. The NMR spectra were obtained on a Hitachi Model R-22 (90 MHz), using tetramethylsilane as an internal standard (δ, ppm). Column chromatography was carried out on Kanto-Kagaku silica gel.

Materials. The preparation of the following compounds has already been reported: manganic acetate dihydrate[2] and benzofuran (I).[5]

The Reaction of Benzofuran (I) with Manganic Acetate. A solution of I (9.44 g, 0.08 mol) in 50 ml of acetic acid was refluxed under nitrogen with 5.36 g (0.02 mol) of manganic acetate dihydrate, in the presence of 12 ml of acetic anhydride, until the brown manganic color disappeared. The reaction mixture was diluted with water and extracted several times with ether. The ether extracts were then dried and evaporated. The residue was chromatographed on silica gel with hexane as the eluent.

The first elution with hexane gave 0.40 g (42%[6]) of **A**, bp 156—157 °C/16 Torr. Found: C, 69.61; H, 5.37%. Calcd for $C_{11}H_{10}O_3$: C, 69.46; H, 5.30%. IR spectrum (oil film): 3030, 1740 (C=O), 1590, 1240 (-OAc), 830, 810, 760, 750 cm^{-1}. NMR spectrum: δ 1.95 (s, 3H, CH_3), 5.10 (s, 2H, CH_2), 6.62 (s, 1H, H on C_3), 7.00—7.50 ppm (m, 4H, H on benzene ring). Mass spectrum *m/e* (rel. intensity): 190 (22) (M^+ for $C_{11}H_{10}O_3$), 148 (10) ($M^+-CH_2=C=O$), 131 (100) (M^+-OAc). The physical constants and IR and NMR spectra were identical with those of 2-(acetoxymethyl)benzofuran, which was prepared by acetylation of 2-benzofuranylmethanol.[7]

The second elution with hexane gave 0.37 g (21%[6]) of **B**, mp 111—112 °C (ethanol). Found: C, 68.03; H, 4.38%. Calcd for $C_{10}H_8O_3$: C, 68.18; H, 4.58%. IR spectrum (KBr): 3050, 3000, 2980, 1770 (C=O), 1610, 1480, 1240 (O-C=O), 1040, 740 cm^{-1}. NMR spectrum: δ 2.95 (s, 1H, H_d), 3.00 (d, 1H, $J_{b,c}$=2 Hz, H_c), 5.35 (d-d, 1H, $J_{a,b}$=6 Hz,

$J_{b,c}$=2 Hz, H_b), 5.99 (d, 1H, $J_{a,b}$=6 Hz, H_d), 7.00—7.50 ppm (m, 4H, H on benzene ring). Mass spectrum *m/e* (rel. intensity); 176 (65) (M^+ for $C_{10}H_8O_3$), 131 (100) (2-benzofuranyl–CH_2^+). After hydrolysis of **B** with potassium hydroxide solution, the treatment of the reaction product with hot acetic anhydride led to 2-benzofuranylacetic acid, mp 97—98 °C.[8] From these results, **B** was identified as 3a,8b-dihydrofuro[3,2-*b*]benzofuran-2(3*H*)-one.

The following elution with hexane–benzene (1: 1) gave 0.042 g (3%[6]) of **C**, mp 73—74 °C (methanol). Found: C, 82.43; H, 4.96%. Calcd for $C_{17}H_{12}O_2$: C, 82.24; H, 4.87%. IR spectrum (KBr): 3050, 2930, 1600, 1580, 1445, 810, 790, 750 cm^{-1}. NMR spectrum: δ 4.18 (s, 2H, CH_2), 6.46 (s, 2H, H, on C_3 and C_3'), 7.10—7.50 ppm (m, 8H, H on benzene rings). Mass spectrum *m/e* (rel. intensity): 248 (15) (M^+ for $C_{17}H_{12}O_2$), 131 (100) (2-benzofuranyl–CH_2^+). **C** is identical in all respects with bis(2-benzofuranyl)methane, which was prepared by Wolff-Kishner reduction of bis(2-benzofuranyl) ketone.[9]

The elution with chloroform gave 0.032 g (0.2%[6]) of **D**, 2-benzofuranylacetic acid, mp 97—98 °C (lit,[7] mp 97—99 °C).

References

1) a) E. I. Heiba, R. M. Dessau, and W. J. Koehl, Jr., *J. Am. Chem. Soc.*, **90**, 5905 (1968); b) E. I. Heiba, R. M. Dessau, and P. G. Rodewald, *ibid.*, **96**, 7977 (1974); c) J. B. Bush, Jr. and H. Finkbeiner, *ibid.*, **90**, 5903 (1968).

2) E. I. Heiba, R. M. Dessau, and W. J. Koehl, Jr., *J. Am. Chem. Soc.*, **91**, 138 (1969).

3) R. E. Van Der Ploeg, R. W. DeKorte, and E. C. Kooyman, *J. Catal.*, **10**, 52 (1968).

4) P. Spagnolo, M. Tiecco, A. Tundo, and G. Martelli, *J. Chem. Soc. Perkin Trans. 1*, **1972**, 556.

5) A. W. Burgstahler and L. R. Worden, *Org. Synth.*, Coll. Vol. V, 251 (1973).

6) This calculation is based on the stoichiometry of 2 mol of manganic acetate/mol of **B** and **D** produced, and 4 mol of manganic acetate/mol of **A** and **C** obtained. This stoichiometry is required by the mechanism presented in this paper.

7) R. Gaertner, *J. Am. Chem. Soc.*, **73**, 4400 (1951).

8) R. B. Wagner and J. M. Tome, *J. Am. Chem. Soc.*, **72**, 3477 (1950).

9) T. Izumi, T. Takeda, and A. Kasahara, *Bull. of Yamagata Univ. Eng.*, **13**, (1), 193 (1974).

BULLETIN OF THE CHEMICAL SOCIETY OF JAPAN, VOL. 49 (12), 3713—3714 (1976)

Photo-induced Reaction of 2-Alkoxy-3-bromo-1,4-naphthoquinones with Acetylenes: Formation of 2-Aryl-substituted Naphtho[2,3-*b*]furan-4,9-diones

Tetsuo OTSUKI

Department of Chemistry, Faculty of Science, Kyoto University, Kyoto 606

(Received July 31, 1976)

Synopsis. 2-Aryl-substituted naphtho[2,3-*b*]furan-4,9-diones **3** were obtained as a major product in the photochemical reaction of 2-alkoxy-3-bromo-1,4-naphthoquinones with acetylenes.

The photochemical reaction of 2-alkoxy-3-bromo-1,4-naphthoquinones with several acetylenes has been investigated. One of the major products in the reaction was product **3**. Interestingly, the reaction product is of a quite different type from that of the reaction of 2-alkoxy-3-bromo-1,4-naphthoquinone with olefins.[1] Pappas and Farid,[2] on the other hand, have reported the photochemical reaction of 2-alkoxy-1,4-naphthoquinones with acetylenes, but their products were cyclobutene derivatives, which are different from those of the present reaction.

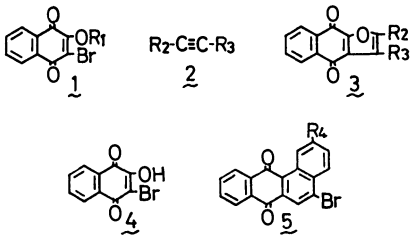

As a typical example, the photochemical reaction of 2-bromo-3-methoxy-1,4-naphthoquinone with phenylacetylene is described. On irradiating the benzene solution of 2-bromo-3-methoxy-1,4-naphthoquinone **1a** ($R_1=CH_3$) and phenylacetylene **2a** ($R_2=C_6H_5$, $R_3=H$) by means of a high pressure Hg arc lamp, 2-phenylnaphtho[2,3-*b*]furan-4,9-dione **3a** ($R_2=C_6H_5$, $R_3=H$) was obtained as a major product (63% yield), accompanying with **4** and **5a** ($R_4=H$). Otherwise, **3a** can be synthesized from 2-hydroxy-1,4-naphthoquinone and phenylacetaldehyde by four reaction steps,[3] but the overall yield is not so good (about 13%). Therefore, this photochemical reaction could provide a new synthetic route to 2-arylnaphtho[2,3-*b*]furan-4,9-diones, though the applicability is rather limited. The reductive acetylation of **3a** gave 4,9-diacetoxy-2-phenylnaphtho[2,3-*b*]furan. Product **4** is likely to be the by-product of a side-reaction since it is formed on irradiation of **1a** in benzene. The structure of **5a** ($R_4=H$), which is produced in trace, was deduced by comparison of its spectral data with those of benz[*a*]anthracene-7,12-diones.[1]

The similar reaction was found to proceed in other combinations of quinones and acetylene derivatives (Table 1). The change of relative yields of **3** against those of **4** would be explicable in terms of the reactivity of the acetylenes used. Diphenylacetylene **2g** ($R_2=R_3=C_6H_5$), for example, may be hard to react with **1**, presumably due to its steric requirements. The alkyl group lost in the course of the photochemical reaction was detected as ethyl bromide (GLC) in the case of the reaction of **1b** ($R_1=C_2H_5$) with **2a**. As mentioned above, Pappas and Farid and their co-workers obtained cyclobutene derivatives in the photochemical reaction of 2-alkoxy-1,4-naphthoquinones with acetylenes.[2] Their products were different from those of the present investigation; the difference probably originates from the presence of the labile C–Br bond in the quinones examined by the present author. The pathway of the present reaction may be formularized as the following:

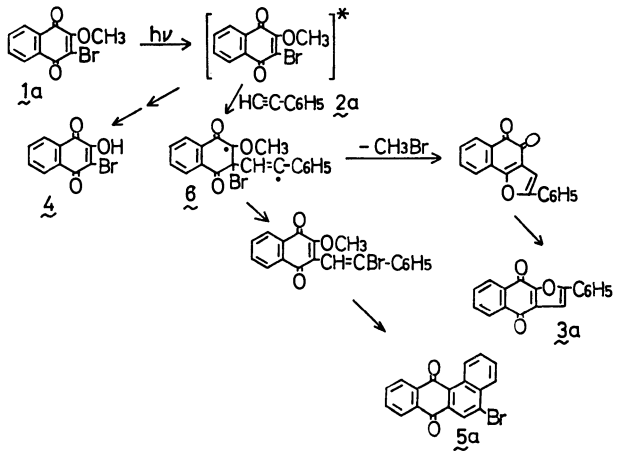

Table 1. The yield of the product in the photochemical reaction

1	2	3	4	5
1a ($R_1=CH_3$)	**2a** ($R_2=C_6H_5$, $R_3=H$)	**3a**: 63% ($R_2=C_6H_5$, $R_3=H$)	8%	**5a**: trace ($R_4=H$)
1a ($R_1=CH_3$)	**2b** ($R_2=p$-CH_3-C_6H_4, $R_3=H$)	**3b**: 38% ($R_2=p$-CH_3-C_6H_4, $R_3=H$)	10%	**5b**: 9% ($R_3=CH_3$)
1a ($R_1=CH_3$)	**2c** ($R_2=p$-C_2H_5-C_6H_4, $R_3=H$)	**3c**: 48% ($R_2=p$-C_2H_5-C_6H_4, $R_3=H$)	15%	**5c**: 4% ($R_4=C_2H_5$)
1a ($R_1=CH_3$)	**2d** ($R_2=p$-C_3H_7-C_6H_4, $R_3=H$)	**3d**: 45% ($R_2=p$-C_3H_7-C_6H_4, $R_3=H$)	16%	**5d**: 5% ($R_4=C_3H_7$)
1a ($R_1=CH_3$)	**2e** ($R_2=p$-*t*-C_4H_9-C_6H_4, $R_3=H$)	**3e**: 31% ($R_2=p$-*t*-C_4H_9-C_6H_4, $R_3=H$)	14%	**5e**: 6% ($R_4=t$-C_4H_9)
1a ($R_1=CH_3$)	**2f** ($R_2=C_4H_9$, $R_3=H$)	**3f**: 5% ($R_2=C_4H_9$, $R_3=H$)	47%	—
1a ($R_1=CH_3$)	**2g** ($R_2=R_3=C_6H_5$)	0	61%	0
1b ($R_1=C_2H_5$)	**2a** ($R_2=C_6H_5$, $R_3=H$)	**3a**: 7% ($R_2=C_6H_5$, $R_3=H$)	36%	**5a**: trace ($R_4=H$)

Experimental

Starting Materials. 2-Bromo-3-methoxy-1,4-naphthoquinone and 2-bromo-3-ethoxy-1,4-naphthoquinone were prepared by the bromination of the corresponding 2-alkoxy-1,4-naphthoquinones.[4] Phenylacetylene, diphenylacetylene, and 1-hexyne were commercially available and subjected to the reaction without further purification. The other acetylenes were synthesized from substituted acetophenones.[5]

General Procedure. The benzene solution (20 ml) of a 2-alkoxy-3-bromo-1,4-naphthoquinone (0.5 mmol) and an acetylene derivative (1.0 mmol) was irradiated by means of a high pressure Hg arc lamp (300 W). After the consumption of the quinone (about 8 h), the reaction mixture was extracted with saturated sodium hydrogencarbonate solution. From the alkaline soluble fraction, 2-bromo-3-hydroxy-1,4-naphthoquinone **4** was isolated.[6] On purification of the alkaline insoluble organic layer by using TLC on silica gel, 2-substituted naphtho[2,3-*b*]furan-4,9-dione **3** and 2-substituted 5-bromobenz[*a*]anthracene-7,12-dione **5** were obtained.

Identification of the Products. *2-Phenylnaphtho[2,3-b]furan-4,9-dione (**3a**)*: Red needles from benzene–hexane, mp 250.0—251.0 °C. Found: C, 78.60; H, 3.57%. Calcd for $C_{18}H_{10}O_3$: C, 78.82; H, 3.68%. Mass: *m/e*=274 (M^+). IR (KBr disk): 1670 cm^{-1} (C=O). NMR ($CDCl_3$): δ; 7.18 (1H, s), 7.34—7.54 (3H, m), 7.64—7.96 (4H, m), 8.14—8.30 ppm (2H, m). UVmax ($CHCl_3$): 421 nm (ε: 4.3×10^3), 290 (2.8×10^4), 270 (2.4×10^4).

*2-p-Tolylnaphtho[2,3-b]furan-4,9-dione (**3b**)*: Yellow plates from benzene–hexane, mp 266.5—267.0 °C. Found: C, 79.32; H, 4.31%. Calcd for $C_{19}H_{12}O_3$: C, 79.15; H, 4.19%. Mass: *m/e*=288 (M^+). IR (KBr disk): 1670 cm^{-1} (C=O). NMR ($CDCl_3$): δ; 2.40 (3H, s), 7.14 (1H, s), 7.16—7.40 (2H, m), 7.70—7.90 (4H, m), 8.16—8.36 ppm (2H, m). UVmax ($CHCl_3$): 437 nm (ε: 5.3×10^3), 295 (3.2×10^4), 273 (2.5×10^4).

*2-p-Ethylphenylnaphtho[2,3-b]furan-4,9-dione (**3c**)*: Yellow crystals, mp 186.0—189.0 °C. Mass: *m/e*=302 (M^+). IR (KBr disk): 1685 cm^{-1} (C=O). NMR ($CDCl_3$): δ; 1.24 (3H, t, J=8 Hz), 2.70 (2H, q, J=8 Hz), 7.16 (1H, s), 7.34 (2H, d, J=10 Hz), 7.70—7.90 (2H, m), 7.84 (2H, d, J=10 Hz), 8.12—8.32 ppm (2H, m).

*2-p-Propylphenylnaphtho[2,3-b]furan-4,9-dione (**3d**)*: Yellow crystals, mp 167.0—169.0 °C. Mass: *m/e*=316 (M^+). IR (KBr disk): 1665 cm^{-1} (C=O). NMR ($CDCl_3$): δ; 0.96 (3H, t, J=6 Hz), 1.70 (2H, m), 2.68 (2H, t, J=8 Hz), 7.16 (1H, s), 7.34 (2H, d, J=6 Hz), 7.72—7.90 (2H, m), 7.84 (2H, d, J=6 Hz), 8.08—8.16 ppm (2H, m).

*2-p-t-Butylphenylnaphtho[2,3-b]furan-4,9-dione (**3e**)*: Yellow crystals, mp 169.0—172.0 °C. Mass: *m/e*=330 (M^+). IR (KBr disk): 1660 cm^{-1} (C=O). NMR ($CDCl_3$): δ; 1.36 (9H, s), 7.16 (1H, s), 7.52 (2H, d, J=8 Hz), 7.68—7.84 (2H, m), 7.86 (2H, d, J=8 Hz), 8.10—8.30 ppm (2H, m).

*2-Butylnaphtho[2,3-b]furan-4,9-dione (**3f**)*: Yellow crystals, mp 160 °C. IR (KBr disk): 1680 cm^{-1} (C=O). NMR ($CDCl_3$): δ; 0.80—2.30 (9H, m), 6.42 (1H, s), 7.68—7.86 (2H, m), 8.04—8.22 ppm (2H, m).

*5-Bromo-2-methylbenz[a]anthracene-7,12-dione (**5b**)*: Yellow crystals from petroleum ether, mp 180.0—182.0 °C. Mass: *m/e*=352, 350 (M^+). IR (KBr disk): 1665 cm^{-1} (C=O). NMR ($CDCl_3$): δ; 2.62 (3H, s), 7.30—8.42 (7H, m), 9.84 ppm (1H, br s). UV max ($CHCl_3$): 414 nm (ε: 2.4×10^3), 364 (sh) (2.5×10^3), 333 (3.4×10^3), 290 (3.1×10^4), 251 (2.6×10^4).

*5-Bromo-2-ethylbenz[a]anthracene-7,12-dione (**5c**)*: Yellow crystals, mp 146.0—151.0 °C (dec). Mass: *m/e*=366, 364 (M^+). IR (KBr disk): 1665 cm^{-1} (C=O). NMR ($CDCl_3$): δ; 1.40 (3H, t, J=8 Hz), 2.98 (2H, q, J=8 Hz), 7.50—8.40 (7H, m), 9.62 ppm (1H, br s).

*5-Bromo-2-propylbenz[a]anthracene-7,12-dione (**5d**)*: Yellow crystals, mp 149.0—151.0 °C. Mass: *m/e*=380, 378 (M^+). IR (KBr disk): 1667 cm^{-1} (C=O). NMR ($CDCl_3$): δ; 1.02 (3H, t, J=6 Hz), 1.80 (2H, m), 2.90 (2H, t, J=8 Hz), 7.50—8.40 (7H, m), 9.80 ppm (1H, br s).

*5-Bromo-2-t-butylbenz[a]anthracene-7,12-dione (**5e**)*: Yellow crystals, mp 161.0—164.0 °C. Mass: *m/e*=394, 392 (M^+). IR (KBr disk): 1667 cm^{-1} (C=O). NMR ($CDCl_3$): δ; 1.52 (9H, s), 7.40—8.40 (7H, m), 9.98 ppm (1H, br s).

*The Reductive Acetylation of **3a**.* **3a** (10 mg) was refluxed with 3 ml of acetic anhydride and 100 mg of zinc dust for 30 min and filtered. The filtrate was poured into 10 ml of water and extracted with 20 ml of ether. Purification by using TLC on silica gel afforded 4,9-diacetoxy-2-phenylnaphtho[2,3-*b*]furan: white needles, mp 211—214 °C (yield: 54%). Mass: *m/e*=360 (M^+). IR (KBr disk): 1765 cm^{-1} (C=O). NMR ($CDCl_3$): δ; 2.56 (3H, s), 2.60 (3H, s), 6.96 (1H, s), 7.32—7.56 (5H, m), 7.76—8.00 ppm (4H, m).

The present author wishes to express his sincere gratitude to Professor Kazuhiro Maruyama, Kyoto University, for his fruitful suggestions and invaluable encouragements; he also thanks the Ministry of Education, Japan, for a Grants-in-Aid (No. 911503 and 943019).

References

1) K. Maruyama and T. Otsuki, *Chem. Lett.*, **1975**, 87. K. Maruyama, T. Otsuki, and K. Mitsui, *Bull. Chem. Soc. Jpn.*, **49**, 3361 (1976).

2) S. P. Pappas and N. A. Portnoy, *J. Org. Chem.*, **33**, 2200 (1968); S. Farid, W. Kothe, and G. Pfundt, *Tetrahedron Lett.*, **1968**, 4147.

3) S. O. Hooker and A. Steyermark, *J. Am. Chem. Soc.*, **58**, 1201 (1936).

4) L. F. Fieser and R. H. Brown, *J. Am. Chem. Soc.*, **71**, 3609 (1949).

5) L. I. Smith and H. H. Hoehn, *J. Am. Chem. Soc.*, **63**, 1175 (1941).

6) Th. Diehl and V. Merz, *Ber.*, **11**, 1066 (1878).

BULLETIN OF THE CHEMICAL SOCIETY OF JAPAN, VOL. 49 (12), 3715 (1976)

Synthesis of 1-Azido-5-methyl-4-hexen-2-one and Its Catalytic Dimerization

Takao KATAGIRI, Akira AGATA, Kunihiko TAKABE, and Juntaro TANAKA

Department of Synthetic Chemistry, Faculty of Engineering, Shizuoka University, Hamamatsu 432

(Received May 28, 1976)

Synopsis. 1-Azido-5-methyl-4-hexen-2-one was synthesized easily from 4-methyl-3-pentenenitrile which was prepared from isoprene. This compound is quite stable. Its catalytic dimerization gave 4,4-bis(3-methyl-2-butenyl)-2-butenolide.

Lokensgard *et al.*[2] studied the decomposition of 1-azido-3-cyclopentenyl-2-propanone and they proposed a mechanism for the decomposition. In this paper, the synthesis and the catalytic dimerization of an acyclic β,γ-unsaturated diazoketone, 1-azido-5-methyl-4-hexen-2-one (**1**), are reported.

The catalytic dimerization of **1** gave a main compound (**2**). The structure of **2** was confirmed to be as follows: The MS showed that **2** was the condensed dimer of **1**. The PMR spectrum showed that the two 3-methyl-2-butenyl groups were equivalent. Since the chemical shifts of the methylene in the above groups were in a higher field than that of **1**, the above groups did not attach to the next carbon of a carbonyl group. Moreover, the coupling constants of the lower olefinic protons (J=6.0 Hz) agreed with that of 2-butenolide.[3] In the IR spectrum, signals at 1750 cm^{-1} for the carbonyl in a five membered lactone and at 1790 cm^{-1} (as the shoulder) were observed, and **2** might be an α,β-unsaturated γ-lactone. From these data, **2** was identified as 4,4-bis(3-methyl-2-butenyl)-2-butenolide (**2**).

The mechanism of the formation of **2** might be as shown in the reaction scheme. Since the acid (**3**) could be obtained when the reaction was quenched with water at the early stage of the reaction, **2** may be produced through the intermediates (ii), (iii), and (iv) as suggested by Lokensgard *et al.*[2]

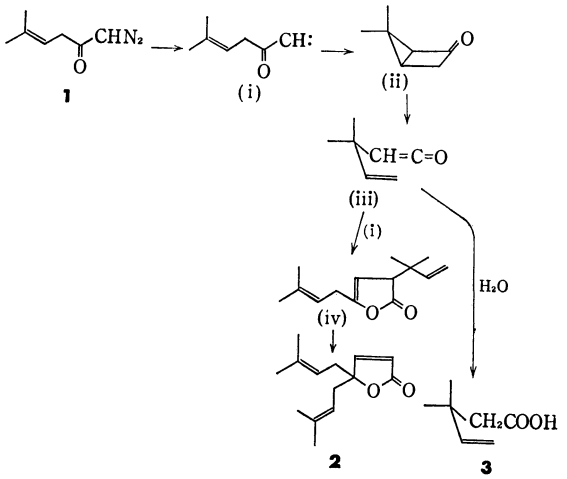

Experimental

Synthesis of 1-Azido-5-methyl-4-hexen-2-one (1). 1-Chloro-3-methyl-2-butene (60 g), which was prepared from isoprene,[4] was reacted with CuCN(45 g) in benzene (30 ml) in the presence of KI (0.5 g) at 10—20 °C for several hours. From the reaction mixture, 4-methyl-3-pentenenitrile was isolated by the fractional distillation (bp 62—63 °C/15 Torr, 26 g). The nitrile was hydrolyzed by 60 g of 30% aqueous KOH, and 23.7 g of 4-methyl-3-pentenoic acid was obtained. This acid was chlorinated with 30 g of thionyl chloride, and 4-methyl-3-pentenoyl chloride was obtained (bp 60—61 °C/20 Torr, 22.4 g). This chloride was dissolved in ether (30 ml) and the solution was added dropwise into an ether solution (50 ml) of diazomethane, which was prepared from 25 g of nitrosomethylurea, under cooling at 0—5 °C for 3 h. After the addition, the solution was kept at room temperature for 12 h. Careful distillation gave a yellow oil (bp 68—69 °C/3 Torr, 5.3 g). The oil was analyzed by GLC (Apiezon L, 100 °C) (98% purity). This showed the following spectral data: PMR (δ, CCl_4) 1.64 (s, 3H, $=CCH_3$), 1.76 (s, 3H, $=CCH_3$), 2.93 (d, 2H, J=7.0 Hz, $-CH_2-$), 5.12 (s, 1H, $-CHN_2$), 5.24 (t, 1H, J=7.0 Hz, $-CH=$). IR (cm^{-1}) 2110, 1640.

Catalytic Dimerization of 1. A benzene solution (30 ml) of **1** (5.8 g) was added dropwise to a suspension of 1.0 g of CuO in 100 ml of benzene under reflux with vigorous stirring. After the evolution of nitrogen ceased and the catalyst was removed by filtration, the product was distilled (bp 98—102 °C/3 Torr, 2.8 g). The GLC showed that this distillate contained 84% of a main compound (**2**).

4,4-Bis(3-methyl-2-butenyl)-2-butenolide (2): MS (*m/e*) 220 (M^+), 69 (Base ion, $C_5H_9^+$). PMR (δ, CCl_4) 1.62 (s, 6H, $=CCH_3$), 1.72 (s, 6H, $=CCH_3$), 2.41 (d, 4H, J=7.0 Hz, $-CH_2-$), 5.00 (t, 2H, J=7.0 Hz, $-CH=$), 5.94 (d, 1H, J=6.0 Hz), 7.23 (d, 1H, J=6.0 Hz). IR (cm^{-1}) 1750, 1790. Found: C, 76.22; H, 9.20%. Calcd for $C_{14}H_{20}O_2$: C, 76.32; H, 9.15%.

In the other run, when water was added to the reaction mixture as soon as the evolution of nitrogen ceased, a different fraction (bp 65—70 °C/3 Torr) than (**2**) was obtained (15% based on (**1**)). This fraction contained 3,3-dimethyl-4-pentenoic acid (**3**) mainly. (**3**): MS (*m/e*) 128 (M^+). PMR (δ, CCl_4) 1.20 (s, 6H, $-C(CH_3)_2$), 2.34 (s, 2H, $-CH_2-$), 5.06 (dd, 1H, J=1.5 Hz, and 10.5 Hz, $\begin{matrix}H\\ \diagdown\\ C=C\\ H\diagup \quad \diagdown H\end{matrix}$), 5.07 (dd, 1H, J=1.5 Hz and 18.0 Hz, $\begin{matrix}\quad H\\ \diagdown\\ C=C\\ H\diagup \quad \diagdown H\end{matrix}$), 6.07 (dd, 1H, J=10.5 Hz and 18.0 Hz, $\begin{matrix}\quad H\\ \diagdown\\ C=C\\ H\diagup \quad \diagdown H\end{matrix}$), 12.27 (s, 1H, $-COOH$). IR (cm^{-1}) 3450, 1710, 995, 915. Found: C, 65.55; H, 10.02%. Calcd for $C_7H_{12}O_2$: C, 65.59; H, 9.94%.

References

1) Studies on the Derivatives of Isoprene. VI. Preceding paper: T. Katagiri, T. Suzuki, K. Takabe, and J. Tanaka, *Nippon Kagaku Kaishi*, **1975**, 2246.

2) J. P. Lokensgard, J. O'Dea, and E. A. Hill, *J. Org. Chem.*, **39**, 3355 (1974).

3) R. Freeman, *Mol. Phys.*, **5**, 499 (1962).

4) J. Tanaka, T. Katagiri, and S. Yamada, *Nippon Kagaku Zasshi*, **87**, 877 (1966).